APPENDIX E

Supporting documents for Regional ASR Study groundwater model

1. **Numerical Model Development Support and Data Collection (CH2M Hill, 2005).**
2. **Bench-Scale Modeling Report (Brown et al., 2006)**
3. **Phase I Modeling Report and Figures (USACE, 2006)**
4. **Phase II Modeling Report, Figures, and Appendices (USACE, 2011)**
5. **ASR Regional Modeling Scenarios Report (USACE 2014)**

ASR Test Well Work Plan and Model Data Collection
Contract No. W912EP-05-D-0004
Delivery Order No. 1

Sub-Task No. 3 - Groundwater Numerical Model Development Support and Data Collection Report

Prepared for

U.S. Army Corps of Engineers, Jacksonville District

Submitted by:
CH2MHILL
4350 W. Cypress St., Ste. 600.
Tampa, FL 33607

December 2005

Contents

List of Appendices

List of Tables

Number

List of Figures

Number

List of Acronyms

APT	Aquifer Performance Test
ASR	Aquifer Storage and Recovery
BZ	Boulder Zone
CERP	Comprehensive Everglades Restoration Project
DWRM	District Wide Regulation Model
EC	East-Central
ETB	Eastern Tampa Bay
FAS	Floridan Aquifer System
ft/day	Feet per day
ft^2/d	Square feet per day
GLAUC	Glauconite marker
IAS	Intermediate Aquifer System
ICU	Intermediate Confining Unit
Kv	Vertical hydraulic conductivity
LEC	Lower East Coast
LFA	Lower Floridan Aquifer
LPZ	Lower permeable zone
LTA	Lower Tamiami Aquifer
MAP	Middle Avon Park
MCU	Middle confining unit
MF	Middle Floridan aquifer
mg/L	Milligrams per liter
MSCU	Middle semiconfining unit
SAS	Surficial Aquifer System
SD	Southern District
SFWMD	South Florida Water Management District
SJRWMD	St. Johns River Water Management District
SWFWMD	Southwest Florida Water Management District
SWUCA	Southern Water Use Caution Area
TDS	Total dissolved solids
TMR	Telescopic mesh refinement
UFA	Upper Florida Aquifer
UPZ	Upper permeable zone
USACE	U.S. Army Corps of Engineers
USGS	United States Geological Survey

Executive Summary

This report has been prepared for the U.S. Army Corps of Engineers (USACE) to convey the results of a technical review of numerical groundwater models, a review of the Preliminary Hydrogeologic Framework document, and a carbonate aquifer dispersion database study in support of the Comprehensive Everglades Restoration Project (CERP).

A document entitled *Preliminary Hydrogeologic Framework, October 4, 2004*, is an interim work product for the Aquifer Storage and Recovery (ASR) Regional Study. The report synthesized major regional works on the Floridan aquifer system (FAS) into a single comprehensive view of the hydrostratigraphy and hydraulic properties of the FAS from Orlando to Key West. It included 770 hydrostratigraphic picks from 392 wells. Eight cross sections were prepared from wells located in central to south Florida that had appropriate drilled depths and adequate geophysical logs for the purpose of this study. This document identified a newly recognized permeable zone in the FAS.

The USACE selected eight models from a list of 32 models submitted by CH2M HILL. The selected models provided an adequate coverage of the area of interest between Orlando and the Florida Keys. The models were evaluated and summarized for general areas corresponding approximately to the northern and southern regions of the Florida peninsula. Model similarities and differences were described. In addition, the models were compared to the hydrogeologic framework previously established through other studies conducted by the USACE, the South Florida Water Management District (SFWMD), and the United States Geological Survey (USGS).

As stated previously, a dispersion research study was conducted under the Subtask 3 scope of work for the USACE. The goal of this research effort was to provide dispersion data from sandstone and carbonate aquifers with a focus on technical sources from Florida and other similar geologic environments from the United States and the world. Based on the USACE's scope of work, technical papers, reports and other sources available to and obtained by CH2M HILL were reviewed and dispersion values were tabulated. In addition to the dispersion data, which were typically presented as longitudinal dispersivity, other pertinent information (where available) was also tabulated in the database for comparative purposes. These supplemental aquifer data include transmissivity, storativity, transverse dispersivity, molecular dispersivity, and aquifer name, matrix, thickness, and type.

Based on the data reviewed, CH2M HILL recommends construction of a 14-layer model to be run using finite-element groundwater modeling software. Of these 14 layers, seven layers will be used to simulate permeable zones. Three of these zones are identified to be studied further for development of potential ASR systems.

SECTION 1

Introduction

This report has been prepared for the U.S. Army Corps of Engineers (USACE) Jacksonville District and the South Florida Water Management District (SFWMD) in support of the Comprehensive Everglades Restoration Project (CERP). The scope of work for this report is based on Subtask 3 of the Aquifer Storage and Recovery (ASR) Test Well Work Plan Development and Model Data Collection (revised June 10, 2005; Contract No. W912EP-05-D-004). The final purpose of the study is to provide the USACE a baseline of conceptual model recommendations to build an initial Florida Peninsular model. This tool will be used to model the potential regional effects and aquifer behaviors of the CERP ASR implementation plan.

The purpose of this report is to convey the results of a technical review of eight numerical groundwater models selected by the USACE and compare this information to the known hydrogeology of Florida. The eight models were selected by the USACE from a list of 32 models prepared by CH2M HILL. Table 1 provides the list of models. The selected models provided an adequate coverage of the area of interest between Orlando and the Florida Keys. The model review areas correspond to the northern and southern regions of Florida, which are generally north or south of Lake Okeechobee, as shown on Figure 1. The reviews describe the similarities and differences between these models, both individually and regionally, and provide key information for USACE's consideration for future development of a peninsula-wide groundwater numerical model from Orlando to the Florida Keys. Table 2 presents a comparison of the reviewed groundwater model layering schemes. Recommendations on numerical model layering are provided in this report based on the model reviews included in Appendices A and B of this report with comparison to the *Draft-Final Report -Task 3.0. Define Preliminary Hydrogeologic Framework, October 4, 2004*, prepared by Ron Reese (USGS – Project lead) and Emily Richardson (SFWMD – Task lead).

Within Subtask 3, the USACE required the development of a groundwater dispersion database. A separate TM has been prepared and is included in Appendix C to document the results of a literature search and development of the groundwater dispersion database. The goal of this research is to provide dispersion data on primarily sandstone and carbonate aquifers with a focus on technical sources from Florida and other similar geologic environments from the United States and the world.

SECTION 2

Hydrogeologic Framework Document Review

Prepared by the USGS with assistance from the SFWMD, the *Draft-Final Report -Task 3.0. Define Preliminary Hydrogeologic Framework, October 4, 2004*, is an interim work product for the ASR Regional Study. The report synthesized major regional works on the Floridan aquifer system (FAS) into a single comprehensive view of the hydrostratigraphy and hydraulic properties of the FAS from Orlando to Key West. It included 770 hydrostratigraphic picks from 392 wells. Figure 2 presents the wells reviewed for this hydrogeological framework study. The sources of information evaluated through the study are included in Section 7, References.

The framework report provides a starting point for development of a hydrologic model of the FAS to plan, predict, and evaluate the potential impacts of future CERP ASR implementation. The objectives of the report were to:

1. Identify the differences in aquifer nomenclature and interpretation across the study area.
2. Establish stratigraphic framework through correlation of geophysical logs from key wells.
3. Correlate major aquifers and confining units, north to south, and east to west, across the study area.
4. Map bounding surfaces (top and bottom) of each hydrostratigraphic unit.
5. Classify available hydraulic parameter data according to the identified hydrostratigraphic units.
6. Map transmissivity and storativity for permeable zones, and vertical hydraulic conductivity for confining units

The interpretation of data assumed that the aquifers were continuous even though there appeared to be some question regarding correlation and aquifer continuity between points. For aquifer model development, a similar approach was recommended, but applying more conservative approaches in areas of greater uncertainty.

The report proposed the inclusion of a new informal hydrogeologic unit for the FAS, the "middle Floridan aquifer" (MF). The report concluded that the MF is regionally continuous, present above the Middle Avon Park (MAP) marker bed, that the permeability is associated with fractured dolostone within the Avon Park Formation (but may not be equally developed across the study area), and that the MF lies below the 10,000 milligrams per liter (mg/L) total dissolved solids (TDS) salinity boundary (in parts of the SWFWMD area). Figure 3 shows the relationship of the hydrogeologic units evaluated and the incorporation of the proposed MF.

The report identified several issues that may require additional resolution. These issues were:

1. Confinement between the MF and Lower Floridan Aquifer (LFA) permeable zones as mapped in this study could be poor in some areas of southern Florida.
2. In the western portion of the study area, particularly along the coast, the "Ocala Limestone-Avon Park Formation moderately permeable zone" was identified to have high transmissivity locally, and is used for injection of treated wastewater. In the study, the zone was often not included within the MF, but rather was included in the confining unit between the Upper Florida Aquifer (UFA) and the MF. The UFA extends only down to the top of or into the upper part of the Ocala Limestone in this area. However, in other areas of the state, treated wastewater injection activities are typically conducted in the Boulder Zone, where present, or in portions of the LF1 where seawater exists.
3. Confinement between the UFA and MF as mapped in this study could be poor in some areas of north-central and northeast Florida, especially in the area of the upper Kissimmee River Basin.
4. In the lower west coast area of the peninsula (i.e., Lee, Hendry, and Collier Counties), the elevation of the top of the UFA exhibits considerable variability with many pronounced high and low areas. Development of a map showing the thickness of the basal portion of the Hawthorn Group included in the UFA was recommended as a future task to identify the variations in the elevation.
5. The scale of the project necessitated that the Intermediate Confining Unit (ICU) or Intermediate Aquifer System (IAS) be mapped as a single unit, but they may contain significant aquifers within much of the study area, particularly along the west coast of the peninsula.

2.1 Hydrostratigraphic Units

As previously shown in Figure 3, the FAS is comprised of two major aquifers, the UFA and LFA, which are separated by the Middle Confining Unit (MCU). The MCU is also known as MC1 as defined by Reese (2004). Within the UFA and LFA are significant permeable zones such as the Lower Hawthorn Producing Zone, the MF, and the Boulder Zone (BZ). The following paragraphs describe the characteristics of each of these units as defined by Reese (2004).

2.1.1 Upper Floridan Aquifer

Good confinement is exhibited above the UFA as noted by artesian pressure. During drilling, lost-circulation zones or sudden increases in the rate of penetration often help to define the top of the UFA. However, smaller flow zones can occur above the large flow zone near the top of the UFA, but may not be included in the UFA due to their head, permeability, and position (thickness and degree of confinement provided by the unit separating them from the main flow zone). The top of the UFA often coincides with a formation boundary, but can occur over a wide range within the geologic section (e.g., from

within the lower part of the Hawthorn Group in southwest Florida to the upper part of the Avon Park Formation).

The base of the UFA or top of the MCU (MC1) can be gradational and difficult to define. The base of the UFA often occurs in the Avon Park Formation, but in the western part of the peninsula it commonly occurs near the top of the Ocala Limestone. In order to fill some large data gaps in the Southwest Florida Water Management District (SWFWMD), the elevation of the top of the Ocala Limestone was used as a surrogate for the top of the MCU in 47 wells evaluated in the study.

South of Lake Okeechobee, there is a notable lack of fully penetrating tests in the UFA primarily resulting from poor water quality and the development of the Surficial Aquifer System (SAS) or IAS in this area. In the lower west coast region, there are no fully penetrating tests south of the Caloosahatchee River. Similarly, eastward from Orlando, in the far northeastern portion of the study area, a rapid decline in water quality has discouraged development and therefore testing in the FAS.

Transmissivity (T) in the UFA decreases from coastal areas inland with an area of low T extending down the center of the peninsula from southern central Florida (T less than 5,000 square feet per day [ft^2/d]) to central southern Florida (T less than 15,000 ft^2/d). T in 4 coastal areas (Lee, Miami-Dade, St. Lucie-Martin, and Pinellas Counties) and in Orange County reaches 50,000 ft^2/d or greater. The area with highest T (greater than 50,000 ft^2/d and up to 100,000 ft^2/d) extends from Pinellas County inland across northeastern Manatee County and into northwestern Polk County.

Measured storativity values from 82 Aquifer Performance Tests (APTs) evaluated in the study from the UFA ranged from a low of $4.5x10^{-8}$ to a high of 0.4. Erroneously high estimates of storativity for highly anisotropic media (e.g., most flow from fractured rock, cavernous zones, or narrow bedding plane flow zones) in the very high transmissivity areas may be an artifact of the standard curve matching procedure for APT analysis. Erroneous estimation of storativity is likely due to high flow zones in the fractured or cavernous intervals that violate the assumption of radial flow to the well bore.

2.1.2 Middle Floridan Aquifer

The MF usually occurs within a thick section of the Avon Park Formation composed primarily of dolomitic limestone and sucrosic dolomite. The permeability in the MF is primarily associated with fracturing, but cavernous permeability can also be present. Lost circulation zones encountered while drilling often marks the MF. The thickness of the MF is commonly 300 or 400 feet, but it can be as thick as 500 or 600 feet. It reduces to 50 feet thick or less in the lower southwest Florida area.

Permeability in the MF appears to decline abruptly south of Lake Okeechobee. The MF has not been extensively evaluated south of Lake Okeechobee. The report indicated that it is particularly important to have values in this area because the closest measured values north of the Caloosahatchee River were very high.

In general, transmissivity in the MF has higher values than in the UFA, and has a T of more than 200,000 ft^2/d in four areas. Transmissivity is minimal (less than 5,000 ft^2/d) in most of southern Florida (south and west of Palm Beach County). The area with highest T is in

southwestern Florida, centered on a well in southern Desoto County (ROMP 12), where a T of 1,600,000 ft^2/d was reported. In Pinellas County, transmissivity was recorded as high as 1,200,000 ft^2/d.

Elimination of extreme values and partially penetrating tests left only 14 data points on which to base storativity. Unlike the UFA, the range and distribution of estimated storativity in the MF exhibits significant difference between fully penetrating and partially penetrating tests. The highest permeability in the MF is associated with a horizon of fractured dolomite. Erroneous estimation of storativity is likely due to high flow zones that violate the assumption of radial flow to the well bore (as previously noted).

2.1.3 Lower Floridan Aquifer

The uppermost permeable zone of the LFA (LF1 as defined by Reese, 2004) is defined as the first major permeable zone developed below the MAP marker, but above the glauconite marker (GLAUC) near the top of the Oldsmar Formation. LF1 occurs in the lower part of the Avon Park Formation in fractured dolostone, but tends to be more dense and massive. In some cases, the MF and LF1 may be separated by only a thin but apparently unfractured dolostone unit, and confinement between the MF and LF1 may not exist in some areas. Confinement can be very good in central and southwest Florida due to the occurrence of pore-filling anhydrite and gypsum.

Outside of greater metropolitan Orlando, where the LF1 is highly utilized for water supply, it is not possible to map the hydraulic properties of this zone with confidence. In Orange and Osceola Counties, transmissivity ranges from a low of 82,000 ft^2/d to a high of 688,000 ft^2/d. East of this area, water quality deteriorates rapidly and the LF1 is generally greater than 10,000 mg/L TDS. As a result, the LF1 production capability has not been tested in this area.

LF1 appears to thin significantly toward the coast in much of the study area. Model derived values for transmissivity of the LFA exhibited a similar eastward decline and a transmissivity of 1,360 ft^2/d was estimated at well BR1217. In general, transmissivity in LF1 is higher in southern Florida (greater than 80,000 ft^2/d). Transmissivity greater than 100,000 ft^2/d and up to almost 700,000 ft^2/d occurs in north-central Florida, centered in northwest Osceola and Orange Counties.

Geophysical logs from the Polk City core hole (POLKC 3_G) and Kaiser injection well (W-11424) in Polk County show little evidence of the high permeability exhibited in the LF (west of Osceola and central Orange County). Lithologic logs from both wells indicated the presence anhydrite infilling of pore spaces and it is assumed there is little to no permeability from that point down to the base of the FAS.

The report indicated that there are no aquifer performance tests in LF1 in southwest Florida (Lee, Collier, Glades, or Hendry Counties). Transmissivity was estimated at a number of wells in the SWFWMD based on the aquifer thickness, from the hydrostratigraphic surfaces generated in this study, and a hydraulic conductivity of 9.6 feet per day (ft/day) (as observed at the South Cross Bayou Injection well, W-17073). The report concluded that there was strong evidence to support poor to non-existent development of permeability in the LFA in SWFWMD, but southward, the LF1 is highly permeable based on observed drilling response, lithologic and geophysical logs. At the South Bay site, the results of an APT of LF1

(72 percent of the permeable zone tested) on the southern end of Lake Okeechobee produced a transmissivity value of almost 70,000 ft^2/d.

There are only two archived values of storativity in LF1 within the DBHYDRO database, with values of $1.2x10^{-5}$ and $2.6x10^{-5}$. In the absence of additional data, use of an average value of $2x10^{-3}$ was recommended.

2.1.4 Boulder Zone

The top of BZ, a zone of very high permeability in the lower part of the LFA, was also mapped in this study. The top of the BZ generally occurs one to several hundred feet below the GLAUC marker in the Oldsmar Formation, although there are some exceptions where the top is slightly above the marker. The BZ is not present in central Florida (north of Lee, Glades, and Okeechobee Counties in central Florida) except along the east coast. Similar to the uppermost permeable zone of the LFA, this zone is not developed along the coast in the northwest portion of the study area. BZ permeability ranges from fractured to cavernous, and both fractured limestone and dolostone can be present. Transmissivity for the BZ is in the order of 10^6 to 10^7 ft^2/d.

2.2 Confining Units

Three confining units were identified: the Middle Confining Unit 1 (MC1), the Middle Confining Unit 2 (MC2) and the Lower Confining Unit (LC). The report provided vertical hydraulic conductivity (Kv) data based on hydraulic well tests of confining units, leakance values determined from hydraulic well test of aquifers and core analysis data.

The MC1 separates the UFA and MF permeable zones. Kv of MC1 increases from the west coast, where it is approximately 0.1 ft/day or less, to the east coast, where it is greater than 1.0 ft/day, but less than 10 ft/day. The wells with core data in MC1 were very limited and were located primarily in the western portion of the peninsula. The MC2 separates the MF from the LFA permeable zones; Kv is lowest along both the east, and west coasts of Florida. Kv values range from less than 0.1 ft/day down to 0.01 ft/day. The LC separates LF1 from the BZ. Kv along the east coast of Florida is generally less than 0.1 ft/day and the data are poorly distributed.

SECTION 3

Numerical Model Review

Research was conducted to determine what models were available for review. The government agencies that assisted in providing information on available models were USACE, SWFWMD, St. Johns River Water Management District (SJRWMD), SFWMD, and USGS. A number of engineering consultant models were previously known or recently identified. Most, however, were not considered for placement on the list because these types of models typically are limited in hydrogeologic calibration outside of study area; limited in geological layering accuracy on a regional scale; and in most cases have not been subject to regulatory peer review. For these reasons, only published models, which were constructed by or for governmental agencies, were listed. The following eight models were selected by the USACE for review from among 32 available models:

- Eastern Tampa Bay Model (Barcelo and Basso, 1993)
- Lee County Model (Bower, et al., 1990)
- Lower East Coast Model (Fairbank, et al., 1999)
- Peninsular Florida Model (Sepulveda, 2002)
- Southern District Model (Beach and Chan, 2003)
- East-Central Model (McGurk and Presley, 2002)
- HydroGeoLogic Model (HydroGeoLogic, 2002)
- SWFWMD District Wide Regulatory Model (ESI, 2004)

The models were divided into two groups for review. The first group included the southwest Florida area. The second model review group included the southeast Florida area. This grouping allowed for better model comparisons in similar areas. These model areas were also compared to the *Draft-Final Report -Task 3.0. Define Preliminary Hydrogeologic Framework, October 4, 2004* document to determine how the model layering compared to actual field information. Two model review TMs were produced, one each for the southwest and southeast areas, and are provided in Appendixes A and B, respectively. The conclusions from these TMs were then also compared to each other and to the *Draft-Final Report -Task 3.0. Define Preliminary Hydrogeologic Framework, October 4, 2004* to provide the study area conceptual model recommendations contained in this report.

3.1 Southwest Florida Region Model Review

The area of focus for four of the five models in this group is generally the SWFWMD jurisdictional area. The fifth model (Sepulveda, 2002) includes most of the Florida peninsula. The five models reviewed for the southwest region of Florida were:

- Eastern Tampa Bay Water Use Caution Area Model (Barcelo and Basso, 1993)

- Peninsular Florida Model (Sepulveda, 2002)
- Southern District of SWFWMD (Beach and Chan, 2003)
- HydroGeoLogic Model (HydroGeoLogic, 2002)
- SWFWMD District Wide Regulatory Model (ESI, 2004)

As presented previously, Table 2 provides a comparison of the reviewed groundwater model layering schemes. The TM prepared for the review of these five models is provided in Appendix A. A brief summary, general observations, and any limitations for each model are provided below.

3.1.1 Peninsular Model (Sepulveda, 2002)

This model is a compilation of 17 local numerical models. The purpose of the Peninsular Model was to: (1) test and refine the conceptual understanding of the regional groundwater flow system; (2) develop a database to support sub regional groundwater flow modeling; and (3) evaluate effects of projected 2020 groundwater withdrawals on groundwater levels. The four-layer model was based on the computer code MODFLOW-96, developed by the USGS. The top layer consists of specified-head cells simulating the SAS as a source-sink layer. The second layer simulates the IAS in southwest Florida and the ICU where it is present. The third and fourth layers simulate the UF and LFA, respectively. Steady-state groundwater flow conditions were approximated for time-averaged hydrologic conditions from August 1993 through July 1994 (1993-1994). This period was selected based on data from UF wells equipped with continuous water level recorders. The grid used for the groundwater flow model was uniform and composed of square 5,000-foot cells, with 210 columns and 300 rows.

The active model area, which encompasses approximately 40,800 square miles in peninsular Florida, includes areas of various physiographic regions classified according to natural features. Hydrogeologic conditions vary among physiographic regions, requiring different approaches to estimating hydraulic properties for different areas. The elevations of water levels for the SAS and heads in the UFA, for time-averaged 1993-1994 conditions, were computed by using multiple linear regressions of measured water levels in each of the physiographic regions. The model documentation should be consulted for additional explanation of the regression technique.

Groundwater flow simulation was limited vertically to depths containing water with chloride concentrations less than 5,000 mg/L. Groundwater flow in areas where chloride concentration exceeds 5,000 mg/L was not considered to be part of the flow system in this study. Flow across the interface represented by this chloride concentration was assumed to be negligible.

The groundwater flow model was calibrated using time-averaged data for 1993-1994 at 1,624 control points, flow measurements or estimates at 156 springs in the study area, and base-flow estimates of rivers in the unconfined areas of the UFA obtained by using a generalized hydrograph separation of recorded discharge data. Transmissivity of the IAS, UFA, and LFA; leakance of the upper and lower confining units of the IAS, the ICU, the MCU, and the MSCU; spring and riverbed conductances; and net recharge rates to

unconfined areas of the UFA were adjusted until a reasonable fit was obtained. The active model area encompasses approximately 40,800 square miles in peninsular Florida from Charlton and Camden Counties in Georgia to near the Palm Beach County – Martin County line in south Florida. The west-to-east extent of the study area spans approximately 200 miles from the Gulf of Mexico to the Atlantic Ocean.

3.1.2 Southern District Model (Beach and Chan, 2003)

The Southern District (SD) Model simulates ground-water flow in the major artesian aquifers of the southern half of the SWFWMD, which covers all or parts of 16 counties in west-central Florida. The model is based on the finite-difference, numerical code MODFLOW. The SD Model described here is calibrated to 1993, annual-average, steady-state conditions with a specified-head water table. A verification of transient response was made with a transient simulation for monthly conditions for the period January 1992 through December 1993. The SD Model represents an enlargement of the Eastern Tampa Bay (ETB) Model that was developed to assess groundwater resources within the Eastern Tampa Bay Water Resource Assessment Project (1993) area of southern Hillsborough, Manatee, and northern Sarasota Counties. The ETB Model was also used by the SWFWMD for analysis of groundwater resource conditions in the Southern Water Use Caution Area (SWUCA), which was comprised of all, or parts of the eight counties in the southern half of the SWFWMD. The SD Model is designed specifically to simulate groundwater resource conditions in the SWUCA, thereby overcoming the major limitations of the ETB Model, particularly with respect to boundary conditions.

3.1.3 Eastern Tampa Bay Model (Barcelo and Basso, 1993)

The ETB Model includes all of Manatee, Hardee, Sarasota and Desoto Counties and parts of Hillsborough, Pinellas, Polk, Charlotte, Glades and Highlands Counties. The ETB Model is an earlier version of the SD Model (Beach and Chan, 2003), which was previously discussed. The SD Model extends beyond the boundaries of the ETB Model to include Pasco and Hernando Counties to the north and Lee County to the south. Groundwater in the study area occurs in three principal aquifers: the SAS, the IAS, and the UFA. The aquifers are separated by clay confining units that restrict the vertical movement of water. Recharge to the UFA primarily results from rainfall that infiltrates the land surface and percolates downward through the SAS and IAS. Leakage occurs across the semiconfining beds that separate the IAS and SAS, and the IAS and the UFA. Although the UFA has two major producing zones, the aquifer is conceptualized as a single hydrologic unit. Regional groundwater flow in the UFA occurs predominantly in the lower permeable zone (LPZ). The IAS and UFA are simulated as single layer isotropic mediums with groundwater moving in horizontal planes. Horizontal flow in the confining beds is negligible compared to horizontal flow in the adjacent aquifers. Storage of water in the confining beds is negligible. Movement of the saltwater interface is assumed to have little effect on calculated heads. Heads in the SAS are assumed insensitive to changes in stress in the underlying aquifers.

The ETB Model is based on the numerical, finite-difference code MODFLOW, which was developed by McDonald and Harbaugh (1984 and 1996). Both steady-state and transient conditions were simulated by the model. Average groundwater resource conditions for the

year 1989 served as the target for the steady-state model. For the transient simulations, the model was calibrated to hydrologic conditions from October 1988 through September 1989.

The SD Model is divided into three layers:

- Layer 1: SAS
- Layer 2: IAS
- Layer 3: UF

The model grid is oriented along the north-south axis with uniform grid spacing of 2 miles x 2 miles, and consisting of 56 rows and 60 columns.

3.1.4 HydroGeoLogic Model (HydroGeoLogic, 2002)

The HydroGeoLogic Model is based upon the SD Model (Beach and Chan, 2003) discussed previously and an uncalibrated, saltwater intrusion model that was developed by Waterstone Environmental Hydrology and Engineering, Inc. (Waterstone). The domain of the HydroGeoLogic Model includes the southern half of Hillsborough County and all of Manatee and Sarasota Counties. The HydroGeoLogic Model is a smaller subset of the SD Model in terms of geographic area. The simulated area coincides with the domain of the Waterstone Model. Hydraulic properties and boundary conditions were assumed from the SD Model, while the model domain, grid spacing, and layer thicknesses were assumed from the Waterstone Model.

The hydrogeologic framework for this model is the same as discussed in the SD Model. The local groundwater flow system is comprised of three, vertically sequenced aquifer systems and their intervening semi-confining units. In descending order, these aquifer systems are the unconfined SAS, the confined IAS, and the confined UFA. Like the SD Model, the LFA is not considered because it contains highly mineralized groundwater and is not utilized for water supply.

The hydrogeologic framework was conceptualized as 10 layers in the HydroGeoLogic Model. In order to simulate density dependant flow and transport, intervening semi-confining layers must be explicitly modeled rather than using arrays of leakance. Hydraulic conductivity and thickness must therefore be specified for each aquifer and semi-confining unit. The Suwannee Limestone, Ocala Limestone, and Avon Park Formation are subdivided into two, three, and five finite-difference layers, respectively. These layers explicitly simulate permeable units and semi-confining units that have been identified in the three formations. The uppermost formation in the HydroGeoLogic Model is the Suwannee Limestone. Only the UFA was simulated in the HydroGeoLogic Model. Rather than explicitly incorporating the SAS and IAS/ICU into the density-dependant model, vertical flow through these aquifers is simulated by specifying a general-head boundary condition at the top of the upper permeable zone (UPZ) within the Suwannee Limestone. Hydraulic heads for the SAS and leakance values in the SD Model were used to calculate the general-head boundary conditions.

3.1.5 SWFWMD District Wide Regulatory Model (ESI, 2004)

The goal of this modeling effort was two-fold. First, develop a District-Wide Regulation Model (DWRM), which is a modified version of the USGS model of the IAS and FAS in Peninsular Florida (Sepulveda, 2002) covering the entire SWFWMD plus a buffer area surrounding the SWFWMD. The USGS model developed by Sepulveda is known as the Peninsular Model and was described previously. The second goal was to develop a modified telescopic mesh refinement (TMR) technique that would streamline the SWFWMD's review of Water Use Permits.

The DWRM approach was to use the Peninsular Model as a starting point and activate the SAS layer, which the USGS treated as an array of constant heads. The boundary of the new model was the SWFWMD boundary plus a buffer area of approximately 10 miles so that permits at the edge of the SWFWMD boundary could be evaluated. Because the original Peninsular Model did not extend fully to the southern boundary of the SWFWMD, 22 rows were added to the DWRM. The southern boundaries of the DWRM were made to coincide with the SD Model.

The hydrogeologic framework is the same as the Peninsular Model. The SAS is the uppermost water-bearing hydrogeologic unit. The SAS extends throughout most of the study area, except where the UFA is unconfined. The IAS underlies the SAS and extends throughout most of southwest Florida. Confining beds that overlie the UFA and underlie the SAS limit the vertical extent of the IAS in west-central Florida.

The FAS is a thick sequence of limestone and dolomitic limestone of Oligocene and Eocene ages with highly variable permeability. The FAS is divided into two aquifers of relatively high permeability, referred to as the UFA and the LFA. These aquifers are separated by a less permeable unit called the MCU in west-central Florida and in the northwest part of the study area, and the MSCU in east-central Florida. The top of the UFA coincides with either the top of the Suwannee Limestone or the top of the Ocala Limestone, depending upon location. Rather than a single-low permeability unit separating the UFA and LFA, several units of regional extent separate the UFA from the LFA. Any of the regionally extensive low-permeability units may contain thin layers of moderate to high permeability. These confining units are not continuous and do not necessarily consist of the same rock type everywhere.

The conceptual ground-water flow system is the same as the Peninsular Model except that the SAS (Layer 1) is actively simulated in the DWRM. In the Peninsular Model, the SAS was simulated as an array of constant heads. The SAS, IAS (or ICU in areas where the IAS is absent), the UF and the LFA were designated layers 1 through 4, respectively. Confining layers were simulated by using vertical leakance arrays. Model-simulated groundwater flow occurs horizontally within the aquifers and vertically through the confining units.

The IAS (Layer 2) in was simulated as a single active aquifer bounded above and below by arrays of leakance values. Because this model is restricted to simulating the movement of freshwater within the aquifers; areas where the IAS, the UFA and the LFA (Layers 2, 3, and 4) contain water with chloride concentrations exceeding 5,000 mg/L are considered inactive. Recharge to or discharge from the IAS is assumed to occur through the upper or lower confining units of the IAS.

The MCU was represented by vertical leakance values that limit water exchange between the UF (Layer 3) and the LFA (Layer 4) in west-central and southwest Florida.

The DWRM is based on the numerical, finite-difference code MODFLOW, which was developed by McDonald and Harbaugh (1984 and 1996). MOPDFLOW96 was the version of MODFLOW used for the DWR Model. Steady-state conditions were simulated by the model. Average groundwater resource conditions from August 1993 through July 1994 served as the target for the steady-state model.

The DWRM is divided into 4 layers.

- Layer 1: SAS
- Layer 2: IAS
- Layer 3: UFA
- Layer 4: LFA

The model grid is oriented along the north-south axis. All model cells are 5,000 feet by 5,000 feet, with 210 columns and 322 rows.

3.2 Comparison of Southwest Group of Models

The Peninsular Model extends from Charlton and Camden Counties in south Georgia to near the Palm Beach County – Martin County line in south Florida. The SD Model encompasses a smaller area, from Hernando County to the north and Lee County to the south and from the Gulf of Mexico on the west to the Kissimmee River on the east. The ETB Model is an earlier version of the SD Model and includes a smaller area, extending from Hillsborough County to the north to Charlotte County in the south, from the Gulf of Mexico on the west to Polk County on the east. The SD Model area includes all of the ETB Model area, while the Peninsular Model includes the areas of both the ETB Model and the SD Model. The DWRM is a smaller subset of the Peninsular Model and coincides with the boundaries of the SWFWMD plus a buffer zone of approximately 10 miles on all sides. The HydroGeoLogic Model is a smaller subset of the SD Model and includes the southern half of Hillsborough County and all of Manatee and Sarasota Counties. Unlike the other models, the HydroGeoLogic Model simulates solute transport and density-driven groundwater movement. All five models are finite-difference models.

Three aquifer systems are present within the area simulated by the five groundwater models. The SAS is the uppermost water-bearing hydrogeologic unit. The SAS mostly consists of variable amounts of sand, clay, sandy clay, shell beds, silt, and clay. The SAS extends throughout most of the study area, except where the UFA is unconfined. The IAS underlies the SAS and extends throughout most of southwest Florida. The unit consists mainly of clastic sediments interbedded with carbonate rocks that generally coincide with the Hawthorn Group. Confining beds that overlie the UFA and underlie the SAS limit the vertical extent of the IAS in west-central Florida. In the absence of significant permeable zones, the IAS is defined as the ICU. The ICU is present outside of west-central Florida, wherever the IAS pinches out. The UFA is considered unconfined in areas where the ICU or IAS is absent or very thin.

The FAS is a thick sequence of limestone and dolomitic limestone of Oligocene and Eocene ages with highly variable permeability. The FAS is generally divided into two aquifers of relatively high permeability, referred to as the UFA and the LFA. These aquifers are separated by a less permeable unit called the MCU in west-central Florida and in the northwest part of the study area, and the MSCU in east-central Florida. The top of the UFA coincides with the top of the Tampa Member, Suwannee Limestone or Ocala Limestone, depending upon location. The bottom of the UF is the top of the shallowest, significant, regional confining unit.

In east-central Florida, the UFA and LFA are separated by the MSCU, a sequence of somewhat permeable, soft, chalky, limestone that locally contains some gypsum and chert and commonly is partially dolomitized. In west-central Florida and in the northwest part of the study area, the UFA and LFA are separated by the MCU, which is composed of gypsiferous dolomite and dolomitic limestone of considerably lower permeability than that of the MSCU in east-central Florida.

Two discrete permeable zones have been defined in the UFA. The UPZ has been identified within sections of the Suwannee Limestone and the Tampa Member of the Arcadia Formation. The LPZ of the UFA has been identified within the lower part of the Ocala Limestone and the upper part of the Avon Park Limestone. The Ocala Limestone occurs between the Suwannee Limestone and the Avon Park Formation and is thought to function as a semi-confining unit between the UPZ and LPZ.

Two discrete permeable zones have been identified in the LFA in northeast Florida. They consist of an upper permeable zone (LF1) and lower Fernandina permeable zone (FPZ). In south Florida, two permeable zones have been identified. The upper producing zone (LF1) is found within the lower portion of the Avon Park Formation below the MCU, while the lower producing zone is found in the Oldsmar Formation. The lower producing zone is known as the Boulder Zone due to drilling characteristics, and is known for extremely high transmissivity.

The Peninsular Model includes four layers: the SAS, IAS (ICU), UFA and LFA. Layer 2 is either the IAS or ICU, depending upon location. The UPZ and LPZ of the UFA are simulated as one layer (Layer 3) given the evidence that there is significant hydraulic connection between the units. Layer 4 is the LFA, which is not simulated in the SD Model or the ETB Model. In west-central Florida where the SD Model and ETB Model are situated, groundwater in the LFA is highly saline. As a result, the LFA is not simulated in those area models.

The SD Model explicitly simulates separate permeable zones found in the IAS in west-central Florida. Permeable zones known locally as PZ2 and PZ3 are simulated as Layers 2 and 3, respectively. In contrast, the Peninsular Model utilizes one layer to simulate the IAS. Layers 4 and 5 of the SD Model simulate the UPZ and LPZ of the UFA. The Peninsular Model utilizes one layer to simulate the UFA. The LFA, which the Peninsular Model simulates, is not simulated by the SD Model.

The ETB Model has three layers, which simulate the SAS, the IAS, and the UFA. The LFA is not simulated nor are multiple zones of permeability in the IAS or UFA. All four models indirectly simulate semi-confining units and confining units with arrays of leakance values.

The DWRM is very similar to and is based on the Peninsular Model. Like the Peninsular Model, the DWRM consists of four layers. Layer 1 is the SAS. Layer 2 is the IAS and Layer 3 is the UFA. Layer 4 is the LFA. Unlike the Peninsular Model, which utilizes constant heads to simulate the SAS, the SAS is actively simulated in the DWRM. Layer 2 of the DWRM simulates PZ3 of the IAS, whereas Layer 2 of the Peninsular Model simulates the average of PZ2 and PZ3 of the IAS. The SD Model simulates PZ2 and PZ3 as separate layers. Another similarity between the Peninsular Model and the DWRM is that the base of the model is the 5,000 mg/L chloride concentration. Strata that contain groundwater with a chloride concentration in excess of 5,000 mg/L are not simulated. In west-central Florida, the LFA is highly mineralized and therefore is not simulated by either model.

The HydroGeoLogic Model is different from the other four models in that it is designed to simulate density-driven, solute transport processes. The HydroGeoLogic Model is based on the SD Model, but covers a smaller geographic area consisting of southern Hillsborough County, Manatee County, and Sarasota County. A notable difference between the two models is that the semi-confining units are explicitly simulated in the HydroGeoLogic Model as separate model layers. The other four models simulate advective groundwater movement and represent semi-confining units with arrays of leakance. The semi-confining units are not directly simulated with model layers. Ten layers are used in the HydroGeoLogic Model to simulate the permeable and less permeable units in the Suwannee Limestone, Ocala Limestone, and Avon Park Formation. The SAS and IAS are not simulated directly in the HydroGeoLogic Model. General-head boundary cells are used instead to simulate the movement of water vertically into the Suwannee Limestone, which is the top of the model. The bottom of the model is the MCU. Two model layers are used to simulate the Suwannee Limestone, while three layers are used to simulate the Ocala Limestone. Five layers are used to simulate the Avon Park Formation. The primary purpose of the HydroGeoLogic Model is to simulate the movement of the saltwater/freshwater interface and the vertical movement of saline water in order to make sound decisions regarding permit applications. Likewise, the primary purpose of the four advective transport models is to simulate potential impacts to the various aquifer systems without consideration of density differences in the groundwater.

3.3 Southeast Florida Region Model Review

The southeast region of Florida generally included the central area around Orange County, southwest Florida around Lee County, and east to Broward County. The area of focus was generally the SFWMD jurisdiction. The three models reviewed for the central and south region of Florida were:

- Lee County Model (Bower, et al., 1990)
- Lower East Coast Model (Fairbank et al., 1999)
- East-Central Model (McGurk and Presley, 2002)

Presented previously, Table 2 provides a comparison of the reviewed groundwater model layering schemes. The TM prepared for the review of these three models is provided in Appendix B. A brief summary, general observations, and any limitations for each model are provided below.

3.3.1 Lee County Model (Bower et al., 1990)

The Lee County Model was created to be used for predictive purposes when evaluating requests for large groundwater withdrawals and to serve as a basis for groundwater management planning in Lee County. The three aquifer systems within the study area are the SAS, IAS, and UFA. The SAS includes the unconfined water table aquifer and the lower Tamiami aquifer. The IAS includes the Sandstone Aquifer and Mid-Hawthorn Aquifer, and associated semi-confining units. The UFA includes the Lower Hawthorn Aquifer and deeper permeable zones.

The Lee County Model extends over 2,000 square miles and consists of seven layers to simulate the SAS, the IAS, and the UFA. Cells in the interior of the model are 1 mile square. Cells on the north and west sides of the model were expanded to reduce boundary effects seen during early calibration attempts.

3.3.2 Lower East Coast Floridan Aquifer Model (Fairbank et al., 1999)

This three-dimensional steady-state model was created for the Lower East Coast (LEC) Planning Area. The LEC Model covers 16,434 square miles and has none layers with a uniform grid spacing of 1 mile. The model simulates three primary flow zones, two within the UFA and a third in the LFA. Flow Zone 1 includes permeable zones at or near the top of the Avon Park Formation and the Ocala Limestone (Layer 3). Flow Zone 2 includes permeable zones within the upper part of the Avon Park Formation (Layer 5). Flow Zone 3 includes the shallowest producing intervals at or near the top of the Oldsmar Formation (Layer 7). Low permeability units between the primary flow zones are included explicitly in this model as individual layers. Additionally, the SAS and the BZ are included as constant head boundaries at the top and bottom of the model. Water quality in the UFA in the area of the model varies, causing density differences which affect groundwater flow. The model utilizes "fresh-water equivalent head values" to account for this water quality variation.

3.3.3 East-Central Floridan Aquifer Model (McGurk and Presley, 2002)

This three-dimensional steady-state model was created, expanding on previous regional models covering all or parts of Orange, Seminole, Brevard, Lake, Osceola, Marion, Polk, Sumter, and Volusia Counties. The East-Central (EC) Model covers 7,568 square miles, has uniform 2,500-foot square cells, and has four layers. The layers corresponded to the SAS, UFA (two layers), and LFA.

In this area, drainage wells provide significant man made source of recharge to the FAS. These injection wells are numerous in the model. Data utilized to create this detailed model came from many sources. Rainfall, surface water data, observation and test well data, groundwater withdrawal data, wastewater treatment plant flows and reuse data were obtained from agencies and reports on previous models and studies.

3.4 Comparison of Southeast Group of Models

The LEC Model utilizes nine layers to simulate the SAS, UFA, and LFA. The IAS is not simulated because it is not present within the model area. Semi-confining units within the LEC Model are explicitly simulated as separate layer, whereas they are implicitly simulated

with leakance arrays in the EC Model and Lee County Model. Two permeable zones in the UFA are simulated in the LEC Model. The LFA is simulated as one permeable zone with one active layer. The EC Model utilizes four layers to simulate the SAS (Layer 1), UFA (Layers 2 and 3) and LFA (Layer 4). As with the LEC Model, the IAS is not present in the model area and is not simulated. The Lee County Model uses seven layers to simulate the SAS, the IAS, and UFA. The LFA is not simulated. In Lee County, the IAS is a significant source of water supply and consists of two permeable zones: mid-Hawthorn Aquifer and Sandstone Aquifer. The SAS also consists of two permeable zones: the unconfined water table aquifer and the confined Lower Tamiami Aquifer. The UFA is simulated as two active permeable zones: Lower Hawthorn Aquifer and the Suwannee Aquifer.

The MF is not simulated in the three models. The Lee County Model simulates two active permeable units in the UFA, whereas the LEC Model simulates two permeable units in the UFA and one active permeable unit in the LFA. The EC Model, like the LEC Model, simulates two permeable units in the UFA and one permeable unit in the LFA. None of the model documentation mentions the MF.

SECTION 4

Dispersion Research and Database

The goal of this research effort was to provide dispersion data on primarily sandstone and carbonate aquifers with a focus on technical sources from Florida and other similar geologic environments from the United States and other areas of the world. Based on the USACE's scope of work, technical papers, reports and other sources available to and obtained by CH2M HILL were reviewed and dispersion values were tabulated. In addition to the dispersion data (which was typically presented as longitudinal dispersivity), other pertinent information, where available, was also tabulated in the database for comparative purposes. This supplemental aquifer data include: transmissivity, storativity, transverse dispersivity, and molecular dispersivity, and aquifer name, matrix, thickness, and type. The dispersion study TM and information database is provided in Appendix C.

Dispersion values for other sedimentary, igneous and metamorphic aquifer matrixes have also been included and may be useful for evaluation of fractured flow through dolomite, where applicable. CH2M HILL was able to obtain dispersion data from primarily domestic technical publications, which were limited in number. To supplement dispersion data from foreign sources, CH2M HILL contracted Nerac, Inc., an outside research service. The combined research effort generated 40 literature sources from which the dispersion data were obtained and tabulated.

Very few of the documents had physical data on dispersivity based on tracer or other in-situ testing. Many of the dispersivity values presented in the cited literature were estimated, established from other sources, or where the results of groundwater model calibration. It was also noted that the differences in the ranges of dispersivity values depended on how the coefficient was being used. The values based on large-scale model calibration were relatively high, while those based on matching results from single-well tracer tests were comparatively low. This illustrates that dispersivity values in the literature are scale-dependent and dependent on their ultimate use in modeling or calculations. Essentially, dispersivity is more of a modeling calibration factor rather than an actual measured aquifer parameter in the available literature. The values in the sited literature appear to depend also on the flow field and the scale at which it is being described.

SECTION 5

Conceptual CERP Model Recommendations

5.1 Common Hydrogeologic Framework

The review of the eight models discussed above indicates that the best approach to simulating the common hydrogeologic framework is to represent the SAS, IAS, FAS and intervening confining and semi-confining layers as discrete layers within the CERP Model. The semi-confining and confining units must be directly simulated via model layers if solute transport processes and density-driven groundwater movement are to be simulated. The following conceptual model is one possibility:

Layer 1 – SAS
Layer 2 – Semi-confining Unit
Layer 3 – IAS ***(potential ASR Zone)***
Layer 4 – Semi-confining Unit
Layer 5 – UPZ of the UFA ***(potential ASR Zone)***
Layer 6 – Semi-confining Unit
Layer 7 – LPZ of the UFA ***(potential ASR zone)***
Layer 8 – MC1 Semi-confining Unit
Layer 9 – MF Middle Floridan Aquifer ***(local potential ASR zone)***
Layer 10 – MC2 Semi-confining Unit
Layer 11 – LF1 UPZ of the LFA
Layer 12 – LC Semi-confining Unit
Layer 13 – BZ Boulder Zone (where present)
Layer 14 – Sub-Floridan Confining Unit

The expected focus of the modeling effort will be to simulate ASR in the UPZ of the UFA and to a lesser extent the LPZ of the UFA, and the IAS. Which permeable zones that are selected will largely depend upon native groundwater quality and the presence of competing groundwater users. Potential ASR zones become less ideal as the TDS concentration increases, which will limit recovery efficiency. Water quality falls within the ideal range for ASR consideration in all three proposed zones depending upon location. With these general criteria in mind, certain layers in the proposed model can be eliminated from consideration as an ASR zone. However, they may still need to be simulated in order to assess potential impacts from ASR activities.

5.2 Potential ASR Storage Zones

The SAS (Layer 1) could be eliminated from ASR consideration due to competing users, the presence of sensitive ecosystems, lack of available storage (i.e., high water table), excellent groundwater quality, and lack of suitable transmissivity and storage volume for ASR. Likewise, the IAS (Layer 3) in west-central Florida can be eliminated for similar reasons. The BZ (Layer 11) can be eliminated from consideration because the transmissivity of this unit is

so large as to preclude development of an ASR storage zone. This unit is also widely used in south Florida as a disposal zone for municipal reclaimed water. Because of these considerations, the SAS, IAS (in west-central Florida), and BZ can be ruled out as potential ASR storage zones.

The UPZ of the UFA is widely used as an ASR storage zone in Florida. It generally coincides with the Tampa member of the Arcadia Formation and the Suwannee Limestone. There are no active ASR systems in Florida that utilize deeper aquifers than the UPZ for ASR storage. There is at least one system in the planning stages that will use the LPZ of the UFA for an ASR storage zone. The LPZ is generally found within the upper portion of the Avon Park Formation. These two zones would be the primary targets for developing the CERP network of ASR wells. Locally in southwest Florida, the Lower Hawthorn Producing Zone (IAS) is currently utilized as a source of groundwater for reverse osmosis water treatment in Lee County and could be utilized as an ASR storage zone. There are few competing users of this zone due to the availability of good quality water in shallower aquifers.

The MF and LF1 of the LFA are not expected to be less favorable potential candidates for ASR system development on a regional scale. Due to formation depth and saline water quality, use of LF1 in central Florida would be precluded because it is a source of good quality water for the Orlando area However, after further investigation, these formations may be found to be locally favorable for ASR development. Elsewhere, the ambient water quality (typically elevated salinity concentrations) in the MF and the LF1 would preclude ASR development. In terms of further investigation, the permeable zones within the UFA should be considered the best candidates for ASR development, followed to a lesser degree by the IAS in southwest Florida. The IAS and the LPZ of the UFA have fewer competing users but have more saline groundwater quality, whereas the UPZ of the UFA has better quality groundwater but a greater number of competing users. These factors (competing users and ambient groundwater quality) are among several that must be carefully evaluated to determine utility for ASR development.

5.3 Discussion of Model Framework

5.3.1 SAS

The SAS is present throughout the area simulated by the five models. Horizontal hydraulic conductivity and thickness are reasonably well known. Vertical hydraulic conductivity is less well known but can be extrapolated in most cases from measured values of horizontal hydraulic conductivity. Through most of peninsular Florida, the SAS consists of unconsolidated deposits of sand, shell, and clay. In south Florida, there is a significant limestone component to the SAS. It is known locally as the Lower Tamiami Aquifer (LTA). In this area, the SAS is composed of an upper unconfined aquifer, which overlies the confined LTA. In southeast Florida, the Biscayne aquifer has a significant limestone component.

5.3.2 Confining and Semi-confining Units

Direct simulation of the confining and semi-confining units will be problematic because little data is available that characterizes their hydraulic properties. In most cases, only leakance is available when vertical hydraulic conductivity and thickness are needed. Hydraulic characteristics of the confining unit below the SAS are fairly well known. This unit retards the flow of groundwater between the SAS and the underlying IAS (where present). Where the IAS is not present, the confining unit is designated as the ICU. The ICU separates the SAS from the underlying UFA. In areas where the IAS or ICU is not present, the UFA is considered unconfined. In areas where the ICU is present, the hydraulic properties of model Layers 2 through 4 must be modified so that they collectively simulate a confining unit, the ICU. In areas where both the ICU and IAS are not present and the UFA is unconfined, Layers 1 through 4 would be rendered inactive. Reese (2004) identified three confining units (MC1, MC2, and LC) in the FAS. MC1 is equivalent to middle confining unit I or II of Miller and separates the UF from the MF. MC2 is equivalent to middle confining unit VI of Miller (1986) and separates the MF from the LFA. LC is found on top of the BZ and is equivalent to middle confining unit VIII (Miller, 1986). The vertical hydraulic conductivity and thickness values of MC1, MC2, and LC are poorly known and will be problematic to define in the CERP Model.

5.3.3 Intermediate Aquifer System

The IAS contains significant permeable zones in west-central Florida and southwest Florida. Three permeable zones, known locally as PZ1, PZ2, and PZ3, have been defined in west-central Florida south of State Road 60 in Hillsborough County. PZ2 and PZ3 are more widespread than PZ1 and are found in Sarasota, Desoto, and Charlotte Counties. In southwest Florida (Lee and Collier Counties) the IAS contains the Sandstone Aquifer and the Mid-Hawthorn Aquifer. Both aquifers are significant sources of potable water supply in these counties. Outside of southwest Florida and west-central Florida, the IAS is not present and consists instead of significant confining units known as the ICU. CH2M HILL recommends that the IAS be simulated as one active layer in west-central Florida and as two active layers in southwest Florida. Outside of these two areas, the IAS layers should be simulated as semi-confining units representing the ICU. The hydraulic characteristics of the IAS and ICU are fairly well known.

5.3.4 Upper Floridan Aquifer

The UFA can be simulated as one discrete permeable unit, which is the approach of the SD Model, Peninsular Model, ETB Model, and DWRM. The LEC Model and EC Model simulated the UFA as two or more active model layers. Two dominant permeable zones have been identified in the UFA within the wider model area. Hydraulic characteristics of the UPZ and LPZ of the UFA are fairly well defined and different in magnitude, with the LPZ being considerable more transmissive. There is ample evidence from APTs in Florida that the two permeable units act as one hydraulic unit with little confinement between them. As a result, the common approach has been to simulate the UFA as one model layer and utilize hydraulic properties as an average of the two units. However, hydraulic properties for both permeable zones are sufficiently well known to warrant delineation as two separate layers. The UPZ of the UFA is commonly found in the Suwannee Limestone and lower

Miocene formations, whereas the LPZ is commonly found at the bottom of the Ocala Limestone, or top of the Avon Park Formation. In central and eastern Florida, the Suwannee Limestone is not present and the UPZ is found at the top of the Ocala Limestone. Based upon the review of all eight models, CH2M HILL recommends that the UFA be simulated with two active layers representing the UPZ and LPZ. Areas where no APTs have been performed will require estimation of hydraulic parameters.

Based on CH2M HILL's ASR and injection well experience concerning horizontal anisotropy, the carbonate formations that typically comprise the storage zones are likely to have varying physical properties (anisotropy) in the horizontal direction around the well. These properties are difficult to quantify at the local level and can only be inferred regionally. The dominant structural fracture pattern in the Eocene sediments suggests two preferential orientations, one NW - SE, and the other SW - NE. It is possible that permeable zones within the Floridan aquifer have similar orientations, however, direct evidence from other wells is lacking. In the typical ASR or DIW facility, the number of monitoring wells is inadequate to evaluate anisotropic conditions and only anecdotal observations are possible. Because the influence of anisotropic conditions may vary from well to well, it is very difficult to predict the local affect on aquifer behavior. Experience suggests that in most cases, any detrimental affects can be overcome with careful selection of open hole intervals and well spacing. However, there will be a certain percentage of sites where local fracture and cavity systems will impact the specific capacity of a particular well and may impact the performance of water supply wells and ASR wells. This is true in Floridan aquifer wells throughout the state. On a regional scale, it is common practice to assume the Floridan aquifer behaves as an isotropic and homogeneous unit with large scale features, such as springs, rivers, recharge areas, coastal discharge, etc., influencing the potentiometric surface and subsequent groundwater flow patterns. This has proven to be a reasonable assumption for regional scale evaluations.

5.3.5 Middle Floridan Aquifer and Lower Floridan Aquifer

The MF is a new informal hydrogeologic unit (Reese, 2004) and as such is not discussed in any of the documentation for the eight models. In the model documentation, the FAS is subdivided into the UFA and LFA, which is consistent with previous USGS reports (Miller, 1986). According to Miller, the MCU separates the UFA from the LFA in west central and southwest Florida. In central and eastern Florida, the MSCU separates the UFA from the LFA. Two permeable zones in the LFA are identified in the model documentation. They consist of an upper permeable zone (typically located with the lower portion of the Avon Park Formation) and the Boulder Zone (BZ), which is located within the Oldsmar Formation. The upper permeable zone of the LFA is designated by Reese (2004) as LF1.

The MF is a permeable zone that appears to be located within the middle portion of the Avon Park Formation above the uppermost permeable zone (LF1) of the LFA. The MF appears to be sandwiched between two confining units that have been defined as MC1 and MC2 by Reese (2004). The lower confining unit (MC2) is also known as middle confining unit VI (Miller, 1986) and is restricted to south Florida. Relatively little information is known about the MF because there has been no need to drill into this unit due to poor water quality.

For the CERP Model, the LFA should therefore be simulated as containing two major permeable zones: LF1 and the BZ. The MF should be simulated as a distinct permeable zone separate from the LFA. Alternatively, the MF could be considered a separate permeable zone of the LFA. However, because there are significant confining units separating the MF from the UFA above and LFA below, it was decided to define it as a separate aquifer. The lowermost permeable zone of the LFA is the BZ and is typically found within the Oldsmar Formation. Relatively little hydraulic data is available for the MF and LFA due to availability of good quality water in shallower aquifers. Groundwater quality in the LFA (LF1) is relatively poor in west-central, southwest, and south Florida. In central and eastern Florida, groundwater quality is relatively good in LF1, which in these areas of Florida is utilized extensively as a source of drinking water.

5.4 Discussion of Model Grid or Mesh Spacings

The USACE intends to use a finite- element approach to the model simulations. It is difficult to determine the number of elements that will be required without knowing the exact geometry of the elements in the proposed finite-element model. Each finite-element model is different and different element configurations can be used (i.e., trapezoid verses triangular). All of the models reviewed utilized the finite-difference mathematical formulation. Most of the models used 2,500-foot to 5,000-foot uniform cell sizes depending on the size of the model study area and the detail the authors were targeting without exceeding the available computing power.

Assuming the model will cover an area from north of Orlando to the Florida Keys and from the east coast to the west coast, the dimensions of the model will be approximately 150 miles from east to west and 300 miles from north to south. Given our level of understanding of the distribution of aquifer properties in peninsular Florida it would be appropriate to assume that cell size or element size should approximate one mile or a significant portion of one mile in dimension. Of course, the greater the resolution required, the greater the processing power required. A compromise must be reached that accounts for the desired resolution of the mathematical model and the availability of processing power and speed. A rough estimate of the number of finite-difference cells required for the model assuming certain cell sizes and 14 model layers is provided below:

Cell Size	No. Columns	No. Rows	No. of Cells or Calculation Points
1 Mile	150	300	45,000
0.5 Mile	300	600	180,000
0.25 Mile	600	1,200	720,000

Square shaped cells are assumed, that is cell dimensions are the same along the X and Y axis. An aspect ratio of up to 5 can be used in most finite-element models so the geometry of the cells/elements can easily deviate from the square. The number of cells or calculation points would increase accordingly if the number of layers used to simulate the hydrogeologic regime is increased. As many of 28 layers (2 model layers per hydrogeologic layer) may be utilized to achieve the desired level of accuracy.

SECTION 6

Recommended CERP Model Framework

Fourteen layers are recommended for the CERP Model to simulate the hydrologic regime of peninsular Florida. This layering scheme (previously presented) includes seven semi-confining/confining units and seven permeable units. The permeable units consist of the SAS (Layer 1), IAS (Layer 3), UPZ of the UFA (Layer 5), LPZ of the UFA (Layer 7), MF (Layer 9), LF1 (Layer 11), and BZ (Layer 13).

Alternatively, the model framework can be reduced to 12 layers if the IAS is not simulated because it is only present in west-central Florida and southwest Florida. The SAS and BZ could also be simulated as arrays of constant heads to further simplify the CERP Model.

SECTION 7

References

Bower, et al. 1990. A Three-Dimensional Finite Difference Ground Water Model of Lee County, Florida. Technical Publication 90-01. South Florida Water Management District. West Palm Beach, Florida.

Fairbank, P., J. Valdes, E. Rectenwald, M. Switaneck, and E. Hopkins. 1999. Documentation for the Lower East Coast Floridan Aquifer Model. South Florida Water Management District. West Palm Beach, Florida.

Florida Geological Survey. 2003. Update of the Hydrogeology of SWFWMD. (FGS, in preparation).

Lukasciewicz, John. 1992. *A Three-dimensional Finite Difference Groundwater Flow Model of the Floridan Aquifer System in Martin, St. Lucie and eastern Okeechobee Counties, Florida.* SFWMD Technical Publication 92-03.

McGurk, B., and P. Fischl Presley. 2002. Simulation of the Effects of Groundwater Withdrawals on the Floridan Aquifer System in East-Central Florida: Model Expansion and Revision. Technical Publication SJ2002-3. St. Johns River Water Management District. Palatka, FL.

Miller, J.A. 1986. *Hydrogeologic Framework of the Floridan Aquifer System in Florida and Parts of Georgia, Alabama and South Carolina.* Professional Paper 1403-B. Washington, D.C.: U.S. Geological Survey.

O'Reilly, A.M., R.M. Spechler, and B.E. McGurk. 2002. *Hydrogeology and Water-Quality Characteristics of the Lower Floridan Aquifer in East-Central Florida.* U.S. Geological Survey WRIR 02-4193.

Randazzo, A. F., and D. S. Jones. 1997. The Geology of Florida, University Press of Florida.

Reese, R.S. & R.J. Memberg. 1999. *Hydrogeology and the Distribution of Salinity in the Floridan Aquifer System, Palm Beach County, Florida.* U.S. Geological Survey. WRIR 99-4061.

Reese, R.S. 1994. *Hydrogeology and the Distribution and Origin of Salinity in the Floridan Aquifer System, Southeastern, Florida.* WRIR 94-4010. U.S. Geological Survey.

Reese, R.S. 2000. *Hydrogeology and the Distribution of Salinity in the Floridan Aquifer System, Southwestern, Florida.* U.S. Geological Survey. WRIR 98-4253.

Reese, R.S. 2003. *Hydrogeology, Water Quality, and the Distribution and Sources of Salinity in the Floridan Aquifer System, Martin and St. Lucie Counties, Florida.* U.S. Geological Survey. WRIR 03-4242.

Tables

Table 1
Groundwater Models Available for Review
Subtask 3 - Groundwater Model Development

Model number	Authors (Organization and year)	Document Source	General location	Number of rows	Number of columns	Grid type	Layering description
1	Grubb and Rutledge (USGS 1979)		Parts of Polk, Lake, Sumter, Hernando, and Pasco Counties	36	40	Uniform cell size of5,400 by 6,075 feet	SAS, layer 1, SH
2	Ryder (USGS 1985)	USGS[1]	West-central Florida	49	32	Uniform cell size of 4 miles by 4 miles	SAS, layer 3, SH IAS, layer 2 UFA, layer 1
3	Fretwell (USGS 1988)	USGS[1]	Pasco County	38	54	Uniform cell size of 1 square mile	SAS, layer 1, SH UFA, layer 2
4	Yobbi (USGS 1989)		Citrus and Hernando Counties	22	18	Uniform cell size of 2 miles by 2 miles	UFA, one-layer model
5	Tibbals (USGS 1990)	USGS[1]	East-central Florida	50	24	Uniform cell size of 4 miles by 4 miles	SAS, layer 3, SH UFA, layer 2 LFA, layer 1
6	Lukasiewicz (SFWMD 1992)	USGS[1]	Martin and St. Lucie Counties	54	53	Uniform cell size of 1 square mile	SAS, layer 1, SH UFA, layer 2 LFA, layer 3 LFA, layer 4, SH
7	Barcelo and Basso (SWFWMD 1993)	USGS[1]	Southwest Florida	56	60	Uniform cell size of 2 miles by 2 miles	SAS, layer 1, SH IAS, layer 2 UFA, layer 3
8	Blanford and Birdie (HydroGeoLogic 1993)	USGS[1]	Hernando County	33	43	Uniform cell size of 1 square mile	UFA, one-layer model
9	Hancock and Basso (SWFWMD 1993)	USGS[1]	Parts of Hemando, Pasco, Hillsborough, and Pinellas Counties	62	69	Variable cell size, ranging from 2,640 by 2,640 feet to 1 square mile	SAS, layer 1 UFA, layer 2 UFA, layer 3
10	Metz (USGS 1995)	USGS[1]	Hardee and DeSoto Counties	47	46	Uniform cell size of 5,390 by 6,050 feet	SAS, layer 1, SH JAS, layer 2 UFA, layer 3
11	Motz (SJRWMD 1995)	USGS[1]	North-central Florida	53	54	Variable cell size, ranging from 5,000 by 5,000 feet to 15,000 by 20,000 feet	SAS, layer 1, SH IAS, layer 2, UT UFA, layer 3 LFA, layer 4 FPZ, layer 5
12	Murray and Halford (USGS 1996)	USGS[1]	Orange, Seminole, and parts of Volusia, Lake, and Osceola Counties	40	55	Uniform cell size of 5,322 by 6,050 feet	SAS, layer 1, SH UFA, layer 2 LFA, layer 3
13	Yobbi (USGE 1996)	USGS[1]	Parts of Polk, Osceola, Hardee, De Soto, Highlands, and Glades Counties	86	41	Uniform cell size of 1 square mile	SAS, layer 1 IAS, layer 2 UFA, layer 3
14	Durden (SJRWMD 1997)	USGS[1]	Northeast Florida	68	35	Variable cell size, ranging from 5,222 by 6,057 feet to 18,280 by 23,499 feet	SAS, layer 1, SH UFA, layer 2 LFA, layer 3 FPZ, layer 4
15	Restrepo, Bevier and Butler (SFWMD 1992)	SFWMD	Broward County	100	134	Cell size 1000 feet (E-W) by 2000 feet (N-S)	SAS discretized into 5 layers
16	Bennett (SFWMD 1992)	SFWMD	Collier County	73	47	Uniform cell size 1 square mile	WT, Layer 1 LT, Layer 2 SS, Layer 3 MH, Layer 4 LH, Layer 5
17	Smith (SFWMD 1990)	SFWMD	Hendry County	48	54	Uniform cell size 1 square mile	WT, Layer 1 LT, Layer 2 SS, Layer 3
18	Hopkins (SFWMD 1991)	SFWMD	Jensen Beach Peninsula, Martin County	96	98	Uniform cell size 240 feet by 240 feet	SAS discretized into 2 layers
19	Bower, Adams and Restrepo (SFWMD 1990)	SFWMD	Lee County	42	48	Uniform cell size 1 square mile	WT, Layer 1 LT, Layer 2 SS, Layer 3 MH, Layer 4 LH, Layer 5 Suwan, Layers 6,7
20	Adams (SFWMD, 1992)	SFWMD	Martin County	59	109	Uniform cell size 2000 feet by 2000 feet	SAS
21	Butler and Padgett (SFWMD 1995)	SFWMD	St. Lucie County	71	109	Uniform cell size 2000 feet by 2000 feet	SAS discretized into 3 layers
22	Fairbank and Others (SFWMD 1999) - LEC Model	SFWMD	Lower East Coast: Palm Beach, Broward, Miami-Dade Counties	166	99	Uniform cell size 1 mile by 1 mile	SAS, Layers 1, 2 UFA, Layers 3,4,5 MCU, Layer 6 LFA, Layers 7,8,9
23	Nair and Others (SFWMD 2000)	SFWMD	South Palm Beach County	NA	NA	Uniform cell size 500 feet by 500 feet	SAS discretized into 5 layers
24	Wilsnack and Others (SFWMD 2000)	SFWMD	North-Miami Dade County	NA	NA	Uniform cell size 500 feet by 500 feet	SAS discretized into 8 layers
25	South Florida Water Management Model (SFWMD) Multiple Authors	SFWMD	Lake Ocheecobee to Florida Bay	62	62	Uniform cell size 2 mile by 2 mile	SAS and surface water features
26	Sepulveda (USGS 2002) - Megamodel	USGS[1]	Peninsular Florida from Northeast Florida to Glades County	300	210	Uniform cell size 5000 feet by 5000 feet	SAS-Layer 1, IAS-Layer 2, UFA-Layer 3, LFA-Layer 4
27	Beach and Chan (SWFWMD 2003)	SWFWMD	Southern portion of SWFWMD - Southern District	NA	NA	Uniform cell size 5000 feet by 5000 feet	SAS-Layer 1, IAS-Layers 2 and 3, UFA-Layers 4 and 5
28	South Florida Regional Simulation Model (SFRSM) Multiple Authors	SFWMD	Lake Ocheecobee to Florida Bay	Not Applicable	Not Applicable	Finite-Element Grid, Triangular elements, 0.5 to 1.0 mile on a side	SAS and surface water features
29	McGurk and Presley (SJRWMD, 2002)	US Army CE[2] Jacksonville District SJRWMD	East-central Florida	174	194	Uniform cell size 2500 feet by 2500 feet	SAS-Layer 1, Upper UFA-Layer 2, Lower UFA-Layer 3, LFA-Layer 4
30	HydroGeoLogic for SWFWMD (2002) [density dependent]	US Army CE[2] Jacksonville District SWFWMD	West-central Florida	123	103	Variable cell size, ranging from 2500 feet by 5000 feet	10-Layer model (UFA only): Suwannee LS layers 1&2, Ocala LS layers 3 to 5, Avon Park Fm layers 6 to 10
31	Durden and Huang (SJRWMD 2002)	US Army CE[2] Jacksonville District	Northeastern Florida	68	35	Finite-Element Grid, Variable cell size, rows from 6,060 feet to 15,200 feet columns from 5,220 feet to 19,600 feet	8-Layer model: SAS layer 4, UFA layer 3, LFA layer 2, Fernandina permeable zone layer 1, plus 3 semi-confining layers
32	Environmental Solutions, Inc (ESI) for SWFWMD (2004)	SWFWMD	SWFWMD District wide	322	210	Uniform cell size 5000 feet by 5000 feet	SAS-Layer 1, IAS-Layer 2, UFA-Layer 3, LFA-Layer 4

Notes:
1 Sepulveda, Nicasio, 2002, *Simulation of Ground-Water Flow in the Intermediate and Floridan Aquifer Syetems in Peninsular Florida:* U.S. Geological Survey Water-Resources Investigations Report 02-4009,

2 U.S. Army Corps of Engineers, *Literature review of Regional Florida Groundwater Modeling for Regional Aquifer Storage & Recovery Study at Florida*. March 2005, Jacksonville District.

SAS - Surficial Aquifer System
UFA - Upper Floridan aquifer
LFA - Lower Floridan aquifer
MCU - Middle Confining Unit
NA - not available

IAS - intermediate aquifer system
MH - Mid Hawthorn
LH - Lower Hawthorn
FPZ - Fernandina Permeability Zone

USACE models selected for CH2M HILL review

Table 2
Groundwater Model Layer Comparisons
Subtask 3 - Groundwater Model Development

	Author Agency Location	Model No. 7 Barcelo & Basso, 1993 SWFWMD Eastern Tampa Bay WUCA	Model No. 19 Bower et. al.. 1990 SFWMD Lee County, FL	Model No. 22 Fairbanks et.al., 1999 SFWMD Lower East Coast FL (LEC)	Model No. 26 Sepulveda, 2002 USGS Peninsular Florida (Megamodel)	Model No. 27 Beach & Chan, 2003 SWFWMD Southern District	Model No. 29 McGurk & Presley, 2002 SJRWMD East-Central Florida (ECF)	Model No. 30 HydeoGeoLogic, Inc 2002 SWFWMD West-Central Florida	Model No. 33 Environmental Simulations, Inc., 2004 SWFWMD District Wide Regulatory Model (DWRM)
Surficial Aquifer	Water-Table/Biscayne Aquifer	Layer 1	Layer 1	Layer 1	Layer 1	Layer 1	Layer 1		Layer 1
	Confining Beds			Layer 2					
	Lower Tamiami Aquifer		Layer 2						
Intermediate Aquifer or Confining Unit	Confining Unit								Layer 2
	Sandstone Aquifer	Layer 2	Layer 3						
	PZ1				Layer 2				
	PZ2				Layer 2	Layer 2			
	PZ3				Layer 2	Layer 2			
	Semi-Confining Unit								
	Mid-Hawthorn Producing Zone		Layer 4						
	Semi-Confining Unit								
Floridan Aquifer System	Lower Hawthorn Producing Zone		Layer 5						
	Upper Floridan Aquifer	Layer 3	Layer 6, Suwanee	Layer 3, Avon Park	Layer 3	Layer 4	Layer 2, AP & Ocala	Layer 1, Suwanee	Layer 3
				Layer 4 (confining)			Layer 3, Avon Park	Layer 2, Suwanee	
				Layer 5, Avon Park				Layer 3, Ocala	
								Layer 4, Ocala	
								Layer 5, Ocala	
								Layer 6, Avon Park	
								Layer 7, Avon Park	
								Layer 8, Avon Park	
								Layer 9, Avon Park	
	Middle Confining Unit/Middle Semi-confining Unit			Layer 6				Layer 10, Avon Park	
	Middle Floridan Producing Zone								
	Lower Floridan Aquifer		Layer 7 Suw. & Deeper	Layer 7, Oldsmar	Layer 4		Layer 4		
				Layer 8 (Confining)					
	Lower Floridan-Boulder Zone			Layer 9					
	Sub-Florida Confining Unit								

Figures

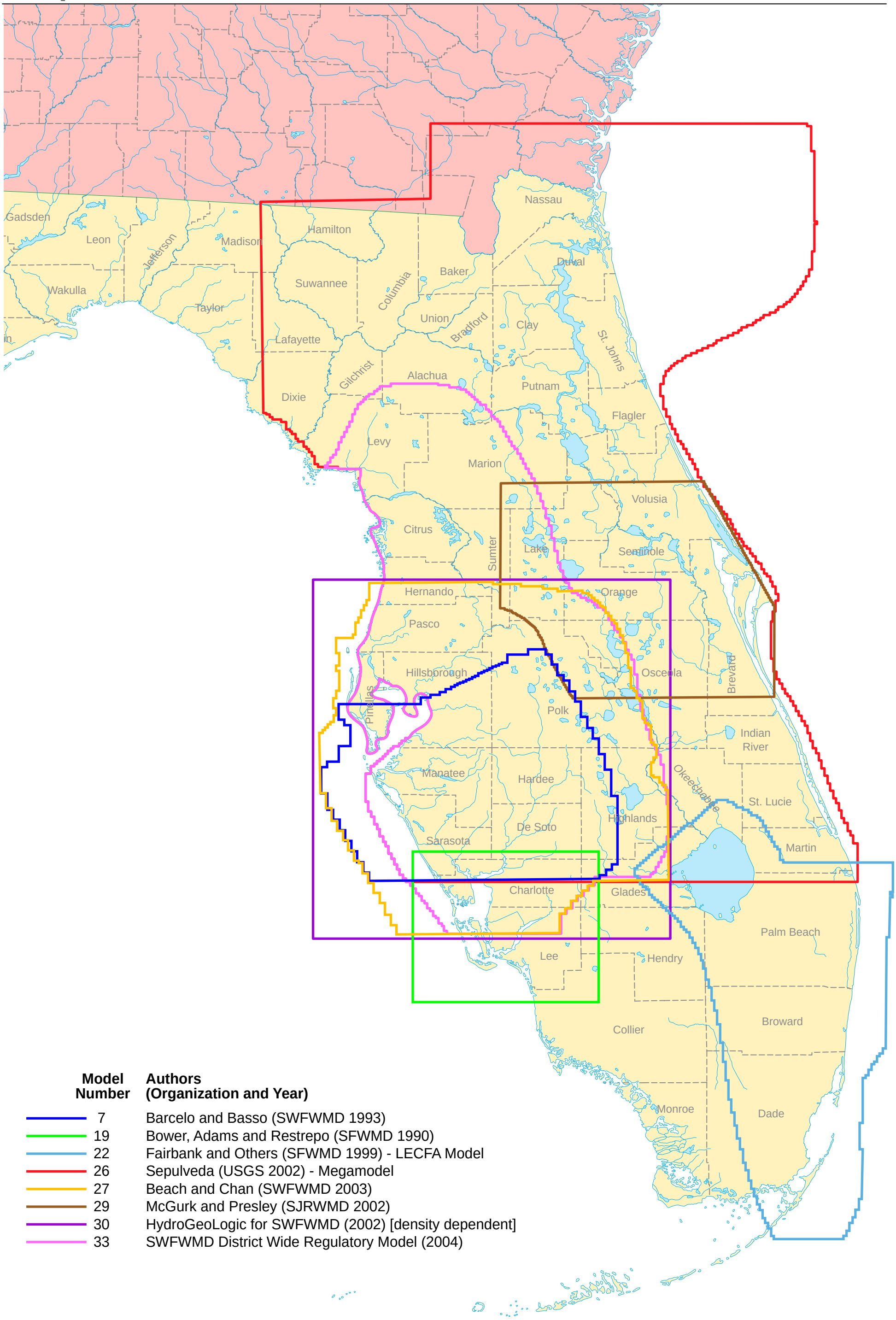

Model Number	Authors (Organization and Year)
7	Barcelo and Basso (SWFWMD 1993)
19	Bower, Adams and Restrepo (SFWMD 1990)
22	Fairbank and Others (SFWMD 1999) - LECFA Model
26	Sepulveda (USGS 2002) - Megamodel
27	Beach and Chan (SWFWMD 2003)
29	McGurk and Presley (SJRWMD 2002)
30	HydroGeoLogic for SWFWMD (2002) [density dependent]
33	SWFWMD District Wide Regulatory Model (2004)

North

0 15 30

Approximate Scale in Miles

FIGURE 1
Reviewed Model Boundaries
USACE - Subtask 3 Model Development

CH2MHILL

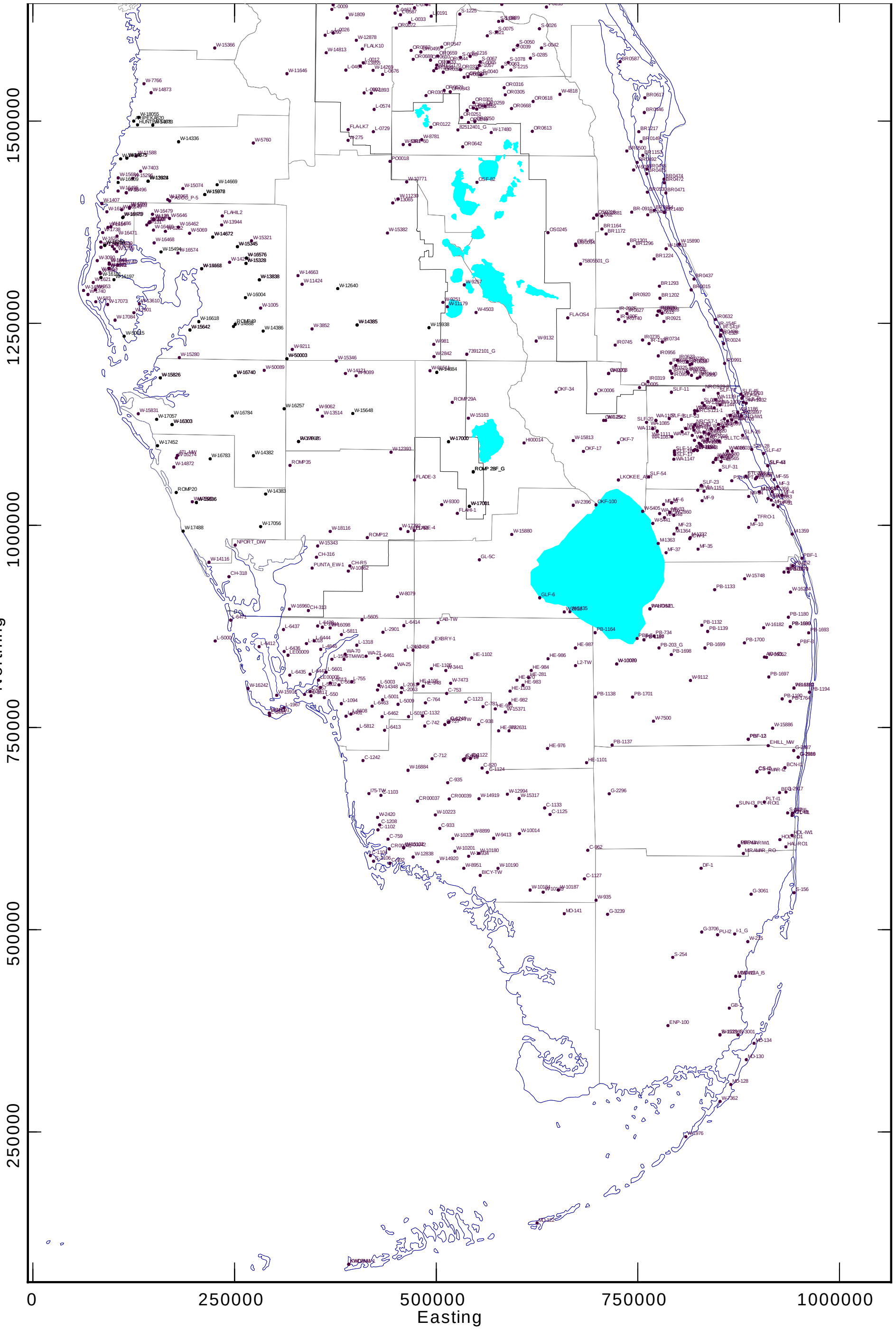

FIGURE 2
Wells considered for the Hydrogeologic Framework
USACE Subtask 3 - Model Development

Series		Geologic Unit		Lithology	Hydrogeologic unit		Approximate thickness (feet)
HOLOCENE TO PLIOCENE		UNDIFFERENTIATED		Quartz sand, silt, clay, and shell	SURFICIAL AQUIFER SYSTEM	WATER-TABLE / BISCAYNE AQUIFER	20-300
		TAMIAMI FORMATION		Silt, sandy clay, micritic limestone, sandy, shelly limestone, calcareous sandstone, and quartz sand		CONFINING BEDS LOWER TAMIAMI AQUIFER	
MIOCENE AND LATE OLIGOCENE		HAWTHORN GROUP	PEACE RIVER FORMATION	Interbedded sand, silt, gravel, clay, carbonate, and phosphatic sand	INTERMEDIATE AQUIFER SYSTEM OR CONFINING UNIT	CONFINING UNIT SANDSTONE AQUIFER CONFINING UNIT MID-HAWTHORN AQUIFER CONFINING UNIT	250-750
			ARCADIA FORMATION	Sandy micritic limestone, marlstone, shell beds, dolomite,phosphatic sand and carbonate, sand, silt, and clay			
EARLY OLIGOCENE		SUWANNEE LIMESTONE		Fossiliferous, calcarenitic limestone	FLORIDAN AQUIFER SYSTEM	LOWER HAWTHORN PRODUCING ZONE UPPER FLORIDAN AQUIFER (UF)	0-300 100-700
EOCENE	LATE	OCALA LIMESTONE		Chalky to fossiliferous, calcarenitic limestone			
	MIDDLE	AVON PARK FORMATION		Fine-grained, micritic to fossiliferous limestone, dolomitic limestone, dolostone, and anhydrite/ gypsum		MIDDLE CONFINING UNIT MF	500-1,300 0-400
	EARLY	? OLDSMAR FORMATION				LF1 LOWER FLORIDAN AQUIFER BZ	1,400-1,800 200-700
PALEOCENE		CEDAR KEYS FORMATION		Dolomite and dolomitic limestone			
				Massive anhydrite beds		SUB-FLORIDAN CONFINING UNIT	1,200?

Note:
? denotes geologic units are missing in some areas

Source:
Reese, 2004

FIGURE 3
Relationship of Hydrogeologic Units Proposed by the Preliminary Hydrogeologic Framework Study
Sub-Task 3 - Model Development

Appendices

APPENDIX A

Southwest Florida Region Model Review TM

Southwest Florida Region Groundwater Model Review: Sepulveda (2002), Beach and Chan (2003), Barcelo and Basso (1993), HydroGeoLogic (2002), and Environmental Simulations, Inc. (2004)

PREPARED FOR: US Army Corp of Engineers

PREPARED BY: CH2M HILL

DATE: December 14, 2005

PROJECT NUMBER: 334350.TW.03

Contents

Introduction and Purpose

The goal of this project is to collect and summarize data from available model documentation and provide recommendations to the U.S. Army Corps of Engineers (USACE) Jacksonville District for the development of a Regional Groundwater Model of Florida. This Technical Memorandum (TM) summarizes the model reviews for northern and west-central Florida. A second TM has been prepared that summarizes three separate models from central and south Florida.

Five models were reviewed:

- Peninsular Model (Sepulveda, 2002)
- Southern District of SWFWMD Model (Beach and Chan, 2003)
- Eastern Tampa Bay Model (Barcelo and Basso, 1993)
- HydroGeoLogic Model (HydroGeoLogic, 2002)
- District Wide Regulatory Model (Environmental Simulations, Inc. [ESI], 2004)

Figure 1 shows the geographic relationship between the five model areas.

Comparison of Model Frameworks

The Peninsular Model developed by Sepulveda (2002) extends from Charlton and Camden Counties in south Georgia to near the Palm Beach County – Martin County line in south Florida. The Beach and Chan Model (2003), known as the Southern District (SD) Model, encompasses a smaller area, from Hernando County in the north to Lee County in the south and from the Gulf of Mexico in the west to the Kissimmee River in the east. The Eastern Tampa Bay (ETB) Model (Barcelo and Basso, 1993) is an earlier version of the SD Model and includes a smaller area, extending from Hillsborough County in the north to Charlotte County in the south, from the Gulf of Mexico in the west to Polk County in the east. The SD Model area includes all of the ETB Model area, while the Peninsular Model includes the areas of both the ETB Model and the SD Model. The District Wide Regulatory (DWR) Model (ESI, 2004) is a smaller subset of the Peninsular Model and coincides with the boundaries of the Southwest Florida Water Management District (SWFWMD) plus a buffer zone of approximately 10 miles on all sides. The southern boundary of the DWR Model was extended past the southern boundary of the Peninsular Model to coincide with the southern boundary of the SWFWMD. The HydroGeoLogic Model (2002) is a smaller subset of the SD Model and includes the southern half of Hillsborough County and all of Manatee and Sarasota Counties. Unlike the other models, the HydroGeoLogic Model simulates solute transport and density-driven groundwater movement. All five models are finite-difference models.

Three aquifer systems are present within the area simulated by the five groundwater models. The surficial aquifer system (SAS) is the uppermost water-bearing hydrogeologic unit. The SAS mostly consists of variable amounts of sand, clay, sandy clay, shell beds, silt, and clay. The SAS extends throughout most of the study area, except where the Upper Floridan aquifer (UFA) is unconfined. The intermediate aquifer system (IAS) underlies the SAS and extends throughout most of southwest Florida. State Road 60 is generally considered the northern boundary of the IAS in western Florida. The unit consists mainly of clastic sediments interbedded with carbonate rocks that generally coincide with the Hawthorn Group. Confining beds that overlie the UFA and underlie the SAS limit the vertical extent of the IAS in west-central Florida. In the absence of significant permeable zones, the IAS is defined as the intermediate confining unit (ICU). The ICU is present outside of west-central Florida, wherever the IAS pinches out. The UFA is considered to be unconfined in areas where the ICU or IAS is absent or very thin.

The Floridan Aquifer System (FAS) is a thick sequence of limestone and dolomitic limestone of Oligocene and Eocene ages with highly variable permeability. The FAS is divided into two aquifers of relatively high permeability, referred to as the UFA and the Lower Floridan aquifer (LFA). These aquifers are separated by a less permeable unit called the Middle

Confining Unit (MCU) in west-central Florida and in the northwest part of the study area, and the middle semi-confining unit (MSCU) in east-central Florida. The top of the UFA coincides with the top of the Tampa Member, Suwannee Limestone or the Ocala Limestone, depending upon location. The bottom of the UFA is the top of the shallowest, significant, regional confining unit.

In east-central Florida, the UFA and LFA are separated by the MSCU, a sequence of somewhat permeable, soft, chalky, limestone that locally contains some gypsum and chert and commonly is partially dolomitized. In west-central Florida and in the northwest part of the study area, the UFA and LFA are separated by the MCU, which is composed of gypsiferous dolomite and dolomitic limestone of considerably lower permeability than that of the MSCU in east-central Florida.

Two discrete permeable zones have been defined in the UFA. The upper permeable zone (UPZ) has been identified within sections of the Suwannee Limestone and the Tampa Member of the Arcadia Formation. The lower permeable zone (LPZ) of the UFA has been identified within the lower part of the Ocala Limestone and the upper part of the Avon Park Limestone. The Ocala Limestone occurs between the Suwannee Limestone and the Avon Park Limestone and is thought to function as a semi-confining unit between the UPZ and LPZ.

Two discrete permeable zones have been identified in the LFA in northeast Florida. They consist of a UPZ also known as LF1, and the lower Fernandina permeable zone (FPZ). In south Florida, two permeable zones have also been identified. The upper producing zone (LF1) is found within the lower portion of the Avon Park Formation below the MCU, while the lower producing zone is found in the Oldsmar Formation. The lower producing zone is known as the "Boulder Zone" due to drilling characteristics and is known for extremely high transmissivity. The Middle Floridan Aquifer identified by Reese (2004) is not discussed in any of the model documentation.

The five models compared for this TM are provided in Table 1. The Peninsular Model includes four layers: the SAS, IAS (ICU), UFA, and LFA. Layer 2 is either the IAS or ICU, depending upon location. The UPZ and LPZ of the UFA are simulated as one layer (Layer 3) given the evidence that there is significant hydraulic connection between the units. Layer 4 is the LFA, which is not simulated in the SD Model or the ETB Model. In west-central Florida where the SD Model and ETB Model are situated, groundwater in the LFA is highly saline. As a result, the LFA is not simulated in those area models.

The SD Model explicitly simulates separate permeable zones found in the IAS in west-central Florida. Permeable zones known locally as PZ2 and PZ3 are simulated as Layers 2 and 3, respectively. In contrast, the Peninsular Model utilizes one layer to simulate the IAS. Layers 4 and 5 of the SD Model simulate the UPZ and LPZ of the UFA. The Peninsular Model utilizes one layer to simulate the UFA. The LFA, which the Peninsular Model simulates, is not simulated by the SD Model.

The ETB Model has three layers, which simulate the SAS, IAS and the UFA. The LFA is not simulated nor are multiple zones of permeability in the IAS or UFA. All four models indirectly simulate semi-confining units and confining units with arrays of leakance values. The DWR Model is very similar to and is based on the Peninsular Model. Like the Peninsular Model, the DWR Model consists of four layers. Layer 1 is the SAS. Layer 2 is the

IAS, and Layer 3 is the UFA. Layer 4 is the LFA. Unlike the Peninsular Model, which utilizes constant heads to simulate the SAS, the SAS is actively simulated in the DWR Model. Layer 2 of the DWR Model simulates PZ3 of the IAS whereas Layer 2 of the Peninsular Model simulates the average of PZ2 and PZ3 of the IAS. The SD Model simulates PZ2 and PZ3 as separate layers. Another similarity between the Peninsular Model and the DWR Model is that the base of the model is considered to be the 5,000 milligrams per liter (mg/L) chloride concentration. Strata that contain groundwater with a chloride concentration in excess of 5,000 mg/L are not simulated. In west-central Florida, the LFA is highly mineralized and therefore is not simulated by either model.

The HydroGeoLogic Model is different from the other four models in that it is designed to simulate density-driven, solute transport processes. The HydroGeoLogic Model is based on the SD Model, but covers a smaller geographic area consisting of southern Hillsborough County, Manatee County, and Sarasota County. A notable difference between the two models is that the semi-confining units are explicitly simulated in the HydroGeoLogic Model as separate model layers. The other four models simulate advective groundwater movement and represent semi-confining units with arrays of leakance. The semi-confining units are not directly simulated with model layers. Ten layers are used in the HydroGeoLogic Model to simulate the permeable and less permeable units in the Suwannee Limestone, Ocala Limestone, and Avon Park Formation. The SAS and IAS are not simulated directly in the HydroGeoLogic Model. General-head boundary cells are used instead to simulate the movement of water vertically into the Suwannee Limestone, which is the top of the model. The bottom of the model is the MCU. Two model layers are used to simulate the Suwannee Limestone, while three layers are used to simulate the Ocala Limestone. Five layers are used to simulate the Avon Park Formation. The primary purpose of the HydroGeoLogic Model is to simulate the movement of the saltwater/freshwater interface and the vertical movement of saline water in order to make sound decisions regarding permit applications. Likewise, the primary purpose of the four advective transport models is to simulate potential impacts to the various aquifer systems without consideration of density differences in the groundwater.

Model Summaries

Sepulveda, 2002. Simulation of Groundwater Flow in the Intermediate and Floridan Aquifer Systems in Peninsular Florida, U.S. Geological Survey Water-Resources Investigations Report 02-4009.

Model Area

The active model area encompasses approximately 40,800 square miles in peninsular Florida, as shown in Figure 2, from Charlton and Camden Counties in Georgia to near the Palm Beach – Martin County line in south Florida. The west-to-east extent of the study area spans approximately 200 miles, from the Gulf of Mexico to the Atlantic Ocean.

Hydrogeologic Framework

The hydrogeologis units of the study area are shown in Figure 3. The SAS is the uppermost water-bearing hydrogeologic unit. The SAS mostly consists of variable amounts of sand,

clay, sandy clay, shell beds, silt, and clay. Limestone units within the SAS are primarily in southwest Florida. The SAS extends throughout most of the study area, except where the UFA is unconfined. The IAS underlies the SAS and extends throughout most of southwest Florida. The unit consists mainly of clastic sediments interbedded with carbonate rocks that generally coincide with the Hawthorn Group. Confining beds that overlie the UFA and underlie the SAS limit the vertical extent of the IAS in west-central Florida. The thickness of the IAS varies from approximately 25 feet in parts of Hillsborough and Polk Counties to approximately 400 feet in Charlotte County.

The hydrogeologic units, ICU and IAS, within the Hawthorn Group are differentiated based upon the permeability of the rock. In contrast to the IAS, the ICU is considerably less permeable. The UFA is considered to be unconfined in areas where the ICU or IAS is absent or very thin.

The FAS is a thick sequence of limestone and dolomitic limestone of Oligocene and Eocene ages with highly variable permeability. The FAS is divided into two aquifers of relatively high permeability, referred to as the UFA and the LFA. These aquifers are separated by a less permeable unit called the MCU in west-central Florida and in the northwest part of the study area, and the MSCU in east-central Florida. The top of the UFA coincides either with the top of the Suwannee Limestone or the top of the Ocala Limestone, depending upon location. Rather than a single-low permeability unit separating the UFA and LFA, several units of regional extent separate the UFA from the LFA. Any of the regionally extensive low-permeability units may contain thin layers of moderate to high permeability. These confining units are not continuous and do not necessarily consist of the same rock type everywhere.

In east-central Florida, the UFA and LFA are separated by the MSCU, a sequence of somewhat permeable, soft, chalky, limestone that locally contains some gypsum and chert and commonly is partially dolomitized. In west-central Florida and in the northwest part of the study area, the UFA and LFA are separated by the MCU, which is composed of gypsiferous dolomite and dolomitic limestone of considerably lower permeability than that of the MSCU in east-central Florida.

In northeast Florida, the LFA is subdivided into two zones, the upper zone of the LFA and the FPZ. In southeast-central Florida, a localized production zone called the Boulder zone occurs within the LFA. Generally low-permeability dolomite and evaporite beds form the sub-Floridan confining unit, or the base of the FAS. These beds of very low permeability serve as the hydraulic base of the FAS and in the study area, and range in elevation from approximately -1,200 feet mean sea level (msl) in the northwest to approximately -4,100 feet msl in south Florida.

Conceptual Model

The conceptual groundwater flow system is shown in cross sections on Figure 4. Both sections are oriented from east to west. The regional groundwater flow system was simulated as a quasi-three-dimensional groundwater flow model with four layers. Figure 5 shows the principal hydrogeologic units and equivalent layers in the regional model. The SAS, IAS (or ICU in areas where the IAS is absent), the UFA and the LFA were designated Layers 1 through 4, respectively. The SAS was simulated as a source-sink layer. Confining

layers were simulated by using vertical leakance arrays. Model-simulated groundwater flow occurs horizontally within the aquifers and vertically through the confining units.

The IAS (Layer 2) in southwest and south-central Florida was simulated as a single active aquifer bounded above and below by arrays of leakance values. Because this model is restricted to simulating the movement of freshwater within the aquifers, areas where the IAS, the UFA and the LFA (Layers 2, 3, and 4) contain water with chloride concentrations exceeding 5,000 mg/L are considered inactive. Recharge to or discharge from the IAS is assumed to occur through the upper or lower confining units of the IAS.

The MCU was represented by vertical leakance values that limit water exchange between the UFA (Layer 3) and the LFA (Layer 4) in west-central and southwest Florida, and in the northwest part of the study area to a greater degree than in areas where the MSCU is present. The MSCU in east-central, southeast, and northeast Florida was represented by an array of vertical leakance values that allowed water exchange between the UFA and LFA.

The River, Drain, and Recharge packages were used in this groundwater model. The River package was used to simulate the discharge of water to and from rivers in unconfined areas of the UFA. The discharge of groundwater to swamps in unconfined areas of the UFA and the flow from UFA springs located outside river cells were simulated by using the Drain package. Flow from springs was simulated as discharge to drain cells using the measured or estimated spring pool altitude as the drain elevation. The net recharge rates to unconfined areas of the UFA were assigned using the Recharge package.

Numerical Model

The Peninsular Model is based on the numerical, finite-difference code MODFLOW, which was developed by McDonald and Harbaugh (1984 and 1996). Steady-state conditions were simulated by the model. Average groundwater resource conditions from August 1993 through July 1994 served as the target for the steady-state model.

Model Description

The Peninsular Model was conceptualized as a quasi-three-dimensional flow model with horizontal flow in the aquifer systems and vertical leakance through the confining layers. The confining units are not explicitly simulated but are represented by arrays of leakance. Groundwater flow is predominantly horizontal in the aquifer systems and vertical in the confining units.

Model Grid and Discretization

The Peninsular Model is divided into four layers.

- Layer 1 – SAS
- Layer 2 – IAS (or ICU)
- Layer 3 – UFA
- Layer 4 – LFA

The model grid is oriented along the north-south axis. All model cells are 5,000 feet by 5,000 feet, with 210 columns and 300 rows.

Boundary Conditions

The SAS (Layer 1) was simulated as a layer of constant heads. A no-flow boundary condition was applied along all lateral boundaries of Layer 2 (IAS or ICU). Flow entering or leaving cells in Layer 2 is assumed to occur as either horizontal flow to neighboring cells or vertical flow to either the SAS (Layer 1) or the UFA (Layer 3). Lateral boundary conditions for the UFA (Layer 3) and the LFA (Layer 4) were either no-flow or specified head. Along the Gulf of Mexico in Citrus, Hernando, and Pasco Counties, most of the lateral flow in the UFA is assumed to be discharged by numerous springs. Based on this observation, no-flow conditions were applied to the boundary of Layer 3 in those areas. Specified heads were used elsewhere along the boundary of Layer 3. No-flow conditions were applied along all lateral boundaries in Layer 4 (LFA). The eastern and western boundaries of the LFA coincided with the location at which the chloride concentration in the LFA exceeded 5,000 mg/L. Specified heads in the UFA along the northeastern boundary of the model were set equal to the equivalent freshwater head.

Transmissivity

Transmissivity in the IAS ranged from 100 square feet per day (ft^2/d) along the northern, eastern and western boundaries of the IAS to 30,000 ft^2/d in Sarasota County (Figure 6). Transmissivity of the UFA ranged from 3,000 ft^2/d in areas where the UFA is thin to 12,000,000 ft^2/d in areas of cavernous limestone near springs (Figure 7). Transmissivity values for the LFA (Figure 8) ranged from 5,000 ft^2/d along parts of the lateral boundaries of the LFA to 760,000 ft^2/d in northeast Florida. High transmissivity values were simulated in parts of Orange County and south Florida.

Leakance

Leakance values for the upper confining unit of the IAS, ICU and MCU/MSCU between the UFA and LFA are shown on Figures 9, 10, and 11, respectively.

Beach and Chan, 2003. Southern District Groundwater Flow Model Version 1.0, Prepared by the Hydrologic Evaluation Section, Resource Conservation and Development Department, Southwest Florida Water Management District.

Model Area

The modeled area was delineated to minimize any boundary effects on the principal area of interest: the Southern Water Use Caution Area (SWUCA). The modeled area generally extends from central Hernando County in the north to central Lee County in the south. The model extends from about 5 to 20 miles into the Gulf of Mexico on the west side and to the Kissimmee River on the east side. The active model area is approximately 12,800 square miles. The SWUCA covers approximately 5,500 square miles of this area. Figure 12 shows the model area and extent of the SWUCA.

Hydrogeologic Framework

The local groundwater flow system is comprised of three vertically sequenced aquifer systems. In descending order, these systems are the unconfined SAS, the confined IAS, and the confined UFA. The SAS is generally shallow and extends from land surface to the upper

confining unit of the IAS. Thickness varies from 5 to 50 feet over most of the southern SWFWMD, but depths as high as 300 feet are reached in the vicinity of the Lake Wales Ridge. Reported hydraulic conductivities range from 5 to 15 ft/day in the northern part of the basin and 10 to 60 ft/d in the southern counties.

The IAS consists of confining units and multiple permeable zones bounded by the SAS above and the UFA below. The IAS functions not only as an aquifer system, but as the ICU between the SAS and UFA. The IAS consists of three principal permeable zones designated as PZ1, PZ2, and PZ3. PZ1 is often well connected hydraulically to the SAS and is of local significance only. PZ2 ranges in thickness from 20 to 190 feet and is more productive than PZ1. PZ2 is generally well separated hydraulically from both the upper and lower permeable zones. PZ3 ranges in thickness from 0 to 300 feet. Transmissivity for PZ1 ranges from 50 to 8,000 ft^2/d; PZ2 ranges from 200 to 13,300 ft^2/d; and PZ3 ranges from 30 to 15,400 ft^2/d. Depending on location, the IAS can be recharged by leakance from the overlying SAS or by upward leakance from the underlying FAS, or both. The geology and hydrogeology of the SD Model are shown on Figure 13.

The UFA consists of a thick sequence of carbonate rocks which range from 2,500 feet to 3,200 feet thick over the model area. The UFA is confined above by the lower confining unit of the IAS and below by the MCU. The UFA is divided into two permeable units: the UPZ and the LPZ. UPZ and LPZ are separated by a semi-confining unit. The UPZ includes most of the Suwannee Limestone and sometimes the overlying Tampa Formation. Transmissivities of the UPZ range from 1,400 ft^2/d to 290,000 ft^2/d. The Ocala Limestone coincides with the semi-confining unit (SCU) between the UPZ and LPZ. The SCU ranges in thickness from approximately 200 feet in the northern area of the model to more than 500 feet in the south.

The LPZ occurs principally in the Avon Park Formation and is sometimes referred to as the "high T zone." Fracturing and secondary porosity are the principal mechanism of this permeability. Transmissivity varies from 5,000 ft^2/d to 1,600,000 ft^2/d.

Conceptual Model

The conceptual model was devised to include the hydrologic units discussed above. Figure 14 is an east-west, hydrogeologic cross-section of the conceptual model. Figure 15 is a north-south hydrogeologic cross section of the conceptual model. Five major permeable zones are simulated from three separate aquifer systems. Intervening semi-confining units are simulated indirectly in the model via leakance arrays. Regional groundwater flow direction is west towards the coast. Equivalent freshwater heads were utilized to simulate the saltwater interface in the LPZ. The aquifer systems generally thicken and dip from north to south. Equivalent porous media conditions are assumed.

Numerical Model

The SD Model is based on the numerical, finite-difference code MODFLOW, which was developed by McDonald and Harbaugh (1984 and 1996). Both steady-state and transient conditions were simulated. Average groundwater resource conditions for the year 1993 served as the target for the steady-state model. For the transient simulations, the model was calibrated to hydrologic conditions from January 1993 through December 1993.

Model Description

The SD Model was conceptualized as a quasi-three dimensional flow model because of the strong horizontal flow in the aquifer systems and the tight confinement between the SAS and the UFA and within the IAS. Groundwater flow is predominantly horizontal in the aquifer systems and vertical in the confining units.

Model Grid and Discretization

The SD Model is divided into five layers:

- Layer 1 – SAS
- Layer 2 – PZ2 of the IAS
- Layer 3 – PZ3 of the IAS
- Layer 4 – UPZ of the UFA
- Layer 5 – LPZ of the UFA

The model grid is oriented along the north-south axis and aligned with the Peninsular Model (Sepulveda, 2002). All model cells are 5,000 feet by 5,000 feet.

Boundary Conditions

The model is bounded above by specified heads which represent the SAS. The bottom of the model is the MCU, which is considered to be impermeable. The lateral boundaries are a combination of specified heads and specified flux (no flow). The lateral boundaries of Layers 2 and 3 are specified as no-flow except along the southern boundary, which is defined as constant heads.

The lateral boundaries of the UFA, Layers 4 and 5, are generally no-flow along the northern and southern boundaries. The east side of the model is subdivided into 5 separate constant head reaches. The offshore boundary is designated as a no-flow boundary in Layer 4 and as equivalent freshwater heads in Layer 5. General head boundaries are not utilized in this model.

Transmissivity

Calibrated transmissivities for Layers 2 through 5 are shown on Figures 16, 17, 18, and 19. The transmissivity for Layer 2 (PZ2) varies from 1 ft^2/d to 66,000 ft^2/d. PZ2 and PZ3 do not extend to the northern part of the model, which is why a transmissivity of 1 ft^2/d is specified. Transmissivity of Layer 3 (PZ3) varies from 1 ft^2/d to 18,000 ft^2/d. Transmissivities are generally higher in Layer 4 (UPZ), ranging from 2,000 ft^2/d to 350,000 ft^2/d. The highest transmissivities in the entire model are found in Layer 5 (LPZ) and ranges from 19,000 ft^2/d to 900,000 ft^2/d.

Leakance

Leakance between Layer 1 (SAS) and Layer 2 (PZ2) and between Layers 2 and 3 (PZ3) range from 0.000001 day^{-1} to 0.003 day^{-1}. Leakance between Layer 3 (PZ3) and Layer 4 (LPZ) ranges from 0.0000018 to 1.0 day^{-1}. Leakance of 1.0 day^{-1} assumes full communication between the layers. Between Layer 4 (UPZ) and Layer 5 (LPZ), only one leakance value is assigned: 0.01 day^{-1}. Figures 20, 21, 22 and 23 show calibrated leakance values for each layer of the SD Model.

Barcelo and Basso, 1993. Computer Model of Groundwater Flow in the Eastern Tampa Bay Water Use Caution Area: Southwest Florida Water Management District.

Model Area

The ETB Model includes all of Manatee, Hardee, Sarasota and Desoto Counties and parts of Hillsborough, Pinellas, Polk, Charlotte, Glades, and Highlands Counties. The ETB Model is an earlier version of the SD Model (Beach and Chan, 2003), which was previously discussed. The SD Model extends beyond the boundaries of the ETB Model to include Pasco and Hernando Counties to the north and Lee County to the south.

Hydrogeologic Framework

Groundwater in the study area occurs in three principal aquifers; the SAS, IAS, and UFA. The aquifers are separated by clay confining units that restrict the vertical movement of water. The geological framework and hydrostratigraphy of the study area are the same as that for the SD Model, as shown on Figure 13 (presented previously).

The SAS is found throughout the study area and consists of marine and non-marine quartz sand, clayey sand, shell, shelly marl and phosphorite, with some marl and limestone. Average thickness is approximately 25 feet, but ranges from less than 10 feet near the coast to several hundred feet in the eastern portion of the study area. Hydraulic properties of the SAS vary widely. Transmissivity varies from 20 ft^2/d in the northern part of the study area to 5,300 ft^2/d in Charlotte and Highlands Counties. Specific yield ranges from 0.05 to 0.30.

The IAS is found throughout the study area and comprises all water bearing units and confining beds between the overlying SAS and underlying UFA. The IAS consists of three principal parts: the upper intermediate confining bed which separates the surficial aquifer from the permeable units of the IAS; one to three permeable units; and the lower intermediate confining bed which separates the IAS from the underlying UFA. Thickness of the IAS ranges from 100 feet in Polk County to greater than 700 feet in Charlotte County. Transmissivity ranges from less than 300 ft^2/d to 15,400 ft^2/d. In the northern portion of the study area, transmissivity is generally less than 4,400 ft^2/d except along the Peace River in Polk County. In the southern portion of the study area, the upper limit for transmissivity is approximately 15,000 ft^2/d.

The upper ICU limits the flow of groundwater between the SAS and the IAS. The lower ICU restricts flow between the IAS and the UFA. The upper ICU is composed of sandy clay, clay, and marl that are part of the Peace River Formation of the Hawthorn Group. The thickness of the upper ICU ranges from 25 feet in northern Hillsborough County and Polk County to about 150 feet in central Desoto County. In the extreme northern part of the study area the confining bed becomes thin and discontinuous due to differential erosion and karst activity. The lower ICU is generally composed of sandy clay and clayey sand that is located near the base of the Tampa Member of the Arcadia Formation. The thickness of the unit ranges from less than 25 feet in Polk County to approximately 250 feet in the southeastern portion of the study area.

The UFA is composed of permeable sections of the Tampa Member, Suwannee Limestone, Ocala Limestone, and Avon Park Formation. The base of the UFA is the top of the MCU,

which is considered to be the first occurrence of vertically persistent, intergranular evaporites. This study does not consider the LFA which exists below the MCU and contains highly mineralized water. Thickness of the UFA ranges from approximately 1,000 feet in the northern portion of the study area to 1,400 feet toward the south.

Within the UFA are two permeable zones. These zones are typically associated with the Tampa Member and Suwannee Limestone, permeable portions of the Ocala Limestone (upper producing zone) and the highly permeable zones (lower producing zone) within the Avon Park Formation. The UPZ and LPZ are separated by the semiconfining portions of the Ocala Limestone.

The significance of two permeable zones is important in areas where the water quality of the LPZ is poor. In the inland part of the study area, highly productive wells are completed into the LPZ. Toward the southwest portion of the study area groundwater in the LPZ becomes increasingly mineralized. As a result, wells are typically constructed into the lower portions of the IAS and the UPZ of the UFA.

Although the Ocala Limestone is regarded as a semiconfining unit, there is evidence to suggest that there is sufficient hydraulic connection across the Ocala Limestone such that the UFA functions as a single hydraulic unit. Transmissivity of the LPZ range from 860,000 ft^2/d in eastern Desoto County to 36,000 ft^2/d in east-central Hillsborough County.

Conceptual Model

The conceptual model is similar to that of the SD Model (Figures 14 and 15, previously presented) and was devised to include the hydrologic units discussed above. Recharge to the UFA primarily results from rainfall that infiltrates the land surface and percolates downward through the SAS and IAS. Leakage occurs across the semiconfining beds that separate the IAS and SAS, and the IAS and the UFA. Although the UFA has two major producing zones, the aquifer is conceptualized as a single hydrologic unit. Regional groundwater flow in the UFA occurs predominantly in the LPZ. The IAS and UFA are simulated as single layer isotropic mediums with groundwater moving in horizontal planes. Horizontal flow in the confining beds is negligible compared to horizontal flow in the adjacent aquifers. Storage of water in the confining beds is negligible. Movement of the saltwater interface is assumed to have little effect on calculated heads. Heads in the SAS are assumed to be insensitive to changes in stress in the underlying aquifers.

Numerical Model

The ETB model is based on the numerical, finite-difference code MODFLOW, which was developed by McDonald and Harbaugh (1984 and 1996). Both steady-state and transient conditions were simulated by the model. Average groundwater resource conditions for the year 1989 served as the target for the steady-state model. For the transient simulations, the model was calibrated to hydrologic conditions from October 1988 through September 1989.

Model Description

The ETB Model was conceptualized as a quasi-three dimensional flow model because of the strong horizontal flow in the aquifer systems and the tight confinement between the SAS

and the UFA and within the IAS. Groundwater flow is predominantly horizontal in the aquifer systems and vertical in the confining units.

Model Grid and Discretization

The SD Model is divided into three layers:

- Layer 1 – SAS
- Layer 2 – IAS
- Layer 3 – UFA

The model grid is oriented along the north-south axis with uniform grid spacing of 2 miles by 2 miles, and consists of 56 rows and 60 columns.

Boundary Conditions

Water levels in Layer 1 (SAS) were held constant during model calibration. Specified heads were utilized through Layer 1. A combination no-flow cells and constant head cells were utilized along the boundary of Layer 2 (IAS). No-flow cells were utilized along the northern, eastern and southern boundaries of the model in Layer 2. Constant head cells were used along the western boundary of the model in Layer 2. A combination of head-dependant flux cells, constant head cells and no-flow cells were utilized along the boundary of Layer 3 (UFA).

Transmissivity

Transmissivity in Layer 2 (IAS) ranges from less than 1 ft^2/d along the northern boundary of the model to 11,000 ft^2/d in Charlotte County. Transmissivity of Layer 3 (UFA) ranges from 33,500 ft^2/d to 400,000 ft^2/d.

Leakance

Five zones were used to define leakance between Layers 1 and 2. Leakance varies between 0.00001 day^{-1} and 0.00067 day^{-1}. Six zones were used to define leakance between Layers 2 and 3.

HydroGeoLogic, Inc., June 2002. Three-Dimensional Density-Dependant Flow and Transport Modeling of Saltwater Intrusion in the Southern Water Use Caution Area

Model Area

The HydroGeoLogic Model is based upon the SD Model (Beach and Chan, 2003) discussed previously and an uncalibrated, saltwater intrusion model that was developed by Waterstone Environmental Hydrology and Engineering, Inc. (Waterstone). The domain of the HydroGeoLogic Model includes the southern half of Hillsborough County and all of Manatee and Sarasota Counties. The HydroGeoLogic Model is a smaller subset of the SD Model in terms of geographic area. The simulated area coincides with the domain of the Waterstone Model. Hydraulic properties and boundary conditions were assumed from the SD Model, while the model domain, grid spacing, and layer thicknesses were assumed from the Waterstone Model.

Hydrogeologic Framework

The hydrogeologic framework for this model is exactly the same as that of the SD Model. The local groundwater flow system is comprised of three vertically sequenced aquifer systems and their intervening semi-confining units. In descending order, these aquifer systems are the unconfined SAS, the confined IAS, and the confined UFA. As with the SD Model, for this model the LFA is not considered because it contains highly mineralized groundwater and is not utilized for water supply.

Conceptual Model

The hydrogeologic framework was conceptualized as 10 layers in the HydroGeoLogic Model. In order to simulate density-dependant flow and transport, intervening semi-confining layers must be explicitly modeled rather than using arrays of leakance. Hydraulic conductivity and thickness must therefore be specified for each aquifer and semi-confining unit. The Suwannee Limestone, Ocala Limestone, and Avon Park Formation are subdivided into two, three, and five finite-difference layers, respectively. These layers explicitly simulate permeable units and semi-confining units that have been identified in the three formations. The geometry of the hydrostratigraphic units assigned in the current model (i.e., top and bottom elevations) was adopted from the Waterstone Model. During their modeling investigation, Waterstone estimated the top and bottom elevations for all of the hydrostratigraphic units based on lithologic data provided by the SWFWMD. The uppermost formation in the HydroGeoLogic Model is the Suwannee Limestone. Only the UFA was simulated in the HydroGeoLogic Model. Rather than explicitly incorporating the SAS and IAS/ICU into the density-dependant model, vertical flow through these aquifers is simulated by specifying a general-head boundary condition at the top of the UPZ within the Suwannee Limestone. Hydraulic heads for the SAS and leakance values in the SD Model were used to calculate the general-head boundary conditions.

Numerical Model

The computer code MODHMS was selected for construction of the flow and solute transport model. MODHMS is a MODFLOW-based code developed by HydroGeoLogic for evaluating complex hydrologic and hydrogeologic settings. The density-dependant transport capabilities of MODHMS have been incorporated from DSTRAM, which is a well established and applied saltwater intrusion model developed by Huyakorn and Panday (1991). The MODFLOW-based structure of MODHMS makes the code fully compatible in terms of numerical approximations, grid structure and input/output data structures with the other MODFLOW based models developed for the SWFWMD. All of the MODFLOW features are available for use within MODHMS, including boundary conditions such as drains, streams, general-head conditions, and those involving water table conditions, infiltration, aquitard leakages, and pumping and injection wells. For contaminant transport simulation, MODHMS accounts for advection, anisotropic hydrodynamic dispersion with separate aerial and vertical components for longitudinal and transverse dispersivities, linear equilibrium sorption and first-order degradation reactions.

MODHMS is capable of simulating density-dependant, single-phase fluid flow and solute transport in saturated porous media. The code is applicable for complex situations where fluid flow is influenced significantly by variations in solute concentration.

Model Description

The HydroGeoLogic Model is fully three-dimensional in that semi-confining layers are explicitly simulated together with the permeable zones that comprise the aquifer systems. Arrays of thickness and hydraulic conductivity are specified for each permeable layer and semi-confining layer. Arrays of leakance are not utilized to implicitly simulate the semi-confining layers. The semi-confining layers must be fully three-dimensional in order to accurately simulate the saltwater interface, which is a physical feature that crosses aquifer systems in the vertical and horizontal directions.

Model Grid and Discretization

Ten layers are utilized to vertically discretize the UFA. The layers discretize the Suwannee Limestone, Ocala Limestone and Avon Park Formation. The top two layers are used to simulate the Suwannee Limestone. The next three layers are used to simulate the Ocala Limestone, and the bottom five layers are used for the Avon Park Formation. Multiple layers were used for each formation in order to explicitly simulate permeable zones and semi-confining layers. Formation boundaries were not necessarily used to delineate layer boundaries but rather contrasts in permeability were used to delineate separate layers.

The density-dependant model grid consists of 103 columns and 123 rows with spacings that range from 2,500 to 5,000 feet. The grid is deformed in the vertical direction to conform to permeability/formation geometries and topography.

Boundary Conditions

General-head boundary conditions were utilized in the top layer to simulate flow from the SAS and IAS, which were not directly simulated. Pre-development heads from the SD Model were used to provide constant heads boundaries along the northern, southern and eastern faces of the HydroGeoLogic Model. Constant heads along these boundaries were assigned to the Suwannee Limestone and the model layers that comprise the Avon Park Formation. The western boundary conditions were also defined as constant heads. The bottom boundary of the model was simulated as no-flow conditions. The bottom boundary coincides with the MCU.

Hydraulic Parameters

Hydraulic conductivity and thickness for each model layer must be specified. Initial values for hydraulic conductivity of the model layers were derived from calibrated transmissivity and leakance values that were assigned to the SD Model. It was assumed that horizontal hydraulic conductivity is isotropic in all model layers. Transmissivity from the SD Model was divided by unit thickness values from the Waterstone Model to yield arrays of hydraulic conductivity for each model layer. A horizontal to vertical anisotropy of 100:1 was assumed for each aquifer unit. Leakance and transmissivity are not specified in the fully three-dimensional modeling approach taken by the HydroGeoLogic Model.

Environmental Simulations, Inc., April 2004. Development of the District Wide Regulation Model for Southwest Florida Water Management District.

Model Area

Environmental Simulations, Inc. (ESI) was retained by the SWFWMD to assist in formulating their approach to regional groundwater modeling. The goal of the project was two-fold. First, develop a District Wide Regulation Model (DWRM), which is a modified version of the USGS model of the IAS and FAS in Peninsular Florida (Sepulveda, 2002) covering the entire SWFWMD plus a buffer area surrounding the SWFWMD. The USGS model developed by Sepulveda is known as the Peninsular Model and was described previously. The second goal was to develop a modified telescopic mesh refinement (TMR) technique that would streamline the SWFWMD's review of Water Use Permits.

The DWRM approach was to use the Peninsular Model as a starting point and activate the SAS layer, which the USGS treated as an array of constant heads. The Peninsular model was also reduced in size to cover an area slightly larger than the SWFWMD. The overall regional modeling approach was subdivided into several tasks.

- Reduce the Peninsular Model to cover only the SWFWMD
- Activate the SAS layer
- Create SWFWMD wide stream coverage for use in the calibration and TMR
- Calibrate the SAS layer
- Create new TMR routine

The area outside the SWFWMD was eliminated from the Peninsular Model. The boundary of the new model was the SWFWMD boundary plus a buffer area of approximately 10 miles so that permits at the edge of the SWFWMD boundary could be evaluated. Because the original Peninsular Model did not extend fully to the southern boundary of the SWFWMD, 22 rows were added to the DWR Model. The southern boundaries of the DWR Model were made to coincide with the SD Model.

Hydrogeologic Framework

The hydrogeologic framework is the same as the Peninsular Model. The SAS is the uppermost water-bearing hydrogeologic unit. The SAS mostly consists of variable amounts of sand, clay, sandy clay, shell beds, silt, and clay. Limestone units within the SAS are primarily in southwest Florida. The SAS extends throughout most of the study area, except where the UFA is unconfined. The IAS underlies the SAS and extends throughout most of southwest Florida. The unit consists mainly of clastic sediments interbedded with carbonate rocks that generally coincide with the Hawthorn Group. Confining beds that overlie the UFA and underlie the SAS limit the vertical extent of the IAS in west-central Florida. The thickness of the IAS varies from approximately 25 feet in parts of Hillsborough and Polk Counties to approximately 400 feet in Charlotte County.

The hydrogeologic units (ICU and IAS) within the Hawthorn Group are differentiated based upon the permeability of the rock. In contrast to the IAS, the ICU is considerably less permeable. The UFA is considered to be unconfined in areas where the ICU or IAS is absent or very thin.

The FAS is a thick sequence of limestone and dolomitic limestone of Oligocene and Eocene ages with highly variable permeability. The FAS is divided into two aquifers of relatively high permeability, referred to as the UFA and the LFA. These aquifers are separated by a less permeable unit called the MCU in west-central Florida and in the northwest part of the study area, and MSCU in east-central Florida. The top of the UFA coincides either with the top of the Suwannee Limestone or the top of the Ocala Limestone, depending upon location. Rather than a single low-permeability unit separating the UFA and LFA, several units of regional extent separate the UFA from the LFA. Any of the regionally extensive low-permeability units may contain thin layers of moderate to high permeability. These confining units are not continuous and do not necessarily consist of the same rock type everywhere.

In west-central Florida, the UFA and LFA are separated by the MCU, which is composed of gypsiferous dolomite and dolomitic limestone of considerably lower permeability than that of the MSCU in east-central Florida.

Conceptual Model

The conceptual groundwater flow system is the same as the Peninsular Model except that the SAS (Layer 1) is actively simulated in the DWRM. In the Peninsular Model, the SAS was simulated as an array of constant heads. The SAS, IAS (or ICU in areas where the IAS is absent), the UFA, and the LFA were designated Layers 1 through 4, respectively. Confining layers were simulated by using vertical leakance arrays. Model-simulated groundwater flow occurs horizontally within the aquifers and vertically through the confining units.

The IAS (Layer 2) in was simulated as a single active aquifer bounded above and below by arrays of leakance values. Because this model is restricted to simulating the movement of freshwater within the aquifers; areas where the IAS, the UFA and the LFA (Layers 2 through 4) contain water with chloride concentrations exceeding 5,000 mg/L are considered inactive. Recharge to or discharge from the IAS is assumed to occur through the upper or lower confining units of the IAS.

The MCU was represented by vertical leakance values that limit water exchange between the UFA (Layer 3) and the LFA (Layer 4) in west-central and southwest Florida.

The River, Drain, and Recharge packages were used in this groundwater model. The River package was used to simulate the discharge of water to and from rivers in unconfined areas of the UFA. The discharge of groundwater to swamps in unconfined areas of the UFA and the flow from UFA springs located outside river cells was simulated by using the Drain package. Flow from springs was simulated as discharge to drain cells using the measured or estimated spring pool altitude as the drain elevation. The net recharge rates to unconfined areas of the UFA were assigned using the Recharge package.

Numerical Model

The DWR Model is based on the numerical, finite-difference code MODFLOW, which was developed by McDonald and Harbaugh (1984 and 1996). MODFLOW96 was the version of MODFLOW used for the DWR Model. Steady-state conditions were simulated by the model. Average groundwater resource conditions from August 1993 through July 1994 served as the target for the steady-state model.

Model Description

Like the Peninsular Model, the DWR Model was conceptualized as a quasi-three-dimensional flow model with horizontal flow in the aquifer systems and vertical leakance through the confining layers. The confining units are not explicitly simulated but are represented by arrays of leakance. Groundwater flow is predominantly horizontal in the aquifer systems and vertical in the confining units.

Model Grid and Discretization

The DWR Model is divided into four layers:

- Layer 1 – SAS
- Layer 2 – Intermediate Aquifer System (IAS)
- Layer 3 – Upper Floridan Aquifer
- Layer 4 – Lower Florida Aquifer

The model grid is oriented along the north-south axis. All model cells are 5,000 feet by 5,000 feet, with 210 columns and 322 rows.

Boundary Conditions

Constant head cells in most of the SAS (Layer 1) were changed to active cells except around the outer edges of the model and within major lakes and streams. Layers 1 and 2 were changed from no-flow cells to active cells in the northern portion of the SWFWMD where the FAS is unconfined. General-head boundaries were placed along boundaries that were continuous within the Peninsular Model. Model properties and boundary conditions in the southern part of the SWFWMD were imported from the SD Model. Heads assigned to the new general head boundaries were taken from the Peninsular Model. Conductance of the GHB cells was computed using hydraulic conductivity and cell thickness of the Peninsular Model.

Hydraulic Parameters

Hydraulic conductivity in the SAS (Layer 1) ranges from about 10 to 80 ft/day with most areas varying between 10 and 30 ft/day. The transmissivity of the IAS (Layer 2) ranges from about 100 ft^2/d to 25,000 ft^2/d with most areas between 1,000 and 10,000 ft^2/d. The transmissivity of the UFA ranges from about 1,000 ft^2/d to 10,000,000 ft^2/d in the calibrated DWR Model. In the southern part of the SWFWMD, the maximum transmissivity was set to 2,000,000 ft^2/d based upon results of aquifer performance tests in the area. UFA transmissivities in the northern portion of the SWFWMD were allowed to be as high as 10,000,000 ft^2/d, which was about the maximum transmissivity in the Peninsular Model. Most the UFA (Layer 3) had a transmissivity on the order of 100,000 ft^2/d. The average transmissivity of the LFA (Layer 4) was about 190,000 ft^2/d. In general, the arrays of transmissivity (Layers 2, 3, 4) and hydraulic conductivity (Layer 1) conform to the range of field values reported in the literature and the SWFWMD's database.

Leakance values for the interface between the SAS and IAS range from about 1.0×10^{-6} day^{-1} to 0.1 day^{-1}. Most of the higher leakance values are for the northern part of the SWFWMD where the SAS is in contact with the UFA. Leakance values between the IAS and UFA range from 1.0×10^{-6} day^{-1} to 0.01 day^{-1} with most areas being around 0.001 day^{-1}.

Table 1
Southwest Groundwater Model Review Layer Comparisons
Subtask 3 - Groundwater Model Development

		Model No. 7	Model No. 26	Model No. 27	Model No. 30	Model No. 33
	Author Agency Location	Barcelo & Basso, 1993 SWFWMD Eastern Tampa Bay WUCA	Sepulveda, 2002 USGS Peninsular Florida (Megamodel)	Beach & Chan, 2003 SWFWMD Southern District	HydeoGeoLogic, Inc 2002 SWFWMD West-Central Florida	Environmental Simulations, Inc., 2004 SWFWMD District Wide Regulatory Model (DWRM)
Surficial Aquifer	Water-Table/Biscayne Aquifer	Layer 1	Layer 1	Layer 1		Layer 1
	Confining Beds					
	Lower Tamiami Aquifer					
Intermediate Aquifer or Confining Unit	Confining Unit					Layer 2
	Sandstone Aquifer	Layer 2				
	PZ1		Layer 2			
	PZ2		Layer 2	Layer 2		
	PZ3		Layer 2	Layer 2		
	Semi-Confining Unit					
	Mid-Hawthorn Producing Zone					
	Semi-Confining Unit					
Floridan Aquifer System	Lower Hawthorn Producing Zone					
	Upper Floridan Aquifer	Layer 3	Layer 3	Layer 4	Layer 1, Suwanee	Layer 3
					Layer 2, Suwanee	
					Layer 3, Ocala	
					Layer 4, Ocala	
					Layer 5, Ocala	
					Layer 6, Avon Park	
					Layer 7, Avon Park	
					Layer 8, Avon Park	
					Layer 9, Avon Park	
	Middle Confining Unit/Middle Semi-confining Unit				Layer 10, Avon Park	
	Middle Floridan Producing Zone					
	Lower Floridan Aquifer		Layer 4			
	Lower Floridan-Boulder Zone					
	Sub-Florida Confining Unit					

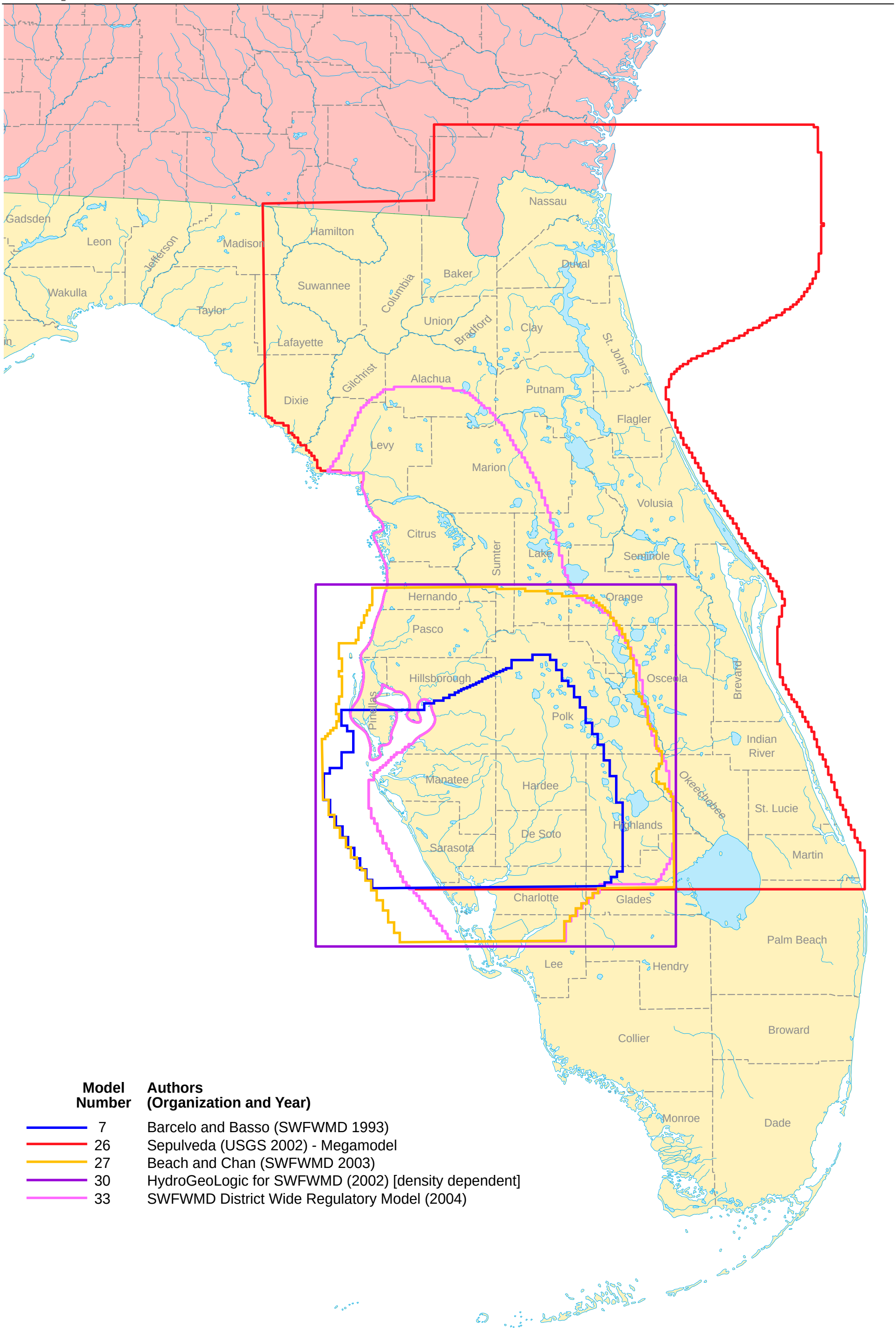

Model Number	Authors (Organization and Year)
7	Barcelo and Basso (SWFWMD 1993)
26	Sepulveda (USGS 2002) - Megamodel
27	Beach and Chan (SWFWMD 2003)
30	HydroGeoLogic for SWFWMD (2002) [density dependent]
33	SWFWMD District Wide Regulatory Model (2004)

North

0 15 30

Approximate Scale in Miles

FIGURE 1
Reviewed Model Boundaries
USACE - Subtask 3 Model Development

CH2MHILL

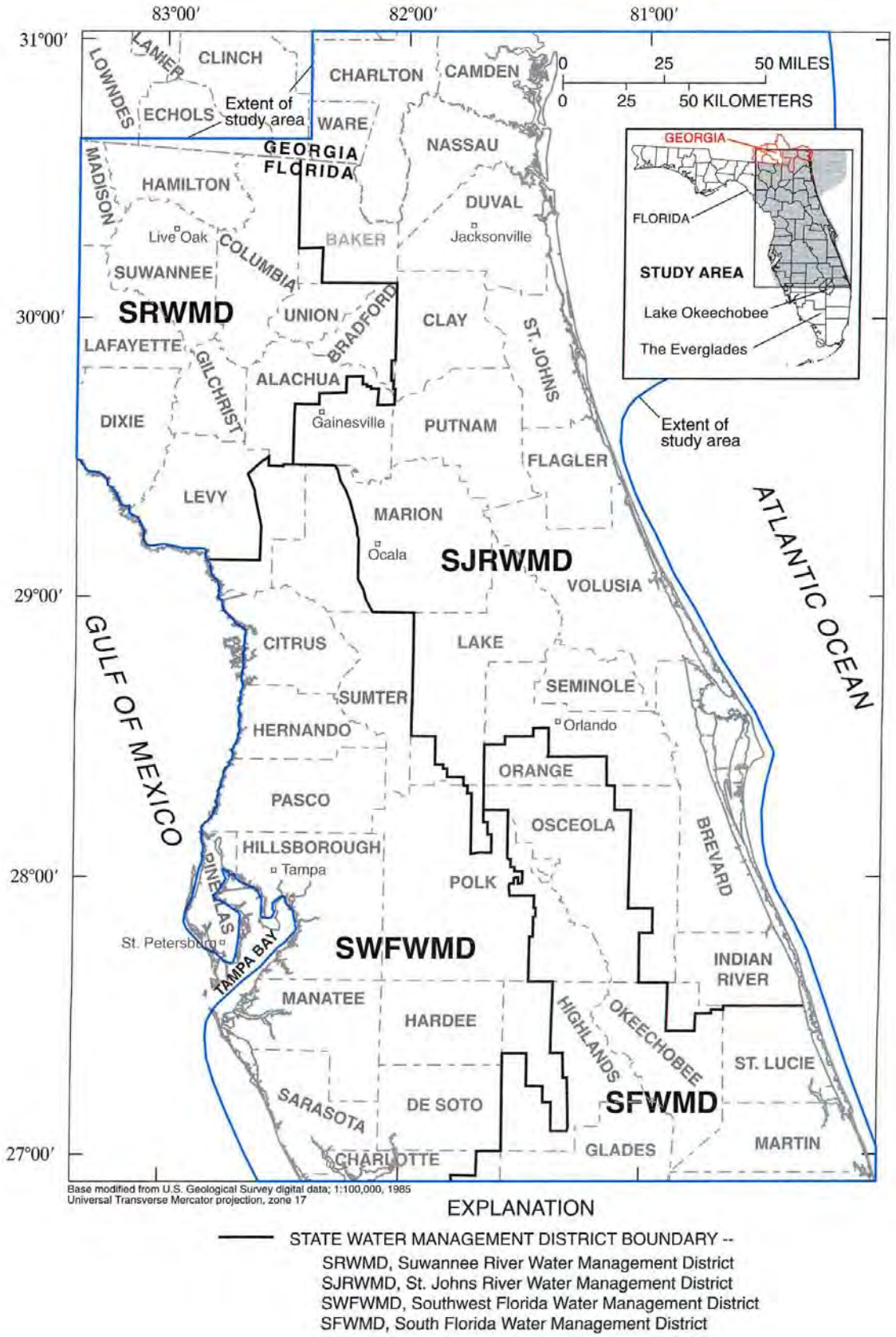

Source:
Simulation of Ground-Water Flow in the Intermediate and Floridan Aquifer Systems in Peninsular Florida
USGS
Water-Resources Investigations Report 02-4009

FIGURE 2
Location of Study Area and
Water Mangement District Boundaries
Sub-Task 3 - Model Development

SYSTEM	SERIES	STRATIGRAPHIC UNIT	GENERAL LITHOLOGY	HYDROGEOLOGIC UNIT
QUATERNARY	HOLOCENE	SURFICIAL DEPOSITS	Undifferentiated fluvial sands and residuum with interbedded clay, shell, and limestone.	SURFICIAL AQUIFER SYSTEM
	PLEISTOCENE	SURFICIAL DEPOSITS	Undifferentiated terrace and shallow marine deposits.	
TERTIARY	PLIOCENE	UNDIFFERENTIATED DEPOSITS (southwest Florida)	Clayey and pebbly sand; clay, marl, shell, phosphatic.	
	MIOCENE	HAWTHORN GROUP (generally absent in north-central Florida)	Highly variable sequence of mostly clay, silt, and sand - all phosphatic, phosphatic limestone, or dolomite, in lower part. In southwest Florida, white to light-gray, sandy, hard to soft, locally clayey, fossiliferous limestone containing phosphate and chert in some places.	INTERMEDIATE AQUIFER SYSTEM OR INTERMEDIATE CONFINING UNIT
	OLIGOCENE	SUWANNEE LIMESTONE (absent in northeast Florida)	Cream to tan, crystalline, highly vuggy limestone containing prominent gastropod and pelecypod cast and molds.	UPPER FLORIDAN AQUIFER
	EOCENE	OCALA LIMESTONE	(UPPER) White, generally soft, somewhat friable, porous coquina composed of large foraminifera bryozoan fragments and whole to broken echinoid remains, all loosely bound by a matrix of micritic limestone. (LOWER) Cream to white, generally fine-grained, soft to semi-indurated micritic limestone containing abundant miliolid remains and scattered large foraminifers.	
		AVON PARK FORMATION	Mainly cream-colored, highly microfossiliferous chalky limestone that locally contains some gypsum and chert that is commonly partially dolomitized.	MIDDLE CONFINING/ MIDDLE SEMICONFINING UNIT
		OLDSMAR FORMATION	Consists mostly of off-white to light-gray micritic to finely pelletal limestone thickly to thinly interbedded with gray to tan to light-brown, fine to medium crystalline, and commonly vuggy, dolomite.	LOWER FLORIDAN AQUIFER
	PALEOCENE	CEDAR KEYS FORMATION	(UPPER) Gray to cream, coarsely crystalline dolomite that is moderately to highly porous. (LOWER) Tan to gray, finely crystalline to microcrystalline dolomite interbedded with white to clear anhydrite.	SUB-FLORIDAN CONFINING UNIT

Source:
Simulation of Ground-Water Flow in the Intermediate and Floridan Aquifer Systems in Peninsular Florida
USGS
Water-Resources Investigations Report 02-4009

FIGURE 3
Stratigraphic Units, General Lithology, and Hydrogeologic Units
Sub-Task 3 - Model Development

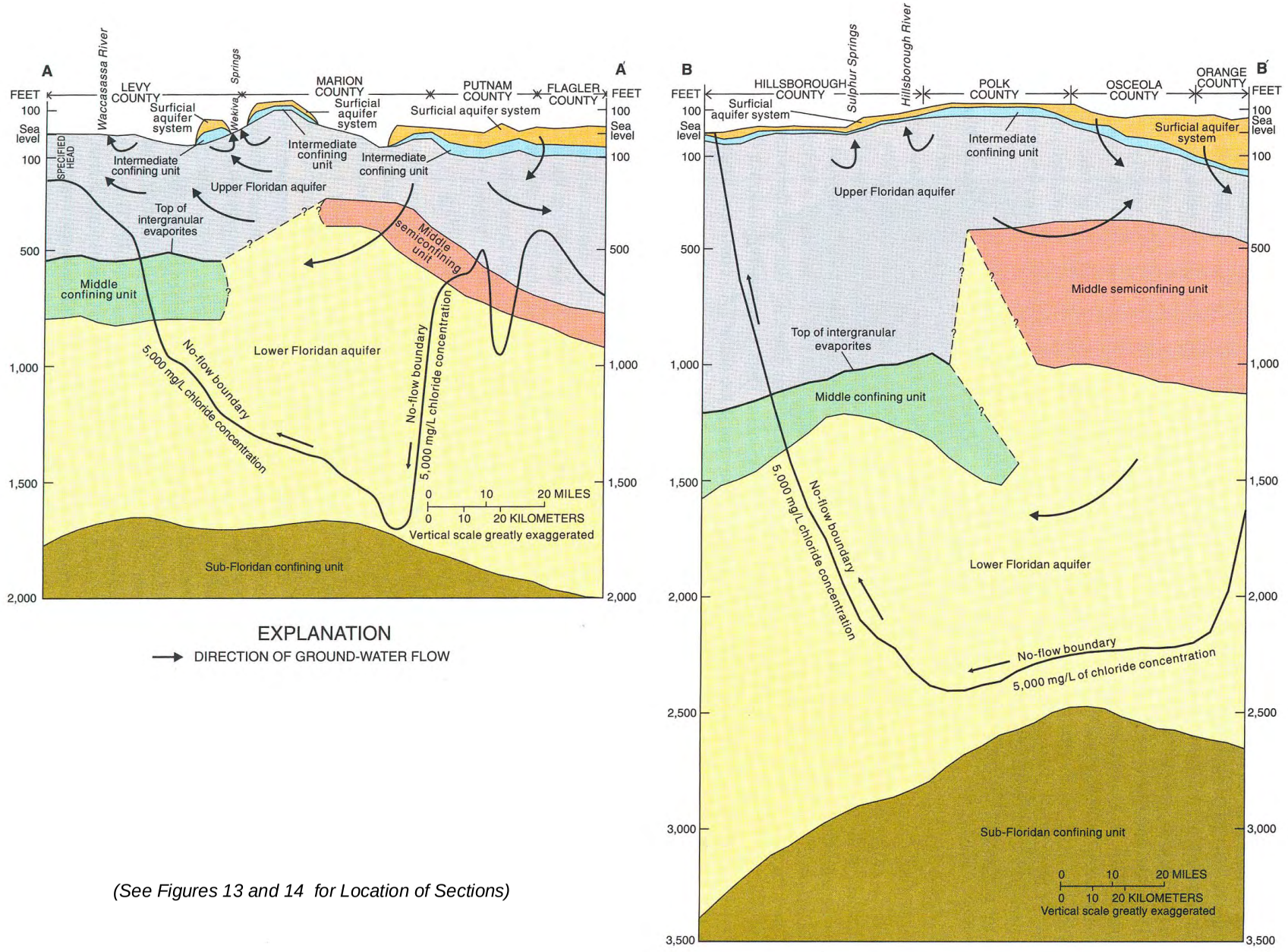

(See Figures 13 and 14 for Location of Sections)

Source:
Simulation of Ground-Water Flow in the Intermediate and Floridan Aquifer Systems in Peninsular Florida
USGS
Water-Resources Investigations Report 02-4009

FIGURE 4
Generalized Hydrogeologic Sections A-A' and B-B' Showing Conceptualized Ground-Water Flow (Modified from Miller, 1986)
Sub-Task 3 - Model Development

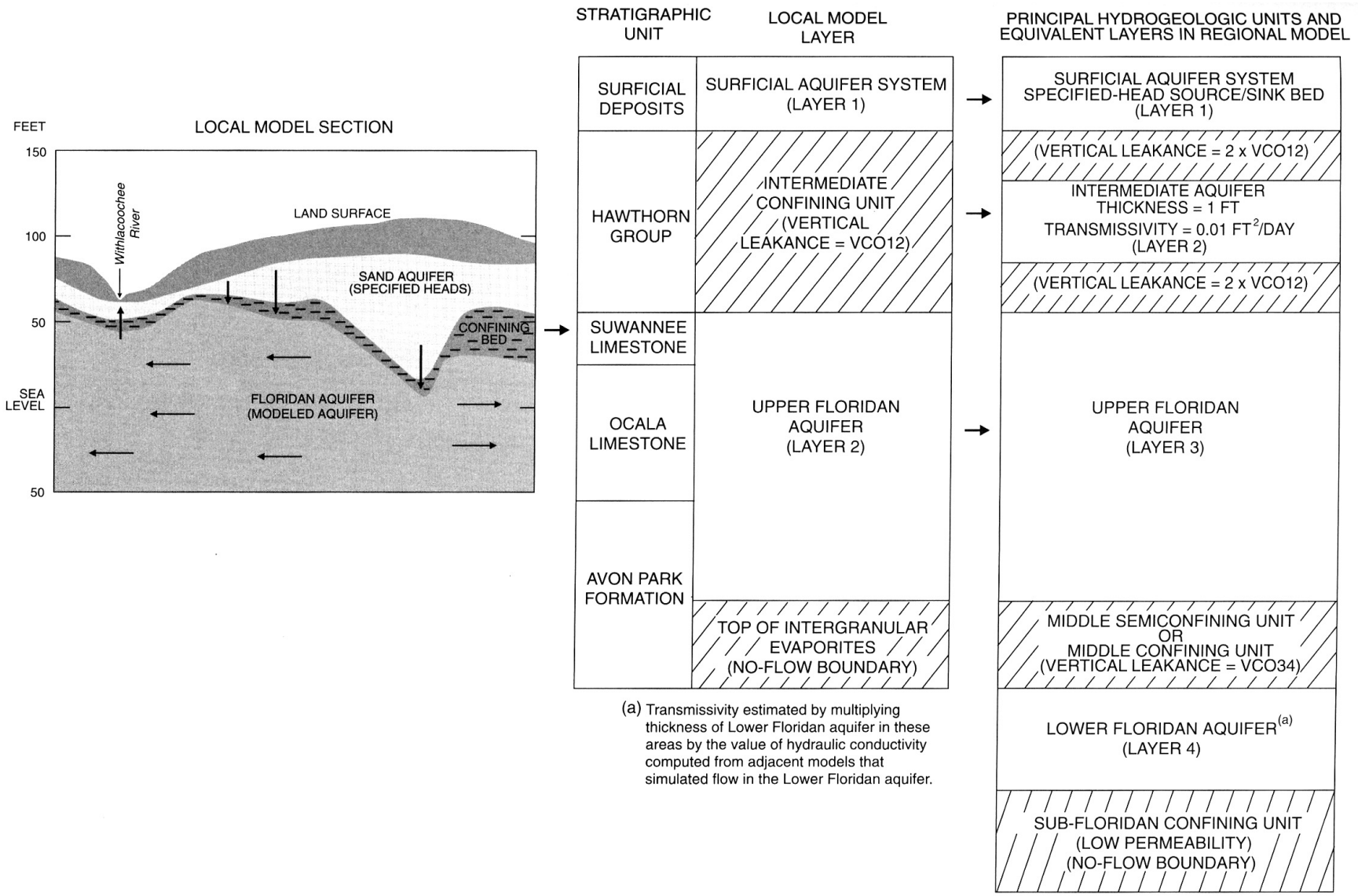

FIGURE 5
Layering Scheme and Representation of Geologic Units in Local Models 1 and 3, and Corresponding Layering Scheme in the Regional Model
Sub-Task 3 - Model Development

Source:
Simulation of Ground-Water Flow in the Intermediate and Floridan Aquifer Systems in Peninsular Florida
USGS
Water-Resources Investigations Report 02-4009

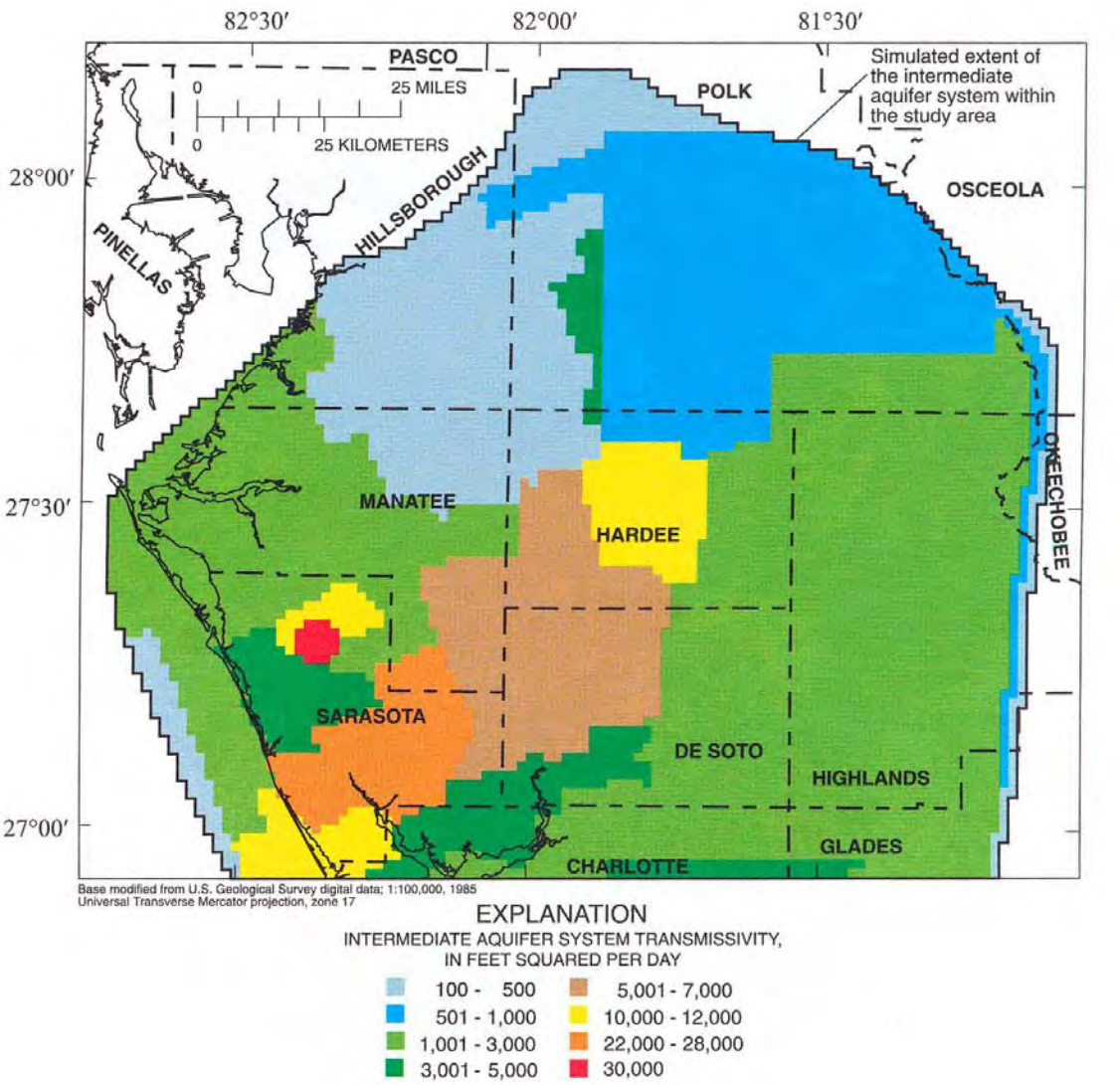

Source:
Simulation of Ground-Water Flow in the Intermediate and Floridan Aquifer Systems in Peninsular Florida
USGS
Water-Resources Investigations Report 02-4009

FIGURE 6
Transmissivity of the Intermediate Aquifer System from the Calibrated Model
Sub-Task 3 - Model Development

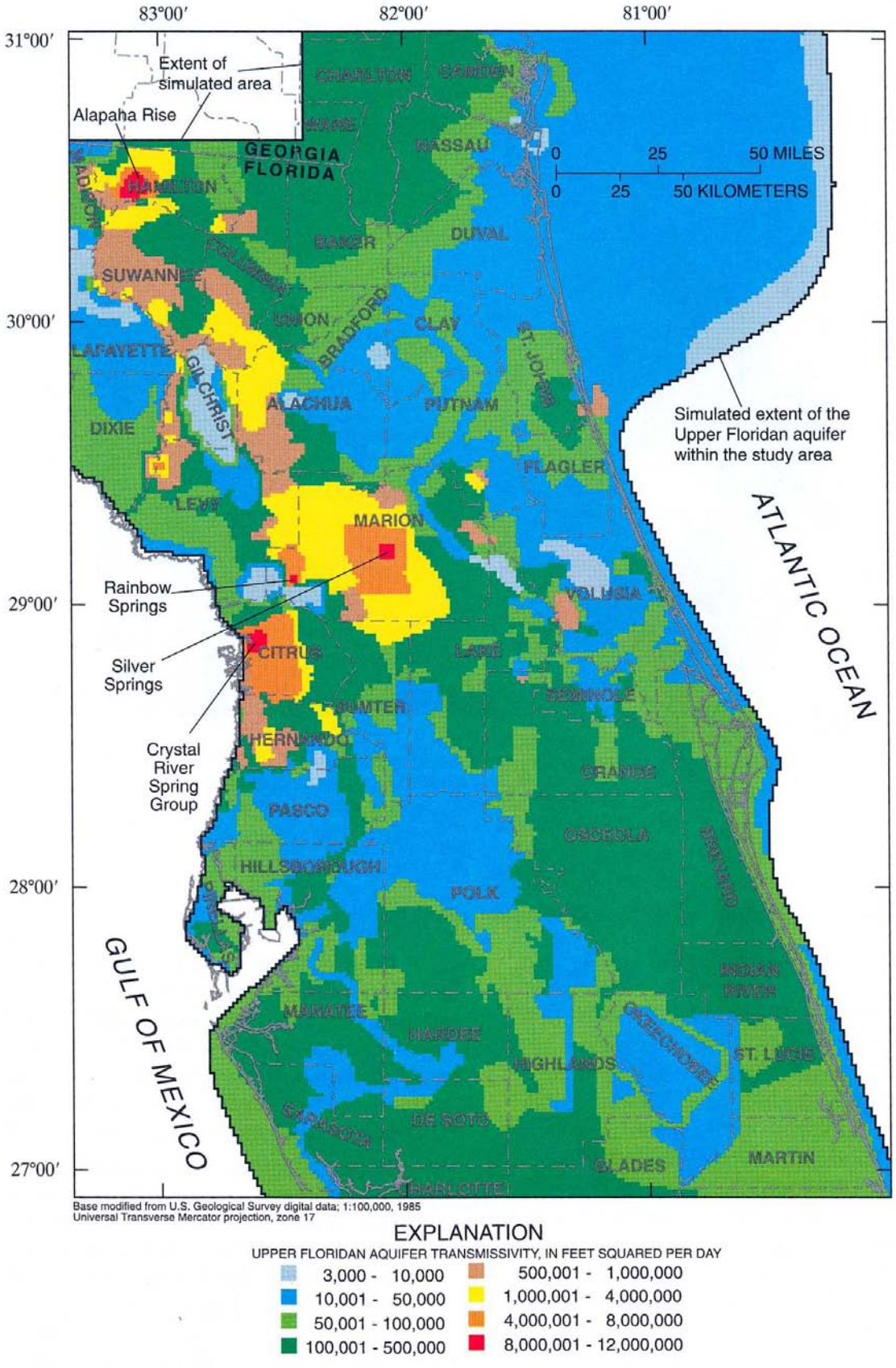

Source:
Simulation of Ground-Water Flow in the Intermediate and Floridan Aquifer Systems in Peninsular Florida
USGS
Water-Resources Investigations Report 02-4009

FIGURE 7
Transmissivity of the Upper Floridan Aquifer System from the Calibrated Model
Sub-Task 3 - Model Development

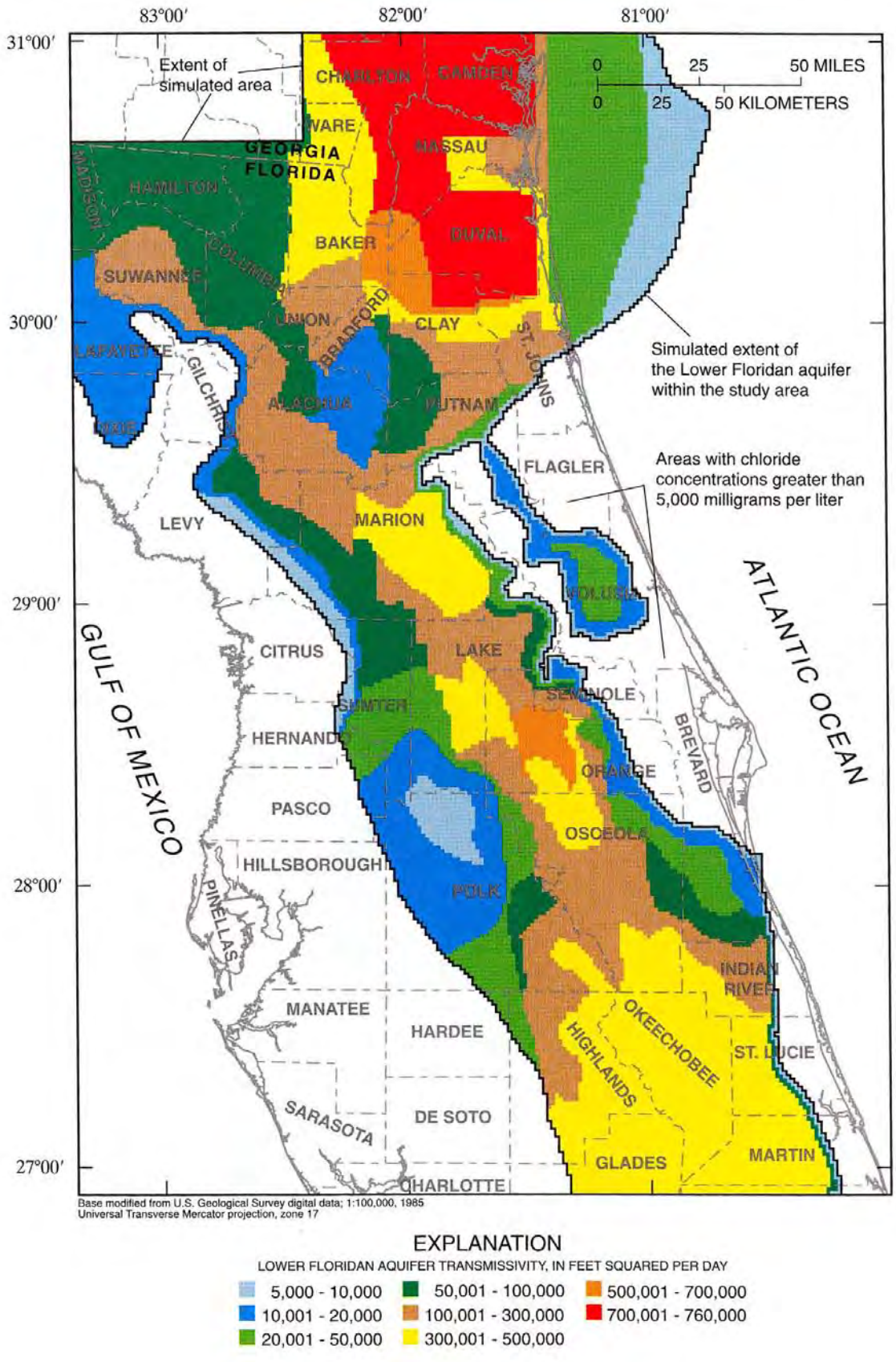

Source:
Simulation of Ground-Water Flow in the Intermediate and Floridan Aquifer Systems in Peninsular Florida
USGS
Water-Resources Investigations Report 02-4009

FIGURE 8
Transmissivity of the Lower Floridan Aquifer System from the Calibrated Model
Sub-Task 3 - Model Development

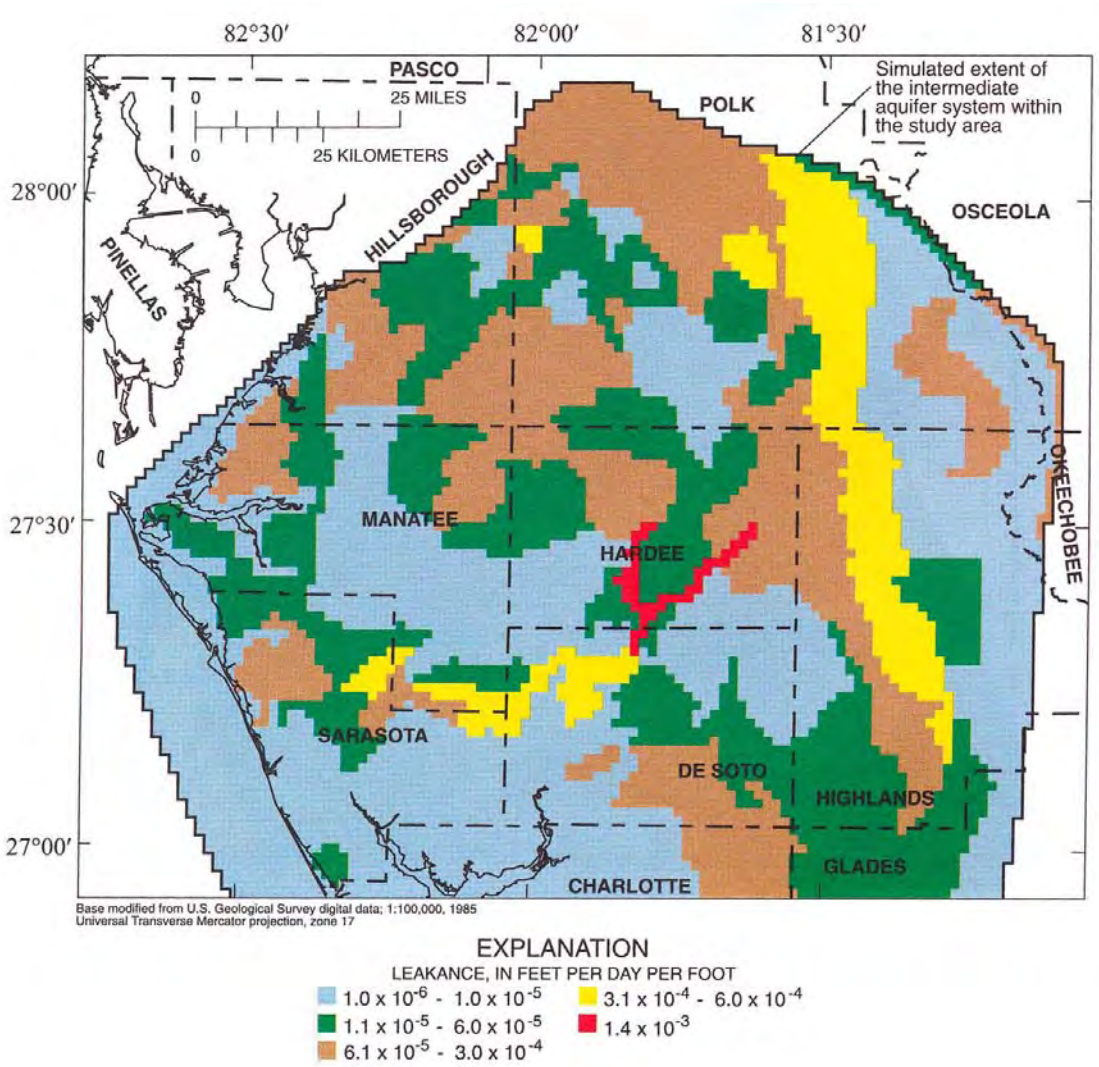

Source:
Simulation of Ground-Water Flow in the Intermediate and Floridan Aquifer Systems in Peninsular Florida
USGS
Water-Resources Investigations Report 02-4009

FIGURE 9
Leakance of the Upper Confining Unit of the Intermediate Aquifer System from the Calibrated Model
Sub-Task 3 - Model Development

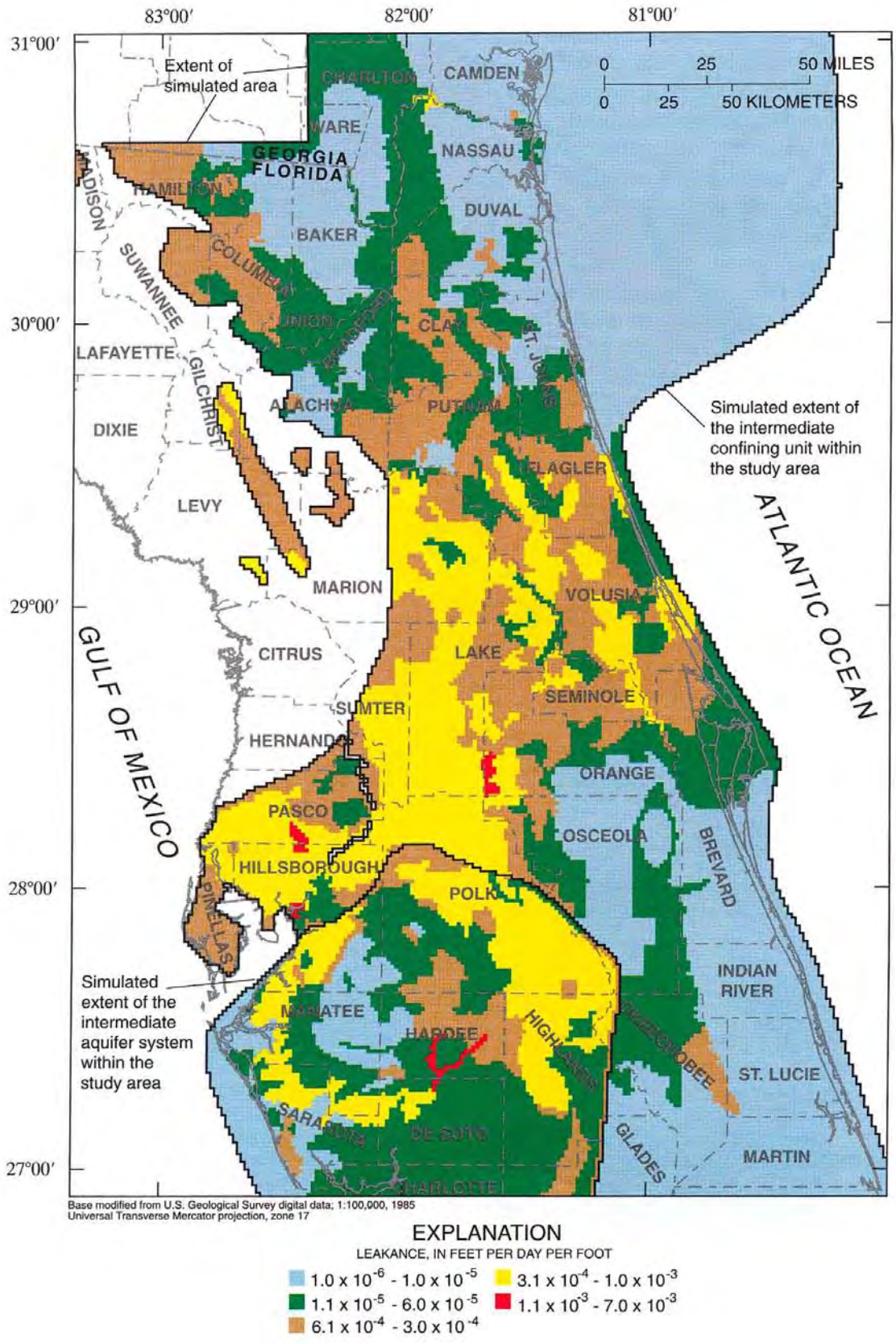

FIGURE 10
Leakance of the Intermediate Confining Unit and the Lower Confining Unit of the Intermediate Aquifer System from the Calibrated Model

Source:
Simulation of Ground-Water Flow in the Intermediate and Floridan Aquifer Systems in Peninsular Florida
USGS
Water-Resources Investigations Report 02-4009

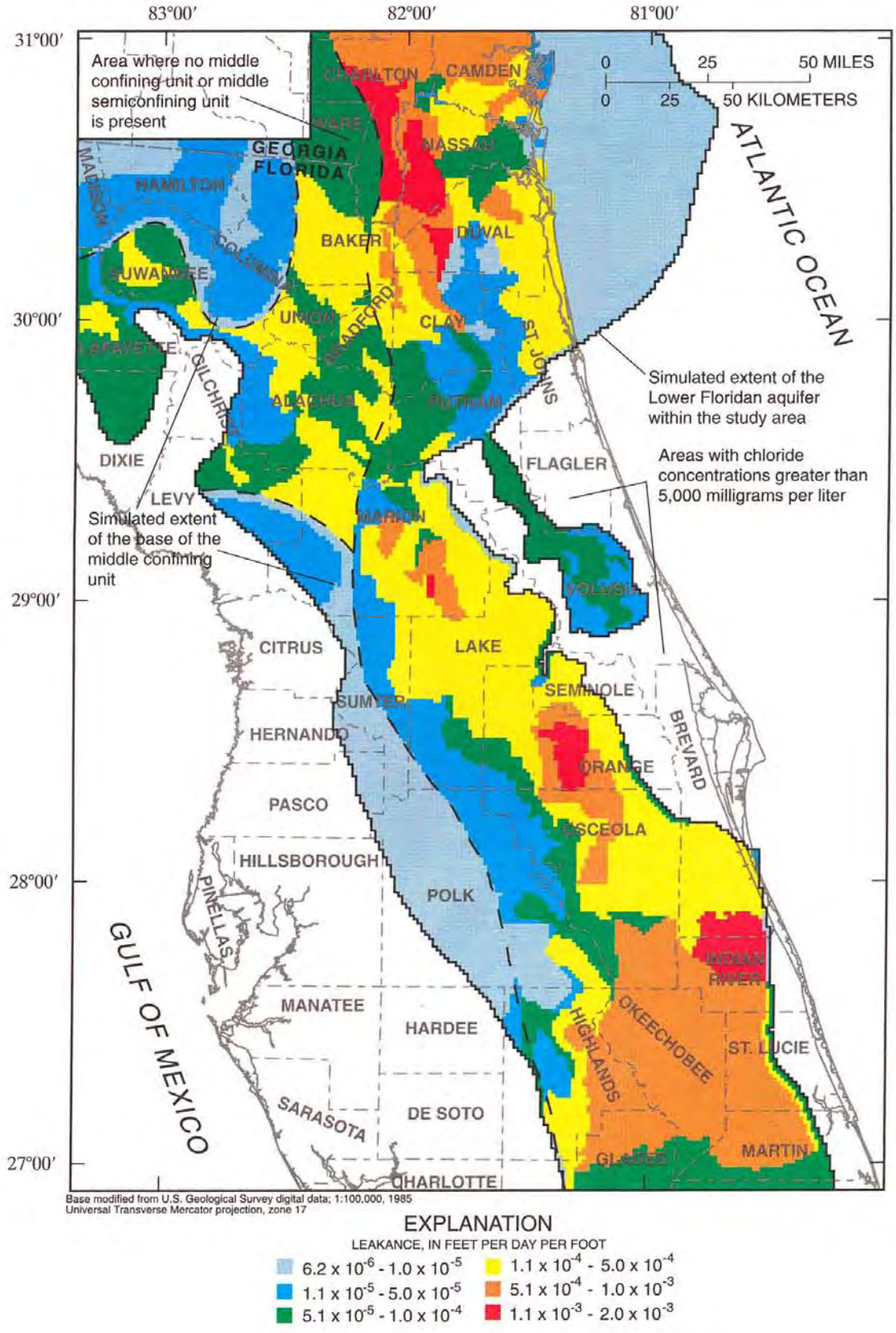

Source:
Simulation of Ground-Water Flow in the Intermediate and Floridan Aquifer Systems in Peninsular Florida
USGS
Water-Resources Investigations Report 02-4009

FIGURE 11
Leakance of the Middle Confining and Middle Semiconfining Units from the Calibrated Model
Sub-Task 3 - Model Development

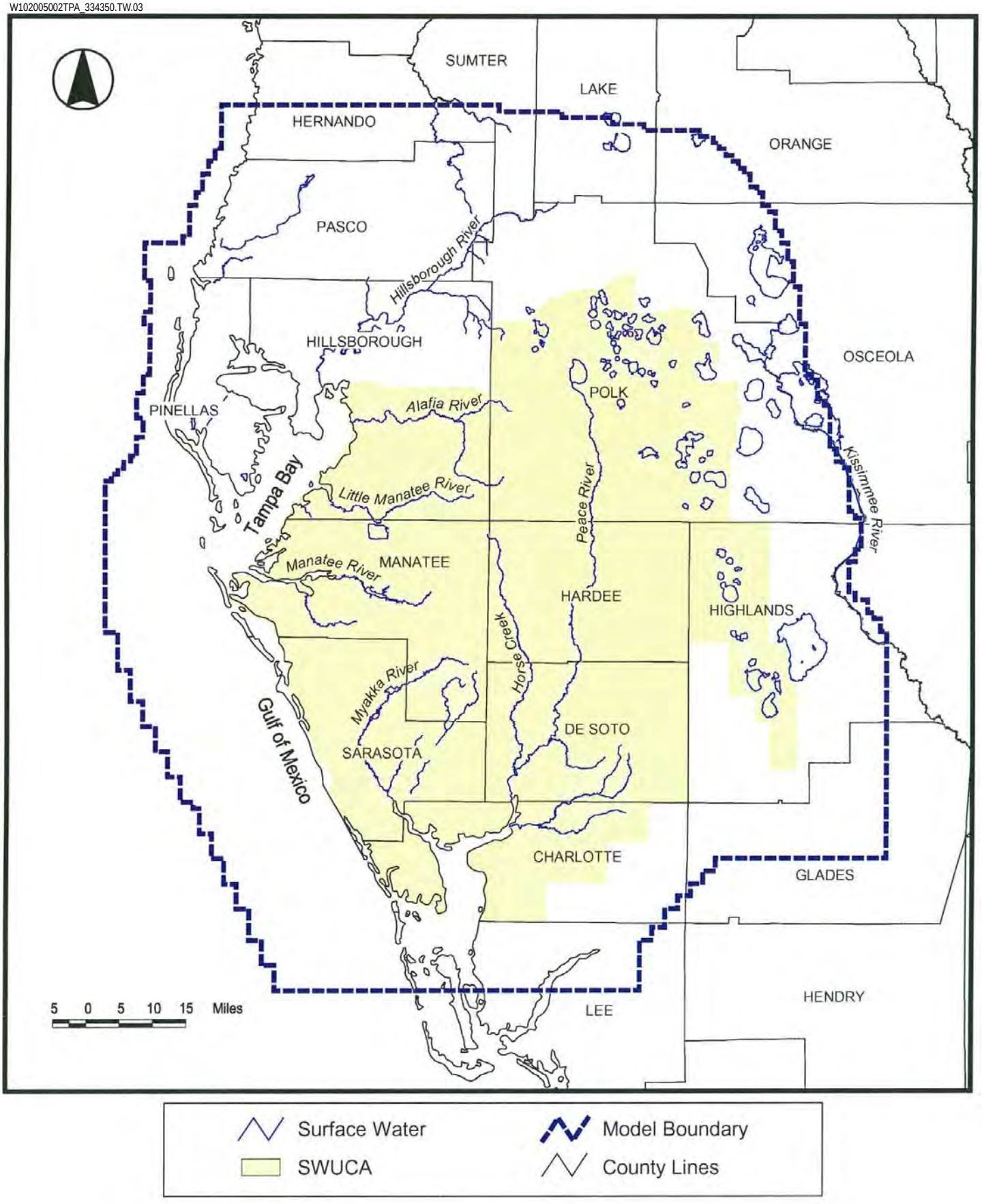

FIGURE 12
Model Area of the Southern District Model
with Major Surface Water Features
Sub-Task 3 - Model Development

Source:
Southern District Ground-Water Flow Model
Version 1.0
SWFWMD, August 2003

Series	Stratigraphic Unit		Hydrogeologic Unit		Lithology
Holocene to Pliocene	Undifferentiated Surficial Deposits		Surficial Aquifer System		Sand, silty sand, clayey sand, peat, and shell
Miocene	Hawthorn Group	Peace River Formation	UICU	Intermediate Aquifer System	Predominantly phosphatic clay, gray to green to brown, plastic, ductile, minor sand, residual limestone and dolostone
			PZ 2		
		Arcadia Formation	MICU		
		Tampa Member	PZ 3		Limestone, gray to tan, sandy, soft, clayey, minor sand, phosphatic. Chert found locally
			SCU		
Oligocene	Suwannee Limestone		UPZ	Upper Floridan Aquifer	Limestone, cream to tan, sandy, vuggy, fossiliferous
Eocene	Ocala Limestone		SCU		Limestone, white to tan, friable to micritic, fine-grained, soft, abundant foraminifera
	Avon Park Formation		LPZ		Limestone and dolomite. Limestone is tan, recrystalized. Dolomite is brown, fractured, sucrosic, hard. Peat found locally at top. Interstitial gypsum in lower part.
			Middle Confining Unit		

Source:
Southern District Ground-Water Flow Model
Version 1.0
SWFWMD, August 2003

FIGURE 13
Geology and Hydrogeology of the Southern District Model Area (from Basso, 2001)
Sub-Task 3 - Model Development

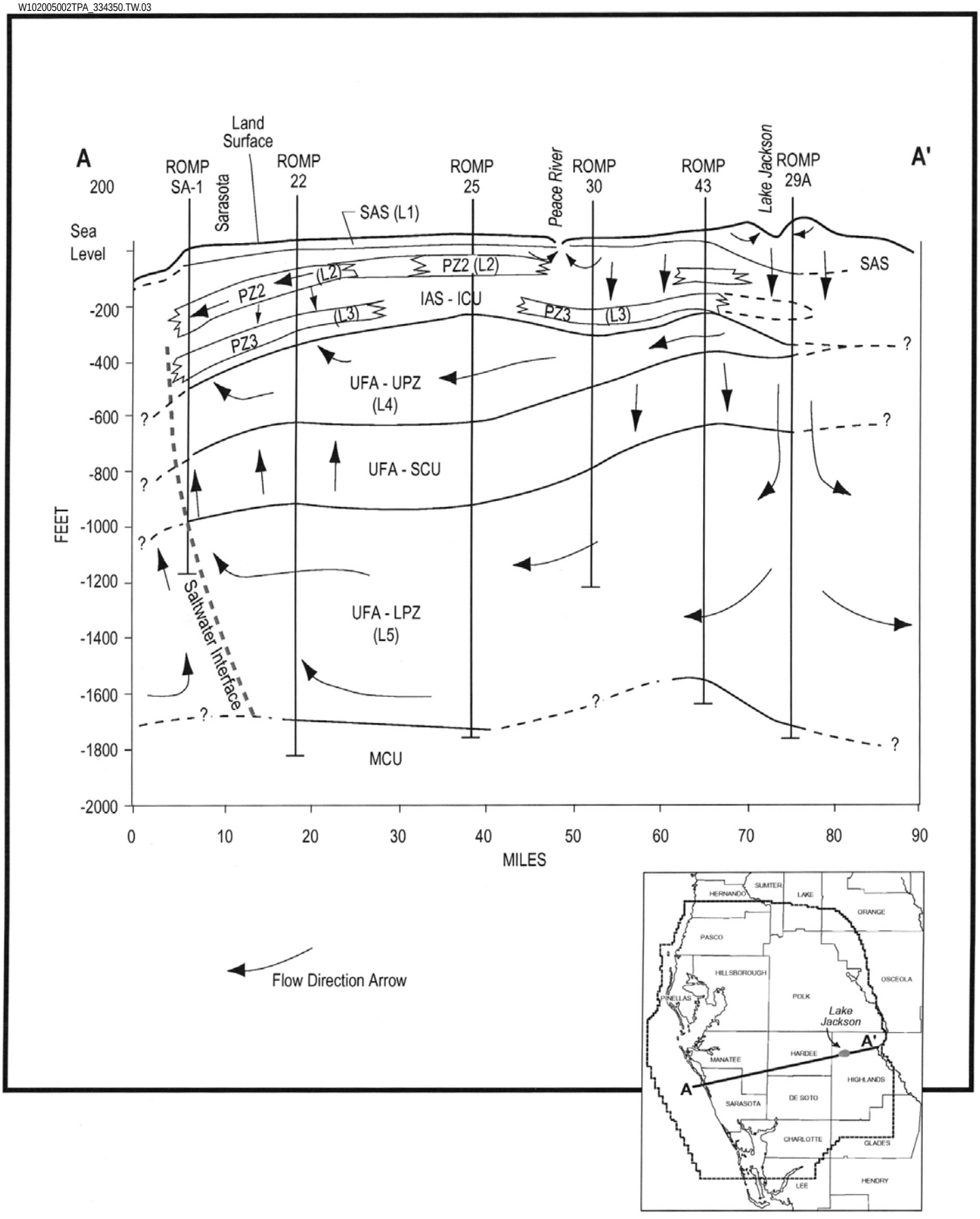

FIGURE 14
Conceptual Model as Hydrogeologic Cross Section from East to West (Section A-A')
Sub-Task 3 - Model Development

Source:
Southern District Ground-Water Flow Model
Version 1.0
SWFWMD, August 2003

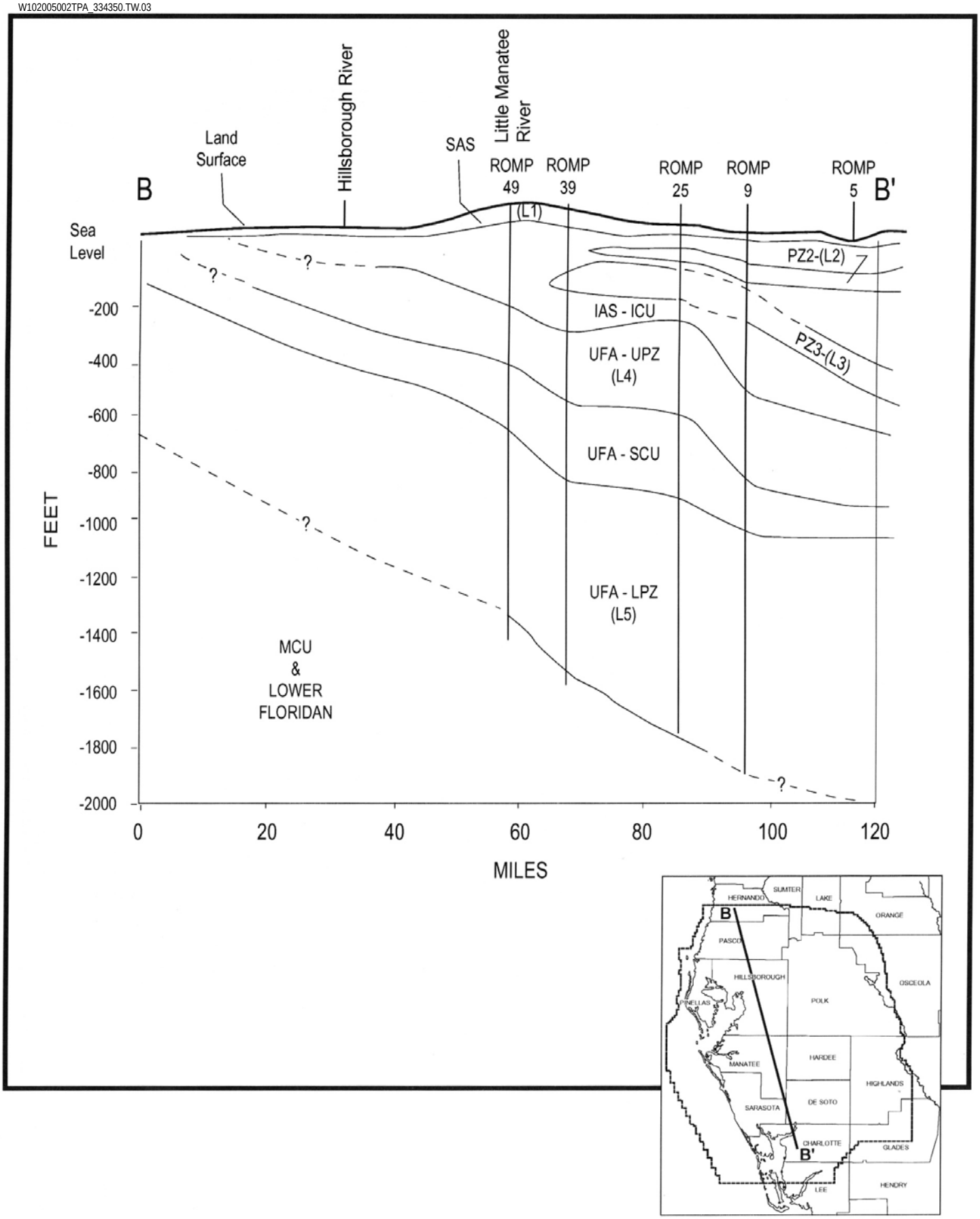

FIGURE 15
Conceptual Model as Hydrogeologic Cross Section from East to West (Section B-B')
Sub-Task 3 - Model Development

Source:
Southern District Ground-Water Flow Model
Version 1.0
SWFWMD, August 2003

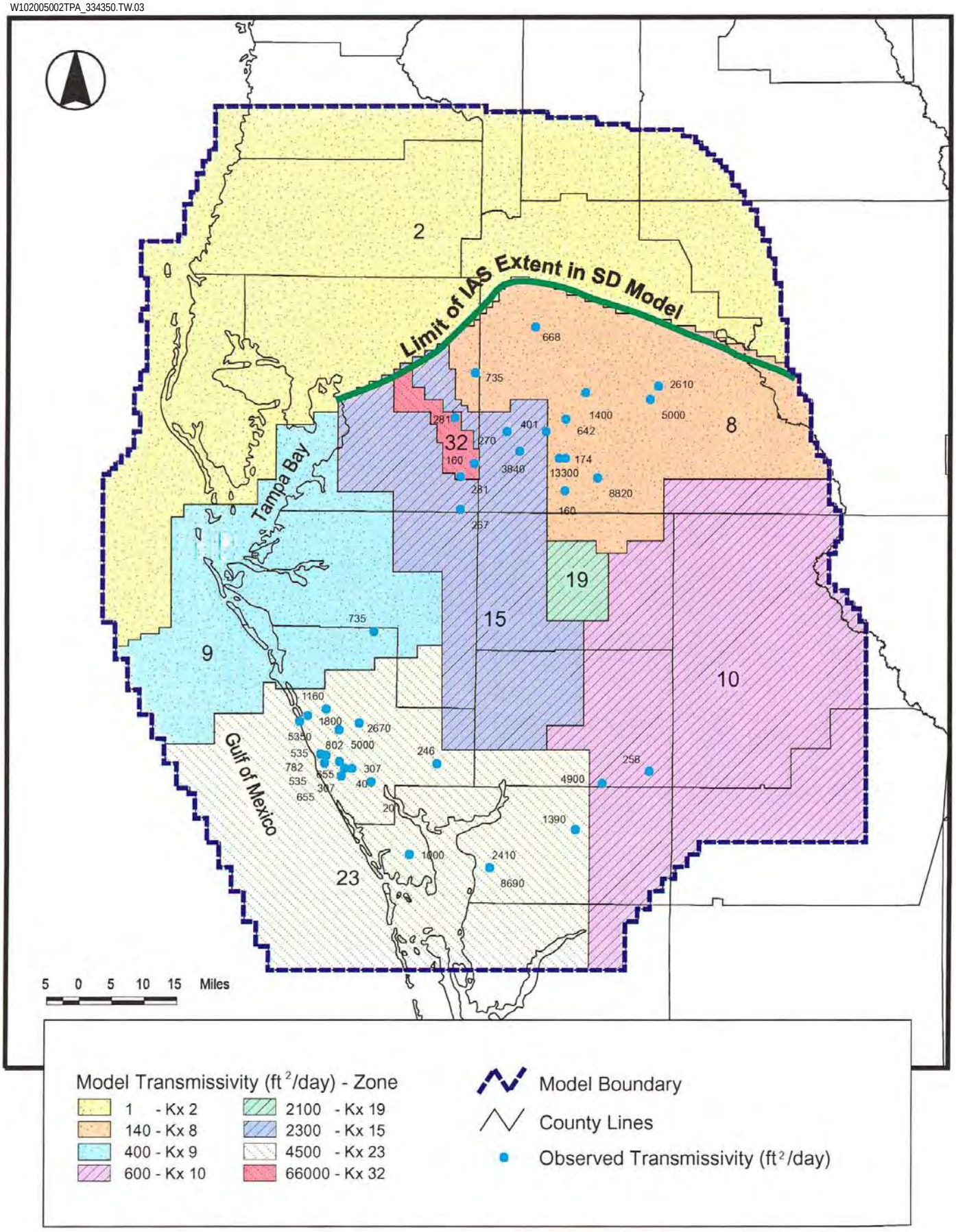

Source:
Southern District Ground-Water Flow Model
Version 1.0
SWFWMD, August 2003

FIGURE 16
Calibrated Transmissivity Distributions with Field Observed Values: Layer 2
Sub-Task 3 - Model Development

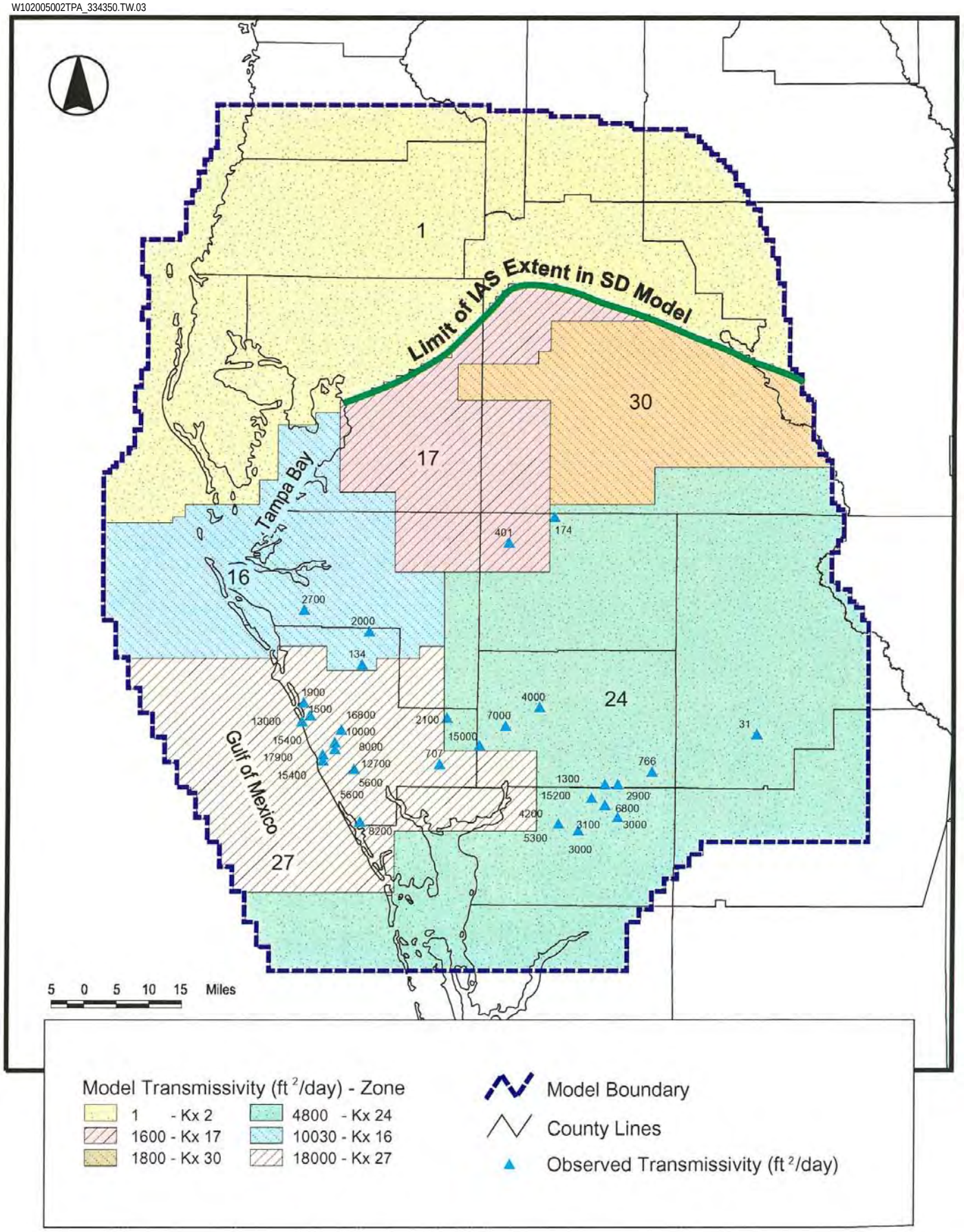

FIGURE 17
Calibrated Transmissivity Distributions with Field Observed Values: Layer 3
Sub-Task 3 - Model Development

Source:
Southern District Ground-Water Flow Model
Version 1.0
SWFWMD, August 2003

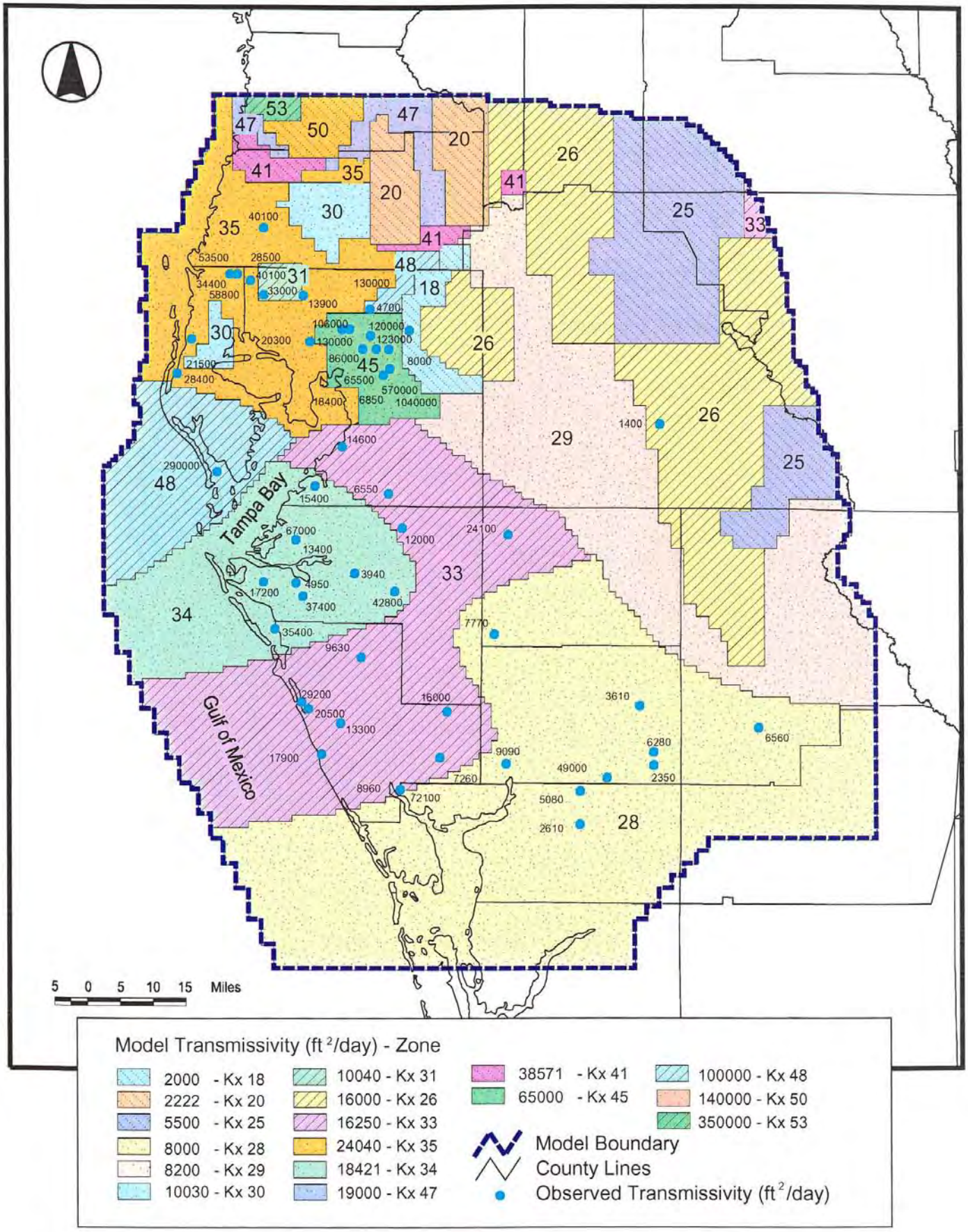

FIGURE 18
Calibrated Transmissivity Distributions with Field Observed Values: Layer 4
Sub-Task 3 - Model Development

Source:
Southern District Ground-Water Flow Model
Version 1.0
SWFWMD, August 2003

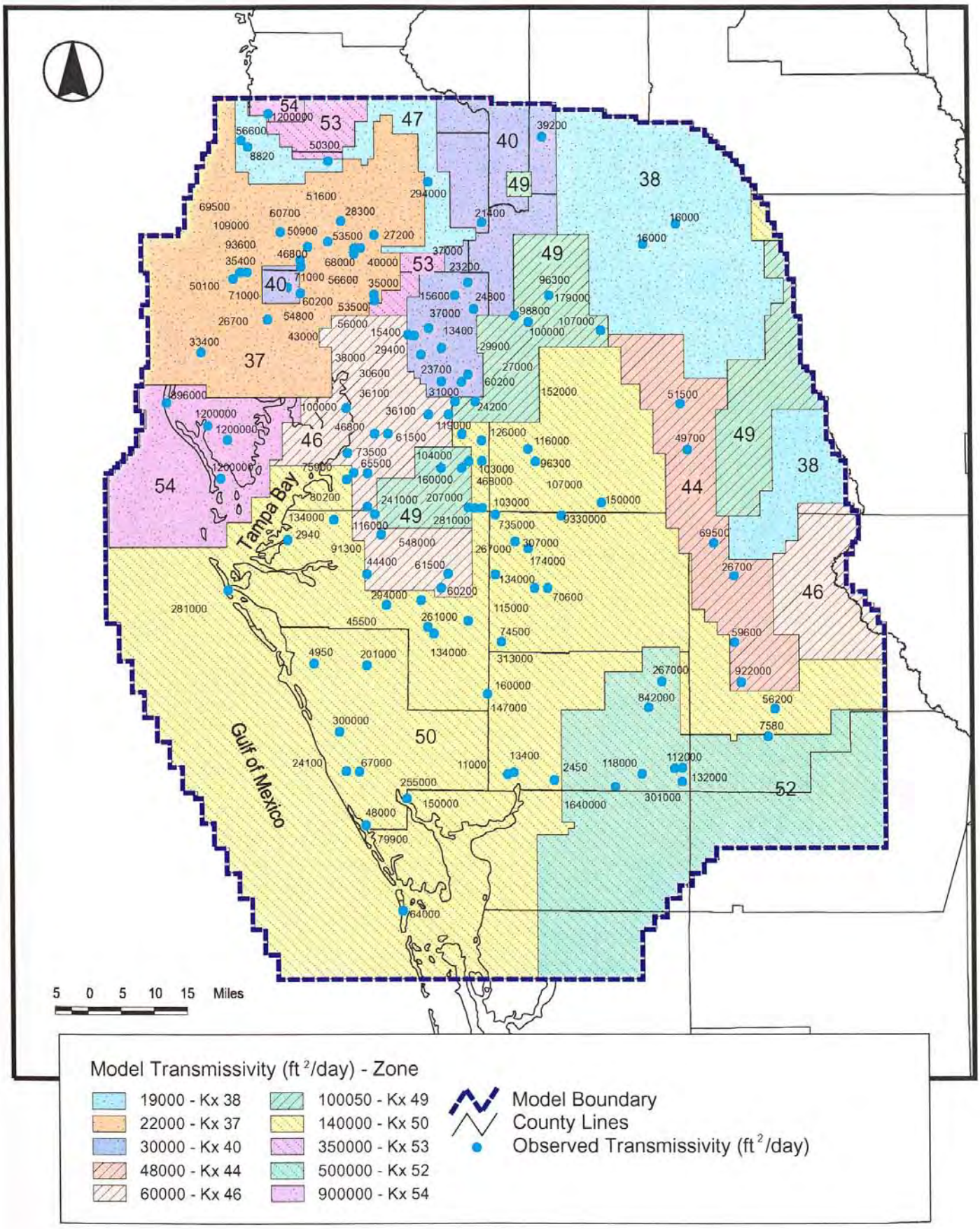

Source:
Southern District Ground-Water Flow Model
Version 1.0
SWFWMD, August 2003

FIGURE 19
Calibrated Transmissivity Distributions with Field Observed Values: Layer 5
Sub-Task 3 - Model Development

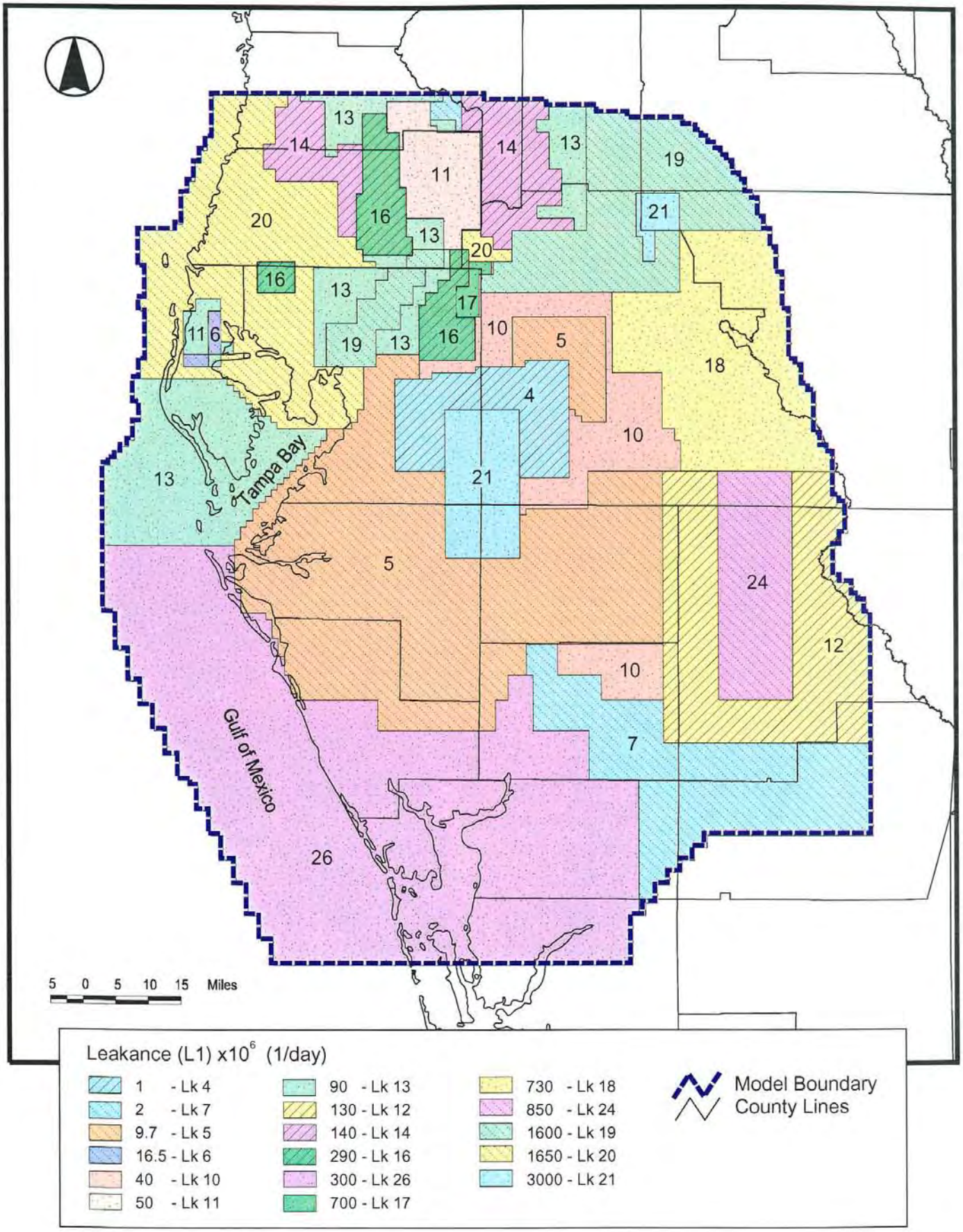

Source:
Southern District Ground-Water Flow Model
Version 1.0
SWFWMD, August 2003

FIGURE 20
Calibrated Leakance Values: Layer 1
(Between Layers 1 and 2)
Sub-Task 3 - Model Development

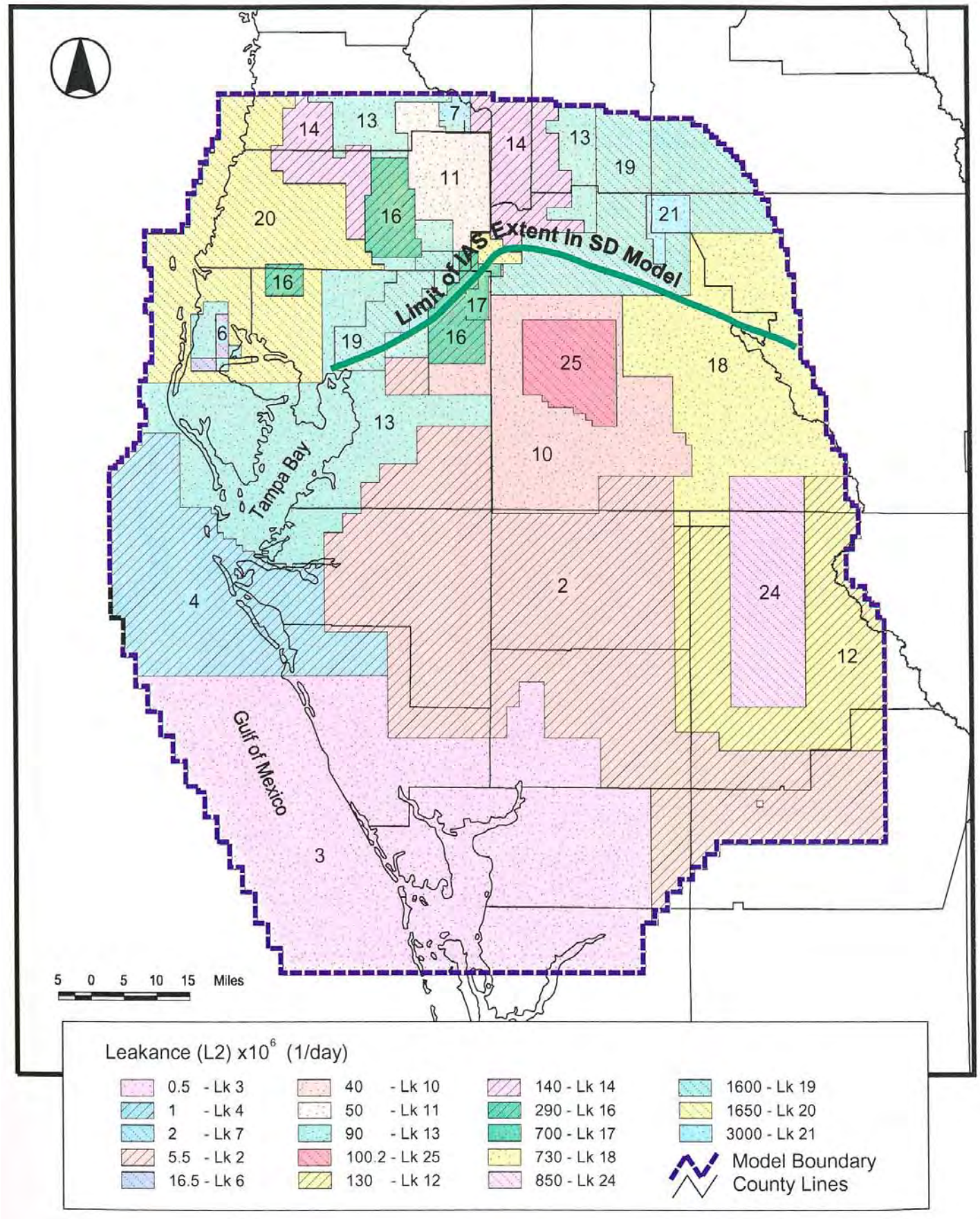

Source:
Southern District Ground-Water Flow Model
Version 1.0
SWFWMD, August 2003

FIGURE 21
Calibrated Leakance Values: Layer 2
(Between Layers 2 and 3)
Sub-Task 3 - Model Development

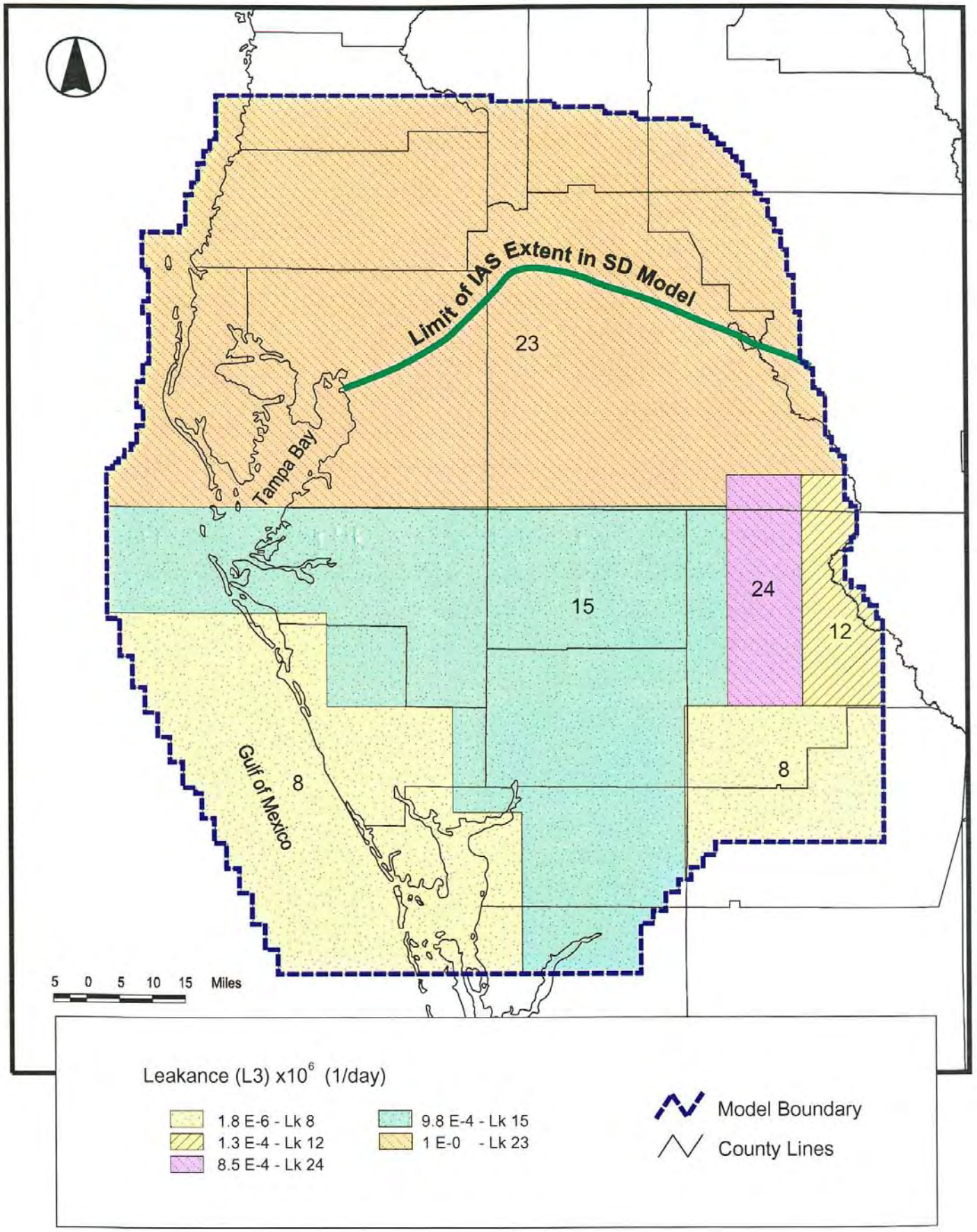

Source:
Southern District Ground-Water Flow Model
Version 1.0
SWFWMD, August 2003

FIGURE 22
Calibrated Leakance Values: Layer 3
(Between Layers 3 and 4)
Sub-Task 3 - Model Development

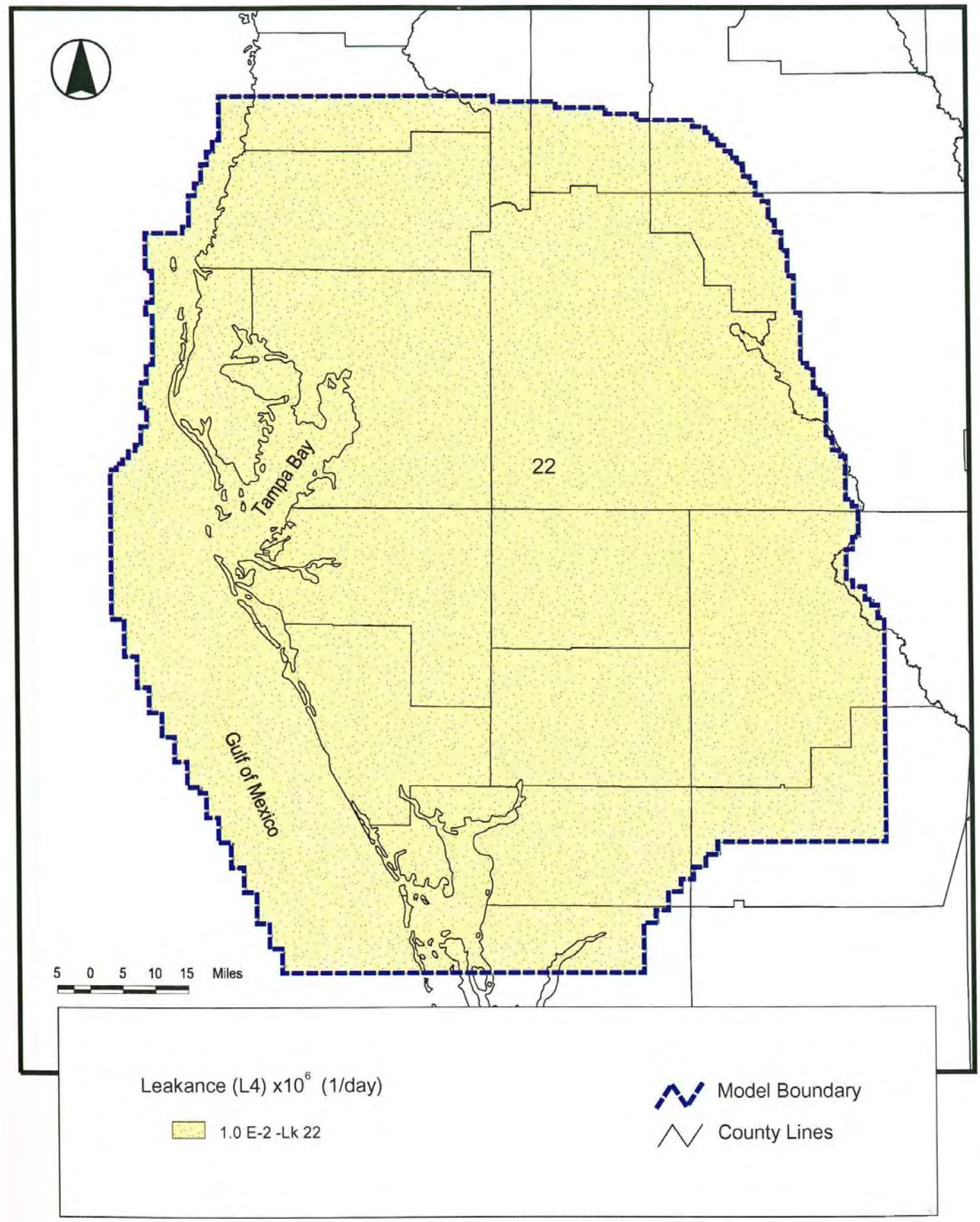

FIGURE 23
Calibrated Leakance Values: Layer 4
(Between Layers 4 and 5)
Sub-Task 3 - Model Development

Source:
Southern District Ground-Water Flow Model
Version 1.0
SWFWMD, August 2003

APPENDIX B

Southeast Florida Region Model Review TM

Southeast Florida Region Groundwater Model Review: Fairbank et al. (1999), McGurk and Presley (2002), and Bower et al. (1990)

PREPARED FOR: USACE Jacksonville District

PREPARED BY: CH2M HILL

DATE: November 21, 2005

PROJECT NUMBER: 334350.TW.03

Contents

Introduction and Purpose

The goal of this project is to collect and summarize data from available model documentation and provide recommendations to the U.S. Army Corps of Engineers (USACE) Jacksonville District for the development of a Regional Groundwater Model of Florida. This Technical Memorandum (TM) summarizes the model reviews for middle and southern Florida.

Three models were reviewed. These models covered the middle and southern part of the Florida peninsula. **Figure 1** shows the extent of the individual models. These models are referenced in this TM as follows:

- Lower East Coast Floridan Aquifer Model (Fairbank et al., 1999)
- East-Central Floridan Aquifer Model (McGurk and Presley, 2002)
- Lee County Model (Bower et al., 1990)

Comparison of Hydrogeology and Model Frameworks

Three principal aquifer systems are present in the area of interest. These aquifer systems include the Surficial Aquifer System (SAS), the Intermediate Aquifer System (IAS), and the Floridan Aquifer System (FAS). These aquifers are represented in each of the models.

The SAS covers most of the area of interest. It consists of unconsolidated sand, shelly sand, and shell with locally important limestone beds. Groundwater is generally under unconfined conditions and is recharged from the surface or, where heads are higher in deeper formations, from below. Transmissivity values vary widely from 1,000 to more than 10,000 square feet per day (ft^2/d). The most productive parts of the undifferentiated SAS occur in Collier and Hendry Counties. In the southeastern part of the state, the SAS is known as the Biscayne Aquifer and is the major source of fresh water for the region. Aquifer tests in the Biscayne Aquifer in Brevard County have resulted in calculated transmissivities of more than 1,000,000 ft^2/d (Randazzo, 1997).

Aquifers that lie below the SAS and above the FAS are referred to as the IAS. The IAS consists of beds of sand, sandy limestone, limestone, and dolomite, and is bounded by clay confining units above and below. Water in the IAS exists under confined conditions. Transmissivity values vary but are generally reported to be less than 10,000 ft^2/d. The system is an important source of water for Sarasota, Charlotte, and Lee Counties, where the FAS beneath the IAS contains brackish water (Randazzo, 1997).

The FAS exists throughout the state of Florida, and has been defined based on its permeability, which is at least an order of magnitude greater than the associated confining units above and below the aquifer. In most of the study area, the FAS can be divided into the Upper Floridan Aquifer (UFA) and Lower Floridan Aquifer (LFA). The UFA is generally the most productive and best known part of the aquifer. The LFA is less well known because it is deeper and generally filled with saltwater. The "Boulder Zone" exists in the LFA in the southeast part of the state. Transmissivity values for the UFA range from less than 50,000 ft^2/d to more than 100,000 ft^2/d in the northern part of the study area (Randazzo, 1997). The transmissivty of the Boulder Zone in the LFA has been estimated to be as high as 24.6×10^6 ft^2/d (Meyer, 1989).

The three models reviewed cover different geographic areas and model the three aquifer systems differently based on the goals of the model, available data, and aquifer characteristics in the area. **Table 1** provides a brief comparison of the model frameworks.

TABLE 1
Comparison of Model Frameworks
Southeast Florida Region Model Review

Layer	Lower East Coast	East Central Florida	Lee County
Layer 1	Surficial Aquifer System	Surficial Aquifer System	Surficial Aquifer System (Water Table)
Layer 2	Semi Confining Units	Upper Floridan (Avon Park, Ocala)	Surficial Aquifer System (Lower Tamiami Aquifer)
Layer 3	Upper Floridan (Avon Park, Ocala)	Upper Floridan (Avon Park)	Intermediate Aquifer System (Sandstone Aquifer)
Layer 4	Semi Confining Units	Lower Floridan	Intermediate Aquifer System (Mid-Hawthorn Aquifer)
Layer 5	Upper Floridan (Avon Park)		Floridian Aquifer System (Lower Hawthorn Aquifer)
Layer 6	Semi Confining Units		Floridian Aquifer System (Suwannee and Deeper Aquifers)
Layer 7	Lower Floridan (Oldsmar)		Floridian Aquifer System (Suwannee and Deeper Aquifers)
Layer 8	Semi Confining Units		
Layer 9	Base of Floridan (Boulder Zone)		

Model Summaries

Lower East Coast Floridan Aquifer Model (Fairbank et al., 1999)

Conceptual Model

A three-dimensional, steady-state model was created for the Lower East Coast Planning Area. Appendix A provides figures from the model documentation. The model includes three primary flow zones; two are within the UFA and a third is in the LFA. Flow Zone 1 includes permeable zones at or near the top of the Avon Park Formation and the Ocala Limestone (Layer 3). Flow Zone 2 includes permeable zones within the upper part of the Avon Park Formation (Layer 5). Flow Zone 3 includes the shallowest producing intervals at or near the top of the Oldsmar Formation (Layer 7). Low permeability units between the primary flow zones are included explicitly in this model. Additionally, the SAS and the Boulder Zone are included as constant head boundaries at the top and bottom of the model, respectively. Figure 2 in Appendix A provides the Flow Zone Conceptualization.

Numerical Model

Model Grid Description

Based on the available documentation, the model covers 16,434 square miles and has a total of nine layers with a uniform grid spacing of 1 mile. The model grid domain is shown in Figure 1 in Appendix A.

Range of Hydraulic Conductivity and Transmissivity

Table 2 presents horizontal and vertical hydraulic conductivity calues reported in the model documentation. Variable layer thickness resulted in variable values of transmissivity. Sensitivity analysis of the model to values of hydraulic conductivity in the model layers is included in the model documentation.

TABLE 2
Model Layers and Hydraulic Conductivity Values
Southeast Florida Region Model Review

Layer	Formation	Layer Type	Horizontal K (ft/day)	Vertical K (ft/day)
Layer 1	Surficial Aquifer System	Constant Head	N/A	N/A
Layer 2	Semi Confining Units	Leakance Layer	0.5	1.0 e-5
Layer 3	Upper Floridan (Avon Park, Ocala)	Active Layer	175	8.0
Layer 4	Semi Confining Units	Leakance Layer	0.09	7.0 e-3
Layer 5	Upper Floridan (Avon Park)	Active Layer	75	9.0
Layer 6	Semi Confining Units	Leakance Layer	9	2.2 e-3
Layer 7	Lower Floridan (Oldsmar)	Active Layer	99	2.2 e-4
Layer 8	Semi Confining Units	Leakance Layer	0.9	1.7 e-3
Layer 9	Base of Floridan (Boulder Zone)	Constant Head	N/A	N/A

Layer thickness varied based on contact elevations collected from test borings and wells drilled in the study area. Table 1 included in Appendix A provides the data used for layer elevations. Hydrostratigraphic picks for model layers are based on data compiled from reports prepared by consultants and SFWMD. The model documentation provides an extensive list of well/test drilling sites and layer elevations.

Recharge

Recharge is not explicitly modeled. Instead, Layer 1 is modeled as a constant head boundary condition which supplies recharge or allows discharge through the semiconfining Layer 2.

Boundary Conditions

The top and bottom layers (Layer 1 and Layer 9) are modeled as constant head boundaries which supply recharge or allows discharge of groundwater through the associated semiconfining units. General head boundaries are utilized laterally around the model domain. Figures 4 and 10 in Appendix A show the locations of model boundaries. The constant head value for Layer 1 was calculated to be 2.5 feet from existing land surface. Lake Okeechobee was modeled at 15.4 feet which represents the average stage for the period of record. Starting head and boundary conditions for lower layers were created using pressure data from the SFWMD monitoring well network and FDEP monitoring wells. A total of 26 District wells and 47 utility wells were used to gather information. Figures 4 through 10 in Appendix A show initial head distributions.

Applied Stresses

Only two prescribed flow conditions (pumping wells) are included in the model. Average values of pumping for the Boynton Beach ASR facility and the Jupiter reverse osmosis (RO) facility were used during calibration of the model. Figure 3 in Appendix A shows the locations of the pumping facilities included in the model.

Calibration

The steady-state calibration period for the model is from 1995 to 1997. Two facilities operated continuously during this period and were included in the model: the Boynton Beach ASR facility and the Jupiter RO facility. Initial values for aquifer parameters were based on representative values collected from wells completed in the intervals included in the model. Table 2 in Appendix A provides the basis for the parameters. Table 10 in Appendix A compares the calculated and model calibrated values.

Water quality in the FAS in the area of the model varies, causing density differences which affect groundwater flow. The model utilizes "fresh-water equivalent head values" to account for this water quality variation.

East-Central Floridan Aquifer Model (McGurk and Presley, 2002)

Conceptual Model

A three-dimensional steady-state model was created, expanding on previous regional models covering all or parts of Orange, Seminole, Brevard, Lake, Osceola, Marion, Polk, Sumter, and Volusia Counties. Appendix B provides figures from the model documentation. Figures 1 and 2 in Appendix B show the location of the modeled area. The model was created to simulate pre-development conditions, modern day post-development conditions, and future flow conditions which incorporate increased water supply demands.

The SAS, the Intermediate Confining Unit (ICU), and the FAS are simulated. The SAS consists of sand, silt, clayey sand, and shell beds, and receives recharge from rainfall, irrigation water, septic tank effluent, rapid infiltration basins and other sources. The ICU separates the SAS from the FAS. The thickness of the confining unit and its hydrogeologic properties are highly variable. The FAS includes the Cedar Key Formation, Oldsmar Formation, Avon Park Formation, and the Ocala Limestone. The FAS is separated into the UFA, the middle semiconfining unit, and the LFA. Figure 7 in Appendix B provides the geologic and hydrostratigraphic units within the project area. Figure 25 in Appendix B shows a cross section with the units and direction of saline and fresh groundwater flow.

Numerical Model

Model Grid Description

The model covers 7,568 square miles. The grid is uniform with 2,500-foot by 2,500-foot square cells. Layer elevations were calculated based on data from data collected from previous studies and an extensive list of wells and test borings is included in the appendix of the model documentation. Figures 4 and 5 in Appendix B show the locations of wells completed in the SAS and FAS utilized for this study. Figures 9 through 14 in Appendix B show layer elevations within the model. At cell locations where the saline water interface

elevation was calculated to be above an aquifer layer bottom elevation, the bottom elevation of the flow domain was recomputed to equal the saline water interface elevation. Cells where the saline water interface was calculated to be within 20 feet of the top of an aquifer layer were considered to be saline and therefore inactive.

Range of Hydraulic Conductivity and Transmissivity

The model includes variable values of hydraulic conductivity and associated transmissivity. Figure 8 in Appendix B provides the locations of aquifer performance tests completed in the study area. Table 3 provides the ranges reported. Additionally, Figures 65 through 76 in Appendix B show the spatial distribution of the aquifer parameters.

TABLE 3
Model Layers and Hydraulic Conductivity Values
Southeast Florida Region Model Review

Layer	Formation	Layer Type	Horizontal K (ft/day)	Vertical K (ft/day)
Layer 1	Surficial Aquifer System	Unconfined Active	20	0.001 - 0.1
Layer 2	Upper Floridan (Avon Park, Ocala)	Confined Active	50-5000	0.25-50
Layer 3	Upper Floridan (Avon Park)	Confined Active	50-5000	0.01 – 1.5
Layer 4	Lower Floridan	Confined Active	15-500	

Recharge

The model utilizes the recharge package to apply recharge to the SAS based on detailed information including precipitation, water applied to rapid infiltration basins, septic tank effluent, and irrigation.

Boundary Conditions

General head boundaries are utilized laterally around the model. The head values are based on estimated predevelopment heads in Layers 2 and 3. Layer 4, the LFA, generally varied from +2 feet to -2 feet from the upper layer elevations depending on known discharge/recharge zones. An exception is noted in the southwest where it was 10 to 20 feet lower based on local data. Figure 28 in Appendix B shows modeled lateral boundaries.

General head boundaries were also used to simulate the water level and flux changes along the seaward boundary between saltwater and freshwater within the interior of the grid. This boundary condition was selected to allow for changes due to the moving transition zone. Lakes, rivers, and other surface water attributes were modeled as constant heads cells and rivers as appropriate.

Applied Stresses

Drainage wells provide significant man made source of recharge to the FAS. These injection wells are numerous in the model. Injection rates were based on detailed evaluation of injection well locations and types from available reports. Pumping wells are shown in Figures 30 through 32 of Appendix B for each of the model layers.

Calibration

The model was calibrated to average 1995 steady-state conditions. Calibration included comparison of observed and modeled groundwater levels as well as evaluation of stream flow and spring flow data.

Data utilized to create this detailed model came from many sources. Rainfall, surface water data, observation and test well data, groundwater withdrawal data, wastewater treatment plant flows, and reuse data were obtained from agencies and reports on previous models and studies. An extensive appendix (more than 400 pages) provided with the model documentation contains much of this information.

Lee County Model (Bower et al., 1990)

Conceptual Model

The Lee County Model was created to be used for predictive purposes when evaluating requests for large groundwater withdrawals and to serve as a basis for groundwater management planning in Lee County. The three aquifer systems within the study area are the SAS (including the water table and lower Tamiami aquifers), the IAS (including the sandstone and Mid-Hawthorn and associated confining units), and the FAS (including the lower Hawthorn, Suwannee, and deeper aquifers). In the study area, the FAS contains water with salinity levels above recommended standards for potable use.

Figure 1 in Appendix C shows the location of the study area. Figure 2 in Appendix C provides the generalized hydrogeologic cross section. Figure 3 in Appendix C provides a cross section showing aquifers and corresponding model layers.

Numerical Model

Model Grid Resolution

The model extends across Lee County and covers more than 2,000 square miles. The model consists of 42 rows and 48 columns. Cells in the interior of the model are 1 mile square. Cells on the north and west sides of the model were expanded to reduce boundary effects seen during early calibration attempts. Figures 5 and 6 in Appendix C show the model domain and grid.

Range of Hydraulic Conductivity and Transmissivity

Values for transmissivity were variable for all layers except Layer 6. Figures A-38 through A-54 provide areal distribution of hydraulic parameters included in the model. Table 4 contains the approximate ranges taken from these figures. Vertical conductance (Vcon) is substituted for vertical conductivity to be consistent with the model documentation. Vertical hydraulic conductivity can be calculated from the Vcon values by multiplying them by the confining layer thickness. However, these data are not available in the documentation.

TABLE 4
Model Layers, Hydraulic Conductivity, Transmissivity and Vertical Conductance Values
South Florida Model Review

Layer	Formation	Layer Type	Horizontal K/T (ft/day)/(ft^2/day)	Transmissivity (ft^2/day)	Vcon (1/day)
Layer 1	Surficial Aquifer System (Water Table)	Active-Unconfined		<500 to 1,500	< 6.0 e-5 to >1.6 e-4
Layer 2	Surficial Aquifer System (Lower Tamiami Aquifer)	Active-Confined		<10,000 to >40,000	<3.6e-5 to >9.0e-5
Layer 3	Intermediate Aquifer System (Sandstone Aquifer)	Active-Confined	.001-100	<2,000 to >10,000	<3.0e-11 to >7.5e-11
Layer 4	Intermediate Aquifer System (Mid-Hawthorn Aquifer)	Active-Confined	10-30	<500 to >3,500	<1.0e-5 to >4.0e-5
Layer 5	Floridan Aquifer System (Lower Hawthorn Aquifer)	Active-Confined	56	<8,000 to >16,000	<7.0e-5 to >1.4e-4
Layer 6	Floridan Aquifer System (Suwannee and Deeper Aquifers)	Active-Confined		10,368	7.0e-5
Layer 7	Floridan Aquifer System (Suwannee and Deeper Aquifers)	Constant Head		N/A	N/A

Range of Storage and Specific Yield

Layer 1 specific yield was set uniformly at 0.2. Storage coefficients in Layers 2 through 5 were set to $1e^{-6}$ multiplied by the layer thickness. Layer 5 storativity was set at a uniform value of $1e^{-4}$.

Recharge

Recharge was calculated for model cells based on net precipitation, surface drainage, and evapotranspiration. Values for each cell were calculated on a monthly basis from April 1985 to September 1986.

Boundary Conditions

Constant head boundaries were used laterally around this model as a vertical boundary layer in Layer 7. The River package was used to simulate rivers and some canals in the study area. Additionally, major canals in the East Coast Water Control District were simulated using the drain package. General head boundaries were not used in this model. Figure 7 in Appendix C shows the locations of specified head boundaries. Figure 8 in Appendix C shows the locations of river and drain cells.

Applied Stresses

The model contains groundwater withdrawals representing public water supplies, irrigation demands, and domestic self-supply wells. Figure 8 in Appendix C shows the locations of public well fields. Figure 9 in Appendix C shows the locations of cells where irrigation

withdrawals are applied to the model. Figure 12 in Appendix C shows locations where domestic self supply is included in the model.

Calibration

Both steady-state and transient calibrations were performed. The steady state run was used as a starting point for the transient run. The transient model run was from April 1985 to September 1986. The 12-month period from October 1985 to September 1986 was used for calibration.

Model Comparison to Hydrogeologic Framework

The aquifer parameters taken from the models were compared to the values in the hydrogeologic framework document. The greatest source of uncertainty in this evaluation is the comparison of values for the Middle Floridan Aquifer, which is not explicitly described in the documentation of these models. Where there are two flow zones modeled in the UFA, the lower zone is assumed to correspond to the Middle Floridan Aquifer. Tables 5, 6, and 7 below compare the values.

TABLE 5
Lower East Coast Floridan Model – Comparison to Hydrogeologic Framework
Southeast Florida Region Model Review

Aquifer Hydrogeologic Parameter	Average Framework Value (ft^2/d)	Approx Model Range (ft^2/d)
UF Transmissivity	24,911	2,800-82,600
MF Transmissivity	109,517	1,900-29,500
LF Transmissivity	63,164	3,100-32,400
UF Storativity	1.15E-03	NA
MF Storativity	5.05E-03	NA
Middle Confining Unit 1	2.52E-01	7.00E-03
Middle Confining Unit 2	7.52E-01	2.20E-03

TABLE 6
East Central Floridan Model – Comparison to Hydrogeologic Framework
Southeast Florida Region Model Review

Aquifer Hydrogeologic Parameter	Average Framework Value (ft^2/d)	Approx Model Range (ft^2/d)
UF Transmissivity	36,226	20,000-1,000,000
MF Transmissivity	229,821	20,000-1,000,000
LF Transmissivity	130,379	2,500-685000
UF Storativity	4.62E-04	NA
MF Storativity	6.24E-04	NA
Middle Confining Unit 1	7.30E-01	
Middle Confining Unit 2	1.00E-01	.05-1

TABLE 7
Lee County Model – Comparison to Hydrogeologic Framework
Southeast Florida Region Model Review

Aquifer Hydrogeologic Parameter	Average Framework Value (ft^2/d)	Approx Model Range (ft^2/d)
UF Transmissivity	15,051	8,000-16,000
MF Transmissivity	306,721	1.04E+04
LF Transmissivity	50,731	NA
UF Storativity	2.11E-04	1.00E-04
MF Storativity	6.40E-05	1.00E-04
Middle Confining Unit 1	2.32E-01	2.57E-03
Middle Confining Unit 2	1.47E-01	NA

References

Bower, R.F., K.M. Adams and J.I. Restrepo. 1990. A Three-Dimensional Finite Difference Ground Water Model of Lee County, Florida. Technical Publication 90-01. South Florida Water Management District. West Palm Beach, Florida.

Fairbank, P., J. Valdes, E. Rectenwald, M. Switaneck, and E. Hopkins. 1999. Documentation for the Lower East Coast Floridan Aquifer Model. South Florida Water Management District.

McGurk, B., and P. Fischl Presley. 2002. Simulation of the Effects of Groundwater Withdrawals on the Floridan Aquifer System in East-Central Florida: Model Expansion and Revision. Technical Publication SJ2002-3. St. Johns River Water Management District. Palatka, Florida.

Randazzo, A. F., and D. S. Jones. 1997. The Geology of Florida, University Press of Florida.

Sepulveda, N. 2001. Comparisons Among Ground-Water Flow Models and Analysis of Discrepancies in Simulated Transmissivities of the Upper Floridan Aquifer in Ground-Water Flow Model Overlap Areas. U.S. Geological Survey Karst Interest Group Proceedings. Water Resources Investigations Report 01-4011. Pp 58-67.

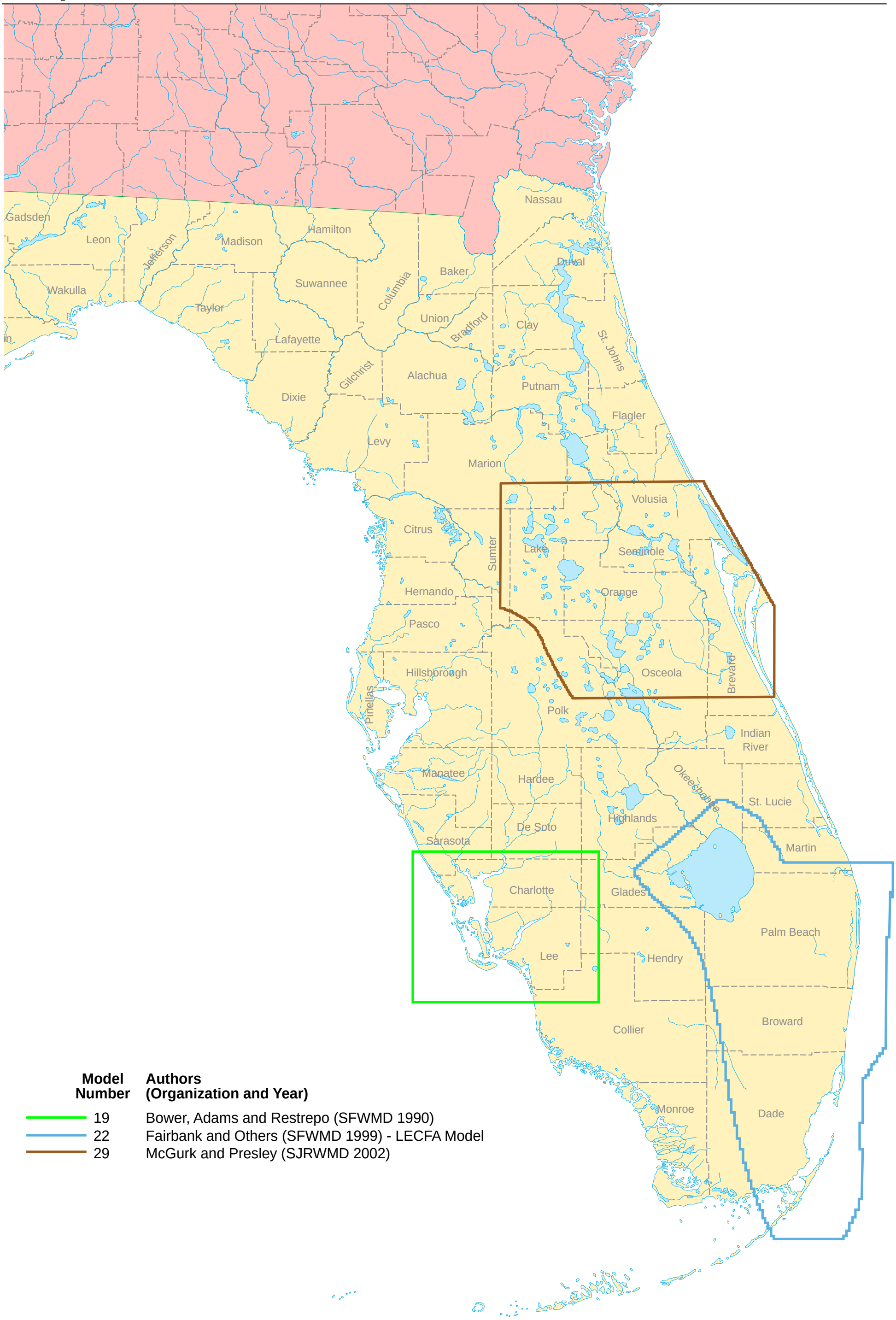

Model Number	Authors (Organization and Year)
19	Bower, Adams and Restrepo (SFWMD 1990)
22	Fairbank and Others (SFWMD 1999) - LECFA Model
29	McGurk and Presley (SJRWMD 2002)

North

0 15 30

Approximate Scale in Miles

FIGURE 1
Reviewed Model Boundaries
USACE - Subtask 3 Model Development

CH2MHILL

Appendix A

Selected Figures and Tables from Documentation of the East Coast Florida model

Table 1. Altitudes Corresponding to Surficial Aquifer and Flow Zone Model Layers.

			SURFICIAL AQUIFER (LAYER 1)	FLOW ZONE #1 (LAYER 3)		FLOW ZONE #2 (LAYER 5)		FLOW ZONE #3 (LAYER 7)		
Site Id.	X Coord.	Y Coord.	Bt. Elev.	Top Elev.	Bt. Elev.	Top Elev.	Bt. Elev.	Top Elev.	Bt. Elev.	Reference
Acme Imp Dist	750942	834288	-180	-805	-1080	-1230	-1480	-1830	-2080	CH2MHILL, 1995
City of Boynton Beach - Disposal Well	786754	799208	-183	-783	-983	-1283	-1583	-1733	-1908	CH2MHILL, 1995
Coral Springs Imp Dist	741441	699813	-190	-940	-1290	-1390	-1440	-2090	-2240	CH2MHILL, 1995 [Picks based on Margate well]
City of Margate	757520	697620	-285	-935	-1285	-1385	-1435	-2085	-2235	CH2MHILL, 1995
PBC System 9	765559	747318	-155	-905	-1180	-1380	-1430	-1830	-2080	CH2MHILL, 1995
PBC Southern Regional	777253	783129	-230	-780	-1080	-1455	-1505	-1780	-1980	CH2MHILL, 1995
Century Village @ Pembroke Pines	720247	606265	-195	-995	-1120	-1595	-1745	-2195	-2295	CH2MHILL, 1995
Pratt & Whitney	723170	938799	-125	-850	-925	-1175	-1575	-1975	-2075	CH2MHILL, 1995
QO Chemicals	613544	867176	-160	-635	-810	-1035	-1385	-1835	-2035	CH2MHILL, 1995
Village of Royal Palm Beach	750942	874484	-130	-880	-1055	-1205	-1430	-2180	-2380	CH2MHILL, 1995
Seacoast Utility Authority	779445	925644	-258	-883	-1033	-1283	-1558	-1983	-2108	CH2MHILL, 1995
City of Sunrise	722439	655962	-195	-995	-1345	-1545	-1695	-2270	-2295	CH2MHILL, 1995
City of WPB #6	786754	880331	-185	-985	-1160	-1285	-1535	-1960	-2085	CH2MHILL, 1995
City of Boynton Beach ASR	809410	799938	-345	-795	-1070	-1295	-1595	-1795	-1895	CH2MHILL, 1995
City of Deerfield Beach	791139	721738	-165	-990	-1165	-1340	-1540	-2090	-2240	CH2MHILL, 1995 [Picks partly based on C-13 well]
City of Hollywood	781638	606265	-293	-943	-1093	-1593	-1743	-2193	-2293	CH2MHILL, 1995 [Picks partly based on Pembroke Pines well]
C-13 Floridan Test Well	789677	676426	-364	-989	-1164	-1339	-1539	-2089	-2239	CH2MHILL, 1995 [Picks partly based on Margate well]
USGS Alligator Alley Test Well	548743	675603	-138	-763	-1238	-1563	-1713	-2063	-2263	CH2MHILL, 1995
Miami-Dade Well I-5	720170	441316	-125	-975	-1055	-1355	-1555	-2395	-2515	CH2MHILL, 1977
MF-1	667937	1043387	-125	-650	-800					Brown & Reece, 1979
MF-3	766873	1047651	-175	-750						Brown & Reece, 1979

Fairbank, P., J. Valdes, E. Rectenwald, M. Switaneck, and E. Hopkins, 1999. Documentation for the Lower East Coast Aquifer Model. Documentation for the Lower East Coast Floridan Aquifer Model. South Florida Water Management District.

Table 1 contd. Altitudes corresponding to surficial aquifer and flow zone model layers.

			SURFICIAL AQUIFER (LAYER 1)	FLOW ZONE #1 (LAYER 3)		FLOW ZONE #2 (LAYER 5)		FLOW ZONE #3 (LAYER 7)		
Site Id.	X Coord.	Y Coord.	Bt. Elev.	Top Elev.	Bt. Elev.	Top Elev.	Bt. Elev.	Top Elev.	Bt. Elev.	Reference
MF-6	635484	1027816	-125	-700	-800	-900				Brown & Reece, 1979
MF-10	731133	997245	-100	-600	-800	-900				Brown & Reece, 1979
OKF-2	593433	1166945	-150	-350	-500	-550				Shaw & Trost, 1984
SLF-5	673614	1151256	-100	-475	-600	-675	-900			Brown & Reece, 1979
SLF-9	632614	1131914	-150	-450	-600	-675	-850			Brown & Reece, 1979
SLF-14	639058	1091948	-125	-550	-850	-950	-1250			Brown & Reece, 1979
SLF-20	604517	1127187	-175	-475	-625	-675	-875			Brown & Reece, 1979
SLF-23	672336	1049363	-100	-625	-800	-825				Brown & Reece, 1979
MF-8	715084	1040781	-150	-575	-850					Brown & Reece, 1979
MF-5	743789	1042558	-225	-850						Brown & Reece, 1979
PBF-1	797129	959196	-250	-850	-1025					Shaw & Trost, 1984
GLF-1	524932	1022450	-200	-600	-775					Shaw & Trost, 1984
GLF-2	494213	983064	-200	-625	-750					Shaw & Trost, 1984
HIF-39	454290	1102237	-125	-375	-675	-875	-1025			Shaw & Trost, 1984
OKF-18	496486	1135331	-150	-375	-600	-650	-900			Shaw & Trost, 1984
OKF-19	511261	1132808	-125	-350	-500	-600	-850			Shaw & Trost, 1984
OKF-29	551354	1129709	-50	-375	-550	-650	-850			Shaw & Trost, 1984
Plantation #1	739972	652373	-218	-1043		-1585	-1648	-2180	-2247	CDM, 1987 & 1991a
Plantation #2	750609	657383	-217			-1572	-1642	-2122	-2222	CDM, 1991b
SLF-50	662955	1092340	-105	-625	-745	-815	-935			Wedderburn & Knapp, 1983
USSC ASR Test Well	674453	890741	-185	-935	-1035	-1160	-1460			ViroGroup, 1993
PU-I1 (Sunset Park)	713777	494534	-135	-895	-1075	-1535	-1725	-2495	-2715	Black, Crow & Eidsness, 1970

Fairbank, P., J. Valdes, E. Rectenwald, M. Switaneck, and E. Hopkins, 1999. Documentation for the Lower East Coast Aquifer Model. Documentation for the Lower East Coast Floridan Aquifer Model. South Florida Water Management District.

Table 1 contd. Altitudes corresponding to surficial aquifer and flow zone model layers.

			SURFICIAL AQUIFER (LAYER 1)	FLOW ZONE #1 (LAYER 3)		FLOW ZONE #2 (LAYER 5)		FLOW ZONE #3 (LAYER 7)		
Site Id.	X Coord.	Y Coord.	Bt. Elev.	Top Elev.	Bt. Elev.	Top Elev.	Bt. Elev.	Top Elev.	Bt. Elev.	Reference
PU-I2 (Kendale Lakes)	692558	493627	-115	-1055	-1095	-1505	-1735	-2495	-2705	Black, Crow & Eidsness, 1972
G-3061 (Hialeah ASR well)	734185	543807		-1019	-1031					Reese, 1994
NP-100	631054	381242		-965	-1005	-1165	-1328			Meyer, 1971
S-524	636935	465655				-1132	-1192			Meyer, 1971
G-1273	695665	287597		-800	-890					Meyer, 1971
W-2912	500053	882046		-1185	-1295	-1605	-1645	-2045	-2085	Puri & Winston, 1974
W-4661	573250	735652		-905	-935	-1215	-1235			Puri & Winston, 1974
W-445	535188	483855		-910	-930	-1440	-1470	-1920	-2050	Puri & Winston, 1974
Jupiter RO facility (multi-well composite)	778291	944693			-1035	-1315	-1645	-1815		ViroGroup, 1994
Stuart Injection Well IW-2	748598	1038851				-975	-1055			Montgomery Watson, 1997
City of Miramar IW-1	724512	594136	-183	-1063	-1133	-1632	-1731	-1913	-1998	Montgomery Watson, 1996
City of WPB ASR	804703	864431	-355	-960	-1185					CH2MHill, 1998b
City of Sunrise ASR	742533	667332	-182	-1102	-1262					Montgomery Watson, 1998
City of Delray Beach ASR	741876	782028		-1006	-1190					CH2MHill, 1998a
West Wellfield ASR	672876	496977	-166	-831	-1241					CH2MHill, 1997b
PBC System 3 Multipurpose Floridan Well	782494	782181	-320	-1040						Kimley-Horn & Assoc., 1998
BCOES ASR facility	792605	713184	-362	-977	-1182					CH2MHill, 1997a
Indiantown Cogeneration Project (IPW-1)	657324	985586	-133	-675	-695	-745	-775	-1435	-1475	Bechtel Corp., 1991 & 1994
SFWMD Okeechobee ASR Demo. Proj.	570202	1053544	-125					-1283	-1605	CH2MHill, 1989a
DBF R0-1/BF-6	786910	720819	-412	-947	-1115					Lukasiewicz, SFWMD (unpublished data)
BF-3/BF-1	769399	669411	-395	-995	-1195	-1495	-1595	-2095	-2145	Lukasiewicz, SFWMD (unpublished data)

Fairbank, P., J. Valdes, E. Rectenwald, M. Switaneck, and E. Hopkins, 1999. Documentation for the Lower East Coast Aquifer Model. Documentation for the Lower East Coast Floridan Aquifer Model. South Florida Water Management District.

Table 1 contd. Altitudes corresponding to surficial aquifer and flow zone model layers.

			SURFICIAL AQUIFER (LAYER 1)	FLOW ZONE #1 (LAYER 3)		FLOW ZONE #2 (LAYER 5)		FLOW ZONE #3 (LAYER 7)		
Site Id.	X Coord.	Y Coord.	Bt. Elev.	Top Elev.	Bt. Elev.	Top Elev.	Bt. Elev.	Top Elev.	Bt. Elev.	Reference
DF1	674672	573207	-195	-1090	-1189	-1690	-1775	-2560	-2635	Lukasiewicz, SFWMD (unpublished data)
PBF-3	792908	852229	-295	-1035	-1237	-1345	-1495	-2325	-2475	Lukasiewicz, SFWMD (unpublished data)
Loxahatchee R. ENCON	780324	942215	-366			-1366	-1686	-2048	-2093	Geraghty & Miller, 1994
N. Port St. Lucie IW	710753	1092359	-135	-585				-2085	-2385	CH2MHill, 1987
N. Martin Ct. IW (DeBartolo Corp. site)	737470	1057769	-335					-1690	-1955	Geraghty & Miller, 1988
FPL Turkey Point (Obs. Well A)	695303	369971	-97	-1097	-1250					Dames & Moore, 1975
Broward N. District Regional WWTP (IW-4)	776937	701266	-435					-1985	-2135	Geraghty & Miller, 1991a,b
Lohmeyer Plant (Ft. Lauderdale)	787166	642468								Geraghty & Miller, 1984
Deerfield Floridan Test/Production Well	786999	721123		-950	-1118					Camp, Dresser & McKee, 1993

Fairbank, P., J. Valdes, E. Rectenwald, M. Switaneck, and E. Hopkins, 1999. Documentation for the Lower East Coast Aquifer Model. Documentation for the Lower East Coast Floridan Aquifer Model. South Florida Water Management District.

Table 2. Geometric Means (GM) of Horizontal (K) and Vertical (K') Hydraulic Conductivity Values Corresponding to Model Layers.

SITE ID.	X COORD.	Y COORD.	K (ft/d)	K'(ft/d)	REFERENCES
LAYER 2					
City of Deerfield Beach	791139	721738		2	CH2M Hill, 1995
City of Hollywood	781638	606265		0.04	CH2M Hill, 1995
City of WPB ASR	804703	864431	0.5	0.4	CH2M Hill, 1998b
Indiantown Cogeneration Project (IPW-1)	657324	985586		0.005	Bechtel Corp., 1991 & 1994
DBF R0-1/BF-6	786910	720819		0.0001	SFWMD (unpublished data)
FPL Turkey Point (Obs. Well A)	695303	369971		0.002	Dames & Moore, 1975
Deerfield Floridan Test/Production Well	786999	721123	***GM = 0.5***	***GM = 0.02***	Camp, Dresser & McKee, 1993
LAYER 3					
Century Village @ Pembroke Pines	720247	606265	118		Geraghty & Miller, 1995
City of Boynton Beach ASR	809410	799938	90		CH2M Hill, 1995
City of Deerfield Beach	791139	721738	140		CH2M Hill, 1995
City of Hollywood	781638	606265	139		CH2M Hill, 1995
C-13 Floridan Test Well	789677	676426	680		CH2M Hill, 1995
MF-6	635484	1027816	169		Brown & Reece, 1979
OKF-2	593433	1166945	576		Shaw & Trost, 1984
SLF-9	632614	1131914	1026		Brown, 1980
SLF-20	604517	1127187	72		Brown, 1980
SLF-50	662955	1092340	94	8	Wedderburn & Knapp, 1983
City of WPB ASR	804703	864431	566		CH2M Hill, 1998b
City of Sunrise ASR	742533	667332	30		Montgomery Watson, 1998
West Wellfield ASR	672876	496977	30		CH2M Hill, 1997b
BCOES ASR facility	792605	713184	1320		CH2M Hill, 1997a
Indiantown Cogeneration Project (IPW-1)	657324	985586	55		Bechtel Corp., 1991 & 1994

Fairbank, P., J. Valdes, E. Rectenwald, M. Switaneck, and E. Hopkins, 1999. Documentation for the Lower East Coast Aquifer Model. Documentation for the Lower East Coast Floridan Aquifer Model. South Florida Water Management District.

Table 2 contd. Geometric Means (GM) of Horizontal (K) and Vertical (K') Hydraulic Conductivity Values Corresponding to Model Layers.

SITE ID.	X COORD.	Y COORD.	K (ft/d)	K'(ft/d)	REFERENCES
LAYER 3 (contd.)					
DBF R0-1/BF-6	786910	720819	144		SFWMD (unpublished data)
BF-3/BF-1	769399	669411	679		SFWMD (unpublished data)
DF1	674672	573207	181		SFWMD (unpublished data)
PBF-3	792908	852229	171		SFWMD (unpublished data)
FPL Turkey Point (Obs. Well A)	695303	369971	80		Dames & Moore, 1975
Deerfield Floridan Test/Production Well	786999	721123	144		Camp, Dresser & McKee, 1993
			GM = 175	***GM = 8***	
LAYER 4					
City of WPB ASR	804703	864431	0.0005		CH2M Hill, 1998b
City of Sunrise ASR	742533	667332	0.4		Montgomery Watson, 1998
Jupiter RO facility	778291	944693		0.003	ViroGroup, 1994
City of WPB ASR	804703	864431		0.0007	CH2M Hill, 1998
BF-3/BF-1	769399	669411		0.13	SFWMD (unpublished data)
			GM = 0.01	***GM = 0.007***	
LAYER 5					
Century Village @ Pembroke Pines	720247	606265	0.2		Geraghty & Miller, 1995
C-13 Floridan Test Well	789677	676426	30		CH2M Hill, 1995
MF-6	635484	1027816	183		Brown, 1980
SLF-9	632614	1131914	0.001		Brown, 1980
SLF-20	604517	1127187	24		Brown, 1980
Plantation #1	739972	652373	40		CDM, 1987 & 1991a
Plantation #2	750609	657383	124		CDM, 1991b
SLF-50	662955	1092340	25		Wedderburn & Knapp, 1983
Jupiter RO facility (multi well composite)	778291	944693	249		ViroGroup, 1994
City of Miramar IW-1	724512	594136	16		Montgomery Watson, 1996
Indiantown Cogeneration Project (IPW-1)	657324	985586	55		Bechtel Corp., 1991 & 1994
BF-3/BF-1	769399	669411	103		SFWMD (unpublished data)
DF1	674672	573207	35		SFWMD (unpublished data)
PBF-3	792908	852229	1667		SFWMD (unpublished data)
			GM = 21		

Fairbank, P., J. Valdes, E. Rectenwald, M. Switaneck, and E. Hopkins, 1999. Documentation for the Lower East Coast Aquifer Model. Documentation for the Lower East Coast Floridan Aquifer Model. South Florida Water Management District.

Table 2 contd. Geometric Means (GM) of Horizontal (K) and Vertical (K') Hydraulic Conductivity Values Corresponding to Model Layers.

SITE ID.	X COORD.	Y COORD.	K (ft/d)	K'(ft/d)	REFERENCES
LAYER 6					
Acme Imp Dist	750942	834288	0.4		CH2M Hill, 1995
Coral Springs Imp Dist	741441	699813	0.04	0.16	Geraghty and Miller, 1986
C-13 Floridan Test Well	789677	676426	0.4		CH2M Hill, 1995
Miami-Dade Well I-5	720170	441316	3		CH2M Hill, 1977; Hydrologic Assoc., 1994
Plantation #1	739972	652373	17	0.1	CDM, 1987 & 1991a
Plantation #2	750609	657383	37	3	CDM, 1991b
City of Miramar IW-1	724512	594136	21	0.09	Montgomery Watson, 1996
BF-3/BF-1	769399	669411	5		SFWMD (unpublished data)
Indiantown Cogeneration Project (IPW-1)	657324	985586		0.96	Bechtel Corp., 1991 & 1994
SFWMD Okeechobee ASR Demo. Proj.	570202	1053544		0.4	CH2M Hill, 1989
Broward N. District Regional WWTP (IW-4)	776937	701266		0.4	Geraghty & Miller, 1991a,b
			GM = 2	***GM = 0.35***	
LAYER 7					
Acme Imp Dist	750942	834288	14		CH2M Hill, 1995
Coral Springs Imp Dist	741441	699813	0.03	0.22	Geraghty & Miller, 1986
PBC Southern Regional	777253	783129	116		CH2M Hill, 1995
C-13 Floridan Test Well	789677	676426	210		CH2M Hill, 1995
Plantation #2	750609	657383	94		CDM, 1991b
City of Miramar IW-1	724512	594136	20		Montgomery Watson, 1996
Indiantown Cogeneration Project (IPW-1)	657324	985586	2055		Bechtel Corp., 1991 & 1994
SFWMD Okeechobee ASR Demo. Proj.	570202	1053544	1470		CH2M Hill, 1989a
BF-3/BF-1	769399	669411	205		SFWMD (unpublished data)
DF1	674672	573207	40		SFWMD (unpublished data)
PBF-3	792908	852229	7		SFWMD (unpublished data)
Loxahatchee R. ENCON	780324	942215	1313		Geraghty & Miller, 1994
N. Martin Ct. IW (DeBartolo Corp. site)	737470	1057769	32		Geraghty & Miller, 1988
			GM = 60	***GM = 0.22***	
LAYER 8					
Acme Imp Dist	750942	834288	7		CH2M HIll, 1995
Coral Springs Imp Dist	741441	699813	0.05		CH2M Hill, 1995; Geraghty & Miller, 1986
Century Village @ Pembroke Pines	720247	606265	2		Geraghty & Miller, 1995
Village of Royal Palm Beach	750942	874484	0.005	0.001	CH2MHILL, 1995
Seacoast Utility Authority	779445	925644	0.003	0.002	CH2M Hill, 1989b
Plantation #1	739972	652373	5	0.07	CDM, 1987 & 1991a

Fairbank, P., J. Valdes, E. Rectenwald, M. Switaneck, and E. Hopkins, 1999. Documentation for the Lower East Coast Aquifer Model.
Documentation for the Lower East Coast Floridan Aquifer Model.
South Florida Water Management District.

Table 2 contd. Geometric Means (GM) of Horizontal (K) and Vertical (K') Hydraulic Conductivity Values Corresponding to Model Layers.

SITE ID.	X COORD.	Y COORD.	K (ft/d)	K'(ft/d)	REFERENCES
LAYER 8 (contd.)					
Plantation #2	750609	657383	4	0.3	CDM, 1991b
City of Miramar IW-1	724512	594136	0.9	0.0009	Montgomery Watson, 1996
N. Port St. Lucie IW	710753	1092359	0.00013	0.000051	CH2MHill, 1987
N. Martin Ct. IW (DeBartolo Corp. site)	737470	1057769	4	0.00041	Geraghty & Miller, 1988
Broward N. District Regional WWTP (IW-4)	776937	701266	1		Geraghty & Miller, 1991a,b
Coral Springs Imp Dist	741441	699813		0.004	Geraghty & Miller, 1986
PBC System 9	765559	747318		0.002	CH2M Hill, 1986
PBC System 3 Multipurpose Floridan Well	782494	782181		0.02	Kimley-Horn, 1998; Geraghty & Miller, 1987
Lohmeyer Plant (Ft. Lauderdale)	787166	642468		0.1	Geraghty & Miller, 1984
			GM = 0.2	***GM = 0.004***	
LAYER 9					
Coral Springs Imp Dist	741441	699813	1000		Geraghty & Miller, 1986
Century Village @ Pembroke Pines	720247	606265	733		Geraghty & Miller, 1995
Miami-Dade Well I-5	720170	441316	58565		Singh et al., 1983
Plantation #2	750609	657383	133	3	CDM, 1991b
PBC System 3 Multipurpose Floridan Well	782494	782181	607		Kimley-Horn, 1998; Geraghty & Miller, 1987
N. Martin Ct. IW (DeBartolo Corp. site)	737470	1057769	804		Geraghty & Miller, 1988
Lohmeyer Plant (Ft. Lauderdale)	787166	642468	19647		Geraghty & Miller, 1984
			GM = 1771	***GM = 3***	

Fairbank, P., J. Valdes, E. Rectenwald, M. Switaneck, and E. Hopkins, 1999. Documentation for the Lower East Coast Aquifer Model. Documentation for the Lower East Coast Floridan Aquifer Model. South Florida Water Management District.

Table 10. Hydraulic Conductivity Comparison (Initial vs. Calibrated).

Initial Parameters					Calibrated Parameters			
Layer	Kx	Ky	Kz	Anisotropy Ratio (Kx/Kz)	Kx	Ky	Kz	Anisotropy Ratio (Kx/Kz)
2	5.00E-01	5.00E-01	2.00E-02	2.50E+01	5.00E-01	5.00E-01	1.00E-05	5.00E+04
3	1.75E+02	1.75E+02	8.00E+00	2.19E+01	1.75E+02	1.75E+02	8.00E+00	2.19E+01
4	1.00E-02	1.00E-02	7.00E-03	1.43E+00	9.00E-02	9.00E-02	7.00E-03	1.29E+01
5	2.10E+01	2.10E+01	1.10E+00	1.91E+01	7.50E+01	7.50E+01	9.00E+00	8.33E+00
6	2.00E+00	2.00E+00	3.50E-01	5.71E+00	9.00E+00	9.00E+00	2.20E-03	4.09E+03
7	6.00E+01	6.00E+01	2.20E-01	2.73E+02	9.90E+01	9.90E+01	2.20E-04	4.50E+05
8	2.00E-01	2.00E-01	4.00E-03	5.00E+01	9.00E-01	9.00E-01	1.70E-03	5.29E+02

Fairbank, P., J. Valdes, E. Rectenwald, M. Switaneck, and E. Hopkins, 1999. Documentation for the Lower East Coast Aquifer Model. Documentation for the Lower East Coast Floridan Aquifer Model. South Florida Water Management District.

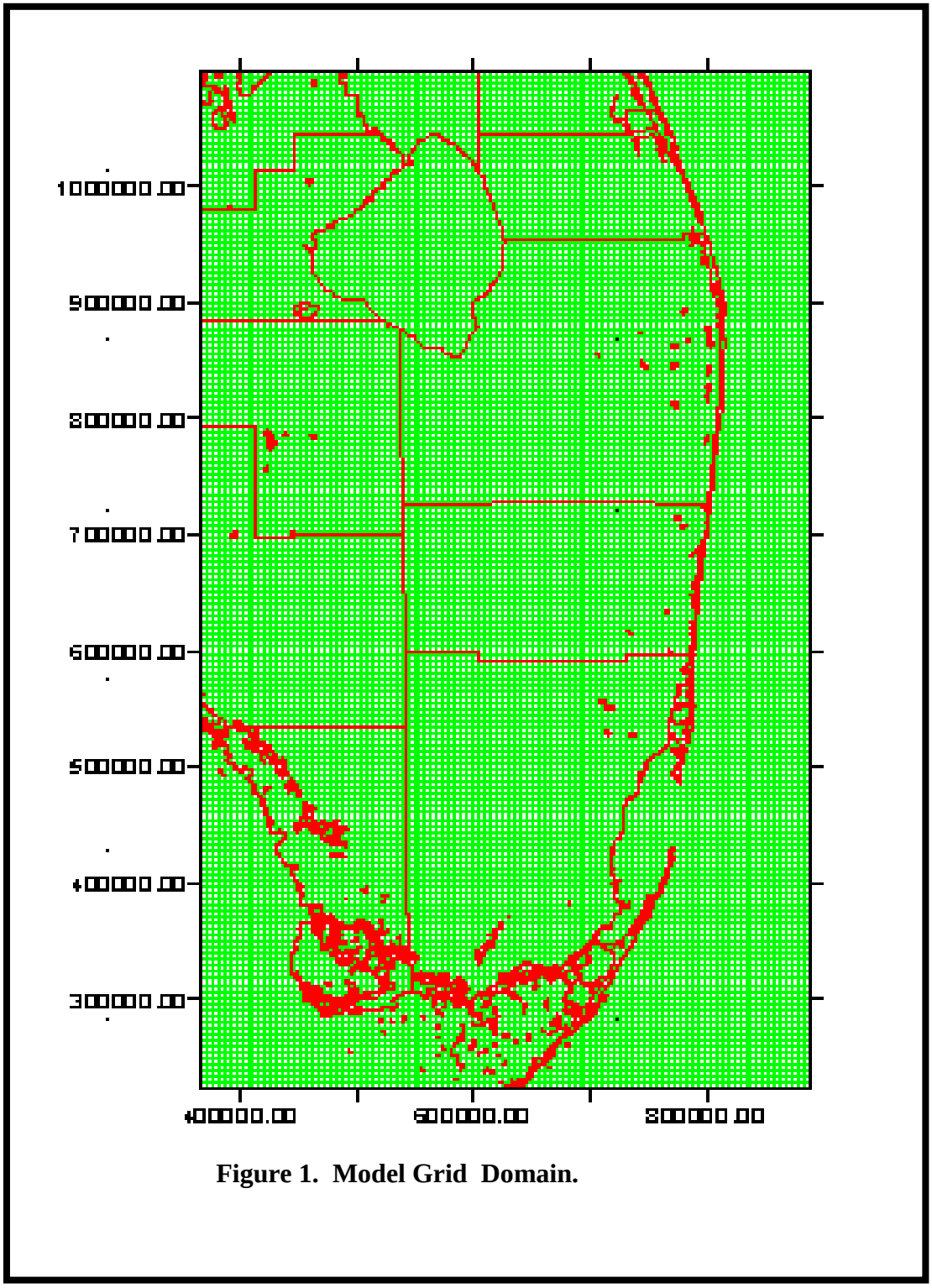

Figure 1. Model Grid Domain.

Fairbank, P., J. Valdes, E. Rectenwald, M. Switaneck, and E. Hopkins, 1999. Documentation for the Lower East Coast Aquifer Model. Documentation for the Lower East Coast Floridan Aquifer Model. South Florida Water Management District.

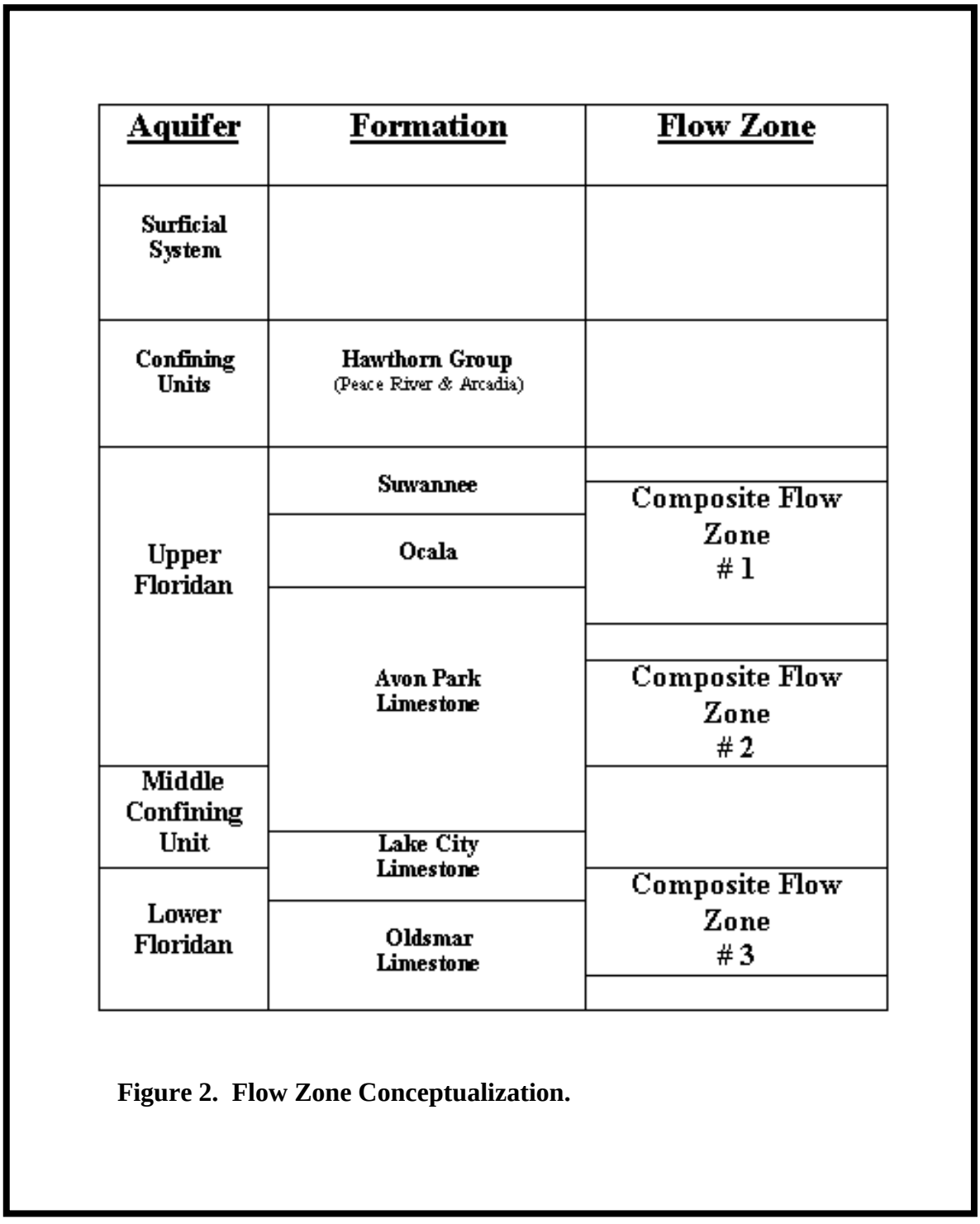

Figure 2. Flow Zone Conceptualization.

Fairbank, P., J. Valdes, E. Rectenwald, M. Switaneck, and E. Hopkins, 1999. Documentation for the Lower East Coast Aquifer Model. Documentation for the Lower East Coast Floridan Aquifer Model. South Florida Water Management District.

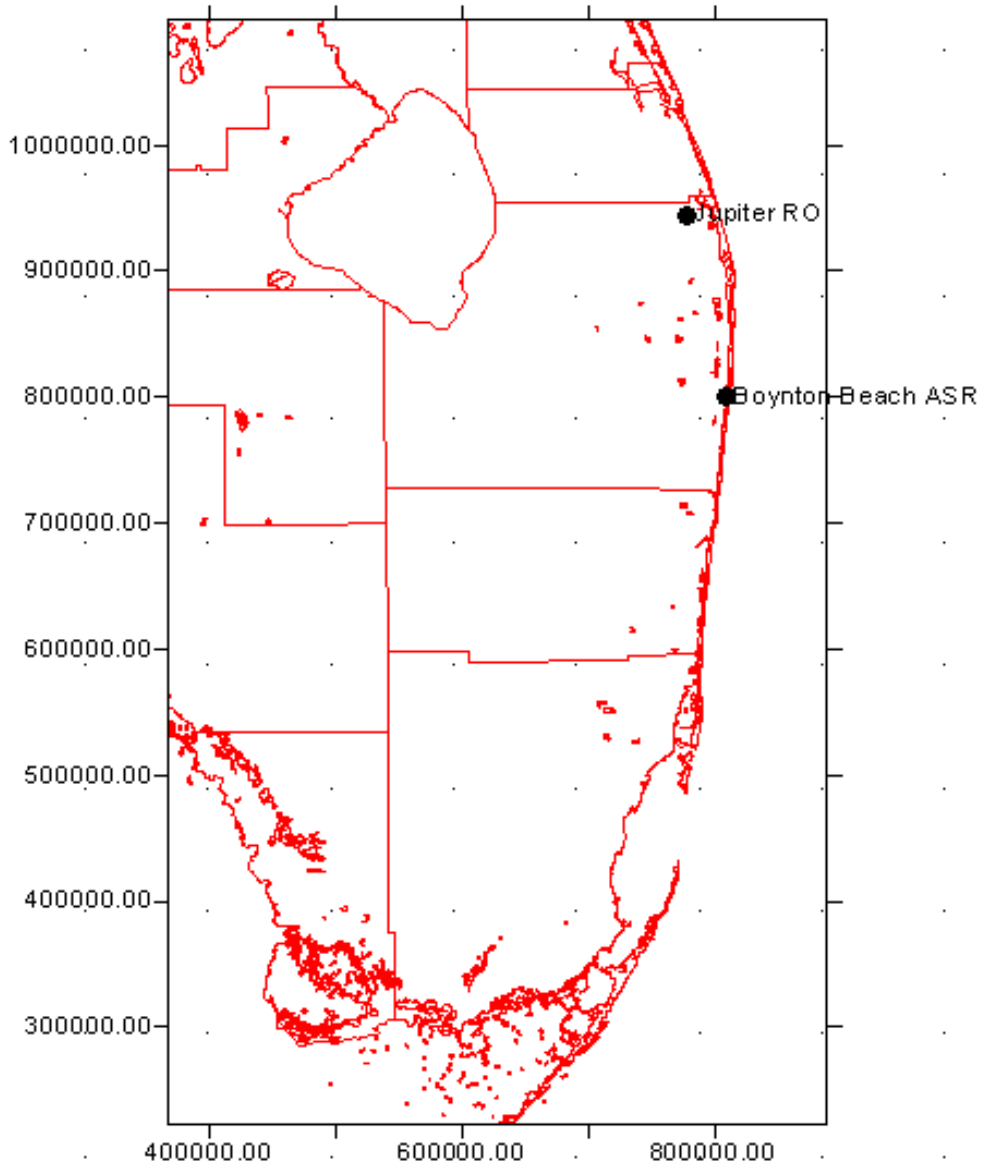

- Well location

Figure 3. Pumping Well Centers.

Fairbank, P., J. Valdes, E. Rectenwald, M. Switaneck, and E. Hopkins, 1999. Documentation for the Lower East Coast Aquifer Model. Documentation for the Lower East Coast Floridan Aquifer Model. South Florida Water Management District.

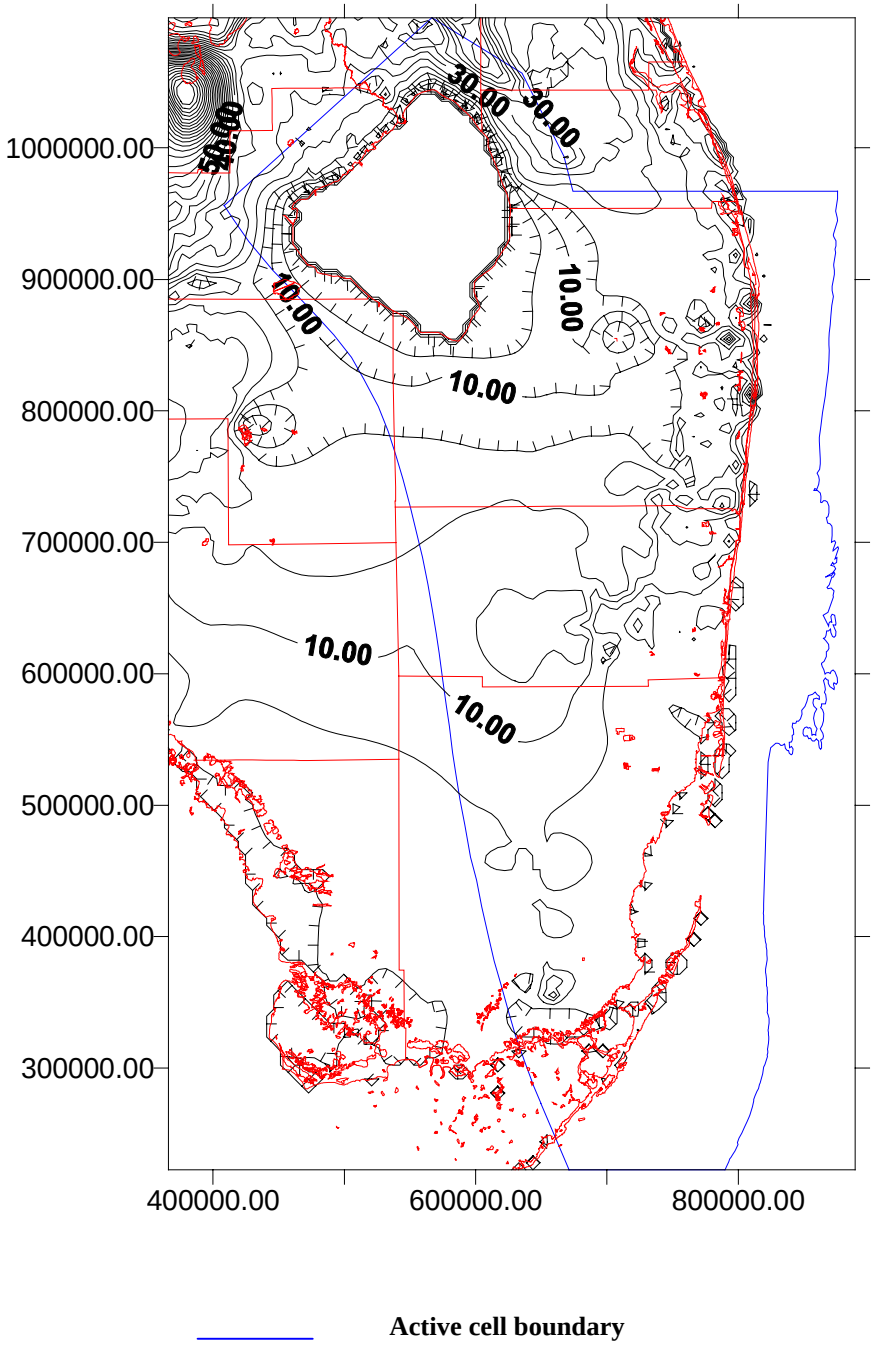

Figure 4. Initial Head Distribution – Layer 1.

Fairbank, P., J. Valdes, E. Rectenwald, M. Switaneck, and E. Hopkins, 1999. Documentation for the Lower East Coast Aquifer Model. Documentation for the Lower East Coast Floridan Aquifer Model. South Florida Water Management District.

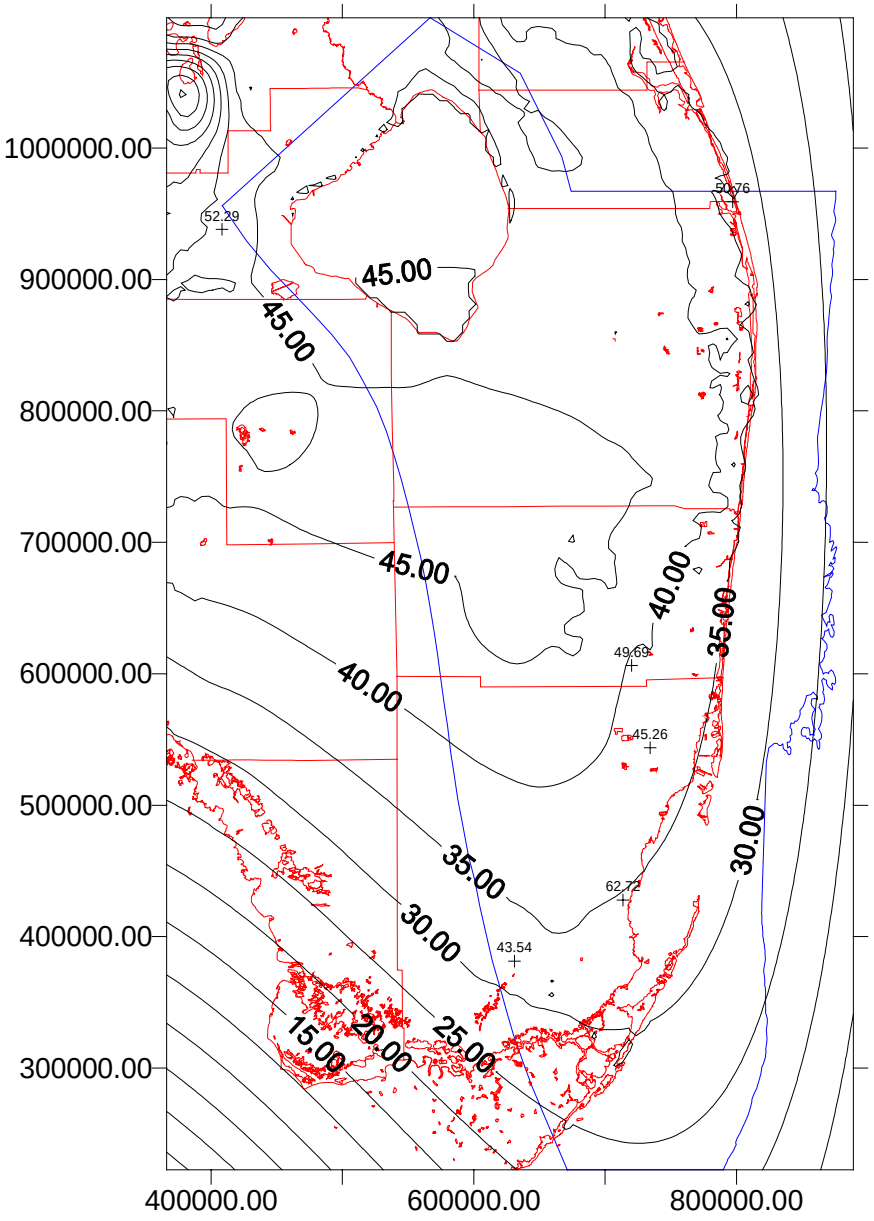

Figure 5. Initial Head Distribution – Layer 2.

Fairbank, P., J. Valdes, E. Rectenwald, M. Switaneck, and E. Hopkins, 1999. Documentation for the Lower East Coast Aquifer Model. Documentation for the Lower East Coast Floridan Aquifer Model. South Florida Water Management District.

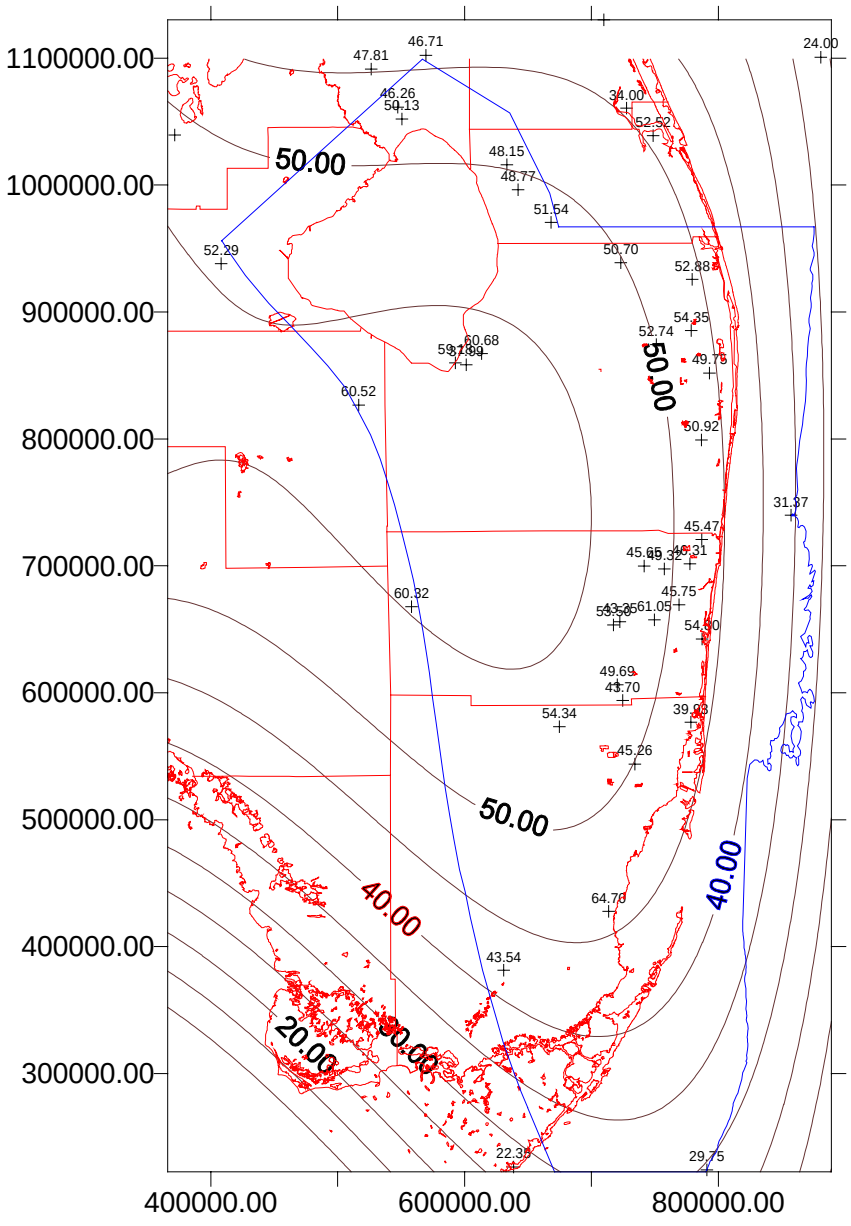

Figure 6. Initial Head Distribution – Layers 3,4,5.

Fairbank, P., J. Valdes, E. Rectenwald, M. Switaneck, and E. Hopkins, 1999. Documentation for the Lower East Coast Aquifer Model. Documentation for the Lower East Coast Floridan Aquifer Model. South Florida Water Management District.

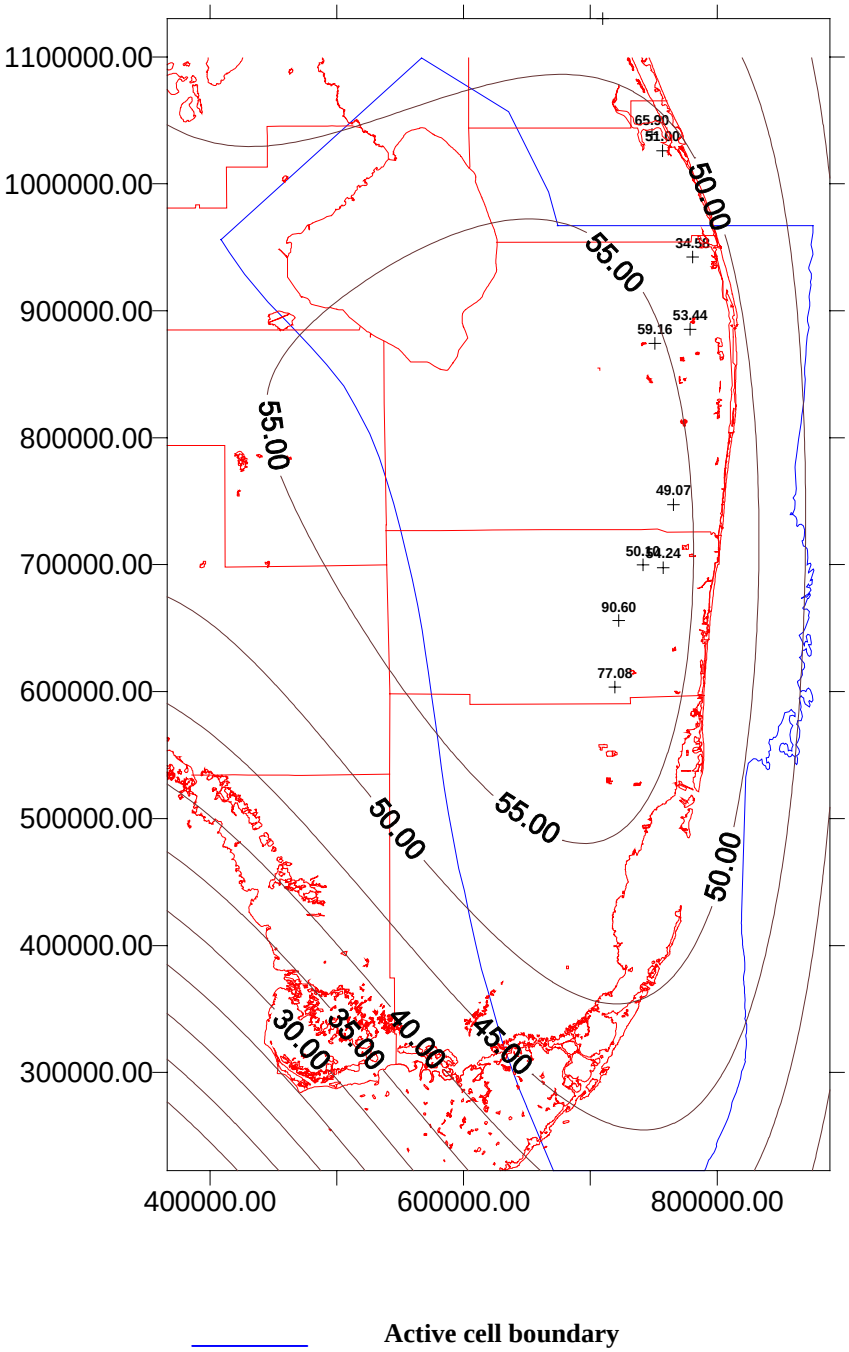

Figure 7. Initial Head Distribution – Layer 6.

Fairbank, P., J. Valdes, E. Rectenwald, M. Switaneck, and E. Hopkins, 1999. Documentation for the Lower East Coast Aquifer Model. Documentation for the Lower East Coast Floridan Aquifer Model. South Florida Water Management District.

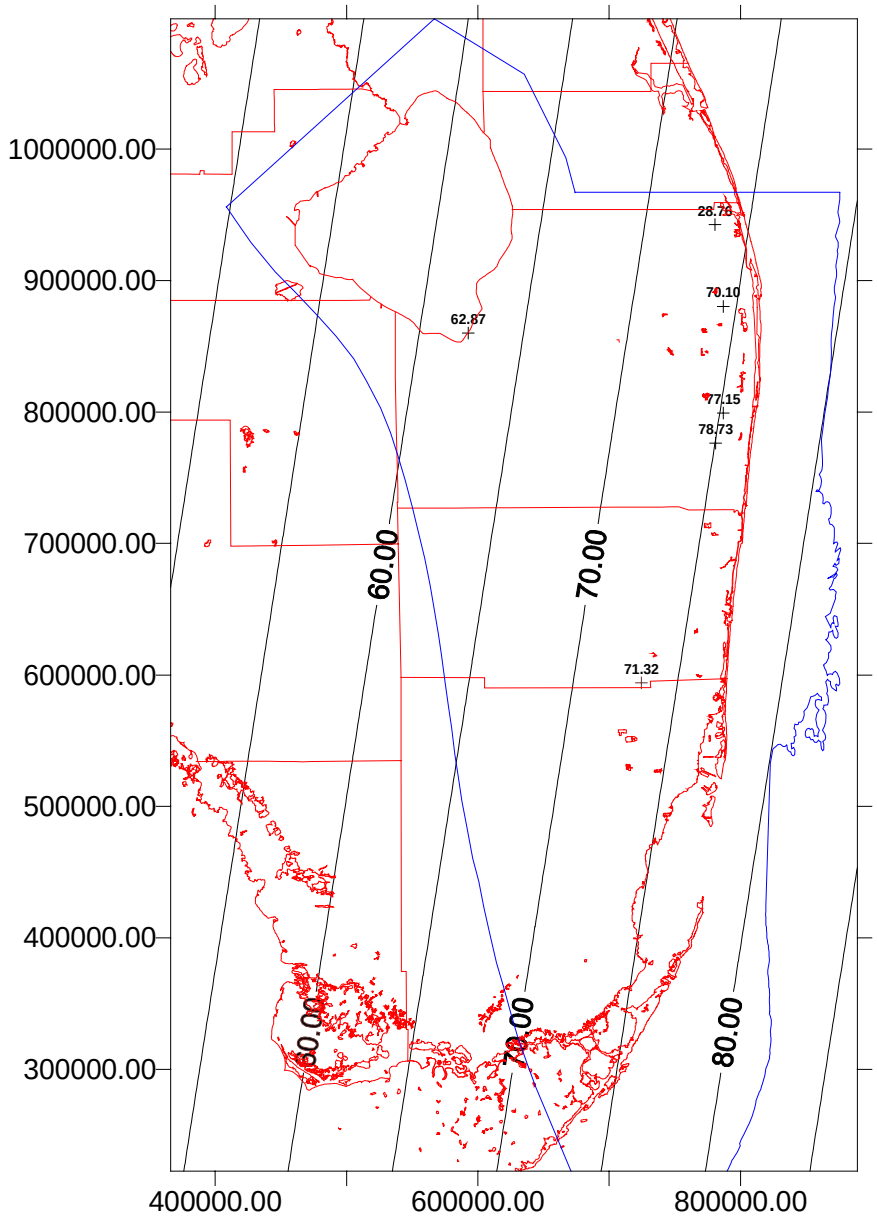

Figure 8. Initial Head Distribution – Layer 7.

Fairbank, P., J. Valdes, E. Rectenwald, M. Switaneck, and E. Hopkins, 1999. Documentation for the Lower East Coast Aquifer Model. Documentation for the Lower East Coast Floridan Aquifer Model. South Florida Water Management District.

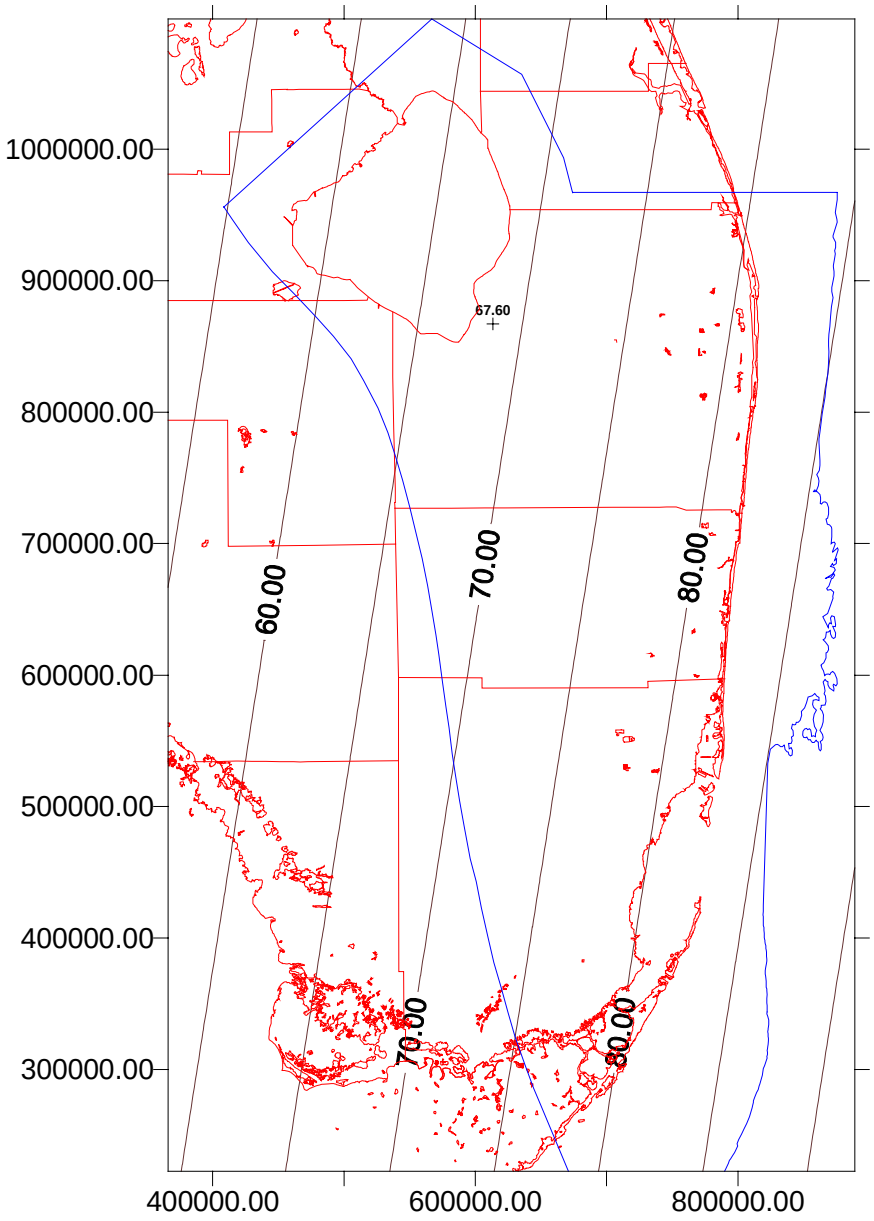

Figure 9. Initial Head Distribution – Layer 8.

Fairbank, P., J. Valdes, E. Rectenwald, M. Switaneck, and E. Hopkins, 1999. Documentation for the Lower East Coast Aquifer Model. Documentation for the Lower East Coast Floridan Aquifer Model. South Florida Water Management District.

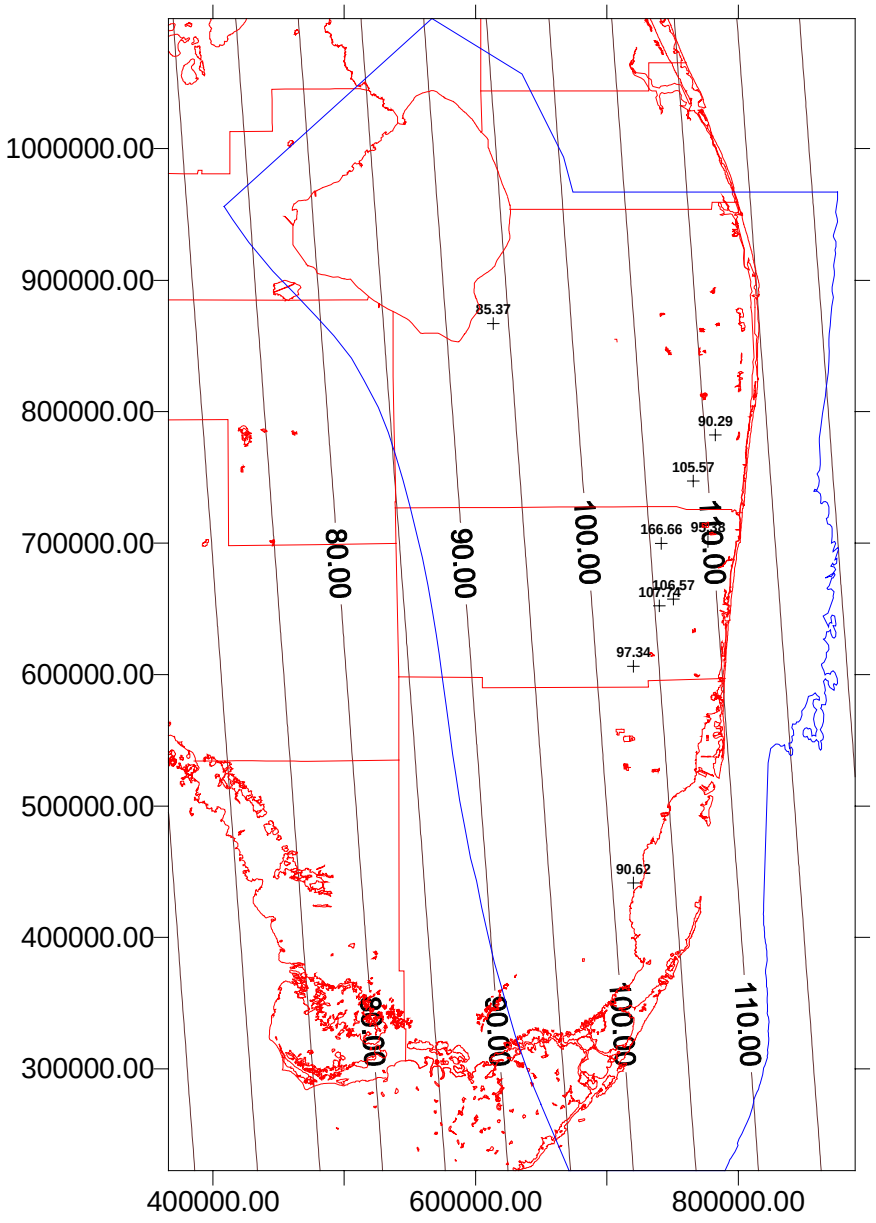

Figure 10. Initial Head Distribution – Layer 9.

Fairbank, P., J. Valdes, E. Rectenwald, M. Switaneck, and E. Hopkins, 1999. Documentation for the Lower East Coast Aquifer Model. Documentation for the Lower East Coast Floridan Aquifer Model. South Florida Water Management District.

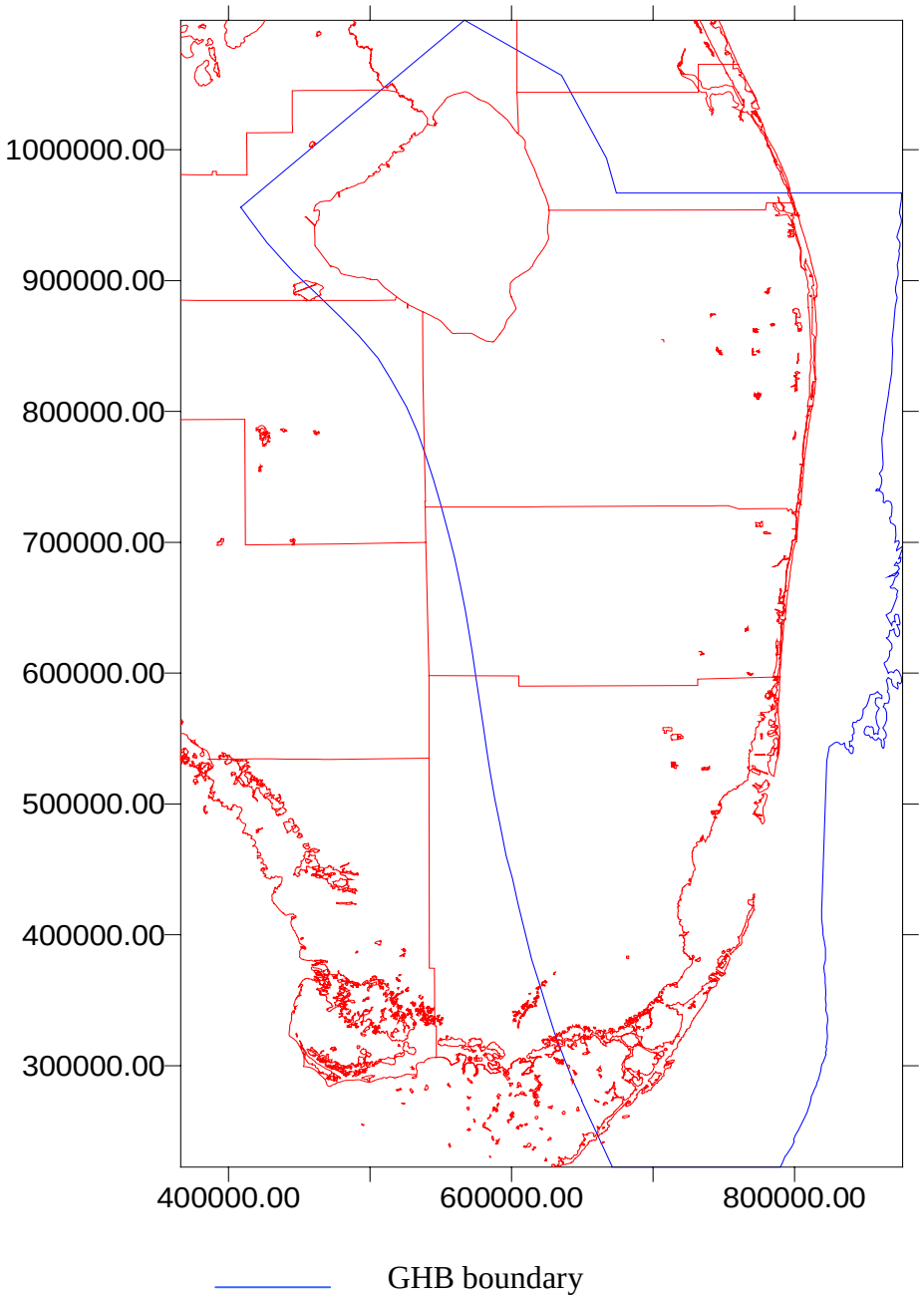

Figure 11. General Head Boundary Delineation.

Fairbank, P., J. Valdes, E. Rectenwald, M. Switaneck, and E. Hopkins, 1999. Documentation for the Lower East Coast Aquifer Model. Documentation for the Lower East Coast Floridan Aquifer Model. South Florida Water Management District.

Appendix B

Selected Figures from Documentation of the Lee County, Florida model

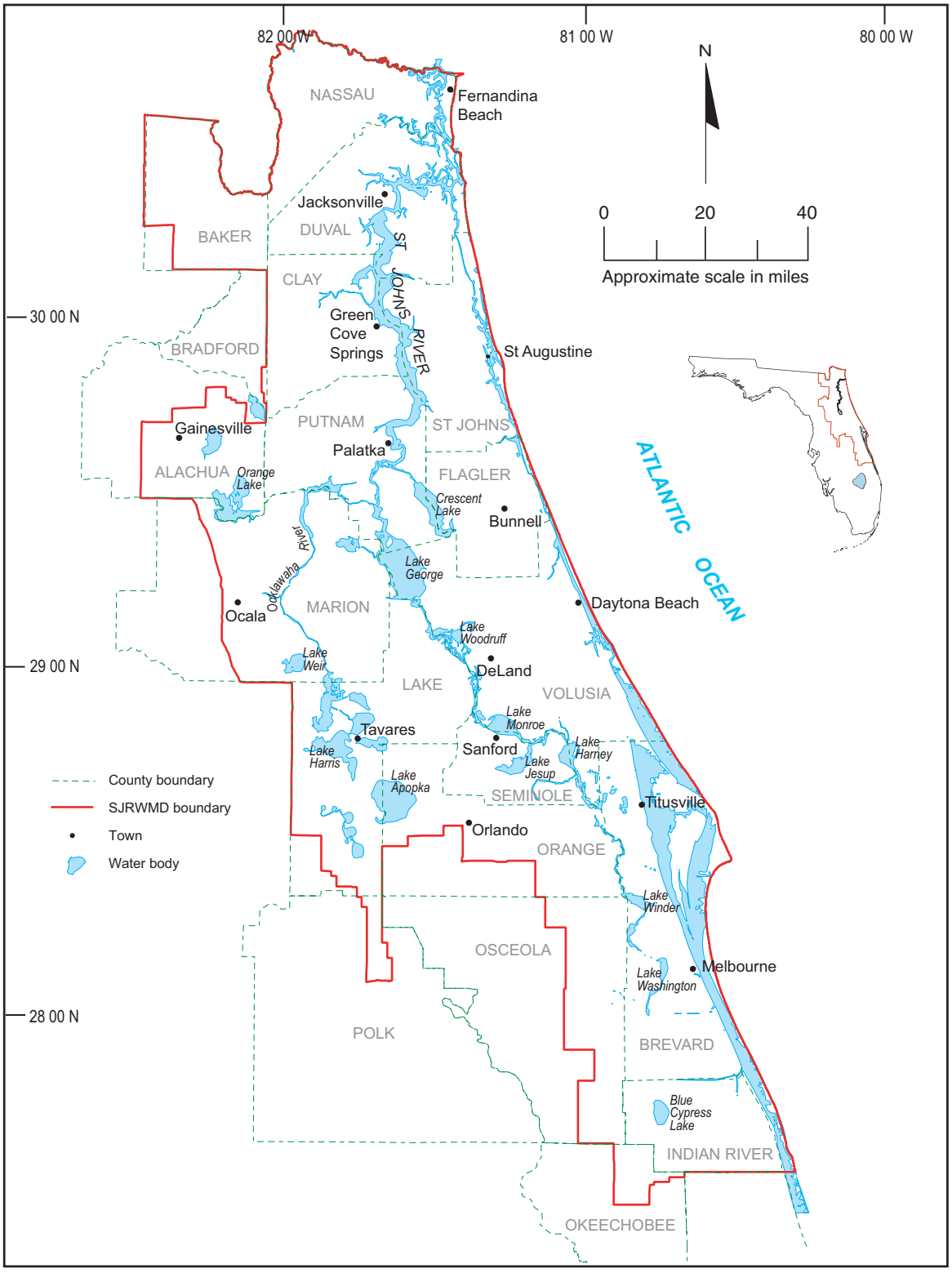

Figure 1. The St. Johns River Water Management District (SJRWMD)

McGurk, B., and P. Fischl Presley, 2002. Simulation of the Effects of Groundwater Withdrawals on the Floridan Aquifer System in East-Central Florida: Model Expansion and Revision. Technical Publication SJ2002-3, St. Johns River Water Management District, Palatka, FL.

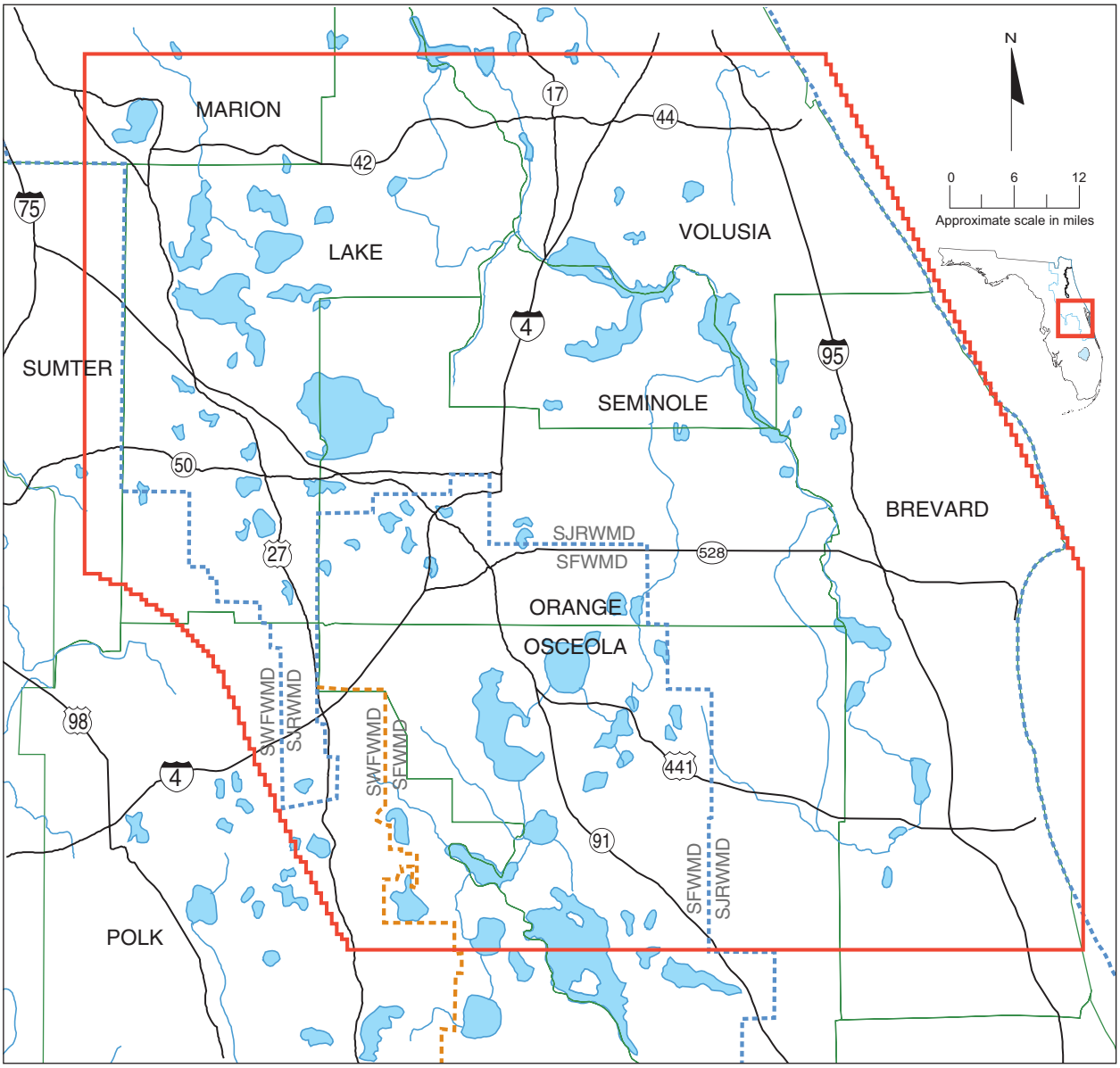

Figure 2. East-central Florida (ECF) project area — includes a portion of the Southwest Florida Water Management District (SWFWMD) and the South Florida Water Management District (SFWMD)

McGurk, B., and P. Fischl Presley, 2002. Simulation of the Effects of Groundwater Withdrawals on the Floridan Aquifer System in East-Central Florida: Model Expansion and Revision. Technical Publication SJ2002-3, St. Johns River Water Management District, Palatka, FL.

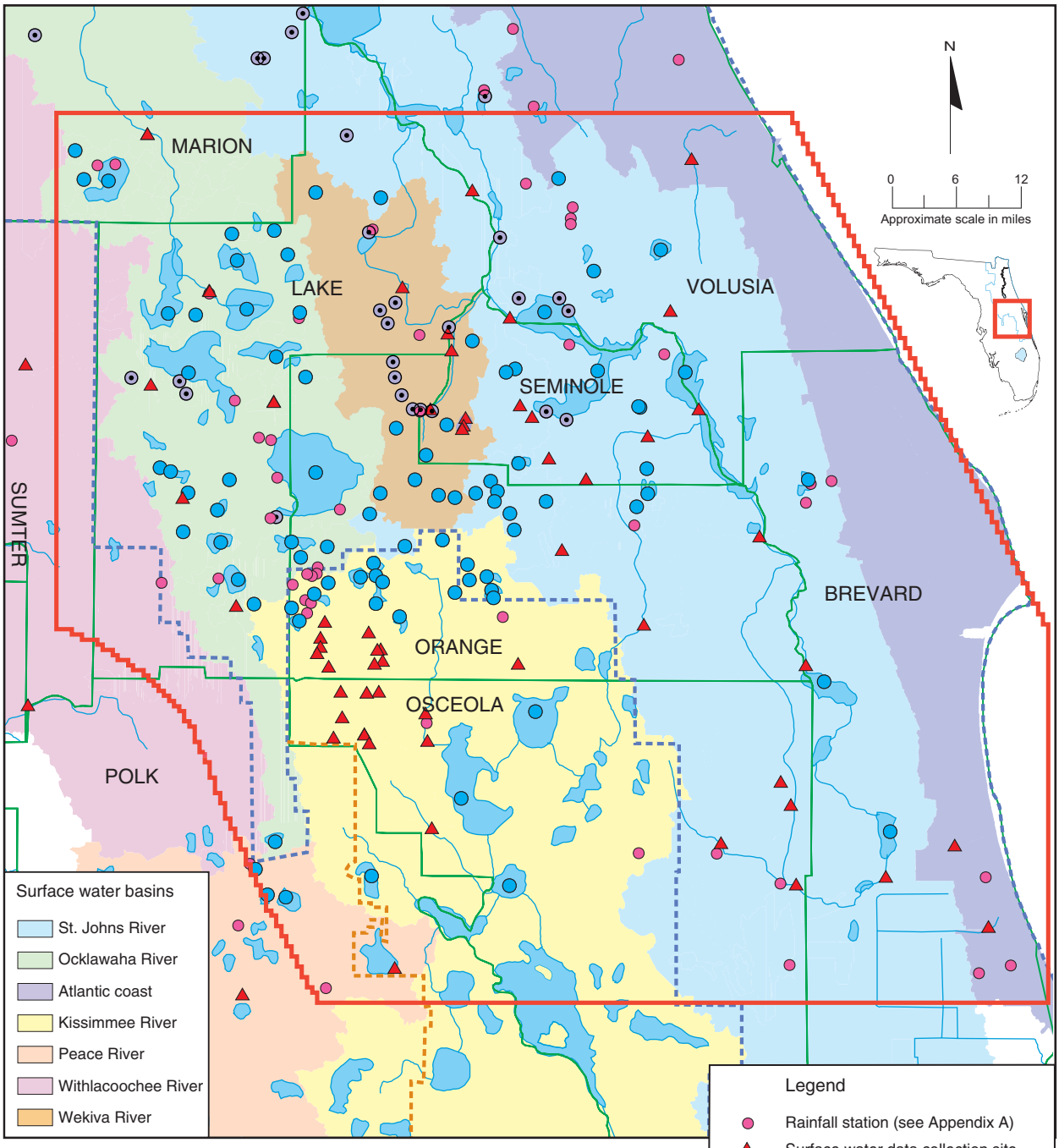

Figure 3. Locations of surface-water features, springs, rainfall stations and surface-water data collection sites

McGurk, B., and P. Fischl Presley, 2002. Simulation of the Effects of Groundwater Withdrawals on the Floridan Aquifer System in East-Central Florida: Model Expansion and Revision. Technical Publication SJ2002-3, St. Johns River Water Management District, Palatka, FL.

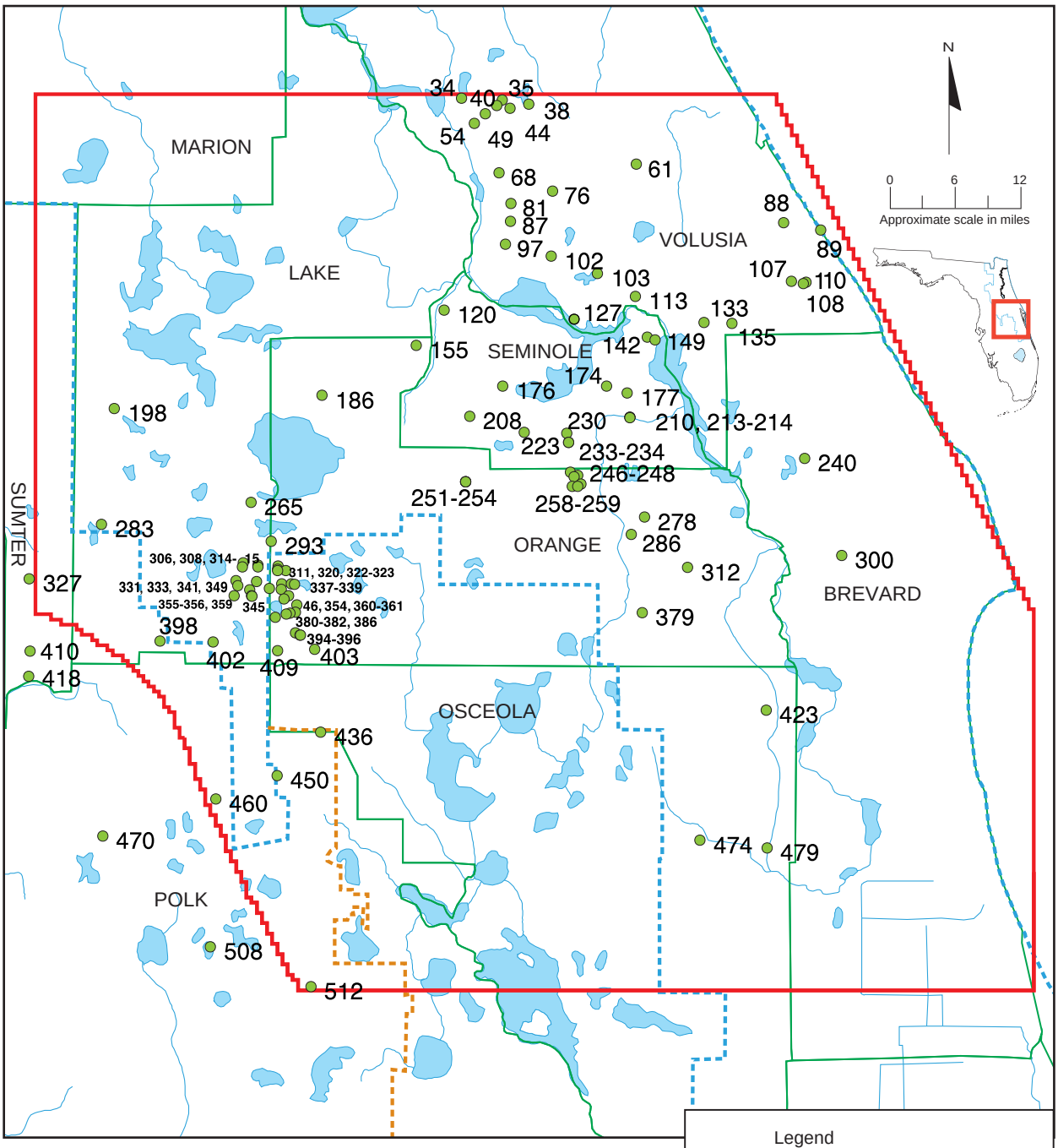

Figure 4. Locations of observation and test wells completed in the surficial aquifer system

McGurk, B., and P. Fischl Presley, 2002. Simulation of the Effects of Groundwater Withdrawals on the Floridan Aquifer System in East-Central Florida: Model Expansion and Revision. Technical Publication SJ2002-3, St. Johns River Water Management District, Palatka, FL.

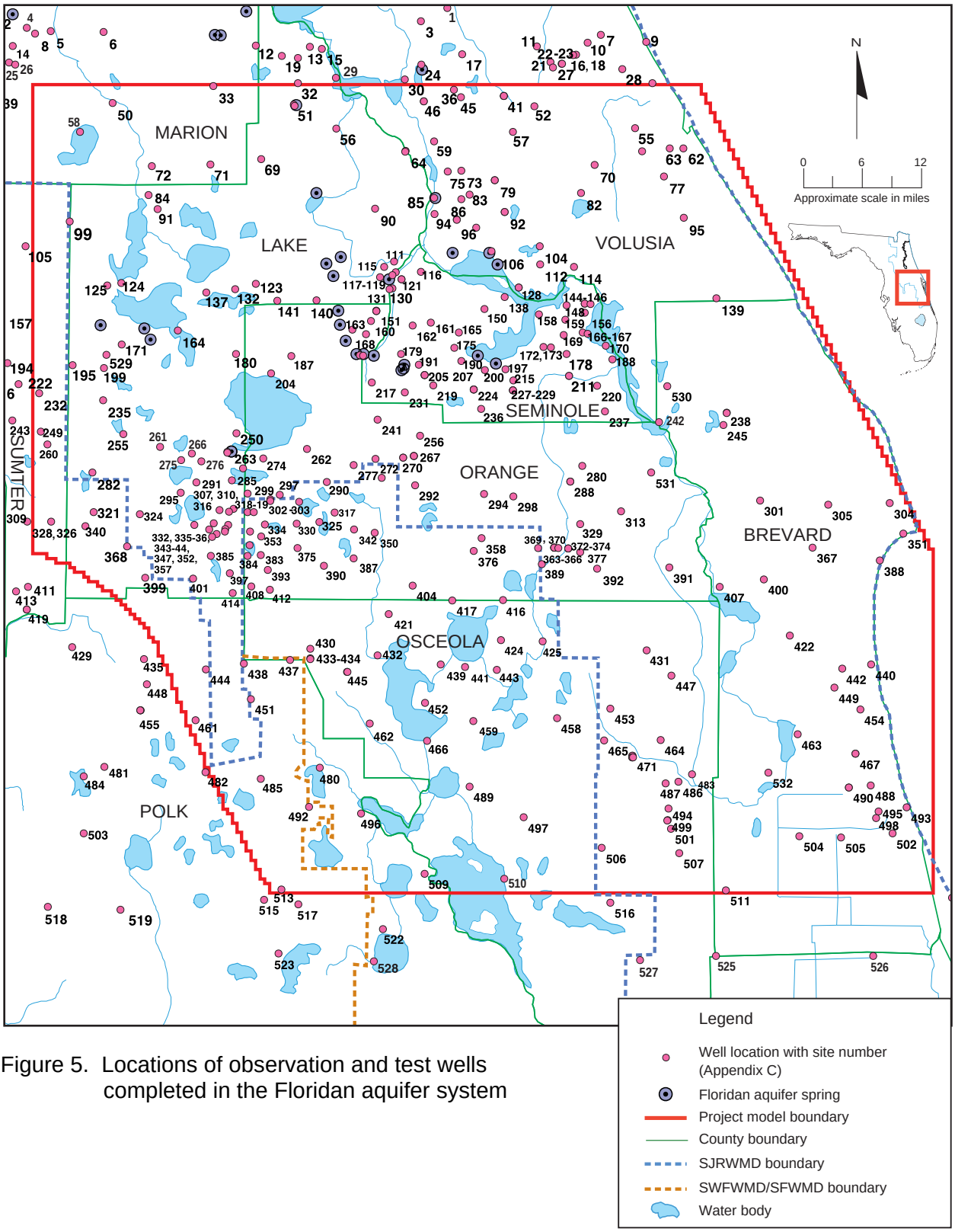

Figure 5. Locations of observation and test wells completed in the Floridan aquifer system

McGurk, B., and P. Fischl Presley, 2002. Simulation of the Effects of Groundwater Withdrawals on the Floridan Aquifer System in East-Central Florida: Model Expansion and Revision. Technical Publication SJ2002-3, St. Johns River Water Management District, Palatka, FL.

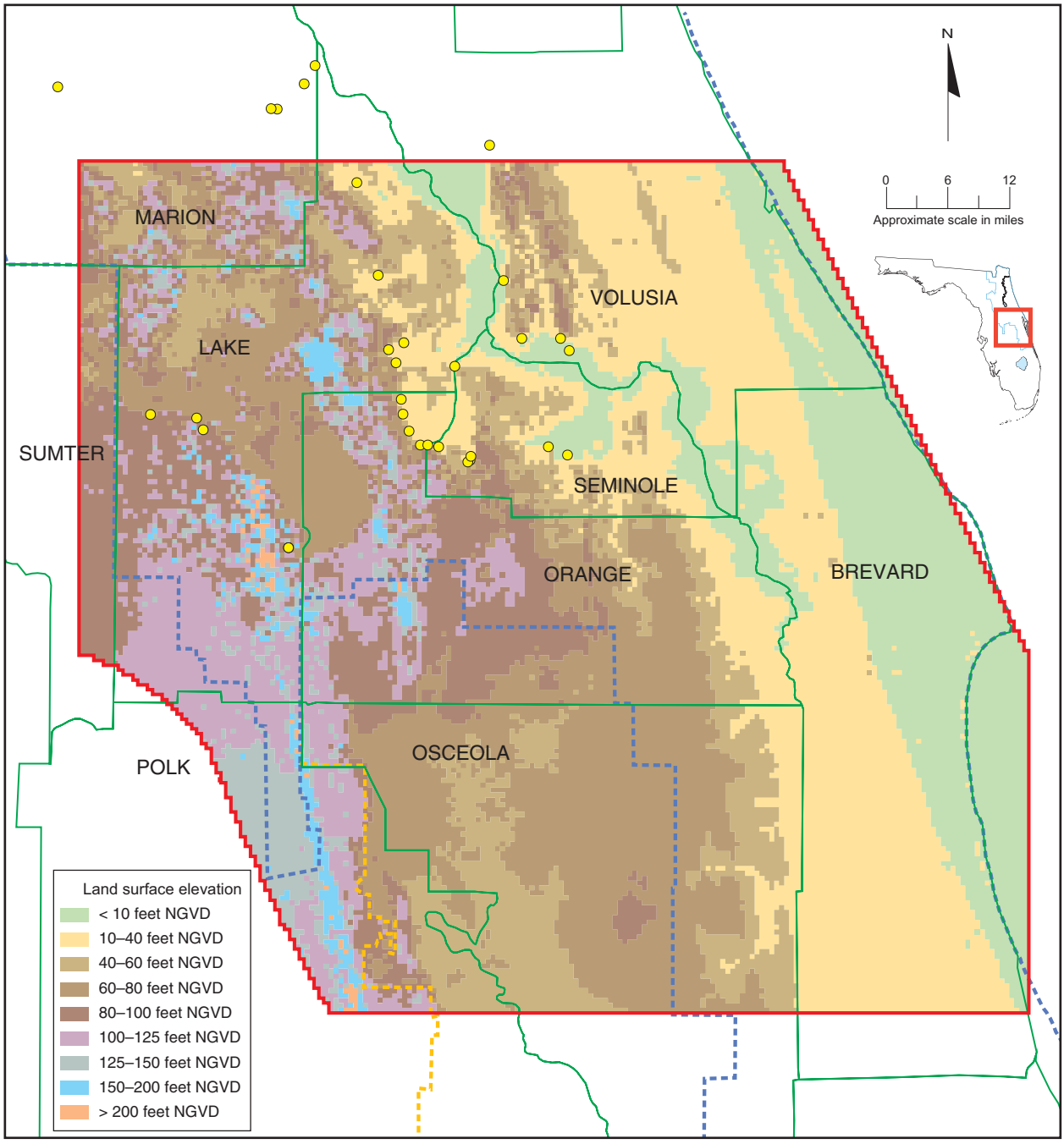

Figure 6. Land surface elevations in the east-central Florida project area

McGurk, B., and P. Fischl Presley, 2002. Simulation of the Effects of Groundwater Withdrawals on the Floridan Aquifer System in East-Central Florida: Model Expansion and Revision. Technical Publication SJ2002-3, St. Johns River Water Management District, Palatka, FL.

<table>
<tr><th>Geologic Series / Stratigraphic Unit</th><th>Lithology and Thickness (feet)</th><th>Hydrostratigraphic Unit</th></tr>
<tr><td>Holocene, Pleistocene / undifferentiated</td><td>Interbedded sand, clay, marl, and peat / 0–150</td><td>Surficial aquifer system</td></tr>
<tr><td>Pliocene, Miocene / undifferentiated sediments, Hawthorn Group</td><td>Interbedded clay, sandy clay, and sand, often phosphatic, with some phosphatic limestone and dolostone / 0–250</td><td>Intermediate confining unit</td></tr>
<tr><td>Upper Eocene / Ocala Limestone</td><td>Predominantly soft to hard porous limestone, minor amounts of hard, crystalline dolostone / 0–300</td><td rowspan="2">Upper Floridan aquifer—upper zone</td></tr>
<tr><td rowspan="4">Middle Eocene / Avon Park Formation</td><td rowspan="3">Upper part: predominantly hard, crystalline dolostone with abundant fractures and solution cavities / 100–200

Middle part: predominantly soft, porous limestone and dolomitic limestone, with minor amounts of hard crystalline dolostone / <100–700

Lower part: soft to hard porous limestone and hard, fractured crystalline dolostone / 600–800</td><td>Upper Floridan aquifer—lower zone</td></tr>
<tr><td rowspan="2">Middle semiconfining unit</td></tr>
<tr><td rowspan="3">Lower Floridan aquifer</td></tr>
<tr><td>Lower Eocene / Oldsmar Formation</td><td>Soft to hard porous limestone and hard, fractured crystalline dolostone; minor amounts of peat, chert, anhydrite, and gypsum / 500–1,000</td></tr>
<tr><td>Paleocene / Cedar Keys Formation</td><td>Interbedded carbonate rocks and evaporites / 500–2,200</td><td>Lower confining unit</td></tr>
</table>

Figure 7. Geologic and hydrostratigraphic units within the east-central Florida project area

McGurk, B., and P. Fischl Presley, 2002. Simulation of the Effects of Groundwater Withdrawals on the Floridan Aquifer System in East-Central Florida: Model Expansion and Revision. Technical Publication SJ2002-3, St. Johns River Water Management District, Palatka, FL.

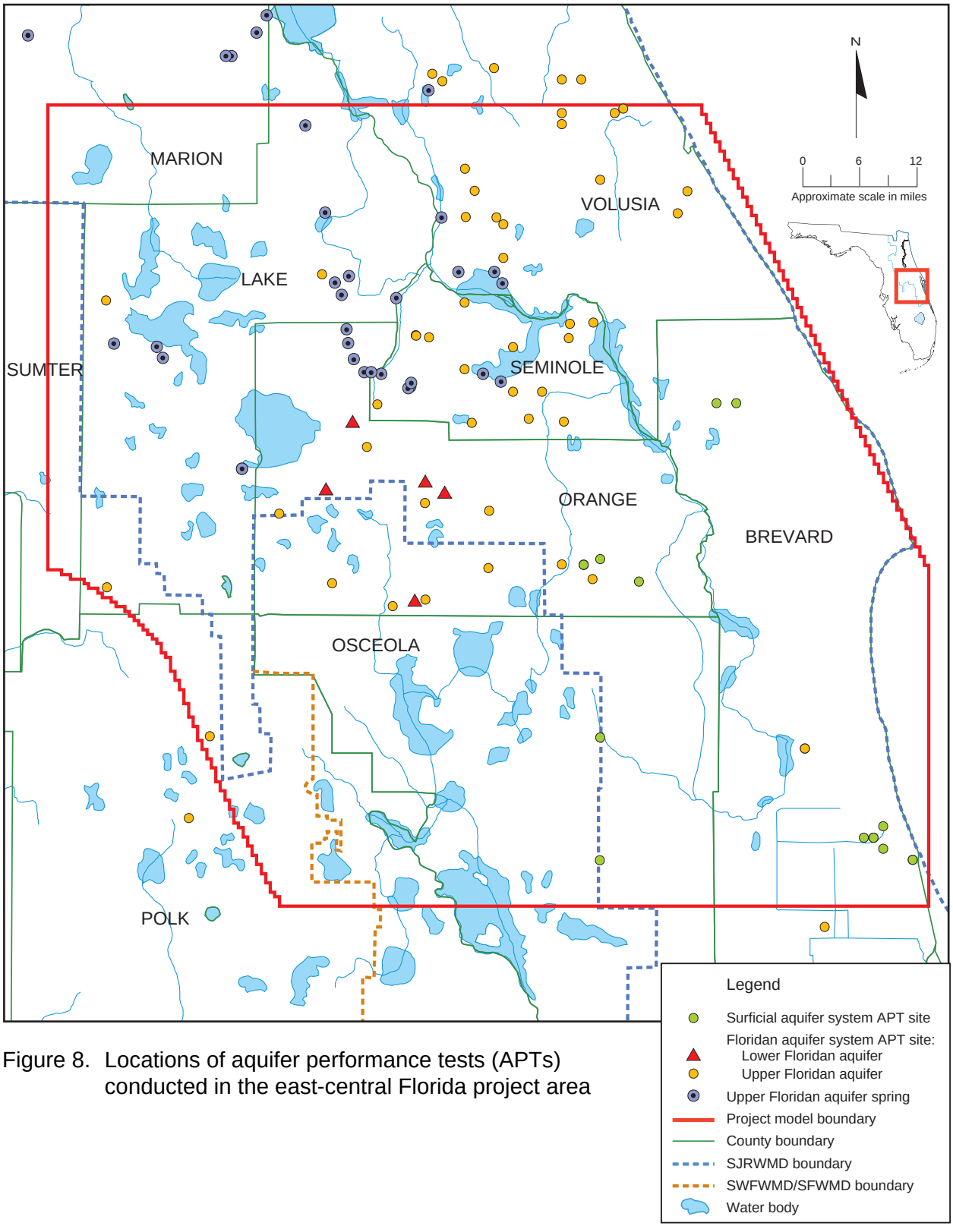

Figure 8. Locations of aquifer performance tests (APTs) conducted in the east-central Florida project area

McGurk, B., and P. Fischl Presley, 2002. Simulation of the Effects of Groundwater Withdrawals on the Floridan Aquifer System in East-Central Florida: Model Expansion and Revision. Technical Publication SJ2002-3, St. Johns River Water Management District, Palatka, FL.

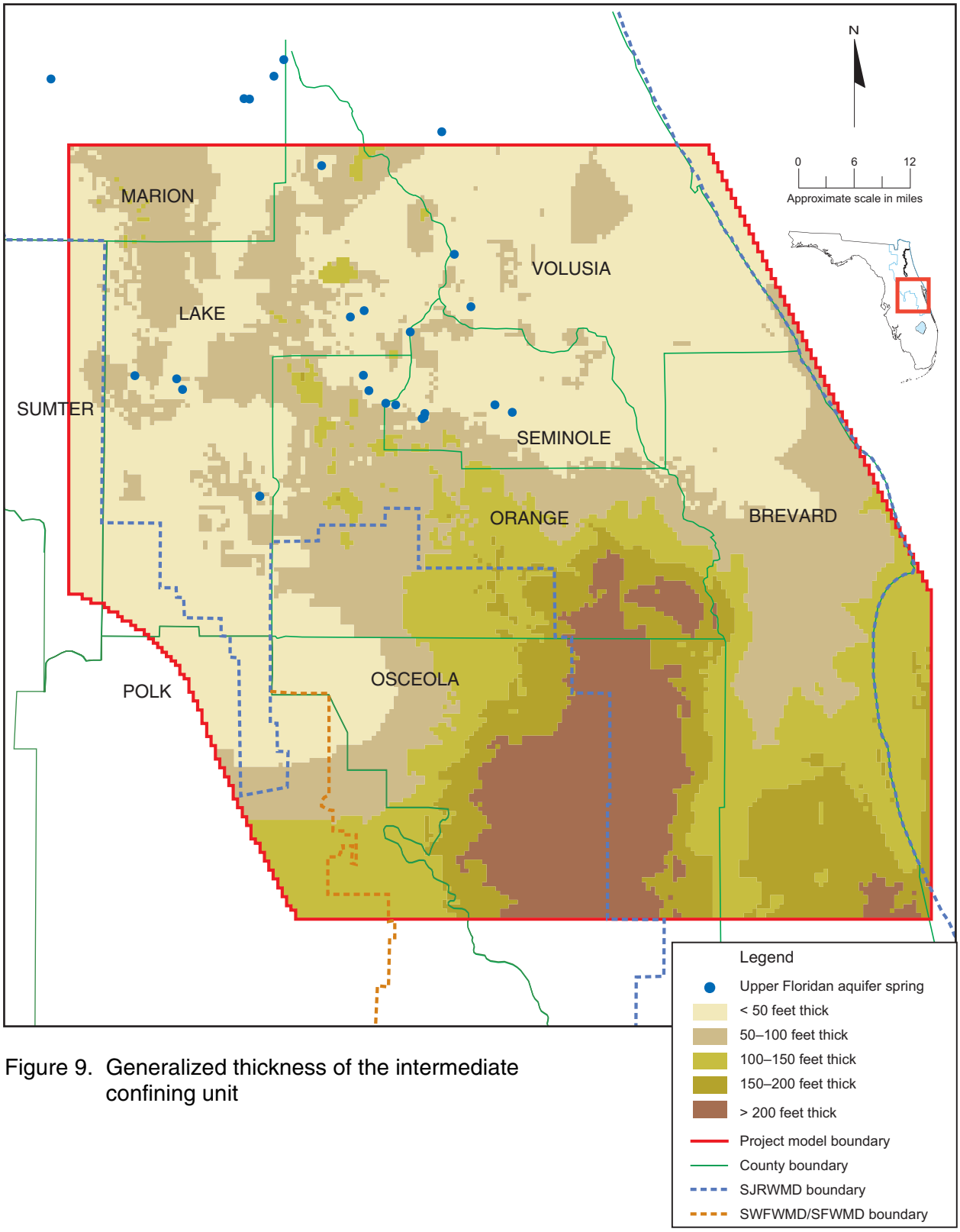

Figure 9. Generalized thickness of the intermediate confining unit

McGurk, B., and P. Fischl Presley, 2002. Simulation of the Effects of Groundwater Withdrawals on the Floridan Aquifer System in East-Central Florida: Model Expansion and Revision. Technical Publication SJ2002-3, St. Johns River Water Management District, Palatka, FL.

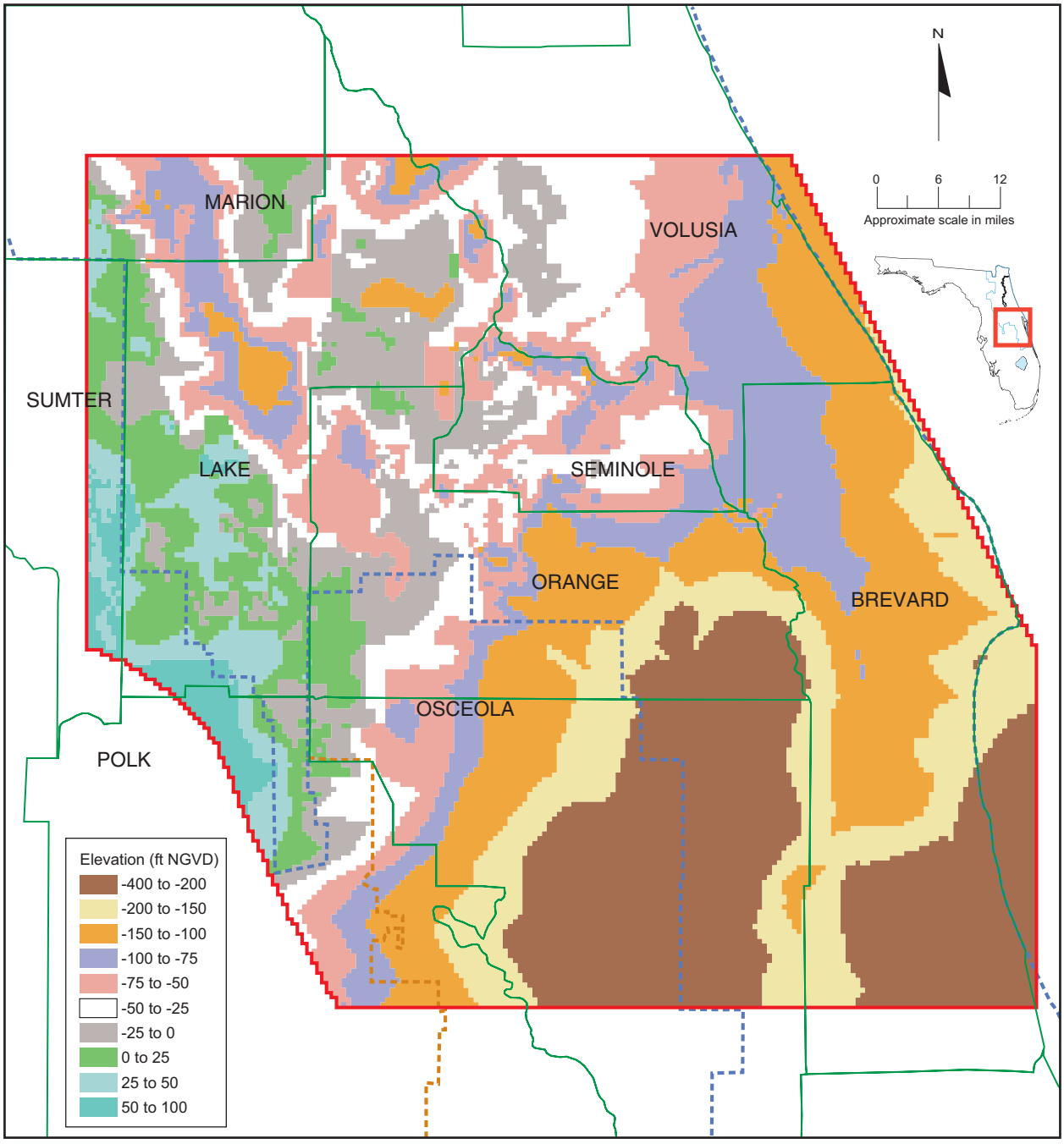

Figure 10. Generalized elevation of the top of the Upper Floridan aquifer (modified from Miller 1986)

McGurk, B., and P. Fischl Presley, 2002. Simulation of the Effects of Groundwater Withdrawals on the Floridan Aquifer System in East-Central Florida: Model Expansion and Revision. Technical Publication SJ2002-3, St. Johns River Water Management District, Palatka, FL.

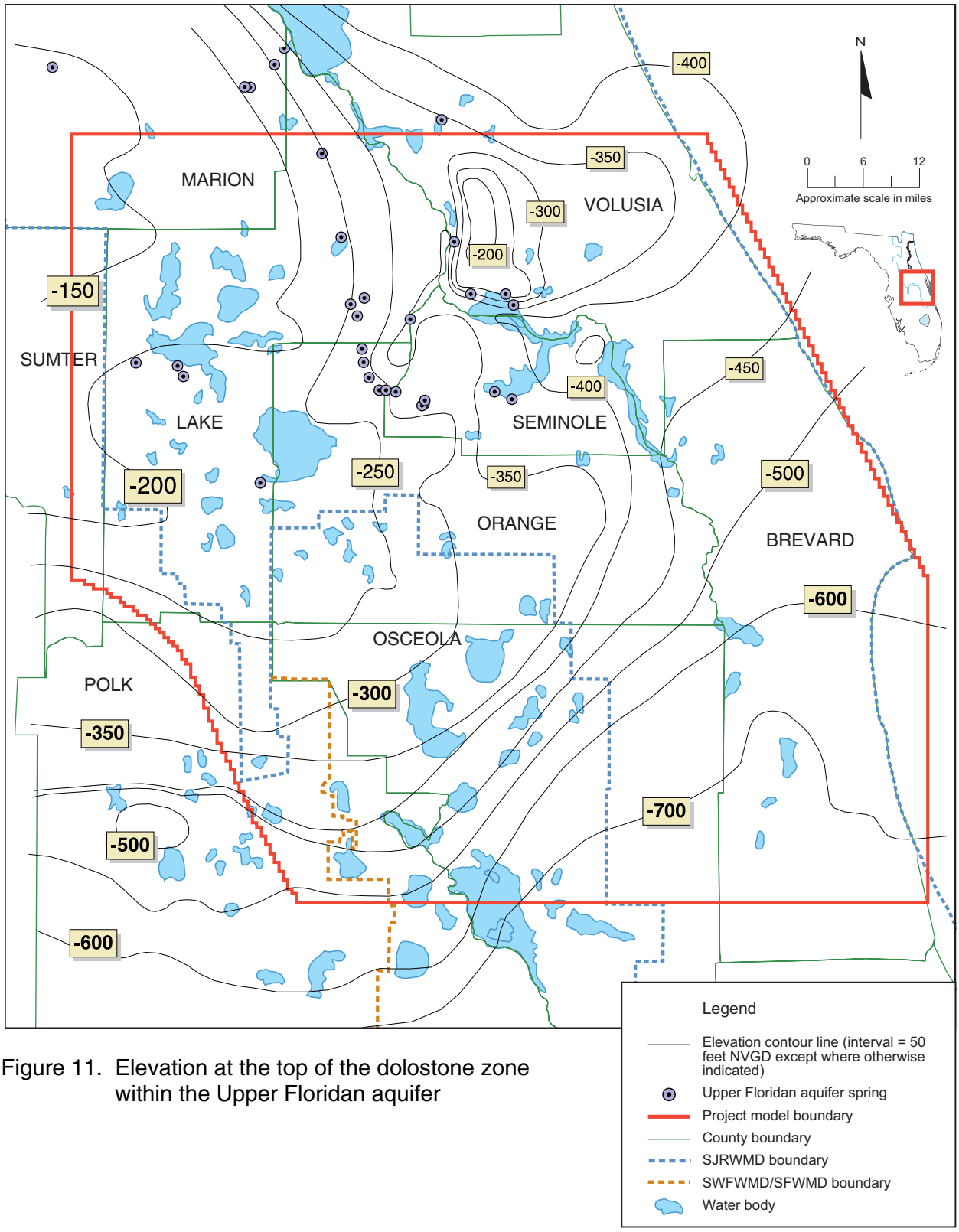

Figure 11. Elevation at the top of the dolostone zone within the Upper Floridan aquifer

McGurk, B., and P. Fischl Presley, 2002. Simulation of the Effects of Groundwater Withdrawals on the Floridan Aquifer System in East-Central Florida: Model Expansion and Revision. Technical Publication SJ2002-3, St. Johns River Water Management District, Palatka, FL.

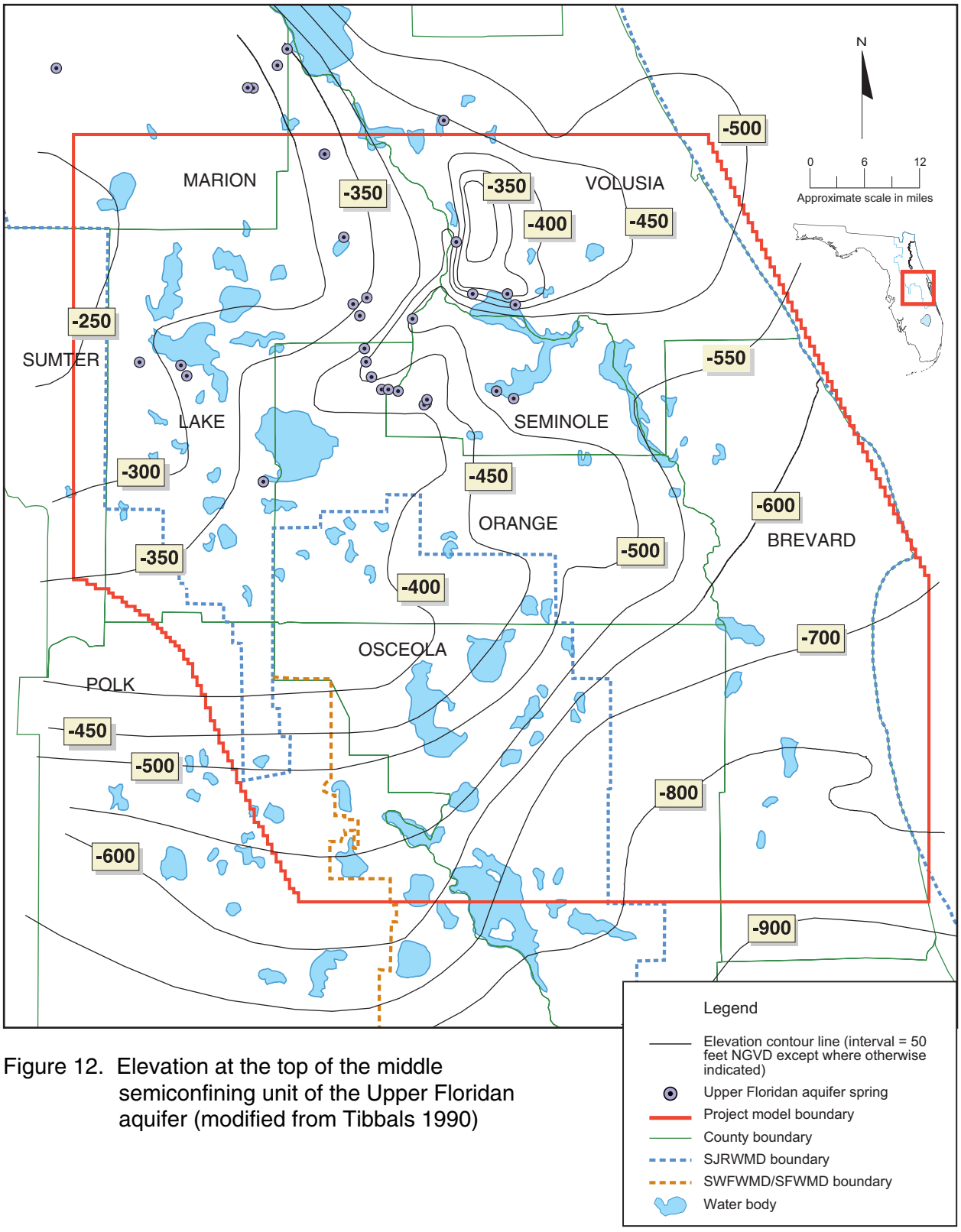

Figure 12. Elevation at the top of the middle semiconfining unit of the Upper Floridan aquifer (modified from Tibbals 1990)

McGurk, B., and P. Fischl Presley, 2002. Simulation of the Effects of Groundwater Withdrawals on the Floridan Aquifer System in East-Central Florida: Model Expansion and Revision. Technical Publication SJ2002-3, St. Johns River Water Management District, Palatka, FL.

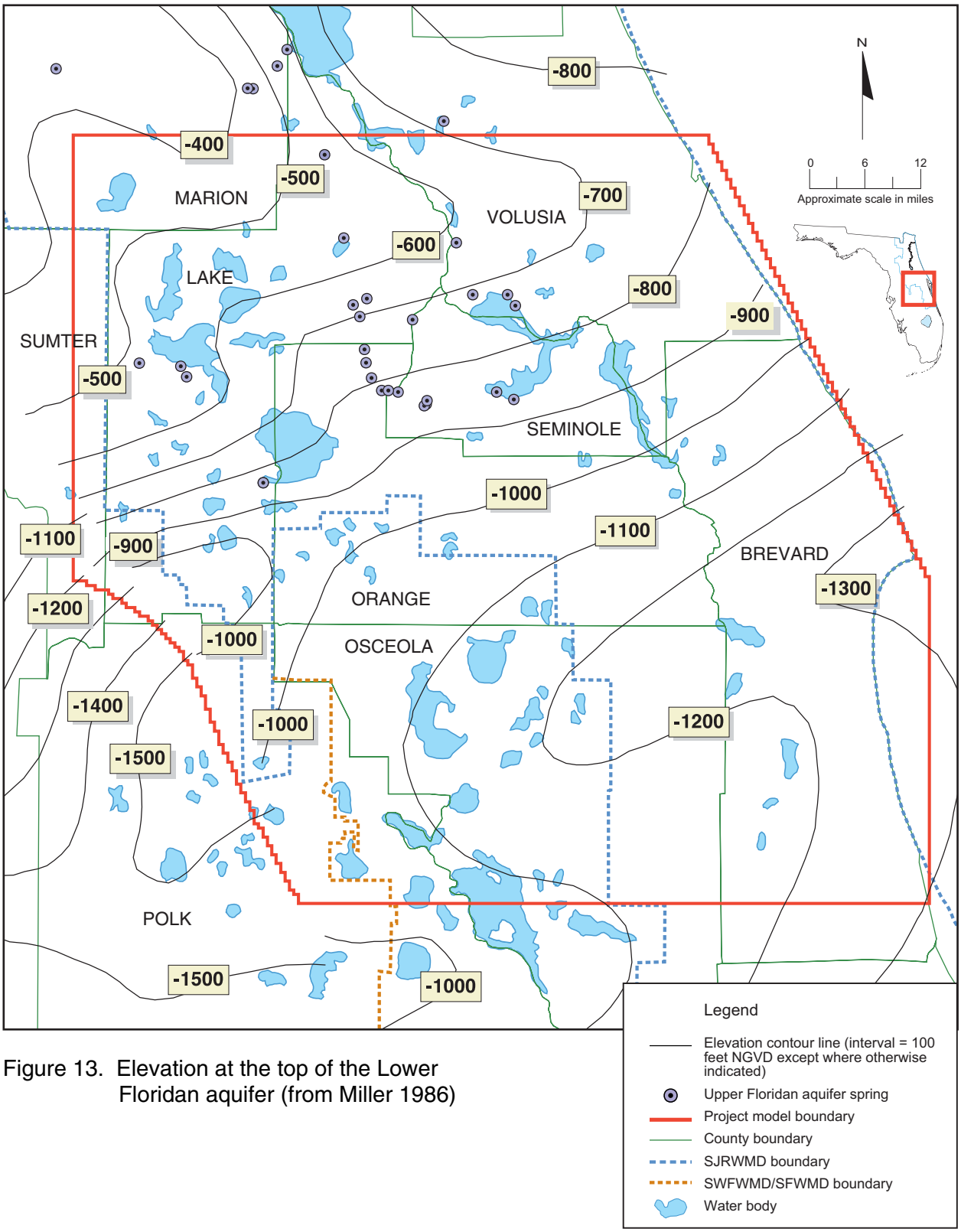

Figure 13. Elevation at the top of the Lower Floridan aquifer (from Miller 1986)

McGurk, B., and P. Fischl Presley, 2002. Simulation of the Effects of Groundwater Withdrawals on the Floridan Aquifer System in East-Central Florida: Model Expansion and Revision. Technical Publication SJ2002-3, St. Johns River Water Management District, Palatka, FL.

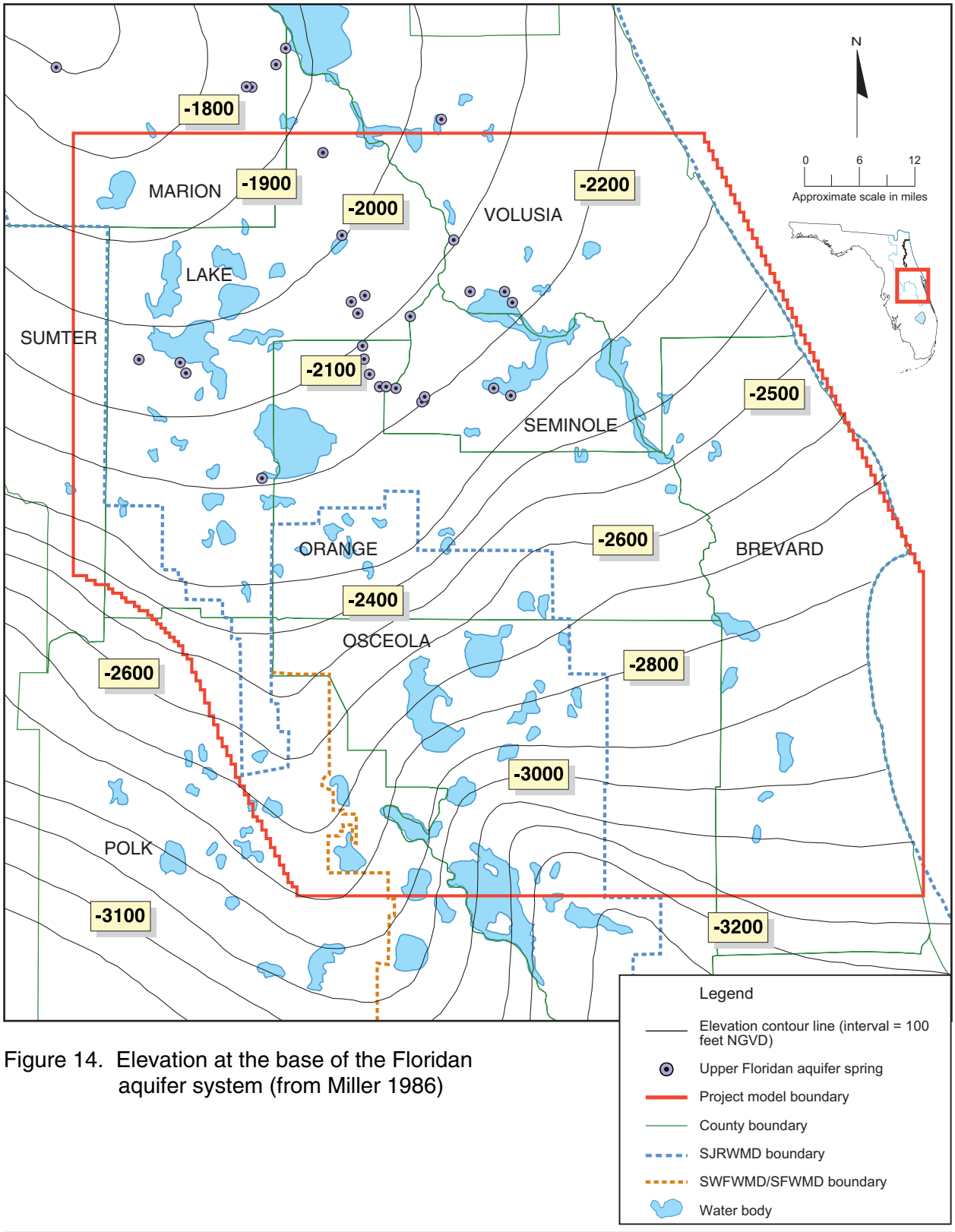

Figure 14. Elevation at the base of the Floridan aquifer system (from Miller 1986)

McGurk, B., and P. Fischl Presley, 2002. Simulation of the Effects of Groundwater Withdrawals on the Floridan Aquifer System in East-Central Florida: Model Expansion and Revision. Technical Publication SJ2002-3, St. Johns River Water Management District, Palatka, FL.

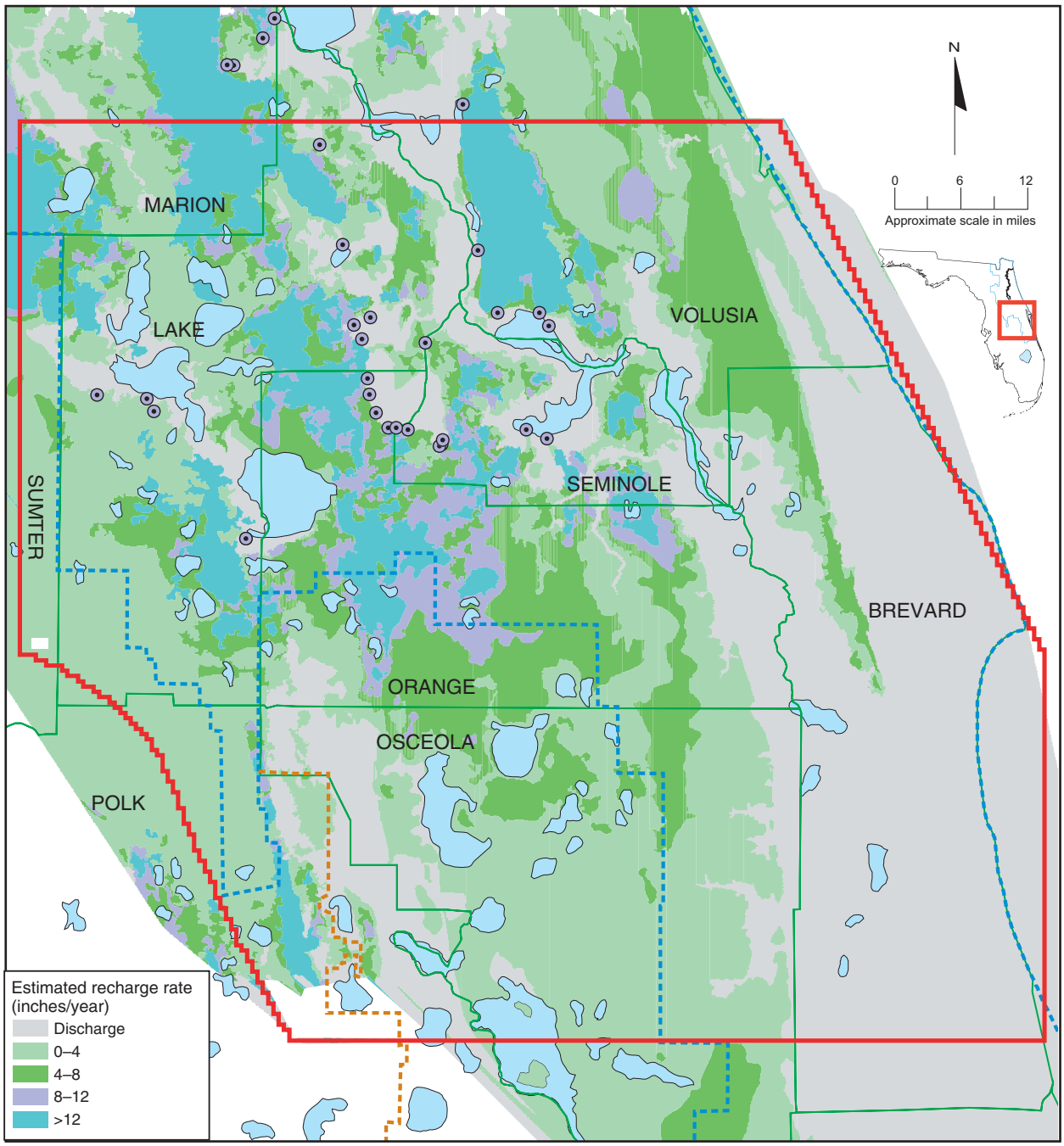

Figure 15. Areas of recharge to and discharge from the Floridan aquifer system (modified from Boniol et al. 1993)

McGurk, B., and P. Fischl Presley, 2002. Simulation of the Effects of Groundwater Withdrawals on the Floridan Aquifer System in East-Central Florida: Model Expansion and Revision. Technical Publication SJ2002-3, St. Johns River Water Management District, Palatka, FL.

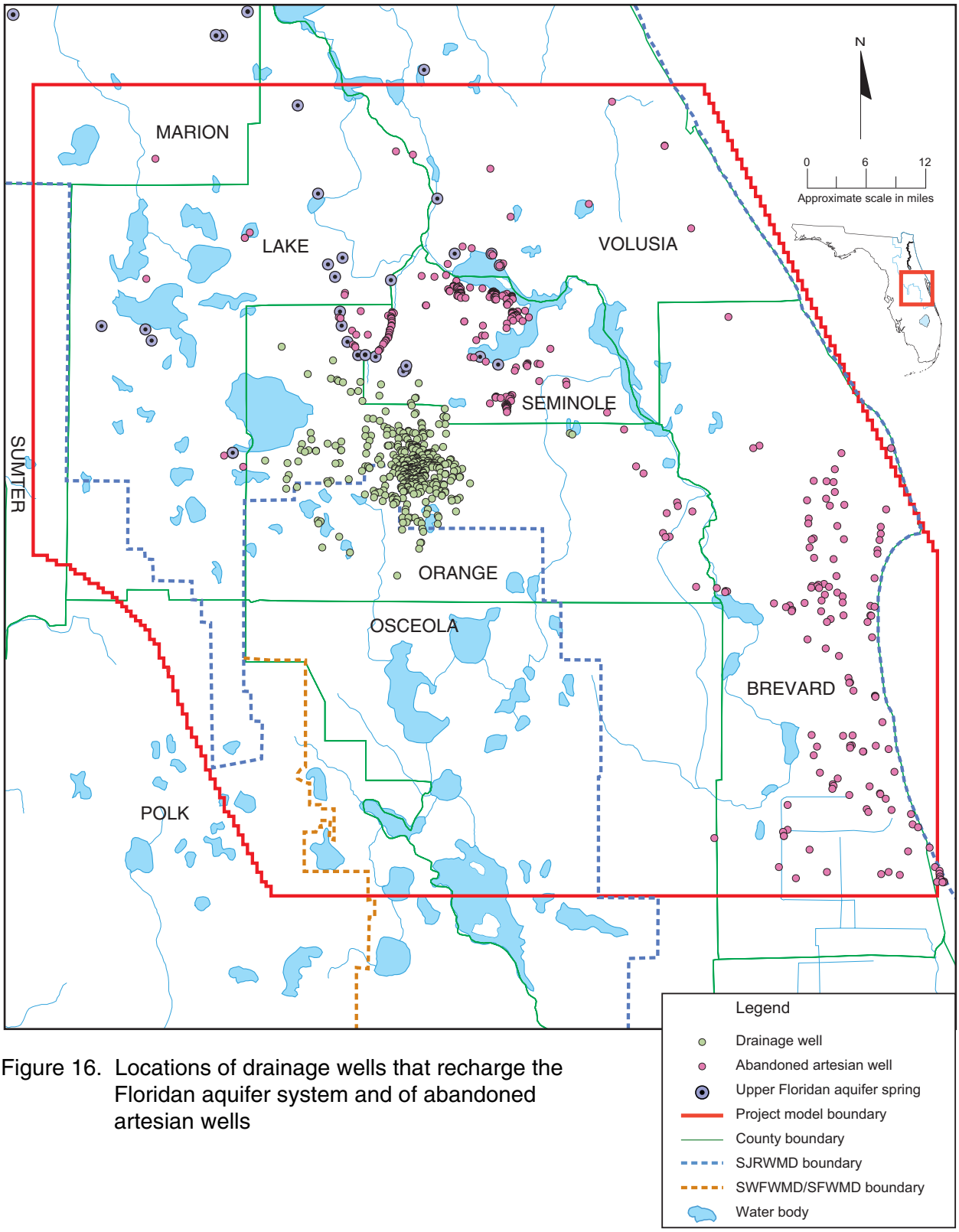

Figure 16. Locations of drainage wells that recharge the Floridan aquifer system and of abandoned artesian wells

McGurk, B., and P. Fischl Presley, 2002. Simulation of the Effects of Groundwater Withdrawals on the Floridan Aquifer System in East-Central Florida: Model Expansion and Revision. Technical Publication SJ2002-3, St. Johns River Water Management District, Palatka, FL.

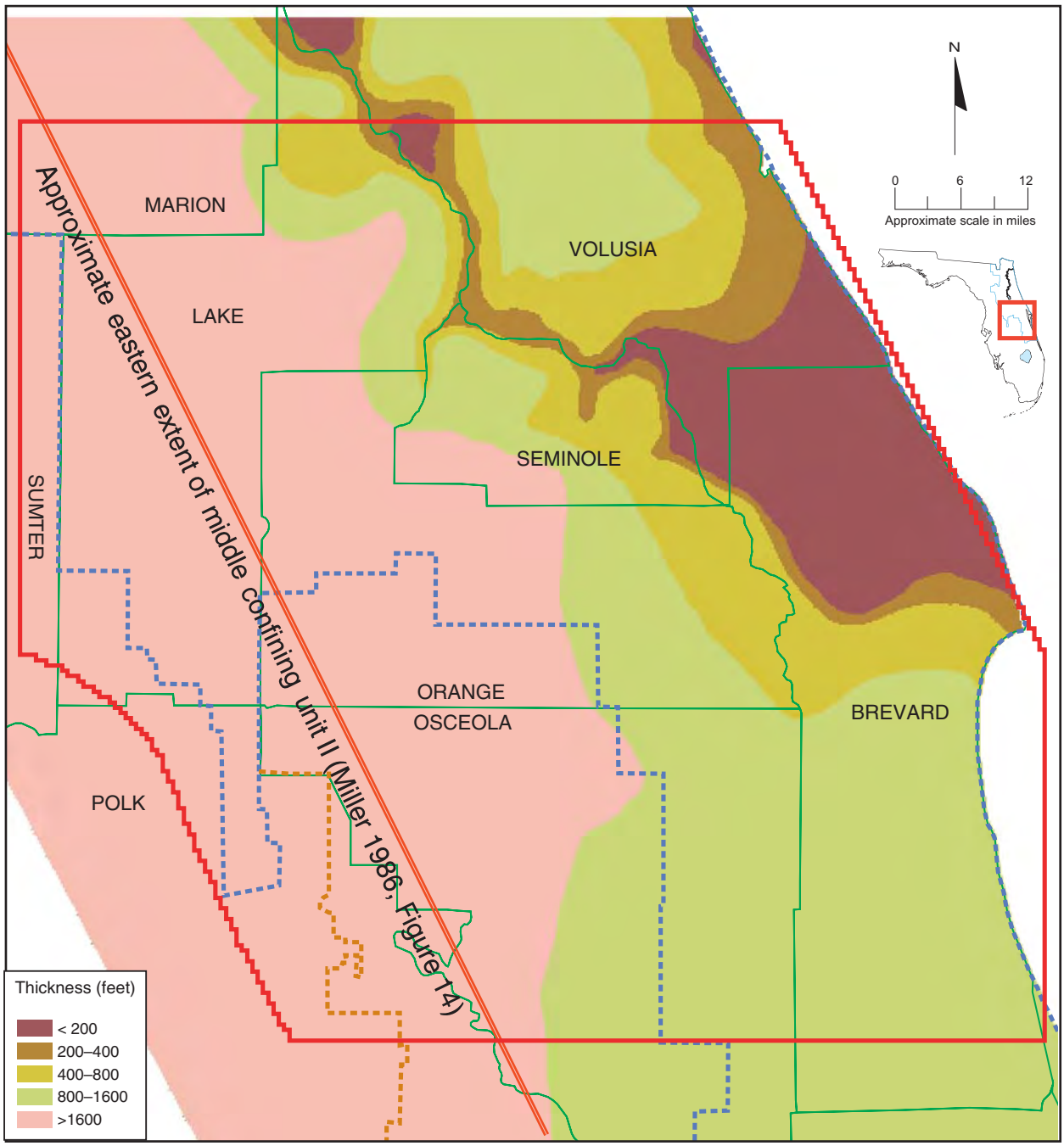

Figure 24. Thickness of the Floridan aquifer system containing chloride concentrations less than 5,000 milligrams per liter (from McGurk et al. 1998)

McGurk, B., and P. Fischl Presley, 2002. Simulation of the Effects of Groundwater Withdrawals on the Floridan Aquifer System in East-Central Florida: Model Expansion and Revision. Technical Publication SJ2002-3, St. Johns River Water Management District, Palatka, FL.

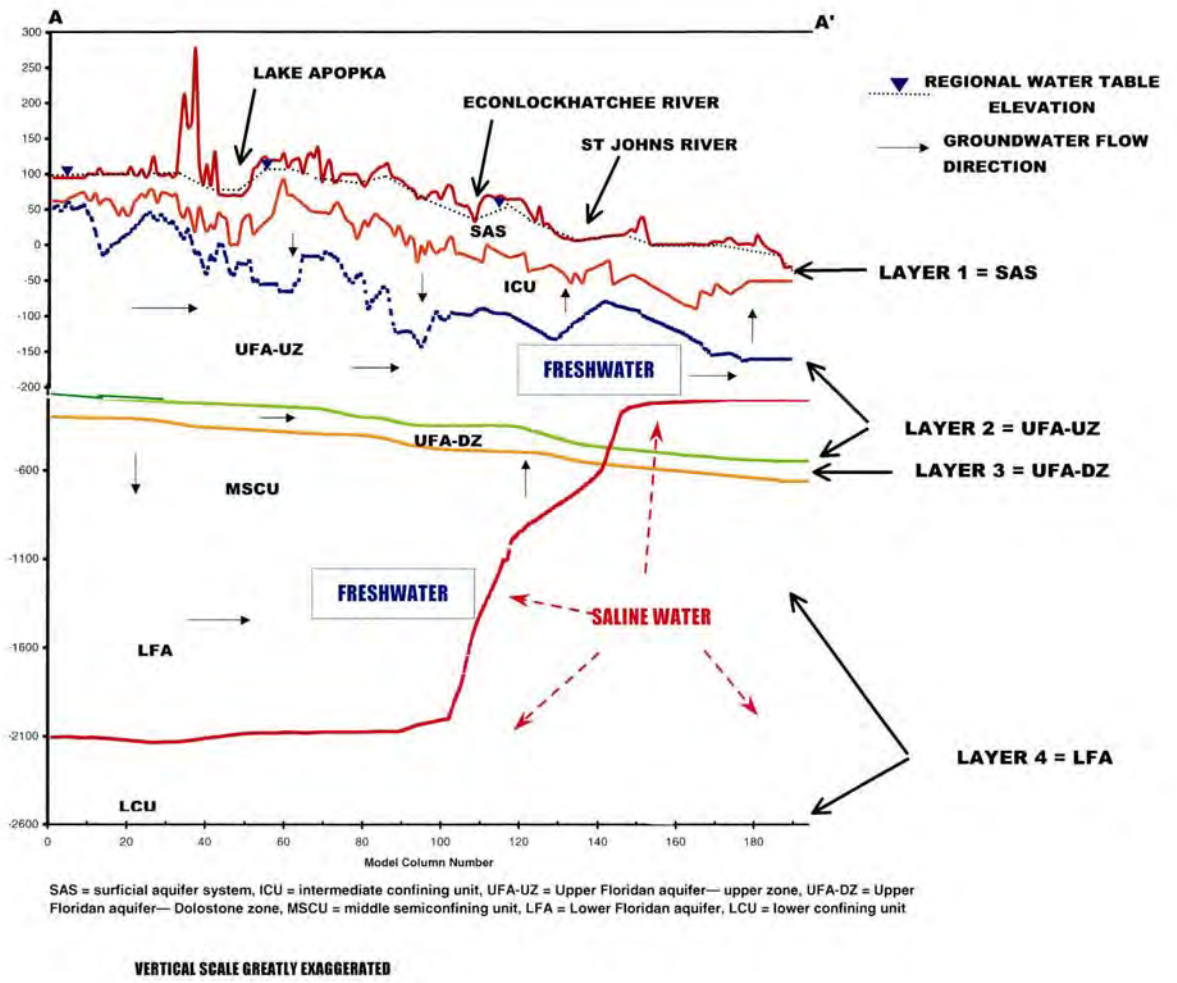

Figure 25. Hydrogeologic cross section along model row 80 showing the conceptual model of regional groundwater flow in east-central Florida

McGurk, B., and P. Fischl Presley, 2002. Simulation of the Effects of Groundwater Withdrawals on the Floridan Aquifer System in East-Central Florida: Model Expansion and Revision. Technical Publication SJ2002-3, St. Johns River Water Management District, Palatka, FL.

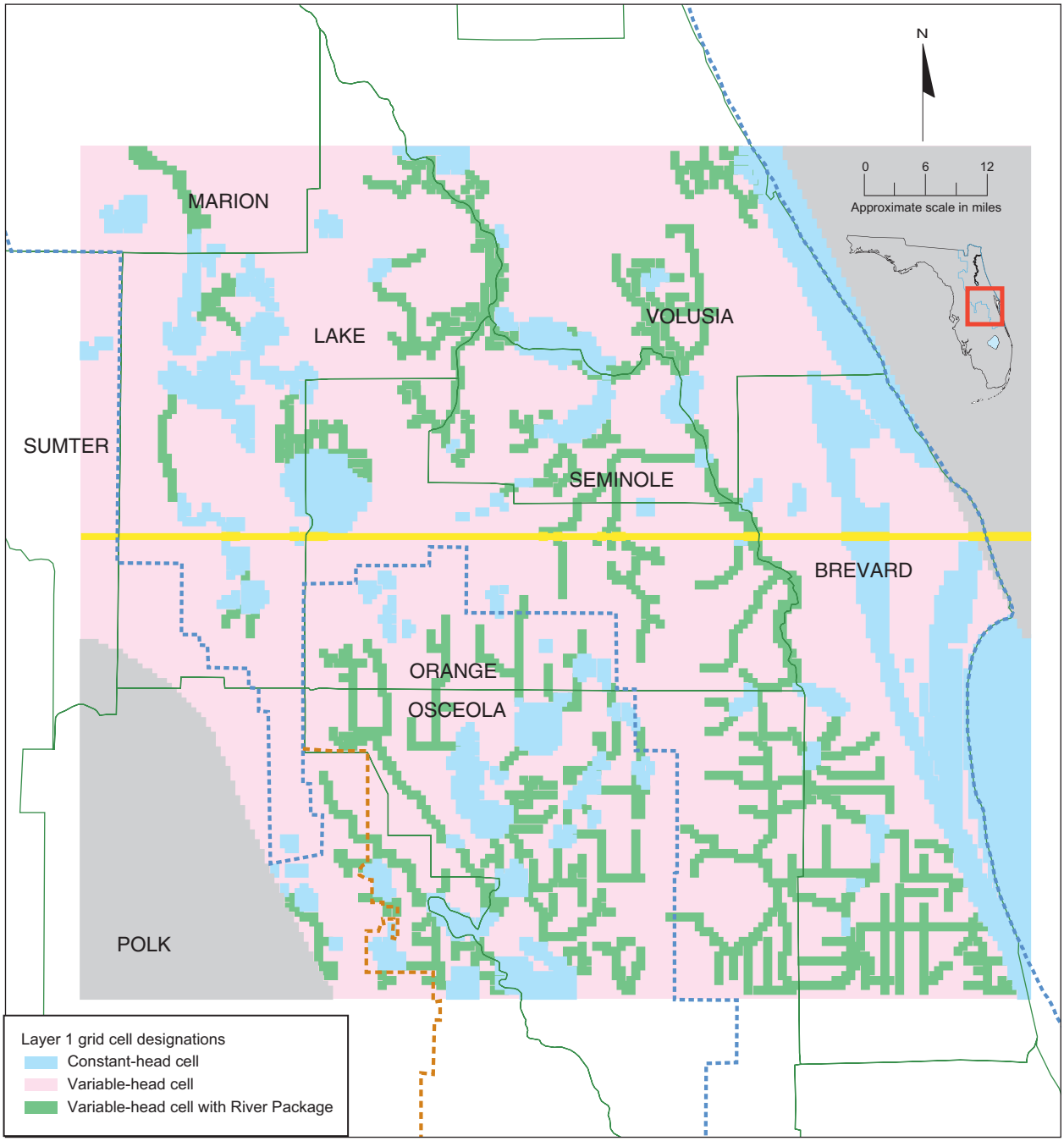

Figure 26. East-central Florida regional model domain showing inactive areas and layer 1 grid cell designations

McGurk, B., and P. Fischl Presley, 2002. Simulation of the Effects of Groundwater Withdrawals on the Floridan Aquifer System in East-Central Florida: Model Expansion and Revision. Technical Publication SJ2002-3, St. Johns River Water Management District, Palatka, FL.

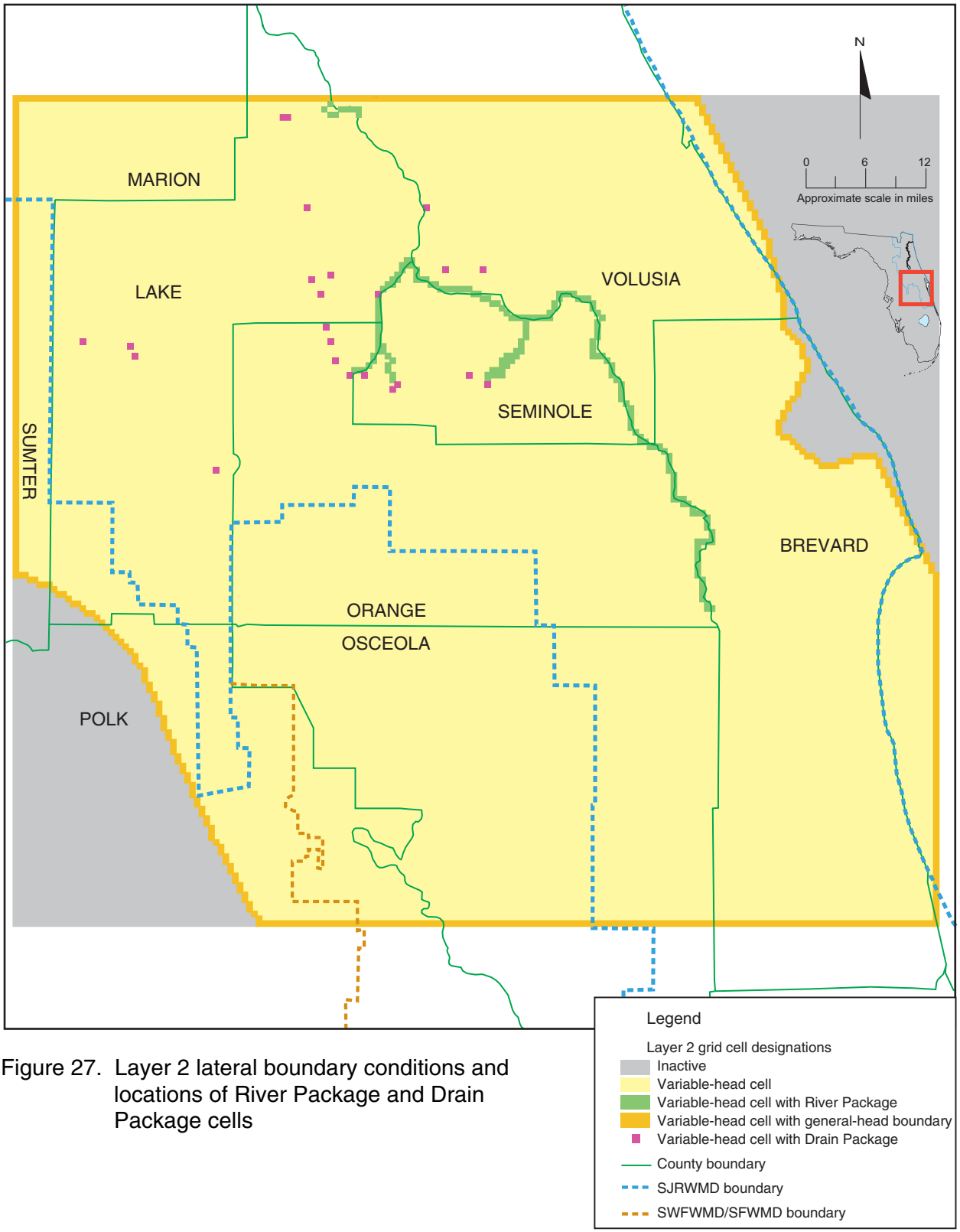

Figure 27. Layer 2 lateral boundary conditions and locations of River Package and Drain Package cells

McGurk, B., and P. Fischl Presley, 2002. Simulation of the Effects of Groundwater Withdrawals on the Floridan Aquifer System in East-Central Florida: Model Expansion and Revision. Technical Publication SJ2002-3, St. Johns River Water Management District, Palatka, FL.

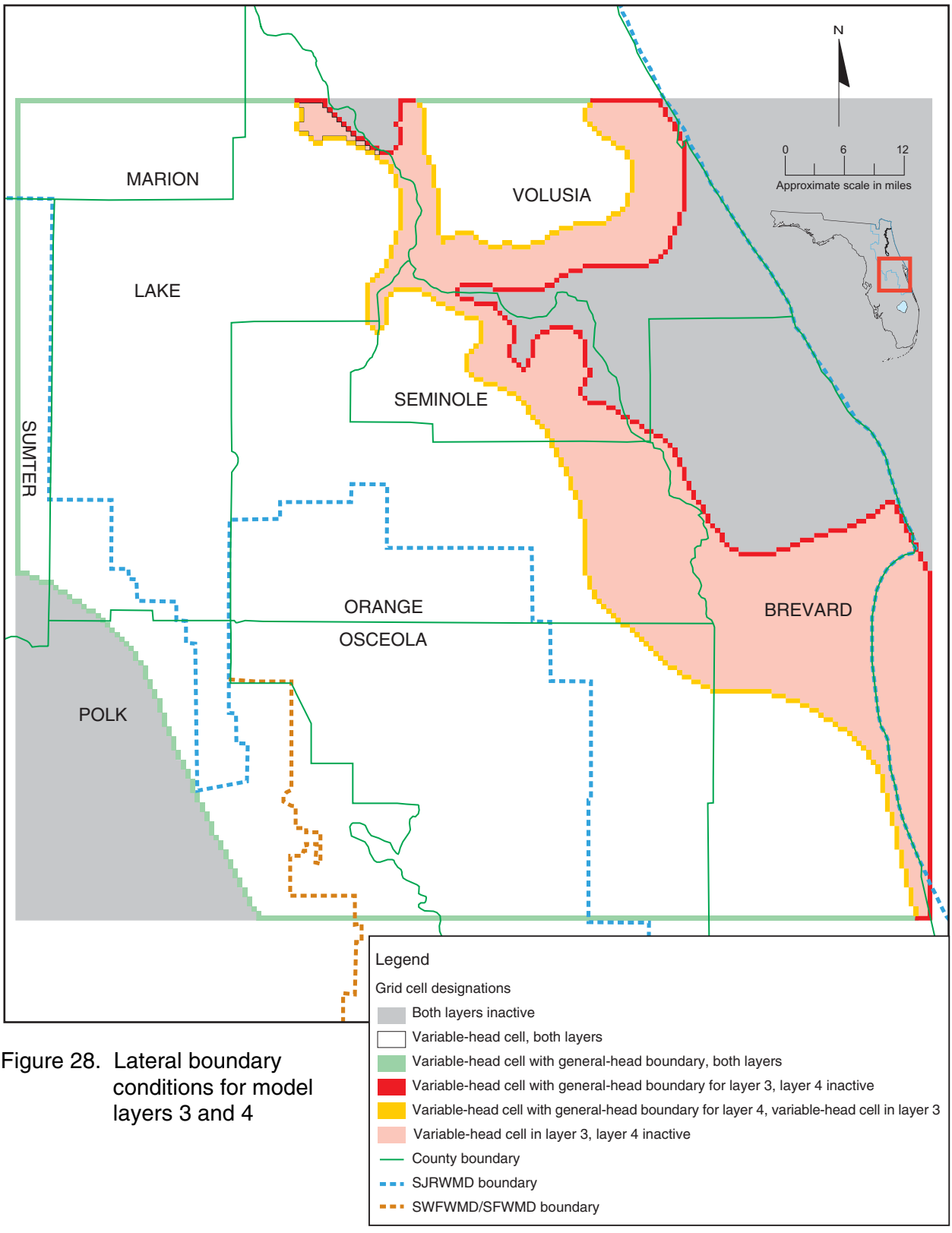

Figure 28. Lateral boundary conditions for model layers 3 and 4

McGurk, B., and P. Fischl Presley, 2002. Simulation of the Effects of Groundwater Withdrawals on the Floridan Aquifer System in East-Central Florida: Model Expansion and Revision. Technical Publication SJ2002-3, St. Johns River Water Management District, Palatka, FL.

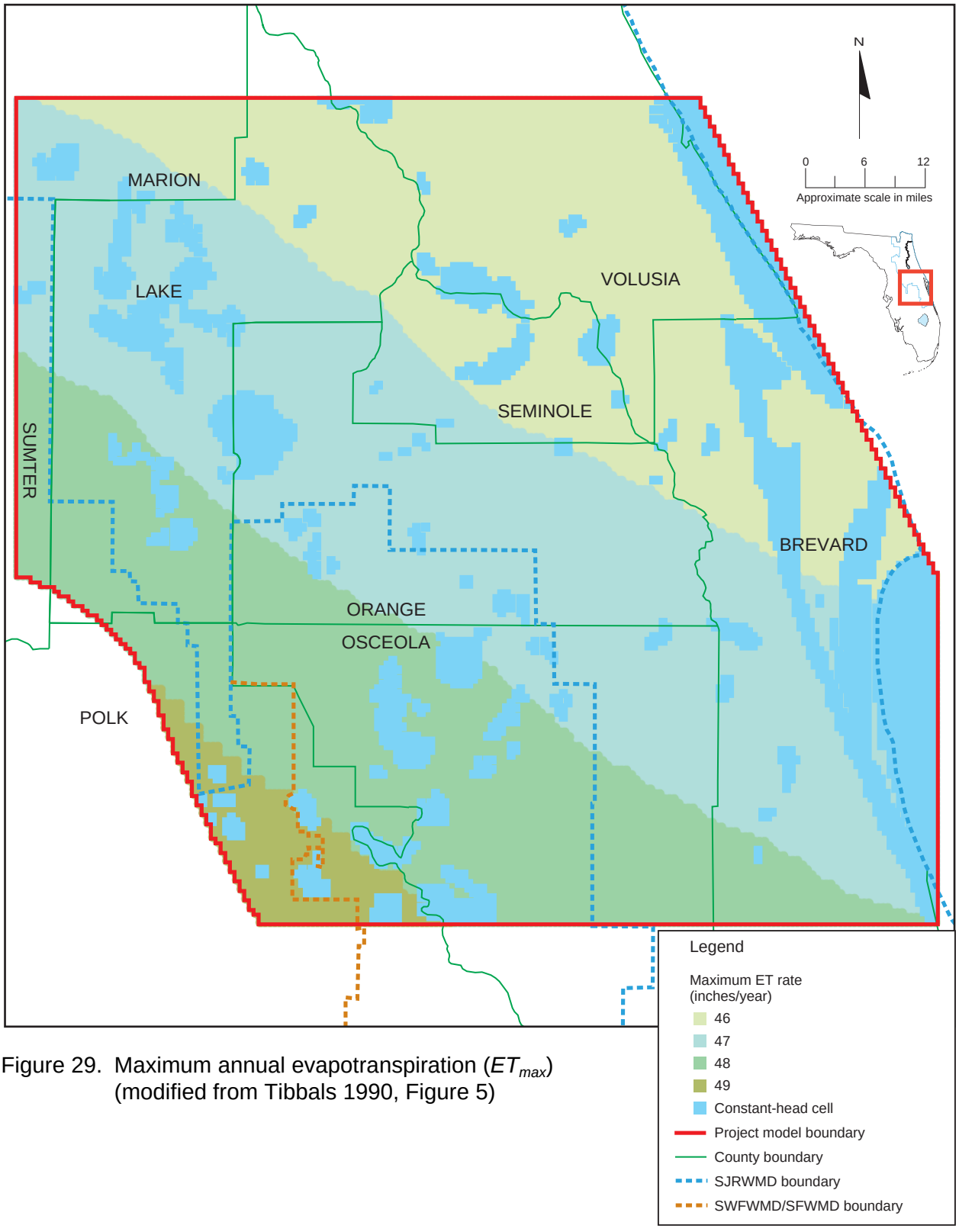

Figure 29. Maximum annual evapotranspiration (ET_{max}) (modified from Tibbals 1990, Figure 5)

McGurk, B., and P. Fischl Presley, 2002. Simulation of the Effects of Groundwater Withdrawals on the Floridan Aquifer System in East-Central Florida: Model Expansion and Revision. Technical Publication SJ2002-3, St. Johns River Water Management District, Palatka, FL.

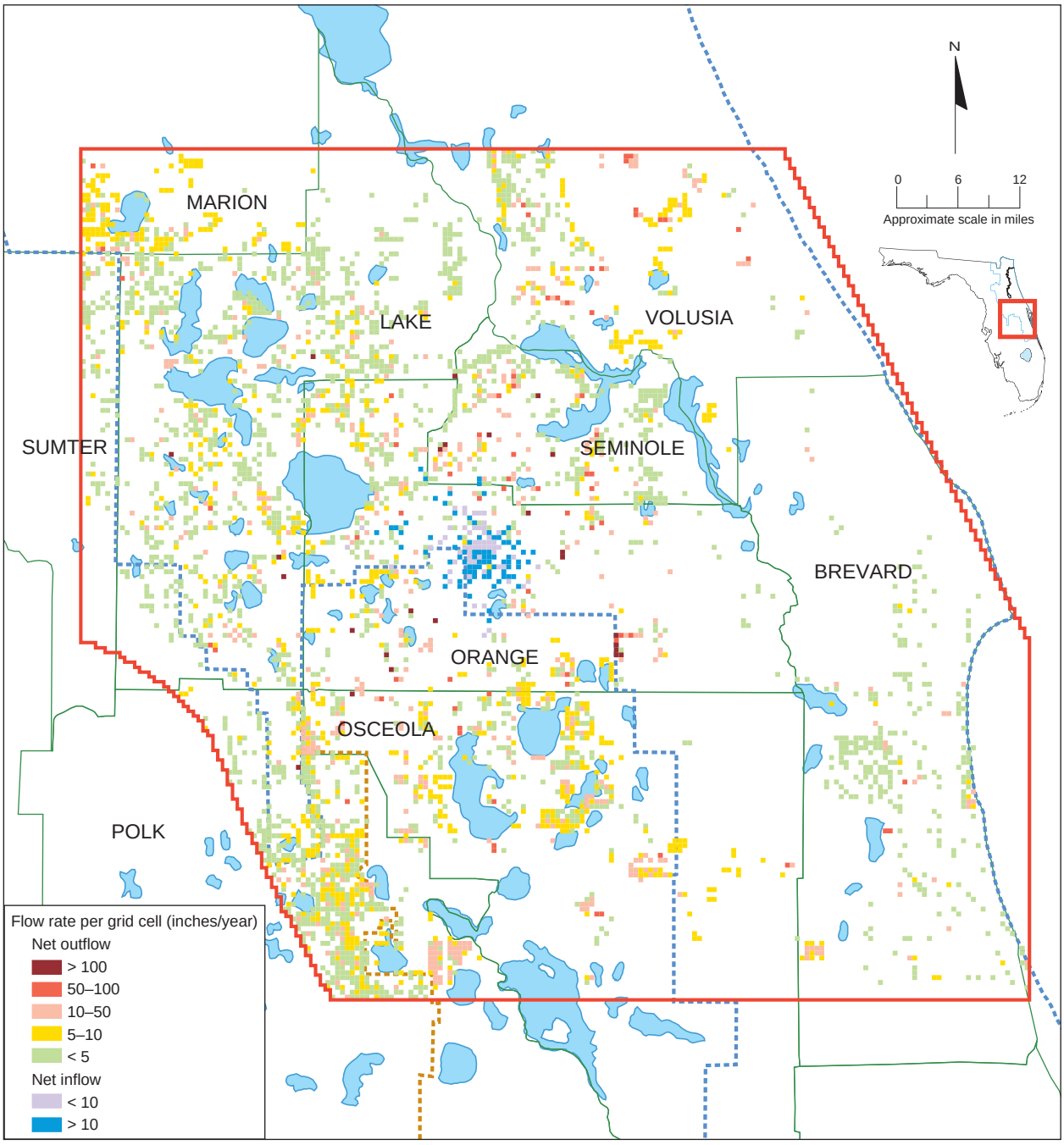

Figure 30. Average 1995 withdrawals applied to model layer 2

McGurk, B., and P. Fischl Presley, 2002. Simulation of the Effects of Groundwater Withdrawals on the Floridan Aquifer System in East-Central Florida: Model Expansion and Revision. Technical Publication SJ2002-3, St. Johns River Water Management District, Palatka, FL.

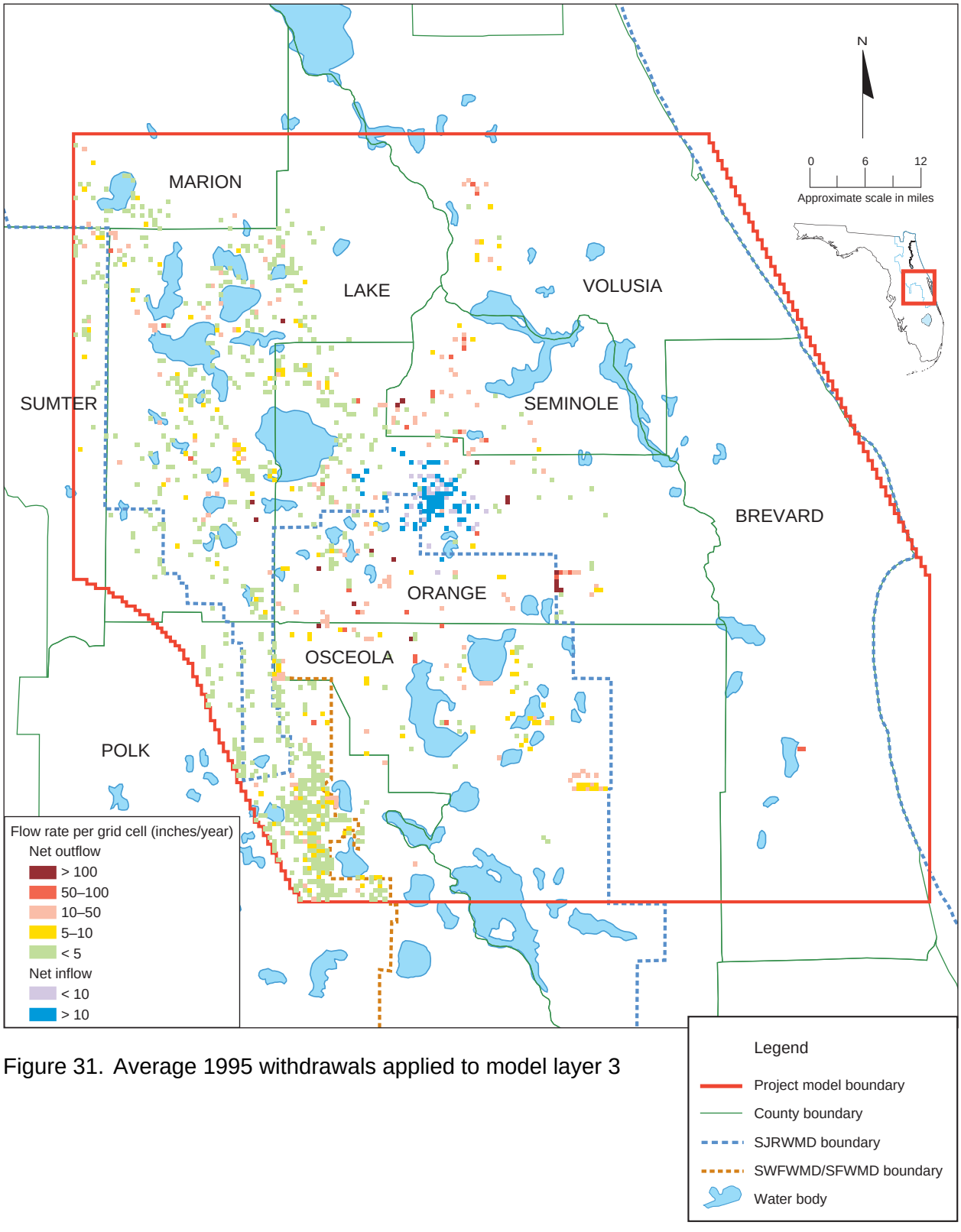

Figure 31. Average 1995 withdrawals applied to model layer 3

McGurk, B., and P. Fischl Presley, 2002. Simulation of the Effects of Groundwater Withdrawals on the Floridan Aquifer System in East-Central Florida: Model Expansion and Revision. Technical Publication SJ2002-3, St. Johns River Water Management District, Palatka, FL.

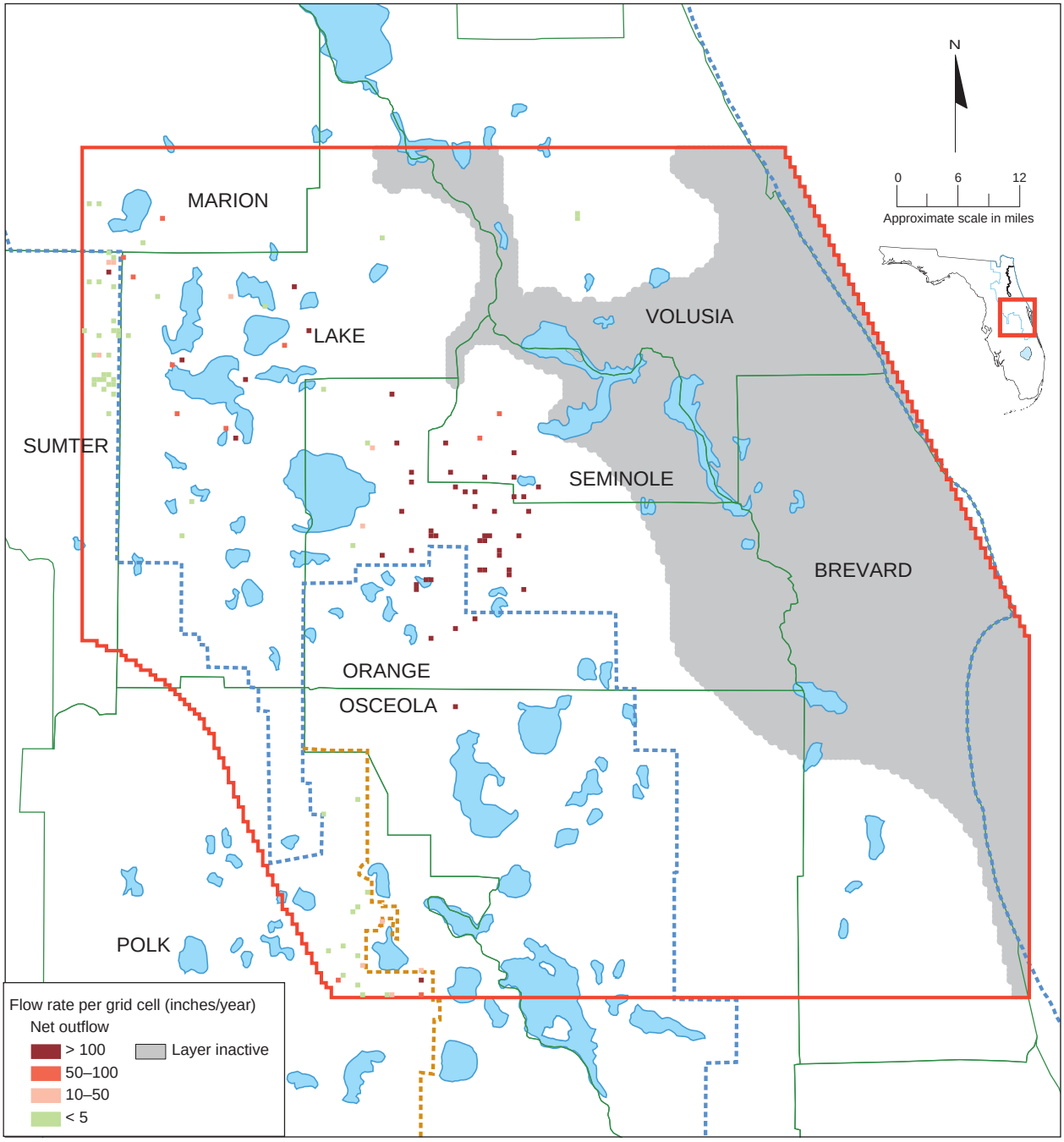

Figure 32. Average 1995 withdrawals applied to model layer 4

McGurk, B., and P. Fischl Presley, 2002. Simulation of the Effects of Groundwater Withdrawals on the Floridan Aquifer System in East-Central Florida: Model Expansion and Revision. Technical Publication SJ2002-3, St. Johns River Water Management District, Palatka, FL.

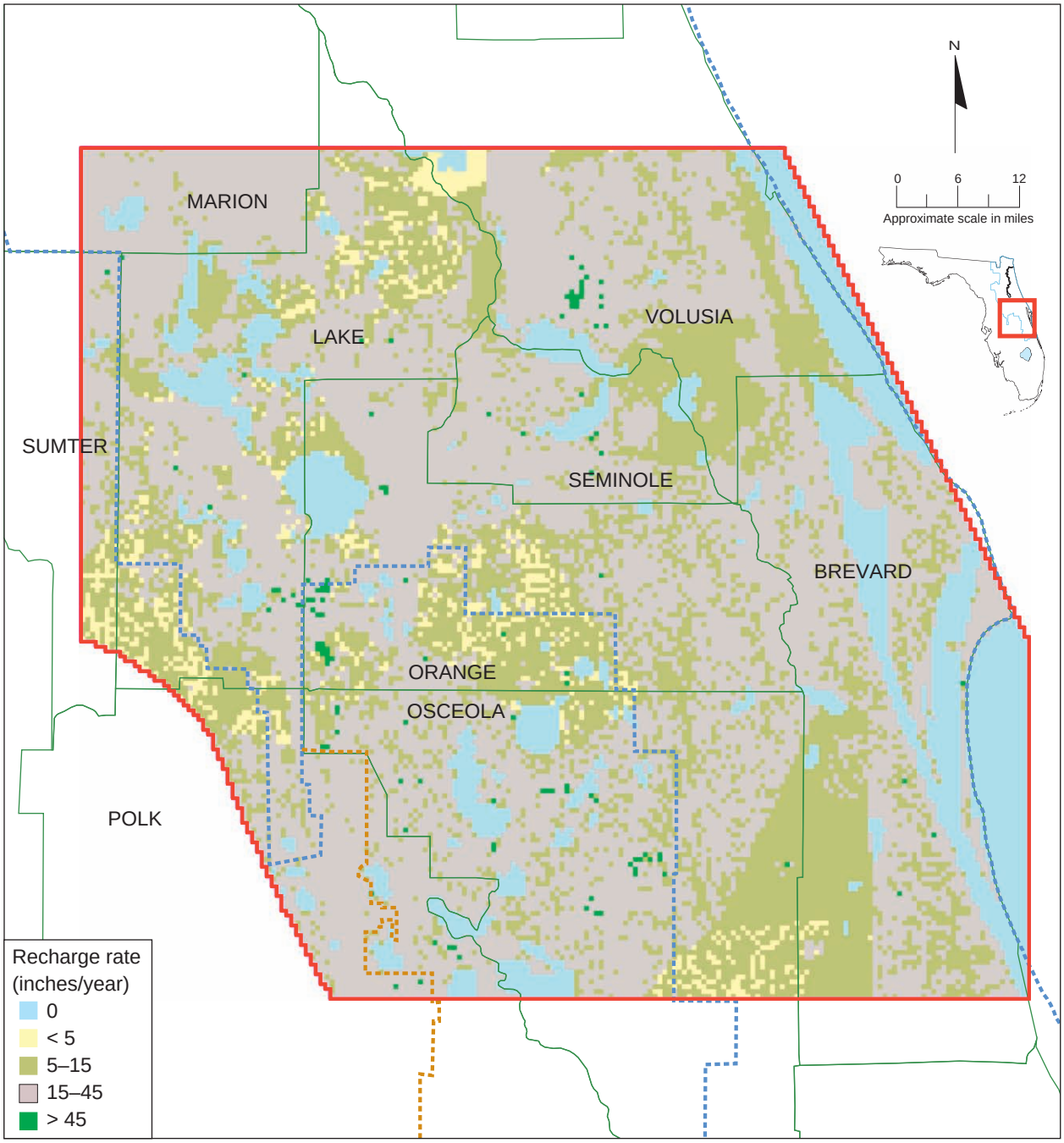

Figure 41. Recharge applied to the surficial aquifer system for average 1995 conditions

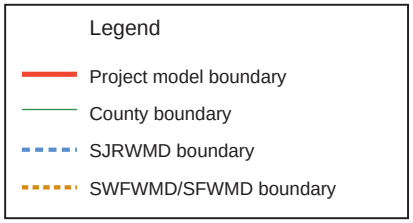

McGurk, B., and P. Fischl Presley, 2002. Simulation of the Effects of Groundwater Withdrawals on the Floridan Aquifer System in East-Central Florida: Model Expansion and Revision. Technical Publication SJ2002-3, St. Johns River Water Management District, Palatka, FL.

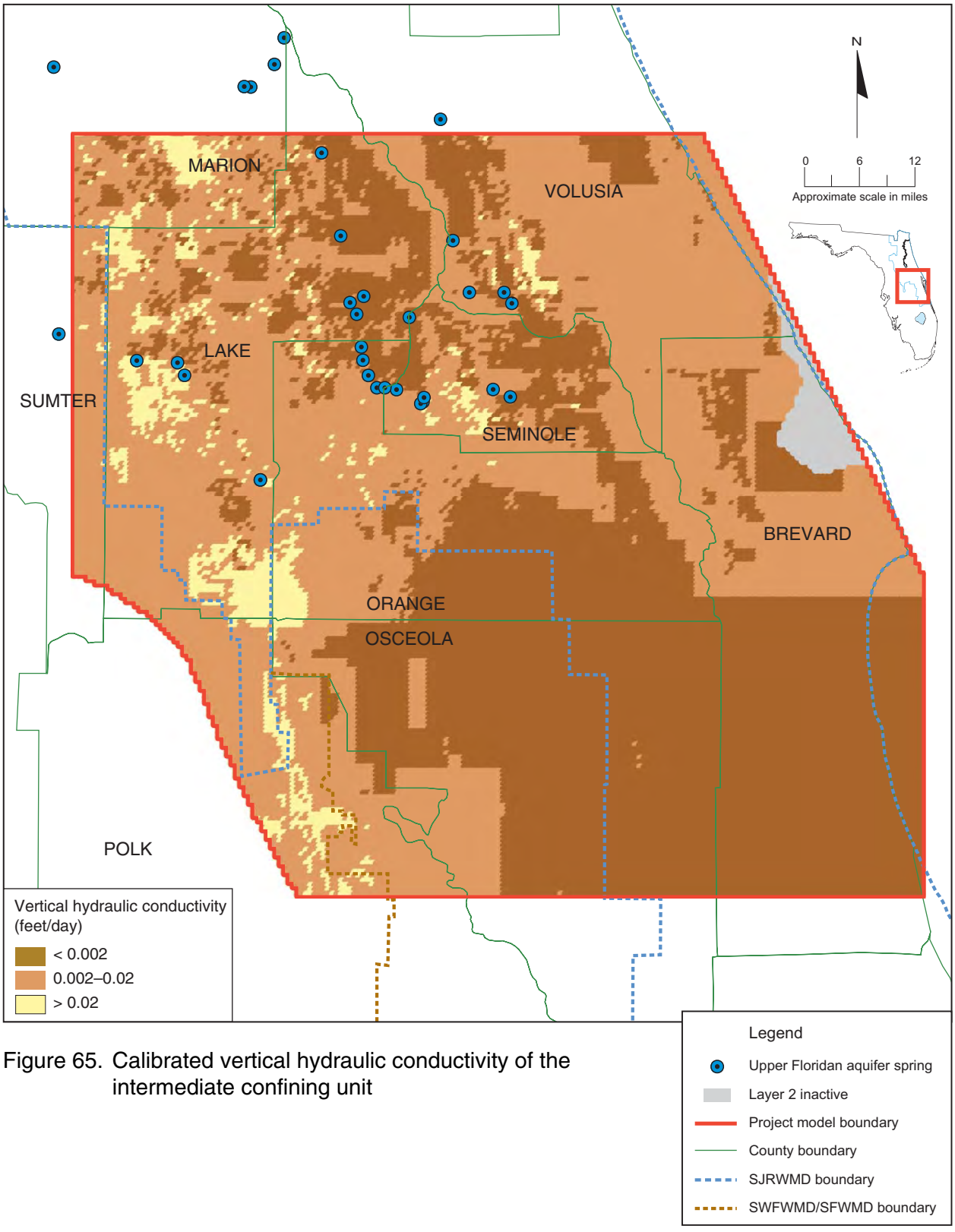

Figure 65. Calibrated vertical hydraulic conductivity of the intermediate confining unit

McGurk, B., and P. Fischl Presley, 2002. Simulation of the Effects of Groundwater Withdrawals on the Floridan Aquifer System in East-Central Florida: Model Expansion and Revision. Technical Publication SJ2002-3, St. Johns River Water Management District, Palatka, FL.

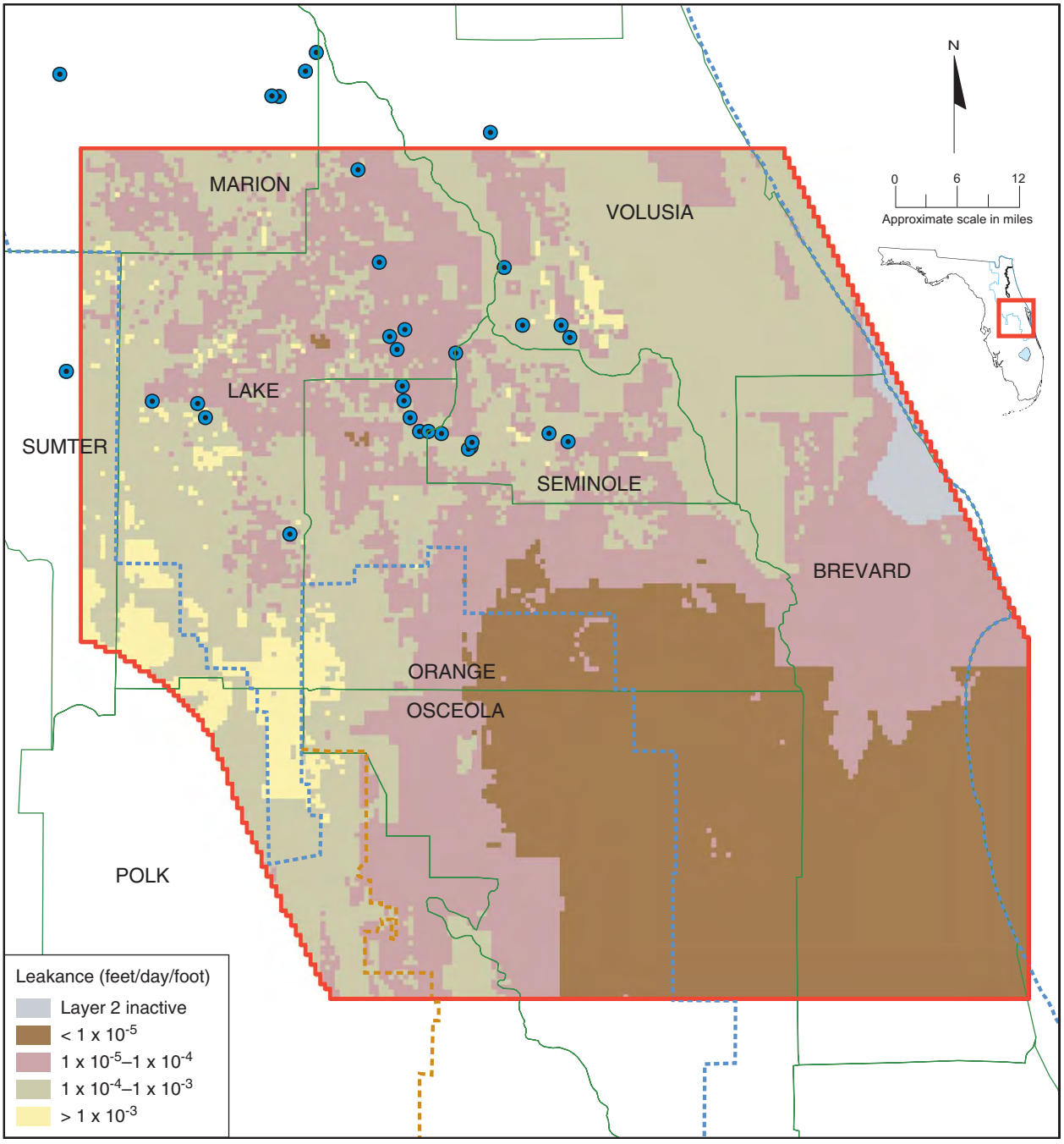

Figure 66. Calibrated leakance of the intermediate confining unit

McGurk, B., and P. Fischl Presley, 2002. Simulation of the Effects of Groundwater Withdrawals on the Floridan Aquifer System in East-Central Florida: Model Expansion and Revision. Technical Publication SJ2002-3, St. Johns River Water Management District, Palatka, FL.

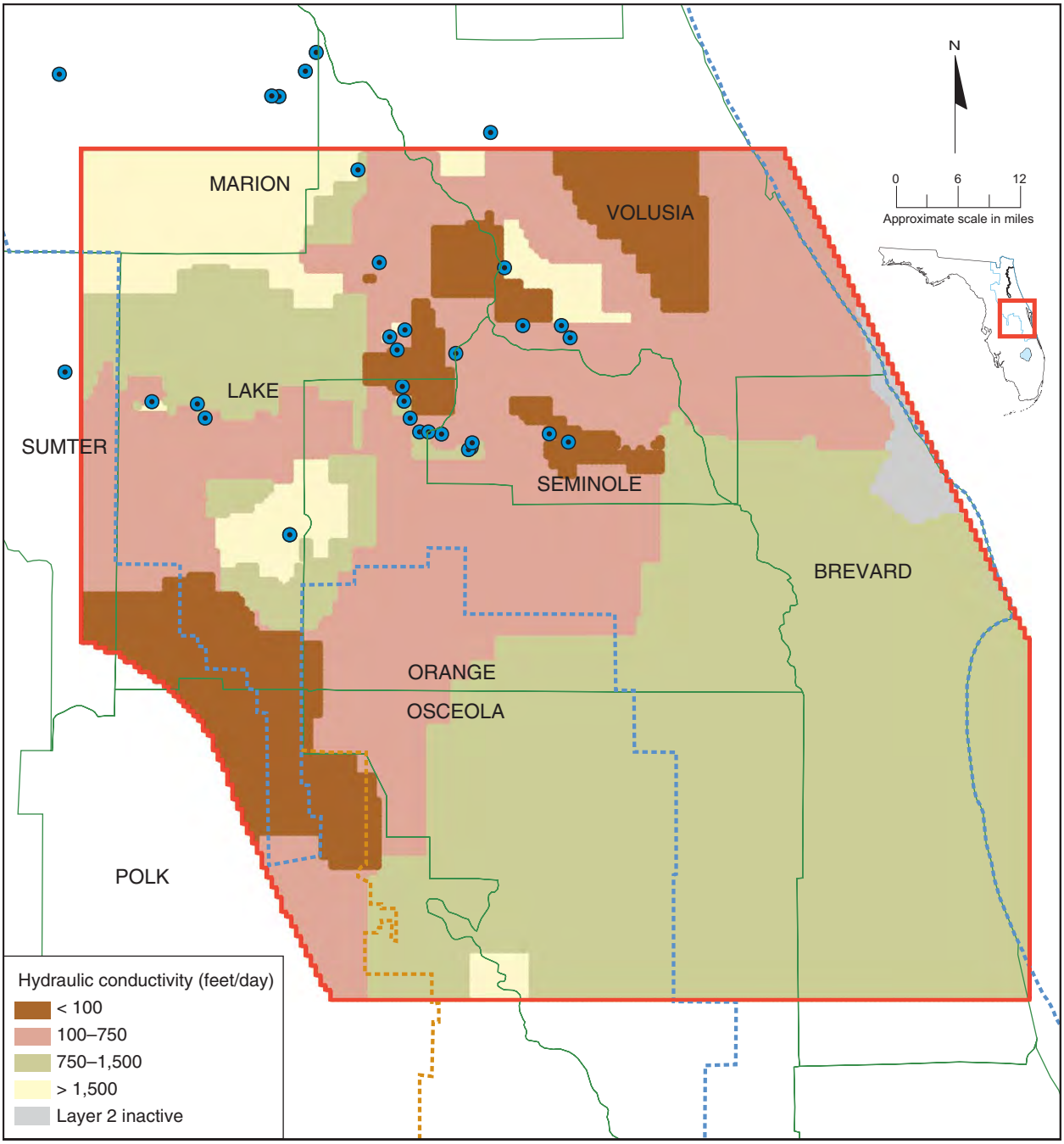

Figure 67. Calibrated layer 2 (Upper Floridan aquifer—upper zone) horizontal hydraulic conductivity

McGurk, B., and P. Fischl Presley, 2002. Simulation of the Effects of Groundwater Withdrawals on the Floridan Aquifer System in East-Central Florida: Model Expansion and Revision. Technical Publication SJ2002-3, St. Johns River Water Management District, Palatka, FL.

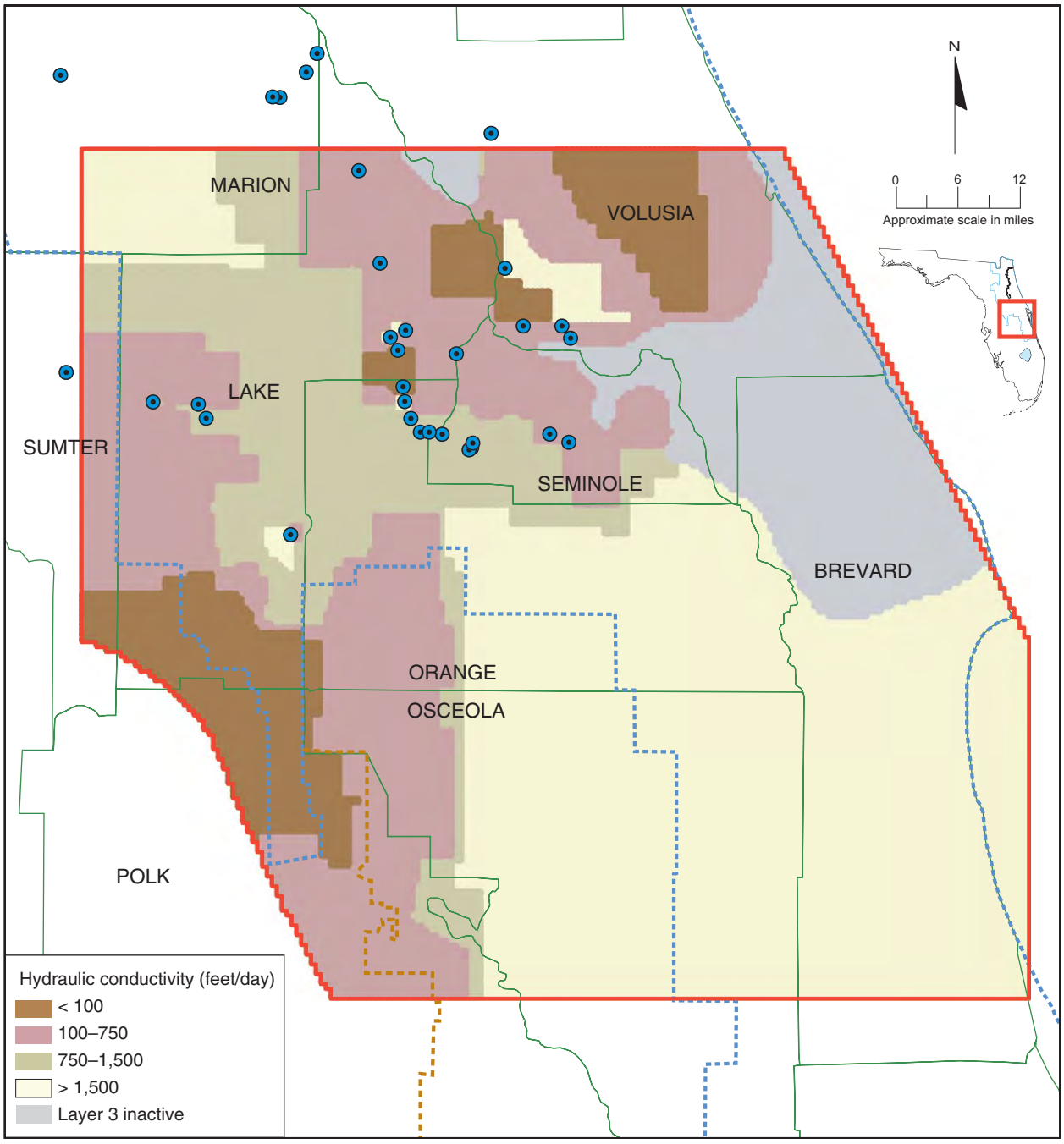

Figure 68. Calibrated layer 3 (Upper Floridan aquifer—lower zone) horizontal hydraulic conductivity

McGurk, B., and P. Fischl Presley, 2002. Simulation of the Effects of Groundwater Withdrawals on the Floridan Aquifer System in East-Central Florida: Model Expansion and Revision. Technical Publication SJ2002-3, St. Johns River Water Management District, Palatka, FL.

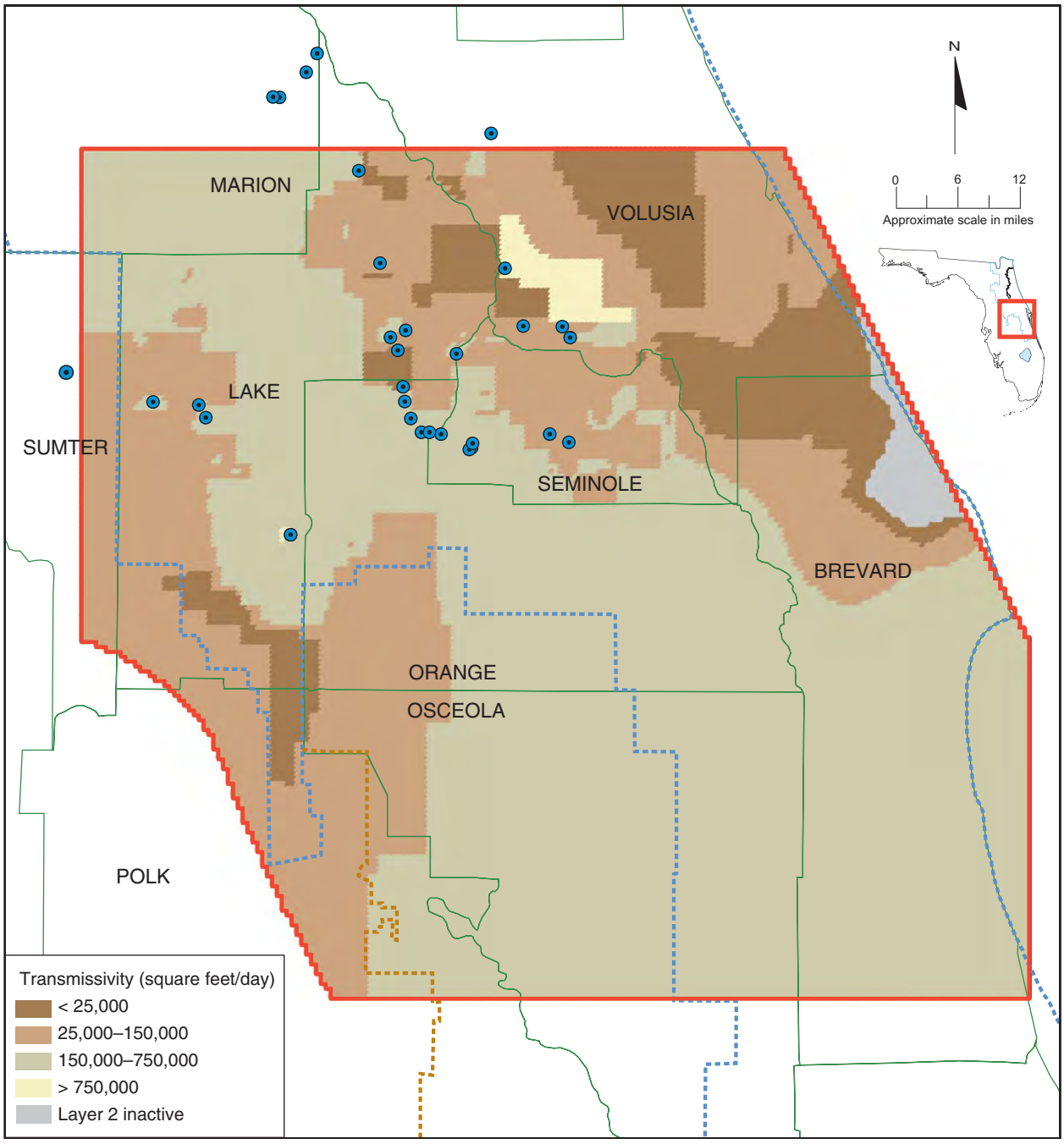

Figure 69. Calibrated transmissivity of the Upper Floridan aquifer (layers 2 and 3)

McGurk, B., and P. Fischl Presley, 2002. Simulation of the Effects of Groundwater Withdrawals on the Floridan Aquifer System in East-Central Florida: Model Expansion and Revision. Technical Publication SJ2002-3, St. Johns River Water Management District, Palatka, FL.

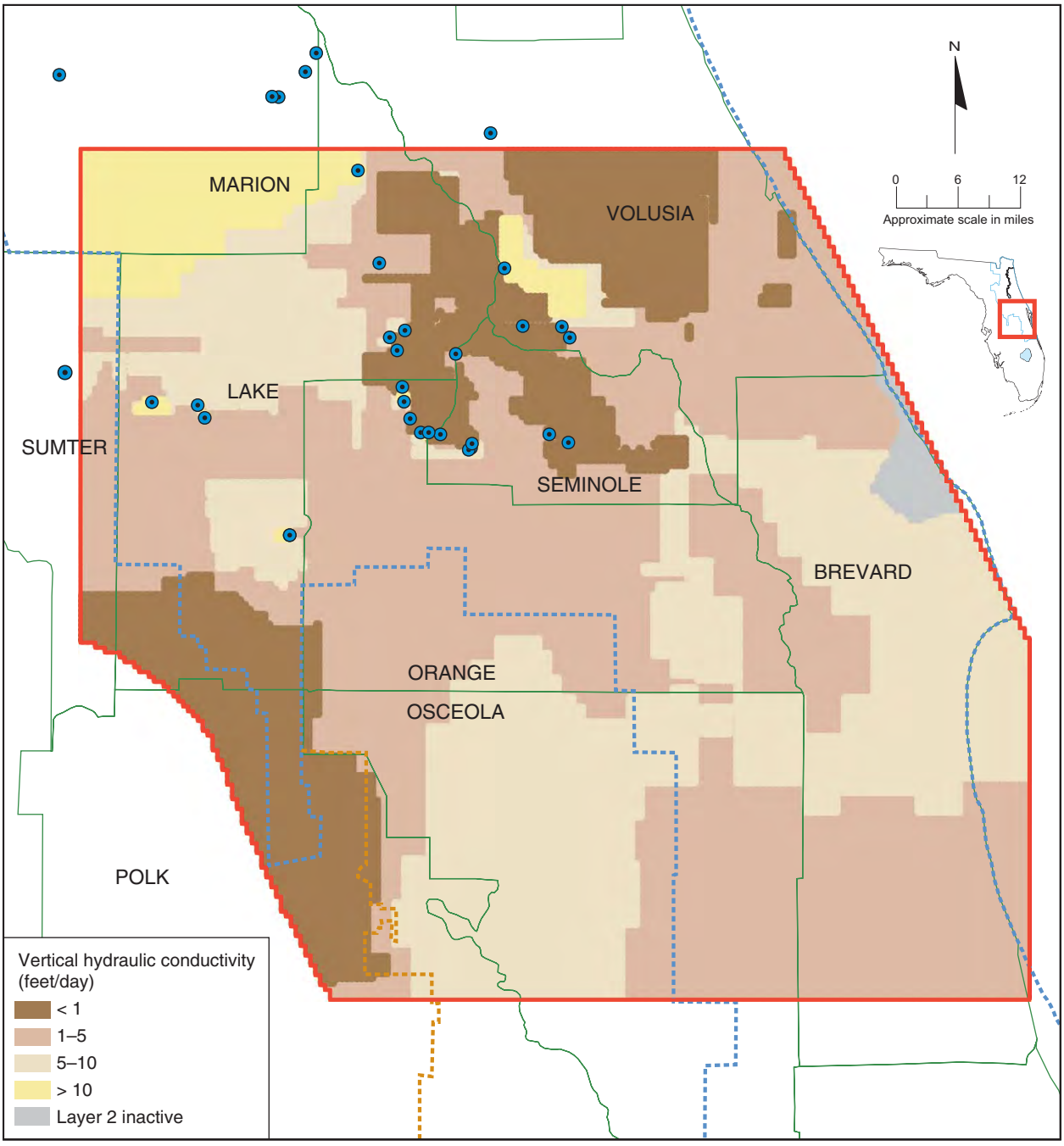

Figure 70. Calibrated vertical hydraulic conductivity of model layer 2 (Upper Floridan aquifer—upper zone)

McGurk, B., and P. Fischl Presley, 2002. Simulation of the Effects of Groundwater Withdrawals on the Floridan Aquifer System in East-Central Florida: Model Expansion and Revision. Technical Publication SJ2002-3, St. Johns River Water Management District, Palatka, FL.

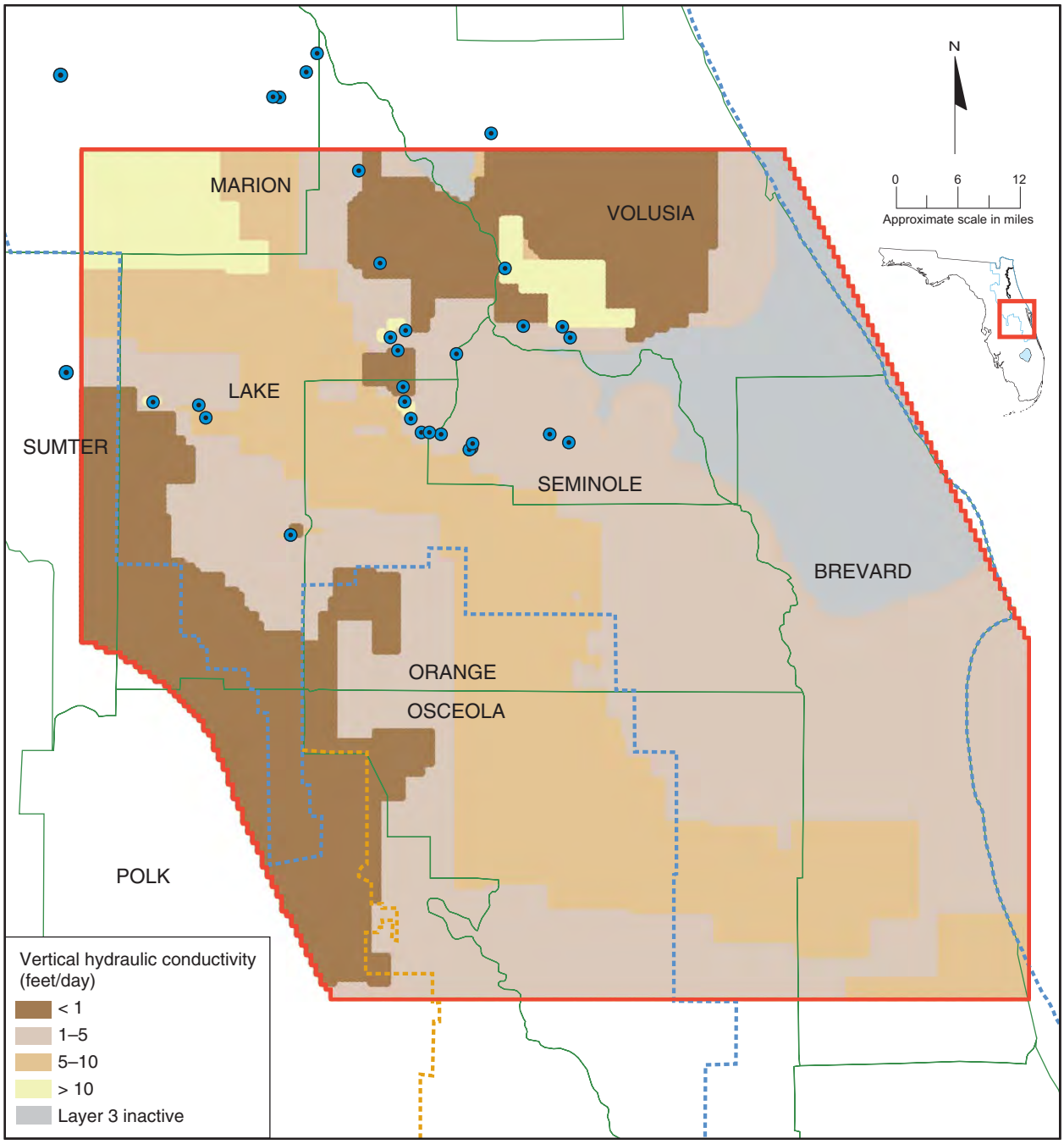

Figure 71. Calibrated vertical hydraulic conductivity of model layer 3 (Upper Floridan aquifer—lower zone)

McGurk, B., and P. Fischl Presley, 2002. Simulation of the Effects of Groundwater Withdrawals on the Floridan Aquifer System in East-Central Florida: Model Expansion and Revision. Technical Publication SJ2002-3, St. Johns River Water Management District, Palatka, FL.

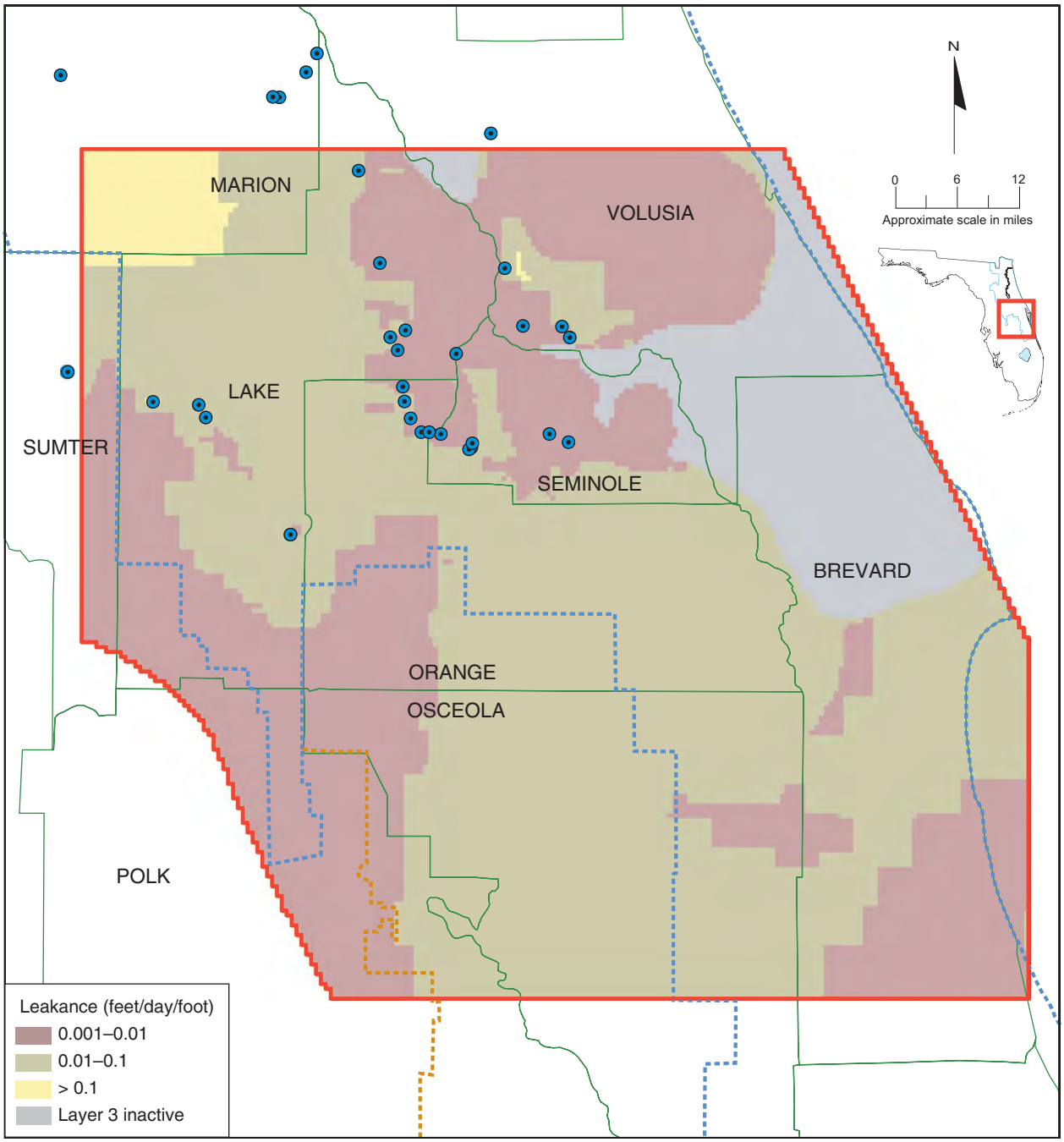

Figure 72. Calibrated leakance between Upper Floridan aquifer layers 2 and 3

McGurk, B., and P. Fischl Presley, 2002. Simulation of the Effects of Groundwater Withdrawals on the Floridan Aquifer System in East-Central Florida: Model Expansion and Revision. Technical Publication SJ2002-3, St. Johns River Water Management District, Palatka, FL.

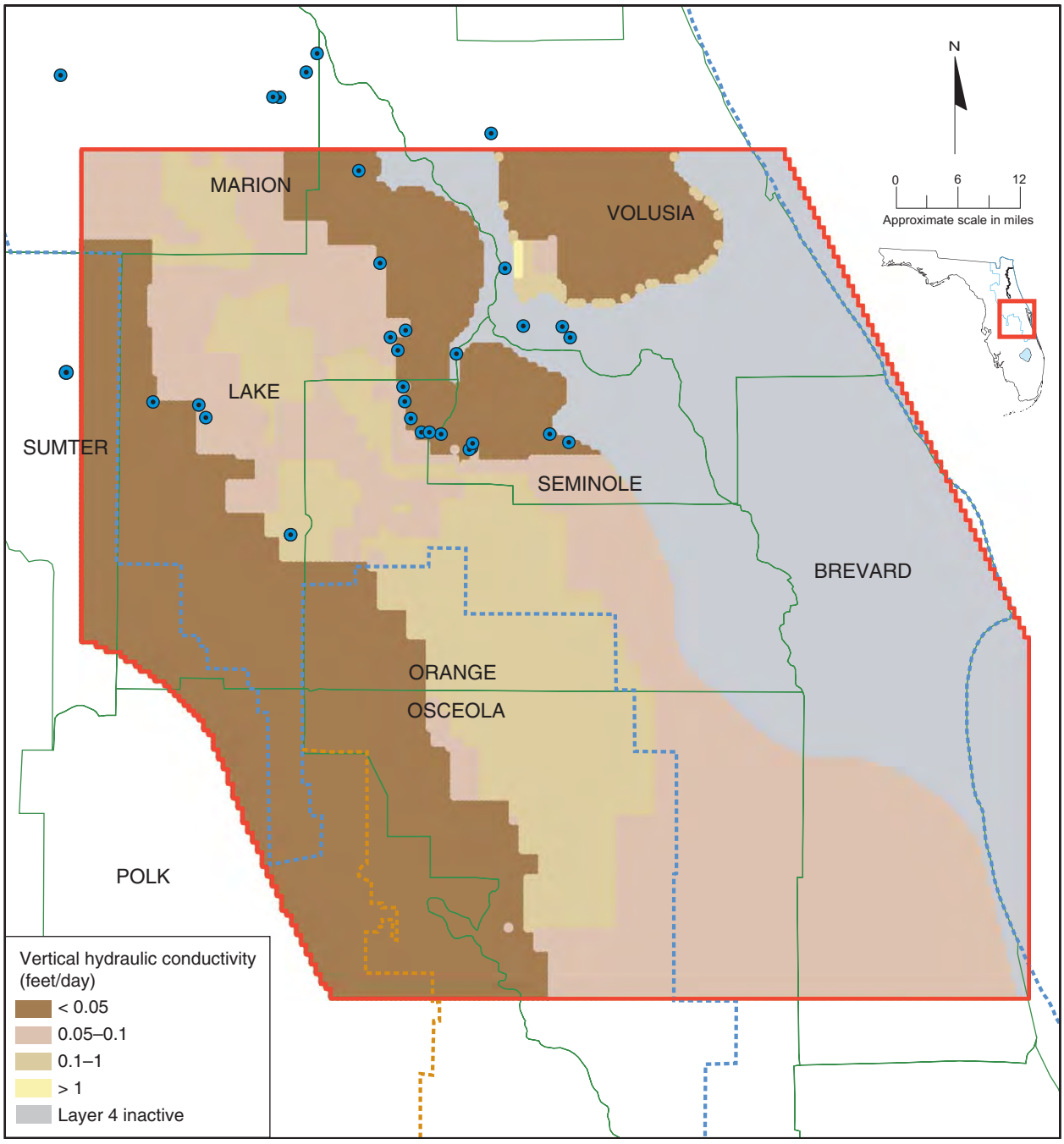

Figure 73. Calibrated vertical hydraulic conductivity of the middle semiconfining unit

McGurk, B., and P. Fischl Presley, 2002. Simulation of the Effects of Groundwater Withdrawals on the Floridan Aquifer System in East-Central Florida: Model Expansion and Revision. Technical Publication SJ2002-3, St. Johns River Water Management District, Palatka, FL.

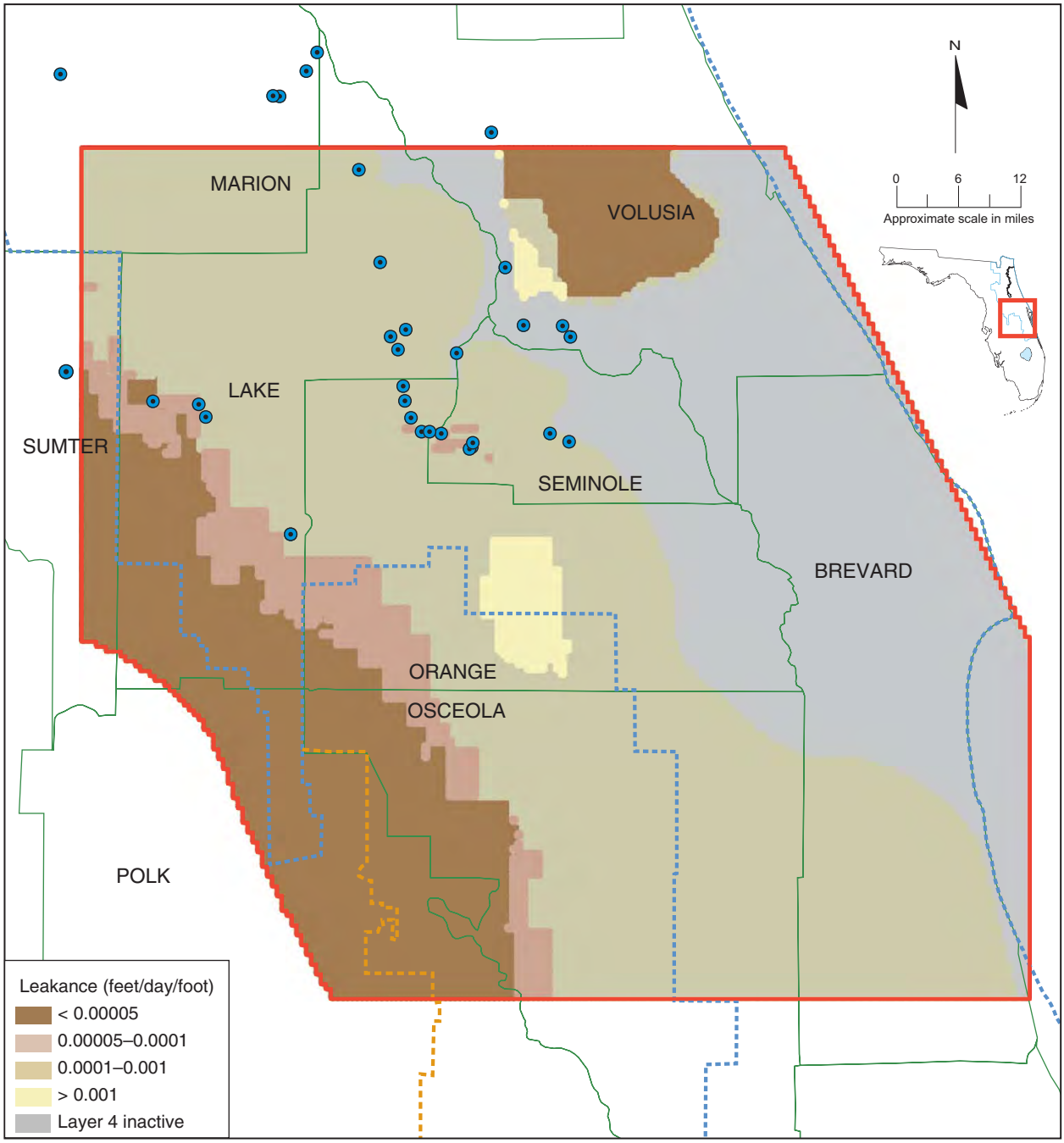

Figure 74. Calibrated leakance of the middle semiconfining unit

McGurk, B., and P. Fischl Presley, 2002. Simulation of the Effects of Groundwater Withdrawals on the Floridan Aquifer System in East-Central Florida: Model Expansion and Revision. Technical Publication SJ2002-3, St. Johns River Water Management District, Palatka, FL.

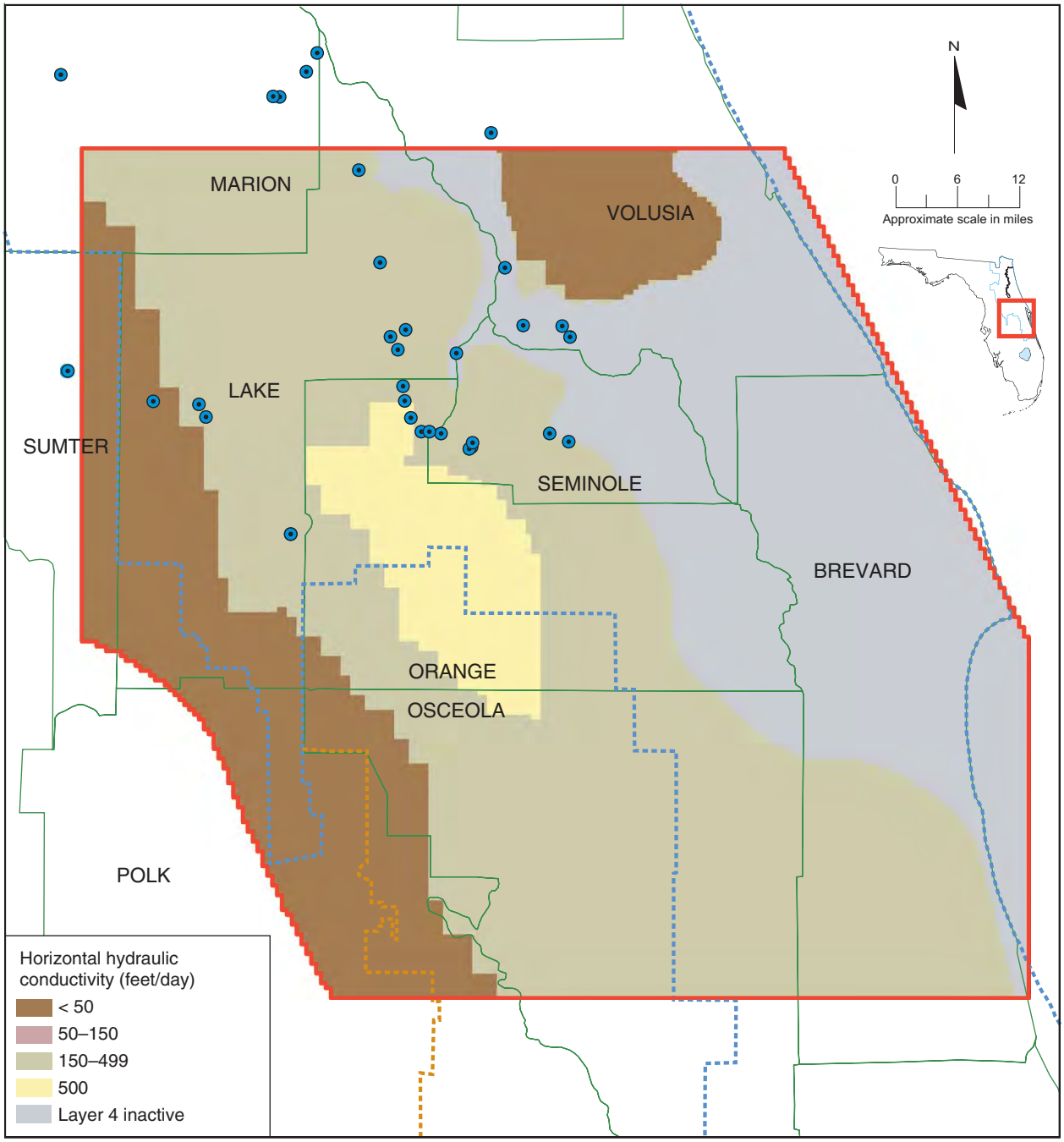

Figure 75. Calibrated layer 4 (Lower Floridan aquifer) horizontal hydraulic conductivity

McGurk, B., and P. Fischl Presley, 2002. Simulation of the Effects of Groundwater Withdrawals on the Floridan Aquifer System in East-Central Florida: Model Expansion and Revision. Technical Publication SJ2002-3, St. Johns River Water Management District, Palatka, FL.

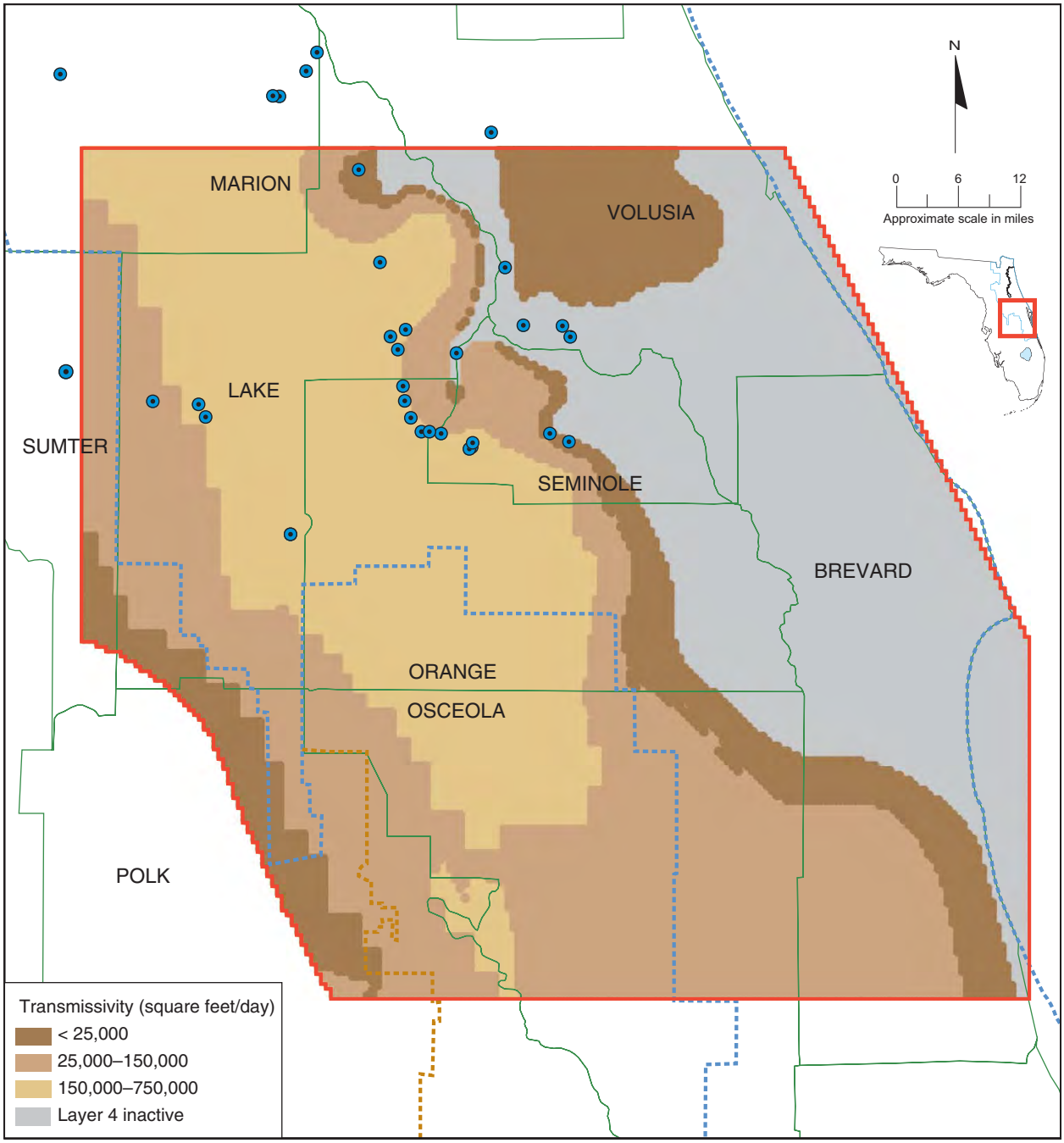

Figure 76. Calibrated transmissivity of the Lower Floridan aquifer (layer 4)

McGurk, B., and P. Fischl Presley, 2002. Simulation of the Effects of Groundwater Withdrawals on the Floridan Aquifer System in East-Central Florida: Model Expansion and Revision. Technical Publication SJ2002-3, St. Johns River Water Management District, Palatka, FL.

Appendix C

Selected Figures from Documentation of Lower East Coast Florida model

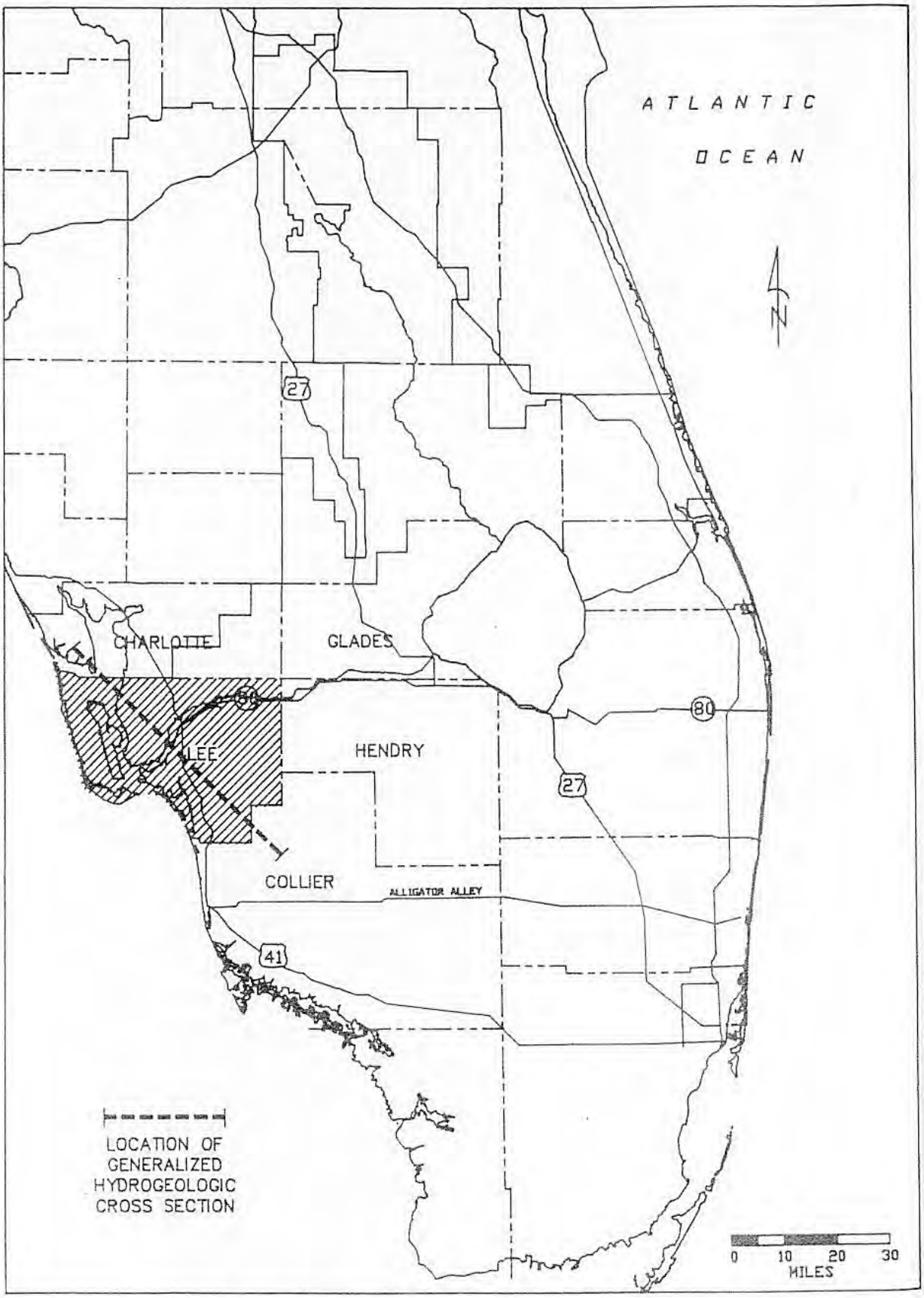

Figure 1. LOCATION OF STUDY AREA

Bower, R.F., K.M. Adams and J.I. Restrepo, 1990. A Three-Dimensional Finite Difference Ground Water Model of Lee County, Florida. Technical Publication 90-01, South Florida Water Management District, West Palm Beach, FL.

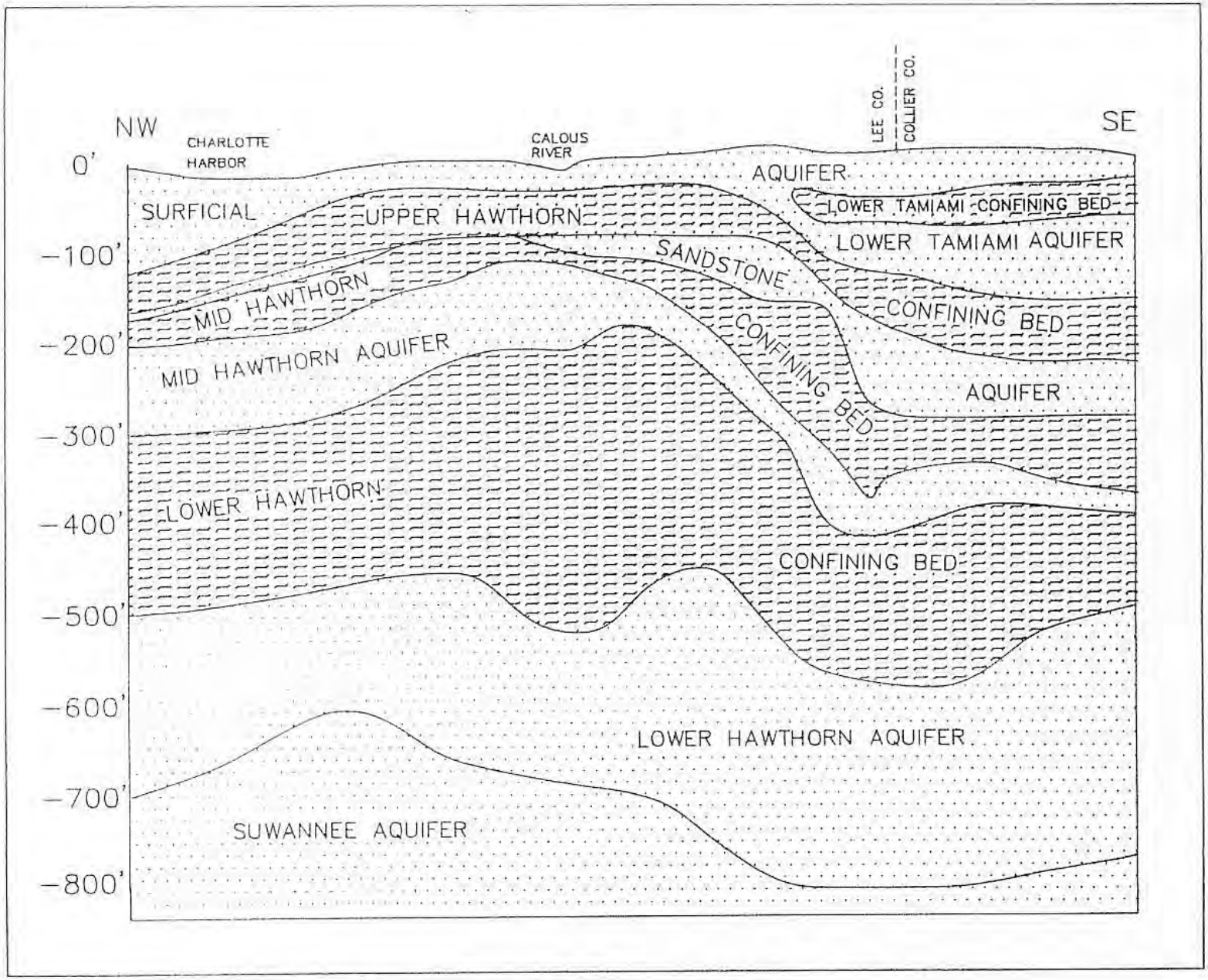

Figure 2. GENERALIZED HYDROGEOLOGIC CROSS SECTION

Bower, R.F., K.M. Adams and J.I. Restrepo, 1990. A Three-Dimensional Finite Difference Ground Water Model of Lee County, Florida. Technical Publication 90-01, South Florida Water Management District, West Palm Beach, FL.

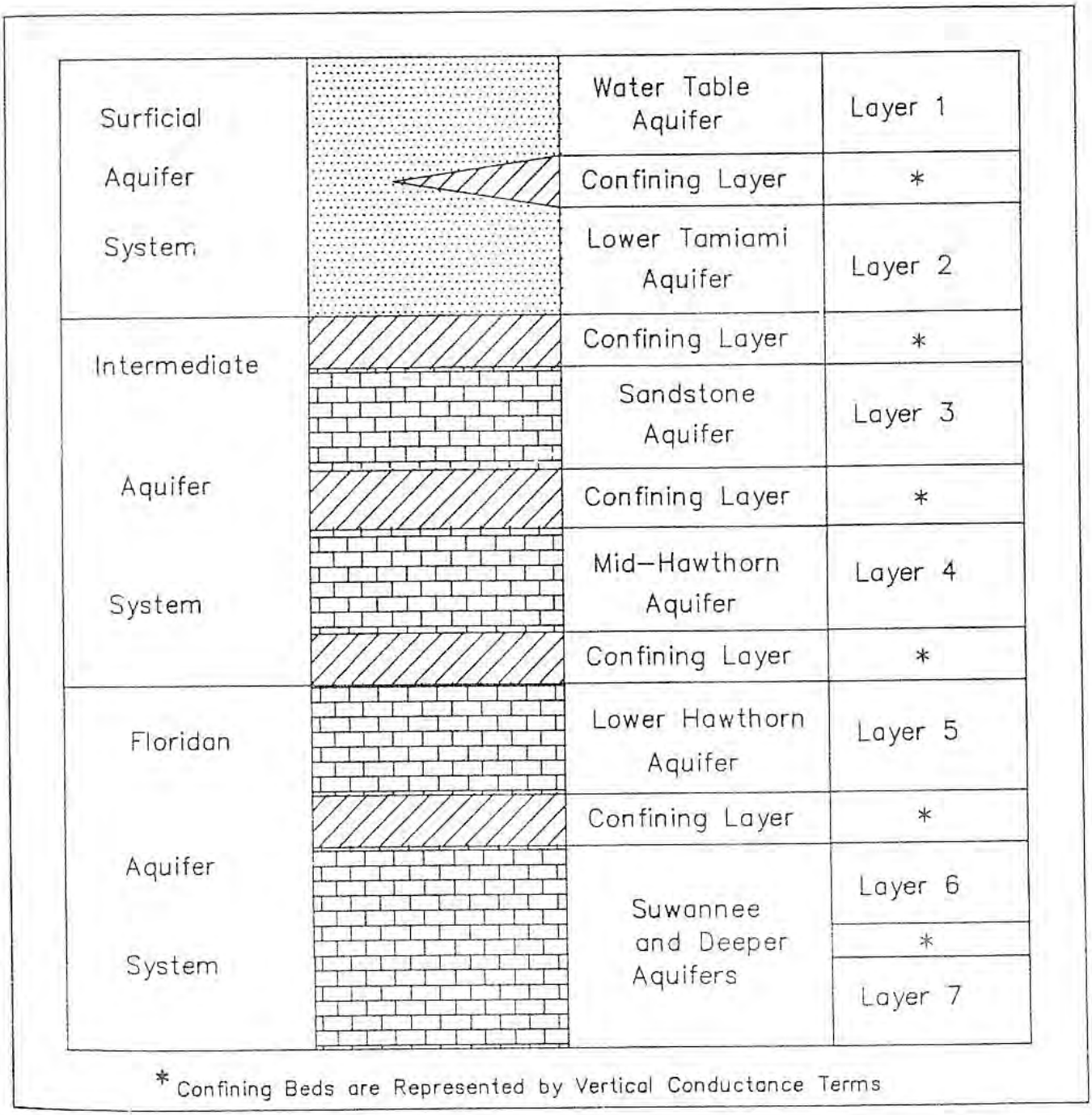

Figure 3. AQUIFERS AND CORRESPONDING MODEL LAYERS

Bower, R.F., K.M. Adams and J.I. Restrepo, 1990. A Three-Dimensional Finite Difference Ground Water Model of Lee County, Florida. Technical Publication 90-01, South Florida Water Management District, West Palm Beach, FL.

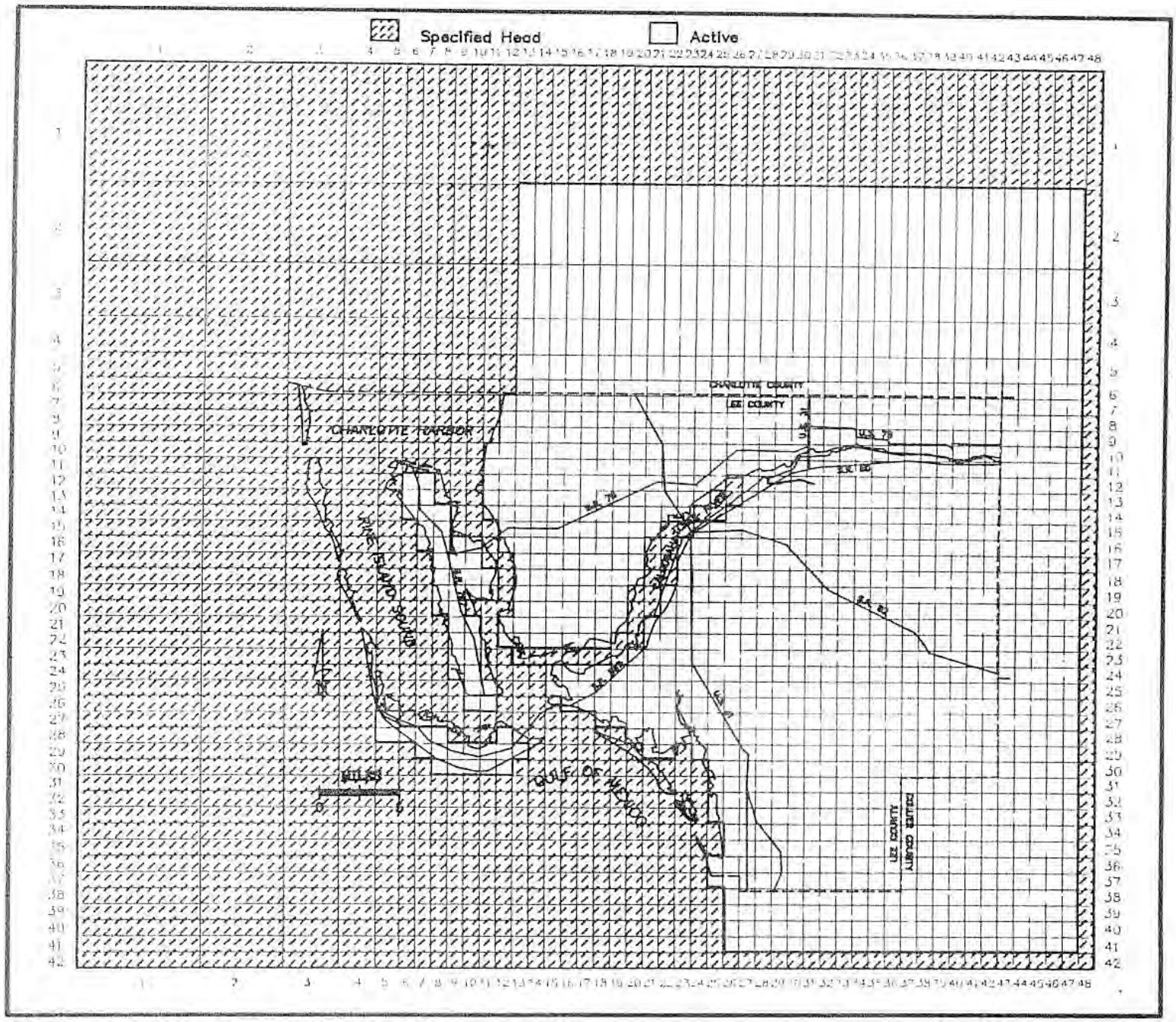

Figure 5. CELL TYPES IN LAYER 1

Bower, R.F., K.M. Adams and J.I. Restrepo, 1990. A Three-Dimensional Finite Difference Ground Water Model of Lee County, Florida. Technical Publication 90-01, South Florida Water Management District, West Palm Beach, FL.

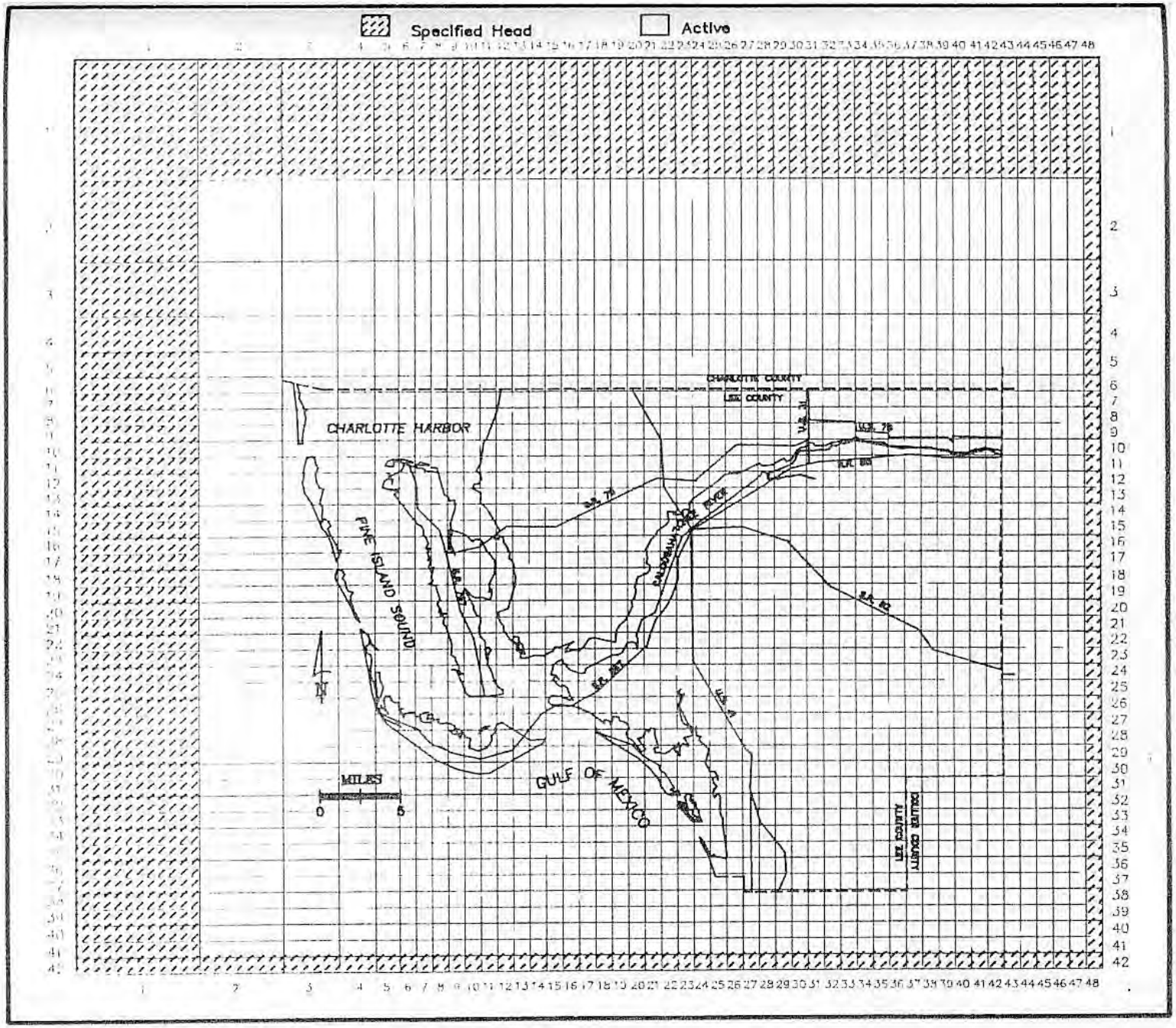

Figure 6. CELL TYPES IN LAYERS 2 THROUGH 6

Bower, R.F., K.M. Adams and J.I. Restrepo, 1990. A Three-Dimensional Finite Difference Ground Water Model of Lee County, Florida. Technical Publication 90-01, South Florida Water Management District, West Palm Beach, FL.

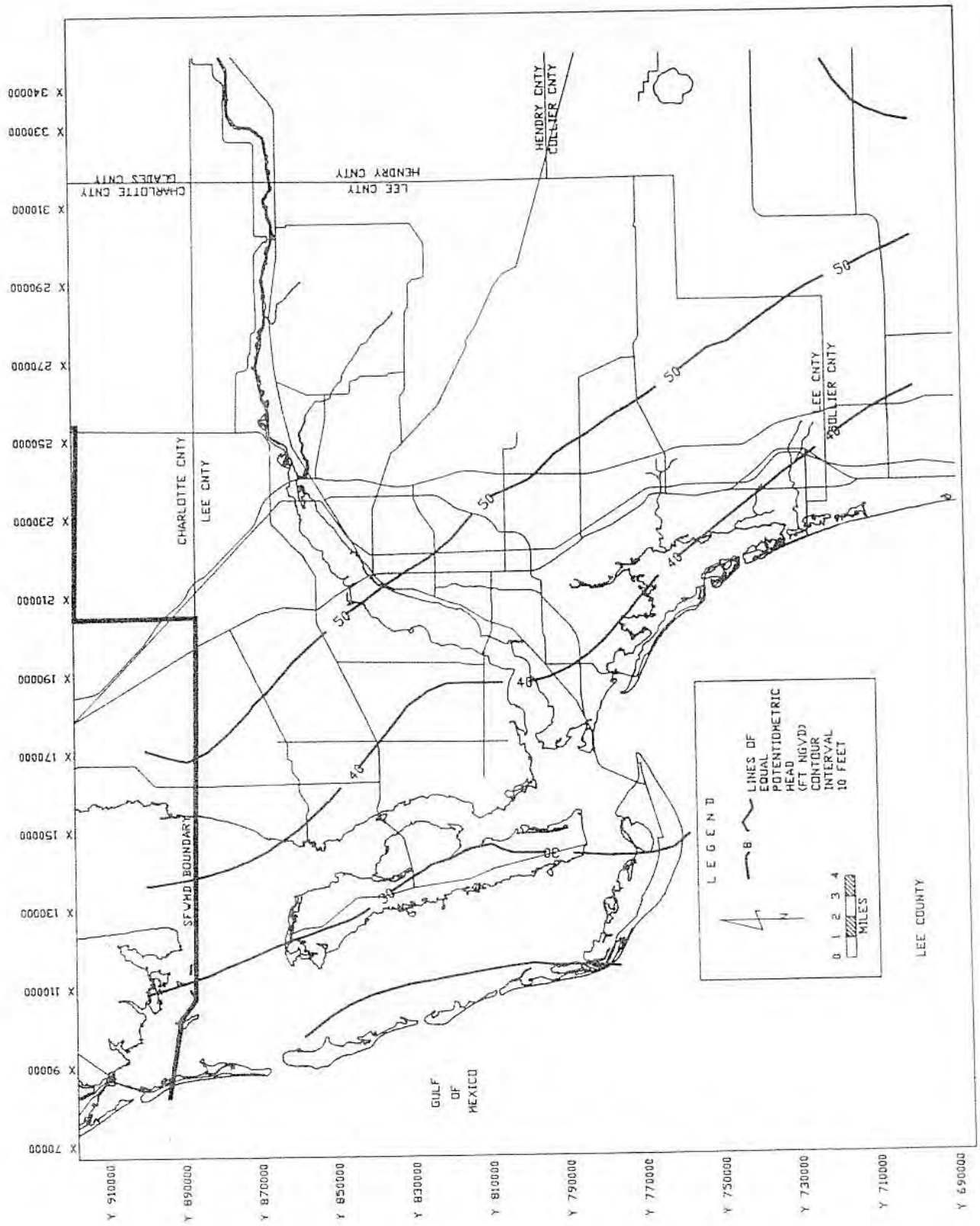

Figure 7. SPECIFIED HEAD USED IN LAYER 7

Bower, R.F., K.M. Adams and J.I. Restrepo, 1990. A Three-Dimensional Finite Difference Ground Water Model of Lee County, Florida. Technical Publication 90-01, South Florida Water Management District, West Palm Beach, FL.

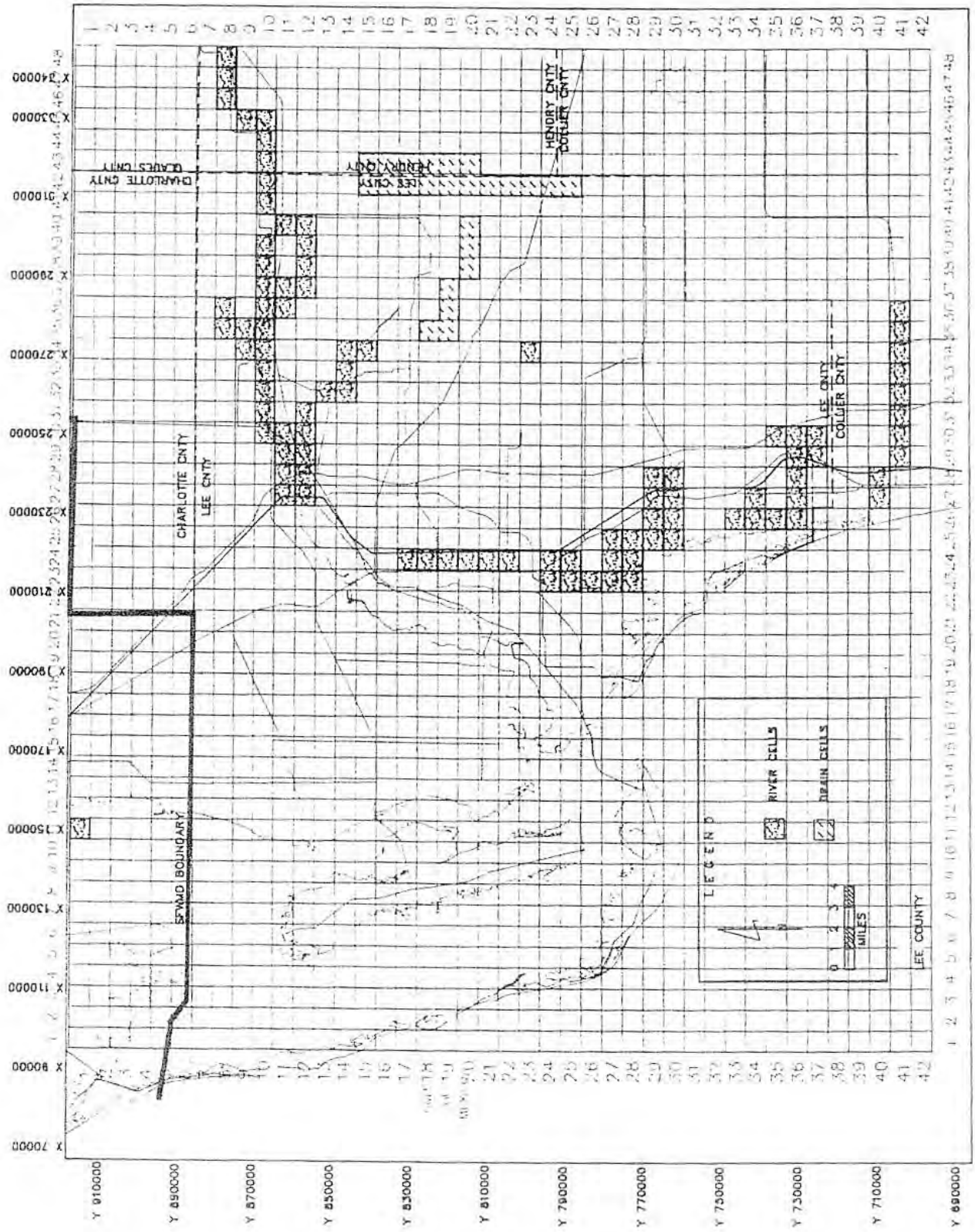

Figure 8. LAYER 1 RIVER AND DRAIN CELLS

Bower, R.F., K.M. Adams and J.I. Restrepo, 1990. A Three-Dimensional Finite Difference Ground Water Model of Lee County, Florida. Technical Publication 90-01, South Florida Water Management District, West Palm Beach, FL.

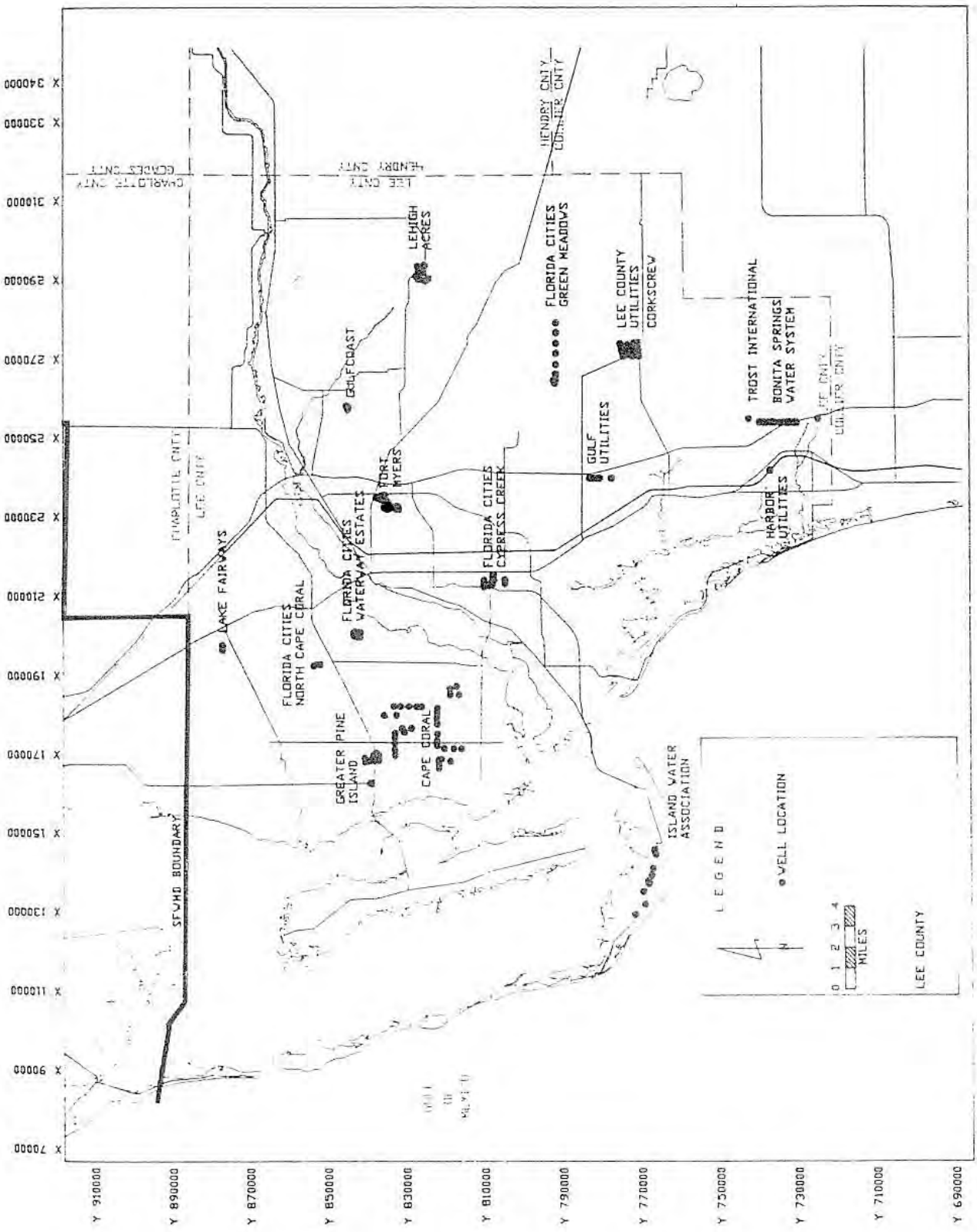

Figure 9. LOCATION OF PUBLIC WATER SUPPLY WELLFIELDS

Bower, R.F., K.M. Adams and J.I. Restrepo, 1990. A Three-Dimensional Finite Difference Ground Water Model of Lee County, Florida. Technical Publication 90-01, South Florida Water Management District, West Palm Beach, FL.

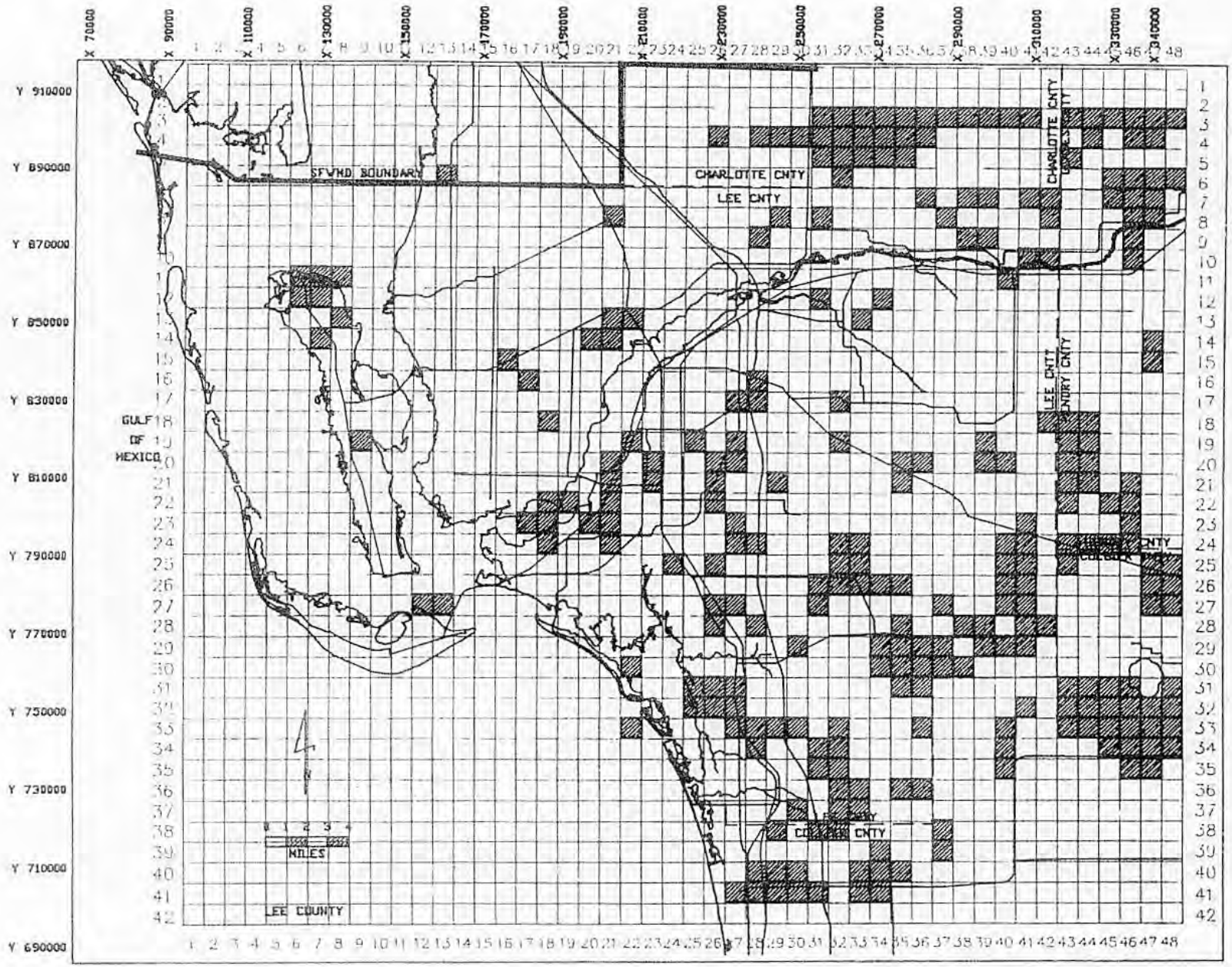

Figure 10. LOCATION OF CELLS WITH IRRIGATION WATER USE, ANY LAYER

Bower, R.F., K.M. Adams and J.I. Restrepo, 1990. A Three-Dimensional Finite Difference Ground Water Model of Lee County, Florida. Technical Publication 90-01, South Florida Water Management District, West Palm Beach, FL.

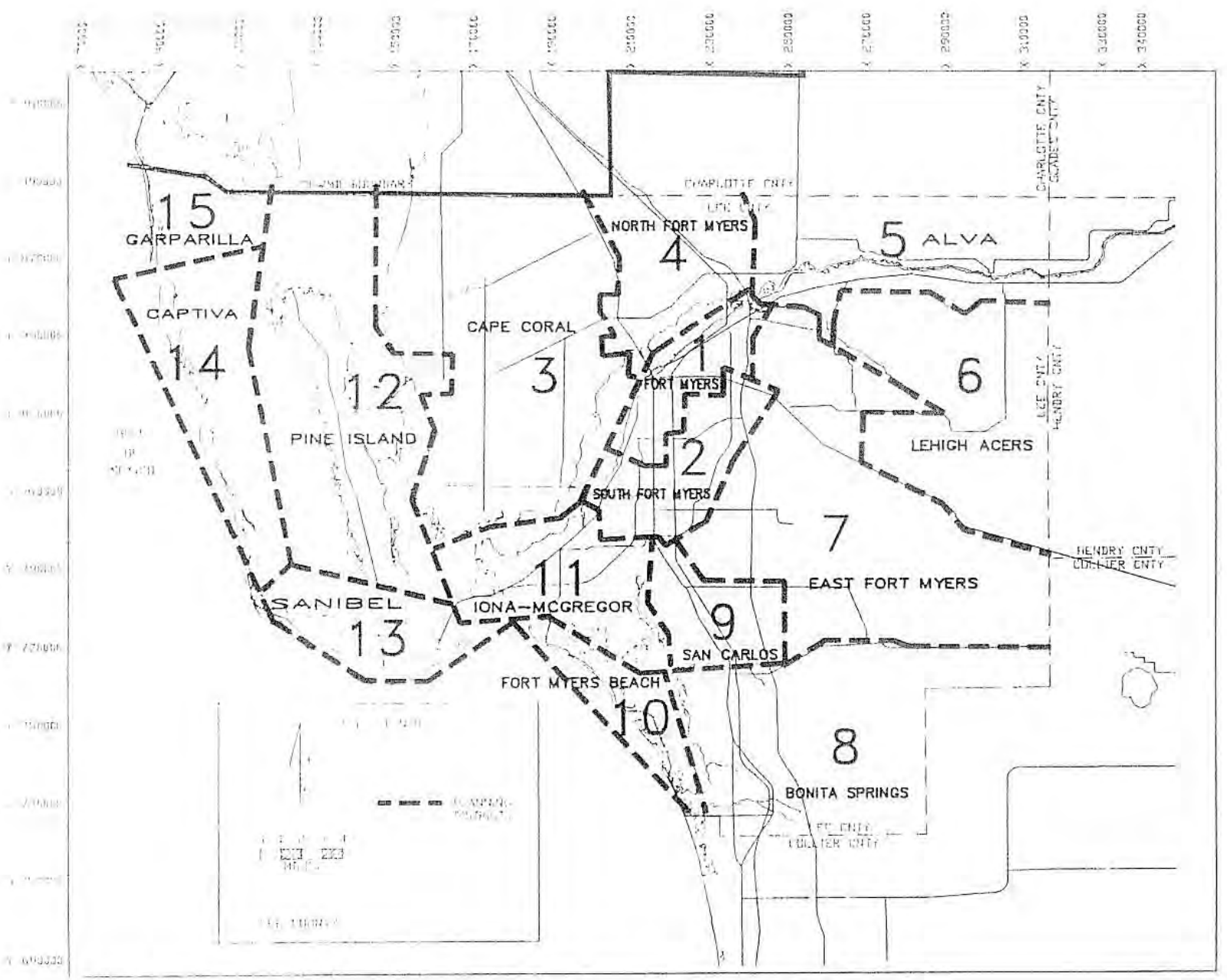

Figure 11. LOCATION OF PLANNING DISTRICTS IN LEE COUNTY

Bower, R.F., K.M. Adams and J.I. Restrepo, 1990. A Three-Dimensional Finite Difference Ground Water Model of Lee County, Florida. Technical Publication 90-01, South Florida Water Management District, West Palm Beach, FL.

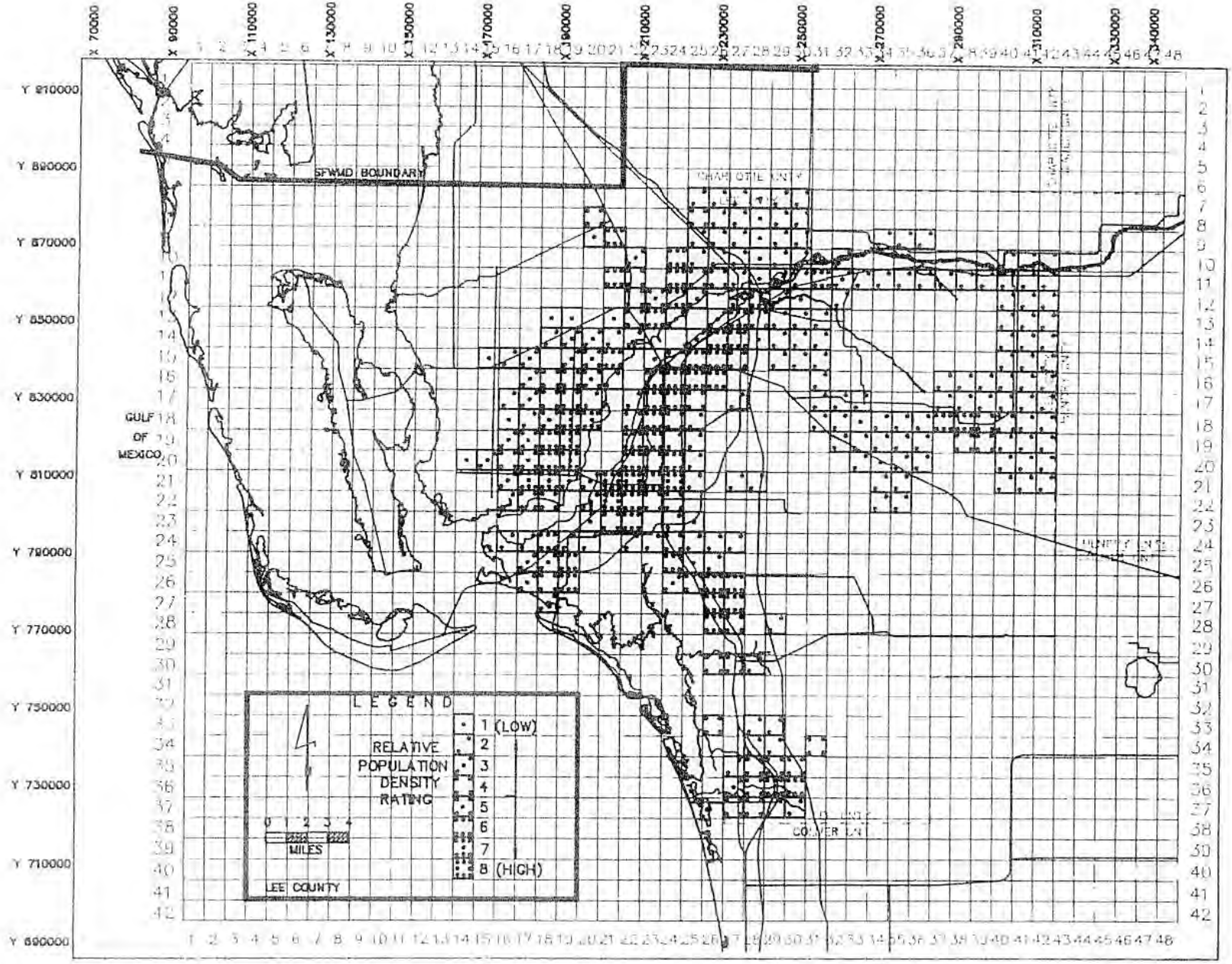

Figure 12. LOCATION OF CELLS WITH DOMESTIC SELF SUPPLY WATER USE

Bower, R.F., K.M. Adams and J.I. Restrepo, 1990. A Three-Dimensional Finite Difference Ground Water Model of Lee County, Florida. Technical Publication 90-01, South Florida Water Management District, West Palm Beach, FL.

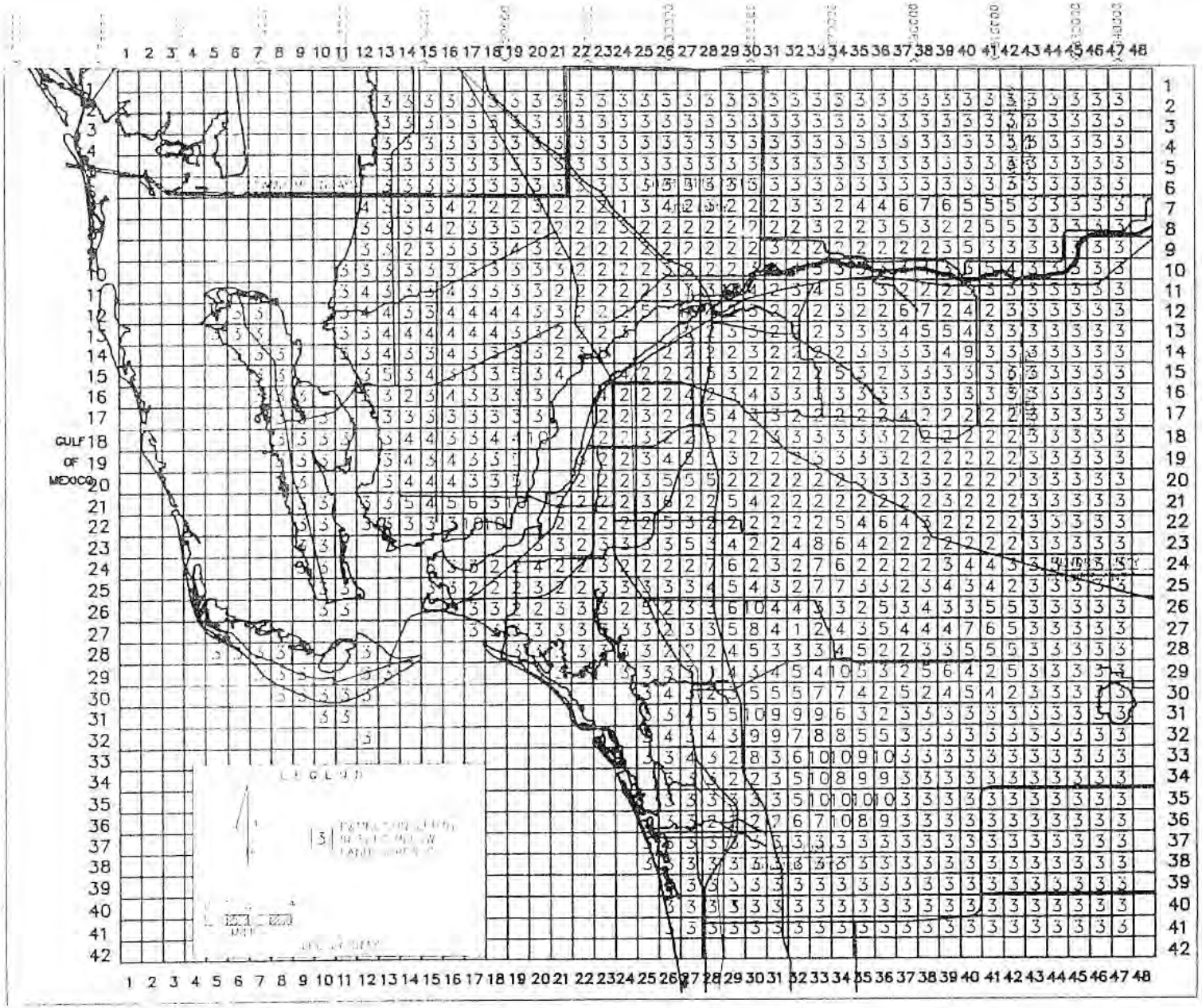

Figure A-37. EVAPOTRANSPIRATION EXTINCTION DEPTH

Bower, R.F., K.M. Adams and J.I. Restrepo, 1990. A Three-Dimensional Finite Difference Ground Water Model of Lee County, Florida. Technical Publication 90-01, South Florida Water Management District, West Palm Beach, FL.

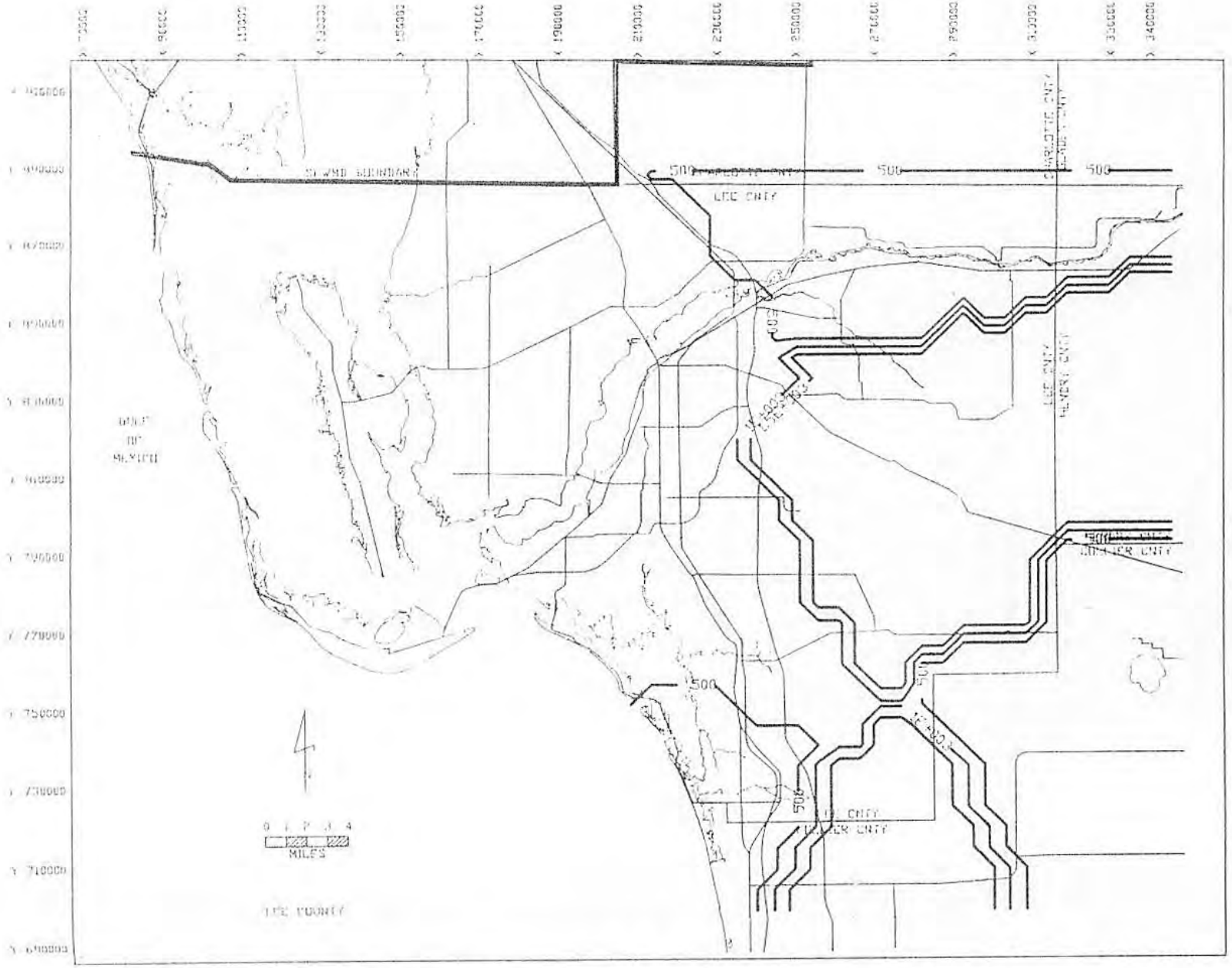

Figure A-38. HYDRAULIC CONDUCTIVITY OF LAYER 1 (WATER TABLE AQUIFER) IN FT/DAY

Bower, R.F., K.M. Adams and J.I. Restrepo, 1990. A Three-Dimensional Finite Difference Ground Water Model of Lee County, Florida. Technical Publication 90-01, South Florida Water Management District, West Palm Beach, FL.

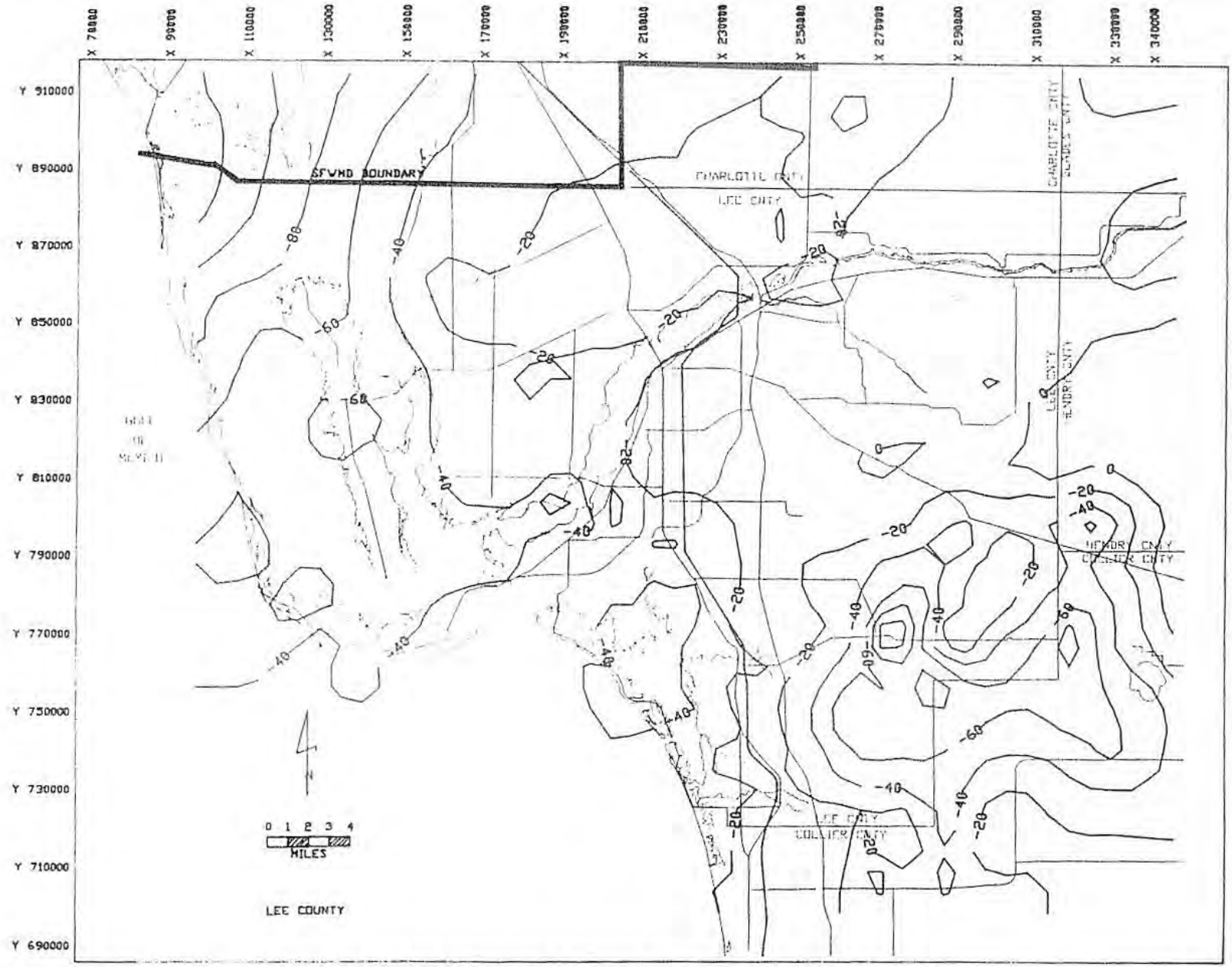

Figure A-39. BOTTOM ELEVATION OF LAYER 1 (WATER TABLE AQUIFER) IN FEET NGVD

Bower, R.F., K.M. Adams and J.I. Restrepo, 1990. A Three-Dimensional Finite Difference Ground Water Model of Lee County, Florida. Technical Publication 90-01, South Florida Water Management District, West Palm Beach, FL.

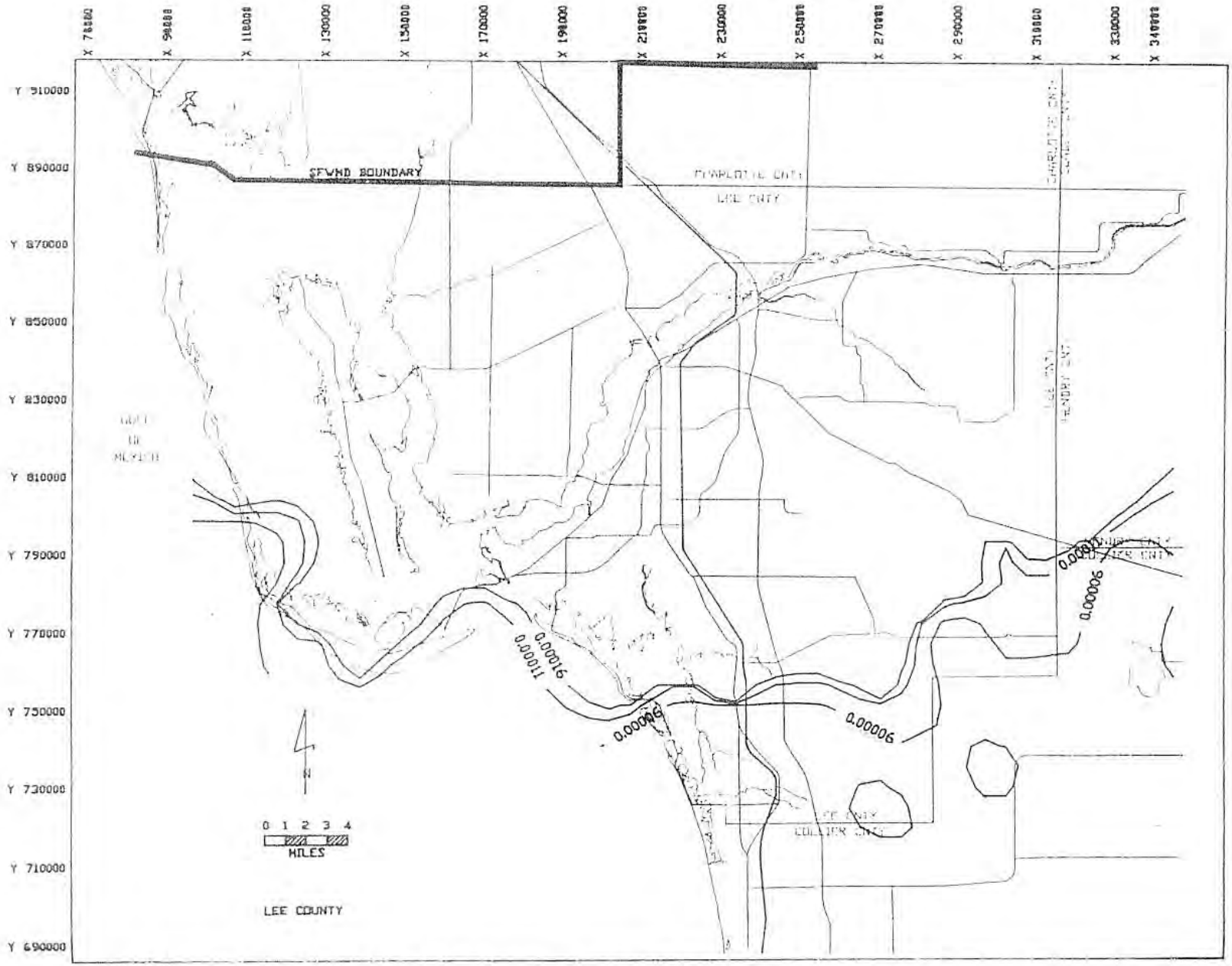

Figure A-40. VERTICAL CONDUCTANCE, BOTTOM OF LAYER 1 (LOWER TAMIAMI CONFINING BED) IN 1/DAY (0.0124 FT./DAY/LOWER TAMIAMI CONFINING BED THICKNESS)

Bower, R.F., K.M. Adams and J.I. Restrepo, 1990. A Three-Dimensional Finite Difference Ground Water Model of Lee County, Florida. Technical Publication 90-01, South Florida Water Management District, West Palm Beach, FL.

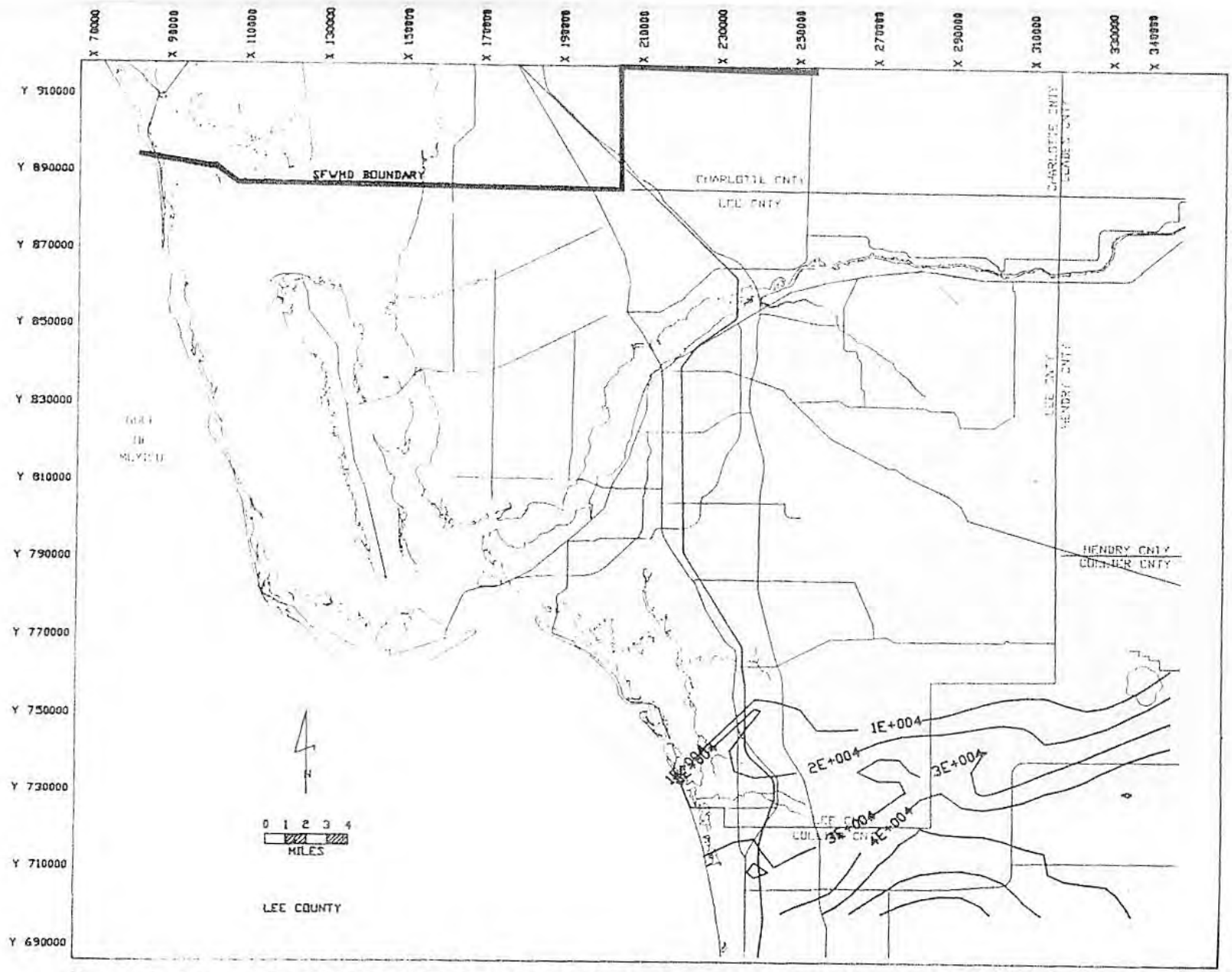

Figure A-41. TRANSMISSIVITY OF LAYER 2 (LOWER TAMIAMI AQUIFER) IN FT.2/DAY

Bower, R.F., K.M. Adams and J.I. Restrepo, 1990. A Three-Dimensional Finite Difference Ground Water Model of Lee County, Florida. Technical Publication 90-01, South Florida Water Management District, West Palm Beach, FL.

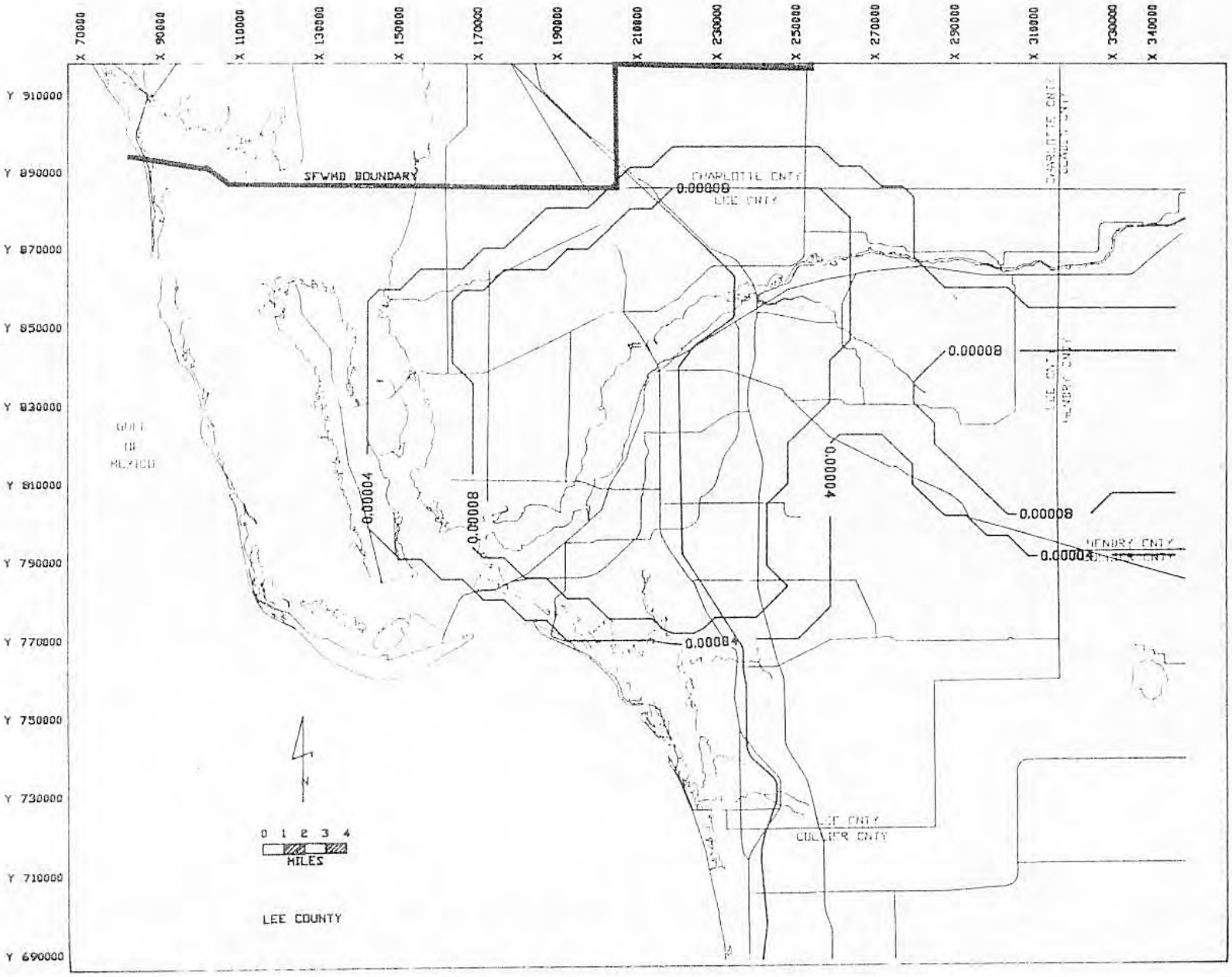

Figure A-42. VERTICAL CONDUCTANCE, BOTTOM OF LAYER 2 (UPPER HAWTHORN CONFINING BED) IN 1/DAY

Bower, R.F., K.M. Adams and J.I. Restrepo, 1990. A Three-Dimensional Finite Difference Ground Water Model of Lee County, Florida. Technical Publication 90-01, South Florida Water Management District, West Palm Beach, FL.

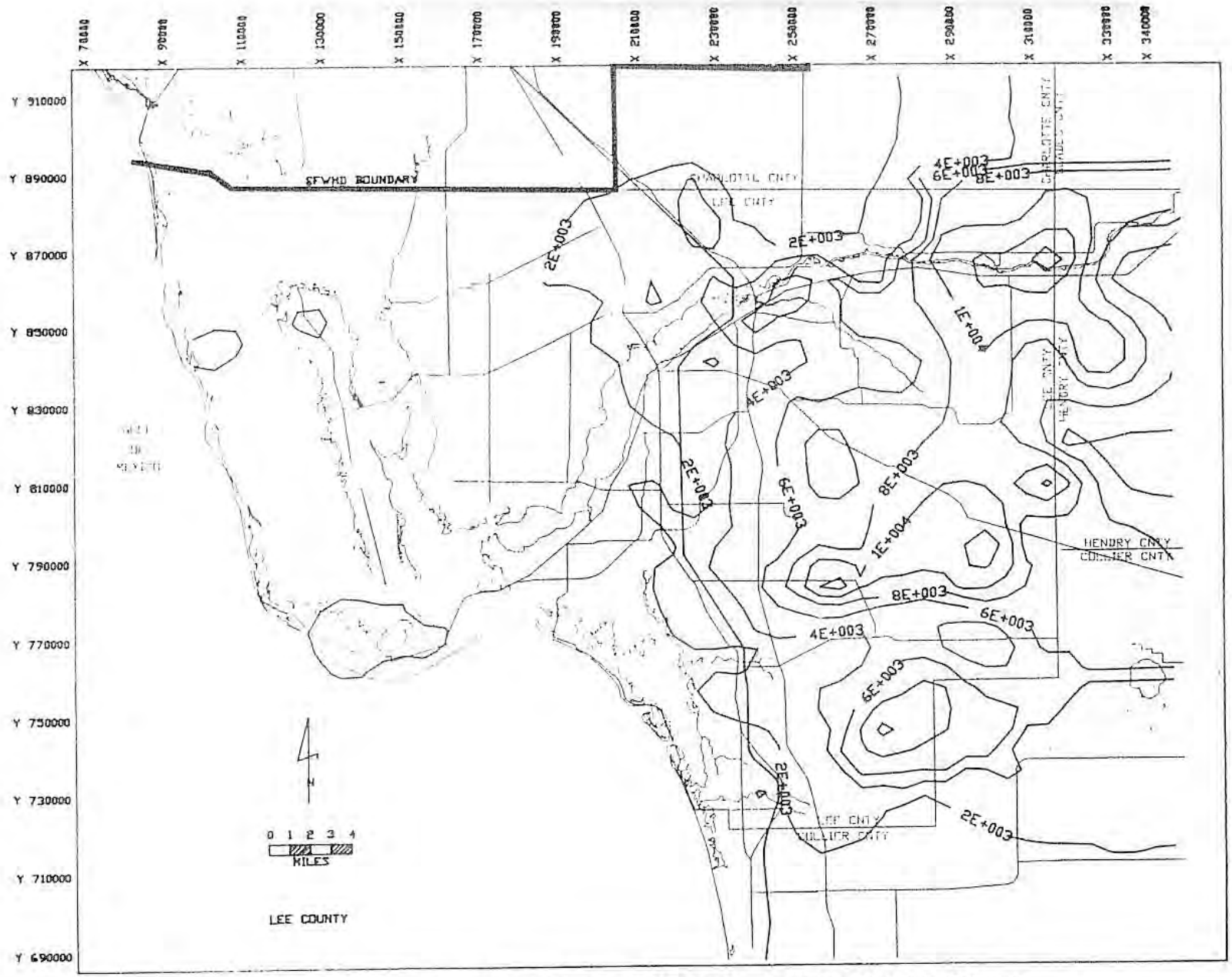

Figure A-43. TRANSMISSIVITY OF LAYER 3 (SANDSTONE AQUIFER) IN FT.2/DAY

Bower, R.F., K.M. Adams and J.I. Restrepo, 1990. A Three-Dimensional Finite Difference Ground Water Model of Lee County, Florida. Technical Publication 90-01, South Florida Water Management District, West Palm Beach, FL.

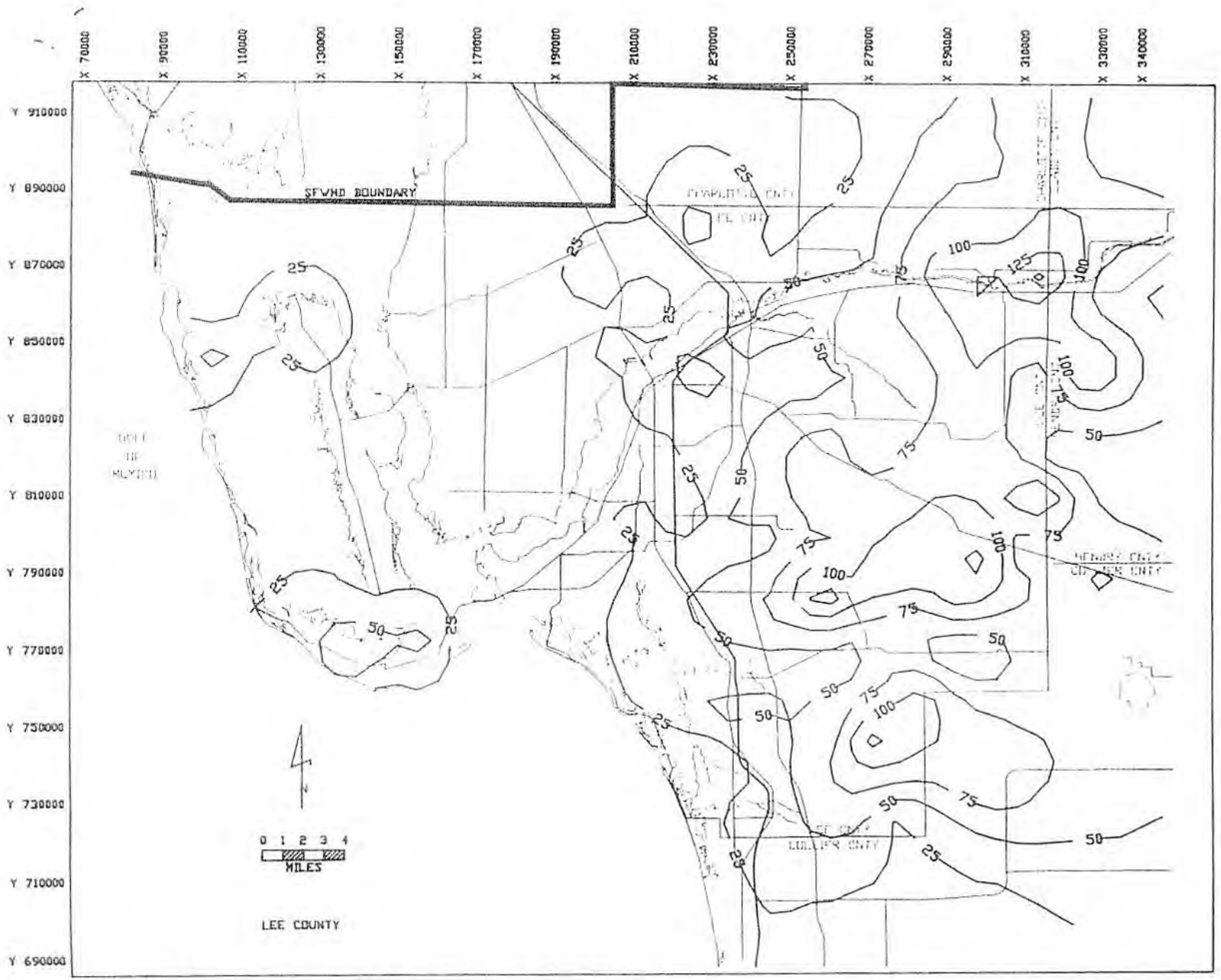

Figure A-44. THICKNESS OF LAYER 3 (SANDSTONE AQUIFER) IN FEET

Bower, R.F., K.M. Adams and J.I. Restrepo, 1990. A Three-Dimensional Finite Difference Ground Water Model of Lee County, Florida. Technical Publication 90-01, South Florida Water Management District, West Palm Beach, FL.

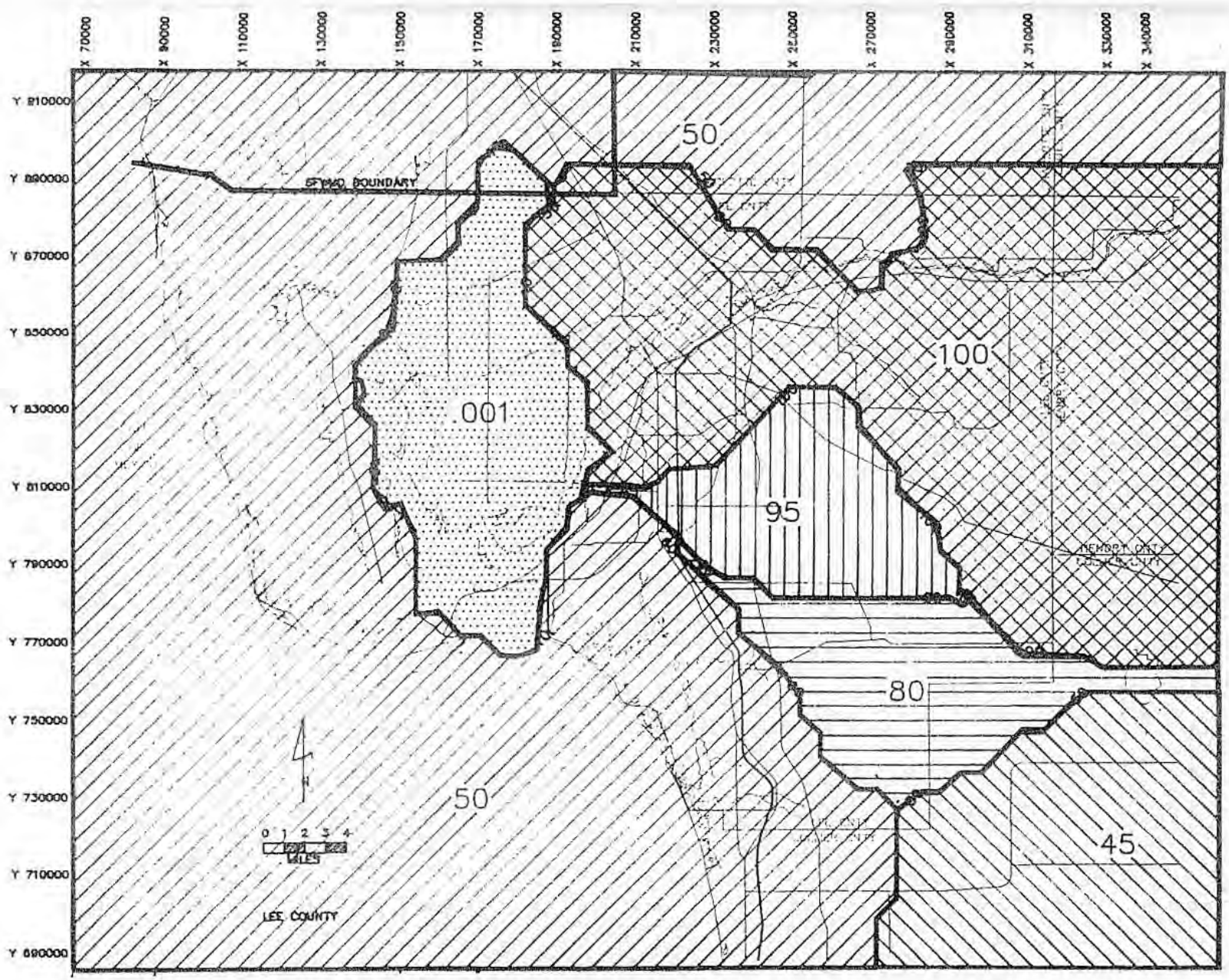

Figure A-45. HYDRAULIC CONDUCTIVITY OF LAYER 3 (SANDSTONE AQUIFER) IN FT./DAY

Bower, R.F., K.M. Adams and J.I. Restrepo, 1990. A Three-Dimensional Finite Difference Ground Water Model of Lee County, Florida. Technical Publication 90-01, South Florida Water Management District, West Palm Beach, FL.

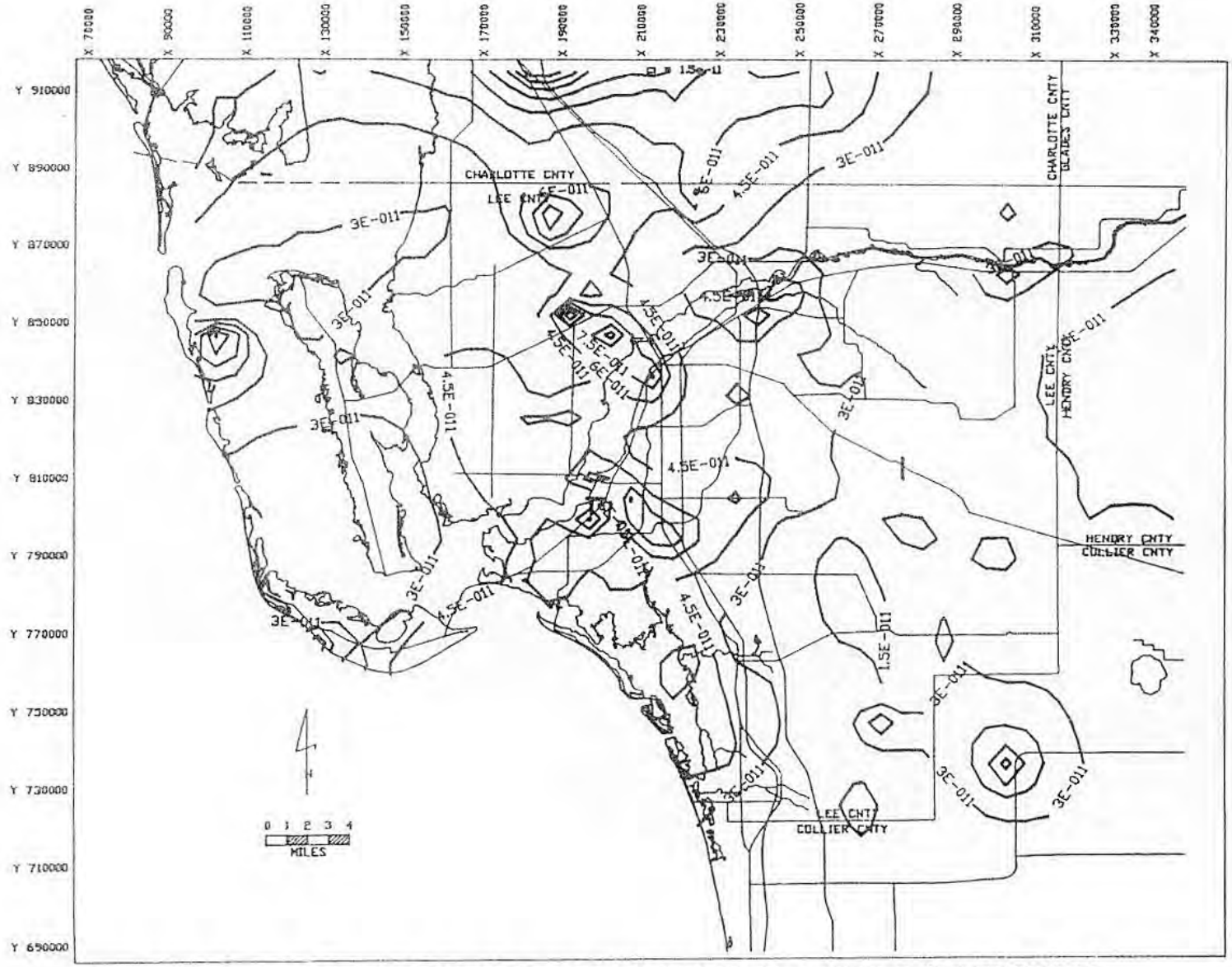

Figure A-46. VERTICAL CONDUCTANCE, BOTTOM OF LAYER 3 (SANDSTONE AQUIFER) IN 1/DAY (0.00017 FT/DAY / MID HAWTHORN CONFINING BED THICKNESS)

Bower, R.F., K.M. Adams and J.I. Restrepo, 1990. A Three-Dimensional Finite Difference Ground Water Model of Lee County, Florida. Technical Publication 90-01, South Florida Water Management District, West Palm Beach, FL.

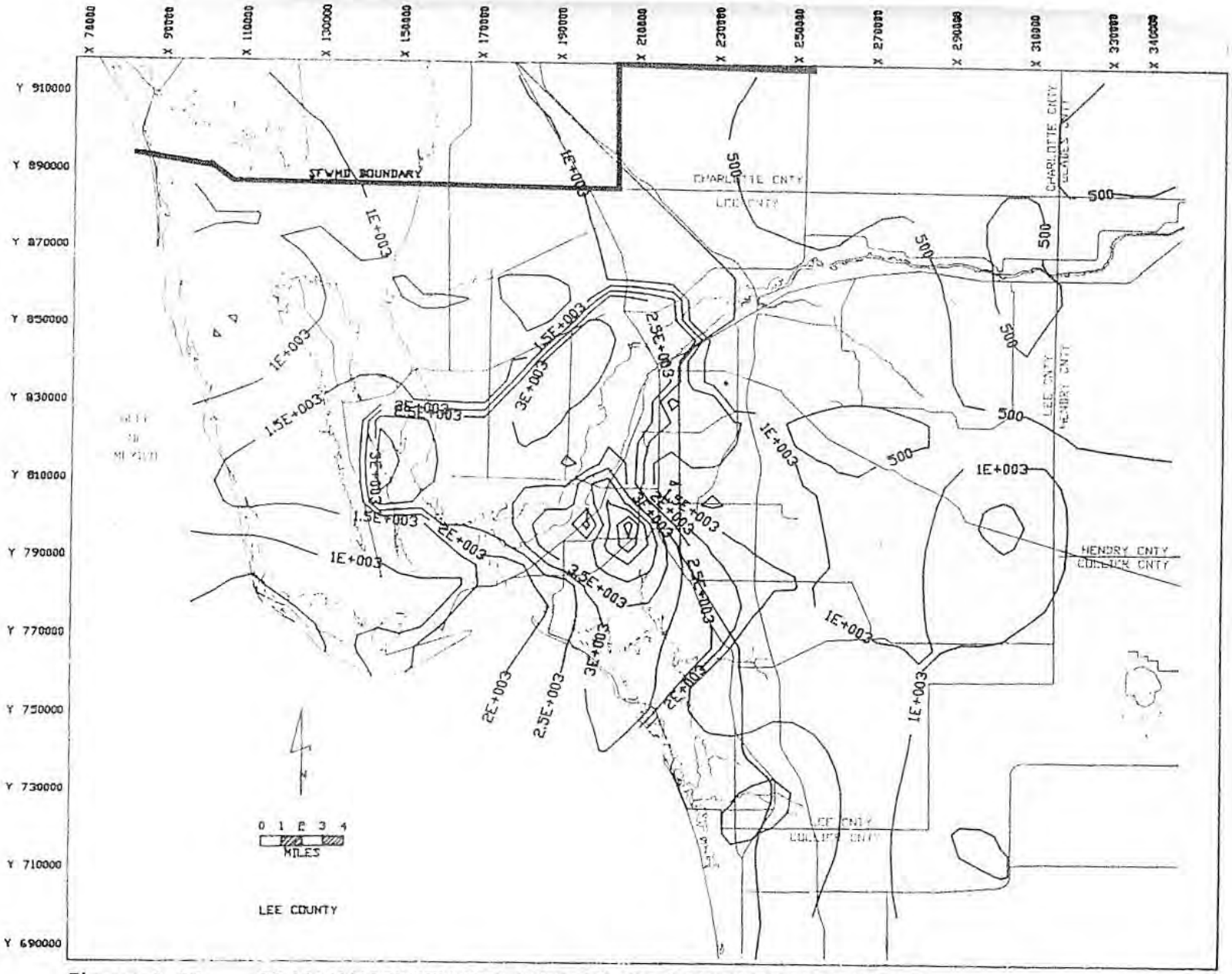

Figure A-47. TRANSMISSIVITY OF LAYER 4 (MID-HAWTHORN AQUIFER) IN FT.2/DAY

Bower, R.F., K.M. Adams and J.I. Restrepo, 1990. A Three-Dimensional Finite Difference Ground Water Model of Lee County, Florida. Technical Publication 90-01, South Florida Water Management District, West Palm Beach, FL.

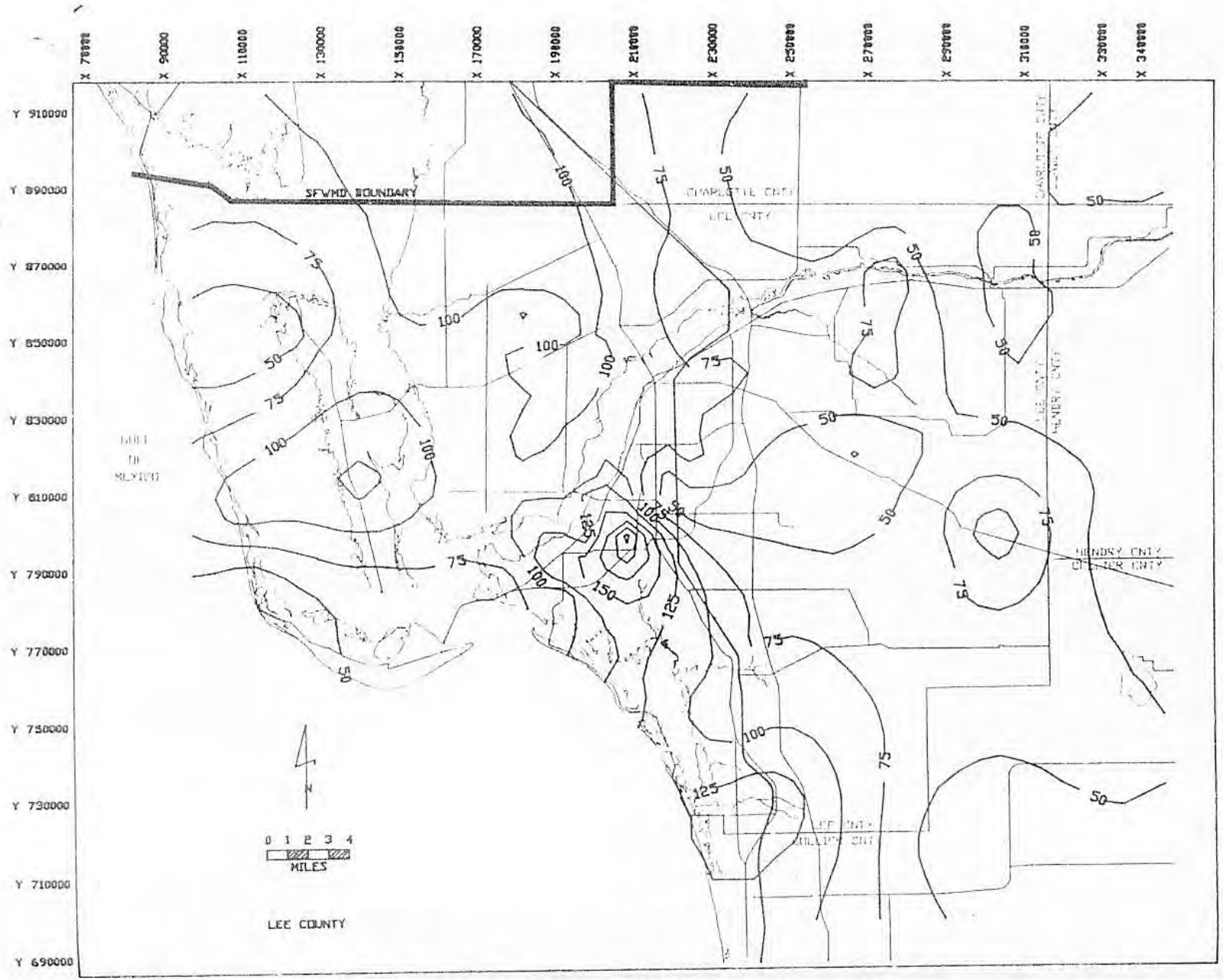

Figure A-48. THICKNESS OF LAYER 4(MID-HAWTHORN AQUIFER) IN FEET

Bower, R.F., K.M. Adams and J.I. Restrepo, 1990. A Three-Dimensional Finite Difference Ground Water Model of Lee County, Florida. Technical Publication 90-01, South Florida Water Management District, West Palm Beach, FL.

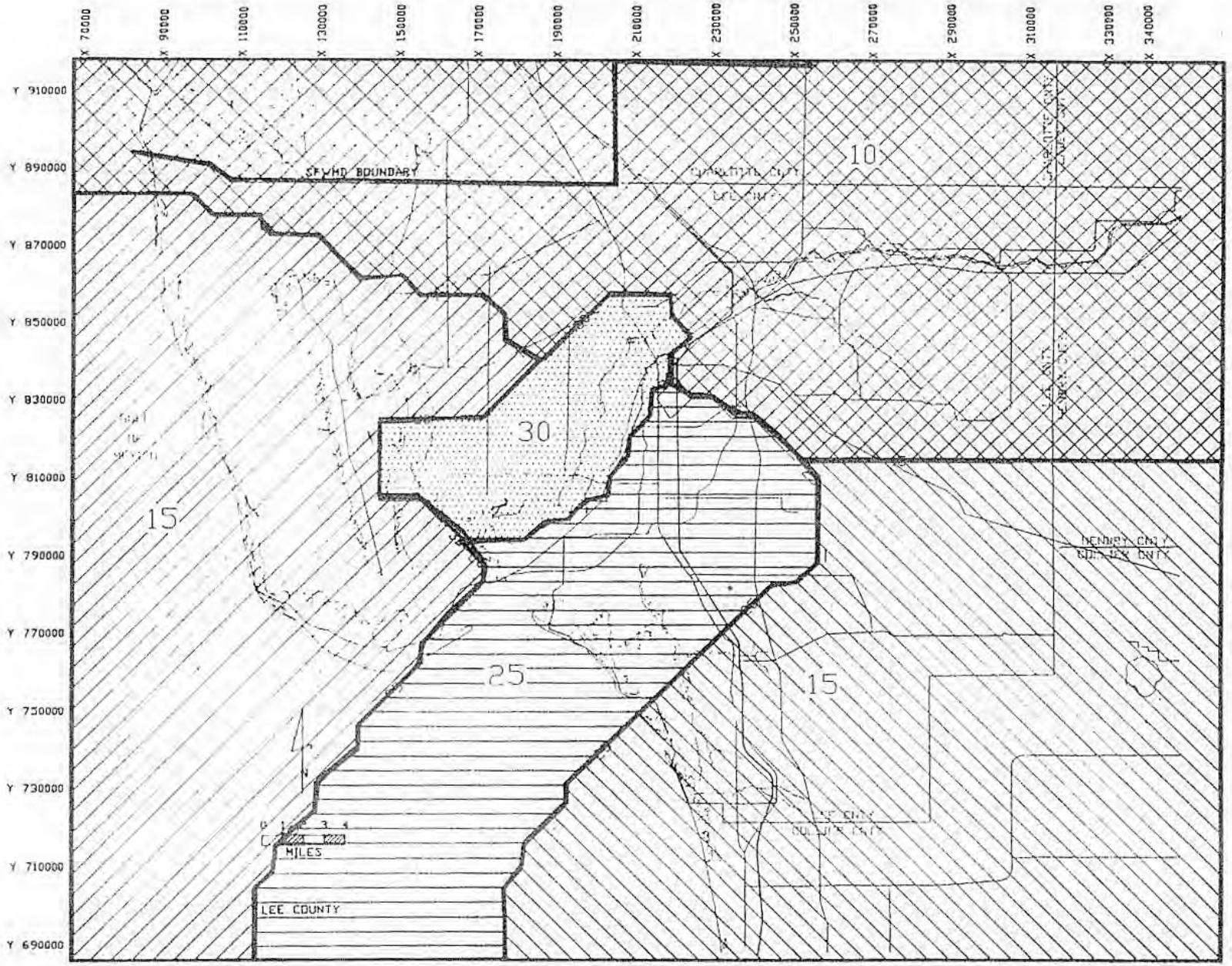

Figure A-49. HYDRAULIC CONDUCTIVITY OF LAYER 4 (MID-HAWTHORN AQUIFER) IN FT./DAY

Bower, R.F., K.M. Adams and J.I. Restrepo, 1990. A Three-Dimensional Finite Difference Ground Water Model of Lee County, Florida. Technical Publication 90-01, South Florida Water Management District, West Palm Beach, FL.

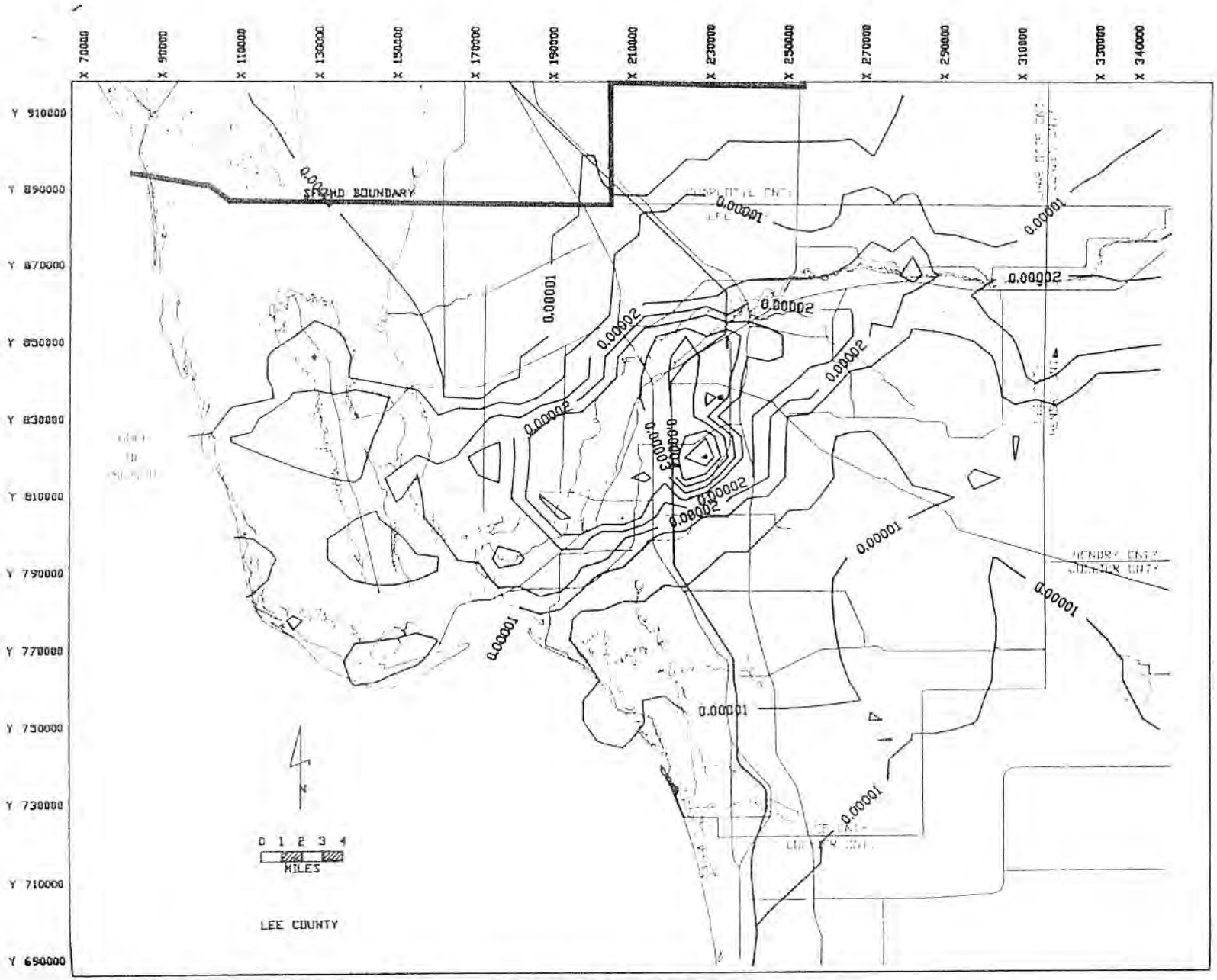

Figure A-50. VERTICAL CONDUCTANCE, BOTTOM OF LAYER 4 (LOWER HAWTHORN CONFINING BED) IN 1/DAY

Bower, R.F., K.M. Adams and J.I. Restrepo, 1990. A Three-Dimensional Finite Difference Ground Water Model of Lee County, Florida. Technical Publication 90-01, South Florida Water Management District, West Palm Beach, FL.

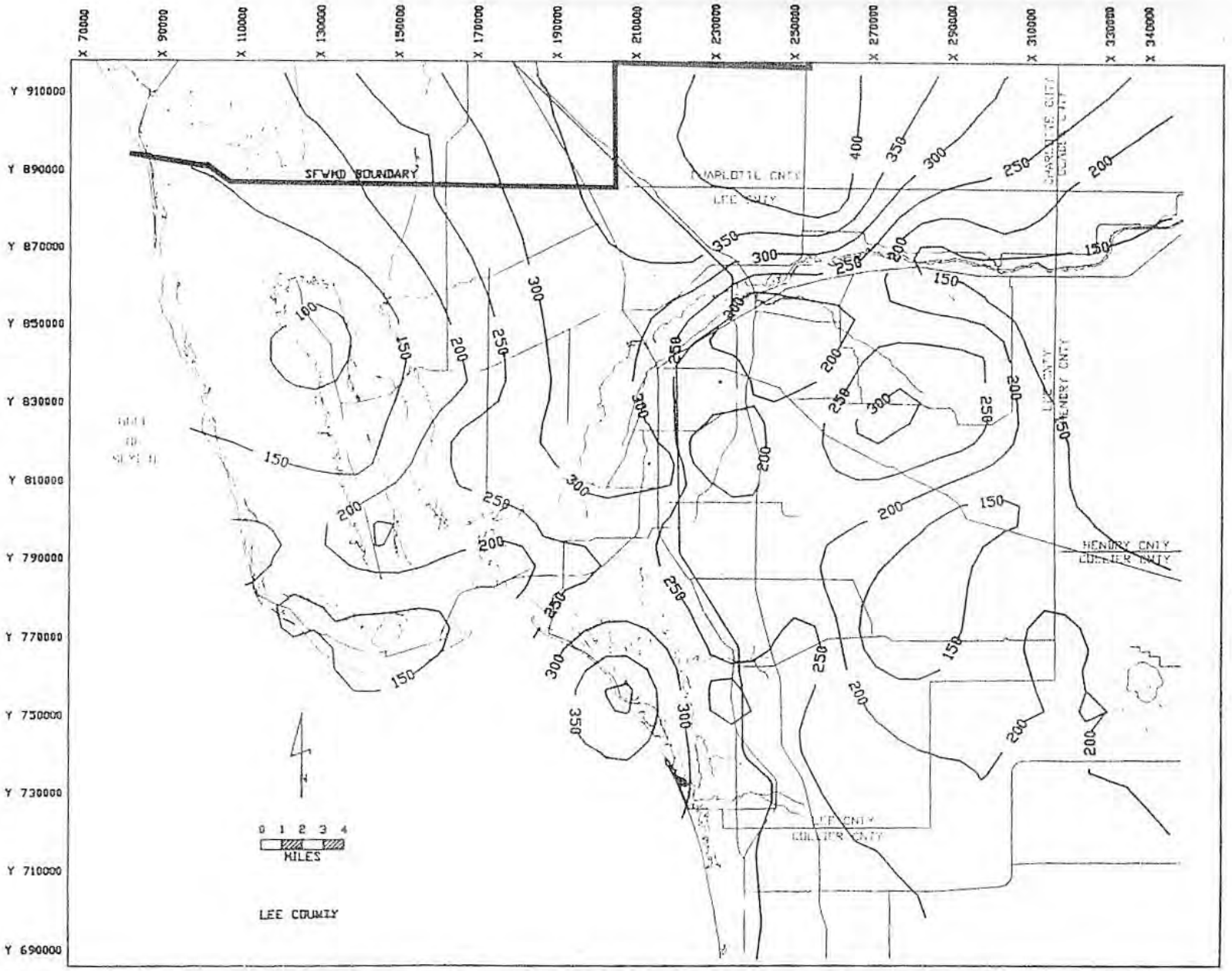

Figure A-51. THICKNESS OF THE LOWER HAWTHORN CONFINING BED (FEET)

Bower, R.F., K.M. Adams and J.I. Restrepo, 1990. A Three-Dimensional Finite Difference Ground Water Model of Lee County, Florida. Technical Publication 90-01, South Florida Water Management District, West Palm Beach, FL.

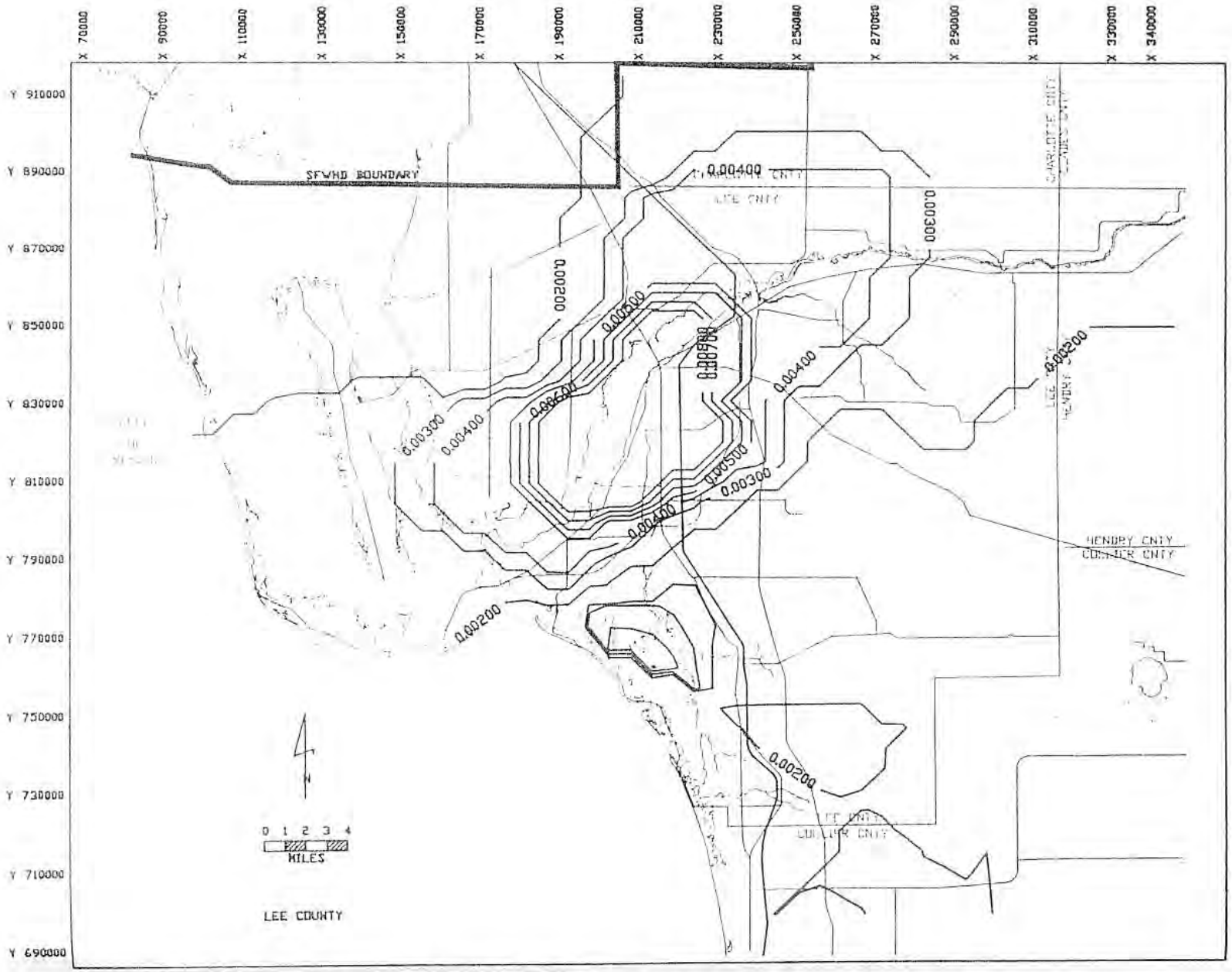

Figure A-52. VERTICAL HYDRAULIC CONDUCTIVITY, BOTTOM OF LAYER 4 (LOWER HAWTHORN CONFINING BED) IN FT/DAY

Bower, R.F., K.M. Adams and J.I. Restrepo, 1990. A Three-Dimensional Finite Difference Ground Water Model of Lee County, Florida. Technical Publication 90-01, South Florida Water Management District, West Palm Beach, FL.

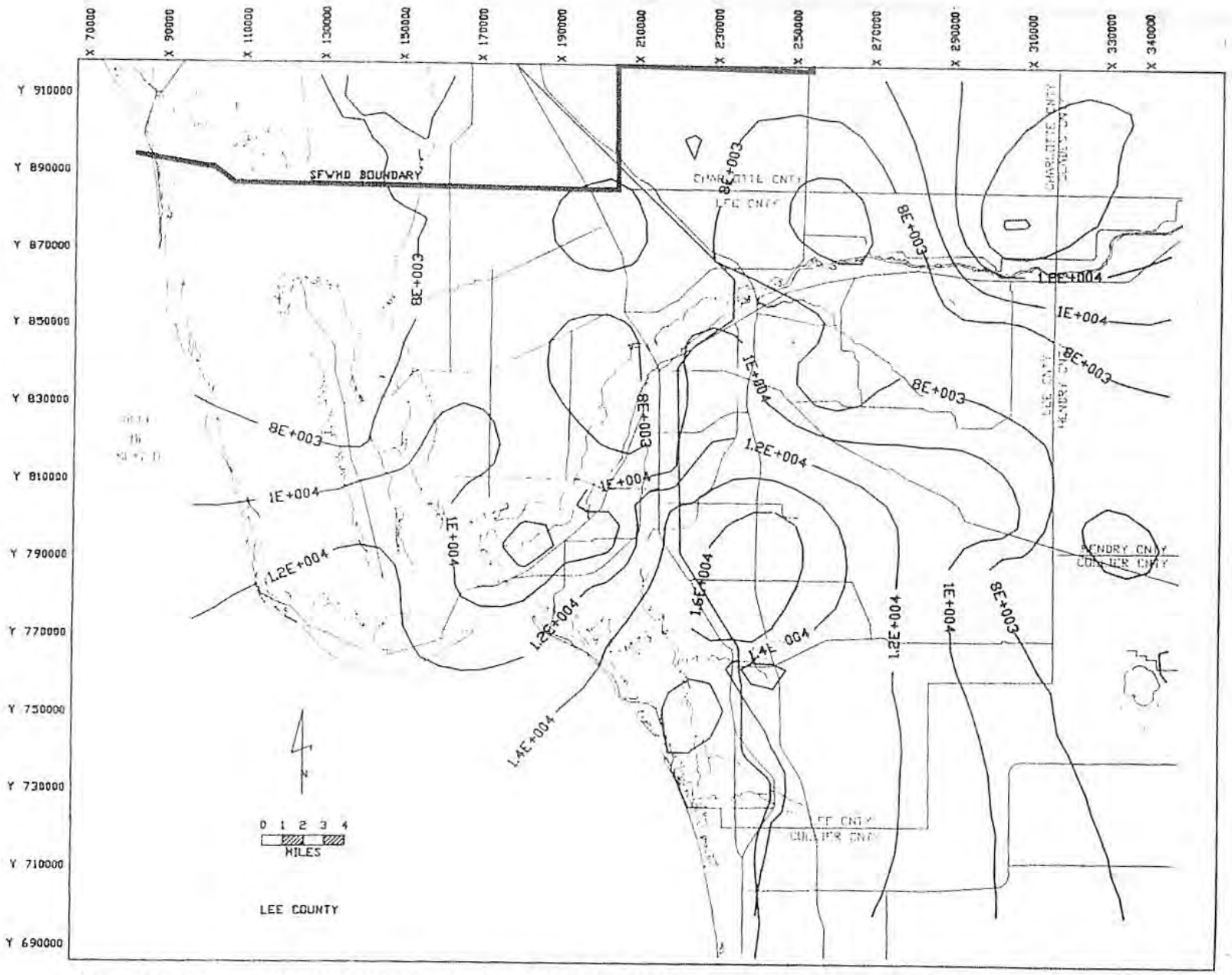

Figure A-53. TRANSMISSIVITY OF LAYER 5 (LOWER HAWTHORN CONFINING BED) IN FT.2/DAY (56 FT./DAY X LOWER HAWTHORN AQUIFER THICKNESS)

Bower, R.F., K.M. Adams and J.I. Restrepo, 1990. A Three-Dimensional Finite Difference Ground Water Model of Lee County, Florida. Technical Publication 90-01, South Florida Water Management District, West Palm Beach, FL.

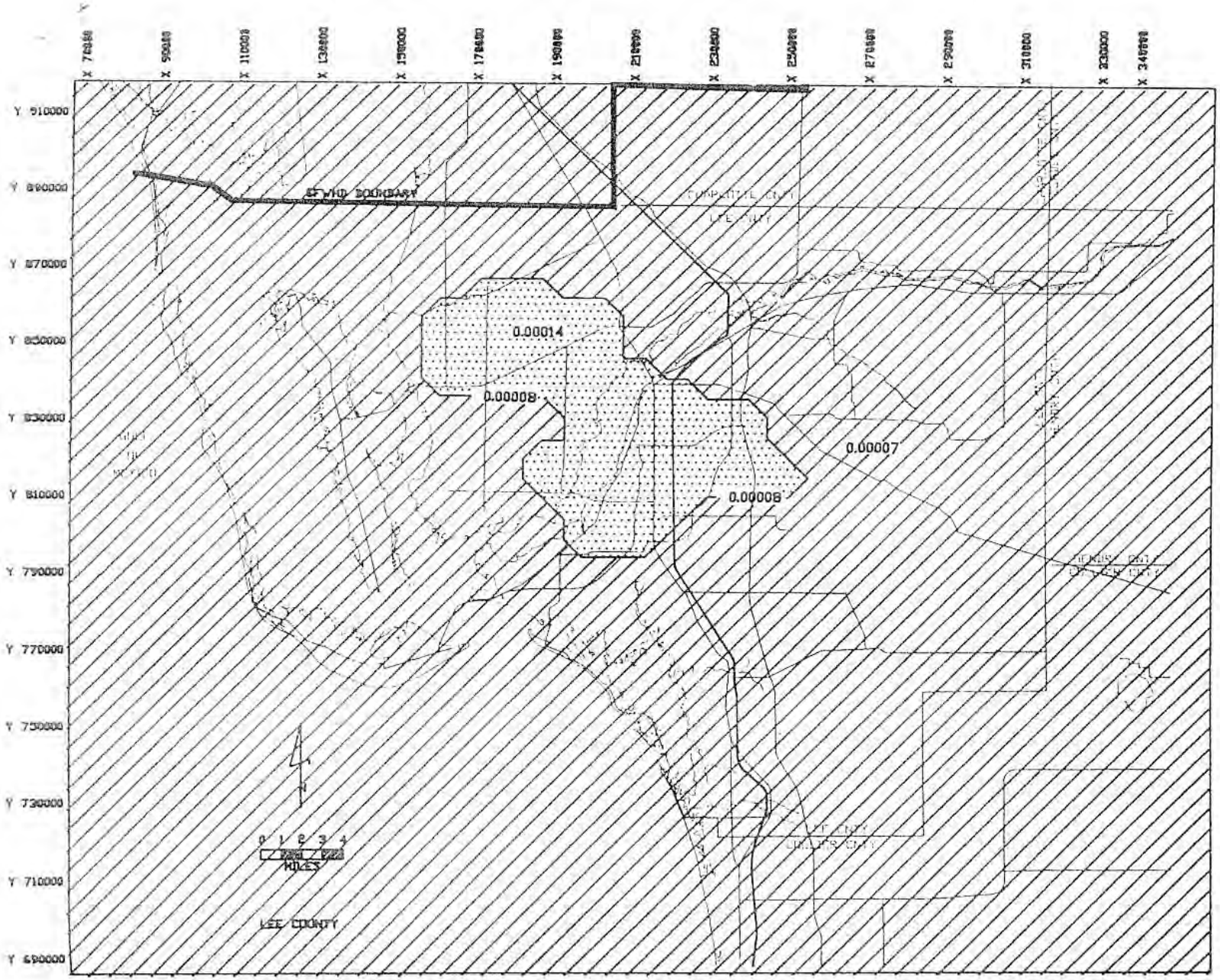

Figure A-54. VERTICAL CONDUCTANCE, BOTTOM OF LAYER 5 (1/DAY)

Bower, R.F., K.M. Adams and J.I. Restrepo, 1990. A Three-Dimensional Finite Difference Ground Water Model of Lee County, Florida. Technical Publication 90-01, South Florida Water Management District, West Palm Beach, FL.

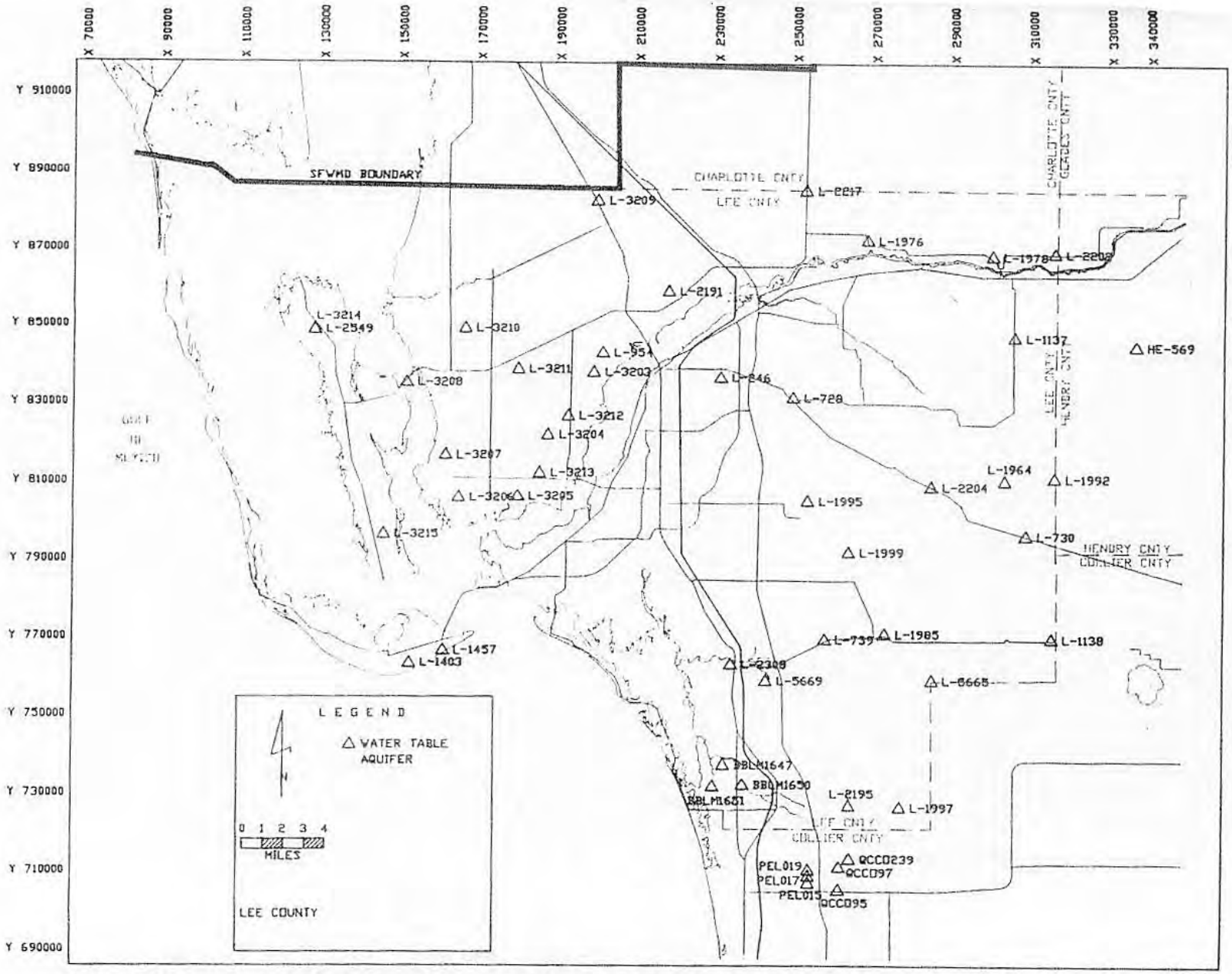

Figure B-1. LOCATION OF WATER LEVEL MONITORING WELLS, WATER TABLE AQUIFER (LAYER 1)

Bower, R.F., K.M. Adams and J.I. Restrepo, 1990. A Three-Dimensional Finite Difference Ground Water Model of Lee County, Florida. Technical Publication 90-01, South Florida Water Management District, West Palm Beach, FL.

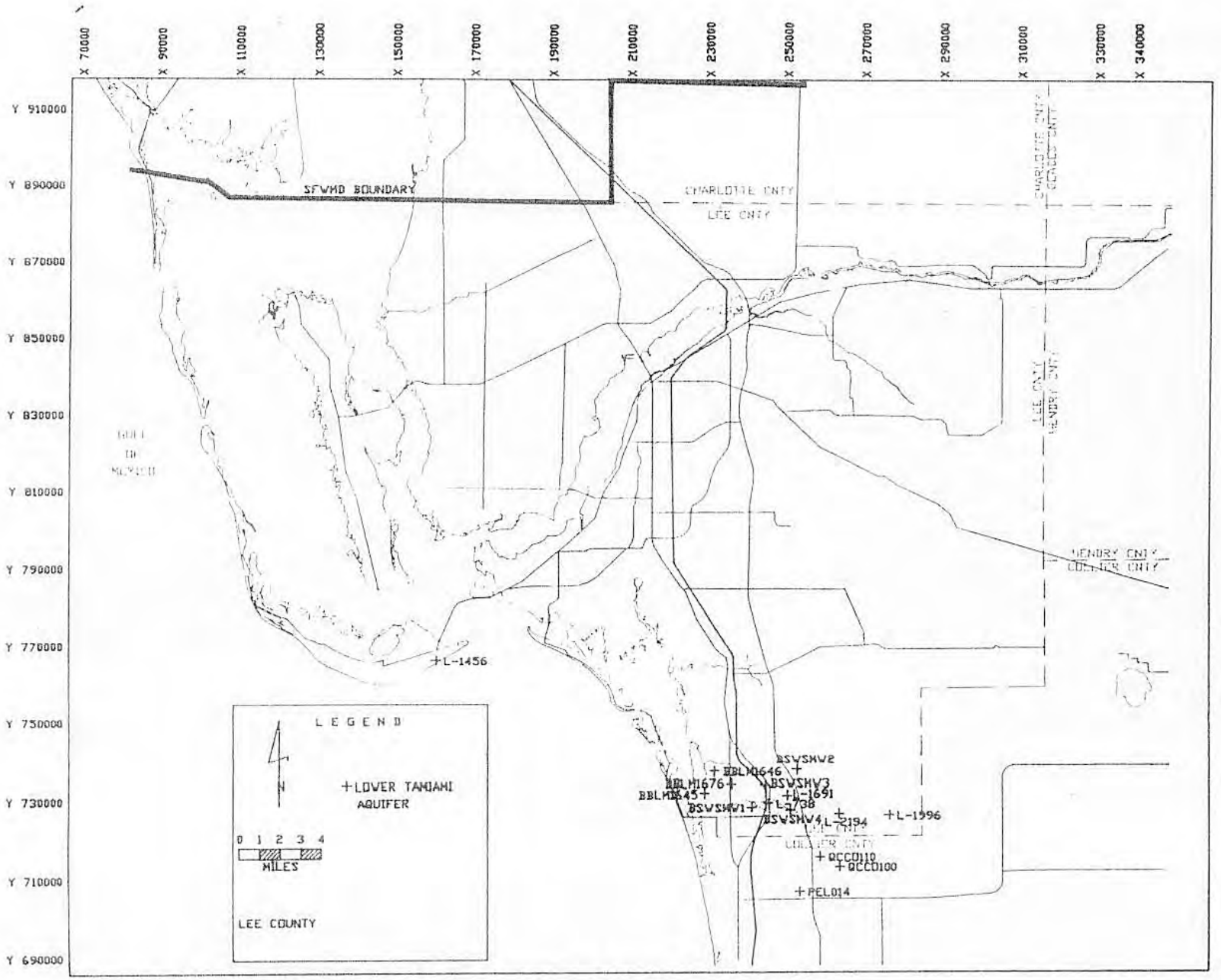

Figure B-2. LOCATION OF WATER LEVEL MONITORING WELLS, LOWER TAMIAMI AQUIFER (LAYER 2)

Bower, R.F., K.M. Adams and J.I. Restrepo, 1990. A Three-Dimensional Finite Difference Ground Water Model of Lee County, Florida. Technical Publication 90-01, South Florida Water Management District, West Palm Beach, FL.

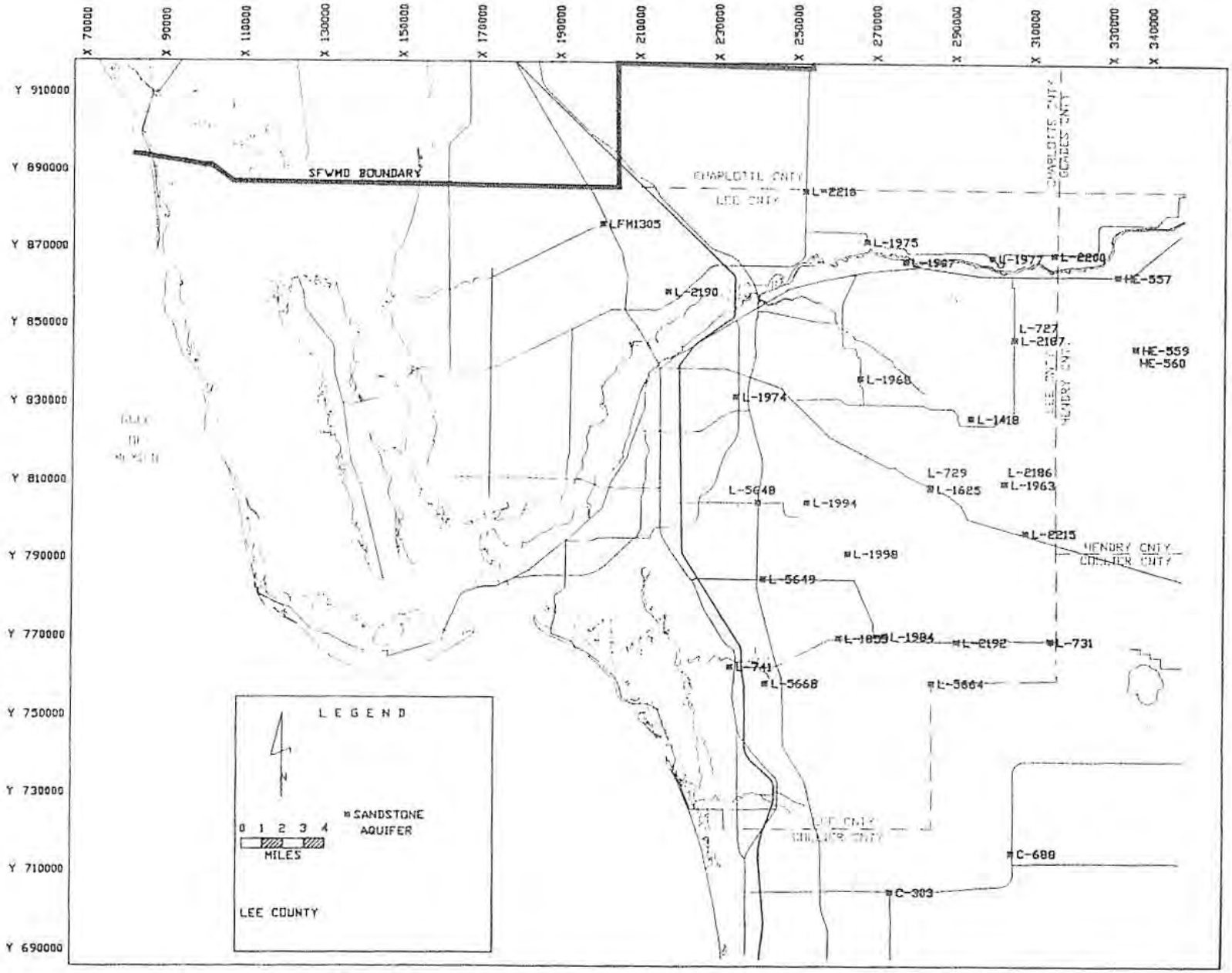

Figure B-3. LOCATION OF WATER LEVEL MONITORING WELLS, SANDSTONE AQUIFER (LAYER 3)

Bower, R.F., K.M. Adams and J.I. Restrepo, 1990. A Three-Dimensional Finite Difference Ground Water Model of Lee County, Florida. Technical Publication 90-01, South Florida Water Management District, West Palm Beach, FL.

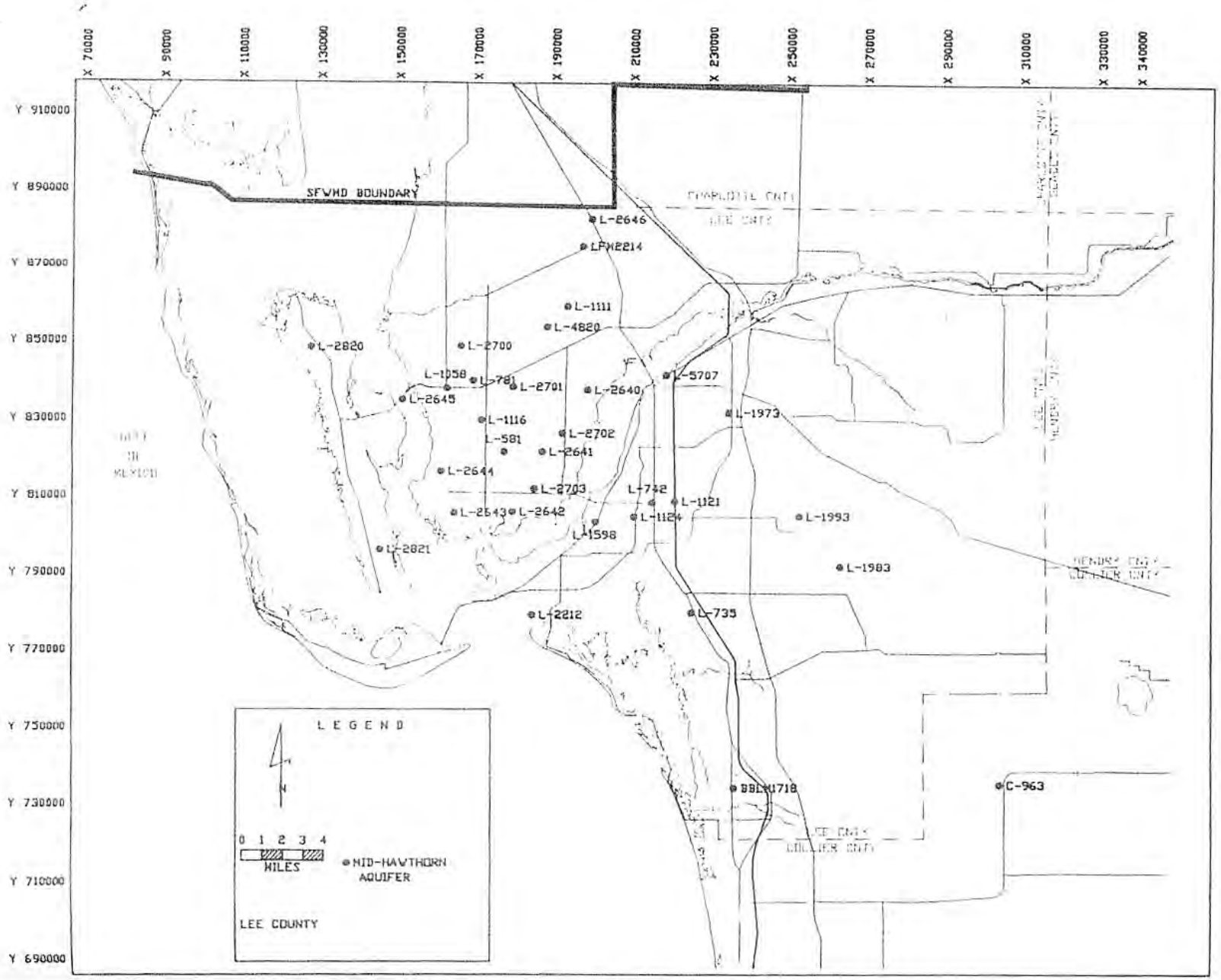

Figure B-4. LOCATION OF WATER LEVEL MONITORING WELLS, MID-HAWTHORN AQUIFER (LAYER 4)

Bower, R.F., K.M. Adams and J.I. Restrepo, 1990. A Three-Dimensional Finite Difference Ground Water Model of Lee County, Florida. Technical Publication 90-01, South Florida Water Management District, West Palm Beach, FL.

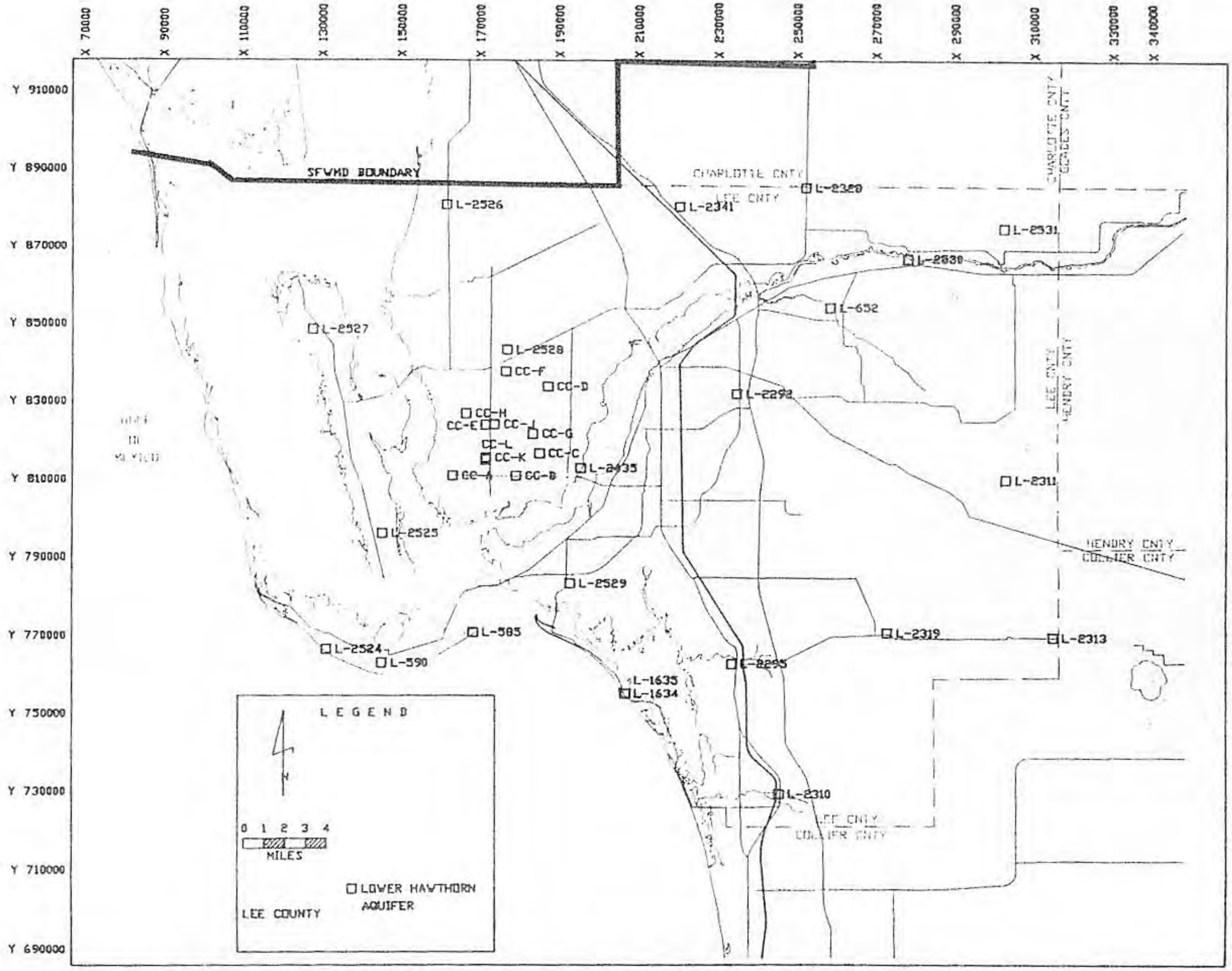

Figure B-5. LOCATION OF WATER LEVEL MONITORING WELLS, LOWER HAWTHORN AQUIFER (LAYER 5)

Bower, R.F., K.M. Adams and J.I. Restrepo, 1990. A Three-Dimensional Finite Difference Ground Water Model of Lee County, Florida. Technical Publication 90-01, South Florida Water Management District, West Palm Beach, FL.

APPENDIX C

Dispersion Database TM

Sub-Task No. 3 - Groundwater Dispersion Literature Search and Database for ASR Regional Study Groundwater Model Development

PREPARED FOR: U.S. Army Corp of Engineers-Jacksonville District and the South Florida Water Management District

PREPARED BY: CH2M HILL/Tampa, Florida

DATE: December 14, 2005

PROJECT NUMBER: 334350.TW.03

This technical memorandum (TM) has been prepared for the U.S. Army Corp of Engineers (USACE), Jacksonville District and the South Florida Water Management District (SFWMD) in support of the Comprehensive Everglades Restoration Project (CERP). The scope of work for this TM is based on Sub-Task 3 of the Aquifer Storage and Recovery (ASR) Test Well Work Plan Development and Model Data Collection (revised June 10, 2005) and provides documentation for the preparation of a groundwater dispersion database, provided herein. The goal of this research effort was to provide dispersion data on primarily sandstone and carbonate aquifers with a focus on technical sources from Florida and other similar geologic environments from the United States and other areas of the world. Based on the USACE's scope of work, technical papers, reports and other sources available to and obtained by CH2M HILL were reviewed and dispersion values were tabulated. In addition to the dispersion data, which was typically presented as longitudinal dispersivity, other pertinent information, where available, was also tabulated in the data base for comparative purposes. This supplemental aquifer data includes: transmissivity, storativity, transverse dispersivity, and molecular dispersivity, and aquifer name, matrix, thickness, and type.

The dispersion database is provided in Exhibit 1. Abstracts for each literature sources used in the development of the database are provided in Exhibit 2 and electronic copies (Adobe format) of published technical papers and reports are provided on compact disk (which includes the entire Sub-Task 3 deliverable) as Exhibit 3.

CH2M HILL conducted the initial literature reviews targeting sources for dispersion data for sandstones and carbonate aquifers. Dispersion values for other sedimentary, igneous and metamorphic aquifer matrixes have also been included and may be useful for evaluation of fractured flow through dolomite, where applicable.CH2M HILL was able to obtain dispersion data from primarily domestic technical publications, which were limited in number. To supplement dispersion data from foreign sources, CH2M HILL contracted Nerac, Inc., an outside research service. The combined research effort generated 40 literature sources from which the dispersion data was obtained and tabulated.

Very few of the documents had physical data on dispersivity based on tracer or other in-situ testing. Many of the dispersivity values presented in the cited literature were estimated, established from other sources, or the results of groundwater model calibration. It is also noted that the differences in the ranges of dispersivity values depend on how the coefficient was being used. The values based on large-scale model calibration were relatively high, while those based on matching results from single-well tracer tests were quite low. This illustrates that dispersivity is scale dependent and also dependent on its ultimate use in modeling or calculations. Essentially, dispersivity is a modeling calibration factor rather than an aquifer parameter. It depends not only on the nature of the aquifer materials, but also on the scale of the flow field and the scale at which it is being mathematically described.

Attachments:

1. Aquifer Dispersion Database
2. Technical Abstracts
3. Published Technical Papers (on Sub-Task 3 Final CD – December 2005)

Exibit 1

Aquifer Dispersion Database

AQUIFER DISPERSION DATABASE - NOVEMBER 2005

								Aquifer Parameters											
								Approx Depth	Thickness		Transmissivity		Storage		Dispersion				
								(m)	(m)		(m^2/d)		(dimensionless)		Longitudinal (m)		Transverse (m)		Molecular (m^2/s)	
No.	Date	Author	Title	Country	Aquifer Name	Aquifer Type	Aquifer Matrix		Min	Max	Min	Max	Min	Max	Min	Max	Min	Max	Min	Max
1	2005	Dirk Schulze-Makuch	*Longitudinal Dispersivity Data and Implications for Scaling Behavior* Abstract See (1)	USA			Fine to medium sand		2.000	3					3.9E-02	2.0E-01				
							Heterogeneous sediments		3,650						1.5E+01	1.5E+01				
				USA			Fluvial heterogeneous gravel & sands		26	234					1.6E+01	3.0E+01				
							Heterogeneous coarse sand and gravel silt & clay		8,800	8800					3.1E+01	3.1E+01				
							Med. Course sand with gravel and cobbles		350	350					1.0E+01	1.0E+01				
							Wausau sand		0.208	0					3.0E-04	3.0E-04				
							Ottawa sand		0.2072	0					1.1E-03	1.1E-03				
							Sand outwash deposits		1,000	1000					3.2E+00	3.2E+00				
							Med to coarse silica sand		0.114	0					1.2E-03	1.2E-03				
							Heterogeneous sediments		20	20					9.1E-02	9.1E-02				
				Denmark			Heterogeneous sand in an outwash plain		125	125					4.5E-01	4.5E-01				
							Sand and zeolite mix		0.9	1					1.2E-01	1.2E-01				
				USA			Coastal sandy aquifer		5	5					5.0E-02	2.5E-01				
							Sandy sediments		5.11	266					1.9E-01	5.5E-01				
				Canada			Fine to med uniform sand		6.5	7					7.0E-02	7.0E-02				
							Poorly sorted alluvial sand and gravel deposits		8.9	120					6.0E-01	1.1E+01				
							Glacio lacustrine sand		45	45					5.0E+01	5.0E+01				
							Sand with minor silt		130	130					1.0E+00	1.0E+00				
							Heterogeneous sand		0.15	2					4.7E-02	1.3E-01				
							Berea sandstone		0.229	0					1.9E-03	3.2E-03				
							Torpedo sandstone		0.235	0					6.4E-04	1.1E-03				
							Berea sandstone		0.6096	1					1.0E-03	5.9E-03				
							Fractured sandstone		0.24	0					6.0E-03	6.0E-03				
							Berea sandstone		1.22	1					2.7E-03	5.9E-03				
							St. Peter sandstone		0.035	0					1.5E-03	1.9E-03				
							Vugular limestone cores		0.094	0					9.4E-01	2.8E+00				
							Karstic limestone		3066	3100					1.2E+01	4.9E+01				
							Silurian dolomite		17.2	20					1.0E-01	6.3E-01				
				USA			Karstic limestone		914	987					2.8E+00	6.8E+00				
							Silurian dolomite		0.035	0					6.0E-03	4.5E-02				
							Silurian dolomite		597	597					3.7E+00	3.7E+00				
							Silurian dolomite		50.1	30					8.7E+00	1.1E+01				
				USA			Flood basalt		1	35000					1.0E-02	3.2E+01				
							Flood basalt		17	17					1.0E+00	1.0E+00				
				USA			Fractured basalt		6.1	21					6.0E-02	2.7E+00				
				USA			Fractured basalt		9.1	81					2.0E-01	5.0E+00				
							Layered basalt		100	100					7.6E+01	7.6E+01				
							Fractured granite		3	15					1.2E-02	1.2E+00				
				Sweden			Precambrian granite & gneiss		22	51					1.1E-01	2.1E-01				
				Spain			Fractured granite		14.5	22					3.4E+00	4.4E+01				
							Fractured granite		10.2	10					5.6E-01	5.6E-01				
				Sweden			Fractured granite		22	22					1.0E+00	1.0E+00				
							Fractured granite		11.2	346					2.5E-01	3.9E+00				
							Fractured granite		0.16	0					4.3E-02	9.5E-02				
							Densely fractured granite		14	26					9.0E-01	8.0E+00				
				Sweden			Fractured granite		10.7	43					1.8E+00	6.8E+00				

AQUIFER DISPERSION DATABASE - NOVEMBER 2005

								Aquifer Parameters											
								Approx Depth	Thickness		Transmissivity		Storage		Dispersion				
								(m)	(m)		(m^2/d)		(dimensionless)		Longitudinal (m)		Transverse (m)		Molecular (m^2/s)	
No.	Date	Author	Title	Country	Aquifer Name	Aquifer Type	Aquifer Matrix		Min	Max	Min	Max	Min	Max	Min	Max	Min	Max	Min	Max
2	1992	Ward, David S. el al	*Analysis of Ground-Water Flow and Injection Fluid Transport In the Floridan Aquifer near Pensacola, FL* Abstract See (2)	USA	Lower Floridan	Confined	Carbonate	450	18	18	7.9E+01	3.3E+02			1.0E+01	1.0E+01				
3	2005	USGS	*Analysis of Tests of Subsurface Injection, Storage, and Recovery in the Lower Floridan Aquifer, Okeechobee County, FL* Abstract See (3)	USA	Lower Floridan	Confined	Carbonate	337	132	132	7.1E+04	7.1E+04			1.0E+00	2.0E+00	1.0E-01	2.0E+00	5.0E-10	5.0E-10
					Middle Semi-confining unit	Semi-confined	Carbonate	350			6.6E+01	2.7E+02								
4	1993	Grubb, Stuart	*Analytical Model for Estimation of Steady-State Capture Zones of Pumping Wells in Confined and Unconfined Aquifers* Abstract See (4)																	
5	1993	Leap, Darrell I.	*Apparent Relative Retardation of Tritium and Bromide in Dolomite* Abstract See (5)	USA	Cambrian Bonanza King dolomite		Fractured Carbonate	191	3.1	3					2.7E+01	3.0E+01			1.0E-09	2.0E-09
6	1992	Lee, R.R. el al	*Aquifer Analysis and Modeling in a Fractured, Hetrogeneous Medium* Abstract See (6)	USA	Cambrian Age Conasauga Group	Unconfined	Interbedded limestone, siltstone, shale	33	6	6	3.1E-01	1.6E-01	0.0E+00	0.0E+00	1.0E+00	1.0E-01				
7	1997	Cohen, Robert M.	*Design guidelines For Conventional Pump-and-Treat Systems* Abstract See (7)	USA																
8	1999	Mallants, Dirk	*Dispersivity Estimates from a Tracer Experiment in a Sandy Aquifer* Abstract See (8)	Belgium	Mol Sands	Unconfirned	Quartz sand	5	20	20					9.0E-02	9.0E-02	8.5E-03	8.5E-03		
9	1999	Zanini, L.	*GroundWater Flow in a Fractured Carbonate Aquifer Inferred from Combined Hydrogeological and Geochemical Measurements* Abstract See (9)	Canada	Lockport Formation	Unconfined	Carbonate		55	55	1.0E-10	1.0E-02								
10	1996	Davis, Hal	*Hydrogeologic Investigation and Simulation of Ground-Water Flow in the Upper Floridan Aquifer of North-Central Florida and Southwestern Georgia and delineation of contributing areas for selected City of Tallahassee, Florida, water supply wells (WRI 95-4296)* Abstract See (10)	USA	Floridan Carbonate		Carbonate				6.6E+02	1.2E+05								
11	1999	Broska, James C.	*Hydrogeology and Analysis of Aquifer Characteristics in West-Central Pinellas County, Florida (OFR-99-18S)* Abstract (See 11)	USA	Upper Floridan	Confined	Carbonate	30.5-122	90	90	2.3E+02	3.5E+03	3.6E-05	3.1E-04	0.0E+00	0.0E+00	0.0E+00	0.0E+00		
12	1991		*Hydrogeology of Effluent Disposal Z ones, Floridan Aquifer, South Florida* Abstract (See 12)	USA	Floridan Boulder Zone	Confined	Carbonate	300-900	100	100	1.2E+04	5.0E+04	3.0E-04	2.0E-03						
13	2003	Shoemaker, W. Barclay	*Important Observations and Parameters for a Salt Water Intrusion Model* Abstract (See 13)	USA	Biscayne	Unconfined	Carbonate	1							5.0E+00	1.5E+01				

AQUIFER DISPERSION DATABASE - NOVEMBER 2005

								Aquifer Parameters											
								Approx Depth	Thickness		Transmissivity		Storage		Dispersion				
								(m)	(m)		(m^2/d)		(dimensionless)		Longitudinal (m)		Transverse (m)		Molecular (m^2/s)	
No.	Date	Author	Title	Country	Aquifer Name	Aquifer Type	Aquifer Matrix		Min	Max	Min	Max	Min	Max	Min	Max	Min	Max	Min	Max
14	1992	Bidaux, Pascal	*Calculation of Low-Range flow Velocities in Fractured Carbonate Media from Borehole Hydrochemical Logging Data Comparison with Thermometric Results* Abstract (See 14)	France	Surficial karst	unconfined	carbonate	60	30	30									2.0E-05	2.0E-05
15	2004	Castro, Maria C.	*Calculation of Ground Water Ages - A Comparative Analysis* *Supplemental Data from Ground-Water Resoources of the Carrizo Aquifer in the Winter Garden Area of Texas, Vol 1, Report 210* Abstract (See 15)	USA	Eocene Carrizo Aquifer	confined	sandstone/shale	170-1700	0	330	5.0E+02	2.5E+03	5.0E-04	5.0E-04	1.3E+02	1.3E+01			1.2E-09 3.8E-09	1.2E-09 3.8E-09
16	2000	Peng, Wei-Shyuan et al	*Can Contaminant Transport Models Predict Breakthrough?* Abstract (See 16)	USA	Unconsolidated sand aquifer	confined	sand	19	21.6	22	1.1E+03	1.1E+03	4.7E-04	6.9E-04	1.5E-01	1.5E-01	1.0E-02	5.0E-02	1.0E-09	1.0E-09
17	1994	Stoessell, Ronald K.	*Dampening of Transverse Dispersion in the Halocline in Karst Limestone in the Northeastern Yucaton Peninsula* Abstract (See 17)	Mexico	Surficial karst	unconfined	carbonate	1	48	56							2.0E-06	2.0E-06	1.5E-09	1.5E-09
18	1993	Jiao, Jiu J.	*Data Analysis Methods for Determining Two-dimensional Dispersive Parameters* Abstract (See 18)	Canada	surficial	unconfined									8.0E-02	3.0E-02				
19	1996	Knochenmus, Lari A.	*Description of Anisotropy and Heterogeneity and Their Effect on Ground-Water Flow and Areas of Contribution to Public Supply Wells in a Karst Carbonate Aquifer System (Water Supply Paper 2475)* Abstract (See 19)																	
20	1991	Leap, Darrell I.	*Influence of Pore Pressure on Apparent Dispersity of a Fissured Dolomitic Aquifer* Abstract (See 20)	USA	Cambrian Bonanza King Dolomite	unconfined	fissured carbonate	193	8.5	9	4.8E+03	1.1E+04	5.0E-04	5.0E-04	2.7E+01	3.1E+01				
21	2002	Reese, Ronald S.	*Inventory and Review of Aquifer Storage and Recovery in Southern Florida* Abstract (See 21)	USA	Upper Floridan	confined	carbonate		152	366	7.4E+01	1.0E+04			6.1E-01 0.0E+00	9.1E+00 3.0E+00	0.0E+00	3.0E+01		
22	1997	Yobbi, Dann K.	*Simulation of Subsurface Storage and Recovery of Effluent Using Multiple Wells, St. Petersburg, Florida* Abstract (See 22)	USA	Upper Floridan	confined	carbonate	50	305	305	4.6E+02	1.1E+05	7.8E-04	3.3E-04	7.6E+00	7.6E+00	1.5E+00	1.5E+00	9.9E-11	9.9E-11
23	1996	Yobbi, Dann K.	*Simulation of Subsurface Storage and Recovery of Treated Effluent Injected in a Saline Aquifer, St. Petersburg, Florida* Abstract (See 23)	USA	Upper Floridan	confined	carbonate	30	55	55	2.0E+03	3.2E+03	4.0E-04	8.0E-04	3.8E+00	3.8E+00	7.6E-01	7.6E-01	9.9E-11	9.9E-11
24	1997	Merritt, Michael L.	*Tests of Subsurface Storage or Freshwater at Hialeah, Dade County, Florida, and Numerical Simulation of the Salinity of Recovered Water* Abstract (See 24)	USA	Upper Florida	confined	carbonate	309	3.7	6	1.0E+03	1.0E+03	7.8E-05	7.8E-05	2.0E+01	2.0E+01			2.1E-05	2.1E-05

AQUIFER DISPERSION DATABASE - NOVEMBER 2005

								Aquifer Parameters											
								Approx Depth	Thickness		Transmissivity		Storage		Dispersion				
								(m)	(m)		(m^2/d)		(dimensionless)		Longitudinal (m)		Transverse (m)		Molecular (m^2/s)	
No.	Date	Author	Title	Country	Aquifer Name	Aquifer Type	Aquifer Matrix		Min	Max	Min	Max	Min	Max	Min	Max	Min	Max	Min	Max
25	1993	Mutch, Robert D.	*The Impact of Matrix Diffusion on the Cleanup of Fractured Igneous, Metamorphic and Sedimentary Rock Aquifers* Abstract (See 25)	USA, UK, Canada, Sweden, Western Europe	Conasauga shale, Nolichvcky shale, Culebra dolomite, Queenston shale	fractured	igneous/metamorphic/sedimentary								5.0E+00	5.0E+00			3.1E-11	3.1E-11
26	1997	Katz, Brian G	*Use of Chemical and Isotopic Tracers to Characterize the Interactions Between Groundwater and Surface Water in Mantled Karst* Abstract (See 26)	USA	Upper Floridan	confined	carbonate karst													
27	2003	Shoemaker, W. Barclay	*Potential for Saltwater Intrusion into the Lower Tamiami Aquifer near Bonita Springs, Southwestern Florida* Abstract (See 27)	USA	surficial	unconfined	carbonate		6	30	2.4E+02	1.8E+04	1.0E-08	1.0E-08	0.0E+00	0.0E+00				
28	1995	Quiñones-Aponte, Vincente	*Preliminary Assessment of Injection, Storage, and Recovery of Freshwater in the Lower Hawthorn Aquifer, Cape Coral, Florida* Abstract (See 28)	USA	Hawthorn Intermediate Aquifer System	confined	carbonate/sandstone	128-188	60	60	7.5E-04	8.6E-04	$1x10^{-4}$	$1x10^{-4}$	3.0E+00	5.0E+00	3.0E-01	5.0E-01	5.0E-10	5.0E-10
29	2004	Birk, Steffn	*Process-Based Interpretation of Tracer Tests in Carbonate Aquifers* Abstract (See 29)	Germany	Gallusquelle Catchment	unconfined	carbonate		5	5	4.3E+01	4.3E+01	1.0E-02	1.0E-02	4.4E+00	6.9E+00			0.010-0.14	0.010-0.14
30	1985	Merritt, Michael L.	*Recovering Fresh Water Stored in Saline Limestone Aquifers* Abstract (See 30)	USA	Floridan	confined	carbonate	291	50	50					1.2E+00	1.2E+00	0.0E+00	0.0E+00	1.0E-09	1.0E-09
31	1998	Dunnivant, Frank M.	*Water and Radioactive Tracer Flow in a Heterogeneous Field-Scale System* Abstract (See 31)	USA	Snake River Plain Aquifer	unconfined	Fractured basalt	190	237	237	1.1E+05	7.3E+05	1.8E-01	2.3E-02	1.0E-01	4.6E+01			7.5E-01	2.1E+02
32	1996	CH2M HILL	*Predictive Modeling Results for the City of St. Petersburg's Deep Injection Well System* (and associated technical memorandums) Abstract (See 32)	USA	Hawthorn Group	confined	carbonate	10	50	50	1.1E+00	1.0E-02	3.1E-05	3.1E-05	1.5E+01	3.8E+00	3.0E+00	7.6E-01	9.6E-13	9.6E-13
					Floridan Aquifer Tampa Member Zone A	confined	carbonate	20	38	38	1.9E+03	1.4E+03	1.6E-06	1.6E-06	1.5E+01	3.8E+00	3.0E+00	7.6E-01	9.6E-13	9.6E-13
					Floridan Aquifer Suwannee Limestone Semi-confining Unit A/B	confined	carbonate	60	40	40	6.0E+00	1.2E+00	1.2E-06	1.2E-06	1.5E+01	3.8E+00	3.0E+00	7.6E-01	9.6E-13	9.6E-13
					Floridan Aquifer Suwannee Limestone Permeable Unit A/BB	confined	carbonate	100	30	30					1.5E+01	3.8E+00	3.0E+00	7.6E-01	9.6E-13	9.6E-13
					Floridan Aquifer Suwannee Limestone Zone B	confined	carbonate	130	10	10	5.5E+02	5.5E+02	1.2E-06	1.2E-06	1.5E+01	3.8E+00	3.0E+00	7.6E-01	9.6E-13	9.6E-13
					Floridan Aquifer Ocala Limestone Semi-confining Unit B/C	confined	carbonate	140	70	70	1.1E+02	1.1E+01			1.5E+01	3.8E+00	3.0E+00	7.6E-01	9.6E-13	9.6E-13
					Floridan Aquifer Avon Park Formation Zone C	confined	carbonate	210	100	100	2.5E+05	7.6E+04	1.0E-06	1.0E-06	1.5E+01	3.8E+00	3.0E+00	7.6E-01	9.6E-13	9.6E-13

AQUIFER DISPERSION DATABASE - NOVEMBER 2005

								Aquifer Parameters											
								Approx Depth	Thickness		Transmissivity		Storage		Dispersion				
								(m)	(m)		(m^2/d)		(dimensionless)		Longitudinal (m)		Transverse (m)		Molecular (m^2/s)	
No.	Date	Author	Title	Country	Aquifer Name	Aquifer Type	Aquifer Matrix		Min	Max	Min	Max	Min	Max	Min	Max	Min	Max	Min	Max
33	1992	Gelhar, Lynn W.	*A Critical Review of Data on Field-Scale Dispersion in Aquifers* Abstract (See 33)	USA			Very heterogeneous sand and gravel		8	8	6.9E+00	6.9E+02			7.5E+00	7.5E+00				
				USA			Glaciofluviatile sand and gravels		64	64	3.2E+03	1.7E+05			3.1E+01	1.8E+01				
				USA			Fractured dolomite		5.5	6					5.2E+00	5.2E+00				
				USA			Glaciofluviatile sands and gravels		64	64	1.5E+05	1.5E+05			6.0E+00	4.6E+02				
				USA			Limestone		50	50	5.6E-02	7.4E-02			1.7E+02	5.2E+01				
				USA			Fractured dolomite and limestone		15	15	4.3E+03	9.5E+03			1.5E+01	1.5E+01				
				USA			Alluvium (tuff)		500	500	7.3E+03	7.3E+03			1.0E+01	3.0E+01				
				France			Fractured granite		20	20	5.2E+03	1.6E+03			5.0E-01	5.0E-01				
				France			Alluvial Deposites		6	6	1.6E+02	1.6E+02			3.0E+00	3.0E+00				
				USA			Glaciofluvial sand		7	27	6.0E-02	2.3E+01			3.0E+01	6.0E+01				
				USA			Limestone		53	53	2.2E+01	2.2E+01			1.2E+01	1.2E+01				
				USA			Glaciofluvial sand		9	9	5.6E+01	5.6E+01			4.3E-01	4.3E-01	3.9E-02	3.9E-02		
				France	Rhine aquifer		sand, gravel and cobbles		12	12					1.1E+01	1.1E+01				
				France	Rhine aquifer		alluvial-sand, gravel & pebbles w clay lenses		125	125	1.1E+04	1.1E+04			1.5E+01	1.0E+00				
				France			gravel and slightly stratified clay lenses		20	20					1.2E+01	4.0E+00				
				USA			med. coarse sand with gravel		70	70	7.9E+02	7.9E+02			9.6E-01	1.8E-02				
				USA			Brecciated basalt interflow zone								6.0E-01	6.0E-01				
				France			Fractured granite		50	50	4.3E+01	4.3E+01			2.0E+00	2.0E+00				
				USA			Basaltic lava and sediments		76	76	1.2E+04	1.2E-06			9.1E+01	9.1E+01				
				USA			Fractured dolomite		12	12					3.8E+01	3.8E+01				
				USA			Sandstone, shale, sand and alluvial sediments								8.0E+01	2.0E+02	8.0E+00	2.0E+01		
				Israel			dolomite		100	100					6.0E+00	6.0E+00				
				USA			Sandstone w/silt and clay layers		90	90					1.0E-01	1.0E+00				
				Switzerland			Layered gravel and silty sand		25	25	2.0E+03	1.4E+04			4.0E-02	7.0E-01				
				Switzerland			Layered gravel and silty sand		25.5	26	1.9E+02	1.6E+04			1.1E+00	5.8E+01				
				USA			Layered med. sand		21.6	22					4.0E+00	4.0E+00				
				France			Alluvial deposits		9	9	3.1E+02	3.1E+02			3.0E+00	1.5E+00				
				England			Fractured chalk								3.1E+00	3.1E+00				
				England			Chalk								1.0E+00	1.0E+00				
				USA			Fluvial Sands								1.6E+00	7.6E-01				
				Germany			Fluvioglacial gravels		14	14					1.9E+00	5.0E+00				
				USA			Alluvium								3.1E+01	3.1E+01				
				USA			Allvium, inhomogeneous clay, silt, sand, and gravel								3.1E+01	9.1E+00				
				Poland			sand		2.5	3	6.7E+00	3.2E+01			1.8E-01	1.8E-01				
				Poland			Fractured dolomite		57	57	1.2E+03	2.3E+03			4.4E+01	1.1E+02				
				Poland			Fractured dolomite		48	48	1.0E+03	1.9E+03			2.1E+00	2.1E+00				
				Poland			Limestone		7	7	6.7E+01	6.7E+01			2.7E+00	2.7E+01				
				Poland			Limestone		7	7	6.7E+01	6.7E+01			2.1E+01	2.1E+01				
				USA			Sand and gravel with clay lenses		1.5	2	1.2E+02	1.2E+02			2.0E+00	3.0E+00				

AQUIFER DISPERSION DATABASE - NOVEMBER 2005

								Aquifer Parameters											
								Approx Depth	Thickness		Transmissivity		Storage		Dispersion				
								(m)	(m)		(m^2/d)		(dimensionless)		Longitudinal (m)		Transverse (m)		Molecular (m^2/s)	
No.	Date	Author	Title	Country	Aquifer Name	Aquifer Type	Aquifer Matrix		Min	Max	Min	Max	Min	Max	Min	Max	Min	Max	Min	Max
				Canada			Sand								5.0E-02	7.0E-02				
				USA			Fine sand and glacial till		0.75	1	1.6E+00	1.9E+00			5.0E-02	7.0E-02				
				Israel			Sand and sandstone with some clay		80	80	1.8E-03	2.1E-03			5.0E-01	1.5E+00				
				South America			Sand		20	20					1.0E-02	4.2E-01				
				France			Sand		3	3	7.2E+01	9.5E+01			1.1E-01	2.7E+00				
				USA			Fluvial sand								6.0E-02	1.6E-01				
				USA			Unconsolidated sand and gravel		27	27	1.9E+03	3.7E+03			2.1E+00	3.4E+00	6.1E-01	9.2E-01		
				New Zealand			Gravel w/cobbles		100	100	2.5E+04	2.5E+04			1.4E+00	1.2E+01	1.0E-01	3.3E+00		
				New Zealand			Alluvium (gravels)		120	120	3.2E+04	3.2E+04			3.0E-01	1.5E+00				
				New Zealand			Alluvium (gravels)								4.1E+01	1.0E+01				
				United Kingdom			Sandstone		44	44	9.1E+00	5.3E+02			1.6E-01	6.0E-01				
				USA			Med. to fine sand interspersed w/clay and silt		2	2	9.1E+02	9.1E+02			1.5E+00	1.5E+00				
				USA			Sand		8.5	9	1.5E+01	1.5E+02			5.0E-01	5.0E-01				
				USA			Sand		8.5	9	1.5E+01	1.5E+02			3.0E-02	3.0E-02				
				USA			Glacial outwash		43	43	2.8E+03	2.8E+03			2.1E+01	4.2E+00				
				USA			Fractured limestone		6	6	9.5E+02	2.5E+04			2.0E+01	2.3E+01				
				USA			Glaciofluvial sand		9	9	5.6E+01	5.6E+01			5.0E-01	5.0E-02				
				USA			Sand, gravel and silt		2	2	4.3E+01	1.1E+02			2.0E+00	1.1E+01				
				USA			Basaltic lava and sediments		76	76	1.2E+04	1.2E+06			9.1E+02	1.4E+03				
				USA			Alluvial sediments		27	27	1.8E+01	8.6E+02			15.2-61	1.8E+01				
				USA			Alluvial sediments		305	305	1.3E+03	1.3E+03			6.1E+01	6.1E+01				
				France			Clay, sand and gravel		12	12	6.7E+03	1.6E+04			3.0E-01	6.9E+00				
				France			Sand and gravel		12	12					1.3E+00	2.5E+01				
				France			Sand		3	3	7.2E+01	9.5E+01			1.0E+00	1.0E+00				
				USA			Fractured limestone and calcareous sandstone		30.5	31	1.2E+04	1.2E+04			6.7E+00	6.7E+00				
				USA			Glaciofluvial sand		7	27	1.1E+02	4.6E+01			1.0E-02	8.0E-01	5.0E-03	3.0E-02		
				USA			sand								7.6E+00	7.6E+00				
				USA			sand, silt and clay		21	21	9.1E+02	9.1E+02			7.6E-01	7.6E-01				
				USA			Glaciofluvial sand and gravel		152	152	7.8E+00	5.6E+05			9.1E+01	2.7E+01				
				USA			Sand, gravel and silt		2	2	4.3E+01	1.1E+02			1.0E+00	1.0E-01				
				USA			Fractured dolomite		7	7	6.9E+00	6.9E+00			1.0E+01	1.5E+01				
				USA			Crystalline, fractured Schist and Gneiss		76	76	2.4E+00	2.4E+00			1.3E+02	1.3E+02				
				Switzerland			Gravel		20	20	1.0E+04	1.0E+04			1.3E+02	2.3E+02				
				Australia			Sand and gravel		6.1	6	2.9E+03	2.9E+03			2.6E-01	2.6E-01				
				USA			Unconsolidated gravel, sand, and silt				5.0E+02	5.0E+02			5.5E-01	1.5E+01				
				USA			Sand		1000	1000	2.5E+01	7.5E+01			5.6E+03	4.0E+04				
				USA			Sand and gravel		17	17	2.8E+02	3.8E+02			1.5E-02	1.5E-02				

AQUIFER DISPERSION DATABASE - NOVEMBER 2005

								Aquifer Parameters											
								Approx Depth	Thickness		Transmissivity		Storage		Dispersion				
								(m)	(m)		(m^2/d)		(dimensionless)		Longitudinal (m)		Transverse (m)		Molecular (m^2/s)	
No.	Date	Author	Title	Country	Aquifer Name	Aquifer Type	Aquifer Matrix		Min	Max	Min	Max	Min	Max	Min	Max	Min	Max	Min	Max
34	2002	Gale, I.N.	ASR-UK: Elucidating the Hydrogeological Issues Associated with Aquifer Storage and Recovery in the UK Abstract (See 34)	UK	Lincolnshire Limestone		Carbonate		10	40									1.0E-09	1.0E-09
					Chalk		Carbonate		50	200									1.0E-09	1.0E-09
					Sherwood Sandstone		Sandstone		50	300									1.0E-09	1.0E-09
					Lower Greensand		Sandstone		10	40									1.0E-09	1.0E-09
35	2001	Bender, A.	*Results from a Forced Gradient Tracer Test in a Fractured Aquifer with Simultaneous Input of Different Tracers*	Germany	Middle Buntsandstein Formation															
					First/Second		Multi-layered sand, clay and siltstones	4	8	10	$8x10^{-4}$	$1x10^{-3}$			5.0E+00	1.0E+01				
					Third		Multi-layered sand, clay and siltstones		10	10	$1x10^{-4}$	$1x10^{-4}$			1.0E+01	5.0E+01				
36	2002	Sanford, William E.	*Analysis of a Vertical Dipole Tracer Test in Highly Fractured Rock*	Australia	Saddleworth formation		Highly Fractured Metadolostone	6	21	21					1.7E-01	2.5E-01			$2.01x10^{-9}$	$7.22x10^{-9}$
37	1981	Gonzalez, D.D.	*Field Test for Efffective Porosity and Dispersivity in Fractured Dolomite, The Wipp Southeastern New Mexico*	USA	Magenta Dolomite Member	confined	fractured dolomite	172			1.0E-02	1.0E-02								
					Culebra dolomite member	confined	fractured dolomite	202			6.0E-02	6.0E-02	1.3x10-5	1.3x10-5	4.0E+00	5.2E+00				
					Rustler-salado contact	confined	Halitic dissolution residue	227			1.0E+00	$1x10^{-5}$								
38	2000	Davis, G.B.	*Deuterated Tracers for Assessing Natural Attenuation in Contaminated Groundwater*	Australia			Sand								3.4E-03	2.6E-02				
39	2000	Vereecken, H.	*Analysis of Solute Transport in a Heterogeneous Aquifer: The Krauthausen Field Experiment*	Germany	RUR sediments, upper rhine sediments, lower rhine sediments	unconfined	Hertergeneous sediments	13	10	13					3.6E+00	7.2E+00				
40	1981	Iserwood, D.	*Geoscience Database Handbook for Modeling A Nuclear Waste Repository*	Canada	Alluvial aquifer												3.4E-02			
				France	Alluvial aquifer												1.0E-01	5.0E-01		
				USA			Fractured dolomite										3.8E+01			
				USA			fractured schistgneiss								1.3E+02					
				USA			alluvial sediments								1.5E+00					
				England			fractured chalk								3.1E+00					
							intack chalk								1.0E+00					
				USA			sand/gravel										2.0E+00	3.0E+00		
				USA			Mississippi limestone								1.2E+01					
				USA			carbonate aquifer								1.5E+01					
				USA			alluvial sediments								3.1E+01		3.1E+01			
				USA			alluvial sediments								3.1E+01		9.1E+00			
				USA											3.1E+01		9.1E+00			
				USA			alluvial sediments								8.0E+01	2.0E+02	8.0E+00	2.0E+01		
				USA			glacial deposits								2.1E+01		4.3E+00			
				USA			limestone								6.1E+01		2.0E+01			
				USA			fractured basalt								9.1E+01		1.4E+02			
				USA			fractured basalt								9.1E+01		9.1E+01			
				USA			fractured basalt								3.1E+01		1.8E+01			
				USA			alluvial sediments								6.1E+01		1.8E-01			
				France			alluvial sediments								1.5E+01		1.0E+00			
				Canada			glacial till								3.0E+00	6.1E+00	6.0E-01	1.2E+00		
				USA											6.7E+00		7.0E-01			
				USA			alluvial deposits								6.1E+01		1.8E+01			
				France			alluvial aquifer								1.2E+01		4.0E+00			
				USA			limestone								2.1E+01					
				USA			lava flows and sediments								9.1E+01		1.4E+02			

AQUIFER DISPERSION DATABASE - NOVEMBER 2005

								Aquifer Parameters											
								Approx Depth	Thickness		Transmissivity		Storage		Dispersion				
								(m)	(m)		(m^2/d)		(dimensionless)		Longitudinal (m)		Transverse (m)		Molecular (m^2/s)	
No.	Date	Author	Title	Country	Aquifer Name	Aquifer Type	Aquifer Matrix		Min	Max	Min	Max	Min	Max	Min	Max	Min	Max	Min	Max
41	2002	HydroGeoLogic, Inc.	*Three-Dimensional Density-Dependant Flow and Transport Modeling of Saltwater Intrusion in the Southern Water Use Caution Area*	USA	Suwannee Limestone	confined	Carbonate								1.0E+02		2.0E+01			
					Ocala Limestone	confined	Carbonate								1.0E+01		5.0E+00			
					Avon Park Formation	confined	Carbonate								8.0E+01		1.5E+01			

Exibit 2

Technical Abstracts

Groundwater Dispersion Literature Search Abstracts

(1) Abstract: Longitudinal Dispersivity Data and Implications for Scaling Behavior. Dirk Schulze-Makuch. 2005.

Longitudinal dispersivity data were compiled from 109 different authors for different types of geological media. The data were subdivided into different subsets. Dispersivity values for consolidated media were subdivided as basalts, granites, sandstones, and carbonate rocks, while unconsolidated sediments were subdivided into three reliability classes. The datasets provided here may provide groundwater practitioners a preliminary guide to estimate dispersivity values at various scales and to guide and verify theories on scaling behavior. Based on the dataset presented here, the relationship that empirically best described the dispersivity data in regard to scale of measurement was in the form of a power law. The scaling exponent for consolidated and unconsolidated geological media varied between 0.40 and 0.92, and 0.44 and 0.94, respectively. Higher reliability subsets of data for the unconsolidated sediments and more frequently tested rock formations indicate that the scaling exponent is at the lower end of the observed range, close to 0.5. No significant difference in scaling exponent was found among different media, and no clear evidence exists for the presence of an upperbound or asymptotic behavior on the relationship for any of the analyzed media.

(2) Abstract: Analysis of Ground-Water Flow and Injection Fluid Transport in the Floridan Aquifer near Pensacola, FL. Ward, David S., et al. 1992.

Liquid waste has been injected into a permeable part of the lower limestone of the Floridan aquifer since 1963, raising hydraulic head in the injection zone throughout a region of northwestern Florida. The injection zone consists of a moderately permeable limestone, hydraulically isolated from overlying aquifers by a thick layer of clay. The formation fluid is saline, but becomes fresher up dip, northward where the limestone crops out. Numerical simulations were performed at regional and local scales to assess the regional pressure increase, to analyze the movement of the 10,000 mg/l total dissolved solids (TDS) isopleth (formation fluid) in the lower limestone of the Floridan aquifer, and to analyze the migration of the injection fluid, both historically and predictively, in the injection formation. This work is based largely on previous work by Merritt (1984), but uses the SWIFT code. Modifications to Merritt's work include increasing the hydraulic conductivity near the injection wells and using more recent injection rates; extensions include particle tracking and solute transport modeling. The simulations indicate that regional pressure increases should be much less than previously predicted. Using the new results, by the year 2033, the average movement of the 10,000 mg/l TDS isopleth due to injection is expected to be approximately 2200 ft (671 in). Additionally, by the year 2033, the undiluted injection fluid (95% of injection concentration) should migrate to an approximate diameter of 2.1 mi (3.4 km) from the injection wells.

(3) Abstract: Analysis of Tests of Subsurface Injection, Storage, and Recovery in the Lower Floridan Aquifer, Okeechobee County, FL. USGS. 2005.

The analysis of capture zones of pumping wells is useful for designing pumping systems and wellhead protection programs. Using discharge potentials, equations are derived that can be applied to confined, unconfined, or combined confined and unconfined aquifers. The transient equations

are transcendental and cannot be solved explicitly. However, infinite-time (steady-state) equations are presented which can be solved. They define an area in which, theoretically, all the water in the aquifer will eventually reach the pumping well, although the equations do not consider the effects of hydrodynamic dispersion. Equations for calculating the stagnation point, upgradient divide, and dividing streamline within the aquifer and an example problem are presented.

(4) Analytical Model for Estimation of Steady-State Capture Zones of Pumping Wells in Confined and Unconfined Aquifers. Grubb, Start. 1993.

The analysis of capture zones of pumping wells is useful for designing pumping systems and wellhead protection programs. Using discharge potentials, equations are derived that can be applied to confined, unconfined, or combined confined and unconfined aquifers. The transient equations are transcendental and cannot be solved explicitly. However, infinite-time (steady-state) equations are presented which can be solved. They define an area in which, theoretically, all the water in the aquifer will eventually reach the pumping well, although the equations do not consider the effects of hydrodynamic dispersion. Equations for calculating the stagnation point, upgradient divide, and dividing streamline within the aquifer and an example problem are presented.

(5) Apparent Relative Retardation of Tritium and Bromide in dolomite. Leap, Darrell I. 1993.

In order to determine the suitability of bromide as a surrogate for tritium for ground-water tracing in fractured and fissured dolomite, apparent relative retardation coefficients of bromide with respect to tritium were computed by the cumulative relative mass-time method from breakthrough curves of both substances, when used simultaneously as tracers in a two-well recirculating tracer test. Throughout the 33.78-day test, relative retardation differences of only a few hundredths were detected for most of the testing time.

Tritium was less retarded in flow through highly transmissive openings than in more diffuse flow. Bromide was generally retarded relative to tritium except at the pumping well where the concentrations of both were diluted an order of magnitude below those in the monitoring wells, and tritium was retarded slightly more than bromide.

Apparent relative retardation was found to change with transmissivity, concentration, flow-path length and time, but not enough to rule out bromide as a suitable surrogate for, or even better than, tritium in dolomite if the limitations of each tracer are known.

(6) Aquifer Analysis and Modeling in a Fractured, Hetrogeneous Medium. Lee, R.R. et al. 1992.

A ground-water flow and contaminant transport modeling study was performed at a proposed low-level radioactive waste disposal site on the Department of Energy's Oak Ridge Reservation to assess the accuracy of a computer simulation of the flow field in the shallow water-table aquifer. The migration of a ground-water tracer, under controlled field conditions, was used as a

comparative benchmark of solute transport simulations assuming different aquifer characteristics. A conventional approach to aquifer analysis and modeling, which assumed the domain to be homogeneous with low anisotropy, resulted in an inaccurate simulation of tracer migration. Alternative conceptual models were formulated which considered the effects of geologic heterogeneities on tracer migration which could be verified by additional data acquisition and analysis. Application of the alternative concepts in numerical modeling resulted in more accurate simulations of tracer migration. These results suggested that local geology created discrete flow pathways oriented oblique to the maximum gradient which were unresolved in conventional aquifer analysis. Results of the study showed that standard approaches to aquifer analysis and computer modeling are crudely representative of the flow field and provide nonconservative estimates of contaminant transport at the scale of a waste disposal unit. By adopting an iterative approach to site characterization, conceptual model formulation, and numerical modeling, the level of resolution provided by a ground-water tracer was accurately simulated.

(7) Design Guidelines for Conventional Pump-and-Treat Systems. Cohen, Robert M. 1997.

The RCRA/Superfund Ground-Water Forum is a group of scientists representing EPA's Regional Superfund Offices, committed to the identification and resolution of ground-water issues affecting the remediation of Superfund sites. Design of conventional ground-water extraction and injection (i.e., pump-and-treat) systems has been identified by the Forum as an issue of concern to decision makers. This issue paper focuses on design of conventional ground-water extraction and injection systems used in subsurface remediation.

(8) Dispersivity Estimates from a Tracer Experiment in a Sandy Aquifer. Mallants, Dirk. 1999.

The success or failure of transport models in predicting the migration of a contaminant plume in ground water depends to a large extent on the quality of flow and transport parameters used. In this study, we investigate the spatial variability in the tracer velocity and dispersivity in a shallow sandy aquifer in northern Belgium. Based on hydraulic conductivity measurements on cores sampled along a vertical profile, the aquifer was found to be mildly heterogeneous, i.e., with the variance of the log-transformed conductivity K, 62i.,K, equal to 0.22. By means of a natural gradient tracer experiment, transport of a chloride tracer was investigated in a three-dimensional network of multilevel point samplers (MLS). Least squares fitting of a two-dimensional transport model to the individual breakthrough curves resulted in an average longitudinal dispersivity that was 10 times larger than the transverse dispersivity. The results further showed the existence of a dispersion-scale effect whereby the depth-averaged longitudinal dispersivity increases with increasing travel distance. The average longitudinal dispersivity corresponding to a travel distance of 10 m was equal to 0.2 m. We finally show that theoretical expressions for the macroscopic dispersivity tensor, which require input on hydraulic conductivity heterogeneity, could be used here to approximate the observed dispersive behavior. These conceptually simple models are useful to estimate macroscopic dispersivities when no tracer data are available.

(9) GroundWater Flow in a Fractured Carbonate Aquifer Inferred from Combined Hydrogeological and Geochemical Measurements. Zanini, L. 1999.

A conceptual model for ground water flow is presented for a fractured Silurian dolomite in the Niagara Escarpment area of southern Ontario. Such a model is necessary to facilitate remedial efforts of a PCB-contaminated site located in Smithville, Ontario. Both physical and chemical hydrogeological observations obtained from field investigations were used to deduce the structure of the ground water flow system in the fracture network. The field study was conducted using observations obtained from six bore holes drilled in the vicinity of the town of Smithville. The boreholes were diamond cored through the entire thickness of the dolomite formation (approximately 45 m), hydraulically tested using a 2 m packer spacing and then completed using multipacker casing strings. Measurements of hydraulic head were obtained on a weekly basis over a period of two years, and ground water from each borehole interval was collected for geochemical analyses for inorganic and isotopic composition. Transmissivity measurements indicate that the dolomite is divided into two ground water flow systems separated by an extensive unit of low transmissivity that is pervasive throughout the region. The upper flow system is characterized by water enriched in Mg^{2+} and $S0_4^{2-}$. Below the low transmissivity zone, ground water increases in salinity and is enriched in Cat^{2+} and $S0_4^{2-}$. Based on the geochemistry, the rate of ground water migration in the lower flow system is surmised to be much less than that in the upper system. Measurements of hydraulic head in conjunction with the results of the analyses of the environmental isotopes ($\delta^{18}O$ and $\delta^{2}H$) suggest that ground water flow is mainly horizontal and likely governed by enlarged bedding plane fractures. The isotope geochemistry and topographical features further suggest that ground water recharge is occurring approximately 2 km to the north of Smithville.

(10) Hydrogeologic Investigation and Simulation of Ground-Water Flow in the Upper Floridan Aquifer of North-Central Florida and Southwestern Georgia and delineation of contributing areas for selected City of Tallahassee, Florida, Water Supply Wells (WRI 95-4296). Davis, Hal. 1996.

A 4-year investigation of the Upper Floridan aquifer and ground-water flow system in Leon County, Florida, and surrounding counties of north-central Florida and southwestern Georgia began in 1990. The purpose of the investigation was to describe the ground-water flow system to delineate the contributing areas to selected City of Tallahassee, Florida, water-supply wells. The investigation was prompted by the detection low levels of tetrachloroethylene in ground-water samples collected from several of the city's water supply wells.

Hydrologic data and previous studies indicate that; ground-water flow within the Upper Floridan aquifer can be considered steady-state; the Upper Floridan aquifer is a single water-bearing unit; recharge is from precipitation; and that discharge occurs as spring flow, leakage rivers, leakage to the Gulf of Mexico, and pumpage. Measured transmissivities of the aquifer ranged from 1,300 ft^2/d (feet squared per day) to 1,300,000 ft^2/d.

Steady-state ground-water flow in the Upper Floridan aquifer was simulated using a three-dimensional ground-water flow model. Transmissivities ranging from less than 5,000 ft^2/d to greater than 11,000,000 ft^2/d were required to calibrate to observed conditions. Recharge rates used

in the model ranged from 18.0 inches per year in areas where the aquifer was unconfined to less than 2 inches per year in broad areas where the aquifer was confined.

Contributing areas to five Tallahassee water-supply wells were simulated by particle-tracking techniques. Particles were seeded in model cells containing pumping wells then tracked backwards in time toward recharge areas. The contributing area for each well was simulated twice, once assuming a porosity of 25 percent and once assuming a porosity of 5 percent. A porosity of 25 percent is considered a reasonable average value for the Upper Floridan aquifer; the 5 percent porosity simulated the movement of ground-water through only solution-enhanced bedding plains and fractures. The contributing areas were generally elliptical in shape, reflecting the influence of the sloping potentiometric surface. The contributing areas delineated for a 5 percent porosity were always much larger than those determined using a 25 percent porosity. The lowest average ground-water velocity computed within a contributing area, using a 25 percent porosity, was 1.0 ft/d (foot per day) and the highest velocity was 1.6 ft/d. The lowest average ground-water velocity, determined using a 5 percent porosity, was 2.4 ft/d and the highest was 7.4 ft/d.

The contributing areas for each of the five wells was also determined analytically and compared to the model-derived areas. The upgradient width of the simulated contributing areas were larger than the upgradient width of the analytically determined contributing areas for four of the five wells. The model could more accurately delineate contributing areas because of the ability to simulate wells as partially penetrating and by incorporating complex, three-dimensional aquifer characteristics, which the analytical method could not.

(11) Hydrogeology and Analysis of Aquifer Characteristics in West-Central Pinellas County, Florida (OFR-99-18s). Broska, James C. 1999.

The U.S. Geological Survey, in cooperation with Pinellas County, Florida, conducted an investigation to describe the hydrogeology and analyze the aquifer characteristics in west-central Pinellas County. A production test well and four monitor wells were constructed in Pinellas County at Walsingham Park during 1996-97. Water-quality sampling, static and dynamic borehole geophysical surveys, and hydraulic tests were conducted at the wells to delineate the hydrogeology at Walsingham Park. A 9-day aquifer test was conducted to determine the hydraulic characteristics of the aquifer system and observe the changes in water quality due to pumping.

A numerical model was constructed to simulate the aquifer test and calculate values for hydraulic conductivity and storage coefficient for permeable zones and confining units at Walsingham Park. Final calibrated values for hydraulic conductivity for the different permeable zones and confining units at the test site were 18 feet per day for Upper Zone A, 750 feet per day for Lower Zone A, 1 foot per day for Zone B, $1x10^{-4}$ feet per day for the intermediate confining unit, and 10 feet per day for the semiconfining unit separating Upper Zone A and Lower Zone A. Final calibrated values for storage coefficient were $3.1x10^{-4}$ for Upper Zone A, $8.6x10^{-5}$ for Lower Zone A, $2.6x10^{-5}$ for Zone B, $3.1x10^{-4}$ for the intermediate confining unit, and $4.3x10^{-5}$ for the semiconfining unit separating Upper Zone A and Lower Zone A. Estimates of transmissivity for Upper Zone A and Lower Zone A were about 2,500 and 37,500 feet squared per day, respectively.

(12) Hydrogeology of Effluent Disposal Zones, Floridan Aquifer, South Florida. Broska, James C. 1991.

The increasing population of south Florida is creating a need for greater waste-water disposal capacity. The people of Florida are dependent on ground water for drinking, irrigation, and other uses. The emphasis on preservation of surface-water quality means that many surface waters are not allowed to receive effluent from municipal or industrial sources. Since the 1940s, the highly transmissive zones of the nonpotable portion of the Floridan aquifer have served as disposal zones for oil field brine and later for industrial and municipal effluent.

The Floridan aquifer of south Florida is a carbonate Cenozoic age aquifer. Transmissivities between 0.5 and 21 million gpd/ft exist in cavernous and fractured sequences in the aquifer. Confining zones that overlie the disposal intervals have transmissivities and hydraulic conductivities one to three orders of magnitude less than the injection intervals. These confining zones prevent low density municipal effluent from rising upward through the overlying saline waters.

This paper provides an integration of previously published work with recent site-specific data collected from deep injection wells drilled in the last two decades.

(13) Important Observations and Parameters for a Salt Water Intrusion Model. Shoemaker, W. Barclay. 2003

Sensitivity analysis with a density-dependent ground water flow simulator can provide insight and understanding of salt water intrusion calibration problems far beyond what is possible through intuitive analysis alone. Five simple experimental simulations presented here demonstrate this point. Results show that dispersivity is a very important parameter for reproducing a steady-state distribution of hydraulic head, salinity, and flow in the transition zone between fresh water and salt water in a coastal aquifer system. When estimating dispersivity, the following conclusions can be drawn about the data types and locations considered. (1) The “toe” of the transition zone is the most effective location for hydraulic head and salinity observations. (2) Areas near the coastline where submarine ground water discharge occurs are the most effective locations for flow observations. (3) Salinity observations are more effective than hydraulic head observations. (4) The importance of flow observations aligned perpendicular to the shoreline varies dramatically depending on distance seaward from the shoreline. Extreme parameter correlation can prohibit unique estimation of permeability parameters such as hydraulic conductivity and flow parameters such as recharge in a density-dependent ground water flow model when using hydraulic head and salinity observations. Adding flow observations perpendicular to the shoreline in areas where ground water is exchanged with the ocean body can reduce the correlation, potentially resulting in unique estimates of these parameter values. Results are expected to be directly applicable to many complex situations, and have implications for model development whether or not formal optimization methods are used in model calibration.

(14) Calculation of Low-Range Flow Velocities in Fractured Carbonate Media from Borehole Hydrochemical Logging Data Comparison with Thermometric results. Bidaux, Pascal. 1992.

Flow rates and concentrations from fractures intersected by a borehole can be estimated by matching simulated concentration profiles to the observed variations in water chemistry along the borehole. Experiments in karstic rocks prove that hydraulic short circuits between fractures yield a very complex flow pattern, and that flow velocities in the borehole may be higher than the velocity at which the piezometric level varies. Combined temperature and concentration studies characterize flow in both high permeability channels and slightly fissured blocks, as chemical profiles detect low velocity flows that cannot be identified on temperature profiles. Such studies are therefore advisable to characterize natural flow in fractured carbonate rocks, but also in other fractured media.

(15) Calculation of Ground Water Ages – A Comparative Analysis. Castro, Maria C. 2004

Ground water age is a fundamental, yet complex, concept in ground water hydrology. Discrepancies between results obtained through different modeling approaches for ground water age calculation have been reported, in particular, between ground water ages modeled by advection and direct simulation of around water ages (e.g., age-mass approach), which includes effects of advection and dispersion. Here, through a series of two-dimensional (2D) simulations, the impact of water mixing through advection and dispersion on modeled ages is systematically stronger in areas where water velocities are smaller and far more pronounced on ^{14}C ages. This effect is also observed in one-dimensional models. 2D simulations show that longitudinal dispersion generally acts as a "source" of ^{14}C, while vertical dispersion acts as a "sink," leading to apparent younger or older modeled ^{14}C ages as compared to advective and directly simulated ground water ages. The presence of permeable and impermeable faults provides an equally important source for discrepancies, leading to major differences in modeled ages among the three methods considered. Overall, our results show that a ^{14}C modeling approach using a solute transport model for calculating ground water age appears to be more reliable in ground water systems without faults and where water velocities are relatively high than in systems that are relatively more heterogeneous and those where faults are present. Among the three modeling approaches considered here, direct simulation of ground water age seems to yield the most consistent results in complex, heterogeneous ground wetter flow systems, giving a vertical age structure consistent with ages expected from consideration of the flow system.

(16) Can Contaminant Transport Models Predict Breakthrough? Peng, Wei-Shyuan et al. 2000.

A solute breakthrough curve measured during a two-well tracer test was successfully predicted in 1986 using specialized contaminant transport models. Water was injected into a confined, unconsolidated sand aquifer and pumped out 125 feet (38.3 m) away at the same steady rate. The injected water was spiked with bromide for over three days; the outflow concentration was monitored for a month. Based on previous tests, the horizontal hydraulic conductivity of the thick

aquifer varied by a factor of seven among 12 layers. Assuming stratified flow with small dispersivities, two research groups accurately predicted breakthrough with three-dimensional (12-layer) models using curvilinear elements following the arc-shaped flowlines in this test.

Can contaminant transport models commonly used in industry, that use rectangular blocks, also reproduce this breakthrough curve? The two-well test was simulated with four MODELOW-based models, LT3D (FD and HMOC options), MODFLOWT, MOC3D, and MODFLOW-SUR-FACT.

Using the same 12 layers and small dispersivity used in the successful 1986 simulations, these models fit almost as accurately as the models using curvilinear blocks. Subtle variations in the curves illustrate differences among the codes. Sensitivities of the results to number and size of grid blocks, number of layers, boundary conditions, and values of dispersivity and porosity are briefly presented. The fit between calculated and measured breakthrough curves degenerated as the number of layers and/or grid blocks decreased, reflecting a loss of model predictive power as the level of characterization lessened. Therefore, the breakthrough curve for most field sites can be predicted only qualitatively due to limited characterization of the hydrogeology and contaminant source strength.

(17) Dampening of Transverse Dispersion in the Halocline in Karst Limestone in the Northeastern Yucatan Peninsula. Stoessell, Ronald K. 1994.

A range of hydrodynamic dispersion coefficients was estimated for fracture-fluid and combined fracture and pore-fluid flow within the halocline of the limestone aquifer forming the surface of the northern Yucatan Peninsula. The coefficients are fit parameters in a model reproducing observed halocline profiles in a sinkhole and in a borehole near the northeastern coast. Fitted coefficients range from 10^{-7} to $10^{-4}cm^2/sec$, of which molecular diffusion, without transverse (vertical) dispersion, can account for 10^{-7} to $10^{-5}cm^2/sec$. The mechanical stability of the vertical density gradient in the halocline dampens transverse dispersion in pore fluids and in fracture fluids that are transitional between laminar and turbulent flow. The dampening is proportional to the ratio of the energy needed for the fluid to rise and displace a less dense fluid to the vertical component of the kinetic energy of the fluid. The ratio of these two energies is at a maximum during the initial stage of development of a halocline and decreases as the halocline widens.

(18) Data Analysis Methods for Determining Two-dimensional Dispersive Parameters. Jiao, Jiu J. 1993.

Two methods for calculating two-dimensional hydrodynamic dispersion parameters by analyzing experimental data, the dispersive-plume-area (DPA) method and the linear-graphic (LG) method, are proposed in this paper. The DPA method determines the dispersive parameters by analyzing the dispersive plume area after injection of a salt-water slug into an aquifer. The transverse and longitudinal dispersivity and even the porosity of an aquifer may be derived. The LG method transforms the concentration-time curve into a straight line. Using the slope of the line, dispersivity and velocity can be obtained. Both methods are examined using theoretical considerations and practical examples.

(19) Descriptions of Anisotropy and Heterogeneity and their Effect on Ground-Water Flow and Areas of Contribution to Public Supply Wells in a Karst Carbonate Aquifer system. Knochenmus, Lari A. 1996.

Delineation of areas of contribution to wells tapping a karst carbonate aquifer system can be extremely difficult using conventional approaches designed for isotropic and homogeneous aquifers, because ground-water flow tends to be through solution-enhanced conduits. Nonradial flow along preferential zones can result in inaccurate estimates of flow paths and travel times. Because of the large variability in factors affecting contributing areas and an imperfect understanding of how these factors can vary, the estimation of contributing areas is an approximation at best.

To better understand the effects of aquifer anisotropy and heterogeneity on areas of contribution, an exploratory modeling approach was used. MODFLOW, a numerical flow model, and MODPATH, a particle tracking program, were used to generate time-related areas of contribution for six hypothetical carbonate aquifer system types. The six types were conceptualized to approximate different types of aquifer anisotropy and heterogeneity. These include: (1) an isotropic and homogeneous single-layer system; (2) an anisotropic in a horizontal plane single-layer system; (3) a discrete vertically fractured single-layer system; (4) a multilayered system; (5) a doubly porous single-layer system; and (6) a vertically and horizontally interconnected heterogeneous system. The simulated aquifer anisotropy was 5:1 (K_{xx}/K_{yy}) determined from TENSORM results. The simulated discrete vertical fracture network represents locations inferred from mapped photolineaments. The simulated enhanced flow zones were determined from borehole video and geophysical logs. Areas of contribution were simulated for two prototype regions. The two prototypes were selected to be representative of the hydrologic diversity within the study area and were designated the Central Swamp and Lake Terrace regions.

Localized conditions in pumping, production well distribution, and aquifer transmissivity affect the size, shape, and orientation of areas of contribution to public supply wells. The simulated areas of contribution are 60 percent larger in the Central Swamp region where pumpage is more than double and transmissivity is about half that of the Lake Terrace region. Although these factors are important, this study focused on the effects from hydrogeologic factors common to karst carbonate aquifer systems.

This study indicates that the distribution and type of aquifer anisotropy and heterogeneity will affect the size, shape, and orientation of areas of contribution in a karst carbonate aquifer system. The size of the 50-year time-related areas of contribution ranged from 8.2 to 39.1 square miles in the Central Swamp region and from 4.0 to 18.3 square miles in the Lake Terrace region. Simulations showed that the size of areas of contribution is primarily affected by simulated withdrawal rates, effective porosity of the carbonate rock, and transmissivity. The shape and orientation of the simulated areas of contribution primarily result from aquifer anisotropy, well distribution, flow along solution-enhanced zones, and short-circuiting of flow through fracture networks.

Comparisons also were made between protection zones delineated using analytical models areas of contribution delineated using numerical models. The size of the 5-year time-related protection zone in the Central Swamp region using analytical model was almost twice as large as numerically simulated area of contribution, and more than eight times larger than the numeric simulated area of contribution in the Lake Terrace region. The differences in size are primarily t result of how the flow field is approximated. The analytical method assumes only lateral fl to wells but numerical

methods allow particle move laterally and vertically. Additionally, multiple-well-interference effects resulting from the close proximity of several pumping wells cal: individual capture zones to converge or diver depending on the difference in pumping rates orientation among the wells. Such an interpretation is not available from analytical methods. simulated distributions of aquifer anisotropy heterogeneity, in this study, were highly conceptualized, but were based on plausible occurrence anisotropy and heterogeneity inherent in carbonate aquifer systems.

(20) Influence of Pore Pressure on Apparent Dispersity of a Fissured Dolomitic Aquifer. Leap, Darrell I. 1991.

The U.S. Geological Survey's Amargosa Tracer Calibration Site in southern Nevada has been used for three different recirculating tracer tests using as tracers: (1) tritium, (2) sulfur-35, and (3) tritium and bromide together. Although the physical setup, well spacings, and thus apparent scale were the same in all tests, the recirculating rates and pore pressures were different. Apparent dispersivities found in the three tests differed considerably, revealing an inverse relationship between computed dispersivity and recirculation rate. These differences are believed to be caused primarily by changes in fissure-aperture widths and thus, hydraulic conductivities, with resulting changes in flow rates and directions caused by changes in pore pressure between different tests in the presence of high ambient pore pressure. The results of this study indicate that forced-gradient tracer tests for determination of dispersivity should not be performed when ambient pore pressure and/or testing pore pressure is a significant percentage of overburden pressure. In addition, apparent dispersivity calculated by forced-gradient tracer tests can differ considerably from that of unstressed natural situations, and consequent solute-transport estimates are likely to be in error.

(21) Inventory and Review of Aquifer Storage and Recovery in Southern Florida. Reese, Ronald S. 2002.

Aquifer storage and recovery in southern Florida has been proposed on an unprecedented scale as part of the Comprehensive Everglades Restoration Plan. Aquifer storage and recovery wells were constructed or are under construction at 27 sites in southern Florida, mostly by local municipalities or counties located in coastal areas. The Upper Floridan aquifer, the principal storage zone of interest to the restoration plan, is the aquifer being used at 22 of the sites. The aquifer is brackish to saline in southern Florida, which can greatly affect the recovery of the freshwater recharged and stored.

Well data were inventoried and compiled for all wells at most of the 27 sites. Construction and testing data were compiled into four main categories: (1) well identification, location, and construction data; (2) hydraulic test data; (3) ambient formation water-quality data; and (4) cycle testing data. Each cycle during testing or operation includes periods of recharge of freshwater, storage, and recovery that each last days or months. Cycle testing data include calculations of recovery efficiency, which is the percentage of the total amount of potable water recharged for each cycle that is recovered.

Calculated cycle test data include potable water recovery efficiencies for 16 of the 27 sites. However, the number of cycles at most sites was limited; except for two sites, the highest number of cycles was five. Only nine sites had a recovery efficiency above 10 percent for the first cycle, and

10 sites achieved a recovery efficiency above 30 percent during at least one cycle. The highest recovery efficiency achieved per cycle was 84 percent for cycle 16 at the Boynton Beach site. Factors that could affect recovery of freshwater varied widely between sites. The thickness of the open storage zone at all sites ranged from 45 to 452 feet. For sites with the storage zone in the Upper Floridan aquifer, transmissivity based on tests of the storage zones ranged from 800 to 108,000 feet squared per day, leakance values indicated that confinement is not good in some areas, and the chloride concentration of ambient water ranged from 500 to 11,000 milligrams per liter. Based on review of four case studies and data from other sites, several hydrogeologic and design factors appear to be important to the performance of aquifer storage and recovery in the Floridan aquifer system. Performance is maximized when the storage zone is thin and located at the top of the Upper Floridan aquifer, and transmissivity and salinity of the storage zone are moderate (less than 30,000 feet squared per day and 3,000 milligrams per liter of chloride concentration, respectively). The structural setting at a site could also be important because of the potential for updip migration of a recharged freshwater bubble due to density contrast or loss of overlying confinement due to deformation.

(22) Simulation of Subsurface Storage and Recovery of Effluent Using Multiple Wells, St. Petersburg, Florida. Yobbi, Dann K. 1997.

The potential for subsurface storage and recovery, otherwise called aquifer storage and recovery, of effluent in the uppermost producing zone of the Upper Floridan aquifer in St. Petersburg, Florida, was studied by the U.S. Geological Survey, in cooperation with the city of St. Petersburg and the Southwest Florida Water Management District. The success of subsurface storage and recovery depends on the recovery efficiency, or the quantity of water, relative to the quantity injected, that can be recovered before the water that is withdrawn fails to meet salinity limits. The viability of this practice will depend upon the ability of the injected zone to receive, store, and discharge the injected fluid.

A three-dimensional numerical model of ground-water flow and solute transport, incorporating available data on aquifer properties and water quality, was developed to evaluate the effects of changing various operational factors on recovery efficiency. The reference case for testing was a base model considered representative of the aquifer system underlying the Southwest St. Petersburg Water Treatment Facility. The base simulation used as a standard for comparison consisted of a single cycle of 90 days of simultaneous injection of effluent in three wells at a rate of 4.0 million gallons per day and then equal rate withdrawal of 4.0 million gallons per day until the pumped water in each well reached a dissolved solids concentration of 1,500 milligrams per liter. A recovery efficiency of 14.8 percent was estimated for the base simulation. Ten successive injection and recovery cycles increased recovery efficiency to about 56 percent. Based on model simulations for hypothetical conditions, recovery efficiency (1) increased with successive injection and recovery cycles; (2) increased when the volume of injectant increased; (3) decreased when storage time increased; (4) did not change significantly when the injection rate or recovery rate increased, or when the ratio of recovery rate to injection rate increased, and (5) was not significantly affected by any particular geometric arrangement of wells or by the number of wells when the volume of water injected remained constant. Recovery efficiency from multiple wells was nearly the same as from a single well. Recovery efficiency ranged from about 7 to 56 percent, in several tests.

Sensitivity of recovery efficiency to variations in selected parameters such as dissolved-solids concentration of the injection zone, permeability, vertical anisotropy, longitudinal and transverse dispersivities, and effective porosity was tested. Changes in the dissolved-solids concentration of the injection zone produced the greatest change in recovery efficiency. Uniform changes in dispersivity values produced the second greatest change in recovery efficiency. Generally, recovery efficiency increased when the above parameter values were decreased and recovery efficiency decreased when these parameter values were increased.

Density difference between native and injected waters was the most important factor affecting recovery efficiency in this study. For the base simulation, sensitivity tests indicated that recovery efficiency increased from about 15 to 78 percent when the dissolved-solids concentration of the native water decreased from about 7,800 to 500 milligrams per liter.

Dispersivity is another important factor affecting recovery efficiency. For the base simulation, sensitivity tests indicated that recovery efficiencies from about 9 to 24 percent can be obtained for difference dispersivity values. A field determination of dispersivity was not made as part of this study, and values used may not be representative of the actual dispersive characteristics of the aquifer system at the study site. However, dispersivity values tested are within the range of values used in previous studies.

(23) Simulation of Subsurface Storage and Recovery of Treated Effluent Injected in a Saline Aquifer, St. Petersburg, Florida. Yobbi, Dann K. 1996.

The potential for subsurface storage and recovery of treated effluent into the uppermost producing zone (zone A) of the Upper Floridan aquifer in St. Petersburg, Florida, is being studied by the U.S. Geological Survey, in cooperation with the city of St. Petersburg and the Southwest Florida Water Management District. A measure of the success of this practice is the recovery efficiency, or the quantity of water relative to the quantity injected, that can be recovered before the water that is withdrawn fails to meet water-quality standards. The feasibility of this practice will depend upon the ability of the injected zone to receive, store, and discharge the injected fluid.

A cylindrical model of ground-water flow and solute transport, incorporating available data on aquifer properties and water quality, was developed to determine the relation of recovery efficiency to various aquifer and fluid properties that could prevail in the study area. The reference case for testing was a base model considered representative of the saline aquifer underlying St. Petersburg. Parameter variations in the tests represent possible variations in aquifer conditions in the area. The model also was used to study the effect of various cyclic injection and withdrawal schemes on the recovery efficiency of the well and aquifer system.

A base simulation assuming 15 days of injection of effluent at a rate of 1.0 million gallons per day and 15 days of withdrawal at a rate of 1.0 million gallons per day was used as reference to compare changes in various hydraulic and chemical parameters on recovery efficiency. A recovery efficiency of 20 percent was estimated for the base simulation. For practical ranges of hydraulic and fluid properties that could prevail in the study area, the model analysis indicates that (1) the greater the density contrast between injected and resident formation water, the lower the recovery efficiency, (2) recovery efficiency decreases significantly as dispersion increases, (3) high formation permeability favors low recovery efficiencies, and (4) porosity and anisotropy have little

effect on recovery efficiencies. In several hypothetical tests, the recovery efficiency fluctuated between about 4 and 76 percent.

The sensitivity of recovery efficiency to variations in the rate and duration of injection (0.25, 0.50, 1.0, and 2.0 million gallons per day) and withdrawal cycles (60, 180, and 365 days) was determined. For a given operational scheme, recovery efficiency increased as the injection and withdrawal rate is increased. Model results indicate that recovery efficiencies of between about 23 and 37 percent can be obtained for different subsurface storage and recovery schemes. Five successive injection, storage, and recovery cycles can increase the recovery efficiency to about 46 to 62 percent. There is a larger rate of increase at smaller rates than at larger rates. Over the range of variables studied, recovery efficiency improved with successive cycles, increasing rapidly during initial cycles then more slowly at later cycles.

The operation of a single well used for subsurface storage and recovery appears to be technically feasible under moderately favorable conditions; however, the recovery efficiency is highly dependent upon local physical and operational parameters. A combination of hydraulic, chemical, and operational parameters that minimize dispersion and buoyancy flow, maximizes recovery efficiency. Recovery efficiency was optimal where resident formation water density and permeabilities were relatively similar and low.

(24) Tests of Subsurface Storage or Freshwater at Hialeah, Dade County, Florida, and Numerical Simulation of the Salinity of Recovered Water. Merritt, Michael L. 1997.

Injection and observation wells were drilled in late 1974 for the purpose of conducting tests of storage and recovery of potable water in the brackish Upper Floridan aquifer. Three tests, involving storage and recovery cycles of varying volumes and storage period lengths, were performed between July 1975 and January 1980. Recovery was by natural artesian flow, and recovery efficiencies were 32.9, 47.8, and 38.5 percent. Wellbore plugging occurred during the injection stages, but injectivity was restored by periodic 2- to 3-hour backflushes at the natural artesian flow rate.

An interval of shelly limestone between 1,015 and 1,050 feet below land surface contained the flow zone. Data from an analysis of 18 spinner flowmeter logs indicated that the principal part of the flow zone extended from 1,024 to 1,036 feet below land surface and that minor amounts of flow occurred to a depth of about 1,047 feet. A neutron porosity log indicated the bulk porosity of both the flow zone and confining layers to be 35 percent. Chloride and dissolved-solids concentrations of water in the flow zone were 1,200 and 2,700 milligrams per liter, respectively.

A three-dimensional, finite-difference flow and solute-transport code was used to simulate pressure data measured during an aquifer test and observed salinity increases in recovered water during storage and recovery cycles. The aquifer test conducted in February 1975 was simulated by using a hydraulic conductivity estimate of 800 feet per day and a rock compressibility estimate of 0.0000400 (pound per square inch). The equivalent transmissivity and storage coefficients were 9,600 cubic feet per day per square foot times foot of aquifer thickness and 7.8×10^{-5}, respectively. Simulation of observed salinity increases during the three recoveries required dispersivities of 65 feet, a molecular diffusivity of 0.0002 foot squared per day, and a regional pore velocity of 260 feet per year. Central differencing in space and time was used for the solute-transport computations as well as an experimental method of computing vertical dispersion that used a scaling factor of 0.013.

Additional simulations of the aquifer-test data and recovery salinities were obtained based on assumptions that (1) the flow zone was 21 feet thick, (2) flow-zone effective porosity was 20 percent, and (3) flow-zone hydraulic conductivity was bipolar anisotropic by a ratio of 10:1. The four sets of simulation values were used in model runs in which 10 years of annual injection, storage, and recovery cycles were simulated. Computed recovery efficiencies increased from 40 percent in the first year to 68 percent in later cycles. The high regional pore velocity required for model calibration substantially limited the recovery efficiency achieved in later cycles.

(25) The Impact of Matrix Diffusion on the Cleanup of Fractured Igneous, Metamorphic and Sedimentary Rock Aquifers. Mutch, Robert D. 1993.

Aquifer restoration has been recognized for many years to be an extremely difficult undertaking. For a variety of reasons, restoration of fractured rock aquifers appears to be especially difficult. One reason is the phenomenon of matrix diffusion. Matrix diffusion refers to the process by which contaminants diffuse into and out of the relatively immobile matrix pore water from the mobile fracture water.

In most (but not all) fractured rock, groundwater moves primarily through the interconnected network of fractures and the pore water within the matrix of the rock is relatively immobile. As contaminated groundwater moves through the fractures, the contamination is also subject to diffusion into the often stagnant matrix pore water of the rock. The diffusion of contaminants into the rock matrix is beneficial in one respect in that it retards the advance of a contaminant plume through a fractured rock aquifer. However, the diffusion-controlled release of contaminants from the rock matrix can substantially prolong aquifer cleanup efforts over what would be possible in a simple porous medium aquifer of equivalent hydraulic conductivity.

In order to evaluate the impact of matrix diffusion upon the cleanup of fractured rock aquifers, a simple mathematical model has been developed which predicts contaminant levels along a representative fracture in the rock as a function of position, time, and past history of contaminant levels in the groundwater. The model takes into account the characteristics of the fractured rock through which the groundwater is moving, specifically fracture porosity, matrix porosity, fracture spacing, matrix diffusivity, groundwater velocity in the fractures, longitudinal dispersion constant, and length of the groundwater flow path.

The model is employed to evaluate the effect of matrix diffusion on the cleanup of typical sedimentary rock aquifers and typical metamorphic or igneous aquifers. Through sensitivity analyses, the modeling reveals the parameters most strongly governing the process. The modeling also looks at the effect of pump and treat systems and specifically the “rebound effect” that can result from premature cessation of pump and treat systems.

(26) Use of Chemical and Isotopic Tracers to Characterize the Interactions Between Groundwater and Surface Water in Mantled Karst. Katz, Brian G. 1997.

In the mantled karst terrane of northern Florida, the water quality of the Upper Floridan aquifer is influenced by the degree of connectivity between the aquifer and the surface. Chemical and isotopic analyses [$^{l8}O/^{16}O$ ($\delta^{18}O$), $^{2}H/^{1}H$ (δD), $^{13}C/^{12}C$ ($\delta^{13}C$), tritium (^{3}H), and strontium-87/strontium-86 ($^{87}Sr/\ ^{86}Sr$)] along with geochemical mass-balance modeling were used to identify the dominant hydrochemical processes that control the composition of ground water as it evolves downgradient in two systems. In one system, surface water enters the Upper Floridan aquifer through a sinkhole located in the Northern Highlands physiographic unit. In the other system, surface water enters the aquifer through a sinkhole lake (Lake Bradford) in the Woodville Karst Plain. Differences in the composition of water isotopes ($\delta^{18}O$ and δD) in rainfall, ground water, and surface water were used to develop mixing models of surface water (leakage of water to the Upper Floridan aquifer from a sinkhole lake and a sinkhole) and ground water. Using mass-balance calculations, based on differences in $\delta^{18}O$ and δD, the proportion of lake water that mixed with meteoric water ranged from 7 to 86% in water from wells located in close proximity to Lake Bradford. In deeper parts of the Upper Floridan aquifer, water enriched in ^{18}O and D from five of 12 sampled municipal wells indicated that recharge from a sinkhole (1 to 24%) and surface water with an evaporated isotopic signature (2 to 32%) was mixing with ground water.

The solute isotopes, $\delta^{13}C$ and $^{87}Sr/^{86}Sr$, were used to test the sensitivity of binary and ternary mixing models, and to estimate the amount of mass transfer of carbon and other dissolved species in geochemical reactions. In ground water downgradient from Lake Bradford, the dominant processes controlling carbon cycling in ground water were dissolution of carbonate minerals, aerobic degradation of organic matter, and hydrolysis of silicate minerals. In the deeper parts of the Upper Floridan aquifer, the major processes controlling the concentrations of major dissolved species included dissolution of calcite and dolomite, and degradation of organic matter under oxic conditions. The Upper Floridan aquifer is highly susceptible to contamination from activities at the land surface in the Tallahassee area. The presence of post-1950s concentrations of ^{3}H in ground water from depths greater than 100 m below land surface indicates that water throughout much of the Upper Floridan aquifer has been recharged during the last 40 years. Even though mixing is likely between ground water and surface water in many parts of the study area, the Upper Floridan aquifer produces good quality water, which due to dilution effects shows little if any impact from trace elements or nutrients that are present in surface waters.

(27) Potential for Saltwater Intrusion into the Lower Tamiami Aquifer near Bonita Springs, Southwestern Florida. Shoemaker, W. Barclay. 2003.

A study was conducted to examine the potential for saltwater intrusion into the lower Tamiami aquifer beneath Bonita Springs in south western Florida. Field data were collected, and constant- and variable-density ground-water flow simulations were performed that: (1) spatially quantified modern and seasonal stresses, (2) identified potential mechanisms of saltwater intrusion, and (3) estimated the potential extent of saltwater intrusion for the area of concern.

MODFLOW and the inverse modeling routine UCODE were used to spatially quantify modern and seasonal stresses by calibrating a constant-density ground-water flow model to field data collected

in 1996. The model was calibrated by assuming hydraulic conductivity parameters were accurate and by estimating unmonitored ground-water pumpage and potential evapotranspiration with UCODE. Uncertainty in these estimated parameters was quantified with 95-percent confidence intervals. These confidence intervals indicate more uncertainty (or less reliability) in the estimates of unmonitored ground-water pumpage than estimates of pan-evaporation multipliers, because of the nature and distribution of observations used during calibration. Comparison of simulated water levels, streamflows, and net recharge with field data suggests the model is a good representation of field conditions.

Potential mechanisms of saltwater intrusion into the lower Tamiami aquifer include: (1) lateral inland movement of the freshwater-saltwater interface from the southwestern coast of Florida; (2) upward leakage from deeper saline waterbearing zones through natural upwelling and upconing, both of which could occur as diffuse upward flow through semiconfining layers, conduit flow through karst features, or pipe flow through leaky artesian wells; (3) downward leakage of saltwater from surface-water channels; and (4) movement of unflushed pockets of relict seawater. Of the many potential mechanisms of saltwater intrusion, field data and variable-density ground-water flow simulations suggest that upconing is of utmost concern, and lateral encroachment is of second-most concern. This interpretation is uncertain, however, because the predominance of saltwater intrusion through leaky artesian wells with connection to deeper, more saline, and higher pressure aquifers was difficult to establish.

Effective management of ground-water resources in southwestern Florida requires an understanding of the potential extent of saltwater intrusion in the lower Tamiami aquifer near Bonita Springs. Variable-density, ground-water flow simulations suggest that when saltwater is at dynamic equilibrium with 1996 seasonal stresses, the extent of saltwater intrusion is about 100 square kilometers areally and 70,000 hectare-meters volumetrically. The volumetric extent of saltwater intrusion was most sensitive to changes in recharge, ground-water pumpage, sea level, salinity of the Gulf of Mexico, and the potentiometric surface of the sandstone aquifer, respectively.

(28) Preliminary Assessment of Injection, Storage, and Recovery of Freshwater in the Lower Hawthorn Aquifer, Cape Coral, Florida. Quinones-Aponte, Vincente. 1995.

A preliminary assessment of subsurface injection, storage and recovery of fresh canal water was made in the naturally brackish lower Hawthorn aquifer in Cape Coral, southwestern Florida. A digital modeling approach was used for this preliminary assessment, incorporating available data on hydrologic conditions, aquifer properties, and water quality to simulate density-dependent groundwater flow and advective-dispersive transport of a conservative ground-water solute (chloride ion).

A baseline simulation was used as reference to compare the effects of changing various operational factors on the recovery efficiency. A recovery efficiency of 64 percent was estimated for the baseline simulation. Based on the model, the recovery efficiency increases if the injection rate and recovery rates are increased and if the ratio of recovery rate to injection rate is increased. Recovery efficiency decreases if the amount of water injected is increased; slightly decreases if the storage time is increased; is not changed significantly if the water is injected to a specific flow zone; increases with successive cycles of injection, storage, and recovery; and decreases if the chloride concentrations in either the injection water or native aquifer water are increased. In everal hypothetical tests, the recovery efficiency fluctuated between 22 and about 100 percent.

Two successive cycles could bring the recovery efficiency from 60 to about 80 percent. Interlayer solute mass movement across the upper and lower boundaries seems to be the most important factor affecting the recovery efficiency. A sensitivity analysis was performed applying a technique in which the change in the various factors and the corresponding model responses are normalized so that meaningful comparisons among the responses could be made. The general results from the sensitivity analysis indicated that the permeabilities of the upper and lower flow zones were the most important factors that produced the greatest changes in the relative sensitivity of the recovery efficiency. Almost equally significant changes occurred in the relative sensitivity of the recovery efficiency when all porosity values of the upper and lower flow zones and the leaky confining units and the vertical anisotropy ratio were changed.

The advective factors are the most important in the Cape Coral area according to the sensitivity analysis. However, the dispersivity values used in the model were extrapolated from studies conducted at the nearby Lee County Water Treatment Plant, and these values might not be representative of the actual dispersive characteristics of the lower Hawthorn aquifer in the Cape Coral area.

29) Process-Based Interpretation of Tracer Tests in Carbonate Aquifers. Birk, Steffin. 2004.

A tracer test in a carbonate aquifer is analyzed using the method of moments and two analytical advection dispersion models (ADMs) as well as a numerical model. The numerical model is a coupled continuum-pipe flow and transport model that accounts for two different flow components in karstified carbonate aquifers, i.e., rapid and often turbulent conduit flow and Darcian flow in the fissured porous rock. All techniques employed provide reasonable fits to the tracer breakthrough curve (TBC) measured at a spring. The resulting parameter estimates are compared to investigate how each conceptual model of flow and transport processes that forms the basis of the analyses affects the interpretation of the tracer test. Numerical modeling results suggest that the method of moments and the analytical ADMs tend to overestimate the conduit volume because part of the water discharged at the spring is wrongly attributed to the conduit system if flow in the fissured porous rock is ignored. In addition, numerical modeling suggests that mixing of the two flow components accounts for part of the dispersion apparent in the measured TBC, while the remaining part can be attributed to Taylor dispersion. These processes, however, cannot reasonably explain the tail of the TBC. Instead, retention in immobile-fluid regions as included in a nonequilibrium ADM provides a possible explanation.

30) Recovering Fresh Water Stored in Saline Limestone Aquifers. Merritt, Michael L. 1985.

Numerical modeling techniques are used to examine the hydrogeologic, design, and management factors governing the recovery efficiency of subsurface fresh-water storage. The modeling approach permitted many combinations of conditions to be studied. A sensitivity analysis was used that consisted of varying certain parameters while keeping constant as many other parameters or processes as possible. The results show that a loss of recovery efficiency resulted from: (1) processes causing mixing of injected fresh water with native saline water (hydrodynamic

dispersion); (2) processes or conditions causing the irreversible displacement of the injected fresh water with respect to the well (buoyancy stratification and background hydraulic gradients); or (3) processes or procedures causing injection and withdrawal flow patterns to be dissimilar (dissimilar injection and withdrawal schedules in multiple-well systems). Other results indicated that recovery efficiency improved considerably during the first several successive cycles, provided that each recovery phase ended when the chloride concentration of withdrawn water exceeded established criteria for potability (usually 250 milligrams per liter). Other findings were that fresh water injected into highly permeable or highly saline aquifers would buoy rapidly with a deleterious effect on recovery efficiency.

(31) Water and Radioactive Tracer Flow in a Heterogeneous Field-Scale System. Dunnivant, Frank M. 1998.

A coupled field-scale aquifer pumping and water infiltration test was conducted at the Idaho National Engineering and Environmental Laboratory in order to evaluate subsurface water and contaminant transport processes in a heterogeneous flow system. The test included an aquifer pumping test to determine the storage properties of the aquifer and the state of confinement of the aquifer (~190 m below land surface), and a vadose zone infiltration test to determine vertical moisture and radioactive tracer migration rates. Pump test results indicated that the Snake River Plain Aquifer was locally unconfined with a transmissivity ranging from 5.57×10^5 to 9.29×10^4 m^2/day. Moisture monitoring with neutron probes indicated that infiltrating water was initially transported vertically through the upper basalt layer of the vadose zone, primarily through fractures and rubble zones, at an average rate of 5 m/day (based on vertical distance traveled and first arrival of water at the monitoring points). Analysis of breakthrough curves for a conservative tracer allowed estimation of the arrival of the peak concentration and yielded an average velocity of 1 m/day. The migration velocities from the neutron probe and tracer tests are in good agreement given the scale of the test and difference in analysis techniques. None of the data sets showed a correlation between migration velocity (arrival time) and distance from the point source, but they strongly indicate preferential flow through discrete fractures. Upon reaching the first continuous sedimentary interbed layer in the basalt formation, water flow was diverted laterally along the interbed surface where it spread outward in primarily three areas corresponding to topographic lows on the interbed surface, and slowly infiltrated into the interbed. The nonpredictable movement of water and tracer through specific fractures underlying the site suggests that a priori prediction of transmissive fractures in this media is not possible. Results do suggest that the continuous sedimentary interbed layers, in general, impede vertical water flow and contaminant migration.

(32) Predictive Modeling Results for the City of St. Petersburg's Deep Injection Well system (and associated technical memorandums). CH2M HILL. 1996.

The City of St. Petersburg is pursuing injection well operating permits for 10 deep injection wells at its four Water Reclamation Facilities (WRFs). Solute transport modeling is being used as a tool to develop a better understanding of historical and projected water quality changes at the City's four injection sites. The City has negotiated consent orders with the Florida Department of Environmental Protection (FDEP) to continue operation of the deep injection wells while outstanding permitting issues are addressed. As part of the consent order process, the City is

developing technical data in support of the injection well operating permits. Technical Memorandum No. STM-3 is the third in a series of technical memoranda related to solute transport modeling conducted in support of the re-permitting process. Technical Memorandum No. STM-1, Development of the Solute Transport Conceptual Model, was submitted to the FDEP Technical Advisory Committee (TAC) in February 1995. Background information and the conceptual approach to the modeling was described in STM-1. Technical Memorandum No. STM-2, Solute Transport Model Calibration for the City of St. Petersburg's Deep Injection Well Systems, was presented to the FDEP TAC in October 1995. In STM-2, the numerical representation of the conceptual model was presented, and simulated and observed water quality and water level trends were compared at each of the four WRFs.

In this Technical Memorandum (STM-3), Predictive Modeling Results for the City of St. Petersburg's Deep Injection Well Systems, the calibrated model simulations presented in STM-2 are extended into the future to evaluate possible changes in water quality in selected hydrogeologic zones. The results of this effort are intended to provide insight to the City and the FDEP TAC to aid in development of an appropriate permitting strategy for each WRF.

(33) A Critical Review of Data on Field-Scale Dispersion in Aquifers. Gelhar, Lynn W. 1992.

A critical review of dispersivity observations from 59 different field sites was developed by compiling extensive tabulations of information on aquifer type, hydraulic properties, flow configuration, type of monitoring network, tracer, method of data interpretation, overall scale of observation and longitudinal, horizontal transverse and vertical transverse dispersivities from original sources. This information was then used to classify the dispersivity data into three reliability classes. Overall, the data indicate a trend of systematic increase of the longitudinal dispersivity with observation scale but the trend is much less clear when the reliability of the data is considered. The longitudinal dispersivities ranged from 10^{-2} to 10^{4}m for scales ranging from 10^{-1} to 10^{5}m, but the largest scale for high reliability data was only 250 m. When the data are classified according to porous versus fractured media there does not appear to be any significant difference between these aquifer types. At a given scale, the longitudinal dispersivity values are found to range over 2-3 orders of magnitude and the higher reliability data tend to fall in the lower portion of this range. It is not appropriate to represent the longitudinal dispersivity data by a single universal line. The variations in dispersivity reflect the influence of differing degrees of aquifer heterogeneity at different sites. The data on transverse dispersivities are more limited but clearly indicate that vertical transverse dispersivities are typically an order of magnitude smaller than horizontal transverse dispersivities. Reanalyses of data from several of the field sites show that improved interpretations most often lead to smaller dispersivities. Overall, it is concluded that longitudinal dispersivities in the lower part of the indicated range are more likely to be realistic for field applications.

(34) ASR-UK: Elucidating the Hydrogeological Issues Associated with Aquifer Storage and Recovery in the UK. Gales, I.N. 2002.

The results of a study, funded by BGS, UKWIR and EA, and undertaken between 1995 and 1998, indicated that there is a large potential for development of Aquifer Storage Recovery (ASR) schemes in the UK at a wide range of scales (Jones et al., 1998). The study stimulated considerable interest and, at that time, three water companies had initiated field trials. Several other schemes were at the desk study stage.

Experience from the United States shows that ASR is frequently a cost-effective solution to a wide variety of water supply, as well as water quality problems. The potential of the technology in Britain needed to be more fully evaluated, in order to optimize the use of our water resources, both fresh and wastewater. However, several uncertainties were highlighted by this study that could constrain the acceptance and utilization of ASR as a component in strategies for sustainable management of water resources.

The project reported here, ASR-UK, addresses some of the issues identified through generic research and the development of guidelines and models to assist in decision-making throughout the investigative, development and implementation stages of schemes. The issues addressed are:

- Research into the controls on dispersion and diffusion of injected water and their impacts on recovery efficiency. Models were developed to predict the extent and movement of "bubbles" of stored water in aquifers as well as changes in water quality with time. Work initially focused on the Chalk aquifer but other aquifers were also investigated.
- The impacts of geochemical interactions between native and injected water as well as water-rock interactions. The adverse as well as the beneficial effects need to be predicted in order to address them in the most cost-effective manner. The project therefore aimed to assess the significance of these reactions on the permeability of aquifers, the quality of recovered water and the efficiency of schemes.
- During the life of the project, the importance of the environmental impacts of ASR schemes, in relation to the operational cycle used, became increasingly apparent. Quantification of these impacts is required throughout all phases of a study, from the initial assessment of the potential of a site, through the staged testing to implementation and commissioning of a scheme.

The project was designed to address these issues through review of current knowledge and the application and development of models, some of which can be used as tools in current and future investigations. It was initially planned that the development of these models would be closely aligned with on-going investigations and field trials, which would provide data to validate the models as well as providing feedback to the investigation. This proved to be the case with the investigations in the Chalk aquifer but little data were available from other aquifers.

(35) Results from a forced Gradient Tracer Test in a Fractured Aquifer with Simultaneous Input of Different Tracers. Bender, A. 2001.

Interpretation of pumping test and tracer test data allowed for the evaluation of capture areas of discharge wells as well as important hydraulic parameters of a multi-layered aquifer system such as longitudinal dispersivity, hydraulic conductivity, effective porosity and leakage flow. Evaluation of the tracer breakthrough curves was realized using a analytical solution of the mass transport equation for radial symmetric flow patterns induced by the forced gradient tracer test. The results of the tracer test yielded important input parameters for subsequent calculations of pollution spreading with a numerical groundwater model to optimize the location and necessary pumping rats of future discharge wells as part of hydraulic remediation measures.

(36) Analysis of a Vertical Dipole Tracer Test in Highly Fractured Rock. Sanford, William E. 2002.

The results of a vertical dipole tracer experiment performed in highly fractured rocks of the Clare Valley, South Australia, are presented. The injection and withdrawal piezometers were both screened over 3 m and were separated by 6 m (midpoint to midpoint). Due to the long screen length, several fracture sets were intersected, some of which do not connect the two piezometers. Dissolved helium and bromide were injected into the dipole flow field for 75 minutes, followed by an additional 510 minutes of flushing. The breakthrough of helium was retarded relative to bromide, as was expected due to the greater aqueous diffusion coefficient of helium. Also, only ~25% of the total mass injected of both tracers was recovered. Modeling of the tracer transport was accomplished using an analytical one-dimensional flow and transport model for flow through a fracture with diffusion into the matrix. The assumptions made include: streamlines connecting the injection and withdrawal point can be modeled as a dipole of equal strength, flow along each streamline is one dimensional, and there is a constant Peclet number for each streamline. In contrast to many other field tracer studies performed in fractured rock, the actual travel length between piezometers was not known. Modeling was accomplished by fitting the characteristics of the tracer breakthrough curves (BTCs), such as arrival times of the peak concentration and the center of mass. The important steps were to determine the fracture aperture (240 um) based on the parameters that influence the rate of matrix diffusion (this controls the arrival time of the peak concentration), estimating the travel distance (11 m) by fitting the time of arrival of the centers of mass of the tracers; and estimating fracture dispersivity (0.5 m) by fitting the times that the inflection points occurred on the front and back limbs of the BTCs. This method works even though there was dilution in the withdrawal well, the amount of which can be estimated by determining the value that the modeled concentrations need to be reduced to fit the data (~50%). The use of two tracers with different diffusion coefficients was not necessary, but it provides important checks in the modeling process because the apparent retardation between the two tracers is evidence of matrix diffusion and the BTCs of both tracers need to be accurately modeled by the best fit parameters.

(37) Field Test for Effective Porosity and Dispersivity in Fractured Dolomite, the WIPP, Southeastern New Mexico. Gonzalez, D.D. 1981.

The Waste Isolation Pilot Plant (WIPP), a demonstration facility 26 mi (41.6 km) east of Carlsbad, New Mexico, used to store transuranic waste in Permiam-bedded salts, has been under field investigation since 1975. Hydrologically, the area is characterized by a typical semiarid environment underlaid by four confined aquifer systems whose transmissivities range from 10 to 10^{-5} ft ^{2}/d (1 to 10^{-6} m^2/d).

Previous local hydrogeologic investigations show a fractured dolomite, whose thickness and depth of burial range from 22 to 24 ft (6.7 to 7.3 m) and 498 to 897 ft (152 to 274 m), respectively, as the most likely groundwater vehicle to transport waste to be biosphere in the event such a repository is breached. To describe adequately and to predict solute transport, certain hydraulic characteristics of the transporting medium need to be estimated along a hypothetical flow path. Effective porosity and dispersivity are two parameters which are most difficult to predict, particularly in fractured rock exhibiting low trransmissivities. This paper describes the results of the first of a series of two-well recirculation tracing tests to be performed. The recirculation tests were performed using an extraction-injection well couplet similar to that described by Grove and Beetem (1971). Tests duration was 270 days and resulted in a well-defined breakthrough curve.

(38) Deuterated Tracers for Assessing Natural Attenuation in Contaminated Groundwater. Davis, G.B. 2000.

Three groundwater tracer tests using deuterium-labelled-benzene, toluene, xylene and naphthalene (BTXN), trichloroethene (TCE) and munitions compounds (e.g. trinitrotoluene-TNT) were carried out in Australia to determine sorption, biodegradation and other transport parameters for contaminant plumes. The BTXN and TCE tests were natural gradient tests in an anaerobic sand aquifer, and the third munitions tracer test was a forced gradient test in a fractured basalt aquifer. Sorption coefficients, biodegradation rates and dispersion coefficients were estimated from multi-depth and location monitoring and modelling. The use of deuterium-labelled tracers is shown to be viable and attractive, although difficulties with in-field operations and environmental policy may limit application of such a technique.

(39) Analysis of Solute Transport in a Heterogeneous Aquifer: The Krauthausen Field Experiment. Vereecken, H. 2002.

A field-scale natural gradient tracer experiment with bromide, uranin and lithium was conducted in a heterogeneous aquifer at Krauthausen, Germany. The temporal and spatial evolution of the solute plumes was monitored over 398 days for bromide and 449 days for uranin and lithium. The spatial variability of basic aquifer parameters, hydraulic conductivity, and sorption parameters of the aquifer material was investigated in detail. Local Darcian velocities were measured using NH_4BR^{82} as a radioactive tracer in 33 observation wells. Vertical and horizontal correlation lengths of hydraulic properties were determined using variogram analysis. The magnitude of the local Darcian velocities was found to be lognormally distributed. In addition, the groundwater flow direction

showed a clear trend in the vertical direction. The horizontal correlation length of the magnitude of Darcian velocity agreed with the correlation length of *K* estimated from grain size data. Batch experiments on aquifer sediments showed that sorption of uranin and lithium could be described by a Freundlich isotherm. The Freundlich *n* parameter of uranin sorption showed little variation with depth. The time evolution of the bromide plume was quantified in terms of spatial moments. The longitudinal effective dispersivity estimated from spatial moment analysis was within the range of calculated effective dispersivities, taking into account the uncertainty of estimates of the ln *K* statistics.

(40) Values for Longitudinal and Transverse Dispersivity, Obtained From Single-Well, Two-Well, and Multi-Well Tracer Tests. Isherwood, 1981.

(none)

(41) Three-Dimensional Density-Dependant Flow and Transport Modeling of Saltwater Intrusion in the Southern Water Use Caution Area. HydroGeoLogic, 2002.

(none)

Exhibit 3

Technical Papers

WATER RESOURCES RESEARCH, VOL. 28, NO. 7, PAGES 1955–1974, JULY 1992

A Critical Review of Data on Field-Scale Dispersion in Aquifers

LYNN W. GELHAR

Department of Civil Engineering, Massachusetts Institute of Technology, Cambridge

CLAIRE WELTY

Department of Civil and Architectural Engineering, Drexel University, Philadelphia, Pennsylvania

KENNETH R. REHFELDT

Illinois State Water Survey, Champaign

A critical review of dispersivity observations from 59 different field sites was developed by compiling extensive tabulations of information on aquifer type, hydraulic properties, flow configuration, type of monitoring network, tracer, method of data interpretation, overall scale of observation and longitudinal, horizontal transverse and vertical transverse dispersivities from original sources. This information was then used to classify the dispersivity data into three reliability classes. Overall, the data indicate a trend of systematic increase of the longitudinal dispersivity with observation scale but the trend is much less clear when the reliability of the data is considered. The longitudinal dispersivities ranged from 10^{-2} to 10^{4} m for scales ranging from 10^{-1} to 10^{5} m, but the largest scale for high reliability data was only 250 m. When the data are classified according to porous versus fractured media there does not appear to be any significant difference between these aquifer types. At a given scale, the longitudinal dispersivity values are found to range over 2–3 orders of magnitude and the higher reliability data tend to fall in the lower portion of this range. It is not appropriate to represent the longitudinal dispersivity data by a single universal line. The variations in dispersivity reflect the influence of differing degrees of aquifer heterogeneity at different sites. The data on transverse dispersivities are more limited but clearly indicate that vertical transverse dispersivities are typically an order of magnitude smaller than horizontal transverse dispersivities. Reanalyses of data from several of the field sites show that improved interpretations most often lead to smaller dispersivities. Overall, it is concluded that longitudinal dispersivities in the lower part of the indicated range are more likely to be realistic for field applications.

INTRODUCTION

The phenomenon of dispersive mixing of solutes in aquifers has been the subject of considerable research interest over the past 10 years. Characterizing the dispersivity at a particular field site is essential to any effort in predicting the subsurface movement and spreading of a contaminant plume at that location. Both theoretical and experimental investigations have found that field-scale dispersivities are several orders of magnitude greater than lab-scale values for the same material; it is generally agreed that this difference is a reflection of the influence of natural heterogeneities which produce irregular flow patterns at the field scale. Consequently, laboratory measurements of dispersivity cannot be used to predict field values of dispersivity. Instead field-scale tracer tests are sometimes conducted to estimate dispersivity at a particular site.

Early efforts to document the scale dependence of dispersivity [*Lallemand-Barres and Peaudecerf*, 1978; *Anderson*, 1979; *Pickens and Grisak*, 1981; *Beims*, 1983; *Neretnieks*, 1985] were based on field values of dispersivity reported in the literature and the test scales associated with those values. These studies were useful in that they indeed documented field evidence of the scale effect, but they were lacking in that they did not assess the reliability of the data presented. Because we felt that the data would be more meaningful if their variable quality was recognized, we assembled the dispersivity data along with related information from the original sources and evaluated the reliability or quality of these data [*Gelhar et al.*, 1985]. The graphical results of that work have been widely used by both practitioners and theoreticians, often without appropriate consideration of the reliability of the data. For example, recent theoretical developments based on fractal concepts [*Philip*, 1986; *Wheatcraft and Tyler*, 1988; *Neuman*, 1990] have relied on information similar to that in the work by *Gelhar et al.* [1985] but those studies disregarded the issue of the reliability of the data. We feel that it is important to update the dispersivity information including results from recent comprehensive field experiments and at the same time focus on the interpretations of the reliability of the data. With these goals in mind, this work develops the following: (1) an outline of the theoretical description of dispersive mixing in porous media; (2) a tabular summary of existing data on values of field-scale dispersivity and related site information reported in the literature; (3) an evaluation of the reliability or quality of these values based on clearly delineated criteria; and (4) discussion and interpretation of the applied and theoretical implications of the data.

Paper number 92WR00607.
0043-1397/92/92WR-00607$05.00

THEORETICAL CONCEPTS OF FIELD-SCALE DISPERSIVE MIXING

The mass balance equation governing the transport of an ideal chemically nonreactive conservative solute by a homo-

geneous fluid (constant density and viscosity) that flows through a rigid saturated porous medium is commonly expressed as [e.g., *Bear*, 1972; *de Marsily*, 1986]

$$\frac{\partial c}{\partial t} + v_i \frac{\partial c}{\partial x_i} = \frac{\partial}{\partial x_i}\left(D_{ij} \frac{\partial c}{\partial x_j}\right) \qquad i, j = 1, 2, 3 \qquad (1)$$

where c is the solute concentration, v_i is the seepage velocity component in the x_i direction, and D_{ij} are the components of the dispersion coefficient tensor. The right-hand side of (1) represents the net dispersive transport which is presumed to be Fickian, i.e., the dispersive mass flux is proportional to the concentration gradient. Some investigators [e.g., *Robertson and Barraclough*, 1973; *Bredehoeft and Pinder*, 1973] alternatively define the dispersion coefficient tensor including the porosity n as $D^*_{ij} = nD_{ij}$. When it was clear that D^*_{ij} was used in a study, we converted to the more common form used in (1). The mean flow direction is taken to be x_1, with $v_1 = v$, $v_2 = v_3 = 0$. Assuming that x_1, x_2, and x_3 are principal directions, the dispersivity is simply the ratio of the appropriate component of the dispersive coefficient tensor divided by the magnitude of the seepage velocity, v. To distinguish the field-scale dispersivities from laboratory values, the field-scale values are designated by the uppercase letter A [see *Gelhar and Axness*, 1983] and, to allow for anisotropy of transverse dispersion, a third dispersivity coefficient is used as follows:

$$D_{11} = A_L v \qquad D_{22} = A_T v \qquad D_{33} = A_V v \qquad (2)$$

where A_L is the longitudinal macrodispersivity (field scale), and A_T is the horizontal transverse macrodispersivity, and A_V is the vertical transverse macrodispersivity.

The classical equation (1) with macrodispersivities (2) is standardly used for applied modeling of field-scale solute transport. The macrodispersivities are considered to be a property of some region of the aquifer. Although the macrodispersivity may be a function of space, in most applications it is assumed constant over a region of the aquifer that encompasses the entire plume both horizontally and vertically. Real solute plumes are observed to be three-dimensional [*LeBlanc*, 1982; *Perlmutter and Lieber*, 1970; *MacFarlane et al.*, 1983] and often of limited vertical extent. Although the classical equation is three-dimensional, the two-dimensional form is most commonly applied. Reasons for the use of the two-dimensional form of the equation include lack of three-dimensional data and in the case of numerical models, restrictions on the size of data arrays in the model. Seldom is the two-dimensional form justified on the basis of site conditions or plume observations.

A number of theoretical studies have proposed methods of describing field-scale dispersive mixing. All of the theories view field-scale dispersion as being produced by some kind of small-scale heterogeneity or variability of the aquifer. At present there is considerable debate concerning how to parameterize the variability and model field-scale solute transport. Assuming a perfectly layered aquifer, one group [*Molz et al.*, 1983, 1986] suggests measuring the variability in detail and modeling the transport in each layer with local-scale dispersivities, thus eliminating the need for a field-scale dispersivity. Again assuming a layered aquifer, a second group suggests the use of a scale-dependent or time-dependent field-scale dispersivity [e.g., *Pickens and Grisak*, 1981; *Dieulin*, 1980]. A third group [e.g., *Gelhar and Axness*, 1983; *Dagan*, 1982; *Neuman et al.*, 1987] has examined more general three-dimensional heterogeneity with stochastic methods and concluded the classical equation with constant field-scale dispersivities is applicable to describe transport over large distances. These stochastic approaches incorporate the effects of practically unknowable small-scale variations in flow by means of macrodispersivities which are used in a deterministic transport model describing the large-scale variations in flow by means of the convection terms. Nonetheless, under what circumstances a field-scale dispersivity can be used to describe field-scale solute transport is still an open question. Until the issue is resolved, the field-scale dispersivity concept can be regarded as a working hypothesis which has a sound theoretical basis and finds wide application.

FIELD DATA ON DISPERSIVITY

Summary of Observations

A literature review was conducted to collect reported values of dispersivity from published analyses of field-scale tracer tests and contaminant transport modeling efforts. The literature sources and pertinent data characterizing each reviewed study are summarized in Table 1 which includes information on 59 different field sites. The information compiled from each study includes site location, description of aquifer material, average aquifer saturated thickness, hydraulic conductivity or transmissivity, effective porosity, mean pore velocity, flow configuration, dimensionality of monitoring network, tracer type and input conditions, length scale of the test or problem, reported values of longitudinal and horizontal and vertical transverse dispersivities, and classification of the reliability of the reported data. Blank entries indicate that the information was not provided in the cited documents. This table summarizes information for purposes of comparison only. More detail regarding a particular study may be found in the original sources.

Aquifer characteristics. As indicated by the second through sixth columns from the left, the study sites represent a wide variety of aquifer conditions and settings. Summarized in these columns is information on aquifer material, saturated thickness, hydraulic conductivity or transmissivity, and velocity. The aquifer thickness for each site is the arithmetic average of the range at that site. Hydraulic conductivity and transmissivity values show the range reported at the site. Reported values for effective porosity vary from 0.5% (for fractured media) to 60% (for porous media). When a value was reported as "porosity," we interpreted this as the effective porosity (interconnected pore space), the value used in analysis of the advection-dispersion equation. Where porosity was reported as "total porosity," we have indicated this in the table. The velocity column indicates the mean pore or seepage velocity at a site. In some cases the values were calculated from information provided on average specific discharge, q, and effective porosity, n, as $v = q/n$. Velocities ranged from 0.0003 to 200 m/d.

Methods of determining dispersivity. The seventh through tenth columns from the left summarize the method used to determine the dispersivity for each site. The seventh, eighth, and ninth columns from the left describe experimental conditions: flow configuration, monitoring, tracer and

input; the tenth column from the left summarizes methods of data interpretation. Dispersivity values were calculated or inferred from one of two types of subsurface solute transport events: large-scale, uncontrolled contamination (naturally occurring or human-induced) events, or controlled tracer tests.

Uncontrolled events are characterized by a source input history that is unknown, transport of contaminants by the ambient flow of groundwater, and solute plumes that often extend over regional scales (hundreds of meters). We describe naturally occurring events as "environmental" tracers, implying chemical constituents associated with uncontrolled natural changes occurring in groundwater before the start of a study. Examples of naturally occurring events include tritium in groundwater from recharge containing atmospheric bomb tritium, seawater intrusion, and mineral dissolution. These events are indicated in the "tracer and input" column by the notation "environmental" along with the type of chemical species reported. Examples of human-induced contamination events include leaks and spills to groundwater from landfills, storage tanks, surface impoundments, and infiltration basins. These types of events are indicated by the notation "contamination" in the tracer and input column. Values of dispersivity for uncontrolled events are commonly determined by fitting a one-, two-, or three-dimensional solute transport model to historical data; i.e., values of dispersivity are altered until model output matches historical solute concentration measurements.

The main features distinguishing controlled tracer tests from uncontrolled ones is that in the former, both the quantity and duration of solute input are known. This is indicated by "step" (continuous input of mass) or "pulse" ("instantaneous" or slug input) in the "tracer and input" column. Controlled tracer tests may be conducted under ambient groundwater flow conditions (also referred to as natural gradient tests), or under conditions where the flow configuration is induced by pumping or recharge. The type of test is reported in the "flow configuration" column. Induced flow configurations include radial, two-well, and forced uniform flow. In radial flow tracer tests, a pulse or step input of tracer is injected at a recharge well and the time distribution of tracer is recorded at an observation well (diverging radial flow test), or the tracer is injected at an observation well and the time distribution is recorded at a distant pumping well (converging radial flow test). In a two-well test, both a recharge well and pumping well are operating; tracer is injected at the recharge well and tracer breakthrough is observed at the pumping well. Recirculation of the water (containing tracer) from the pumping well to the recharge well is often employed. "Forced uniform flow" refers to the flow regime at the Bonnaud site in France, where a uniform flow field was generated between two lines of equally spaced wells, one line recharging and one line pumping, with both screened to the full depth of the aquifer. A discussion of the advantages and disadvantages of different types of tracer tests is presented by *Welty and Gelhar* [1989].

A number of methods have been used to evaluate the data from controlled tracer tests, as indicated by column headed "method of data interpretation." These include fitting of one-, or two- or three-dimensional solute transport analytical solutions, and the method of spatial moments. It should be noted that since the velocity is nonuniform for both radial and two-well tracer tests, analysis of the data must account for this effect to determine dispersivity properly for such cases. Nonuniform velocity effects have also been observed in ambient flow tracer tests.

The types of tracers used to determine dispersivity at each site are summarized in the "tracer and input" column along with the input conditions. A variety of chemical and microbiological tracers have been employed for controlled tracer tests. Discussions of the suitability of different chemical and microbial species for tracer tests are presented by *Davis et al.* [1980, 1985] and *Betson et al.* [1985]. A primary consideration in designing a controlled tracer test is whether the species is conservative or nonconservative. A conservative tracer is one that moves with the same velocity as the groundwater and does not undergo radioactive decay, adsorption, degradation, chemical reaction (or in the case of microorganisms, death). If any of these effects are present, they must be accounted for in evaluation of the dispersivity. Another factor important in the choice of a tracer is that it is not present in naturally occurring groundwater, or that it is injected at concentrations much higher than natural background levels.

The "monitoring" column indicates whether two- or three-dimensional monitoring was employed at a site. By two-dimensional monitoring we mean depth-averaged (vertically mixed). Three-dimensional monitoring implies point samples with depth. This information is noted because vertical mixing in an observation well influences the concentration of tracer in a water sample. Several studies [*Meyer et al.*, 1981; *Pickens and Grisak*, 1981] have shown that when a tracer is not injected over the full aquifer depth, vertically mixed samples underestimate the tracer concentration and as a result the longitudinal dispersivity is overestimated. This occurs because the tracer occupies only a portion of the vertical thickness. When a sample from the entire thickness is taken, the true tracer concentration is diluted in the well with tracer-free water. If an attempt is made to interpret the diluted ("measured") concentration, the dispersivity will be overestimated. At many sites there was no indication whether point or fully mixed sampling was performed. From examination of the cases where three-dimensional measurements of solute concentrations were made, it is clear that vertical mixing of the tracer as it travels through the aquifer is often very small [*Sudicky et al.*, 1983; *LeBlanc*, 1982; *Freyberg*, 1986; *Garabedian et al.*, 1988, 1991].

Field dispersivities and scale. The "scale of test" column represents the distance traveled from the source for ambient conditions, or the distance between injection and observation wells for the case of an induced flow configuration. The values of dispersivity reported at the indicated scale are given in the second column from the right. Data from the 59 sites yielded 106 values of longitudinal dispersivity, since often multiple investigations or multiple experiments by one investigator were performed at one site. A plot of the longitudinal dispersivity values as a function of scale is presented in Figure 1. The arithmetic average was plotted in cases where a range was reported either for the scale or dispersivity in Table 1. In some cases, values of dispersivity for individual layers were reported as well as an average "aquifer" value. In these cases the latter value was plotted for the given scale. The symbols on Figure 1 indicate whether the dispersivity value is for fractured media (open symbols, 18 values) or porous media (solid symbols, 88

TABLE 1. Summary of

Reference and Site Name	Aquifer Material	Average Aquifer Thickness, m	Hydraulic Conductivity (m/s) or Transmissivity (m^2/s)	Effective Porosity, %	Velocity, m/d	Flow Configuration
Adams and Gelhar [1991],§ Columbus, Mississippi	very heterogeneous sand and gravel	8	10^{-5} to 10^{-3} m/s	35	0.03–0.5	ambient
Ahlstrom et al. [1977], Hanford, Washington	glaciofluviatile sands and gravels	64	5.7×10^{-4} to 3.0 $\times 10^{-2}$ m/s			ambient
Bentley and Walter [1983], WIPP	fractured dolomite	5.5		18	0.3	two-well recirculating
Bierschenk [1959] and *Cole* [1972], Hanford, Washington	glaciofluviatile sands and gravels	64	1.7×10^{-1} m^2/s	10	26 31	ambinet
Bredehoeft and Pinder [1973], Brunswick, Georgia	limestone	50	6.5×10^{-7} to 8.6 $\times 10^{-7}$ m^2/s	35		radial converging
Claasen and Cordes [1975], Amargosa, Nevada	fractured dolomite and limestone	15	5×10^{-2} to 11 $\times 10^{-2}$ m^2/s	6–60	0.14–3.4	two-well recirculating
Daniels [1981, 1982], Nevada Test Site	alluvium derived from tuff	500	1.7×10^{-5} m/s		0.04	radial converging
Dieulin [1981], Le Cellier (Lozere, France)	fractured granite	20	3×10^{-4} to 9 $\times 10^{-4}$ m/s	2–8	3	radial converging
Dieulin [1980], Torcy, France	alluvial deposits	6	3×10^{-4} m/s		0.5	ambient
Egboka et al. [1983], Borden	glaciofluvial sand	7–27	10^{-5} to 10^{-7} m/s	38	0.01–0.04	ambient
Fenske [1973], Tatum Salt Dome, Mississippi	limestone	53	4.7×10^{-6} m/s	23	1.2	radial diverging
Freyberg [1986], Borden	glaciofluvial sand	9	7.2×10^{-5} m/s	33 (total)	0.09	ambient
Fried and Ungemach [1971], Rhine aquifer	sand, gravel, and cobbles	12			9.6	radial diverging
Fried [1975], Rhine aquifer (salt mines) southern Alsace, France	alluvial; mixture of sand, gravel, and pebbles with clay lenses	125	10^{-3} m/s			ambient
Fried [1975], Lyons, France (sanitary landfill)	alluvial, with sand and gravel and slightly stratified clay lenses	20			5.0	ambient
Garabedian et al. [1988] Cape Cod, Massachusetts	medium to coarse sand with some gravel overlying silty sand and till	70	1.3×10^{-3} m/s	39	0.43	ambient
Gelhar [1982], Hanford, Washington	brecciated basalt interflow zone					two-well without recirculation
Goblet [1982], site B, France	fractured granite	50	10^{-5} to 10^{-7} m/s		84	radial converging
Grove [1977], NRTS, Idaho	basaltic lava and sediments	76	1.4×10^{-1} to 1.4 $\times 10^{1}$ m^2/s	10		ambient
Grove and Beetem [1971], Eddy County (near Carlsbad), New Mexico	fractured dolomite	12		12	3.5	two-well recirculating
Gupta et al. [1975], Sutter Basin, California	sandstone, shale, sand, and alluvial sediments					ambient
Halevy and Nir [1962] and *Lenda and Zuber* [1970], Nahal Oren, Israel	dolomite	100		3.4	4.0	radial converging
Harpaz [1965], southern coastal plain, Israel	sandstone with silt and clay layers	90			14	radial diverging
Helweg and Labadie [1977], Bonsall subbasin, California						ambient
Hoehn [1983], lower Glatt Valley, Switzerland	layered gravel and silty sand	25	9.2×10^{-4} to 6.6 $\times 10^{-3}$ m/s		3.4 1.8 1.2 8.6 4.1 1.7	ambient

Field Observations

Monitoring	Tracer and Input*	Method of Data Interpretation	Scale of Test, m	Dispersivity $A_L/A_T/A_V$,† m	Classification of Reliability of $A_L/A_T/A_V$ (I, II, III)‡
three-dimensional	Br^- (pulse)	spatial moments	200	7.5	II
two-dimensional	^3H (contamination)	two-dimensional numerical model	20,000	30.5/18.3	III
two-dimensional	PFB, SCN (step)	one-dimensional quasi-uniform flow solution [*Grove and Beetem*, 1971]	23	5.2	III
two-dimensional	fluorescein (pulse)	one-dimensional uniform flow solution	3,500 4,000	6 460	III III
two-dimensional	Cl^- (contamination)	two-dimensional numerical model	2,000	170/52	III
two-dimensional	^3H (pulse)	one-dimensional quasi-uniform flow solution [*Grove and Beetem*, 1971]	122	15	III
two-dimensional	^3H (contamination)	radial flow type curve [*Sauty*, 1980]	91	10–30	III
two-dimensional	Cl^-, I^- (pulse)	radial flow type curve [*Sauty*, 1980]	5	0.5	II
two-dimensional (resistivity)	Cl^- (pulse)	one-dimensional uniform flow solution	15	3	III
three-dimensional	^3H (environmental)	one-dimensional uniform flow solution	600	30–60	III
	^3H (pulse)	one-dimensional uniform flow solution	91	11.6	III
three-dimensional	Br^-, Cl^- (pulse)	spatial moments	90	0.43/0.039	I
	Cl^- (pulse)	one-dimensional radial flow numerical model	6	11	III
three-dimensional	Cl^- (contamination)	two-dimensional numerical model	800	15/1	III
two-dimensional	EC (contamination)	two-dimensional numerical model	600–1000	12/4	III
three-dimensional	Br^- (pulse)	spatial moments	250	0.96/0.018/ 0.0015	I
two-dimensional	^{131}I (pulse)	one-dimensional nonuniform flow solution along streamlines [*Gelhar*, 1982]	17.1	0.60	I
two-dimensional	RhWt, SrCl (pulse)	one-dimensional uniform flow solution including borehole flushing effects	17	2	III
two-dimensional	Cl^- (contamination)	two-dimensional numerical model	20,000	91/91	III
two-dimensional	^3H (step)	one-dimensional quasi-uniform flow solution [*Grove and Beetem*, 1971]	55	38.1	III
	Cl^- (environmental)	three-dimensional numerical model	50,000	80–200/ 8–20	III
two-dimensional	^{60}Co (pulse)	one-dimensional uniform flow solution	250	6	II
two-dimensional	Cl^- (step)	one-dimensional radial flow solution	28	0.1–1.0	II
	TDS (contamination)	two-dimensional numerical model	14,000	30.5/9.1	III
two-dimensional	uranine (pulse)	one-dimensional uniform flow solution for layers	4.4 4.4 4.4 10.4 10.4 10.4	0.1 0.01 0.2 0.3 0.04 0.7	III III

TABLE 1.

Reference and Site Name	Aquifer Material	Average Aquifer Thickness, m	Hydraulic Conductivity (m/s) or Transmissivity (m^2/s)	Effective Porosity, %	Velocity, m/d	Flow Configuration
Hoehn and Santschi [1987], lower Glatt Valley, Switzerland	layered gravel and silty sand	27.5	8.1×10^{-5} to 6.6×10^{-3} m/s		1.5 3.2 5.6 3.9 3.2	ambient ambient
Huyakorn et al. [1986], Mobile, Alabama	layered medium sand	21.6		0.35		two-well without recirculation
Iris [1980], Campuget (Gard), France	alluvial deposits	9	3.6×10^{-3} m^2/s		0.05	radial diverging
Ivanovitch and Smith [1978], Dorset, England	fractured chalk		2.2×10^{-3} m/s (fast pulse)	0.5	57.6	radial converging
	chalk		3.6×10^{-4} m/s (slow pulse)	2.3	9.6	radial converging
Kies [1981], New Mexico State University, Las Cruces	fluvial sands		9.55×10^{-5} m/s	42 (total)		ambient
Klotz et al. [1980], Dormach, Germany	fluvioglacial gravels	14			20	radial converging
Konikow [1976], Rocky Mountain Arsenal	alluvium			30		ambient
Konikow and Bredehoeft [1974], Arkansas River valley (at La Junta, Colorado)	alluvium, inhomogeneous clay, silt, sand and gravel		2.4×10^{-4} to 4.2×10^{-3} m/s	20		ambient
Kreft et al. [1974], Poland	sand	2.5	3.1×10^{-5} to 1.5×10^{-4} m/s; 1.2×10^{-4} m^2/s	24	29	radial converging
Kreft et al. [1974], Zn-Pb deposits, Poland	fractured dolomite	57	2.5×10^{-4} to 4.7×10^{-4} m/s	2.4	7.5 100	radial converging
	fractured dolomite	48	2.5×10^{-4} to 4.7×10^{-4} m/s	2.4	60.1 22.7	radial converging
Kreft et al. [1974], sulfur deposits, Poland	limestone	7	1.1×10^{-4} m/s	12.3	10 10.8	radial converging
	limestone	7	1.1×10^{-4} m/s	12.3	8.6	radial converging
Lau et al. [1957], University of California, Berkeley	sand and gravel with clay lenses	1.5	9×10^{-4} m/s	30	7	radial diverging
Lee et al. [1980], Perch Lake, Ontario, (lake bed)	sand		3.2×10^{-5} m/s		0.14	ambient
Leland and Hillel [1981], Amherst, Massachusetts	fine sand and glacial till	0.75	2.4 to 3×10^{-5} m/s	40	0.3–0.6	ambient
Mercado [1966], Yavne region, Israel	sand and sandstone with some silt and clay	80	2.1×10^{-8} to 2.4×10^{-6} m^2/s	23.3	0.84–3.4	radial diverging/converging
Meyer et al. [1981]; Koeberg Nuclear Power Station, South Africa	sand	20			0.12	ambient
Molinari and Peaudecerf [1977] and *Sauty* [1977], Bonnaud, France	sand	3	8.3×10^{-4} to 1.1×10^{-3} m^2/s		2.7 1.0 2.4 1.0 2.0 2.0	forced uniform
Moltyaner and Killey [1988*a*, *b*], Twin Lake aquifer (Chalk River)	fluvial sand			40.8 (total)	1.2	ambient
Naymik and Barcelona [1981], Meredosia, Illinois (Morgan County)	unconsolidated sand and gravel	27	2.2×10^{-2} to 4.3×10^{-2} m^2/s			ambient

(continued)

Monitoring	Tracer and Input*	Method of Data Interpretation	Scale of Test, m	Dispersivity $A_L/A_T/A_V$,† m	Classification of Reliability of $A_L/A_T/A_V$ (I, II, III)‡
two-dimensional	uranine (pulse)	temporal moments	4.4	1.1	II
			10.4	1.2	II
two-dimensional	^3H (environmental)	temporal moments	100	6.7	III
			110	10.0	III
			500	58.0	III
two-dimensional	Br^- (pulse)	two-dimensional numerical model	38.3	4.0	I
three-dimensional	heat (pulse)	two-dimensional radial numerical model	40	3/1.5	II
	^{82}Br (pulse)	one-dimensional uniform flow solution	8	3.1	III
	^{82}Br (pulse)	one-dimensional uniform flow solution	8	1.0	III
two-dimensional	NO_3^- (pulse)	two-dimensional uniform flow solution	25	1.6/0.76	III
two-dimensional	^{82}Br, uranine (pulse)	one-dimensional uniform flow solution	10	5, 1.9	II
	Cl^- (contamination)	two-dimensional numerical model	13,000	30.5	III
two-dimensional	dissolved solids (contamination)	two-dimensional numerical model	18,000	30.5/9.1	III
two-dimensional	^{131}I (pulse)	one-dimensional uniform flow solution	5–6	0.18	II
	^{131}I (pulse)	one-dimensional uniform flow solution	22	44–110	II
	^{131}I (pulse)	one-dimensional uniform flow solution	21.3	2.1	II
	^{58}Co (pulse)	one-dimensional uniform flow solution	27	2.7–27	II
	^{58}Co (pulse)	one-dimensional uniform flow solution	41.5	20.8	II
	Cl^- (step)	one-dimensional radial numerical model	19	2–3	I
three-dimensional	Cl^- (pulse)	one-dimensional uniform flow solution	≤6	0.012	II
three-dimensional	Cl^- (pulse)	two-dimensional uniform flow solution	4	0.05–0.07	III
three-dimensional	^{60}Co, Cl^- (step)	one-dimensional radial flow solution	≤115 (observation wells)	0.5–1.5 (injection phase)	I
three-dimensional	^{131}I (pulse)	one-dimensional uniform flow solution for layers	2–8	0.01, 0.03, 0.01, 0.05 for layers; 0.42 for depth average	III
two-dimensional	I^-	two-dimensional uniform flow solution	13	0.79	I
	^3H		13	1.27	I
	^{131}I		13	0.72	I
	^{131}I		26	2.23	I
	^{131}I		33.2	1.94/0.11	I
	^{131}I (pulse)		32.5	2.73/0.11	I
three-dimensional	^{131}I (pulse)	two-dimensional uniform flow solution	40	0.06–0.16/ 0.0006–0.002	II
two-dimensional	NH_3 (contamination)	two-dimensional numerical model	16.4	2.13–3.35/ 0.61–0.915	III

TABLE 1.

Reference and Site Name	Aquifer Material	Average Aquifer Thickness, m	Hydraulic Conductivity (m/s) or Transmissivity (m^2/s)	Effective Porosity, %	Velocity, m/d	Flow Configuration
New Zealand Ministry of Works and Development [1977] Heretaunga aquifer, New Zealand:						
Roys Hill site	gravel with cobbles	100	0.29 m^2/s	22	150–200	ambient
Flaxmere site 2	alluvium (gravels)	120	0.37 m^2/s	22	20–25	ambient
Hastings City rubbish dump	alluvium (gravels)		0.14, 0.35 m^2/s		20	ambient
Oakes and Edworthy [1977], Clipstone, United Kingdom	sandstone	44	2.4×10^{-6} to 1.4×10^{-4} m/s	32–48	5.6, 4.0 9.6	radial diverging
					2.4, 3.6	radial converging
Papadopulos and Larson [1978], Mobile, Alabama	medium to fine sand interspersed with clay and silt	21	5×10^{-4} m/s (horizontal) and 5.1×10^{-5} m/s (vertical)	25	0.05	radial diverging
Pickens and Grisak [1981], Chalk River	sand	8.5	2×10^{-5} to 2×10^{-4} m/s	38	0.15	two-well recirculating
	sand	8.5	2×10^{-5} to 2×10^{-4} m/s	38	0.15	radial diverging/converging
Pinder [1973], Long Island	glacial outwash	43	7.5×10^{-4} m/s	35	0.43	regional
Rabinowitz and Gross [1972], Roswell Basin, New Mexico	fractured limestone	61	1.1×10^{-2} to 2.9×10^{-1} m^2/s	1	11–21	regional
Rajaram and Gelhar [1991], Borden	glaciofluvial sand	9	7.2×10^{-5} m/s	33 (total)	0.09	ambient
Roberts et al. [1981], Palo Alto bay lands	sand, gravel, and silt	2	1.25×10^{-3} m^2/s (lower aquifer); 5.0×10^{-4} m^2/s (upper aquifer)	25	15.5 12.0 3.5 25.6 7.9	radial diverging
Robertson [1974] and *Robertson and Barraclough* [1973], NRTS, Idaho	basaltic lava and sediments	76	1.4×10^{-1} to 1.4×10^{1} m^2/s	10	1.5–8	regional
Robson [1974, 1978], Barstow, California	alluvial sediments	27	2.1×10^{-4} to 1×10^{-2} m^2/s	40		two-well recirculating
				40	3	regional
Robson [1978], Barstow, California	alluvial sediments	30.5	5×10^{-4} m/s	40		regional
Rousselot et al. [1977], Byles–Saint Vulbas near Lyon, France	clay, sand, and gravel	12	6.5×10^{-3} to 1.5×10^{-2} m/s	14 2.1–18 1.8–5.9 11–24	18 11.5, 3.8 46.7, 16 24	radial converging
Sauty [1977], Corbas, France	sand and gravel	12			125, 100 15.5, 78 6.9	radial converging
Sauty et al. [1978], Bonnaud, France	sand	3	8.3×10^{-4} to 1.1×10^{-3} m^2/s			radial diverging
Segol and Pinder [1976], Cutler area, Biscayne Bay aquifer, Florida	fractured limestone and calcareous sandstone	30.5	0.45×10^{-2} m/s (horizontal) and 0.09×10^{-4} m/s (vertical)	25	20	ambient
Sudicky et al. [1983], Borden	glaciofluvial sand	7–27	4.8×10^{-5} to 7.6×10^{-5} m/s	38	0.07–0.25	ambient
Sykes et al. [1982, 1983], Borden	sand		5.8 to 7.2×10^{-5} m/s	35		ambient
Sykes et al.[1983], Mobile, Alabama	sand, silt, and clay	21	5×10^{-4} m/s (horizontal) and 2.5×10^{-5} m/s (vertical)	25	0.05	radial diverging

(continued)

Monitoring	Tracer and Input*	Method of Data Interpretation	Scale of Test, m	Dispersivity $A_L/A_T/A_V$,† m	Classification of Reliability of $A_L/A_T/A_V$ (I, II, III)‡
three-dimensional	^{131}I, RhWt, ^{82}Br, Cl^-, *E. Coli* (pulse)	three-dimensional uniform flow solution	54–59	1.4–11.5/ 0.1–3.3/ 0.04–0.10	II
three-dimensional	RhWt, ^{82}Br (pulse)	three-dimensional uniform flow solution	25	0.3–1.5/ · · ·/0.06	II
three-dimensional	Cl^- (contamination)	three-dimensional uniform flow solution	290	41/10/0.07	III
two-dimensional	^{82}Br (pulse)	radial flow numerical model	6	0.16, 0.38	II
			3	0.31	II
two-dimensional	Cl^-, I^- (pulse)		6	0.6	II
			3	0.6	II
two-dimensional	heat (step)	two-dimensional numerical model	57.3	1.5	II
three-dimensional	^{51}Cr (step)	one-dimensional quasi-uniform flow solution	8	0.5	III
three-dimensional	^{131}I (step)	one-dimensional radial flow solution	3	0.03	III
three-dimensional	Cr^{+6} (contamination)	two-dimensional numerical model	1,000	21.3/4.2	III
two-dimensional	^3H (environmental)	one-dimensional uniform flow solution	32,000	20–23	III
three-dimensional	Br^-, Cl^- (pulse)	spatial moments	90	0.50/0.05/ 0.0022	I
two-dimensional	Cl^- (step)	one-dimensional uniform flow solution	11	5	III
			20	2	III
			40	8	III
			16	4	III
			43	11	III
two-dimensional	Cl^- (contamination)	two-dimensional numerical model	20,000	910/1370	III
two-dimensional	Cl^- (step)	one-dimensional quasi-uniform flow solution	6.4	15.2	III
two-dimensional	TDS (contamination)	two-dimensional numerical model	10,000	61/18	III
three-dimensional	TDS (contamination)	two-dimensional numerical model (vertical section)	3,200	61/· · ·/0.2	III
two-dimensional	I^- (pulse)	one-dimensional uniform flow solution for layers	9.3	6.9	II
			5.3	0.3, 0.7	III
			10.7	0.46, 1.1	III
			7.1	0.37	II
two-dimensional	I^- (pulse)	one-dimensional uniform flow solution for layers	25	11, 1.25	III
			50	25, 6.25	III
			150	12.5	II
two-dimensional	heat (step)	one-dimensional radial flow solution	13	1.0	II
three-dimensional	Cl^- (environmental)	two-dimensional numerical model	490	6.7/· · ·/0.67	III
three-dimensional	Cl^- (pulse)	three-dimensional uniform flow solution	11	0.08/0.03	II
			0.75	0.01/0.005	II
three-dimensional	Cl^- (pulse)	two-dimensional numerical model	700	7.6/· · ·/0.31	III
three-dimensional	heat (step)	three-dimensional numerical model	57.3	0.76/· · ·/0.15	II

TABLE 1.

Reference and Site Name	Aquifer Material	Average Aquifer Thickness, m	Hydraulic Conductivity (m/s) or Transmissivity (m^2/s)	Effective Porosity, %	Velocity, m/d	Flow Configuration
Vaccaro and Bolke [1983], Spokane aquifer, Washington and Idaho	glaciofluvial sand and gravel	152	9×10^{-5} m^2/s to 6.5 m^2/s	7–40	0.003–2.8	ambient
Valocchi et al. [1981], Palo Alto bay lands	sand, gravel, and silt	2	1.25×10^{-3} m^2/s (lower aquifer); 5.0×10^{-4} m^2/s (upper aquifer)	25	27	radial diverging
Walter [1983], WIPP	fractured dolomite	7	8.0×10^{-5} m^2/s	0.7 and 11 (along separate paths)	4.7, 2.4	radial converging
Webster et al. [1970], Savannah River Plant, South Carolina	crystalline, fractured schist and gneiss	76	3.6×10^{-7} m/s		1.3 21.4	two-well recirculating
Werner et al. [1983], Hydrothermal Test Site, Aefligen, Switzerland	gravel	20	6×10^{-3} m/s	17	9.1	ambient
Wiebenga et al. [1967] and *Lenda and Zuber* [1970], Burdekin Delta, Australia	sand and gravel	6.1	5.5×10^{-3} m/s	32	29	radial converging
Wilson [1971] and *Robson* [1974], Tucson, Arizona	unconsolidated gravel, sand, and silt		5.75×10^{-3} m^2/s	38		two-well without recirculation radial diverging
Wood [1981], Aquia Formation, southern Maryland	sand	1,000	2.9×10^{-4} to 8.7×10^{-4} m^2/s	35	0.0003–0.0007	ambient
Wood and Ehrlich [1978] and *Bassett et al.* [1980], Lubbock, Texas	sand and gravel	17	3.2×10^{-3} to 4.4×10^{-3} m^2/s		78	radial converging

*TDS denotes total dissolved solids; EC, electrical conductivity; PFB, pentafluorobenzoate; MTFMB, metatrifluoromethylbenzoate; MFB, metafluorobenzoate; Para-FB, parafluorobenzoate; RhWT, rhodamine-WT dye; and SCN, thiocyanate.

†A_L denotes longitudinal dispersivity; A_T, horizontal transverse dispersivity; and A_V, vertical transverse dispersivity. Reported values for A_L, A_T, and A_V are separated by slashes. Absence of slashes means that values were reported for A_L only. A comma or a dash separating entries means that multiple values or a range of values, respectively, were reported for a particular dispersivity component.

‡For description of classification criteria, see text.

§E. E. Adams and L. W. Gelhar, Field study of dispersion in a heterogeneous aquifer: Spatial moments analysis (submitted to *Water Resources Research*, 1991).

‖Porosity-corrected dispersivity value.

values). The type of event evaluated is indicated by a circle (tracer test, 83 values), triangle (contamination event, 15 values), or square (environmental tracer, eight values). The total numbers of values of dispersivity for each type of medium and test are shown in Table 2. Any reported values of horizontal transverse dispersivity or vertical transverse dispersivity are also listed in the dispersivity column of Table 1. For the cases examined, 24 values of horizontal transverse dispersivity and nine values of vertical transverse dispersivity were reported. In nearly all cases, the horizontal values were found to be 1–2 orders of magnitude less than the longitudinal values, and the vertical values smaller by another order of magnitude.

Evaluation of Dispersivity Data

From Figure 1, it appears that longitudinal dispersivity increases with scale. Field observations of dispersivity ranged from 0.01 m to approximately 5500 m at scales of 0.75 m to 100 km. The longitudinal dispersivity for the two types of aquifer material (porous versus fractured media) tends to scatter over a similar range, although at a smaller scale fractured media seem to show higher values. At each scale there is at least a two-order-of-magnitude range in dispersivity. Because we noted a number of problems with data and their interpretation as we gathered them for Table 1, we would regard any conclusions about Figure 1 with skepticism until further qualifying statements can be made about the data points. Typical problems that we found with the studies reported in Table 1 include the following: data analysis not matched to flow configuration; mass input history unknown; nonconservative effects of tracer not accounted for; dimensionality of the monitoring not matched to the dimensionality of the analysis; and assumption of distinct geologic layers in analysis when their actual presence was not documented. Based on these problems, we decided to rate the data as high (I), medium (II), or low (III) reliability according to the criteria set forth below. Table 3 lists the criteria used to designate either high- or low-reliability data. No specific criteria were defined for the intermediate classification; it encompasses the dispersivity

(continued)

Monitoring	Tracer and Input*	Method of Data Interpretation	Scale of Test, m	Dispersivity $A_L/A_T/A_V$,† m	Classification of Reliability of $A_L/A_T/A_V$ (I, II, III)‡
	Cl^- (contamination)	two-dimensional numerical model	43,400	91.4/27.4	III
	Cl^- (step)	two-dimensional numerical model	16	1.0/0.1	I
two-dimensional	MTFMB, PFB, MFB, para-FB (pulse)	one-dimensional uniform flow solution	30	10–15	III
two-dimensional	^{85}Sr ^{85}Br (pulse)	one-dimensional quasi-uniform flow solution	538	134	III
three-dimensional	heat (step)	one-dimensional numerical model	700	130–234	III
			37	131	III
			105	208	III
			200	234	III
	^{131}I, ^3H (pulse)	one-dimensional uniform flow solution	18.3	0.26	II
three-dimensional	Cl^- (step)	one-dimensional quasi-uniform flow solution	79.2	15.2	III
two-dimensional	Cl^- (step)	one-dimensional radial flow solution	4.6	0.55	III
	Na^+ (environmental)	one-dimensional uniform flow solution	10^5	5,600–40,000	III
two-dimensional	I^- (pulse)	one-dimensional radial flow solution	1.52	0.015	II

values that do not fall into the high or low groups. These classifications do not place strict numerical confidence limits on reported dispersivities, but rather are intended to provide an order-of-magnitude estimate of the confidence we place on a given value. In general, we consider high-reliability dispersivity values to be accurate within a factor of 2. Low-reliability values are considered to be no more accurate than within 1 or 2 orders of magnitude. Intermediate reliability falls somewhere between the extremes. We wish to make a distinction between the judgment of the reliability of the reported dispersivity and the worth of a study. Often, the purpose of a study was for something other than the determination of dispersivity. Our classification of dispersivity is not intended as a judgment on the quality of a study as a whole, but rather to provide us with some criteria with which to screen the large number of data values obtained. By then examining the more reliable data, conclusions which evolve from the data will be more soundly based and alternative interpretations may become apparent.

High-reliability dispersivity data. For a reported dispersivity value to be classified as high reliability, each of the following criteria must have been met.

1. The tracer test was either ambient flow with known input, diverging radial flow, or a two-well pulse test (without recirculation). These three test configurations produce breakthrough curves which are sensitive to the dispersion coefficient and appear to work well in field applications [*Welty and Gelhar*, 1989]. The radial converging flow test is generally considered less satisfactory than the diverging test because breakthrough curves at the pumping well for the converging test frequently exhibit tailing, which complicates the interpretation of these tests. Some researchers attribute this behavior to two or more discrete geologic layers and try to reproduce the observed breakthrough curve by superposition of breakthrough curves in each layer, where the properties of each layer may differ [e.g., *Ivanovitch and Smith*, 1978; *Sauty*, 1977]. The problem with this interpretation is that there are typically numerous heterogeneities on a small scale that cannot be attributed solely to identifiable layers. One possible explanation of the tailing in radial convergent tests is sometimes termed "borehole flushing," where the tail of the breakthrough curve is attributed to the slow flushing of the input slug of tracer out of the injection borehole by the ambient groundwater flow. *Goblet* [1982] measured the slow flushing of tracer out of the

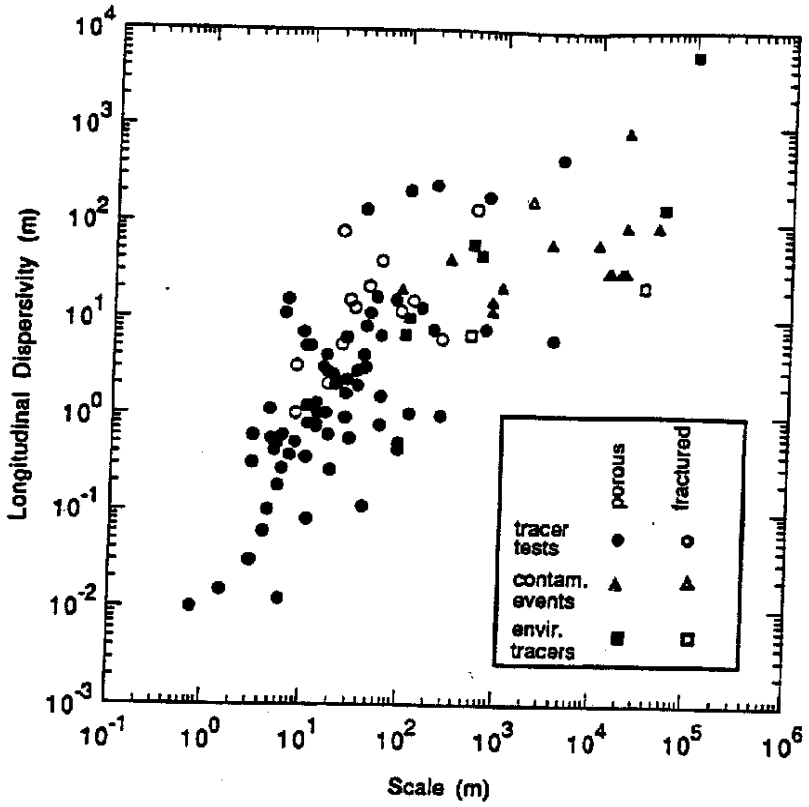

Fig. 1. Longitudinal dispersivity versus scale of observation identified by type of observation and type of aquifer. The data are from 59 field sites characterized by widely differing geologic materials.

borehole and modeled the effect as an exponentially decreasing input. His solution reproduced the tailing observed at the pumping well. In cases where borehole flushing was observed and accounted for, dispersivities obtained from a radial convergent flow test were not excluded from the high-reliability category.

2. The tracer input must be well defined. Both the input concentration and the temporal distribution of the input concentrations must be known (measured). If not, the input is another unknown in the solution of the advection-dispersion equation, and we are less confident in the resulting value of dispersivity.

3. The tracer must be conservative. A reactive or nonconservative tracer complicates the governing equations and resulted in additional parameters that must be estimated. Consequently, we are less confident in the resulting dispersivity. Tracers such as Cl^-, I^-, Br^-, and tritium were considered to be conservative.

4. The dimensionality of the tracer concentration measurements was appropriate. A tracer introduced into an aquifer will spread in three spatial dimensions. High-reliability dispersivities were judged to be those where three-dimensional monitoring was used in all cases except where the aquifer tracer had been injected and measured over the full depth of the aquifer; in this case two-dimensional monitoring was acceptable. In all other cases, where the dimension of the measurement was either not reported or where two-dimensional measurements were used where three-dimensional measurements should have been used, the dispersivity values were judged to be of lower reliability.

5. The analysis of the concentration data was appropriate. Since the interpretation of the tracer data is necessarily linked to the type of tracer test to which the interpretation method is applied, these two features of the field studies were evaluated together. The three general categories of data interpretation can be grouped as follows: (1) breakthrough curve analysis, usually applied to uniform ambient flow tests and radial flow tests [e.g., *Sauty*, 1980]; (2) method of spatial moments, applied to uniform ambient flow tests [*Freyberg*, 1986]; and (3) numerical methods, applied to contamination events [e.g., *Pinder*, 1973; *Konikow and Bredehoeft*, 1974].

A common difficulty with the interpretation of concentration data using breakthrough curve matching to determine dispersivity is the assumption that the dispersivity is constant. The field data assembled in this review suggest that this assumption is not valid, at least for small-scale tests (tens of meters). At larger scales (hundreds of meters) an asymptotic constant value of dispersivity is predicted by some theories. However, at most sites the displacement distance after which the dispersivity is constant is not

TABLE 2. Numbers of Dispersivities for Different Types of Tests and Media

	Tracer Type			
Media Type	Artificial	Contamination	Environmental	Total
Porous	68	14	6	88
Fractured	15	1	2	18
Total	83	15	8	106

TABLE 3. Criteria Used to Classify the Reliability of the Reported Dispersivity Values

Classification	Criteria
High reliability	Tracer test was either ambient flow, radial diverging flow, or two-well instantaneous pulse test (without recirculation). Tracer input was well defined. Tracer was conservative. Spatial dimensionality of the tracer concentration measurements was appropriate. Analysis of the tracer concentration data was appropriate.
Low reliability	Two-well recirculating test with step input was used. Single-well injection-withdrawal test with tracer monitoring at the single well was used. Tracer input was not clearly defined. Tracer breakthrough curve was assumed to be the superposition of breakthrough curves in separate layers. Measurement of tracer concentration in space was inadequate. Equation used to obtain dispersivity was not appropriate for the data collected.

known. Data for which no a priori assumptions were made regarding the dispersivity were considered to be highly reliable.

A second major problem with many of the analyses reviewed was that a one- or two-dimensional solution to the advection-dispersion equation was used when the spreading of the plume under consideration was three-dimensional in nature. High-reliability dispersivities were those for which the dimensionality of the solute plume, the solute measurements, and the data analyses were consistent.

Low-reliability dispersivity data. A reported dispersivity was classified as being of low reliability if one of the following criteria was met.

1. The two-well recirculating test with a step input was used. The problem with this configuration is that, except for very early time where concentrations are low, the breakthrough curve is not strongly influenced by dispersion, but rather is determined by the different travel times along the flow paths established by injection and pumping wells [*Welty and Gelhar*, 1989]. As a result, the two-well test with a step input is generally insensitive to dispersion. For this reason all tests of this type were considered to produce data of low reliability.

2. The single-well injection-withdrawal test was used with tracer monitoring at the pumping well. A difficulty encountered in the small-scale, single-well, injection-withdrawal test (where water is pumped into and out of one well) is that if observations are made at the production well, the dispersion process observed is different from one of unidirectional flow. The problem stems from the fact that macrodispersion near the injection well is due to velocity differences associated with layered heterogeneity of the hydraulic conductivity. In the single-well test with observations made at the production well, the effect observed is that of reversing the velocity of the water. If the tracer travels at different velocities in layers as it radiates outward, it will also travel with the same velocity pattern as it is drawn back to the production well. As a result, the mixing process is partially reversible and the dispersivity would be underestimated relative to the value for unidirectional flow. *Heller* [1972] has carried out experiments which demonstrate the reversibility effect on a laboratory scale.

3. The tracer input was not clearly defined. When a contamination event or environmental tracer is modeled, the tracer input (both quantity and temporal distribution) is not well defined and becomes another unknown in solving the advection-dispersion equation.

4. The tracer breakthrough curve was assumed to be the superposition of breakthrough curves in separate layers when there was little or no evidence of such layers at the field site. These studies generally assume that the porous medium is perfectly stratified, which, especially at the field scale, may not be a valid assumption. At a small scale (a few meters) where the existence of continuous layers may be a reasonable assumption, the dispersivity of each layer does not represent the field-scale parameter. The field-scale dispersivity is a result of the spreading due to the different velocities in each layer.

5. The measurement of tracer concentration in space was inadequate. Under ambient flow conditions the tracer is usually distributed in three-dimensional space, but if the measurements are two-dimensional then the actual tracer cloud cannot be analyzed lacking the appropriate data. If the tracer is introduced over the entire saturated thickness, then two-dimensional measurements would be adequate.

6. The equation used to obtain dispersivity was not appropriate for the data collected. Various assumptions regarding flow and solute characteristics are made in obtaining a solution to the advection-dispersion equation. To apply a particular solution to the data from a field experiment, the assumptions in that solution must be consistent with the experimental conditions. One common example is the case of applying a one-dimensional (uniform velocity) flow solution to a radial flow test in which the converging (or diverging) flow field around the pumping or injection well is clearly nonuniform.

Results of classification. From the classification process, 14 dispersivity values were judged to be of high reliability. The sites where these values were determined include Borden, Ontario, Canada; Otis Air Force Base, Cape Cod, Massachusetts; Hanford, Washington; Mobile, Alabama; University of California, Berkeley; Yavne region, Israel; Bonnaud, France (six tests); and Palo Alto bay lands. There were 61 values judged to be of low reliability for one or more of the reasons discussed above; 31 sites provided data judged to be of intermediate value. Figure 2 depicts the longitudinal dispersivity data replotted with symbols reflecting the reliability classification; the largest symbols indicate data judged to be of highest reliability.

The general compilation of all dispersivity data in Figure 1 indicates that dispersivity might increase indefinitely with scale, but after critically evaluating the data in terms of reliability as shown in Figure 2, it is evident that this trend cannot be extrapolated with confidence to all scales. The largest high-reliability dispersivity value is 4 m (Mobile, Alabama) and the largest scale of high-reliability values is 250 m (Cape Cod, Massachusetts). It is not clear from these data whether dispersivity increases indefinitely with scale or whether the relationship becomes constant for very large scales, as would be predicted by some theories. This points

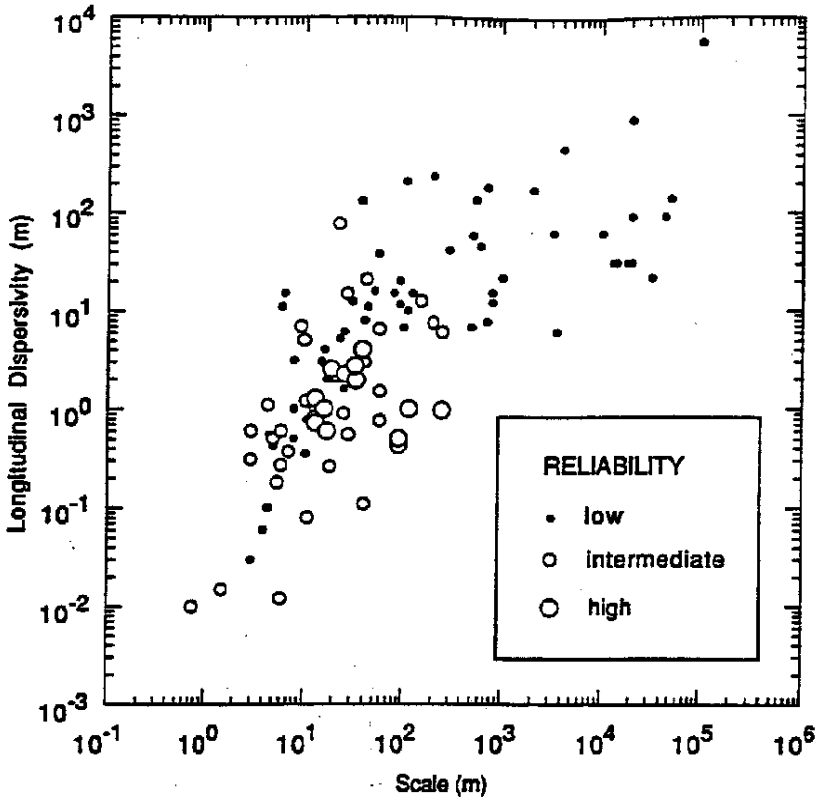

Fig. 2. Longitudinal dispersivity versus scale with data classified by reliability.

to a need for reliable data at scales larger than 250 m. Whether conducting controlled tracer tests at these very large scales is feasible is open to question.

When the reliability of the data is considered, the apparent difference between fractured and porous media at small scales (Figure 1) is regarded to be less significant because none of the fractured media data are of high reliability.

Reanalyses of Selected Dispersivity Data

In cases where the concentration data collected were of high reliability but the method of analysis could be improved, we reevaluated the data to determine a dispersivity value which we judged to be of higher reliability. The details of these analyses are reported by *Welty and Gelhar* [1989]. The results are summarized here.

Corbas, France. The data from this converging radial flow tracer test are reported by *Sauty* [1977]. These data are of particular interest because tests were conducted at three different scales in the same aquifer material; tracer was injected at 25, 50, and 150 m from a pumping well. *Sauty* [1977] evaluated these data using uniform flow solutions to the one-dimensional advection-dispersion equation. At the two smaller-scale tests, he assumed a two-layer scheme, although this assumption was not supported by geologic evidence. For this reason the data at the smaller scales were rated to be of lower reliability than the data at 150 m. We reevaluated these data using a solution that accounts for nonuniform, convergent radial flow effects and that makes no assumptions about geologic layers [*Welty and Gelhar*, 1989]. The values of dispersivity reported by Sauty at 25 m are 11 m and 1.25 m for the two hypothesized layers; we calculated a value of 2.4 m without the assumption of layers. At 50 m, Sauty calculated dispersivity values of 25 m and 6.25 m for the two layers; we calculate an overall value of 4.6 m. At a scale of 150 m, Sauty calculated a dispersivity value of 12.5 m without the assumption of layers; our calculation of 10.5 m is in close agreement. Our calculations indicate that dispersivity increases with scale, accounting for nonuniform flow effects and without the arbitrary assumption of geologic layers.

Savannah River Plant, Georgia. *Webster et al.* [1970] evaluated data from a two-well recirculating test using the methodology of *Grove and Beetem* [1971]. This analysis assumes uniform flow along stream tubes and sums individual breakthrough curves along the stream tubes to obtain a composite breakthrough curve. A dispersivity value of 134 m at a scale of 538 m was obtained using this method. We reevaluated the data using the methodology of *Gelhar* [1982] which accounts for nonuniform flow effects. We obtained a dispersivity value of 47 m from our analysis. We have more confidence in this value because the analysis more accurately represents the actual flow configuration.

Tucson, Arizona. The data reported by *Wilson* [1971] for a two-well test were also evaluated by *Robson* [1974] using a Grove and Beetem–type analysis. Wilson reported a value of longitudinal dispersivity of 15.2 m at a scale of 79.2 m. Using a nonuniform flow solution based on that of *Gelhar* [1982], we calculated a value of longitudinal dispersivity of 1.2 m, an order of magnitude smaller than that of Robson. Again, we have more confidence in this value because the analysis more accurately reflects the actual flow situation.

Columbus, Mississippi. The natural gradient tracer test at the Columbus site (E. E. Adams and L. W. Gelhar, Field

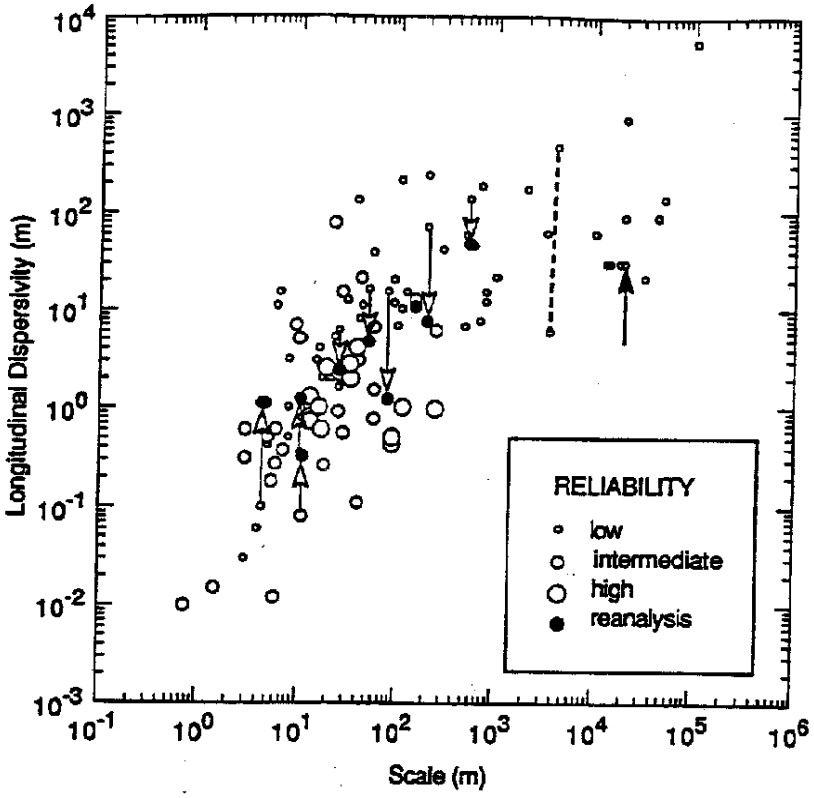

Fig. 3. Longitudinal dispersivity versus scale of observation with adjustments resulting from reanalyses. Arrows indicate reported values at tails and corresponding values from reanalyses at heads. Dashed line connects two dispersivity values determined at the Hanford site.

study of dispersion in a heterogeneous aquifer: Spatial moments analysis, submitted to *Water Resources Research*, 1991; hereinafter Adams and Gelhar, submitted manuscript, 1991) is unique in that the large-scale ambient flow field exhibits strong nonuniformity and the aquifer is very heterogeneous. A superficial spatial moments interpretation, ignoring the flow nonuniformity, indicated a longitudinal dispersivity of around 70 m, whereas a more refined analysis that explicitly includes the influence of flow nonuniformity yields a dispersivity of around 7 m (Adams and Gelhar, submitted manuscript, 1991). This refined estimate is regarded to be of intermediate reliability because of the uncertainty regarding the mass balance at the Columbus site.

From the above reanalyses, all values of dispersivity calculated were smaller than the original values. We have higher confidence in these values because they are associated with solutions to the advection-dispersion equation with more realistic assumptions. In all cases we would rate the new values to be of intermediate reliability instead of low reliability. The reevaluated data are shown as solid symbols on Figure 3 connected to their original values by vertical arrows.

Based on the above reanalyses, we suspect that it is most likely that improved analyses would reduce many of the lower-reliability dispersivities in Figure 2. However, there are a few cases for which more appropriate observations and/or interpretations would most likely lead to larger dispersivities. For example, the Twin Lake natural gradient tracer test [*Moltyaner and Killey*, 1988*a*, *b*] was interpreted by using breakthrough curves at individual boreholes constructed as the average of breakthrough curves in three somewhat arbitrarily defined layers. We suspect that this kind of localized observation will produce a significantly lower dispersivity than would result from a spatial moments analysis which considers the overall spreading of the plume. The magnitude of the possible increase in the dispersivity cannot be assessed because the sampling network did not completely encompass the plume at the Twin Lake site.

Another example is that of the first Borden site natural gradient experiment [*Sudicky et al.*, 1983] which was analyzed using an analytical solution with spatially constant dispersivities. In the near-source region where dispersivities are actually increasing with displacement, this approach will tend to underestimate the magnitude of the dispersivity. *Gelhar et al.* [1985] reanalyzed the first Borden experiment using the method of spatial moments and found that the longitudinal dispersivity at 11 m was 2–4 times that found by *Sudicky et al.* [1983]. The resulting increase in the dispersivity is illustrated in Figure 3 connected to the original point by a vertical line. Because of the incomplete plume sampling and plume bifurcation in this test (only the "slow zone" was analyzed), this point is still regarded to be of intermediate reliability.

Dispersivities at small displacements will also be underestimated if based on breakthrough curves measured in localized samplers in individual layers. Such effects are likely, for example, in the Perch Lake [*Lee et al.*, 1980] and Lower Glatt Valley [*Hoehn*, 1983] interpretations. Later interpretation of the Lower Glatt Valley data using temporal moments [*Hoehn and Santschi*, 1987] shows values an order of

magnitude larger; these are connected with the original values by vertical lines in Figure 3.

As a further illustration of the uncertainty in the longitudinal dispersivity values in Figure 2, consider the data for the Hanford site. The tracer test [*Bierschenk*, 1959; *Cole*, 1972] interpreted from breakthrough curves at two different wells at roughly the same distance (around 4000 m) from the injection point produced values differing by 2 orders of magnitude (see dashed line in Figure 3). This difference illustrates the difficulty in interpreting point breakthrough curves in heterogeneous aquifers, even at this large displacement. The numerical simulations of the contamination plume [*Ahlstrom et al.*, 1977] extending to 20,000 m used a dispersivity of 30.5 m (100 feet) as identified by the bold arrow in Figure 3. Evidently this round number (100 feet) was popular in several different simulations of contaminant plumes.

In none of the cases of simulations of contamination events is there any explicit information on how the dispersivity values were selected or in what sense the values may be optimal. Consequently it is not possible to quantify the uncertainty in dispersivity values based on contamination event simulations. However, experience suggests that, because of the possible tendency to select large dispersivities which avoid the numerical difficulties associated with large grid Peclet numbers, some of the dispersivity values based on contaminant plumes are likely to be biased toward higher values. Such overestimates would occur mainly at larger scales.

The results of these reanalyses provide an explicit indication of the uncertainty in the dispersivity values in Figure 2 and suggest that for large displacements the low-reliability dispersivities are likely to decrease whereas for small displacements some increases can be expected.

Transverse Dispersivities

Although the data on transverse dispersivity are much more limited, they reveal some features which are important in applications. The data on horizontal and vertical transverse dispersivities are summarized in Figures 4 and 5, which show these parameters as a function of scale of observation. The data are portrayed in terms of reliability classification with the largest symbols identifying the high-reliability points.

In the case of the horizontal dispersivity, there appears to be some trend of increasing dispersivity with scale but this appearance results from low-reliability data which finds their origin largely in contaminant event simulations using two-dimensional depth-averaged descriptions. In these contamination situations the sources are often ill-defined; if the actual source area is larger than that represented in the model there will be greater transverse spreading which would incorrectly be attributed to transverse dispersion.

In the case of vertical transverse dispersion (Figure 5), the data are even more limited and certainly do not imply any significant trend with overall scale. Note that there are only two points of high reliability, those corresponding to the Borden [*Freyberg*, 1986] and Cape Cod [*Garabedian et al.*, 1988, 1991] sites. The estimate of the vertical transverse dispersivity for the Borden site is from the recent three-dimensional analysis of *Rajaram and Gelhar* [1991]. The vertical transverse dispersivity is seen to be much smaller than the horizontal transverse dispersivity, apparently reflecting the roughly horizontal stratification of hydraulic conductivity encountered in permeable sedimentary materials. All of the vertical dispersivities are less than 1 m and high-reliability values are only a few millimeters, this being the same order of magnitude as the local transverse dispersivity for sandy materials.

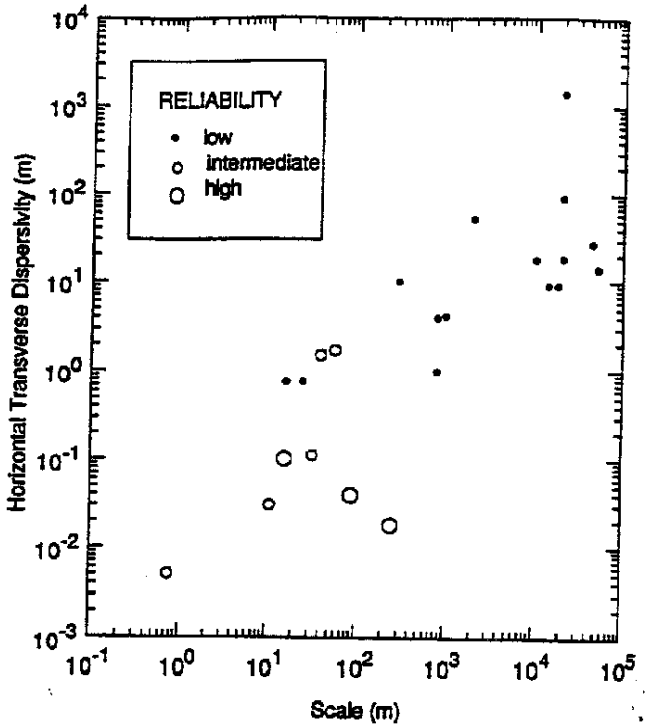

Fig. 4. Horizontal transverse dispersivity as a function of observation scale.

The ratio of longitudinal dispersivity to the horizontal and vertical transverse dispersivities is shown in Figure 6. This form of presentation is used because it is common practice to select constant values for the ratio of longitudinal to transverse dispersivities. For one thing, this plot illustrates the popularity of using, in numerical simulations, a horizontal transverse dispersivity which is about one third of the longitudinal dispersivity (the horizontal dashed line in Figure 6). There does not appear to be any real justification for using this ratio. We are not aware of any simulation work which systematically demonstrates the appropriateness of this value for the horizontal transverse dispersivity. The two high-reliability points show an order of magnitude higher ratio of longitudinal to horizontal transverse dispersivities. The vertical dashed lines in Figure 6 are used to identify three-dimensionally monitored sites for which all three principal components of the dispersivity tensor have been estimated. In all of these cases, the vertical transverse dispersivity is 1–2 orders of magnitude smaller than the horizontal transverse dispersivity. This behavior further emphasizes the small degree of vertical mixing which is frequently encountered in naturally stratified sediments. This small degree of vertical mixing is clearly an important consideration in many applications, such as the design of observation networks to monitor contamination plumes and the development of remediation schemes. Consequently, in order to model many field situations realistically, it will be necessary to use three-dimensional transport models which adequately represent the small but finite vertical mixing.

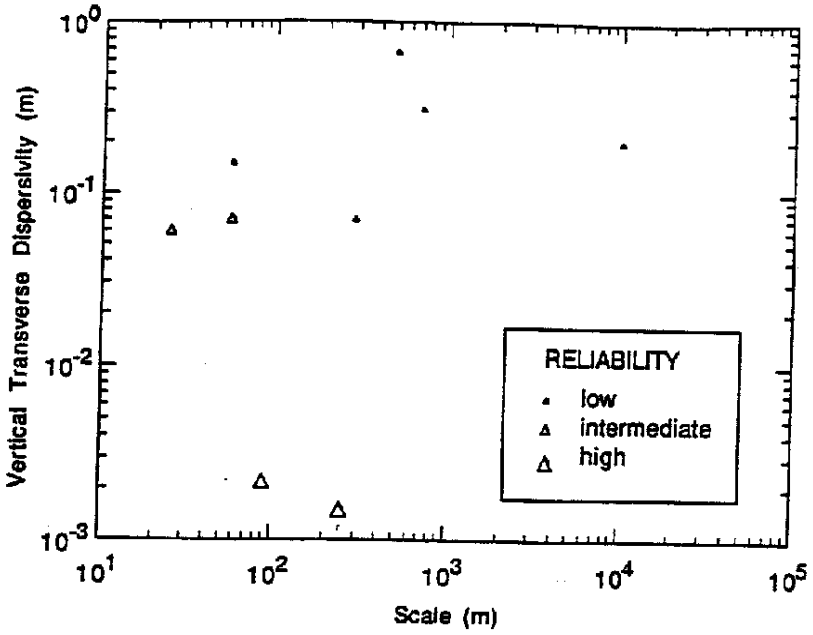

Fig. 5. Vertical transverse dispersivity as a function of observation scale.

INTERPRETATIONS

This review of field observations of dispersive mixing in aquifers demonstrates several overall features which are evident from the graphical and tabular information developed here. Taken in aggregate, without regard for reliability, the data indicate a clear trend of systematic increase of longitudinal dispersivity with scale. In terms of aquifer type (porous versus fractured media) the data at smaller scale may seem to be higher for fractured media but, in view of the lower reliability of the fractured media data, this difference is of minimal significance.

When the data on longitudinal dispersivity are classified according to reliability, the pattern regarding scale dependence of dispersivity is less clear (see Figure 2). There are no high-reliability points at scales greater than 300 m and the high-reliability points are systematically in the lower portion of the scattering of data. The lack of high-reliability data at scales greater than 300 m reflects the fact that the data beyond that scale are almost exclusively from contamination simulations or environmental tracer studies for which the solute input is typically ill-defined. Because of the very long period of time required to carry out controlled input tracer experiments at these larger scales, such experiments have not been undertaken.

Although the data shown in Figure 2 suggest that some overall trend of increasing dispersivity with scale is plausible, it does not seem reasonable to conclude that a single universal line [*Neuman*, 1990] can be meaningfully identified

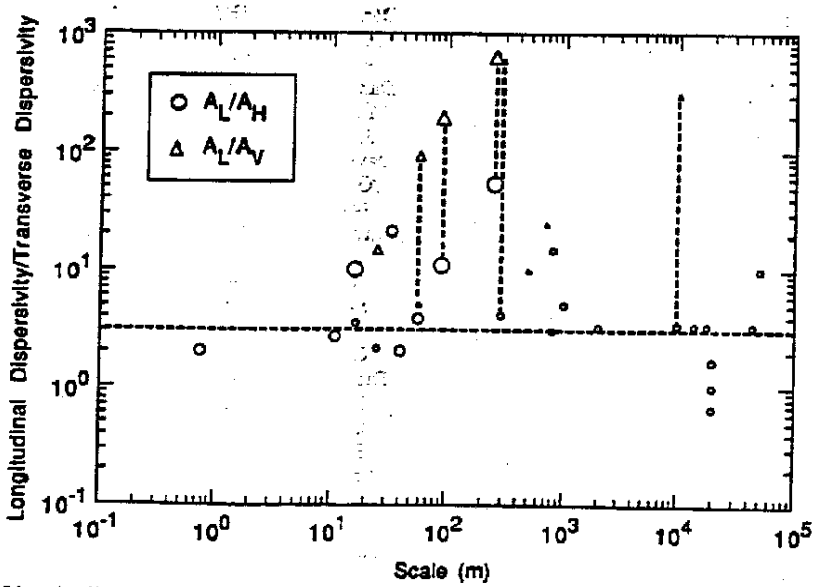

Fig. 6. Ratio of longitudinal to horizontal and vertical transverse dispersivities; largest symbols are high reliability and smallest symbols are low reliability. Vertical dashed lines connecting two points indicate sites where all three principal components of the dispersivity tensor have been measured. Horizontal dashed line indicates a ratio of A_L/A_T = 1/3, which has been widely used in numerical simulations.

by applying standard linear regression to all of the data. Rather we would expect a family of curves reflecting different dispersivities in aquifers with different degrees of heterogeneity. At a given scale, the longitudinal dispersivity typically ranges over 2–3 orders of magnitude. This degree of variation can be explained in terms of the established stochastic theory [e.g., *Gelhar and Axness*, 1983; *Dagan*, 1984] which shows that the longitudinal dispersivity is proportional to the product of the variance and the correlation scale of the natural logarithm of hydraulic conductivity. A compilation of data on these parameters [*Gelhar*, 1986] shows that they vary over a range that can easily explain the range of variation in Figure 2. The theoretical results for the developing dispersion process [*Gelhar et al.*, 1979; *Dagan*, 1984; *Gelhar*, 1987; *Naff et al.*, 1988] show that the longitudinal dispersivity initially increases linearly with displacement distance and gradually approaches a constant asymptotic value [see *Gelhar*, 1987, Figure 9]. One could visualize the behavior of Figure 2 as being the result of superimposing several such theoretical curves with different parameters characterizing aquifer heterogeneity.

The results of reanalyses for several of the individual sites serve to illustrate explicitly the uncertainty involved in the estimates of longitudinal dispersivity. The reanalyses indicate that, for the most part, improved analysis will lead to decreases in the longitudinal dispersivity except possibly for very small displacements where limited localized sampling can produce underestimates of the bulk spreading and mixing. In cases where the dispersivity estimates were based on numerical simulations of contamination events, the degree of uncertainty is likely large and ill-determined, but bias in some of the estimates toward the high side seems most likely.

From an applications perspective, the information assembled here should serve as a strong cautionary note about routinely adopting dispersivities from Figure 2 or a linear regression representation through the data. We feel that the preponderance of evidence favors the use of dispersivity values in the lower half of the range at any given scale. If values in the upper part of the range are adopted, excessively large dilution may be predicted and the environmental consequences misrepresented. In the case of transverse dispersivities, it is particularly important to recognize the very low vertical transverse dispersivities that have been observed at several sites. As a result, many contamination plumes will exhibit very limited vertical mixing with high concentrations at a given horizon. The recognition of such features is of obvious importance in designing monitoring schemes and implementing aquifer remediation. Horizontal transverse dispersivities are typically an order of magnitude smaller than the longitudinal dispersivity whereas vertical transverse dispersivities are another order of magnitude lower.

From a research perspective, the data reviewed here suggest a need for some skepticism regarding "universal" models which represent the scattered data of varying reliability by a single straight line. The presumption of such a universal model ignores the fact that different aquifers will have different degrees of heterogeneity at a given scale. The data suggest that there is a scale dependence of longitudinal dispersivity but reliable data must be developed at larger scales in order to establish the nature of the dependence. Clearly, there is a need for very large scale, long-term, carefully planned experiments extending to several kilometers.

Acknowledgments. The work was supported in part by the Electric Power Research Institute (EPRI), project 2485-5, which was a joint effort of the Massachusetts Institute of Technology (MIT) and the Tennessee Valley Authority (TVA). This portion of the work was done at MIT under contract TV-61664A with TVA. The work was also supported by the National Science Foundation, grant CES-8814615.

REFERENCES

Ahlstrom, S. W., H. P. Foote, R. C. Arnett, C. P. Cole, and R. J. Serne, Multicomponent mass transport model: Theory and numerical implementation (discrete-particle-random-walk-version), *Rep. BNWL-2127*, Battelle Pac. Northwest Lab., Richland, Wash., 1977.

Anderson, M. P., Using models to simulate the movement of contaminants through groundwater flow systems, *CRC Crit. Rev. Environ. Control*, *9*, 97–156, 1979.

Bassett, R. L., et al., Preliminary data from a series of artificial recharge experiments at Stanton, Texas, *U.S. Geol. Surv. Open File Rep.*, *81-0149*, 1980.

Bear, J., *Dynamics of Fluids in Porous Media*, Elsevier Scientific, New York, 1972. (Reprinted by Dover, New York, 1988.)

Beims, U., Planung, Durchführung und Auswertung von Gütepumpversuchen, *Z. Angew. Geol.*, *29*(10), 482–490, 1983.

Bentley, H. W., and G. R. Walter, Two-well recirculating tracer tests at H-2: Waste Isolation Pilot Plant (WIPP), southwest New Mexico, draft paper, Hydro Geochem., Inc., Tucson, Ariz., 1983.

Betson, R. P., J. M. Boggs, S. C. Young, W. R. Waldrop, and L. W. Gelhar, Macrodispersion experiment (MADE): Design of a field experiment to investigate transport processes in a saturated groundwater zone, *Rep. EPRI EA-4082*, Elec. Power Res. Inst., Palo Alto, Calif., June 1985.

Bierschenk, W. H., Aquifer characteristics and ground-water movement at Hanford, *Rep. HW-60601*, Hanford At. Products Oper., Richland, Wash., 1959.

Bredehoeft, J. D., and G. F. Pinder, Mass transport in flowing groundwater, *Water Resour. Res.*, *9*(1), 144–210, 1973.

Claasen, H. C., and E. H. Cordes, Two-well recirculating tracer test in fractured carbonate rock, Nevada, *Hydrol. Sci. Bull.*, *20*(3), 367–382, 1975.

Cole, J. A., Some interpretations of dispersion measurements in aquifers, *Groundwater Pollution in Europe*, edited by J. A. Cole, pp. 86–95, Water Research Association, Reading, England, 1972.

Dagan, G., Stochastic modeling of groundwater flow by unconditional and conditional probabilities, 2, The solute transport, *Water Resour. Res.*, *18*(4), 835–848, 1982.

Dagan, G., Solute transport in heterogeneous porous formations, *J. Fluid Mech.*, *145*, 151–177, 1984.

Daniels, W. R. (Ed.), Laboratory field studies related to the radionuclide migration project, *Progress Rep. LA-8670-PR*, Los Alamos Sci. Lab., Los Alamos, N. M., 1981.

Daniels, W. R. (Ed.), Laboratory field studies related to the radionuclide migration project (draft), *Progress Rep. LA-9192-PR*, Los Alamos Sci. Lab., Los Alamos, N. M., 1982.

Davis, S. N., G. M. Thompson, H. W. Bentley, and G. Stiles, Groundwater tracers—A short review, *Ground Water*, *18*(1), 14–23, 1980.

Davis, S. N., D. J. Campbell, H. W. Bentley, and T. J. Flynn, An introduction to groundwater tracers, *Rep. EPA/600/2-85/022*, Environ. Prot. Agency, Washington, D. C., 1985. (Available as *NTIS PB86-100591* from Natl. Tech. Inf. Serv., Springfield, Va.)

de Marsily, G., *Quantitative Hydrogeology*, Academic, San Diego, Calif., 1986.

Dieulin, A., Propagation de pollution dans un aquifere alluvial: L'effet de parcours, doctoral dissertation, Univ. Pierre et Marie Curie-Paris VI and l'Ecole Natl. Super. des Mines de Paris, Fontainebleau, France, 1980.

Dieulin, A., Lixiviation in situ d'un gisement d'uranium en milieu granitique, *Draft Rep. LHM/RD/81/63*, Ecole Natl. Super. des Mines de Paris, Fontainebleau, France, 1981.

Egboka, B. C. E., J. A. Cherry, R. N. Farvolden, and E. O. Frind, Migration of contaminants in groundwater at a landfill: A case study, 3, Tritium as an indicator of dispersion and recharge, *J. Hydrol.*, *63*, 51–80, 1983.

Fenske, P. R., Hydrology and radionuclide transport, monitoring well HT-2m, Tatum Dome, Mississippi, *Proj. Rep. 25, Tech. Rep.*

NVD-1253-6, Cent. for Water Resour. Res., Desert Res. Inst., Univ. of Nev. Syst., Reno, 1973.

Freyberg, D. L., A natural gradient experiment on solute transport in a sand aquifer, 2, Spatial moments and the advection and dispersion of nonreactive tracers, *Water Resour. Res.*, *22*(13), 2031–2046, 1986.

Fried, J. J., *Groundwater Pollution*, Elsevier, New York, 1975.

Fried, J. J., and P. Ungemach, Determination in situ du coefficient de dispersion longitudinale d'un milieu poreux naturel, *C. R. Acad. Sci., Ser. 2*, *272*, 1327–1329, 1971.

Garabedian, S. P., L. W. Gelhar, and M. A. Celia, Large-scale dispersive transport in aquifers: Field experiments and reactive transport theory, *Rep. 315*, Ralph M. Parsons Lab. for Water Resour. and Hydrodyn., Mass. Inst. of Technol., Cambridge, 1988.

Garabedian, S. P., D. R. LeBlanc, L. W. Gelhar, and M. A. Celia, Large-scale natural gradient tracer test in sand and gravel, Cape Cod, Massachusetts, 2, Analysis of tracer moments for a nonreactive tracer, *Water Resour. Res.*, *27*(5), 911–924, 1991.

Gelhar, L. W., Analysis of two-well tracer tests with a pulse input, *Rep. RHO-BW-CR-131 P*, Rockwell Intl., Richland, Wash., 1982.

Gelhar, L. W., Stochastic subsurface hydrology from theory to applications, *Water Resour. Res.*, *22*, 135S–145S, 1986.

Gelhar, L. W., Stochastic analysis of solute transport in saturated and unsaturated porous media, *NATO ASI Ser., Ser. E*, *128*, 657–700, 1987.

Gelhar, L. W., and C. L. Axness, Three dimensional stochastic analysis of macrodispersion in aquifers, *Water Resour. Res.*, *19*(1), 161–180, 1983.

Gelhar, L. W., A. L. Gutjahr, and R. L. Naff, Stochastic analysis of macrodispersion in a stratified aquifer, *Water Resour. Res.*, *15*(6), 1387–1397, 1979.

Gelhar, L. W., A. Mantaglou, C. Welty, and K. R. Rehfeldt, A review of field-scale physical solute transport processes in saturated and unsaturated porous media, *EPRI Rep. EA-4190*, Elec. Power Res. Inst., Palo Alto, Calif., Aug. 1985.

Goblet, P., Interpretation d'experiences de tracage en milieu granitique (site B), *Rep. LHM/RD/82/11*, Cent. d'Inf. Geol., Ecole Natl. Super. des Mines de Paris, Fontainebleau, France, 1982.

Grove, D. B., The use of Galerkin finite-element methods to solve mass transport equations, *Rep. USGS/WRD/WRI-78/011*, U.S. Geol. Surv., Denver, Colo., 1977. (Available as *NTIS PB 277-532* from Natl. Tech. Inf. Serv., Springfield, Va.)

Grove, D. B., and W. A. Beetem, Porosity and dispersion constant calculations for a fractured carbonate aquifer using the two-well tracer method, *Water Resour. Res.*, *7*(1), 128–134, 1971.

Gupta, S. K., K. K. Tanji, and J. N. Luthin, A three-dimensional finite element ground water model, *Rep. UCAL-WRC-C-152*, Calif. Water Resour. Cent., Univ. of Calif., Davis, 1975. (Available as *NTIS PB 248-925* from Natl. Tech. Inf. Serv., Springfield, Va.)

Halevy, E., and A. Nir, Determination of aquifer parameters with the aid of radioactive tracers, *J. Geophys. Res.*, *67*(5), 2403–2409, 1962.

Harpaz, Y., Field experiments in recharge and mixing through wells, *Underground Water Storage Study Tech. Rep. 17, Publ. 483*, Tahal–Water Plann. for Isr., Tel Aviv, 1965.

Heller, J. P., Observations of mixing and diffusion in porous media, *Proc. Symp. Fundam. Transp. Phenom. Porous Media, 2nd*, 1–26, 1972.

Helweg, O. J., and J. W. Labadie, Linked models for managing river basin salt balance, *Water Resour. Res.*, *13*(2), 329–336, 1977.

Hoehn, E., Geological interpretation of local-scale tracer observations in a river-ground water infiltration system, draft report, Swiss Fed. Inst. Reactor Res. (EIR), Würenlingen, Switzerland, 1983.

Hoehn, E., and P. H. Santschi, Interpretation of tracer displacement during infiltration of river water to groundwater, *Water Resour. Res.*, *23*(4), 633–640, 1987.

Huyakorn, P. S., P. F. Anderson, F. J. Motz, O. Güven, and J. G. Melville, Simulations of two-well tracer tests in stratified aquifers at the Chalk River and the Mobile sites, *Water Resour. Res.*, *22*(7), 1016–1030, 1986.

Iris, P., Contribution à l'étude de la valorisation energetique des aquifères peu profonds, thèse de docteur-ingenieur, Ecole des Mines de Paris, Fontainebleau, France, 1980.

Ivanovitch, M., and D. B. Smith, Determination of aquifer parameters by a two-well pulsed method using radioactive tracers, *J. Hydrol.*, *36*(1/2), 35–45, 1978.

Kies, B., Solute transport in unsaturated field soil and in groundwater, Ph.D. dissertation, Dep. of Agron., N. M., State Univ., Las Cruces, 1981.

Klotz, D., K. P. Seiler, H. Moser, and F. Neumaier, Dispersivity and velocity relationship from laboratory and field experiments, *J. Hydrol.*, *45*(3/4), 169–184, 1980.

Konikow, L. F., Modeling solute transport in ground water, in *Environmental Sensing and Assessment: Proceedings of the International Conference*, article 20-3, Institute for Electrical and Electronic Engineers, Piscataway, N. J., 1976.

Konikow, L. F., and J. D. Bredehoeft, Modeling flow and chemical quality changes in an irrigated stream-aquifer system, *Water Resour. Res.*, *10*(3), 546–562, 1974.

Kreft, A., A. Lenda, B. Turek, A. Zuber, and K. Czauderna, Determination of effective porosities by the two-well pulse method, *Isot. Tech. Groundwater Hydrol., Proc. Symp.*, *2*, 295–312, 1974.

Lallemande-Barres, A., and P. Peaudecerf, Recherche des relations entre la valeur de la dispersivité macroscopique d'un milieu aquifère, ses autres caractéristiques et les conditions de mesure, *Bull. Bur. Rech. Geol. Min., Sect. 3, Ser. 2, 4*, 1978.

Lau, L. K., W. J. Kaufman, and D. K. Todd, Studies of dispersion in a radial flow system, Canal Seepage Research: Dispersion Phenomena in Flow Through Porous Media, *Progress Rep. 3, I.E.R. Ser. 93, Issue 3*, Sanit. Eng. Res. Lab., Dep. of Eng. and School of Public Health, Univ. of Calif., Berkeley, 1957.

LeBlanc, D. R., Sewage plume in a sand and gravel aquifer, Cape Cod, Massachusetts, *U.S. Geol. Surv. Open File Rep., 82-274*, 35 pp., 1982.

Lee, D. R., J. A. Cherry, and J. F. Pickens, Groundwater transport of a salt tracer through a sandy lakebed, *Limnol. Oceanogr.*, *25*(1), 46–61, 1980.

Leland, D. F., and D. Hillel, Scale effects on measurement of dispersivity in a shallow, unconfined aquifer, paper presented at Chapman Conference on Spatial Variability in Hydrologic Modeling, AGU, Fort Collins, Colo., July 21–23, 1981.

Lenda, A., and A. Zuber, Tracer dispersion in groundwater experiments, in *Isot. Hydrol. Proc. Symp. 1970*, 619–641, 1970.

MacFarlane, D. S., J. A. Cherry, R. W. Gilham, and E. A. Sudicky, Migration of contaminants at a landfill: A case study, 1, Groundwater flow and plume delineation, *J. Hydrol.*, *63*, 1–29, 1983.

Mercado, A., Recharge and mixing tests at Yavne 20 well field, *Underground Water Storage Study Tech. Rep. 12, Publ. 611*, Tahal–Water Plann. for Isr., Tel Aviv, 1966.

Meyer, B. R., C. A. R. Bain, A. S. M. DeJesus, and D. Stephenson, Radiotracer evaluation of groundwater dispersion in a multilayered aquifer, *J. Hydrol.*, *50*(1/3), 259–271, 1981.

Molinari, J., and P. Peaudecerf, Essais conjoints en laboratoire et sur le terrain en vue d'une approach simplefiée de la prévision des propagations de substances miscibles dans les aquifères réels, paper presented at Symposium on Hydrodynamic Diffusion and Dispersion in Porous Media, Int. Assoc. for Hydraul. Res., Pavis, Italy, 1977.

Moltyaner, G. L., and R. W. D. Killey, Twin Lake tracer tests: Longitudinal dispersion, *Water Resour. Res.*, *24*(10), 1613–1627, 1988*a*.

Moltyaner, G. L., and R. W. D. Killey, Twin Lake tracer tests: Transverse dispersion, *Water Resour. Res.*, *24*(10), 1628–1637, 1988*b*.

Molz, F. J., O. Güven, and J. G. Melville, An examination of scale-dependent dispersion coefficients, *Ground Water*, *21*, 715–725, 1983.

Molz, F. J., O. Güven, J. G. Melville, R. D. Crocker, and K. T. Matteson, Performance, analysis, and simulation of a two-well tracer test at the Mobile site, *Water Resour. Res.*, *22*(7), 1031–1037, 1986.

Naff, R. L., T.-C. J. Yeh, and M. W. Kemblowski, A note on the recent natural gradient tracer test at the Borden site, *Water Resour. Res.*, *24*(12), 2099–2103, 1988.

Naymik, T. G., and M. J. Barcelona, Characterization of a contaminant plume in ground water, Meredosia, Illinois, *Ground Water*, *19*(5), 517–526, 1981.

Neretnieks, I., Transport in fractured rocks, paper presented at the

17th International Congress on the Hydrology of Rock of Low Permeability, Intl. Assoc. of Hydrogeol., Tucson, Ariz., Jan. 7–12, 1985.

Neuman, S. P., Universal scaling of hydraulic conductivities in geologic media, *Water Resour. Res.*, *26*(8), 1749–1758, 1990.

Neuman, S. P., C. L. Winter, and C. M. Newman, Stochastic theory of field-scale dispersion in anisotropic porous media, *Water Resour. Res.*, *23*(3), 453–466, 1987.

New Zealand Ministry of Works and Development, Water and Soil Division, Movement of contaminants into and through the Heretaunga Plains aquifer, report, Wellington, 1977.

Oakes, D. B., and D. J. Edworthy, Field measurement of dispersion coefficients in the United Kingdom, in *Ground Water Quality, Measurement, Prediction, and Protection*, pp. 327–340, Water Research Centre, Reading, England, 1977.

Papadopulos, S. S., and S. P. Larson, Aquifer storage of heated water: II, Numerical simulation of field results, *Ground Water*, *16*(4), 242–248, 1978.

Perlmutter, N. M., and M. Lieber, Dispersal of plating wastes and sewage contaminants in the groundwater and surface water: South Farmingdale–Massapequid area, Nassau County, New York, *U.S. Geol. Surv. Water Supply Pap.*, *1879-G*, 1970.

Philip, J. R., Issues in flow and transport in heterogeneous porous media, *Transp. Porous Media*, *1*, 319–338, 1986.

Pickens, J. F., and G. E. Grisak, Scale dependent dispersion in a stratified granular aquifer, *Water Resour. Res.*, *17*(4), 1191–1211, 1981.

Pinder, G. F., A Galerkin–finite element simulation of groundwater contamination on Long Island, *Water Resour. Res.*, *9*(6), 1657–1669, 1973.

Rabinowitz, D. D., and G. W. Gross, Environmental tritium as a hydrometeorologic tool in the Roswell Basin, New Mexico, *Tech. Completion Rep. OWRR:A-037-NMEX*, N. M. Water Resour. Res. Inst., Las Cruces, 1972.

Rajaram, H., and L. W. Gelhar, Three-dimensional spatial moments analysis of the Borden tracer test, *Water Resour. Res.*, *27*(6), 1239–1251, 1991.

Roberts, P. V., M. Reinhard, G. D. Hopkins, and R. S. Summers, Advection-dispersion-sorption models for simulating the transport of organic contaminants, paper presented at *International Conference on Ground Water Quality Research*, Rice Univ., Houston, Tex., 1981.

Robertson, J. B., Digital modeling of radioactive and chemical waste transport in the Snake River Plain aquifer of the National Reactor Testing Station, Idaho, *U.S. Geol. Surv. Open File Rep.*, *IDO-22054*, 1974.

Robertson, J. B., and J. T. Barraclough, Radioactive and chemical waste transport in groundwater of National Reactor Testing Station: 20-year case history and digital model, *Underground Waste Manage. Artif. Recharge Prepr. Pap. Int. Symp. 2nd*, *1*, 291–322, 1973.

Robson, S. G., Feasibility of digital water quality modeling illustrated by application at Barstow, California, *U.S. Geol. Surv. Water Resourc. Invest.*, *46-73*, 1974.

Robson, S. G., Application of digital profile modeling techniques to ground-water solute transport at Barstow, California, *U.S. Geol. Surv. Water Supply Pap.*, *2050*, 1978.

Rousselot, D., J. P. Sauty, and B. Gaillard, Etude hydrogéologique de la zone industrielle de Blyes-Saint-Vulbas, rapport préliminaire no. 5: Caracteristiques hydrodynamiques du système aquifère, *Rep. Jal 77/33*, Bur. de Rech. Geol. et Min., Orleans, France, 1977.

Sauty, J. P., Contribution à l'identification des paramètres de dispersion dans les aquifères par interprétation des expériences de tracage, dissertation, Univ. Sci. et Med. et Inst. Natl. Polytech. de Grenoble, Grenoble, France, 1977.

Sauty, J. P., An analysis of hydrodispersive transfer in aquifers, *Water Resour. Res.*, *16*(1), 145–158, 1980.

Sauty, J. P., A. C. Gringarten, and P. A. Landel, The effects of thermal dispersion on injection of hot water in aquifers, paper presented at Invitational Well-Testing Symposium, Lawrence Berkeley Lab., Berkeley, Calif., 1978.

Segol, G., and G. F. Pinder, Transient simulation of saltwater intrusion in southeastern Florida, *Water Resour. Res.*, *12*(1), 65–70, 1976.

Sudicky, E. A., J. A. Cherry, and E. O. Frind, Migration of contaminants in groundwater at a landfill: A case study, 4, A natural-gradient dispersion test, *J. Hydrol.*, *63*, 81–108, 1983.

Sykes, J. F., S. B. Pahwa, R. B. Lantz, and D. S. Ward, Numerical simulation of flow and contaminant migration at an extensively monitored landfill, *Water Resour. Res.*, *18*(6), 1687–1704, 1982.

Sykes, J. F., S. B. Pahwa, D. S. Ward, and D. S. Lantz, The validation of SWENT, a geosphere transport model, in *Scientific Computing*, edited by R. Stapleman et al., pp. 351–361, IMAES/North-Holland, Amsterdam, 1983.

Vaccaro, J. J., and E. L. Bolke, Evaluation of water quality characteristics of part of the Spokane aquifer, Washington and Idaho, using a solute transport digital model, *U.S. Geol. Surv. Open File Rep.*, *82-769*, 1983.

Valocchi, A. J., P. V. Roberts, G. A. Parks, and R. L. Street, Simulation of the transport of ion-exchanging solutes using laboratory-determined chemical parameter values, *Ground Water*, *19*(6), 600–607, 1981.

Walter, G. B., Convergent flow tracer test at H-6: Waste isolation pilot plant (WIPP), southeast New Mexico (draft), Hydro Geochem, Inc., Tucson, Ariz., 1983.

Webster, D. S., J. F. Procter, and J. W. Marine, Two-well tracer test in fractured crystalline rock, *U.S. Geol. Surv., Water Supply Pap.*, *1544-I*, 1970.

Welty, C., and L. W. Gelhar, Evaluation of longitudinal dispersivity from tracer test data, *Rep. 320*, Ralph M. Parsons Lab. for Water Resour. and Hydrodyn., Mass. Inst. of Technol., Cambridge, 1989.

Werner, A., et al., Nutzung von Grundwasser fur Warmepumpen, Versickerrungstest Aefligen, Versuch 2, 1982/83, Water and Energy Manage. Agency of the State of Bern, Switzerland, 1983.

Wheatcraft, S. W., and S. W. Tyler, An explanation of scale-dependent dispersivity in heterogeneous aquifers using concepts of fractal geometry, *Water Resour. Res.*, *24*(4), 566–578, 1988.

Wiebenga, W. A., et al., Radioisotopes as groundwater tracers, *J. Geophys. Res.*, *72*(16), 4081–4091, 1967.

Wilson, L. G., Investigations on the subsurface disposal of waste effluents at inland sites, *Res. Develop. Progress Rep. 650*, U.S. Dep. of Interior, Washington, D. C., 1971.

Wood, W., A geochemical method of determining dispersivity in regional groundwater systems, *J. Hydrol.*, *54*(1/3), 209–224, 1981.

Wood, W. W., and G. G. Ehrlich, Use of baker's yeast to trace microbial movement in ground water, *Ground Water*, *16*(6), 398–403, 1978.

L. W. Gelhar, Ralph M. Parsons Laboratory, Department of Civil Engineering, Massachusetts Institute of Technology, Cambridge, MA 02139.

K. R. Rehfeldt, Illinois State Water Survey, 2204 Griffith Drive, Champaign, IL 61820.

C. Welty, Department of Civil and Architectural Engineering, Drexel University, Philadelphia, PA 19104.

(Received April 8, 1991;
revised March 4, 1992;
accepted March 12, 1992.)

ground water

Analysis of a Vertical Dipole Tracer Test in Highly Fractured Rock

by William E. Sanford[1], Peter G. Cook[2], and John C. Dighton[2]

Abstract/

The results of a vertical dipole tracer experiment performed in highly fractured rocks of the Clare Valley, South Australia, are presented. The injection and withdrawal piezometers were both screened over 3 m and were separated by 6 m (midpoint to midpoint). Due to the long screen length, several fracture sets were intersected, some of which do not connect the two piezometers. Dissolved helium and bromide were injected into the dipole flow field for 75 minutes, followed by an additional 510 minutes of flushing. The breakthrough of helium was retarded relative to bromide, as was expected due to the greater aqueous diffusion coefficient of helium. Also, only ~25% of the total mass injected of both tracers was recovered. Modeling of the tracer transport was accomplished using an analytical one-dimensional flow and transport model for flow through a fracture with diffusion into the matrix. The assumptions made include: streamlines connecting the injection and withdrawal point can be modeled as a dipole of equal strength, flow along each streamline is one dimensional, and there is a constant Peclet number for each streamline. In contrast to many other field tracer studies performed in fractured rock, the actual travel length between piezometers was not known. Modeling was accomplished by fitting the characteristics of the tracer breakthrough curves (BTCs), such as arrival times of the peak concentration and the center of mass. The important steps were to determine the fracture aperture (240 μm) based on the parameters that influence the rate of matrix diffusion (this controls the arrival time of the peak concentration); estimating the travel distance (11 m) by fitting the time of arrival of the centers of mass of the tracers; and estimating fracture dispersivity (0.5 m) by fitting the times that the inflection points occurred on the front and back limbs of the BTCs. This method works even though there was dilution in the withdrawal well, the amount of which can be estimated by determining the value that the modeled concentrations need to be reduced to fit the data (~50%). The use of two tracers with different diffusion coefficients was not necessary, but it provides important checks in the modeling process because the apparent retardation between the two tracers is evidence of matrix diffusion and the BTCs of both tracers need to be accurately modeled by the best fit parameters.

Introduction

Many tracer tests in fractured rocks are performed in well-defined fractured zones (Maloszewski and Zuber 1985; Himmelsbach et al. 1998; Jardine et al. 1999) where the injection and sampling occur in this zone and it is generally assumed that the tracer travels only through this zone. In this paper, we present the results of a tracer test using helium and bromide performed in the flow field of a vertical dipole established in a highly fractured metadolostone in the Clare Valley of South Australia (Figure 1). In this system, there exist five sets of fractures (Figure 2). With the injection and withdrawal occurring in relatively large screened sections (3 m), the analysis of the breakthrough data needs to account for tracer being injected into fractures not connected to the withdrawal well and tracer-free water mixing with tracer-tagged water in the withdrawal well. In addition, unlike most other tests, we do not know the actual length of the fracture connecting the two piezometers.

The purpose of this paper is to present a method to analyze breakthrough curves (BTCs) in highly fractured rock. We will show: (1) by fitting the characteristics of the BTCs, estimates of the effective field-scale flow and transport parameters can be made; (2) the use of multiple tracers is important to constrain the flow and transport parameters; and (3) the amount of dilution in the withdrawal well can be estimated.

Model Development

To model the transport of the two tracers, several assumptions need to be made at the beginning. First, it will

[1]Department of Earth Resources, Colorado State University, Fort Collins, CO 80523-1482; (970) 491-5929; fax (970) 491-6307; bills@cnr.colostate.edu

[2]CSIRO Land and Water, Private Bag 2, Glen Osmond SA 5064, Australia; 61 8 83038744; fax 61 8 83038750; peter.cook@adl.clw.csiro.au

Received April 2001, accepted April 2002.

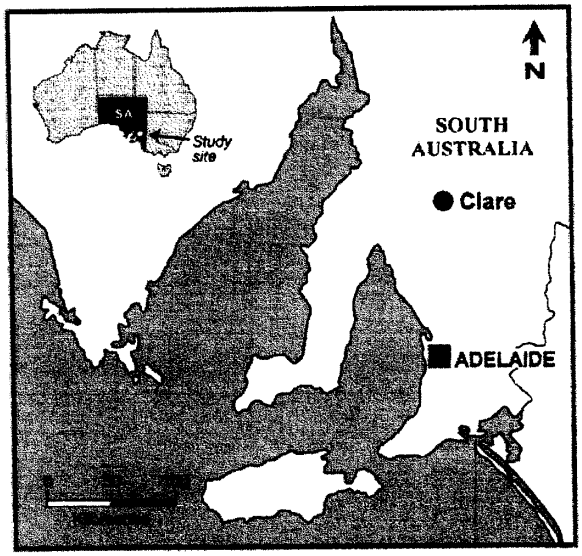

Figure 1. Location of study site in South Australia.

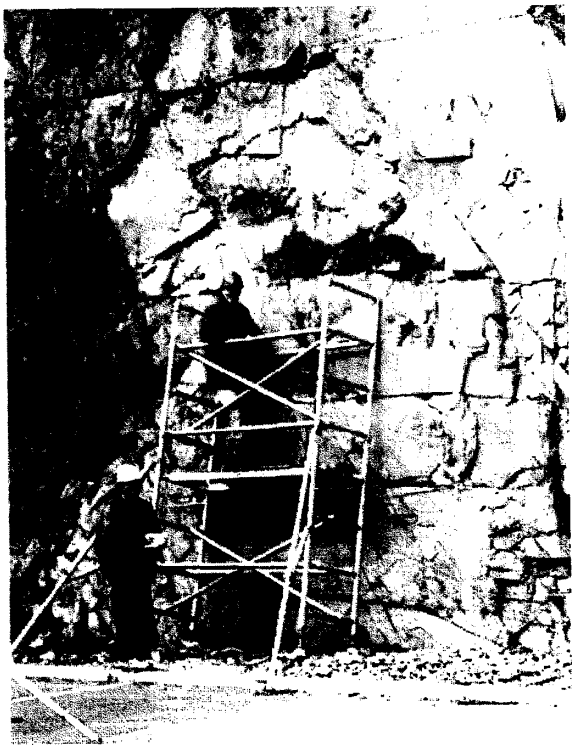

Figure 2. Photo of outcrop showing fracture patterns.

be assumed that the transport between the two piezometers is through a single fracture. Maloszewski and Zuber (1985, 1993) concluded that for short-term experiments on the order of tens of hours, the assumption of a single fracture is applicable. In several other works (Grove and Beetem 1971; Himmelsbach et al. 1998; Jardine et al. 1999) the tracer data was modeled as a single fracture partly because the tracer was injected and withdrawn from a well-defined fractured interval. A second assumption, following Grove and Beetem (1971) and Himmelsbach et al. (1998), is that the flow through the single fracture will follow a series of streamlines that would develop between a dipole of equal strength. A third assumption will be that the flow along each streamline will be considered at a constant velocity. This third assumption will be discussed in more detail later.

As shown in Figure 2, the rock is quite fractured. Each piezometer is screened over a 3 m section. (The height of the person on the scaffold in Figure 2 is approximately 2 m.) Therefore, it is likely that each piezometer intersects fractures that are not connected to the other piezometer. As a result, some of the tracer-tagged injection water may flow out fractures that are not connected to the withdrawal piezometer and the withdrawal piezometer may pull in water from nonconnecting fractures, causing a dilution of the tracer-tagged water that flows between each piezometer.

Another complicating factor for the situation at the field site is that the actual length of the fracture connecting the two piezometers is not known. It can be as small as 6 m (the distance from the bottom of the screened section of the upper piezometer and the top of the screened section of the lower piezometer) or any length greater than that.

To model the flow, we follow methods outlined in Grove and Beetem (1971) and Himmelsbach et al. (1998). In these papers, the flow was assumed to be through a single fracture and was modeled as a series of streamlines following the arcs of circles of different radii connecting the injection and withdrawal points. Grove and Beetem (1971) gave solutions for calculating the length and travel time along each streamline. The length (L) is given by

$$L = \frac{2\,a\,\alpha}{\sin\alpha} \tag{1}$$

where 2a is the spacing between injection and withdrawal points, and α varies between zero and π and is related to the angle at which each streamline leaves the injection point and enters the withdrawal point. The travel time along each streamline is given by

$$t = \frac{\pi\,m\,\theta_f\,(2a)^2}{Q\sin^2\alpha}\,[\alpha\cot\alpha - 1] \tag{2}$$

where Q is the pumping rate, θ_f is the fracture porosity, and m is the thickness of the aquifer.

Grove and Beetem (1971) and Himmelsbach et al. (1998) both modeled the transport through the fracture with one-dimensional analytical solutions. Each streamline represents the same proportion of flow between the wells and, assuming no flow across streamlines, each can be treated as a single flowpath. Himmelsbach et al. (1998) state that 35 streamlines are sufficient to accurately model the flow field of the dipole. Therefore, transport is calculated for each of the 35 streamlines with each contributing 1/35 of the flow. The contribution from each is summed at the times of interest in order to model the BTCs.

Transport modeling was done following the analytical solution of Sudicky and Frind (1982) for parallel fractures in the computer code CRAFLUSH. In this solution, steady-state flow occurs only in the fractures with diffusive exchange with the matrix. The values that are required for

specification are fracture aperture, ground water velocity, fracture spacing, dispersivity in the fracture, effective diffusion coefficient, fracture and matrix retardation, and matrix porosity. To model as a single fracture, we need to use a fracture spacing that is far enough to prevent interaction of neighboring fractures over the time scale of the experiment. Therefore, we chose a spacing of 10.25 m for use in the model, which is more than adequate to prevent the influence of neighboring fractures.

Typically, analytical solutions require the assumption of a constant velocity along the entire flowpath. The velocity along a streamline is not constant. Both Grove and Beetem (1971) and Himmelsbach et al. (1998) used analytical solutions but got around the need for a constant velocity by assuming that each streamline had a unique and constant Peclet number given by dividing the length of the streamline by the dispersivity in the fracture (dispersivity constant for all flowpaths). For the transport modeling in this paper, we will also assume a constant Peclet number along each streamline by using an average velocity determined by dividing the length of the streamline found using Equation 1 by the travel time found using Equation 2. These two approaches are essentially identical.

Accurate modeling of flow and transport through a fracture requires the coupling of the terms required for both. The fracture aperture can be calculated following Novakowski et al. (1985) and Himmelsbach et al. (1998) from

$$2b = \sqrt{\ln \frac{X}{r_w} \frac{4 \nu \tau_f X^2}{g\, t_0\, \Delta H}} \tag{3}$$

where

- X = length of shortest streamline, equal to 2a in Equation 1 (L)
- r_w = radius of bore (L)
- ν = kinematic viscosity of water (L^2/T)
- τ_f = fracture tortuosity (assumed as 1)
- t_0 = mean travel time along path X (distance between poles) (T)
- ΔH = difference in hydraulic head between piezometers (L).
- g = gravitational acceleration (L/T^2)

From Himmelsbach et al. (1998), the fracture porosity is determined by

$$\theta_f = \frac{3\, Q\, t_0}{\pi\, m\, X^2} \tag{4}$$

Substituting Equation 4 into Equation 2, we find that the travel time along a streamline is

$$t = \frac{3\, t_0}{\sin^2 \alpha} (\alpha \cot \alpha - 1) \tag{5}$$

Therefore, the average travel time between the wells along each streamline can be calculated independently of the proportion of the pumping rate that actually flows between wells.

Another term we need to estimate is the straight line distance between wells (X = 2a). To arrive at a first estimate, we will use an equation developed by Lever and Bradbury (1985) that calculates the time for the arrival of the peak concentration at a distance L for a pulse injection of tracer traveling through a single fracture (with parallel streamlines) in which matrix diffusion is occurring (their Equation 5.1):

$$t_{max} = \frac{K\, L}{v} + \frac{D_{eff}\, \theta_m\, L^2}{6\, v^2\, b^2} \tag{6}$$

where

- t_{max} = time of arrival of peak concentration (T)
- K = fracture retardation (here taken as 1)
- v = ground water velocity (L/T)
- D_{eff} = effective aqueous diffusion coefficient in the matrix (L^2/T)
- θ_m = matrix porosity
- b = half aperture of the fracture (L).

Letting L/v equal t_0 and K = 1, Equation 6 becomes

$$t_{max} = t_0 + \frac{D_{eff}\, \theta_m\, t_0^2}{6\, b^2} \tag{7}$$

The values for t_{max} and t_0 are selected from the tracer breakthrough data. The effective diffusion coefficient and matrix porosity are known, so Equation 7 is solved for the fracture aperture, 2b. The use of Equation 7 is important in that it relates the separation of the peak arrive time from the plug-flow time to the matrix diffusion parameters and to the contact time of the tracer with the rock matrix. This value of 2b is then used in Equation 3 to get a first estimate of the distance X.

There currently is no method to address the amount of dilution to be expected either in the modeling approach we have used or in a finite-element model because the entire fractured system would need to be known, which would be virtually impossible to do in this or other field sites. However, we can get around the effects of dilution by modeling characteristics of the BTCs of both tracers by reproducing the relative behavior of the two tracers. This is a similar approach to the use of partitioning tracers to examine NAPL concentrations in aquifers (Jin et al. 1995). It is not the total masses of tracers recovered that are important, it is the differences in their relative breakthroughs that provide information on the transport parameters between the injection and withdrawal wells. Therefore, our approach was to model the timing of the peak concentrations of both tracers, the times for the centers of mass of both tracers to arrive, and the inflection times on the leading and trailing edges of the BTCs. If there is dilution, the model will consistently produce relative concentrations higher than the data. Because dilution is affecting the concentrations only in the withdrawal well and not along the flowpath, an estimate of the amount of dilution can be made by determining the factor needed to reduce the modeled concentrations to fit the data.

Methods

Site Description

The Clare Valley is one of South Australia's wine-producing regions. Located 100 km north of Adelaide (Figure 1), it receives an average of 600 mm of rainfall per year. Ground water is used for irrigation of vineyards and, with an expanding wine industry, the demand is likely to increase. This increase has necessitated research into understanding the hydrogeology of the fractured rock aquifer to allow planning for sustainable use of ground water resources in the region. The Department of Water Resources, SA, installed a number of wells in the region to determine the water balance. Studies include natural ground water fluxes, use of environmental tracers to determine recharge, and examination of fracture connectivity (Cook et al. 1999; Cook and Simmons 2000).

The Clare Valley consists of low-grade metamorphosed, folded, and faulted sedimentary rocks of Proterozoic age (Morton et al. 1998). The major lithologies are sandstone, shale, quartzite, and dolomite. In this paper, data is presented from a field site (Wendouree) in the Saddleworth Formation (silty dolomite). The primary porosity of the dolomite has been measured to be 4.8% using mercury porosimetry. Outcrop mapping in an exposure approximately 70 m long and 6 m deep, located 3 km north-northwest of the field site, indicates five sets of fractures (Figure 2). For this site, on the western limb of the Hill River Syncline, the aquifers are on end, with the majority of fractures and bedding planes oriented vertically. The bedding comprises one vertical fracture set that strikes 151°. A second set of vertical fractures strikes 59°. A set of conjugate shear fractures has the same trend as the second set of vertical fractures with dips of ~60°. The only shallow dipping fracture set has a strike of 345° and a dip of 27°. The largest apertures measured in the outcrop are 600 μm. The highly fractured nature of the bedrock as seen in outcrop suggested that the vertical hydraulic conductivity of the aquifer due to vertical fracturing could be greater than the horizontal hydraulic conductivity.

At the field site, a 250 mm bore was drilled to 37.4 m depth, and a nest of six 50 mm PVC piezometers were installed in the bore, separated by bentonite and cement plugs. This paper discusses data from the three upper piezometers in this nest: 41497-6, 41497-5, and 41497-4, with screens at 9 to 12, 18 to 21, and 27 to 30 m below land surface (bls), respectively. Water levels vary seasonally between ~4 m depth in October–November and 7 m depth in July–August. At the time of the experiment, the water level was 6.0 m bls. Under ambient conditions, there is no measurable vertical head gradient at this site, indicating little or no vertical flow under nonpumping conditions.

Pumping Test

To first determine the approximate degree of connectedness of the piezometer levels, a pumping test was performed in which water was extracted with a submersible pump from piezometer 41497-5 at a rate of 15 L/min. Hydraulic heads were monitored in the piezometers located directly above (41497-6) and below (41497-4). Pumping continued until the heads in all three wells stabilized. The final drawdown in each piezometer was 0.26 m in 41497-4, 2.29 m in 41497-5, and 0.17 m in 41497-6. This difference in head response in the upper and lower piezometers suggests that there are fractures that intercept the withdrawal piezometer and one of the monitoring locations but not the other.

Tracer Test

The tracer test was designed to determine the actual volumetric flow rate between the two piezometers and to put constraints on field parameters such as average aperture size, ground water velocity, and the effects of matrix diffusion. The two tracers chosen were bromide and helium because of their conservative nature, ease of sampling and analysis, and their different aqueous diffusion coefficients (7.22×10^{-5} cm^2/sec for He vs. 2.01×10^{-5} cm^2/sec for Br^-). The bromide solution was made by dissolving approximately 750 g of KBr in 500 L of water in a rain water tank, achieving a bromide concentration of 864 ppm.

Helium was infused into the water through 100 m of 0.32 cm diameter silicon tubing following the method described by Sanford et al. (1996). Due to the length of time needed to charge the tracer water in this manner, the flow of helium was started five days before the tracer test. The water in the tank was mixed by turning on a submersible pump for a few minutes several times per day. The helium concentration in the injection water reached approximately 20% saturation. Complete saturation was avoided because of the concerns of the formation of bubbles due to degassing as the tracer solution came into contact with the slightly warmer ground water.

The injection system consisted of two 500 L tanks. One tank contained the tracer solution and the other contained local ground water. An outlet was placed near the bottom of each tank and fitted with 1.27 cm outer diameter (O.D.) copper tubing. Copper tubing was used to prevent the diffusive loss of the dissolved helium that can occur through the walls of plastic-type tubing. The tubing from each tank connected to a valve and then the two lines met at a tee. One line from the tee rose vertically through an in-line flowmeter. At the top of the flowmeter, a short section of tubing ran horizontally and was equipped with a septum port for collecting samples of the injection water. After this horizontal length, 1.27 cm O.D. copper tubing was used down to the screened section of 41497-5. At the bottom, a 60 cm length of 0.64 cm O.D. copper tubing was fitted to restrict the flow, with the outlet placed in the midpoint of the screened interval. Injection took place under gravity flow, with the valves being used to switch injection water between tanks. The flow rate was maintained at a constant rate of 4.7 L/min during the entire injection period.

The withdrawal portion of the doublet was established with an MP1 Grundfos® submersible pump centered on the midpoint of the screened interval of piezometer 41497-4. Attached to the pump was 1.27 cm O.D. copper tubing that ran to the surface. At the surface, the exit of the tubing was placed at a slightly upward angle to keep the outlet section completely filled with water at all times. The pumping rate was calibrated to equal that of the injection system.

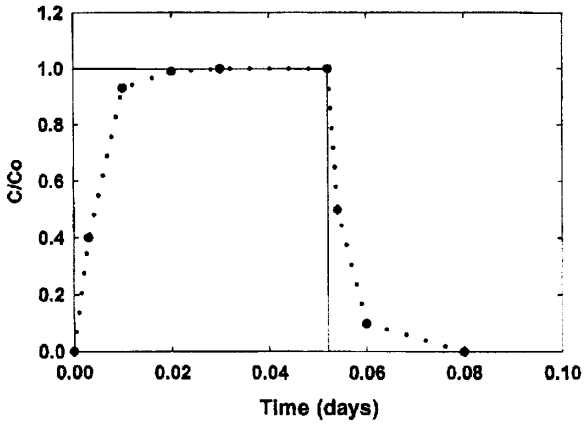

Figure 3. Injection pulse used in model to account for mixing in the injection bore. Solid line represents the theoretical injection with no mixing and the dotted line represents the modeled injection with mixing.

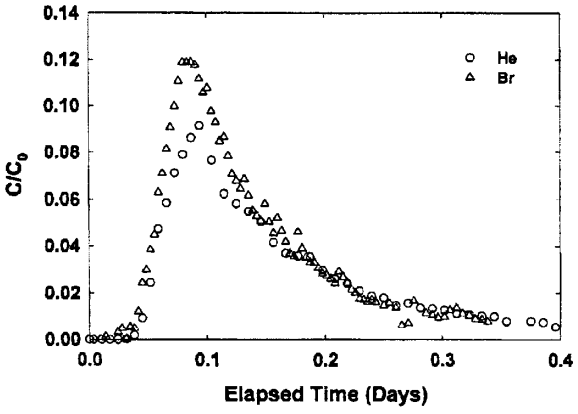

Figure 4. The breakthrough curves for helium and bromide.

The dipole was established prior to injection of the tracers by injecting tracer-free water until the hydraulic heads stabilized (approximately 30 minutes). The tracer solution was then injected for a total of 75 minutes, after which time the valves were switched so that only tracer-free water was injected. The test continued for an additional 510 minutes to recover the injected tracer. The total head difference between the two piezometers during the test remained constant at 0.6 m.

Samples of the tracer water were collected periodically during the injection through the port at the top of the injection line. Glass syringes fitted with needles were used to collect the water. For bromide samples, approximately 20 mL were collected and placed in a 100 mL plastic bottle. Helium samples were collected by slowly drawing water into the glass syringe to avoid the formation of bubbles. Once approximately 10 mL of water was collected, the needle was removed and a small rubber vial cap was placed over the luer-lock tip on the syringe.

Bromide samples from the withdrawal line were collected by placing 100 mL plastic bottles into the outlet stream and filling to approximately two-thirds full. Helium samples were collected by placing the needle on the glass syringe into the outlet pipe and slowly drawing in the sample, again avoiding the formation of bubbles. The syringes were capped as described previously. Sampling frequency was initially every five minutes for bromide and 15 minutes for helium for the first three hours of the test. After this time, helium was sampled every 20 minutes and bromide every 15 minutes.

The samples were taken to a nearby temporary laboratory for analysis. Bromide analyses were performed on 10 mL aliquots using an Orion® solid-state, ion-selective electrode with an Orion double-junction reference electrode. To extract helium from the water samples, water was removed from the syringe by placing a needle through the rubber cap until the volume left in the sampling syringe was equal to 8 mL. A headspace of 2 mL of high purity nitrogen (carrier gas) was added and the sample was shaken for 30 to 60 seconds. A 1 mL sample of the headspace was extracted and injected into a gas chromatograph equipped with a thermal conductivity detector and an 8 m molecular sieve column. See Sanford et al. (1996) for details on the gas chromatograph settings.

Wellbore Mixing

To handle the effects of wellbore mixing, an assumption of complete, instantaneous mixing within the volume was made. The concentration in the well volume at any time is given by

$$\frac{\partial C_w}{\partial t} = \frac{Q}{V}(C_i - C_w) \qquad (8)$$

where

C_w = concentration in well at time t (M/L^3)
t = time (T)
V = well volume (L^3)
Q = injection rate (L^3/T)
C_i = concentration of water entering the well (M/L^3).

The effect of wellbore mixing on the concentration in the injection well is shown in Figure 3. To account for this in the transport modeling, the source concentration was varied with time in such a way as to represent this modified injection pulse. The total amount of mass injected remained the same.

The distances, aperture, and velocities calculated from the preceding are used in the transport model with iterations made on the dispersivity and well spacing to find the best fit to the BTCs. The effects of dilution are handled as mentioned previously.

Results

The effects of matrix diffusion on the transport of the tracers are clearly evident in that the breakthrough of helium (the tracer with the largest effective diffusion coefficient) is retarded relative to the breakthrough of bromide (Figure 4). The center of mass of the bromide arrived at a relative volume (RV) of 2.59 and the center of mass of helium arrived at RV = 2.97. Mass recoveries of the tracers were determined to be 24.5% for helium and 28.4% for bromide.

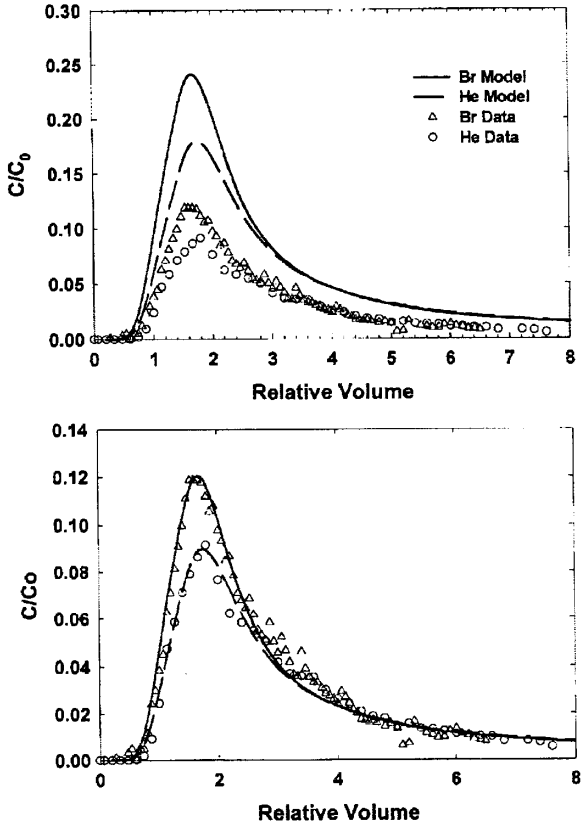

Figure 5. Best-fit results of the modeling. Relative volume is related to the volume of the injection pulse: (a) fit to the centers of mass, peak times, and inflection points; (b) fit to data by dividing concentrations in Figure 5a by 2.

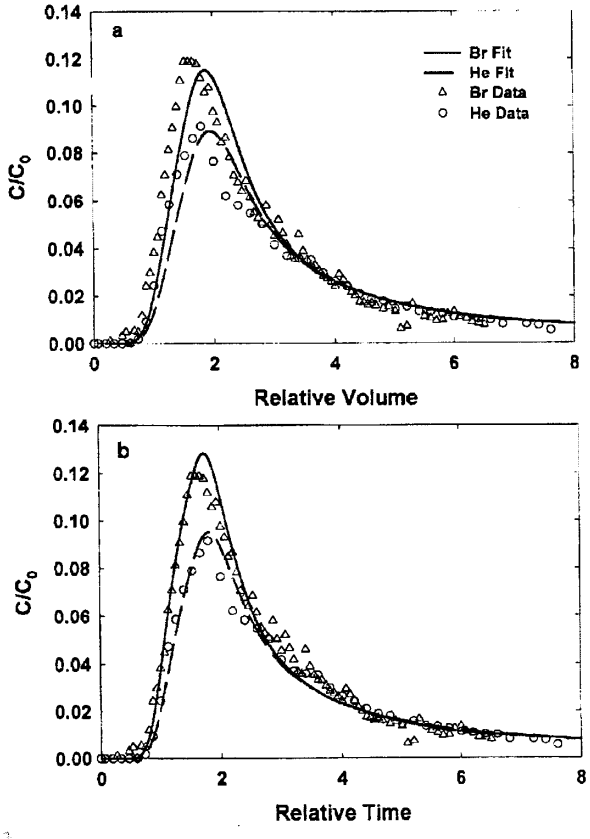

Figure 6. (a) Modeling of the data using a t_0 = 0.05 day; (b) Modeling of data using a dispersivity value of 0.2 m.

Modeling

The first step in modeling was to use Equation 7 to solve for the half width of the aperture. Again, the aim was to minimize the use of assumptions in producing the best modeling fit to the tracer data. The arrival time of the peak concentration was taken from the breakthrough data for the tracer with the largest diffusion coefficient, helium; hence, t_{max} = 0.094 day (Figure 4). The effective diffusion coefficients were taken from previous work (Sanford et al. 1996) and were given previously. The matrix porosity used was that measured (5%). The average travel time along the straight line path between the injection and withdrawal wells (t_0) was selected from the BTCs (Figure 4) as the time of first arrival of the tracers, resulting in t_0 = 0.04 day. Solving Equation 7 yields an aperture (2b) of 240 μm. This aperture value was then used in Equation 3 to solve for the length of the fracture, with the radius of the bore equal to 0.125 m. This resulted in a calculated length of 8.5 m and a velocity of 212 m/day. This length was substituted for 2a in Equation 1 to calculate the lengths of the streamlines and in Equation 2 to calculate the arrival times.

The calculated aperture, lengths, and velocities were used in the transport modeling. The only parameter not known, chosen from the BTC, or calculated for the transport modeling was the fracture dispersivity. Himmelsbach et al. (1998) present tracer data from dipole tests along a fracture with well spacings of 11.2 and 16.2 m. Their best fit dispersivities ranged from 0.17 to 0.25 m. Based on their results, the initial value of dispersivity used in the modeling was 0.2 m.

Centers of Mass Fit

The centers of mass of the modeled BTCs were compared to those of the tracers. With the spacing of 8.5 m, the modeled time for the peak to arrive for both tracers was too early, as were the centers of mass (RV = 2.08 for bromide and RV = 2.27 for helium). The next step then was to increase the fracture length, recalculate the streamlines, and remodel the BTCs.

Figure 5a presents the best fit to the breakthrough characteristics for both tracers using a spacing of 11 m, an aperture of 240 μm, a maximum velocity of 275 m/day, and a dispersivity of 0.5 m. For bromide, the center of mass of the model arrived at RV = 2.58. For helium, the center of mass of the model was RV = 2.96. Also note how the peak times and inflection points also correspond. The modeled concentrations are greater than the actual concentrations, with twice as much mass recovery modeled. If we divide the modeled concentrations by two, the resulting BTCs fit the data very well (Figure 5b). This indicates that there was an approximate 50% dilution in the withdrawal well.

Discussion

The fit to the data achieved by the method used here is a result of modeling the characteristics of the tracer BTCs and the relative differences between each tracer. Maloszewski and Zuber (1985) and Himmelsbach et al. (1998) stress the importance of the parameter that describes the matrix diffusion process, given by

$$a = \frac{\theta D^{1/2}}{2b} \tag{9}$$

during the fitting process. For our approach, we arrive at this relationship through the use of Equation 7. It can be shown that identical BTCs can be generated using the transport model as long as the value in Equation 9 is kept constant. For example, if the matrix porosity is doubled and the aperture is doubled and all other terms kept constant, identical BTCs will result. However, by doubling the aperture, the hydraulic relationship between the head difference and the arrival time is violated (Equation 3); for our case, the matrix porosity is known, so doubling it is not valid.

Obviously, the choice of t_0 is important. Because there is no other method available, it is best to choose the value from the BTC. An example of using a greater value of t_0 = 0.05 day is shown in Figure 6a. Here, the peak arrivals are late, as are the centers of mass (RV = 2.78 for bromide, RV = 3.12 for helium). The time difference between the first arrival and the peak concentration is too large compared to the data.

Figure 6b shows the results of using all the same parameters as in the best fit model except with a dispersivity of 0.2 m. For this representation, the timing of the peaks and arrival of the centers of mass are the same as the data, but the modeling fit is not as good.

Dilution

Once the breakthrough characteristics were fit for both tracers, it was necessary to reduce the modeled concentrations by half. This reduction suggests that half the water being drawn into the withdrawal well is from fractures not connected to the injection well. Reinspection of Figure 2 allows us to conclude that this is not unreasonable. For the tracers, only 25% of their injected mass was recovered. Two reasons account for this loss: First, in all models that were run, only 50% of the mass was recovered because, by using the streamline approach, some of the flowpaths have long distances and slow velocities. Therefore, some of the tracer injected into the fracture is traveling long distances and at slow velocities, so it never arrives at the withdrawal well during the time frame of the experiment. As a result, the maximum amount of tracer to be recovered if all mass was injected into the fracture would be about 50%. Himmelsbach et al. (1998) present the results of one of their dipole tracer tests and found that the mass recovery curve becomes asymptotic to 50% recovery. For our test, because only 25% was recovered, this suggests that only 50% of the tracer mass was injected into the fracture connecting the two piezometers. Second, with the streamline approach, the presence of a regional hydraulic gradient can result in additional mass loss.

Conclusions

A methodology for the analysis of a vertical tracer test in a highly fractured rock under dipole conditions was presented for conditions in which the injection and withdrawal occur over relatively large screen lengths. The assumptions made include streamlines connecting the injection and withdrawal point can be modeled as a dipole of equal strength, flow along each streamline is one dimensional, and there is a constant Peclet number for each streamline.

Because of the screen length (3 m), multiple fracture sets were intersected, some of which are not continuous between piezometers, and the actual travel length between piezometers was not known. By fitting the characteristics of the tracer BTCs, effective fracture aperture and the travel distance were estimated. The important steps were to determine the fracture aperture based on the parameters that influence the rate of matrix diffusion, which causes the lag between the arrival of the peak concentration and the average water velocity. The travel distance was then estimated by fitting the time of arrival of the centers of mass of the tracers. Dispersivity was determined by fitting the times that the inflection points occurred on the front and back limbs of the BTCs. An estimate of the amount of tracer that actually traveled between the two piezometers was estimated by determining the amount that the modeled concentration had to be reduced to fit the data. This step was a result of there being dilution in the withdrawal piezometer due to water being pulled in from fractures not connected to the injection piezometer.

The best fit modeling results for the active fracture connecting the two piezometers are a separation of 11 m, a fracture aperture of 240 μm, a maximum velocity of 275 m/day, a dispersivity of 0.5 m, and only approximately 50% of the injected tracer traveled through the connecting fracture and, of that, only 50% was recovered. These parameter values are not necessarily those to be used for every fracture in the system, but rather they provide a first approximation of the actual values.

Finally, the use of two tracers with differing diffusion coefficients was not necessary but was important for two reasons: First, the apparent retardation between the two tracers is evidence of matrix diffusion. Second, the BTCs of both tracers need to be accurately modeled by the best fit parameters. Therefore, multiple tracers provide important checks in the modeling process.

Acknowledgments

Partial support was provided for W. Sanford as a visiting fellow by Land & Water Resources R&D Corp., Adelaide, Australia. The authors wish to thank the several reviewers who provided invaluable comments and insights on earlier versions of this manuscript.

Editor's Note: The use of brand names in peer-reviewed papers is for identification purposes only and does not constitute endorsement by the authors, their employers, or the National Ground Water Association.

References

Cook, P.G., A.J. Love, and J.C. Dighton. 1999. Inferring ground water flow in fractured rock from dissolved radon. *Ground Water* 37, no. 4: 606-610.

Cook, P.G., and C.T. Simmons. 2000. Using environmental tracers to constrain flow parameters in fractured rock aquifers; Clare Valley, South Australia. In *Dynamics of Fluids in Fractured Rock*, ed. B. Faybishenko, P. A. Witherspoon, and S. M. Benson, 337-347. American Geophysical Union.

Grove, D.B., and W.A. Beetam. 1971. Porosity and dispersion constant calculations for fractured carbonate aquifer using two well tracer method. *Water Resources Research* 7, no. 1: 128-134.

Himmelsbach, T., H. Hotzl, and P. Maloszewski. 1998. Solute transport processes in a highly permeable fault zone of Lindau Fractured Rock Test Site (Germany). *Ground Water* 36, no. 5: 792-800.

Jardine, P.M., W.E. Sanford, J.P. Gwo, O.C. Reedy, D.S. Hicks, J.S. Riggs, and W.B. Bailey. 1999. Quantifying diffusive mass transfer in fractured shale bedrock. *Water Resources Research* 35, 2015-2030.

Jin, M., M. Delshad, V. Dwarakanath, D.C. McKinney, G.A. Pope, K. Sepehrnoori, C.E. Tilberg, and R.E. Jackson. 1995. Partitioning tracer test for detection, estimation, and remediation performance assessment of subsurface nonaqueous phase liquids. *Water Resources Research* 31, 1201-1211.

Lever, D.A., and M.H. Bradbury. 1985. Rock-matrix diffusion and its implications for radionuclide migration. *Mineralogical Magazine* 49, 245-254.

Maloszewski, P., and A. Zuber. 1985. On the theory of tracer experiments in fissured rocks with a porous matrix. *Journal of Hydrology* 79, 333-358.

Maloszewski, P., and A. Zuber. 1993. Tracer experiments in fractured rock: Matrix diffusion and the validity of models. *Water Resources Research* 29, no. 8: 2723-2735.

Morton D., A.J. Love, D. Clarke, R. Martin, P.G. Cook, and K. McEwan.1998. Clare Valley groundwater resources. Progress report 1: Hydrogeology, drilling and groundwater monitoring. Primary Industries and Resources South Australia. Report Book 98/00015.

Novakowski, K.S., G.B. Evans, D.A. Lever, and K.G. Raven. 1985. A field example of measuring hydrodynamic dispersion in a single fracture. *Water Resources Research* 21, no. 8: 1165-1174.

Sanford, W.E., R.G. Shropshire, and D.K. Solomon. 1996. Dissolved gas tracers in groundwater: Simplified injection, sampling and analysis. *Water Resources Research* 32, no. 6: 1635-1642.

Sudicky, E.A., and E.O. Frind. 1982. Contaminant transport in fractured porous media: Analytical solutions for a system of parallel fractures. *Water Resources Research* 18, no. 6: 1634-1642.

Analysis of Ground-Water Flow and Injection Fluid Transport in the Floridan Aquifer Near Pensacola, Florida

by David S. Ward, James W. Mercer, and Lisa L. August[a]

Abstract

Liquid waste has been injected into a permeable part of the lower limestone of the Floridan aquifer since 1963, raising hydraulic head in the injection zone throughout a region of northwestern Florida. The injection zone consists of a moderately permeable limestone, hydraulically isolated from overlying aquifers by a thick layer of clay. The formation fluid is saline, but becomes fresher up dip, northward where the limestone crops out. Numerical simulations were performed at regional and local scales to assess the regional pressure increase, to analyze the movement of the 10,000 mg/l total dissolved solids (TDS) isopleth (formation fluid) in the lower limestone of the Floridan aquifer, and to analyze the migration of the injection fluid, both historically and predictively, in the injection formation. This work is based largely on previous work by Merritt (1984), but uses the SWIFT code. Modifications to Merritt's work include increasing the hydraulic conductivity near the injection wells and using more recent injection rates; extensions include particle tracking and solute transport modeling. The simulations indicate that regional pressure increases should be much less than previously predicted. Using the new results, by the year 2033, the average movement of the 10,000 mg/l TDS isopleth due to injection is expected to be approximately 2200 ft (671 m). Additionally, by the year 2033, the indiluted injection fluid (95% of injection concentration) should migrate to an approximate diameter of 2.1 mi (3.4 km) from the injection wells.

Introduction

Liquid injection began near Pensacola, Florida in 1963. Today two facilities are injecting waste liquids, derived from the manufacture of synthetic fibers, into the Floridan aquifer (Vecchioli, 1979). Both sites are shown in Figure 1, which depicts both the injection wells and nearby monitor wells. This study is primarily concerned with Injection Site 1, where injection began in July 1963. Injection Site 2 is 8.5 mi (13.7 km) east-southeast of the first and began operation in June 1975; it is included in this study because the pressure buildup at Injection Site 2 affects the flow field.

After review of the site hydrogeology, including water quality, this paper describes three steps performed to estimate the environmental impact of injection: (1) numerical simulation of the regional ground-water flow system in the Pensacola area, (2) quantitative analysis of the movement of the 10,000 mg/l total dissolved solids (TDS) isopleth (i.e., the formation fluid) in the lower limestone of the Floridan aquifer, and (3) numerical simulation of the movement of the injection fluid, both historically and predictively, in the injection formation. This work is based largely on previous work by Merritt (1984), who performed numerical simulations of the regional ground-water flow system. His work was recreated using an updated version of the code (Ward, 1988) he used. The flow model was refined and used as the basis for subsequent analysis of the 10,000 mg/l TDS isopleth and injection fluid migration.

The purpose of this work is to refine the work of Merritt and to extend his work by considering solute transport. Specifically, the goal is to reasonably estimate the impact injection has on the natural flow system. This includes estimating injection fluid migration, as well as migration of saline water as defined by the 10,000 mg/l TDS isopleth (a regulatory consideration). The Pensacola area offers an opportunity to better understand the impacts of deep-well injection because the existing data base is much more extensive than those existing at most deep-well injection sites.

Site Description

Hydrogeology

The hydrogeology of this portion of northwest Florida has been studied extensively and is described by Barraclough (1966), Goolsby (1971), Foster and Goolsby (1972), Faulkner and Pascale (1975), and Pascale and Martin (1978). Regional data have been collected by the U.S. Geological Survey, with a summary provided by Hull and Martin (1982). The

[a]GeoTrans, Inc., 46050 Manekin Plaza, Suite 100, Sterling, Virginia 22170.

Received September 1990, revised May and July 1991, accepted August 1991.

Discussion open until November 1, 1992.

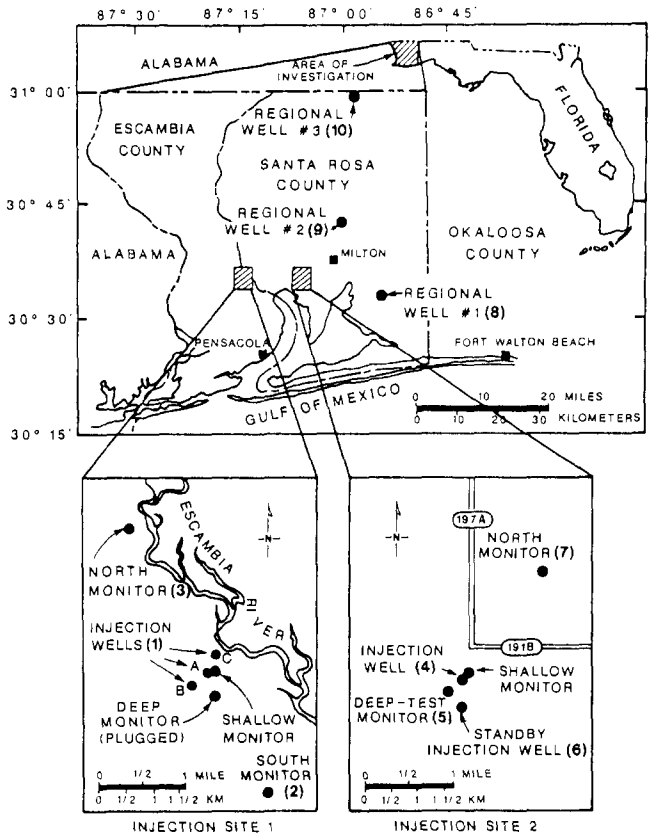

Fig. 1. Well location map for injection sites and vicinity (modified from Merritt, 1984).

geology of Escambia and Santa Rosa Counties is discussed by Marsh (1966). Early assessment of the two counties' water resources by Musgrove et al. (1961 and 1965) indicated that is was feasible to use the lower limestone portion of the Floridan aquifer for waste injection. As the hydrogeology of this region is discussed in these references and in Merritt (1984), only a brief description is provided here.

Waste is injected into the lower limestone of the Floridan aquifer, which dips southwest and, prior to injection, contained saline water in excess of 10,000 mg/l total dissolved solids at Site 1. Figure 2 provides a generalized north-south geological section showing Site 1. At this location, the top of the lower limestone is about 1,400 ft (427 m) below land surface. It is overlain by the 200-ft (61-m) thick Bucatunna Clay, which serves as a confining bed. The clay is overlain by the upper limestone of the Floridan aquifer, which also contains saline water at Site 1. Above the 230-ft (70-m) thick upper limestone lies the Pensacola Clay, a 400- to 500-ft (120-150-m) thick confining bed that separates a fresh-water aquifer above the Pensacola Clay from the saline upper limestone aquifer (Vecchioli, 1979). Fresh-water supplies for the area are obtained from the 300-400+-ft (90-120+-m) thick sand and gravel aquifer that overlies the Pensacola Clay and extends to land surface.

As shown in Figure 3, the Bucatunna Clay pinches out toward the east near Fort Walton Beach. It subcrops toward the south under the Gulf of Mexico and is offset by vertical faulting toward the west in Alabama. Toward the north, recharge occurs where the Floridan aquifer outcrops. Natural flow is generally from the recharge areas in the

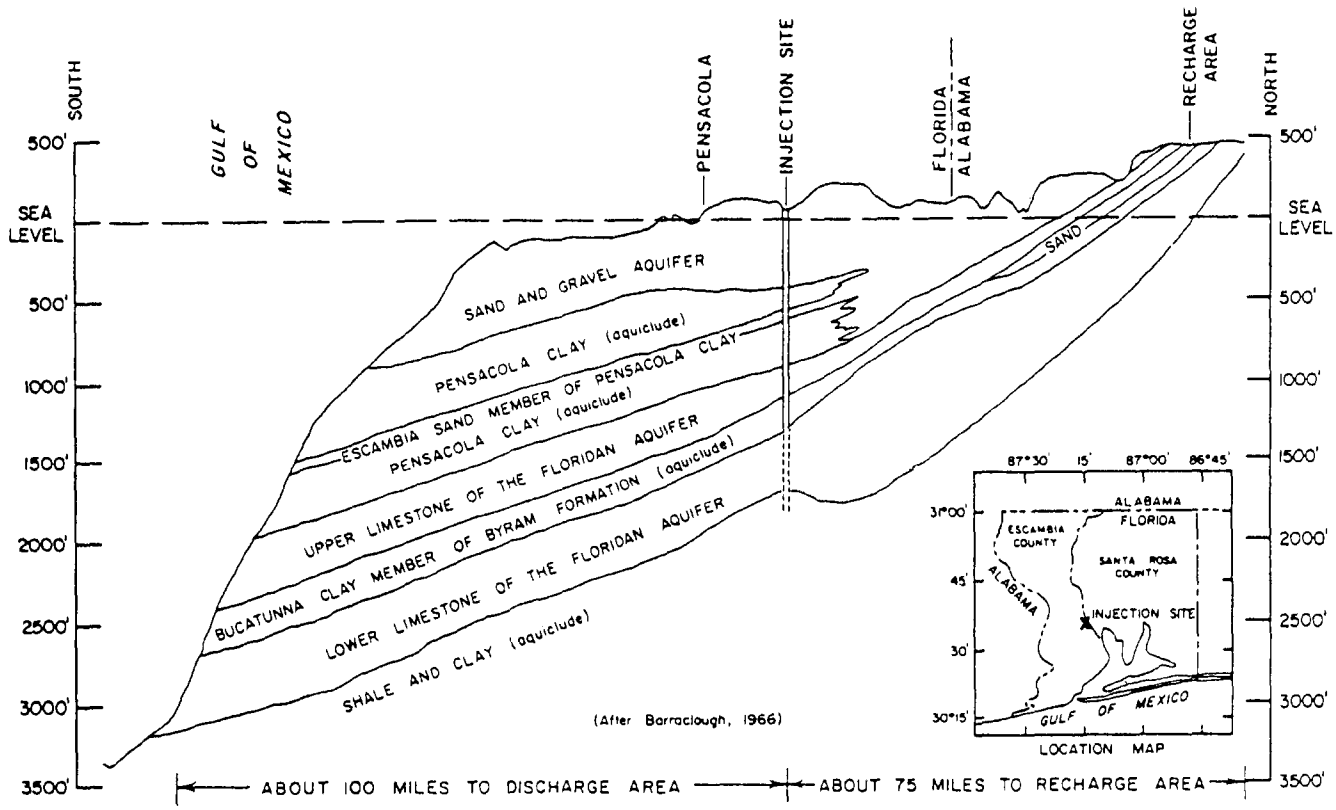

Fig. 2. Generalized north-south geological section through southern Alabama and northwestern Florida. The injection site indicated is Site 1 (from Goolsby, 1971).

north toward the Gulf of Mexico. Indications of the displacement of the limestone by faulting in an area northwest of the injection sites and of its thinning to the west and southwest of the injection sites suggest a partial or complete barrier to flow in these directions (Merritt, 1984).

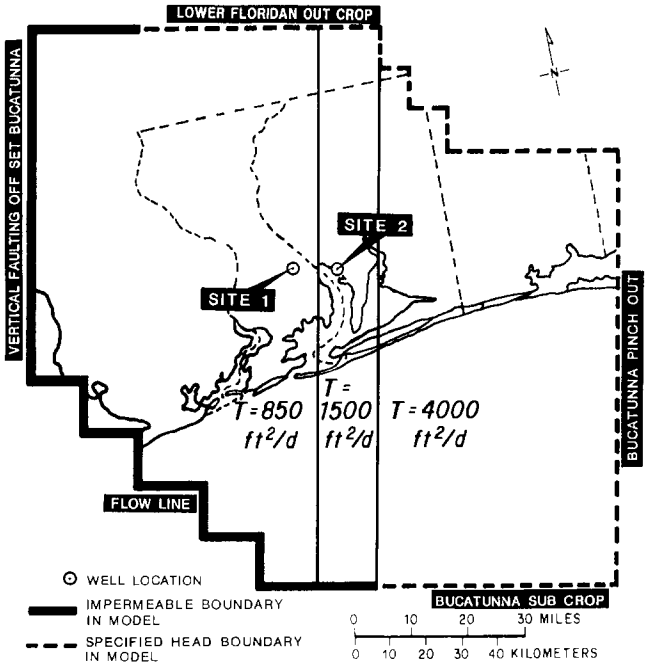

Fig. 3. Boundary conditions and transmissivity zones used in the regional flow model.

Water Quality

Beginning in 1963, the USGS conducted a ground-water sampling program in the lower limestone of the Floridan aquifer to collect data related to the geochemistry of subsurface injection. Chemical analyses are reported for ground-water samples from the wells shown in Figure 1. In addition, analyses are reported for both companies' injection fluids. Based on this information, viscosity and density differences between formation and injection fluids at Site 1 are negligible. Data collected from 1963 to 1980 are available for all sample points (Hull and Martin, 1982). Data for the 1981-1987 period also are available from USGS annual reports. Not all wells have a complete history of data, and only a fraction of the analyses are complete with respect to major cations and anions used in the classification and chemical characterization of ground water.

As a result, data from only nine sample sites of interest were selected for analysis. These included injection fluid from Site 1, and the site's north and south monitor wells; injection fluid from Site 2, and the site's deep-test and north monitor wells; and regional wells 1, 2, and 3. Although a limited number of samples from discrete zones have been reported, in general, the samples collected from well sites represent average water quality over an unknown aquifer interval.

The water-quality data are used to classify the water type at the sample sites. The major cations and anions, which define the water type (or facies), are plotted on Durov diagrams (Zaporozec, 1972; Katz and Choquette, 1991). The Durov plots created for samples from Injection Sites 1 and 2 are shown in Figures 4 and 5, respectively. A Durov plot for

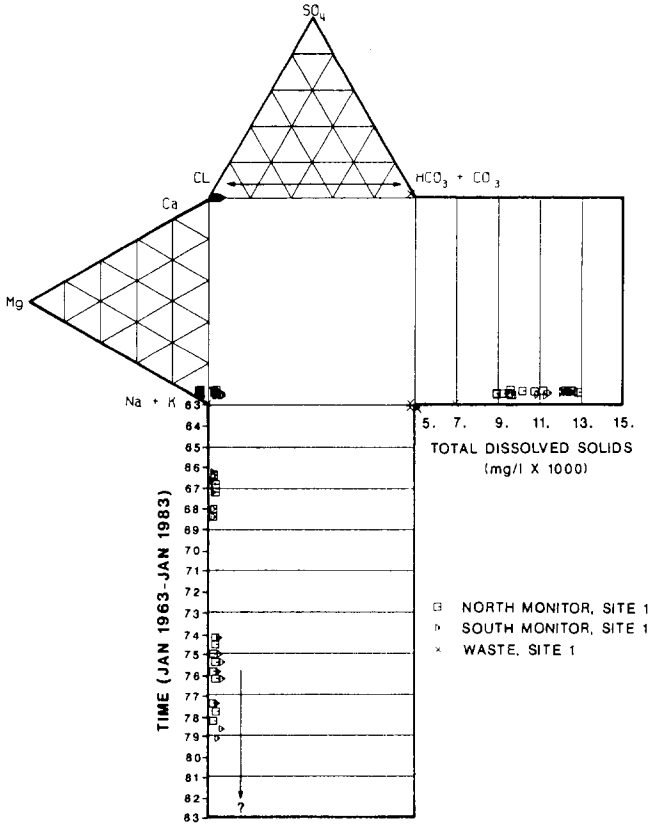

Fig. 4. Durov plots for Site 1 injection (1) fluid and monitor wells (2 and 3); time scale in years.

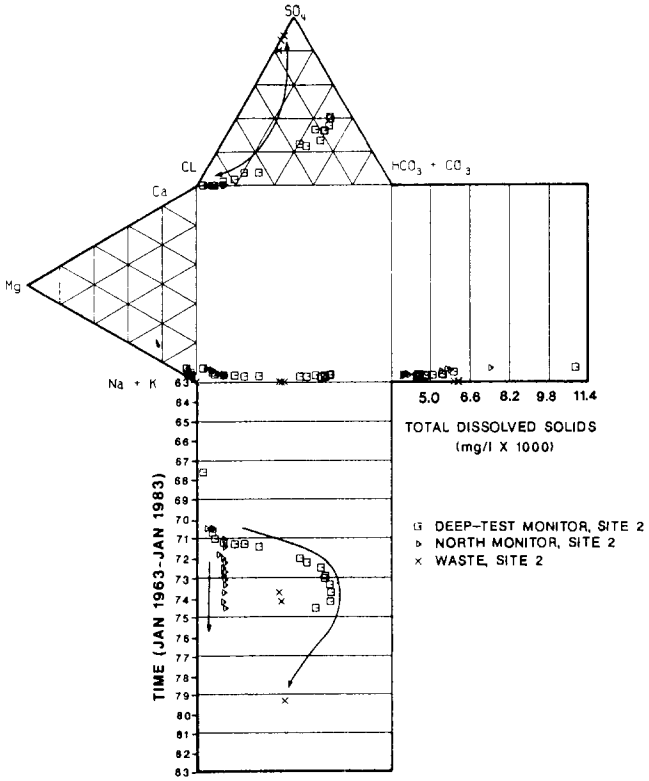

Fig. 5. Durov plots for Site 2 injection (4) fluid and monitor wells (5 and 7); time scale in years.

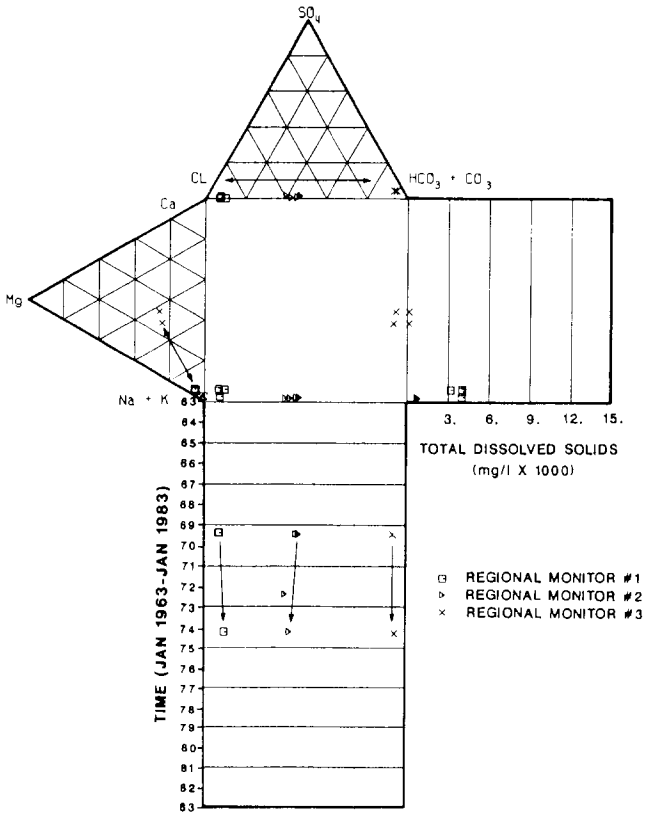

Fig. 6. Durov plots for regional wells #1(8), #2(9), and #3(10); time scale in years.

each regional well is shown in Figure 6. Total dissolved solids (TDS) in mg/l and the date of the sample are plotted on the adjacent rectangles. The date of the sample is plotted to illustrate possible changes in water composition over time.

As shown, the Durov plot consists of two triangles and three rectangles. The top triangle represents the anion composition, where the corners are 100% sulfate (SO_4), 100% chloride (Cl), and 100% bicarbonate ($CO_3 + HCO_3$). The triangle to the left represents the cation composition, where the corners are magnesium (Mg), sodium or potassium (Na + K), and calcium (Ca). Once a water analysis has been made, the percentage of the various cations and anions may be calculated and plotted as a point on the cation triangle and a point on the anion triangle. Multiple data may be plotted on the same plot. The water type is designated by the location of the sample points on the triangles. The points on the triangles may be projected onto the adjoining rectangles. The lines will intersect in the central rectangle, yielding a point that represents the major-ion composition for that sample on a percentage basis. These lines can be extended further into the adjacent rectangles. The rectangles are scaled and are used to compare changes in various samples. These two rectangles may be scaled in terms of two parameters selected from a number of possibilities, including total dissolved solids, ionic strength, hardness, pH, etc. For this application, the two rectangles are scaled in terms of total dissolved solids (right rectangle) and time (lower rectangle). Thus, an observance of these rectangles indicates how these parameters change with each sample or, in the case of the time scale, how the sample composition changes with time.

In Figure 4, the plots for the north and south monitor wells at Site 1 represent the native ground water as a sodium chloride water. The injection fluid (a slightly acidic waste) is represented as a sodium bicarbonate water. These two water types may be considered end members for water quality throughout the area of aquifer affected by injection. That is, the chemical composition of the ground water between the monitor wells and the injection well will plot along a line connecting the two end-member points. Because neither monitor well shows any significant change in composition over time, it is suggested that components of the injection fluid have not reached these wells. Pascale and Martin (1978), however, point out that the water samples from the south monitor well showed increases in bicarbonate concentrations from 282 mg/l to 636 mg/l and that dissolved organic carbon increased from 9 mg/l to 47 mg/l between September 1973 and March 1977. They further state that these increases at the south monitor well were accompanied by an increase in dissolved gas concentration and a distinctive odor like that of the injection fluid. Thus, it is not clear if waste components have reached the south monitor well.

It should also be pointed out that geochemical effects were detected in the deep monitor well (see Figure 1) about 0.25 mi (0.4 km) from the injection wells about 10 months after injection began (Goolsby, 1972). The geochemical effects included increases in calcium, total alkalinity, and the formation of nitrogen and methane gas. This well was subsequently plugged to prevent communication with overlying aquifers.

By contrast, in Figure 5, the deep-test monitor well at Site 2 changes in chemical composition over time. In this case, the north monitor well and the injection fluid represent the end-member water types as sodium chloride and sodium sulfate, respectively. The Durov plot shows the invasion of waste constituents at the deep-test monitor well by the movement of the composition point in the central rectangle along a line between the end members. As a general comparison of the two injection sites, it should be noted that the north monitor well at Site 2 shows a slightly lower chloride/bicarbonate ratio and a lower TDS content than the Site 1 monitor wells.

Figure 6 demonstrates the change in water quality over the region from a sodium chloride water at regional well 1 to a sodium bicarbonate water at regional well 3. The increase in calcium and magnesium and decrease in chloride at regional well 3 indicates an increase in fresh water due to the proximity of recharge waters where the lower limestone of the Floridan aquifer crops out. Note that waters from the Site 1 injection fluid and regional well 3 are classified under the same water type, although representative points on the composition triangles are significantly different. This emphasizes the broad range of this classification system.

In addition to Durov plots, time series plots of specific constituents were plotted to assess injection fluid movement and formation fluid movement. Although not presented, Site 1 monitor wells showed a scatter of points that suggests the variation is due to inconsistencies in sampling methods

and not individual analyses. Regional wells demonstrated a lack of data but did show that the chloride content of each well differs by an order of magnitude with chloride increasing to the south, down dip from the aquifer outcrop and recharge area.

In summary, the water-quality analysis is helpful in characterizing water types and provides general conclusions concerning injection fluid movement at Site 2 and trends in water salinity. Unfortunately, the water-quality analysis is not sufficient to indicate the movement of the injection fluid at Site 1 or movement of formation fluid.

Regional Flow Modeling

In this section, the work of Merritt (1984) is extended to simulate both steady-state and transient flow fields in the lower limestone of the Floridan aquifer using injection conditions representative of 1986 and projected for future years. The results of this work are used to define flow conditions and to assess the relative movement of the waste plume (injection fluid) and 10,000 mg/l TDS isopleth (formation fluid). In addition, the model is used to provide an estimate of the extent of pressure effects in the ground-water system resulting from injection. The computer code used in this application is Sandia Waste-Isolation Flow and Transport Code (SWIFT), a fully three-dimensional, finite-difference algorithm (Cranwell and Reeves, 1981; Reeves et al., 1986a, b). The code has been applied to a variety of geohydrologic problems (Finley and Reeves, 1982; Reeves et al., 1986c) and was developed under a rigorous quality assurance program (Ward et al., 1984).

Simulation Description

The pertinent data used for the regional flow model are listed in Table 1. Merritt's conceptual model was used with the following changes: Merritt assumes a minor density variation between native and injection fluids, but states that the assumption did not affect the regional hydraulic solution (Merritt, 1984, p. 43). Based on the negligible effect, a uniform equivalent fresh-water density [i.e., 62.4 lb/ft^3 (1 gm/cm^3)] is used throughout the system. The model developed by Merritt reproduced the effects of injection fairly accurately on a regional scale. Near-well pressure buildup, however, was overstimated because increased permeability near the injection well(s) (based on field measurement taken in 1982) was not incorporated into his model. A modification was made to the near-well permeability distribution in order to reproduce more accurately observed pressure buildup at the injection well(s). Except for the above changes, the assumptions of the regional flow model are consistent with Merritt's model.

The model developed herein is a two-dimensional, single-layer representation with flow confined from above and below. The finite-difference grid used for the model is shown in Figure 7. The boundary conditions, taken directly from Merritt's model, are illustrated in Figure 3. A specified head boundary (based on extrapolation of limited preinjection head data) is assigned to the eastern half of the grid, which represents the outcrop and pinchout boundary of the confining layer to the north and east, and the subcrop boundary to the south. The remaining boundary is considered impermeable and specified as a zero-flux boundary. This corresponds to permeability barriers to the northwest and west resulting from facies changes and faults. Figure 3 also shows the delineation of three transmissivity zones based on aquifer tests.

In addition to the three transmissivity zones presented in Figure 3 and Table 1, the model was modified to include near-well transmissivity zones. These zones are characterized by regions exhibiting increased transmissivity. The increases are assumed to have resulted from dissolution of the limestone as a result of the injection fluids and may extend several hundred feet into the formation. A field test performed at Site 1 in 1982, after 19 years of injection, indicated a permeability of 22 darcies, or a hydraulic conductivity of approximately 60 ft/d (18 m/d). Assuming an effective formation thickness of 60 ft (18 m), the corresponding transmissivity is 3600 ft^2/d (334 m^2/d). This value is approximately 4.2 times greater than the 850 ft^2/d (79 m^2/d) value determined in the early 1960s and used by Merritt.

A total of seven flow simulations were made and are summarized in Table 2. As shown, the first three simulations (cases 1, 2, and 3) were made to reproduce Merritt's regional simulation results. The next three simulations were sensitivity runs used to account for the increased hydraulic conductivity near the injection wells. The cases considered are described in Table 3 as cases A, B, and C. The final flow simulation uses information gained from the previous simulations and incorporates transient conditions with variable injection rates. This final flow simulation is used for the subsequent solute transport analysis. All seven simulations are described below.

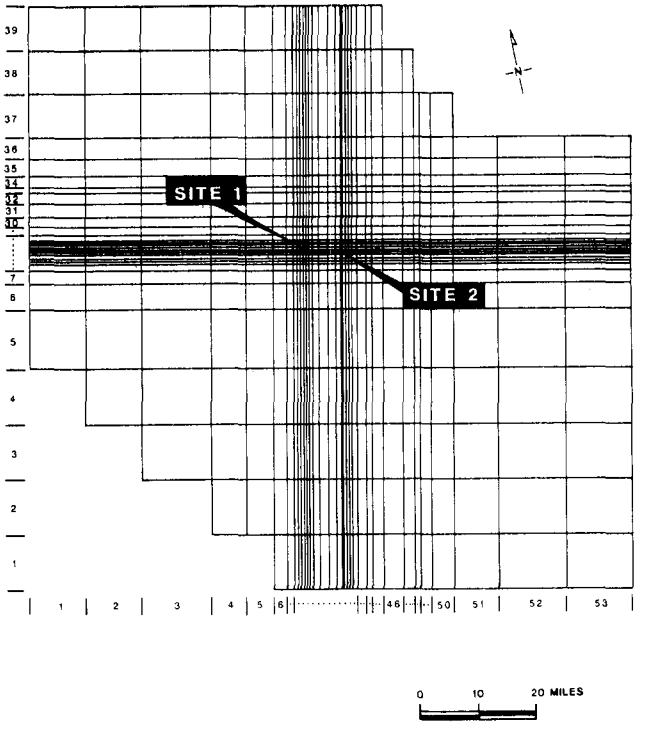

Fig. 7. Finite-difference grid used for regional flow model.

Table 1. Data Used for Regional Flow Model

Parameter	*Value*	*Source*
Porosity	0.28	Merritt (1984, p. 44)
Transmissivity[1]		Merritt (1984, p. 35)
Strip 1	850 ft^2/d (79 m^2/d)	
Strip 2	1500 ft^2/d (139 m^2/d)	
Strip 3	4000 ft^2/d (372 m^2/d)	
Water viscosity	0.76 cp	Merritt (1984, p. 18)
Water density[2]	62.4 lb/ft^3 (1 gm/cm^3)	
Well Index[3]		
Site 1	1406.8 ft^2/d (130.7 m^2/d)	
Site 2	2479.2 ft^2/d (230.2 m^2/d)	
Rock compressibility	3.5×10^{-5} psi^{-1} (5.07×10^{-9} Pa^{-1})	
Water compressibility	3.0×10^{-6} psi^{-1} (4.35×10^{-10} Pa^{-1})	

[1] The x-direction and y-direction transmissivities are equivalent. Location of the strips are presented in Figure 2. Transmissivity is based on the product of hydraulic conductivity and layer thickness.
[2] A uniform equivalent fresh-water density assumed throughout the system.
[3] See Reeves et al. (1986b) for method of calculation.

Table 2. Summary of Simulations Performed for the Regional Flow Modeling Study

Simulation type	*Injection condition*	*Transmissivity condition*	*Purpose*
Steady-state (case 1)	Preinjection	No near-well zones	Reproduce Merritt's regional results
Steady-state (case 2)	1978 rates	No near-well zones	Reproduce Merritt's regional results
Steady-state (case 3)	1986 rates	No near-well zones	Reproduce Merritt's regional results
Steady-state	1986 rates	No near-well zones (case A)[2]	Sensitivity to est. near-well K increase
Steady-state	1986 rates	No near-well zones (case B)[2]	Sensitivity to est. near-well K increase
Steady-state	1986 rates	No near-well zones (case C)[2]	Sensitivity to est. near-well K increase
Transient	Step-wise[1]	No near-well zones (case C)[2]	Account for variation in injection rates

[1]Refer to Figure 7.
[2]Refer to Table 3.

In an effort to reproduce Merritt's results, three steady-state simulations are performed in which injection rates were varied to assess the changes in regional pressure (or head) distribution since the initiation of injection at Site 1. Case 1 represents preinjection conditions, where injection rates are set to zero. Case 2 represents steady-state conditions from 1963 to 1978. As discussed by Merritt (1984, p. 6), for the period 1963-1978, the Site 1 rate varied from a low of 550 gpm (2.1 m^3/min) in 1963 to a high of 2,605 gpm (9.9 m^3/min) in 1972. For this reason, Merritt simulated this time period using transient conditions. He points out, however, that most available water-level data were measured after 1971, so that history matching during this time period was difficult. From the commencement of injection at Site 2 in June 1975 until 1978, injection rates remained at nearly the same level at both sites, so a single average at each site was used during that period. For case 2, these average values were used and are referred to as the 1978 injection rates. They were determined from Merritt (1984) to be 2,295 gpm (8.7 m^3/min) and 550 gpm (2.1 m^3/min) for Sites 1 and 2, respectively. Because of the responsiveness of the limestone aquifer, the average rates provide a final pressure (head) result similar to the resultant head in Merritt's transient simulation. For case 3, average rates were also used and are referred to as the 1986 injection rates. These rates are 1,250

Table 3. Factors by Which Transmissivity was Increased Within Concentric Circles Around Site 1 Injection Well(s)

	Radius (ft) [m]		
Case	*120 [37]*	*300 [91]*	*800 [244]*
A	8.0	4.0	2.0
B	27.0	10.0	3.0
C*	4.2	2.1	1.0
Merritt	1.0	1.0	1.0

*Interpretation is based on field test performed in 1982 (oral communication from L. Brown, 1987).

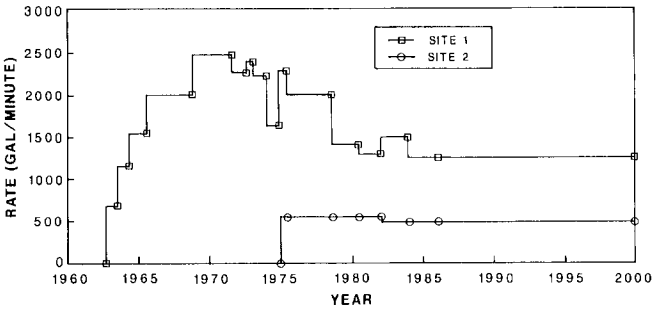

Fig. 8. Waste injection rates used in the transient flow simulations with 16 pumping periods. Data from Merritt (1984), with future rates at Sites 1 and 2 assumed to be 1250 gpm (4.7 m^3/min) and 500 gpm (1.9 m^3/min), respectively.

gpm (4.7 m^3/min) and 500 gpm (1.9 m^3/min) for Sites 1 and 2, respectively (oral communication, L. Brown, 1987). Due to source reduction efforts at Site 1, future injection rates are expected to decrease. The flow system responds very rapidly, thus calculating the steady-state potentiometric surface is a good approximation of the flow system. In the final simulations, this approximation is improved by using additional pumping periods.

To account for increased permeability near the injection wells, three refined steady-state cases are simulated, as presented in Table 3. The injection wells at Site 1 are assumed to be situated in the center of concentric zones that increase in transmissivity with proximity to the well. Three cases (A, B, and C) are used to simulate the steady-state flow field with 1986 injection rates. The three cases, presented in Table 3, are based on history matching against the observed pressure buildups at the injection wells. These refined cases were simulated after reproducing Merritt's regional results (i.e., cases 1, 2, and 3).

To more accurately account for variations in the injection rates, transient flow simulations also are performed using step-wise changes in the injection rates at Sites 1 and 2. The injection rates for each pumping period are time-averaged values and are provided in Figure 8. A summary of all simulations performed for the regional flow modeling is given in Table 2.

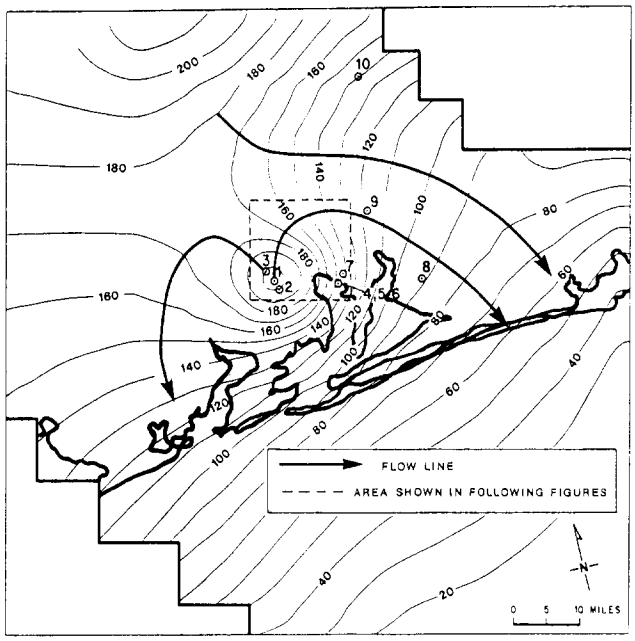

Fig. 9. Steady-state hydraulic head distribution (ft MSL) for 1986 injection conditions and case C transmissivity distribution.

Simulation Results

Results for steady-state cases 1 and 2 are not shown. The main purpose for simulating these cases was to reproduce the results of Merritt (1984). For both cases, head distributions showed good agreement with Merritt's results and the observed data. For preinjection conditions, the hydraulic gradient trends south-southeast over the region and grades approximately 3.8×10^{-4} ft/ft in the area of Site 1. Case 2 demonstrates a head increase over the region as a result of the injection. The head distribution for case 3, presented in Figure 9, shows a reduction in head (as compared to case 2) as a result of the decrease in injection rates. Also shown are generalized flow lines.

The data sets for the steady-state simulations were modified to include the refined transmissivity zones described in Table 3. The results of these simulations are reported for 10 locations, representing wells in the Floridan aquifer (see Table 4). The increased transmissivity zone locally impacts

Table 4. Computed Hydraulic Head Values (ft MSL) at Nodes Representing Selected Wells of the Regional Flow Model Using 1986 Steady-State Injection Rates

Well name (number)[1]	*Case A*[3]	*Case B*[3]	*Case C*[3]	*Merritt*	*Observed*
Site 1					
Injection cluster (1)	390	365	437	529	225-325
South monitor (2)	231	231	231	231	215-225
North monitor (3)	228	228	228	228	215-225
Site 2					
Injection (5)	176	176	176	176	120-160
North monitor (7)	150	150	149	155	157-167
Regional					
No. 1 (8)	90	90	90	91	80+
No. 2 (9)	116	116	116	116	135+
No. 3 (10)	138	138	138	138	115+

[1]Well number corresponds to index on Figure 1.
[2]Observed data are based on actual monthly measurement during the period 1983-1986 data files and published reports.
[3]See Table 3.

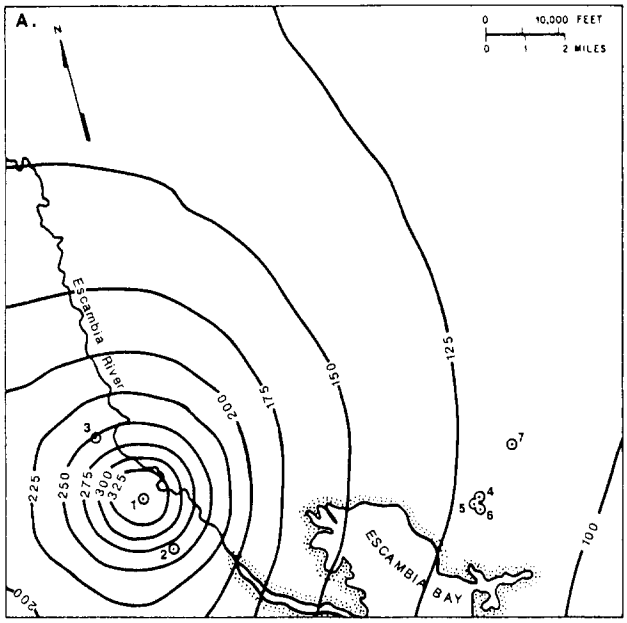

Fig. 10a. Partial display of the computed 1974 hydraulic head distribution (ft MSL) based on transient injection conditions (see Figure 8 for inset location).

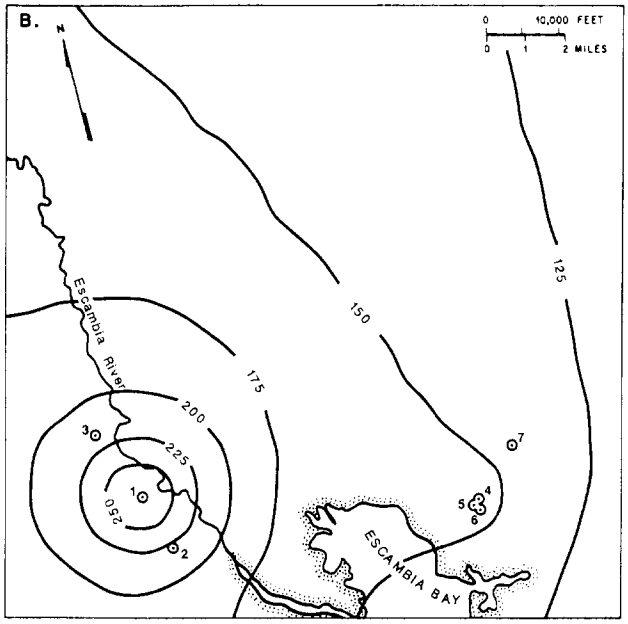

Fig. 10b. Partial display of the computed 1987 hydraulic head distribution (ft MSL) based on transient injection conditions (see Figure 8 for inset location).

the pressure buildup at the Site 1 injection well(s) only. Case B represents the greatest local increase in transmissivity and yields the smallest simulated head at Site 1. While case C yields the greatest buildup, it is thought to most accurately represent the near-well zone transmissivity based on comparison with field test (Table 3).

Model calibration was limited to near-well zone transmissivity. Calibration of transmissivity in other portions of the modeled area performed by Merritt (1984) appeared correct and were not changed. The steady-state calibration is good at Site 1 north and south monitor wells (2) and (3) and at Site 2 north monitor well (7). The difference in the observed and simulated heads at the regional wells is due to assumptions of steady flow and the effects of imposing a prescribed head boundary along the northern edge of the model.

Transient ground-water flow was simulated using the stepwise injection rates given in Figure 8. The computed hydraulic head in the lower limestone of the Floridan aquifer, for the beginning of years 1974, 1987, and 2033, is presented in Figures 10a-10c. These dates correspond to the year prior to beginning of Site 2 operation, the date of this study, and 70 years of operation at Site 1, respectively. Only a portion of the modeled grid is shown such that pressure buildups at both Sites 1 and 2 can be seen. Regionally (away from the area shown in Figure 10), the computed heads are similar to those computed in the steady-state simulations (Figure 9). By the year 1974 (Figure 10a), the pressure buildup at Site 1 exceeds 340 ft above sea level. By 1987 (Figure 10b), the head at Site 1 is reduced as a result of the decrease in the injection rate, and a buildup is evident at Site 2. In the year 2033 (Figure 10c), the predicted heads are similar to those in 1987 because the injection rates are the same.

The results of these simulations may be used to assess the extent of the hydraulic pressure effects of injection under different conditions. Though there are different ways to estimate the extent of pressure effects, one conservative way is to use the distance to the stagnation point, that is, the point where the hydraulic gradient reverses direction (see Figure 9, northwest of Site 1). On the southeast side of the saddle point, the gradient, hence flow direction, is toward

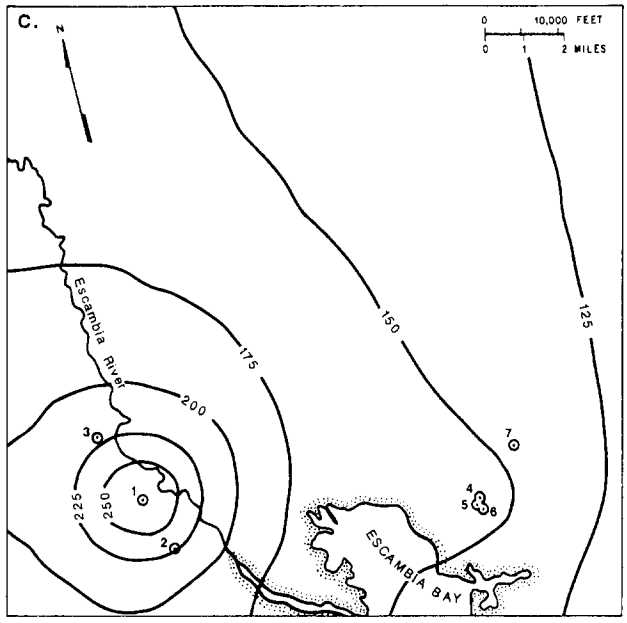

Fig. 10c. Partial display of the computed 2033 hydraulic head distribution (ft MSL) based on transient injection conditions (see Figure 8 for inset location).

the northwest. This flow changes direction at the stagnation point. The extent or distance of pressure effects would be different toward the northeast, but the stagnation point does provide a means to compare the relative extent of the head changes produced by different injection rates. Using the 1978 injection rates and steady-state conditions, the pressure front (defined by the saddle point and not shown) extends to the northwest approximately 25 mi (40 km) from the Site 1 injection wells. This is significantly less than the estimate of approximately 40 mi (64 km) made by Faulkner and Pascale (1975), who used an analytical approach with uniform properties and infinite boundaries. Using the 1986 injection rates and steady-state conditions, the current pressure front (defined by the saddle point) extends only 15 mi (24 km) (see Figure 9).

The extent of the pressure front using transient injection conditions is similar to, yet more accurate than, that produced by the steady-state simulations. Using transient analysis, the position of the stagnation point moves from the point of injection to the northwest. In 1987, the calculated pressure front using the transient simulation extends less than 15 mi (24 km) to the northwest. Because it is a more accurate representation, the transient flow analysis is used as the basis for salt-water front and waste plume movement described in the following sections.

After 2033, injection was assumed to be discontinued. The transient simulation was continued for another 100 years to 2133 with zero injection rates. Later results of this simulation are not shown; however, the head decreases rapidly and, within 10 years after stopping injection, the preinjection flow field is reestablished.

To account for possible future changes in the injection rates, a limited sensitivity analysis was conducted using the transient simulation. After 1986, the injection rate at Site 1 was assumed to increase 10% to 1375 gpm. Using this new rate, the head at the injection well increased from 437 feet to 471 feet. The increase of 34 feet relative to a preinjection head of 90 feet corresponds to approximately 10%.

Modeling the 10,000 mg/l Total Dissolved Solids Isopleth

The results obtained from modeling the salt-water front (formation fluid) in the lower limestone of the Floridan aquifer near Site 1 are presented in this section. The goal is to estimate the effects of injection on the formation fluid; more specifically, to estimate the relative movement of the salt-water front (as defined by the 10,000 mg/l TDS isopleth) caused by the injection. The 10,000 mg/l TDS isopleth is used because of regulatory considerations, where less than 10,000 mg/l TDS is defined as an underground source of drinking water. Definition and movement of the 10,000 mg/l total dissolved solids isopleth is complicated by data limitations and uncertainty associated with the processes of dispersion and density tilting (the tendency to have the denser salt water undercut the lighter fresh water, causing an interface between the two fluids to tilt). In addition, its location may vary with depth and the isopleth may move in response to recharge, regional pumping, and even as a result of past changes in sea-level elevation. In places, the natural water-quality contours are perpendicular to the preinjection flow system (Faulkner and Pascale, 1975). That is, the preinjection flow direction is toward the southeast, whereas chloride concentrations increase toward the southwest. This could be the result of complex subcropping of the Floridan aquifer under the Gulf of Mexico combined with changes in concentrations that are still occurring as a result of the last change in sea level. Due to these uncertainties, movement of the 10,000 mg/l TDS isopleth was simulated using particle tracking in the horizontal plane.

For the purpose of this study, the isopleth is defined as a vertical plane (ignoring significant density tilting) that separates ground water in the lower limestone of the Floridan aquifer that is less than 10,000 mg/l from ground water that is greater than 10,000 mg/l of total dissolved solids. There is considerable uncertainty as to where the isopleth occurs due to the sparseness of water-quality measurements. Because this interface was actually in dynamic equilibrium prior to 1963, an approach is taken in which the density-driven movements are assumed to be relatively insignificant and are, therefore, not considered. In this analysis, only hydraulically induced movement or forced convection is examined and only the relative or incremental movement of the isopleth, caused by injection, is computed.

The approach used is an extension of the regional flow model where calculated ground-water velocities are used to integrate the movement of the 10,000 mg/l TDS isopleth. Conservative assumptions include using the stepwise transient velocity field based on the injection rates presented in Figure 8. The movement of the 10,000 mg/l TDS isopleth was calculated by moving discrete particles. Twelve particle locations along the isopleth are initialized and calculations performed for 70 years. The initial 1963 10,000 mg/l TDS isopleth position is based on the inferred chloride distribution in Faulkner and Pascale (1975), where chloride is assumed to represent approximately 55% of the total dissolved solids. In this simulation, each particle trace is calculated for a given time step and the particles translated. Over the simulation period, the particles are translated hundreds of times. The model is based on the assumption that the aquifer is 60 ft (18 m) thick and has a porosity of 0.28. These are conservative estimates of the formation properties in that they represent a minimum volume for injection fluid to fill, causing the 10,000 mg/l TDS isopleth to migrate further for a given injection volume. As discussed in the next section, an aquifer thickness of 100 ft is a more representative value at Site 1.

Results of isopleth movement are shown in Figure 11. The 12 particles move at different rates and in different directions in response to the local ground-water velocity and direction of flow. Prior to injection, the regional flow in the Pensacola area was approximately to the south-southeast. Within a few years, the movement of each particle begins to be impacted by the injection wells. Another change in direction results from injection effects at Site 2, which began in 1975. This is demonstrated by the movement of the southeasternmost particle in Figure 11. The current (1987) average movement (average of the particles used in this analysis) of the 10,000 mg/l TDS isopleth is calculated to be approxi-

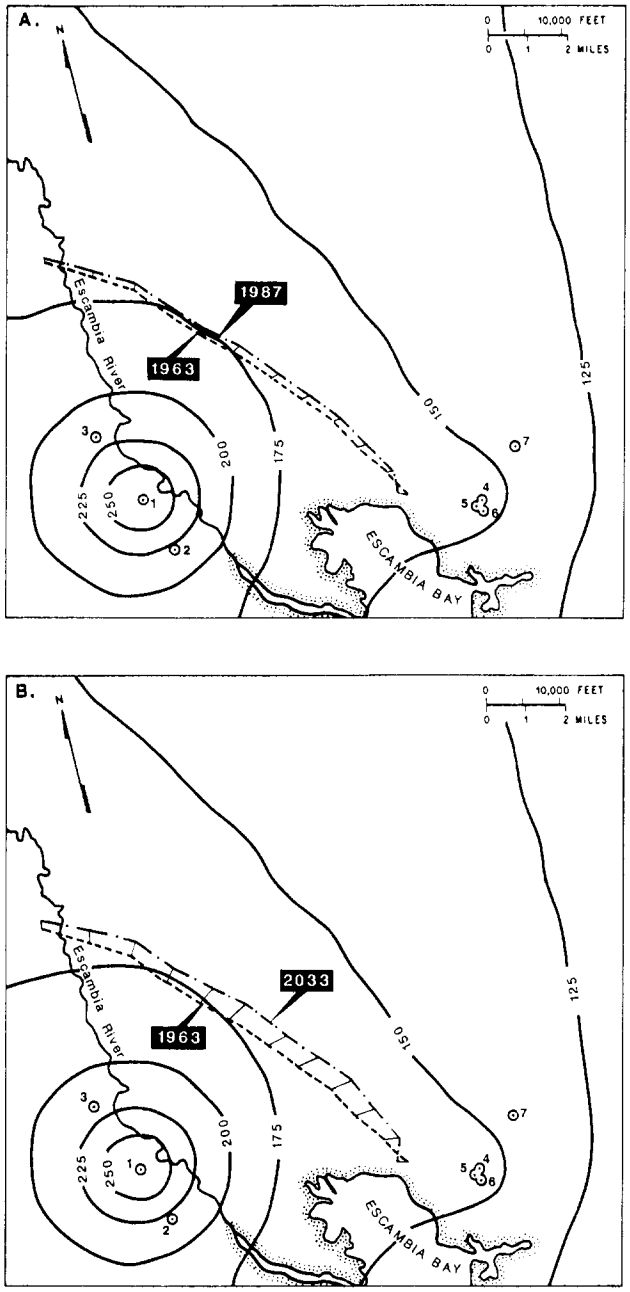

Fig. 11. Simulated movement of 10,000 mg/l TDS isopleth from 1963-1987(A) and 1963-2033(B). Potentiometric surface based on transient simulation with results shown for 1987.

mately 900 ft (274 m) from the initial position. By the year 2033, the average movement will be 2200 ft (671 m). These distances are substantially less than the average radius of the waste plume (discussed in the next section) because they are further from the region of head buildup near the injection wells.

Using a 10% higher injection rate at Site 1 after 1986 caused an increase in the integrated (1963-2033) particle travel distance of 6 to 9%, depending on the locations of the particles. Using velocities (from the flow modeling) after 2033 and cessation of injection, the particles drift slowly in a southeasterly direction in response to reestablishment of preinjection flow conditions. Therefore, the maximum displacement of the 10,000 mg/l TDS isopleth is observed in 2033.

Modeling Injection Fluid

A modeling study was performed to simulate the position of the injection fluid at Site 1. This study is based on the hypothesis that injection will continue for several more decades, probably at the current rate. Predictive simulations are performed from 1963 to 2033. The assumptions used in this study are conservative, i.e., adsorption and degradation are assumed to be negligible.

The approach used here is twofold, employing (1) a nested grid and (2) a radial grid. The first step is to nest a refined transport grid within a subsection of the regional flow grid (Figure 7). The regional flow effects are passed directly into the local transport grid through boundary conditions. This is based on the telescopic mesh refinement method (see Ward et al., 1987). For this study, three mesh refinements (not shown) were performed to create three local grids and to obtain an accurate transport solution. The local grids were square and measured 2500 ft (762 m), 5000 ft (1524 m), and 21,000 ft (6401 m) on a side. For each of these grids, steady-state ground-water velocities from the regional simulation (Figure 9) were interpolated on the local transport grids. Preliminary transport analyses were performed for 10 yrs of injection, and the waste plume evolved in a symmetric, radial pattern. As exhibited in the head distribution contours (e.g., see Figure 9), the symmetric pattern in hydraulic head extends over 5 mi (8 km) before regional impact is experienced. These results support and justify the use of a radial grid approach (described below) as the injection fluid is not expected to extend beyond a few miles.

Based on the above results, the final step in this analysis was simplified by using a radial grid. The assumption of radial symmetry is justified, based on the results from the nested gridding approach. The propagation of the pressure front from the injection well precedes that of the injection fluid. In Figures 10a-10c, the simulated 1974, 1987, and 2033 head contours for the lower limestone of the Floridan aquifer are presented, respectively. Based on volume calculations, the injected fluid is not expected to travel beyond the computed radial hydraulic head distribution by the year 2033, further supporting the radial transport analysis.

A transient simulation of the injection operations is performed using the rates in Figure 8. In this approach, ground-water velocities were calculated that vary with time and location. The radial grid is designed using 50 grid blocks ranging in width from approximately 80 ft (24 m) near the injection well(s) to 780 ft (238 m) near the perimeter of the 14,000-ft radius grid. Based on the work of Merritt (1984), an aquifer thickness of 60 ft (18 m) and a porosity of 28 percent were used. An additional simulation using a 100-ft (30-m) thickness was also performed, because studies at Site 1 indicate 100 ft (30 m) to be more representative of actual local conditions (oral communication, L. Brown, 1987).

The value of dispersivity in the hydrodynamic dispersion tensor used in the model was based on experience and, in part, a field test made at Site 2 for which a value of 33 ft (10 m) was determined. However, Beekman and Appelo

(1991) recently observed that during salt-water displacement by fresh ground water, the dispersivity was three times larger than for the reverse situation. Therefore, a value of 100 ft (30 m) is used and subject to some unknown degree of uncertainty. No attempts were made to calibrate the model because, as discussed in the section on water quality, waste breakthrough at the monitoring wells has not yet been observed to allow calibration.

Because the strata overlying and underlying the lower limestone of the Floridan aquifer are assumed to be impermeable, only waste concentration profiles for the injection zone are simulated. Results for the time periods displayed demonstrate the dispersed waste plume concentration as a function of distance from the injection well.

The undiluted waste body, defined as 95% of injection concentration, is predicted to enlarge to almost 3 mi (4.8 km) in diameter by the year 2033 for the case of the conservative estimate for aquifer thickness [60 ft (18 m)]. In the second case, an aquifer thickness of 100 ft (30 m) is used. Because of the greater thickness, the extent of the undiluted waste body is reduced by the ratio of the thicknesses in the two cases. By the year 2033, the undiluted body diameter is approximately 2.1 mi (3.4 km) in diameter. In both cases, by 1987, dispersed portions of the plume are in the vicinity of the south monitor well, which is consistent with some evidence discussed in the section on water quality. Plume contour plots are presented for 1987 for the 100-ft (30-m) aquifer thickness case in Figure 12. This shows the current waste body size relative to the regional monitor wells.

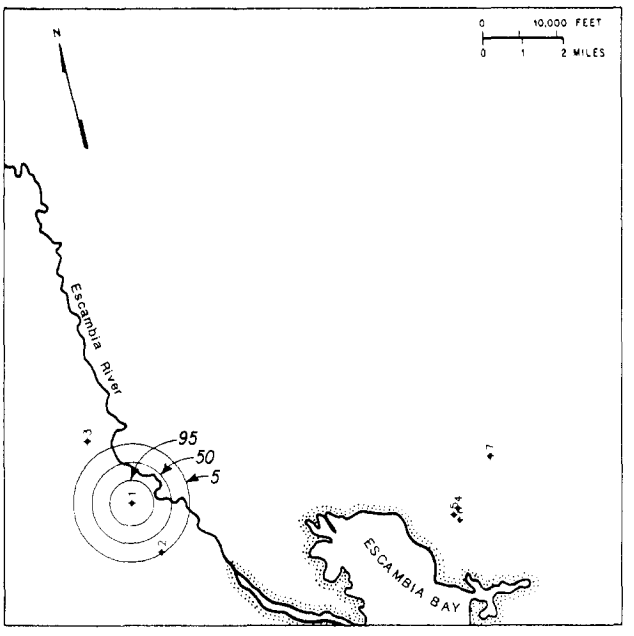

Fig. 12. Simulated plume contours (5, 50, 95% of injection concentration) in 1987 within a 100-ft thick injection zone.

Conclusions

Liquid injection in northwestern Florida has been analyzed. Water-quality data were helpful in defining water types and general trends, but did not show changes in water quality with time (except at Site 2), and therefore could not be used in transport model calibration. Flow model calibration had previously been performed by Merritt (1984), and his results were reproduced prior to making model refinements. These refinements consisted of increasing the hydraulic conductivity near the injection wells and using present injection rates.

Both steady-state and transient flow simulations were performed, with a transient flow simulation forming the basis for salt-water front (formation fluid) and injection fluid movement analysis. The salt-water front movement was analyzed using particle tracking, whereas injection fluid movement was analyzed using solute transport assuming cylindrical symmetry. The numerical simulations of groundwater flow and solute transport are used to support the following conclusions concerning injection Site 1 and vicinity:

- Based on the history match of available data, a two-dimensional transient representation of the regional groundwater flow system of the limestone aquifer provides an appropriate basis for subsequent analysis of injected waste transport.
- In order to match hydraulic head buildup near injection wells more accurately, increased zones of transmissivity were incorporated into the work of Merritt (1984) to represent zones of dissolutioning.
- For practical purposes, the pressure front associated with injection probably extends less than 15 mi (24 km). Because of reduced injection rates and a more accurate aquifer representation, the pressure buildup is much less than the 40 mi (64 km) extent predicted by Faulkner and Pascale (1975).
- The relative movement of the 10,000 mg/l TDS isopleth resulting from injection at Site 1 is very small, on a regional basis.
- Although the exact position of the 10,000 mg/l TDS isopleth is not known, the calculated average relative movement between 1963 and 1987 is approximately 900 ft (274 m) and between 1963 and 2033 is 2200 ft (671 m).
- The calculated undiluted injection fluid (95% of injection concentration) diameters range from 1.1 mi (2 km) to 1.5 mi (2.4 km) in 1987 and from 2.1 mi (3.4 km) to 3.0 mi (4.8 km) in the year 2033.

This modeling application demonstrates how various analysis tools are used to address different problems. Flow analysis required a regional model. Because the waste fluid migration was more limited geographically than the flow analysis, a simplified radial solute transport model was adequate to address waste migration issues (compare Figure 11 with Figure 10). Finally, the movement of formation fluid as represented by the 10,000 mg/l TDS isopleth was addressed using particle tracking. An attempt was made in each analysis to use an approach consistent with analysis goals and data availability. The simulation and analysis was motivated in response to regulatory concerns. Unlike many deep-well injection sites, however, the Pensacola area has relatively good spatial and temporal data coverage. Although each site is unique, the approach utilized in this study is applicable to other deep-well injection sites.

Acknowledgments

We would like to acknowledge the help of Laura Brown (formerly Monsanto, now U.S. Environmental Protection Agency) and Jerry Rinaldi (Monsanto) for their help in preparing this manuscript. We also acknowledge Mike Merritt (U.S. Geological Survey) for providing data sets used in Merritt (1984).

References

Barraclough, J. T. 1966. Water injection into a deep limestone aquifer in northwestern Florida. Ground Water. v. 4, no. 1, pp. 22-24.

Beekman, H. E. and C.A.J. Appelo. 1991. Ion chromatography of fresh- and salt-water displacement: Laboratory experiments and multicomponent-transport modelling. Journal of Contaminant Hydrology. v. 7, pp. 21-37.

Cranwell, R. M. and R. Reeves. 1981. User's Manual for the Sandia Waste-Isolation Flow and Transport Model (SWIFT). NUREG/CR-2234, SAND81-2516, Sandia National Laboratories, Albuquerque, NM.

Faulkner, G. L. and C. A. Pascale. 1975. Monitoring regional effects of high pressure injection of industrial waste water in a limestone aquifer. Ground Water. v. 13, no. 2, pp. 197-208.

Finley, N. C. and M. Reeves. 1982. SWIFT Self-Teaching Curriculum. NUREG/CR-1968, SAND81-0410, Sandia National Laboratories, Albuquerque, NM.

Foster, J. B. and D. A. Goolsby. 1972. Construction of waste injection monitor wells near Pensacola, Florida. Florida Bureau of Geology Information Circular 74. 34 pp.

Goolsby, D. A. 1971. Hydrochemical effects of injecting wastes into a limestone aquifer near Pensacola, Florida. Ground Water. v. 9, no. 1, pp. 13-19.

Goolsby, D. A. 1972. Geochemical effects and movement of injected industrial waste in a limestone aquifer. In: Underground Waste Management and Environmental Implications. Memoir No. 18, Am. Assoc. Pet. Geol. pp. 355-368.

Hull, R. W. and J. B. Martin. 1982. Data on sub-surface storage of liquid waste near Pensacola, Florida, 1963-1980. U.S. Geological Survey Open File Report 82-689. 179 pp.

Katz, B. G. and A. F. Choquette. 1991. Aqueous geochemistry of the sand-and-gravel aquifer, northwest Florida. Ground Water. v. 29, no. 1, pp. 47-55.

Marsh, O. T. 1966. Geology of Escambia and Santa Rosa Counties, western Florida panhandle. Florida Geological Survey Bulletin 46. 140 pp.

Merritt, M. L. 1984. Digital simulation of the regional effects of subsurface injection of liquid waste near Pensacola, Florida. U.S. Geological Survey Water Resources Investigations Report 84-4042. 73 pp.

Musgrove, R. H., J. T. Barraclough, and O. T. Marsh. 1961. Interim report on the water resources of Escambia and Santa Rosa Counties, Florida. Florida Geological Survey Information Circular 30. 89 pp.

Musgrove, R. H., J. T. Barraclough, and R. G. Grantham. 1965. Water resources of Escambia and Santa Rosa Counties, Florida. Florida Division of Geology Report of Investigations 40. 102 pp.

Pascale, C. A. and J. B. Martin. 1978. Hydrologic monitoring of a deep-well waste-injection system near Pensacola, Florida, March 1970-March 1977. U.S. Geological Survey Water-Resources Investigations 78-27. 61 pp.

Pascale, C. A. 1976. Construction and testing of two waste-injection monitor wells in northwest Florida. U.S. Geological Survey Water-Resources Investigations 76-1. 42 pp.

Reeves, M., D. S. Ward, N. D. Johns, and R. M. Cranwell. 1986a. Data Input Guide for SWIFT II, The Sandia Waste-Isolation Flow and Transport Model for Fractured Media. NUREG/CR-3162, SAND83-0242, Sandia National Laboratories, Albuquerque, NM.

Reeves, M., D. S. Ward, N. D. Johns, and R. M. Cranwell. 1986b. Theory and Implementation for SWIFT II, The Sandia Waste-Isolation Flow and Transport Model for Fractured Media. NUREG/CR-3328, SAND83-1159, Sandia National Laboratories, Albuquerque, NM.

Reeves, M., D. S. Ward, P. A. Davis, and E. J. Bonano. 1986c. SWIFT II Self-Teaching Curriculum: Illustrative Problems for the Sandia Waste-Isolation Flow and Transport Model for Fractured Media. NUREG/CR-3925, SAND84-1586, Sandia National Laboratories, Albuquerque, NM.

Vecchioli, J. 1979. Monitoring of subsurface injection of wastes, Florida. Ground Water. v. 17, no. 3, pp. 244-249.

Ward, D. S., M. Reeves, and L. E. Duda. 1984. Verification and Field Comparison of the Sandia Waste-Isolation Flow and Transport Model (SWIFT). NUREG/CR-3316, SAND83-1154, Sandia National Laboratories, Albuquerque, NM.

Ward, D. S. 1988. Data Input Guide for SWIFT III, Version 2.25. GeoTrans Technical Report, Herndon, VA.

Ward, D. S., D. R. Buss, J. W. Mercer, and S. S. Hughes. 1987. Evaluation of a corrective action at the Chem-Dyne hazardous waste site using a telescopic mesh refinement modeling approach. Water Resources Research. v. 23, no. 4, pp. 603-617.

Zaporozec, A. 1972. Graphical interpretation of water quality data. Ground Water. v. 10, no. 2, pp. 32-43.

* * * * *

David S. Ward is Vice President, Research and Development, at GeoTrans, Inc. He received his M.S. degree in Civil Engineering from Princeton University in 1977. His expertise is in hydrogeologic analysis with special emphasis on numerical simulation of hazardous waste, remedial action, deep well injection, and radioactive waste disposal. Ward has developed, documented, benchmarked, and applied numerous computer codes for projects related to hazardous waste disposal and remediation, deep well injection, water resources, sea-water intrusion, and performance assessment of nuclear waste repositories. He has extensive experience modeling complex hydrogeologic systems involving fluid flow and transport in fractured and porous media, partially saturated and multiphase flow, and head, brine, and radionuclide transport. His broad experience also includes implementing and refining procedures for validation, documentation, and technology transfer of numerical and technical analyses.

James W. Mercer received a bachelor's degree in Geology from Florida State University in 1969 and an M.S. and Ph.D. in Geology from the University of Illinois in 1971 and 1973, respectively. For eight years he was a Research Hydrologist with the U.S. Geological Survey. Since 1979, he has been President of GeoTrans, Inc. In 1985, Mercer received the Wesley W. Horner Award of the American Society of Civil Engineers for work performed at the Love Canal hazardous waste site. He is a former secretary of the hydrology section of the American Geophysical Union and a former member of the National Research Council's Water Science and Technology Board. He is a Fellow of the Geological Society of America, is an associate editor of the ***Journal of Contaminant Hydrology****, and is vice president of institution development, American Institute of Hydrology.*

Lisa L. August received a B.A. degree in Geology in 1980 from Smith College, Northampton, Massachusetts and an M.S. degree in Geology in 1986 from George Washington University, Washington, D.C. She has been a Hydrogeologist with GeoTrans, Inc. since 1981. August is a Certified Professional Geologist in Florida and the Commonwealth of Virginia.

ELSEVIER

Journal of Contaminant Hydrology 45 (2000) 329–358

JOURNAL OF
Contaminant
Hydrology

www.elsevier.com/locate/jconhyd

Analysis of solute transport in a heterogeneous aquifer: the Krauthausen field experiment

H. Vereecken*, U. Döring, H. Hardelauf, U. Jaekel, U. Hashagen, O. Neuendorf, H. Schwarze, R. Seidemann

Institute of Chemistry and Dynamics of the Geosphere, ICG-4, Forschungszentrum Jülich GmbH (KFA), Postfach 1913, D-52425 Jülich, Germany

Received 9 September 1999; received in revised form 24 March 2000; accepted 24 March 2000

Abstract

A field-scale natural gradient tracer experiment with bromide, uranin and lithium was conducted in a heterogeneous aquifer at Krauthausen, Germany. The temporal and spatial evolution of the solute plumes was monitored over 398 days for bromide and 449 days for uranin and lithium. The spatial variability of basic aquifer parameters, hydraulic conductivity, and sorption parameters of the aquifer material was investigated in detail. Local Darcian velocities were measured using NH_4Br^{82} as a radioactive tracer in 33 observation wells. Vertical and horizontal correlation lengths of hydraulic properties were determined using variogram analysis. The magnitude of the local Darcian velocities was found to be lognormally distributed. In addition, the groundwater flow direction showed a clear trend in the vertical direction. The horizontal correlation length of the magnitude of Darcian velocity agreed with the correlation length of K estimated from grain size data. Batch experiments on aquifer sediments showed that sorption of uranin and lithium could be described by a Freundlich isotherm. The Freundlich n parameter of uranin sorption showed little variation with depth. The time evolution of the bromide plume was quantified in terms of spatial moments. The longitudinal effective dispersivity estimated from spatial moment analysis was within the range of calculated effective dispersivities,

* Corresponding author.
E-mail address: h.vereecken@fz-juelich.de (H. Vereecken).

0169-7722/00/$ - see front matter
PII: S0169-7722(00)00107-8

taking into account the uncertainty of estimates of the $\ln K$ statistics.

Keywords: Tracer tests; Freundlich sorption; Heterogeneous aquifers; Hydraulic conductivity; Dispersion; Groundwater velocity

1. Introduction

Mathematical models are increasingly used to describe the fate and mobility of pollutants in soils and groundwater, and to perform risk assessment of potentially hazardous substances. An accurate prediction of pollutant transport, however, requires knowledge of the spatial and temporal variation of transport properties, such as hydraulic, physico-chemical, and biological parameters. The spatial variation of soil and aquifer properties causes considerable fluctuations in solute concentrations in soils and aquifers, and leachate quantities from unsaturated soils (Dagan, 1989; Russo and Dagan, 1991). Theoretical and experimental investigations have shown that spatial variability of hydraulic conductivity, K, causes dispersive spreading of solutes, which is much larger than the spreading expected when using transport models with parameters determined from column experiments (Pickens and Grisak, 1981; Gelhar, 1986; Arya et al., 1988). Stochastic theories have been developed to relate this dispersive spreading to statistical properties of K (Gelhar and Axness, 1983; Dagan, 1984; Dagan, 1989; Gelhar, 1993; Jaekel and Vereecken, 1996, 1997). Some of these theories were compared with data obtained from large-scale field experiments, e.g., the Borden site tracer experiment (Sudicky, 1986), the Cape Cod tracer experiment (LeBlanc et al., 1991), and the Columbus tracer experiment (Boggs et al., 1992). Most of these studies and experiments investigated the transport of conservative tracers or substances assumed to undergo linear equilibrium or linear nonequilibrium sorption (Thorbjarnarson and Mackay, 1994; Zhang et al., 1998) in heterogeneous aquifers.

The tracer experiments at the Krauthausen field site were conceived to provide information on the transport of bromide as inert tracer and uranin and lithium as reactive tracers in a heterogeneous aquifer. Laboratory batch experiments and column displacement studies with sediment from the Krauthausen test site indicated that sorption of uranin and lithium may be described either by a Freundlich isotherm equation, hysteretic Freundlich sorption or linear nonequilibrium sorption (Vereecken et al., 1999b). Asymptotic analysis of uranin transport showed, e.g., that the value of the Freundlich n exponent derived from field breakthrough curves (BTCs) differed considerably from the values obtained in batch experiments. This indicates that a simple nonlinear equilibrium model is not appropriate to describe the field-scale behaviour of uranin. Which of the above sorption processes observed in column experiments is controlling the solute transport at the test site is presently not clear? Identification of the field-scale processes affecting transport of uranin and lithium requires, therefore, in a first step, detailed knowledge on the characteristics of the groundwater velocity field and the spatial variability of sediment properties.

In this study, the spatial variability of hydraulic conductivity, Darcian velocities, sediment properties and sorption parameters for lithium and uranin at the test site is

analyzed. Results of the large scale bromide tracer experiment are presented and evaluated using stochastic transport theory. In further work, the field-scale transport of lithium and uranin will be analyzed.

2. The field site

The Krauthausen test site is situated approximately 10 km northwest of the city of Düren and 6 km from the research center Jülich, Germany. The field site is located in the Lower Rhine Embayment and has an extension of 200×70 m (Fig. 1). A site specific geological profile was established on the basis of four drillings. These were conducted to a depth of 15 to 20 m (78–83 m above mean sea level (MSL)). The local base of the aquifer in which the tracer experiments were conducted is situated at a depth of 11–13 m (85–87 m above MSL) and consists of intermitting thin layers of clay and silt. Three different layers were distinguished in the aquifer (Döring, 1997): layer 1 corresponding to the Rur sediments (93–95 m above MSL); layer 2 corresponding to the upper part of the Rhine sediments (90–93 m above MSL); and layer 3 corresponding to the lower Rhine sediments (88–90 m above MSL).

The regional direction of groundwater flow is towards the NE with a hydraulic gradient of about 0.002. This gradient remained relatively constant in the period where tracer experiments conducted. Mean yearly precipitation in the area is about 690 mm. The groundwater table at the test site showed a significant seasonal variation. During summer, the groundwater level may be as low as 2.5 m below surface (95.5 m above MSL); and during winter, the level may rise up to approximately 1.0 m below surface (97 m above MSL).

Analysis of the groundwater quality (Fig. 1) showed high concentrations of chloride (70–100 ppm) prohibiting its use as a conservative tracer. The high nitrate concentrations (90–100 ppm) were caused by the intense agricultural activity in this region. The water is of the calcium-bicarbonate type with a relatively high amount of sulfate, the pH value is 6.7.

In order to ensure sufficient monitoring of the spatial and temporal distribution of the tracer substances as well as to obtain representative sediment materials for aquifer characterization, 68 observation wells with a diameter of 50 mm were installed to an elevation of 87 m above MSL (Fig. 1). A detailed specification of the installation procedure and observation well construction is given by Vereecken et al. (1999a). 58 observation wells were equipped with Multi-Level-Samplers (MLS) consisting of a bundle of 24 PE tubes (diameter 0.5 cm) attached to the outside wall of the observation well. The drilling diameter for all wells was 328 mm. The boreholes used for the installation of MLS were sealed at the bottom with clay and backfilled with gravel. The top part of the borehole was sealed with clay. Vertical distances between samplers range between 0.22 and 0.35 m. In order to prevent vertical mixing of the tracer substances in the fully screened wells (34 in total), large flexible silicon hoses were installed and operated under pressure in the course of the tracer experiments. These flexible tubes sealed the inside of the screened observation wells to prevent mixing and short cuts

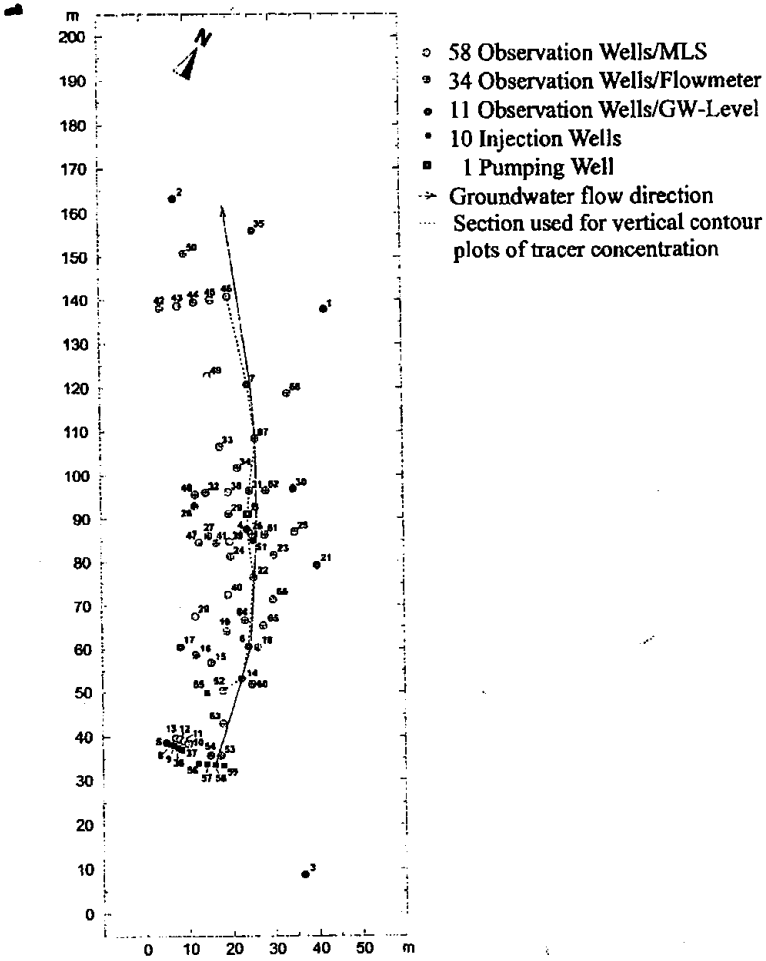

Fig. 1. Locations and category of the wells at the Krauthausen field site.

inside the wells. In various tests (Döring, 1997) the presence of these hoses showed no sorptive effect.

Two natural gradient field tracer experiments, one with lithium and uranin and one with bromide, were conducted at the test site Krauthausen. Evolution of the solute plumes was characterized by calculating spatial moments from 7 (bromide) and 12 (uranin and lithium) complete sampling rounds. In addition, BTCs were determined for 24 depths at each of 15 locations for a period of 449 days for the reactive tracers and 398 days for the bromide tracer. The number of data for the BTC ranged between 20 and 60. The heterogeneity of the aquifer material was characterized in terms of the spatial variation of sediment properties, hydraulic conductivity and sorption related parameters.

3. Determination of basic aquifer properties

3.1. Sediment properties

At the field site, 392 sediment samples were collected between soil surface and 87 m above MSL and analyzed for grain size distribution (12 fractions), organic carbon content (Corg), cation exchange capacity (CEC) and specific surface area (SSA). Of these 392 sediment samples, 250 samples (10 and 20 cm depth intervals) were obtained from undisturbed cores at locations 7, 22 and 32, while the remaining 142 sediment samples (20 cm depth intervals) were taken at 31 locations at three different elevation intervals (92–92.2, 91–91.2 and 90.4–90.6 m above MSL), which correspond to the depth of injection of the tracers.

Total porosity was determined on 83 soil cores collected at nine locations at the tracer site (Table 1). The majority of these 83 soil cores were taken at an elevation between 90 and 92 m above MSL. Total porosity was calculated from $\phi = 1 - (\rho/d)$ where ρ is the bulk density [ML^{-3}] and d is the sediment density [ML^{-3}]. Picnometer measurements on selected samples with varying porosity gave a mean value of 2.65 g/cm^3 for d with a standard deviation of 0.008 g/cm^3. The bulk density was obtained by drying and weighing the aquifer material at 10 cm core intervals. Since the top and bottom samples of each sediment core were disturbed during drilling, these samples were not considered.

The determination of the Corg was performed according to the method of Walkley–Black (Metson et al., 1979) on 1.2 g of sediment with a particle size < 2 mm. The CEC was determined by extracting 5 g sediment (< 2 mm) with an ammonium-acetate solution of pH 7. SSA was determined using a five-point BET method with nitrogen gas. Three to five replicate measurements on each sample were conducted. For one sample, 3.5 g sediment (< 2 mm) was used. Parameter values for the complete sediment fraction were obtained by correcting them by the weight percentage of the sediment fraction < 2 mm.

3.2. Hydraulic conductivity

Local scale variation of the hydraulic conductivity, K, was determined from flowmeter measurements and grain size data. Grain size data were determined from sieve analysis for the fractions larger than 50 μm (> 5 mm, 5–2 mm, 2–1 mm, 1 mm–500

Table 1
Statistics of the porosity for the different layers

	Height above mean sea level [m]	Mean porosity [%]	Standard deviation [%]	N
Layer 1	93–95	20	8	11
Layer 2	90–93	28	6	57
Layer 3	88–90	22	6	15
Layer 2+3	88–93	27	7	72
Overall	88–95	26	7	83

μm, 500–200 μm, 200–100 μm, 100–50 μm), while the pipette method was used to determine the silt and clay fractions (50–20, 20–10, 10–2 and <2 μm). K values were estimated from the grain size distribution data using two methods of Seiler (Seiler-I, Seiler-II) [1973], given by Eqs. (1) and (2):

$$K = c_1(u)\, d_{10}^2, \tag{1}$$

$$K = c_1(u)\, d_{25}^2, \tag{2}$$

where c_1 and c_2 are coefficients depending on the uniformity coefficient u, which is defined as d_{60}/d_{10}, where d_i is the ith percentile or quartile of the cumulative grain size distribution. Eqs. (1) and (2) are derived from experiments conducted by Seiler (1973) on glacial–fluvial sediments of aquifer located in Germany with an u-value ranging between 1 and 110. For values of u larger than 17, Eq. (2) (referred to as Seiler-II) proved to provide better estimates of the hydraulic conductivity than Eq. (1) and vice versa (Döring, 1997). The u-values of the sediments of the Krauthausen test site ranged between 5 and 30, suggesting that both Seiler methods may be equally suitable for the test site. The formula of Hazen was not used in this study because it only applies to sediments with u-values smaller than 5. Estimates of hydraulic conductivity using both equations of Seiler were, therefore, included in the analysis.

In addition to k-values estimated from grain size data, the borehole flowmeter method was used to characterize the small-scale variability of hydraulic conductivity. This method measures the vertical flow in a screened pumping well at different depth intervals. Details concerning the method can be found in Rehfeldt et al. (1992) and Molz et al. (1989). The layer-wise hydraulic conductivity was calculated from:

$$K_i = \frac{\Delta q_i}{\Delta q_d} K_p \tag{3}$$

where K_p is the hydraulic conductivity obtained from a large-scale pumping test, Δq_i is the inflow from the depth interval i, and Δq_d is the average of all inflow values obtained within one well. Similar approaches were successfully used by Molz et al. (1989), Rehfeldt et al. (1989) and Teutsch et al. (1991).

In the field, a mean pumping rate of 1500 l/h was imposed and the flowmeter measurements were started after the pumping rate became constant within an accuracy of ±4%. This was typically achieved after 15 min. This time duration is sufficient to warrant the use of Eq. (3) (Kabala, 1994). Measurements started at the deepest accessible point in the well and were made every 10 cm. For every depth, the average of 20 to 50 measurements was calculated subsequently.

3.3. Determination of local velocities

Single borehole measurements with a radioactive tracer (Fried et al., 1979; Klotz et al., 1979) were used to determine the variability in magnitude and direction of horizontal Darcian velocities at the field site. The procedure consisted of the following stages. $^{82}Br^-$ was injected and homogenized in a defined volume of a screened well, which was isolated by packers. This volume in our study was 1.0 dm^3 corresponding to a probed

layer thickness of 0.5 m. Due to the natural groundwater flow, $^{82}Br^-$ was transported and the dilution was measured with a scintillation detector as a function of time. From the dilution curve, the magnitude of the Darcian velocity was calculated. After the tracer had left the measuring volume, the flow direction was determined by locating the radioactive tracer plume. This was done with a lead-shielded scintillator, where a notch was left to allow radiation from a narrow sector to reach the detector. By rotating this arrangement, the direction with the maximum intensity gave the local flow direction.

Borehole measurements were performed in 33 out of the 34 wells designed for flowmeter measurements (Fig. 1) in the period from 12 to 14 March 1996. In 30 wells, the Darcian velocity was determined in two horizontal planes at 90.8 and 89.8 m above MSL. The packers were centered around these two depths. The elevation for measurement, thus, varied from 90.55 to 91.05 m and from 89.55 to 90.05 m above MSL. In addition, vertical velocity profiles were measured in locations 22, 32 and 53. Measurements started at 94.8 m above MSL with vertical increments of 0.5 m. In total, 82 measurements of groundwater velocity were performed. In some cases, the measuring device for flow direction could not be lowered to the required depth so that only 68 velocity measurements yielded data for flow direction.

3.4. Determination of sorption parameters

Sorption isotherms were determined on 47 samples using three equilibrium concentrations measured on eight batch samples. These samples were collected in layers 2 and 3. Uranin isotherms were determined using initial concentrations of 5 μg/l (three replicates), 50 μg/l (two replicates) and 500 μg/l (three replicates), the initial lithium concentrations were 90, 900 and 9000 μg/l with the same number of replicates as for uranin. Kinetic experiments showed that equilibrium conditions were obtained within 24

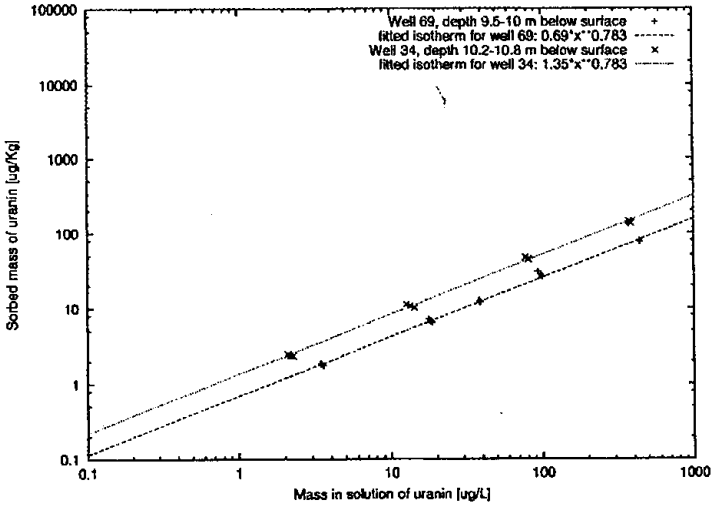

Fig. 2. Measured and fitted sorption isotherms for uranin.

h. This time scale was used to determine the sorbed concentration of uranin. Best fits of the measured isotherms for uranin and lithium were obtained with the Freundlich equation $s = kc^n$ where s is the sorbed mass and c is the solute concentration. This is shown in Fig. 2 for uranin for sediment taken at two different depths. The Freundlich equation was fitted to the 47 isotherms in order to derive the spatial variation of the Freundlich parameters in layer 2 + 3. Döring (1997) showed that the estimated k and n parameter values were not significantly different compared to estimates derived from batch experiments with six equilibrium concentrations. Details concerning the batch procedure, the selection of initial concentrations and the comparison of the two batch isotherm measurement procedures are given in Döring, (1997) and Döring et al. (1999). The k value of the complete sediment fraction was obtained by correcting it by the weight percentage of the fraction less than 2 mm of the whole sediment fraction.

To quantify the effect of differing Freundlich parameters on sorption and to facilitate comparison of sediment and sorption properties, the sorption capacity, S, was introduced. S is defined as the sorbed mass of lithium or uranin for a chosen solute concentration. For uranin and lithium, S was calculated for solute concentrations of 50 and 800 μg/l, respectively. These concentration values were assumed to be representative of concentrations observed at the field site after a travel distance of about 20 m.

4. Statistics of porosity and hydraulic conductivity

Results of the total porosity measurements are given in Table 1. The overall mean total porosity is 26%. Layer 2 has the highest mean porosity of 28% with a standard deviation of 6%. Lower values were found for layers 1 and 3. Table 2 lists the mean and variance of the estimated hydraulic conductivities using grain size data for the different layers of the aquifer. Both methods of Seiler (Section 3.2) gave comparable results for the mean and variance of $\ln K$ ($\sigma^2_{\ln K}$) on the complete dataset. Evaluating the layers separately, the Rur gravel (layer 1) is more heterogeneous than the other layers as indicated by large values of $\sigma^2_{\ln K}$. The $\sigma^2_{\ln K}$ value for the Rhine gravel (layer 2 + 3) is equal to 1.08 (Seiler-I) and 0.84 (Seiler-II). It is through this part of the aquifer that most of the tracer masses were transported. Layer 3 seems to be the most homogeneous with $\sigma^2_{\ln K}$ equal to 0.56 (Seiler-I) and 0.64 (Seiler-II). Vertical contour plots show that most of the tracer mass was probably transported through this part of the aquifer (see Section 10).

Table 2
The mean and variances of the hydraulic conductivities (m/s) of different layers using two indirect methods. The mean value $\langle K \rangle_g$ was calculated as the geometric mean

	$\langle K \rangle_g$	$\sigma^2_{\ln K}$	$\langle K \rangle_g$	$\sigma^2_{\ln K}$	$\langle K \rangle_g$	$\sigma^2_{\ln K}$	$\langle K \rangle_g$	$\sigma^2_{\ln K}$	$\langle K \rangle_g$	$\sigma^2_{\ln K}$
Layer	overall	overall	1	1	2	2	2+3	2+3	3	3
N	279		42		193		237		44	
Seiler-I	1.3×10^{-3}	1.3	7.3×10^{-4}	2.2	1.7×10^{-3}	1.07	1.4×10^{-3}	1.08	7.2×10^{-4}	0.56
Seiler-II	1.0×10^{-3}	1.3	8.4×10^{-4}	3.1	1.3×10^{-3}	0.87	1.2×10^{-3}	0.84	9.4×10^{-4}	0.64

5. Spatial variation of hydraulic conductivity

5.1. Variogram analysis of hydraulic conductivities from grain size data

5.1.1. Vertical analysis

Vertical variograms of estimated hydraulic conductivities using the Seiler-I and Seiler-II method were calculated using the GEOPACK software by Yates (1989). The vertical variograms were based on 120 grain size distributions at locations 7, 22 and 32 for the layers 2 and 3. Layer 1 (Rur sediment) as well as the data points from the aquifer base below 88 m above MSL were excluded from the analysis. The exponential model as described by Journel and Huijbregts (1978) was fitted to the data points and gave a good description of the experimental variograms (Fig. 3). The estimated ranges were 0.6 and 0.4 m for the Seiler-I and Seiler-II methods, respectively, with a standard error of 0.3 m for both methods. The sill variance corrected for the nugget was 0.32 and 0.33 for Seiler-I and Seiler-II. The standard error of estimate was equal to 0.072 and 0.14, respectively. Both variograms showed a clear nugget of 0.32 and 0.24 with standard error of estimates of 0.076 and 0.15, respectively.

5.1.2. Horizontal analysis

3-D isotropic variograms of estimated hydraulic conductivities were calculated for layers 2 and 3 with GAMV3 (Deutsch and Journel, 1992) for irregularly spaced 3-D data. Variogram analysis of the data was done using an unit separation distance of 3.5 m and a lag tolerance of 1.75 m. The dip angle and the maximum acceptable horizontal deviation from the direction vector were set equal to 0.0 and 0.1 m, respectively.

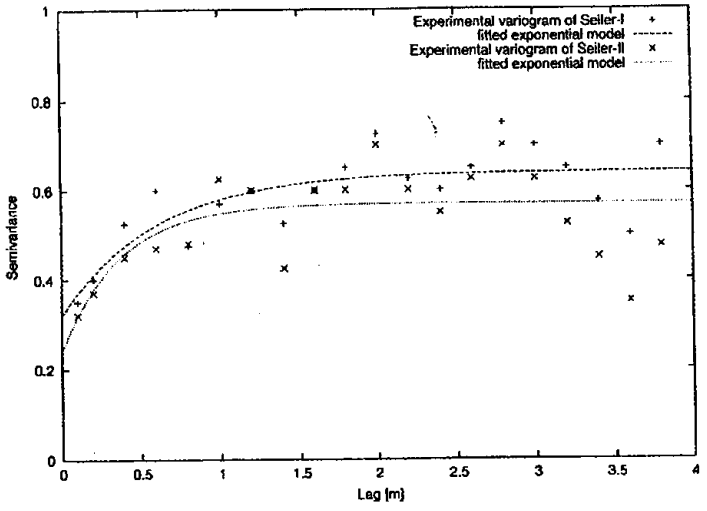

Fig. 3. Experimental and fitted exponential variogram of the estimated hydraulic conductivity in the vertical direction using the Seiler-I and Seiler-II method.

Analysis of the spatial variation of hydraulic conductivity estimates showed the presence of a linear trend, which could be described by:

$$\ln K(x,y,z) = 1.6 - 0.04x - 0.007y + 0.05z \tag{4}$$

where x, y and z are the space coordinates of the flow domain (y corresponds to the main flow direction of the groundwater). After substraction of this trend, an exponential variogram model with nugget was fitted to the hydraulic conductivity data obtained by the Seiler methods. Only for the Seiler-I model, a spatial correlation structure could be identified (Fig. 4). The estimated value of horizontal correlation length was 6.66 m with a standard error of estimate of 4.7 m. The estimated nugget value was equal to zero. The estimated sill variance was 0.88 with a standard error of estimate of 0.1.

5.2. Vertical variogram analysis of flowmeter data

Variogram calculations for separate vertical profiles are often inaccurate due to limited number of measurement points. This leads to a large uncertainty in the calculated semivariances, which are reflected by large scatter especially for large lag values. To overcome this limitation an overall vertical variogram was calculated using the K-values of all wells (not including replicate measurements). This was done by projecting the vertical profiles on to one transect where they were separated by a large lag distance to eliminate spurious correlations. In total 710 data points obtained from 23 wells were used to calculate the experimental variogram. The fitted exponential model gave a

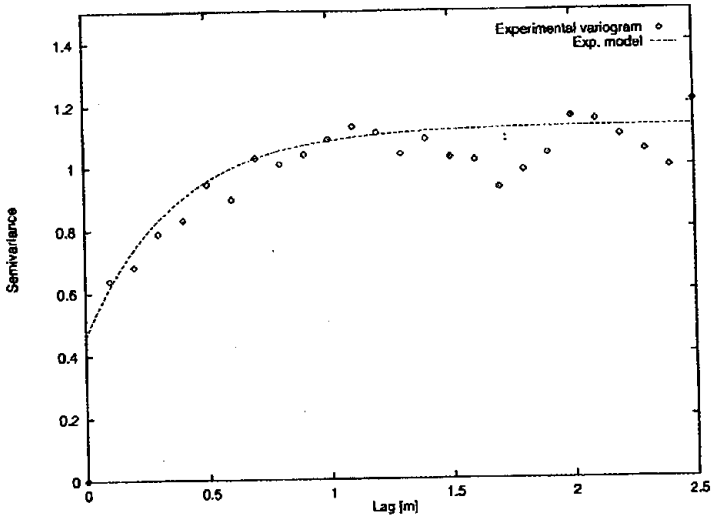

Fig. 4. Experimental and fitted exponential variogram of the hydraulic conductivity in the vertical direction using all locations projected on a transect.

correlation length of 0.37 m with a standard error of estimate of 0.09 m (Fig. 5). The value of the sill variance is 1.13, which is somewhat smaller than the sample variance of 1.3. The standard error of estimate is 0.11. The nugget is 0.46 with an standard error of estimate of 0.11. The estimated vertical correlation length is in good agreement with the value estimated from the Seiler-II (0.4 m) method. The Seiler-I method gave a correlation length that was a factor two times larger. This means that the vertical correlation length obtained from flowmeter measurements and grain size data estimates are quite similar. This is also supported by the findings of Rehfeldt et al. (1992).

5.3. Horizontal variogram analysis of flowmeter data

3-D experimental variograms of K values from flowmeter measurements were calculated using GAMV3 (Deutsch and Journel, 1992) in order to identify the horizontal correlation lengths of K. Numerous search schemes with different search directions, lag widths, dipping and tolerance angles were evaluated, but no spatial structure could be identified. The semivariances at small and large lag distances were of the same order of magnitude. This finding is in contrast to results of Rehfeldt et al. (1992), who succeeded in estimating the horizontal correlation length from flowmeter measurements. In their work, the ratio of vertical measurement interval and vertical correlation length was equal to 11, whereas, in our case, the ratio ranges between 2 and 3. At Cape Cod (Hess et al., 1992), the ratio ranged between 1 and 2.5. This small ratio may be one of the reasons why the experimental horizontal variograms presented in Hess et al. (1992) do not show such a clear spatial structure as those of Rehfeldt et al. (1992).

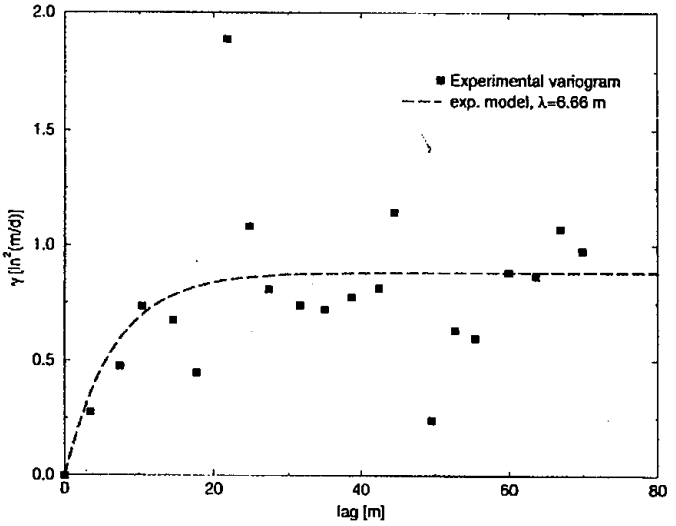

Fig. 5. 3-D experimental and fitted exponential variogram of estimated hydraulic conductivity using the Seiler-I method.

6. Spatial variation of local Darcian velocities

6.1. Univariate statistics of the local velocities

In Table 3, we show the statistics of the measured Darcian velocity U for two datasets (sets 1 and 2). Set 1 contains all data for which the magnitude of the Darcian velocity was available. In set 2, measurements were analyzed, which yielded both magnitude and direction of flow. The velocity components U_1 and U_2 were calculated by decomposing U along the mean flow path (340°N) and the direction perpendicular to it. Both datasets provide similar statistics of U. The Shapiro–Wilk test values for $\ln U$ are larger than 0.95 indicating that the observed data might come from a lognormal distribution. The geometric mean of U and overall variance of $\ln U$ in set 1 is 0.47 m/day and 1.86, respectively. Using an average porosity of 28% (layer 2), an average groundwater flow velocity of about 1.7 m/day is obtained. For set 2, the average groundwater flow velocity is 1.5 m/day. The calculated groundwater velocities on the basis of Table 2 (Seiler-I and Seiler-II, layer 2 + 3, layer 3, horiz.) range between 0.58 and 1.54 m/day. This indicates that the estimated groundwater velocities from the Seiler methods and the direct velocity measurements are of the same order of magnitude. Especially, the Seiler-II method is in good agreement.

The direction of measured groundwater velocities varied between 210°N and 90°N. The mean flow direction was at 340°N. Table 4 shows the change in magnitude and direction of U for the three wells for which a vertical profile was monitored. Large variations in the magnitude of the Darcian velocity occurred with depth. The values ranged between 0.47 and 7.87 m/day at location 22 and between 0.08 and 4.34 m/day at location 32. In addition, variations up to a factor of 9 occurred over a distance of 0.5 m. Further, the geometric mean of U varies considerably between wells with the lowest value of 0.24 m/day ($\exp(\ln K)$) at location 53 (Table 4). A second important observation is related to the direction of flow in the three observation wells. In these three wells, a systematic change in the flow direction was present. In layer 1, the direction of flow was towards the NNE and changed to N–W direction in layer 2. In

Table 3
Statistical properties of the magnitude of groundwater velocity for two different cases. S–W test represents the Shapiro–Wilk test. Values in parentheses give the probability of finding a smaller value

	Data with reliable directional information, set 2 ($N = 61$)	All measurements, set 1 ($N = 82$)
$\langle U \rangle$ (m/day)	1.1	1.21
Median U	0.32	0.44
Variance U	4.47	4.64
S–W test	0.52 (0.0001)	0.56 (0.0001)
$\langle \ln U \rangle$	−0.89	−0.75
Median $\ln U$	−1.14	−0.82
Variance $\ln U$	1.91	1.86
S–W test	0.96 (0.11)	0.97 (0.14)

Table 4
Change in magnitude and direction of Darcian velocities with depth in three wells. The numbers in parentheses indicate the deviation in degrees from the mean flow direction

Depth below surface (m)	Elevation above MSL (m)	B22, U (m/day)	B32, U (m/day)	B53, U (m/day)
3.6	94.8	0.78 (80)	4.34 (20)	0.12 (40)
4.1	94.3	0.47 (30)	2.72 (−25)	0.27 (25)
4.6	93.8	1.77 (20)	0.85 (−90)	0.20 (−70)
5.6	92.8	1.02 (−5)	1.50 (−80)	0.16 (−35)
6.1	92.3	3.11 (5)	0.80 (−110)	0.30 (−50)
6.6	91.8	2.66 (−40)	0.65 (−30)	0.30 (−20)
7.6	90.8	1.76 (−25)	0.62 (−35)	0.27 (−75)
8.1	90.3	4.17 (−85)	0.42 (−5)	0.31 (15)
8.6	89.8	0.86 (−60)	0.47 (25)	0.30 (105)
9.6	88.8	7.87 (85)	0.08 (30)	
10.1	88.3	1.74 (60)	0.10 (50)	
$\langle U \rangle$ (m/day)		2.38	1.14	0.247
var(U)		4.54	1.67	0.005
$\langle \ln U \rangle$		0.56	−0.44	−1.44
var($\ln U$)		0.67	1.46	0.12

layer 3, the flow direction was towards NNE again. The change in flow direction corresponds to the three different hydrogeological layers distinguished on the basis of the geological survey. This variation is shown in more detail in Table 5. This table contains the means and variances of U_1 and U_2 ($\sigma^2_{U_1}$, $\sigma^2_{U_2}$) for the different hydrogeological layers (layer 1–3) and for the whole aquifer. U_1 is the velocity component in the direction of flow (340°N) and U_2 is the velocity component perpendicular to it. These components are obtained by straightforward decomposition of the measured groundwa-

Table 5
Mean and variance for the longitudinal and transversal velocity components U_1 and U_2 for different layers and layer 2+3. S–W test represents the Shapiro–Wilk test. Values in parentheses give the probability of finding a smaller value

		U_1, parallel to 340°	U_2, orthogonal to 340°
Layer 1 (10)	mean (m/day)	0.96	0.08
	σ^2 ((m/day)^2)	1.85	0.60
	SW	0.73 (0.0026)	0.97 (0.93)
Layer 2 (31)	mean (m/day)	0.63	−0.38
	σ^2 ((m/day)^2)	1.36	0.89
	SW	0.51 (0.0001)	0.61 (0.0001)
Layer 3 (20)	mean (m/day)	0.70	0.90
	σ^2 ((m/day)^2)	3.8	6.7
	SW	0.34 (0.0001)	0.49 (0.0001)
Overall (61)	mean (m/day)	0.70	0.12
	σ^2 ((m/day)^2)	2.2	3.0
	SW	0.48 (0.0001)	0.56 (0.0001)

ter velocities on the mean flow direction. Striking is the very high value of $\sigma^2_{U_2}$ (3.0) for the whole aquifer, which is even larger than $\sigma^2_{U_1}$ (2.2). In addition, the overall mean value of U_2 is positive, indicating a bias of the measurements of flow direction towards the eastern direction. The large variance in U_2 is a direct consequence of the trend present in the direction of the velocity. This trend may partly be removed by analysing the data according to the hydrogeological layers. For layer 1, the variance in U_2 is 0.6, which is about 31% of the variance in U_1. The mean value U_2 (0.08) is positive indicating that the flow directions were slightly biased in the eastern direction. For layer 2, the variance of U_2 (0.89) is larger than in layer 1 and its mean value is negative (-0.38), which indicates that the direction of the velocities was biased in the western direction. Finally, for layer 3, the velocity directions were heavily biased to the eastern direction again with a mean value of U_2 of 0.9. In addition, $\sigma^2_{U_2}$ (6.7) is almost twice as large as $\sigma^2_{U_1}$, showing that there was a considerable variation in the direction of flow. Thus, the high value for $\sigma^2_{U_2}$ in the whole aquifer was mainly caused by the strong variations in velocity magnitudes occurring in layer 3.

The above analysis shows that the main flow direction differs between the different hydrogeological layers. This variation seems to lead to large variances in velocity component perpendicular to the mean flow and may cause additional transverse dispersive effects. This may also partly explain the underestimation of transverse dispersivities observed at other test sites (at the Introduction) based on stochastic theories, which assume a constant mean velocity both in magnitude and direction.

6.2. *Spatial analysis of the local velocities*

Although the analysis of the direct velocity measurements showed a clear trend in the direction of the velocity (Section 6.1), the mean magnitude did not differ considerably between measurement planes. This was verified by comparing the mean velocity values of the two measurement planes combined with a trend analysis. Experimental variograms of $\ln U$ were, therefore, calculated using data from both measurement planes. Two experimental variograms were calculated using GAMV3 with a search angle of 340°N (case 1) and 310°N (case 2), respectively. The search direction of 340°N was motivated by the mean flow direction of the solute plumes (Section 12.4). The other search angle was chosen arbitrarily. The tolerance angle was 45°. An exponential correlation model was fitted through the experimental variograms of U (case 1, case 2). The correlation lengths are 4.2 m for case 1 and 6.9 m for case 2 (Table 6). Fig. 6 shows

Table 6
Results of variogram analysis for the magnitude of the measured Darcian velocities. Both exponential and spherical models are fitted. SSE is the sum of squared errors which is a measure for the goodness of fit; S.E. is the standard error of estimate, N is the number of data points; and L is the horizontal correlation length. The mentioned direction refers to the search angle of the variogram analysis

	L (m)	S.E.	Sill	S.E.	SSE	N
Case 1 (340°, magnitude)	4.19	2.16	2.10	0.18	2.63	53
Case 2 (310°, magnitude)	6.86	2.50	2.07	0.15	1.49	53

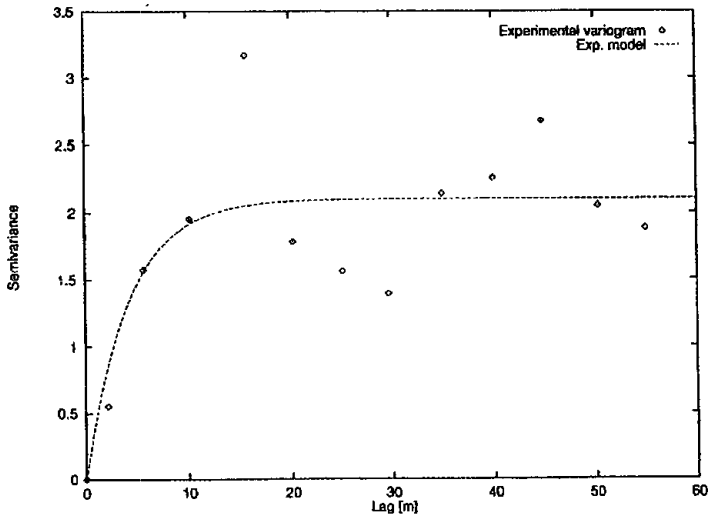

Fig. 6. Experimental and fitted exponential variogram of the horizontal velocity magnitude for a search direction of 340°N.

a fit of the exponential model to the experimental variogram obtained for case 1 (340°N). The experimental variogram was calculated for lag distances of 5 m centered at 2.5 m. Compared to the K-values of the flowmeter measurements for which no horizontal spatial structure could be found (Section 5.3), a clear spatial correlation was found for the Darcian velocities. As discussed previously for the flowmeter data, this may be due to the fact that the measurement interval of 0.5 m was more appropriate than the interval used in the flowmeter measurements to detect the horizontal correlation length.

The variogram analysis of the local velocities showed that the spatial dependence may be described by an exponential variogram function with a correlation length of 4.2 m. This correlation length is similar to the correlation length obtained from the K-values from grain size distribution (6.66 m, Section 5.1).

7. Spatial variation of Freundlich parameters for uranin and lithium

Mean (M), standard deviation (ST.DEV.) and measurement errors (ME.ER) for k and n of uranin and lithium in the Rhine gravel (layer 2 + 3) are listed in Table 7. For both substances, the measurement errors of k and n parameters are considerably lower than their observed spatial variation expressed by ST.DEV. Therefore, the measured variation is due to spatial variation in the estimated sorption parameters. For uranin in layer 2 + 3, the mean value of n and k (total sediment) are 0.83 and 0.35, respectively. The mean values of n for layer 2 (0.85) and 3 (0.81) are significantly (at 95% confidence interval) different. The mean value of k differs by a factor two to three between layers and is

Table 7
Mean and standard deviation (ST.DEV) for Freundlich k and n parameters of uranin and lithium in layer 2+3. ME.ER is the mean measurement error

Number of samples	Rhine gravel, layer 2+3		Upper rhine gravel, layer 2		Lower rhine gravel, layer 3	
	k	n	k	n	k	n
	$N=47$		$N=31$		$N=16$	
Uranin, tot. sed.						
M	0.35	0.83	0.25	0.85	0.55	0.81
ST.DEV.	±0.20	±0.06	±0.11	±0.07	±0.18	±0.03
ME.ER.	±0.03	±0.02	±0.03	±0.02	±0.03	±0.01
Lithium, tot. sed.						
M	6.7	0.53	8.4	0.49	3.2	0.61
ST.DEV.	±4.5	±0.08	±4.8	±0.06	±1.0	±0.05
ME.ER.	±1.3	±0.02	±1.6	±0.02	±0.6	±0.02

statistical different at 95% confidence. Lithium sorption is strongly nonlinear as indicated by the low values of n, ranging between 0.49 and 0.61 (Table 7). Mean k values of the total sediment range between 3.2 and 8.4. The mean values of k and n for layer 2 and layer 3 are statistically different at a confidence level of 95%. Due to the limited number of data and the clear difference in mean values between layers, no spatial analysis of n and k was performed.

8. Correlation analysis of sorption and aquifer parameters

8.1. Correlation between hydraulic conductivity and sorption parameters

Correlation coefficients are calculated between hydraulic conductivity, K, and sorption parameters, n and k, for lithium and uranin (Table 8). Hydraulic conductivities were estimated from grain size data using the method of Seiler-II (Section 3.2). The

Table 8
Correlation coefficients for uranin and lithium sorption parameters and hydraulic conductivity K

Number of samples	Rhine gravel, layer 2+3			Upper rhine gravel, layer 2			Lower rhine gravel, layer 3		
	$N=47$			$N=31$			$N=16$		
	k	n	S	k	n	S	k	n	S
Uranin									
$\ln K$, fract. < 2 mm	−0.05	0.30	0.00	−0.20	0.65	0.15	−0.45	0.40	−0.30
$\ln K$, tot. sed.	−0.45	0.30	−0.40	−0.50	0.65	−0.35	−0.65	0.40	−0.60
Lithium									
$\ln K$, fract. < 2 mm	−0.40	−0.35	0.20	−0.30	−0.65	−0.35	0.45	−0.50	−0.15
$\ln K$, tot. sed.	−0.40	−0.35	−0.40	−0.55	−0.65	−0.50	0.00	−0.50	−0.50

correlation coefficients are very low both for uranin and lithium and this for both types of sediment fraction. The largest correlations were found between n and $\ln K$ with values ranging between 0.30 and 0.65 for uranin and between -0.35 and -0.65 for lithium. The difference in correlation signs between uranin and lithium may indicate that different sorbents are responsible for the interaction. By recalculating the data for the whole sediment the correlation between k and $\ln K$ increased to values ranging between -0.40 and -0.65 for uranin and lithium. Only in one case (lithium, total sediment, layer 2) no correlation was found. Similar results were found using the method of Seiler-I. The low correlations agree with the findings of Robin et al. (1991), who reported weak negative correlations between the log transformed distribution coefficient of strontium, $\ln K_d$, and $\ln K$.

8.2. Correlations between Freundlich parameters and sediment properties

Correlation coefficients between k, n, S of uranin and sediment properties are given in Table 9. The sediment sorption capacity, S, mainly determined by k, was investigated for all layers. The n parameter does not show any significant correlation with the aquifer properties for layer 2 + 3. The sorption capacity determined for the whole sediment fraction is positively correlated with log transformed values of clay content, CEC and the amount of fines. No correlation with Corg was found. The correlation coefficients between parameters differed for layers 2 and 3 when analysed separately. The values of the coefficients for layer 3 were similar to those found for layers 2 and 3 together (Rhine gravel). For layer 2, n was, however, negatively correlated with all measured sediment properties, especially with the fine sediment fraction. This is probably due to the fact that uranin sorption occurs at different sorption sites in layers 2 and 3. The larger correlation coefficient between k and the log transformed clay fraction for layer 3 compared to layer 2 indicates that the clay fraction is the major sorbent for layer 3. For layer 2, other properties than clay minerals, such as oxides, most likely control the sorption of uranin.

Table 9
Correlation coefficients for uranin sorption parameters and physico-chemical properties of aquifer. SSA is the specific surface area; CEC, the cation exchange capacity; and Corg, organic carbon content

Number of samples	Rhine gravel, layer 2+3			Upper rhine gravel, layer 2			Lower rhine gravel, layer 3		
	$N=47$			$N=31$			$N=16$		
Uranin	k	n	S	k	n	S	k	n	S
k		−0.20			−0.05			−0.50	
S	0.90	0.25		0.90	−0.20		0.90	0.45	
ln(Clay)	0.85	0.00	0.75	0.45	−0.20	0.45	0.70	0.20	0.70
ln(Fines)	0.60	−0.30	0.70	0.60	−0.75	0.35	0.50	0.20	0.60
ln(CEC)	0.75	0.02	0.75	0.45	−0.15	0.50	0.55	0.35	0.65
ln(SSA)	0.50	0.05	0.55	0.70	−0.40	0.50	0.60	0.00	0.50
ln(Corg)	0.05	−0.15	0.00	−0.25	−0.15	−0.35	0.20	−0.20	0.10

Table 10

Correlation coefficients for lithium sorption parameters and physico-chemical properties of aquifer. SSA is the specific surface area; CEC, the cation exchange capacity; and Corg, organic carbon content

Number of samples	Rhine gravel, layer 2 + 3			Upper rhine gravel, layer 2			Lower rhine gravel, layer 3		
	$N = 47$			$N = 31$			$N = 16$		
Lithium	k	n	S	k	n	S	k	n	S
k		−0.85			−0.60			−0.80	
S	−0.05	0.75		0.15	0.55		−0.60	0.25	
ln(Clay) (< 2 μm)	−0.25	0.75	0.75	0.10	0.55	0.85	−0.50	0.85	0.20
ln(Fines) (< 0.2 mm)	−0.50	0.75	0.65	−0.10	0.25	0.40	−0.20	0.85	0.30
ln(CEC)	−0.15	0.75	0.85	0.10	0.50	0.75	0.10	0.40	0.50
ln(SSA)	−0.35	0.45	0.25	−0.45	0.40	0.50	−0.40	0.40	−0.10
ln(Corg)	−0.25	−0.05	−0.15	−0.30	−0.05	−0.35	−0.15	0.15	0.00

Table 10 gives the correlation coefficients for lithium sorption data with the sediment properties. The values of k and n are negatively correlated. For layer 2 + 3, n is positively correlated with the log transformed sediment properties and S. The largest correlations coefficients for n are found in layer 3 with log transformed clay content and fines. These values are different from the values found for uranin. First, only weak correlations (Table 9) were found in layer 3 for n of uranin with clay and fines. Secondly, only negative correlations for n of uranin were found with sediment parameters in layer 2. The value of k for lithium sorption is weakly correlated with the log transformed properties of the sediment. This is again in contradiction with the observation made for uranin.

The differences in correlation coefficients of uranin and lithium sorption parameters with sediment properties may be explained by different sorbing materials in the sediment layers and the chemical nature of uranin and lithium. Uranin is a large organic anion with carboxylic groups whereas lithium is a small cation. Therefore, it is expected that uranin sorption occurs on positively charged oxides (e.g., Goethite), which from their size may belong to the clay fraction. On the basis of the correlation coefficient with Corg, there was no evidence of uranin sorption with organic carbon. For lithium, sorption probably occurs on the basis of ion exchange processes with clay minerals.

9. Tracer injections

Three different tracers were injected into groundwater: uranin ($C_{20}H_{20}Na_2O_5$) and lithium chloride (LiCl) on 30 August 1994 and sodium bromide (NaBr) on 3 April 1996. Eosin ($C_{20}H_6Br_4Na_2O_5$) was used in a pretest to obtain estimates of groundwater flow direction and velocity with the purpose of defining the locations of observation wells (Döring, 1997). The spatial and temporal evolution of Li^+ (hereafter referred to as lithium) and uranin were then monitored for 449 days. Chloride was not used as a tracer substance due to the high background concentration in the groundwater. The spatial and temporal evolution of Br^- (hereafter referred to as bromide) was monitored for 398

days. Preliminary batch experiments with sediment from different depths showed that bromide behaved as an inert (conservative) tracer. Uranin and lithium were used as reactive tracer substances.

120 kg LiCl and 2 kg uranin (55% purity) dissolved and well mixed in 4500 l of groundwater were injected. The tracer solution was equally distributed over the three injection wells (57, 58, 59) (Fig. 1) and injected at a depth between 6 and 7 m below the surface (91.4–92.4 m above MSL). The injection lasted for 5 h. During this time, concentration and temperature of the injection solution were monitored. The initial concentrations of uranin and lithium were 240 and 4100 mg/l, respectively. The water temperature was constant at about 17.2°C, the groundwater temperature was 10°C. The injected solution had a density of 1.015 g/cm^3, which was about 1.5% higher than the density of the groundwater.

The injection of 135.9 kg of NaBr dissolved in 8000 l of groundwater lasted for 10.8 h. To minimize downward movement of the solute plume due to a higher mass density compared to the groundwater, the solution volume and injection time were doubled compared to our earlier tracer experiments with LiCl and uranin.

10. Monitoring of solute concentrations

During the tracer tests with uranin and lithium, which were monitored for 15 months, 7468 lithium and 19,386 uranin samples were collected and analyzed. For the bromide, 12,616 samples were analyzed. To characterize the spatial extent of the uranin and lithium clouds, 12 sampling rounds were done. For bromide, seven measurement rounds were done. Uranin BTCs were measured for every sampler at 15 locations. Bromide and lithium concentrations were determined on every second sample. The number of lithium and bromide samples analysed were smaller than uranin because their detection was more complicated and expensive than uranin. Groundwater samples were collected with a 12-channel peristaltic pump. Two volumes of a sampler tube (200 ml) were removed before a sample of 10 ml was taken. Testing of the PE tubes showed that no sorption of the substances occurred. The samples were stored at the field site in dark conditions at 8°C and transported to the laboratory at the end of the day.

Bromide was measured using ion-chromatography with a detection limit of 0.02 mg/l and a relative measurement error of 5%. The natural background concentration of bromide was about 0.25 mg/l. Uranin was analyzed using fluorescence spectroscopy with synchron scan (Schaefer, 1995). Concentrations of 200 ng/l could be detected but due to the antecedent use of eosin, an uranin detection level of 2 μg/l was set. Samples containing both uranin and eosin were analyzed by fitting two Gaussian curves, one for uranin and one for eosin, to the observed spectrum. The area below the uranin curve was then determined and transformed into concentrations using calibration curves. Lithium was analyzed using ICP-MS. This method allows the detection of lithium to about 20 μg/l. But since the natural background of lithium varied between 2 and 20 μg/l, a cutoff value of 50 μg/l was set.

As previously stated, this paper focuses on the analysis of bromide transport using spatial moment analysis. The measured bromide BTCs will be discussed and interpreted

in a paper by Vanderborght and Vereecken (2000) using classical CDE analysis and temporal moment analysis. Field BTCs of uranin were analysed by Vereecken et al. (1999b) using asymptotic analysis. The results of the field-scale analysis were compared with results from local scale BTCs. In addition to the determination of the tracers, the major cation and anion concentration were determined in samples collected along the tracer flow path. Work is on its way to interpret the transport behaviour of lithium using observed BTCs of these anions and cations.

11. Contour plots of bromide plume

Horizontal and vertical contour plots were calculated using the SURFER software (Version 5.02, 1994). Horizontal interpolation was performed by Kriging using a linear variogram model without nugget, a rotation angle of $-30°$ and an anisotropic ratio of 0.5. Interpolation in the vertical plane was done with Kriging using a linear variogram. Horizontal contour plots of vertically averaged bromide concentrations are shown in Figs. 7 and 8. After 138 days, the longitudinal extension of the plume is about 100 m.

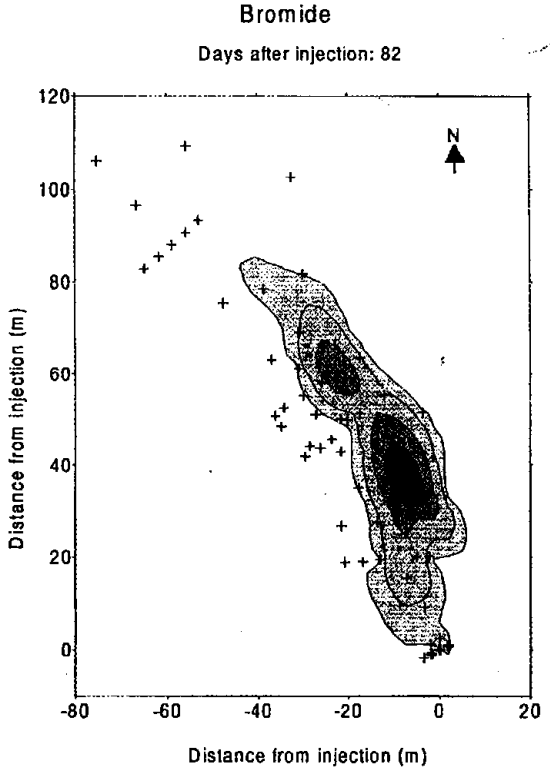

Fig. 7. Horizontal contour plots of the vertical averaged concentrations of bromide for 82 days after injection.

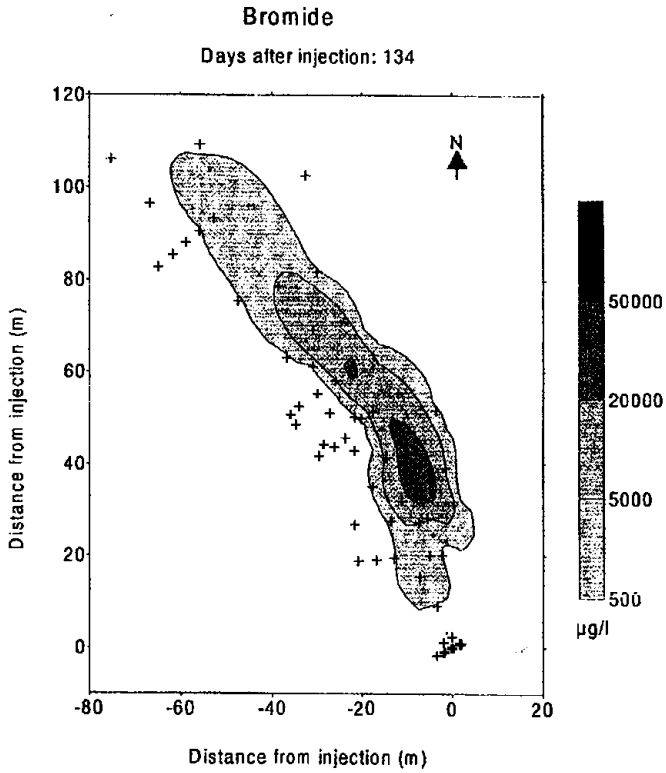

Fig. 8. Horizontal contour plots of the vertical averaged concentrations of bromide for 134 days after injection.

For larger times, a part of the bromide mass is transported beyond the field site. This is also illustrated by the steady decrease of the total recovered mass (see Section 12.2.1). Vertical contour plots (between 88.4–95.4 m and 87.4–95.4 m above MSL) of the solute concentrations along a transect in the mean groundwater flow direction were constructed for four sampling dates (Fig. 1). The vertical contour plot (Fig. 9) shows that bromide partly sank below the depth of injection (91.4–92.4 m above MSL). In addition, the contour lines are not closed at the bottom suggesting that tracer mass was lost below the deepest sampler. This sinking of the plume was most likely caused by the higher density of about 1.5% of the injected solute than groundwater.

12. Spatial moment analysis

12.1. Calculation of the spatial moments

The calculation of spatial moments of the tracer plumes is one of the most frequently used methods to compare experimental data with predictions from stochastic theories

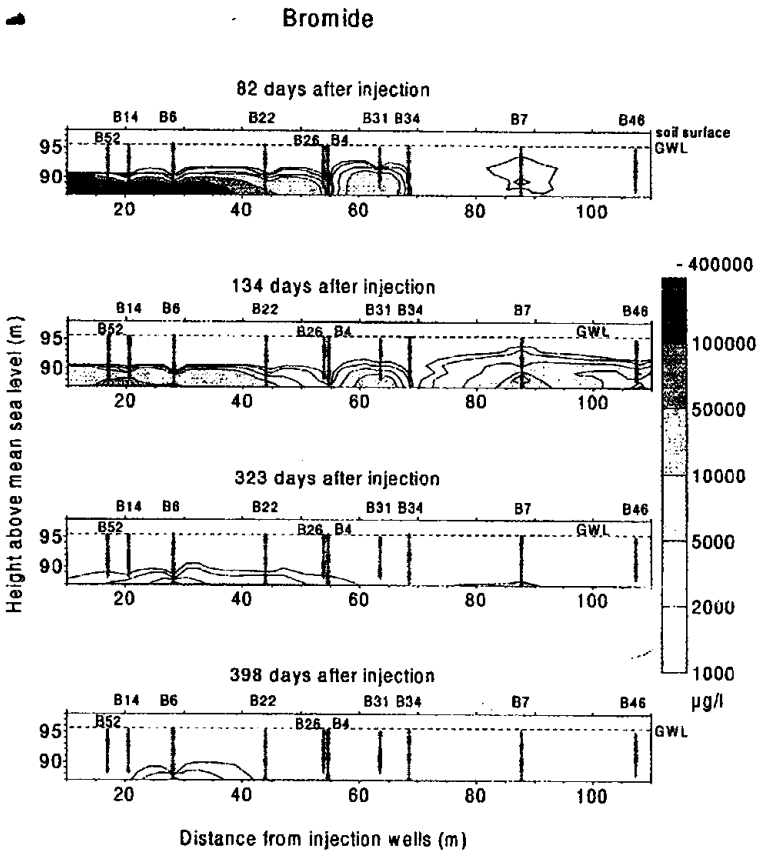

Fig. 9. Vertical contour plots of bromide concentrations along a transect in the direction of groundwater flow.

(Freyberg, 1986; Garabedian et al., 1991). Spatial moments for the dissolved phase are defined as:

$$M_0 = \int\int\int n(\vec{x})\, c(\vec{x},t)\, \mathrm{d}\vec{x}, \tag{5}$$

$$M_1 = \frac{1}{M_0}\int\int\int \vec{x} n(\vec{x})\, c(\vec{x},t)\, \mathrm{d}\vec{x}, \tag{6}$$

$$\Sigma = \frac{1}{M_0}\int\int\int (\vec{x} - M_1)(\vec{x} - M_1)^T n(\vec{x})\, c(\vec{x},t)\, \mathrm{d}\vec{x}, \tag{7}$$

where M_0 is the zeroth-order moment representing the mass of solute; M_1 is the first-order moment representing the position of the center of mass; Σ is the second-order central moment representing the spread of the plume, $c(\vec{x},t)$ is the concentration of the dissolved phase at time t and spatial coordinate $\vec{x}$ and n is the porosity of the medium.

The integrals in Eqs. (5)–(7) were evaluated numerically. The vertical direction of the integration domain extended from 87.0 to 95.5 m above MSL. Extrapolation of concentration values was needed in a few samplers to assign values to nodal points belonging to wells, which did not reach the lower boundary of the integration domain. We used the extrapolation algorithm proposed by Freyberg (1986), which involved halving the concentration for each stepwise increase in vertical sampling distance. Eigenvalues and eigenvectors of Σ (Eq. (7)) were calculated using routines from the NAGlib to obtain the principal components of the variance tensor. Eigenvectors can be used to calculate the orientation of the plume axis with respect to the original coordinate system. In this study, we only considered the orientation of the plume in the horizontal plane with respect to the original coordinate system.

12.2. Analysis of spatial moments

12.2.1. Zeroth-order spatial moment

The zeroth-order moment representing the mass of dissolved substance in the domain was calculated using a mean porosity of 26% for the whole aquifer. The bromide tracer shows a systematic decrease of mass in solution (Fig. 10). The recovered mass remains roughly constant over a period of 110 days after injection. The decrease in dissolved mass was most likely caused by a density driven downward movement of the tracers. Similar downward driven movements due to higher densities of the injected volume were observed at the Cape Cod (LeBlanc et al., 1991) and Columbus (Boggs et al., 1992) tracer experiments. The zeroth-order moments for uranin and lithium (not shown) indicated an even more drastic decrease of the recovered mass with time. It is anticipated that in addition to the downward movement of the plumes, sorption of

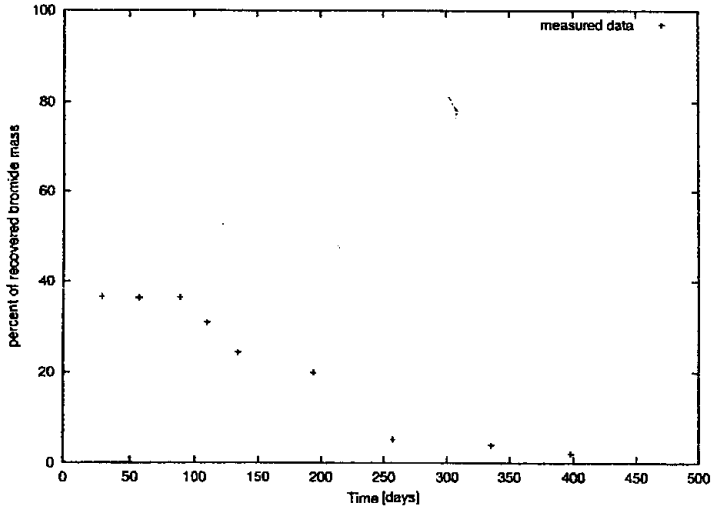

Fig. 10. Variation of mass recovery of bromide with time.

lithium and uranin occurs on the sediment. This is supported by the findings from the batch experiments (Section 3.4). However, it is not clear whether nonlinear equilibrium sorption is the main driving sorption process. Column experiments conducted on sediments from the field site with uranin and lithium showed that other sorption mechanisms may play a role. Interpretation of the uranin and lithium field-scale transport will be subject of further work. In the following, we focus on the spatial moments of bromide and restrict our evaluation to the period of constant mass recovery of bromide.

12.3. First-order spatial moments

From the first spatial moment, the mean solute velocity of the bromide tracer was determined (Fig. 11). 110 days after injection, the mean average solute plume velocity of bromide was 0.5 m/day. This velocity is in agreement with the effective velocities derived by time moment analysis of bromide BTCs, which range between 0.41 and 0.84 m/day, depending on the method of calculating flux-averaged concentrations (Vanderborght and Vereecken, 2000), but is lower than the estimates obtained from local velocities (1.7 m/day) and grain size data methods using Seiler-I and Seiler-II (0.72 and 0.92 m/day). The estimates from the grain size data are in good agreement with the velocities derived from the field BTCs of bromide. The velocities derived from the grain size data were obtained by multiplying the K-values with the mean hydraulic gradient (0.002) and dividing the product by the mean overall porosity (0.26). Evaluation of the orientation of the tracer cloud main axes calculated from the first spatial moment showed that the mean flow direction of the bromide plume was 330°N.

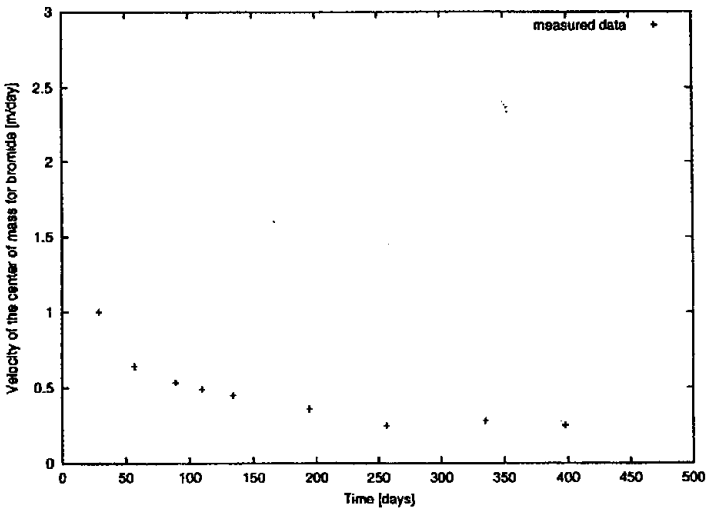

Fig. 11. Change of mean velocity from spatial moment analysis for bromid.

12.4. Second-order spatial moments

The second-order centered longitudinal moment (longitudinal variance) of bromide is shown in Fig. 12. An almost linear increase of the moment with time is observed up to a value of 470 m^2 after 134 days. Thereafter, the calculated values of the moment are fluctuating with two large values above 1100 m^2 on days 323 and 398. For the initial 110 days after injection, the longitudinal dispersion and the mean velocity were 1.82 m^2/day and 0.5 m/day, respectively. This results in a longitudinal dispersivity, α_L, of 3.64 m. This value should be considered as a lower estimate because asymptotic behaviour may not have been reached yet. This value is of the same order of magnitude as observed at the Columbus field site experiment, which was found to range between 5 and 10 m (Adams and Gelhar, 1992). The variance of $\ln K$ at this site was 4.5 with a correlation length of 4.8 m. Lower longitudinal dispersivities were observed at the Borden site ($\alpha_L = 0.43$ m) and the Cape Cod site ($\alpha_L = 0.96$ m). Both test sites are less heterogeneous with variances of $\ln K$ ranging between 0.14 (Borden site) and 0.29 (Cape Cod). The variance of $\ln K$ at the Krauthausen test site obtained from grain size data for layer 2 + 3 ranges between 0.84 and 1.08 (Table 2). This is larger than the values from Borden (0.29) and Cape Cod (0.14–0.24), but smaller than the value from the Columbus site. Correlation lengths for K at Borden and Cape Cod were 2.8 m and 5.1 m. Our estimated horizontal correlation length on the basis of grain size data was equal to 6.7 m with a standard error of estimate of 4.7 m.

Using the theory of Gelhar and Axness (1983), an estimate of α_L for the Krauthausen field site is obtained from the equation $\alpha_L = \sigma^2_{\ln K} I_{\ln K}$ where $\sigma^2_{\ln K}$ is the variance of $\ln K$ and $I_{\ln K}$ is the correlation length. With $\sigma^2_{\ln K} \approx 1.08$ (Table 2, Seiler-I) and a correlation length of 6.7 m, we obtain a dispersivity $\alpha_L \approx 7.2$ m. This is twice as large

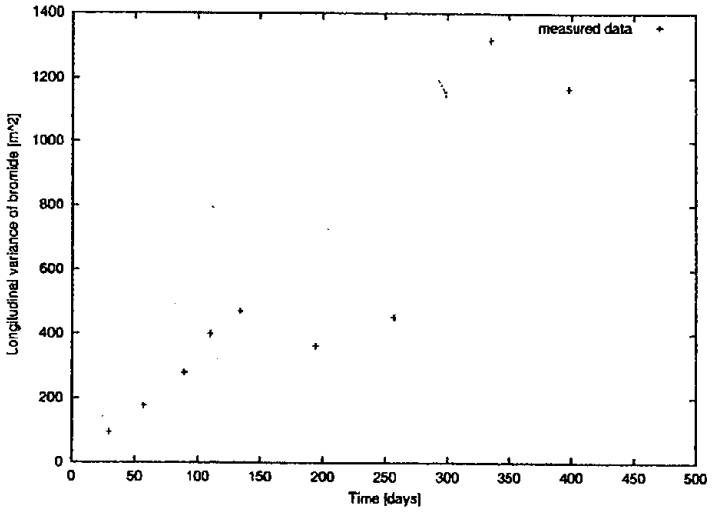

Fig. 12. Change of longitudinal variance of the bromide solute plume with time.

as the observed value of 3.64 m. Two reasons can be invoked to explain this difference. One possibility may be that the asymptotic regime is not yet obtained. The maximum travel distance for the plume was about 170 m, which corresponds to 25 correlation lengths of $\ln K$. The evaluation of the spatial moments was, however, restricted to a smaller distance due to mass loss. This may have provided too few correlation lengths needed to obtain asymptotic behaviour. The other reason may be the overestimation of $\sigma^2_{\ln K}$. The vertical contour plots of bromide suggest that most of the solute mass travelled through the bottom part of the flow domain, which corresponds to layer 3. The estimates of $\sigma^2_{\ln K}$ for this layer are smaller than for the layer 2 + 3 with a value of 0.56 (Seiler-I, Table 2). Using this value would give an estimate for α_L of 3.75, which is in better agreement with the value obtained from spatial moments. The observed dispersivity value of 3.64 m is, however, within the range of estimated dispersivity values when the standard error of estimate for the correlation length of $\ln K$ is taken into account. Due to this large uncertainty, the evaluation of stochastic solute transport theories becomes difficult. In addition, truncation of the solute plume may affect the reliability of the moments based on spatial moment evaluation in terms of an underestimation of effective dispersivities (Miralles-Wilhelm and Gelhar, 1996).

The second-order centered transverse moment (transverse variance) (Fig. 13) provides information on the transverse macrodispersivity. The transverse variance of bromide increased to a value of 9.8 m^2 after 29 days and reached an almost constant value of about 20 m^2 after 57 days. These values need to be corrected for the initial extent of the plume in the horizontal direction. The plume was injected over a width of about 6 m, which corresponds to a variance of about 3.0 m^2 in the transverse direction. The transverse variance was, therefore, equal to about 17 m^2 after 57 days. This almost constant tranverse variance suggests that a small or even zero asymptotic value for the

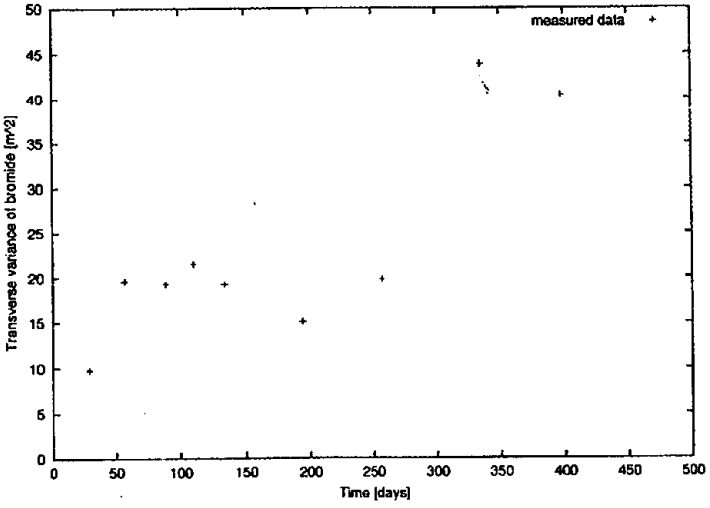

Fig. 13. Change of transversal variance of the bromide solute plume with time.

effective horizontal dispersivity may be appropriate. This finding is in agreement with the Borden site experiment where a small or zero asymptotic value for horizontal dispersivity was found also not to be inappropriate (Freyberg, 1986). At the Borden site, this asymptotic behaviour occurred after 300 to 650 days of travel time, which corresponds to a travelled distance of 27 to 59 m and corresponds to 9.6 to 21 correlation lengths of $\ln K$. For the range of groundwater velocities (0.4 to 0.92 m/day) observed at the Krauthausen test site and using $I_{\ln K} = 6.7$ m, an asymptotic regime seems to be obtained after 3.4 to 7.8 correlation lengths of $\ln K$. The results at the Borden and Krauthausen site differ from the findings at Cape Cod. At this site, the transverse horizontal variance was found to increase linearly over a travel distance of 200 m suggesting that a zero asymptotic value for the horizontal macrodispersivity was not yet obtained after 39 correlation lengths. In terms of statistics of $\ln K$, the Cape Cod site is the most homogeneous ($\sigma^2_{\ln K} = 0.14$–0.24) with $I_{\ln K} = 5.1$ m, which is close to the value for the Krauthausen site (6.7 m). A straight forward comparison between the sites in terms of asymptotic behaviour is, however, frauded with difficulties and can only be indicative because these estimates are uncertain due to estimation errors in the values of $\sigma^2_{\ln K}$ and $I_{\ln K}$. These uncertainties are caused by the limited spatial resolution of the sampling grid and the different results provided by the various methods used to derive the statistics of $\ln K$. In addition, mass loss of bromide at the Krauthausen combined with a trend in the groundwater flow direction complicates the picture. Further research at the test site will, therefore, focus on the use of new geophysical techniques (Kulessa et al., 2000) to monitor in a noninvasive manner the spreading of solutes and to avoid the limitations of spatial resolution.

13. Conclusions

The following findings were obtained from the experimental work conducted at the tracer field site Krauthausen.

(1) The vertical spatial correlation of hydraulic conductivity, K, derived from grain size data was described with an exponential variogram model with a correlation length of 0.4 and 0.6 m, depending on the choosen grain size data method. The vertical correlation length of K values obtained from flowmeter measurements was 0.37 m and agrees with the estimates from grain size data methods.

(2) The horizontal correlation length of K from grain size data based on the Seiler-I method was 6.7 m. No horizontal correlation length for K could be derived from flowmeter measurements.

(3) The magnitude of local Darcian velocities at the test site was found to be lognormally distributed with a geometric mean value of 0.47 m/day and a variance of 1.86. The local flow direction measurements showed a clear trend in the groundwater flow direction. This trend may lead to an enlarged dispersive effect on solute transport, which is not accounted for in stochastic theories. The spatial dependence of local velocities was described by an exponential variogram with a correlation length of 4.2 m. This correlation length is in good agreement with the correlation length obtained from the K-values from grain size distribution (6.7 m).

(4) The sorption isotherms of uranin measured in batch experiments could be described by a Freundlich equation with an n exponent varying between 0.71 and 0.95 within two standard deviation in layer 2 + 3. The lithium isotherms determined in batch experiments could also be described by a Freundlich isotherm. The value of the n parameter varied within one standard deviation between 0.37 and 0.69. In contrast to uranin, the n exponent of lithium sorption showed a clear correlation with clay content and CEC.

(5) Weak correlations between Freundlich sorption parameters obtained for the sediment fraction < 2 mm and $\ln K$, estimated from grain size data, were obtained both for uranin and lithium. This is in agreement with earlier findings in literature. A negative correlation $\ln K$, and Freundlich k of uranin pertaining to the whole sediment fraction was found, in which values ranged between -0.5 and -0.65. For lithium, both the k and n parameters were negatively correlated with $\ln K$.

(6) Spatial moment analysis showed a systematic decrease of the mass recovery for bromide. This is explained by the density driven vertical movement of the plumes below the MLS and mass loss due to the fact that the plume left the field site.

(7) The calculated longitudinal dispersivity at the test site was 3.64 m. Using the theory of Gelhar and Axness (1983), $\sigma^2_{\ln K} = 1.08$ and a correlation length of 6.7 m, the estimated longitudinal dispersivity is 7.2 m. Due to large uncertainties in the estimated correlation length and variance of $\ln K$ and the tracer mass loss, the quality of the estimates based on the theory of Gelhar and Axness could not be verified.

References

Adams, E., Gelhar, L.W., 1992. Field study of dispersion in a heterogeneous aquifer: 2. Spatial moment analysis. Water Resour. Res. 28 (12), 3293–3307.

Arya. A., Hewett, T.A., Larson, R.G., Lake, L.W., 1988. Dispersion and reservoir heterogeneity. SPE Reservoir Eng. 3 (1), 139–148.

Boggs, M.J., Young, S.C., Beard, L.M., Gelhar, L.W., Rehfeldt, K.R., Adams, E.E., 1992. Field study of dispersion in a heterogeneous aquifer: 1. Overview and site description. Water Resour. Res. 28 (12), 3281–3291.

Dagan, G., 1984. Solute transport in heterogeneous porous formations. J. Fluid Mech. 145, 151–177.

Dagan, G., 1989. Flow and transport in porous formations. Springer Verlag, Berlin.

Deutsch, C.V., Journel, A.G., 1992. GSLIB, Geostatistical Software Library and User's Guide. Oxford Univ. Press, New York.

Döring, U., 1997. Transport der reaktiven Stoffe Eosin, Uranin und Lithium in einem heterogenen Grundwasserleiter, PhD thesis, Christian-Albrechts Universität, Kiel, Germany, p. 118.

Döring, U., Jaekel, U., Neuendorf, O., Seidemann, R., Vereecken, H., 1999. Analysis of reactive solute transport in a heterogeneous aquifer: The Krauthausen field experiment. 3. Characterization of sorption heterogeneity and its impact on solute transport, Forschungszentrum Jülich, Internal report Nr. 500899.

Freyberg, D.L., 1986. A natural gradient experiment on solute transport in a sand aquifer: 2. Spatial moments and the advection and dispersion of nonreactive tracers. Water Resour. Res. 22 (13), 2031–2046.

Fried, J.J., Moser, H., Muntzer, P., Poulet, J.B., Trimborn, P., Zilliox, L., 1979. Determination of the range of velocities of groundwater movement by the method of punctual dilution. In 'Protection des eaux souterraines captees pour l'alimentation humaine; conditions naturelles de propagation des pollutions. Bur. Geol. Min., Serv. Geol. Nat., Orleans, France, 175–182.

Garabedian, S.P., LeBlanc, D.R., Gelhar, L.W., Celia, M.A., 1991. Large-Scale natural gradient tracer test in sand and gravel, Cape Cod, Massachusetts: 2. Analysis of spatial moments for a nonreactive tracer. Water Resour. Res. 27 (5), 911–924.

Gelhar, L.W., 1986. Stochastic subsurface hydrology from theory to application. Water Resour. Res. 22 (9), 135S–145S.

Gelhar, L.W., 1993. Stochastic Subsurface Hydrology. Prentice-Hall, Englewood Cliffs, NJ.

Gelhar, L.W., Axness, C.L., 1983. Three dimensional stochastic analysis of macrodispersion in aquifers. Water Resour. Res. 19 (1), 161–180.

Hess, K.M., Wolf, S.H., Celia, M.A., 1992. Large scale natural gradient tracer test in sand and gravel, Cape Cod, Massachusetts: 3. Hydraulic conductivity and calculated macrodispersivities. Water Resour. Res. 28 (8), 2011–2027.

Jaekel, U., Vereecken, H., 1996. Asymptotic analysis of nonlinear equilibrium solute transport in porous media. Water Resour. Res. 32 (10), 3093–3098.

Jaekel, U., Vereecken, H., 1997. Renormalization group analysis of macrodispersion in a directed random flow. Water Resour. Res. 33 (10), 2287–2299.

Journel, A., Huijbregts, J.L., 1978. Mining Geostatistics. Academic Press, London, p. 600.

Kabala, Z.J., 1994. Measuring distributions of hydraulic conductivity and specific storativity by the double flowmeter test. Water Resour. Res. 30 (3), 685–690.

Klotz, D., Moser, H., Trimborn, P., 1979. Single-borehole techniques, present status and examples of recent applications. Proc. Int. Symp. Isot. Hydrol., 1978 vol. 1 International Atomic Agency, Vienna, pp. 159–179.

Kulessa, B., Jaekel, U., Bick, M., Hashagen, U., Vereecken, H., 2000. Towards high resolution imaging of subsurface pollution: an introduction to the magneto-electrical resitivity imaging tool (MERIT). In: Powers, M.H., Ibrahim, A.B., Cramer, L. (Eds.), Proc. Symp. Appl. Geophys. Eng. Environ. Probl., Environmental and Engineering Geophysical Society, Arlington, VA, pp. 925–934.

LeBlanc, D.R., Garabedian, S.P., Hess, K.M., Gelhar, L.W., Quadri, R.D., Stollenwerk, K.G., Wood, W.W., 1991. Large scale natural gradient tracer test in sand and gravel, Cape Cod, Massachusetts: 1. Experimental design and observed tracer movement. Water Resour. Res. 27 (5), 895–910.

Metson, A.J., Blakemore, L.C., Rhoades, D.A., 1979. Methods for the determination of soil organic carbon; a review, and application to New Zealand soils. N. Z. J. Soil Sci. 22, 205–228.

Miralles-Wilhelm, F., Gelhar, L.W., 1996. Stochastic analysis of sorption macrokinetics in heterogeneous aquifers. Water Resour. Res. 32 (6), 1541–1549.

Molz, F., Morin, R.H., Hess, A.E., Melville, J.G., Goven, O., 1989. The impeller meter for measuring aquifer permeability variations: evaluation and comparison with tests. Water Resour. Res. 25 (7), 1677–1686.

Pickens, J.F., Grisak, G.E., 1981. Scale-dependent dispersion in a stratified granular aquifer. Water Resour. Res. 17 (4), 1191–1211.

Rehfeldt, K.R., Hufschmiedt, P., Gelhar, L.W., Schaefer, M.E., 1989. Measuring hydraulic conductivity with the borehole flowmeter. Elec. Power Res. Inst., (Palo Alto, Calif.), Rep. EN-6511.

Rehfeldt, K.R., Boggs, J.M., Gelhar, L.W., 1992. Field study of dispersion in a heterogeneous aquifer: 3. Geostatistical analysis of hydraulic conductivity. Water Resour. Res. 28 (12), 3309–3324.

Robin, M.J.L., Sudicky, E.A., Gillham, R.W., Kachanoski, R.G., 1991. Spatial variability of strontium distribution coefficients and their correlation with hydraulic conductivity in the Canadian Forces Borden Aquifer. Water Resour. Res. 27 (10), 2619–2632.

Russo, D., Dagan, G., 1991. On solute transport in a heterogeneous porous formation under saturated and unsaturated water flows. Water Resour. Res. 27 (3), 285–292.

Schaefer, R.G., 1995. Verhalten von Schadstoffen in geologischen Systemen. I. Quantifizierung von Farbtracern in Grundwasser: Dokumentation des Fluoreszens-spektroskopischen Analysenverfahrens für Eosin und Uranin. KFA/ICG-4 Interner Bericht Nr. 500695, Forschungszentrum Jülich GmbH, Germany.

Seiler, K.-P., 1973. Durchlässigkeit, Porosität und Kornverteilung quartärer Kies-Sand-Ablagerungen des bayerischen Alpenvorlandes. GWF 114 (8), 353–358, München.

Sudicky, E.A., 1986. A natural gradient experiment on solute transport in a sand aquifer: spatial variability of hydraulic conductivity and its role in the dispersion process. Water Resour. Res. 22 (13), 2069–2082.

Teutsch, G., Hofmann, B., Kobus, B., Ptak, Th., Schad, H., 1991. Testfeld Wasser/Boden, Teilprojekt II Schadstofftransport im Untergrund, Erkundungs- und Bewachungsmethoden. Abschlussbericht zum Projekt Wasser-Abfall-Boden, PW 87044. p. 128, Karlsruhe.

Thorbjarnarson, K.W., MacKay, D.M., 1994. A forced-gradient experiment on solute transport in the Borden

aquifer. 3. Nonequilibrium transport of the sorbing organic compound. Water Resour. Res. 30 (2), 401–419.

Vanderborght, J., Vereecken, H., 2000. Analyses of locally measured bromide breakthrough curves from a natural gradient tracer experiment at Krauthausen. J. Contam. Hydrol., Submitted.

Vereecken, H., Döring, U., Hardelauf, H., Jaekel, U., Neuendorf, O., Schwarze, H., Seidemann, R., 1999a. Analysis of reactive solute transport in a heterogeneous aquifer: The Krauthausen field experiment. 1. Experimental set-up, sediment characterization and moment analyses. Forschungszentrum Jülich GmbH, Internal report Nr.500798.

Vereecken, H., Jaekel, U., Esser, O., Nitzsche, O., 1999b. Solute transport analysis of bromide, uranin and LiCl using breaktbrough curves from aquifer sediment. J. Contam. Hydrol. 39, 7–34.

Yates, S.R., 1989. Geopack; a geostastical software system. In: Ports-Michael, A. (Ed.), Proc. 1989 Natl. Conf. Hydraul. Eng., American Society of Civil Engineering, Hydraulics Division, New York, pp. 693–698.

Zhang, H., Schwartz, F.W., Wood, W.W., Garabedian, S.P., LeBlanc, D.R., 1998. Simulation of variable-density flow and transport of reactive and nonreactive solutes during a tracer test at Cape Cod, Massachusetts. Water Resour. Res. 34 (1), 67–82.

Analysis of Tests of Subsurface Injection, Storage, and Recovery of Freshwater in the Lower Floridan Aquifer, Okeechobee County, Florida

U.S. GEOLOGICAL SURVEY

Open-File Report 95-765

Prepared in cooperation with the
SOUTH FLORIDA WATER MANAGEMENT DISTRICT

Analysis of Tests of Subsurface Injection, Storage, and Recovery of Freshwater in the Lower Floridan Aquifer, Okeechobee County, Florida

By Vicente Quiñones-Aponte, Kevin Kotun, and Joseph F. Whitley

U.S. GEOLOGICAL SURVEY

Open-File Report 95-765

Prepared in cooperation with the

South Florida Water Management District

Tallahassee, Florida
1996

U.S. DEPARTMENT OF THE INTERIOR
BRUCE BABBITT, Secretary

U.S. GEOLOGICAL SURVEY
Gordon P. Eaton, Director

For additional information, write to:

District Chief
U.S. Geological Survey
Suite 3015
227 N. Bronough Street
Tallahassee, Florida 32301

Copies of this report can be purchased from:

U.S. Geological Survey
Earth Science Information Center
Open-File Reports Section
Box 25286, MS 517
Denver, CO 80225

CONTENTS

FIGURES

TABLES

GLOSSARY OF TERMS

A	Area [L^2]
A_{eff}	Effective area [L^2]
b	Thickness of the flow zone [L]
C	Solute concentration [M/L^3]
C_i	Solute concentration in injected water [M/L^3]
C_n	Solute concentration in native water [M/L^3]
c	Volumetric solute concentration in the aquifer fluid [M/L^3]
c'	Volumetric solute concentration in the injected fluid [M/L^3]
D_d	Molecular diffusion coefficient [L^2/T]
$\underline{D}_m$	Dispersion tensor [L^2/T]
d	Characteristic length [L]
dh_i	Head change in the *i-th* high-permeability zone [L]
d_r	Change in distance from the pumping well [L]
g	Gravitational acceleration vector [L/T^2]
$\underline{I}$	Identity tensor [dimensionless
K_i	Hydraulic conductivity of the *i-th* high-permeability zone [L/T]
k	Intrinsic permeability of the aquifer [L^2]
k_H	Horizontal permeability of the aquifer material [L^2]
k_V	Vertical permeability of the aquifer material [L^2]
n	Apparent porosity of the aquifer [dimensionless]
p	Fluid pressure [M/LT^2]
ρ	Fluid density [M/L^3]
ρ_i	Density of injected water [M/L^3]
ρ_n	Density of native water [M/L^3]
Pgh	Hydrostatic pressure [M/LT^2]
Q	Flow rate through the flow zone [L^3/T]
Q'	Volumetric injection rate per unit area of aquifer [L/T]
Q_i	Representation of flow components from the different aquifer high-permeability zones where $i = 1,2,3$ [L^3/T]
Q_p	Mass of fluid injected or withdrawn per unit time per unit volume of aquifer [M/L^3T]
Q_T	Total flow rate through the well [L^3/T]
q	Specific discharge [L/T]
R_e	Reynolds number [dimensionless]
r	Radial distance [L]
T_i	Transmissivity of the aquifer [L^2/T]
t	Time [T]
μ	Dynamic viscosity of the fluid [M/LT]
V	Fluid kinematic viscosity [L^2/T]
v	Average pore-water velocity [L/T]
z	Elevation above a reference datum [L]
α_L	Longitudinal dispersivity of the aquifer [L]
α_T	Transverse dispersivity of the aquifer [L]
Δt	Time step [T]
∇	Gradient operator [1/L]

Analysis of Tests of Subsurface Injection, Storage, and Recovery of Freshwater in the Lower Floridan Aquifer, Okeechobee County, Florida

By Vicente Quiñones-Aponte, Kevin Kotun, *and* Joseph F. Whitley

Abstract

A series of freshwater subsurface injection, storage, and recovery tests were conducted at an injection-well site near Lake Okeechobee in Okeechobee County, Florida, to assess the recoverability of injected canal water from the Lower Floridan aquifer. At the study site, the Lower Floridan aquifer is characterized as having four local, relatively independent, high-permeability flow zones (389 to 398 meters, 419 to 424 meters, 456 to 462 meters, and 472 to 476 meters below sea level). Four subsurface injection, storage, and recovery cycles were performed at the Lake Okeechobee injection-well site in which volumes of water injected ranged from about 387,275 to 1,343,675 cubic meters for all the cycles, and volumes of water recovered ranged from about 106,200 to 484,400 cubic meters for cycles 1, 2, and 3. The recovery efficiency for successive cycles 2 and 3 increased from 22 to 36 percent and is expected to continue increasing with additional cycles.

A comparison of chloride concentration breakthrough curves at the deep monitor well (located about 171 meters from the injection well) for cycles 1, 4, and test no. 4 (from a previous study) revealed unexpected findings. One significant result was that the concentration asymptote, expected to be reached at concentration levels equivalent or close to the injected water concentration, was instead reached at higher concentration levels. The injection to recovery rate ratio might affect the chloride concentration breakthrough curve at the deep monitor well, which could explain this unexpected behavior. Because there are four high-permeability zones, if the rate of injection is smaller than the rate of recovery (natural artesian flow), the head differential might not be transmitted through the entire open wellbore, and injected water would probably flow only through the upper high-permeability zones. Therefore, observed chloride concentration values at the deep monitor well would be higher than the concentration of the injected water and would represent a mix of water from the different high-permeability zones.

A generalized digital model was constructed to simulate the subsurface injection, storage, and recovery of freshwater in the Lower Floridan aquifer at the Lake Okeechobee injection-well site. The model was constructed using a modified version of the Saturated-Unsaturated **TRA**nsport code (SUTRA), which simulates variable-density advective-dispersive solute transport and variable-density ground-water flow. Satisfactory comparisons of simulated to observed dimensionless chloride concentrations for the deep monitor well were obtained when using the model during the injection and recovery phases of cycle 1, but not for the injection well during the recovery phase of cycle 1 even after several attempts. This precluded the determination of the recovery efficiency values by using the model.

The unsatisfactory comparisons of simulated to observed dimensionless chloride concentrations for the injection well and failure of the model to represent the field data at this well could

be due to the characteristics of the Lower Floridan aquifer (at the local scale), which is cavernous or conduit in nature. To test this possibility, Reynolds numbers were estimated at varying distances from the injection well, taking into consideration two aquifer types or conceptual systems, porous media and cavernous. For the porous media conceptual system, the Reynolds numbers were greater than 10 at distances less than 1.42 meters from the injection well. Thus, application of Darcy's law to ground-water flow might not be valid at this distance. However, at the deep monitor well (171 meters from the injection well), the Reynolds number was 0.08 which is indicative of laminar porous media flow. For the cavernous conceptual system, the Reynolds numbers were greater than 2,000 at distances less than 1,000 meters from the well. This number represents the upper limit of laminar flow, which is the fundamental assumption for the application of Darcy's law to free flow.

Results from the study suggest that to simulate recovery efficiency for the Lower Floridan aquifer at the Lake Okeechobee injection-well site might require the application of a free-flow type model (conduit flow or fracture flow). This type of model may produce a more realistic representation of the actual fluid motion in the Lower Floridan aquifer and could provide appropriate estimates of the recovery efficiency.

INTRODUCTION

Lake Okeechobee is the second largest natural freshwater lake in the United States, encompassing about 1,813 km^2 (square kilometers). The lake is the principal source of potable water for southern Florida and is part of the flood-control system for the area (fig. 1). A serious contamination problem to Lake Okeechobee is posed by phosphate loads from tributary canals, such as Taylor Creek and Nubbin Slough (fig. 1), which might accelerate eutrophication of the lake (Lake Okeechobee Technical Advisory Committee, 1986). The Lake Okeechobee Technical Advisory Committee proposed a study to determine the feasibility of reducing phosphate loads into Lake Okeechobee.

From April 1991 to September 1994, the U.S. Geological Survey, in cooperation with the South Florida Water Management District, conducted a study to: (1) assess the feasibility of subsurface injection, storage, and recovery as a mechanism for reducing phosphate loads in the canal water; (2) examine the chemical behavior of the canal-water and native aquifer water mix during subsurface injection, storage, and recovery, focusing on the fate of orthophosphate; and (3) estimate the recovery efficiency of injected canal water from the Lower Floridan aquifer. A report by Quiñones-Aponte and Whitley (1996, in press) analyzed the application of phosphate mass-balance approaches to assess the feasibility of subsurface injection, storage, and recovery as a tool for reducing phosphate loads in the canal water. This report assesses the recoverability of injected canal water from the Lower Floridan aquifer.

Purpose and Scope

The purposes of this report are to: (1) describe a series of freshwater subsurface injection, storage, and recovery tests conducted at an injection-well facility near Lake Okeechobee; (2) present the analyses of the subsurface injection, storage, and recovery tests; and (3) assess the recoverability of injected canal water from the Lower Floridan aquifer using field data and digital model analyses. This report combines information and results from a previous study (CH_2M Hill, 1989) and the present study to characterize the Lower Floridan aquifer at the Lake Okeechobee injection-well site; these characteristics include lithostratigraphic units, hydrogeologic units, aquifer properties, potentiometric levels, and ambient water quality. Recovery efficiencies from actual field subsurface injection, storage, and recovery tests were estimated and are included in this report to measure the success of a subsurface injection, storage, and recovery cycle. A summary of the governing ground-water flow and solute transport equations is also included with a description of the digital model development and its application to evaluate recovery efficiency at the Lake Okeechobee injection-well site. Finally, simulations were made using a digital model code (QSUTRA) to study the effects of the aquifer characteristics on the recoverability of the injected canal water.

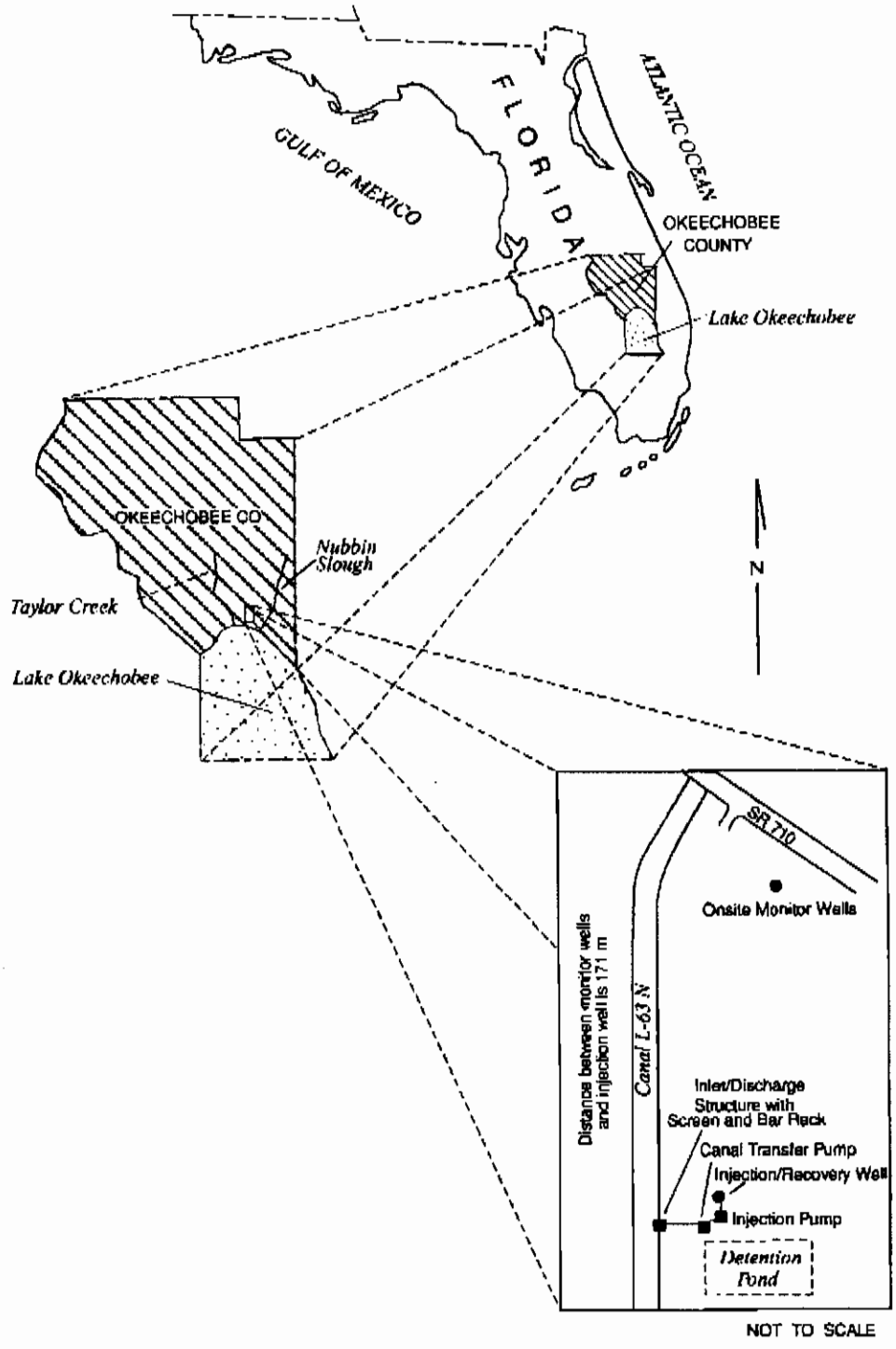

Figure 1. Location of the Lake Okeechobee injection-well site and the contributing canals.

Description of Study Area

The study area is located at existing well facilities near the northern shore of Lake Okeechobee at the intersection of State Road 710 and Canal L-63N in Okeechobee County, Fla. (fig. 1). The facilities were designed and constructed by CH_2M Hill (1989), under an agreement with the South Florida Water Management District, and consist of a canal inlet/discharge structure to withdraw water from Canal L-63N, chlorination facilities (not used for the present study), a detention pond, an injection well, pumps, and two nested monitor wells located about 171 m (meters) from the injection well (fig. 1). All the wells are characterized by artesian heads. Initial testing at this well site was conducted by CH_2M Hill (1989).

The general hydrogeologic characteristics of the injection well site are briefly described in the subsequent sections, including lithostratigraphic and hydrogeologic units. The description of the aquifer hydraulic characteristics focuses on the Lower Floridan aquifer, which is the hydrogeologic unit considered in this study.

Hydrogeologic Setting

The geology of Okeechobee County and the Lake Okeechobee injection-well site has been described by previous investigators, including Sellards (1912), Parker and others (1955), Puri and Vernon (1964), Miller (1986), CH_2M Hill (1989), and Lukasiewicz (1992). The upper 550 m of sediments at the injection-well site are comprised of the upper part of the Oldsmar Formation of lower Eocene age, the Avon Park Formation (formerly termed the Lake City Limestone) of middle Eocene age, the Ocala Limestone of upper Eocene age, the Tampa Limestone of Miocene age, the Hawthorn Formation of Miocene age, the Tamiami Formation of Pliocene age, and the Anastasia Formation of Pleistocene age (fig. 2).

The Oldsmar Formation, Avon Park Formation, and Ocala Limestone are present in the Floridan aquifer system (fig. 2). The Ocala Limestone and the upper part of the Avon Park Formation constitute the Upper Floridan aquifer, the middle part of the Avon Park Formation constitutes the middle semiconfining unit, and the lower part of the Avon Park Formation and the upper part of the Oldsmar Formation constitute the Lower Floridan aquifer (Miller, 1986). The middle semiconfining unit separates the Upper Floridan aquifer from the Lower Floridan aquifer within the Floridan aquifer system. The Oldsmar Formation is characterized by off-white to light-gray, micritic to finely pelletal limestone interbedded with gray to tan to light-brown, fine to medium crystalline, commonly vuggy dolomite (Miller, 1986). The Avon Park Formation is characterized by pelletal but locally micritic cream, tan, or light-brown, soft to well-indurated limestone sediments (Miller, 1986) with fauna typical of Eocene age and also contains large amounts of lignite and carbonaceous plant material (Puri and Vernon, 1964). Overlying the Avon Park Formation is the Ocala Limestone containing marine fauna and foraminifera throughout and chert beds in places. The cavernous Ocala Limestone produces large volumes of water and is the source of many springs in Florida that originate from the Floridan aquifer system (Parker and others, 1955).

The Tampa Limestone and Hawthorn Formation are present in a confining unit (about 162 m thick) between the surficial aquifer and the Floridan aquifer system (fig. 2) and consist of sand, silts, and limestones of marine origin. Limestones are predominant in the lower part of the Tampa Limestone (Puri and Vernon, 1964). At the Lake Okeechobee injection-well site, the Tampa Limestone is characterized as a soft loosely consolidated limestone, rich in phosphorite (fig. 2). The base of the Tampa Limestone is considered the top of the Floridan aquifer system and is identified by increased consolidation and occurrence of arenaceous limestone. The Hawthorn Formation overlying the Tampa Limestone contains many types of deposits, including carbonate with quartz sand and phosphatic clayey dolostones. The Tamiami Formation and Anastasia Formation are present in the surficial aquifer (fig. 2). At the Lake Okeechobee injection-well site, the Tamiami Formation consists of fine silty sand, shell fragments, low phosphorite, and interbedded clay (CH_2M Hill, 1989). The Anastasia Formation is generally composed of coquina, quartz sand, calcareous quartz sandstone, and shelly marl (Sellards, 1912) but consists of unconsolidated sand with fine shell fragments at the injection-well site (CH_2M Hill, 1989).

Hydraulic Characteristics of the Lower Floridan Aquifer

The Lower Floridan aquifer at the Lake Okeechobee injection-well site is characterized by two flow zones under confined conditions isolated from each other by an intermediate dolomite confining unit (CH_2M Hill, 1989; and Lukasiewicz, 1992). The upper

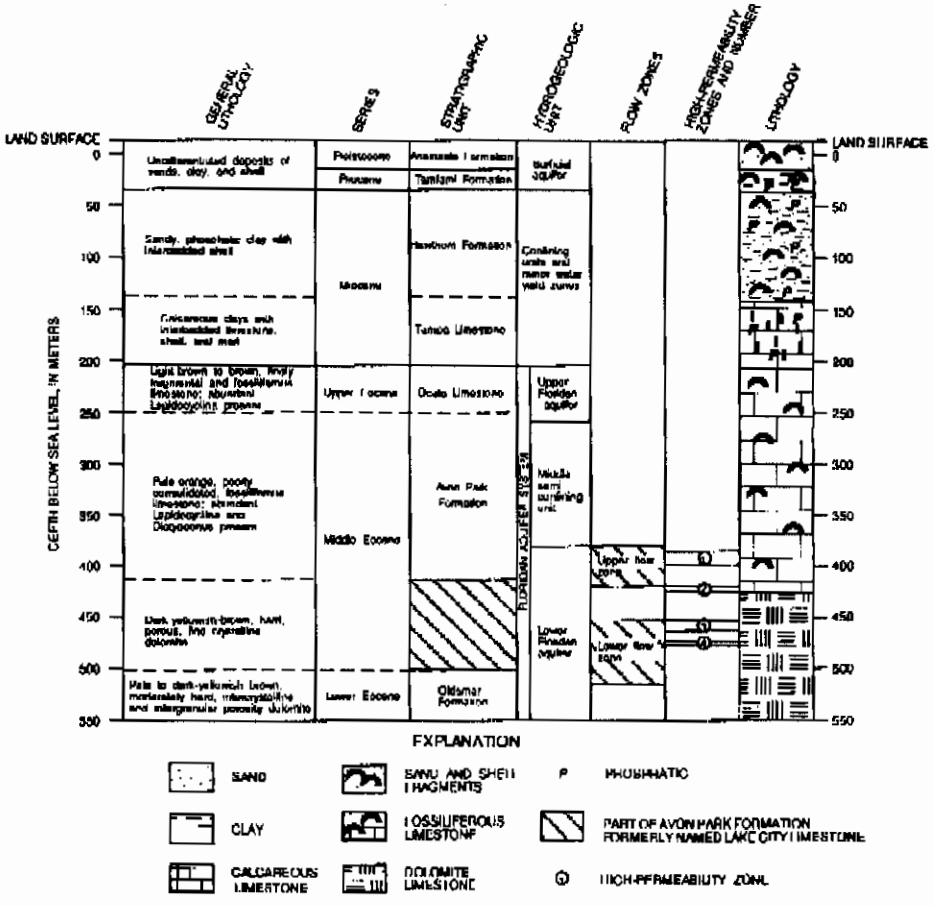

Figure 2. Geologic column of the Lake Okeechobee injection-well site showing stratigraphic units, hydrogeologic units, and lithology. Modified from CH_2M Hill (1989).

flow zone occurs from about 380 to 419 m below sea level, the intermediate confining unit occurs from about 419 to 456 m below sea level, and the lower flow zone occurs from about 456 to 518 m below sea level (fig. 2). At local scale, high-permeability zones occur along some intervals in the upper and lower flow zones (CH_2M Hill, 1989). Local high-permeability zones were present along two intervals in the upper flow zone (389 to 398 m below sea level and 419 to 424 m below sea level) and along two intervals in the lower flow zone (456 to 462 m below sea level and 472 to 476 m below sea level).

Field data and model simulation results from Lukasiewicz (1992) were used to estimate the direction and magnitude of the regional ground-water flow gradient at the Lake Okeechobee injection-well site. The direction of flow was estimated at about 45 degrees northeast from true north and the background hydraulic gradient was about 0.047 m/km (meter per kilometer). The four local high-permeability zones occurring within the upper and lower flow zones were identified by CH_2M Hill (1989) using data from geophysical logs (caliper, flow velocity, fluid resistivity, and fluid temperature) during pumping conditions. The percent of flow from the individual local high-permeability zones (table 1) was estimated from caliper/velocity (flow meter) borehole logs conducted during pumping or flowing conditions (CH_2M Hill, 1989).

CH_2M Hill (1989) estimated the hydraulic characteristics of the open-hole interval of the injection well and the middle semiconfining unit above the flow zones. The estimated transmissivity of the aquifer at the injection well was about 71,000 m^2/d (meters squared per day) for the interval between 377 and 509 m below sea level, which is equivalent to an average hydraulic conductivity of 540 m/d (meters per day).

Table 1. Hydraulic characteristics of the Lower Floridan aquifer at the Lake Okeechobee injection-well site

[Percent of flow estimated using caliper and flow-meter borehole logs]

High-permeability zone	Depth interval (meters below sea level)	Thickness (meters)	Percent of flow from this zone	Horizontal hydraulic conductivity (meters per second)	Horizontal intrinsic permeability (square meters)
1	389-398	9.0	60	5.48×10^{-2}	5.57×10^{-9}
2	419-424	5.0	11	1.81×10^{-2}	1.84×10^{-9}
3	456-462	6.0	22	3.01×10^{-2}	3.06×10^{-9}
4	472-476	4.0	7	1.44×10^{-2}	1.46×10^{-9}

The hydraulic characteristics of the middle semiconfining unit were estimated from a packer test conducted at a depth interval of between 349 and 365 m below sea level. This middle semiconfining unit (fig. 2) confines the aquifer considered in the subject study at its upper limit. Transmissivity values in this unit ranged from 65.6 to 273.2 m^2/d, which is equivalent to a hydraulic conductivity range of between 4.1 and 17.2 m/d.

The hydraulic characteristics of the individual high-permeability zones of the two flow zones in the Lower Floridan aquifer at the Lake Okeechobee injection-well site can be estimated using the following mathematical procedure:

$$Q_T = Q_1 + Q_2 + Q_3 + Q_4 \qquad (1)$$

where:

Q_T is the total flow rate through the well, and

Q_i (i = 1,2,3,4) represents the flow components from the different aquifer high-permeability zones.

For radial flow through each flow zone, Darcy's law can be expressed as:

$$Q_i = 2\pi r T_i \frac{dh_i}{dr} \qquad (2)$$

where:

r is the radial distance from the pumping well,

T_i is the transmissivity in the *i-th* high-permeability zone,

dh_i is the head change in the *i-th* high-permeability zone, and

dr is the change in distance from the pumping well.

Assuming a very small difference in head gradient among the high-permeability zones, $dh_i/dr = dh/dr$, and uniform head distribution in the well-bore, equation *(2)* becomes:

$$Q_T = 2\pi r\left(T_1 + T_2 + T_3 + T_4\right)\frac{dh}{dr} = 2\pi r T \frac{dh}{dr} \qquad (3)$$

and:

$$T = T_1 + T_2 + T_3 + T_4 = K_1 b_1 + K_2 b_2 + K_3 b_3 + K_4 b_4 \qquad (4)$$

Based on the previous assumptions, $Q_i/Q_T = T_i/T$ and $T_i = K_i b_i$. The average hydraulic conductivity of each high-permeability interval i can be estimated if the thicknesses (b_i) of the high-permeability zones are known. The hydraulic conductivity values K_i for the four high-permeability zones, given in table 1, were estimated using the flow terms Q expressed as a percentage (where Q_T = 100), assuming that all flow comes from the four high-permeability zones, and using the transmissivity value estimated at the injection well (71,000 m^2/d).

Aquifer matrix permeability (k_i, intrinsic permeability) values, given in table 1, were computed using:

$$k_i = \frac{\mu K i}{\rho g} \qquad (5)$$

where:

μ is the dynamic viscosity of the fluid [M/LT],

ρ is fluid density [M/L^3], and

g is the gravitational acceleration vector [L/T^2].

Subsurface Injection, Storage, and Recovery Concept

Subsurface injection, storage, and recovery of freshwater in brackish or saline aquifers is a water supply storage strategy that has received increased attention in recent years. The subsurface injection, storage, and recovery concept is suited for southern Florida where there is: (1) a surplus of freshwater during the wet season; and (2) a lack of suitable surface storage reservoirs because of the cost of land, limits of topography, and high rates of evapotranspiration and seepage losses. The suitability of a particular aquifer to store surface water is determined through subsurface injection, storage, and recovery tests from which the recovery efficiency (ability of the well/aquifer system to retrieve some fraction of the injected water) is determined.

The success of subsurface injection, storage, and recovery of freshwater is measured by the recovery efficiency. The recovery efficiency is defined as the volume of mixed injected and native aquifer waters recovered that meets a prescribed chemical standard, expressed as a percentage of the volume of water initially injected (Meyer, 1989). Most recent studies of subsurface injection, storage, and recovery have assumed the recommended level of 250 mg/L (milligrams per liter) for chloride concentration as the standard (Florida Department of Environmental Protection, 1993). However, in this study a limit of 1,385 mg/L of chloride and a limit of specific conductance of 5,000 µS/cm (microsiemens per centimeter) were established because the potential use (agricultural irrigation) of the recovered water tolerates this salinity level. This salinity level is the upper limit that can be tolerated by most crop types.

Merritt and others (1983) and Merritt (1985) describe a number of physical mechanisms that control the recoverability of freshwater injected into the Floridan aquifer system. They determined that buoyancy stratification, mixing due to hydrodynamic dispersion, and downgradient displacement of the injected freshwater with the native water were the three dominant processes that affected the recovery efficiency.

Buoyancy stratification is the process in which the lighter freshwater rises through the aquifer while moving outward from the injection well and overrides the denser, native saltwater or brackish water. Buoyancy stratification can be very significant especially during long storage periods. During recovery, native saltwater in the lower part of the injection zone is drawn into the well, whereas freshwater remains in the upper part of the zone. Buoyancy stratification is controlled by the density contrast between native and injected waters, permeability of the injection zone, and thickness of the injection zone (Merritt, 1985). Studies by Merritt and others (1983) and Merritt (1985) indicate that thin aquifers of moderate permeability are less affected by buoyancy stratification, and therefore, best suited for subsurface injection, storage, and recovery of freshwater. Confinement of the injection zone by low-permeability hydrogeologic units can also aid in limiting the upward movement of freshwater.

Hydrodynamic dispersion describes the mixing of solutes due to molecular diffusion and mechanical dispersion. Molecular diffusion is the process that describes the movement of solute particles from areas of high solute concentration to areas of low solute concentration. The effect of molecular diffusion is independent of the fluid velocity. Mechanical dispersion is caused by mixing of solutes due to variations in fluid velocities at the microscopic scale. Enhanced mechanical dispersion or macrodispersion is caused by velocity variations resulting from local differences in hydraulic conductivity. At the relatively large velocities during injection and recovery, the effects due to mechanical dispersion are generally far greater than those due to molecular diffusion. During long-term storage, however, molecular diffusion may become the dominant mixing process.

A transition zone is created during the mixing of the native and injected waters. The extent of the transition zone depends on the rate of injection, length of injection period, and the difference in solute concentration between the native and injected waters. Because velocities are higher near the well, most of the mixing occurs at the start of the injection process. As injection continues, the transition zone moves outward at continually decreasing velocities, leading to decreasing dispersive mixing at the interface between the native and injected water.

The effect of downgradient displacement of the injected freshwater body on recovery efficiency depends on the length of the injection-recovery cycle and the regional ground-water flow velocities. For subsurface injection, storage, and recovery cycles of relatively short duration (with respect to the size (scale) of the aquifer system), this effect can be considered negligible because the local hydraulic gradient due to injection is much greater than the regional gradient.

Clogging of the aquifer around the injection wellbore is another factor that can affect the recovery efficiency. Clogging can be caused by bacterial growth, suspended sediments in the injected water, and chemical precipitation of solutes due to reactions between the injected water and the aquifer matrix or native water. At the Lake Okeechobee well facilities (fig. 1), the injection well is open hole from 377 to 509 m below sea level and the aquifer is characterized as cavernous. None of the aforementioned clogging problems are likely to occur for such a well-aquifer system. However, geochemical models can be used to predict the reactions that would most likely occur during rock-water interaction and mixing of injected and native waters.

Acknowledgments

The authors wish to thank the personnel of the South Florida Water Management District for their extraordinary effort in coordinating the fieldwork. Special thanks to Keith Smith and Marty Braun of the Hydrogeology Division and Scott Burns formerly of the Hydrogeology Division.

TESTS OF SUBSURFACE INJECTION, STORAGE, AND RECOVERY OF FRESHWATER

A series of freshwater subsurface injection, storage, and recovery tests were conducted at the Lake Okeechobee injection-well site to assess the recoverability of injected canal water from the Lower Floridan aquifer. The injected water was withdrawn from the L-63N canal, which collects water from Taylor Creek and Nubbin Slough (fig. 1). The canal water is composed of runoff and local ground-water discharge from shallow infiltration. According to Quiñones-Aponte and Whitley (1996, in press), the injected canal water and the water in the Lower Floridan aquifer are of similar major inorganic composition.

The subsurface injection, storage, and recovery facilities have been previously described in this report and consist of an injection well that is 60.96 cm (centimeters) in diameter and a nest of two monitor wells, one shallow and one deep, located about 171 m from the injection well (fig. 1). The injection well is cased to a depth of 377 m below sea level and open hole to 509 m below sea level in the Lower Floridan aquifer. The shallow and deep monitor wells were used to observe water-quality changes due to mixing of the injected canal water and native aquifer water in the Lower Floridan aquifer. The shallow well is 15.2 cm in diameter and open to the middle semiconfining unit of the Floridan aquifer system from 292 to 318 m below sea level. The deep well completed in the Lower Floridan aquifer is 3.8 cm in diameter and is open to the aquifer from 379 to 539 m below sea level.

Background water-quality data were collected prior to the subsurface injection, storage, and recovery cycles. CH_2M Hill (1989) used a straddle packer to conduct hydraulic testing and collect water samples from four depth intervals (349 to 365 m, 383 to 403 m, 401 to 450 m, and 460 to 497 m below sea level). These depth intervals do not necessarily coincide with the high permeability zones included in table 1, but some may include the high-permeability zones. The data, presented in table 2, indicate that chloride, specific conductance, and total dissolved solids values were significantly different between zones and increased with depth. This suggests that there is some degree of semiconfinement among the high-permeability zones.

Initial testing was conducted by CH_2M Hill (1989) at the Lake Okeechobee injection-well site to: (1) estimate the maximum feasible injection rate, (2) determine if pretreatment by chlorination would be necessary to eliminate potential fecal coliforms in the injected water, and (3) evaluate the recoverability of the injected canal water. Results indicated that water can be injected into the Lower Floridan aquifer through the injection well at a rate from 18,925 to 37,850 m^3/d (cubic meters per day). Chlorination had little effect on coliform concentrations in the brackish environment of the Lower Floridan aquifer. CH_2M Hill (1989) further reported that water can be withdrawn from the well (under the natural and built-up artesian pressures of the aquifer) at a rate from 10,976.5 to 16,275.5 m^3/d. CH_2M Hill also indicated that the recoverability of the injected canal water could be enhanced by increasing the volume to be stored and/or backplugging the deeper saline zone of the aquifer that is open to the injection well (456 to 509 m below sea level). However, actual testing of this hypothesis was beyond the scope of the study (CH_2M Hill, 1989). CH_2M Hill (1989) indicated that density might affect the recovery efficiency. Most of their tests were affected by the relatively small volumes injected, about 94,600 to 344,185 m^3 (cubic meters), and the duration of the storage period (0 to 28 days). Such

Table 2. Background water-quality data for the canal water and native-aquifer water at the Lake Okeechobee injection-well site

[Data from CH_2M Hill (1989); straddle packer used to conduct tests in monitor well test hole]

Water type	Straddle packer test depth interval (meters below sea level)	Representative high-permeability zones (from table 1)	Chloride (milligrams per liter)	Field specific conductance (microsiemens per centimeter)	Total dissolved solids (milligrams per liter)	Static water-level altitude (meters, sea level)
Canal			290	1,140	729	
Native aquifer	349-365	Middle semiconfining unit	131	1,155	656	13.3
	383-403	1	1,800	7,850	4,000	12.4
	401-450	2	2,500	10,890	5,740	12.1
	460-497	3,4	2,920	12,763	6,710	11.9

conditions precluded recovery of meaningful quantities and impeded the interpretation of the test results in terms of the recovery efficiency. When the amount of injected water is small (relative to the size of the aquifer), the conditions represented by the data do not actually represent the aquifer, but the well/aquifer interface. CH_2M Hill (1989) could not make any projections or a conclusive assessment of the recovery efficiency potential because of the relatively small volume injected.

Four subsurface injection, storage, and recovery cycles were conducted for the present study, as was the case for the study by CH_2M Hill (1989). Cycle 1 consists of injection and recovery phases; cycles 2 and 3 consist of injection, storage, and recovery phases; and cycle 4 consists only of an injection phase. The injection, storage, and recovery phases are explained below:

- Injection: Phase in which canal water is injected through the well into the formation using a pump.
- Storage: Period in which the well is shut-in, and
- Recovery: Phase in which water is withdrawn from the aquifer (through the injection/recovery well) by natural artesian flow. A 35.6-cm diameter valve was open, discharging at rates ranging from 16,460 to 18,532 m^3/d. The water was discharged into a detention pond and later released into the L-63N canal (fig. 1).

The volumes of water injected ranged from 387,275 to 1,343,675 m^3 in the present study and ranged from 94,600 to 344,185 m^3 in the study by CH_2M Hill (1989). A preestablished water-quality limit (5,000 µS/cm of specific conductance, which is equivalent to a chloride concentration of 1,385 mg/L) was used to end the recovery cycle and determine the recoverability of water. Recovery was terminated when these water-quality criteria were met at the injection well. The results of the four injection, storage, and recovery cycles for the present study are discussed in the subsequent sections of this report.

Cycle 1

Cycle 1 consisted of injection and recovery phases. A preinjection phase was conducted for cycle 1, during which background water-quality conditions were established when specific conductance and chloride values were 10,400 µS/cm and 3,100 mg/L in the injection well, 7,930 µS/cm and 2,200 mg/L in the deep monitor well, and 1,280 µS/cm and 210 mg/L in the shallow monitor well. The amount of water discharged from the flowing well into the detention pond before reaching the background water-quality conditions was about 1,890 m^3. Corresponding constituents in water samples collected from the injection well and from the straddle packer test at an interval of between 383 and 403 m below sea level in the deep monitor well (table 2) were similar to background chloride and specific conductance values.

The injection phase of cycle 1 was conducted over a 35-day period in spring 1991 (April 17 to May 22), and the volume of water injected was 686,324 m^3. During this period, the injection rate ranged from 16,400 to 21,700 m^3/d and averaged 20,186 m^3/d (fig. 3A and table 3). The specific conductance and chloride values in the injected water were 709 µS/cm and 150 mg/L, respectively. All water samples were collected at the wellhead; the reason being that water

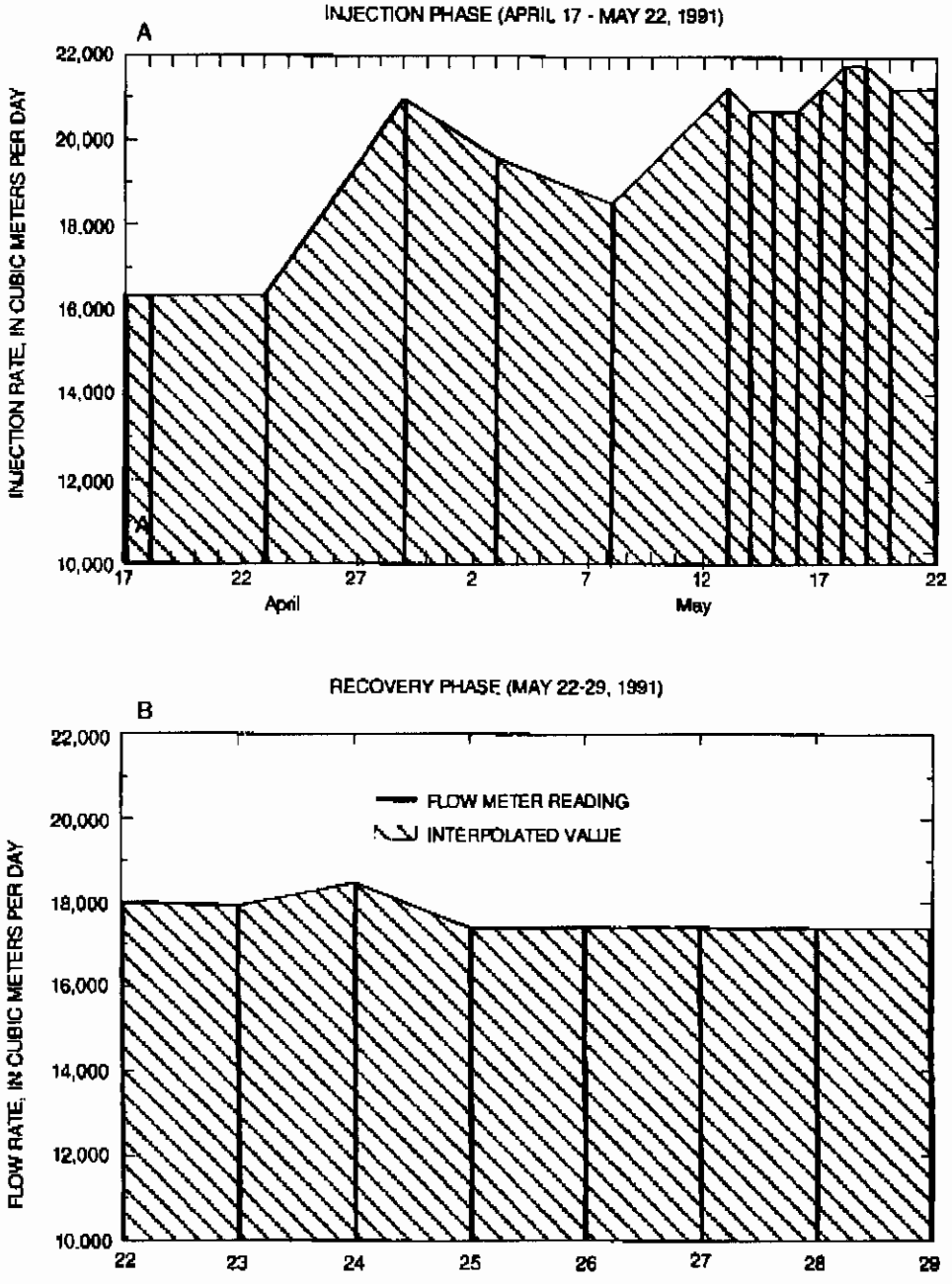

Figure 3. Rates of injection and recovery for cycle 1.

Table 3. Summary of results from subsurface injection, storage, and recovery cycles at the Lake Okeechobee injection-well site

Cycle number	Volume of water injected (cubic meters)	Volume of water recovered (cubic meters)	Storage period (days)	Average injection rate (cubic meters per day)	Average recovery rate (cubic meters per day)	Recovery efficiency (percent)
CH_2M Hill[1]	344,185		0	17,201	13,693	24
1	686,324	106,200	0	20,186	17,700	15
2	1,294,784	287,162	8	20,552	16,892	22
3	1,343,675	484,400	5	21,043	[2]17,300	36
4	387,275	--	--	14,549	--	--

[1]Data from CH_2M Hill (1989) test no. 4

[2]Estimated using flow-meter readings from cycles 1 and 2.

levels in the injection, deep, and shallow monitor wells rise above land surface due to the artesian condition of the respective aquifers.

The recovery phase was conducted over a 7-day period (May 22-29, 1991) when the preestablished water-quality limit (5,000 µS/cm of specific conductance, which is equivalent to a chloride concentration of 1,385 mg/L) was reached at the injection well. Chloride concentrations in the injection well (and the shallow and deep monitor wells) for the injection and recovery phases of cycle 1 are shown in figure 4. During the recovery phase, an average flow rate of about 17,700 m^3/d was maintained (fig. 3B and table 3). The volume of water recovered prior to achieving the preestablished chloride concentration limit (fig. 4B) was 106,200 m^3, and the estimated recovery efficiency was about 15 percent (table 3).

Cycle 2

Cycle 2 consisted of injection, storage, and recovery phases. Background water-quality conditions were not preestablished for this cycle. The buffer zone, which was created by the mixing of native aquifer water and residual water injected during cycle 1, served as reference conditions for cycle 2. This procedure is described in the literature as a "successive cycle" (Merritt, 1985). Preinjection sampling indicated that specific conductances and chloride concentrations were 4,220 µS/cm and 1,100 mg/L in the injection well, 2,020 µS/cm and 480 mg/L in the deep monitor well, and 959 µS/cm and 140 mg/L in the shallow monitor well.

The injection phase of cycle 2 was conducted over a 63-day period in summer 1991 (June 24 to August 26), and the volume of water injected was 1,294,784 m^3. During this period, the injection rate ranged from 19,077 to 21,800 m^3/d and averaged 20,552 m^3/d (fig. 5A and table 3).

A storage period of about 8 days (August 26 to September 3, 1991) was allowed before the beginning of the recovery phase of cycle 2. The recovery phase was conducted over a 17-day period (September 3-20, 1991) prior to achieving the preestablished water-quality limit (5,000 µS/cm of specific conductance which is equivalent to a chloride concentration of 1,385 mg/L). Chloride concentrations in the injection well (and the shallow and deep monitor wells) for the injection and recovery phases of cycle 2 are shown in figure 6. During the recovery phase, the flow rate ranged from 16,460 to 17,545 m^3/d and averaged 16,892 m^3/d (fig. 5B and table 3). The volume of water recovered prior to exceeding the preestablished chloride limit at the injection well (fig. 6B) was 287,162 m^3 and the estimated recovery efficiency was about 22 percent (table 3).

Cycle 3

Cycle 3 also consisted of injection, storage, and recovery cycles. Background water-quality conditions were not preestablished for this cycle. The buffer zone water quality established by previous successive cycles of injection and recovery (described in the previous section) served as reference conditions for cycle 3. Preinjection sampling indicated that specific conductances and chloride concentrations were 5,020 µS/cm and

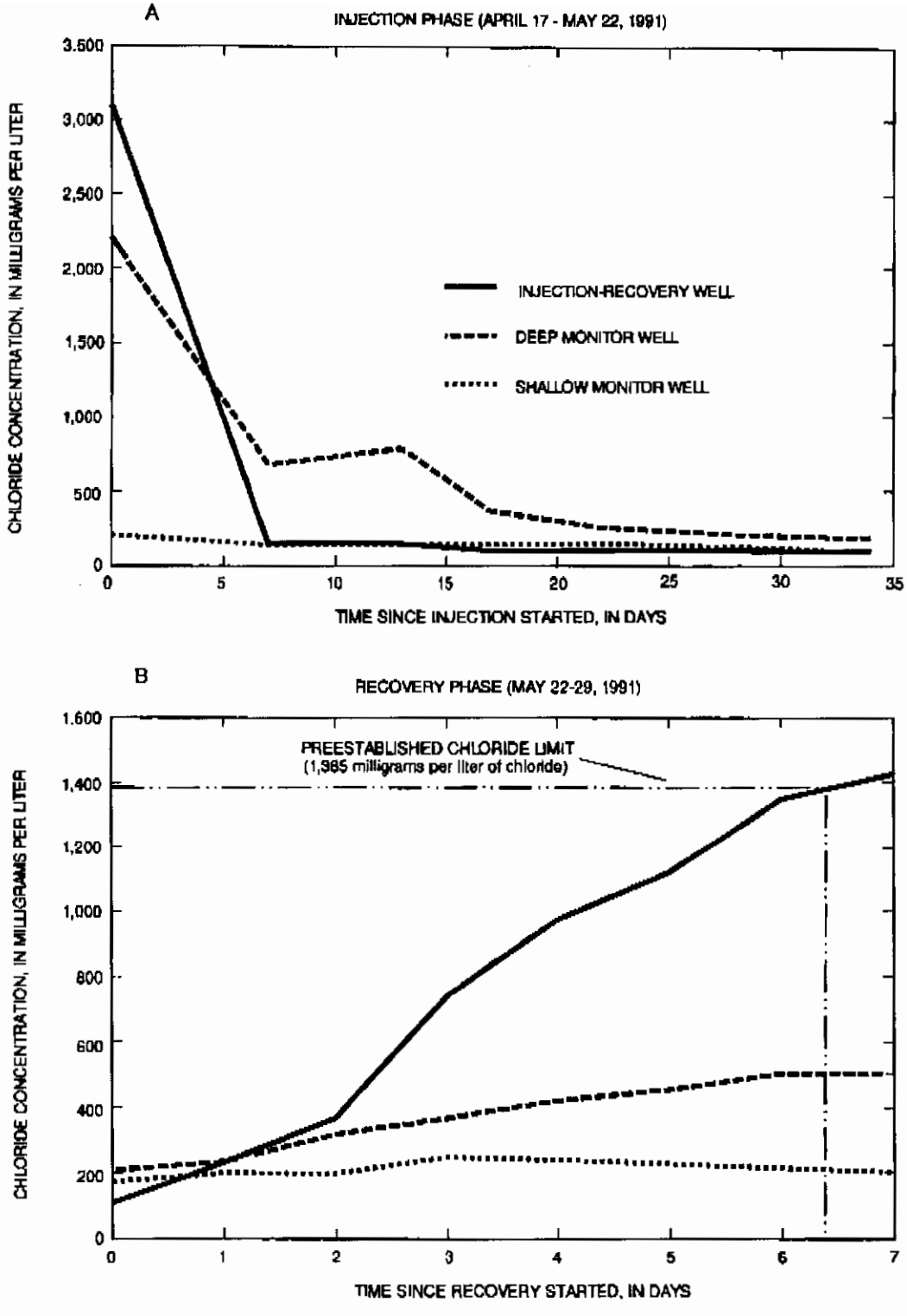

Figure 4. Chloride concentrations in the injection-recovery well and shallow and deep monitor wells during the injection and recovery phases of cycle 1.

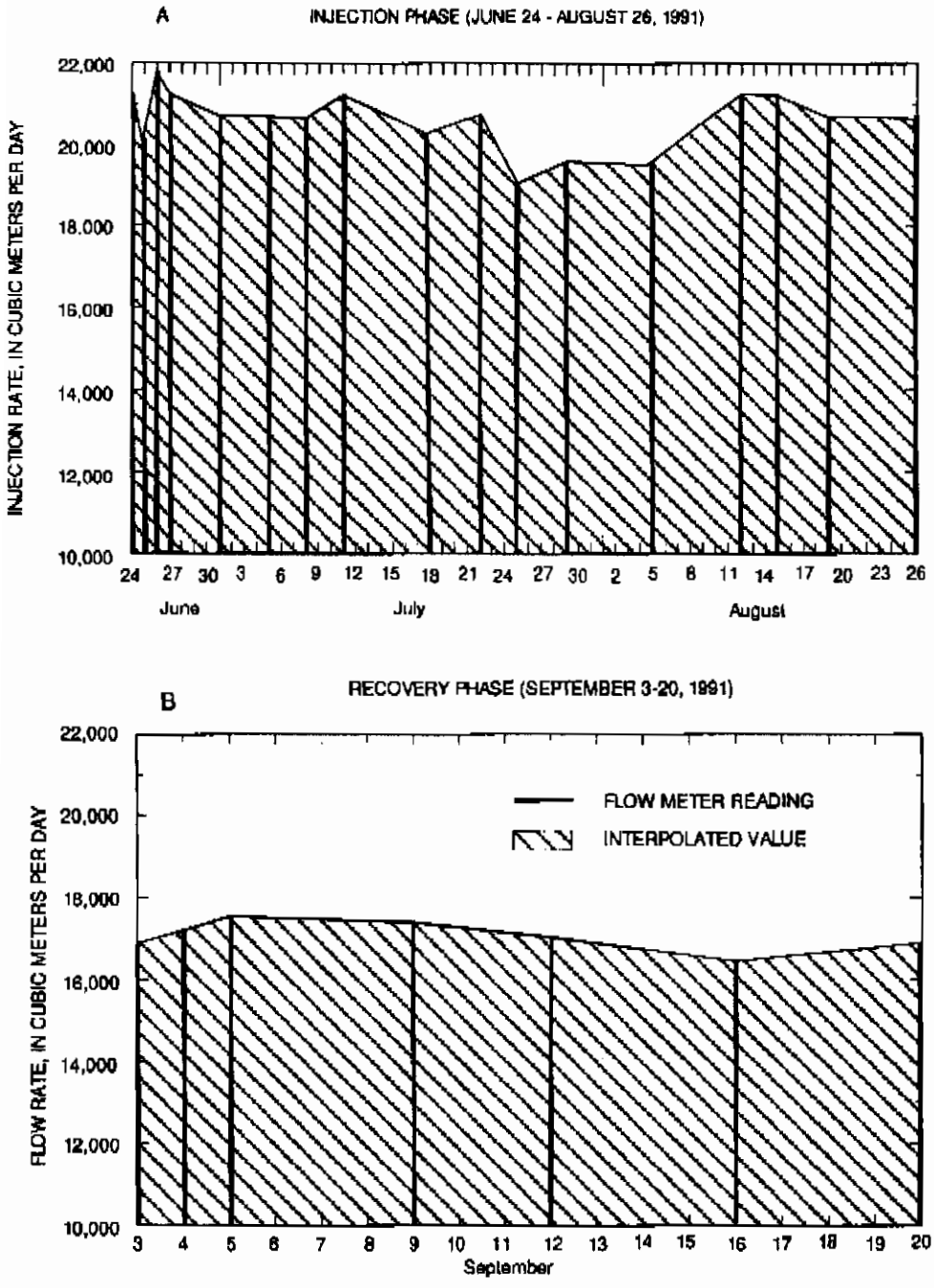

Figure 5. Rates of injection and recovery for cycle 2.

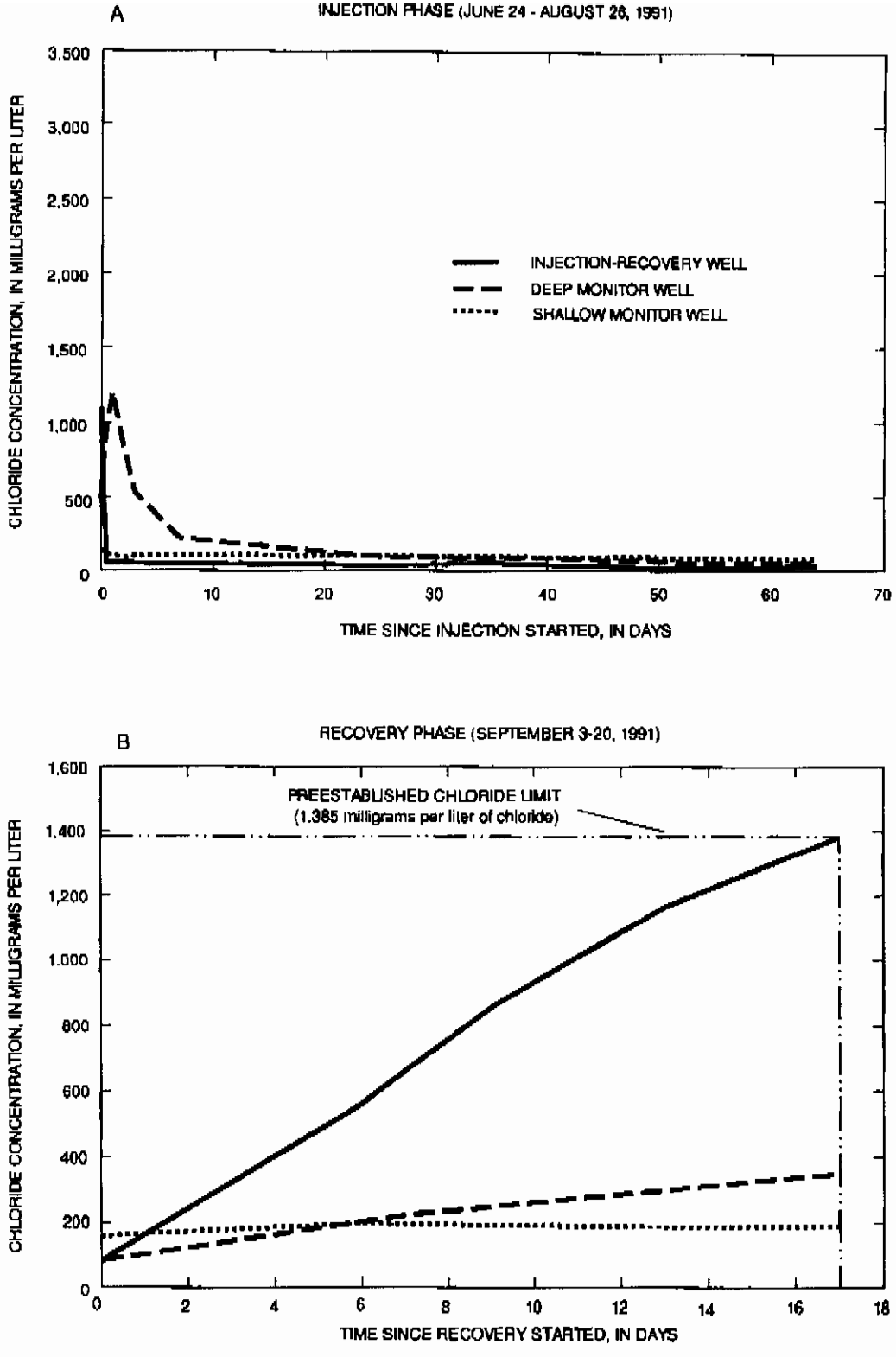

Figure 6. Chloride concentrations in the injection-recovery well and shallow and deep monitor wells during the injection and recovery phases of cycle 2.

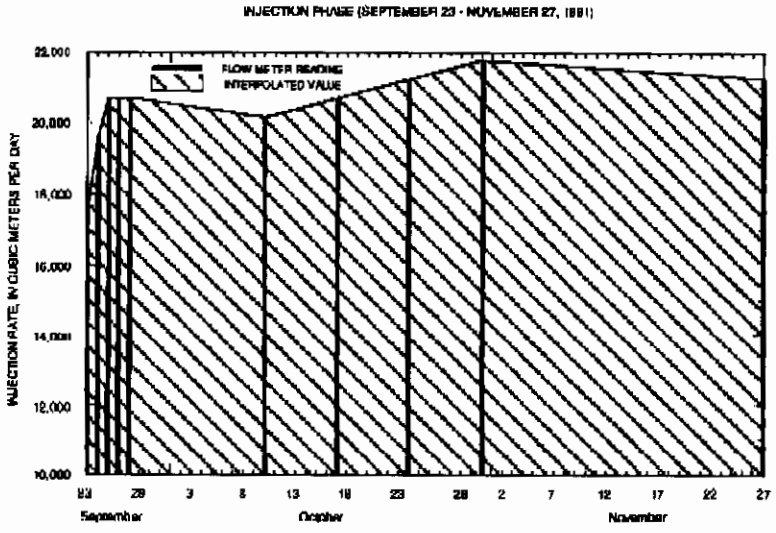

Figure 7. Rates of injection for cycle 3.

1,400 mg/L in the injection well, 1,410 µS/cm and 300 mg/L in the deep monitor well, and 929 µS/cm and 150 mg/L in the shallow monitor well.

The injection phase of cycle 3 was conducted over a 65-day period in autumn 1991 (September 23 to November 27), and the volume of water injected was 1,343,675 m^3. During this period, the injection rate ranged from 17,400 to 21,800 m^3/d and averaged 21,043 m^3/d (fig. 7 and table 3).

A storage period of about 5 days (November 27 to December 2, 1991) was allowed before the beginning of the recovery phase of cycle 3. The recovery phase was conducted over a 28-day period (December 2-30, 1991). Specific conductances and chloride concentrations at the end of the recovery period were about 4,700 µS/cm and 1,297 mg/L at the injection well. Chloride concentrations in the injection well (and the shallow and deep monitor wells) for the injection and recovery phases of cycle 3 are shown in figure 8. The recovery flow rate was not measured because of mechanical problems with the flow meter, but an average rate of 17,300 m^3/d was estimated using flowmeter readings from cycles 1 and 2. The specific conductance and chloride data were extrapolated through time because the chloride concentration limit of 1,385 mg/L was not reached at the end of the cycle. The volume of water recovered for the preestablished chloride limit (fig. 8B) was 484,400 m^3, and the estimated recovery efficiency was about 36 percent (table 3).

Cycle 4

Cycle 4 was used to define the dynamics of the aquifer system during the injection phase. Before injection, the valve at the wellhead was opened and water began flowing under natural artesian conditions. This backflow phase was conducted in an attempt to reestablish background water-quality conditions. Natural artesian flow was maintained for 161 days (January 27 to July 6, 1992). The natural artesian flow rate decreased with time during the test from more than 16,000 m^3/d to about 6,500 m^3/d. This may be an indication of pressure buildup in the aquifer during the injection phase. After 161 days of natural artesian flow, background water-quality conditions had not yet been reestablished at the injection and deep and shallow monitoring wells (fig. 9). The attempt to reestablish background water-quality conditions was abandoned because at least five additional months might have been required, and time constraints precluded continuation of the process (fig. 9). As a result, the reference water-quality conditions for cycle 4 consisted of lower chloride concentrations than those representing native aquifer water. The reference chloride concentrations (estimated from specific conductance readings) were about 2,700 mg/L at the injection well, 1,750 mg/L at the deep monitor well, and 240 mg/L at the shallow monitor well.

The injection phase of cycle 4 was conducted over a 26-day period in summer 1992 (July 8 to August 3), and the volume of water injected was 387,275 m^3.

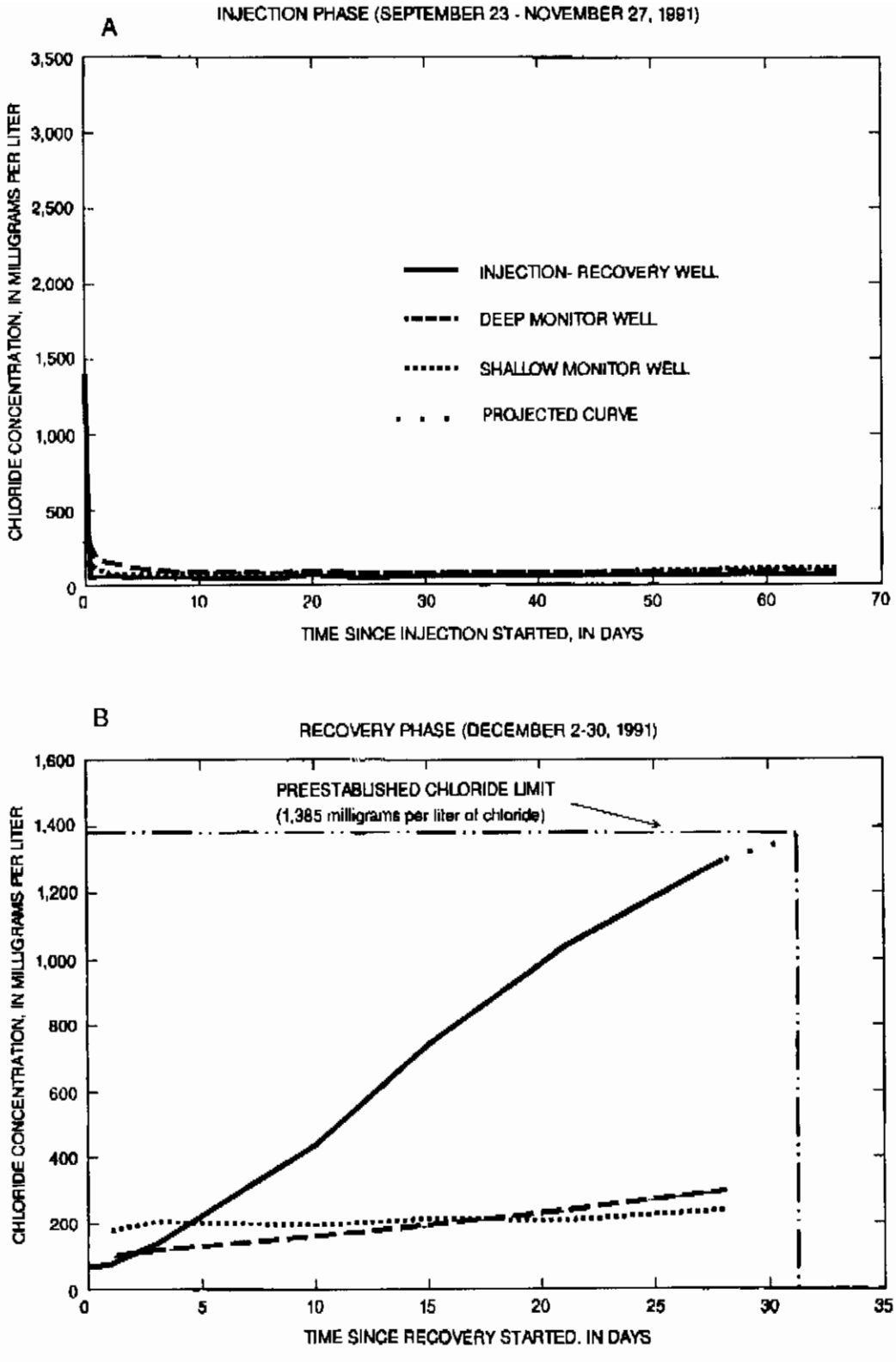

Figure 8. Chloride concentrations in the injection-recovery well and shallow and deep monitor wells during the injection and recovery phases of cycle 3.

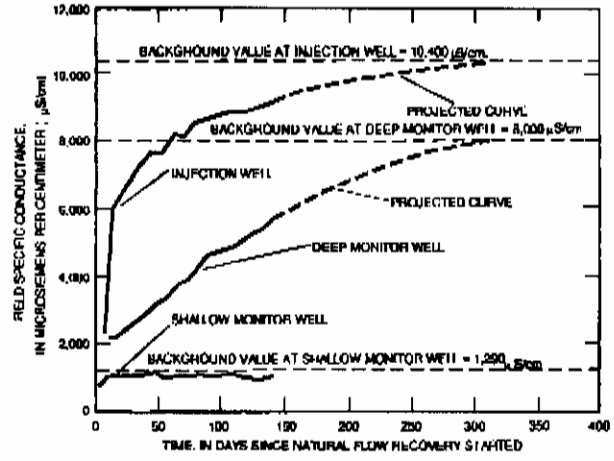

Figure 9. Specific conductance at the injection, deep monitor, and shallow monitor wells during the natural flow recovery period for reestablishing background water-quality conditions.

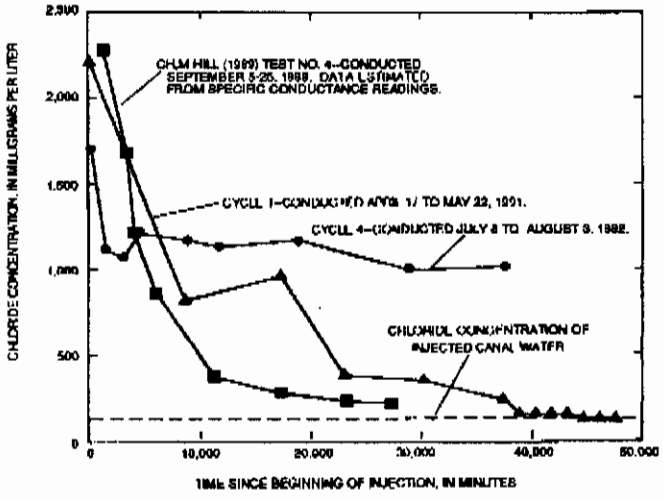

Figure 10. Chloride concentration breakthrough curves at the deep monitor well for the injection phase of cycles 1 and 4 from the present study and test no. 4 from a previous study.

An average injection rate of 14,549 m^3/d was maintained during this period (table 3). A storage period and a recovery phase were not conducted for cycle 4 due to the nature of the test.

Chloride concentration breakthrough curves were developed for the injection phase of cycles 1 and 4 (at the deep monitor well) from the present study data and test no. 4 from previous study data (CH_2M Hill, 1989). A comparison of the curves (fig. 10) reflects unexpected differences, especially considering that all three tests were conducted under similar background conditions. For example, it is expected that the chloride concentration curve reach an asymptote at a chloride concentration equal to that representative of canal water. Although it could be expected that the asymptote was reached at different times, for a conservative ion such as chloride, the asymptote should reach the same canal-water chloride concentration (chloride concentration of the injected water, approximately 120 mg/L). Several explanations of the hydrogeologic and hydraulic conditions at the injection well that may help explain this unexpected behavior are provided below.

1. Background chloride concentrations increased significantly with depth in the four high-permeability, relatively independent zones of the Lower Floridan aquifer. Chloride concentrations were 1,800 mg/L from 389 to 398 m below sea level (high-permeability zone 1),

2,500 mg/L from 419 to 424 m below sea level (high-permeability zone 2), 2,900 mg/L from 456 to 462 m below sea level (high-permeability zone 3), and 2,900 mg/L from 472 to 476 m below sea level (high permeability zone 4). These differences in background concentrations may have contributed to the anomalous patterns of the breakthrough curves (fig. 10).

2. Water-level altitudes, representative of the high permeability zones, were estimated from measurements using a straddle packer (CH_2M Hill, 1989) (table 2) and indicated a hydraulic gradient from the upper to the lower high-permeability zones. These data suggest that water from the upper high-permeability zone (1,800 mg/L of chloride concentration) might be flowing through the wellbore into the lower high-permeability zones (2,920 mg/L of chloride concentration). Hence, a mixing of the waters from the different high-permeability zones would occur, and the chloride concentration at which the asymptote of the breakthrough curve is reached would change (affected by the degree of mixing between the waters from the different zones).
3. The fact that the average injection rate for cycle 4 (14,549 m^3/d) was less than the natural artesian discharge rate (16,000 to 17,000 m^3/d) may have produced a greater degree of mixing at the deep monitor well (fig. 11). Figure 11A shows that if the injection rate (QINJECTED) were equal to or greater than the natural artesian flow (QNATURAL), all four high-permeability zones would transmit the injected water to the deep monitor well, and therefore, the chloride concentration value observed at the monitor well would be similar to that of the injected water. However, if QINJECTED were less than QNATURAL, the head differential might not be transmitted through the entire open wellbore, and injected water would probably flow only through the upper high-permeability zones (fig. 11B). As a result, chloride concentration values observed at the deep monitor well would represent a mix of water from the different high-permeability zones (fig. 11B), and therefore, would be higher than the concentration of the injected water.

ANALYSIS AND SUMMARY OF TEST CYCLES

Four subsurface injection, storage, and recovery cycles were conducted at the Lake Okeechobee injection-well site. Cycle 1 included injection and recovery phases; cycles 2 and 3 included injection, storage, and recovery phases; and cycle 4 included only an injection phase. The injection phases of each cycle were conducted over selected time periods in 1991 and 1992, and the volumes of water injected ranged from 387,275 to 1,343,675 m^3. The injection rate for cycles 1, 2, and 3 was similar and averaged about 20,600 m^3/d. The injection rate for cycle 4 was 14,549 m^3/d.

The recovery phases of cycles 1, 2, and 3 were conducted during variable time periods in 1991 when the preestablished water-quality limit was achieved at the injection well. The preestablished water-quality limit (5,000 µS/cm of specific conductance, which is equivalent to 1,385 mg/L of chloride concentration) was achieved for cycles 1 and 2 and projected for cycle 3. The average recovery flow rate ranged from 16,892 to 17,700 m^3/d for the three cycles. The volume of water recovered prior to achieving the preestablished water-quality limit ranged from 106,200 to 484,400 m^3, and the resulting recovery efficiency ranged from 15 to 36 percent.

The variability of the injection and recovery rates is shown in figures 3, 5, and 7 and can be due to several factors. Three of these factors include measurement device error (flow meter), change in background pressure, and electrical power failure (for the case of injection).

A comparison of the recovery efficiency for cycles 1, 2, and 3 in this study and test no. 4 from a previous study (CH_2M Hill, 1989) has been made, and the results are shown in figure 12. The recovery efficiency for successive cycles 2 and 3 increased from 22 to 36 percent and is expected to continue increasing with additional cycles. Cycle 1 and test no. 4 were conducted under similar background conditions (background conditions equal to native-aquifer water conditions or no residual injected water from a previous test). The volume of water injected for cycle 1 was 686,324 m^3 and the volume injected for test no. 4 was 344,185 m^3. Results indicated that the recovery efficiency was 24 percent for test no. 4 and 15 percent for cycle 1, suggesting that the recovery efficiency decreases with increasing injected volumes of water for tests conducted with no residual injected water from previous tests (background conditions equal to native-aquifer water conditions). All of these results are in agreement with those from previous studies by Tibbals and Frazee (1976) and Quiñones-Aponte and others (1989).

Cycle 4 was conducted in 1992 to define the dynamics of the aquifer system during the injection phase. A comparison of chloride concentration breakthrough curves at the deep monitor well (about 171 m from the injection well) for cycles 1 and 4 and test no. 4 reflects unexpected differences, especially considering that all three tests apparently were conducted under similar background conditions. One major difference was that the asymptote, expected to be reached at

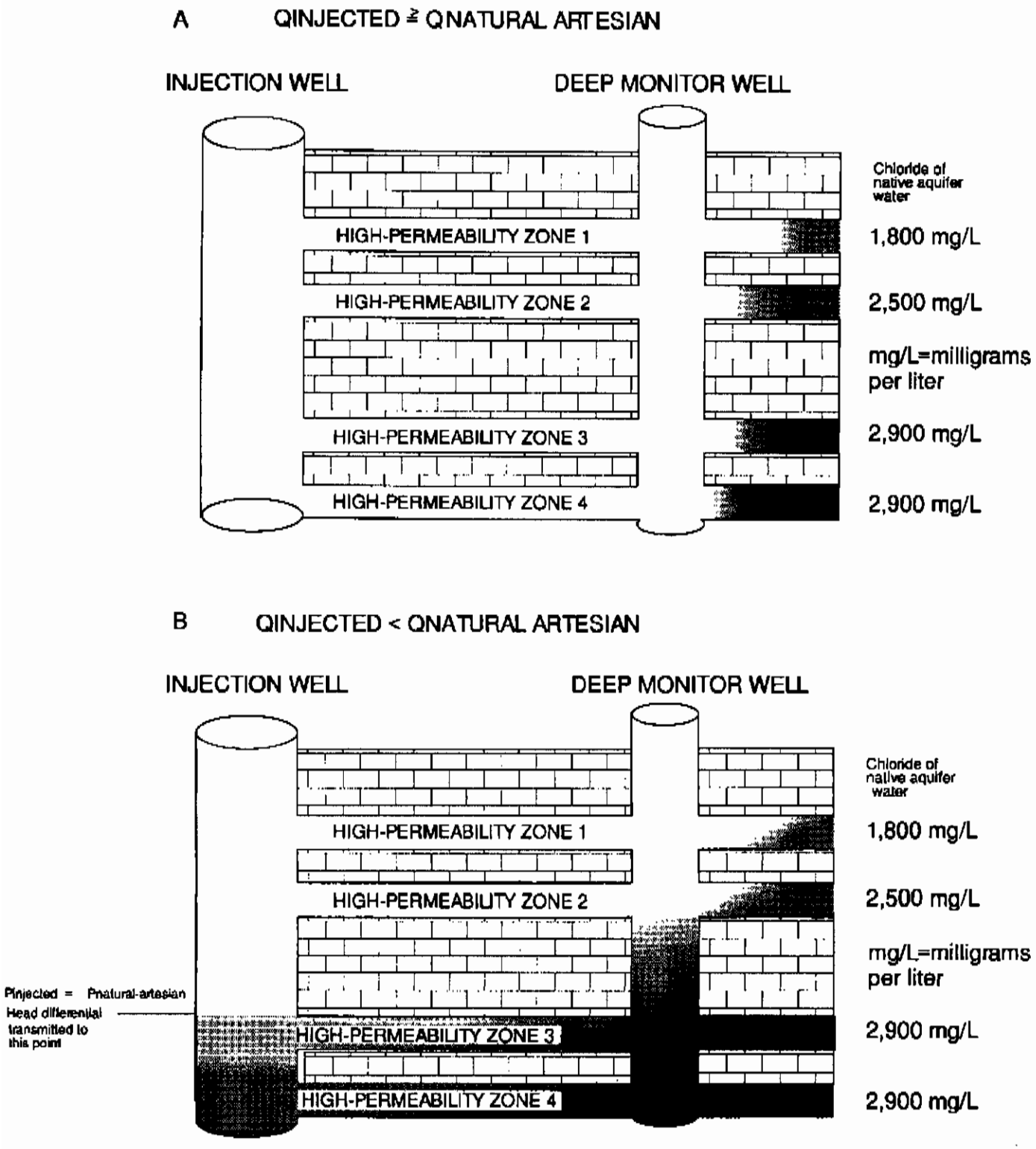

Figure 11. The injection process for two injection/recovery rate ratios: (A) QINJECTION/QNATURAL ARTESIAN is greater than or equal to 1.0, and (B) QINJECTION/QNATURAL ARTESIAN is less than 1.0.

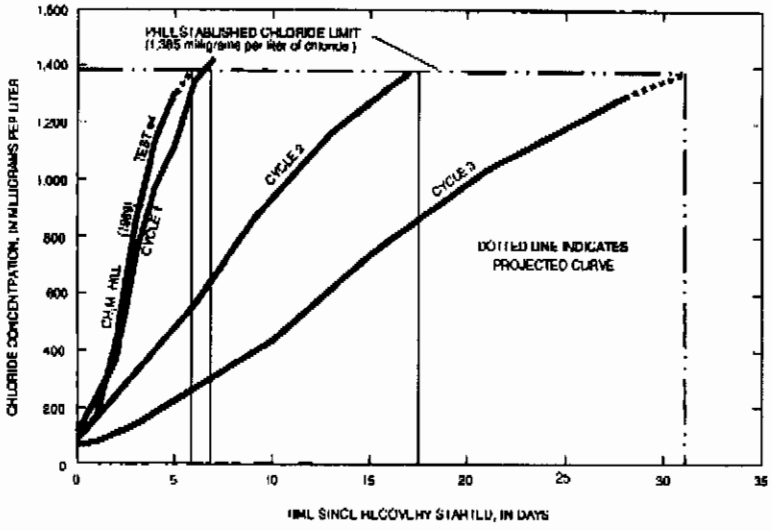

Figure 12. Chloride concentrations in the injection well during the recovery phase of cycles 1, 2, and 3 from the present study and test no. 4 from a previous study.

concentration levels equivalent or close to the injected water concentration, was instead reached at higher concentration levels.

Analysis of chloride concentrations in water at the injection-recovery well and at the deep monitor well (figs. 4, 6, and 8) indicates that flow through the Lower Floridan aquifer is not representative of a simple uniform-isotropic outflow of freshwater in a confined aquifer followed by a similar type of backflow. For the simple freshwater case of uniform-isotropic outflow and backflow within a porous media, changes in chloride concentration in water at the monitor well during recovery would precede changes in chloride concentration at the injection-recovery well. At some time during recovery, conditions at the monitoring well would return to background levels of chloride concentration because the bubble of injected water would clear the monitor well location while some freshwater still remained around the injection-recovery well. However, chloride concentrations returned to background levels at the injection-recovery well prior to achieving background conditions at the deep monitor well (figs. 4, 6, and 8). This suggests that the aquifer system is not characterized by a simple uniform-isotropic type flow, but instead responds as a conduit or cavernous type flow system. This hypothesis is illustrated by figure 11 and supports the corresponding discussion of cases where QINJECTED is less than QNATURAL. Figures 4, 6, and 8 also show that there were no significant changes in chloride concentration in water recovered from the shallow monitor well during the study, indicating that the injected freshwater did not reach this location vertically.

At the beginning of the recovery phase of cycle 1, chloride concentrations in water at the deep and shallow monitor wells were similar (fig. 4B). However, for cycles 2 and 3 (at the beginning of the tests), the chloride concentration in water at the deep monitor well was lower than in water at the shallow monitor well (figs. 6B and 8B). Additionally, the chloride concentration in water at the deep monitor well water at the beginning of cycles 2 and 3 was very similar to concentrations in water at the injection-recovery well (figs. 6B and 8B), indicating that injected water reached the deep monitor well during cycle 1 operations.

SIMULATION ANALYSIS OF SUBSURFACE INJECTION, STORAGE, AND RECOVERY OF FRESHWATER

The movement of solutes through porous media is controlled by both advection and hydrodynamic dispersion. Advective transport describes the movement of solute particles along the average direction of fluid flow at a rate equal to the mean pore-water velocity. Hydrodynamic dispersion describes the spread of solute particles along and transverse to the direction of average fluid flow in response to molecular diffusion and mechanical dispersion.

The following variable-density advective dispersive solute-transport equation was modified by

Quiñones-Aponte and Wexler (1995) for saturated flow and conservative solute species from a more general form presented by Voss (1984):

$$\frac{\partial(n\rho c)}{\partial t} = \nabla\cdot(n\rho v c) + \nabla\cdot[n\rho(D_d I + \underline{D}_m)\cdot\nabla c] + Q' c' \quad (6)$$

where:

n is the apparent porosity of the aquifer [dimensionless],

c is volumetric solute concentration in aquifer fluid [M/L^3],

t is time [T],

∇ is the gradient operator [1/L],

v is the average pore-water velocity [L/T],

D_d is the molecular diffusion coefficient [L^2/T],

I is the identity tensor (ones on diagonal, zero elsewhere),

$\underline{D}_m$ is the dispersion tensor [L^2/T],

Q' is the volumetric injection rate per unit area of aquifer [L/T], and

c is volumetric solute concentration in the injected fluid [M/L^3].

In equation *(6)*, the term $Q' c'$ represents only sources of fluid. Withdrawals of fluid from the aquifer are not considered in equation *(6)* because the concentration of solute in the fluid being withdrawn, c', is identical to the solute concentration c in the aquifer.

The average pore-water velocity (v) needed to solve equation *(6)* can be determined by:

$$v = -\frac{q}{n} \quad (7)$$

where q is specific discharge (flow rate per unit cross-sectional area) [L/T].

The rate of ground-water flow (specific discharge) is represented by Darcy's law:

$$q = -k(\nabla p - \rho g z)/\mu \quad (8)$$

where:

k is the intrinsic permeability of the aquifer materials [L^2],

p is the fluid pressure [M/LT^2], and

z is the altitude above a reference datum [L].

The variable-density flow equation is developed using Darcy's law *(8)* and the principle of conservation of fluid mass:

$$\frac{\partial(n\rho)}{\partial t} = -\nabla\cdot(\rho q) \pm Q_p \quad (9)$$

where:

Q_p is the mass of fluid injected (+) or withdrawn (-) per unit time per unit volume of aquifer [M/L^{3}T].

A generalized digital model was constructed to simulate the subsurface injection, storage, and recovery of freshwater in the Lower Floridan aquifer at the Lake Okeechobee injection-well site. The model was constructed using a modified version of the Saturated-Unsaturated TRAnsport (SUTRA) code (Voss, 1984), which simulates variable-density advective-dispersive solute-transport and variable-density ground-water flow. This modified version of SUTRA for a regular rectangular grid, QSUTRA (Quiñones-Aponte and Wexler, 1995), reduces computer storage and time, allowing for more-detailed discretization. Like the original code (SUTRA), QSUTRA uses the Galerkin finite-element technique (Voss, 1984) to compute the solution of the ground-water flow and solute-transport equations. The ground-water flow equation *(9)* is solved using the Incomplete Cholesky-Conjugate Gradient method (Kuiper, 1987), and the solute-transport equation *(6)* is solved using the Line Successive Overrelaxation method (Young, 1954).

The simulations of freshwater injection, storage, and recovery in the Lower Floridan aquifer were made using the radial flow option of the QSUTRA code. Because of a lack of information on the spatial variability of the hydraulic and transport characteristics, several assumptions had to be made: (1) the effect of the background hydraulic gradient is negligible, (2) the aquifer is divided into vertically adjacent layers characterized in the model as homogeneous with respect to their hydraulic and transport characteristics, (3) the hydraulic and transport characteristics are homogeneous along the radial direction of flow, and (4) the aquifer characteristics are isotropic along the horizontal (radial) direction.

Model Concept and Construction

The conceptual model represents a generalized version of the Lower Floridan aquifer at the Lake Okeechobee injection-well site (fig. 1). It was developed on the basis of data obtained from geophysical logs, straddle packer tests, pumping tests, and injection tests during a previous study (CH_2M Hill, 1989). According to the data by CH_2M Hill (1989) and several

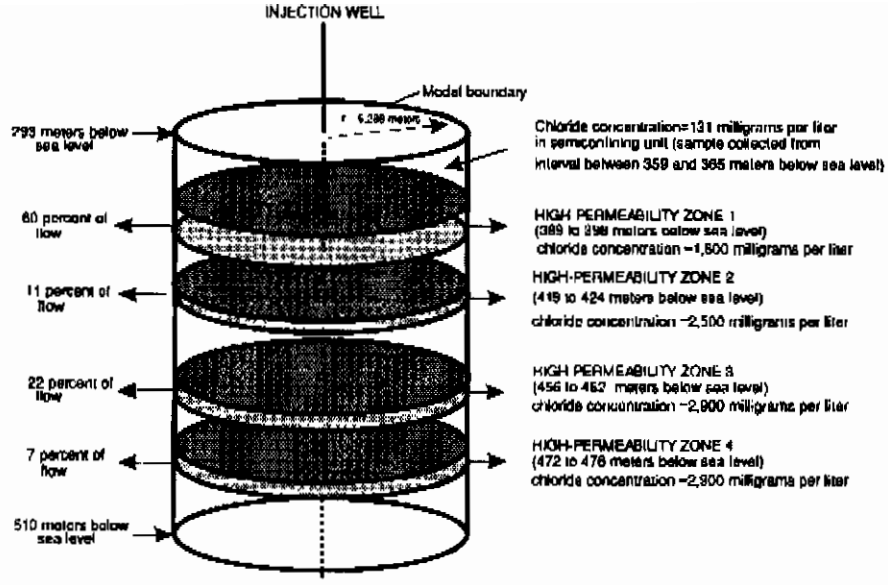

Figure 13. Generalized conceptual model of the Lower Floridan aquifer at the Lake Okeechobee injection-well site.

assumptions described previously, a generalized representation of the aquifer conditions at the site can be produced using a cylindrical coordinate system. This representative system can be justified for the case of injection or pumping from a single well where regional hydraulic gradients are small and aquifer hydraulic and transport characteristics are isotropic.

As previously discussed, the Lower Floridan aquifer can be visualized as containing four relatively independent high-permeability flow zones: high-permeability zone 1 (389 to 398 m below sea level), high-permeability zone 2 (419 to 424 m below sea level), high-permeability zone 3 (456 to 462 m below sea level), and high-permeability zone 4 (472 to 476 m below sea level). The high-permeability zones are characterized by fracture or cavernous type flow and are partly isolated from each other by hydrogeologic units of relatively low hydraulic characteristics. Sixty percent of the flow travels along high-permeability zone 1, 11 percent travels along high-permeability zone 2, 22 percent travels along high-permeability zone 3, and 7 percent travels along high-permeability zone 4 (fig. 13 and table 1). A very small percentage of the flow is transported as diffuse flow throughout the semiconfining units that are present between the high-permeability zones.

Water samples collected using a straddle packer (CH_2M Hill, 1989) indicated large differences in total dissolved solids, chloride concentrations, and water level altitude between the representative high permeability zones (table 2). High-permeability zone 1 had a total dissolved solids concentration of about 4,000 mg/L, a chloride concentration of about 1,800 mg/L, and a water-level altitude of 12.4 m. High-permeability zone 2 had a total dissolved solids concentration of about 5,740 mg/L, a chloride concentration of about 2,500 mg/L, and a water-level altitude of 12.1 m. High-permeability zones 3 and 4 had a total dissolved solids concentration of about 6,710 mg/L, a chloride concentration of about 2,920 mg/L, and a water-level altitude of 11.9 m. Although the high-permeability zones are relatively close to each other, the differences in water-quality data and water-level altitude indicated some degree of confinement between the zones. Additionally, an analysis of a water sample collected from 349 to 365 m, which represents a segment of the middle semiconfining unit (fig. 2), indicated that the total dissolved solids concentration was 656 mg/L and the chloride concentration was 131 mg/L (table 2). This result suggests that the degree of hydraulic connection among the high-permeability zones is relatively small.

Grid Design

A cylindrical coordinate finite-element grid was constructed (fig. 14) to study the subsurface injection, storage, and recovery cycles in the Lower Floridan aquifer at the Lake Okeechobee injection-well site. The model grid represents a radial extension of 6,288 m out

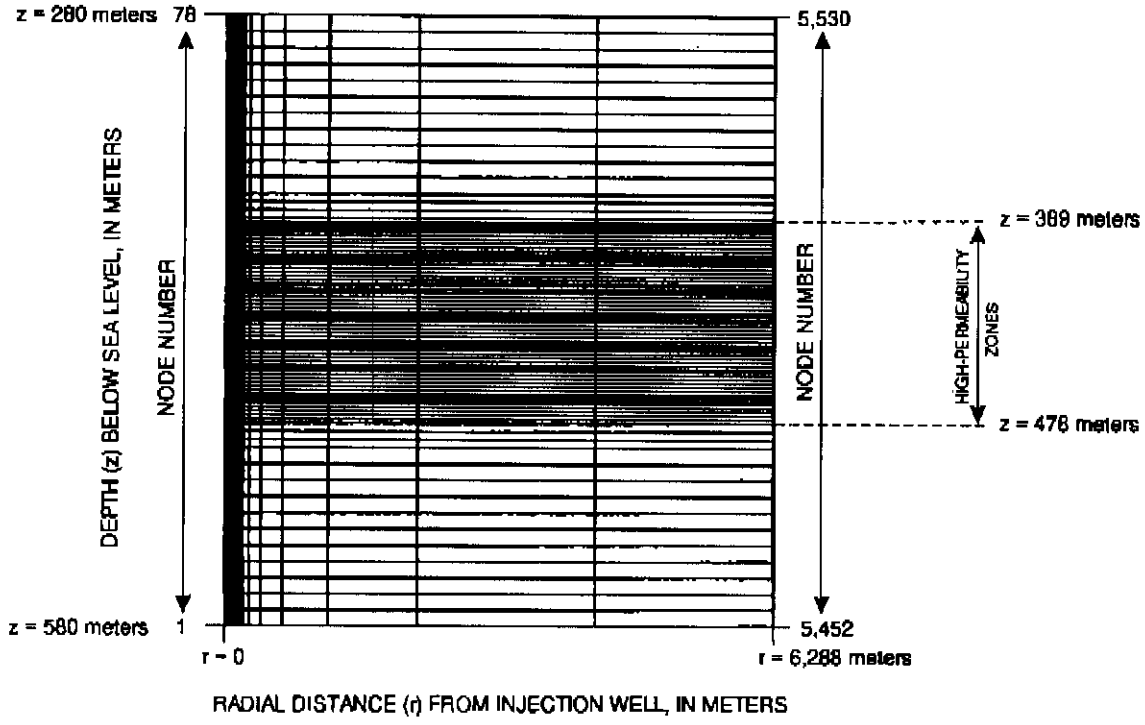

Figure 14. The cylindrical coordinate finite-element grid of the Lower Floridan aquifer at the injection-well site.

from the injection well into the aquifer. The grid is finer in the vicinity of the injection well to avoid errors associated with numerical dispersion (artificial dispersion due to inadequate discretization) and large differences between sides of a model-grid element. Elements represent a 2-m thickness and 2-m length near the well but vary elsewhere. Elements represent 4-m lengths at a distance of 100 m from the well, 8-m lengths at a distance of 120 m from the well, and lengths as much as 2,048 m beyond a distance of 160 m. Element thickness varied from 2 to 8 m, with 4-m thick elements providing a transition. Elements representing 8 m of aquifer thickness are used for the first 11 and last 11 rows of the model grid. Elements representing 2 m of aquifer thickness are used for 50 rows of the grid, corresponding to the aquifer interval that would be affected by injected canal water. Elements representing 4 m of aquifer thickness are used for 6 rows of the grid and correspond to a transition between the element rows representing thicknesses of 2 and 8 m (fig. 14).

Boundary and Initial Conditions

Boundary and initial conditions were determined for the generalized model of the Lower Floridan aquifer at the Lake Okeechobee injection-well site. Boundary conditions were set from $r = 0$ to $r = 6{,}288$ m at $z = 280$ m and $z = 580$ m below sea level, the limits of the finite-element grid (fig. 14). Specified pressure nodes were set at the top and bottom of the Lower Floridan aquifer with specified chloride concentration for any inflow across these boundaries (upper and lower limits of the modeled zone). Specified pressures were set equal to hydrostatic pressure ($P = h\rho g$). The chloride concentration was set equal to the concentration of the native water at these boundaries, which was obtained from in-situ samples. The boundary condition at the well ($r = 0$) was applied by specifying the mass flux equal to the injection rate. The flux was distributed among the boundary nodes along the length of the injection zone using an analysis from packer test data (fig. 13 and tables 1 and 2). The analysis showed that the flow distribution was 60, 11, 22, and 7 percent for high-permeability zones 1, 2, 3, and 4, respectively. The aquifer hydraulic characteristics (K and k) were determined in a similar manner using field determined transmissivity values and procedures described earlier in the report. A chloride concentration corresponding to the injected water during injection was specified at the well boundary ($r = 0$). A flux-average chloride concentration (weighted average concentration using flux as weighting factor) for water withdrawn during recovery was calculated using simulated chloride concentration values at boundary nodes representing the well (fig. 14, $r = 0$). The vertical lateral boundary (external boundary) was represented as a no-flow/

no-transport condition with the assumption that this boundary is sufficiently far away from the area of interest. At the upper and lower model limits, the constant pressure and concentration boundaries can be justified because of the distance from the injection source and the permeability gradients that exist throughout the 300-m thickness.

The initial pressures were assumed to be hydrostatic ($P = h\rho g$) and set equal to the equivalent freshwater head that corresponded to static conditions prior to injection. Initial chloride concentration was set equal to solute concentration in the native aquifer water at the different flow zones and boundaries (table 2). The fluid density ρ was assumed to depend only on solute concentration C and was calculated by the model based on initial solute concentrations and the following functional relation between density and solute concentration at each node:

$$\rho = \rho_i + (\rho_n \quad \rho_i)\,[(C - C_i)/(C_n - C_i)] \qquad (10)$$

where:

ρ_i is density of injected water [M/L^3],

ρ_n is density of native water [M/L^3],

C_i is solute concentration in injected water [M/L^3], and

C_n is solute concentration in native water [M/L^3].

Time Steps

To avoid numerical dispersion associated with a large time-step size, initial time-step sizes were set at or less than 100 seconds. The time-step size was increased during the injection phase so that the injected water front (neglecting dispersion) moved a constant distance with each successive time step. In the simulation of the mixing of two water bodies in a radial flow field, it is important to require that the time step, Δt, satisfies the condition:

$$\frac{v\ \Delta t}{2.0} \ll \alpha_L \qquad (11)$$

where α_L is the longitudinal dispersivity of the aquifer [L] (Kipp, 1987).

The time step must be of such size to permit the simulated movement of the injected water front inside a model element without an abrupt transition from one element to the next. For the radial coordinate system, water velocity increases as the water particles move closer to the well, and therefore, the time-step size must be increased during injection and decreased during recovery to meet the stability criterion established by equation *(11)*.

The final time-step size from the injection phase was used and maintained uniformly for the entire simulation of the storage period. During the recovery phase, the time-step size was gradually reduced from its maximum value as the injected water front moved closer to the well.

Calibration and Testing

The calibration and testing of the model was performed by changing the model variables within realistic limits, until a satisfactory comparison between the observed and simulated solute breakthrough data was obtained. Initial model variables were set according to data presented in tables 1 and 4. Other model constants are listed in table 5. A vertical anisotropy (k_H/k_V) ratio of 100:1 was assumed for the high-permeability zones and the semiconfining units that are present between the zones. For the semiconfining units, a horizontal intrinsic permeability value (k_H) of 1.53×10^{-11} m^2 (square meters) and a vertical intrinsic permeability value (k_V) of 1.53×10^{-13} m^2 were assigned. These values were derived using equation *(5)*, a k_H/k_V ratio of 100:1, and data from a CH_2M Hill (1989) straddle packer test in the middle semiconfining unit (349 to 365 m below sea level). The porosity for the semiconfining units between the high-permeability zones was assumed to be 0.15. The apparent effective porosity value listed in table 4 for the high-permeability zones was the result of calibration trials. Although conceptually this apparent effective porosity value (5 percent) seems to be too low for the high-permeability zones, it was the highest value (combined with the calibrated intrinsic permeabilities) to yield acceptable results in modeling the chloride concentration breakthrough curve at the deep monitor well.

Because the open intervals of the injection and monitor wells include more than one node, composite chloride concentration values representative of the wells were computed using simulated chloride concentrations at nodes representing the well. The computation was determined using a weighted average value (with permeability as a weighting factor) from nodes representing the open interval of the monitor wells and a flux-weighted average concentration value from nodes representing the injection well. Composite

Table 4. Aquifer characteristics used in the model of the Lower Floridan aquifer at the Lake Okeechobee injection-well site.

High-permeability zone	Depth interval (meters below sea level)	Horizontal permeability (square meters)	Vertical permeability (square meters)	Apparent effective porosity (percent)	Specific pressure storativity (kilograms per meter per second squared^{-1})	Longitudinal dispersivity (meters)	Transverse dispersivity (meters)
1	389-398	5.894×10^{-9}	5.894×10^{-11}	5	1.36×10^{-10}	1.0	0.1
2	419-424	1.945×10^{-9}	1.945×10^{-11}	5	1.36×10^{-10}	1.0	.1
3	456-462	3.242×10^{-9}	3.242×10^{-11}	5	1.36×10^{-10}	1.0	.1
4	472-476	1.547×10^{-9}	1.547×10^{-11}	5	1.36×10^{-10}	1.0	.1

Table 5. Fluid, solute, and rock matrix properties used in the simulations

[kg/m/s, kilograms per meter per second; kg/m^3, kilograms per cubic meter; m^2/s, square meters per second; (kg/m•sec^2)$^{-1}$, kilograms per meter per second squared^{-1}]

Property	Value
Dynamic viscosity of native water, in kg/m/s	0.001
Dynamic viscosity of injected water, in kg/m/s	0.00089
Density of native water, in kg/m^3	1,004.4
Density of injected water, in kg/m^3	1,000.1
Coefficient of molecular diffusion, in m^2/s	5.0×10^{-10}
Fluid compressibility, in (kg/m•sec^2)$^{-1}$	4.4×10^{-10}
Rock matrix compressibility, in (kg/m•sec^2)$^{-1}$	1.2×10^{-10}

chloride concentration values determined using the flux-weighted method are more accurate than composite concentration values from the permeability-weighted method. However, at the time of this study, the computer model (QSUTRA) does not provide for the computation of flux-weighted average concentrations at nodes representing an observation well.

Satisfactory comparisons of simulated to observed dimensionless chloride concentrations for the deep monitor well were obtained when using the model to simulate the injection and recovery phases of cycle 1 (fig. 15) using the parameters listed in table 4. Several attempts were made, changing the hydraulic and transport parameters by two or three orders of magnitude and changing the boundary conditions. Different combinations of no-flow and specified pressure boundary conditions were tested for the model limits. However, no acceptable comparison of simulated to observed dimensionless chloride concentrations for the injection well during the recovery phase of cycle 1 was obtained (fig. 16). A dimensionless version of chloride data obtained in the field (observed data) compared to dimensionless chloride data obtained from four calibration attempts (simulated data) for the injection well is shown in figure 16. The simulated data in figure 16 represent model results using the parameters in table 4 and represent the simulated values for different longitudinal and transverse dispersivities (α_L = 1.0 m and α_T = 0.1 m, α_L = 2.0 m and α_T = 2.0 m, α_L = 1.0 m and α_T = 1.0 m, and α_L = 1.0 m and α_T = 0.6 m).

Although many other calibration attempts were made, only the results for which the model input

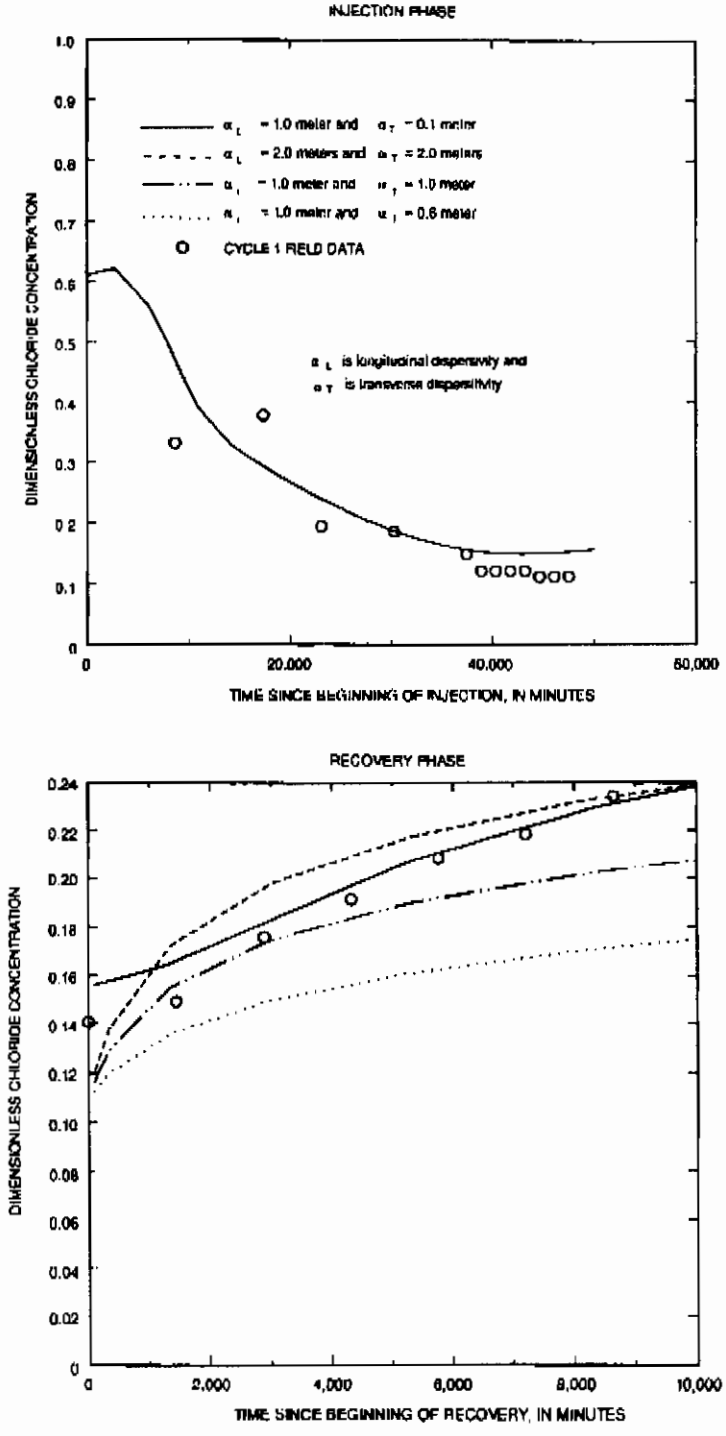

Figure 15. Observed and simulated dimensionless chloride concentration breakthrough curves at the deep monitor well during the injection and recovery phases of cycle 1.

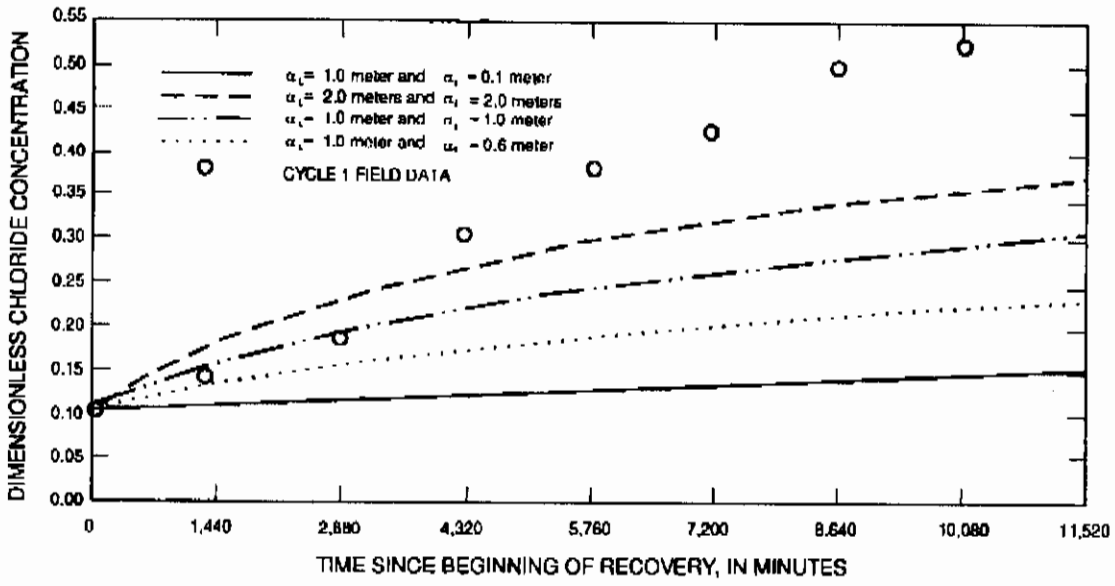

Figure 16. Observed and simulated dimensionless chloride concentrations in the injection well during the recovery phase of cycle 1.

variables were close to the parameters listed in table 4 are presented in this report. It was suspected that the cavernous/conduit nature of the Lower Floridan aquifer would allow for very high velocities (relative to typical ground-water velocities) to develop near the injection well. Such velocities would preclude an appropriate representation of flow and solute transport using the QSUTRA model, which is based on porous media assumptions. Porous media type models are based on Darcy's law which assumes a linear proportionality between specific discharge (discharge per unit measured of aquifer thickness) and hydraulic gradient. This proportionality is characteristic of laminar ground-water flow. The Reynolds number, defined below, is used to determine limits between laminar and turbulent flow regimes. For turbulent flow, the linear proportionality between specific discharge and hydraulic gradient is not valid. Where turbulent flow occurs, a porous media based flow model would compute hydraulic gradient distributions smaller than actual field gradients. Therefore, to test for the occurrence of turbulent flow, Reynolds numbers were estimated for different distances from the injection well using two different conceptual models, porous media and cavernous conceptual models. The Reynolds number (R_e) is defined as the ratio of inertial forces to viscous forces:

$$R_e = \frac{v\ d}{V} \qquad (12)$$

where:

d is a characteristic length (in this case, thickness of flow zone for cavernous conceptual system or $k^{1/2}$ [the square root of the intrinsic permeability] for the porous media conceptual system) [L], and

V is the fluid kinematic viscosity [L^2/T].

Reynolds numbers were only estimated for high-permeability zone 1 (9-m thick), which constituted 60 percent of the flow (fig. 13). The Reynolds numbers were estimated for two different conceptual systems in radial or cylindrical coordinates, a cavernous system and a porous media system (table 6). To estimate Reynolds numbers of actual field conditions at different distances from the injection source, it was necessary to determine or approximate the actual pore-water velocity at the different locations, the effective thickness of the flow zone (cavernous conceptual system) or intrinsic permeability (porous media conceptual system), and the fluid kinematic viscosity.

The actual radial ground-water flow velocity at a location from the injection source (the deep monitor well, located 171 m from the source) was determined from a chloride concentration breakthrough curve. This was accomplished by identifying the inflection point of the chloride concentration breakthrough curve, which usually coincides with the 50 percent concentration change from native to injected water. Data from test no. 4 by CH_2M Hill (1989) was used to estimate the pore-water velocity at the deep monitor well (fig. 17 and

Table 6. Sectional area, velocity, and Reynolds number estimated at different distances from the injection source

Radius (meters)	Area[1] (square meters)	Actual velocity (meters per second)	Reynolds number cavernous conceptual system (dimensionless)	Reynolds number porous media conceptual system (dimensionless)
0.1	0.0919	1.29961	13,539,167	112.3
.25	.2298	.51984	5,415,667	44.9
.5	.4596	.25992	2,707,833	22.4
1	.9191	.12996	1,353,917	11.2
2	1.84	.06498	676,958	5.6
4	3.67	.03249	338,479	2.8
6	5.51	.02166	225,653	1.8
8	7.35	.01624	169,240	1.4
10	9.19	.01300	135,392	1.1
12	11.02	.01083	112,826	.94
16	14.7	.00812	84,620	.70
20	18.4	.00650	67,696	.56
30	27.6	.00433	45,131	.37
40	36.8	.00325	33,848	.28
50	45.9	.00260	27,078	.22
100	91.9	.00130	13,539	.11
171	157	[2].00076	7,917	.066
200	184	.00065	6,770	.056
500	460	.00026	2,708	.022
1,000	919	.00013	1,354	.011
5,000	4,596	.00003	271	.0022

[1]The cavernous conceptual system is $2\pi rb \cdot correction\ factor$ and the porous media conceptual system is $2\pi rbn \cdot correction\ factor$ where r is the radial distance from the injection source, b is the thickness of the flow zone, and n is the apparent porosity of the aquifer (dimensionless). The correction factor was applied to adjust the thickness area of the flow zone in order to approximate actual field velocities. The correction factor was determined using the actual ground-water flow velocity estimated at the deep monitor well located 171 meters from the injection well.

[2]Actual field velocity estimated from a concentration breakthrough curve at the deep monitor well (fig. 17).

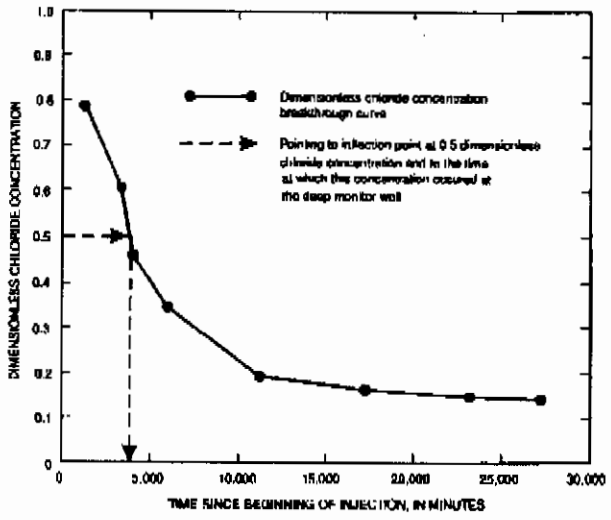

Figure 17. Dimensionless chloride concentration breakthrough curve of data from test no. 4. Test data from CH_2M Hill (1989).

table 3). These test data were selected for velocity determination because the subject test background concentration (native water concentration) was well established. This is important in determining the actual inflection point of the breakthrough curve (50 percent concentration change). The estimated pore-water velocity at the deep monitor well was 0.000760 m/s (meter per second). The area perpendicular to the flow for the case of radial flow is defined as $A = 2\pi rb$ where A is the area, r is the radial distance from the injection source, and b is the thickness of the flow zone. The effective area was first estimated at the location of the deep monitor well for which a velocity value was previously determined. The effective area was estimated by using the relation:

$$Q = v \cdot A_{eff} \cdot correction\ factor \qquad (13)$$

or:

$$A_{eff} = \frac{Q}{v \cdot correction\ factor} \qquad (14)$$

where Q is the flow through the flow zone. The correction factor was applied to the areas determined for different distance r to obtain an effective area (A_{eff}) for each location, and the effective area was used alone with flow rate to determine velocities at the different distances.

For the case of the porous media conceptual system, the square root of the intrinsic permeability of the high-permeability zone 1 (table 1) was used as the characteristic length as recommended by Bear (1979). Fluid kinematic viscosity in this zone was assumed as 8.639×10^{-7} m^2/s (square meters per second) at a water temperature of 26.7 degrees Celsius. For the case of the cavernous conceptual system, an effective thickness was determined using the same correction factors that were applied to the area to determine A_{eff} and used in equation *(12)* as the characteristic length.

For the porous media conceptual system, the Reynolds numbers were greater than 10 at distances less than 1.42 m from the injection well (fig. 18). This number (Reynolds number equal to 10) represents the upper limit of laminar porous media flow, which is the fundamental assumption for the application of Darcy's law to ground-water flow (Bear, 1979). At the deep monitor well located about 171 m from the injection well, the Reynolds number was about 0.08 which indicates laminar ground-water flow (porous media flow) at that location (fig. 18). The Reynolds number was about 100 at a distance of 0.1 m from the injection well (fig. 18). Thus, application of Darcy's law to ground-water flow is not valid at this distance nor is the transport solution, which is affected by the head gradient in the advection terms of the governing solute-transport equation. This may explain why the QSUTRA model produced good results for the deep monitor well, but was not able to produce acceptable results for the injection well. For the cavernous conceptual system, Reynolds numbers less than about 2,000 that are representative of laminar flow in circular tubes (Rouse,

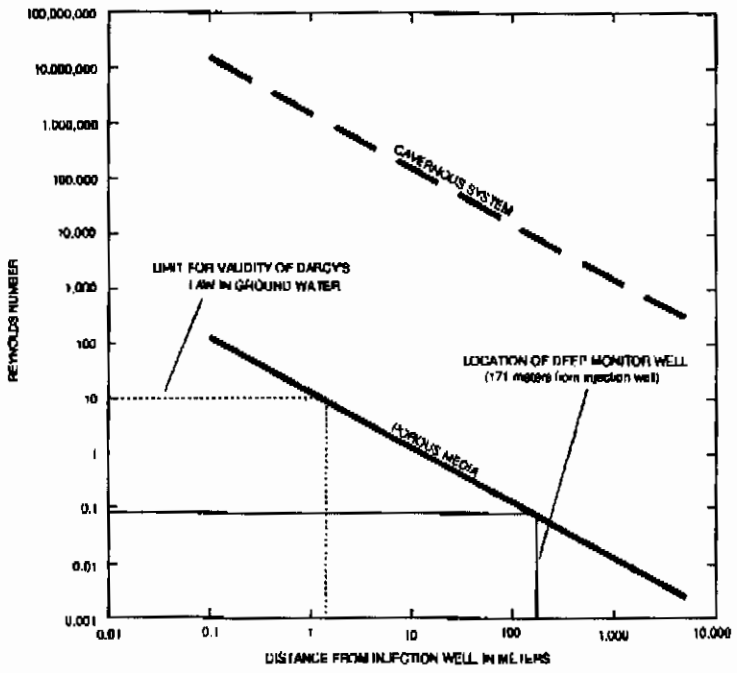

Figure 18. Reynolds number for a cavernous conceptual system and a porous media conceptual system as a function of distance from the injection well

1956, p. 174) were obtained at distances greater than 800 m (fig. 18). The Reynolds number was greater than 2,000 at distances less than 1,000 m from the injection well. This number represents the upper limit of laminar flow.

SUMMARY AND CONCLUSIONS

A series of freshwater subsurface injection, storage, and recovery tests were conducted at an injection-well site near Lake Okeechobee in Okeechobee County, Florida, to assess the recoverability of injected canal water from the Lower Floridan aquifer. Initial testing at the Lake Okeechobee injection-well site was previously conducted by a private consultant, and some of their results have been included as part of the U.S. Geological Survey study. At the study site, the Lower Floridan aquifer is characterized as having four local, relatively independent, high-permeability flow zones (389 to 398 m, 419 to 424 m, 456 to 462 m, and 472 to 476 m below sea level). The transmissivity of the aquifer at the injection well was estimated to be about 71,000 m^2/d from 377 to 509 m below sea level (equivalent to an average hydraulic conductivity of 540 m/d).

Four subsurface injection, storage, and recovery test cycles were conducted at the Lake Okeechobee injection-well site. Cycle 1 included injection and recovery phases; cycles 2 and 3 included injection, storage, and recovery phases; and cycle 4 included only an injection phase. The volumes of water injected ranged from 387,275 to 1,343,675 m^3 and the average injection rates ranged from 14,549 to 21,043 m^3/d for all the cycles. The volumes of water recovered, prior to achieving (or projecting) the preestablished water-quality limit (5,000 µS/cm of specific conductance, which is equivalent to about 1,385 mg/L of chloride concentration), ranged from 106,200 to 484,400 m^3 and the average recovery flow rates ranged from 16,892 to 17,700 m^3/d for cycles 1, 2, and 3. The recovery efficiency for successive cycles 2 and 3 increased from 22 to 36 percent and is expected to continue increasing with additional cycles. Cycle 1 and test no. 4 (from a previous study) were conducted under similar background conditions (background conditions equal to native-aquifer water conditions or no residual injected water from a previous test). The volumes of water injected were 686,324 m^3 for cycle 1 and 344,185 m^3 for test no. 4. The recovery efficiency was 24 percent for test no. 4 and 15 percent for cycle 1, indicating that the value decreases with increasing volumes of injected water. All these results are in agreement with those from previous studies.

Cycle 4 was conducted to define the dynamics of the aquifer system during the injection phase. A comparison of chloride concentration breakthrough curves at the deep monitor well (about 171 m from the injection well) for cycles 1 and 4 and test no. 4 reflects unexpected differences, especially considering that all three tests were conducted under similar background conditions. One major difference was that the concentration asymptote, expected to be reached at concentration levels equivalent or close to the injected water concentration, was instead reached at higher concentration levels. One factor that may explain the unexpected differences suggests that the ratio of injection to recovery rates could affect the chloride concentration breakthrough curves at the deep monitor well. For cases where the injection rate is smaller than the natural artesian flow rate, the head differential might not be transmitted to the deeper high-permeability zones. The injected water would probably reach the deep monitor well only through the upper high-permeability zones, and the chloride concentration values observed at this well would represent a mix of water from the different upper and lower high-permeability zones. Hence, the asymptote would be reached at a higher chloride concentration level in cases where the injection rate is smaller than the natural artesian flow rate.

A generalized digital model was constructed to simulate the subsurface injection, storage, and recovery of freshwater in the Lower Floridan aquifer at the Lake Okeechobee study site. The model was constructed using a modified version of the SUTRA code (QSUTRA). QSUTRA uses the Incomplete Cholesky-Conjugate Gradient method to solve the ground-water flow equation and the Line Successive Overrelaxation method to solve the solute-transport equation. A cylindrical coordinate finite-element grid was constructed to study the subsurface injection, storage, and recovery cycles in the Lower Floridan aquifer, and boundary and initial conditions were determined for the generalized model.

The calibration and testing of the model was performed by changing the model variables within realistic limits, until a satisfactory comparison between the observed and simulated solute breakthrough data was obtained. Satisfactory comparisons of simulated to observed dimensionless chloride concentrations for the deep monitor well were obtained when using the model during the injection and recovery phases of cycle 1, but not for the injection well during the recovery phase of cycle 1 even after several attempts. This precluded the determination of the recovery efficiency values by using the model. The cavernous or conduit nature of the Lower Floridan aquifer at the local scale permits very high velocities (relative to typical ground-water velocities) to develop near the injection well. Such velocities could explain the unsatisfactory comparisons of simulated to observed dimensionless chloride concentrations for the injection well and failure of the model to represent the field data at this well. To test this possibility, Reynolds numbers were estimated at varying distances from the injection well, taking into consideration two aquifer conceptual systems: porous media and cavernous.

For the porous media conceptual system, the square root of the permeability value was used as a characteristic length to estimate Reynolds numbers. The Reynolds numbers were greater than 10 at distances less than 1.42 m from the injection well. Thus, application of Darcy's law to ground-water flow might not be valid at this distance. At the deep monitor well located about 171 m from the injection well, the Reynolds number was about 0.08 which is representative of laminar porous media flow conditions.

For the cavernous conceptual system, the thickness (9 m) of high-permeability zone 1 was used as a characteristic length to estimate Reynolds numbers. The Reynolds numbers were greater than 2,000 at distances less than 1,000 m from the well. This number represents the upper limit of laminar flow, which is the fundamental assumption for the application of Darcy's law to free flow.

In conclusion, the simulation of recovery efficiency for the Lower Floridan aquifer at the Lake Okeechobee injection-well site might require the application of a free-flow type model (conduit flow or fracture flow model). This type of model may produce a more realistic representation of the actual fluid motion in the aquifer and will provide appropriate estimates of the recovery efficiency.

Analytical Model for Estimation of Steady-State Capture Zones of Pumping Wells in Confined and Unconfined Aquifers

by Stuart Grubb[a]

Abstract

The analysis of capture zones of pumping wells is useful for designing pumping systems and wellhead protection programs. Using discharge potentials, equations are derived that can be applied to confined, unconfined, or combined confined and unconfined aquifers. The transient equations are transcendental and cannot be solved explicitly. However, infinite-time (steady-state) equations are presented which can be solved. They define an area in which, theoretically, all the water in the aquifer will eventually reach the pumping well, although the equations do not consider the effects of hydrodynamic dispersion. Equations for calculating the stagnation point, upgradient divide, and dividing streamline within the aquifer and an example problem are presented.

1. Introduction

A capture zone is defined as the area of an aquifer in which all the water will be removed by a pumping well or wells within a certain time period. Capture zone analysis has been recognized as an important consideration in the design of ground-water remediation systems and wellhead protection programs (Javandel and Tsang, 1986; Lee and Wilson, 1988). Bear and Jacobs (1965) investigated the movement of water particles injected into aquifers, and their analytical model is often used for determining capture zones as well. Several standard ground-water texts have simple equations for determining the infinite-time (steady-state) capture zone of a single well in a confined aquifer with uniform regional flow (for example, Bear, 1979; Todd, 1980). Equations can be superimposed to calculate the capture zone of multiple well systems (Javandel and Tsang, 1986), and computer models have been developed for analyzing multiple wells and heterogeneous aquifers (for example, McElwee, 1991). These models include the EPA's wellhead protection area (WHPA) package (EPA, 1990).

This paper presents a model for determining capture zones which is applicable not only to confined aquifers, but to unconfined and combined confined and unconfined aquifers as well. Portions of the model development were presented in Javandel and others (1985) and Bear and Jacobs (1965). These authors used the potential ($K\phi$) and the specific discharge to develop the equations. The primary difference in the model presented here is that the equations are generalized in terms of discharge potential so they can be used for confined aquifers, unconfined aquifers, and combined confined and unconfined aquifers by simply using the appropriate definition of one parameter, the discharge potential. The discharge potential concept was developed over 20 years ago and is fully documented in Strack (1989) and discussed by Marsily (1986), but it is not widely used.

2. Analytical Model

The assumptions for this model are as follows:

- The aquifer is homogeneous, isotropic, and infinite in horizontal extent.
- Uniform flow (steady-state) conditions prevail.
- A confined aquifer has a uniform transmissivity and no leakage through the upper or lower confining layers. An unconfined aquifer has a horizontal lower confining layer with no leakage, rainfall infiltration, or other vertical recharge. The effect of these assumptions is discussed later.
- Because the equations assume steady-state conditions, the storativity of a confined aquifer and the specific yield of an unconfined aquifer have been neglected. Hydrodynamic dispersion is also neglected.
- Dupuit assumption, i.e. vertical gradients are negligible.

[a]Grubb Environmental Services, 2233 15th Avenue, North St. Paul, Minnesota 55109.

Received October 1991, revised February 1992, accepted March 1992.

Discussion open until July 1, 1993.

• The well is fully penetrating, is open over the thickness of the confined or unconfined aquifer at the well, and pumps at a constant rate.

Complex potentials are used to describe the distribution of discharge potentials throughout the aquifer. For background on the mathematics of complex potentials, Strack (1989, p. 269) gives a good, concise overview of the theory of complex functions. The complex potential for uniform regional flow in the (x, y) plane is

$$\Omega = -Q_0 z e^{-i\alpha} + C \tag{1}$$

and the complex potential for a well is (Strack, 1989, p. 279)

$$\Omega = \frac{Q_w}{2\pi} \ln(z - z_w) + C \tag{2}$$

where Q_0 = discharge vector of uniform flow; z = complex potential = $x + iy$; z_w = complex potential at the well; α = angle between the x axis and uniform flow; Q_w = discharge from the well; and C = constant which corresponds to the elevation of the bottom of the aquifer. Assume that $C = 0$. Note that

$$e^{-i\alpha} = \cos\alpha - i\sin\alpha \tag{3}$$

and

$$Q_0 = Q_{x0} + Q_{y0} = \frac{d\Phi}{dx} + \frac{d\Phi}{dy} \tag{4}$$

where Q_{x0} = x component of uniform flow; Q_{y0} = y component of uniform flow; and Φ = discharge potential.

The discharge potential is defined differently for confined, unconfined, and combined confined and unconfined aquifers as follows (Strack, 1989, p. 49):

Confined aquifer:	$\Phi = Kb\phi$
Unconfined aquifer:	$\Phi = \frac{1}{2}K\phi^2$
Combined confined and unconfined aquifer:	$\Phi = Kb\phi - \frac{1}{2}Kb^2$ for confined part
	$\Phi = \frac{1}{2}K\phi^2$ for unconfined part

where K = hydraulic conductivity; b = confined aquifer thickness; and ϕ = hydraulic head (or phreatic head) above the bottom of the aquifer. Writing equations in terms of discharge potentials is useful because the same equations may be used for all three types of aquifers by simply using the appropriate definition for Φ.

Because the complex potentials and the boundary conditions considered are linear and homogeneous, any linear combination of complex potentials can also be solved according to the principle of superposition. Superimposing (adding) the complex potentials for uniform flow and for flow to the pumping well gives

$$\Omega = \Phi + \Psi_i = -Q_0 z e^{-i\alpha} + \frac{Q_w}{2\pi} \ln(z - z_w) \tag{5}$$

where Ψ = stream function.

The real and imaginary parts of (5) are

$$\Phi = -Q_0([x - x_w]\cos\alpha + [y - y_w]\sin\alpha) + \frac{Q_w}{4\pi} \ln([x - x_w]^2 + [y - y_w]^2) \tag{6}$$

$$\Psi = Q_0([x - x_w]\sin\alpha + [y - y_w]\cos\alpha) + \frac{Q_w}{2\pi} \tan^{-1}\left(\frac{y - y_w}{x - x_w}\right) \tag{7}$$

where x_w, y_w = x and y coordinates of the well.

The velocity components v_x and v_y in the x and y directions, respectively, along a particular streamline are

$$v_x = \frac{dx}{dt} = \frac{1}{Bn}\frac{d\Phi}{dx} = \frac{-Q_0\cos\alpha}{Bn} + \frac{Q_w[x - x_w]}{2\pi Bn([x - x_w]^2 + [y - y_w]^2)} \tag{8}$$

$$v_y = \frac{dy}{dt} = \frac{1}{Bn}\frac{d\Phi}{dy} = \frac{-Q_0\sin\alpha}{Bn} + \frac{Q_w[y - y_w]}{2\pi Bn([x - x_w]^2 + [y - y_w]^2)} \tag{9}$$

where n = porosity; t = time since pumping began; and B = aquifer thickness defined for different aquifers as follows

Confined aquifer:	$B = b$	
Unconfined aquifer:	$B = \phi$	
Combined confined and unconfined aquifer:	$B = b$	for confined part
	$B = \phi$	for unconfined part

For this problem assume that the uniform flow is in the direction of the x axis so that $\alpha = 0$. Equation (7) can then be written

$$x - x_w = [y - y_w]\,\text{cotan}\,\frac{2\pi}{Q_w}(\Psi - Q_0[y - y_w]) \tag{10}$$

Substituting (10) into (9) yields

$$dt = \frac{2\pi Bn}{Q_w}[y - y_w]\csc^2\frac{2\pi}{Q_w}(\Psi - Q_0[y - y_w])\,dy \quad \ldots . (11)$$

After integrating,

$$t = \frac{Bn[y - y_w]}{Q_0}\cot\frac{2\pi}{Q_w}(\Psi - Q_0[y - y_w]) + \frac{BnQ_w}{2\pi Q_0^2}\ln\sin\frac{2\pi}{Q_w}(\Psi - Q_0[y - y_w]) + f(\Psi) \tag{12}$$

where $f(\Psi)$ is a constant dependent on the particular streamline considered. Equation (12) describes the time when water particles starting at a specific (x, y) coordinate along the streamline will reach the pumping well. When pumping first begins, the particles closest to the well will be captured

immediately. In other words, $x = x_w, y = y_w, t = 0$ will be a solution to the equation. Therefore

$$f(\Psi) = \frac{-BnQ_w}{2\pi Q_0^2} \ln \sin \frac{2\pi}{Q_w} \Psi \quad (13)$$

Substituting (13) into (12) yields

$$t = \frac{Bn[y - y_w]}{Q_0} \cot \frac{2\pi}{Q_w} (\Psi - Q_0[y - y_w]) + \frac{Bn}{2\pi Q_0^2} \ln \frac{\sin \frac{2\pi}{Q_w} (\Psi - Q_0[y - y_w])}{\sin \frac{2\pi}{Q_w} \Psi} \quad (14)$$

Substituting (7) into (14) yields

$$t = \frac{Bn[x - x_w]}{Q_0} - \frac{BnQ_w}{2Q_0^2} \ln \frac{\sin\left(\frac{2\pi}{Q_w} Q_0[y - y_w] + \theta\right)}{\sin \theta} \quad (15)$$

where $\theta = \tan^{-1}([y - y_w]/[x - x_w])$.

Three dimensionless parameters may be introduced:

$$\bar{x} = \frac{2\pi Q_0}{Q_w}[x - x_w]; \quad \bar{y} = \frac{2\pi Q_0}{Q_w}[y - y_w]; \quad \bar{t} = \frac{2\pi Q_0^2}{BnQ_w} t \quad \ldots . (16)$$

Substituting (16) into (15) yields

$$\bar{t} = \bar{x} + \ln \frac{\sin\theta}{\sin(\bar{y} + \theta)} \quad (17)$$

or

$$e^{\bar{x} - \bar{t}} = \sin\bar{y} \frac{\bar{x}}{\bar{y}} + \cos\bar{y} \quad (18)$$

Bear and Jacobs (1965) provide additional analysis of equation (18) and its implications for ground-water transport in confined aquifers. Unfortunately, equation (18) is transcendental and cannot be solved explicitly for either x or y. Iterative solutions have been developed for solving special cases of the equation (for example, McElwee, 1991). These solutions are valid for unconfined aquifers as well if the dimensionless parameters introduced in equation (16) are used in equation (18).

3. Single Well in Uniform Flow at Infinite Time (Steady State)

A quick and simple analysis which is useful for many hydrogeologic projects is determining the capture zone of a single well in uniform flow at infinite time, or steady state. This will define an area in which all the water in the aquifer will reach the well if the well pumps for a sufficiently long time. At infinite time equation (18) can be simplified considerably and solved for x. The equations below give three critical parameters, the stagnation point, the upgradient divide, and the equation for the dividing streamline.

For simplicity, consider $x_w = 0$, $y_w = 0$, and $\alpha = 0$ as shown in Figure 1. The stagnation point is where $v_x = v_y = 0$. From equation (9) it is clear that $v_y = 0$ when $y = y_w = 0$. Substituting into equation (8) and solving for x yields

$$x_{STAG} = \frac{Q_w}{2\pi Q_0} \quad (19)$$

where x_{STAG} is the distance from the well to the downgradient stagnation point. As $\bar{t} \to \infty$, the equation for a streamline [equation (18)] becomes

$$\bar{x} = \frac{-\bar{y}}{\tan\bar{y}} \quad (20)$$

As $x \to \infty$ then $\tan y \to 0$, and $y \to N\pi$ where N = integer. Therefore, by equation (16), as $x \to \infty$

$$\bar{y} \to \frac{NQ_w}{2Q_0} \quad (21)$$

Substituting equation (21) into equation (7) with $x \to \infty$ yields

$$\Psi = \frac{NQ_w}{2} \quad (22)$$

The dividing streamline will approach the stagnation point. Substituting equation (22) and the coordinates of the stagnation point into equation (7) yields N = 1. Therefore, as $x \to \infty$, the dividing streamline will approach the line

$$y_{DIV} = \pm \frac{Q_w}{2Q_0} \quad (23)$$

which represents half the width of the capture zone far upgradient of the well. Considering that N = 1, substituting equation (16) into equation (20) yields the equation for the dividing streamline

$$x = \frac{y}{\tan\left(\frac{2\pi Q_0}{Q_w} y\right)} \quad (24)$$

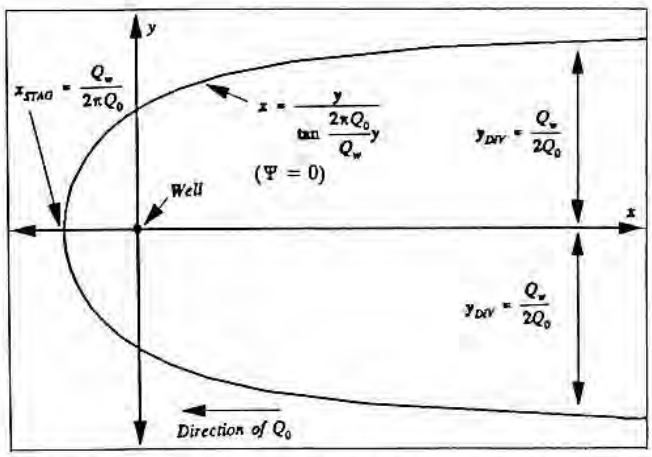

Fig. 1. Stagnation point, upgradient divide, and dividing streamline at infinite time (steady state).

The stagnation point, upgradient divide, and dividing streamline are shown on Figure 1. Because the direction of uniform flow for this problem is aligned with the x axis, $d\Phi/dy = 0$ and

$$Q_0 = \frac{d\Phi}{dx} \cong \frac{\Phi_1 - \Phi_2}{L} \tag{25}$$

where Φ_1 and Φ_2 = downgradient and upgradient discharge potentials, respectively, along a streamline before pumping begins; and L = distance between the locations where Φ_1 and Φ_2 were measured. The equations for the stagnation point, upgradient divide, and dividing streamline can be simplified into more common terms by substituting the above definition for Q_0 and the appropriate definitions for Φ. For a confined aquifer

$$x_{STAG} = \frac{Q_w}{2\pi Ti} \tag{26}$$

where i = natural hydraulic gradient = $d\phi/dx$ and T = aquifer transmissivity = Kb,

$$y_{DIV} = \pm \frac{Q_w}{2Ti} \tag{27}$$

and the dividing streamline is

$$x = \frac{y}{\tan\left(\frac{2\pi Ti}{Q_w}\, y\right)} \tag{28}$$

For an unconfined aquifer

$$x_{STAG} = \frac{Q_w L}{\pi K(\phi_1^2 - \phi_2^2)} \tag{29}$$

$$y_{DIV} = \pm \frac{Q_w L}{K(\phi_1^2 - \phi_2^2)} \tag{30}$$

and the dividing streamline is

$$x = \frac{y}{\tan\left[\frac{\pi K(\phi_1^2 - \phi_2^2)}{Q_w L}\, y\right]} \tag{31}$$

Equations (19), (23), and (24) can also be applied to combined confined and unconfined aquifers. To calculate Q_0 for this scenario, substitute the appropriate definition for Φ into equation (25) based on whether Φ was measured in the confined or unconfined part of the aquifer. For example, if Φ_1 is measured in the unconfined portion of the aquifer and Φ_2 is measured in the confined portion of the aquifer, then $\Phi_1 = \frac{1}{2}K\phi_1^2$ and $\Phi_2 = Kb\phi_2 - \frac{1}{2}Kb^2$. Substituting into equation (25) yields

$$Q_0 = \frac{K(\phi_1^2 - 2b\phi_2 + b^2)}{2L} \tag{32}$$

Note also that equation (6) may be used to obtain values of Φ throughout the aquifer by substituting the appropriate x and y coordinates. The effect of several pumping (or injection) wells on the value of Φ at any point in the aquifer may also be determined by using equation (6) and the principle of superposition. A separate equation for Φ is written for each well being considered based on its x_w, y_w, and Q_w. The separate equations are then added to yield one equation for Φ for any point in the aquifer.

4. Example Problem

The data for this example problem were adapted from a site in Wisconsin which formerly had a leaking underground storage tank. The leak had been detected shortly after it occurred, and a pumping well was to be installed to contain the spread of petroleum hydrocarbon contamination in the aquifer. The project hydrogeologist needed to determine the capture zone of the well as part of the pumping system design and evaluation.

In this example, the problem will be solved assuming the aquifer is confined [using equations (26)-(28)] and unconfined [using equations (29)-(31)], and the results will be compared. A site map is shown on Figure 2. Note that the x-axis has been aligned with the ground-water flow direction.

The aquifer and well characteristics are: Hydraulic conductivity (K) (determined from aquifer tests): 72 ft/day; Elevation of the lower confining layer: 1618.00 ft; Elevation of the upper confining layer (confined aquifer only): 1629.00 ft; Measured ground-water elevations in piezometers: P-1 = 1630.50 ft and P-2 = 1629.50 ft; Distance between P-1 and P-2 (L): 235 ft; Pumping rate (Q_w): 963 ft^3/day (5 gpm); ϕ_1 = 1630.50 ft − 1618.00 ft = 12.50 ft; and ϕ_2 = 1629.50 ft − 1618.00 ft = 11.50 ft. A cross section of the aquifer is shown on Figure 3.

For the confined aquifer:

$$b = 1629.00 \text{ ft} - 1618.00 \text{ ft} = 11.00 \text{ ft}$$

$$T = Kb = 790 \text{ ft}^2/\text{day}$$

$$i = \frac{\Phi_1 - \Phi_2}{L} = 0.00425$$

$$x_{STAG} = \frac{Q_w}{2\pi Ti} = 46 \text{ ft}$$

$$y_{DIV} = \pm \frac{Q_w}{2Ti} = \pm 140 \text{ ft}$$

and the dividing streamline is

$$x = \frac{y}{\tan\left(\frac{2\pi Ti}{Q_w}\, y\right)} = \frac{y}{\tan 0.022y}$$

For the unconfined aquifer:

$$x_{STAG} = \frac{Q_w L}{\pi K(\phi_1^2 - \phi_2^2)} = 42 \text{ ft}$$

$$y_{DIV} = \pm \frac{Q_w L}{K(\phi_1^2 - \phi_2^2)} = \pm 130 \text{ ft}$$

and the dividing streamline is

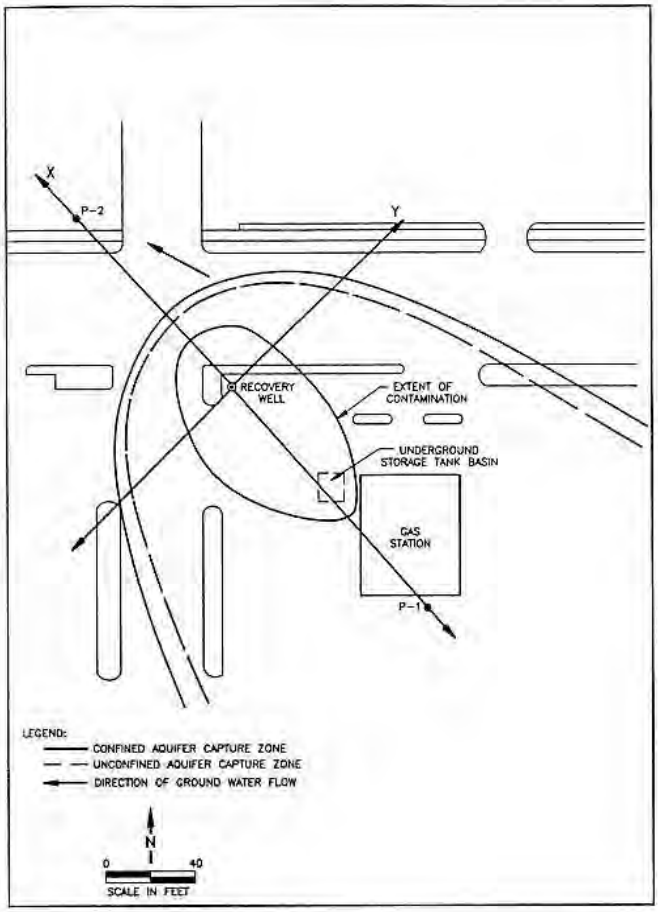

Fig. 2. Site map for the example problem showing the calculated capture zones.

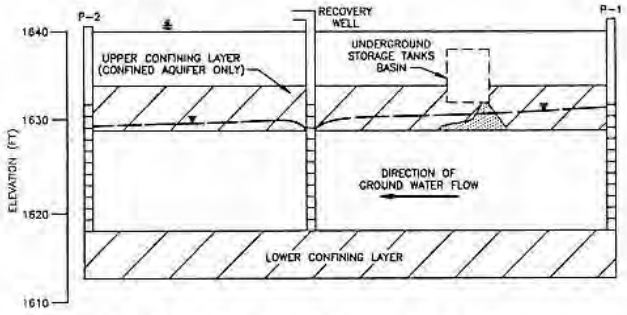

Fig. 3. Cross section of the aquifer along the x-axis.

$$x = \frac{y}{\tan\left[\dfrac{\pi K(\phi_1^2 - \phi_2^2)}{Q_w L}\, y\right]} = \frac{y}{\tan 0.024y}$$

The results of the analyses are shown on Figure 2.

5. Limitations of the Model

The steady-state equations presented in Section 1 neglect the influence of storativity and specific yield. The significance of this assumption decreases as pumping continues, and by definition storativity and specific yield = 0 at infinite time (steady state). Bear and Jacobs (1965) present a discussion of the effect of neglecting storativity for a confined aquifer with an injection well. They state that the actual front of the water injected from the well will lag behind the calculated front due to the storativity of the well and the aquifer. Similarly, in a pumping situation the actual capture zone will be somewhat smaller than the calculated capture zone due to the water being removed from storage.

The influence of water naturally added to or subtracted from the aquifer system other than regional uniform flow (leakage and infiltration) is not included in the equations. For unconfined aquifers, this may be a good assumption in urban areas or other areas where drainage systems prevent rainfall infiltration. If the addition of water to the aquifer through leakage and infiltration were considered in the equations, the result would be a smaller calculated capture zone.

The model is based on the Dupuit assumption, i.e., vertical gradients are negligible. For this reason, the model may not be accurate in areas of aquifer recharge or discharge, including the area near a well.

Hydrodynamic dispersion is commonly neglected from capture zone analyses. If dispersion were included in the analysis, there would not be a sharp capture zone boundary but rather a wide boundary with width proportional to the dispersion coefficient. Within the boundary only some fraction of the water particles would be captured by the well after a given time.

While the capture zone equations are clearly useful for solving problems related to contaminant transport or wellhead protection, it should be noted that the equations consider only advective flow. The solution to a contaminant transport problem must also incorporate the effects of dispersion, diffusion, sorption, degradation, and retardation.

6. Conclusions

Despite the assumptions and simplifications necessary to derive these equations, the equations can provide useful information for designing pumping systems or wellhead protection programs. Although they do not consider hydrodynamic dispersion, equations (26) through (31) are particularly useful for a quick analysis of critical properties of an aquifer and pumping system. While the many assumptions greatly restrict its applicability, users of the model should find many hydrogeologic problems of limited scope which could benefit from this analysis. The model presented in Section 2 is developed in terms of discharge potentials, which makes the equations applicable to confined, unconfined, and combined confined and unconfined aquifers. Previously derived capture zone equations (and computer programs) could also be modified and written in terms of discharge potentials to make them applicable to both confined and unconfined aquifers.

Computer Programs

A computer program is available which will solve and graph the capture zone equations in this paper. Included on the same computer diskette are spreadsheets for Lotus 1-2-3 and Quattro Pro which solve and graph these equations and other equations commonly used for well design and groundwater modeling. To order these programs, send a check or money order for $20 to Grubb Environmental Services, 2233 15th Avenue, North St. Paul, MN 55109. Please indi-

cate whether you prefer 5.25-inch or 3.5-inch IBM formatted diskettes.

Acknowledgments

Thanks to Stephen Smith of GeoHydroCycle, Inc., John Baxter, Barry O'Flanagan, and Jim Prieur for reviewing this paper and to Linda Sax for drafting the figures.

Nomenclature

- B aquifer thickness [L];
- b confined aquifer thickness [L];
- C constant which corresponds to the elevation of the bottom of the aquifer;
- i natural ground-water gradient [L/L];
- K hydraulic conductivity [L/T];
- L distance between locations where Φ_1 and Φ_2 were measured [L];
- n porosity;
- N integer constant;
- Q_0 discharge vector of uniform flow (L^2/T];
- Q_w discharge from the well [L^3/T];
- Q_{x0} x component of uniform flow [L^2/T];
- Q_{y0} y component of uniform flow [L^2/T];
- t time since pumping began [T];
- T aquifer transmissivity [L^2/T];
- v_x velocity component in the x direction [L/T];
- v_y velocity component in the y direction [L/T];
- x_{STAG} distance from the well to the downgradient stagnation point [L];
- x_w x coordinate of the well [L];
- y_{DIV} y coordinate of the dividing streamline far upgradient of the well [L];
- y_w y coordinate of the well [L];
- z complex potential $x + iy$;
- z_w complex potential at the well;
- α angle between the x axis and uniform flow;
- θ $\tan^{-1}([y - y_w]/[x - x_w])$;
- Φ discharge potential [L^3/T];
- Φ_1 downgradient discharge potential [L^3/T];
- Φ_2 upgradient discharge potential [L^3/T];
- ϕ hydraulic head (or phreatic head) above the bottom of the aquifer [L]; and
- Ψ stream function [L^3/T].

References

Bear, J. 1979. Hydraulics of Groundwater. McGraw-Hill, NY. 569 pp.

Bear, J. and M. Jacobs. 1965. On the movement of water bodies injected into aquifers. Journal of Hydrology. v. 3, pp. 37-57.

EPA (U.S. Environmental Protection Agency). 1990. WHPA: A Modular Semi-Analytical Model for the Delineation of Wellhead Protection Areas. Office of Ground-Water Protection, Washington, DC.

Javandel, I., C. Doughty, and C.-F. Tsang. 1985. Groundwater Transport: Handbook of Mathematical Models. American Geophysical Union, Washington, DC. Water Resources Monograph Series 10. 228 pp.

Javandel, I. and C.-F. Tsang. 1986. Capture-zone type curves: A tool for aquifer cleanup. Ground Water. v. 24, no. 5, pp. 616-625.

Lee, K.H.L. and J. L. Wilson. 1986. Pollution capture zones for pumping wells in aquifers with ambient flow. EOS. v. 67, p. 966.

Marsily, G. de. 1986. Quantitative Hydrogeology. Academic Press, Inc. 440 pp.

McElwee, C. D. 1991. Computer notes: Capture zones for simple aquifers. Ground Water. v. 29, no. 4, pp. 587-590.

Strack, O.D.L. 1989. Groundwater Mechanics. Prentice Hall, Englewood Cliffs, NJ. 732 pp.

Todd, D. K. 1980. Groundwater Hydrology. John Wiley and Sons, NY. 535 pp.

Apparent Relative Retardation of Tritium and Bromide in Dolomite

by Darrell I. Leap[a]

Abstract

In order to determine the suitability of bromide as a surrogate for tritium for ground-water tracing in fractured and fissured dolomite, apparent relative retardation coefficients of bromide with respect to tritium were computed by the cumulative relative mass-time method from breakthrough curves of both substances, when used simultaneously as tracers in a two-well recirculating tracer test. Throughout the 33.78-day test, relative retardation differences of only a few hundredths were detected for most of the testing time.

Tritium was less retarded in flow through highly transmissive openings than in more diffuse flow. Bromide was generally retarded relative to tritium except at the pumping well where the concentrations of both were diluted an order of magnitude below those in the monitoring wells, and tritium was retarded slightly more than bromide.

Apparent relative retardation was found to change with transmissivity, concentration, flow-path length and time, but not enough to rule out bromide as a suitable surrogate for, or even better than, tritium in dolomite if the limitations of each tracer are known.

Introduction

The Problem

Tritium has been touted by references below as one of the best substances for tracing ground-water movement because it is a constituent of water and behaves very conservatively. Tritiated water acts very much like normal water in ground-water flow systems. Because of its radioactive nature (a low-level beta emitter) with a half-life of 12.43 years (Mann et al., 1982), regulations usually prohibit its use except under very restrictive conditions, and usually with hard-to-obtain permission from regulatory agencies.

Therefore, suitable surrogate tracers are often needed which behave as closely as possible to tritium, but which are not radioactive or chemically hazardous. In addition, there is a need to quantify, as precisely as possible, the in situ behavior of such surrogates relative to tritium for various geologic media. This information is needed for (1) tracer-testing aquifers in order to gain information about their hydraulics and solute-transport properties in general; and (2) tracer-testing for the same purposes aquifers already contaminated by tritium or other radioactive substances, but into which injection of additional radioactive substances for tracing purposes would be undesirable or prohibited.

In order to quantify such relative tritium-surrogate behavior so that the information can be properly applied in field tests, and the test results understood, the following questions must be answered about the apparent retardation of the bromide surrogate relative to that of tritium:

1. How conservative is bromide with respect to tritium over a range of normalized concentrations?
2. What are the retardation characteristics of tritium and bromide in flow in open fractures and fissures versus flow in lower-transmissivity media?
3. How does retardation of bromide relative to retardation of tritium change over time during flow?
4. How does the relative retardation change with flow-path length? And finally,
5. How does bromide compare to tritium as a surrogate?

This information was of great interest to the U.S. Geological Survey and the U.S. Department of Energy, especially in the Amargosa Desert of southern Nevada, in the fractured and fissured Cambrian dolomite downgradient of the Nevada Test Site.

This study has for the first time precisely quantified the relative retardation differences to be expected between tritium and bromide tracers in fractured and fissured dolomite on the field scale. This information and the newly developed methodology reported herein can help investigators better plan future tests of a similar kind and interpret the results therefrom, using different tracer combinations in different lithologies.

Background and Literature Review

Numerous tracer tests using bromide and tritium have been performed to study movement of surface water, ground water, and soil moisture. Clayton and Smith (1963) reported that the radioactive bromide-82 ion was not adsorbed at all in river-tracing experiments. Payne (1968) found bromide to give results identical to tritium when both were used as tracers in karst conduits. Payne (1988) also

[a]Department of Earth and Atmospheric Sciences, Purdue University, West Lafayette, Indiana 47907-1397.

Received July 1991, revised January 1992, accepted January 1992.

Discussion open until January 1, 1993.

states that tritium is the "ideal tracer" in a review of isotope hydrology. Comparison of bromide and nitrate in unsaturated soils showed that both behaved identically (Smith and Davis, 1974). Schmotzer et al. (1973), after tracing water through limestone caverns, reported, "bromide does not appear to be lost by precipitation, adsorption or absorption, and is biologically stable." Similar results in karst studies were reported by Jester and Uhler (1974).

Miettinen (1978) studied the movement of tritium in soils and suggested that slight retardation of tritium might occur due to hydrogen exchange on clay micelles attached to magnesium. This process would only be important in water with low pH, and not in dolomitic aquifers. Tennyson and Settergren (1980) used nonradioactive bromide to trace water through the root zone of two silt loams and found that bromide was not retained on soil particles by ion exchange. Hamill (1980) considered bromide as the next best tracer to tritium after finding no adsorption of bromide as a river tracer.

Murray et al. (1981) used lithium bromide (LiBr) solution as a tracer to verify the hydraulic connection between a sanitary landfill and a downgradient spring in carbonate rocks. Bromide proved very useful because of (1) its low background concentration; (2) existence of a sensitive analytical procedure (neutron activation); (3) its lack of toxicity; and (4) its conservative nature, especially in the presence of organics which rendered rhodamine WT unusable in this case.

Moreno and Neretnieks (1985) considered tritium and bromide both to be nonsorbing tracers when both were used individually in laboratory experiments in fractured granite. They found that (1) dispersion in channels within the fracture wall can be greater than dispersion along the nonchanneled part of the fracture; (2) diffusion and sorption into the rock matrix may be two important processes in retardation; and (3) diffusion increases with increasing contact time of tracer and rock.

Wierenga and Van Genuchten (1989) performed unsaturated-flow tracer experiments with tritium and chloride in columns 30 cm and 6 m long; both were filled with loamy fine sand containing 4.7% clay, and less than 1% organic matter. Their research showed that for both column lengths, (1) dispersivity using tritium breakthrough data averaged 0.88, and 0.87 for chloride; (2) the mean retardation factor or coefficient R_d for tritium was 0.94 ($R_d = 1.0$ indicates no retardation), and that for chloride was 0.87, indicating less retardation for chloride (meaning it traveled faster than both tritium and the advective water velocity; (3) this value in turn was due to the effects of anionic exclusion of the chloride from clay particles which caused chloride to move ahead of the advective front. They concluded that chloride and bromide may not be ideal tracers for unsaturated fine-grained soils because they can move faster than the advective front. Anionic exclusion is also discussed in detail in Bolt et al. (1978).

Research Objectives

Although Payne (1968) studied bromide and tritium together in a karst system, it was decided that a higher degree of quantification was needed of the possible subtle differences in behavior that might not be apparent from inspection of breakthrough curves alone, especially since normalized concentrations are generally plotted on a logarithmic scale which compresses differences between curves. This decision was also motivated by the varying conclusions in the literature about the efficacies of bromide versus tritium.

More detailed behavioral information was felt to be especially necessary in the aquifer of interest—the Cambrian Bonanza King dolomite in the Amargosa Desert of southern Nevada, because of its wide range of fracture apertures (from less than one mm to several cm).

Because of its numerous fractures and fissures, this aquifer would be expected to contain much more rock surface area and discrete pore spaces in which more retardation could take place than in a karst system with only large, open conduits.

This particular study, utilizing data and information from a 33.78-day, two-well recirculating tracer test that was run to determine aquifer dispersivity (Leap and Belmonte, 1992), was initiated with the objectives of answering the five questions asked earlier.

Research Approach

The research approach consisted of running a two-well recirculating test with an injection well, a pumping well, and three sampling or monitoring wells (Figure 1) in an aquifer between 191 and 218 meters from the surface. Ammonium bromide (NH_4Br) and tritiated water (HTO) were simultaneously used as tracers and subsequently compared in behavior.

Each ground-water sample retrieved was split into aliquots—one for tritium analysis and one for bromide. Tritium was analyzed by liquid scintillation at the National Water Quality Laboratory of the U.S. Geological Survey, in Denver, Colorado, and the results corrected for radioactive decay. Bromide was analyzed by neutron-activation analysis at the Breazeale TRIGA nuclear reactor facility of the Pennsylvania State University.

The normalized concentration of each tracer was computed as (C/C_o) where C = concentration at any time, and C_o = initial concentration of the initial injected tracer pulse or spike. The results were plotted as breakthrough curves of normalized concentration vs time to obtain estimates of the apparent longitudinal dispersivity by the method of Grove (1971) (Leap and Belmonte, 1992). Further analyses of the curves were conducted for this study to determine apparent relative retardation of bromide with respect to tritium at each sampling well at each sampling time by the Cumulative Relative Mass-Time Method, developed for this study and described in a subsequent section.

Retardation of bromide relative to tritium was then studied to determine its variation with respect to concentration, transmissivity, time of flow, and flow-path length. A comparison was then made of bromide as a general surrogate for tritium by assessing the range of relative retardation determined during the 33.78-day test.

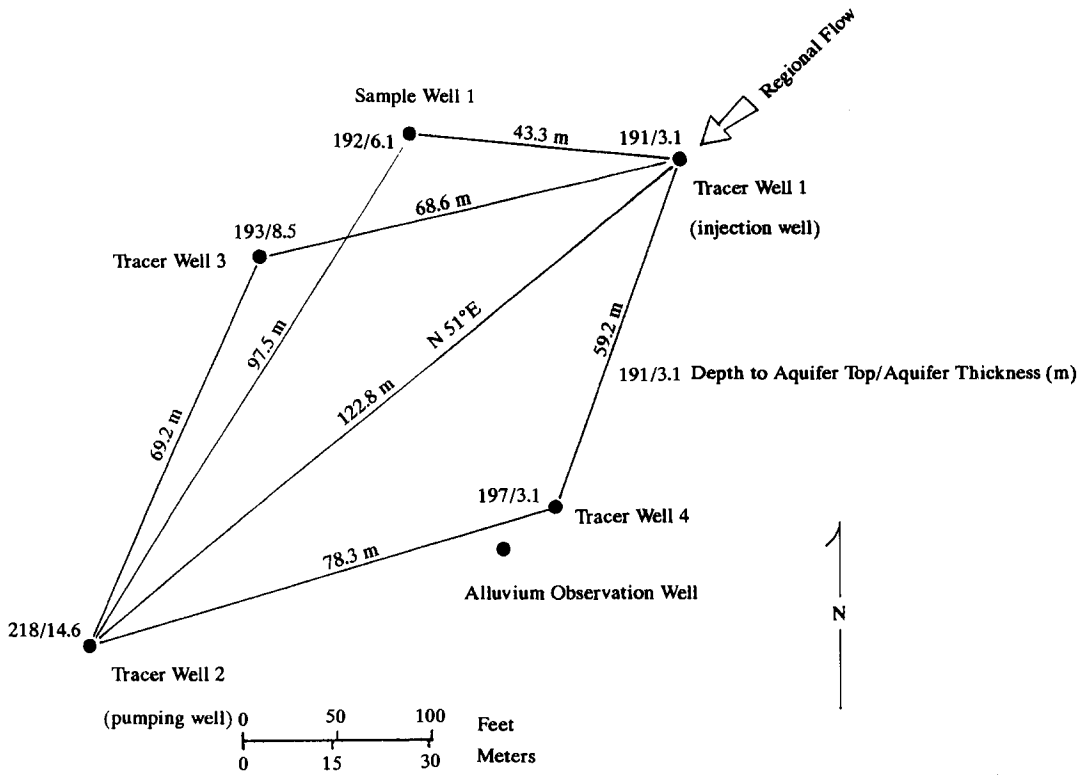

Fig. 1. Map showing locations of wells, aquifer depths, and aquifer thicknesses at the Tracer Site (after Leap and Belmonte, 1992).

Basic Theory

Retardation

Retardation of a dissolved chemical tracer species is due to sorption, chemical reactions with porous media or fracture walls, and movement into dead-end pores by diffusion. As a result, the tracer mass will not move as fast as the average advective velocity of ground water which carries it. The retardation coefficient in porous media is expressed as (Freeze and Cherry, 1979; Prickett et al., 1981)

$$R_d = \frac{v}{v_c} \tag{1}$$

$$R_d = 1 + \frac{\rho_b K_d}{n} \tag{2}$$

and in fractured media (Burkholder, 1976) as

$$R_d = 1 + AK_a \tag{3}$$

where v = average ground-water velocity; v_c = average velocity of the tracer mass; ρ_b = bulk mass density of the porous medium; n = effective porosity; K_d = distribution coefficient of the porous medium; K_a = fractured-rock distribution coefficient; and A = ratio of fracture-wall surface area to void space (volume).

In a normalized breakthrough curve of a tracer with a constant-concentration source, v_c is the velocity of the point where $C/C_o = 0.5$ on the breakthrough-curve front (Figure 2). In a normalized breakthrough curve resulting from a rectangular pulse source (constant concentration over finite injection time), v_c is the velocity of the center of mass of the pulse as shown in Figure 3.

Equations (1)-(3) could not be used to analyze the results of this experiment because (1) it was impossible to accurately assess A, K_d, K_a, or ρ_b; and (2) the recycled pulses of tracers made the curve tails too high and long to obtain a center of mass. The apparent retardation of bromide, relative to that of tritium (Apparent Relative Retardation) had to be estimated by another method developed

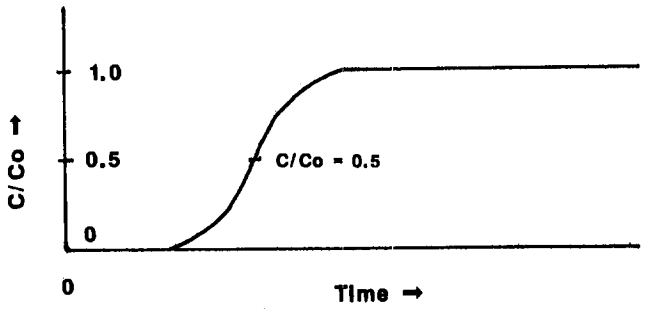

Fig. 2. Normalized breakthrough curve resulting from transport of a tracer from a constant-concentration source.

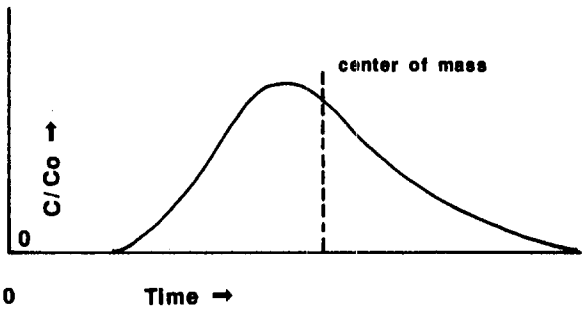

Fig. 3. Normalized breakthrough curve resulting from transport of a tracer from a rectangular-pulse source.

below—the Cumulative Relative Mass-Time (CRMT) method. The modifier, "Apparent," is used because in the absence of absolute retardation coefficients, what may appear to be differences in retardation of two tracers may be partly due to their different anionic exclusion rates as well as actual retardation.

Computing Relative Retardation by the Cumulative Relative Mass-Time Method

The mass-time area under the breakthrough curve between two sampling times (t_{i-1} and t_i) can be computed as

$$a_i = \int_{t_{i-1}}^{t_i} (r_i t + b)dt \tag{4}$$

where $i \geq 2$; r_i = slope of the curve between two consecutive sampling times, i.e.,

$$r_i = \frac{(m_i - m_{i-1})}{(t_i - t_{i-1})} \tag{5}$$

assuming a linear change in mass per unit time between closely spaced sampling points; b = intercept of the curve; N = total number of sampling times; $t_1 = 0$, i.e., the first or zero sampling time; t_N = last sampling time; and m_i = mass detected in one unit volume (i.e., concentration at sampling time, i).

Evaluation of the integral yields

$$a_i = (\frac{r_i}{2})(t_i - t_{i-1})^2 + b(t_i - t_{i-1}) \tag{6}$$

The sum of the mass-time increments, or Cumulative Area of Mass-Time (CAMT) from the beginning of the curve to any subsequent sampling time is given by

$$CAMT_k = \sum_2^k a_i \tag{7}$$

where $k \leq N$.

$CAMT_k$ can be normalized to obtain the dimensionless Cumulative Relative Mass-Time (CRMT), as shown

$$CRMT_k = \frac{CAMT_k}{(C_o \times T_o)} \tag{8}$$

where C_o = original concentration of initial pulse, and T_o = time duration of the initial-pulse injection; or

$$CRMT_k = \frac{\sum_2^k a_i}{(C_o \times T_o)} \tag{9}$$

The difference, $DIFF_i$, between the CRMT curves of tritium and bromide at any sampling time, t_i, is simply

$$DIFF_i = CRMT(T)_i - CRMT(Br)_i \tag{10}$$

This number is used to observe subtle differences between CRMT values of two different tracers which may not be readily apparent visually when plotted on a logarithmic scale due to compression of the vertical axis.

The Apparent Relative Retardation Coefficient, ARR_d, of bromide (relative to tritium) up to a certain sampling-time point, k, is found by

$$ARR_{dk} = \frac{CRMT(T)_k}{CRMT(Br)_k} \tag{11}$$

If $ARR_{dk} > 1.0$, bromide is retarded relative to tritium; if $ARR_{dk} < 1.0$, tritium is retarded relative to bromide; if $ARR_{dk} = 1.0$, neither is retarded relative to the other.

Determining an absolute retardation coefficient of a particular tracer (a unique R_d) is not possible with this method in the case of recirculation, because a unique center of mass of the breakthrough curve is not obtainable. In the absence of recirculation, the center of mass for a discrete pulse would simply be the point on the breakthrough curve corresponding to $CRMT_N/2$, assuming $CRMT_N$ were computed for the entire pulse breakthrough curve.

Factors and Processes Affecting Relative Retardation in Dolomite

(A) Anionic Exclusion

Clays, because of their negatively charged surfaces, tend to anionically exclude negatively charged halide ions (Bolt et al., 1978; Wierenga and Van Genuchten, 1989). This process would be expected to be most significant in low-transmissivity zones and clay-rich pores. Anionic exclusion would cause some bromide to move faster than normal through water, and faster than tritium, to produce a lower apparent relative retardation of bromide with respect to tritium.

(B) Molecular Diffusion

Tritium diffuses through normal water as tritiated water (HTO), with a molecular weight of approximately 20, and a diffusion coefficient at 25°C, variously reported in 10^{-5} cm^2/sec as ranging from 2.25 (Devell, 1962), to 2.44 (Wang et al., 1953).

Ammonium bromide diffuses through water as an ion pair such as (NH_4^+-Br^-) as required to maintain electroneutrality. The molecular weight of NH_4Br is approximately 98, or 4.9 times that of tritiated water. The diffusion coefficient of NH_4Br at 25°C is calculated from Cussler (1984) to be 2.02×10^{-5} cm^2/sec, or 0.90 to 0.83 times that of HTO.

Although the values of the diffusion coefficients of HTO and NH_4Br for a purely aqueous phase do not differ greatly, tritiated water will diffuse into small dead-end pores more readily than the larger and heavier (NH_4^+-Br^-) ion pair, under the same concentration gradient. The expected effect of greater tritium diffusion into dead-end pores would be increased actual tritium retardation and less apparent retardation of bromide relative to tritium in low-transmissivity zones, where more dead-end pores would be expected.

In flow through large conduits with minimal interaction of tritium and bromide with dead-end pores, clays, or conduit walls, tritium would be expected to move faster than bromide because of its lower molecular weight and higher diffusion coefficient, providing the concentration gradients were the same for both tracers. The expected effects would be lower actual retardation of both tracers, but increased

relative retardation of bromide with respect to tritium, as opposed to effects in less transmissive areas.

(C) Concentration Effects

In general, the higher the concentration, the greater will be the rate of anionic exclusion of bromide and diffusion of both species.

(D) Effects of Flow-Path Length

Increasing the flow-path length (which is affected by recirculation) will in general increase the effective surface upon which the above actual processes can take place.

In very long flow paths, within low-transmissivity media, one would expect the effects to include greater actual retardation of tritium by dead-end pore diffusion, with lesser retardation of bromide by dead-end pore diffusion with respect to tritium, but more anionic exclusion of bromide due to an increased ratio of residual clay volume to pore volume. As a result, the apparent relative retardation of bromide with respect to tritium should decrease. In open-conduit flow, long flow paths should allow more tritium diffusion in the direction of flow with greater apparent relative retardation of bromide with respect to tritium.

(E) Effects of Residence Time

In general, the effects of longer residence time of a tracer in the system is similar to those resulting from longer flow paths because it allows a tracer to be in contact with retarding media for longer periods.

Field Research Site and Experimental Setup

The field research was carried out at the U.S. Geological Survey's Amargosa Tracer Calibration Site (hereafter called the "Tracer Site") in the Amargosa Desert of southern Nevada, approximately 121 km northwest of Las Vegas, and 24 km southwest of Mercury (Leap and Belmonte, 1992). A two-well recirculating system was already installed at the site, consisting of an injection well, a pumping well, and four monitoring wells (Figure 1), denoted as follows: Tracer Well 1 (TW1), the injection well; Tracer Well 2 (TW2), the pumping well; and monitoring wells, Tracer Well 3 (TW3), Tracer Well 4 (TW4), Sample Well 1 (SW1); and the Alluvium Observation Well (AOW)—the latter was not used for the test. Samples were taken during the test from all the wells except TW1 and AOW.

The aquifer is a highly fractured and fissured zone confined within the dolomitic Cambrian Bonanza King formation. The thicknesses and the elevations of the top and bottom of the aquifer are shown in Figure 1. Thickness ranges from 3.1 m at TW1 and TW4 to 14.6 m at TW2.

Examination of drilling logs (Johnston, 1968) and cores (in the U.S. Geological Survey's core library at Mercury, Nevada) revealed fractures, vugs, and fissures ranging in width from less than one mm to 45 cm, with no preferred orientation. Borehole flowmeter tests precisely defined the top, bottom, and thicknesses of the permeable fractured and fissured zone constituting the aquifer.

A six-inch (15-cm) diameter PVC pipeline connected TW2 and TW1. A separate injection trailer positioned near TW1 contained a glove box and injection pump for injecting radioactive tracers into TW1. Bromide was injected from a mixing tank and pumped directly into the recirculating pipeline, 1.2 m upstream from TW1 (Leap and Belmonte, 1992).

The monitoring wells, TW3, TW4, and SW1, were each equipped with submersible pumps positioned midway between the top and bottom of the aquifer, which were connected to PVC sample-delivery lines. A delivery line was also connected to the recirculating pipeline near TW1 to retrieve samples of effluent from TW2 (Leap and Belmonte, 1992).

All delivery lines entered a sampling trailer where samples were periodically collected by automatic samplers. All pumps and samplers were activated to take samples automatically at preselected times. Travel times of samples from sampling pumps to samplers were negligible.

Description of Field Tracer Experiments

The recirculating system was started and allowed to run for three days before injection in order to check it for problems. At zero time, $t_1 = 0$, the beginning of tracer injection, tritium and bromide were injected as rectangular pulses (constant concentrations throughout finite injection times), essentially simultaneously with each other. Bromide was injected from a mixing tank containing 414 kg of ammonium bromide (NH_4Br) dissolved in 860 liters of water from the aquifer. The injection rate was such that the injection time period (T_o) lasted 15.6 minutes (0.011 day), to produce a rectangular pulse in the aquifer with an initial bromide concentration (C_o) of 20,425 mg/l.

Tritium injection began 40 seconds later and lasted for a T_o of 14.4 minutes (0.010 day). A total of 12.2 curies (Ci) of tritiated water in a volume of one liter was injected at such a rate as to produce a rectangular pulse entering the aquifer with a C_o of 0.797 μCi/ml. The 40-second time lag between injection start times of the two tracers was considered negligible.

The entire tracer test, running with an average recirculation rate of 15.5 l/s, lasted for 33.78 days, and samples were taken from TW2, TW3, TW4, and SW1 over the entire test period.

Frequency of Sample Analysis

Analyses of bromide and tritium were made of samples taken at the same times. Samples were taken more frequently before peak times, and less frequently afterward.

From TW2, 129 samples each of bromide and tritium were analyzed over a period of 33.78 days to give an average frequency of 3.8 samples per day. From the other three wells, 52 analyses were made each of bromide and tritium over 33.78 days to yield an average of 1.5 samples per day.

Each tritium concentration reported herein represents the average of five separate analyses with an analytical error generally between 1 and 2.5 percent. The analytical error of bromide concentrations from five separate analyses ranged between 1 and 1.75 percent. These errors were not great enough to cause any significant effects upon the calculated DIFF and ARR_d curves below.

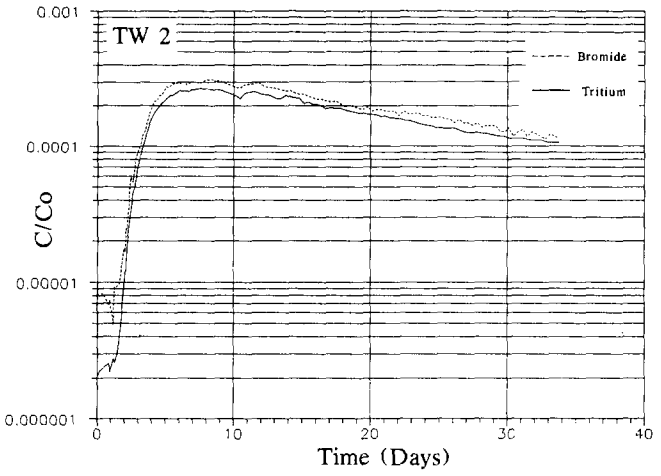

Fig. 4a. Tritium and bromide breakthrough curves from TW2.

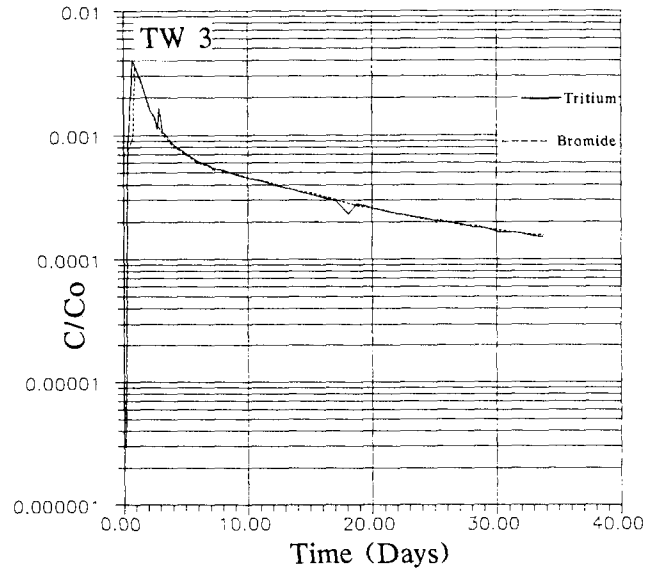

Fig. 4b. Tritium and bromide breakthrough curves from TW3.

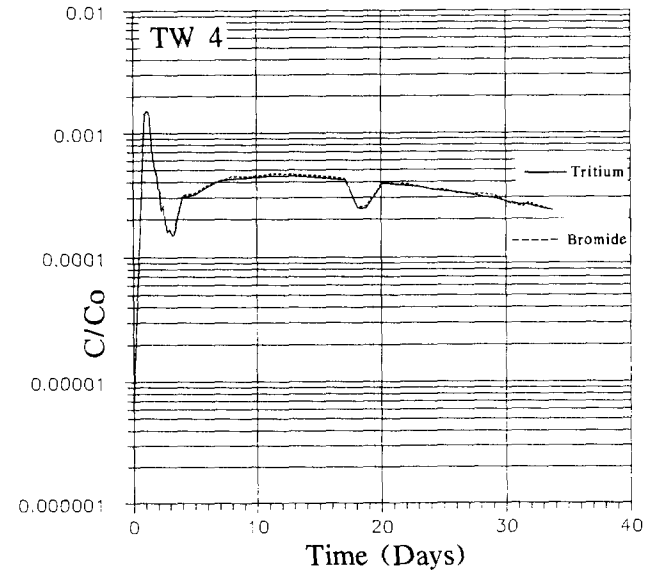

Fig. 4c. Tritium and bromide breakthrough curves from TW4.

Results and Discussion of Data Analysis

Visual Inspection of Breakthrough Curves

Normalized breakthrough curves (C/C_o) of both tritium and bromide were constructed from sample analyses from all four sampled wells. Figures 4 (a, b, c, and d) show the curves from TW2, TW3, TW4, and SW1, respectively. Arrival times of breakthrough-curve peaks are summarized in Table 1. All curves show the effects of recirculation, i.e., the falling limbs or tails of the curves do not drop as fast as one would expect in the case of a dispersed finite tracer pulse without recirculation.

At TW2, both tritium and bromide curves peaked at 8.03 days and the curves show recirculation beginning at approximately 10.44 days, as evidenced by dips in both curves, but later recirculated pulses are impossible to ascertain. The particular curve shapes (long drawn-out tails), and order-of-magnitude dilution when compared to curves from other wells described below, are due to the wider total area of flow of tracer-spiked water to TW2, mass loss, and the introduction of unspiked water by TW2 to the spiked mass (Figure 5).

The tritium and bromide breakthrough curves from TW2 were analyzed by the method of Grove (1971) to estimate values of average aquifer porosity of 10 percent, longitudinal dispersivity of 27.4 m using the tritium curve, and 30.3 m using bromide (Leap and Belmonte, 1992). Only at TW2 was the normalized concentration of bromide consistently higher than that of tritium. Both the higher concentration and higher dispersivity of bromide is due to greater apparent retardation of tritium relative to bromide at TW2, as explained later. The ratio of bromide dispersivity to tritium dispersivity was 1.1, which is very close to the ratio of chloride dispersivity to tritium dispersivity of 1.09 reported by Wierenga and Van Genuchten (1989).

Wells SW1 and TW3 are on the same side of the flow system, in the thicker, more transmissive part of the aquifer, but TW4 is on the opposite side in the thinner, less transmissive part (Figure 1). Bromide and tritium curves from these three wells lie on top of each other.

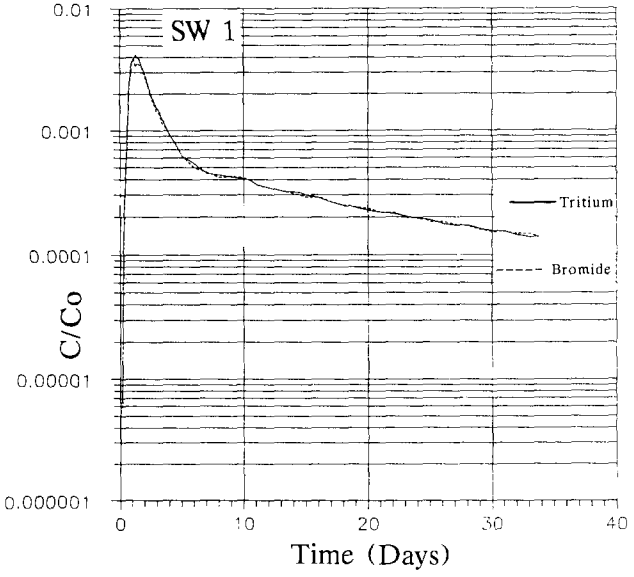

Fig. 4d. Tritium and bromide breakthrough curves from SW1.

Table 1. Summary of CRMT, DIFF, and ARR_d Data at Selected Times from Each Well Sampled

Well	*Sampling times (in days)*		*CRMT(T)*	*CRMT(Br)*	*DIFF*	*ARR_d*	*Distance from TW1 (in m)*
TW2	peak	8.03	0.11035	0.11488	−0.00453	0.961	122.8
	(both)	10.19	0.16437	0.17159	−0.00722	0.958	
		20.11	0.37161	0.37846	−0.00685	0.982	
		30.11	0.50896	0.51588	−0.00662	0.987	
	last	33.78	0.54867	0.55341	−0.00400	0.991	
TW3	peak(T)	0.78	0.10587	0.03738	0.06849	2.832	68.6
	peak(Br)	0.94	0.16761	0.07016	0.09746	2.389	
		10.44	1.07020	0.86605	0.20415	1.236	
		20.11	1.38630	1.15730	0.22900	1.198	
		30.11	1.58910	1.33940	0.24970	1.186	
	last	33.78	1.64620	1.39130	0.25490	1.183	
TW4	peak(T)	1.28	0.08691	0.07886	0.00805	1.102	59.2
	peak(Br)	1.11	0.06140	0.05581	0.00559	1.100	
		10.44	0.42978	0.39399	0.03579	1.091	
		20.11	0.80642	0.74430	0.06212	1.084	
		30.11	1.13720	1.04700	0.09020	1.086	
	last	33.78	1.22840	1.12900	0.09940	1.088	
SW1	peak(T)	1.28	0.23976	0.20337	0.03639	1.179	43.3
	peak(Br)	1.11	0.17167	0.14720	0.02447	1.166	
		10.44	1.15270	0.99507	0.15763	1.158	
		20.11	1.42870	1.24670	0.18200	1.146	
		30.11	1.60860	1.41220	0.19640	1.139	
	last	33.78	1.65960	1.46000	0.19960	1.137	

At SW1, tritium peaked at 1.28 days, 0.17 days behind the bromide peak at 1.11 days. Recirculation appears to have begun between 5 and 6 days at SW1, and between 6 and 7 days at TW3, as evidenced by rather sudden changes in curve slopes. Tritium peaked at TW3 at 0.78 days, and bromide at 0.94 days (a difference of 0.16 days).

The TW4 curve shows a tritium peak at 1.28 days, 0.17 days behind the bromide peak at 1.11 days. One pulse began almost immediately, and two recirculated pulses came through afterward—one began at 3.2 and the other at 18.1 days, respectively.

TW3 is 25.3 m further from TW1 than is SW1 (Figure 1 and Table 1). Yet, peaks of tritium and bromide arrived at TW3 at 0.5 and 0.17 days, respectively, earlier than at SW1 because of a more permeable pathway between TW1 and TW3 than between TW1 and SW1. Peak arrival times at TW4 were the same as those at SW1 which is 15.9 m closer to the injection well (TW1).

It is important to note that only at TW3 did tritium peak before bromide. This phenomenon, as explained later, is believed to suggest that the more open pathway to TW3 caused increased relative retardation of bromide with respect to tritium because of less actual retardation of and perhaps more diffusion of tritium along the path to TW3. Such is not the case in other wells located in less transmissive flow paths.

Cumulative Relative Mass-Time and Relative Retardation Data

Computed values of CRMT and DIFF are shown graphically in Figures 6 (a, b, c, and d) for TW2, TW3, TW4, and SW1, respectively. Figure 7 shows ARR_d curves from all four wells. Table 1 summarizes the data at selected sampling times.

As in the case of the breakthrough curves, tritium and bromide CRMT curves are nearly parallel in all cases. This closeness belies small and subtle differences between the CRMT's of both tracers plotted on a logarithmic scale, which compresses deviations between the curves. Therefore, one must examine the DIFF curve for each tritium-bromide pair to notice the true differences between the CRMT curves

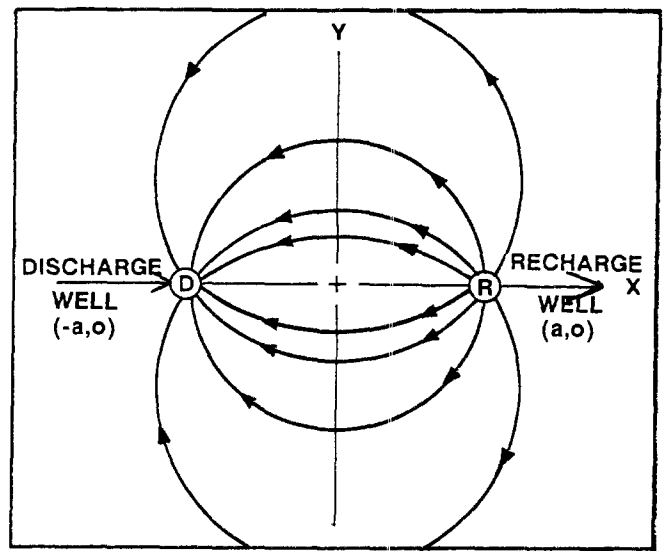

Fig. 5. Generalized ground-water flow system of a homogeneous, isotropic aquifer during a two-well recirculating tracer test (after Grove and Beetem, 1971).

of each. In all curves except those from TW2, CRMT(T) > CRMT(Br).

A DIFF curve is not shown for TW2 because CRMT(Br) is greater than CRMT(T) after the peak time, due to higher normalized concentrations of bromide than of tritium over time, resulting from slight retardation of tritium with respect to bromide and ionic exclusion of bromide during transport through generally less transmissive pathways to that well. Thus, equation (10) yields negative values for DIFF, which cannot be shown on a logarithmic scale. Table 1 lists negative DIFF values from TW2 for selected times.

In all cases, the CRMT and DIFF curves from TW3 and SW1 are generally smooth and gradually increase after peak arrival times. Both CRMT and DIFF curves for TW4 show distinct perturbations beginning at the same time as the trough between the breakthrough-curve peaks and the first recirculated pulse. CRMT curves from TW2 also increase smoothly, but the DIFF values (Table 1) show very small differences between them (not exceeding −0.00722). The absolute value of this number is less than those from the other wells.

Table 1 shows that except for TW4, the CRMT values of both tracers decreased with increasing distance from TW1 (the injection well). The distance from TW1 to TW4 is between that from TW1 to SW1, and TW1 to TW3, and the CRMT values of TW4 are lower than those of either of the other two wells.

This was due to the fact that longer flow distances allowed concentrations to be lowered by more retardation and dilution. This was also pronounced in TW4 because of low transmissivity. Recirculation also added the factors of irretrievable mass loss and dilution, decreasing the concentration.

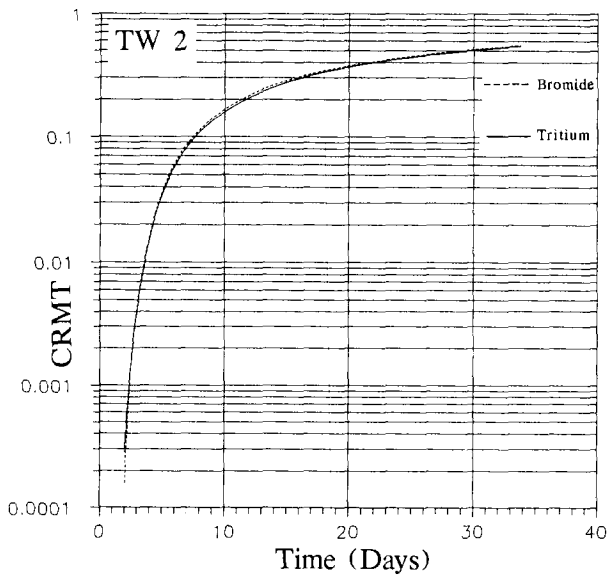

Fig. 6a. CRMT curve from TW2.

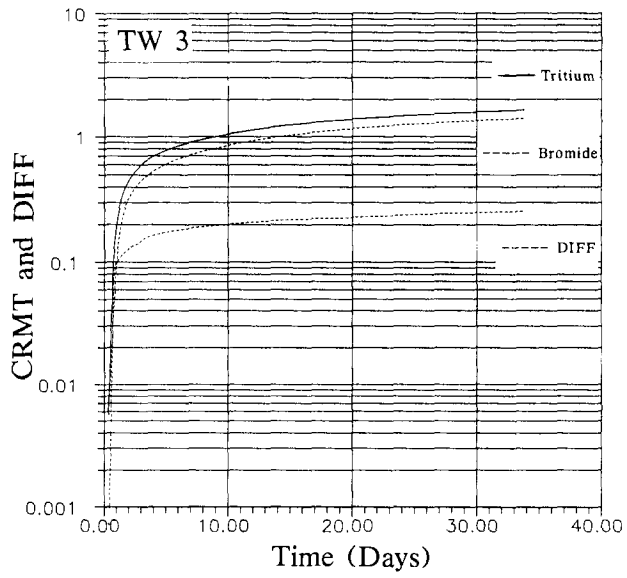

Fig. 6b. CRMT and DIFF curves from TW3.

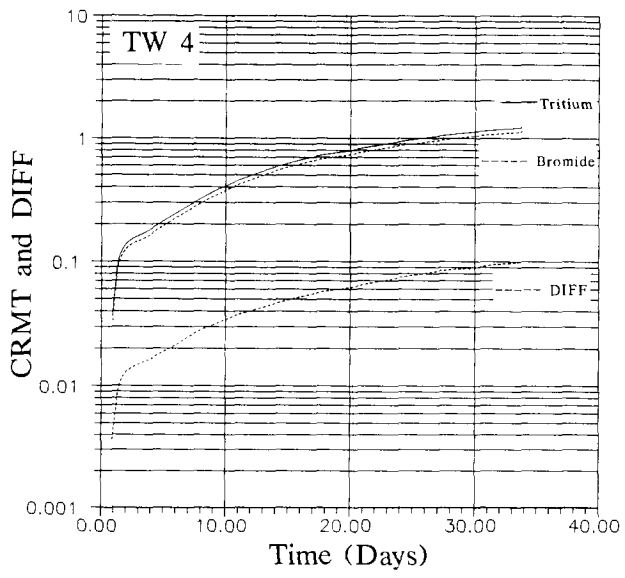

Fig. 6c. CRMT and DIFF curves from TW4.

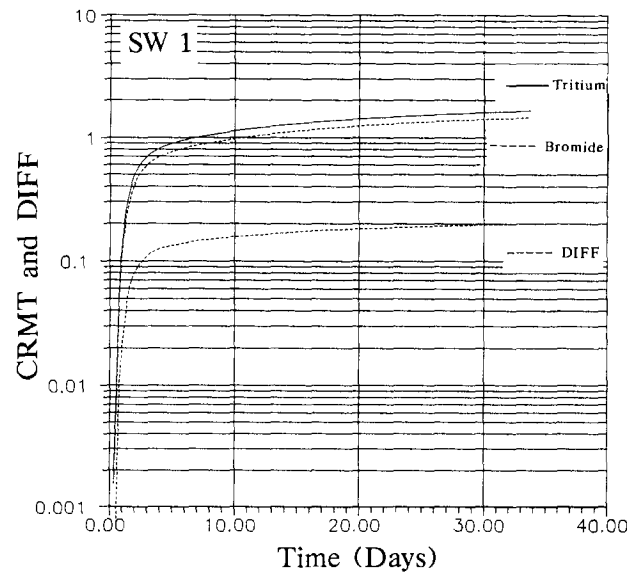

Fig. 6d. CRMT and DIFF curves from SW1.

ARR_d values after peak times, from highest to lowest, are found in the following order: TW3, SW1, TW4, and TW2 (Figure 7 and Table 1). ARR_d values from the first three wells are always greater than 1.0, and decrease in value after peak times, but the ARR_d curve of TW2 increases after the peak time and remains less than 1.0. From Figure 7 and Table 1, it is apparent that with the exception of TW3, ARR_d values decrease in general with increasing distance from the injection well (TW1).

After peak times, in flow to TW3, TW4, and SW1, bromide was apparently relatively retarded over time more than tritium, but at a decreasing rate, because at first, tritium was more mobile than bromide, but over time, tritium retardation and anionic exclusion of bromide decreased the rate. On the other hand, in flow to TW2, tritium was relatively retarded by an amount slightly greater than that of bromide, but bromide continued to be retarded at a slightly greater rate relative to that of tritium because the tritium concentration had become low enough that its retardation rate slowed to slighly less than the rate of bromide. These explanations are evidenced by the decreasing ARR_d curves over time from TW3, SW1, and TW4; and increase with time in the curve from TW2.

This argument is strengthened by study of Figures 6 (a, b, c, and d) and equation (11), from which it can be deduced that decreasing values of ARR_d from TW3, TW4, and SW1 over time could only be due to a decreasing **rate** of increase of CRMT(T) with respect to the **rate** of increase of CRMT(Br), i.e.,

$$\frac{\partial^2 CRMT(T)}{\partial t^2} < \frac{\partial^2 CRMT(Br)}{\partial t^2} \qquad (12)$$

This is because neither the rate of increase of CRMT(T) nor that of CRMT(Br) could have increased over time unless one appeals to some hitherto unknown and unobserved process of desorption and/or deretardation which would not have been likely to occur because of fairly constant values of pH and temperature during the test.

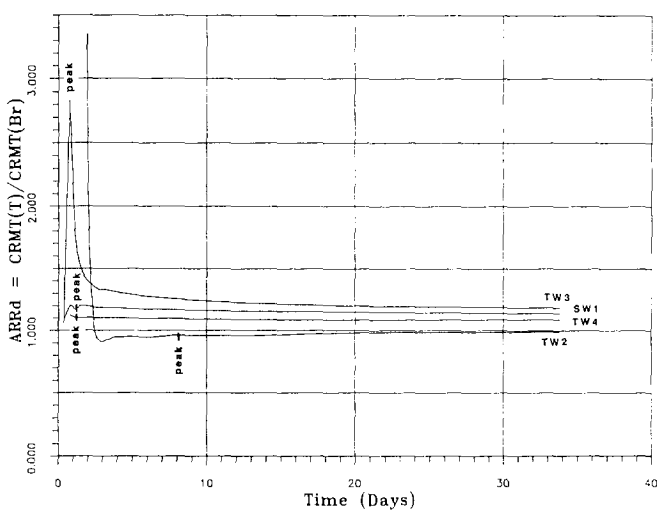

Fig. 7. ARR_d curves from TW2, TW3, TW4, and SW1.

Bromide concentration was also an order of magnitude less at TW2 than at other wells; yet, the increase in the ARR_d curve at TW2 toward a value of unity indicates that the rate of tritium retardation was continuing to decrease relative to the rate of bromide retardation, even though tritium was still more retarded than bromide.

This behavior at TW2, very different than at the other wells, was due to an order-of-magnitude dilution below that at the other wells. This in turn was caused by pumping unspiked water at TW2, a wider area of flow to TW2 through less transmissive media, and injection of mass out of the system at TW1. As a result, there was greater opportunity for greater relative apparent retardation of tritium with respect to bromide than at the other wells.

Suitability of Bromide as a Tritium Surrogate

From the previous discussions, it is apparent that bromide is a better surrogate for tritium (i.e., bromide behaves more like tritium) in lower transmissivity diffuse flow (as at TW2 and TW4) than in flow in more transmissive media in dolomite. This is because tritium is actually retarded more in diffuse flow and therefore, relative retardation of bromide is less than in more transmissive flow (as at TW3 and SW1). Flow-path length and residence time do not appear to be as important in higher transmissivity flow as they are in lower transmissivity flow.

The ARR_d values do not appear large enough to rule out bromide as a general tritium surrogate in either flow environment because of (1) the generally low relative retardation of bromide, and (2) the small change in ARR_d values from all wells over the last 30 days of the test. In fact, this argument suggests that bromide may be a more suitable tracer than tritium in dolomite of widely varying transmissivity over a long time because bromide appears to be less sensitive to variations in concentration, residence time, flow-path length and transmissivity. This recommendation may seem contrary to the suggestion of Wierenga and Van Genuchten (1989), that chloride and bromide may not be the best tracers in sandy soil, but this research has shown that in low-transmissivity dolomite, bromide behaves essentially like tritium.

Conclusions

Using two tracers simultaneously revealed properties of apparent relative retardation not discernible with only one. From the results of this research, the following conclusions are evident as answers to the five original questions in the "Introduction."

1. Neither tritium nor bromide are completely conservative tracers in fissured and fractured dolomite, but tritium can be relatively retarded very slightly with respect to bromide at very low normalized concentrations (at or less than 3×10^{-4}). At higher normalized concentrations (from 3×10^{-4} to 3×10^{-3}), tritium was relatively less retarded than bromide, but the rate of apparent relative bromide retardation decreased over time.

2. Tritium is retarded more readily than bromide when flowing through low-transmissivity dolomitic media with large total surface area, such as sets of microfractures, vugs,

and other pores which produce diffuse flow and dead-end porosity, but it was apparently relatively less retarded than bromide in more transmissive open fractures and fissures, perhaps due in part to greater tritium mobility in these zones than in the less transmissive zones. Bromide retardation did not appear to vary as much as tritium retardation with changes in transmissivity.

3. The apparent relative retardation coefficient of bromide with respect to tritium changed no more than a few hundredths over 30 days after peak arrival at any well.

4. Retardation was also exacerbated by increasing flow-path length because the longer the path, the greater was the rock-fracture surface area in contact with the water to provide surface for retardation. Therefore, similar tests performed on longer scale systems would be likely to yield greater retardation values.

5. In general, differences in apparent relative retardation were so slight that bromide can indeed be considered a suitable surrogate for tritium in tracing ground-water flow in fractured and fissured dolomite, in diffuse and/or open-conduit flow. Bromide may actually be a better tracer than tritium in a widely varying flow environment.

Acknowledgments

The author wishes to thank the following for their assistance: The U.S. Geological Survey: Ren Jen Sun, Hans Claassen, Bert Wier, Wayne Everett, James Nelson, William Smith, Charles Washington, and Leonard Wollitz, for technical and field assistance; Vic Janzer, Leroy Schroeder, and Doug Manigold, for liquid-scintillation analysis. The Pennsylvania State University, School of Nuclear Engineering: William Jester and Dale Raupach, for neutron-activation analysis. Purdue University, Department of Earth and Atmospheric Sciences: Pam Mai Belmonte, for data analysis; William R. Smith, for help with data plotting; and Steven J. Fritz for careful peer review of the manuscript.

The support of the Water Resources Division of the U.S. Geological Survey (with funding from the U.S. Department of Energy), and its permission to publish the paper are gratefully acknowledged.

"Contents of this publication do not necessarily reflect the views and policies of the U.S. Department of the Interior, nor does mention of trade names or commercial products constitute their endorsement by the U.S. Government."

References

Bolt, G. H., M.G.M. Bruggenwert, and A. Kamphorst. 1978. Adsorption of cations by soil. In: Soil Chemistry, A. Basic Elements, Chapt. 4, G. H. Bolt and M.G.M. Bruggenwert (eds.). Elsevier Inc., New York. 281 pp.

Burkholder, H. C. 1976. Methods and data for predicting nuclide migration in geologic media. In: Proceedings of International Symposium, Management of Wastes from the LWR Fuel Cycle, Denver, CO.

Clayton, C. G. and D. B. Smith. 1963. A comparison of radioactive methods for river-flow measurement. In: Proceedings of International Symposium, Applications of Radioisotopes in Hydrology. International Atomic Energy Agency, Vienna. pp. 1-24.

Cussler, E. L. 1984. Diffusion: Mass Transfer in Fluid Systems. Cambridge University Press, New York. 525 pp.

Devell, L. 1962. Measurements of the self-diffusion of water in pure water, H_2O-D_2O mixtures and solutions of electrolytes. Acta Chemica Scandinavica. v. 16, no. 9, pp. 2177-2188.

Freeze, R. A. and J. A. Cherry. 1979. Groundwater. Prentice-Hall, Inc. 604 pp.

Grove, D. B. 1971. An analysis of the flow field of a discharging-recharging pair of wells. U.S. Geological Survey Report 474-99. Springfield, VA. 56 pp.

Grove D. B. and W. A. Beetem. 1971. Porosity and dispersion-constant calculations for a fractured carbonate aquifer using the two-well tracer method. Water Resources Research. v. 7, no. 1, pp. 128-134.

Hamill, L. 1980. A note on the performance of a bromide-82 radioactive tracer in the River Skerne, England. Journal of Hydrology. v. 47, no. 314, pp. 307-315.

Jester, W. A. and K. A. Uhler. 1974. Identification and evaluation of water tracers amenable to post-sampling neutron activation analysis. Pennsylvania State Univ. Research Publication 85. 92 pp.

Johnston, R. H. 1968. U.S. Geological Survey tracer study, Amargosa Desert, Nye County, Nevada, Part I: Exploratory drilling, tracer-well construction and testing, and preliminary findings. U.S. Geological Survey Open-File Report. 64 pp.

Leap, D. I. and P. M. Belmonte. 1992. Influence of pore pressure on apparent dispersivity of a fissured dolomitic aquifer. Ground Water. v. 30, no. 1, pp. 87-95.

Mann, W. B., M. P. Urterweger, and B. M. Coursey. 1982. Comments on the NBS tritiated-water standards and their use. Int. J. Appl. Radiat. Isot. v. 33, pp. 383-386.

Miettinen, J. K. 1978. Transfer and uptake mechanism of tritium in soil. In: Proceedings of International Symposium, Behavior of Tritium in the Environment. International Atomic Energy Agency, San Francisco. pp. 339-347.

Moreno, L. and I. Neretnieks. 1985. Analysis of some laboratory tracer runs in natural fissures. Water Resources Research. v. 21, no. 7, pp. 951-958.

Murray, J. P., J. V. Rouse, and A. B. Carpenter. 1981. Groundwater contamination by sanitary landfill leachate and domestic wastewater in carbonate terrain: Principal source diagnosis, chemical transport characteristics and design implications. Water Research. v. 15, pp. 745-757.

Payne, B. R. 1968. Flow through fractures and tubular openings. In: Guidebook on Nuclear Techniques in Hydrology. International Atomic Energy Agency, Vienna. Technical Report Series. no. 91, pp. 197-201.

Payne, B. R. 1988. Status of isotope hydrology today. Journal of Hydrology. v. 100, no. 1/3, pp. 207-237.

Prickett, T. A., T. G. Naymik, and Carl G. Lonnquist. 1981. A "random-walk" solute transport model for selected groundwater quality evaluations. Illinois State Water Survey, Champaign, IL. Bulletin 65.

Schmotzer, J. K., W. A. Jester, and R. R. Parizek. 1973. Groundwater tracing with post-sampling activation analysis. Journal of Hydrology. v. 20, no. 3, pp. 217-236.

Smith, S. J. and R. J. Davis. 1974. Relative movement of bromide and nitrate through soils. Journal of Environmental Quality. v. 3, no. 2, pp. 152-155.

Tennyson, L. C. and C. D. Settergren. 1980. Percolate water and bromide movement in the root zone of effluent irrigation sites. Water Resources Bulletin. v. 16, no. 3.

Wang, J. H., C. V. Robinson, and I. S. Edelman. 1953. Self diffusion and structure of liquid water. III: Measurement of the self diffusion of liquid water with ^2H, ^3H and ^{18}O as tracers. Journal of the American Chemical Society. v. 75, pp. 466-470.

Wierenga, P. J. and M. Th. Van Genuchten. 1989. Solute transport through small and large unsaturated soil columns. Ground Water. v. 27, no. 1, pp. 35-42.

Aquifer Analysis and Modeling in a Fractured, Heterogeneous Medium

by R. R. Lee[a], R. H. Ketelle[a], J. M. Bownds[a], and T. A. Rizk[b]

Abstract

A ground-water flow and contaminant transport modeling study was performed at a proposed low-level radioactive waste disposal site on the Department of Energy's Oak Ridge Reservation to assess the accuracy of a computer simulation of the flow field in the shallow water-table aquifer. The migration of a ground-water tracer, under controlled field conditions, was used as a comparative benchmark of solute transport simulations assuming different aquifer characteristics. A conventional approach to aquifer analysis and modeling, which assumed the domain to be homogeneous with low anisotropy, resulted in an inaccurate simulation of tracer migration. Alternative conceptual models were formulated which considered the effects of geologic heterogeneities on tracer migration which could be verified by additional data acquisition and analysis. Application of the alternative concepts in numerical modeling resulted in more accurate simulations of tracer migration. These results suggested that local geology created discrete flow pathways oriented oblique to the maximum gradient which were unresolved in conventional aquifer analysis. Results of the study showed that standard approaches to aquifer analysis and computer modeling are crudely representative of the flow field and provide nonconservative estimates of contaminant transport at the scale of a waste disposal unit. By adopting an iterative approach to site characterization, conceptual model formulation, and numerical modeling, the level of resolution provided by a ground-water tracer was accurately simulated.

Introduction

In general, there is a need to calibrate/validate the results of ground-water flow and contaminant transport models with field data. In some relatively simple flow systems, this process may be straightforward; however, the reliability of simplistic flow and transport estimates decreases in relation to system complexities and spatial and temporal extrapolation beyond available site data for model calibration. To determine the level of data collection and analysis effort required to achieve a reasonably accurate computer simulation at a moderately complex site, a field and modeling study was performed. This paper describes the process used to calibrate a numerical ground-water flow and contaminant transport model. Through iterative conceptual model formulation and testing, model application, and field testing, numerical simulation results were obtained which accurately approximated the migration of a ground-water tracer.

Site Description

The study site is located in the Valley and Ridge Province of the southern Appalachians on the Department of Energy's Oak Ridge Reservation (Figure 1). The site encompasses about an acre of hillside terrain bordered on the southwest by a small perennial stream. Interbedded (about 1 m scale) limestone, siltstone, and shale lithologies of the Cambrian age Conasauga Group, Maryville Limestone underlie the site. The orientation of bedrock strike is N 55° E, and the rocks dip 45° SE, consistent with the regional structural setting. Fractures are ubiquitous, and soil is thin to essentially absent. Weathered bedrock (regolith) extends from just beneath the ground surface to depths ranging from about 3 to 10 m. The piezometric surface fluctuates approx-

[a]Energy Division, Oak Ridge National Laboratory, Oak Ridge, Tennessee 37831-6185.

[b]Tennessee Valley Authority Engineering Laboratory, Norris, Tennessee 37828.

Received November 1990, revised July and November 1991, January and March 1992, accepted April 1992.

Discussion open until January 1, 1993.

imately 0.3 to 1 m in response to normal seasonal precipitation, and is generally coincident with the bedrock weathering interface.

Site Characterization Methods and Interpretations

Geologic and hydrogeologic characterization studies included rock core drilling, lithologic and geophysical logging, construction of individual and cluster piezometers, discrete zone straddle packer testing, falling head testing, performance of two pumping tests drawing water from different aquifer zones, and continuous and periodic water-table monitoring. Aquifer tests were performed to depths of about 55 m. Drilling was performed by coring, augering, or rotary methods using low pressure water as the drilling fluid to reduce artificial fracture dilation.

Geologic Investigations

Rock coring was performed at four locations in the immediate site periphery from depths of 10 to 60 m to establish stratigraphic control and to perform straddle packer tests. Core hole locations are illustrated in Figure 1. Bedrock consisted of three irregularly interbedded lithologic units of about 1 m thickness each. Two units consisted of relatively homogeneous limestone and shale, and the third unit consisted of calcareous siltstone with planar to wavy laminated, coalesced lenses of silty limestone or 2 to 5 cm thick limestone beds. Lithologic correlations, in some cases to the bedding plane level of resolution, indicated overall lateral continuity, particularly of the shale units, with minor lateral character change in the limestone units. With the exception of a limited zone of intense deformation, on-site bedrock attitude was uniformly 45° SE. While bedding plane fractures were presumed to be laterally extensive, joints and fractures which crossed lithologies generally did not penetrate adjacent lithologies. Such joints and fractures were generally separable into two strike and two dip sets. Occasional vertically extensive fractures (as much as about 15 cm long) were filled with calcite. Fracture density ranged from about 15 to 30 fractures/m, occurring more frequently in heterogeneous, thin-bedded lithologies.

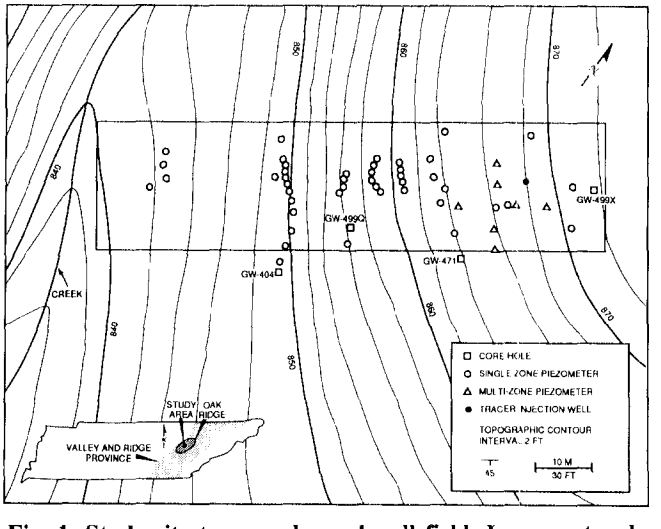

Fig. 1. Study site topography and well field. Large rectangle represents computational domain boundary.

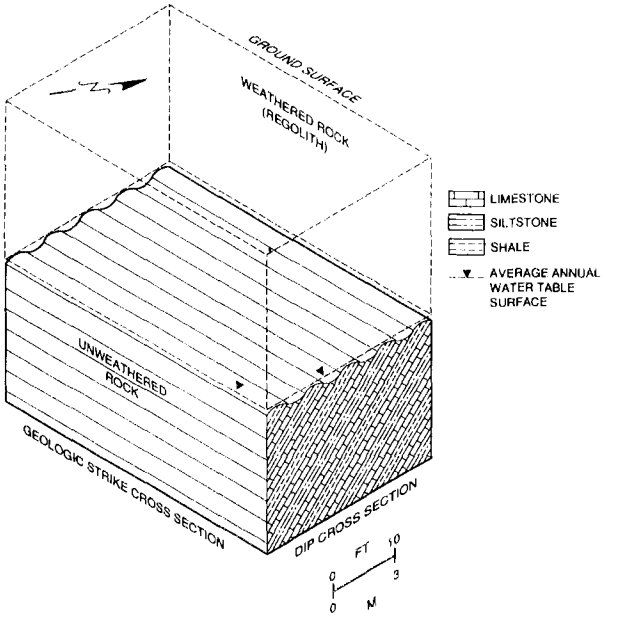

Fig. 2. Simplified block diagram of subsurface geology and piezometric surface.

Geophysical logs were obtained from each core hole to document stratigraphic control and for correlation with rock core. Such logs included natural gamma, neutron, neutron porosity, compensated density, density porosity, single point resistivity, long and short normal resistivity, and temperature. Logs were also used for comparison with results from straddle packer testing (discussion to follow) to investigate potential geophysical evidence of lithologic and/or fracture-related flow.

Depth to the bedrock weathering interface, based on the depth to machine auger refusal, was used for comparison with the rock core and geophysical log data to achieve more precise stratigraphic control. Auger refusal data indicated strike-normal relief on the bedrock weathering interface which was interpreted to be related to differential weathering of the approximately 1 m thick limestone and shale-dominated lithologic units. Figure 2 is a simplified block diagram depicting subsurface geologic conditions and the interpreted strike-normal corrugated aspect to the bedrock weathering interface. The average annual water-table surface is included for reference.

Hydrogeologic Investigations

Site hydrogeologic studies were performed to obtain both overall and discrete zone aquifer properties. Aquifer testing included pumping tests, straddle packer tests performed above and below the water table, slug tests, and the performance of a ground-water tracer test.

Pumping Tests

Two 24 hr pumping tests were performed in the shallow and deep portions of the aquifer (from nominal 6 to 33 m depths). Because previous pumping tests at Oak Ridge sug-

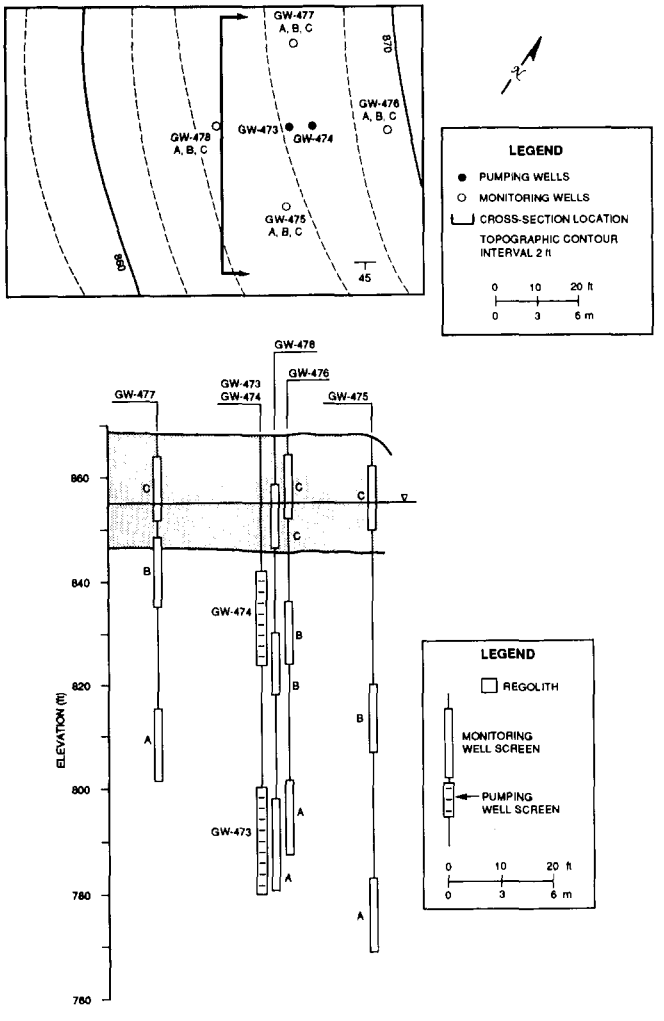

Fig. 3. Pumping test plan layout and stike-normal cross section.

gested aquifer anisotropy parallel to geologic strike (Davis et al., 1984; and Lozier et al., 1986), the plan view pumping test well field was oriented parallel and perpendicular to geologic strike. The plan and cross-sectional pumping test layout are shown in Figure 3. Each monitoring well cluster consisted of three wells. Shallow wells were located within the water table above the bedrock weathering interface. Intermediate and deep monitoring wells were located at different depths but in the same strata to investigate lithologic or structural influences on aquifer response to pumping. Shallow and deep pumping wells were located in the same strata as the intermediate and deep monitoring wells, respectively. Figure 4 illustrates the 24 hr drawdown isopleths for the shallow wells during the shallow pumping test as representative of both tests.

Pumping test data were analyzed for transmissivity and storage coefficient using the methods described by Chow (1952), Neuman (1975), and Theis (1935). Estimates of bulk hydraulic conductivity were obtained from the geometric mean of the transmissivity data assuming a 6 m aquifer thickness based on the pumping test setup. In general, the Theis and Neuman analytical methods provided slightly higher values of hydraulic conductivity (factor of 2 to 3). The geometric mean hydraulic conductivity value for the deep and shallow pumping tests was 1×10^{-5} and 7×10^{-5} cm/s, respectively, with both tests exhibiting a one order-of-magnitude range of values. These data suggested a weak relationship between hydraulic conductivity and depth.

The data were analyzed for aquifer anisotropy using the Gringarten and Witherspoon (1972) fractured aquifer solution and the Papadopulos (1965) infinite aquifer solution. In both analyses, the major and minor hydraulic conductivity axes were parallel and normal to bedding, respectively. Using iterative methods, the Gringarten and Witherspoon solution suggested an hydraulic conductivity anisotropy ratio of about 2:1 parallel to geologic strike. Parameters obtained from the Papadopulos solution using a nonlinear optimization technique (Crane et al., 1980) indicated an anisotropy ratio of 38:1 parallel to strike (Rizk, 1990). In similar settings at Oak Ridge, Davis et al. (1984) report an anisotropy value of about 4:1 parallel to strike, Smith and Vaughn (1985) obtained values of 5:1, and Geraghty and Miller (1990a) report an optimum value of 3:1 in model calibration. Use of the Papadopulos solution in the analysis of an NaCl tracer pumping test in the same stratigraphic unit but in another location at Oak Ridge yielded an average value of about 30:1 parallel to strike (Lozier et al., 1986).

Straddle Packer and Slug Tests

Slug tests were performed in 19 piezometers in the pumping test area at depths ranging from 5 to 26 m to obtain values of bulk hydraulic conductivity. Piezometer screen lengths ranged from 1.2 m in wells located near the water table to 4 m in deeper wells. Data were analyzed by the procedure described by Hvorslev (1951). Hydraulic conductivity values ranged from 2×10^{-4} to 8×10^{-7} cm/s with a geometric mean value of 1×10^{-5} cm/s. Values of hydraulic conductivity were not found to be related to screen length or well depth.

Two stages of straddle packer tests were performed, one before and one after the tracer test. In both stages of testing, correlative stratigraphic intervals in two core holes were tested. The first stage consisted of 19 tests performed to depths of 55 m using a 4 m interpacker spacing. These tests were performed to investigate relationships between values of hydraulic conductivity and depth, fracture density, and

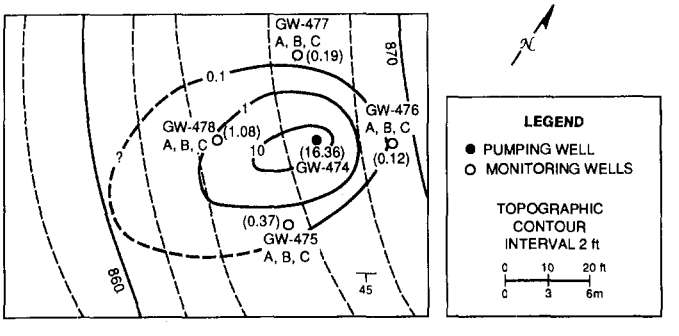

Fig. 4. Drawdown isopleths at completion of the 24 hr shallow pumping test.

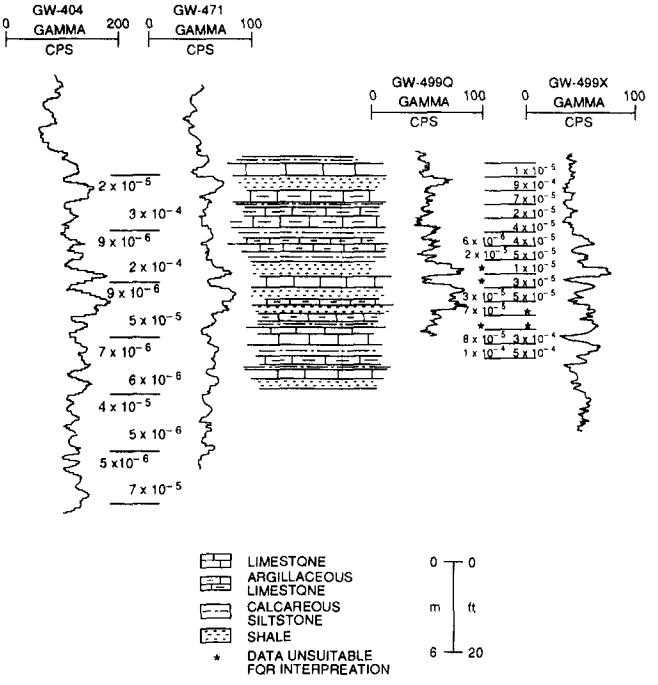

Fig. 5. 1 and 4 m straddle packer and falling head test results in correlative stratigraphic intervals.

geophysical evidence of flow and for comparison with test results from the pumping and slug tests. In the second stage, another 23 packer tests were performed in two additional core holes to depths of 14 m using a 1 m interpacker spacing. These tests, which included 10 falling head tests in the vadose zone (in regolith), were performed to investigate hypotheses relating values of hydraulic conductivity with lithology, test scale, test method, and weathered vs. unweathered bedrock.

The straddle packer test setup consisted of two inflatable packers with pressure transducers located between packers and above and below the straddle packer string. A predetermined interpacker spacing was set above ground. After positioning the packer string and inflating the packers at the designated core hole depth, water was removed from the interpacker space by swabbing. For the falling head tests, water was pumped through the drilling rods to a level close to ground surface. For all tests, care was taken to remove or introduce water to minimize alterations to natural formation properties.

Preliminary data analyses were performed on-site with portable computers, and reanalyses were performed in the office. Tests performed below the water table were analyzed by methods described by Horner (1951), Hvorslev (1951), and Gringarten et al. (1979). Falling head tests performed above the water table were analyzed by the methods described by Stephens and Neuman (1982a and 1982b) and Hvorslev (1951). Figure 5 shows lithologically correlated core hole natural gamma logs and straddle packer and falling head test hydraulic conductivity values from correlative test intervals for both the 4 and 1 m tests to depths of about 30 m.

Analysis of the test results revealed a weak relationship between values of hydraulic conductivity and test scale, fracture density, and/or depth, and no systematic relationship with lithology or test method. Hydraulic conductivity values from vadose zone falling head tests were indistinguishable from straddle packer tests performed below the water table. Qualitative predictions of the outcome of test results based on rock core and geophysical log data were reasonably accurate in about 25% of the tests. The geometric mean hydraulic conductivity value of the 4 m tests was 3×10^{-5} cm/s ranging from 3×10^{-4} to 3×10^{-6} cm/s. The geometric mean hydraulic conductivity value of the 1 m tests was 4×10^{-5} cm/s ranging from 9×10^{-4} to 6×10^{-6} cm/s. With the exception of one vadose zone test, values of hydraulic conductivity obtained from all test methods were within the range of values reported by Connell and Bailey (1989) for the Maryville Formation in Bear Creek Valley elsewhere at Oak Ridge.

Tracer Test

The tracer test was performed under ambient conditions (natural site gradient). Based on water elevation data from the pumping test cluster wells, additional tracer detection well clusters and single piezometers were constructed in the immediate vicinity, downgradient from the selected tracer injection well location. Well clusters were constructed similar to those for the pumping test, and single piezometers were constructed similar to the shallow wells in the pumping test clusters. Background wells were constructed to more accurately describe the piezometric surface and to define the tracer plume boundaries.

Following the removal of 10 l of water from the injection well, 10 l of 40% Rhodamine-WT dye solution was introduced to the upper 0.3 m of the water-table surface. As tracer migration progressed, 39 additional shallow detection wells were constructed in the shallow portion of the aquifer in front of the tracer plume to obtain tracer arrival data and to describe detailed plume evolution. To avoid disturbances to plume migration, drilling for the additional detection wells was performed by augering to the bedrock weathering interface, and the wells were not developed. Depending on sampling location and migration behavior, samples were obtained from between 8 hr and biweekly intervals and immediately following precipitation events. Biweekly water elevation data were obtained from all detection wells. Daily precipitation data were obtained from a nearby meteorological station. Tracer analysis at 1 ppb resolution was performed on-site using fluorimetric techniques.

Figure 6 illustrates the 10 ppb tracer concentration contour at three months superimposed on the piezometric surface described by shallow wells at locations shown. Because the piezometric surface in the immediate vicinity of the injection well on the day of injection was essentially the same as shown in Figure 6, tracer was anticipated to migrate along the maximum gradient. Instead, observed tracer migration was parallel to geologic strike in a narrow, slightly meandering, and fingering plume. This indicated the presence of flow field heterogeneities which were unresolved in the initial aquifer analysis. Local irregularities in the piezo-

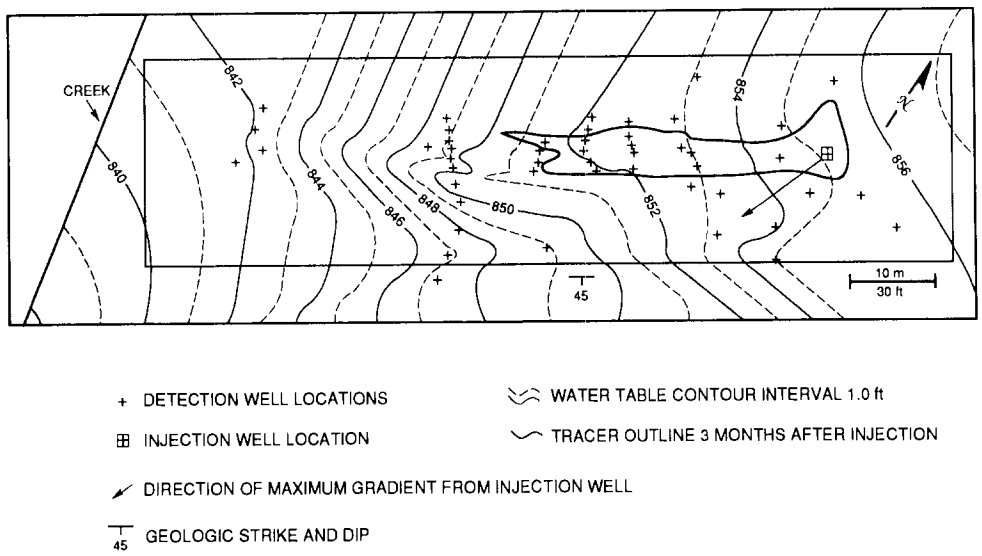

Fig. 6. 10 ppb tracer concentration contour three months after injection superimposed on water-table surface.

metric surface, which were considered artifacts prior to the tracer test and discounted, were found to strongly influence migration. These irregularities in the piezometric surface, strike-parallel ridges of elevated head, flanked the southern boundary of the tracer plume. Despite minor variations in the elevation of the piezometric surface throughout the year, its shape and the position of the plume with respect to the surface remained essentially unchanged.

Early time (one month) tracer migrated in a plume less than 2.5 m wide which reached a maximum width of 6 m after 12 months and a length:width aspect ratio of 7.5:1. Monitoring wells positioned across the plume axis, and sometimes less than 1 m apart, often showed two order-of-magnitude differences in tracer concentration. The tracer boundary was clearly defined; at peripheral locations, repeated concentrations of 10 ppb and less were outside the plume boundary.

In the first two weeks, a high concentration plume migrated as rapidly as 1.0 m/day for about 14 m in the near-field, but another 9 m of migration in the mid-field required an additional 230 days (0.04 m/day). Total migration distance of 33 m (the far-field) for the 100 ppb front required 370 days (0.09 m/day average). Data analysis could not attribute the erratic rate of migration to the presence of a concentration gradient induced by the slug dye injection, and no consistent correlation could be found with changes in the water-table gradient profile or with precipitation. Rather, the migration rate, narrow overall plume shape, and slightly meandering and fingering plume all suggested the presence of lithologic and/or fracture-related pathways of preferred flow.

Average vertical head gradients to depths of 20 to 30 m below ground surface in a hydrogeologic cross section oriented perpendicular to local geologic strike at the site are shown in Figure 7. As shown, the average vertical gradient at the site indicates upward leakage of ground water from deeper zones of elevated head toward the water-table surface. A similar cross section (not shown) oriented parallel to strike, and parallel to the tracer path, shows similar upward leakage conditions from the tracer injection point toward the local stream. The general upward vertical gradient observed at the site explains the observation of tracer only in

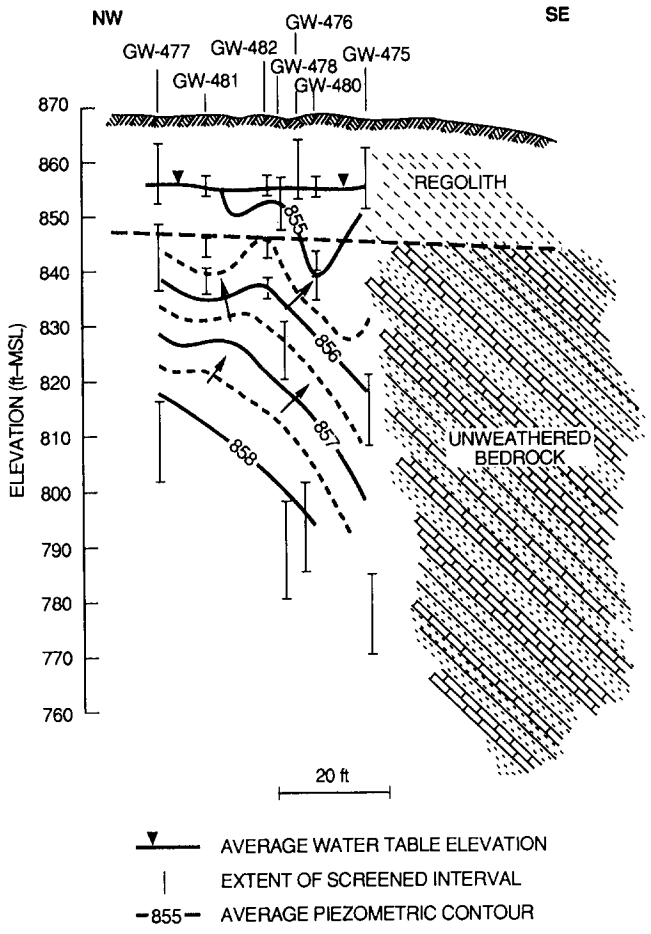

Fig. 7. Strike-normal cross section of the vertical head profile in the vicinity of the pumping test.

the water-table zone of the aquifer. Tracer was never detected at depth despite long-term monitoring at various depths in bedrock within the tracer pathway and in stratigraphically correlative core holes downdip and downslope of the tracer injection zone. Tracer detection and observed vertical gradients at the site demonstrate that neutral density solutes introduced at the water table mix in a thin zone below the water table and migrate through the bedding plane dominated fracture system. This thin mixing zone which is recharged by local precipitation infiltration from above and by upward leakage from below approximates a two-dimensional solute mixing domain.

Numerical Modeling

Because of the vertical head profile and tracer migration confined to the uppermost portions of the aquifer, the aquifer was assumed to be two-dimensional and of uniform thickness throughout. Because of low precipitation during the period of the test and negligible water-table variation, annual average values of hydraulic head data, including creek data, were applied to a continuously differentiable quintic spline for irregularly spaced data (Renka, 1982) to establish constant head boundaries and to generate interpolated head values at all nodes for comparison with computed values. This method, which was used throughout modeling, allowed for calibration throughout the entire spline-generated head surface which provided a more global calibration than simple comparison at selected data locations. Areal recharge of 2.5 cm was applied uniformly over the domain which accommodated the three-dimensional nature of the problem by allowing leakance from any direction. Because of little change in the piezometric surface during the test, the velocity field was assumed to be steady state. Hydraulic conductivity, porosity, and dispersivity parameters (characteristic length) were assumed to remain constant. The code was run in weekly time steps for a period of 12 months.

Because of the overall regular shape of the domain and the flexibility to allow spatially variable hydraulic parameter coefficients in the hydraulic head equation, the USGS Method of Characteristics (MOC) code (Konikow and Bredehoeft, 1988) was used. The computational domain represented a strike-parallel rectangle encompassing the area of tracer migration at the bedrock weathering interface (the water-table surface) with 1×4 m finite difference grid cells (long dimension parallel to strike) to resolve details of tracer plume evolution.

To the extent possible, input parameter values were constrained by analysis of site data. Aquifer studies at Oak Ridge (Geraghty and Miller, 1990b; Lozier et al., 1986; and Davis et al., 1984) have estimated effective porosity values ranging from 1 to 10%. Selection of a relatively low value (3%) seemed plausible for geologic conditions and provided a reasonable scaling factor to simulate tracer migration velocity. While a 6 m aquifer thickness was assumed based on the pumping test setup, tracer migration essentially at the water-table surface suggested that aquifer thickness could be used as a velocity tuning parameter within a 1 to 6 m range, and a 3 m thickness was used. Because flow was assumed to be advective, dispersivity parameters and their anisotropy were varied among cases but kept low within the scale of the problem. Descriptions of the concepts of the flow field which evolved during the study, corresponding differences in model input, and results are described below.

Conceptual Model Descriptions and Modeling Results

For purposes of describing the flow field and providing input parameter values for numerical modeling, the data were equivocal and could be interpreted in several ways. Based on reinterpretations of the data, three conceptual models of the flow field were formulated. As additional field data analysis and/or numerical modeling results dictated, conceptual models were modified or abandoned. A description of each conceptual model and the result of its application in numerical modeling are presented below. Table 1 provides the input parameter values used for each concept. Table 2 compares calibration and results of each concept with tracer data using the evaluation criteria migration direction, migration distance, plume length:width aspect ratio, and average annual velocity. Figure 8 compares the tracer plume configuration at 12 months [Figure 8(a)] with simulations at the same time for the homogeneous, low anisotropic [Figure 8(b)], geologic-based [Figure 8(c)] and hydrogeologic-based [Figure 8(d)] cases described below.

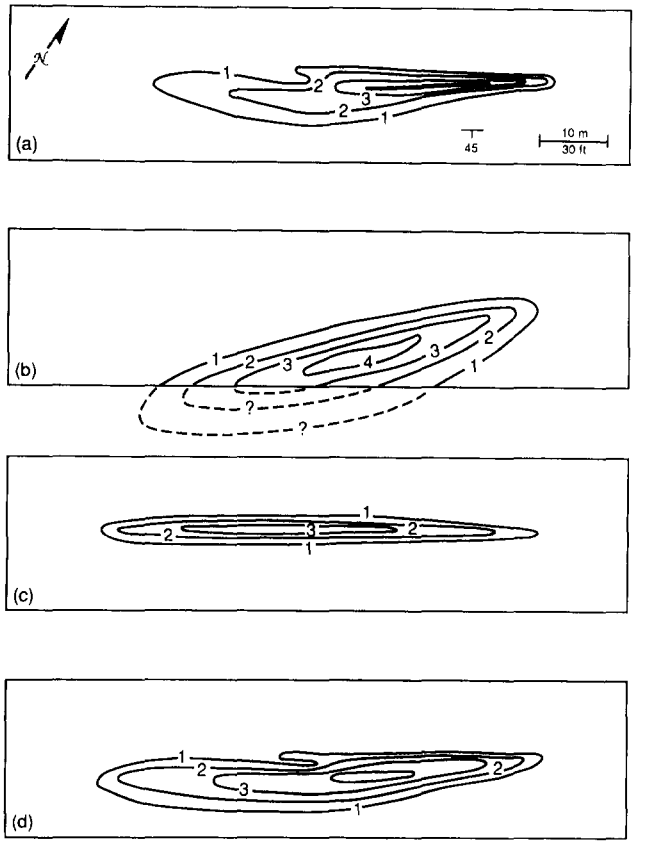

Fig. 8. Log tracer concentration at 12 months (a); and simulation results for the homogeneous, low anisotropy case (b); the geologic-based case (c); and the hydrogeologic-based case (d). Rectangular border represents computational domain boundary in all cases.

Table 1. Input Parameter Values for All Cases

Simulation parameters	Value (by case) Homogeneous	Geologic	Hydrogeologic
Grid parameters			
Number of nodes (x)	20	20	20
Number of nodes (y)	20	20	20
Cell length (x) (m)	4	4	4
Cell width (y) (m)	1	1	1
Hydrologic parameters			
Storage coefficient (steady state)	0	0	0
Hydraulic conductivity (x) (cm/s)	6×10^{-5}	6×10^{-5} (limestone) 6×10^{-7} (shale)	CDF[1]
Hydraulic conductivity (y) (cm/s)	3×10^{-5}	6×10^{-6} (limestone) 6×10^{-8} (shale)	CDF[1] × .03
Medium parameters			
Effective porosity (%)	3	3	3
Saturated thickness (m)	3	3	3
Dispersivity (x) (characteristic length)	1	10^{-3}	1
Dispersivity (y) (characteristic length)	0.1	10^{-3}	0.1
Tracer source parameters			
Number of injection wells	1	1	1
Injection rate (m^3/s)	3×10^{-10}	3×10^{-10}	3×10^{-10}
Concentration (ppb)	10^4	10^4	10^4

[1]Random sampling of the cumulative distribution function (CDF) of field measured values.

Homogeneous, Low Anisotropy Case

The initial conceptual model was developed prior to the tracer test and was based on results of larger scale (4 m) straddle packer tests, slug tests, and pumping tests. These aquifer tests suggested the aquifer could be modeled as a homogeneous, equivalent porous medium with low anisotropy. The concept was supported by the slightly elliptical but generally uniform drawdown observed during both pumping tests which suggested an absence of significant fracture influence and the general agreement in hydraulic conductivity values obtained from all aquifer test methods. A hydraulic conductivity value of 6×10^{-5} cm/s was assigned to all cells, and a hydraulic conductivity anisotropy ratio of 2:1 parallel to strike was used based on the results of the shallow pumping test. Dispersivity parameters were established at the smallest dimension of the problem (1 m) with a longitudinal:transverse dispersivity ratio of 10:1. Calibration was obtained with a root mean square (rms) error slightly greater than 0.1 m and an average difference between computed and spline-generated head values of 0.04 m.

Contrary to subsequent tracer migration, application of the homogeneous, low anisotropy concept in numerical modeling predicted tracer migration 14 degrees from strike, a plume length:width aspect ratio of 2.6:1, and distance of 69 m. Increases in the anisotropy of hydraulic conductivity to 10:1 and 30:1 improved the direction of migration to within 3 degrees of strike and the plume length:width aspect ratio to 5.4 but resulted in increasing migration distance and loss of calibration. Incremental increases in porosity (to 4%) improved the migration distance but provided no improvements in length:width aspect ratio or migration direction. Tuning of dispersivity parameters and their anisotropy to the limits of the problem scale provided little improvement to previous plume configurations. When no reasonable combination of parameter values could approximate the tracer plume and maintain head calibration, modeling efforts were terminated, and the concept was reevaluated.

Geologic-Based Case

An alternative geologic-based concept was developed while the tracer test was ongoing. The concept considered

Table 2. Calibration and Comparison of Tracer Plume at One Year with Modeling Results for Each Concept

Concept	Calibration: Drawdown (m)	Calibration: RMS error (m)	Evaluation criteria: Migration direction (degrees from strike)	Migration distance (m)	Aspect ratio (length/width)	Velocity (m/d)
Tracer	—	—	1	46	7.5	0.13
Homogeneous	0.04	0.1	14	69	2.6	0.19
Geologic	0.06	0.2	0	51	18.7	0.14
Hydrogeologic	0.02	0.2	3	52	7.4	0.14

that tracer migration was related to a systematic hydraulic conductivity contrast between limestone and shale-dominated lithologies which was unresolved by larger scale aquifer testing and/or by physical restriction of tracer caused by the corrugated shape of the bedrock weathering interface. The concept was supported by geologic, auger drilling, hydraulic head, and tracer data. For model input, strike-parallel cells representing limestone lithologies were assigned two order-of-magnitude higher hydraulic conductivity values than cells representing shale lithologies (6×10^{-5} vs. 6×10^{-7} cm/s). Because of the results of the homogeneous, low anisotropy case, a hydraulic conductivity anisotropy ratio of 10:1 was selected for use based on a compromise between high and low values obtained from previous pumping test results. Because of strong directional influences inherent in the conceptual model, dispersivity parameters were kept very low (10^{-3} m). Calibration was achieved with a 0.2 m rms error and an average difference between computed and spline-generated head values of 0.06 m.

Application of the geologic-based concept to modeling resulted in reasonably accurate transport simulations in terms of migration distance, direction, and velocity but a length:width aspect ratio of 18.7:1. As parameter tuning (hydraulic conductivity and dispersivity) to improve the aspect ratio was ongoing, results of the 1 m straddle packer and falling head tests, which were designed to verify the concept, became available. The results indicated an absence of hydraulic conductivity contrast between limestone and shale-dominated lithologies. Despite the intuitively satisfying nature of the concept and the promising modeling results, the inability to verify the concept with field data resulted in its abandonment.

Hydrogeologic-Based Case

A third hydrogeologic-based conceptual model was formulated as the tracer test continued. The concept assumed that the widely varying hydraulic conductivity data were a valid representation of a randomly heterogeneous flow field. Irregularities in the piezometric surface (preferred tracer migration pathways) which flanked the plume on the south, were assumed to represent discrete zones of enhanced discharge flux, possibly fractures. These zones effectively functioned, and could be realistically represented, as conduits of elevated hydraulic conductivity. For model input, hydraulic conductivity values were assigned to each cell by randomly sampling the cumulative distribution function of field measured values. In contrast to a Monte Carlo study, one set (one value/node) of randomly selected hydraulic conductivity values was used. A value at the upper end of measured values (1×10^{-4} cm/s) was assigned to conduits. A hydraulic conductivity anisotropy value at the upper bound of those measured at Oak Ridge (30:1) was used. Despite this seemingly high value of anisotropy, it was thought that in combination with the random values of hydraulic conductivity a more satisfactory result could be obtained. Dispersivity coefficients and their anisotropy were established as in the homogeneous case. Calibration was achieved with a 0.2 m rms error and 0.02 m average difference between computed and spline-generated head values.

Application of the hydrogeologic-based concept in modeling resulted in an accurate simulation of the tracer with highly favorable comparisons in all evaluation criteria. While a robust tracer data set was available for calibration when the simulations were performed, the favorable comparison with the plume shape and evolution using only head data for calibration adds further validity to the concept. Although the 1 m straddle packer tests did not identify conduits of elevated hydraulic conductivity, tracer migration rate data, plume fingering, and hydraulic head data suggest their presence. Their inclusion is required at the 1 to 10 m scale for accurate simulations of the rate of tracer migration in early time steps (two weeks) and to simulate plume fingering, but they have little effect on the accuracy of the position of the 100 and 1000 ppb isopleths at longer times.

Concept Comparison

The aquifer analysis conducted prior to the tracer test was designed to be comprehensive to obtain both overall and detailed aquifer characteristics data using a conventional approach to data collection and analysis. Results of that analysis indicated the flow field could be represented as a homogeneous equivalent porous medium with low anisotropy. Application of that interpretation in numerical modeling, however, resulted in inaccurate simulations of tracer migration. Tracer data clearly indicated that simplifying assumptions in the homogeneous, low anisotropy concept failed to account for system heterogeneities and were not applicable to the shallow aquifer at Oak Ridge.

The alternative geologic and hydrogeologic-based concepts were formulated when tracer data demonstrated the heterogeneous and strongly anisotropic nature of the flow field. While neither concept is wholly supported by interpretations of all site data, both are supported by the bulk of the empirical data. While modeling results indicate the hydrogeologic-based concept most accurately describes the flow field, both alternative concepts provided superior results over the initial homogeneous, low anisotropy concept when applied in numerical modeling. This suggests that modeling at the scale of this test should reflect the strongly heterogeneous character of the flow field by possibly including selected regions resembling fractured porous flow.

Conclusions

Results of this study demonstrate that application of conventional methods of hydrogeologic data collection, data analysis, and numerical modeling to the complex natural setting at Oak Ridge results in only crude estimates of the flow field. In contrast, the level of resolution provided by a ground-water tracer can be accurately simulated while constraining input parameter values to those obtained from interpretations of field data and by adopting an iterative approach to site characterization, conceptual model formulation, and numerical modeling.

Reliance upon the analyses and interpretations of initial site data and modeling results, which assumed homogeneous, slightly anisotropic conditions and domi-

nantly gradient driven flow, would also result in nonconservative estimates of contaminant transport. Tests documented in this study show that a ground-water contaminant will likely not be detected in locations down maximum gradient from a waste disposal unit at this site. In complex hydrogeologic settings, the use of ground-water tracer tests to verify solute transport model results provides an effective means of deterministically evaluating those system characteristics which most influence flow.

References

Chow, V. T. 1952. On the determination of transmissivity and storage coefficient from pumping test data. Trans. Am. Geophysical Union. v. 33.

Connell, J. F. and Z. C. Bailey. 1989. Statistical and simulation analysis of hydraulic-conductivity data for Bear Creek and Melton Valleys, Oak Ridge Reservation, Tennessee. U.S.G.S. Water Resources Investigations Report 89-4062. 49 pp.

Crane, R. L., K. E. Hillstrom, and M. Minkoff. 1980. Solution of the general nonlinear programming problem with subroutine VMCON. National Technical Information Service, Springfield, VA. Argonne National Laboratory Report No. ANL-80-64.

Davis, E. C., et al. 1984. Site characterization techniques used at a low-level waste shallow land burial field demonstration facility. Oak Ridge National Laboratory, Oak Ridge, TN. ORNL/TM-9146.

Geraghty and Miller, Inc. 1990a. Development of ground-water flow models for the S-3 waste management area, Y-12 Facility, Oak Ridge, Tennessee. Oak Ridge Y-12 Plant, Oak Ridge, TN. Y/Sub/89-00206C/1.

Geraghty and Miller, Inc. 1990b. Development of contaminant transport models for four constituents at the S-3 site, Y-12 plant, Oak Ridge, Tennessee. Oak Ridge Y-12 Plant, Oak Ridge, TN. Y/Sub/89-00206C/3.

Gringarten, A. C., D. P. Bourdet, P. A. Landell, and V. J. Kniazeff. 1979. A comparison between different skin and wellbore storage type curves for early-time transient analysis. SPE-AIME 54th Annual Fall Technical Conference and Exhibition, Las Vegas, NV, September 23-26. Society of Petroleum Engineers Reprint SPE-8205.

Gringarten, A. C. and P. A. Witherspoon. 1972. A method of analyzing pump test data from fractured aquifers. Proc. Symposium on Percolation Through Fissured Rock, Stuttgart, Inst. Soc. Rock Mechanics and Intl. Assn. Engineering Geology. T3-B-1 to T3-B-8.

Horner, D. R. 1951. Pressure build-up in wells. Proc. Third World Petroleum Congress, The Hague. Section II, pp. 503-523.

Hvorslev, M. J. 1951. Time lag and soil permeability in groundwater observations. Waterways Experiment Station, Corps of Engineers, Vicksburg, MS. Bull. No. 36.

Konikow, L. F. and J. D. Bredehoeft. 1988. Computer model of two-dimensional solute transport and dispersion in ground water, version 2.5. USGS. Book 7, Chapter C-2.

Lozier, W. B., C. A. Spiers, and R. Pearson. 1986. Aquifer pump test with tracers. Oak Ridge National Laboratory, Oak Ridge, TN. ORNL/Sub/86-32136/2.

Neuman, S. P. 1975. Analysis of pumping test data from anisotropic unconfined aquifers considering delayed gravity response. Water Resources Research. v. II, no. 2, pp. 329-342.

Papadopulos, I. S. 1965. Nonsteady flow to a well in an infinite anisotropic aquifer. Hydrology of Fractured Rocks, Proc. Dubrovnik Symposium. v. I.

Renka, R. J. 1982. A storage-efficient method for construction of a Thiessen triangulation. Oak Ridge National Laboratory, Oak Ridge, TN. ORNL/CSD-101.

Rizk, T. A. 1990. Ground water flow and contaminant transport in geologic media. Ph.D. dissertation. North Carolina State Univ., Raleigh, NC. 244 pp.

Smith, E. D. and N. D. Vaughn. 1985. Aquifer test analysis in nonradial flow regimes: A case study. Ground Water. v. 23, no. 2, pp. 167-175.

Stephens, D. B. and S. P. Neuman. 1982a. Vadose zone permeability tests: Summary. Proc. ASCE. v. 108, no. HY5, pp. 623-639.

Stephens, D. B. and S. P. Neuman. 1982b. Vadose zone permeability tests: Steady state results. Proc. ASCE. v. 108, no. HY5, pp. 640-659.

Theis, C. V. 1935. The relation between the lowering of the piezometric surface and the rate and duration of discharge of a well using groundwater storage. Trans. Am. Geophysical Union, 16th Annual Meeting. Pt. 2, pp. 519-524.

ground water

Calculation of Ground Water Ages—A Comparative Analysis

by Maria Clara Castro[1] and Patrick Goblet[2]

Abstract

Ground water age is a fundamental, yet complex, concept in ground water hydrology. Discrepancies between results obtained through different modeling approaches for ground water age calculation have been reported, in particular, between ground water ages modeled by advection and direct simulation of ground water ages (e.g., age-mass approach), which includes effects of advection and dispersion. Here, through a series of two-dimensional (2D) simulations, the impact of water mixing through advection and dispersion on modeled ^{14}C and directly simulated ground water ages is assessed. Impact of dispersion on modeled ages is systematically stronger in areas where water velocities are smaller and far more pronounced on ^{14}C ages. This effect is also observed in one-dimensional models. 2D simulations show that longitudinal dispersion generally acts as a "source" of ^{14}C, while vertical dispersion acts as a "sink," leading to apparent younger or older modeled ^{14}C ages as compared to advective and directly simulated ground water ages. The presence of permeable and impermeable faults provides an equally important source for discrepancies, leading to major differences in modeled ages among the three methods considered. Overall, our results show that a ^{14}C modeling approach using a solute transport model for calculating ground water age appears to be more reliable in ground water systems without faults and where water velocities are relatively high than in systems that are relatively more heterogeneous and those where faults are present. Among the three modeling approaches considered here, direct simulation of ground water age seems to yield the most consistent results in complex, heterogeneous ground water flow systems, giving a vertical age structure consistent with ages expected from consideration of the flow system.

Introduction

The concept of "ground water age" is one of the most fundamental in ground water hydrology. Fundamental because it is critical to effective management of ground water resources, prediction of the rate at which a contaminant migrates, or yet, reconstruction of the past climate through the use of noble gases dissolved in ground water. Knowing the age of ground water implies knowing precisely how a particular ground water system functions, i.e., its hydrodynamic parameters (e.g., hydraulic head distribution, hydraulic conductivity field, and porosity), recharge rates, and cross-formational rates of flow and mass within the system of interest.

Traditionally, two approaches have been used to estimate the age of ground water: estimation of ground water ages through application of the piston flow model concept and through the use of radioisotope tracers (e.g., ^{3}H, ^{14}C, ^{36}Cl; see Phillips and Castro 2003). The first approach considers the age of ground water as corresponding simply to the time elapsed along a streamline since recharge took place. The basic assumption is the presence of a closed system and absence of water mixing of different ages both across formations and within the aquifer itself. The second method, as traditionally employed assuming that all necessary geochemical corrections have been applied (e.g., Plummer et al. 1991), is used under the assumption that radioactive decay is the dominant process causing a reduction/change in the tracer concentration. Although concentrations of these tracers are also affected by ground water mixing through advection, dispersion, and/or diffusion, the impact of such

[1]Corresponding author: University of Michigan, Department of Geological Sciences, C. C. Little Building, 425 E. University Ave., Ann Arbor, MI 48109-1063; tel (734) 615-3812; fax (734) 763-4690; mccastro@umich.edu

[2]Ecole des Mines de Paris, Centre d'Informatique Géologique, 77305 Fontainebleau, France.

Received July 9, 2004; accepted December 18, 2004.

processes on the tracer's concentration is often neglected and is not taken into account in the age calculation (e.g., Stute et al. 1992; Castro et al. 2000). Thus, when such processes are not considered, radioisotope ages will correspond to the "true" water ages only in the presence of a closed system and total absence of water mixing. This is, however, not the case for most ground water systems (Pint et al. 2003). Movement of water in porous media is, in addition to advection and like any other tracer, also affected by kinematic dispersion, molecular diffusion, and cross-formational flow, which leads to mixing of water molecules with different ages. Independent of the chosen approach, more accurate ground water ages should be obtained by considering transport by advection, dispersion, and diffusion.

The concept of ground water age has been recently reexamined by hydrogeologists in order to derive model ages that can be compared to field measurements (Goode 1996; Varni and Carrera 1998; Bethke and Johnson 2002a, 2002b). In this approach, a parallel is made between water age and solute concentration. Ground water age is directly simulated by taking into account not only advection but also dispersion and diffusion, and the quantity conserved is the product of water age and its mass. Thus, if ground water mixing processes are non-negligible, direct simulation of ground water age (e.g., age-mass approach), which incorporates mixing of water molecules in the age calculation, should provide more realistic ages than the more traditional methods in which mixing is typically neglected. This is expected to be particularly true in complex ground water systems.

With respect to ^{14}C, which is the tracer of choice for late Pleistocene and Holocene paleoclimatic reconstructions through the use of noble gases dissolved in ground water (e.g., Stute et al. 1992; Weyhenmeyer et al. 2000), issues dealing with loss of ^{14}C by diffusion toward neighboring aquitards leading to apparent older ^{14}C ages have been addressed (e.g., Sudicky and Frind 1981; Walker and Cook 1991; Sanford and Buapeng 1996; Sanford 1997). On the contrary, with the exception of a theoretical analysis on the impact of longitudinal dispersion (Johnson and DePaolo 1996), influence of mixing of water of different ages through advection alone and that of longitudinal and transverse dispersion in particular on ^{14}C ages has received more limited attention.

Here, through a series of two-dimensional (2D) simulations carried out for a complex real ground water flow system, the impact of water mixing through advection as well as that of dispersion is assessed by comparing ground water ages calculated using an advective model, ages based on ^{14}C simulated using a solute transport model, and directly simulated ages. It will be shown how these different modeling approaches respond to changes in hydraulic conductivity and the presence of permeable and impermeable faults in the system. The combined influence of horizontal and vertical dispersion on modeled ages and the resulting vertical and horizontal age distribution are discussed. Through a one-dimensional (1D) analysis, impact of horizontal dispersion on ^{14}C ages as well as its dependency on ground water velocities is illustrated.

For comparative purposes, our starting point will be a 2D ground water flow model of flow in the Carrizo Aquifer and surrounding formations in southwest Texas that has been calibrated with ^{4}He and ^{3}He concentrations (Castro and Goblet 2003a; Castro 2004) and for which advective and directly simulated ground water ages (Castro and Goblet 2003a, 2003b) have been calculated. In this system, based on C isotope measurements available in a number of water samples, ^{14}C ages were previously estimated following the traditional approach in which mixing processes are not considered (Castro et al. 2000). Only radioactive decay and chemical interactions were taken into account in this ^{14}C age calculation, and no attempt to simulate ^{14}C transport in the system with incorporation of mixing processes was made. Subsequent comparison of these calculated ^{14}C ages with modeled advective ages (Castro and Goblet, 2003a) and those obtained through direct simulation of ground water age (Castro and Goblet 2003b) shows lack of agreement at several locations. Here, we attempt to shed some light on possible physical processes that can lead to such discrepancies when different model approaches are considered for the age calculation.

Regional and Hydrogeological Setting

The Eocene Carrizo Aquifer is a major ground water flow system exposed on the northwestern margin of the Gulf Coast Basin in South Texas (Figure 1a). In Atascosa, McMullen, and portions of surrounding counties (Figure 1b), the Carrizo Aquifer lies unconformably on the Lower-Wilcox Formation, a confining layer composed of mudstones and clay (Figure 1c; Hamlin 1988). The confining Recklaw Formation conformably overlies the Carrizo Aquifer and is in turn overlain by the Queen City Aquifer. These formations crop out subparallel to the present-day coastline and dip to the southeast (Figures 1b and 1c). The Carrizo Aquifer terminates at a major growth-fault system, the Wilcox Geothermal Corridor (Figures 1a and 1b). The presence of minor faults is also known in these formations.

Carrizo and Recklaw hydraulic conductivities decrease exponentially over 4 orders of magnitude with increased distance from the recharge area and depth, a decrease that reflects the combined influences of differential compaction of the media as well as down-dip lithological change (Patriarche et al. 2004) giving origin to a complex velocity field (Figure 1c). Calibrated hydraulic conductivities in the recharge area for the Carrizo and Recklaw are 5×10^{-4} and 3×10^{-8} m/s, respectively (Castro and Goblet 2003a). Calibration was obtained by applying exponentially decreasing factors $F_c = \exp -((x_c - 6633)/12{,}000)$ and $F_r = \exp -((x_r - 19{,}133)/12{,}000)$ to the Carrizo and Recklaw, respectively, where x_c and x_r represent any point at a distance x from the origin of the Carrizo and Recklaw outcrop areas, respectively. Hydraulic conductivity values for the Carrizo and Recklaw in the discharge area are 3×10^{-8} and 6.4×10^{-12} m/s, respectively. For the Queen City and Lower-Wilcox formations, we have adopted uniform hydraulic

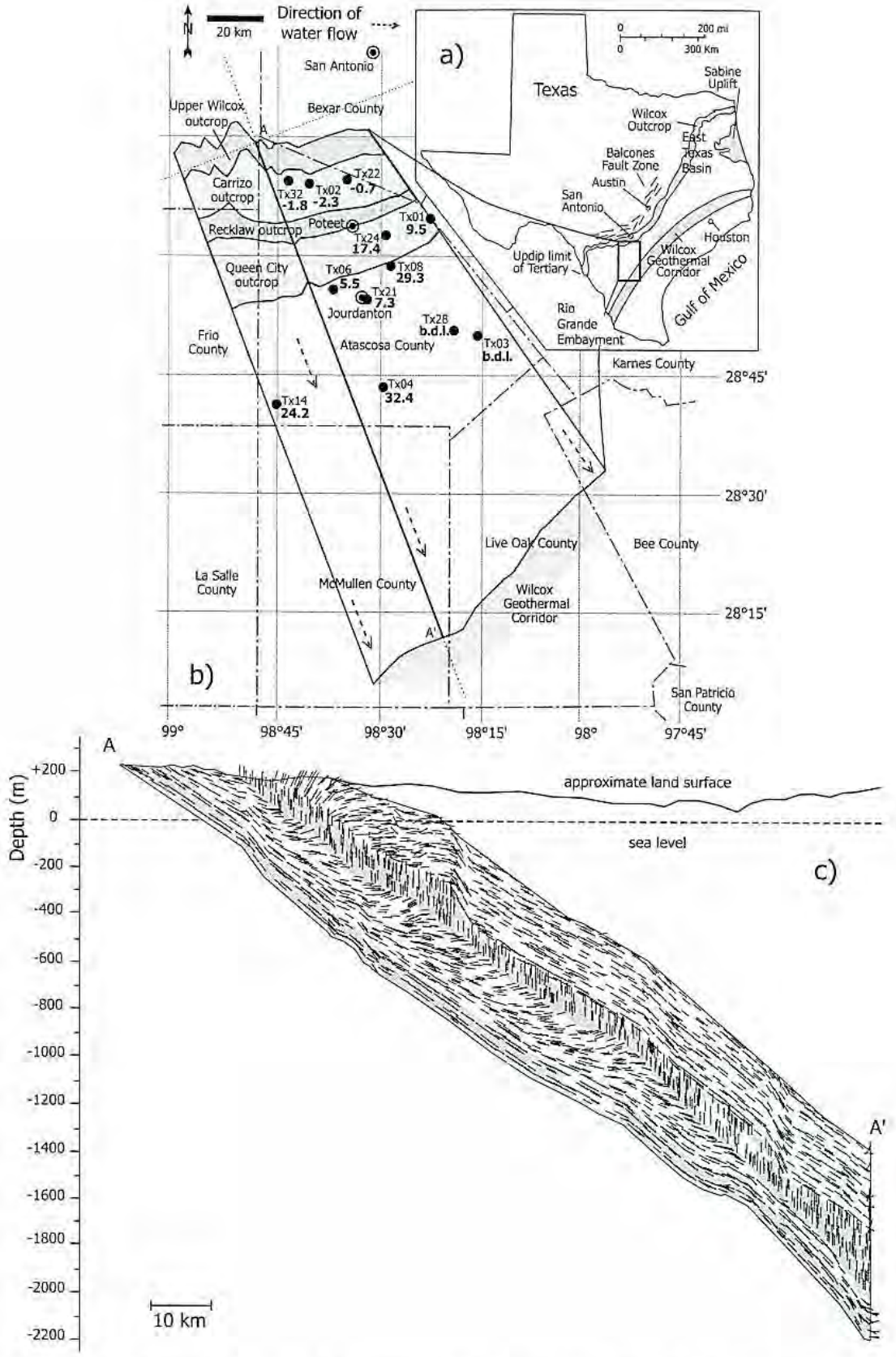

Figure 1. Study area and formation outcrops in southwestern Texas. (a) Geographical and tectonic setting (after Hamlin, 1988). (b) Detailed setting of the area with location of cross section AA′ along which simulations of ground water flow, transport, and age were carried out; sample locations for which ^{14}C ages based on C isotope measurements are available (Castro et al. 2000) indicated as closed circles; ^{14}C ages (kyr) in bold; ^{14}C is below detection limit (b.d.l.) at samples TX28 and TX03. (c) Normalized Darcy velocity vectors in place for the ground water flow model calibrated with ^{4}He (Castro and Goblet 2003a).

conductivities of 5×10^{-5} and 1×10^{-11} m/s, respectively. Average porosity values used in the simulations presented here are 20%, 12.5%, 35%, and 26% for the Queen City, Recklaw, Carrizo, and Wilcox formations, respectively (Castro and Goblet 2003a). Water infiltrates in the Carrizo outcrop area and flows toward the southeast. Discharge occurs by cross-formational upward leakage through the Recklaw. Ground water flow simulations

(Castro and Goblet 2003a) clearly show the presence of semivertical directions of water velocities toward the Recklaw Formation at the top of the Carrizo Aquifer, illustrating the effectiveness of indirect recharge for this confining layer. Near the outcrop, water movement in the Queen City is semivertical due to the strong upward leakage into the Recklaw. Elsewhere, direct influence of upward leakage in the Queen City is not detected and flow in this aquifer becomes essentially horizontal in response to the rapid decrease in hydraulic conductivities of the Recklaw.

Calculation of Ground Water Ages

All steady-state ground water flow simulations presented here were conducted as described by Castro and Goblet (2003a) along cross section AA′ (Figure 1c). The finite-element model is represented by a triangular mesh corresponding to a 120.6-km-long stratigraphic cross section between 220 and −2210 m of elevation, and it comprises 58,968 elements and 31,949 nodes. The mesh is composed of triangles uniformly distributed over the entire length of the cross section with maximum element length of 50 m. The mesh size was chosen to meet three objectives: (1) proper discretization of the different formations and, particularly, of the Carrizo Aquifer; (2) the possibility to introduce sufficiently small values of dispersivity (Table 1); and (3) the ability to extend the 2D mesh into a three-dimensional one (Patriarche et al. 2004). For most of the calculations, the element size conforms to the classical stability criterion for the numerical approximation of the advection-dispersion equation such that longitudinal dispersivity is more than twice the element size. Sensitivity tests with much smaller dispersivity values (α_L = 12.5 m, α_T = 1.25 m) yield results that are not significantly different from the results presented here. In addition, sensitivity tests conducted using a much finer mesh (2.5 m) show that no important bias was introduced by not strictly conforming to the criterion. It is important to note, however, that in the following discussion, emphasis is not on absolute ages; rather, it is on differences in behavior displayed by three different modeling approaches under the same geological and hydrogeological conditions and physical parameters.

Table 1
Diffusion and Dispersivity Parameters Used in ^{14}C and Ground Water Age Simulations

Parameter	Value	Reference
Diffusion coefficients		
$H^1H^3O^{16}$	3.83×10^{-9} m²/s	Wang et al. (1953)
HCO_3^-	1.18×10^{-9} m²/s	Li and Gregory (1974)
Tortuosity coefficients		
Aquifers	0.1	
Confining layers	0.05	
Dispersivity coefficients		
Longitudinal	125 m	
Transverse	12.5 m	

Boundary conditions for the 2D ground water flow model include hydraulic head values prescribed on the outcrop areas of all formations as well as on top of the Queen City Aquifer. At the base of the Wilcox, a no-flow boundary condition was imposed. In addition, a high hydraulic conductivity value of 10^{-5} m/s was imposed at the top of the Queen City in the Wilcox Geothermal Corridor area allowing water to be evacuated upward, representing the situation occurring at the major growth-fault system.

Subsequently, we describe the procedure used for age calculations with the three different modeling approaches: (1) application of the piston flow model principle referred to here as "advective ages"; (2) direct simulation of ground water ages; and (3) simulation of ^{14}C transport and corresponding modeled ages referred to here as "^{14}C Ages."

Advective Ages

For all ground water flow simulations, advective ages were calculated taking into account the established hydraulic gradients, hydraulic conductivity values, porosities, and Darcy velocities. Water travel times were calculated along streamlines as follows:

$$t = \int_{x_0}^{x} \frac{dx}{v} \tag{1}$$

where x_0 represents the origin of a particular streamline; x, a point at any distance x from the origin of the streamline; and v, the modeled pore water velocity. Only advection is taken into account in this age estimation. Thus, mixing of ground water both cross-formational and within the different formations is not considered.

Direct Simulation of Ground Water Age

For all ground water flow simulations presented here, all ground water age simulations were carried out in steady state and calculated as follows:

$$\mathrm{div}[(\omega d + \alpha |U|)\mathrm{grad}\vec{\tau} - \vec{U}\tau] = \omega \tag{2}$$

where ω is the porosity, d is the tritiated water diffusion coefficient in porous media multiplied by the tortuosity coefficient (Table 1), α is the dispersivity tensor (m) expressed in the two main directions of anisotropy by α_L and α_T, respectively, in the longitudinal and the transverse directions of flow (Table 1), τ is the age, and U is the Darcy velocity (m/s).

To account for ground water mixing, we treat water age as one would treat a solute concentration; water age (in seconds) is simulated by considering the product of water mass (ρV) and age (τ) (Goode 1996), where ρ is the water density (kg/m³) and V is the water volume (m³). This quantity, referred to as "age-mass" (kg s), is conserved and is equivalent to moles of a solute tracer. Boundary conditions included zero–age-mass flux across all no-flow and inflow boundaries of the domain (AA′;

Figures 1b and 1c) and no age-mass dispersive flux across outflow boundaries.

Directly simulated water age can be compared to the concentration of a conservative tracer that is not affected by chemical reactions and that accumulates in ground water due to in situ production as well as an external deeper source. Helium is probably the closest example of such a tracer (Castro and Goblet 2003a).

^{14}C Ages

For all ground water flow simulations presented, transport of ^{14}C was simulated in the entire system (cross section AA', Figure 1c) in steady state by taking into account advection, dispersion, diffusion, and radioactive decay following:

$$\mathrm{div}[(\omega d + \bar{\alpha}\,|U|)\mathrm{grad}\vec{\ } \ C - \vec{U}\ \ C] = \omega\lambda C \qquad (3)$$

where d is the diffusion coefficient for HCO_3^- multiplied by the tortuosity coefficient (Table 1), and λ (T^{-1}) is the radioactive decay constant for ^{14}C of 3.84×10^{-12}/s taking into account its half-life of 5730 years (Mann et al. 1961). In a similar approach to that of Sudicky and Frind (1981) and for the sake of simplicity, concentrations of the stable carbonate species are assumed to be uniform throughout the system, with variations of ^{14}C due only to radioactive decay and transport processes. In this situation, the ^{14}C concentration C is expressed as percent modern carbon (pmc). Boundary conditions include a prescribed pmc of 90 (C_0) in all outcrop areas, which corresponds to the measured percent modern ^{14}C value in the Carrizo recharge area (Castro et al. 2000). For all other external boundaries, in particular the top of the Queen City, an outlet condition was prescribed that allows ^{14}C to exit the system by advection. At the bottom of the Wilcox, however, water is devoid of ^{14}C content due to the very low hydraulic conductivities in place. Here, diffusion is the dominant transport mechanism and ^{14}C exits the Carrizo toward the Wilcox in an attempt to reach isotopic equilibrium. Migration of ^{14}C into the Wilcox is, however, very limited in distal extent due to its relatively short half-life. In all formations, waters are also devoid of ^{14}C at the southernmost limit of the system.

After simulation of ^{14}C transport in the system, ^{14}C ages were then calculated following the traditional approach in which ^{14}C is assumed to be transported only by advection, and where dispersion, diffusion, and ground water mixing (cross-formational and within each formation) is neglected. In this case, the water age A (T) that results from simulated ^{14}C concentrations is given by:

$$A = -\frac{1}{\lambda}\ln\frac{C}{C_0} \qquad (4)$$

If ^{14}C concentrations changed (were reduced) as a result of radioactive decay alone and ^{14}C transport was only by advection in total absence of ground water mixing, then the obtained ^{14}C ages should correspond to the calculated advective ages in the entire system. In the examples given and analysis that follows, we will see that this is not the case. More importantly, it will be shown that, for a diversity of natural settings, ^{14}C ages calculated following this approach do not respond to changes in the hydrogeological system in a similar manner to modeled advective ages, nor to ages obtained through direct simulation of ground water age, which portrays the behavior of the water molecule. The most important distinction between simulated water ages and a tracer such as ^{14}C lies in the conservative vs. nonconservative nature of these two tracers.

Although in our ^{14}C transport simulations all mixing processes due to advection, dispersion, and diffusion were accounted for, which is what happens in a real system, it is important to note that our calculated ^{14}C ages, following the most common approach taken for ^{14}C ground water dating, are unadjusted to account for both "losses" and/or "additions" of ^{14}C that have occurred in the system due to mixing processes (e.g., dispersion). As a result, ^{14}C ages determined using this procedure will yield, in certain cases, apparent older or younger ages than one would expect the real age of ground water to be, further reinforcing the argument that such modeled ^{14}C ages do not always accurately portray the dynamics of the ground water system itself.

Simulation Results and Discussion

We proceed to illustrate how the three different modeling approaches lead to differences in calculated ages under distinct hydrogeological conditions. We also illustrate how ground water mixing through advection and dispersion impacts differently the calculation of ages obtained through direct simulation of ground water age and those obtained through transport of ^{14}C. Results of simulations presented here are meant to compare how each modeling approach behaves under different scenarios in one complex aquifer system that represents the Carrizo Aquifer and surrounding formations. When employing these modeling approaches in other complex systems where fluvial, deltaic, and marine depositional environments are present, relative behavior similar to the results presented here is expected. However, these results and, in particular, the observed differences in absolute modeled age values should not be generalized and directly applied to other systems.

Impact of Horizontal Dispersion

Although our goal is not to discuss results in terms of absolute modeled ages, we start by showing the horizontal distribution of these ages in the Carrizo Aquifer (Figure 2a) as calculated from Equations 1 and 2 and by combining Equations 3 and 4 for our original ground water flow model calibrated with ^4He concentrations (Castro and Goblet 2003a). All calculated ages are shown down to 60 km from the recharge area where ^{14}C content reaches ~1 pmc. Further away, the ^{14}C content becomes negligible.

It is clear that these ages differ in absolute values and evolve differently with respect to each other along the ground water flowpath. ^{14}C ages are the youngest along the entire flowpath, while ages obtained through direct simulation of ground water age are younger than advective ages down to 20 km, to become progressively older than

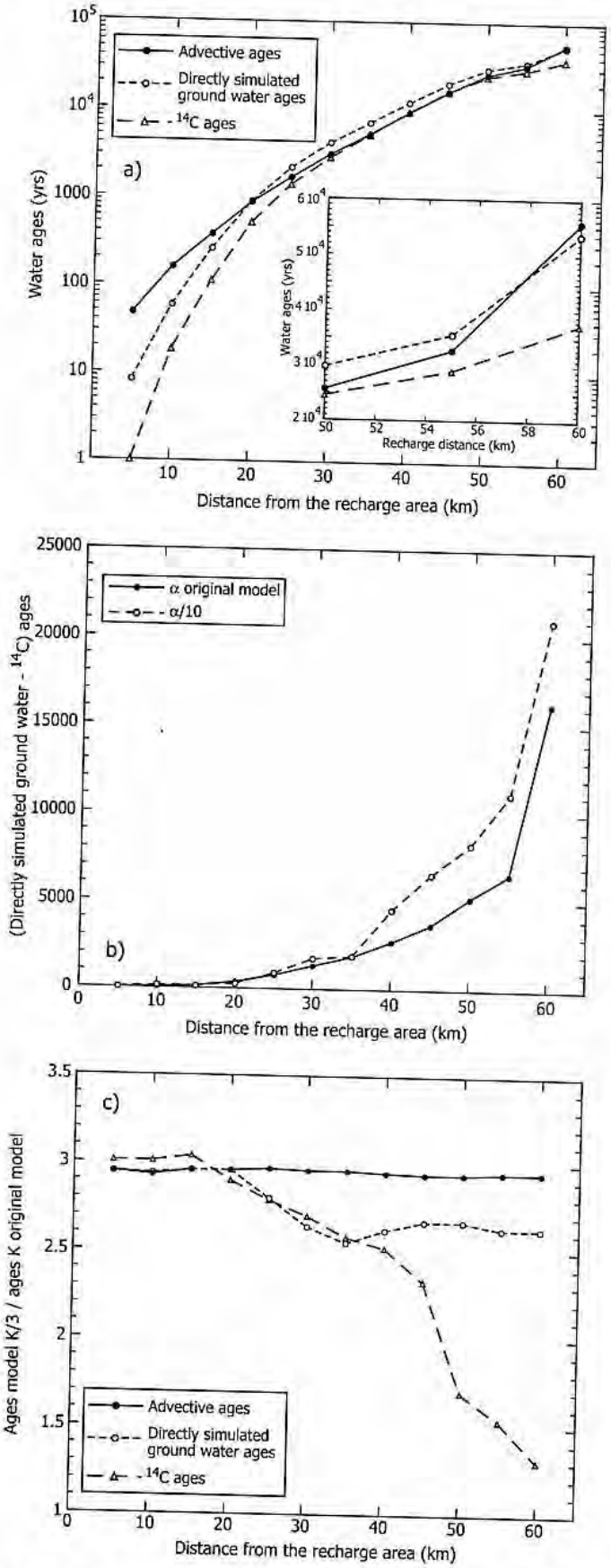

Figure 2. (a) Calculated advective, ^{14}C, and directly simulated ground water ages in the Carrizo Aquifer for a regional 2D ground water flow model calibrated with ^{4}He (Castro and Goblet 2003a) as a function of distance from the recharge area; detail between 50 and 60 km from the recharge area is also shown in a linear scale. (b) Absolute age difference between ^{14}C and directly simulated ground water ages as a function of recharge distance corresponding to the original model for both the original dispersivity tensor value and one which is 1 order of magnitude smaller. (c) Calculated advective, ^{14}C, and directly simulated ground water ages ratios in the Carrizo Aquifer between the original ground water flow model for which hydraulic conductivities in the Carrizo and Recklaw outcrop were reduced threefold ($K/3$), while maintaining all other parameters unchanged, and that one of the original model (K), as a function of distance from the recharge area.

the latter up to 50 km from the recharge area. This trend is then reversed, with directly simulated ages becoming progressively younger than advective ages at ~60 km from the recharge area (Figure 2a). Although not shown, it should be noted that as distance from the recharge area increases, this trend is accentuated, with directly simulated ages becoming younger than advective ages up to tens of thousand years. For example, ~80 km from the recharge area, directly simulated ages are about 22,000 years younger than the latter. Similarly, with increased recharge distance, ^{14}C ages become progressively younger than both advective and directly simulated ages (~18.5 and ~16.2 kyr younger at 60 km, respectively). This increasing age gap with increased recharge distance among all ages is the major feature observed.

The major hydrogeological change taking place along the ground water flowpath in this system is a strong and progressive reduction of the horizontal velocity component, and therefore of the horizontal dispersive flux, up to 2 orders of magnitude 60 km from the recharge area (from 8.5×10^{-7} to 1.7×10^{-9} m/s). Tests carried out in total absence of diffusion show that, with the exception of the Wilcox, diffusion plays a negligible role in this portion of the system, due to the relatively high hydraulic conductivities in all formations. Diffusion impacts directly simulated ground water ages at farther distances, where ^{14}C is no longer detected and where hydraulic conductivities in the Recklaw are $\leq 10^{-10}$ m/s. Thus, diffusion will not be part of our discussion.

To assess the impact of horizontal dispersion on calculated ^{14}C and directly simulated ages, a number of tests were carried out. For example, by reducing the dispersivity tensor 1 order of magnitude while maintaining all other parameters unchanged, the gap between ages increased (Figure 2b), with ^{14}C ages ~22 kyr younger than directly simulated ages, as opposed to ~16 kyr in the original ground water flow system, at 60 km from the recharge area.

On a separate set of simulations, hydraulic conductivities in the Carrizo and Recklaw outcrop areas were reduced threefold as compared to our original ground water flow model. All other parameters remained unchanged. By creating the same decrease of hydraulic conductivities in these two formations, we have roughly maintained the original hydraulic head gradient in the system (see discussion by Patriarche et al. 2004), and the observed increase in advective ages should be proportional to this reduction in hydraulic conductivity and, therefore, velocity. This is what is observed when looking at the ratios between ages obtained in this particular ground water flow system and those in the original one (Figure 2c). The observed increase in advective ages is roughly constant and threefold along the entire domain. The same, however, is not true with respect to ^{14}C and directly simulated ages. Specifically, all three modeling approaches display a similar behavior in areas where the water velocity is greater than $\sim 3 \times 10^{-8}$ m/s, i.e., up to ~20 km from the recharge area (Figure 2c), where advection is dominant. For larger distances from the recharge area (~20 to 35 km) and lower velocity values ($\sim 3 \times 10^{-8}$ to 7×10^{-9} m/s), the observed increase in ^{14}C and directly simulated ages is similar and smaller than the one observed on advective ages. The most remarkable effect, however, is observed on ^{14}C ages. Although in the first portion of the flowpath ^{14}C ages, like advective and directly simulated ages, display a threefold increase, as distance from the recharge area increases and velocities decrease, ^{14}C ages display a smaller and smaller age increase compared to the original flow system, to almost entirely "recover" and display ages that are very close to the original ones (~1.3 times higher) 60 km from the recharge area. Furthermore, the gap that was initially almost nonexistent between ^{14}C and directly simulated ages up to 35 km from the recharge area became far more pronounced with increased recharge distance and decreasing velocities (less than $\sim 7 \times 10^{-9}$ m/s).

From this set of simulations, a few important observations can be made: (1) kinematic dispersion impacts both ^{14}C and directly simulated ground water ages for velocities less than $\sim 3 \times 10^{-8}$ m/s; (2) the influence of dispersion on both ages increases with decreasing velocities; and (3) the influence of longitudinal dispersion is far greater on ^{14}C ages as compared to directly simulated ages for velocities less than $\sim 7 \times 10^{-9}$ m/s. Observations 1 and 2 are in agreement with conclusions reached by Goode (1996) based on a set of simulations carried out in a hypothetical and simpler system. Dispersive and diffusive mixing of water (as verified here on directly simulated ages farther from the recharge area) tends to limit the maximum water ages. With respect to directly simulated ground water ages, this is because, by analogy to Fick's law applied to solutes, dispersive flux of age-mass occurs in the direction of decreasing ages, thus inducing a reduction in the water ages. As pointed out in Observation 3, however, this effect is more visible on ^{14}C ages due to the presence of significant concentration gradients along the flowpath. Such gradients induce more ^{14}C to move from higher to lower concentration areas, resulting in ^{14}C ages that are much younger than the real water age. In this situation, where there is a very strong reduction of the horizontal velocity field, horizontal dispersion acts as a "source" of ^{14}C. This "source effect" is particularly important in low–water velocity areas where the role of dispersion becomes more prominent. Figure 2c shows that in this particular case, horizontal dispersion becomes an important source of ^{14}C at distances $\geq$40 km where the horizontal velocity is less than or equal to $\sim 7 \times 10^{-9}$ m/s. For higher velocity values, i.e., areas closer to the recharge area, the use of our modeling approach to determine ground water ages based on ^{14}C could be, in this situation, reliable.

This example shows that care must be taken when using ^{14}C as a ground water age indicator while neglecting the impact of dispersion. It also shows evidence for the higher reliability of this particular ^{14}C ground water dating method in ground water systems where water velocities are relatively high, thus diminishing the role horizontal dispersion plays, in this particular case, as a source of ^{14}C. Results presented here also seem to indicate that the modeling approach followed to determine ^{14}C ages is likely to be less reliable in highly heterogeneous ground water systems where hydraulic conductivities and

thus water velocities vary over several orders of magnitude, and reach low values, compared to more homogenous ones where velocities are high with only small variations (e.g., 1 order of magnitude or less). A similar conclusion concerning the use of chlorofluorocarbon-based ages for very young water (tens of years) was reached by Weissmann et al. (2002).

This degree of reliability of ^{14}C ages in high— vs. low—water velocity areas due to the impact of horizontal dispersion can also be observed in 1D models as illustrated subsequently.

Impact of Horizontal Dispersion on ^{14}C Ages—High vs. Low Horizontal Velocities

The general steady-state, 1D differential equation incorporating advection, dispersion, and radioactive decay along the flowpath with boundary conditions $C(0) = C_0$ and $C(\infty) = 0$ is as follows:

$$U\frac{dC}{dx} - D^*\frac{d^2C}{dx^2} + \omega\lambda C = 0 \quad 0 \le x \le \infty \tag{5}$$

where D^* is the coefficient of hydrodynamic dispersion, which includes molecular diffusion.

The analytical solution to Equation 5 is given by:

$$C(x) = C_0 \exp\left(\frac{\left(U - \sqrt{U^2 + 4\omega\lambda D}\right)x}{2D}\right) \tag{6}$$

where

$$D = \alpha U \tag{7}$$

and, therefore, molecular diffusion is not taken into account.

Equation 6 can be rewritten as:

$$C(x) = C_0 \exp\left(\frac{x}{2\alpha}\left(1 - \sqrt{1 + \frac{4\omega\alpha\lambda}{U}}\right)\right) \tag{8}$$

Depending on the value of the dimensionless number

$$N = \frac{4\omega\alpha\lambda}{U} \tag{9}$$

which incorporates the combined effects of advection, dispersion, and radioactive decay, a different approximation to Equation 8 can be obtained, thus emphasizing the driving mechanism:

1. For $N << 1$, the approximate solution is:

$$C = C_0 \exp\left(-\frac{x\omega\lambda}{U}\right) \tag{10}$$

This solution is valid for high water velocity values and is not dependent on the dispersivity. Here, radioactive decay is not significant, which leads to a quasi-linear concentration profile and thus absence of dispersion.

2. For $N >> 1$, the approximate solution is:

$$C = C_0 \exp\left(-x\sqrt{\frac{\omega\lambda}{\alpha U}}\right) \tag{11}$$

This solution is valid for low water velocity values and depends directly on the dispersivity. Radioactive decay plays a dominant role here leading to an exponential concentration profile and hence the presence of a dispersive flux.

Using $\lambda = 3.84 \times 10^{-12}$/s and $\omega = 0.35$, ^{14}C concentrations were calculated through Equation 6 for high (8.5×10^{-7} m/s) and low (1×10^{-10} m/s) water Darcy velocities, respectively. For both cases, three different dispersivity values (12.5, 125, and 1250 m) were tested. ^{14}C ages were subsequently calculated using Equation 4.

1D simulation results clearly show (Figure 3a) that, for the high water velocity value, ^{14}C age profiles obtained using Equation 6 for the three different dispersivities are undistinguishable, and thus that dispersion does not impact ^{14}C concentrations and resulting ^{14}C ages as previously shown in the 2D simulations. In contrast, and as previously shown through the 2D model, 1D simulations conducted for lower velocity values clearly illustrate the impact of dispersion on ^{14}C concentrations and resulting ^{14}C ages (Figure 3b).

This 1D analysis further supports the idea that the modeling approach used here to determine ^{14}C ages yields more reliable results in high water velocity areas where ^{14}C ages are not affected by dispersion.

It can also be shown that impact of dispersion on ^{14}C concentration profiles and resulting ^{14}C ages is directly related to the ratio of advective to dispersive flux, not on the absolute dispersive flux value alone. Specifically, this impact is negligible for high values of this ratio. Impact of dispersion on ^{14}C ages increases progressively as the advective/dispersive flux ratio decreases and becomes significant for low values of the latter. This dependency can be directly illustrated in a 1D analysis by using our derived solutions for high (Equation 10) and low (Equation 11) water velocity values and the corresponding parameter values used in both examples. We illustrate this subsequently.

From Equation 10, the advective and dispersive fluxes are given by

$$UC = UC_0 \exp\left(-\frac{x\omega\lambda}{U}\right) \tag{12}$$

and

$$\alpha U\frac{\partial C}{\partial x} = \alpha C_0\omega\lambda\exp\left(-\frac{x\omega\lambda}{U}\right) \tag{13}$$

respectively. Thus, for high water velocities the advective/dispersive flux ratio is:

$$\frac{U}{\alpha\omega\lambda} \tag{14}$$

Similarly, from Equation 11, advective and dispersive fluxes are given by:

$$UC = UC_0 \exp\left(-x\sqrt{\frac{\omega\lambda}{\alpha U}}\right) \tag{15}$$

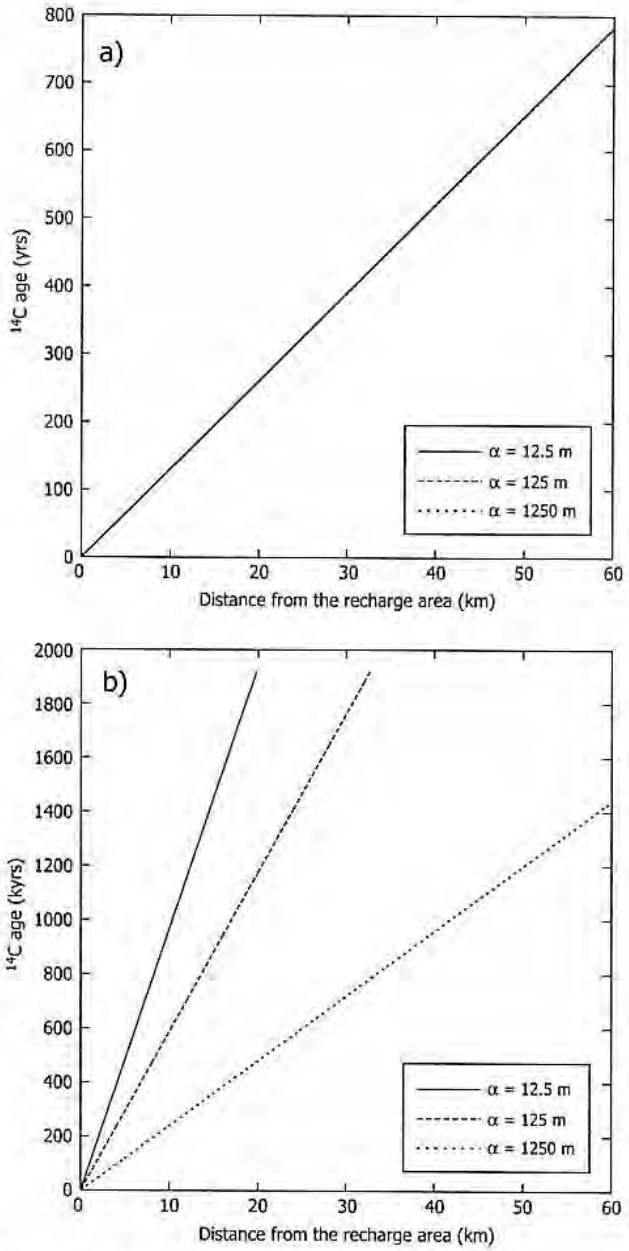

Figure 3. ^{14}C ages calculated using 1D simulations for three different dispersivity values (12.5, 125, and 1250 m): (a) for a high water velocity value ($U = 8.5 \times 10^{-7}$ m/s); (b) for a low water velocity value ($U = 1 \times 10^{-10}$ m/s).

and

$$\alpha U \frac{\partial C}{\partial x} = C_0 \sqrt{\alpha U \omega \lambda} \exp\left(-x\sqrt{\frac{\omega\lambda}{\alpha U}}\right) \qquad (16)$$

respectively. Thus, for low water velocities the advective/dispersive flux ratio is:

$$\sqrt{\frac{U}{\alpha\omega\lambda}} \qquad (17)$$

For α = 125 m, the advective/dispersive flux ratios calculated using Equations 14 ($U = 8.5 \times 10^{-7}$ m/s) and 17 ($U = 1 \times 10^{-10}$ m/s) yield 5000 and 0.8, respectively. This shows that impact of dispersion on ^{14}C ages is indeed dependent on the advective/dispersive flux ratio and is only significant when this ratio is small.

The 1D analysis presented here is simply meant to illustrate theoretically how the impact of horizontal dispersion on ^{14}C ages is dependent on the horizontal velocity value. It is also meant to illustrate how this impact, through its dependency on the coupled advective-dispersive fluxes, becomes more prominent with decreasing velocities and thus with decreasing dispersive fluxes. However, through a 1D analysis it is not possible to evaluate simultaneously the role of horizontal and transverse dispersion as well as the impact of mixing due to cross-formational flow, mixing mechanisms that impact concentration profiles and ground water ages. We thus proceed to analyze the impact of all mixing processes on our three modeling approaches through a 2D analysis.

Vertical Age Structure

A detailed analysis of the age structure along a vertical plane of all calculated ages in our original ground water flow system (Figure 2a) 50 km from the recharge area reveals some interesting results (Figure 4). This includes the Carrizo Aquifer, the overlying confining layer (Recklaw), and the Queen City Aquifer. This complex vertical age structure is essentially the result of the combined effects of mixing due to advection and horizontal and vertical dispersion.

As expected, vertical advective ages in the Carrizo Aquifer display an almost total absence of age gradient. This is because horizontal velocities are similar throughout the entire thickness of the aquifer along a same vertical, with water moving as "packets" along streamlines downgradient (see discussion by Bethke and Johnson 2002b) without exchanging water with neighboring formations (closed system). By contrast, ^{14}C and directly simulated ground water ages show a strong vertical age gradient. Ground water becomes progressively younger from bottom to top (Figure 4). At the bottom of the Carrizo, mixing with older water from the neighboring confining layer is occurring through vertical dispersion, in addition to some ^{14}C exiting the system toward the Wilcox through diffusion. Toward the top of the Carrizo, the vertical dispersion component carrying older water from the bottom becomes smaller, allowing horizontal dispersion to dominate over the vertical component rendering younger ^{14}C and directly simulated ground water ages. Comparison between ages shows once again the influence of horizontal dispersion on ^{14}C ages, the latter being younger than directly simulated ages throughout the entire thickness of the Carrizo due to this artificial source of ^{14}C.

At the interface of the confining layer, cross-formational flow is greatly facilitated through vertical dispersion as opposed to advection (Figure 4). Advective ages in the Recklaw Formation are higher than those in the Carrizo, which is opposite to ^{14}C and directly simulated ground water ages. At the interface with the Queen City, however, the situation is reversed compared to that observed in the Carrizo. In the Queen City, ^{14}C ages are now the oldest throughout most of the thickness and a vertical age gradient is absent (Figure 4). The dominant age

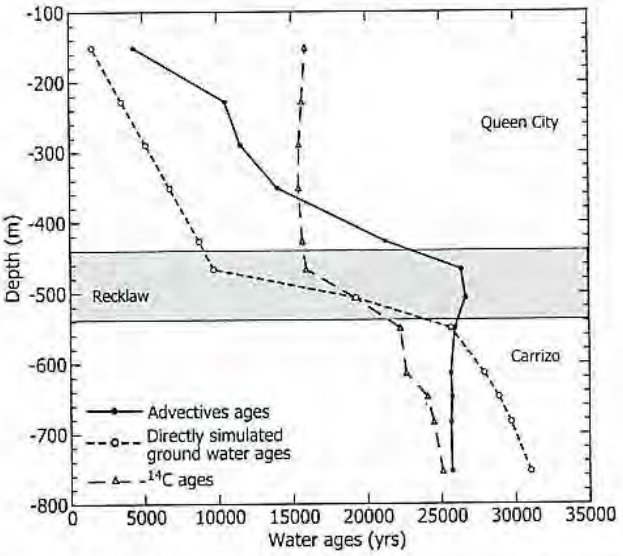

Figure 4. Vertical age structure of calculated advective, ^{14}C, and directly simulated ground water ages corresponding to the original ground water flow model calibrated with ^{4}He concentrations (Castro et al. 2003a) within the Carrizo, Recklaw, and Queen City, 50 km away from the Carrizo recharge area.

factor on ^{14}C ages in the Queen City is now the combined effect of vertical dispersion and advection through vertical upward leakage in the Recklaw, which brings a constant flux of older water with lower ^{14}C content originating in the Carrizo. Here, vertical dispersion acts as a "sink" of ^{14}C. By contrast, and as streamlines in the Queen City (which originate in the Carrizo recharge area) become shorter and shorter toward the top of the aquifer, advective ages display a vertical age gradient here, becoming progressively younger toward the surface. In addition to younger advective water arriving into the Queen City, horizontal dispersion also renders directly simulated ground water ages younger upward. This results in directly simulated ages younger than advective ages, which is the reverse of what is observed in the Carrizo.

Analysis of the vertical age structure in this complex system is important as it illustrates how the combined effect of mixing processes (e.g., advection, horizontal and vertical dispersion, as well as cross-formational flow) might cause very different vertical age structures in different areas/formations of one particular system while using the same dating method. It also illustrates, depending on the formation of interest, how these ages might evolve with respect to each other in unexpected ways.

One last important observation to note is that unlike modeled advective and ^{14}C ages, directly simulated ground water ages display a consistent behavior in the Carrizo and Queen City aquifers, with older ages at the bottom, younger toward the top. Such consistency likely indicates that, when mixing processes are relevant in a particular ground water flow system, direct simulation of ground water age will yield more realistic results than the advective and ^{14}C modeling approaches as described here.

Impact of Faults on Calculated Ages

We also investigated the potential impact of both high- and low-permeability faults that might be present not only within one particular aquifer but also in surrounding confining layers. The presence of faults in sedimentary systems is not uncommon, and a number of local faults are well documented in the Carrizo Aquifer and surrounding formations in our study area (Figure 1b). We carried out a series of simulations in which a fault with a length of ~12.5 m (the smallest element length in our original mesh) was placed ~27 km from the Carrizo recharge area in different formations. Through this set of simulations, variable hydraulic conductivity values were attributed to this fault. With the exception of this newly introduced fault, all other parameters and boundary conditions remained unchanged (Figure 1c; Castro and Goblet 2003a). Here, we present results of two different sets of simulations, the first representing a low-permeability fault placed in the Carrizo, and the second representing a high-permeability fault located in the overlying confining layer, the Recklaw Formation. Low- and high-permeability faults with hydraulic conductivities several orders of magnitude different from the values used in the simulations presented here all reveal similar trends.

Low-Permeability Fault in the Carrizo Aquifer

A hydraulic conductivity of 5×10^{-9} m/s was assigned to a fault introduced in the Carrizo Aquifer. The presence of this low-permeability fault gave origin to a ground water flow system far more complex than the original one (Figure 1c), complexity that is directly translated to calculated ground water ages (Figure 5a). Changes in the ground water flow system induced by the presence of this fault, from the recharge area down to its location, include a relatively small reduction of the horizontal velocity component simultaneously with an increase of the vertical velocity. The most remarkable changes, however, are observed on the opposite side of the fault. Here, a strong reduction of the hydraulic gradient, and therefore of the velocity field, is observed. In addition, in the vicinity of the fault, the direction of vertical leakage in the Recklaw Formation was reversed and is now downward and much smaller (~2 orders of magnitude) than that of the original ground water flow system. The new modeled water ages show these changes in a clear fashion. Between the recharge area and up to the fault location, all ages follow a similar aging trend, and no important differences between advective, ^{14}C, and directly simulated ground water ages behavior can be observed. This is because between the recharge area and the fault location, horizontal advection is by far the dominant transport process affecting all calculated ages. This behavior is consistent with previous results (e.g., Figure 2c). On the opposite side of the fault, however, and due to the strong reduction of the velocity field, all ages are now much older than the original ones, and important discrepancies between their aging behavior are observed (Figure 5a): (1) advective ages display the highest aging rate along the entire trajectory, down to 60 km from the recharge area and (2) near the fault, between ~27 and 35 km, aging of ^{14}C ages is more pronounced than that of directly simulated ground water ages. Simulated ^{14}C concentration distribution shows that a local concentric area with unusually low ^{14}C concentrations has now

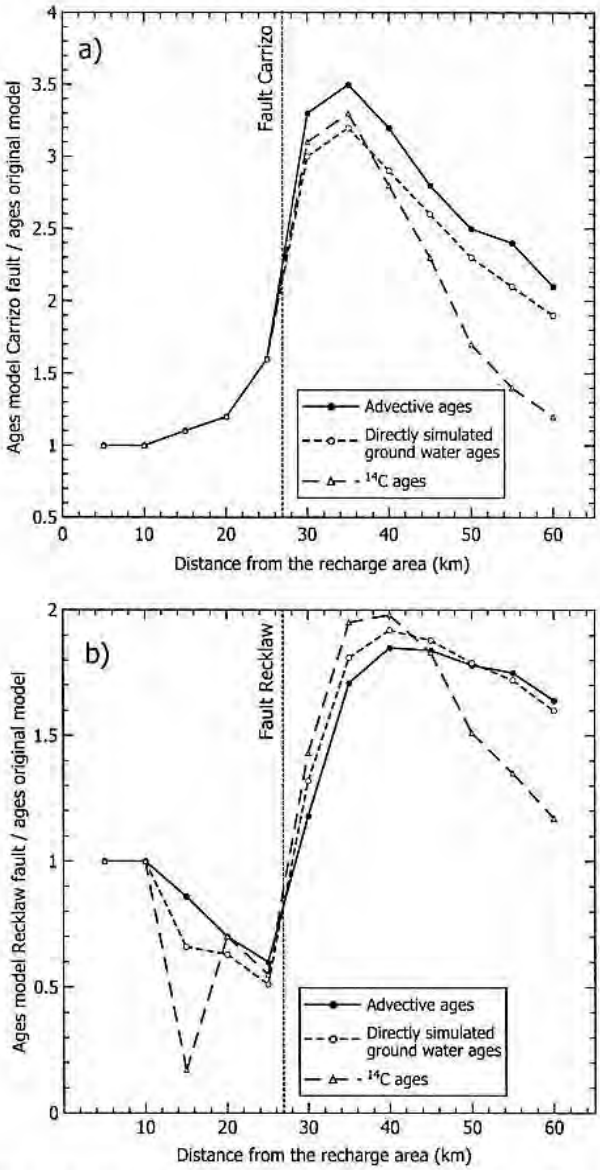

Figure 5. Calculated advective, ^{14}C, and directly simulated ground water age ratios in the Carrizo Aquifer: (a) between the original ground water flow model in which a low-permeability fault was placed in the Carrizo Aquifer (K_{fault} = 5×10^{-9} m/s) and that one of the original model (Figure 2a), as a function of distance from the recharge area. The location of the fault is indicated; (b) between the original ground water flow model in which a high-permeability fault was placed in the Recklaw Formation ($K_{fault} = 1 \times 10^{-2}$ m/s) and that one of the original model (Figure 2a), as a function of distance from the recharge area.

developed in the Recklaw Formation, near the fault. These unusually low ^{14}C concentrations are due to the very slow water movement in this confining layer. As leakage is now downward, almost stagnant water with very low ^{14}C content mix with Carrizo water, resulting in a higher aging rate than directly simulated ground water ages. Further away, at ~40 km and as previously verified, horizontal dispersion plays once again an important role on ^{14}C and directly simulated ground water ages, and the expected behavior is observed, with ^{14}C ages becoming progressively younger than directly simulated ages with increased distance from the recharge area and decreasing velocities.

High-Permeability Fault in the Recklaw Formation

To assess the potential impact on calculated water ages of a permeable fault located in a neighboring confining layer, a hydraulic conductivity value of 10^{-2} m/s was assigned to a fault placed in the Recklaw Formation. Once again, the presence of such a fault gave rise to major changes in the ground water flow system, which, in turn, resulted in important changes and distinct behavior on calculated water ages (Figure 5b). Here, horizontal flow between the recharge area and the fault is greatly enhanced, resulting in advective, ^{14}C, and directly simulated ground water ages that are now younger compared to those of the original ground water flow system. As upward leakage flux in the Recklaw Formation is smaller, less water exits the Carrizo vertically, rendering directly simulated ages and, particularly, ^{14}C ages younger compared to advective ones. On the opposite side of the fault, at ~30 km, the situation is reversed. The presence of the fault has now induced a very strong upward water movement through the Recklaw, in addition to an important reduction of water velocities in the Carrizo. As a result, ^{14}C now exits the Carrizo Aquifer upwards at a much higher rate in the fault area, leading to a much lower ^{14}C content in this aquifer on the opposite side of the fault as compared to the original ground water flow system. Consequently, between the fault location and ~40 km from the recharge area, ^{14}C ages now at a higher rate than advective and directly simulated ground water ages (Figure 5b). This upward water movement affects also the directly simulated ground water ages, although not to the same extent, as previously discussed. In this particular case, and for a relatively short distance, between ~27 and 40 km from the recharge area, advective ages are less affected by aging, while directly simulated ground water ages occupy an intermediate position. Note that despite the fact that advective ages are considerably older here compared to the original ground water flow system due to a reduction of the velocity field, the observed increase of ^{14}C and directly simulated ages is well in excess relative to advective ages due simply to mixing processes. As observed in previous situations, at further distances from the recharge area and with decreasing velocities, ^{14}C ages become younger than directly simulated ground water ages.

Calculated ^{14}C Ages Based on C Isotope Measurements

Simulations presented here were carried out in a complex ground water flow system, the Carrizo Aquifer and surrounding formations, in which the presence of local faults is well known. As pointed out earlier, in this system, based on C isotope measurements available in a number of water samples (Figure 1b; Castro et al. 2000), ^{14}C ages were previously estimated following the traditional approach in which mixing processes are not considered (Castro et al. 2000). Only radioactive decay and chemical interactions were taken into account, and no attempt was made to simulate ^{14}C transport in the system with incorporation of mixing processes (Castro et al.

2000). Subsequent comparison of these calculated ^{14}C ages with modeled advective ages (Castro and Goblet 2003a), and those obtained through direct simulation of ground water age (Castro and Goblet 2003b), shows strong discrepancies at several locations (Figure 6). Such discrepancies are particularly strong between calculated ^{14}C ages based on C isotope measurements (Castro et al. 2000) and modeled advective and directly simulated ground water ages. It is clear that at certain locations (samples TX01, TX24, and TX08, Figure 6), ^{14}C yields apparent ages that are far older than advective and directly simulated ages. In addition, at two locations (TX28 and TX03) where the presence of ^{14}C was expected based on modeling results, ^{14}C was below detection limit (Figure 6). Importantly, farther from the recharge area (samples TX04 and TX14; Figure 1b), where velocities are smaller and the impact of dispersion is more prominent, ^{14}C ages are younger than modeled advective and directly simulated ground water ages (Figure 6). Here, our simulations suggest that mixing with younger water takes place as directly simulated ground water ages become younger than advective ages (sample TX14; Figure 6). Although we cannot be fully confident that these observed discrepancies in the Carrizo Aquifer are the combined result of ground water mixing due to the presence of faults, cross-formational flow through advection, and the impact of both longitudinal and transverse dispersion, the situation observed in the field appears to be consistent with some of the simulation results presented here.

Concluding Remarks

With the set of 2D simulations presented here, we have shown how, due to mixing processes and particularly due to advection and dispersion, modeled advective, ^{14}C, and directly simulated ground water ages evolve differently with respect to each other. The impact of dispersion is particularly strong on ages obtained through simulation of ^{14}C as this mixing process may act as an important source or sink for ^{14}C in the presence of significant concentration gradients. Mixing processes due to advection and dispersion may also give rise to unexpected modeled vertical age profiles. Impact of dispersion on modeled ^{14}C and directly simulated ground water ages is systematically stronger in areas where velocities are smaller, as dispersive flux will occur in the direction of either decreasing ages (direct simulation of ground water age) or decreasing concentrations (modeled ^{14}C ages). Specifically, in the system considered here, impact of dispersion on these calculated ages becomes nonnegligible for water velocities less than $\sim 3 \times 10^{-8}$ m/s, and is particularly pronounced on modeled ^{14}C ages for velocities less than $\sim 7 \times 10^{-9}$ m/s. We also illustrate through a 1D analysis the effect of horizontal dispersion on ^{14}C ages, which depends directly on the ratio of advective to dispersive flux, not on the dispersive flux value alone. Impact of dispersion becomes more prominent with decreasing velocities and thus with decreasing dispersive fluxes. Specifically, this impact is significant for low ratios of advective to dispersive flux and decreases as the ratio increases. Longitudinal dispersion acts generally as a source of ^{14}C within a particular aquifer, while vertical dispersion acts as a sink for ^{14}C both within a single aquifer by enhancing mixing with older water located at greater depths or when crossing confining layers. Thus, depending on how dispersion contributes to additions or losses of ^{14}C, older or younger apparent modeled ^{14}C ages relative to the actual age of ground water might be observed.

The impact of faults on modeled water ages was also assessed. Depending on fault locations (aquifers vs. aquitards) and on its degree of permeability, advective, ^{14}C, and directly simulated ground water ages will evolve in very different ways, leading potentially to local differences in modeled ages up to many thousands of years. Our modeling approach for ^{14}C dating (i.e., ^{14}C ages) has a particularly distinct behavior in complex ground water flow systems where extremely strong variations of the velocity field are present, in addition to the presence of local faults. Here, mixing due to cross-formational flow as well as dispersion may impact significantly the modeled ^{14}C concentrations.

Simulations presented here were carried out in a complex ground water flow system, the Carrizo Aquifer and surrounding formations, in which the presence of local faults is well known. Here, previous calculations of advective (Castro and Goblet 2003a), ^{14}C (Castro et al. 2000), and directly simulated ground water ages (Castro and Goblet 2003b) show the presence of strong discrepancies at several locations. Specifically, discrepancies are particularly strong between ^{14}C calculated based on C isotope measurements neglecting mixing processes (Castro et al. 2000) and modeled advective and directly simulated ground water ages. Although we cannot be fully confident that these observed discrepancies in the Carrizo Aquifer are the combined result of mixing processes due to advection and dispersion enhanced locally by the

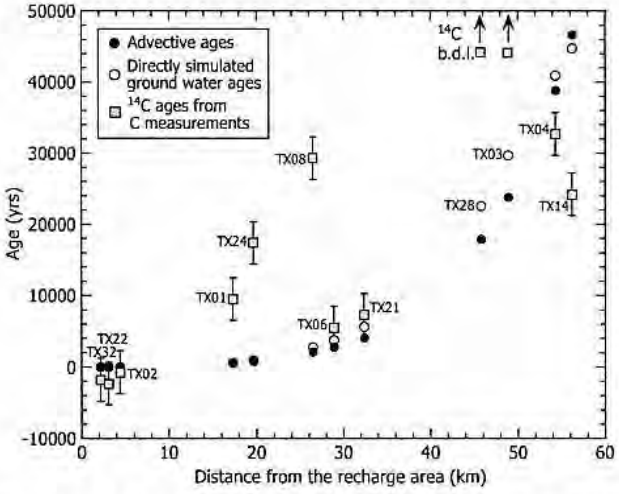

Figure 6. Calculated advective and directly simulated ground water ages (Castro and Goblet 2003a, 2003b, respectively), as well as geochemically corrected ^{14}C ages determined directly from measured ^{14}C concentrations (closed squares) (Castro et al. 2000) in the Carrizo Aquifer at sampling locations in the study area (Figure 1b), as a function of distance from the recharge area. ^{14}C is below detection limit (b.d.l.) at samples TX28 and TX03.

presence of faults, the situation observed in the field is certainly consistent with some of the simulation results presented here. Ideally, ^{14}C ages should be estimated by taking into account all physical and chemical processes affecting its concentration in order to systematically obtain ^{14}C ages that are close to the real age of ground water.

Overall, direct simulation of ground water ages seems to yield more consistent results than the modeling approaches employed here for calculation of advective and ^{14}C ages when mixing processes in a particular ground water flow system are nonnegligible and water velocities vary over several orders of magnitude within one single aquifer. Specifically, and unlike the two other modeling approaches, directly simulated ages display a consistent (or expected) vertical age structure in all formations, with older ages at the bottom, younger toward the top. The modeling approach employed here for calculation of ^{14}C ages will yield more consistent results in systems where ground water velocities are high and exhibit small variation, in addition to systems where faults are absent. Modeled advective ages will yield water ages that are representative of the real system only when mixing processes can be neglected. The latter are thus the most restrictive.

Acknowledgments

The authors thank M. P. Anderson, W. Sanford, G. Weissmann, and P. Binning for their insightful and thorough reviews, which lead to a much improved final version of this manuscript. Financial support by the National Science Foundation grant EAR-03087 07 and the Elizabeth Caroline Crosby Research Award (NSF ADVANCE at University of Michigan) is greatly appreciated.

References

Bethke, C.M., and T.M. Johnson. 2002a. Paradox of groundwater age. *Geology* 30, no.2: 107–110.

Bethke, C.M., and T.M. Johnson. 2002b. Ground water age. *Ground Water* 40, no. 4: 337–339.

Castro, M.C. 2004. Helium sources in passive margin aquifers—New evidence for a significant mantle ^{3}He source in aquifers with unexpectedly low in-situ $^{3}He/^{4}He$ production. *Earth Planetary Science Letters* 222, no. 3–4: 897–913.

Castro, M.C., and P. Goblet. 2003a. Calibration of regional groundwater flow models—Working toward a better understanding of site-specific systems. *Water Resources Research* 39, no. 6: 13-1–13-24.

Castro, M.C., and P. Goblet. 2003b. Noble gas thermometry and hydrologic ages: Evidence for late Holocene warming in Southwest Texas. *Geophysical Research Letters* 30, no. 24: 2-1–2-4.

Castro, M.C., M. Stute, and P. Schlosser. 2000. Comparison of ^{4}He and ^{14}C ages in simple aquifer systems: Implications for groundwater flow and chronologies. *Applied Geochemistry* 15, no. 8: 1137–1167.

Goode, D.J. 1996. Direct simulation of groundwater age. *Water Resources Research* 32, no. 2: 289–296.

Hamlin, H.S. 1988. Depositional and groundwater flow systems of the Carrizo-Upper Wilcox, South Texas. Austin, Texas: Bureau of Economic Geology, Report of Investigations, 175.

Johnson, T.M., and D.J. DePaolo. 1996. Reaction-transport models for radiocarbon in groundwater: The effects of longitudinal dispersion and the use of Sr isotope ratios to correct for water-rock interaction. *Water Resources Research* 32, no. 7: 2203–2212.

Li, Y.-H., and S. Gregory. 1974. Diffusion of ions in sea water and in deep sea sediments. *Geochimica et Cosmochima Acta* 38: no. 5: 703–714.

Mann, W.B., W.F. Marlow, and E.E. Hughes. 1961. Half-life of carbon-14. *International Journal of Applied Radiation and Isotopes* 11, no. 1: 57.

Patriarche D., Castro M.C., and Goblet P. 2004. Large-scale hydraulic conductivities inferred from three-dimensional groundwater flow and ^{4}He transport modeling in the Carrizo aquifer, Texas. *Journal of Geophysical Research* 109, 1–19.

Phillips, F.M., and M.C. Castro. 2003. Groundwater dating and residence-time measurements. In *Treatise on Geochemistry*, ed. H.D. Holland and K.K. Turekian, vol. . 5: *Surface and Ground Water, Weathering, and Soils*, ed. J.I. Drever, 451–497. Oxford, U.K.: Elsevier.

Pint, C.D., R.J. Hunt, and M.P. Anderson. 2003. Flowpath delineation and ground water age, Allequash Basin, Wisconsin. *Ground Water* 41, no. 7: 895–902.

Plummer, L.N., E.C. Prestemon, and D.L. Parkhurst. 1991. An interactive code (NETPATH) for modeling net geochemical reactions along a flow path. Reston, Virginia: USGS Water-Resources Investigations Report 91–4078.

Sanford. W.E. 1997. Correcting for diffusion in carbon-14 dating of ground water. *Ground Water* 35, no. 2: 357–361.

Sanford W.E., and S. Buapeng. 1996. Assessment of a groundwater flow model of the Bangkok Basin, Thailand, using carbon-14-based ages and paleohydrology. *Hydrogeology Journal* 4, no. 4: 26–40.

Stute, M., P. Schlosser, J.F. Clark, and W.S. Broecker. 1992. Paleotemperatures in the southwestern United States derived from noble gas measurements in groundwater. *Science* 256, no. 5059: 1000–1003.

Sudicky, E.A., and E.O. Frind. 1981. Carbon 14 dating of groundwater in confined aquifers: Implications of aquitard diffusion. *Water Resources Research* 17, no. 4: 1060–1064.

Varni, M., and J. Carrera. 1998. Simulation of groundwater distributions. *Water Resources Research* 34, no. 12: 3271–3281.

Walker G.R., and P.G. Cook. 1991. The importance of considering diffusion when using carbon-14 to estimate groundwater recharge to an unconfined aquifer. *Journal of Hydrology* 128, no. 1–4: 41–48.

Wang, J.H., C.V. Robinson, and I.S. Edelman. 1953. Self-diffusion and structure of liquid water. III. Measurement of self-diffusion of liquid water with H^{2}, H^{3} and O^{18} as tracers. *Journal of American Chemical Society* 75, no. 2: 466–470.

Weissmann, G.S., Y. Zhang, E.M. LaBolle, and G.E. Fogg. 2002. Dispersion of groundwater age in an alluvial aquifer system. *Water Resources Research* 38, no. 10: 16-1–16-13.

Weyhenmeyer C.E., S.J. Burns, H.N. Waber, W. Aeschbach-Hertig, R. Kipfer, H.H. Loosli, and A. Matter. 2000. Cool glacial temperatures and changes in moisture source recorded in Oman groundwaters. *Science* 287, no. 5454: 842–845.

Calculation of Low-Range Flow Velocities in Fractured Carbonate Media from Borehole Hydrochemical Logging Data Comparison with Thermometric Results

by Pascal Bidaux and Claude Drogue[a]

Abstract

Flow rates and concentrations from fractures intersected by a borehole can be estimated by matching simulated concentration profiles to the observed variations in water chemistry along the borehole. Experiments in karstic rocks prove that hydraulic short circuits between fractures yield a very complex flow pattern, and that flow velocities in the borehole may be higher than the velocity at which the piezometric level varies. Combined temperature and concentration studies characterize flow in both high permeability channels and slightly fissured blocks, as chemical profiles detect low velocity flows that cannot be identified on temperature profiles. Such studies are therefore advisable to characterize natural flow in fractured carbonate rocks, but also in other fractured media.

Introduction

As the "equivalent porous medium" concept (Bear, 1972) is generally not applicable at the local scale in fractured media (Long, 1983; Long and Witherspoon, 1985), large scale hydraulic measurements (Witherspoon et al., 1980) only provide a basis for more detailed flow analysis. Specific borehole techniques have been developed to characterize, localize, and quantify ground-water flow precisely. For example, hydrothermal properties of fractures in granite have been determined by injecting water between packers (Hosanski and Ledoux, 1982), but no information on natural flow is obtained because the high pressure modifies the system. Radioisotope methods provide information on natural flow (Moser and Drost, 1986), but these methods are expensive and highly regulated to avoid any negative impact on the environment. Fracture inflow parameters into a borehole produced at a low flow rate also have been characterized by fluid conductivity logging (Tsang, 1987; Tsang and Hale, 1989).

Hydrochemical logging, introduced by Bidaux et al. (1986) to identify microcirculations in granites, consists of determining the variations in water chemistry along an open borehole. It is somewhat similar to fluid conductivity logging, but provides more precise information, as conductivity only gives an indication on the overall mineralization of water. For example, hydrochemical logs along boreholes in a karstic aquifer in Southern China (Yuan et al., 1990), unveiled a simultaneous increase in magnesium concentration and decrease in calcium concentration with no significant conductivity change.

The present paper analyzes hydrochemical logs under their transient aspect. Successive logs are used to estimate fracture inflow parameters (flow rates and concentrations into and out of a borehole). The transient behavior of a concentration profile, resulting from hydraulic short circuits between fractures and from differences in the chemical composition of water inflows, is simulated for a given set of fracture inflow parameters. A field application is given for a 51 m deep borehole at an experimental site in a karstic aquifer in Southern France. Field data processing involves an inverse problem, as the inputs of the model (fracture inflow parameters) are unknown and the outputs (simulated logs) must be adjusted to experimental data. Successive bicarbonate concentration logs are obtained by analyzing water samples taken along the borehole at various depths; then simulations are performed to find the set of fracture inflow parameters which gives the best fit. Finally, the obtained values of fracture inflow parameters are discussed along with the structural context, other hydraulic observations, and thermometric data.

Formulation

A succession of hydrochemical logs is described by a function C(z,t) (concentration in a given element at depth z and time t). Prior to solving the inverse problem (determining fracture inflow parameters from experimental data which are discrete values of C), let us consider the direct problem (generating logs for a given set of fracture inflow parameters). Concentration (in the borehole profile) is

[a]Laboratoire d'Hydrogéologie, Université des Sciences et Techniques, Place E. Bataillon, 34095 Montpellier Cedex 05, France.

Received September 1990, revised February and May 1992, accepted June 1992.

Discussion open until July 1, 1993.

assumed to obey the following equation:

$$D \frac{\partial^2 z}{\partial z^2} - \frac{\partial}{\partial z}(VC) + \phi_f = \frac{\partial C}{\partial t} \quad (1)$$

where D is the apparent longitudinal dispersion coefficient, V is the "through flow" velocity as defined by Moser and Drost (1986), and ϕ_f is the source term related to fracture inflow or outflow. Dissolution/precipitation, adsorption/desorption at the well walls, and chemical reactions within the aqueous phase, depend on the considered element. In the present work, they are neglected as justified previously (Bidaux et al., 1986).

V and ϕ_f directly derive from fracture inflow parameters. Inflows and outflows are assumed to occur only at discrete locations z_{fj} (fractures), and the "through flow" velocity is given by the continuity equation:

$$V(z,t) = \frac{1}{S} \sum_{j,\, z_{fj} < z} Q_{fj}(t) \quad (2)$$

in which $Q_{fj}(t)$ represents the algebraic value of the flow into the borehole at fracture j (positive for an inflow). The horizontal cross section S of the borehole is assumed to be constant. Hence, at each time t, $V_t(z) = V(z,t)$ is a step function of z with a discontinuity $\Delta V = Q_{fj}/S$ at each fracture j. Positive values of V correspond to flow toward the top of the borehole. The source term ϕ_f has a distinct formulation whether it concerns an inflow or an outflow, as concentration in water flowing out from the borehole into a fracture is given by its value in the borehole in front of the fracture, while inflow concentration is set by conditions inside the fracture and not in the borehole. For an inflow, we have:

$$\phi_f(t) = \frac{Q_{fj}(t)}{S} C_{fj}(t)\, \delta(z_{fj}) \quad (3a)$$

in which $C_{fj}(t)$ represents the inflow concentration, and δ is the Dirac function. The expression for an outflow does not involve C_{fj}:

$$\phi_f(t) = \frac{Q_{fj}(t)}{S} C(z_{fj}, t)\, \delta(z_{fj}) \quad (3b)$$

In order to avoid numerical dispersion and oscillations, advection and dispersion are solved separately at each time step. Karasaki (1988) used a similar technique to simulate transport in fracture networks. Instead of calculating the profile $C_t(z)$ at time t from $C_{t-\Delta t}(z)$ directly, using (1), an intermediate fictive profile $C^{(a)}{}_t(z)$ is first calculated, that is obtained from $C_{t-\Delta t}(z)$ by pure advection. Then $C_t(z)$ is obtained from $C^{(a)}{}_t(z)$ by pure dispersion during the time interval Δt. Using a Lagrangian description, advection can be solved exactly for any depth z and within any time interval Δt, by backtracking the fluid particle located at depth z without time or space discretization. The advected concentration $C^{(a)}{}_t(z)$ can be simply calculated from the initial profile and fracture inflow parameters by distinguishing four cases, whether water comes from the borehole, from a fracture, or is a mixture of both borehole and fracture water (Figure 1). Using an Eulerian description,

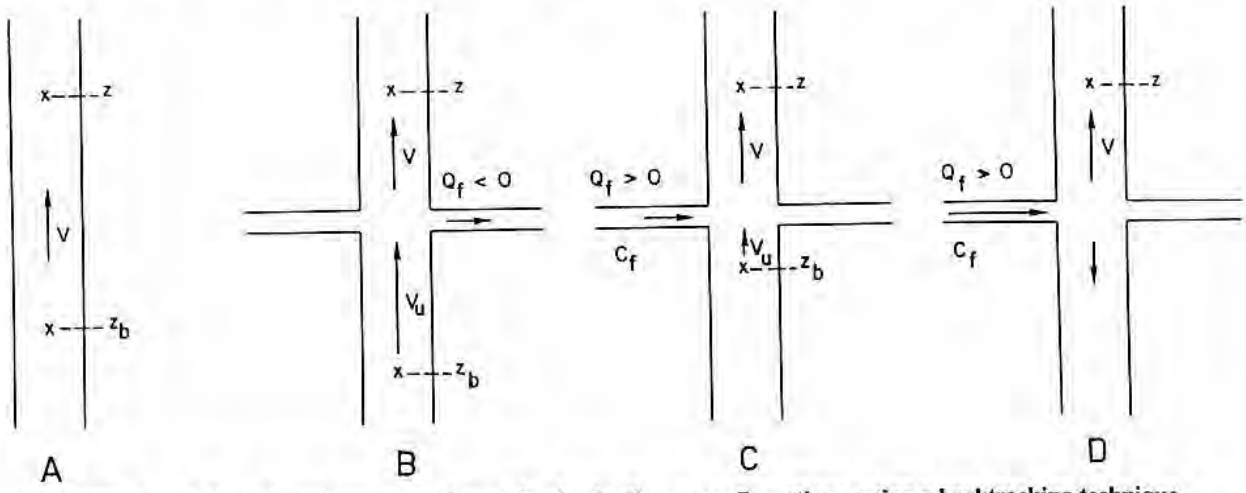

Fig. 1. Determination of the advected concentration at depth z in diverse configurations, using a backtracking technique.

A. No fracture exists between z and z-VΔt. Water at z is unmixed borehole water:

$$C^{(a)}{}_t(z) = C_{t-\Delta t}(z_b), \text{ with } z_b = z - V\Delta t$$

B. An outflow exists at z_f between z and $z - V\Delta t$, and the throughflow velocity upstream is V_u ($|Vu| > |V|$). Water at z is still unmixed borehole water, but the expression of z_b has changed:

$$C^{(a)}{}_t(z) = C_{t-\Delta t}(z_b), \text{ with } z_b = z_f - V_u(\Delta t - (z - z_f)/V)$$

C. An inflow exists at z_f between z and $z - V\Delta t$, and the throughflow velocity has the same direction on both sides of z_f. Water at z is a mixture of fracture water and borehole water from upstream:

$$C^{(a)}{}_t(z) = [Q_f C_f + V_u S C_{t-\Delta t}(z_b)]/VS, \text{ with } z_b = z_f - V_u(\Delta t - (z - z_f)/V)$$

D. An inflow exists at z_f between z and $z - V\Delta t$, and the flow diverges from the fracture. Water at z is unmixed fracture water:

$$C^{(A)}{}_t(z) = C_f$$

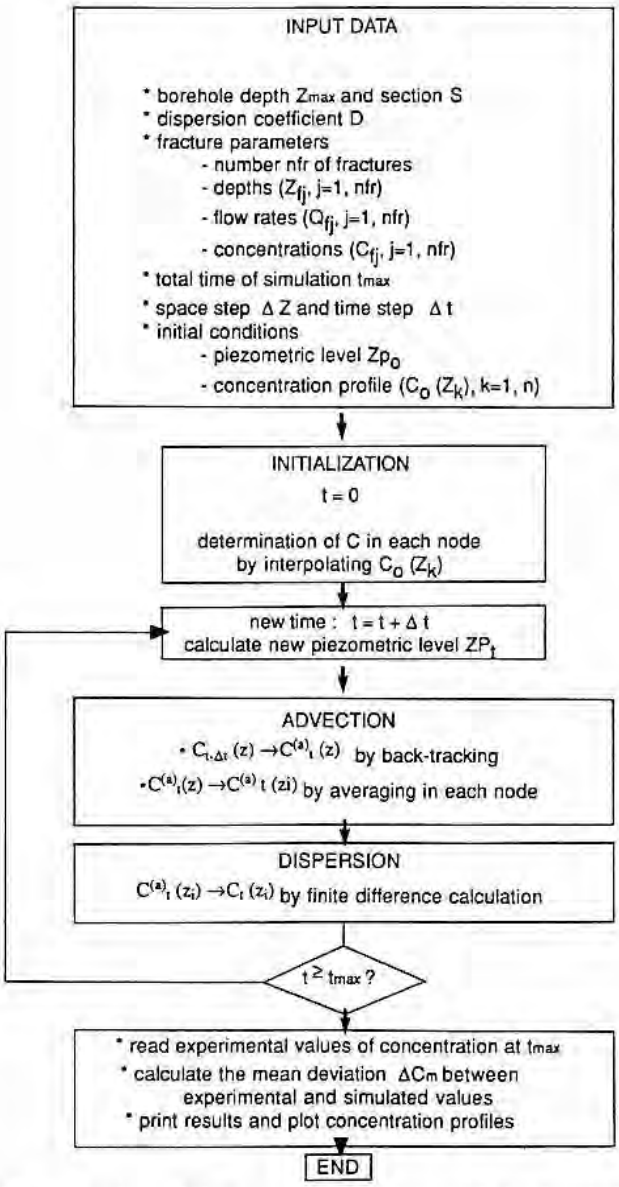

Fig. 2. Structure of the computer code for simulating borehole hydrochemical logging. At each time step, the advective and dispersive problem are solved separately.

dispersion is solved by an implicit finite-difference technique. Because of the discretization, the advected concentration profile is averaged in each node before the calculation of dispersion (Figure 2).

Procedure and Field Results

The Experimental Site

The field measurements concern an experimental site located in the lower Cretaceous limestones and marly limestones at Terrieu, Southern France. The site has been developed since 1975 to study the saturated zone of a karstic aquifer at the scale of the interfractural distance (Drogue and Grillot, 1976). On the site, 20 open boreholes have been drilled on a 5 m × 5 m square grid (Figure 3), whose axes are oriented parallel to the directions for which the intensity of fracturing is maximum (N020 and N110), based on both outcrop mapping and aerial photographs. The boreholes are 60 m deep and reach the saturated zone of the karst. The water table is about 30 m below the ground surface in the dry season. During the rainy season, it is typically 15 to 20 m below the ground surface. Sporadically, some boreholes may become artesian or the whole site may be flooded, as a result of the most violent rains.

Previous measurements on the site have already emphasized a strong correlation between structure and hydraulic behavior. Among them, pumping tests disclose anisotropy. The flow is preferentially oriented parallel to the directions of maximum intensity of fracturing (Pitard,

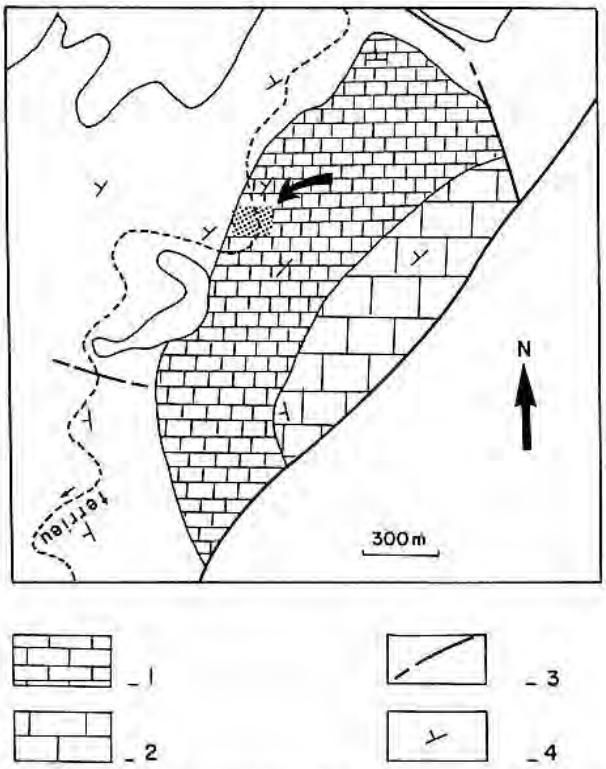

Fig. 3a. The Terrieu experimental site—location and geological setting (1: Lower Cretaceous; 2: Upper Jurassic; 3: fault; 4: dip).

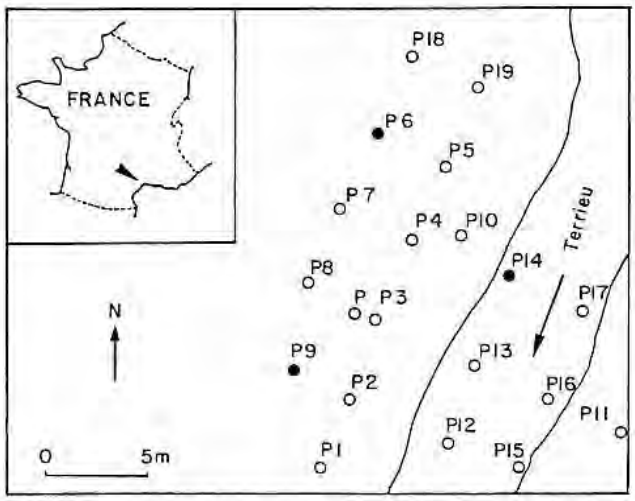

Fig. 3b. The Terrieu experimental site—the boreholes marked by black circles are those mentioned in the present study: P6 (estimation of the longitudinal dispersion); P9 (continuous recording of water level); P14 (time series of hydrochemical logs).

1976). Temperature profiles along the boreholes exhibit a strong horizontal heterogeneity: the mean low-water temperature gradient may differ up to a two-to-one ratio from one borehole to another (Drogue, 1985). Significant variations in the geothermal flux or in rock thermal conductivity are unlikely to occur at such a small scale, and the unperturbed temperature profiles show that the effect of natural convection is unimportant. Thus, vertical advection is the most reasonable explanation for the observed disparity in the temperature gradients. Besides, the deformation of thermal profiles during a high-water period, which is specific to each borehole, indicates the main inflow of water just infiltrated, which has not reached temperature equilibrium with the rock matrix (Figure 4).

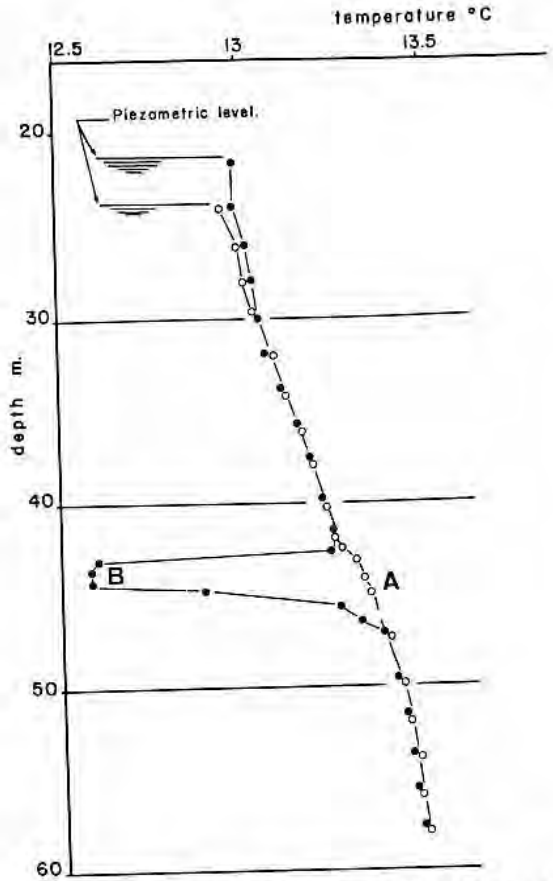

Fig. 4. Typical unperturbed (A) and perturbed (B) temperature profiles in a borehole with a major fracture at Terrieu.

Estimation of Advection Flow Velocities Along the Borehole

The experimental hydrochemical logs concern borehole P14, during the period between November 13 and December 14, 1984. On November 14-15 and November 30-December 1, heavy rains were followed by an abrupt increase in the water level. The water level on P14 is fairly similar to that on P9, which is continuously recorded (Figure 5). The hydrochemical logs (Figure 6) extend to a depth of 50 m, below which the borehole has collapsed. For each log, water samples are taken out of the borehole at a variable step (1 to 4 m) and passed through a 0.45 μm filter. The sampling volume is small (250 cm^3) to minimize any

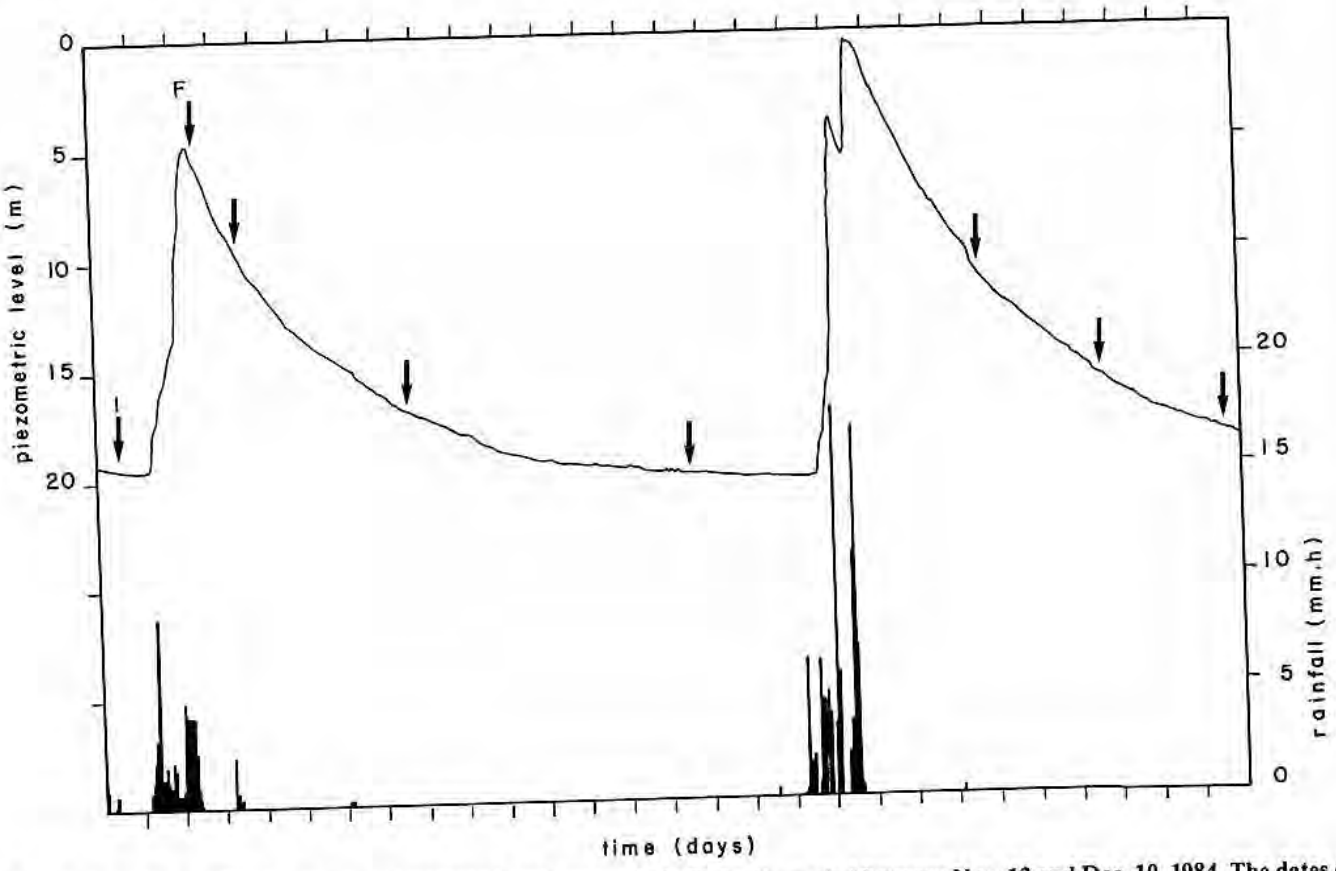

Fig. 5. Rainfall at the Terrieu site and piezometric level on borehole P9 for the period between Nov. 13 and Dec. 10, 1984. The dates of hydrochemical logs are shown by arrows. The dates of initial and final profiles used for the adjustment of fracture flow parameters are indicated by the letters "I" and "F," respectively.

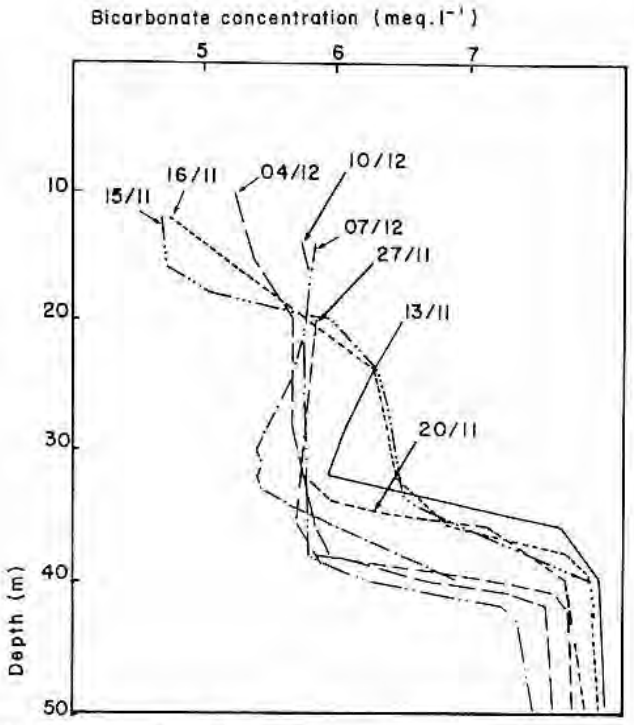

Fig. 6. Observed bicarbonate concentration profiles in borehole P14 at eight different dates.

perturbation to the system. Bicarbonate concentration is immediately determined by a potentiometric titration, using the Gran method (reproducibility: 0.5% accuracy: 1%). The following analysis is based on bicarbonate that has proved to be a good indicator of ground-water flow. It may seem paradoxical to choose such a reactive element, but concentration in less reactive elements does not differ significantly enough from one inflow to another and hence exhibits flats, uninterpretable profiles. At the time scale of a rainy episode (several days), it is reasonable to assume that calcite dissolution mainly occurs in the fractures, where the contact area is large, rather than at the well wall. Nonlinearities in mixing are expected to be unimportant, because inflows with composition of similar types are involved.

The dispersion coefficient D has been estimated by observing the spread of deionized water in a borehole at the same site (Bidaux, 1987). This second borehole does not cross any major fracture, and the experiment has been carried out during a low-water period (summer) so that the advective transport can be neglected. The obtained value, $2 \times 10^{-5} m^2.s^{-1}$, is four orders of magnitude larger than ion diffusion in water. Such difference can be explained by the existence of thermal convection cells (Sammel, 1968). Small cells, even if they do not appear on temperature profiles, may drastically enhance large-scale dispersion by generating recirculation (Pomeau, 1985). The parabolic flow velocity distribution may also contribute to longitudinal dispersion, the borehole diameter (115 mm) and the inflow values estimated below yield Reynolds numbers from less than 1 to the 100 range. In addition, dispersion effects related to the flow velocity distribution in a horizontal cross section are probably increased by the irregularity of the borehole walls. However, a detailed analysis of dispersion along a borehole falls beyond the scope of the present paper. The experimentally determined dispersion coefficient is considered as a macroscopic, 1D number that globally integrates the several possible small-scale phenomena mentioned hereabove.

The piezometric variations considered on P14 to constrain the fit are based on both discrete measurements on P14 and the continuous recording on P9 (Figure 7). Five periods are so distinguished; each one has its specific set of constant fracture inflow parameters and hence exhibits a linear variation in the piezometric level. An indicator of the quality of the match is given by the following expression:

$$\Delta C_m = \sqrt{\frac{1}{n} \sum_{i=1}^{n} [C_{exp}(i) - C_{sim}(i)]^2} \qquad (4)$$

in which $[C_{exp}(i), i = 1,n]$ are the n experimental final values and $[C_{sim}(i), i = 1,n]$ are the corresponding simulated values. In the present case, a simple set of fractures (approximate depths: 10 m, 20 m, 35 m, and other fractures in the lower part of the borehole, below 42 m and may be in the collapsed section, between 51 and 60 m) and the fracture inflow parameters given in Table 1 yield a satisfactory value of ΔC_m (below 0.04 $meq.l^{-1}$). Experimental and simulated concentrations for the final date (Nov. 15) are in good agreement (Figure 8). Let us mention that the circulation in the lower part of the borehole can be quantified, but not localized with precision, because it occurs in a portion where the concentration gradient is very low.

Hydraulic Interpretation and Discussion

The values given in Table 1 have been obtained by trial and error, and there is no evidence that the provided solution is unique. Other sets of inflow parameters may yield equally good matches. However, our results for the analysis of the hydrochemical logs hereabove will be validated by the following discussion, in which a consistent schema is proposed for the hydraulic evolution of the system during the studied time interval. The piezometric level h results from the hydraulic potential values h_f in the fractures, near their

Table 1. Fracture Inflow/Outflow Parameters Giving the Best Fit for the Hydrochemical Evolution of P14 for the Studied Time Interval

Fracture depth Z_f (m)	*Bicarbonate concentration C_f ($meq.l^{-1}$)*	*Fracture inflow Q_f (cm^3S^{-1})*				
		first 15 h	*next 17 h*	*next 3 h*	*next 4 h*	*next 2 h*
10	4.68	0	0.95	5.16	3.78	0.84
20		0	-1.21	-2.25	-0.98	-0.95
34	6.40	0	1.38	2.51	-0.66	-0.58
under 42	8.00	-0.01	-0.12	-1.10	0.03	0.98

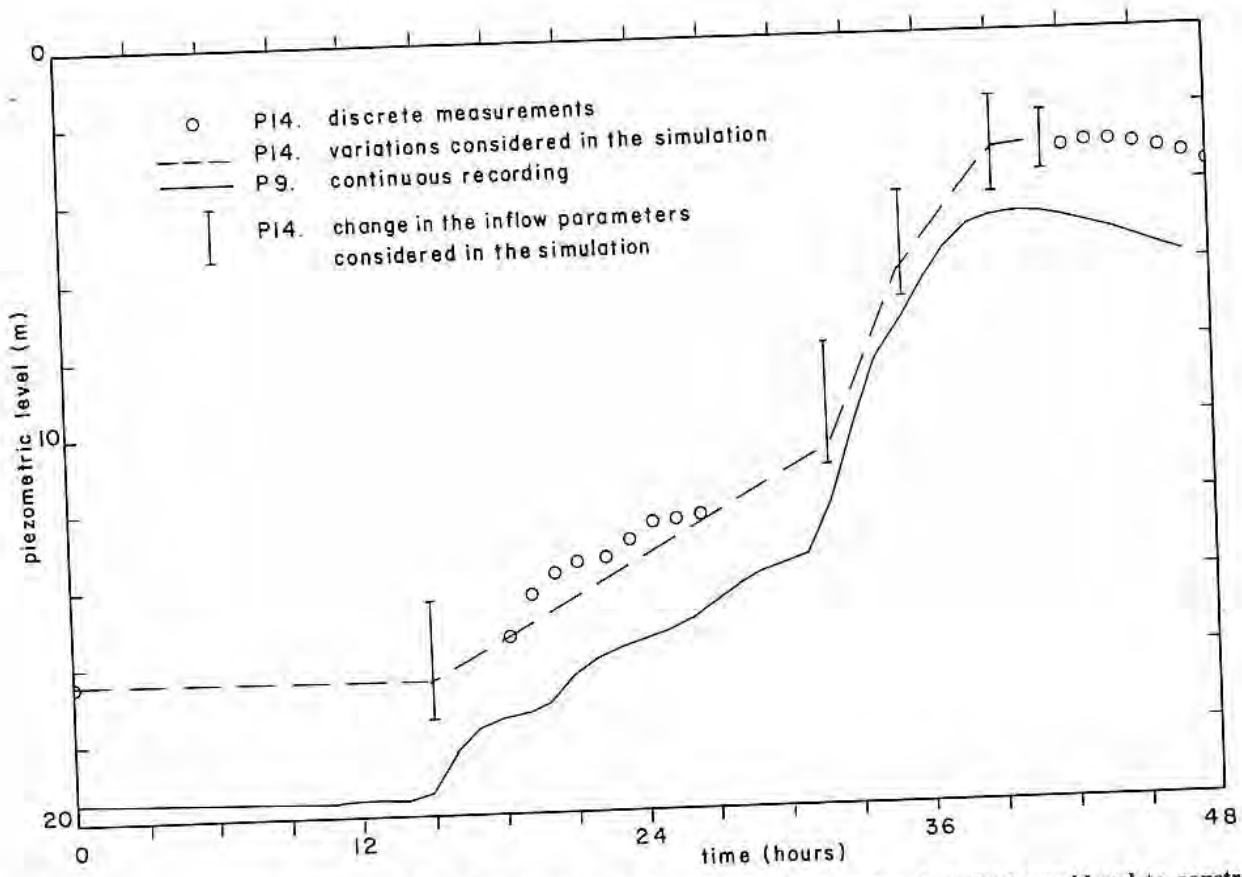

Fig. 7. Discrete piezometric measurements and hypothetical continuous variations on borehole P14 considered to constrain the simulation: comparison with the continuous record from borehole P9.

intersection with the borehole. A given fracture discharges water if $h_f > h$ and absorbs water if $h_f < h$. The rain causes a rise in the h_f values, but each fracture behaves distinctly, because it is more or less sensitive to the rain, reacts after some delay, and has specific hydraulic parameters. In light of these considerations, the four main fractures intersecting the borehole can be characterized. The top fracture ($z_f = 10$ m) responds sharply and rapidly to rainfall, which attests a good connection with the ground surface. The sudden increase in the inflow value (from 0.95 to 5.16 $cm^3 s^{-1}$) corresponds approximately to the time at which the water level in the borehole reaches the fracture and may be linked to the fact that a permeable zone at that level becomes saturated and hence exhibits a higher hydraulic conductivity. The second fracture ($z_f = 20$ m), on the contrary, absorbs water during the whole time interval. This behavior corresponds to a good connection with the drainage system and a rather poor connection with surface fractures. The third fracture ($z_f = 34$ m) and the fourth fracture (below 42 m) have symmetric behaviors: both exhibit inversions. The former discharges, then absorbs water while the latter absorbs, then discharges. That may result from the distinction between the two types of porosity that characterize a karstic aquifer: conductive channels in which the pressure perturbation occurs immediately after rainfall; and capacitive, finely fissured blocks in which the pressure wave is delayed and damped. Hence, the fracture at $z_f = 34$ m, which responds at once, is probably more conductive than the lower fracture.

Also, the bicarbonate concentration in fractures appears to remain stable throughout the studied episode, but differs

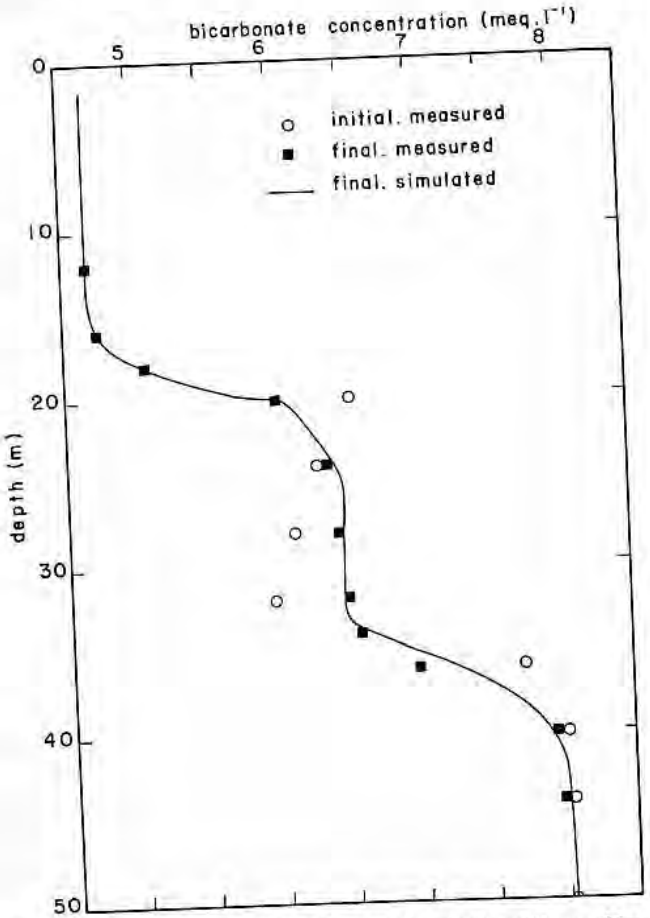

Fig. 8. Measured and simulated hydrochemical profiles on Nov. 15 (final values), and measured profile on Nov. 13. The best simulated log is obtained with the fracture flow parmeters given in Table 1 using the measured values on Nov. 13 as initial conditions.

from one fracture to another: the deeper the fracture, the more mineralized is the water. A longer residence time and flow in narrow fractures for the deeper water may explain that higher concentration, while inflows in the upper part correspond to water just infiltrated, flowing in wide channels, therefore dissolves a moderate quantity of carbonate rock.

Another explanation may be a heterogeneous context of CO_2 pressures, that results in a heterogeneous distribution of bicarbonate concentrations at saturation. Deep CO_2 forming would be in line with the tectonic context and temperature anomalies observed at the regional scale (Champagne, 1984). This would also account for the very high measured bicarbonate concentrations: lower values are found in karsts in Southern China (Bidaux et al., 1988), although the surface CO_2 pressures are presumably much higher there than at Terrieu, according to the climate and to the vegetation. These hydrochemical considerations are also in agreement with the hydraulic scheme discussed above; because the structure of the karst is strongly heterogeneous and discontinuous, the effects of deep CO_2 would be expected to have an irregular spatial distribution.

Comparison Between Hydrochemical and Thermometric Data

The observations hereabove are consistent with the previously mentioned heterogeneity in the temperature gradients of the boreholes at the site. At a larger depth scale, temperature profiles are distorted by ascending or descending water flow, which induces respectively an increase or a decrease of the temperature gradient near the ground surface (Drogue, 1985). Such vertical flows do exist, as shown for borehole P14 which intersects fractures with distinct hydraulic potentials. Besides, two out of the four zones of fracture flow revealed by hydrochemical logs in P14 coincide with thermometric results. According to temperature profiles (Figure 9), inflows occur in the upper part of the borehole and other flows are observed at about a depth of 35 m. However, the fracture flows at a depth of 20 m and deeper than 42 m do not appear.

The following development discusses how hydrochemical and thermal logs complement each other and how their combined use provides the optimal information on groundwater flow. The main point is the difference between heat and solute transfer processes, although both obey a similar mathematical formulation. At the well wall, chemical fluxes between water and rock matrix are very small and can be neglected, as the kinetics of chemical processes are very slow and the contact area is small. But heat conduction through rock matrix is the main factor which controls the temperature of water in the borehole. Therefore, a thermal reference profile can be defined which corresponds to an equilibrium between borehole water and the surrounding rock whose temperature is given by the geothermal gradient. Conversely, no hydrochemical reference profile exists because the water in the borehole does not reach a chemical equilibrium with the minerals in the surrounding rock. For that reason, a single hydrochemical log does not generally provide reliable information concerning fracture flow into and out of the borehole. Successive logs should be run in order to identify fracture flow parameters by studying advection in the borehole. On the other hand, from a single temperature profile, it is possible to observe directly whether the borehole is perturbed or not. As a consequence of heat conduction through rock matrix, a thermally perturbed borehole is rapidly brought back to equilibrium after the perturbing inflow stops (between 3 and 10 days if the flood is not too strong). But a chemical perturbation in the borehole, caused by an inflow of water of another composition, does not dissipate so easily. The anomaly may move upwards or downwards, mix with water previously in the borehole and spread by dispersion. It does not disappear until it is completely flushed out of the borehole. The hydrochemical profile remains in a modified status for a very long time and another perturbation may occur before the first one has disappeared. A steady state may never be reached. Besides, the thermal diffusion coefficient in water is about 100 times larger than the diffusion coefficient of ions. Hence, a temperature perturbation vanishes more quickly than a chemical perturbation.

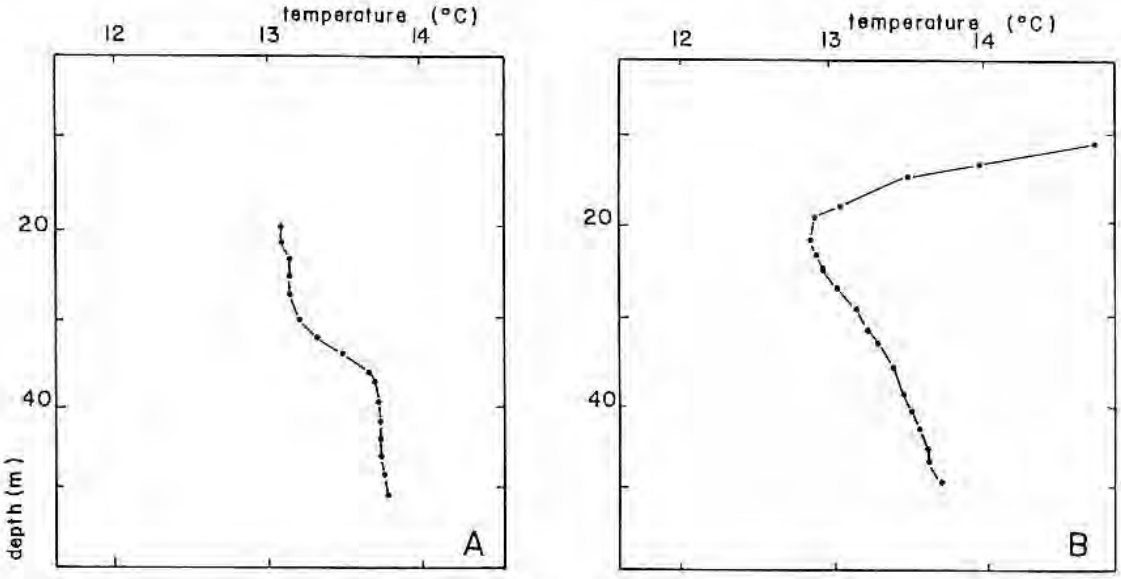

Fig. 9. Temperature profiles from borehole P14. A: Oct. 19, 1977 (before rainstorm). B: Oct. 26, 1977 (after rainstorm).

Conclusion

Although the sampling technique and the assumptions of the model are quite simplistic, and the degree of uniqueness of the solution needs further investigation, hydrochemical logging provides valuable information concerning the location and the intensity of ground-water flow in karstic rocks. Hydrochemical logging is also applicable to other types of fissured or fractured media, and the results of its processing may be used as an input to constrain sophisticated three-dimensional simulators of transient flow and transport in fracture networks, such as Karasaki's (1988). The model also could be easily extended in order to take regional flow inside the fractures into account. Flow patterns in fractures would be similar to those studied by Bidaux and Tsang (1989, 1991) for a porous aquifer.

The analysis of hydrochemical logs in a borehole during a rainy episode has allowed flow rates and bicarbonate concentrations from and into the intersected fractures to be evaluated. The connections of the fractures with the ground surface, the drainage system, and the deep karst, have been characterized.

While temperature appears to be an instant indicator of high velocity flow, hydrochemistry can identify low velocity flow, which cannot be detected by temperature measurements. Thus, the combined use of thermal and hydrochemical logs seems to be a suitable tool for the study of groundwater flow in karstic rocks. High velocity flow, which occurs in high permeability channels, and low velocity flow, which occurs in low secondary permeability, slightly fissured blocks, can be characterized. Consequently, the proposed technique consists in a quantitative approach of the karst model that has already been recognized qualitatively by several authors (Milanovic, 1981; Cui Guangzhong et al., 1988; Drogue, 1988; White 1988).

Acknowledgments

The authors are grateful to Chin-Fu Tsang of Lawrence Berkeley Laboratory for fruitful discussions and comments on the manuscript.

References

Bear, J. 1972. Dynamics of Fluids in Porous Media. Elsevier. 764 pp.

Bidaux, P. 1987. Méthode hydrochimique pour localiser et mesurer les écoulements naturels en milieu fissuré peu perméable. Hydrogéologie. no. 3, pp. 169-176.

Bidaux, P., C. Drogue, A. Dai, and J. S. Tang. 1988. The main chemical features of groundwater in carbonate Devono-Carboniferous rocks in Southern China. Rev. Sc. de l'Eau. I, no. 3, pp. 253-276.

Bidaux, P., G. Michard, C. Drogue, and C. Beaucaire. 1986. Nouvelle méthode pour l'identification des écoulements en roches fissurées peu perméables. C. R. Acad. Sc. Paris. t. 302, Série II, no. 11, pp. 751-754.

Bidaux, P. and C.-F. Tsang. 1989. An analytic solution relating wellbore and formation velocities with application to tracer dilution problem. Proc. Conf. "New Field Techniques for Quantifying the Physical and Chemical Properties of Heterogeneous Aquifers," Dallas, Texas, March 20-23, 1989. National Water Well Association. pp. 585-604.

Bidaux, P. and C.-F. Tsang. 1991. Fluid flow patterns around a well or an underground drift with complex skin effects. Water Resour. Res. v. 27, no. 11, pp. 2993-3008.

Champagne, P. 1984. Utilisation des mesures de température des eaux souterraines pour une meilleure connaissance des écoulements d'une nappe phréatique. Thèse, 3e cycle, Univ. Montpellier II. 150 pp.

Cui Guangzhong, Shu Yuan Feng, Qin Xiaogun. 1988. Hybrid simulation for karst water systems. Exemplified by Beishan Karst Water Systems. IAH 21st Congress, Karst Hydrology and Karst Environment Protection. October, Guilin-China. v. XXI, part 2, pp. 655-662.

Drogue, C. 1985. Geothermal gradients and groundwater circulations in fissured and karstic rocks: The role played by the structure of the permeable network. J. Geodyn. no. 4, pp. 219-231.

Drogue, C. 1988. Scale effect of rock fissuration porosity. Environ. Geol. Water Sci. v. 11, no. 2, pp. 135-140.

Drogue, C. and J. C. Grillot. 1976. Structure géologique et premières observations piézométriques à la limite du sous-système karstique de Terrieu (périmètre expérimental). In: Ann. Sc. Univ. Besançon (France), Géologie. fasc. 25, 3è série, pp. 195-210.

Hosanski, J.-M. and E. Ledoux. 1982. In situ determination of the hydrothermal properties of a deep fractured medium by a single well technique. J. Hydrol. v. 56, pp. 39-47.

Karasaki, K. 1988. Modifiaction to TRINET: A three-dimensional advection-dispersion code for fracture networks. Earth Sciences Division Annual Report 1987, Lawrence Berkeley Laboratory. Report no. 24200, pp. 175-176.

Long, J.C.S. 1983. Investigation of equivalent porous medium permeability in networks of discontinuous fractures. Ph.D. thesis, Univ. of California, Berkeley.

Long, J.C.S. and P. A. Witherspoon. 1985. The relationship of the degree of interconnection to permeability in fractured networks. J. Geophys. Res. v. 90, no. 34, pp. 3087-3098.

Milanovic, P. T. 1981. Karst Hydrology. Water Res. Publications. pp. 116-150.

Moser, H. and W. Drost. 1986. Application of single and multi-well techniques in fractured rocks. Proc. Meeting "Isotope Techniques in the Study of the Hydrology of Fractured and Fissured Rocks," Vienna, Nov. 17-21, 1986. International Atomic Energy Agency. pp. 223-237.

Pitard, J. 1976. Contribution à l'interprétation des essais par pompage dans les roches fissurées. Doct. thesis, Univ. Montpellier II, France. 98 pp.

Pomeau, Y. 1985. Dispersion dans un écoulement en présence de zones de recirculation. C. R. Acad. Sc., Paris. t.301, série II, no. 6, pp. 1004-1012.

Sammel, E. A. 1968. Convective flow and its effects on temperature logging in small diameter wells. Geophysics. v. 33, no. 6, pp. 1004-1012.

Tsang, C.-F. 1987. A borehole fluid conductivity logging method for the determination of fracture inflow parameters. Lawrence Berkeley Laboratory. Report no. 23096.

Tsang, C.-F. and F. V. Hale. 1989. A direct integral method for the analysis of borehole conductivity logs to determine fracture inflow parameters. Proc. Conf. "New Field Techniques for Quantifying the Physical and Chemical Properties of Heterogeneous Aquifers," Dallas, Texas, March 20-23, 1989. National Water Well Association. pp. 133-153.

Witherspoon, P. A., C. R. Wilson, J.C.S. Long, A. O. Dubois, R. M. Galbraith, J. E. Gale, and M. McPherson. 1980. Mesures de perméabilité en grand dans les roches cristallines fracturées. Bull. BRGM. (2), sec. III, no. 1, 1980-81, pp. 53-61.

White, W. B. 1988. Geomorphology and Hydrology of Karst Terrains. Oxford Univ. Press. pp. 150-183.

Yuan, D., C. Drogue, A. Dai, W. Lao, W. Cai, P. Bidaux, and M. Razack. 1990. Hydrology of the karst aquifer at the experimental site of Guilin in Southern China. J. Hydrol. v. 115, pp. 285-296.

Can Contaminant Transport Models Predict Breakthrough?

by Wei-Shyuan "Stone" Peng, Duane R. Hampton, Leonard F. Konikow, Kiran Kambham, and Jeffrey J. Benegar

Abstract

A solute breakthrough curve measured during a two-well tracer test was successfully predicted in 1986 using specialized contaminant transport models. Water was injected into a confined, unconsolidated sand aquifer and pumped out 125 feet (38.3 m) away at the same steady rate. The injected water was spiked with bromide for over three days; the outflow concentration was monitored for a month. Based on previous tests, the horizontal hydraulic conductivity of the thick aquifer varied by a factor of seven among 12 layers. Assuming stratified flow with small dispersivities, two research groups accurately predicted breakthrough with three-dimensional (12-layer) models using curvilinear elements following the arc-shaped flowlines in this test.

Can contaminant transport models commonly used in industry, that use rectangular blocks, also reproduce this breakthrough curve? The two-well test was simulated with four MODFLOW-based models, MT3D (FD and HMOC options), MODFLOWT, MOC3D, and MODFLOW-SURFACT.

Using the same 12 layers and small dispersivity used in the successful 1986 simulations, these models fit almost as accurately as the models using curvilinear blocks. Subtle variations in the curves illustrate differences among the codes. Sensitivities of the results to number and size of grid blocks, number of layers, boundary conditions, and values of dispersivity and porosity are briefly presented. The fit between calculated and measured breakthrough curves degenerated as the number of layers and/or grid blocks decreased, reflecting a loss of model predictive power as the level of characterization lessened. Therefore, the breakthrough curve for most field sites can be predicted only qualitatively due to limited characterization of the hydrogeology and contaminant source strength.

Introduction

The flow of contaminated ground water at many sites is simulated using computer models. These models are used to calculate the concentration of a contaminant at an exposure point where a potential receptor exists. This concentration is compared with regulatory standards to determine whether human health or the environment is at risk.

Many of the computer models used for this purpose are based on MODFLOW (McDonald and Harbaugh 1988), a ground water flow model that has become a true industry standard because it is comprehensive, widely available, accepted by courts and government agencies, well-documented, supported, and easily modified. MT3D (Zheng 1990) is a full-featured three-dimensional (3D) transport model that links with MODFLOW. MODFLOW-SURFACT (HydroGeoLogic 1995) is an enhanced version of MODFLOW linked with a transport model. MODFLOWT (GeoTrans 1996) and MOC3D (Konikow et al. 1996) are 3D flow and transport models that incorporate MODFLOW. These numerical models are versatile and powerful. In this study we use one well-controlled field experiment as the basis for evaluating the viability of these models for quantifying contaminant transport.

Our ultimate goal is to assess whether such sophisticated numerical models can be used "off the shelf" by modelers in industry, many having limited prior contaminant modeling experience, and still have any predictive value. Many factors complicate this assessment of the potential

Pages 104–113

of modeling for predictive power, including adequacy of site data, budget for modeling effort, and modeler training. Therefore, we would like to narrow our focus, and ask an easier question. Given sufficient time, budget, training, hardware and software, and an ideally characterized site with a well-quantified contaminant source, can experienced ground water modelers use these numerical models to successfully predict contaminant transport? If we cannot successfully predict contaminant transport using these models under ideal conditions, we doubt that contaminant transport predictions resulting from time- and resource-limited studies of less-well characterized sites and contaminant sources will be reliable.

Field Test

Site Description

This study focuses upon a best-case scenario, a site where the hydrogeology is thoroughly characterized and the contaminant input was measured over time. It is also an appropriate site because two groups (Huyakorn et al. 1986; Molz et al. 1986) have independently predicted the contaminant breakthrough with success using sophisticated models without using the previously measured breakthrough curve to calibrate their models and adjust their predictions. Thus, we know that predicting breakthrough within a reasonable confidence interval is achievable. A two-well tracer test was conducted in a confined aquifer near Mobile, Alabama (Molz et al. 1986). The surficial deposits at this site along the western flank of the Mobile River consist of a Quaternary fluvial terrace deposit comprised of interbedded sand and clay units. The 71-foot (21.6 m) thick unconsolidated sand aquifer is confined between clayey units. In the experiment by Molz et al. (1986), two wells that fully penetrate this confined stratum were used. Water was pumped out of one well and disposed at a safe distance from the test area. Water was simultaneously injected at the same rate within ± 1%, 250 gallons per minute (0.9464 m^3/min), in the other well, 125 feet (38.3 m) away. After a steady flow pattern was established, the injected water was spiked with a bromide tracer solution for 76.6 hours. Tracer-free water was injected thereafter. The bromide concentration in the pumping well was measured for 32.5 days.

This confined sand aquifer had been characterized previously during experiments investigating seasonal hot water storage underground. Parr et al. (1983) calculated an average transmissivity of 12,160 to 12,270 ft^2/day (1130 to 1140 m^2/day), a longitudinal dispersivity of 0.3 feet (9.1 cm), a ratio of horizontal to vertical hydraulic conductivity of 6.71, and a storage coefficient ranging from 0.00047 to 0.00069. Parr et al. (1983) also reported without justification the following values: a regional gradient of 3.3×10^{-4}, an *estimated* porosity of 0.33, and a hydraulic conductivity of 176 ft/day (53.6 m/day). This reported hydraulic conductivity differs slightly from the values calculated using the transmissivities of 12,160 to 12,270 ft^2/day (1130 to 1140 m^2/day) divided by the aquifer thickness, 71 feet (21.6 m), or 171 to 173 ft/day (52.3 to 52.8 m/day). The aquifer is composed of medium to fine sand

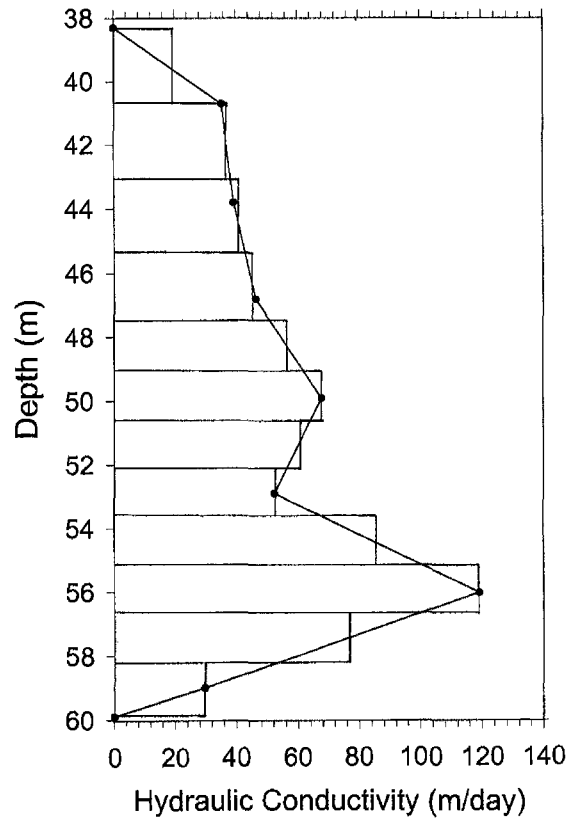

Figure 1. Twelve-layer hydraulic conductivity discretization of measured values.

containing from 1% to 15% silt and clay (Molz et al. 1985). The aquifer appears to coarsen slightly downward, with a horizon at a depth of 184 feet (56 m) having fewer fines than the other depths sampled (Molz et al. 1985).

Single-well tracer tests were performed to determine the vertical distribution of horizontal hydraulic conductivity (Molz et al. 1985). In these tests, a conservative tracer solution was injected into the aquifer for a period and then withdrawn through the same well. The tracer concentration was measured periodically at the injection/withdrawal well and at a nearby observation well with seven distinct monitoring levels. Tracer concentration and electrical conductivity data from the fourth test were used to infer tracer breakthrough times for different aquifer depths. These breakthrough times were the basis of the vertical distribution of horizontal hydraulic conductivity, K_h, shown as a jagged line with seven nonzero data points in Figure 1. The K_h values in this aquifer varied by up to a factor of four among seven different vertical intervals reported in Molz et al. (1985). Molz et al. (1986) and Huyakorn et al. (1986) represented this variation in K_h using 12 discrete layers whose normalized conductivity values are presented in Table 1 and are depicted in Figure 1. The K_h values in this aquifer varied by up to a factor of seven among 12 different vertical intervals, which were 4.9 to 7.2 feet (1.5 to 2.5 m) thick.

Previous Simulations

The two-well test was simulated by the two independent groups cited previously using the models described

Table 1
Two-Well Test Parameters Used to Predict Breakthrough Curves

Layer (i)	Thickness (m)	K_i/K_{max} Normalized K_i	Q_i/Q_{Total} Normalized Q_i	$K_z = K_i/6.71$ m/day
1	2.4	0.15	0.037	2.66
2	2.46	0.31	0.078	5.50
3	2.24	0.34	0.078	6.03
4	2.25	0.38	0.088	6.74
5	1.5	0.48	0.074	8.52
6	1.5	0.57	0.088	10.12
7	1.5	0.51	0.079	9.05
8	1.5	0.44	0.068	7.81
9	1.5	0.72	0.111	12.78
10	1.5	1.00	0.154	17.75
11	1.5	0.65	0.100	11.54
12	1.75	0.25	0.045	4.44

K_{max} = 391 ft/day (119.1 m/day)
Q_{Total} = 250 gpm (0.9464 m^3/min)

Table 2.
Additional Two-Well Test Parameters Used to Predict Breakthrough Curves

Additional Parameters	Value
Longitudinal dispersivity	0.5 ft (0.15 m)
Transverse (horizontal) dispersivity	0.16 ft (0.05 m)
Transverse (vertical) dispersivity	0.033 ft (0.01 m)
Tracer injection time	3.19 days
Total injection time	32.5 days
One-half well spacing	62.8 ft (19.14 m)
Radius of injection and production wells	3 in (0.08 m)
Injection and production rates	250 gpm (0.9464 m^3/min)
Porosity	0.35
Aquifer thickness	71 ft (21.6 m)
Molecular diffusion coefficient	1.1×10^{-8} ft^2/s (1×10^{-9} m^2/s)

by Huyakorn et al. (1986) and Guven et al. (1986). Data supplied to the modelers came directly from field measurements or calculations derived from field measurements, with the exceptions of dispersivity and porosity (Table 2). Molz et al. (1986) explained how they arrived at a porosity estimate of 0.35 (instead of the previously estimated value of 0.33), and justified using an estimated longitudinal dispersivity of 0.5 feet (15 cm) (instead of the measured value of 0.3 feet, or 9.1 cm). The dispersivity of 0.3 feet (9.1 cm) was measured for an injection test over a distance of 50 feet (15.2 m) from the injection well. This experiment, with the wells 125 feet (38.3 m) apart, would likely be described by a larger dispersivity. Pickens and Grisak (1981) measured dispersivities that increased with the scale of the tracer test. Note that a longitudinal dispersivity of 0.5 feet (15 cm) is much smaller relative to the transport distance of 125 feet (38.3 m) than dispersivities commonly used in models, which are usually a percentage of the block size (e.g., 33% to 50%) or of the plume length (e.g., 10% as proposed by Pickens and Grisak 1981). Hence, this situation is dominated by advection as one would expect in a forced-gradient tracer test. The modelers were also given the measured injected bromide concentrations shown in Figure 2.

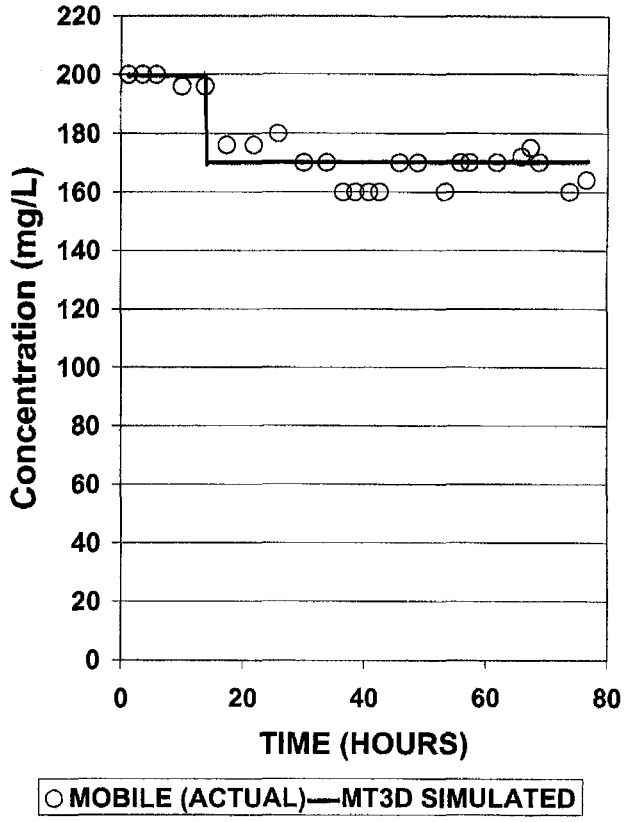

Figure 2. Bromide concentrations in injection well.

The first model was a 3D finite-element flow and transport model specially adapted by GeoTrans to follow the arc-shaped flowline pattern (Figure 3) created by a pumping/injection well pair (Huyakorn et al. 1986). It was based on 3D curvilinear coordinates so the element sides coincided with ground water flowlines. This coincidence of the element boundaries and flowlines minimizes numerical dispersion. To simulate the two-well tracer test, stratified and steady horizontal flow was assumed within each layer. By representing the measured permeability variations explicitly in the 12 layers, dispersion could be accounted for using the small value in Table 2. The model evaluated the ground water velocity distribution based on the pattern for steady flow between an injection and production well, and used it to solve the advection-dispersion equation written in 3D curvilinear coordinates.

The second model used to simulate the two-well test, called the Two-Well Advection Model, was described by Guven et al. (1986). This model assumes steady horizontal flow in perfectly stratified layers. This finite-difference model is based on the velocity field obtained from a steady-state analytical solution, ignoring completely any local hydrodynamic dispersion. Again, the finite-difference grid "blocks" consist of arc-shaped crescents that follow the flowlines. The results of applying this model to the Mobile site were reported by Molz et al. (1986).

Both simulations did a remarkable job of predicting the bromide breakthrough curve (Figure 4). Each group predicted the bromide concentration versus time, or breakthrough curve, at the production well without access

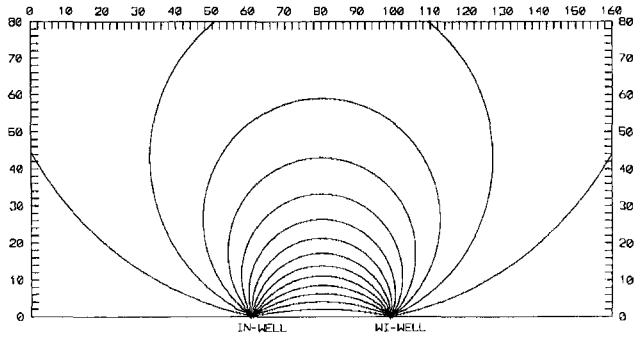

Figure 3. Flowlines linking injection and production well pair.

to the previously measured curve. The results were not calibrated. The agreement between these simulations and the measured breakthrough curve suggests that the spreading of the tracer slug over the distances involved in the two-well test depended largely on velocity variations that were controlled by the 12-layer hydraulic conductivity distribution. The use of a small dispersivity by Huyakorn et al. (1986) or no dispersivity in the model of Guven et al. (1986) assured that the computed breakthrough curve was dominated by advection.

Methods

We simulated this two-well test using four model combinations: MODFLOW with MT3D (version 1.85 from S.S. Papadopulos & Associates Inc.), MODFLOWT (version 1.13 from HSI GeoTrans), MODFLOW-SURFACT (M-S) (version 1.0 from HydroGeoLogic), and MOC3D (version 1.2 from the U.S. Geological Survey). The models were run on microcomputers. More recent versions of these models have become available since we performed this work. For example, MT3D is now available as MT3D96 or MT3DMS.

The model discretization and boundary conditions are described in the following paragraphs. In all cases, the domain simulated was half of the real domain. We exploited the symmetry of the problem, which has a straight flowline linking the pumping and injection wells, by modeling only one side of that flowline and diminishing the pumping and injection rates by 50%. The wells were both fully penetrating. Well flow rates were allocated among layers in the 3D simulations by dividing the total flow into layer-by-layer flows proportional to the transmissivity of each layer (Table 1). For the MOC3D, MODFLOWT, M-S, and most MT3D simulations, the domain was 525 feet (160 m) long parallel to the flowline linking the two wells on one side, and 262.5 feet (80 m) wide (Figure 3). Each grid block measured 6.6 feet (2 m) on each side, requiring an 80 × 40 grid. No-flow boundary conditions were used on all four sides for the simulations reported here, but other runs were made using constant-head boundaries on three sides for comparison purposes. (The boundary passing through the two wells must always be a no-flow boundary.) The constant-head breakthrough curves were lower than the curves obtained using no-

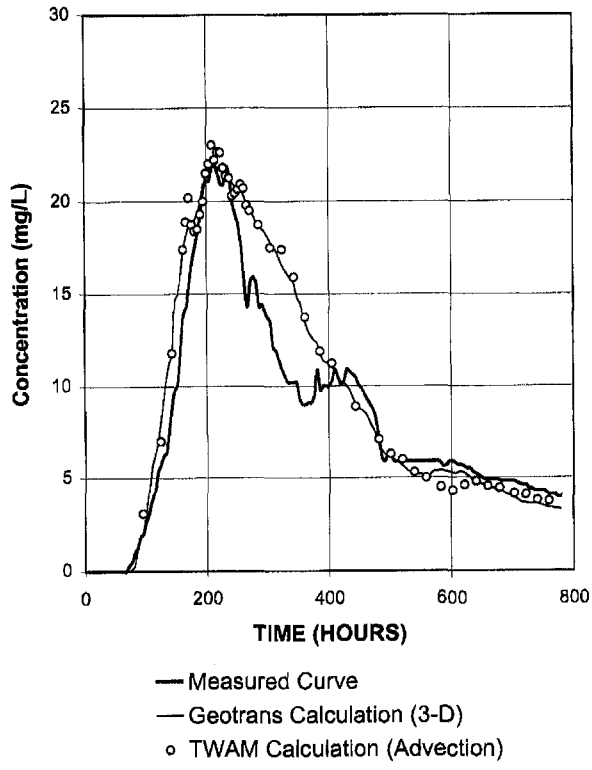

Figure 4. Measured and predicted bromide breakthrough curves for two-well test.

flow boundaries, showing that mass was lost out of the system (about 12%). Further runs using a 1063 × 531.5 foot (324 × 162 m) domain showed only 3% mass was lost out the constant-head boundaries.

MT3D (Zheng 1990) features four different solution schemes: explicit finite-difference (FD), method of characteristics (MOC), modified MOC (MMOC), and hybrid MOC (HMOC), which is a combination of MOC and MMOC exploiting the advantages of each method. All four of these methods were used initially. After comparing the results of these four methods, we used only FD and HMOC since the MOC and MMOC methods had later peaks and more numerical dispersion than HMOC results. We report here primarily the FD results to facilitate a fair comparison with the two other models that use finite-difference methods. The explicit FD method incorporates upstream weighting of the advective terms, which leads to more numerical dispersion than the other three methods. The FD method has two important advantages over the other three MT3D methods in this comparitive study. It is much faster, and produces smooth curves that are visually more satisfactory and that facilitate comparison. The alternate MT3D methods produce noisy breakthrough curves having seemingly nonphysical spikes, which is characteristic of particle-tracking methods in general, but is more severe in this problem due to its point source and sink and the problem geometry. The most recent version of MT3D-MT3DMS-has another option available besides the FD and MOC options: total variation diminishing (TVD), which is an advanced finite-difference option.

MODFLOWT (GeoTrans 1996) simulates ground water flow and advective-dispersive transport through the implicit finite-difference technique. Model users may choose between upstream weighting and central differencing for the advective terms in the finite-difference approximation of the partial differential equation for solute transport. In this study, central differencing is used because it introduces no numerical dispersion into the approximation of the advective terms. The simulation was run using sufficiently small constant time steps to maintain the Courant number criterion (less than one). The implicit time discretization employed in MODFLOWT allows for larger time steps to be used than in MT3D, which uses an explicit time discretization. Also, the Orthomin (Vinsome 1976) solver package option of MODFLOWT was used. This iterative solution scheme is similar to conjugate gradient (CG) methods for solving systems of linear equations. However, unlike CG techniques, the ORTHOMIN procedure guarantees convergence for unsymmetric matrices, such as those generated in solving the transport equation.

MODFLOW-SURFACT (M-S) (HydroGeoLogic 1995) is an enhancement of MODFLOW. M-S simulates advective-dispersive transport of up to five chemical species with linear/nonlinear retardation and first-order degradation with generation of transformation products. Time discretization may be performed using fully implicit, fully explicit, or Crank-Nicolson schemes. Spatial discretization of the advective terms is performed using the TVD scheme with a van Leer flux limiter (van Leer 1979; Harten 1983; Osher and Chakravarthy 1984). Upstream weighting, central differencing, and mixed spatial weighting schemes are also available. This study uses the TVD scheme with Crank-Nicolson time discretization to minimize numerical errors. Grid-block and time-step sizes were the same as for the other models to permit comparisons.

MOC3D (Konikow et al. 1996) is an updated version of the classic USGS 2D model of flow and transport, MOC. It is integrated with MODFLOW to simulate the transient, 3D transport and dispersion of a solute subject to decay and retardation. This implementation of the method of characteristics uses particle tracking to represent advective transport and explicit finite-difference methods to calculate the effects of other processes. MOC3D can be applied to a subgrid (of uniform rectangles) of the primary MODFLOW grid that is used to solve the flow equation. This method is most accurate and efficient for advection-dominated problems such as the one studied here.

Predictive power of the different models could be assessed several ways. The most straightforward way was to visually compare the model-predicted breakthrough curve with the measured breakthrough curve as was done in Figure 4 by previous researchers. Another option we might have chosen was to measure goodness-of-fit of the modeled to the measured breakthrough curves using a metric like root mean squared error or mean absolute error (Anderson and Woessner 1992). These metrics would sum up measures of the deviations between the two curves at many specific times. We did not choose to use these quantitative measures of prediction quality because each model produced concentration predictions over time based on their time-stepping schemes, and those times did not match the times from other models or when measured concentrations were available. Hence, the comparisons between models using these metrics would not have been fair or accurate, nor could we apply these metrics to the previous studies shown in Figure 4. Finally, one could argue that there are more important points in the breakthrough curve, such as when the first nonzero concentration is measured (or the breakthrough time), and the time and concentration at which the breakthrough curve peaks. Accurately predicting these two points is most important from a regulatory viewpoint. Another important part of the curve to fit from a remediation viewpoint is the falling limb of the curve that follows the peak. We elected to present the curve comparisons visually so each reader can assess the quality of the curve fit according to his or her own criteria.

Results and Discussion

The results from MT3D (FD option), MODFLOWT, and MODFLOW-SURFACT simulating the 12-layer data set closely match the observed breakthrough curve (Figure 5). These results are based on using a dispersivity of 0.5 feet (15 cm) and a porosity of 0.35 as well as all other parameters as specified in Table 2. Sensitivity studies of MT3D (HMOC option primarily; also FD option) showed that changing the porosity values by 0.05 made a noticeable difference (a bigger difference with HMOC

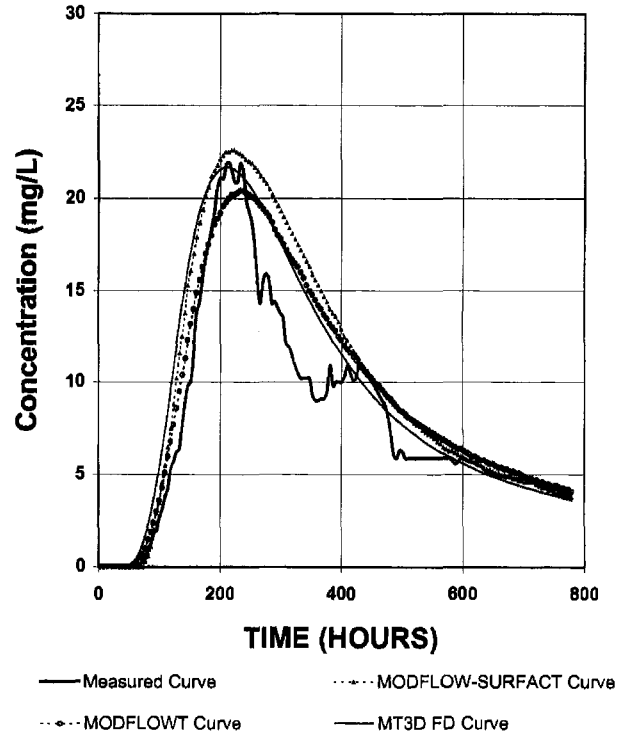

Figure 5. Comparison of bromide breakthrough curves calculated by MT3D (FD option), MODFLOWT, and MODFLOW-SURFACT with the measured breakthrough curve.

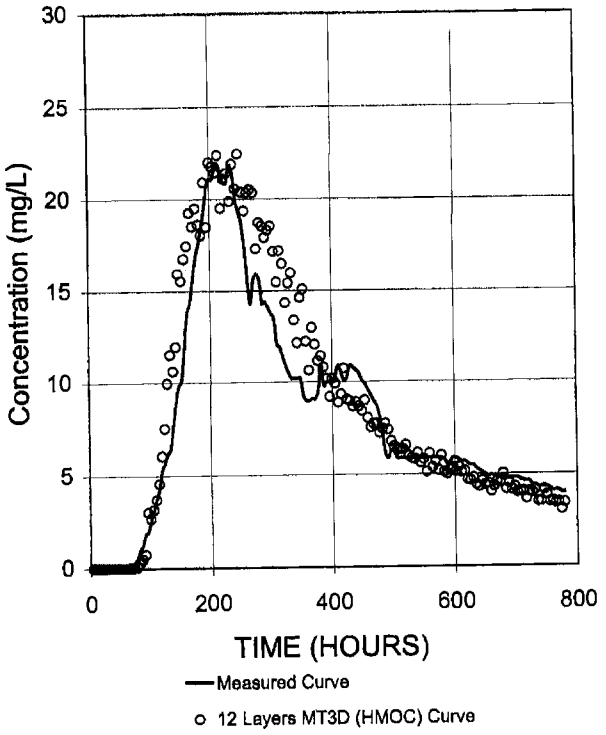

Figure 6. Comparison of bromide breakthrough curves calculated by MT3D (HMOC option) with the measured breakthrough curve.

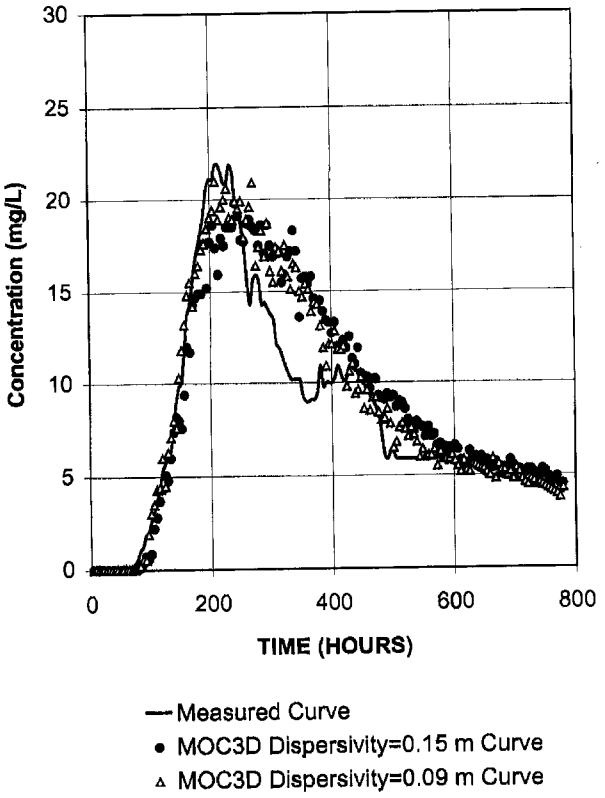

Figure 7. Breakthrough curves calculated by MOC3D using (porosity, dispersivity) of (0.33, .09 m) and (0.35, 0.15 m) versus the measured curve.

than with FD, perhaps due to the damping inherent in FD). Changing the dispersivity values from 0.5 to 3 feet (15 to 90 cm) for this advectively-dominated case resulted in only minor changes in the breakthrough curve. The MT3D curve exhibits early breakthrough due to numerical dispersion caused by upstream weighting used in the FD solver, but fits best the peak and lag portions of the bromide breakthrough. The HMOC results from MT3D, shown in Figure 6, fit as well. The 12-layer results from all three "off-the-shelf" models with rectangular blocks were almost as close to the measured curve as those obtained with the specialized computer models using arc-shaped grid "blocks."

The results obtained using the USGS MOC3D model to simulate this problem also fit the observed breakthrough curve well (Figure 7). The better-fitting curve of the two results shown is based on using the previously measured value of dispersivity, 0.3 feet (9 cm), and earlier estimate of porosity, 0.33. The MOC3D breakthrough curve did not match as well (Figure 7) when the larger dispersivity (0.5 feet, or 15 cm) and porosity (0.35) values were used, the same values used for the simulations shown in Figures 4, 5, and 6. As stated before, MOC solutions are more sensitive to porosity variations than are finite-difference solutions. Note that the concentrations shown in Figures 6 and 7 fluctuate more than in the finite-difference curves shown in Figure 5. This is a characteristic of results from particle-tracking models, such as MOC3D and MT3D (any of the three MOC options), because of the discrete nature of particles. In a sense these non-smooth results reflect the fluctuations of the measured curve better than the smooth finite-difference solutions do (but they are numerical artifacts).

For the MT3D, MOC3D, MODFLOWT, and M-S simulations the domain was 525 feet (160 m) long parallel to the flowline linking the two wells on one side, and 262.5 feet (80 m) wide (Figure 3). Each grid block measured 6.6 feet (2 m) on each side, requiring an 80 × 40 grid. No-flow boundary conditions were used on all four sides for the simulations previously shown in Figures 5, 6, and 7, as well as those shown subsequently. A larger domain of 1880 by 938 feet (573 by 286 m) also was modeled using an expanding 80 by 40 grid surrounded by impermeable boundaries. The results were essentially identical with those for the 525 by 262.5 feet (160 by 80 m) domain (Figure 8), validating the use of a smaller domain.

An important factor affecting the curves is dispersivity. The longitudinal, transverse, and vertical dispersivities were all kept small (Table 2), less than 0.2 m. Some numerical methods inherently introduce numerical dispersion. This numerical dispersivity adds to the specified dispersivity parameters to produce larger overall dispersivities, resulting in faster breakthrough times, lower peak concentrations and longer tailing of the breakthrough curve. For example, the finite-difference method typically adds numerical dispersion about equal to half of the grid block size, which was 2 m for most simulations. Therefore, the numerical dispersion greatly increased the overall longitudinal dispersion. Nevertheless, in this advectively dominated problem, dispersion has a

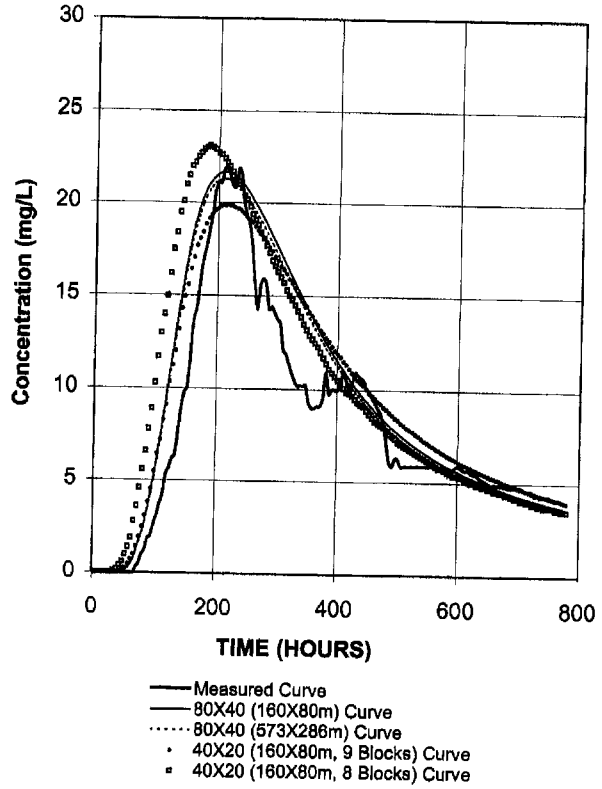

Figure 8. MT3D FD 12-layer breakthrough curves for different grids versus measured curve.

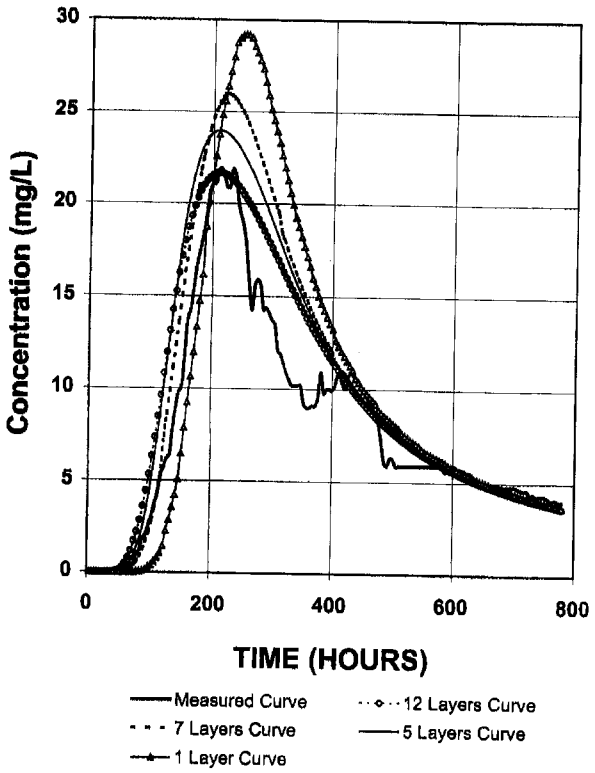

Figure 9. MT3D FD breakthrough curves for different numbers of layers versus measured curve.

secondary impact on the breakthrough curve because of the limited travel time and distance during which dispersion could spread out the tracer.

When the grid block size for the 525 by 262.5 feet (160 by 80 m) domain was increased to 13.1 feet (4 m) on a side, leading to a 40 by 20 grid, the peak height decreased significantly (Figure 8) due to the increased numerical dispersion, especially using the HMOC option (not shown). The injection and production wells are supposed to be 125 feet (38.3 m) apart. In the 80 by 40 grid, the grid blocks containing these wells are separated by 18 6.6-foot (2-m) blocks. In the 40 by 20 grid, the grid blocks containing these wells could be separated by eight or nine 13.1-foot (4 m) blocks. Using nine blocks provides a better match with the results from the 80 by 40 grid. Using eight 13.1-foot (4 m) blocks between the well blocks leads to an earlier breakthrough time, increased peak height, and earlier peak time. All subsequent 40 by 20 grid simulations were based on using nine 13.1-foot (4 m) blocks between the wells. Decreasing the grid block size from 6.6 feet (2 m) to 3.3 feet (1 m) resulted in a slight delay in breakthrough time due to decreased numerical dispersion and a slight decrease in the peak concentration.

To see if having detailed geologic data was necessary to achieve predictive power, we simulated this problem using MT3D with 12 layers, seven composite layers, five layers, and a single, average layer. While the curve calculated using MT3D with 12 layers closely matched the measured curve, the seven- and one-layer simulations (Figure 9) resulted in curves that exhibited late breakthroughs, late peaks, and high peak concentrations. The results would normally show a better fit as the number of layers increases. In Figure 9, the predicted breakthrough curve for five layers was better than that for seven layers because the hydraulic conductivity discretization we chose for five layers captured the high and low conductivity values better than our seven-layer discretization did. For this problem, with source and sink wells closely spaced in a confined aquifer and the resulting advectively dominated transport of bromide, using 12 layers (rather than seven, five, or one) was a hydrogeologic detail necessary for predictive power. Most of the natural dispersion present in this aquifer was due to the tracer traveling at different speeds in layers of different hydraulic conductivities.

For simulations using less than 12 layers, the measured peak height could be better matched when the dispersivity was increased by a large multiplicative factor. This increased dispersivity substitutes for the dispersion introduced by multiple layers with different hydraulic conductivities. The ASTM recommendation is to use a dispersivity that is one-tenth the plume length or distance of travel. Because the two wells are separated by 125 feet (38.3 m), the dispersivity resulting from adopting this recommendation would be 12.5 feet (3.83 m). We simulated this problem on an 80 by 40 grid using a single layer with this 12.5-foot (3.83 m) dispersivity as well as six other dispersivity values ranging from 1.64 feet (0.5 m) to 32.8 feet (10 m). The best curve match was achieved with a dispersivity of 12.5 feet (3.83 m) using the HMOC option (not shown). Using the FD option, the smaller 8.2-foot (2.5 m) dispersivity produced as good a fit as 12.5 feet (3.83 m) (Figure 10), implying that the optimal value

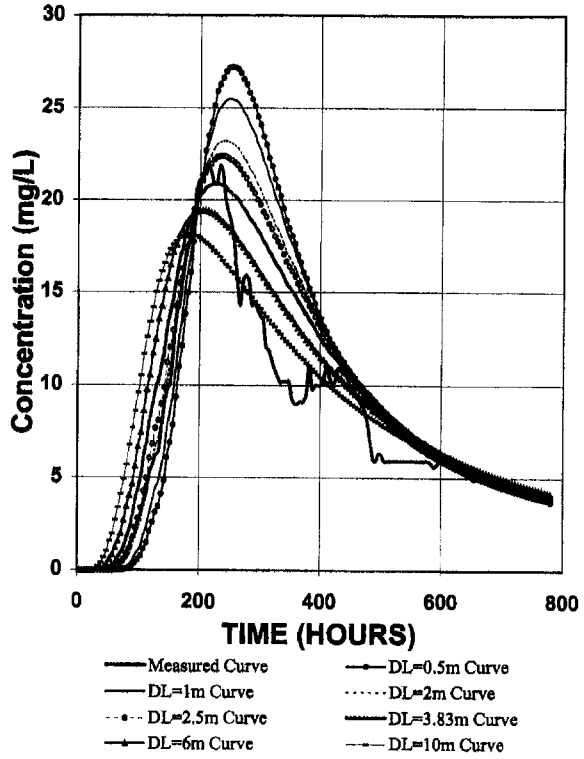

Figure 10. MT3D FD one-layer breakthrough curves for different dispersivities on 80 × 40 grid versus measured curve.

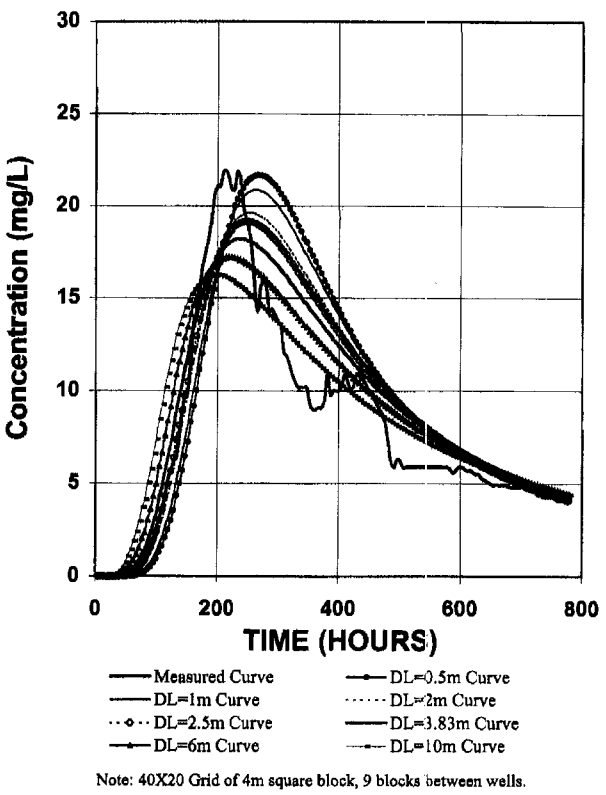

Figure 11. MT3D FD one-layer breakthrough curves for different dispersivities on 40 × 20 grid versus measured curve.

was somewhere between these two values. This slight disparity in the optimal dispersivity values makes sense given that the FD option has more inherent numerical dispersion than does the HMOC option, bringing the total dispersivity using the FD option into agreement with that used in the HMOC option.

To test whether we could use the ASTM standard dispersivity with a one-layer model and thereby dispense with characterizing the layering, we decreased the grid density to 40 by 20 (with nine blocks between the well blocks) and repeated these runs. After all, a modeler does not automatically know how many grid blocks to use in modeling a particular domain. Figure 11 shows that peak times are later and peak heights are lower for the curves from the 40 by 20 grid than those for corresponding curves on an 80 by 40 grid. The lower peak heights are due to increased numerical dispersion caused by the larger grid blocks. The shift in the predicted breakthrough curves caused by using a different grid density resulted in a different best-fitting curve on the 40 by 20 grid than on the 80 by 40 grid. (Although none is a good fit, the curve for a dispersivity of 1.64 feet [0.5 m] seems closest.) While these assessments of the best-fitting curves are qualitative, the important point is that one cannot arbitrarily pick a dispersivity for a one layer simulation and achieve a good fit. The dispersivity that produces the best fit at one grid density will not always be the best choice at a different grid density. Hence, the use of too few layers leads to loss of predictive power.

Decreasing the number of layers used to describe the vertical variation of horizontal hydraulic conductivity in the aquifer while trying to match the measured curve required increasing the dispersivity (e.g. for a one-layer simulation, multiplying by a factor of 3 to 26). This multiplicative factor depended strongly upon the number of layers, the grid spacing and the numerical transport simulation option chosen. Predictive power was lost when the model used insufficient hydrogeological detail.

The breakthrough curve was sensitive to changes in the rate of pumping and injection. When this rate was increased by 20%, the peak height increased by about 20% and the breakthrough occurred earlier. When the rate was decreased by 20%, the peak height decreased by about 20% and breakthrough was delayed.

This forced-gradient tracer test in a confined aquifer is perhaps the simplest tracer test to simulate with predictive power. A natural-gradient tracer test conducted over longer times and distances would be a greater challenge to successfully predict because one would also have to account for changes in the hydraulic gradient and for lateral changes in horizontal hydraulic conductivity. If a natural-gradient test were conducted in a water-table aquifer one would also have to account for recharge as a function of space and time. A tracer test in a fractured aquifer or in a karst setting would be even more challenging to simulate given the difficulty of characterizing the hydrogeology. Perhaps the most challenging conservative tracer test to simulate would be a multiphase flow situation with tracers in both the water and NAPL phases. The likelihood

of successfully predicting tracer movement in the multiphase case would be small given the difficulty of characterizing the multiphase flow relationships in heterogeneous aquifers. If the tracers used were nonconservative due to biodegradation, sorption, or other abiotic processes, the tracer test breakthrough curves would become virtually impossible to predict quantitatively.

Interestingly, the results of the most complicated tracer experiment are probably easier to predict than the breakthrough curves at typical contaminant sites. At many sites the contaminant source strength over time and space is unknown, and the hydrogeology can only be inferred using boring logs from the dozen or so wells present and the past plume positions over a few years. We often use a snapshot of the contaminant concentration as an instantaneous source because we cannot accurately reconstruct the contaminant input as a function of time and space. But even in an optimal case with a dense 3D network of more than 5000 sampling points—Waterloo's Borden aquifer site—Freyberg (1986) and Roberts et al. (1986) could only partially reconstruct the known masses of the original release using the detailed snapshot of two conservative salt tracers. Using an assumed constant concentration or flux source in a model without corroborating data is likely to be even less accurate than using a snapshot of the concentrations.

Summary and Conclusions

In conclusion, given sufficient time, budget, training, hardware, and an ideally characterized site with known contaminant input, all four MODFLOW-based transport models tested can predict breakthrough as accurately as a previous generation of research software. Predictive power is possible in a model only if it captures sufficient hydrogeologic details. If we have adequately characterized the hydraulic conductivity distribution for a 3D case, a small estimated dispersivity value can be used while preserving predictive power because the advective flow field can be modeled in detail and dispersion represents only a small part of the overall contaminant movement. Aquifers are often inadequately characterized, necessitating use of a larger dispersivity to compensate for ignorance of the true velocity field. Predictive power is lost when a large estimated dispersivity is used. Another difficulty for modelers is that we rarely know the contaminant input function at real sites. When the hydrogeological and chemical characterization data are less than ideal, transport models are less able to predict breakthrough and therefore should be used more qualitatively.

Acknowledgments

Thanks to Kathy Hewitt Grindstaff for initiating this project, and to Brett Coulter of C.C. Johnson & Malhotra, P.C., for his contributions. Thanks also to Alan Kehew of Western Michigan University, Sorab Panday of HydroGeoLogic, Chuck Newell of Groundwater Services, and an anonymous reviewer for their detailed reviews of previous drafts. We appreciate the reviews of this draft by John Shafer of the University of South Carolina and Scott Potter of ARCADIS Geraghty & Miller.

References

Anderson, M.P., and W.W. Woessner. 1992. *Applied Groundwater Modeling*. Boston, Massachusetts: Academic Press.

Freyberg, D.L. 1986. A natural gradient experiment on solute transport in a sand aquifer—2. Spatial moments and the advection and dispersion of nonreactive tracers. *Water Resources Research* 22, no. 13: 2031–2046.

GeoTrans Inc. 1996. MODFLOWT, a modular three-dimensional groundwater flow and transport model. Sterling, Virginia: GeoTrans.

Guven, O., R.W. Falta, F.J. Molz, and J.G. Melville. 1986. A simplified analysis of two-well tracer tests in stratified aquifers. *Ground Water* 24, no. 1: 63–71.

Harten, A. 1983. High resolution schemes for hyperbolic conservation laws. *J. Computational Physics* 49: 357–393.

Huyakorn, P.S., P.F. Andersen, F.J. Molz, O. Guven and J.G. Melville. 1986. Simulations of two-well tracer tests in stratified aquifers at the Chalk River and the Mobile sites. *Water Resources Research* 22, no. 7: 1016–1030.

HydroGeoLogic Inc. 1995. MODFLOW-SURFACT, an enhanced, MODFLOW based groundwater flow and transport model. Herndon, Virginia: HydroGeoLogic.

Konikow, L.F., D.J. Goode, and G.Z. Hornberger. 1996. A three-dimensional method-of-characteristics solute-transport model (MOC3D). U.S. Geological Survey Water-Resources Investigations Report 96-4267. Denver, Colorado: USGS.

McDonald, M.G. and A.W. Harbaugh. 1988. A modular three-dimensional finite-difference ground-water flow model. In Techniques of Water-Resources Investigations of the U.S.Geological Survey, Book 6, chapter A1. Denver, Colorado: USGS.

Molz, F.J., J.G. Melville, O. Guven, R.D. Crocker and K.T. Matteson. 1985. Design and performance of single-well tracer tests at the Mobile site. *Water Resources Research* 21, no. 10: 1497-1502.

Molz, F.J., O. Guven, J.G. Melville, R.D. Crocker, and K.T. Matteson. 1986. Performance, analysis, and simulation of a two-well tracer test at the Mobile site. *Water Resources Research* 22, no. 7: 1031–1037.

Osher, S., and S. Chakravarthy. 1984. High resolution schemes and the entropy condition. *SIAM J. Numerical Analysis* 21, no. 5: 955–984.

Parr, A.D, F.J. Molz and J.G. Melville. 1983. Field determination of aquifer thermal energy storage parameters. *Ground Water* 21, no. 1: 22–35.

Peng, W.S., D.R. Hampton, and K.M. Grindstaff. 1996. *Can groundwater contaminant transport models predict breakthrough*? ModelCare 96 Poster Papers. Golden, Colorado: International Ground Water Modeling Center.

Pickens, J.F., and G.E. Grisak. 1981. Scale-dependent dispersion in a stratified granular aquifer. *Water Resources Research* 17, no. 4: 1191–1211.

Roberts, P.V., M.N. Goltz, and D.M. Mackay. 1986. A natural gradient experiment on solute transport in a sand aquifer—3. Retardation estimates and mass balances for organic solutes. *Water Resources Research* 22, no. 13: 2047–2058.

van Leer, B. 1979. Towards the ultimate conservative difference scheme V. A second order sequel to Godunov's method. *J. Computational Physics* 32: 101–136.

Vinsome, P.K.W. 1976. Orthomin, an iterative method for solving sparse banded sets of simultaneous linear equations. Paper SPE 5729 read at the SPE-AIME Fourth Symposium on Numerical Simulation of Reservoir Performance, February, at Los Angeles, California.

Zheng, C. 1990. MT3D, a modular three-dimensional transport model. Rockville, Maryland: S.S. Papadopulos & Assoc.

Biographical Sketches

Jeffrey J. Benegar *received a B.S. in environmental sciences from the University of Virginia in 1987 and an M.S. in environmental engineering from Virginia Tech in 1995. He has been employed at HSI GeoTrans (HSI GeoTrans, 46050 Manekin Plaza, Ste. 100, Sterling, VA 20166; phone [703] 444-7000; fax [703] 444-1685;* Jeff@hsigeotrans.com; http://www.hsigeotrans.com*) in Sterling, Virginia, the last 10 years and has performed numerous ground water flow and transport projects.*

Duane R. Hampton *is an associate professor of geology at Western Michigan University, (Dept. of Geosciences, 1201 Oliver St., Western Michigan University, Kalamazoo, MI 49008; phone [616] 387-5496; fax [616] 387-5513;* duane.hampton@wmich.edu.*) where he has worked since 1986. He has a B.S. in geology from Michigan State and an M.S. and Ph.D. in civil engineering from Auburn and Colorado State, respectively. He taught two years in civil engineering at Auburn. He also worked as a hydrogeologist/modeler for ENSR in Fort Collins, Colorado. His research interests include: NAPL monitoring, recovery and tracing; well construction methods; ground water and surface water interactions; coupled heat and multiphase flow in unsaturated soils; and determining the applicability of transport models to heterogeneous sites.*

Kiran K. R. Kambham *received a B.S. in civil engineering from S.V. University, India, in 1986. He earned an M.S. in public health and environmental engineering from Andhra University, India, in 1988. He then worked as an environmental engineer at State Pollution Control Board, Andhra Pradesh. In 1995, he received a Ph.D. in environmental engineering from Texas A & M University. Since then Dr. Kambham has worked as a hydrogeologist/project engineer for HydroGeoLogic Inc., in Herndon, Virginia. He is a programmer/analyst contractor with Mobil Oil Corp. (Rite Click Consulting Inc., 9555 Blake Lane #T2, Fairfax, VA 22031; phone [703] 591-2041;* kkambham@worldnet.att.net.*) in Fairfax, Virginia, where his work involves GIS and software implementation.*

Leonard F. Konikow *has worked as a research hydrologist with the U.S. Geological Survey (U.S. Geological Survey, 431 National Center, Reston, VA 20192; phone [703] 648-5878; fax [703] 648-5274;* lkonikow@usgs.gov.*)since 1972. He received a B.A. in geology from Hofstra University (1966) and an M.S. (1969) and Ph.D. (1973) from Pennsylvania State University. His research interests include the development and application of solute-transport models to ground water contamination problems. He received the M. King Hubbert science award from the National Ground Water Association in 1989, and the O.E. Meinzer Award from the Geological Society of America in 1997.*

Wei-Shyuan "Stone" Peng *completed a B.S. in geology at Chinese Culture University in Taiwan in 1984. He completed an M.S. in environmental earth science at Western Michigan University in 1991. He worked for Dell Engineering Inc. in Holland, Michigan until 1996. Currently, he is a project hydrogeologist/modeler for Horizon Environmental Corp. (4595 Broadmoor SE, Suite 200, Grand Rapids, MI 49512; phone [616] 554-3210, ext. 320; fax [616] 554-3211;* speng@horizonenv.com.*)*

Dampening of Transverse Dispersion in the Halocline in Karst Limestone in the Northeastern Yucatan Peninsula

by Ronald K. Stoessell[a]

Abstract

A range of hydrodynamic dispersion coefficients was estimated for fracture-fluid and combined fracture and pore-fluid flow within the halocline of the limestone aquifer forming the surface of the northern Yucatan Peninsula. The coefficients are fit parameters in a model reproducing observed halocline profiles in a sinkhole and in a borehole near the northeastern coast. Fitted coefficients range from 10^{-7} to 10^{-4} cm^2/sec, of which molecular diffusion, without transverse (vertical) dispersion, can account for 10^{-7} to 10^{-5} cm^2/sec. The mechanical stability of the vertical density gradient in the halocline dampens transverse dispersion in pore fluids and in fracture fluids that are transitional between laminar and turbulent flow. The dampening is proportional to the ratio of the energy needed for the fluid to rise and displace a less dense fluid to the vertical component of the kinetic energy of the fluid. The ratio of these two energies is at a maximum during the initial stage of development of a halocline and decreases as the halocline widens.

Introduction

The northern Yucatan Peninsula (Figure 1) is a flat, low-lying, semitropical, Cenozoic limestone platform, having karst topography and lacking through-flowing rivers. Annual rainfall ranges from 0.5 m along the northern coast to 1.5 m along the eastern coast. The dimensions of the region are about 320 km east-west and 200 km north-south, with a maximum surface elevation of about 30 m (Back and Hanshaw, 1976). The peninsula is the site of rapid growth in population due to the developing tourist industry.

The surface limestone aquifer serves as the fresh-water aquifer for the peninsula. This aquifer contains a narrow fresh-water lens overlying saline water (sea water modified by water-rock interactions). The hydraulic head of the ground-water table at Chichen Itza, in the center of the peninsula (Figure 1) and 150 km from the eastern coast, was only 1.2 and 1.4 m above mean sea level in 1924 and 1966 (Back and Hanshaw, 1976). These hydraulic heads correspond, respectively, to 48 and 56 m thick fresh-water lenses in static, isostatic equilibrium with underlying sea water; although, the actual thickness will differ because the system is not static and perhaps not in isostatic equilibrium (Moore et al., 1992). The fresh-water lens thickness decreases towards the coast, becoming 30 and 18 m thick at Cenote Angelita and cenote Chemuyil, respectively, which are 12 and 6 km inland from the northeastern coast (Figure 1).

The coastal water-table elevation varies on the order of 0.1 to 0.2 m between rainy and nonrainy seasons; however, the total thickness of the coastal fresh-water lens does not vary significantly between seasons or on a yearly basis (Moore et al., 1992; Stoessell et al., 1993). The daily tidal range along the Caribbean coast is about 0.3 m and does not appear to affect the water-table elevation or the thickness of the fresh-water lens at distances greater than 2 km inland from the coast (Moore et al., 1992).

The limestone aquifer is a dual-porosity rock containing fractures and pores. In agreement with Wilson (1989), the author envisions fracture-fluid flow dominating over pore-fluid flow in the ground-water system. Fluids within the pores are likely to intersect fractures and join the fracture flow. Although some fracture fluids move out of the fractures into pores, the bulk of fracture fluids move within the fractures towards the coast. Fluids within the rock pores in the coastal region may have had significant fracture-flow portions of their travel path from the interior of the peninsula.

[a]Department of Geology and Geophysics, University of New Orleans, New Orleans, Louisiana 70148.

Received October 1993, revised April 1994, accepted October 1994.

Recently, Moore et al. (1992) reported measured average linear ground-water velocities in large fractures along the northeastern coast of the Yucatan Peninsula. The maximum measured fracture-flow velocities in fresh water increased from 1 cm/sec to 12 cm/sec along a 10 km coastward traverse, from Cenote Carwash to Cenote Tancah, along the Caribbean coast (Figure 1). This increase is presumed to result from the coastal wedging-out of the fresh-water lens as well as increased funneling of ground water from smaller fractures into larger fractures as the coast is approached (Moore et al., 1992). The fracture-fluid velocities are high values for ground-water flow; however, Worthington (1993) argues that the velocities within the fractures should be even higher.

Moore et al. (1992) also estimated average linear water velocities in pore fluids from point-dilution tests in an uncased borehole 2.6 km from the coast. These represented maximum velocity estimates and were 0.02 cm/sec in the fresh-water lens and 0.08 cm/sec in the underlying sea water, reflecting the nearby presence of a fracture. These two pore-fluid velocities are point measurements and are not necessarily representative of the pore-fluid environment.

The zone of brackish water separating the fresh water from the underlying saline water is called the halocline. The halocline thickness is surprisingly narrow, only 1 and 1.5 meters in width in Cenotes Angelita and Chemuyil, about 12 and 6 km, respectively, from the coast and 150 km from the interior of the peninsula (Figure 1). The narrowness of the haloclines suggests that diffusion, a slower process than transverse dispersion, is primarily responsible for their development. A less dense fluid (fresh water) overlying a more dense fluid (saline water) may act to dampen transverse dispersion.

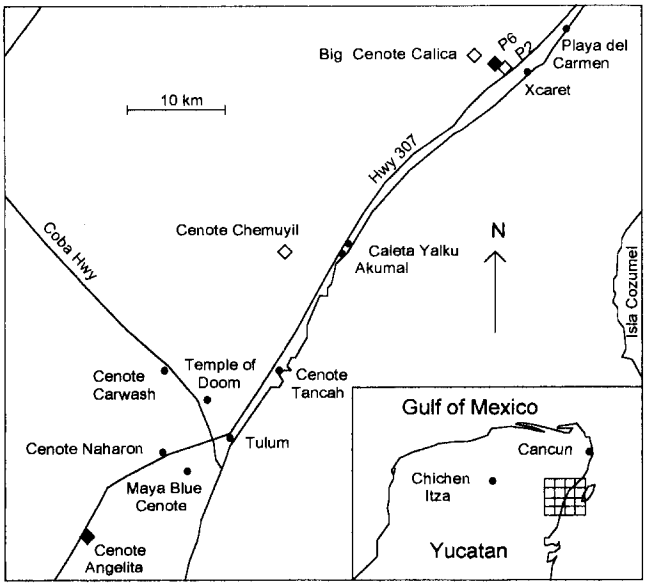

Fig. 1. Location map of the study area showing the sampling sites (marked with a diamond) for the depth-salinity profiles in Figure 3.

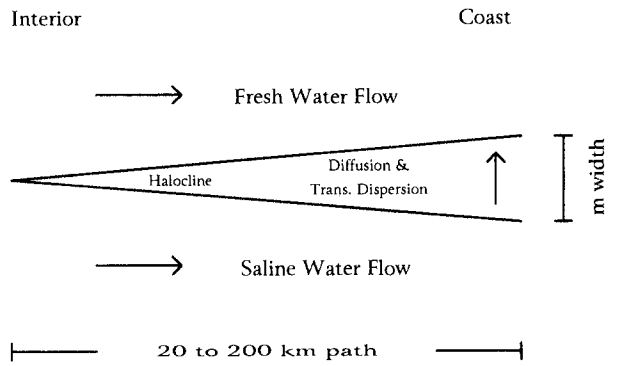

Fig. 2. Schematic model of the development of the halocline between underlying saline waters and overlying fresh waters.

Pollution problems are expected to increase in the fresh-water aquifer as the population increases. Pollutants injected in saline waters below the halocline may cross into the overlying fresh waters. In the absence of vertical advection, the rate of crossover will be controlled by transverse dispersion and molecular diffusion. For modeling purposes, the effects of these two processes are usually combined into the hydrodynamic dispersion coefficient, the parameter estimated in this study.

There are two purposes to this study. The first is to use the observed depth-salinity in a sinkhole and within a coastal borehole to estimate hydrodynamic dispersion coefficients. The second is to use these coefficients to assess the relative importance of diffusion versus transverse dispersion in developing the halocline and explain the apparent dampening of transverse dispersion.

Model Description and Assumptions

The simple molecular diffusion and transverse dispersion model is shown schematically in Figure 2. The fresh water and underlying saline water are assumed to flow horizontally towards the coast, from the interior of the peninsula, at equal velocities. Initially, the two ground-water zones are separated by a sharp interface. As the ground water flows coastward, molecular diffusion and transverse dispersion widen the interface into a brackish zone or halocline. Aquifer heterogeneity produces transverse dispersion during pore-fluid flow, and transitional turbulent flow produces transverse dispersion during fracture-fluid flow. Because transverse dispersion involves nonhorizontal fluid movement, a minor amount of vertical movement is included in the model in transverse dispersion.

Estimated path lengths of ground-water movement and a range of average linear flow velocities, constrained by field measurements, set limits on the time available for developing the brackish zone. The model is not intended to be used within a few km of the coast where wedging-out of the fresh-water lens has significantly increased fresh-water velocity, and tidal pumping causes vertical mixing.

The assumption that the underlying saline waters are not static and move towards the Caribbean Sea is consistent

with the saline waters, near the halocline, acting as the return arm of a sea-water convection cell (Cooper, 1959; Whitaker and Smart, 1990; Moore et al., 1992). The assumption of equal velocities of the underlying saline waters and the overlying fresh waters is an approximation suggested by the observed salinity-depth profiles at some of the field sites. If the saline waters are static or moving significantly more slowly than the fresh waters, diffusivity processes will result in a steeper depth-salinity gradient in the saline portion compared to the fresh-water portion of the halocline.

The depth-salinity gradient in the halocline can be modeled independently of horizontal flow if the saline waters and overlying ground water are moving at nearly equal velocities. Longitudinal dispersion can be neglected because of the large flux of solutes in the horizontal direction (Sudicky and Frind, 1981; 1982). The distribution of dissolved salts in a vertical column of water, at a given point along the horizontal ground-water flow path, is assumed to have resulted from molecular diffusion plus transverse dispersion. The model calculates the halocline width and vertical salinity gradient using estimated flow-path times.

Observed Salinity-Depth Profiles

Salinity-depth profiles, taken near the end of the dry season from 1990 to 1993, are shown in Figure 3 for several cenotes and for two coastal boreholes, located approximately 150 km from the center of the peninsula. The data are from the hydrology study by Moore et al. (1992), the water-quality studies by Stoessell et al. (1993) and Marcella (1994) and an unpublished 1992 study by Ron Stoessell. The salinities have been computed from conductivity measurements and calibrated with analytical measurements of the compositions of water samples. The salinity-depth profiles do not vary from year to year, indicating stable steady-state conditions.

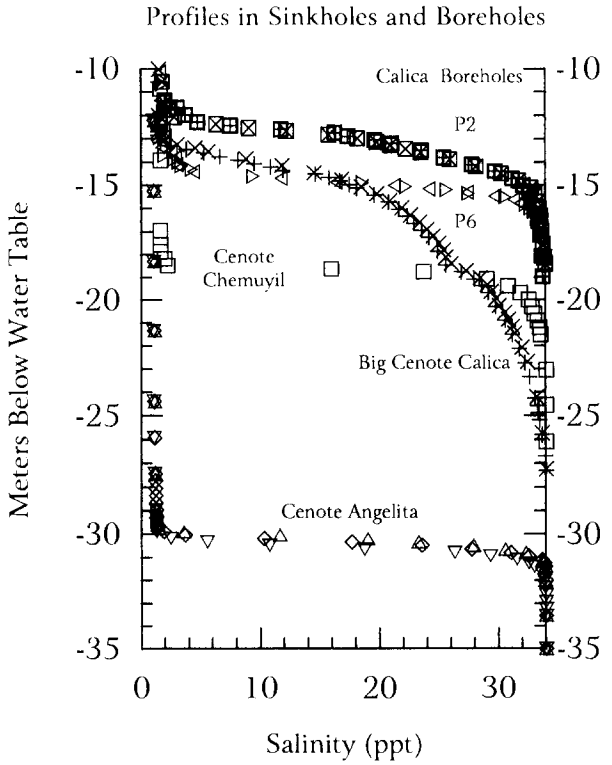

Fig. 3. Depth-salinity profiles at the following sites: Cenote Angelita (5/91, ▽; 4/92, △; 4/93, ◇), Cenote Chemuyil (4/92, □), Big Cenote Calica (4/92, ×; 4/93, +), Calica Borehole P2 (8/90, ⊞; 5/91, ⊠), and Calica Borehole P6 (8/90, ▷; 5/91, ◁).

The halocline profiles have similar shapes in Cenotes Angelita and Chemuyil and in Calica Boreholes P2 and P6. The distances from the coast for Cenotes Angelita and Chemuyil and Calica Boreholes P6 and P2 are about 12, 6, 3.6, and 2.6 km, respectively, and the halocline widths are approximately 1, 1.5, 2, and 3 m, respectively. The increased width in the halocline in the boreholes is generally due to the slower pore-fluid flow rates, providing more time for the haloclines to develop and perhaps to increased mixing in the less saline portion of the halocline as the fresh-water flow velocity increases towards the coast. Tidal effects would increase mixing in the more saline portion of the halocline and may be important in Borehole #2 which is the site closest to the coast.

At all sites, the average depth-salinity gradient is slightly steeper to much steeper in the more saline halocline zones, indicating the fresh-water flow velocity is greater than the saline-water flow velocity. In this study, the author has used the Cenote Angelita and Calica Borehole P6 sites where the gradients are **approximately the same** in both fresh-water and saline-water portions of the halocline. For these two locations, the resulting fit of the model to the data suggests the saline-water flow velocity approaches the fresh-water flow velocity in the vicinity of the halocline.

The data from Big Cenote Calica are included to show situations where simple diffusion and transverse dispersion cannot account for the salinity-depth distribution. Big Cenote Calica lies about 6 km inland from the coast (Figure 1). The discontinuity in the profile of the Big Cenote Calica is thought to reflect channeling of high salinity water in fractures within the halocline. The simple model used in this study does not fit the flow system at Big Cenote Calica.

Estimated Flow-Path Lengths, Average Flow Velocities and Flow-Path Times, and Turbulent Flow

The linear distance from the coastal region to the interior of the peninsula is about 150 km. Because the starting point for ground water reaching the northeastern coastal region is not known, a range in linear path lengths must be assumed. A range of path lengths of 20 to 200 km has been used in this study.

The measured average linear fracture-flow velocity 10 km from the coast was about 1 cm/sec which was the lower detection limit of the flow meter used by Moore et al. (1992). This value is greater than the average linear fracture-flow velocity from the interior, because it includes the effect of the coastal wedging-out of the fresh-water lens. For this study, I have assumed a range of average linear fracture-flow velocities from 0.05 to 0.5 cm/sec for ground water reaching Cenote Angelita. The range in time for ground water to

reach Cenote Angelita through fractures along pathways of 20 to 200 km is 0.1268 to 12.68 years.

As previously mentioned, less information is available on pore-fluid velocities. Complicating the problem is that a significant amount of the flow-path to a pore-fluid site probably occurred in fractures. For this study, the author has assumed the range of average linear flow velocities in the combined pore and fracture path leading to Calica Borehole P6 is an order of magnitude lower than in the fractures alone, or 0.005 to 0.05 cm/sec. The range of time for ground water to reach Calica Borehole P6 through the combined fracture and pore path along pathways of 20 to 200 km is 1.268 to 126.8 years.

The range in linear fracture-flow velocities of 0.05 to 0.5 cm/sec corresponds to 25° C Reynolds numbers for pure water of 55 to 555, respectively, assuming a fracture width of 1 cm. These values represent transition conditions between laminar and turbulent flow which occur at Reynolds numbers between 60 and 600 (Fetter, 1988). Within fractures the transverse dispersion results from turbulent flow.

Mathematical Model

The analytical solution to the diffusion plus transverse dispersion model for developing the halocline is given by Crank (1970, p. 12 and Fig. 2.3).

$$C_{(z,t)} - C_f = 0.5\,(C_s - C_f)\ \mathbf{erfc}[z/(4Dt)^{0.5}] \qquad (1)$$

where $C_{(z,t)}$ is the salinity at time t (sec) at a distance z (cm) from the original interface at time zero. The interface fluid maintains the average salinity of the two end-member fluids. C_s is 34 ppt, the initial salinity of the saline water. C_f is the initial salinity of the fresh water and is 1 ppt in Cenote Angelita and 2 ppt in Calica Borehole P6. D is the **fit parameter** in the model, the hydrodynamic dispersion coefficient which is the sum of the molecular diffusion coefficient plus the transverse dispersion coefficient. Selected values for **erfc**[z], the error-function complement are listed in Crank (1970, Table 2.1).

Results

The salinity data from Cenote Angelita and Calica Borehole P6 in Figure 3 have been replotted, respectively, in Figures 4 and 5 as a function of distance from the interface. The interface fluid has the average composition of the fresh water and saline water. The curves on Figures 4 and 5 have been computed from equation (1) for constant values, in cm units, of the equation parameter $(4Dt)^{0.5}$.

Curve b on Figure 4 provides the best fit to the Angelita data with an equation parameter of 40 cm. The parameter is used, with the previously estimated range in time for the ground water to reach Cenote Angelita of 0.1268 to 12.68 years, to calculate a range in D of 1×10^{-6} to 1×10^{-4} cm^2/sec. The estimated value of D is proportional to the linear ground-water velocity so that the maximum value corresponds to the maximum velocity of 0.5 cm/sec used in this study.

Curve b on Figure 5 provides the best fit to the Calica Borehole P6 data with an equation parameter of 65 cm. The parameter is used, with the previously estimated range in

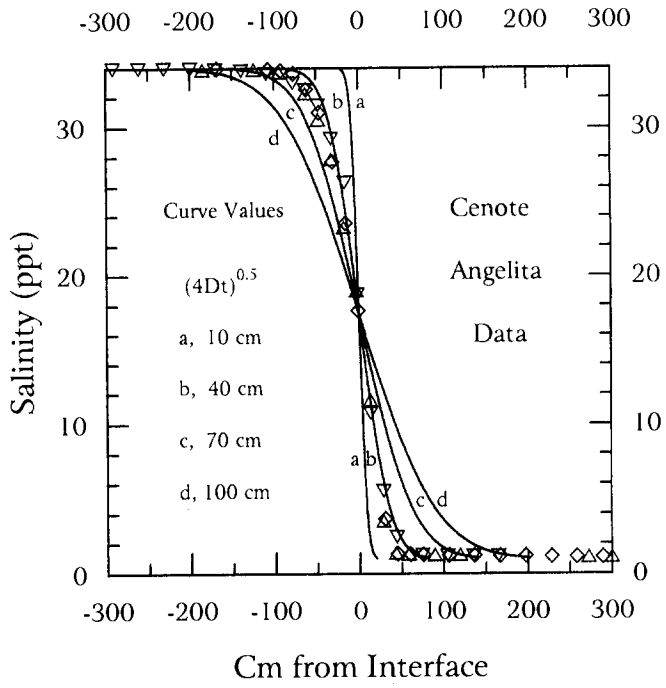

Fig. 4. Cenote Angelita salinities (5/91, ▽; 4/92, △; 4/93, ◇) plotted as a function of distance from the interface marking the average composition of fresh and saline waters. The solid curves were computed from equation (1) for constant values of $(4Dt)^{0.5}$.

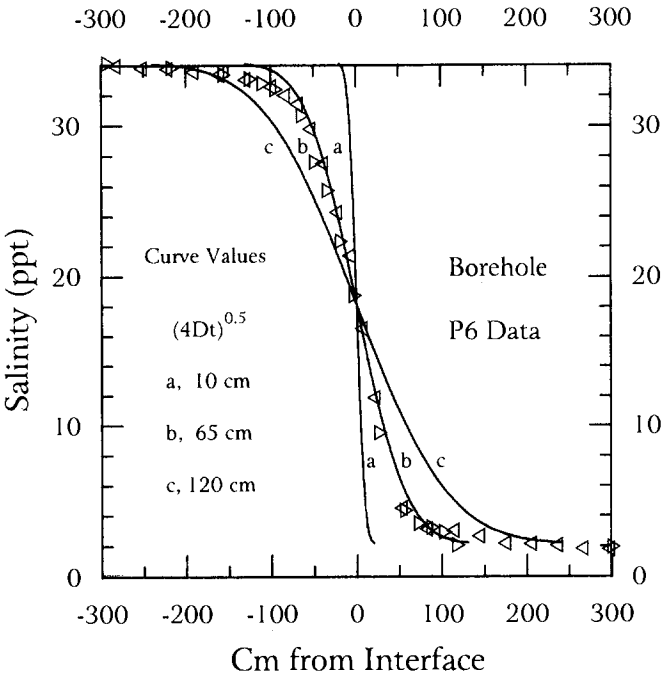

Fig. 5. Calica Borehole P6 salinities (8/90, ▷; 5/91, ◁) plotted as a function of distance from the interface marking the average composition of fresh and saline waters. The solid curves were computed from equation (1) for constant values of $(4Dt)^{0.5}$.

time for the ground water to reach Borehole P2 of 1.268 to 126.8 years, to calculate a range in D of 2.6×10^{-7} to 2.6×10^{-5} cm^2/sec.

The variability in the curves as a function of the equation parameter leads to an estimated error of less than 5 cm in picking the equation parameter which best fits the data. Taking this error into account increases the range in D to 2.3×10^{-7} to 1.3×10^{-4} cm^2/sec.

Discussion

The hydrodynamic dispersion coefficient can be split into the molecular diffusion coefficient D_m and the transverse dispersion coefficient D_t.

$$D = D_m + D_t \quad (2)$$

D_m in fluids has an expected value of about 1.5×10^{-5} cm^2/sec in an aqueous solution of 25° C which is the coefficient for NaCl diffusion in a 0.5 molar solution (Lerman, 1979). D_m in a porous or fractured medium has to be corrected for the solid matrix through which diffusion cannot occur. The correction involves multiplying the aqueous diffusion coefficient by the porosity fraction and dividing by the tortuosity squared (Stoessell, 1987). In the open-fracture pathway leading to Cenote Angelita, the porosity fraction is taken as one, the maximum possible value. In the combination fracture and pore system pathway leading to Calica Borehole P6, the average porosity fraction is taken as 0.5, an intermediate value between open fractures and the pores of the rock. The tortuosity, the ratio of the true path-length distance to the shortest distance, is assumed to range from 1 to 2 in the linear fracture system pathway leading to Cenote Angelita (Weidie, 1985) and between 2 and 3 in the combination fracture and pore system pathway leading to Calica Borehole P6. The overall tortuosity and porosity range corresponds to an overall range in D_m from 1.5×10^{-5} to 8.3×10^{-7} cm^2/sec. This range covers the lower portion of the estimated range in D, the hydrodynamic dispersion coefficient.

The maximum value of D_t, computed from equation (2) with the maximum estimate of D and the estimates of D_m, would be of the order of magnitude of 10^{-4} cm^2/sec. Hydrologists usually estimate D_t from the relation

$$D_t = a_t v \quad (3)$$

where a_t is the transverse dispersivity in cm, and v is the longitudinal (horizontal in this study) velocity.

Sanford and Konikow (1989a, 1989b) modeled Yucatan ground-water movement along the northeastern coast in a two-dimensional flow of a fluid of variable density through a heterogeneous, anisotropic, confined aquifer. Their model coupled equilibrium calcite dissolution with fluid flow to predict porosity development over tens of thousands of years. Sanford and Konikow used values of 50 cm for a_t, predicting steady-state vertical dimensions of the coastal haloclines between 20 and 40 m thick. These vertical dimensions are much larger than in the observed haloclines shown in Figure 3 and by Stoessell et al. (1989, Figure 3; 1993, Figure 2).

The maximum value of a_t, consistent with the maximum estimated value of D_t (for v equal to 0.5 cm/sec) is only 2×10^{-4} cm. This low value of a_t reflects the reduced effect of transverse dispersion, consistent with the observed haloclines having vertical dimensions of only a few meters.

The process of transverse dispersion in the halocline fluids requires packets of fluids to undergo vertical displacement. The path of the fluid packets is probably not vertical, but inclined at a small angle to the horizontal, resulting in a vertical displacement. However, the vertical density gradation in the halocline fluids is mechanically stable, with less dense fluids overlying more dense fluids. This mechanical stability dampens transverse dispersion, reducing the transverse dispersion coefficient.

The dampening effect on transverse dispersion in the halocline can be related to an energy ratio. Let N be the ratio of the displacement energy needed, for a unit volume of fluid to rise vertically a characteristic distance z and displace an equivalent volume of less dense fluid, to the vertical component of the kinetic energy possessed by the fluid.

$$N = g(p_f - p_{ldf})\, z/[0.5p_f(v_h \tan \alpha)^2] \quad (4)$$

p_f and p_{ldf} are the densities of the fluid and the less dense fluid respectively, g is the acceleration due to gravity, v_h is the horizontal fluid velocity, and α is the angle between the horizontal component of the flow velocity and the actual flow direction of the fluid packet undergoing dispersion. The term ($v_h \tan \alpha$) is the vertical component of the fluid velocity.

The larger the value of N, the greater the dampening effect on transverse dispersion. In this study N is at a maximum during the initial stage of formation of the halocline whan a sharp interface separates the overlying fresh water from the saline water (i.e., modified sea water). The maximum density difference would be between modified sea water and fresh water (with 1 ppt) with densities of about 1.025 and 1.001 g/cm^3, respectively. The angle α will be some small angle, assumed to be about 1 degree. For this situation with z equal to 1 micron (0.0001 cm), N ranges from 600,000 to 60 over the range of ground-water velocities used in this study, 0.005 cm/sec to 0.5 cm/sec. N is decreased by increasing the angle α and increased by increasing the vertical distance z. In a pore fluid, z would correspond to the grain diameter. Assuming α is 45 degrees and that z is one mm results in a range of N of 180,000 to 18 over the velocity range of 0.005 to 0.5 cm/sec.

As the halocline widens, the density difference decreases across z. At a density difference of 0.0001 g/cm^3, the range in N decreases from 2,500 to 0.25, assuming α is 1 degree and z is a micron. This decrease in N, as the halocline widens, reduces the dampening effect on dispersion, increasing the importance of transverse dispersion relative to molecular diffusion.

Acknowledgments

The author thanks Yolanda Moore for discussions on ground-water flow in the Yucatan and Dale Easley for discussions on diffusion and dispersion processes. The

author appreciates the time spent by three unknown journal reviewers who provided detailed comments that were used in revising the manuscript.

References

Back, W. and B. B. Hanshaw. 1976. Hydrogeochemistry of the northern Yucatan Peninsula, Mexico, with a section on Mayan water practices. In: Guide Book, Field Trip to Peninsula of Yucatan (revised), New Orleans Geological Society. pp. 211-243.

Cooper, H. H., Jr. 1959. A hypothesis concerning the dynamic balance of freshwater and saltwater in a coastal aquifer. Journal of Geophysical Research. v. 64, pp. 461-467.

Crank, J. 1970. The Mathematics of Diffusion. Oxford University Press, London. 347 pp.

Fetter, C. W. 1988. Applied Hydrogeology. Macmillan Publishing Company, New York, NY. 592 pp.

Lerman, A. 1979. Geochemical Processes Water and Sediment Environments. John Wiley and Sons, New York, NY 481 pp.

Marcella, L. M. 1994. Potential for dolomitization occurring in sea-water salinity fluids in the northeastern Yucatan Peninsula, Mexico (M.S. thesis). Univ. of New Orleans, New Orleans, LA. 55 pp.

Moore, Y. H., R. K. Stoessell, and D. H. Easley. 1992. Groundwater flow along the northeastern coast of the Yucatan Peninsula. Ground Water. v. 30, pp. 343-350.

Moore, Y. H., R. K. Stoessell, and D. H. Easley. 1993. Reply to Discussion of "Fresh-water/sea-water relationship within a ground-water flow system, northeastern coast of the Yucatan Peninsula." Ground Water. v. 31, pp. 321-322.

Sanford, W. E. and L. F. Konikow. 1989a. Porosity development in coastal carbonate aquifers. Geology. v. 17, pp. 249-252.

Sanford, W. E. and L. F. Konikow. 1989b. Simulation of calcite dissolution and porosity changes in saltwater mixing zones in coastal aquifers. Water Resources Research. v. 25, pp. 655-667.

Stoessell, R. K. 1987. Mass transport in sandstones around dissolving plagioclase grains. Geology. v. 15, pp. 295-298.

Stoessell, R. K., Y. H. Moore, and J. G. Coke. 1993. The occurrence and effect of sulfate reduction and sulfide oxidation on coastal limestone dissolution in Yucatan cenotes. Ground Water. v. 31, pp. 566-575.

Stoessell, R. K., W. C. Ward, B. H. Ford, and J. D. Schuffert. 1989. Water chemistry and $CaCO_3$ dissolution in the saline portion of an open-flow mixing zone, coastal Yucatan Peninsula, Mexico. Geological Society of America Bulletin. v. 101, pp. 159-169.

Sudicky, E. A. and E. O. Frind. 1981. Carbon 14 dating of groundwater in confined aquifers: Implications of aquitard diffusion. Water Resources Research. v. 17, pp. 1060-1064.

Sudicky, E. A. and E. O. Frind. 1982. Contaminant transportation in fractured porous media: Analytical solution for a system of parallel fractures. Water Resources Research. v. 18, pp. 1634-1642.

Weidie, A. E. 1985. Geology of the Yucatan Platform. In: Geology and Hydrogeology of the Yucatan and Quaternary Geology of Northeastern Yucatan Peninsula. New Orleans Geological Society, New Orleans, LA. 160 pp.

Whitaker, F. F. and P. L. Smart. 1990. Active circulation of saline ground waters in carbonate platforms: Evidence from the Great Bahama Bank. v. 18, pp. 20-203.

Wilson, W. L. 1989. Comment on "Porosity development in coastal carbonate aquifers." Geology. v. 18, pp. 200-203.

Worthington, S.R.H. 1993. Discussion of "Fresh-water/sea-water relationship within a ground-water flow system, northeastern coast of the Yucatan Peninsula." Ground Water. v. 31, p. 321.

Data-Analyses Methods for Determining Two-Dimensional Dispersive Parameters

by Jiu J. Jiao[a]

Abstract

Two methods for calculating two-dimensional hydrodynamic dispersion parameters by analyzing experimental data, the dispersive-plume-area (DPA) method and the linear-graphic (LG) method, are proposed in this paper. The DPA method determines the dispersive parameters by analyzing the dispersive plume area after injection of a salt-water slug into an aquifer. The transverse and longitudinal dispersivity and even the porosity of an aquifer may be derived. The LG method transforms the concentration-time curve into a straight line. Using the slope of the line, dispersivity and velocity can be obtained. Both methods are examined using theoretical considerations and practical examples.

1. Introduction

Two methods of determining two-dimensional dispersive parameters are described in this paper: the dispersive-plume-area (DPA) method and the linear-graphic (LG) method. The DPA method uses concentration contours of a dispersive plume to estimate dispersive parameters. The concentration contours can be obtained from a multiple well observation system or through surface geophysical methods. If the plume is traceable by surface measurements, only a tracer injection well is needed, which could be more economical than the traditional multiwell monitoring network. This method is demonstrated using the data from a tracer test at a landfill near Borden, Ontario, Canada. The LG method requires concentration-time data from two wells, one along the main axis of flow and one off the main axis of plume migration. Using the values for maximum concentration and time, the method transforms the concentration-time curve into a straight line. From the slope of the line, dispersivity and velocity can be obtained. This method is demonstrated using tracer test data from a laboratory experiment.

2. Basic Equations

For this development, the aquifer is assumed to be homogenous and isotropic, and ground-water flow is one-dimensional. If the direction of flow is taken as parallel to the x-axis and a tracer injection point (well) is located at the origin, then the movement of the tracer plume after instantaneous injection into the aquifer can be described in rectangular coordinates by (Fried, 1975):

$$C(x, y, t) = \frac{m/\mu}{4\pi t(D_l D_t)^{1/2}} \exp\left[-\frac{(x - ut)^2}{4D_l t} - \frac{y^2}{4D_t t}\right] \quad (1)$$

where C is the concentration of the tracer point (x, y) and time t (ML^{-3}); D_l, D_t are the longitudinal and transverse dispersive coefficients, respectively (L^2/T); μ is porosity (dimensionless); m is the mass of the tracer injected instantaneously over unit thickness of the aquifer (M/L); u is the flow velocity (L/T).

The dispersive coefficients and dispersivities are assumed to conform to the relationship:

$$D_l = \alpha_l u \qquad D_t = \alpha_t u \quad (2)$$

where α_l, α_t are the longitudinal and transverse dispersivities, respectively (L).

3. Dispersion-Plume-Area Method

There have been several methods proposed to obtain two-dimensional hydrodynamic dispersion parameters from field experimental data (Fried, 1975), but each of these methods requires that the data be from a multiple well monitoring network in which one well is used for tracer injection and the other wells for collection of water samples.

[a]School of Civil Engineering, Birmingham University, P.O. Box 363, Birmingham B15 2TT, United Kingdom.

Received April 1991, revised August 1991 and March 1992, accepted April 1992.

Discussion open until July 1, 1993.

The disadvantages are that observation wells are expensive, and the process of obtaining concentration data is complicated. Also, monitoring wells should be located in a distribution downgradient of the injection well. Precise determination of the direction of the flow is difficult. Once a monitoring array is established and a tracer is injected into a well, if the estimated flow direction is incorrect, the tracer may move in a direction away from the observation wells.

The data-analysis method proposed in this section is called the dispersive-plume-area (DPA) method. This method does not require direct concentration data at given points, but only the overall movement of the dispersive plume of the tracer. The movement of the plume could be followed by surface electrical resistivity measurements which are cheaper than multiple well observation systems and can be easily adjusted for changes in direction of tracer movement. Surface resistivity measurements have been well-established by previous researchers. Fried (1975) used field examples to describe single well geophysical methods to determine ground-water velocities. MacFarlane et al. (1983) used an electrical conductance method to delineate the plume near a landfill in Borden, Ontario, Canada. White (1988) used surface resistivity measurements to determine the direction and velocity of ground-water flow and the hydraulic conductivity of an aquifer.

The DPA method is illustrated by using the data from a tracer test completed at a landfill near Borden, Ontario, Canada. The tracer test was made by Sudicky et al. (1983) who obtained the dispersive parameters using traditional analytical methods. The agreement between the parameters acquired by the DPA method and those by Sudicky et al. (1983) shows the new method is applicable.

3.1 Theoretical Development

Rearranging equation (1) yields:

$$\frac{(x-ut)^2}{4D_l t}+\frac{y^2}{4D_t t}=\ln\frac{m/\mu}{4\pi tC(D_lD_t)^{1/2}} \qquad (3)$$

This equation shows that the distribution of tracer in an aquifer takes the shape of an ellipse with its center at the point (ut, 0). The ellipse is moving forward with the speed u. Rearranging equation (3) expressions for lengths of the major and minor axes of the ellipse can be obtained:

$$a=[4D_l t\ln\frac{m/\mu}{4\pi tC(D_lD_t)^{1/2}}]^{1/2} \qquad (4)$$

$$b=[4D_t t\ln\frac{m/\mu}{4\pi tC(D_lD_t)^{1/2}}]^{1/2} \qquad (5)$$

where a, b are half lengths of the major and minor axes of the ellipse, respectively.

From equations (4) and (5), it is easy to determine:

$$a/b=(D_l/D_t)^{1/2} \qquad (6)$$

Equation (6) indicates that the ratio of the lengths of the two axes is a constant and reflects the difference in magnitude between the longitudinal and transverse dispersion coefficients.

The area of the ellipse enclosed by the contour with concentration C at time t can be described as:

$$S=\pi ab=4\pi t(D_lD_t)^{1/2}\ln\frac{m/\mu}{4\pi tC(D_lD_t)^{1/2}} \qquad (7)$$

Equation (7) can be rearranged as:

$$S=4\pi t(D_lD_t)^{1/2}\ln\frac{m/\mu}{4\pi t(D_lD_t)^{1/2}}-4\pi t(D_lD_t)^{1/2}\ln C \qquad (8)$$

Equation (8) indicates that at time t the relationship between the area S and the concentration C is linear in a semilogarithmic coordinate system. The slope of the line is:

$$k=-4\pi t(D_lD_t)^{1/2} \qquad (9)$$

Equation (9) can be rewritten as:

$$-k/4\pi t=(D_lD_t)^{1/2} \qquad (10)$$

Solving equations (6) and (10), D_l, D_t can be obtained. If one also measures the S = 0 intercept (let it be d = lnC) of the line, then equation (8) becomes:

$$-k\ln\frac{m/\mu}{-k}+kd=0 \qquad (11)$$

From equation (11), an expression for porosity can be obtained:

$$\mu=-m/(ke^d) \qquad (12)$$

If the value of porosity is known, equation (12) can be used to estimate the mass injected into the aquifer.

In addition, equation (7) can also be rewritten as:

$$S/t=4\pi(D_lD_t)^{1/2}\ln\frac{m/\mu}{4\pi C(D_lD_t)^{1/2}}-4\pi(D_lD_t)^{1/2}\ln t \qquad (13)$$

This shows that if the areas enclosed by contours of a given concentration can be obtained, the relationship between S/t and t is linear in a semilogarithmic coordinate system. A method similar to that described above can be used to estimate the dispersive coefficients after measuring the slope and intercept of the line.

3.2 Field Example

Near Borden, Ontario, Canada, a tracer test was conducted to investigate the migration of contaminants in ground water near a landfill by Sudicky et al. (1983). Approximately 0.7 m^3 of salt water with a chloride concentration of 580.7 mg/l was injected into the ground water. After injection, the tracer slug gradually split into two plumes moving forward with different velocities. One of them, with an average ground-water flow rate of 2.9×10^{-6} m/s, evolved into a Gaussian form. The spatial distribution of chloride after 121 days of transport is shown in Figure 1. The injection and observation well system, shown in Figure 1, consisted of nearly 70 monitoring points. After all the point concentration data was collected, Sudicky et al. (1983)

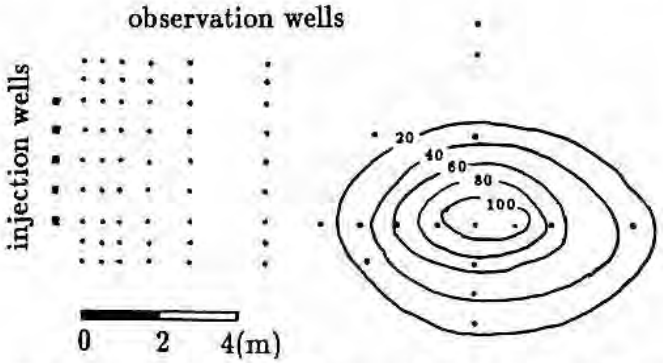

Fig. 1. Chloride distribution in ground water at the Borden Site 121 days after tracer injection [after Sudicky et al. (1983)].

obtained aquifer dispersivities by trial-and-error matching of observed data using an analytical solution:

$$\alpha_l = 0.08 \text{ m}, \qquad \alpha_t = 0.03 \text{ m}$$

The same problem can be solved by the DPA method. First, the lengths of the major and minor axes of the ellipse corresponding to different contours with different concentrations can be measured from Figure 1. After converting the scaled measurements to actual dimensions, the areas and ratios between the major and minor axes of the plume can be calculated. All these data are enumerated in Table 1.

A semilogarithmic plot of the calculated plume area versus concentration produced the relationship shown in Figure 2. The slope of the S-ln C line is measured as $k = -18.45$. Using equation (10) with $t = 121$ days yields:

$$D_l D_t = 3.102530 \tag{14}$$

From Table 1, an average value for a/b can be obtained. Then by using equation (6), one can have:

$$D_l / D_t = 0.000147 \tag{15}$$

Coupling equations (14) and (15), D_l and D_t can be calculated as:

$$D_l = 0.2138 \text{ (m}^2\text{/d)} \qquad D_t = 0.0069 \text{ (m}^2\text{/d)}$$

From field measurements the average velocity is known to be:

$$u = 2.9 \times 10^{-6} \text{ (m/s)} = 0.2506 \text{ (m/d)}$$

Then by using equations (2), one can have:

longitudinal dispersivity:

$$\alpha_l = D_l / u = 0.09 \text{ (m)}$$

transverse dispersivity:

$$\alpha_t = D_t / u = 0.03 \text{ (m)}$$

These results are very similar to those obtained by Sudicky et al., but the method is much simpler and more easily understood than the method used by Sudicky et al. (1983).

Table 1. Data for the DPA Method

a/b	C(mg/l)	a(m)	b(m)	lnC	$S(m^2)$
2.239	100	1.119	0.500	4.605	1.758
1.732	80	1.642	0.948	4.382	4.890
1.667	60	2.239	1.343	4.094	9.447
1.604	40	3.172	1.978	3.689	19.711
1.565	20	4.040	2.575	2.996	32.601

The concentration contours were obtained by analyzing water samples from the observation wells because the test monitoring network was designed for conventional tracer tests and other purposes of researching the aquifer. If the contours were obtained by surface resistivity measurements, then the whole process of data collection and analysis could be much more economical and simple.

4. Linear-Graphic Method

The method outlined in this section is called the linear-graphic (LG) method. It is also based on the use of equation (1) and is designed to estimate dispersivity and velocity. Wang et al. (1987) also developed a line graphical method to estimate dispersive parameters. After rearranging equation (1), Wang et al. found that there is a linear relationship between $H' [= d(\ln(Ct))/dt]$ and $T (= 1/t^2)$. The disadvantage of this method is that it is very difficult to perform the derivative computation H′ from actual data, which is usually very erratic and noisy. The LG method discussed in this paper uses the values of maximum C_m and corresponding time t_m and then, using much simpler procedures, transforms the observed concentration-time curve into a straight line.

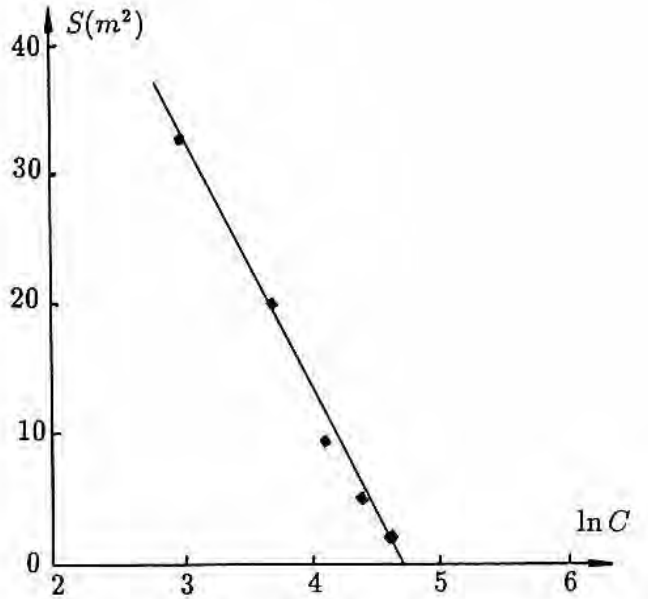

Fig. 2. Plot of S verse lnC developed from Sudicky et al. (1983) tracer dispersion study at the Borden site.

4.1 Theory Development

The theoretical development of the LG method requires taking the derivative of equation (1) with respect to t

$$C' = \frac{m/\mu}{4\pi t^2 (D_l D_t)^{1/2}} \left[\frac{x^2 - u^2 t^2}{4 D_l t} + \frac{y^2}{4 D_t t} - 1 \right] \exp\left[- \frac{(x - ut)^2}{4 D_l t} - \frac{y^2}{4 D_t t} \right] \quad (16)$$

The local maximum values for (1) are found by setting $C' = 0$:

$$\frac{x^2 - u^2 t^2}{4 D_l t} + \frac{y^2}{4 D_t t} - 1 = 0 \quad (17)$$

or

$$(x^2 - u^2 t^2) D_t + y^2 D_l - 4 D_l D_t t = 0 \quad (18)$$

If the time corresponding to $C' = 0$ is designated as t_m, then equation (18) becomes

$$t_m = \frac{D_l}{u^2} \left[\left(4 + \frac{u^2 x^2}{D_l^2} + \frac{u^2 y^2}{D_l D_t}\right)^{1/2} - 2 \right] \quad (19)$$

The concentration corresponding to t_m is noted as C_m. From equation (1), C_m can be solved as:

$$C_m = \frac{m/\mu}{4\pi t_m (D_l D_t)^{1/2}} \exp\left[- \frac{(x - ut_m)^2}{4 D_l t_m} - \frac{y^2}{4 D_t t_m} \right] \quad \ldots . (20)$$

If the observation point is located on the x-axis, then equation (18) is simplified as:

$$x^2 - u^2 t_m^2 - 4 D_l t_m = 0 \quad (21)$$

or

$$D_l = (x^2 - u^2 t_m^2)/4 t_m \quad (22)$$

which can be rewritten as

$$D_l = \frac{x^2}{4 t_m [u^2 t_m^2/(x^2 - u^2 t_m^2) + 1]} \quad (23)$$

letting

$$k = u^2 t_m/(x^2 - u^2 t_m^2) \quad (24)$$

equation (23) then becomes

$$D_l = \frac{x^2}{4 t_m (k t_m + 1)} \quad (25)$$

Substituting (24) into (22) and solving for u yields:

$$u = 2(D_l k)^{1/2} \quad (26)$$

Equations (25) and (26) indicate that D_l and u can be obtained if k is known. The parameter k can be obtained in the following manner:

Using equations (1) and (20) (letting $y = 0$) and rearranging,

$$\frac{C_m t_m}{Ct} = \exp\left[\frac{(x - ut)^2}{4 D_l t} - \frac{(x - ut_m)^2}{4 D_l t_m} \right] \quad (27)$$

or

$$\ln \frac{C_m t_m}{Ct} = \frac{(t - t_m)(u^2 t t_m - x^2)}{4 D_l t t_m} \quad (28)$$

Substituting (22) into (28),

$$\ln \frac{C_m t_m}{Ct} = \left(\frac{t - t_m}{t} \right) \left(\frac{u^2 t t_m - x^2}{x^2 - u^2 t_m^2} \right) \quad (29)$$

adding $(t - t_m)/t$ to both sides of the above equation and then rearranging the right-hand side, the following equation is obtained:

$$\ln \frac{C_m t_m}{Ct} + \frac{t - t_m}{t} = \frac{u^2 t_m}{x^2 - u^2 t_m^2} \frac{(t - t_m)^2}{t} \quad (30)$$

Equation (30) is the equation of a straight line of the form

$$Y = kX \quad (31)$$

where

$$\left.\begin{aligned} X &= (t - t_m)^2/t \\ Y &= \ln(C_m t_m/Ct) + (t - t_m)/t \end{aligned}\right\} \quad (32)$$

k is the slope of the straight line.

Procedures to estimate dispersive parameters using the LG method can be summarized as follows: read t_m and C_m from a C-t curve; calculate values of X and Y using equation (32); plot the transformed data and measure the slope k; calculate D_l and u using equations (25) and (26); then use data from an observation point (x', y') (not located on the x-axis) to obtain t_m'. The value of D_t can then be obtained from equation (18):

$$D_t = -y'^2 D_l/(x'^2 - u^2 t_m'^2 - 4 D_l t_m') \quad (33)$$

It should be noted that the relationship involving C_m and C in equation (32) is independent of the units used. Therefore, if the measured data are conductivity or resistivity instead of concentration, it is not necessary to transform the data to concentration values as long as the values are directly proportional to concentration.

4.2 Laboratory Example

Two-dimensional dispersion experiments were conducted at China University of Geosciences in 1986, using salt water as a tracer [for details see Jiao et al. (1988)]. The electrical conductivity (G) and time (t) data from one of the experiments is shown in Table 2. The corresponding curve is shown in Figure 3. The value of t_m can be read as 159.8 (min.). The distance from the tracer injection point to the observation point is 80 cm. The G-t data is transformed to X-Y data using equation (32).

The ascending and descending portions of the G-t curve (Figure 3) correspond to the two straight lines in the X-Y plane (Figure 4). The points a, o, b in Figure 3 correspond to the points a', o', b' in Figure 4. Theoretically, if the movement of the tracer does not violate any of the assumptions behind development of equation (1), the two straight lines should coincide. For this example, deviation of the

Table 2. Observed Time-Conductivity Data and Transformed X, Y Data for LG Example

t(min.)	G(μΩ/cm)	X	Y
146.17	0.04	1.28	2.81
146.67	0.07	1.18	2.26
147.33	0.09	1.06	2.00
148.17	0.12	0.92	1.72
149.55	0.18	0.71	1.31
150.00	0.21	0.64	1.16
150.50	0.24	0.58	1.03
151.00	0.26	0.52	0.95
152.50	0.37	0.35	0.59
153.18	0.42	0.29	0.47
153.50	0.44	0.26	0.42
154.07	0.48	0.22	0.33
156.00	0.59	0.09	0.13
157.00	0.63	0.05	0.06
158.00	0.66	0.02	0.02
160.00	0.67	0.00	0.00
161.50	0.65	0.02	0.03
163.67	0.59	0.09	0.13
164.50	0.56	0.13	0.18
165.00	0.54	0.16	0.22
166.00	0.51	0.23	0.27
166.50	0.49	0.27	0.31
167.00	0.47	0.31	0.35
167.50	0.45	0.35	0.40
169.50	0.40	0.50	0.51
169.87	0.37	0.59	0.59
170.67	0.34	0.67	0.68
171.50	0.30	0.79	0.80
173.00	0.25	1.00	0.98
173.50	0.23	1.08	1.07
174.00	0.21	1.15	1.17
174.50	0.19	1.23	1.26
176.33	0.14	1.54	1.56
180.23	0.07	2.31	2.25
185.52	0.03	2.82	3.10
194.10	0.03	3.20	3.10

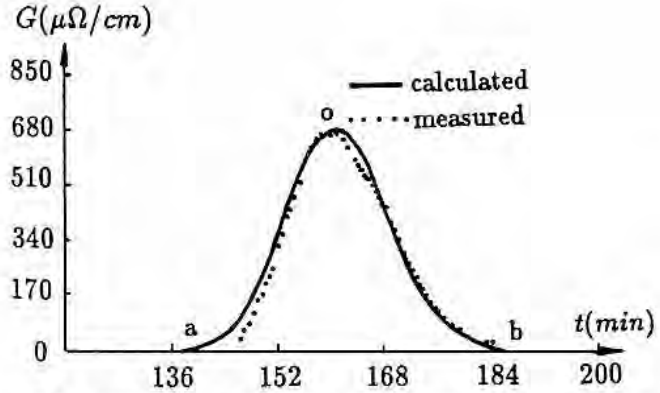

Fig. 3. Comparison of calculated and experimental conductivity changes as a function of time during a laboratory tracer dispersion study.

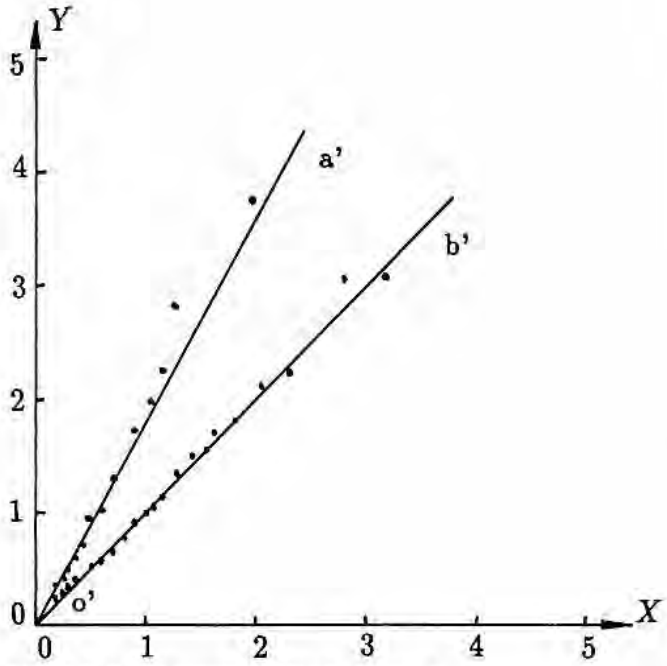

Fig. 4. X-Y line corresponding to Figure 3.

data points from the lines increases as X and Y increase. The deviation is an indication of the difference between the theoretical equation and the real situation. There are three possible explanations: (1) some of the assumptions for equation (1) may not be valid for this case; (2) the values t_m and C_m read from the C-t curve are not the exact values of t_m and C_m; or (3) the data are more erroneous at the time when the tracer first appears and at the time when it finally disappears at the observation point compared with the observed data near time t_m.

In this case, two slope values k_a (= 1.86) and k_b (= 1.0) are used. Employing equation (25) yields:

$$D_l = 80^2/[4 \times 159.8(159.8k_a + 1)] = 0.0335$$

Using equation (31):

$$u = 2(0.0335 \times k_a)^{1/2} = 0.4997$$

If k_b is used, then:

$$D_l' = 0.0622 \qquad u' = 0.4990$$

Averaged values of D_l and D_l', and u and u' are used as the final values $\bar{D}_l$ and $\bar{u}$

$$\bar{D}_l = (D_l + D_l')/2 = 0.0479(cm^2/min.)$$

$$\bar{u} = (u + u')/2 = 0.4993(cm/min.)$$

For this dispersion experiment, the observation points in the y direction were too far and did not intercept the tracer, so the data in the y direction were not available. D_t could not be obtained by using equation (33). Another method (Jiao et al. 1988) is used to obtain D_t to be 0.015 (cm^2/min.). Figure 4 shows that the fit between the real data and the calculated data is generally good.

5. Conclusion

Two methods of estimating dispersive parameters are described in the paper. The most interesting point in the DPA method is that for the first time it demonstrates that the aquifer dispersivities may be estimated by the shape of the dispersive plume, not necessarily the actual concentration. The example data in the text were collected with actual ground-water measurements, but the paper treats them in a way as if they were from resistivity measurements. So it may be reasonable to modify surface resistivity measurement methods to estimate aquifer dispersive parameters using the DPA method. This could be much more economical than using the traditional multiwell monitoring network to determine aquifer dispersive parameters. It may also be worthwhile to note that the DPA method does not necessarily need historical observation data (concentration-time data) which are often not available for field problems. In addition, it seems that this method can be used with data defining any plume resulting from instantaneous injection of a conservative material, even if the initial mass is not known. But it should be noted that the DPA method can only be used when the assumptions associated with equation (1) are valid, and the surface geophysical methods are applicable if the plume data are to be obtained through the surface measurements.

The LG method transforms the concentration-time curve into a straight line. Dispersivity and velocity can be estimated after measuring the slope of the line. This method is more economical and easier to perform compared to the method by Wang et al. (1987) which may suffer from the influence of erratic experiment data points on the derivative computation. On the other hand, the method in this paper is sensitive to the values of C_m and t_m. Attention should be paid to choose C_m and t_m properly.

Acknowledgment

The author gratefully acknowledges the advice given by Professor C. X. Chen in writing this paper. My thanks also to A. Hughes and B. Patel, as their comments resulted in an improved text. Comments from three anonymous reviewers were extremely helpful and appreciated.

References

Fried, J. J. 1975. Groundwater Pollution, Developments in Water Science, 4. Elsevier. pp. 92-113.

Jiao, J. J., D. G. Weng, and X. B. Li. 1988. Study on hydrodynamic dispersion theory in porous media by experiments. In: Environmental Geology Study in China, edited by C. Y. Sun. China Science Press, Beijing. pp. 188-199.

MacFarlane, D. S., J. A. Cherry, R. W. Gillham, and E. A. Sudicky. 1983. Migration of contaminants in groundwater at a landfill: A case study, 1. Groundwater flow and plume delineation. J. Hydrol. v. 63, pp. 1-29.

Sudicky, E. A., J. A. Cherry, and E. O. Frind. 1983. Migration of contaminants in groundwater at a landfill: A case study, 4. A natural-gradient dispersion test. J. Hydrol. v. 63, pp. 81-108.

Wang, H. Q., N. Crampon, S. Huberson, and J. M. Garnier. 1987. A linear graphical method for determining hydrodispersive characteristics in tracer experiments with instantaneous injection. J. Hydrol. v. 95, pp. 143-154.

White, P. A. 1988. Measurement of groundwater parameters using salt-water injection and surface resistivity. Ground Water. v. 26, no. 2, pp. 188-199.

Descriptions of Anisotropy and Heterogeneity and Their Effect on Ground-Water Flow and Areas of Contribution to Public Supply Wells in a Karst Carbonate Aquifer System

United States Geological Survey Water-Supply Paper 2475

Prepared in cooperation with the Florida Department of Environmental Protection

AVAILABILITY OF BOOKS AND MAPS OF THE U.S. GEOLOGICAL SURVEY

Instructions on ordering publications of the U.S. Geological Survey, along with prices of the last offerings, are given in the current-year issues of the monthly catalog "New Publications of the U.S. Geological Survey." Prices of available U.S. Geological Survey publications released prior to the current year are listed in the most recent annual "Price and Availability List." Publications that may be listed in various U.S. Geological Survey catalogs (**see back inside cover**) but not listed in the most recent annual "Price and Availability List" may be no longer available.

Order U.S. Geological Survey publications **by mail** or **over the counter** from the offices given below.

BY MAIL

Books

Professional Papers, Bulletins, Water-Supply Papers, Techniques of Water-Resources Investigations, Circulars, publications of general interest (such as leaflets, pamphlets, booklets), single copies of Earthquakes & Volcanoes, Preliminary Determination of Epicenters, and some miscellaneous reports, including some of the foregoing series that have gone out of print at the Superintendent of Documents, are obtainable by mail from

U.S. Geological Survey, Information Services
Box 25286, Federal Center, Denver, CO 80225

Subscriptions to periodicals (Earthquakes & Volcanoes and Preliminary Determination of Epicenters) can be obtained ONLY from the

Superintendent of Documents
Government Printing Office
Washington, DC 20402

(Check or money order must be payable to Superintendent of Documents.)

Maps

For maps, address mail orders to

U.S. Geological Survey, Information Services
Box 25286, Federal Center, Denver, CO 80225

OVER THE COUNTER

Books and Maps

Books and maps of the U.S. Geological Survey are available over the counter at the following U.S. Geological Survey Earth Science Information Centers (ESIC), all of which are authorized agents of the Superintendent of Documents:

- **ANCHORAGE, Alaska**—Rm. 101, 4230 University Dr.
- **LAKEWOOD, Colorado**—Federal Center, Bldg. 810
- **MENLO PARK, California**—Bldg. 3, Rm. 3128, 345 Middlefield Rd.
- **RESTON, Virginia**—USGS National Center, Rm. 1C402, 12201 Sunrise Valley Dr.
- **SALT LAKE CITY, Utah**—Federal Bldg., Rm. 8105, 125 South State St.
- **SPOKANE, Washington**—U.S. Post Office Bldg., Rm. 135, West 904 Riverside Ave.
- **WASHINGTON, D.C.**—Main Interior Bldg., Rm. 2650, 18th and C Sts., NW.

Maps Only

Maps may be purchased over the counter at the following U.S. Geological Survey offices:

- **ROLLA, Missouri**—1400 Independence Rd.
- **STENNIS SPACE CENTER, Mississippi**—Bldg. 3101

Descriptions of Anisotropy and Heterogeneity and Their Effect on Ground-Water Flow and Areas of Contribution to Public Supply Wells in a Karst Carbonate Aquifer System

By LARI A. KNOCHENMUS and JAMES L. ROBINSON

Prepared in cooperation with the
Florida Department of Environmental Protection

U.S. GEOLOGICAL SURVEY WATER-SUPPLY PAPER 2475

U.S. DEPARTMENT OF THE INTERIOR
BRUCE BABBITT, Secretary

U.S. GEOLOGICAL SURVEY
Gordon P. Eaton, Director

UNITED STATES GOVERNMENT PRINTING OFFICE, WASHINGTON: 1996

For sale by the
U.S. Geological Survey
Branch of Information Services
Box 25286
Denver, CO 80225–0286

Library of Congress Cataloging in Publication Data

By Knochenmus, Lari A., and Robinson, James L.
Descriptions of anisotropy and heterogeneity and their effect on ground-water flow and areas of contribution to public supply wells in a karst carbonate aquifer system
46 p. cm.—(U.S. Geological Survey Water-Supply Paper 2475)
QE12345 91–4303CIP
[151.7209792] ISBN 0-607-86216-5

CONTENTS

FIGURES

TABLES

CONVERSION FACTORS, VERTICAL DATUM, AND ACRONYMS

Multiply	By	To obtain
	Length	
foot (ft)	0.3048	meter
	Area	
square mile (mi^2)	2.590	square kilometer
	Volume	
cubic foot per day (ft^3/d)	0.02832	cubic meter per day
	Flow	
million gallons per day (Mgal/d)	0.04381	cubic meters per day
	Transmissivity	
foot squared per day (ft^2/d)	0.0929	meter squared per day
	Hydraulic conductivity	
foot per day per foot [(ft/d)/ft]	1.00	meter per day per meter

Sea level: In this report, "sea level" refers to the National Geodetic Vertical Datum of 1929 (NGVD of 1929)—a geodetic datum derived from a general adjustment of the first-order level nets of the United States and Canada, formerly called Sea Level Datum of 1929.

Acronyms

FDEP = Florida Department of Environmental Protection
MODFLOW = U.S. Geological Survey modular ground-water flow model
MODPATH = U.S. Geological Survey postprocessor particle tracker
NWHWRAP = Northwest Hillsborough Water Resources Assessment Project
ROMP = Regional observation monitoring well program
VCONT = Vertical conductance

ASR – UK: ELUCIDATING THE HYDROGEOLOGICAL ISSUES ASSOCIATED WITH AQUIFER STORAGE AND RECOVERY IN THE UK

UKWIR Report Ref. No. 02/WR/09/2

BGS Report No. CR/02/156/N

This report summarizes the results of a 3-year project undertaken by the BGS in collaboration with UCL. The project was co-funded by a Foresight LINK award and UK Water Industry Research Ltd. (UKWIR).

Printed copies of this report may be obtained from UKWIR

British Geological Survey
NATURAL ENVIRONMENT RESEARCH COUNCIL

Project Title and Reference	**Water Resources – Groundwater – WR/22**
Report Title	**ASR - UK: Elucidating the hydrogeological issues associated with Aquifer Storage and Recovery in the UK**
Managing Company	**Thames Water Utilities plc.**
Collaborator	**Co-funded by a Foresight LINK award. Collaboration with University College, London**
Contractor	**British Geological Survey (Natural Environment Research Council)**
Author of Report	**Gale, I N. Williams, A T. Gaus, I. Jones, H K**
Principal Researcher	**Gale, I N**
Report Type	**Final**
Period Covered	**1998 - 2001**
Acknowledgements	**Prof J A Barker (UCL) for contributions to Chapter 3. Mr S Fletcher and Mr J Ellis (Environment Agency) for Chapter 7. Members of the Steering Committee and other BGS staff who contributed.**

This report constitutes BGS Report No. CR/02/156/N.

UK Water Industry Research Limited provides a framework for a common research programme to undertake projects which are considered to be fundamental to water operators on 'one voice' issues. Its contributors are the water and sewerage companies and the water supply companies of England and Wales, the Scottish Water Authorities and Northern Ireland's Water Service.

Published by UK Water Industry Research Limited
1 Queen Anne's Gate, London SW1H 9BT

First published 2002

ISBN 1 84507 263 9

Printed by Webree.com Ltd.

UK WATER INDUSTRY RESEARCH LIMITED

ASR - UK: ELUCIDATING THE HYDROGEOLOGICAL ISSUES ASSOCIATED WITH AQUIFER STORAGE AND RECOVERY IN THE UK

FOREWORD

The term Aquifer Storage Recovery (ASR) was originally coined by David Pyne of CH2M-Hill in the 1980's to describe the technique of creating additional storage at existing water treatment works by injecting surplus potable, treated water into aquifers underlying the works. Injection is via dual-purpose, recharge/abstraction boreholes, often by adapting existing abstraction boreholes. The technique caught on in the US because it provided answers to questions, including:

- How do we meet growing demand without large capital investment in new surface reservoirs?
- How can we design schemes with acceptable impacts on the environment?
- How can we be confident of regulatory approval and avoid lengthy public enquiries?

The steadily increasing number of ASR projects across the US since the late 1980s is testament to the cost-effectiveness of the technique and its operational flexibility.

In the UK, the water industry became interested in ASR* as a real option in the latter part of the 1990s. This was partly, but not wholly, as a result of the higher national profile water resource planning took on since the summer of 1995 and the associated pre-AMP3 regulatory guidance on water resource options. Thus, from OFWAT, we had the useful guideline that options should be small-scale and cost-effective and from the Environment Agency the threefold criteria of sustainability, sustainability and sustainability.

Interest in ASR also came from UK hydrogeologists who realised that because the injected potable water displaces the native groundwater to create a "bubble," the technique could work successfully in unused, non-potable aquifers. Successful development of ASR schemes into saline aquifers in the Florida Keys ably demonstrated this principle. Clearly, an innovative way of utilising the storage potential in hitherto untapped UK aquifers had now opened up. In the era of planning for climate change this indeed represents a huge opportunity for creating sustainable storage.

ASR in the UK is currently progressing up the steep part of the learning curve. To date there have been several ASR pilot investigations but, as yet, no schemes have been commissioned. This initial phase of work has met with mixed success and has drawn out several technical issues and uncertainties, most of which have become the focus of this study.

From the water resource planning perspective, ASR has many plus points and is a key option in the Environment Agency's Water Resources Strategy for England and Wales. However, from an asset investment perspective the current technical uncertainties

around ASR mean that other options, more certain of success,** albeit possibly more costly and environmentally less sustainable, may be given higher priority. The outputs from this project will help greatly in providing a better understanding of the technical problems that may be encountered and thereby enable the design of an appropriate feasibility study, and staged development programme, to minimise risk of failure.

The outputs from this project consist of this summary report, a web site, interim technical reports and models on the web site and the attached CD, as well as several scientific publications. Together these provide greater understanding and analytical elucidation of the environmental impacts, yield potential and quality changes associated with ASR in UK aquifers.

Finally, for those water companies who believe that they will not need to develop new water resources over the next 25 years this project will be of academic interest only. However, for the rest of us I would suggest that assimilating the outputs of the project is a compulsory exercise. Whilst water resource strategists and planners need to understand the key messages herein, it will be the front-line practitioners, largely hydrogeologists, who will gain most from the project's technical findings and analytical tools. With AMP4 on the horizon, this jointly-funded project represents not only good value for money but is also a timely and needed addition to our planning armoury.

Brian Connorton

UKWIR technical member of project Steering Committee

---

* The term ASR has been adopted by UK hydrogeologists to describe recharging, hitherto unused or under-used aquifers, via dual-purpose, abstraction/recharge boreholes to create an ASR "bubble." In this regard ASR is a sub-set of artificial recharge. The latter is the generic term applied to any technique for transferring water into aquifers (intentionally or as a result of other activities) either indirectly through surface recharge basins or directly by borehole injection. Thus hydrogeologists tend not to refer to the large scheme in North London (NLARS) as an ASR scheme but rather as an artificial recharge scheme. This is because it has numerous injection points into a widely-used potable aquifer and the management principle is not so much to create a recharge bubble under each site, but to manage the aggregated recharge mound over a large extent of the confined Chalk aquifer.

** Success is here regarded as having achieved the designed deployable output at the budgeted cost and with the necessary regulatory approvals.

Executive Summary

Objectives

- Promote ASR through research into generic issues related to risks that are currently constraining development of ASR to British aquifers, namely:

  – impacts of the dual-porosity behaviour of the Chalk and other aquifers on recovery efficiency

  – geochemical interactions; water/water and water/rock in different aquifers

  – environmental impacts in relation to operational cycles

- Facilitate the exchange of information through the usual media as well as the Internet. Convene annual national symposia on ASR for the water suppliers, regulators and researchers and support a strong presence at international fora.

Conclusions

- British aquifers can be considered as part of a continuum ranging from single porosity unconsolidated aquifers (e.g. Lower Greensand) to fractured dual-porosity aquifers (Chalk).

- The response of these aquifers to ASR varies in a predictable manner that is controlled by the proportion of fracture and matrix porosity, both from the physical mixing and geochemical interaction perspectives. This aquifer 'continuum' and the impact trends are illustrated below.

Increasing <u>single</u> porosity Character

- "bubble" of injected water
- mixing limited to edges of "bubble"
- less interaction with native water
- stronger injection water-rock interaction

Increasing <u>dual</u> porosity Character

- more diffusive exchange
- larger mixing area
- strong native component in recovered water
- stronger chemical interaction between the two waters

- The conclusions from the work undertaken in this study give generic indications of how aquifers will respond to ASR. Because of geological variability, it must be stressed that this is only intended to act as a basis for site-specific assessments. Some modelling tools have been developed to assist in these assessments.

Recommendations

- As data become available from trials in the Sherwood Sandstone and Lower Greensand aquifers it should be used to refine the physical and geochemical models, provide relevant feedback and compare results with those from the trials.

- Apply relevant models developed by this project to current and prospective ASR schemes to assist in decision making, particularly in relation to the environmental impact assessment.

- The modelling has identified the parameters that are of most significance in a variety of hydrogeological environments. There are very few measurements of some key parameters, such as aquitard properties, and a database needs to be compiled in order to facilitate future developments.

Benefits

- A clearer understanding has been gained of the response of British aquifers to ASR from both the physical and geochemical perspectives.

- Simple modelling tools have been developed (supplied with this report) to assist in decision-making from the early stages of ASR schemes. These tools are designed to help assess the environmental impacts of the scheme and to identify the parameters that need to be determined in order to proceed.

- Physical (SWIFT) and geochemical (PHREEQC) models have been applied to ASR schemes and an initial attempt to link the two was made. This will form the basis for improved understanding of the processes determining the efficiency of ASR scheme as more are developed in different aquifers.

- Regulatory considerations have been reviewed with respect to ASR in the light of new and forthcoming EU Directives and their implementation.

For further information please contact UK Water Industry Research Limited, 1 Queen Anne's Gate, London SW1H 9BT quoting the report reference number

Contents

1 Background and aims of the project

The results of a study, funded by BGS, UKWIR and EA, and undertaken between 1995 and 1998, indicated that there is a large potential for development of Aquifer Storage Recovery (ASR) schemes in the UK at a wide range of scales (Jones et al., 1998). The study stimulated considerable interest and, at that time, three water companies had initiated field trials. Several other schemes were at the desk study stage.

Experience from the United States shows that ASR is frequently a cost-effective solution to a wide variety of water supply, as well as water quality problems. The potential of the technology in Britain needed to be more fully evaluated, in order to optimise the use of our water resources, both fresh and wastewater. However, several uncertainties were highlighted by this study that could constrain the acceptance and utilisation of ASR as a component in strategies for sustainable management of water resources.

The project reported here, ASR-UK, addresses some of the issues identified through generic research and the development of guidelines and models to assist in decision-making throughout the investigative, development and implementation stages of schemes. The issues addressed are:

- Research into the controls on dispersion and diffusion of injected water and their impacts on recovery efficiency. Models were developed to predict the extent and movement of "bubbles" of stored water in aquifers as well as changes in water quality with time. Work initially focused on the Chalk aquifer but other aquifers were also investigated.

- The impacts of geochemical interactions between native and injected water as well as water-rock interactions. The adverse as well as the beneficial effects need to be predicted in order to address them in the most cost-effective manner. The project therefore aimed to assess the significance of these reactions on the permeability of aquifers, the quality of recovered water and the efficiency of schemes.

- During the life of the project, the importance of the environmental impacts of ASR schemes, in relation to the operational cycle used, became increasingly apparent. Quantification of these impacts is required throughout all phases of a study, from the initial assessment of the potential of a site, through the staged testing to implementation and commissioning of a scheme.

The project was designed to address these issues through review of current knowledge and the application and development of models, some of which can be used as tools in current and future investigations. It was initially planned that the development of these models would be closely aligned with on-going investigations and field trials, which would provide data to validate the models as well as providing feedback to the investigation. This proved to be the case with the investigations in the Chalk aquifer but little data were available from other aquifers.

2 ASR – using aquifers to store water in the UK

2.1 Introduction

Artificial Recharge (AR) is a means of supplementing natural infiltration into an aquifer; it involves storing water in an aquifer at times when there is a surplus, potentially for use at times of scarcity. Traditionally, the technique has utilised aquifers containing potable water.

Artificial recharge is defined here to include any technique used to introduce water into an aquifer, via boreholes or basins, for any purpose. It can be used strategically where an aquifer is already over-exploited, such that no further abstraction would be allowed without artificial recharge taking place, or where lack of natural recharge prevents its utilisation. In these cases, the water could be abstracted from the same wells as used for injection, or from additional wells or natural discharges down hydraulic gradient. This technique is employed only in potable aquifers, as the water being abstracted is not necessarily the same water that was injected. The net water balance would however be zero or positive.

Artificial recharge has been carried out in many forms for centuries. A more recent development occurred around 50 years ago, when the first investigations of injecting potable water into saline aquifers were carried out (Cederstrom, 1957). This involved recharge of freshwater into the brackish aquifers of the coastal plains of Virginia in 1946; the injected water forming a lens or bubble of potable water within the saline body of groundwater. This practice has become known as Aquifer Storage Recovery (ASR).

Pyne (1995) defines ASR as:

> The storage of water in a suitable aquifer through a well during times when water is available, and recovery of the water from the same well during times when it is needed.

The use of non-potable aquifers greatly increases the potential for using artificial recharge, and in the last couple of decades, the concept has been developed widely in the United States. However ASR is not a proven technology for UK aquifers, which can be quite distinct from aquifers that are used in the USA. The risks have been perceived as being too great to consider development of such schemes in the UK but, in recent years, several trial schemes have been undertaken, and the data and experience gained from these, are providing valuable support for the technique.

Areas where ASR are most likely to be considered in Britain would be in confined parts of aquifers that have not been used for productive water supply because of poor quality. It follows that little hydrogeological information is available, so embarking on a scheme becomes more speculative and the risk factors increase. Use of potable aquifers at outcrop for ASR schemes is less likely to occur as the aquifer may be fully licensed, natural recharge will occur and the groundwater-surface water interaction will be more immediate, and hence have environmental impacts. However, each case needs to be judged on its individual merits as ASR schemes can store valuable quantities of water in relatively small volumes of aquifer, so local hydrogeological environments could prove to be suitable.

2.2 Application of ASR

There are a large number of possible applications for ASR, some of which are listed in Table 2.1. It is envisaged that in the UK, ASR will typically be used to meet short-term peaks in demand by recharging aquifers during periods of low demand and recovering the water during periods of high demand. ASR should always be viewed in the context of alternative methods of resolving water supply or quality issues, as part of a broader strategy. In particular, the environmental benefits should be factored into the decision process.

Table 2.1 Applications of ASR (adapted from Pyne 1995)

Category	Application
Water storage	- Seasonal storage and recovery
	- Long term storage
	- Emergency storage
	- Diurnal storage
Water quality	- Chlorination by-product removal
	- Nitrate removal
	- Stabilisation of aggressive water
	- Control of contaminant plumes
Environmental improvement	- Restoration of groundwater levels, 'low flow' rivers and groundwater fed wetlands
	- Reduction of subsidence
	- Reduce/prevent saline intrusion
	- Enhancement of baseflow to streams
Operational advantages	- Maintenance of distribution system pressure and flow
	- Deferment of the expansion of treatment facilities
	- Deferment of the development of new sources

Ideally, ASR sites should be located in a confined, single porosity aquifer at sufficient distance from the outcrop to have an acceptable impact on flows in streams. The delay of this impact can be engineered to have maximum effect during periods of high stream flow, when it becomes insignificant. Sub-vertical hydraulic boundaries or a moderate value of transmissivity, are needed to constrain the distance at which the effects of injection and recovery are significant. A readily accessible source of water for injection is also needed and access to an existing treatment works could be important if the recovered water is not wholly potable. As with the development of a conventional groundwater supply, the site-specific factors determine its impact on the environment, the resource and other users. These issues also need to be addressed in ASR schemes,

together with those specifically pertinent to ASR, in order to optimise the management and use of water resources.

2.3 Drivers for the use of ASR in the UK

The aquatic environment is regulated by the Environment Agency in England and Wales, the Scottish Environment Protection Agency (SEPA) and the Department of the Environment for N. Ireland. Their agendas are determined by implementation of the regulations established by government, in order to comply with EC Directives, notably the Water Framework Directive (2000) and the Habitats Directive (1997).

Demands for water from a wide variety of users have to be accommodated. These include not only the Water Companies for potable supply and effluent dilution but also navigation, fisheries, irrigation as well as private and industrial abstractions. Environmental demands also have to be met to ensure acceptable river flows and maintenance of wetland habitats.

Demand management techniques such as leakage reduction, metering, industrial reuse, consumer use reduction and other water saving techniques have been successful but become less applicable as the cost/benefit ratio increases. In many areas the available water resources are fully licensed and in some cases the impacts of abstraction will result in the need to reduce or surrender a licence to abstract groundwater.

The options for replacement of these sources are limited, particularly where environmental concerns are valued highly. Construction of surface impoundments tend to meet strong opposition on the grounds of loss of land, habitats and negative environmental impacts and can take decades to come to fruition. Although construction of an additional borehole source can be relatively rapid, this option is often precluded on the grounds that aquifers are fully licensed or that the impacts on surface water and wetlands are unacceptable. Construction of pipelines to improve distribution networks, or importing water from considerable distances need to be assessed on their cost-effectiveness. The number of viable schemes will tend to diminish with time as the most cost-effective schemes are implemented.

Schemes such as desalination and wastewater reuse are high cost options that are usually only viable in small, limited and exceptional circumstances. In comparison, ASR becomes an increasingly attractive option, the main advantages being:

- Minimum environmental impact as the net water abstraction is zero or negative
- Installations can usually be located at or near where storage/demand problems need to be addressed
- Staged development to spread costs and to meet increasing demand
- Costs are usually less than alternative schemes
- *In-situ* improvements in water quality can reduce the need for treatment on abstraction

ASR is therefore a sustainable water resources and quality management technique that can be applied to address a wide range of problems as part of a broader water management strategy.

2.4 Potential for ASR in the UK

2.4.1 Introduction

There is a limited history of artificial recharge schemes in Britain. These include trial schemes on the Triassic sandstones at Clipstone and Edwinstowe (IWES, 1986) and at Stourbridge (Jones, 1983), and on the Lower Greensand at Hardham (O'Shea, 1984). However, the North London Artificial Recharge Scheme (NLARS), which recharges the Chalk and the overlying Tertiary sands, is the only major operational scheme. In more recent years, trial ASR schemes have provided data and experience on British aquifers, most notably the trials in the Chalk in East Anglia and the extensive testing programme in the Chalk at Lytchett Minster, Dorset.

Currently trials are being undertaken on the Sherwood Sandstone aquifer at Loftsome Bridge in Yorkshire and on the Lower Greensand aquifer at Stockbury in Kent. In addition, several agricultural supply schemes have been developed in the Nottinghamshire where groundwater is abstracted from the Permian limestone and stored in the overlying Sherwood Sandstone for later use as irrigation water. Yeilds from boreholes in the limestone are insufficient to meet the short-term intensive requirements and, as the Sherwood Sandstone aquifer is fully licensed, abstraction can only be permitted subsequent to addition of water; the net abstraction being zero or negative.

A regional assessment of ASR potential of the aquifers in England and Wales was carried out by Jones et al. (1998). Within the scale of the assessment, it was not possible to consider the potential for ASR in each of the minor aquifers, and therefore the study focused on the majors aquifers (Table 2.2). This does not mean that all minor aquifers should be dismissed, as they can be important on a local scale. Figure 2.1 shows the locations of the major aquifers in the UK together with the locations of ASR, and other Artificial Recharge investigations.

2.4.2 Chalk and Upper Greensand

The Chalk, in hydraulic connection with the Upper Greensand in some areas, is an important aquifer over much of southern and central England. Although porosity is high (up to 40%), the pore throats are narrow, and most of the usable storage is within the fractures and larger pores. As a result, the Chalk frequently has high transmissivity, but low storage coefficient, resulting in high diffusivity, so the impact of ASR schemes on the aquifer at outcrop needs to be carefully assessed. Where the Chalk is in hydraulic continuity with overlying deposits (e.g. the drift in East Anglia, or the Palaeogene in the London Basin) or underlying formations (e.g. the Upper Greensand), storage is increased, and the combined aquifer may have enhanced potential for ASR.

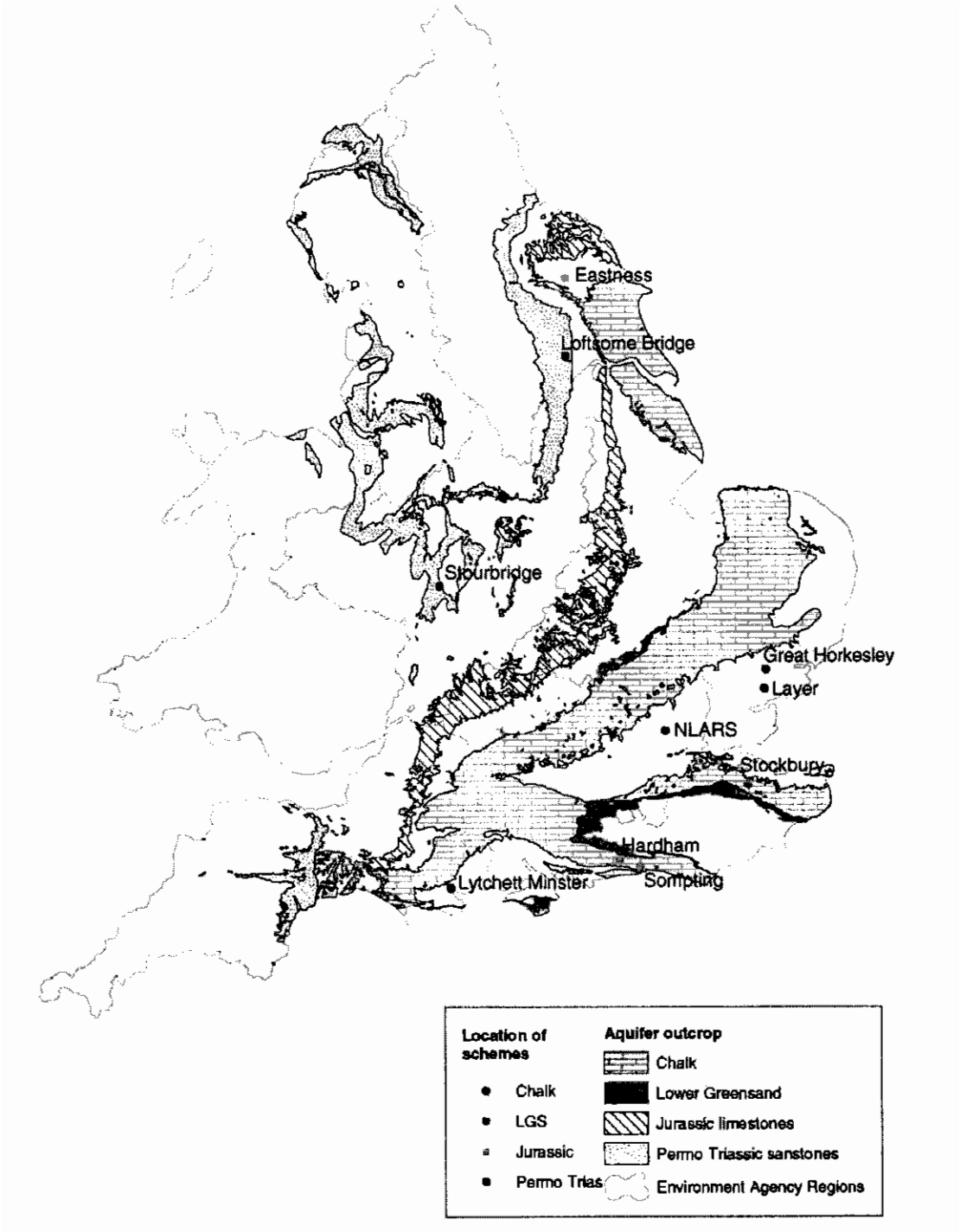

Figure 2.1 The location of ASR and other artificial recharge schemes in relation to the major aquifers in the UK

ASR may be constrained in the Chalk aquifer where the native groundwater is saline or brackish. When fresh water is injected it will tend to flow through the fractures, rather than through the matrix of the rock. Saline native groundwater in the matrix will then diffuse across a large interface and thus reduce the quality of the water subsequently recovered from the fractures. The significance of this process is discussed further in Section 4.3 of this report. In some cases the lack of environmental impacts of ASR may outweigh this water quality issue, which can be dealt with through treatment or dilution on recovery. Where the native groundwater has no serious limitations in terms of water quality, and the hydraulic parameters are satisfactory, the Chalk aquifer will have good potential, as illustrated by the success of the North London Artificial Recharge Scheme (NLARS) (O'Shea et al., 1995).

The Upper Greensand may also have potential for ASR due to its high storage capacity. Impermeable horizons within the formation can act as confining layers, thus creating a multi-layered aquifer and offering the opportunity for stacking. The degree of hydraulic continuity between the Chalk and Upper Greensand varies but where there is continuity, the combined aquifer may have greater potential. High iron in solution in some areas could pose a problem with plugging of boreholes due to the precipitation of iron oxides when injecting oxygenated water into a reducing environment. However, if this process is understood, it can be controlled and managed.

Table 2.2 Potential for ASR in England and Wales

Region (Env. Agency)	Chalk	Lower Greensand	Jurassic Limestones	Permo-Triassic Sandstone
Anglian	Moderate	Good (south of Region)	Lincs Lst: Mod. in south	
Midlands				Moderate to good
North East	Moderate to low (south of Region)		Corallian: Low to moderate	Moderate to good (best in south)
North West				Moderate to good
Southern	Moderate UGS: good in southwest	Good (southwest of Region)		
South West	Moderate to good (east of Region)		Moderate to low (east of Region)	Moderate to good (east of Region)
Thames	Good (East London)	Good (west of Region)	Moderate?	
Welsh				Low

n.b. Empty cells indicate absence of, or insignificant aquifer in region

2.4.3 Lower Greensand

The Lower Greensand is an important aquifer in parts of southern England, mainly in Bedfordshire and Cambridgeshire, and to the south of London around the Weald and on the Isle of Wight, as well as other smaller outliers elsewhere. It has a limited area of outcrop, although its high storage and generally good water quality render it important locally. Water quality can be exceptionally good, even where the aquifer is deeply confined, for example at Slough.

The Lower Greensand has good potential for ASR as transmissivity values, even where confined, are generally reasonable, and storage coefficients are high. It is most likely to be of use where it attains maximum thickness, and where intergranular flow is dominant, for example in the west of the Weald.

2.4.4 Jurassic Limestones

The Jurassic sediments outcrop in a broad band from the southwest to the northeast of England. The two main limestones are the Great Oolite Limestone and the Inferior Oolite. The minor limestones are frequently relatively thin, and rarely extend over large areas. Intergranular permeabilities are generally low, and the dominant flow mechanism is through solution-enlarged fractures. The high transmissivity combined with low storage results in the aquifers having a high diffusivity and hence rapid response times to pumping or injection. This may result in impacts in the unconfined part of an aquifer, even where boreholes are several kilometres from outcrop.

Water quality is good close to outcrop, but tends to becomes more saline down dip, beneath confining strata. Thus, although the limestones may have some potential for ASR, the potential is only likely to occur at a local scale.

2.4.5 Permo-Triassic Sandstones

The Permo-Triassic sandstones crop out across southwest, central, northeast and northwest England, and the Vale of Clwyd. They comprise a thick (up to 1000 m), variable sequence of predominantly sandstone, with inter-layered fine-grained horizons. Although matrix porosity and permeability are fairly high, the aquifer frequently relies on fractures for much of the groundwater flow close to boreholes. Although fractures generally close with increasing depth of burial, they have been reported even at depth, to be sufficiently open to maintain a high transmissivity. For example, during investigations for the Stourbridge scheme, Jones (1983) reported a fracture at 158 m depth in the recharge borehole. Faults have been reported to compartmentalise the aquifer in some areas, for example the West Midlands. Such isolated aquifer blocks could be particularly useful in terms of ASR.

The great thickness of the sandstones combined with their high matrix porosity and the influence of fractures, may result in injected water being "lost" unless very large quantities are injected. To minimise this loss, ASR schemes should be located in sections of aquifer that are confined by marl, or other low permeability strata, with as few fractures as possible. The injected water will then tend to displace inter-granular water around the borehole, thus increasing recovery efficiency.

2.4.6 Magnesian Limestone

The Magnesian Limestone occurs in a narrow north-south strip from Sunderland to Nottingham. It comprises two or three limestone horizons, separated by marls and siltstones. In the north, the aquifer is divided into three, with the Middle Magnesian Limestone having the greatest porosity. The transmissivity of the Magnesian Limestone is controlled by fracturing, hence aquifer properties are very variable and unpredictable. The reliance on fracture flow may limit its potential for ASR.

2.4.7 Carboniferous Limestone

The Carboniferous Limestone occurs in Derbyshire, the Mendips, north and south Wales, and in northwest Yorkshire. The matrix of the Carboniferous Limestone has a very low porosity and permeability, and the formation functions only as an aquifer by virtue of the secondary network of solution-enlarged fractures. It is characterised by very rapid groundwater flow, the direction of which may be difficult to predict. Boreholes yields are unpredictable and may have very high yields if they intercept fractures, and be non-productive if they fail to do so. Much of the yield from the aquifer is from spring discharge so, in general, the aquifer is unsuitable for ASR.

2.4.8 Minor aquifers

Other **minor aquifers** should be considered on an individual basis. ASR schemes require areas of aquifers in the order of tens of hectares so suitable, local geological settings can be adequate. Aquifers identified as having some potential include the **Fell Sandstone, Millstone Grit, Kellaways Rock** and some **Upper Lias Sands.** When considering these aquifers their potential can by reviewed in respect of the "aquifer continuum", ranging from unconsolidated arenaceous deposits with high matrix porosity (Lower Greensand), through consolidated sandstone aquifer with high matrix porosity and some fracture flow (Sherwood Sandstone), fracture-flow dominated, high diffusivity aquifers (Jurassic Limestone) to fracture flow dominated aquifers with dual porosity mixing being the dominant process (Chalk).

3 Environmental benefits and constraints

3.1 Introduction and modelled scenarios

ASR schemes can utilise aquifers, at relatively small cost, that would otherwise be considered as marginal or useless. ASR can also have benefits when used in conjunction with potable aquifers in situations where the resource within the aquifer is limited. Examples of these situations are when an aquifer has limited recharge, or where an aquifer is already being exploited fully and where environmental impacts may restrict the amount of groundwater that can be abstracted during certain seasons. In this chapter, the factors that might affect the operation of an ASR scheme are examined and methods for their quantification presented.

Of particular concern is the impact that an ASR scheme may have on water levels in adjacent aquifers or in the unconfined zone of the target aquifer. As ASR schemes are designed to not result in a net abstraction from the aquifer, the normal water resources considerations about environmental impacts are not relevant and different factors need considering. In the long-term, there may be some net addition of water to the aquifer, but this should be small in relation to the overall resource. However, it does not necessarily follow that environmental impacts (e.g. water levels at outcrop) are negligible during the injection or abstraction phases.

A scheme that injects and then abstracts the same volume of water will, as a long-term steady state average, have no impact on local or regional groundwater levels. However, the seasonality of the scheme means that the local water levels will first be increased and then reduced. The timing and absolute value of these changes are of importance in assessing the eventual impact of a scheme. The work described here investigates the short-term effect on water levels and flows caused by the addition of water to the aquifer, and its subsequent removal.

Several situations have been considered and numerical and analytical models have been developed to examine these situations. The first is the case when the target aquifer is confined but is overlain (above the confining layer) by another aquifer (in this case, an unconfined aquifer). The impact that injecting water into the underlying aquifer has on the upper aquifer will be considered in terms of a change in flow between the two aquifers. Another case, which is investigated, is that of a target (confined) aquifer which outcrops at some distance from the proposed ASR scheme. The effect on water levels at the point where the aquifer becomes confined is estimated using a numerical model, for a range of transmissivity values and aquifer dimensions. Consideration has also been given to the time at which the maximum effect occurs. Descriptions of the models that have been used to investigate these situations are included in this report. It is anticipated that they will be used at an initial stage of ASR investigations, using parameters appropriate to the particular hydrogeological setting. The software is appended on disk and the models are discussed in greater detail in Williams et al. (2001).

It is envisaged that these 'first-pass' hydrogeological models will give one of three indications for a particular site:

- The impact on the adjacent water table is negligible
- The impact is definitely significant and the site is not suitable

- Further investigation is required; perhaps including more detailed modelling.

3.2 Confined ASR aquifer overlain by unconfined aquifer

Before work on assessing 'environmental impact' can be started it is important to decide what exactly is meant by the term and how it is best measured. On initial inspection it would appear that the best way to measure the 'impact' on an overlying aquifer (as depicted in Figure 3.1) would be in terms of a change in head caused by the operation of the ASR scheme. However, further consideration suggests that this may not be the case. The first problem that is encountered is the question of where this change in head should be calculated. It is obvious that the maximum change will be directly above the abstraction point i.e. at the ASR well. However it is equally obvious that the change at this point is not of any great interest as not only will it be in an area controlled by the operators of the ASR scheme but it will also be very much the worst case.

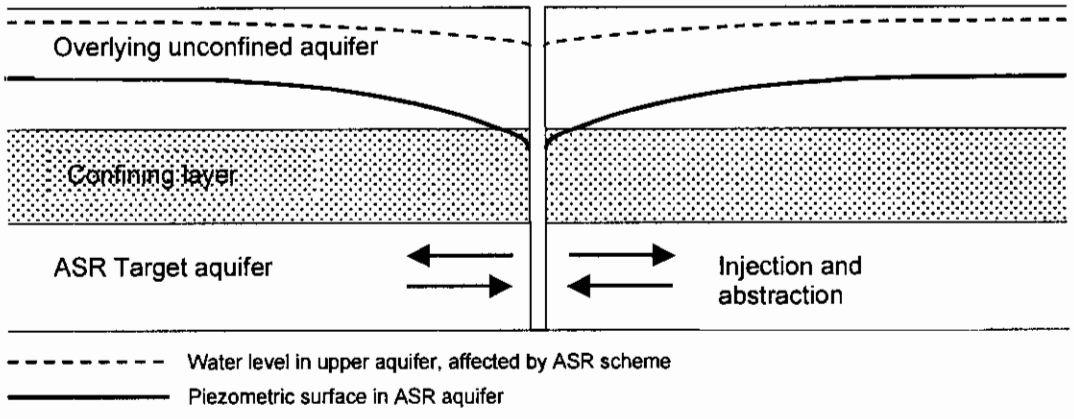

Figure 3.1 Schematic of modelled situation

The change in head at a specified distance (say 100 m), or distances, from the ASR well might be more useful and appropriate. The choice of distance should probably be influenced by the hydraulic properties of the overlying aquifer, as a cone of depression will have a different shape depending on the permeability (a lower permeability aquifer will have a deeper, less extensive cone than a higher permeability aquifer). The estimated effect, in metres, at the chosen point could then be used to decide whether or not the ASR scheme would have a significant impact on the overlying aquifer and the surface environment. The significance of the impact would probably be compared to the natural groundwater level fluctuations expected on an annual basis, or some similar criterion. Thus the decisions, which have to be taken are: a) where to estimate the change in head and b) with what to compare it?

Both of these decisions depend in part on the properties of the overlying aquifer. It would be more convenient to have a measure of the environmental impact of an ASR scheme that is independent of these properties. An ASR scheme will 'impact' on the overlying aquifer if it alters the water resources available in that aquifer or alters surface water features such as streams and wetlands. Thus a useable measure of impact would be the flux created into or out of the upper aquifer as a consequence of operating the ASR scheme. This value could sensibly be compared with the water resource available

in the upper aquifer before starting the ASR scheme, as measured by the annual recharge rate, for instance. Alternatively, the leakage out of the upper aquifer could be considered as a new 'abstraction' within the aquifer, where the magnitude of the leakage is compared to an abstraction rate.

The equations, which describe the flow of water within the aquifer system, have been solved analytically and the solution (effectively an extension of the Theis solution) has been incorporated into a spreadsheet. The spreadsheet allows the impact of an ASR scheme operating under variable cycling regimes to be estimated. The relevant parameters, which are required, are the storage coefficient of the aquifer containing the ASR well, and the vertical permeability, thickness and specific storage of the intervening aquitard.

Interestingly, the transmissivity of the target (ASR) aquifer is not a required parameter. This is because the focus is on *total* leakage through the aquitard, and not on how it is distributed areally. Another point of interest is that it is the properties of the aquitard that dominate. This is important, as these parameters are often not well known and this suggests that some effort should be focussed towards measuring these parameters, as there is no database of aquitard parameters for the UK.

The spreadsheet model has been used to show how the leakage from the upper aquifer varies during an ASR scheme run for five annual cycles (Williams et al. 2001). The effect of different aquitard hydraulic parameters and physical parameters can also be shown. The key findings are:

- Aquitards with low vertical hydraulic conductivity (k_v of less than 10^{-3} m/d) result in an impact in the upper aquifer which is of the same magnitude as that in the target aquifer with effectively no time delay, i.e. the system behaves as one aquifer.

- The higher the storage coefficient of the ASR aquifer, the less the impact on the upper aquifer.

- If the aquitard is compressible (i.e. high aquitard specific storage) the impact on the upper aquifer becomes negligible.

3.3 Effect of an ASR scheme on the outcrop area of the target aquifer.

In order to give an indication of the effect that an ASR scheme might have in the outcrop area of a target aquifer, a numerical model has been developed. It is possible that an ASR scheme may have an adverse environmental effect on streams or wetlands in the area where the target aquifer becomes unconfined.

Streams and wetlands are influenced by the water level in the aquifer that feeds them. Therefore, in this case, the head change within the aquifer near where it becomes unconfined ***is*** a useful measure of environmental impact of an ASR scheme. This can be related easily to the heads required to maintain stream flow or wetland function. The numerical model has been used to show the drawdown (i.e. the lowering of the water level) which will occur at the outcrop at the closest point to the ASR well. This will give a worst-case as the drawdown will be smaller further from the ASR well. Figure

3.2 shows the layout simulated in the numerical model. This is described in more detail in Williams et al. (2001).

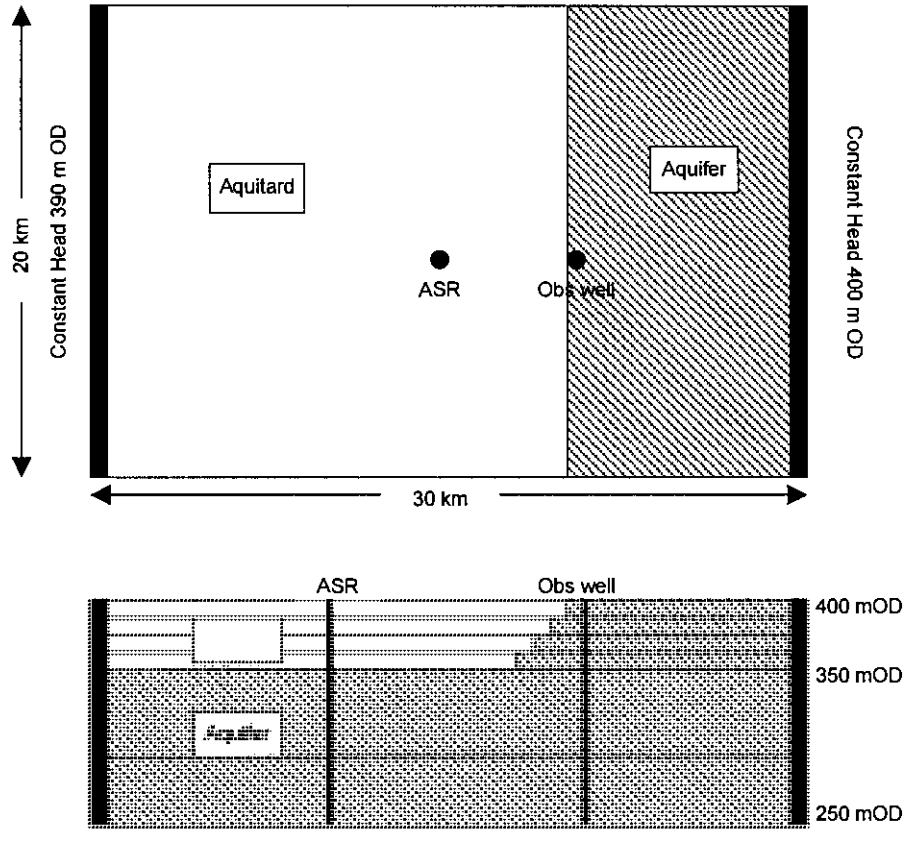

Figure 3.2 Schematic plan and cross-section of the modelled scenario.

The numerical model makes it possible to estimate the drawdown at the edge of the outcrop for different values of the aquifer and aquitard properties. It is also possible to change the thickness of the layers within the model. This makes it a very useful tool for initial investigations of the potential environmental impacts. Examples of the influence of the various aquifer parameters are given in Williams et al. (2001) and the model itself is appended to this report on disk.

For example, the modelling shows that the ***distance*** from the ASR well to the outcrop makes a significant difference to the potential impact of the ASR scheme. The estimated drawdown at the edge of the outcrop area, after five annual ASR cycles, changes from 0.25 m to 0.04 m as the ASR well is moved from 2 km to 15 km from the outcrop (Figure 3.3).

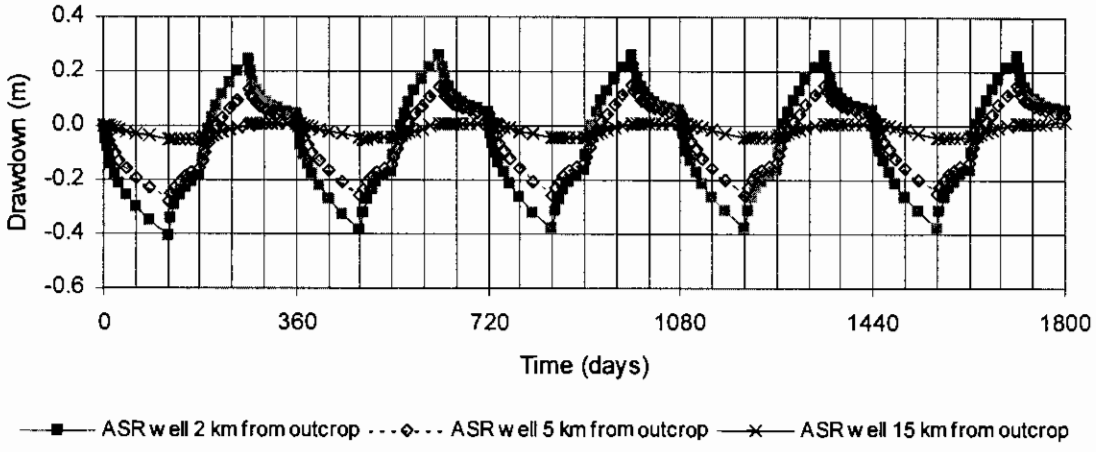

Figure 3.3 The impact of changing the position of the ASR well relative to the outcrop of the aquifer over five annual ASR cycles

It is also interesting to note that the maximum drawdown at the outcrop area occurs sometime after the maximum effect at the ASR well, i.e. the maximum impact of the ASR scheme is delayed beyond the end of pumping. The magnitude of this delay is greater when the aquifer transmissivity is smaller and when the storage coefficient is larger. The delay may be more than several months for an ASR well 10 km from the outcrop area in an aquifer with a transmissivity of 100 m^2/d and a storage coefficient of 10^{-3} (Figure 3.4). This factor may be very important when considering whether a change in head in the aquifer is significant in relation to annual variations. A change in water level that is significant in the summer months, when stream flows are low, may be insignificant in the winter.

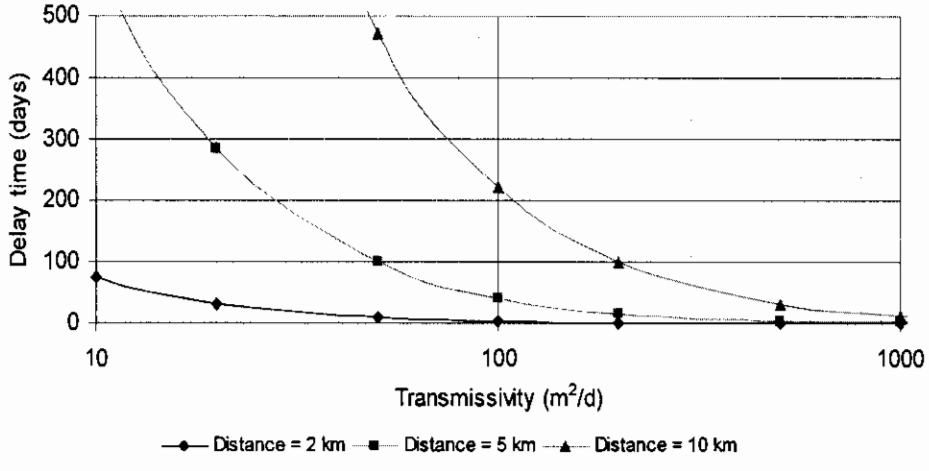

Figure 3.4 Time after the end of a 60-day pumping period when the maximum effect occurs ($S=10^{-3}$).

The model has also been used to demonstrate the difference between an ASR scheme and a conventional abstraction-only scheme (Figure 3.5). The model was set-up with some effective recharge across the outcrop area, and so may not be representative of

regions where ASR might be used (where it is assumed that all the available water resources are already 'allocated' to abstractions or environmental requirements). However, even in this 'best-case' (for the abstraction-only scheme), it is clear that abstraction-only results in much greater drawdown at the outcrop compared to the ASR scheme. The maximum drawdown simulated is 0.3 m at the end of the fifth year of abstraction and this drawdown is slowly increasing year-on-year. However, as the net abstraction with the ASR scheme is zero, the maximum drawdown does not increase year-on-year and is only half that of the abstraction-only scheme.

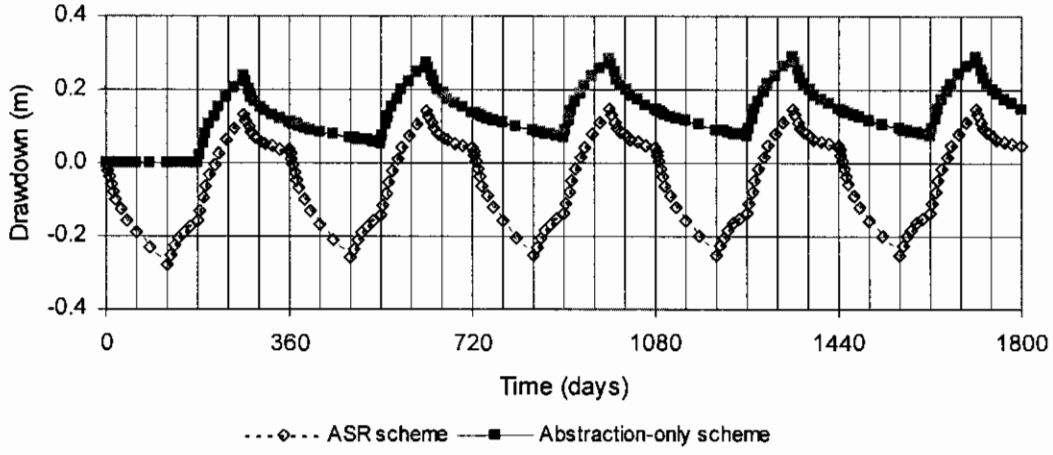

Figure 3.5 Comparison of ASR scheme with an abstraction only scheme.

3.4 Conclusions

Modelling tools have been developed which can give a useful insight into the possible effect of an ASR scheme in a variety of different hydrogeological settings. These first-pass tools can be used to indicate which aquifer parameters have the greatest effect on the impact and thus which parameters it is important to measure. As the tools are easy to use they can be applied to a wide variety of possible ASR sites very simply and thus reduce the cost of initial investigations.

Using the models has shown that under some circumstances there is a significant time delay between the maximum drawdown at the abstraction well and the maximum effect at outcrop. This means that in some cases ASR schemes could well have an advantageous environmental impact. This would occur when the drawdown at outcrop was delayed by several months so that maximum drawdown occurred at high river flow, possibly inducing recharge, and maximum water level rise occurs during low flow periods, contributing to river flow.

4 Significance of aquifer parameters in major aquifers

4.1 Introduction

The main mechanisms for the 'loss' of injected fresh water are dispersion (hydrodynamic mixing and molecular diffusion), density stratification (gravitational segregation) and lateral movement down hydraulic gradient. Mixing occurs at the interface of injected and native waters, and a dispersion or buffer zone develops. The degree of mixing is partly dependent on the type of flow in the aquifer. Harpaz (1971) showed that sandstones are likely to have higher recovery efficiencies than limestones due to the relatively slow groundwater movement in sandstones. The recharging water follows a radial expansion pattern and tends to retain the shape of a coherent water body, except in highly stratified formations.

The amount of mixing between native and injected water in an ASR-scheme, and the quality changes that occur as a consequence of this mixing, will largely depend on the physical properties of the aquifer in which the ASR-scheme is carried out. Building up a bubble of injected water in the aquifer in which little or no mixing with the native water occurs is one of the key aims of a successful ASR-scheme. If extensive mixing occurs, the recovered water will be influenced by the native water quality, which can be undesirable.

In order to assess the suitability of the main aquifers in Britain for ASR in terms of mixing, a sensitivity analysis has been carried out. The aquifers considered are the Chalk, Lincolnshire Limestone, Lower Greensand and Sherwood Sandstone, these being the aquifers most likely to be used for ASR (Figure. 2.1).

For each aquifer, a range in values of the major parameters (e.g. porosity, permeability, thickness) was defined based on the known properties of the aquifer. The impact of this variation on the amount of mixing between native and injected water was then assessed. using a 3D-dual porosity model, SWIFT (see Box). The impacts of operational and test cycles on the recovered water quality were also modelled. No chemical reactions between the injected water and the native groundwater and the aquifer material were included. The changes therefore solely reflect mixing processes and are what would be expected of a non-reactive solute such as chloride. The results (represented by the concentrations measured in the well) show the possible ranges in recovered water qualities and the differences between the four main aquifer types.

The SWIFT Model

SWIFT is a fully transient three-dimensional model, which simulates the flow and transport of fluids (brines), heat (energy) and radionuclides in fractured geologic media. It is particularly appropriate for modelling ASR in fractured media because of its ability to model dual porosity aquifers. Such aquifers are widespread in the UK (Chalk and Lincolnshire Limestone) and where present are likely to be important in controlling the recovered water quality in an ASR-scheme. When a dual porosity medium is modelled in SWIFT, the modelled system is described in two parts: the fractures and the porous blocks. Both parts have their own properties and must be fully defined.

4.2 Impacts of the main British aquifers on mixing during ASR

The Chalk and the Lincolnshire Limestone are both best described as dual porosity aquifers. The main difference between them is the matrix porosity (2 to 40 times greater in the Chalk). In dual porosity aquifers, the bulk of the flow takes place in the fractures while storage is provided by the matrix. The important parameters in this type of aquifer, as far as solute transport is concerned, are the fracture and matrix porosity, the spacing between fractures and the diffusion coefficient. This is a measure of the rate at which solutes can penetrate the matrix blocks as a result of concentration gradients. Of these parameters, only matrix porosity is readily measured, although estimates of fracture porosity and fracture spacing can be made from pumping tests and from geophysical logging. The diffusion coefficient of some solutes into clean chalk samples have been measured and so estimates (order of magnitude) for this parameter are available. However the relevance of laboratory measurements on clean uniform surfaces to processes occurring at natural fracture surfaces is still poorly understood.

In contrast to the Chalk and the Lincolnshire Limestone, the Lower Greensand behaves as a single porosity medium. This means that the same void spaces (as reflected by the porosity) control both the permeability and the storage. In this case, the parameters that are of most relevance to transport of solutes, are the porosity and dispersivity. Dispersivity is a measure of how much a plume of solute will spread as it moves and is controlled by the heterogeneity of the aquifer. Dispersivity can be measured in the laboratory under controlled conditions but the values obtained are often found to be much smaller than those estimated from field data. This is a because of the large-scale heterogeneities present in the aquifer but not represented in the small blocks of aquifer material that can be tested in the laboratory. The dispersivity is therefore usually derived during model calibration with field data.

The behaviour of the Sherwood Sandstone lies somewhere between the dual-porosity and single-porosity ideals and is probably best described as a dual-permeability medium. This is because the matrix is permeable enough to transmit water at the low rates which are relevant in regional flow systems, but probably not in the near-well situation where fracture flow is likely to dominate. The SWIFT model cannot simulate this type of aquifer, and in the work reported here, the Sherwood Sandstone has been modelled as a dual-porosity medium.

4.3 The dual-porosity issue

4.3.1 Conceptual model

In some cases, the effects of molecular diffusion may be highly significant and this is considered to be the dominant mixing process in the Chalk aquifer in the UK (Jones et al., 1998). The Chalk is unusual in that it has a high porosity (up to 40%) and may contain saline or brackish water in the pore spaces. Due to the small pore throat diameters, groundwater flow is dominantly through fractures (1-2% porosity) and not through the pores. The ratio of matrix water to fracture water is high and so diffusion of solutes from the matrix water can therefore have a strong influence on the chemistry of the mobile fracture water.

If a Chalk aquifer contains poor quality water then injection of potable water will mix with and displace water from the fractures. However, diffusive mixing will be the

dominant process between the fracture and the matrix waters. The rate at which this occurs depends on the surface area of contact between the two waters, their relative volumes and the concentrations and ionic species under consideration. The scale and rate of this process is therefore a key to the success of ASR schemes in aquifers that contain non-potable native groundwater.

It is therefore worthwhile examining the processes that occur during an injection-recovery cycle in some detail. This has been modelled by considering a cylinder of fractured aquifer centered around a well. The numerical grid used for these calculations extended to a radius of 2000 m about the well and has a variable mesh spacing beginning at 0.25 m close to the borehole and increasing logarithmically with distance away from the well. Initially, the aquifer was assumed to be full of water, both in the fractures and the matrix, with a nominal solute concentration ('salinity') of 1.0 representing native groundwater. The injected water was assumed to have a concentration of 0.0. Therefore the relative concentration in the recovered water lies between 0 and 1 and is a direct measure of the fraction of the native water found in the recovered water – this is one measure of the efficiency (or inefficiency) of an ASR scheme. The response of the model to a typical annual cycle is shown in Figure 4.1. The relative concentration plotted is that found at the well.

During the injection phase (Figure 4.1A), the concentration at the well is 0.0, that is, the injected water concentration. If the well is left standing after injection stops (Figure 4.1B), the concentration in the well gradually increases due to diffusive exchange between the injection water in the fractures and the native groundwater in the matrix. When the recovery (pumping) phase starts (Figure 4.1C), the concentration in the well increases further as higher salinity water from greater distances in the aquifer is drawn into the well along fractures. This is the key phase of the cycle as predictions can be compared directly with measured concentrations in the recovered water. When the recovery stops, the now relatively fresh water in the matrix close to the well causes a dilution of the fracture water by diffusive mixing. As soon as injection starts again, the salinity in the well drops to 0.0, i.e. back to the concentration in the injected water. If the volume of injected water is greater than that taken out during recovery, such a cycle builds up a 'bubble' or buffer zone of injected water in the aquifer, albeit with considerable mixing with native groundwater at the interface.

It is the moderately slow rate of exchange between matrix and fracture water that is the problem with dual porosity aquifers such as the Chalk. If this exchange were either very fast or very slow then the ideal for ASR – a distinct bubble of injected water close to the well – could be established. When significant exchange takes place within a few months or years, the timescale of a typical ASR scheme, this ideal is prevented.

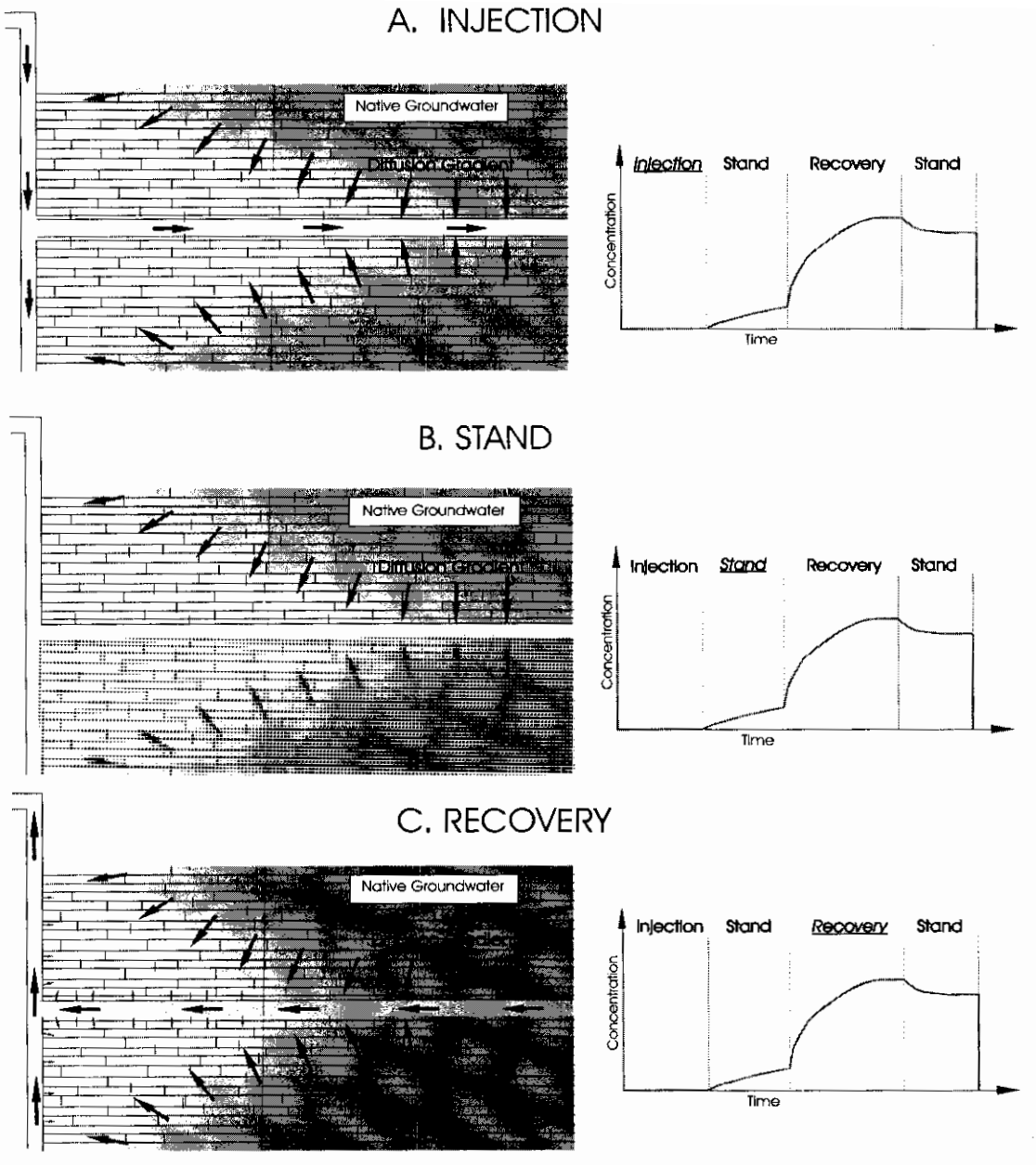

Figure 4.1 Modelled response of a dual-porosity aquifer to a typical injection-stand-recovery cycle. The relative concentration plotted is a measure of the fraction of the native water in the recovered water

4.3.2 Calibration of a dual porosity model against field data collected from a trial in the Chalk aquifer

The modelled results were calibrated against data collected during an extensive cycle-testing programme undertaken by Wessex Water Services at their site in the confined Chalk aquifer at Lytchett Minster in Dorset. Water from a supply main was injected at a constant rate of 2 to 3.2 Ml/d in cycles ranging in duration from a few days initially and increasing to over four months in Cycle 9. Apart from the first cycle, less water was

recovered than was injected in order to build up a buffer zone. The water injected over nine cycles totaled about 980 Ml of which 360 Ml was recovered. Using a fracture porosity of 0.01, the maximum radius of the residual 'bubble' in the fractures is estimated to be about 700 m.

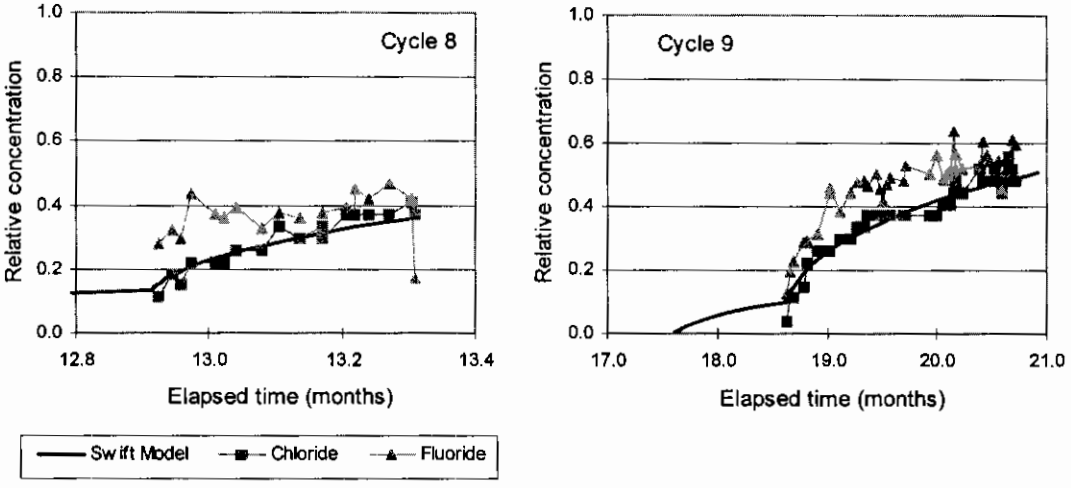

Figure 4.2. Results of dual porosity modelling from Cycles 8 and 9 of the testing programme in the Chalk aquifer at Lytchett Minster. Data for the observed variation in chloride and fluoride concentrations are also shown

The model was matched to the non-reactive solute, chloride. The match between the modelled and observed concentrations is good for Cycle 8 and 9 (Figure 4.2). A good match was also found for the preceding seven cycles. Also shown in Figure 4.2 are the relative concentrations for what proved to be a reactive solute, fluoride. The measured relative concentration of fluoride is greater than the modelled concentration indicating that some fluoride must be dissolving from the aquifer. The impacts of geochemical reactions on the recovered water quality are discussed further in Chapter 5.

4.4 Impact of mixing in British aquifers

In order to assess the impact of ASR-schemes on the recovered water quality in British aquifers, a sensitivity analysis was carried out using the SWIFT-model. The impact of operational and test cycles on the recovered water quality were modelled assuming a plausible range of aquifer parameters (Table 4.1). No chemical reactions between the injected water and the native groundwater and the aquifer material were included in the model. The changes therefore solely reflect mixing processes, both advective and diffusive.

For the sensitivity analysis, two ASR regimes were tested. One regime represents a typical series of test cycles (short cycles), while the second represents a typical series of operational cycles, i.e. long cycles. This was done to determine whether the timescale was important or not.

Table 4.1 Estimated values or ranges of values for some physical properties of the main aquifers in the UK

Aquifer	Permeability (m/d)		Porosity (%)		Storativity (m^{-1})	Thickness (m)
	Matrix	Fracture	Matrix	Fracture		
Lincolnshire Limestone (Jurassic)	10^{-3}	10 to100	1-10	0.5 to 5	10^{-6}	10-40
Chalk (Cretaceous)	10^{-3}	1 to100	20-40	0.5 to 2	10^{-6}	50-200
Sherwood Sandstone (Triassic)	1 to 50	10 to 500	10-25	1	10^{-5}	50-300
Lower Greensand (Cretaceous)	1 to 100		10-25		10^{-5}	10-40

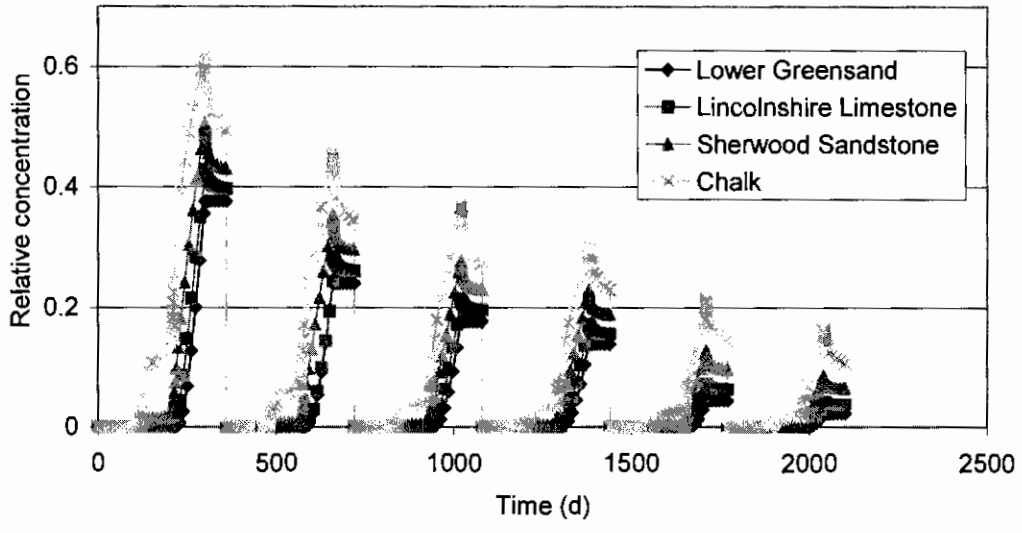

Figure 4.3 Predicted responses of the four major aquifers in the UK to ASR over six annual cycles. Each trace represents a series of injection-stand-recovery cycles of the type illustrated in Figure 4.1

For each aquifer a base case was modelled. The selected parameter values were chosen to be in the middle of the estimated parameter range (if a range was indicated). The base case was calculated for each aquifer over six annual cycles (Figure 4.3). The peak concentration declines with successive cycles because of the gradual increase in the size of the freshwater bubble close to the well. The relative concentration in a given cycle increases in the sequence: Lower Greensand < Lincolnshire Limestone < Sherwood Sandstone < Chalk, reflecting the increasing influence of fracture flow in drawing in native groundwater and reducing the compactness of the freshwater bubble around the well.

As an example of the sensitivity of the results to variations in aquifer properties, a detailed analysis of the Chalk aquifer was undertaken (Figure 4.4). These analyses were

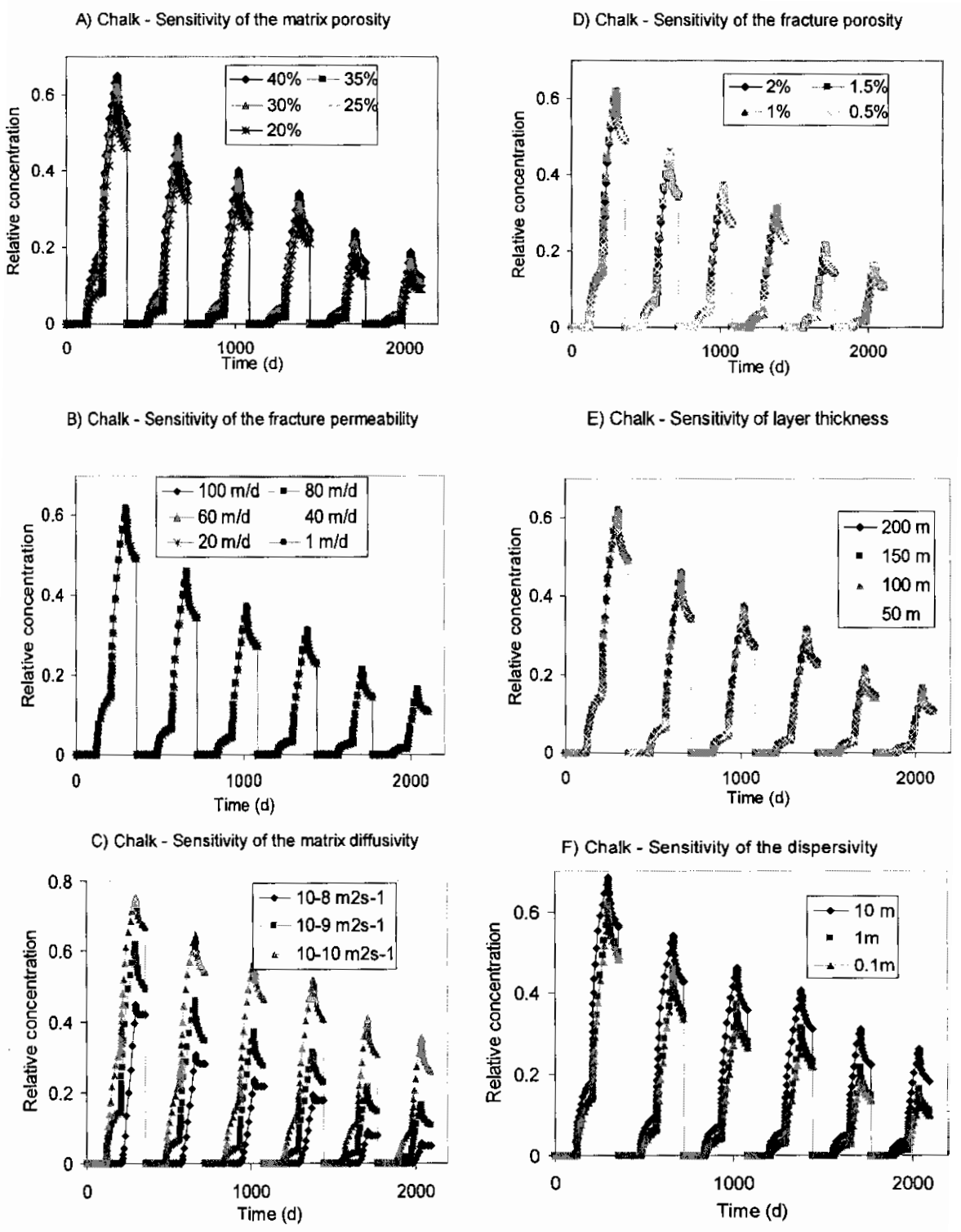

Figure 4.4 Sensitivity analysis of ASR-cycle testing in the Chalk to various aquifer properties: matrix porosity, fracture permeability, fracture porosity and layer thickness, matrix diffusivity and dispersivity

also carried out for the other aquifers except for the influence of matrix diffusivity and dispersivity, which were only evaluated in the case of the Chalk aquifer. These two parameters were assumed to be constant for the Sherwood Sandstone, the Lincolnshire

Limestone and the Lower Greensand because their dependency on the other parameters was unknown. It is, in general, difficult to measure the matrix diffusivity and dispersivity of aquifers.

Varying the parameter values over the plausible ranges expected for the dual-porosity Chalk aquifer, the Sherwood Sandstone and the Lincolnshire Limestone aquifers showed that the effect on the relative concentration of a non-reactive solute was small. Because of these low sensitivities, the conclusions drawn from the short-term test cycles can reasonably be extrapolated to longer-term operational cycles. Of the parameters examined, the matrix porosity had the greatest influence on the modelled relative concentrations. Variations in the other parameters (fracture permeability, fracture porosity and thickness of the aquifer) were negligible and variations in the matrix diffusivity and aquifer dispersivity were small.

However, the sensitivity to the parameters that are difficult to measure (matrix diffusivity, dispersivity) might be greater than shown in Figure 4.4. For example, it cannot necessarily be concluded from these calculations that these parameters never influence the modelled concentrations since they also depend on the values of other parameters such as fracture permeability, rock porosity and matrix porosity. A matrix diffusivity of 10^{-9} m^2/s and a fracture dispersivity of 10 m were found to be appropriate for all of the aquifers modelled.

The lack of sensitivity of the mixing to the aquifer thickness and permeability is not unexpected since the same volume of water had been injected in each of the model runs. This, of course, leads to very different imposed heads on the aquifer, some of which would be unlikely in reality. However the volume of the aquifer (and thus the volume of the native groundwater), which comes into contact with the injected water is the same in all cases in which only the permeability or the thickness were changed. For dual-porosity aquifers, the matrix permeability has little effect on predicted concentrations because it has been assumed that there is no flow in the matrix except perpendicular to the fractures. This is a reasonable assumption for the Chalk and the Lincolnshire Limestone, but for the Sherwood Sandstone this assumption might not hold and therefore the results for the Sherwood Sandstone aquifer should be viewed with caution.

Based on the parameter estimates given in Table 4.1 and the calculations described above, the Chalk seems to be the least suitable aquifer for ASR in terms of recovered water quality. This is due to its high matrix porosity in comparison to the other aquifers, leading to a high degree of mixing between injected and native water. Due to the low matrix porosity of the Lincolnshire Limestone, matrix effects are less important. Because of the combination of good matrix porosity and fracture permeability in the Sherwood Sandstone (a dual-permeability aquifer), the response largely depends on the presence or absence of fractures in the target aquifer. If fractures are present, the response tends towards that of a Chalk aquifer, whereas if fractures are absent, then the response tends towards that of the Lower Greensand aquifer.

The absence of dual-porosity effects in the Lower Greensand aquifer means that the quality of the native groundwater has a minimal influence on the quality of the recovered water as it is simply displaced by the injected water with little mixing.

If the quality of the native groundwater in an aquifer is already good, then the extent of mixing is not important and other quality issues and the efficiency of the scheme in terms of recovery of injected water will determine the likely overall benefits.

The main conclusion of this modelling is that where an ASR scheme is to be used in an aquifer with poor quality native groundwater then, all other things being equal, dual-porosity aquifers will need more conditioning (injection of non-recoverable water to build up a buffer zone of mixed waters) than single porosity aquifers. However the suitability of any particular aquifer depends on its physical (dispersive and diffusive parameters) and chemical characteristics (native groundwater and injected water quality) Local variations can be great and will need to be determined on a site-by-site basis from field trials.

5 Water – groundwater – rock interactions

5.1 Introduction

The geochemical processes involved in an ASR scheme involve a range of chemical reactions between the injection waters, the native groundwater and the aquifer (Figure 5.1). Therefore the chemical changes that occur are determined by three end-members:

- chemical composition of the injected water;
- chemical composition of the native groundwater;
- chemical (mineralogical) characteristics of the aquifer.

There are large potential variations in the chemical compositions of both the injection and the native waters, as well as the rock matrix. The source of the injected water can include drinking water, untreated or treated surface water, untreated or treated groundwater or reclaimed water. Native groundwater quality can vary from fresh through brackish water to saline water. The major element chemistry is often dominated by reactions involving carbonate or silicate mineral phases. The redox status may be either oxidising or reducing. In addition, large regional differences exist in native groundwater quality related to land use, residence time and differences in aquifer mineralogy.

The simplest estimate of recovered water quality is that it will lie somewhere between that of the injection water and that of the native groundwater. If there are no chemical reactions, then the recovered water quality will merely reflect the mixing ratio. This would be true of an ion such as chloride and is what has been modelled in Chapter 4. Most solutes do react to some extent with the aquifer – the solid/solution ratio is extremely high in aquifers so that even a small amount of dissolution, for example, can have a major effect on groundwater quality. In most cases, native groundwater will have equilibrated with the host aquifer and so this should give an indication of the presence of relatively soluble minerals such as halite (NaCl), gypsum ($CaSO_4.2H_2O$), calcite (CaCO3), dolomite ($CaMg(CO_3)_2$) and fluorite (CaF_2). Geochemical modelling can help to establish which of these minerals is present in the aquifer.

Occasionally, the injection of water may cause 'new' reactions to take place, which could lead to the quality of the recovered water quality being outside the range of quality spanned by the injection and native water. For example, if oxidising water is put into a reducing aquifer containing pyrite (FeS_2) then this could lead to pyrite oxidation with the release of sulphate, and probably more significantly, dissolved iron. Other minor elements could also be released. The extent of this oxidation is controlled by both the amount of dissolved oxygen and nitrate in the injection water. Injecting reducing water into an oxidising aquifer could also lead to the release of iron and manganese by dissolving iron and manganese oxides. There can also be some surprising effects when mixing two waters – for example, the mixing of two calcite-saturated waters can lead to a calcite-unsaturated water and thereby lead to further calcite dissolution from the

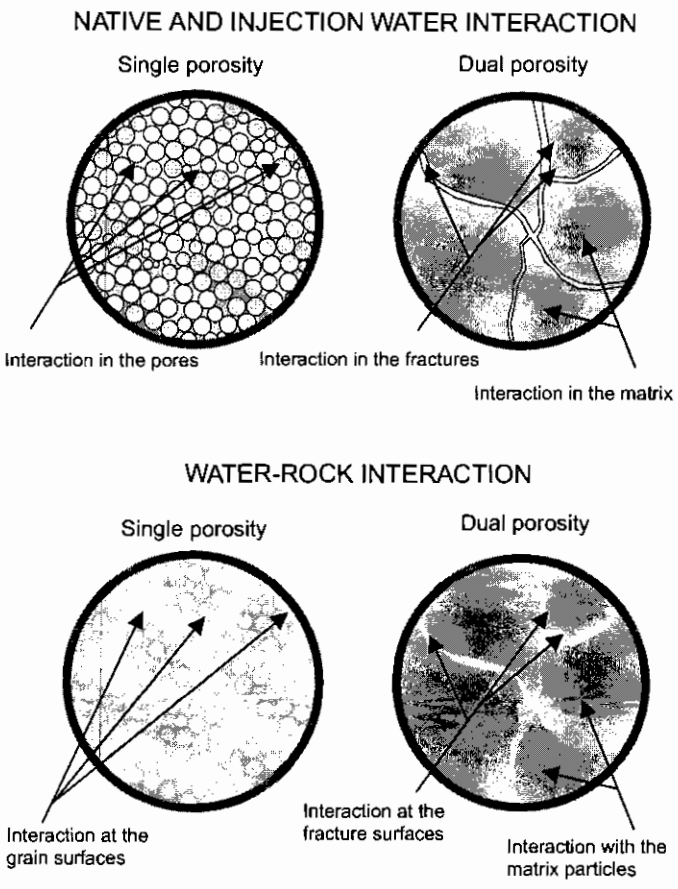

Figure 5.1 Situations in which chemical interactions between groundwater and aquifer can take place during ASR

Aquifer material. Similar effects can occur with other minerals. The danger with these additional reactions is that they may put the recovered waters outside the acceptable range for drinking water or may lead to the development of precipitates that may clog the well. Geochemical modelling can provide estimates of these effects but the rate of most of these dissolution/precipitation reactions in British aquifers is poorly understood and so these estimates are likely to be only approximate.

The PHREEQC Model (originally developed by the USGS)

PHREEQC is based on an ion-association aqueous model and has capabilities for (1) speciation and saturation-index calculations; (2) reaction-path and 1D-transport calculations involving reversible reactions, which include aqueous, mineral, gas, solid-solution, surface-complexation, and ion-exchange equilibria, and irreversible reactions, which include specified mole transfers of reactants, kinetically controlled reactions, mixing of solutions and temperature changes and (3) inverse modelling, which finds sets of mineral and gas mole transfers that account for differences in composition between given waters, i.e. how the water quality may have evolved from one place to another (Parkhurst and Appelo, 1999).

Modelling of the likely major impacts of ASR on the recovered water quality in the four main aquifers in Britain was carried out using various plausible combinations of

injection water quality, aquifer type and native water quality. The aquifers investigated were the Chalk, the Lower Greensand, the Sherwood Sandstone and the Jurassic Limestone. The PHREEQC geochemical speciation and transport model (see Box) was used for these calculations. The objective of this modelling was to provide guidance on possible water quality issues that should be considered when investigating the development of new ASR-schemes. More detailed modelling based on site-specific data is necessary to assess any probable water quality problems in specific situations since conditions are likely to vary greatly from site to site.

Table 5.1 The range of injection and native water combinations tested during the geochemical modelling for various British aquifers

Chalk	Lincolnshire Limestone
• Injection of treated Upper Chalk water into the confined Upper Chalk at Lytchett Minster • Injection of treated Upper Chalk water into the confined Upper Chalk at Holton Heath • Injection of treated Blashford Lakes surface water into the confined Upper Chalk at Lytchett Minster • Injection of treated Blashford Lakes surface water into the confined Upper Chalk at Holton Heath	• Injection of River Trent water into the Lincolnshire Limestone at Spalding Bulb Company • Injection of River Trent water into the Lincolnshire Limestone at Lenton PS
Sherwood Sandstone	**Lower Greensand**
• Injection of River Derwent water into the Sherwood Sandstone aquifer at Budby. • Injection of River Derwent water into the Sherwood Sandstone aquifer at Gainsborough B.P. • Injection of Magnesian Limestone water into the Sherwood Sandstone aquifer at Gainsborough B.P. • Injection of Magnesian Limestone water into the Sherwood Sandstone aquifer at Budby.	• Injection of treated Upper Chalk water into the Lower Greensand at Stockbury • Injection of River Medway water into the Lower Greensand at Stockbury

The main geochemical processes relevant to ASR include mixing, adsorption-desorption, ion-exchange, oxidation-reduction and dissolution-precipitation reactions

(Jones et al., 1999). In addition, microbially-mediated reactions (not modelled here) may occur, particularly related to the degradation of organic chemicals and the reduction of nitrate. An overview of the different types of injection and native waters used for the exploratory modelling is given in Table 5.1. The end members were selected to be representative of scenarios that have been, or are likely to be utilised. Details of the water chemistries used are given in Gaus (2001).

Major chemical changes to the quality of the injected water during recovery are to be expected when one or more of the following conditions are met:

- there is a large difference in chemical quality between the injected and the native water; this can cause large differences in pH or redox status.
- the native water or the sediment do not possess a sufficient pH buffering capacity (e.g. in the case of acidic waters where no calcite or dolomite is present for dissolution)
- there is a large difference in elemental concentrations between the injection and the native water (e.g. fluoride) and significant mixing occurs (e.g. in dual porosity aquifers)
- a change in chemical condition of the water having contact with the sediment is able to trigger major (e.g. dissolution of gypsum) or minor (e.g. dissolution of heavy metals) reactions.

5.2 Geochemical assessment for the different aquifers

Depending on the flow regime in the aquifer, different types of chemical interactions are likely to dominate and determine the quality of the recovered water.

In cases where the aquifer has a dual porosity character (as is the case for the Chalk and the Lincolnshire Limestone), the following factors might influence the quality of the recovered water:

- during ASR, the native water in the fractures will be replaced quickly with injected water. However, diffusional interchange between the matrix and fractures is relatively slow with the matrix retaining the native water signature for a long time. This diffusional mixing might lead to additional geochemical reactions.
- the water quality in the matrix pores may differ significantly from that of the water in the fractures. Such differences may have significant effects.

When the aquifer is a single porosity aquifer (e.g. the Lower Greensand) in which intergranular flow predominates, then it is more likely that a 'bubble' of injected water will form around the ASR-injection well. This bubble, of almost 100 % injected water, will be surrounded by a mixing zone of native and injected water. The creation of such a bubble (reservoir) of injected water in the aquifer has two major consequences:

- simple mixing between the injected water and the native water will be restricted to the mixing zone, as will the impact of geochemical reactions between the waters, leaving the injected water in the bubble relatively unaffected.

- largely unmixed injected water in the bubble will be able to trigger more intense geochemical reactions with the sediment when there is a large difference in quality between injected and native waters.

Although the behaviour of the Sherwood Sandstone lies somewhere between dual-porosity (the bulk of the flow takes place in the fractures and storage is provided by the matrix) and single-porosity (flow takes place in the matrix), it is probably best described as a dual-permeability medium. The matrix is permeable enough to transmit water at the low rates relevant to regional flow systems, but is probably not permeable enough to affect water flow in some near-well situations where rapid fracture flow is likely to be dominant. Because the extent of mixing will be even greater in the dual porosity case, this is seen as the worst case and was therefore assumed in the modelling.

The main chemical reactions for each aquifer have been classified into issues related to the native water quality, issues related to the injected water quality and issues related to the chemical reactions within the aquifer. Interactions with the sediment are based on the anticipated major components from geochemical descriptions for the different aquifers. The results of the modelling study are discussed in detail, and tabulated in Gaus (2001) and are summarised here in Table 5.2

These conclusions are based on the modelled cases only, and highlight the main chemical reactions likely to occur when implementing an ASR-scheme. Other chemical interactions may determine the quality of the recovered water when other injection waters are used, when the native water has a different quality, or when the geochemistry of the aquifers is different from that assumed here. Also reactions involving some minor elements such as cadmium, nickel and arsenic have not been considered.

In general the changes in the quality of injected water which may occur following recovery will depend strongly on the injected water quality and the native groundwater quality as well as the physical (transport) and chemical properties of the aquifer concerned. Recovered water quality will usually lie somewhere between the two end-members and for reactive solutes, may be closer to the native groundwater quality. Rarely, there may be interactions between injected groundwater and the aquifer that give rise to poorer recovered water quality than found in either of the two end-members. The most likely example of this is where aerated, high-nitrate groundwater is injected into a reducing aquifer containing pyrite (FeS_2). This can lead to the release of significant quantities of iron, sulphate and other minor elements.

Geochemical modelling can be used at different levels when planning and developing an ASR-scheme. During the initial desk study, it can be used to provide an initial assessment of the chemical viability of the scheme. During the trial and implementation stages of an ASR scheme as additional water quality data become available, geochemical modelling can be used to assess the impact of specific geochemical reactions. This is illustrated for the case of fluoride, which was monitored during an ASR trial in the Chalk in southern England (see Section 5.3).

Table 5.2. Possible impacts of ASR on recovered water quality in the UK

Inorganic chemical parameter	Possible groundwater reactions which may change the injected water quality
pH	In aquifers containing free calcium carbonate (all Chalk limestone aquifers and usually the Sherwood Sandstone and Lower Greensand), the pH of the recovered water is likely to be close to that of the native groundwater.
Chloride (Cl)	Expect injected water to mix with native groundwater and the final Cl concentration will reflect the extent of this mixing and the two concentrations, i.e. conservative mixing. This should be relatively rapid in well-mixed aquifers but will be slow (months to years) in dual porosity aquifers such as the Chalk.
Sodium and potassium (Na and K)	As for Cl but some cation exchange will occur on clays, which will tend to buffer concentrations to be closer to those in the aquifer. The effect will be greatest where the clay content is greatest, e.g. Lower Chalk and parts of the Lower Greensand.
Calcium and magnesium (Ca and Mg)	In the presence of free calcium carbonates, these concentrations are likely to be controlled by carbonate equilibria but cation exchange may also be important where the clay content is high. Generally concentrations will tend to approach those of the native groundwater.
Iron, manganese, ammonium and nitrite (Fe, Mn, NH_4 and NO_2)	Most injected waters will be aerobic and therefore low in these constituents but may be injected into a reducing aquifer where they are elevated (in the UK, most confined aquifers are reducing). This will increase their concentration in the recovered water but it should not be greater than in the native groundwater and will tend to be less if the injected water contains dissolved oxygen.
Sulphate (SO_4)	Similar to Fe and Mn but injection of aerated or high nitrate water into a reducing aquifer containing pyrite could lead to release of sulphate and acidity (which could lead to enhanced release of CO_2 when it reacts with carbonates).
Fluoride (F)	Similar to Cl but there can be an additional slow release from fluoride-containing minerals, especially where Ca concentrations are low. High native concentrations of fluoride are occasionally found in carbonate aquifers in the UK, but not in the sandstone aquifers.
Trace constituents	Most metals (Zn, Cd, Pb, Al etc) which are present as cations or carbonate complexes tend to be present at low concentrations at the near-neutral pH's of most UK groundwaters. Exceptions can arise in slightly acidic (some shallow Sherwood Sandstone and Lower Greensand groundwaters) and strongly reducing waters but such instances are relatively rare. Arsenic can be enhanced near mineralised areas and close to the redox boundary in semi-confined aquifers, both in the Chalk and Sherwood Sandstone. Boron can be high particularly in areas associated with residual salinity.
Nitrate (NO_3)	Likely to be reduced if high nitrate, aerobic water is injected into a reducing aquifer due to denitrification.

Although beyond the scope of the modelling undertaken, the potential improvements in water quality, resulting from ASR, are considerable. Reduction of nitrate, when injected into a reducing aquifer may be microbially mediated, as may many other reactions involving organic chemicals. Attenuation of these chemicals during artificial recharge, is poorly understood and is the topic of much current research. Examples of attenuation of disinfection-by-products (DBP) (Pyne et al., 1996) and the capacity of aquifers for adsorbtion and biodegradation of organic carbon (Dillon and Pavelic, 1996) have been documented. However the sustainable treatment processes occurring in aquifers need further investigation, particularly in relation to pathogens, natural and synthetic organic chemicals, including endocrine disruptors.

5.3 Case Study: fluoride modelling of the ASR trial in Lytchett Minster

The SWIFT model, applied to the ASR trial in the Chalk aquifer at Lytchett Minster, Dorset, (see Section 4.3.2) demonstrated that the increase in fluoride concentration in the recovered water could not be attributed solely to dual-porosity mixing. An additional chemical reaction must have taken place to give the observed increase of about 10 % above that predicted for mixing alone. Geochemical modelling was used to help to identify the geochemical processes leading to this additional increase in fluoride in the recovered water. A full description of the fluoride modelling at Lytchett Minster can be found in Gaus,et al. (2001).

An example of the excess fluoride in the recovered water is shown in Figure 5.2 (right) for Cycle 9. Data from other cycles showed the same pattern. Chloride (which shows conservative behaviour) was used to calculate the amount of mixing between injection and native water and is shown on the x-axis. The ratio between mixing based on fluoride to that based on chloride is plotted on the y-axis. If fluoride also behaved conservatively, the fitted line would be horizontal; intersecting the y-axis at 1.0. The fact that this ratio is much greater than 1 at the beginning of each recovery cycle, and reduces during the recovery phase, indicates that processes other than simple mixing control the fluoride concentration. Where the main component of the recovered water is injection water, the fluoride concentration is much greater than would be expected from simple mixing alone. With an increasing fraction of native water in the mixture, excess fluoride due to geochemical reactions will influence the fluoride mixing ratio to a lesser degree because of the high fluoride concentration in the native groundwater.

Three mechanisms that could cause the observed increase in fluoride concentrations were postulated and the results expected from each mechanism was modelled and then compared with the field observations. The three mechanisms are:

1. the fluoride concentration in the matrix water is higher than in the fracture water: the recovered water will reflect the difference between the fracture water and the matrix water in the Chalk even with no geochemical reactions

2. the mineral fluorite (CaF_2) is available for dissolution in the matrix and in the fractures, but only a limited amount is present: the concentration of fluoride in the recovered water will be limited by the amount of fluorite in the sediment that is available for dissolution

3. fluorite is available in sufficient quantities for the fluoride concentration to reach saturation but the dissolution kinetics are slow: the rate of fluorite dissolution therefore determines the fluoride concentration in the recovered water (a simple kinetic equation was used to describe the dissolution kinetics).

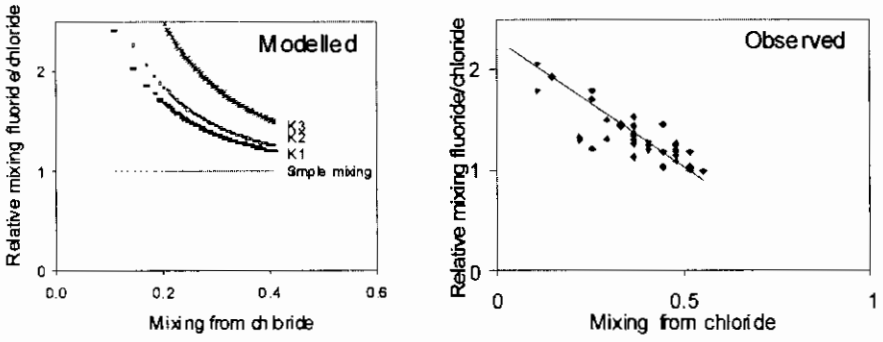

Figure 5.2 Comparison of modelled and observed relative mixing ratios for fluoride and chloride versus the amount of mixing between injection and native groundwater. Left: modelled ratios based on fluorite dissolution kinetics (mechanism 3) for three parameter sets (K1, K2 and K3); Right: optimal fit (line) through observed ratios (crosses) from Cycle 9.

The modelling results according to mechanism 3 are shown in Figure 5.2 (right). Modelling showed that the mechanisms 1 and 2 were not able to fit the observed data. Therefore, it is concluded that the increase in fluoride is probably controlled by the dissolution kinetics of a mineral, probably fluorite, which is present in excess in the Chalk sediments.

If this is the case, a significant decrease in fluoride concentration in subsequent cycles is unlikely to occur until the available fluorite is exhausted and mechanism 2 becomes the dominant process. However, the amount of fluoride dissolved and removed during ASR-cycles is likely to be small compared with that present within the solid phases in the aquifer. No data are available for the amount of fluorite present in the Chalk sediment at the site.

This case study demonstrated the broader view that must be taken when including an ASR scheme as part of a water resources strategy. The cost implications of the additional treatment, or blending, need to be compared to alternative sources of supply, remembering to include the environmental benefits (Eastwood and Stanfield, 2001). The Chalk and Lincolnshire Limestone are known to contain occasional high-fluoride groundwaters (Edmunds et al., 1989). The Sherwood Sandstone aquifer is normally low in fluoride (<0.1 mg/l). Fluorapatite, another F-containing mineral, is known to be present in some Chalk sediments and could provide an additional source of fluoride but it is likely to be released at a much slower rate than from fluorite.

6 Regulatory considerations

6.1 Regulations affecting Artificial Recharges to groundwater

Under the Groundwater Regulations, 1998 (GWR) an authorisation is required for discharges of listed substances to groundwater (the saturated zone). Regulation 6 of the GWR makes provision for the authorisation of artificial recharges, subject to there being no risk of pollution of groundwater. (Note: under the GWR it is not just actual pollution but the risk of such pollution that has to be considered). Direct discharges to groundwater (directly to the water table) may be consented under the Water Resources Act, 1991- these consents also act as authorisations under the GWR.

The GWR, which reflect the EU Groundwater Directive, require that there should be no entry of List I substances into groundwater and no pollution by List II substances. Listed substances (List I and List II) are given in the Schedule attached to the GWR. There is a formal process by which the Environment Agency, as the responsible body in England & Wales, determines whether a substance is listed. The Ecotox Centre should be consulted regarding the status of any particular substance.

Under Regulation 2, the Environment Agency can determine whether a discharge can be excluded from the GWR by virtue of the quantity and concentration of listed substances in the discharge. This is a case-specific assessment, which must be undertaken with no prior investigation of the hydrogeology of the site (following a European Court decision several years ago) it must be obvious from the nature of the source material that it could not cause entry into groundwater of List I substances or pollution by List II substances. The DETR guidance on the GWR makes it clear that although there are no specific concentration limits for pollutants, the drinking water and other similar standards may be used as a benchmark for such assessments.

If a discharge is found to be outside the remit of the Groundwater Regulations by virtue of the ***de minimis*** provision above, it is unlikely to require any other form of consent under water quality legislation. If the discharge contains only non-listed but nevertheless potentially polluting matter (e.g. bacteriological contamination), it may still possibly require a discharge consent under the Water Resources Act, 1991.

List I substances can be allowed to enter groundwater if the groundwater body can be declared as being "permanently unsuitable for other uses". There is a detailed procedure that describes this within the Agency's Groundwater Regulations Process Manual. This is publicly accessible but is not a published procedure. It can be obtained via Environment Agency offices.

6.2 Guidance on dealing with authorisations for artificial recharge and recovery (ARR) schemes

As part of a project assessing the potential for ASR in England and Wales, the regulatory issues associated with development of schemes were reviewed in the context of the existing guidance. The conclusions of this review are given in Appendix J of the project report (Jones et al. 1998), the main points of which are summarised below.

The purpose of Appendix J was to provide guidance on the licensing and consenting requirements associated with Artificial Recharge and Recovery (ARR) schemes. These can range between:

- Aquifer Storage and Recovery (ASR) schemes as developed in the USA, involving recharge of water into relatively deep, possibly poor quality and little-used aquifers to create a bubble of fresh groundwater for subsequent re-abstraction, and

- Artificial recharge schemes involving injection of water into good quality, generally well-utilised, aquifers to enable better or increased use of water resources (e.g. to store excess winter resources for re-abstraction to meet summer demand, or to support use of an aquifer with limited or heavily-utilised natural resources, etc).

The guidance covers a range of situations encompassed by such schemes, all of which will require authorisations from the Environment Agency.

Nothing in the guidelines modifies the abstraction licensing best practice set out in the Environment Agency's National Abstraction Licensing Manual, to which reference should be made for detailed explanation of Agency requirements, policy and procedures. Unless otherwise stated, references to sections in the legislation relate to the Water Resources Act 1991 ("WRA1991").

The phased and individual nature of ARR scheme development (which can extend over several years) makes it difficult to produce guidelines which will cover every eventuality but in general, the developer should ensure that :

a) Abstraction of water from any aquifer or surface water source is authorised either by an existing licence or by a Section 32 consent, as appropriate, having been discussed with the Agency beforehand.

b) The recharge of any water to the receiving aquifer is authorised in accordance with legislative and Agency requirements.

c) The discharge of any water to controlled waters (either surface or groundwater) is authorised in accordance with legislative and Agency requirements.

Discharge consenting requirements for b) and c) above will depend upon whether or not the discharge is classed as trade effluent. Where in doubt, Agency staff should consult their Regional legal departments.

The Agency will seek to control all recharge and subsequent re-abstraction to ensure effective development of water resources whilst protecting the environment and other abstractors. In particular, it will expect schemes to be sustainable in terms of quantities recharged and re-abstracted and may wish to apply water level or water quality conditions to any authorisations issued.

The developer should be aware that, for most schemes, the Agency will issue separate authorisations relating to each main phase of development/implementation, since the monitoring, abstraction and discharge requirements for the initial testing, operational

testing and final scheme implementation phases will differ. It is therefore important that the developer continues to keep in close contact with the Agency as each phase progresses.

Whilst the Agency appreciates that developers will want to know at the outset about the likelihood of obtaining all necessary authorisations for all phases, it is unlikely to be able to give firm indications at that stage. Much will depend upon the findings of investigations as each phase of the scheme progresses. It is possible that later phases will not be able to go ahead if, for example:

- earlier phases show there are insufficient resources to provide the donor water, or
- there are incompatibilities in quality between the donor and receiving waters that cannot be resolved, or
- there are adverse effects on lawful abstractions, or
- the Agency believes that the recharge of water will be environmentally damaging.

6.3 Phased development/authorisations

The phased and individual nature of ARR scheme development (which can extend over several years) makes it difficult to produce guidelines that will cover every eventuality. In general, the developer should obtain the necessary authorisations throughout the six phases of development and ensure that the required Environmental Impact Appraisals (EAPs) are carried out.

Phased development of Artificial Recharge and Recovery Schemes	
Phase 1	preliminary discussions
Phase 2	development/construction of donor source(s)
Phase 3	construction/initial development of recharge borehole(s)
Phase 4	operational testing of recharge borehole(s) and re-abstraction source(s)
Phase 5	applications for authorisations for operational scheme
Phase 6	determination and issue of licences and consent

6.4 Environmental Impact Appraisals (EAPs)

The Agency will require that the effects of the proposed development on the environment are considered. The scope of the impact appraisal will be affected by the nature of the aquifer, the two extremes of which are shown below.

Aquifer Type	Nature of the Aquifer	Type of EAP
Shallow Unconfined (Traditional Artificial Recharge Schemes)	Good quality water present Probability that surface water may be affected Probable impact on existing abstraction rights Limited spread of level changes	Full EAP probably required
Deep Confined (Aquifer Storage and Recovery Schemes)	Poor quality water No direct connection with surface water Existing abstractors likely to be absent Level changes can be widespread	Relatively restricted EAP probably sufficient

In addition to the normal requirements necessary for abstraction licences, environmental impact appraisals for ARR schemes should include consideration of, amongst others, the following effects as appropriate. Some of these issues have been considered further in the ASR-UK project. Discussion of the possible environmental impacts is in Chapter 3 of this report. A series of models are described that can be used to assess and quantify the likely impacts. These models are of varying complexity so they can be applied at appropriate phases of development.

Feature	Possible effects	Possible problems
Existing abstraction boreholes	Increase or decrease in rest water level in the borehole	Existing installation becomes inappropriate
Existing abstraction boreholes where rest water level is close to surface	Increase in level to give artesian conditions	Flooded pump chambers Electrical problems Flooding of nearby farmland
Low lying areas	Increase in groundwater level	Water logged ground Flooding Increased flow of land drains (loss of recharged water)
Springs	Increase in spring flow; Changes in quality of groundwater discharged	Insufficient overflow capacity for new flows Flooding of chamber and pumping equipment Flooding of receiving water course

		Loss of recharge water
		Change in habitats
Streams	Increase in streamflow/flow in ditches;	Flooding
		Increase in depth of cattle watering areas
	Changes in quality of groundwater discharged	Loss of recharge water
		Change in habitats
Water bodies	Change in level	Change in habitats
		Changes in overflow quantities
		Loss of recharge water
Change in groundwater quality	Deterioration in quality	Loss of potability or suitability of water for use
		Corrosion or encrustation on water system - pumps and household systems
		Quality effects on habitats
Ground instabilities	Wetting of Clays;	Subsidence as clays swell
	Lubrication of strata boundaries	Instability of slopes

ANNEX J3 – The Potential for Aquifer Storage and Recovery in England and Wales. (from Jones et al. 1998)

DECISION MATRIX FOR ABSTRACTION CONSENTING & LICENSING

Details of source					Scheme development stage							
					Initial testing			Operational testing			Operational use	
					Approval needed			Approval needed			Approval needed	
Source of supply?	Does abstraction point already exist?	Is it already in use?	Is it already licenced?	Will proposal increase authorised or actual quantities abstracted or alter pattern of abstraction?	S32 consent	New licence	Licence variation	S32 consent	New licence	Licence variation	New licence	Licence variation
Groundwater	Yes	No	No	Yes	✓	×	×	See Note 1		×	See Note 2	
			Yes	No	× (Note 3)	×	×	× (Note 4)	×	×	×	× (Note 5)
				Yes	✓	×	×	See Note 1			×	✓(Note 7)
		Yes	No	No	✓	×	×	See Note 1		×	See Note 2	
				Yes	✓	×	×	See Note 1		×	See Note 2	
			Yes	No	× (Note 3)	×	×	× (Note 4)	×	×	×	× (Note 5)
				Yes	✓	×	×	See Note 1			×	✓(Note 7)
	No	N/A	N/A	Yes	✓	×	×	See Note 1		×	See Note 2	
SurfaceWater (Note 10)	Yes	No	No	Yes	N/A	✓(Note 6)	×	N/A	×	✓(Note 7)	×	✓(Note 7)
			Yes	No	N/A	×	×(Note 8)	N/A	×	×(Note 9)	×	× (Note 5)
				Yes	N/A	×	✓(Note 6)	N/A	×	✓(Note 7)	×	✓(Note 7)
		Yes	No	No	N/A	✓(Note 6)	×	N/A	×	✓(Note 7)	×	✓(Note 7)
				Yes	N/A	✓(Note 6)	×	N/A	×	✓(Note 7)	×	✓(Note 7)
			Yes	No	N/A	×	×(Note 8)	N/A	×	×(Note 9)	×	× (Note 5)
				Yes	N/A	×	✓(Note 6)	N/A	×	✓(Note 7)	×	✓(Note 7)
	No	N/A	N/A	Yes	N/A	✓(Note 6)	×	N/A	×	✓(Note 7)	×	✓(Note 7)

✓ = Normally required × = Normally not required (but subject also to note where indicated)

Notes:

1. A Section 32 Consent should be issued at the operational testing stage if initial testing has failed to provide sufficient information to enable a formal licence application to be properly assessed. Otherwise, issue a time-limited licence or variation as appropriate (time limit may need to be shorter than policy would normally indicate).

2. Either new licence or licence variation, depending on type of approval given for operational testing. If licence was issued at that stage, a variation may be needed.

3. If characteristics of source or understanding of impact not properly known (e.g. current licence was determined as a Licence of Right or source was never properly tested), or it is necessary to control the testing to be carried out/specify special monitoring, it would be best to persuade potential operator to accept a Section 32 Consent, otherwise the Agency's requirements should be defined in a formal agreement (either under Section 20 (for water companies), or Section 158 of WRA, 1991).

4. If characteristics of source or understanding of impact still not properly known, you will need to persuade potential operator to accept a further Section 32 Consent, or define the Agency's requirements in another formal agreement (either under Section 20 or Section 158 of WRA, 1991).

5. The ARR operator will need to apply for a variation if it wishes to take advantage of reduced charges associated with any transfer of water or if earlier testing reveals current licence is inappropriate for the operational scheme.

6. New or varied licence will usually need to be for a shorter time limit than normal policy dictates, since the conditions included are likely to be test-specific.

7. Where a licence has been issued/varied for testing purposes, it may need varying for subsequent phases of development/operational use.

8. If it is necessary to control the testing to be carried out /specify special monitoring in such a way that is not covered by any existing licence, the Agency's requirements should be defined in a formal agreement (either under Section 20 or Section 158 of the WRA, 1991).

9. If it is necessary to further control testing/specify monitoring, the Agency's requirements will need to be defined in another formal agreement as for Note 8 above.

10. "Surface water" source of supply refers to those sources for which abstraction must be licensed (i.e. those that are non-exempt). The Water Resources Act 1991 defines those that are exempt (see 3.2.2.1(a) in guidance notes).

11. ✓= Normally required, ×=Normally not required (subject also to note where indicated).

7 Summary and conclusions

1. Aquifer Storage Recovery (ASR) is viable water management technique that has the potential to resolve a wide variety of supply issues in an environmentally sustainable manner. The main advantages are:

   - Net abstraction is zero or negative so minimal impact on the surface water environment.
   - Small land area required to store relatively large quantities of water at the point where it is available for injection and needed for supply.
   - Staged development possible to spread costs and at the same time keep up with demand.
   - Improvements in water quality can occur during storage and, once understood, water quality problems can be addressed, on recovery, through treatment or dilution. Cost implications need to be assessed in relation to alternative schemes

2. Several aquifers in the UK are suitable for ASR schemes, their advantages and disadvantages are summarised below. These comments are generic and because the scale of schemes can be of the order of a few hundred metres, local geological conditions may be different. Minor aquifers, or blocks of major aquifers may prove to be ideal for ASR at particular localities even where they are not generally considered to have a high potential.

   - The **Sherwood Sandstone and some Permian sandstone** aquifers appears to have the greatest potential due to their wide geographical distribution, great thickness and high inter-granular porosity. Care is needed to select a section of the aquifer with high porosity and few fractures in order to constrain the bubble of injected water, displace indigenous groundwater and thus obtain a high recovery efficiency
   - **Lower Greensand** aquifer is limited in areal extent and thickness but, in suitable locations, this high matrix porosity aquifer will be a good ASR target. Injected bubbles will displace the native groundwater thus minimising the zone of mixing and hence geochemical problems
   - The **Chalk** aquifer has been demonstrated to be an effective hydraulic target for ASR but if the native groundwater quality is non-potable then diffusion from the matrix will be a long-term problem. This does not preclude the use of these parts of the aquifer where environmental impact considerations may still make the scheme attractive. However, the economic implications of additional treatment or dilution will need to be factored in. Where the Chalk is in hydraulic contact with overlying **Palaeogene** or **Quaternary** arenaceous deposits or the underlying **Upper Greensand**, then the storage in these aquifers can make an ASR scheme potentially more viable.
   - The variability of the **Jurassic limestones** will make their suitability for ASR equally variable. However, the aquifer may be able to provide a

reservoir for ASR where the local hydrogeological conditions are suitable. The high diffusivity of these aquifers means that the environmental impacts need to be evaluated at distances of several kilometres.

- Other **minor aquifers** should be considered on an individual basis. ASR schemes require areas of aquifers of the order of only tens of hectares so suitable, local geological settings can be adequate. Aquifers identified as having some potential include the **Fell Sandstone, Millstone Grit, Kellaways Rock** and some **Upper Lias Sands.** When considering these aquifers their potential can by reviewed in respect of the "aquifer continuum" described in this report. This continuum ranges from unconsolidated arenaceous deposits with high matrix porosity (Lower Greensand), through consolidated sandstone aquifer with high matrix porosity and some fracture flow (Sherwood Sandstone), fracture flow dominated, high diffusivity aquifers (Jurassic Limestone) to fracture flow dominated aquifers with dual porosity mixing being the dominant process (Chalk).

3. The environmental impacts of schemes will be crucial in determining their success or failure and should be assessed at the earliest stages of a scheme. Key issues are the impacts on water levels in overlying aquifers and in the unconfined part of the target aquifer, even at distances of several kilometres. Of particular concern are the impacts on stream-flow and wetlands and these need to be assessed in relation to the time delay of response of the aquifer at outcrop in relation to injection or recovery at the ASR well. Simple models have been developed to address some of these issues and to act as tools to assist decision-making on how to proceed and what additional information is required throughout the review, field trial and implementation phases of a scheme. Optimisation of the operational cycle can be demonstrated to minimise the impacts.

4. The recovery efficiencies of ASR schemes will be determined by the amount of mixing between the native groundwater and the injected water and this is controlled by the physical properties of the aquifers. In addition to physical mixing, both advective and diffusive, geochemical reactions between different waters and the rock matrix will determine the quality of the recovered water. The physical aspects have been modelled using the SWIFT/486 modelling package to test the sensitivity of the systems to ranges of aquifer properties as well as testing and operational cycles. Within the limitations and assumptions inherent in the model, the main conclusion is that dual-porosity aquifers will need more conditioning (injection of non-recoverable water to build up a buffer zone of mixed waters) than single porosity aquifers before they are suitable for use for ASR. However the suitability of any aquifer depends on the site-specific dispersive and diffusive parameters, which can generally only be obtained from field trials.

5. Geochemical models have been used to predict likely impacts of injecting a variety of waters into different aquifers containing different groundwaters. The selection of the different components was constrained by the most likely scenarios in the four major aquifers. The PHREEQC model was used and it was

found that, depending on the flow regime in different aquifers (matrix flow or fracture flow dominated), different chemical reactions dominate

- In dual porosity aquifers the injected water in the fissures will continue to react with the matrix water as well as the rock matrix whereas in a single porosity aquifer the pore water is displaced and reactions are restricted to the peripheral mixing zone, the bulk of the injected water being unaffected. However, in the latter case, the reactions, if any, between the injected water and the rock matrix will dominate.

- Geochemical reactions can be expected to be significant if there are:

    i. Large differences in pH and redox potential between the native and injected water

    ii. Little buffering capacity in the native water and/or the sediment

    iii. Large differences in concentrations between native and injected waters, combined with intensive mixing

    iv. The water mixture triggers dissolution reactions leading to the sediment releasing significant quantities of major or minor elements.

8 References

Cederstrom, D. J. Geology and ground-water resources of the York-James peninsula, Virginia, US Geological Survey: 237 (1957)

Dillon, P J and Pavelic, P. Guidelines on the quality of stormwater and treated wastewater for injection into aquifers for storage and reuse. Urban Water Research Association of Australia. Research Report No. 109. (1996).

Eastwood, J C, and Stanfield, P J. Key success factors in an ASR scheme. Quarterly Journal of Engineering Geology and Hydrogeology. 34. p. 399-409. Geological Society, London. (2001).

Edmunds W M, Cook J M, Kinniburgh D G, Miles, D L and Trafford J M, Trace-element occurrence in British groundwaters, BGS Research Report SD/89/3 (1989)

Gaus, I. Physical and geochemical modelling (SWIFT-PHREEQC) of British aquifers for aquifer storage and recovery purposes. Part 2: Geochemical Modelling. BGS Commissioned Report CR/01/54 (2001).Groundwater Regulations (1998).

Gaus I, Williams A T & Shand P. Physical and geochemical modelling (SWIFT-PHREEQC) of British aquifers for aquifer storage and recovery purposes. Part 1. Physical modeling and model calibration. BGS Technical Report WD/00/08 (2000).

Harpaz, Y. "Artificial groundwater recharge by means of wells in Israel." Proc. of American Society Civil Engineers, Journal of Hydraulics Division: 1947-1964. (1971).

IWES Development of groundwater (Chapter 14). Groundwater: Occurrence, development and protection. IWES: 485-542. (1986).

Jones, H. H. Investigations for artificial recharge of the Triassic Sandstone aquifer near Stourbridge, U.K. Journal of Institution of Water Engineers and Scientists **37**(1): 9-27. (1983)

Jones H K, Gaus I, Williams A T, Shand P and Gale 1 N, ASR-UK. A review of status of research and investigations, BGS Technical Report WD/99/54 (1999)

Jones H K, Macdonald D M J and Gale I N, The potential for aquifer storage and recovery in England and Wales, BGS Technical Report WD/98/26 (1998)

O'Shea M J. Borehole recharge of the Folkestone Beds at Hardham, Sussex, 1980-81. Journal of the Institute of Water Engineers and Scientists, 38 (1), p.9-24. (1984)

O'Shea M J, Baxter K M, and Charalambous A N. The hydrogeology of the Enfield-Haringay artificial recharge scheme, North London. Quarterly Journal of Engineering Geology, 28, S115-S129 (1995)

Parkhurst D L and Appelo C A J, User's guide to PHREEQC (version 2) – A computer program for speciation, reaction-path, 1-D transport, and inverse geochemical calculations, U.S. Geol. Survey Water Resources Inv (1999)

Pyne, R D G Groundwater recharge and wells: A guide to Aquifer Storage Recovery. Florida, USA., CRC Press (1995).

Pyne, R D G, Singer, P C and Miller, C T. Aquifer storage recovery of treated drinking water. AWWARF Report No. 90689. (1996)

Williams, A T, Barker, J A & Griffiths, K J. The environmental impacts of Aquifer Storage Recovery Schemes. BGS Commissioned Report CR/01/153 (2001).

Descriptions of Anisotropy and Heterogeneity and Their Effect on Ground-Water Flow and Areas of Contribution to Public Supply Wells in a Karst Carbonate Aquifer System

By Lari A. Knochenmus *and* James L. Robinson

Abstract

Delineation of areas of contribution to wells tapping a karst carbonate aquifer system can be extremely difficult using conventional approaches designed for isotropic and homogeneous aquifers, because ground-water flow tends to be through solution-enhanced conduits. Nonradial flow along preferential zones can result in inaccurate estimates of flow paths and traveltimes. Because of the large variability in factors affecting contributing areas and an imperfect understanding of how these factors can vary, the estimation of contributing areas is an approximation at best.

To better understand the effects of aquifer anisotropy and heterogeneity on areas of contribution, an exploratory modeling approach was used. MODFLOW, a numerical flow model, and MODPATH, a particle tracking program, were used to generate time-related areas of contribution for six hypothetical carbonate aquifer system types. The six types were conceptualized to approximate different types of aquifer anisotropy and heterogeneity. These include: (1) an isotropic and homogeneous single-layer system; (2) an anisotropic in a horizontal plane single-layer system; (3) a discrete vertically fractured single-layer system; (4) a multilayered system; (5) a doubly porous single-layer system; and (6) a vertically and horizontally interconnected heterogeneous system. The simulated aquifer anisotropy was 5:1 (K_{xx}/K_{yy}) determined from TENSOR2D results. The simulated discrete vertical fracture network represents locations inferred from mapped photolineaments. The simulated enhanced flow zones were determined from borehole video and geophysical logs. Areas of contribution were simulated for two prototype regions. The two prototypes were selected to be representative of the hydrologic diversity within the study area and were designated the Central Swamp and Lake Terrace regions.

Localized conditions in pumping, production well distribution, and aquifer transmissivity affect the size, shape, and orientation of areas of contribution to public supply wells. The simulated areas of contribution are 60 percent larger in the Central Swamp region where pumpage is more than double and transmissivity is about half that of the Lake Terrace region. Although these factors are important, this study focused on the effects from hydrogeologic factors common to karst carbonate aquifer systems.

This study indicates that the distribution and type of aquifer anisotropy and heterogeneity will affect the size, shape, and orientation of areas of contribution in a karst carbonate aquifer system. The size of the 50-year time-related areas of contribution ranged from 8.2 to 39.1 square miles in the Central Swamp region and from 4.0 to 18.3 square miles in the Lake Terrace region. Simulations showed that the size of areas of contribution is primarily affected by simulated withdrawal rates, effective porosity of the carbonate rock, and transmissivity. The shape and orientation of the simulated areas of contribution primarily result from aquifer anisotropy, well distribution, flow along solution-enhanced zones, and short-circuiting of flow through fracture networks.

Comparisons also were made between protection zones delineated using analytical models and areas of contribution delineated using numerical models. The size of the 5-year time-related protection zone in the Central Swamp region using an analytical model was almost twice as large as the numerically simulated area of contribution, and more than eight times larger than the numerically simulated area of contribution in the Lake Terrace region. The differences in size are primarily the result of how the flow field is approximated. The analytical method assumes only lateral flow to wells but numerical methods allow particles to move laterally and vertically. Additionally, multiple-well-interference effects resulting from the close proximity of several pumping wells cause individual capture zones to converge or diverge, depending on the difference in pumping rates and orientation among the wells. Such an interpretation is not available from analytical methods. The simulated distributions of aquifer anisotropy and heterogeneity, in this study, were highly conceptualized, but were based on plausible occurrences of anisotropy and heterogeneity inherent in carbonate aquifer systems.

INTRODUCTION

The 1986 Safe Drinking Water Act Amendments require States to establish wellhead protection programs to delineate protective areas (areas of contribution) around existing and future public supply wells and well fields. The contributing area includes the geographical extent from which ground-water flow is diverted to the pumping well (Morrissey, 1989, p. 7-8). Traditional strategies to protect ground-water resources have been through land-use regulation within a prescribed radial area around each well. At times, little regard has been given to localized hydrogeologic factors common to karstic aquifers that can affect the size, shape, and orientation of areas of contribution to supply wells. Public supply wells in karst carbonate aquifers are particularly vulnerable to contamination. This is because permeability in carbonate aquifers is enhanced by circulation of water and dissolution of rock, creating higher permeability along preferred flow paths.

Historically, carbonate aquifers have been treated as diffuse-flow aquifers, in that ground-water movement virtually follows Darcy's law. This assumption, although adequate for defining flow in regional ground-water studies, is inadequate for local studies based on the inaccuracies inherent in the conceptual model. For example, the effects of nonradial, non-Darcian flow due to preferential flow paths through enhanced secondary-porosity zones, such as fractures, is a complicating aspect for developing useful strategies for ground-water protection in carbonate terranes. Therefore, a better understanding of the effects of aquifer heterogeneity on the size, shape, and orientation of contributing areas to supply wells is needed to understand ground-water flow to pumped wells. In 1990, the U.S. Geological Survey, in cooperation with the Florida Department of Environmental Protection (FDEP), began a study to illustrate the effects of aquifer anisotropy and heterogeneity, inherent to karst carbonate aquifers, on the size, shape, and orientation of contributing areas around public supply wells and well fields.

Purpose and Scope

This report describes aquifer anisotropy and heterogeneity in a karst carbonate aquifer, how these heterogeneities affect ground-water flow, and their effect on the size, shape, and orientation of contributing areas to well fields. To evaluate how areas of contribution might be affected by aquifer anisotropy and heterogeneity, a study area in west-central Florida (fig. 1) underlain by the Floridan aquifer system was selected because adequate existing data were available. Within the study area, two prototype carbonate aquifer systems were defined for detailed study. The specific purposes of the report are to:

1. Describe the anisotropy and heterogeneity typical of a karst carbonate aquifer system.
2. Present effects of aquifer anisotropy and heterogeneity on ground-water flow.
3. Show the effects of aquifer anisotropy and heterogeneity on areas of contribution to supply wells.
4. Compare delineation of protection zones determined using analytical methods and areas of contribution determined using numerical methods.

Spatial distributions of aquifer anisotropy and heterogeneity, examined in this report, were based on the results of previous studies. Historical aquifer test data were used as input to a computer program, TENSOR2D (Maslia and Randolph, 1986), to identify the possible range in magnitude and direction of anisotropy (K_{xx}/K_{yy}) in a horizontal plane. Results of a photolineament study (Culbreath, 1988) were used to

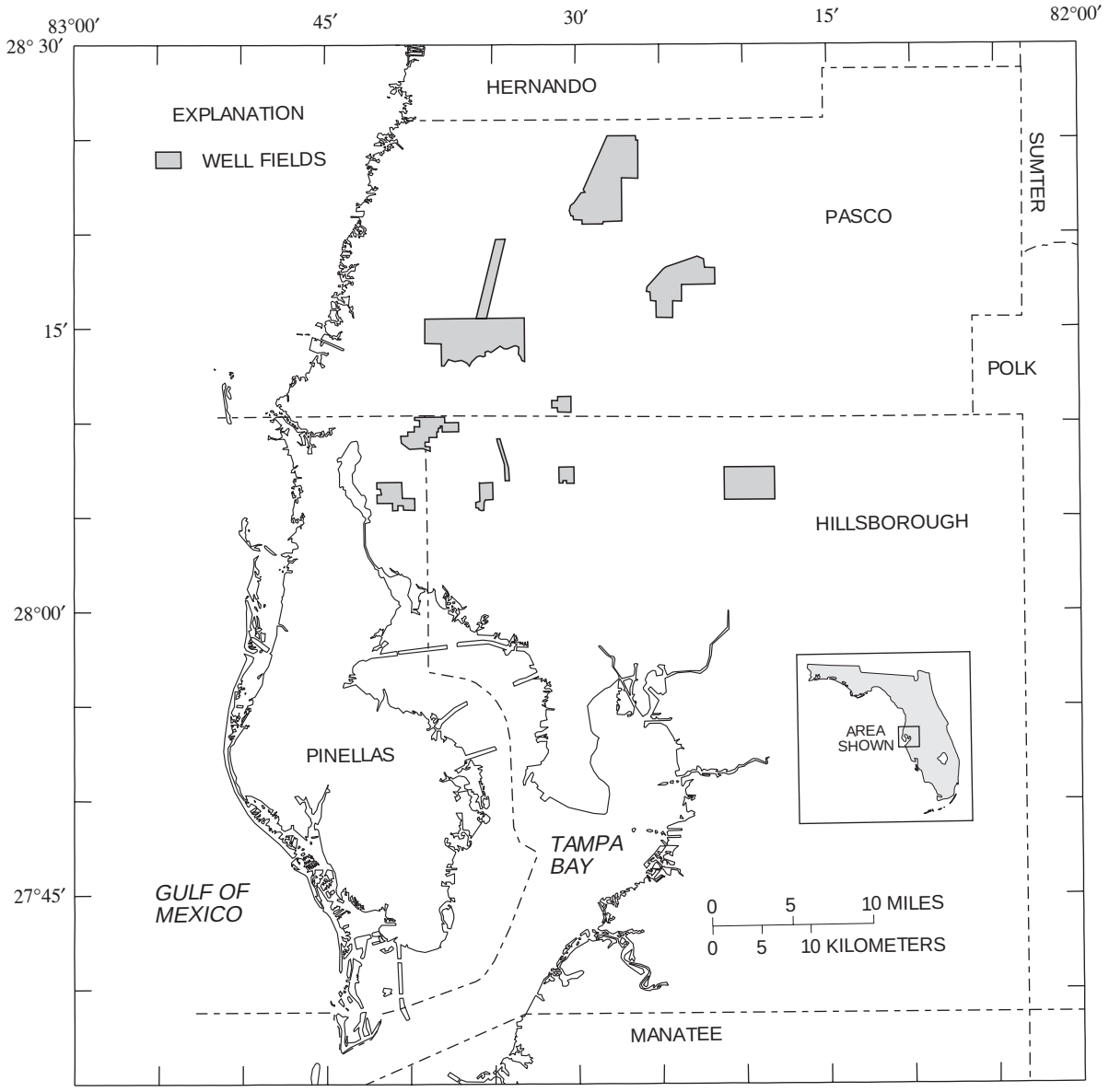

Figure 1. Location of the study area and well fields.

estimate locations of vertical fracture zones. Borehole video and geophysical logs were used to estimate locations of enhanced flow zones (Safko and Hickey, 1992). The data were then used to construct various hypothetical carbonate aquifer system types to be tested at two prototype regions, using the U.S. Geological Survey modular ground-water flow model (MODFLOW) and particle tracking program (MODPATH). This report is based on work done in west-central Florida, but the investigative techniques presented are applicable to similar hydrogeologic settings elsewhere.

Hydrogeology of the Upper Floridan Aquifer, a Typical Karst Carbonate Aquifer System

The most productive carbonate sequence in Florida and the southeastern Coastal Plain is the Floridan aquifer system, composed of limestones and dolomites with enhanced permeability caused by tectonic fracturing and karstification. These processes created secondary porosity, resulting in significant aquifer heterogeneity. Secondary porosity is defined in the Dictionary of Geologic Terms (Bates and Jackson, 1984) as porosity

developed in rock after its deposition or emplacement through such processes as solution or fracturing. The mechanisms for secondary porosity development in the Upper Floridan aquifer system are mechanical fracturing and chemical dissolution.

Vertical fracturing in a carbonate aquifer system can occur from propagation of basement structures through the overlying carbonates in response to crustal flexing caused by earth tides (Blanchet, 1957). Surface lineaments have long been recognized as surface manifestations of underlying vertical to near-vertical zones of fracture concentrations (Lattman and Parizek, 1964). Previous investigators recognized the occurrence of fracture traces and surface lineaments in west-central Florida as systematic patterns and correlated these patterns to fractures observed in limestone outcrops (Vernon, 1951, p. 47-52). Culbreath (1988) investigated the correlation between surface lineaments and major faults in the crystalline basement rocks using gravity surface geophysical methods. The surface lineaments that had corresponding gravity anomalies were orthogonally and bimodally distributed, and their preferred orientation is between 45 and 55 degrees east and west of north (fig. 2). Culbreath (1988) hypothesized that geologic structures occurring in this preferred orientation are more likely to be manifested at the surface as lineaments because they parallel the stress fields associated with earth tides.

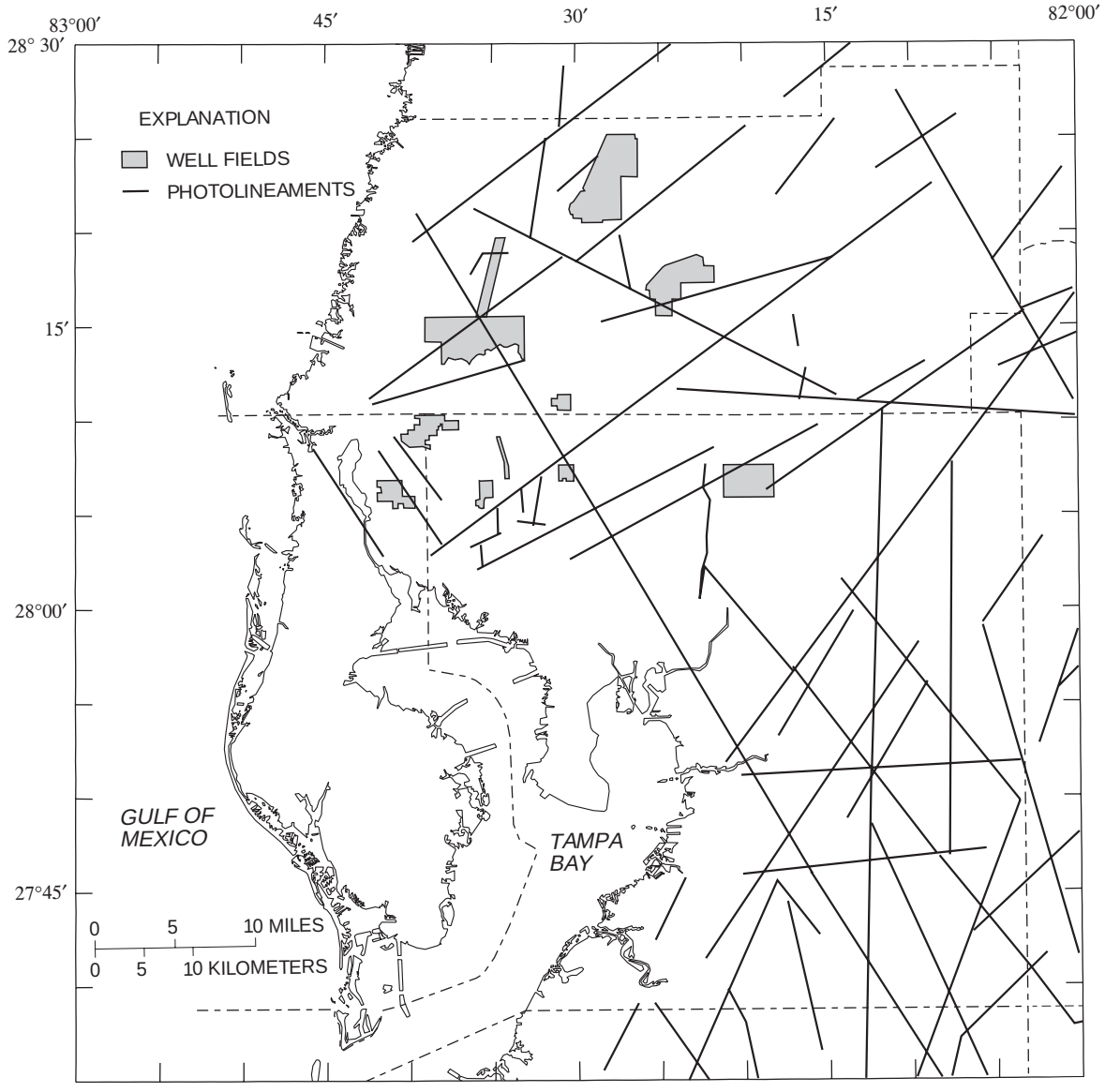

Figure 2. Location of photolineaments that have corresponding gravity anomalies. (Modified from Culbreath, 1988.)

In karst carbonate aquifer systems, fracture zones can be enlarged by chemical dissolution. Fractures channel ground-water flow along discrete paths, resulting in increased solution activity. Lattman and Parizek (1964) observed that karst features and associated highly transmissive zones are related to differential dissolution of the carbonate rock along linear fractures, faults, and joints in the rocks. Within the surface expressions of vertical to near-vertical fractures, narrow zones have been detected where porosity can be 10 to 100 times that of the intergranular matrix (Stewart and Wood, 1984). These narrow zones are highly heterogeneous discrete zones of increased vertical permeability within the carbonate aquifer system.

One mechanism for development of the heterogeneous layering of higher permeability zones in carbonate aquifer systems is chemical dissolution in response to changes in sea level. As water levels in the ocean rise and fall, base-levels change and subaerial karstification is cyclically renewed, creating various horizons of extensive secondary porosity development throughout the carbonate sequence. Chemical dissolution is most aggressive along zones of weakness in carbonate sequences. Horizontal zones of weakness tend to be at lithologic interfaces of differing types, at a specific lithologic boundary where a concentration of impurities such as sand, silt, and shell exists, and where cyclic changes such as laminations occur within a lithology. The lithologic heterogeneity within the Floridan aquifer system resulted from deposition in warm shallow seas over periods of geologic time where even slight changes in depositional conditions and diagenetic alterations resulted in textural and mineralogical changes described above. Vertical fracturing and heterogeneous layering of the carbonate rocks have resulted in variable horizontal and vertical permeabilities in the Upper Floridan aquifer (Williams, 1985). Subtle variations can affect porosity and permeability, resulting in a highly heterogeneous carbonate aquifer system.

Hydrogeologic Setting

The hydrogeologic framework in the study area comprises two aquifers, the clastic surficial aquifer system and the carbonate Floridan aquifer system that are separated by the intermediate confining unit (fig. 3). The Floridan aquifer system consists of the Upper and Lower Floridan aquifers that are separated by a middle confining unit (Miller, 1986). The middle confining unit and Lower Floridan aquifer generally contain saltwater in the study area. The Upper Floridan aquifer contains all or parts of the Avon Park Formation, the Ocala Group, the Suwannee Limestone, and the Tampa Member of the Arcadia Formation of the Hawthorn Group. In this report, the Tampa Member will be used to designate the Tampa Member of the Arcadia Formation of the Hawthorn Group. The formation names used in this report are based upon the geologic definitions of Scott (1988) and are the usage of the Florida Geological Survey.

Transmissivity

In general, the majority of water supplied to municipal wells open to the entire Upper Floridan aquifer is from two 50- to 100-ft thick, areally persistent, highly fractured zones in the dolomitic section of the Avon Park Formation (Ryder, 1978; Ryder and others, 1980; CH2M Hill, 1990a,b). The overlying Ocala Group, Suwannee Limestone, and the Tampa Member, where present, also are characterized by discrete producing zones that occur locally and less predictably near formational contacts. Although most of the water is derived from discrete producing zones, the intergranular matrix of the Upper Floridan aquifer also is a source of ground water.

Transmissivity of the Upper Floridan aquifer is highly variable and ranges from 29,400 to 130,000 ft^2/d within the study area. This is a direct result of the anisotropic and heterogeneous nature of the aquifer. Transmissivities determined from aquifer tests for the Upper Floridan aquifer vary widely because: (1) some wells do not penetrate the highly permeable (fractured) dolomites in the Avon Park Formation, (2) the wells may or may not intersect locally occurring permeability zones related to secondary porosity, and (3) the highly heterogeneous and anisotropic nature of the carbonate aquifer system makes the application of standard methods of aquifer test analysis uncertain and the results questionable (Wolansky and Corral, 1985, p. 28). Table 1 lists the ranges in transmissivity in the study area as reported by other investigators and compiled by Bengtsson (1987).

Porosity

The following definitions, of different porosity types, are the terminology used in this report. The porosity classification in based on the size, shape, distribution, and volume of voids compared to the overall volume of rock. Porosity may be microscopic or macroscopic.

<table>
<tr><th rowspan="2">SYSTEM</th><th rowspan="2">SERIES</th><th rowspan="2" colspan="3">STRATIGRAPHIC UNIT</th><th colspan="2">HYDROGEOLOGIC UNIT</th></tr>
<tr><th>GENERAL UNIT NAMES</th><th>UNITS IN THE STUDY AREA</th></tr>
<tr><td rowspan="2">QUATERNARY</td><td rowspan="2">HOLOCENE
PLEISTO-
CENE</td><td colspan="3">TERRACE DEPOSITS</td><td rowspan="2">SURFICIAL AQUIFER SYSTEM</td><td rowspan="2">ABSENT OR SURFICIAL AQUIFER SYSTEM</td></tr>
<tr><td colspan="3" rowspan="2">CALOOSAHATCHEE MARL AND TAMIAMI FORMATION</td></tr>
<tr><td rowspan="8">TERTIARY</td><td>PLIOCENE</td><td rowspan="3">INTERMEDIATE AQUIFER SYSTEM OR INTERMEDIATE CONFINING UNIT[2]</td><td rowspan="3">ABSENT OR INTERMEDIATE CONFINING UNIT[2]</td></tr>
<tr><td rowspan="3">MIOCENE</td><td rowspan="3">HAWTHORN GROUP[1]</td><td>PEACE RIVER FORMA-TION</td><td>BONE VALLEY MEMBER</td></tr>
<tr><td colspan="2">ARCADIA FORMATION</td></tr>
<tr><td></td><td>TAMPA MEMBER</td><td rowspan="5">FLORIDAN AQUIFER SYSTEM[3]</td><td rowspan="3">UPPER FLORIDAN AQUIFER[3]</td></tr>
<tr><td>OLIGOCENE</td><td colspan="3">SUWANNEE LIMESTONE</td></tr>
<tr><td rowspan="3">EOCENE</td><td colspan="3">OCALA GROUP</td></tr>
<tr><td colspan="3">AVON PARK FORMATION</td></tr>
<tr><td rowspan="2">PALEOCENE</td><td colspan="3" rowspan="2">OLDSMAR AND CEDER KEYS FORMATIONS</td><td>MIDDLE CONFINING UNIT[3]</td></tr>
<tr><td>LOWER FLORIDAN AQUIFER[3]</td></tr>
</table>

[1]Based on nomenclature of Scott (1988).
[2]Based on nomenclature of Southeastern Geological Society (1986).
[3]Based on nomenclature of Miller (1986).

Figure 3. Hydrogeologic framework.

Microscopic porosity includes intercrystalline porosity, interstitial porosity, and microfissure porosity. Intercrystalline porosity is defined as the voids between mineral crystals. Interstitial porosity is defined as the voids between loose or poorly cemented granular material. Microfissure porosity is defined as the voids formed by microjoints, microfissures, and bedding and schistosity planes. Macroscopic or channel porosity is the porosity occurring as large fissures, conduits, and channels. In carbonate sequences, porosity is often a combination of microscopic and macroscopic porosity and therefore, two additional porosity types are defined. Rock porosity is defined as the porosity of unfissured blocks or volumes of rock. Massive or formation/aquifer scale porosity is defined as the combined porosity from both interstitial pores (rock porosity) and fissures (channel porosity) (LaMoreaux and others, 1984, p. 47). Effective porosity is defined as the amount of interconnected pore space available for fluid transmission (Lohman and others, 1972, p. 10).

Table 1. Ranges in transmissivity values by well field from aquifer test analyses

[ft^2/d, feet squared per day. Modified from Bengtsson (1987)]

Well Field	Transmissivity (ft^2/d)
Cross Bar Ranch	47,500 to 115,000
Cypress Creek	31,500 to 53,600 78,610
Starkey	[1]40,000 60,700
South Pasco	53,600 47,000 51,000 to 71,000
Eldridge Wilde	[1]33,000 34,400 to 58,800 35,500
East Lake	40,000
Cosme-Odessa	[1]53,500
Section 21	29,400 to 87,000 60,000 71,000
Morris Bridge	53,000 to 130,000 35,000 to 56,000

[1]Wells do not penetrate the major producing zones in the Avon Park Formation.

Some aquifers can be characterized by diffuse-flow where water moves more or less uniformly through the interconnected pore space of the rocks (rock porosity). Unconsolidated clastic aquifers are in this category. Karst carbonate aquifers can be characterized by conduit flow along irregularly distributed, solution-enlarged fissures (channel porosity) in combination with diffuse flow through the more uniformly distributed, interconnected pores (rock porosity). The Floridan aquifer system of west-central Florida is in this category (Vecchioli and others, 1989, p. 33)

Twenty-two core samples from four wells were selected for laboratory analysis of effective porosity to characterize the matrix properties of the Upper Floridan aquifer. The core samples were supplied by the Florida Geological Survey. Samples were selected as representative of a specific hydrogeologic unit within the study area. Laboratory analyses for effective porosity were completed by a commercial laboratory. The four wells from which cores were selected are ROMP 99 (Regional Observation Monitoring Well Program), ROMP TR12-3, ROMP TR14-2, and Brantley #1 (fig. 4). The effective porosity values, corresponding lithologic unit, and sample depths are listed in table 2. The average effective porosity values for the Tampa Member, Suwannee Limestone, and Ocala Group are 29, 36, and 38 percent, respectively. Cores were not selected for evaluating the effective porosity of the Avon Park Formation because of its highly fractured nature. A well-indurated core selected to be representative of the Avon Park Formation would disproportionately represent the least permeable zones. Additional effective porosity values, determined from cores from selected wells (fig. 4), in the proximity of the study area are listed in table 2.

Effective porosities typical of clastic aquifers reflect the interstitial porosity, which can be measured at the rock-core scale, whereas effective porosities typical of karst carbonate aquifers are massive porosities and reflect both rock porosity and channel porosity that cannot be satisfactorily measured at the rock-core scale. Generally, the effective porosity associated with fractured aquifers is much less than that of porous media aquifers. Therefore, the range of effective porosity values presented in this study include values associated with channel and interstitial porosity and represent the massive porosity of a karst carbonate aquifer system.

DESCRIPTIONS OF ANISOTROPY AND HETEROGENEITY IN THE STUDY AREA

Field data collected from wells in the study area indicate the presence of aquifer anisotropy and heterogeneity. Anisotropy and heterogeneity in carbonate aquifer systems is largely attributed to aquifer stratification, localized solution channeling, and discontinuous confining beds.

Anisotropy

Anisotropy is defined as the condition of having different properties in different directions (Bates and Jackson, 1984, p. 21). A fractured carbonate aquifer system can often be modeled as an anisotropic aquifer, because the permeability inherent in a carbonate aquifer can result from preferential dissolution of rock along fractures producing directional dependent aquifer properties. Experiments by Hushey and Crawford (1967) indicated that the overall permeability is greater when fractures are aligned with the predominant flow direction. Analytical solutions were developed for use in conjunction with aquifer test data to determine aquifer anisotropy and components of the anisotropic transmissivity tensor. These components define the principal directions of anisotropy corresponding to the

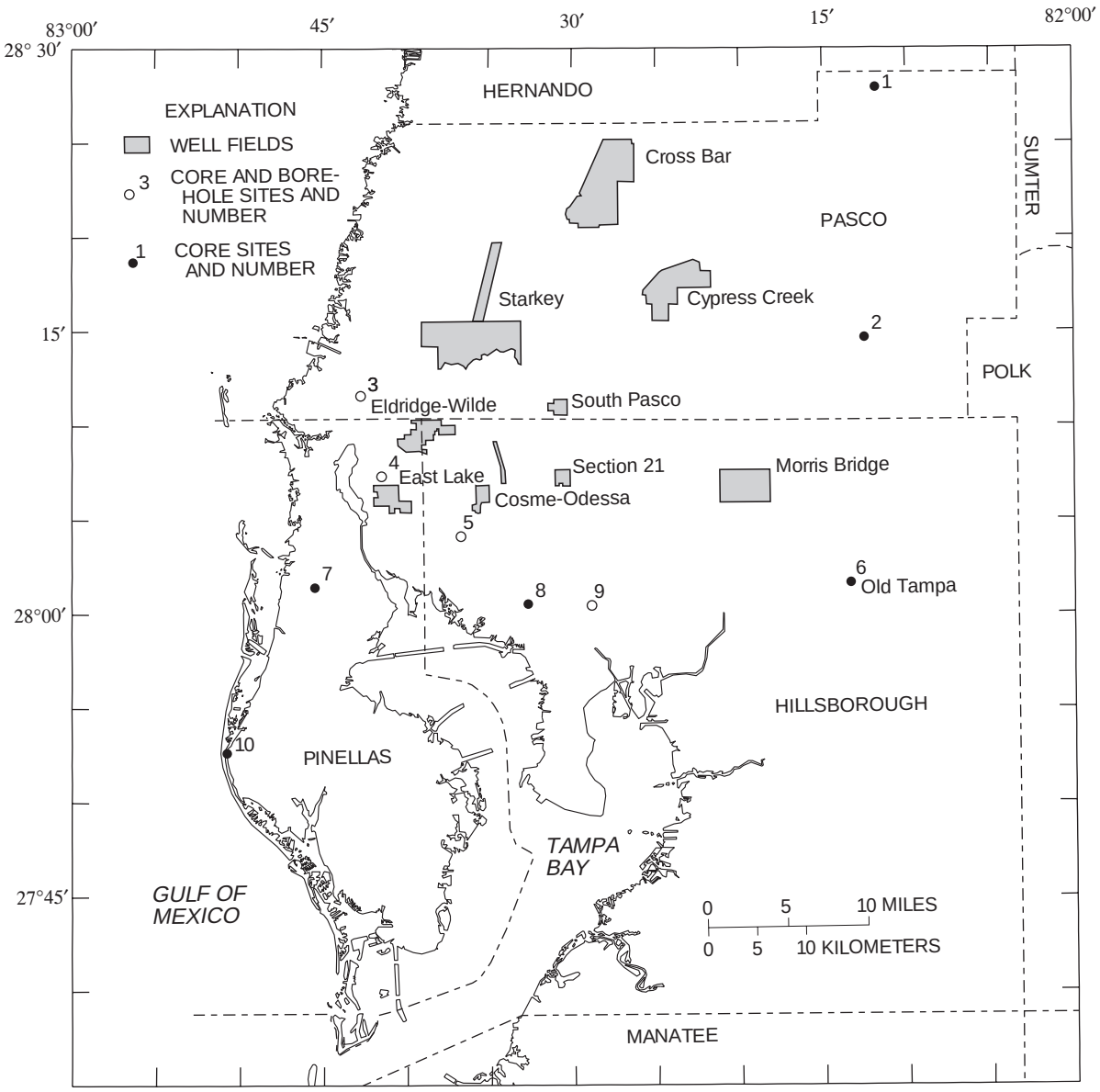

Figure 4. Location of the study area, well fields, and selected wells.

directions in space at which transmissivity (or hydraulic conductivity) attains its maximum and minimum values. The value of the ratio of the maximum and minimum transmissivities defines the magnitude of anisotropy. Based on indications of nonisotropic and nonhomogeneous porous-media ground-water flow, the TENSOR2D computer program (Maslia and Randolph, 1986) was used to evaluate the magnitude and direction of aquifer anisotropy. The TENSOR2D program automates the solution of hydraulic parameters and tensor components for an anisotropic aquifer using the Papadopulos method (1965). The rigorous application of the Papadopulos method requires data from a pumping well and a minimum of three observation wells. Transmissivities are determined for both the major ($T_{\varepsilon\varepsilon}$) and minor ($T_{\eta\eta}$) components of the anisotropic transmissivity tensor. Aquifer test data from wells, shown in figure 4, that tap a karst carbonate aquifer system were used as input to the program.

Aquifer test data sets for seven well fields within the study area were analyzed by using the TENSOR2D program. The results were highly variable within and among the well fields. In several instances, multiple wells were tested within the same well field, and TENSOR2D results did not indicate the same magnitude or direction of aquifer anisotropy; therefore, even at a local scale, the aquifer is not homogeneous, and the results were considered qualitative. Sometimes, the

Table 2. Laboratory analyses of effective porosity from rock cores from selected wells

[Locations shown on fig. 4]

Map number	County	Well name	Other name	Latitude longitude	Stratigraphic units	Sample depth (ft)	Effective porosity (percent)	Source
1	Pasco	—	W-16304	282756 821149	Ocala	112 172 214	45 36 34	This study
2	Pasco	Brantley 1	W-15957	281446 821225	Suwannee	59 80 129 141	43 34 39 27	This study
3	Pasco	NWHWRAP 3-D	—	281142 824241	Ocala Avon Park	348 388 438 1,051	37 38 39 12	CH2M Hill, (1990b)
4	Pinellas	NWHWRAP 1-D	—	280923 824123	Ocala Avon Park 	436 452 490 1,155 1,174	40 27 34 11 24	CH2M Hill (1990a)
5	Hillsborough	NWHWRAP 4-D	—	280411 823643	Ocala Avon Park	425 485 530 1,166	45 32 21 11	CH2M Hill (1990b)
6	Hillsborough	Tampa 19	—	280145 821324	Suwannee Ocala	105 240	21 46	Robinson, 1995
7	Pinellas	ROMP TR14-2	W-15204	280132 824528	Tampa Suwannee Ocala 	99 137 203 232 273 397 419 500 540	41 21 30 30 42 39 38 49 25	This study
8	Hillsborough	ROMP TR12-3	W-15494	280034 823237	Tampa Suwannee Ocala	106 158 198 319 445 491	29 24 29 40 36 48	This study
9	Hillsborough	NWHWRAP 2-D	—	280033 822848	Ocala Avon Park 	404 444 472 1,119 1,137	44 38 17 25 13	CH2M Hill (1990b)
10	Pinellas	McKay Creek	—	275241 825039	Ocala Avon Park 	616 892 957 1,028	48 20 7 2	Hickey (1977)

components of transmissivity could not be determined by using TENSOR2D analysis because of one or a combination of several possible factors: (1) the observation well distribution was insufficient to characterize the transmissivity tensor; (2) the assumptions of Papadopulos were violated because observation wells were too close together, too near the pumping well, or too far from the pumping well; and (3) the horizontal anisotropy did not adequately account for all of the variability in aquifer properties. The magnitude of aquifer anisotropy from the aquifer test data sets ranged from 2.5:1 to 25:1. Aquifer anisotropy for well fields increased toward the north, coinciding with a thinning of the confining materials. The average aquifer anisotropy from all TENSOR2D results was 5:1. The directions of apparent anisotropy ranged from 40 to 130 degrees and generally coincided with the orientation of the photolineaments. If the anisotropy is due to persistent fracture sets of relatively consistent orientation, it could be inferred that the principal directions are a result of fracture orientation. However, there is no guarantee that regional scale fractures would be indicative of density, persistence, and orientation of fractures at a local scale.

Layered Heterogeneity

Although the Floridan aquifer system is basically a vertically continuous sequence of generally permeable carbonates, extremely high permeabilities occur as discrete zones within the aquifer. Geophysical logs and borehole television surveys from regionally dispersed wells indicate that the aquifer system contains several highly permeable zones. These zones, which contribute most of the water to wells, generally conform to bedding planes and commonly contain enhanced secondary porosity caused by solution or fracturing and are separated by rocks of lower permeability that display relatively few secondary porosity features. Borehole television surveys have demonstrated that, in places, the Floridan aquifer system contains thin to moderately thick horizontal openings connected by nearly vertical fractures, some of which have been enlarged by chemical dissolution.

An approach that uses borehole data for characterizing secondary porosity of carbonate rocks was applied to this study. A detailed description of the methodology can be found in a report by Safko and Hickey (1992). Generally, the distribution of effective secondary porosity is determined from concurrent interpretation of lithologic logs, drillers' comments, borehole geophysical logs, and television surveys. The term "effective secondary porosity" is defined as observed secondary porosity from the borehole television surveys supported by interpretations of the caliper, pumping flowmeter, and pumping temperature logs, which indicates that the observed secondary porosity extends beyond the immediate vicinity of the borehole. Such secondary porosity features would be principally related to geologic processes rather than drilling activities (Safko and Hickey, 1992, p. 1).

Effective secondary porosity distributions in the study area were characterized in a general way from four test wells in northwest Hillsborough, northeast Pinellas, and southern Pasco Counties (fig. 4). The wells were constructed and tested under supervision of CH2M Hill as part of the Northwest Hillsborough Water Resources Assessment Project (NWHWRAP). The wells penetrate the entire thickness of the Upper Floridan aquifer. Figure 5 shows the lithologic, apparent secondary porosity, driller comments, caliper, pumping flowmeter, pumping temperature, and effective secondary porosity logs for each of the four wells. All logs, except the effective secondary porosity logs, were constructed from observed data. The apparent secondary porosity log was constructed from the television survey by classifying observed secondary porosity types for 10-ft segments of the borehole. Secondary porosity was classified into three types—vugs, cavities, and fractures—based on definitions proposed by Safko and Hickey, (1992). Cavity porosity designation was further restricted only to those zones in which the driller comment logs specified a bit drop. No bit drops were reported during the drilling of the NWHWRAP test holes; therefore, all observed cavities from the borehole television surveys (fig. 5, col. B) were interpreted as resulting from borehole collapse during the drilling process. The term "dredging" (fig. 5, col. B) refers to the removal of rock fragments from a borehole before drilling can continue. Dredging is required as a consequence of the collapse of poorly indurated lithologies during drilling and often results in enlargement of the borehole diameter. Miller (1986) states that the fractured nature of dolomite commonly causes chunks of dolomite to be dislodged during the drilling process. Corroborative data from pumping flowmeter and temperature logs were used to verify flow zones. Where appreciable flow enters the well, as indicated from flowmeter and temperature log response, apparent secondary porosity was considered to be effective secondary porosity.

Effective secondary porosity for each of the NWHWRAP wells are described below. Effective secondary porosity for NWHWRAP site 1-D (fig. 5) is characterized by vug porosity from 425 to 485 ft and by large vugs intersected by high angle fractures from 585 to 675 ft and at 816 ft. Because borehole television survey data were not available for the bottom 379 ft of the borehole, the secondary porosity could not be characterized for the flow zone from 1,085 to 1,187 ft. Effective secondary porosity for NWHWRAP site 2-D (fig. 5) is characterized by fracture porosity from 262 to 272 ft and from 312 to 332 ft and by large vugs intersected by high angle fractures from 700 to 822 ft, from 942 to 982 ft, and from 992 to 1,072 ft. Effective secondary porosity for NWHWRAP site 3-D (fig. 5) is characterized by fracture porosity from 198 to 218 ft, from 558 to 638 ft, and from 828 to 878 ft and by large vugs intersected by high angle fractures from 638 to 768 ft and from 890 to 1,018 ft. Because borehole television survey data were not available for the interval from 258 to 558 ft, secondary porosity could not be characterized for the flow zone from 290 to 320 ft and from 405 to 455 ft. Effective secondary porosity for NWHWRAP site 4-D (fig. 5) is characterized by vug and fracture porosity from 309 to 405 ft. Because borehole television survey data were not available for the bottom 389 ft, the secondary porosity could not be characterized for the flow zone from 990 to 1,120 ft. The effective secondary porosity interpretations are shown in figure 5, column G, and are interpreted to be distributed spatially and interconnected beyond the vicinity of the borehole and to be the result of geologic processes. The secondary porosity types associated with the prominent flow zones are probably intersections of near vertical fractures with horizontal planes of weakness that have been enlarged by solution.

Analysis of the distribution of the effective secondary porosity indicates that the Upper Floridan aquifer is a layered aquifer system. In general, the producing zones occur near lithologic contacts where horizontal zones of weakness tend to occur. The majority of water enters the borehole from the fractured dolomitic units of the Avon Park Formation. Dolomite beds tend to be severely fractured along zones of weakness. The types of secondary porosity are different in the limestone and dolomite sequences (fig. 5, col. B), possibly the result of the response of different lithologies to stress. Limestone is ductile and the apparent secondary porosity types tends to be vugs and cavities. Because of less induration in the limestone, drilling processes can create cavities from washouts. Dolomite is harder and more brittle and the apparent secondary porosity type tends to be fractures.

Prototype Regions

Within the study area, two prototype carbonate aquifer systems were characterized for detailed analysis. The hydrogeologic framework of these two prototypes represent the end-members of the hydrologic diversity in the study area and were designated the Central Swamp and Lake Terrace regions. The names of these regions were derived from the physiographic units where they are located. The physiographic units north of Tampa Bay are shown in figure 6. Each physiographic unit encompasses one or more well fields. The hydrogeologic framework and aquifer characteristics for the Central Swamp and Lake Terrace regions are those for the Cypress Creek and Cosme-Odessa well fields, respectively.

Descriptions of the hydrogeologic framework and aquifer characteristics of the prototype regions are based on existing data compiled from previous studies by the U.S. Geological Survey, the Southwest Florida Water Management District, the Florida Geological Survey, and private consulting firms. The hydrogeologic framework is composed of two aquifer systems separated by the intermediate confining unit. Aquifer heterogeneity, including vertical fracture zones and horizontal enhanced flow zones, has been observed in both the Central Swamp and Lake Terrace regions. The vertical fracture network is based on the actual locations identified by Culbreath (1988). Horizontal layering of the Upper Floridan aquifer in the Central Swamp and Lake Terrace regions is supported by drillers' logs, specific-capacity data, and borehole geophysical logs for selected wells in the regions. Locations of selected wells (fig. 7) and generalized hydrogeologic sections constructed from well data (figs. 8 and 9) show the observed distribution of aquifer heterogeneity.

There are several hydrologic differences between the two prototype regions. Topography in the Central Swamp region is flat and swampy, and land surface ranges from 60 to 70 ft above sea level. In the Lake Terrace region, land surface ranges from 10 to 70 ft above sea level. The surficial aquifer system is 25 ft thick or less in the Central Swamp region and ranges from 50 to 100 ft in the Lake Terrace region. In the Central Swamp and Lake Terrace region, the intermediate confining unit ranges from 25 to 50 ft thick and 25 ft or less, respectively. The Upper Floridan aquifer is about 900 and 1,125 ft thick, respectively. The Central

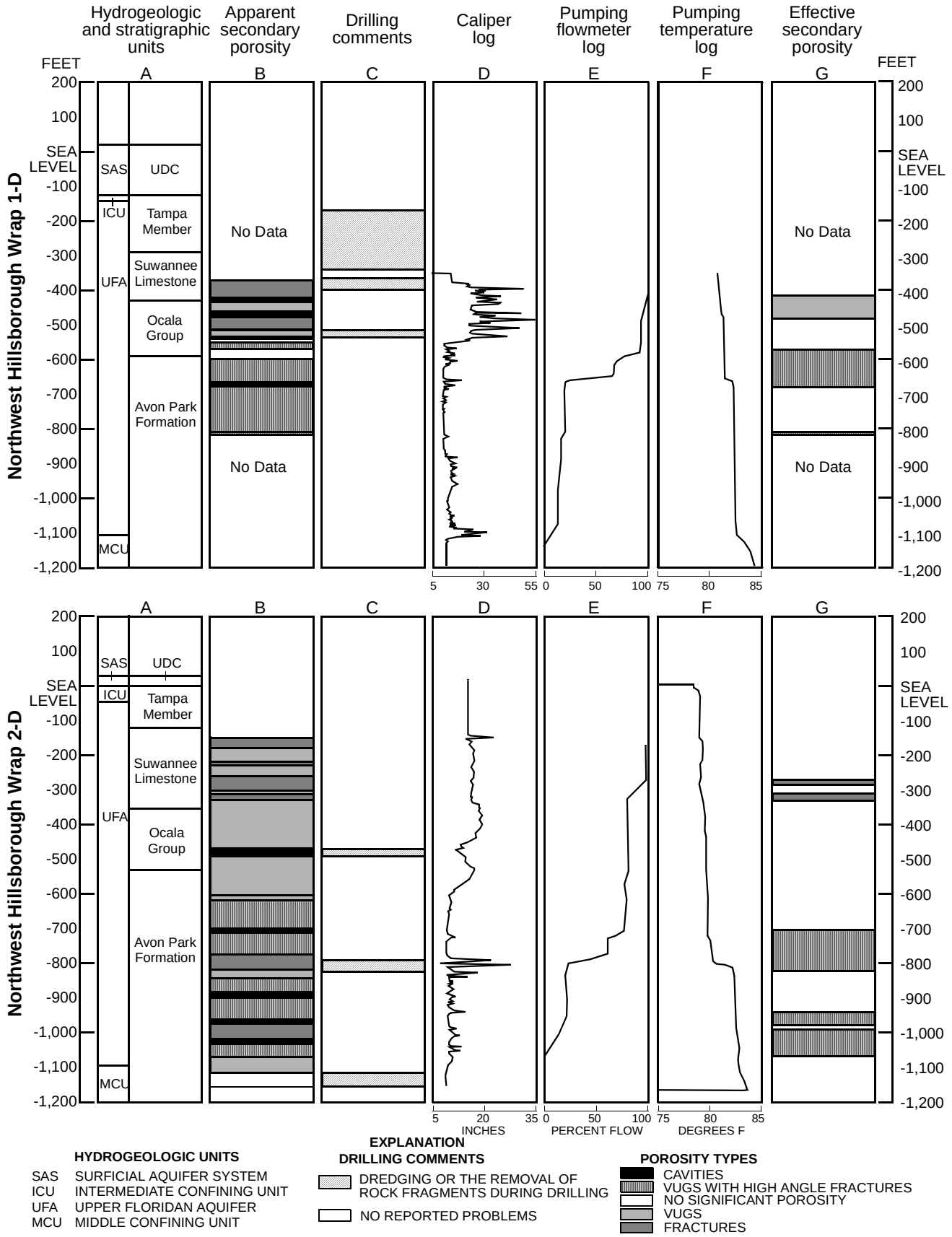

Figure 5. Comprehensive borehole interpretation for the Northwest Hillsborough Water Resources Assessment Project: sites 1-D, 2-D, 3-D, and 4-D.

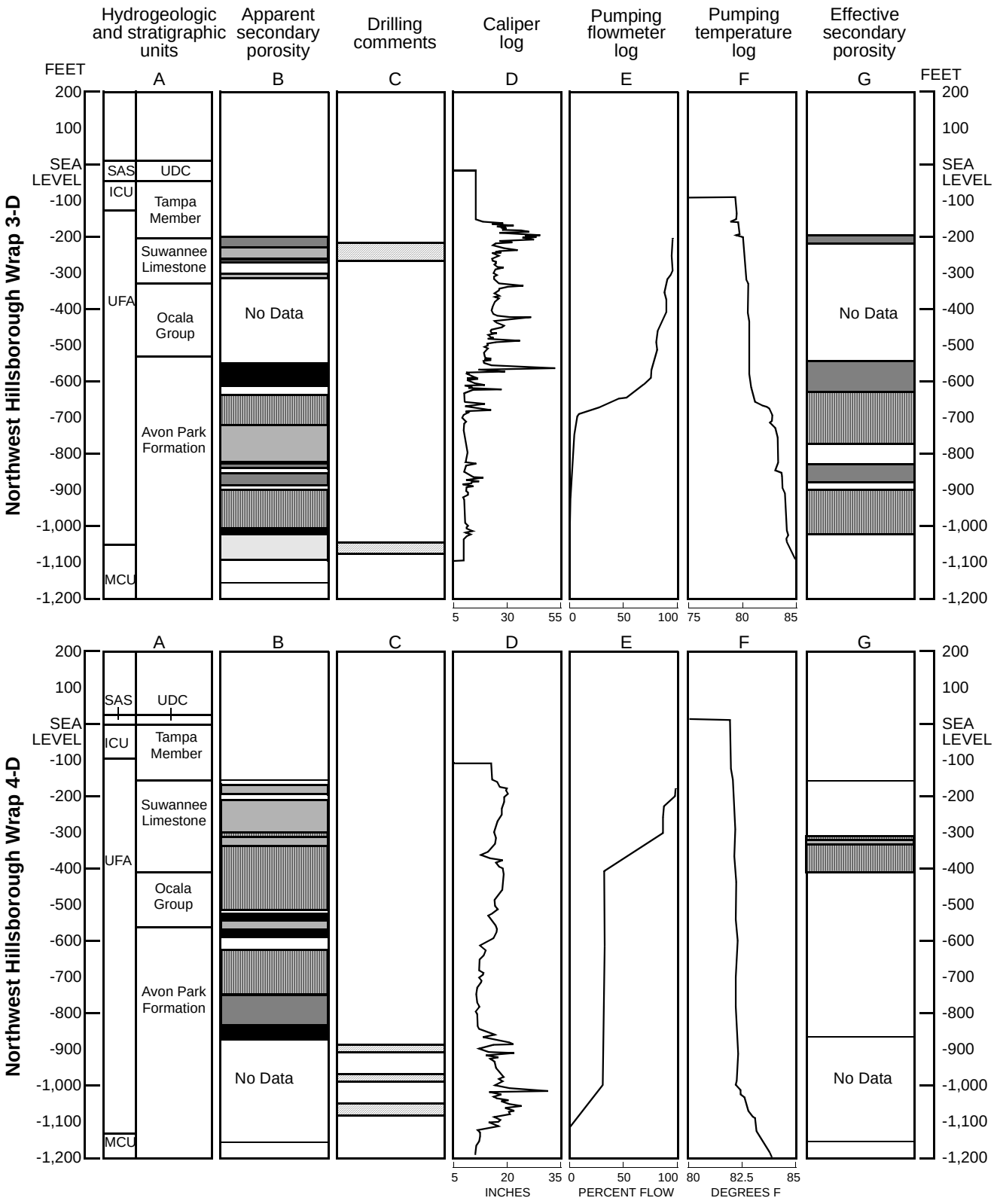

Figure 5. (Continued) Comprehensive borehole interpretation for the Northwest Hillsborough Water Resources Assessment Project: sites 1-D, 2-D, 3-D, and 4-D.

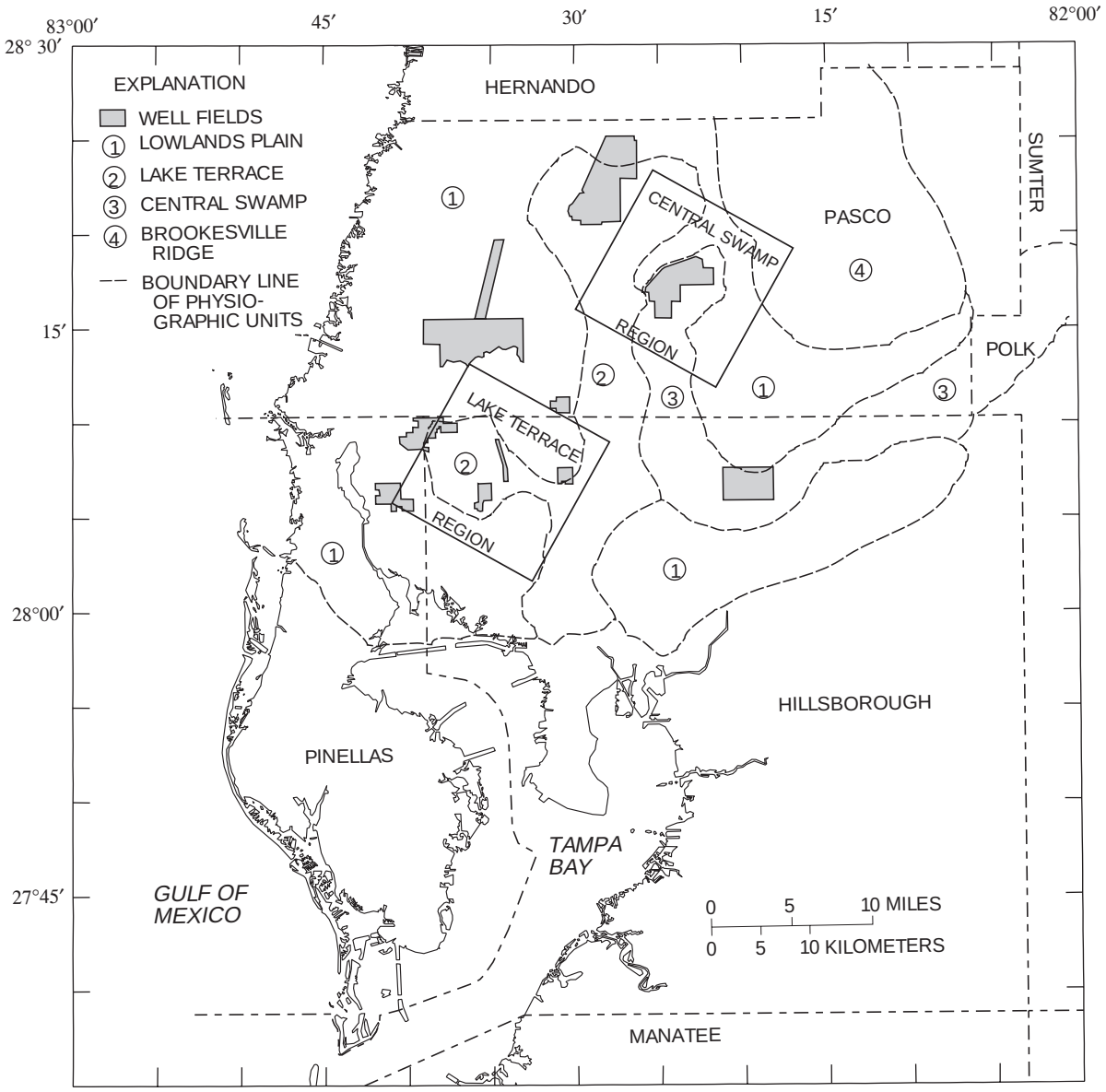

Figure 6. Physiographic units and regions.

Swamp and Lake Terrace regions are in zone 2 and zone 4 of sinkhole types classified by Sinclair and others (1985). Zone 2 is characterized by bare or thinly covered limestone where sinkhole development is rare. Zone 4 is characterized by a 25- to 100-ft thick clastic cover where sinkholes are numerous. Layering of the secondary porosity zones in the Central Swamp region is highly variable (fig. 8). Ryder (1978) states that, in the vicinity of Cypress Creek well field, movement of ground water is primarily along solution-enhanced joints and fractures, and water enters the well from discrete flow intervals.

Two major water-bearing zones occur in the dolomitic zone of the Avon Park Formation. The Tampa Member, Suwannee Limestone, and Ocala Group can contain solution-enhanced permeable zones that generally occur near formational contacts. In the Lake Terrace region, specific-capacity data from wells in the vicinity of the Cosme-Odessa well field, indicate the existence of three flow zones. These enhanced flow zones are at depths from 360 to 420 ft, from 780 to 840 ft, and from 1,000 to 1,155 ft below sea level. Borehole interpretation methods indicate an effective secondary porosity zone from 290 to 390 ft (fig. 9).

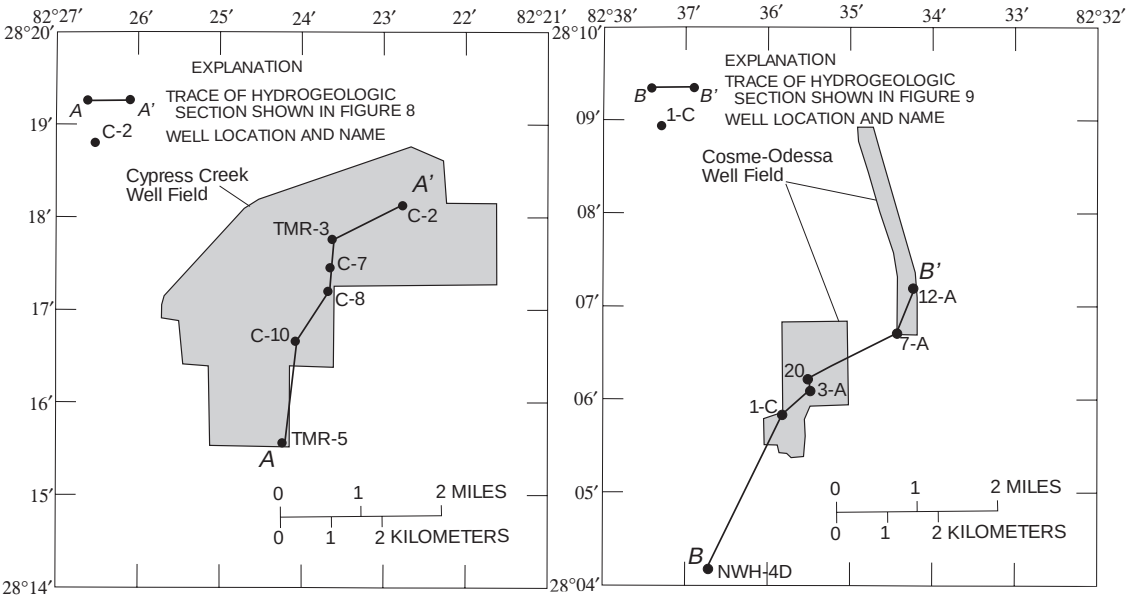

Figure 7. Location of selected wells used for the hydrogeologic sections *A-A′* across the Cypress Creek well field and *B-B′* across the Cosme-Odessa well field.

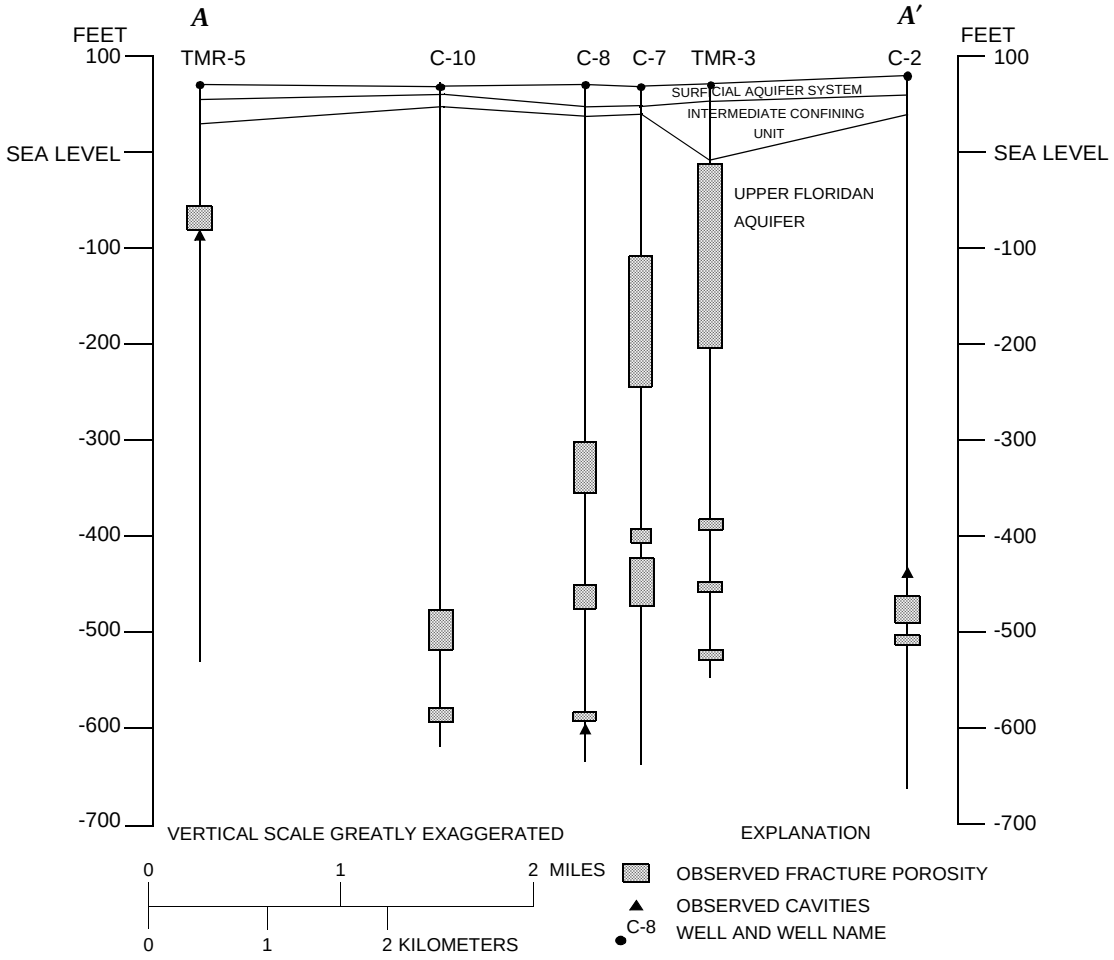

Figure 8. Generalized hydrogeologic section *A-A′*, showing vertical distribution of observed secondary porosity across the Cypress Creek well field.

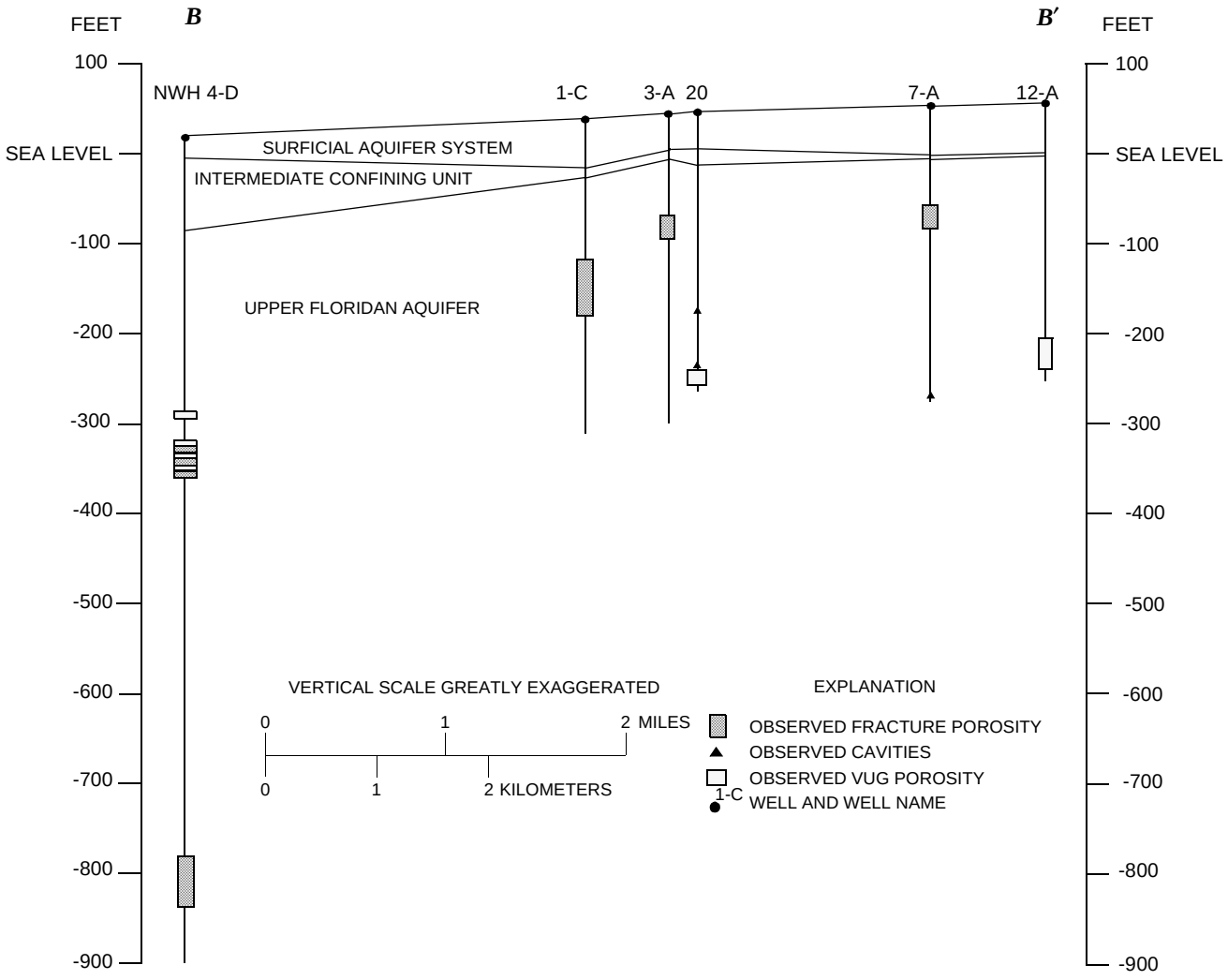

Figure 9. Generalized hydrogeologic section *B-B′*, showing vertical distribution of observed secondary porosity across the Cosme-Odessa well field.

A highly fractured zone from 980 to 1,130 ft is indicated by the caliper log. Pumping temperature logs indicate borehole flow from 1,000 to 1,030 ft (CH2M Hill, 1990a,b).

Generally, the depth interval from 425 to 780 feet within the Ocala Group has lower permeability and acts as a semiconfining unit within the Upper Floridan aquifer. Permeable zones overlie and underlie this zone. As shown in figures 8 and 9, the sources of water to wells, in both the Central Swamp and Lake Terrace regions, are derived from multiple, vertically spaced, and discrete permeable zones.

HYPOTHETICAL CARBONATE AQUIFER SYSTEMS

Observations of anisotropy and heterogeneity, based on field data, in the Central Swamp and Lake Terrace regions led to the development of six hypothetical carbonate aquifer systems. These systems were conceptualized to illustrate generalized types of carbonate aquifer systems. The systems were developed to incorporate increasingly complex representations of aquifer anisotropy and heterogeneity. In addition, an isotropic and homogeneous carbonate aquifer system was developed for comparison with the more complex carbonate aquifer systems.

The first carbonate aquifer system is that of a single isotropic and homogeneous unit, where aquifer properties are uniform (fig. 10, case 1).

The second carbonate aquifer system incorporates horizontal anisotropy (fig. 10, case 2) where aquifer properties differ by direction. The anisotropy was found to vary from site to site. This is most likely caused by the orthogonal distribution of the fracture network.

The third carbonate aquifer system includes a fully penetrating vertical fracture network in a single layer carbonate unit (fig. 10, case 3). The fracture network is based on the work of Culbreath (1988). Fractures in carbonate aquifer systems can behave as impermeable barriers to flow or as highly permeable conduits for flow (Stewart and Wood, 1984). Both impermeable and highly permeable fractures are known to occur in the Upper Floridan aquifer system.

The fourth carbonate aquifer system includes heterogeneous layering of hydraulic properties as a result of carbonate dissolution, thereby creating enhanced flow zones (fig. 10, cases 4a and 4b). Case 4a shows the layering of the carbonate aquifer system by using lithostratigraphic boundaries. Field data indicates that these units have different hydraulic properties. Case 4b shows the redistribution of layers by further defining the relatively thin flow zones found within specific lithostratigraphic units. Enhanced flow zones in carbonate terranes are indicated from specific-capacity data, borehole geophysical logs, and drillers' logs.

The fifth carbonate aquifer system was that of a doubly porous system (fig. 10, case 5). In a double porous system, the aquifer porosity consists of two types, the postdepositional secondary porosity, such as fractures and solution channels and the syndepositional primary porosity of the intergranular matrix, both having distinctive characteristics. Two coexisting porosities and hydraulic conductivities are recognized: those of lower storage capacity (low porosity) and higher hydraulic conductivity (permeability) of the fracture dominated rock volumes, and those of higher storage capacity (high porosity) and lower hydraulic conductivity (permeability) of the unfractured rock volumes. Field evidence supports this double porosity behavior. The core data suggests that primary porosity is significant; however, borehole geophysical log and television survey interpretations indicate that appreciable flow enters the well along discrete zones characterized by secondary porosity features. Transmissivity values determined from aquifer test analysis within a single well field vary significantly. The highest calculated transmissivities are probably from areas where the pumped well intersected fractured (secondary porosity) zones. Both secondary and primary porosity contribute to the total porosity in the aquifer; however, if movement of water within pores isolated from solution channels were insignificant relative to movement within the solution channels, then transmissivity and effective porosity values would be ascribed to the flow properties and channel porosity volume of the solution conduits. Channel porosity volume relative to the total rock volume is typically much less than the measured 30 percent from core samples.

The sixth carbonate aquifer system (fig. 10, case 6) combines the effects of both the enhanced vertical interconnection between hydrogeologic layer and the horizontal, solution-enhanced flow zones.

EFFECTS OF AQUIFER ANISOTROPY AND HETEROGENEITY ON GROUND-WATER FLOW

Aquifer anisotropy and heterogeneity, inherent in carbonate aquifer systems, can affect both the direction and velocity of ground-water flow. Fluid flow in karst carbonate aquifers can be highly variable and difficult to measure or predict with a reasonable degree of certainty, because flow regimes can range from almost entirely diffuse to predominantly conduit flow. Over brief periods of time, where small volumes of the aquifer are tested, such as during aquifer testing, a carbonate aquifer system might be dominated by flow in fractures. Yet, with longer periods of time, a larger volume of the aquifer is tested and the overall flow might tend to behave as if it were an equivalent porous medium. A karst carbonate aquifer system might behave as an equivalent porous medium when the secondary porosity features are numerous and spatially interconnected such that the aquifer effectively assumes hydraulic characteristics of a porous medium. Additionally, the volume of aquifer material tested or scale of the problem determines how heterogeneities must be taken into account in evaluating the flow system. Although Darcian flow assumptions might be acceptable for estimating the general head gradient, the average linear velocities might be inaccurate due to the directional dependence and strong discontinuity of fractures.

The influence of aquifer anisotropy and heterogeneity on the movement of ground water often can be inferred from aquifer and tracer test data and from

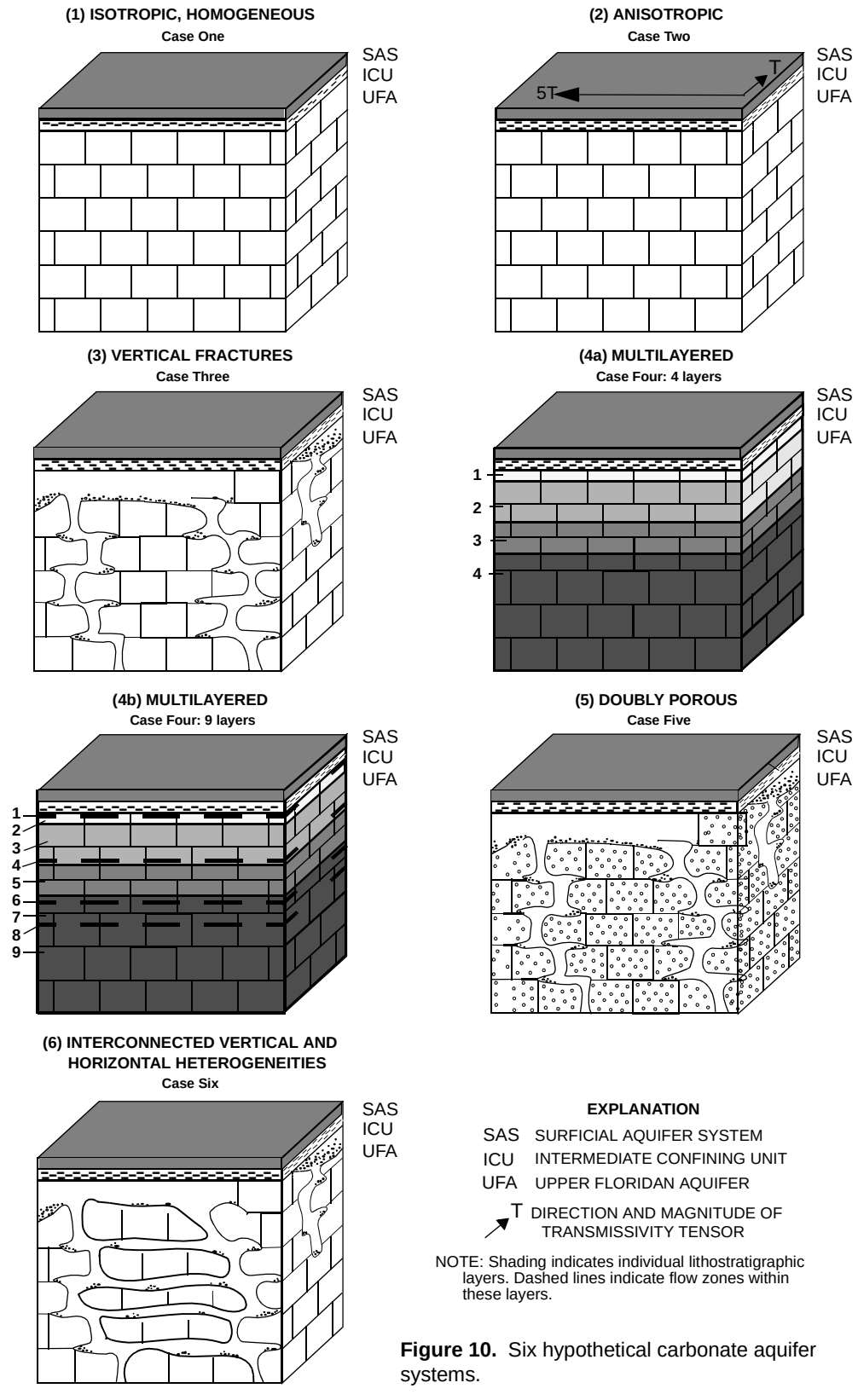

Figure 10. Six hypothetical carbonate aquifer systems.

borehole geophysical logs. Aquifer test data for the Upper Floridan aquifer have been collected by the U.S. Geological Survey, local and State agencies, and private consultants. Selected aquifer tests conducted from 1952 to 1976 were analyzed and presented in a report by Wolansky and Corral (1985). The purpose of that study was to obtain a probable range of values of transmissivity, storage coefficient or specific yield, and leakance for the surficial aquifer system, the intermediate confining unit, and the Upper Floridan aquifer. In several instances, analyses of aquifer test data from the Upper Floridan aquifer system provided ambiguous results and were excluded from the report. These aquifer tests, which indicated a wide variation in hydraulic properties at a site, as determined by inconsistent responses in several observation wells, indicated that the basic assumptions of the analytical solutions were not entirely met. The authors surmise that heterogeneity, anisotropy, and hydrologic boundaries may be responsible for the apparent variation in aquifer properties (Wolansky and Corral, 1985, p. 27).

Tracer tests were performed at the Old Tampa well field in 1992 (fig. 4). Rapid fluid flow between widely separated wells was observed, indicating that flow is through conduits rather than through porous media (Robinson, 1995). Prior to tracer test initiation, tracer arrival time of 46 days was calculated based on porous media flow assumptions, a distance between wells of 200 ft and a porosity of 25 percent. Initial tracer arrival occurred after 4 hours, a second arrival occurred after 36 days, and a peak concentration occurred after 48 days. The bimodal distribution of tracer arrival suggests that the porous media assumptions are not strictly obeyed in the aquifer. Conclusions from the reports by Wolansky and Corral (1985) and Robinson (1995) are that aquifer and tracer test data indicate that the hydraulic response of the carbonate aquifer system to stresses in west-central Florida deviates from isotropic and homogeneous porous media behavior. These assumptions are used for most area of contribution calculations.

MODEL DESIGN AND SIMULATION OF THE PROTOTYPE CENTRAL SWAMP AND LAKE TERRACE REGIONS

A finite-difference flow model was used to evaluate the effects of simulated aquifer anisotropy and heterogeneity on areas of contribution to supply wells in the Central Swamp and Lake Terrace regions. The models are highly conceptual and were not calibrated because of the hypothetical nature of the simulation and because no data exists for comparison with the model results. The analysis implemented an exploratory modeling approach where models are constructed to simulate a wide range of possible solutions. It is used to better understand a system filled with hydrologic uncertainties. This modeling approach permitted many combinations of aquifer anisotropy and heterogeneity types to be simulated. To compare the effects of aquifer anisotropy and heterogeneity on contributing areas, particle tracking was used to delineate the size, shape and orientation of these areas. Contributing area analysis delineates the two-dimensional surface area that corresponds to the area of influence of a pumping well. The area of influence of a pumping well is the area around a well where captured water balances well discharge. The carbonate aquifer system types were simulated by emphasizing anisotropy and heterogeneity typical of karst carbonate terranes.

The models selected to analyze ground-water flow in the study area are the U.S. Geological Survey MODFLOW program (McDonald and Harbaugh, 1984) and MODPATH program (Pollock, 1988). MODFLOW is a three-dimensional, finite-difference flow model. The flow fields generated by MODFLOW are used as input to MODPATH. The MODPATH program is a post-processing, particle-tracking program designed for use with output from flow simulations obtained using MODFLOW. MODPATH is used to delineate pathlines and position of particles at specific time intervals within the simulated flow system. Pathlines and particles can be tracked forward (in the direction of future locations) or backward (in the direction of past locations) from specified model cells.

MODFLOW and MODPATH numerical models were used to generate time-related areas of contribution in the Central Swamp and Lake Terrace regions and were each simulated as the six hypothetical carbonate aquifer system discussed in a previous section of the report. Particles were backtracked from simulated well locations toward the recharge areas to delineate pathlines along which ground-water would flow toward the well. The areal extent of the simulated pathlines defines the approximate area of capture from which the well field draws its water. If the hydrologic system is at equilibrium, the resulting particle paths delineate the total capture zone. Lengths of pathlines are proportional to ground-water flow velocity. Velocities increase as particles approach the simulated wells and is indicated by progressively longer spacing between positions of particles plotted along pathlines.

Boundary Conditions and Grid Design

The two prototype regions were assigned identical boundary conditions and model size so that comparisons between the regions were similarly constrained. Although the boundary conditions do not correspond to natural hydrologic boundaries, if the model area were sufficiently large such that effects of simulated well field pumping would not cause measurable head changes at the boundaries, constant-head boundaries could then be used (Bush, 1978). This criterion was used to define the location of the lateral, hypothetical boundaries for the Central Swamp and Lake Terrace regions. The procedure used to determine this area was to utilize the MODPATH program to evaluate the configuration of particle paths delineating sources of water to well fields. MODPATH was used in conjunction with a calibrated flow model (Fretwell, 1988), that coincides with the study area of this project. The area around each well field encompassed by the pathlines was used as general guidelines for locating the lateral boundaries beyond which well field pumping effects are minimized. An adequate model extent of 100-mi^2 was selected and the lateral boundaries were specified as constant-head boundaries. The upper boundary condition, the water table, was also assigned a specified head. The lower boundary condition was designated a no-flow boundary and represents the hydrologic boundary between the Upper Floridan aquifer and the middle confining unit. Discretization of the 100-mi^2 model area created 1,600, 1/16-mi^2 uniform grid blocks per layer. Both the Central Swamp and Lake Terrace regions were assigned equivalent boundary condition types and discretizations (fig. 11) and these conditions were not changed during simulation. The main objective of the digital simulation was to illustrate how the incorporation of conceptualized distributions of aquifer anisotropy and heterogeneity effect the size, shape, and orientation of areas of contribution to supply wells. The areas of contribution for this study are based on a "traveltime" distance, not on a capture zone defined by a potentiometric surface; therefore, a gradient for neither the water table nor pumped aquifer was simulated.

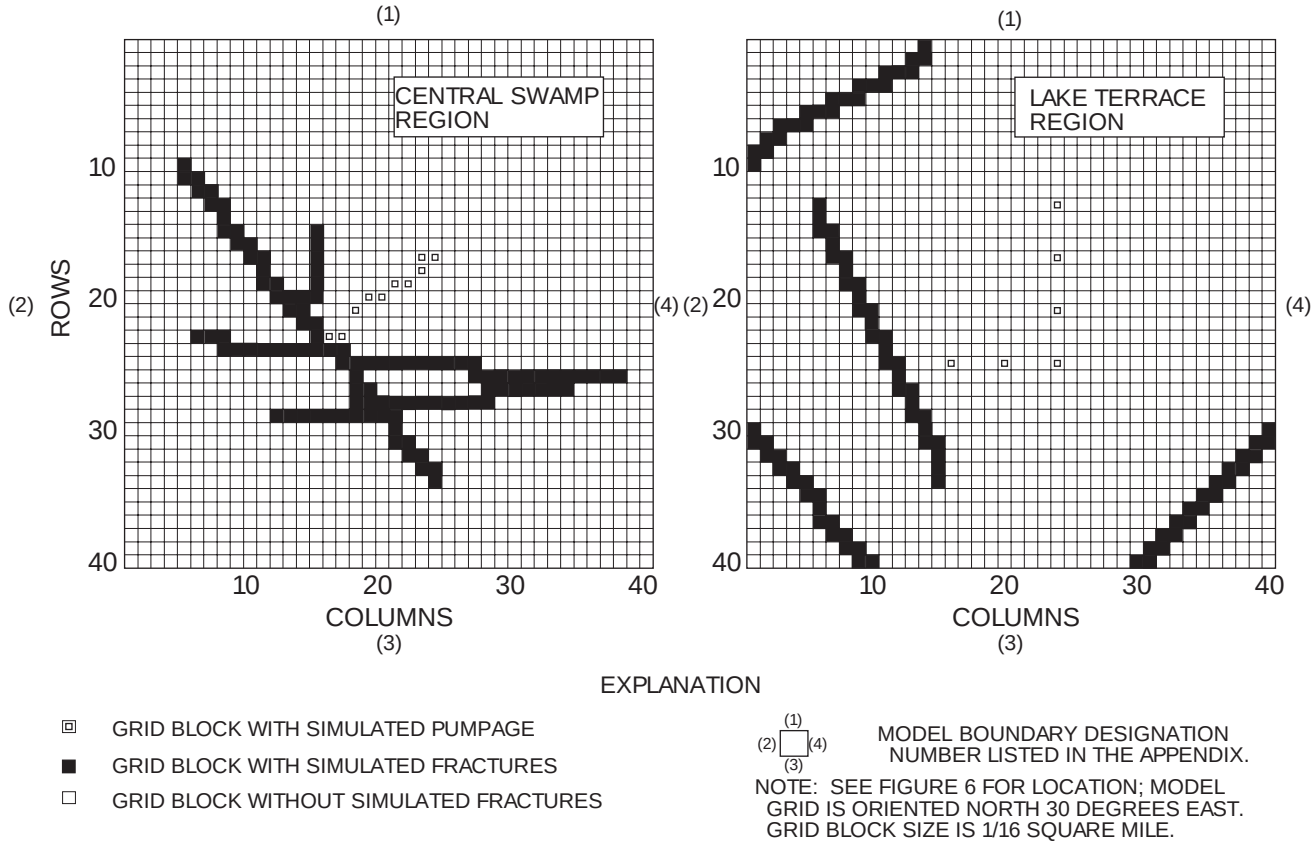

Figure 11. Model grid of 40 rows and 40 columns per layer, showing grid blocks, simulated fractures, and wells in the Central Swamp and Lake Terrace regions.

Model Input Parameters

The quasi-three-dimensional flow systems of the Central Swamp and Lake Terrace regions were constructed to include an unconfined aquifer system (surficial aquifer system) and a confined aquifer system (Upper Floridan aquifer) separated by a confining unit (intermediate confining unit). Model input parameters were compiled from data gathered during previous investigations and are defined for each of the hypothetical carbonate aquifer system types in the following sections of the report. The input parameters were derived from specific capacity tests, aquifer tests, laboratory core analyses, surface and borehole geophysical log data, and calibrated model information (Hutchinson, 1984; Bengtsson, 1987; Fretwell, 1988). Input data for the regions for each of the carbonate aquifer system types are shown in figures 12 and 13.

Simulated pumpage are 30 and 13 Mgal/d, which are the withdrawals used in previously calibrated models for the Cypress Creek and Cosme-Odessa well fields, respectively (Hutchinson, 1984; Fretwell, 1988). Well locations and grid distributed pumpage approximates the configuration of the Cypress Creek and Cosme-Odessa production wells (fig. 11).

Case 1: Isotropic and Homogeneous Single-Layer System

The input data selected for simulating an isotropic, homogeneous, single-layer, carbonate aquifer system for the Central Swamp and Lake Terrace regions are described below. The transmissivity values selected for simulation of the Central Swamp and Lake Terrace regions are 30,000 and 57,000 ft^2/d, respectively. Reported transmissivities in the vicinity of these regions are listed in table 1.

The thickness of the aquifer penetrated by test wells in the Central Swamp region for which transmissivity values are reported is 700 ft. Even though these wells are not fully penetrating, the major water-bearing zones designated by Ryder (1978) have been penetrated. Therefore, the reported transmissivity values should be considered representative of the Upper Floridan aquifer in the region. Reported transmissivity values from published calibrated models for the Cypress Creek well field ranged from 26,000 to 41,000 ft^2/d (Fretwell, 1988) and from 31,500 to 53,600 ft^2/d (Ryder, 1978).

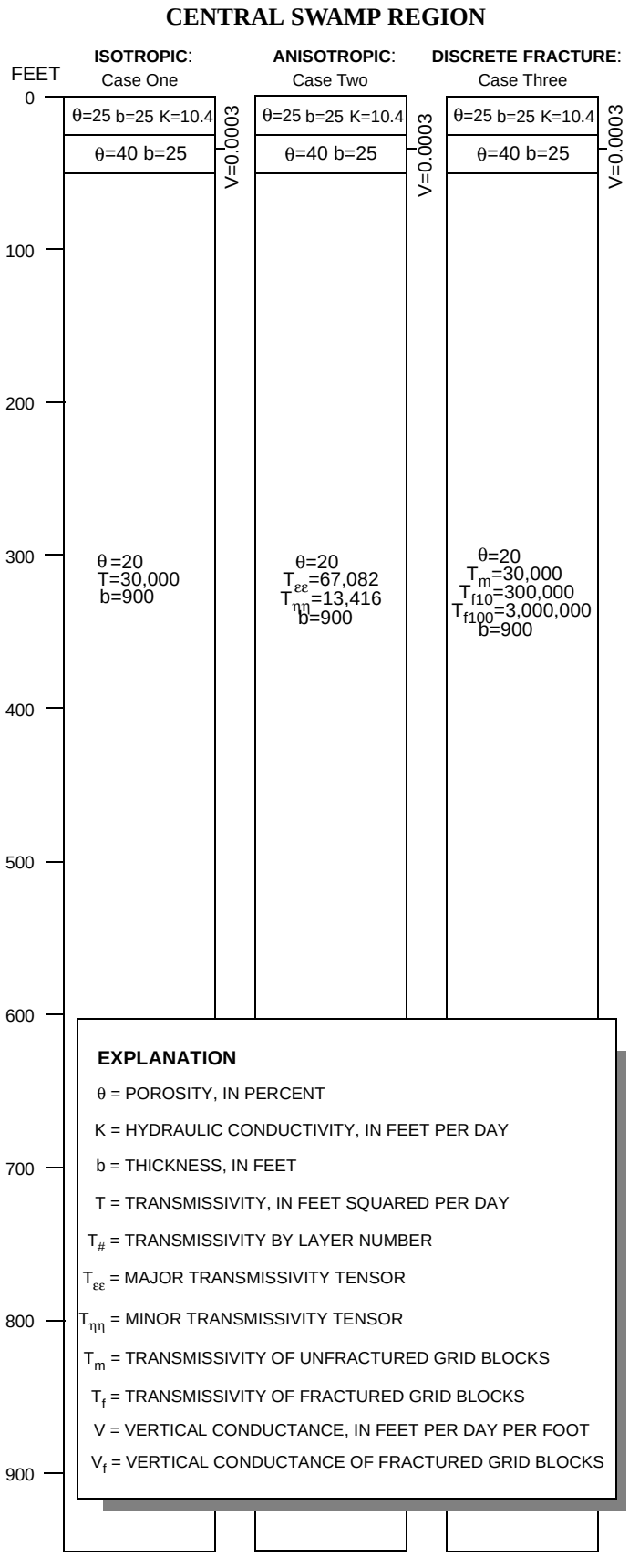

Figure 12. Distribution of input data for the Central Swamp region for the hypothetical carbonate aquifer systems.

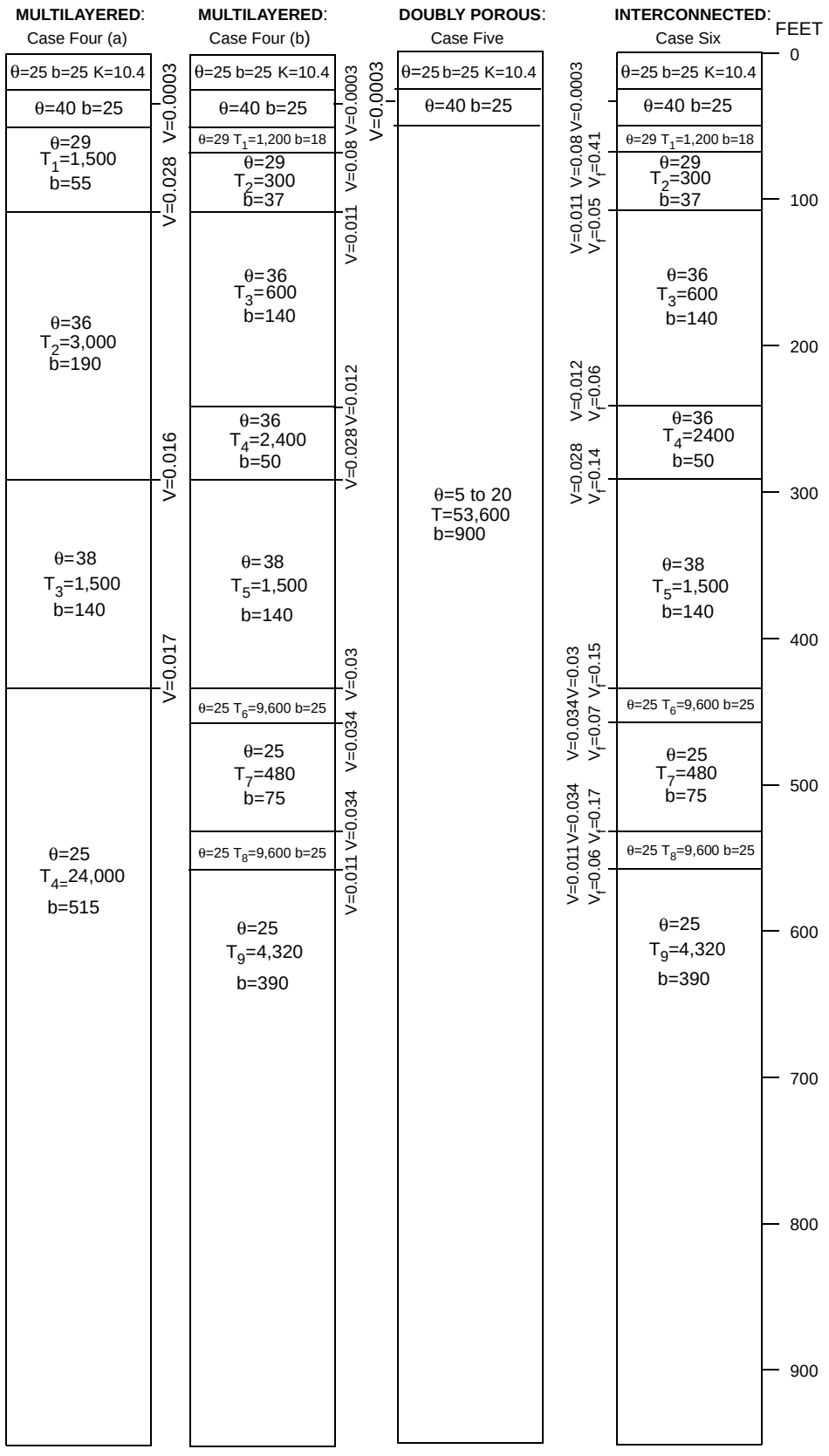

Figure 12. (Continued) Distribution of input data for the Central Swamp region for the hypothetical carbonate aquifer systems.

LAKE TERRACE REGION

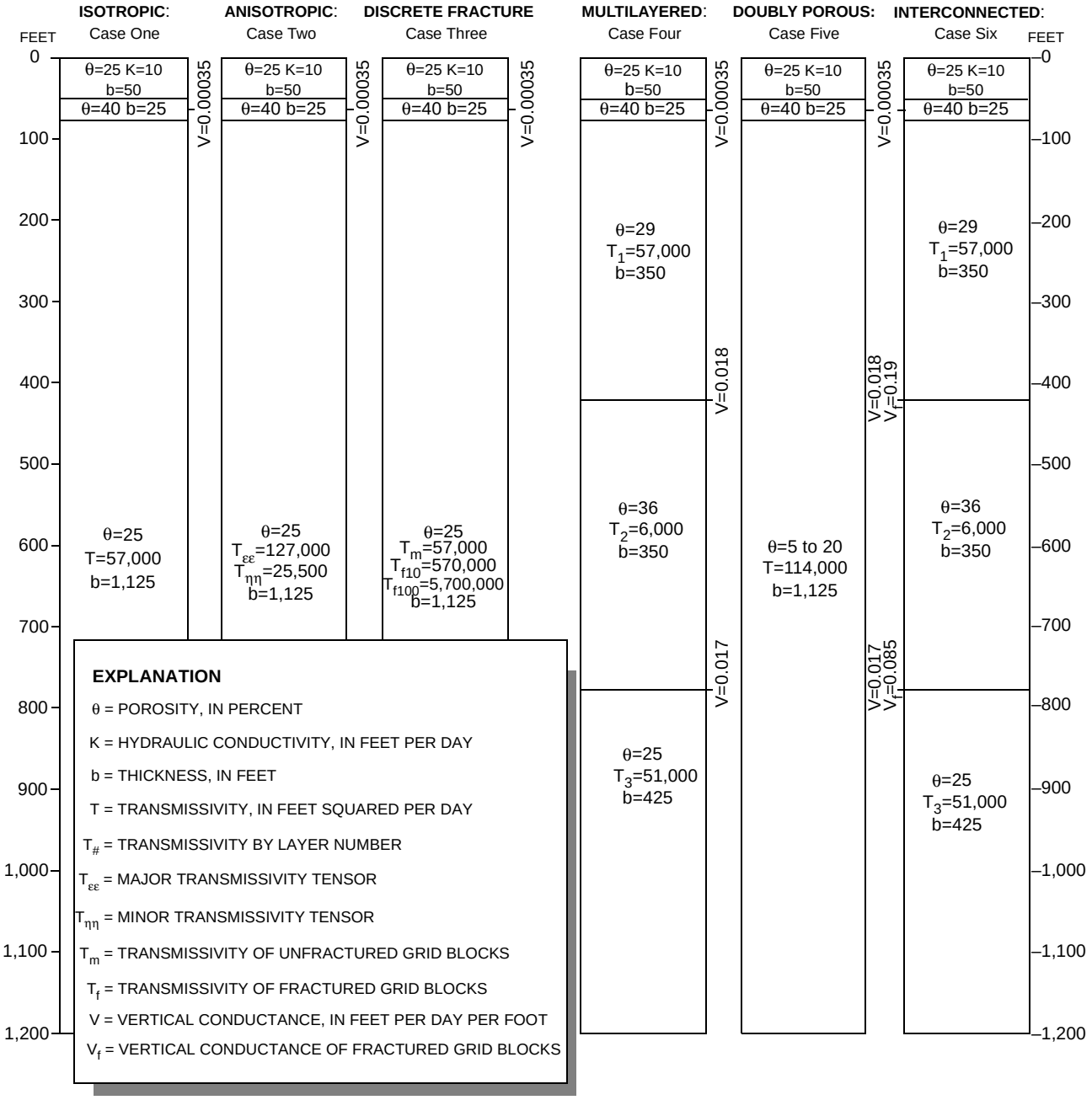

Figure 13. Distribution of input data for the Lake Terrace region for the hypothetical carbonate aquifer systems.

Reported transmissivities from published calibrated models for the Cosme-Odessa well field are 57,000 ft^2/d (Hutchinson, 1984; Bengtsson, 1987) and 66,000 ft^2/d (Fretwell, 1988). However, the aquifer thickness penetrated by the test wells in the Lake Terrace region for which transmissivity values are reported ranges from 200 to 600 ft and represents only 18 to 53 percent of the estimated 1,125-ft total thickness of the Upper Floridan aquifer in the region. Reported transmissivity values should be considered a minimum for the Upper Floridan aquifer in the Lake Terrace region.

The effective porosity values selected for simulation in the Central Swamp and Lake Terrace regions are 20 and 25 percent, respectively. These values are representative of the rock or primary porosity of the Upper Floridan aquifer system.

Case 2: Anisotropy in a Horizontal Plane for a Single-Layer System

The transmissivity values for an anisotropic carbonate aquifer system in the Central Swamp and Lake Terrace regions were computed by assuming an anisotropy ratio of 5:1 and effective transmissivities (T_e) of 30,000 and 57,000 ft^2/d, respectively. The term "effective transmissivity" is defined as the average of the transmissivities in the two principal directions corresponding to the greatest and least preferred flow directions. These directions defined the principal transmissivity tensors. The selected anisotropy ratio is the average of the TENSOR2D results from aquifer tests in west-central Florida. Anisotropy was simulated by using the MODFLOW program with two transmissivity tensors designated $T_{\varepsilon\varepsilon}$ and $T_{\eta\eta}$, which are the maximum and minimum transmissivities, respectively. The equation used to compute the transmissivity tensors is:

$$T_e = (T_{\varepsilon\varepsilon} \times T_{\eta\eta})^{1/2}.$$

Maximum transmissivities probably coincide with fracture locations. Because the fractures are orthogonally distributed, two possible orientations of maximum transmissivity are possible. Therefore, the maximum transmissivity tensor was independently simulated, first along rows and then along columns. The input values for the maximum and minimum transmissivities are about 67,000 and 13,400 ft^2/d in the Central Swamp region and 127,500 and 25,500 ft^2/d in the Lake Terrace region.

Case 3: Discrete, Vertically Fractured, Single-Layer System

Simulation of a carbonate aquifer system with discrete, fully penetrating, permeable vertical fractures was approximated by incorporating differing permeabilities for the fractured and unfractured grid blocks. The influence of permeable vertical fractures in a carbonate aquifer system can be grossly approximated by enhancing the transmissive properties of the fractures. Studies have indicated that fracture permeability may be 10 to 100 times greater than unfractured rock permeability (Stewart and Wood, 1984). Fractures can act as conduits for flow as well as barriers to flow. Both types, conduits and barriers, have been observed in the Upper Floridan aquifer in west-central Florida (Wood and Stewart, 1985). Fractures that are barriers to flow have been recrystallized or filled in with clastic material and are simulated as no-flow grid blocks. Fractures that are conduits for flow are simulated by increasing the transmissivity in the fractures grid blocks relative to the unfractured blocks. The fracture locations in the Central Swamp and Lake Terrace regions, based on the work of Culbreath (1988), are shown in figure 11. The simulated fracture-influenced transmissivity values for the Central Swamp and Lake Terrace regions range from 300,000 to 3,000,000 ft^2/d and 570,000 to 5,700,000 ft^2/d, and the simulated porosities are 20 and 25 percent, respectively. The transmissivity and porosity selected for simulation of the unfractured part of the aquifer in the Central Swamp and Lake Terrace regions are 30,000 ft^2/d and 20 percent and 57,000 ft^2/d and 25 percent, respectively. These transmissivity values fall within the range of published data for west-central Florida. The porosity values are average values from core samples from this study and published reports in west-central Florida.

Case 4: Multilayered System

Carbonate aquifer systems with multiple layers of differing hydraulic properties was simulated by subdividing the single layer aquifer into separate lithostratigraphic units. In addition, discrete flow zones occur within these lithostratigraphic units. Data indicate that, in the study area, the Upper Floridan aquifer contains multiple, thin, flow zones that supply most of the water to wells. The occurrence of flow zones are at varying depths but are generally associated with locations of lithologic contacts. The layered carbonate aquifer system in the Central Swamp region was simulated, both as a four- and nine-layer system on the basis of specific-capacity data and the work of Ryder (1978). The layered carbonate aquifer system in the Lake Terrace region was simulated as a three-layer system.

The four-layer aquifer system in the Central Swamp region was simulated by redistributing aquifer properties by lithostratigraphic unit based on the assumption, supported by physical data, that the lithostratigraphic units do not equally supply water to wells. The four layers of the carbonate aquifer system represent the lithostratigraphic units of the Tampa Member, Suwannee Limestone, Ocala Group, and Avon Park Formation. These lithostratigraphic units are 55, 190, 140, and 515 ft thick and contribute 5, 10, 5, and 80 percent of the flow, respectively. Multilayered models of differing hydraulic characteristics require vertical-conductance data (VCONT) that define the interaction between layers. VCONT is a calculated input parameter and is defined as the vertical hydraulic conductivity divided by the thickness from one layer to the next

lower layer (McDonald and Harbaugh, 1984, p. 155). The simulated ratio of horizontal to vertical hydraulic conductivity is 5:1. This ratio falls within the range of published values determined from core analyses. Porosities were assigned to each layer based on effective porosities determined from core analyses for specific lithostratigraphic units of the carbonate aquifer system. Input values are shown in figure 12.

A nine-layer aquifer system in the Central Swamp region was simulated also because, within these distinct lithostratigraphic units, discrete flow zones occur that supply most of the water to wells. Aquifer properties were redistributed by assuming that 80 percent of the flow in each lithostratigraphic unit, with the exception of the Ocala Group, was derived from the discrete flow zones. The Ocala Group tends to behave as a semiconfining unit within the study area. The lithostratigraphic units were relayered to incorporate the discrete flow zones. The location and thickness of the flow zones in the Tampa Member, Suwannee Limestone, and Avon Park Formation generally conform to descriptions by Ryder (1978). The Tampa Member has an 18-ft-thick flow zone that supplies 80 percent of the flow from the unit. The flow zone occurs near the contact with the intermediate confining unit. The remaining 37 ft of the Tampa Member supplies the remaining 20 percent of the flow from the unit. The Suwannee Limestone has a 50-ft thick flow zone that supplies 80 percent of the flow from the unit. The flow zone occurs near the contact with the underlying Ocala Group. The remaining 150 ft of the Suwannee Limestone supplies 20 percent of the flow from the unit. The Ocala Group was simulated without a discrete flow zone and the entire 140-ft thickness supplies 5 percent of the total water to the well. Two discrete flow zones, each with a thickness of 25 ft, were simulated in the Avon Park Formation. The combined flow supplied from the Avon Park Formation to wells from the two zones is equivalent to 80 percent of the flow from the unit. The flow was equally divided between them. The remaining 20 percent of flow from the unit was attributed to the two less permeable, unfractured units separating the producing zones. Input values are shown in figure 12.

The VCONT values simulated for the nine-layer carbonate aquifer system are a calculated parameter (McDonald and Harbaugh, 1984, p. 155). The porosities were assigned by lithostratigraphic unit as described for the four-layer model. Although the nine-layer model is highly conceptualized, many authors have alluded to the heterogeneous layering observed.

A three-layer aquifer system in the Lake Terrace region was simulated. Specific-capacity data and borehole geophysical log interpretations for the NWHWRAP test well 4-D (CH2M Hill, 1990b) indicate that, in the vicinity of the Lake Terrace region, the Upper Floridan aquifer contains two units of high permeability that are separated by a unit of low permeability. Pumping flowmeter logs from the test well indicate that slightly more than half of the flow enters the well from the upper 300 ft of the carbonate aquifer, and most of the remaining flow enters the well from the lower 300 ft. Based on the discussion of well penetration depth, published transmissivity values of 57,000 and 51,000 ft^2/d were used to characterize the upper and lower producing zones, respectively. The selected horizontal to vertical hydraulic conductivity ratio is 5:1. The input values for VCONT are a calculated parameter. Porosities were assigned to each layer based on average effective porosities determined by core analysis for specific lithostratigraphic units. Input values are shown in figure 13.

Case 5: Doubly Porous, Single-Layer System

Doubly porous systems consist of two media: the high porosity, low permeability of the unfractured parts of the aquifer; and the low porosity, and high permeability of the fractured parts of the aquifer. Generally, fluid transmission occurs through the fractures; therefore, a doubly porous aquifer system can be approximated by using porous media models and by increasing the effective transmissivity (permeability) and by decreasing the effective porosity (Gordon, 1986). The rationale of increasing the overall transmissivity in the simulation is because fractures transmit the water and typically have higher transmissivities than unfractured parts of the aquifer. The rationale for decreasing the porosity in the simulation is because, in an aquifer system consisting of both primary and secondary porosity, fluid flow tends to be through the secondary porosity solution features which make up only a small part of the total aquifer porosity. Therefore, the rate of fluid movement can be more accurately estimated by using a porosity value only associated with the conduits. The doubly porous carbonate aquifer system was approximated by simulating the aquifer as a single layer with a higher transmissivity and lower porosity value for both the Central Swamp and Lake Terrace regions. The transmissivity value selected for the Central Swamp region is the largest transmissivity value determined from aquifer test analyses. The transmissivity value selected for the Lake Terrace region is

equivalent to the total transmissivity of the multilayered model. The wide range of effective porosities is measured in carbonate aquifer systems, and the effective porosity that is solely related to the volume of the fractures is unknown. Therefore, a range of porosities was tested. Input values are shown in figures 12 and 13.

Case 6: Vertically and Horizontally Interconnected Heterogeneous System

The carbonate aquifer system incorporating vertical fracture zones and horizontal, solution-enhanced conduits, was simulated to investigate the effects of a hypothetically distributed, three-dimensional heterogeneity. The distribution of transmissivity values for the Central Swamp and Lake Terrace regions is identical to the distribution used to simulated the multilayered aquifer system, thereby incorporating horizontal, solution-enhanced flow zones. Vertical fractures were simulated by increasing the vertical hydraulic conductivity in fractured blocks relative to the unfractured blocks to simulate the enhanced connectivity between layers. The calculated VCONT values used in the layered model were used to simulate the unfractured blocks. The calculated VCONT values for the fractured blocks were simulated as being five times as permeable as the unfractured blocks, thereby short-circuiting the porous media flow. The term "short-circuiting" is used to describe the interconnection between fractures enhancing fluid movement. This short circuiting was observed at the Old Tampa well field (Robinson, 1995). The effective porosity values are those used for the layered model. Input values are shown in figures 12 and 13.

Simulated Areas of Contribution to Supply Wells, Using Particle Tracking Techniques

Ground-water flow was modeled by using particle tracking techniques to derive the area contributing water to supply wells. The area around each well encompassed by pathlines defines the approximate area of contribution that supplies water to pumping wells. Areas of contribution were delineated for the hypothetical carbonate aquifer systems by placing particles within the grid block containing wells and by running the MODPATH program in the backward-tracking mode. Particle locations were plotted at 10-year intervals and terminated after 50 years. Particle locations were also plotted for a 5-year delineation of the area of contribution. The particle paths were plotted in plane and cross-sectional view. Plane view particle paths were used to estimate time-related areas of contribution to supply wells for the Central Swamp and Lake Terrace regions. Plane views were created by projecting all of the particle paths onto a two-dimensional slice and, therefore, represents the composite area of contribution for the entire thickness of the simulated regions. The extent of the particle paths represents the maximum area from which water is supplied to the wells. Cross-sectional view particle paths are presented to show the effects of aquifer heterogeneity on the vertical flow fields. Cross-sectional views were created by projecting particle paths for supply wells located along a specified row onto that particular row. Therefore, particle paths in the cross section and in the plane view cannot be readily correlated. The sizes of the simulated areas of contribution are those for 50- and 5-year time-related areas.

The Central Swamp Region

The size, shape, and orientation of the areas of contribution in the Central Swamp region for the hypothetical carbonate aquifer systems were delineated by seeding cells containing production wells with particles and by analyzing the flow path patterns in plane view (fig. 14). In addition, boundary fluxes were calculated using the computer program ZONEBUDGET. ZONEBUDGET can be used to calculate the subregional water budgets using results from MODFLOW (Harbaugh, 1990). The appendix contains a list of inflow percentages from each of the constant-head boundaries. Inflow from the constant-head water table ranged from 58 to 81 percent. A brief discussion of the ZONEBUDGET results is included in the discussion of the individual cases.

Case 1.—The isotropic, homogeneous single-layer carbonate aquifer system has a 12.7-mi^2 area of contribution in the shape of an elongated oval. The orientation is slightly northeast-southwest, roughly following the supply well orientation. The ZONEBUDGET results for Case 1 indicates that about 75 percent of the boundary inflow is derived from the water table. The lateral boundaries contribute varying percentages ranging from 5.5 to 7 percent. The differences among percentages derived from the individual lateral boundaries is probably the result of well locations relative to the boundaries.

Cases 2A and 2B.—The simulated areas of contribution are approximately 12.4 mi^2 for the anisotropic, single-layer, carbonate aquifer system. The shape and orientation are elliptical and elongated in the direction of the maximum transmissivity tensor. The ZONEBUDGET results for Cases 2A and 2B indicate that about 63 percent of the boundary inflow is derived from the water table. This is 12 percent less than in the isotropic case (Case 1) and is probably the result of enhanced direction-dependent lateral transmissivity in the pumped aquifer. The combined inflow from the lateral boundaries normal to the maximum transmissivity tensor contribute about 35 percent.

Case 3A.—The simulated area of contribution is approximately 8.2 mi^2 for the impermeable, discrete, fractured, carbonate aquifer system. The shape is roughly circular and without apparent orientation. The shift to a more circular area of contribution is probably due to the flow field attenuation at the fracture network and greater velocities of the particles not intersecting fractures. The ZONEBUDGET results for Case 3A indicates that about 81 percent of the boundary inflow is derived from the water table. This is 6 percent more than in the isotropic case and is probably the result of the flow field attenuation by the simulated impermeable fractures in the pumped aquifer. Lateral inflow is contributed almost exclusively from lateral boundaries 1 and 4, which are located away from the impermeable fracture blocks.

Cases 3B and 3C.—The simulated areas of contribution for the permeable, discrete, fractured, carbonate aquifer system ranged from 10.7 to 12.1 mi^2. The size of the area of contribution for various values of fracture-influenced transmissivity is not greatly affected; but, as the ratio of transmissivities in the fractured and unfractured blocks increases, particle paths deviate from radial flow. Particles travel two to three times farther in the simulated fractured blocks than in the unfractured blocks. The ZONEBUDGET results for Cases 3B and 3C indicate that about 69 and 63 percent of the boundary inflow is derived from the water table, respectively. This is 6 and 12 percent less than in the isotropic case and is probably the result of enhanced transmissivity of the simulated permeable fractures. The lateral boundaries closest to the fractured blocks contribute a greater percentage, and this percentage increases as the ratio of transmissivities in the fractured to unfractured blocks is increased.

Case 4A.—The simulated area of contribution for the four-layer carbonate aquifer system is the same size (12.7 mi^2), shape, and orientation as the simulated area of contribution for the Case 1 model. This indicates that the distribution of transmissivity values by layer does not affect the composite area of contribution to supply wells. However, these alterations do affect the individual particle paths. The vertical component of flow is enhanced by simulating a layered aquifer system with variable hydraulic properties. The ZONEBUDGET results for Case 4A indicates that about 72.5 percent of the boundary inflow is derived from the water table. The lateral boundaries contribute varying percentages ranging between 5.6 and 7.5 percent.

Case 4B.—The simulated area of contribution for the nine-layer carbonate aquifer system is 23.0 mi^2. The shape is irregular, but roughly circular. There appears to be no preferred orientation. This hypothetical carbonate aquifer system incorporated discrete producing zones of higher permeability. The particle paths are horizontal in the permeable zones and more vertical in the lower permeability layers. The particles travel four times farther in these zones, generating a larger composite area of contribution. The ZONEBUDGET results for Case 4B indicates that about 75 percent of the boundary inflow is derived from the water table and is nearly equivalent to the isotropic case. The lack of preferred orientation of the composite area of contribution is supported by the budget results because nearly equivalent percentages are contributed from each of the lateral boundaries.

Case 5.—The simulated area of contribution for the doubly porous, carbonate aquifer system are 12.7, 16.0, and 39.1 mi^2 for porosities of 20, 10, and 5 percent, respectively. The area of contribution for the doubly porous model with an effective porosity of 20 percent is not shown in figure 14 because it is identical to Case 1. The doubly porous model with an effective porosity of 5 percent is almost circular in shape. No orientation was evident. The ZONEBUDGET results for Case 5 when using a 5 percent porosity indicates that about 57 percent of the boundary inflow is derived from the water table. This is 18 percent less than in the isotropic case and is probably the result of the higher simulated transmissivity in the pumped aquifer. The lack of preferred orientation of the area of contribution is supported by the budget results because nearly equivalent percentages are contributed from each of the lateral boundaries.

Case 6.—The simulated area of contribution for the vertically and horizontally interconnected heterogeneous carbonate aquifer system is 23.6 mi^2.

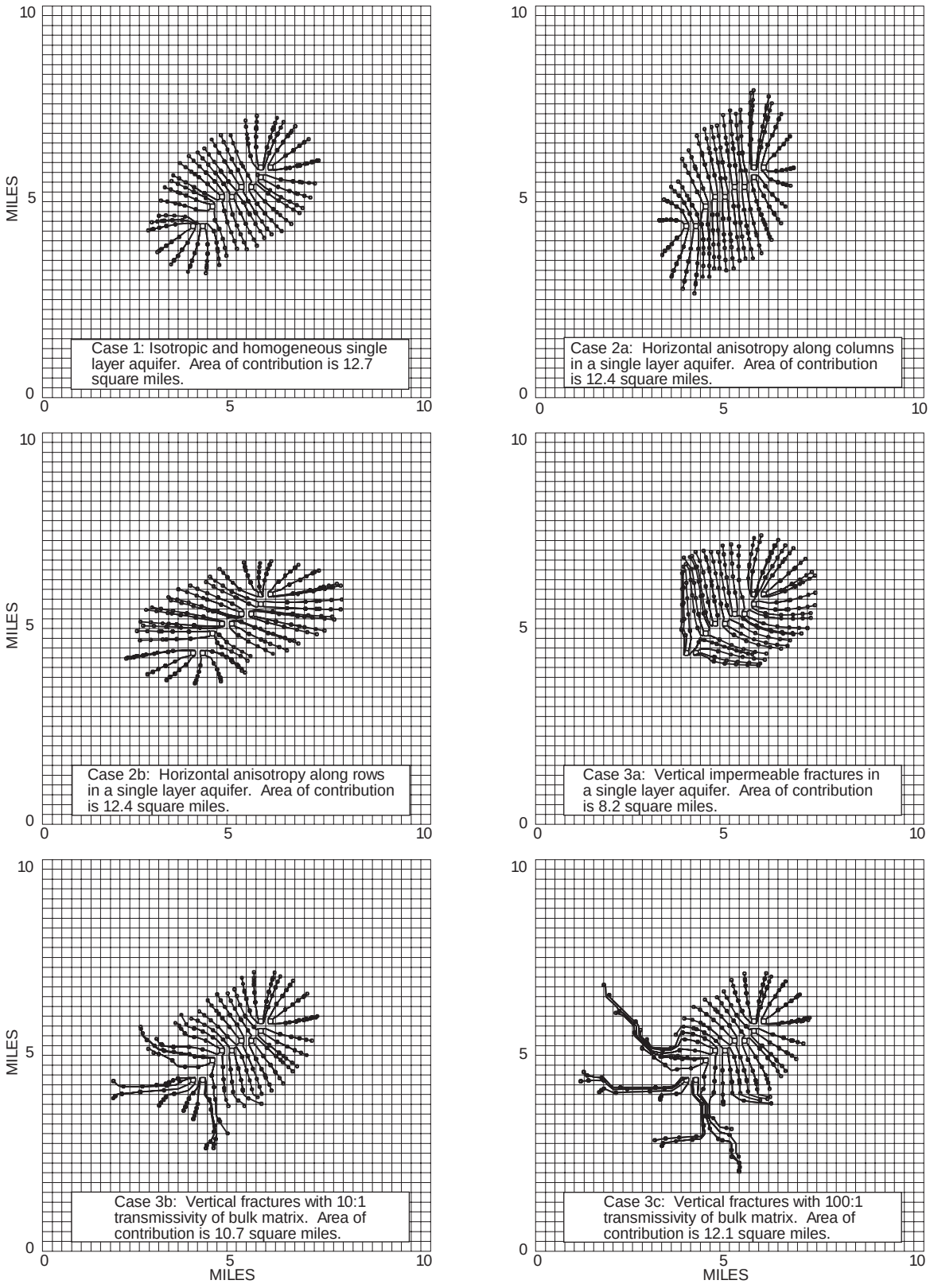

Figure 14. Fifty-year time-related area of contribution for the hypothetical carbonate aquifer systems in the Central Swamp region.

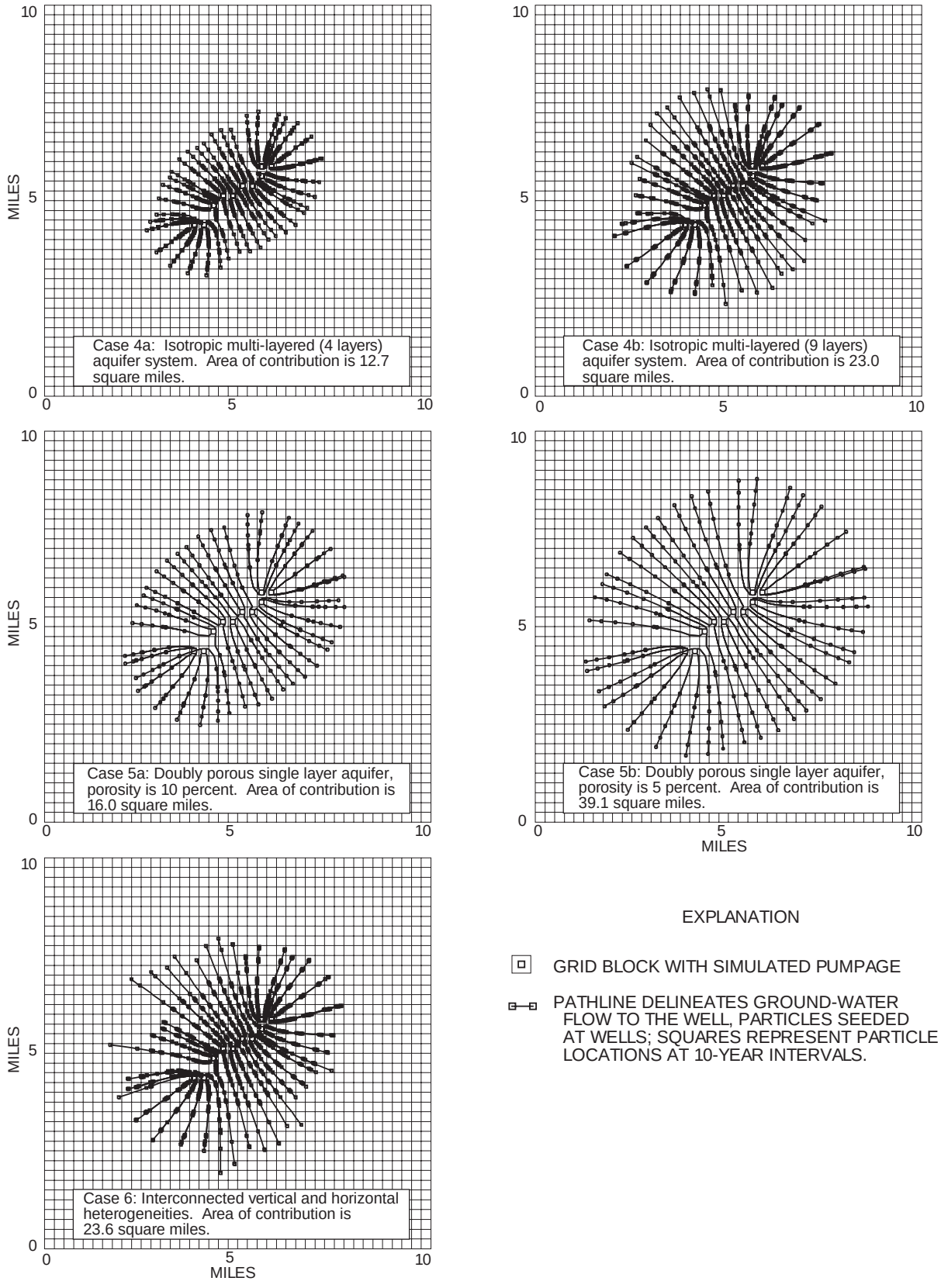

Figure 14. (Continued) Fifty-year time-related area of contribution for the hypothetical carbonate aquifer systems in the Central Swamp region.

The shape is irregular, especially in the vicinity of the simulated fracture network. The ZONEBUDGET results for Case 6 indicate that boundary inflows are nearly the same as for Case 4B. This indicates that enhanced lateral flow zones in the pumped aquifer control the source of boundary inflow to a greater extent than enhanced vertical interconnection between flow zones even though the shape of the area of contribution is affected by these simulated vertical fractures.

Figure 15 is included in the report to show the effects of aquifer heterogeneity in cross section. The cross-section view is along row 20 in the Central Swamp region and particle paths are projected onto a two-dimensional slice corresponding to row 20. Particles were seeded in each well in row 20, and all wells were pumped during simulation. The projection can be misleading in that particles that do not travel in the specified row are projected onto that row. However, the figure does present the vertical flow deviations not readily discernible in plane view. The vertical flow deviations shown in figure 15 are discussed in terms of observed variations for the particular row.

Case 1.—The particle paths are evenly spaced and become more vertical near the top of the simulated carbonate aquifer system.

Cases 2A and 2B.—The predominant direction of aquifer anisotropy is readily apparent. By using the cross-section projection along a row, lateral spread of pathlines is small when flow is predominantly along columns and large when flow is predominantly along rows.

Cases 3A, 3B, and 3C.—Discrete fracture networks influence the lateral spread of pathlines by limiting pathline length when intersecting closed fractures and increasing lateral spread in the direction of high permeability fractures.

Case 4A.—Simulation of a multilayered aquifer system with contrasting hydraulic properties had a pronounced effect on flowlines and simulated particle paths. The particles tend to move more horizontally in permeability layers and more vertically in low permeability layers.

Case 4B.—Simulation of discrete producing zones has an even more pronounced effect because of the greater contrasts in hydraulic properties among the hydrologic units. Flow is predominantly horizontal in the enhanced flow zones and nearly vertical in the less permeable zones.

Cases 5A and 5B.—Selection of simulated porosity affects the lateral spread of pathlines. The lower the porosity the larger the spread.

Case 6.— The distribution of pathlines in the cross section does not appear to be affected by enhanced vertical connectivity between zones and is identical to case 4B.

All of the hydrogeologic factors tested had some effect on the simulated flow fields that defined the areas of contribution in the Central Swamp region. Generally, the simulated areas of contribution represent a composite area that results from pumping interference among supply wells. Well orientation, distribution, and pumping rates have an underlying effect on the size, shape, and orientation of the areas of contribution. Differing types of simulated aquifer anisotropy and heterogeneity affected the areas of contribution in a variety of ways. The size of the simulated areas of contribution is mostly affected by heterogeneous layering of aquifer properties and the selection of effective porosity. The shape of simulated areas of contribution to supply wells is mostly affected by the location of the discrete fracture network, and the orientation of simulated areas of contribution is mostly affected by aquifer anisotropy.

The Lake Terrace Region

The size, shape, and orientation of the areas of contribution in the Lake Terrace region for the hypothetical carbonate aquifer systems were delineated by seeding cells containing production wells with particles and by analyzing the flow path patterns in plane view (fig. 16). In addition, boundary fluxes were calculated by using the computer program ZONEBUDGET. ZONEBUDGET can be used to calculate the subregional water budgets using results from MODFLOW (Harbaugh, 1990). The appendix contains a list of inflow percentages from each of the constant-head boundaries. Inflow from the constant-head water table ranged from 38 to 65 percent. A brief discussion of the ZONEBUDGET results among the various cases is included in the discussion of the individual cases.

Case 1.—The isotropic, homogeneous, single-layer, carbonate aquifer system has a 4.0-mi^2 area of contribution. The shape and orientation that were delineated are roughly radial particle paths surrounding an individual grid block containing wells. The combined areas of contribution for the well field roughly follow the orientation of the supply wells. The ZONE

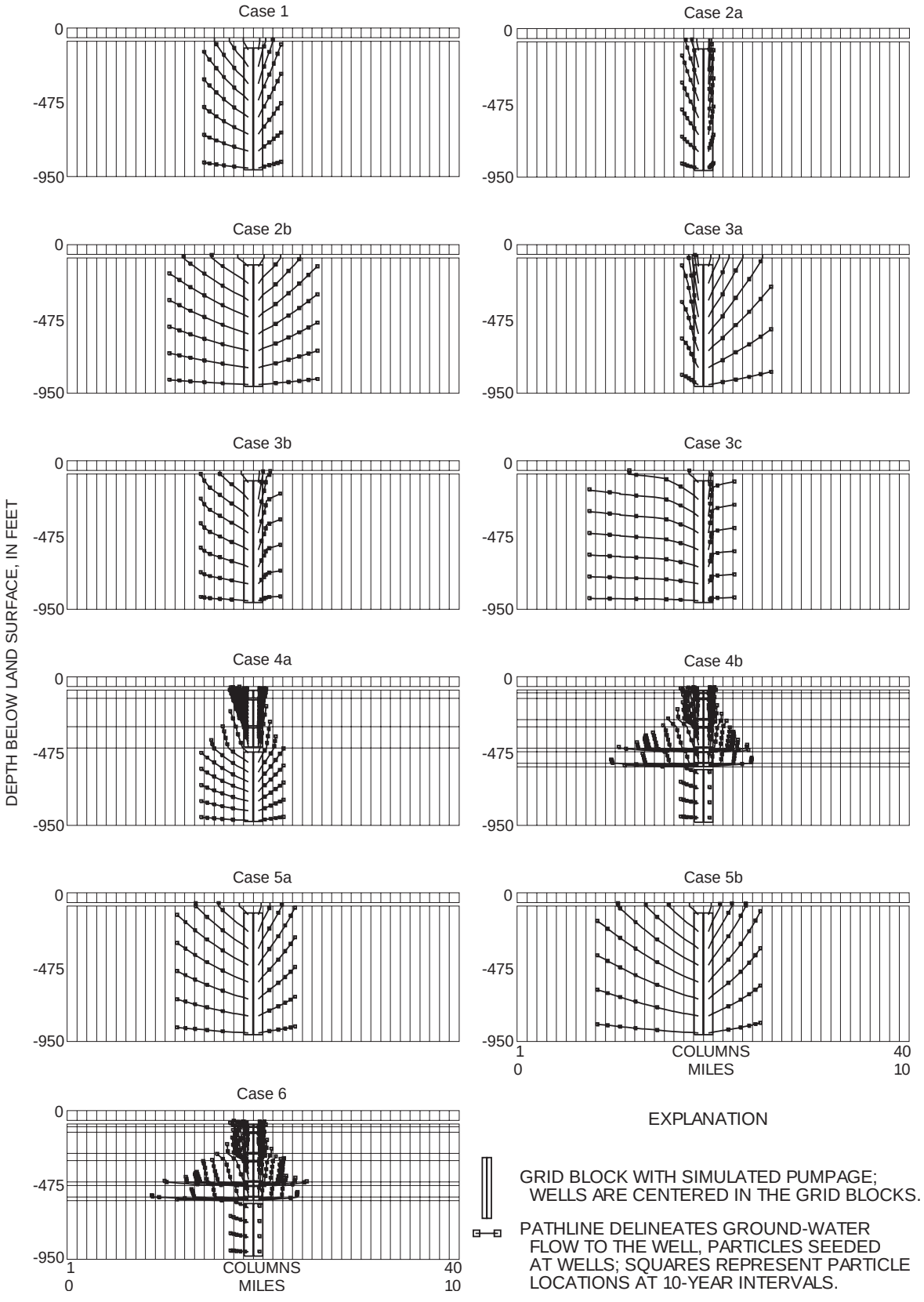

Figure 15. Fifty-year traveltimes for particles projected onto a two-dimensional slice corresponding to row 20 for the hypothetical carbonate aquifer systems in the Central Swamp region.

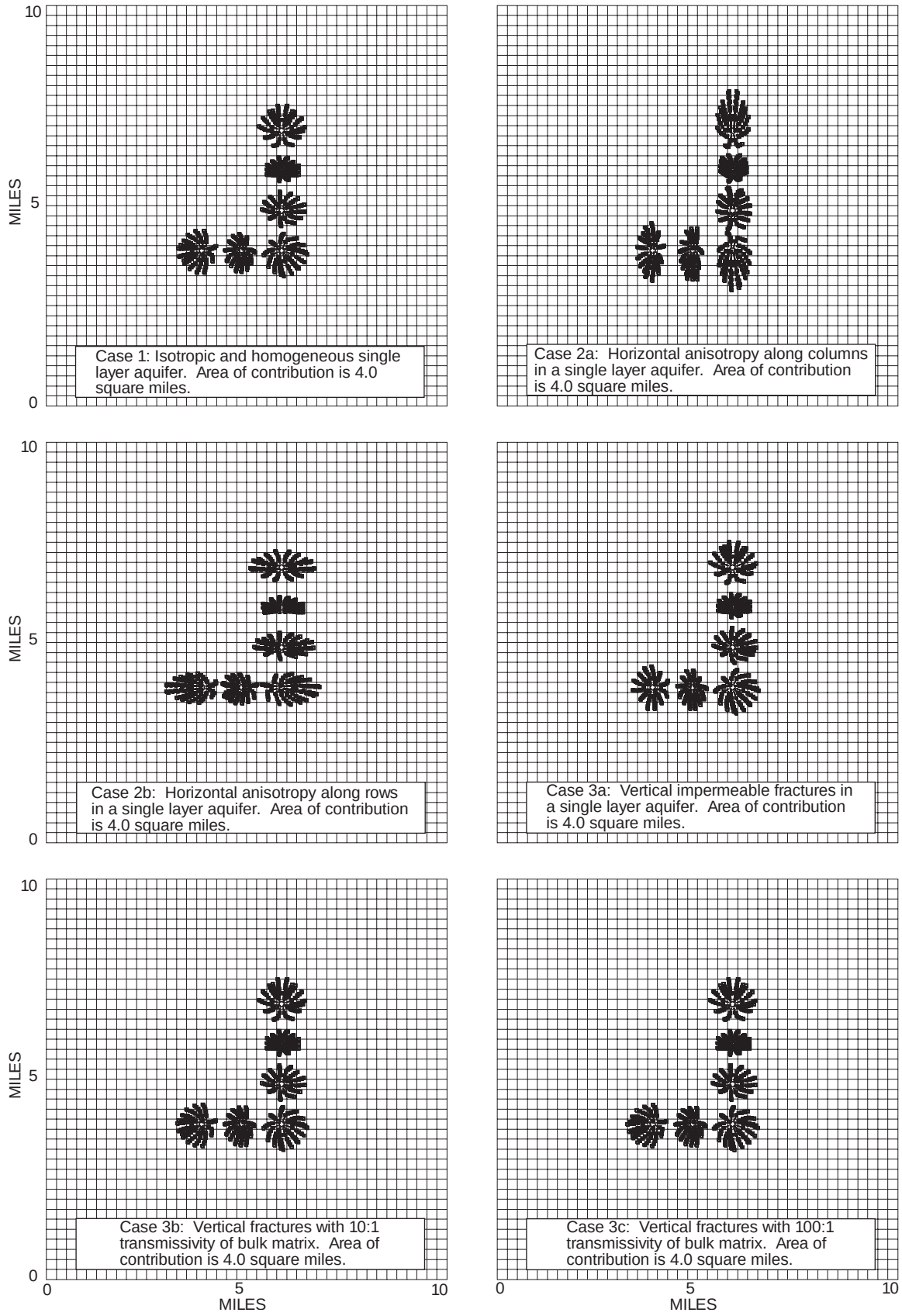

Figure 16. Fifty-year time-related areas of contribution for the hypothetical carbonate aquifer systems in the Lake Terrace region.

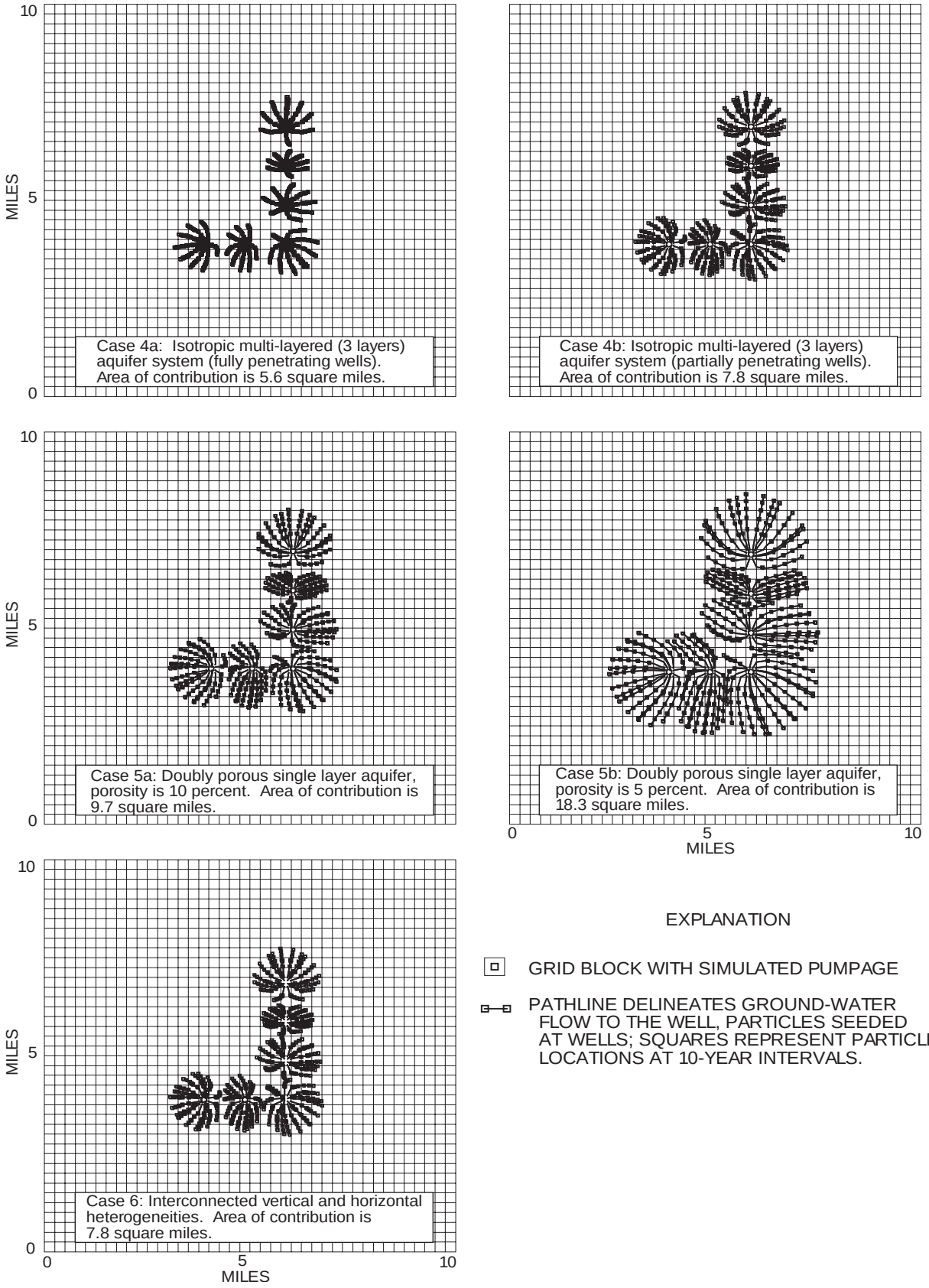

Figure 16. (Continued) Fifty-year time-related areas of contribution for the hypothetical carbonate aquifer systems in the Lake Terrace region.

BUDGET results for Case 1 indicate that about 58 percent of the boundary inflow is derived from the water table. The lateral boundaries contribute varying percentages ranging between 8 and 12 percent. The differences among percentages derived from the individual lateral boundaries is probably the result of well locations relative to the boundaries.

Cases 2A and 2B.—The anisotropic, single-layer, carbonate aquifer system also has a 4.0 mi^2 area of contribution. The shape and orientation of particle paths are elliptical and elongated in the direction of the maximum transmissivity tensor. The ZONEBUDGET results for Cases 2A and 2B indicate that about 48 percent of the boundary inflow is derived from the water table. This is 10 percent less than in the isotropic case (Case 1) and is probably the result of enhanced direction-dependent lateral transmissivity in the pumped aquifer. The combined inflow from the lateral boundaries normal to the maximum transmissivity tensor contribute 50 percent.

Cases 3A, 3B, and 3C.—Neither the simulated impermeable nor permeable, fractured, single-layer, carbonate aquifer system affected the size, shape, or orientation of the simulated areas of contribution. The 50-year particle paths do not intersect the simulated fracture locations. The area of contribution is the same as for Case 1. Whereas simulated fracture locations did not affect the size, shape, or orientation of the areas of contribution, the ZONEBUDGET results were affected. The ZONEBUDGET results for Case 3A indicate that about 66 percent of the boundary inflow is derived from the water table. This is 8 percent more than in the isotropic case and is probably the result of the flow field attenuation by the simulated fractures in the pumped aquifer. A combined lateral inflow of about 32 percent is almost equally contributed from boundaries 1, 3, and 4. Lateral boundary 2 contributes only about 2 percent. This is probably due to the close proximity of an impermeable fracture to the wells. The ZONEBUDGET results for Case 3B and 3C indicate that about 56 and 55 percent of the boundary inflow is derived from the water table, respectively. This is 2 and 3 percent less than in the isotropic case and is probably the result of the enhanced transmissivity of the simulated permeable fractures; however, the lateral inflow is not significantly increased because the fractures blocks are located distant from the pumped wells. The greatest increase in contribution between impermeable and permeable fracture simulations is from lateral boundary 2.

Case 4.—Two scenarios of well construction, fully and partially penetrating, were simulated in the multilayered carbonate aquifer system. The simulated areas of contribution for the fully and partially penetrating wells tapping a multilayered carbonate aquifer system are 5.6 and 7.8 mi^2, respectively. The general shape and orientation is the same as for the previous cases. The difference between the sizes in areas for case 4A and 4B is the result of greater well interference, as exhibited by the particle paths in case 4B. The representation of the partial penetrating wells coincide with actual well depths in the Cosme-Odessa well field. The ZONEBUDGET results for Cases 4A and 4B indicate that between 38 and 40 percent of the boundary inflow is derived from the water table and is nearly 20 percent less than in the isotropic case. The effects of partial penetration did not substantially change inflow from the water table (<2 percent). Inflow from the lateral boundaries for Case 4A ranges from about 13 to 18 percent and in Case 4B from about 12 to 17 percent.

Cases 5A, 5B, and 5C.—The simulated areas of contribution for the doubly porous carbonate aquifer system with an effective porosity of 20 and 10 percent are 5.6 and 9.7 mi^2, respectively. The simulated areas of contribution for the doubly porous carbonate aquifer system with an effective porosity of 5 percent is 18.3 mi^2. As the simulated effective porosity decreased, the area of contribution increased. The composite shape and orientation are similar but the particle paths around individual wells are less radial due to competition among the wells. The area of contribution for 20 percent porosity is not shown in figure 16. The ZONEBUDGET results for Case 5 when using a 5 percent porosity indicate that about 38 percent of the boundary inflow is derived from the water table. This is 20 percent less than in the isotropic case and is probably the result of the higher simulated transmissivity in the pumped aquifer.

Case 6.—The simulated areas of contribution for the fully and partially penetrating wells tapping an vertically and horizontally interconnected heterogeneous, carbonate aquifer system are 5.6 and 7.8 mi^2, respectively. The simulated areas of contribution are nearly identical to Case 4; therefore, only the partially penetrating well simulation is shown in figure 16. The enhanced vertical connection between layers in the simulated fractured grid blocks did not affect the areas of contribution. The ZONEBUDGET results for Case 6 indicate that boundary inflows are nearly the same as for Case 4B. This indicates that enhanced lateral flow

zones in the pumped aquifer control the source of boundary inflow to a greater extent than enhanced vertical interconnection between flow zones even though the shape of the area of contribution is affected by these simulated vertical fractures.

Figure 17 is included in the report to show the effects of aquifer heterogeneity in cross section. The cross-section view is along row 25 in the Lake Terrace region and particle paths are projected onto a two-dimensional slice corresponding to row 25. Slight variations in the flow fields can be observed that are not readily apparent in plane view.

Case 1.—The particle paths are evenly spaced and become more vertical near the top of the simulated carbonate aquifer system.

Cases 2A and 2B.—The predominant direction of anisotropy is readily apparent. The lateral spread of pathlines is small when flow is predominantly along columns and large when flow is predominantly along rows.

Cases 3A, 3B, and 3C.—Particle paths closest to the simulated impermeable fracture network (Case 3A) reflect slight effects from the no-flow grid blocks by becoming more vertical. Slight variations in the flow field as represented by particle paths (case 3B and 3C) are the result of location and permeability of the discrete fracture network, but, because the fracture network is not intersected directly, effects are minimal.

Case 4A and 4B.—Layering and well penetration affect the flow field by creating variations in fluid movement direction and velocity. The lateral spread of particles is small in the simulated semiconfining unit relative to the more permeable units (Case 4A). When only the upper producing zone is being stressed, flow paths are predominantly horizontal in the high permeability layers and vertical in the low permeability layer (Case 4B). The flow velocities vary by layer due to differing effective porosities and permeabilities.

Case 5.—Selection of simulated porosity affects the lateral spread of pathlines. The lower the porosity, the larger the spread, which results in competition for flow among wells.

Case 6.—The particle paths are identical to those for Case 4. The fracture network is not intersected and, therefore, has little effect on particle paths.

In the Lake Terrace region, the hydrogeologic factors tested affected the areas of contribution to supply wells. The well distribution, orientation, and pumping rates resulted in the distinct shape of the areas of contribution. Pumping interference is minimal, and each well is characterized by an individual contributing area for isotropic, homogeneous conditions (Case 1). Incorporation of aquifer anisotropy and heterogeneity does affect the size, shape, and orientation of areas of contribution, but not as dramatically as expected. The size of the simulated areas of contribution is mostly affected by heterogeneous layering of aquifer properties (Cases 4 and 6) and by the selection of effective porosity (Case 5). The shape of simulated areas of contribution is mostly affected by well orientation and distribution, and the orientation is mostly affected by aquifer anisotropy (Case 2).

Comparisons Between Simulated Areas of Contribution in the Central Swamp and Lake Terrace Regions

The simulated areas of contribution for the prototype regions were compared to illustrate the effects of withdrawal rates, well distribution, and hydrogeologic differences on size, shape, and orientation of the areas. The major difference between the simulated areas of contribution in the Central Swamp and Lake Terrace regions is size. Generally, the simulated areas of contribution are about 60 percent larger in the Central Swamp region where the pumping rate is more than double and transmissivity is about half that of the Lake Terrace region. However, the difference in contributing area size between the two regions was not constant for all the hypothetical carbonate aquifer systems simulated. The largest difference in simulated contributing area size between the Central Swamp and Lake Terrace regions was 64 percent, a result of the simulation of the vertically and horizontally interconnected heterogeneities (Case 6). The smallest difference in contributing area size between the regions was 31 percent, a result of the simulation of a multilayered system (Case 4).

The shapes of the simulated areas of contribution in the Lake Terrace region are predominantly controlled by well location and distribution and generally follow the outline of supply wells at the Cosme-Odessa well field. The shapes of simulated areas of contribution in the Central Swamp region are primarily affected by locations of simulated fracture networks. The larger the ratio of fracture to bulk matrix permeability, the more linear the flow field becomes. The shapes of particle paths for the multilayered carbonate aquifer system in the Central Swamp region were irregular, rosette-shaped areas of contribution because of the variability in flow direction and velocity between high

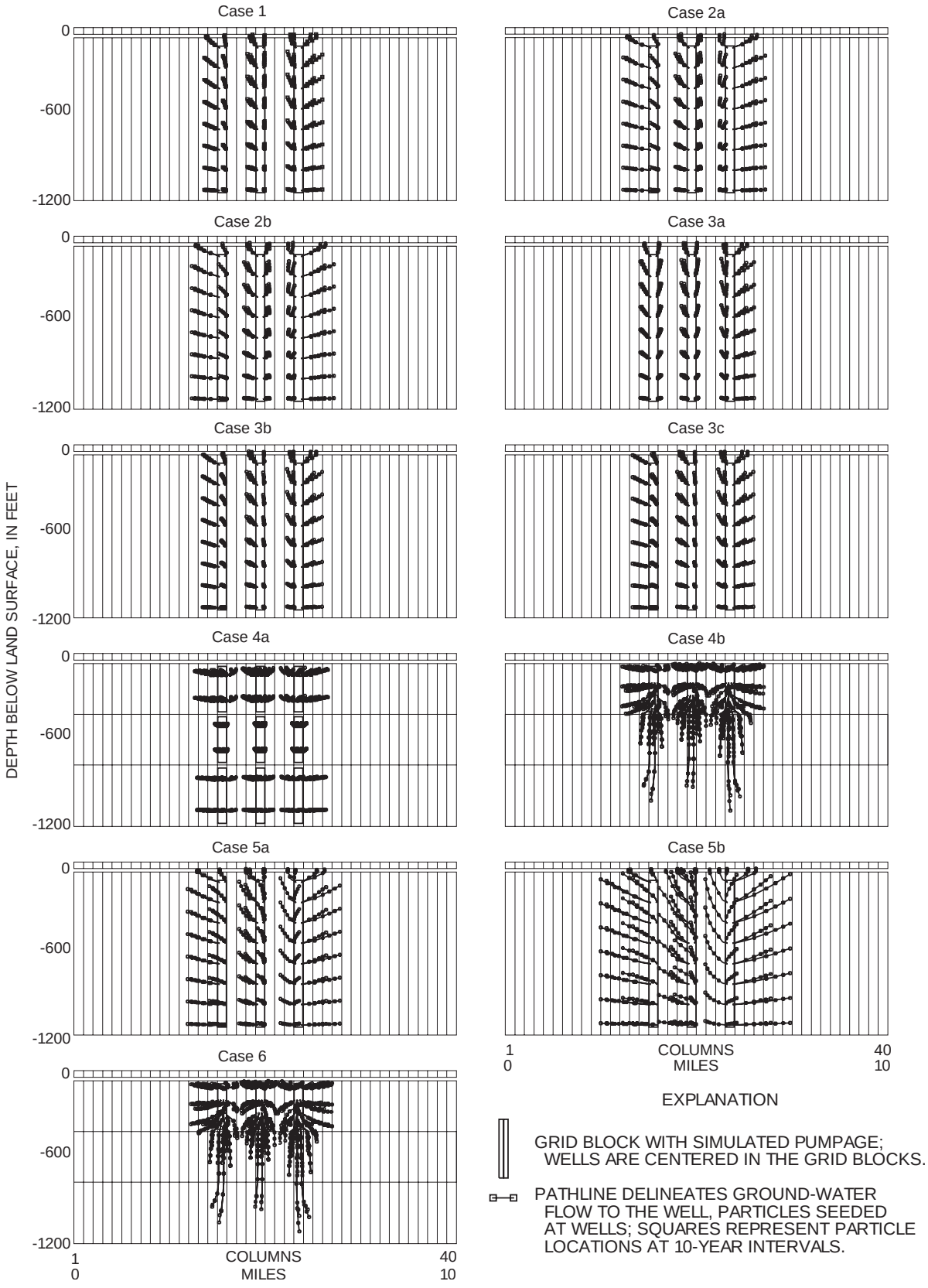

Figure 17. Fifty-year traveltimes for particles projected onto a two-dimensional slice corresponding to row 25 for the hypothetical carbonate aquifer systems in the Lake Terrace region.

and low permeability layers. The shapes of the areas of contribution for simulations incorporating aquifer anisotropy in both regions are elongated ellipses. Aquifer anisotropy has similar effects on the orientation of simulated areas of contribution in the Central Swamp and Lake Terrace regions. The orientation of these areas of contribution is controlled by the maximum transmissivity tensor. In the Central Swamp region, orientation of particle paths is affected by the fracture network. Flow deviates from radial to linear paths once the fracture network is intersected. The 50-year traveltimes in the Lake Terrace region are unaffected by the simulated fracture network, because the 50-year traveltimes of particle paths do not intersect the discrete fracture network. The first particles just reach the fracture network after 100 years.

Simulations incorporating generalized representations of nonisotropic and nonhomogeneous aquifer behavior including anisotropy, vertical fractures, and multiple layers do affect the size, shape, and orientation of areas of contribution. Therefore, local-scale heterogeneities should be considered when delineating areas of contribution for karst carbonate aquifer systems.

COMPARISON OF NUMERICAL SIMULATION RESULTS WITH RESULTS USING ANALYTICAL METHODS

Major differences in the methodology between analytical and numerical delineation of protection zones to supply wells result from the strict limiting assumptions when implementing analytical techniques. Analytical models are typically one-dimensional. Consequently, three-dimensional aquifer anisotropy and heterogeneity cannot be incorporated. The numerical models developed for this study were designed to approximate varying degrees of aquifer anisotropy and heterogeneity.

Vecchioli and others (1989) used a radial, volumetric displacement, analytical method to delineate protection zones at well fields in the Upper Floridan aquifer in west-central Florida. The analytical method used was based on equations derived from Darcy's law and assumes uniform, radial flow. A porosity of 5 percent was selected for the analysis. The selection of a 5 percent porosity value is based on the characterization of the Upper Floridan aquifer system as a doubly porous system having both primary and secondary porosity. Fluid flow tends to be through the solution features (secondary porosity) which make up only a small part of the total porosity. Therefore, the rate of fluid movement can be more accurately estimated by using a porosity value only associated with the conduits. Protection zones were delineated for a specified traveltime of 5 years, flow was assumed to be lateral in the aquifer, and the aquifer thickness was taken equal to the well penetration. Where the protection zones overlapped, composite protection zones were delineated. Limitations of the analytical method include the inability to incorporate the natural slope of the potentiometric surface, complex hydrologic boundaries, and variations in porosity and aquifer thickness (Vecchioli and others, 1989, p. 33).

The numerical model that most closely approximates the conditions used in the analytical model is the doubly porous model when using an aquifer porosity of 5 percent (Case 5). To make comparisons with the analytically derived protection zones, 5-year time related areas of contribution were numerically simulated for the Central Swamp and Lake Terrace regions. The numerically simulated contributing areas for the two regions and the analytically delineated protection zones for the Cypress Creek and Cosme-Odessa well fields (from Vecchioli and others, 1989) are shown in figure 18.

The areas of contribution that were delineated using numerical methods are different in both shape and size from protection zones that were delineated using analytical methods. The protection zones that were delineated for the Cypress Creek and Cosme-Odessa well fields using the analytical model are 7.85 and 8.24 mi^2, respectively. The contributing areas that were delineated for the Central Swamp and Lake Terrace regions are about 4 and 1 mi^2, respectively. This discrepancy in size can be the result of various factors. The most critical factor is that the analytically derived protection zone size was determined for a 5-year lateral traveltime, which does not correspond to a 5-year traveltime for seeded particles because particles can move both laterally and vertically. Some of the assumptions of analytical methods that may affect the size, shape, and orientation of delineated protection zones are that ground-water flow to wells is uniform and that the aquifer is bounded by nonleaky confining beds. The assumption of uniform, radial flow is only approximated near the well bore and the deviation from radial flow increases as the distance from the well is increased. The assumption of nonleaky confining beds is a poor assumption, because relatively few confined

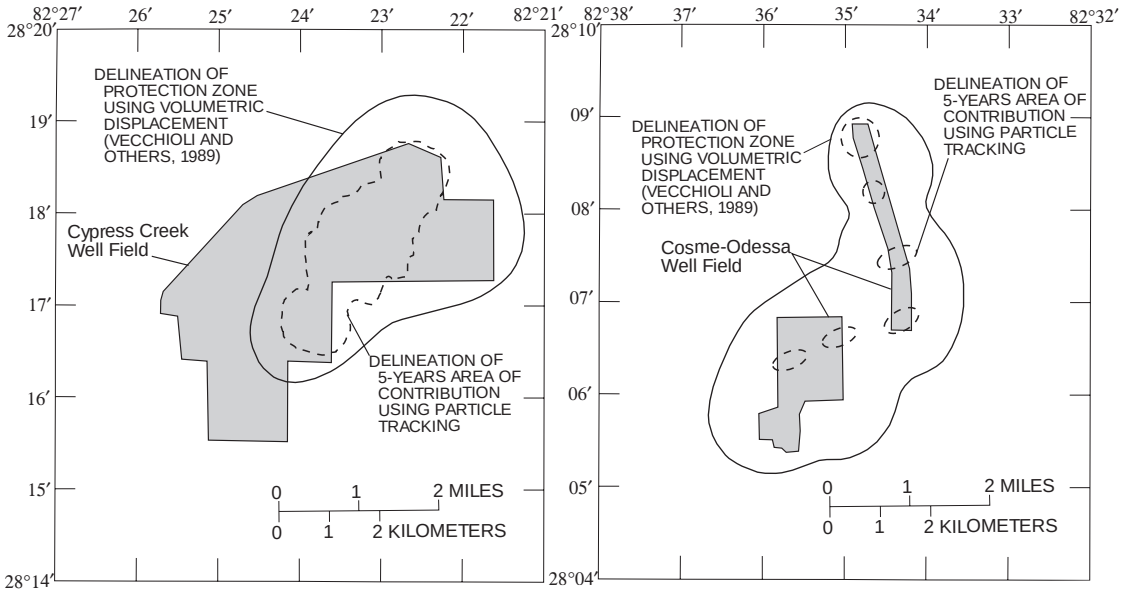

Figure 18. Delineation of protection zones using analytical methods, and areas of contribution using numerical methods for the Central Swamp and Lake Terrace regions.

aquifers do not receive water from adjacent beds. In addition the analytically derived protection zones do not account for changes in the flow field caused by changes in the local hydraulic gradient in response to pumping.

Numerical models should be more accurate than analytical models simply because greater aquifer complexities can be incorporated in the model. However, these numerical models are hypothetical in that distributions and behaviors of aquifer heterogeneities are not well understood. The analytically derived protection zones are very conservative when compared with the contributing areas delineated by numerical modeling.

SUMMARY AND CONCLUSIONS

The highly permeable, karst carbonate Floridan aquifer system underlies Florida and much of the southeastern Coastal Plain and is a principal source of drinking water. Public supply wells in karst carbonate aquifers are particularly vulnerable to contamination. Estimation of areas of contribution in karst carbonate aquifers can be extremely difficult, because permeability in carbonate aquifers is greatly enhanced by dissolution of rock, which creates an uneven distribution of permeability along preferred flow paths.

Traditional strategies to protect ground-water resources have been through land-use regulation within a prescribed radial area around supply wells. Hydrogeologic factors operating at a site that may affect the size, shape, and orientation of areas of contribution to supply wells often are not considered. Ground-water flow to wells in karst carbonate aquifer systems tends to be through solution-enhanced conduits. Nonradial flow along preferential zones can result in inaccurate estimations of flow paths and traveltimes. A better understanding of the effects of aquifer heterogeneity on flow fields is needed to protect the ground-water resources.

The influence of aquifer anisotropy and heterogeneity on the movement of ground water can often be inferred from aquifer and tracer test data. Evaluation of aquifer test, tracer test, and borehole geophysical log data available for the study area indicate various nonuniform flow conditions. Based on field evidence of nonuniform flow, six hypothetical carbonate aquifer systems were conceptualized. These conceptualized systems were designed to approximate anisotropic and heterogeneous aquifer behavior and to evaluate how incorporation of aquifer anisotropy and heterogeneity may affect the size, shape, and orientation of areas of contribution.

Although many hydrogeologic factors affect the estimation of contributing areas to well fields, this report focused primarily on the effects of aquifer heterogeneity and anisotropy on the size, shape, and orientation of the simulated areas. The method used to estimate contributing areas was a three-dimensional numerical flow model and particle tracking subroutine used as a postprocessor. MODFLOW and MODPATH numerical models were used to generate time-related areas of contribution for six carbonate aquifer system types. These include: an isotropic and homogeneous single-layer system; an anisotropic in a horizontal plane single-layer system; a discrete vertically fractured single-layer system; a multilayered system; a doubly porous single-layer system; and a vertically and horizontally interconnected heterogeneous system. The simulated aquifer anisotropy was 5:1 and was determined from TENSOR2D results. The simulated vertical discrete fracture network represents locations of photolineaments. The simulated enhanced flow zones were determined from borehole video and geophysical logs. The hypothetical carbonate aquifer systems were simulated for two prototype regions. The two regions, Central Swamp and Lake Terrace, were selected to be representative of the hydrologic diversity within the study area.

The simulated distributions of aquifer heterogeneity and anisotropy are highly conceptualized, but are based on plausible carbonate aquifer heterogeneities observed in west-central Florida that are typical of carbonate aquifers everywhere. This study indicates that the distribution and nature of aquifer heterogeneities will affect the size, shape, and orientation of areas of contribution in a karst carbonate aquifer system. The size of the 50-year time-related areas of contribution ranged from 8.2 to 39.1 square miles in the Central Swamp region. The size of the 50-year time-related areas of contribution ranged from 4.0 to 18.3 square miles in the Lake Terrace regions. The differences in size between the regions are primarily the results of variability in withdrawal rates, well distribution, and aquifer transmissivity. The simulated areas of contribution are 60 percent larger in the Central Swamp region where pumpage is more than double and transmissivity is about half that of the Lake Terrace region. Simulations showed that the size of areas of contribution is primarily affected by simulated withdrawal rates, effective porosity of the carbonate rock, and transmissivity. The shape and orientation of the simulated areas of contribution primarily result from aquifer anisotropy, well distribution, flow along solution-enhanced zones, and short-circuiting of flow through fracture networks. Flow velocities and particle path length respond to withdrawal rates, simulated effective porosity, short-circuiting of flow by fractures, and effective transmissivity.

Results of simulations incorporating aquifer heterogeneity indicate that oversimplification of the flow system may result in erroneous definition of flow fields. For example, aquifer anisotropy typical of many carbonate aquifers creates elliptical flow fields. Circular protection zones do not adequately characterize the elliptical areas of contribution. Also, areas of contribution were larger when the carbonate aquifer system was simulated as a multilayered system with discrete flow zones. This type of carbonate aquifer system is observed in west-central Florida. Simulated areas of contribution are significantly influenced by the choice of effective porosity. However, accurate, quantitative values of effective porosity in a carbonate aquifer system like the Upper Floridan aquifer are extremely difficult to measure.

Although the effective porosity from core analyses can characterize the primary porosity of the Upper Floridan aquifer, fluid flow tends to be through solution features that make up only a small part of the total porosity. The inclusion of a vertical fracture network may or may not affect the delineation of areas of contribution. In the Lake Terrace region, the simulated fractures had little effect on the short term (50-year) area of contribution. In the Central Swamp region, the simulated fractures have a large effect, because the simulated flow field intersected these fractures. Flow in fractures is linear rather than radial and velocities increase. Areas of contribution are difficult to precisely determine where a high degree of aquifer anisotropy and heterogeneity exists. The anisotropies and heterogeneities were simulated to show their possible effects on the size, shape, and orientation of areas of contribution.

SELECTED REFERENCES

Barenblatt, G.I., Zheltov, I.P., and Kochina, N., 1960, Basic concepts in the theory of seepage of homogeneous liquids in fissured rocks: Journal of Applied Mathematics and Mechanics, v. 24, no. 5, p. 1286-1303.

Bates, R.L., and Jackson, J.A., eds, 1984, Dictionary of geologic terms (3d ed.): American Geological Institute: Garden City, N.Y., Anchor Press, 571 p.

Beck, B.F., and others, 1984, Field guide to some illustrative examples of karst hydrogeology in central and northern Florida: A field trip guidebook produced in conjunction with the first multidisciplinary conference on sinkholes: Orlando, Florida Sinkhole Research Institute, College of Engineering, University of Central Florida, 43 p.

Bengtsson, T., 1987, Development and documentation of a transient, quasi-three-dimensional finite-difference model of the tri-county well-field area: Brooksville, Southwest Florida Water Management District, 95 p.

Benson, R.C., and Scaife, J., 1987, Assessment of flow in fractured rock and karst environments: Proceedings, Second Multidisciplinary Conference on Sinkholes and the Environmental Impacts of Karst, Orlando, Fla., p. 237-245.

Blanchet, P.H., 1957, Development of fracture analysis as an exploration method: American Association of Petroleum Geologists Bulletin, v. 41, p. 1748-1759.

Blandford, N.T., and Huyakorn, P.S., 1990, A modular semi-analytical model for the delineation of wellhead protection areas: U.S. Environmental Protection Agency.

Boulton, N.S., and Streltsova, T.D., 1977a, Unsteady flow to a pumped well in a fissured water-bearing formation: Journal of Hydrology, v. 34, p. 257-270.

——— 1977b, Unsteady flow to a pumped well in a two-layered water-bearing formation: Journal of Hydrology, v. 35, p. 245-256.

Bush, P.W., 1978, Hydrologic evaluation of part of central Volusia County, Florida: U.S. Geological Survey Water-Resources Investigations 78-89, 50 p.

CH2M Hill, Inc., 1990a, Drilling and testing of well no. 1-D, Northwest Hillsborough Water Resources Assessment Project: Brooksville, Southwest Florida Water Management District.

——— 1990b, Drilling and testing of wells 2-D, 3-D, and 4-D, Northwest Hillsborough Water Resources Assessment Project: Brooksville, Southwest Florida Water Management District.

Conaway, J., 1987, Temperature logging as an aid to understanding groundwater flow in boreholes: Proceedings, Second MGLS Symposium, p. 51-57.

Culbreath, M.A., 1988, Geophysical investigation of lineaments in south Florida: Master's thesis, Department of Geology, University of South Florida, Tampa, 97 p.

Eagon, H.B., Jr., and Johe, D.E., 1972, Practical solutions for pumping tests in carbonate rock aquifers: Ground Water, v. 10, no. 4, p. 6-13.

Endo, H.K., Long, J.C.S., Wilson, C.R., and Witherspoon, P.A., 1984, A model for investigating mechanical transport in fracture networks: Water Resources Research, v. 20, no. 10, p. 1390-1400.

Fretwell, J.D., 1988, Water resources and effects of groundwater development in Pasco County, Florida: U.S. Geological Survey Water-Resources Investigations Report 87-4188, 209 p.

Gerhart, J.M., 1984, A model for regional ground-water flow in secondary-permeability terrane: Ground Water, v. 22, no. 2, p. 168-175.

Gilboy, A.E., 1987, Ground penetrating radar: Its application in the identification of subsurface solution features—A case study in west-central Florida: Proceedings, Second Multidisciplinary Conference on Sinkholes and the Environmental Impacts of Karst, Orlando, Fla., p. 197-203.

Gordon, M.J., 1986, Dependence of effective porosity on fracture continuity in fractured media: Ground Water, v. 24, no. 4, p. 446-452.

Gringarten, A.C., 1982, Flow-test evaluation of fractured reservoirs: Geological Society of America, Special Paper 189, p. 237-263.

Harbaugh, A.W., 1990, A computer program for calculating subregional water budgets using results from the U.S. Geological Survey Modular Three-Dimensional Finite-Difference Ground-Water Flow Model: U.S. Geological Survey Open-File Report 90-392, 46 p.

Hickey, J.J., 1977, Hydrogeologic data for the McKay Creek subsurface waste-injection test site, Pinellas County, Florida: U.S. Geological Survey Open-File Report 77-802, 94 p.

——— 1984, Field testing the hypothesis of Darcian flow through a carbonate aquifer: Ground Water, v. 22, no. 5, p. 544-547.

Hushey, W.L., and Crawford, P.B., 1967, Performance of petroleum reservoirs containing vertical fractures in the matrix: Society of Petroleum Engineers Journal, v. 19, no. 6, p. 221.

Hutchinson, C.B., 1984, Hydrology of well-field areas near Tampa, Florida, phase 2—Development and documentation of a quasi-three-dimensional finite-difference model for simulation of steady-stage ground-water flow: U.S. Geological survey Water-Resources Investigations Report 84-4002, 174 p.

Hutchinson, C.B., 1985, Hydrogeology of the Cross Bar Ranch well-field area and projected impact of pumping, Pasco County, Florida: U.S. Geological Survey Water-Resources Investigations Report 85-4001, 89 p.

——— 1990, Analysis of ground-water flow in the A-sand aquifer at Paramaribo, Surinam, South America: U.S. Geological Survey Water-Resources Investigations Report 90-4036, 65 p.

Jenkins, D.N., and Prentice, J.K., 1982, Theory for aquifer test analysis in fractured rocks under linear (non-radial) flow conditions: Ground Water, v. 20, no. 1, p. 12-21.

Jordan, R.H., 1958, An interpretation of Floridan karst: Journal of Geology, p. 261-270.

Joyner, B.F., and Gerhart, J.M., 1980, Hydrologic monitoring program in Eldridge-Wilde and East Lake Road well-field areas, Pinellas and Hillsborough Counties, Florida, 1977 Water Year: U.S. Geological Survey Open-File Report 80-345, 34 p.

Keys, W.S., 1988, Borehole geophysics applied to groundwater investigations: U.S. Geological Survey Open-File Report 87-539, p. 258-275.

Kiraly, L., 1971, Ground-water flow in heterogeneous, anisotropic, fractured media: Journal of Hydrology, v. 12, no. 3, p. 225.

Kruseman, G.P., and de Ridder, N.A., 1991, Analysis and evaluation of pumping test data: International Institute for Land Reclamation and Improvement Publication 47, 377 p.

LaMoreaux, P.E., Wilson, B.M., and Memon, B.A., eds., 1984, Guide to the hydrology of carbonate rocks: Studies and Reports in Hydrology, no. 41, Paris, UNESCO, 345 p.

Lane, E., 1986, Karst in Florida: Florida Geological Survey Special Publication 29, 100 p.

Lattman, L.H., and Parizek, R.R., 1964, Relationship between fractures traces and the occurrence of groundwater in carbonate rocks: Journal of Hydrology, v. 2, p. 73-91.

LeGrand, H.E., and Stringfield, V.T., 1971, Development and distribution of permeability in carbonate aquifers: Water Resources Research, v. 7, no. 5, p. 1284-1294.

Lohman, S.W., and others, 1972, Definitions of selected ground-water terms—Revisions and conceptual refinements: U.S. Geological Survey Water-Supply Paper 1988, 21 p.

Long, J.C., Remer, J.S., Wilson, C.R., and Witherspoon, P.A., 1982, Porous media equivalents for networks of discontinuous fractures: Water Resources Research, v. 18, no. 3, p. 645-658.

Maini, Y.N.T., 1971, Insitu hydraulic parameters in jointed rock-fluid measurement and interpretation: Ph.D. dissertation, Imperial College, London.

Marine, I.W., 1980, Determination of the location and connectivity of fractures in metamorphic rock with in-hole tracers: Ground Water, v. 18, no. 3, p. 252-261.

Maslia, M.L., and Randolph, R.B., 1986, Methods and computer program documentations for determining anisotropic transmissivity tensor components of two-dimensional ground-water flow: U.S. Geological Survey Open-File Report 86-227, 64 p.

McDonald, M.G., and Harbaugh, A.W., 1984, A modular three-dimensional, finite-difference ground-water flow model: U.S. Geological Survey Open-File Report 83-875, 528 p.

Miller, J.A., 1986, Hydrogeologic framework of the Floridan aquifer system in Florida and parts of Georgia, Alabama, and South Carolina: U.S. Geological Survey Professional Paper 1403-B, 91 p.

Mills, L.R., 1980, Hydrologic monitoring program in Eldridge-Wilde and East Lake Road well-field areas, Pinellas and Hillsborough Counties, Florida, 1978: U.S. Geological Survey Open-File Report 80-1195, 23 p.

Moench, A.F., 1984, Double-porosity models for a fissured groundwater reservoir with fracture skin: Water Resources Research, v. 20, no. 7, p. 831-846.

Moore, D.L., and Stewart, M.T., 1983, Geophysical signatures of fracture traces in a karst aquifer (Florida, U.S.A.): Journal of Hydrology, v. 61, p. 325-340.

Morrissey, D.J., 1989, Estimation of the recharge are contributing water to a pumped well in a glacial-drift river-valley aquifer: U.S. Geological Survey Water-Supply Paper 2338, 41 p.

Paillet, F.L., Hess, A.E., Cheng, C.H., and Hardin, E., 1987, Characterization of fracture permeability with high-resolution vertical flow measurements during borehole pumping: Ground Water, v. 25, no. 1, p. 28-40.

Palmer, A.N., 1984, Geomorphic interpretation of karst features, *in* LaFleur, R.G., ed., Groundwater as a geomorphic agent: London, Allen and Unwin, p. 173-209.

Papadopulos, I.S., 1965, Nonsteady flow to a well in an infinite anisotropic aquifer: International Association of Hydrology, Roches Fissures, Proceedings Dubrovinid Symposium, p. 21-31.

Parizek, R.R., 1976, On the nature and significance of fracture traces and lineaments in carbonate and other terranes: *in* Proceedings, Karst Hydrology and Water Resources: Ft. Collins, Colo., v. 1, p. 3.1-3.108.

Parsons, R.W., 1966, Permeability of idealized fractures rock: Society of Petroleum Engineers Journal, v. 6, no. 2, p. 126.

Pollock, D.W., 1988, Semianalytical computation of path lines for finite-difference models: Ground Water, v. 26, no. 6, p. 743-750.

——— 1989, Documentation of computer programs to compute and display pathlines using results from the U.S. Geological Survey modular three-dimensional finite-difference ground-water flow model: U.S. Geological Survey Open-File Report 89-381, 188 p.

Randazzo, A.F., 1989, Model of porosity development in a coastal carbonate aquifer system: Gainesville, University of Florida, Water Resources Research Center Publication no. 109.

Robinson, J.L., 1995, Hydrogeology and results of tracer tests at the Old Tampa well field in Hillsborough County, with implications for wellhead-protection strategies in west-central Florida: U.S. Geological Survey Water-Resources Investigations Report 93-4171.

Ryan, K.W., 1989, Two-dimensional numerical simulation of the relationship between sinkhole lakes and ground water along the central Florida ridge, *in* Proceedings, Third Multidisciplinary Conference on Sinkholes: St. Petersburg Beach, Fla., p. 33-45.

Ryder, P.D., 1978, Model evaluation of the Cypress Creek well field in west-central Florida: U.S. Geological Survey Water-Resources Investigations 78-79, 68 p.

——— 1982, Digital model of predevelopment flow in the Tertiary limestone (Floridan) aquifer system in west-central Florida: U.S. Geological Survey Water-Resources Investigations 81-54, 61 p.

Ryder, P.D., Johnson, D.M., and Gerhart, J.M., 1980, Model evaluation of the hydrogeology of the Morris Bridge well field and vicinity in west-central Florida: U.S. Geological Survey Water-Resources Investigations 80-29, 100 p.

Safko, P.S., and Hickey, J.J., 1992, A preliminary approach to the use of borehole data, including television surveys, for characterizing secondary porosity of carbonate rocks in the Floridan aquifer system: U.S. Geological Survey Water-Resources Investigations Report 91-4168, 70 p.

Sagar, B., and Runchal, A., 1992, Permeability of fractured rock: Effect of fracture size and data uncertainties: Water Resources Research, v. 18, no. 2, p. 266-274.

Schmidt, W., and Scott, T.M., 1984, Florida karst—its relationship to geologic structure and stratigraphy, *in* Proceedings, First Multidisciplinary Conference on Sinkholes: Orlando, Fla., p. 11-16.

Schmoker, J.W., and Halley, R.B., 1982, Carbonate porosity versus depth: A predictable relation for south Florida: American Association of Petroleum Geologists Bulletin, v. 66, no. 12, p. 2561-2570.

Schreuder and Davis, Inc., 1991, Pemberton Creek site well construction and aquifer testing: Consultant's report prepared for and in the files of West Coast Regional Water Supply Authority.

Scott, T.M., 1988, The lithostratigraphy of the Hawthorn Group (Miocene of Florida: Florida Geological Survey Bulletin 59, 148 p.

Sen, Z., 1986, Aquifer test analysis in fractured rocks with linear flow patterns: Ground Water, v. 24, no. 1, p. 72-78.

Shapiro, A.M., 1989, Interpretation of oscillatory water levels during aquifer tests in fracture rock: Water Resources Research, v. 25, no. 10, p. 2129-2137.

Sinclair, W.C., and Stewart, J.W., 1985, Sinkhole type, development, and distribution: Florida Bureau of Geology Map Series 110, 1 sheet.

Sinclair, W.C., Stewart, J.W., Knutilla, R.L., Gilboy, A.E., and Miller, R.L., 1985, Type, features, and occurrence of sinkholes in the karst of west-central Florida: U.S. Geological Survey Water-Resources Investigations Report 85-4126, 81 p.

Smart, C.C., 1988, Artificial tracer techniques for the determination of the structure of conduit aquifers: Ground Water, v. 26, no. 4, p. 445-453.

Smith, D.I., Atkinson, T.C., and Drew, D.P., 1976, The hydrology of limestone terranes, *in* Ford, T.D., and Cullingford, C.H.D., eds., The science of speleology: chap. 6, p. 179-212.

Smith, E.D., and Vaughan, N.D., 1985, Aquifer test analysis in nonradial flow regimes: A case study: Ground Water, v. 23, no. 2, p. 167-175.

Snow, D.T., 1965, A parallel plate model of fractured permeable media: Ph.D. dissertation, University of California, Berkeley.

Southeastern Geological Society, 1986, Hydrogeological units of Florida: Florida Geological Survey Special Publication no. 28, 8 p.

Southwest Florida Water Management District, 1988, Ground-water resource availability inventory, Hillsborough County, Florida: Brooksville, Resource Management and Planning Departments, 203 p.

Stewart, J.W., 1968, Hydrologic effects of pumping from the Floridan aquifer in northwest Hillsborough, northeast Pinellas, and southwest Pasco Counties, Florida: U.S. Geological Survey Open-File Report 68-005, 241 p.

——— 1987, Potential recharge and ground-water contamination from selected sinkholes in west-central Florida, *in* Proceedings, Second Multidisciplinary Conference on Sinkholes and Environmental Impacts of Karst: Orlando, Fla., p. 247-252.

Stewart, M.T., and Wood, J., 1984, Geophysical characteristics of fracture zones in the carbonate Floridan aquifer, *in* Proceedings, Conference sponsored by the Florida Sinkhole Institute, University of Central Florida, College of Engineering: Orlando, p. 225-229.

Streltsova, T.D., 1975, Hydrodynamics of groundwater flow in a fractured formation: Water Resources Research, v. 12, no. 3, p. 405-414.

Stringfield, V.T., 1966, Artesian water in tertiary limestone in southeastern states: U.S. Geological Survey Professional Paper 517, 226 p.

Taylor, M.D., Riordan, P.J., and Harley, B.M., 1989, Two methods for representing sinkholes in a three-dimensional ground water flow model, *in* Proceedings, Third Multidisciplinary Conference on Sinkholes: St. Petersburg Beach, Fla., p. 53-58.

Thrailkill, J., 1968, Chemical and hydrologic factors in the excavation of limestone caves: Geological Society of America Bulletin, v. 79, p. 19-46.

———1986, Models and methods for shallow conduit-flow carbonate aquifers: Proceedings, Environmental Problems in Karst Terranes and Their Solutions, Bowling Green, Ky., p. 17-31.

Tibbals, C.H., Anderson, Warren, and Laughlin, C.P., 1980, Ground-water hydrology of the Dade City area, Pasco County, with emphasis on the hydrologic effects of pumping from the Floridan aquifer: U.S. Geological Survey Water-Resources Investigations 80-33, 64 p.

Upchurch, S.B., and Littlefield, J.R., Jr., 1987, Evaluation of data for sinkhole-development risk models, *in* Proceedings, Second Multidisciplinary Conference on Sinkholes and the Environmental Impacts of Karst: Orlando, Fla., p. 359-364.

U.S. Environmental Protection Agency, 1990, Wellhead protection area delineation methods for confined aquifer and unconfined, fractured aquifer settings: A training workshop: Washington, D.C., Office of Ground-Water Protection.

van der Kamp, G., 1976, Determining aquifer transmissivity by means of well response test: Water Resources Research, v. 12, p. 71-77.

Vecchioli, John, Hunn, J.D., and Aucott, W.R., 1989, Evaluation of methodology for delineation of protection zones around public-supply wells in west-central Florida: U.S. Geological Survey Water-Resources Investigations Report 88-4051, 36 p.

Veni, G., 1987, Fracture permeability: Implications on cave and sinkhole development and their environmental assessments, *in* Proceedings, Second Multidisciplinary Conference on Sinkholes and the Environmental Impacts of Karst: Orlando, Fla., p. 101-105.

Vernon, R.O., 1951, Geology of Citrus and Levy Counties, Florida: Florida Geological Survey Bulletin no. 33, p. 47-52.

Ward, D.S., Skipp, D.C., Griffin, D., and Barcelo, M.D., 1987, Dual-porosity and discrete fracture simulation of ground-water flow in west-central Florida, *in* Proceedings, Fourth International Conference on the Use of Models, Association of Ground Water Scientists and Engineers: Indianapolis, Indiana, p. 135-139.

Warren, J.E., and Root, P.J., 1963, The behavior of naturally fractured reservoirs: Society of Petroleum Engineering Journal, v. 3, p. 245-255.

White, W.B., 1969, Conceptual models for carbonate aquifers: Ground Water, v. 7, p. 15-21.

Williams, S.R., 1985, Relationship of ground water chemistry to photolineaments in a karst aquifer: Master's thesis, University of South Florida, Tampa, 137 p.

Wilson, W.E., and Gerhart, J.M., 1980, Simulated effects of ground-water development on potentiometric surface of the Florida aquifer, west-central Florida: U.S. Geological Survey Water-Resources Investigations Report 79-1271, 119 p.

Wolansky, R.M., and Corral, M.A., Jr., 1985, Aquifer tests in west-central Florida, 1952-76: U.S. Geological Survey Water-Resources Investigations Report 84-4044, 127 p.

Wood, J.H., and Stewart, M.T., 1985, The geophysical and geologic characteristics of fracture zones in the carbonate Floridan aquifer: Gainesville, University of Florida, Florida Water Resources Research Center publication no. 88.

APPENDIX

Boundary Fluxes Calculated by Using the ZONEBUDGET Computer Program for the Central Swamp and Lake Terrace Regions

Appendix. Boundary fluxes calculated using ZONEBUDGET computer program for the Central Swamp and Lake Terrace regions

Central Swamp			Lake Terrace		
Case Number	**Boundary Designation**	**Inflow (percent)**	**Case Number**	**Boundary Designation**	**Inflow (percent)**
	Water Table	74.7		Water Table	58.0
	1	7.0		1	11.0
1	2	6.6	1	2	8.0
	3	5.5		3	11.0
	4	6.2		4	12.0
	Water Table	63.8		Water Table	48.1
	1	18.5		1	24.0
2a	2	0.9	2a	2	0.9
	3	16.0		3	26.0
	4	6.2		4	1.0
	Water Table	63.4		Water Table	48.0
	1	1.0		1	2.0
2b	2	18.0	2b	2	21.0
	3	0.6		3	2.0
	4	17.0		4	27.0
	Water Table	81.0		Water Table	66.0
	1	10.0		1	10.0
3a	2	1.0	3a	2	2.0
	3	0.0		3	10.0
	4	8.0		4	12.0
	Water Table	69.3		Water Table	56.0
	1	6.5		1	11.0
3b	2	9.2	3b	2	9.0
	3	6.8		3	12.0
	4	8.2		4	12.0
	Water Table	63.2		Water Table	55.0
	1	6.5		1	10.0
3c	2	11.5	3c	2	11.0
	3	7.0		3	12.0
	4	11.8		4	12.0
	Water Table	72.5		Water Table	37.8
	1	7.5		1	14.8
4a	2	6.8	4a	2	12.6
	3	5.6		3	16.9
	4	6.8		4	17.9
	Water Table	74.4		Water Table	39.8
	1	6.6		1	14.8
4b	2	6.4	4b	2	11.6
	3	6.2		3	15.9
	4	6.4		4	17.4
	Water Table	57.0		Water Table	38.0
	1	12.0		1	16.0
5c	2	11.0	5c	2	12.0
	3	10.0		3	17.0
	4	10.0		4	17.0
	Water Table	74.5		Water Table	38.0
	1	6.6		1	14.8
6	2	6.3	6b	2	11.6
	3	6.2		3	15.9
	4	6.4		4	17.9

SELECTED SERIES OF U.S. GEOLOGICAL SURVEY PUBLICATIONS

Periodicals

Earthquakes & Volcanoes (issued bimonthly).
Preliminary Determination of Epicenters (issued monthly).

Technical Books and Reports

Professional Papers are mainly comprehensive scientific reports of wide and lasting interest and importance to professional scientists and engineers. Included are reports on the results of resource studies and of topographic, hydrologic, and geologic investigations. They also include collections of related papers addressing different aspects of a single scientific topic.

Bulletins contain significant data and interpretations that are of lasting scientific interest but are generally more limited in scope or geographic coverage than Professional Papers. They include the results of resource studies and of geologic and topographic investigations, as well as collections of short papers related to a specific topic.

Water-Supply Papers are comprehensive reports that present significant interpretive results of hydrologic investigations of wide interest to professional geologists, hydrologists, and engineers. The series covers investigations in all phases of hydrology, including hydrogeology, availability of water, quality of water, and use of water.

Circulars present administrative information or important scientific information of wide popular interest in a format designed for distribution at no cost to the public. Information is usually of short-term interest.

Water-Resources Investigations Reports are papers of an interpretive nature made available to the public outside the formal USGS publications series. Copies are reproduced on request unlike formal USGS publications, and they are also available for public inspection at depositories indicated in USGS catalogs.

Open-File Reports include unpublished manuscript reports, maps, and other material that are made available for public consultation at depositories. They are a nonpermanent form of publication that may be cited in other publications as sources of information.

Maps

Geologic Quadrangle Maps are multicolor geologic maps on topographic bases in 7.5- or 15-minute quadrangle formats (scales mainly 1:24,000 or 1:62,500) showing bedrock, surficial, or engineering geology. Maps generally include brief texts; some maps include structure and columnar sections only.

Geophysical Investigations Maps are on topographic or planimetric bases at various scales; they show results of surveys using geophysical techniques, such as gravity, magnetic, seismic, or radioactivity, which reflect subsurface structures that are of economic or geologic significance. Many maps include correlations with the geology.

Miscellaneous Investigations Series Maps are on planimetric or topographic bases of regular and irregular areas at various scales; they present a wide variety of format and subject matter. The series also includes 7.5-minute quadrangle photogeologic maps on planimetric bases that show geology as interpreted from aerial photographs. Series also includes maps of Mars and the Moon.

Coal Investigations Maps are geologic maps on topographic or planimetric bases at various scales showing bedrock or surficial geology, stratigraphy, and structural relations in certain coal-resource areas.

Oil and Gas Investigations Charts show stratigraphic information for certain oil and gas fields and other areas having petroleum potential.

Miscellaneous Field Studies Maps are multicolor or black-and-white maps on topographic or planimetric bases for quadrangle or irregular areas at various scales. Pre-1971 maps show bedrock geology in relation to specific mining or mineral-deposit problems; post-1971 maps are primarily black-and-white maps on various subjects such as environmental studies or wilderness mineral investigations.

Hydrologic Investigations Atlases are multicolored or black-and-white maps on topographic or planimetric bases presenting a wide range of geohydrologic data of both regular and irregular areas; principal scale is 1:24,000, and regional studies are at 1:250,000 scale or smaller.

Catalogs

Permanent catalogs, as well as some others, giving comprehensive listings of U.S. Geological Survey publications are available under the conditions indicated below from the U.S. Geological Survey, Information Services, Box 25286, Federal Center, Denver, CO 80225. (See latest Price and Availability List.)

"Publications of the Geological Survey, 1879–1961" may be purchased by mail and over the counter in paperback book form and as a set of microfiche.

"Publications of the Geological Survey, 1962–1970" may be purchased by mail and over the counter in paperback book form and as a set of microfiche.

"Publications of the U.S. Geological Survey, 1971–1981" may be purchased by mail and over the counter in paperback book form (two volumes, publications listing and index) and as a set of microfiche.

Supplements for 1982, 1983, 1984, 1985, 1986, and for subsequent years since the last permanent catalog may be purchased by mail and over the counter in paperback book form.

State catalogs, "List of U.S. Geological Survey Geologic and Water-Supply Reports and Maps For (State)," may be purchased by mail and over the counter in paperback booklet form only.

"Price and Availability List of U.S. Geological Survey Publications," issued annually, is available free of charge in paperback booklet form only.

Selected copies of a monthly catalog "New Publications of the U.S. Geological Survey" are available free of charge by mail or may be obtained over the counter in paperback booklet form only. Those wishing a free subscription to the monthly catalog "New Publications of the U.S. Geological Survey" should write to the U.S. Geological Survey, 582 National Center, Reston, VA 22092.

Note—Prices of Government publications listed in older catalogs, announcements, and publications may be incorrect. Therefore, the prices charged may differ from the prices in catalogs, announcements, and publications.

United States Environmental Protection Agency | Office of Research and Development | Office of Solid Waste and Emergency Response | EPA/540/S-97/504 September 1997

Ground Water Issue

Design Guidelines for Conventional Pump-and-Treat Systems

Robert M. Cohen[1], James W. Mercer[1], Robert M. Greenwald[1], and Milovan S. Beljin[2]

The RCRA/Superfund Ground-Water Forum is a group of scientists representing EPA's Regional Superfund Offices, committed to the identification and resolution of ground-water issues affecting the remediation of Superfund sites. Design of conventional ground-water extraction and injection (i.e., pump-and-treat) systems has been identified by the Forum as an issue of concern to decision makers. This issue paper focuses on design of conventional ground-water extraction and injection systems used in subsurface remediation.

For further information contact Steve Acree (405) 436-8609 or Randall Ross (405) 436-8611 at the Subsurface Remediation and Protection Division of the National Risk Management Research Laboratory, Ada, Oklahoma.

Introduction

Containment and cleanup of contaminated ground water are among the primary objectives of the CERCLA (Comprehensive Environmental Response, Compensation, and Liability Act; also known as Superfund) and RCRA (Resource Conservation and Recovery Act) remediation programs. Ground-water contamination problems are pervasive in both programs; over 85 percent of CERCLA National Priority List sites and a substantial portion of RCRA facilities have some degree of ground-water contamination (U.S. EPA, 1993a). A common approach to deal with contaminated ground water is to extract the contaminated water and treat it at the surface prior to discharge or reinjection as illustrated in Figure 1. This is referred to as conventional pump-and-treat (P&T) remediation.

Conventional pump-and-treat is an applicable component of many remedial systems. However, such a system will not be appropriate to achieve restoration in portions of many sites due to hydrogeologic and contaminant-related limitations such as those presented by significant accumulations of DNAPLs (denser-than-water nonaqueous phase liquids) trapped below the water table. Such limitations will directly impact the effectiveness of P&T at many sites and the selection of remedial actions. Detailed discussion of the contaminant transport and fate processes that limit the potential for subsurface restoration using P&T and their characterization is beyond the scope of this document.

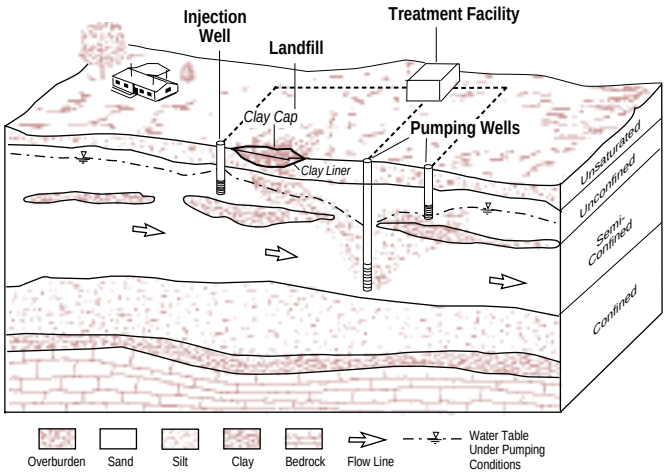

Figure 1. Example of a P&T system (after Mercer et al., 1990).

[1] *GeoTrans, Inc., Sterling, VA*
[2] *National Risk Management Research Laboratory, Office of Research and Development, U.S. EPA, Ada, OK*

Superfund Technology Support Center for Ground Water

National Risk Management Research Laboratory
Subsurface Protection and Remediation Division
Robert S. Kerr Environmental Research Center
Ada, Oklahoma

Technology Innovation Office
Office of Solid Waste and Emergency Response, US EPA, Washington, DC

Walter W. Kovalick, Jr., Ph.D.
Director

Inadequate design and implementation also may severely impact the performance of a P&T system. Examples of design inadequacies include too few recovery wells, insufficient pumping rates, deficient well locations or completion intervals, and failure to account for complex chemistry of contaminants. Similarly, poor system operation, exemplified by excessive downtime or failure to manipulate pumping schemes to limit ground-water stagnation, will restrict P&T effectiveness. This document provides guidance on designing conventional ground-water P&T systems. Chemical enhancements to P&T and immiscible contaminant recovery methods are addressed elsewhere (e.g., American Petroleum Institute, 1989, 1992; Palmer and Fish, 1992; U.S. EPA, 1992a, 1995; Grubb and Sitar, 1994; NRC, 1994).

P&T Remediation Strategies

In order to determine an appropriate strategy to manage contaminated ground water, it is necessary first to evaluate site conditions and define remediation goals. Historically, the goal of ground-water remediation has been to protect human health and the environment and to restore ground water to beneficial uses where practicable. For ground water that is or may be used for drinking, clean-up goals under CERCLA and RCRA generally are set at drinking water standards such as Maximum Contaminant Levels (MCLs) established under the Safe Drinking Water Act. Other clean-up requirements may be appropriate for ground water that is not used for drinking.

It has long been recognized that chemical transport from contaminant source/release areas, such as abandoned landfills and leaking tanks, contaminates ground water and other media in downgradient areas (e.g., OTA, 1984). As such, a common strategy for managing contaminated ground water has been to remove or contain contaminant sources (e.g., by excavation, construction of physical barriers, and/or pumping) and to address downgradient contamination using P&T technology.

Strategies for managing ground-water contamination (Figure 2) using P&T technology include: (1) hydraulic/physical containment, (2) ground-water quality restoration, and (3) mixed objective strategies. Several innovative technologies, such as air sparging, engineered bioremediation, and permeable treatment walls, can be used in conjunction with P&T, or alone, to address these ground-water remediation objectives. At some sites, natural attenuation processes may limit the need for P&T. The management strategy selected depends on site-specific hydrogeologic and contaminant conditions, and remediation goals.

Hydraulic Containment

P&T systems are frequently designed to hydraulically control the movement of contaminated ground water in order to prevent continued expansion of the contamination zone. At sites where the contaminant source cannot be removed (e.g., a landfill or bedrock with DNAPLs), hydraulic containment is an option to achieve source control. Hydraulic containment of dissolved contaminants by pumping ground water from wells or drains has been demonstrated at numerous sites. The concept is illustrated in Figure 3. Properly controlled fluid injection using wells, drains, or surface application (e.g., along the downgradient periphery of the proposed containment area) and physical containment options (e.g., subsurface barrier walls and surface covers to limit inflow) can enhance hydraulic containment

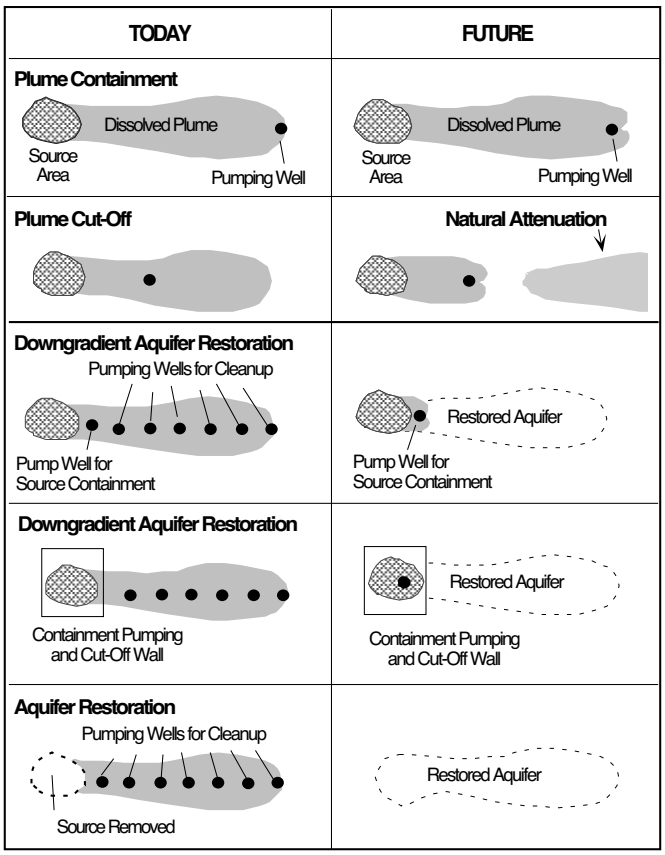

Figure 2. Several ground-water contamination management strategies using P&T technology (after NRC, 1994; Cherry et al., 1992).

systems by reducing the pumping rate required to maintain containment. In many cases, hydraulic containment systems are designed to provide long-term containment of contaminated ground water or source areas at the lowest cost by optimizing well, drain, surface cover, and/or cutoff wall locations and by minimizing pumping rates.

Cleanup/Restoration

For sites where the contaminant source has been removed or contained, it may be possible to clean up the dissolved plume. P&T technology designed for aquifer restoration generally combines hydraulic containment with more aggressive manipulation of ground water (i.e., higher pumping rates) to attain clean-up goals during a finite period. Ground-water cleanup is typically much more difficult to achieve than hydraulic containment. Hydrogeologic and contaminant conditions favorable to cleanup (e.g., degradable dissolved contaminants in uniform, permeable media) are summarized in Figure 4.

Mixed Objective Strategies

At many sites, P&T systems can be used to contain contaminant source areas and attempt restoration of downgradient dissolved plumes (Figure 2). A mixed P&T strategy is appropriate, therefore, at sites where different portions of the contaminated

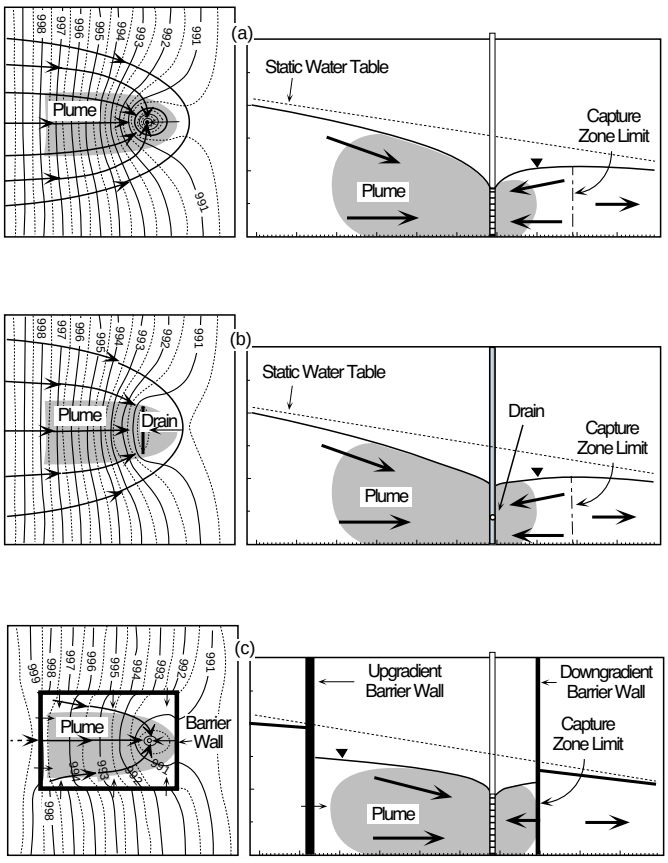

Figure 3. Examples of hydraulic containment in plan view and cross section using an extraction well (a), a drain (b), and a well within a barrier wall (c).

region are amenable to remediation using different methods. At sites contaminated with LNAPLs (lighter-than-water NAPLs), for example, a mixed remedial strategy may include: (1) vacuum-enhanced pumping to recover free product, affect hydraulic containment, and stimulate bioremediation in the LNAPL release area; and (2) restoring downgradient ground water via natural attenuation, P&T, and/or air sparging.

Characterizing Sites for P&T Design

The main goal of site characterization should be to obtain sufficient data to select and design a remedy (NRC, 1994). This is accomplished by investigating: (1) the nature, extent, and distribution of contaminants in source areas and downgradient plumes; (2) potential receptors and risks posed by contaminated ground water; and (3) hydrogeologic and contaminant properties that affect containment, restoration, and system design in different site areas. Categories of data used to formulate a site conceptual model for remedy evaluation are identified in Figure 5. The conceptual model is used to formulate remedial strategies such as restoration and/or containment.

Inadequate site characterization can lead to flawed P&T design and poor system performance. A complete understanding of a contamination site is unobtainable, however, due to subsurface complexities and investigation cost. Thus, characterization efforts must develop sufficient data to select and design an effective remedy while recognizing that significant uncertainties about subsurface conditions will persist.

Site characterization for remedial design is an extensive subject, key aspects of which are addressed briefly below. Additional information regarding procedures and strategies for investigating contamination sites is provided by U.S. EPA (1988a, 1991a, 1993b), Nielsen (1991), Cohen and Mercer (1993), Sara (1994), CCME (1994), and Boulding (1995).

Using a Phased and Integrated Approach

Due to slow contaminant transport and interphase transfer, many P&T systems will operate for decades to contain and clean up contaminated ground water. Data collected during investigation and remediation should be reviewed periodically to refine the site conceptual model and identify modifications that will improve P&T system performance. Thus, as depicted in Figure 6, a phased and integrated approach should be taken to site characterization and remediation. For example, given significant uncertainty regarding well locations and pumping rates needed to achieve remedial objectives, it may be prudent to initiate pumping at several locations and then determine system expansion requirements based on performance monitoring data. This phased approach to system installation may be more cost effective than grossly overdesigning the system to account for uncertainty in subsurface characterization at many sites.

During the initial phase of site investigation, prior studies and background information are reviewed to identify likely

CONTAMINANT AND HYDROGEOLOGIC CHARACTERISTICS	GENERALIZED RESTORATION DIFFICULTY SCALE — Increasing Difficulty →
SITE USE	
Nature of Release	Small volume, Short duration, Slug release → Large volume, Long duration, Continual
CONTAMINANT PROPERTIES	
Biotic/Abiotic Decay Potential	High → Low
Volatility	High → Low
Contaminant Sorption Potential	Low → High
CONTAMINANT DISTRIBUTION	
Contaminant Phase	Aqueous, Gaseous → LNAPL → DNAPL
Volume of Contaminated Media	Small → Large
Contaminant Depth	Shallow → Deep
GEOLOGIC CONDITIONS	
Stratigraphy	Simple → Complex
Unconsolidated Media Texture	Coarse-grained → Fine-grained
Degree of Heterogeneity	Low → High
GROUNDWATER FLOW PARAMETERS	
Hydraulic Conductivity	High (> 0.01 cm/s) → Low (< 0.0001 cm/s)
Temporal Variation	Little → High
Vertical Flow	Little → High downward

Figure 4. Generalized ground-water restoration difficulty scale (modified from U.S. EPA, 1993a).

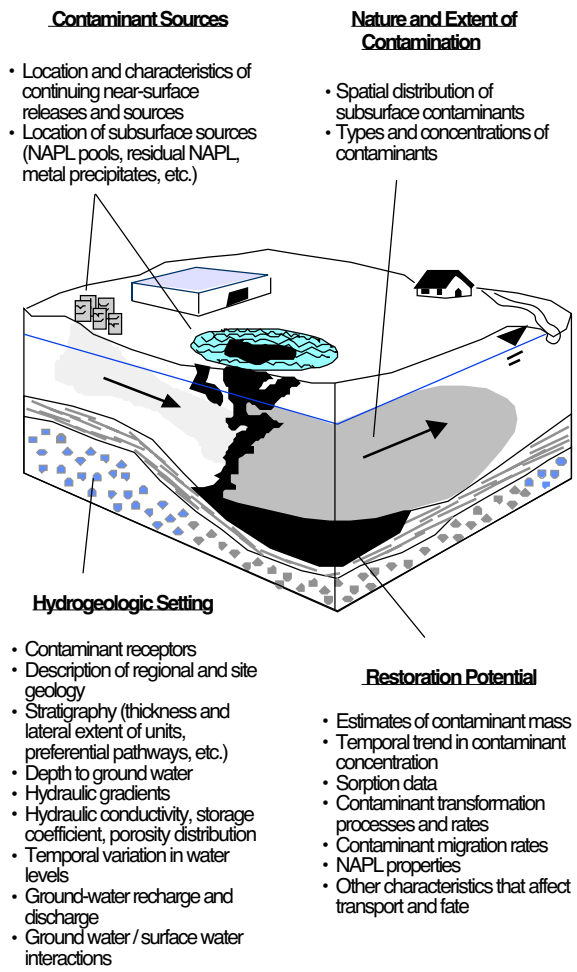

Figure 5. Types of data used to develop a site conceptual model for remedy assessment (modified from U.S. EPA, 1993a).

contaminant sources, transport pathways, and receptors. Based on this initial conceptualization, a data collection program is devised to better define the nature and extent of contamination and provide information (i.e., hydraulic conductivity distribution, aquifer boundary conditions, and initial hydraulic gradients) for remedy design. Contaminant source and downgradient dissolved plume areas should be delineated early during the characterization process to clarify site management strategies. P&T systems can often be designed to contain source and downgradient plume areas based on data acquired during the early and intermediate phases of investigation. Additional studies, including monitoring of actual P&T performance, are usually required, however, to assess the potential to restore ground-water quality in different site areas.

Mathematical models representing aspects of the site conceptual model should be used to evaluate alternative extraction/injection schemes, perform sensitivity analysis, and identify additional data needs. Integrating P&T operation and monitoring data can lead to model refinements and design enhancements.

P&T performance is typically assessed by measuring hydraulic heads and gradients, ground-water flow directions and rates, pumping rates, pumped water and treatment system effluent quality, and contaminant distributions in ground water and porous media. Guidance on methods for monitoring P&T performance is provided by Cohen et al. (1994). Careful examination of system performance, considering transient effects, is commonly warranted during the first months after start-up, and after subsequent major changes to P&T operation. Remediation, therefore, should be considered part of site characterization, yielding data that may lead to improved P&T system design and operation.

In recognition of inherent uncertainty and the potential for phased remediation, a reasonable degree of flexibility should be incorporated in P&T design to accommodate modifications. This may involve overdesign of certain system components (e.g., pipe or electric wire size), use of modular equipment (e.g., package treatment units), and strategic placement of junction boxes. Overdesign may allow system modifications such as

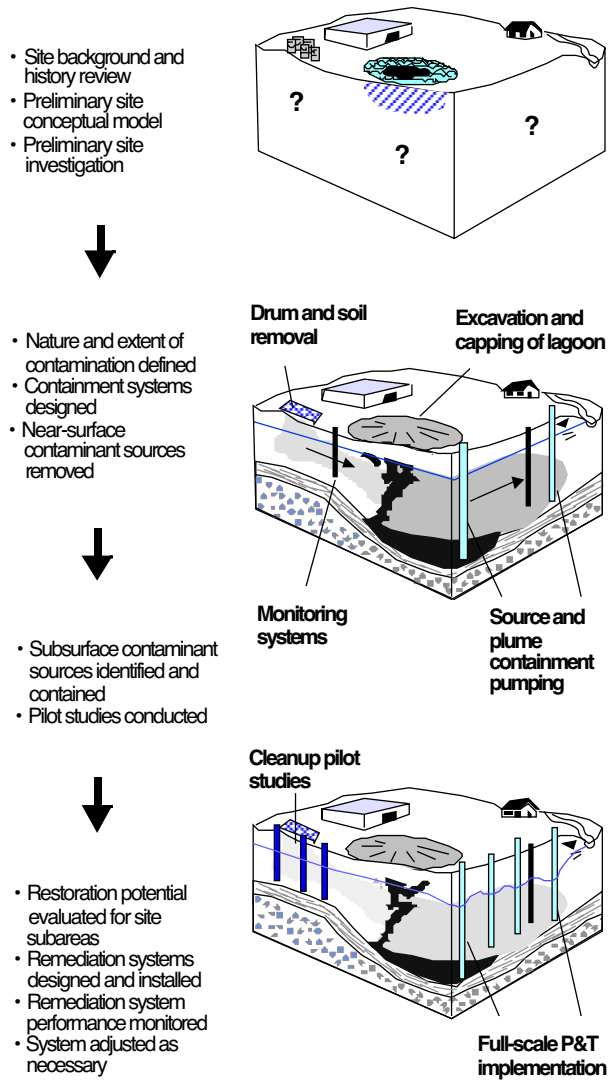

Figure 6. Iterative phases of site characterization and remediation (modified from U.S. EPA, 1993a; NRC, 1994).

incorporation of additional extraction wells or higher flow rates at relatively minimal expense. The degree of overdesign required as a contingency for uncertainties in subsurface conditions will be site specific and largely dependent on the level of site characterization performed prior to design. Estimates of potential ranges of required flowrates may be obtained at many sites during design-stage ground-water flow modeling.

Contaminant Characterization

Contaminant characterization is a key element of remedial evaluations. The nature, distribution, and extent of contamination will influence the selection of remedial actions and specific system designs. Contaminant characterization data needed to select and design a P&T system are listed in Figure 5. Important goals include: (1) delineating contaminant source areas and release characteristics; (2) defining the nature and extent (horizontal and vertical) of contamination; (3) characterizing contaminant transport pathways, processes, and rates; (4) estimating risks associated with contaminant transport; and (5) assessing aquifer restoration potential (see below). Contaminant characterization efforts generally involve document review, indirect and direct field characterization methods (e.g., soil, soil gas analysis and ground-water sampling), and data analysis.

Assessing Potential Limitations to P&T

Monitoring contaminant concentrations in ground water with time at P&T sites often reveals "tailing" and "rebound" phenomena. "Tailing" refers to the progressively slower rate of dissolved contaminant concentration decline observed with continued operation of a P&T system (Figures 7 and 8). The tailing contaminant concentration may exceed clean-up standards. Another problem is that dissolved contaminant concentrations may "rebound" if pumping is discontinued after temporarily attaining a clean-up standard (Figure 7).

If aquifer restoration is a potential remediation goal, then site characterization should investigate the physical and chemical phenomena that cause tailing and rebound. At many sites, most of the contaminant mass is not dissolved in ground water, but is present as NAPL, adsorbed species, and solids. Slow mass transfer of contaminants from these phases to ground water during P&T will cause tailing and prolong the clean-up effort. Physical causes of tailing include ground-water velocity and flowpath variations, and the slow diffusion of contaminants from low permeability zones during P&T operation. These phenomena are briefly discussed in Appendix A.

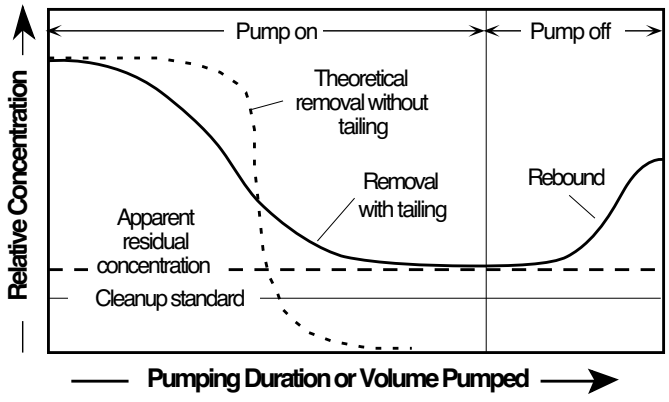

Figure 7. Concentration versus pumping duration or volume showing tailing and rebound effects (modified from Keely, 1989).

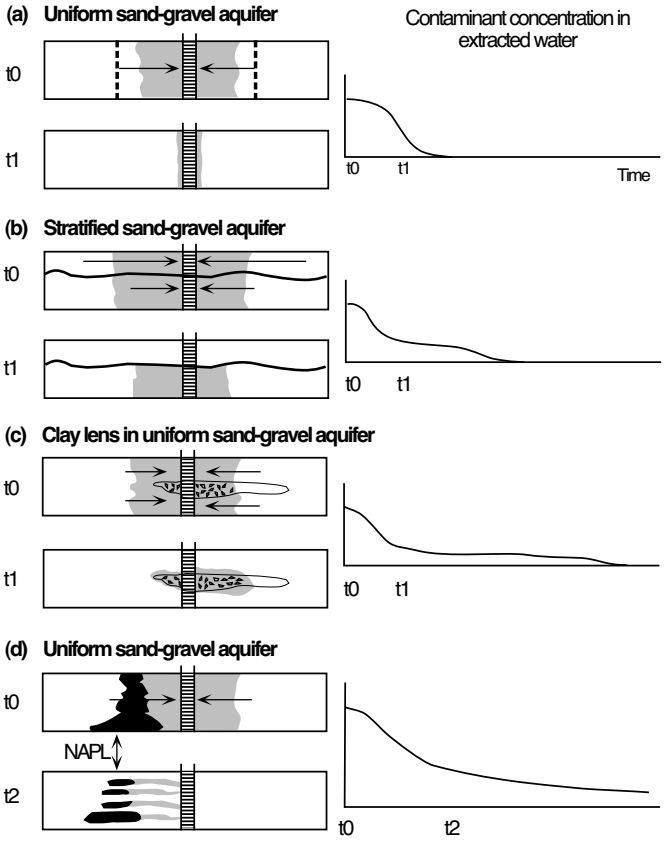

Figure 8. Hypothetical examples of contaminant removal using P&T (modified from Mackay and Cherry, 1989). Black indicates NAPL; stippling indicates contaminant in dissolved and sorbed phases (with uniform initial distribution); and arrows indicate relative ground-water velocity. Ground water is pumped from the well at the same rate for each case. The dotted lines in (a) represent the volume of water that would have to be pumped to flush slightly retarded contaminants from the uniform aquifer.

Tailing and rebound patterns associated with different physical and chemical processes are similar. Multiple processes (i.e., dissolution, diffusion, and desorption) will typically be active at a P&T site. Diagnosis of the cause of tailing and rebound, therefore, requires careful consideration of site conditions and usually cannot be made by examining concentration-versus-time data alone. Quantitative development of the conceptual model using analytical or numerical methods may help estimate the relative significance of different processes that cause tailing and rebound. Knowledge of the potential limitations at each site may allow more detailed analyses of the potential effectiveness of different P&T remediation strategies and different system configurations.

Hydrogeologic Characterization

Components of hydrogeologic investigation needed for P&T design are listed in Figure 5. Care must be taken to avoid exacerbating the contamination problem as a result of field work (e.g., inducing unwanted migration via drilling or pumping), or performing investigations not needed for risk or remedy assessment. Characterizing ground-water flow and contaminant transport is particularly challenging in heterogeneous media, especially where contaminants have migrated into fractured rock. Methods for characterizing fractured rock settings include drilling/coring, aquifer tests, packer tests, tracer tests, surface and borehole geophysical surveys, borehole flowmeter surveys, and air photograph fracture trace analysis (Sara, 1994). At the scale of many contaminated sites, complete characterization of fractured rock (and other heterogeneous media) may be economically infeasible (Schmelling and Ross, 1989), and not needed to design an effective P&T system (NRC, 1994). The appropriate characterization methods and level-of-effort must be determined on a site-specific basis.

Long-term aquifer tests and phased-system installations are often cost-effective means for acquiring field-scale hydrogeologic and remedial design data. Aquifer tests should be conducted to acquire field-scale measurements of hydrogeologic properties, such as formation transmissivity and storage coefficient, that are critical to extraction system design. Test results are used to: (1) determine well pumping rates and drawdowns; (2) assess well locations and pumping rates needed for full-scale operation; (3) evaluate the design of well and treatment system components; and (4) estimate capital and O&M costs. Recommended procedures for conducting aquifer tests are described by Osborne (1993) and others.

The number and duration of tests required to obtain sufficient data to design a P&T system depends on many factors, including plume size, the distribution of hydrogeologic units, their hydraulic properties, and hydrogeologic boundary conditions. In general, multiple tests are warranted at large and heterogeneous sites. Test design parameters (including specification of observation well locations, test duration, and pumping rate) can be assessed using well hydraulics solutions, ground-water flow models, and/or by conducting short-term step tests.

Observation wells should be located close enough to the pumping well to ensure adequate responses to pumping stress. Drawdowns will depend on site-specific hydrologic conditions that influence ground-water elevations during the test. Wells should also be located so that data may be used to evaluate heterogeneity and anisotropy, if warranted.

Although reasonable estimates of formation transmissivity can generally be obtained using data acquired during the first several hours of pumping (if observation wells are close to the pumping well), it may be advisable to extend aquifer tests to days or weeks to evaluate capture zones, boundary conditions, and ground-water treatability issues. Slug tests can also be used to augment aquifer test results. However, short-term aquifer and slug tests generally are not as reliable indicators of system performance as long-term aquifer tests.

Disposal options for aquifer test water are subject to site conditions and regulations but may include: discharge to a storm or sanitary sewer, discharge to the ground, discharge to surface water, reinjection to the subsurface, and transport to an off-site disposal facility. Regulatory agencies should be contacted to determine disposal requirements.

Ground-Water Treatability Studies

Treatability data needed for design of ground-water treatment systems generally should be acquired by conducting chemical analyses and treatability studies on contaminated ground water extracted during aquifer tests. Analysis of water samples obtained at different times during an aquifer test often will provide data regarding the initial range of contaminant concentrations in influent water to the treatment plant. Bench- and pilot-scale treatability studies are valuable means for determining the feasibility of candidate processes for treating contaminated ground water (U.S. EPA, 1989, 1994a). Laboratory bench-scale tests use small quantities of extracted ground water to provide preliminary data on various treatment processes, pretreatment requirements, and potential costs. During pilot-scale tests, skid-mounted or mobile pilot equipment is operated to study the effect of varying system parameters (e.g., flow rate) on treatment results and to identify potential problems, such as chemical precipitation of dissolved iron (Fe) and manganese (Mn) in an air stripper.

Air stripping and granular activated carbon (GAC) units may be used to remove organic compounds from ground water during aquifer tests; ion exchange/adsorption can be used to remove most metals (U.S. EPA, 1996). Air stripping is generally more cost-effective than GAC for treating volatile organic compounds when flow rates exceed 3 gpm (Long, 1993), but may require additional vapor phase treatment.

Potential for Fluid Injection

Artificial fluid injection/recharge is used to enhance hydraulic control and flushing of contamination zones. Treatment plant effluent or public supply water can be injected above or below the water table via wells, trenches, drains, or surface application (sprinkler, furrow, or basin infiltration). The applied water can be amended to stimulate bioremediation or to minimize well and formation clogging problems. Recharge is typically controlled by maintaining the water level in injection wells or drains or by pumping at specified rates. Regulatory agencies should be contacted to determine injection permit requirements. Potential problems with the use of injection include undesired horizontal or vertical contaminant migration due to the increased hydraulic gradients. Sites where injection is to be used should be carefully characterized and monitored to ensure that environmental problems are not exacerbated.

Aspects of site characterization critical to fluid injection design include determination of: (1) site stratigraphy and permeability distribution, (2) hydrogeologic boundary conditions, (3) possible injection rates and resulting hydraulic head and ground-water flow patterns, and (4) the potential for well and formation clogging due to injection.

Hydraulic parameters estimated from analysis of standard aquifer tests are often used to design injection systems. Constant-head, constant-rate, and stepped rate or head injection tests can also be conducted to evaluate hydraulic properties and injection potential using standard aquifer test procedures (Driscoll, 1986; Kruseman and deRidder, 1990). More discrete

techniques (e.g., packer tests, borehole flowmeter surveys) may be desirable to identify high permeability zones. Hydraulic heads and ground-water flow patterns resulting from injection can be examined and predicted using well or drain hydraulics equations and ground-water flow models. Such analysis can also be used to determine potential injection rates, durations, and monitoring locations for injection tests. In addition to helping estimate formation hydraulic properties, injection tests provide information on water compatibility and clogging issues that are critical to injection design.

The most common problem associated with fluid injection is permeability reduction due to clogging of screen openings. This causes a decline in injection rates. Clogging results from physical filtration of solids suspended in injected water, chemical precipitation of dissolved solids, and the excessive growth of microorganisms (also known as biofouling). Less frequently, well or formation damage results from air entrainment, clay swelling, and clay dispersion due to injection. In general, the injection capacity of a system is often overdesigned by a significant factor (e.g., 1.5 to 2) to account for loss of capacity under operating conditions due to such problems as permeability reduction and the temporary loss of capacity during well maintenance. The optimal degree of overdesign is site specific and will depend on such factors as the rate at which clogging occurs and the cost of maintenance.

The potential for well clogging and mitigative measures can be examined by analysis of the injected fluid and bench scale testing. In general, injection water should contain: (1) no suspended solids to minimize clogging; (2) little or no dissolved oxygen, nutrients, and microbes to minimize biofouling; and (3) low concentrations of constituents that are sensitive to changes in pH, redox, pressure, and temperature conditions (e.g., Fe and Mn) to minimize precipitation. Column permeameter tests can be conducted to examine changes in hydraulic conductivity resulting from injection. Due to the potential significance of many hydrogeologic, physical, and chemical factors, however, fluid injection is best evaluated by conducting extended injection tests during which injection rates and hydraulic heads are monitored carefully. Results of field tests help define formation hydraulic properties, potential injection rates, injection well spacings, mounding response, and clogging potential.

Dissolved or suspended solids may need to be removed from water by aeration, flocculation, and filtration prior to injection. Similarly, nutrients and/or dissolved oxygen may need to be removed to prevent biofouling. Water should be injected below the water table through a pipe to prevent its aeration in the well. Injecting warm water can also promote biofouling. Clogging problems can be minimized by overdesigning injection capacity (e.g., by installing more wells, longer screens, etc.) and implementing a regular well maintenance program.

Extraction and injection rate monitoring and well inspection, using a downhole video camera or other means, can help identify wells in need of treatment or replacement. Periodic rehabilitation of wells or drains (by surging, jetting, chlorination, or acid treatment) may be required to restore declining injection rates (Driscoll, 1986). Chemical incrustation can be addressed by acid treatment, backwashing, mechanical agitation (with a wire brush or surge block), and pumping. Strong oxidizing agents, such as a chlorine solution, can be used in conjunction with backwashing, mechanical agitation, and pumping to treat wells damaged by slime-producing bacteria. Acidification and chlorination, however, may interfere with interpretation of ground-water chemistry data. Fine particles can be removed (to some extent) using standard well development techniques. Experienced well drillers should be contacted for advice on rehabilitation methods. These potential problems need to be considered when projecting P&T costs. Significant maintenance may be required at many sites to retain desired injection capacity. More detailed discussions of the engineering aspects of water injection are provided by Pyne (1995).

Data Presentation

Complete discussion of methods for characterization and remedial design analyses and supporting data is beyond the scope of this document. In general, such information should be presented graphically and accompanied by supporting calculations and analyses. Tools for electronic storage, manipulation, analysis, and display of data and designs are generally available and often provide a convenient format for storage and access of this information (e.g., database, CAD, and/or GIS programs). Characterization data such as three-dimensional contaminant distribution are best presented on site maps and in representative cross sections. Hydraulic properties and hydraulic head data may also be presented in similar fashion. Pertinent features such as well locations (i.e., monitoring, production, injection), surface water bodies, potential source areas, and relevant structures should be included, as appropriate. Supporting data should be provided in tabular or spreadsheet form and accompany the maps and cross sections.

Capture Zone Analysis for P&T Design

P&T design is refined by performing field tests, modeling alternative injection/extraction schemes, and monitoring system performance. The first step in establishing design criteria, after characterizing pre-remedy ground-water flow patterns and contaminant distributions, is to determine the desired containment and/or restoration area (two-dimensional) and volume (three-dimensional). These should be clearly specified in the remedial design and monitoring plans. After defining the proposed containment area, a capture zone analysis is conducted to design the P&T system and a performance monitoring plan is developed based on the predicted flow field.

The capture zone of an extraction well or drain refers to that portion of the subsurface containing ground water that will ultimately discharge to the well or drain (Figures 3 and 9). It should be noticed that the capture zone of a well is not coincident with its drawdown zone of influence (ZOI) (Figure 9). The extent of the ZOI depends largely on transmissivity and pumping rate under steady-state conditions. However, the shape of the capture zone depends on the natural hydraulic gradient as well as pumping rate and transmissivity. Relatively high natural hydraulic gradients result in narrow capture zones that do not extend far in the downgradient direction. Therefore, some sidegradient and downgradient areas within the ZOI of a recovery well will be beyond its capture zone, and “rules-of-thumb” regarding overlapping drawdown zones should not be used to determine well spacings or pumping rates for P&T design.

In recent years, many mathematical models have been developed or applied to compute capture zones, ground-water pathlines, flushing rates, and associated travel times to extraction

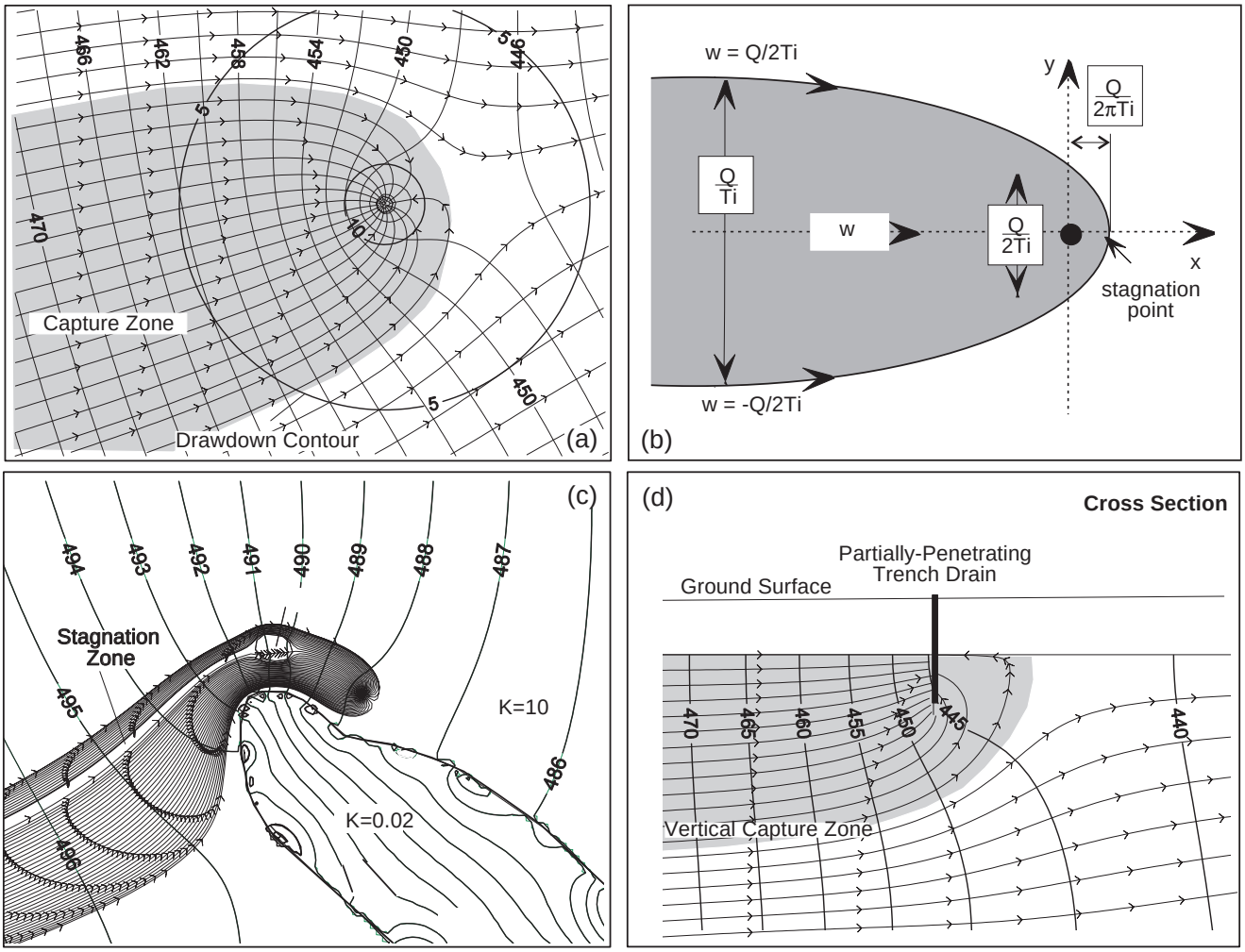

Figure 9. ***(a) Illustration of drawdown contours (i.e., zone of influence) and the capture zone of a single pumping well in a uniform medium. Equations for the dividing streamlines (w = Q/2Ti) that separate the capture zone of a single well from the rest of an isotropic, confined aquifer with a uniform regional hydraulic gradient are given in (b) where T = transmissivity, Q = pumping rate, and i = initial uniform hydraulic gradient. Simplified capture zone analysis methods may provide misleading results when applied to more complex problems, such as those dealing with heterogeneous media, as depicted in (c) where K = relative hydraulic conductivity, and three-dimensional flow (d).***

wells or drains (Javandel et al., 1984; Javandel and Tsang, 1986; Shafer, 1987a,b; Newsom and Wilson, 1988; Fitts, 1989,1994; Strack, 1989; Bonn and Rounds, 1990; Bair et al., 1991; Rumbaugh, 1991; Bair and Roadcap, 1992; Blandford et al., 1993; Gorelick et al., 1993; Pollock, 1994; Strack et al., 1994). These models provide insight into flow patterns generated by alternative P&T schemes and the selection of monitoring locations and frequency. Additionally, linear programming methods are being used to optimize P&T design (Ahlfeld and Sawyer, 1990; Gorelick et al., 1993; Hagemeyer et al., 1993) by specifying an objective function subject to various constraints (e.g., minimize pumping rates but maintain inward hydraulic gradients).

Model selection for P&T design analysis depends on the complexity of the site, available data, and the familiarity of the analyst with different codes. In general, the simplest tool applicable to site conditions and the desired degree of uncertainty should be used in design. However, conditions at many sites will be sufficiently complex that screening level characterizations and design tools will result in significant uncertainty. Regardless of the design tools which are used, capture zone analysis should also be conducted, and well locations and pumping rates optimized, by monitoring hydraulic heads and flow rates during aquifer tests and system operation. Conceptual model refinements gained by monitoring lead to enhanced P&T design and operation. In some cases, these refinements are incorporated in a mathematical model that is used to reevaluate and improve system design.

Capture Zone Analysis Tools

Many types of tools are available for capture zone analysis and system design (Table 1). Graphical methods are useful screening level design tools in many situations. Based on this approach, the simple graphical method shown in Figure 9 can be used to locate the stagnation point and dividing streamlines, and then

Table 1. P&T Design Tools (modified from van der Heijde and Elnawawy, 1993)

Method	*Example*	*Description*
Aquifer Tests and Pilot Testing		Controlled and monitored pilot tests are conducted to assist P&T design. Suggested operating procedures for aquifer tests and analytical methods are described by Osborne (1993) and many others. Test results should be used to improve P&T design modeling, where applicable.
Graphical - Capture Zone Type Curves	(Javandel and Tsang, 1986)	A simple graphical method can be used to determine minimum pumping rates and well spacings needed to maintain capture using 1, 2, or 3 pumping wells along a line perpendicular to the regional direction of ground-water flow in a confined aquifer.
Semi-analytical Ground-Water Flow and Pathline Models	WHPA (Blandford et al., 1993) WHAEM (Strack et al., 1994; Haitjema et al., 1994)	These models superposition analytic functions to simulate simple or complex aquifer conditions including wells, line sources, line sinks, recharge, and regional flow (Strack, 1989). Advantages include flexibility, ease of use, speed, accuracy, and no model grid. Generally limited to analysis of 2-D flow problems.
Numerical Models of Ground-Water Flow	MODFLOW (McDonald and Harbaugh, 1988)	Finite-difference (FD) and finite element (FE) ground-water flow models have been developed to simulate 2-D areal or cross-sectional and quasi- or fully- 3-D, steady or transient flow in anisotropic, heterogeneous, layered aquifer systems. These models can handle a variety of complex conditions allowing analysis of simple and complex ground-water flow problems, including P&T design analysis. Various pre- and post-processors are available. In general, more complex and detailed site characterization data are required for simulation of complex problems.
Pathline and Particle Tracking Post-Processors	MODPATH (Pollock, 1994) GPTRAC (Blandford et al., 1993)	These programs use particle tracking to calculate pathlines, capture zones, and travel times based on ground-water flow model output. Programs vary in assumptions and complexity of site conditions that may be simulated (e.g., 2-D or 3-D flow, heterogeneity, anisotropy).
Numerical Models of Ground-water Flow and Contaminant Transport	MT3D (Zheng, 1992) MOC (Konikow and Bredehoeft, 1989)	These models can be used to evaluate aquifer restoration issues such as changes in contaminant mass distribution with time due to P&T operation.
Optimization Models	MODMAN (Greenwald, 1993)	Optimization programs designed to link with ground-water flow models yield answers to questions such as: (1) where should pumping and injection wells be located, and (2) at what rate should water be extracted or injected at each well? The optimal solution maximizes or minimizes a user-defined objective function and satisfies all user-defined constraints. A typical objective may be to maximize the total pumping rate from all wells, while constraints might include upper and lower limits on heads, gradients, or pumping rates. A variety of objectives and constraints are available to the user, allowing many P&T issues to be considered.

Software is available from a variety of sources including the Center for Subsurface Modeling Support at the U.S. EPA's Robert S. Kerr Environmental Research Center in Ada, Oklahoma (405-436-8594).

sketch the capture zone of a single well in a uniform flow field. This analysis is extended by Javandel and Tsang (1986) to determine the minimum uniform pumping rates and well spacings needed to maintain a capture zone between two or three pumping wells along a line perpendicular to the regional direction of ground-water flow. Their capture zone design criteria and type curves can be used for capture zone analysis, but more efficient P&T systems can be designed with nonuniform pump well orientations, spacings, and extraction rates. The extent to which the results of these simple models represent actual conditions depends on the extent to which the assumptions vary from actual site conditions.

More complex tools are often necessary to optimize P&T design and reduce uncertainty. Several semianalytical models employ complex potential theory to calculate stream functions, potential functions, specific discharge distribution, and/or velocity distribution by superimposing the effects of multiple extraction/injection wells using the Thiem equation on an ambient uniform ground-water flow field in a two-dimensional, homogeneous, isotropic, confined, steady-state system (e.g., RESSQC, Blandford et al., 1993). Streamlines, flushing rates, and capture zones associated with irregular well spacings and variable pumping rates can be simulated by these models. Many of these models support reverse and forward particle tracking to trace capture zones and streamlines. For example, reverse particle tracking is implemented in RESSQC to derive steady-state capture zones by releasing particles from the stagnation point(s) of the system and tracking their advective pathlines in the reversed velocity field. Similarly, time-related captures zones (Figure 10) are obtained by tracing the reverse pathlines formed by particles released around each pumping well (Shafer, 1987a; Blandford et al., 1993).

Application of semianalytical models to field problems requires careful evaluation of their limiting assumptions (e.g., isotropic and homogeneous hydraulic conductivity, fully-penetrating wells, no recharge, no vertical flow component, and constant transmissivity). Several analytical models relax these restrictive assumptions by superposition of various functions to treat recharge, layering, heterogeneity, three-dimensional flow, etc. Examples of two-dimensional time-related capture zones determined using TWODAN (Fitts, 1994; 1995) are shown in Figure 10. Given their ease of use and inherent uncertainties regarding the ground-water flow field, the more robust semianalytical models are ideal tools for evaluating alternative injection/extraction well locations and pumping rates at many sites. Where field conditions do not conform sufficiently to model assumptions, the simulation results will be invalid.

Numerical models are generally used to simulate ground-water flow in complex three-dimensional hydrogeologic systems (e.g., MODFLOW, McDonald and Harbaugh, 1988; and SWIFT/486, Ward et al., 1993). For example, the benefits of using partially-penetrating recovery wells to minimize pumping rates and unnecessary vertical spreading of contaminants can be examined using a three-dimensional flow model. Numerical flow model output is processed using reverse or forward particle-tracking software such as MODPATH (Pollock, 1994), GWPATH (Shafer, 1987b), and PATH3D (Zheng, 1990) to assess pathlines and capture zones associated with P&T systems at sites that cannot be adequately modeled using simpler techniques. Solute transport models are primarily run to address aquifer restoration issues such as changes in contaminant mass distribution with time due to P&T operation.

Ground-water flow models can be coupled with linear programming optimization schemes to determine the most effective well placements and pumping rates for hydraulic containment. The optimal solution maximizes or minimizes a user-defined objective function subject to all user-defined constraints. In a P&T system, a typical objective function may be to minimize the pumping rate to reduce cost, while constraints may include specified inward gradients at key locations, and limits on drawdowns, pumping rates, and the number of pumping wells. Gorelick et al. (1993) present a review of the use of optimization techniques in combination with ground-water models for P&T system design. Available codes include AQMAN (Lefkoff and Gorelick, 1987), an optimization code that employs the Trescott et al. (1976) two-dimensional ground-water flow model, and MODMAN (Greenwald, 1993), which adds optimization capability to the three-dimensional USGS MODFLOW model (McDonald and Harbaugh, 1988). A case study of optimization code use to assist P&T design is given by Hagemeyer et al. (1993).

Techniques have been presented in the literature for combining nonlinear optimization methods with contaminant transport simulation models (Gorelick, 1983; Wagner and Gorelick, 1987; Ahlfeld et al., 1988). These techniques are intended to provide solutions to problems formulated in terms of predicted concentrations (e.g., minimize pumping such that TCE is below the required clean-up level within five years at target locations). However, such analysis requires the use of a solute transport model and solution of a relatively difficult nonlinear problem. As a result, computation effort is large and uncertainty in results is high compared to optimization based on ground-water flow. Nonlinear optimization methods using solute transport models have not yet been packaged into commercial software and have rarely been applied to ground-water contamination problems.

Extraction / Injection Scheme Design

For a successful hydraulic containment, contaminants moving with ground water in the desired containment zone must follow pathlines that are captured by the P&T system. An appropriate remedial objective might be to minimize the total cost required to maintain perpetual containment and satisfy regulatory requirements. Given this objective, installing low permeability barriers (Figure 3c) to reduce pumping rates might be cost-effective. At sites with an objective of contaminant mass removal (i.e., where the containment area size may be diminished or P&T discontinued if clean-up goals are met), a more complex cost-effectiveness trade-off exists between minimizing hydraulic containment costs and maximizing contaminant mass removal rates.

Unless natural attenuation mechanisms are being relied upon to limit plume migration, hydraulic containment is generally a prerequisite for aquifer restoration. Restoration P&T design will typically reflect a compromise among objectives that seek to: (1) reduce contaminant concentrations to clean-up standards, (2) maximize mass removal, (3) minimize clean-up time, and (4) minimize cost. Due to the limitations described in Appendix A, P&T for aquifer restoration requires a high degree of performance monitoring and management to identify problem areas and improve system design and operation.

Restoration P&T ground-water flow management involves optimizing well locations, depths, and injection/extraction rates to maintain an effective hydraulic sweep through the

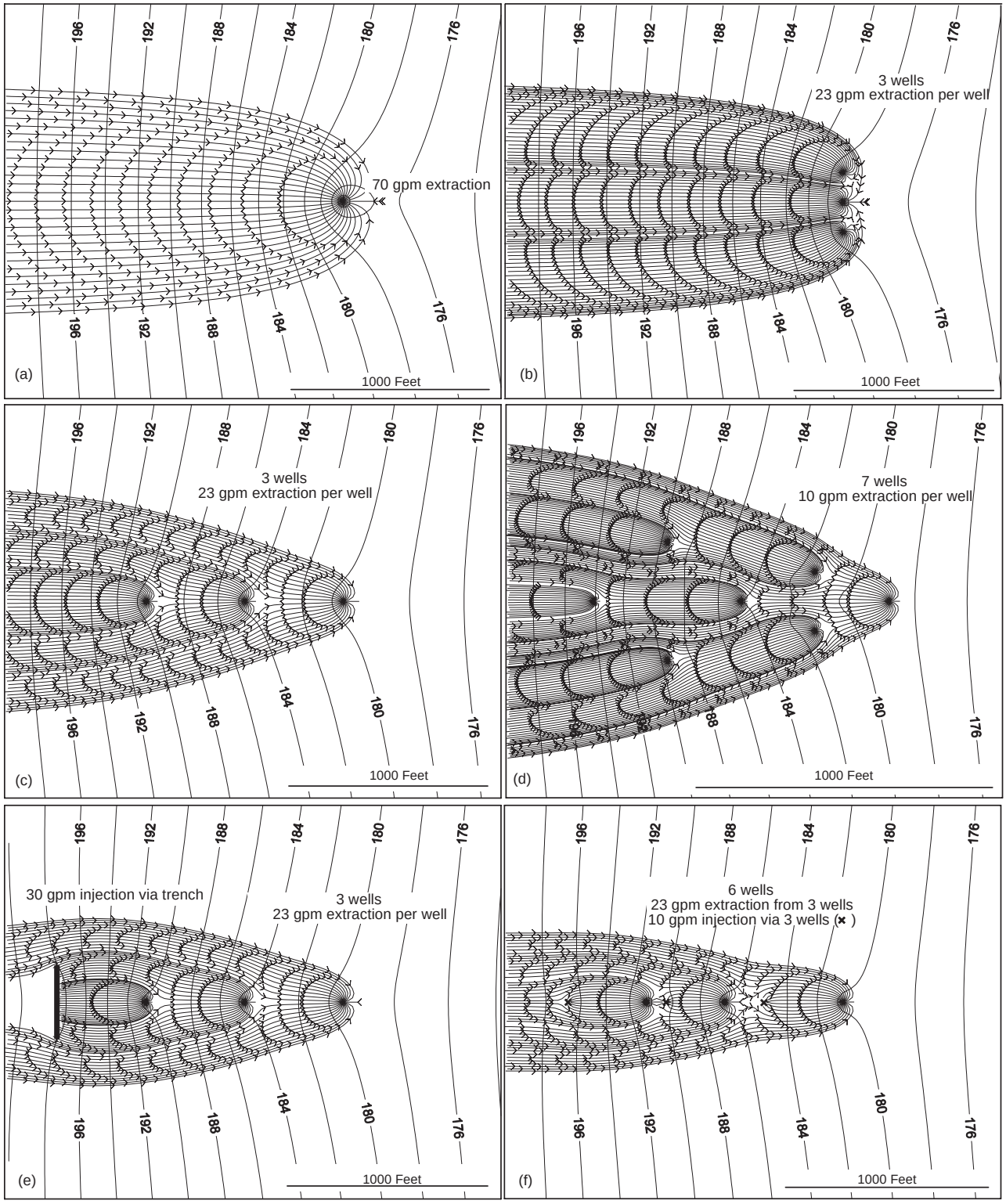

Figure 10. Hydraulic head contours and capture zones simulated using TWODAN (Fitts, 1995) for several extraction/injection schemes in an aquifer with a uniform transmissivity of 1000 ft²/d, and an initial hydraulic gradient of 0.01. Pathline time intervals of one year are marked by arrows. Note the stagnation zones that develop downgradient of extraction wells and upgradient of injection wells.

contamination zone, minimize stagnation zones, flush pore volumes through the system, and contain contaminated ground water. Wells are installed in lines and other patterns to achieve these objectives (Figure 10). Horizontal wells and drains are constructed to create ground-water line sinks and mounds, and thereby affect linear hydraulic sweeps.

Pore Volume Flushing

Restoration requires that sufficient ground water be flushed through the contaminated zone to remove both existing dissolved contaminants and those that will continue to desorb from porous media, dissolve from precipitates or NAPL, and/or diffuse from low permeability zones. The sum of these processes and dilution in the flow field yields persistent acceptable ground-water quality at compliance locations.

The volume of ground water within a contamination plume is known as the pore volume (PV), which is defined as

$$PV = \int_A bn \, dA \qquad (1)$$

where b is the plume thickness, n is the formation porosity, and A is the area of the plume. If the thickness and porosity are relatively uniform, then

$$PV = BnA \qquad (2)$$

where B is the average thickness of the plume.

Assuming linear, reversible, and instantaneous sorption, no NAPL or solid contaminants, and neglecting dispersion, the theoretical number of PVs required to remove a contaminant from a homogeneous aquifer is approximated by the retardation factor, R, which is the ground-water flow velocity relative to velocity of dissolved contaminant movement. An example of the relationship between the number of PVs and R, that also accounts for dispersion, is demonstrated by a numerical model used to evaluate a P&T design at the Chem-Dyne site in Ohio (Ward et al., 1987). Due to simulation of linear sorption, a nearly linear relationship was found to exist between retardation and the duration of pumping (or volume pumped) needed to reach the ground-water clean-up goal. Batch flush models (e.g., U.S. EPA, 1988b; Zheng et al., 1992) often assume linear sorption to calculate the number of PVs required to reach a clean-up concentration, C_{wt} in ground water as a function of the retardation factor, R, and the initial aqueous-phase contaminant concentration, C_{wo}:

$$\text{No. of PVs} = -R \ln (C_{wt} / C_{wo}) \qquad (3)$$

Though useful for simple systems, the representation of linear, reversible, and instantaneous sorption in contaminant transport models can lead to significant underestimation of P&T clean-up times. For example, the desorption of most inorganic contaminants (e.g., chromium and arsenic) is nonlinear. In addition, much of the pore space in aquifer materials may not be available for fluid flow. In such situations, flushing is not efficient and removal of a greater number of pore volumes of water will be required.

Kinetic limitations often may prevent sustenance of equilibrium contaminant concentrations in ground water (Bahr, 1989; Brogan, 1991; Haley et al., 1991; Palmer and Fish, 1992). Such effects occur in situations where contaminant mass transfer to flowing ground water is slow relative to ground-water velocity. For example, contaminant mass removal from low permeability materials may be limited by the rate of diffusion from these materials into more permeable flowpaths. In this situation, increasing ground-water velocity and pore volume flushing rates beyond a certain point would provide very little increase in contaminant removal rate. Kinetic limitations to mass transfer are likely to be relatively significant where ground-water velocities are high surrounding injection and extraction wells.

The number of PVs that must be extracted for restoration is a function of the clean-up standard, the initial contaminant distribution, and the chemical/media phenomena that affect cleanup. Screening-level estimates of the number of PVs required for cleanup can be made by modeling and by assessing the trend of contaminant concentration versus the number of PVs removed. At many sites, numerous PVs (i.e., 10 to 100s) will have to be flushed through the contamination zone to attain clean-up standards.

The number of PVs withdrawn per year is a useful measure of the aggressiveness of a P&T operation. Many current systems are designed to remove between 0.3 and 2 PVs annually. For example, less than 2 PVs per year were extracted at 22 of the 24 P&T systems studied by U.S. EPA (1992b) and reviewed by NRC (1994). Low permeability conditions or competing uses for ground water may restrict the ability to pump at higher rates. As noted above, kinetic limitations to mass transfer also may diminish the benefit of higher pumping rates. The potential significance of such limitations should be evaluated prior to installation of aggressive systems designed for relatively high flushing rates. If limiting factors are not present, pumping rates may be increased to hasten cleanup.

The time required to pump one pore volume of ground water from the contaminated zone is a fundamental parameter that should be calculated for P&T systems. NRC (1994), however, determined that the number of PVs withdrawn at P&T sites is rarely reported. Restoration assessments should include estimates of the number of PVs needed for cleanup. However, it must be noted that such analyses generally oversimplify highly complex site conditions. It may often be impracticable to characterize the site in sufficient detail to reduce uncertainty in estimates of restoration time frames to insignificant levels. Uncertainty in these estimates should be considered during remedial evaluations.

Poor P&T design may lead to low system effectiveness and contaminant concentration tailing. Poor design factors include low pumping rates and improper location of pumping wells and completion depths. A simple check on the total pumping rate is to calculate the number of PVs per year. Inadequate location or completion of wells or drains may lead to poor P&T performance even if the total pumping rate is appropriate. For example, wells placed at the containment area perimeter may withdraw a large volume of clean ground water from beyond the plume via flowlines that do not flush the contaminated zone. Similarly, pumping from the entire thickness of a formation in which the contamination is limited vertically will reduce the fraction of water that flushes the contaminated zone. In general, restoration pumping wells or drains should be placed in areas of relatively high contaminant concentration as well as locations suitable for achieving hydraulic containment.

Well placement can be evaluated by: (1) using ground-water flow and transport models; (2) comparing contaminant mass removed to contaminant mass dissolved in ground water; and (3) applying expert knowledge. P&T system modifications should be considered if any of these methods indicate that different pumping locations or rates will improve system effectiveness.

Minimize Ground-Water Stagnation

Ground-water flow patterns need to be managed to minimize stagnation during P&T operation. Stagnation zones develop in areas where the P&T operation produces low hydraulic gradients (e.g., downgradient of a pumping well and upgradient of an injection well) and in low permeability zones regardless of hydraulic gradient. Ground-water flow modeling can be used to assess ground water and solute velocity distributions, travel times, and stagnation zones associated with alternative pumping schemes. During operation, stagnation zones can be identified by measuring hydraulic gradients, tracer movement, ground-water flow rates (e.g., with certain types of downhole flowmeters or in situ probes), and by modeling analysis. Low permeability heterogeneities should be delineated as practicable during the site characterization and P&T operation. Stagnation zones associated with different pumping schemes are evident in Figure 10.

Once identified, the size, magnitude, and duration of stagnation zones can be diminished by changing pumping (extraction and/or injection) schedules, locations, and rates. Again, flow modeling based on field data may be used to estimate optimum pumping locations and rates to limit ground-water stagnation. An adaptive pumping scheme, whereby extraction/injection pumping is modified based on analysis of field data, should result in more expedient cleanup.

Guidance from Modeling Studies

Several modeling studies have been conducted to examine the effectiveness of alternative extraction and injection well schemes with regard to hydraulic containment and ground-water clean-up objectives (e.g., Freeberg et al., 1987; Satkin and Bedient, 1988; Ahlfeld and Sawyer, 1990; Tiedeman and Gorelick, 1993; Marquis, Jr. and Dineen, 1994; Haggerty and Gorelick, 1994). Although the optimum extraction/injection scheme depends on site-specific conditions, objectives, and constraints, consideration should be given to guidance derived from simulation studies of P&T performance.

A conceptual modeling analysis using FTWORK (Faust et al., 1993) of three alternative pumping strategies for an idealized site with a uniform medium, linear equilibrium sorption, a single non-degrading contaminant, and a continuing release is presented in Figure 11. The plume management strategies include: (1) downgradient pumping, (2) source control with downgradient pumping, and (3) source control with mid-plume and downgradient pumping. As shown, downgradient pumping by itself allows and increases the movement of highly contaminated ground water throughout the flowpath between the release area and the downgradient recovery well. This alternative results in expansion of the highly contaminated plume and makes it more difficult to achieve cleanup. The importance of source control is clearly demonstrated by comparing the management alternatives. Source control pumping prevents continued offsite migration and thereby facilitates downgradient cleanup of contaminated ground water. The combined source control, mid-plume, and downgradient pumping alternative reduces the flowpath and travel time of contaminants to extraction wells and diminishes the impact of processes which cause tailing. As such, with more aggressive P&T, cleanup is achieved more quickly and the volume of ground water that must be pumped for cleanup is less than for the other alternatives.

The effectiveness of seven injection/extraction well schemes shown in Figure 12 at removing a contaminant plume was evaluated by Satkin and Bedient (1988) using the MOC transport model (Konikow and Bredehoeft, 1989). The performance of each scheme was assessed for eight different hydrogeologic conditions, which were simulated by varying maximum drawdown, dispersivity, and regional hydraulic gradient. Effectiveness was judged based on simulated cleanup, flushing rate, and the volume of water requiring treatment. Findings of this study include (Satkin and Bedient, 1988): (1) multiple extraction wells located along the plume axis (the center line scheme) reduce clean-up time by shortening contaminant travel paths and allowing higher pumping rates; (2) the three-spot, double-cell, and doublet schemes were effective under low hydraulic gradient conditions, but require onsite treatment and reinjection; (3) the three-spot pattern outperformed the other schemes for simulations incorporating a high regional hydraulic gradient; and, (4) the center line pattern was effective under all simulated conditions. Andersen et al. (1984) and Satkin and Bedient (1988) showed that the five-spot pattern (Figure 12) may be a relatively inefficient scheme for cleanup.

Brogan (1991) and Gailey and Gorelick (1993) used simulations to demonstrate that the best single recovery well location is somewhat downgradient of a plume's center of mass. The optimum location (requiring the lowest pumping rate) for a single extraction well to remediate a plume within a given time period increases in distance downgradient from the center of contaminant mass with increasing remediation time (Gailey and Gorelick, 1993; Haggerty and Gorelick, 1994). Thus, optimum pumping locations and rates depend on the specified clean-up time frame.

The relative merits of conventional extraction/injection well schemes, in-situ bioremediation, and P&T enhanced by injecting oxygenated water to stimulate biodegradation for containing and cleaning up a hypothetical naphthalene plume in a uniform aquifer were examined by Marquis and Dineen (1994). Nineteen remediation alternatives were modeled using BIOPLUME II (Rifai et al., 1987), a modified version of the MOC code (Konikow and Bredehoeft, 1989) that simulates oxygen transport and oxygen-limited biodegradation. Key findings made by Marquis and Dineen (1994) include the following: (1) ground-water extraction was more effective at preventing offsite migration than bioremediation; (2) P&T enhanced by injecting highly oxygenated water (with 50 mg/L dissolved oxygen) provided the most effective plume control and cleanup; (3) greater contaminant mass reductions occurred when extraction or injection wells were located in the more contaminated portions of the plume; (4) cleanup is hastened by minimizing the distances that contaminants must travel to extraction wells or that dissolved oxygen must travel to reach degradable contaminants; (5) to maximize containment, P&T schemes should be designed to produce convergent flow toward a central extraction location and to minimize divergent flow along the plume periphery; and (6) extraction/injection schemes should be designed to minimize the presence of upgradient and intraplume stagnation areas.

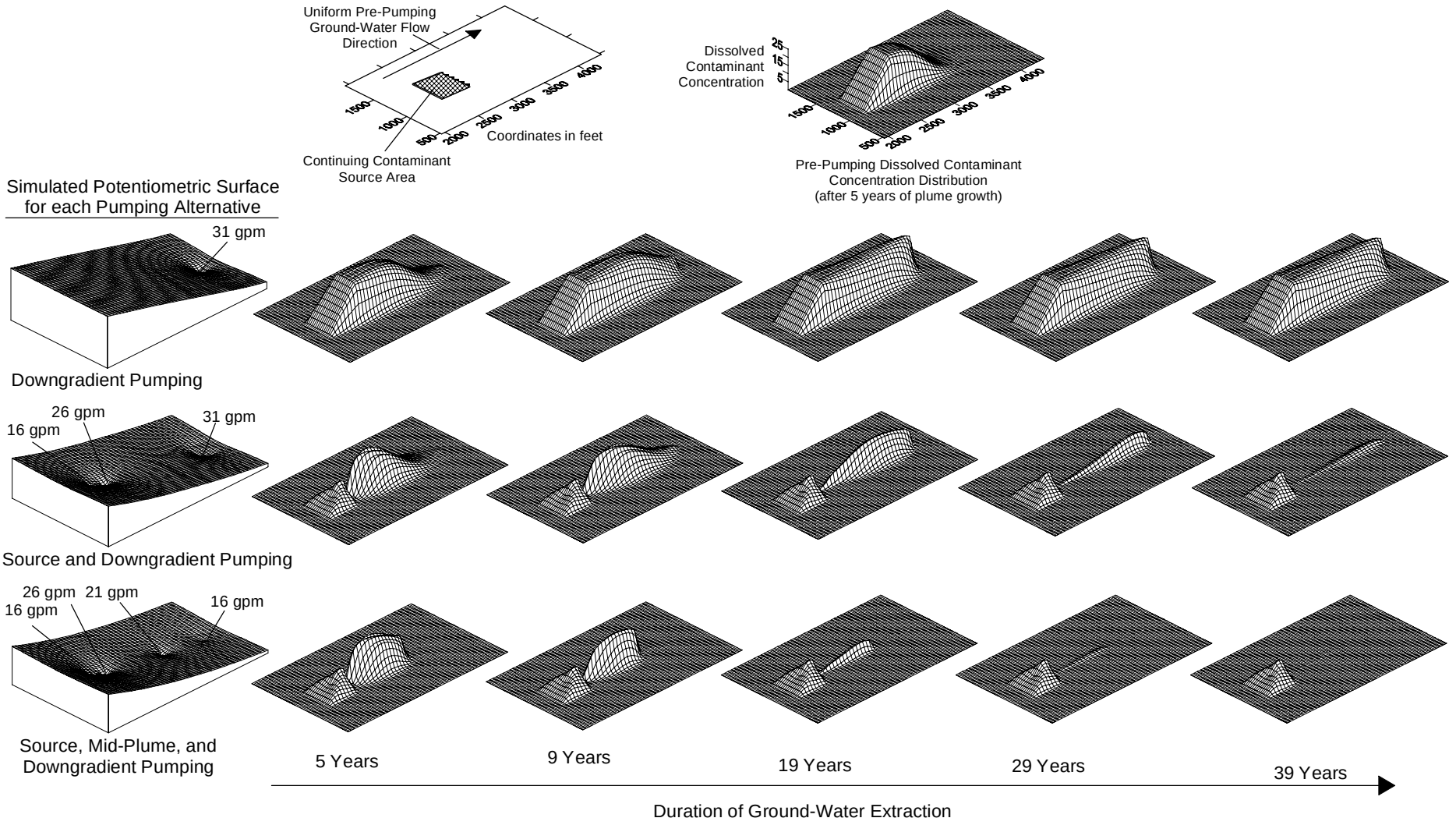

Figure 11. Results of FTWORK (Faust et al., 1993) simulation analysis of three P&T alternatives for an idealized site (with uniform media, linear equilibrium sorption, and a single non-degrading contaminant) showing dissolved contaminant concentrations with time of pumping.

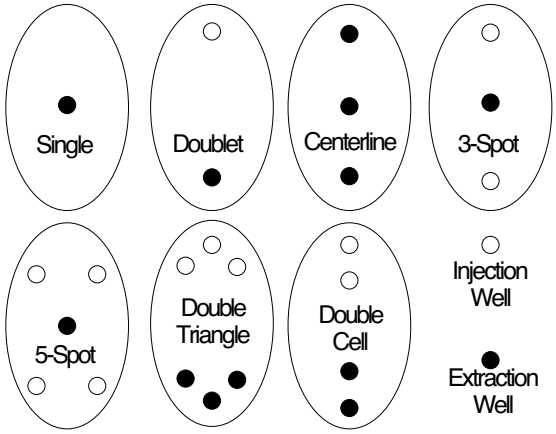

Figure 12. Well schemes evaluated by Satkin and Bedient (1988).

Pulsed Pumping

Pulsed pumping, with alternating pumping and resting periods as illustrated in Figure 13, has been suggested as a means to address tailing, flush stagnation zones by selective well cycling, and increase P&T efficiency (Keely, 1989; Borden and Kao, 1992; Gorelick et al., 1993). Dissolved contaminant concentrations increase due to diffusion, desorption, and dissolution in slower-moving ground water during the resting phase of pulsed pumping. Once pumping is resumed, ground water with higher concentrations is removed, thus increasing the rate of mass removal during active pumping. Due to slow mass transfer from immobile phases to flowing ground water, however, contaminant concentrations decline with continued pumping until the next resting phase begins.

Several simulation studies have been conducted to evaluate the effectiveness of pulsed pumping (Powers et al., 1991; Brogan, 1991; Borden and Kao, 1992; Armstrong et al., 1994; Rabideau and Miller, 1994; and Harvey et al., 1994). Harvey et al. (1994) found that: (1) for equal volumes of ground water extracted, pulsed pumping does not remove more contaminant mass than pumping continuously at the lower equivalent time-averaged rate; (2) if the resting period is too long, pulsed pumping will remove much less mass than pumping continuously at an equivalent time-averaged rate; and, (3) if pulsed and continuous pumping rates are the same, pulsed pumping will take longer to achieve clean-up goals, but will require significantly less time of pump operation. At many sites with significant tailing and rebound, it will be preferable, therefore, to pump continuously at a lower average rate than to initiate pulsed pumping. Cost savings associated with less time of pump operation, however, may make pulsed pumping advantageous.

If used, pulsed pumping schedules can be developed based on pilot tests, modeling analysis, or ongoing performance monitoring of hydraulic heads and contaminant concentrations. The pumping period should be long enough to remove most of the contaminant mass in the mobile ground water. The resting period should not be so long that the dissolved concentration in mobile ground water exceeds 70% to 90% of its equilibrium value. Additional resting becomes inefficient as equilibrium is approached because the rate of mass transfer from immobile to mobile phases is driven by the concentration gradient. Care must be taken to ensure that the hydraulic containment objective is met during pump rest periods. Further guidance on interpreting field data to designate pulsed pumping parameters is provided by Harvey et al. (1994). Simulation results showing the sensitivity of pulsed pumping performance to rest period duration are shown in Figure 13.

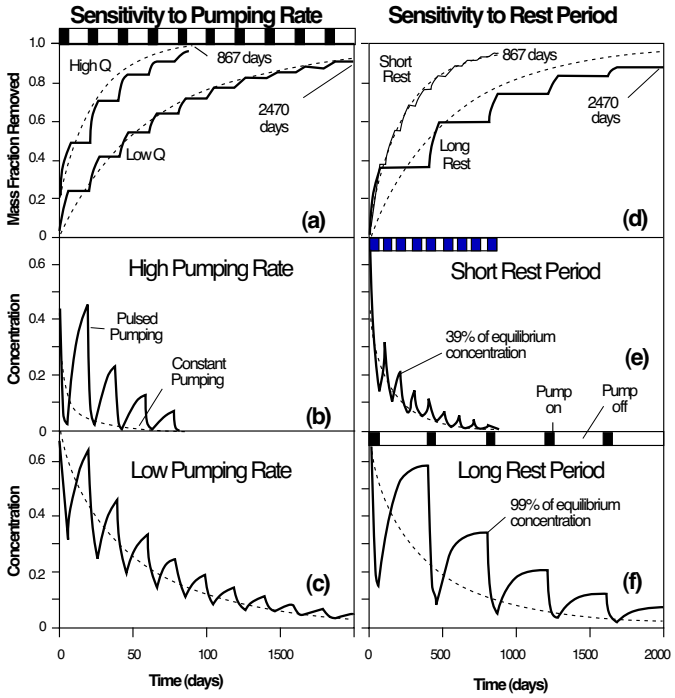

Figure 13. Effects of varying pulsed pumping parameters (after Harvey et al., 1994). The fraction of total mass removed with time is shown in (a) and (d); pumping well concentrations are shown in (b), (c), (e), and (f). Dashed lines represent equivalent constant pumping rates. Black bars at top of figures represent pumping periods and white bars represent rest periods.

Dealing with Multiple Contaminant Plumes

Multiple contaminants that migrate at different velocities in ground water are commonly encountered at contamination sites. Compounds that partition more strongly to the solid phase are transported more slowly, remain closer to source areas, and are more difficult to extract from the subsurface by pumping than the more mobile compounds. Thus, a P&T design that is ideal for a single contaminant plume might perform poorly at a site with multiple contaminants.

Haggerty and Gorelick (1994) used a solute transport model and optimization analysis to examine the ability of five pumping schemes to simultaneously remediate three contaminant plumes that were chromatographically separated during ground-water transport. The simulated problem and alternative extraction schemes are shown in Figure 14.

In the single well scheme, one well is placed along the plume axis at one of the indicated locations. For the other schemes,

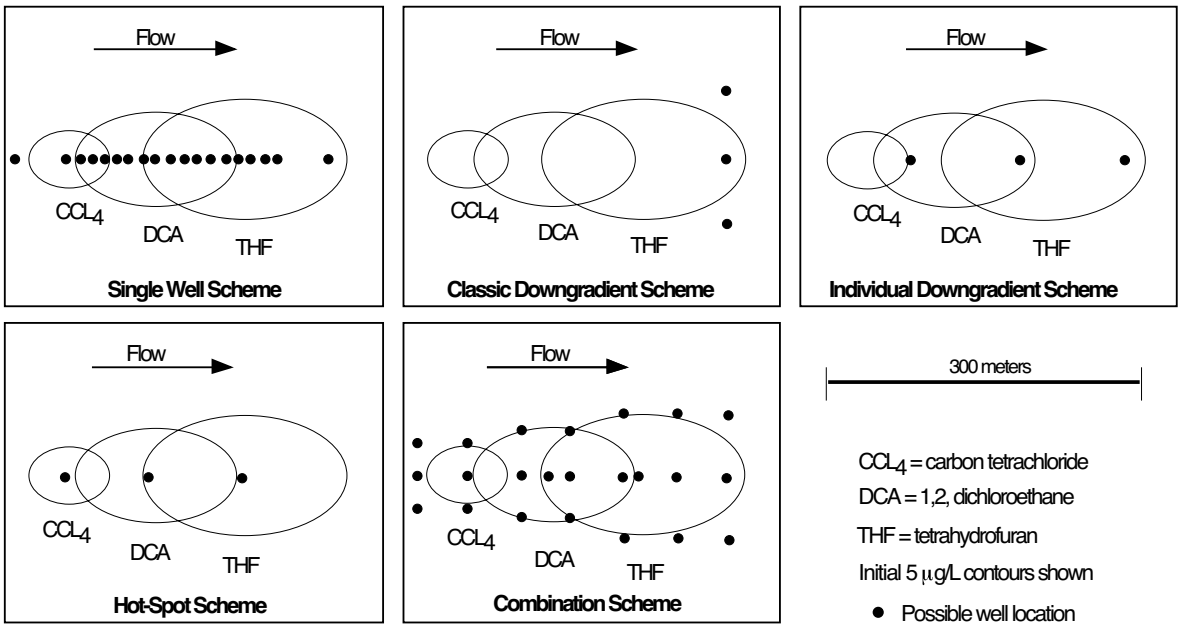

Figure 14. Map view of five pumping schemes studied by Haggerty and Gorelick (1994) overlain on the initial 5 µg/L contours of simulated CCl_4, DCA, and THF plumes. Many of the possible well locations were not used because the optimization analysis determined pumping at some locations to be 0 liters/sec. Only the optimum single well location was used for pumping under the single well scheme (modified from Haggerty and Gorelick, 1994).

wells can be placed at any number of the sites shown. The optimum number, location, and pumping rates of wells in each scheme were determined using the optimization model to achieve cleanup at the lowest possible pumping rate within a specified remediation period. Sensitivity analyses were conducted to examine the influence of mass transfer rate limitations on contaminant mobilization and removal. Findings presented by Haggerty and Gorelick (1994) for each pumping scheme are summarized in Figure 15.

For the smallest mass transfer rate parameter, $\xi = 0.005$ day^{-1}, none of the schemes can achieve cleanup within three years regardless of pumping rate due to mass transfer rate limitations. Assuming that the site is cleaned up everywhere with no dilution caused by mixing with uncontaminated ground water, then the minimum remediation time due to mass transfer limitations can be calculated as,

$$t_{min} = -(\rho_b \lambda_k / \xi) \ln (s_k^* / s_k') \qquad (4)$$

where ρ_b is the formation bulk density (M/L^3), λ_k is the distribution coefficient for compound k (L^3/M), ξ is a first-order mass transfer rate parameter (1/T), s_k^* is the immobile domain concentration standard (M/M), and s_k' is the initial maximum immobile concentration of contaminant k found at the site (M/M). Rate-limited mass transfer hinders short-term cleanup, but may have negligible impact on long-term P&T. Desorption or diffusion rate limitations may make it impossible to achieve cleanup within a short time.

For the combination scheme shown in Figure 14, seven or eight wells are optimal to achieve cleanup within three years to sufficiently reduce the distance contaminants must travel within the short remediation period. Ground water is pumped at the highest rates along the plume axis and in the location of the most retarded compounds to compensate for their low velocities.

The combination scheme essentially reduces to an individual downgradient well design for longer remediation periods. Only two or three wells along the plume axis are needed for cleanup and the ideal well locations approximate those of the individual downgradient scheme (e.g., one well cleans up the most retarded plume and the other cleans up the more mobile, downgradient plumes). The individual downgradient scheme, which requires fewer wells, therefore, is well-suited for longer-term P&T efforts.

For fast cleanup, the hot spot scheme requires less pumping than all but the combination scheme. More pumping, however, is required using the hot spot wells for a 15-year clean-up period compared to the individual downgradient scheme. This is because individual downgradient wells take advantage of the plume migration via slow regional ground-water flow during the longer clean-up period.

The classic downgradient scheme (Figure 14) is the least desirable alternative shown for attaining cleanup because the contaminants must travel completely across the multiplume site to reach the recovery wells. As a result, the more retarded contaminant plumes are smeared to the wells, an excessive volume of ground water must be extracted for cleanup, and short-term cleanup is infeasible. The single recovery well option also has significant drawbacks. It will generally require pumping more ground water and result in more contaminant smearing than all of the other schemes except the classic downgradient design.

A good P&T design must address mobile, weakly-sorbed and slow-moving, highly-sorbed contaminants to be effective at

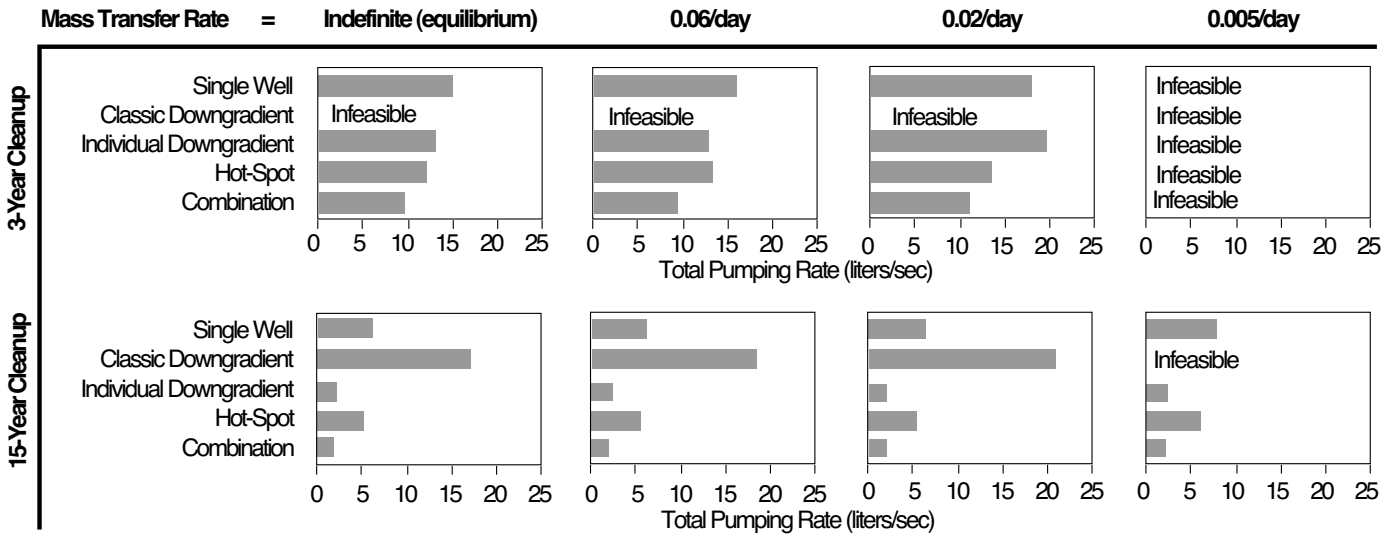

Figure 15. Optimal pumping rates for each well scheme (Figure 14) showing the minimum rate needed to capture and clean up the contaminants for the 3-year and 15-year pumping periods and mass transfer rates ranging from infinite (at equilibrium) to 0.005/day (modified from Haggerty and Gorelick, 1994).

cleanup. Substantial pumping should occur in the upgradient portion of a multiplume site to minimize both the smearing of strongly sorbed contaminants and the total volume of ground water that must be extracted for cleanup.

Other Considerations

Cyclic water-level fluctuations — Ground-water levels near surface water respond to changes in surface water stage. Cyclic stage fluctuations occur in tidal waters and in some streams that are regulated by pumping or discharge control. Where the surface water fluctuates as a harmonic motion, as occurs due to tides, a series of sinusoidal waves is propagated into the aquifer (Ferris, 1963). The amplitude of each transmitted wave decreases and the time lag of a given wave peak increases with distance from the surface water. Hydraulic gradients between contamination sites and nearby tidal water bodies, therefore, increase at low tide and decrease (or may be locally reversed) at high tide. As a result, these cyclic water-level fluctuations tend to enhance ground-water capture during high tide periods and inhibit capture during low tide periods. The impact of cyclic water-level fluctuations can be examined using analytical solutions (Jacob, 1950; Ferris, 1963) or numerical models with highly refined time steps and boundary conditions. At contamination sites that are influenced by cyclic water-level fluctuations, consideration should be given to adopting a variable rate pumping schedule, with higher extraction rates during low stage periods, to provide cost-effective hydraulic containment throughout the surface water stage cycle.

Dewatering — Water flushing will be limited to infiltration rates where P&T operation has lowered the water table and partially dewatered contaminated media. As a result, dissolved contaminant concentrations may rebound when the water table rises after pumping is reduced or terminated. Water can be injected or infiltrated, and pumping locations and rates can be varied, to both minimize this potential problem and increase the rate of flushing. Where injection is not feasible, soil vapor extraction or other vadose zone remedial measures might be needed to remove contaminant mass above the water table.

Drawdown limitations — Under some conditions, hydraulic containment cannot be maintained unless barrier walls are installed and/or water is injected (or infiltrated) downgradient of, or within, the contaminated zone. Limited aquifer saturated thickness, a relatively high initial hydraulic gradient, a sloping aquifer base, and low permeability are factors that can prevent hydraulic containment using wells or drains (Saroff et al., 1992). Where these conditions exist and hydraulic containment is planned, particular care should be taken during pilot tests and monitoring to assess this limitation.

Fractured and karst media — Fractured and solution-channeled geologic materials often represent highly heterogeneous and anisotropic systems to which techniques developed for characterization and evaluation of porous media are not readily applicable. Characterization techniques in such systems are an area of continuing research and beyond the scope of this document. Contaminant transport and P&T design/operation will be largely controlled by such factors as orientation, density, and connectivity of transmissive fracture systems. Techniques used to evaluate potential capture zones and remedial time frames based on porous-media assumptions often will not be applicable. Evaluations of capture zones will generally be based on site-specific characterization of the fractured or karst system and may involve use of tracer tests, observations during aquifer tests, and other specialized techniques such as borehole flowmeter investigations to define transmissive fracture systems and evaluate connectivity.

Information required for extraction well design will include characterization of transmissive, contaminated areas and intervals in fractured/karst systems and characterization of flow and transport parameters in any overlying porous materials (e.g., overburden, saprolite). At some sites where overburden and fractured rock are contaminated, extraction wells screened/

open across both units may be acceptable with adjustments in filter pack/screen specification for each unit. Conversely, it may be practical to screen wells only in the more transmissive unit to capture contaminants in both units. Such determinations depend on the distribution of hydraulic parameters in each affected unit. Ultimately, pilot testing of wells with careful monitoring generally will be required to evaluate the effectiveness of such systems.

In some situations, rock units may be sufficiently fractured as to approximate porous media behavior (de Marsily, 1986) allowing use of more traditional design evaluations discussed elsewhere in this document. In other situations, contaminants may be moving only in very discrete fracture systems rendering characterization difficult and necessitating careful delineation of dominant fractures and design of wells with very discrete screen/open intervals for optimum operation. The usual design approach in this situation is to locate and screen wells to intersect as many contaminated, transmissive fractures as possible (Gorelick et al., 1993). Testing of each well will be required to determine specific drawdown/flowrate relationships and evaluate potential gradient control.

The optimal well design for each of these situations will depend on the site-specific distribution of contaminants and hydraulic properties of each rock and overburden unit. However, similar design principles apply to fractured systems as to heterogeneous porous media. Design should be based on three-dimensional contaminant distribution and three-dimensional analysis of hydrologic properties of each unit within the system. In general, there still will be a significant degree of uncertainty associated with determinations of flow/transport in fractured/karst systems at most sites due to the impracticability of defining contaminant distribution and transport parameters in sufficient detail using available characterization techniques. A flexible design approach and performance monitoring can be used to minimize the effect of these uncertainties.

Highly permeable and heterogeneous media — In highly permeable media, high pumping rates are usually required to attain demonstrable hydraulic containment. Barrier walls and low-permeability surface covers installed to reduce the rate of pumping needed for containment also facilitate demonstration of inward hydraulic gradients (Figure 3). Hydraulic containment and site characterization can also be enhanced in heterogeneous media by installing barrier drains and walls, particularly if done in a manner that allows subsurface examination during construction.

Horizontal anisotropy — Significant horizontal anisotropy may be present at some sites, particularly where strata are inclined or fractured. The directions of maximum and minimum permeability are usually aligned parallel and perpendicular, respectively, to foliation or fractures. In anisotropic media, the flow of ground water (and contaminants moving with ground water) is offset from the hydraulic gradient in the direction of maximum permeability. Interpretation of hydraulic head data and capture zone analysis must account for anisotropy to evaluate extraction/injection wellfield effectiveness. Various well hydraulics equations (Papadopulos, 1965; Kruseman and deRidder, 1990) and numerical models can be employed to account for anisotropic conditions during P&T design.

Injection/extraction cells — Recharging upgradient of the contaminant plume and flushing the contaminant toward a downgradient extraction well can be designed to create a ground-water recirculation cell that isolates the plume from the surrounding ground water (Figure 16). Injection and extraction rates and locations can be adjusted to minimize the volume of ground water requiring treatment, increase flushing rates through the contamination zone (thereby reducing the flushing time), and provide additional containment (Wilson, 1984). If permitted and properly designed, water injection can greatly enhance hydraulic control and contamination zone flushing. Of course, due to water balance considerations (i.e., recharge from the land surface), it is generally not possible to reinject and recapture all of the extracted ground water. Poorly designed and inadequately monitored injection can lead to unintended horizontal and/or vertical contaminant migration.

Partial penetration — Construction of wells that only partially penetrate the aquifer may be desirable or undesirable in different situations. Contaminated ground water emanating from shallow source areas frequently is limited to the upper portion of a hydrogeologic unit. For this case, partially-penetrating recovery wells should be constructed to limit the downward spread of contaminants and the extraction of clean deep ground water. In situations where extraction wells or drains partially penetrate a contaminant plume capture may not extend to the lower limits of the plume. Three-dimensional data (e.g., hydraulic head, hydraulic conductivity distribution, contaminant distribution) are required to evaluate and monitor three-dimensional capture. In such situations, construction of wells or drains that fully penetrate the contaminated interval may reduce uncertainty and costs associated with monitoring vertical capture.

Physical barriers — Physical barriers to ground-water flow (e.g., slurry walls, grout curtains, sheet piling, etc.) reduce inflow into the system and often allow use of lower ground-water extraction and treatment rates to achieve a particular hydraulic head distribution (e.g., inward hydraulic gradient or significant dewatering). Surface caps may also be used to reduce infiltration and further reduce extraction requirements. In addition, use of such barriers and maintenance of an inward hydraulic gradient will generally reduce the complexity of adequately monitoring capture zones.

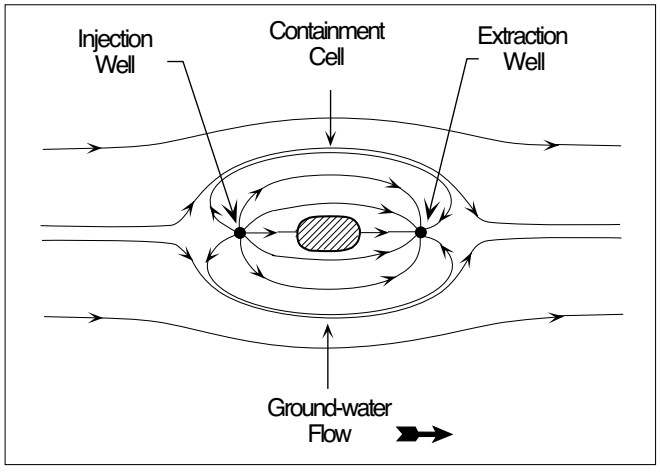

Figure 16. Plan view of a single-cell hydraulic containment, showing flow lines and a hatched contaminant plume (modified from Wilson,1984).

Situations in which use of physical barriers may be advantageous or cost effective include sites where treatment capacity for extracted ground water is limited, reductions in treatment costs outweigh barrier construction costs, and heterogeneous sites or sites with relatively high pre-design hydraulic gradients where uncertainty in capture zone determinations is high. Additional details regarding design and construction aspects of physical barriers may be found in U.S. EPA (1984), Evans (1991), Grube (1992), and Rumer and Ryan (1995).

Although these features may be used as enhancements to a P&T system, they often will not be appropriate replacements for P&T. Physical barriers without the use of P&T to lower hydraulic head within the enclosure will generally result in increasing hydraulic head within the wall. This may result in leakage over the wall, under the wall, or through relatively minor imperfections in the wall.

Physical constraints — Many ground-water contamination sites are located in developed areas where the presence of roads, buildings, and other structures constrain the placement of P&T components (i.e., wells, pipelines, and treatment plants). Such constraints should be identified early in the design process and incorporated into the analysis of feasible remedies. In some cases, it will be necessary to assess potential for subsidence that may result from pumping.

Surface-water interactions — Streams, rivers, lakes, and other surface water bodies frequently act as discharge boundaries to local and regional ground-water flow systems (and dissolved contaminants migrating therein). A variety of complex leakage and discharge relationships, however, exist spatially and temporally between surface water and ground water. Interaction between ground water and surface water may help or hinder P&T operations. At some sites, P&T design can take advantage of induced infiltration along stream line sinks to enhance hydraulic containment and flushing rates. Elsewhere, it may be desirable to limit streambed leakage (e.g., using physical barriers) to minimize requisite pumping rates or the inflow of surface water that has been contaminated at upstream locations. Consideration should also be given to potential hydraulic benefits of discharging treated ground water at alternative stream locations. Relatively complex interactions between surface water and ground water can best be analyzed by numerical model analysis and monitoring system performance.

Timeliness of remedial action — Research has shown that contaminants that have been in contact with porous media for long times are much more resistant to desorption, extraction, and degradation (Brusseau, 1993). As the residence time of a contaminant plume increases, so do potential contaminant tailing and rebound problems associated with sorption/desorption and matrix diffusion. Old plumes are likely to exhibit significant nonideal behavior, making cleanup difficult. Remedial efforts should be implemented as soon as practicable following a release to limit the difficulty of removing contaminant mass from low permeability zones and sorbed phases.

Well completion interval — Well completion intervals are selected based on site conditions and P&T strategy. Maximum well yield can generally be obtained by screening 80 percent to 90 percent of the thickness of a confined aquifer. In an unconfined formation, the screen should be placed low enough in the contaminated section so that the pumping level is not drawn into the screen. This will prevent aeration of the screen and extend the service life of the screen and pump. Longer screens may be needed in thick contamination zones and in low permeability formations to achieve an acceptable yield.

An individual well (with zone-dependent screen and sandpack characteristics) may be completed in multiple transmissive zones and hydrogeologic units if such a construction will not exacerbate vertical contaminant migration or prevent the cost-effective cleanup of individual layers. In general, (1) screens should not be constructed to hydraulically connect transmissive zones across an aquitard; (2) it is undesirable to pump ground water directly from uncontaminated intervals; and (3) partially-penetrating recovery wells can be used to limit the downward contaminant spreading and recovery pumping rates at sites where contaminants are limited to the upper portion of a thick hydrogeologic unit. Open-hole bedrock well completions are usually acceptable, but care must be taken to not promote contaminant migration (e.g., by completing an open-hole well across an effective aquitard).

Site characterization activities (such as interval-specific packer-aquifer tests, borehole flowmeter testing, and ground-water sampling) and three-dimensional simulation analysis can be used to help evaluate complicated cost-benefit trade-offs between alternative well designs in vertically heterogeneous media.

P&T Components

Ground-water extraction/injection systems are tailored to site-specific conditions and remediation goals. As a result, system component combinations yield a large variety of P&T configurations. A conceptual process flow diagram for a typical P&T system where volatile organic contaminants are removed from ground water by air stripping (and carbon adsorption polishing, as needed) is shown in Figure 17. Selected P&T system components are described below and in Table 2. Specific guidance regarding component selection and monitoring treatment system discharge compliance with appropriate regulations is beyond the scope of this document. Guidance regarding monitoring system effectiveness with respect to remedial design objectives is provided in Cohen et al. (1994).

Vertical Wells

Vertical wells are integral components of most P&T systems. Extraction wells are intended to capture and remove contaminated ground water; injection wells are used to enhance hydraulic containment and ground-water flushing rates. Basic component considerations include drilling/installation method, well diameter, screen and casing specifications, completion depth interval, and pump specifications. Detailed guidance on well drilling, construction, and development methods is provided by Repa and Kufs (1985), Driscoll (1986), Bureau of Reclamation (1995), and others.

Well yield and efficiency are of prime concern when designing extraction and injection wells. Yield is the rate at which ground water can be pumped under site-specific conditions (e.g., desired drawdown limits). Well losses caused by poor design or construction decrease well efficiency and result in increased drawdown within the well to maintain a particular yield. This is one reason that hydraulic head measurements taken in a pumping well are often poor indicators of hydraulic head in the formation immediately adjacent to the well. Within

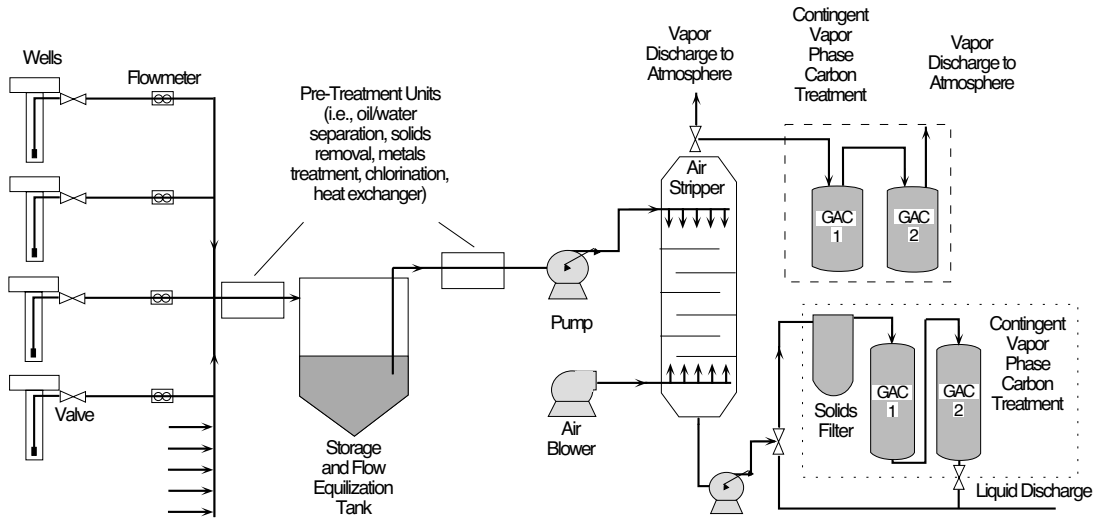

Figure 17. Example conceptual treatment diagram for a P&T system using air-stripping and optional granular activated carbon polishing treatment of liquid and vapor phase effluent from the air stripper.

Table 2. Appurtenant Pump-and-Treat Equipment

Equipment	*Description*
Piping	Conveys pumped fluids to treatment system and/or point of discharge. Piping materials will dictate if the system may be installed above or below grade with or without secondary containment measures. Piping materials (i.e., steel, HDPE, PVC, etc.) are selected based on chemical compatibility and strength factors.
Flowmeters	Measures flow rate at given time and/ or the cumulative throughput in a pipe. Typically installed at each well, at major piping junctions, and after major treatment units. Some designs allow for the instrument to act as an on/off switch or flow regulator. Many different types are available.
Valves	The primary use of valves (i.e., gate, ball, check, butterfly) is to control flow in pipes and to connections in the pipe manifold. Valves may be operated manually or actuated by electrical or magnetic mechanisms. Check valves are used to prevent backflow into the well after pumping has ceased and siphoning from tanks or treatment units. Other uses for valves include sample ports, pressure relief, and air vents.
Level Switches Sensors	Float, optical, ultrasonic, and conductivity switches/sensors are used to determine the level of fluids in a well or tank. Used to actuate or terminate pumping and to indicate or warn operators of rising or falling fluid levels in wells and tanks.
Pressure Switches	Used to shut off pumps after detecting a drop in discharge pressure caused by a loss in suction pressure.
Pressure and Vacuum Indicators	Used to measure the pressure in pipes, across pipe connections, and in sealed tanks and vessels.
Control Panels	Device which provides centralized, global control of P&T system operation and monitors and displays system status. Control panels are typically custom designed for specific applications.
Remote Monitoring, Data Acquisition, & Telemetry Devices	Provides interactive monitoring and control of unattended P&T systems. Allows for real-time data acquisition. Alerts operators to system failures and provides an interface for remote reprogramming of operations. Remote monitoring devices should also be accessible from the Control Panel.
Pull and Junction Boxes	Above and/or below grade installations that allow access to connections in the piping manifold, electric wiring, and system controls. Strategic placement provides flexibility for system expansion.
Pitless Adaptor Unit	Allows for the transfer of extracted ground water from the well to buried piping outside of the well casing.
Well Cover	Available with padlock hasps, with and without a connection to the electrical conduit for submersible pumps.

limits, such parameters as screen diameter, screened interval, and screen open area are specified to optimize yield and maximize efficiency. Increased yield results in minimizing the number of wells required to attain specific system design objectives.

The well diameter must be large enough to accommodate the pump and other downhole instrumentation. The size of the pump required to obtain the desired yield, within the site-specific hydrogeologic limits, will determine the size of the casing. Although several different types of pumps may be selected, standard electric submersible pumps are most commonly used for extracting ground water at contamination sites. A close fit between the pump and casing promotes cooling of the submersible pump motor; but can lead to insertion or removal difficulties. Commonly, the casing diameter is sized two standard pipe sizes larger than the pump. For example, a 4-inch diameter pump is set in a 6-inch diameter well. The well diameter generally should be no less than one pipe size larger than the nominal pump diameter. Except for well point systems, pumping wells are usually at least four inches in diameter. The casing size should also be selected to ensure that the uphole velocity during pumping is <5 ft/sec (Driscoll, 1986) to prevent excessive head losses.

Pump selection depends on the desired pumping rate, well yield, and the total hydraulic head lift required. Designers should consult performance curves and data provided by pump manufacturers. Pneumatic pumps are used in some P&T applications, particularly at sites where providing electrical service is problematic, combustible vapors are present, or excessive drawdown might damage electric submersible pumps. Electric and pneumatic pumps that extract total fluids or separate liquid phases (e.g., LNAPL, water, and DNAPL) are readily available.

Extraction wells may be driven (or jetted) well points, naturally developed wells, or filter-packed wells. Screens and filter packs should be appropriately sized to the native media. Grain-size analyses of unconsolidated formation samples are highly recommended to determine appropriate slot and sandpack sizes. Wells can often be developed with natural packs in areas where the formation materials are permeable and relatively coarse grained. In naturally developed wells, the slot size is chosen so that most fines adjacent to the borehole are pumped through the screen during development. Custom screen design using sections with different slot sizes based on the grain size distribution of the different materials in the screened interval may be useful at sites where the highest possible specific capacity is desired.

Use of an artificial filter pack is advantageous when the geologic materials are highly laminated; highly uniform, fine-grained deposits; or in situations where a small screen slot size (e.g., <0.010 inch) dictated by natural pack criteria would significantly reduce the water transmitting capability of the screen (Driscoll, 1986). Filter pack materials generally are composed of clean, well-rounded, uniformed-sized, siliceous grains and designed to retain most of the natural formation materials. The screen slot size is then typically selected to retain 90 percent of the sandpack. Grading of the filter pack is based on the finest-grained layer in the screened interval. Such a design generally does not restrict flow from coarser-grained layers as the hydraulic conductivity of the filter pack is significantly higher than the conductivity of these layers.

Filter packs mechanically retain formation particles. The factor controlling formation retention is the ratio of pack grain size to that of the formation, not pack thickness. Pack thickness recommendations from the literature for production wells range from approximately 3 inches to 8 inches (U.S. EPA, 1975). Pack thickness in the lower end of the recommended range will often be required to allow sufficient development for maximum well efficiency. Two common errors in filter packed wells that lead to low yields are use of a standard filter pack regardless of formation characteristics and use of screens with improper slot sizes for given filter pack characteristics (Driscoll, 1986).

Bedrock wells can be completed as open-holes; but screen and sandpack may be desirable to prevent caving and limit sand pumping. Well development by surging, jetting, backwashing, and pumping improves well efficiency. Driscoll (1986) provides a comprehensive treatise on well design, construction, and development and should be consulted prior to design.

Well screen and casing are frequently constructed of black low-carbon steel, Type 304 or Type 316 stainless steel, and PVC. Although low-carbon steel is frequently used for well casing, serious iron oxidation problems may occur when sodium hypochlorite is used to redevelop the wells. Iron flaking may cause clogging in injection wells. Manufacturers can provide advice on material compatibility with ground water and contaminants regarding the potential for corrosion, incrustation, and chemical attack. Material compatibility guidance is also available in various documents (e.g., Driscoll, 1986; McCaulou et al., 1995). The physical strength of the screen and casing materials is a concern for very deep wells. PVC casing may not be suitable for depths exceeding 300 feet, especially for large-diameter wells. Screens do not need to be as strong as casing because their openings relieve hydrostatic pressure, but must be able to withstand stresses associated with well installation and development. Screens are more susceptible to corrosion failure than steel casing. Whereas casing can suffer substantial corrosion and still function, minor screen corrosion can enlarge slot openings and result in severe sand pumping. This accounts for the use of stainless steel screens in conjunction with mild steel casing. For an economical well installation that resists degradation due to high concentrations of organic chemicals, stainless screen and casing can be threaded to PVC riser above the water table. Properties and dimensions of selected well casing products are highlighted in Table 3.

Generally, well screen diameter is selected to provide sufficient open area so that the velocity of water entering the screen is less than 0.1 ft/s to minimize friction losses, corrosion, and incrustation (Driscoll, 1986). Screen diameter influences well yield but to a lesser extent than does screen length. The potential increase of well yield with increasing screen diameter depends on site-specific conditions. Potential increases in some situations may be relatively insignificant. For example, in relatively conductive material where yields are high, increasing the screen diameter from 6 inches to 12 inches may only result in yield increases of several percent. In materials with low hydraulic conductivity, potential yield increases resulting from increased screen diameter may be significant and should be considered.

Open area of the screen affects entrance velocity and well efficiency. Limited open area limits well development and results in increased drawdown within the well for a specific yield.

Table 3. Properties and Dimensions of Selected Well Casing Products

Casing Material	Size (in.)	OD (in.)	ID (in.)	Wall thickness (in.)	Weight (lb/ft)	Collapse Strength (psi)	Comments
Black Steel Thin Wall Water Well Casing	4	4.500	4.216	0.142	6.60		+ Stronger, more rigid, and less temperature sensitive than PVC.
	6	6.625	6.249	0.188	12.9	1030	+ Much less expensive than stainless steel.
Black Steel Schedule 40	4	4.500	4.026	0.237	10.8		- Rusts easily, providing sorptive and reactive capacity for metals and organic chemicals.
	6	6.625	6.065	0.280	19.0	2286	- Subject to corrosion (given low pH, high dissolved oxygen, H_2S presence, >1000 mg/L TDS, >50 mg/L Cl^-).
PVC Schedule 40 (PVC 12454)	4	4.500	4.026	0.237	2.0	158	+ Lightweight, easy workability, inexpensive.
	6	6.625	6.065	0.280	3.6	78	+ Completely resistant to galvanic and electrochemical corrosion.
							+ High strength-to-weight ratio.
PVC Schedule 80 (PVC 12454)	4	4.500	3.826	0.337	2.8	494	+ Resistant to low concentrations of most organic contaminants.
	6	6.625	5.761	0.432	5.4	314	- Poor chemical resistance to high concentrations of aromatic hydrocarbons, esters, ketones, and organic solvents.
							- Lower strength than steel; may not be suitable for very deep applications.
Stainless Steel Schedule 5	4	4.500	4.334	0.083	3.9	315	+ Stronger, more rigid, and less temperature sensitive than PVC.
	6	6.625	6.407	0.109	7.6	129	+ Good chemical resistance to organic chemicals.
							+ Resistant to corrosion and oxidation.
Stainless Steel Schedule 40	4	4.500	4.026	0.237	10.8	2672	- Expensive.
	6	6.625	6.065	0.280	19.0	1942	- May corrode if exposed to long-term corrosive conditions.

Open area for different slot configurations (e.g., machine slotted vs. continuous slot) varies significantly. Continuous slot screens have significantly more open area per foot of screen than other slot configurations. Manufacturers should be consulted regarding open area of their screens. If the entrance velocity is calculated to be too high (i.e., > 0.1 ft/s), longer screens with greater open area, or larger diameter screens, where practical, should be considered.

The pump intake generally should not be placed in the well screen. Such placement may result in high screen entrance velocity, increased incrustation or corrosion rates, sand pumping, or dewatering of the screen (Driscoll, 1986). In general, the pump intake position does not greatly affect the relative volumes of water produced by different formation materials in the screened interval. In most situations, this distribution is predominantly controlled by the hydraulic properties (e.g., hydraulic conductivity) of the various materials.

Due to their tendency to clog, injection wells are typically overdesigned in terms of well diameter or screen length to reduce maintenance activities. Rather than using vertical wells, artificial recharge may be better accommodated by surface spreading, infiltration galleries, trenches, or horizontal wells. These options have greater surface area and are less likely to clog than vertical wells.

Vertical Well Point Systems

Well point systems are comprised of multiple closely spaced wells that are connected via a main pipe header to a suction lift pump. Suction lift systems are limited to pumping shallow ground water at depths of less than approximately 25 feet. Such systems are based on construction dewatering technology. Well point systems are often used at sites where the hydraulic conductivity of aquifer materials is relatively low and large numbers of wells would be required to meet design objectives, particularly hydraulic containment or dewatering objectives. Where applicable, such systems may be more cost-effective than conventional wells. Well point systems are described in more detail in Bureau of Reclamation (1995).

Horizontal and Slant Wells

During recent years, directional drilling rigs from the utility, mining, and petroleum industries have been adapted to install horizontal wells at contaminated sites (Kaback et al., 1989;

Karlsson and Bitto, 1990; Langseth, 1990; Kaback et al., 1991; Morgan, 1992; Conger and Trichel, 1993; WSRC, 1993; U.S. EPA, 1994b; and CCEM, 1995). As of January 1996, more than 370 horizontal wells had been drilled at contamination sites in the United States for ground-water extraction (33%), soil vapor extraction (35%), air sparging (21%) and other purposes (11%) including petroleum recovery, ground-water infiltration, and bioventing (CCEM, 1996). Most of these wells (73%) were installed less than 26 feet deep by utility type contractors.

Horizontal wells can be drilled in soil or rock as continuous holes with surface access at each end or as blind holes (Figure 18). Slant wells are completed in straight angle borings. As shown in Figure 18, slant or horizontal wells can be strategically installed to: (1) allow injection or extraction in inaccessible areas such as beneath buildings, ponds, or landfills; (2) intercept multiple vertical fractures; and (3) provide hydraulic control along the leading edge of a plume or elsewhere by creating hydraulic line sinks (extraction) or pressure ridges (injection) without the need to excavate trenches. Horizontal wells with long screens may be more cost-effective than vertical wells, particularly at sites where contaminated ground water is extensive horizontally, but not vertically. The higher cost of horizontal wells, compared to vertical wells, may be offset by savings derived from more efficient remediation, drilling fewer wells, the purchase of fewer pumps, etc.

Horizontal well construction methods are described by U.S. EPA (1994b), CCEM (1995), and in drilling contractor literature. Continuous holes are typically drilled as inverted arcs from a surface entry point to a surface exit point. Using an adjustable angle, slant rotary drill rig, a pilot boring may be advanced at an angle to the desired subsurface elevation, directed along the completion path using a steerable drill head and a walkover radio-frequency (or other) guidance system, and then angled upward to exit the ground. Following completion of the pilot hole, the boring is cut to the final diameter using reamers. Rock holes may be advanced using a steerable tungsten carbide bit with a downhole air hammer, air rotary, or mud motor assembly. Drilling fluids, consisting of water, air, bentonite slurries, or polymeric solutions, are typically recycled through a closed-loop system to remove cuttings from the borehole. Well screen, casing, risers, filter fabric and/or pre-packed filter media are assembled at the exit end of a continuous hole and pulled into place behind the reamer. Pre-packed stainless steel screens have been selected for wells requiring a filter pack, but less expensive materials, including PVC, HDPE, steel, and fiberglass have also been used for well screen. Similar to conventional water wells, horizontal well screen and filter pack sizes are designed to optimize well yield and limit fine particle entry. Much greater compressive and tensile strength are required of horizontal well materials, however, to prevent failure during emplacement or wellbore collapse. Pre-packed filter materials are used due to the difficulty of placing sand, plugs, and grout in a horizontal well bore. Horizontal wells may be developed by pumping, swab/surging, and jetting. For blind wells, a washover bit and pipe are used to allow horizontal well construction within a temporary casing.

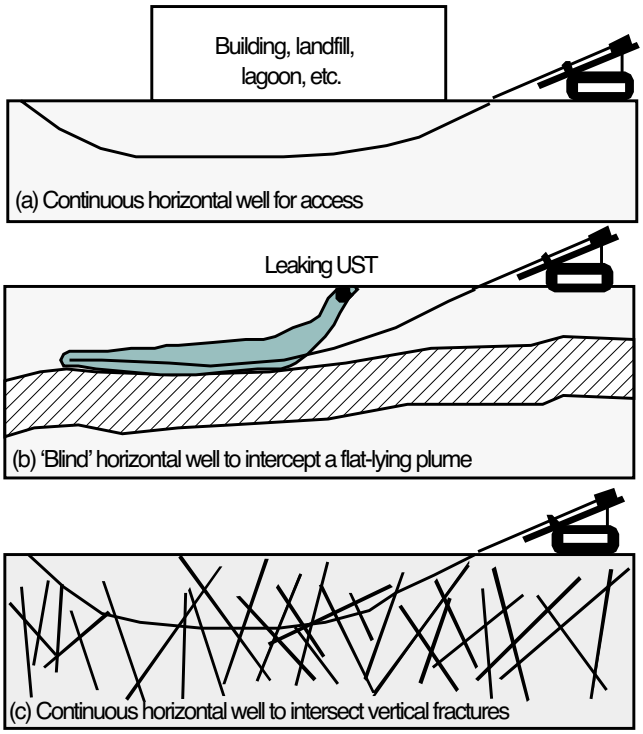

Figure 18. Several applications of horizontal wells (modified from U.S. EPA, 1994b).

Trench Drain Systems

Trench drain systems are typically constructed perpendicular to the direction of ground-water flow to cut off and contain contaminant migration by creating a continuous hydraulic sink (Figure 19). A trench drain installed along the plume axis, however, will provide more effective contaminant mass removal (but may not provide complete containment). Designers should assess the potential for downgradient mounding of ground water transmitted along the length of a drain system, particularly if the drain is not oriented perpendicular to the natural flow direction. It may be appropriate to construct segmented drains to restrict flow along the drain length.

Trench drains are typically constructed using a backhoe to shallow depth in heterogeneous, low permeability media where many wells would be needed to obtain the required yield for capture of a specific area, but may also be suitable in moderate and high permeability soil. Although the depth limit for conventional excavation techniques is about 20 feet, specialized equipment can be used to install trench drains as deep as approximately 70 feet or deeper. The saturated zone of the trench is backfilled with a highly-permeable granular material such as sand or gravel. Geotextile filter fabric is placed around the permeable backfill to prevent fine particles from clogging the drain system. The upper few feet of the trench should be backfilled with low permeability material to reduce infiltration. Ground water that enters the granular backfill flows through the fill, and/or through perforated pipe installed near the trench bottom, to an extraction sump or sumps pumped to maintain a hydraulic sink along the drain.

Consideration should be given to pipe cleanout access and the installation of monitor wells along the drain length. At some locations, it may be advantageous to install an impermeable synthetic membrane on the downgradient side of a cutoff trench to prevent fluid bypass. Trench drain systems can also be used to inject treated or clean water to create pressure ridges and

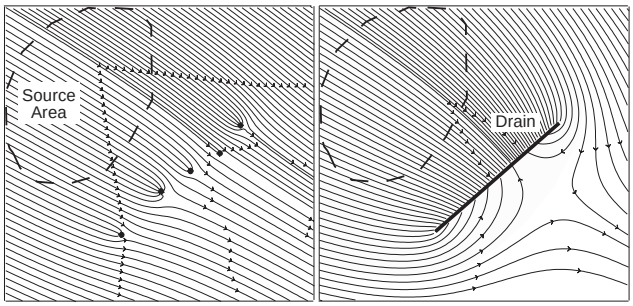

Figure 19. A trench drain constructed perpendicular to the direction of ground-water flow may provide more effective containment than extraction wells (e.g., for shallow contamination in heterogeneous, low-permeability media).

thereby enhance hydraulic containment and flushing rates. Drain depth, spacing, location, and other design criteria can be assessed using the computational tools described in Table 1 and various analytical solutions (Cohen and Miller, 1983).

The cost of excavating drains into bedrock is usually prohibitive. Drain construction also may be impractical due to access restrictions, building stability concerns, and costs associated with excavating large quantities of contaminated materials. Potential excavation stability problems can be addressed by using a trench box or other shoring methods, minimizing both the time that excavated sections are kept open and the length of open sections, and/or by use of guar guam or other gels (U.S. EPA, 1992c). Alternatively, 'one pass' trenching techniques may be applicable. For example, a 'one-pass' trencher can be used to excavate a 12-inch wide trench to a maximum depth of 22 feet, install a HDPE perforated collection pipe, and place granular backfill in a simultaneous operation (Gilbert and Gress, 1987). This method minimizes contaminant exposure during trenching, quantities of contaminated material requiring disposition, and stability problems. Additional information on trench drain systems is provided by Repa and Kufs (1985), Meini et al. (1990), Day (1991), and U.S. EPA (1991b, 1994b).

Treatment Technology Selection

Ground-water treatment technologies rely on physical, chemical, and/or biological processes to reduce contaminant concentrations to acceptable levels. Presumptive treatment technologies include use of: air stripping, granular activated carbon (GAC), chemical/UV oxidation, and aerobic biological reactors for dissolved organic contaminants; chemical precipitation, ion exchange/adsorption, and electrochemical methods for treatment of metals; and a combination of technologies to treat ground water containing both organic and inorganic constituents (U.S. EPA, 1996). Widely-used ground-water treatment technologies that are available as package plants are described in Appendix B .

The evaluation and selection of treatment alternatives for a particular P&T system is based on technical feasibility and costs (capital and operational) of achieving remediation goals. Key parameters that influence treatment design and efficacy include flow rate, ground-water constituents requiring treatment (including naturally occurring dissolved metals that may foul or interfere with a treatment system), influent concentrations, and discharge requirements. Relationships between these parameters and treatment design are discussed briefly below, and in more detail by AWWA (1990), Nyer (1992), U.S. EPA (1994a), WEF (1994), and Noyes (1994).

The treatment flow rate, influent concentrations, and desired effluent concentrations influence the applicability of potential treatment methods. Flow rate is usually based on a projection of the pumping rate needed to achieve remediation goals. Treatment plant capacity may need to be increased where effluent is reinjected or where aggressive P&T is employed to hasten cleanup. The degree of contaminant concentration reduction required for each constituent is crucial to treatment design. For example, although GAC adsorption may reduce the concentration of a particular contaminant more than air stripping, depending on the discharge requirements, air stripping may be utilized as the sole technology, as pretreatment to GAC, or not at all. The discharge requirements often depend on the final disposal method for the treated water. Options include discharge to surface water, reinjection, discharge to another treatment system, or direct use. Regulations may preclude some options due to effluent concentrations, flow rate, or potential impacts to the ground water. Discharge to an existing treatment system (POTW or industrial treatment system) is generally the least restrictive option, but each system will have specific flow rate and concentration requirements. Effluent discharge to surface water and reinjection below the water table require permits.

The first step in selecting a treatment strategy is to exclude methods that are not implementable based on contaminant type, concentrations, flow rate, and site characteristics. Where multiple contaminants are present, some technologies may be excluded as complete solutions, but considered as a pretreatment or polishing step in a 'treatment train'. Thus, to effectively use air stripping for volatile organic contaminants, it may be necessary to pretreat the influent by chemical precipitation to remove dissolved metals that could foul the stripping unit. Examples of unit processes and sequences in ground-water treatment trains are listed in Table 4. At some sites, it may be beneficial to split ground water that is extracted from different areas into more than one treatment train (e.g., highly contaminated water from a source area may be treated differently than dilute downgradient ground water).

The technically implementable methods are then assessed with regard to effectiveness, relative implementability, and cost. An evaluation of effectiveness should consider the projected rate and duration of flow, the level of treatment required for each constituent, and the reliability of each method. Reliability may be difficult to assess for innovative technologies based on readily available data. In the absence of adequate performance data, treatability and pilot-scale testing should be conducted to yield critical data for use in technology selection, design of full-scale facilities, estimating costs, and identifying potential problems. The time element of treatment can be addressed during pilot studies by appropriate scaling of treatment units, flow rates, and concentrations (e.g., smaller capacity GAC units can be used to determine constituent breakthrough times more quickly). An evaluation of relative implementability should consider technical and administrative aspects, including permits, space limitations, storage and disposal options, availability of equipment, availability of skilled workers to implement the technology, visual impacts, and community relations. Cost estimates should include capital costs, annual costs, and an estimate of treatment duration; and cost comparisons should incorporate a discount rate for future costs and a cash flow analysis.

Treatment strategies should be designed and implemented in a manner that will accommodate changing conditions over the life cycle of a P&T project. At many sites, modifying treatment capacity or methods to match changing influent chemistry or flow rate over time can improve system performance and reduce cost. As with pumping, treatment optimization requires ongoing monitoring.

Proposed designs (e.g., extraction/injection well construction and placement, piping diagrams, treatment system design) should be presented in drawings and accompanied by detailed text discussion with appropriate tables. Discussion should include such topics as materials selection, proposed processes, and installation procedures. Rationale for design choices should also be discussed with supporting calculations presented and supporting data presented or referenced.

Technology Integration

Under favorable conditions (Figure 4), P&T technology can achieve clean-up goals. However, most, if not all, remedial methods will have difficulty rapidly restoring ground-water quality to meet low concentration standards in the presence of highly sorbing contaminants, NAPL, and heterogeneous media. In these cases, remedial performance may be improved by integrating P&T operation with other clean-up technologies. This integration can occur spatially (e.g., where P&T is applied to the dissolved plume and other technologies are applied to source areas) and temporally (e.g., where multiple technologies are applied in series).

Remedial technology integration has occurred at many sites contaminated with petroleum product LNAPLs. Although mobile LNAPL may be pumped via extraction wells, immobile product will remain in the subsurface. Excavation is a candidate technology to remove shallow LNAPL. Due to their volatility and degradability, many petroleum products, such as gasoline, can also be remediated using SVE and enhanced bioremediation. Alternatively, natural attenuation may be demonstrated to be an effective petroleum contaminant management strategy at some sites.

Table 4. Common Treatment Train Unit Processes [1] and Sequence (modified from U.S. EPA, 1996)

Ground-Water Treatment Train Unit Processes

Solid or Liquid Separation Technologies	*Primary Treatment Technologies*	*Effluent Polishing Technologies[2]*	*Vapor Phase Treatment Technologies[3]*
• Oil/grease separation[4] • Filtration[5] • Coagulation or flocculation[5] • Clarification or sedimentation[5]	For Organics: • Air stripping • Granular activated carbon • Chemical/UV oxidation • Aerobic biological reactors For Metals: • Chemical precipitation • Ion exchange/adsorption • Electrochemical methods	• Activated carbon • Ion exchange • Neutralization	• Activated carbon • Catalytic oxidation • Thermal incineration • Acid gas scrubbing • Condensation

General Sequence of Ground-Water Treatment Train Unit Processes

Sequence	*Unit Treatment Process*	*Treatment Stage*
Begin	Equalize inflow	Pre-treatment
	Separate solid particles	Pre-treatment
	Separate oil/grease (NAPLs)	Pre-treatment
	Remove metals	Treatment
	Remove volatile organic contaminants	Treatment
	Remove other organic contaminants	Treatment
	Polish organics[2]	Post-treatment
	Polish metals	Post-treatment
End	Adjust pH, if required	Post-treatment

Notes: [1] Technologies that may be required for treatment residuals, such as spent carbon, are not listed.
[2] Effluent polishing technologies are used for the final stage of treatment prior to discharge, and can include pH adjustment (neutralization) as well as additional removal of aqueous constituents.
[3] Vapor phase contaminants released during water treatment may need to be contained and treated. These include organic contaminants volatilized during air stripping, from biological treatment, or other gases released from chemical oxidation, reduction, or biologic processes (e.g., hydrochloric acid, hydrogen sulfide, methane, etc.).
[4] Methods for separating oil and/or grease from water include, but are not limited to, gravity separation and dissolved air floatation. These methods can be used to remove NAPLs from extracted water.
[5] These technologies can be used to remove solid particles at the start of the treatment train or to remove other solids resulting from chemical precipitation, chemical/UV oxidation, or biological treatment.

These same technologies (extraction, excavation, SVE, air sparging and, to a lesser extent, bioremediation) have also been applied to DNAPL source areas where the chemicals have the appropriate properties. Additional technologies are being evaluated for NAPL recovery (i.e., surfactant flushing, steam flushing, alcohol flooding, hot water flooding, and surfactant-enhanced solubilization). Except for excavation, however, there are no proven technologies to remove sufficient DNAPL to fully restore a DNAPL-contaminated aquifer (U.S. EPA, 1992a). Therefore, hydraulic containment will remain an important management option for the DNAPL-contaminated portion of the subsurface.

Away from source areas, bioremediation also can be combined with P&T. Various solutions, including dissolved oxygen and nutrients, can be injected upgradient or within the contaminant plume to enhance biodegradation. At some sites, natural attenuation may be used in conjunction with or following ground-water extraction.

Natural attenuation refers to natural biological, chemical, and physical processes that reduce contaminant concentrations and mass. Also known as intrinsic remediation, it includes destructive chemical transformation processes (radioactive decay, biodegradation, and hydrolysis) and nondestructive partitioning and dilution processes (sorption, volatilization, and dispersion). At many sites, contaminant plume growth is restricted by biodegradation, partitioning, and/or dilution. For example, the limited mobility of many soluble petroleum hydrocarbons, such as BTEX compounds, in ground water due to biodegradation has been particularly well-documented (e.g., Barker et al., 1987).

Natural attenuation processes may be significant factors in contaminant removal and limitations to aqueous-phase contaminant migration at many sites. Field evaluation of such processes and rates is an area of continuing research. Proposed methodologies for evaluating natural attenuation of fuel contaminants are discussed in Wiedemeier et al. (1995) and McAllister and Chiang (1994).

Potentially cost-effective, innovative enhancements and alternatives to P&T (NRC, 1994) are being pilot-tested at many contamination sites. Permeable treatment walls using the funnel-and-gate approach are leading candidate remedial technologies (Starr and Cherry, 1994). These systems are designed to reduce contaminant concentrations in ground water that is passively funneled through a permeable reaction wall, which contains abiotic or biologically reactive media, an air sparge system, or some other enhancement.

Design of Operations and Maintenance

Detailed plans for evaluation of maintenance requirements should be established prior to installation. Establishment of the plan during the design stage allows for incorporation of features to simplify maintenance procedures (e.g., access ports for cleaning distribution piping in infiltration galleries). Maintenance such as pump replacement and well development may be performed on an as needed basis. The required frequency will depend on site conditions and equipment. Equipment manuals may be consulted regarding maintenance requirements for specific system components.

The major causes of decreased well performance include reduction in yield due to incrustation or biofouling of the screen or adjacent materials, formation plugging by fine-grained materials, corrosion or incrustation resulting in increased water velocity and sand pumping, structural failure of the casing or screen, and pump damage (Driscoll, 1986). Periodic monitoring of total depth, pumping rate, drawdown, specific capacity, and efficiency may be used as indicators of maintenance requirements for extraction or injection wells. Injection wells and galleries are particularly susceptible to blockage or fouling and may require frequent maintenance. Maintenance schedules should be sufficiently frequent so as not to compromise system performance with respect to the established design objectives (e.g., maintain capture, maintain specified pore volume flushing rates). Additional discussion of operation and maintenance issues is provided in Driscoll (1986) and Bureau of Reclamation (1995).

Performance Monitoring

P&T performance is monitored by measuring hydraulic heads and gradients, ground-water flow directions and rates, pumping rates, pumped water and treatment system effluent quality, and contaminant distributions in ground water and porous media. These data are evaluated to interpret P&T capture zones, flushing rates, contaminant transport and removal, and to improve system operation. Detailed guidance on methods for monitoring P&T performance is provided by Cohen et al. (1994).

Restoration progress can be assessed by comparing the rate of contaminant mass removal (e.g., plotted as cumulative mass removed) to estimates of the dissolved and/or total contaminant mass-in-place. If the rate of contaminant mass extracted approximates the rate of dissolved mass-in-place reduction, then the contaminants removed by pumping are primarily derived from the dissolved phase. Conversely, a contaminant source (i.e., NAPL, sorbed contaminant, or a continuing release) is indicated where the mass removal rate greatly exceeds the rate of dissolved mass-in-place reduction. Site hydrogeology and contaminant properties should be evaluated to determine if source removal or containment, or P&T system modifications, could improve P&T performance.

The time needed to remove dissolved mass-in-place can be projected by extrapolating the trend of the mass removal rate curve or the cumulative mass removed curve. Future concentration tailing, however, may extend the extrapolated clean-up time. If the mass removal trend indicates a significantly greater clean-up duration than estimated originally, system modification may be necessary. The effect (or lack of effect) of P&T system modifications will be evidenced by the continuing mass removal rate and cumulative mass removed trends.

Progress inferred from mass removal rates can be misleading, however, where NAPL and solid phase contaminants are present (e.g., the mass removed will exceed the initial estimate of dissolved mass-in-place). Interpretation suffers from the high degree of uncertainty associated with estimating NAPL or solid contaminant mass-in-place. Stabilization of dissolved contaminant concentrations while mass removal continues may be an indication of NAPL or solid phase contaminant presence. Methods for evaluating the potential presence of NAPL are provided by Feenstra et al. (1991), Newell and Ross (1992), and Cohen and Mercer (1993).

Mass removal rates are also subject to misinterpretation where dissolved contaminant concentrations decline rapidly due to:

(1) mass transfer rate limitations to desorption, NAPL or precipitate dissolution, or matrix diffusion; (2) dewatering a portion or all of the contaminated zone; (3) dilution of contaminated ground water with clean ground water flowing to extraction wells from beyond the plume perimeter; or (4) the removal of a slug of highly contaminated ground water. Contaminant concentration rebound will occur if pumping is terminated prematurely in response to these conditions.

The projected restoration or clean-up time is site specific and varies widely depending on contaminant and hydrogeologic conditions and the clean-up concentration goal. Estimating clean-up time is complicated by difficulties in quantifying the initial contaminant mass distribution and processes that limit cleanup. Guidance for estimating ground-water restoration times using batch and continuous flushing models is provided by U.S. EPA (1988b). The batch flushing model is based on a series of consecutive discrete flushing periods during which contaminated water in equilibrium with adsorbed contaminants is displaced from the aquifer pore space by clean water. Values of contaminant concentration in soil and water are calculated after each flush. An example of an analogous method (and corrections) to this batch flushing model are provided by Zheng et al. (1991, 1992). The batch and continuous models assume that: (1) zero-concentration influent water displaces contaminated ground water from the contamination zone by simple advection with no dispersion; (2) the clean ground water equilibrates instantaneously with the remaining adsorbed contaminant mass; (3) the sorption isotherm is linear; and (4) chemical reactions do not affect the sorption process. Care must be taken to avoid relying on misleading estimates of restoration time that may be obtained by using these simplified models. Although more sophisticated modeling techniques are available (i.e., contaminant transport models), their application often suffers from data limitations, resulting in uncertain predictions. Nevertheless, clean-up time analyses are useful for assessing alternative remedial options and determining whether or not clean-up goals are feasible.

Disclaimer

The U.S. Environmental Protection Agency through its Office of Research and Development partially funded and collaborated in the research described here under Contract No. 68-C4-0031 to Dynamac Corporation. It has been subjected to the Agency's peer and administrative review and has been approved for publication as an EPA document. Mention of trade names or commercial products does not constitute endorsement or recommendation for use.

Quality Assurance Statement

All research projects making conclusions or recommendation based on environmentally related measurements and funded by the Environmental Protection Agency are required to participate in the Agency Quality Assurance Program. This project did not involve physical measurements and as such did not require a QA plan.

References

Ahlfeld, D.P., J.M. Mulvey, G.F. Pinder, and E.F. Wood, 1988. Contaminated groundwater remediation design using simulation, optimization and sensitivity theory, 1 Model development, *Water Resources Research*, 24(3):431-442.

Ahlfeld, D.P., and C.S. Sawyer, 1990. Well location in capture zone design using simulation and optimization techniques, *Ground Water*, 28(4):507-512.

Allen, H.E., E.M. Perdue, and D.S. Brown, 1993. *Metals in Groundwater*, Lewis Publishers, Boca Raton, FL.

American Petroleum Institute, 1989. A Guide to the Assessment and Remediation of Underground Petroleum Releases, API Publication No. 1628, Washington, DC.

American Petroleum Institute, 1992. Pump and Treat: The Petroleum Industry Perspective, API Publication No. 4561, Washington, DC.

Armstrong, J.E., E.O. Frind, and R.D. McClellan, 1994. Nonequilibrium mass transfer between vapor, aqueous, and solid phases in unsaturated soils during vapor extraction, *Water Resources Research*, 30(2):355-368.

Andersen, P.F., C.R. Faust, and J.W. Mercer, 1984. Analysis of conceptual design for remedial measures at Lipari Landfill, New Jersey, *Ground Water*, 22:176-190.

AWWA, 1990. *Water Quality and Treatment*, American Water Works Association, McGraw-Hill, Inc., New York, NY.

Bahr, J., 1989. Analysis of nonequilibrium desorption of volatile organics during a field test of aquifer decontamination, *Journal of Contaminant Hydrology*, 4(3):205-222.

Bair, E.S., A.E. Springer, and G.S. Roadcap, 1991. Delineation of travel time-related capture areas of wells using analytical flow models and particle tracking analysis, *Ground Water*, 29(3):387-397.

Bair, E.S., and G.S. Roadcap, 1992. Comparison of flow models used to delineate capture zones of wells: Leaky-confined fractured-carbonate aquifer, *Ground Water*, 30(2):199-211.

Barker, J.F., G.C. Patrick, and D. Major, 1987. Natural attenuation of aromatic hydrocarbons in a shallow sand aquifer, *Ground Water Monitoring Review*, 7(1):64-71.

Bear, J., 1972. *Dynamics of Fluids in Porous Media*, American Elsevier Publishing Co., New York, NY.

Blandford, T.N., P.S. Huyakorn, and Y. Wu, 1993. WHPA - A Modular Semi-Analytical Model for the Delineation of Wellhead Protection Areas, U.S. EPA Office of Drinking Water and Ground Water, Washington, DC.

Bonn, B.A., and S.A. Rounds, 1990. *DREAM — Analytical Ground Water Flow Programs*, Lewis Publishers, Boca Raton, FL.

Borden, R.C., and C.M. Kao, 1992. Evaluation of groundwater extraction for remediation of petroleum-contaminated aquifers, *Water Environ. Res.*, 64(1):2836.

Boulding, J.R., 1995. *Practical Handbook of Soil, Vadose Zone, and Ground-Water Contamination Assessment, Prevention, and Remediation*, Lewis Publishers, Boca Raton, FL.

Brogan, S.D., 1991. Aquifer Remediation in the Presence of Rate-Limited Sorption, Masters Thesis, Stanford University, Palo Alto, CA.

Brusseau, M.L., 1993. Complex Mixtures and Groundwater Quality, Environmental Research Brief, EPA/600/S-93/004, U.S. EPA, ORD, R.S. Kerr Environmental Research Laboratory, Ada, OK.

Bureau of Reclamation, 1995. *Ground Water Manual*, U.S. Government Printing Office, Washington, DC.

Carslaw, H.S., and J.C. Jaeger, 1959. *Conduction of Heat in Solids*, Oxford University Press, London, England.

CCEM, 1995. Horizontal News, Vol. 1, No. 1, Colorado Center for Environmental Management for the Department of Energy Office of Technology Development, Denver, CO.

CCEM, 1996. Horizontal drilling survey results. Colorado Center for Environmental Management for the Department of Energy Office of Technology Development, Denver, CO.

CCME, 1994. Subsurface Assessment Handbook for Contaminated Sites, Canadian Council of Ministers of the Environment Report CCME EPC-NCSRP48E.

Cherry, J.A., S. Feenstra, and D.M. Mackay, 1992. Developing rational goals for in situ remedial technologies, *In:* Subsurface Restoration Conference Proceedings, Third International Conference on Ground Water Quality Research, National Center for Ground Water Research Dallas, TX, June 21-24, 1992.

Cohen, R.M., and J.W. Mercer, 1993. *DNAPL Site Evaluation*, C.K. Smoley Press, Boca Raton, FL.

Cohen, R.M., and W.J. Miller, 1983. Use of analytical models for evaluating corrective actions at hazardous waste disposal facilities, *Proceedings of the Third National Symposium on Aquifer Restoration and Ground Water Monitoring*, NWWA, Dublin, OH, pp. 85-97.

Cohen, R.M., A.H. Vincent, J.W. Mercer, C.R. Faust, and C.P. Spalding, 1994. Methods for Monitoring Pump-and-Treat Performance, EPA/600/R-94/123, U.S. EPA, ORD, R.S. Kerr Environmental Research Laboratory, Ada, OK.

Conger, R.M., and K. Trichel, 1993. A ground water pumping application for remediation of a chlorinated hydrocarbon plume with horizontal well technology, *Proceedings of the Seventh National Outdoor Action Conference and Exposition*, NGWA, Dublin, OH, pp. 47-61.

Day, S.R., 1991. Extraction/interception trenches by the bio-polymer slurry drainage trench technique, *Hazardous Materials Control*, Sept/Oct, pp. 27-31.

de Marsily, G., 1986. *Quantitative Hydrogeology: Groundwater Hydrology for Engineers*, Academic Press, Orlando, FL.

Domenico, P.A., and F.W. Schwartz, 1990. *Physical and Chemical Hydrogeology*, John Wiley & Sons, New York, NY.

Driscoll, F.G., 1986. *Ground Water and Wells*, Johnson Division, UOP, St. Paul, MN.

EPRI, 1989. Techniques to Develop Data for Hydrogeochemical Models, Electric Power Research Institute Report EA-6637, Palo Alto, CA.

Evans, J.C., 1991. Geotechnics of hazardous waste control systems, Chapter 20, *Foundation Engineering Handbook*, 2nd ed., H.Y. Fang, ed., Van Nostrad-Reinhold Co., New York, NY.

Faust, C.R., P.N. Sims, C.P. Spalding, P.F. Andersen, B.H. Lester, M.G. Shupe, and A. Harrover, 1993. FTWORK: Groundwater Flow and Solute Transport in Three Dimensions, Version 2.8, GeoTrans, Inc., Sterling, VA.

Feenstra, S., D.M. Mackay, and J.A. Cherry, 1991. A method for assessing residual NAPL based on organic chemical concentrations in soil samples, *Ground Water Monitoring Review*, 11(2):128-136.

Felmy, A.R., D.C. Girvin, and E.A. Jenne, 1984. MINTEQ: A Computer Program for Calculating Aqueous Geochemical Equilibria, EPA/600/3-84/032, U.S. EPA, Washington, DC.

Ferris, J.G., 1963. Cyclic water-level fluctuations as a basis for determining aquifer transmissivity, in Methods for Determining Permeability, Transmissibility and Drawdown, U.S. Geological Survey Water-Supply Paper 1536-I, pp. 305-318.

Fetter, C.W., 1993. *Contaminant Hydrogeology*, Macmillan Publishing Company, New York, NY.

Fitts, C.R., 1989. Simple analytic functions for modeling three-dimensional flow in layered aquifers, *Water Resources Research*, 25(5):943-948.

Fitts, C.R., 1994. Well discharge optimization using analytic elements, *Ground Water*, 32(4):547-550.

Fitts, C.R., 1995. TWODAN manual, Scarborough, ME.

Freeberg, K.M., P.B. Bedient, and J.A. Connor, 1987. Modeling of TCE contamination and recovery in a shallow sand aquifer, *Ground Water*, 25:70-80.

Gailey, R.M., and S.M. Gorelick, 1993. Design of optimal, reliable plume capture schemes: Application to the Gloucester landfill ground-water contamination problem, *Ground Water*, 31(1):107-114.

Gilbert, S.G., and J.J. Gress, 1987. Interceptor trenches for positive ground-water control, *Ground Water Monitoring Review*, 7(2):55-59.

Gillham, R.W., E.A. Sudicky, J.A. Cherry, and E.O. Frind, 1984. An advective-diffusive concept for solute transport in heterogeneous unconsolidated geologic deposits, *Water Resources Research*, 20(3):369-378.

Gorelick, S.M., 1983. A review of distributed parameter groundwater management modeling methods, *Water Resources Research*, 19(2):305-319.

Gorelick, S.M., R.A. Freeze, D. Donohue, and J.F. Keely, 1993. *Groundwater Contamination Optimal Capture and Containment*, Lewis Publishers, Boca Raton, FL.

Greenwald, R.M., 1993. MODMAN - An Optimization Module for MODFLOW, Version 2.1, Documentation and User's Guide, GeoTrans, Inc., Sterling, VA.

Grisak, G.E., and J.F. Pickens, 1980. Solute transport through fractured media: 1. The effect of matrix diffusion, *Water Resources Research*, 16:719-730.

Grube, W.E., Jr., 1992. Slurry trench cut-off walls for environmental pollution control, *Slurry Walls: Design, Construction and Quality Control*, ASTM STP 1129, D.B. Paul, R.R. Davidson, and N.J. Cavalli, eds., American Society for Testing and Materials, Philadelphia, PA.

Grubb, D.G., and N. Sitar, 1994. Evaluation of Technologies for In-Situ Cleanup of DNAPL Contaminated Sites, EPA/600/R-94/120, U.S. EPA, ORD, R.S. Kerr Environmental Research Laboratory, Ada, OK.

Hagemeyer, R.T., P.F. Andersen, R.M. Greenwald, and J.L. Clausen, 1993. Evaluation of alternative plume containment designs at the Paducah Gaseous Diffusion Plant Using MODMAN, a well pumpage optimization module for MODFLOW, *Proceedings of the 1993 Ground Water Modeling Conference*, IGWMC, Colorado School of Mines, Golden, CO, pp. 2-42 to 2-51.

Haggerty, R., and S.M. Gorelick, 1994. Design of multiple contaminant remediation: Sensitivity to rate-limited mass transport, *Water Resources Research*, 30(2):435-446.

Haitjema, H.M., J. Wittman, V. Kelson, and N. Bauch, 1994. WhAEM: Program Documentation for the Wellhead Analytical Element Model, EPA/600/R-94/210, U.S. EPA, ORD, R.S. Kerr Environmental Research Laboratory, Ada, OK.

Haley, J.L., B. Hanson, C. Enfield, and J. Glass, 1991. Evaluating the effectiveness of ground water extraction systems, *Ground Water Monitoring Review*, 11(1):119-124.

Harvey, C.F., R. Haggerty, and S.M. Gorelick, 1994. Aquifer remediation: A method for estimating mass transfer rate coefficients and an evaluation of pulsed pumping, *Water Resources Research*, 30(7):1979-1991.

Jacob, C.E., 1950. Flow of ground water, in *Engineering Hydraulics*, Rouse, H., ed., John Wiley & Sons, New York, NY, pp. 321-386.

Javandel, I., C. Doughty, and C.F. Tsang, 1984. *Groundwater Transport: Handbook of Mathematical Models*, American Geophysical Union Water Resources Monograph No. 10, Washington, DC.

Javandel, I., and C.F. Tsang, 1986. Capture-zone type curves: A tool for aquifer cleanup, *Ground Water*, 24:616-625.

Kaback, D.S., B.B. Looney, J.C. Corey, L.M. Wright, and J.L. Steele, 1989. Horizontal wells for in situ remediation of ground water and soils, *Proceedings of the Third National Outdoor Action Conference on Aquifer Restoration, Ground Water Monitoring, and Geophysical Methods*, NWWA, Dublin, OH, pp. 121-135.

Kaback, D.S., B.B. Looney, C.A. Eddy, and T.C. Hazen, 1991. Innovative ground-water and soil remediation: In situ air-stripping using horizontal wells, *Proceedings of the Fifth National Outdoor Action Conference on Aquifer Restoration, Monitoring, and Geophysical Methods, NWWA*, Dublin, OH, pp. 47-58.

Karlsson, H., and R. Bitto, 1990. New horizontal wellbore system for monitoring and remedial wells, *Proceedings of the 11th National Superfund Conference*, HMCRI, Silver Spring, MD, pp. 357-362.

Keely, J.F., 1989. Performance Evaluation of Pump-and-Treat Remediations, EPA/540/4-89/005, U.S. EPA, ORD, R.S. Kerr Environmental Research Laboratory, Ada, OK.

Kharaka, Y.K., W.D. Gunter, P.K. Aggarwal, and E.H. Perkins, 1988. SOLMINEQ.88 - Solution-mineral equilibrium computations., U.S. Geological Survey, Menlo Park, CA.

Konikow, L.F., and J.D. Bredehoeft, 1989. Computer Model of Two-Dimensional Solute Transport and Dispersion in Ground Water, U.S. Geological Survey, Reston, VA.

Kruseman, G.P., and N.A. deRidder, 1990. *Analysis and Evaluation of Pumping Test Data*, International Institute of Land Reclamation and Improvement, Bulletin 11, 2nd ed., Wageningen, The Netherlands.

Langseth, D.E., 1990. Hydraulic performance of horizontal wells, *Proceedings of the 11th National Superfund Conference*, HMCRI, Silver Spring, MD, pp. 398-408.

Lefkoff, L.J., and S.M. Gorelick, 1987. AQMAN: Linear and Quadratic Programming Matrix Generator Using Two-dimensional Groundwater Flow Simulation for Aquifer Management Modeling, U.S. Geological Survey Water Resources Investigations Report 87-4061.

Long, G.M., 1993. Clean up hydrocarbon contamination effectively, *Chemical Engineering Progress*, 89(5).

Mackay, D.M., and J.A. Cherry, 1989. Groundwater contamination: Pump-and-treat remediation, *Environmental Science and Technology*, 23(6):620-636.

Marquis, Jr., S.A., and D. Dineen, 1994. Comparison between pump and treat, biorestoration, and biorestoration/pump and treat combined: Lessons from computer modeling, *Ground Water Monitoring and Remediation*, 14(2):105-119.

McAllister, P.M., and C.Y. Chiang, 1994. A practical approach to evaluating natural attenuation of contaminants in ground water, *Ground Water Monitoring and Remediation*, 14(2):161-173.

McCaulou, D.R., D.G. Jewett, and S.G. Huling, 1995. Nonaqueous Phase Liquids Compatibility with Materials Used in Well Construction, Sampling, and Remediation, EPA/540/S-95/503, Ground Water Issue Paper, U.S. EPA, ORD, R.S. Kerr Environmental Research Laboratory, Ada, OK.

McDonald, M.G., and A.W. Harbaugh, 1988. A Modular Three-Dimensional Finite-Difference Groundwater Flow Model, U.S. Geological Survey Techniques of Water-Resources Investigations, Book 6, Chapter A1, Reston, VA.

McKay, L.D., R.W. Gillham, and J.A. Cherry, 1993. Field experiments in a fractured clay till: 2. Solute and colloid transport, *Water Resources Research*, 29:3879-3890.

Meini, D., M. Ghiasi, R.J. Patterson, N. Ramanujam, and M.P. Tyson, 1990. Extraction of TCE-contaminated ground water by subsurface drains and a pumping well, *Ground Water*, 28(1):17-24.

Mercer, J.W., D.C. Skipp, and D. Giffin, 1990. Basics of Pump-and-Treat Groundwater Remediation, EPA/600/8-90/003, U.S. EPA, ORD, R.S. Kerr Environmental Research Laboratory, Ada, OK.

Montgomery, J.H., and L.M. Welkom, 1990. *Groundwater Chemicals Desk Reference*, Lewis Publishers, Boca Raton, FL.

Morgan, J.H., 1992. Horizontal drilling applications of petroleum technologies for environmental purposes, *Ground Water Monitoring Review*, 12(3):98-101.

Myrand, D., R.W. Gillham, E.A. Sudicky, S.F. O'Hannesin, and R.L. Johnson, 1992. Diffusion of volatile organic compounds in natural clay deposits: Laboratory tests, *Journal of Contaminant Hydrology*, 10:159-177.

NRC, 1994. *Alternatives for Ground Water Cleanup*, National Research Council, National Academy Press, Washington, DC.

Newell, C.J., S.D. Acree, R.R. Ross, and S.G. Huling, 1995. Light Nonaqueous Phase Liquids, EPA/540/S-95/500, U.S. EPA, ORD, R.S. Kerr Environmental Research Laboratory, Ada, OK.

Newell, C.J., and R.R. Ross, 1992, Estimating potential for occurrence of DNAPL at Superfund sites, U.S. EPA Quick Reference Fact Sheet, U.S. EPA, ORD, R.S. Kerr Environmental Research Laboratory, Ada, OK.

Newsom, J.M., and J.L. Wilson, 1988. Flow of ground water to a well near a stream — Effect of ambient ground-water flow direction, *Ground Water*, 26(6):703-711.

Nielsen, D.M., ed., 1991. *Practical Handbook of Ground-Water Monitoring*, Lewis Publishers, Boca Raton, FL.

Noyes, R., 1994. *Unit Operations in Environmental Engineering*, Noyes Publications, Park Ridge, NJ.

Nyer, E.K., 1992. *Groundwater Treatment Technology*, Van Nostrand-Reinhold, New York, NY.

Osborne, P.S., 1993. Suggested Operating Procedures for Aquifer Pumping Tests, Ground Water Issue Paper, EPA/540/S-93/503, U.S. EPA, ORD, R.S. Kerr Environmental Research Laboratory, Ada, OK.

OTA, 1984. Protecting the Nation's Groundwater from Contamination, U.S. Congressional Office of Technology Assessment, OTA-O-276, Volumes I and II, Washington, DC.

Palmer, C.D., and W. Fish, 1991. Physicochemical processes: Inorganic contaminants, in Site Characterization for Subsurface Remediation, U.S. EPA Seminar Publication, EPA/925/4-91/026, U.S. EPA, ORD, R.S. Kerr Environmental Research Laboratory, Ada, OK, pp. 179-192.

Palmer, C.D., and W. Fish, 1992. Chemical Enhancements to Pump-and-Treat Remediation, U.S. EPA Ground Water Issue Paper, EPA/540/S-92/001, U.S. EPA, ORD, R.S. Kerr Environmental Research Laboratory, Ada, OK.

Pankow, J.F., and J.A. Cherry, eds, 1995. *Dense Chlorinated Solvents and Other DNAPLs in Groundwater: History, Behavior, and Remediation*, Waterloo Press, Waterloo, Ontario, Canada.

Papadopulos, S.S., 1965. Nonsteady flow to a well in an infinite anisotropic aquifer, *Proceedings of Symposium International Association of Scientific Hydrology*, Dubrovnik, pp. 21-31.

Parker, B.L., R.W. Gillham, and J.A. Cherry, 1994. Diffusive disappearance of immiscible phase organic liquids in fractured geologic media, *Ground Water*, 32(5):805-820.

Parkhurst, D.L., D.C. Thorstenson, and L.N. Plummer, 1980. PHREEQE - A Computer Program for Geochemical Calculations, U.S. Geological Survey Water Resources Investigation 80-96, USGS, Reston, VA.

Pollock, D.W., 1994. User's Guide for MODPATH, MODPATH-PLOT, Version 3: A Particle Tracking Post-Processing Package for MODFLOW, U.S. Geological Survey Open-File Report 94-464, USGS, Reston, VA.

Powers, S.E., C.O. Loureiro, L.M. Abriola, and W.J. Weber, Jr., 1991. Theoretical study of the significance of nonequilibrium dissolution of nonaqueous phase liquids in subsurface systems, *Water Resources Research*, 27(4):463-477.

Pyne, R.D.G., 1995. *Groundwater Recharge and Wells, A Guide to Aquifer Storage Recovery*, Lewis Publishers, Boca Raton, FL.

Rabideau, A.J., and C.T. Miller, 1994. Two-dimensional modeling of aquifer remediation influenced by sorption nonequilibrium and hydraulic conductivity heterogeneity, *Water Resources Research*, 30(5):1457-1470.

Repa, E., and C. Kufs, 1985. Leachate Plume Management, EPA/540/2-85/004, U.S. EPA, Hazardous Waste Engineering Research Laboratory, Office of Research and Development, Cincinnati, OH.

Rifai, H.S., P.B. Bedient, R.C. Borden, and J.F. Haasbeek, 1987. BIOPLUME II - Computer model of two-dimensional contaminant transport under the influence of oxygen limited biodegradation in ground water, Version 1.0, EPA/600/8-88-093, February 1989.

Rumbaugh, J.O., 1991. Quick Flow: Analytical ground-water flow model, Version 1.0, Geraghty and Miller, Plainview, NY.

Rumer, R.R. and M.E. Ryan, eds., 1995. *Barrier Containment Technologies for Environmental Remediation Applications*, John Wiley & Sons, Inc., New York, NY.

Runnells, 1993. Inorganic chemical processes and reactions, in Regional Ground-Water Quality, W.M. Alley, ed., Van Nostrand-Reinhold, New York, pp. 131-153.

Sara, M.N., 1994. *Standard Handbook for Solid and Hazardous Waste Facility Assessments*, Lewis Publishers, Boca Raton, FL.

Saroff, S.T., H. He, and G. Powell, 1992. Hydrogeological implications of saprolite aquifer remediation at Fairfax, Virginia, oil spill, *Proceedings of HMCRI's 13th Annual National Conference and Exhibition*, Hazardous Materials Control Research Institute, Silver Spring, MD, pp. 407-412.

Satkin, R.L., and P.B. Bedient, 1988. Effectiveness of various aquifer restoration schemes under variable hydrogeologic conditions, *Ground Water*, 26(4):488-498.

Schmelling, S.G., and R.R. Ross, 1989. Contaminant Transport in Fractured Media: Models for Decision Makers, U.S. EPA Ground Water Issue Paper, EPA/540/4-89/004, U.S. EPA, ORD, R.S. Kerr Environmental Research Laboratory, Ada, OK.

Shafer, J.M., 1987a. Reverse pathline calculation of time-related capture zones in nonuniform flow, *Ground Water*, 25(3):282-289.

Shafer, J.M., 1987b. GWPATH: Interactive Groundwater Flow Path Analysis, Illinois State Water Survey, Bulletin 69.

Starr, R.C., and J.A. Cherry, 1994. In situ remediation of contaminated ground water: The funnel-and-gate system, *Ground Water*, 32(3):465-476.

Strack, O.D.L., 1989. *Groundwater Mechanics*, Prentice Hall, Englewood Cliffs, NJ.

Strack, O.D.L., E.I. Anderson, M. Bakker, W.C. Olsen, J.C. Panda, R.W. Pennings, and D.R. Steward, 1994. CZAEM User's Guide: Modeling Capture Zones of Ground-Water Using Analytic Elements, EPA/600/R-94/174, Office of Research and Development, Cincinnati, OH.

Stumm, W., 1992. *Chemistry of the Solid-Water Interface*, John Wiley & Sons, New York, NY.

Tiedeman, C., and S.M. Gorelick, 1993. Analysis of uncertainty in optimal groundwater contaminant capture design, *Water Resources Research*, 29(7):2139-2153.

Trescott, P.C., G.F. Pinder, and S.P. Larson, 1976. Finite-Difference Model for Aquifer Simulation in Two Dimensions with Results of Numerical Experiments, U.S. Geological Survey Techniques of Water Resource Investigations Book 7, Chapter C1, USGS, Reston, VA.

Truesdell, A.H., and B.F. Jones, 1974. WATEQ: A Computer Program for Calculating Chemical Equilibria of Natural Waters, U.S. Geological Survey Journal of Research, 2:233-248.

U.S. EPA, 1975. Manual of Water Well Construction Practices, EPA-570/9-75/001, Office of Water Supply, Washington, DC.

U.S. EPA, 1984. Slurry Trench Construction for Pollution Migration Control, EPA-540/2-84/001, U.S. EPA, Municipal Environmental Research Laboratory, Office of Research and Development, Cincinnati, OH.

U.S. EPA, 1988a. Guidance for Conducting Remedial Investigations and Feasibility Studies under CERCLA, EPA/540/G-89/004, U.S. EPA, Washington, DC.

U.S. EPA, 1988b. Guidance on Remedial Actions for Contaminated Ground Water at Superfund Sites, EPA/540/G-99/003, OSWER Directive 9283.1-2, U.S. EPA, Washington, DC.

U.S. EPA, 1989. Guide for Conducting Treatability Studies Under CERCLA, EPA/540/2-89/058, U.S. EPA, Office of Research and Development, Cincinnati, OH.

U.S. EPA, 1991a. Site Characterization for Subsurface Remediation, Seminar Publication, EPA/625/4-91/026, U.S. EPA, Center for Environmental Research Information, Office of Research and Development, Cincinnati, OH.

U.S. EPA, 1991b. Handbook — Stabilization Technologies for RCRA Corrective Actions, EPA/625/6-91/026, U.S. EPA, Office of Research and Development, Washington, DC.

U.S. EPA, 1992a. Dense nonaqueous phase liquids — A workshop summary, Dallas, Texas, April 17-18, 1991, EPA/600/R-92/030, U.S. EPA, ORD, R.S. Kerr Environmental Research Laboratory, Ada, OK.

U.S. EPA, 1992b. Evaluation of Ground-Water Extraction Remedies, U.S. EPA, Office of Emergency and Remedial Response, Washington, DC.

U.S. EPA, 1992c. RCRA Corrective Action Stabilization Technologies, EPA/625/R-92/014, U.S. EPA, Office of Research and Development, Washington, DC.

U.S. EPA, 1993a. Guidance for evaluating the technical impracticability of ground-water restoration, Directive 9234.2-25, Interim Final, U.S. EPA, Office of Solid Waste and Emergency Response, Washington, DC.

U.S. EPA, 1993b. Subsurface Characterization and Monitoring Techniques, A Desk Reference Guide, Volumes I and II, EPA/625/R-93/003, U.S. EPA, Washington, DC.

U.S. EPA, 1994a. Manual - Ground-Water and Leachate Treatment Systems, EPA/625/R-94/005, U.S. EPA, Office of Research and Development, Cincinnati, OH.

U.S. EPA, 1994b. Alternative Methods for Fluid Delivery and Recovery, EPA/625/R-94/003, U.S. EPA, Center for Environmental Research Information, Cincinnati, OH.

U.S. EPA, 1995. How to Evaluate Alternate Cleanup Technologies for Underground Storage Tank Sites, EPA/510/B-94/003, U.S. EPA, Office of Underground Storage Tanks, Washington, DC.

U.S. EPA, 1996. Presumptive Response Strategy and Ex-Situ Treatment Technologies for Contaminated Ground Water at CERCLA Sites, U.S. EPA, Office of Solid Waste and Emergency Response, EPA/540/R-96/023.

van der Heijde, P.K.M., and O.A. Elnawawy, 1993. Compilation of Ground-Water Models, EPA/600/R-93/118, U.S. EPA, ORD, R.S. Kerr Environmental Research Laboratory, Ada, OK.

Wagner, B.J., and S.M. Gorelick, 1987. Optimal groundwater quality management under parameter uncertainty, *Water Resources Research*, 23(7):1162-1174.

Ward, D.S., D.R. Buss, J.W. Mercer, and S.S. Hughes, 1987. Evaluation of a groundwater corrective action at the Chem-Dyne hazardous waste site using a telescopic mesh refinement modeling approach, *Water Resources Research*, 23(4):603-617.

Ward, D.S., A.L. Harrover, A.H. Vincent, and B.H. Lester, 1993. Data Input Guide for SWIFT/486, GeoTrans, Inc., Sterling, VA.

WEF, 1994. Pretreatment of Industrial Wastes, Manual of Practice No. FD-3, Water Environment Federation, Alexandria, VA.

Wiedemeier, T.H., J.T. Wilson, D.H. Kampbell, R.N. Miller, and J.E. Hansen, 1995. Technical Protocol for Implementing Intrinsic Remediation with Long-Term Monitoring for Natural Attenuation of Fuel Contamination Dissolved in Groundwater, Volume I, Air Force Center for Environmental Excellence, Brooks AFB, San Antonio, TX.

Wilson, J.L., 1984. Double-cell hydraulic containment of pollutant plumes, *Proceedings of the Fourth National Symposium and Exposition on Aquifer Restoration and Ground Water Monitoring*, NWWA, Dublin, OH, pp. 65-70.

Wolery, T.J., 1979. Calculations of Chemical Equilibrium between Aqueous Solutions and Minerals: The EQ3/6 Software Package, UCRL-52658, Lawrence Livermore Laboratory, Livermore, CA.

WSRC, 1993. Summary Report of the Drilling Technologies Tested at the Integrated Demonstration Site, WSRC-TR-93-565, Westinghouse Savannah River Company, Aiken, SC.

Zheng, C., 1990. PATH3D - A Ground-Water Path and Travel-Time Simulator, Version 2.0, User's Manual, S.S. Papadopulos and Associates, Bethesda, MD.

Zheng, C., 1992. MT3D - A Modular Three-Dimensional Transport Model for Simulation of Advection, Dispersion, and Chemical Reactions of Contaminants in Groundwater Systems, S.S. Papadopulos and Associates, Bethesda, MD.

Zheng, C., G.D. Bennett, and C.B. Andrews, 1991. Analysis of ground-water remedial alternatives at a Superfund site, *Ground Water*, 29(6):838-848.

Zheng, C., G.D. Bennett, and C.B. Andrews, 1992. Reply to discussion of analysis of ground-water remedial alternatives at a Superfund site, *Ground Water*, 30(3):440-442.

Appendix A

Limitations for Conventional P&T Technology

Widespread experience with P&T systems during the past 15 years indicates that their ability to reduce and maintain dissolved contaminant concentrations below clean-up standards in reasonable time frames is hindered at many sites due to complex hydrogeologic conditions, contaminant chemistry factors, and inadequate system design (Keely, 1989; Mercer et al., 1990; U.S. EPA, 1993a; NRC, 1994; and Cohen et al. 1994). Hydrogeologic conditions that confound ground-water cleanup include the presence of complex sedimentary deposits, low permeability formations, and fractured bedrock. Chemical processes that cause contaminant concentration tailing and rebound during and after P&T operation, respectively, and thereby impede complete aquifer restoration, include: (1) the presence and slow dissolution of nonaqueous phase liquids (NAPLs); (2) contaminant partitioning between ground water and porous media; and (3) contaminant diffusion into low permeability regions that are inaccessible to flowing ground water. These limitations may render restoration using only conventional P&T technology impracticable at some sites.

NAPL Dissolution

NAPLs that are denser than water (DNAPLs), in particular, exacerbate ground-water restoration efforts. This is due to their prevalence at contamination sites, their complex subsurface migration behavior and distribution, their low aqueous solubility, and limits to DNAPL removal using available technologies (U.S. EPA, 1992a; Grubb and Sitar, 1994; and Pankow and Cherry, 1995). Greater success has been achieved remediating petroleum hydrocarbon LNAPLs using conventional methods and enhanced technologies such as soil vapor extraction, bioremediation, and air sparging.

Subsurface NAPL trapped as ganglia at residual saturation or contained in pools can be a long-term source of ground-water contamination, as illustrated in Figure 8-d, due to its limited aqueous solubility that may greatly exceed drinking water standards. At many sites, NAPL pools will continue to contaminate ground water long after residual fingers and ganglia have dissolved completely (Cohen and Mercer, 1993). If NAPLs are not removed (e.g., by excavation) or contained (as depicted in Figure 2), then tailing and rebound will occur during and after P&T operation, respectively, in and downgradient of the NAPL zone. Above residual saturation, NAPL will flow unless it is immobilized in a stratigraphic trap or by hydrodynamic forces. NAPL movement can greatly expand the subsurface volume where restoration is impractical. A critical element of site characterization, therefore, is to delineate the nature and extent of mobile and residual NAPL so that these source areas can be removed or contained. Detailed guidance on NAPL site characterization is provided by American Petroleum Institute (1989), U.S. EPA (1992a), Cohen and Mercer (1993), and Newell et al. (1995).

Contaminant Sorption and Desorption

Sorption/desorption also cause tailing, concentration rebound, and slow ground-water restoration. As dissolved contaminant concentrations are reduced by P&T operation, contaminants sorbed to subsurface media desorb from the matrix and dissolve in ground water. The volume of ground water that must be passed through a contamination zone to attain clean-up standards increases with contaminant sorption and kinetic limitations to the rate of desorption.

Equilibrium contaminant partitioning between porous media and ground water can be described by the Langmuir or Freundlich isotherms (Figure A-1). For the linear isotherms (N = 1) and for limited ranges of C_w (particularly at low concentration) where N $\neq$ 1, the Freundlich constant, K_f, can be identified as a soil-water distribution coefficient, K_d:

$$K_d = C_s / C_w \qquad \text{(A-1)}$$

where C_s and C_w are the equilibrium contaminant concentrations in soil and water, respectively.

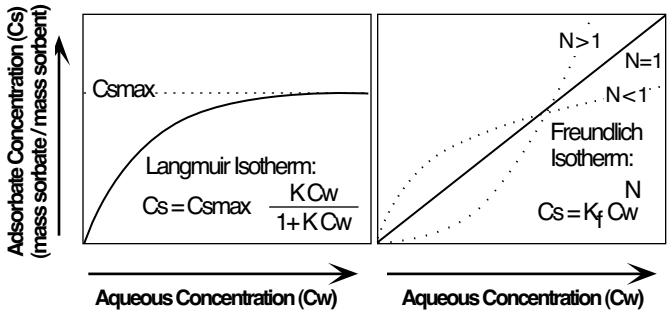

Figure A-1 The Langmuir and Freundlich adsorption isotherms (modified from Palmer and Fish, 1992).

Contaminant K_d values must be characterized to predict ground-water restoration times for different P&T schemes or for natural ground-water flushing. By assuming that sorption is instantaneous, reversible, and linear, K_d values can be used to estimate: (1) the retardation factor, R,

$$R = 1 + K_d \rho_b / n \qquad \text{(A-2)}$$

and (2) the equilibrium distribution of contaminant mass between the solid and aqueous phases

$$f_w = C_w V_w / [(C_w V_w)+(C_s M_s)] = V_w / (V_w + K_d M_s) \quad \text{(A-3)}$$

where ρ_b is the dry bulk density of the media, n is the media porosity, V_w is the volume of water in the total subject volume, M_s is the mass of solids in the total subject volume, and f_w is the fraction of mass residing in the aqueous phase.

Although the ratio of bulk density to porosity is typically within a range of four to six, K_d values for different contaminants vary over orders-of-magnitude (e.g., Montgomery and Welkom, 1990). Thus, contaminant velocity and P&T restoration time are particularly sensitive to soil-water partitioning (K_d values) of ground-water contaminants.

The nonlinearity of contaminant desorption and difficulty of contaminant removal appear to increase with the duration of contaminant presence in the subsurface (Brusseau, 1993). Thus, old plumes are likely to exhibit significant nonideal behavior. Conversely, ground-water cleanup may be simplified if remedial efforts are undertaken quickly after the occurrence of a contaminant release.

Sorption and retardation values vary between different contaminants at a given site and between different sites for a given contaminant (Mackay and Cherry, 1989). As depicted in Figure 8, desorption and retardation increase the volume of ground water that must be pumped to attain dissolved contaminant concentration reductions. Tailing and rebound effects will be exacerbated where desorption is slow relative to ground-water flow and kinetic limitations prevent sustenance of equilibrium contaminant concentrations in ground water (Bahr, 1989; Brogan, 1991; Haley et al., 1991; and Palmer and Fish, 1992). This concept is illustrated in Figure A-2.

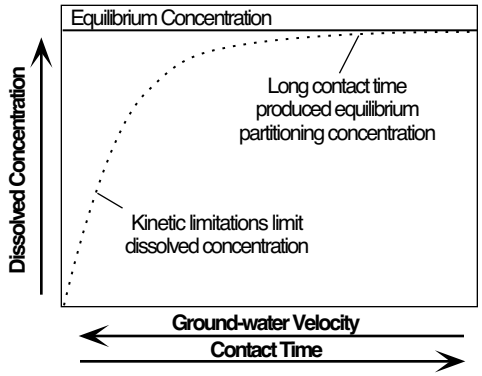

Figure A-2. Relationship between ground-water velocity and the concentration of dissolved contaminants that (a) desorb from porous media, (b) dissolve from precipitates, or (c) dissolve from NAPL (modified from Keely, 1989). Kinetic limitations to dissolution exacerbate tailing.

Solids Dissolution

Important physicochemical processes that affect the solubility, reactivity, mobility, and toxicity of inorganic contaminants include: (1) chemical speciation, (2) oxidation/reduction, (3) dissolution/ precipitation, (4) ion exchange and sorption, and (5) particle transport (Palmer and Fish, 1991). Inorganic contaminants occur in many different chemical forms or "species." Knowing the total concentration of an inorganic element in ground water or soil, as commonly provided by laboratory analysis, may be of little value (alone) in assessing its subsurface behavior. Rather, it is often more important to determine contaminant speciation which depends on several factors including pH, Eh, ion and gas concentrations, and temperature. For example, metal cations combine with different anions to form aqueous complexes that increase the solubility, mobility, and risk associated with potentially toxic metals such as chromium and arsenic.

Given the complex interaction between solid minerals, inorganics, and environmental factors (such as Eh-pH relations), computer codes are used to assess the solubility and geochemical behavior of inorganic species in ground water. Codes used to evaluate mineral solubility, saturation, and chemical speciation include WATEQ (Truesdell and Jones, 1974), SOLMINEQ88 (Kharaka et al., 1988) and mass transfer codes, such as PHREEQE (Parkhurst et al., 1980), EQ3/EQ6 (Wolery, 1979), and MINTEQ (Felmy et al., 1984), that can also be used to deduce equilibrium chemical reactions. Data requirements for these codes typically include field analysis of ground-water samples for pH, temperature, Eh or dissolved oxygen, and alkalinity, and a complete inorganic chemical analysis for all major and minor ions and all metals and anions under investigation.

Besides conducting thorough chemical analyses for speciation studies, investigations should be conducted to delineate inorganic contaminant plumes and estimate plume migration rates. Mineralogical characterization efforts can be used to identify solid phases (e.g., clay minerals and Fe and Mn oxyhydroxides) that control inorganic contaminant partitioning (EPRI, 1989). Sorption-desorption and other tests can be conducted to assess inorganic contaminant partitioning, solubility, and mobility as a function of pH and other factors, and the potential for aquifer restoration. Additional information relevant to assessing inorganic ground-water contamination is given by EPRI (1989), Domenico and Schwartz (1990), Palmer and Fish (1991), Stumm (1992), Fetter (1993), Runnells (1993), and Allen et al. (1993).

Ground-Water Velocity Variation

Tailing and rebound also result from variable travel times associated with different flowpaths taken by contaminants to extraction wells. Ground water at the edge of a capture zone travels a greater distance under a lower hydraulic gradient than ground water closer to the center of the capture zone. Travel times also vary as a function of initial contaminant distribution and hydraulic conductivity differences. If pumping is stopped, rebound will occur wherever the resulting flowpath modification diminishes contaminant dilution. Permeability and contaminant distributions should be characterized to facilitate analysis of ground-water stagnation and velocity variations that would be induced by alternative pumping schemes.

Matrix Diffusion

As contaminants advance through relatively permeable pathways in heterogeneous media, concentration gradients cause diffusion of contaminant mass into the less permeable media and thereby retard solute velocity relative to ground water (Gillham et al., 1984). During a P&T operation, dissolved contaminant concentrations in the relatively permeable zones may be quickly

reduced by advective flushing relative to the less permeable zones. This causes a reversal in the initial concentration gradient and the slow diffusion of contaminants from the low to high permeability media. This slow process can cause long-term tailing and rebound after the termination of pumping.

Matrix diffusion may dictate the time necessary for complete remediation, particularly in heterogeneous and fractured media where transport via preferential pathways results in large concentration gradients (Grisak and Pickens, 1980; McKay et al., 1993; and Parker et al., 1994). For example, consider a sand aquifer with clay lenses that was contaminated for a long time before commencing P&T operation. Advective transport induced by pumping may quickly reduce contaminant concentrations in the sand. Concentrations in the clay lenses, however, will decrease slowly as contaminants slowly diffuse from the clay to the sand. The areal extent of the clay is such that an approximation of one-dimensional diffusion out of each lens can be used to estimate the time needed to reduce contaminant concentrations in the clay. If (C_o) is a uniform initial contaminant concentration in a clay lens of thickness m, and that P&T maintains a very low concentration in the sand, then the time required for diffusion to reduce the average relative contaminant concentration (C/C_o) in a clay lens can be estimated by (Carslaw and Jaeger, 1959, p. 97):

$$\frac{C}{C_0} = \frac{8\,C_0}{\pi^2} \sum_{n=0}^{\infty} \frac{1}{(2n+1)^2} \exp\left(-\frac{D^0}{\alpha R m^2} (2n+1)^2 \pi^2 t \right) \qquad \text{(A-4)}$$

where R is the retardation factor, α is tortuosity (typically = 1.6 to 1.3 in granular media; Bear, 1972), D^o is the free water diffusion coefficient, and t is time. Considering typical free water diffusion coefficients for organic contaminants (1×10^{-5} to 1×10^{-6} cm ^{2}/sec), changes in C/C_o in clay lenses of different thickness are shown as a function of time in Figure A-3, and indicate that matrix diffusion can greatly increase aquifer clean-up time.

The potential for matrix diffusion to cause tailing and rebound can be assessed based on (1) knowledge of the contaminant concentration history in the subsurface, (2) site stratigraphy, (3) chemical analyses conducted on vertical core samples taken from low-permeability matrix material, (4) diffusion modeling, and (5) review of P&T monitoring data. Estimates of water diffusion coefficients for various contaminants and media are available in the literature (Parker et al., 1994) or can be, but rarely are, measured in a laboratory (Myrand et al., 1992).

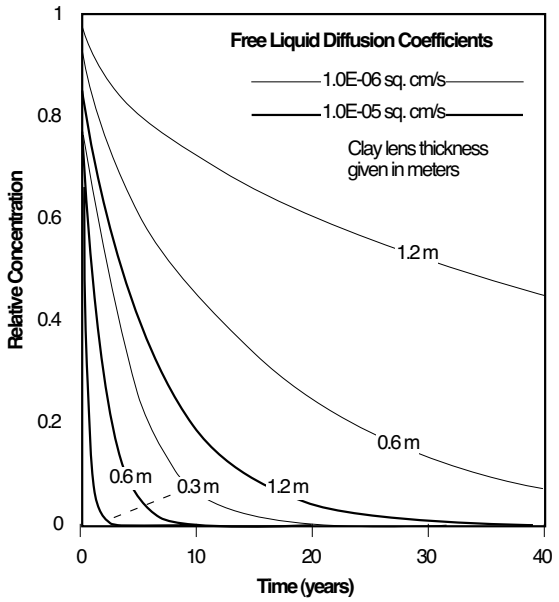

Figure A-3. Changes in average relative contaminant concentration in clay lenses of specified thickness due to diffusion to adjacent clean zones during P&T (based on typical diffusion coefficient and tortuosity values).

Appendix B

Selected Ground-Water Treatment Technologies Available as Package Plants

(modified from U.S. EPA, 1994a; Boulding, 1995)

Method	*Process Description*	*Package Plant Components and Sizes* *(Dimensions are for overall plant envelope)*	*Advantages and Limitations*
Air Stripping Widely used to remove volatile contaminants from ground water.	Volatile contaminants are transferred from water to gas phase by passing air or steam through water in a tall packed tower, shallow tray tower, or stripping lagoons. The air stream containing volatile contaminants may require treatment (e.g., with vapor-phase carbon). Stripping with steam may be cost-effective for water containing a mix of relatively nonvolatile and volatile compounds, particularly at industrial facilities where steam is readily available.	Package plants include tall packed tower or compact low profile diffuser tray units, feed pump, air blower, and effluent pump. Flow meters for influent and air flow are required. An influent throttle valve and blower damper are required to adjust the air/water ratio. Acid or chlorine is used to wash the tower packing (e.g., of Fe precipitates). Heights are for packed tower units. 1-10 gpm — 4'x4'x20' — 2 HP 10-50 gpm — 6'x8'x25' — 5 HP 50-100 gpm — 7'x10'x30' — 8 HP 100-400 gpm— 8'x12'x40' —20 HP	Effective for VOCs. Equipment is relatively simple. Startup and shutdown can be accomplished quickly. Modular design is well-suited for contaminant P&T. Package systems widely available. Dissolved Fe and Mn can be precipitated and foul the packed media resulting in headloss and reduced system effectiveness. Pretreatment (oxidation, precipitation, sedimentation) of influent may be required. Biological fouling may also occur (requiring cleaning via chlorination or a biocide). Sensitive to pH, temperature, and flow rate. May be cost-prohibitive at temperatures below freezing (may need to heat). May need GAC polishing of water effluent and treatment of air stream.
Granular Activated Carbon (GAC) Adsorption Widely used to remove metals, volatile and semi-volatile organics, pesticides, PCBs, etc. from ground water and leachate.	Aqueous contaminants are sorbed to GAC or synthetic resin packed in vessels in parallel or series. Used sorbent is regenerated or replaced. Extent of adsorption depends on strength of molecular attraction, molecular weight of contaminants, type and characteristics of adsorbent, pH, and surface area.	Package systems include 1 to 3 pressure vessels on a skid, interconnecting piping, a feed pump, optionally a backwash pump, pressure gauges, differential pressure gauges, influent flow meter, backwash flow meter, and control panel. Spent adsorbers are disconnected and sent to regeneration centers or landfills. 1-10 gpm - 12'x8'x8' - 2 HP 10-50 gpm - 14'x8'x8' - 7 HP 50-100 gpm - 20'x10'x8' - 10 HP 100-200 gpm - 20'x20'x8' - 20 HP	Effective for low solubility organics. Useful for a wide range of contaminants over a broad concentration range. Not adversely affected by toxics. High O&M costs. Intolerant of suspended solids (will clog). Pretreatment required for oil and grease greater than 10 mg/L. Synthetic resins intolerant of strong oxidizing agents.
Chemical Precipitation, Flocculation, Sedimentation Widely used to remove metals from contaminated ground water and landfill leachate.	Metals are precipitated to insoluble metal hydroxides, sulfides, carbonates, or other salts by the addition of a chemical (e.g., to raise pH), oxidation, or change in water temperature. Flocculent aids may be added to hasten sedimentation.	Package plants include a rapid-mix tank, flocculation chamber, and settling tank. Inclined plate gravity separation or circular clarifiers are used for settling. Typical equipment includes a rapid mixer, flocculator and drive, feed pump, sludge pump, acid and caustic soda pumps for pH control, and a polymer pump. 1-10 gpm - 8'x4'x9' - 3 HP 10-50 gpm - 10'x4'x13' - 5 HP 50-100 gpm - 11'x6'x14' - 7 HP	Useful for many contaminated ground-water streams, particularly as a pretreatment step. Effectiveness limited by presence of complexing agents in water. Precipitate sludge may be a hazardous waste.

Appendix B (continued)

Method	Process Description	Package Plant Components and Sizes (Dimensions are for overall plant envelope)	Advantages and Limitations
UV Oxidation Used increasingly to remove organic contaminants from ground water and other wastewaters.	Ultraviolet (UV) oxidation involves adding an oxidant, such as hydrogen peroxide, to contaminated water and then irradiating the solution with UV light. This splits the hydrogen peroxide, producing hydroxyl radicals which react with organic contaminants, causing their breakdown to non-toxic products (e.g., low weight aldehydes, carbon dioxide and water).	An oxidant (hydrogen peroxide) is injected upstream of the reactor vessel and mixed with the contaminated water in line. The fluid then flows sequentially through 1 or more reactors containing UV lamps where treatment occurs. 1x10 kW - 2'x6'x6' 1x30 kW - 4'x4'x8' 4x30 kW - 12'x5'x8'	UV oxidation can treat a broad range of soluble organics and is particularly effective for destroying chloroalkanes such as TCE and vinyl chloride and aromatic compounds such as benzene and toluene. Pretreatment may be needed to remove suspended solids, NAPL, and iron concentrations > 100 mg/L. Treatability studies needed.
Filtration Widely used to remove fine suspended solids from ground water and landfill leachate.	A fixed or moving bed of media traps and removes suspended solids from water passing through the media. Monomedium filters usually contain sand, while multimedia filters include granular anthracite over sand possibly over very fine garnet sand. Filters are used upstream of other treatment processes.	Package filters consist of one or more pressure vessels on a skid. A feed pump, backwash pump, piping, and valves complete the system. 1-10 gpm - 10'x4'x8' - 2 HP 10-50 gpm - 14'x6'x8' - 3 HP 50-100 gpm - 18'x8'x8' - 5 HP 100-250 gpm - 24'x10'x8' - 15 HP	Reliable and effective means of removing low levels of solids. Equipment is readily available and easy to operate and control. Filters clog if suspended solids concentration is high. Backwash water requires further treatment.
Ion Exchange Widely used to remove metal cations, TDS, and anions (e.g., nitrate, sulfate, chromate) from drinking water and for various other applications.	Ion exchange is an adsorption process that uses a resin media to remove dissolved ion contaminants (by exchanging sorption sites held by harmless ions). Cation resins adsorb metals while anion resins adsorb such contaminants as nitrate and sulfate. Systems consist of pressure vessels containing beds of resin pellets and strainers to retain the pellets. The resin bed is regenerated by flushing with acid and/or caustic soda.	Package plants include resin-filled pressure vessels, regeneration chemical tanks, and waste brine storage tanks. Acid and caustic soda solution pumps are provided to regenerate the resin. Resins can be selected that are ion-specific. 1-10 gpm - 8'x3'x6' - 3 HP 10-50 gpm - 14'x5'x8' - 10 HP 50-100 gpm - 17'x6'x10' - 12 HP	Removes a broad range of ionic species. Units are compact and not energy intensive. Must monitor effluent for contaminant breakthrough. High concentrations of Fe and Mn, hardness cations (Ca and Mg), suspended solids, and certain organics will foul ion exchangers. These constituents are often present at much higher concentration than the targeted contaminants. One option is to use ion-specific resins to remove heavy metals in the presence of Ca and Mg.
Reverse Osmosis (RO) Widely used for removing dissolved solids from drinking water and other applications.	RO is a separation process that uses selective semipermeable membranes to remove dissolved solids from water. A high-pressure pump forces the water through a membrane, overcoming the natural osmotic pressure, to divide the water into a dilute (treated) stream and a concentrated (residual brine) stream.	RO package plants include cartridge prefilters, a high-pressure feed pump, RO modules, pressure vessels, and a backpressure valve. 1-10 gpm - 8'x3'x6' - 13 HP 10-50 gpm - 12'x6'x6' - 35 HP 50-100 gpm - 14'x12'x8' - 85 HP	Can reduce both inorganic and organic dissolved solids. Some brine must flow out of the RO module to remove concentrated contaminants. This rejected flow may be 10% to 50% of the feed flow. Units are subject to chemical attack, fouling, and plugging. Pretreatment needs (e.g., to remove Fe, Ca, Mg) may be great.

Appendix B (continued)

Method	Process Description	Package Plant Components and Sizes (Dimensions are for overall plant envelope)	Advantages and Limitations
Fluidized Bed Biological Reactor (FBR) Widely used to remove soluble organics (e.g., BTEX, aromatics, halogenated aliphatics, etc.) from ground water, but not landfill leachate.	An aerobic FBR is a fixed-film biological treatment technology using microbes grown on GAC or sand media. Dedicated pumps provide desired fluidization and control the reactor internal flux. Influent enters the reactor bottom. The media bed expands as the biofilm grows thicker and reduces the media density. An internal growth control system intercepts the rising bed at a desired height, removes most biomass from the media, and returns the media to the reactor. Aerobic GAC FBR integrates biological removal with GAC sorption.	Package plants include an enclosed vertical cylindrical vessel, influent pump, air compressor or blower, air diffuser, effluent recycle pump, and media/biomass separation tank. 1-10 gpm - 12'x7'x15' - 7 HP 10-50 gpm - 18'x10'x15' - 10 HP 50-100 gpm - 18'x12'x15' - 12 HP 100-400 gpm - 18'x16'x15' - 40 HP	Expected to have a high process and mechanical reliability. Single or dual reactor design provides on-line flexibility. GAC FBR provides stable performance under fluctuating loading conditions. NAPL may pass through or cover the biofilm surface. Iron levels > 20 mg/L may require pretreatment to avoid plugging. Ca and Mg may cause scaling problems. Not designed for removing suspended solids. GAC FBR is not efficient for low-yield, nonbiodegradable organics because it is often operated as a high loading system with a short retention time.
Activated Sludge System Widely used to remove biodegradable organic contaminants and inorganic nutrients (e.g., N and P) from landfill leachate, but not from ground water.	This is a suspended-growth, biological treatment system that uses aerobic microbes to biodegrade organic contaminants. Influent is pumped into an aeration tank, mixed with bacteria, and kept in suspension. In the presence of oxygen, nutrients, organic compounds, and acclimated biomass, organic contaminants are biodegraded. After a treatment period, the fluid and biomass are passed to a settling tank, where cells are separated from treated water. A portion of the settled cells are recycled to the next treatment batch and the remaining sludge is disposed.	Package plants include cylindrical or rectangular aeration tanks and clarifiers, positive displacement blower, air diffusers, sludge recycle pump, sludge waste pump, chemical feed pumps, and control panel. 1-10 gpm - 23'x12'x12' - 5 HP 10-50 gpm - 45'x24'x12' - 15 HP 50-100 gpm - 45'x50'x12' - 25 HP 100-200 gpm- 45'x100'x12'- 47 HP	Effective and reliable if there are no shock loads. Technology is highly developed. Can tolerate higher organic loads than most biological treatment processes. High degree of flexibility. High capital costs. Generates sludge that may be high in metals and refractory organics. Sensitive to high concentrations of heavy metals or toxic organics. Fairly energy intensive. Has difficulty with low concentrations of contaminants, relatively long time needed for organism acclimation. Long detention times for some complex contaminant degradation.
Sequencing Batch Reactor (SBR) Widely used to remove biodegradable organics and inorganic nutrients from LF leachate, but not from ground water.	The SBR is a periodically operated, suspended growth, activated sludge process. It is different from the continuous activated sludge process in that the treatment steps are carried out in a single reactor tank in sequential steps.	Package plants include 1 or 2 rectangular or cylindrical SBR tanks, blowers, air diffusers, influent pumps, waste sludge pump, effluent pump, and chemical pumps. A floating decanter removes clear water from the reactor water at the end of the treatment cycle. 1-10 gpm - 20'x10'x12' - 7 HP 10-50 gpm - 30'x15'x14' - 40 HP 50-100 gpm - 40'x20'x14' - 80 HP	See above. By using a single tank, SBR saves land requirements and provides flexibility in changeable time and mode of aeration in each stage.

Tracers and Modelling in Hydrogeology (Proceedings of the TraM'2000 Conference held at Liège, Belgium, May 2000). IAHS Publ. no. 262, 2000.

Deuterated tracers for assessing natural attenuation in contaminated groundwater

G. B. DAVIS, B. M. PATTERSON

Centre for Groundwater Studies, CSIRO Land and Water, PO Box 5, Wembley, Western Australia 6913, Australia

e-mail: greg.davis@per.clw.csiro.au

J. THIERRIN

CSD Colombi Schmutz Dorthe AG, Avenue Cuenin 2,CH-2900 Porrentruy, Switzerland

E. BENKER

IT Environmental, Level 2, 33 Longland Street, Newstead, Queensland 4006, Australia

Abstract Three groundwater tracer tests using deuterium-labelled benzene, toluene, xylene and naphthalene (BTXN), trichloroethene (TCE) and munitions compounds (e.g. trinitrotoluene—TNT) were carried out in Australia to determine sorption, biodegradation and other transport parameters for contaminant plumes. The BTXN and TCE tests were natural gradient tests in an anaerobic sand aquifer, and the third munitions tracer test was a forced gradient test in a fractured basalt aquifer. Sorption coefficients, biodegradation rates and dispersion coefficients were estimated from multi-depth and location monitoring and modelling. The use of deuterium-labelled tracers is shown to be viable and attractive, although difficulties with in-field operations and environmental policy may limit application of such a technique.

INTRODUCTION

Quantifying the natural attenuation of hazardous chemicals in groundwater environments is non-trivial (Wiedemeier *et al.*, 1999). Direct *in situ* estimates of sorption coefficients, biodegradation rates and dispersion coefficients are needed to assess natural attenuation, and to parameterize models of contaminant fate. Laboratory-derived estimates are often not representative of field conditions. Summary results of three in-field groundwater tracer tests using deuterium-labelled compounds are presented and compared to laboratory and other estimates. The advantages and difficulties of the technique are also discussed. One tracer test involved the injection of deuterium-labelled benzene, toluene, xylene and naphthalene (BTXN) compounds into a gasoline plume in anaerobic sulphate-rich groundwater. The second tracer test involved the injection of deuterium-labelled trichloroethene (TCE) into a TCE plume, and the third tracer test involved injection of deuterium-labelled munition compounds (e.g. trinitrotoluene—TNT) into a mixed contaminant plume in a fractured basalt aquifer.

BTXN TRACER TEST

Fully deuterated BTXN were used with bromide as groundwater pollutant tracers inside a plume of gasoline components to determine *in situ* retardation (R) and biodegradation rates ($t_{½}$) for a sand aquifer (Thierrin *et al.*, 1995). The benzene plume at the site was greater than 420 m long while the toluene and *o*-xylene plumes were typically 100–200 m. Variable attenuation was apparent for individual BTEX components (Davis *et al.*, 1999). Sulphate reduction was also observed. The tracer test was carried out over 17 m in the mid-region of the plume. Monitoring occurred at 19 stainless steel multi-port boreholes. Prior to injection, the deuterated BTXN and bromide were mixed into 400 l of groundwater pumped from the injection well under anaerobic conditions. The injected mass of bromide, benzene-d_6, toluene-d_8, *p*-xylene-d_{10}, and naphthalene-d_8, was 82.8, 2.1, 1.83, 1.55 and 0.5 g, respectively, with mass recoveries of 68, 69, 48, 56 and 15%. The total injected mass of 6 g compared with 100 kg dissolved in the plume.

Depth-averaged $t_{½}$ and R values were calculated (Table 1) from the breakthrough curves (Fig. 1). The data show increasing retardation from benzene, to toluene, to *p*-xylene, to naphthalene. R values from laboratory batch tests (Table 1) were much greater than tracer test values. Except for naphthalene, tracer test estimates of $t_{½}$ were comparable to simple whole-of-plume modelling (Thierrin *et al.*, 1993). The additional mass loss of naphthalene was possibly due to nonlinear sorption or biodegradation. The latter seems unlikely (Wiedemeier *et al.*, 1999). Also, tracer test dispersivity estimates of 0.0034–0.026 m, indicating limited dilution due to dispersion.

Table 1 Half-lives (days) from the tracer test and whole-of-plume modelling (assuming first-order rates), and R values from the tracer test and laboratory batch tests.

Parameter	Tracer test (half-life in days)	Modelling (half-life in days)	Tracer test (R)	Batch test (R)
Benzene	>800	>800	1.02 ± 0.04	1.3
Toluene	90 ± 30	120 ± 25	1.04 ± 0.02	1.9
p-xylene	225 ± 75	–	1.12 ± 0.10	–
m- and *p*-xylene	–	170 ± 10	–	2.0
o-xylene	–	125 ± 10	–	1.9
Naphthalene	33 ± 6	160 ± 20	1.32 ± 0.14	2.6

TCE TRACER TEST

The transport characteristics of a TCE plume in anaerobic, ammonium and sulphate-rich groundwater were determined through a small-scale (13 m) natural-gradient tracer test using deuterium-labelled TCE (TCE-d_1) and bromide (Benker *et al.*, 1997). The plume was approximately 100–150 m wide and 3–9 m thick, with TCE, ammonium and sulphate concentrations up to 1300 µg l^{-1}, 90 and 470 mg l^{-1}, respectively. Dichloroethene was detected. The tracer test was carried out in the plume ~600 m downgradient of the source area. The tracer solution, consisting of 400 l of groundwater spiked with 30 g of KBr and 42.5 µl of TCE-d_1 (plume mass was 60–100 l of TCE), was injected at a rate of 80 l min^{-1}, 15–16 m below ground (mid-

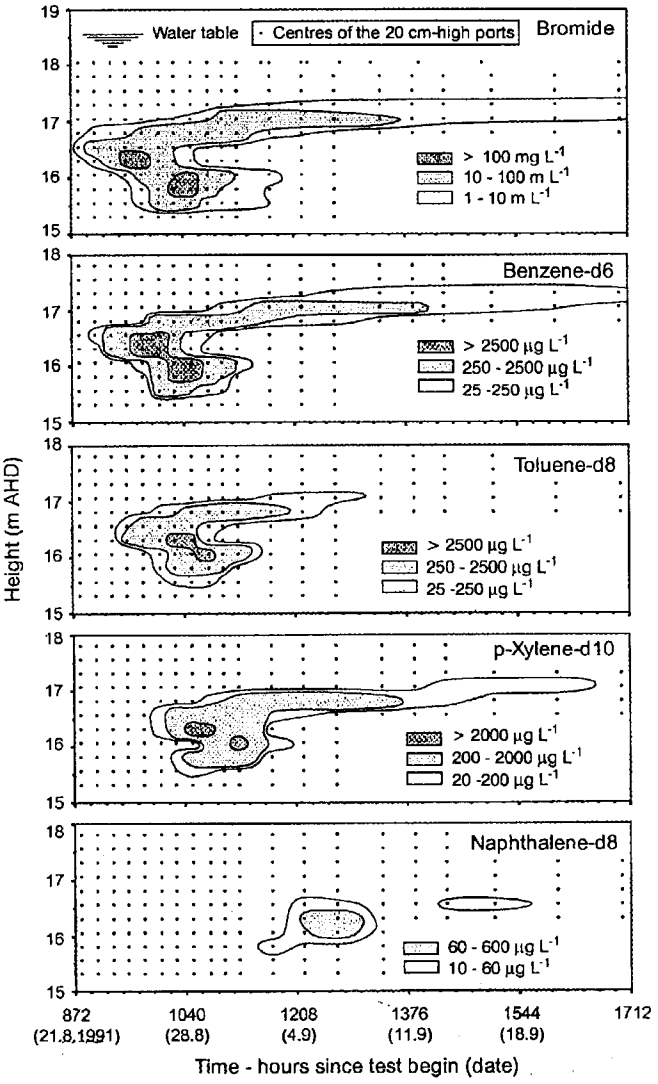

Fig. 1 Tracer test data depicted as depth–time contour plots (after Thierrin *et al.*, 1995).

plume). Monitoring occurred in seven multi-port bores, each with nine 0.2 m long screens placed vertically 0.1 m apart, 14.3–16.9 m below ground.

The field experiment showed TCE-d_1 to be stable and non-retarded (Fig. 2). Commonly used correlation equations (Benker *et al.*, 1998) overestimated R values for TCE. Batch experiments were more accurate but still overestimated TCE sorption. Column experiments were most suitable for predicting TCE sorption. Tracer test modelling also indicated a longitudinal dispersivity of 0.005 m. The tracer test indicated that TCE within the aquifer moves conservatively, is highly mobile, and that high concentrations will be preserved to substantial distances downgradient of the source.

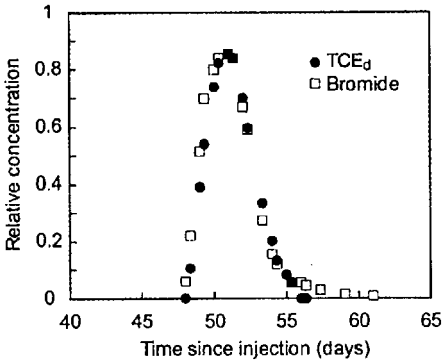

Fig. 2 Bromide and TCE-d_1 breakthrough 13 m from the injection location.

MUNITIONS TRACER TEST

A forced-gradient tracer experiment using deuterated munition compounds (2-nitrotoluene-d_7, 2-NTd_7; 4-nitrotoluene-d_7, 4-NTd_7; 2,6-dinitrotoluene-d_6, 2,6-DNTd_6; 2,4-dinitrotoluene-d_6, 2,4-DNTd_6; 2,4,6-trinitrotoluene-d_5, TNTd_5; and hexahydro-1,3,5-trinitro-1,3,5-triazine-d_6, RDXd_6) and bromide was conducted to determine *in situ* retardation and biodegradation rates in a fractured basalt aquifer at a munitions factory in Melbourne Victoria (Toze *et al.*, 1997). The tracers were mixed into 400 l of groundwater pumped from the injection bore T1 under anaerobic conditions. Bore T14, 24 m downgradient of T1, was pumped (at 3.8 m^3 h^{-1}) prior to injection to stabilize groundwater flows and drawdowns (0.17 m in T1, 0.37 m in T14). The tracers were injected into T1 (12–14 m below ground) over 35 min. Groundwater was sampled from T1 and six other bores each with 2–5 sampling ports, 11.5–15.5 m below ground.

Table 2 Injected concentrations of bromide and deuterated munitions compounds at bore T1, and calculated *R* values from the tracer test and laboratory soil columns.

Compound	Injected concentration ($\mu g\ l^{-1}$)	Field *R* values	Laboratory *R* values
bromide	1 120 000	–	–
2-NTd_7	2 400	1.1	1.0
4-NTd_7	1 200	1.0	1.4
2,6-DNTd_6	470	1.1	1.5
2,4-DNTd_6	1 460	1.2	8.2
TNTd_5	750	–	8.8
RDXd_6	690	–	2.1

Injected concentrations are shown in Table 2. The tracers moved laterally and vertically, e.g. 2-NTd_7 took up to 70 h to peak at T1-5 (500 $\mu g\ l^{-1}$), possibly due to density effects of the added bromide (T1-5 indicates port 5). Deuterated munition compounds were detected almost immediately in three bores ~2 m away from T1, and after about 3 h, peak 2-NTd_7 concentrations were 710, 930 and 1600 $\mu g\ l^{-1}$ in these bores. The tracers were detected at two bores 6 m away (e.g. Fig. 3), although TNTd_5 and RDXd_6 were not detected. Peak 2-NTd_7 concentrations (65 $\mu g\ l^{-1}$ and 50 $\mu g\ l^{-1}$)

occurred after 42 and 50 h at these 6-m bores. No significant degradation of the deuterated munitions compounds could be inferred. The R values determined from breakthrough curves at bore T9-4 (Fig. 3) were generally significantly less than laboratory-derived R values (Table 2; Patterson *et al.*, 1996). The greater values of R may be due to fresh basalt surfaces from packing of columns. The contaminated plumes have the potential to travel significant distances off-site from the initial source areas.

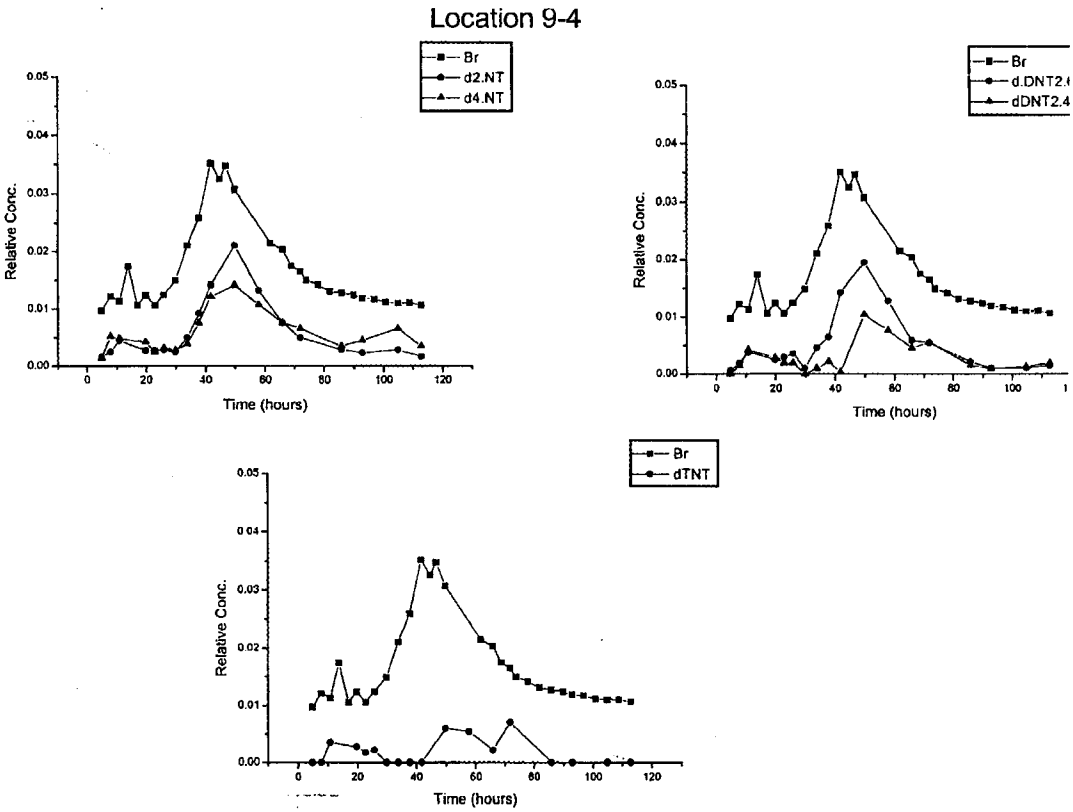

Fig. 3 Breakthrough curves at sampling port 4 of borehole T9 (6 m from T1).

ADVANTAGES AND DISADVANTAGES

In each tracer test, key contaminants (benzene, TCE and munitions) were shown not to be degrading significantly, however, the munitions experiment was inconclusive. *In situ* measurement of sorption and biodegradation avoids *ex situ* variability and disturbance in laboratory experimentation, as exemplified by the comparison between batch, column and tracer scale estimates (Tables 1, 2 and Benker *et al.*, 1998). A difficulty however, is preserving groundwater geochemical (inorganic and organic) conditions when extracting groundwater for mixing of tracers and re-injection, especially where anaerobic conditions and volatile constituents need to be preserved.

Defining the shape and zone of radius of the injected tracer volume is also difficult—this may lead to mis-estimation of some of the transport parameters. Groundwater hydraulic changes during tracer tests may confuse analysis. Prior to the BTXN tracer experiment, a bromide tracer test was carried out to define flow directions and velocities. Between the end of the bromide tracer test and the start of the BTXN tracer test, the flow direction changed by 20°, complicating monitoring bore locations and the frequency of monitoring.

The stability of deuterated compounds is also a concern, and how well the deuterated compounds mimic the actual compounds of interest. The munitions compounds were tested to determine their hydrogen/deuterium exchange rates under various pH conditions (pH values of ~4.5, 6.8–7.0 and ~9.1). Analysis of characteristic ions indicated no change in isotope ratios (and hence no deuterium/hydrogen exchange) under acidic, neutral or basic conditions for all the compounds apart from TNT. For TNT, exchange occurred under neutral and basic conditions (Fig. 4). The NTs and DNTs are less acidic than TNT with fewer nitro groups to share a negative charge, and so are less prone than TNT to hydroxide ion attack. Despite the instability of the $TNTd_5$ under basic and neutral conditions, all the deuterated compounds were able to be used confidently because of the slightly acidic nature of the groundwater at the site.

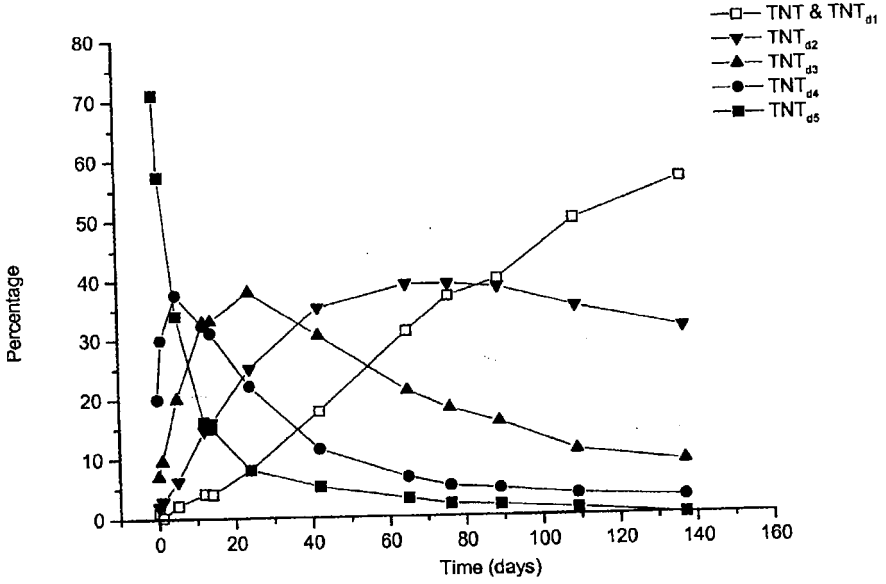

Fig. 4 Transformation of deuterated TNT under basic conditions.

The value of *in situ* deuterium-labelled tracer tests for measuring transport and natural attenuation characteristics far outweighs the disadvantages, especially when contending with the uncertainties of conventional measurements on disturbed samples in batch, column and microcosm experiments. A greater limitation however, may be the prohibition in some countries of the injection of any amount of hazardous compounds into the subsurface, regardless of benefit/impact ratios.

REFERENCES

Benker, E., Davis, G. B. & Barry, D. A. (1997) Factors controlling the distribution and transport of trichloroethene in a sandy aquifer: hydrogeology and results of an *in situ* transport experiment. *J. Hydrol.* **202**(1–4), 315–340.

Benker, E., Davis, G. B. & Barry, D. A. (1998) Estimating the retardation coefficient of trichloroethene for a sand aquifer low in sediment organic carbon—a comparison of methods. *J. Contam. Hydrol.* **30**(1–2), 157–178.

Davis, G. B., Barber, C., Power, T. R., Thierrin, J., Patterson, B. M., Rayner, J. L. & Qinglong Wu (1999) The variability and intrinsic remediation of a BTEX plume in anaerobic sulphate-rich groundwater. *J. Contam. Hydrol.* **36**(3–4), 265–290.

Patterson, B. M., Davis, G. B., Zappia, L. & Power, T. R. (1996) Sorption of munition compounds in a weathered basalt aquifer material from Victoria, Australia. In: *Environmentally Responsible Defence* (ed. by P. Crabb, J. Kesby & L. Olive), 361–370. Australian Defence Studies Centre, Canberra, Australia.

Thierrin, J., Davis, G. B. & Barber, C. (1995) A ground-water tracer test with deuterated compounds for monitoring *in situ* biodegradation and retardation of aromatic hydrocarbons. *Ground Water* **33**(3), 469–475.

Thierrin, J., Davis, G. B., Barber, C., Patterson, B. M., Pribac, F., Power, T. R & Lambert, M. (1993) Natural degradation rates of BTEX compounds and naphthalene in a sulphate reducing groundwater environment. *Hydrol. Sci. J.* **38**(4), 309–322.

Toze, S., Patterson, B. M., Briegel, D., Power, T. R., Zappia, L. & Davis, G. B. (1997) Mobility and degradation of munition residues in fractured rock aquifers at the Albion explosives factory, Melbourne. *Department of Defence/CSIRO MoU Project: Final Report: July 1993 to June 1996*, vol. I: *Main Report*; vol. II: *Attachments*. CSIRO Land and Water Report no. 96–51.

Wiedemeier, T. H., Rifai, H. S., Newell, C. J. & Wilson, J. W. (1999) *Natural Attenuation of Fuels and Chlorinated Solvents in the Subsurface*. John Wiley Inc., New York.

Dispersivity Estimates from a Tracer Experiment in a Sandy Aquifer

by Dirk Mallants[a,c], Armando Espino[a], Marijke Van Hoorick[a], Jan Feyen[a], Noel Vandenberghe[b], and Walter Loy[b]

Abstract

The success or failure of transport models in predicting the migration of a contaminant plume in ground water depends to a large extent on the quality of flow and transport parameters used. In this study, we investigate the spatial variability in the tracer velocity and dispersivity in a shallow sandy aquifer in northern Belgium. Based on hydraulic conductivity measurements on cores sampled along a vertical profile, the aquifer was found to be mildly heterogeneous, i.e., with the variance of the log-transformed conductivity K, $\sigma^2_{\ln K}$, equal to 0.22. By means of a natural gradient tracer experiment, transport of a chloride tracer was investigated in a three-dimensional network of multilevel point samplers (MLS). Least squares fitting of a two-dimensional transport model to the individual breakthrough curves resulted in an average longitudinal dispersivity that was 10 times larger than the transverse dispersivity. The results further showed the existence of a dispersion-scale effect whereby the depth-averaged longitudinal dispersivity increases with increasing travel distance. The average longitudinal dispersivity corresponding to a travel distance of 10 m was equal to 0.2 m. We finally show that theoretical expressions for the macroscopic dispersivity tensor, which require input on hydraulic conductivity heterogeneity, could be used here to approximate the observed dispersive behavior. These conceptually simple models are useful to estimate macroscopic dispersivities when no tracer data are available.

Introduction

Prediction of subsurface contaminant spreading requires information on the site-specific mixing behavior. The process of dispersive mixing in the direction of mean ground water flow is characterized by the longitudinal dispersivity parameter, whereas transverse dispersion is governed by the transverse dispersivity. Common methods to estimate the dispersivity at a particular site are based on the analysis of controlled field-scale tracer tests (e.g., Freyberg 1986; Garabedian et al. 1988; Jensen et al. 1993) or on uncontrolled migration events such as large contaminant plumes (e.g., van der Kamp et al. 1994; Engesgaard et al. 1996).

The analysis of tracer data from small and large plumes has revealed that the longitudinal dispersivity increases with increasing transport distance (e.g., Gelhar et al. 1992). This so-called dispersion-scale effect may be explained by considering a contaminant plume that encounters a large number of small-scale heterogeneities within a sedimentary unit of the aquifer. These heterogeneities cause spatial variations of fluid velocities, which in turn are responsible for mixing of solutes (Freeze and Cherry 1979).

Several theoretical models have been developed that predict the scale dependence of the dispersivity parameter on the basis of more easily measurable properties, such as the variance and the correlation scale of the hydraulic conductivity (Gelhar and Axness 1983; Dagan 1989). These stochastic models are useful in that they provide estimates of the field-scale dispersivity where direct determination in the field is impossible. However, there is a continuous need to evaluate the predictive capacity of such models for different sediments.

The objectives of the present study are: (1) to map the hydraulic conductivity heterogeneity in the top layer of a sand aquifer; (2) to determine the dispersivity-scale relationship on the basis of a field tracer test; and (3) to test several theoretical models of dispersivity using the field data of the first two objectives.

Materials and Methods

Description of the Experimental Site

The experimental site is located in the northern part of the province of Antwerp, close to the village of Mol, Belgium (Figure 1). At the study site the top 20 m of the aquifer are mainly composed of well-sorted fine, white quartz sands, generally referred to as the Mol sands. The underlying Kasterlee sands (20 to 32 m) contain glauconite-rich silt and clay lenses and are considered to behave as an aquitard (Patijn 1981). The stratigraphy of the top of the sandy aquifer was determined from particle size analysis and the presence of specific minerals such as tourmaline and zircon. Contiguous core sampling (56 cores in total) along a vertical pro-

[a]Institute for Land and Water Management, University of Leuven, Vital Decosterstraat 102, B-3000 Leuven, Belgium.

[b]Institute for Earth Sciences, University of Leuven, Redingenstraat 14, B-3000 Leuven, Belgium.

[c]Current address: Belgian Nuclear Research Centre, Boeretang 200, B-2400 Mol, Belgium.

Received February 1999, accepted November 1999.

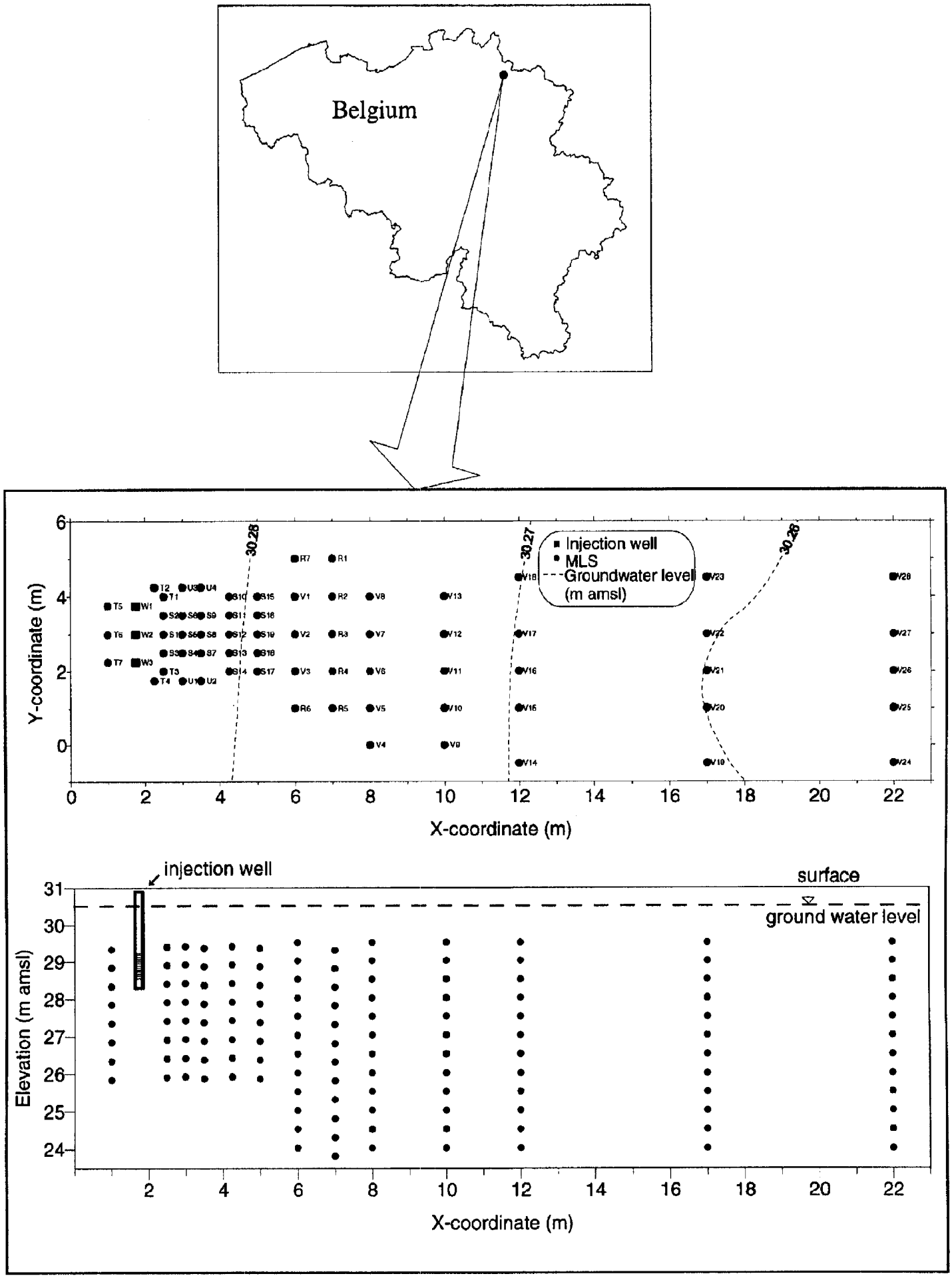

Figure 1. Location of experimental site (top), MLS-network (middle) and cross section of aquifer with sampling ports indicated as closed circles.

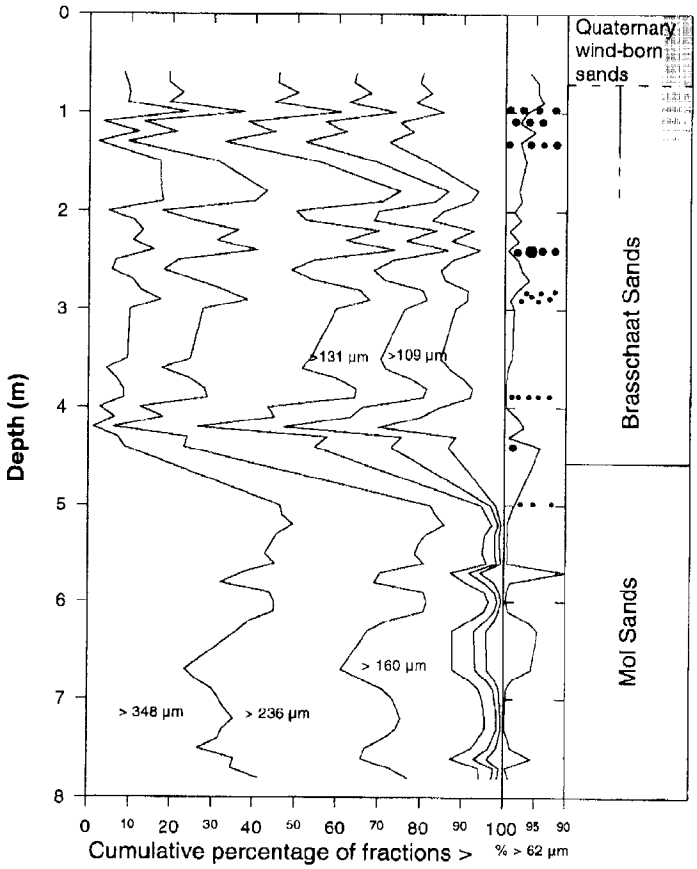

Figure 2. Particle size distribution and stratigraphic analysis of core samples. The left part shows all fractions, whereas the middle part shows only fractions larger than 62 µm. Closed circles represent small stones.

file of 8 m depth and particle size analysis allowed us to construct continuous particle size distribution curves (Figure 2). The cumulative percentage of particles larger than 62 µm is consistently above 90% and, at most depths, even larger than 95%. Between 4 and 5 m, the deeper sands become coarser compared with the shallow ones, with a relatively sharp boundary between the two sediments. Also of importance to the tracer experiment are the Brasschaat sands (from 0.6 to 4.5 m depth) overlying the Mol sands. The former are of Quaternary age (early Pleistocene) and will be referred to hereafter as sediment 1; whereas the latter are marine deposits of Tertiary age (Pliocene), referred to hereafter as sediment 2. The Brasschaat sands are covered by Quaternary wind-borne sands.

Prior to the determination of the particle size and the porosity, we determined the hydraulic conductivity, K, on the same 56 undisturbed core samples. K was measured using a laboratory constant head permeameter. Vertical variability in K is given in Figure 3, together with porosity and estimated transport velocity, v (to be discussed later). The increase in K with increasing depth is consistent with the sands becoming coarser at greater depths, i.e., when moving from sediment 1 to sediment 2. Geometric mean values of K (variance of ln K between parenthesis) for sediment 1 and 2 are, respectively, 7.64×10^{-5} m/s (0.60) and 2.89×10^{-4} m/s (0.33). The global K value for both sediments was 1.83×10^{-4} m/s and the overall variance of ln K was 0.22. The horizontal correlation length for hydraulic conductivity, L, was determined on additional cores collected within the Brasschaat sands (at a depth of approximately 1.5 m). Variogram analysis revealed a value of L = 1 m. Absence of detailed data on the horizontal variability in

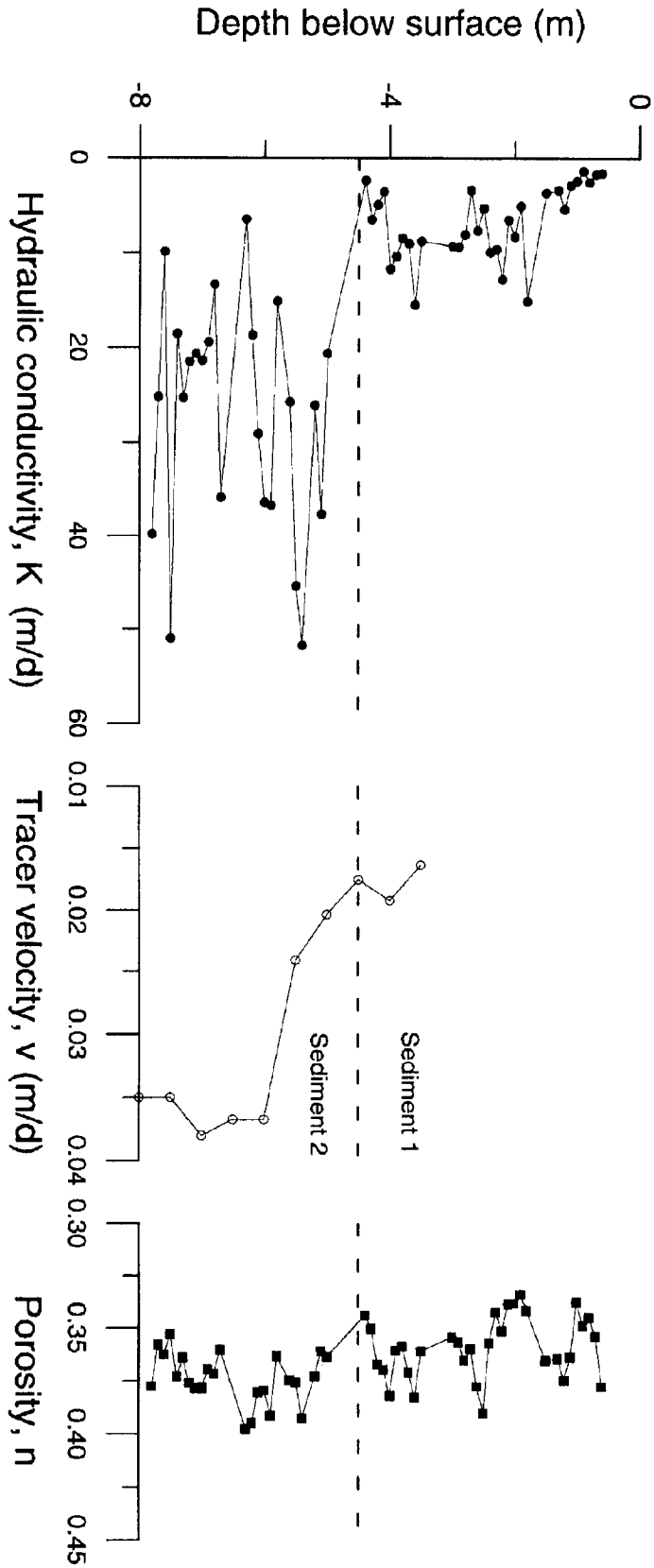

Figure 3. Vertical variability in hydraulic conductivity, K, estimated tracer velocity, v, and porosity, n. Dashed line indicates boundary between sediment 1 and 2.

hydraulic conductivity for the lower layer necessitated the use of data from the upper layer as being representative for the lower one. This may be justified because the spatial structure of sedimentary aquifers is usually controlled by large-scale depositional processes that can be expected to generate a larger continuity in the horizontal

than the vertical direction (Koltermann and Gorelick 1996). It is reasonable to assume that for this mildly heterogeneous sedimentary aquifer the horizontal spatial structure will not change dramatically within a few meters. Values for porosity determined on the same core samples ranged between 0.33 and 0.40, with an average of 0.37.

Tracer Experiment

An array of 65 multilevel samplers was installed to monitor the migration of a tracer (Figure 1). Each MLS had sampling ports every 0.5 m and the ground water was sampled between 1.5 and 7 m beneath the water table. The sampling ports were similar in design to the ones described by Domenico and Schwartz (1998).

A 540 L chloride solution (1.5 g/L) was injected in three injection wells over 17 hours. By means of the spatial arrangement of the three injection wells on a line, the initially contaminated volume of the aquifer may be approximated by a parallelepiped. The spacing of 0.75 m between the injection wells was considered to be close enough to achieve an overlap of the injected tracer volume before the first samplers would be reached. The estimated size of the parallelepiped was $0.72 \times 1 \times 2.2 = 1.58$ m^3. The injection wells were screened from 1 to 1.5 m below water level. There was no noticeable increase in water level at the time of injection. Sampling of the MLS started immediately after injection and continued for more than 200 days. Chloride concentrations were determined by means of potentiometric titration. The central line of MLS (S1-S5-S8-etc.) was sampled most frequently, whereas snapshots of the three-dimensional plume behavior were taken approximately every month. The average hydraulic gradient for the entire sampling period ranged between 0.0024 and 0.0035 (Figure 1).

Dispersion Models

Chloride breakthrough curves were constructed for sampling ports that had been monitored almost weekly. Transport parameters were obtained by fitting a two-dimensional transport model to the individual breakthrough curves. For a two-dimensional uniform flow field and an instantaneous injection of a tracer, the model is given by Bear (1979):

$$C(x,y,t) = \frac{M}{4\pi nbt(D_L D_T)^{0.5}} \exp\left(-\frac{(x - vt)^2}{4D_L t} - \frac{y^2}{4D_T t}\right) \quad (1)$$

where C is concentration, M is the injected mass, n is porosity, b is the thickness of the aquifer, v is flow velocity in x direction, D_L and D_T are the local scale longitudinal, respectively transverse dispersion coefficient owing to small-scale velocity variations, x and y are spatial coordinates, and t is time since start of injection. The velocity in the y direction is assumed to be zero, and the x axis is oriented in the direction of flow.

Several solutions to the advection-dispersion equation exist. For instance, Sudicky et al. (1983) and Moltyaner and Killey (1988a, 1988b) applied an analytical solution describing the movement of a contaminant released as a rectangular parallelepiped. Others such as Leland and Hillel (1982) have applied the solution for an instantaneous point injection to a tracer test similar in layout to ours. All these analytical solutions are based on the assumption of unidirectional and uniform flow. Regardless of the analytical model applied, it will provide only an approximate description of the transport and dispersion process. As a result, dispersivities thus obtained may be considered only approximate. Furthermore, when the size of the injection volume is small relative to the sampled part

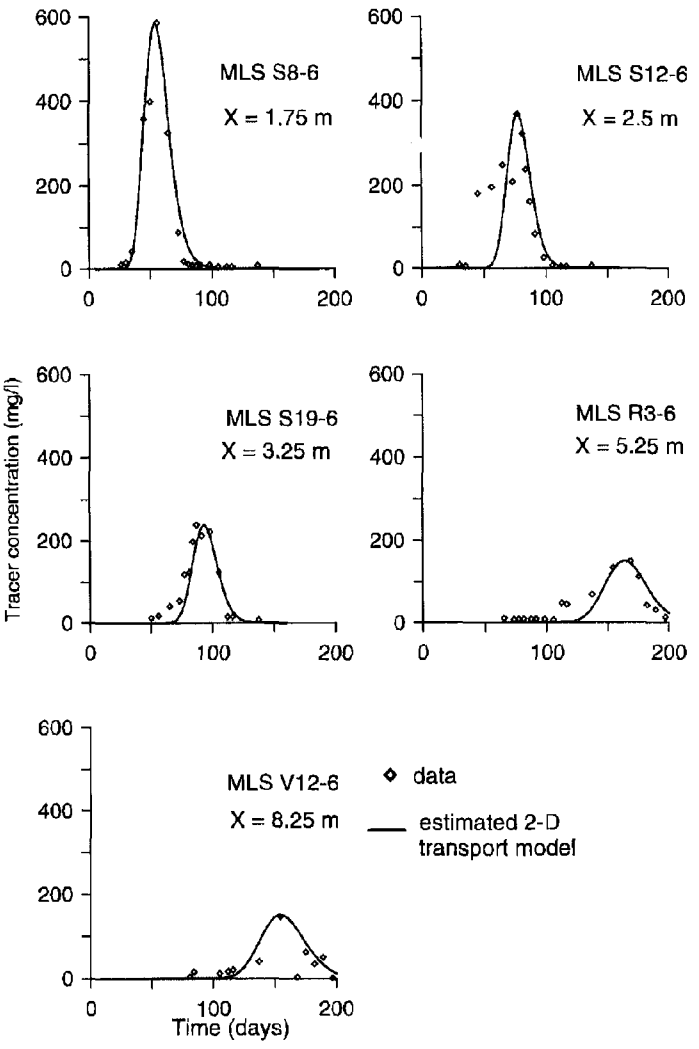

Figure 4. Observed and estimated tracer concentrations in five MLS located on a central line in the direction of ground water flow (at a depth of 4 m below surface). MLS S8-6, MLS12-6, etc., indicates the code of each sampler (for location, see Figure 1), with the second number referring to the sampling port (in this case the sixth). Distance from injection well is also indicated.

of the aquifer, the solution to the two-dimensional transport model for an instantaneous point injection given by Bear (1979) may be used to a parallelepiped source. Finally, because the 17-hour injection time is still small relative to the travel time to the different samplers, we considered the injection to be effectively instantaneous.

The parameter estimation code of Sauty and Kinzelbach (1988) was used to obtain the flow velocity and the longitudinal and transverse dispersion coefficients by minimizing the differences between the calculated and observed tracer concentrations. Application of Equation 1 further assumes a uniform vertical solute concentration. On the basis of the depth distribution of the hydraulic conductivity (Figure 3) it was evident that a more conductive layer was underlying the top layer starting approximately at 4 m below surface. This vertical inhomogeneity in hydraulic conductivity suggested that an injected tracer could migrate differently (i.e., faster) in the lower layer compared with the upper one. Therefore, the multilevel samplers were used to obtain a profile of estimated pore water velocities and dispersivities across the vertical dimension of the aquifer. Accordingly, rather than fitting Equation 1 to vertically averaged breakthrough curves, we first used Equation 1 to describe transport at different depths and then averaged the dispersivities with

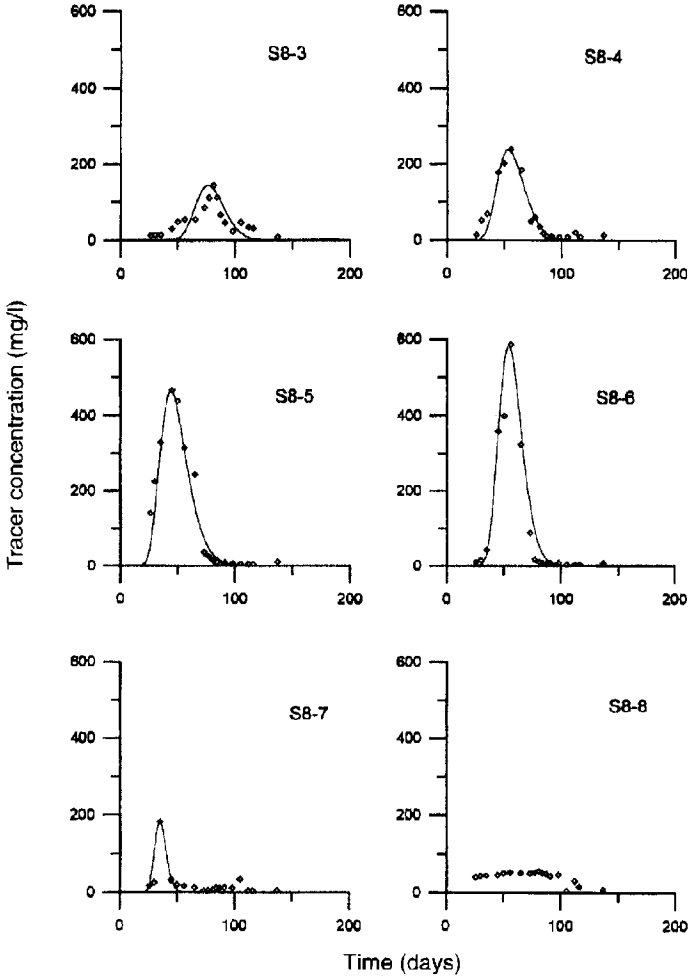

Figure 5. Observed and estimated tracer concentrations in MLS S8 located at 1.75 m from the injection wells. Distance between depth intervals is 0.5 m, with S8-3 at 2.5 m below surface.

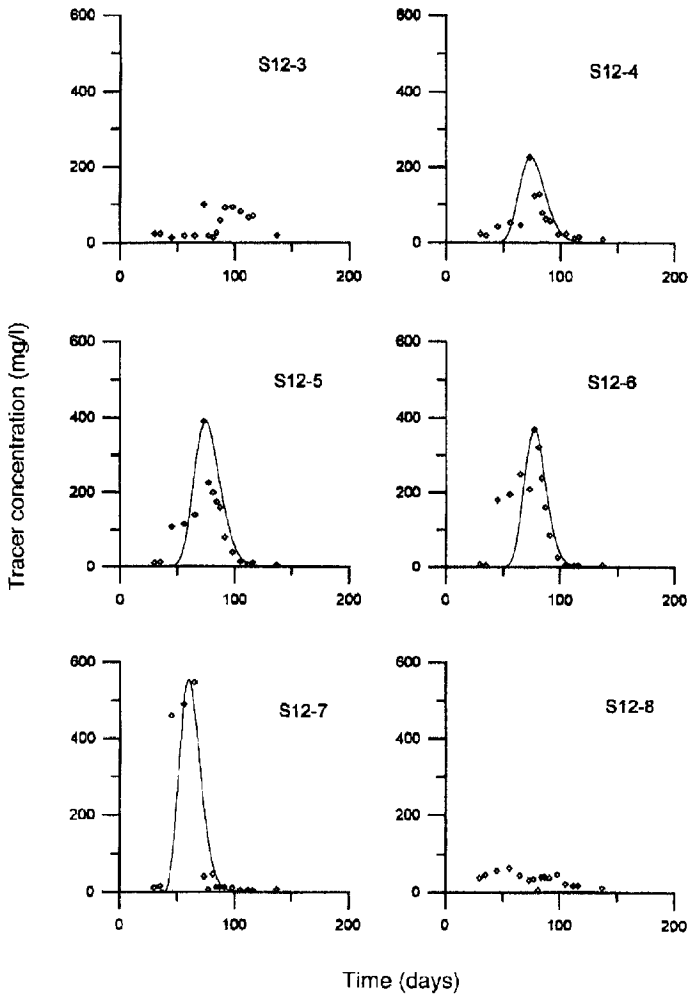

Figure 6. Observed and estimated tracer concentrations in MLS S12 located at 2.5 m from the injection wells. Distance between depth intervals is 0.5 m, with S12-3 at 2.5 m below surface.

depth.

The depth b = 30 m and the porosity n were adjusted dependent upon depth (Figure 3). From the estimated dispersion coefficients, D_L and D_T, we calculated the longitudinal and transverse dispersivities, α_L and α_T, as

$$\alpha_L = \frac{D_L}{v}$$
$$\alpha_T = \frac{D_T}{v} \qquad (2)$$

Results and Discussion

Estimating Dispersivity Parameters

Typical breakthrough curves measured at a depth of 3 m below the water table are given in Figure 4, with the fitted two-dimensional model. All five multilevel samplers are located on one line in the direction of the main flow, with the first one at a distance of x = 1.75 m from the middle injection well. The vertical distribution of the pore water velocities that were estimated by fitting of Equation 1 to the breakthrough curves is shown in Figure 3. Each value represents the average of all values estimated at that particular depth. As could be expected from the hydraulic conductivity distributions with depth, v also increases with increasing depth: from 0.016 m/d at 4 m to 0.035 m/d at 8 m depth. Note that although the average hydraulic conductivity of sediment 2 is almost four times larger than that of sediment 1, the pore water velocity in sediment 2 is only twice as large as that of sediment 1. This discrepancy may indicate the presence of a vertical flow component not accounted for in the model, leading to an underestimation of the true velocity and/or an overestimation of the measured K values because of the use of small diameter samples that may have exhibited flow along the core wall. Additional explanations could be the uncertainties due to the parameter optimization approach and the use of straight line distances from the injection wells to the different samplers in calculating the velocities.

Observed and fitted breakthrough curves at different depths along the same vertical line for two multilevel samplers (MLS S8 and MLS S12) are shown in Figure 5 and 6, respectively. For multilevel sampler S8, at 1.75 m from the injection wells, the center of the plume is somewhat in between sampling port 5 and 6. The maximum concentration occurs at sampling port 6, approximately 4 m below surface. At 2.5 m from the injection wells (MLS S12), the center of the plume has slightly stretched in the vertical direction and now also includes sampling port 7, where the tracer maximum is. These observations suggest that there is a small but noticeable vertical movement between the depth intervals, possibly the combined result of density effects, short-circuiting between different

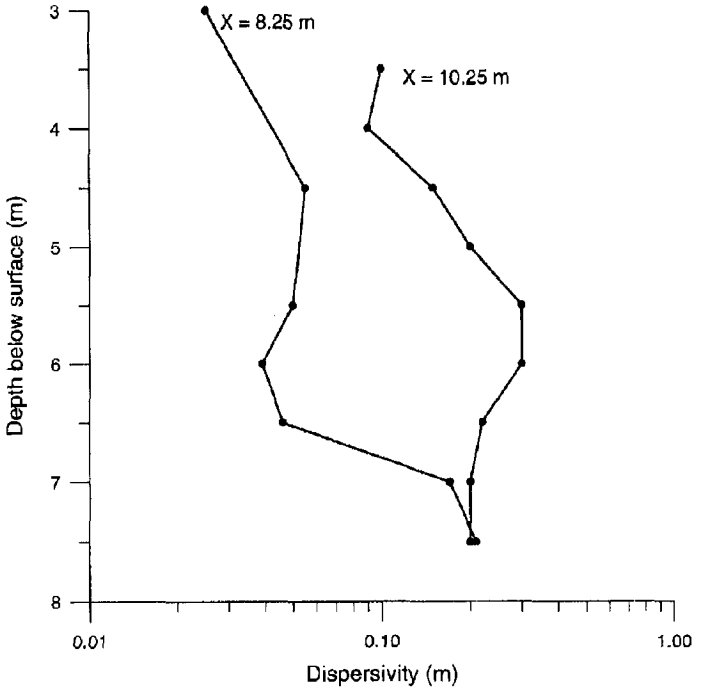

Figure 7. Longitudinal dispersivity versus depth below surface (based on data for MLS V12 and V17).

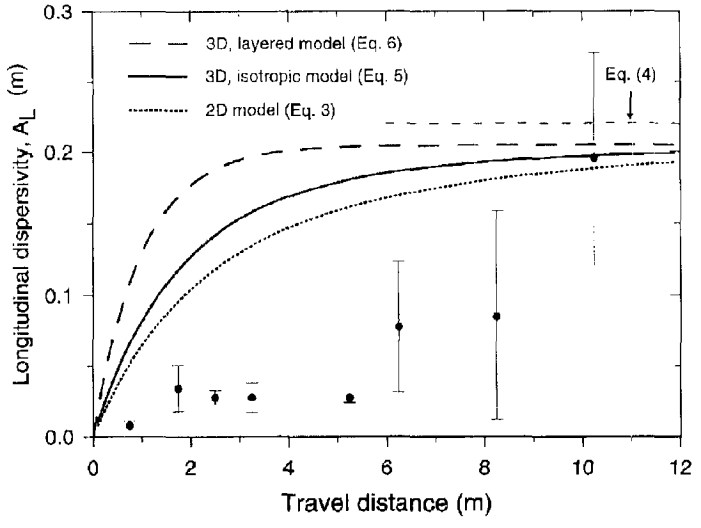

Figure 8. Behavior of dispersivity with increasing travel distance. Average observed longitudinal dispersivities are indicated as closed circles (error bars are one standard deviation). Theoretical models are based on Equations 3 through 6.

depth intervals as a result of higher permeabilities around the multilevel samplers, or some other reason. The effect of this vertical movement on the estimated transport parameters is small, i.e., an increase in dispersivity with increasing depth was found to exist but it was small and not systematic. For instance, Figure 7 shows the vertical variability in the dispersivity parameter for two multilevel samplers at 8.25 and 10.25 m, respectively, from the injection wells. In the first profile at x = 8.25 m, the dispersivity varies between 0.03 m at 3 m depth and 0.05 m at 6.5 m depth. A significant increase occurs at the 7 and 7.5 m depths, where a maximum value of 0.20 m was found. The second profile shows a somewhat different behavior, with an increasing dispersivity from 0.1 m at 4 m depth to 0.3 m at 5.5 and 6 m depth. At greater depths, it decreases again to 0.2 m. From these data it is clear that the dispersivity behaves rather erratically with depth, presumably caused by variability in hydraulic conductivity in both vertical and horizontal directions. Since the purpose of the study was to investigate the effects of small-scale heterogeneities on flow and transport parameters, the analysis was done using the individual breakthrough curves rather than composite curves calculated as the average of the concentrations measured at all depths of a particular sampler. The latter tend to average out the effect of small-scale heterogeneities.

A statistical analysis of the transport parameters v, α_L, and α_T revealed a lognormal probability density function for all three parameters. The mean (and standard deviation) values were v = 0.025 (0.014) m/d, α_L = 0.09 (0.093) m, and α_T = 0.0085 (0.047) m, respectively. The ratio α_L/α_T is approximately equal to 10, which is well within the range of five to 100 proposed by de Marsily (1986).

All calculated dispersivities with approximately the same distance traveled from the source were averaged. These values are shown in Figure 8 with their standard deviation. The average dispersivity increases from 0.01 m for x = 0.75 m to 0.2 m for a travel distance of 10.15 m. According to the compilation by Gelhar et al. (1992) of dispersivity values taken from the literature, observed dispersivities for a travel distance of 10 m range from 0.01 to 10 m. From Figure 8 we further note the presence of a dispersion scale effect, but there is insufficient data to conclude whether or not the plume traversed sufficient heterogeneities such that the dispersion would remain constant.

Testing of Macro-Dispersion Models

The property of the aquifer that characterizes the macrodispersive spreading owing to spatial variations of macroscopic pore water velocities is the macro-dispersivity, A. These velocity variations are caused primarily by hydraulic conductivity heterogeneities, although they also may be attributed in part to spatial variability in effective porosity or the transient nature of flow directions (this mainly affects the transverse macro-dispersion [Rehfeldt and Gelhar 1992]). Because spatial variability in hydraulic conductivity is generally orders of magnitude larger than variability in porosity (Koltermann and Gorelick 1996), the effect of the latter is often neglected. Considering our data set, the coefficient of variation CV for hydraulic conductivity was 0.49, whereas that for total porosity was 0.04. From Figure 3, we further note that differences in total porosity across the boundary between layer one and two are small. For sandy materials, total porosity is nearly identical to effective porosity (de Marsily 1986). Therefore, the observed variability in total porosity presumably contributes little to the dispersion process.

Several theoretical models exist to predict the macro-dispersion. Most of these models make use of the variability of the hydraulic conductivity (in terms of the variance of lnK, σ^2_{lnK}) and the correlation length of lnK, L, the latter being the distance for which the spatial correlation between K values becomes zero. In case of two-dimensional ground water flow in an isotropic aquifer (the assumption is that the correlation length in the x and y directions is the same), the following models may be used to predict the longitudinal macro-dispersivity A_L for intermediate travel distance (Sposito and Barry 1987):

$$A_L = L\,\sigma^2_{lnK_s}[1 - 3(2x/L)^{-1} - 3(x/L)^{-2}\exp(-x/L) + 3(x/L)^{-3}(1 - \exp(-x/L))] \quad (3)$$

and long travel distance ($x \rightarrow \infty$) (Gelhar 1993):

$$A_L = \sigma^2_{lnK_s} L$$

(4)

In case of three-dimensional ground water flow and an intermediate travel distance, the following model exists for an isotropic aquifer (Gelhar 1993):

$$A_L = \frac{L\,\sigma^2_{\ln K}}{\gamma^2}[1 - 4(x/L)^{-2} + 24(x/L)^{-4} - 8[(x/L)^{-2} + 3(x/L)^{-3} + 3(x/L)^{-4}]\exp(-x/L)] \quad (5)$$

where $\gamma = \exp(\sigma^2_{\ln K}/6)$.

The model for a stratified aquifer (the horizontal correlation length is much larger than the vertical) is

$$A_L = \frac{L\,\sigma^2_{\ln K}}{\gamma^2}(1 - \exp(-x/L)) \quad (6)$$

The theoretical behavior of A_L was calculated for all four models using the previously determined values of $\sigma^2_{\ln K} = 0.22$ and L = 1 m (Figure 8). The two-dimensional model for long travel distance clearly is an asymptotic model, which only slightly overestimates the average measured dispersivity. Moreover, the value for A_L predicted by the long-distance model (i.e., 0.22 m) is close to the measured one, i.e., 0.2 m. The two-dimensional model for intermediate distance overpredicts the measured values at intermediate distance, but it is nearly identical to the measured value at x = 10.15 m. The three-dimensional models also overpredict the measurements at early and intermediate distance, but their behavior at x = 10.15 m is close to the data. The difference between the two- and three-dimensional models at long travel distance is that the latter reach their constant value at x = 10 L (i.e., at x = 10 m, when L = 1 m), whereas the former becomes constant only after approximately 60 correlation lengths (i.e., at x = 60 m, when L = 1 m; Dagan 1989).

Although the theoretical dispersivity models use only data on hydraulic conductivity heterogeneity, their predictions are within a factor of 2 to 3 from the measurements for distances larger than 5 m. Closer to the origin, differences are larger, probably owing to the small distance traveled and the relatively small number of heterogeneities encountered by the solute plume. Nevertheless, the power of the theoretical models to predict macro-dispersivities in the absence of tracer data warrants further development and testing under different hydrogeological conditions.

Conclusions

A ground water tracer test was conducted in which the solute plume traveled through fairly homogeneous sandy sediments where the lower part was more permeable than the upper part. The results revealed a vertical distribution of the tracer velocity, which showed the same trend as the vertical variability of hydraulic conductivity measurements. However, the average tracer velocity for the lower sediment was only twice as large as that of the upper sediment, whereas the average conductivity for the lower sediment was four times larger than that of the upper. Based on a two-dimensional transport model, average estimated values for the longitudinal and transverse dispersivity were 0.09 and 0.0085 m, respectively. At the maximum travel distance of 10.15 m the average dispersivity was 0.2 m. Theoretical macro-dispersion models that use the variance and correlation length of hydraulic conductivity measurements as inputs predicted the dispersivity at x = 10.15 m fairly well. For shorter travel distances, the predictions were less accurate. This study illustrates how important good estimates of hydraulic conductivity are in contaminant transport research.

References

Bear, J. 1979. *Hydraulics of Groundwater.* New York: McGraw-Hill.

Dagan, G. 1989. *Flow and Transport in Porous Formations.* New York: Springer Verlag.

de Marsily, G. 1986. *Quantitative Hydrogeology.* New York: Academic Press.

Domenico, P.A., and F.W. Schwartz. 1998. *Physical and Chemical Hydrogeology*, 2nd ed. New York: John Wiley & Sons.

Engesgaard, P., K.H. Jensen, J. Molsen, E.O. Frind, and H. Olsen. 1996. Large-scale dispersion in a sandy aquifer: Simulation of subsurface transport of environmental tritium. *Water Resources Research* 32, no. 11: 3253-3266.

Freeze, R.A., and J.A. Cherry. 1979. *Groundwater.* Englewood Cliffs, New Jersey: Prentice-Hall.

Freyberg, D.L. 1986. A natural gradient experiment on solute transport in sand aquifer, 2. Spatial moments and the advection and dispersion of nonreactive tracers. *Water Resources Research* 22, no. 13: 2031-2046.

Garabedian, S.P.L., L.W. Gelhar, and M.A. Celia, 1988. Large-scale dispersive transport in aquifers: Field experiments and reactive transport theory. Report 315. Cambridge: Ralph M. Parsons Laboratory, Massachusetts Institute of Technology.

Gelhar, L.W. 1993. *Stochastic Subsurface Hydrology.* Englewood Cliffs, New Jersey: Prentice Hall.

Gelhar, L.W., and C.L. Axness. 1983. Three-dimensional stochastic analysis of macrodispersion in aquifers. *Water Resources Research* 19, no. 1: 161-180.

Gelhar, L.W., C. Welty, and K.R. Rehfeldt, 1992. A critical overview of data on field-scale dispersion in aquifers. *Water Resources Research* 28, no. 7: 1955-1974.

Jensen, K.H., K. Bitsch, and P.L. Bjerg, 1993. Large-scale dispersion experiments in a sandy aquifer in Denmark: Observed tracer movements and numerical analysis. *Water Resources Research* 29, no. 3: 673-696.

Koltermann, C.E., and S.M. Gorelick. 1996. Heterogeneity in sedimentary deposits: A review of structure-imitating, process-imitating, and descriptive methods. *Water Resources Research* 32, no. 9: 2617-2658.

Leland, D.F., and D. Hillel. 1982. A field study of solute dispersion in a shallow, unconfined aquifer. *Soil Science Society of America Journal* 46, 905-912.

Moltyaner, G.L., and R.W.D. Killey. 1988a. Twin Lake tracer tests: Longitudinal dispersion. *Water Resources Research* 24, no. 10: 1613-1627.

Moltyaner, G.L., and R.W.D. Killey. 1988b. Twin Lake tracer tests: Transverse dispersion. *Water Resources Research* 24, no. 10: 1628-1637.

Patijn, J. 1981. Grain-size analysis on the samples of the experimental shaft at the SCK•CEN site. Report S81/46/352/JP/ls-b/R-48. Mol, Belgium: Belgian Nuclear Research Centre.

Rehfeldt, K.R., and L.W. Gelhar. 1992. Stochastic analysis of dispersion in unsteady flow in heterogeneous aquifers. *Water Resources Research* 28, no. 7: 2085-2089.

Sauty, J.P., and W. Kinzelbach. 1988. Computer aided tracer test interpretation code "CATTI," Users Manual. Stuttgart, Germany: IFN Inst. für Wasserbau.

Sposito, G., and D.A. Barry. 1987. On the Dagan model of solute transport in groundwater: Foundational aspects. *Water Resources Research* 23, no. 10: 1867-1875.

Sudicky, E. A., J.A. Cherry, and E.O. Frind. 1983. Migration of contaminants in ground water at a landfill: A case study, 4, A natural gradient dispersion test. *Journal of Hydrology* 63, 81-108.

Van der Kamp, G., L.D. Luba, J.A. Cherry, and H. Maathuis. 1994. Field study of a long and very narrow contaminant plume. *Ground Water* 32, no. 6: 1008-1016.

Field Test for Effective Porosity and Dispersivity in Fractured Dolomite, the WIPP, Southeastern New Mexico

D. D. Gonzalez
Sandia National Laboratories, Albuquerque, New Mexico 87185

H. W. Bentley
Hydro Geo Chem, Inc., Tucson, Arizona 85716

Introduction

The Waste Isolation Pilot Plant (WIPP), a demonstration facility 26 mi (41.6 km) east of Carlsbad, New Mexico, used to store transuranic waste in Permian-bedded salts, has been under field investigation since 1975. Hydrologically, the area is characterized by a typical semiarid environment underlaid by four confined aquifer systems whose transmissivities range from 10 to 10^{-5} ft^2/d (1 to 10^{-6} m^2/d).

Previous local hydrogeologic investigations show a fractured dolomite, whose thickness and depth of burial range from 22 to 24 ft (6.7 to 7.3 m) and 498 to 897 ft (152 to 274 m), respectively, as the most likely groundwater vehicle to transport waste to the biosphere in the event such a repository is breached. To describe adequately and to predict solute transport, certain hydraulic characteristics of the transporting medium need to be estimated along a hypothetical flow path. Effective porosity and dispersivity are two parameters which are most difficult to predict, particularly in fractured rock exhibiting low transmissivities. This paper describes the results of the first of a series of two-well recirculation tracing tests to be performed. The recirculation tests were performed using an extraction-injection well couplet similar to that described by Grove and Beetem [1971]. Test duration was

270 days and resulted in a well-defined breakthrough curve. Specific test configurations are described in detail in a later section of this paper.

H-2 Site Description

The regional hydrogeology of the WIPP area has been described by Hiss [1976], Powers et al. [1978], and Mercer and Orr [1979]. Hydrologic testing at the H-2 site has concentrated on the three liquid-bearing zones above the proposed waste repository horizons. These are the Permian Rustler-Salado contact and the two beds within the Rustler Formation: the Culebra and the Magenta Dolomite members.

The H-2 wells were drilled by the U.S. Geological Survey (USGS) and Sandia National Laboratories in 1977. H-2A was completed to the Magenta at a depth of 563 ft (172 m). H-2B was drilled to the Culebra at 661 ft (202 m), then perforated in the Magenta, and completed as a dual-observation well. H-2C was drilled to the Rustler-Salado contact at 743 ft (227 m), perforated in the Culebra, and also completed as a dual-observation well [Mercer and Orr, 1979]. Figure 1 shows the three-well configuration, the zones each is open to, and their general orientation.

The three liquid-bearing zones were cored and analyzed by the USGS. A description of these cores, taken from Mercer and Orr [1979], is given in Tables 1a - 1c.

Hydrologic testing of the Rustler-Salado contact and of the Magenta Dolomite Member consisted of bailing each well dry and observing the recovery response. Estimates of transmissivity in the Rustler-Salado contact were between 10^{-1} and 10^{-4} ft^2/d (1 and 10^{-5} m^2/d). The transmissivity in the Magenta averaged about 0.1 ft^2/d (0.01 m^2/d) [Mercer and Orr, 1979].

Three aquifer tests with observation wells were made to determine hydraulic properties of the Culebra. The average transmissivity from these tests is 0.6 ft^2/d (0.06 m^2/d); storage coefficient is about 1.3×10^{-5} [Bentley and Walter, 1983].

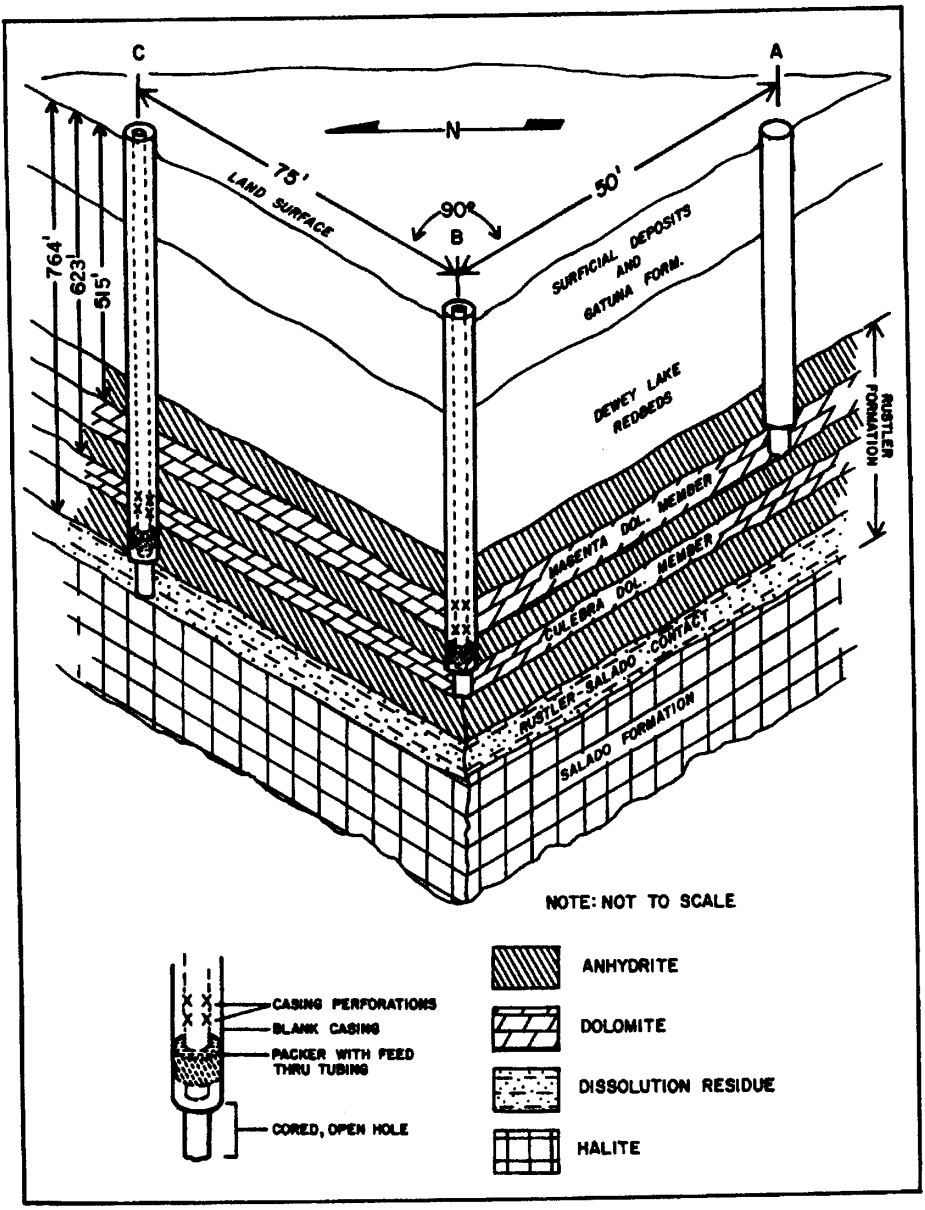

Fig. 1. Cross section through wells H-2A, H-2B, and H-2C.

TABLE 1a. Well H-2C

Depth, ft	Description
743-762.2	gray mudstone with pink halite vugs and clear halitic fracture fillings, gradational downward to banded, red, halitic mudstone
762.2-764.1	red-brown halitic mudstone
764.1-767.3	red-brown, argillaceous halite
767.3-772.5	red-orange polyhalitic halite with polyhalite blebs and bands
772.5-773.5	red-brown halitic clay and red-brown argillaceous halite
773.5-795.6	light pink to light red-orange polyhalitic halite, minor clay partins, with brown halitic clay at base

Rustler-Salado cored interval: 743-795 ft; top of Rustler-Salado contact: 764 ft.

Tracing Test Configuration

Test 1

The pumping and injecting system for test 1 included H-2B as the pumping well and H-2C as the injecting well (Figure 1). Pumping was begun on February 13, 1980, to allow the aquifer to approach steady state flow conditions. Injection of sodium benzoate (SBA), pentafluorobenzoate (PFB), and a suite of halocarbon tracers (CCl_4, $CFCl_3$, and CF_2Cl_2) was begun at 2330 hours on February 22, 1980, at

TABLE 1b. Well H-2B

Depth, ft	Description
611-624.2	dense gray anhydrite, massive to banded
624.2-642.0	brown silty dolomite with selentic fracture fillings and crystals, pitted and fractured from 629.5 to 642.0 ft
642.0-644.0	gray mudstone
644.0-652.0	red-brown selenitic siltstone
652.0-660.7	dense gray anhydrite

Culebra Dolomite cored interval: 611-661 ft; Culebra Dolomite thickness: 624-642 ft.

TABLE 1c. Well H-2A

Depth, ft	Description
511.7-513	cement
513.0-514.6	dense gray anhydrite
514.6-539.6	gray-brown silty dolomite with some fractures in the interval 537.5-539.6 ft
539.6-563	brown-gray banded anhydrite

Magenta Dolomite cored interval: 513-563 ft; Magenta Dolomite thickness: 515-540 ft.

which time the water flow rate through the system was 1140 ml/min. Injection continued until some time between 1200 hours on February 24 and 1200 hours on February 25, when the tracer injection line ruptured and the remainder of the tracers were lost.

Pumping continued in an attempt to complete the test successfully; however, sediment accumulation affected the injection system and the performance of the injection well, H-2C, until the test was terminated June 18, 1980.

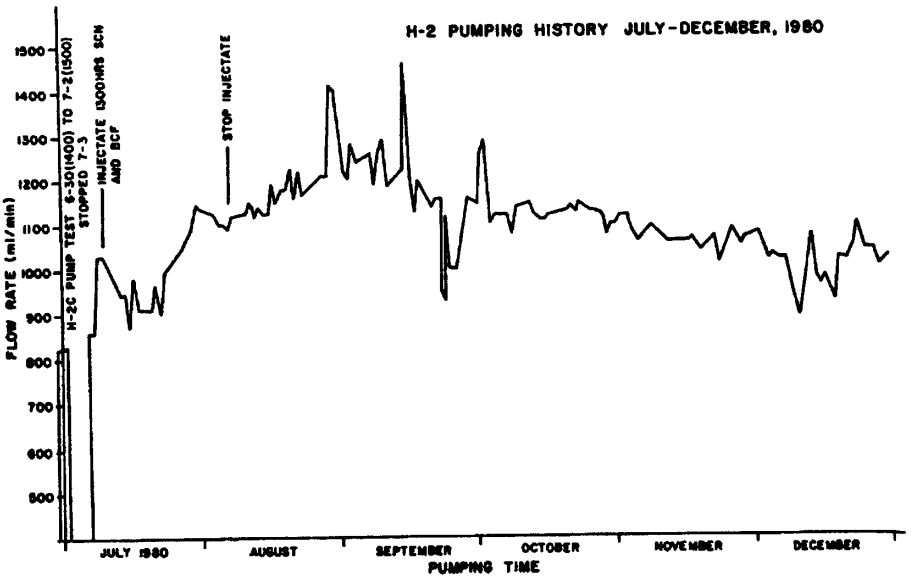

Fig. 2. H-2 pumping history July-December 1980.

Test 2

After the abortion of test 1 the site was reconfigured with H-2C as the pumped well and H-2B as the injection well. A combination of in-line filters and a settling tank alleviated almost all problems with sedimentation. After pumping to steady state, tracer injection was begun on July 10, 1980, with sodium thiocyanate (SCN) and bromochlorodifluoromethane (BCF) and continued for 28 days at rates of 1.9 ml/min for SCN and 0.75 ml/min for BCF.

Pumping of H-2C continued for 274 days until the test was terminated when the data suite was completed on April 7, 1981. The discharge from H-2C varied from 930 to 1460 ml/min, as shown in Figure 2.

Tracer Injection

Analysis of the two-well recirculating test [Grove and Beetem, 1971] depends on a constant concentration of tracer having been injected for a significant fraction of the test period. This constant injection was accomplished by the use of a MPL Micrometering Pump equipped with three pumping units capable of pumping at rates of 0.092 to 60 ml/min with 2% accuracy. In the case of the volatile tracers, which were dissolved in isopropanol, the potential changes in concentration due to volatilization or variable head space were eliminated by injecting from a 40-gal. pressure tank equipped with an internal neoprene diaphragm. Figure 3 is a schematic of the tracer injection system. Recirculation and injection was accomplished by a 3/4-in. (1.9 cm) pipe string connecting the pumping well and the injection well. At the injection well the pipe was connected to a 1/2-in. (1.3 cm) polyethylene tubing which was run down to the well perforations at the Culebra. Thus the volatiles were introduced at a maximum water depth, which minimized losses. Both the volatile and anion tracers were injected into the formation with little dilution by the water stored in the well bore.

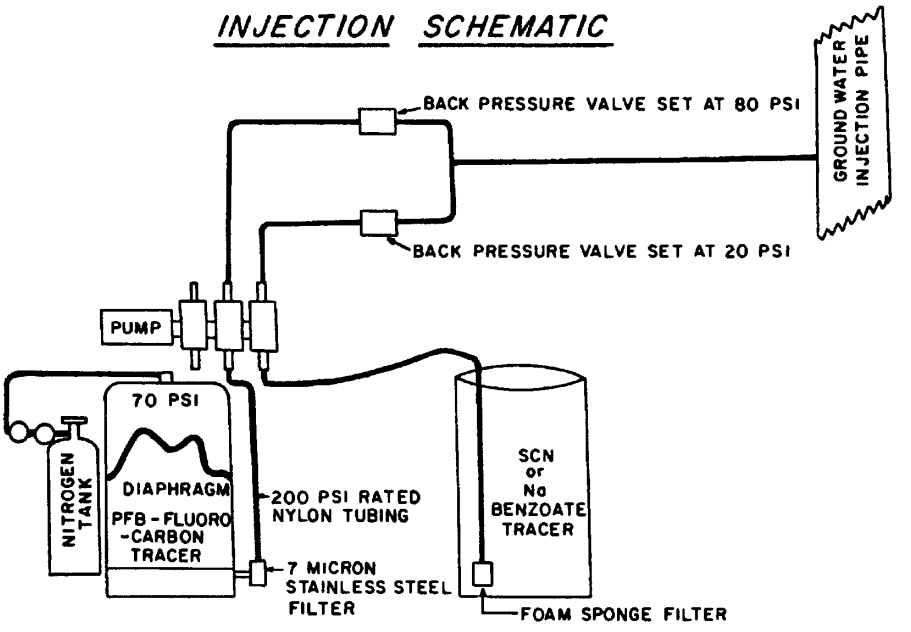

Fig. 3. Schematic of tracer injection circuit.

Tracer Collection

Anion tracers were collected from a faucet at the pumping head and stored in 250-ml polyethylene bottles and, later, in 30-ml plastic scintillation counting bottles. Volatiles were collected in 30-ml melt seal vials which were sealed within 5 min with a butane torch.

Tracer Analysis

Volatile tracer injectate concentrations were estimated at the site by direct injection into a Varian 3000 gas chromatograph equipped with a 6-ft (1.8 m) Carbopak 1/8-in. (0.3 cm) column and an electron capture detector. These analyses were qualitative, made only to establish that the tracers were in the proper range, approximately 1 mg/l. No subsequent analyses of these tracers were made. Anion tracer injectate concentrations were analyzed by

TABLE 2. H-2 SCN Tracer Test Analyses

Date	SCN^-, mg/l	Date	SCN^-, mg/l
Sept. 22, 1980	0.012	Nov. 28, 1980	4.61
Sept. 23, 1980	0.018	Nov. 29, 1980	3.79
Sept. 24, 1980	0.024	Nov. 30, 1980	4.59
Sept. 25, 1980	0.030	Dec. 2, 1980	5.84
Sept. 26, 1980	0.041	Dec. 3, 1980	5.62
Sept. 27, 1980	0.055	Dec. 5, 1980	6.02
Sept. 29, 1980	0.076	Dec. 6, 1980	5.96
Sept. 30, 1980	0.095	Dec. 7, 1980	6.12
Oct. 1, 1980	0.142	Dec. 8, 1980	6.26
Oct. 2, 1980	0.245	Dec. 9, 1980	6.06
Oct. 3, 1980	0.228	Dec. 10, 1980	5.80
Oct. 4, 1980	0.343	Dec. 11, 1980	6.12
Oct. 5, 1980	0.371	Dec. 14, 1980	5.42
Oct. 8, 1980	0.576	Dec. 15, 1980	6.60
Oct. 9, 1980	0.624	Dec. 16, 1980	6.57
Oct. 10, 1980	0.661	Dec. 17, 1980	6.80
Oct. 13, 1980	0.866	Dec. 19, 1980	5.31
Oct. 14, 1980	1.39	Dec. 20, 1980	6.65
Oct. 15, 1980	1.63	Dec. 22, 1980	6.76
Oct. 16, 1980	1.68	Dec. 23, 1980	7.38
Oct. 17, 1980	1.82	Dec. 24, 1980	7.53
Oct. 21, 1980	1.99	Dec. 26, 1980	7.54
Oct. 22, 1980	2.61	Dec. 28, 1980	7.49
Oct. 23, 1980	2.74	Dec. 29, 1980	7.72
Oct. 24, 1980	2.89	Dec. 31, 1980	8.07
Oct. 27, 1980	3.33	Jan. 4, 1981	7.94
Oct. 28, 1980	3.45	Jan. 5, 1981	8.23
Oct. 29, 1980	3.49	Jan. 7, 1981	7.75
Oct. 30, 1980	3.67	Jan. 8, 1981	7.98
Oct. 31, 1980	3.76	Jan. 11, 1981	6.94
Nov. 1, 1980	3.16	Jan. 12, 1981	7.89
Nov. 2, 1980	3.72	Jan. 14, 1981	7.42
Nov. 4, 1980	4.26	Jan. 16, 1981	6.66
Nov. 5, 1980	4.41	Jan. 20, 1981	10.31
Nov. 6, 1990	4.41	Jan. 21, 1981	10.28
Nov. 9, 1980	3.52	Jan. 22, 1981	10.31
Nov. 11, 1980	4.55	Jan. 23, 1981	10.36
Nov. 12, 1980	4.54	Jan. 27, 1981	10.26
Nov. 13, 1980	4.65	Jan. 28, 1981	10.49
Nov. 17, 1980	4.80	Jan. 29, 1981	10.71
Nov. 18, 1980	4.91	Jan. 30, 1981	11.14
Nov. 19, 1980	4.88	Jan. 31, 1981	7.09
Nov. 20, 1980	4.97	Feb. 2, 1981	12.11
Nov. 23, 1980	5.12	Feb. 3, 1981	9.04
Nov. 24, 1980	4.76	Feb. 4, 1981	11.89
Nov. 27, 1980	5.41	Feb. 5, 1981	12.24

TABLE 2. (continued)

Date	SCN^-, mg/l	Date	SCN^-, mg/l
Feb. 6, 1981	12.31	March 12, 1981	13.00
Feb. 12, 1981	12.47	March 13, 1981	12.88
Feb. 13, 1981	12.60	March 16, 1981	12.84
Feb. 15, 1981	12.60	March 17, 1981	7.81
Feb. 17, 1981	12.55	March 18, 1981	10.23
Feb. 18, 1981	12.51	March 22, 1981	12.39
Feb. 20, 1981	12.63	March 23, 1981	12.35
Feb. 22, 1981	12.25	March 24, 1981	12.33
Feb. 25, 1981	12.39	March 26, 1981	12.23
Feb. 26, 1981	12.63	March 27, 1981	12.20
Feb. 27, 1981	12.70	March 28, 1981	12.60
March 2, 1981	12.59	April 1, 1981	11.26
March 4, 1981	12.28	April 2, 1981	8.82
March 6, 1981	12.31	April 5, 1981	10.21
March 9, 1981	12.34	April 6, 1981	10.83
March 10, 1981	12.43	April 7, 1981	11.11

Injection July 10, 1980; average concentration 721 $\pm$ 27 mg/l.

high performance liquid chromatography (HPLC). HPLC was used onsite for the first tracing test for PFB and SBA tracer injection. Average injection well concentrations were 721 $\pm$ 27 mg/l for SCN^-, 650 mg/l for SBA, and 213 mg/l for PFB.

As the tracing test proceeded, tracer samples were sent to the Hydro Geo Chem laboratory in Tucson, Arizona, for further analysis. Laboratory analysis included HPLC measurement of SCN^- and PFB.

Table 2 shows the SCN^- results. Table 3 represents the PFB data. Standards were analyzed every fifth to tenth chromatogram, and two analyses were made for each sample. If the results did no agree within 2% or less, a third analysis was performed.

Tracer Stability

Both SCN^- and PFB appear to be refractory in the Culebra. Moreover, neither has shown any degradation at mg/l levels in Culebra H-2

TABLE 3. H-2 SCN Two-Well Pump Back Test

Date	PFB, mg/l	Date	PFB, mg/l
July 10, 1980	0.32	Aug. 24, 1980	8.85
July 15, 1980	0.21	Aug. 25, 1980	6.40
July 21, 1980	0.33	Aug. 30, 1980	8.19
July 25, 1980	1.26	Sept. 2, 1980	7.40
July 30, 1980	3.71	Sept. 5, 1980	5.64
Aug. 1, 1980	5.09	Sept. 10, 1980	3.92
Aug. 4, 1980	2.56	Sept. 15, 1980	3.28
Aug. 5, 1980	7.11	Sept. 18, 1980	2.23
Aug. 8, 1980	3.62	Oct. 5, 1980	0.70
Aug. 11, 1980	9.12	Oct. 10, 1980	0.40
Aug. 13, 1980	10.05	Oct. 15, 1980	0.50
Aug. 15, 1980	11.36	Oct. 21, 1980	0.29
Aug. 17, 1980	11.36	Oct. 24, 1980	0.24
Aug. 18, 1980	9.00	Oct. 30, 1980	0.19
Aug. 19, 1980	10.40	Nov. 5, 1980	0.20
Aug. 20, 1980	11.08	Nov. 20, 1980	0.13
Aug. 21, 1980	10.70	Dec. 10, 1980	0.30
Aug. 22, 1980	10.00	Dec. 20, 1980	0.20
Aug. 23, 1980	9.51		

water when stored in the laboratory for several months. PFB was first injected at H-2C on February 13, 1980, recovered in August 1980, and analyzed in September 1981, with no apparent losses occurring in the formation or in the laboratory. Studies with mixtures of barnyard soils and water yield similar results [H.W. Bentley, personal communication, 1983].

Results and Interpretation of H-2 Recirculation Test 2

A numerical analysis of the H-2 recirculation test was performed using the Grove and Beetem [1971] model. The model consists of a recharging-discharging well pair with a pattern of streamlines and treats the aquifer as uniform and isotropic and pumping as constant. To calculate the movement of the tracer, the model approximates the infinite number of streamlines by a finite number

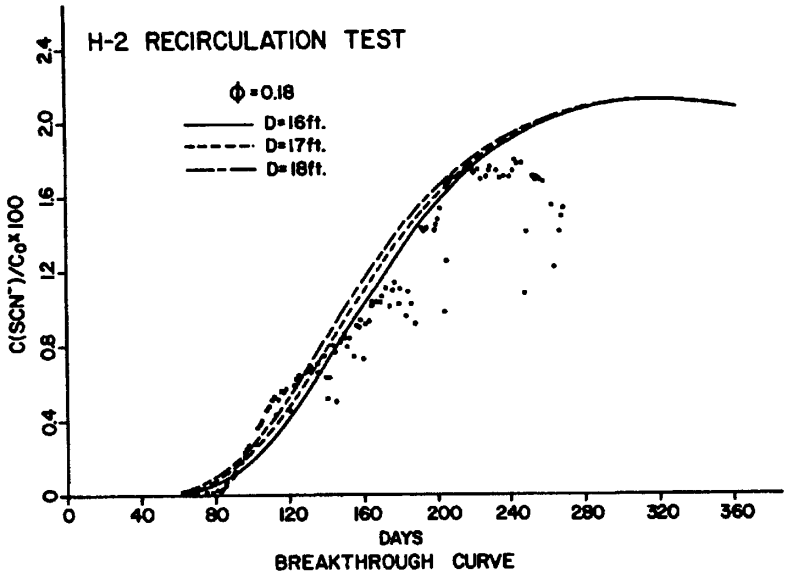

Fig. 4 Two-well recirculation SCN^- tracing test at the H-2 well pad, WIPP, SE New Mexico. Lines are output from the Grove and Beetem [1971] model with porosity ϕ fixed and varying dispersivities α.

of crescents. Each crescent is treated as a one-dimensional flow tube with only longitudinal dispersivity defined. This model uses the one-dimensional solution to the convective-dispersive equation for a finite column:

$$\frac{\partial c}{\partial t} = - v \frac{\partial c}{\partial x} + D \frac{\partial^2 c}{\partial x^2}$$

as presented by Brenner [1962]. The boundary conditions used by Brenner are

$$qC_o = vc - D \frac{\partial c}{\partial x}$$

at $x = 0$ borehole surface of injection well and

$$\frac{\partial c}{\partial x} = 0$$

at $x = L$ borehole surface of extraction well, where $x = 0$ and $x = L$ are the coordinates of the injection and pumping wells, respectively, and

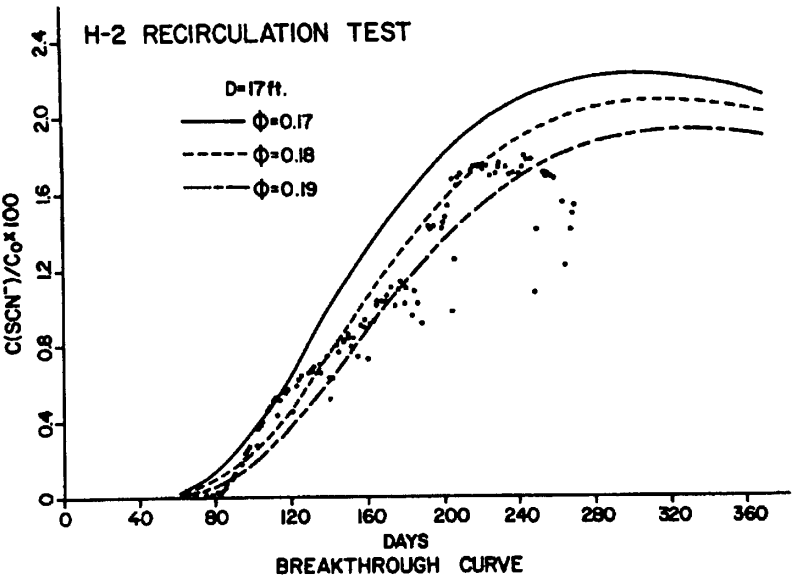

Fig. 5. Two-well recirculation SCN^- tracing test at the H-2 well pad, WIPP, SE New Mexico. Grove-Beetem curves show effects of changes in porosity ϕ by 0.01 with dispersivity α fixed at 17 ft.

q Darcy velocity, L/T;

C_o initial concentration, M/L^3;

v seepage velocity, L/T;

c observed concentration, M/L^3;

D coefficient of hydrodynamic dispersion, L^2/T;

x distance, L;

α dispersivity;

D αv.

The boundary condition used by Brenner at the extraction well implies no dispersive flux. Although this boundary condition has often been used to represent finite length columns, its physical validity is questionable.

An attempt was made to fit the observed data from the H-2 recirculation test with the Grove and Beetem model using a range of porosities, ϕ, and dispersivities, α. The result of variations in

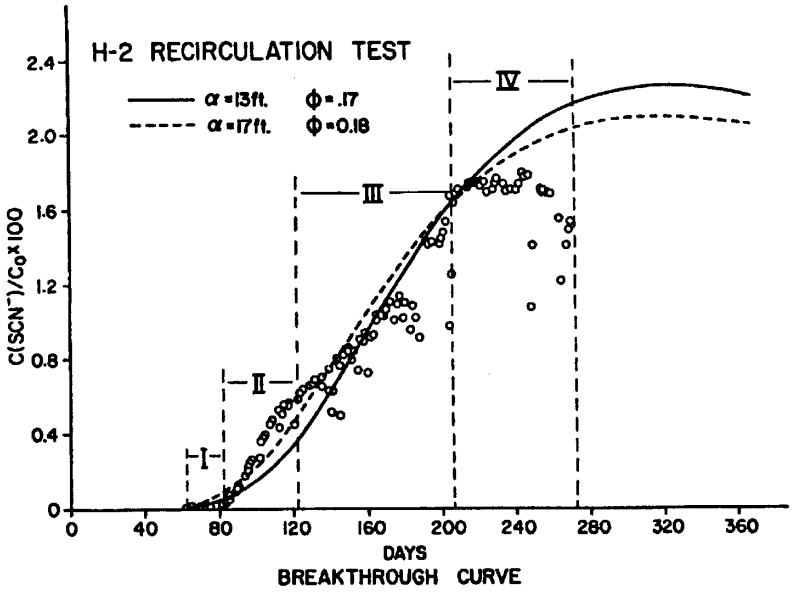

Fig. 6. Attempts to fit various parts of the SCN^- tracer breakthrough curve with varying dispersivity α and porosity ϕ.

α with a given ϕ is shown in Figure 4. Increases in α displace the curves toward earlier times. However, they have little effect on the curve slope or maximum.

Figure 5 demonstrates the variation in curves when α is fixed and ϕ is allowed to change. The porosity variations produce much larger effects in the first appearance time, slope of limb, peak time, and value of peak. For the values of α and ϕ shown, changes in porosity have a much larger effect on the breakthrough curve than changes in dispersivity.

Simplifying, the observed breakthrough curve was divided into four segments, as shown in Figure 6. Segment I extends from about 60 to 80 days after injection during which time the tracer first reached detectable concentrations. Segment II extends from 80 to 120 days during which time the concentration rose rapidly. Segment III includes that portion of the curve between 120 and 200 days where the curve is concave upward. Finally, segment IV begins at

200 days when the tracer curve becomes convex, reaches a maximum, and finally declines.

Two curves are shown in Figure 6 corresponding to α = 13 ft (4 m) with ϕ = 0.17 and α = 17 ft (5.2 m) with ϕ = 0.18. The solid line for α = 13 ft (4 m) and ϕ = 0.17, fits segment I and the early part of segment IV reasonably well but does not fit segments II and III. The dashed line in Figure 6, corresponding to α = 17 ft (5.2 m) and ϕ = 0.18, is considered to be the best fit for the first three segments of the breakthrough curve. Although this curve also matches the very early portion of segment IV, it does not match the late time data. The Grove-Beetem model cannot be used to generate a breakthrough curve matching the decline in concentration after about 220 days. Given the shape of the observed breakthrough curve in segments II and III, neither the Grove-Beetem model nor any other solution to the two-well problem that treats the formation as uniform and discharge as constant can be expected to represent accurately the observed breakthrough curve.

Conclusions

As a result of tracer performance and simplicity in handling and analysis, the anions PFB and SCN are the tracers of choice for use in evaluating aquifer parameters in dolomites at the WIPP.

Porosity and dispersivity at H-2 have been estimated at 18% and 17 ft (5.2 m), respectively. The data obtained from recirculating tests are valuable in establishing the flow and solute transport regime in the Culebra Dolomite of the Rustler Formation in the vicinity of the H-2 location. The type curves generated by the Grove-Beetem model fit the early portions of the data, however, do not match late-time data. The model cannot match the decline in concentrations without modification to include anisotropy, variable pumping rates and boundary conditions, and solute retardation in terms of matrix permeability.

A site specific numerical model is indicated, utilizing both recirculation and convergent flow tracer test for calibration. At

H-2, for instance, convergent flow tracer tests and aquifer tests for anisotropy should be performed. These results coupled with the H-2 recirculating tests will provide the basis to generate a model which describes these local phenomena and will provide guidance in establishing the field operations plan. Presently, anisotropy and tracer tests are planned at six hydropads along a hypothetical flow path originating at the center of the WIPP proposed facility and leading towards the discharge area near the Pecos River, 17 mi (27.4 km) away. Hydropad modeling will serve as the basis for a regional flow and solute transport model.

References

Bentley, H. W., and G. R. Walter, H-2 two-well recirculating tracer test, the proposed Waste Isolation Pilot Plant (WIPP), southeast New Mexico, Sandia Nat. Lab. Contract Report Sand 83-7014, Albuquerque, N. M., 1983.

Brenner, H., The diffusion model of longitudinal mixing in beds of finite length: Numerical values, Chem. Eng. Sci., 17, 229-243, 1962.

Grove, D. B., and W. A. Beetem, Porosity and dispersion constant calculations for a fractured carbonate aquifer using the two-well tracer method, Water Resour. Res., 7(1), 125-134, 1971.

Hiss, W. I., Structure of the Permian Guadalupian Capitan aquifer, southeast New Mexico and west Texas, Resour. Map 6, N. M. Bur. of Mines and Miner. Resour., Scorro, 1976.

Mercer, J. W., and B. R. Orr, Interim data report on geohydrology of the proposed water isolation pilot plant site, southeastern New Mexico, U. S. Geol. Surv. Water Resour. Invest., 79-98, 1979.

Powers, D. W., et al. (Eds.), Geological characterization report, Waste Isolation Pilot Plant (WIPP) site, southeastern New Mexico, Sandia Nat. Lab., Albuquerque, N. M., 1978.

Thompson, G. M., and J. M. Hayes, Trichlorofluoromethane in ground water--A possible tracer and indicator of groundwater age, Water Resour. Res., 15(3), 546, 1979.

Ground Water Flow in a Fractured Carbonate Aquifer Inferred from Combined Hydrogeological and Geochemical Measurements

by L. Zanini[a], K.S. Novakowski[b], P. Lapcevic[c], G.S. Bickerton[a], J. Voralek[c], and C. Talbot[c]

Abstract

A conceptual model for ground water flow is presented for a fractured Silurian dolomite in the Niagara Escarpment area of southern Ontario. Such a model is necessary to facilitate remedial efforts of a PCB-contaminated site located in Smithville, Ontario. Both physical and chemical hydrogeological observations obtained from field investigations were used to deduce the structure of the ground water flow system in the fracture network. The field study was conducted using observations obtained from six boreholes drilled in the vicinity of the town of Smithville. The boreholes were diamond cored through the entire thickness of the dolomite formation (approximately 45 m), hydraulically tested using a 2 m packer spacing and then completed using multipacker casing strings. Measurements of hydraulic head were obtained on a weekly basis over a period of two years, and ground water from each borehole interval was collected for geochemical analyses for inorganic and isotopic composition. Transmissivity measurements indicate that the dolomite is divided into two ground water flow systems separated by an extensive unit of low transmissivity that is pervasive throughout the region. The upper flow system is characterized by water enriched in Mg^{2+} and SO_4^{2-}. Below the low transmissivity zone, ground water increases in salinity and is enriched in Ca^{2+} and SO_4^{2-}. Based on the geochemistry, the rate of ground water migration in the lower flow system is surmised to be much less than that in the upper system. Measurements of hydraulic head in conjunction with the results of the analyses of the environmental isotopes ($\delta^{18}O$ and δ^2H) suggest that ground water flow is mainly horizontal and likely governed by enlarged bedding plane fractures. The isotope geochemistry and topographical features further suggest that ground water recharge is occurring approximately 2 km to the north of Smithville.

Introduction

The Niagara Escarpment is an extensive geological structure that extends along the western shoreline of Lake Ontario (Figure 1). This feature is composed of a stratigraphic sequence of dolostone and shale units that includes the Lockport Formation as the cap rock (Tesmer 1981). The Lockport Formation is an important source of water for many of the farming communities in the Niagara region. It also underlies numerous industrialized cities and towns. As a result, chlorinated solvents have contaminated the ground water at several locations (Masalia and Johnson 1984; Yager et al. 1997).

During the late 1970s and early 1980s a PCB management site was operated on the outskirts of the town of Smithville, located approximately 15 km south of Lake Ontario, on the Niagara escarpment (Figure 1). In 1985, it was discovered that PCB oils and associated solvents had penetrated the overburden and pervaded the upper horizons of the Lockport Formation. This resulted in the closure of a local water supply well, which used ground water from this aquifer. The full impact of the PCB contamination into the lower horizons is yet to be resolved. However, it was determined that a conceptual model for ground water flow in the region was necessary to develop a remedial strategy for the site.

The primary purpose of this study is to use both physical and geochemical hydrogeological observations in the construction of the conceptual model. Physical hydrogeological observations include measurement of the distribution of transmissivity and measurement of hydraulic head at selected depth intervals in the Lockport Formation. Geochemical observations include measurements of the inorganic ionic content, stable isotopic ($\delta^{18}O$, δD) and tritium (^3H) composition of the ground water, as well as determination of the chemical composition of the rock units. The inorganic composition of the ground water is used in conjunction with hydraulic measurements to determine preferential flowpaths in the fracture network. Trends in the concentrations of dissolved inorganic compounds are used to define differing ground water flow regimes. Isotopic composition is used as an indicator of ground water recharge. Thus, the geochemical data provides information on the ground water flow system that cannot be deduced using hydraulic information alone. Recent application of a similar approach was used in the development of a conceptual ground water flow model for granitic rock in Aspo, Sweden (Smellie et al. 1995) and for the fractured Chalk Aquifer in the United Kingdom (Hisock et al. 1996).

Site Geology and Hydrogeology

The contaminated site is just north of the town of Smithville, Ontario (Figure 1). The surface topography in the area (Figure 1) indicates the presence of a swale oriented in the east-west direction, located approximately 1.5 km to the north of the site. A river (20

[a]The University of Waterloo, Department of Earth Sciences, Waterloo, Ontario, N2L 3G1

[b]Department of Earth Science, Brock University, 500 Glenridge Ave., St. Catherines, Ontario, L2S 3A1; Kent@craton.geol.brocku.ca (corresponding author)

[c]National Water Research Institute, 867 Lakeshore Rd., Burlington, Ontario, N2J 3B7 Canada

Received September 1998; accepted November 1999.

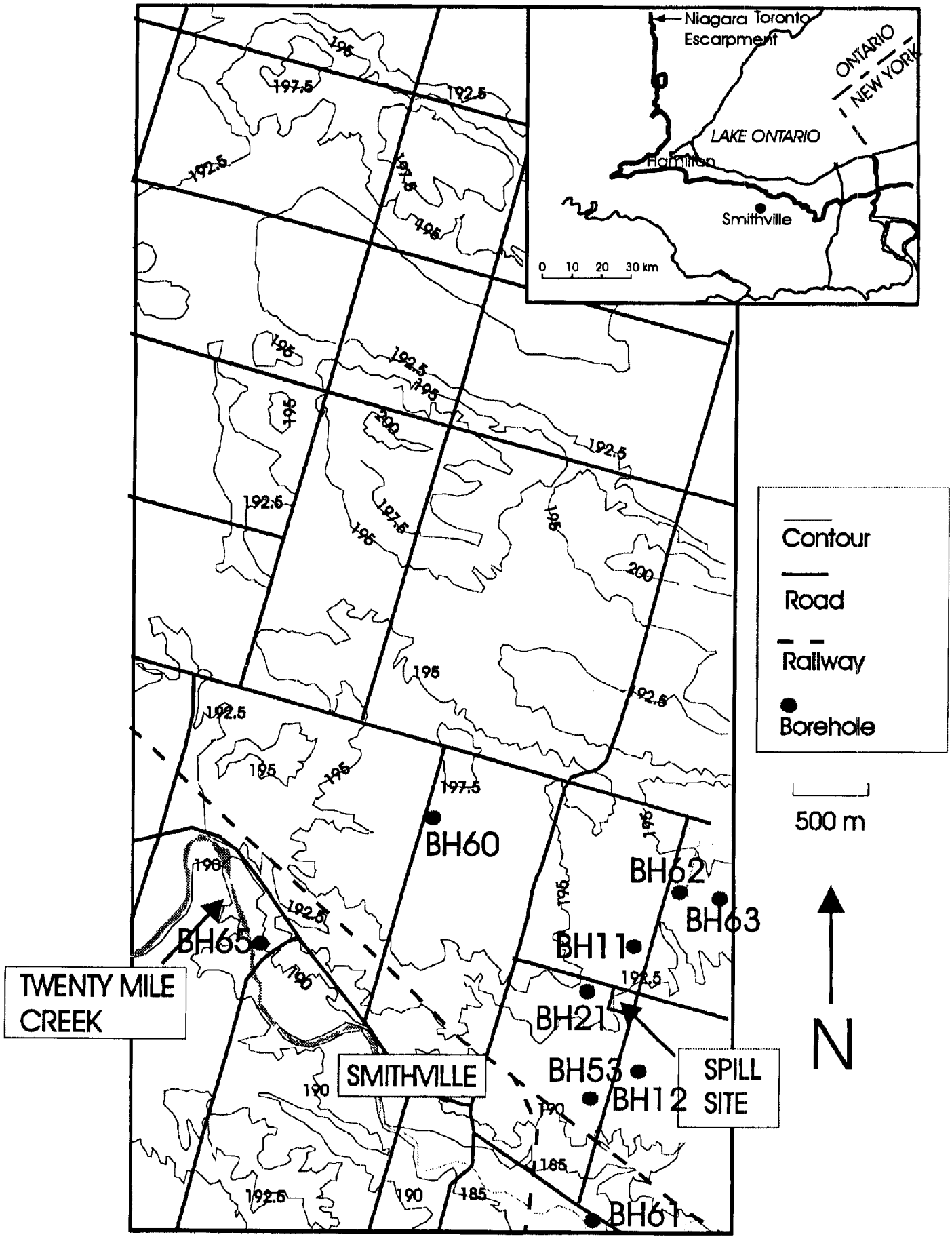

Figure 1. Topographical map of the Smithville field site and borehole locations.

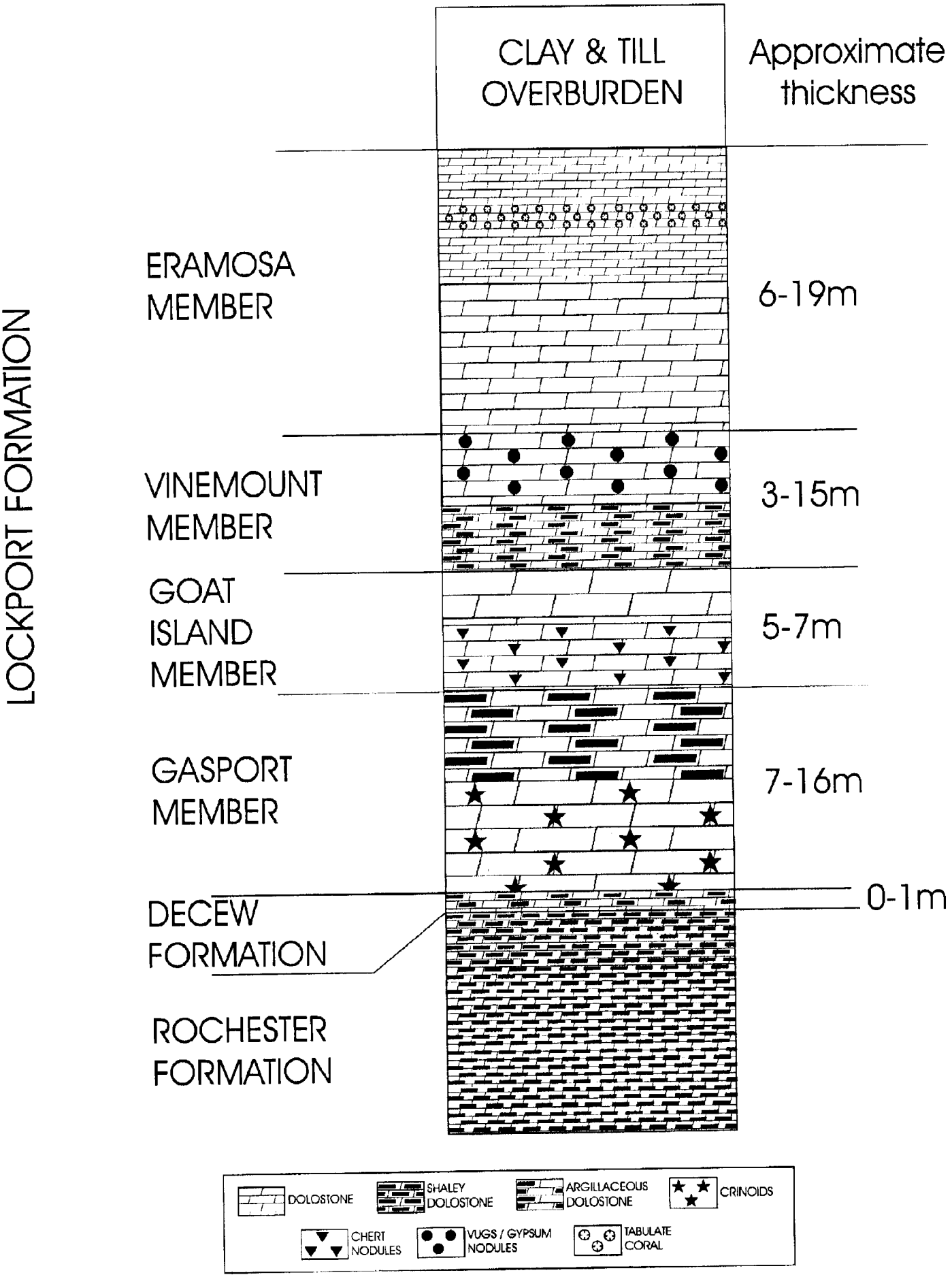

Figure 2. General stratigraphy of the Lockport Formation including average thickness (m) of the units.

Mile Creek), flowing from the northwest to the southeast, is approximately 1 km to the south of the site. The topographical gradient in the vicinity of the site has a slight inclination of approximately 10 m/km to the south. Approximately 5 to 10 m of glaciolacustrine clay and clay till underlies the site (Figure 2). The overburden is of minimal permeability (K is approximately equal to 10^{-9} to 10^{-11} m/s) although pervaded by sparse vertical fractures, some of which may be fully penetrating (Golder Associates 1995). The Lockport Formation (Figure 2) underlying the clay till is composed of four geological members consisting of fine to medium grained dolostone that dip in a southeasterly direction at an angle of 0.5 degrees (Golder Associates 1995). The upper member (Eramosa) of the Lockport Formation is 10 to 20 m in thickness and contains a fairly uniform distribution of vertical fractures (Lapcevic et al. 1996). Transmissivity of the fractures can be as high as 10^{-2} m^2/s (Golder Associates 1995). The Vinemount member, which underlies the Eramosa, is characterized by a weathered vuggy zone (1 to 4 m thick) and a zone of unfractured rock of relatively low transmissivity (3 to 4 m in thickness). The lower members (Goat Island and Gasport) are 6 to 7 m and 8 to 10 m in thickness, respectively. Fracture frequency in these units is sparser, although transmissivity is no less than that observed in the Eramosa member. The Lockport Formation is underlain by an impermeable shale (the Rochester Formation) of up to 17 m in thickness and is considered a regional aquitard (Golder Associates 1995).

Ground water flow in the fracture system is generally to the southeast, following the stratigraphic dip of the geological units (Golder Associates 1995). Based on previous studies of the Lockport Formation conducted at this site and elsewhere in the region, it is inferred that ground water flow is primarily governed by bedding plane fractures that are laterally extensive and have limited vertical interconnection (Novakowski and Lapcevic 1988; Riechart 1992; Golder Associates 1995). Thus, it was initially assumed that ground water flow in the Lockport Formation underlying the contaminated site is primarily in the horizontal direction, controlled by bedding plane fractures of unknown lateral extent and unknown vertical interconnectivity. Previous site investigations (Golder Associates 1995) indicate that some fractures, at least in the upper Lockport members, are laterally connected over a distance of 1 km as evidenced by the downgradient transport of aqueous-phase contamination emanating from the PCB source. Hydraulic gradients in these members have been estimated to be 0.02 with initial estimates of ground water velocity ranging 20 to 6000 m/a. Hydraulic gradients in some of the lower dolostone members were estimated at values ranging from 0.001 to 0.007 m/a (Golder Associates 1995).

Field Investigation

To conduct the field study, six 76 mm diameter boreholes were drilled in the vicinity of the site (Figure 1) using a diamond core and triple-tube wireline techniques. The boreholes were drilled to penetrate the entire thickness of the Lockport Formation; a depth of approximately 55 m below ground surface. Five of the boreholes are inclined at angles ranging from 55 to 57 degrees with respect to the ground surface, and one borehole (borehole 65) is vertical. Boreholes were drilled at an angle in order to intercept vertical fractures.

Once drilling was completed, hydraulic tests using the constant-head injection method (Novakowski 1988) were performed on each borehole to obtain measurements of transmissivity over continuous 2 m depth intervals. Because the majority of the testing was conducted in inclined boreholes, an inherent error is imparted to the interpretation of the hydraulic testing results. This is because the actual flow around the borehole is slightly elliptical, rather than radial as assumed for the analysis. The degree of error accrued was calculated to be no more than a few percent. Standard sliding-head packers with steel-reinforced glands were used for the testing. Periodic leak and inflation tests were conducted to ensure that the packers were obtaining a competent seal against the borehole wall. Minimum and maximum values of transmissivity ranging between 10^{-10} m^2/s and 10^{-2} m^2/s can be determined using the constant-head method.

After completion of the hydraulic testing, the boreholes were instrumented with a series of permanently emplaced packer systems (Black et al. 1987). There are five to nine isolated intervals with respect to depth in each borehole. Values of hydraulic head in each interval were calculated from pressure measurements obtained using a pressure transducer. Measurements of hydraulic head were obtained on a weekly basis over a two-year period.

A total of 31 rock samples, collected from each of the stratigraphic units of the Lockport Formation, were submitted for mineralogical analyses. The samples were prepared by crushing the sample to a powder (less than 100 μm size fraction) using a ceramic ball mill. Samples were analyzed for mineral content using X-ray diffraction (XRD).

Ground water samples were collected in November 1997 from zones isolated using the permanently emplaced packer systems. The samples were collected using a stainless-steel sampling chamber (volume of 500 mL) connected to an electronic actuating device that draws ground water from the isolated zone outside the borehole casing. Ground water in the borehole annulus is subject to mixing and diffusional processes that equilibrate the geochemical parameters with those of the surrounding ground water. Since ground water is not sampled from within the borehole casing, the need to purge the borehole of standing water is eliminated (Black et al. 1987).

After drawing the sample to ground surface, electrical conductivity, Eh, and pH were measured in the field on unfiltered samples in enclosed containers. Electrical conductivity was measured using a conductivity probe. A combination electrode with an Ag/AgCl internal reference, calibrated against the buffers 4 and 7 were used to determine pH. Eh was measured using a combination platinum redox and Ag/AgCl reference electrode. Alkalinity was measured immediately following sample collection by titrating a known volume of filtered sample with 0.16N sulfuric acid using a HACH digital titrator. Ground water samples collected for the analyses of inorganic ions and dissolved organic carbon (DOC) were filtered in the field using a 0.45 μm nylon filter. Samples submitted for cation analyses were preserved at the time of collection with ultrapure HCl.

Analyses for metals were performed at the National Laboratories for Environmental Testing in Burlington, Ontario, Canada, using inductively coupled plasma spectroscopy (ICP-MS). Anions (Cl^-, SO_4^{2-} and SiO_2) were determined using ultraviolet photometry (COBAS). Concentrations of ammonia (NH_3-N) and nitrate (NO_3-N) were analyzed using a Bran+Luebbe TRAACS-800 continuous flow analyzer. Analyses for DOC were performed using ultraviolet digestion. Charge imbalances for the inorganic ions are less than 10% with the exception of two samples.

In July and November of 1997, ground water samples were also collected for stable isotope analyses (^{18}O and ^{2}H). Analyses were performed at the National Hydrology Institute in Saskatoon, Saskachewan, Canada, using standard CO_2/water and H_2/water

Table 1
X-ray Diffraction Analyses of Rock Samples Collected from Various Geological Units

Formation (Member)	Elevation (masl)	Dolomite (%)	Quartz (%)	Gypsum (%)
Eramosa	183.3	97.3	2.7	ND
Eramosa	179.9	93.7	2.5	ND
Eramosa	176.1	97.1	2.9	ND
Eramosa	171.6	87.0	0.0	ND
Eramosa	168.5	97.6	2.4	ND
Vinemount 2	173.5	94.0	6.0	ND
Vinemount 2	165.6	96.9	3.1	ND
Vinemount 2	139.7	91.1	5.5	3.4
Vinemount 1	173.9	91.6	8.4	ND
Vinemount 1	172.9	89.3	3.0	7.7
Vinemount 1	171.6	87.6	8.7	3.6
Vinemount 1	161.6	89.8	2.8	7.4
Vinemount 1	159.5	92.4	7.6	ND
Vinemount 1	156.0	96.3	3.7	ND
Goat Island	169.7	93.7	6.3	ND
Goat Island	168.2	96.7	3.3	ND
Goat Island	168.1	91.7	2.0	6.3
Goat Island	157.6	96.4	3.6	ND
Goat Island	154.4	96.7	3.3	ND
Goat Island	150.8	96.6	3.4	ND
Gasport	163.9	93.2	2.1	4.6
Gasport	163.1	90.0	3.0	ND
Gasport	160.3	84.5	15.5	ND
Gasport	155.7	97.6	2.4	ND
Gasport	153.8	96.3	3.7	ND
Gasport	151.5	92.1	7.9	ND
Gasport	145.4	91.2	2.3	6.5
Rochester	154.6	92.1	7.9	ND
Rochester	153.1	93.0	7.0	ND
Rochester	147.1	87.5	12.5	ND
Rochester	141.3	73.3	6.2	ND

*ND = not detected.

equilibration techniques. $\delta^{18}O$ and $\delta^{2}H$ data were normalized to VSMOW/SLAP and are reported relative to VSMOW with reproducibility of ±0.1 and ±2.0, respectively. Samples were analyzed for ^{3}H at the University of Waterloo, Waterloo, Ontario, Canada, by using direct scintillation methods obtaining a detection limit of 6TU, with a reproducibility of ±8TU. Eleven samples were reanalyzed for enriched ^{3}H analyses in order to refine the estimate of concentration of ^{3}H in the ground water at a few locations. The enriched 3H analyses have a reproducibility ranging between ±0.6 to ±1.3 TU.

Saturation indices of various mineral phases were calculated using ground water chemistry and the geochemical speciation program PHREEQC (Parkhurst 1995). Thermodynamic data used for these calculations were provided in the PHREEQC database.

Results

Mineralogy

X-ray diffraction analyses (Table 1) indicate that the three principal minerals present in the units are dolomite (86 to 98 wt%), quartz (2 to 15 wt%), and gypsum (3 to 8 wt%). However, none of the samples from the Eramosa member are observed to contain any measurable gypsum.

Water Chemistry

The ground water underlying the Smithville site (Table 2) is mainly reducing (Eh < 0) at depths greater than 20 to 30 m below ground surface (approximately < 170 meters above sea level [masl]). At shallow depths, conditions are more aerobic (Eh > 0 mV). Increased concentrations of HS^- in solution and subsequent decrease in Fe^{2+} concentrations suggest that redox conditions change from iron reducing to sulfate reducing with increasing depth. The pH of the ground water is near neutral (6.8) to slightly alkaline (7.6). Temperature of the ground water ranges from approximately 10°C to 11°C. Concentrations of Ca^{2+}, N^{a+}, K^+, HS^-, Cl^-, and SO_4^{2-} increase with depth and Mg^{2+} and Fe^{2+} decrease with depth. Alkalinity also decreases slightly with depth.

Hydraulic Properties

The results of the constant head injection tests indicate that the transmissivity of the Lockport formation ranges between the testing limits of 10^{-10} m^2/s and 10^{-2} m^2/s with a few exceptions. Highest transmissivities measured at the maximum level (10^{-2} m^2/s) of the transmissivity test (3% of the total number of tests) are observed in boreholes 61, 63, and 65 at approximately 165, 155, and 170 masl, respectively. Nine percent of the zones tested had transmissivities below the minimum testing limit (10^{-10} m^2/s). Most of these zones are concentrated in the lower Vinemount and upper Rochester units. However, a few low transmissivity zones are observed at the top of the Goat Island (boreholes 60 and 62) adjacent to the Vinemount/Goat Island bedrock contact. The Eramosa, upper Vinemount and Gasport units are characterized by high transmissivities ranging from 10^{-5} to 10^{-2} m^2/s, whereas many low transmissivity measurements (10^{-10} to 10^{-7} m^2/s) are observed in the lower Vinemount unit and the Rochester Formation.

Hydraulic head measurements range from 181 to 192 masl. The highest hydraulic head measurements are observed in the Eramosa member of boreholes 60, 62, and 63. In these boreholes, hydraulic head decreases sharply below the Eramosa member. Hydraulic head is observed to be almost uniform with depth in boreholes 53 and 65 with values ranging between 184 and 185 masl. In borehole 61, hydraulic head is observed to be highest at an intermediate depth (at 160 masl), reflecting an artesian condition.

Environmental Isotopes

In general, the stable isotopic composition of the ground water ranges widely from −9 to −14 ‰ and −50 to −110 ‰ for $\delta^{18}O$ and $\delta^{2}H$, respectively. The isotopic composition of the ground water is enriched (−9 to −11 ‰ and −50 to −80 ‰ for $\delta^{18}O$ and $\delta^{2}H$, respectively) and changes little with depth in boreholes 60, 61, 62, and 63 whereas values become significantly depleted at approximately 165 masl and below in boreholes 53 and 65. Tritium values vary from below detection to values greater than 25TU.

Discussion

Major ion analyses of the ground water indicate that three chemically distinct zones are present in the flow system (Table 2,

Table 2
Geochemical Analyses of Ground Water Samples Collected from Boreholes at Selected Depths

Borehole	Bottom Zone (masl)	Top Zone (masl)	pH	Eh (mV)	Alkalinity (mg/L $CaCO_3$)	Ca (mg/L)	Mg (mg/L)	Na (mg/L)	K (mg/L)	Fe (mg/L)	SO_4 (mg/L)	Cl (mg/L	HS (mg/L)	SiO_2 (mg/L)
53	176.4	191.8	6.9	320	300	268	477	127	7.00	1.67	2810	64.2	ND*	16.3
	173.9	175.7	7.2	259	160	214	72	32.2	2.40	0.35	628	6.70	0.02	12.7
	167.6	173.2	7.2	195	125	132	97	41.0	2.60	0.46	519	16.2	ND	13.3
	162.6	166.9	7.2	29	257	250	125	53	4.20	0.16	847	34.7	0.79	12.9
	157.6	161.9	7.3	−30	138	662	178	451	25.3	0.13	1840	1290	3.42	7.46
	151.3	156.8	6.6	−100	209	558	154	116	12.5	0.09	2105	216	4.48	7.06
	146.3	150.5	7.0	−80	127	575	153	206	10.5	0.07	1920	514	5.86	8.32
	142.5	145.5	6.9	−94	292	663	164	407	5.91	0.05	1495	1061	5.56	8.50
	139.0	141.7	6.3	−103	180	2900	847	7000	137	0.05	1457	18917	5.68	26.4
60	183.1	197.0	6.9	98	400	400	520	260	5.70	10.60	2943	19.4	0.09	15.9
	175.7	182.4	7.2	155	291	140	110	31.3	2.20	0.01	616	11.4	0.04	13.0
	168.2	174.9	7.0	−78	234	338	136	119	8.10	0.05	1185	315	5.81	10.2
	159.9	167.4	7.1	−53	248	173	122	51.9	5.20	0.09	794	72.5	2.31	12.7
	156.6	159.2	7.0	93	268	342	90	45.1	5.40	1.13	1172	80.6	0.27	13.7
	153.0	155.8	7.0	−62	255	507	127	370	19.3	0.06	1679	864	3.64	11.7
61	175.0	182.2	7.0	−9	300	248	285	92.9	6.20	1.00	1430	34.8	0.29	14.9
	170.1	174.3	6.9	−13	310	387	83	44.4	4.40	0.09	1265	58.0	3.35	12.5
	165.2	169.4	7.0	−25	218	447	103	56	3.80	0.06	1120	56.5	3.07	12.3
	155.4	164.5	7.0	−22	237	278	112	51.7	4.00	0.03	763	38.7	1.77	12.8
	151.7	154.6	6.9	−65	204	465	91	70.8	6.50	0.06	1443	163	6.13	9.83
	145.5	150.9	6.8	−63	232	538	121	127	6.90	0.07	1450	373	5.81	9.38
	141.9	144.8	7.0	−28	230	562	107	100	6.70	0.09	1678	224	2.13	11.0
	138.4	141.1	7.1	10	231	600	125	324	13.7	2.08	1196	1025	0.13	9.42
62	175.0	195.4	7.4	118	285	392	341	129	5.00	9.69	2270	164	ND	12.7
	171.3	173.4	7.7	47	245	551	197	85.0	10.2	5.20	2350	75.2	ND	7.46
	163.9	170.6	7.1	−92	206	537	127	36.0	10.2	0.05	1745	44.5	5.35	7.90
	155.2	163.1	7.1	−95	176	520	120	30.4	7.70	0.06	1933	67.5	5.11	7.41
	151.4	154.5	7.6	28	204	710	238	704	25.5	4.52	1903	1654	—	7.42
63	179.6	194.3	7.3	162	214	149	177	65	2.80	1.83	672	11.1	0.01	14.5
	174.7	178.6	7.3	153	204	139	167	53.9	2.60	1.7	742	14.3	ND	13.9
	171.4	173.7	6.9	103	224	376	88.7	32.4	4.50	1.77	1310	17.4	0.02	13.0
	167.7	170.4	7.3	92	231	352	129	43.1	4.40	5.95	1334	31.1	0.12	11.8
	161.6	166.7	7.3	101	216	323	117	39.1	4.50	5.43	923	37.4	0.10	11.9
	153.4	160.6	7.3	94	193	359	134	43.5	4.30	3.38	1176	31.0	0.22	11.1
65	175.2	180.5	7.1	14	204	114	86	32.0	2.60	0.232	418	8.2	0.76	15.6
	164.7	174.0	7.0	179	229	268	170	72.0	5.40	2.98	912	70.0	0.49	12.9
	159.2	163.5	6.9	−115	177	753	191	624	32.0	0.053	1390	1410	4.93	6.84
	153.7	158.0	6.9	−80	—	1010	273	1500	31.6	0.045	1440	1300	4.42	6.24
	149.2	152.5	6.7	−105	145	798	225	2190	42.6	0.049	1450	5490	3.56	6.27
	145.6	148.0	6.8	−105	144	1650	340	2900	57.1	0.051	1280	7700	—	6.65

*ND = not detected.
— = not measured.

Figure 3). At shallow depths (elevations greater than 170 masl) corresponding to the Eramosa and upper Vinemount units (Table 2, Figure 3, boreholes 53, 61, 62, 63, and 65), Mg^{2+} and SO_4^{2-} are observed to be the ions of highest concentration in solution. At elevations between approximately 150 to 170 masl, corresponding to the lower Vinemount, Gasport, and Goat Island members, Ca^{2+} and SO_4^{2-} ions dominate. At greatest depth (elevations less than 150 masl, Rochester Formation) in boreholes 53, 61, 63, and 65, the ground water chemistry approaches brine conditions, characterized by high concentrations of Na^+ and Cl^-.

The location of these chemical zones can be readily explained as a consequence of mineral dissolution/precipitation reactions and the interaction of the ground water with formation members. For example, calculated saturation indices (SI) (Figure 3) indicate that ground water in most boreholes is undersaturated (SI approximately −0.5 to −1.0) with respect to gypsum at shallow depths (Eramosa and upper Vinemount). At greater depths ground water is observed to be close to equilibrium with gypsum (SI is approx-

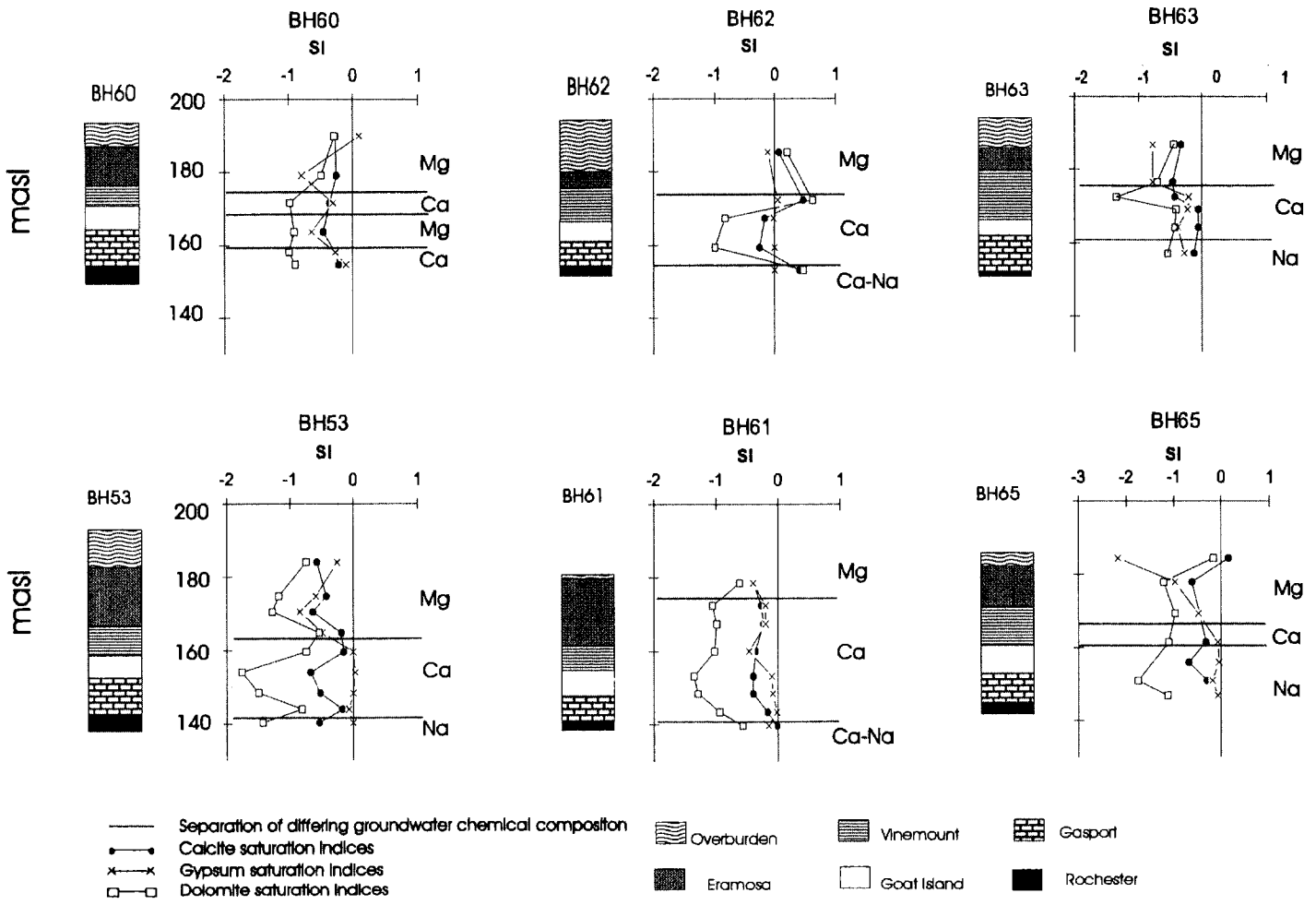

Figure 3. Calculated saturation indices (PHREEQC) for dolomite, gypsum, and calcite using chemistry from ground water samples collected at selected borehole depths in (a) boreholes 60, 62, and 63 upgradient from the PCB-contaminated site, and in (b) boreholes 53, 61, and 65 downgradient from the PCB-contaminated site.

imately 0) suggesting that the amount of Ca in the ground water is controlled by chemical equilibration reactions with gypsum observed to be present in the Vinemount, Goat Island, and Gasport members (Table 1). At elevations corresponding to the Rochester Formation, ground water tends to be undersaturated or near saturation with respect to both dolomite and calcite (Figure 3).

X-ray diffraction analyses indicate that almost all members of the Lockport Formation contain a small percentage of gypsum whereas no gypsum was observed in the Eramosa member. Thus, the dissolution of dolomite and calcite alone will control the amount of Ca concentrations in the ground water located in this member. The presence of gypsum in the lower formation members and the observation that ground water is in equilibrium with gypsum at depth in most boreholes, suggests that relative to ground water observed in the Eramosa, undersaturated water (i.e., recharge water) has not extensively reached this horizon. This is also evidenced by the diminished frequency of the vertical fractures observed in the lower members as compared to the Eramosa member (approximately three times lower frequency at depth; Lapcevic et al. 1996). The high Na concentrations and overall salinity observed in ground water at greater depth (elevations of approximately 150 masl or less; Figure 3, Table 2) also suggest high residence time and therefore sluggish ground water velocity.

The measured hydraulic parameters (transmissivity and hydraulic head) in each borehole are compared with measured geochemical parameters in Figure 4. The boreholes are arranged based on their position relative to the location upgradient (boreholes 60, 62, and 63; Figure 4a), in an area of possible ground water recharge, versus those located either immediately adjacent to the contaminated site (borehole 53, Figure 4b), or in possible areas of discharge along the river (boreholes 61 and 65; Figure 4b). Superimposed on these figures are the distribution of the three chemically distinct ground water zones previously discussed.

Upgradient Boreholes

Although the overburden is relatively thick in the vicinity of boreholes 60, 62, and 63 (Figure 4a), it was initially surmised that these boreholes are situated immediately downgradient from a potential zone of recharge. These boreholes are located approximately 1 km south of a swale that trends east-west. Due to a slight southward dip in the bedding planes, the thickness of the Eramosa member in these boreholes is less than that observed in the downgradient boreholes. The distribution of transmissivity follows the general observations (i.e., high transmissivity in the Eramosa, Goat Island, and Gasport members). Lower transmissivities are observed in the middle to lower Vinemount member. An exception to this is borehole 62, which exhibits lower transmissivity throughout the base of the Eramosa, Vinemount, and Goat Island members, with higher transmissivity evident only in the Gasport member.

The distribution of hydraulic head indicates a downward gradient with increasing depth in all three boreholes. In each case, the transition between higher and lower hydraulic head occurs at the

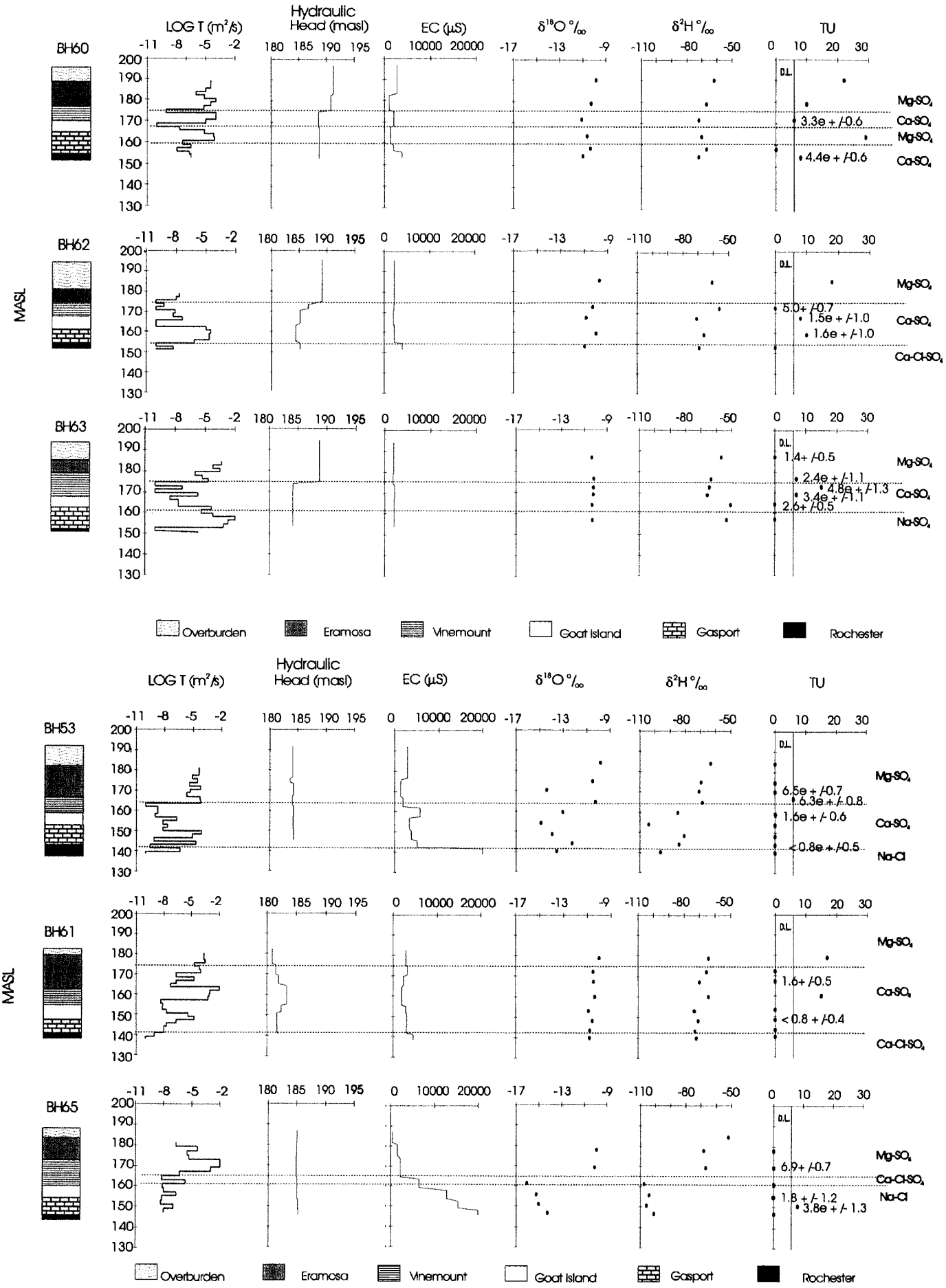

Figure 4. Composite diagram of measured parameters in (a) boreholes 60, 62, and 63 located upgradient from the PCB-contaminated site, and (b) boreholes 53, 61, and 65 located downgradient from the PCB-contaminated site.

base of the Eramosa member or top of the Vinemount member, across a discrete zone of low transmissivity. In the case of boreholes 60 and 63, the hydraulic head below the low transmissivity zone is uniform. The steady decrease in hydraulic head with depth (downward gradient) observed in borehole 62 may indicate weak vertical fracture connection through these units in the immediate vicinity of this borehole.

Electrical conductivity is relatively uniform with depth, ranging from approximately 2000 to 4000 µs. Similarly, the stable isotopic composition of the ground water is also uniform with depth, ranging from −9 ‰ to −11 ‰ and −60 ‰ and −80 ‰ for $\delta^{18}O$ and $\delta^{2}H$, respectively. Average $\delta^{18}O$ and $\delta^{2}H$ values in precipitation collected in Simco, Ontario, (located approximately 100 km to the east) during the period from 1975 to 1982, are approximately −10 ‰ and −70 ‰, respectively (IAEA/WMO 1988). Thus the ground water is of recent origin. In addition, many of the sampled zones contain measurable concentrations of ^{3}H indicating that ground water in these zones is of post WWII age. In boreholes 60 and 62, ^{3}H concentrations are highest in the shallow depths (elevations greater than 165 masl). However, high transmissivity zones in the lower Vinemount and Goat Island to upper Gasport also exhibit moderate to high ^{3}H concentrations.

The fact that there is little change in electrical conductivity and in the stable isotopic signature with respect to depth suggests that in the upgradient boreholes, ground water in both the upper Eramosa member and in the lower members are of a common origin. The presence of ^{3}H at various depths (i.e., shallow and deep) further indicates that younger water is infiltrating all depths of the flow system. On a local scale, recharge water may infiltrate through fractures in the thick overburden immediately above the boreholes. Alternatively, a large portion of recharge water may originate from the swale (Figure 1) and a bedrock ridge that lies immediately to the north of the site. The bedrock ridge has a topographic high of 10 to 15 m above the swale and is composed of Eramosa member rock, which outcrops in several places. Thus on a larger, more regional scale, the source of recharge water for the area most likely originates from exposed fractures in the ridge and swale areas.

Downgradient Boreholes

In general, the lithology logs for boreholes 53, 61, and 65 show a diminished overburden thickness and an increase in the thickness of the Eramosa member in the downgradient direction (Figure 4b). The elevation of the top of the Rochester Formation (the underlying aquitard) is 8 to 9 m below that of the upgradient boreholes.

The distribution of transmissivity in these boreholes is similar to that for the upgradient boreholes. Low transmissivity zones in the middle to lower Vinemount and high transmissivity zones in the Eramosa/Upper Vinemount, Goat Island, and Gasport members are observed. The exception is borehole 65, which has more sparsely distributed zones of limited transmissivity (10^{-7} to 10^{-8} m^2/s) in the Goat Island and Gasport members.

Contrary to the boreholes located upgradient, boreholes 53 and 65 have a relatively uniform distribution of hydraulic head with depth. The slightly lower hydraulic head observed at 175 masl (middle of the Eramosa member) in borehole 53 may be attributed to the ongoing pumping from a water treatment facility at the contaminated site that pumps ground water from only a few meters into the upper bedrock. The hydraulic head distribution in borehole 61 is dissimilar to all other boreholes in that the highest hydraulic head is observed in the high transmissivity feature that straddles the Eramosa-Vinemount member contact. This zone is artesian, resulting in vertically upward and downward gradients emanating from this horizon.

The electrical conductivity in boreholes located downgradient generally increases with depth (Figure 4b) with the exception of borehole 61. The most profound change in electrical conductivity is observed in boreholes 53 and 65, where measured values range from 1500 µs in the shallow zones to values greater than 20,000 µs in the deepest zones. Electrical conductivity in borehole 65 is observed to steadily increase with depth, whereas in borehole 53 electrical conductivity mainly increases below the Eramosa-Vinemount contact located at 162 masl. In borehole 61 electrical conductivity increases only slightly from approximately 2000 to 5000 µs.

In boreholes 53 and 65, $\delta^{18}O$ and $\delta^{2}H$ concentrations are relatively enriched in ground water located in the Eramosa and Upper Vinemount members (greater than 165 masl) with values ranging between −9 ‰ and −11 ‰ and −50 ‰ to −80 ‰, respectively. Below the Vinemount member, the isotopic signature becomes significantly more depleted with values ranging between −13 ‰ to −17 ‰ and −80 ‰ to −110 ‰ for $\delta^{18}O$ and $\delta^{2}H$, respectively. The change in isotopic signature occurs below the low transmissivity zone in the Vinemount member. In boreholes 53 and 65, ^{3}H (analyzed by direct methods) is not observed in any of the sampled ground water. However, enriched ^{3}H values obtained subsequently from borehole 53 indicate that the presence of ^{3}H (6.3TU ± 0.8TU) at 175 masl, close to the contact between the Eramosa and Vinemount units. The isotopic composition of the ground water in borehole 61 varies little with $\delta^{18}O$ and $\delta^{2}H$ ranging from −9 ‰ to −11 ‰ and −55 ‰ to −80 ‰ throughout the borehole depth. This signature is similar to that for the upgradient boreholes. As with the upgradient boreholes, substantial ^{3}H concentrations are also observed in borehole 61, particularly at the shallowest interval and the high transmissivity zone located in the middle of the Eramosa member. In borehole 65, a small amount of ^{3}H is observed at 150 masl. A second sample from this zone obtained five months later confirmed the presence of ^{3}H (3.8TU enriched ± 1.3TU). However, this zone is of low transmissivity (approximately 10^{-8} m^2/s), and it is likely that drill water was entrapped during installation of the permanent packer system.

The pronounced shift with depth in isotopic composition and electrical conductance observed in boreholes 53 and 65 suggests that two distinct flow systems are present. As with the upgradient boreholes, the low transmissivity zone in the Vinemount member appears to be the dividing horizon between the two individual flow systems.

Tritium, $\delta^{18}O$ and $\delta^{2}H$ concentrations in borehole 53 show the presence of recent water in the high transmissivity zone at the base of the Eramosa and the upper Vinemount. A value of 6.3 (± 0.8 TU) for enriched ^{3}H was obtained for this interval. The source for this water is likely through connection with the upgradient recharge area. Considering that ground water velocities in the fractures within the lower Eramosa range from 10 to 30 m/day (Radcliffe 1997) and matrix porosities range from 5% to 15% (unpublished data), transport of the ^{3}H from the recharge area in a horizontal flow system can be simulated. Using the Tang et al. (1981) solution, simulation of transport in a discrete fracture having an aperture of 500 µm, a velocity of 30 m/day and adjacent matrix porosity of 5% shows that ^{3}H concentrations as high as 15TU are possible at borehole 53 when input conditions at borehole 60 (i.e., 30TU) are employed.

The results for borehole 61 are complicated by the presence of the artesian hydraulic head in the high transmissivity zone in the

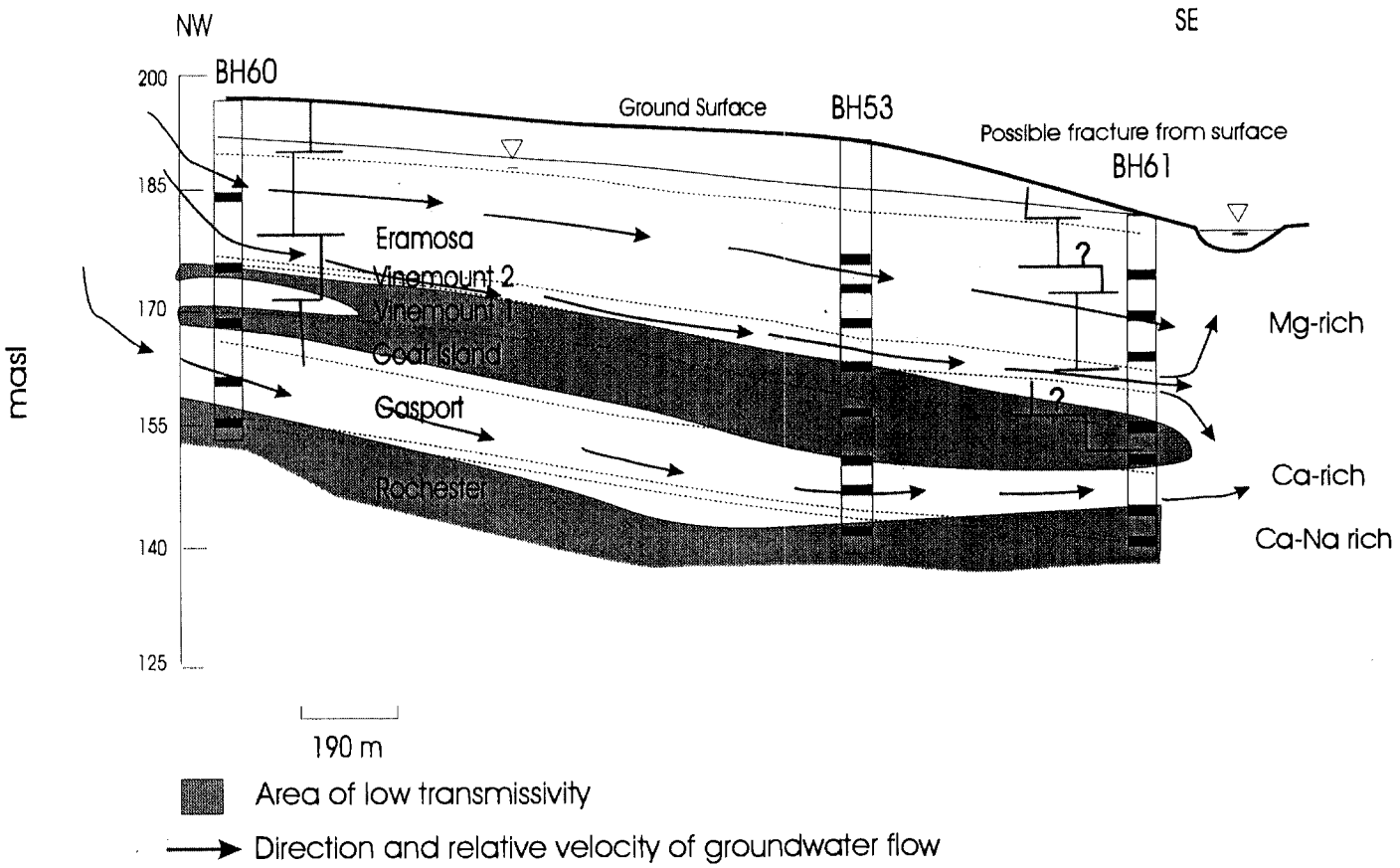

Figure 5. Conceptual model of two-dimensional flow at the Smithville site in the general direction of ground water flow (length of arrow indicates ground water velocity).

Lower Eramosa and Vinemount units. The water in this zone is observed to contain ^3H (15TU ± 8) and shows a similar isotopic signature to ground water located near the upgradient boreholes. The source of this water is uncertain. The strong discharging (upward gradients) observed in this highly transmissive zone suggests that the recharge is occurring from some distance away. Thus, hydraulic connection from the recharge area may be present. However, the upper Eramosa is exposed on the river bottom at several locations both upstream and downstream from borehole 61. Approximately 2 km upstream from borehole 61, river flow decreases with a significant volume discharging through the river bed. Thus, it is also possible that the source of recharge water in borehole 61 is through hydraulic connection with river water entering the subsurface at an upstream location.

Ground water in the stratigraphic intervals and below the artesian zone have stable isotopic signatures similar to that in the artesian zone. Although these waters do not contain measurable ^3H, it is likely that they originate from the artesian zone, through vertical connections, or are recharged at locations further up the river valley.

Conceptual Model and Conclusions

Since fracture networks are, in general, complex with the nature of fracture interconnection being uncertain, interpretation of ground water flow from borehole to borehole using hydraulic parameters is difficult. Indeed, the large variations in transmissivity values noted in all boreholes suggest that variability in ground water flow are common in the fracture system. The previous discussion supplements the hydrological data with geochemical data to provide evidence for hydraulic interconnection on a large scale. The conceptual model (Figure 5) represents a two-dimensional cross section, using three selected boreholes located in the direction of ground water flow (northwest to southeast).

Hydraulic head and measurements of transmissivity can provide only a general idea of ground water flow in the immediate vicinity of a particular borehole. For example, the uniform distribution of hydraulic head in boreholes 53 and 65 coupled with large variations observed in transmissivity measurements may indicate that ground water flow is primarily horizontal in the vicinity of these boreholes, with little interaction between the individual fracture planes. Alternatively, the uniformity of the hydraulic head distribution could imply that the horizontal fracture planes are extremely well connected such that vertical gradients are immeasurable. However, the chemistry and isotopic composition of the ground water in these boreholes shows the water above the Vinemount to be markedly different from that below, suggesting that little interaction between the water in these two horizons has occurred. We can also infer from the uniformity in hydraulic head that there are no local ground water sources (recharge zones) or drains (discharge zones) nearby.

Conversely, in the upgradient boreholes and borehole 61, transmissivity measurements are equally varied, yet distribution of hydraulic head with depth is not uniform. Evidence for predominantly horizontal flow is provided by the sharp change in hydraulic head distribution occurring at approximately 175 masl in the upgradient boreholes (60, 62, and 63) indicating that a unit of low permeability divides two separate flow systems. The uniform distribution of the geochemical parameters with depth and the presence of ^3H at depths below the low transmissive zone (e.g., borehole 60) suggests that on a small scale surrounding each borehole, local vertical hydraulic interconnections exist to allow for the penetration of recharge water across the low transmissive barrier.

In both the upgradient and downgradient vicinities, ground water flow is predominantly horizontal. Flow is likely controlled by

large bedding plane fractures that have been observed in the Lockport Formation (Tesmer 1981; Novakowski and Lapcevic 1988; Yager and Kappel 1998). The presence of bedding-plane partings is common in sedimentary rock sequences and is usually caused by stress changes. Enlarged bedding plane partings have been found to control ground water flow in the Lockport Formation at Niagara Falls Ontario, and in the Newark Basin, New Jersey (Novakowski and Lapcevic 1988; Michalski and Britton 1997).

The uniformity of the stable isotope composition with depth in the upgradient holes (60, 62, and 63) and the overall similarity to that of recent precipitation values suggest that ground water recharge is occurring just upgradient of these boreholes. Ground water recharge for the area likely occurs through fractures in the Eramosa unit from the swale and ridge located immediately north of the upgradient boreholes, where the Eramosa is observed to outcrop.

In all boreholes, a zone of low transmissivity is located in the middle to lower Vinemount member. This zone of low transmissivity varies in thickness yet appears ubiquitously. It is this horizon of low transmissivity that separates ground water flow into the upper and lower flow regimes in the region. The upper flow regime is present in the Eramosa member. The lower flow regime is present mainly in the Gasport and Goat Island members (Figure 5).

Inorganic ion concentrations of ground water and geochemical speciation modeling suggest that these regimes are physically and chemically related to the bedrock. Shallow ground water is found to be dominated by high Mg^{2+} concentrations due to equilibrium reactions with dolomite, which control the amount of Ca^{2+} and Mg^{2+} in solution. However, in the lower flow regime, ground water is dominated by high Ca^{2+} and SO_4^{2-} concentrations due to the higher amount of gypsum minerals present in the rocks.

Transmissivity measurements in the lower flow regime are observed to be just as high as that in the upper. Thus, calculations based on equivalent aperture width suggest that ground water velocity in both flow regimes are similar (Novakowski 1988). However, the high electrical conductivity and overall salinity observed at depth in the downgradient boreholes 53 and 65 suggest that ground water residence time in this zone may be greater than in the upper zone. Also, the observed depletion in stable oxygen and hydrogen isotopes at depth in these boreholes indicates that there is relatively less dilution from younger recharge water. As recharge is observed to penetrate all depths in the upgradient boreholes, it is therefore implied that fracture connectivity in the lower flow regime is less than that of the upper. This decrease in fracture connectivity allows for a greater period of time for recharge water to be transported downgradient (i.e., decreased velocity). Thus, the high transmissivity measurements observed in the lower flow regime are likely a result of increased fracture connectivity on a local scale only.

Ground water discharge from the flow system is less well defined. At borehole 65, located upstream of the town of Smithville along the banks of 20 Mile Creek, ground water in both the upper and lower flow systems appears to completely underflow the river. However, at borehole 61 located downstream from the town center, ground water appears to interact with the river water, at least within the upper flow system. In borehole 61, a high transmissivity zone in the Goat Island/Gasport exhibits the lowest hydraulic head at depth of any of the boreholes. This indicates significant underflow of the lower flow system.

Acknowledgments

Gratitude is extended to Kelly Millar, Susan Brown, and Andrea Brown for their assistance in the laboratory and the field. Also appreciated are editing suggestions from Jos Beckers and suggestions from Amy Sheldon in the interpretation of the tritium analyses. Funding for this research was provided by the Smithville Phase IV project.

Editor's Note: The use of brand names in peer-reviewed papers is for identification purposes only and does not constitute endorsement by the authors, their employers, or the National Ground Water Association.

References

Black, W.H., H.R. Smith, and F.D. Patton. 1987. Multiple-level groundwater monitoring with the MP system. In *Proceedings of the NWWA-AGU Conference. Surface and Borehole Geophysical Methods and Ground Water Instrumentation,* by National Water Well Association. Dublin, Ohio: NWWA.

Golder Associates Ltd. 1995. Hydrogeologic data compilation and assessment, CWML site. Smithville, Ontario. Golder Associates Ltd. Report No. 941-9033.

Hissock, K.M., P.F. Dennis, P.R. Saynor, and M.O. Thomas. 1996. Hydrochemical and stable isotope evidence for the extent and nature of the effective Chalk Aquifer of north Norfolk, UK. *Journal of Hydrology* 180, 79-107.

IAEA/WMO. 1998. Global network for isotopes in precipitation. The GNIP database, Release 2. Simco, Ontario. See Web site at www.iaea.org

Lapcevic, P., K.S. Novakowski, G. Bickerton, and J. Voralek. 1996. Preliminary results of the fall 1995 drilling and hydraulic testing program at the Smithville phase IV bedrock remediation site. National Water Research Institute. Burlington, Ontario, Canada, Technical Report, Contribution Number 96-50.

Maslia, M.L., and R.H. Johnston. 1984. Use of a digital model to evaluate hydrogeologic controls on groundwater flow in a fractured rock aquifer at Niagara Falls, New York, U.S.A. *Journal of Hydrology* 75, 167-194.

Michalski, A., and R. Britton. 1997. The role of bedding fractures in the hydrogeology of sedimentary bedrock—Evidence from the Newark Basin, New Jersey. *Ground Water* 35, no. 2: 318 -327.

Novakowski, K.S. 1988. Comparison of fracture aperture widths determined from hydraulic measurements and tracer experiments. In *Fluid Flow, Heat Transfer and Mass Transport in Fractured Rocks,* 68-80. *Proceedings of the 4th Canadian/American Conference on Hydrogeology,* ed. B. Hitchon and S. Bachu by National Water Well Association. Dublin, Ohio: NWWA.

Novakowski, K.S., and P.A. Lapcevic. 1988. Regional hydrogeology of the Silurian and Ordovician sedimentary rock underlying Niagara Falls, Ontario, Canada. *Journal of Hydrology* 104, 211-236.

Parkhurst, D.L. 1995. User's guide to PHREEQC—A computer program for speciation, reaction-path, advective-transport and inverse geochemical calculations. U.S. Geological Survey, Water-Resources Investigations Report 95-4227.

Radcliffe, A. 1997. Determination of groundwater velocities in discrete fractures using point dilution methods. B.Sc. thesis, Department of Earth Sciences, University of Waterloo, Ontario.

Riechart, T. M. 1992. Influence of vertical fractures in horizontally stratified rocks. Unpublished M.Sc. thesis, Department of Earth Sciences, University of Waterloo, Ontario.

Smellie, J.A.T., M. Laaksoharju, and P. Wikberg. 1995. Aspo, SE Sweden: A natural groundwater flow model derived from hydrogeochemical observations. *Journal of Hydrology* 172: 127-146.

Tang, D.H., E.D. Frind, and E.A. Sudicky. 1981. Contaminant transport in fractured porous media. Analytical solution for a single fracture. *Water Resources Research* 17, no. 3: 555-564.

Tesmer, I.H. 1981. *Colossal Cataract, the Geological History of Niagara Falls.* Albany, New York: State University of New York Press.

Yager, R.M., S.E. Bilotta, C.L. Mann, and E.L. Madsen. 1997. Metabolic adaptation and in situ attenuation of chlorinated ethenes by naturally occurring microorganisms in a fractured dolomite aquifer near Niagara Falls, New York. *Environmental Science and Technology* 31, 3138-3147.

Yager, R.M., and W.M. Kappel. 1998. Infiltration and hydraulic connections from the Niagara River to a fractured-dolomite aquifer in Niagara Falls, New York. *Journal of Hydrology* 206, 84-97.

TEXAS
WATER
DEVELOPMENT
BOARD

Report 210

GROUND-WATER RESOURCES OF THE CARRIZO AQUIFER IN THE WINTER GARDEN AREA OF TEXAS

VOLUME 1

September 1976

TEXAS WATER DEVELOPMENT BOARD

REPORT 210

GROUND-WATER RESOURCES OF THE CARRIZO AQUIFER IN THE WINTER GARDEN AREA OF TEXAS

VOLUME I

By

William B. Klemt
Gail L. Duffin
Glenward R. Elder
Geologists, Texas Water Development Board

September 1976

TEXAS WATER DEVELOPMENT BOARD

Published and distributed
by the
Texas Water Development Board
Post Office Box 13087
Austin, Texas 78711

TABLE OF CONTENTS

TABLE OF CONTENTS (Cont'd.)

TABLE OF CONTENTS (Cont'd.)

GROUND-WATER RESOURCES OF THE CARRIZO AQUIFER IN THE WINTER GARDEN AREA OF TEXAS

ABSTRACT

The Winter Garden Area of Texas lies southwest of the San Marccos River and within the Guadalupe, San Antonio, Nueces, and Rio Grande basins. It consists of all or parts of Atascosa, Bexar, Caldwell, Dimmit, Frio, Gonzales, Guadalupe, Karnes, La Salle, Live Oak, McMullen, Maverick, Medina, Uvalde, Webb, Wilson, and Zavala Countie:;. Within the Winter Garden Area is found the Winter Garden District which includes Dimmit and Zavala Counties; and eastern Maverick County.

The Carrizo aquifer is the most continuous, permeable, and most developed (heavily pumped) water-bearing unit in the Winter Garden Area. Throughout most of the Winter Garden Area, the Carrizo aquifer yields ground water which is acceptable for most irrigation, public supply, and industrial purposes.

Recharge to the Carrizo aquifer enters by infiltration from rainfall and from streams which flow across the outcrop. The average rate of recharge to the Carrizo aquifer in the Winter Garden Area is about 100,000 acre-feet per year or 89 mgd (million gallons per day). In addition, leakage to the aquifer from other formations occurs in Dimmit, Frio, and Zavala Counties; an estimated 9,500 acre-feet per year (8.5 mgd) leaked into the Carrizo through confining beds and down uncemented well bores during the period 1963-1969. Average annual pumpage for the period 1963-1969 was approximately 272,000 acre-feet (243 mgd). Thus, for this period about 162,500 acre-feet per year (145 mgd) was removed annually from storage. These large annual withdrawals of ground water from storage have caused declines in Carrizo aquifer water levels, which directly affect the cost of pumping water and are also related to water-quality changes within the aquifer, particularly in the Winter Garden District (Dimmit, Zavala, and eastern Maverick Counties).

One of the primary objectives of this study was to simulate the Carrizo aquifer in the Winter Garden Area with a digital computer mathematical model. The simulations for the period 1970 through 2020 indicate the following: (a) in the heavily irrigated areas near Batesville and east of Carrizo Springs and Crystal City in Dimmit and Zavala Counties, water levels will continue to decline rapidly; (b) elsewhere in the Winter Garden Area, water levels will slowly decline if pumpage remains unregulated and occurs at predicted rates; (c) a firm water supply of 20,000 to 40,000 acre-feet per year (18 to 36 mgd) of ground water from wells can be developed in Wilson County for municipal use in the San Antonio region; (d) approximately 330,000 acre-feet per year (294 mgd) of ground water can be developed annually from the Carrizo aquifer and not lower water levels below a 400-foot level below land surface or below the top of the water-bearing sands until the year 2020, representing an increase of 58,000 acre-feet per year (52 mgd) over the withdrawals of 1963-l 969; and (e) the areas most favorable for development of additional ground-water supplies are in Wilson and Gonzales Counties.

GROUND-WATER RESOURCES OF THE CARRIZO AQUIFER IN THE WINTER GARDEN AREA OF TEXAS

INTRODUCTION

Purpose and Scope

Field study was begun in October 1967 to determine the ground-water resources of the Winter Garden Area of Texas with emphasis on the Carrizo aquifer. The primary objectives of this study were: (a) to determine the regional geohydrologic characteristics of the Carrizo aquifer; (b) to establish monitoring programs for pumpage, water levels, and water quality with respect to the Carrizo aquifer for continuous evaluation of ground-water availability and dependability on a regional basis; (c) to examine the feasibility of artificially recharging the Carrizo aquifer; and (d) to use a digital computer model of the Carrizo aquifer to evaluate the aquifer's response to pumping and the probable future ground-water conditions. Field work for this study was completed in the spring of 1970.

Volume I summarizes the results of this investigation, and contains information on the amounts of water that have been and can be produced from the Carrizo aquifer, its hydrologic characteristics, and the chemical quality of its water. The water-bearing strata of the Wilcox Group and other aquifers of the Claiborne Group are also discussed. Volume II contains supporting basic data: records of 3,214 water wells, records of water levels in 474 wells, and chemical analyses of water samples from 1,553 wells. Also available for reference in the files of the Texas Water Development Board are drillers' logs of 711 wells that were used in the study.

Location and Population

The area covered by this report, which will be referred to as the Winter Garden Area, is the area southwest of the San Marcos River in which the Carrizo aquifer contains fresh to slightly saline water. It consists of all or parts of Atascosa, Bexar, Dimmit, Frio, Gonzales, Guadalupe, Karnes, La Salle, Live Oak, McMullen, Maverick, Medina, Uvalde, Webb, Wilson, and Zavala Counties. Data were also collected east of the San Marcos River (Caldwell and eastern Guadalupe Counties), in order to minimize boundary effects of a computer simulation of the Carrizo aquifer. Although most of the maps in this report extend well east of the San Marcos River, all figures in the report concerning volume of ground water apply only to areas west of the San Marcos. The Winter Garden Area (west of the San Marcos River) consists of approximately 11,800 square miles and represents approximately 4.5 percent of the State's total area. Within the Winter Garden Area is the Winter Garden District, an irrigated region which produces vegetables in late winter and early spring in Dimmit, Zavala, and eastern Maverick Counties (Figure 1).

According to data in the 1970-71 Texas Almanac, the Winter Garden Area has a population of approximately 140,000, or about 1.2 percent of the State's population.

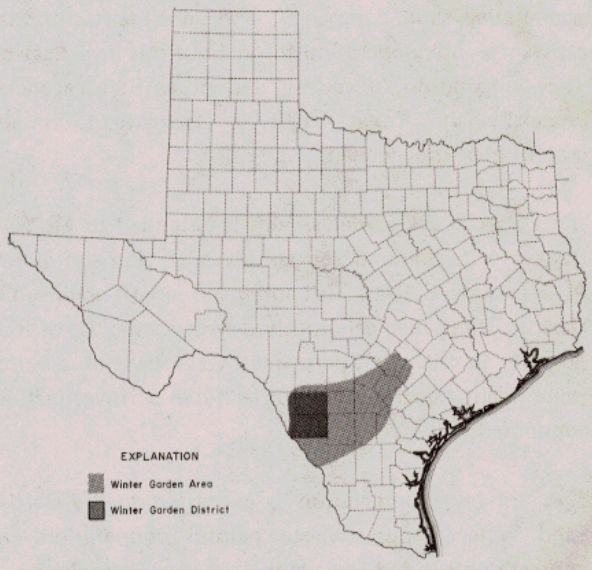

Figure 1.—Location and Extent of the Winter Garden Area and the Winter Garden District

Personnel

This report was prepared by the authors under the general direction of Lewis Seward, Principal Engineer-Project Development, and Robert Bluntzer, director, Water Availability Division. Tommy Barnes, geologist, assisted in assembling the data.

The digital computer mathematical model used to simulate the Carrizo aquifer was developed by George F. Pinder of the United States Geological Survey, and was modified by staff of the Board's Systems Engineering Division, under the direction of Lial Tischler and assisted by Al Austin, Tommy Knowles, and Allen White. Core drilling and the laboratory testing of drill cuttings and cores were done by staff of the Board's Materials Testing Laboratory and Core Drill Branch under the direction of James Sansom and Henry Sampson.

Acknowledgements

The authors appreciate the cooperation extended by the property owners in the Winter Garden Area who supplied information concerning their wells and, in many instances, also allowed access to their property and the use of their wells to monitor water-level changes and production capabilities. Acknowledgement is also extended to the water well drillers of the area, city officials, water superintendents, officials of independent water districts, electric and natural gas distribution cooperatives and companies, and consultants for their assistance and cooperation throughout this investigation. The cooperation of fede-al and other State agencies, especially the Texas Highway Department, is also gratefully acknowledged.

Special acknowledgement is extended to Mr. Billy Deagan of Sutherland Springs, Mr. J. D. Harrison of Palo Alto, and Mr. Calvin Hardt and Mr. George Thompson of Devine. These men generously permitted the use of their property in order that perrnanent water-level observation wells might be drilled and other types of investigations conducted.

Finally, appreciation is expressed to the Carrizo Sand Water Group, whose helpful cooperation and interest contributed toward the successful completion of this investigation and a better understanding of the ground-water resources of the Winter Garden Area.

WATER-BEARING STRATA OF THE WILCOX AND CLAIBORNE GROUPS

The Wilcox and Claiborne Groups contain the major aquifers within the study area. The strata of these units are marine and continental in origin and consist mainly of clay, cross-bedded river sand, beach sand, silt, and lignite. The stratigraphic units of the Wilcox and Claiborne, their approximate thickness, lithologic description, and water-bearing characteristics are given in Table 1. Their position in the subsurface is illustrated in the geohydrologic sections, Figures 27, 28, and 29. Estimates of the amount of ground water obtained from the aquifers for irrigation, public supply, and industrial purposes are given in Table 4.

For the purpose of this report, the Wilcox Group will be considered as an undifferentiated geologic unit. The upper section of the Wilcox contains some massive sand beds which are continental in origin. The middle portion is composed principally of nonmarine sand, clay, and lenticular beds of lignite. The basal portion contains mainly sand and clay of shallow marine origin. The Wilcox reaches a maximum thickness of about 2,800 feet and contains fresh to very saline water in the Winter Garden Area. Figure 2 illustrates the extent of sands containing fresh to slightly saline water-having less than 3,000 mg/l (milligrams per liter) dissolved solids--in the Wilcox aquifer (Wilcox Group). The approximate depth to and altitude of the top of the Wilcox aquifer are shown on Figure 10.

Overlying the Wilcox is the Carrizo Sand, the lowermost formation of the Claiborne Group. The Carrizo is composed mainly of very permeable, massive, cross-bedded, medium-grained sand and ranges in thickness from 150 to 1,200 feet in the report area. It is the principal and most developed (heavily pumped) water-bearing unit in the Winter Garden Area.

The general extent of fresh to slightly saline water in the Carrizo aquifer (Carrizo Sand) is given in Figure 2. The approximate depth to and altitude of the top of the Carrizo aquifer are illustrated in Figure 8. The total thickness and net sand thickness of the Carrizo aquifer are shown on Figure 9. The depth to and altitude of the base of the Carrizo aquifer are illustrated in Figure 10.

Because some of the sands in the Wilcox Group may be hydraulically connected with the Carrizo Sand,

Table 1.—Water-Bearing Characteristics of the Wilcox and Claiborne Groups in the Winter Garden Area

Yield, in gallons per minute : small, less than 50; moderate, 50 to 500; large, over 500.
Salinity (total dissolved solids), in milligrams per liter: fresh, less than 1,000; slightly saline, 1,000 to 3,000; moderately saline, 3,000 to 10,000; very saline, 10,000 to 35,000; brine, over 35,000.

SYSTEM	SERIES	GROUP	GEOLOGIC UNIT		APPROXIMATE THICKNESS (FT)		CHARACTER OF ROCKS		WATER-BEARING PROPERTIES	
Tertiary	Eocene	Claiborne	Yegua Formation		700-1,000+		Clay, silt with interbedded thin lignites and sandstones. Some minor beds of limestone and oyster shells are found.		Yields small quantities of slightly to moderately saline water to wells in the outcrop area.	
			Laredo Formation	Cook Mountain Formation	600-700	400-500	Glauconitic sand and clay. Some gypsiferous clay and impure limestones.	Fossiliferous clay and shale. Some interbedded sandstone and limestone.	Yields small to moderate quantities of fresh to moderately saline water to wells.	Yields small quantities of slightly to moderately saline water to wells.
				Sparta Sand		40-200		Medium to fine sand. Some interbedded clay.		Yields small to moderate quantities of fresh to moderately saline water to wells.
			El Pico Clay	Weches Formation	700-1,500	50-200	Clay with interbedded sandstones, claystones, and lignite coal lenses.	Fossiliferous, glauconitic shale and sand.	Yields small quantities of slightly to moderately saline water to wells.	Not known to yield water to wells.
				Queen City Sand		500-1,400		Marine, medium to fine sand with interbedded clay and shale.		Yields small to moderate quantities of fresh to slightly saline water to wells.
			Bigford Formation	Reklaw Formation	200-900	200-400	Sands with interbedded silts and shales. Plant remains are abundant.	Clay with interbedded glauconitic sand.	Yields small to moderate quantities of fresh to very saline water to wells.	Yields small quantities of slightly to moderately saline water to wells in or near the outcrop.
			Carrizo Sand		150-1,200		Coarse to fine sand, massive, cross-bedded with a few partings of carbonaceous clay.		Principal aquifer in the report area. Yields moderate to large quantities of fresh to slightly saline water to wells.	
		Wilcox			0-2,800		Interbedded sand, clay, and silt with discontinuous beds of lignite. The shale and clay sometimes contain gypsum.		Yields small to moderate quantities of fresh to slightly saline water to wells in the northern and western parts of the report area.	

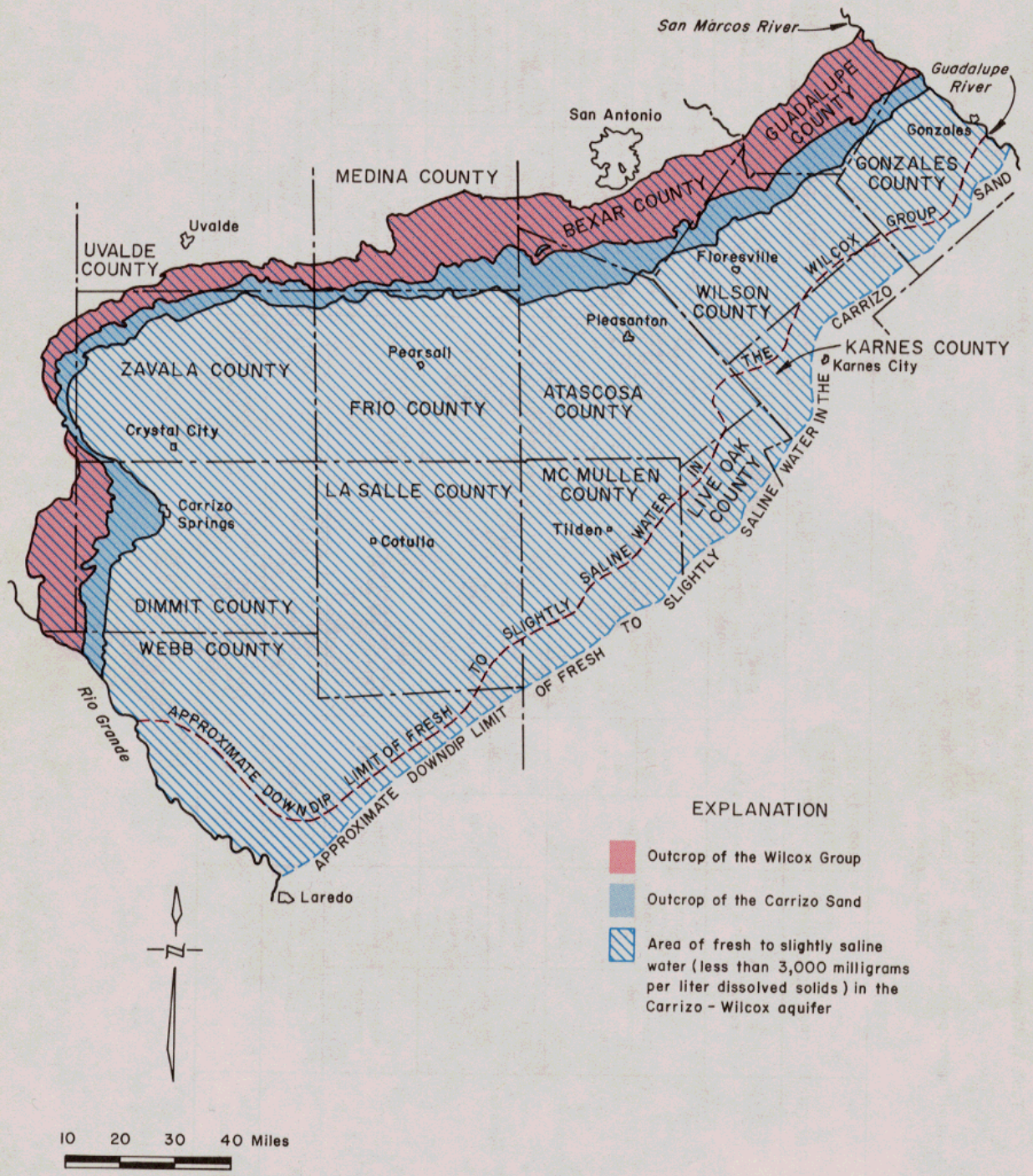

Figure 2
Extent of Fresh to Slightly Saline
Water in the Carrizo-Wilcox Aquifer

the term "Carrizo-Wilcox aquifer" is often used. The waters probably comingle to a degree, although most of the sand beds in the Wilcox Group are less permeable and most contain poorer quality water than the Carrizo Sand. Within the Wilcox, also, water quality in most areas generally diminishes with greater depth. The depth to and altitude of the base of fresh to slightly saline water in the Carrizo-Wilcox aquifer (Carrizo Sand and Wilcox Group) are shown on Figure 11. A better understanding of the extent of fresh to slightly saline water in the aquifer can be had by referring to the geohydrologic sections (Figures 27, 28, and 29). The total saturated thickness, and net saturated sand thickness, of the Carrizo-Wilcox aquifer above the base of fresh to slightly saline water are illustrated in Figure 12.

Above the Carrizo in areas west and southwest of the Frio River are the Bigford, El Pico Clay, Laredo, and Yegua Formations, which differ in lithologic character and fossil content from their equivalent counterparts northeast of the Frio River—the Reklaw, Queen City Sand, Weches, Sparta Sand, and Cook Mountain. Nomenclature of these and other formations of the Claiborne Group is detailed by Eargle (1968). The predominantly sandy units—the Queen City Sand, Bigford Formation, Sparta Sand, and Laredo Formation—interfinger in the vicinity of the Frio River to form two aquifers. These are the Queen City-Bigford and the Sparta-Laredo aquifers, which yield fresh to slightly saline water in the study area. The interfingering relationships of the formations in the vicinity of the Frio River are illustrated in Figure 3.

The Queen City-Bigford aquifer includes the water-bearing sands of the Queen City Sand and Bigford Formation. The Bigford Formation consists of sand, silt, and thin beds of shale, with the shale making up about 25 percent of the formation in the outcrop (Eargle, 1968). The Queen City Sand is a thick unit of sand, clay, and sandy clay. The Queen City-Bigford aquifer ranges in thickness from approximately 200 feet in Zavala

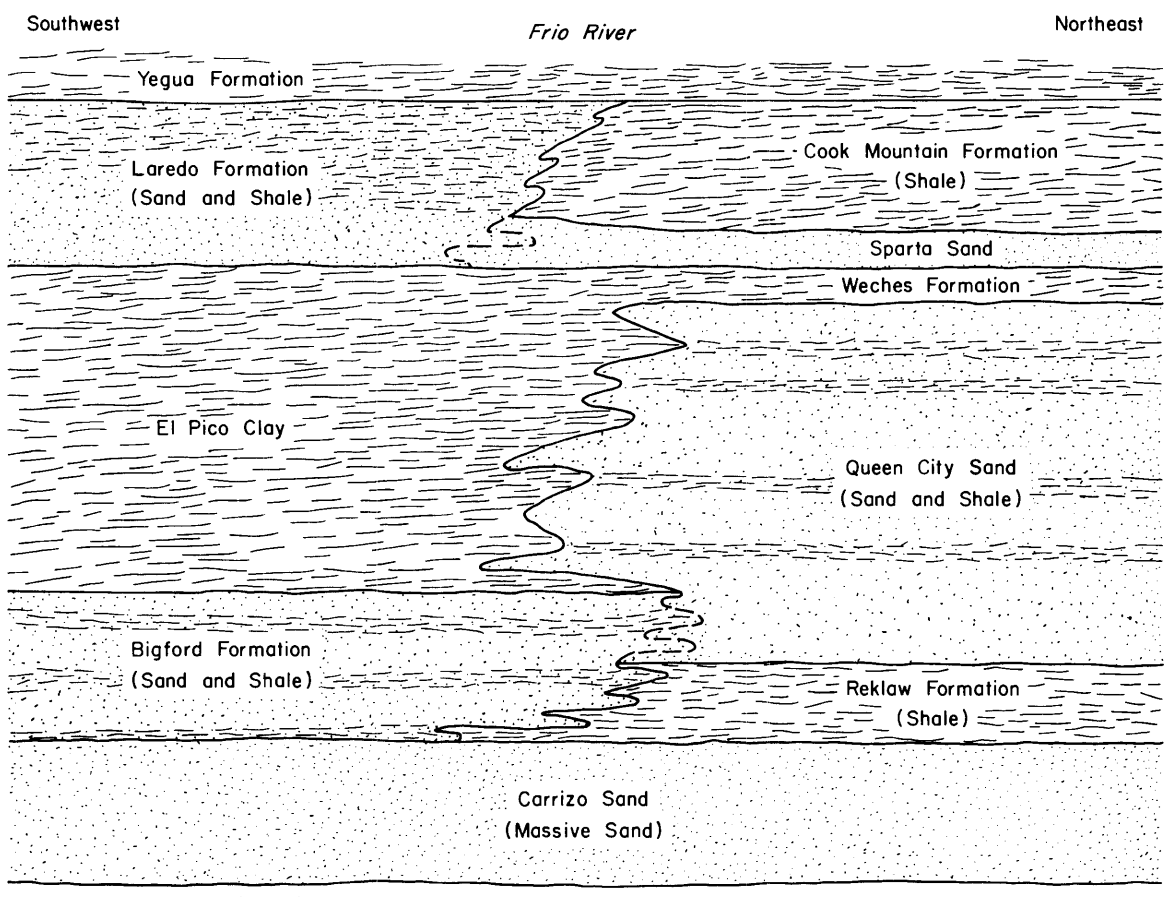

Modified from Eargle (1968)

Figure 3.—Idealized Geologic Section Illustrating the Interfingering of Sands and Shales of the Claiborne Group in the Vicinity of the Frio River

County to 1,400 feet in Frio County. Figure 4 shows the general extent of fresh to slightly saline water in the Queen City-Bigford aquifer in the study area.

The Sparta-Laredo aquifer contains the water-bearing sands of the Sparta Sand and Laredo Formation. The Sparta Sand ranges from 40 to 200 feet in thickness and consists of sand with minor amounts of clay. The Laredo Formation, consisting of sand and sandstone at the base and grading into sandy clay and clay at the top, attains a maximum thickness of 600 to 700 feet. The general extent of fresh to slightly saline water in the Sparta-Laredo aquifer in the study area is shown in Figure 5.

The uppermost formation of the Claiborne Group is the Yegua, consisting of fine sand, silt, and clay. The Yegua Formation generally yields small amounts of slightly to moderately saline water (1,000 to 10,000 mg/l dissolved solicls) east of the Frio River. West of the Frio River, the Yegua yields highly mineralized water that is generally unfit for livestock use.

THE CARRIZO AQUIFER

The name "Carrizo" was first applied by Owen (1889) to the thick, massive sand beds that unconformably overlie the sand, silt, and clay of the Wilcox Group in the vicinity of Carrizo Springs, Texas. Plummer (Sellards, Adkins, and Plummer, 1932) suggests that the type locality for the Carrizo Sand be designated at Brand Rock on the east bank of Pena Creek, which is about 5 miles west of Carrizo Springs. The development of the Carrizo aquifer dates back to 1884 when S. D. Frazier completed the first flowing well at Carrizo Springs in Dimmit County at a depth of 165 feet (Roesler, 1890). Today, the Carrizo aquifer is the most prolific source of fresh ground water in the Winter Garden Area.

Recharge, Discharge, and Movement

Annual recharge to the Carrizo aquifer in Dimmit, Zavala, and Maverick Counties according to Turner and others (1948) averages about 25,000 acre-feet. Alexander and White (1966) estimated the annual average recharge to the Carrizo aquifer in Atascosa and Frio Counties to be 13,000 and 10,000 acre-feet, respectively. Barnes (1956) reported approximately 26,000 acre-feet per year being recharged in Wilson County. These areas account for about 75 percent of the Carrizo outcrop in the Winter Garden Area. From these data it was estimated that the remaining outcrop areas would receive about 26.000 acre-feet annually, based upon the higher permeability of the aquifer and the higher amount of precipitation in the eastern portion of the study area. Thus, the average rate of recharge to the Carrizo aquifer in the Winter Garden Area is about 100,000 acre-feet per year or 89 mgd (million gallons per day).

In some local areas of the Carrizo aquifer's extent, some of the sands containing fresh to slightly saline water in the Wilcox Group, Bigford Formation, and Reklaw Formation may be hydrologically connected with the Carrizo Sand. Leakage into the Carrizo aquifer is known to occur in the regions of intensive irrigation in Dimmit, Frio, and Zavala Counties where water of higher mineral content in other formations leaks through confining beds or percolates down well bores of poorly constructed and abandoned wells. Computer simulations of the aquifer, which will be discussed later, have indicated that much greater water-level declines should have occurred during the period 1963-1969 than actually occurred except as may be accounted for by interformational leakage. The computer simulations indicate that about 9,500 acre-feet per year (8.5 mgd) leaked into the Carrizo during the period 1963-1969.

The estimated amount of water pumped for irrigation, public supply, and industrial use from the Carrizo aquifer in the study region and in the Winter Garden District (Dimmit, Zavala, and eastern Maverick Counties) is given in Figure 7. The graph shows that pumpage in the Winter Garden Area averaged about 272,000 acre-feet per year (243 mgd) for the period 1963-I 969.

Ground water in the Carrizo aquifer moves downward from the recharge zone to the zone of saturation and then generally in the direction of the slope of the piezometric surface. The piezometric surface is an imaginary surface that everywhere coincides with the static water level in the aquifer. The piezometric surfaces of the Carrizo aquifer in 1929-30 and in 1970 are illustrated in Figures 13 and 14, respectively.

Hydraulic Characteristics

An aquifer's hydraulic characteristics are generally described in terms of its coefficients of transmissibility and storage. These were determined for the Carrizo aquifer by conducting pumping tests in selected wells, and from the well performance tests that had been made by water well drilling and servicing companies. The tests consist of pumping a well for a period of time and taking periodic water-level measurements in the pumping well and in one or more nearby observation wells if available.

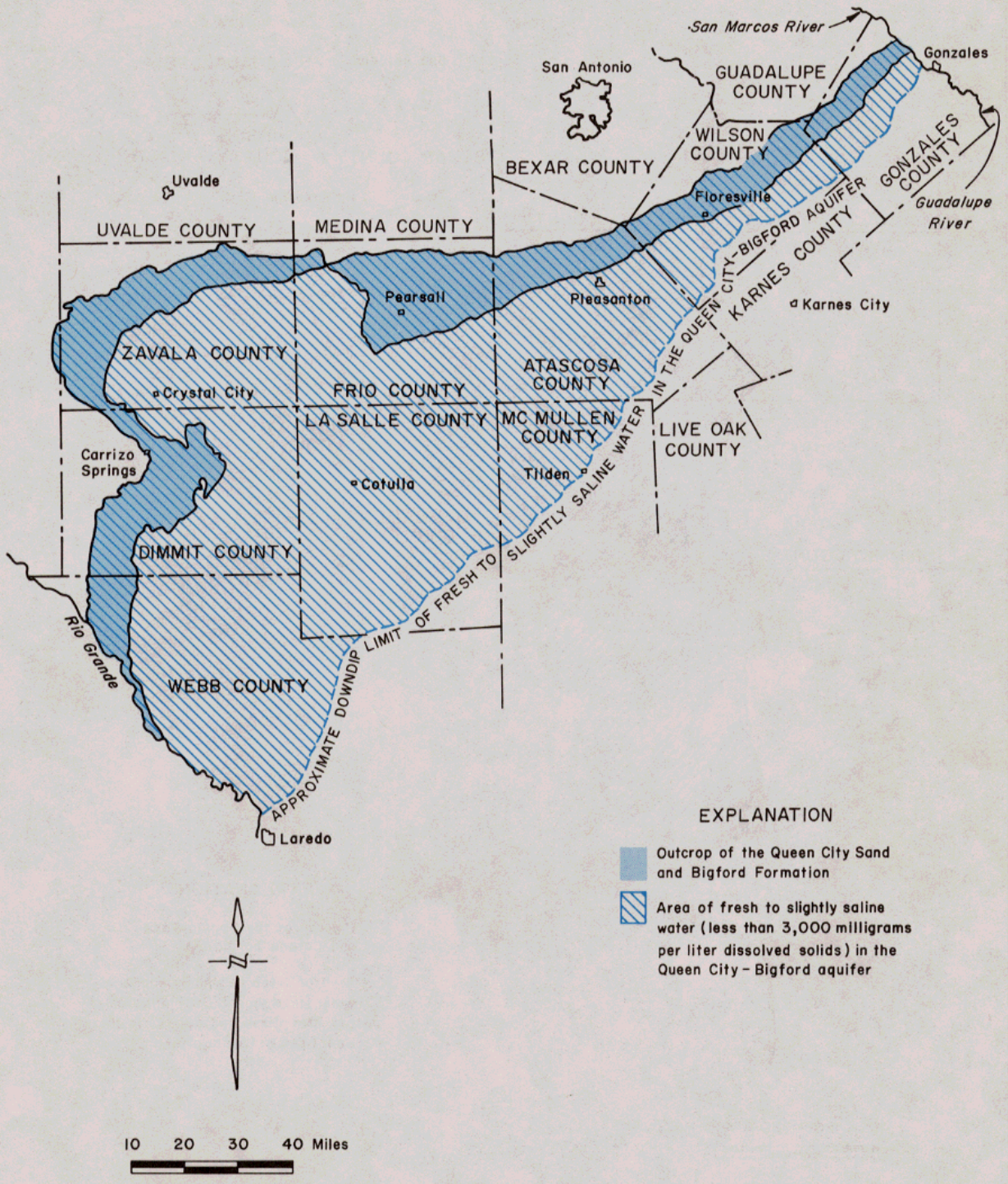

Figure 4

Extent of Fresh to Slightly Saline Water in the Queen City-Bigford Aquifer

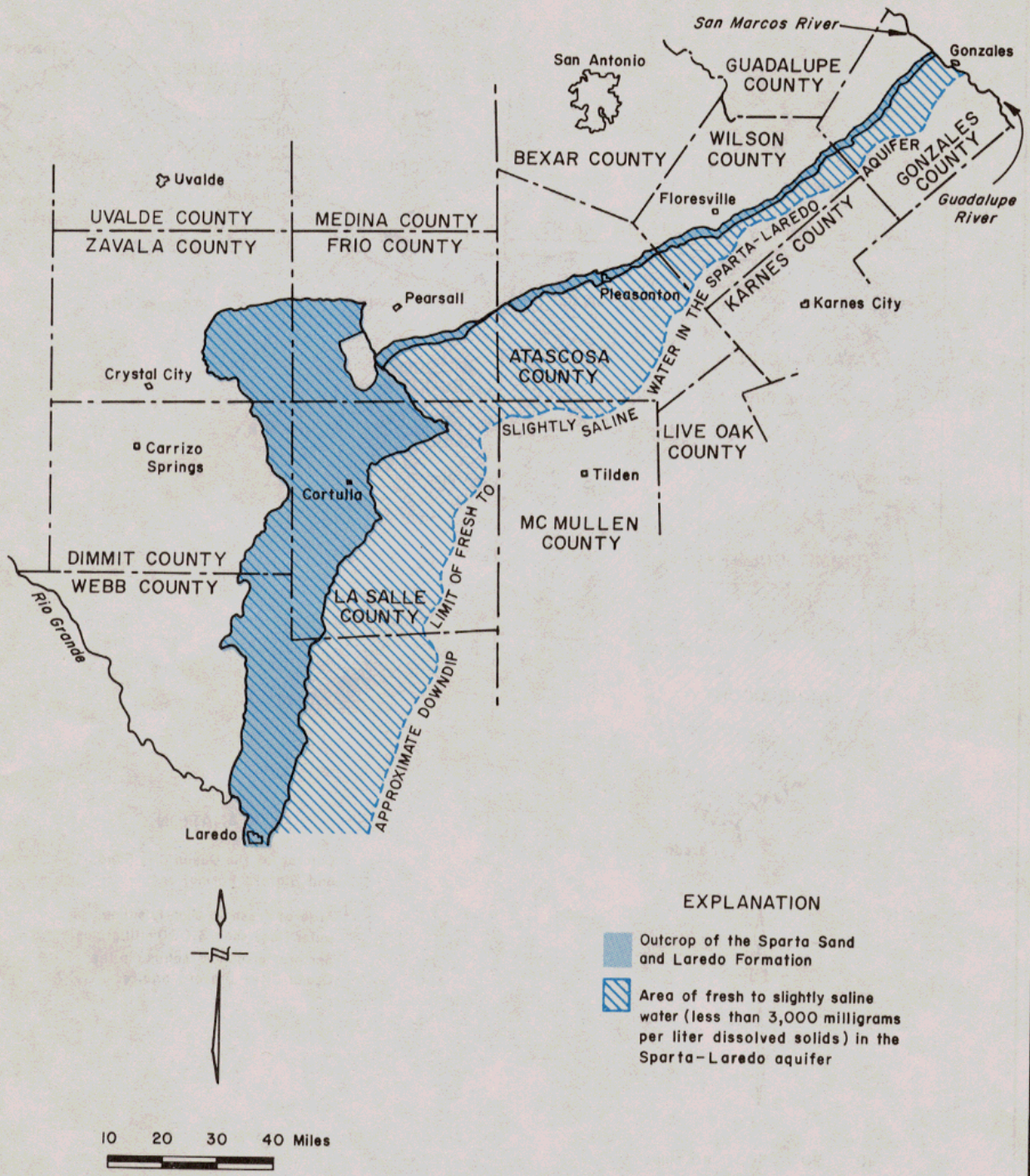

Figure 5

Extent of Fresh to Slightly Saline Water in the Sparta-Laredo Aquifer

Data obtained from pumping tests were analyzed using the Theis (1935) nonequilibrium formula. For tests conducted under water-table conditions, the water-level drawdown data were corrected in the manner described by Jacob (1944) for the decrease in aquifer transmissibility that accompanies the decrease in its saturated thickness during the test. Performance test data were analyzed by the modified Thiem formula as presented by Thomasson (1960) and with further modification by the authors to consider well completion efficiencies. Specific capacities of wells were also determined, by dividing the well's yield by the total water-level drawdown measured in the well.

Each well test provided transmissibility data for only that portion of the aquifer screened by the well. These transmissibility values were divided by the effective sand thickness utilized by the well, to obtain a coefficient of aquifer permeability. The permeability coefficients were then multiplied by an estimate of the aquifer's total net thickness of sand containing fresh to slightly saline water to obtain approximate coefficients of transmissibility for the aquifer's total fresh to slightly saline water section.

The coefficients of permeability determined for the aquifer are shown in Figure 15, and the coefficients of transmissibility are given in Figure 16. The specific capacities of individual water wells are given in Figure 17.

The largest permeability and transmissibility coefficients found in selected counties are presented below:

COUNTY	MAXIMUM COEFFICIENT OF PERMEABILITY (GPD/FT^2 AT FORMATION TEMPERATURE)	MAXIMUM COEFFICIENT OF TRANSMISSIBILITY (GPD/FT AT FORMATION TEMPERATURE)
Atascosa	475	317,000
Dimmit	410	65,000
Frio	500	230,000
Gonzales	300	200,000
La Salle	170	110,000
McMullen	90	100,000
Webb	70	7,000
Wilson	500	30 1,000
Zavala	425	75,000

The average coefficient of storage in the outcrop, under water-table conditions, is approximately 0.25. Downdip, where the aquifer is under artesian conditions, the average coefficient of storage is approximately 5×10^{-4} or 0.0005. The coefficient of storage is a dimensionless term which indicates the volume of water that an aquifer releases from or takes into storage per unit surface area of the aquifer per unit change in the component of head normal to that surface. For water-table conditions the coefficient of storage is the same as the specific yield of the material dewatered during pumping, and for artesian conditions it reflects the amount of aquifer compression and water expansion when the head or pressure is reduced during pumping.

An aquifer's permeability depends on the shape, sorting, arrangement, and cementation of its component sediment grains. To obtain permeability data for the Carrizo aquifer in the outcrop, a test-hole drilling program was initiated. Test holes were drilled with the Texas Water Development Board's drilling rig in the outcrop of the Carrizo Sand in seven counties, and the cores obtained from these test holes were analyzed by the Board's Materials Testing Laboratory to obtain information on sand particle diameters and to determine coefficients of grain-size uniformity and permeability. Permeability coefficients, in gallons per day per square foot (gpd/ft^2), were determined by using a falling head permeameter and correcting the results to 60°F (16°C).

The results of laboratory determinations for selected test holes in the Carrizo Sand outcrop are summarized by county below. The coefficients of permeability shown are generally higher than those obtained from analyses of pumping tests of wells in the Carrizo Sand outcrop.

COUNTY	NUMBER OF TEST HOLES	AVERAGE SAND GRAIN DIAMETER 50 PERCENT RETAINED (INCHES)	AVERAGE SAND GRAIN DIAMETER 90 PERCENT RETAINED (INCHES)	AVERAGE UNIFORMITY COEFFICIENT	AVERAGE COEFFICIENT OF PERMEABILITY (GPD/FT² AT 60°F)	
					CORES	CUTTINGS
Atascosa	2	0.0115	0.0066	2.00	487	555
Dimmit	1	.0092	.0048	2.09	40	479
Frio	1	.0106	.0064	1.82	–	
Maverick	1	.0122	.0063	2.24	–	685
Medina	2	.0086	.0051	1.85	748	626
Wilson	4	.009 1	.0047	2.11	475	556
Zavala	4	.0088	.0055	1.72	944	539

Chemical Quality

All ground water contains minerals carried in solution, the type and concentration of which depend upon the surface and subsurface environment, rate of ground-water movement, and source of the ground water. Precipitation is relatively free of minerals until it comes in contact with the various constituents which make up the soils and component rocks of the aquifer. As a result of the water's solvent power, minerals are dissolved and carried into solution as the water moves through the aquifer. The concentration depends upon the solubility of the minerals present, the length of time water is in contact with the rocks, and the amount of dissolved carbon dioxide the water contains. Concentrations of dissolved minerals in ground water generally increase with depth where circulation has been restricted due to various geologic conditions.

The source, significance, and range in concentration of selected chemical constituents in ground water in the Carrizo aquifer are given in Table 2. Dissolved-solids concentrations and sodium adsorption ratios (SAR) in water samples collected from the Carrizo aquifer are illustrated in Figures 18 and 19.

The characteristics of an irrigation water that seem to be most important in determining its quality are as follows: (a) total concentration of soluble salts; (b) relative proportion of sodium to other principal cations (magnesium, calcium, and potassium); (c) concentration of boron or other elements that may be toxic; and (d) under some conditions, the bicarbonate concentration as related to the concentration of calcium plus magnesium. These have been termed, respectively, the salinity hazard, the sodium (alkali) hazard, the boron hazard, and the bicarbonate ion hazard.

For the purposes of diagnosis and classification of irrigation waters, the total concentration of soluble salts (salinity hazard) in the water can be adequately expressed in terms of specific conductance. Specific conductance is the measure of the ability of the ionized inorganic salts in solution to conduct an electrical current and is usually expressed in terms of micromhos per cubic centimeter at 25°C. In general, water having a conductance below 750 micromhos per cubic centimeter is satisfactory for irrigation; however, salt-sensitive crops, such as strawberries and green beans, may be adversely affected by irrigation water having a conductance in the range of 250 to 750 micromhos per cubic centimeter. The specific conductance of water samples collected from the Carrizo aquifer ranged from 94 to 4,990 micromhos per cubic centimeter at 25°C.

In the past, irrigation waters were divided into the three following classes based on the percent sodium: (a) water with a percent sodium less than 60, excellent

Table 2.—Source, Significance, and Concentration Range of Selected Chemical Constituents in Ground Water in the Carrizo Aquifer

(Concentration ranges shown are in milligrams per liter except specific conductance, pH, percent sodiu sodium-adsorption ratio, and residual sodium carbonate.)

CONSTITUENT OR PROPERTY	SOURCE OR CAUSE	SIGNIFICANCE	CONCENTRATION RANGE
Silica (SiO_2)	Dissolved from practically all rocks and soils, commonly less than 30 mg/l. High concentrations, as much as 100 mg/l, generally occur in highly alkaline waters.	Forms hard scale in pipes and boilers. Carried over in steam of high pressure boilers to form deposits on blades of turbines. Inhibits deterioration of zeolite-type water softeners.	4 - 95
Iron (Fe)	Dissolved from practically all rocks and soils. May also be derived from iron pipes, pumps, and other equipment.	On exposure to air, iron in ground water oxidizes to reddish-brown precipitate. More than about 0.3 mg/l stains laundry and utensils reddish-brown. Objectionable for food processing, textile processing, beverages, ice manufacture, brewing, and other processes. U.S. Public Health Service (1962) drinking-water standards state that iron should not exceed 0.3 mg/l. Larger quantities cause unpleasant taste and favor growth of iron bacteria.	<1 - 68.62
Calcium (Ca) and Magnesium (Mg)	Dissolved from practically all soils and rocks, but especially from limestone, dolomite, and gypsum. Calcium and magnesium are found in large quantities in some brines. Magnesium is present in large quantities in sea water.	Cause most of the hardness and scale-forming properties of water; soap consuming (see hardness). Waters low in calcium and magnesium desired in electroplating, tanning, dyeing, and in textile manufacturing.	(Ca) 2 - 323 (Mg) <1 - 103
Sodium (Na) and Potassium (K)	Dissolved from practically all rocks and soils. Found also in oilfield brines, sea water, industrial brines, and sewage.	Large amounts, in combination with chloride, give a salty taste. Moderate quantities have little effect on the usefullness of water for most purposes. Sodium salts may cause foaming in steam boilers and a high sodium content may limit the use of water for irrigation.	(Na) 8 - 1,310 (K) <1 - 23
Bicarbonate (HCO_3) and Carbonate (CO_3)	Action of carbon dioxide in water on carbonate rocks such as limestone and dolomite.	Bicarbonate and carbonate produce alkalinity. Bicarbonates of calcium and magnesium decompose in steam boilers and hot water facilities to form scale and release corrosive carbon dioxide gas. In combination with calcium and magnesium, cause carbonate hardness.	(HCO_3) <1 - 2,760
Sulfate (SO_4)	Dissolved from rocks and soils containing gypsum, iron sulfides, and other sulfur compounds. Commonly present in some industrial wastes.	Sulfate in water containing calcium forms hard scale in steam boilers. In large amounts, sulfate in combination with other ions gives bitter taste to water. U.S. Public Health Service (1962) drinking-water standards recommend that the sulfate content should not exceed 250 mg/l.	<1 - 1,160

Table 2.—Source, Significance, and Concentration Range of Selected Chemical Constituents in Ground Water in the Carrizo Aquifer—Continued

CONSTITUENT OR PROPERTY	SOURCE OR CAUSE	SIGNIFICANCE	CONCENTRATION RANGE
Chloride (Cl)	Dissolved from rocks and soils. Present in sewage and found in large amounts in oil-field brines, sea water, and industrial brines.	In large amounts in combination with sodium, gives salty taste to drinking water. In large quantities, increases the corrosiveness of water. U.S. Public Health Service (1962) drinking-water standards recommend that the chloride content should not exceed 250 mg/l.	.9 - 970
Fluoride (F)	Dissolved in small to minute quantities from most rocks and soils. Added to many waters by fluoridation of municipal supplies.	Fluoride in drinking water reduces the incidence of tooth decay when the water is consumed during the period of enamel calcification. However, it may cause mottling of the teeth depending on the concentration of fluoride, the age of the child, amount of drinking water consumed, and susceptibility of the individual (Maier, 1950, p. 1120-1132).	<1 - 10.7
Nitrate (NO_3)	Decaying organic matter, sewage, fertilizers, and nitrates in soil.	Concentration much greater than the local average may suggest pollution. U.S. Public Health Service (1962) drinking-water standards suggest a limit of 45 mg/l. Waters of high nitrate content have been reported to be the cause of methemoglobinemia (an often fatal disease in infants) and therefore should not be used in infant feeding (Maxcy, 1950, p. 271). Nitrate has been shown to be helpful in reducing inter-crystalline cracking of boiler steel. It encourages growth of algae and other organisms which produce undesirable tastes and odors.	<1 - 120
Boron (B)	A minor constituent of rocks and of natural waters.	An excessive boron content will make water unsuitable for irrigation. Wilcox (1955, p. 11) indicated that a boron concentration of as much as 1.0 mg/l is permissible for irrigating sensitive crops; as much as 2.0 mg/l for semitolerant crops; and as much as 3.0 mg/l for tolerant crops. Crops sensitive to boron include most deciduous fruits and nut trees and navy beans; semitolerant crops include most small grains, potatoes and some other vegetables, and cotton; and tolerant crops include alfalfa, most root vegetables, and the date palm.	<1 - 1.5
Dissolved solids	Chiefly mineral constituents dissolved from rocks and soils.	U.S. Public Health Service (1962) drinking-water standards recommend that waters containing more than 500 mg/l dissolved solids not be used if other less mineralized supplies are available. For many purposes the dissolved-solids content is a major limitation on the use of water. A general classification of water based on dissolved-solids	6 - 3,139

Table 2.—Source, Significance, and Concentration Range of Selected Chemical Constituents in Ground Water in the Carrizo Aquifer—Continued

CONSTITUENT OR PROPERTY	SOURCE OR CAUSE	SIGNIFICANCE	CONCENTRATION RANGE
		content, in mg/l, is as follows (Winslow and Kister, 1956, p. 5): Waters containing less than 1,000 mg/l of dissolved solids are considered fresh; 1,000 to 3,000 mg/l, slightly saline; 3,000 to 10,000 mg/l, moderately saline; 10,000 to 35,000 mg/l, very saline; and more than 35,000 mg/l, brine.	
Hardness as $CaCO_3$	In most waters nearly all the hardness is due to calcium and magnesium. All the metallic cations other than the alkali metals also cause hardness.	Consumes soap before a lather will form. Deposits soap curd on bathtubs. Hard water forms scale in boilers, water heaters, and pipes. Hardness equivalent to the bicarbonate and carbonate is called carbonate hardness. Any hardness in excess of this is called non-carbonate hardness. Waters of hardness up to 60 mg/l are considered soft; 61 to 120 mg/l, moderately hard; 121 to 180 mg/l, hard; and more than 180 mg/l, very hard.	1 - 2,027
Specific conductance (micromhos per cubic centimeter at 25°C)	Mineral content of the water.	Indicates degree of mineralization. Specific conductance is a measure of the capacity of the water to conduct an electric current. Varies with concentration and degree of ionization of the constituents.	94 - 4,990
Hydrogen ion concentration (pH)	Acids, acid-generating salts, and free carbon dioxide lower the pH. Carbonates, bicarbonates, hydroxides, phosphates, silicates, and borates raise the pH.	A pH of 7.0 indicates neutrality of a solution. Values higher than 7.0 denote increasing alkalinity; values lower than 7.0 indicate increasing acidity. pH is a measure of the activity of the hydrogen ions. Corrosiveness of water generally increases with decreasing pH. However, excessively alkaline waters may also attack metals.	3.3 - 8.8
Percent sodium (% Na)	Sodium in water.	A ratio (using milliequivalents per liter) of the sodium ions to the total sodium, calcium, and magnesium ions. A sodium percentage exceeding 50 percent is a warning of a sodium hazard. Continued irrigation with this type of water will impair the tilth and permeability of the soil.	2.0 - 99.7
Sodium-adsorption ratio (SAR)	Sodium in water.	A ratio for soil extracts and irrigation waters used to express the relative activity of sodium ions in exchange reactions with soil (U.S. Salinity Laboratory Staff, 1954, p. 72, 156). Defined by the following equation: $$SAR = \frac{Na^{+}}{\sqrt{\frac{Ca^{++} + Mg^{++}}{2}}},$$ where Na^{+}, Ca^{++}, and Mg^{++} represent the concentrations, in milliequivalents per liter (me/l), of the respective ions.	.06 - 161.28

Table 2.—Source, Significance, and Concentration Range of Selected Chemical Constituents in Ground Water in the Carrizo Aquifer—Continued

CONSTITUENT OR PROPERTY	SOURCE OR CAUSE	SIGNIFICANCE	CONCENTRATION RANGE
Residual sodium carbonate (RSC)	Sodium and carbonate or bicarbonate in water.	As calcium and magnesium precipitate as carbonates in the soil, the relative proportion of sodium in the water is increased (Eaton, 1950, p. 123-133). Defined by the following equation: $RSC = (CO_3^{--} + HCO_3^-) - (Ca^{++} + Mg^{++})$, where CO_3^{--}, HCO_3^-, Ca^{++}, and Mg^{++} represent the concentrations, in milliequivalents per liter (me/l), of the respective ions.	<1 - 45.02

to good; (b) water with a percent sodium between 60 and 75, good to injurious, and (c) water with a percent sodium greater than 75, injurious to unsatisfactory. The percent sodium in water samples collected from the Carrizo aquifer ranged from 2.0 to 99.7.

A better measure of the sodium hazard of water for irrigation is the sodium-adsorption ratio (SAR) which is used to express the relative activity of sodium ions in exchange reactions with soil. The SAR is easily computed from the data determined in the usual water analysis by using the following equation:

$$SAR = \frac{Na^+}{\sqrt{\frac{Ca^{++} + Mg^{++}}{2}}},$$

where Na^+, Ca^{++}, and Mg^{++} represent the concentrations of sodium, calcium, and magnesium ions in milliequivalents per liter (me/l). The SAR of water samples collected from the Carrizo aquifer ranged from 0.06 to 161.28.

When the SAR and the specific conductance of a water are known, the classification of the water for irrigation can be determined by graphically plotting these values on the diagram shown in Figure 6. Low-sodium water (S1) can be used for irrigation on almost all soils with little danger of the development of harmful levels of exchangeable sodium. Medium-sodium water (S2) will present an appreciable sodium hazard in certain fine-textured soils having high cation-exchange capacity, especially under low-leaching conditions, unless gypsum is present in the soil. This water may be used on coarse-textured or organic soils having good permeability. High-sodium water (S3) may produce harmful levels of exchangeable sodium in most soils and will require special soil management such as good drainage, leaching, and addition of organic matter. Very

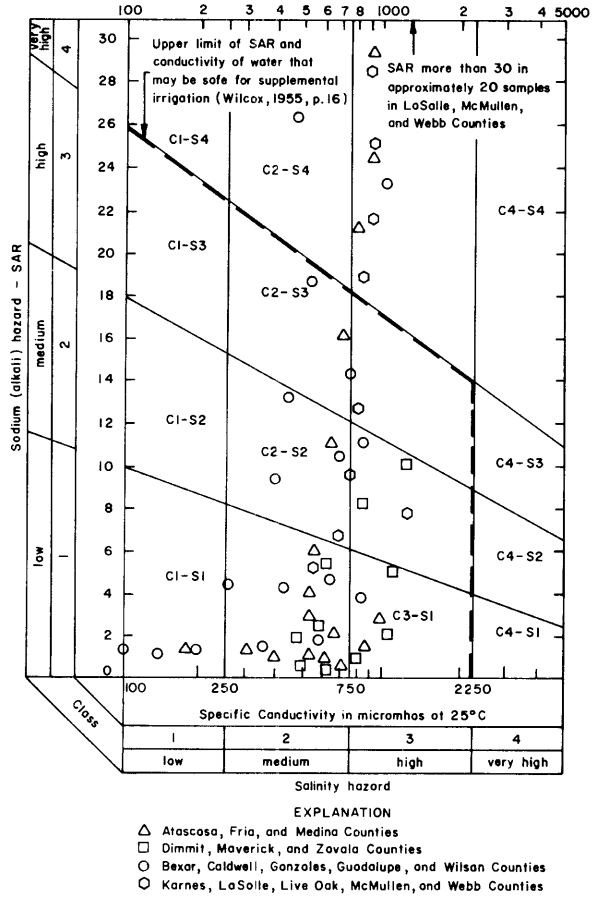

Figure 6.—Classification of Irrigation Waters, and Quality of Water From Representative Wells in the Carrizo Aquifer (After U.S. Salinity Laboratory Staff, 1954, p. 80)

high sodium water (S4) is generally unsatisfactory for irrigation unless special action is taken, such as addition of gypsum to the soil.

Low-salinity water (Cl) can be used for irrigation of most crops on most soils with little likelihood that soil salinity will develop. Medium-salinity water (C2) can be used if a moderate amount of leaching occurs. High salinity water (C3) cannot be used on soils with restricted drainage.

The classification of ground water from representative wells completed in the Carrizo aquifer, sampled throughout the Winter Garden Area, shows low to high salinity hazard (specific conductivity 100 to 1,300 micromhos per cubic centimeter at 25°C) while the sodium (alkali) hazard is generally low to medium (SAR 0.06 to 13) as illustrated in Figure 6.

In appraising the quality of an irrigation water, first consideration must be given to salinity and sodium hazards (Figure 6). Then consideration should be given to independent characteristics such as boron and bicarbonate, either of which may change the quality rating. The use of water of any quality must take into account such factors as land and crop management practices and soil drainage.

In the Winter Garden Area most public and domestic ground-water supplies are obtained from the Carrizo aquifer. Concentration limits recommended by the U.S. Public Health Service (1962, p. 7-8) for chemical constituents in public and domestic water supplies are shown in the following table. It should be noted that these concentration limits will prevail except where suitable water supplies are not available or cannot be made available at a reasonable cost.

SUBSTANCE		CONCENTRATION (MG/L)
Chloride	(Cl)	250
Fluoride	(F)	.8*
Iron	(Fe)	.3
Manganese	(Mn)	.05
Nitrate	(NO^3)	45
Sulfate	(SO_4)	250
Dissolved-solids		500

*Upper limit based on annual average of maximum daily air temperature range of 79.3 – 90.5°F. The recommended control limits of fluoride concentration in mg/l are: lower, 0.6; optimum, 0.7; and upper, 0.8.

Water samples from wells completed in the Carrizo aquifer were examined for chloride, sulfate, and dissolved solids. The chloride content ranged from 0.9 to 970 mg/l in 819 samples; only 5 percent of the samples contained water having greater than 250 mg/l chloride. Sulfate content ranged from less than 1 to 1,160 mg/l in 807 samples; only 4 percent of the samples contained water having greater than 250 mg/l sulfate. The dissolved-solids content in Carrizo aquifer samples ranged from 6 to 3,139 mg/l in 772 samples; only 18 percent of the samples contained water having greater than 500 mg/l dissolved solids.

Water containing less than 1,000 mg/l of dissolved solids is regarded in this report as fresh and more than 1,000 mg/l as saline. Less than 500 mg/l is recommended by the U.S. Public Health Service (1962) in potable water where water of this quality is available. However, it must be recognized that in many areas of Texas the only available water supply may have a dissolved-solids concentration greatly in excess of 1,000 mg/l. Only 7 percent of the Carrizo samples contained water having more than 1,000 mg/l dissolved solids.

Water having a dissolved-solids concentration of 1,000 to 3,000 mg/l is classified as slightly saline and is used by many small communities, farms, and ranches. Water of this class has been recognized as somewhat unsatisfactory but generally not harmful. Less than 1 percent of the Carrizo wells within the Winder Garden Area contained water having greater than 3,000 mg/l dissolved solids.

The chemical quality of ground water from the Carrizo aquifer is generally favorable for industrial use throughout most of the Winter Garden Area. The tolerance in chemical quality of water for industrial use differs widely for different industries and different processes. Table 3 illustrates some of the suggested tolerances for a number of industries (American Water Works Association, 1950, p. 66-67).

Aquifer Development and the Decline of Water Levels

Development of ground water from the Carrizo aquifer in the Winter Garden Area prior to 1900 was mainly for domestic, livestock, and public supply purposes. One of the earlier irrigation wells was completed at Carrizo Springs, Dimmit County, in 1884, at a depth of 165 feet. This was a flowing well that was used for both domestic and irrigation purposes (Roesler, 1890). During the period 1900-1930, large-scale irrigation development took place in Dimmit and Zavala Counties due to introduction of the efficient deep-well turbine pump. Later irrigation development spread northeast to many of the other counties in the Winter Garden Area.

Pumpage from the Carrizo aquifer during 1930-1969 is shown in Figure 7. The pumpage data in Figure 7 are based in part on power and yield tests conducted on selected irrigation wells, in part on questionnaires mailed annually by the Texas Water Development Board to municipalities and industries, and in part on various earlier studies in the region. The amount of ground water pumped from the Carrizo

Table 3.—Water-Quality Tolerances for Industrial Applications[1]

[Allowable Limits in Milligrams Per Liter Except as Indicated]

INDUSTRY	TURBIDITY	COLOR	COLOR $+O_2$ CONSUMED	DISSOLVED OXYGEN (ml/l)	ODOR	HARDNESS	ALKALINITY (AS $CaCO_3$)	pH	TOTAL SOLIDS	Ca	Fe	Mn	Fe+Mn	Al_2O_3	SiO_2	Cu	F	CO_3	HCO_3	OH	$CaSO_4$	Na_2SO_4 TO Na_2SO_3 RATIO	GENERAL[2]
Air Conditioning[3]	--	--	--	--	--	--	--	--	--	--	0.5	0.5	0.5	--	--	--	--	--	--	--	--	--	A,B
Baking	10	10	--	--	--	(4)	--	--	--	--	.2	.2	.2	--	--	--	--	--	--	--	--	--	C
Boiler feed:																							
0-150 psi	20	80	100	2	--	75	--	8.0+	3,000-1,000	--	--	--	--	5	40	--	--	200	50	50	--	1 to 1	--
150-250 psi	10	40	50	.2	--	40	--	8.5+	2,500-500	--	--	--	--	.5	20	--	--	100	30	40	--	2 to 1	--
250 psi and up	5	5	10	0	--	8	--	9.0+	1,500-100	--	--	--	--	.05	5	--	--	40	5	30	--	3 to 1	--
Brewing:[5]																							
Light	10	--	--	--	Low	--	75	6.5-7.0	500	100-200	.1	.1	.1	--	--	--	1	--	--	--	100-200	--	C,D
Dark	10	--	--	--	Low	--	150	7.0+	1,000	200-500	.1	.1	.1	--	--	--	1	--	--	--	200-500	--	C,D
Canning:																							
Legumes	10	--	--	--	Low	25-75	--	--	--	--	.2	.2	.2	--	--	--	--	--	--	--	--	--	C
General	10	--	--	--	Low	--	--	--	--	--	.2	.2	.2	--	--	--	1	--	--	--	--	--	C
Carbonated beverages[6]	2	10	10	--	0	250	50	--	850	--	.2	.2	.3	--	--	--	.2	--	--	--	--	--	C
Confectionary	--	--	--	--	Low	--	--	(7)	100	--	.2	.2	.2	--	--	--	--	--	--	--	--	--	--
Cooling[8]	50	--	--	--	--	50	--		--	--	.5	.5	.5	--	--	--	--	--	--	--	--	--	A,B
Food, general	10	--	--	--	Low	--	--	--	--	--	.2	.2	.2	--	--	--	--	--	--	--	--	--	C
Ice (raw water)[9]	1-5	5	--	--	--	--	30-50	--	300	--	.2	.2	.2	--	10	--	--	--	--	--	--	--	C
Laundering	--	--	--	--	--	50	--	--	--	--	.2	.2	.2	--	--	--	--	--	--	--	--	--	--
Plastics, clear, undercolored	2	2	--	--	--	--	--	--	200	--	.02	.02	.02	--	--	--	--	--	--	--	--	--	--
Paper and pulp:[10]																							
Groundwood	50	20	--	--	--	180	--	--	--	--	1.0	.5	1.0	--	--	--	--	--	--	--	--	--	A
Kraft pulp	25	15	--	--	--	100	--	--	300	--	.2	.1	.2	--	--	--	--	--	--	--	--	--	--
Soda and sulfite	15	10	--	--	--	100	--	--	200	--	.1	.05	.1	--	--	--	--	--	--	--	--	--	--
Light paper, HL-Grade	5	5	--	--	--	50	--	--	200	--	.1	.05	.1	--	--	--	--	--	--	--	--	--	B
Rayon (viscose) pulp:																							
Production	5	5	--	--	--	8	50	--	100	--	.05	.03	.05	<8.0	<25	<5	--	--	--	--	--	--	--
Manufacture	.3	--	--	--	--	55	--	7.8-8.3	--	--	.0	.0	.0	--	--	--	--	--	--	--	--	--	--
Tanning[11]	20	10-100	--	--	--	50-135	135	8.0	--	--	.2	.2	.2	--	--	--	--	--	--	--	--	--	--
Textiles:																							
General	5	20	--	--	--	20	--	--	--	--	.25	.25	--	--	--	--	--	--	--	--	--	--	--
Dyeing[12]	5	5-20	--	--	--	20	--	--	--	--	.25	.25	.25	--	--	--	--	--	--	--	--	--	--
Wool scouring[13]	--	70	--	--	--	20	--	--	--	--	1.0	1.0	1.0	--	--	--	--	--	--	--	--	--	--
Cotton bandage[13]	5	5	--	--	Low	20	--	--	--	--	.2	.2	.2	--	--	--	--	--	--	--	--	--	--

1/ American Water Works Association, 1950.
2/ A—No corrosiveness; B—No slime formation; C—Conformance to Federal drinking water standards necessary; D-NaCl, 275 mg/l.
3/ Waters with algae and hydrogen sulfide odors are most unsuitable for air conditioning.
4/ Some hardness desirable.
5/ Water for distilling must meet the same general requirements as for brewing (gin and spirits mashing water of light-beer quality; whiskey mashing water of dark-beer quality).
6/ Clear, odorless, sterile water for syrup and carbonization. Water consistent in character. Most high quality filtered municipal water not satisfactory for beverages.
7/ Hard candy requires pH of 7.0 or greater, as low value favors inversion of sucrose, causing sticky product.
8/ Control of corrosiveness is necessary as is also control of organisms, such as sulfur and iron bacteria, which tend to form slimes.
9/ $Ca(HCO_3)_2$ particularly troublesome. $Mg(HCO_3)_2$ tends to greenish color. CO_2 assists to prevent cracking. Sulfates and chlorides of Ca, Mg, Na should each be less than 300 mg/l (white butts).
10/ Uniformity of composition and temperature desirable. Iron objectionable as cellulose adsorbs iron from dilute solutions. Manganese very objectionable, clogs pipelines and is oxidized to permanganates by chlorine, causing reddish color.
11/ Excessive iron, manganese, or turbidity creates spots and discoloration in tanning of hides and leather goods.
12/ Constant composition; residual alumina 0.5 mg/l.
13/ Calcium, magnesium, iron, manganese, suspended matter, and soluble organic matter may be objectionable.

Table 4.-Estimated Use of Ground Water for Irrigation, Public Supply, and Industrial Purposes From the Carrizo-Wilcox, Queen City-Bigford, and Sparta-Laredo Aquifers, 1969

AQUIFER	PUMPAGE, IN ACRE-FEET			
	PUBLIC SUPPLY	INDUSTRIAL	IRRIGATION	TOTAL'
Carrizo-Wilcox	–	–	–	273,000
a) Carrizo	8,900	3,100	255,000	–
b) Wilcox	2,000	480	3,700	–
Queen City-Bigford	1,100	31	4,000	5,130
Sparta- Laredo	120	–	850	97
			Total *	279,000

*Figures are approximate because some of the pumpage is estimated. Totals are rounded to three significant figures. In addition to the amounts shown in the table, approximately 3,000 acre-feet was lost from uncontrolled flowing wells and approximately 11,000 acre-feet was used for domestic and livestock purposes from these aquifers.

aquifer from 1930 to 1938 remained nearly constant. Since the late 1930's or early 1940's, the aquifer has undergone generally steady development to provide increasingly larger amounts of ground water, mostly for irrigation needs. Other causes for this increase include population growth, industrial expansion, and widespread drought conditions in early 1950's.

Table 4 provides estimates of the amounts of ground water obtained from the Carrizo and other aquifers in 1969 in the Winter Garden Area. The total irrigation, public supply, and industrial ground-water pumpage in 1969 in the Winter Garden Area was approximately 279,000 acre-feet or 249 mgd. Irrigation pumpage accounted for about 264,000 acre-feet (235 mgd), with about 255,000 acre-feet (228 mgd) coming from the Carrizo aquifer. These figures indicate that the Carrizo aquifer supplied 97 percent of the total irrigation pumpage, and that the irrigation pumpage amounts to 95 percent of the total irrigation, public supply, and industrial ground-water pumpage of the Winter Garden Area.

Large Carrizo water-level declines have taken place in the Winter Garden District (Dimmit, Zavala, and eastern Maverick Counties) where large amounts of ground water have been used in the production of garden vegetables. Figure 20 shows declines of 240 feet in this area for the period 1929-30 to 1970. Water-level declines in Atascosa, Wilson, and Gonzales Counties have not been as severe as in the Winter Garden District; however, south of Pearsall in Frio County, water levels have declined approximately 180 feet during this same period.

Availability of Ground Water for Future Development

Application of the Digital Computer Mathematical Model

One of the primary objectives of this study was to simulate the Carrizo aquifer in the Winter Garden Area with a digital computer mathematical model. The simulation process allows the prediction of water-level declines in the Carrizo aquifer based on projected pumpage, and the predicted water-level declines provide a means for evaluating the ability of the Carrizo aquifer to meet anticipated ground-water withdrawal requirements.

Three sets of aquifer simulations were made with the Carrizo aquifer model. First, the model was provided with data on the estimated past and projected future pumping rates and was programmed to compute and print out the amounts of resulting water-level decline for the periods 1970-l 980, 1970-l 990, and 1970-2020. County Agricultural Extension Agents furnished projections of irrigation pumpage requirements for these periods and studies conducted by the Board were used to project public supply and industrial

The following table summarizes the average annual pumpage that was programmed into the model for the periods 1963-1970, 1970-1980, 1980-1990, and 1990-2020:

PERIOD	FRIO COUNTY		WINTER GARDEN DISTRICT (DIMMIT, ZAVALA, AND EASTERN MAVERICK COUNTIES)		WINTER GARDEN AREA (REPORT AREA)	
	ACRE-FEET PER YEAR	MGD	ACRE-FEET PER YEAR	MGD	ACRE-FEET PER YEAR	MGD
1963-1970	72,700	64.86	121,400	108.31	272,000	242.65
1970-1980	74,200	66.20	120,600	107.59	306,000	272.99
1980-1990	76,300	68.06	119,600	106.69	314,000	280.12
1990-2020	79,000	70.48	119,000	106.16	332,000	296.19

Recharge and leakage to the Carrizo aquifer were assumed for these studies to approximate 100,000 acre-feet per year (89 mgd) and 9,500 acre-feet per year (8.5 mgd), respectively, in the Winter Garden Area.

Next, it was desired to know whether the Carrizo aquifer southeast of San Antonio in Wilson County could provide a firm municipal water supply of 20,000 to 40,000 acre-feet per year (18 to 36 mgd) for the San Antonio metropolitan area. The model was made to simulate two alternative lines of pumping wells or well fields, one under water-table conditions (Line A, shown on Figure 24) and the other under artesian conditions (Line B, shown on Figure 25). Wells along Line A were placed just southeast of the outcrop of the Carrizo Sand. Those along Line B were located approximately 5 miles downdip from the outcrop. Each of these lines of wells was simulated to produce 20,000 acre-feet per year (18 mgd), 30,000 acre-feet per year (27 mgd), and 40,000 acre-feet per year (36 mgd). This pumpage was in addition to the predicted irrigation, public supply, and industrial pumpage which had been forecast for the Winter Garden Area. Recharge to the Carrizo aquifer in the area of investigation was estimated to be approximately 26,000 acre-feet annually (23 mgd). This recharge area includes the Carrizo Sand outcrop in Wilson County and parts of Atascosa, Bexar, and Guadalupe Counties.

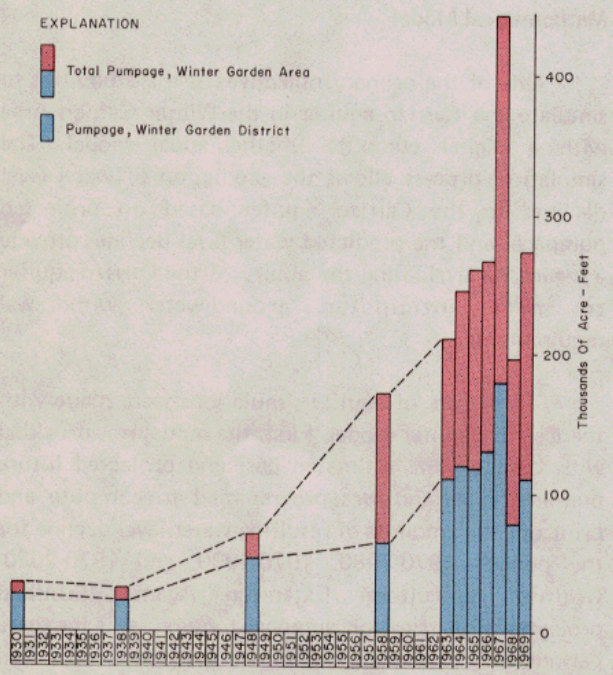

Figure 7.—Approximate Pumpage From the Carrizo Aquifer for Irrigation, Public Supply, and Industrial Use, 1930-1969

Last, simulations were made with the aquifer model to determine the annual withdrawal or pumping rate per unit area which would lower the Carrizo aquifer water levels to 400 feet below land surface throughout the Winter Garden Area. The pumping and lowering of water levels would occur from 1970 to 2020 and generally in the area between the outcrop and the downdip limit of fresh to slightly saline water (less than 3,000 mg/l dissolved solids). For the purpose of this study, ground-water development of the Carrizo aquifer in the downdip areas was considered economically feasible as long as water levels were 400 feet or less below land surface. Under these conditions, the following criteria were used as a basis for data input into the model prior to the simulation: (a) recharge and leakage to the Carrizo aquifer were assumed to approximate 100,000 acre-feet per year (89 mgd) and 9,500 acre-feet per year (8.5 mgd), respectively; (b) in the area where the Carrizo aquifer contains water having a dissolved-solids content greater than 1,000 mg/l, pumpage was not increased above the 1963-1969

average; and (c) pumpage was regulated so that water-level declines would be minimized in the outcrop and not fall below the top of the aquifer in the downdip area. The simulation provided data in the form of annual pumpage rates per unit area, which were used to determine the areas where the Carrizo aquifer is most and least favorable for future development.

Results of Aquifer Simulation

The simulation studies of the Carrizo aquifer indicate that, if pumpage remains unregulated and occurs at predicted rates, water levels will continue to decline rapidly in the heavily irrigated areas near Batesville and east of Carrizo Springs and Crystall City in Dimmit and Zavala Counties; elsewhere, water levels will slowly decline throughout the Winter Garden Area, including the downdip areas of interface between slightly saline and moderately saline ground water. The predicted water-level changes for the periods 1970-l 980, 1970-l990, and 1970-2020 are presented in the form of contour maps in Figures 21, 22, and 23.

The simulations of lines of pumping wells in areas of water-table and artesian conditions indicate that a firm water supply of 20,000 to 40,000 acre-feet (18 to 36 mgd) can be developed from the Carrizo aquifer in Wilson County for municipal use in the San Antonio region. The lines of pumping wells and their associated cones of water-level depression for the period 1970-2020 are illustrated in Figures 24 and 25. The maximum water-level drawdowns obtained from the simulations are summarized in the following table:

LINE OF PUMPING WELLS	PUMPAGE, 1970-2020 (ACRE-FEET)	MAXIMUM DRAWDOWN, 1970-2020 (FEET)
Line A	20,000 (18 mgd)	80
Line B	20,000 (18 mgd)	100
Line A	30,000 (27 mgd)	100
Line B	30,000 (27 mgd)	120
Line A	40,000 (36 mgd)	160
Line B	40,000 (36 mgd)	160

The annual recharge to the Carrizo aquifer in the area southeast of San Antonio is estimated to be approximately 26,000 acre-feet (23 mgd). The recharge area, for the most part includes the Carrizo Sand outcrop in Wilson County and parts of Atascosa, Bexar, and Guadalupe Counties. Recharge to the Carrizo aquifer would be increased as water levels are drawn down in the outcrop by the proposed well fields. The drawdown of water levels would reduce evapotranspiration losses and spring discharge into the San Antonio River and Cibolo Creek. The amount of increase in recharge which would result from the lowering of water levels in the vicinity of the outcrop was not estimated or used in the simulation studies.

Figure 26 illustrates pumpage patterns for optimizing development of ground water in the Carrizo aquifer in the Winter Garden Area. This rnap is a product of the 50-year aquifer simulation to determine the maximum constant pumping rates per unit area for the period 1970-2020, which would not bring water levels more than 400 feet below land surface or below the top of the aquifer. Possible water-quality changes due to the additional development of ground water were not considered in the analysis.

The aquifer simulation indicates that, under the constraints mentioned, approximately 330,000 acre-feet of water per year (294 mgd) could be pumped during the period 1970 to 2020 from the Carrizo aquifer in the Winter Garden Area. This is an increase of about 58,000 acre-feet per year (52 mgd) over the average annual withdrawals by large-capacity wells for the period 1963- 1969.

As shown in Figure 26, the areas favorable for future development of ground water from the Carrizo aquifer are generally located in (a) the Floresville, Stockdale, and Nixon areas of Wilson and Gonzales Counties; (b) northeast La Salle County; (c) an area west of Pearsall in Frio and Zavala Counties; (d) central and western Zavala County; and (e) central and southwestern Dimmit and northwestern Webb Counties. In these areas, approximately 118,000 acre-feet per year (105 mgd) could be developed in addition to the 1963-1969 average withdrawal rate without bringing water levels more than

400 feet below land surface or below the top of the water-bearing sands until the year 2020. The average annual withdrawal for the period 1963-1969 in these areas was approximately 22,500 acre-feet (20 mgd). The best locations for additional development generally correspond with the areas where the thickest accumulations of water-bearing sand occur within the aquifer (Figure 12j. Also, additional development must be distributed widely in order to avoid concentrated withdrawals of ground water in small areas.

Within the extensive area that is fully developed (Figure 26), ground-water withdrawal ideally should not be increased over the 1963-1969 rate, which was approximately 133,000 acre-feet per year (119 mgd).

The areas least favorable for future ground-water development from the Carrizo aquifer are the overdeveloped areas, shown in Figure 26 to be located: (a) in the outcrop of the Carrizo Sand in northern Frio, northern Atascosa, and southeastern Medina Counties; (b) at and southeast of Pearsall in Frio County; (c) near Batesville and in the outcrop of the Carrizo in northeastern Zavala County; (d) northeast, east, and southeast of Crystal City in Zavala and Dimmit Counties; and (e) near Carrizo Springs in Dimmit County. The 1963-1969 average annual withdrawal in these areas, approximately 117,000 acre-feet (104 mgd), should be reduced by approximately 59,800 acre-feet (53 mgd) if excessive water-level declines are to be avoided.

Artificial Recharge

Artificial recharge occurs when natural recharge is augmented so as to increase the amount of water entering the aquifer. The means of artificial recharge may include increasing the rate of infiltration through the soil profile, increasing the area in which surface runoff is in contact with the aquifer outcrop, and increasing the time during which the surface water is in contact with the aquifer outcrop. In addition to modifications to increase recharge in the aquifer's outcrop, water can be injected into the aquifer in downdip areas through injection wells.

Barnes (1956) estimated that a permanent water supply of 112,000 acre-feet per year (100 mgd) could be developed from the Carrizo aquifer in Wilson County for the San Antonio region by lowering water levels in the Carrizo outcrop in Atascosa, Bexar, and Wilson Counties, which would increase the amount of direct streambed infiltration from the San Antonio River and Cibolo Creek, and by spreading other waters over the outcrop. Barnes assumes that most of the water brought in for artificial recharge would be surplus water generated by the city of San Antonio. In order to lower the water table in the outcrop, Barnes proposes drilling 18 wells along a line parallel with the lower Carrizo outcrop edge. These wells would be spaced one mile apart and each produce 1,000 gpm (gallons per minute).

When evapotranspiration losses and spring flows have ceased in the aquifer outcrop due to water-level declines, other steps to increase the amount of recharge in the outcrop appear feasible. The Winter Garden District (Dimmit, Zavala, and eastern Maverick Counties) offers excellent possibilities, as large water-level declines have taken place in the outcrop in this region. Similarly, the well field proposed by Barnes (1956) or the well fields studied in this report in Wilson County would offer excellent possibilities for artificial recharge by creating large water-level declines in the outcrop.

Artificial recharge to the Carrizo aquifer in the outcrop could be achieved by: (a) constructing a series of diked basins, superimposed on the natural stream drainage to retard runoff and promote infiltration; (b) scarifying, leveling, and widening the beds of intermittent streams to increase infiltration; and (c) transporting to the outcrop the surplus water of cities, industry, or flood runoff.

Getzendaner (1953) describes an injection well experiment on the Byrd Ranch near Crystal City. Initially the injection rate was estimated at 1,800 gpm for 38 minutes, at which time the Carrizo aquifer ceased to take water at this rate and the injection rate was reduced to approximately 900 gpm. This lower injection rate was continued for 4 hours and 45 minutes until the experiment was terminated because of darkness. Getzendaner wrote:

> Many experiments with such wells, in California and elsewhere, have had little success. But excepting in Brooklyn and Queens, Long Island, where water is injected into gravel, there has been no attempt, so far as the literature discloses, to inject water through wells into as porous and permeable, nor as thick a formation as the Carrizo Sand in this district.

Clogging of the aquifer and low injection rates are problems which must be overcome if injection wells are to function successfully. Some of the causes of clogging are algea, silt, and entrained air. Poor recharge well design and completion of recharge wells in zones of low permeability in the aquifer may also contribute to low injection rates.

The amount and cost of water which can be recharged into the Carrizo aquifer depend on the

availability of recharge water, methods used, frequency of use, maintenance (clogging, weeds, sedimentation or flocculation, etc.) land costs, and capital works investment. The cost of artificial recharge projects may be reduced in part through the operation of sand pits or possibly by joint use of a recreation area. For example, sand excavated from the artificial recharge puts could be sold for construction purposes; and municipal recreational facilities such as parks, golf courses, baseball diamonds, football fields, public hunting and fishing areas, and skeet and trap ranges could be incorporated into an artificial recharge project.

Ground-Water Development Problems

Problems associated with the development of ground water from the Carrizo aquifer can be related to (a) improper well completion, (b) water-level declines, and (c) contamination of native ground water.

Improper well completion can usually be attributed to insufficient casing, open-hole rather than screened completion, slotted or perforated casing as a substitute for screen, improper gravelpacking, or lack of cement in the annulus between the casing and the borehole. The following are recommendations for the proper construction and completion of high-capacity wells in sand and gravel aquifers: (a) wells should be drilled to the base of the zone containing desirable quality water, thereby utilizing maximum saturated thickness; (b) all wells should be cased (including screen) from ground level to total depth; (c) gravel packing, when used, should be preceded by a sieve analysis of the aquifer to determine the proper size of the pack material to be used; and (d) the well should be completed with a properly designed well screen.

Large, concentrated withdrawals of ground water from storage in the Carrizo aquifer have caused large-scale water-level declines and possible contamination problems in the Winter Garden District (Dimmit, Zavala, and eastern Maverick Counties) where the aquifer has comparatively low transmissibility. This district is famous for its production of garden vegetables and has experienced a large amount of irrigation development since the late 1930's. As a result of these large water-level declines, well yields have decreased. In order to meet increased water demands, well pumps must be set deeper and larger motors installed. In some cases, new wells are needed to meet the demands for water supplies. These improvements cause operating costs to spiral upward as ground-water users attempt to meet demands and, in doing so, cause additional water-level declines.

Prior to large-scale development of ground water in Dimmit and Zavala Counties, the hydrostatic head of the Carrizo aquifer was considerably higher than the hydrostatic head of the highly mineralized waters of the overlying sands. As the hydrostatic head of the Carrizo dropped with development in Dimmit and Zavala Counties, the mineralized waters from these sands began moving into the Carrizo as leakage through the confining beds or down the well bores in which the casing was defective, improperly installed, or had not been cemented. This water mingles with the native Carrizo water, thus deteriorating its chemical quality. Although the problem is confined to individual wells at present, continued increase in development of the Carrizo in Dimmit and Zavala Counties could result in more wide spread aquifer contamination due to interformational leakage.

Developing and utilizing ground water from a well or well field require adequate planning. Future development of ground water in the Winter Garden Area should be based on a program of test drilling, test pumping, and chemical analysis of water from the producing aquifer. Such preliminary data can be used to determine the most efficient well completion, optimum pumping rate, efficient pump setting, optimum well spacing, and feasibility of drilling additional wells. Large, concentrated withdrawals of ground water in small areas should be avoided.

GROUND-WATER AVAILABILITY IN THE WILCOX, QUEEN CITY-BIGFORD, AND SPARTA-LAREDO AQUIFERS

Estimates of the amount of water available from the Wilcox, Queen City-Bigford, and Sparta-Laredo aquifers are based on the transmission and storage capacities of the aquifers. The transmission capacity of an aquifer can be approximated for any proposed development scheme by using the formula

$$Q=TWI,$$

where

Q = the average quantity of water in gallons per day moving through the aquifer;

T = the average coefficient of transmissibility in gallons per day per foot of aquifer width;

W = the width of the aquifer in miles, parallel to the strike of the formation; and

I = the average hydraulic gradient in feet per mile.

The development scheme considered is based on the following conditions: (a) the effect of pumping is such that static water levels are drawn down to a maximum depth of 400 feet below land surface, but not below the top of the aquifer; (b) the line along which the static water levels are 400 feet below the land surface is located about midway between the outcrop and the downdip limit of fresh to slightly saline water in the aquifer; and (c) lowering of water levels within the outcrop does not occur. The average coefficient of transmissibility in gallons per day per foot (gpd/ft) was determined from the average net sand thickness and the estimated permeability along the line described above; and the average artesian storage coefficient was estimated by multiplying the average net saturated sand thickness, in feet, by 10^{-6} per foot, which is proper for most confined aquifers (Lohman, 1972, p. 8).

In determining the quantity of water available, (a) a total amount of water obtained from artesian storage by lowering the static water level to a depth of 400 feet below land surface was calculated, and (b) the amount of water that the aquifer will transmit annually after static water levels have been lowered to a depth of 400 feet below land surface was calculated.

The following table summarizes the coefficients used to estimate the amount of water which can be developed from the Wilcox, Queen City-Bigford, and Sparta-Laredo aquifers. Only the portions of the Wilcox and Queen City-Bigford aquifers east of the Frio River are included in this determination since it is doubtful that these aquifers will be developed to any great extent west of the river.

AQUIFER	COEFFICIENT OF TRANSMISSIBILITY (GPD/FT)	WIDTH OF AQUIFER (MILES)	HYDRAULIC GRADIENT (FT/MILE)	ARTESIAN STORAGE COEFFICIENT
Wilcox	44,000	123	33	5×10^{-4}
Queen City-Bigforcl	14,000	111	88	5×10^{-4}
Sparta-Laredo	5,000	197	81	1×10^{-4}

Based on the above figures, east of the Frio River 200,000 acre-feet of water per year (178 mgd) can theoretically be transmitted by the Wilcox aquifer and 153,000 acre-feet annually (136.5 mgd) by the Queen City-Bigford aquifer to pumping wells in the Winter Garden Area. Approximately 89,000 acre-feet per year (79 mgd) can be transmitted by the Sparta-Laredo aquifer. These are the computed amounts which can be pumped annually without lowering the static water levels below the top of the aquifer or more than 400 feet below land surface, providing that the aquifer recharge in the outcrop is sufficient. In the opinion of the authors, the areas of aquifer outcrop may be too small to supply these estimated transmission capacities and they should be reduced by a factor of 2 or 3 for judging the amount of water continuously available.

The amount of water available from storage was calculated to be 244,000 acre-feet in the Wilcox, 100,000 acre-feet in the Queen City-Bigford, and 40,000 acre-feet for the Sparta-Laredo, should static water levels be lowered 400 feet below land surface along a line midway between the outcrop and the downdip limit of fresh to slightly saline water in the aquifers. These amounts can be pumped from storage only once, not annually, and should not be considered in long-range planning.

SUMMARY

The Winter Garden Area consists of approximately 11,800 square miles and lies within the Guadalupe, San Antonio, Nueces, and Rio Grande basins. It includes all or part of Atascosa, Bexar, Dimmit, Frio, Gonzales, Guadalupe, Karnes, La Salle, Live Oak, McMullen, Maverick, Medina, Uvalde, Webb, Wilson, and Zavala Counties. Within the Winter Garden Area is found the Winter Garden District which includes Dimmit and Zavala Counties and the eastern part of Maverick County.

The Carrizo aquifer (Carrizo Sand) is the most continuous and permeable aquifer in the area and therefore is the most developed water-bearing formation. In local areas of the aquifer's extent, some of the sands containing fresh to slightly saline water in the Reklaw Formation, Bigford Formation, and Wilcox Group may be hydrologically connected to the Carrizo Sand. The Carrizo aquifer ranges in thickness from about 150 to 1,200 feet. The transmissibility of the Carrizo ranges from less than 1,000 gallons per day per foot in Webb County to 317,000 gallons per day per foot in Atascosa County. The average coefficient of storage in the outcrop of the Carrizo aquifer is approximately 0.20. Downdip, where the aquifer is under artesian conditions,

the average coefficient of storage approximates 0.0005 or 5×10^{-4}.

Throughout the Winter Garden Area, the Carrizo aquifer yields fresh to slightly saline water which is acceptable for most irrigation, public supply, and industrial purposes. In the outcrop, the Carrizo aquifer contains hard water which is otherwise low in dissolved solids. Downdip the water is softer, has a higher temperature, and contains more dissolved solids. Carrizo aquifer water has a low to high salinity hazard for irrigation use, and the sodium (alkali) hazard is generally low to medium.

The average rate of recharge to the Carrizo aquifer in the Winter Garden Area is about 100,000 acre-feet per year or 89 mgd. In the heavily irrigated areas of Dimmit, Zavala, and Frio Counties, leakage into the Carrizo from other aquifers is occurring; an estimated 9,500 acre-feet per year (8.5 mgd) leaked into the Carrizo during the period 1963-1969. The approximate average annual pumpage from large wells (irrigation, public supply, and industrial) from the Carrizo aquifer in the Winter Garden Area during the period 1963-1969 was about 272,000 acre-feet (243 mgd); thus, about 162,500 acre-feet (145 mgd) of ground water was removed annually from storage in the aquifer. Although the water stored in the aquifer is in no danger of being depleted for many years, the increased pumping lifts caused by water-level declines will make it more costly to pump water for irrigation.

Contamination of native ground water in the Carrizo aquifer by water of higher mineral content from overlying sands is a serious problem in Dimmit and Zavala Counties. The water from these sands moves into the Carrizo as leakage through confining beds or down the well bores in which the casing is defective, improperly installed, or has not been cemented. At present the problem is confined to individual wells, but a continued increase in development of the Carrizo in Dimmit and Zavala Counties could result in more widespread contamination due to interformational leakage.

The digital computer simulation of the Carrizo aquifer for the period 1970 through 2020 indicates that: (a) water levels near Batesville and east of Carrizo Springs and Crystal City in the Winter Garden District will continue to decline rapidly; (b) elsewhere throughout the Winter Garden Area, water levels will slowly decline if pumpage remains unregulated and occurs at predicted rates; (c) a firm water supply of 20,000 to 40,000 acre-feet per year (18 to 36 mgd) of ground water from wells can be developed in Wilson County for municipal use; (d) approximately 330,000 acre-feet per year (294 mgd) of ground water can be developed from the Carrizo aquifer and not lower water levels below a 400-foot level below land surface or below the top of the water-bearing sands until the year 2020, representing an increase of 58,000 acre-feet per year (52 mgd) over the average withdrawals of 1963-1969; and (e) the areas most favorable for the development of additional ground-water supplies are in Wilson and Gonzales Counties.

Developing and utilizing ground water from a well or well field require adequate planning. Future development of ground water in the Winter Garden Area should be based on a program of test drilling, test pumping, and chemical analyses of water from the producing aquifer. Such preliminary data can be used to determine the most efficient well completion, optimum pumping rate, efficient pump setting, optimum well spacing, and feasibility of drilling additional wells. Large, concentrated withdrawals of ground water in small areas should be avoided.

REFERENCES

Alexander, W. H., Jr., and White, D. E., 1966, Ground-water resources of Atascosa and Frio Counties, Texas: Texas Water Devel. Board Rept. 32, 211 p.

Alexander, W. H., Jr., and others, 1964, Reconnaissance investigation of the ground-water resources of the Guadalupe, San Antonio and Nueces River basins, Texas: Texas Water Comm. Bull. 6409, 106 p.

Altgelt, E. S., and Michal, E. J., 1937, Records of wells and springs, logs of wells and test holes and analyses of water from wells, springs and test holes, and map showing location of wells, Guadalupe County, Texas: Texas Board of Water Engineers duplicated rept., 66 p.

American Water Works Association, 1950, Water quality and treatment: Am. Water Works Assoc. Manual, 2d ed., tables 3-4, p. 66-67.

Anders, R. B., 1957, Ground-water geology of Wilson County, Texas: Texas Board Water Engineers Bull. 5710, 66 p.

–1960, Ground-water geology of Karnes County, Texas: Texas Board Water Engineers Bull. 6007, 110p.

Anders, R. B., and Baker, E. T., Jr., 1961, Ground-water geology of Live Oak County, Texas: Texas Board Water Engineers Bull. 6105, 128 p.

Arnow, Ted, 1959, Ground-water geology of Bexar County, Texas: Texas Board Water Engineers Bull. 5911, 62 p.

Baldwin, H. L., and McGuiness, C. L., 1963, A primer on ground water: Washington, U.S. Govt. Printing Office, 26 p.

Barnes, J. R., 1956, Availability of ground water from Carrizo Sand in Wilson County, Texas: Consultant's rept. to the Guadalupe-Blanco River Authority, 13 p. (Reference copy available at Texas Water Development Board)

Broadhurst, W. L., and others, 1950, Public water supplies in southern Texas: U.S. Geol. Survey Water-Supply Paper 1070, 114 p.

Brown, J. B., and others, 1965, Reconnaissance investigation of the ground-water resources of the Rio Grande basin, Texas: Texas Water Comm. Bull. 6502, 213 p.

Carr, J. T., 1967, The climate and physiography of Texas: Texas Water Devel. Board Rept. 53, 27 p.

Chow, Ven Te, Ed., 1964, Handbook of applied hydrology: New York, McGraw-Hill Book Co., Inc., 1418 p.

Dallas, Morning News, 1933, Texas almanac and state industrial guide 1933: A. H. Belo Corp., 384 p.

Dallas Morning News, 1941, Texas almanac and state industrial guide 1941-42: A. H. Belo Corp., 576 p.

–1953, Texas almanac 1954-55: A. H. Belo Corp., 672 p.

–1961, Texas almanac 1961-62: A. H. Belo Corp. 704 p.

–1969, Texas almanac and state industrial guide 1970-71: A. H. Belo Corp., 704 p.

Davis, S. M., and Dewiest, R. J. M., 1966, Hydrogeology: New York, John Wiley & Sons, Inc., 463 p.

Deussen, Alexander, 1924, Geology of the coastal plain of Texas west of the Brazos River: U.S. Geol. Survey Prof. Paper 126, 139 p.

Deussen, Alexander, and Dole, R. B., 1916, Ground water in La Salle and McMullen Counties, Texas: U.S. Geol. Survey Water-Supply Paper 375, p. 141-177.

Dewiest, R. J. M., 1965, Geohydrology: New York, John Wiley & Sons, inc., 366 p.

Doll, W. L., and others, 1963, Water resources of West Virginia: West Virginia Dept. of Nat. Resources, Div. Water Resources, 134 p.

Eargle, D. H., 1968, Nomenclature of formations of Claiborne Group, Middle Eocene Coastal Plain of Texas: U.S. Geol. Survey Bull. 1251-D, 25 p.

Eaton, F. M., 1950, Significance of carbonates in irrigation waters: Soil Sci., v. 59, p. 123-l 33.

Follett, C. R., 1956a, Records of water-level measurements in Bexar County, Texas: Texas Board Water Engineers Bull. 5606, 61 p.

_1956b, Records of water-level measurements in Medina County, Texas, 1930 to March 1956: Texas Board Water Engineers Bull. 5609, 25 p.

_1956c, Records of water-level measurements in Dimmit, Maverick, and Zavala Counties, Texas, 1920, 1928 to Sept. 1956: Texas Board Water Engineers Bull. 5617, 76 p.

-1966, Ground-water resources of Caldwell County, Texas: Texas Water Devel. Board Rept. 12, 141 p.

Frazier, J. M., Jr., 1939, Records of wells and springs, drillers' logs, water analyses, and map showing location of wells and springs in Gonzales County, Texas: Texas Board Water Engineers duplicated rept., 58 p.

Getzendaner, F. M., 1953, Supplement to replenishing Carrizo Sand Water: Consultant's rept., 13 p., (Reference copy available at Texas Water Development Board)

Gillett, P. T., and Janca, I. G., 1965, Inventory of Texas irrigation, 1958 and 1964: Texas Water Comm. Bull. 6515, 323 p.

Harris, H. B., 1965, Ground-water resources of La Salle and McMullen Counties, Texas: Texas Water Comm. Bull. 6520,96 p.

Hem, J. D., 1959, Study and interpretation of the chemical characteristics of natural water: U.S. Geol. Survey Water-Supply Paper 1473, 269 p.

Hill, R. T., and Vaughan, T. W., 1898, Geology of the Edwards Plateau and Rio Grande Plain adjacent to Austin and San Antonio, Texas, with reference to underground water: U.S. Geol. Survey 18th Ann. Rept., pt. 2, p. 193-323.

Holt, C. L. R., Jr., 1956, Geology and ground-water resources of Medina County, Texas: Texas Board Water Engineers Bull. 5601, 289 p.

Howard, J. W., 1968, Water-level data from observation wells in the northwestern Gulf Coastal Plain of Texas: Texas Water Devel. Board Rept. 70, 209 p.

Howell, J. V., 1957, Glossary of Geology and related Sciences: Am. Geol. Inst., 325 p.

Jacob, C. E., 1944, Notes on determining permeability by pumping tests under water-table conditions: U.S. Geol. Survey open-file rept.

Johnson, E. E., 1963, Basic principles of water well design, pt. 3: Johnson Drillers' Jour., v. 35, no. 6, p. 4-5, 8.

Johnson, Edward E., Inc., 1966, Ground water and wells (A reference book for the water-well industry): Saint Paul, Minnesota, Edward E. Johnson, Inc., 440 p.

Kane, J. W., 1967, Monthly reservoir evaporation rates for Texas 1940 through 1965: Texas Water Devel. Board Rept. 64, 111 p.

Klemt, W. B., and others, 1972, Board's San Antonio office conducting two aquifer studies, *in* Water for Texas: Texas Water Devel. Board, v. 2, no. 8, p. 5-10.

Layden, R. L., 1971, The story of Big Wells: Gulf Coast Assoc. of Geol. Sot. Trans., v. 21, p. 245-255.

Leopold, L. B., and Langbein, W. B., 1960, A primer on water: Washington, U.S. Govt. Printing Office, 50 p.

Lohman, S. W., 1972, Ground-water Hydraulics: U.S. Geol. Survey Prof. Paper 708, 70 p.

Livingston, Penn, 1947, Ground-water resources of Bexar County, Texas: Texas Board Water Engineers duplicated rept., 240 p.

Lonsdale, J. T., 1935, Geology and ground-water resources of Atascosa and Frio Counties, Texas: U.S. Geol. Survey Water-Supply Paper 676,90 p.

Lonsdale, J. T., and Day, J. R., 1937, Geology and ground-water resources of Webb County, Texas: U.S. Geol. Survey Water-Supply Paper 778, 104 p.

Lyerly, P. J., and Longenecker, D. E., 1957, Salinity control in irrigation agriculture: Texas Agr. Expt. Sta. Bull. 876, 20 p.

Magistad, 0. C., and Christiansen, J. E., 1944, Saline soils, their nature and management: U.S. Dept. Agriculture Circ. 707.

Maier, F. J., 1950, Fluoridation of public water supplies: Am. Water Works Assoc. Jour., v. 42, pt. 1, p. 66-67, 1120-l 132.

Marek, E. L., 1936, Records of wells and springs, drillers' logs, and water analyses and a map showing

the location of wells and springs in Wilson County, Texas: Texas Board Water Engineers duplicated rept., 73 p.

Mason, C. C., 1960, Geology and ground-water resources of Dimmit County, Texas: Texas Board Water Engineers Bull. 6003, 234 p.

Maxcy, K. F., 1950, Report on the relation of nitrate concentrations in well waters to the occurrence of methemoglobinemia: Natl. Research Council Bull. Sanitary Eng., p. 265-271, app. D.

Meinzer, 0. E., and others, 1942, Physics of the Earth, v. 9, Hydrology: New York, McGraw-Hill Book Co., Inc., 712 p.

Moore, E. W., 1940, Progress report of the committee on quality tolerances of water for industrial uses: New England Water Works Assoc. Jour., v. 54, p. 261-272.

Morris, D. A., and Johnson, A. I., 1966, Summary of hydrologic and physical properties of rock and soil materials as analyzed by the hydrologic laboratory of the U.S. Geological Survey, 1948-60: U.S. Geol. Survey open-file rept., 60 p.

Moulder, E. A., 1957, Development of ground water from the Carrizo Sand and Wilcox Group in Dimmit, Zavala, Maverick, Frio, Atascosa, Medina, Bexar, Live Oak, McMullen, La Salle, and Webb Counties, Texas: U.S. Geol. Survey open-file rept., 21 p.

Myers, B. N., 1969, Compilation of results of aquifer tests in Texas: Texas Water Devel. Board Rept. 98, 532 p.

Outlaw, D. E., and others, 1952, Records of wells, drillers' logs, water analyses, and map showing locations of wells in Winter Garden district, Dimmit and Zavala Counties, and eastern Maverick County, Texas: Texas Board Water Engineers Bull. 5203, 59 p.

Owen, J., 1889, Report of geologists for southern Texas: Texas Geol. Survey Prog. Rept. 1.

Peckham, R. C., 1965, Availability and quality of ground water in Leon County, Texas: Texas Water Comm. Bull. 6513,44 p.

Peckham, R. C., and others, 1963, Reconnaissance investigation of the ground-water resources of the Trinity River basin, Texas: Texas Water Comm. Bull. 6309, 110 p.

Pinder, G. F., and Bredehoeft, J. D., 1968, Application of the digital computer for aquifer evaluation: Water Resources Research, v. 4, no. 5, p. 1069-1093.

Rainwater, F. H., and Thatcher, L. L., 1960, Methods for collection and analysis of water samples: U.S. Geol. Survey Water-Supply Paper 1454,301 p.

Rasmussen, W. C., 1947, Geology and ground-water resources of Caldwell County, Texas: Texas Board Water Engineers duplicated rept., 62 p.

Roesler, F. E., 1890, Report (on the underground water supply of Texas): U.S. 51st. Cong., 1st Sess., Ex. Doc. 222, v. 12 (U.S. Serial no. 26891, p. 243-319.

Sayre, A. M., 1936, Geology and ground-water resources of Uvalde and Medina Counties, Texas: U.S. Geol. Survey Water-Supply Paper 678, 146 p.

Scalapino, R. A., 1963, Ground-water conditions in the Carrizo Sand in Texas: Ground Water Jour. of the Natl. Water Well Assoc., v. 1, no. 4, p. 26-32.

Sellards, E. H., Adkins, W. S., and Plummer, F. B., 1932, The geology of Texas, v. I., Stratigraphy: Univ. Texas Bull. 3232, Bur. Econ. Geology, 1007 p., [1933].

Shafer, G. H., 1965, Ground-water resources of Gonzales County, Texas: Texas Water Devel. Board Rept. 4, 89 p.

-1966, Ground-water resources of Guadalupe County, Texas: Texas Water Devel. Board Rept. 19, 95 p.

Smith, H. F., 1954, Gravel packing water wells: Water Well Jour., 4 p.

Smith, 0. M., Dott, R. H., and Warkentin, E. C., 1942, The chemical analysis of the waters of Oklahoma: Oklahoma A&M Coll. Div. Eng. Pub. no. 52, v. 12, p. 15.

Stearman, Jack, 1960, Water levels in observation wells in Atascosa and Frio Counties, Texas, 1955-1960: Texas Board Water Engineers Bull. 6015, 10 p.

Sundstrom, R. W., and Follett, C. R., 1950, Ground-water resources of Atascosa County, Texas: U.S. G eo l. Survey Water-Supply Paper 1079-C, p. 107-l 53.

Swartz, B. W., 1954, Records of water-level measurements in Atascosa and Frio Counties, Texas: Texas Board Water Engineers Bull. 5416, 24 p.

-1957, Records of water levels in Bastrop and Caldwell Counties, Texas, 1937 through Dec. 1956: Texas Board Water Engineers Bull. 5702, 24 p.

Swenson, H. A., and Baldwin, H. L., 1965, A primer on water quality: Washington, U.S. Govt. Printing Office, 27 p.

Texas, Board Water Engineers, 1956, Chemical quality standards for irrigation waters: Texas Board Water Engineers duplicated rept., 7 p.

Texas Water Development Board, 1971, Inventories of irrigation in Texas 1958, 1964, and 1969: Texas Water Devel. Board Rept. 172,229 p.

Theis, C. V., 1935, The relation between the lowering of piezometric surface and the rate and duration of discharge of a well using ground-water storage: Trans. Am. Geophys. Union 16th Ann. Meeting, pt. 2.

Thomasson, H. G., Jr., Olmstead, F. H., and Le Roix, E. F., 1960, Geology water resources, and usable ground-water storage capacity of part of Solano County, California: U.S. Geol. Survey, Water-Supply Paper 1464, p. 207-209, 220-223.

Thornthwaite, C. W., 1952, Evaportranspiration in the hydrologic cycle, *in* The physical and economic foundation of natural resources, v. 2, The physical basis of water supply and its principal uses: U.S. Cong., House of Representatives, Comm. on Interior and Insular Affairs, p. 25-35.

Tolman, C. F., 1937, Ground water: New York, McGraw-Hill Book Co., Inc., 593 p.

Trowbridge, A. C., 1923, Tertiary stratigraphy in the lower Rio Grande region [abs.] : Geol. Soc. America Bull. 34.

Turner, S. F., and others, 1940, Records of wells, drillers' logs, water analyses and maps showing location of wells in Winter Garden district in Dimmit and Zavala Counties and eastern Maverick County, Texas: Texas Board Water Engineers duplicated rept., 125 p.

._1948, Geology and ground-water resources of the Winter Garden district, Texas: U.S. Geol. Survey Water-Supply Paper 1481, 248 p.

U.S. Bureau of Reclamation, 1947, Laboratory tests on protective filters for hydraulic and static structures, Earth materials: U.S. But-. of Reclamation Rept. EM-1 32.

U.S. Geological Survey, 1955a, Handbook for hydrologists: U.S. Geol. Survey, 49 p.

U.S. Geological Survey, 1955b, Quality of surface waters for irrigation, Western United States, 1952: U.S. Geol. Survey Water-Supply Paper 1362, 179 p.

U.S. Public Health Service, 1962, Public Health Service drinking water standards: Public Health Service Pub. 956, 61 p.

U.S. Salinity Laboratory Staff, 1954, Diagnosis and improvement of saline and alkaline soils: U.S. Dept. of Agr. Handb. 60, 160 p.

Walton, W. C., 1962, Selected analytical methods for well and aquifer evaluation: Illinois State Water Survey Rept. 49, 81 p., 76 figs., 4 pls.

-1970, Ground-water resource evaluation: New York, McGraw-Hill Book Co., Inc., 664 p.

White, W. N., and Meinzer, 0. E., 1931, Ground water in the Winter Garden and adjacent districts in southwestern Texas: U.S. Geol. Survey open-file rept.

Wilcox, L. V., 1955, Classification and use of irrigation waters: U.S. Dept. of Agriculture Circ. 969, 19 p.

Wilcox, L. V., Blair, G., and Bower, C. A., 1954, Effect of bicarbonate on suitability of water for irrigation: Soil Sci., v. 77, no. 4, p. 259-266.

Winslow, A. G., and Kister, L. R., Jr., 1956, Saline-water resources of Texas: U.S. Geol. Survey Water-Supply Paper 1365, 105 p.

Wisler, C. O., and Brater, E. F., 1959, Hydrology: New York, John Wiley & Sons, Inc., 408 p.

The following Texas Railroad Commission publications, *A Survey of Secondary Recovery and Pressure Maintenance Operations* contain data used in estimating part of the industrial pumpage:

YEARS COVERED	TEXAS RAILROAD COMMISSION BULLETIN NO.
Beginning of operations to 1952	
1952 to 1954	47
1954 to 1956	–
1956 to 1958	–
1958 to 1960	60
1960 to 1962	62

YEARS COVERED	TEXAS RAILROAD COMMISSION BULLETIN NO.	YEARS COVERED	TEXAS RAILROAD COMMISSION BULLETIN NO.
1962 to 1964	64	1966 to 1968	68
1964 to 1966	66	1968 to 1970	70

TEXAS
WATER
DEVELOPMENT
BOARD

Report 210

GROUND-WATER RESOURCES OF THE CARRIZO AQUIFER IN THE WINTER GARDEN AREA OF TEXAS

VOLUME 2

April 1977

TEXAS WATER DEVELOPMENT BOARD

REPORT 210

GROUND WATER RESOURCES OF THE CARRIZO AQUIFER IN THE WINTER GARDEN AREA OF TEXAS

VOLUME 2

Records of Wells; Water Levels in Wells; Chemical Analyses of Water; and Well Location Maps

BY

Glenn Marquardt
and
Eulogio Rodriguez, Jr.

April 1977

Published and distributed
by the
Texas Water Development Board
Post Office Box 13087
Austin, Texas 78711

TABLE OF CONTENTS

TABLES AND MAPS

GROUND-WATER RESOURCES OF THE CARRIZO AQUIFER

IN THE WINTER GARDEN AREA OF TEXAS

VOLUME 2

INTRODUCTION

This report is prepared in two volumes. Volume 1 contains interpretive information on the ground-water resources of the Carrizo aquifer presented as text and related illustrations and tables. Volume 2 contains supporting basic data including well location maps, records of 3,214 water wells, records of water levels in 474 wells, and chemical analyses of water samples from 1,553 wells. Also used in the study were drillers' logs of 711 wells which are available for reference in the files of the Texas Water Development Board.

The well-numbering system used in this report is one adopted by the Texas Water Development Board for use throughout the State and is shown in the accompanying figure. This system facilitates the location of wells and prevents duplication of well numbers in present and future studies. Each well is assigned a seven-digit number which is derived by using the following system.

The State is divided into l-degree quadrangles of latitude and longitude. There are 89 such quadrangles, numbered 01 through 89. Each l-degree quadrangle is further subdivided into sixty-four 7½-minute quadrangles numbered 01 through 64. Finally, each 7½-minute quadrangle is subdivided into nine 2½-minute quadrangles, numbered 1 through 9. Within these 2½-minute quadrangles, each well is assigned a two-digit number beginning with 01.

The first two digits of each well number identify the l-degree quadrangle; the third and fourth digits indicate the 7½-minute quadrangle; the fifth digit identifies the 2½-minute quadrangle; and the last 2 digits identify the well within the 2½-minute quadrangle.

In addition to the seven-digit well number, a two-letter prefix is used to identify the county. The prefixes for the counties entirely or partially covered by this report are:

PREFIX	COUNTY	PREFIX	COUNTY
AL	Atascosa	SJ	Live Oak
AY	Bexar	su	McMullen
BU	Caldwell	TB	Maverick
HZ	Dimmit	TD	Medina
KB	Frio	YP	Uvalde
KR	Gonzales	VZ	Webb
KX	Guadalupe	ZL	Wilson
PZ	Karnes	ZX	Zavala
RX	La Salle		

For example, well AL-68-62-703 is in Atascosa County (AL); l-degree quadrangle 68; 7½-minute quadrangle 62; 2½-minute quadrangle 7; and was the third well inventoried in that 2½-minute quadrangle.

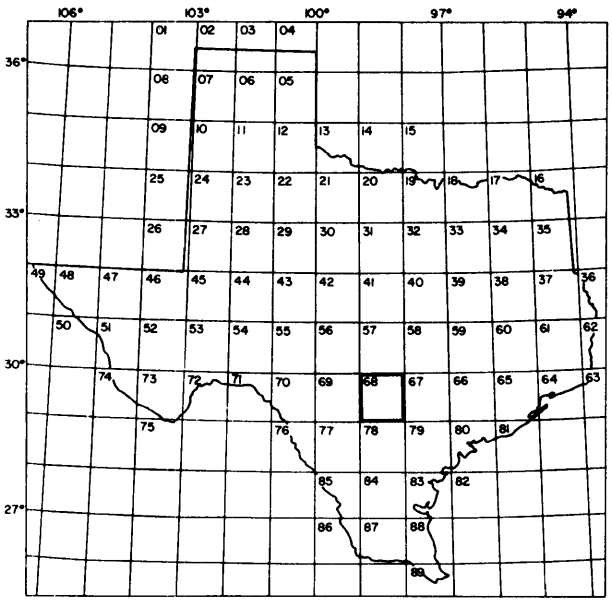

1 - degree Quadrangles

Location of Well AL-68-62-703

68 1 - degree quadrangle

62 7 1/2 - minute quadrangle

7 2 1/2 - minute quadrangle

03 Well number within 2 1/2 - minute quadrangle

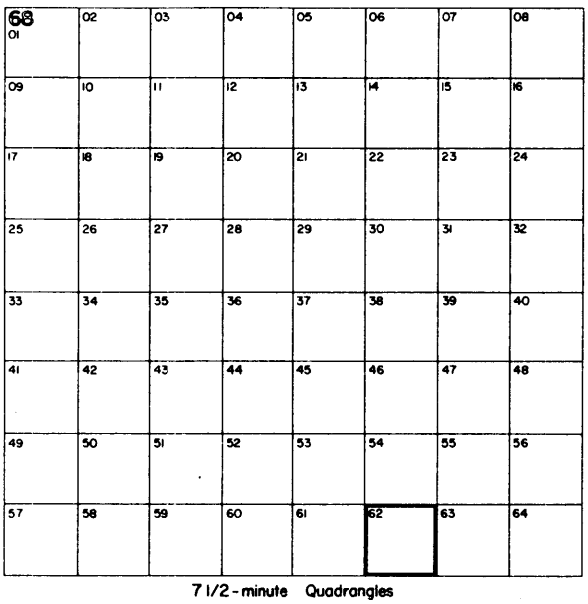

7 1/2 - minute Quadrangles

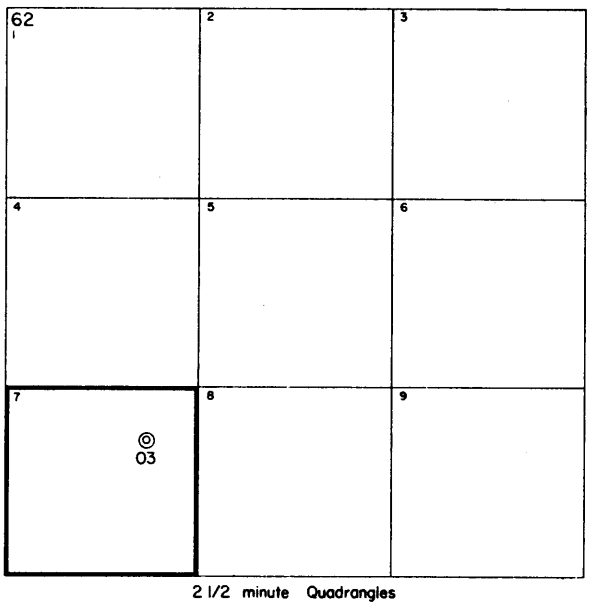

2 1/2 minute Quadrangles

Well-Numbering System

ATASCOSA COUNTY

Table 2.-Selected Oil, Gas, and Stratigraphic Tests

Type Log: D, Drillers'; E, Electric; R, Radioactive; S, Sample.
Logs in Texas Water Development Board files

WELL	OPERATOR	LEASE AND WELL	DATE DRILLED	DEPTH (FT)	APPROXIMATE LAND SURFACE ELEVATION (FT)	TYPE LOG
AL-68-50-601	Gilcrease Oil Co., George Coates and M. L. Wise	F. T. Henderson No. 1	1955	2,495	662	E
901	J. W. Baton	– Granberg No. 1	1961	2,778	664	E
51-504	Brazos Oil and Gas co.	Edward Hartung, et al. No. 1	1966	1,577	736	E
902	CAFRE Research Ltd.	Charles Simmang Heirs No. 1	1951	2,009	660	E
52-714	Texas Water Development Board	Texas Water Development Board	1970	392	676	D, S
58-301	Ray Clark	F. 2. Jones Trustee No. 1	1948	3,335	656	E
303	Caddo Oil Co. Inc.	Thompson No. D-7	1963	2,450	651	E
601	Sutton Drilling Co.	T. A. Crawford No. 1	1956	2,501	582	E
806	Shell Oil Co.	Jane Burns No. A-4	1954	3,619	573	E
807	The Texas Co.	Theo Rogers No. A-5	1953	3,584	616	E
808	do.	Jane Burns No. 8-4	1954	3,625	580	E
901	Sun Oil Co.	C. D. Johnson No. 1	1954	3,551	555	E
903	The Texas Co.	Theo Rogers No. A-10	1954	3,606	583	E
904	do.	Theo Rogers No. C-2	1954	3,570	573	E
59-I 01	J. C. McCabe and Pegg Brothers	Nellie Smith No. 1	1948	3,542	595	E
204	do.	Leonor Galindo No. 2	1948	2,341	556	E
210	George Parker	A. N. Langston No. 1	1953	2,310	568	E
305	Frank Frohnhoefer	E. C. Rogers Estate No. 1	1947	2,606	550	E
402	Sullivan and Garrett	Ike Cowley No. 1	1948	2,669	537	E
505	Amerada Petroleum Corp.	– Finch No. 1	1958	2,804	552	E
803	Inca Drilling Co.	T. C. Byrom No. 1	1958	3,661	516	E
60-115	Tenneco Oil Co.	Cleo Rogers No. 1	1966	6,500	570	
205	Herman Brown, et al.	Marv Stanush No. 1	1949	4,020	542	E
208	H. H. McFarland and I. R. Patton	V. A. Doumch No. 1	1947	3,557	543	E
209	McFarland Drilling co.	Henrietta Estate No. 1	1956	3,978	580	E

Table 2.-Selected Oil, Gas, and Stratigraphic Tests in Atascosa County-Continued

WELL	OPERATOR	LEASE AND WELL	DATE DRILLED	DEPTH (FT)	APPROXIMATE LAND SURFACE ELEVATION (FT)	TYPE LOG
A L-68-60- 306	Eugene W. Gill	Lawrence Katormorak No. 1	1947	4,166	485	E
61-101	George K. Mery	– Ward No. 1	1959	2,000	493	E
208	Arkansas Fuel Oil co.	I. A. Jasik No. 1	1947	4,316	518	E
303	Selbv-Walker Corp. and McFarland Drilling Co.	L. 8. Palmer No. 1	1954	4,444	566	E
411	Wilcox Oil Co.	Isabel Huizar No. 1	1950	5,207	405	E
908	The Texas Co.	Allen Witten No. 1	1965	4,226	422	E
62-804	Barry and Lack	N. S. Richter No. 1	1956	1,300	430	E
78-02-302	Hvdro-Carbons Co.	Theo Rogers No. 1	1948	3,210	565	E
506	Diamond Drilling co.	A. G. Cumpian	1957	3,945	555	E
601	Rodney DeLange, et al.	A. W. Dirmuke No. 1	1955	4,172	562	E
605	Lone Star Producing co.	R. D. Booth No. 4	1955	4,335	504	E
805	F. William Carr and Louis H. Haring, Jr.	Victor W. Marsch No. 1	1951	4,611	568	E
806	F. William Carr	Victor Marsh No. A-l	1955	4,991	581	E
807	do.	– Thompson No. 2	1954	4,933	567	E
906	Humble Oil and Refining Co.	E. J. Pruitt No. D-l	1951	4,983	486	E
909	Carter and Carter	Stanley Brauchle No. 1	1954	4,312	465	E
910	Magnolia Petroleum co.	L. 8. Finch No. 1	1952	5,160	511	E
03-203	Lone Star Producing co.	Nellie B. Alvarado No. 1	1956	4,292	546	E
204	Glen A. Martin	R. B. Davidson No. 1	1955	4,258	554	E
301	A. J. Kuenstler	R. W. Brite No. 1	1955	4,256	525	E
305	Morgan Minerals	– Walton No. 1	1955	4,304	530	E
309	Lone Star Producing co.	R. R. Meadows No. 3	1956	4,344	499	E
402	Rodney DeLange	– Wilson No. 3	1955	4,309	547	E
406	0. N. Neatherlv, Jr.	J. A. Wilson No. 1	1954	4,352	548	E
410	Rodney DeLange, et al.	J. W. Smellev No. 1	1955	4,311	540	E
411	do.	– Wilson No. 2	1955	4,355	557	E
412	0. N. Neatherlv, Jr., et al.	R. D. Booth No. 1	1954	4,070	512	E
413	Rodney DeLange, et al.	J. A. Wilson No. 8	1955	4,300	552	E

Table 2.-Selected Oil, Gas, and Stratigraphic Tests in Atascosa County-Continued

WELL	OPERATOR	LEASE AND WELL	DATE DRILLED	DEPTH (FT)	APPROXIMATE LAND SURFACE ELEVATION (FT)	TYPE LOG
AL-78-03-414	Lone Star Producing co.	Weir Unit No. 1	1955	4,250	536	E
415	do.	Luke 8. Weir No. 6	1955	4,290	546	E
501	Drilling and Exploration Co.	Cyril Dalkowitz, et al. No. 1	1955	4,317	560	E
511	Lone Star Producing co.	M. Aguilar No. 1	1956	4,310	538	E
512	do.	A. Salazar No. 1	1956	4,375	540	E
513	do.	A. L. Gustomente No. 2	1955	4,400	564	E
514	do.	Charlie Pena No. 1	1956	4,415	554	E
712	Carter and Carter	Dick Prassel No. 1	1954	4,730	525	E
713	Armstrong and Horn, et al.	Dave Guerra No. 1	1954	5,142	513	E
714	Alaska Steamship Co. and Texita Oil co.	Dick Prassel No. 2	1954	5,094	512	E
715	Armstrong and Horn Drilling Co.	Ernest Guerra No. 1	1953	5,021	518	E
717	do.	Frank Geyer No. 1	1954	5,078	541	E
802	Alaska Steamship Co. and Newman Brothers	J. F. Chupick No. 1	1954	5,264	543	E
806	Humble Oil and Refining Co.	Edward Matocha No. 1	1946	7,249	493	E
04-603	Security Drilling Co.	Fred Frank No. 1	1955	4,667	432	E
609	H. A. Pagenkope and Caleb Adams	Mary Rosa Whitfield No. 1	1961	1,552	428	E
610	do.	– Palmer No. 2	1961	1,558	381	E
611	do.	George and Douglas Weatherston No. 1	1961	1,527	390	E
706	Humble Oil and Refining Co.	Alamo Lumber Co. No. 2	1947	7,400	462	
707	do.	0. H. Pfeil No. 3	1947	7,407	469	E
708	do.	John Sanders No. 4	1947	7,392	448	E
806	do.	A. N. Moursund No. 1	1946	7,375	425	E
807	do.	Henry Schorsch No. 1	1945	7,405	442	E
816	do.	Henry Schorsch No. 3	1946	7,373	435	E
817	do.	Henry Schorsch No. 7	1948	7,369	421	E
909	do.	H. H. Coward No. 6	1946	7,665	479	E
910	do.	J. A. Walton No. 1	–	–	402	E
911	do.	W. M. Avant No. B-l	1945	7,589	403	E

Table 2.-Selected Oil, Gas, and Stratigraphic Tests in Atascosa County-Continued

WELL	OPERATOR	LEASE AND WELL	DATE DRILLED	DEPTH (FT)	APPROXIMATE LAND SURFACE ELEVATION (FT)	TYPE LOG
AL-78-04-912	Humble Oil and Refining Co.	Ford and Hock, et al. No. 1	1944	7,635	451	E
913	do.	Coward and Lutgen No. 1	1944	1,843	465	E
914	do.	W. M. Avant No. 1	1945	7,591	404	E
915	R. A. R. Special and Tom Crews	S. P. Finch No. 3	1955	1,589	403	E
05-213	Davidor and Davidor, Inc.	Guy S. Combs, Jr. No. 1	1966	6,823	354	E
303	Jergins of Texas Ltd.	L. J. Wiseman No. 1	1955	4,527	405	E
311	Davidor and Davidor, Inc.	– Byrd No. 3	1966	6,853	400	E
401	Continental Oil Co., Taylor and Brown	Nell Sutton No. 1	1955	7,435	418	E
607	Thomas Brothers and M. L. Wise	M. F. Flores No. 1	1954	1,947	316	E
608	J. E. Hillier and M. 0. Turner	Stanley Coughran No. 1	1961	5,506	310	E
704	Martin, Shelley and Thomas	Kate Richter No. 1	1951	1,903	425	E
706	Humble Oil and Refining Co.	Duren and Richter No. 5	1944	7,573	383	E
707	Wherry and Green	– Richter No. 1	1952	1,783	421	E
708	Humble Oil and Refining Co.	Ralph Richter No. 1	1943	7,625	435	E
799	H. and J. Drilling co.	H. H. Coward No. 1	1963	3,940	445	E
710	Humble Oil and Refining Co.	Rogerson and Doren No. 1	1946	7,565	378	E
711	do.	Duren and Richter No. 4	1944	7,603	408	E
714	do.	Coward and Klein No. 1	1946	5,315	439	E
716	Shell Oil Co.	– Bomba No. 2	1952	1.786	410	E
805	Humble Oil and Refining Co.	Joseph Courand No. B-l	1946	7,738	402	E
806	Thomas Brothers and Forney and Winn	C. T. Troell No. 3	1953	1,859	398	E
808	Sid Katz, et al.	C. T. Troell No. 6	1953	1,931	444	E
899	Humble Oil and Refining Co.	R. D. Quillian No. 1	1944	7,67 1	410	E
810	Magnolia Petroleum co.	J. A. Courand No. 10	1954	1,853	390	E
901	Robert Mosbacher and W. T. Mendell	Butts and Sawyer No. 1	1956	7,489	410	E
903	Willard Shuart	C. A. Thorp No. 1	1958	2,200	389	E
904	Frio Producing Co.	C. S. Slaytton No. 1	1963	2,207	326	E

Table 2.-Selected Oil, Gas, and Stratigraphic Tests in Atascosa County-Continued

WELL	OPERATOR	LEASE AND WELL	DATE DRILLED	DEPTH (FT)	APPROXIMATE LAND SURFACE ELEVATION (FT)	TYPE LOG
AL-78-05-905	Sid Katz	Claudia Krueger No. 1	1952	2,079	345	E
06-101	Shell Oil Co.	D. D. Heinen No. 1	1959	5,507	366	E
506	Lone Star Producing co.	Sarah E. Ferry No. 2	1951	8,216	355	E
604	Farenthold and Pitcarin and Minton	– Harris No. 1	1956	5,364	364	E
605	Rowan and Hope and E. W. Gill	Charles H. Brown No. 1	1952	5,820	303	E
701	Humble Oil and Refining Co.	Nellie Gordon and C. G. Dinsmore No. 1	1947	8,120	305	E
703	Pan Tex Corp.	N. G. Dinsmoore No. 1	1951	5,968	348	E
704	Humble Oil and Refining Co.	Nellie Gordon and C. G. Dinsmore No. 8-I	1947	8,093	286	E
705	J. R. McDonald	Bob Hinds No. 2 8R	1964	2,096	285	E
706	Humble Oil and Refining Co.	C. P. Korus No. B-2	1949	8,135	305	E
804	Barry and Moore	Sarah Ferry No. 1	1954	2,166	331	E
904	Magnolia Petroleum co.	E. A. Kinsel No. 1	1946	3,010	315	E
07-702	Monterey Exploration Co.	Guv Smith No. 1	1953	6,064	280	E
703	Newman Brothers. et al.	– Friesenhahn No. 1	1947	5,738	331	E
1 O-301	The Texas Co.	Sesario Tijerina No. 1	1956	5,082	512	E
306	Magnolia Petroleum co.	B. K. Nixon No. 11	1957	5,165	483	E
307	Humble Oil and Refining Co.	W. E. Pound No. 2	1946	5,094	446	E
308	Texas Eastern Production Co.	Claude 8. Finch No. 1	1966	5,138	498	E
311	Humble Oil and Refining Co.	W. W. Clement No. 1	1946	5,210	452	E
312	do.	A. K. McBride No. 8	1947	5,176	454	E
313	do.	Cesario No. 1	1948	5,075	458	E
314	do.	A. M. Lockwood No. 2	1946	6,909	459	E
503	Burleson and Biggers	Marrs McLean No. A-l	1945	5,009	509	E
504	Humble Oil and Refining Co.	8. K. Nixon No. 8-3	1948	5,195	480	E
604	Arnold Oil Well Service	M. M. Davis No. 1	1955	5,449	428	E
609	Humble Oil and Refining Co.	M. M. Davis No. B-1	1947	5,212	453	E

Table 2.—Selected Oil, Gas, and Stratigraphic Tests in Atascosa County—Continued

WELL	OPERATOR	LEASE AND WELL	DATE DRILLED	DEPTH (FT)	APPROXIMATE LAND SURFACE ELEVATION (FT)	TYPE LOG
AL-78-10-610	Kirkwood and Morgan Inc.	Marrs McLean No. 4	1949	5,259	482	E
613	The Texas Co.	State National Bank of Corpus Christi No. 1	1947	5,143	452	E
614	Humble Oil and Refining Co.	— Rivas No. B-1	1948	5,163	452	E
616	Kirkwood and Morgan Inc.	Marrs McLean No. 2	1947	5,502	474	E
901	Milam Drilling Co.	Milton Davis No. 1	1951	6,002	502	E
11-102	Armstrong and Horn and M. E. Andrews	G. L. Tullos No. 1	1954	5,282	528	E
107	Third M. E. Andrews, Ltd.	W. E. Holbrecht No. 1	1956	5,330	520	E
109	Humble Oil and Refining Co.	E. J. Pruitt No. 11	1946	7,108	517	E
112	do.	A. K. McBride No. 5	1946	5,106	443	E
113	do.	J. T. Eppright No. 1	1947	7,000	532	E
114	do.	W. R. Johnson No. 2	1947	5,215	464	E
115	The Bering Co.	J. J. Koemel No. 4	1947	5,192	459	E
116	Humble Oil and Refining Co.	Hugh Favor No. 1	1947	5,305	533	E
117	do.	E. M. Chylek No. 2	1947	5,215	466	E
118	do.	M. M. Davis No. 2	1948	5,200	436	E
120	The Texas Co.	E. D. Scott No. 1	1946	5,404	508	E
123	Humble Oil and Refining Co.	Earl D. Scott No. 1 Unit A	1947	5,250	535	E
209	R. L. Lynd	— Raussean No. 2	1952	4,549	508	E
210	Humble Oil and Refining Co.	M. M. Davis No. E-1	1947	5,315	548	E
211	do.	Emilia Lujan No. C-4	1948	5,300	542	E
212	do.	Emilia Lujan No. C-2	1947	5,276	528	E
214	do.	Emilia Lujan No. C-5	1950	5,306	550	E
216	do.	J. B. Henry No. 2	1947	5,268	509	E
304	do.	S.P.J.S.T. Lodge No. 1	1947	7,390	453	E
306	Magnolia Petroleum Co.	J. C. Wallace No. 1	1949	7,411	453	E
307	do.	Claire Pearlstone No. 1	1947	7,402	445	E
405	Phillips Petroleum Co.	— Alene No. 6	1948	5,207	443	E
406	Humble Oil and Refining Co.	M. M. Davis No. 4	1948	5,220	442	E

Table 2.—Selected Oil, Gas, and Stratigraphic Tests in Atascosa County—Continued

WELL	OPERATOR	LEASE AND WELL	DATE DRILLED	DEPTH (FT)	APPROXIMATE LAND SURFACE ELEVATION (FT)	TYPE LOG
AL-78-11-407	The Texas Co.	Nellie Chamberlain No. 1	1947	5,215	461	E
601	E. V. McCright	G. A. Schroeder No. 1	1954	2,024	502	E
602	General Crude Oil Co.	Esther H. Klingeman No. 1	1955	6,314	493	E
802	Forney and Winn Co.	Allen Hime No. 1	1952	2,070	419	E
12-102	J. C. Hawkins	P. F. Tudyk No. 3	1947	7,412	472	E
106	Stanolind Oil and Gas Co.	A. W. Schwarz No. 4	1948	7,403	450	E
107	do.	— Kitchens No. 1	1947	7,368	423	E
108	Magnolia Petroleum Co.	Augustin Orta No. 1	1947	7,390	453	E
109	do.	Nixon and Steinie No. 1	1946	7,380	443	E
110	Humble Oil and Refining Co.	John Sandeen No. 1	1946	7,386	442	E
113	Plymouth Oil Co.	E. L. Powell No. 4	1949	7,390	455	E
114	do.	K. T. Darby No. 1	1949	7,411	472	E
115	Curtis R. Inman	— Pluto No. 1	1952	1,571	424	E
206	R.A.R. Special and Tom Crews	J. E. Walton No. 7	1958	3,079	392	E
207	Humble Oil and Refining Co.	Henry Schorsch No. 4	1947	7,367	421	E
208	F. B. Cochran	R. Ermis No. 1	1953	1,708	411	E
303	Wherry and Green	— Terrell No. 5	1952	1,687	406	E
702	Tynan and Yonker	Herbert F. Vandiver No. 1	1953	2,099	470	E
14-104	Tri-Mark and Texita Oil Co.	Joe K. Williams No. 1	1953	2,572	266	E
502	E. W. Gill	D. C. McAda No. 1	1947	5,808	249	E
15-101	Payne and Mead	J. A. Bruner No. 1	1947	5,911	345	E
102	Southern Minerals Corp.	Rosana Campbell No. 1	1947	5,898	303	E
103	Sun Oil Co.	— Lancaster No. 1	1960	6,205	352	E
201	Southern Minerals Corp.	Mattie Corbitt No. 1	1951	6,083	322	E
202	H. R. Smith, et al.	E. F. Jendrusch No. 1	1948	3,356	389	E
203	Carrl Oil and Dan Auld	Tom Campbell No. 1	1961	10,322	370	E
503	Gulf Oil Corp.	Emma Tartt No. 1 (SWD)	1961	6,800	404	E
506	Lone Star Producing Co.	L. T. Urbanczyk No. A-1	1956	10,921	399	E

Table 2.—Selected Oil, Gas, and Stratigraphic Tests in Atascosa County—Continued

WELL	OPERATOR	LEASE AND WELL	DATE DRILLED	DEPTH (FT)	APPROXIMATE LAND SURFACE ELEVATION (FT)	TYPE LOG
AL-78-15-507	Lone Star Producing Co.	John L. Tom No. A-3	1957	10,990	404	E
510	do.	— Tom No. 1	1956	10,470	373	E
512	do.	John L. Tom No. A-4	1957	11,050	403	E
604	Caroline Hunt Trust Estate	Felix Frenzel No. 1	1949	4,506	400	E
607	H. R. Smith, et al.	Jessie Henderson No. 3	1947	3,838	477	E
609	Lone Star Producing Co.	H. A. Schuman No. 1	1957	11,065	471	E
610	do.	Otto Lieke No. 1	1958	11,000	449	E
611	do.	H. E. Richter No. 1	1958	10,980	431	E
612	H. R. Smith, et al.	C. M. Kent No. 2	1948	3,858	470	E
616	do.	Gus Stolle No. 1	1949	3,928	509	E
702	Appell Drilling Co.	Jake Pollok No. 1	1947	3,560	355	E
703	Alaska Steamship Co. and Newman Brothers	Smith and Mowinckle No. 1	1948	3,802	346	E
704	Appell Drilling Co.	Smith and Mowinckle No. 1	1947	3,615	314	E
801	H. R. Smith, et al.	Hurt and Tartt No. 6	1946	3,790	433	E
802	do.	Smith and Mowinckle No. 1	1947	3,856	363	E
803	Appell Drilling Co.	J. L. Tom No. 1	1948	3,974	373	E
808	F. William Carr	Lytle Tom No. 2	1955	4,075	409	E
809	Gulf Oil Corp.	Emma Tartt No. 1	1945	2,033	423	E
901	H. R. Smith and Skinner and Eddy	Hurt and Tartt No. 1	1946	3,928	445	E
903	Appell Drilling Co.	H. R. Kellner No. 1	1947	4,040	420	E
18-603	Zander, Liston and Foster, et al.	Nana D. Newton No. 1	1950	6,435	451	E
19-302	Ray McDonald and H & J Drilling Co.	L. C. Berry No. 2	1957	2,255	371	E
701	Morgan Minerals, et al.	M. T. Flanagan No. 1	1956	6,788	373	E
901	S. F. Hurlburt	H. D. Countiss No. 1-A	1944	5,372	341	E
20-201	Sun Oil Co.	Ruth Hagen Unit No. 1	1959	5,393	388	E
302	Varn Petroleum Co.	Tilton-Peeler No. 1	1966	5,528	316	E
21-101	Sun Oil Co.	A. M. Peeler No. 1	1958	5,532	297	E
102	do.	A. M. Peeler No. 3	1958	4,600	307	E
401	Thomas Drilling Corp.	A. B. Peeler No. B-1	—	6,186	369	E

Table 2.—Selected Oil, Gas, and Stratigraphic Tests in Atascosa County—Continued

WELL	OPERATOR	LEASE AND WELL	DATE DRILLED	DEPTH (FT)	APPROXIMATE LAND SURFACE ELEVATION (FT)	TYPE LOG
AL-78-21-403	Sun Oil Co.	A. M. Peeler No. C-3	1963	3,268	338	E
701	Engeo Oil and Gas Co.	Eva Coe Lewis No. 1	1960	3,311	391	E
22-101	Don B. Megahan	Donna Farms No. 2	1935	4,005	380	D, E
301	Appell Drilling Co.	L. May No. 1	1948	3,605	294	E
302	Newman Brothers, et al.	Ada Tom No. 1	1948	3,851	290	E
303	J. D. Medley and Burt Oil Co.	Phil Tom No. 1	1953	6,606	323	E
601	Appell Drilling Co.	Phillip Tom No. 1	1947	4,019	248	E
602	Calvin Michelson	Minnie Lee Tom No. 2	1963	6,688	250	E
23-104	Southern Minerals Corp.	J. L. Tom No. 1	1946	6,505	279	E
105	Hartmann Drilling Co.	Smith and Mowinckle No. 1	1938	4,622	392	E
205	W. H. Appell	Smith and Mowinckle No. 2	1948	4,112	365	E

BEXAR COUNTY (SOUTHERN PART)

Table 2.—Selected Oil, Gas, and Stratigraphic Tests

Type Log: D, Drillers'; E, Electric; R, Radioactive; S, Sample.
Logs in Texas Water Development Board files

WELL	OPERATOR	LEASE AND WELL	DATE DRILLED	DEPTH (FT)	APPROXIMATE LAND SURFACE ELEVATION (FT)	TYPE LOG
AY-68-43-704	Bur-Kan Petroleum Co., et al.	Lee Hubbard No. 1	1948	5,140	700	E
44-601	Hillsman and Greenburg	— Russell No. 1	1956	1,480	563	E
45-303	Anderson-Prichard Oil Corp.	E. H. Yturri No. 2	1948	1,550	580	E
503	Southton Oil Co.	San Antonio Cotton Mill No. 22	1961	2,007	500	E
801	Karl Arnold	C. A. Goeth	—	—	530	E
52-301	C. E. McCaughey	R. W. DeVilbiss No. 1	1948	2,555	582	E
53-103	J. A. Tarver	F. Lamm No. 1	1930	1,581	517	E
202	H. & J. Drilling Co.	George D. Wright No. 1	—	—	525	E
601	W. W. Lynch	W. Whitt No. 1	1966	1,815	545	E
602	F. M. Frasher-P. G. Northrup, et al.	W. I. Whitt No. 1	1949	3,109	543	E
54-101	Star Oil Co.	J. J. Leop No. 1	1949	3,020	472	E
207	C. O. Hagan	Charles J. Griesenbeck No. 1	1954	2,850	484	E
405	—	Esperanza Ranch No. 1	—	3,490	571	E
61-215	H. & J. Drilling Co. and Wilson Brothers Oil Co.	Annie Chapaty No. 1	—	—	535	E

CALDWELL COUNTY

Table 2.—Selected Oil, Gas, and Stratigraphic Tests

Type Log: D, Drillers'; E, Electric; R, Radioactive; S, Sample.
Logs in Texas Water Development Board files

WELL	OPERATOR	LEASE AND WELL	DATE DRILLED	DEPTH (FT)	APPROXIMATE LAND SURFACE ELEVATION (FT)	TYPE LOG
BU-67-19-111	Ashley and Co.	State of Texas, San Marcos River Bed No. 1	1958	2,040	430	E
113	Fisk and Morehead Oil Interests	Eva Shanklin No. 1	1957	2,514	439	E
208	A-Bear Oil Co.	G. C. Walker No. 1	1969	2,670	400	E
403	Forrest C. Lattner	Dr. J. T. O'Banion No. 7	1961	2,241	391	E
641	Claude V. Brown	Matthews and E. I. Moses No. 5	1957	2,646	370	E
20-405	Sam Macco Oil Operations	Gus T. Brown No. 1	1949	3,372	360	E
406	Luling Oil and Gas Co.	J. F. Webb No. 1	1948	3,232	400	E
709	E. Constantin, Jr.	— Watson No. 1	1965	1,450	370	E
803	Walter T. Brown and James C. Callaway	H. M. Ainsworth, et al. No. 1	1959	1,795	451	E
804	J. Kenneth Blackmar	H. N. Ainsworth No. 1	1965	1,707	372	E

DIMMIT COUNTY

Table 2.—Selected Oil, Gas, and Stratigraphic Tests

Type Log: D, Drillers'; E, Electric; R, Radioactivity; S, Sample.
Logs in Texas Water Development Board files

WELL	OPERATOR	LEASE AND WELL	DATE DRILLED	DEPTH (FT)	APPROXIMATE LAND SURFACE ELEVATION (FT)	TYPE LOG
HZ-76-32-201	Wellington Oil Co.	D. J. Sullivan No. B-1	1941	2,748	685	E
302	Sutton Producing Co.	NCT-B-6 No. 5 Fee	1957	2,241	716	E
501	Wellington Oil Co.	Sullivan No. B-2	1942	2,819	680	E
48-101	Humble Oil and Refining Co.	Fitzsimons No. 323	1967	2,950	705	E
201	The Shamrock Oil and Gas Corp.	H. A. Fitzsimons, et al. No. 2	1958	1,015	731	E
601	do.	Hugh Fitzsimons, et al. No. 31	1969	3,600	822	E
77-18-908	C. C. Winn and Texas Seaboard Oil Co.	G. C. Jackson No. 1	1958	4,535	576	E
910	I. K. Howeth, et al.	Travis O. Box No. 1	1955	3,659	562	E
911	Howeth and Mason	Rosa E. Crenshaw, Estate No. 6	1954	3,629	576	E
912	Howeth and Mason, et al.	G. C. Crenshaw No. 1	1956	4,600	576	E
913	do.	E. L. Dismukes No. 2	1955	3,580	570	E
19-902	Bennett Brothers Drilling Co.	Mary Bachman No. 1	1945	3,309	557	E
904	do.	E. R. Jones "A" No. 6	1970	5,600	590	E
25-304	Big Springs Exploration Co.	George Dewey Speer No. 1	1960	3,680	614	E
503	Anderson and Prichard Oil Corp.	S. E. McKnight No. 2	1948	2,280	678	E
607	Renwar Oil Corp., et al.	Eva D. Williams No. A-1	1955	3,110	624	E
912	Sutton Drilling Co.	J. F. Cleveland No. 3	1955	2,803	653	E
913	do.	J. F. Cleveland No. 4	1955	2,895	651	E
914	Henderson Coquat, O. N. Beer and Gus Canalles	E. Dolan No. 1	1955	2,650	622	E
26-112	Howeth and Mason	C. Zedler No. 1	1953	4,222	600	E
206	McCabe, Turner and Pronto Drilling Co.	J. S. Ward No. 1	1955	3,300	539	E
311	Pronto Drilling Co. and Foster Hinson	H. P. Hunnicutt	1956	3,910	520	E
607	W. W. Oatman, et al.	F. R. Van Hoozer No. 1	1962	4,014	520	E

Table 2.—Selected Oil, Gas, and Stratigraphic Tests in Dimmit County—Continued

WELL	OPERATOR	LEASE AND WELL	DATE DRILLED	DEPTH (FT)	APPROXIMATE LAND SURFACE ELEVATION (FT)	TYPE LOG
HZ-77-26-608	W. W. Oatman	Ruth McLean Bowman No. 1	1963	4,018	526	E
719	Antler Drilling Co., Inc.	A. Votaw No. 1	1955	2,998	627	E
721	E. C. McRorey and Pronto Drilling Co.	Mary Blanche Vernor No. A-1	1957	2,791	593	E
907	J. C. McCabe and Bowman Cattle Co.	Ruth McLean Bowman No. 1	1959	8,667	497	E
27-405	Howeth and Mason and Intex Oil Co.	Dee Davenport No. 2	1954	4,505	576	E
406	do.	Dee Davenport No. 1	1952	4,145	596	E
707	W. W. Oatman	Ruth McLean Bowman No. 1	1963	4,018	526	E
708	W. J. Dick	Frost National Bank No. 2	1964	3,875	519	E
28-301	Howeth and Mason	R. L. Bach No. 1	1962	4,878	610	E
403	Deep Rock Oil Corp.	C. W. Barker No. 1	1951	8,517	518	E
602	Sun Oil Co.	Frost National Bank, Trustee No. 1	1970	6,465	510	E
902	do.	Frost National Bank and Trust No. 44	1971	5,800	496	E
903	do.	J. H. Bagby, et al. No. 4	1970	5,565	482	E
29-101	Amerada Petroleum Corp.	Odus Waldrum No. 1	1955	8,845	547	E
501	The Texas Co.	E. T. Standifer No. 1	1947	8,171	510	E
604	Kirkwood and Morgan	Y. C. Strait No. 1	1952	5,138	514	E
701	Cockrell and Continental Oil Co.	O. C. Rogers No. 1	1948	6,183	554	E
801	Adams and Haggarty	Anna and R. B. Vesper No. 1	1954	5,205	466	E
33-101	Michel T. Halbouty	Damon White No. 1	1956	3,201	765	E
205	W. J. Walton	– McKnight No. 1	1943	2,837	677	E
206	Calatexia Co.	S. E. McKnight No. 1	1945	2,960	698	E
315	Pronto Drilling Co. and Reiner Oil Co.	J. C. Johnson, et al. No. 1	1958	3,007	627	E
318	Humble Oil and Refining Co.	S. E. McKnight No. 1	1945	5,017	655	E
320	do.	J. C. Johnson No. B-1	1946	3,193	637	E
512	Sun Oil Co.	Joe R. Straus No. 1	1958	3,600	722	E
513	Michel T. Halbouty, et al.	Robert Shook No. 4	1959	3,600	735	E

Table 2.-Selected Oil, Gas, and Stratigraphic Tests in Dimmit County-Continued

WELL	OPERATOR	LEASE AND WELL	DATE DRILLED	DEPTH (FT)	APPROXIMATE LAND SURFACE ELEVATION (FT)	TYPE LOG
HZ-77-33 612	Sun Oil Co.	Joe R. Straus No. 2	1959	3,850	722	E
613	do.	Joe R. Straus No. 4	1960	3,500	685	E
614	Allen and Schumate, inc.	Joe Straus No. 1	1963	3,610	707	E
34-317	Sutton Drilling Co.	Dr. Asher McComb No. 3	1956	3,720	524	E
318	The Texas Co.	Ethel Payne No. 1	1947	4,015	522	E
35-301	Spartan Drilling Co.	N. C. King No. 1	1952	4,716	530	E
702	Howeth and Mason	– McLaren No. 1	1953	5,065	630	E
903	The Texas Co.	Catarina Farms No. 1	1946	4,810	568	E
36 101	J. Frank Stringer and Petroleum Inc., et al.	Oliver Addison Taylor, et al. No. 1	1960	9,012	465	E
402	Sun 0i1 Co.	David W. Bouldin No. 1	1953	4,953	506	E
37 103	Stanross Production Corp.	Geo. W. Henrichson No. 1	1954	5,231	499	E
104	Barnsdall Oil Co.	H. W. Henrichson No. 1	1946	5,284	491	E
105	DeLange and Milam Drilling Co.	Walter Herbst No. 1	1947	5,505	482	E
41 301	W. J. Steeger	Leroy C. Jones No. 1	1956	4,022	739	E
601	Sutton Drilling Co.	Bill George No. 1	1956	4,338	701	E
42 302	Howeth and Mason	J. R. Marmion No. 1	1953	5,015	647	E
43 501	Henderson Coquat and Algond 0i1 Co.	H. A. Dillon No. 2	1948	5,210	570	E
601	Armstrong and Horn	do.	1955	5,095	569	E
44 301	Howeth and Mason	Geo. Light, Jr. No. 6	1953	5,556	543	E
45 101	Union Producing co.	– Light No. 1	1958	5,900	543	E
201	Sun Oil Co.	George E. Light No. 1	1955	6,072	604	E

FRIO COUNTY

Table 2.—Selected Oil, Gas, and Stratigraphic Tests

Type Log: D, Drillers'; E, Electric; R, Radioactive; S, Sample.
Logs in Texas Water Development Board files

WELL	OPERATOR	LEASE AND WELL	DATE DRILLED	DEPTH (FT)	APPROXIMATE LAND SURFACE ELEVATION (FT)	TYPE LOG
KB-68-57-409	C. C. Winn	Frank Wall No. 1	1956	3,401	599	E
803	Rock Hill Oil Co.	A. Hitzfelder No. 1	1955	3,625	599	E
807	Mason Fargason and Mineral Estate, Inc.	Mae Ussery, et al. No. 1	1963	3,165	559	E
909	Miller Royalty Co. and C. C. Dauchy	F. H. McFarren No. 1	1949	3,138	592	E
914	Lewis Oil Co.	C. R. Thompson No. B-2	1954	3,065	569	E
915	Shell Oil Co.	T. W. Bain No. 22	1954	3,078	567	E
916	G. A. Schimel	A. E. Williams No. 1	1951	2,870	641	E
58-201	Theljohn Oil Co.	C. A. Davidson No. 1	1954	2,429	570	E
705	Shell Oil Co.	— Burns No. 1	—	—	654	E
804	Wherry and Green	W. E. Dickerson No. 1	1953	3,262	635	E
805	The Texas Co.	— Burnes No. B-17	1954	3,587	609	E
69-61-907	Wilcox Oil and Gas Co.	R. H. Harris No. 1	1939	4,065	655	E
62-603	Don F. Tobin	J. B. McMahan No. 1	1968	3,320	635	E
63-301	Gillespie, Rossman and White	J. W. Ward No. 1	1959	2,226	673	E
64-702	P. G. Lake, Inc.	E. G. Gracey and Oscar Wegenhoff No. 1	1954	3,829	651	E
802	Lone Star Producing Co.	L. F. Sirianni No. 1	1955	2,752	716	E
77-05-302	Kirkwood and Alsabrook	Mark L. Brown No. 1-A	1961	4,840	757	E
901	R. L. Kirkwood	Griffith Williams No. 1	1949	4,265	601	E
06-801	C. C. Dunwoody, Jr.	Halff and Oppenheimer No. 1	1953	4,023	740	E
08-606	Howeth and Mason	Ernest Berry No. 1	1953	3,737	603	E
717	Pronto Drilling Co.	Halff and Oppenheimer No. 1	1955	4,399	618	E
805	Newman Brothers Drilling Co. and Alaska Steamship Co.	— Cudd No. 1	1949	4,342	642	E
807	Jergins Oil Co.	L. Padgett No. 1	1948	4,318	638	E
811	Martin, Shelly and Thomas	Virgil Toalson No. 1	1950	4,375	650	E

Table 2.-Selected Oil, Gas, and Stratigraphic Tests in Frio &unty-Continued

WELL	OPERATOR	LEASE AND WELL	DATE DRILLED	DEPTH (FTI	APPROXIMATE LAND SURFACE ELEVATION (FT)	TYPE LOG
K8-77-08-901	Oil and Gas Properties Management Inc.	J. M. Riggan No. 1	1961	4,130	614	E
904	Martin, Shelly and Thomas	Leo Newsom No. 1	1951	4,410	628	E
908	do.	Leo Newsom No. 2	1951	4,270	620	E
14-101	Skinner, et al.	A. Hauser Estate No. 1-A	1947	4,563	610	E
401	Humble Oil and Refining Co.	Wm. Talasek No. 1	1949	6,701	581	E
502	do.	Sid Katz No. 1	1950	6,478	542	E
503	do.	Ruth Harlan No.	1949	6,494	590	E
701	do.	Frank Doering No. 1	1948	6,647	577	E
703	do.	Frank Doering No. 3	1950	4,115	580	E
802	Katz Oil Co. and Lone Star Producing co.	J. H. Calvert No. 1	1958	10,993	552	E
806	Humble Oil and Refining Co.	Ora Park No. 1	1949	6,452	510	E
15-203	W. 6. Osborn, et al.	– Davies No. 2	1941	3,915	535	E
204	Amerada Petroleum Corp.	Elgin 0. Kothman No. 2	1949	5,650	525	E
305	do.	– Melms No. 1	1937	3,887	555	E
309	Highland Oil Co.	Nat M. Johnson No. 1	1944	3,957	550	E
310	do.	Halff and Oppenheimer No. 8	1944	3,920	536	E
311	Falcon, Seaboard and Dunwoodey	M. Tschirhart No. 1	1940	3,941	548	E
313	do.	G. H. Bever No. 1	1960	9,666	650	E
401	J. C. Hawkins, W. M. Nichold and Henshaw Brothers	C. H. Miller No. 1	1948	5,484	610	E
403	do.	Corv and McWilliams No. 3	1948	5,693	570	E
404	do.	Corv and McWilliams No. 6	1949	5,413	541	E
405	Star Oil Co.	– Smith No. A-l	1949	5.785	570	R
406	do.	W. A. Smith No. 1	1949	5,410	602	E
407	Amerada Petroleum Corp. and Rvcade Oil Corp.	W. H. Smith No. 5	1949	5,770	600	E
408	Star Oil Co.	W. H. Smith No. B-l	1949	5,204	555	E
503	Forrest Oil Corp., et al.	Lillie H. Oppenheimer, et al. No. 1	1949	5,350	500	E

Table 2.—Selected Oil, Gas, and Stratigraphic Tests in Frio County—Continued

WELL	OPERATOR	LEASE AND WELL	DATE DRILLED	DEPTH (FT)	APPROXIMATE LAND SURFACE ELEVATION (FT)	TYPE LOG
KB-77-15-604	Carrl Oil Co.	— Cude No. 1	1954	5,421	531	E
16-204	Sun Oil Co.	G. F. Toalson, et al. No. 1	1948	4,799	712	E
208	H. & J. Drilling Co.	Ed Mann No. 1	1965	4,216	665	E
503	O. W. Killiam	W. W. McKinley No. 1	1953	4,914	559	E
601	Producers Corp. of Nevada	Irma Mills No. 1	1954	4,842	673	E
707	Dunwoody and Alaska Steamship Co.	Jesse Dobbs No. 1	1954	5,068	529	E
21-302	Pan American Petroleum Corp.	Lena Buerger No. 1	1966	11,689	622	E
601	Sun Oil Co.	Harry F. Thompson, Jr. No. 1	1969	6,012	616	E
22-202	Kirkwood and Morgan	Roberts and Speer No. 1	1948	7,448	629	E
904	do.	— Cox No. 1	1952	5,136	539	E
23-104	do.	R. H. and H. E. Gill No. 1	1948	5,495	581	E
806	do.	A. H. McLean No. 1	1952	5,236	560	E
24-304	Hassie Hunt Trust	Emma F. Shiner No. 1	1951	5,767	495	E
78-01-102	George Parker	M. Berry No. 1	1953	3,000	590	E
108	A. T. Jergins and Sons	— Berry No. 1	1952	3,409	580	E
301	W. G. Darsey, Jr., et al.	Travis W. Bain No. 1	1950	3,289	582	E
304	C. L. Wright and and Kewanee Oil Co.	Ruth Bowman No. 1	1963	3,439	563	E
305	Shell Oil Co.	A. F. Meyer No. 20	1953	3,333	588	E
306	C. C. Dauchy and Miller Royalty Co.	— Bowman No. 1	1950	3,393	585	E
307	Shell Oil Co.	T. W. Bain No. 35	1954	3,216	620	E
308	Lloyd H. Smith	Ruth Bowman No. 1	1963	3,330	557	E
401	Magnolia Petroleum Co.	W. W. McKinley No. 1	1947	11,944	601	E
402	Howeth and Mason	J. E. Berry Estate No. 1	1953	3,649	542	E
403	do.	T. B. Riggs No. 1	1953	3,661	580	E
404	Magnolia Petroleum Co.	H. L. Smith No. 1	1947	3,715	580	E
504	H. & J. Drilling Co. and F. C. Gaines, Jr.	W. T. Youngblood No. 1	1958	3,778	506	E

Table 2.—Selected Oil, Gas, and Stratigraphic Tests in Frio County—Continued

WELL	OPERATOR	LEASE AND WELL	DATE DRILLED	DEPTH (FT)	APPROXIMATE LAND SURFACE ELEVATION (FT)	TYPE LOG
KB-78-01-702	Newman Brothers Drilling Co. and Alaska Steamship Co.	Oppenheimer and Lang No. 1	1949	4,195	507	E
706	Harry Parker and M. O. Turner	Riggan-Breazeal Unit No. 2, No. 1	1963	4,118	588	E
803	Athens and Fitzgerald	M. C. Peters No. 1	1954	5,388	497	E
903	Magnolia Petroleum Co.	Oppenheimer Estate No. A-1	1949	4,504	567	E
905	Newman Brothers Drilling Co. and Alaska Steamship Co.	Oppenheimer and Lang No. 1-C	1949	4,271	523	E
02-101	Miller Royalty Co. and Milam Drilling Co.	C. R. Thompson No. 1	1949	3,300	562	E
102	George W. Graham and F. William Carr	T. P. Nowlin No. 1	1951	3,449	571	E
103	C. C. Dauchy and Miller Royalty Co.	Tom P. Nowlin No. 2	1950	3,331	600	E
104	Shell Oil Co.	Emma Richter No. 7	1952	3,260	612	E
105	do.	Jane Burns No. 19	1953	3,277	622	E
107	do.	Jane Burns No. 17	1953	3,411	605	E
108	do.	C. S. Thompson No. 1	1953	3,483	640	E
201	Stanolind Oil and Gas Co.	T. B. Stuart No. 5	1954	3,747	593	E
205	Goldston Oil	W. J. Sinks No. 1	1954	3,597	598	E
206	Shell Oil Co.	C. S. Thompson No. A-3	1954	3,540	644	E
208	do.	Webb Thompson No. B-26	1953	3,668	643	E
209	do.	Jane Burns No. C-6	1954	3,692	617	E
210	do.	C. S. Thompson No. A-5	1954	3,571	617	E
211	Goldston Oil Corp.	Anna Witting No. 7	1954	3,644	591	E
403	Big Six Drilling Co.	Tony Mann No. 1	1956	3,989	569	E
507	Gasoline Production Corp.	G. L. Avant No. 1	1953	3,861	559	E
703	Sutton Production Co.	— Peters No. 18-C	1961	4,146	530	E
801	Texita Oil Co. and E. W. Gill	— Sanchez No. 1	1955	4,360	550	E
802	Kirkwood and Morgan	Candelario Luna No. 1	1949	4,610	538	E
809	Miller Royalty Co.	Marion Rodgers	1953	4,916	541	E
810	Sun Oil Co.	R. Mejia No. 3	1952	4,947	520	E

Table 2.-Selected Oil, Gas, and Stratigraphic Tests in Frio County-Continued

WELL	OPERATOR	LEASE AND WELL	DATE DRILLED	DEPTH (FT)	APPROXIMATE LAND SURFACE ELEVATION (FT)	TYPE LOG
KB-78-02-811	Sun Oil Co.	–	–	4,960	527	E
812	F. William Carr	Marion Rodgers No. 1	1954	4,963	546	E
813	do.	– Dunmore No. 1	1954	4,955	540	E
09-201	Plymouth Oil co.	J. D. Oppenheimer No. 1	1949	4,516	523	E
401	Sun Oil Co.	Sam Johnson No. 1	1953	4,777	583	E
802	W. L. Pickens	J. D. Oppenheimer No. 1	1948	5,138	488	E
901	Humble Oil and Refining Co.	F. C. McKinnev No. 1	1950	5,800	442	E
1 O-502	Lewis Oil Co.	Marrs McLean No. 22	1949	5,295	550	E
505	Lewis Oil Co.	Marrs McLean No. 21	1949	5,287	517	E
701	Schimmel Drilling Co., et al.	Oppenheimer and Lang No. 1	1954	5,673	556	E
702	J. C. McCabe	Oppenheimer and Lang No. 1	1954	5,174	492	E
704	Humble Oil and Refining Co.	F. 8. Kothmann No. 3	1965	5,635	462	E
17-302	Argo Oil Corp. Edwin L. Cox	F. 8. Thompson No. 1	1953	6,212	527	E
304	Amerada Petroleum Corp.	F. C. McKinnev No. 1	1955	8,728	454	E
501	Carlee Oil Co.	Emma Shiner No. 1	1951	6,089	492	E
601	Humble Oil and Refining Co.	W. F. Smith No. 1	1949	6,449	495	E
603	F. William Carr	W. F. Smith No. 1	1951	6,309	521	E
18-203	Milam Drilling Co.	W. L. Pickens No. 1	1950	5,616	475	E
205	The Texas Co.	W. L. Pickens No. 8-I	1956	5,798	448	E

GONZALES COUNTY

Table 2.—Selected Oil, Gas, and Stratigraphic Tests

Type Log: D, Drillers'; E, Electric; R, Radioactive; S, Sample.
Logs in Texas Water Development Board files

WELL	OPERATOR	LEASE AND WELL	DATE DRILLED	DEPTH (FT)	APPROXIMATE LAND SURFACE EVELATION (FT)	TYPE LOG
KR-67-20-613	Cecil V. Hagen	C. B. Gray Estate No. 1	1967	2,215	460	E
701	North Central Oil Corp.	J. F. Webb No. 1	1956	4,001	347	E
901	The Texas Co.	S. W. Hendershot, et al. No. 1	1941	4,641	375	E
907	Aztec Oil and Gas Co.	S. W. Hendershot No. 1	1965	2,110	369	E
21-702	J. K. Adair	E. R. Jobe No. 1	1954	2,033	445	E
704	Michel T. Halbouty	Aurelia Mitchell Trust No. 1	1966	7,565	450	E
22-401	J. W. Gorman	G. W. Parr No. 2	1954	4,993	390	E
27-302	Turner and Eddy	J. F. Webb No. 1	1948	3,440	395	E
303	Bill Perryman Drilling Co. and Ken Blackmar	— Eckols No. 1	1967	1,100	400	E
501	W. Stewart Boyle	— Ottine No. 1	1943	3,803	513	E
601	Quintana Petroleum Corp.	A. Schnabel No. 1	1951	7,435	382	E
603	Aztec Oil and Gas Co.	J. C. Barfield No. 1	1965	2,258	397	E
604	do.	Neal Barfield No. 1	1965	1,921	414	E
704	Alfred C. Glassell, Jr.	Alfred C. Meyer No. 1	1966	2,086	463	E
802	Jack Clark	H. R. Ritchie No. 1	1955	4,361	367	E
804	J. S. Futch	J. E. Goss No. 1	1956	2,023	400	E
908	Aztec Oil and Gas Co.	— Allen No. 1	1965	2,299	363	E
28-301	S. A. Olson, Pat H. Baker and Sons	W. L. Botts No. 1-A	1958	2,509	342	E
404	Jergins of Texas, Ltd.	J. Briesemeister No. 1	1955	4,880	394	E
601	Magnolia Petroleum Co.	Walter Spahn No. 1	1952	9,000	320	E
29-102	Gulf Coast Leaseholds, Inc. and F. Glassel Jr., et al.	J. Lamar Johnson No. 1	1955	8,078	405	E
401	Quintana Petroleum Corp.	Anna Spahn No. 1	1946	9,316	302	E
601	Sutton Drilling Co.	D. M. Christian Estate No. 1	1951	2,725	310	E
704	A. E. Mabry	L. V. Nichols No. 1	1955	1,460	284	E

Table 2.—Selected Oil, Gas, and Stratigraphic Tests in Gonzales County—Continued

WELL	OPERATOR	LEASE AND WELL	DATE DRILLED	DEPTH (FT)	APPROXIMATE LAND SURFACE ELEVATION (FT)	TYPE LOG
KR-67-30-101	O. Neathery, Jr., et al.	W. H. Baldridge No. 2	1954	4,699	386	E
104	do.	W. H. Baldridge No. 1	1954	5,553	380	E
105	Carl D. Lang, et al.	Adolf Kolar No. 1	1966	4,250	315	E
202	W. E. Bakke	— Steiner No. 1	1960	8,495	289	E
505	Kirkwood and Co. and Forest Oil Co.	Ethel Wright No. 1	1950	5,204	333	E
34-611	Fred Shield and General Crude Oil Co.	— Seelingson No. 1-C	1964	4,433	450	E
805	Gulf Coast Leaseholds, Inc. and Alfred C. Glassell, Jr.	W. E. Davenport No. 1	1955	4,625	443	E
906	Don Williamson	— Littlefield No. 1	1965	2,500	420	E
35-104	United North and South Development Co.	Albert Soefje No. 1	1950	4,050	379	E
106	West Petroleum Corp.	Walter Soefje No. 1	1965	1,890	440	E
108	Aztec Oil and Gas Co.	— Littlefield No. 1	1965	2,150	457	E
202	S. A. Brewster	S. A. Brewster No. 1	1965	2,300	395	E
301	Lecuna Oil Corp.	M. K. Townes No. 1	1959	5,721	443	E
407	Bridwell Oil Co. and Jergins of Texas	Z. C. Davis No. 1	1955	2,651	445	E
501	Cecil V. Hagen and A. C. Glassell, Jr.	Arnold Lay No. 1	1960	3,654	414	E
36-801	Travis Drillers, Inc. and Glen A. Martin	Robert Jurica No. 1	1956	2,648	315	E
903	Cecil V. Hagen	— Heinemeyer No. 1	1961	8,560	292	E
37-202	Corder Drilling Co., Inc.	J. S. Lewis No. 1	1959	1,713	276	E
401	Armstrong and Horn and Gail A. Barry	Kent E. Gardien No. 1	1955	3,515	327	E
502	Kirkwood and Morgan, Inc.	E. A. Shrader No. 1	1956	5,528	285	E
703	Continental Oil Co.	Edwin P. Bruns No. 1	1942	5,779	302	E
705	Jergins of Texas, Ltd.	G. Tenberg No. 1	1955	3,389	274	E
706	Southern Oil Well Service Co.	— Tenbery No. 1	1964	3,846	291	E
707	Maguire Industries, Inc.	Rudolph Valenta No. 1	1944	2,512	284	E
708	Continental Oil Co.	J. J. Gatlin No. 1	1959	3,611	285	E

Table 2.—Selected Oil, Gas, and Stratigraphic Tests in Gonzales County—Continued

WELL	OPERATOR	LEASE AND WELL	DATE DRILLED	DEPTH (FT)	APPROXIMATE LAND SURFACE ELEVATION (FT)	TYPE LOG
KR-67-37-801	F. B. Lefevre, et al.	Carl DuBose, et ux. No. 1	1959	4,061	304	E
802	Randon Production Co.	Lillie Dunning No. 1	1951	2,704	327	E
901	Bay City Drilling Co.	D. B. Ploeger No. 1	1958	6,085	299	E
42-201	Southwest Workover Co.	J. W. Heneley No. 1	1956	4,849	483	E
203	Barron Kidd	J. A. Hewell No. 1	1965	2,850	421	E
301	Petro-Tex Oil Corp.	— Metz No. 1	1956	2,893	372	E
302	Carl D. Lang, et al.	Derwood Mahan No. 1	1967	3,503	375	E
501	Skinner Corp., et al.	U. C. Pattillo No. 1	1959	3,716	372	E
502	Gulf Coast Leaseholds, Inc.	S. Kelly No. 1	1956	5,610	404	E
601	Producers Corp. of Nevada	J. T. Anderson No. 1	1949	6,218	331	E
605	do.	— Williams No. 1	1950	5,926	362	E
606	Rock Hill Oil Co.	— Chessher No. 1	1952	5,953	365	E
607	Texas Gas Exploration Corp.	John Respondek No. 1	1967	2,108	385	E
43-102	Leland L. Palmer et al.	R. H. Allison No. 1	1959	2,153	313	E
202	M. O. Turner	C. P. Bouldin No. 1	1962	6,731	377	E
408	Producers Corp. of Nevada	E. S. Austin No. 1	1950	6,248	383	E
505	Mrs. James R. Dougherty	Patteson Estate No. 2-B	1962	7,045	315	E
602	do.	M. Robinson No. 1	1957	1,652	310	E
603	C. C. Winn	T. D. Manford No. 1	1956	4,982	263	E
704	Texita Oil Co.	Estella Manford, et al. No. 1	1953	1,430	365	E
803	Mrs. James R. Dougherty	Patteson Estate No. 1	1957	4,617	311	E
808	do.	Patteson Estate No. 5	1958	1,919	324	E
44-102	J. C. Barnes	J. R. Tinsley No. 1	1957	7,502	301	E
302	Humble Oil and Refining Co.	Allie Barnett No. 1	1947	8,686	279	E
501	J. E. Hillier	Oscar Baker No. 1	1959	5,518	300	E
502	H. and J. Drilling Co. and S. E. Thomas	Paul Barnhart No. 1	1964	5,610	246	E
604	Continental Oil Co.	Otis Cardwell No. 1	1954	6,045	227	E
45-201	Mr. James R. Dougherty	R. Frisbie No. 1	1963	3,202	263	E

Table 2.—Selected Oil, Gas, and Stratigraphic Tests in Gonzales County—Continued

WELL	OPERATOR	LEASE AND WELL	DATE DRILLED	DEPTH (FT)	APPROXIMATE LAND SURFACE ELEVATION (FT)	TYPE LOG
KR-67-45-202	L. G. Shelly and W. L. Dugger, Jr.	Pearl Young No. 1	1955	6,820	270	E
401	B. Coleman Renick and Union Oil and Gas Co.	Dunnie Edwards No. 1	1957	11,054	235	E
501	Tenneco Oil Co.	Ann Hamilton Cusack No. 1	1962	10,113	251	E
503	Amerada Petroleum Corp.	Morgan and Kunetka No. 1	1943	6,740	240	E
504	Owen and Beauchamp	Frank Kunetka No. 1	1946	6,655	253	E
46-101	W. O. Woodward, Jr.	Tilda DuBose No. 1	1949	6,014	340	E
402	Hunt Oil Co.	E. L. Stoeltje No. 1	1960	12,529	301	E
403	Harkins and Co.	— Zappe No. 1	1962	11,860	234	E
51-104	G. W. Strake	H. K. Weber No. 1	1943	4,808	307	E
302	Danciger Oil and Refining Co.	H. K. Weber No. 1	1944	4,217	275	E
52-101	Newman Brothers and American Republic Corp, et al.	W. C. Billings No. 1	1949	6,002	250	E
201	W. A. Richardson, Jr. Trustee	— Buethe No. 1	1952	6,812	281	E
302	Skinner Corp. - Armstrong and Horn Drilling Co.	Harry Chandler No. 1	1958	6,603	226	E
402	Tex Harvey Oil Co.	Ura D. Lord No. 1	1942	6,532	325	E
403	A. Edmiston	Dan Billings No. 1	1941	5,230	371	E
404	Southern Minerals Corp.	Mrs. Frank Duderstadt No. 1	1963	6,891	325	E
501	Gulf Coast Leaseholds, Inc. and A. C. Glassell, Jr.	William Jacobs No. 1	1956	7,020	296	E
503	South Basin Oil Co.	Frank Duderstadt No. 1	1944	5,260	334	E
53-201	Hunt Oil Co.	W. R. Miller No. 1	1960	13,354	219	E

GUADALUPE COUNTY

Table 2-Selected Oil, Gas, and Stratigraphic Tests.

Type Log: D, Drillers'; E, Electric; R, Radioactive; S, Sample.
Logs in Texas Water Development Board files

WELL	OPERATOR	LEASE AND WELL	DATE DRILLED	DEPTH (FT)	APPROXIMATE LAND SURFACE ELEVATION (FT)	TYPE LOG
KX-67-18-507	Ohio Oil Co.	Elizabeth Wilke No. 2	1956	2,166	565	E
802	Harry Henderson	F. Schmidt No. 1	1954	2,237	603	E
803	J. L. Ashen, et al.	– Noack No. 1	1955	2,424	575	E
906	L.W. Powell	C. B. Appling Estate No. 1	1966	2,345	470	E
907	L. 0. Tarrant, et al.	J. I. Cash Estate No. 2	1956	2,235	578	E
19-705	Lewis Hart	J. R. Tiller Estate No. 1	1955	2,358	400	E
25-601	C. R. England	R. J. Govett No. 1	1953	2,334	515	E
809	Pryor Dillard	Nolte Estate No. 2	1949	1,943	478	E
906	Hughes and Hebert	Virgil Halm No. 1	1952	2,983	490	E
26-202	Texas Southern Oil Producing Co.	Jesse A. Turner No. 1	1957	5,455	498	E
203	Weigand Brothers	Paul and Emma Baumert No. 1	1944	2,530	546	E
306	Sun Oil Co.	C. Knobloch No. 16	1952	2,697	478	E
308	Gulf Oil Corp.	C. Anderson No. 7	1954	2,735	490	E
310	Humble Oil and Refining Co.	L. G. Denman No. A-42	1952	2,720	500	E
404	Sam Macco Oil Operations	August G. Bode No. 1	1949	2,086	485	E
407	W. B. Head	– Janecka No. 1	1955	2,124	485	E
408	R. L. Turner and James H. Eddy	August G. Bode No. 1	1948	2,394	475	E
409	R. L. Turner	Frank Schmidt No 1	1952	2,500	495	E
501	E. H. Stickney	Adolph Hoffman No. 1	1956	2,479	418	E
502	Humble Oil and Refining Co.	Dan J. Denman No. 6	1961	2,655	453	E
510	Bert R. Smith and Hugh Nichols	Tom Anderson No. 1	1950	2,313	450	E
511	Mrs. James R. Dougherty	Tom Anderson No. B-l	1964	2,681	525	E
601	The Texas Co.	L. Anderson No. 17	1957	2,703	483	E
602	Humble Oil and Refining Co.	Sue E. Denman No. 1 SWD	1948	2,706	450	E
606	do.	Mrs. A. E. Dowdy No. 4	1939	2,537	440	E

Table 2.—Selected Oil, Gas, and Stratigraphic Tests in Guadalupe County—Continued

WELL	OPERATOR	LEASE AND WELL	DATE DRILLED	DEPTH (FT)	APPROXIMATE LAND SURFACE ELEVATION (FT)	TYPE LOG
KX-67-26-607	Humble Oil and Refining Co.	D. D. Baker No. 1 SWD	1947	3,151	450	E
701	Bradco Oil and Gas Co.	A. Zoboroski No. 1	1955	2,468	470	E
801	Travis Drillers Inc.	Vivroux Hardware Co., Inc. No. 1	1957	3,555	548	E
806	W. C. Silver	Theodore Jahns No. 1	1967	2,478	435	E
27-102	Magnolia Petroleum Co.	Erwin Forsage No. 2	1952	2,643	466	E
106	The Texas Co.	Pauline Roamel No. 6	1950	2,670	450	E
108	Gulf Oil Corp.	Dix and McKean No. 23	1950	2,630	470	E
109	The Texas Co.	— Knoblock No. A-23	1953	2,608	466	E
202	Hall, et al.	— Manford No. 2	1958	2,355	458	E
203	Allen and Shumate, Inc.	C. D. McEver No. 1	1962	5,013	373	E
402	Riddle Oil Co.	Pegg and Lorentzson No. 1	1967	1,395	403	E
33-106	A. T. Jergins	Ella Harris Greenwood No. 1	1955	1,031	550	E
305	Allen Burr, et al.	W. J. Blanks Estate No. 1	1957	3,225	639	E
309	Leon V. Manry	Effie Williams, et al. No. 1	1945	3,004	588	E
406	Herbert C. Wenske	J. W. Massey No. 1	1955	1,142	592	E
804	Varn Petroleum Co.	Edgar A. Vaughn No. 1	1966	1,672	559	E
34-201	Wellington Oil Co.	Gus B. Mauerman No. 1	1940	3,649	656	E
404	do.	C. M. Wells No. 1	1940	3,789	624	E
702	M. L. Wise, et al.	H. H. Weinert Estate No. 1	1954	4,413	501	E
68-39-601	Utah Oil Corp.	E. J. Zuehl No. 1	1949	1,699	510	E
40-104	Joe Carlson	E. Theiss No. 1	1955	679	570	E
107	Wellington Oil Co.	Albert Koepp No. 1	1937	1,628	570	E
306	Lake Rice Mills, Inc.	Ben Stein No. 1	1953	1,979	567	E
308	do.	Edwin H. Gerdes No. 1	1953	2,006	580	E
409	Bruin Oil Co.	— Rosenbrock No. 1-A	1938	1,886	512	E
505	Diamond Half Oil Corp.	William J. Strey No. 1	1940	800	534	E
506	Maples C. Hughes	— Poenitz No. 3	1954	900	498	E

Table 2.-Selected Oil, Gas, and Stratigraphic Tests in Guadalupe County-Continued

WELL	OPERATOR	LEASE AND WELL	DATE DRILLED	DEPTH (FT)	APPROXIMATE LAND SURFACE ELEVATION (FT)	TYPE LOG
KX-59-39-704	Froemsn O. Crenshaw	I. A. Echels No. 1	1950	785	491	E
705	W. O. Fortenborry	Alfred L. Doege No. 1	1955	954	494	E
706	do.	C. E. Scull No. 2	1955	769	455	E
707	do.	Erk Koepp No. 2	1955	1,040	463	E
708	H. H. Weinert	– Mattke No. 1	1949	2,013	510	E
712	W. O. Fortenberrv	Elam Scull No. 1	1954	1,434	450	E
713	do.	Eric Koepp No. 1	1935		460	E
714	Parks Brothers and R. A. Voight	Ed. Lee No. 1	1955	923	536	E
715	J. H. Burt	– Hartfield No. 1	1944	2,050	483	E
904	c. M. s. Oil co.	– Feiselman No. 1	1955	1,365	554	E
905	W. M. Hauser, ot al.	– Hoerman No. 4	1956	2,010	595	E

KARNES COUNTY

Table 2.-Selected Oil, Gas, and Stratigraphic Tests

Type Log: D, Drillers'; E, Electric; R, Radioactive; S, Sample.
Logs in Texas Water Development Board files

WELL	OPERATOR	LEASE AND WELL	DATE DRILLED	DEPTH (FT)	APPROXIMATE LAND SURFACE ELEVATION (FT)	TYPE LOG
PZ-67-60-901	Kirkpatrick-Coates, et al.	B. M. Brockman No. 1	1950	5,820	389	E
902	Producers Corp. of Nevada and Cosden Petroleum Corp.	W. S. Cochran, Jr. No. 1	1954	6,376	370	E
57-302	Dan and Jack Auld	V. Cambers No. 1	1955	6,026	416	E
303	Martin, Shelly, and Thomas	Alex Pawelek No. 1	1952	6,119	396	E
601	Sutton Producing co.	– Pawelek No. 1	1960	11,014	359	E
58-701	W. Earl Rowe	T. W. Roberts No. 1	1951	5,272	353	E
59501	Tennessee Production Co.	Paul Seidel No. 1	1952	7,747	463	E
78-08-203	Shell Oil Co.	Ben Korzekwa No. 1	1950	6,430	344	E
601	Seaboard Oil Co.	Nick Gabrysch No. 1	1948	11,180	384	E
602	W. Earl Rowe and Glenn Mortimer	P. J. Manka No. 1	1955	6,600	397	E
901	Seaboard Oil Co.	Tom Kolodziejezyk No. 1	1943	7,455	445	E
16-101	H.R. Smith, et al.	V. M. Butler No. 1	1947	4,012	484	E
501	Southern Minerals Corp.	Alice Ryan No. 1	1960	4,486	448	E
602	Pan American Production Co.	Fritz Fenner No. 1	1949	7,889	448	E
603	Kirkwood Co. and W. G. Darsey, Jr.	V. S. Kowalik No. 1	1949	7.882	457	E
604	Seaboard Oil Co.	Rudolph Best No. 2	1945	7,938	479	E
901	Lone Star Producing co.	D. E. Moore No. 1	1954	7,974	429	E
79-01-201	Standard Oil Co. of Texas	Lucy Manka Gdn. No. 2, Well No. 1	1960	11,450	352	E
02-201	Federal Royalty Co. and Rio Grande Drilling Co.	Mary Yanta No. 1	1946	7,278	272	E
302	Indiola Oil Co.	Mary Mika No. 1	1943	6,514	335	E
09-101	Luling Oil and Gas Co., Inc.	J. O. Faith No. 1	1943	4,642	410	E
501	Ernest Fletcher	Annie Zamzow No. 1	1952	8,504	390	E
701	John J. Coyle	Ernest Esse No. 1	1954	6,520	482	E
17-201	Blanco Oil Co. and Al Buchanan	Carl 0. Carlson No. 1	1943	6,260	435	E
202	Al Buchanan and Slick Oil Co.	Mary K. Wolfe No. 1	1944	6,265	443	E

LA SALLE COUNTY

Table 2.-Selected Oil, Gas, and Stratigraphic Tests

Type Log: D, Drillers'; E, Electric; R, Radioactive; S, Sample.
Logs in Texas Water Development Board files

WELL	OPERATOR	LEASE AND WELL	DATE DRILLED	DEPTH (FT)	APPROXIMATE LAND SURFACE ELEVATION (FT)	TYPE LOG
RX-77-23-704	8. G. Byars and C. G. Dunwoody, Jr.	J. L. Barkley No. 1	1954	5,400	533	E
29-902	Shell Oil Co.	J. L. Matthews No. 1	1956	10,742	483	E
30-l 01	W. J. Steeger	Joe McMillien No. 1	1958	5,354	544	E
402	Sutton Producing co.	Ben Alexander No. 1	1963	5,385	519	E
501	Marty Freedman	M. C. Smith No. 1	1952	5,535	605	E
902	Henderson Coquat and 0. R. Mitchell	Carlos Pena No. 1	1951	5,767	518	E
31-504	Kirkwood and Morgan, Inc.	Will Nagy No. 1	1952	4,255	473	E
32-901	Lann and McClanahan	Storev and Reed No. 1	1955	6,732	406	E
38-301	George H. Echols	Ben Alexander No. 1	1951	5,785	492	E
905	Siznod Oil Corp., et al.	M. L. Girard No. 1	1950	6,911	480	E
801	Howeth and Mason	A. U. Knaggs No. 1	1952	4,805	459	E
40-902	Continental Oil Co.	Fred L. Klattenhoff No. 1	1958	4,725	408	E
46-401	0. W. Killam	L. Otis Cox No. 1	1957	4,468	505	E
47-301	Jergins Oil Co.	J. E. Bishop No. 1	1947	5,000	357	E
804	Navillus Oil Well Servicing Co.	Sam Evans No. 1	1947	5,505	400	E
902	Sutton Producing co.	C. N. Cooke No. 2-A	1962	5,339	340	E
903	Champlin Petroleum co.	Albert Martin No. 1	1966	5,515	340	E
48-302	Sutton Producing co.	– Buckholdt No. 2	1958	5,429	362	E
503	Stanolind Oil and Gas co.	C. N. Cooke No. 1	1955	5,665	365	E
505	A. D. Sossaman	do.	1964	4,998	350	E
506	H. 8. Lively	C. N. Cooke No. 2	1964	5,373	350	E
507	E. J. McCurdy	Cartwright Ranch No. 1	1941	5,512	362	E
508	Ralph Evans	C. N. Cooke Estate No. 1	1966	5,389	353	E
601	Sutton Producing co.	F. J. Buckholt No. 1	1958	5,655	375	E
603	Frank Kallina and Ralph Evans	H. Cartwright No. B-l	1960	5,711	376	E

Table 2.-Selected Oil, Gas, and Stratigraphic Tests in La Salle County-Continued

WELL	OPERATOR	LEASE AND WELL	DATE DRILLED	DEPTH (FT)	APPROXIMATE LAND SURFACE ELEVATION (FT)	TYPE LOG
RX-77-48-604	Sutton Producing co.	Preston Stone No. 1	1959	5,603	375	E
605	Frank Kallina and Ralph Evans	H. Cartwright No. 1	1959	5,650	400	E
606	do.	Cartwright No. 2	1959	5,510	376	E
607	Charles E. Fraser	D. C. Reed No. 1	1944	5,718	405	E
608	Quintana Petroleum Corp.	F. G. Gausemeier No. I-8	1.943	4,307	440	E
701	Sutton Producing co.	C. N. Cooke No. 1-A	1960	10,404	398	E
702	Joe G. Gibson and J. B. Clark	C. N. Cooke No. 1	1961	5,500	332	E
703	Davidor and Davidor, Inc.	Albert Martin No. 1	1967	5,468	344	E
704	Champlin Petroleum co.	Albert Martin No. A-l	1966	5,515	355	E
53601	San Jacinto Petroleum Corp.	A. L. Krause No. 1	1952	10,463	540	E
54-502	Security Drilling Co.	Albert Martin No. 1	1956	5,008	496	E
503	Stanolind Oil and Gas Co.	do.	1953	4,955	542	E
601	Thomas Brothers	H. M. Gutierrez No. 1	1955	5,010	502	E
602	Ginther, Warren and Ginther	Albert Martin No. 1	1950	5,118	500	E
701	Barnsdall Oil Co. and Trinity Petroleum Co.	Gustav Sager No. 1	1941	5,514	599	E
55-201	Sutton Producing co.	Joe Amberson, Jr. No. 1-A	1955	5,221	438	E
202	do.	Joe Amberson No. 1	1955	5,204	434	E
601	R. M. Ranger	Jeffries Ranch No. 1	1948	5,640	408	E
56-50 1	Magnolia Petroleum co.	Burks Ranch No. 1	1942	6,202	304	E
901	Petroleum, Inc. and Sutton	St. Louis Union Trust Co. No. 1	1959	6,261	292	E
902	Flamingo Ventures and J. M. Taylor	Robert Coquat No. 1	1959	6,132	304	E
63-602	J. E. Hillier	R. J. Nunlev No. 1	1961	6,102	353	E
64- 103	Sohio Petroleum co.	Callahan Land and Cattle Co. No. B-1	1944	6,211	335	E
601	Henderson Coquat and Amerada Petroleum Co.	St. Louis Union Trust Co. No. 1	1950	6,508	365	E
78- 17-802	Skelly Oil Co.	John J. Schorp No. 1	1951	6,310	459	E
901	James M. Anderson	R. 8. Pumphrey	1952	6,375	461	E

Table 2.-Selected Oil, Gas, and Stratigraphic Tests in La Salle County-Continued

WELL	OPERATOR	LEASE AND WELL	DATE DRILLED	DEPTH (FT)	APPROXIMATE LAND SURFACE ELEVATION	TYPE LOG
RX-78-18-704	Rock Hill Oil Co. and Twin Oil Co.	La Salle Co. No. 1	1949	6,321	460	E
25-201	Geo. Parker and Chas. McCune	Mable I. Wilson No. 1	1949	6,352	430	E
301	Service Contracting co.	E. L. Sturm No. 1	1955	6,808	426	E
302	C. C. Winn	Mabel Wilson No. 1	1960	6,500	435	E
303	Dan Auld and W. S. Shipman, Jr.	Mable I. Wilson No. 1	1962	12,500	421	E
805	L. V. Chenoweth	– Fee No. 1	1942	5,002	355	E
26-101	The Texas Co.	The La Salle Co. No. 1	1948	9,050	415	E
401	C. C. Winn and C. W. McCurdy	The La Salle Co. No. 1	1957	4,973	375	E
703	Quintana Petroleum Corp.	R. W. Kostroun No. 1	1942	5,365	380	E
803	Jess McNeel	Jess McNeel No. 1	1945	3,060	365	E
33- 104	Thomas Brothers and C. C. Winn	Mathilde 011e, et al. No. 1	1955	5,010	360	E
105	Engeo Oil and Gas Co. and Sam Larue, et al.	Margaret Ann Kimball No. 1	1960	5,100	351	E
201	Sun Oil Co.	Naylor and Jones No. 1	1952	4,377	349	E
301	do.	Naylor and Jones No. 2	1955	5,303	333	E
501	Gulf Oil Corp.	Naylor and Jones No. 1	1959	10,960	364	E
704	Sutton Producing Co. and 0. W. McCurdy	W. E. Pfluger No. 1	1958	5,510	408	E
705	Sutton Producing co.	– Pfluger No. 2	1958	4,730	405	E
706	Sun Ray Mid-Continent Oil co.	E. Gerbert No. 1	1958	4,749	408	E
901	Quintana Petroleum Corp.	Naylor and Jones No. 1	1942	5,582	418	E
34-204	Appell Petroleum Corp.	Naylor and Jones Ranch Co., et al. No. 2	1961	5,665	299	E
501	do.	Naylor and Jones Ranch Co., et al. No. 1	1961	5,675	356	E
41-103	Navarro Oil Co.	Ray L. Talbert No. 1	1942	5,750	445	E
106	Lee Brothers Oil co.	H. D. Storev, Sr. No. 2	1956	10,705	444	E
107	Sixth M. E. Andrews, LTD.	Sforey and Reed No. 1	1956	5,420	458	E

Table 2.-Selected Oil, Gas, and Stratigraphic Tests in La Salle County-tintinued

WELL	OPERATOR	LEASE AND WELL	DATE DR I LLED	DEPTH (FT)	APPROXIMATE LAND SURFACE ELEVATION (FT)	TYPE LOG
RX-78-41-I 08	Progress Petroleum, Inc.	Maria Zuehl No. I	1943	5,723	440	E
199	Esgen and Manry	Talbert No. 1	1942	5,616	440	E
I10	Transwestern Oil co.	Reed and Storey No. 1	1944	5,707	443	E
111	Lloyd H. Smith and co.	D. C. Reed, et al. No. 1	1949	5,590	465	E
204	Quintana Petroleum Corp.	South Texas 'Syndicate No. 15	1942	5,100	442	E
207	do.	South Texas Syndicate No. 16	1942	5,752	455	E
209	do.	South Texas Syndicate No. 12	1942	5,733	445	E
303	do.	South Texas Syndicate No. 8		5,651	430	E
304	Standard Oil Co. of Texas	South Texas Syndicate No. 1	1954	11,525	435	E
305	Quintana Petroleum Corp.	South Texas Syndicate No. 6	1942	5,660	460	E
307	do.	Washburn Ranch No. B-1	1941	5,695	442	E
308	H. R. Cullen	Washburn Ranch No. 2	1940	5,561	459	E
310	Quintana Petroleum Corp.	Washburn Ranch No. 3	1941	5,708	440	E
37 1	do.	South Texas Syndicate No. 23	1943	5,543	445	E
312	do.	South Texas Syndicate No. 25	1943	5,579	465	E
343	do.	South Texas Syndicate No. 26	1945	5,567	450	E
3I4	do.	South Texas Syndicate No. 27	1943	5,573	445	E
3f5	do.	South Texas Syndicate No. 9	1942	5,827	445	E
316	do.	South Texas Syndicate No. 7	1942	5,573	465	E
321	do.	South Texas Syndicate No. 11	1942	5,571	465	E
402	Sun Ray Mid-Continent Oil co.	– Yarbrough No. 1	1961	6,786	425	E
403	Kallina, Evans Jane Oil and Gas Co., et al.	Storey and Reed No. 2	1962	5,554	417	E
404	Sun Oil Co.	do.	1961	5,631	408	E
405	do.	Storev and Reed No. 3	1962	5,666	415	E

Table 2.-Selected Oil, Gas, and Stratigraphic Tests in La Salle County-Continued

WELL	OPERATOR	LEASE AND WELL	DATE DRILLED	DEPTH (FT)	APPROXIMATE LAND SURFACE ELEVATION (FT)	TYPE LOG
RX-78-41-502	Newman Brothers, Skinner and Eddy Corp.	South Texas Syndicate No. E-I	1947	3,148	461	E
42-101	Alaska Steamship Co. and Newman Brothers	South Texas Syndicate No. 3-D	1948	5,685	465	E
102	Sutton Producing co.	South Texas Syndicate No. 1	1964		422	E
103	Newman Brothers, Skinner and Eddy Corp.	South Texas Syndicate No. D-2	1947	5,716	452	E
104	do.	South Texas Syndicate No. D-I	1947	5,253	451	E
105	Quintana Petroleum Corp.	South Texas Syndicate No. 31	1944	5,741	423	E
501	Jack Frost	South Texas Syndicate No. 1	1963	6,000	404	E
49-203	Newman Brothers, Skinner and Eddy Corp.	South Texas Syndicate No. F-I	1947	3,402	430	E
301	do.	South Texas Syndicate No. C-4	1947	5,525	378	E
302	Alaska Steamship Co. and Newman Brothers	South Texas Syndicate No. F-3	1949	3,906	400	E
303	Newman Brothers, Skinner and Eddy Corp.	South Texas Syndicate No. c-3	1947	3,813	458	E
304	do.	South Texas Syndicate No. c-2	1947	5,496	458	E
305	Quintana Petroleum Corp.	South Texas Syndicate No. F-I	1945	6,634	460	E
801	Hill, Spice, Miller and Pierce	Nueces Land and Livestock Co. No. 1	1957	6,016	385	E
803	Parr and Delaney Oil Co.	– Dobie No. 1	1952	6,042	314	E
902	A. F. Scott	Nueces Land and Livestock Co. No. 1	1955	4,074	360	E
50-203	Quintana Petroleum Corp.	South Texas Syndicate No. D-2	1943	5,461	442	E
204	Newman Brothers, Skinner and Eddy Corp.	South Texas Syndicate No. B-7	1947	5,706	405	E
205	Quintana Petroleum Corp.	South Texas Syndicate No. 1	1943		445	E
401	Seaboard Oil Co.	Nueces Land and Livestock Co. No. 1	1953	6,410	326	E
57401	Coastal States Gas Producing Co.	St. Louis Union Trust Co. No. 1	1959	6,450	299	E

LIVE OAK COUNTY (NORTHERN PART)

Table 2.-Selected Oil, Gas, and Stratigraphic Tests

Type Log: D, Drillers'; E, Electric; R, Radioactive; S, Sample.
Logs in Texas Water Development Board files.

WELL	OPERATOR	LEASE AND WELL	DATE DRILLED	DEPTH (FT)	APPROXIMATE LAND SURFACE ELEVATION (FT)	TYPE LOG
SJ-78-23-206	H. R. Smith and Gulf Oil Corp.	J. M. Ponder No. 1	1947	4,329	373	E
701	H.L. Massingill and Wilcox Oil Co.	P. Taylor No. 1	1948	6,250	280	E
24-l 02	Ryan, Hays and Burke	– Stolte No. 1	1950	8,006	329	E
701	Henderson Coquat	C. Nelson Estate No. 1	1944	7,015	341	E
31-401	Ryan and Abbott	Etta Terrell No. 1	1950	7,517	155	E
901	Argo Oil Corp.	– Schulz No. 1	1949	9,507	283	E
32-802	Kirkwood Drilling co.	W. J. Templin No. 1	1964	7,285	281	E
38-201	Charles E. Fraser	Atkinson No. 1		7,018	180	E
40-701	F. William Carr	Albert West No. 8-I	1958	7,963	135	E

MC MULLEN COUNTY

Table 2.—Selected Oil, Gas, and Stratigraphic Tests

Type Log: D, Drillers'; E, Electric; R, Radioactive; S, Sample.
Logs in Texas Water Development Board files

WELL	OPERATOR	LEASE AND WELL	DATE DRILLED	DEPTH (FT)	APPROXIMATE LAND SURFACE ELEVATION (FT)	TYPE LOG
SU-78-20-701	S. F. Hurlbut, et al.	H. D. Countiss No. 1	1944	5,782	309	E
702	Kirkwood and Morgan	H. D. Countis 1-32	1952	6,022	321	E
21-802	Santa Clara Oil Co.	Volney M. Brown, et al. No. 1-A	1945	6,310	371	E
803	Hassie Hunt Trust	Adolph Poenisch No. 1	1952	6,524	386	E
901	Santa Clara Oil Co.	V. M. Brown No. 1	1945	6,415	365	E
26-503	Jess McNeel	Jess McNeel No. 2	1946	3,205	355	E
27-201	Shell Oil Co.	M. Franklin, Jr. No. 1	1952	5,700	422	E
301	Kirkwood and Morgan	Lena Franklin No. 1	1958	5,556	388	E
302	Hamill and Smith	R. S. Franklin No. 1	1938	3,510	354	E
401	Maguire and Del Mar Drilling Co.	Lena Franklin, et al. No. 1	1958	10,506	373	E
601	Homer S. Head, et al.	Wheeler and Wheeler No. 1	1948	6,017	356	E
901	Crown Central Petroleum Co.	D. J. Dolan No. 1	1941	5,516	316	E
902	Sutton Producing Co.	E. J. Dolan No. 1-A	1962	11,009	325	E
28-201	Rowan and Hope and M. L. Massingill	Tom Franklin No. 1	1949	4,432	296	E
304	Humble Oil and Refining Co.	Louis Gubbels No. B-1	1954	11,010	271	E
305	do.	Louis M. Gubbels No. 3	1954	5,842	267	E
306	do.	Louis M. Gubbels No. 10	1960	6,304	273	E
307	The Atlantic Refining Co.	M. A. Lewis No. 1	1949	6,000	276	E
309	The Atlantic Refining Co. and Newman Brothers, et al.	Clifton Wheeler No. 1	1948	6,476	277	E
503	S. M. Nesser	R. S. Franklin No. 1	1938	3,030	360	E
605	R. H. Hedge and J. C. Wynne	H. M. Roark No. 1	1951	6,505	302	E
606	Arnold Well Service	J. F. Roark, et al. No. 1	1962	3,485	302	E
607	Gilcrease Operating Co., Blanco Oil Co. and H. L. Rymal	H. M. and J. F. Roark No. 1-A	1963	6,110	325	E

Table 2.—Selected Oil, Gas, and Stratigraphic Tests in McMullen County—Continued

WELL	OPERATOR	LEASE AND WELL	DATE DRILLED	DEPTH (FT)	APPROXIMATE LAND SURFACE ELEVATION (FT)	TYPE LOG
SU-78-28-608	Clarie Bentz-Stoddard and J. C. Drilling Co.	H. M. Roark No. 2	1963	6,012	281	E
609	J. C. Drilling Co.	— Roark No. 4	1964	5,975	280	E
610	Davis and Bates, Inc. and Edwin L. Cox	James F. Roark No. 1	1965	5,910	301	E
611	Stanolind Oil and Gas Co.	H. M. Roark No. 1	1949	5,205	301	E
613	Arnold Well Service	Jessie Morgan No. A-1	1962	5,995	263	E
614	Afroma Oil and Co., Inc.	M. A. Tyler No. 1	1967	6,012	260	E
701	Stanolind Oil and Gas Co.	E. M. Henry No. 1	1943	7,942	323	E
703	do.	J. F. Henry No. 1	1945	6,802	316	E
704	Arnold Well Service	J. C. Dolan No. 1	1963	6,015	316	E
705	Standard Oil Co. of Texas	E. M. Henry Unit No. 2 Well No. 1	1957	11,420	327	E
802	Frio Production Co.	E. M. Henry No. 1	1961	3,732	372	E
803	Harris S. Stahl	Sara M. Lester, et al. No. 2	1967	3,784	329	E
29-101	Humble Oil and Refining Co.	Louis M. Gubbels No. 14	1961	10,506	285	E
201	Gordon Street, Inc.	Graves Peeler No. 1	1964	6,405	341	E
202	Haynes and V. T. Drilling Co.	— Brown No. 1	1966	6,513	355	E
301	Sun Oil Co.	Brown Ranch No. 1	1955	6,503	348	E
303	Union Producing Co.	G. Jambers No. 1	1950	5,930	287	E
402	Continental Oil Co.	Richard Horton No. 1	1964	12,120	285	E
501	Bravado Oil Co. and Harris-Funk	Marie G. McCampbell No. 1	1949	6,014	249	E
605	Tenneco Oil Co.	Jambers Ranch No. A-1	1964	11,464	277	E
701	J. T. DeGrazier	Rose T. Quinn No. 1	1953	7,015	245	E
30-401	Loma Oil Co.	Leonard Jacob Corp. No. A-1-D	1955	6,864	305	E
402	Bridwell Oil Co.	Mabel Brownson No. 11	1955	6,776	257	E
403	Leonard Jacob Corp.	Mabel New No. 1	1960	6,617	305	E
34-801	Phillips Petroleum Co.	Mula No. 1	1952	6,006	367	E
901	do.	J. T. Pearson No. 3	1953	6,205	375	E

Table 2.—Selected Oil, Gas, and Stratigraphic Tests in McMullen County—Continued

WELL	OPERATOR	LEASE AND WELL	DATE DRILLED	DEPTH (FT)	APPROXIMATE LAND SURFACE ELEVATION (FT)	TYPE LOG
SU-78-34-902	Quintana Petroleum Corp.	South Texas Syndicate No. F-8	1943	5,848	338	E
35-101	Hassie Hunt Trust	R. B. Lowe No. 1	1952	6,010	291	E
103	David Faskin	Allye Henry No. 1	1960	11,334	284	E
301	J. E. Mowinkel, et al.	T. R. Kuykendall No. 1	1948	6,555	336	E
603	Humble Oil and Refining Co.	J. C. Dilworth, Jr. No. 1	1955	11,916	268	E
604	Forest Oil Corp., et al.	J. C. Dilworth No. 2	1949	6,026	272	E
606	Humble Oil and Refining Co.	J. C. Dilworth, Jr. No. 3	1962	11,052	280	E
607	do.	J. C. Dilworth, Jr. No. 2	1957	11,471	315	E
803	Producers Corp. of Nevada and Argo Oil Corp.	J. C. Dilworth, Jr. No. 1	1955	6,187	287	E
901	Texas Eastern Transmission Corp.	S. Von Lackum	1956	11,915	305	E
36-102	W. R. Thomas	Bernice Franklin Willis No. 1	1965	6,157	284	E
301	Sunray Oil Corp.	J. A. Bracken No. 1	1945	6,515	241	E
401	Texas Eastern Transmission Corp. and Producers Corp. of Nevada	G. L. Hayes No. 1	1956	11,550	254	E
402	Humble Oil and Refining Co.	J. B. Dilworth No. 1	1943	5,900	275	E
501	do.		1943	6,775	283	E
602	Standard Oil Co. of Texas	J. H. Dickinson No. 1	1955	11,560	348	E
702	do.	Moore-Wheeler Unit No. 1	1959	11,296	275	E
904	Theo Hamm Brewing Co.	J. H. Dickinson No. 1	1953	6,009	330	E
905	Amerada Petroleum Corp.	F. B. Horton No. 1	1956	11,854	359	E
906	Bright and Schiff	R. F. Horton No. 1	1959	6,725	324	E
37-703	Blair-Vreeland	L. S. McClaugherty No. 1	1963	6,514	298	E
38-103	Thomas Drilling Corp.	W. O. and L. T. Stevenson No. 1	1960	5,050	179	E
104	do.	Donald Stephenson No. 1	1960	4,809	238	E
105	Paul DeCleva	— Brown, et al. No. 1	1966	4,830	221	E
401	E. M. Jones	— Ezzell No. 3	1937	5,301	227	E
701	Holly Development Co., et al.	Hays-Ezzell Ranch No. 1	1952	7,512	231	E

Table 2.—Selected Oil, Gas, and Stratigraphic Tests in McMullen County—Continued

WELL	OPERATOR	LEASE AND WELL	DATE DRILLED	DEPTH (FT)	APPROXIMATE LAND SURFACE ELEVATION (FT)	TYPE LOG
SU-78-42-601	Shamrock Oil and Gas Corp.	Alamo National Bank and Trustee No. 1	1961	6,200	380	E
801	Quintana Petroleum Corp.	South Texas Syndicate No. D-3	1945	15,301	372	E
803	Newman Brothers and Skinner and Eddy Corp.	South Texas Syndicate No. B-4	1947	4,109	332	E
901	Quintana Petroleum Corp.	South Texas Syndicate No. C-2	1942	6,911	377	E
903	do.	South Texas Syndicate No. C-1	1942	7,623	338	E
904	do.	South Texas Syndicate No. C-4	1942	7,141	305	E
905	Newman Bros. and Alaska Steamship Co.	South Texas Syndicate No. B-13	1942	4,171	350	E
906	do.	South Texas Syndicate No. B-12	1949	4,045	360	E
907	Newman Brothers and Skinner and Eddy Corp.	South Texas Syndicate No. A-4	1947	3,957	331	E
908	Quintana Petroleum Corp.	South Texas Syndicate No. C-8	1944	6,426	327	E
43-101	Gilcrease Operating Co.	Alamo National Bank Trustee No. 1	1963	6,032	354	E
201	Kirkwood and Morgan	E. L. Craig No. 1	1956	6,158	329	E
501	Quintana Petroleum Corp.	Mabel Lowe Grimes No. 1	1943	7,524	348	E
602	Newman Brothers and Jergins Oil and Alaska Steamship Co.	do.	1948	5,904	306	E
701	Alaska Steamship Co. and Newman Brothers	South Texas Syndicate No. AA-5	1952	6,178	341	E
703	Newman Brothers and Skinner and Eddy Corp.	South Texas Syndicate No. A-6	1947	3,949	328	E
704		South Texas Syndicate No. AA-1	1947	3,956	283	E
801	Quintana Petroleum Corp.	South Texas Syndicate-Washburn No. F-7	1945	6,044	265	E
44-101	H. R. Smith	James Walker No. 1	1955	6,714	325	E
903	Miller and Fox Minerals Corp.	H. P. Brown No. 1	1959	5,737	255	E
46-105	Plymouth Oil Co.	Harry Ezzell No. 1-A	1945	7,215	305	E
701	Edwin M. Jones	— Ezzell No. C-2	1944	7,260	293	E

Table 2.—Selected Oil, Gas, and Stratigraphic Tests in McMullen County—Continued

WELL	OPERATOR	LEASE AND WELL	DATE DRILLED	DEPTH (FT)	APPROXIMATE LAND SURFACE ELEVATION (FT)	TYPE LOG
704	Edwin M. Jones	H. Ezzell No. C-4	1944	7,060	335	E
705	Estate of Edwin M. Jones	— Shiner No. 1	1948	7,617	351	E
706	do.	H. Ezzell No. C-6	1948	7,669	320	E
51-202	Howell Oil Corp. and Durham Sales Co.	Don Martin No. 1	1937	3,510	260	E
52-604	W. Ridley Wheeler, Estate	— Rives No. 1	1963	8,507	320	E
605	Humble Oil and Refining Co.	Cow Creek Gas Unit No. 2 Well No. 1	1964	6,597	330	E
902	Southern Petroleum Exploration Co., Inc. and Blair-Vreeland	Sol Winter Estate No. 1	1961	6,652	396	E
907	Ramada Oil and Gas Co.	Atkinson Estate No. 1	1961	6,801	395	E
53-103	Dee Davenport	Annie Roves Dolph, et al. No. 1-A	1945	7,237	315	E
204	John W. Pace and Blair-Vreeland	Continental Fee No. 1	1965	7,010	318	E
205	do.	La Jolla Corp. No. 1	1965	7,014	293	E
404	Amerada Petroleum Corp.	Murray Holland No. 1	1966	7,025	375	E
604	Atlantic Refining Co.	D. W. Rhode No. 1	1950	7,709	350	E
54-105	Skinner Corp. and L. B. Horn	— Lowrance No. 1	1961	7,510	357	E
701	The Atlantic Refining Co.	D. W. Rhode, Sec. 9 No. 1	1955	7,831	438	E
58-301	Gulf Oil Corp.	Nueces Land and Livestock Co. No. 1	1942	7,465	292	E
59-106	Southern Minerals Corp.	Nueces Land and Livestock Co. No. 1-171	1966	7,465	335	E
107	Mortex Oil Co.	Nueces Land and Livestock Co. No. 2	1957	7,477	269	E
60-202	M. L. Wise Drilling Co., et al.	Hagist Ranch No. 1	1954	8,010	462	E
208	Amerada Petroleum Corp.	do.	1962	7,720	437	E
303	Ramada Oil and Gas Co.	Gordon-Murphy No. 1	1960	6,880	462	E
304	Moody Properties and Knox Miller, Jr.	Whitley and Lanier-State No. 1	1960	6,750	440	E

MEDINA COUNTY (SOUTHERN PART)

Table 2.—Selected Oil, Gas, and Stratigraphic Tests

Type Log: D, Drillers'; E, Electric; R, Radioactive; S, Sample.
Logs in the Texas Water Development Board files

WELL	OPERATOR	LEASE AND WELL	DATE DRILLED	DEPTH (FT)	APPROXIMATE LAND SURFACE ELEVATION (FT)	TYPE LOG
TD-68-57-306	Texas Water Development Board	Texas Water Development Board No. 4-1	1971	192	635	E,R, D,S
69-63-101	Humble Oil and Refining Co.	E. Wilson No. 1	1948	7,167	680	E

UVALDE COUNTY (SOUTHEASTERN PART)

Table 2-Selected Oil, Gas, and Stratigraphic Tests

Type Log: D, Drillers'; E, Electric; R, Radioactive; S, Sample.
Logs in Texas Water Development Board files

WELL	OPERATOR	LEASE AND WELL	DATE DR I LLED	DEPTH (FT)	APPROXIMATE LAND SURFACE ELEVATION (FT)	TYPE LOG
Y P-69-59-301	Tiger Oil and Gas co.	Lilian Saidel No. 1	1967	805	847	E
60-101	W. J. Steeger	F. T. Kincaid No. 2	1961	4,000	775	E
61-101	Tiger Oil and Gas co.	E. D. Kincaid, Sr. No. A-4	1965	1,505	730	E
103	do.	– Woodlev No. 2	1965	1,210	720	E
104	Western Oil and Development Co.	E. D. Kincaid, Sr. et al. No. 1	1964	1,510	724	E
201	Ike Howeth	E. D. Kincaid No. 1	1963	5,629	718	E

WEBB COUNTY

Table 2.—Selected Oil, Gas, and Stratigraphic Tests

Type Log: D, Drillers'; E, Electric; R, Radioactive; S, Sample.
Logs in Texas Water Development Board files.

WELL	OPERATOR	LEASE AND WELL	DATE DRILLED	DEPTH (FT)	APPROXIMATE LAND SURFACE ELEVATION (FT)	TYPE LOG
YZ-77-50-401	Fred W. Shield and General Crude Oil Co.	Dolph Briscoe, Jr. No. 1	1962	4,615	800	E
53-402	Dan J. Harrison, Jr.	E. Fee No. 1	1963	7,000	633	E
501	Kirkwood and Morgan	A. E. Schletez No. 2	1955	4,611	524	E
703	Sutton Producing Co.	Sam Kone No. 1	1959	10,330	599	E
57-101	L. A. Nordan	Dolph Briscoe, Jr. No. 1	1959	8,205	625	E
201	Fred W. Shield, et al.	do.	1958	4,507	752	E
502	O. N. Beer, et al.	Dolph Briscoe, Jr. No. 2	1958	4,750	700	E
901	Copano Oil Co.	Dolph Briscoe, Jr. No. 1	1959	10,473	604	E
58-102	William H. Spice, Jr., Trustee	O. S. Petty No. 1	1955	3,350	795	E
60-701	W. C. McBride, Inc.	W. V. Booth No. 1	1948	3,050	771	E
61-702	R. G. Rice	B. B. Dunbar No. 1	1961	4,505	736	E
703	Universal Petroleum Corp.	do.	1961	5,490	730	E
801	Robert Mosbacher	Webb Co. Commissioners Court No. 1	1960	5,309	695	E
901	Sohio Petroleum Co.	Robert Sanchez No. 1	1944	—	566	E
62-801	do.	Maria G. Martin No. 1	1944	5,460	478	E
64-602	Seaboard Oil Co. and Sunray Oil Co.	Mary K. Withers No. 1	1950	6,725	410	E
78-57-701	Humble Oil and Refining Co.	Mary K. Withers No. 2	1945	7,375	376	E
58-502	do.	Lewis Yeager No. B-1	1947	8,026	339	E
84-01-301	Union Sulphur Co.	—	1949	6,527	326	E
702	Mrs. James R. Dougherty and F. W. Holbrook	W. R. Nicholson Estate No. 1	1962	7,514	358	E
09-101	The Texas Co.	— Nicholson No. 1	1945	7,014	427	E
85-01-901	Copano Oil Co.	Ed Rachal No. A-2	1960	3,055	565	E

Table 2.—Selected Oil, Gas, and Stratigraphic Tests in Webb County—Continued

WELL	OPERATOR	LEASE AND WELL	DATE DRILLED	DEPTH (FT)	APPROXIMATE LAND SURFACE ELEVATION (FT)	TYPE LOG
YZ-85-02-401	Copano Oil Co., et al.	Desiderio Trevino No. 1	1958	9,100	545	E
03-302	Hughes and Hughes	— Booth No. 1-A	1967	3,810	663	E
401	Ryan-Hayes and Burke	La Mesa Land and Cattle Co. No. 1	1950	3,730	656	E
601	Magnolia Petroleum Co.	Hamilton Ranch No. A-1	1941	9,181	604	E
801	W. C. McBride, Inc. and Mid-Continent Petroleum Corp.	Anna L. Connevy	1947	3,963	575	E
903	McCartney and Ross	E. T. Laubscher No. 1	1946	4,770	708	E
904	Frank J. Gravis, et al.	do.	1943	5,004	700	E
05-701	Mid-Continent Petroleum Corp.	— Laubscher No. 1	1936	3,508	790	E
07-101	Brown and Wheeler	Maria Martin, et al. No. 1	1949	5,526	434	E
801	Transwestern Oil Co. and Seaboard Oil Co.	Callaghan Land and Pastoral Co. No. 1	1943	6,260	469	E
08-201	Sohio Production Co.	Callaghan Land and Pastoral Co. No. A-1	1944	7,228	449	E
403	Kirkwood Drilling Co.	Olmitos Ranch No. 1	1960	7,050	444	E
10-301	Windsor Oil Co.	La Mesa Land and Cattle Co. No. 1	1949	3,839	659	E
11-501	Ammann and McNab, LTD.	Rosa Vela Benavides No. 1	1949	3,875	615	E
701	Magnolia Petroleum Co.	Santo Tomas Ranch No. 1	1941	6,812	614	E
12-501	Amerada Petroleum Corp.	— Benavides No. 1	1949	11,678	571	E
903	Russell Maguire and Kirkwood and Morgan	Louis Puig No. 1	1956	5,247	669	E
15-502	Sun Oil Co.	Issac Hirsch No. 1-A	1946	7,051	469	E
601	Tucker Drilling Co. and Peter Henderson Oil Corp.	W. P. Lincoln No. 1	1952	8,761	465	E
701	Sinclair Oil and Gas Co.	Dix Ranch No. 1	1956	7,501	477	E
901	Gulf Oil Corp.	Issac Hirsch No. 1	1959	8,010	525	E
19-901	Appell Drilling Co.	Stockbridge No. 1	1951	4,422	443	E
22-201	Rodney DeLange and O. Neathery, Jr.	Callaghan Land and Pastoral Co. No. 1	1962	7,050	532	E
29-101	T. J. Ahern	Hubbard No. A-1	1953	2,605	629	E

WILSON COUNTY

Table 2.—Selected Oil, Gas, and Stratigraphic Tests

Type Log: D, Drillers'; E, Electric; R, Radioactive; S, Sample.
Logs in Texas Water Development Board files

WELL	OPERATOR	LEASE AND WELL	DATE DRILLED	DEPTH (FT)	APPROXIMATE LAND SURFACE ELEVATION (FT)	TYPE LOG
ZL-67-33-702	E. L. Fulton and J. S. Celaya	Carlos D. Browner	1965	1,500	583	E
41-103	Monsanto Co.	Fred W. Hartwick No. 1	1965	1,800	584	E
104	Weco Petroleum Co., Inc.	Richard Lee Hubbard No. 1	1965	1,600	603	E
105	do.	Richard Lee Hubbard No. 6	1966	1,650	612	E
106	E. L. and F. T. Brahaney	Roger Wright No. 1	1966	1,806	593	E
302	Sun Oil Co.	J. H. Bain, Jr. No.2	1955	4,625	543	E
303	do.	J. H. Bain, Jr. No. 1	1954	4,600	510	E
402	R. P. Holland	J. H. Imken, et al. No. 4	1959	1,892	523	E
403	The Young Co.	Jessie Allison No. 1	1965	2,393	453	E
404	H. & J. Drilling Co.	James T. Reddy No. 1	1965	2,310	487	E
504	do.	W. Earl Lynn No. 1	1964	2,730	534	E
505	do.	Sam Wiley No. 1	1966	2,445	522	E
602	Texas Southern Oil and Gas Co.	R. L. Rice No. 1	1954	2,876	481	E
603	Frio Production Co., et al.	E. E. Spear No. 2	1964	2,507	475	E
604	H. & J. Drilling Co.	— Holstein No. 1	1965	2,392	478	E
605	Sun Oil Co.	F. G. Wake No. 1	1965	2,500	477	E
703	Paul F. Danielson	John Richter No. 1	1956	1,701	440	E
704	The Young Co.	Craig Smith No. 1	1965	2,416	480	E
802	Eddy and Vaughn and McShane	J. S. Cone No. 1	1952	5,252	517	E
803	Patterson Drilling Co., et al.	W. W. Lorenz No. 1	1959	2,840	474	E
804	Skinner Corp.	— Whitten No. 1	1959	1,648	506	E
805	Rowan and Hope, Inc.	W. B. Hardin No. 1	1946	5,326	520	E
806	W. O. Fortenberry	E. B. Deason No. 1	1954	3,043	498	E
807	do.	— Beasley No. 1	1954	1,658	514	E
808	Sutton Drilling Co.	A. T. Hardin No. 1	1954	1,628	491	E
901	A. W. Phillips	J. P. Lorenz No. 1-A	1950	3,112	467	E

Table 2.—Selected Oil, Gas, and Stratigraphic Tests in Wilson County—Continued

WELL	OPERATOR	LEASE AND WELL	DATE DRILLED	DEPTH (FT)	APPROXIMATE LAND SURFACE ELEVATION (FT)	TYPE LOG
ZL-67-41-902	Frio Production Co.	E. S. Austin No. 1	1957	4,008	429	E
903	K. B. Absher	— Wiley No. 1	1965	5,428	484	E
42-102	Robert J. Hewitt	H. H. Weinert No. 2	1964	2,253	483	E
402	J. B. Blanchard Co.	H. O. Wiley No. 1	1954	1,688	498	E
403	L. H. and S. A. Olson Drilling Co.	— Davis No. 1	1956	3,098	480	E
49-104	B. and G. Well Service Co.	A. T. Hardin No. 1	1952	2,914	426	E
203	Sutton Drilling Co.	H. C. Stroud No. 1	1954	2,861	463	E
204	do.	H. C. Stroud No. 2	1954	1,622	469	E
801	Humble Oil and Refining Co.	Edmond Lyssy No. 1	1952	4,676	400	E
802	Sun Oil Co.	Leon Laskowski No. 1	1956	4,241	385	E
902	Diamond Half Oil Corp.	— Korzekwa No. 1	1942	4,651	381	E
50-202	H. H. Howell	H. H. Weinert No. 1	1953	4,708	356	E
301	Midwest Oil Corp.	J. C. Peebles No. 1	1953	4,639	334	E
401	Southern Minerals Corp.	Tom Manford No. 1	1953	4,606	391	E
501	H. H. Howell	G. N. Evans No. 1-A	1952	4,619	406	E
502	do.	H. H. Weinert No. 3-A	1953	4,826	386	E
601	Shell Oil Co.	C. M. Wells No. 1	1941	5,000	335	E
51-103	George H. Coates	T. C. Cobb No. 1	1956	4,891	341	E
57-202	F. B. Cochran, Jr.	Constant Jarzombek No. 1	1953	5,174	325	E
301	M. O. Turner	Mary Lyssy No. 1	1963	5,542	365	E
68-39-902	Hoxey Oil Co.	— Mitchum No. 1	1955	2,304	483	E
40-804	R. H. Norton	— Scull No. 1	1954	1,578	555	E
47-201	G. I. Reasor	— Haese No. 1	1958	2,116	561	E
402	Sun Oil Co.	Gus Dylla No. 1	1958	2,124	675	E
505	Weco Petroleum Co., Inc.	Theodore Stanusch No. 1	1966	1,410	696	E
603	Richard F. Bailey	J. H. Walsh No. 1	1954	3,146	700	E
604	James M. Anderson, et al.	L. H. Stroud No. 1	1960	1,203	623	E
801	Caddo Oil Co.	— Gilliland No. 1	1966	1,578	573	E
48-106	Nueces Oil and Development Co.	— Wiseman No. 1	1954	1,420	474	E
203	Maple C. Hughes	— Scull No. 1	1953	1,527	461	E

Table 2.-Selected Oil, Gas, and Stratigraphic Tests in Wilson County-Continued

WELL	OPERATOR	LEASE AND WELL	DATE DRILLED	DEPTH (FT)	APPROXIMATE LAND SURFACE ELEVATION (FT)	TYPE LOG
Z L-68-48-204	Maple C. Hughes	Ed Mattke No. 2	1953	2,801	534	E
205	Gasoline Production Corp.	R. J. Huebinger No. 1	1953	1,763	500	E
206	Maple C. Hughes	C. E. Scull Estate No. 7	1954	3,064	440	E
207	do.	Scull Estate No. 1	1953	2,788	460	E
208	C. C. Winn	– Duelm No. A-2	1955	1,307	489	E
209	R. L. Turner	– Hildt No. 1	1955	1,872	510	E
504	W. R. Johnston, Trustee	Theodore Gerlick No. A-l	1955	1,292	440	E
609	L. H. and S. A. Olson Drilling Co.	– Linne No. 17	1955	1,450	505	E
610	Sun Oil Co.	Georgia Lucas No. 1	1965	1,726	573	E
611	Pierce and Davis 67 Limited	W. A. Childreos No. 1	1967	1,800	535	E
704	Fred Nicholson, et al.	A. G. Mathews No. 1	1955	1,752	560	E
705	Alamo Royalty, Inc.	L. H. Mills No. 2	1956	1,682	505	E
808	Fenner and Koloya, et al.	– Tidwell No. 1	1952	2,660	451	E
809	Gasoline Production Corp. and Patterson Drilling Co.	Martin Vorpahl No. 1	1956	2,641	455	E
910	A. T. Slavid	James 0. Bishop No. 1	1963	1,423	448	E
54-204	Jergins Oil Co.	A. C. Oefinger No. 1	1948	3,487	451	E
205	W. R. Quin, Mowinckle and Katz	do.	1948	3,250	455	E
303	J. E. Mowinckle	Franklin Plato No. 1	1947	3,414	505	E
304	A. W. Phillips	Tom Guajardo No. 1	1950	2,980	450	E
305	Sid Katz	P. 0. Rodriguez No. 1	1954	3,511	409	E
306	W. R. Guin and Son	Emil V. Ploch No. 1	1948	3,257	426	E
403	Riddle Oil Co.	Phil and John Shook No. 1	1963	3,589	450	E
464	Francis J. Hynes	Manuel 8. Tarin No. 1	1952	3,580	460	E
504	Varn Petroleum co.	Carlos Flores No. 1	1966	1,465	427	E
505	Texas Water Development Board	Texas Water Development Board No. 2-2	1970	336	422	D,S. E. R
505	H. & J. Drilling co.	Howard Tom No. 1	1956	4,299	497	E

Table 2.—Selected Oil, Gas, and Stratigraphic Tests in Wilson County—Continued

WELL	OPERATOR	LEASE AND WELL	DATE DRILLED	DEPTH (FT)	APPROXIMATE LAND SURFACE ELEVATION (FT)	TYPE LOG
ZL-68-54-708	Hankamer Investment Co.	Travis E. Longley No. 1	1953	4,603	550	E
804	Gorman and DeLange, et al.	D. A. McKenzie No. 1	1952	5,209	527	E
55-105	J. S. Hillsman	Bruno R. Johns No. 1	1964	1,505	468	E
106	do.	Bruno R. Johns No. 2	1965	1,510	502	E
205	S. A. Olson	Ida Roemer No. B-5	1962	1,456	479	E
408	H. & J. Drilling Co.	Arnold Nitsche No. 1	1956	2,647	422	E
606	Pegg Brothers and Bode	Mike Lopez No. 1	1949	2,756	510	E
804	L. & N. Oil Co.	J. L. Dennis No. 1	1954	564	405	E
905	Texas Southern Oil and Gas Co.	Alvin Jung No. 2	1954	2,869	487	E
56-107	Ray McDonald and H. & J. Drilling Co.	S. R. Donaho No. 1	1955	2,182	518	E
203	Trio Oil Co.	— Ridout No. 1	1941	5,308	490	E
204	L. D. Ormsby	— Williamson No. 1	1944	5,072	483	E
311	R. P. Holland	Click and White No. 1	1962	4,820	381	E
406	Tom Schmitz	W. T. Donaho No. 1	1963	5,188	498	E
407	George Parker and Charles McCune	J. V. Blake No. 1	1950	2,881	489	E
504	Sunray Oil Corp., et al.	Ruth McCurdy Underhill No. 3	1950	2,763	468	E
505	Sunray Oil Corp.	F. P. Burton No. 2	1950	2,715	453	E
506	W. G. Darsey, Jr.	W. B. Whitehead No. 1	1949	2,744	475	E
507	Ralph E. Fair	— Teague No. 1	1963	7,487	463	E
601	S. M. Messer	J. H. Spruce No. 1	1949	3,247	458	E
602	Sutton Producing Co.	— Maryfield No. 1	1965	3,300	417	E
603	Ledge Petroleum Co., Inc.	Mrs. O. J. Weber, et al. No. 1	1965	3,325	429	E
604	W. B. Yarborough	Fannie C. Spruce No. 1	1966	3,200	480	E
903	C. Andrade, III	Phaddeus Kopecki No. 1	1947	6,354	426	E
62-504	M. L. Wise and O. W. Killam	Stanley Bench No. 1	1954	5,670	509	E
505	M. L. Wise, et al.	Kate Higgins No. 2	1951	6,004	435	E
606	Siznod Oil Corp.	Hal V. Warren No. 1	1953	6,164	462	E

Table 2.—Selected Oil, Gas, and Stratigraphic Tests in Wilson County—Continued

WELL	OPERATOR	LEASE AND WELL	DATE DRILLED	DEPTH (FT)	APPROXIMATE LAND SURFACE ELEVATION (FT)	TYPE LOG
ZL-68-63-102	Rowan and Hope and E. W. Gill	L. N. Mitchell No. 1	1952	5,738	476	E
103	M. L. Wise and O. W. Killam	— Watson No. 1	1953	5,417	387	E
205	Henshaw Brothers	Julius Ewing No. 1	1948	6,487	400	E
206	do.	Dr. H. C. Woods No. 1	1948	3,912	396	E
403	D. O. Wade	— Brundrech No. 1	1955	1,105	496	E
703	J. C. McCabe	Charlie F. Fuller No. 1	1953	1,830	399	E
64-104	C. C. Winn	— McCracken No. 1	1953	2,750	443	E
302	Sutton Drilling Co.	Joe Keller No. 1	1954	4,230	377	E
303	Wise Drilling Co.	— Kolodziez No. 1	1949	4,213	428	E
501	Frank J. Garvis, et al.	J. H. McDaniel No. 1	1949	5,200	367	E
901	Sullivan and Garnett	— Moczygemba No. 1	1944	3,820	373	E
78-07-502	The Superior Oil Co.	J. C. Merchant No. 1	1954	6,271	348	E
503	H. H. Howell and William I. Lee and Raymond M. Peeler, et al.	do.	1956	4,345	374	E
504	M. O. Turner and H. & J. Drilling Co.	E. G. Casares No. 1	1960	6,310	388	E
506	H. & J. Drilling Co.	D. W. Raabe No. 1	1964	5,565	374	E
704	O. G. McClain	S. V. Houston No. 1	1953	6,215	307	E
801	Morris Cannan	Baptist Foundation of Texas No. 1	1954	6,433	382	E
08-101	L. H. Armer, et al.	Ignatz Pawlik No. 1	1952	6,114	381	E
102	Mid-Continent Petroleum Corp. and W. C. McBride, Inc.	W. F. Gabrysch No. 1	1947	6,515	387	E
103	Henshaw Brothers	E. W. Schneider No. 1	1940	3,381	315	E
202	Luling Oil and Gas Co.	— Rutkowski No. 1	1948	6,105	349	E

ZAVALA COUNTY

Table 2.-Selected Oil, Gas, and Stratigraphic Tests

Type Log: D, Drillers'; E, Electric; R, Radioactive; S, Sample.
Logs in Texas Water Development Board files

WELL	OPERATOR	LEASE AND WELL	DATE DRILLED	DEPTH (FTI	APPROXIMATE LAND SURFACE ELEVATION (FTI	TYPE LOG
ZX-69-58-501	W. J. Steeger, et al.	Mary C. Smyth No. 1	1961	4,699	786	E
602	Jergins Oil Co.	Ike T. Pryor No. 1	1947	3,519	784	E
603	Serba Oil Co.	Ike T. Pryor No. 6-7	1962	1,476	850	E
714	Texas Water Development Board	Texas Water Development Board No. 7-2	1971	231	800	D, R, E. S
59-702	Serba Oil Co.	Ike T. Pryor No. C-2	1961	929	825	E
703	Quintin Little	Lee Estate No. 5	1967	1,751)	902	E
60-706	Intex Oil Co.	Joe W. Vanham, Jr. No. 1	1963	2,277	775	E
904	J. J. Cody	W. Ft. Capps No. 1	1961	1,243	826	E
905	Magnolia Petroleum co.	Roy Capps No. 1	1948	3,894	790	E
61-401	Humble Oil and Refining Co.	E. D. Kincaid, Sr. No. 2	1962	2,063	780	E
820	Wilcox Oil and Gas Co.	W. D. Kincaid No. 1	1939	3,549	735	E
76-l 6-302	Norton Oil Co. and V. P. Grage	R. W. Norton No. 6	1958	3,387	644	E
806	Sutton Producing co.	– Van Cleve No. 1	1955	2,760	623	E
24-301	Petroleum Investment Co.	J. C. Flanagan No. 1	1962	3,225	588	E
613	W. J. Steeger, et al.	Norvel Chittim No. 2	1963	3,344	642	E
77-01-202	W. J. Steeger	J. L. Matthews, et al. No. 1	1960	2,197	751	E
406	F. M. Ginther	Bebe Mathews No. 1	1945	2,503	727	E
801	Jones and O'Erlen, Inc.	Joseph L. Matthews No. 3	1959	3,500	671	E
901	San Miguel Lease and Royalty Co.	James L. Matthews No. C-l	1958	2,870	709	E
02.510	Humble Oil and Refining Co.	Ike Pryor Estate No. 1	1944	5,867	726	E
511	Serba Oil and Gas co.	Emma Pryor-Mangum No. 43 1	1962	2,846	705	E
03-501	S. H. Howell	T. A. Price No. 1	1948	4,403	780	E
801	Lipan Oil Co.	Elizabeth Bartlett No. 2	1963	5,866	718	E
04-205	Seaboard Oil Co.	J. F. Webb No. 1	1956	3,004	742	E
438	C. C. Winn	– Caldwell No. 1	1962	3,332	682	E

Table 2.—Selected Oil, Gas, and Stratigraphic Tests in Zavala County—Continued

WELL	OPERATOR	LEASE AND WELL	DATE DRILLED	DEPTH (FT)	APPROXIMATE LAND SURFACE ELEVATION (FT)	TYPE LOG
ZX-77-04-439	C. C. Winn	— Baxter No. 1	1962	3,345	690	E
519	do.	R. Kirchner No. 1	1956	3,050	685	E
520	do.	— Boykin No. 1	1962	3,416	698	E
720	do.	Jack Lee No. 1	1962	3,545	686	E
721	do.	— Truitt No. 1	1963	3,649	660	E
05-801	Northern Natural Gas Producing Co. and Phillips and Stringer	Russell K. Dunbar No. 2	1959	4,300	650	E
09-602	General Crude Oil Co.	Sam Guyler No. 1	1959	4,512	680	E
603	C. C. Winn	John Scoggins No. 1	—	2,333	698	E
604	do.	— Scroggins No. 5	1962	3,521	716	E
710	Calvin Michelson	A. Von Rosenberg, et al. No. 1	1963	3,410	620	E
901	O. N. Beer and Mel Dar Corp.	H. G. Alexander No. 1	1962	3,655	642	E
902	Sun Oil Co.	Cross S Ranch No. 1	1963	3,637	659	E
10-107	Paul Little	John Scogging No. 1	1961	3,700	679	E
201	C. C. Winn	Ike T. Pryor, Jr., et al. No. 1	1961	3,495	636	E
303	do.	— Pryor No. 11	1962	3,185	664	E
501	The Texas Co.	— Spencer No. 1	1947	3,800	605	E
703	Colton and Colton, et al.	Cross S Ranch No. 1-B	1960	3,710	635	E
704	The Texas Co.	Cross S Ranch No. 3	1947	3,750	621	E
705	do.	Cross S Ranch No. 1	1946	4,302	634	E
707	do.	Northeastern Farming Co. No. 1	1946	3,372	635	E
709	do.	Moore Farm Unit No. 1	1947	3,401	674	E
806	Adams and Lyles	Holsombach and Butler No. 1	1947	1,413	595	E
807	The Texas Co.	Frank Newton No. 1	1947	4,096	589	E
908	C. C. Winn	R. G. Havens No. 1	—	4,050	609	E
909	do.	Bracero No. 7	1961	3,952	610	E
11-101	Texaco, Inc.	Head and Farenthold No. 1	1963	3,810	680	E
301	The Superior Oil Co.	S. S. Cassin No. 1	1965	5,020	696	E
302	do.	Ada Hammond No. 1	1965	4,000	706	E
303	do.	Ada Hammond No. A-1	1965	3,500	716	E

Table 2.-Selected Oil, Gas, and Stratigraphic Tests in Zavala County-Continued

WELL	OPERATOR	LEASE AND WELL	DATE DRILLED	DEPTH (FT)	APPROXIMATE LAND SURFACE ELEVATION (FT)	TYPE LOG
2x-77-1 I-407	C. C. Winn	H. & F. Properties No. 33-1	1961	3,835	644	E
801	do.	– Holdsworth No. 4-36	–	1,744	609	E
901	General Crude Oil co.	– Holdsworth No. 1	1960	5,518	658	E
12-801	Rock Hill Oil Co., et al.	E. Holdsworth	1950	7,253	702	E
901	R. L. Scheig, et al.	E. Howett No. 1	1962	4,349	720	E
13-201	Northern Natural Gas Producing Co. and Phillips and Stringer	Russell K. Dunbar No. 1	1959	4,373	618	E
801	The Texas Co.	National Bank of Commerce No. 1	1945	4,933	659	E
802	do.	George W. West No. 5	1946	4,380	688	E
803	do.	George W. West No. 4	1946	4,445	654	E
17 108	W. J. Steeger, et al.	J. K. Ware No. 1	1958	3,512	587	E
109	do.	J. K. Ware No. 2	1958	3,350	587	E
110	Skelly Oil Co.	J. K. Ware No. 1	1958	3,764	592	E
111	do.	J. K. Ware No. 3	1958	3,329	599	E
112	W. J. Steeger, et al.	J. K. Ware No. 7	1959	3,425	581	E
113	Skelly Oil Co.	J. C. Flanagan No. 1	1958	3,430	599	E
114	C. C. Winn	Flanagan and Kirk No. 1	1961	3,095	585	E
115	do.	W. 0. Kirk No. 1	1961	3,736	585	E
205	W. J. Steeger	Ben Wilson No. 2	1962	3,600	575	E
503	Garr and Wooley	F. D. Keller No. 1	1952	6,324	588	E
18 205	William H. Spice, Jr., Trustee	J. R. Gulick No. 1	1958	3,947	593	E
609	C. C. Winn and George Musselman	Compton No. 1	1958	4,475	564	E
610	Humble Oil and Refining Co.	Marrs McLean No. 1	1946	5,000	581	E
19 115	C. C. Winn	Cross S Ranch No. 1	1961	4,394	583	E
116	do.	Cross S Ranch No. 91 1	1962	4,445	620	E
117	do.	M. D. Ray No. 1	1960	4,514	585	E
501	do.	Delhi Von Atta No. 77 2	1963	4,101	570	E
601	do.	– Delhi No. 5	1962	4,268	615	E
808	Paul Little	Ray McGlothlin No. 1	1961	4,711	555	E
809	C. C. Winn	– Delhi No. 77 1	1963	4,736	550	E

Table 2.—Selected Oil, Gas, and Stratigraphic Tests in Zavala County—Continued

WELL	OPERATOR	LEASE AND WELL	DATE DRILLED	DEPTH (FT)	APPROXIMATE LAND SURFACE ELEVATION (FT)	TYPE LOG
ZX-77-20-102	Ancon Oil and Gas Co. and Robert Beamon	N. W. Gates No. 1	1962	4,813	636	E
901	Sun Oil Co.	Jeff Baggett No. 1	1969	5,600	643	E
902	do.	Erin Bain Jones No. 1	1969	5,500	595	E
903	do.	Erin Bain Jones "A" No. 1	1969	5,875	628	E
21-101	Rio Gas Gathering Co., et al.	W. D. Glasscock No. 1	1961	4,366	658	E
202	Frank C. Kallina and Ralph Evans and L. B. Horn, et al.	Alphonse Krawetz No. 1	1962	4,652	644	E
701	Sun Oil Co.	Mollie Lasater No. 1	1970	5,905	662	E
702	do.	John Baggett No. 2	1970	5,650	643	E
802	do.	John N. Garner Estate No. 2	1971	6,000	617	E

Hydrogeologic Investigation and Simulation of Ground-Water Flow in the Upper Floridan Aquifer of North-Central Florida and Southwestern Georgia and Delineation of Contributing Areas for Selected City of Tallahassee, Florida, Water-Supply Wells

By Hal Davis

U.S. GEOLOGICAL SURVEY
WATER-RESOURCES INVESTIGATIONS REPORT 95-4296

Prepared in cooperation with the
CITY OF TALLAHASSEE and
FLORIDA DEPARTMENT OF ENVIRONMENTAL PROTECTION

Tallahassee, Florida
1996

U.S. DEPARTMENT OF THE INTERIOR
BRUCE BABBITT, Secretary

U.S. GEOLOGICAL SURVEY
Gordon P. Eaton, Director

For additional information write to:

District Chief
U.S. Geological Survey
Suite 3015
227 North Bronough Street
Tallahassee, FL 32301

Copies of this report may be purchased from:

U.S. Geological Survey
Earth Science Information Center
Open-File Reports Section
Federal Center, MS 517
Box 25286
Denver, CO 80225

CONTENTS

FIGURES

TABLES

CONVERSION FACTORS, VERTICAL DATUM, ABBREVIATIONS, AND ACRONYMS

Multiply	By	To obtain
inch (in.)	2.54	centimeter
inches per year (in/yr)	2.54	centimeters per year
foot (ft)	0.3048	meter
gallon (gal)	0.003785	cubic meter
gallon (gal)	3.785	liter
mile (mi)	1.609	kilometer

Equations for temperature conversion between degrees Celsius (°C) and degrees Fahrenheit (°F):

$$°C = 5/9\ (°F - 32)$$
$$°F = (9/5\ °C) + 32$$

Sea level: In this report, "sea level" refers to the National Geodetic Vertical Datum of 1929-- a geodetic datum derived from a general adjustment of the first-order level nets of both the United States and Canada, formerly called Sea Level Datum of 1929.

ADDITIONAL ABBREVIATIONS

ft = feet
in = inch
in/yr = inches per year
gal/min = gallons per minute
Mgal/d = million gallons per day
ft/d = feet per day
ft^2/d = feet squared per day
ft^3/s = feet cubed per second

ACRONYMS

MODFLOW = USGS modular three-dimensional finite-difference ground-water flow model
MODPATH = USGS particle-tracking program
PCE = tetrachloroethylene
RASA = Regional Aquifer System Analysis
USGS = U.S. Geological Survey

Hydrogeologic Investigation and Simulation of Ground-Water Flow in the Upper Floridan Aquifer of North-Central Florida and Southwestern Georgia and Delineation of Contributing Areas for Selected City of Tallahassee, Florida, Water-Supply Wells

By Hal Davis

Abstract

A 4-year investigation of the Upper Floridan aquifer and ground-water flow system in Leon County, Florida, and surrounding counties of north-central Florida and southwestern Georgia began in 1990. The purpose of the investigation was to describe the ground-water flow system and to delineate the contributing areas to selected City of Tallahassee, Florida, water-supply wells. The investigation was prompted by the detection of low levels of tetrachloroethylene in ground-water samples collected from several of the city's water-supply wells.

Hydrologic data and previous studies indicate that; ground-water flow within the Upper Floridan aquifer can be considered steady-state; the Upper Floridan aquifer is a single water-bearing unit; recharge is from precipitation; and that discharge occurs as spring flow, leakage to rivers, leakage to the Gulf of Mexico, and pumpage. Measured transmissivities of the aquifer ranged from 1,300 ft^2/d (feet squared per day) to 1,300,000 ft^2/d.

Steady-state ground-water flow in the Upper Floridan aquifer was simulated using a three-dimensional ground-water flow model. Transmissivities ranging from less than 5,000 ft^2/d to greater than 11,000,000 ft^2/d were required to calibrate to observed conditions. Recharge rates used in the model ranged from 18.0 inches per year in areas where the aquifer was unconfined to less than 2 inches per year in broad areas where the aquifer was confined.

Contributing areas to five Tallahassee water-supply wells were simulated by particle-tracking techniques. Particles were seeded in model cells containing pumping wells then tracked backwards in time toward recharge areas. The contributing area for each well was simulated twice, once assuming a porosity of 25 percent and once assuming a porosity of 5 percent. A porosity of 25 percent is considered a reasonable average value for the Upper Floridan aquifer; the 5 percent porosity simulated the movement of ground-water through only solution-enhanced bedding plains and fractures. The contributing areas were generally elliptical in shape, reflecting the influence of the sloping potentiometric surface. The contributing areas delineated for a 5 percent porosity were always much larger than those determined using a 25 percent porosity. The lowest average ground-water velocity computed within a contributing area, using a 25 percent porosity, was 1.0 ft/d (foot per day) and the highest velocity was 1.6 ft/d. The lowest average ground-water velocity, determined using a 5 percent porosity, was 2.4 ft/d and the highest was 7.4 ft/d.

The contributing areas for each of the five wells was also determined analytically and

compared to the model-derived areas. The upgradient width of the simulated contributing areas were larger than the upgradient width of the analytically determined contributing areas for four of the five wells. The model could more accurately delineate contributing areas because of the ability to simulate wells as partially penetrating and by incorporating complex, three-dimensional aquifer characteristics, which the analytical method could not.

INTRODUCTION

Ground water from the Upper Floridan aquifer is the source of water-supply for Tallahassee, Fla., and for parts of the surrounding area. In most areas, the aquifer yields an ample supply of good quality water; however, in recent years low levels of tetrachloroethylene (PCE) have been detected in ground-water samples obtained from seven of the city's water-supply wells. PCE is attributed to past disposal practices of dry cleaners, service stations, and other businesses within the downtown area. The City of Tallahassee removes PCE from the water by passing it through granular-activated carbon units before distribution. This recent experience has increased the awareness of local authorities that ground-water resources need to be protected. To ensure that water-supply wells, presently free of contamination, remain clean, it is necessary to protect that portion of the aquifer from which the wells derive water. The delineation of areas contributing to supply wells requires an understanding of ground-water flow within the Upper Floridan aquifer. To gain this understanding, the U.S. Geological Survey (USGS), in cooperation with the City of Tallahassee and the Florida Department of Environmental Protection (FDEP), conducted an investigation of the Upper Floridan aquifer.

Purpose and Scope

The purpose of this report is to present the results of an investigation of that part of the Upper Floridan aquifer which underlies Tallahassee and Leon County, Fla., and the surrounding counties in north-central Florida and southwestern Georgia. The specific objectives of the investigation were to 1) determine the hydrogeologic framework of the Upper Floridan aquifer, 2) collect additional hydrogeologic data needed to characterize ground-water flow, 3) simulate ground-water flow using the USGS modular three-dimensional finite-difference ground-water flow model (MODFLOW) (McDonald and Harbaugh, 1988), 4) delineate contributing areas for selected City of Tallahassee water-supply wells, and 5) compare simulated contributing areas to analytically determined contributing areas. The contributing area of a pumping well, defined by Morrissey (1987), is the land area that has the same horizontal extent as that part of an aquifer..., from which ground-water flow is diverted to wells.

This report is organized to focus on the project objectives listed above and the following items are presented: 1) a description of the general hydrogeologic framework of the Upper Floridan aquifer in north-central Florida and southwestern Georgia, 2) a potentiometric-surface map of the Upper Floridan aquifer based on water levels measured during the fall of 1991, 3) river-discharge measurements made to estimate the volume of ground water discharging from the Upper Floridan aquifer in the fall of 1991, 4) an evaluation of the transmissivity of the Upper Floridan aquifer within downtown Tallahassee, determined with a multiple-well aquifer test, 5) a conceptual model of ground-water flow within the Upper Floridan aquifer describing flow directions, hydrologic boundaries, and ground-water sources and sinks, 6) the results of computer simulations of ground-water flow using MODFLOW (McDonald and Harbaugh, 1988), 7) a delineation of contributing areas to selected Tallahassee water-supply wells using the particle-tracking program MODPATH (Pollock, 1989), and 8) a comparison of the simulated and analytically determined contributing areas.

Study Area

The study area encompasses approximately 11,000 square miles in north-central Florida and southwestern Georgia (fig.1) and is within the Coastal Plain physiographic province. The topography is characterized by rolling hills and land-surface altitudes that range from about 350 ft above sea level in the north to sea level in the south. The study area extends to the major ground-water flow boundaries in the regional ground-water flow system, and thus encompasses the entire recharge area for ground water that moves beneath Leon County, Fla. The climate is humid subtropical with relatively high rainfall. From

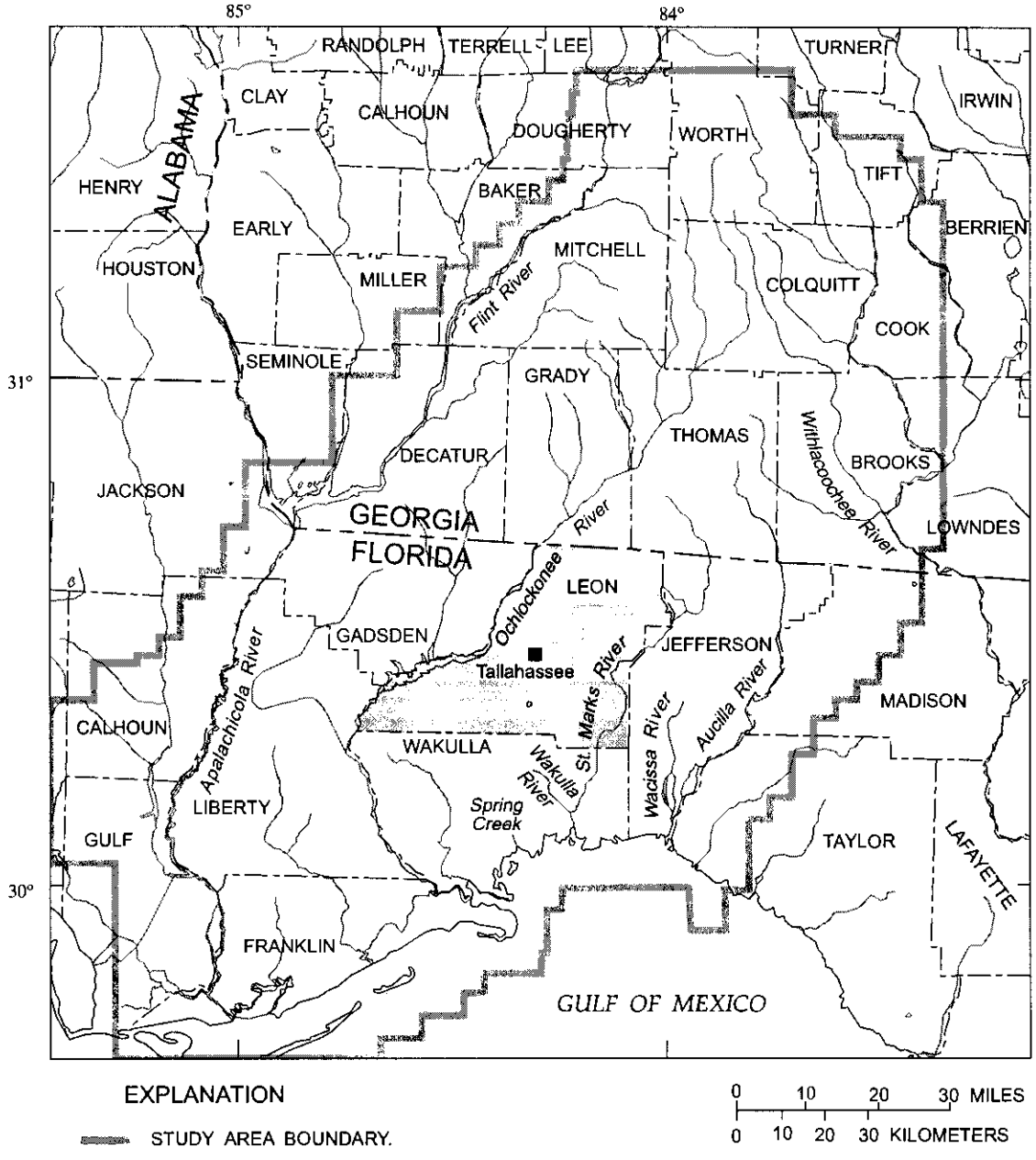

Figure 1. Study area in north-central Florida and southwestern Georgia.

1961 - 1990, the average annual temperature in Tallahassee was 67° F and the average precipitation was 66 in/yr (National Oceanic and Atmospheric Administration, oral commun., 1995).

The major physiographic features of the study area, delineated and described by Clark and Zisa (1976) for Georgia and by Brooks (1981) for Florida, were the Dougherty Plain District, Tifton Upland District, Apalachicola Delta District, and Ocala Uplift District (fig. 2). The topography of the Dougherty Plain District consists of gently rolling hills that are interrupted by numerous sinkholes. Karst topography prevails with many sinkholes still forming. The altitude within the Tifton Upland District ranges from about 480 ft in the north to 150 ft in the southeast, resulting in a gentle slope. This district contains a well

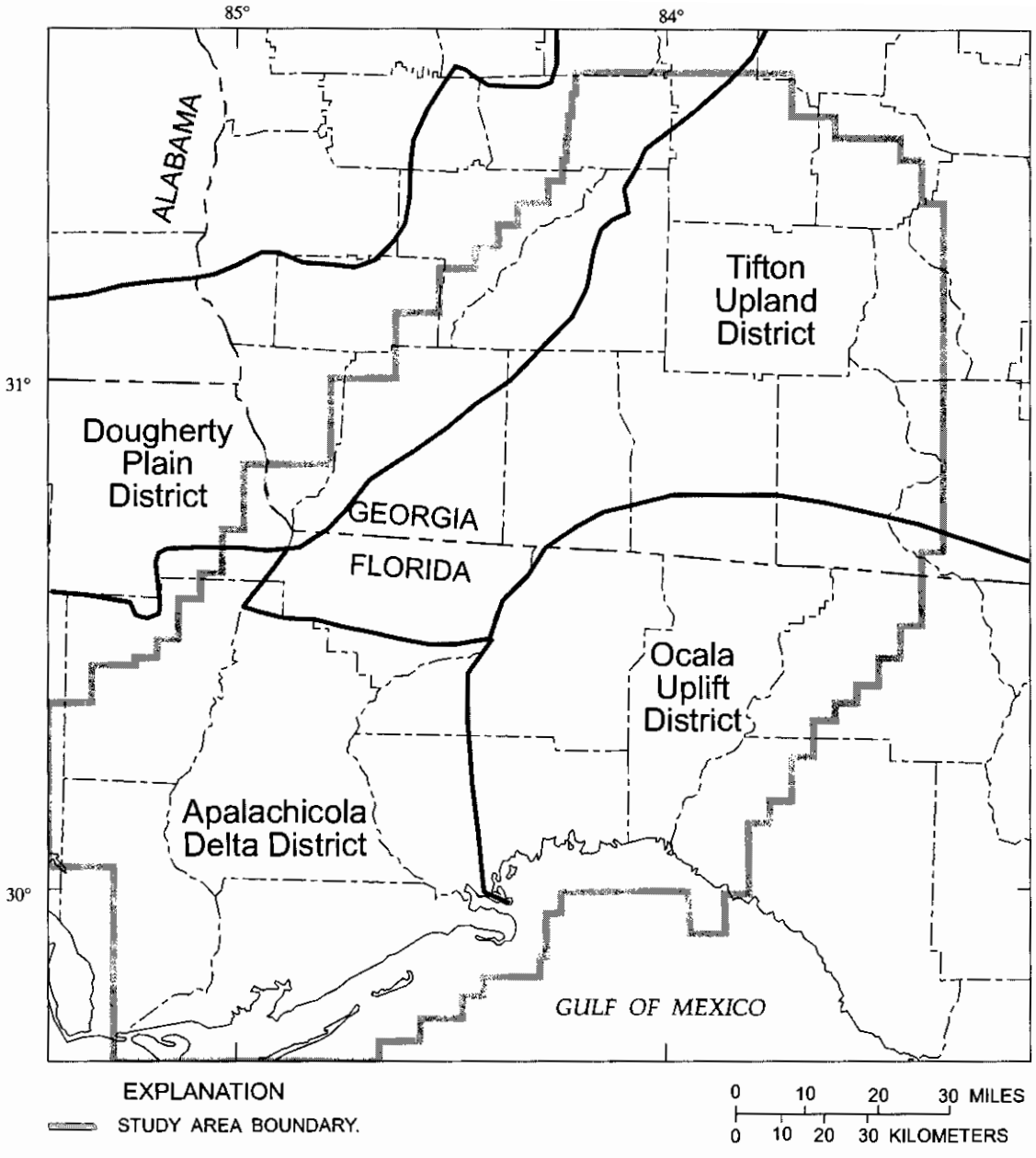

Figure 2. Major physiographic features in north-central Florida and southwestern Georgia (modified from Clark and Zisa, 1976, and Brooks, 1981).

developed dendritic drainage system. The Apalachicola Delta District contains river terraces and deltas, past and present, of the Apalachicola River and is a clastic terrain with no karst features. The topography of the Ocala Uplift District consists of gently rolling hills and in many places limestone occurs at or near land surface. The southward draining streams are continually modified by solution of the underlying limestones.

Previous Investigations

Hendry and Sproul (1966) investigated the geology and ground-water resources of Leon County. They described the geology and hydrology of the Upper Floridan aquifer, the overlying units, and the general water quality. Miller (1986) described the geology of the Floridan aquifer system that underlies all of Florida and parts of Georgia and South Carolina. Within the study area, Miller mapped the top, bottom, and

thickness of the Upper Floridan aquifer and described the geology of the formations that comprise the aquifer. His investigation was part of the Regional Aquifer System Analysis (RASA) program of the USGS. Bush and Johnston (1988) simulated ground-water flow in the entire Floridan aquifer system using a finite-difference model as part of the RASA program. During their investigation, model-derived transmissivities were determined for the Upper Floridan aquifer in the study area, as well as rates of recharge and discharge. A relatively coarse grid with spacing of 8 by 8 mi was used for these simulations.

GEOLOGIC SETTING

The study area is underlain by sedimentary rocks of Tertiary through Quaternary age that consist of limestone, dolostone, clay, and sand of varying degrees of lithification (Miller, 1986). The geologic units from oldest to youngest are: the Clayton Formation of Paleocene age, the Oldsmar Formation of early Eocene age, the Avon Park Formation of middle Eocene age, the Ocala Limestone of late Eocene age, the Suwannee Limestone of Oligocene age, the St. Marks and Chattahoochee Formations of early Miocene age, the Hawthorn Group of Miocene age, the Jackson Bluff, Miccosukee, and Citronelle Formations of Pliocene age, and the undifferentiated sediments of Pleistocene and Holocene age. A list of geologic units, their relation to the principal hydrogeologic units (aquifers and confining units), and corresponding model layers is shown in figure 3. The characteristics of the aquifers, confining units, and model layers are described in later sections. This report uses the terms St. Marks Formation, Chattahoochee Formation, and Hawthorn Group, because they are the currently accepted terminology of the Georgia and Florida Geological Surveys. The geologic descriptions in this section are based on work by Miller (1986), unless otherwise cited.

Sediments of Paleocene Age

The Paleocene-age Clayton Formation underlies the entire study area. The altitude at the top of this formation ranges from about 300 ft below sea level in the north to greater than 3,000 ft below sea level in the extreme south. The formation occurs as a massive calcareous marine clay in the southern part of the study area. Updip, it occurs as a fine- to medium-grained glauconitic sand and clayey sand with smaller amounts of medium- to dark-gray clay.

Sediments of Eocene Age

Eocene-age sediments can be subdivided into the Oldsmar and Avon Park Formations, and Ocala Limestone. The Oldsmar Formation underlies the entire study area, but consists of permeable limestones only in Wakulla, Leon, Jefferson, Taylor, and Madison Counties, Fla. Westward, the Oldsmar becomes increasingly argillaceous and less permeable as it interfingers with calcareous clastic rock. Northward, the Oldsmar grades from limestone to argillaceous limestone and calcareous clay into glauconitic calcareous sand. The altitude of the top of the permeable part of the Oldsmar Formation ranges from about 1,700 ft to greater than 2,500 ft below sea level and is approximately 500 feet thick.

The Avon Park Formation underlies the entire study area and ranges in thickness from about 300 ft in the north to about 1,200 ft in the south. The Avon Park consists of a permeable and relatively pure limestone only in parts of Wakulla, Leon, Jefferson, Taylor, and Madison Counties, Fla. Within these counties, the Avon Park Formation consists of a cream, tan, or light-brown, soft- to well-indurated limestone that is pelletal but locally micritic. To the west and north of these counties, the formation quickly grades into a low-permeability argillaceous, micritic, glauconitic limestone that, in turn, grades updip into calcareous, glauconitic, often shelly sand and clay beds. The altitude of the top of the permeable part of the Avon Park Formation ranges between 800 and 1,000 ft below sea level.

The Ocala Limestone is permeable through the entire study area and ranges in thickness from about 200 ft in the north to about 500 ft in the south. The altitude of the top of the Ocala is about 200 ft above sea level in the northwest where it outcrops in the Dougherty Plain. The Ocala slopes gently to the south, where it reaches depths of between 500 and 1,000 ft below sea level. The Ocala Limestone consists of two different rock types. The upper portion is a white, generally soft and friable, porous coquina consisting of foraminifera, bryozoan fragments, and whole to broken echinoid remains. The lower part of the Ocala Limestone is composed of cream to white, generally fine-grained, soft to semi-indurated, micritric limestone containing abundant miliolid remains and large foraminifers (Applin and Applin, 1944).

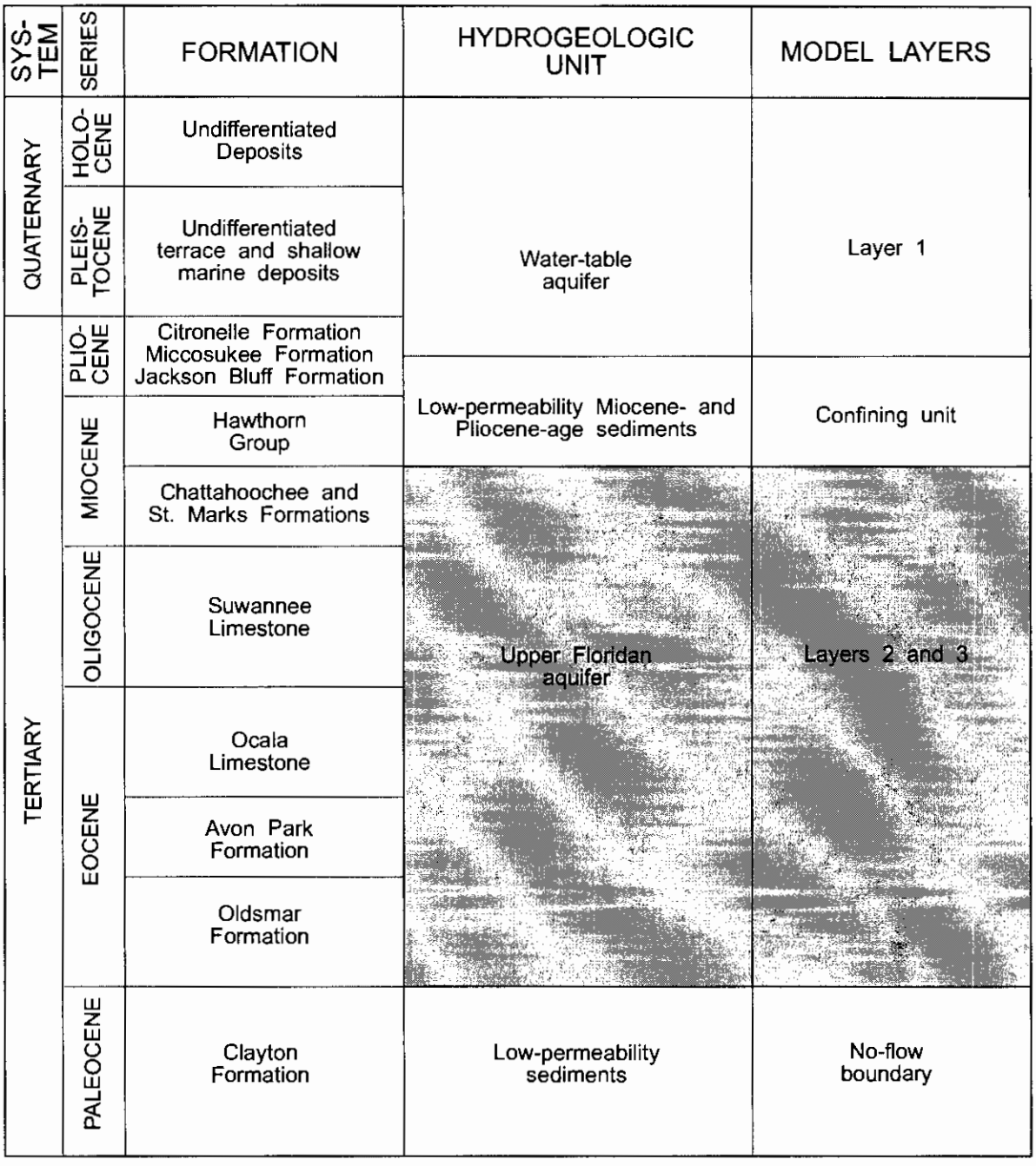

Figure 3. Relation of geologic units, hydrogeologic units, and model layers in north-central Florida and southwestern Georgia.

Sediments of Oligocene Age

The thickness of the Suwannee Limestone reaches a maximum of about 600 ft in the southwestern part of the study area and thins to less than 100 ft in the southeast, where it outcrops. The Suwannee also outcrops along the southern and western edge of the Dougherty Plain, but has been removed by erosion from most of the interior of the Dougherty Plain. The altitude of the top of the Suwannee ranges from just over 200 ft in the north to greater than 500 below sea level in the southwest. The Suwannee usually consists of two permeable rock types: 1) cream to tan, crystalline, highly vuggy limestone containing prominent

gastropod and pelecypod casts and molds and 2) white to cream, finely pelletal limestone containing small foraminifers and pellets of micrite bound to a finely crystalline limestone matrix.The two facies are interbedded and cannot be recognized at all locations.

Sediments of Miocene Age

The Miocene-age sediments can be subdivided into the St. Marks Formation, Chattahoochee Formation, and the Hawthorn Group. The St. Marks outcrops, or subcrops at shallow depths, in the western part of the Ocala Uplift Physiographic District. Northward, the St. Marks grades laterally into the Chattahoochee Formation. The Chattahoochee is not present in the Dougherty Plain due to lack of deposition or removal by erosion. The St. Marks is a predominantly fine- to medium-grained, partially recrystallized, silty to sandy limestone that has undergone degrees of secondary dolomitization (Hendry and Sproul, 1966). The Chattahoochee is primarily a dolostone containing quartz sand, clay, calcite, limestone, chert, mica, heavy minerals, phosphate, and fossils (Huddlestun, 1988). The permeability of the St. Marks and Chattahoochee Formations ranges from very permeable to relatively impermeable.

The Hawthorn Group is thin or absent in the Dougherty Plain and in parts of the Ocala Uplift due to lack of deposition or later removal by erosion. The group is thickest in the Apalachicola Delta Physiographic District and within the Tifton Uplands, where the thickness can exceed several hundred feet. The Hawthorn is predominantly sand and clay; subordinate components include dolomite, dolostone, calcite, limestone, phosphorite, phosphate, silica in the forms of claystone, chert, and siliceous microfossils, feldspar, heavy minerals, carbonaceous material and lignite, zeolites, and fossils (Huddlestun, 1988). Locally, in beds and lenses, dolostone, limestone, phosphorite, clay, or claystone can make up the dominant lithologies.

Sediments of Pliocene Age

The Pliocene-age sediments can be subdivided into several formations including the Jackson Bluff Formation, the Miccosukee Formation, and the Citronelle Formation. The Jackson Bluff and Citronelle Formations occur only in the southwestern part of the study area. The Jackson Bluff is composed of clayey sands and sandy clays that are very macrofossiliferous; the Miccosukee Formation is composed of interbedded and cross-bedded clays, silts, sands and gravels of varying coarseness and mixtures (Hendry and Sproul, 1966). The Citronelle Formation is composed of medium to coarse sand containing many stringers of gravel and a few thin clay beds. Similar in distribution to the Hawthorn Group, the Pliocene-age sediments are thin or absent in the Dougherty Plain and parts of the Ocala Uplift, and Tifton Uplands due to lack of deposition or later removal by erosion. Sediments of the Hawthorn Group and the clay, silts, and sandy clays of the Miccosukee and Jackson Bluff Formations form a continuous low-permeability unit that is referred to in this report as the low-permeability Miocene- and Pliocene-age sediments (fig. 3).

Sediments of Pleistocene and Holocene Age

Pleistocene-age sediments consist of medium- to coarse-grained, tan, white, and brown sand that locally contains trace amounts of carbonaceous material and shell fragments. The Holocene deposits include thin sand and gravel accumulations deposited mostly adjacent to streams, estuaries, and lagoons.

HYDROLOGIC SETTING

Aquifers in the study area include the water-table aquifer and Upper Floridan aquifer, which are separated by low-permeability Miocene- and Pliocene-age sediments (figs. 3 and 4). The water-table aquifer yields only small amounts of water when pumped and generally is not utilized. Some water, usually for domestic supply, is produced from the sandy units within the low-permeability Miocene- and Pliocene-age sediments. The Upper Floridan aquifer is utilized for municipal, industrial, agricultural, and domestic water supply. The transmissivity of the Upper Floridan aquifer ranges over several orders of magnitude within the study area. Where transmissivities are high, the Upper Floridan aquifer generally yields large quantities of good-quality water.

Water-Table Aquifer

The water-table aquifer lies within the shallow sediments exposed at land surface. The age of these sediments ranges from Holocene to Pliocene. The transmissivity ranges from very low where the

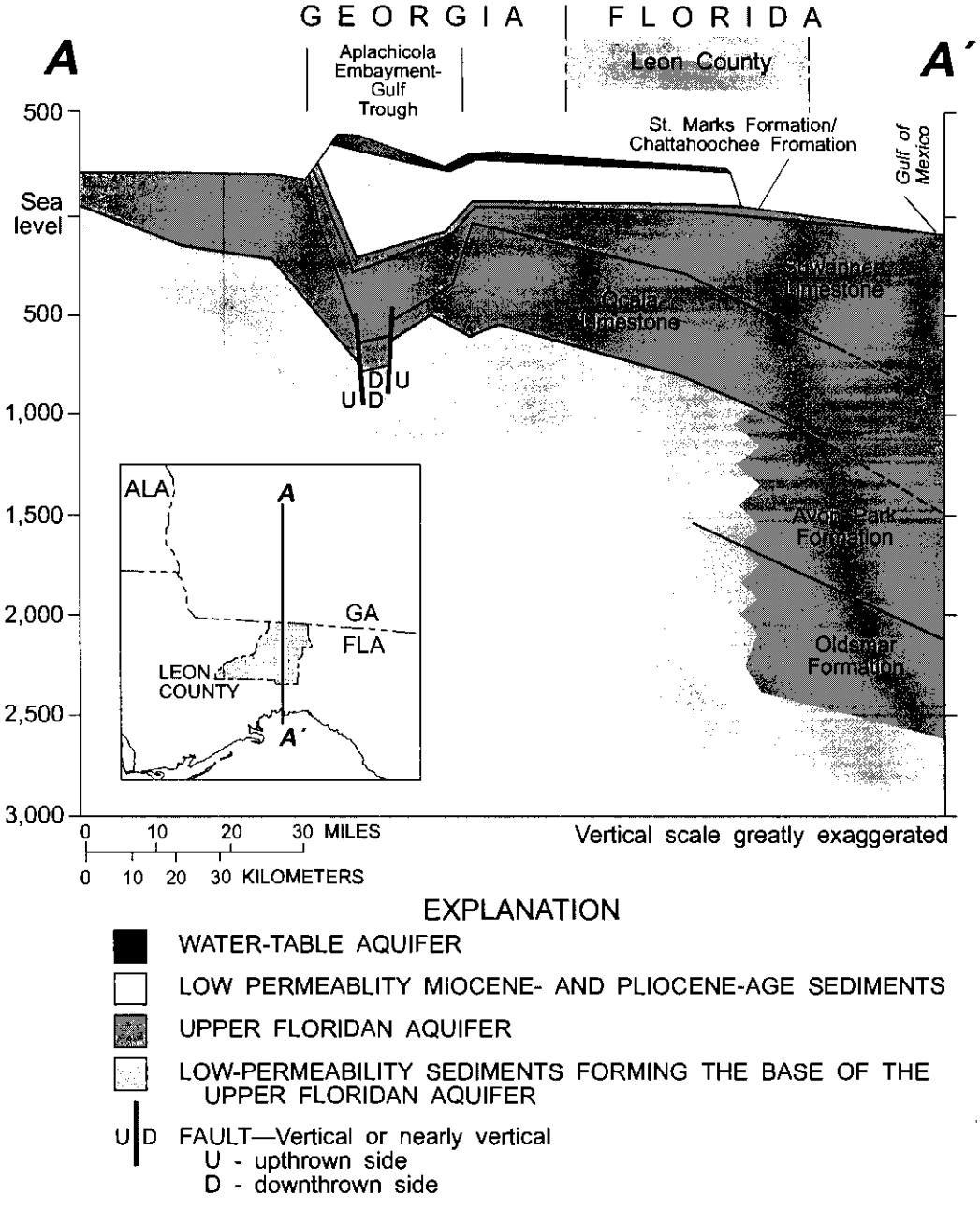

Figure 4. Generalized hydrogeologic section showing aquifers and geologic formations of the Upper Floridan aquifer in north-central Florida and southwestern Georgia.

sediments are fine grained, to moderately high where significant thicknesses of sand and gravel are present. The water-table aquifer is present through most of the study area and generally is less than 50 ft thick. It is generally absent from the Dougherty Plain and parts of the Ocala Uplift. In areas where the water-table aquifer is absent, the water table lies within the Upper Floridan aquifer.

Low-Permeability Miocene- and Pliocene-Age Sediments

The low-permeability Miocene- and Pliocene-age sediments overlie and in some areas confine the Upper Floridan aquifer. These sediments are several hundred feet thick in the Apalachicola Embayment-Gulf Trough feature (figs. 4 and 5). This feature has

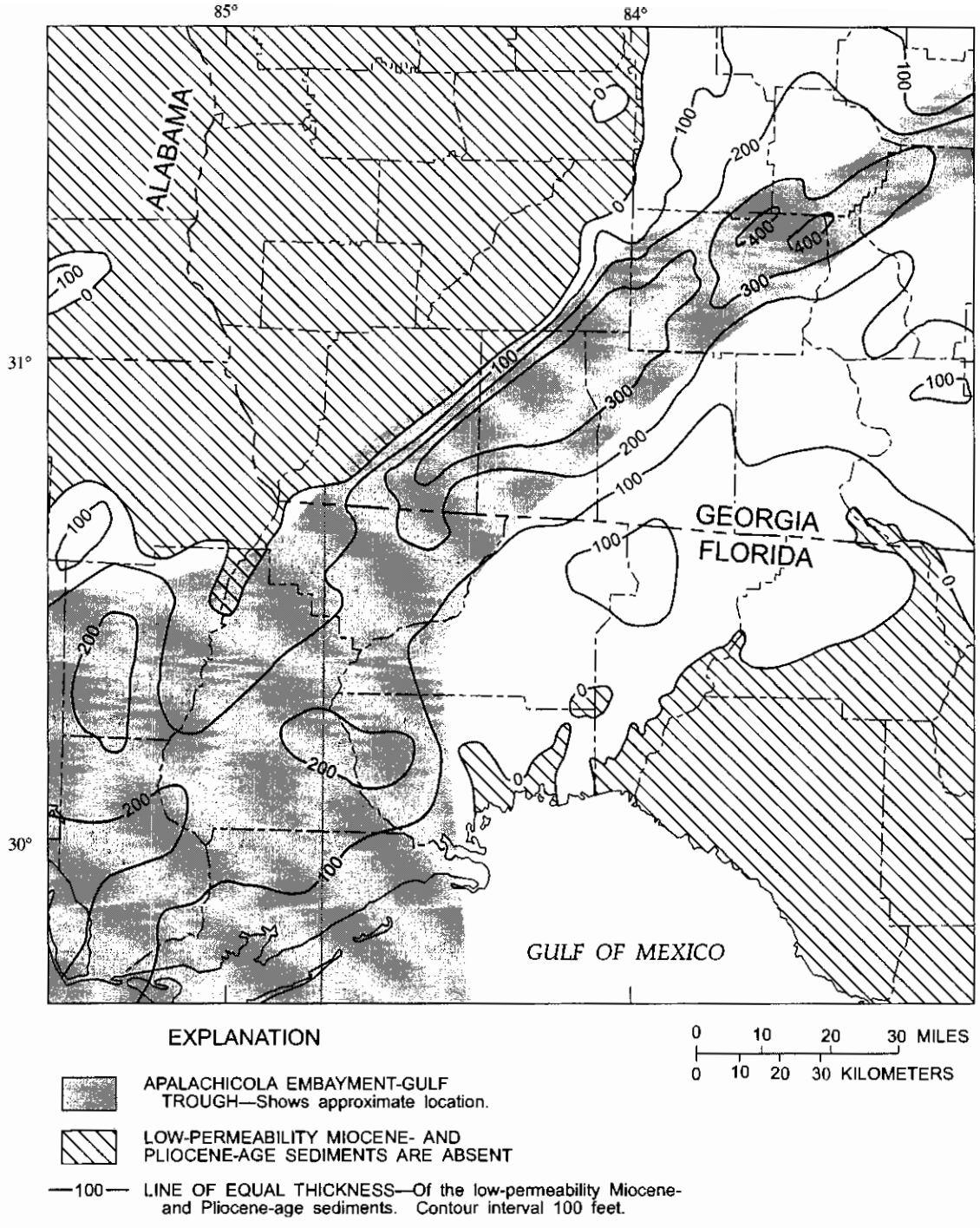

Figure 5. Thickness of low-permeability Miocene- and Pliocene-age sediments (modified from Miller, 1986).

been described as a marine channel that linked the Gulf of Mexico to the Atlantic Ocean during the early Tertiary (Huddlestun, 1988). Falling sea levels restricted circulation within this channel, allowing deposition of thick accumulations of fine grained material. The low-permeability Miocene- and Pliocene-age sediments are generally not present in the Dougherty Plain and are less than 100 ft thick in the Ocala Uplift District (fig.5) (Miller, 1986).

Upper Floridan Aquifer

The Upper Floridan aquifer is part of the Floridan aquifer system that occurs in Florida and parts of Georgia, South Carolina, and Alabama. Miller (1986) defined the Floridan aquifer system as a vertically continuous sequence of carbonate rocks of generally high permeability that are hydraulically connected in varying degrees and whose permeability is, in general, an order of magnitude to several orders of magnitude greater than those of the rocks that bound the system. Within the study area, the Upper Floridan aquifer includes all or parts of the Oldsmar Formation, Avon Park Formation, Ocala Limestone, Suwannee Limestone, St.Marks Formation, and Chattahoochee Formation (fig. 4).

Miller delineated the Upper Floridan aquifer based on the permeability characteristics of the rocks, thus neither the top nor bottom of the aquifer necessarily conforms to formation or time-stratigraphic boundaries. The altitude of the top of the Upper Floridan aquifer (fig. 6) ranges from about 200 ft above sea level in the Dougherty Plain to greater than 400 ft below sea level in parts of the Apalachicola Delta District and Tifton Uplands. The Upper Floridan aquifer is uplifted along the Barwick Arch (Sever, 1966), a subregional feature that lies southeast of the Apalachicola Embayment-Gulf Trough. The altitude of the base of the aquifer (fig. 7) ranges from 200 ft above sea level in the north, where it pinches out, to greater than 2,200 ft below sea level in the south. The aquifer thickens from about 100 ft in the north (fig. 8) to greater than 2,000 ft in the south.

Hydraulic Properties of the Upper Floridan Aquifer

Bush and Johnston (1988) conducted an investigation of the entire Floridan aquifer system and observed that carbonate rocks are nearly always characterized by an uneven distribution of permeability. Throughout much of the area where the Upper Floridan aquifer occurs, the water-bearing openings consist of one or more of the following: 1) openings in loosely cemented fossil hashes that are similar to the interstices of sands, 2) mosaics of many fractures and solution-widened joints, and 3) solution cavities ranging in size from less than 1 in to tens of feet or more. Large solution cavities generally occur near large springs and some sinkholes where dissolution of the limestone is greatest, but these areas represent only a small part of the aquifer on a regional scale. In areas away from the large solution openings, the fist two conditions dominate. The transmissivity of the Upper Floridan aquifer is directly related to the thickness and lithology of the overlying low-permeability sediments. Thinner and more permeable overlying sediments allow greater rates of infiltration and increased dissolution of the limestones. The removal of these sediments from some areas during Pleistocene time is largely responsible for the current distribution of karst, and, therefore, the current distribution of transmissivity.

Transmissivity values determined by aquifer tests for the Upper Floridan aquifer vary greatly within the study area, ranging from 1,300 ft^2/d to 1,300,000 ft^2/d (fig. 9). The highest transmissivity values generally occur within the Dougherty Plain, Ocala Uplift, and parts of the Tifton Uplands where the overlying low-permeability sediments are thinnest or absent. The lowest transmissivity values generally occur within the Apalachicola Embayment - Gulf Trough where the overlying low-permeability sediments are thickest.

Bush and Johnston (1988) simulated ground-water flow using a finite difference model. Their investigation indicated that transmissivity values were as high as 1,000,000 ft^2/d in the Dougherty Plain, ranged between 10,000 and 50,000 ft^2/d along the axis of the Apalachicola Embayment - Gulf Trough, and were greater than 1,000,000 ft^2/d in parts of the Ocala Uplift and Tifton Uplands. Assigned transmissivities in some areas near large springs were as high as 10,000,000 ft^2/d. Kellam and Gorday (1990) also recognized that the Upper Floridan aquifer, within the Apalachicola Embayment - Gulf Trough, consisted of poorly permeability limestones. They attributed the lower permeabilities to a combination of factors: 1) the lower primary permeability of the deeper-water limestones deposited in the feature, 2) the greater thickness of overburden which limits development of secondary porosity, and 3) possibly a lack of joints and fractures to enhance ground-water movement. They further postulated that ground-water movement was sluggish in parts of the feature based on high levels of dissolved ions in the water.

Ground-Water Pumpage

Wells and water-supply systems that withdraw water from the Upper Floridan aquifer are listed in table 1 and locations are shown in figure 10. Generally, the list contains wells or systems that pump, on

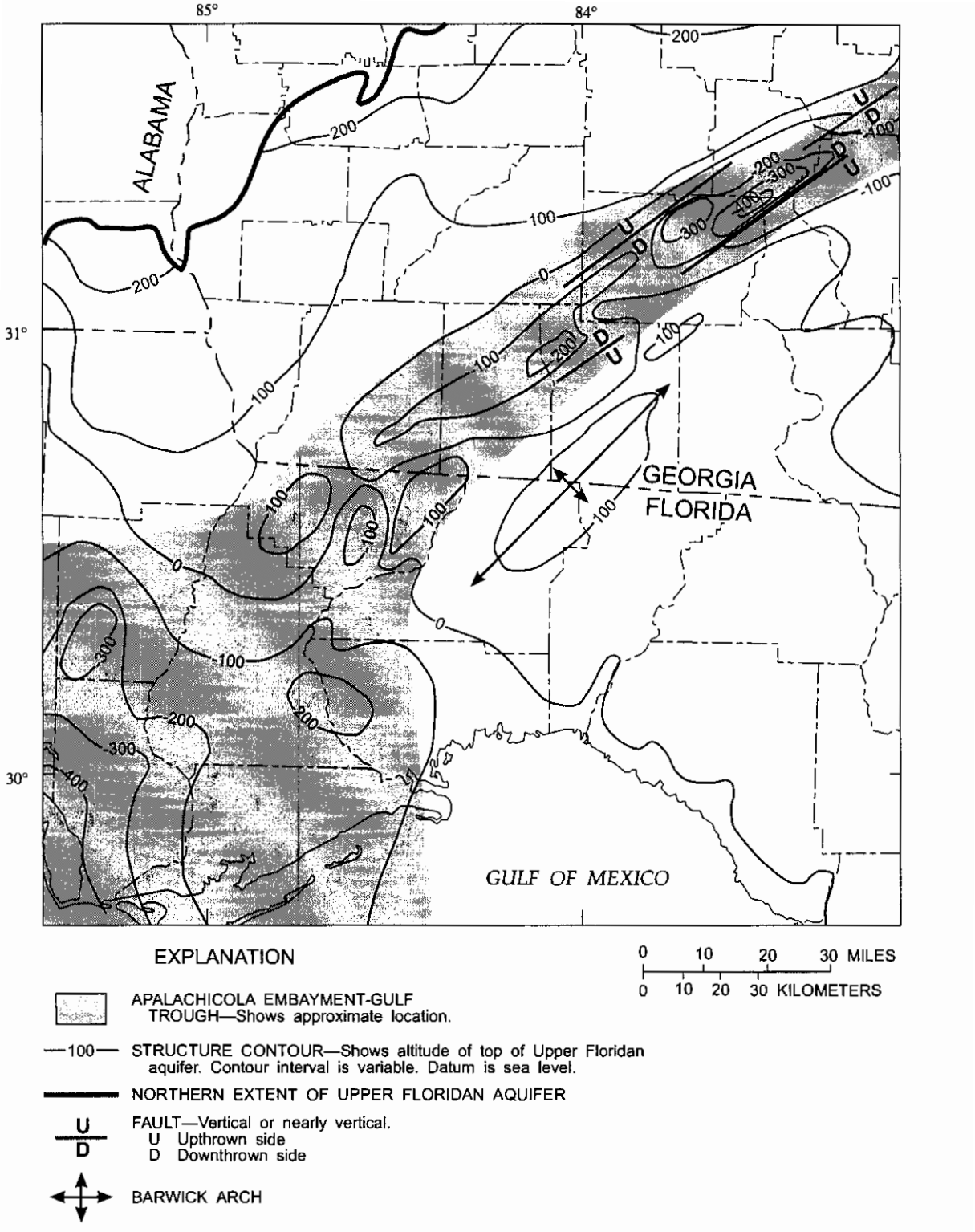

Figure 6. Structure at the top of the Upper Floridan aquifer (modified from Miller, 1986).

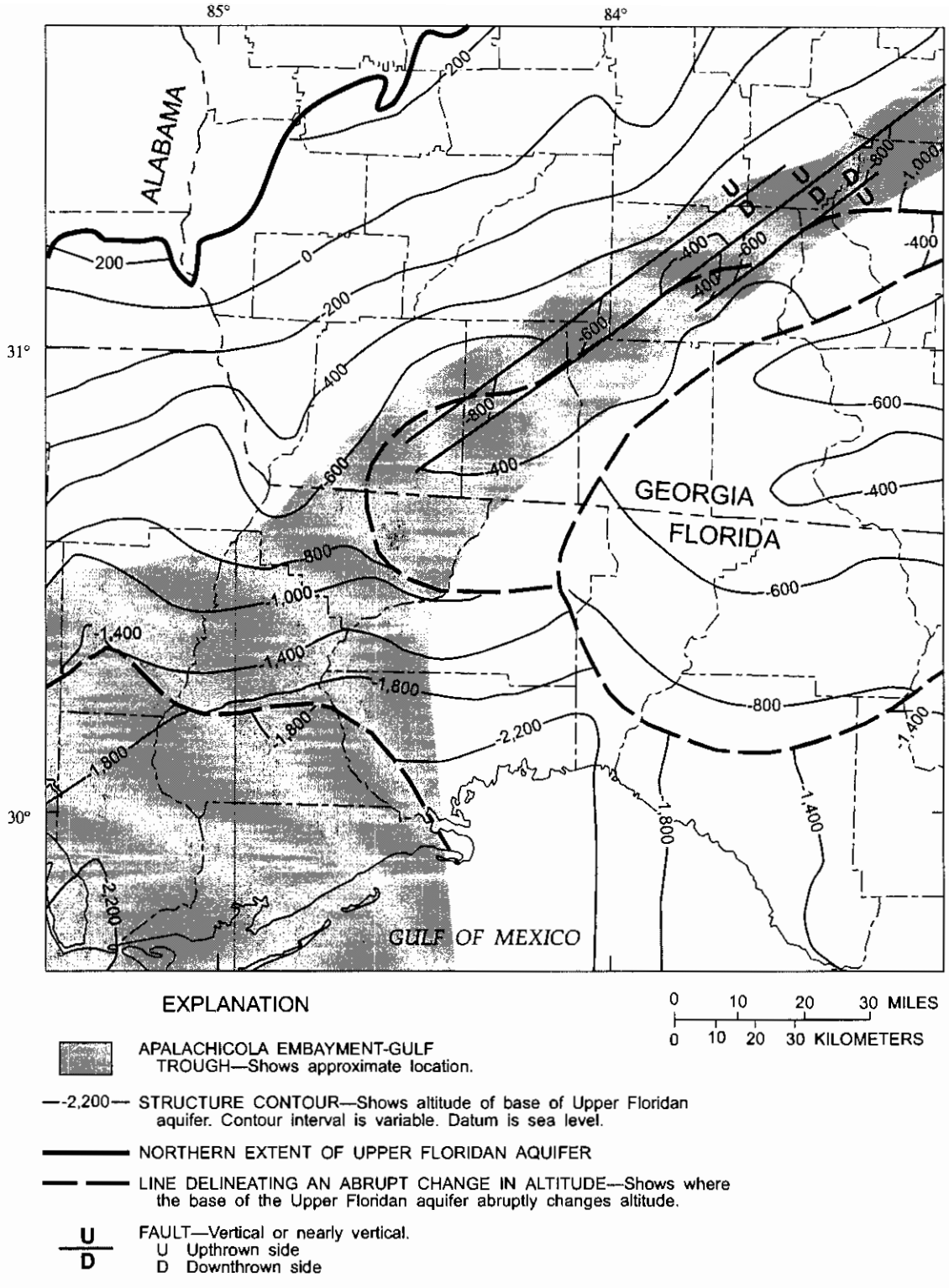

Figure 7. Structure at the base of the Upper Floridan aquifer (modified from Miller, 1986).

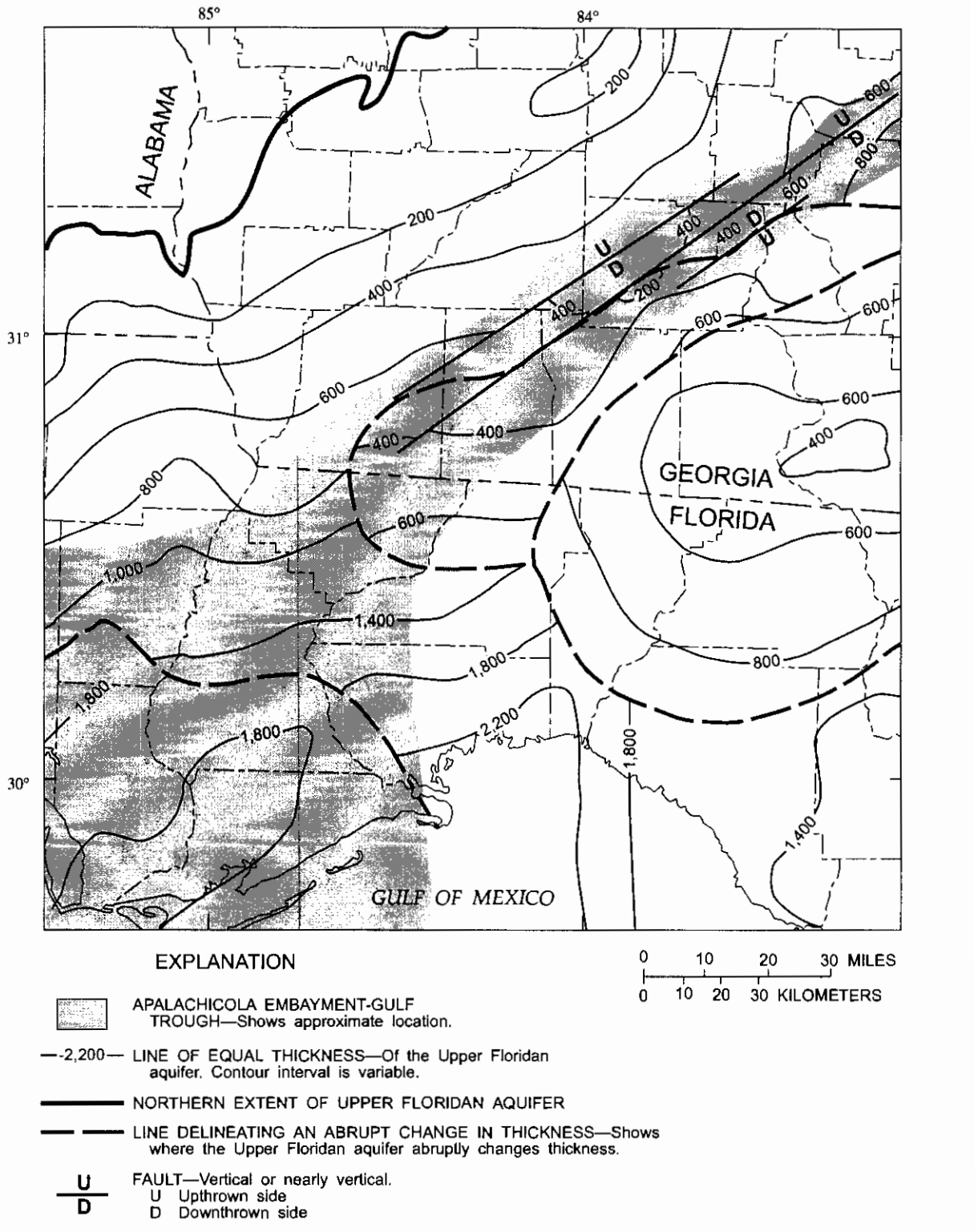

Figure 8. Thickness of the Upper Floridan aquifer (modified from Miller, 1986).

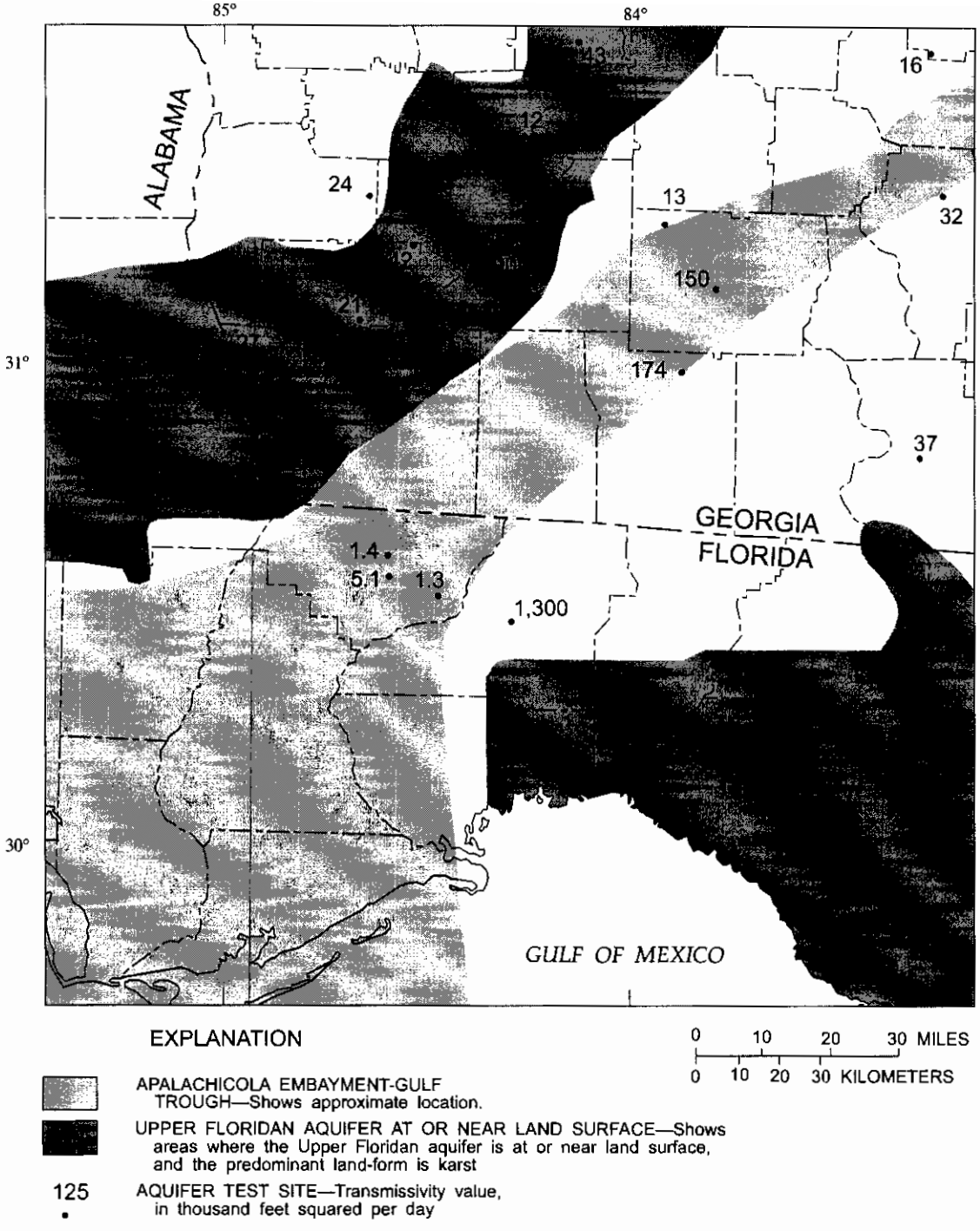

Figure 9. Values of transmissivity of the Upper Floridan aquifer as determined by aquifer testing (modified from Bush and Johnson, 1988).

average, greater than 70 gal/min, although systems that pump lower rates were included if the information was readily available. This list does not include any domestic supply wells, because they pump much less than 70 gal/min. Although individual domestic supply wells pump relatively small amounts of ground water, the number of these wells can be large. Within Leon County, Fla., more than 6,000 domestic supply wells have been drilled since 1976 (Jay Johnson, City of Tallahassee, oral commun., 1995).

Table 1. Pumpage from the Upper Floridan aquifer in north-central Florida and southwestern Georgia

[Source of pumping data for wells in Florida is the Northwest Florida Water Management District unless otherwise cited. Source for wells in Georgia is the U.S. Geological Survey unless otherwise cited; gal/min, gallons per minute]

Site	Owner	Pumping rate for well or well system, in gal/min[1]	County
	STATE OF FLORIDA		
1	CHATTAHOOCHEE- CITY OF	422	GADSDEN
2	SNEADS- TOWN OF	146	JACKSON
3	FL. DEPT OF CORRECTIONS	389	JACKSON
4	STATE OF FLORIDA	685	GADSDEN
5	GULF POWER PLANT	264	JACKSON
6	HAVANA- TOWN OF	363	GADSDEN
7	GRETNA- TOWN OF	116	GADSDEN
8	TALQUIN ELECTRIC	138	LEON
9	TALQUIN ELECTRIC	150	LEON
10	TALQUIN -LK JACKSON-9	64[2]	LEON
11	ROWE DRILLING	347	LEON
12	MONTICELLO- CITY OF	484[3]	JEFFERSON
13	TALQUIN -LK JACKSON-8	236[2]	LEON
14	TALQUIN -SHILOH	84[2]	GADSDEN
15	TALQUIN -LK JACKSON-5	56	LEON
16	TALQUIN -LK JACKSON-1	152	LEON
17	TALQUIN -LK JACKSON-4	79	LEON
18	TALQUIN -SHILOH	64[2]	GADSDEN
19	ROWE DRILLING	556	LEON
20	ROWE DRILLING	556	LEON
21	ROWE DRILLING	556	LEON
22	ROWE DRILLING	625	LEON
23	BELL- PEARLE MAE	625	LEON
24	ROWE DRILLING	694	LEON
25	TALLAHASSEE- POWER PLANT	2932	LEON
26	BRISTOL- CITY OF	123	LIBERTY
27	TALLAHASSEE- CITY OF	17,153	LEON
28	GREENVILLE- TOWN OF	81	MADISON
29	BLOUNTSTOUN- CITY	278	CALHOUN
30	U.S. DEPT. OF JUSTICE	144	LEON
31	DEERTREE HILLS	417	LEON
32	POSEY, HOMER	556	LEON
33	TALQUIN ELECTRIC	75	LEON
34	TALQUIN ELECTRIC	80	LEON
35	NOVAK- BILL	556	LEON
36	TIMBER ENERGY	394	LIBERTY
37	TALQUIN ELECTRIC	134	WAKULLA
38	OLIN BALL POWDER	556	WAKULLA
39	TALLAHASSEE- CITY OF	229	WAKULLA
40	SOPCHOPPY- CITY OF	185	WAKULLA
41	PANACEA WATER SYSTEM	116	WAKULLA
42	ALLIGATOR POINT	69	FRANKLIN
43	LANARK WATER & SEWER	104	FRANKLIN
44	CARABELLE- CITY OF	130	FRANKLIN
45	LEISURE PROPERTIES	111	FRANKLIN
46	APALACHICOLA- CITY	465	FRANKLIN
	STATE OF GEORGIA		
1	MILLER BREWING CO	590	DOUGHERTY
2	US MARINE CORPS LOGISTICS	548	DOUGHERTY
3	PROCTOR&GAMBLE PROD	253[4]	DOUGHERTY
4	CITY OF SYLVESTER WAT&LT	479[4]	WORTH
5	ABRAHAM BALDWIN AG COLLEG	69	TIFT
6	MERCK & CO INC	3271	DOUGHERTY
7	CITY OF TIFTON	3701	TIFT
8	TIFT CO WATER SYSTEM	131[4]	TIFT
9	CITY OF OMEGA	90	TIFT
10	CITY OF NEWTON	69[4]	BAKER
11	TOWN OF NORMAN PARK	104[4]	COLQUITT
12	CITY OF CAMILLA	35[4]	MITCHELL
13	SWIFT INDEPENDENT PACKING	385[4]	COLQUITT
14	CITY OF MOULTRIE	1625	COLQUITT
15	CITY OF ADEL	1062	COOK
16	CITY OF PELHAM	1513[4]	MITCHELL
17	CITY OF MEIGS	83	THOMAS
18	CITY OF CECIL	69[4]	COOK
19	WAVERLY MINERAL PRODUCTS	69[4]	THOMAS
20	OIL DRI CORP OF GA	90[4]	THOMAS
21	AMOCO FABRICS	389	DECATUR
22	CITY OF BAINBRIDGE	1590[4]	DECATUR
23	DECATUR CO INDUST AIR PK	125	DECATUR
24	CITY OF BARWICK	48[4]	BROOKS
25	CITY OF CAIRO	1631	GRADY
26	SUNNYLAND FOODS INC	83[4]	THOMAS
27	CITY OF THOMASVILLE	2489	THOMAS
28	CITY OF BOSTON	76	THOMAS
29	CITY OF QUITMAN	632	BROOKS
30	CITY OF ATTAPULGUS	69[4]	DECATUR

[1]Average pumping rate during November 1991, unless otherwise cited.

[2]Source: Florida Department of Environmental Protection sanitary well permits.

[3]Source: Suwannee River Water Management District.

[4]Average pumping rate for November 1990.

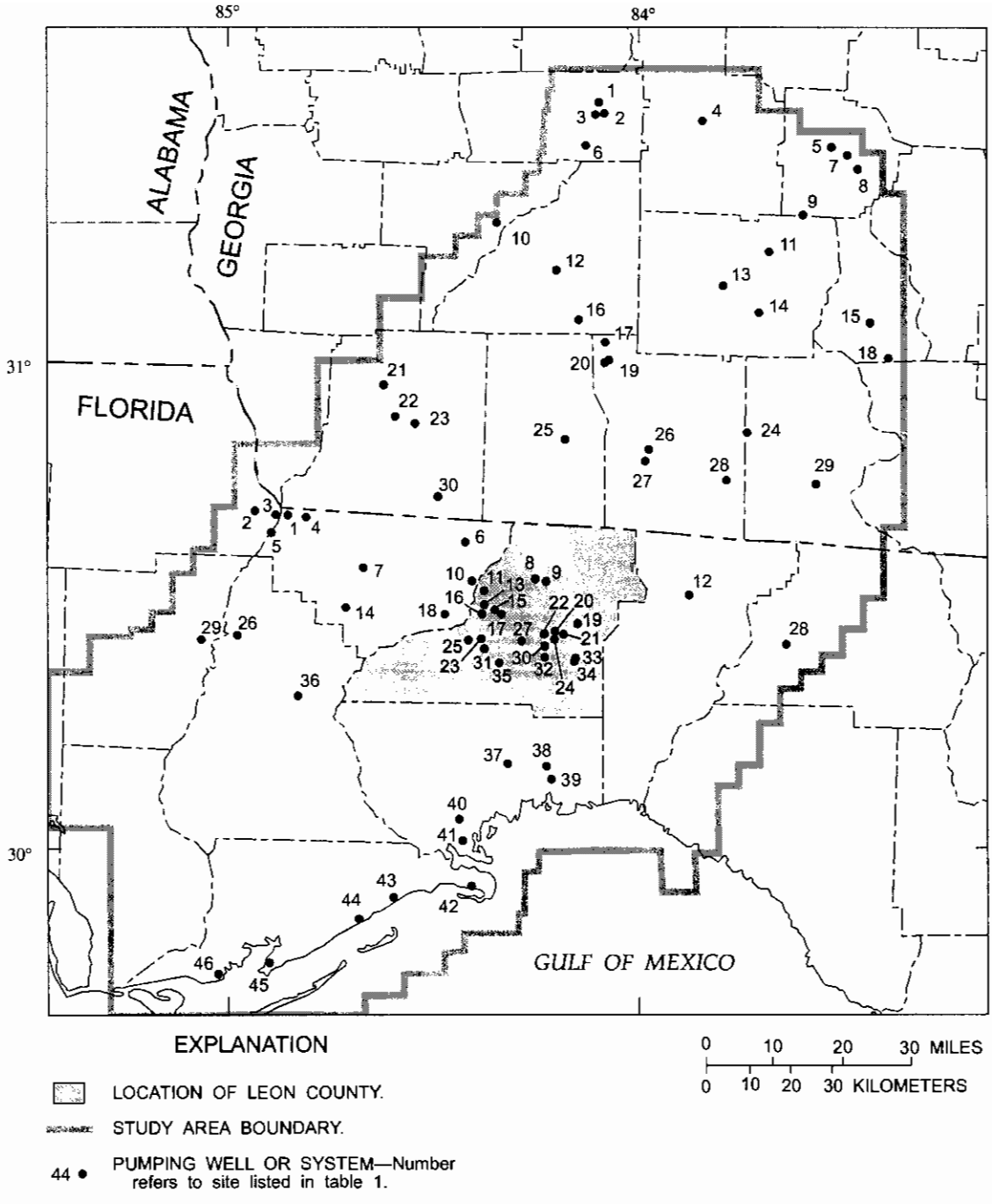

Figure 10. Water-supply wells and systems that withdraw water from the Upper Floridan aquifer (numbers refer to wells or systems listed in table 1).

DATA COLLECTION

A data-collection program was undertaken to quantify hydrologic conditions needed for calibration of a ground-water flow model. Model calibration involves successfully simulating measured hydrologic conditions within acceptable limits of error, as will be discussed later. The potentiometric surface of the Upper Floridan aquifer was estimated by measuring ground-water levels in a network of wells. The rate of ground-water discharge to rivers from the Upper

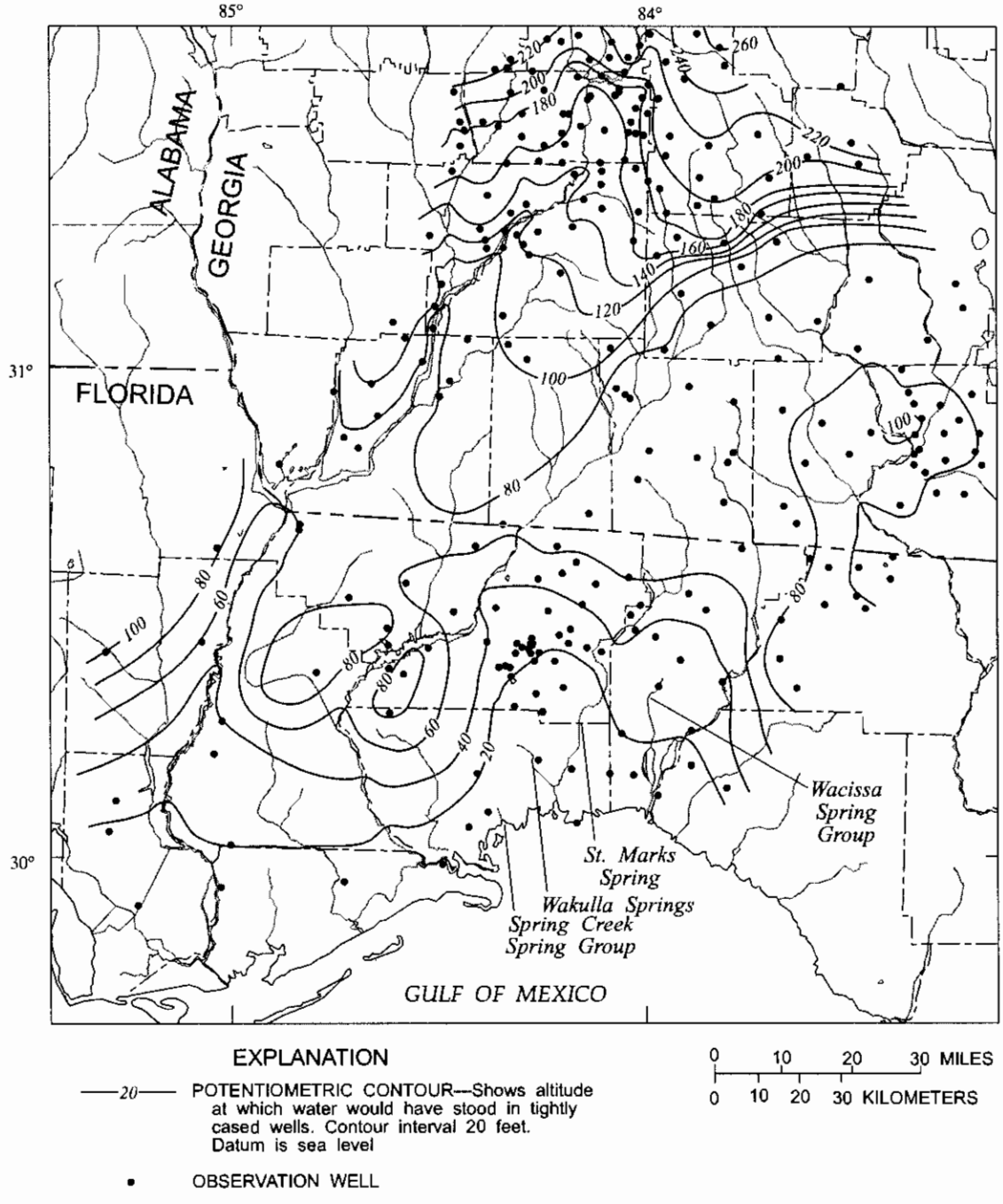

Figure 11. Altitude of the potentiometric surface of the Upper Floridan aquifer during October- November 1991.

Floridan aquifer was quantified by measuring river-discharge rates under base-flow conditions. One aquifer test was conducted to determine the transmissivity of the Upper Floridan aquifer that underlies downtown Tallahassee.

Water-Level Measurements

A potentiometric surface map of the Upper Floridan aquifer (fig. 11) was constructed from ground-water measurements made in 274 wells during the period October 21 to November 8, 1991. Wells

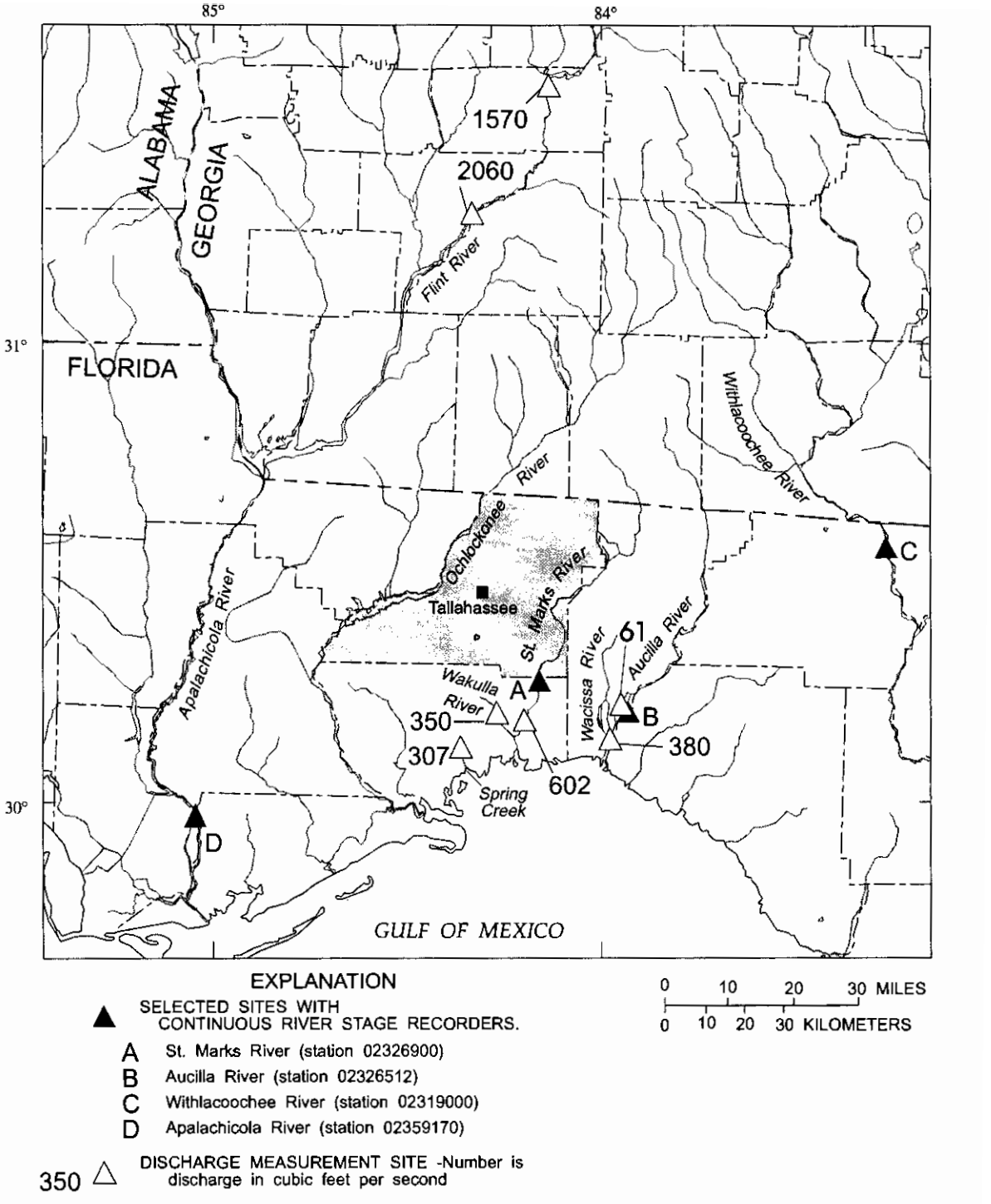

Figure 12. River-discharge measurement sites and related discharge rates on November 1, 1991.

were selected from data bases of agencies that included the USGS, Northwest Florida Water Management District, City of Tallahassee, and Florida Department of Environmental Protection.

River-Discharge Measurements

River-discharge measurements were made at seven locations, on November 1, 1991 (fig. 12) and were made concurrently with the ground-water level

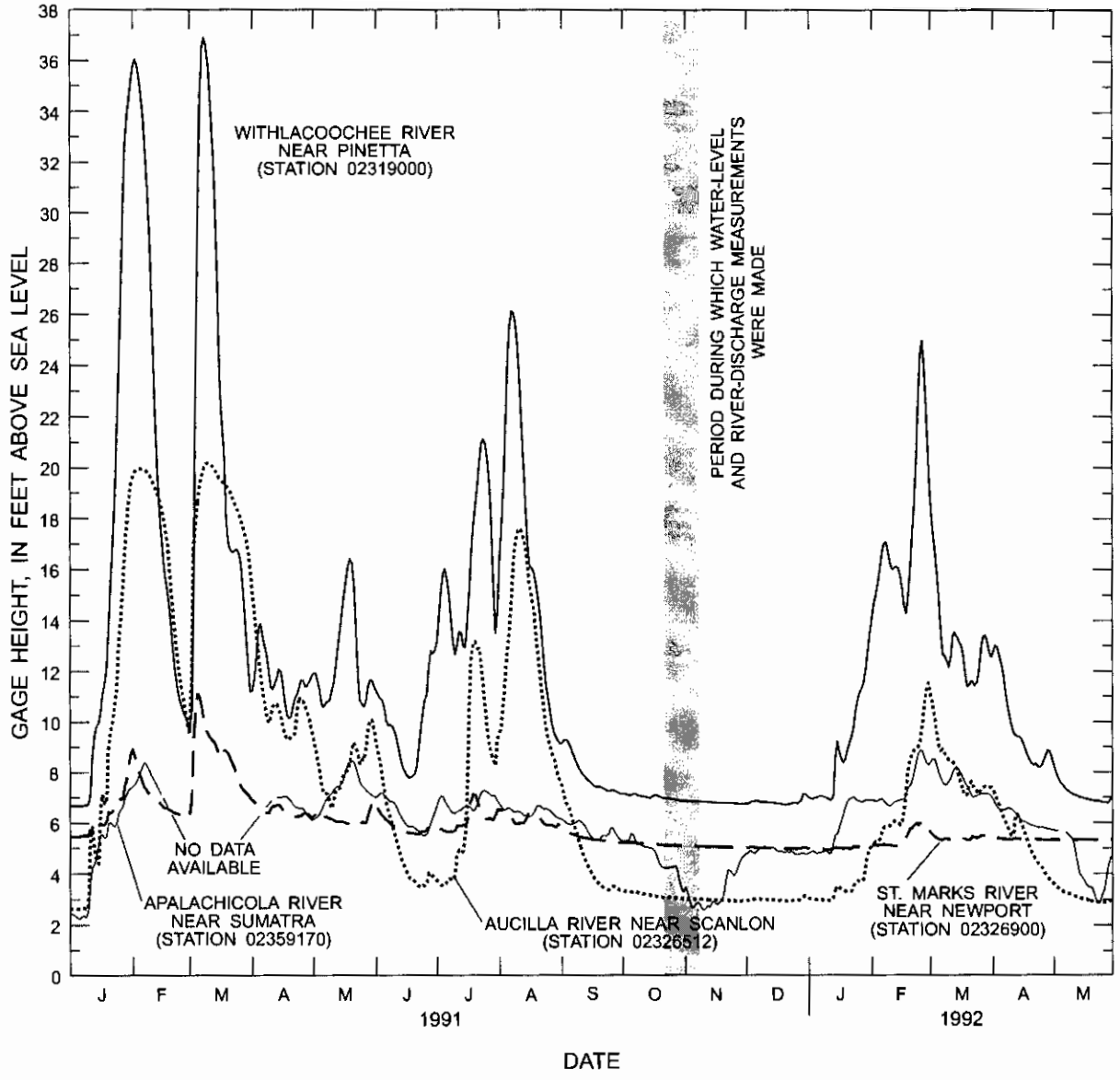

Figure 13. River stages at stations on the St. Marks, Aucilla, Withlacoochee, and Apalachicola Rivers from January 1991 through May 1992.

measurements. Three of the discharge measurements were obtained at established USGS gaging stations. Discharges of the Aucilla, St. Marks, and Wakulla Rivers, and Spring Creek were measured directly using a Price current meter and standard USGS flow-measuring techniques. The amount of error in measuring river discharges varies from station to station and measurement quality can range from very good (within 5 percent) to good (5 - 8 percent) to poor (greater than 10 percent). The error in the discharge measurements of the Aucilla, St. Marks, and Wakulla Rivers, and Spring Creek was estimated at about 10 percent; the other measurements ranged from very good to good. Discharge in the Apalachicola River and the Ochlockonee River and its tributaries was not measured because they are separated from the Upper Floridan aquifer by low-permeability sediments, and are not considered lines of discharge from the Upper Floridan aquifer.

Rivers in the study area were at base-flow conditions during field-data collection due to several months of low rainfall. Base-flow conditions were indicated by constant and low river stages in the Withlacoochee, St. Marks, Aucilla, and Apalachicola Rivers (fig. 13). Variability in stage in the

Apalachicola River is due to dams upstream storing and releasing water and not the variability caused by base flow.

Aquifer Testing

An aquifer test was conducted during November 1992. The purpose of the test was to: 1) determine the transmissivity of the Upper Floridan aquifer at a site within Tallahassee, 2) determine if the aquifer is a single vertically connected hydraulic unit, and 3) to determine if the aquifer acted as porous medium at the aquifer test scale. The test was conducted using the following methodology: City of Tallahassee well 2 was pumped at 1,400 gal/min for 8 days while water levels were measured in five monitoring wells (table 2, fig. 14). After 8 days, the pumping well was turned off and recovery was monitored for 5 hours in well 4, which was equipped with a pressure transducer.

Table 2. Description of pumping and monitoring wells used for aquifer test analysis

[--, not applicable. Locations of wells are shown on fig. 14.]

Monitoring well number	Altitude, in feet above sea level	Well depth, in feet below land surface	Casing depth, in feet below land surface	Distance from pumping well, in feet
Pumping Well:				
City #2	187	415	213	--
Monitoring Wells:				
1	213.32	300	220	1,127
2	212.60	602	485	1,108
3	195.89	340	189	1,220
4	205.47	320	210	805
5	185.99	300	190	1,325

Monitoring wells 1, 3, 4, and 5 had been installed prior to this investigation. Monitoring well 2 was drilled as part of this study. One purpose of the deep well (well 2) was to allow observation of the aquifer response in the lower part of the Upper Floridan aquifer during the aquifer test. Many existing wells penetrate the upper part of the aquifer, but very few penetrate the lower part. Consequently, little is known about the vertical hydraulic connection between the upper and lower parts of the Upper Floridan aquifer. Caliper, natural-gamma, acoustic-velocity, gamma-gamma, salt-tracer, fluid-resistivity, electric long- and short-normal resistivity, focused-resistivity, and spontaneous-potential geophysical logging was performed on the deep well. The geophysical logs showed numerous small openings of several inches in the upper 300 ft of the limestone. The openings are attributed to circulating ground water which dissolved the limestone as it moved along bedding planes and fractures. Such openings were not observed in the limestone in the lower 100 ft of the well; however, this section was believed to be very porous due to the loss of circulation during mud-rotary drilling. Based on the geophysical logs, the permeability of the Upper Floridan aquifer at the test site is considered the result of a mosaic of many fractures and solution-widened joints and openings in loosely cemented fossil hashes that are similar to the interstices of sands.

The aquifer-test data were analyzed by the Theis method (Lohman, 1979). A composite log-log plot of the water-level drawdown data and fitted Theis curve is shown in figure 14. Only data from the first 24 hours of the test were used in the calculation of transmissivity because the later data were affected by city pumpage occurring in areas away from the test and by rainfall. The drawdown data from wells 3, 4, and 5 plotted near a single line (the fitted Theis curve). Using these wells, a transmissivity of 1,300,000 ft^2/d was computed for the Upper Floridan aquifer. Although this is a large transmissivity value, it falls well within the range of values determined by Bush and Johnston (1988).

Wells 1 and 2 are located side-by-side, with well 1 completed in the upper third of the aquifer and well 2 completed in the lower half. The drawdown data from well 2 plotted slightly to the right of the fitted Theis curve, whereas drawdown data from well 1 plotted farther to the right. The delayed response of water levels at these wells could be due to an increase in aquifer storage in the direction of these wells. An increase in storage could be caused by greater dissolution of the limestone creating, a greater volume of void space than elsewhere in the aquifer.

During the aquifer test, water levels at well 2 (the deep well) responded to pumping slightly more quickly than well 1 (the shallow well), even though the pumping well is open at approximately the same interval as well 1 and above well 2. This indicates that a good vertical connection exists between the upper and lower parts of the aquifer and that the Upper Floridan aquifer does act as a single vertically connected unit. Long-term water-level measurements made in these two wells from May 1992 through October 1993

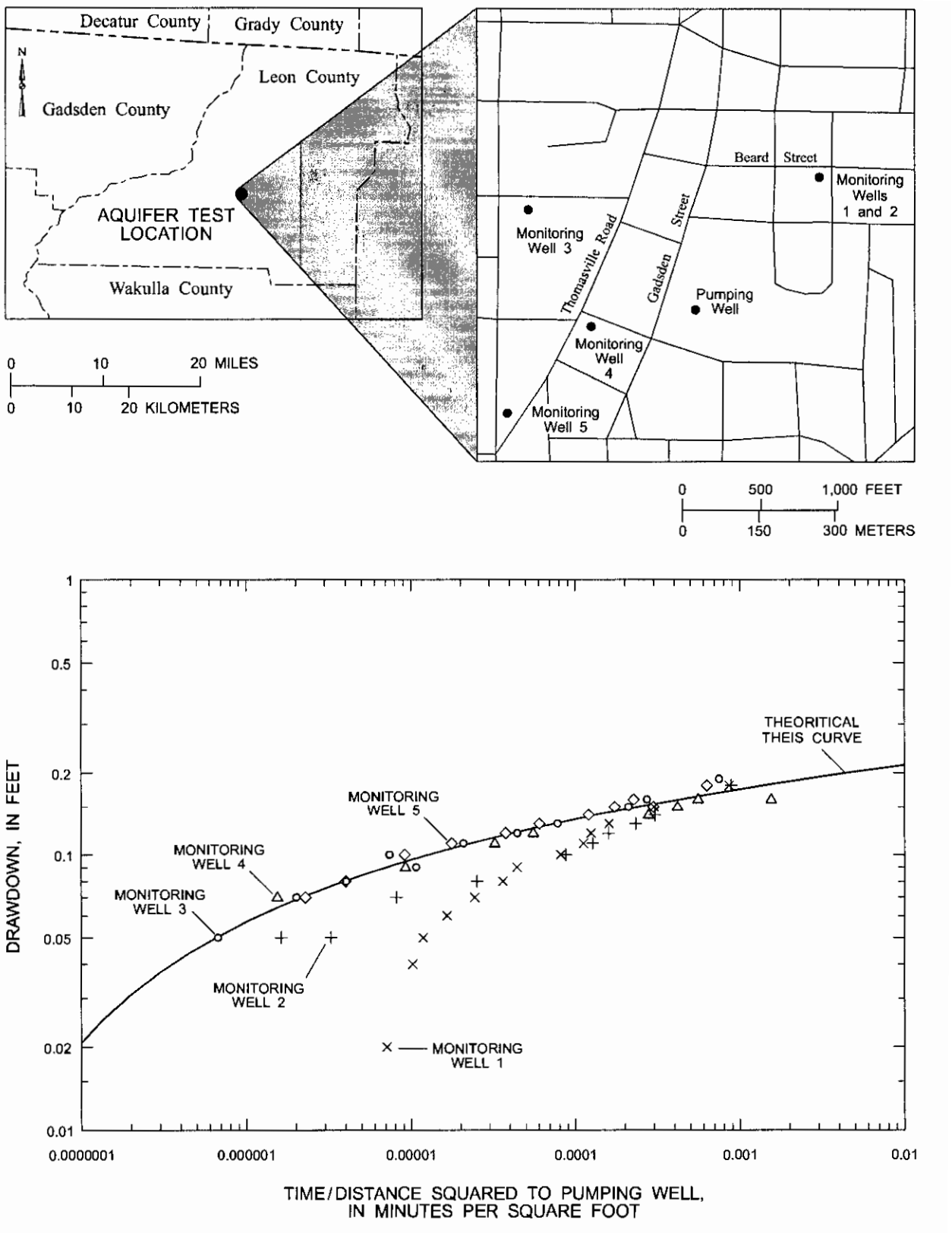

Figure 14. Aquifer response during testing conducted in November 1992, Tallahassee, Fla.

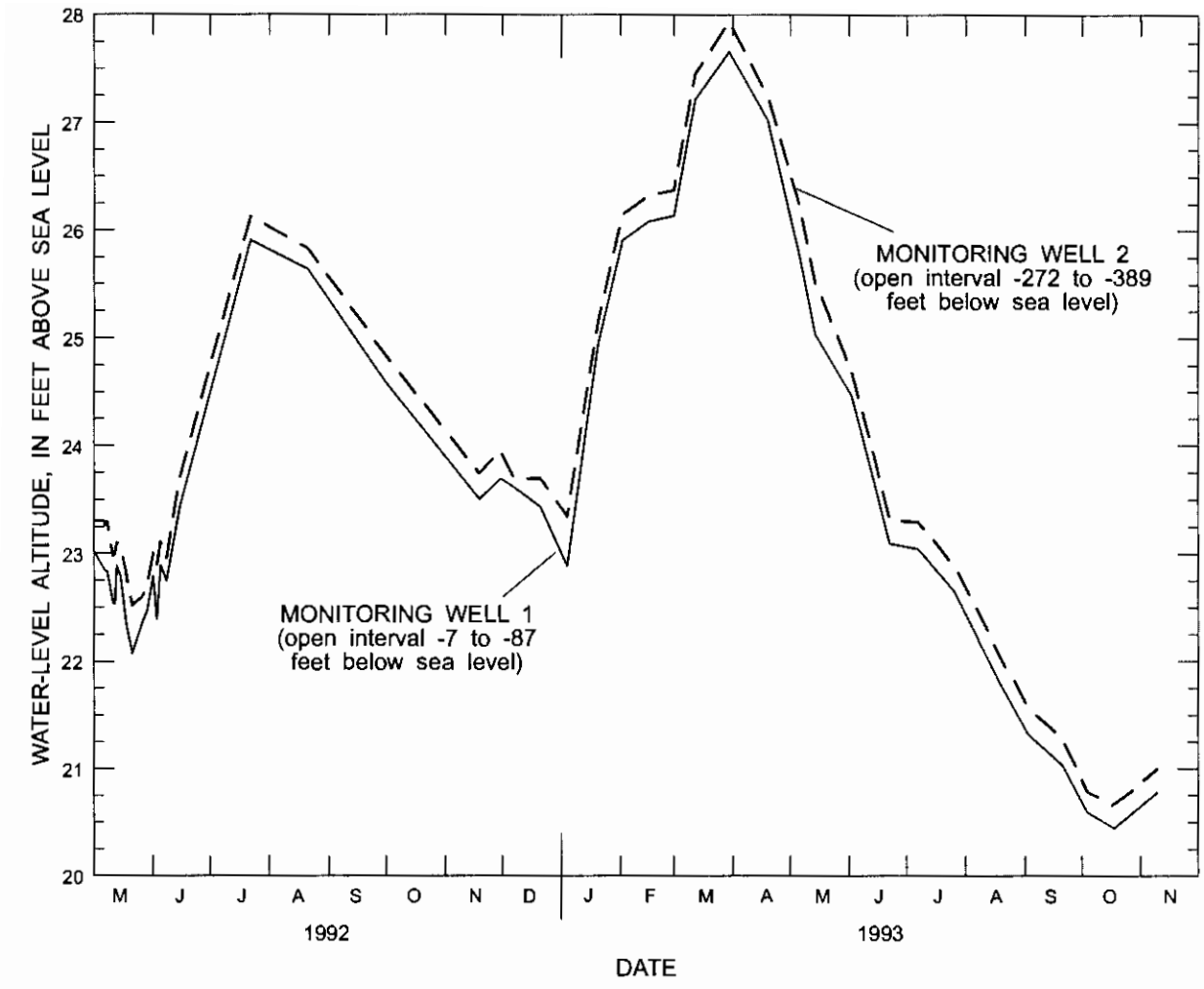

Figure 15. Water-level altitudes in monitoring wells 1 and 2 in Tallahassee, Fla., May 1992 through October 1993.

(fig. 15) show a close correlation of water-level altitudes, further indicating a good vertical connection.

Bush and Johnston (1988) reviewed many Floridan aquifer tests and found that data for many of these tests could be matched to the classic nonleaky, leaky, or delayed-yield response curves, even though the methods are based strictly on porous media assumptions. However, they further argued that porous media assumptions are probably valid in the Upper Floridan aquifer on the scale of the typical aquifer test where the cone of depression is hundreds if not thousands of feet across and where the aquifer response curves matched theoretical curves. For the Tallahassee test, the match between the theoretical Theis curve and the aquifer test data indicated that at the aquifer test scale, the Upper Floridan aquifer responded as a porous medium.

CONCEPTUAL MODEL OF THE GROUND-WATER FLOW SYSTEM

Developing a conceptual model of the aquifer system is an important step in constructing a computer model that accurately simulates ground-water flow. The Upper Floridan aquifer is conceptualized as having the following characteristics: 1) ground-water flow is in a state of dynamic equilibrium and thus can be investigated by assuming steady-state conditions during long term periods, 2) the aquifer acts a single water-bearing unit, 3) the aquifer is recharged by precipitation, and 4) discharge occurs as spring flow, leakage to rivers, leakage to the Gulf of Mexico, and pumpage. Developing a conceptual model also includes locating ground-water divides, determining

ground-water flow directions, and determining areas of recharge and discharge.

The location of the ground-water divides and general directions of ground-water flow were determined from the potentiometric surface map (fig. 16). The most prominent ground-water divide is positioned almost parallel to the axis of the Apalachicola Embayment-Gulf Trough feature. Ground water, on the western side of this divide, will discharge directly into the Flint River or discharge as upward diffuse leakage in the region of the Apalachicola River and Gulf of Mexico. Ground water east of this divide moves generally south toward either the large springs in and around Leon County or toward the Withlacoochee River near the Florida-Georgia border. The exact location of the dividing line between the ground-water basin drained by the large springs in and around Leon County and the basin drained by the Withlacoochee River is not readily apparent and was not drawn. Ground water in the Upper Floridan aquifer, moving beneath Leon County, could have entered the aquifer in counties to the west and north as shown in figures 16 and 17.

The position of the ground-water divides are not necessarily fixed and could move with changing recharge and discharge rates. The position of the divide along the Apalachicola Embayment-Gulf Trough probably fluctuates very little whereas the position of the divide that separates flow to the large springs in and around Leon County and flow to the springs in the Withlacoochee River could fluctuate significantly. For this reason, the study area boundaries were chosen to coincide with rivers, where possible, because their locations are fixed.

As indicated on the regional potentiometric maps for May 1985 (Bush and others, 1987) and May 1980 (Bush and Johnston, 1988), a saddle in the potentiometric surface occurs in Georgia along the eastern part of the study area. Only the westward half of this saddle is indicated on figure 16, the eastward half would occur outside the study area. A ground-water divide would occur at the low point of the saddle. However, the exact location of this divide is difficult to determine because the gradients are so low. Accordingly, ground-water flow out of the study area could occur, and because the transmissivity is high, this outflow could be significant.

The Upper Floridan aquifer within the study area is considered to be in a state of dynamic equilibrium. Dynamic equilibrium is indicated because there have been no known long term changes in the potentiometric surface of the Upper Floridan aquifer, although it has fluctuated seasonally and yearly in response to variations in rainfall (fig. 18). As shown in the figure, water levels rise in this Leon County well during extended periods of high rainfall and slowly decline during periods of low rainfall, but there appears to be no long-term trend of rising or declining water levels in the period from 1984 to 1992. Other studies agree with this finding. Hydrographs were examined from wells located in Leon and Wakulla Counties, Florida, and Seminole, Decatur, Miller, Mitchell, and Dougherty Counties, Georgia. These hydrographs also indicated only seasonal variation and no long-term water-level declines; consequently, the Leon County hydrograph is considered representative of Upper Floridan aquifer hydrographs in the study area and is the only one presented. Bush and Johnston (1988) found that the net decline between the estimated predevelopment potentiometric surface and the observed potentiometric surface in May 1980, was less than 10 ft (and could have been zero). The potentiometric surface shown on figure 16 was similar to the potentiometric surface measured in May 1985 (Bush and others, 1897) and in May 1980 (Bush and Johnston, 1988). The minor differences that occurred were attributed to different data point densities or minor seasonal fluctuations. Hendry and Sproul (1966) plotted the water-level altitudes of two Upper Floridan aquifer wells and one water-table aquifer well (located in Leon County) for the time period 1946 to 1965. The water levels showed seasonal and yearly fluctuations, but no long-term changes were apparent.

Ground-water flow in the Upper Floridan aquifer can be evaluated using steady-state methods, which are a special case of dynamic equilibrium. Assuming long-term steady-state conditions, the net recharge rate to the aquifer is the flux necessary to maintain the head in the aquifer at a constant level. This implies that the average recharge rate is equal to the average discharge rate over the long term, and that the volume of ground water stored in the aquifer does not change. No ground-water system will ever be at true steady-state. Freeze and Cherry (1979, p. 194) stated that if fluctuations in water-level altitudes are small in comparison with the total vertical thickness of the aquifer and the relative configuration of the potentiometric surface remains the same, then the system can be considered steady state. Hendry and Sproul (1966), after examining water-level records for 20 wells within Leon County, determined the maximum range in water-levels (the difference between the highest and lowest) was

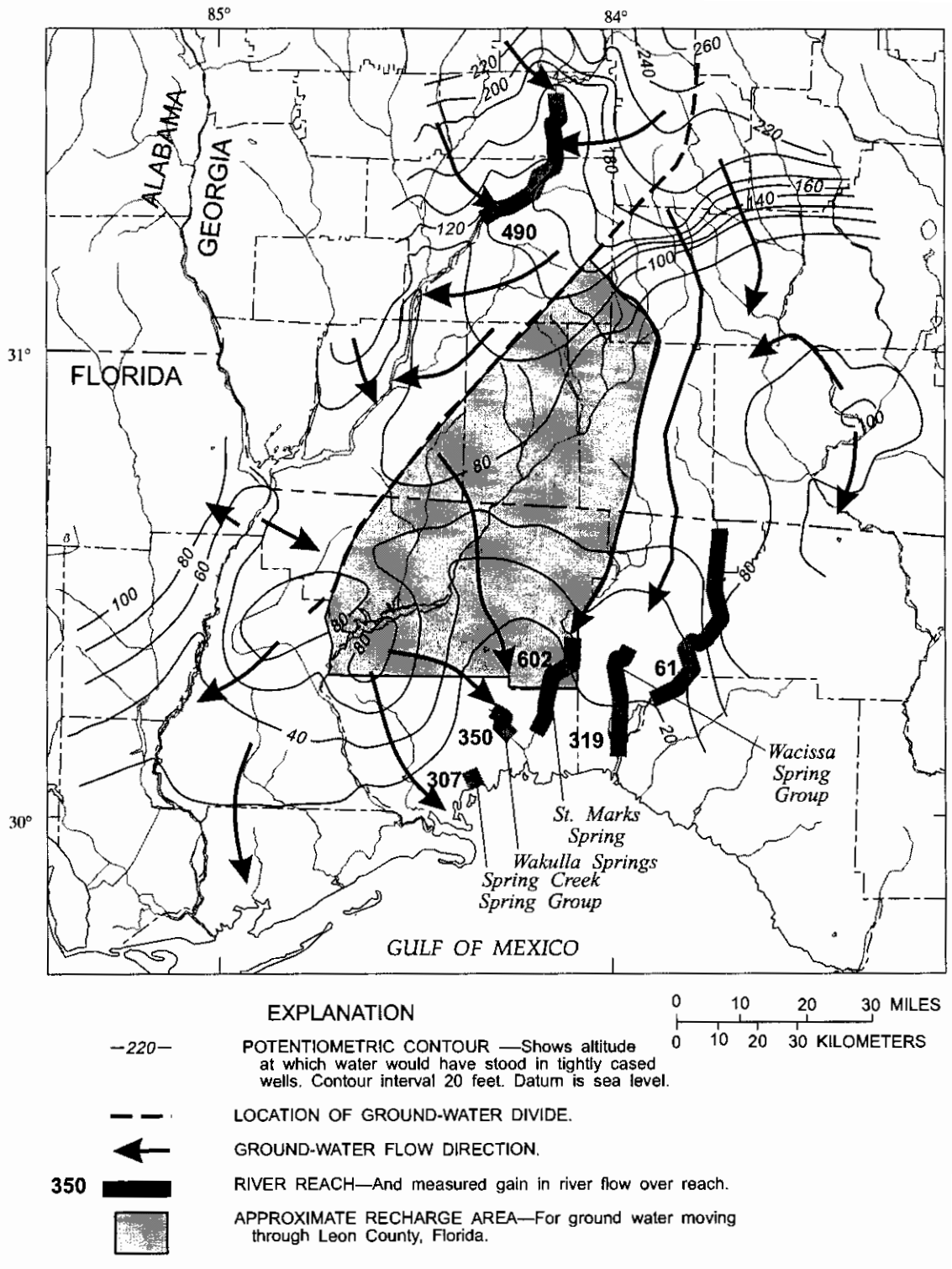

Figure 16. Ground-water flow directions, and net gain in river flow during October-November 1991.

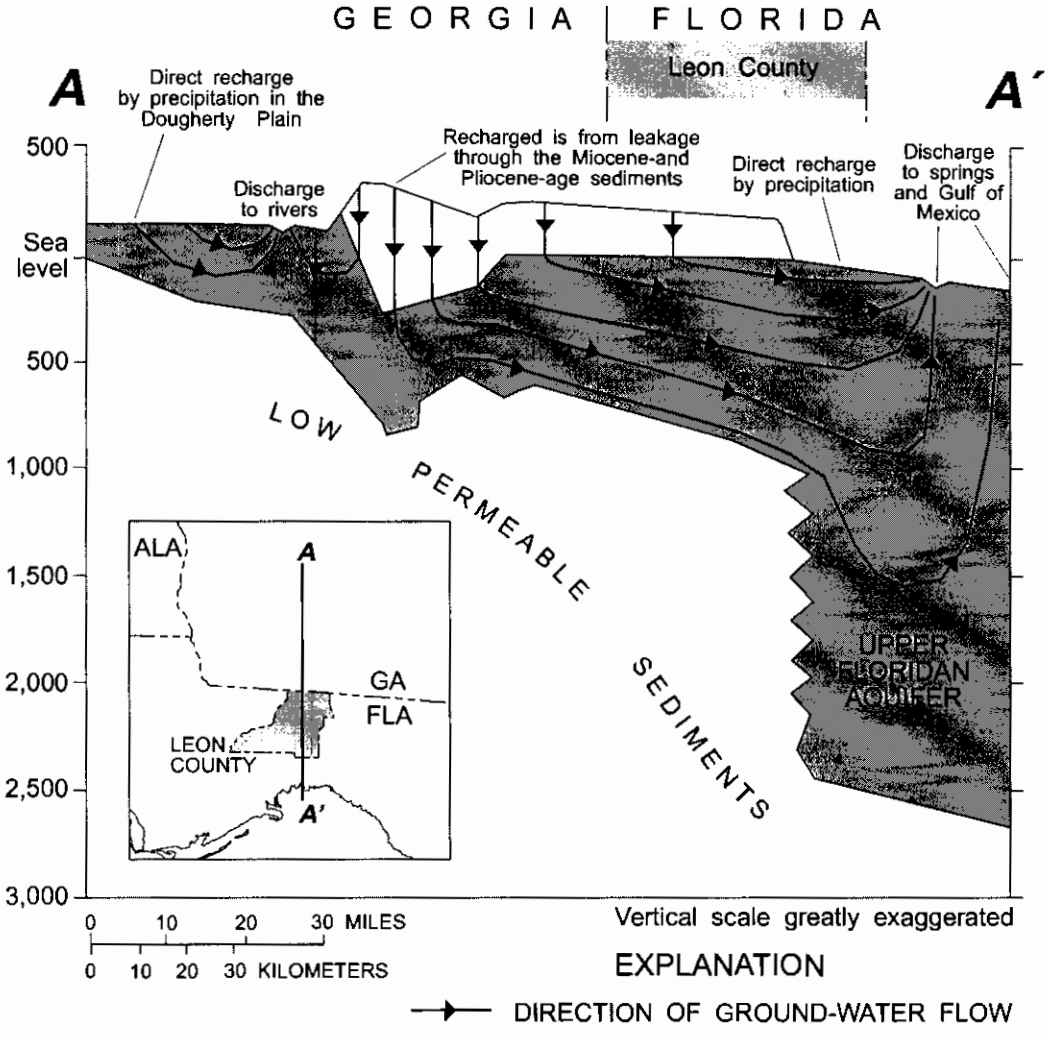

Figure 17. Conceptual model of the Upper Floridan aquifer system showing ground-water flow directions.

less than 14 ft between the years 1959 and 1965. A similar range was observed between 1984 and 1992 (fig. 18). Within Leon County, the Upper Floridan aquifer ranges in thickness between 500 ft in the north and 1,800 ft in the south. Using the argument of Freeze and Cherry (1979) and the fact that the maximum change in water levels in relation to aquifer thickness is about 3 percent, then long-term average conditions of ground-water flow within the Leon County area can be considered to be at steady state. Steady-state conditions were also indicated by the relatively constant stages of rivers that drained ground water from the Upper Floridan aquifer during the period September 1991, to January 1992 (fig.13).

The head in the Upper Floridan aquifer in Tallahassee, during field data collection, was very close to the average head for the period 1984 to 1992 (fig. 18). The average water-level altitude in well FSU 1 during October 21 to November 8, 1991, was 26.8 ft and the average water-level altitude from 1984 to 1992 was 26.2 ft, indicating that aquifer conditions were near a long-term average.

The Upper Floridan aquifer probably acts locally as well as regionally as single water-bearing unit within the study area. That is, there are no zones of sufficient areal extent and low permeability to divide the aquifer into distinct permeable units (Miller, 1986; and Bush and Johnston, 1988). Such assumptions are supported within the Tallahassee area by water-level data collected from two adjacent wells (discussed earlier) and shown in figure 15. The small upward gradient of between 0.2 and 0.5 ft could be caused by City of Tallahassee pumpage from the upper third of the aquifer.

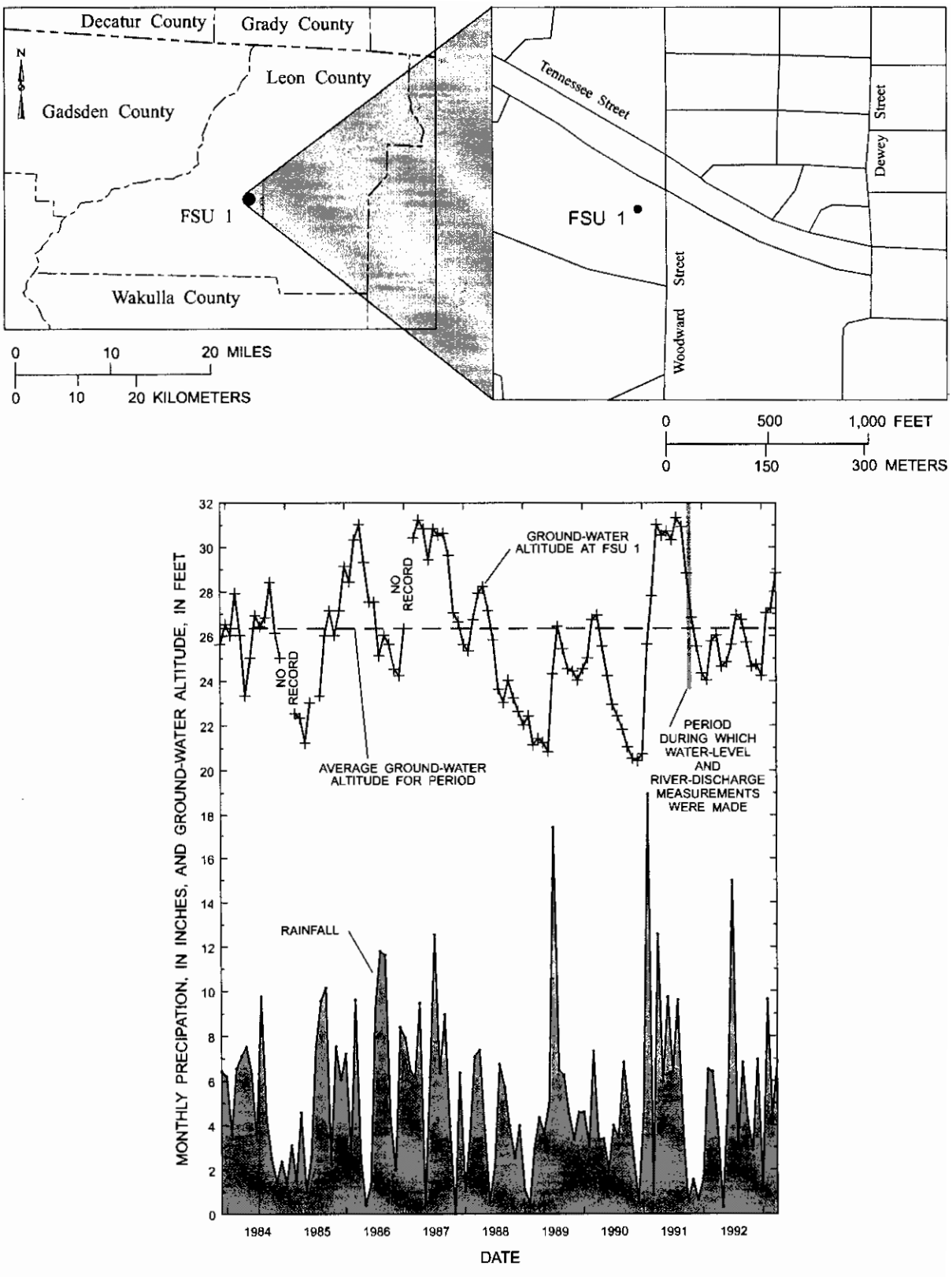

Figure 18. Rainfall and ground-water altitude fluctuations in the Upper Floridan aquifer in well FSU 1, Tallahassee, Fla., 1984 - 1992.

The ultimate source of recharge to the Upper Floridan aquifer is precipitation. Net recharge rates are relatively high in the karst areas (fig. 9) because the aquifer is exposed at land surface or covered only by a thin veneer of sediments. Precipitation falling in these areas can rapidly infiltrate through the overlying sediments or directly enter the aquifer through sinkholes and sumps. Outside the karst areas, the aquifer is overlain by low-permeability Miocene-and Pliocene-age sediments. Net recharge rates in these areas are less than in the karst areas because the low-permeability sediments cause a large proportion of precipitation to become runoff to streams. Model calibrated recharge rates determined by Bush and Johnston (1988) ranged from as high as 20 in/yr in the Ocala Uplift District to less than 1 in/yr in parts of the Apalachicola Embayment - Gulf Trough area.

The Upper Floridan aquifer is confined in some areas and unconfined in others (fig. 19). Unconfined conditions exist in the karst areas and in the area of the Barwick Arch. Near the center of the arch, the limestones comprising the Upper Floridan aquifer reach an elevation of about 150 ft and the potentiometric surface is about 60 ft (Sever, 1966). In this region, the limestones in the uppermost part of the Upper Floridan aquifer are unsaturated and unconfined conditions exist. A large part of Leon County lies within this area. Although the Upper Floridan aquifer is unconfined in the Barwick Arch area, the limestones comprising the aquifer are overlain by the low-permeability sediments which limits recharge to the aquifer. Outside the karst and Barwick Arch areas, the Upper Floridan aquifer is confined by the low-permeability Miocene-and Pliocene-age sediments.

In areas where the low-permeability sediments confine the Upper Floridan aquifer, the rate of recharge (leakage downward) is proportional to the difference in head between the water table and Upper Floridan aquifer. The rate of recharge is also proportional to the vertical hydraulic conductivity of the low-permeability sediments and inversely proportional to the thickness of these sediments. In the Barwick Arch area, the Upper Floridan aquifer is unconfined but overlain by the low-permeability sediments, here the rate of leakage is not dependent on the head in the Upper Floridan aquifer. In these areas, fluctuations in the head of the Upper Floridan aquifer do not change the rate of leakage through the overlying sediments.

Discharge of water from the Upper Floridan aquifer occurs as spring flow, seepage into rivers and the Gulf of Mexico, and withdrawals from wells. Rivers (or reaches of rivers) within the karst areas are directly hydraulically connected with the Upper Floridan aquifer, but rivers (or reaches of rivers) not in the karst areas are generally separated from the aquifer by the low-permeability Miocene- and Pliocene-age sediments. Rivers in the karst areas receive large volumes of water from the Upper Floridan aquifer, mostly as spring flow. A net gain in flow of 490 ft^3/s was measured for one reach of the Flint River in southern Lee and Dougherty County, Georgia (fig.16). In the karst areas of the Ocala Uplift, water is drained from the aquifer by several large springs and spring groups. The major springs in the southern part of the study area are Spring Creek Spring group, Wakulla Spring, St. Marks Spring, and the Wacissa Spring group. These four are among the eight largest springs in Florida (Rosenau and others, 1977). Discharges measured on November 1, 1991, in the rivers directly downstream of these springs were: Spring Creek (307 ft^3/s), Wakulla River (350 ft^3/s), St. Marks River (602 ft^3/s), and Wacissa River (319 ft^3/s). When the measurements were made, the rivers derived most, if not all, of their flow from spring discharges. Some discharge also occurs in smaller springs along the coast and directly to the Gulf of Mexico; however, the rate of discharge from these springs is unknown.

SIMULATION OF GROUND-WATER FLOW IN THE UPPER FLORIDAN AQUIFER

Ground-water flow in the Upper Floridan aquifer was simulated using the USGS modeling software MODFLOW (McDonald and Harbaugh, 1988). The modeling software requires that the aquifer system be divided into a horizontal grid of rows and columns and vertically into layers, creating a three- dimensional matrix of cells. Aquifer properties are assigned to cells (such as top of aquifer, base of the aquifer, hydraulic conductivity of the aquifer, and so forth) so that the cell matrix is tailored to represent known conditions present in the Upper Floridan aquifer. MODFLOW then uses finite-difference equations to simulate three-dimensional ground-water flow. The software iteratively solves the system of equations for hydraulic head at each active model cell and calculates the rate of ground-water flow between cells.

To ensure that the model simulation accurately reflects conditions present in the Upper Floridan aquifer, the model must be calibrated. Calibration is the

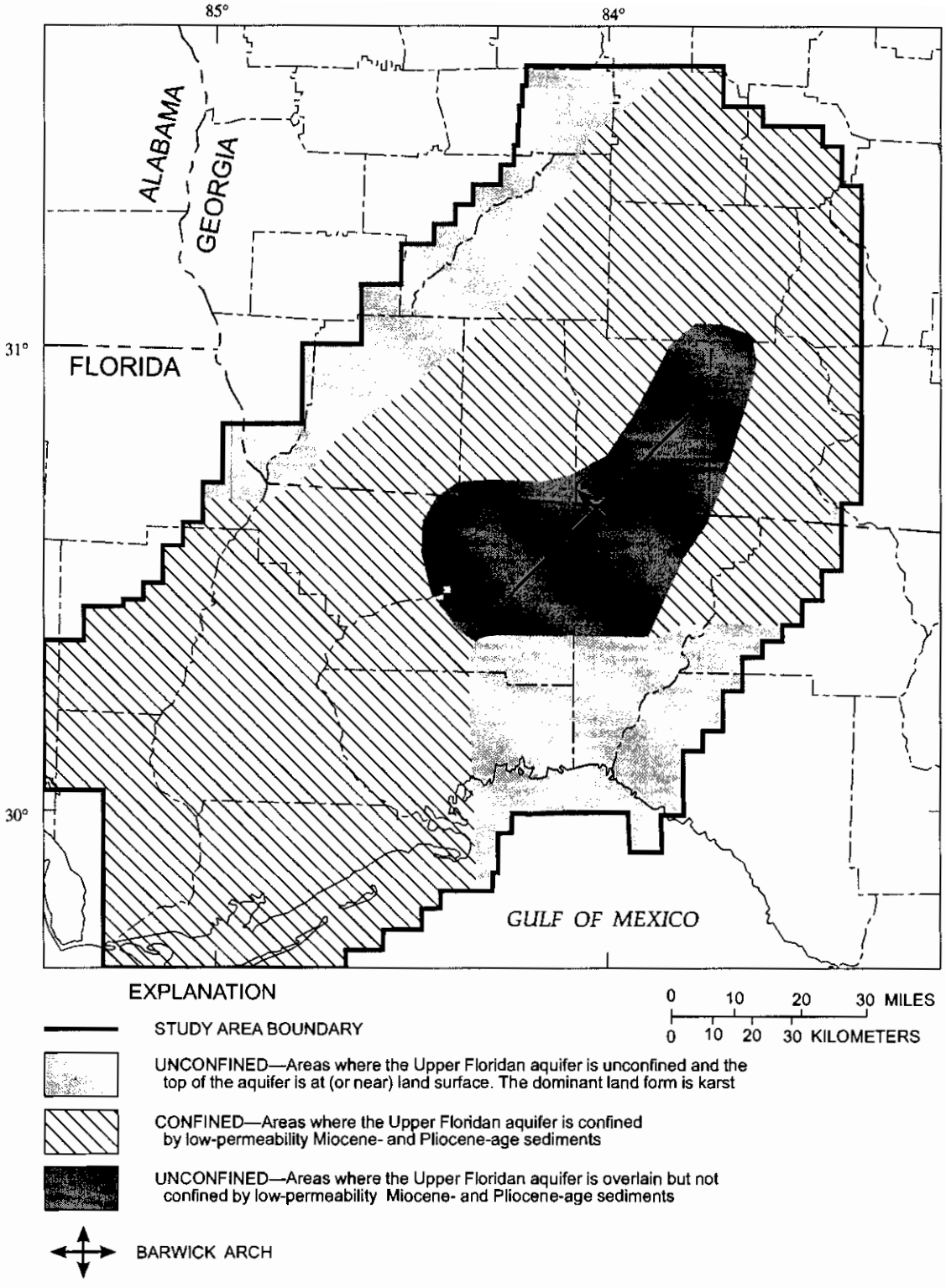

Figure 19. Areas where the Upper Floridan aquifer is confined and unconfined.

process of varying aquifer properties assigned to cells until the computer-simulated aquifer conditions match measured-aquifer conditions. The model was calibrated to hydrologic conditions measured during the data collection part of this investigation, which was late October to early November 1991. Ground-water flow was simulated as steady state, which assumes that the volume of ground-water recharge equals the volume of ground-water discharge. Once calibrated, the model was coupled with particle-tracking techniques to delineate the contributing areas to five City of Tallahassee municipal supply wells.

The model simulates the aquifer as an heterogeneous porous medium and assumes that ground-water flow is uniformly distributed within each active model cell. As discussed earlier, this assumption is valid over most of the study area. However, conduit flow occurs near large springs and near some sinkholes where cave systems are present. In these areas, the aquifer does not behave like a porous medium and the model may predict average ground-water flow velocities that are slower than those that actually occur within the conduits.

Grid Design

The first step in simulating ground-water flow was to divide the entire study area into a grid of cells. The grid consisted of 176 rows and 162 columns (fig. 20), resulting in 28,512 model cells per layer (fig.21). The aquifer system was simulated using 3 layers. Orientation of the grid was north-south. Cell size is variable with the smallest cells occurring near the center of the study area and larger cells occurring near the perimeter. Row and column spacing was chosen so that the water-supply wells, in which contributing areas were to be determined, would be positioned in the smallest model cells. The smallest cells are 30 by 30 ft and the largest cells are 3 by 3 mi. Not all cells in the matrix were used during the simulation of ground-water flow. Some cells were inactive, which allowed the study area to conform to irregular boundaries.

Model Layer 1

Layer 1 in the model represents the water-table aquifer. Layer 1 model cells are utilized only where the low-permeability Miocene- and Pliocene-age sediments confine the Upper Floridan aquifer (figs. 21 and 22). In these areas, layer 1 cells are treated as a specified-head boundary. For this type boundary condition, each cell in the layer can either provide water to or drain water from the cell in the next layer below, while maintaining a head at a specified altitude. If the head in a layer 1 cell is higher than the head in a layer 2 cell, water will flow from layer 1 to layer 2, and vice-versa. During ground-water flow simulation, the head of layer 1 cells was specified to represent the average head for the water-table aquifer located within that cell. The head within the water-table aquifer, in most places, reflects the land-surface topography and generally is a few feet below land surface (but can be tens of feet in some places). For most layer 1 cells, the head was specified to be a few feet below average land-surface altitude. However, in some highland areas the head was specified to be as much as 50 ft below land surface. The low-permeability Miocene- and Pliocene-age sediments were generally several hundred feet thick where the water-table aquifer was simulated, so small errors in the estimated head had a negligible effect on simulated leakage rates.

The movement of water to and from the water-table aquifer is restricted by low-permeability sediments. This resistance to flow between cells in layer 1 and layer 2 is a model input parameter designated Vcont 1. Vcont 1 is calculated for layer 1 cells using the following formula:

$$\text{Vcont } 1 = 1/(b_1/VK_1) \qquad (1)$$

where: b_1 is the thickness of the low-permeability Miocene- and Pliocene-age sediments (ft), and

VK_1 is the vertical hydraulic conductivity of the low-permeability Miocene- and Pliocene-age sediments (ft/d),

The thickness of the low-permeability Miocene- and Pliocene-age sediments is shown on figure 5 and the vertical hydraulic conductivities are discussed with the description of model calibration. An initial value of 0.00005 ft/day was assumed for the vertical hydraulic conductivity. However, this value was changed during model calibration.

Model Layers 2 and 3

The Upper Floridan aquifer is represented in the simulation by model layers 2 and 3 (fig. 21 and 22). Layer 2 represents the upper 230 ft of the aquifer, which, on average, is the zone penetrated by City of Tallahassee water-supply wells. Layer 3 represents the difference between the total thickness of the Upper

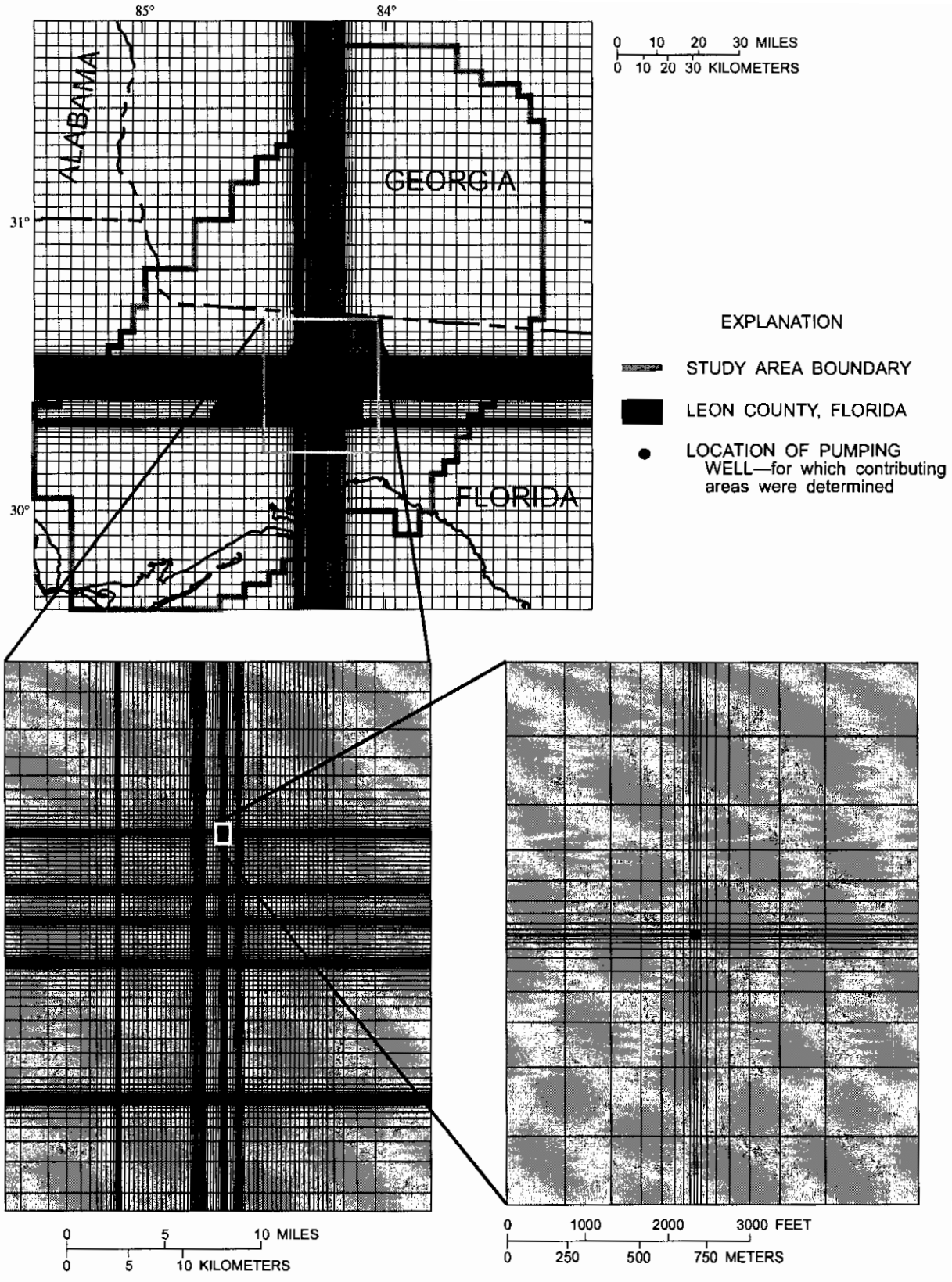

Figure 20. Location and orientation of finite-difference model grid.

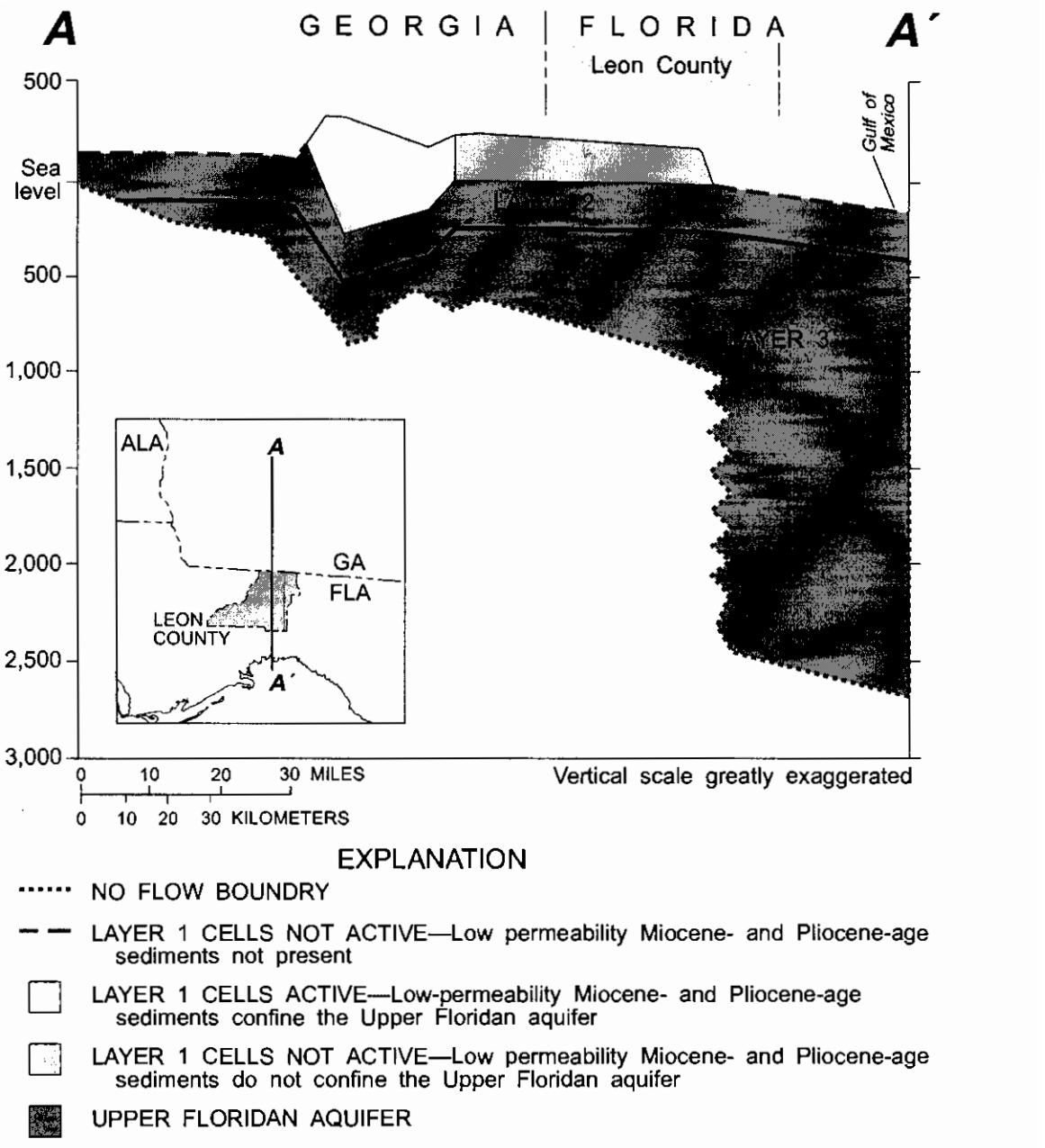

Figure 21. Generalized hydrogeologic section showing model layers.

Floridan and the thickness of layer 2. The Upper Floridan aquifer acts as a single water-bearing unit within the study area. The sole purpose for dividing the aquifer into two layers is to simulate withdrawals from water-supply wells at approximately their actual depths. This is important for accurate delineation of contributing areas (discussed in a later section). Layer 2 is the most areally extensive layer and defines the maximum lateral extent of the model. In the northwestern part of the study area, the Upper Floridan aquifer thins to less than 230 ft and the aquifer is represented completely by layer 2. The Upper Floridan aquifer is bounded below by low-permeability sediments so the base of the model is a no-flow boundary.

The resistance to vertical ground-water movement between layers 2 and 3 is a model input parameter designated Vcont 2, and was calculated by the equation:

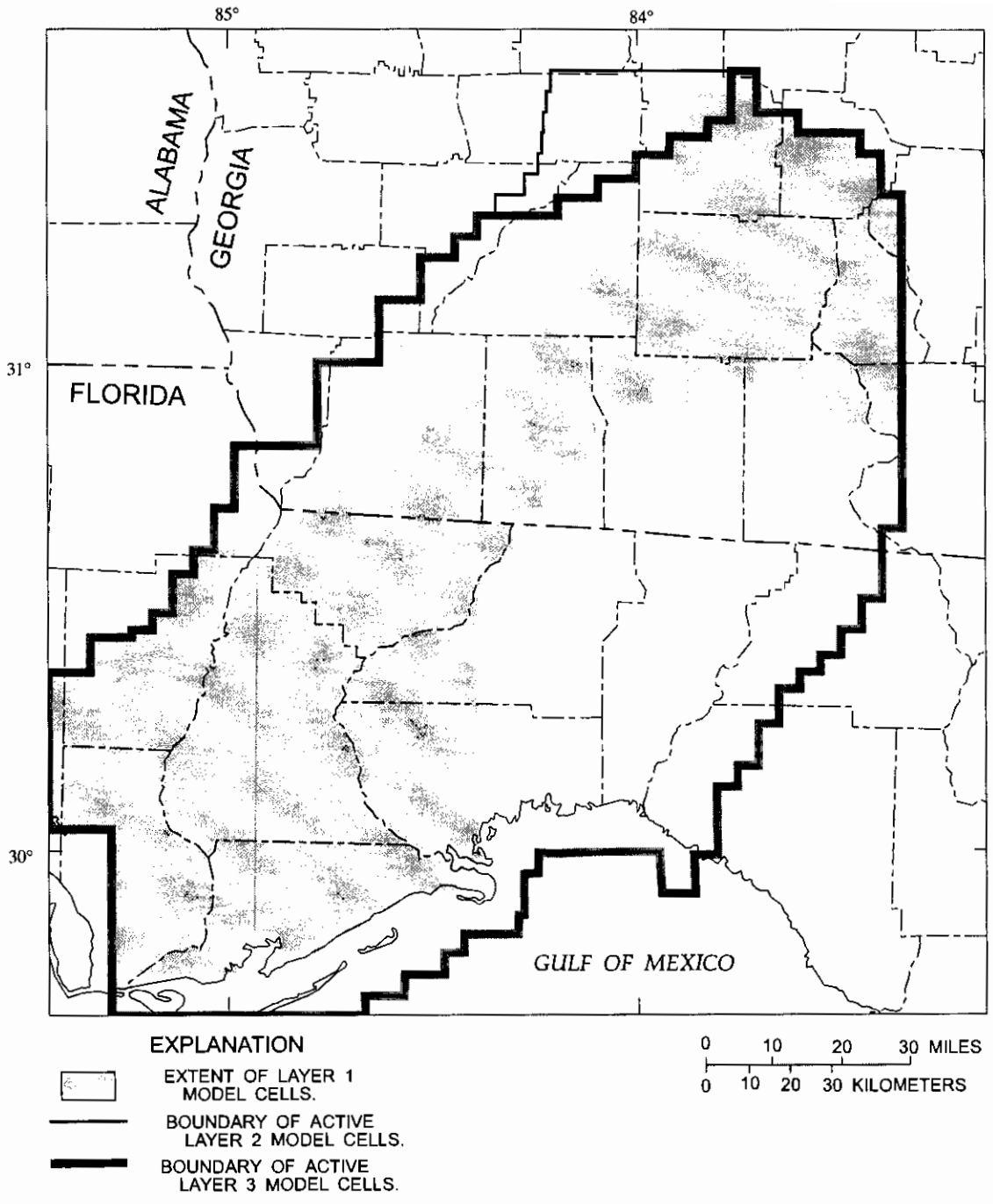

Figure 22. Location of model areas for layers 1, 2, and 3.

$$\text{Vcont 2} = 1/[(230\text{ ft}/2/VK_{UF}) + ([(b_{UF} - 230\text{ ft})/2]/VK_{UF})] \quad (2)$$

where:

VK_{UF} is the vertical hydraulic conductivity of the Upper Floridan aquifer (ft/d), and

b_{UF} is the thickness of the Upper Floridan aquifer (ft).

In calculating Vcont 2, the vertical hydraulic conductivity was set equal to the horizontal hydraulic conductivity of the Upper Floridan aquifer. Under this assumption, ground water can move both horizontally and vertically with equal resistance.

Model Input Parameters and Boundary Conditions

Model input parameters are specified and spatially distributed at active cells before simulation of ground-water flow begins. MODFLOW uses the input parameters to tailor the finite-difference equations to the particular aquifer being investigated. The model input parameters used for this investigation are altitude of the water-table which defines the top of layer 1, altitude at the base of layer 1, Vcont 1, altitude at the top of layer 2, altitude at the base of layer 2, hydraulic conductivity of layer 2, transmissivity of layer 3, and net recharge rates.

Initial estimates of transmissivity for the Upper Floridan aquifer were computed by contouring the transmissivity values (fig. 9) and assigning a transmissivity to each model cell from the contoured data. Values of horizontal hydraulic conductivity for layer 2 were calculated by dividing transmissivity by the total thickness of the aquifer. The transmissivity for each cell of layer 3 was computed by multiplying the thickness of layer 3 at each cell by the corresponding hydraulic conductivity.

An initial estimate of direct recharge to the Upper Floridan aquifer of 7 in/yr was calculated by dividing the net river gains by the approximate area of the aquifer drained by the rivers. This constant recharge rate was applied directly to layer 2 in areas where the Upper Floridan aquifer was unconfined (fig. 23) and was varied separately during model calibration.

Model boundaries were selected and located to approximate natural hydrologic boundaries of the Upper Floridan aquifer. Where feasible, the model boundaries were located at or slightly beyond the major rivers that drain water from the aquifer because these are permanent hydrologic boundaries. The result of the hydraulic connection between the aquifer and river is that stresses imposed on the aquifer (such as pumping) are unlikely to propagate beyond the rivers, both in the natural system and in the simulated system.

The western model boundary is located just west of the Apalachicola and Flint Rivers (fig.24). The eastern boundary is located approximately parallel to ground-water flow paths in the northeastern third of the study area, along the Withlacoochee River and its tributaries in the middle third of the study area, and just east of the Aucilla River at a natural ground-water divide in the lower third of the study area. The southern boundary is located just offshore to simulate diffuse upward leakage to the Gulf of Mexico.

The boundary conditions along the perimeter of the modeled area were either specified head or no flow. Specified-head cells were placed in areas where the potentiometric surface of the Upper Floridan aquifer indicated that ground water could potentiality enter or leave the modeled area due to lateral flow (fig. 24). Specified-head cells were placed west of the Flint River. Specified-head cells were placed in the Gulf of Mexico to simulate diffuse upward leakage of ground water at and near the coastline. The head in these cells was specified at sea level and the placement of the boundary was determined by projecting the onshore gradient offshore to zero. Specified-head cells were placed in two locations on the eastern model boundary. The southern specified heads were used to simulate the flow of ground water out of the model toward large springs located along the Withlacoochee River just outside the modeled area. The northern specified heads were similarly used where the potentiometric surface map indicated possible movement of ground-water out of the modeled area (fig. 16).

The modeled location of rivers that drain ground water from the Upper Floridan are shown in figure 24. A model cell containing a river reach is referred to as a river cell and was assigned a river stage, a river bottom elevation, and riverbed conductance. The volume of water flowing into or out of a river cell is dependent on the difference in altitude between the river stage and simulated head in the aquifer, and on the riverbed conductance. The higher the riverbed conductance, the larger the volume of water that will move between the river and the aquifer per unit head difference. The model input parameter, riverbed conductance, was calculated by the equation:

$$\text{riverbed conductance} = K*L*W / M$$

(McDonald and Harbaugh, 1988)

where:

- K is the vertical hydraulic conductivity of riverbed material (ft per day),
- L is the length of the river reach (ft),
- W is the width of river (ft), and
- M is the thickness of the riverbed material (ft).

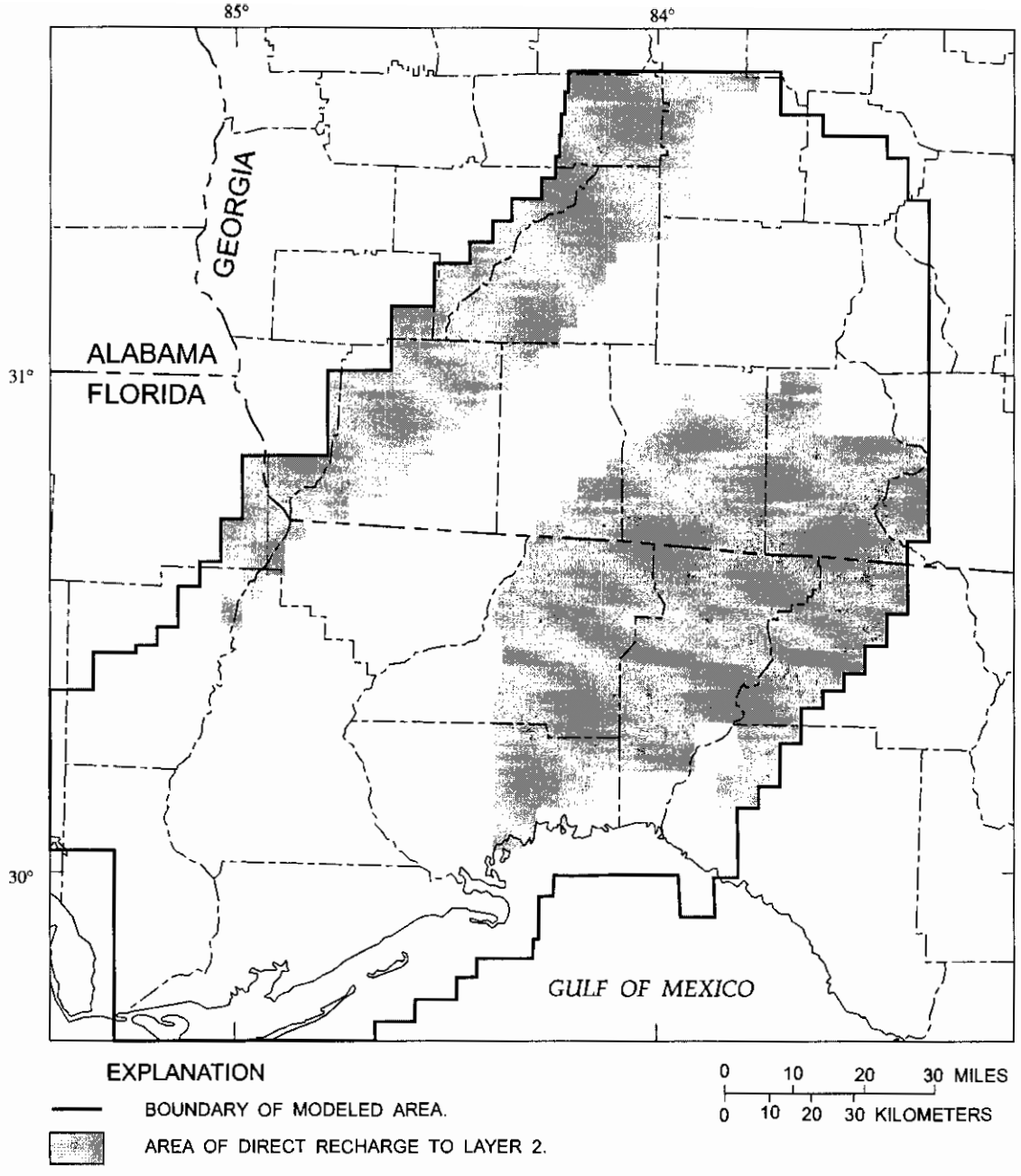

Figure 23. Areas of direct recharge to model layer 2.

Rivers in both the Ocala Uplift and Dougherty Plains are fed by springs. These springs, typically, are the terminal ends of conduit systems that extend for short distances (typically less than 2 miles) into the Upper Floridan aquifer. The riverbed conductances were calculated using a hydraulic conductivity equal to the conductivity of the aquifer material where the river cell resided. Rivers outside the karst areas are separated from the Upper Floridan aquifer by the low-permeability Miocene- and Pliocene-age sediments, do not interact directly with the aquifer, and were not simulated using river cells.

Municipal and industrial pumpage included in the simulation is listed in table 1. Generally,

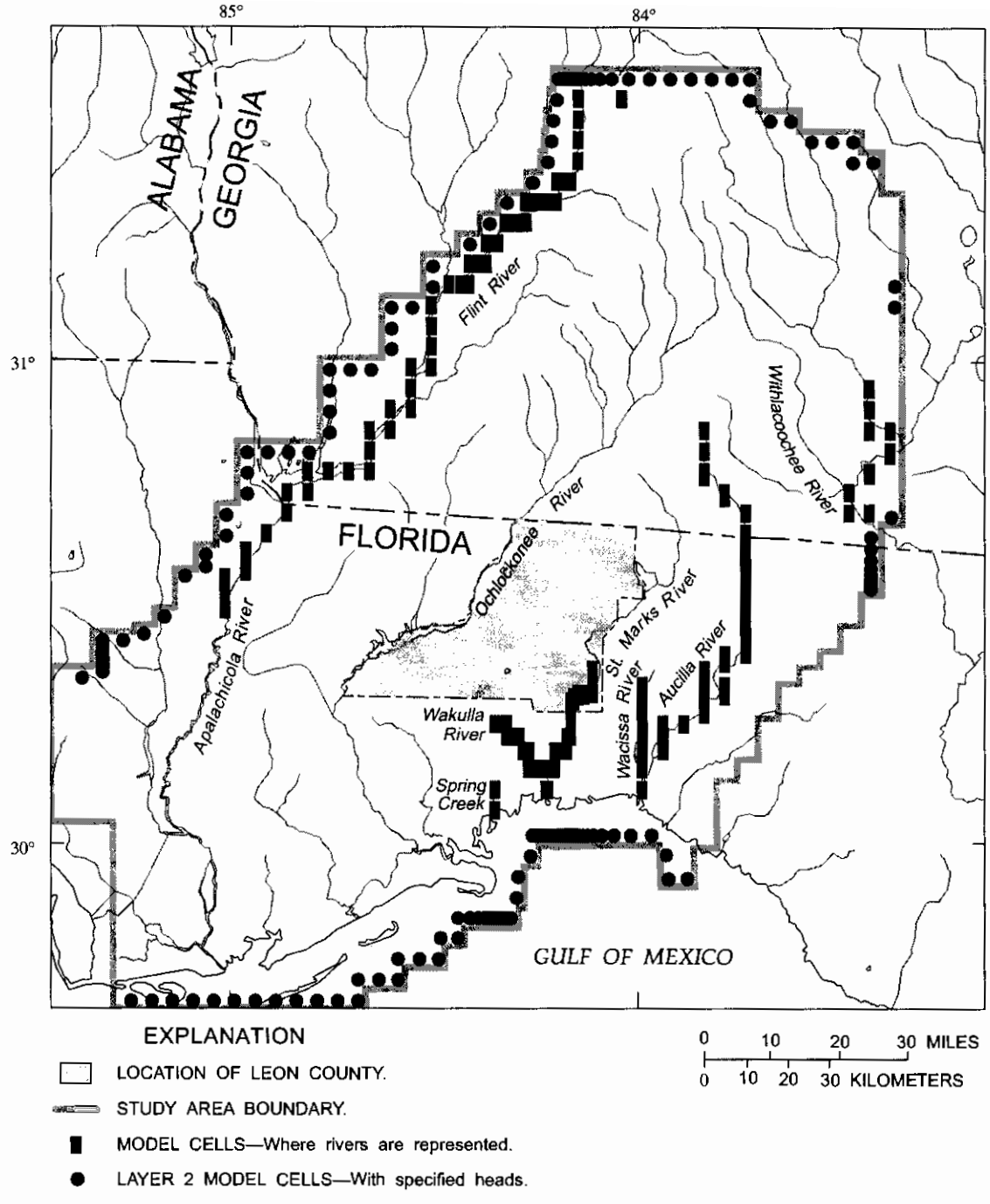

Figure 24. Location of model boundaries, specified-head cells, and cells representing rivers.

only wells at which average pumping is greater than 70 gal/min were included in the simulation; however, wells pumping lower rates were included if the information were readily available. The total pumpage used to calibrate the model was 53,000 gal/min (118 ft^3/s).

Model Calibration

The model calibration process consisted of 1) selecting input parameters, 2) simulating ground-water flow using MODFLOW, 3) comparing simulated heads with measured heads, 4) comparing simulated

river discharges with measured river discharges, and then 5) selecting new values for the input parameters aimed at minimizing the difference between simulated values and measured values. The calibration criteria established for simulated heads was arbitrarily chosen at plus or minus 10 feet of the measured values. The calibration criteria for simulated river gains was established as plus or minus 8 percent of the measured values, which is the accuracy of these measurements. The model was calibrated to the streamflow and water-level conditions observed during late October to early November 1991. Of the 274 water-levels measured to define the potentiometric surface of the Upper Floridan aquifer, 199 were within the boundary of the modeled area.

The input parameters varied during calibration were: transmissivity of the Upper Floridan aquifer, Vcont 1, and direct recharge to layer 2. The parameter Vcont 2 was changed as an artifact of changing the transmissivity of the Upper Floridan aquifer, but it was not independently changed during calibration. Riverbed conductance was recalculated between simulations using the same hydraulic conductivity as the Upper Floridan aquifer. The other input parameters were not varied because they were sufficiently constrained by measured values.

Calibration Results

After calibration, 197 simulated heads were within 10 ft of the 199 measured values and 132 of these were within 5 ft. Simulated and measured heads are compared in figure 25. Simulated and measured river discharge gains are listed in table 3 and shown on figure 26. All simulated river gains were within 6 percent of the measured values and well within the established calibration criteria of 8 percent. The simulated potentiometric surface of the Upper Floridan aquifer is shown in figure 27. Simulated conditions are considered equivalent to long-term average conditions.

The calibration-derived transmissivity distribution of the Upper Floridan aquifer (fig. 28) is the sum of the transmissivities for layers 2 and 3. The sum represents the transmissivity for the entire thickness of the Upper Floridan aquifer. The model-derived transmissivity distribution ranged from less than 5,000 ft^2/d in the region of the Apalachicola Embayment—Gulf Trough to greater than 10,000,000 ft^2/d in the area surrounding the large springs in extreme southern Leon County and west and south of Leon County. The low transmissivity applied to the Apalachicola Embayment—Gulf Trough was necessary to match the rapid potentiometric gradient change in the central and northern parts of the study area and to match the mounding of ground water in western Leon County and Gadsden County. Very high transmissivity values were necessary to match the very low potentiometric gradients in the areas around the large springs. The complex transmissivity distribution applied in and around Leon County was necessary to match the measured potentiometric surface changes which ranged from greater than 80 ft in western Leon County to less than 10 ft in the south.

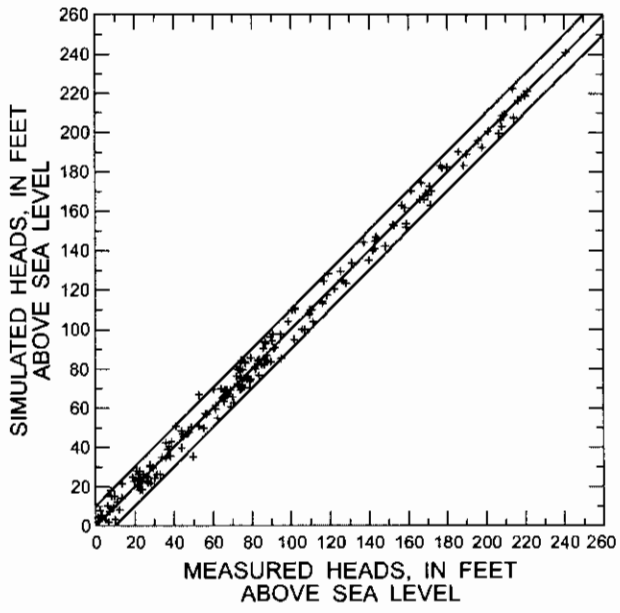

Figure 25. Simulated heads and measured heads.

Table 3. Comparison of measured net river gains, November 1991, and simulated net river gains

[ft^3/s, in cubic feet per second]

River	Measured gain in river reach, in ft^3/s	Model-derived gain in river reach, in ft^3/s	Difference, in percent
Aucilla	61	58	5
Wacissa	319	338	-6
St. Marks	602	601	0
Flint	490	499	-2
Wakulla	350	355	-1
Spring Creek	307	290	6

The calibration-derived vertical hydraulic conductivity distribution of the low-permeability Miocene- and Pliocene-age sediments is shown in figure 29. The vertical hydraulic conductivities were 2.0×10^{-3} ft/d and 2.0×10^{-2} ft/d in the southern part of the study area, 2.0×10^{-6} ft/d in the central part, and

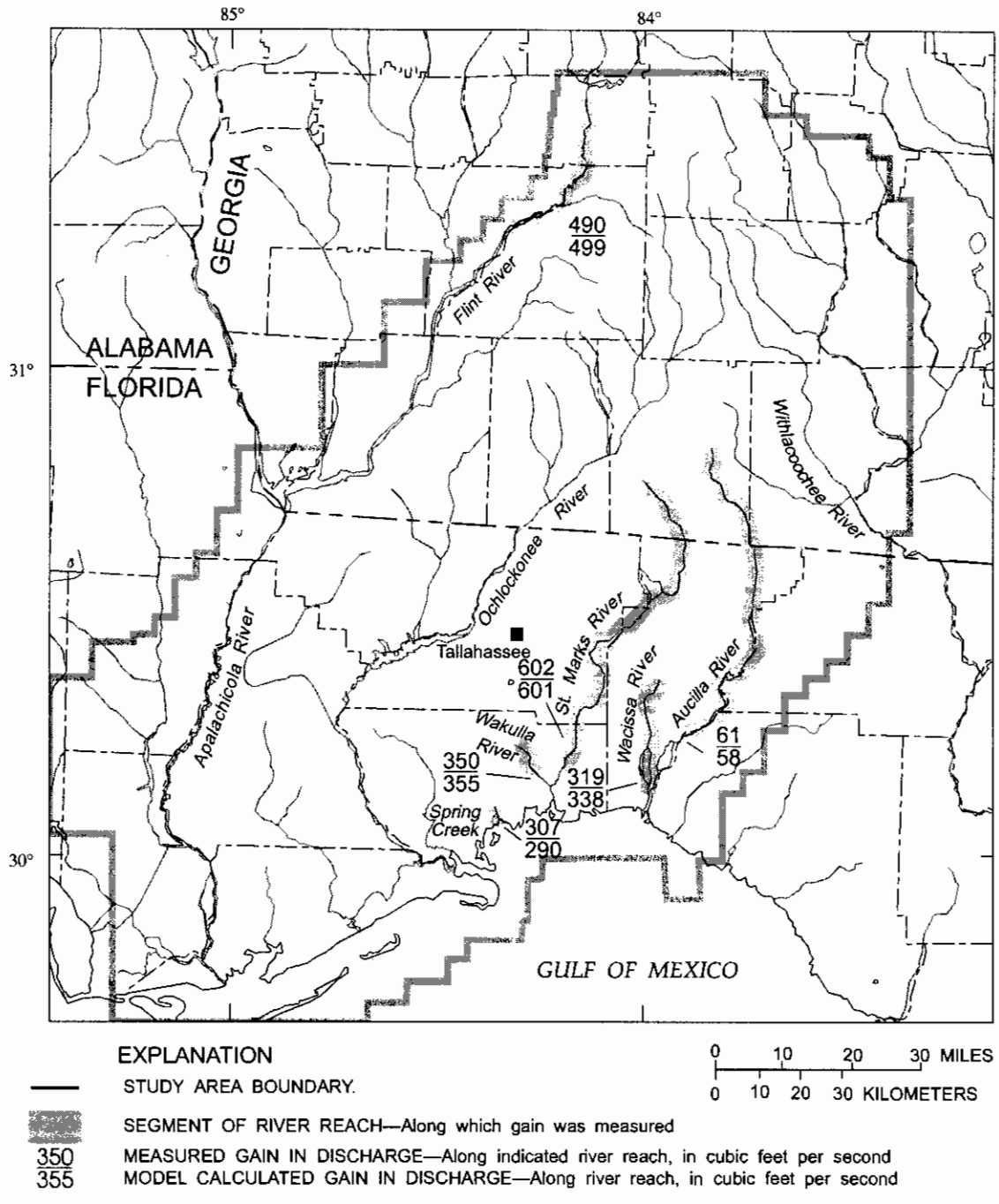

Figure 26. Measured net river gains, November 1991, and simulated net river gains.

7.8×10^{-4} ft/d in the northern part. The variability in the vertical hydraulic conductivity distribution is probably due to changes in the complex lithology of the sediments. In the two narrow zones in the southern part of the study area (darker areas in fig. 29) the vertical hydraulic conductivity is 2.0×10^{-2} ft/d. Rivers are present here, but are separated from the Upper Floridan aquifer by the low-permeability sediments. The relatively high vertical hydraulic conductivity allowed greater upward leakage in the vicinity of these rivers. The upward leakage rates were relatively small, a few cubic feet per second over distances of several miles.

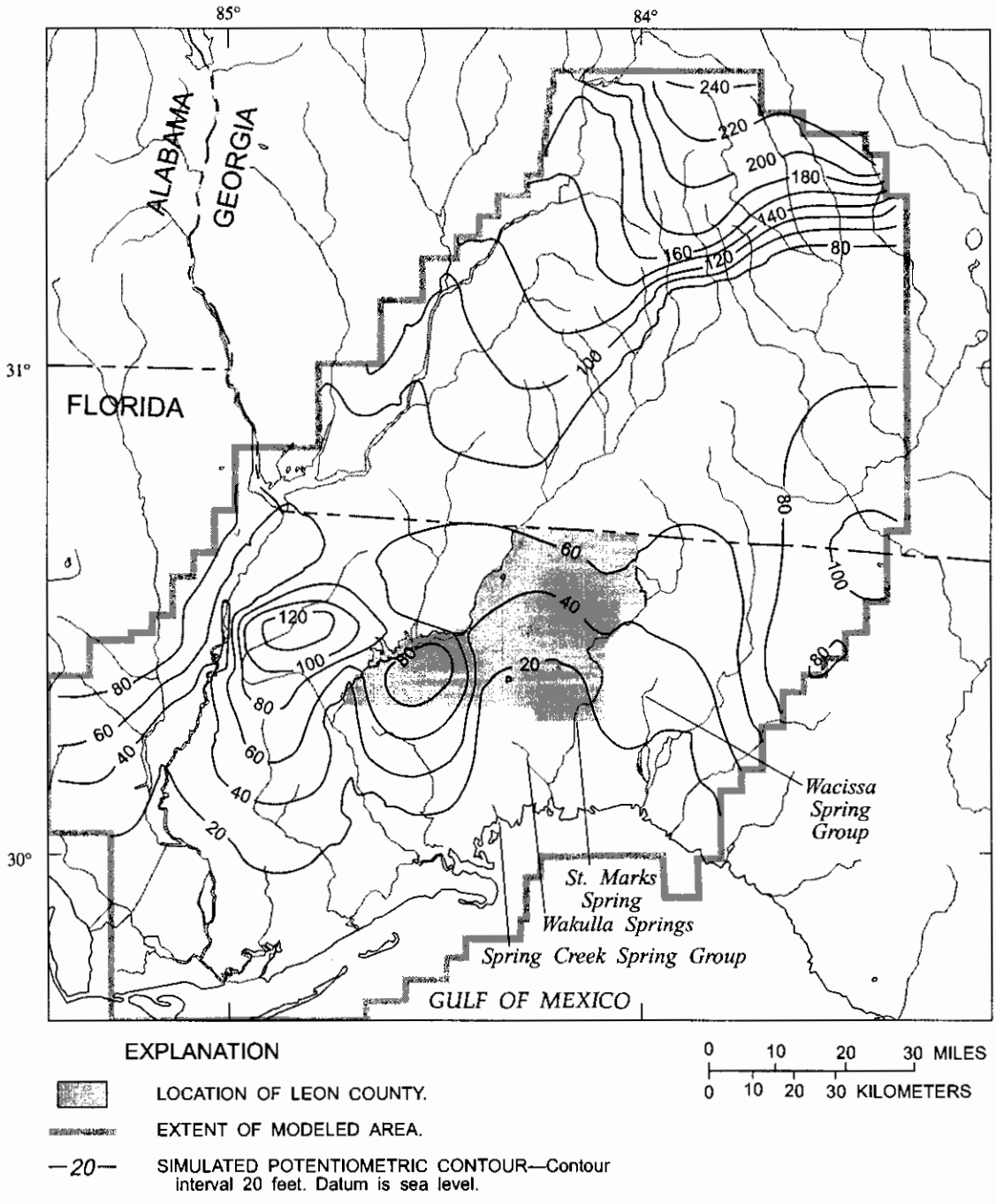

Figure 27. Simulated potentiometric surface of the Upper Floridan aquifer.

However, this leakage was needed to simulate the measured heads in the area. The calibration-derived vertical hydraulic conductivities fall within the range of expected values. The hydraulic conductivity of marine clay ranges from 3×10^{-7} ft/d to 3×10^{-4} ft/d and silt ranges from 3×10^{-4} ft/d to 3 ft/d (Freeze and Cherry, 1979).

The distribution of calibration-derived net recharge and leakage rates are shown in figure 30. The leakage rates between layers 1 and 2 were computed by MODFLOW and were dependent on Vcont 1 and the head difference between the layers. The relatively low rates of leakage were due to the low vertical hydraulic conductivities associated with the thick accumulations of

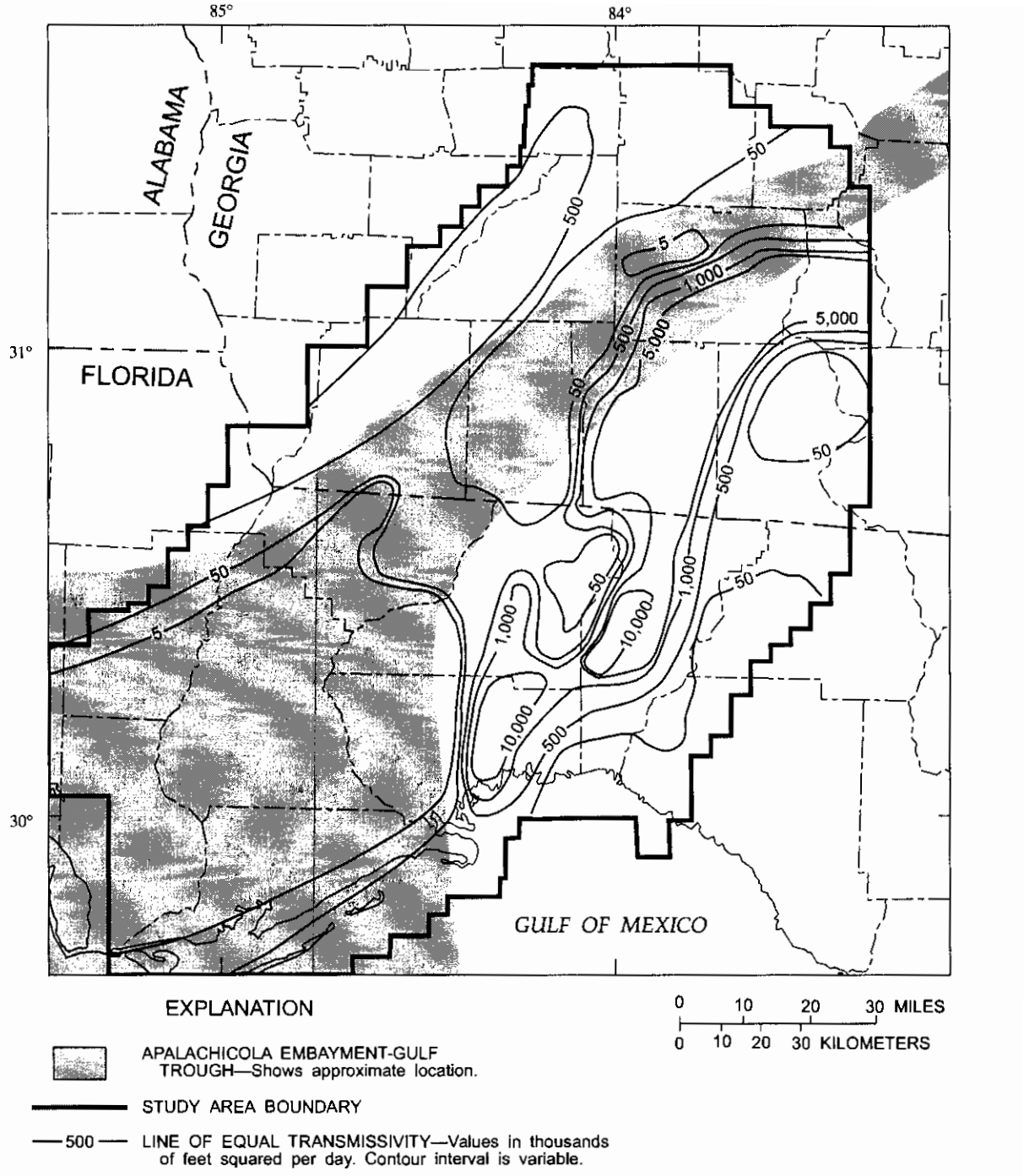

Figure 28. Calibration-derived transmissivities of the Upper Floridan aquifer.

low-permeability sediments in the Apalachicola Embayment - Gulf Trough area. The rates of direct net recharge were higher and occurred in karst areas and where the low-permeability Miocene- and Pliocene- age sediments were relatively thin. The highest rate was 62.0 in/yr and occurred at the Tallahassee wastewater sprayfields. The next highest net recharge rate of 18.0 in/yr occurred in the karst area in and south of Leon County. In this area, the Upper Floridan aquifer is covered by only a thin veneer of sand or directly exposed at land surface. The net recharge rate was 7.5 in/yr in the Dougherty Plain and 7.9 in/yr in most of the Ocala Uplift.

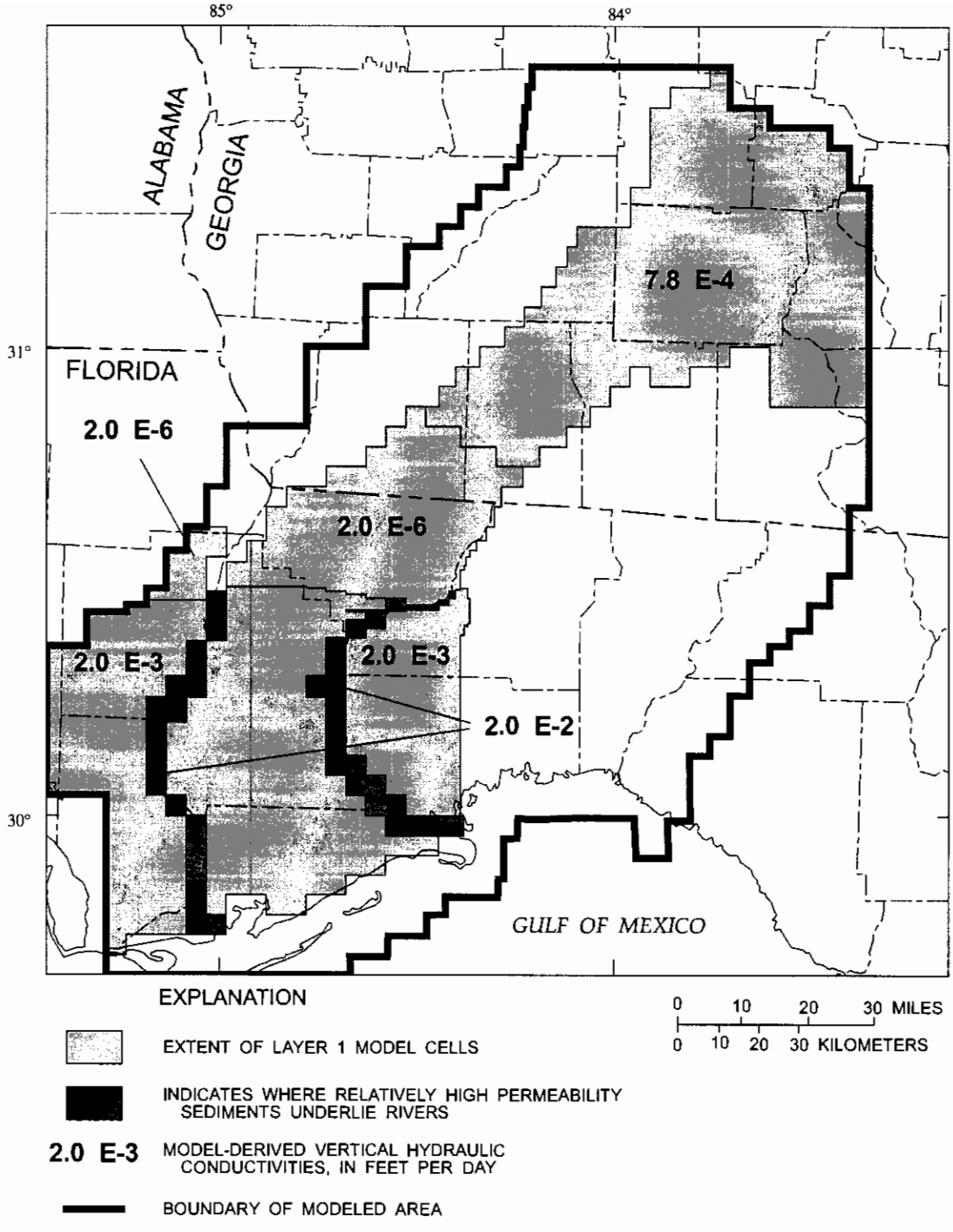

Figure 29. Calibration-derived vertical hydraulic conductivities for layer 1.

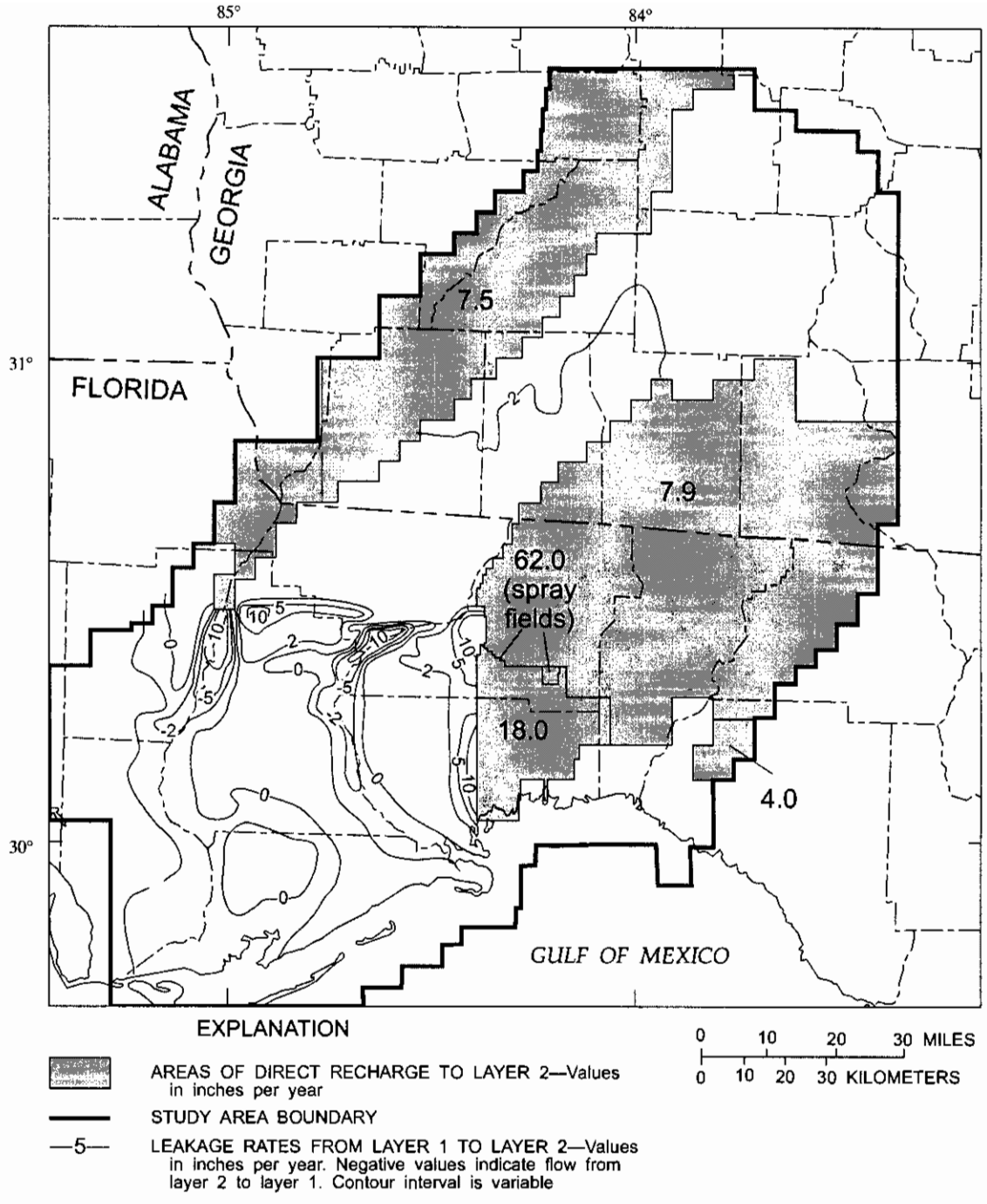

Figure 30. Calibrated leakage and recharge rates to the Upper Floridan aquifer.

Simulation-Derived Water Budget

The ground-water flow simulation was steady state, so the rate of inflow to the Upper Floridan aquifer in the study area (4,334 ft^3/s) was equal to the outflow. The sources of inflow were: direct net recharge to layer 2 (2,413 ft^3/s), subsurface inflow from specified-head cells in layer 2 (1,392 ft^3/s), and vertical leakage from specified-head cells in layer 1 (529 ft^3/s). The outflows were: subsurface discharge to river cells (3,555 ft^3/s), subsurface outflow to specified-head cells in layer 2 (582 ft^3/s), pumpage (118 ft^3/s), and upward leakage to layer 1 (79 ft^3/s). Ground-water inflows and outflows were summed for subregions of the modeled area (fig. 31). Direct net recharge to layer 2 was the largest source of water to the Upper Floridan

BOUNDARY CONDITION TYPE (Values in cubic feet per second)	INFLOW	OUTFLOW
Direct recharge to layer 2	2,413	0
Leakage from specified-head cells in layer 1	529	79
Flow from specified-head cells in layer 2	1,392	582
River cells	0	3,555
Pumpage	0	118
Total	4,334	4,334

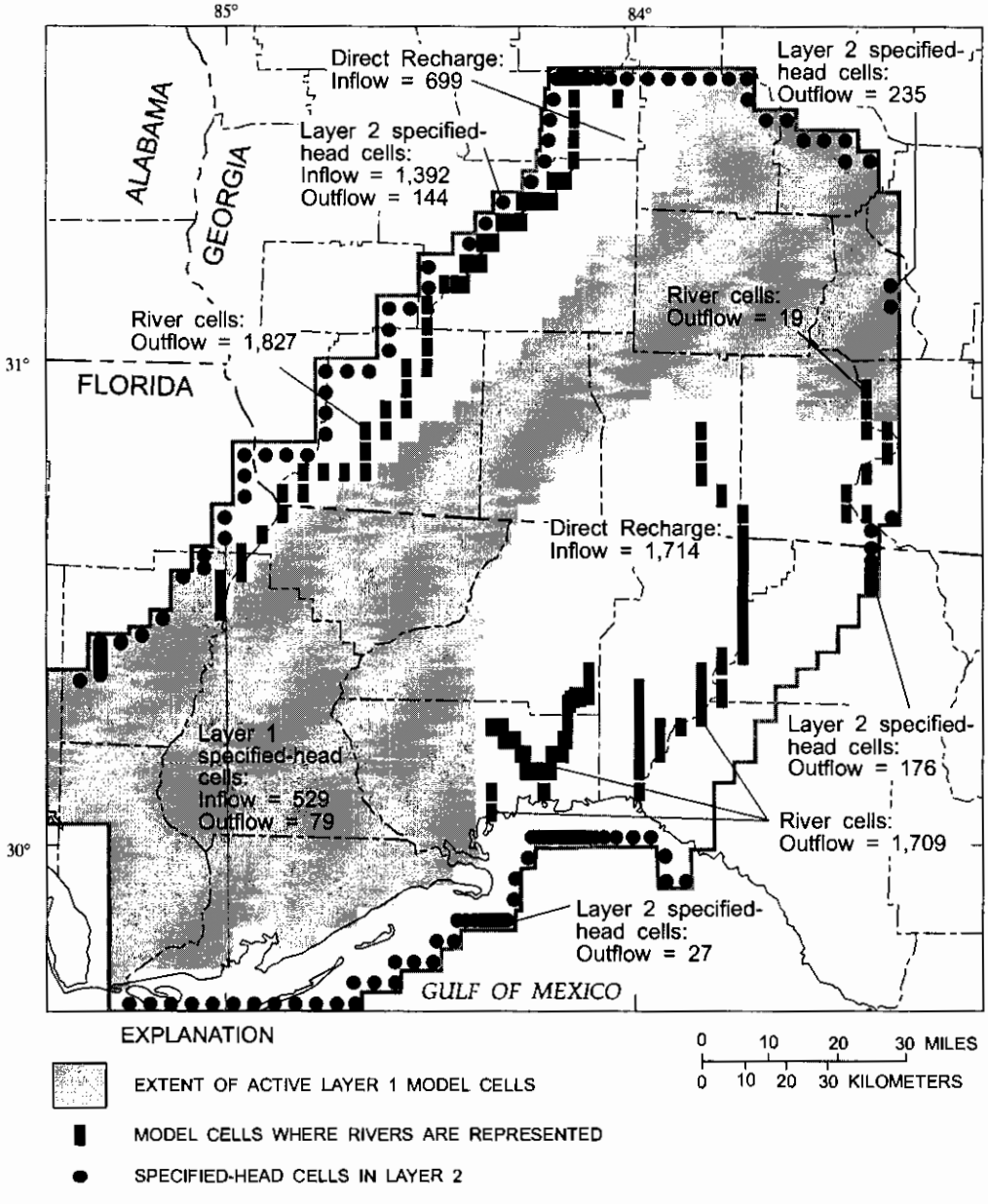

INFLOW = 529 - Rate of inflow to the Upper Floridan aquifer, in cubic feet per second.
OUTFLOW = 79 - Rate of outflow from the Upper Floridan aquifer, in cubic feet per second.

Figure 31. Simulated inflow and outflows in subregions of the study area.

aquifer with 1,714 ft^3/s occurring in the eastern part of the study area and 699 ft^3/s occurring in the Dougherty Plain. The specified-head cells in layer 2, located along the west and north perimeter of the modeled area, provided 1,392 ft^3/s to the aquifer. Almost all of this water later discharged to the Flint River. River cells accounted for most of the ground water discharged, with 1,827 ft^3/s being drained by rivers in the Dougherty Plain and 1,728 ft^3/s by rivers in the southeastern part of the modeled area. The northern set of specified-head cells on the eastern study area boundary drained 235 ft^3/s. The southern set of specified-head cells on the eastern boundary (in the vicinity of the Withlacoochee River) drained 176 ft^3/s. The rate of discharge to the Gulf of Mexico (27 ft^3/s) was relatively low because the large springs in the south-central part of the modeled area effectively drained ground water from the aquifer before it reached the coastline. Upward leakage from the Upper Floridan aquifer to layer 1 (79 ft^3/s) occurred in the southern areas of the Apalachicola Delta District.

Sensitivity Analysis

Sensitivity tests were conducted to assess the response of the calibrated model to a change in one input parameter while the calibrated values of other parameters were unchanged. The input parameters tested were the overall transmissivity of the Upper Floridan aquifer, direct net recharge to layer 2, Vcont 1, Vcont 2, and riverbed conductance. The sensitivity tests were conducted by: 1) changing an input parameter by plus or minus 50 percent from the calibrated value, 2) calculating the number of simulated heads exceeding the error criteria, and 3) comparing the simulated rate of ground-water discharge to rivers with the measured values. The greater the number of heads that exceeded the error criteria (by not being within 10 ft of the measured values) and the larger the difference between simulated-river discharges and measured discharges, the greater the sensitivity of the model to changes in that particular parameter. The results of the sensitivity analysis are listed in table 4.

The model was most sensitive to changes in transmissivity. A decrease in transmissivity of 50 percent caused the number of simulated heads exceeding the error criteria to increase from 2 to 85; simulated ground-water discharge to rivers also fluctuated substantially from the measured values. An increase in transmissivity of 50 percent caused the number of simulated heads exceeding the error criteria to increase to 25.

Table 4. Results of model sensitivity analysis

[trans, transmissivity; Vcont 1, layer 1 vertical conductance; river, river bed conductance; Vcont 2, layer 2 vertical conductance; %, percent]

Parameter changed	Number of cells where the difference between simulated head and measured head exceeded 10 feet	Difference between measured river gain and simulated ground-water discharge, in percent					
		Acuilla River	Wacissa River	St. Marks River	Flint River	Wakulla River	Spring Creek
Calibrated	2	-4	6	0	2	1	5
Trans - 50 %	85	--	29	--	--	--	--
Trans + 50 %	25	--	--	19	--	--	--
Vcont 1 - 50 %	14	-7	-2	2	-3	-2	-7
Vcont 1 + 50 %	18	-3	13	1	6	4	-4
Recharge - 50 %	28	--	--	--	20	--	--
Recharge + 50 %	35	--	--	--	--	--	--
River - 50 %	3	-13	8	-5	1	10	-6
River + 50 %	3	-2	5	2	2	-2	6
Vcont 2 - 50 %	3	--	7	--	--	--	--
Vcont 2 + 50 %	3	--	6	--	--	--	--

The model also was sensitive to changes in direct recharge to layer 2. A decrease in recharge of 50 percent caused the number of simulated heads exceeding the error criteria to increase from 2 to 28. The corresponding simulated ground-water discharge to rivers decreased substantially compared to the measured values. An increase in recharge of 50 percent caused the number of simulated heads exceeding the error criteria to increase to 35 and the simulated ground-water discharges to rivers increased substantially compared to the measured values. Simulations were sensitive to recharge rate because it is the largest source of water to the Upper Floridan aquifer.

Another source of water to the Upper Floridan aquifer was leakage from layer 1. A decrease in Vcont 1 of 50 percent caused the number of simulated heads exceeding the error criteria to increase from 2 to 14; an increase of 50 percent caused the number of simulated heads exceeding the error criteria to increase to 18. Simulated ground-water discharge to rivers did not fluctuate significantly from the measured values because leakage from layer 1 was not a substantial part of the overall water budget.

The model was not sensitive to changes in the riverbed conductance. Both an increase and decrease of 50 percent caused the number of simulated heads exceeding the error criteria to increase from 2 to 3. Simulated ground-water discharge to rivers was only slightly different than the measured values. The riverbed conductances were relatively high because they were calculated using the same hydraulic conductivity as the Upper Floridan aquifer (for reasons discussed earlier). With these high conductances, the simulated volume of ground water leaking into the rivers was controlled by the potentiometric gradients in the surrounding aquifer and not the riverbed conductance. Overall changing the riverbed conductance by plus or minus 50 percent did not greatly affect the simulation results.

The model also was not sensitive to changes in Vcont 2. A decrease of 50 percent caused the number of simulated heads exceeding the error criteria to increase from 2 to 3; an increase in Vcont 2 of 50 percent caused no change in the number of simulated heads exceeding the error criteria. Simulated ground-water discharges to rivers were not substantially different than the measured values. Vcont 2 values were calculated using a vertical hydraulic conductivity equal to the horizontal hydraulic conductivity (for reasons discussed earlier) resulting in relatively high values. The high Vcont 2 values allowed water to move easily from layer 2 to layer 3, and changing this value by plus or minus 50 percent did not sufficiently restrict the movement of water to affect the ground-water flow simulation.

PARTICLE-TRACKING ANALYSIS OF CONTRIBUTING AREAS

The calibrated model was used in combination with the post-processing-program MODPATH (Pollock, 1989) to delineate the contributing areas of five City of Tallahassee water-supply wells. The five wells were chosen because their locations span the range of transmissivities present in the Tallahassee area (fig. 32). Table 5 lists the characteristics of the wells, including the depth, open-hole interval, pumping rate, and relation of well depth and open-hole interval to the thickness of the Upper Floridan aquifer. All of the wells listed partially penetrate the aquifer, and the percent of penetration ranges from 19 percent for well 12 to 28 percent for well 23. The contributing areas were delineated assuming steady-state flow conditions. In reality, the City of Tallahassee operates its wells as needed to meet demand. Only one well was modeled at a time, thus the effects of well interference were not simulated.

Procedure for Delineation of Contributing Areas

The post-processing program MODPATH uses the intercell flow rates (the flow rate at the face of each cell in the model) calculated by MODFLOW to compute ground-water flow directions and velocities. The contributing area to a water-supply well was delineated by "seeding" the simulated pumping well location with particles and then tracking the particles backward toward areas of recharge. Particle tracking was arbitrarily stopped at a time-of-travel of 5 years, thus the time-related contributing area is a fraction of the overall contributing area. The contributing area includes only the time-of-travel within the Upper Floridan aquifer. The time-of-travel of a water particle from land surface, through the water-table aquifer and the low-permeability Miocene- and Pliocene-age sediments, was not included. MODPATH requires the same input parameters as MODFLOW and, additionally requires that porosity be specified for each active

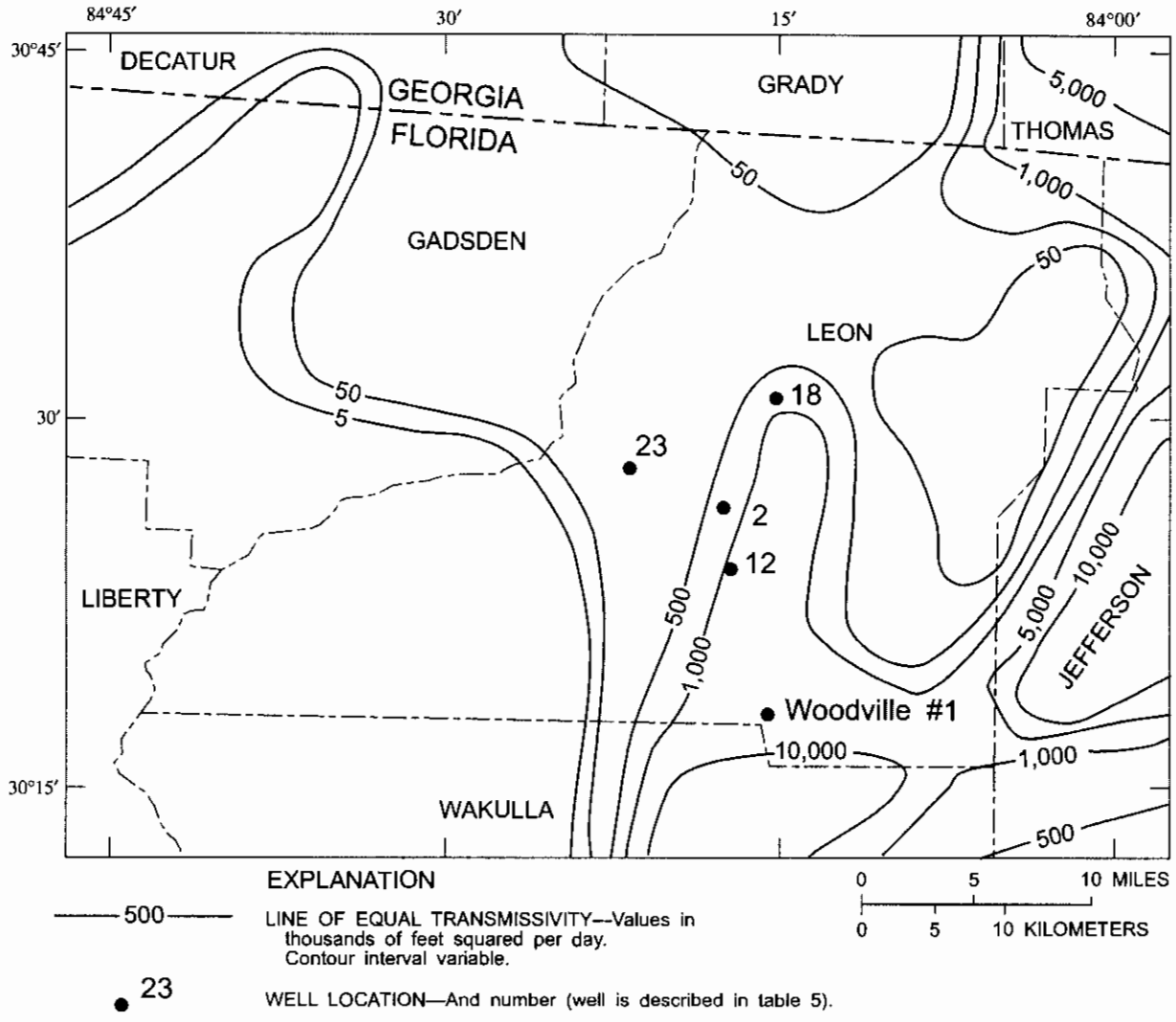

Figure 32. City of Tallahassee, Fla., water-supply wells for which contributing areas were delineated.

cell. The porosity is necessary for the calculation of ground-water velocity.

Porosity within the Upper Floridan aquifer is variable and the distribution is not accurately known. For this reason, the contributing areas were delineated twice, using porosities of 25 and 5 percent. The 25 percent porosity represents an approximate average value for the total porosity in a limestone. The porosity of 5 percent represents only the void space present in interconnected zones created by the dissolution of limestone along bedding planes and fractures. These interconnected zones would have a much higher permeability than the other, much larger, fraction of the aquifer that had not undergone dissolution. A pumping well would draw most of its water from the high-permeability zones where the resistance to ground-water flow is less than the remainder of the aquifer, which would be largely bypassed. The 5 percent porosity is not intended to represent the total porosity present in the Upper Floridan aquifer, but instead represents an estimate of the effective porosity where dissolution has occurred.

The contributing area for a 5 percent porosity is always much larger than the contributing area for a 25 percent porosity. For a lower porosity, the well has to draw water from greater distances to meet the pumping rate because there is less water per unit volume of aquifer. The contributing areas in Leon County are generally elliptical in shape, which reflects the influence of the slope of the potentiometric surface.

Table 5. Characteristics of City of Tallahassee, Florida, water-supply wells for which contributing areas were delineated

Well	Altitude of top of casing, in feet	Depth of well, in feet	Open hole interval, feet below sea level	Pumping rate, in gpm	Altitude of top of Upper Floridan aquifer, in feet above sea level	Altitude of base of Upper Floridan aquifer, in feet below sea level	Depth of penetration of well into the saturated thickness of the Upper Floridan aquifer, in feet[1]	Penetration of well into the saturated thickness of the Upper Floridan aquifer, in percent[2]
2	187	415	-26 to -228	2,050	61	-1,241	248	20
12	125	365	-67 to -240	3,000	55	-1,346	260	19
18	185	388	-82 to -203	2,900	100	-948	223	23
23	120	410	-130 to -290	3,800	34	-1,091	310	28
Woodville 1	35	199	-82 to -157	575	10	-1,575	167	21

[1]Calculated distance from the top of the Upper Floridan aquifer to the bottom of the well.
[2]Calculated by dividing adjacent column by the saturated thickness of the Upper Floridan aquiifer.

Simulated Contributing Areas

The two simulated contributing areas delineated for Tallahassee well 23 are shown in figure 33. The transmissivity in the vicinity of this well is about 100,000 ft^2/d, which is the lowest of the five wells (fig. 32). The pumping rate was 3,800 gal/min. This well penetrates approximately the upper 28 percent of the aquifer. However, because of the relatively low transmissivity and high pumping rate, ground water is drawn from the total thickness of the aquifer (fig. 34). The average ground-water velocity within the contributing area was 1.0 ft/d assuming a 25 percent porosity and 2.4 ft/d assuming a 5 percent porosity.

The two contributing areas simulated for the City of Tallahassee well Woodville 1 are shown in figure 35. The transmissivity in the vicinity of this well is about 10,000,000 ft^2/d, the highest of all the wells. The pumping rate was 575 gal/min. This well penetrates approximately the upper 21 percent of the aquifer. However, ground water is drawn from about the upper 25 percent of the aquifer (fig. 36), because of the high transmissivity and low pumping rate. The average ground-water velocity within the contributing area was 1.6 ft/d assuming a 25 percent porosity, and 7.4 ft/d assuming a 5 percent porosity.

The simulated contributing areas for wells 2, 12 and 18 are shown in figures 37, 38, and 39, respectively. The transmissivities at these wells are intermediate to that of the two wells previously discussed. The transmissivities at wells 2 and 12 are about 1,000,000 ft^2/d and the transmissivity at well 18 is about 750,000 ft^2/d. The pumping rates were 2,050 gal/min for well 2, 3,000 gal/min for well 12, and 2,900 gal/min for well 18. The ground-water velocities within the contributing areas of these wells were between those of well 23 and Woodville 1.

Comparison of Simulated and Analytically Derived Contributing Areas

Contributing areas to pumping wells can also be computed using analytical methods. This methodology is quick compared to the numerical modeling approach; however, the analytical method does not have the flexibility to incorporate a variety of hydrologic conditions. For this reason, simplifying assumptions about the aquifer must be made. For the purpose of comparison, the maximum upgradient width of the contributing area for each of the five Tallahassee wells was determined analytically and compared to the width delineated by particle tracking. The equation used to calculate the contributing area widths was (modified from Todd, 1980):

$$Y_L = Q / T\,i \qquad (3)$$

where:

- Y_L is the upgradient maximum width of the contributing area (ft),
- Q is the discharge rate of the well, (ft^3/s),
- T is transmissivity (ft^2/d), and
- i is the slope of the water table (dimensionless).

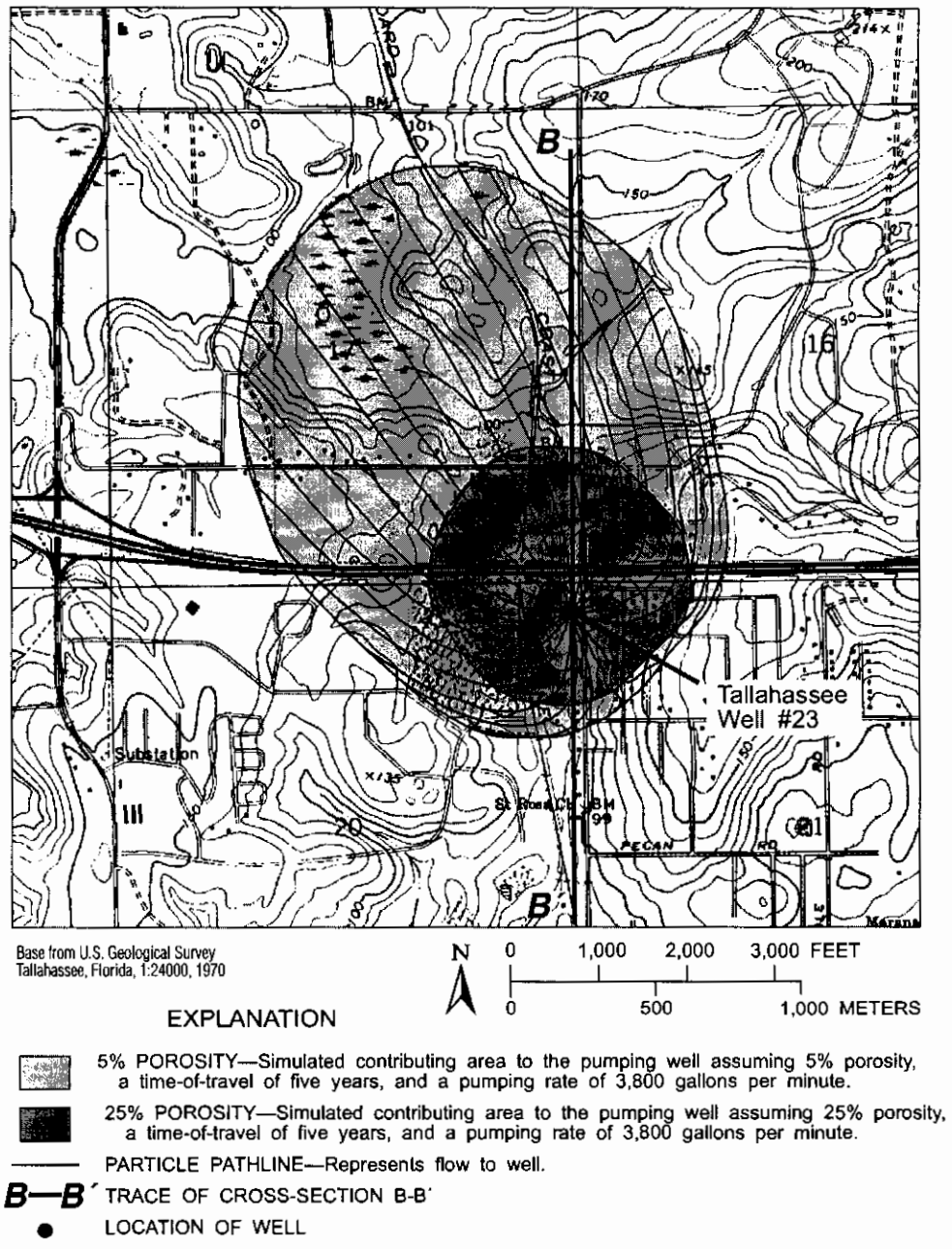

Figure 33. Simulated contributing areas to City of Tallahassee well 23.

This equation is commonly used to calculate contributing areas where a sloping water table is present (U.S. Environmental Protection Agency, 1987). The simplifying assumptions made when using this equation are: steady-state flow conditions, uniformly sloping potentiometric surface, constant pumping rate, uniform constant transmissivity, and a fully penetrating well. Over relatively small areas of 1 to 2 mi^2 within the Tallahassee area, all of these simplifying assumptions are probably valid except the last one.

Simulated and analytically derived contributing-area widths are listed in table 6. The analytically derived width for well 23 was 7,536 ft and the model-derived width was 7,500 ft. These values compare closely because well 23 draws water from the full thickness of the aquifer (even though the well was not fully penetrating, as discussed earlier). The analytically derived contributing-area width for Woodville 1 was 161 ft and the model-derived width was 900 ft. For this well, the analytical equation underestimates

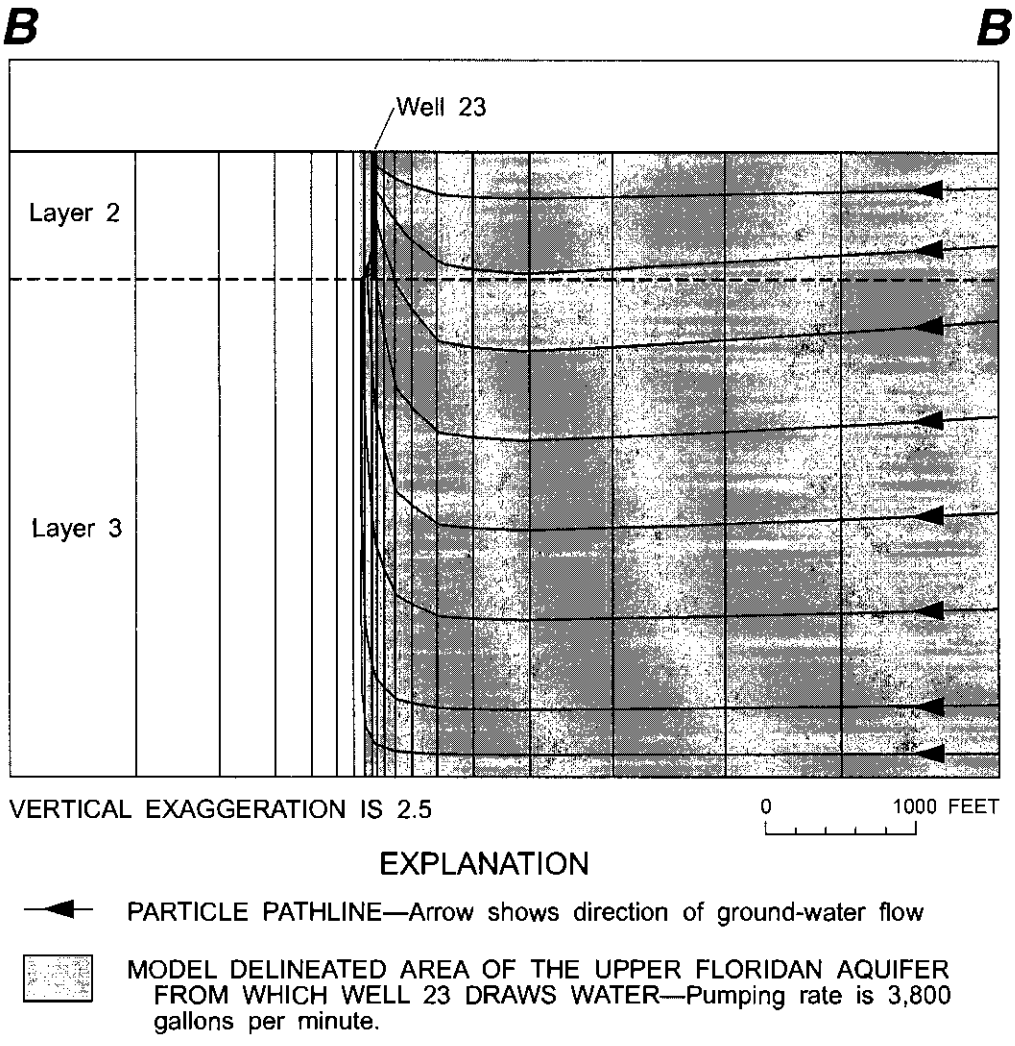

Figure 34. Particle pathlines showing the extent of the Upper Floridan aquifer from which City of Tallahassee well 23 draws water (line of section shown on figure 33).

the width of the contributing area because it assumes that ground water is drawn from the full thickness of the aquifer. The numerical model, which was able to simulate the well as partially penetrating, determined a shallower, wider contributing area which is more accurate. The vertical extent of the aquifer from which wells 2, 12, and 18 drew water was intermediate between those of well 23 and Woodville 1. Thus the differences between the simulated widths and the analytically derived widths were also intermediate between these two wells.

Determination of the contributing areas by model simulation is a more accurate method than analytical approaches because complex, three-dimensional aquifer characteristics can be incorporated into the solution. However, if the characteristics of a particular aquifer match the assumptions of the analytical methods, then these methods could produce good results for considerably less effort. The complexity of the ground-water system must be assessed to determine whether contributing areas should be calculated using numerical ground-water flow models or by simpler analytical methods.

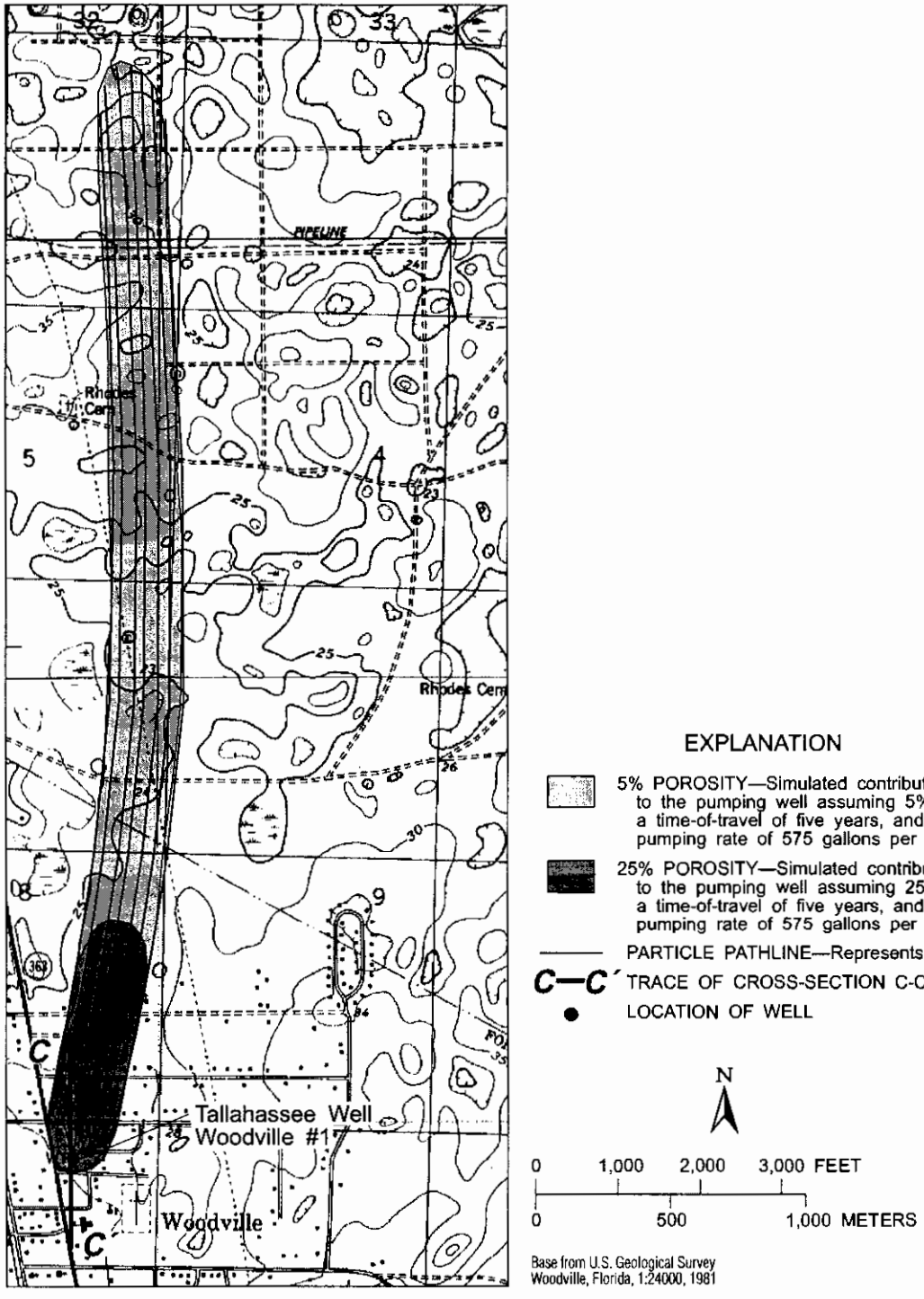

Figure 35. Simulated contributing areas to City of Tallahassee well Woodville 1.

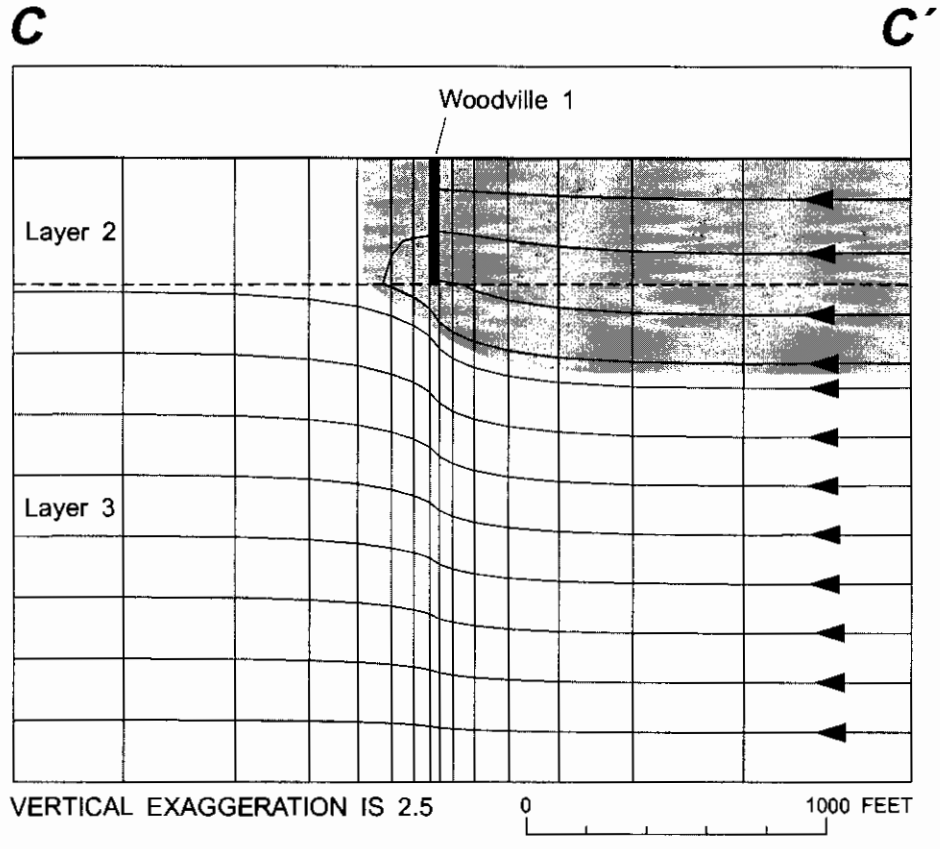

Figure 36. Particle pathlines showing the extent of the Upper Floridan aquifer from which City Tallahassee well Woodville 1 draws water (line of section shown on figure 35).

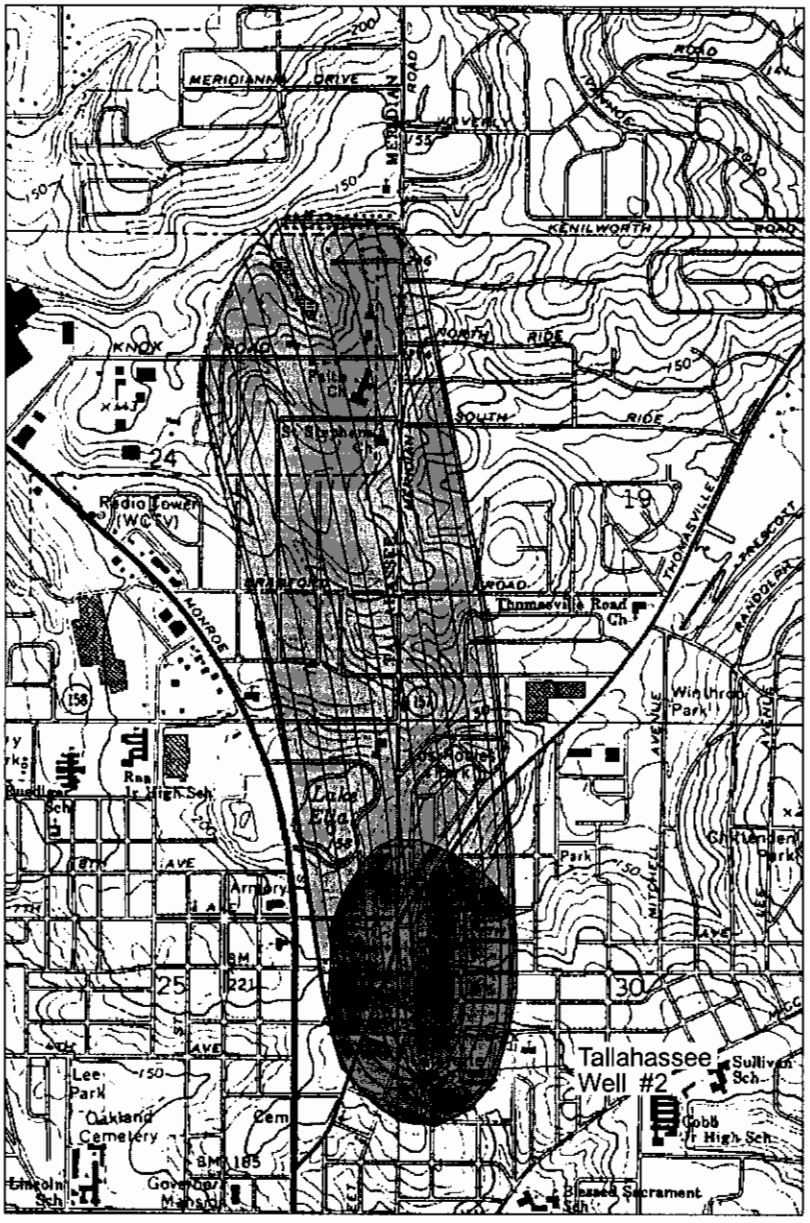

Figure 37. Simulated contributing areas to City of Tallahassee well 2.

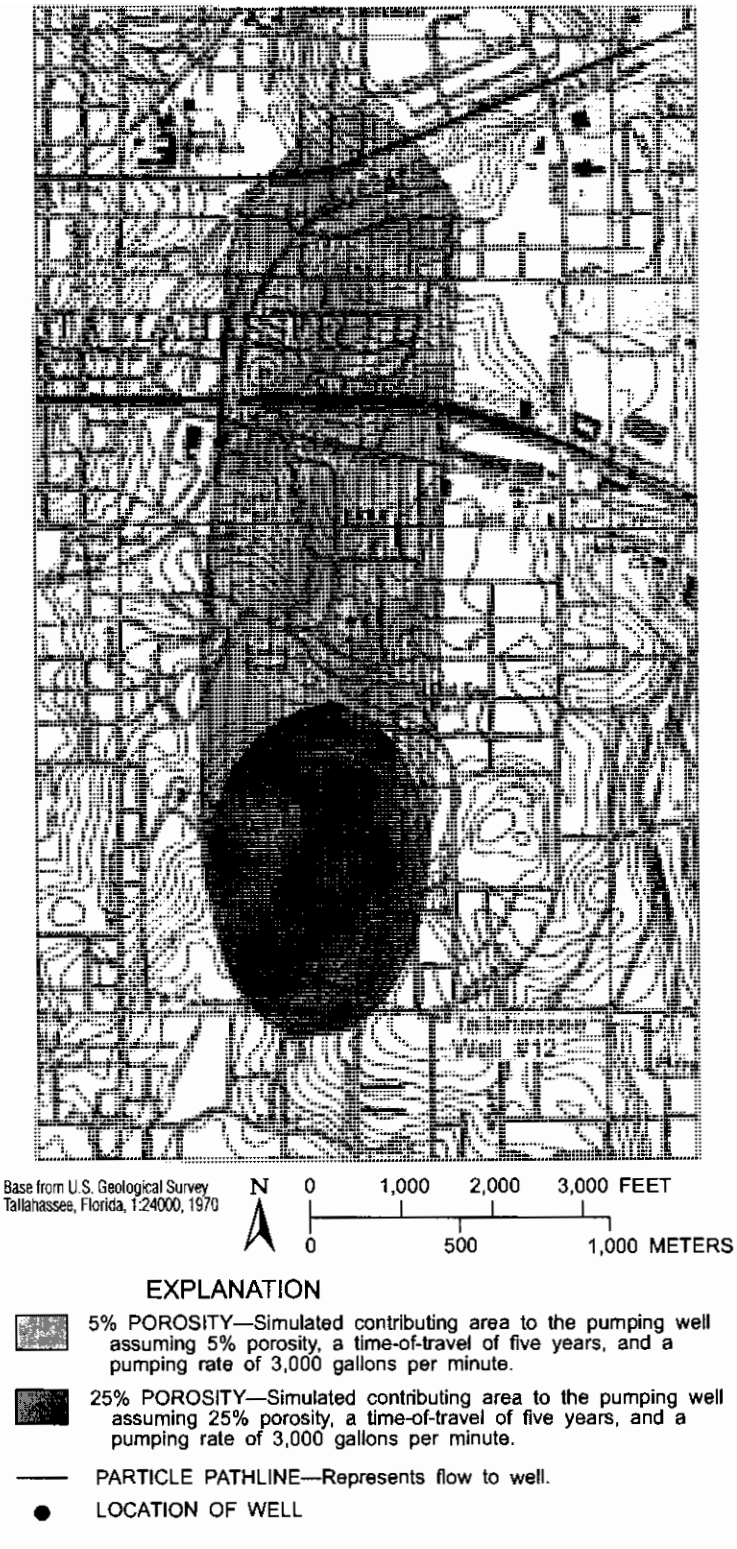

Figure 38. Simulated contributing areas to City of Tallahassee well 12.

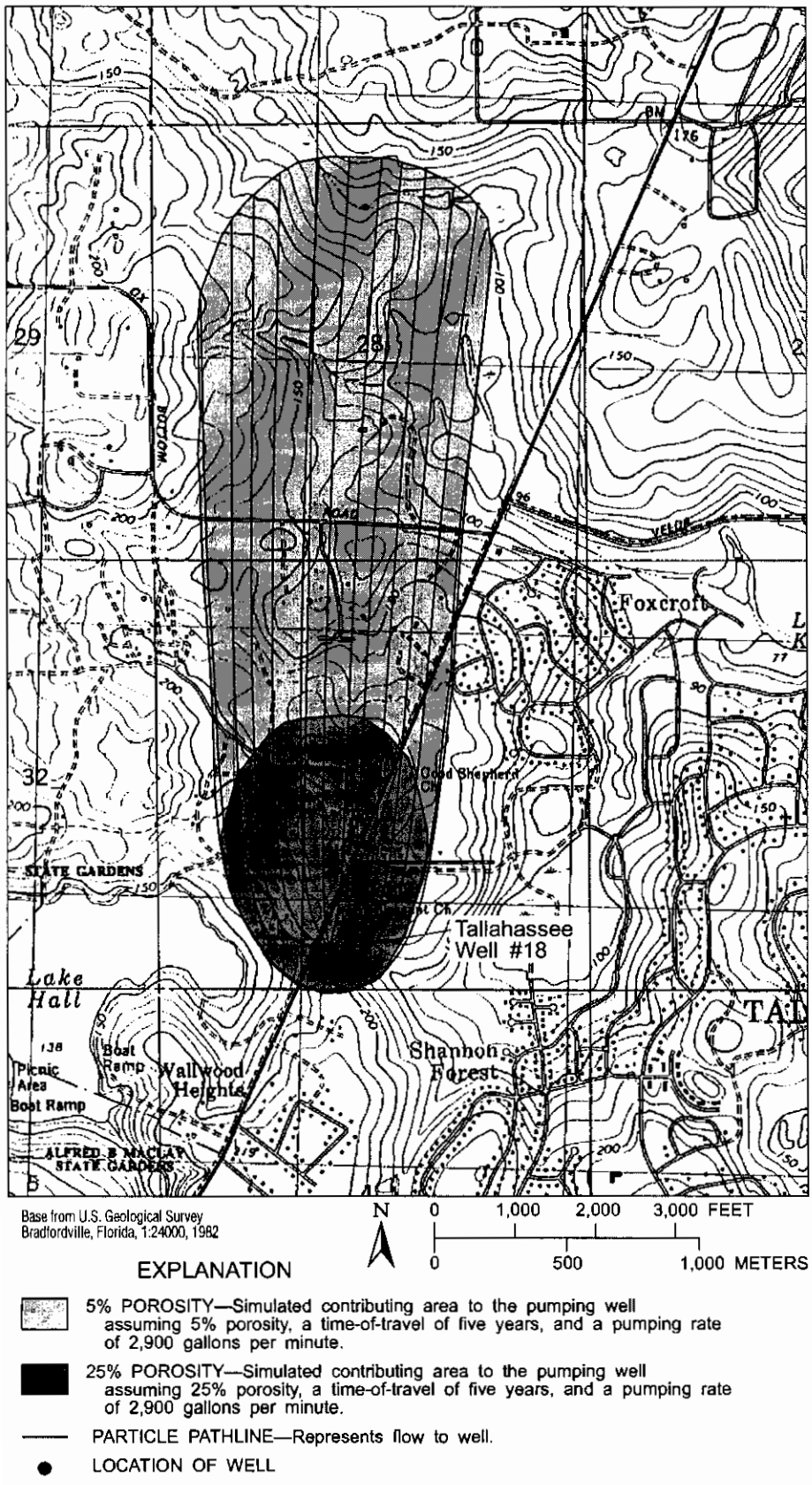

Figure 39. Simulated contributing areas to City of Tallahassee well 18.

Table 6. Contributing area widths determined by numerical and analytical models for five Tallahassee, Florida, water-supply wells

Well	Width of simulated contributing area, in feet	Width of analytically calculated contributing area, in feet
2	2,700	1,067
12	2,500	1,561
18	3,500	2,044
23	7,500	7,536
Woodville 1	900	161

SUMMARY AND CONCLUSIONS

Ground water from the Upper Floridan aquifer is the source of water supply for Tallahassee, Fla., and for many parts of the surrounding area. In most areas, the aquifer yields an ample supply of good quality water; however, in recent years low levels of tetrachloroethylene (PCE) have been detected in ground-water samples taken from seven City of Tallahassee water-supply wells. The PCE is attributed to past disposal practices of dry cleaners, service stations, and other businesses within the downtown area. The City of Tallahassee removes PCE from the water by passing it through granular-activated carbon units before distribution. To ensure that water-supply wells, presently free of contamination, remain clean, it is necessary to understand the ground-water flow system in sufficient detail to protect the contributing areas. The contributing area of a pumping well is the land area that has the same horizontal extent as that part of the aquifer from which ground-water flow is diverted. To gain an understanding of the ground-water flow system, a 4-year investigation of the Upper Floridan aquifer was conducted. The study area was centered in Leon County, Fla., and extended to surrounding counties in north-central Florida and southwestern Georgia.

The study area is underlain by sedimentary rocks of Tertiary through Quaternary age that consists of limestone, dolostone, clay, and sand of varying degrees of lithification. Aquifers in the study area include the water-table aquifer and Upper Floridan aquifer, which are separated by low-permeability sediments. The water-table aquifer yields only small amounts of water when pumped and generally is not used. The Upper Floridan aquifer is utilized for municipal, industrial, agricultural, and domestic water supply. The transmissivity of the Upper Floridan aquifer ranges over several orders of magnitude.

The potentiometric surface of the Upper Floridan aquifer was defined by measuring ground-water levels in a network of 274 wells. The rate of ground-water discharge from the Upper Floridan aquifer to rivers was quantified by measuring river-discharge rates in area rivers. One aquifer test was conducted that determined a transmissivity of 1,300,000 ft^2/d for the Upper Floridan aquifer in downtown Tallahassee.

A conceptual model describing ground-water flow was developed to aid in building a computer model that accurately simulates ground-water flow. The Upper Floridan aquifer is conceptualized as having the following characteristics: ground-water flow is at steady state; the aquifer acts as a single water-bearing unit; and recharge is by precipitation and discharge occurs as spring flow, leakage to rivers, leakage to the Gulf of Mexico, and pumpage. The recharge area for ground-water moving beneath Leon County extends to counties to the west and north.

Steady-state ground-water flow in the Upper Floridan aquifer was simulated using the USGS modeling software MODFLOW. The model was calibrated to hydrologic data collected from late October to early November 1991. The model grid consisted of 176 rows, 162 columns, and 3 layers with 28,512 model cells per layer. Cell size was variable with the smallest cells being near the center of the study area and larger cells being near the perimeter. Row and column spacing was chosen so that water-supply wells, in which contributing areas were to be determined, would be positioned in the smallest model cells. The smallest cells are 30 ft on each side and the largest cells are 3 mi on each side.

The calibrated model was used in combination with the post-processing program MODPATH to simulate the contributing areas of five Tallahassee water-supply wells. The five wells were chosen because their locations spanned the range of transmissivities present in the Tallahassee area. All of the wells partially penetrated the aquifer and penetration ranged from 19 to 28 percent. The contributing area was delineated by "seeding" the simulated pumping well location in the model with particles and then tracking the particles backward toward areas of recharge.

Porosity within the Upper Floridan aquifer is variable and the distribution not accurately known. For this reason, the contributing areas were simulated twice, using a porosity of 25 and 5 percent. The

Hydrogeology and Analysis of Aquifer Characteristics in West-Central Pinellas County, Florida

By James C. Broska *and* Holly L. Barnette

U.S. Geological Survey

Open-File Report 99–185

Prepared in cooperation with

PINELLAS COUNTY

Tallahassee, Florida
1999

U.S. DEPARTMENT OF THE INTERIOR
BRUCE BABBITT, Secretary

U.S. GEOLOGICAL SURVEY
Charles G. Groat, Director

For additional information write to:

District Chief
U.S. Geological Survey
Suite 3015
227 North Bronough St.
Tallahassee, FL 32301

Copies of this report can be purchased from:

U.S. Geological Survey
Branch of Information Services
Box 25286
Denver, CO 80225
888-ASK-USGS

CONTENTS

Figures

Tables

CONVERSION FACTORS, VERTICAL DATUM, AND ADDITIONAL ABBREVIATIONS

Multiply inch-pound unit	By	To obtain
inch per year (in/yr)	25.4	millimeter per year
inches squared per pound (in^2/lb)	$1.45x10^{-4}$	square meter per Newton
foot (ft)	0.3048	meter
foot per day (ft/d)	0.3048	meter per day
foot per day per foot (ft/d)/ft	0.3048	meter per day per meter
foot squared per day (ft^2/d)	0.093	meter squared per day
cubic feet per day (ft^3/d)	0.02832	cubic meter per day
pound per cubic foot (lb/ft^3)	16.02	kilogram per cubic meter
gallon per minute (gal/min)	5.45	cubic meter per day
million gallons per day (Mgal/d)	0.04381	cubic meters per second

Temperature can be converted between degrees Fahrenheit (°F) and degrees Celsius (°C) as follows:

$$°F = 9/5 (°C) + 32$$

$$°C = 5/9 (°F - 32)$$

Sea level: In this report, “sea level” refers to the National Geodetic Vertical Datum of 1929 (NGVD of 1929)—a geodetic datum derived from a general adjustment of the first-order level nets of the United States and Canada, formerly called Sea Level Datum of 1929.

ADDITIONAL ABBREVIATIONS

ICU	=	Intermediate confining unit
SAS	=	Surficial aquifer system
LZA	=	Lower Zone A
UZA	=	Upper Zone A
USGS	=	U.S. Geological Survey
mg/L	=	milligrams per liter
µS/cm	=	microsiemens per centimeter

Hydrogeology and Analysis of Aquifer Characteristics in West-Central Pinellas County, Florida

By James C. Broska *and* Holly L. Barnette

ABSTRACT

The U.S. Geological Survey, in cooperation with Pinellas County, Florida, conducted an investigation to describe the hydrogeology and analyze the aquifer characteristics in west-central Pinellas County. A production test well and four monitor wells were constructed in Pinellas County at Walsingham Park during 1996-97. Water-quality sampling, static and dynamic borehole geophysical surveys, and hydraulic tests were conducted at the wells to delineate the hydrogeology at Walsingham Park. A 9-day aquifer test was conducted to determine the hydraulic characteristics of the aquifer system and observe the changes in water quality due to pumping.

A numerical model was constructed to simulate the aquifer test and calculate values for hydraulic conductivity and storage coefficient for permeable zones and confining units at Walsingham Park. Final calibrated values for hydraulic conductivity for the different permeable zones and confining units at the test site were 18 feet per day for Upper Zone A, 750 feet per day for Lower Zone A, 1 foot per day for Zone B, $1x10^{-4}$ feet per day for the intermediate confining unit, and 10 feet per day for the semiconfining unit separating Upper Zone A and Lower Zone A. Final calibrated values for storage coefficient were $3.1x10^{-4}$ for Upper Zone A, $8.6x10^{-5}$ for Lower Zone A, $2.6x10^{-5}$ for Zone B, $3.1x10^{-4}$ for the intermediate confining unit, and $4.3x10^{-5}$ for the semiconfining unit separating Upper Zone A and Lower Zone A. Estimates of transmissivity for Upper Zone A and Lower Zone A were about 2,500 and 37,500 feet squared per day, respectively.

INTRODUCTION

Pinellas County, located in west-central Florida, has limited potable water supplies and is dependent on water delivered from Tampa Bay Water (formerly called the West Coast Regional Water Supply Authority) which withdraws water from neighboring inland counties to meet the water demands of a large population. Although the population of Pinellas County has not increased significantly since 1990, during the period from 1970 to 1990 the population of Pinellas County increased from 552,329 to 851,659 (University of Florida, 1991). In 1990, the county received a total of 78 Mgal/d of water from Hillsborough and Pasco Counties (Marella, 1992). To alleviate some of the demand for this delivered water, Pinellas County is exploring the possibility of using the brackish-water resources within the Upper Floridan aquifer underlying the county.

Brackish waters (water with dissolved-solids concentrations between 1,000 and 10,000 mg/L) are found in the Upper Floridan aquifer at depths ranging from about 100 to 400 ft below land surface in central Pinellas County (Cherry and others, 1970). The development of these brackish-water resources through low-pressure reverse osmosis could provide a source of potable water. Low-pressure reverse osmosis is a process of forcing water through a membrane to remove dissolved solids, thus purifying the water; however, the process is economically practical only when dissolved-solids concentrations are less than 7,000 mg/L (D. Slonena, Pinellas County Utilities, written commun., 1998).

A production test well and four monitor wells were constructed in 1996-97 at Walsingham Park in west-central Pinellas County. The wells were subjected to various geologic investigation methods to determine the hydrogeology at the test site and the viability of brackish-water development in the area.

Purpose and Scope

This report presents the results of a study by the U.S. Geological Survey (USGS), in cooperation with Pinellas County, to evaluate the brackish-water resources underlying the Walsingham Park study area in west-central Pinellas County. Results from the field investigation and numerical simulation to determine aquifer characteristics at the Walsingham Park test site could provide valuable information for future development of brackish water in Pinellas County and in other coastal counties in west-central Florida. The report includes: descriptions of the hydrogeologic framework of the study site, hydraulic characteristics of the aquifer system, and description of the ground-water quality.

The objectives of this report are to
1.) describe the hydrogeology at the test site, and
2.) evaluate an aquifer test conducted in the Upper Floridan aquifer at the test site.

Description of the Study Area

Pinellas County is a peninsula in west-central Florida bounded by Tampa Bay to the east and the Gulf of Mexico to the west (fig. 1). The county is part of the Gulf Coastal Lowlands physiographic region described by White (1970) which consists of low angle scarps and terraces formed during several Pleistocene sea-level stands. The climate of Pinellas County is subtropical with an average rainfall of 53 inches per year (in/yr). Most rainfall occurs during the summer months between June and September (Causseaux and Fretwell, 1983). Land surface elevation at the Walsingham Park test site is about 55 ft above sea level.

HYDROGEOLOGIC FRAMEWORK

The geology of Florida consists of a pre-Mesozoic igneous and metamorphic basement and an overlying thick sequence of sedimentary units deposited during transgressive and regressive episodes (Heath and Smith, 1954). The hydrogeologic framework underlying the study area consists of Eocene or younger-age rocks and makes up the surficial aquifer system, the intermediate confining unit, and the Floridan aquifer system (fig. 2). This multilayered system consists of several permeable zones interbedded with zones of variable permeability that function as either confining units or semiconfining units. A semiconfining unit in this report refers to lower-permeability carbonate units that do not produce large quantities of water to wells when pumped (Knochenmus and Swenson, 1996). The hydrogeologic information compiled from wells at the test site was correlated with hydrogeologic information from previous studies in west-central Pinellas County. A generalized hydrogeologic section, oriented north-south, was constructed from natural-gamma geophysical logs (fig. 3).

Surficial Aquifer System

The surficial aquifer system (SAS) in Pinellas County is the shallowest water-bearing formation in the study area and consists of undifferentiated sands and clays which change in composition laterally and vertically (Causseaux, 1985). The post-Miocene age surface deposits in Pinellas County lie unconformably above the Hawthorn Group. Surface deposits are characterized by a base of marginal marine beds overlain by sandy, marine terrace deposits and capped by aeolian sand deposits. The thickness of the SAS, which ranges from a few feet to 50 ft, restricts the amount of potable water the aquifer supplies; however, the nonpotable water is utilized for irrigation (Gilboy, 1985). The SAS at the Walsingham Park site is about 35 ft thick. Throughout Pinellas County, the water table is less than 15 ft below land surface during dry periods and close to land surface during wet periods. Precipitation is the main source of recharge.

Hydraulic properties of the SAS are highly variable due to the diversity in physical characteristics of the sediments. Grain size, sorting, and thickness vary throughout the system and greatly influence the permeability and porosity of the system. Values for specific yield range from 0.1 to 0.35 (Causseaux, 1985). Horizontal hydraulic conductivity is estimated to range from 13 to 33 ft/d (Cherry and Brown, 1974; Sinclair, 1974) and vertical hydraulic conductivity is estimated to range from 0.36 to 13 ft/d (Sinclair, 1974; Hutchinson and Stewart, 1978).

Intermediate Confining Unit

The surficial and Floridan aquifer systems are separated by the low-permeability intermediate confining unit (ICU). The ICU occurs within the upper Miocene undifferentiated Arcadia Formation of the Hawthorn Group. The formation consists of interbedded quartz sands, clays, and carbonates. The clay beds in the Arcadia Formation act as confining beds

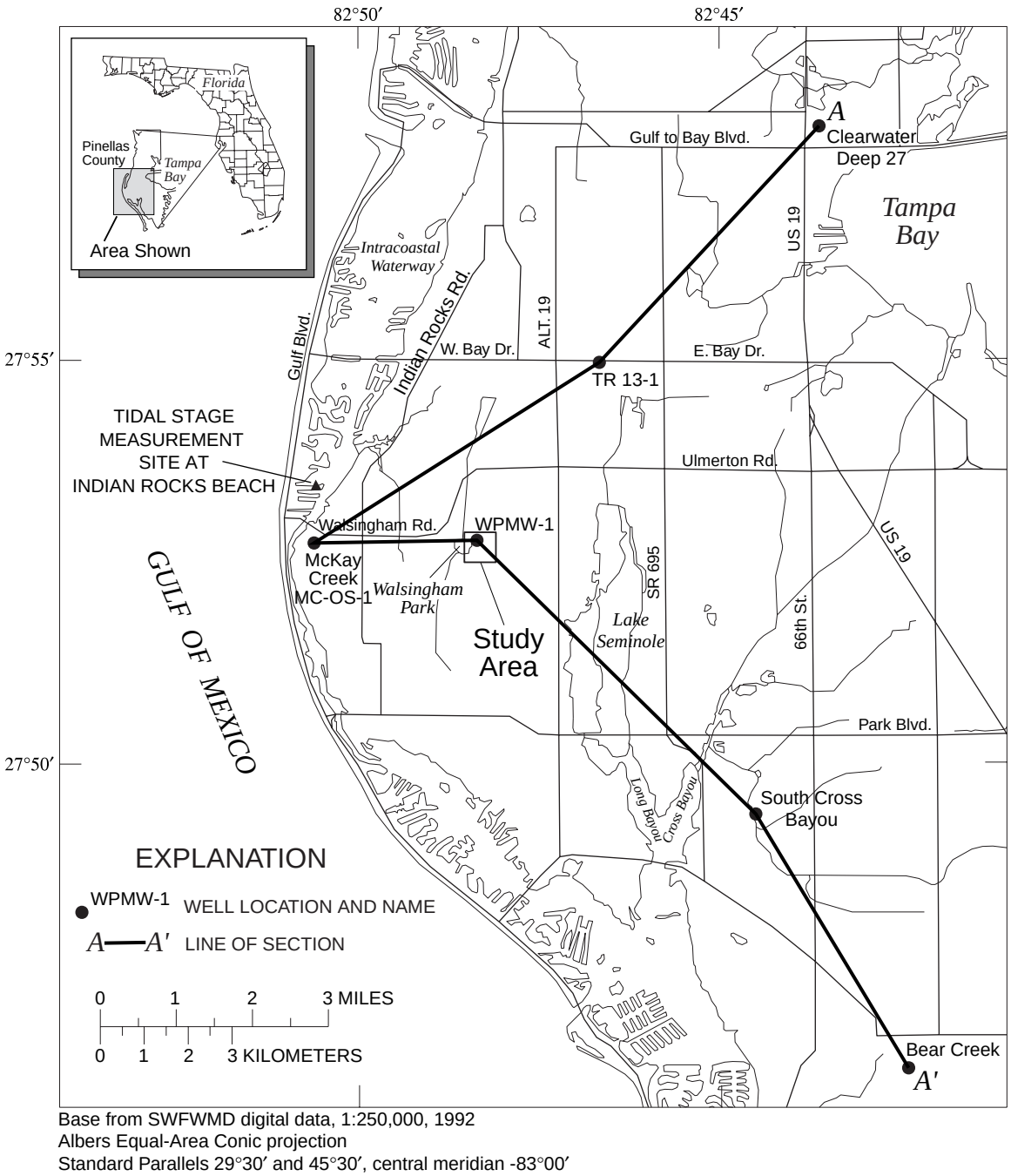

Base from SWFWMD digital data, 1:250,000, 1992
Albers Equal-Area Conic projection
Standard Parallels 29°30′ and 45°30′, central meridian -83°00′

Figure 1. Location of the study area in west-central Pinellas County, well names, and hydrogeologic section *A-A′*.

throughout Pinellas County (Heath and Smith, 1954). The thickness of the ICU averages about 90 ft and ranges from 50 to 140 ft. At the Walsingham Park site, the ICU is about 100 ft thick. Due to the heterogeneous nature of the unit, a wide range of hydraulic properties has been reported. Vertical hydraulic conductivity for the ICU ranges from 1.3×10^{-4} to 6.9×10^{-3} ft/d (Sinclair, 1974; Black, Crow and Eidness, Inc., 1978). Leakance values reported in previous investigations range from 1×10^{-5} to 1.5×10^{-2} (ft/d)/ft (Black, Crow and Eidness, Inc., 1978; Seaburn and Robertson, Inc., 1983; Brown and Associates, Inc., 1986).

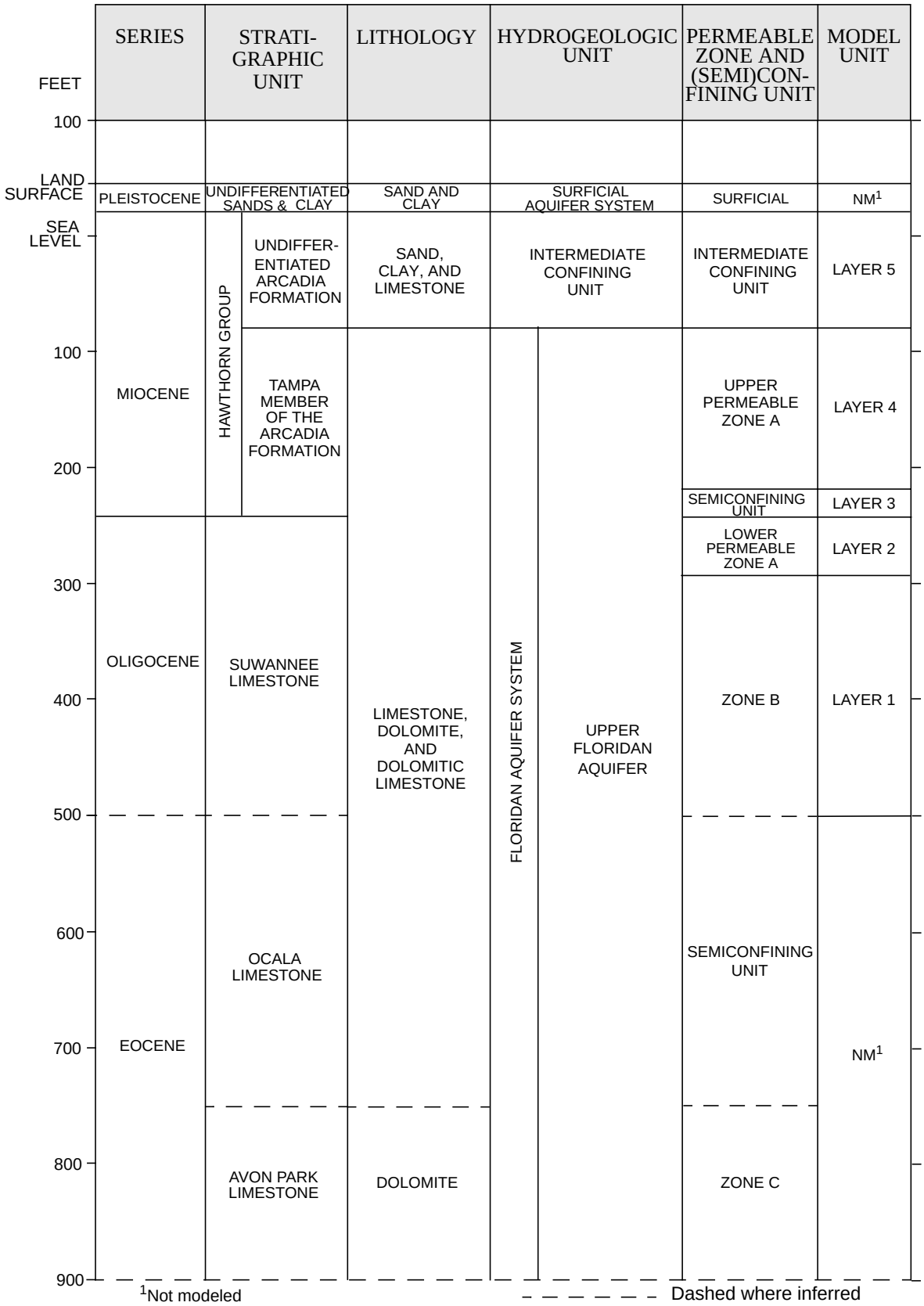

Figure 2. Generalized stratigraphic and hydrogeologic section underlying the Walsingham Park test site, Pinellas County, and equivalent model units (modified from Knochenmus and Swenson, 1996).

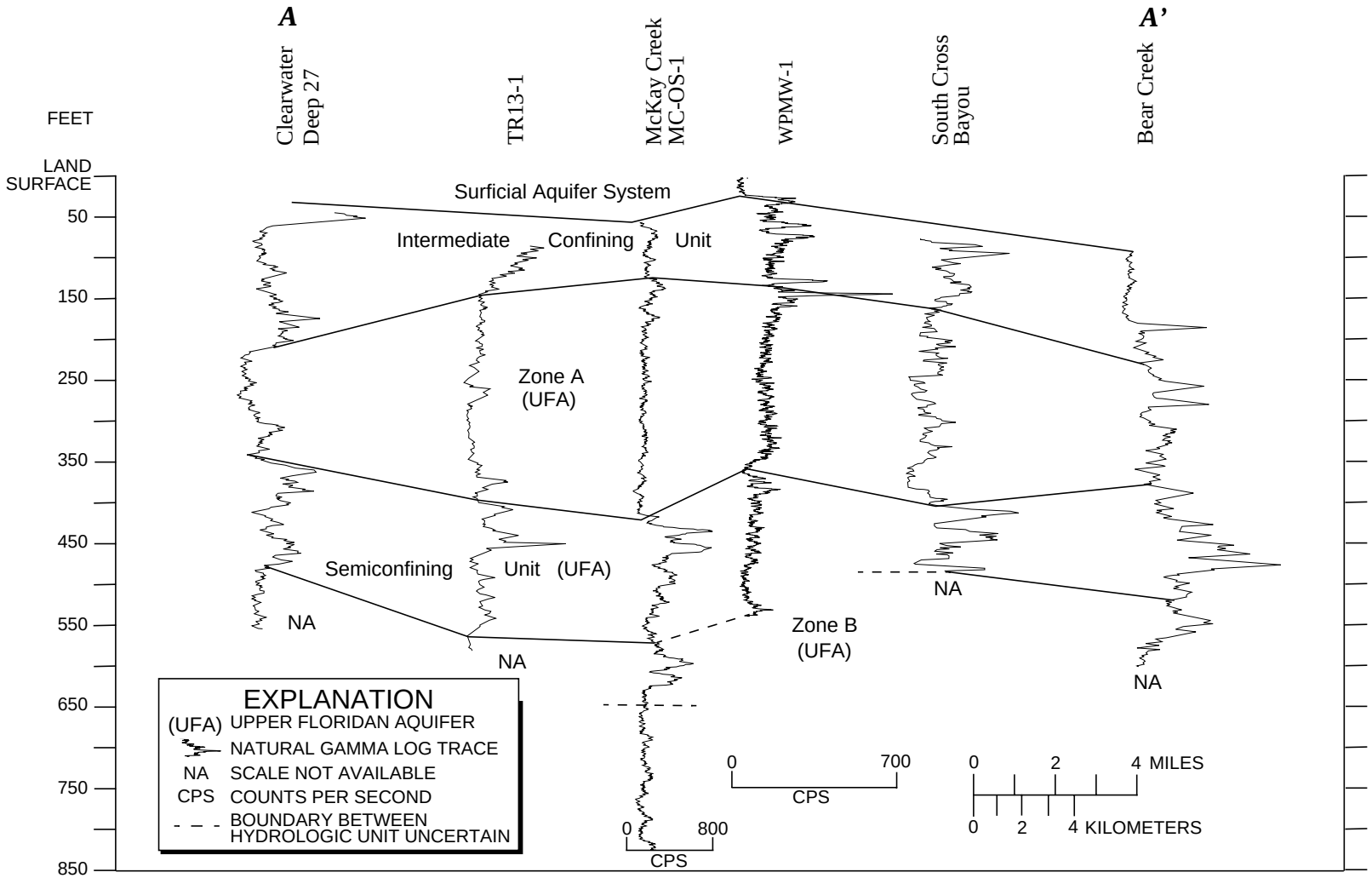

Figure 3. Hydrogeologic units underlying the study area correlated to natural-gamma ray log traces for section *A-A'* in Pinellas County (location of section shown in fig. 1).

Floridan Aquifer System

The Floridan aquifer system consists of limestones and dolomites and includes the Upper Floridan aquifer, the middle confining unit, and the Lower Floridan aquifer. The Upper Floridan aquifer in Pinellas County is composed of the Avon Park Formation, the Ocala Limestone, the Suwannee Limestone, and the Tampa Member of the Arcadia Formation (fig. 2). The Avon Park Formation consists of marine limestones interbedded with dolostones. The limestones are predominantly well indurated packstones which are highly fossiliferous. Overlying the Avon Park Formation is the Ocala Limestone. The Ocala Limestone consists of moderately indurated grainstones and packstones. The foraminiferal limestones in the unit commonly contain benthic foraminifera, bryozoan, echinoid, and mollusk fossils. The Ocala Limestone has a gradational contact with the overlying Suwannee Limestone. The Suwannee Limestone is predominantly foraminiferal packstone to grainstone with abundant mollusk and microfaunal remains (Miller, 1986). Overlying the Suwannee Limestone is the Tampa Member of the Arcadia Formation, which is the lower Miocene unit of the Hawthorn Group (Miller, 1986). The Tampa Member lies unconformably on the Suwannee Limestone and consists of limestone with dolostone, sands, and clays present in minor amounts. Mollusks, foraminifera, and algae are the common fossil molds present in the unit. The unit varies from mudstones to packstones, but is predominately wackestones.

In Pinellas County, the Upper Floridan aquifer is subdivided into four permeable zones generally separated by semiconfining units as defined by Hickey (1982). The zones are labeled alphabetically with increasing depth from A to D. The focus of this report is the uppermost part of the Upper Floridan aquifer, specifically the Tampa Member of the Arcadia Formation of the Hawthorn Group (Zone A) and the Suwannee Limestone (Zones A and B) because these are the only zones that contain brackish water at concentrations suitable for low-pressure reverse osmosis. Further discussions will be restricted to Zones A and B.

Zone A

Zone A, the shallowest and freshest permeable zone in the Upper Floridan aquifer, is made up of the Tampa Member and the upper part of the Suwannee Limestone. In Pinellas County, the thickness of Zone A averages 180 ft and ranges from approximately 115 to 250 ft. Reported transmissivities for Zone A throughout Pinellas County range from 10,000 to 40,000 ft^2/d (Hickey, 1982; Seaburn and Robertson, Inc., 1983; Brown and Associates, Inc., 1986). Values for storativity range from $4x10^{-4}$ to $8x10^{-4}$ (Hickey, 1982). Hickey (1982) divided Zone A into Upper Zone A (UZA) and Lower Zone A (LZA), separated by a discontinuous semiconfining unit. At the Walsingham Park site, a 25-ft thick semiconfining unit consisting of an abundance of marine clay separates the 140 ft thick UZA from LZA, which is about 50 ft thick (fig. 2).

Zone B

In Pinellas County, Zone B underlies Zone A. Thickness of Zone B averages about 150 ft and ranges from about 125 to 170 ft. The upper part of Zone B functions as a semiconfining unit in some parts of Pinellas County and is considered a nonproducing zone in these areas (Hickey, 1982; Knochenmus and Swenson, 1996). Reported hydraulic properties for this sequence are $1.3x10^{-3}$ to 2 ft/d for vertical hydraulic conductivity, 0.1 ft/d for horizontal hydraulic conductivity, and $7x10^{-3}$ (ft/d)/ft for leakance (Hickey, 1982; Seaburn and Robertson, Inc., 1983; and Brown and Associates, Inc., 1986). The lower part of Zone B is more permeable and is comprised of the lower part of the Suwannee Limestone. Thickness of this section of Zone B averages about 62 ft and ranges from 50 to 75 ft. Transmissivity estimates by Hickey (1982) suggest a value of about 5,000 ft^2/d. At the study site, Zone B was encountered between 350 and 547 ft below land surface. However, no apparent changes in permeability in the upper and lower parts of Zone B could be determined during drilling.

Delineation of Hydrogeologic Units Underlying the Study Area

The delineation of hydrogeologic units and their associated hydraulic properties at the Walsingham Park test site was accomplished through the collection and interpretation of lithologic and stratigraphic data, water-quality data, borehole geophysical data, and hydraulic data. During the well construction, rock core description, discrete water-quality sampling, borehole geophysical logging, and specific capacity tests were performed. Upon completion of the well construction, a 9-day aquifer test was performed. In total, one test production well 3 and four monitor wells were installed at the test site (fig. 4).

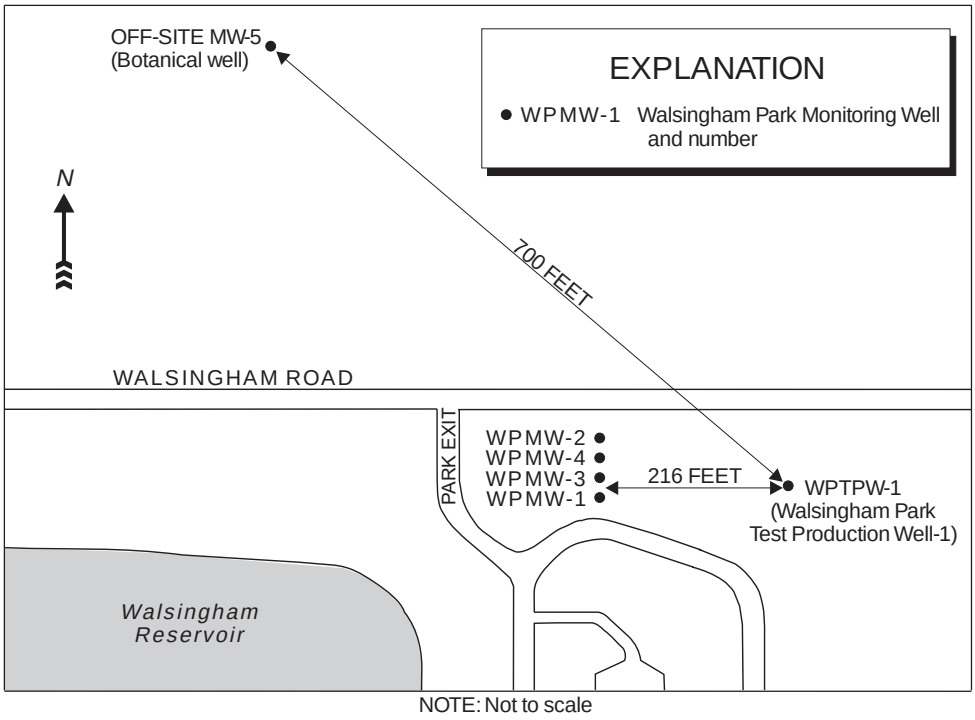

Figure 4. Walsingham Park test site, including location of wells drilled during the field investigation, and location of off-site monitor well (general location is shown in fig. 1).

A production test well and four monitor wells were drilled by using a dual-wall reverse-circulation rotary drilling method. With this drilling method, pressurized air is forced down between the inner and outer barrels of the drilling stem. Rock and/or sediment is cut by the drill bit, and core samples rise to land surface through the inner barrel. The first well drilled was originally designed to function as a deep exploratory well and was drilled to a depth of 547 ft. This well was drilled to define the geology, water quality, and vertical distribution of producing zones and confining units at the test site. Data collected from the deep exploratory well were used to determine the total depths and casing depths of the test production well and monitor wells. After drilling and data collection, the deep exploratory well was backplugged to a depth of 266 ft and converted into the Walsingham Park UZA monitor well 1 (WPMW-1). The WPMW-1 and all other monitor wells were constructed to monitor a specific producing zone or lower permeability unit to evaluate the responses of various zones to pumping. The other wells drilled as part of this study are hereafter referred to as the test production well 1 (WPTPW-1), the LZA brackish-water monitor well 2 (WPMW-2), the intermediate confining unit monitor well 3 (WPMW-3), and the surficial aquifer system monitor well 4 (WPMW-4). Total depths and casing depths of all the wells constructed during this study are provided in figure 5.

Water-Quality Sampling

Water-quality samples were collected by the USGS and Pinellas County personnel during drilling of WPMW-1 to determine vertical distribution of water quality at the site. Water samples were collected at discrete intervals every 10 ft during drilling and tested onsite for specific conductance, temperature, and pH. When abrupt changes in field measurements occurred, water samples were collected and analyzed for major ions and physical properties at the Pinellas County Utilities laboratory. A vertical water-quality profile showing variations in dissolved solids with depth during drilling of WPMW-1 is presented in figure 6. As illustrated, the dissolved-solids concentration begins increasing approximately 350 ft below land surface. Although some water samples collected between 360 and 425 ft below land surface contained a lower concentration of dissolved solids, this anomaly may have been caused by drilling constraints as water samples were collected over a period of 3 consecutive days.

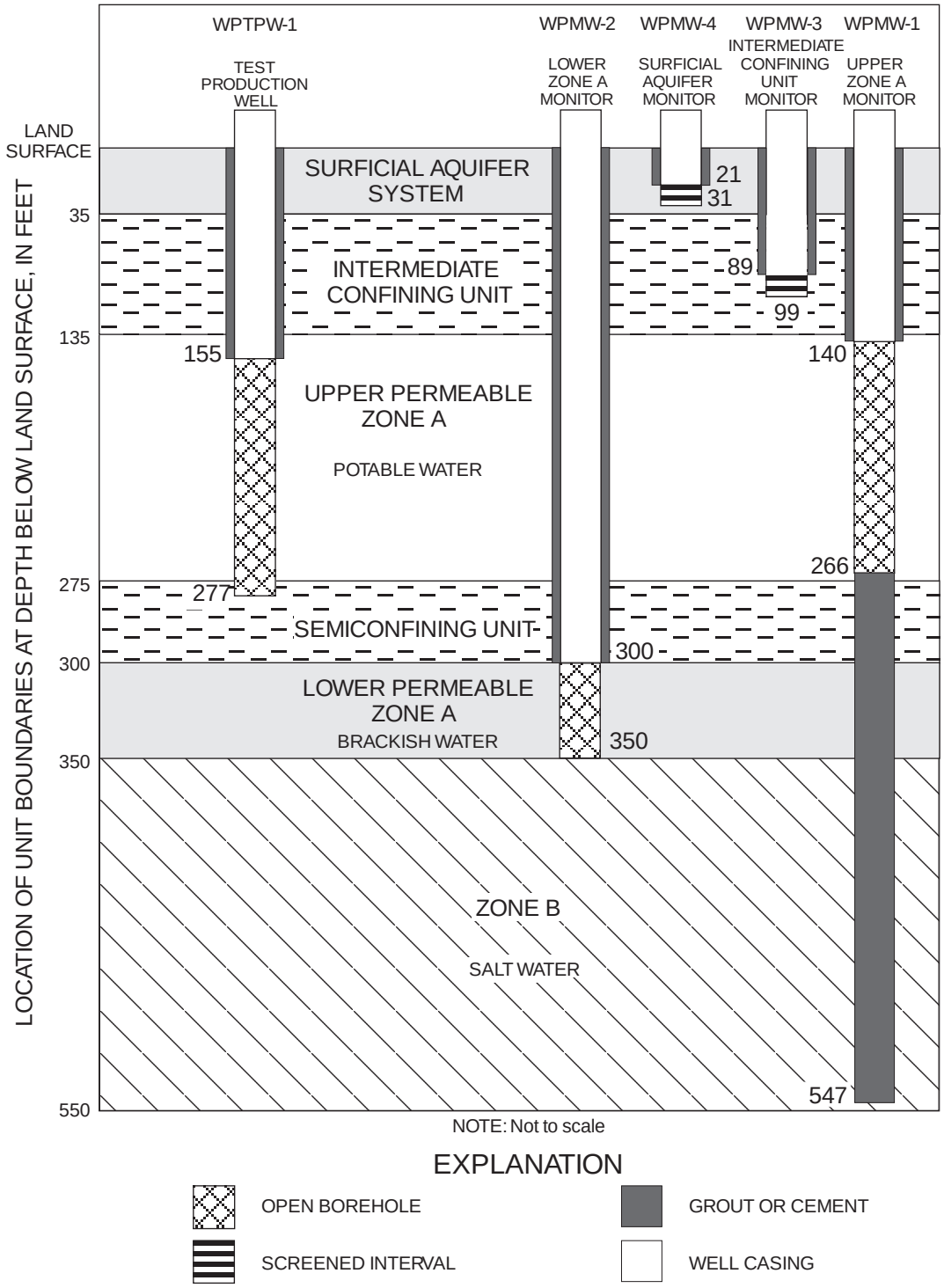

NOTE: Before backplugging to 266 feet, WPMW-1 was referred to as the deep exploratory well.

Figure 5. Generalized section view of casing depths and final depths of wells at the Walsingham Park test site.

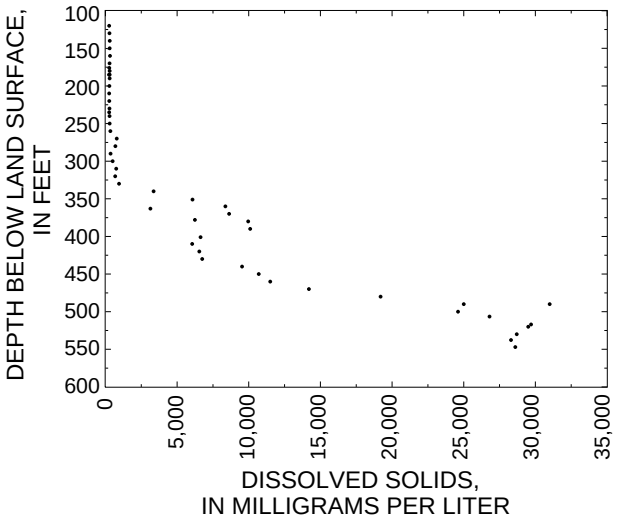

Figure 6. Relation of dissolved solids and depth from water samples collected during drilling of Walsingham Park deep exploratory well (WPMW-1).

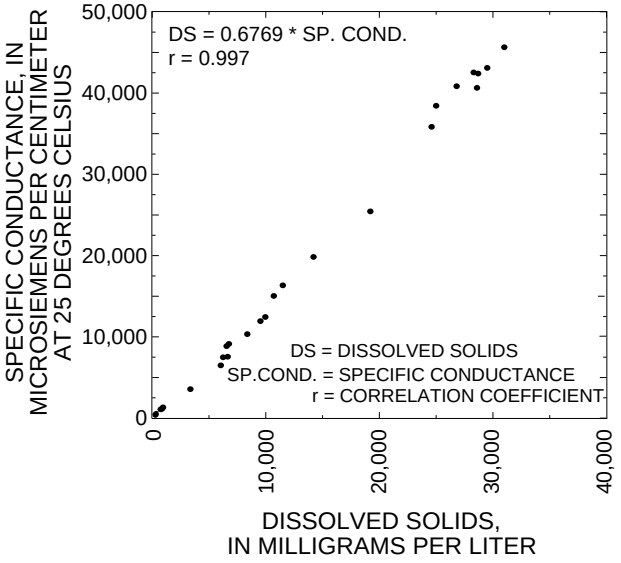

Figure 7. Relation between dissolved solids and specific conductance of selected water samples collected during drilling of Walsingham Park deep exploratory well (WPMW-1).

The freshening of water samples between drilling days may have been the result of mixing of waters in the borehole. However, previous investigations in northern Pinellas County have shown that layering of water with higher dissolved-solids concentrations can occur over water with lower dissolved-solids concentrations (Knochenmus and Swenson, 1996). The nature of this water-quality anomaly at the Walsingham Park test site could not be determined upon completion of drilling.

Additionally, selected samples were used to show the correlation between specific conductance and dissolved-solids concentrations for ground water representative of the study site (fig. 7). The linear regression closely fits a straight line with a correlation coefficient (r) of 0.997. The correlation of the two parameters was later used to estimate changes in dissolved-solids concentration under pumping conditions; however, the relation of dissolved solids to specific conductance would not be constant for the entire range of samples (Hem, 1985). As figure 7 illustrates, the slope of the linear regression is different for specific ranges of conductance values. Changes in water quality that occurred during hydraulic testing are discussed further in the aquifer test section of this report.

Geophysical Logging

Borehole geophysical logging was used to delineate hydrogeologic units, flow zones, and water-quality changes at the test site. Geophysical logs were collected by a Pinellas County contractor under static and pumping conditions on WPMW-1. A lithologic log from WPMW-1 was also compiled during drilling. Logs collected during static conditions included caliper, natural-gamma radiation, fluid resistivity, and fluid temperature. Logs collected under pumping conditions included ascending and descending flow meter with the pump placed 120 ft below land surface. A schematic of the geophysical logs collected from WPMW-1 is shown in figure 8.

Interpretations of the geophysical logs in conjunction with the lithologic log were used to determine the distribution of flow zones and semiconfining units. Natural-gamma radiation logs are used to delineate clay and phosphate-bearing deposits by recording the naturally occurring radiation coming from the formation adjacent to the borehole. The natural-gamma log, when correlated with the WPMW-1 lithologic log, confirmed the presence of clay and phosphate deposits from 35 to 135 ft below land surface. This sequence corresponded to the ICU at the study site. The decrease in the natural-gamma values at about 340 ft below land surface indicates a region of low phosphate content within the Suwannee Limestone.

Flow logs measured under pumping conditions are used in conjunction with caliper logs to delineate flow zones. Within a relatively uniform borehole diameter, an increase in counts per second indicates an increase in fluid velocity, thus an increase in flow. The flow meter logs collected at WPMW-1 indicate the presence of a major flow zone from around 300 to 350 ft below land surface, corresponding to LZA.

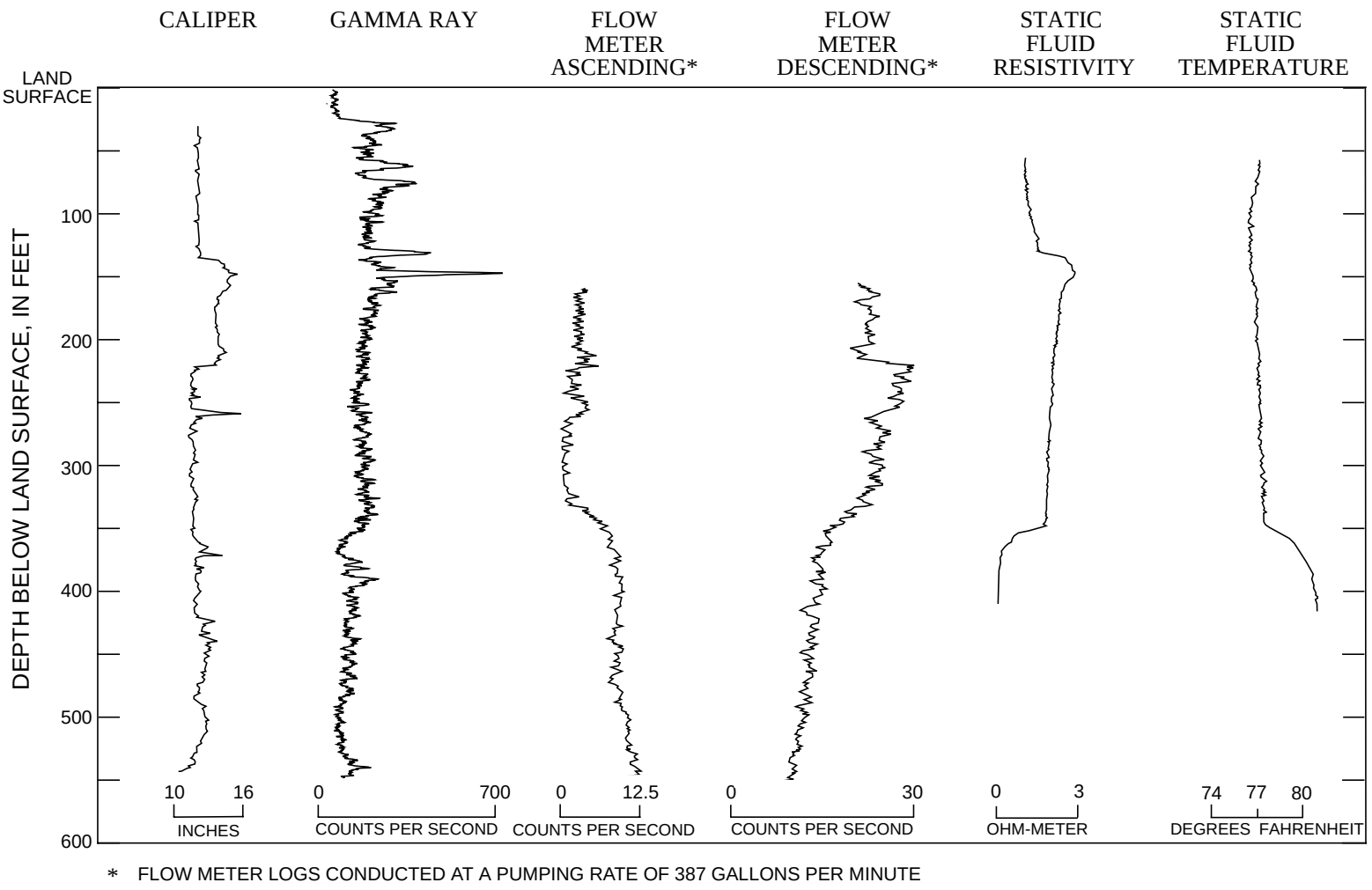

Figure 8. Geophysical logs of Walsingham Park deep exploratory well (WPMW-1).

Fluid resistivity and temperature logs are used to identify zones of water-quality change. The fluid resistivity and fluid temperature logs indicate a rapid water-quality change approximately 350 ft below land surface as fluid resistivity decreases and fluid temperature increases. The change in water quality at 350 ft below land surface was noted in the water-quality profile developed from water samples taken during drilling. However, unlike the water-quality profile, neither the fluid resistivity nor temperature logs suggest a freshening of water from 360 ft below land surface to the lowest extent of the logs at about 415 ft below land surface (fig. 8).

Specific-Capacity Tests

Specific-capacity tests were performed on WPMW-1 to evaluate the various hydrogeologic units at the study site. Water-level data, collected under a range of pumping rates, were analyzed to estimate hydraulic parameters of the system. Specific-capacity tests measure well yield per unit of drawdown for specific intervals of individual hydrogeologic units. Results were used to estimate hydraulic properties of specific intervals, locate permeable zones, and determine the well and casing depths of the monitor and production wells. In addition to specific-capacity tests, packer tests were performed upon completion of WPMW-1 (prior to backplugging) to further identify permeable zones at the site. Transmissivity and hydraulic conductivity values, estimated from specific-capacity and packer tests performed on the deep exploratory well (WPMW-1), are listed in table 1.

Table 1. Results from specific capacity and packer tests from the deep exploratory well

[ft, feet; ft^3/d, cubic feet per day; (gal/min)/ft, gallons per minute per foot; ft^2/d, feet squared per day; ft/d, feet per day]

Depth interval below land surface (ft)	Pump rate (ft^3/d)	Total change in head (ft)	Specific capacity (gal/min)/ft	Transmissivity (ft^2/d)	Hydraulic conductivity (ft/d)
135-185	11,744	9.73	6.3	1,675	34
135-235	11,934	8.87	7.0	1,870	19
135-235	59,864	59.64	5.2	1,400	14
205-235	9,336	9.59	5.1	1,350	45
230-282[a]	17,901	13.74	6.8	1,810	35
268-285[a]	9,182	4.63	10.3	2,750	162
288-340[a]	18,289	14.50	6.6	1,750	34
338-355[a]	9,624	4.31	11.6	3,100	182
385-542[a]	9,124	5.77	8.2	2,195	33

[a]Packer test interval.

The values were estimated by applying specific-capacity and packer-test data to empirical equations developed from the modified Jacob nonequilibrium equation for a single-well test (Driscoll, 1986, p. 1021). Due to the difficulty in placing packers in the borehole and leakage problems detected around the packers, confidence in the packer-test data was low for determining hydraulic parameters. However, UZA from about 135 to 270 ft below land surface and LZA from about 300 to 350 ft below land surface were determined to be the primary flow zones contributing ground water to the wells. Although LZA had a higher specific capacity, it was located directly above a highly mineralized water-quality zone. Therefore, UZA was more suitable for a longer-term aquifer test.

Aquifer Test

A 9-day aquifer test was conducted at the test site from July 29 to August 7, 1997, to estimate the hydraulic parameters of Zone A and determine changes in water quality due to long-term pumping. The four onsite and one offsite monitor wells were used to observe responses in various zones to pumping from UZA at WPTPW-1. Background water-level data collected before and after pumping showed that head differences between zones at the test site reflected a downward head gradient (fig. 9). At the onset of the aquifer test, the water level in the SAS monitor (WPMW-4) was about 2.5 ft above the water level in the ICU monitor (WPMW-3), whereas the water level in the ICU monitor was more than 36 ft higher than the water level in the UZA monitor (WPMW-1). Moreover, the water level in the UZA monitor was 0.15 ft higher than the water level in the LZA monitor (WPMW-2). The test production well (WPTPW-1) was pumped at a rate of 220 gal/min for the length of the test. After the initiation of pumping, responses were noted for the various monitor wells. WPMW-1 responded immediately with a lowering of water level in the first minute of pumping. WPMW-2 also responded quickly with the first drawdown noted after 4 minutes of pumping. Contrasting the changes in water levels at these two wells, the water level in WPMW-1 decreased by 1.0 ft, whereas the water level in WPMW-2 decreased by 0.02 ft after 4 minutes of pumping. Furthermore, a “reverse water-level fluctuation” (Andreasen and

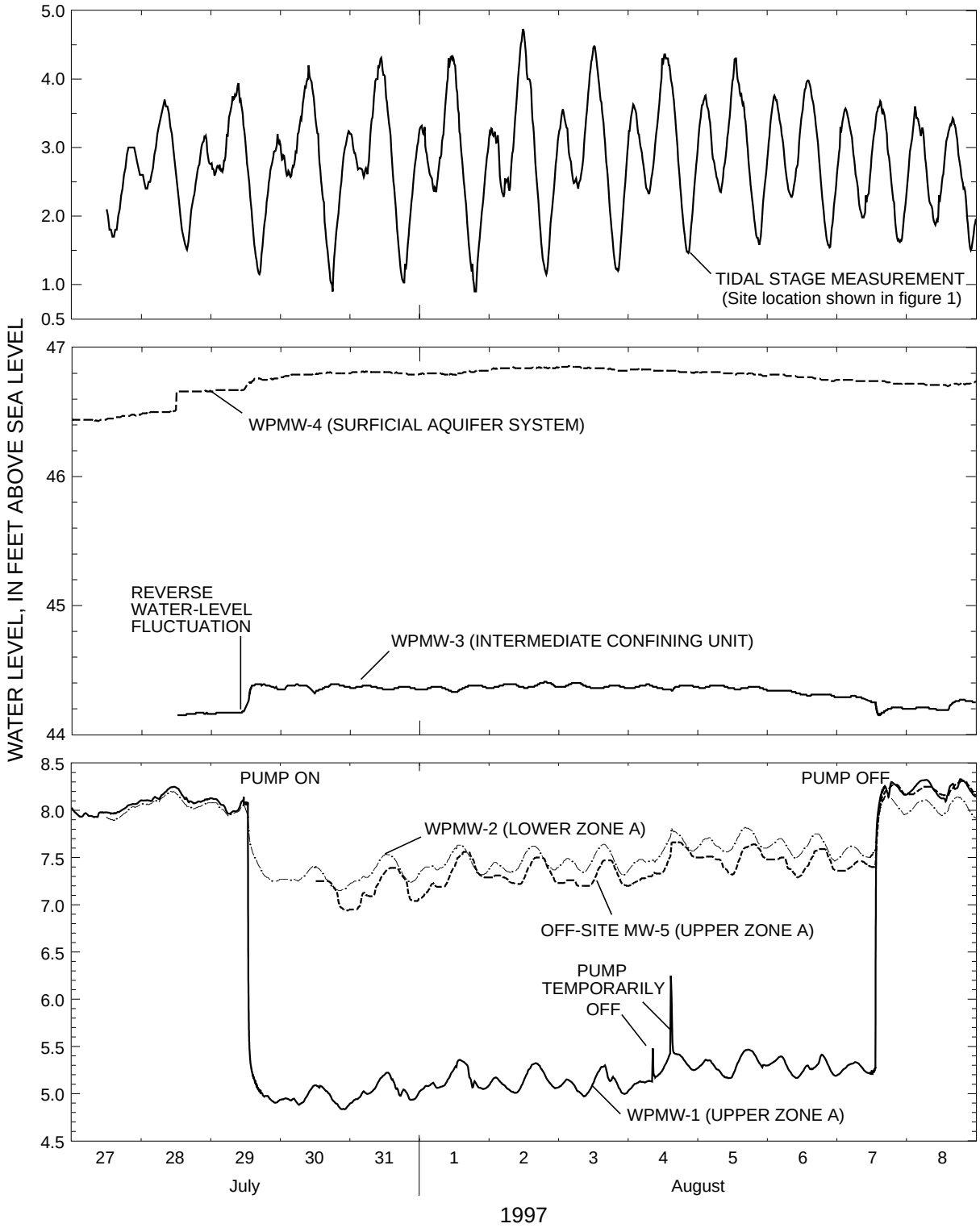

Figure 9. Water levels in all monitor wells before, during, and after the 9-day aquifer test.

Brookhart, 1963) was observed in the ICU monitor well WPMW-3. The water level in the ICU began to rise immediately after pumping began and declined when pumping ended (fig. 9). A possible explanation for this occurrence is that the release of water from compressive storage produced by pumping in UZA caused a reduction in aquifer volume of UZA, which in turn caused both horizontal and vertical deformations in the overlying ICU. These deformations of the ICU subsequently induced the measured water-level rise. This phenomenon has been documented and is often referred to as the Noordbergum Effect (Hsieh, 1996). No response due to pumping was denoted in the surficial aquifer system monitor well WPMW-4. Although water levels were monitored in the five wells for the duration of the test, drawdowns reached steady-state within the first 3 hours of pumping when tidal effects began to interfere with drawdown measurements (fig. 9).

Water-quality data were collected for the duration of the 9-day aquifer test. Specific conductance probes were placed in WPMW-1 and WPMW-2 at depths of 250 ft and 330 ft, respectively. Discharge water from WPTPW-1 was monitored hourly for specific conductance for the duration of the aquifer test. The changes in specific conductance measured during the test are shown in figure 10. Interestingly, water-quality changes noted in the UZA and the LZA monitor wells exhibited opposite trends. By using the relation between dissolved solids and specific conductance developed earlier (fig. 7), an inference can be made regarding the changes in dissolved solids concentrations during the aquifer test. The specific conductance in WPMW-1 in UZA increased from about 1,050 to 1,600 µS/cm corresponding to an increase in dissolved- solids concentration of about 372 mg/L. By contrast, the specific conductance in WPMW-2 in LZA decreased from about 11,900 to 11,200 µS/cm corresponding to a decrease in dissolved-solids concentrations of about 440 mg/L over the 9 days of the test. The specific conductance of the composite sample collected from WPTPW-1 increased from 470 to 488 µS/cm. Although this slight increase in measured specific conductance can be considered to be within the error of measurement of the conductance probe, the data showed a consistent trend (fig. 10).

The opposite trends in water-quality changes noted between the UZA and the LZA monitor wells during the 9-day aquifer test are difficult to explain. The upward hydraulic gradient between LZA and UZA induced during the aquifer test may have resulted in upward movement of more saline water. However, the freshening of water in the LZA monitor well (WPMW-2) during the aquifer test is anomalous. As figure 10 illustrates, the rate of change of measured specific conductance appears to decrease from the time pumping began. It is possible that mineralized water may have invaded LZA during drilling of the deep exploratory well and may have evacuated LZA during the aquifer test, thus returning to native conditions. Since the aquifer test lasted only 9 days, no data are available to determine the specific conductance values at longer pumping times.

Data and the results of the aquifer test are on file and available at the USGS Tampa office. Because analytical methods are constrained by limitations in the simplification of a flow system into one- or two-dimensional flow, the 9-day aquifer test was analyzed by using numerical methods. Numerical methods can simultaneously calculate changes in head and advective transport in a variable-density flow system for multiple observation points.

ANALYSIS OF AQUIFER CHARACTERISTICS

A numerical modeling approach was used to simulate the effects of pumping the variable-density ground-water flow system at the test site. The model was constructed to simulate the 9-day aquifer test conducted at the site and to refine estimates of hydraulic parameters such as hydraulic conductivity and storage coefficient determined from specific-capacity tests and previous investigations.

Numerical Methods

The USGS computer code HST3D (Kipp, 1987) was used to solve the equation for ground-water flow and solute transport using backward-in-space and backward-in-time finite-difference approximation methods. Mass-fractional concentrations and total fluid pressures were simulated using the model. The reader is referred to the original report that documents the computer code (Kipp, 1987) for a complete discussion of the numerical methods and model code.

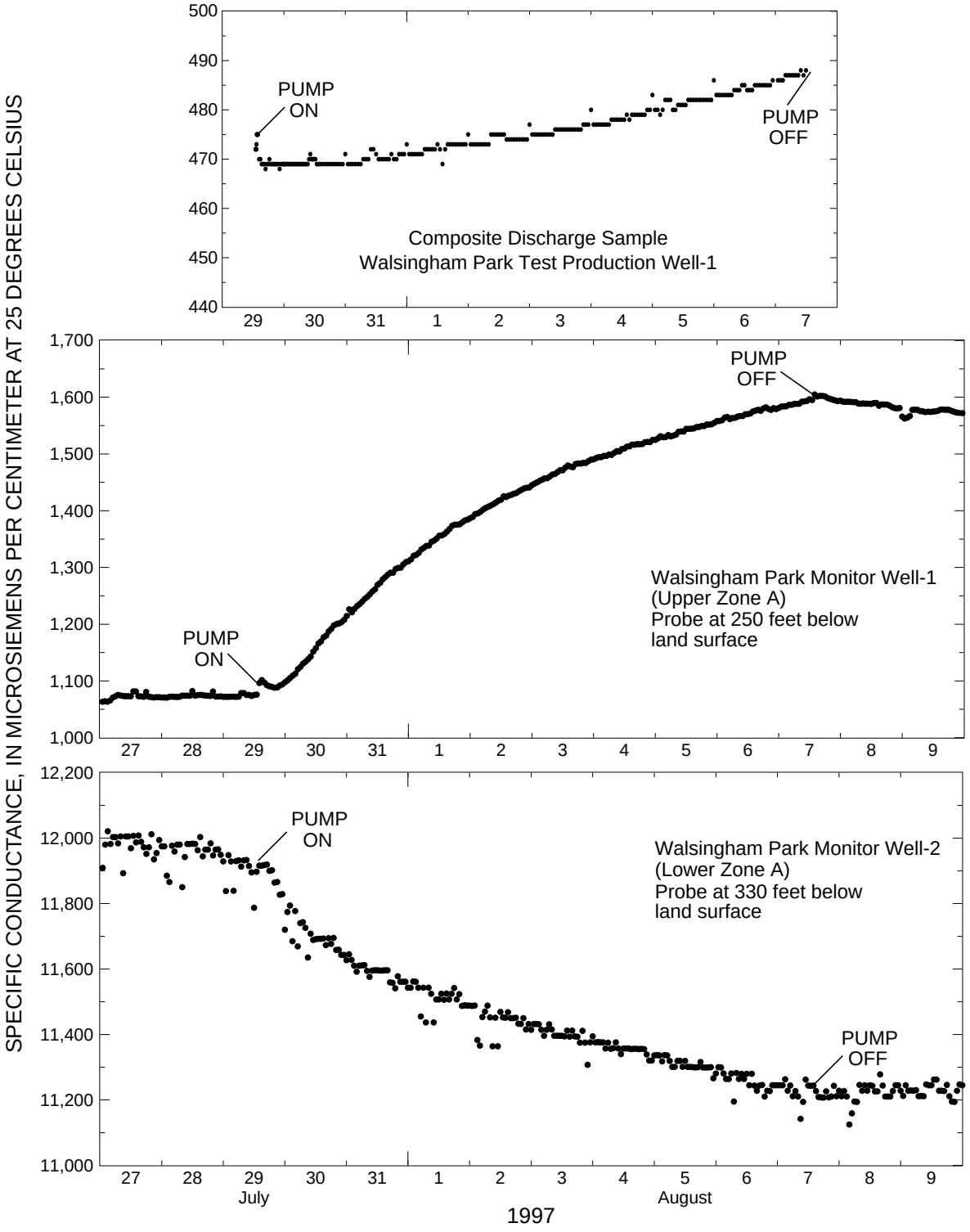

Figure 10. Changes in specific conductance during the 9-day aquifer test at Walsingham Park Test Production Well and Walsingham Park Monitor Wells 1 and 2.

Conceptual Model

The hydrogeologic system of the study area is conceptualized as a multilayered aquifer system encompassing various permeable zones separated by confining and semiconfining units extending from the surficial aquifer system downward through the Suwannee Limestone of the Upper Floridan aquifer (fig. 2). Ground-water flow is considered to be lateral in permeable zones and vertical in confining and semiconfining zones. Ground-water quality changes from fresh to saline with depth as ground water becomes increasingly dense with higher concentrations of dissolved solids. Several assumptions were made regarding the conceptualized hydrogeologic system to effectuate numerical simulation:

1. The aquifer system is assumed to act as an equivalent porous medium,
2. All aquifer layers are homogeneous and isotropic,
3. Initial conditions are hydrostatic,
4. Initial fluid density is constant in each model row, and
5. The water-quality profile is laterally homogeneous for the entire model area.

Design of Numerical Model

The numerical model subdivides the conceptualized hydrogeologic system from the ICU through Zone B at the test site into an organized network of grid blocks, each with assigned fluid and matrix properties representing a 500-ft thick section underlying the test site. The model was constructed by using a cylindrical-coordinate grid of 124 columns and 12 rows (fig. 11), and was designed to simulate the responses of UZA and LZA to brackish-water development. The columns are variable in width with radial spacing expanding logarithmically from 0.3 ft at the test production well up to a maximum width of 328 ft extending out to 11,500 ft. Radial widths extending to 12,500 and 14,500 ft were also simulated, but the additional simulation area in the horizontal direction had no affect on model results. The 12 model rows were grouped together as five distinct hydrogeologic layers. Layer 1 corresponds to model rows 1-3, is 175 ft thick, and represents Zone B of the Upper Floridan aquifer. Layer 2 corresponds to model rows 4 and 5, is 50 ft thick, and represents LZA of the Upper Floridan aquifer. Layer 3 corresponds to model row 6 and represents a discrete, 25-ft section within Zone A with an increased occurrence of green clays. This section was modeled to determine the hydraulic properties of the unit separating UZA and LZA. Layer 4 corresponds to model rows 7-9, is 150 ft thick, and represents UZA of the Upper Floridan aquifer. Layer 5 corresponds to model rows 10-12, is 100 ft thick, and represents the ICU.

Initial and Boundary Conditions

Initial conditions refer to pressure and fluid property distributions established prior to the initiation of the model simulation. Hydrostatic conditions are established in HST3D from a distribution of dissolved solids and fluid densities for each model row. Values for dissolved-solids concentrations and fluid densities, based on water-quality parameters defined from samples taken during drilling, were used to establish initial conditions (table 2). The model calculates the starting fluid pressures based on the user-specified fluid property distribution for all model rows as well as at model boundaries. Under these hydrostatic conditions, the aquifer response to pumping is determined by model simulated changes in pressure relative to the initial hydrostatic conditions (Anderson and Woessner, 1992).

Boundary conditions delimit the model domain by constraining the lateral and vertical extent of the simulated flow system at the model periphery. The inner cylindrical boundary represents the production well and was defined by allocating well information to the various rows that represent the open-hole interval of the pumped well. Model rows not open to the production well were assigned a no-flow condition, whereas the outer cylindrical boundary was defined as a specified-pressure condition (fig. 11). The assigned pressure distribution along the vertical plane of the outer boundary was calculated by using water-level and dissolved-solids concentration data obtained during drilling of the test production well. The lower model boundary was defined as a specified-pressure boundary equivalent to the pressure exerted by a column of stratified saltwater and freshwater in the overlying strata determined from the density of water samples acquired during drilling (fig. 11). The outer and lower specified-boundaries were used to simulate an infinitely extensive aquifer while eliminating the modeling of indefinite regions outside the study area. The upper model boundary was assigned a no-flow boundary coinciding with the top of the ICU. Because no drawdown occurred in either the SAS or the ICU monitor wells during the aquifer test, a no-flow boundary condition at the top of the ICU was deemed appropriate. However, row 11 (corresponding to the

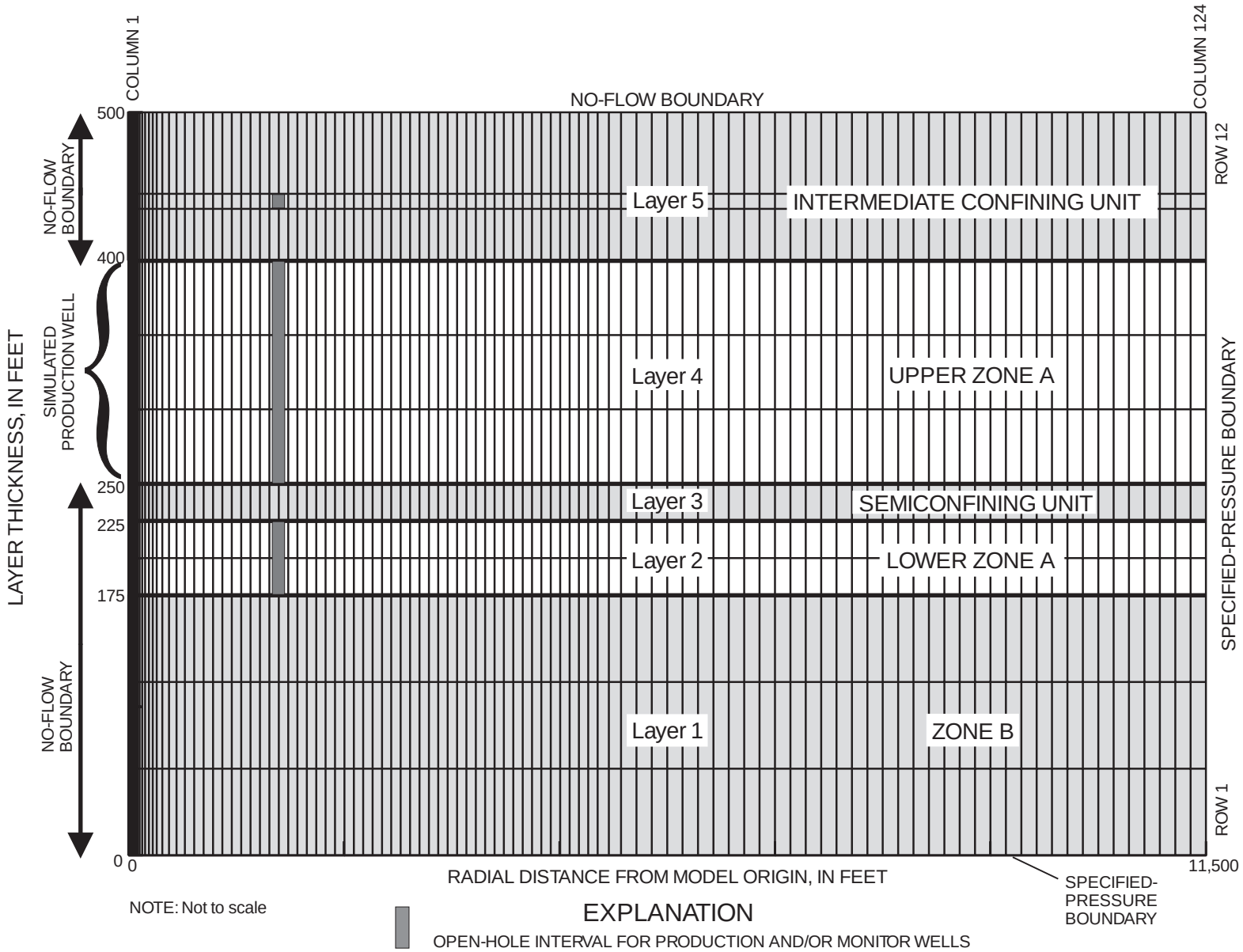

Figure 11. Model grid, simulated open-hole intervals, and boundary conditions used in the HST3D simulation.

Table 2. Values for model parameters used to establish initial conditions and values for calibrated model parameters

[lb/ft^3, pound per cubic foot; mg/L, milligrams per liter; ft^2, feet squared; ft/d, feet per day]

Hydrogeologic unit	Initial conditions		Calibrated model		
	Density (lb/ft^3)	Scaled-solute mass fraction / dissolved solids (mg/L)	Intrinsic permeability (ft^2) / hydraulic conductivity (ft/d)	Storage coefficient	Effective porosity (percent)
Intermediate confining unit	62.38	0.0089 / 250	$3.9x10^{-15}$ / 0.0001	$3.1x10^{-4}$	35
Upper Zone A	62.38	0.0098 / 275	$7.0x10^{-11}$ / 18	$2.6x10^{-4}$	30
Semiconfining unit	62.41	0.0250 / 700	$3.9x10^{-11}$ / 10	$4.3x10^{-5}$	35
Lower Zone A[a] (Row 6)	62.61	0.1786 / 5,000	$2.9x10^{-9}$ / 750	$8.6x10^{-5}$	30
Lower Zone A (Row 5)	62.72	0.2679 / 7,500	$2.9x10^{-9}$ / 750	$8.6x10^{-5}$	30
Zone B	63.65	1.0 / 28,000	$3.9x10^{-12}$ / 1	$2.6x10^{-5}$	30

[a] Input parameters varied between the two rows representing Lower Zone A.

open-hole interval of WPMW-3) was used as an indictor for the upper limit of hydraulic parameters that would simulate a no-response condition in the ICU. Although the lack of a drawdown in the ICU made it impossible to accurately estimate hydraulic properties of the unit, model parameters in rows representing the ICU were adjusted to eliminate drawdown during the simulation.

Model Parameters

Model parameters including bulk matrix properties, fluid properties, and well information were defined for the five hydrogeologic units simulated (table 2). Although some adjustments were made to the parameters during calibration, initial values were carefully selected based on data collected during this investigation and previous studies (Hickey, 1982, 1989; Knochenmus and Swenson, 1996; Yobbi, 1996). Each model parameter is discussed in detail below:

1. *Bulk matrix properties.*—Bulk matrix properties include effective porosity, hydraulic conductivity (as a function of intrinsic permeability), storage coefficient (as a function of matrix compressibility), and dispersivity. Bulk matrix properties (except dispersivity) for each hydrogeologic layer are listed in table 2. Because values of dispersivity are poorly known within the study area, a conservative approach was used by setting longitudinal and transverse dispersivity to zero.

2. *Fluid properties.*—Fluid properties include viscosity, density, compressibility, temperature, and dissolved-solids concentration. Dissolved-solids concentration is expressed as a scaled-solute mass fraction ranging from 0 to 1 in HST3D. A value of 0 represents pure freshwater whereas a value of 1 represents water with the highest dissolved-solids concentration (28,000 mg/L) in the model. Values for density and dissolved solids for each hydrogeologic layer are summarized in table 2. Fluid viscosity was held constant for the entire model at $1.0x10^{-3}$ centipoise. Likewise, fluid temperature and fluid compressibility were held constant with values of 77 ^{o}F, and $3.03x10^{-6}$ in^2/lb, respectively.

3. *Well information.*—Well information needed for model input includes the withdrawal rate of the pumping well and is distributed equally over the three rows representing the pumped zone. The test production well open to UZA was simulated in model rows 7-9. The simulated pumpage was discretized with a constant withdrawal rate assigned to each of the three rows. The total pumpage assigned for all three rows for the aquifer test simulation equaled 220 gal/min. Pumpage was varied thereafter from 200 to 700 gal/min during the brackish-water development simulations.

Simulation of Aquifer Test

Numerical analysis of the 9-day aquifer test data provided a method for calculating hydraulic properties of various hydrogeologic units at the test site. The numerical model was calibrated by simulating the aquifer system's response to pumping UZA during the aquifer test. The model analysis of the 9-day aquifer test consisted of meeting two calibration objectives within acceptable limits: (1) simulate the drawdown and recovery of water levels in selected wells measured during the test, and (2) simulate the overall response of the system to pumping.

The first objective involved matching the initial drawdown part of the aquifer test. The initial 139 minutes of the aquifer test was used because nearly all drawdown effects occurred during this time and monitor well drawdowns could be separated from tidal effects. Tidal effect corrections were made by calculating the tidal efficiency for the monitor zone and adjusting drawdown and recovery data accordingly. Tidal efficiency is the ratio of the water-level amplitude measured in a well to the oceanic tidal amplitude (Ferris and others, 1962). Tidal data were collected at a gage located on the intracoastal waterway at Indian Rocks Beach, 2 mi west of the study site (fig. 1). The calculated tidal efficiency for Zone A averaged 10 percent for ebbing tides and 16 percent for flooding tides. After tidal corrections were made to the observed data, the corrected drawdowns were compared to simulated drawdowns.

Model parameters were adjusted until a reasonable match was derived where simulated drawdowns closely paralleled the observed drawdowns. A reasonable match was considered less than 0.10 ft difference between simulated and observed drawdown data. Final calibrated values for hydraulic conductivity were 18 ft/d for UZA, 750 ft/d for LZA, 1 ft/d for Zone B, $1x10^{-4}$ ft/d for the ICU, and 10 ft/d for the semiconfining unit separating UZA and LZA. Final calibrated values for storage coefficient were $3.1x10^{-4}$ for UZA, $8.6x10^{-5}$ for LZA, $2.6x10^{-5}$ for Zone B, $3.1x10^{-4}$ for the ICU, and $4.3x10^{-5}$ for the semiconfining unit separating UZA and LZA. Calibrated model parameters were further checked by comparing the observed recovery data of the aquifer test to the simulated recovery water levels (fig. 12). Values of the corrected, observed drawdown and recovery and simulated values are provided in table 3.

Table 3. Simulated and corrected observed drawdown and recovery for selected monitor wells during the 9-day aquifer test

[UZA, upper zone A; LZA, lower zone A; NA, data not available; all values are in feet]

Zone and well	Corrected observed drawdown[a]	Simulated drawdown	Corrected observed recovery[b]	Simulated recovery
UZA WPMW-1	2.69	2.66	2.79	2.66
LZA WPMW-2	0.29	0.30	0.36	0.31
UZA Botanical Well	NA	0.59	0.54	0.60

[a]Corrected drawdown for first 139 minutes of pumping.
[b]Corrected recovery for first 136 minutes of recovery in WPMW-1 and Botanical Well, and first 192 minutes of recovery in WPMW-2.

The second objective involved matching the long-term pattern of drawdown and recovery for the length of the 9-day aquifer test. As figure 9 shows, after the initial 139 minutes of pumping, observed drawdowns stabilized (excluding tidal effects) for the remainder of the 9-day test until the pump was turned off and recovery effects occurred. A reasonable match was accomplished when simulated drawdowns functioned in a similar fashion with drawdowns decreasing after the initial drop in water levels and stabilizing throughout the simulation until the recovery part of the test (fig. 13). It should be noted that the simulated hydrographs are superimposed over the uncorrected field hydrographs. No attempt was made to simulate the variations in water levels due to tidal effects.

Sensitivity Analysis

Sensitivity analysis was used to determine the effect of each parameter on the calibrated model results. Input parameters were individually varied over a reasonable range of values to determine the sensitivity of the model to that particular parameter over the entire simulation period. Ranges were based on values from previous investigations discussed in the hydrogeologic framework section of this report. Changes in certain parameters had no effect on the model, whereas others noticeably affected the model results. For example, a one order of magnitude increase and decrease in the value of matrix compressibility in model rows representing both UZA and LZA had no effect on the model results. Furthermore, a one order of magnitude increase and decrease in the intrinsic permeability of model rows representing the ICU had

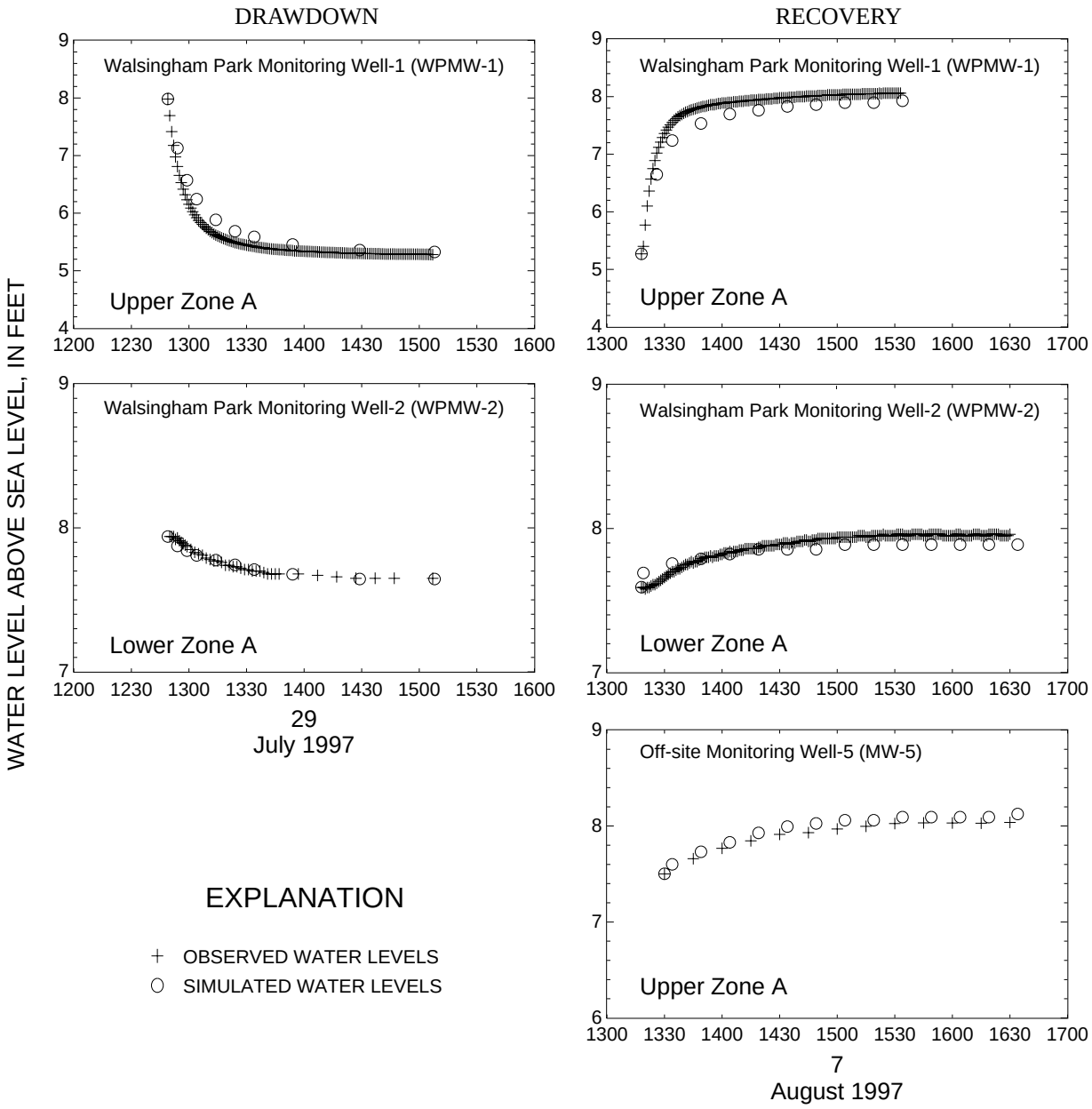

Figure 12. Simulated and observed water levels during drawdown and recovery periods at selected wells during the 9-day aquifer test.

no effect on the model results. Conversely, the largest changes to the model results occurred from changes in intrinsic permeability values assigned to both UZA and LZA (figs. 14a thru 14d). Model rows representing UZA were increased and decreased by one order of magnitude, whereas model rows representing LZA were changed by a factor of 2 and 0.5. Additionally, the value of matrix compressibility assigned to model rows representing the ICU were increased and decreased by one order of magnitude (figs. 14e and 14f). An increase in the matrix compressibility of the ICU resulted in a slight response in only UZA. Furthermore, this response occurs in the early part of the drawdown graph, but the overall magnitude of drawdown in UZA did not change. The model was generally sensitive to changes of intrinsic permeability and insensitive to changes of matrix compressibility; therefore, more confidence was placed on estimates of transmissivity than on estimates of storativity.

Model Limitations

Results from model simulations outlined in this report are approximations of the actual hydrogeologic system. Confidence in model results is dependent on the assumptions outlined earlier in this report and the extent that the hydrogeologic system is simplified for mathematical representation. Simplification of the conceptual model is necessary to simulate a very complex natural system; however, the extent to which the system is simplified represents a source of error in model results. The major limiting factor in the model simulations is that the hydrogeologic system was simulated as a five-layered system with isotropic, homogeneous, and porous-medium individual layers. The actual hydrogeologic system may, however, be anisotropic, heterogeneous, and possess properties of secondary porosity due to dissolution and fracturing. Although alternate combinations of model parameters may provide similar results to those outlined in this report, the model incorporated the best estimates of the unknown parameters, the local geology, and hydrologic conditions.

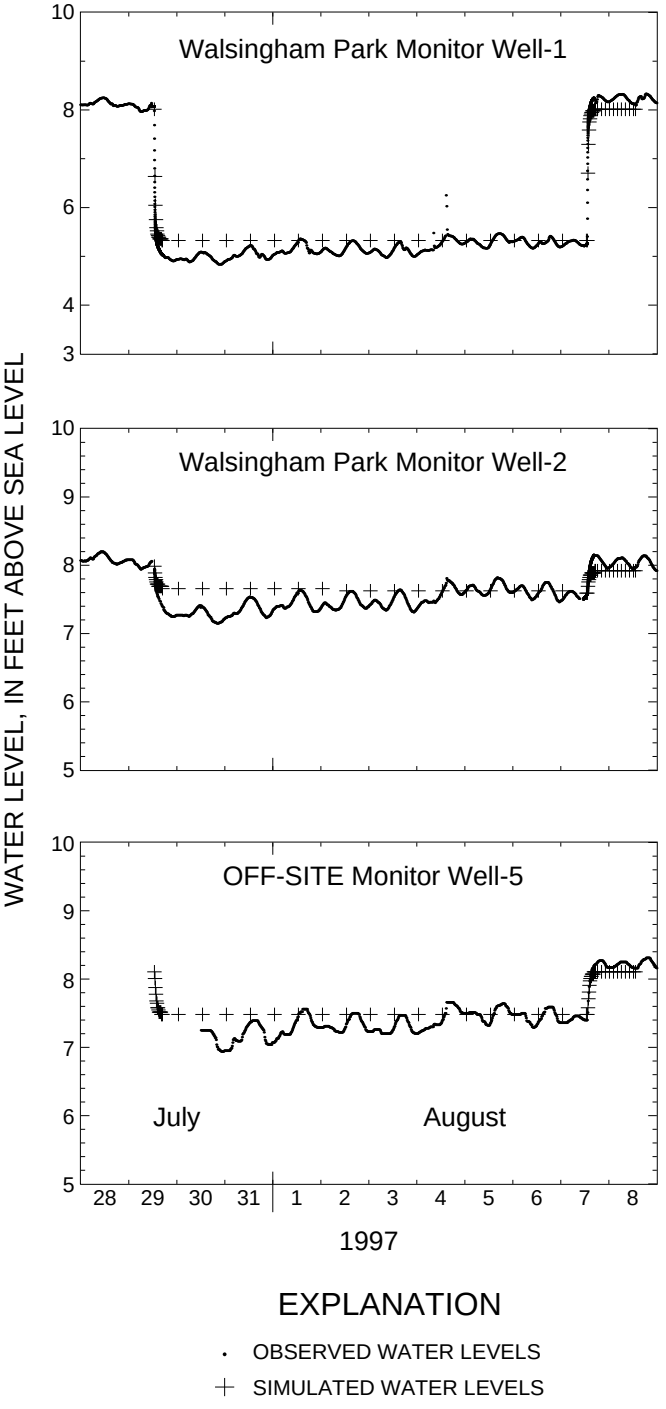

Figure 13. Simulated and observed water levels in selected monitor wells during the 9-day aquifer test.

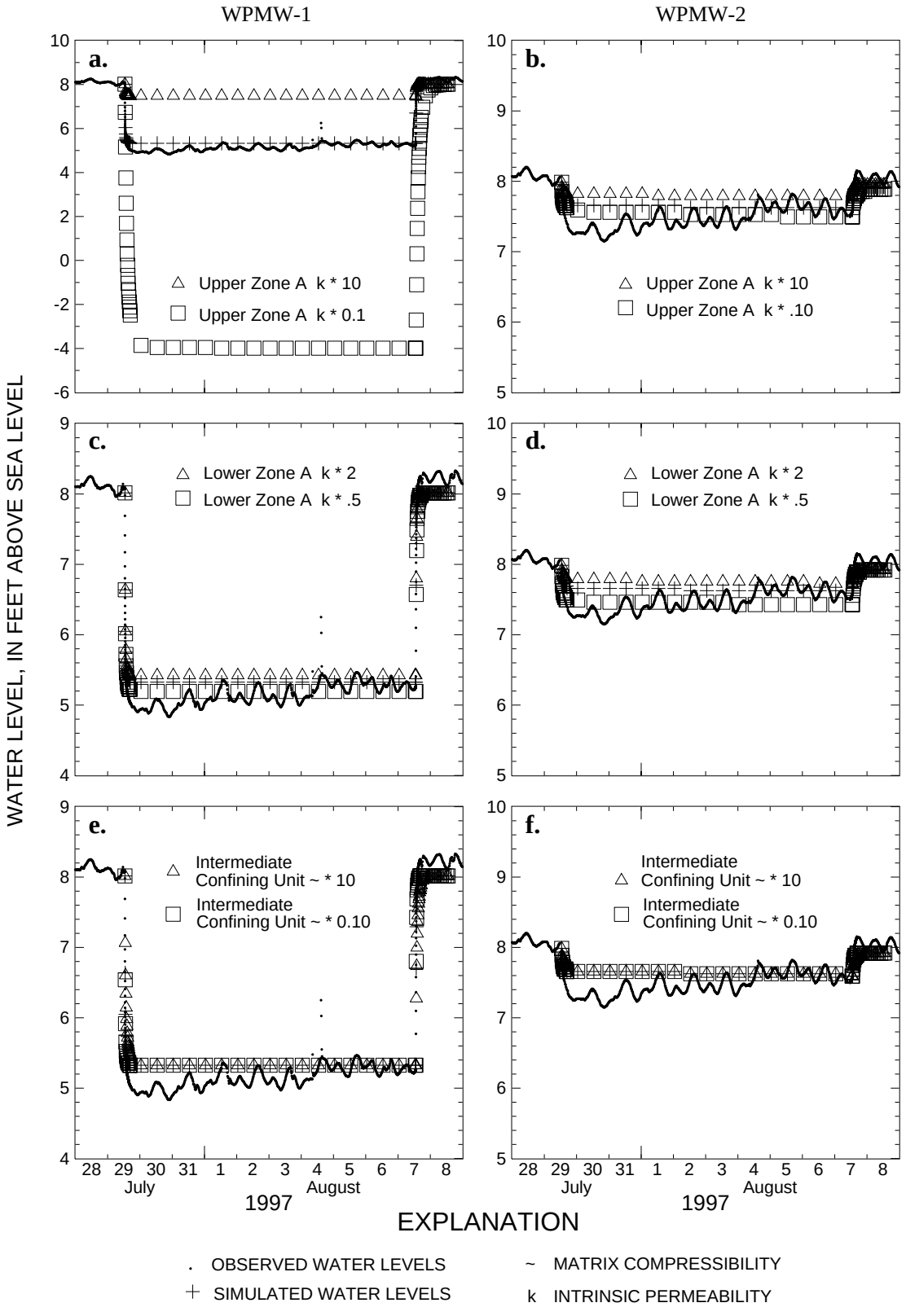

Figure 14. Sensitivity of simulated water levels to changes in selected model input parameters.

SUMMARY

This report presents the results of a study to evaluate the brackish-water resources in the Upper Floridan aquifer underlying west-central Pinellas County, Florida. A production test well and four monitor wells were constructed at a location in Walsingham Park in 1996-97. The wells were sampled for water-quality parameters and investigated using borehole geophysical methods and hydraulic testing. The data collected were analyzed by using numerical techniques to delineate the hydrogeologic framework at the test site.

Collected data indicate that a multilayered aquifer system consisting of two permeable zones underlies Walsingham Park. One zone extends from about 135 to 275 ft below land surface and corresponds to UZA of the Upper Floridan aquifer. Another permeable zone extends from about 300 to 350 ft below land surface and corresponds to LZA of the Upper Floridan aquifer. Analysis of water-quality data indicates that LZA may not provide water of consistent quality because of rapidly increasing dissolved-solids concentrations occurring around 350 ft below land surface. UZA was deemed more appropriate for production pumping and was tested during a 9-day aquifer test.

A numerical model was developed to simulate the 9-day aquifer test performed at the Walsingham Park test site. The model was calibrated to the drawdown and recovery water levels of selected monitor wells at the test site. Final calibrated values for hydraulic conductivity were 18 ft/d for UZA, 750 ft/d for LZA, 1 ft/d for Zone B, $1x10^{-4}$ ft/d for the ICU, and 10 ft/d for the semiconfining unit separating UZA and LZA. Final calibrated values for storage coefficient were $3.1x10^{-4}$ for UZA, $8.6x10^{-5}$ for LZA, $2.6x10^{-5}$ for Zone B, $3.1x10^{-4}$ for the ICU, and $4.3x10^{-5}$ for the semiconfining unit separating UZA and LZA.

REFERENCES CITED

Anderson, M.P., and Woessner, W.W., 1992, Applied groundwater modeling: Simulation of flow and advective transport: San Diego, Calif., Academic Press, 381 p.

Andreasen, G.E., and Brookhart, J.W., 1963, Reverse water-level fluctuations: Methods of collecting and interpreting ground-water data: U.S. Geological Survey Water-Supply Paper 1544-H, p. 30-35.

Black, Crow and Eidness, Inc., 1978, Drilling and testing of the monitoring and injection wells at the Southwest Wastewater Treatment Plant for the city of St. Petersburg, Florida: Brooksville, Consultant's report in the files of the Southwest Florida Water Management District.

Brown and Associates, Inc., 1986, Hydrological investigation for the development and management of the Floridan aquifer, city of Dunedin: Consultant's report in the files of the city of Dunedin, Florida

Causseaux, K.W., 1985, The surficial aquifer in Pinellas County, Florida: U.S. Geological Survey Water-Resources Investigations Report 84-4289, 26 p.

Causseaux, K.W., and Fretwell, J.D., 1983, Chloride concentrations in the coastal margin of the Floridan aquifer, southwest Florida: U.S. Geological Survey Water-Resources Investigations Report 82-4070, 33 p.

Cherry, R.N., and Brown, D.P., 1974, Hydrogeologic aspects of a proposed sanitary landfill near Old Tampa Bay, Florida: Florida Bureau of Geology Report of Investigations 68, 25 p.

Cherry, R.N., Stewart, J.W., and Mann, J.A., 1970, General hydrology of the middle Gulf area, Florida: Florida Bureau of Geology Report of Investigations 56, 96 p.

Driscoll, F.G., 1986, Groundwater and wells (2d ed.): St. Paul, Minn., Johnson Filtration Systems, Inc., 1089 p.

Ferris, J.G., Knowles, D.B., Brown, R.H., and Stallman, R.W., 1962, Theory of aquifer tests: U.S. Geological Survey Water-Supply Paper 1536-E, 174 p.

Gilboy, A.E., 1985, Hydrogeology of the Southwest Florida Water Management District: Southwest Florida Water Management District: Regional Analysis Section Technical Report 85-01, 18 p.

Heath, R.C., and Smith, P.C., 1954, Ground water resources of Pinellas County Florida: Florida Geological Survey Report of Investigations 12, 139 p.

Hem, J.D., 1985, Study and interpretation of the chemical characteristics of natural water: U.S. Geological Survey Water-Supply Paper 2254, 263 p.

Hickey, J.J., 1982, Hydrogeology and results of injection tests at waste-injection test sites in Pinellas County, Florida: U.S. Geological Survey Water Supply Paper 2183, 42 p.

----- 1989, Circular convection during subsurface injection of liquid waste, St. Petersburg, Florida: Water Resources Research, v. 25, no. 7, 1481-1494 p.

Hsieh, P.A., 1996, Deformation-induced changes in hydraulic head during ground-water withdrawal: Ground Water, v. 34, no. 6, p. 1082-1089.

Hutchinson, C.B., and Stewart, J.W., 1978, Geohydrologic evaluation of a landfill in a coastal area, St. Petersburg, Florida: U.S. Geological Survey Water-Resources Investigations Report 77-78, 40 p.

Kipp, K.L., Jr., 1987, HST3D: A computer code for simulation of heat and solute transport in three-dimensional ground-water flow systems: U.S. Geological Survey Water-Resources Investigations Report 86-4095, 519 p.

Knochenmus, L.A., and Swenson, E.S., 1996, Assessment of the fresh- and brackish-water resources underlying Dunedin, Florida: U.S. Geological Survey Water-Resources Investigations Report 96-4164, 40 p.

Marella, R.L., 1992, Water withdrawals, use, and trends in Florida: U.S. Geological Survey Water-Resources Investigations Report 92-4140, 38 p.

Miller, J.A., 1986, Hydrogeologic framework of the Floridan aquifer system in Florida and in parts of Georgia, Alabama, and South Carolina: U.S. Geological Survey Professional Paper 1403-B, 91 p.

Seaburn and Robertson, Inc., 1983, Results of the hydrologic testing program for the city of Clearwater water supply investigation: Consultant's report in the files of the city of Clearwater.

Sinclair, W.C., 1974, Hydrogeologic characteristics of the surficial aquifer in northwest Hillsborough County, Florida: Florida Bureau of Geology Information Circular 86, 98 p.

University of Florida, 1991, Florida population: Census summary 1990: Gainesville, University of Florida, Bureau of Economic and Business Research, 55 p.

White, W.A., 1970, The geomorphology of the Florida Peninsula: Florida Bureau of Geology Bulletin 51, 164 p.

Yobbi, D.K., 1996, Simulation of subsurface storage and recovery of treated effluent injected in a saline aquifer, St. Petersburg, Florida: U.S. Geological Survey Water-Resources Investigations Report 95-4271, 29 p.

Hydrogeology of Effluent Disposal Zones, Floridan Aquifer, South Florida

by Joseph L. Haberfeld[a]

Abstract

The increasing population of south Florida is creating a need for greater waste-water disposal capacity. The people of Florida are dependent on ground water for drinking, irrigation, and other uses. The emphasis on preservation of surface-water quality means that many surface waters are not allowed to receive effluent from municipal or industrial sources. Since the 1940s, the highly transmissive zones of the nonpotable portion of the Floridan aquifer have served as disposal zones for oil field brine and later for industrial and municipal effluent.

The Floridan aquifer of south Florida is a carbonate Cenozoic age aquifer. Transmissivities between 0.5 and 21 million gpd/ft exist in cavernous and fractured sequences in the aquifer. Confining zones that overlie the disposal intervals have transmissivities and hydraulic conductivities one to three orders of magnitude less than the injection intervals. These confining zones prevent low density municipal effluent from rising upward through the overlying saline waters.

This paper provides an integration of previously published work with recent site-specific data collected from deep injection wells drilled in the last two decades.

Introduction

The Floridan aquifer is the principal aquifer in the southeastern United States. It is comprised of rocks of Paleocene through Miocene age and is found in Florida, Georgia, Alabama, and South Carolina. Although its major resource is a potable-water supply, the nonpotable part of the aquifer in south Florida serves as a disposal zone for municipal and industrial waste water. The hydrogeologic setting of the Floridan aquifer is generally favorable for the disposal of effluent in south Florida. The construction and testing of deep injection wells provides hydrogeologic information on the portions of the aquifer containing saline water, leading to a better understanding of aquifer and confining zone properties and flow dynamics. The types of data that yield important information include water quality analyses, geophysical logs, cores, packer tests, and withdrawal and injection tests.

Previous Studies

Numerous characteristics of the disposal zones in south Florida have been studied over the past three decades. Flow characteristics were studied by Meyer (1988), Hickey (1989a, 1989b), Smith and Griffin (1977), and Kohout (1965). General aquifer properties and geologic setting were discussed by Meyer (1989), Puri and Winston (1974), Puri et al. (1973), and Vernon (1970). In addition, numerous studies of individual wells are on file with the Florida Department of Environmental Regulation as support of operating permit applications.

History of Deep Well Injection in Florida

The injection of liquid waste into the Floridan aquifer in south Florida began in 1943. Brine produced from the Sunniland oil field was disposed of in the cavernous zone of the lower Floridan aquifer of Eocene age. This interval is referred to as the "Boulder Zone" due to the difficulty oil field drillers had getting through this zone in search of oil at greater depths. Drillers typically encountered boulders dislodged by the drill bit from cavities, lost circulation, or had

[a]Florida Department of Environmental Regulation, 2600 Blairstone Rd., Tallahassee, Florida 32399.

Received February 1990, revised May 1990, accepted June 1990.

Discussion open until September 1, 1991.

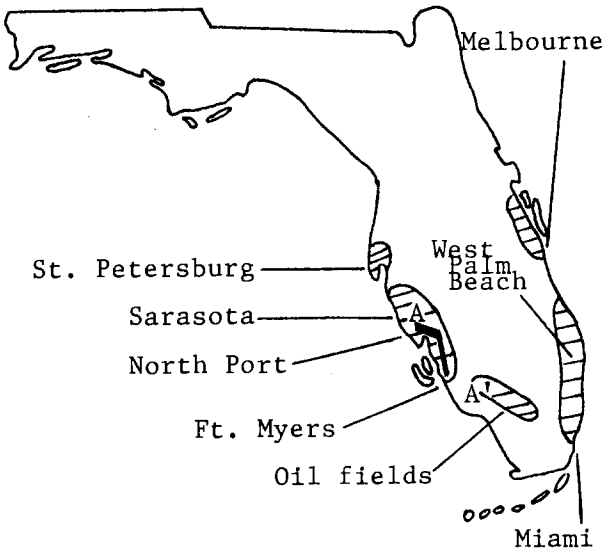

Fig. 1. Locations of the majority of deep injection wells depicted by hatched areas. Location of cross section A-A' is shown.

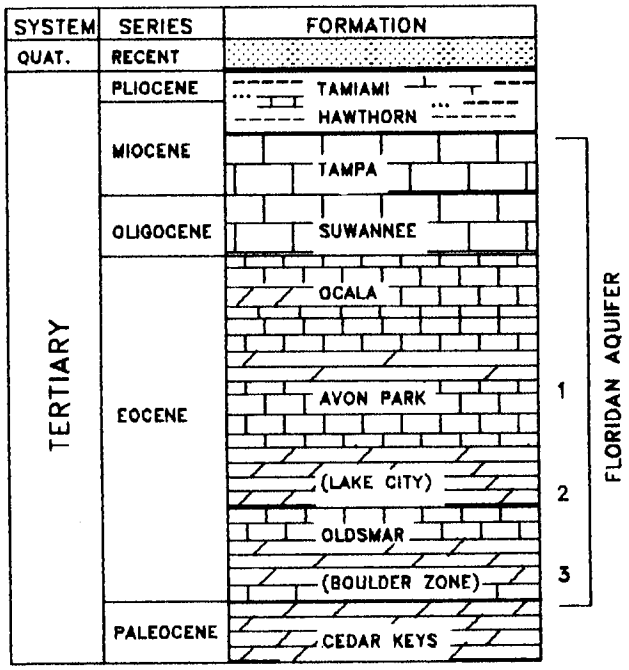

Fig. 2. General stratigraphic column, south Florida (adapted from Puri and Winston, 1974). Standard symbols are shown for lithology. St. Petersburg, Sarasota and North Port areas inject into zone 1; Ft. Myers area injects into zone 2; all other wells inject into zone 3.

the drill string drop several feet through a cavern (Puri and Winston, 1974). The first injection of municipal (domestic) effluent began in 1959 into the upper Floridan aquifer. This zone was abandoned in the 1970s when waste-water treatment plants disposed of their effluent in the more transmissive "Boulder Zone." The majority of effluent now disposed of into deep injection wells in Florida is secondarily treated municipal waste water. Finally, smaller volumes of industrial (nonpetroleum related) waste water have been disposed of in the "Boulder Zone" since 1966.

The establishment and implementation of U.S. Environmental Protection Agency regulations have resulted in the accumulation of data on the Floridan aquifer in south Florida (Figure 1). The municipal wells, as expected, are located in population centers near the coasts. Oil field disposal wells are located between Ft. Myers and Miami.

Hydrogeologic Setting

The Cenozoic section of Florida is dominated by carbonate rocks, particularly in south Florida (Meyer, 1989). The general stratigraphic column shows the vertical extent of the Floridan aquifer, formation names, and lithologies (Figure 2). Limestones and dolomites comprise nearly the entire aquifer. The upper boundary of the Floridan aquifer is defined by the top of the Tampa or Suwannee Formation. The lower boundary is defined by the base of the Oldsmar Formation, although part of the Cedar Keys Formation may be included in the aquifer (Meyer, 1989).

While the occurrence of injection and confining zones is relatively predictable within each highlighted area of Figure 1, there is stratigraphic variation within each area and especially between areas (Figure 3). The "Boulder Zone" of the Oldsmar Formation is the injection interval for the area on the east coast between Miami and Melbourne and for the oil fields of south Florida. On the west coast between St. Petersburg and Ft. Myers, the "Boulder Zone" loses its highly transmissive development, but the younger Avon Park Formation develops both cavernous and fractured characteristics. Hence, injection intervals are between approximately 2,000-3,500 feet on the southeast coast, and are between approximately 600-2,000 feet on the southwest coast.

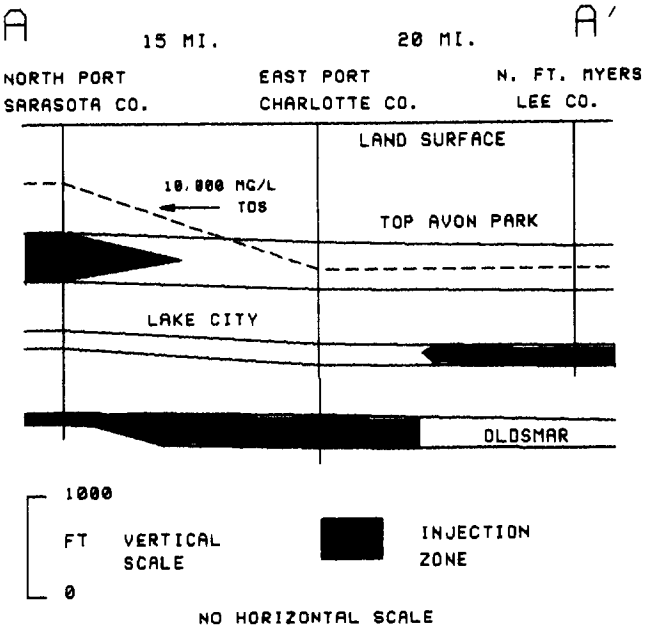

Fig. 3. Cross section A-A' showing stratigraphic variability of permeable injection zones in southwest Florida. Salinity gradually increases from surface to 10,000 mg/l interface. Each well encountered only one usable injection zone. Location of section shown on Figure 1.

Hydrogeologic Characteristics

Aquifer Properties

Withdrawal and injection tests reveal that the cavernous and fractured injection zones of the Floridan aquifer have extremely high transmissivities, ranging from 0.5 to 21 million gpd/ft. The "Boulder Zone" of Eocene age has transmissivities ranging from 1.0 to 4.0 million gpd/ft on the east coast based on injection test data (Geraghty and Miller, 1988). The only "Boulder Zone" well with available data on the west coast, near Ft. Myers, has a transmissivity of 0.51 million gpd/ft. This well, along with available geophysical logs of other southwest coast wells, indicates "Boulder Zone" transmissivity is less on the southwest coast. Quantitative data from oil field disposal wells between Ft. Myers and Miami are unavailable, but transmissivity is very high in this region (Vernon, 1970).

Transmissivity of the Avon Park Formation greatly increases from the east coast to the west coast. This formation serves as a confining sequence on the east coast while serving as the primary disposal zone on the west coast. Avon Park wells in the St. Petersburg area have transmissivities ranging from 9 to 21 million gpd/ft (CH2M Hill, 1987), while Avon Park wells in the Sarasota area have values from 0.5 to 2.8 million gpd/ft (CH2M Hill, 1988). Storage coefficients for the Avon Park in the St. Petersburg area are typical for confined aquifers, from .0002 to .00003 (CH2M Hill, 1987). Storage coefficients are unavailable at nearly all other injection sites owing to the lack of observation wells in the disposal zone.

Several million gallons of effluent per day are injected into the disposal zones with only a minimal increase in wellhead pressure (recorded on a gauge at the wellhead). Most of the increase is due to frictional loss as the effluent travels through the casing down into the injection zone (CH2M Hill, 1988). A typical well in southeast Florida injecting into the "Boulder Zone" might have a static (shut-in) wellhead pressure of 25 psi and an injection wellhead pressure of 30 psi at a rate of 2,000 gpm. Bottom hole pressure (recorded at the top of the injection zone) typically rises only a few psi during injection even at high rates. Figure 4 shows a typical time-drawdown plot for an injection well and the aquifer characteristics at the site.

The highly permeable zones are recognized on geophysical logs by greatly enlarged hole sizes on the caliper log, exceedingly long sonic (acoustic) transit times beyond measurable limits, very low resistivity indicating high porosity and saline water, changes on temperature logs, and flow into or out of zones on flowmeter (fluid velocity) logs (Figure 5). In addition, television video inspections show the caverns and fractures. Cavities are usually 2 to 6 feet high, but can be larger (Puri and Winston, 1974). The caverns alternate vertically with dense, noncavernous limestone and dolomite.

While previous studies emphasized cavern development, there is strong evidence suggesting the disposal zones are highly fractured, and that cavities develop after drill bit penetration (Hickey, 1990). Fractures are evident on television surveys, and drillers often do not report bit drops as would be expected in cavernous zones. The Avon Park injection zone in Pinellas County (St. Petersburg) is dominated by high concentrations of small aperture fractures which "shatter" and collapse during drilling (Hickey, 1989b).

Confining Zone Properties

The municipal effluent has a specific gravity (about 1.000 g/cc) less than the formation water in the injection zones (about 1.025 g/cc, approximately the same as sea water), which causes an additional force of upward flow. Confining rocks must offset this effect. The confining rocks of the Floridan aquifer typically have transmissivities less than 5,000 gpd/ft, and selected short intervals (approximately 10 feet thick) have transmissivities less than 50 gpd/ft (CH2M Hill, 1988). Vertical hydraulic conductivity ranges from .03 to .0003 ft/d. Transmissivity is determined by withdrawal tests or straddle packer pumping tests (Figure 6), and hydraulic conductivity is obtained from cores. Porosity is typically greater than 30%. Lack of interconnection between pore spaces, resulting in lower vertical hydraulic conductivity than might be expected, is how confining beds counteract the effluents' buoyancy in the injection zone.

When injection zones are pumped or used for injection, there are corresponding responses in the potentiometric surfaces of overlying zones in the confining unit. Monitor wells completed in intervals from 560-600 feet and 730-750 feet and located about 80 feet from the North Port injection well in Sarasota County exhibited an average of 0.42 and 0.78 feet of change in water levels respectively during withdrawal and injection tests of the injection well, which is completed open hole from 1,105-3,200 feet (CH2M Hill, 1988). Injection caused a rise in overlying water levels, while pumping caused a fall in water levels. Monitoring of long-term injection has shown no changes in water quality of overlying aquifers. Pressure in overlying aquifers changes because the confining zone rocks are compressible (porosity is about 30%), and a low vertical hydraulic conductivity

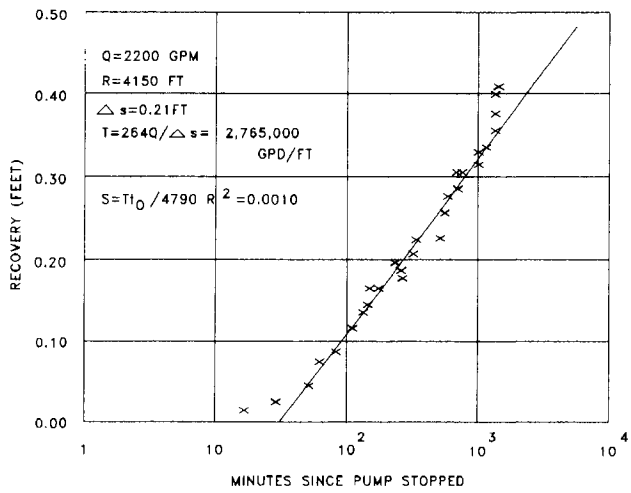

Fig. 4. Plot of observation well recovery data after 24-hour withdrawal test, North Port injection site, Sarasota County. Observation well is 4,150 feet from pumped well and both are completed in the injection zone at a depth of approximately 1,100 feet. (Modified from CH2M Hill, 1988).

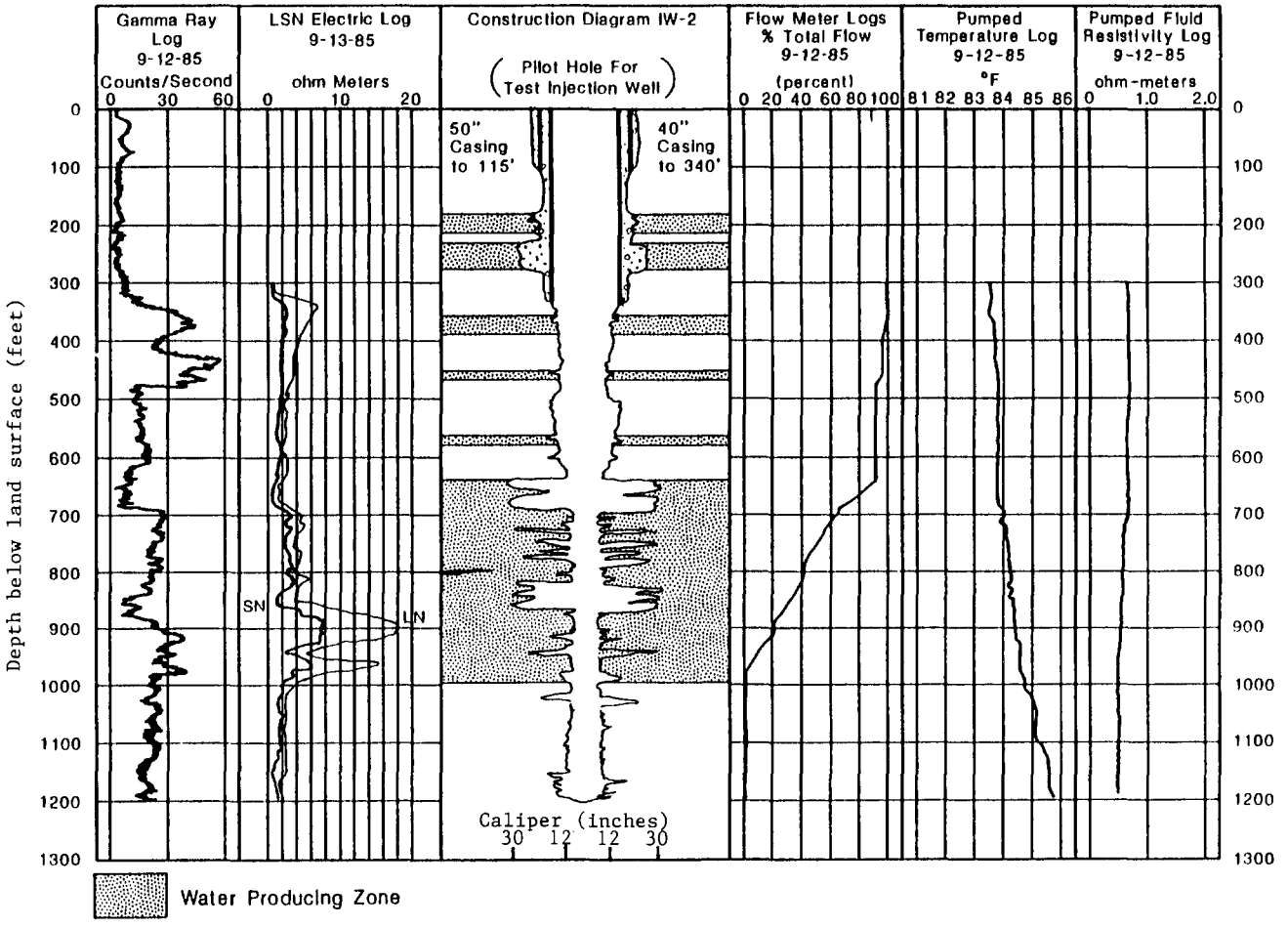

Fig. 5. Log responses for Albert Whitted Injection well no. 2, St. Petersburg, Pinellas County. Top of fractured injection zone at 640 feet below land surface. Notice lower resistivity opposite enlarged borehole below 640 feet. (From CH2M Hill, 1987).

prevents chemical contamination of overlying aquifers (Post, Buckley, Schuh and Jernigan, 1989).

Water Chemistry

South Florida is surrounded by bodies of sea water, which induces a fresh-water/salt-water interface along the Florida coast. Excessive fresh-water withdrawal leads to salt-water intrusion along the coast. The bulk of the population near the coasts makes maintenance of the hydrologic balance a delicate matter.

The federal and state programs allow deep wells for the injection of water not meeting drinking-water standards only if the receiving zone has a total dissolved solids (TDS) concentration greater than or equal to 10,000 mg/l. Such conditions exist beneath the fresh-water/salt-water interface but vary depending on distance from the coast.

The water of the upper Floridan aquifer is generally brackish (between 1,000-5,000 mg/l TDS) and grades downward to become chemically similar to sea water (35,000 mg/l TDS) in the middle or lower Floridan aquifer (Meyer, 1989). Confining rocks overlying the injection zones, located within these saline portions, serve to keep effluent out of brackish and potable waters.

Native formation water and typical secondarily treated

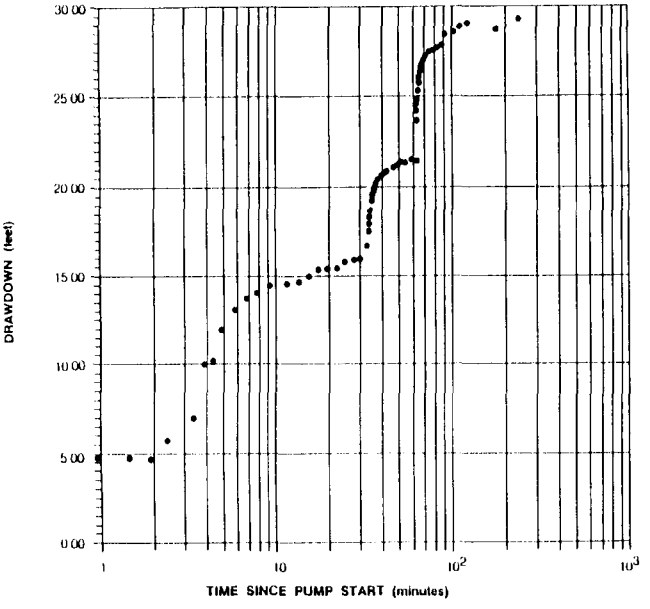

Fig. 6. Time-drawdown plot of confining interval from 560-1,100 feet during variable rate pump-out test, North Port injection well, Sarasota County. Estimated transmissivity of 65,000 gpd/ft reflects influence of thin permeable zones within confining sequence. (From CH2M Hill, 1988).

Table 1. Comparison of Injected Municipal Effluent and Native Formation Water (Data from North Port well, Sarasota County)

Concentrations (mg/l unless stated otherwise)		
Parameter	*Effluent (sampled 7/6/88)*	*Formation water (sampled 11/6/87)*
Sodium	82	9,870
Chloride	87	17,200
Sulfate	175	3,590
Total dissolved solids	604	29,300
Conductivity (μmhos/cm)	863	37,900
pH	7.25	7.15
Fluoride	0.29	1.4
Iron	0.06	0.41
Magnesium	13.8	408
Potassium	11	306
Calcium hardness	228	5,200
Nitrate (as N)	4.41	0.03
Total nitrogen	7.68	1.09
Total phosphorus	3.48	0.42
Total coliform (#/100 ml)	<2	—
Gross alpha (pCi/l)	<0.5	8.3
Turbidity (NTU)	0.9	0.63
Specific gravity (g/cc)	0.99	1.02

municipal effluent are compared in Table 1. The waters of the injection zone are dominated by the sodium and chloride ions, and to a lesser extent by sulfate, calcium, and magnesium. The infiltration of ocean water into the Floridan aquifer at the edge of the Floridan Plateau accounts for the sodium and chloride dominance (Smith and Griffin, 1977; Vernon, 1970; Kohout, 1965). Magnesium is derived from the solution of dolomite. Injection zone water chemistry does not vary significantly from east coast to west coast or from the "Boulder Zone" to the Avon Park Formation. The effluent is typically fresh to very slightly brackish water, depending on the water-supply source. The only significant constituents are elevated levels of nitrogen and phosphorus, and sometimes elevated biochemical oxygen demand and coliform bacteria concentrations. The municipal effluent has no significant effect upon either the native formation water or the carbonate rocks. However, the low density effluent rises to the top of the injection zone and spreads laterally. Modeling done by the U.S. Geological Survey shows circular convection and mixing of the two different liquids (Hickey, 1989b).

Summary

Numerous studies of individual deep injection wells have provided information on hydrogeological characteristics of injection zones in the Floridan aquifer of south Florida and also the confining characteristics of overlying intervals. Site-specific data agree with and add to previous studies. The highly permeable zones of the Floridan aquifer continue to be favorable for effluent disposal as long as each site has an effective confining bed.

Acknowledgments

The author would like to thank Richard J. Deuerling, Florida Department of Environmental Regulation, and Maureen R. Haberfeld, consultant, for critically reviewing this paper.

References

CH2M Hill. 1987. Construction and testing of the injection and monitoring wells at the Albert Whitted Wastewater Treatment Plant. Tampa, FL. v. 1, 78 pp.

CH2M Hill. 1988. Drilling and testing of the deep injection well system at North Port, Florida. Deerfield Beach, FL. v. 1, 119 pp.

Deuerling, R. J. 1983. Class I injection well inventory. Florida Dept. of Environmental Regulation. 66 pp.

Geraghty & Miller. 1988. Construction and testing of an injection well, north Martin County area wastewater treatment plant, Jensen Beach, Florida. Palm Beach Gardens, FL. 39 pp.

Hickey, J. J. 1989a. An approach to the field study of hydraulic gradients in variable-salinity ground water. Ground Water. v. 27, no. 4, pp. 531-539.

Hickey, J. J. 1989b. Circular convection during subsurface injection of liquid waste, St. Petersburg, Florida. Water Resources Research. v. 25, no. 7, pp. 1481-1494.

Hickey, J. J. 1990. Use of borehole video surveys to describe secondary porosity of carbonate rocks of the Floridan aquifer. Oral presentation. Underground Injection Control Workshop, Tallahassee, FL.

Hickey, J. J. and J. Vecchioli. 1986. Subsurface injection of liquid waste with emphasis on injection practices in Florida. U.S. Geological Survey Water Supply Paper 2281. 25 pp.

Kohout, F. A. 1965. A hypothesis concerning cyclic flow of salt water related to geothermal heating in the Floridan aquifer. New York Academy of Sciences. v. 28, no. 2, pp. 249-271.

Meyer, F. W. 1988. Summary of well construction, testing, and preliminary findings from the Alligator Alley test well, Broward County, Florida. U.S. Geological Survey Open-File Report 87-551. 68 pp.

Meyer, F. W. 1989. Subsurface storage of liquids in the Floridan aquifer system in south Florida. U.S. Geological Survey Open-File Report 88-477. 28 pp.

Post, Buckley, Schuh and Jernigan. 1987. Deep test/injection well, North Fort Myers Utility. Miami, FL. v. 1, 261 pp.

Post, Buckley, Schuh and Jernigan. 1988. Deep test/injection well, Atlantic Utilities of Sarasota. Miami, FL. v. 1, 246 pp.

Puri, H. S., G. L. Faulkner, and G. O. Winston. 1973. Hydrogeology of subsurface liquid-waste storage in Florida. Underground Waste Management and Artificial Recharge. v. 2, pp. 825-850.

Puri, H. S. and G. O. Winston. 1974. Geologic framework of the high transmissivity zones in south Florida. Florida Bureau of Geology Special Publication 20. 101 pp.

Smith, D. L. and G. M. Griffin, eds. 1977. The geothermal nature of the Floridan Plateau. Florida Bureau of Geology Special Publication 21. 161 pp.

Vernon, R. O. 1970. The beneficial uses of zones of high transmissivities in the Florida subsurface for water storage and waste disposal. Florida Bureau of Geology Information Circular 70. 39 pp.

* * * * *

Joseph L. Haberfeld has worked in the Underground Injection Control section of the Florida Department of Environmental Regulation (FDER) since 1987. His current interests include the hydrostratigraphy and geophysical log interpretation of injection and confining intervals in the Floridan aquifer. He earned a B.S. degree in Geology at the State University of New York, Fredonia (1975) and an M.S. degree in Geology at Southern Illinois University, Carbondale (1977). Before working at FDER he worked for nine years as a petroleum geologist for Gulf Oil and Chevron.

ground water

Important Observations and Parameters for a Salt Water Intrusion Model

by W. Barclay Shoemaker[1]

Abstract

Sensitivity analysis with a density-dependent ground water flow simulator can provide insight and understanding of salt water intrusion calibration problems far beyond what is possible through intuitive analysis alone. Five simple experimental simulations presented here demonstrate this point. Results show that dispersivity is a very important parameter for reproducing a steady-state distribution of hydraulic head, salinity, and flow in the transition zone between fresh water and salt water in a coastal aquifer system. When estimating dispersivity, the following conclusions can be drawn about the data types and locations considered. (1) The "toe" of the transition zone is the most effective location for hydraulic head and salinity observations. (2) Areas near the coastline where submarine ground water discharge occurs are the most effective locations for flow observations. (3) Salinity observations are more effective than hydraulic head observations. (4) The importance of flow observations aligned perpendicular to the shoreline varies dramatically depending on distance seaward from the shoreline. Extreme parameter correlation can prohibit unique estimation of permeability parameters such as hydraulic conductivity and flow parameters such as recharge in a density-dependent ground water flow model when using hydraulic head and salinity observations. Adding flow observations perpendicular to the shoreline in areas where ground water is exchanged with the ocean body can reduce the correlation, potentially resulting in unique estimates of these parameter values. Results are expected to be directly applicable to many complex situations, and have implications for model development whether or not formal optimization methods are used in model calibration.

Introduction

Numerical models that account for the effects of fluid density on ground water flow are being used more frequently to address scientific, engineering, and water resource management problems (Voss and Wood 1993; Voss 1999; Voss and Andersson 1993; Simmons et al. 1999; Simmons et al. 2002; Shoemaker and Edwards 2003; Langevin 2001). Also being used more frequently are inverse modeling routines based on nonlinear regression methods documented by Hill (1992, 1998), Hill et al. (2000), Poeter and Hill (1998), and Doherty (1990, 2002). However, there has been little application of inverse modeling sensitivity methods to density-dependent ground water flow simulators because of limitations in computing power and the unique technical skills individuals must learn. As computing power increases and expertise grows, modeling studies will likely use both inverse methods and density-dependent ground water flow simulations to solve complicated water resource or ground water contamination problems. Both technologies contain powerful capabilities that can help modelers better understand complex flow systems and make better use of available data.

A practical problem that could benefit from the combined use of these methods is salt water intrusion. Salt water intrusion is important because (1) ~70% of the earth's population lives near a coast, and (2) ~95% of the earth's water lies in the oceans and seas at high levels of salinity (Freeze and Cherry 1979). To study salt water intrusion, density-dependent ground water flow dynamics are needed to simulate flow in the transition zone between fresh water and salt water. Nonlinear regression methods for calibrating and

[1]U.S. Geological Survey, Florida Integrated Science Center, Center for Water and Restoration Studies, 9100 NW 36th St., Suite 107, Miami, FL 33178; (305) 717–5856; fax (305) 717–5801; bshoemak@usgs.gov

Received March 2003, accepted November 2003.
Published in 2004 by the National Ground Water Association.

evaluating models offer many advantages over trial and error methods (Hill 1998). For example, in the context of salt water intrusion models, these methods can be used to (1) estimate flow and transport parameter values that provide the best fit to simulated heads, flows, and salinity to their observed equivalents; (2) calculate sensitivity measures for determining the flow and transport parameters most important to reproducing salt water intrusion observations and for assessing whether the observations are sufficient to estimate parameters of interest; and (3) compute measures of parameter and predictive uncertainty.

The work in this paper is partly motivated by a recent salt water intrusion investigation in which inverse modeling methods were applied to a density-dependent ground water flow simulation. In this study, the U.S. Geological Survey (USGS), in cooperation with the South Florida Water Management District (SFWMD), examined the physics of salt water intrusion in southwestern Florida (Shoemaker and Edwards 2003). During this study, the universal inverse modeling routine UCODE (Poeter and Hill 1998) was applied to the flow model to accomplish the following. (1) Identify flow and transport parameters representing aquifer properties and boundary conditions that could not be estimated accurately and uniquely with the available observations. (2) Determine parameter values that produced the best fit between observations and their simulated equivalents. (3) Quantify uncertainty in parameter estimates through linear confidence intervals. In addition, prediction-scaled sensitivities (Hill 1998) suggested that the extent of salt water intrusion, as reflected by salinity predictions, was most affected by recharge, followed in order of declining importance by ground water pumpage, sea level, and the salinity of the Gulf of Mexico. This insight was more quickly and clearly obtained than would have been possible using traditional calibration and sensitivity methods.

The initial success of the combined use of inverse modeling sensitivity methods with a density-dependent ground water flow simulator was encouraging, but motivated further investigation. For example, the SFWMD/USGS cooperative project did not directly consider potential extreme correlations between flow and transport parameters given observations typically available for calibration of salt water intrusion models. Parameter correlation is measured using correlation coefficients calculated as the covariance between two parameters divided by the product of their standard deviations (Hill 1998). Parameter correlation coefficients with values of +1.00 or –1.00 indicate parameter values that are extremely correlated and generally cannot be estimated uniquely with the observations involved; values < ~0.95 indicate that unique estimates can likely be obtained.

The purpose of this paper is to investigate what insight and understanding of salt water intrusion calibration problems can be attained by combined use of the sensitivity analysis methods suggested by Hill (1998) with a density-dependent ground water flow simulator, and what numerical difficulties are to be expected. This is accomplished using results from five simulations based on a simple two-dimensional, cross sectional model (Langevin 2001) that represents coastal ground water flow within the transition zone between fresh water and salt water. The five simulations differ in the number and type of observations used to compute sensitivities and correlation coefficients. The simple model and approach also demonstrate (1) some challenges of attempting to calibrate a density-dependent ground water flow model with various types of observations, (2) the relative importance of some flow and transport parameters in simulating the types of quantities commonly observed in coastal aquifer systems, and (3) observation types and locations within the transition zone between fresh water and salt water that provide the most information for estimating important flow and transport parameters. Though a simple model is used for the analysis, results are expected to be applicable to more complex situations because the simple model captures the basic dynamics.

Methods

Two modeling codes were selected for this study. SEAWAT–2000 (Langevin et al. 2003) was chosen as the density-dependent ground water flow simulator and UCODE (Poeter and Hill 1998) was chosen as the inverse modeling routine.

SEAWAT–2000 is a new version of the SEAWAT program (Guo and Bennett 1998; Guo and Langevin 2002) that combines MODFLOW–2000 (Harbaugh et al. 2000; Hill et al. 2000) and MT3Dms (Zheng and Wang 1999) to solve the coupled ground water flow and solute transport equations. SEAWAT–2000 contains considerably more functionality than the prior release of the code. This code was chosen primarily because it compares well with other density-dependent flow models in terms of accuracy and execution time. In fact, new solvers for the flow equation (Harbaugh et al. 2000; Mehl and Hill 2001) that may reduce model execution times are available. In addition, the model selected for experimentation in this paper (Langevin 2001) was built and run with a prior version of SEAWAT (Guo and Bennett 1998). As such, little reformatting of model input datasets was necessary.

The UCODE inverse modeling routine was used in this study to compute sensitivities and parameter correlation coefficients. MODFLOW–2000 (Hill et al. 2000) capabilities were not used because they do not support the transport parameters and salinity observations being considered. This was a disadvantage because the sensitivities computed by MODFLOW–2000, which uses the sensitivity-equation method, are more accurate than those computed by UCODE, which uses a perturbation approach. The perturbation sensitivities are expected to be sufficiently accurate to produce robust scaled sensitivity measures for evaluating observation and parameter importance. However, Hill and Østerby (2003) show that the less accurate perturbation sensitivities can affect the utility of the correlation coefficients. In particular, values that should be near +1.00 or –1.00 may be smaller in absolute value, so that extreme parameter correlation may not be detected when actually present. Extreme correlation means coordinated linear changes in parameter values would produce the same simulated results at observation locations (Poeter and Hill 1997). In this situation, estimating unique values of extremely correlated parameters using nonlinear regression will likely be

problematic. Thus, in this work, parameter correlation coefficients that are smaller than +1.00 in absolute value may reflect a lack of correlation, or may reflect the inaccuracies in the perturbation sensitivities. Absolute values that round to +1.00, however, clearly indicate extreme parameter correlation.

Because calculating and interpreting sensitivities and correlation coefficients are an important part of this paper, the equations that compute these quantities (Hill 1998; Poeter and Hill 1998) are presented here. Dimensionless-scaled sensitivities (ss_{ij}) are computed as

$$ss_{ij} = \left(\frac{\partial y_i'}{\partial b_j}\right)\left|\underline{b}\right|\left|b_j\right|\omega_i^{1/2} \quad (1)$$

where y_i' is the simulated value associated with the ith observation; b_j is the jth estimated parameter; $(\partial y_i'/\partial b_j)$ is the sensitivity of the simulated value associated with the ith observation with respect to the jth parameter, and is evaluated at the set of parameter values in $\underline{b}$ is a vector that contains parameter values for which the sensitivities are evaluated; and ω_i is the weight of the ith observation.

Dimensionless-scaled sensitivities are used to determine observation types and locations likely to be most effective for estimating a given parameter value. Composite-scaled sensitivities (css_j) are computed as

$$css_j = \left[\sum_{i=1}^{ND}\left(ss_{ij}\right)^2\Big|_{\underline{b}}/ND\right]^{1/2} \quad (2)$$

where ND is the number of observations. Composite-scaled sensitivities are used to determine the relative importance of various flow and transport parameters for reproducing observed values, and as a measure of the amount of information provided by the set of observations for estimating a parameter value. Correlation coefficients, $cor(i, j)$, are calculated as

$$cor\left(i, j\right) = \frac{cov\left(i, j\right)}{var\left(i\right)^{1/2}\, var\left(j\right)^{1/2}} \quad (3)$$

where cov(i, j) is the covariance between parameter i and j; var(i) is the variance of parameter i; and var(j) is the variance of parameter j.

Correlation coefficients are used to identify parameters that are extremely correlated given the observations used in experimental simulations.

Experimental Density-Dependent Model and Observations

The model used in this study was designed to simulate local submarine ground water discharge to Biscayne Bay in southwestern Florida, and is described in detail by Langevin (2001). The model has one row, 149 columns, and 33 layers (Figure 1). Boundary conditions were assigned to the model domain (Figure 1, Table 1) based on general knowledge, field data, and results from some regional ground water models. Boundary conditions include a constant flux of ground water to each cell in column 1 (Q/m) representing the general flow of ground water toward the coast that originates from recharge on inland areas not represented by the model grid. The constant-flux was computed using hydraulic conductivities and hydraulic gradients similar to those observed in the Biscayne Aquifer (Merritt 1996; Sonenshein and Koszalka 1996). Net recharge (rch) is applied to the inland portion of layer 1. In the context of this model, net rch is the amount of rainfall that exceeds evapotranspiration and runoff and reaches the water table. Net rch was assigned a reasonable value of 38 cm/yr based on studies of rainfall, evapotranspiration, and runoff in a coastal area (Parker et al. 1955; Merritt 1996; German 2000). A no-flow boundary exists along the base of model layer 33 representing a less permeable clastic confining or semiconfining unit that underlies more permeable limestone. This type of hydrostratigraphic sequence is common in coastal environments due to changes in sea level. Constant-head and constant-salinity boundaries are used to represent an ocean body. The constant-head and constant-salinity boundaries were assigned values roughly equal to sea level (0 m), and the salinity of sea water (35 kg/m^3), respectively.

Aquifer permeability and transport properties (Table 1) also were assigned to the cross sectional model based on general knowledge, field data, and prior calibration results. These aquifer properties were initially assigned using results from previous studies (Fish and Stewart 1991; Merritt 1996) and were adjusted by Langevin (2001) while calibrating to match hydraulic head and salinity observations. These properties include longitudinal dispersivity, transverse vertical dispersivity, effective porosity, and horizontal and vertical hydraulic conductivity. Diffusion was assumed to be negligible. The model has one stress period, and initial conditions of head and salinity were used to compute a steady-state distribution of hydraulic head, flow, and salinity within the model domain (Figure 2).

An important modification to the model documented in Langevin (2001) was made for the purposes of this study. During preliminary simulations, the implicit finite difference transport solver (GCG) in MT3Dms produced slightly inaccurate solutions due to the time length of transport steps. This time length is computed internally by the program using various stability criteria. The small inaccuracies in the transport solution resulted in large inaccuracies in perturbation sensitivities calculated for horizontal and vertical hydraulic conductivity. Setting the time length of transport steps to 0.5 the value computed by MT3Dms resulted in more accurate transport solutions and perturbation sensitivities. This was confirmed using the highly accurate, mass conservative total-variation-diminishing (TVD) scheme in MT3Dms. With this change in time step length, transport solutions and sensitivities calculated using the GCG solver were essentially the same as those calculated using the TVD scheme. The GCG solver produced results twice as quickly as the TVD solver and therefore was used for the experimental simulations described hereafter.

Hydraulic head, salinity, and flow observations were generated using the final steady-state results from the cross

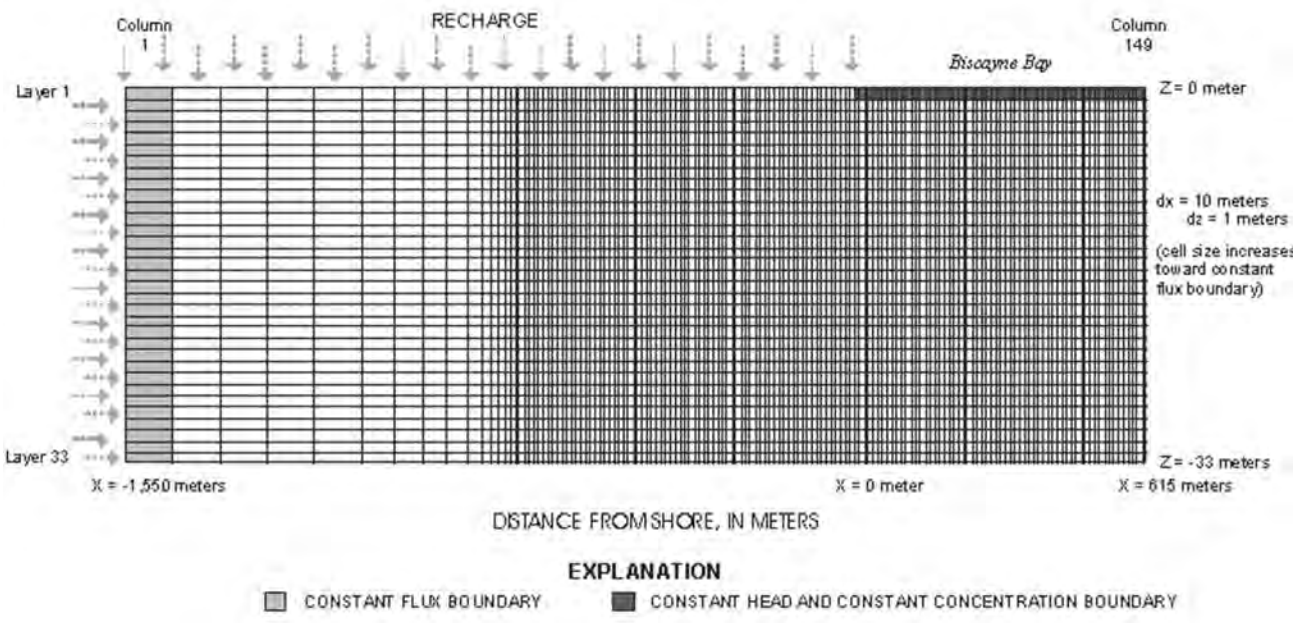

Figure 1. Cross section showing model grid and boundary conditions.

sectional model (Table 2). Measurement error that would likely occur in the field was added to these observations. The measurement error is necessary to calculate the observation weights, which, in turn, are used to calculate the scaled sensitivities and correlation coefficients (weights are used in the calculation of the variance and covariance terms in Equation 3) (Hill 1998). In this study, weights are calculated as the inverse of the variance of likely measurement error. This variance can be computed from the standard deviation or coefficient of variation of measurement error.

For the 23 hydraulic head observations, measurement error was assumed to be normally distributed with a mean of zero (Hill 1992; Cooley 1997) and a standard deviation of ~0.003 m. This standard deviation was based on standard error estimates for water levels measured in wells by the USGS in southern Florida (Prinos et al. 1996). For the 23 salinity observations, measurement error was assumed to be normally distributed with a mean of zero and a standard deviation of ~0.1 kg/m^3. Salinities range from ~3 to 35 kg/m^3, and for this range using a 0.1 kg/m^3 standard deviation was thought to be appropriate based on discussions with USGS water quality personnel. For the five flow observations, measurement error was assumed to be normally distributed with a mean of zero and a coefficient of variation of 30%. These observations are likely to be obtained by seepage meters, which are known to produce relatively large measurement errors (Shinn et al. 2002). Measurement error was randomly sampled from these distributions and added to the simulated results to create the values used as observations in this work (Table 2). For all of the observations used, the errors imposed may be lower than normally expected in field situations in which many types of errors can occur. Their value relative to one another, however, is thought to be representative of field problems, so that the results of the sensitivity analysis conducted in this work should be applicable to most field studies.

The five experimental simulations differed only by the observations used by UCODE to compute correlation coefficients, dimensionless-scaled sensitivities, and composite-scaled sensitivities. The observation sets included 23 hydraulic heads (simulation 1), 23 salinities (simulation 2), 23 hydraulic heads and 23 salinities (simulation 3), 23 hydraulic heads and five flows (simulation 4), and 23 hydraulic heads, 23 salinities, and five flows (simulation 5). All of the observations were located within the transition zone (Figure 3) because this region of the flow system has proven to be particularly difficult to understand based on previous studies (Konikow and Reilly 1999).

Execution time is often a problem when considering density-dependent, ground water flow and transport simulations. A single forward run of this simple model required ~30 min of execution time on a personal computer, with a Pentium II 550 MHz processor and 384 MB RAM. To solve for sensitivities took ~1 h for each defined parameter.

Table 1
Parameter Values and Boundary Stresses Assigned to the Model Domain

Parameter/ Stress	Value (Units)
Q/m[a]	15 (m/d)
dsp[b]	dsp = α L = 10: α T = α L/10 (both in m)
por[c]	0.2 (dimensionless)
Kh[d]	1000 (m/d)
Kv[e]	100 (m/d)
rch[f]	38 (cm/day)

[a](Q/m) is regional ground water flow.
[b](dps) is dispersivity.
[c](por) is effective porosity.
[d](Kh) is horizontal conductivity.
[e](Kv) is vertical hydraulic conductivity.
[f](rch) is recharge.

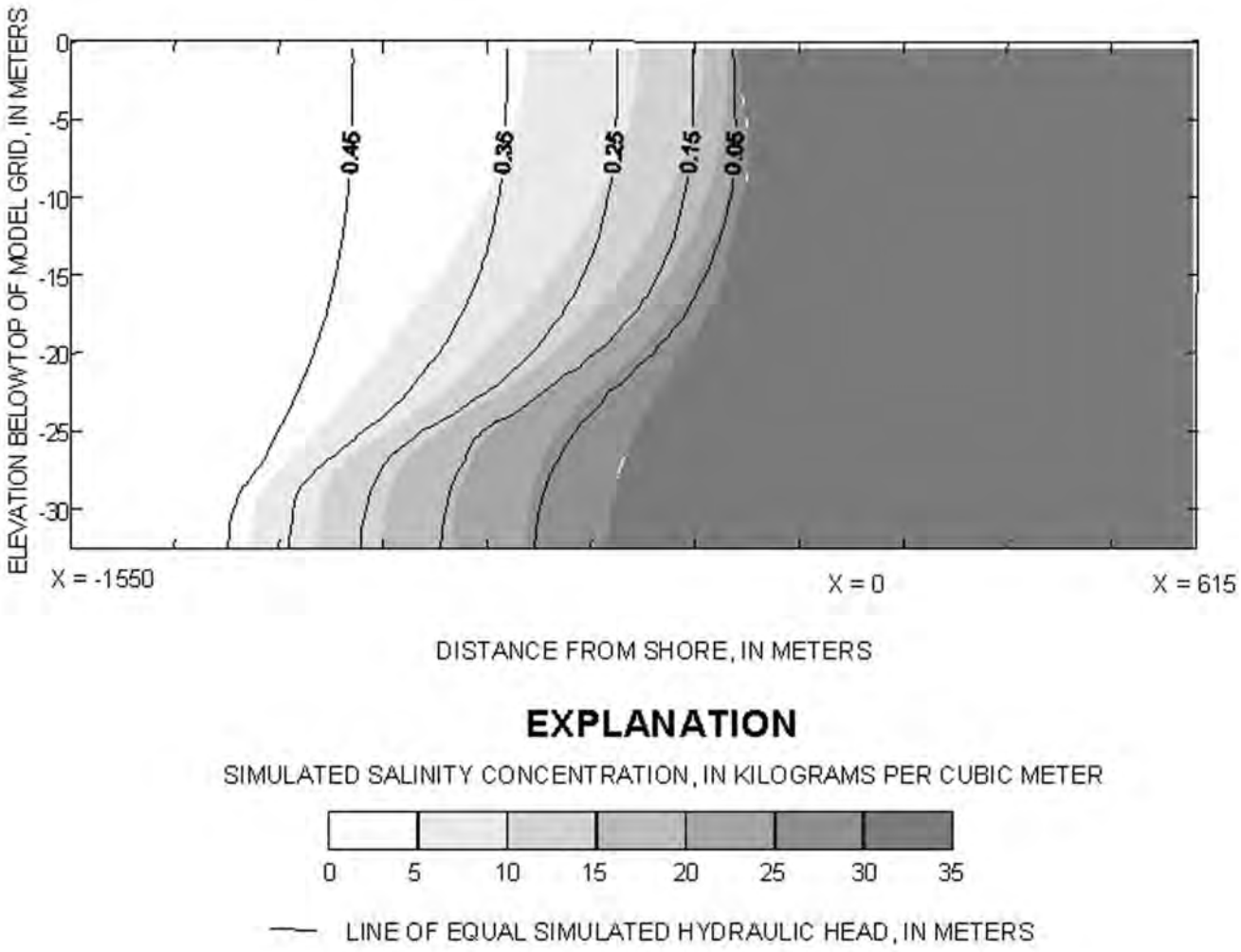

Figure 2. Cross section of steady-state hydraulic heads and salinity in the model domain.

Thus, ~6 h of execution time was necessary for the parameters considered in this paper. To attain this execution time, the longitudinal and vertical components of dispersivity were grouped together by setting the vertical dispersivity equal to 0.1 of the longitudinal dispersivity (Table 1).

Souza and Voss (1987, 1989), Voss and Souza (1998), and Langevin (2001) indicate that simulated hydraulic heads, salinities, and flow are more sensitive to transverse dispersivities (in either the vertical or horizontal directions) than to longitudinal dispersivities because ground water flows mostly parallel to lines of equal solute concentration in the transition zone. The latter makes the density-dependent flow model insensitive to longitudinal dispersivities, but highly sensitive to transverse dispersivities. Additionally, although sea level can be very important for reproducing head, salinity, and flow observations in the transition zone between fresh water and salt water, this parameter is not included. Sea level is typically less uncertain than the other parameters considered in this study (Table 1). For example, sea level and tides are generally well known relative to aquifer properties, recharge, and ground water flow. Composite and dimensionless-scaled sensitivities and correlation coefficients were computed for each experimental simulation for the six parameters listed in Table 1. The sensitivities were calculated by perturbing the parameter value by 1% of its value.

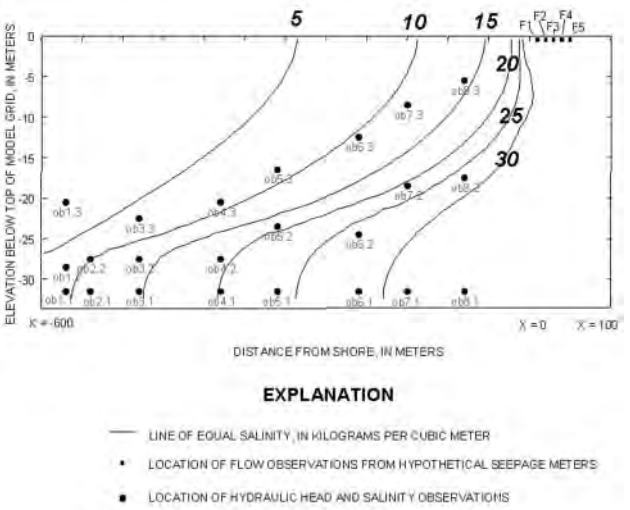

Figure 3. Cross section of observation types and locations in relation to the transition zone between fresh water and salt water.

Results and Discussion

Composite-Scaled Sensitivities

Composite-scaled sensitivities for the five experimental simulations are shown in Figure 4. This figure shows that

Table 2
Observation Types, Locations, Values, and Estimated Measurement Error

Name	Type	Units	Model Output	Error Sample	Observed Values
F1	Flow	m^3/d	–136500	–40967	–177467
F2	Flow	m^3/d	1470	–401	–1871
F3	Flow	m^3/d	61780	18595	80375
F4	Flow	m^3/d	86600	26033	112633
F5	Flow	m^3/d	84920	25518	110438
ob1.1	Head	m	0.3102	–0.0009	0.3093
ob1.2	Head	m	0.3283	–0.0004	0.3279
ob1.3	Head	m	0.4446	0.0035	0.4481
ob2.1	Head	m	0.2786	–0.0006	0.2780
ob2.2	Head	m	0.3073	0.0045	0.3118
ob3.1	Head	m	0.2195	0.0028	0.2223
ob3.2	Head	m	0.2431	0.0081	0.2512
ob3.3	Head	m	0.3727	0.0012	0.3739
ob4.1	Head	m	0.1297	0.0014	0.1283
ob4.2	Head	m	0.1495	–0.0037	0.1458
ob4.3	Head	m	0.3242	–0.0005	0.3237
ob5.1	Head	m	0.0737	0.0004	0.0741
ob5.2	Head	m	0.1680	–0.0009	0.1670
ob5.3	Head	m	0.3123	0.0037	0.3160
ob6.1	Head	m	0.0065	0.0007	0.0073
ob6.2	Head	m	0.0464	0.0006	0.0469
ob6.3	Head	m	0.2636	–0.0004	0.2632
ob7.1	Head	n	–0.0223	0.0035	–0.0188
ob7.2	Head	m	0.1312	–0.0006	0.1306
ob7.3	Head	m	0.2290	0.0045	0.2335
ob8.1	Head	m	–0.0402	0.0028	–0.0374
ob8.2	Head	m	0.0561	0.0081	0.0643
ob1.1	Salinity	kg/m^3	11.05	–0.01	11.03
ob1.2	Salinity	kg/m^3	10.26	0.10	10.36
ob1.3	Salinity	kg/m^3	3.22	0.21	3.44
ob2.1	Salinity	kg/m^3	12.64	–0.05	12.59
ob2.2	Salinity	kg/m^3	11.40	–0.06	11.38
ob3.1	Salinity	kg/m^3	15.82	0.05	15.88
ob3.2	Salinity	kg/m^3	14.78	–0.25	14.53
ob3.2	Salinity	kg/m^3	7.17	0.04	7.21
ob4.1	Salinity	kg/m^3	20.95	–0.06	20.89
ob4.2	Salinity	kg/m^3	19.97	–0.21	19.77
ob4.3	Salinity	kg/m^3	9.48	0.03	9.51
ob5.1	Salinity	kg/m^3	24.41	–0.21	24.20
ob5.2	Salinity	kg/m^3	19.21	–0.07	19.15
ob5.3	Salinity	kg/m^3	9.18	0.07	9.24
ob6.1	Salinity	kg/m^3	28.96	0.06	290.03
ob6.2	Salinity	kg/m^3	26.89	0.03	26.92
ob6.3	Salinity	kg/m^3	10.76	0.16	10.92
ob7.1	Salinity	kg/m^3	31.32	0.10	31.42
ob7.2	Salinity	kg/m^3	21.13	0.11	21.25
ob7.3	Salinity	kg/m^3	11.48	0.24	11.71
ob8.1	Salinity	kg/m^3	33.49	–0.15	33.33
ob8.2	Salinity	kg/m^3	26.91	0.08	26.99
ob8.3	Salinity	kg/m^3	14.24	–0.03	14.21

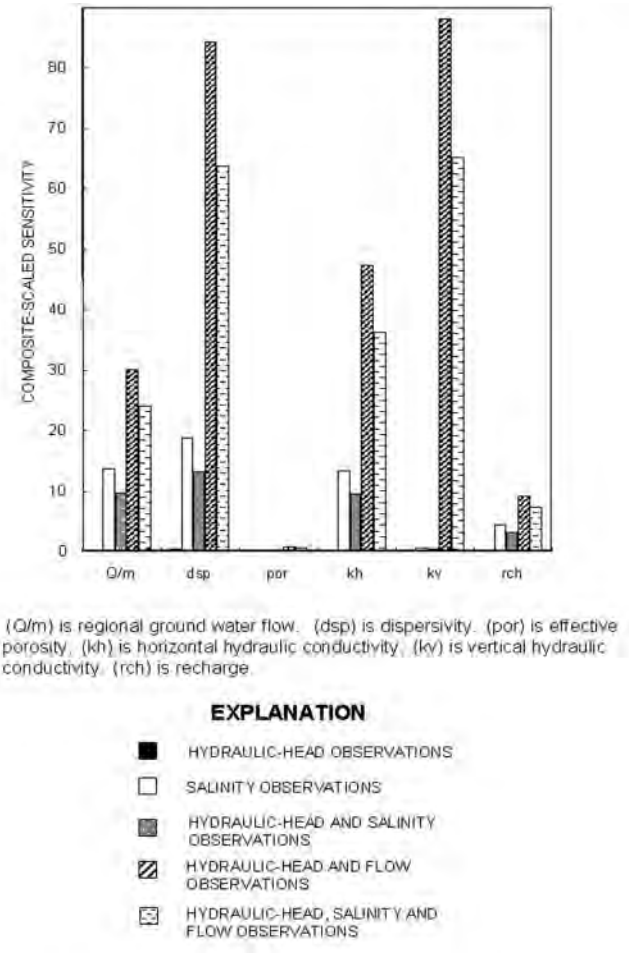

(Q/m) is regional ground water flow, (dsp) is dispersivity, (por) is effective porosity, (kh) is horizontal hydraulic conductivity, (kv) is vertical hydraulic conductivity, (rch) is recharge.

Figure 4. Bar graph of composite-scaled sensitivity for each experimental simulation.

the hydraulic head observations alone provide little information about any of the model parameters. When salinity observations are included (experimental simulations 2 and 3), a consistent pattern is evident. Dispersivity is most important, followed by regional ground water flow, horizontal hydraulic conductivity, recharge, vertical hydraulic conductivity, and effective porosity. Vertical hydraulic conductivity becomes the most important parameter in experimental simulations 4 and 5, which use flow observations. This means the flow observations provide substantial information about vertical hydraulic conductivity.

Dispersivity is clearly a very important parameter in this study, being either the most sensitive or second most sensitive when flow observations are used in the analysis. The importance of dispersivity to the different type of observations is discussed next using dimensionless-scaled sensitivities.

Dimensionless-Scaled Sensitivities

Dimensionless-scaled sensitivities for dispersivity are plotted in Figure 5. Two aspects of these results are discussed in the following sections—(1) the implications of a positive or negative dimensionless-scaled sensitivity value, and (2) observation locations and types likely to be most effective for estimating dispersivity.

Sign Implications of Dimensionless-Scaled Sensitivities

Dimensionless-scaled sensitivities of hydraulic head observations to dispersivity are all positive (Figure 5), meaning that increasing dispersivity increases heads and decreasing dispersivity decreases heads. This reflects the underlying physics. Increasing dispersivity increases the process of salt water mixing with fresh water. This causes the salt water to become less dense and to rise toward the sea, and causes the transition zone to be more vertically oriented and to have a somewhat broader top and a much less pronounced "toe" (Figure 6a). The latter allows more fresh water from recharge to move seaward, resulting in higher hydraulic heads in the vicinity of observation locations. Decreasing dispersivity decreases the mixing process, which produces a much more pronounced salt water toe and allows less fresh water from recharge to move seaward (Figure 6b), resulting in lower hydraulic heads in the vicinity of observation locations.

Dimensionless-scaled sensitivities of salinity observations to dispersivity are negative in most of the transition zone and are positive only at the top of the seaward part of the zone (Figure 5). This means increasing dispersivity decreases salinity in most of the transition zone and increases salinity at the top of the transition zone. Conversely, decreasing dispersivity increases salinity in most of the transition zone and decreases salinity at the top of the transition zone. These changes in salinity are explained by the flow system responses to the changes in dispersivity as shown in Figure 6 and described in the prior paragraph.

Dimensionless-scaled sensitivities of flow observations to dispersivity are mostly negative (Figure 5). An exception is flow observation F5, which has a positive sensitivity. Table 3 was designed to help explain the sign implications of these dimensionless-scaled sensitivities. For clarity, only the implications and results of increasing dispersivity are discussed in this paragraph. When the dimensionless-scaled sensitivity is negative and ground water is discharging to the sea (flow observations F1 and F2), increasing dispersivity increases the amount of ground water discharge. When the dimensionless-scaled sensitivity is negative and sea water is flowing into the aquifer (flow observations F3 and F4), increasing dispersivity decreases the amount of sea water inflow. When the sensitivity is positive and sea water is flowing into the aquifer (flow observation F5), increasing dispersivity increases in the amount of sea water inflow.

Effective Observation Locations for Estimating Dispersivity

Dimensionless-scaled sensitivity of hydraulic head observations to dispersivity range from 0.01 in the top third of the transition zone to 0.52 toward the toe of the transition zone (Figure 5). This result indicates that hydraulic head observations located toward the toe of the transition zone provide more information for estimating dispersivity than head observations located in the middle or top third of the transition zone. The control exerted by the sea, as simulated by the constant-head boundary condition in Biscayne Bay (Figure 1), probably explains this trend in sensitivity. Dimensionless-scaled sensitivities near this boundary are low because the constant heads prevent

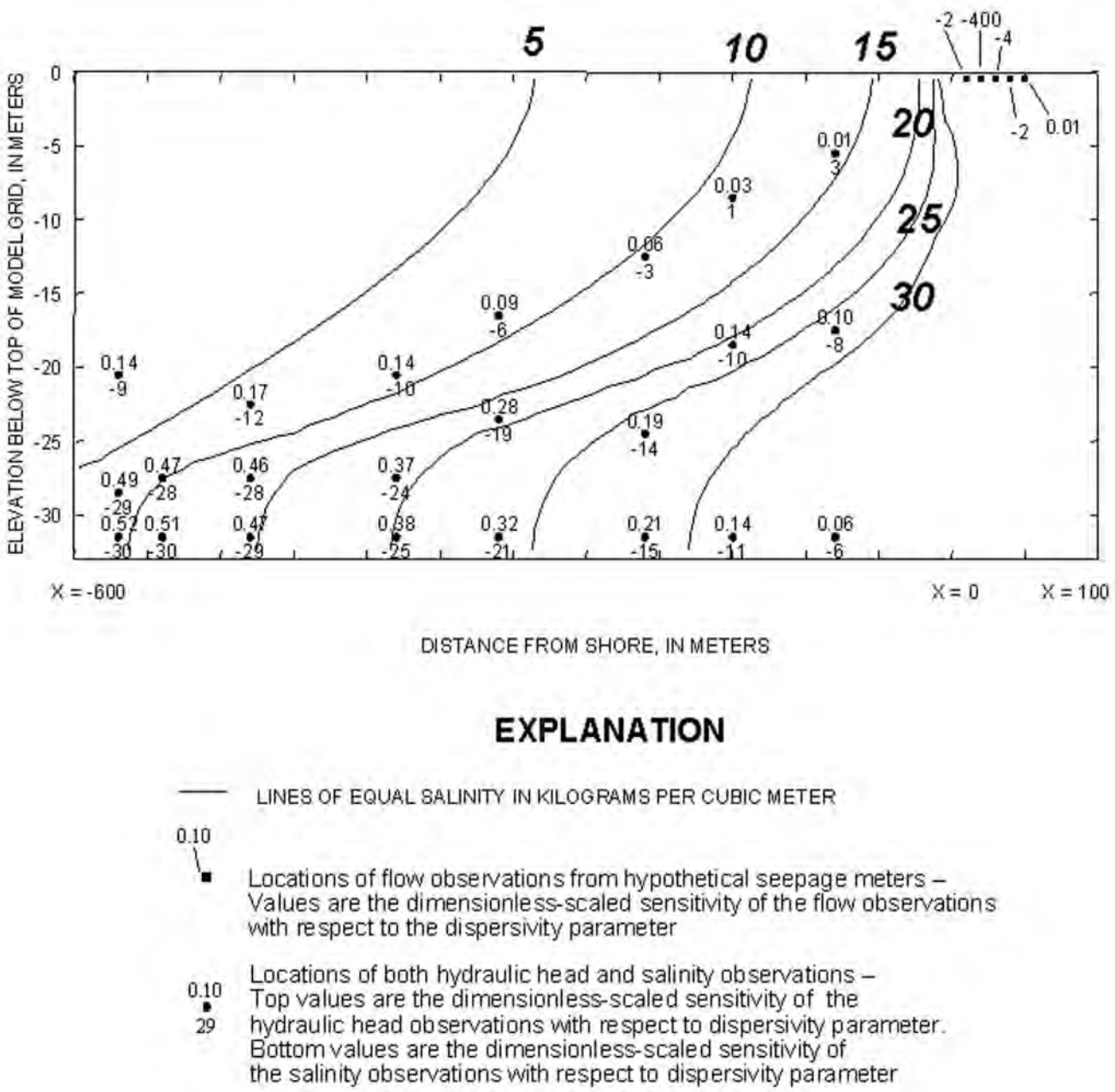

Figure 5. Cross section of dimensionless-scaled sensitivities for dispersivity.

simulated heads from changing when dispersivity is perturbed from an initial value.

Dimensionless-scaled sensitivity of salinity observations to dispersivity range from +3 to –30 (Figure 5). The large absolute values in the toe of the transition zone between fresh water and salt water suggest salinity observations in this location are most effective for estimating dispersivity. This evidence is consistent in that the toe of the transition zone seems most volatile in response to changing dispersivity values (Figure 6). For example, small values of dispersivity result in a toe of the transition zone that moves farther inland. Conversely, large values of dispersivity result in a toe of the transition zone that moves farther seaward. The top third of the transition zone changes only slightly with different values of dispersivity because of the control exerted by the sea, represented as a constant-concentration boundary condition (Figure 1).

Dimensionless-scaled sensitivities of flow observations to dispersivity range from–400.0 to +0.01 (Figure 5). In this model, flow observations within ~50 m of the coastline are most effective for estimating dispersivity (Figure 7). In other coastal aquifer systems, the distance would depend on the distance over which flow to the ocean diminished. This often can be evaluated using temperature sensors or by preliminary flow measurements or modeling. The large differences in the dimensionless-scaled sensitivities for the flow observations can be partly explained by the weights for these observations (recall from Equation 1 that the square root of the weight, $w^{1/2}$, is a term in the calculation of dimensionless-scaled sensitivity). This is illustrated using flow observations F1, F2, and F3. Table 3 shows that when dispersivity is increased to 10.1 from the base case value of 10.0, the magnitude of flow change is about the same at F1, F2, and F3, meaning that the sensitivity dy/db

Table 3
Changes in Flow Caused by Changes in the Dispersion Parameter

dsp = 9.9					
Flow Observation	**F1**	**F2**	**F3**	**F4**	**F5**
Flow change	~1% less	~85% less	~2% more	~0.5% more	Very small decrease
Direction of flow	Discharge to sea	Discharge to sea	Flow into aquifer	Flow into aquifer	Flow into aquifer
dsp = 10.0 (base case)					
Flow (m^3/d)	–136,500	–1470	61,780	86,600	84,920
Dimensionless-scaled sensitivity value	–2	–400	–4	–2	0.01
dsp = 10.1					
Flow Observation	**F1**	**F2**	**F3**	**F4**	**F5**
Flow change (%)	~1% more	~85% more	~2% less	~0.5% less	Very small increase
Flow change (m^3/d)	1220	1250	1080	430	–6
Direction of flow	Discharge to sea	Discharge to sea	Flow into aquifer	Flow into aquifer	Flow into aquifer

is about the same for each of the three observations. However, the dimensionless-scaled sensitivity at F2 is much larger than that at F1 or F3 because of the differences in the weights for these observations. These differences in the weights are related to differences in the magnitudes of observed flows at the three locations. Weights for the flows were defined using coefficients of variation (equal to 0.3), which means that each weight is inversely proportional to the magnitude of the observed flow. For example, the discharge to the sea at F1 is 136,500 m^3/d (Table 3), and $w^{1/2}$ for F1 is thus equal to $1 / (0.3 \times 136{,}500\ m^3/d) = 0.000024\ d/m^3$. The discharge to the sea at F2 is 1470 m^3/d (Table 3), and $w^{1/2}$ is thus equal to $1 / (0.3 \times 1470\ m^3/d) = 0.0023\ d/m^3$. Thus, the difference in the $w^{1/2}$ term for these two observations is clearly the primary reason for the differences in the dimensionless-scaled sensitivity.

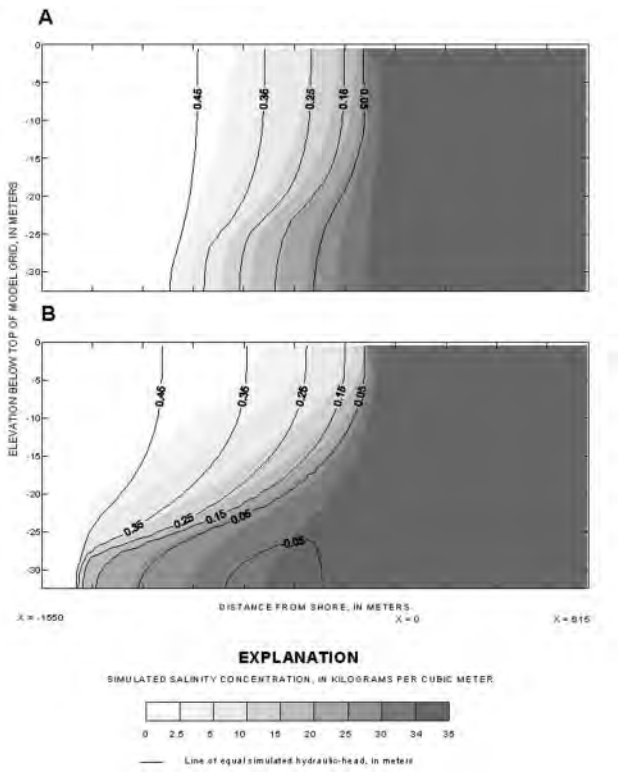

Figure 6. Cross sections showing the change in the geometry of the transition zone resulting from changes in the dispersivity parameter. The dispersivity parameter equals 15 m in cross section (a), and 5 m in cross section (b).

This analysis of the effect of the weights on the dimensionless-scaled sensitivity values also is applicable when considering the importance of the different flow observations in the context of calibrating this model using weighted least-squares regression. The weighting used would cause the F2 observation to have a greater influence in the regression and, thus, a greater influence on the estimated model parameter values compared to the observations at F1 and F3.

Although the weights clearly have a large influence on the relative importance of different flow observations, it is important to also consider the magnitudes of the changes in flux in response to a change in dispersivity when determining flow observation importance. For the five different flow observations considered in this study, these changes in flux suggest that observations at, and just landward of, the flow reversal location are likely to be most important to estimating dispersivity values.

Observation Types Likely to Be Important for Estimating Dispersivity

Examining the absolute magnitude of observation dimensionless-scaled sensitivities to dispersivity can give some insight into the observation types likely to be most effective for estimating dispersivity. Figure 5 shows that salinity observations are always more important than hydraulic head observations. Flow observations near the coastline can be effective, but observations too far from shore are ineffective for estimating dispersivity (Figure 7). As previously mentioned for this model, flow observations within ~50 m of the coastline and near the flow reversal zone appear to be most effective for estimating dispersivity. In other coastal aquifer systems, the locations of important

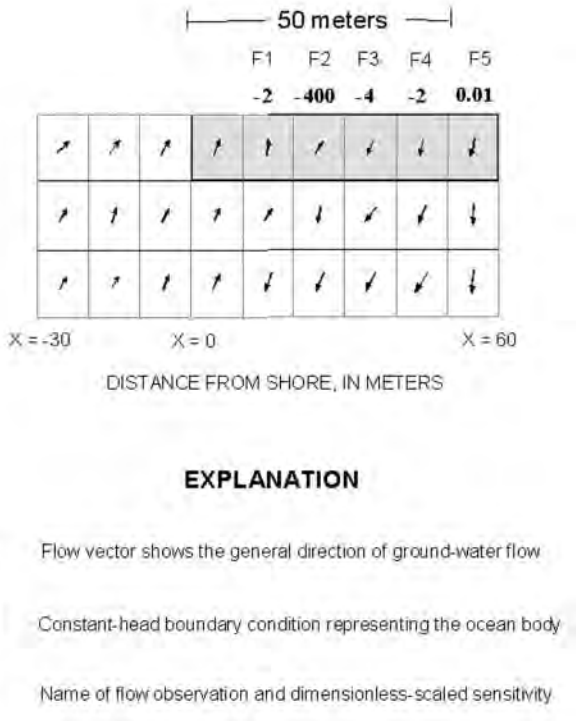

Figure 7. Cross section of the location and dimensionless-scaled sensitivity of flow observations in relation to ground water flow directions.

flow observations would likely depend on the magnitudes and variability of fluxes near the coastline.

Parameter Correlation Coefficients

Parameter correlation coefficients for six parameters in the five experimental simulations were calculated. The absolute values of the correlations for all parameter pairs were < 0.85 for all observation sets. The correlation coefficient for horizontal hydraulic conductivity and regional ground water flow was 0.84 when salinity observations (simulation 2) or hydraulic head and salinity observations (simulation 3) were used.

It is already well established that hydraulic-conductivity parameters and flow parameters representing, for example, recharge or ground water pumpage are correlated when calibrating a density-independent flow model solely using hydraulic head observations (Hill et al. 1998; Emsellem and de Marsily 1971). Therefore, the questions arise as to whether the hydraulic-conductivity and flow parameters are correlated in this density-dependent flow model when using solely hydraulic head observations, and how salinity observations affect the correlations. That is, are the calculated correlation coefficients reliably identifying all extreme parameter correlations in this problem? As previously mentioned, UCODE computes perturbation sensitivities that are less accurate than, for example, the derivative sensitivities computed by MODFLOW–2000. This loss of accuracy may produce unreliable correlation coefficients.

To test this concern, the model was run again with both hydraulic-conductivity and flow parameters in Table 1 multiplied by 100. The simulated heads and salinities in this additional scenario were the same as those in the baseline model (Figure 2). This means that if only head and/or salinity observations are available for calibration, these permeability and flow parameters are extremely correlated. In other words, 100 times more water flowing through a system that is 100 times more permeable produces the same simulated head and salinity results. This is consistent with the small sensitivity of all observations to porosity (Figure 4) as follows. Density would only affect the correlation between the hydraulic conductivity and flow parameters if the salinities were sensitive to the flow rate. This dependence would be indicated by a sensitivity of salinity to porosity. The result shown in Figure 4—that the sensitivity of salinity to porosity is very small relative to its sensitivity to the other parameters—indicates insensitivity to velocity.

In density-independent models, previous research suggests flow observations are useful for dramatically reducing extreme correlations between conductivity and flow parameters (Poeter and Hill 1998; Emsellem and de Marsily 1971; Barth and Hill in review). Apparently, flow observations serve the same role in density-dependent models. As previously mentioned, the correlation coefficient for hydraulic conductivity and ground water flow was ~0.84 when solely using salinity observations, or using hydraulic head and salinity observations. The value of these coefficients changed to–0.17 and 0.79, respectively, when flow observations were included in simulations 4 and 5. This suggests flow observations reduce correlation for this parameter pair. The prior statement is confirmed by results of running the model with both hydraulic-conductivity and flow parameters multiplied by 100. In this additional scenario, simulated flows at observation locations were ~100 times larger in absolute value than simulated flows in the baseline scenario. The hydraulic heads and salinities were basically the same.

A Short Note on Nonlinearity

This density-dependent flow model was nonlinear with respect to the dispersivity parameter in the transition zone between fresh water and salt water. In other words, parameter sensitivities and correlation coefficients changed with different values for dispersivity. For example, when using hydraulic head, salinity, and flow observations, while setting the dispersivity parameter equal to 15 m, the composite scaled sensitivities of effective porosity, ground water flow, and dispersivity are ~0.887, 27.6, and 9.77, respectively. When the dispersivity parameter is set equal to 5 m, the composite scaled sensitivities of effective porosity, ground water flow, and dispersivity are ~2.28, 16.5, and 58.4, respectively. The largest change in composite-scaled sensitivity occurred for the dispersivity parameter.

Apparently, the conclusions about preferable observation locations and types are robust in the presence of the nonlinearity in dispersivity. Simulations that were run with the dispersivity parameter set equal to 15 m/d and 5 m/d support this statement. Despite the dispersivity changes, dimensionless-scaled sensitivities still suggested that when estimating dispersivity: (1) hydraulic-head and salinity observations located in the toe of the transition zone are most favorable; (2) salinity values provide more information than hydraulic-head observations; and (3) flow observations located just landward of the area where the flow direction reverses at the bottom of the ocean are most effective.

Conclusions

A sensitivity analysis with a density-dependent ground water flow simulator was conducted to produce insight and understanding of salt water intrusion calibration problems. The approach used here clearly and defensibly shows (1) the relative importance of various flow and transport parameters for reproducing hydraulic head, salinity, and flow observations, (2) observation locations and observation types likely to be most effective for estimating a dispersivity parameter, (3) parameters that may not be uniquely estimated with a given set of observations because of extreme parameter correlation, and (4) the types of observations that may reduce correlation between parameter values and encourage unique estimates. These results were obtained for the transition zone between fresh water and salt water, a natural feature of coastal ground water flow systems that has previously proven to be very difficult to model and understand. The results apply regardless of how model calibration is pursued; that is, observations provide the same amount of information whether using gradient, global search, or manual trial-and-error methods. The methods investigated here clearly show the information provided by observations.

The following more specific conclusions can be drawn from this study.

1. Dispersivity was a very important parameter for reproducing the distribution of hydraulic head, salinity, and flow in the transition zone between fresh water and salt water, as indicated by composite-scaled sensitivities. It is expected that dispersivity is equally important in many field investigations.
2. The toe of the transition zone between fresh water and salt water, and areas near the coastline where submarine ground water discharge occur, are effective locations for (a) hydraulic head and salinity observations, and (b) flow observations collected on the ocean bottom with, for example, seepage meters. For layered systems in which toes occur at the base of multiple permeable layers, each of the toe locations is likely to be important.
3. Salinity observations are more effective than hydraulic head observations for estimating important dispersivity parameter values in the transition zone between fresh water and salt water. For the same purpose, flow observations located within or near areas of submarine ground water discharge are most effective. Flow observations located just landward of the area where the flow direction reverses at the bottom of the ocean (to the sea vs. from the sea) appear to be most effective for estimating important dispersivity parameter values. Flow observations located farther offshore generally are not useful.
4. As in density-independent models, flow parameters and permeability parameters were extremely correlated when calibrating this density-dependent model solely to hydraulic head and salinity observations. Adding flow observations perpendicular to the shoreline in areas where ground water is exchanged with the ocean reduced the correlation, potentially resulting in unique estimates of these parameter values.
5. The density-dependent flow model was nonlinear with respect to the dispersivity parameter. Thus, different values for dispersivity resulted in different parameter sensitivities and correlations. However, the conclusions about preferable observation locations and types were robust in the presence of the nonlinearity in dispersivity studied here.

Acknowledgments

This article was mostly inspired through collaborate development of research proposals with Mary Hill (USGS, Boulder, Colorado) and Matthew Ely (USGS, Tacoma, Washington). Paul Barlow (USGS, Reston, Virginia) provided support and guidance. This work was funded in part by the USGS Office of Ground Water in Reston, Virginia, and is an extension of work funded by the SFWMD and the USGS Cooperative Work Program in Miami, Florida. Raul Patterson and Chris Langevin (USGS, Miami, Florida) developed the cross section model used for experimental simulations. Mary Hill, Eve Kuniansky and Sandy Cooper (both with USGS, Norcross, Georgia), Rhonda Howard and Mike Deacon (both with USGS, Miami, Florida), and Matthew Tonkin (S.S. Papadopulos and Associates Inc.) generously reviewed initial drafts. Claire Tiedeman (USGS, Menlo Park, California) and one anonymous reviewer for *Ground Water* also provided many insightful comments.

Editor's Note: The use of brand names in peer-reviewed papers is for identification purposes only and does not constitute endorsement by the author, his employer, or the National Ground Water Association.

References

Barth, G., and M.C. Hill. In review. Parameter and observation importance in modeling virus transport in saturated systems—Investigations in one and two dimensions.

Cooley, R.L. 1997. Confidence intervals for ground water models using linearization, likelihood, and bootstrap methods. *Ground Water* 35, no. 5: 869–880.

Doherty, J. 1990. *MODINV—Suite of Software for MODFLOW Preprocessing, Postprocessing, and Parameter Optimization User's Manual*. Queensland, Australia: Australian Centre for Tropical Freshwater Research, James Cook University.

Doherty, J. 2002. PEST—Model independent parameter estimation, version 6. Queensland, Australia: Watermark Numerical Computing.

Emsellem, Y., and G. de Marsily. 1971. An automated solution for the inverse problem. *Water Resources Research* 7, no. 5: 1264–1283.

Fish, J.E., and M. Stewart, 1991. Hydrogeology of the surficial aquifer system, Dade County, Florida. U.S. Geological Survey Water Resources Investigations Report 90–4108.

Freeze, A.R., and J.A. Cherry. 1979. *Groundwater*. Englewood Cliffs, New Jersey: Prentice Hall.

German, E.R. 2000. Regional evaluation of evapotranspiration in the Everglades. U.S. Geological Survey Water Resources Investigations Report 00–4217.

Guo, W., and G.D. Bennett. 1998. SEAWAT version 1.1—A computer program for simulations of ground water flow of variable density. A report prepared by Missimer International Inc.

Guo, W., and C.D. Langevin. 2002. User's guide to SEAWAT: A computer program for simulation of three-dimensional variable-density ground water flow. U.S. Geological Survey Open-File Report 01–434.

Harbaugh, A.W., E.R. Banta, M.C. Hill, and M.G. McDonald. 2000. MODFLOW–2000, the U.S. Geological Survey modular ground water model—User guide to modularization concepts and the ground water flow process. U.S. Geological Survey Open-File Report 00–92.

Hill, M.C. 1992. A computer program (MODFLOWP) for estimating parameters of a transient, three-dimensional, ground water flow model using non-linear regression. U.S. Geological Survey Open File Report 91–484.

Hill, M.C. 1998. Methods and guidelines for effective model calibration. U.S. Geological Survey Water-Resources Investigations Report 98–4005.

Hill, M.C., E.R. Banta, A.W. Harbaugh, and E.R. Anderman. 2000. MODFLOW–2000, the U.S. Geological Survey modular ground water model—User guide to the observation, sensitivity, and parameter estimation processes and three post processing programs. U.S. Geological Survey Open File Report 00–184.

Hill, M.C., and O. Østerby. 2003. Determining extreme parameter correlation in ground water models. *Ground Water* 41, no. 4: 420–430.

Konikow, L.F, and T.E. Reilly. 1999. Seawater intrusion in the United States. In *Seawater Intrusion in Coastal Aquifers—Concepts, Methods, and Practices*, ed. J. Bear, A.H.-D. Cheng, S. Sorek, D. Ouazar, and I Herrera. Dordrecht, Netherlands: Kluwer Academic Publishers.

Langevin, C.D. 2001. Simulation of ground water discharge to Biscayne Bay, southeastern Florida. U.S. Geological Survey Water-Resources Investigations Report 00–4251.

Langevin, C.D., W.B. Shoemaker, and W. Guo. 2003. MODFLOW–2000, the U.S. Geological Survey modular groundwater model—Documentation of the SEAWAT–2000 version with the variable density flow process (VDF) and the integrated MT3Dms transport process (IMT). U.S. Geological Survey Open-File Report 03–426.

Mehl, S.W., and M.C. Hill. 2001. MODFLOW–2000, the U.S. Geological Survey modular ground water model—User guide to the link-AMG (LMG) package for solving matrix equations using an algebraic multigrid solver. U.S. Geological Survey Open-File Report 01–177.

Merritt, M.L. 1996. Simulation of the water table altitude in the Biscayne Aquifer, southern Dade County, Florida, water years 1945–89. U.S. Geological Survey Water-Supply Paper 2458.

Parker, G.G., G.E. Ferguson, and S.K. Love. 1955. Water resources of southeastern Florida. U.S. Geological Survey Water-Supply Paper 1255.

Poeter, E.P., and M.C. Hill. 1997. Inverse models: A necessary next step in ground water modeling. *Ground Water* 35, no. 2: 250–260.

Poeter, E.P., and M.C. Hill. 1998. Documentation of UCODE, a computer code for universal inverse modeling. U.S. Geological Survey Water-Resources Investigations Report 98–4080.

Prinos, S., T. Richards, and R. Krulikas. 1996. Water resources data Florida water year 1996. U.S. Geological Survey Water-Data Report FL–96–2B.

Shoemaker W.B., and K.M. Edwards. 2003. Potential for saltwater intrusion into the lower Tamiami Aquifer near Bonita Springs, southwestern Florida. U.S. Geological Survey Water-Resources Investigation Report 03–4262.

Shinn E.A., C.D. Reich, D. Hickey, and A. Tihansky. 2002. Geology and hydrology of the Florida Keys: Ground water flow and seepage. Abstract presented on the South Florida Information Access web page, http://sofia.usgs.gov/projects/grndwtr_flow/grflowab1.html.

Simmons, C.T., J.M. Sharp Jr., and N.I. Robinson. 1999. Density-driven free convection in zones of inverted salinity through fractured low permeability units in the Gulf of Mexico Basin, Texas, USA. In *Proceedings of the Water 99 Joint Congress*, July 6–8, Brisbane, Queensland, Australia. Australia: Institute of Engineers.

Simmons, C.T., K.A. Narayan, J.A. Woods, and A.L. Herczeg. 2002. Ground water flow and solute transport at the Mourquong saline-water disposal basin, Murray Basin, southeastern Australia. *Hydrogeology Journal* 10, 278–295.

Sonenshein, R.S., and E.J. Koszalka. 1996. Trends in the water table altitude (1984–93) and salt water intrusion (1974–93) in the Biscayne Aquifer, Dade County, Florida. U.S. Geological Survey Open-File Report 95–705.

Souza, W.R., and C.I. Voss. 1987. Analysis of an anisotropic coastal aquifer system using a variable-density flow and solute transport simulation. *Journal of Hydrology* 92, 17–41.

Souza, W.R., and C.I. Voss. 1989. Assessment of potable ground water in a fresh water lens using a variable-density flow and solute transport simulation. In *Proceedings of the NWWA Conference on Solving Ground Water Problems with Models*, February 7–9, 1989, Indianapolis, Indiana. Dublin, Ohio: National Water Well Association.

Voss, C.I. 1999. USGS SUTRA code—History, practical use, and application in Hawaii. In *Seawater Intrusion in Coastal Aquifers—Concepts, Methods, and Practices*, ed. J. Bear, A.H.-D. Cheng, S. Sorek, D. Ouazar, and I Herrera. Dordrecht, Netherlands: Kluwer Academic Publishers.

Voss, C.I., and J. Andersson. 1993. Regional flow in the Baltic Shield during Holocene coastal regression. *Ground Water* 31, no. 6: 989–1006.

Voss, C.I., and W.R. Souza. 1998. Dynamics of a regional fresh water-salt water transition zone in an anisotropic coastal aquifer system. U.S. Geological Survey Open-File Report 98–398.

Voss, C.I., and W.W. Wood. 1993. Synthesis of geochemical, isotopic, and ground water modeling analysis to explain regional flow in a coastal aquifer of southern Oahu, Hawaii. In *Proceedings of the International Atomic Energy Agency Final Research Coordination Meeting*, June 1–4, Vienna, Austria, 147–178. Vienna, Austria: International Atomic Energy Agency.

Zheng, C., and P.P. Wang. 1999. MT3Dms—A modular three-dimensional multispecies transport model for simulation of advection, dispersivity and chemical reactions of contaminants in ground water systems: Documentation and user's guide. U.S. Army Corps of Engineers Contract Report SERDP–99–1.

Influence of Pore Pressure on Apparent Dispersivity of a Fissured Dolomitic Aquifer

by Darrell I. Leap[a] and Pamela Mai Belmonte[b]

Abstract

The U.S. Geological Survey's Amargosa Tracer Calibration Site in southern Nevada has been used for three different recirculating tracer tests using as tracers: (1) tritium, (2) sulfur-35, and (3) tritium and bromide together. Although the physical setup, well spacings, and thus apparent scale were the same in all tests, the recirculating rates and pore pressures were different. Apparent dispersivities found in the three tests differed considerably, revealing an inverse relationship between computed dispersivity and recirculation rate. These differences are believed to be caused primarily by changes in fissure-aperture widths and thus, hydraulic conductivities, with resulting changes in flow rates and directions caused by changes in pore pressure between different tests in the presence of high ambient pore pressure. The results of this study indicate that forced-gradient tracer tests for determination of dispersivity should not be performed when ambient pore pressure and/or testing pore pressure is a significant percentage of overburden pressure. In addition, apparent dispersivity calculated by forced-gradient tracer tests can differ considerably from that of unstressed natural situations, and consequent solute-transport estimates are likely to be in error.

Background

Hydraulic testing of fractured or fissured rocks in the presence of high ambient or high induced pore pressures is known to often yield erroneous values of hydraulic conductivity, or values not characteristic of the natural unstressed aquifer. Several field and laboratory investigations have verified such phenomena.

Tsang, Noorishad, and Witherspoon (1985), after studying a mathematical simulation of pressure-permeability relationships in a single fracture, concluded: "Pressure dependence of rock permeability due to fracture deformation may have a major effect on fluid flow behavior of fractured porous systems." They also concluded that traditional testing procedures are most likely to be valid when testing pressure does not exceed 10 percent of the overburden pressure.

Wood et al. (1985) noted greatly increased spring flow from fractured rocks in Idaho after an earthquake and concluded that pore pressures of 2.3 MPa are greater than horizontal compressional stresses in most sedimentary basins up to a depth of 488 m, and would be sufficient to cause widening of vertical fractures and thus increase flow rates.

Cruz et al. (1982) found that in field studies of pressure tests in wells, fractures 1 mm in width could allow a 120-percent increase in flow rate with a pressure increase of 1 kg/cm^2, but the flow rate for the same pressure increase lessened quite significantly with decreasing aperture size. This phenomenon can be explained by the "Cubic Law" as proven by Witherspoon et al. (1980) from laboratory experiment, i.e.,

$$Q/\Delta h = C(2b)^3 \quad (1)$$

where Q = flow rate; Δh = incremental change in head; $2b$ = fracture aperture width; and C = empirical constant.

[a]Department of Earth and Atmospheric Sciences, Purdue University, West Lafayette, Indiana 47907.

[b]852 A, Nevada Oval, Plattsburg, New York 12903-5366.

Received August 1989, revised March and July 1991, accepted July 1991.

Discussion open until July 1, 1992.

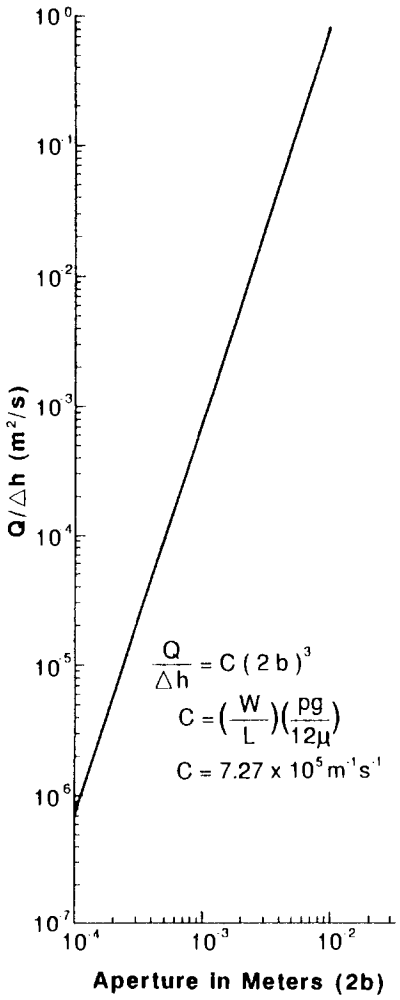

Fig. 1. Relationship of flow rate per-unit-head-drop to fracture-aperture width according to the "Cubic Law," for straight, linear flow.

This relationship shows that flow rate per unit increase in head (and consequently, increasing pore pressure) increases greatly with increasing aperture width. This is illustrated graphically in Figure 1, where for straight linear flow, the fracture width (W) and length (L) are both one meter; the product of density (ρ) and gravitational acceleration (g) is 9.8×10^3 N/m^3; and dynamic viscosity (μ) is 1.1×10^{-3} Nsm^{-2}.

Although the theoretical and experimental studies discussed below have been performed on solute transport in fractures, there is still no universal agreement about the true nature and quantification of dispersivity in fractured and fissured rocks. Dispersivity has been accepted traditionally as a function only of the aquifer, and dispersion is assumed to increase linearly with increasing velocity for constant values of dispersivity and diffusion constants

$$D_L = \alpha_L U + D^* \quad (2)$$

where D_L = longitudinal dispersion coefficient; α_L = longitudinal dispersivity (characteristic length); U = mean interstitial ground-water velocity; D* = coefficient of molecular diffusion for porous media; where

$$D^* = wD \quad (3)$$

and D = diffusion constant in water; $w < 1.0$ and is dependent upon tortuosity, packing, and other shape factors.

It could be assumed that in a single fracture with significant wall asperities, dispersivity would increase with decreasing aperture width, which would bring the asperities closer together to cause greater tortuosity and heterogeneity.

In complex natural systems containing many fractures and fissures of different size, orientation, and connectivity, dispersivity is far more complex. In complex, fractured systems dispersivity could be a function of not only aperture width, but also of scale (distance from source to measurement point) and velocity variations; all of these, in turn, are functions of fracture width, orientation, and connectivity as well as asperity distributions (Marsily, 1986).

Guinn, Kessler, and Greenkorn (1972), using a mathematical model based on the random walk approach, found that the dispersivity tensor may be a function of the average flow direction. They also concluded that the effects of velocity and medium properties are inseparable.

Freeze and Cherry (1979) and Marsily (1986) discussed the variations of flow types and dispersion within fractured and fissured rocks. They reported that the velocity of ground water within a fracture may deviate from the average velocity (computed by Darcy's Law) by orders of magnitude. Marsily summarized five types of flow velocities, described by Louis (1974), which depend upon the values of the Reynolds number and roughness of fracture walls—namely smooth laminar, smooth turbulent, rough turbulent, rough laminar, and very rough laminar.

Although average velocities through fractured and fissured rock masses can be computed by Darcy's Law, it provides no indication of velocities in individual fissures and fractures. The actual velocity in individual fissures and fractures depends not only on the gradients, but also on fracture aperture and wall roughness. Therefore, there are often wide ranges in flow velocities within single fractures and within a group of fractures; very high velocities can even be nonlinear, and therefore can affect computed apparent dispersion values by mechanisms not explainable by classical dispersion theories such as equation (2).

An additional complicating factor addressed by these authors is the frequent deviation of the principal directions of the dispersivity tensor from the principal directions of fracture orientation and, consequently, from the hydraulic-conductivity principal directions in fractured rocks, such that the longitudinal dispersivity constant will not necessarily have a single value regardless of the direction of the velocity vectors, as is often assumed in granular porous media.

Similarly, Molz, Güven, and Melville (1983), through a series of field experiments, concluded that macrodispersivity, and therefore dispersion, is caused primarily by velocity variations that result from natural hydraulic-conductivity variations between strata at different elevations within the flow regime.

Huyakorn and Anderson (1986) came to similar conclusions as the above investigators by modeling flow in a two-well recirculating test with curvilinear coordinates and

testing the numerical model against a physical model. They also concluded that large apparent dispersion is caused by lateral fluid spreading, caused in turn by natural hydraulic-conductivity variations over the aquifer thickness; they concluded that dispersivity is really not a function of velocity itself, but rather, of velocity distribution.

Finally, Hull, Miller and Clemo (1987) concluded, from a series of laboratory experiments, that development of a velocity profile within fractures and transverse diffusion across streamlines is sufficient to explain dispersion and thus, dispersivity is not only a function of fracture geometry and interconnection, but also of velocity.

In the last six references quoted above, the investigators assumed that structural properties of the aquifer, such as fracture-aperture width and orientation, as well as conductivity stratification, were static and intrinsic properties of the aquifer. We believe our study to be the first that has ever attributed changes in computed solute-transport parameters to changes in aquifer structure caused by pressure variations due to testing, with resultant changes in hydraulic properties and hydrodynamics.

This work is significant not only to understanding pressure-dispersivity relationships, but also to the understanding of pitfalls inherent in field-scale tracer studies of fractured and fissured rocks. It vividly illustrates the care that must be taken in performing such tests, especially with high ambient and/or induced pressures which can cause significant changes in solute-transport parameters.

Objectives

Two-well, recirculating tests reported herein were run in order (1) to determine the apparent longitudinal dispersivity of a fissured and fractured aquifer within the Cambrian Bonanza King dolomite draining the Nevada Test Site in southern Nevada; and (2) to study the usefulness of tritium, sulfur-35, and bromide as tracers in this aquifer.

Description of the Amargosa Tracer Calibration Site

The tests were performed at the U.S. Geological Survey's Amargosa Tracer Calibration Site (hereafter called the Tracer Site), located in the Amargosa Desert in southern Nevada, approximately 121 km northwest of Las Vegas and approximately 24 km southwest of Mercury, Nevada (Figure 2).

The facility was constructed as an experimental site for using various kinds of tracers and tracer tests to (1) determine effective porosity of a fissured carbonate aquifer draining the Nevada Test Site; (2) determine ambient, regional velocity of ground water; (3) evaluate sorption phenomena for different radioactive nuclides; and (4) determine apparent longitudinal dispersivity values.

The aquifer itself is believed to be a solution-modified, low-angle reverse fault zone within the Cambrian Bonanza King dolomite. Five wells completely penetrate this aquifer, whose thickness varies from 3.1 m at Tracer Wells 1 and 4 to 13.7 m at Tracer Well 2 (Figure 3). Transmissivity determined by a pumping test ranges from 4,800 m^2day to 10,900 m^2day (unpublished data in files of USGS, Water Resources

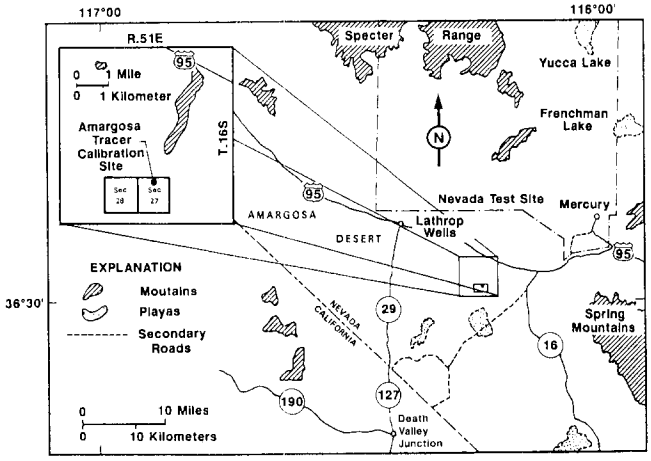

Fig. 2. Map showing location of Amargosa Tracer Calibration Site, southern Nevada.

Division, Denver, Colorado). The storage coefficient is approximately 5×10^{-4}, and the hydraulic gradient is between 10^{-4} and 10^{-5} (Claassen and Cordes, 1975).

Examination of drilling logs and cores taken during drilling of wells [in U.S. Geological Survey Core Library, Mercury, Nevada, and in Johnston (1968)], revealed permeable fractures ranging in width from less than one mm to 45 cm. The fracture-surface roughness, fracture connectivity, and nature of fracture asperities were impossible to assess between the wells, across the area of interest. Borehole flow-meter tests precisely defined the top and thickness of the permeable fissured and fractured zone which constitutes the aquifer thickness as shown in Figure 3.

Tracer Well 2, the pumping well, contained a high-capacity turbine pump driven by an external electric motor which was connected by a polyvinyl chloride (PVC) pipe, 15.0 cm in diameter, to Tracer Well 1 (the injection well) during two-well recirculating tests (Figure 4). These two wells were aligned parallel to the direction of regional

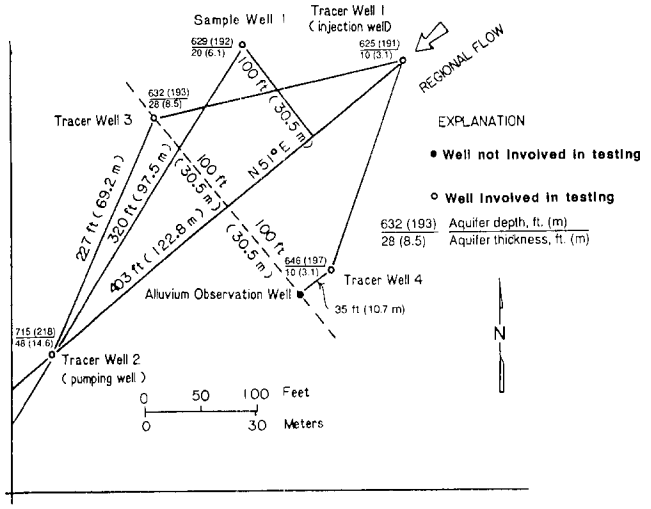

Fig. 3. Map showing locations of wells, aquifer depths, and thicknesses at Tracer Site.

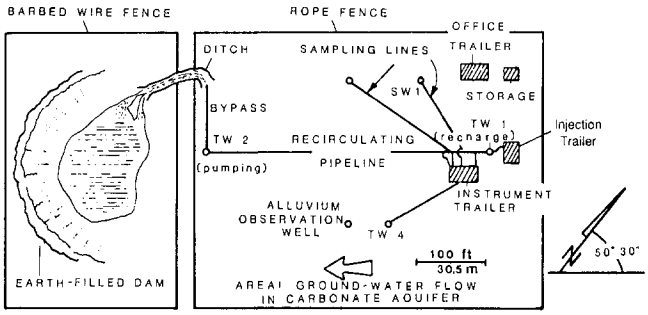

Fig. 4. Physical layout of Tracer Site (after Claassen and Cordes, 1975).

hydraulic gradient in order to minimize asymmetry of tracer flow paths caused by ambient ground-water flow. During tests reported here, samples were taken for analysis from the recirculating line downstream from Tracer Well 2; submersible pumps positioned within the aquifer were used for taking samples from Sample Well 1 and Tracer Well 3. All wells completely penetrated the aquifer and received water from only the aquifer.

Approach

Rectangular pulses (constant concentration over injection-time intervals) of tracer solution were injected into Tracer Well 1 during recirculation. Tracer-laden water was pumped from the sampling wells to automatic samplers in the Instrument Trailer (Figure 4). All pumps and samplers were activated automatically at preset times for sampling.

Breakthrough curves were constructed from analyses of effluent samples pumped from Tracer Well 2, taken from the recirculating pipeline downstream from the well. These curves were matched and compared to synthetic curves constructed for various combinations of porosity and dispersivity by the method of Grove (1971). Apparent dispersivities (characteristic lengths) of the aquifer were taken to be those of the best-fit synthetic curves, within an accuracy of ±3.0 m.

Three two-well recirculating tests were performed at the Tracer Site. The first, (Test 1, using tritium) was reported by Claassen and Cordes (1975). The second (Test 2, employing sulfur-35) and the third (Test 3, tritium and bromide together), were performed by the senior author of this paper. Test 3 was designed to: (1) mimic Test 1 as closely as possible to determine if multiple peaks on the Tracer Well 2 breakthrough curve could be obtained again, and (2) determine if the bromide ion could be used as a suitable surrogate for tritium in this aquifer.

Tritium and sulfur-35 were analyzed by liquid scintillation at the National Water Quality Laboratory of the U.S. Geological Survey, in Denver, Colorado, and decay corrected. Bromide was analyzed by neutron activation at the TRIGA reactor facility at the Pennsylvania State University. Data from all tests were analyzed, studied, and compared by Mai (1986) in order to determine any relation between recirculation rate and apparent dispersivity.

Theory of Two-Well, Recirculating Tracer Tests

Figure 5 shows a typical two-dimensional ground-water flow field of a two-well recirculating system in a homogeneous, isotropic aquifer, assuming negligible ambient regional velocity (Da Costa and Bennett, 1960; Webster et al., 1970). Each of the crescentic arcs can be visualized as a longitudinal dispersion column, and a tracer pulse added to the injection well will disperse longitudinally along the crescents. Assuming a constant hydraulic conductivity, the actual magnitude of longitudinal dispersion will depend upon the relative velocity of flow through each crescent. Transverse or lateral dispersion is not accounted for here and is not obtainable by this method.

The mathematical development of Grove's method for a homogeneous, isotropic aquifer, based on work in above references follows:

The Fickian model for one-dimensional longitudinal dispersion is given as

$$\partial C/\partial t = D_L\, \partial^2 C/\partial L^2 - U\partial C/\partial L \qquad (4a)$$

where L = distance along flow path; C = solute concentration; and t = time.

Boundary conditions are given as

$$C(O,t) = C_o \qquad t \geq O, \qquad (4b)$$

$$C(\infty,t) = O \qquad t \geq O; \qquad (4c)$$

and the initial condition as

$$C(L,O) = \qquad t \geq O. \qquad (4d)$$

Two solutions to equations (4) were given by Grove (1971), following Brenner (1962), as

$$C/Co = 1 - \exp[P(2-\bar{t})] \cdot \sum_{K=1}^{\infty} \frac{\lambda_k \sin(2\lambda_k)}{(\lambda_k^2 + P^2 + P)} \exp(-\lambda_k^2 \bar{t}/P), \qquad (5a)$$

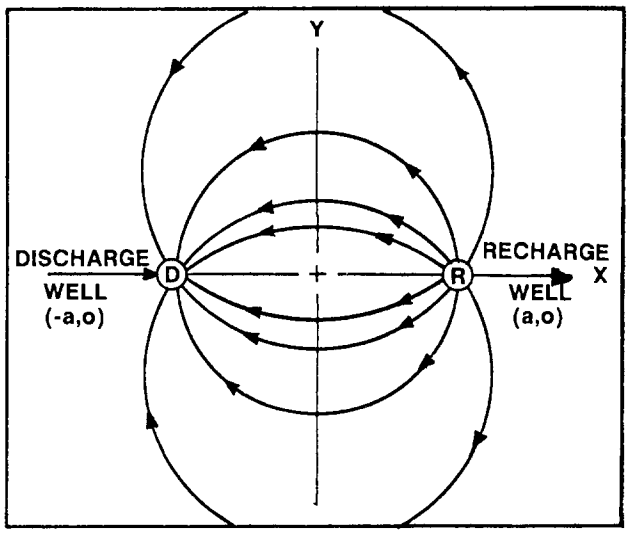

Fig. 5. Ground-water flow paths of an ideal, two-well, recirculating tracer test (after Grove and Beetem, 1971).

and

$$C/Co = \tfrac{1}{2}\mathrm{erfc}[(P/\bar{t})^{1/2}(1-\bar{t})] + (4P\bar{t}/\pi)^{1/2}[3 + 2P(1+\bar{t})]\exp[-P(1-\bar{t})^2/\bar{t}] - [\tfrac{1}{2} + 2P(3+4\bar{t}) + 4P^2(1+\bar{t})^2] \cdot \exp(4P)\,\mathrm{erfc}[(P/\bar{t})^{1/2}(1+\bar{t})] \quad (5b)$$

where Co = original concentration;

$$P = UL/4D_L, \text{ the Peclet Number;} \quad (6a)$$

which also can be written as

$$P = L/4\alpha_L \quad (6b)$$

because the dispersion coefficient is directly proportional to the velocity by a linear relationship when D* is small.

$\lambda_k = K^{th}$ positive root of the equation,

$$\tan 2\lambda = 2\lambda P(\lambda^2 - P^2); \quad (7)$$

$$\lambda_{2n-1} = \beta_n; \quad (8)$$

$$\lambda_{2n} = \gamma_n; \quad (9)$$

where β_n and γ_n are positive roots of the transcendental equations

$$\beta_n \tan \beta_n - P = 0 \text{ for } n \geq 1; \quad (10)$$

$$\gamma_n \cot \gamma_n + P = 0 \text{ for } n \geq 1; \quad (11)$$

$$\bar{t} = T/t, \text{ a dimensionless time variable;} \quad (12)$$

where T = time of interest. For computational purposes, Grove (1971) recommended use of equation (5a) when the value of P/t is less than 1.0 (when U is smaller or t is large), and equation (5b) otherwise. Both equations were used to generate a series of synthetic breakthrough curves for trial fitting to real breakthrough curves.

In Grove's actual computational procedure performed by computer, the two-well flow field was divided into 179 arcs, each of which was treated as a longitudinal dispersion column. For selected values of longitudinal dispersivity and porosity, a Peclet number and time of plug flow through each arc were computed for a particular pumping rate per unit aquifer thickness, porosity, and well spacing. Afterward, the relative concentration from each arc at a particular time was calculated and these relative concentrations were summed. This procedure was repeated for increasing values of time and a complete synthetic breakthrough curve was developed of concentration versus time.

Methodology and Results of the Three Tests

The potentiometric head of the aquifer is approximately 13.7 m below the ground surface and about 168 to 183 m above the top of the aquifer. Taking into account the overburden pressure of approximately 4.4 MPa exerted by both saturated and unsaturated materials above the aquifer, the ambient aquifer pore pressure was calculated to be 1.8 MPa, or 41 percent of the overburden pressure. During the tests, the pressure of actual injection (0.45 MPa) plus the pressure resulting from filling the casing of Tracer Well 1 with water to the land surface was added to the pore pressure in the aquifer at Tracer Well 1. As a result, the actual

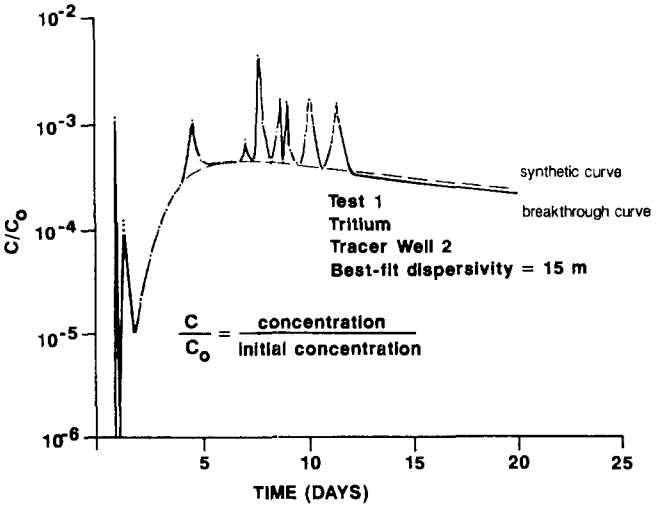

Fig. 6. Best-fit match of tritium breakthrough curve to synthetic curve: Tracer Well 2, Test 1 (after Claassen and Cordes, 1975).

pore pressures in the aquifer at Tracer Well 1 during the two-well recirculating tests were 2.2 MPa in Test 1, 2.4 MPa in Test 2, and 2.3 MPa in Test 3. These are 50, 55, and 52 percent, respectively, of overburden pressure; and 122, 133, and 128 percent, respectively, of ambient pore pressure.

During Test 1 the average recirculation rate was 22.5 L/s. The tracer pulse consisted of 14.1 Ci of tritiated water injected into Tracer Well 1 over a period of 14.4 minutes (0.01 day). The test lasted 30 days; a match of the breakthrough curve to synthetic curves (Figure 6) yielded an apparent dispersivity of 15 m and a porosity-thickness product of 0.88 m (Claassen and Cordes, 1975). Claassen and Cordes did not report thickness and porosity separately. Numerous sharp peaks are superimposed upon the base curve in this breakthrough curve and are discussed in the next section.

Test 2 ran for 38 days at an average recirculation rate of 13.7 L/s, the maximum that could be obtained for this test. Sulfur-35 in the form of sodium sulfate (Na_2SO_4) was injected into Tracer Well 1 over a 48-minute (0.03 day) time span at a constant rate. Apparent dispersivity of 22.9 m, porosity of 10 percent, and a porosity-thickness product of 0.84 m were the values obtained by fitting the breakthrough curve to a synthetic curve (Figure 7), but no sharp peaks

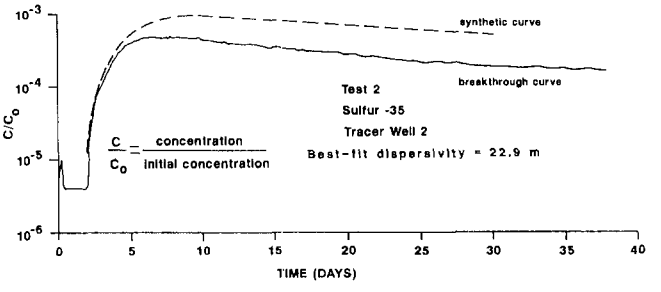

Fig. 7. Best-fit match of sulfur-35 breakthrough curve to synthetic curve: Tracer Well 2, Test 2.

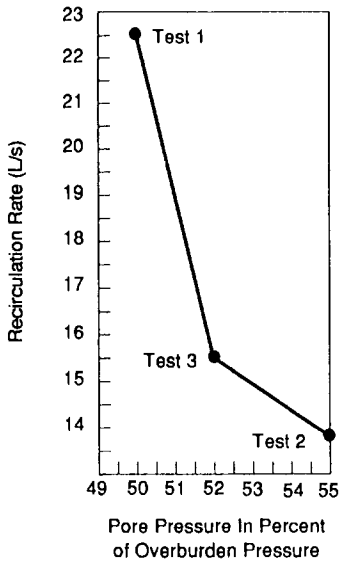

Fig. 8. Relation of recirculation rate to pore pressure in the three tests.

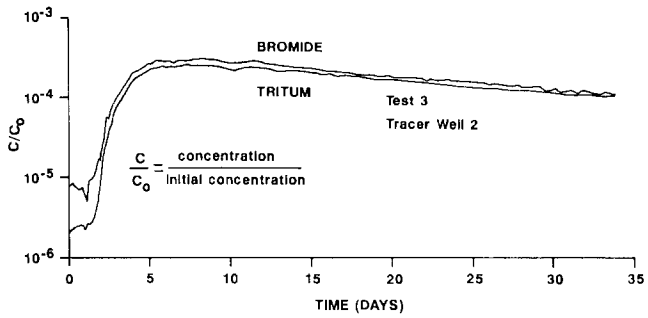

Fig. 9. Comparison of tritium and bromide breakthrough curves: Tracer Well 2, Test 3.

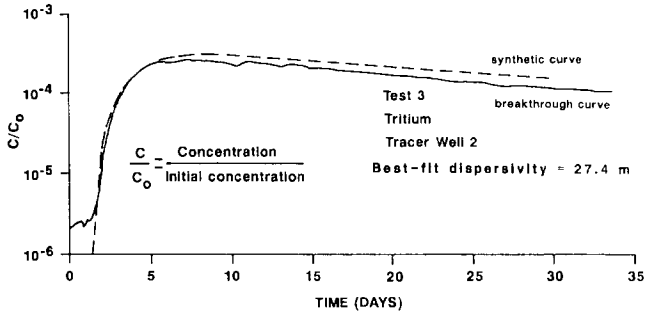

Fig. 10. Best-fit match of tritium breakthrough curve to synthetic curve: Tracer Well 2, Test 3.

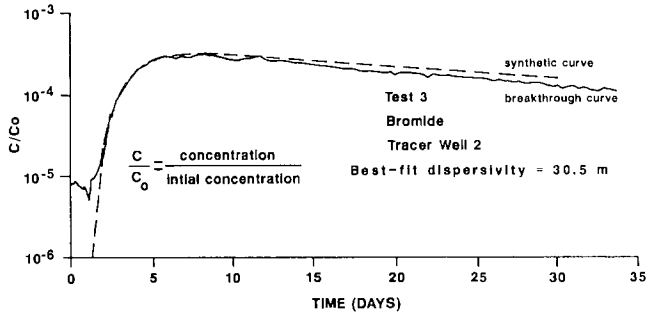

Fig. 11. Best-fit match of bromide breakthrough curve to synthetic curve: Tracer Well 2, Test 3.

were found as in Test 1. In Test 2, the recirculation rate was 39 percent less than in Test 1, but gave a computed apparent dispersivity 153 percent that of Test 1.

The low recirculation rate of Test 2 was believed to be the result of siltation in the aquifer immediately surrounding the borehole of Tracer Well 1, which reduced the hydraulic conductivity in the vicinity of the well. Subsequently, Tracer Well 1 was surged and pumped several times to clean out sediment and to increase its productivity. As a result, it was possible to perform Test 3 at a maximum recirculation rate of 15.5 L/s, but not at the earlier rate of 22.5 L/s of Test 1. An inverse relation of flow rate to pressure for the various tests was found (Figure 8).

Test 3 was run at a recirculation rate of 31 percent less than that of Test 1, but yielded a computed apparent dispersivity for tritium 83 percent greater than that determined by Test 1. The tritium pulse in Test 3 consisted of 12.2 Ci of tritiated water injected evenly over a period of 14.4 minutes (0.01 day). The bromide was also injected as a rectangular pulse of concentration versus time, over a period of 15.6 minutes, almost simultaneously with the tritium, and consisted of a solution of 414 kg of ammonium bromide (NH_4Br) in 860 liters of water. Breakthrough curves of the two tracers were nearly parallel (Figure 9); best-fit curve matching yielded apparent dispersivity of 27.4 m, porosity of 10 percent, and porosity-thickness product of 0.84 for tritium (Figure 10). The bromide curve fit yielded an apparent dispersivity of 30.5 m, porosity of 10 percent and porosity-thickness product of 0.84 (Figure 11). Neither curve showed sharp peaks for this test, which ran for 34 days. These results are summarized in Figure 12, which illustrates the inverse relationship between computed apparent dispersivity and recirculation rate in the case of tritium.

Examination of the closeness of fit of the breakthrough curves to synthetic curves in Tests 1, 2, and 3 (Figures 6, 7 and 10, and 11 respectively) shows how poorly the sulfur-35 data fit the closest synthetic curve. However, the tritium and bromide curves fit very closely.

The method of Grove (1971) used for breakthrough curve analysis for dispersivity was designed for application to only the breakthrough curve of the pumping well (Tracer Well 2 in this case). Therefore, breakthrough curves of Sample Well 1 and Tracer Well 3 could not be used for analysis and are not included. However, the arrival times of the breakthrough-curve peaks at these wells are plotted as functions of recirculation rate and pore pressure in Figures 13 and 14, respectively.

Sample Well 1 is located approximately 45 m from the injection well (Tracer Well 1). Tracer Well 3 is 70 m from

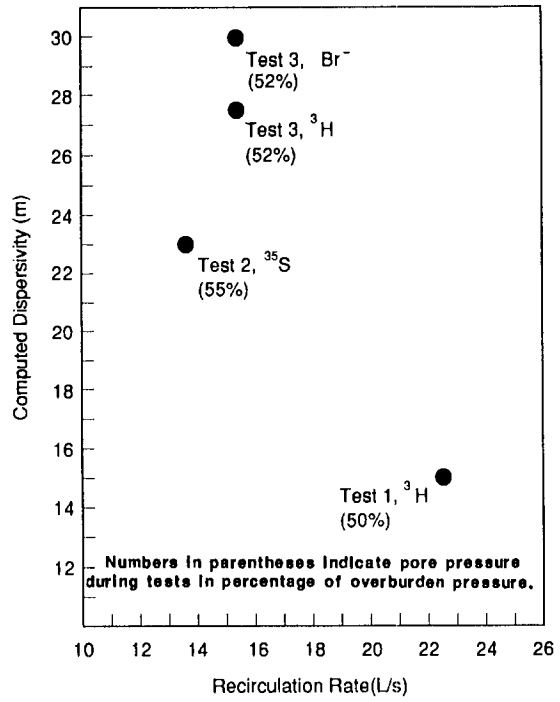

Fig. 12. Computed apparent dispersivity in each test versus recirculation rate of each test.

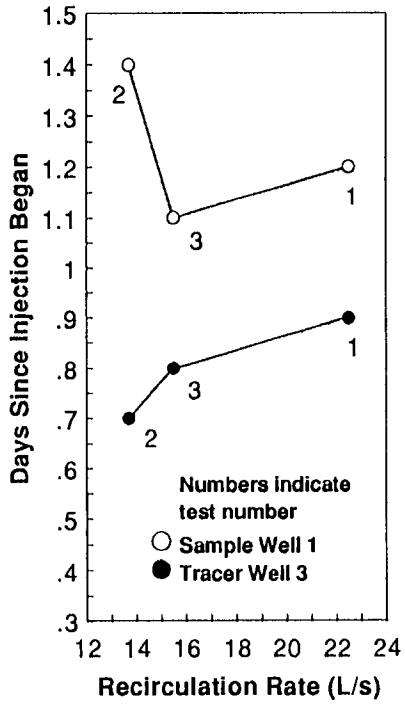

Fig. 13. Arrival times of breakthrough-curve peaks at Sample Well 1 and Tracer Well 3, versus recirculation rates during the three tests.

Tracer Well 1, or 1.6 times the distance of Sample Well 1. Yet, examination of Figures 13 and 14 reveals peak arrival times at Tracer Well 3 as much as 0.3 day earlier than at Sample Well 1 in Tests 1 and 3, and as much as 0.7 day earlier in Test 2.

Figure 13 shows a direct relationship between recirculation rate and peak arrival times at Tracer Well 3 in all three tests. The relationship for Sample Well 1 is inverse between Tests 2 and 3, and 2 and 1, but direct between Tests 3 and 1.

Figure 14 reveals for peak arrival times at Tracer Well 3, an inverse relationship with respect to pore pressure. In the case of Sample Well 1, the relationship is inverse between Tests 1 and 3, but direct between Tests 1 and 2, and also between tests 3 and 2.

The significance of all these relationships is discussed in the next section.

Interpretation and Discussion of Test Results

The most obvious relationship from the test results is the inverse relationship between apparent dispersivity and recirculation rate in the tritium tests, which is shown graphically in Figure 12. It is impossible to determine from only two tritium tests whether or not the relationship between computed apparent dispersivity and recirculation rate is linear at this site, but from observation of Figure 12 it is clear that neither the results of the sulfur-35 test (Test 2) nor bromide results of Test 3 fall on a straight line connecting the tritium results.

The relatively large difference in apparent dispersivity between the sulfur-35 and tritium tests is likely caused in large part by greater adsorption and/or retardation of the more active sulfate ion (SO_4^{--}) than that of either the

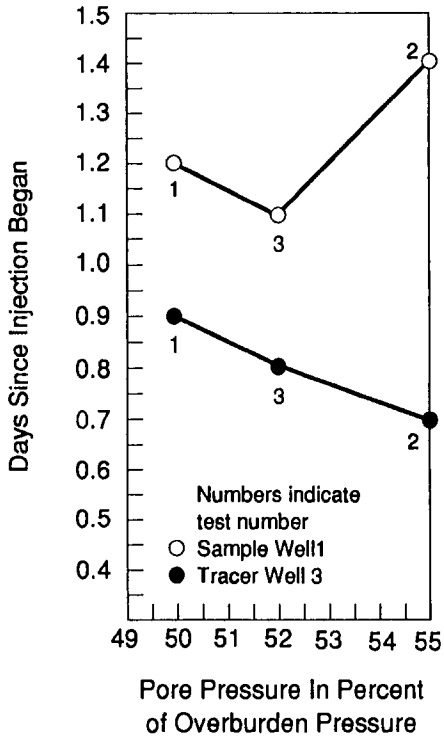

Fig. 14. Arrival times of breakthrough-curve peaks at Sample Well 1 and Tracer Well 3, versus pore pressures during the three tests.

bromide ion (Br^-) or tritiated water. Adsorption or retardation differences between tritium and bromide can explain the 10-percent difference in computed apparent dispersivity between the two tracers for the same recirculation rate in Test 3 (Figure 12). The analytical method of Grove (1971) used here assumes that no retardation or adsorption occurs; these phenomena, if real, probably cancel out when studying the relative change in apparent dispersivity with recirculation rate for two different tritium tests, as discussed below.

Explanation of Differences in Tritium-Test Dispersivities

The 83-percent increase in apparent tritium dispersivity concurrent with a decrease in recirculation rate of 31.3 percent between Tests 1 and 3 cannot be explained by sorption because the same tracer substance was used in both cases. If one assumes the classical independence of dispersivity from velocity, then a change in recirculation rate (and hence a change in advective velocity) cannot explain the dispersivity difference either, if the flow directions were the same in all three tests. However, a different flow regime with different advective transport should result in a different apparent dispersivity value.

The most likely explanation for the phenomenon, considering the discussion in the references earlier, is changes in the aquifer properties such as fissure-aperture width and hence, changes in hydraulic conductivity, local flow rates, and directions which were caused by differences in pore pressure between tests. If the ambient pore pressure of a fissured or fractured aquifer is already relatively high, then a slight artificial increase or decrease in testing pore pressure can cause small changes in aperture width and, thus, large changes in hydraulic conductivity.

High pore pressures during the tests, when compared to pressures reported in the earlier references, would likely be more than adequate to open or enlarge passageways less important under natural pressures and gradients, and therefore shunt ground-water flow in different directions at different flow rates from those of natural unstressed conditions.

It then is very probable that any hydraulic conductivity stratification, and consequent velocity stratification that exists under natural conditions, can be greatly altered by testing pressures. Lateral spreading as well as velocity and hydraulic conductivity stratifications were likely to have been altered significantly from one test to another by different pressures, causing the large difference in computed apparent dispersivities.

There appears to be direct physical evidence of this phenomenon from two observations. In the first place, the sharp peaks observed on the Tracer Well 2 breakthrough curve in Test 1 (Figure 6) do not appear on the curves of subsequent tests, probably indicating changes in transport directions and speeds from those of the first test (Figures 6, 7, 10, and 11). It is very probable that increasing pore pressures in later tests widened individual fissures and fractures that were important transport pathways in the first test, and which produced the spikes; additional fissures and fractures could have been opened wider so that the total effect of additional and/or wider pathways would have caused a smoothing of the breakthrough curves from the later tests.

Second, a direct fracture or fissure pathway seems evident between the injection well (Tracer Well 1) and Tracer Well 3 (Figure 3), for which arrival times of tracer-pulse peaks decreased with increasing pore pressures during the three tests (Figure 14). Such a pathway would likely be widened by increasing pore pressure.

The fact that peaks arrived at Tracer Well 3 before arriving at Sample Well 1 (Figures 13 and 14) which is much closer to the injection well, also strongly indicates such a direct pathway between Tracer Well 1 and Tracer Well 3 which is not apparent between Tracer Well 1 and Sample Well 1. The latter pathway is obviously more diffuse than the first.

The inverse-then-direct relationships between peak arrival times in Sample Well 1, and both recirculation rate and pore pressure (Figures 13 and 14) are not clear, unless they are related to the effects of surging and cleaning of Tracer Well 1 between Tests 2 and 3. This activity apparently affected the permeability of the pathway between the two wells.

Conclusions

1. Differences in computed apparent dispersivities for different recirculating tests with tritium were caused by differences in speed and directions of flow resulting from changes in pore pressure between one test and another, which in turn caused changes in aperture widths and thus in hydraulic conductivities.

2. This penomenon was especially pronounced in tests where the sum of ambient and testing pore pressures was a significant percent of the overburden pressure. More tests of this kind should be run at different pressures in order to determine the acceptable pressure range for accuracy.

3. For this reason, apparent dispersivities, determined by forced-gradient tests run under such high pressures, do not appear to be equivalent to the natural dispersivities existing under nonstressed conditions. In addition, natural changes in potentiometric-surface elevation, with consequent pore-pressure changes, can affect dispersivity over time. Therefore, solute-transport models of such systems, using dispersivity obtained in the above manner at excessive pressures, are likely to yield erroneous estimates of predicted solute-transport rates and concentrations.

Acknowledgments

The authors wish to thank the following for their assistance: **The U.S. Geological Survey:** Ren-Jen Sun, Hans Claassen, Bert Wier, Wayne Everett, James Nelson, William Smith, Charles Washington, Leonard Wollitz, for technical and field assistance; Vic Janzer, Leroy Schroeder, and Doug Manigold, for liquid-scintillation analysis. **The Pennsylvania State University**, School of Nuclear Engineering: William Jester and Dale Raupach, for neutron-activation analysis. **Purdue University**, Department of Earth and Atmospheric Sciences: Wanda Curtis, for typing; James Gardner, for editing; Giovanni Soto, for drafting.

The support of the Water Resources Division of the U.S. Geological Survey (with funding from the U.S. Department of Energy), and its permission to publish this paper are gratefully acknowledged.

"Contents of this publication do not necessarily reflect the views and policies of the U.S. Department of the Interior, nor does mention of trade names or commercial products constitute their endorsement by the U.S. Government."

References

Brenner, H. 1962. The diffusion model of longitudinal mixing in beds of finite length. Numerical values. Chem. Eng. Sci. v. 17, pp. 229-243.

Claassen, H. C. and E. H. Cordes. 1975. Two-well recirculating tracer test in fractured carbonate rock, Nevada. Hydrological Sciences Bulletin. v. xx, no. 3-9, pp. 367-382.

Cruz, P. T., E. F. Quadros, D. C. Fo, and H. Marrano. 1982. Evaluation of openings and hydraulic conductivity of rock discontinuities. In: Proceedings of 23rd Symposium on Rock Mechanics, AIME. pp. 769-777.

Da Costa, J. A. and R. R. Bennett. 1960. The pattern of flow in the vicinity of a recharging and discharging pair of wells in an aquifer having areal parallel flow. I.A.S.H. Committee on Subterranean Waters. Pub. no. 52, pp. 524-536.

Freeze, R. A. and J. A. Cherry. 1979. Groundwater. Prentice Hall, Inc. 604 pp.

Grove, D. B. 1971. An analysis of the flow field of a discharging-recharging pair of wells. U.S. Geological Survey Report 474-99. NTIS, Springfield, VA. 56 pp.

Grove, D. B. and W. A. Beetem. 1971. Porosity and dispersion constant calculations for a fractured carbonate aquifer using the two well tracer method. Water Resources Research. v. 7, no. 1, pp. 128-134.

Guinn, J. A., D. P. Kessler, and R. A. Greenkorn. 1972. The dispersion tensor in anisotropic porous media. Ind. Engr. Chem. Fundamentals. v. 11, no. 4, pp. 447-482.

Hull, L. C., J. D. Miller, and T. M. Clemo. 1987. Laboratory and simulation studies of solute transport in fracture networks. Water Resources Research. v. 23, no. 8, pp. 1505-1513.

Huyakorn, D. S. and D. F. Anderson. 1986. A curvilinear finite element model for simulating two-well tracer tests and transport in stratified aquifers. Water Resources Research. v. 22, no. 5, pp. 663-678.

Johnston, R. H. 1968. U.S. Geological Survey tracer study, Amargosa Desert, Nye County, Nevada, Part I: Exploratory drilling, tracer well construction and testing, and preliminary findings. U.S. Geological Survey Open File Report. 64 pp.

Louis, C. 1974. Introduction âl'hydraulique des roches. Bull. Bur. Rech. Geol. Min. Ser. 2, Sect. III, no. 4.

Mai, P. A. 1986. Estimating porosity and dispersivity of a fissured dolomitic aquifer with two-well recirculating tracer tests. Thesis B.S. degree with Honors, Purdue Univ., Dept. of Earth and Atmospheric Sciences. 42 pp. (unpublished).

Marsily, G. de. 1986. Quantitative Hydrogeology. Academic Press, Inc. 440 pp.

Molz, F. J., O. Güven, and J. G. Melville. 1983. An examination of scale-dependent dispersion coefficients. Ground Water. v. 21, no. 6, pp. 715-732.

Tsang, C. F., J. Noorishad, and P. A. Witherspoon. 1985. The effect of deformability on fluid flow through a fractured porous medium. In: I.A.H. Symposium Proceedings, Tucson. v. XVII, pp. 473-485.

Webster, D. S., J. F. Proctor, and I. W. Marine. 1970. Two-well tracer test in fractured crystalline rock. U.S. Geological Survey Water Supply Paper, 1544-I. 22 pp.

Witherspoon, P. A., J.S.Y. Wang, K. Iwai, and J. E. Gale. 1980. Validity of cubic law for fluid flow in a deformable rock fracture. Water Resources Research. v. 16, no. 6, pp. 1016-1024.

Wood, S. H., C. Wurts, T. Lane, N. Ballenger, M. Shalleen, D. Totorica, and C. Waag. 1985. Increased groundwater discharge caused by the 1983 Idaho earthquake. In: I.A.H. Symposium Proceedings, Tuscon. v. XVII, pp. 741-750.

* * * * *

Darrell I. Leap received the B.S., M.A., and Ph.D. degrees from Marshall, Indiana, and Penn State, respectively. He has worked for state and federal surveys in the areas of glacial geology, hydrogeology, ground-water tracing, and nuclear-waste isolation. He is presently an Associate Professor of Hydrogeology at Purdue University where he teaches and researches in the areas of hydrogeology, modeling, aquifer analysis, tracer studies, ground-water contamination, and hazardous-site assessment.

Pamela Mai Belmonte received the B.S. with Honors in Geology from Purdue University. She now resides in Plattsburg, New York, where she has assumed the very important roles of wife and mother.

U.S. Department of the Interior
U.S. Geological Survey

Inventory and Review of Aquifer Storage and Recovery in Southern Florida

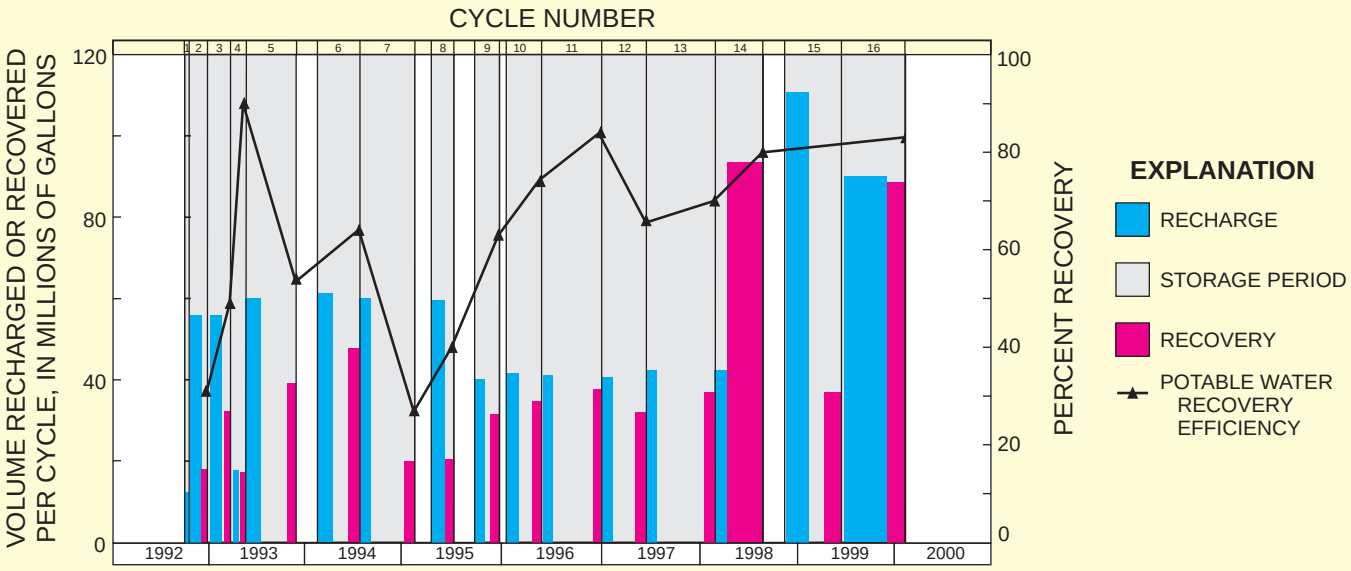

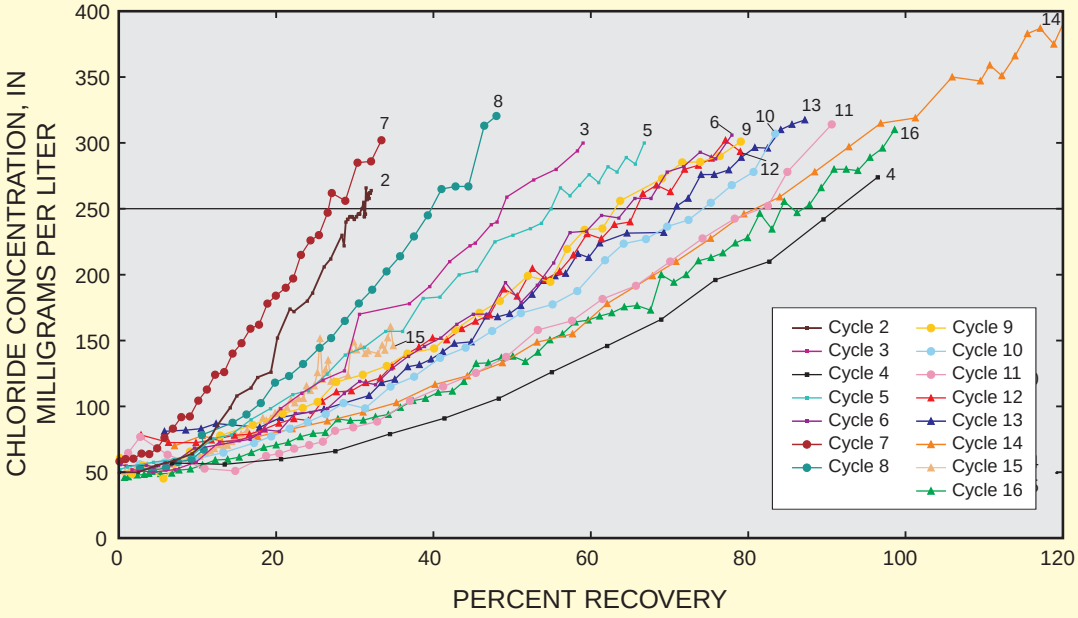

Water-Resources Investigations Report 02–4036

Prepared as part of the U.S. Geological Survey Place-Based Studies Program

Inventory and Review of Aquifer Storage and Recovery in Southern Florida

By Ronald S. Reese

U.S. GEOLOGICAL SURVEY
Water-Resources Investigations Report 02-4036

Prepared as part of the
U.S. GEOLOGICAL SURVEY PLACE-BASED STUDIES PROGRAM

Tallahassee, Florida
2002

U.S. DEPARTMENT OF THE INTERIOR
GALE A. NORTON, Secretary

U.S. GEOLOGICAL SURVEY
Charles G. Groat, Director

For additional information write to:

District Chief
U.S. Geological Survey
227 North Bronough Street
Suite 3015
Tallahassee, Florida 32301

Copies of this report can be purchased from:

U.S. Geological Survey
Branch of Information Services
Box 25286
Denver, CO 80225-0286

888-ASK-USGS

Additional information about water resources in Florida is available on the World Wide Web at
http://fl.water.usgs.gov

CONTENTS

FIGURES

TABLES

Conversion Factors, Vertical Datum, Abbreviations and Acronyms

Multiply	By	To Obtain
inch (in.)	25.4	millimeter
foot (ft)	0.3048	meter
mile (mi)	1.609	kilometer
gallon per minute (gal/min)	3.785	liter per minute
gallon per minute per foot (gal/min/ft)	12.418	liter per minute per meter
million gallons (Mgal)	3,785	cubic meter
million gallons per day (Mgal/d)	3,785	cubic meter per day
square feet per day (ft^2/d)	0.0929	square meter per day
square feet per day (ft^2/d)	7.48	gallon per day per foot
inverse day (1/d)	7.48	gallon per day per cubic foot

Sea level: In this report, “sea level” refers to the National Geodetic Vertical Datum of 1929 (NGVD of 1929)—a geodetic datum derived from a general adjustment of the first-order level nets of both the United States and Canada, formerly called Sea Level Datum of 1929.

ACRONYMS AND ADDITIONAL ABBREVIATIONS USED IN REPORT

ASR	aquifer storage and recovery
CERP	Comprehensive Everglades Restoration Plan
FDEP	Florida Department of Environmental Protection
FKAA	Florida Keys Aqueduct Authority
GPS	global positioning system
GWSI	Ground-Water Site Inventory (U.S. Geological Survey database)
µs/cm	microsiemens per centimeter
mg/L	milligrams per liter
MOR	monthly operating report
SFWMD	South Florida Water Management District
USGS	U.S. Geological Survey
WTP	Water Treatment Plant
WWTP	Wastewater Treatment Plant

Inventory and Review of Aquifer Storage and Recovery in Southern Florida

By Ronald S. Reese

Abstract

Aquifer storage and recovery in southern Florida has been proposed on an unprecedented scale as part of the Comprehensive Everglades Restoration Plan. Aquifer storage and recovery wells were constructed or are under construction at 27 sites in southern Florida, mostly by local municipalities or counties located in coastal areas. The Upper Floridan aquifer, the principal storage zone of interest to the restoration plan, is the aquifer being used at 22 of the sites. The aquifer is brackish to saline in southern Florida, which can greatly affect the recovery of the freshwater recharged and stored.

Well data were inventoried and compiled for all wells at most of the 27 sites. Construction and testing data were compiled into four main categories: (1) well identification, location, and construction data; (2) hydraulic test data; (3) ambient formation water-quality data; and (4) cycle testing data. Each cycle during testing or operation includes periods of recharge of freshwater, storage, and recovery that each last days or months. Cycle testing data include calculations of recovery efficiency, which is the percentage of the total amount of potable water recharged for each cycle that is recovered.

Calculated cycle test data include potable water recovery efficiencies for 16 of the 27 sites. However, the number of cycles at most sites was limited; except for two sites, the highest number of cycles was five. Only nine sites had a recovery efficiency above 10 percent for the first cycle, and 10 sites achieved a recovery efficiency above 30 percent during at least one cycle. The highest recovery efficiency achieved per cycle was 84 percent for cycle 16 at the Boynton Beach site.

Factors that could affect recovery of freshwater varied widely between sites. The thickness of the open storage zone at all sites ranged from 45 to 452 feet. For sites with the storage zone in the Upper Floridan aquifer, transmissivity based on tests of the storage zones ranged from 800 to 108,000 feet squared per day, leakance values indicated that confinement is not good in some areas, and the chloride concentration of ambient water ranged from 500 to 11,000 milligrams per liter.

Based on review of four case studies and data from other sites, several hydrogeologic and design factors appear to be important to the performance of aquifer storage and recovery in the Floridan aquifer system. Performance is maximized when the storage zone is thin and located at the top of the Upper Floridan aquifer, and transmissivity and salinity of the storage zone are moderate (less than 30,000 feet squared per day and 3,000 milligrams per liter of chloride concentration, respectively). The structural setting at a site could also be important because of the potential for updip migration of a recharged freshwater bubble due to density contrast or loss of overlying confinement due to deformation.

INTRODUCTION

Aquifer storage and recovery (ASR) in southern Florida has been proposed as a cost-effective water-supply alternative that can help meet the needs of agricultural, municipal, and recreational users and can be used for Everglades ecosystem restoration. Plans have been made to utilize ASR on an unprecedented scale

in the Central and Southern Florida Comprehensive Review Study as proposed by the U.S. Army Corps of Engineers and the South Florida Water Management District (1999). This review study is also known as the Comprehensive Everglades Restoration Plan (CERP). About 330 ASR wells have been proposed for southern Florida, each with an assumed capacity of 5 Mgal/d during recharge or recovery. Pyne (1995) has described ASR as "the storage of water in a suitable aquifer through a well during times when water is available, and recovery of the water from the same well during times when it is needed."

ASR technology has been tested and implemented in some areas of southern Florida; 26 ASR sites have been constructed and 1 is under construction (fig. 1 and table 1). The status for 10 of the sites is "operational testing," which is a multi-year period of regulatory review during the first phase of operation.

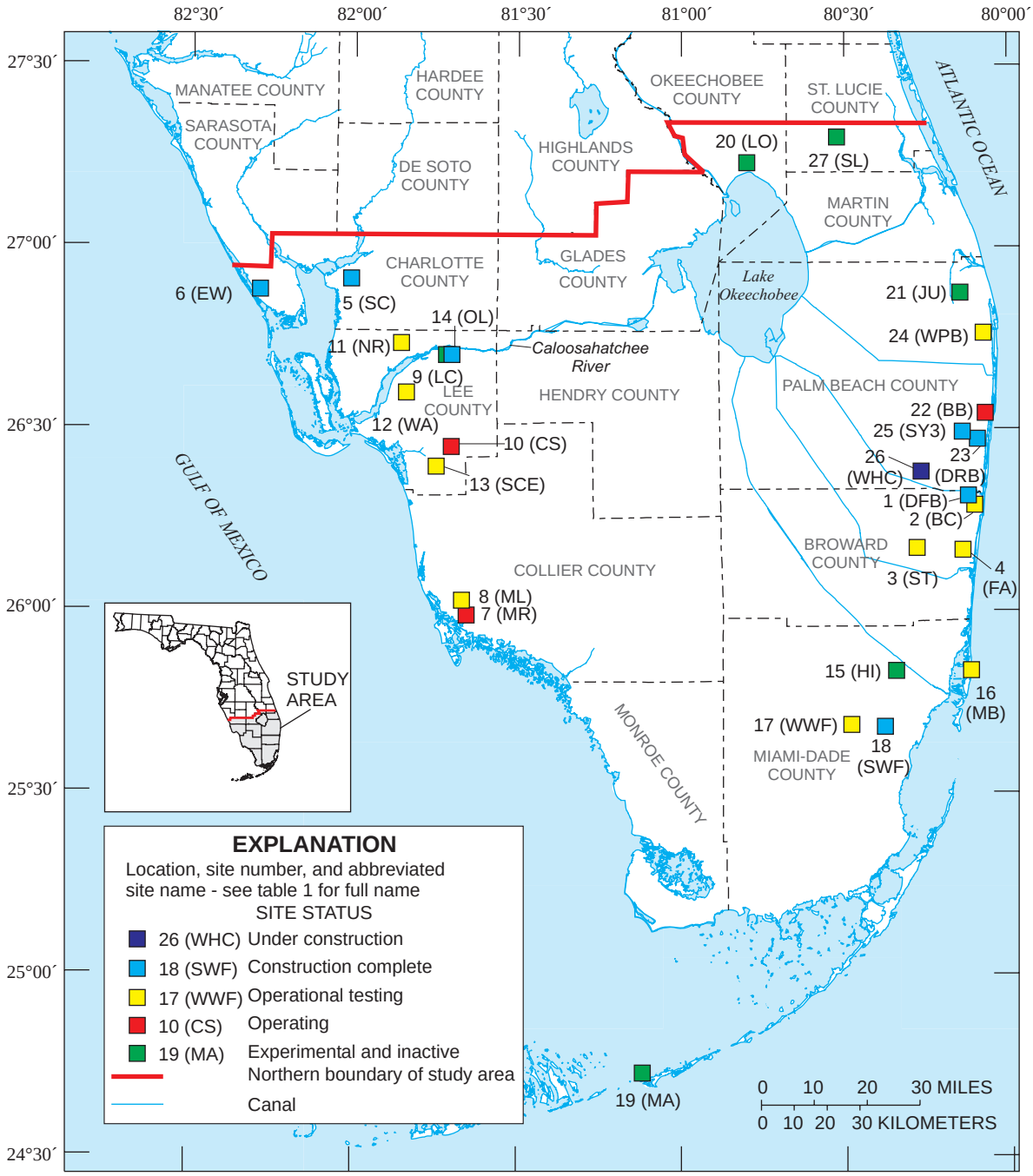

Figure 1. Study area and locations and status of aquifer storage and recovery sites. Status is as of April 2001.

Table 1. Historical and current aquifer storage and recovery sites in southern Florida

[County: B, Broward; CH, Charlotte; CO, Collier; L, Lee; MD, Miami-Dade; MO, Monroe; OK, Okeechobee; PB, Palm Beach; STL. St. Lucie. Utility or operator: BCOES, Broward County Office of Environmental Services; USGS, U.S. Geological Survey; LCRWSA, Lee County Regional Water Supply Authority; MDWSD, Miami-Dade Water and Sewer Department; FKAA, Florida Keys Aqueduct Authority; SFWMD, South Florida Water Management District; FDEP, Florida Department of Environmental Protection; PBCWUD, Palm Beach County Water Utilities Department. Storage zone aquifer: B, Biscayne aquifer; LFA, Lower Floridan Aquifer; MHA, mid-Hawthorn aquifer; SS, sandstone aquifer; UFA, Upper Floridan aquifer. Other abbreviations: WTP, water treatment plant; WWTP, wastewater treatment plant]

Site No.[1]	Site name and abbreviation	County	Utility or operator	Storage zone aquifer	Status	Source water	No. of injection wells	No. of monitoring wells in storage zone
1	Deerfield Beach West WTP (DFB)	B	Deerfield Beach	UFA	Construction complete	Treated drinking water	1	1
2	Broward County WTP 2A (BC)	B	BCOES	UFA	Operational testing	Raw ground water	1	1
3	Springtree WTP (ST)	B	Sunrise	UFA	Operational testing	Treated drinking water	1	0
4	Fiveash WTP (FA)	B	Fort Lauderdale	UFA	Operational testing	Treated drinking water (future raw ground water)	1	1
5	Shell Creek WTP (SC)	CH	Punta Gorda	UFA	Construction complete	Treated drinking water	1	0
6	Englewood South Regional WWTP (EW)	CH	Englewood Water District	UFA	Construction complete	Reclaimed water	1	1
7	Manatee Road (MR)	CO	Collier County	MHA	Operating	Treated drinking water	1	3
8	Marco Lakes (ML)	CO	Florida Water Services	UFA	Operational testing	Partially treated surface water	3	2
9	Lee County WTP (LC)	L	USGS	UFA	Experimental and inactive	Raw and treated surface water	1	2
10	Corkscrew WTP (CS)	L	LCRWSA	MHA	Operating	Treated drinking water	5	5
11	North Reservoir (NR)	L	Lee County	UFA	Operational testing	Treated drinking water	1	1
12	Winkler Avenue (WA)	L	Fort Myers	UFA	Operational testing	Treated drinking water	1	1
13	San Carlos Estates (SCE)	L	Bonita Springs	UFA	Operational testing	Treated drinking water	1	1
14	Olga WTP (OL)	L	Lee County	UFA	Construction complete	Treated drinking water	1	2
15	Hialeah (HI)	MD	USGS	UFA	Experimental and inactive	Raw ground water	1	1

Table 1. Historical and current aquifer storage and recovery sites in southern Florida --(Continued)

[County: B, Broward; CH, Charlotte; CO, Collier; L, Lee; MD, Miami-Dade; MO, Monroe; OK, Okeechobee; PB, Palm Beach; STL. St. Lucie. Utility or operator: BCOES, Broward County Office of Environmental Services; USGS, U.S. Geological Survey; LCRWSA, Lee County Regional Water Supply Authority; MDWSD, Miami-Dade Water and Sewer Department; FKAA, Florida Keys Aqueduct Authority; SFWMD, South Florida Water Management District; FDEP, Florida Department of Environmental Protection; PBCWUD, Palm Beach County Water Utilities Department. Storage zone aquifer: B, Biscayne aquifer; LFA, Lower Floridan Aquifer; MHA, mid-Hawthorn aquifer; SS, sandstone aquifer; UFA, Upper Floridan aquifer. Other abbreviations: WTP, water treatment plant; WWTP, wastewater treatment plant]

Site No.[1]	Site name and abbreviation	County	Utility or operator	Storage zone aquifer	Status	Source water	No. of injection wells	No. of monitoring wells in storage zone
16	Miami Beach (MB)	MD	Miami Beach	B	Operational testing	Treated drinking water	1	Unknown
17	West Well Field (WWF)	MD	MDWSD	MHA, UFA	Operational testing	Raw ground water	3	1
18	Southwest Well Field (SWF)	MD	MDWSD	UFA	Construction complete	Raw ground water	2	0
19	Marathon (MA)	MO	FKAA	SS	Inactive	Treated drinking water	1	1
20	Taylor Creek/Nubbin Slough (Lake Okeechobee) (LO)	OK	SFWMD	LFA	Experimental and inactive	Raw surface water	1	1
21	Jupiter (JU)	PB	FDEP	UFA	Experimental and inactive	Raw surface water	1	1
22	Boynton Beach East WTP (BB)	PB	Boynton Beach	UFA	Operating	Treated drinking water	1	0
23	Delray Beach North Storage Reservoir (DRB)	PB	Delray Beach	UFA	Construction complete	Treated drinking water	1	0
24	West Palm Beach WTP (WPB)	PB	West Palm Beach	UFA	Operational testing	Treated surface water (future raw surface water)	1	1
25	System 3 Palm Beach County (SY3)	PB	PBCWUD	UFA	Construction complete; waiting on permit	Treated drinking water (future raw ground water)	1	1
26	Western Hillsboro Canal, Site 1 (WHC)	PB	SFWMD	UFA	Under construction	Not yet determined	1	1
27	St. Lucie County (SL)	STL	SFWMD	UFA	Experimental and inactive	Raw ground water	1	2

[1] Site numbers refer only to this report. Site locations are shown in figure 1.

During this time, the ASR well system is tested prior to being given a full operating permit by the Florida Department of Environmental Protection (FDEP). Three of the sites have been given an operating permit. Additionally, six sites are no longer active after experimental testing was completed (fig. 1). These sites were operated by government agencies including the U.S. Geological Survey (USGS), South Florida Water Management District (SFWMD), FDEP, and the Florida Keys Aqueduct Authority (FKAA). ASR is a relatively recent development in southern Florida, in terms of its use as a municipal or countywide source of water; 20 active sites in this category were constructed in the 1990's (with 14 of these sites having been constructed since 1996). The strategy for this use of ASR in southern Florida has been to store excess water available during the wet season and recover this water during the dry season when it is needed.

Existing and historical ASR sites in southern Florida are mostly located along the east and west coasts (fig. 1). At most sites, the proposed or planned purpose of the recovered water is to serve as a supplemental supply for municipalities. Under CERP, ASR wells will be constructed in inland areas around Lake Okeechobee, in central Palm Beach County, and along the Caloosahatchee River in Hendry County (U.S. Army Corps of Engineers and South Florida Water Management District, 2001). Recovered water is to be used for additional purposes that include maintaining water levels in Lake Okeechobee and wetland areas and reduction of surface-water flows to tide (estuarine and bay areas) during storm events.

The storage zone being used at most ASR sites is in the Floridan aquifer system (fig. 2). Shallower storage zones are in the mid-Hawthorn and sandstone aquifers of the intermediate aquifer system and the Biscayne aquifer of the surficial aquifer system. The proposed storage zone aquifer in the CERP ASR program is also in the Floridan aquifer system. This aquifer system is continuous throughout southern Florida, and its overlying confinement is generally good.

ASR wells are evaluated and operated through a cyclical process. Each cycle includes periods of injection (recharge) of freshwater into the ASR well, storage, and then withdrawal (recovery) with each period lasting days or months. In southern Florida, the recovery phase may commence immediately after the cessation of recharge with no period of storage, and depending on the source of water supply, municipal supply, or operational problems, the time between cycles may be extensive (months or years). After initial testing and under fully operational conditions, cycles continue but the duration of cycles and storage periods and the volume of water recharged during each cycle usually increase.

In southern Florida, ASR is largely used to store water in an aquifer that contains brackish water. Ambient ground water in the storage zone at most of the ASR sites in the study area is brackish (greater than 1,000 mg/L dissolved-solids concentration) to saline (greater than 10,000 mg/L dissolved-solids concentration); salinity appears to greatly affect the recovery of the recharged freshwater. The salinity of the recharged and recovered water is closely monitored, usually on a daily basis. Because of the high ambient water salinity of the storage zone, much of the recharged freshwater is not recovered largely due to dispersive mixing in the aquifer.

The recovery efficiency for each cycle is the total volume of water recovered, expressed as a percentage of the volume of water recharged. The salinity of water during recovery increases with time, and recovery is terminated at a salinity level that is predetermined by operational considerations. Generally, this limiting salinity level is at the potable water limit of 250 mg/L chloride concentration, or slightly higher if the recovered water is mixed with potable water at a water-treatment plant (WTP).

Few regional investigations of the hydrogeology of the Floridan aquifer system in southern Florida have been conducted, and those studies focused on issues unrelated to ASR. Lacking a regional ASR framework to aid the decision-making process, placement of ASR well sites in southern Florida have primarily been based on factors such as land availability, source-water proximity (preexisting surface-water canal systems or surficial aquifer system well fields), or proximity to a WTP. Little effort has been made to link information collected from each site into a regional hydrogeologic analysis. Additional tools and data are needed to make informed decisions that incorporate constraining hydrogeologic factors in the placement and construction of ASR sites in southern Florida.

This study is part of the USGS South Florida Place-Based Studies Program, which was established for the purpose of providing physical and biological science data and information on which to base ecosystem restoration management decisions. The purpose of

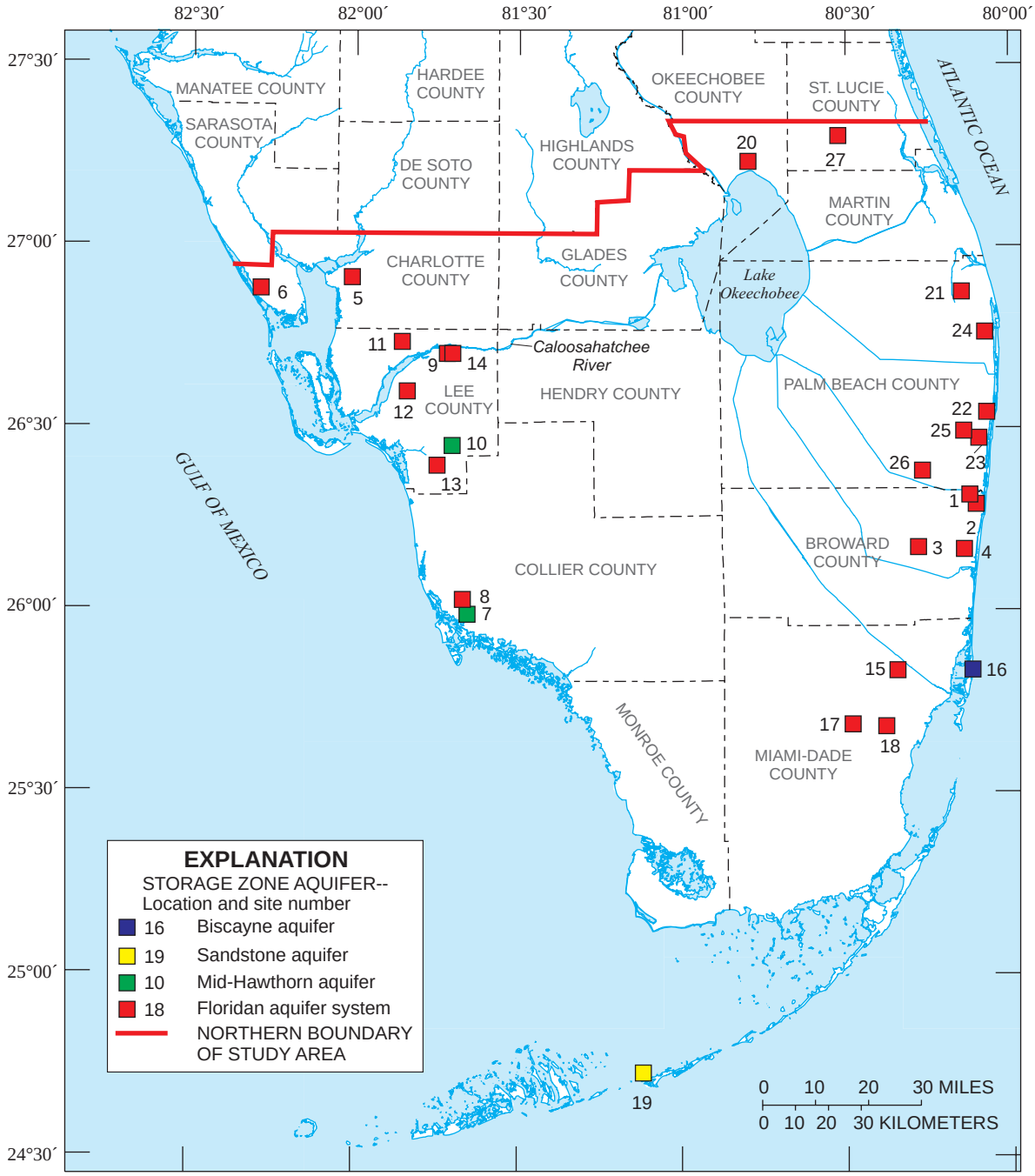

Figure 2. Storage zone aquifers for aquifer storage and recovery sites in southern Florida.

this study was to compile data on existing ASR sites in southern Florida and identify various hydrogeologic, design, and management factors that control the recovery of freshwater recharged into ASR wells.

Purpose and Scope

The purpose of this report is to inventory well construction, hydrogeologic, and operational data on ASR sites in southern Florida and assess site performance. A secondary purpose is to identify hydrogeologic, design, or management factors that influence the success of ASR. Recovery efficiency, defined as the percent of recharged freshwater that is recovered for each cycle, is used to evaluate this performance. Four ASR case studies are described to determine possible technical factors that influence the success of ASR.

The study area includes all of southern Florida and includes Charlotte, Glades, Lee, Hendry, Collier, Monroe, Miami-Dade, Broward, Palm Beach, and Martin Counties, and parts of Okeechobee and St. Lucie Counties (fig. 1). The 27 ASR sites located in the study area represent the source of data for this study. However, this report focuses on the 23 ASR sites in which the Floridan aquifer system serves as the storage zone. Principal hydrogeologic and construction related attributes determined for each ASR site are graphically and spatially illustrated to provide a comparative analysis.

Previous Studies

It has been nearly 20 years since Merritt and others (1983) provided a retrospective overview and status of ASR well development in southern Florida. Merritt and others (1983) presented data from three experimental ASR sites that are also included in this report, and Meyer (1989b) published additional data on experimental ASR sites in southern Florida. Other experimental ASR test data were obtained in reports or written communications for the Jupiter site (fig. 1, map no. 21; J.J. Plappert, Florida Department of Environmental Protection, written commun., 1977), the St. Lucie County site (fig. 1, map no. 27; Wedderburn and Knapp, 1983), the Lee County site (fig. 1, map no. 9; Fitzpatrick, 1986), the Hialeah site (fig. 1, map no. 15; Merritt, 1997), and the Taylor Creek/Nubbin Slough – Lake Okeechobee site (fig. 1, map no. 20; Quiñones-Aponte and others, 1996). Theoretical investigations into the feasibility of cyclic injection of freshwater in southern Florida have been described in reports by Khanal (1980) and Merritt (1985). Merritt (1997) also included numerical simulations of the salinity of recovered water in his study of Hialeah ASR site.

Some regional or local hydrogeologic studies of the Upper Floridan aquifer that encompass or include part of southern Florida are Bush and Johnston (1988), Meyer (1989a), Miller (1986), Reese (1994), Reese (2000), and Reese and Memberg (2000). The reports by Meyer (1989a), Reese (1994; 2000), and Reese and Memberg (2000) are specific to southern Florida.

Factors Affecting Optimal Recovery of Freshwater in Aquifer Storage and Recovery

Recovery of freshwater stored in brackish- to saline-water aquifers is controlled by a wide variety of factors that pertain to hydrogeologic conditions, well or well field design, and operational management. The hydrogeologic factors of a storage zone that are important to recoverability include (1) ambient salinity, (2) aquifer permeability and distribution, (3) aquifer thickness, (4) confinement, (5) ambient hydraulic gradient, and (6) structural setting. Important design and management factors to consider are (1) thickness and location of the storage zone within the aquifer, (2) volume of injected water, (3) duration and frequency of cycles and cycle storage periods, (4) well performance problems such as wellbore plugging, and (5) multiple-well configurations. Most of these factors and their control on recoverability have been numerically simulated (Merritt and others, 1983; Merritt, 1985); however, conclusions on some factors, 95 discussed in the following sections, came from consulting reports and other literature.

Hydrogeologic Factors

During recharge of water by an ASR well, a radial zone of mixing forms around the well in the aquifer. This zone, referred to as the transition zone (Merritt, 1985), separates native water from an inner flushed zone containing mostly injected water, and this inner zone can be described as a freshwater bubble

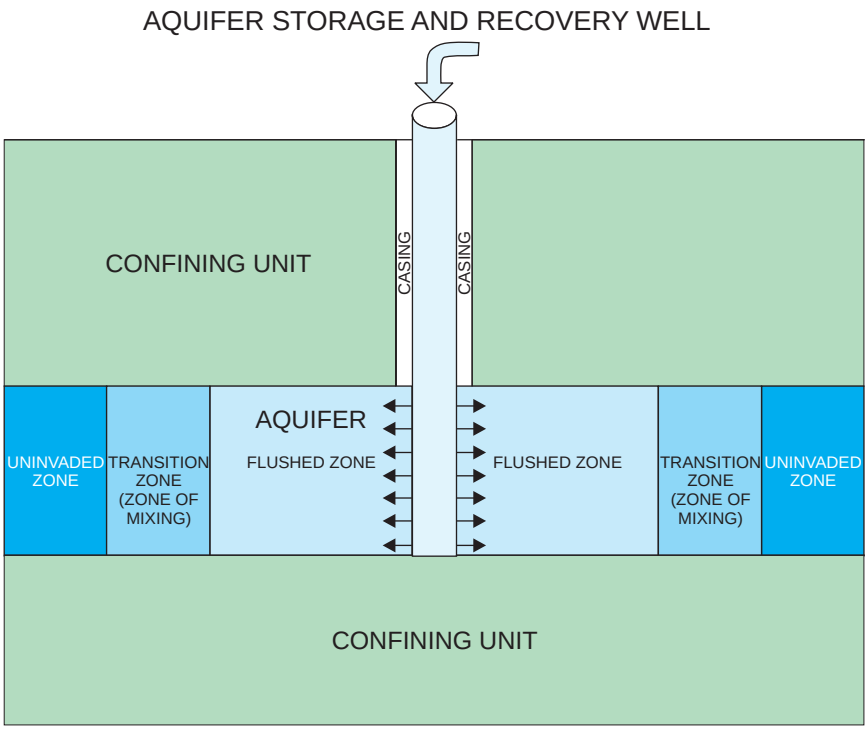

Figure 3. Aquifer storage and recovery well in a confined aquifer depicting idealized flushed and transition zones created by recharge. Flushed zone contains mostly recharged water.

(fig. 3). The degree of mixing between the injected and native water and the width of the transition zone is primarily controlled by hydrodynamic dispersion. Hydrodynamic dispersion or dispersive mixing refers to the effects of molecular diffusion and mechanical dispersion. Mechanical dispersion results from the unevenness of flow through porous media, and at flow velocities occurring during ASR recharge and recovery, this dispersion will dominate over diffusion.

The ambient salinity of water in the storage zone is of primary importance in controlling recovery of freshwater because of mixing with this water and potential buoyancy stratification. Buoyancy stratification occurs where the ambient salinity is high, provided permeability in the aquifer is also high (Merritt, 1985); the injected freshwater moves upward and flows out over the native ground water. During the recovery phase, such stratification increases mixing. Buoyancy stratification should be considered possible when the ambient ground water has a dissolved-solids concentration greater than 5,000 mg/L (Pyne, 1995); in the Floridan aquifer system of southern Florida this equates to about 2,500 mg/L chloride concentration (Reese, 1994). On the basis of numerical simulation, recovery efficiency has been shown to decrease with increasing salinity in saline aquifers only because of dispersive mixing in the transition zone – no buoyancy stratification (Merritt, 1985). Ambient water salinities modeled in Merritt's study, as defined by chloride concentration, were 2,000, 7,000 to 8,000, and 19,000 mg/L (seawater-like salinity).

The permeability or hydraulic conductivity of the storage zone may greatly affect recoverability. The probability of buoyancy stratification increases as permeability increases (Merritt, 1985). Additionally, mechanical dispersion is related to the distribution of permeability within the storage zone. Higher permeability can equate to higher dispersive mixing, and an increase in this dispersion lowers recovery efficiency (fig. 3). Thus, recovery could be better in a sand aquifer of uniform permeability where dispersion results primarily from flow through intergranular pore spaces, as opposed to a limestone aquifer having diffuse and conduit flow components, particularly if thin zones of high permeability occur within the limestone aquifer.

Loss of injected freshwater could occur if a storage zone is not well confined. Injected water may move upward or downward out of the storage zone, or saline water may move up into the storage zone during recovery.

Recovery efficiency is greater in a thin aquifer than in a thick aquifer because of the lower vertical extent of the transition zone along which mixing occurs. However, this effect can be partially offset by increasing the volume of water recharged during a cycle. Minimizing the thickness of the storage zone within a thick aquifer can also be beneficial depending on the aquifer's distribution of vertical hydraulic conductivity.

Downgradient movement of a bubble of recharged water due to the background hydraulic gradient could reduce recovery efficiency. Based on an estimated gradient at the Hialeah ASR site in the Upper Floridan aquifer, reduction in recovery due to this effect was simulated to be minor for a storage period of 6 months, but not for 5 years (Merritt and others, 1983). The average velocity of ambient flow, referred to as the average linear velocity, is a function of both hydraulic conductivity and porosity as well as the background hydraulic gradient (Freeze and Cherry, 1979).

The structural setting of the storage zone at an ASR site could be important to recovery (Water Resources Solutions, Inc., 1999a). Freshwater recovery at a site located in an area that is structurally high or where the dip is low could be more favorable than in an area that is in a structural depression or where the dip is relatively high due to the tendency of the bubble of recharged water to move updip because of buoyancy forces. This factor is likely to be more important as the contrast in salinity and fluid density increases. Structural deformation may influence storage zone confinement due to fracturing, faulting, or vertical dissolution features.

Design and Management Factors

The location of the storage zone relative to the aquifer may be important. If a storage zone extends over only a portion of an aquifer's thickness, this could negatively affect recovery. Merritt (1985) simulated recovery in a case where the ASR storage zone extended only over the lower part of the important flow zone (zone with high permeability) near the top of the Upper Floridan aquifer. Results indicated that recovery efficiency was virtually unaffected compared to the case with the well open to the full thickness of the zone. However, the low ambient salinity (1,200 to 1,300 mg/L chloride concentration) and the moderate hydraulic conductivity values that were used in the simulation prevented any appreciable buoyancy effects from occurring (effects that could cause vertical flow and mixing to increase).

The volume of injected water affects the recovery efficiency. On a per cycle basis, recovery efficiency generally increases as the total volume of injected water increases (Merritt, 1985). However, the effect is much less beneficial when interlayer dispersion (the transverse dispersion between layers of differing hydraulic conductivity in the aquifer) increases. Interlayer dispersion causes mixing between injected and ambient waters in addition to the mixing in the transition zone.

Recovery efficiency increases with repeated cycles. Twelve successive cycles of injection and recovery, with recovery of up to only 250 mg/L chloride concentration for each cycle, were simulated for a variety of longitudinal and transverse dispersivity coefficients. Recovery efficiency improved substantially for all cases with repeated cycles, but the rate of improvement diminished with increasing cycles (fig. 4). Recovery efficiency improves with repeated cycles because much of the recharged water from a previous cycle is left in the aquifer, and during the next cycle, recharged water mixes with water of a lower salinity.

Well plugging can occur during recharge in the Upper Floridan aquifer, reducing the recharge rate and freshwater recovery. This plugging is usually caused by deposition of particulate matter in the injected water or by the formation of a precipitate or sludge caused by reactions that occur at the wellbore face or in the aquifer. One method used to restore formation injectivity is periodic backflushing of the well during the recharge phase. At the Hialeah site, well backflushing produced very fine particles of calcite and an iron compound that had precipitated (Merritt, 1997). Plugging at the Lee County site is attributed to suspended material in the injected water and bacteriological growth at the open borehole face (Fitzpatrick, 1986). Well plugging may affect one flow zone in an open-hole interval more than another, reducing overall recovery. During recovery, the less affected zone contributes most of the flow, and the salinity of water from this zone exceeds the limiting salinity level before all the recoverable freshwater from the plugged zone is obtained.

Various numbers and configurations of multiple storage wells at a site were modeled by Merritt (1985). In that study, the number of wells were varied from one to nine, and the well patterns were varied from a linear array to eight wells in an octagonal pattern with an additional well in the center. Greatest recovery efficiencies were attained in arrays consisting of a central well surrounded by perimeter wells. Though in all cases, the recovery efficiencies for the multiple-well configurations were no better than the single-well case injecting the same total volume as the array of wells. Recovery efficiency could improve, however, when the total volume injected increases as the number of wells injecting at a site increases.

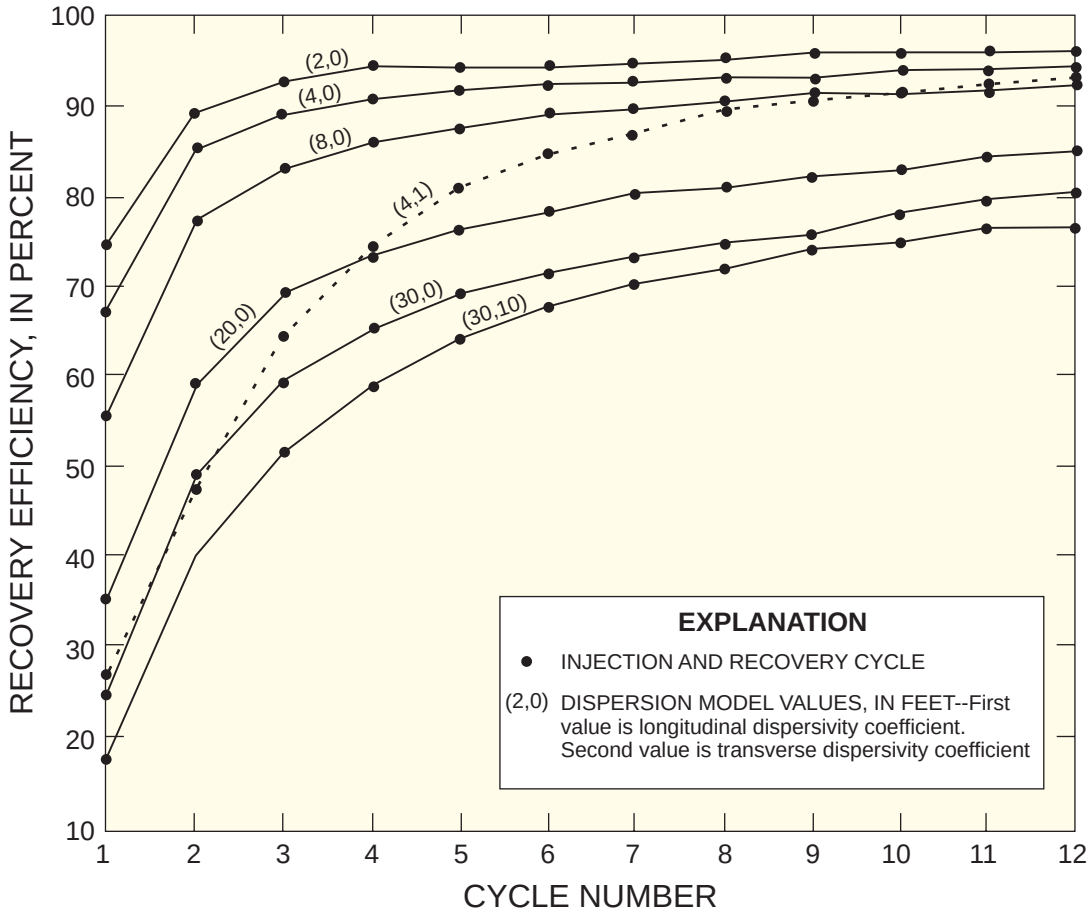

Figure 4. Simulated improvement of potable water recovery efficiency with successive injection and recovery cycles for a variety of dispersion models. The Upper Floridan aquifer at the Hialeah aquifer storage and recovery site was used in the design of the model (modified from Merritt, 1985).

Hydrogeology

The three principal hydrogeologic units in southern Florida are the surficial, intermediate, and Floridan aquifer systems. These aquifer systems in the western part of the study area (Lee, Hendry, and Collier Counties) are described in figure 5. Water-bearing rocks in the intermediate aquifer system grade or pinch out to the east, and in southeastern Florida the intermediate aquifer system becomes the intermediate confining unit. The Floridan aquifer system consists of the Upper Floridan aquifer, middle confining unit, and Lower Floridan aquifer. Three of the aquifers used for ASR in southern Florida are shown in figure 5; namely, the sandstone and mid-Hawthorn aquifers of the intermediate aquifer system and the Upper Floridan aquifer.

The Upper Floridan aquifer is 500 to 1,200 ft thick in southern Florida (fig. 5; Reese, 1994 and Reese and Memberg, 2000). This aquifer is well confined above by thick units in the Hawthorn Group consisting of clay, marl, silt, or clayey sand; hydraulic head in the aquifer is above land surface. The middle confining unit of the Floridan aquifer system underlies the Upper Floridan aquifer and provides good to leaky confinement. This confining unit consists of micritic limestone (wackstone to mudstone), dense dolomite, and in some areas, beds of gypsum (fig. 5). The upper and lower boundaries of the middle confining unit are difficult to define, but its thickness has been estimated to range from 500 to 800 ft in southwestern Florida.

In southwestern Florida, the Upper Floridan aquifer includes the lower part of the Hawthorn Group, Suwannee Limestone, Ocala Limestone, and in some areas, the upper part of the Avon Park Formation (fig. 5). In southeastern Florida, the Suwannee Limestone and Ocala Limestone are commonly absent (Reese, 2000; Reese and Memberg, 2000). In both eastern and western areas, the top of the Upper Floridan aquifer usually is contained within a basal

Series		Geologic Unit		Approximate thickness (feet)	Lithology	Hydrogeologic unit		Approximate thickness (feet)
HOLOCENE TO PLIOCENE		UNDIFFERENTIATED		0-70	Quartz sand, silt, clay, and shell	SURFICIAL AQUIFER SYSTEM	WATER-TABLE AQUIFER	20-100
		TAMIAMI FORMATION		0-175	Silt, sandy clay, micritic limestone, sandy, shelly limestone, calcereous sandstone, and quartz sand		CONFINING BEDS	0-60
							LOWER TAMIAMI AQUIFER	25-160
MIOCENE AND LATE OLIGOCENE		HAWTHORN GROUP	PEACE RIVER FORMATION	50-400	Interbedded sand, silt, gravel, clay, carbonate, and phosphatic sand	INTERMEDIATE AQUIFER SYSTEM	CONFINING UNIT	20-100
							SANDSTONE AQUIFER	0-100
							CONFINING UNIT	10-250
			ARCADIA FORMATION	400-550	Sandy limestone, shell beds, dolomite, phosphatic sand and carbonate, sand, silt, and clay		MID-HAWTHORN AQUIFER	0-130
							CONFINING UNIT	100-400
EARLY OLIGOCENE		SUWANNEE LIMESTONE		0-600	Fossiliferous, calcarenitic limestone	FLORIDAN AQUIFER SYSTEM	LOWER HAWTHORN PRODUCING ZONE	0-300
EOCENE	LATE	OCALA LIMESTONE		0-400	Chalky to fossiliferous, calcarenitic limestone		UPPER FLORIDAN AQUIFER	700-1,200
	MIDDLE	AVON PARK FORMATION		900-1,200	Fine-grained, micritic to fossiliferous limestone, dolomitic limestone, dense dolomite, and gypsum		MIDDLE CONFINING UNIT	500-800
		?—		—?				
	EARLY	OLDSMAR FORMATION		800-1,400			LOWER FLORIDAN AQUIFER	1,400-1,800
							BOULDER ZONE	400
PALEOCENE		CEDAR KEYS FORMATION		500-700	Dolomite and dolomitic limestone			
				1,200?	Massive anhydrite beds		SUB-FLORIDAN CONFINING UNIT	1,200?

Figure 5. Generalized geology and hydrogeology of Lee, Hendry, and Collier Counties (modified from Reese, 2000).

Hawthorn unit, which is defined by an overlying marker unit composed of micritic limestone or marl (fig. 5; Reese and Memberg, 2000). In some areas along the east coast, the Suwannee Limestone is either interpreted as being absent (Miller, 1986; Reese and Memberg, 2000) or present in the lower part of this basal Hawthorn unit.

The Upper Floridan aquifer generally consists of several thin water-bearing zones of high permeability (flow zones) interlayered with thick zones of much lower permeability. Commonly, only one or two major flow zones provide the bulk of the productive capacity. These flow zones are often less than 20 ft thick each and tend to be in the upper part of the Upper Floridan aquifer, typically at or near the top of the Suwannee Limestone, Ocala Limestone, and Avon Park Formation. Unconformities that formed at the end of the Oligocene and Eocene Epochs are present at these contacts (Miller, 1986), and zones of dissolution occur in association with these unconformities in southern Florida (Meyer, 1989a). In southwestern Florida, the most important flow zone tends to be associated with the top of the Suwannee Limestone, whereas in southeastern Florida it is the top of the Avon Park Formation or, if present, the top of the Ocala Limestone. In both of these areas, the basal Hawthorn unit lies above this contact.

The basal Hawthorn unit is shown in an east-west hydrogeologic section that extends across Palm Beach County near the southern end of Lake Okeechobee (figs. 6 and 7). This unit is thickest along

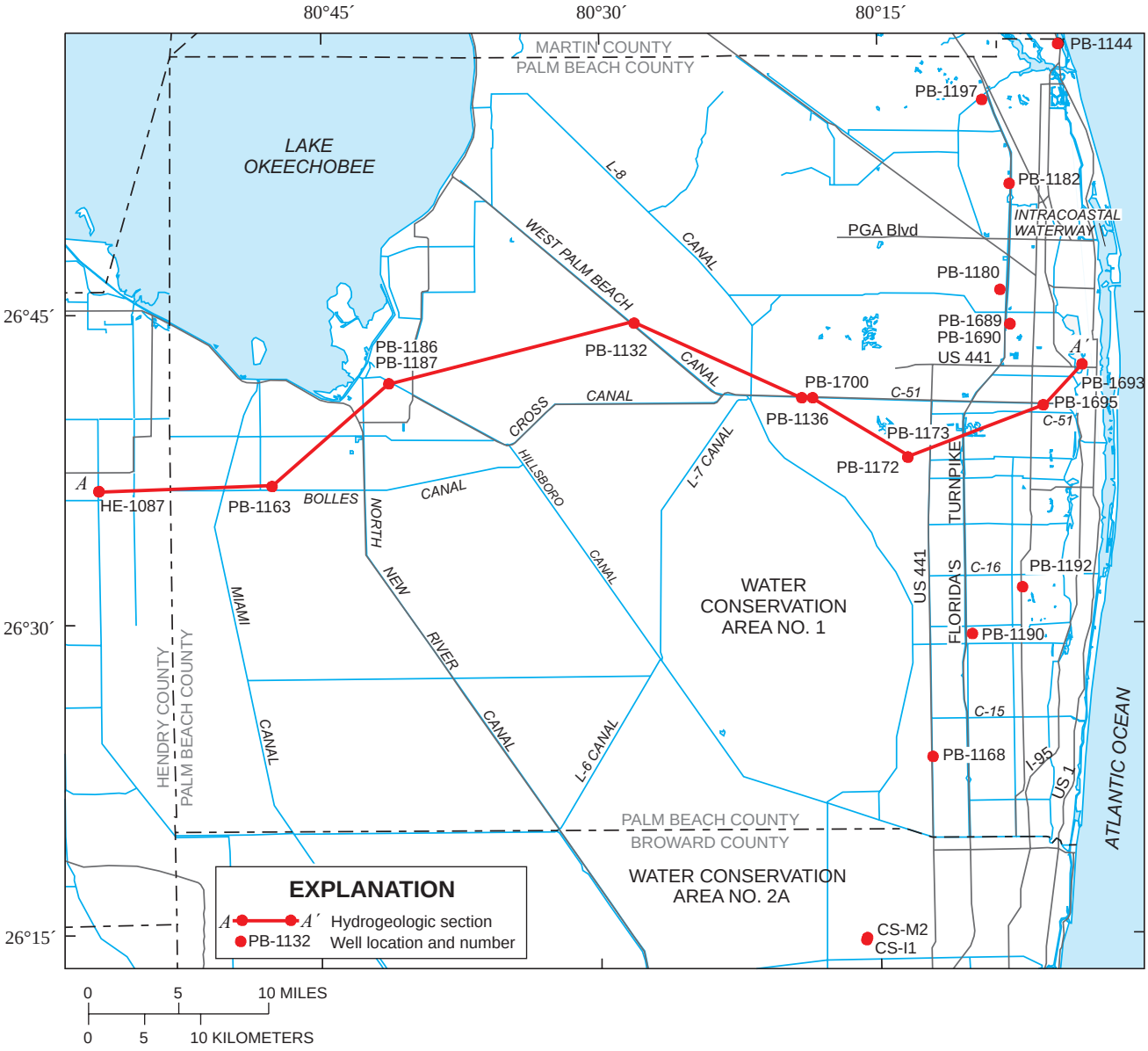

Figure 6. Trace of hydrogeologic section in Palm Beach County (modified from Reese and Memberg, 2000).

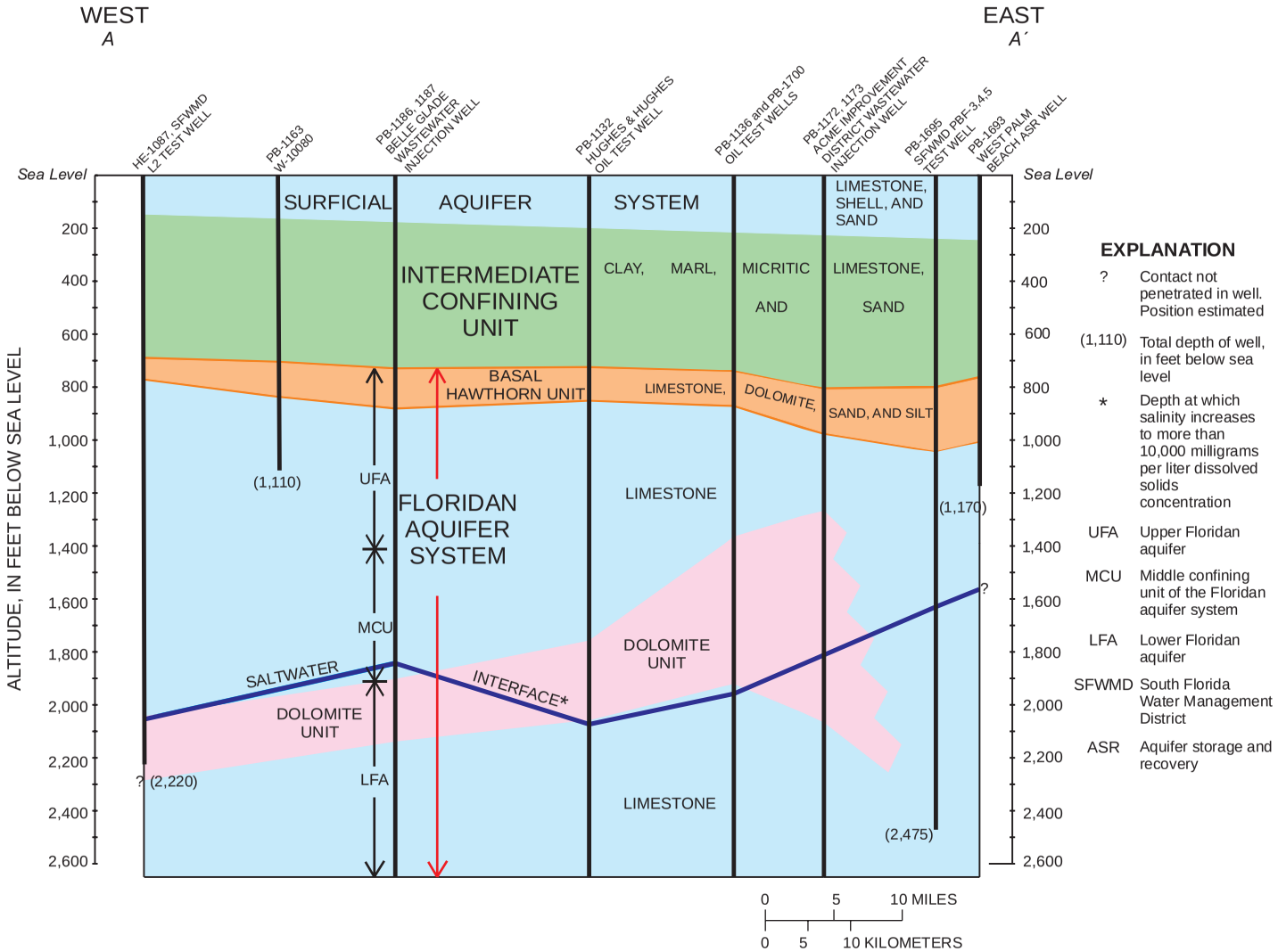

Figure 7. Hydrogeologic section extending east-west across Palm Beach County (modified from Reese and Memberg, 2000).

the coast and thins toward the center of the peninsula. Also shown on the section (fig. 7) are the depths of the saltwater interface in the Floridan aquifer system and a unit composed mostly of dolomite and dolomitic limestone referred to as the dolomite unit (Reese and Memberg, 2000). The saltwater interface (fig. 7) is defined as the depth below which total dissolved solids concentration is greater than 10,000 mg/L.

The dolomite unit of the Floridan aquifer system generally is considered to be within the uppermost permeable unit of the Lower Floridan aquifer in southern Florida (fig. 7; Meyer, 1989a). In some areas of Palm Beach County, however, the top of this unit is as high as 1,200 to 1,300 ft below sea level, as shown (for example) by wells PB-1172 and PB-1173 in figure 7. In these areas, it is uncertain whether all of the dolomite unit would be included in the Lower Floridan aquifer.

The altitude of the basal contact of the Hawthorn Group (same as the base of the basal Hawthorn unit) was mapped for most of southern Florida in three previous studies (Reese, 1994, fig. 6; Reese, 2000, fig. 7; and Reese and Memberg, 2000, fig. 6). Determination of the depth of this contact was primarily based on lithology and gamma-ray geophysical log patterns. As described above, this contact does not necessarily correspond with the top of the Upper Floridan aquifer, but the most important flow zone(s) in the Upper Floridan aquifer is typically associated with the contact. The altitude of this contact varies considerably in southern Florida, ranging from less than 600 ft to greater than 1,200 ft below sea level. Local relief can be as much as several hundred feet, particularly in southwestern Florida.

Complex structure in the Hawthorn Group has been identified in Lee and Hendry Counties along the Caloosahatchee River (Cunningham and others, 2001). The wavy configuration patterns of seismic reflection data show this structure, and these patterns are probably related to karstic collapse of deeper limestone that could be in the Floridan aquifer system.

Acknowledgments

A number of individuals, private consulting firms, water utilities, and regulatory agencies assisted in this study by providing data and technical input. Maintenance supervisor John Reynolds of the Boynton Beach East WTP and lead operators Guy Bartolotta (Broward County WTP 2A), John Cargill (Fiveash WTP), and Howard Erlick (Springtree WTP) were very helpful in providing information and conducting tours of their sites. Steve Evans, Water Quality Supervisor at the Boynton Beach East WTP, was especially helpful in providing detailed water-quality records of all cycles for the ASR well. Offices of the Underground Injection Control Program of FDEP in West Palm Beach, Ft. Myers, and Tallahassee graciously provided additional ASR technical information and data. Mark Pearce of Water Resource Solutions, Inc., Cape Coral, Fla., provided helpful technical input.

INVENTORY OF WELL AND TEST DATA

Well data were inventoried and compiled for all wells at existing and historical ASR sites in southern Florida, and cycle test data (also available for many sites) were synthesized. Consulting reports on the construction and testing of wells and on cycle testing provided much of these data. The consulting reports used to compile these data are listed in the selected references section at the back of this report.

Historical and current ASR sites are listed in table 1 along with the utility or operator of the site, the aquifer being used for the storage zone, site status, type of source water used for injection, and number of wells drilled at each site. The locations of these sites are shown in figure 1. The number of injection (storage) wells at each site ranges from one to five, and most sites have at least one monitoring well in the storage zone.

The type of source water used for injection in southern Florida has included treated drinking water, raw ground or surface water, and reclaimed water (table 1). Treated drinking water is the most common source water type, but raw ground water also is used, or has been proposed for use, at a number of sites on the east coast. The source water planned for the CERP ASR program is raw or partially treated ground water or surface water (table 1, Western Hillsboro Canal, site 1). Special permits, obtained through the FDEP Underground Injection Control program and the U.S. Environmental Protection Agency, are required to inject raw surface or ground water because these waters sometimes exceed maximum contaminant levels for primary or secondary drinking water standards for some constituents.

Construction and Testing Data

Construction and testing data were compiled into three main categories. These categories are well identification, location, and construction data; hydraulic well-test data; and ambient formation water-quality data.

Well Identification and Construction Data

For the purpose of this study, all ASR storage and associated monitoring wells were assigned a USGS number, and data from these wells have been stored as part of the USGS Ground-Water Site Inventory (GWSI) database. Well identification, location, and construction data are given in table 2 (at end of report). The construction information includes total hole depth, ending date of construction, casing depth and diameter, type of each casing string set in the well, and the completed (constructed) open interval and its diameter. In most cases, the completed interval is open hole, but a gravel-packed screen was installed in a few wells. At many sites, the first well drilled was plugged back to the selected storage zone after being drilled deeper to test other potential zones or to determine water-quality changes with depth. In many instances, the latitude and longitude provided herein were obtained from the construction permit, and this location is representative of the storage well only; however, in some instances, the latitude and longitude were more precisely determined for all wells at a site by the use of a hand-held global positioning system (GPS) (see footnote 1 in table 2 at end of report).

The thickness of the open interval ranges from 45 ft at the Marco Lakes (well C-1206) and Marathon (well MO-189) sites to 452 ft at the West Well Field site (well G-3706) (fig. 8; table 2 at end of reort). Open intervals for ASR wells in the Floridan aquifer system average 172 ft thick. The diameter of the open interval ranges from 5.125 in. at the St. Lucie County site to 29 in. at the West Well Field site in Miami-Dade County. Large diameter open intervals are constructed for the purpose of obtaining a high rate of flow. Each of the storage wells at the West Well Field site is designed for a pumping rate of up to 5 Mgal/d.

Hydraulic Well-Test Data

Reported data describing hydraulic tests were compiled for ASR well systems. The data include the reported results of packer tests conducted during drilling, step drawdown tests, single-well constant rate recovery tests, and multiwell constant rate tests (table 3 at end of report). Tests of other permeable intervals at a site that are shallower or deeper than the interval selected to be the storage zone are also included (table 3 at end of report). Water-level data were not analyzed as part of this study; rather, all of the analytical results given in table 3 (at end of report) came from consulting reports in the selected references listed at the back of this report.

Some tests reported in table 3 (at end of report) are single-well step drawdown tests run to determine the specific capacity of a well. These tests provide insight into the productive capacity of a well and are used to determine the size and depth of a pump to be used in the well for a multiwell test or for long-term operation. At some sites, the transmissivity of the tested interval was estimated from a step drawdown test using the specific capacity at each step. At the Marco Lakes ASR site, transmissivity was determined during a step drawdown test of ASR-3 by analyzing the resulting drawdown data from nearby wells using the Cooper and Jacob (1946) solution. Transmissivity was estimated at the Boynton Beach East WTP site from a step drawdown test of ASR-1 using the Cooper and Jacob (1946) solution, but without any monitoring wells. Specific capacity determined from step drawdown tests of storage zones range from 2.7 gal/min/ft at the Marathon site to 390 gal/min/ft at the West Palm Beach site, well ASR-1 (table 3 at end of report). Specific capacity was reported to be 1,600 gal/min/ft on the basis of a multiwell test at the Taylor Creek/Nubbin Slough (Lake Okeechobee) site.

Packer tests are tests of open-hole intervals conducted during drilling using inflatable packers set on a string of drill pipe for the purpose of isolating the interval to be tested. Often, only specific capacity data are reported for packer tests (table 3 at end of report). However, transmissivity can be estimated either from the specific capacity results, or from analysis of the recovery of water level after a period of constant rate pumping during a packer test. This latter method, known as the Theis (1935) residual drawdown or recovery analysis, gives a more reliable estimate than the specific capacity method. Packer test results can be unreliable because of partial penetration, a low pumping rate, a short pumping period, or incomplete isolation of the interval tested (leaky packers).

Hydraulic properties determined from a multiwell, constant rate, drawdown test include transmissivity, storage coefficient, and leakance. Solutions commonly used to analyze water-level data from this type of test include Theis (1935) and Cooper and Jacob (1946) for confined aquifers and Hantush and Jacob (1955) and Walton (1962) for semiconfined, leaky aquifers. Depending on the amount of drawdown (pumping rate) and the degree of background variations in water level, such as tidal fluctuations,

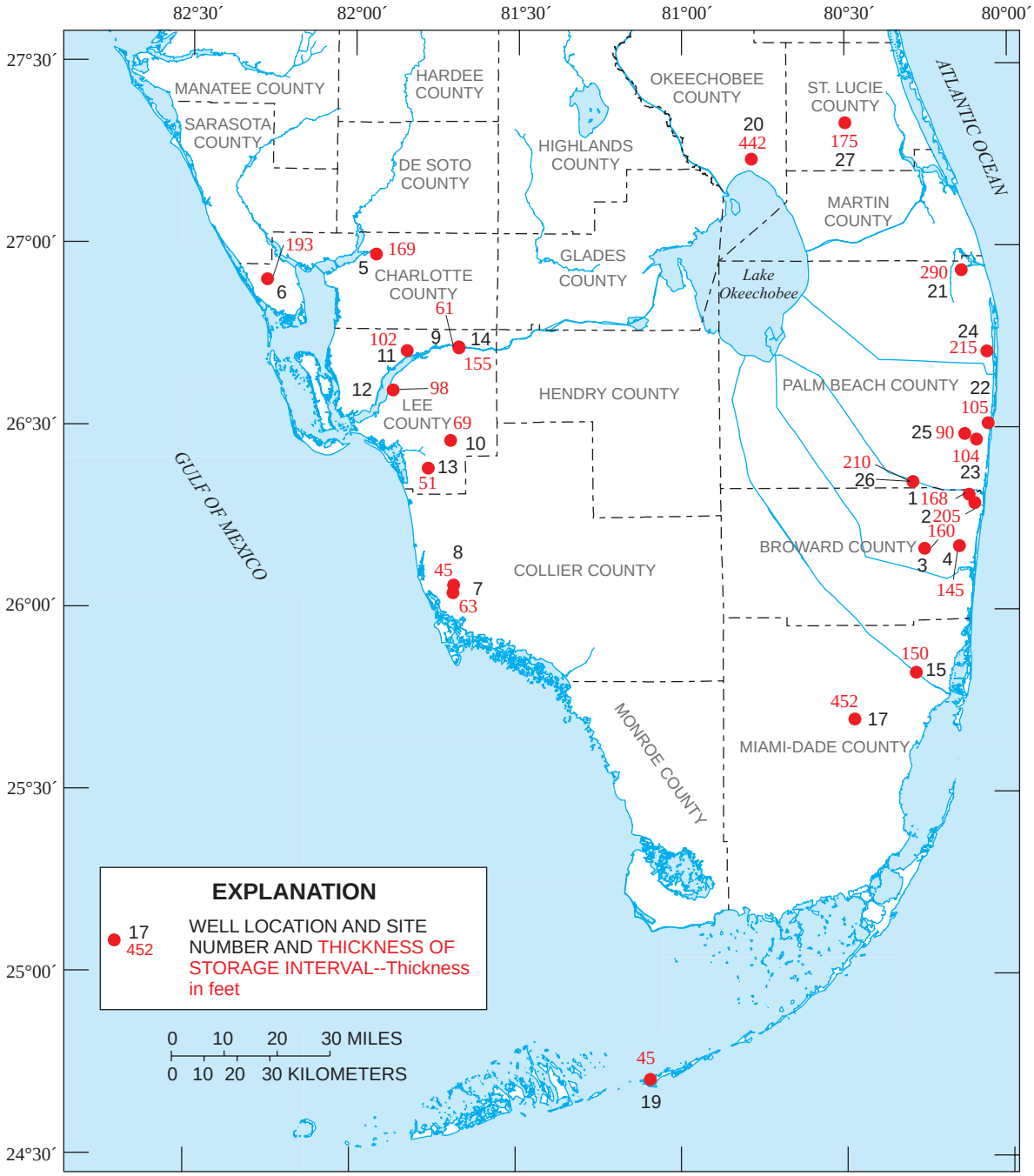

Figure 8. Thickness of open interval in storage wells at aquifer storage and recovery sites in southern Florida. All wells represent first storage well at each site (see table 2).

background water-level measurements should be made for at least 1 day prior to the beginning of the pumping test, and these measurements should be subtracted from the drawdown water-level data collected during the test. Single-well constant rate tests usually provide only an estimate of transmissivity, and solutions used to analyze the recovery water-level data from these tests include the Theis (1935) solution for residual drawdown and the Cooper and Jacob (1946) solution.

Multiwell constant rate tests of the storage zone were performed at 16 of the ASR sites (table 3 at end of report), and not including packer tests, single-well constant rate recovery tests of the storage zone were run at 4 sites, 2 of which also had a multiwell-test run. Constant rate test results could be affected by pretest well treatment designed to increase specific capacity. Acidization of the ASR well prior to the multiwell test was done at the Springtree WTP and West Well Field sites. The Western Hillsboro site planned recharge well (EXW-1) also was acidized after the reported step drawdown test (table 3 at end of report).

Hydraulic properties determined from tests of storage zones may apply only to the storage zone or to a thicker interval if the aquifer containing the storage zone is thicker than the storage zone. In the case where the aquifer is thicker than the storage zone, the hydraulic conductivity of a storage zone will be less than that obtained by dividing the transmissivity determined from a test by the thickness of the storage zone. However, in the Upper Floridan aquifer where thick zones of relatively low permeability separate flow zones, tests of part of the aquifer are typically not influenced by the entire thickness of the aquifer. Thus, the value of transmissivity obtained is less than the total transmissivity of the aquifer (Wedderburn and Knapp, 1983).

For 18 sites where the storage zone is in the Floridan aquifer system, the most reliable or representative values for transmissivity from storage zone tests were selected and then plotted on a map of southern Florida (fig. 9). In most cases, these values came from drawdown analysis of constant rate multiwell tests; if performed, the leaky aquifer solution was used. The storage zone is in the Upper Floridan aquifer in all cases, except at the Taylor Creek/Nubbin Slough (Lake Okeechobee) and the West Well Field sites. At the Lake Okeechobee site, this zone is in the Lower Floridan aquifer (Quiñones-Aponte and others, 1996), and at the West Well Field site, some of the mid-Hawthorn aquifer in addition to the upper part of the Upper Floridan aquifer is included in the storage zone. Transmissivity values range from 800 ft^2/d at the Lee County site to nearly 590,000 ft^2/d at the Lake Okeechobee site. The highest value in the Upper Floridan aquifer is 108,000 ft^2/d at the West Palm Beach WTP site. The average value for sites in the Upper Floridan aquifer is 21,100 ft^2/d, and values greater than 30,000 ft^2/d are considered to be high in this study.

The high transmissivity estimate at the Lake Okeechobee site (fig. 9) is a function of the large thickness of the open interval and the dominant lithology in this interval, which is dolomite. The storage zone contains several highly permeable flow zones that may have secondary fracture permeability. The open interval in the ASR well for the Lee County WTP site is confined to the lower Hawthorn producing zone of the basal Hawthorn unit (Reese, 2000). A second ASR site was later constructed at the same location (Olga WTP site). The Olga WTP site storage zone is deeper in the Upper Floridan aquifer and is contained within the Suwannee Limestone, about 150 ft below the top of this formation (Water Resources Solutions, Inc., 2000a). The estimated transmissivity for the Olga storage zone is 9,400 ft^2/d (fig. 9; table 3 at end of report).

Leakance of the tested aquifer was determined at eight sites in the Floridan aquifer system by multiwell aquifer tests, and values are higher than expected (table 3 at end of report). Leakance is a measure of the degree of aquifer confinement and is defined as the vertical hydraulic conductivity of a confining unit, *divided* by the thickness of the confining unit. However, leakance determined from an aquifer test applies to both the upper and lower confining units of the aquifer, unless it is known that one of the confining units is nonleaky. Leakance estimates ranged from 3.9×10^{-5} 1/d at the West Well Field site to 6.3×10^{-2} 1/d at the Deerfield Beach West WTP site. Leakance estimates less than 1×10^{-3} 1/d have been used to indicate confining conditions in the surficial aquifer system in southern Florida (Reese and Cunningham, 2000). Of the eight values determined for leakance (table 3 at end of report), five exceed this limiting value. Leakance was greater than 4.0×10^{-2} 1/d at the Deerfield Beach West WTP, Olga WTP, and the St. Lucie County sites. Leakance may also be high at the West Palm Beach WTP site. The confined aquifer Theis (1935) solution was used to analyze the multiwell-test data collected at this site, despite a large observed departure below the type curve during the latter part of the test indicating a leaky aquifer.

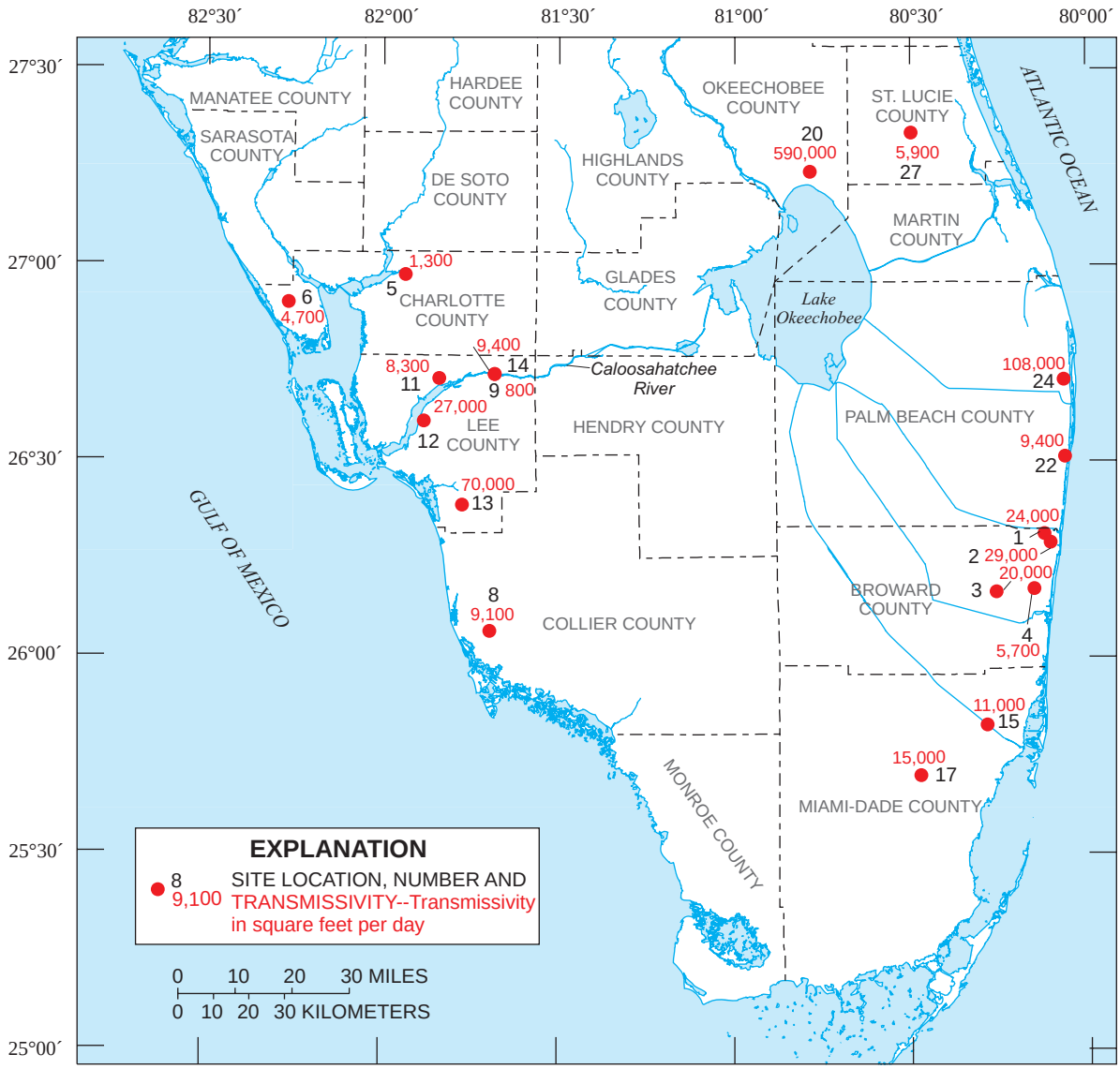

Figure 9. Transmissivity determined for storage zones in the Floridan aquifer system at aquifer storage and recovery sites in southern Florida. The production well used for the test at all sites was ASR-1, except for sites 15 and 27 where MW-1 was used.

The high leakance estimates from the Upper Floridan aquifer are probably best attributed to leakage from below the tested interval rather than from above because of the good confinement generally accepted as being present above the aquifer in southern Florida (Bush and Johnston, 1988). This leakage either originated from intervals lower in the Upper Floridan aquifer or from the middle confining unit of the Floridan aquifer system.

Ambient Water-Quality Data

Ambient water-quality data were collected from storage and monitoring wells at ASR sites (table 4). The inventoried data describe formation water salinity and include the sampled interval, sample date, specific conductance, dissolved chloride concentration, dissolved solids concentration, temperature, and dissolved sulfate concentration. The sampling methods, listed in order of increasing reliability, include (1) collected during drilling by the reverse-air rotary method, (2) collected from packer tests, (3) collected from a pump out test of an open interval below casing before final construction of the well, and (4) collected from a completed open interval. Intervals sampled include the storage zone, intervals deeper and shallower than the storage zone, and intervals that include more than the

Table 4. Ambient water-quality data collected from aquifer storage and recovery well systems in southern Florida

[USGS, U.S. Geological Survey; WTP, water treatment plant; WWTP, wastewater treatment plant; PD, post development; --, not determined or not reported. Type of interval: C, constructed (completed) open interval; O, pump out test of open interval below casing during drilling; P, packer test interval; R, sample collected during reverse-air rotary drilling with top of interval being the base of casing]

Site name	Other identifier	USGS local number	Interval sampled (feet below land surface)	Type of interval	Date sampled	Specific conductance (microsiemens per centimeter)	Dissolved chloride (milligrams per liter)	Dissolved solids (milligrams per liter)	Temperature (degrees Celsius)	Dissolved sulfate (milligrams per liter)
Broward County										
Deerfield Beach West WTP	ASR-1	G-2887	960-1,128[1]	C	09-30-92	5,400	2,000	3,800	25.0	400
			960-1,120[1]	C	09-03-92	5,430	1,850	3,800	22.7	--
			960-1,128[1]	C	09-09-92	6,000	1,600	3,400	--	400
			960-1,128[1]	C	09-30-92	5,400	2,000	3,800	25.0	400
			960-1,128[1]	C	12-11-92	--	1,800	3,700	--	--
Broward County WTP 2A	ASR-1	G-2889	995-1,200[1]	C	12-03-96	--	1,900	3,200	--	380
	MW-1	G-2916	990-1,200[1]	C	03-12-97	--	1,900	2,600	--	250
Springtree WTP	ASR-1	G-2914	1,110-1,340	R	--	4,300	2,200	--	--	--
			1,110-1,270[1]	C	07-31-97	7,310	2,449	4,520	31.0	644
			1,110-1,270[1]	C	01-13-98	9,300	3,600	6,030	28.0	774
Fiveash WTP	ASR-1	G-2917	1,055-1,300	R	--	7,800	4,000	--	--	--
	FMW-1	G-2918	1,055-1,175[1]	C	03-17-98	9,345	3,524	7,880	--	725
	SMW-1	G-2919	180-200	C	01-15-98	--	24	279	--	21
Charlotte County										
Shell Creek WTP	ASR-1	CH-315	700-1,040	R	--	3,540	--	2,020	--	--
			700-755	P	11-05-97	--	837	2,090	--	--
			700-764	C	11-18-97	--	850	1,918	--	--
			764-933[1]	C	08-07-99	--	900	1,900	--	380
Englewood South Regional WWTP	TPW	CH-318	295-808	O	03-02-00	16,800	5,200	10,267	--	664
			563-583	P	02-26-00	31,600	12,000	21,100	--	881
			630-808	P	03-06-00	50,100	17,500	31,133	--	--
			507-700[1]	C	03-31-00	27,000	11,595	19,350	24.2	1,279
	SZMW-1	CH-319	510-700[1]	C	04-20-00	21,600	10,997	22,100	21.0	1,106
	IMW-1	CH-320	280-320	C	04-18-00	11,780	4,458	8,040	21.0	535
	SMW-1	CH-321	170-205	C	04-18-00	8,410	2,875	6,000	21.0	204
Collier County										
Manatee Road	ASR-1	C-1202	465-528[1]	C	10-15-91	8,030	2,754	5,032	--	--
			320-398	P	12-18-90	--	2,450	5,287	--	723
	MW-A	C-1102	970-1,110	P	11-90	--	10,000	--	--	--
			1,220-1,270	P	11-90	--	17,000	--	--	--
			1,330-1,610	P	11-90	--	18,000	--	--	--
			360-500	C	11-90	--	--	--	--	--
			650-770	C	11-90	--	4,000	--	--	--

Table 4. Ambient water-quality data collected from aquifer storage and recovery well systems in southern Florida --(Continued)

[USGS, U.S. Geological Survey; WTP, water treatment plant; WWTP, wastewater treatment plant; PD, post development; --, not determined or not reported. Type of interval: C, constructed (completed) open interval; O, pump out test of open interval below casing during drilling; P, packer test interval; R, sample collected during reverse-air rotary drilling with top of interval being the base of casing]

Site name	Other identifier	USGS local number	Interval sampled (feet below land surface)	Type of interval	Date sampled	Specific conductance (microsiemens per centimeter)	Dissolved chloride (milligrams per liter)	Dissolved solids (milligrams per liter)	Temperature (degrees Celsius)	Dissolved sulfate (milligrams per liter)
Collier County--Continued										
Marco Lakes	ASR-1	C-1206	745-790[1]	C	--	6,000	2,520	6,620	--	--
			745-790[1]	C	06-24-97	--	3,740	5,500	--	744
	DZMW	C-1207	293-352	C	07-01-97	--	3,260	6,180	--	800
			745-817[1]	C	07-01-97	--	2,590	5,620	--	718
	ASR-2	C-1208	735-780[1]	C	PD	8,500	2,480	--	--	--
			735-780[1]	C	09-20-99	6,860	2,449	4,280	--	663
	MHZ2MW	C-1209	440-470	C	09-20-99	8,700	2,999	5,665	25.8	758
	ASRZMW	C-1210	725-774[1]	C	10-01-99	9,120	2,958	5,816	29.8	699
	ASR-3	C-1211	735-780[1]	C	PD	9,120	2,680	--	--	--
			735-780[1]	C	11-24-99	8,860	2,774	3,920	26.3	686
Lee County										
Lee County WTP	MW-1	L-2530	475-615[1]	C	09-25-79	2,500	500	1,520	26.5	270
Corkscrew WTP	ASR-1 LM3982	L-5855	328-397[1]	C	09-09-95	--	39	336	27.0	18
	MW-A	L-5856	524-578	P	08-17-94	640	100	--	--	--
			744-778	P	08-24-94	1,930	600	--	--	--
			340-402[1]	C	04-04-97	-	42	348	--	34
North Reservoir	ASR-1 LM-6210	L-5810	540-642[1]	C	03-02-99	2,400	700	--	--	--
			540-642[1]	C	03-04-99	2,450	740	--	--	--
			540-642[1]	C	03-10-99	2,450	750	--	--	--
	MW-1 LM-6208	L-5811	480-518	P	12-07-98	3,230	890	--	--	--
			529-619[1]	P	12-09-98	2,640	700	--	--	--
			640-703	P	12-11-98	2,710	740	--	--	--
			808-890	P	12-16-98	2,450	720	--	--	--
			904-977	P	12-18-98	3,244	1,000	--	--	--
Winkler Avenue	ASR-1		455-574[1]	P	06-16-99	3,860	972	--	28.5	--
			455-575[1]	P	06-17-99	3,240	770	--	28.5	--
			455-553[1]	C	11-01-99	--	1,240	1,770	--	354
	SZMW-1		455-553[1]	C	09-16-99	--	1,282	2,998	--	414
	MHMW-1		150-200	C	11-01-99	--	1,540	2,410	--	323

Table 4. Ambient water-quality data collected from aquifer storage and recovery well systems in southern Florida --(Continued)

[USGS, U.S. Geological Survey; WTP, water treatment plant; WWTP, wastewater treatment plant; PD, post development; --, not determined or not reported. Type of interval: C, constructed (completed) open interval; O, pump out test of open interval below casing during drilling; P, packer test interval; R, sample collected during reverse-air rotary drilling with top of interval being the base of casing]

Site name	Other identifier	USGS local number	Interval sampled (feet below land surface)	Type of interval	Date sampled	Specific conductance (microsiemens per centimeter)	Dissolved chloride (milligrams per liter)	Dissolved solids (milligrams per liter)	Temperature (degrees Celsius)	Dissolved sulfate (milligrams per liter)
Lee County--Continued										
San Carlos Estates	ASR-1	L-5812	650-687[1]	R	--	4,660	1,100	2,800	31.5	560
			650-718[1]	R	--	4,680	1,110	2,900	32.2	560
			650-701[1]	C	06-07-99	4,700	1,100	3,000	--	520
	SZMW-1R	L-5814	659-721[1]	R	--	4,590	1,100	3,000	31.2	520
			659-721[1]	C	07-29-99	4,570	1,100	2,800	--	580
	SMW-1	L-5815	234-321	R	--	1,681	370	920	28.5	83
			234-321	C	08-02-99	1,694	340	950	--	77
Olga WTP	ASR-1 LM-6086	L-5816	859-920[1]	C	10-21-99	2,677	1,000	--	--	--
			859-920[1]	C	11-09-99	2,690	1,000	--	--	--
	MW-1 LM-6209	L-5817	520-610	P	01-05-99	1,988	540	--	--	--
			617-694	P	01-06-99	1,427	260	--	--	--
			840-940[1]	P	02-30-99	3,420	1,000	--	--	--
			840-940[1]	P	02-04-99	3,461	1,140	--	--	--
			715-940	P	02-04-99	2,928	900	--	--	--
			950-1,106	P	02-08-99	2,793	850	--	--	--
	MW-3 LM-6615	L-5818	826-945	P	03-25-99	2,350	790	--	--	--
			857-945[1]	P	03-25-99	2,948	970	--	--	--
Miami-Dade County										
Hialeah	ASR-1	G-3061	955-1,105[1]	C	12-04-74	4,750	1,200	2,920	--	500
	MW-1	G-3062	840-844	C	07-24-75	6,600	1,900	--	--	--
		G-3062	953-1,060[1]	C	11-20-74	4,200	1,200	2,830	--	480
West Well Field	ASR-1	G-3706	850-1,302[1]	C	01-26-97	8,980	2,000	5,980	25.0	238
	ASR-2	G-3707	845-1,250[1]	C	02-25-97	6,650	2,449	4,390	23.0	615
	ASR-3	G-3708	835-1,210[1]	C	04-09-97	6,750	2,349	4,040	--	595
	MW-1	G-3709	855-1,010	C	02-06-97	6,520	2,499	4,300	25.0	662
			1,370-1,390	C	02-06-97	10,590	4,649	7,220	25.0	466
Monroe County										
Marathon	ASR-1	MO-189	387-432[1]	C	05-04-90	49,000	20,800	37,200	--	2,910

Table 4. Ambient water-quality data collected from aquifer storage and recovery well systems in southern Florida --(Continued)

[USGS, U.S. Geological Survey; WTP, water treatment plant; WWTP, wastewater treatment plant; PD, post development; --, not determined or not reported. Type of interval: C, constructed (completed) open interval; O, pump out test of open interval below casing during drilling; P, packer test interval; R, sample collected during reverse-air rotary drilling with top of interval being the base of casing]

Site name	Other identifier	USGS local number	Interval sampled (feet below land surface)	Type of interval	Date sampled	Specific conductance (microsiemens per centimeter)	Dissolved chloride (milligrams per liter)	Dissolved solids (milligrams per liter)	Temperature (degrees Celsius)	Dissolved sulfate (milligrams per liter)
Okeechobee County										
Taylor Creek/Nubbin Slough (Lake Okeechobee)	ASR-1	OK -9000	1,268-1,710[1]	C	11-04-89	9,270	2,910	5,730	--	--
			1,268-1,710[1]	C	04-17-91	--	3,100	7,180	35.0	--
	MW-1	OK -9001	1,175-1,227	P	04-20-88	800	131	656	28.5	210
			1,288-1,354	P	04-25-88	4,800	1,680	4,000	28.0	570
			1,347-1,370	P	04-25-88	4,800	1,900	4,230	30.0	630
			1,358-1,508	P	04-24-88	7,500	2,510	5,740	29.0	760
			1,540-1,662	P	04-23-88	7,500	2,920	6,710	28.0	930
			990-1,075	C	04-17-91	--	210	820	27.5	--
	MW-1	OK -9002	1,275-1,700[1]	C	04-17-91	--	2,200	5,230	27.0	--
Palm Beach County										
Jupiter	ASR-1	PB-747	990-1,280[1]	C	06-19-74	6,400	1,800	4,060	--	400
Boynton Beach East WTP	ASR-1	PB-1194	804-909[1]	C	05-21-92	6,670	1,920	3,910	25.0	436
	MW-1	PB-1195	300-320	C	05-21-92	33,100	12,100	21,900	--	617
Delray Beach North Storage Reservoir	ASR-1	PB-1702	849-899	P	06-05-96	9,160	2,630	5,670	--	--
			900-952	P	06-11-96	8,480	2,669	5,529	--	--
			974-1,020	P	06-14-96	7,440	2,143	4,363	--	--
			1,020-1,100	P	06-18-96	6,800	2,057	4,255	--	--
			1,020-1,120	O	07-26-96	6,930	2,069	4,752	--	--
			1,020-1,200[1]	O	09-06-96	6,810	2,556	4,234	--	--
			1,016-1,200[1]	C	09-20-96	--	2,300	8,000	--	430
West Palm Beach WTP	ASR-1	PB-1692	985-1,200[1]	C	07-17-97	7,600	2,800	5,056	--	--
	MW-1	PB-1693	975-1,091	P	08-22-96	7,700	2,600	3,800	--	--
			975-1,090	O	08-29-96	7,700	2,600	3,800	--	--
			975-1,190[1]	O	09-01-96	8,290	2,750	4,150	--	--
			975-1,290	O	09-04-96	7,970	2,300	4,270	--	--
			975-1,384	O	09-06-96	7,120	2,520	3,830	--	--
			1,304-1,384	P	09-14-96	6,860	2,060	3,650	--	--
			975-1,191[1]	C	11-16-96	7,350	2,381	3,550	--	--
System 3 Palm Beach County	ASR-1	PB-1763	1,065-1,155[1]	C	01-28-99	7,820	2,100	4,080	23.7	467

Table 4. Ambient water-quality data collected from aquifer storage and recovery well systems in southern Florida --(Continued)

[USGS, U.S. Geological Survey; WTP, water treatment plant; WWTP, wastewater treatment plant; PD, post development; --, not determined or not reported. Type of interval: C, constructed (completed) open interval; O, pump out test of open interval below casing during drilling; P, packer test interval; R, sample collected during reverse-air rotary drilling with top of interval being the base of casing]

Site name	Other identifier	USGS local number	Interval sampled (feet below land surface)	Type of interval	Date sampled	Specific conductance (microsiemens per centimeter)	Dissolved chloride (milligrams per liter)	Dissolved solids (milligrams per liter)	Temperature (degrees Celsius)	Dissolved sulfate (milligrams per liter)
Palm Beach County--Continued										
Western Hillsboro Canal, Site 1	EXW-1	PB-1765	1,160-1,225	P	04-05-00	3,898	1,390	--	23.9	--
			1,015-1,150	P	04-07-00	8,223	2,706	--	23.8	--
			1,015-1,225[1]	C	11-18-00	6,900	--	--	--	--
	PBF-10R	PB-1767	1,015-1,225[1]	C	01-24-01	9,440	--	--	--	--
St. Lucie County										
St. Lucie County	ASR-1	STL-356	600-766[1]	P	03-11-82	3,400	888	2,058	27.8	--
			770-1,000	P	03-12-82	3,200	1,015	1,888	27.8	--
			600-775[1]	C	03-12-82	3,325	955	2,379	27.8	--
	MW-1	STL-357	600-775[1]	C	03-12-82	3,500	1,022	2,143	27.8	--

[1]Interval tested is the same (or about the same) as the storage zone.

selected storage zone (table 4). Upper Floridan aquifer ASR sites in southwestern Florida were usually sampled from shallower permeable zones of the intermediate aquifer system.

The chloride concentration of ambient water in ASR storage zones in the Floridan aquifer system is shown on a map of southern Florida (fig. 10). Samples used for this map were selected from table 4 based on the most reliable sampling method as described above. Chloride concentrations ranged from 500 mg/L at the Lee County WTP site to 11,000 mg/L at the Englewood South Regional WWTP site. At most sites, the chloride concentration ranged from about 1,000 to 3,000 mg/L, and the average concentration was about 2,300 mg/L. Storage zones containing water with 3,000 mg/L or greater were considered to have high chloride concentration in this study. The highest value found in the east coast area was 3,600 mg/L at the Springtree WTP site. The highest chloride concentration found in the upper part of the Upper Floridan aquifer in southern Florida based on three previous studies was 8,000 mg/L in northeastern Palm Beach County; the lowest concentration found was 400 mg/L in Lee County (Reese, 1994; Reese, 2000; and Reese and Memberg, 2000).

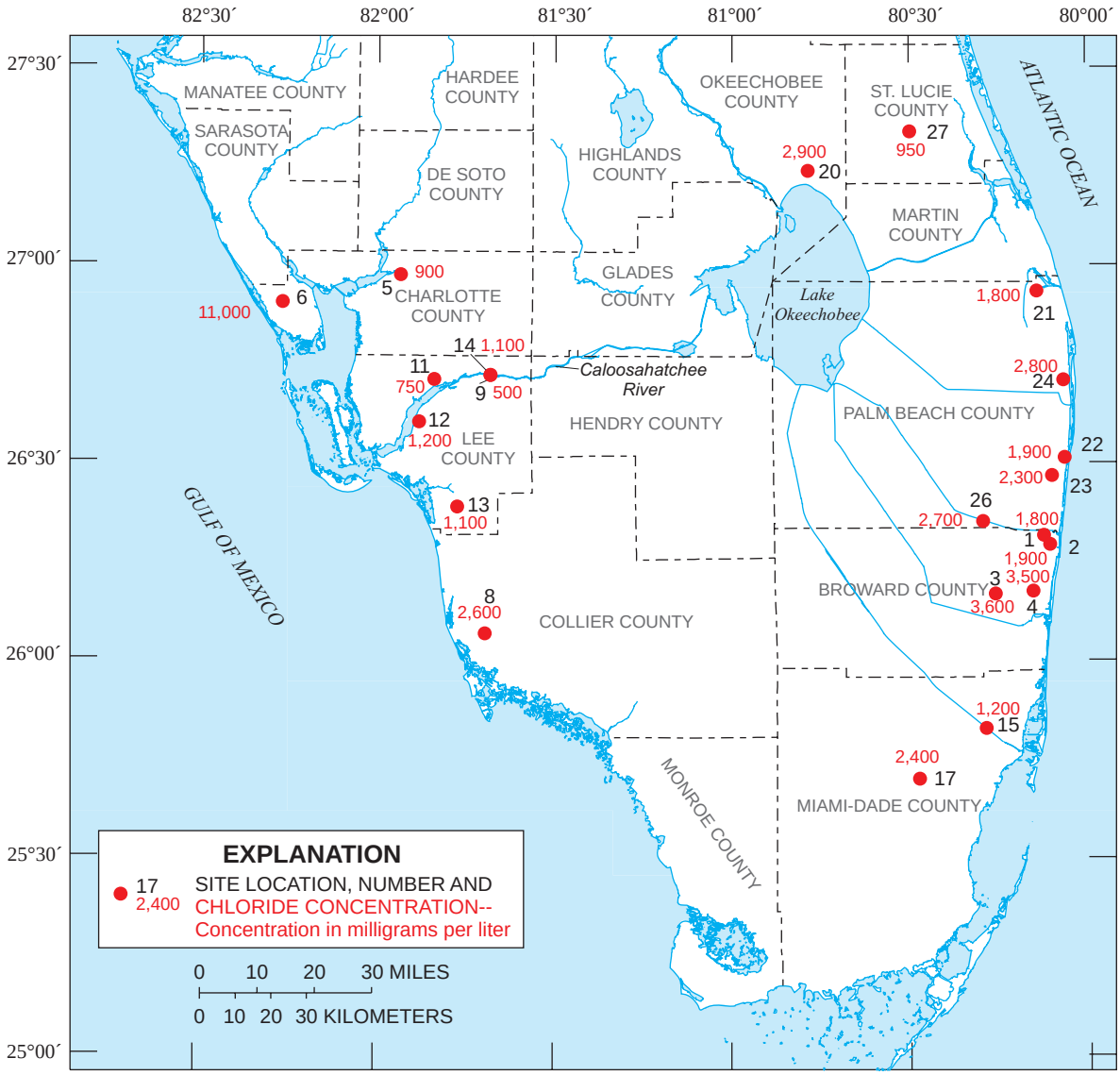

Figure 10. Ambient water salinity of storage zones in the Floridan aquifer system at aquifer storage and recovery sites in southern Florida.

Cycle Test Data

Cycle test information was obtained from consulting reports, other published reports, monthly operating reports (MOR) required by the FDEP as part of the permitting process during operational testing, and in several cases, from daily records provided by a WTP. These data were compiled and are given in table 5. All of the test data given are only for the first storage well (ASR-1) at a site, except for the West Well Field site. Only 18 of the 27 ASR sites listed in table 1 are included in table 5; other ASR sites have not initiated operational testing or test data were not available. Cycle testing at the Olga WTP and North Reservoir sites was postponed due to inadequate treated drinking water supplies that will be used for recharge. The number of days of storage in table 5 includes only the time between the recharge and recovery periods; it does not include days during the recharge period in which injection ceased due to a lack of source water or other operational problems. The MOR provided insufficient data to calculate recovery efficiencies at some ASR sites because the water quality of recharged and recovered water was not reported; these data are not required by the FDEP in the report.

Two recovery efficiency numbers were determined for each cycle (table 5). The first is total recovery efficiency, and it is the percent recovery at the end of the cycle. The chloride concentration of the recovered water at this point is also given in table 5. The chloride concentration at the end of the cycle is usually in the range of 250 to 400 mg/L. The second recovery efficiency number is the potable water recovery efficiency. It is the percent recovery when the chloride concentration of the recovered water reaches only 250 mg/L. Potable water recovery efficiency numbers (potable recovery efficiencies) are used in this report for performance comparisons between sites.

Chloride concentrations of recharged and recovered water for the West Palm Beach WTP site were not reported or made available, and only the total recovery efficiencies are given in table 5. At the West Well Field site, two storage wells were active during the second cycle and all three storage wells were active during the third cycle. However, water was not recovered from well ASR-3 during the cycle 3 recovery period. For cycle 3, recovery efficiencies were determined for individual storage wells and also for all three wells combined (table 5).

The Boynton Beach East WTP site underwent 16 recharge-recovery cycles (table 5). The Marathon site had 11 cycles, and the Marco Lakes and Springtree WTP sites had 5 cycles each; the number of cycles was 4 or less at all other sites. Additional cycles were conducted at the Manatee Road site, but were not reported. Recharge volume per cycle ranged from as low as 0.6 Mgal for cycle 1 at the Lee County WTP site, to as high as 714.33 Mgal during cycle 3 at the West Well Field site. The longest storage period was 181 days for cycle 3 at the Hialeah site.

The highest reported first cycle potable recovery efficiency was 47 percent for the Boynton Beach ASR site. The first cycle recovery efficiency of the Corkscrew WTP site is greater but is not considered here due to the potable nature of water in its storage zone. Except for the Jupiter site where no potable water was reported to be recovered on the first cycle, the lowest potable recovery efficiency was 2 percent at the San Carlos Estates site. Of the 16 sites in table 5 with potable recovery efficiencies calculated, 9 sites had a potable recovery efficiency of well over 10 percent during the first cycle. The seven exceptions include Fiveash WTP, Manatee Road, North Reservoir, San Carlos Estates, Lake Okeechobee, Jupiter, and St. Lucie County sites. Two of these, the Manatee Road and Jupiter sites, showed improvement to a level substantially higher than 10 percent in succeeding cycles. The Fiveash, San Carlos Estates, and Lake Okeechobee sites did not; however, few cycles were conducted at these three sites (two, two and four, respectively). Only one cycle was run at the North Reservoir and St. Lucie County sites.

Ten sites achieved a potable recovery efficiency exceeding 30 percent during at least one cycle; however, at the Shell Creek WTP site, the recovery efficiency diminished to 9 percent during the third cycle when the recharge volume was greatly increased. The highest potable recovery efficiency of 90 percent was during cycle 4 at the Boynton Beach East WTP site, but the recharge volume reported for this cycle could be too low. This recharge volume is based on flow totalizer equipment readings, but calculation of the recharge volume based on reported daily flow rates gives a higher number. The second highest recovery efficiency was 84 percent for cycle 16 at the Boynton Beach site. Recovery efficiency was 72 percent for cycle 4 at the Marathon site; however, the storage zone at this site is within a siliciclastic sandstone aquifer. Because of lower dispersive mixing, recovery from a siliciclastic aquifer may be larger, having only intergranular porosity as compared to carbonate rock storage zones that probably also have secondary, conduit type porosity (Merritt, 1985).

Table 5. Cycle test data from aquifer storage and recovery wells in southern Florida

[Test data at all sites, excluding the West Well Field site, are only for the first storage well at the site (ASR-1). *Data extracted from monthly operating reports and daily records provided by the water treatment plant. All other cycle test data are from consulting reports or other published reports. DS, dissolved solids concentration in mg/L (milligrams per liter); Mgal, million gallons; NA, not applicable; NR, not reported; WTP, Water Treatment Plant; >, greater than]

Site name	Ambient chloride concentration (mg/L)	Cycle			Recharge, storage, recovery periods (days)	Recharge volume (Mgal)	Recovery volume (Mgal)	Chloride concentration of recharge water (mg/L)	Chloride concentration of recovered water at end of cycle (mg/L)	Recovery efficiency at end of cycle (percent)	Recovery efficiency at recovered water chloride concentration of 250 mg/L (percent)
		No.	Beginning date	End date							
Broward County											
Broward County WTP 2A	2,000	Test	07-09-98	07-21-98	10, 1, 2	20	4	30	225	20	>20
		1	07-27-98	11-12-98	91, 0, 17	171	36	35	225	21.1	>21.1
		2	11-13-98	03-11-99	87, 9, 22	196	52	35	225	26	>26
Springtree WTP	3,600	1	07-29-09	08-17-99	20, 0, 4	20	4	70	61	20	>20
		2	08-22-99	10-12-99	40, 1, 10	40	11	65	213	28	>28
		3	10-13-99	12-09-99	42, 1, 14	40	15	60	225	38	>38
		4*	12-10-99	03-27-00	62, 32, 14	40	15	60	222	37.5	>37.5
		5*	03-28-00	11-23-00	[1]178, 31, 31	120	33	NR	225	27.5	>27.5
Fiveash WTP	3,520	1*	10-12-99	10-23-99	10, 0, 1	11.04	1.2	60	225	10.9	>10.9
		2*	10-25-99	12-06-99	39, 1, 2	70.3	4.38	59	225	6.23	>6.23
Charlotte County											
Shell Creek WTP	830	1	07-01-99	08-07-99	21, 0, 9	4.9	1.47	100	250	30	30
		2	08-16-99	09-08-99	17, 0, 8	1.6	.59	75	250	37	37
		3	01-10-00	02-08-00	24, 1, 3	20.3	1.8	180-230	250	9	9
		3	01-10-00	02-08-00	24, 1, 3	20.3	NA	[2]80	250	[2]15	[2]15
Collier County											
Manatee Road	2,750	1	10-16-91	11-06-91	14, 6, 2	6.98	.33	60	300	5	NR
		2	11-11-91	01-14-92	46, 19, 6	30.38	2.57	60	300	8	6.8
		3	07-28-92	09-06-92	20, 20, 6	10	3.02	60	300	30	24
		4	09-15-92	10-25-92	20, 20, 8	10	3.94	60	300	39	32

Table 5. Cycle test data from aquifer storage and recovery wells in southern Florida --(Continued)

[Test data at all sites, excluding the West Well Field site, are only for the first storage well at the site (ASR-1). *Data extracted from monthly operating reports and daily records provided by the water treatment plant. All other cycle test data are from consulting reports or other published reports. DS, dissolved solids concentration in mg/L (milligrams per liter); Mgal, million gallons; NA, not applicable; NR, not reported; WTP, Water Treatment Plant; >, greater than]

Site name	Ambient chloride concentration (mg/L)	Cycle			Recharge, storage, recovery periods (days)	Recharge volume (Mgal)	Recovery volume (Mgal)	Chloride concentration of recharge water (mg/L)	Chloride concentration of recovered water at end of cycle (mg/L)	Recovery efficiency at end of cycle (percent)	Recovery efficiency at recovered water chloride concentration of 250 mg/L (percent)
		No.	Beginning date	End date							
Collier County--Continued											
Marco Lakes	2,600	1	06-26-97	08-19-97	39, 3, 12	19.763	6.04	NR	350	31	22
		1*	06-26-97	08-19-97	39, 3, 12	19.763	6.045	110	384	30.6	22.26
		2	08-21-97	02-25-98	88, 63, 37	86.686	25.7	NR	350	30	5.0
		2*	08-21-97	02-25-98	88, 63, 37	86.686	30.222	115	398	34.9	4
		3	03-05-98	04-29-98	26, 2, 27	21.054	15.8	NR	350	75	38
		3*	03-05-98	04-29-98	26, 2, 27	21.054	17.242	130	370	81.9	33.2
		4	09-01-98	06-10-99	134, 83, 68	110	55	NR	350	50.0	34.5
		4*	09-01-98	06-20-99	121, 98, 73	111	64.391	130	420	58.0	NR
		5	08-19-99	07-03-00	140, 102, 77	132	67	110	350	50.8	35.6
		5*	08-19-99	07-02-00	132, 109, 77	132.303	74	110	395	55.9	NR
Lee County											
Lee County WTP	550	1	10-14-80	NR	1.7, 0, 1.4	0.6	0.22	60	250	38.7	38.7
		2	03-26-81	NR	16, 47, 2.8	6.83	.66	150-350	250	9.7	9.7
		3	08-18-81	NR	79, 98, 40.8	29.03	8.82	60-100	250	30.4	30.4
Corkscrew WTP	39	1	10-25-95	11-14-95	7, 1, 12	2.001	2.963	NR	DS=330	150	NA
		2	02-14-96	10-04-96	76, 35, 122	31.3	22.8	NR	DS=300	73	NA
		3	10-07-96	02-12-97	63, 31, 34	26.1	19.8	NR	DS=225	76	NA
North Reservoir	670	1*	02-26-00	03-18-00	13, 7, 1	6.179	.607	155	250	9.8	9.8
San Carlos Estates	1,150	Test	10-25-99	11-15-99	10, 6, 5	28	7	90	600	25	2
		1	11-30-99	06-28-00	175, 0, 36	138	13	90	466	9.4	3.3
Miami-Dade County											
Hialeah	1,200	1	07-17-75	12-17-75	53, 2, 98	41.9	[3]13.8	65	NR	NR	32.9
		2	01-05-76	07-21-76	65, 54, 79	85	[3]40.7	65	NR	NR	47.8
		3	07-23-76	01-30-80	179, 181, 926	208	[3]80.1	65	NR	NR	38.5

Table 5. Cycle test data from aquifer storage and recovery wells in southern Florida --(Continued)

[Test data at all sites, excluding the West Well Field site, are only for the first storage well at the site (ASR-1). *Data extracted from monthly operating reports and daily records provided by the water treatment plant. All other cycle test data are from consulting reports or other published reports. DS, dissolved solids concentration in mg/L (milligrams per liter); Mgal, million gallons; NA, not applicable; NR, not reported; WTP, Water Treatment Plant; >, greater than]

Site name	Ambient chloride concentration (mg/L)	Cycle			Recharge, storage, recovery periods (days)	Recharge volume (Mgal)	Recovery volume (Mgal)	Chloride concentration of recharge water (mg/L)	Chloride concentration of recovered water at end of cycle (mg/L)	Recovery efficiency at end of cycle (percent)	Recovery efficiency at recovered water chloride concentration of 250 mg/L (percent)
		No.	Beginning date	End date							
Miami-Dade County--Continued											
West Well Field	2,400	1* (ASR-1)	02-18-99	07-21-99	146, 0, 7	359.7	27.8	48	164	7.7	>7.7
		2* (ASR-1)	07-31-99	02-15-00	187, 0, 12	212.2	53.3	43	80	25.1	>25.1
		2* (ASR-2)	09-03-99	02-15-00	153, 0, 12	276.1	61.7	43	212	22.3	>22.3
		3* (ASR-1)	02-15-00	03-23-01	299, 18, 85	338.56	359.37	41	500	106.1	57.4
		3* (ASR-2)	03-27-00	03-23-01	153, 123, 85	175.3	446.563	41	1,150	254.7	54.2
		3* (ASR-3)	02-15-00	03-23-01	Recharge = 299	200.47	No recovery	41	No recovery	NA	NA
		3* (ASR-1, ASR2, ASR-3 combined)	See dates above	See dates above	See values above	714.33	805.933	41	See values above	112.8	40.5
Monroe County											
Marathon	20,800	1	08-12-90	09-17-90	17, 0, 19	4.528	5.132	42	16,200	113	33
		2	09-17-90	12-13-90	43, 34, 11	9.698	3.458	NR	290	35	28
		3	12-13-90	01-25-91	27, 0, 16	5.322	4.181	NR	NR	79	68
		4	01-28-91	02-20-91	14, 0, 10	3.623	2.752	NR	NR	76	72
		5	NR	NR	51, 39, 26	15	6.5	NR	NR	NR	43
		6	NR	NR	56, 36, 43	15.1	7.7	NR	NR	NR	51
		7	NR	NR	56, 35, 30	15..8	8.9	NR	NR	NR	55
		8	NR	NR	76, 21, 34	15.4	10.1	NR	NR	NR	65
		9	NR	NR	54, 0, 44	15	10.1	NR	NR	NR	65
		10	NR	NR	56, 35, 31	15.3	8.6	NR	NR	NR	56
		11	NR	NR	63, 81, 25	[4]14	10.4	NR	NR	NR	71

Table 5. Cycle test data from aquifer storage and recovery wells in southern Florida --(Continued)

[Test data at all sites, excluding the West Well Field site, are only for the first storage well at the site (ASR-1). *Data extracted from monthly operating reports and daily records provided by the water treatment plant. All other cycle test data are from consulting reports or other published reports. DS, dissolved solids concentration in mg/L (milligrams per liter); Mgal, million gallons; NA, not applicable; NR, not reported; WTP, Water Treatment Plant; >, greater than]

Site name	Ambient chloride concentration (mg/L)	Cycle			Recharge, storage, recovery periods (days)	Recharge volume (Mgal)	Recovery volume (Mgal)	Chloride concentration of recharge water (mg/L)	Chloride concentration of recovered water at end of cycle (mg/L)	Recovery efficiency at end of cycle (percent)	Recovery efficiency at recovered water chloride concentration of 250 mg/L (percent)
		No.	Beginning date	End date							
Okeechobee County											
Taylor Creek/Nubbin Slough (Lake Okeechobee)	3,100	[5]4	09-05-89	11-04-89	20, 0, 40	90.94	NR	NR	[6]1,385	24	NR
		[7]1	04-17-91	05-29-91	35, 0, 7	181.35	28.06	150	[6]1,385	15	3.1
		[7]2	06-24-91	09-20-91	63, 8, 17	342.1	75.9	100 or less	[6]1,385	22	2.7
		[7]3	09-23-91	12-02-91	65, 5, 0	355	128	70 or less	[6]1,385	36	7.2
Palm Beach County											
Jupiter	1,980	1	NR	NR	Storage=15	[8]20.5	[8]0	65	250	0	0
		2	NR	NR	Storage=30	[8]100	[8]4.7	65	250	4.7	4.7
		3	NR	NR	Storage=30	[8]306	[8]55.5	65	250	18	18
		4	NR	NR	Storage=120	[8]102	[8]36.1	65	250	35.2	35.2
Boynton Beach East WTP	1,920	1	10-21-92	11-10-92	14, 0, 8	12.52	9.58	60	760	76.5	47
		2	11-10-92	01-22-93	44, 0, 31	57.32	26.1	50	420	45.5	30
		3	01-25-93	04-06-93	43, 5, 25	58.34	32.24	50	NR	55.3	47
		3*	01-25-93	04-06-93	41, 8, 22	54.31	32.04	47	300	59	49
		4*	04-20-93	05-28-93	16, 8, 14	[9]17.87	17.237	51	274	96.5	90
		5*	06-02-93	12-06-93	55, 98, 34	60.16	39.302	46	300	65.3	53.7
		6*	02-24-94	07-25-94	55, 57, 39	61.24	47.713	47	306.5	77.9	64
		7*	07-25-94	02-13-95	44, 124, 35	60.058	20.052	48	302	33.4	26.7
		8*	04-20-95	07-03-95	46, 2, 26	42.906	20.598	52	320.5	48	40
		9*	09-27-95	12-20-95	33, 22, 29	40.091	31.701	52	301	79.1	63
		10*	01-18-96	05-22-96	46, 52, 27	41.764	34.841	48	307	83.4	75
		11*	06-04-96	12-31-96	34, 149, 27	41.218	37.347	41	314	90.6	82
		12*	01-03-97	06-16-97	42, 81, 41	40.586	32.062	49	302	79	66
		13*	06-19-97	02-23-98	35, 174, 40	42.496	37.061	48	317.5	87.2	70
		14*	02-24-98	08-20-98	45, 1, 131	33.36	95.84	62	1,004	287	81
		15*	11-13-98	06-03-99	83, 57, 62	110.83	37.56	46	146	33.9	>33.9
		16*	06-15-99	01-28-00	156, 4, 67	89.98	88.724	NR	310	98.6	84

Table 5. Cycle test data from aquifer storage and recovery wells in southern Florida --(Continued)

[Test data at all sites, excluding the West Well Field site, are only for the first storage well at the site (ASR-1). *Data extracted from monthly operating reports and daily records provided by the water treatment plant. All other cycle test data are from consulting reports or other published reports. DS, dissolved solids concentration in mg/L (milligrams per liter); Mgal, million gallons; NA, not applicable; NR, not reported; WTP, Water Treatment Plant; >, greater than]

Site name	Ambient chloride concentration (mg/L)	Cycle			Recharge, storage, recovery periods (days)	Recharge volume (Mgal)	Recovery volume (Mgal)	Chloride concentration of recharge water (mg/L)	Chloride concentration of recovered water at end of cycle (mg/L)	Recovery efficiency at end of cycle (percent)	Recovery efficiency at recovered water chloride concentration of 250 mg/L (percent)
		No.	Beginning date	End date							
Palm Beach County--Continued											
West Palm Beach WTP	2,800	1*	10-04-97	01-22-98	93, 0, 17	270.7	40	NR	NR	14.8	NR
		2*	01-23-98	03-27-98	40, 1, 22	110.7	46	NR	NR	41.5	NR
		3*	04-01-98	06-08-98	37, 3, 28	102.6	58	NR	NR	56.5	NR
		4*	08-10-98	11-10-98	53, 3, 36	143.1	73.32	NR	NR	51.2	NR
St. Lucie County											
St. Lucie County	955	1	10-19-82	02-04-83	3, 38, 67	1.5	3.41	200	NR	NR	3
		1	10-19-82	02-04-83	3, 38, 67	1.5	NA	[2]50	NR	NR	[2]33

[1]Cycle 5 had 52 days of down time during the recharge period.
[2]Recovery efficiency estimated using a fictitious value for recharge chloride concentration.
[3]Recovery continued past the reported recovery volume, which had an ending chloride concentration of 250 mg/L.
[4]An additional 5.2 million gallons were recharged during the last 57 days of the storage period by trickle flow (50 gallons per minute).
[5]Conducted by CH_2M Hill.
[6]A specific conductance of 5,000 microsiemens per centimeter was used to terminate recovery for all cycles, which equals 1,385 milligrams per liter chloride concentration.
[7]Conducted by the U.S. Geological Survey.
[8]Injection rate for all cycles was 2,000 gallons per minute, and recovery rate was 1,000 gallons per minute.
[9]The recharge volume for cycle 4 could be too low, which would make the recovery efficiencies too high.

CASE STUDIES OF SELECTED AQUIFER STORAGE AND RECOVERY SITES

Detailed information regarding four sites is presented in this section. For the most part, the sites were selected on the basis of the number of cycles that were conducted. Two sites are located in southeastern Florida, and two are in southwestern Florida. The selected sites illustrate the contrast in hydrogeology between the coastal areas. Each case study includes a graphical representation of the hydrogeology at the site and well construction information.

Boynton Beach East Water Treatment Plant

The Boynton Beach East WTP ASR site located on the east coast in Palm Beach County is operated by Boynton Beach Utilities. The source of water for recharge is treated drinking water from the WTP. The location of the storage zone in relation to lithology, geophysical log signatures, and hydrogeologic units at the Boynton Beach site is shown in figure 11. Also shown are the location of flow zones as determined by flowmeter, fluid resistivity, and caliper logs for the interval extending from a depth of 804 to 1,200 ft below land surface. The flow zones in this interval primarily occur in the basal Hawthorn unit (Reese and Memberg, 2000) or near its base. The flow zones are thin, they tend to coincide with formation resistivity peaks possibly indicating cementation and secondary porosity, and they occur just below intervals of higher gamma-ray response. These intervals of higher gamma-ray response indicate beds high in phosphate sand content. The base of the Upper Floridan aquifer was not penetrated in the ASR well but is estimated to be at a depth of at least 1,500 ft below land surface.

The thickness of the storage zone open interval at the Boynton Beach site is 105 ft (fig. 9); transmissivity is reported to be about 9,400 ft^2/d (fig. 9; CH_2M Hill 1993), and ambient water had a chloride concentration of 1,900 mg/L (fig. 10). The site is located in a structurally high area along the east coast where the altitude of the Hawthorn Group basal contact is 930 ft below sea level (Reese and Memberg, 2000).

Cycle testing at the Boynton Beach site began in late 1992, and by early 2000, 16 recharge-recovery cycles had been conducted for an average of about 2 cycles per year (fig. 12). Potable recovery efficiency increased rapidly during the first four cycles to 90 percent per cycle; however, as noted previously, the 90 percent recovery for cycle 4 is questionable. During the next three cycles, recovery efficiency decreased to less than 30 percent, possibly because of longer storage periods. Recovery efficiency for cycles 8 to 16 generally increased to greater than 80 percent.

Percent recovery is plotted against the chloride concentration of recovered water during each cycle in figure 13. For most cycles, water was recovered until the chloride concentration in the recovered water slightly exceeded 300 mg/L (also see table 5). During cycle 14, however, recovery continued until chloride concentration increased to about 1,000 mg/L, contributing to a lower recovery rate for cycle 15. The data points for cycle 15 are shifted to substantially lower recovery percentages than for cycle 14 (fig. 13). The recovery efficiency for cycle 16 is the best obtained, with the exception of cycle 4, which has a recharge volume that could be higher than reported. However, the storage period for cycle 16 was only 4 days, and the recovery efficiency for this cycle could have benefited from the large recharge volume (111 Mgal) and incomplete recovery (recovery up to a chloride concentration of only 146 mg/L) for cycle 15.

Potable water recovery efficiencies for test and operational cycles at the Boynton Beach site appear to be greater than for all other Floridan aquifer system ASR sites in southern Florida. However, the number of cycles conducted at most other sites are limited, and the chloride concentration of the recharge water used at the Boynton Beach site is only about 50 mg/L (table 5). Several hydrogeologic, and design and management factors are favorable at this site that may explain the higher recovery efficiencies. The storage zone is located at the top of the Upper Floridan aquifer and is thin in comparison to the average storage zone thickness (about 180 ft) for wells in the Floridan aquifer system (fig. 8). Transmissivity and ambient salinity of the storage zone are moderate, being less than 30,000 ft^2/d and 3,000 mg/L of chloride concentration, respectively, and the site is located in a structurally high area.

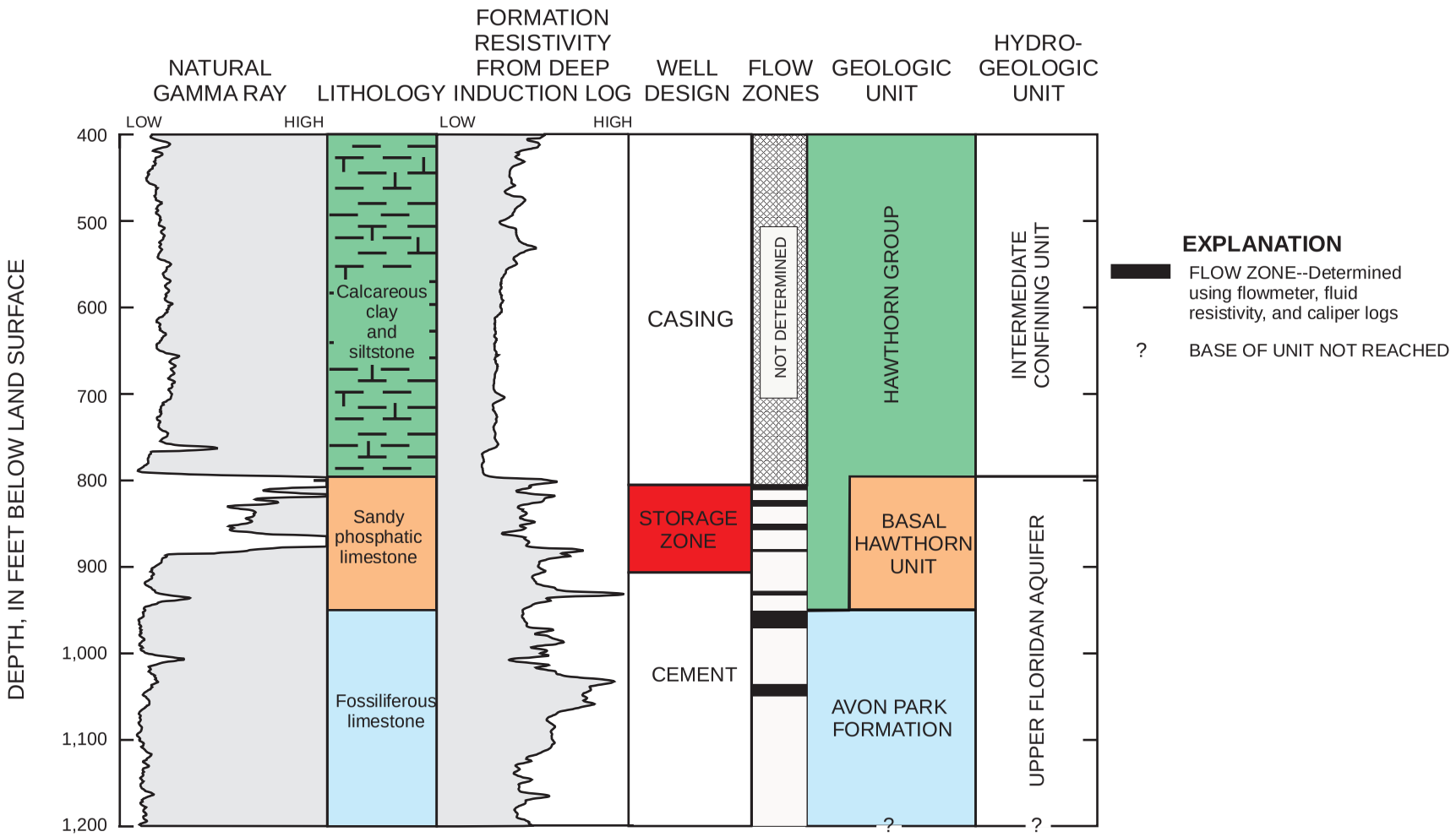

Figure 11. Location of the storage zone in relation to geophysical logs, lithology, flow zones, and geologic and hydrogeologic units for aquifer storage and recovery well PB-1194 at the Boynton Beach East Water Treatment Plant site in Palm Beach County.

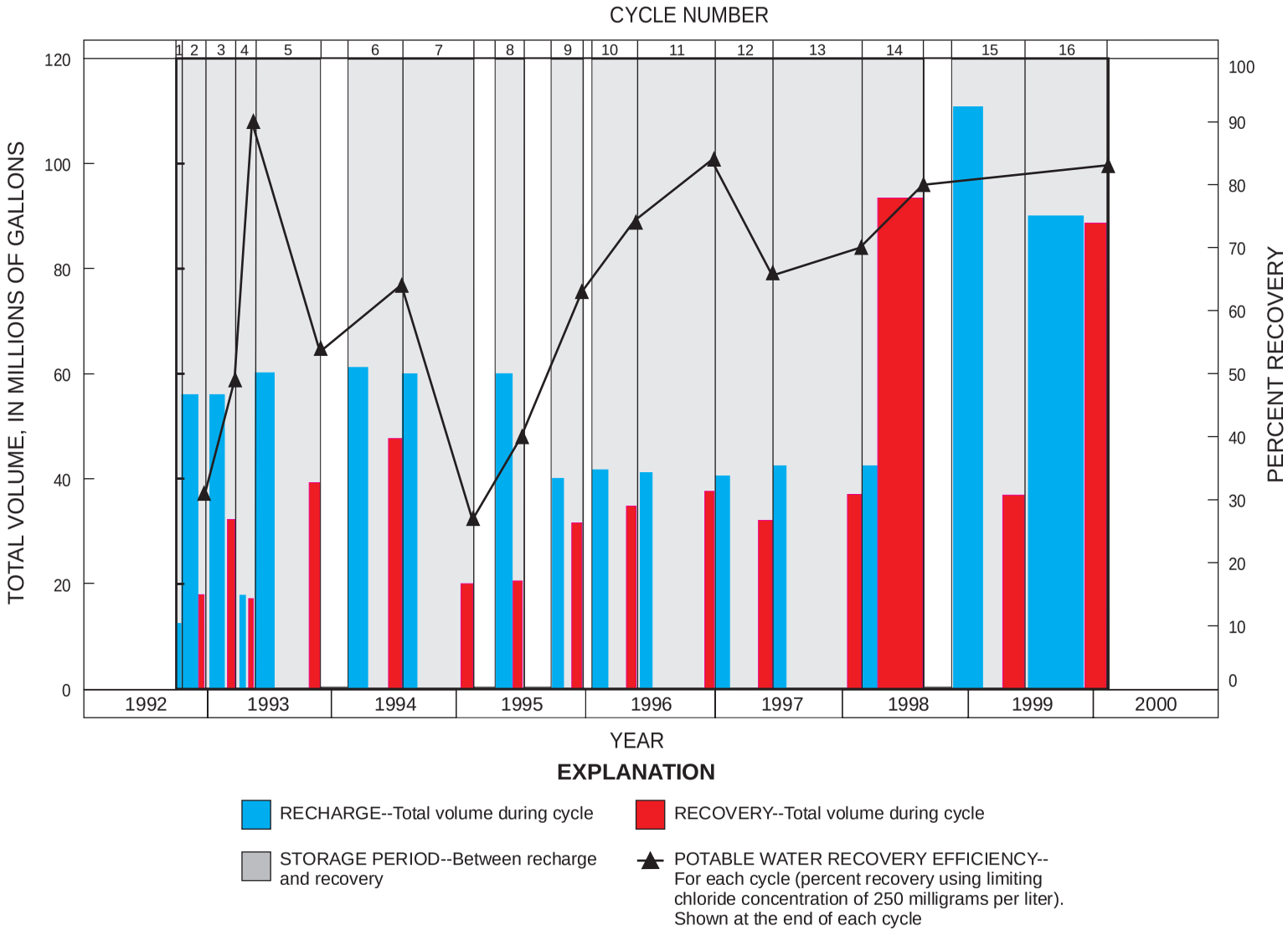

Figure 12. Operational cycles at the Boynton Beach East Water Treatment Plant site in Palm Beach County and relations of volumes recharged and recovered, time, and percent recovery for each cycle. Recovery for cycle 15 was 34 percent for an ending chloride concentration of 146 milligrams per liter.

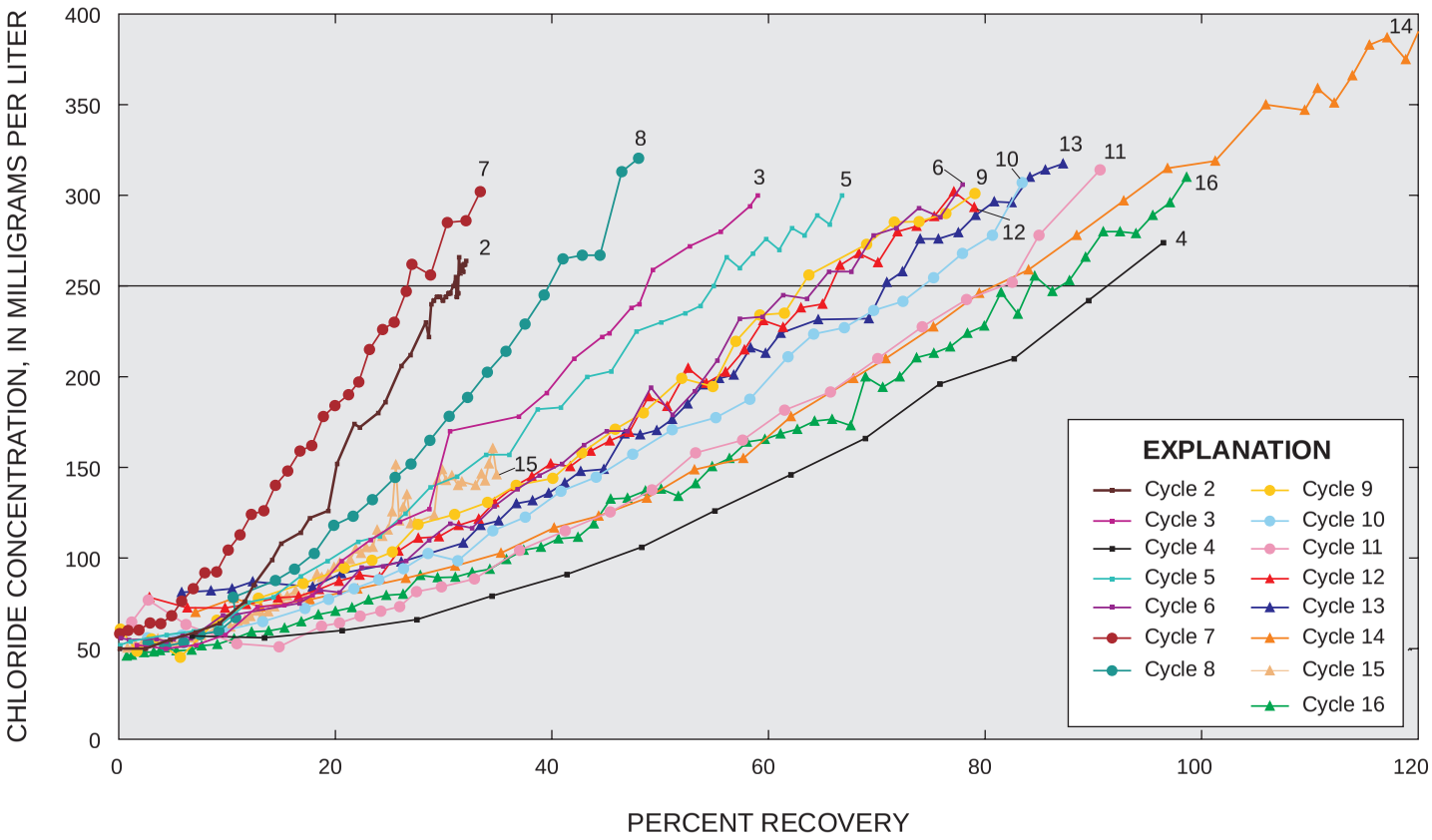

Figure 13. Percent recovery of recharged water during operational cycles in relation to chloride concentration of recovered water at the Boynton Beach East Water Treatment Plant site in Palm Beach County. Recovery for cycle 14 was continued until reaching a chloride concentration of about 1,000 milligrams per liter.

Springtree Water Treatment Plant

The Springtree WTP ASR site located in Broward County is operated by the City of Sunrise. Treated drinking water is used for recharge. The location of the storage zone in relation to lithology, geophysical log signatures, and hydrogeologic units at the Springtree site is shown in figure 14. Geophysical logs, such as the flowmeter, used to identify flow zones in the well were not run. Unlike the Boynton Beach site, the storage zone is not located at the top of the Upper Floridan aquifer. Casing was set through virtually all of the basal Hawthorn unit. The thickness of the storage zone open interval at the Springtree site is 160 ft (fig. 8). A photograph of the Springtree site wellhead site is shown in figure 15.

Storage zone transmissivity at the Springtree site is reported to be about 5,700 ft^2/d (table 3 at end

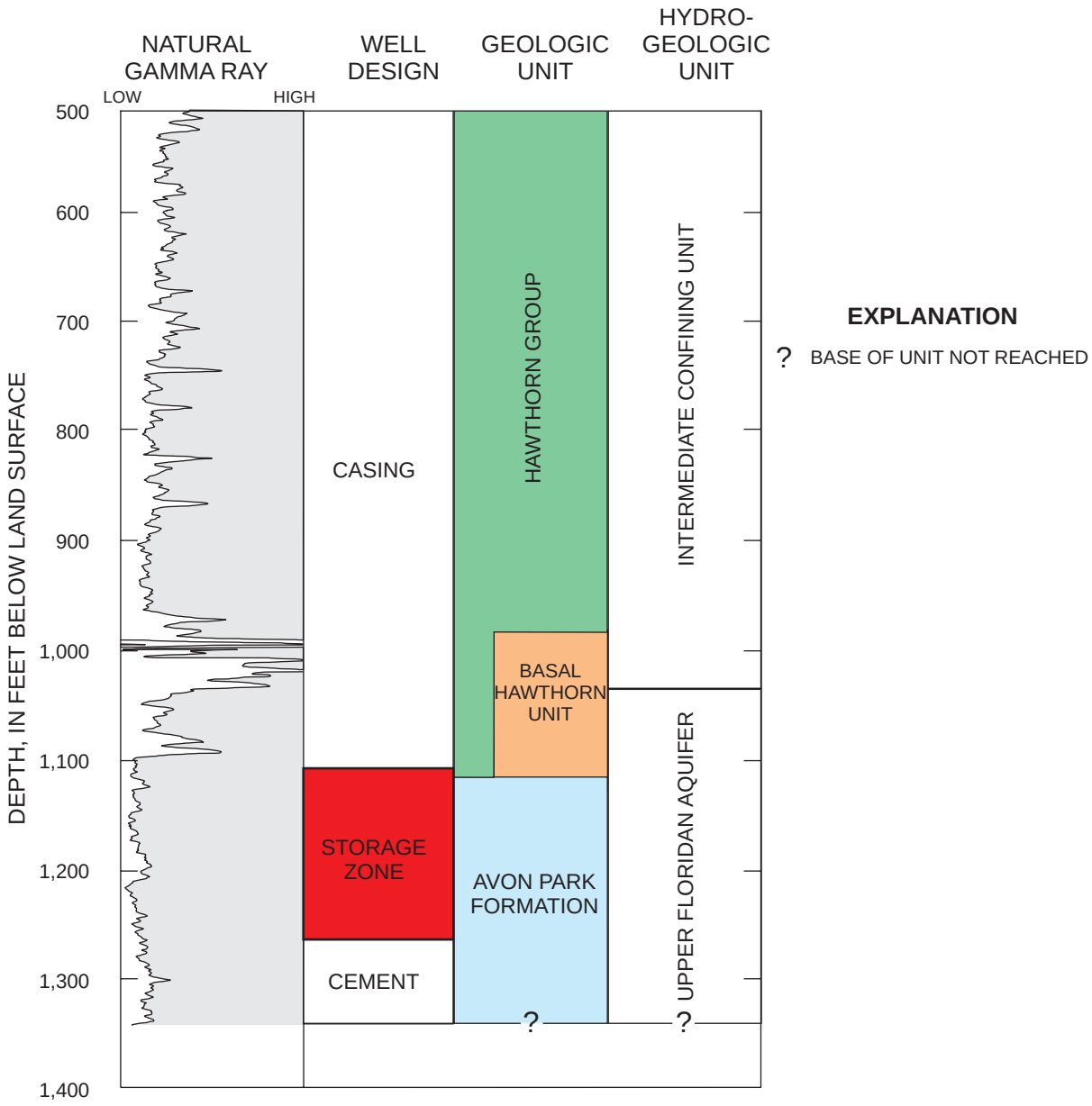

Figure 14. Location of the storage zone in relation to gamma-ray geophysical log and geologic and hydrogeologic units for aquifer storage and recovery well G-2914 at the Springtree Water Treatment Plant site in Broward County.

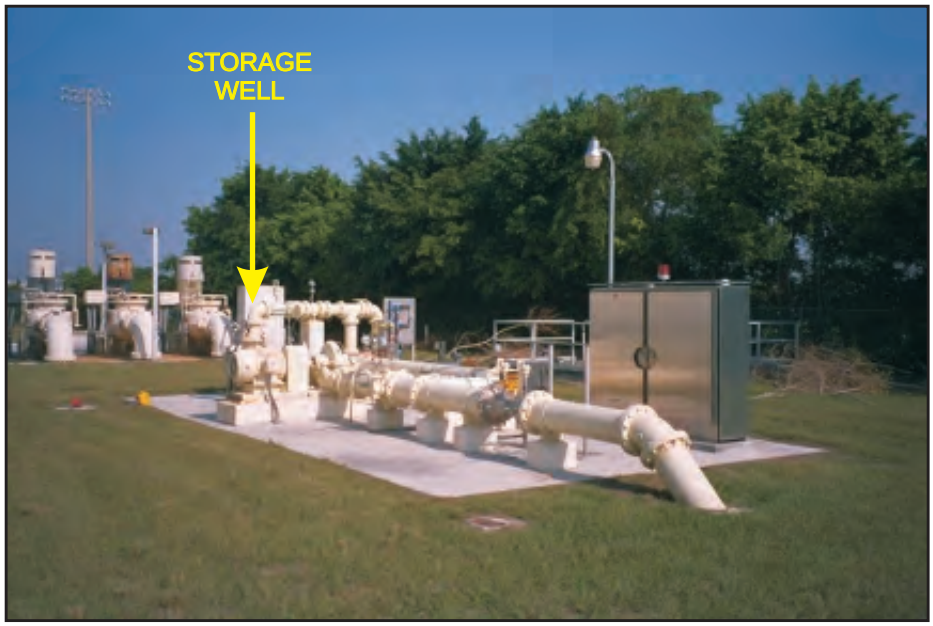

Figure 15. Wellhead piping, valves, and control system for the aquifer storage and recovery well at the Springtree Water Treatment Plant site in Broward County. Storage well on left side of concrete pad as shown by arrow.

of report; Montgomery Watson, 1998a). This value is lower than at surrounding sites (fig. 9), perhaps because only a small part of the basal Hawthorn unit is included in the open interval. The chloride concentration of ambient water in the storage zone is 3,600 mg/L (fig. 10). The altitude of the Hawthorn Group basal contact is 1,105 ft below sea level, and the site is located at the edge of a structurally low area (Reese, 1994).

Cycle testing at the Springtree site began at the end of July 1999, and five recharge-recovery cycles had been completed by the end of November 2000 (table 5). The ending chloride concentration for all cycles was 225 mg/L or less. The increase in recovery efficiency during the first four cycles was not as great as the Boynton Beach East WTP site, increasing from 20 percent for the first cycle to 37.5 for the fourth cycle. Although the volume recharged for the fifth cycle (120 Mgal) was at least three times that recharged in each of the first four cycles, recovery efficiency diminished to 27.5 percent. The lower recovery efficiencies at the Springtree site relative to the Boynton Beach East WTP site could be explained by high storage zone ambient water salinity and the storage zone position relative to the top of the aquifer.

Marco Lakes

The Marco Lakes ASR site located on the west coast in Collier County is operated by Florida Water Services for the City of Marco Island. The source of recharge water is partially treated surface water. The storage zone at the site straddles the contact between the basal Hawthorn unit and the Suwannee Limestone (fig. 16). The Suwannee Limestone is thick and well developed in the area, unlike southeastern Florida where the formation is thin or absent. The thickness and diameter of the open interval for the storage zone in well ASR-1 at the Marco Lakes site are 45 ft and 10 in., respectively (fig. 8; table 2 at end of report). By comparison, these dimensions are 44 ft and 12.25 in., respectively, for well ASR-2 (fig. 16; table 2 at end of report).

Transmissivity of the storage zone is reported to be about 9,100 ft^2/d (fig. 9; ViroGroup, Inc., 1998b). Storage zone ambient water is brackish; the reported chloride concentration is about 2,600 mg/L (fig. 10; well DZMW, table 4). Chloride concentration ranged from about 2,500 to about 3,700 mg/L in other wells completed in the storage zone at the Marco Lakes site (table 4). The site is located in a structurally high area where the altitude of the Hawthorn Group basal contact is 742 ft below sea level (Reese, 2000).

Five recharge-recovery cycles were conducted at the Marco Lakes site in ASR-1 between June 1997 and July 2000 (table 5). The ending chloride concentration for the recovery period used for comparison of cycles was 350 mg/L (Water Resources Solutions, Inc., 2000d), and the recovery efficiencies at this chloride concentration level increased from 31 percent for the first cycle to about 51 percent for the fifth cycle. The total volume of water recharged per cycle

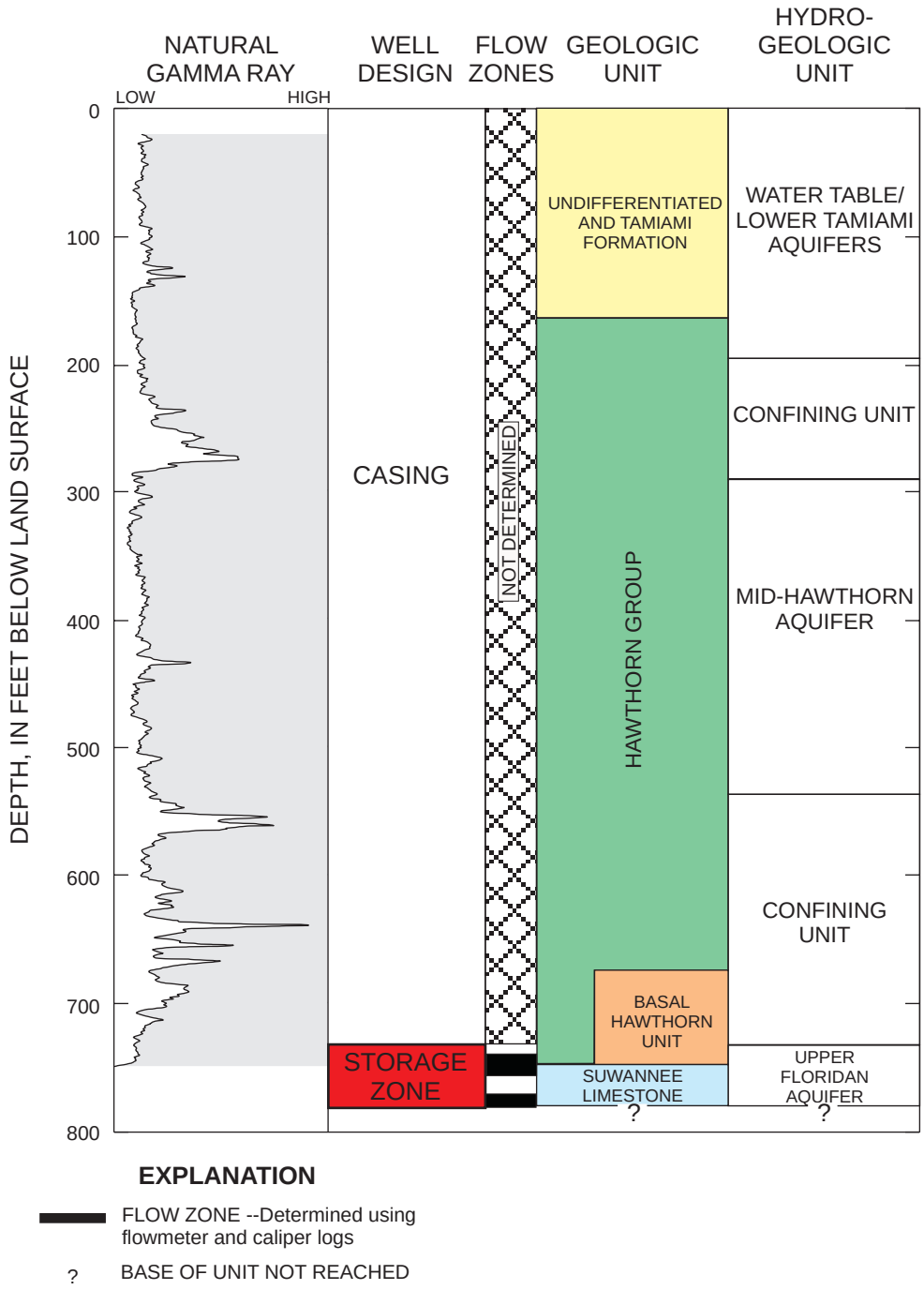

Figure 16. Location of storage zone in relation to gamma-ray geophysical log, flow zones, and geologic and hydro-geologic units for aquifer storage and recovery well C-1208 (ASR-2) at the Marco Lakes site in Collier County

increased from about 20 to 132 Mgal, respectively. The potable water recovery efficiency increased from 22 to almost 36 percent for the same two cycles.

Percent recovery was compared with the chloride concentration of recovered water during each cycle at the Marco Lakes site (fig. 17). On the basis of numerical simulation, the erratic recovery curve and poor recovery efficiency for cycle 2 is attributed to preferential well plugging during recharge of one of two receiving intervals (flow zones) in the storage zone (Water Resources Solutions, Inc., 1999c). Calcium carbonate is the likely precipitate causing plugging, and acidification of the recharge water prior to injection has reduced or eliminated the problem in later cycles.

The Marco Lakes recovery efficiencies at an ending chloride concentration of 350 mg/L rather than those at 250 mg/L concentration could serve as a better comparison with the Boynton Beach East WTP site potable recovery efficiencies. The chloride concentration of the recharge water at Marco Lakes averages

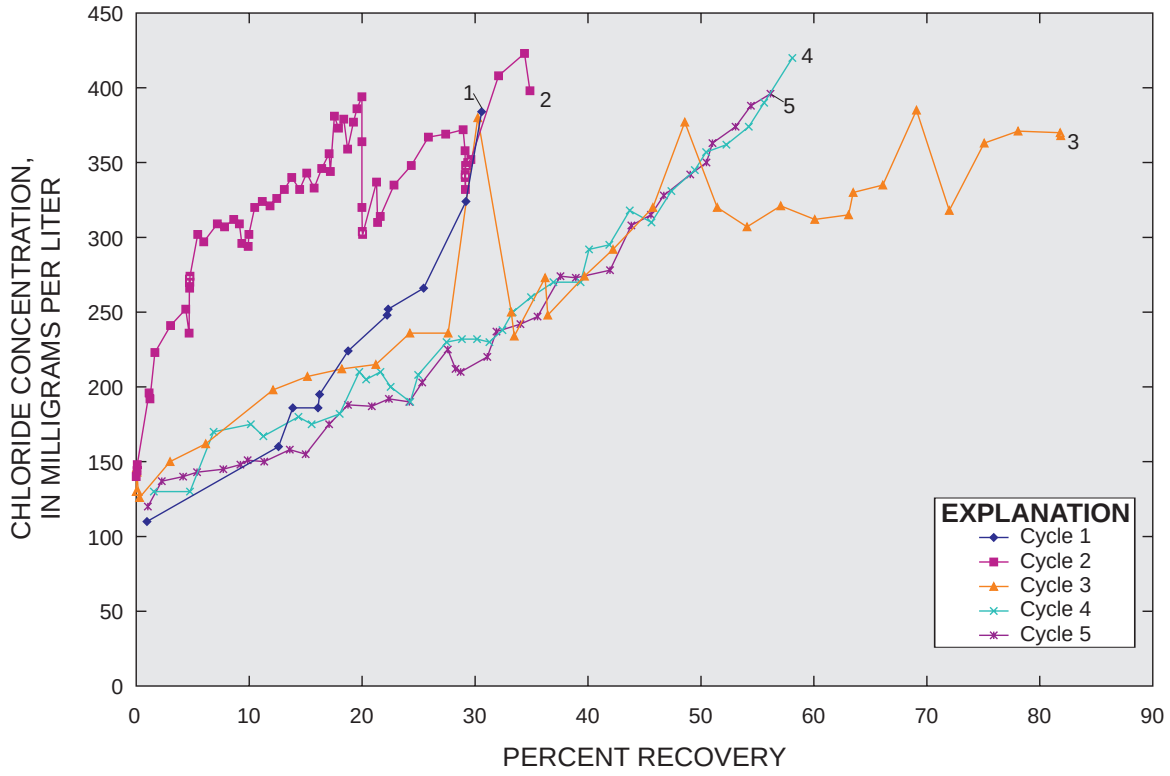

Figure 17. Percent recovery of recharged water during operational cycles in relation to chloride concentration of recovered water at the Marco Lakes site in Collier County.

120 mg/L (table 5), whereas the concentration at Boynton Beach averages about 50 mg/L. Perhaps calculations of recovery efficiencies based on a mass-balance approach would provide a better means of comparison between these two sites. These calculations would include the chloride concentrations of both the ambient and recharged water. Although the Marco Lakes site is in early phases of testing and operation, several factors could explain the moderate to good recovery efficiencies. The storage zone is thin and located near the top of the Upper Floridan aquifer (fig. 16). The storage zone has moderate transmissivity, and the site is located on a structural geologic high.

San Carlos Estates

The San Carlos Estates ASR site located near the west coast in Lee County is operated by Bonita Springs Utilities. Treated drinking water is used as the recharge water source. The storage zone at the site is located within the basal Hawthorn unit (fig. 18). The top of the Suwannee Limestone was not reached in any of the wells at the site. The thickness of the ASR well storage zone is only 51 ft (fig. 8).

Compared to the Marco Lakes site, transmissivity of the storage zone at the San Carlos Estates site is high; it is reported to be about 70,000 ft^2/d (fig. 9; CH_2M Hill, 1999b). The chloride concentration of ambient water in the storage zone is only 1,100 mg/L (fig. 10). The site may be located in a slightly low area structurally (Reese, 2000); however, additional wells that intersect the basal contact of the Hawthorn Group are required to confirm this setting.

Two cycles, one a short test cycle, were conducted at the San Carlos Estates ASR site (table 5). Despite a second cycle recharge volume of 138 Mgal, potable recovery efficiency has been no greater than about 3 percent. High transmissivity of the storage zone and the distribution of permeability within it may explain the poor recovery efficiency obtained thus far. Flowmeter log data indicate that most flow in the storage zone occurs within a 4-ft-thick interval between 698 and 702 ft below land surface (fig. 18). The high permeability of this thin flow zone may cause high dispersive mixing within the storage zone resulting in the poor recovery.

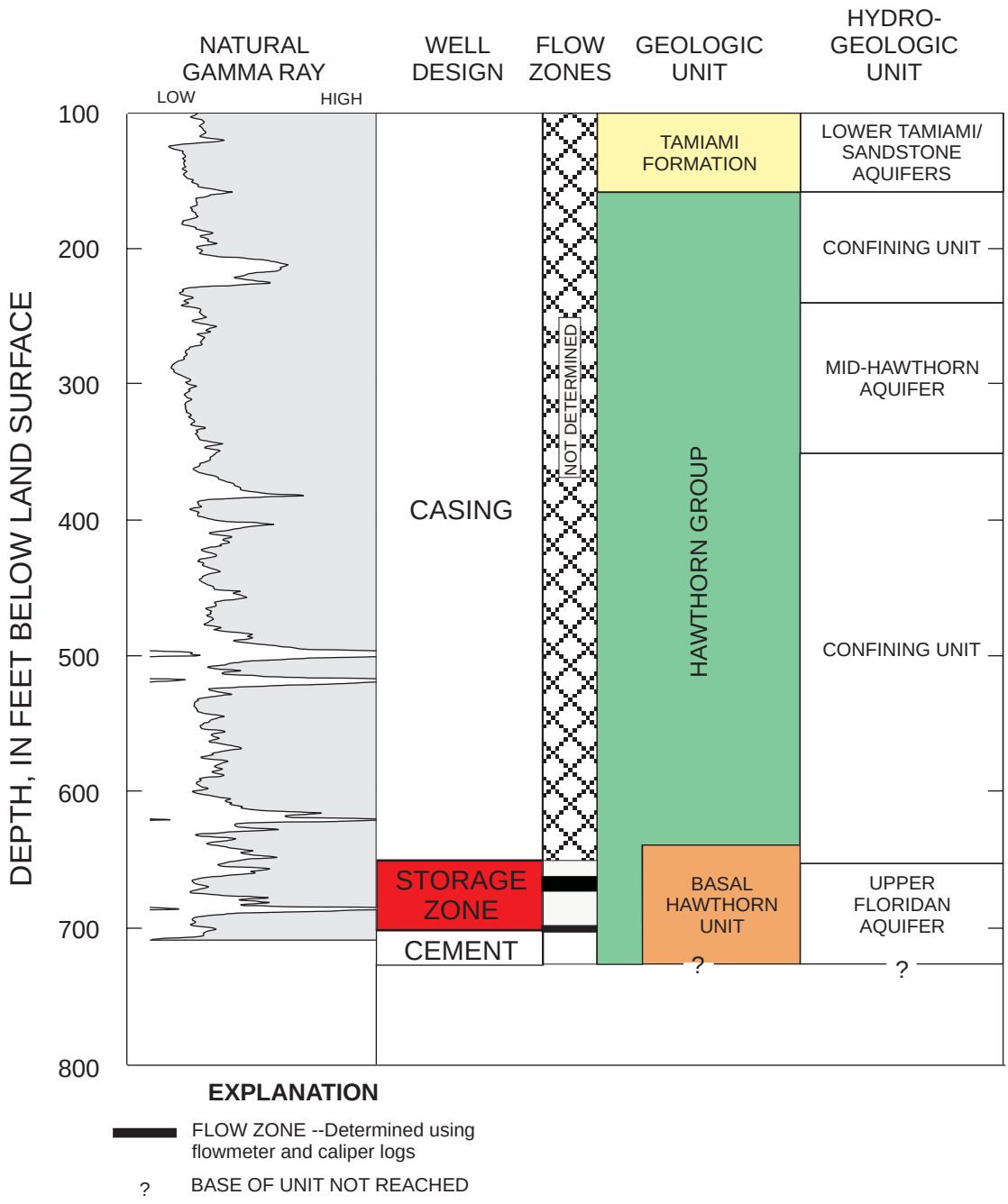

Figure 18. Location of storage zone in relation to gamma-ray geophysical log, flow zones, and geologic and hydrogeologic units for aquifer storage and recovery well L-5812 at the San Carlos Estates site in Lee County.

SUMMARY AND CONCLUSIONS

Aquifer storage and recovery (ASR) wells were constructed at 27 sites in southern Florida with most sites located in coastal areas. Twenty ASR were constructed by local municipalities or counties in southern Florida in the 1990's and 14 since 1996. Six of the 27 sites were experimental in nature and are no longer active. The storage zone at 23 of the 27 sites is contained within the Floridan aquifer system; of these 23 sites, 22 are in the Upper Floridan aquifer and 1 is in the Lower Floridan aquifer

Regional ASR in southern Florida has been proposed in the Comprehensive Everglades Restoration Plan (CERP) as a cost-effective water-supply alternative that can help meet needs of agricultural, municipal, and recreational users and help provide ecological benefits. About 330 high capacity wells have been proposed for southern Florida, with most to be sited inland, such as around Lake Okeechobee. Water salinity in the Upper Floridan aquifer, the hydrogeologic unit of interest in the CERP, is brackish to saline at all current ASR sites in southern Florida. The ambient salinity of water contained in the storage zone can substantially affect recovery of water recharged and stored.

This study was performed to inventory construction, hydrogeologic, and operational data on ASR sites in southern Florida and to compare site performance to hydrogeologic, design, or management factors that may influence their degree of success. Each ASR cycle includes periods of injection of freshwater, storage, and recovery, with each period lasting days or months. Potable water recovery efficiency of individual cycles at a site is the primary measure used to evaluate the performance of sites, and this efficiency is the volume of water recovered when chloride concentration reaches 250 as a percent of the volume recharged.

The basal contact of the Hawthorn Group lies close to the top of the Upper Floridan aquifer, and the most important flow zones in this aquifer commonly occur at or near this contact. The altitude of this contact varies considerably in southern Florida, ranging from less than 600 ft to greater than 1,200 ft below sea level. Local relief on this contact can be as much as several hundred feet.

Well data were inventoried and complied for all wells at existing and historical ASR sites in southern Florida. Construction and testing data were compiled into four categories: (1) well identification, location, and construction data; (2) hydraulic well-test data; (3) ambient formation water-quality data; and (4) cycle testing data. Intervals for which data were inventoried and compiled include the ASR storage zone interval and deeper and shallower intervals.

Factors important to efficient ASR operation vary widely between the sites. The thickness of the open storage zone ranged from 45 to 452 ft. Open intervals in the 150 to 200 ft range are most common. Transmissivity of the Upper Floridan aquifer storage zone for 17 sites ranged from 800 to 108,000 ft^2/d. Transmissivity at the Taylor Creek/Nubbin Slough (Lake Okeechobee) site, completed in the Lower Floridan aquifer, was reported to be 590,000 ft^2/d. Storage zone transmissivity for most sites ranged from 5,000 to 30,000 ft^2/d; greater than 30,000 ft^2/d is considered high. Leakance of storage zone confining units, determined from multiwell aquifer tests at seven sites in the Upper Floridan aquifer, ranged from 3.9×10^{-5} to 6.3×10^{-2} 1/d; of these, five had leakance greater than 1×10^{-3} 1/d, indicating that confinement is poor in some areas. These high leakance estimates are probably best attributed to leakage from below the storage zone rather than from above. Chloride concentration of ambient water from storage zones in the Upper Floridan aquifer ranged from 500 to 11,000 mg/L. At most sites, the chloride concentration ranged from about 1,000 to 3,000 mg/L; greater than 3,000 mg/L is considered to be high.

Cycle test data were compiled for 18 ASR sites, and potable water recovery efficiencies were calculated at 16 of these sites. To date, the Boynton Beach East WTP site has experienced the highest number of recharge-recovery cycles (16 cycles). Recharge volume per cycle ranged from as low as 0.6 to as high as 714 Mgal. Cycle 3 at the Hialeah site had the longest storage time (181 days). The highest potable water recovery efficiency for the first cycle was 47 percent at the Boynton Beach East WTP site, and except for one site with incomplete information, the lowest was 2 percent at the San Carlos Estates site. Nine of the 16 sites had a recovery efficiency above 10 percent for the first cycle, and 10 sites achieved a recovery efficiency above 30 percent during at least one cycle. The highest recovery efficiency achieved was 84 percent for cycle 16 at the Boynton Beach East WTP site. Recovery efficiencies for test and operational cycles at Boynton Beach appeared to be better than all other Floridan aquifer system sites. However, the number of cycles conducted at most other sites was limited, and the

chloride concentration of the recharge water used at Boynton Beach was low (about 50 mg/L).

The increase in potable water recovery efficiency during the first five cycles at the Springtree WTP site was not as favorable as at the Boynton Beach East WTP site. Recovery started at 20 percent for the first cycle and ended at 27.5 percent for the fifth cycle, despite a recharge volume for the fifth cycle (120 Mgal) that was three or more times greater than in all previous cycles. Recovery efficiencies at the Marco Lakes site for the first five cycles increased from 22 to 36 percent, with 132 Mgal recharged during cycle 5. However, these numbers may not be comparable to those from the Boynton Beach and Springtree sites because the chloride concentration of the recharged water at the Marco Lakes site was two or more times higher than at the other two sites, lowering the potable water recovery efficiencies.

Based on review of four case studies and review of data from other sites, several hydrogeologic and design factors appear to play a substantial role in the performance of ASR in the Floridan aquifer system in southern Florida. Recovery efficiency appears to be maximized if the storage zone is thin and located within the uppermost part of the Upper Floridan aquifer, and transmissivity (less than about 30,000 ft^2/d) and ambient salinity (less than 3,000 mg/L chloride concentration) of the ASR storage zone are moderate. The structural setting of a site could also be important because of the potential for updip migration of recharged freshwater or the lessening of overlying confinement due to deformation. Avoiding areas that lie within a structural low or which are structurally complex or have higher dip could improve recovery efficiency.

SELECTED REFERENCES

Bush, P.W., and R.H. Johnston, 1988, Ground-water hydraulics, regional flow, and ground-water development of the Floridan aquifer system in Florida and in parts of Georgia, South Carolina, and Alabama: U.S. Geological Survey Professional Paper 1403-C, 80 p.

Camp, Dresser, and McKee, Inc., 1993, Floridan aquifer test/production well and monitor well: Completion report prepared for the City of Deerfield Beach, Florida, and South Florida Water Management District, 29 p.

CH_2M Hill, 1989, Construction and testing of the aquifer storage and recovery (ASR) demonstration project for Lake Okeechobee, Florida: Engineering report prepared for South Florida Water Management District, p. 1-1 to 4-9, appendixes, 3 v.

——— 1991, Preliminary results of the Florida Keys aquifer storage recovery test program at Marathon: Final report prepared for Florida Keys Aqueduct Authority, 46 p. 12 app.

——— 1993, Boynton Beach aquifer storage and recovery system: Engineering report prepared for the City of Boynton Beach, Florida, p. 1-1 to 7-1, 13 app.

——— 1997, Construction and testing of the aquifer storage and recovery (ASR) system at the BCOES 2A Water Treatment Plant: Engineering report prepared for the Broward County Office of Environmental Services and Montgomery Watson, p. 1-1 to 6-3, 13 app.

——— 1998a, Construction and testing of the aquifer storage and recovery facility at the West Palm Beach Water Treatment Plant: Engineering report prepared for the City of West Palm Beach, Florida, p. 1-1 to 7-1, 15 app.

——— 1998b, Construction and testing of the aquifer storage and recovery (ASR) system at the MDWASD West Wellfield: Engineering report prepared for Miami-Dade Water and Sewer Department, p. 1-1 to 6-2, 13 app.

——— 1998c, Construction and testing of the aquifer storage and recovery facility at the City of Delray Beach's North Storage Reservoir: Engineering report prepared for the City of Delray Beach, Florida, p. 1-1 to 5-1, app.

——— 1999a, Cycle testing report for the BCOES 2A Water Treatment Plant ASR facility: Report prepared for Underground Injection Control Program Manager of Florida Department of Environmental Protection, 4 p., figures and attachments.

——— 1999b, Potable water aquifer storage recovery phase II drilling and testing at the San Carlos Estates ASR site, Bonita Springs, Florida: Well completion report prepared for Bonita Springs Utilities, Inc., p. 1-1 to 7-2, 9 app.

——— 2000a, San Carlos Estates potable water ASR 5-day aquifer performance test, water quality and aquifer characteristic data: Technical memorandum TM-5 prepared for Bonita Springs Utilities, Inc., 14 p. and attachments.

——— 2000b, San Carlos Estates potable water ASR, cycle test 1 recovery water quality results: Technical memorandum TM-7 prepared for Bonita Springs Utilities, Inc., 15 p. and attachments.

Cooper, H.H., Jr., and Jacob, C.E., 1946, A generalized graphical method for evaluating formation constants and summarizing well-field history: American Geophysical Union Transactions, v. 27, no. 4, p. 526-534.

Cunningham, K.J., Locker, S.D., Hine, A.C., and others, 2001, Surface-geophysical characterization of groundwater systems of the Caloosahatchee River Basin, southern Florida: U.S. Geological Survey Water-Resources Investigations Report 01-4084, 76 p.

Fitzpatrick, D. J., 1986, Tests for injecting, storing and recovering freshwater in a saline artesian aquifer, Lee County, Florida: U.S. Geological Survey Water-Resources Investigations Report 85-4249, 53 p.

Freeze, R.A., and Cherry, J.A., 1979, Groundwater: Englewood Cliffs, N.J., Prentice-Hall, Inc., 604 p.

Hantush, M.S., and Jacob, C.E., 1955, Nonsteady radial flow in an infinite leaky aquifer: American Geophysical Union Transactions, v. 36, no. 1, p. 95-100.

Jacob, C.E., and Lohman, S.W., 1952, Nonsteady flow to a well of constant drawdown in an extensive aquifer: American Geophysical Union Transactions, v. 33, p. 559-569.

Khanal, N.N., 1980, Advanced water-supply alternatives for the Upper East Coast Planning Area; Part I – feasibility of cyclic storage of freshwater in a brackish aquifer and Part II – desalination alternative: South Florida Water Management District Technical Publication no. 80-6, 75 p.

Lukasiewicz, John, Switanek, M.P., and Verrastro, R.T., 2001, Floridan aquifer system test well program, city of South Bay, Florida: South Florida Water Management District Technical Publication WS-2, 34 p., appendixes.

Merritt, M.L., 1985, Subsurface storage of freshwater in south Florida: a digital model analysis of recoverability: U.S. Geological Survey Water-Supply Paper 2261, 44 p.

——— 1997, Tests of subsurface storage of freshwater at Hialeah, Dade County, Florida, and numerical simulation of the salinity of recovered water: U.S. Geological Survey Water-Supply Paper 2431, 114 p., 2 pls.

Merritt, M.L., Meyer, F.W., Sonntag, W.H., and Fitzpatrick, D. J., 1983, Subsurface storage of freshwater in south Florida: a prospectus: U.S. Geological Survey Water-Resources Investigations Report 83-4214, 69 p.

Meyer, F.W., 1989a, Hydrogeology, ground-water movement, and subsurface storage in the Floridan aquifer system in southern Florida: U.S. Geological Survey Professional Paper 1403-G, 59 p.

——— 1989b, Subsurface storage of liquids in the Floridan aquifer system in south Florida: U.S. Geological Survey Open-File Report 88-477, 25 p

Miller, J.A., 1986, Hydrogeologic framework of the Floridan aquifer system in Florida and in parts of Georgia, Alabama, and South Carolina: U.S. Geological Survey Professional Paper 1403-B, 91 p.

Missimer & Associates, Inc., 1991a, Phase I – deep aquifer hydrogeologic study, Collier County, Florida, preliminary report: Addendum to report prepared for Collier County Utilities Division, 5 p., 5 app.

——— 1991b, Phase I – deep aquifer hydrogeologic study, Collier County, Florida: Final report prepared for Collier County Utilities Division, 61 p., 5 app.

——— 1993, Phase II Collier County aquifer storage and recovery project: Preliminary report prepared for Collier County Utilities Division, 47 p.

Montgomery Watson, 1998a, Springtree Water Treatment Plant aquifer storage and recovery system: Well construction report prepared for the City of Sunrise, Florida, p. 1-1 to 5-1, 13 app.

——— 1998b, Exploratory ASR well drilling and testing at the Shell Creek Water Treatment Plant: Interim report prepared for the City of Punta Gorda, Florida, and Southwest Florida Water Management District, p. 1-1 to 5-4, appendixes.

——— 1998c, Fiveash Water Treatment Plant aquifer storage and recovery system: Well construction report prepared for the City of Fort Lauderdale, Florida, p. 1-1 to 6-1, 14 app.

——— 2000a, Exploratory ASR well drilling and testing at the Shell Creek Water Treatment Plant: Final report prepared for the City of Punta Gorda, Florida, and Southwest Florida Water Management District, p. 1-1 to 5-5, appendixes.

——— 2000b, Springtree Water Treatment Plant aquifer storage and recovery (ASR) system: Cycle testing report prepared for the City of Sunrise, Florida, 27 p., 2 app.

PBS&J and CH_2M Hill, 2000, Reclaimed water ASR well construction and testing summary at the South Regional Wastewater Treatment Plant: Final report prepared for Englewood Water District and Southwest Florida Water Management District, p. 1-1 to 6-1, 14 app.

Pyne, R.D.G., 1995, Groundwater recharge and wells, a guide to aquifer storage recovery: Boca Raton, Fla., Lewis Publishers, 376 p.

Quiñones-Aponte, Vicente, Kotun, Kevin, and Whitley, J. F., 1996, Analysis of tests of subsurface injection, storage, and recovery of freshwater in the Lower Floridian aquifer, Okeechobee County, Florida: U.S. Geological Survey Open-File Report 95-765, 32 p.

Reese, R.S., 1994, Hydrogeology and the distribution and origin of salinity in the Floridan aquifer system, southeastern Florida: U.S. Geological Survey Water-Resources Investigations Report 94-4010, 56 p.

——— 2000, Hydrogeology and the distribution of salinity in the Floridan aquifer system, southwestern Florida: U.S. Geological Survey Water-Resources Investigations Report 98-4253, 86 p., 10 pls.

Reese, R.S., and Cunningham, K.J., 2000, Hydrogeology of the gray limestone aquifer in southern Florida: U.S.

Geological Survey Water-Resources Investigations Report 99-4213, 244 p.

Reese, R.S., and Memberg, S.J., 2000, Hydrogeology and the distribution of salinity in the Floridan aquifer system, Palm Beach County, Florida: U.S. Geological Survey Water-Resources Investigations Report 99-4061, 52 p., 2 pls.

Theis, C.V., 1935, The relation between the lowering of the piezometric surface and the rate and duration of discharge of a well using ground-water storage: American Geophysical Union Transactions, v. 16, p. 519-524.

U.S. Army Corps of Engineers and South Florida Water Management District, 1999, Central and Southern Florida Project Comprehensive Review Study: Final Integrated Feasibility Report and Programmatic Environment Impact Statement, 27 p.

——— 2001, Lake Okeechobee aquifer storage and recovery pilot project, project management plan, final draft: Central and Southern Florida Comprehensive Everglades Restoration Plan, 66 p.

ViroGroup, Inc., 1998a, Lee County Corkscrew Water Treatment Facility aquifer storage and recovery pilot well: Well completion report prepared for Lee County Utilities, figures and appendixes.

——— 1998b, Marco Lakes aquifer storage and recovery pilot project: Final report prepared for Florida Water Services, Inc., 51 p., 8 app.

ViroGroup, Inc., and Camp, Dresser, and McKee, Inc., 1994, Lee County Regional Water Supply Authority ASR test well #LM-3982, east Lee County, Florida: Completion report prepared for Lee County Regional Water Supply Authority, 37 p., 6 appendixes.

——— 1997, Corkscrew Water Treatment Facility aquifer storage and recovery pilot project: Final report prepared for Lee County Regional Water Supply Authority, 108 p. and appendixes, 2 v.

Walton, W.C., 1962, Selected analytical methods for well and aquifer evaluation: Illinois State Water Survey Bulletin no. 49, 81p.

——— 1970, Groundwater water resources evaluation: New York, McGraw-Hill, 664 p.

Water Resources Solutions, Inc., 1999a, Lee County Utilities observation well #1 (LM-6208) at the North Reservoir site, Lee County, Florida: Completion report prepared for Hole, Montes & Associates, Inc., 27 p., 9 app.

——— 1999b, Lee County Utilities ASR Well #1 (LM-6210) at the North Reservoir site, Lee County, Florida: Completion report prepared for Hole, Montes & Associates, Inc., 26 p., 9 app.

——— 1999c, Marco Lakes aquifer storage and recovery project cycle 4: Report prepared for Florida Water Services, Inc., 33 p., 1 app.

——— 2000a, Lee County Utilities observation wells #1 (LM-6209) and #3 (LM-6615) at the Olga WTP site, Lee County, Florida: Completion report prepared for Hole, Montes & Associates, Inc., 39 p., 9 app.

——— 2000b, Lee County Utilities ASR Well #1 (LM-6086) at the Olga WTP site, Lee County, Florida: Completion report prepared for Hole, Montes & Associates, Inc., 32 p., 9 app.

——— 2000c, Marco Lakes ASR expansion project: Well completion report prepared for Florida Water Services, Inc., 24 p., 3 v., app.

——— 2000d, Marco Lakes aquifer storage and recovery project cycle 5: Summary report prepared for Florida Water Services, Inc., 17 p.

Water Resources Solutions, Inc., and Pitman Hartenstein & Assoc., Inc., 1999, Corkscrew ASR expansion project: Well completion report prepared for Lee County Utilities, 40 p., 2 v., appendixes.

Wedderburn, L.A., and Knapp, M.S., 1983, Field investigation into the feasibility of storing fresh water in saline portions of the Floridan aquifer system, St. Lucie County, Florida: South Florida Water Management District Technical Publication 83-7, 71 p.

Table 2. Well Identification, location, and construction data for aquifer storage and recovery system wells in southern Florida

[Depths are in feet below land surface. Completed open intervals are open hole unless noted otherwise. Diameter of open interval for open-hole completions is size of bit used to drill or ream out hole. Abbreviations and annotations: USGS, U.S. Geological Survey; WTP, water treatment plant; WWTP, wastewater treatment plant; PVC, polyvinyl chlorinated; ?, unknown; NR, not reported]

Site name	USGS local well no.	Other well identifier	Land-net location	Latitude and longitude	Altitude of land surface (feet)	Total hole depth (feet)	Date at end of construc-tion	Depth to top and bottom of casing (feet)	Casing diam-eter (inches)	Type of casing	Completed open interval (feet)	Diameter of open interval (inches)
Broward County												
Deerfield Beach West WTP	G-2887	ASR-1	Same as for MW-1	261857 800726	13.17	1,128	10-92	0-400 0-960	26.00 12.00	Steel PVC	960-1,128	10.63
	G-2888	MW-1	SENE S2, 48S,42E; 370 feet north of ASR-1	261901 800726	12	1,128	12-10-92	0-42 0-402 0-960	24.00 16.00 6.00	Steel Steel Steel	960-1,128	5.875
Broward County WTP 2A	G-2889	ASR-1	SE S12, 48S, 42E	261735 800625	16.6	1,200	12-03-96	0-40 0-397 0-995	36.00 26.00 16.00	Steel Steel Steel	995-1,200	16
	G-2916	MW-1			17	1,200	09-25-96	0-40 0-400 0-990	24.00 14.00 6.63	Steel Steel Steel	990-1,200	6
Springtree WTP	G-2914	ASR-1	NW S21,49S,41E	261033 [1]801540	10	1,345	07-97	0-170 0-1,110	26.00 16.00	Steel Steel	1,110-1,270	16
Fiveash WTP	G-2917	ASR-1		261030 800915	NR	1,300	12-30-97	0-198 0-1,055	26.00 16.00	Steel Steel	1,055-1,200	16
	G-2918	FMW-1			NR	1,175	03-15-98	0-370 0-1,055	14.00 6.63	Steel Steel	1,055-1,175	13
	G-2919	SMW-1			NR	210	01-11-98	0-20 0-180 [2]180-200	12.00 2.00 2.00	Steel PVC PVC	[3]180-200	2
Charlotte County												
Shell Creek WTP	CH-315	ASR-1	S29, 40S, 24E	265831 815607	19.4	1,043	04-99	0-34 0-700 650-764	24.00 16.00 12.00	Steel	764-933	12.25
Englewood South Regional WWTP	CH-318	TPW-1 (ASR-1)	S16, 41S, 20E	265415 821604	6	807	03-30-00	0-37 0-295 0-507	30.00 24.00 16.00	Steel Steel Steel	507-700	15
	CH-319	SZMW-1	400 feet west of TPW-1		NR	700	04-17-00	0-42 0-290 0-510	20.00 14.00 6.00	Steel Steel PVC	510-700	6
	CH-320	IMW-1	2,200 feet northwest of TPW-1		NR	320	04-06-00	0-40 0-280	14.00 4.00	Steel PVC	280-320	4
	CH-321	SMW-1	150 feet east of TPW-1		NR	205	03-23-00	0-40 0-170	14.00 6.00	Steel PVC	170-205	6

Table 2. Well Identification, location, and construction data for aquifer storage and recovery system wells in southern Florida --(Continued)

[Depths are in feet below land surface. Completed open intervals are open hole unless noted otherwise. Diameter of open interval for open-hole completions is size of bit used to drill or ream out hole. Abbreviations and annotations: USGS, U.S. Geological Survey; WTP, water treatment plant; WWTP, wastewater treatment plant; PVC, polyvinyl chlorinated; ?, unknown; NR, not reported]

Site name	USGS local well no.	Other well identifier	Land-net location	Latitude and longitude	Altitude of land surface (feet)	Total hole depth (feet)	Date at end of construc-tion	Depth to top and bottom of casing (feet)	Casing diam-eter (inches)	Type of casing	Completed open interval (feet)	Diameter of open interval (inches)
Collier County												
Manatee Road	C-1202	ASR-1	400 feet southeast of MW-A	260247 814141	NR	528	1991	0-40 0-100 100-465	24.00 16.00 12.00	Steel ? ?	465-528	12
	C-1102	MW-A CO-2080	SWNE S10, 51S, 26 E	260249 814145	5	1,608	11-90	0-360 0-650	12.00 4.00	NR NR	360-500 650-770	8 8
	C-1203	MW-B		260247 814141	NR	520	1991	0-465	4.00	PVC	465-520	
	C-1204	MW-C		260247 814141	NR	520	1991	0-465	4.00	PVC	465-520	
	C-1205	MW-D		260247 814141	NR	150	1991	0-110	4.00	PVC	110-150	
Marco Lakes	C-1206	ASR-1	NE S3, 51S, 26E	260356 [1]814136	NR	790	7-8-96	0-40 0-152 152-745	24.00 16.00 12.00	Steel PVC PVC	745-790	10
	C-1207	DZMW	375 feet southeast of ASR-1	260353 814133	NR	817	04-26-96	0-293 0-745	10.00 6.00	PVC Steel	293-352 745-817	9.625 9.625
	C-1208	ASR-2	SE S34, 50S, 26E		7.5	780	08-26-99	0-27 0-736	26.00 16.00	Steel PVC	736-780	12.25
	C-1209	MHZ2MW	S34, 50S, 26E		7.5	470	09-10-99	0-31 0-440	16.00 6.90	PVC	440-470	12.25
	C-1210	ASRZMW	1,750 feet northeast of ASR-2		9.25	774	10-01-99	0-38 0-725	16.00 6.90	PVC	725-774	12.25
	C-1211	ASR-3	S34, 50S, 26E		7.5	780	11-08-99	0-30 0-736	26.00 16.00	Steel PVC	736-780	12.25
Lee County												
Lee County WTP	L-2530	MW-1	NESE S23, 43S, 26E	264308 814049	7.2	614	1977	0-475	4.00	NR	475-615	2
	L-2901	Deep test	SE S23, 43S, 26E	264309 814051	8	705	12-05-78	0-60	6.00	NR	60-705	4
	L-3224	MW-2	NESE S23, 43S, 26E	264309 814057	9.99	622	04-79	0-460	4.00	NR	460-620	4
	L-3225	ASR-1	NESE S23, 43S, 26E	264309 814052	10.72	602	1980	0-445	10.00	PVC	445-600	9

Table 2. Well Identification, location, and construction data for aquifer storage and recovery system wells in southern Florida --(Continued)

[Depths are in feet below land surface. Completed open intervals are open hole unless noted otherwise. Diameter of open interval for open-hole completions is size of bit used to drill or ream out hole. Abbreviations and annotations: USGS, U.S. Geological Survey; WTP, water treatment plant; WWTP, wastewater treatment plant; PVC, polyvinyl chlorinated; ?, unknown; NR, not reported]

Site name	USGS local well no.	Other well identifier	Land-net location	Latitude and longitude	Altitude of land surface (feet)	Total hole depth (feet)	Date at end of construc-tion	Depth to top and bottom of casing (feet)	Casing diam-eter (inches)	Type of casing	Completed open interval (feet)	Diameter of open interval (inches)
Lee County--Continued												
Corkscrew WTP	L-5855	ASR-1 LM-4627	NENW S22, 46S, 26E	262752 814216	23.31	397	06-23-95	0-30 0-328	18.00 12.00	Steel PVC	328-397	12
	L-5856	MW-A LM-3982	NENW S22, 46S, 26E	262752 814211	24.37	780	09-06-94	0-340	8.00	PVC	340-402	8
	L-5857	MW-B	NENW S22, 46S, 26E	262749 814218	25.29	504	02-27-95	0-452	4.00	PVC	452-504	4
	L-5858	MW-C	NENW S22, 46S, 26E	262752 814220	24.55	400	03-03-95	0-330	4.00	PVC	330-400	4
	L-5859	ASR-2	NENW S22, 46S, 26E	262744 814216	27.18	397	06-23-99	0-33 0-337	20.00 12.00	Steel PVC	337-397	10.63
	L-5860	ASR-3	SW S15, 46S, 26E	262818 814232	27.32	347	02-11-99	0-41 0-285	20.00 12.00	Steel PVC	285-347	10.63
	L-5861	ASR-4	SW S15, 46S, 26E	262805 814226	27.03	368	06-10-99	0-40 0-310	20.00 12.00	Steel PVC	310-368	10.63
	L-5862	ASR-5	NE S16, 46S, 26E	262831 814238	29.14	329	05-25-99	0-21 0-253	20.00 12.00	Steel PVC	253-291	10.63
	L-5863	MW-1	SW S22, 46S, 26E	262720 814215	23.44	410	02-01-99	0-41 0-358	16.00 6.00	Steel PVC	358-410	5.5
	L-5864	MW-2	SW S15, 46S, 26E	262821 814233	28.64	354	01-20-99	0-39 0-283	16.00 6.00	Steel PVC	283-354	5.5
	L-5865	MW-3	NENW S22, 46S, 26E	262735 814217	25.15	411	02-23-99	0-41 0-355	16.00 6.00	Steel PVC	355-411	5.5
North Reservoir	L-5810	ASR-1 LM-6210	SWSW S20, 43S, 25E	264238 815019	12	642	03-02-99	0-40 0-499 0-540	30.00 24.00 16.00	Steel Steel PVC	540-642	12
	L-5811	MW-1 LM-6208	260 feet south of ASR-1		12	980	01-27-99	0-42 0-495 0-537	18.00 12.00 6.00	Steel Steel PVC	537-615	8
Winkler Avenue	L-5871	ASR-1	S35, 44S, 24E	263608 815253	NR	647	06-23-99	0-91 0-455	20.00 12.00	Steel PVC	455-553	9.625
	L-5872	SZMW-1	~220 feet southwest of ASR-1		NR	553	08-05-99	0-16 0-455	16.00 6.00	Steel PVC	455-553	5.5
	L-5873	MHMW-1	~80 feet south of ASR-1		NR	200	08-06-99	0-150	6.00	PVC	150-200	5.5

Table 2. Well Identification, location, and construction data for aquifer storage and recovery system wells in southern Florida --(Continued)

[Depths are in feet below land surface. Completed open intervals are open hole unless noted otherwise. Diameter of open interval for open-hole completions is size of bit used to drill or ream out hole. Abbreviations and annotations: USGS, U.S. Geological Survey; WTP, water treatment plant; WWTP, wastewater treatment plant; PVC, polyvinyl chlorinated; ?, unknown; NR, not reported]

Site name	USGS local well no.	Other well identifier	Land-net location	Latitude and longitude	Altitude of land surface (feet)	Total hole depth (feet)	Date at end of construction	Depth to top and bottom of casing (feet)	Casing diameter (inches)	Type of casing	Completed open interval (feet)	Diameter of open interval (inches)
Lee County--Continued												
San Carlos Estates	L-5812	TPW-1 (ASR-1)	S14, 47S, 25E	262321 [1]814625	NR	718	08-03-99	0-93 0-650	20.00 12.00	Steel PVC	650-701	11
	L-5813	SZMW-1	~200 feet south of ASR-1, abandoned		NR	657	07-26-99	0-19 0-655	16.00 6.00	Steel PVC	Abandoned	12
	L-5814	SZMW-1R	~200 feet south of ASR-1, replacement well	262319 814625	NR	721	07-29-99	0-19 0-659	16.00 6.00	Steel PVC	659-721	5.5
	L-5815	SMW-1	~100 feet east of ASR-1		NR	321	08-02-99	0-19 0-234	16.00 6.00	Steel PVC	234-321	5.5
Olga WTP	L-5816	ASR-1 LM-6068	NESE S23, 43S, 26E	264312 [1]814056	6	920	10-22-99	0-35 0-737 0-859	34.00 24.00 16.00	Steel Steel PVC	859-920	13
	L-5817	MW-1 LM-6209	470 feet southwest of ASR-1	264309 [1]814100	6	1,200	09-08-99	0-30 0-525.5 0-674.5 0-850	18.00 12.00 8.00 4.00	Steel Steel PVC PVC	850-895	8
	L-5818	MW-3 LM-6615	370 feet west-northwest of ASR-1	264313 [1]814100	6	945	05-13-99	0-35 0-742 0-864	18.00 12.00 6.00	Steel Steel PVC	864-945	8
Miami-Dade County												
Hialeah	G-3061	ASR-1	NWSW S18, 53S, 41E	254941 801717	8.4	1,105	12-09-74	0-201 0-955	24.00 14.00	Steel Steel	955-1,105	12
	G-3062	MW-1	289 feet north-northwest of ASR-1	254944 801718	5.43	1,064	11-19-74 06-04-80	0-198 0-953 0-862	14.00 6.63 2.38	Steel Steel Steel	840-844 953-1,060	
West Well Field	G-3706	ASR-1		254200 802830	NR	1,302	12-23-96	0-170 0-850	40.00 30.00	Steel Steel	850-1,302	29
	G-3707	ASR-2	975 feet north of ASR-1		NR	1,350	02-14-97	0-170 0-845	40.00 30.00	Steel Steel	845-1,250	29
	G-3708	ASR-3	1,955 feet north of ASR-1		NR	1,300	03-11-97	0-170 0-835	40.00 30.00	Steel Steel	835-1,210	29
	G-3709	MW-1 Test 711	270 feet north-northwest of ASR-1		NR	1,643	01-03-97	0-170 0-855 0-1,370 [2]1,370-1,390	24.00 12.00 12.00 2.00	Steel Steel PVC PVC	855-1,010 [3]1,370-1,390	12 2

Table 2. Well Identification, location, and construction data for aquifer storage and recovery system wells in southern Florida --(Continued)

[Depths are in feet below land surface. Completed open intervals are open hole unless noted otherwise. Diameter of open interval for open-hole completions is size of bit used to drill or ream out hole. Abbreviations and annotations: USGS, U.S. Geological Survey; WTP, water treatment plant; WWTP, wastewater treatment plant; PVC, polyvinyl chlorinated; ?, unknown; NR, not reported]

Site name	USGS local well no.	Other well identifier	Land-net location	Latitude and longitude	Altitude of land surface (feet)	Total hole depth (feet)	Date at end of construction	Depth to top and bottom of casing (feet)	Casing diameter (inches)	Type of casing	Completed open interval (feet)	Diameter of open interval (inches)
Monroe County												
Marathon	MO-189	ASR-1	S8, 66S, 32E	244239 810538	NR	450	05-01-90	0-36 0-387 362-387 [2]387-427	30.00 16.00 10.00 10.00	Steel PVC Steel Steel	[3]387-432	12
	MO-190	OW-1	126 feet south of ASR-1		NR	428	03-17-90	0-19 0-388 [2]388-428	12.00 4.00 4.00	Steel PVC PVC	[3]356-428	8
	MO-191	OW-2 Test well	258 feet southeast of ASR-1		NR	550	1989	0-22 0-400 375-413 [2]413-435	16.00 10.00 4.00 4.00	Steel Steel Steel Steel	[3]400-450	10
Okeechobee County												
Taylor Creek/Nubbin Slough-(Lake Okeechobee)	OK-9000	ASR-1	S24, 37S, 35E	271420 804709	16	1,710	06-19-88	0-65 0-200 0-1,268	42.00 34.00 24.00	Steel Steel Steel	1,268-1,710	22
	OK-9001	MW-1	560 feet north of ASR-1		16	1,800	07-22-88	0-82 0-200 0-990 0-1,270	24.00 12.00 6.00 1.50	Steel Steel Steel ?	990-1,075 1,275-1,700	8 6
	OK-9002	Deep monitoring tube in MW-1			16						1,275-1,700	
Palm Beach County												
Jupiter	PB-747	ASR-1	S3, 41S, 42E	265604 800826	13	1,280	06-74	0-400 0-990	20.00 12.00	Steel Steel	990-1,280	NR
	PB-1145	MW-1	500 feet from ASR-1	265608 800823	13	1,270	1975	0-400 0-990	12.00 5.00	NR NR	995-1,270	
Boynton Beach East WTP	PB-1194	ASR-1	NE S33, 45S, 43E	263050 [1]800346	18.9	1,260	04-13-92	0-38 0-399 0-804	36.00 26.00 16.00	Steel Steel Steel	804-909	16
	PB-1195	MW-1	~50 feet south of ASR-1		18.9	435	05-21-92	0-300 [2]300-320	4.00 4.00	PVC PVC	[3]300-320	4
Delray Beach North Storage Reservoir	PB-1702	ASR-1	S17, 46S, 43E	262800 800600	21.2	1,200	08-24-96	0-400 352-1,016	20.00 14.00	Steel Steel	1,016-1,120	18.5

Table 2. Well Identification, location, and construction data for aquifer storage and recovery system wells in southern Florida --(Continued)

[Depths are in feet below land surface. Completed open intervals are open hole unless noted otherwise. Diameter of open interval for open-hole completions is size of bit used to drill or ream out hole. Abbreviations and annotations: USGS, U.S. Geological Survey; WTP, water treatment plant; WWTP, wastewater treatment plant; PVC, polyvinyl chlorinated; ?, unknown; NR, not reported]

Site name	USGS local well no.	Other well identifier	Land-net location	Latitude and longitude	Altitude of land surface (feet)	Total hole depth (feet)	Date at end of construc-tion	Depth to top and bottom of casing (feet)	Casing diam-eter (inches)	Type of casing	Completed open interval (feet)	Diameter of open interval (inches)
Palm Beach County--Continued												
West Palm Beach WTP	PB-1692	ASR-1	~100 feet east of MW-1	264259 [1]800349	19.13	1,200	01-29-97	0-56 0-389 0-985	42.00 36.00 24.00	Steel Steel Steel	985-1,200	22
	PB-1693	MW-1	NW S21, 43S, 43E	264257 [1]800350	18.97	1,410	11-13-96	0-65 0-379 0-975	30.00 24.00 12.75	Steel Steel Steel	975-1,191	12
System 3 Palm Beach County	PB-1763	ASR-1	S?, 46S, 42E	262859 800811	NR	1,155	01-99	0-60 0-365 0-223	36.00 24.00 18.00	Steel PVC Steel	1,065-1,155	14
	PB-1764	MW-1			NR	1,500	01-98	215-1,065 0-155 0-1,050 0-1,052	16.00 16.00 10.00 5.00	PVC Steel Steel PVC	1,052-1,270	10
Western Hillsboro Canal, Site 1	PB-1765	EXW-1 (ASR-1)	NR	262119 [1]801743	NR	1,225	03-31-00	0-205 0-1,015	36.00 24.00	Steel Steel	1,015-1,225	24
	PB-1766	PBF-10	300 feet northwest of EXW-1	262120 [1]801746	NR	2,370	?	0-375 0-1,000 0-1,505 0-2,130	24.00 18.00 12.00 2.38	Steel Steel Steel ?	1,505-1,670 2,130-2,260	12 12
	PB-1767	PBF-10R[4]	300 feet northwest of EXW-1	262120 [1]801746	NR	1,225	08-00	0-1,015	3.00	NR	1,015-1,225	8
St. Lucie County												
St. Lucie County	STL-356	ASR-1 SLF-50	SE S14, 36S, 39E	272017 802953	31.75	1,000	02-82	0-130 0-600	12.00 6.00	PVC PVC	600-775	5.125
	STL-357	MW-1 SLF-51	148 feet northeast of ASR-1	272019 802053	25.56	775	02-82	0-130 0-600	12.00 6.00	PVC PVC	600-775	5.125
	STL-355	MW-2 SLF-49	420 feet northwest of ASR-1	272020 802954	25.09	893	?	0-560	NR	NR	560-893	NR

[1]Latitude-longitude determined in the field using a hand held global positioning system accurate to ± 0.2 seconds.
[2]Top and bottom depth of screen.
[3]Screened interval plus gravel pack above or below screen.
[4]Replacement well to PBF-10, upper zone.

Table 3. Hydraulic test data from aquifer storage and recovery well systems in southern Florida

[Depths are in feet below land surface. Test type: M, multiwell constant rate; P, Packer test; R, single well constant rate recovery; S, step drawdown. Method of analysis: SC, specific capacity; Theis, Theis (1935) confined aquifer; C-J, Cooper and Jacob (1946) confined aquifer; Theis Rec, Theis (1935) residual drawdown recovery; H-J, Hantush and Jacob (1955) leaky aquifer; Walton, Walton (1962) leaky aquifer; J-L, Jacob and Lohman (1952). Other annotations: WTP, water treatment plant; WWTP, wastewater treatment plant; -, not applicable; NR, not reported]

Test date	Production well identifier	Open interval tested (feet)	Test type	Monitoring well	Pumping rate (gallons per minute)	Length of test (hours)	Transmissivity (square feet per day)	Storage coefficient (unitless)	Leakance (1/day)	Method of analysis	Specific capacity (gallons per minute per foot)	Background measurements	Problems and comments
Broward County													
Deerfield Beach West WTP													
NR	ASR-1	956-1,130[1]	S	--	950-2,100	NR	--	-	--	--	42.6-32.0	NR	Step-drawdown test was performed prior to multiwell, but date of test was not given in report
12-10-92	ASR-1	956-1,130[1]	M	MW-1	1,200	5.7	24,200	$1.33x10^{-6}$	$6.3x10^{-2}$	H-J	--		
Broward County WTP 2A													
11-21-96	ASR-1	995-1,200[1]	S	--	1,050-2,950	8	-	--	--	--	90.6-51.1	Data collected for multi-well test but no information on whether corrections were made	Walton method should give same transmissivity if no leakance as C-J method(?) Curve matches look okay
11-26-96	ASR-1	995-1,200[1]	M	MW-1	1,000	24	28,900	$1.1x10^{-4}$	None	Walton	--		
11-26-96	ASR-1	995-1,200[1]	M	MW-1	1,000	24	37,200	$5.3x10^{-5}$	--	C-J	--		
11-26-96	ASR-1	995-1,200[1]	M	ASR-1	1,000	24	44,000	--	--	Theis Rec	NR		
09-19-96	MW-1	990-1,200[1]	S	--	480	6	--	--	--	--	20		
Sprintree WTP													
06-06-97	ASR-1	1,110-1,270[1]	S	--	700-1,900	8	--	--	--	--	18.4-16.5	NR	Acidization of well done after step test and before constant rate test. Interpretation of recovery data favored late time data
07-28-97	ASR-1	1,110-1,270[1]	R	--	2,115	48	5,700	--	--	Theis Rec	22.75		
Fiveash WTP													
01-12-98	FMW-1	998-1,028	P, R	--	160	4	4,700	--	--	Theis Rec	4.7	NR	Third packer test showed apparent failure after about 10 minutes, which may have affected data. FMW-1 apparently not used in 24-hour test of ASR-1
01-13-98	FMW-1	998-1,042	P, R	--	160	4	8,000	--	--	Theis Rec	5		
01-15-98	FMW-1	1,058-1,175[1]	P	--	600	10 min	23,500	--	--	C-J	46		
03-16-98	FMW-1	1,055-1,175[1]	S	--	100-160	4	--	--	--	--	3.8-3.6		
03-17-98	FMW-1	1,055-1,175[1]	S	--	164	24	NR	--	--	--	~3.5		
03-25-98	ASR-1	1,055-1,200[1]	S	--	968-2,104	4	--	--	--	--	25.5-17.7		
03-30-98	ASR-1	1,055-1,200[1]	R	--	2,100	24	19,500	--	--	Theis Rec	~17.5		
Charlotte County													
Shell Creek WtP													
11-05-97	ASR-1	700-755	P	--	300-550	NR	--	--	--	--	10.0-5.6	NR	
11-17-97	ASR-1	700-764	S	--	231-597	12	--	--	--	--	5.3-4.6		
11-18-97	ASR-1	700-764	R	--	546	54	1,300	--	--	SC	4.4		
06-28-99	ASR-1	764-933[1]	S	--	610-600	8	--	--	--	--	10.6		
Englewood South Regional WWTP													
NR	TPW-1	563-583	P, R	--	10	1.33	450	--	--	Theis Rec	1	NR	Multiwell aquifer test planned in the future
03-07-00	TPW-1	630-807	P	--	131	4.00	1,300	--	--	SC	5		
03-31-00	TPW-1	507-700[1]	S	--	490-1,050	NR	4,700	--	--	SC	17.34 (avg)		
04-20-00	SZMW-1	510-700[1]	S	--	31-101	NR	3,700	--	--	SC	13.87 (avg)		
04-18-00	IMW-1	280-320	S	--	28.3-59.5	NR	2,300	--	--	SC	5.5-4.0		
04-18-00	SMW-1	170-205	S	--	9.3-17.7	NR	300	--	--	SC	1 (avg)		

Table 3. Hydraulic test data from aquifer storage and recovery well systems in southern Florida --(Continued)

[Depths are in feet below land surface. Test type: M, multiwell constant rate; P, Packer test; R, single well constant rate recovery; S, step drawdown. Method of analysis: SC, specific capacity; Theis, Theis (1935) confined aquifer; C-J, Cooper and Jacob (1946) confined aquifer; Theis Rec, Theis (1935) residual drawdown recovery; H-J, Hantush and Jacob (1955) leaky aquifer; Walton, Walton (1962) leaky aquifer; J-L, Jacob and Lohman (1952). Other annotations: WTP, water treatment plant; WWTP, wastewater treatment plant; -, not applicable; NR, not reported]

Test date	Production well identifier	Open interval tested (feet)	Test type	Monitoring well	Pumping rate (gallons per minute)	Length of test (hours)	Transmissivity (square feet per day)	Storage coefficient (unitless)	Leakance (1/day)	Method of analysis	Specific capacity (gallons per minute per foot)	Background measurements	Problems and comments
Collier County													
Manatee Road													
11-90	MW-A	360-460	P, S	--	NR	NR	2,400	--	--	See comment	NR	NR	All of the step-drawdown tests are indicated to be packer tests; however, some could have been a test of an open interval below casing. For step test, transmissivity was determined at each step by an unspecified method in Walton (1970). Then an adjusted estimated value of transmissivity was obtained by plotting transmissivity against flow rate for each step. For the multiwell test, 670 gallons per minute was an injection rate
11-90	MW-A	465-530[1]	P, S	--	NR	NR	20,000	--	--	See comment	NR		
11-90	MW-A	680-760	P, S	--	NR	NR	15,000	--	--	See comment	NR		
11-90	MW-A	930-1020	P, S	--	NR	NR	6,700	--	--	See comment	NR		
11-90	MW-A	1,180-1,220	P, S	--	NR	NR	6,300	--	--	See comment	NR		
11-90	MW-A	1,345-1,606	P, S	--	NR	NR	5,700	--	--	See comment	NR		
NR	ASR-1	465-528[1]	M	MW-B	670	17	9,400	$1.00x10^{-4}$	$3.7x10^{-4}$	H-J	--		
NR	ASR-1	465-528	M	MW-B	670	17	12,000	--	--	Theis Rec	--		
Marco Lakes													
NR	DZMW	296-399	S	--	220-600	NR	67,000	--	--	Walton	220-170	NR	Estimated transmissivity in lower Hawthorn zone I (550 to 622 feet) was too low for consideration as an aquifer storage and recovery interval. No dates were reported for any tests. Good agreement between tests
NR	DZMW	296-399	R	--	600	3	42,400	--	--	Theis Rec	NR		
NR	DZMW	550-622	P, R	--	5	4	47	--	--	Theis Rec	NR		
NR	DZMW	745-811[1]	R	--	187	4.5	8,200	--	--	Theis Rec	NR		
NR	ASR-1	745-790[1]	M	ASR-1	463	8.3	16,300	--	--	Theis Rec	NR		
NR	ASR-1	745-790[1]	M	DZMW	463	8.3	9,100	$6.5x10^{-5}$	$7x10^{-4}$	H-J	--		
NR	ASR-1	745-790[1]	M	DZMW	463	8.3	12,000	--	--	Theis Rec	--		
NR	ASR-2	736-780[1]	S	ASR-1	400-650	NR	--	--	--	--	25-24		
NR	ASR-3	736-780[1]	S, M	ASR-2, ASRZMW	400-820	NR	8,000 to 8,100	--	--	C-J	17.4-15		
Lee County													
Lee County WTP													
NR	ASR-1	445-600[1]	M	NR	350	48	800	$1.00x10^{-4}$	$1.0x10^{-2}$	H-J	NR	NR	Storage zone in ASR-1 is located in the lower Hawthorn producing zone of the Upper Floridan aquifer as defined by Reese (2000)

Table 3. Hydraulic test data from aquifer storage and recovery well systems in southern Florida --(Continued)

[Depths are in feet below land surface. Test type: M, multiwell constant rate; P, Packer test; R, single well constant rate recovery; S, step drawdown. Method of analysis: SC, specific capacity; Theis, Theis (1935) confined aquifer; C-J, Cooper and Jacob (1946) confined aquifer; Theis Rec, Theis (1935) residual drawdown recovery; H-J, Hantush and Jacob (1955) leaky aquifer; Walton, Walton (1962) leaky aquifer; J-L, Jacob and Lohman (1952). Other annotations: WTP, water treatment plant; WWTP, wastewater treatment plant; -, not applicable; NR, not reported]

Test date	Production well identifier	Open interval tested (feet)	Test type	Monitoring well	Pumping rate (gallons per minute)	Length of test (hours)	Transmissivity (square feet per day)	Storage coefficient (unitless)	Leakance (1/day)	Method of analysis	Specific capacity (gallons per minute per foot)	Background measurements	Problems and comments
Lee County--Continued													
Corkscrew WTP													
08-94	MW-A	428-515	P	--	NR	NR	500	--	--	SC	2.5		
08-17-94	MW-A	524-578	P	--	39	5 min.	500	--	--	SC	NR		
08-24-94	MW-A	744-778	P, S	--	15-72	4	13,000	--	--	SC	1.3-0.6		
NR	MW-B	452-504	NR	--	NR	NR	100	NR	NR	NR	NR		
09-95	ASR-1	328-397[1]	M	MW-C	400	115.5	3,410	$7.70x10^{-5}$	$1.6x10^{-5}$	Hantush	--		Test of MW-A, interval 744 to 778 feet, was of upper 34 of 240 feet thick Suwannee Limestone.Second multi-well test of ASR-1 followed back-plugging of MW-A to injection zone.Transmissivity values for step-drawdown test of ASR-2, 3, 4, and 5 were obtained by modified Walton method. Second step test of ASR-5 was post-acidization of the well. Additional multiwell tests of ASR-1 and ASR-3 were conducted during the expansion project
09-95	ASR-1	328-397[1]	M	MW-C	400	115.5	3,380	$6.70x10^{-5}$	--	C-J	--		
09-95	ASR-1	328-397[1]	M	MW-C	400	115.5	3,460	--	--	Theis Rec	--		
06-96	ASR-1	328-397[1]	M	MW-A	415	120	1,760	$2.30x10^{-4}$	--	Theis	--	Data collected for multi-well test in September 1995	
06-96	ASR-1	328-397[1]	M	MW-A	415	120	1,900	$1.70x10^{-4}$	--	C-J	--		
06-96	ASR-1	328-397[1]	M	MW-C	415	120	3,180	$5.70x10^{-5}$	--	Theis	--		
06-96	ASR-1	328-397[1]	M	MW-C	415	120	3,410	$4.90x10^{-5}$	--	C-J	--		
07-13-99	ASR-2	337-397[1]	S	--	115-410	NR	2,040	--	--	SC	7.8-6.6		
02-12-99	ASR-3	285-347[1]	S	--	129-497	NR	7,350	--	--	SC	26.9-19.4		
06-25-99	ASR-4	310-368[1]	S	--	153-450	NR	4,020	--	--	SC	15.0-11.7		
07-08-99	ASR-5	253-291[1]	S	--	163-380	NR	-	--	--	-	7.4-5.2		
07-20-99	ASR-5	253-291[1]	S	--	130-490	NR	13,400	--	--	SC	50.0-36.1		
North Reservoir													
12-07-98	MW-1	480-518	S	--	92-430	NR	14,400	--	--	SC	44.4-41.3		
12-09-98	MW-1	529-619[1]	P, S	--	73-295	NR	5,200	--	--	SC	9.7-3.5		
12-11-98	MW-1	640-703	P, S	--	79-281	NR	2,040	--	--	SC	6.6-2.8		
12-16-98	MW-1	808-890	P, S	--	55-190	NR	680	--	--	SC	2.8-1.8		
12-18-98	MW-1	904-977	P, S	--	85-322	NR	9,590	--	--	SC	10.5-3.1		
03-03-99	ASR-1	540-642[1]	S	--	162-590	4	2,220	--	--	SC	8.65-7.00	Data collected for 3 days prior to the multiwell test	Fit of line to ASR-1 recovery data for multiwell test is poor
03-08-99	ASR-1	540-642[1]	M	MW-1	379	72	8,290	$3.27x10^{-4}$	$7.33x10^{-4}$	H-J	--		
03-08-99	ASR-1	540-642[1]	M	MW-1	379	72	8,740	$4.64x10^{-4}$	- -	C-J (recovery)	--		
03-08-99	ASR-1	540-642[1]	M	ASR-1	379	72	8,570	--	- -	C-J (recovery)	NR		

Table 3. Hydraulic test data from aquifer storage and recovery well systems in southern Florida --(Continued)

[Depths are in feet below land surface. Test type: M, multiwell constant rate; P, Packer test; R, single well constant rate recovery; S, step drawdown. Method of analysis: SC, specific capacity; Theis, Theis (1935) confined aquifer; C-J, Cooper and Jacob (1946) confined aquifer; Theis Rec, Theis (1935) residual drawdown recovery; H-J, Hantush and Jacob (1955) leaky aquifer; Walton, Walton (1962) leaky aquifer; J-L, Jacob and Lohman (1952). Other annotations: WTP, water treatment plant; WWTP, wastewater treatment plant; -, not applicable; NR, not reported]

Test date	Production well identifier	Open interval tested (feet)	Test type	Monitoring well	Pumping rate (gallons per minute)	Length of test (hours)	Transmissivity (square feet per day)	Storage coefficient (unitless)	Leakance (1/day)	Method of analysis	Specific capacity (gallons per minute per foot)	Background measurements	Problems and comments
Lee County--Continued													
Winkler Avenue													
NR	ASR-1	455-554[1]	S	--	135	15 min	--	--	--	--	59.7	Ninety hours collected prior to multiwell test, but apparently not used to correct drawdown data	Pumping rate for multiwell test was 1,540 for first 6.5 hours, then changed to 1,400. No attempt was made to analyze multiwell test data for storage coefficient or leakance. Storage zone is located in the lower Hawthorn producing zone of the Upper Floridan aquifer
NR	ASR-1	455-647	S	--	160	15 min	--	--	--	--	86.3		
6-16-99	ASR-1	455-574[1]	P	--	479	70 min	29,100	--	--	C-J (recovery)	NR		
6-17-99	ASR-1	455-575[1]	P	--	483	18 min	26,600	--	--	C-J (recovery)	NR		
10-23-99	ASR-1	455-553[1]	M	ASR-1	1540-1400	27	24,700	--	--	C-J	NR		
10-23-99	ASR-1	455-553[1]	M	ASR-1	1540-1400	27	25,400	--	--	C-J (recovery)	--		
10-23-99	ASR-1	455-553[1]	M	SZMW-1	1540-1400	27	27,400	NR	NR	C-J	--		
10-23-99	ASR-1	455-553[1]	M	SZMW-1	1540-1400	27	29,000	--	--	C-J (recovery)	--		
San Carlos Estates													
06-07-99	TPW-1	650-701[1]	S	--	710-1,480	8	--	--	--	--	250-130	Unknown for multiwell test. Test followed 10 days of recharge at 1,955 gallons per minute and then 6-day static period.	High specific capacity in TPW-1 due to two pilot holes in open interval. Pumping rate for test on 11/10/99 of 985 gallons per minute was natural flow. C-J solution for drawdown in SZMW-1R is suspect. Solution is for very late time only, and background changes due to prior recharge may have affected response
07-29-99	SZMW-1R	659-721[1]	S	--	170-350	8	--	--	--	--	15-9.0		
08-02-99	SMW-1	234-321	S	--	150-220	8	--	--	--	--	8.9-6.5		
11-10-99	TPW-1	650-701[1]	M	SZMW-1R	985	8	39,000	$1.00x10^{-2}$	--	C-J	--		
11-10-99	TPW-1	650-701[1]	M	SZMW-1R	985	8	70,000	--	--	Theis Rec	--		
Olga WTP													
01-05-99	MW-1	515-605	S	--	110-400	NR	2,500	--	--	SC	NR	Measured for multiwell test, but unknown if used to correct drawdown	H-J results for multiwell test agree better with single well and packer test than C-J results. A second constant rate test was run but is not reported here. Storage zone is about 150 feet below top of Suwannee Limestone
01-07-99	MW-1	612-689	P	--	70-200	NR	1,300	--	--	SC	NR		
02-03-99	MW-1	835-935[1]	P	--	70-355	NR	7,600	--	--	SC	NR		
02-04-99	MW-1	710-935	P	--	70-350	NR	7,600	--	--	SC	NR		
02-04-99	MW-1	835-935[1]	P	--	70-350	NR	7,600	--	--	SC	NR		
02-08-99	MW-1	945-1,101	P	--	6 to 15	NR	33	--	--	SC	NR		
03-17-99	MW-3	740-820	S	--	78-480	NR	1,900	--	--	SC	NR		
03-25-99	MW-3	830-945[1]	P	--	80-340	NR	9,000	--	--	SC	NR		
03-25-99	MW-3	854-945[1]	P	--	75-350	NR	6,400	--	--	SC	NR		
03-26-99	MW-3	857-945[1]	R	--	300	NR	8,700	--	--	Theis Rec	NR		
11-01-99	ASR-1	859-920[1]	S	--	112-545	5	5,000	--	--	SC	14.9-8.5		
11-03-99	ASR-1	859-920[1]	M	MW-1	500	60	7,200	$5.10x10^{-5}$	$5.2x10^{-3}$	H-J	--		
11-03-99	ASR-1	859-920[1]	M	MW-1	500	60	12,000	$4.10x10^{-5}$	--	C-J	--		
11-03-99	ASR-1	859-920[1]	M	MW-3	500	60	9,400	$5.50x10^{-5}$	$6.0x10^{-2}$	H-J	--		
11-03-99	ASR-1	859-920[1]	M	MW-3	500	60	11,000	$4.20x10^{-4}$	--	C-J	--		

Table 3. Hydraulic test data from aquifer storage and recovery well systems in southern Florida --(Continued)

[Depths are in feet below land surface. Test type: M, multiwell constant rate; P, Packer test; R, single well constant rate recovery; S, step drawdown. Method of analysis: SC, specific capacity; Theis, Theis (1935) confined aquifer; C-J, Cooper and Jacob (1946) confined aquifer; Theis Rec, Theis (1935) residual drawdown recovery; H-J, Hantush and Jacob (1955) leaky aquifer; Walton, Walton (1962) leaky aquifer; J-L, Jacob and Lohman (1952). Other annotations: WTP, water treatment plant; WWTP, wastewater treatment plant; -, not applicable; NR, not reported]

Test date	Production well identifier	Open interval tested (feet)	Test type	Monitoring well	Pumping rate (gallons per minute)	Length of test (hours)	Transmissivity (square feet per day)	Storage coefficient (unitless)	Leakance (1/day)	Method of analysis	Specific capacity (gallons per minute per foot)	Background measurements	Problems and comments
Miami-Dade County													
Hialeah													
02-10-75	MW-1	953-1,060[1]	M	ASR-1	250	1.66	11,000	$8.4x10^{-5}$	--	J-L	--	NR	Transmissivity estimate from Meyer (1989b). Storage coefficient estimated by model simulation of pumping test
West Well Field													
01-26-97	ASR-1	850-1,302[1]	S	--	1,400-4,000	8	--	--	--	--	269-52.1	Measured for multiwell test. Correction was not done, due to negligibility.	All three aquifer storage and recovery wells were heavily acidized prior to all tests. Late time drawdown data problematic because of pump going down several times.
02-25-97	ASR-2	845-1,250[1]	S	--	1,500-3,800	8	--	--	--	--	126.6-51.1		
04-08-97	ASR-3	835-1,210[1]	S	--	1,500-3,800	8	--	--	--	--	46.1-38.2		
12-09-97	ASR-1	850-1,302[1]	M	ASR-1	3,500	72	10,300	N/A	N/A	C-J	NR		
12-09-97	ASR-1	850-1,302[1]	M	ASR-2	3,500	72	15,400	$3.90x10^{-4}$	$1.6x10^{-3}$	Walton	--		
12-09-97	ASR-1	850-1,302[1]	M	ASR-2	3,500	72	18,200	$2.90x10^{-4}$	N/A	C-J	--		
12-09-97	ASR-1	850-1,302[1]	M	ASR-3	3,500	72	15,400	$4.40x10^{-4}$	$3.9x10^{-5}$	Walton	--		
12-09-97	ASR-1	850-1,302[1]	M	ASR-3	3,500	72	19,700	$3.30x10^{-4}$	N/A	C-J	--		
Monroe County													
Marathon													
05-03-90	ASR-1	387-432[1]	M	OW-1	105	25	2,290	$3.20x10^{-4}$	NR	Walton	--	Measured for 3 weeks prior to multiwell test. A regional increasing trend in water level was determined	Leakance using Walton (1962) method not determined
05-03-90	ASR-1	387-432[1]	M	OW-1	105	25	2,510	$3.70x10^{-4}$	--	C-J	--		
05-03-90	ASR-1	387-432[1]	M	OW-1	105	25	1,760	--	--	Theis-Rec	--		
05-03-90	ASR-1	387-432[1]	M	OW-2	105	25	2,180	$5.20x10^{-4}$	NR	Walton	--		
05-03-90	ASR-1	387-432[1]	M	OW-2	105	25	4,090	--	--	Theis-Rec	--		
05-06-90	ASR-1	387-432[1]	S	--	95-350	NR	--	--	--	--	3.9-2.7		
Okeechobee County													
Taylor Creek-Nubbin Slough (Lake Okeechobee)													
04-20-98	MW-1	1,175-1,227	P	--	10	6.4	706	NR	--	C-J	NR	Water-level data taken for 5 days prior to constant rate test; corrections made using a long-term increasing trend	Leakance derived by extrapolation; longer pumping period required for more accurate value
04-20-98	MW-1	1,175-1,227	P, R	--	10	6.4	2,940	--	--	Recovery	NR		
08-02-98	ASR-1	1,268-1,710[1]	M	ASR-1	6,500	24	620,000	N/A	N/A	C-J (recovery)	1,600		
08-02-98	ASR-1	1,268-1,710[1]	M	MW-1	6,500	24	586,000	$1.25x10^{-3}$	0.01-0.001	H-J	1,600		
08-02-98	ASR-1	1,268-1,710[1]	M	MW-1	6,500	24	765,000	$1.90x10^{-4}$	N/A	C-J (recovery)	1,600		

Table 3. Hydraulic test data from aquifer storage and recovery well systems in southern Florida --(Continued)

[Depths are in feet below land surface. Test type: M, multiwell constant rate; P, Packer test; R, single well constant rate recovery; S, step drawdown. Method of analysis: SC, specific capacity; Theis, Theis (1935) confined aquifer; C-J, Cooper and Jacob (1946) confined aquifer; Theis Rec, Theis (1935) residual drawdown recovery; H-J, Hantush and Jacob (1955) leaky aquifer; Walton, Walton (1962) leaky aquifer; J-L, Jacob and Lohman (1952). Other annotations: WTP, water treatment plant; WWTP, wastewater treatment plant; -, not applicable; NR, not reported]

Test date	Production well identifier	Open interval tested (feet)	Test type	Monitoring well	Pumping rate (gallons per minute)	Length of test (hours)	Transmissivity (square feet per day)	Storage coefficient (unitless)	Leakance (1/day)	Method of analysis	Specific capacity (gallons per minute per foot)	Background measurements	Problems and comments
Palm Beach County													
Boynton Beach East WTP													
04-09-92	ASR-1	804-900[1]	S	--	320-2,100	NR	6,800-13,000	NR	--	C-J	18-28	NR	Second step test is with permanent equipment installed in well. Average of estimates for transmissivity was 70,000 gallons per day per foot
10-15-92	ASR-1	804-909[1]	S	--	798-1,723	NR	Not calculated	--	--	C-J	29-27		
Delray Beach North Storage Reservoir													
06-05-96	ASR-1	849-899	P	--	49	NR	--	--	--	--	0.37	NR	Second step test performed after acidization of well. For the second step test, pump malfunctioned after about 10 minutes of pumping during the last step at 2,550 gallons per minute
06-11-96	ASR-1	900-952	P	--	83	NR	--	--	--	--	0.90		
06-14-96	ASR-1	974-1,020	P	--	90	NR	--	--	--	--	2.40		
06-18-96	ASR-1	1,020-1,100	P	--	98	NR	--	--	--	--	2.00		
09-20-96	ASR-1	1,020-1,200[1]	S	--	575-1,100	24	--	--	--	--	10.8-7.8		
02-24-98	ASR-1	1,020-1,200[1]	S	--	760-2,550	13.2	--	--	--	--	17.2-15.7		
West Palm Beach WTP													
08-22-96	FAMW	975-1,091	P, S	--	64-142	NR	--	--	--	--	194-86	NR	Recovery was allowed following step test of ASR-1 before multiwell test was begun. Large deviation from Theis curve during late time, but leaky aquifer solution not used
09-14-96	FAMW	1,304-1,384	P, S	--	55-110	NR	--	--	--	--	220-110		
08-29-96	FAMW	975-1,090	S	--	300-584	NR	--	--	--	--	75-58		
09-01-96	FAMW	975-1,190[1]	S	--	300-584	NR	--	--	--	--	110-101		
09-04-96	FAMW	975-1,290	S	--	550-740	NR	--	--	--	--	116-105		
09-06-96	FAMW	975-1,384	S	--	550-740	NR	--	--	--	--	116-99		
11-19-96	FAMW	975-1,191[1]	S	--	550-732	NR	--	--	--	--	62-42		
01-30-97	ASR-1	985-1,200[1]	S	--	508-704	24	--	--	--	--	390-306		
02-01-97	ASR-1	985-1,200[1]	M	FAMW	700	24	138,000	1.00×10^{-4}	--	C-J	--		
02-01-97	ASR-1	985-1,200[1]	M	FAMW	700	24	108,000	8.00×10^{-4}	--	Theis	--		
Western Hillsboro Canal, Site 1													
04-05-00	EXW-1	1,160-1,225	P	--	95	NR	--	--	--	--	22.6	NR	Acidized EXW-1 with 4,300 gallons of 36 percent HCl on 6-2-00
04-10-00	EXW-1	1,015-1,150	P	--	105	NR	--	--	--	--	10.9		
05-25-00	EXW-1	1,015-1,225[1]	S	--	1,000-3,000	NR	--	--	--	--	31.1-26.6		
St. Lucie County													
08-24-82	MW-1	600-775[1]	M	ASR-1	388	72	5,910	1.64×10^{-4}	4.3×10^{-2}	H-J (drawdown)	--	NR	Also conducted four pump tests of ASR-1 during drilling with total depth ranging from 627 to 1,000 feet and casing at 600 feet. Transmissivity was calculated from these tests based on recovery data from ASR-1
08-24-82	MW-1	600-775[1]	M	ASR-1	388	72	6,430	2.67×10^{-4}	4.7×10^{-2}	H-J (recovery)	--		

[1]Open interval tested is the same (or about the same) as the storage zone.

ground water

Review Paper/

Longitudinal Dispersivity Data and Implications for Scaling Behavior

by Dirk Schulze-Makuch[1]

Abstract

Longitudinal dispersivity (α) data were compiled from 109 different authors for different types of geological media. The data were subdivided into different subsets. Dispersivity values for consolidated media were subdivided as basalts, granites, sandstones, and carbonate rocks, while unconsolidated sediments were subdivided into three reliability classes. The data sets provided here may provide ground water practitioners a preliminary guide to estimate dispersivity values at various scales and to guide and verify theories on scaling behavior. Based on the data set presented here, the relationship that empirically best described the dispersivity data in regard to scale of measurement was in the form of a power law. The scaling exponent for consolidated and unconsolidated geological media varied between 0.40 and 0.92, and 0.44 and 0.94, respectively. Higher reliability subsets of data for the unconsolidated sediments and more frequently tested rock formations indicate that the scaling exponent is at the lower end of the observed range, close to 0.5. No significant difference in scaling exponent was found among different media, and no clear evidence exists for the presence of an upper bound or asymptotic behavior on the relationship for any of the analyzed media.

Introduction

Longitudinal dispersivity (α) is used to represent the local variations in the velocity field of a ground water solute in the direction of fluid flow, if a Gaussian solution to subsurface transport is assumed. In a one-dimensional flow field, longitudinal dispersivity is multiplied by the average linear velocity, v, to describe solute dispersion. Then, the dispersion coefficient is the sum of the quantity αv and the effective diffusion coefficient. Longitudinal dispersivity has been frequently shown to increase with the scale of measurement (Pickens and Grisak 1981; Gelhar et al. 1985; Neuman 1990; Schulze-Makuch and Cherkauer 1997; Neuman and Federico 2003), owing to many independent processes, including advection, local dispersion and diffusion, the nonstationary nature of hydraulic conductivity fields, and sampling bias. While some general relationships have previously been proposed to quantify the dependence of dispersivity on measurement scale (e.g., Neuman 1990), none has been accepted in the scientific community because none provides a satisfactory solution. In this review paper, dispersivity data from 109 different authors were used to establish a relationship of longitudinal dispersivity with scale of measurement for specific types of geological media. It is beyond this study to describe the processes that result in the observed scale effect. The objective is rather to summarize data and subsets of data to guide and verify theories on scaling behavior and to provide a tool for practitioners and ground water modelers to help estimate the range of dispersivities to expect when performing "upscaling" procedures. In addition, the paper considers whether the observed increase in dispersivity with scale is related to the type of geological medium.

Methodology

Dispersivity data were accumulated from laboratory experiments, aquifer tests, and modeling results conducted by various authors. Dispersivities obtained from modeling results are not measurements in a physical sense but were included in the analysis if no other measurements on larger scales were available. The base data set for this investigation was formed from the data compilations by Gelhar et al. (1985, 1992). These data are briefly characterized in Appendix A; for additional information the reader is referred to the original data source. Additional data sources that were included in the analysis are presented in Table 1,

[1]Department of Geology, Washington State University, Webster Physical Sciences Building, Pullman, WA 99164; 1-509-335-1180; fax 1-509-335-7816; dirksm@wsu.edu

Received October 21, 2003; accepted October 30, 2004.

Table 1
Partial Summary of Data and Sources (Also see Appendix 1, Table A1)

Type of Medium	Description	Scale (m)	α (m)	Tracer; Description of Test, and Analysis Method	Overall Reliability
A. *Unconsolidated sediments*					
Atakan et al. (1974)	Fine to medium sand	2.0 3.1 3.1 2.9	0.039 0.0034 0.196 0.185	Uranin, rhodamine B; pulse injection, analytical solution assuming Gaussian distribution, uncertainty about scale of experiment (between 2 and 5 m)	III
Avon and Bredehoeft (1989)	Heterogeneous sediments	3650	15.2	Trichloroethylene; model, 2D numerical solute transport model	III
Boesel et al. (2000)	Fluvial heterogeneous gravel and sands	26.6 28.6 44.2 30.0 58.0 26.0 63.1 43.3 80.0 91.5 234 223	1.5 1.5 2.2 4.0 4.0 1.0 6.0 5.0 5.0 3.5 30 30	Fluorescein, eosin, sodium naphthionate, NaBr; natural gradient multiwell tracer test, analysis by fitting a 2D analytical solution to measured breakthrough curves (MODFLOW and MT3D)	II
Chapelle (1986)	Heterogeneous coarse sand with gravel, silt, and clay	8800	30.5	Cl; model, simulation of brackish water intrusion, 2D solute transport code developed and documented by Konikow and Bredehoeft (1978)	III
Chiang et al. (1989)	Medium coarse sand with gravel and cobbles	350	10	Benzene, toluene, and xylenes conc.; Bioplume II simulating the transport of soluble BTX and dissolved oxygen including first-order decay function	III
Coats and Smith (1964)	Wausau sand	0.208	0.00030	CaCl; continuous source, analytical solution, unclear whether horizontal or vertical dispersivity was measured	III
	Ottawa Sand	0.2072	0.0011	CaCl; continuous source, analytical solution, unclear whether horizontal or vertical dispersivity was measured	III
Engesgaard et al. (1996)	Sandy outwash deposits	1000	3.2	Tritium; pulse injection, 2D transport analysis using a modified version of FLOTRANS, a finite-element model capable of simulating steady-state ground water flow and advective-dispersive mass transport with linear decay	II
Hendry et al. (1999)	Medium to coarse silica sand	0.114	0.0012	Cl and bacteria; pulse injection, 1D mathematical model for advective transport accounting for irreversible and reversible sorption	II
Hyndman and Gorelick (1996)	Heterogeneous sediments	20	0.091	Fluorescein; pulse injection, Split Inversion Method, which combines seismic, hydraulic, and tracer data to estimate the 3D zonation of aquifer properties along with hydraulic properties	II

Table 1 (Continued)
Partial Summary of Data and Sources (Also see Appendix 1, Table A1)

Type of Medium	Description	Scale (m)	α (m)	Tracer; Description of Test, and Analysis Method	Overall Reliability
Jensen and Bitsch (1993)	Heterogeneous sand in an outwash plain	125	0.45	Cl, tritium; natural gradient dispersion experiment, analysis optimized model to observed breakthrough curves representing depth-averaged concentration plus 3D numerical flow and transport model applied for better quantification of dispersivity parameter	II
Lehner (2004)	Sand and zeolite mix	0.9	0.124	Microspheres; pulse injection in a model aquifer, analytical solution from concentration breakthrough	III
Mas-Pla et al. (1992)	Coastal sandy aquifer	5 5 5	0.10 0.25 0.05	Cl; continuous injection and withdrawal of ground water in a two-well experiment artificially creating steady-state flow conditions, 2D flow and transport model to simulate tracer migration, 1D advection-dispersion model that considers the nonuniform velocity field	III
Moltyaner et al. (1993)	Sandy sediments	5.11 25.8 71.5 80 94.8 93.4 101.6 116.2 266	0.24 0.19 0.19 0.34 0.34 0.21 0.23 0.51 0.55	Tritium; tracer test between injection well and wetland in the ground water discharge area, statistical moments analysis, various 2D and 3D modeling including method of characteristics and random walk method	I
Palmer and Nadon (1986)	Fine to medium uniform sand	6.5	0.07	Cl; injection tracer experiment, analysis of data by an approximate solution developed by Lau et al. (1959)	III
Ptak and Teutsch (1994)	Poorly sorted alluvial sand and gravel deposits	12.82 8.9 9.9 12.36 12.21 8.93 17.07 9.9 17.07 120.36 52.15 32.66 34.10 40.98 56.41 44.49 32.66 34.10 40.98 56.41 44.49	1.5 0.71 1.33 6.61 2.0 1.38 2.5 1.02 0.6 0.6 11.0 4.35 3.99 3.83 5.52 10.59 5.0 4.0 5.92 6.0 7.09	Fluorescein; forced-gradient tracer tests, transport parameters were calculated form the breakthrough curves using the 1D analytical solution by Sauty (1980) in a steady-state, radially symmetric divergent flow field at the observation scale Fluorescein; natural gradient tracer test, transport parameters were calculated form the breakthrough curves using the 1D analytical solution by Sauty (1980) in a steady-state, radially symmetric divergent flow field at the observation scale	II
Rivett et al. (1994)	Glaciolacustrine sand	45	50	Sulfate and organic solvents; multiple-well tracer test, 3D analytical solution for contaminant transport in a finite-thickness aquifer (PATCH3D)	II

Table 1 (Continued)
Partial Summary of Data and Sources (Also see Appendix 1, Table A1)

Type of Medium	Description	Scale (m)	α (m)	Tracer; Description of Test, and Analysis Method	Overall Reliability
Robertson et al. (1991)	Sand with minor silt	130	1	Br; multiple-well, steady-state natural gradient tracer test, analysis by 3D analytical model	I
Silliman and Simpson (1987)	Heterogeneous sand	0.15	0.058	NaCl; continuous source displacement; analytical moment analysis based on probability distribution, dispersivities were calculated by dividing the variance of parameter $[(x\text{-}vt)/2t)^{1/2}]$ at the electrode column by the velocity calculated for that column	I
		0.46	0.047		
		0.91	0.076		
		1.37	0.094		
		1.83	0.093		
		0.15	0.054		
		0.46	0.071		
		0.91	0.073		
		1.37	0.075		
		1.83	0.127		
B. *Sandstones*					
Baker (1977)	Berea Sandstone	0.229	0.00186	Benzene and metaxylene; displacement tests, concentration profiles by gas chromatographic analysis, unclear whether long or vertical dispersivity was measured, use of nonconservative tracer	III
		0.229	0.00320		
		0.229	0.00305		
Coats and Smith (1964)	Torpedo Sandstone	0.235	0.00064	CaCl; continuous source, analytical solution, unclear whether horizontal or vertical dispersivity was measured	III
		0.235	0.00078		
		0.235	0.00111		
Delshad (1986)	Berea Sandstone	0.6096	0.0059	Brine; single-phase displacement, analytical solution, unclear whether horizontal or vertical dispersivity was measured	III
		0.6096	0.0030		
		0.6096	0.0030		
		0.6096	0.0010		
Himmelsbach and Wendland (2000)	Fractured sandstone	0.24	0.006	Pyranine, Cd, Pb; numerical modeling of a tracer experiment (double-porosity approach)	III
Kasraie and Farouq Ali (1984)	Berea Sandstone	1.22	0.00599	CaCl, toluene, iso-octane; displacement tests. Procedure by Brigham (1974) for data analysis, unclear whether longitudinal or vertical dispersivity was measured, use of nonconservative tracer	III
		1.22	0.00361		
		1.22	0.00271		
		1.22	0.00535		
		1.22	0.00480		
		1.22	0.00523		
Schulze-Makuch (1996)	St. Peter Sandstone	0.035	0.0016	KBr; continuous source displacement, analytical solution matched to concentration profile, horizontally drilled core	II
		0.035	0.0015		
		0.035	0.0019		
C. *Carbonate rocks*					
Baker (1977)	Vugular limestone cores	0.094	0.94	Benzene and metaxylene; concentration profiles by gas chromatographic analysis, unclear whether longitudinal or vertical dispersivity was measured, use of nonconservative tracer	III
		0.094	1.95		
		0.094	2.79		
		0.094	1.45		
		0.094	2.06		
		0.094	1.41		
		0.094	2.27		
Maloszewski et al. (1992)	Karstic limestone	3100	12.3	Chloride, uranine, amidor; multiflow model fitted to experimental results, scale (distance) calculated by dividing mean water velocity by mean transit time	II
		3100	19.0		
		3100	18.4		
		3100	24.1		
		3100	15.1		
		3100	29.1		
		3100	14.0		
		3100	23.7		
		3100	11.9		
		3100	29.7		
		3100	21.2		
		3066	48.7		
		3066	26.6		

Table 1 (Continued)
Partial Summary of Data and Sources (Also see Appendix 1, Table A1)

Type of Medium	Description	Scale (m)	α (m)	Tracer; Description of Test, and Analysis Method	Overall Reliability
Maloszewski and Zuber (1993)	Silurian dolomite	19.8 19.8 17.2	0.63 0.10 0.29	Cl; single-fracture dispersion model applied to tracer test in a convergent radial flow zone in a horizontal fracture	II
Mull et al. (1988)	Karstic limestone	916 987 983 919 920 930 914	6.8 3.64 2.78 6.1 4.25 4.18 3.84	Fluorescein; tracer tests using springs, analytical solution based on equations by Fischer (1968), with the assumptions of constant velocity and uniform flow characteristics between injection and sampling points	III
Schulze-Makuch (1996)	Silurian dolomite	0.035 0.035 0.035 0.035 0.035 0.035	0.036* 0.045 0.038* 0.032 0.006 0.010	KBr; continuous source displacement, analytical solution matched to concentration profile, two of the samples (marked with an asterisk) exhibited double-porosity flow behavior	II
	Silurian dolomite	597	3.7	Cl; total dissolved solids, lake water intrusion into dolomite aquifer, analytical solution, 2D, porous medium breakthrough	I
Schulze-Makuch (1996) from MMSD (1983) data	Silurian dolomite	50.1 30.2	11.2 8.7	Rhodamine WT; pulse, analytical solution using procedure from Cole (1974), multiple-well tracer tests, tracer breakthrough from early fracture response, formation exhibited double-porosity behavior	II
D. *Basalts*					
Lavenue and Domenico (1986)	Flood basalt	1 2000 35,000	0.01 3.16 31.6	Cl; natural water chemistry, analysis by Domenico and Robbins (1985) model, not much known about source concentrations and dimensions	III
Leonhart et al. (1983)	Flood basalt	17	1.0	^{131}I and K-thiocyanate; two well recirculating tracer technique within paired boreholes. Analytical solution by matching type curves that simulate concentration variations at the pumping well	III
Nimmer (1998)	Fractured basalt	6.1 6.1 21.3	0.10 0.06 2.67	Fluorescein, iodide, benzoic acid, alcohol, *B. thermoruber* spores; microbeads; multiple-well radial convergent tests, curve matching method after Sauty (1980)	II
Steele et al. (1989)	Fractured basalt	9.1 9.1 80.5 33.5 14.6 12.8	1.7 1.8 0.2 1.6 4.0 5.0	NaCl, KCl; pulse injection, analytical solution matched to concentration profile	III
Souza and Voss (1987)	Layered basalt	100	76	Salt water intrusion into the coastal basalt (Oahu, Hawaii), 2D finite-element method to simulate variable-density ground water flow and transport of total dissolved solids (code SUTRA)	II
E. *Granites*					
Baeumle et al. (2000)	Fractured granite	3 3 15	0.9 1.2 0.012	Cl, eosin; forced-gradient tracer tests, analysis with single-fissure dispersion model and single-fissure piston flow model	II III II
Carlsson et al. (1979)	Precambrian granite and gneiss	51 22 35	0.21 0.19 0.11	^{82}Br, rhodamine WT; pulse injection, 1D analytical solution, assuming 1 fissure per meter, injection of tracer in a fracture system between two boreholes	III

Table 1 (Continued)
Partial Summary of Data and Sources (Also see Appendix 1, Table A1)

Type of Medium	Description	Scale (m)	α (m)	Tracer; Description of Test, and Analysis Method	Overall Reliability
D'Alessandro et al. (1997)	Fractured granite	22.0 22.0 14.5	3.4 4.0 4.4	Fluorescein, iodide, eosin; multiple-well test with packed-off intervals, radial advective-dispersive transport with and without matrix diffusion, code TRAZADOR, which analytically solves transport equations for conservative tracers following the inverse problem approach	II
Einsiedl et al. (2000)	Fractured granite	10.2	0.56	Fluorescent dye; multiple-well tracer test, pulse injection, analysis by single-fissure dispersion model	II
Gutierrez et al. (1997)	Fractured granite	22	1	Deuterium, uranine, DTPA-Gd; 2D radial advection-dispersion model, code TRANSIN III for automatic calibration of ground water flow and solute transport parameters (3D)	II
Himmelsbach et al. (1998)	Fractured granite	346 235 49 21.4 11.2 11.2 11.2 11.2 11.2 16.2 16.2	3.46 3.91 2.45 2.14 0.3 0.3 0.3 0.17 0.17 0.9 0.25	Deuterium and dye tracers (eosin, pyranine, uranine); large-scale tracer tests under natural-flow field conditions (21 to 346 m) and small-scale tracer tests (11 to 16.2 m) under artificial induced radial convergent and injection-withdrawal flow fields, analysis by 1D single-fissure dispersion model, modeling advective-dispersive transport in the fractures coupled with diffusive transport in the adjacent rock matrix	II
Keller et al. (1999)	Fractured granite	0.16 0.16 0.16	0.043 0.078 0.095	Iodide; first value is experimental, second value is based on geostatistics of fracture zone, third value is by numerical model, transport of solute is imaged using CT scanning, model uses small perturbation approach	II
Maloszewski and Zuber (1993)	Densely fractured granite	14 18 26 16	1.2 0.9 2.1 8.0	Na-fluorescein; Cr-ethylene-diaminetetraacetic acid; tracer tests between section of wells, single-fissure dispersion model applied to tracer test	II
Tsang et al. (1991)	Fractured granite	10.7 24.6 33.3 36.4 42.8	4.7 2.3 6.8 2.7 1.8	Elbenyl, eosin Y, eosin B, uranine, iodide; reanalysis of multiyear tracer tests performed by Neretnieks (1987) and Abelin et al. (1987), analytical solution approximating the early part of the injection history by an exponential decay function	III
		10.7 24.6 33.3 36.4 42.8	1.7 2.9 2.0 0.6 1.5	Elbenyl, eosin Y, eosin B, uranine, iodide; reanalysis of multiyear tracer tests performed by Neretnieks (1987) and Abelin et al. (1987). Analysis applies a deconvolution procedure involving the use of Toeplitz matrices	II

Note: If a range in scale is provided, the arithmetic mean is provided in the table. If a range in dispersivity is reported, then the geometric mean is provided in the table. Rating system for reliability is adopted from Gelhar et al. (1992). Reliability assignments are valid for the whole data set associated with a reference unless indicated otherwise.

which includes a brief characterization of aquifer material tested, type of test and tracer, and analysis method. The data were also grouped according to reliability, adopting the system used by Gelhar et al. (1992). Briefly, high-reliability data are assigned to group I, and the dispersivity values in that group are thought to be accurate within a factor of two. Low-reliability data are assigned to group III and are thought to be no more accurate than within one or two orders of magnitude. Intermediate reliabilities are assigned to group II. For a reported dispersivity value to be assigned to group I, each of the following criteria must have been met: (1) the tracer test was ambient flow with known input, diverging radial flow, or a two-well pulse test; (2) the tracer input was well defined; (3) the tracer was conservative (e.g., Cl^-, I^-, Br^-, tritium); and (4) the dimensionality of the tracer concentration measurements and the analysis of the concentration data were appropriate. Reported dispersivity values were assigned to group III if (1) the two-well recirculating test with a step input was used; (2) the single-well injection-withdrawal test was used with tracer monitoring at the pumping well; (3) the tracer input was not clearly defined; (4) the tracer breakthrough curve was assumed to be the superposition of breakthrough curves in separate layers when there was little or no evidence of such layers at the test site; (5) the measurement of tracer concentrations in space was inadequate; or (6) the equation used to obtain dispersivity was not appropriate for the data collected. For detailed information on the reliability criteria, please see Gelhar et al. (1992). Typical problems encountered in the dispersivity data analyses were mass input history unknown, nonconservative effect of tracer not accounted for, dimensionality of the monitoring not matched to the dimensionality of the analysis, and assumption of distinct geologic layers in analysis when their actual presence was not or not sufficiently documented. The assignment of reliability classes should not be taken as a judgment of the conducted tracer test and its analysis; it is intended simply to provide some quality assessment in regard to the parameter of longitudinal dispersivity (i.e., many tests were not conducted with the primary objective to characterize longitudinal dispersivity with the highest possible accuracy).

Since longitudinal dispersivity is a one-dimensional parameter, flow distance was chosen as an appropriate scale of measurement. For a laboratory experiment, flow distance was generally determined by measuring the length of the horizontally oriented core through which the tracer traveled (e.g., Schulze-Makuch 1996); for a field tracer test, by determining the distance between the injection and the withdrawal well (e.g., D'Alessandro et al. 1997); and for a computer simulation, by the horizontal flow distance between a ground water source and a sink. The scale for single-well injection tests and packer tracer tests was obtained by determining the radius of influence, which was calculated from the volume of water introduced (i.e., discharge or injection rate multiplied by the time interval) by assuming cylindrical flow to the well screen or packed interval, respectively. Many references provided the appropriate scale measure in the cited paper (e.g., Gelhar et al. 1985). If a range in scale of measurement was provided (generally ranges were small), the arithmetic mean was chosen for the analysis. If a range in longitudinal dispersivity was provided, the geometric mean was used (Table 1). The geometric mean was thought to represent a more suitable mean for dispersivity because the values varied commonly by an order of magnitude or more. Also, dispersivity, which is related to variations in hydraulic conductivity, is variable in space due to local heterogeneities, and it is generally recognized that the probability density function of hydraulic conductivity is lognormal (e.g., Freeze and Cherry 1979). If no scale of measurement was provided, it was calculated from the description of the experimental or aquifer test setup whenever possible. The obtained longitudinal dispersivity/scale of measurement data pairs were then sorted by type of geological medium to identify a relationship of dispersivity with geological medium as has been found for hydraulic conductivity data (Schulze-Makuch et al. 1999). Geological media analyzed were unconsolidated sediments, sandstones, carbonate rocks, basalts, and granites.

Results

Longitudinal dispersivity values obtained from laboratory tests, aquifer tests, and computer models were plotted vs. scale of measurement for each analyzed geological medium (e.g., Figure 1 for unconsolidated media). The plot shows that longitudinal dispersivity increases exponentially with scale of measurement. Plots for consolidated media show a similar scaling behavior (Figure 2). According to the conventional explanation for this scaling behavior as a tracer moves through the geological medium, more and more heterogeneities are encountered, and dispersivity increases with scale of measurement due to a combination of advective and diffusion-related processes. Results from a total of 307 longitudinal dispersivity determinations from a total of 109 authors are given in Table 1 and Table A1 in Appendix A. The scaling exponent for all data from the unconsolidated sediments was 0.81, with a 95% confidence interval of 0.11. The larger scale data appear to level off somewhat (Figure 1), and if an upper bound is interpreted to exist at a scale of ~2000 m the slope increases to 0.94. However, the resulting regression coefficient and 95% confidence interval is lower. Also, if the whole data set is subdivided into reliability classes, then the scaling exponent decreases with higher reliability classes (Table 2). Not enough tracer tests were conducted in consolidated rocks to allow an evaluation in reliability classes. Scaling exponents range here between 0.40 and 0.92, with a lower 95% confidence interval and higher regression coefficients generally associated with the lower scaling exponents (e.g., a scaling exponent of 0.40 for carbonates with a 95% confidence interval of 0.09; Table 3). High 95% confidence intervals are a result of too few data pairs and large dispersivity variations that can be expected from data that are derived from different aquifers at different locations. No statistically significant difference between unconsolidated and consolidated geological media could be shown.

The parameter c in Tables 2 and 3 equals the longitudinal dispersivity value of a specific medium at a flow

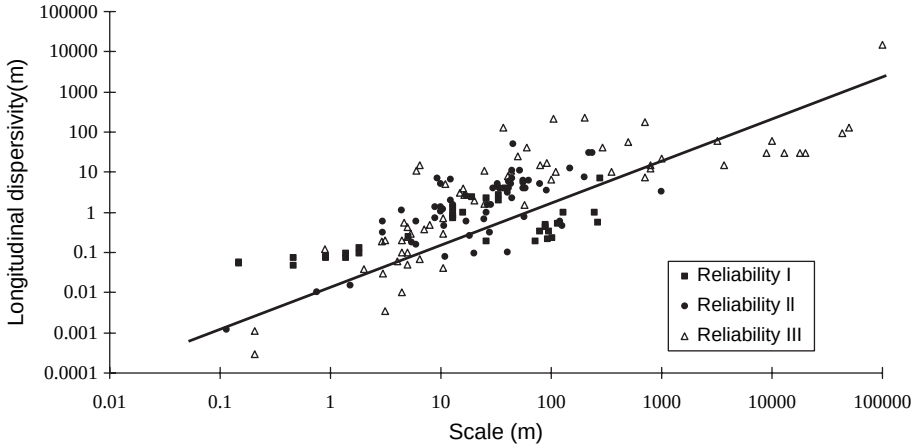

Figure 1. Relationship of longitudinal dispersivity to scale of measurement for unconsolidated sediments. The line represents the regression line for all data points (regardless of assigned reliability class) with a scaling exponent of 0.81 and a *c* value of 0.085 m.

distance of 1 m. This parameter can be considered to be a characteristic value for the geological medium, which is related to interconnectivity, type, and size of pores in porous-flow media, and fracture aperture and interconnectivity in fracture-flow media. Longitudinal dispersivities for a flow distance of 1 m are highest for carbonates with a *c* value of 80 cm.

The upper bound represents the volume at which a porous medium becomes the equivalent of a homogeneous medium, and thus longitudinal dispersivity remains constant with scale. This volume has also been referred to as the representative elementary volume. The determination of an upper bound is problematic because (1) the upper bound is strongly affected by values obtained from computer simulations, which are not physical measurements; and (2) each individual aquifer could have a unique upper bound, and the upper bound as determined from the method used here provides a mean value of an upper bound for a specific type of aquifer only. Based on the data analysis performed, none of the media appeared to exhibit an upper bound (Tables 2 and 3; Figures 1 and 2), at least not within the scale range for which the relationships were established.

Discussion

The scaling relationship of longitudinal dispersivity with scale of measurement below the upper bound can be described by the empirical power law

$$\alpha = c(L)^m \tag{1}$$

where α is longitudinal dispersivity (L), c a parameter characteristic for a geological medium (L^{1-m}), L the flow distance (L), and m the scaling exponent (slope of the line on the log-log plot). The mathematical model used here is simply based on the best fit found by the author, but it is consistent with (1) power law relationships of dispersivity with scale as suggested by others (e.g., Neuman 1990, 1995); (2) theoretical developments based on fractal concepts (e.g., Wheatcraft and Tyler 1988); and (3) relationships developed for the related parameter of hydraulic conductivity (e.g., Schulze-Makuch and Cherkauer 1997; Schulze-Makuch et al. 1999). The scaling exponent for all geological media analyzed lies between 0.40 and 0.94. This value is subject to several uncertainties. One is the limited number of data points available. Only a few

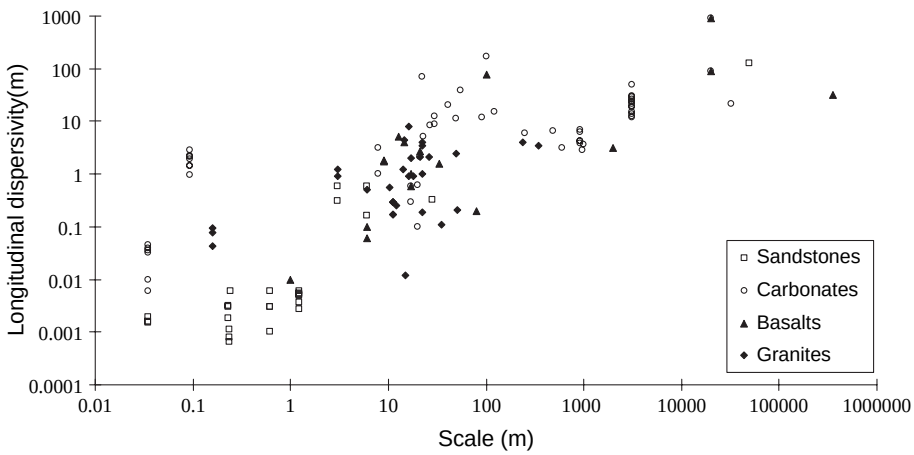

Figure 2. Relationship of longitudinal dispersivity to scale of measurement for various rock types. The scaling behavior for each rock type is quantified in Table 3.

Table 2
Scaling Behavior of Longitudinal Dispersivity in Unconsolidated Sediments

Type of Medium	N[1]	n[2]	Slope of Exponent, m	Regression coefficient[3]	95% Confidence Interval about Mean	c[4]	Upper Bound[5] (m)
Unconsolidated	156	62	0.81	0.77	0.11	0.085	none
(all reliabilities)	146	55	0.94	0.74	0.14	0.063	2000
Unconsolidated (reliabilities I and II only)	93	31	0.70	0.67	0.15	0.112	none or >1000
Unconsolidated (reliability I only)	32	10	0.44	0.71	0.15	0.20	none or >100

[1]Number of single values of longitudinal dispersivity in specified type of geological medium.
[2]Number of different sources (authors).
[3]Regression coefficient of the relationship based on all single data points below the identified upper bound.
[4]Medium-characteristic parameter c (m).
[5]Upper bound of the relationship.
Note: Two interpretations are provided for unconsolidated sediments of all reliabilities. One with no upper bound, one with an upper bound. All large-scale values are of reliability III, thus not included in reliabilities I and II, and reliability I values only.

aquifer tests are designed to measure dispersivity in addition to the hydraulic conductivity or transmissivity of an aquifer. This uncertainty is quantified for each of the geological media analyzed by the 95% confidence interval about the exponent provided in Tables 2 and 3. The 95% confidence interval is typically high for media with few data points (e.g., sandstones) and low for media with many data points (e.g., unconsolidated sediments and carbonates). Another factor that introduces bias on the scaling exponent is the position of an upper bound. An upper bound (fractal cutoff limit) was proposed by Wheatcraft and Tyler (1988) on theoretical grounds in their model describing dispersion in a set of fractal streamtubes. It was also observed by Schulze-Makuch et al. (1999) for the scaling behavior of hydraulic conductivity data. The upper bound represents the scale at which the geological medium approaches the properties of a homogeneous medium. It is inferred by plotting dispersivity vs. scale of measurement (e.g., Figure 1) and validated by calculating regression coefficients and 95% confidence intervals for subsections of the data. Only the data for the unconsolidated sediments indicate the possible presence of an upper bound at ~2000 m (Table 2). However, this is thought to be unlikely, since it would widen the 95% confidence interval and increase the scaling exponent, while higher reliability data actually show that the scaling exponent is most likely lower. Gelhar et al. (1992) observed that reanalyses of data showed that improved interpretations most often lead to smaller dispersivities, which will lead to a smaller scaling exponent. This is exactly what was observed here as well.

Neuman and Federico (2003) proposed that the scaling behavior of dispersivity is observed because of the heterogeneous nature of the medium and because dispersivities are determined on the basis of traditional Fickian advection-dispersion models of solute transport, where dispersivity is treated as a constant. The observed increase of dispersivity with scale of measurement due to the heterogeneous nature of the medium is sometimes referred to anomalous or non-Fickian dispersion, while the increase based on inadequate modeling is referred to as "apparent" dispersivity. Neuman (1995) suggested a scaling exponent of 1.5 for longitudinal dispersivity, and Neuman and Federico (2003) attributed this value in part to non-Fickian dispersion (m = 1) and apparent dispersion (m = 0.5). They also hypothesized that longitudinal dispersivity eventually stabilizes at a constant Fickian asymptote, terming its earlier increase with travel distance preasymptotic. This type of behavior was also supported by stochastic analyses and numerical simulations

Table 3
Scaling Behavior of Longitudinal Dispersivity in Consolidated Rocks

Type of Medium	N[1]	n[2]	Slope of Exponent, m	Regression Coefficient[3]	95% Confidence Interval about Mean	c[4]	Upper Bound[5] (m)
Sandstones	29	9	0.92	0.88	0.77	0.01	none or >10,000
Carbonates	54	19	0.40	0.74	0.09	0.80	none or >10,000
Basalts	17	8	0.61	0.75	0.23	0.15	none or >10,000
Granites	41	11	0.51	0.53	0.13	0.21	none or >100

[1]Number of single values of longitudinal dispersivity in specified type of geological medium.
[2]Number of different sources (authors).
[3]Regression coefficient of the relationship based on all single data points.
[4]Medium-characteristic parameter c (m).
[5]Upper bound of the relationship.

performed by Gelhar and Axness (1983), Schwarze et al. (2001), Janković et al. (2003), and Dagan and Fiori (2003), among others. The data set analyzed here, which constitutes the largest data set of which the author is aware, does not support those claims. Moreover, the empirical scaling exponents found here are much lower than those previously reported, ~0.5 for this study vs. 1.5 found by Neuman (1995). The lower scaling exponent may be explained in part by more sophisticated and higher reliability methods used by various authors that reduce or eliminate apparent dispersivity (e.g., causing the observed trend of decreasing scaling exponents in higher reliability data; Table 2). An asymptotic behavior might be suspected in the unconsolidated sediment for all reliability classes above a scale of 2000 m, but it cannot be substantiated (Table 2). However, this study appears to be consistent with Neuman (1990) in that there appears to be no strong dependence on the type of geological medium in which the test was conducted. Hydraulic conductivity does exhibit a strong dependence on geological medium, of course (Schulze-Makuch et al. 1999), and longitudinal dispersivity should in theory do so as well because heterogeneities encountered in different geological media are different, and thus should be reflected by different scaling exponents. However, no statistically significant difference can be observed among the different media.

A significant difference among geological media, though, can be observed for the medium-characteristic parameter c, which is a measure of heterogeneity at a unit flow distance (1 m). It is largest for carbonate rocks with a value of 0.8 m, and lowest for unconsolidated sediment and sandstones with values of 0.01 m and ~0.009 m, respectively. This finding appears reasonable as carbonates can be extremely heterogeneous on small scales, exhibiting a wide range of porosities caused by vugs, fractures, and flow conduits with various types of fluid flow behaviors (porous flow, fracture flow, conduit flow, and combinations of these). Sandstones and sandy sediments, on the other hand, are quite often homogeneous on this scale but will exhibit major heterogeneities on larger scales due to facies changes, channel deposits etc.

Any analysis like this must be considered with caution. Large intrinsic errors are incorporated by using dispersivity values from different aquifers at different localities. It is necessary to keep in mind that each geological medium is unique with unique geometries that a solute will encounter along its flowpath, and thus each site will display its characteristic scaling behavior. Also, various authors use different assumptions and methods of analysis, which will cloud any effort to discern a generalized scaling behavior. Even if a generalized scaling rule is found, it cannot represent local expressions of geological facies such as channeling of flow, and thus detailed geologic mapping is required to quantify heterogeneities in the geological record (Anderson 1991; Neuman 1991). In addition, the analysis presented here did not try to achieve a representative poll of different geological media, as some geological types were overrepresented in the data sample considered here. However, given that most aquifer tests do not measure transport properties such as longitudinal dispersivity and the general paucity of tracer tests, the number of data accumulated here is thought to provide a valuable contribution to stimulate further investigations into the scaling behavior of dispersivity.

Conclusions

The scaling relationship of longitudinal dispersivity with scale of measurement below the upper bound can be described by the empirical power law $\alpha = c(L)^m$, where α is longitudinal dispersivity (L), c is a parameter characteristic of a geological medium (L^{1-m}), L is the flow distance (L), and m is the scaling exponent. Based on the 307 data pairs analyzed, the mean scaling exponent appears to be ~0.5, with no statistically significant difference between various geological media. The parameter c varies between ~0.01 m for sandstones and unconsolidated media, and 0.8 m for carbonate rocks. No upper bound on the relationships was apparent for a flow distance up to ~10,000 m for all media except for granites where this statement can only be extended to a flow distance of 100 m due to lack of data on regional-scale transport.

Acknowledgments

I appreciate the valuable comments made by the two anonymous reviewers on previous versions of this manuscript. Their constructive input significantly improved this work. I also thank Huade Guan, currently at the New Mexico Institute of Mining and Technology, and Colleen Rust, Washington State University, for data collection for this study.

References

Abelin, H., L. Birgersson, J. Gidlund, L. Moreno, I. Neretnieks, H. Widen, and J. Agren. 1987. 3D migration experiments, results and evaluation, Stripa Project Technical Report 87-21. Stockholm, Sweden: Sweden Nuclear Fuel and Waste Management Co. (SKB).

Adams, E.E., and L.W. Gelhar. 1992. Field study of dispersion in a heterogeneous aquifer: 2. Spatial moments analysis. *Water Resources Research* 28, no. 12: 3293–3307.

Anderson, M.P. 1991. Comment on "universal scaling of hydraulic conductivities and dispersivities in geological media" by S.P. Neuman. *Water Resources Research* 27, no. 6: 1381–1382.

Atakan, Y., W. Roether, G. Matthess, and K.-O. Muennich. 1974. Felduntersuchungen von Fliessvorgaengen in einem Porengrundwasserleiter mittels Farbstoffindikatoren. *GWF-Wasser/Abwasser* 115, no. 4: 159–164.

Avon, L., and J.D. Bredehoeft. 1989. An analysis of trichloroethylene movement in groundwater at Castle Air Force Base, California. *Journal of Hydrology* 110, no. 1–2: 23–50.

Baeumle, R., H. Hoetzl, and K. Witthueser. 2000. Flow pattern and transport behavior of granitic rock intersected by a highly permeable fault zone. *IAHS Publ*. no. 262: 283–288.

Baker, L.E. 1977. Effects of dispersion and dead-end pore volume in miscible flooding. *Society of Petroleum Engineering Journal*, June: 219–227.

Boesel, D., M. Herfort, T. Ptak, and G. Teutsch. 2000. Design, performance, evaluation, and modeling of a natural gradient multitracer transport experiment in a contaminated heterogeneous porous aquifer. *IAHS Publ*. no. 262: 45–52.

Brigham, W.E. 1974. Mixing equation in short laboratory cores. *Society of Petroleum Engineers Journal, Transactions of the American Institute of Mining, Metallurgical, and Petroleum Engineers* 257, February: 91–99.

Carlsson, L., G. Gridlund, K. Hansson, and C.-E. Klockars. 1979. Estimation of hydraulic conductivity in Swedish Precambrian crystalline bedrock. In *Proceedings of the Workshop on Low-Flow, Low-Permeability Measurements in Largely Impermeable Rocks, OECD*. Paris, France, 97–115. Vienna, Austria: International Atomic Energy Agency.

Chapelle, F.H. 1986. A solute-transport simulation of brackish-water intrusion near Baltimore, Maryland. *Ground Water* 24, no. 3: 304–311.

Chiang, C.Y., J.P. Salanitro, E.Y. Chai, J.D. Colthart, and C.L. Klein. 1989. Aerobic biodegradation of benzene, toluene, and xylene in a sandy aquifer—Data analysis and computer modeling. *Ground Water* 27, no. 6: 823–834.

Coats, K.H., and B.D. Smith. 1964. Dead-end pore volume and dispersion in porous media. *Society of Petroleum Engineers Journal, Transactions of the American Institute of Mining, Metallurgical, and Petroleum Engineers* 231, *March*: 73–84.

Cole, J.A. 1974. Some interpretations of dispersion measurements in aquifers: Groundwater pollution in Europe. In *Proceedings of a Conference Organized by the Water Research Association, Reading, England*, ed. J.A. Cole, 86–93. New York: Water Information Center, Inc.

Dagan, G., and A. Fiori. 2003. Time dependent transport in heterogeneous formations of bimodal structures. Part 1, *Theory. Water Resources Research* 39, no. 5: 465–472.

D'Alessandro M., F. Mousty, G. Bidoglio, J. Guimera, I. Benet, X. Sanchez-Vila, M. Garcia-Gutierrez, and A.Y. DeLlano. 1997. Field tracer experiment in a low permeability fractured medium; results from El Berrocal site. *Journal of Contaminant Hydrology* 26, no. 1–4: 189–201.

Delshad, M. 1986. A study of transport of micellar fluids in porous media. Ph.D. diss., Department of Chemical Engineering, University of Texas at Austin.

Domenico, P.A., and G.A. Robbins. 1985. A new method of contaminant plume analysis. *Ground Water* 23, no. 4: 476–485.

Einsiedle, F., H. Langhals, P. Maloszewski, K. Witthueser, and S. Wohnlich. 2000. Application of two fluorescent dyes and fluorescent particles in a horizontal and vertical fracture. *International Association of Hydrological Sciences Publications* no. 262: 175–180.

Engesgaard, P., H.K. Jensen, J. Molson, E.O. Frind, and H. Olsen. 1996. Large-scale dispersion in a sandy aquifer: Simulation of subsurface transport of environmental tritium. *Water Resources Research* 32, no. 11: 3253–3266.

Fischer, H.B. 1968. Dispersion predictions in natural streams. *Journal of the Sanitary Engineering Division* 94, no. SA5: 927–943.

Freeze, R.A., and J.A. Cherry. 1979. *Groundwater*. Englewood Cliffs, New Jersey: Prentice-Hall Inc.

Gelhar, L.W., and C. Axness. 1983. Three-dimensional stochastic analysis of macrodispersion in Aquifers. *Water Resources Research* 19, no. 1: 161–180.

Gelhar, L.W., A. Mantoglou, C. Welty, and K.R. Rehfeldt. 1985. A review of field-scale physical solute transport processes in saturated and unsaturated porous media. Palo Alto, California: Electric Power Research Institute EPRI EA-4190 Project 2485–5.

Gelhar, L.W., C. Welty, and K.R. Rehfeldt. 1992. A critical review of data on field-scale dispersion in aquifers. *Water Resources Research* 28, no. 7: 1955–1974.

Gutierrez, M.G., Y.A. DeLlamo, B.A. Hernandez, J. Humm, and M. Saltink. 1997. Tracer test at El Berrocal Site. *Journal of Contaminant Hydrology* 26, no. 1–4: 179–188.

Hendry, M.J., J.R. Lawrence, and P. Maloszewski. 1999. Effects of velocity on the transport of two bacteria through saturated sand. *Ground Water* 37, no. 1: 103–112.

Himmelsbach, T., H. Hoetzl, and P. Maloszewski. 1998. Solute transport processes in a highly permeable fault zone of Lindau fractured rock test site. *Ground Water* 36, no. 5: 792–800.

Himmelsbach, T., and E. Wendland. 2000. Transport of heavy metals in a fractured porous block: Experiments and a 3-D model. *International Association of Hydrological Sciences Publications* 262: 325–332.

Hyndman, D.W., and S.M. Gorelick. 1996. Estimating lithologic and transport properties in three dimension using seismic and tracer data: The Kesterson Aquifer. *Water Resources Research* 32, no. 9: 2659–2670.

Janković, I., A. Fiori, and G. Dagan. 2003. Flow and transport through two-dimensional isotropic media of binary conductivity distribution. Part 2: Numerical simulations and comparison with theoretical results. *Stochastic Environmental Research and Risk Assessment* 17, no. 6: 384–393.

Jensen, K.H., and K. Bitsch. 1993. Large-scale dispersion experiments in a sandy aquifer in Denmark: Observed tracer movements and numerical analysis. *Water Resources Research* 29, no. 3: 673–696.

Kasraie, M., and S.M. Farouq Ali. 1984. Role of immobile phase saturations in tertiary oil recovery. In *Paper 12635 Presented at the SPE/DOE Fourth Symposium on Enhanced Oil Recovery*, Tulsa, Oklahoma, April 15–18. Tulsa, Oklahoma: American Association of Petroleum Geologists.

Keller, A.A., P.V. Roberts, and M.J. Blunt. 1999. Effect of fracture aperture variations on the dispersion of contaminants. *Water Resources Research* 35, no. 1: 55–63.

Konikow, L.F., and J.D. Bredehoeft. 1978. *Computer Model of Two-dimensional Solute Transport and Dispersion in Ground Water.* Techniques of water-resources investigations of the United States Geological Survey, Book 7. Alexandria, Virgina: U.S. Geological Survey

Lau, L.K., W.J. Kaufman, and D.K. Todd. 1959. Dispersion of a Water Tracer in a Radial Laminar Flow Through Homogeneous Porous Media. Berkeley, California: Hydraulic Laboratory and Sanitary Engineering Research Laboratory, University of California.

Lavenue, A.M., and P. Domenico. 1986. A preliminary assessment of the regional dispersivity of selected basalt flows at the Hanford site, Washington, USA. *Journal of Hydrology* 85, no. 1–2: 151–167.

Lehner, T.J. 2004. Removal of pathogenic parasites using surfactant-modified zeolite barriers in a model aquifer. M.S. thesis, Department of Geological Sciences, University of Texas at El Paso.

Leonhart, L.S., R.L. Jackson, D.L. Graham, G.M. Thompson, and L.W. Gelhar. 1983. Groundwater flow and transport characteristics of flood basalt as determined from field tracer experiments. *EOS, Transactions, American Geophysical Union* 64, no. 9: 88–89.

Maloszewski, P., T. Harum, and B. Benischke. 1992. Application of tracer models. *Steirische Beitraege zur Hydrogeologie*, no. 43: 116–157.

Maloszewski, P., and A. Zuber. 1993. Tracer experiments in fractured rocks: Matrix diffusion and the validity of methods. *Water Resources Research* 29, no. 8: 2723–2735.

Mas-Pla, J., T.C.J. Yeh, J.F. McCarthy, and T.M. Williams. 1992. A forced gradient tracer experiment in a coastal sandy aquifer, Georgetown Site, South Carolina. *Ground Water* 30, no. 6: 958–964.

Milwaukee Metropolitan Sewage District (MMSD). 1983. Infiltration/exfiltration analysis: Milwaukee pollution abatement program. Milwaukee, Wisconsin: MMSD.

Moltyaner, G.L., M.H. Klukas, C.A. Wills, and R.W.D. Killey. 1993. Numerical simulations of Twin Lake natural gradient tracer tests: A comparison of methods. *Water Resources Research* 29, no. 10: 3433–3452.

Mull, D.S., T.D. Liebermann, J.L. Snoot, and L.H. Woosley. 1988. Application of dye-tracing techniques for determining solute transport characteristics of ground water in karst terranes. Atlanta, Georgia: EPA region 4 report 904/6-88-001.

Neretnieks, I. 1987. Channeling effects in flow and transport in fractured rocks—Some recent observations and models. In Paper Presented at GEOVAL-87. International Symposium, Swedish Nuclear Inspectorate. Stockholm, Sweden: Swedish Nuclear Inspectorate.

Neuman, S.P. 1995. On advective dispersion in fractal velocity and permeability fields. *Water Resources Research* 31, no. 6: 1455–1460.

Neuman, S.P. 1991. Reply (on M.P. Anderson's comment on "universal scaling of hydraulic conductivities and dispersivities in geologic media" by S.P. Neuman). *Water Resources Research* 27, no. 6: 1383–1384.

Neuman, S.P. 1990. Universal scaling of hydraulic conductivities and dispersivities in geologic media. *Water Resources Research* 26, no. 8: 1749–1758.

Neuman, S.P., and V.D. Federico. 2003. Multifaceted nature of hydrogeologic scaling and its interpretation. *Review of Geophysics* 41, no. 3: 4.1–4.31.

Nimmer, R.E. 1998. Ground water tracer studies in Columbia River Basalt. M.S. thesis, Department of Geological Sciences, University of Idaho.

Palmer, C.D., and R.L. Nadon. 1986. A radial injection tracer experiment in a confined aquifer, Scarborough, Ontario, Canada. *Ground Water* 24, no. 3: 322–331.

Pickens, J.F., and G.E. Grisak. 1981. Scale-dependent dispersion in a stratified granular aquifer. *Water Resources Research* 17, no. 4: 1191–1211.

Ptak, T., and G. Teutsch. 1994. Forced and natural gradient tracer tests in a highly heterogeneous porous aquifer: Instrumentation and measurements. *Journal of Hydrology* 159, no. 1–4: 79–104.

Rivett, M.O., S. Feenstra, and J.A. Cherry. 1994. Transport of a dissolved-phase plume from a residual solvent source in a sand aquifer. *Journal of Hydrology* 159, no. 1–4: 27–41.

Robertson, W.D., J.A. Cherry, and E.A. Sudicky. 1991. Groundwater contamination from two small septic systems on sand aquifers. *Ground Water* 29, no. 1: 82–92.

Sauty, J.P. 1980. An analysis of hydrodispersive transfer in aquifers. *Water Resources Research* 16, no. 1: 145–158.

Schulze-Makuch, D. 1996. Facies dependent scale behavior of hydraulic conductivity and longitudinal dispersivity in the carbonate aquifer of SE Wisconsin. Ph.D. diss., Department of Geological Sciences, University of Wisconsin–Milwaukee.

Schulze-Makuch, D., D.A. Carlson, D.S. Cherkauer, and P. Malik. 1999. Scale dependency of hydraulic conductivity in heterogeneous media. *Ground Water* 37, no. 6: 904–919.

Schulze-Makuch, D., and D.S. Cherkauer. 1997. Method developed for extrapolating scale behavior. *EOS, Transactions, American Geophysical Union* 78, no. 1: 3.

Schwarze, H., U. Jaekel, and H. Verreecken. 2001. Estimation of macrodispersion by different approximation methods for flow and transport in randomly heterogeneous media. *Transport in Porous Media* 43, no. 2: 265–287.

Silliman, S.E., and E.S. Simpson. 1987. Laboratory evidence of the scale effect in dispersion of solutes in porous media. *Water Resources Research* 23, no. 8: 1667–1673.

Souza, W.R., and C.I. Voss. 1987. Analysis of an anisotropic coastal aquifer system using variable-density flow and solute transport simulation. *Journal of Hydrology* 92, no. 1–2: 17–41.

Steele, T.D., J.R. Kunkel, S.C. Way, and R.A. Koenig. 1989. Flow of groundwater and transport of contaminants through saturated fractured geologic media. NUREG/CR-5391. Washington, DC: U.S. Nuclear Regulatory Commission.

Tsang, C.F., Y.W. Tsang, and F.V. Hale. 1991. Tracer transport in fractures: Analysis of field data based on a variable-aperture channel model. Technical Report 91–24. Stockholm, Sweden: Swedish Nuclear Fuel and Waste Management Co.

Wheatcraft, S.W., and S.W. Tyler. 1988. An explanation of scale-dependent dispersivity in heterogeneous aquifers using concepts of fractal geometry. *Water Resources Research* 24, no. 4: 566–578.

Appendix A

Table A1: Data Evaluated by Gelhar et al. (1985, 1992)

Author	Description of Medium	Scale (m)	α (m)	Assigned Reliability
A. *Unconsolidated sediments*				
Ahlstrom et al. (1977)	Glaciofluvial sands and gravel	20,000	30.5	III
Adams and Gelhar (1991)	Very heterogeneous sand and gravel	200	7.5	II
Daniels (1981, 1982)	Alluvium derived from tuff	91	17.3	III
Dieulin (1980)	Alluvial deposits	15	3	III
Egboka et al. (1983)	Glaciofluvial sand	60	42.4	III
Freyberg (1986)	Glaciofluvial sand	90	0.43	I
Fried and Ungemach (1971)	Sand, gravel, and cobbles	6	11	III
Fried (1975), Rhine Aquifer	Alluvial; mixture of sand, gravel, and pebbles with clay lenses	800	15	III
Fried (1975), Lyons, France	Alluvial; with sand and gravel, and slightly stratified clay lenses	800	12	III
Garabedian et al. (1988)	Medium to coarse sand with some gravel overlying silty sand and till	250	0.96	I
Hoehn (1983)	Layered gravel and silty sand	4.4	0.1	III
		4.4	0.01	III
		4.4	0.2	III
		10.4	0.3	III
		10.4	0.04	III
		10.4	0.7	III
Hoehn and Santschi (1987)	Layered gravel and silty sand	4.4	1.1	II
		10.4	1.2	II
		100	6.7	III
		110	10.0	III
		500	58.0	III

Appendix A (Continued)
Data Evaluated by Gelhar et al. (1985, 1992)

Author	Description of Medium	Scale (m)	α (m)	Assigned Reliability
Huyakorn et al. (1986)	Layered medium sand	38.3	4.0	I
Iris (1980)	Alluvial deposits	40	3	II
Kies (1981)	Fluvial sands	25	1.6	III
Klotz et al. (1980)	Fluvioglacial gravels	10	5	II
Konikow (1976)	Alluvium	13,000	30.5	III
Konikow and Bredehoeft (1974)	Alluvium, inhomogeneous clay, silt, sand, and gravel	18,000	30.5	III
Kreft et al. (1974)	Sand	5.5	0.18	II
Lau et al. (1957)	Sand and gravel with clay lenses	19	2.45	I
Leland and Hillet (1981)	Fine sand and glacial till	4	0.06	III
Meyer et al. (1981)	Sand	5	0.42	III
Molinari and Peaudecerf (1977)	Sand	13	0.79	I
and Sauty (1977)		13	1.27	I
		13	0.72	I
		26	2.23	I
		33.2	1.94	I
		33.2	2.73	I
Moltyaner and Killey (1988a, 1988b)	Fluvial sand	40	0.10	II
Naymik and Barcelona (1981)	Unconsolidated sand and gravel	16.4	2.67	III
New Zealand Ministry of	Gravel with cobbles	56.5	4.0	II
Works and Development (1977)		25	0.67	II
		290	41	III
Papadopulos and Larson (1978)	Medium to fine sand with clay	57.3	1.5	III
Pickens and Grisak (1981)	Sand	8	0.5	III
		3	0.03	III
Pinder (1973)	Glacial outwash	1000	21.3	III
Rajaram and Gelhar (1991)	Glaciofluvial sand	90	0.5	I
Roberts et al. (1981)	Sand, gravel, silt	11	5	III
		20	2	III
		40	8	III
		16	4	III
		43	11	III
Robson (1974,1978)	Alluvial sediments	6.4	15.2	III
		10,000	61	III
		3,200	61	III
Rousselot et al. (1977)	Clay, sand, and gravel	9.3	6.9	II
		5.3	0.3	III
		10.7	0.46	II
		7.1	0.37	III
Sauty (1977)	Sand and gravel	25	11	III
		50	25	III
		150	12.5	II
Sauty et al. (1978)	Sand	13	1.0	II
Sudicky et al. (1983)	Glaciofluvial sand	11	0.08	II
		0.75	0.01	II
Sykes et al. (1982, 1983)	Sand	700	7.6	III
Sykes et al. (1983)	Sand, silt, and clay	57.3	0.76	II
Vaccaro and Bolke (1983)	Glaciofluvial sand and gravel	43,400	91.4	III
Valocchi et al. (1981)	Sand, gravel, silt	16	1.0	I
Werner et al. (1983)	Gravel	700	174	III
		37	131	III
		105	208	III
		200	234	III
Wiebenga et al. (1967) and Lenda and Zuber (1970)	Sand and gravel	18.3	0.26	II
Wilson (1971) and Robson (1974)	Unconsolidated	79.2	15.2	III
	gravel, sand, and silt	4.6	0.55	III
Wood (1981)	Sand	100,000	14,970	III
Wood and Ehrlich (1978) and Bassett et al. (1980)	Sand and gravel	1.52	0.015	II
B. *Sandstones*				
Gupta et al. (1975)	Sandstone, shale, sand, and alluvial sediments	50,000	127	III
Harpaz (1965)	Sandstone with silt and clay layers	28	0.32	II

Appendix A (Continued)
Data Evaluated by Gelhar et al. (1985, 1992)

Author	Description of Medium	Scale (m)	α (m)	Assigned Reliability
Oakes and Edworthy (1977)	Sandstone	6	0.16	II
		3	0.31	II
		6	0.6	II
		3	0.6	II
C. *Carbonate rocks*				
Kreft et al. (1974)	Limestone	27	8.54	II
		41.5	20.8	II
Kreft et al. (1974)	Fractured dolomite	22	70	II
		21.3	2.1	II
Walter (1983)	Fractured dolomite	30	12.2	III
Fenske (1973)	Limestone	91	11.6	III
Bredehoeft and Pinder (1973)	Limestone	100	170	III
Bentley and Walter (1983)	Fractured dolomite	23	5.2	III
Clasen and Cordes (1975)	Fractured dolomite	122	15	III
Grove and Beetem (1971)	Fractured dolomite	55	38.1	III
Halevy and Nir (1962)	Dolomite	250	6	II
Ivanovitch and Smith (1978)	Fractured chalk	8	3.1	III
Ivanovitch and Smith (1978)	Chalk	8	1	III
Rabinowith and Gross (1972)	Fractured limestone	32,000	21.4	III
Segol and Pinder (1976)	Fractured limestone and calcarous sandstone	490	6.7	III
D. *Basalts*				
Robertson (1974) and Robertson and Barraclough (1973)	Basaltic lava and sediments	20,000	910	III
Gelhar (1982)	Brecciated basalt, interflow zone	17.1	0.6	I
Grove (1977)	Basaltic lava and sediments	20,000	91	III
E. *Granite*				
Dieulin (181)	Fractured granite	6	0.5	II
Goblet (1982)	Fractured granite	17	2	III

Note: If a range was provided for scale, the arithmetic mean was used, for a dispersivity range the geometric mean was used. References are listed in the original documents by Gelhar et al. (1985, 1992).

Potential for Saltwater Intrusion into the Lower Tamiami Aquifer near Bonita Springs, Southwestern Florida

By W. Barclay Shoemaker and K. Michelle Edwards

U.S. GEOLOGICAL SURVEY

Water-Resources Investigations Report 03-4262

Prepared in cooperation with the

South Florida Water Management District

Tallahassee, Florida
2003

U.S. DEPARTMENT OF THE INTERIOR
GALE A. NORTON, Secretary

U.S. GEOLOGICAL SURVEY
CHARLES G. GROAT, Director

For additional information write to:

U.S. Geological Survey
2010 Levy Avenue
Tallahassee, FL 32310

Copies of this report can be purchased from:

U.S. Geological Survey
Branch of Information Services
Box 25286
Federal Center
Denver, CO 80225
888-ASK-USGS

Additional information about water resources in Florida is available on the Internet at http://fl.water.usgs.gov

CONTENTS

PLATES

FIGURES

TABLES

CONVERSION FACTORS, ACRONYMS, ABBREVIATIONS, AND VERTICAL DATUM

Multiply	By	To obtain
millimeter per year (mm/yr)	0.03937	inch per year
meter (m)	3.281	foot
meter per day (m/d)	3.281	foot per day
meter per year (m/yr)	3.281	foot per year
square meter (m^2)	10.76	square foot
cubic meter per day (m^3/d)	35.31	cubic foot per day
cubic meter per second (m^3/s)	35.31	cubic foot per second
kilometer (km)	0.6214	mile
square kilometer (km^2)	0.3861	square mile
centimeter (cm)	0.3937	inch
centimeter (cm)	3.281×10^{-2}	foot
centimeter per day (cm/d)	3.281×10^{-2}	foot per day
centimeter per year (cm/yr)	3.281×10^{-2}	foot per year
kilogram per cubic meter (kg/m^3)	0.06243	pound per cubic foot

OTHER UNITS OF ABBREVIATION

MHz	megahertz
mg/L	milligram per liter

ACRONYMS

ADAPS	Automated Data Processing System
CSS	composite-scaled sensitivities
DBHYDRO	Hydrometeorologic Database (South Florida Water Management District)
DC	direct current
HMOC	hybrid method of characteristics
MAE	mean absolute error
MOC	method of characteristics
MMOC	modified method of characteristics
NGVD	National Geodetic Vertical Datum
NOAA	National Oceanic and Atmospheric Administration
NWIS	National Water Information System (U.S. Geological Survey database)
PSS	prediction-scaled sensitivities
QWDATA	Water Quality Database
SFWMD	South Florida Water Management District
USGS	U.S. Geological Survey
VCONT	vertical conductance

Vertical coordinate information is referenced to the National Geodetic Vertical Datum of 1929 (NGVD of 1929); horizontal coordinate information is referenced to the North American Datum of 1983 (NAD83).

Potential for Saltwater Intrusion into the Lower Tamiami Aquifer near Bonita Springs, Southwestern Florida

By W. Barclay Shoemaker *and* K. Michelle Edwards

Abstract

A study was conducted to examine the potential for saltwater intrusion into the lower Tamiami aquifer beneath Bonita Springs in southwestern Florida. Field data were collected, and constant- and variable-density ground-water flow simulations were performed that: (1) spatially quantified modern and seasonal stresses, (2) identified potential mechanisms of saltwater intrusion, and (3) estimated the potential extent of saltwater intrusion for the area of concern.

MODFLOW and the inverse modeling routine UCODE were used to spatially quantify modern and seasonal stresses by calibrating a constant-density ground-water flow model to field data collected in 1996. The model was calibrated by assuming hydraulic conductivity parameters were accurate and by estimating unmonitored ground-water pumpage and potential evapotranspiration with UCODE. Uncertainty in these estimated parameters was quantified with 95-percent confidence intervals. These confidence intervals indicate more uncertainty (or less reliability) in the estimates of unmonitored ground-water pumpage than estimates of pan-evaporation multipliers, because of the nature and distribution of observations used during calibration. Comparison of simulated water levels, streamflows, and net recharge with field data suggests the model is a good representation of field conditions.

Potential mechanisms of saltwater intrusion into the lower Tamiami aquifer include: (1) lateral inland movement of the freshwater-saltwater interface from the southwestern coast of Florida; (2) upward leakage from deeper saline water-bearing zones through natural upwelling and upconing, both of which could occur as diffuse upward flow through semiconfining layers, conduit flow through karst features, or pipe flow through leaky artesian wells; (3) downward leakage of saltwater from surface-water channels; and (4) movement of unflushed pockets of relict seawater. Of the many potential mechanisms of saltwater intrusion, field data and variable-density ground-water flow simulations suggest that upconing is of utmost concern, and lateral encroachment is of second-most concern. This interpretation is uncertain, however, because the predominance of saltwater intrusion through leaky artesian wells with connection to deeper, more saline, and higher pressure aquifers was difficult to establish.

Effective management of ground-water resources in southwestern Florida requires an understanding of the potential extent of saltwater intrusion in the lower Tamiami aquifer near Bonita Springs. Variable-density, ground-water flow simulations suggest that when saltwater is at dynamic equilibrium with 1996 seasonal stresses, the extent of saltwater intrusion is about 100 square kilometers areally and 70,000 hectare-meters volumetrically. The volumetric extent of saltwater intrusion was most sensitive to changes in recharge, ground-water pumpage, sea level, salinity of the Gulf of Mexico, and the potentiometric surface of the sandstone aquifer, respectively.

INTRODUCTION

Urbanization is proceeding rapidly along the coast of southwestern Florida, with cities and communities springing up from Fort Myers to Naples. In fact, the coast around Bonita Springs is one of the Nation's fastest growing areas. The expanded population has resulted in increased public-supply withdrawals from the lower Tamiami aquifer that have lowered ground-water levels and reversed hydraulic gradients in the aquifer between Bonita Springs and the coastline. Long-term movement of saltwater into coastal aquifers is often attributed to declines in ground-water levels, thus limiting the future availability of potable-water supplies.

Saltwater intrusion is defined by Stewart (1999) as the mass transport of saline waters into zones previously occupied by fresher waters. This definition is broad because natural processes (such as sea level rise and drought) and anthropogenic processes (such as ground-water pumpage and construction of canals) can cause saltwater intrusion. Thus, the investigator is faced with a "classic" inverse problem because an observed distribution of saltwater could be explained equally well by one or more mechanisms of saltwater intrusion. Under these circumstances, multiple sources of information are useful to help identify the predominant mechanisms of saltwater intrusion, including ground-water levels and pumpage, geochemical data (such as chloride concentrations and strontium isotope analysis), surface and borehole geophysical data, research from previous studies, and numerical modeling tools.

Water managers need a clear understanding of the saltwater intrusion process to ensure protection of the fresh ground-water resources in southwestern Florida. In 1999, the U.S. Geological Survey (USGS), in cooperation with the South Florida Water Management District (SFWMD), initiated a study to: (1) quantify modern (stresses with the desired characteristics) and seasonal stresses; (2) help identify potential mechanisms of saltwater intrusion; and (3) estimate the potential extent of saltwater intrusion in the lower Tamiami aquifer near Bonita Springs. Field data and numerical methods were used in this effort.

Purpose and Scope

The purpose of this report is to describe the results of numerical simulation procedures that represent the movement of saltwater in the lower Tamiami aquifer beneath Bonita Springs in southwestern Florida. Water-budget components were characterized and mathematically represented to help simulate ground-water flow and saltwater intrusion in the surficial aquifer system, which includes the lower Tamiami aquifer. A modular, three-dimensional, finite-difference, ground-water flow model was used to represent modern and seasonal stresses during March and September 1996 when ground-water levels are generally at their lowest and highest, respectively. Field data were collected and variable-density, ground-water flow simulations were performed to help identify mechanisms of saltwater intrusion of utmost concern and estimate the potential extent of saltwater intrusion in the lower Tamiami aquifer beneath Bonita Springs. The extent of saltwater intrusion was simulated from predevelopment distribution to dynamic equilibrium with calibrated March and September 1996 conditions.

Description of Study Area

The study area encompasses about 860 km^2 in Lee and western Collier Counties (fig. 1), and is characterized by low topographic relief and a high water table. The physiographic provinces that comprise the study area (fig. 2) are the Gulf Coastal Lowlands, Caloosahatchee Incline, Desoto Plain, Southwestern Slope, Immokalee Rise, Everglades, Okeechobee Plain, Big Cypress Spur, and the Reticulate Coastal Swamps (Fernald and Purdum, 1998). The Immokalee Rise, a sandy ridge formed during high sea-level stands, occupies the highest part of the study area to the northeast (at an elevation of about 12 m) and borders the Caloosahatchee River and Big Cypress watersheds.

The Caloosahatchee River, Estero Bay, and Big Cypress watersheds are located in the study area (fig. 2). The Caloosahatchee River watershed extends from Lake Okeechobee to San Carlos Bay and passes through parts of Charlotte, Glades, Hendry, and Lee Counties and dips slightly into Collier County. The lower reaches of the watershed are characterized by a shallow bay, extensive seagrass beds, and sand flats.

The Estero Bay watershed (fig. 2) occupies central and southern Lee County and parts of northern Collier and western Hendry Counties. The principal surface-water features are Estero River, Spring Creek, Kehl Canal, Imperial River, and Cocohatchee River. The low gradients in these channels result in sluggish and tidally induced flow that is probably much greater than freshwater flow. Channel stages fluctuate

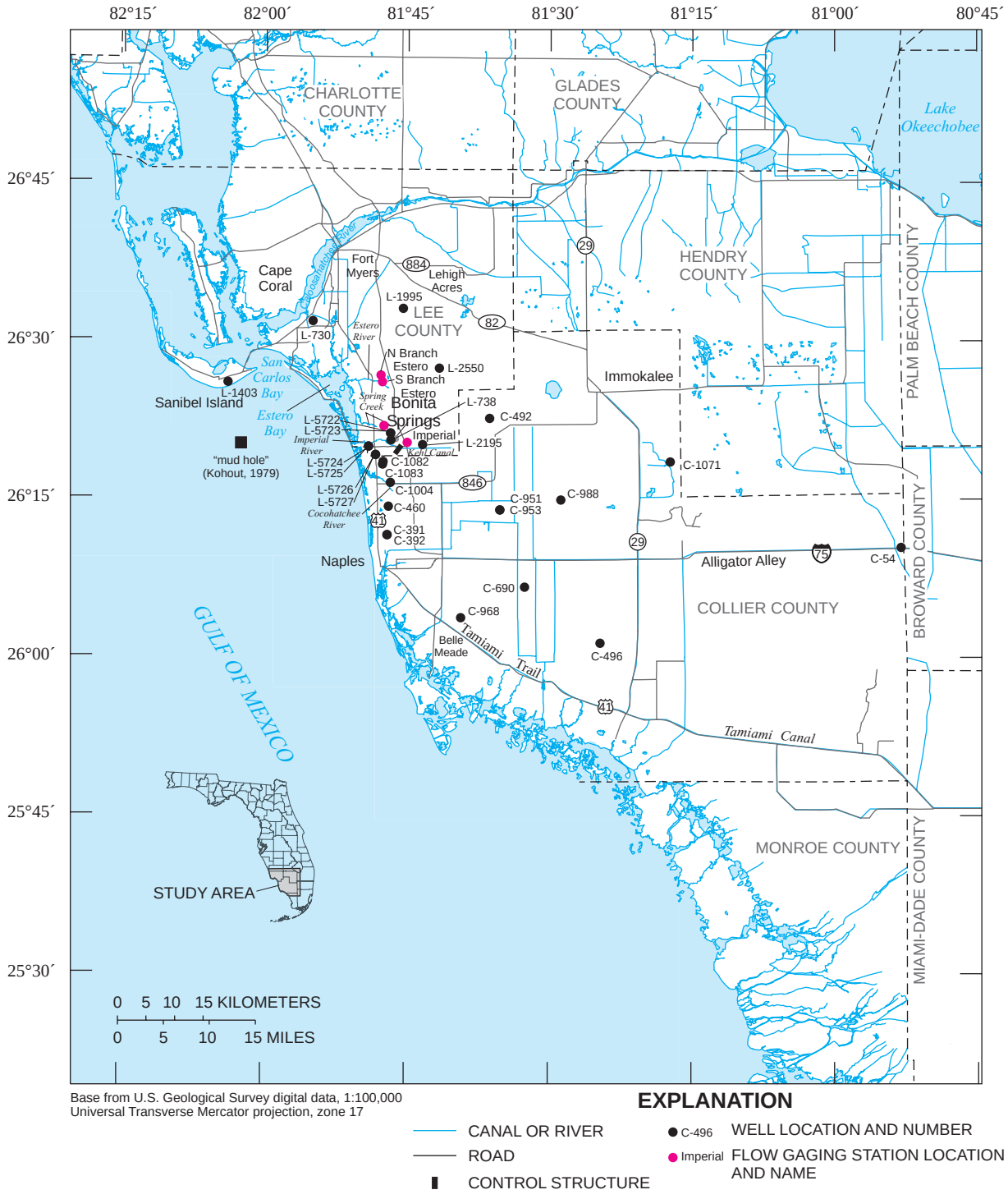

Figure 1. Location of the study area in southwestern Florida.

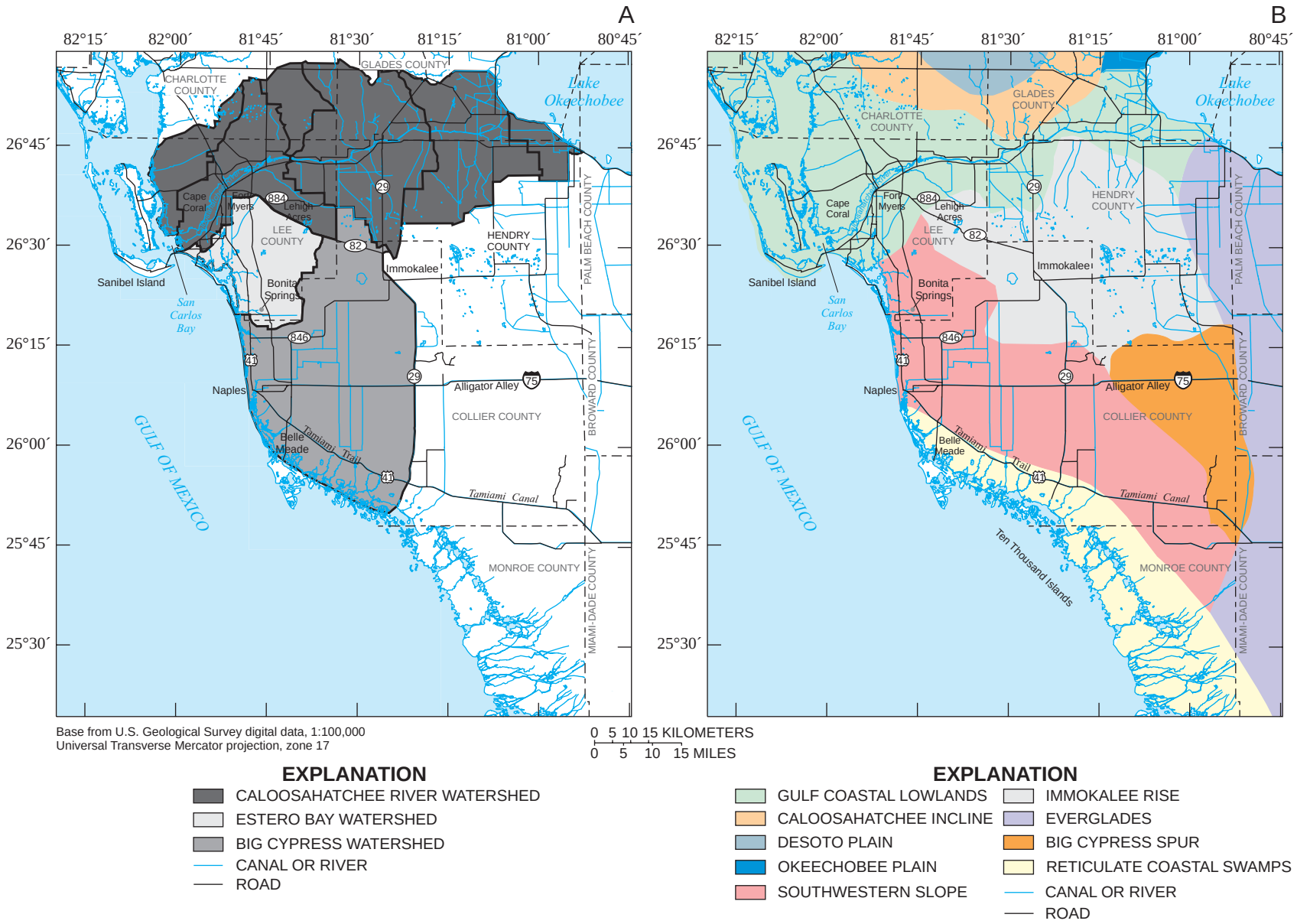

Figure 2. (A) Major watersheds (South Florida Water Management District, 1989), and (B) physiographic features (modified from Fernald and Purdum, 1998) in study area. The Big Cypress watershed includes the Corkscrew Swamp Sanctuary northeast of Naples, Florida.

seasonally with the highest and lowest levels occurring during summer and winter, respectively. The flora and fauna of the Estero Bay watershed are varied and abundant.

The Big Cypress watershed (fig. 2) drains a wide area through a large network of man-made canals and natural sloughs in southern Lee and Hendry Counties and western Collier County. A variety of grasses, shrubs, and small cypress trees dominate the Big Cypress watershed, which includes the Corkscrew Swamp Sanctuary located northeast of Naples. South of Naples, freshwater sloughs and rivers mix with Gulf of Mexico bays and tidal creeks.

Development in the study area is primarily urban and agricultural. Urban development is greatest along the coast west of I-75 (Interstate 75) in Lee and Collier Counties. Agricultural development, located between wetland systems, increases to the east and south in the study area. The undeveloped regions consist of flatwoods, sloughs, swamps, and estuaries. Predevelopment sheetflow in the study area probably was slow due to the vegetation, geomorphology, and low land-elevation gradients. Canals and roads resulting from urban and agricultural development have nearly eliminated the natural sheetflow across the land surface and altered the natural drainage patterns by concentrating stormwater runoff in canals and ditches.

Previous Studies

Many studies of saltwater intrusion have been conducted over the years, and a comprehensive record can be found in Bear and others (1999). Two "classic" studies were completed by Badon-Ghyben (1888) and Herzberg (1901) in which the depth of the saltwater interface below sea level was predicted to be 40 times the freshwater head above sea level in the aquifer of interest, given hydrostatic conditions in a homogeneous unconfined aquifer with a seaward sloping water-table surface. Kohout (1964) recorded that the saltwater front in the Biscayne aquifer in southeastern Florida is as much as 13 km seaward of the position predicted by the Ghyben-Herzberg equation due to ground-water circulation patterns near the saltwater interface. Later research of saltwater intrusion in southeastern Florida was accomplished by Hull and Meyer (1973), Klein and Waller (1985), Klein and Ratzlaff (1989), Sonenshein and Koszalka (1996), Merritt (1996), Sonenshein (1997), Konikow and Reilly (1999), and Langevin (2001). Merritt (1996) used a sensitivity analysis of numerical simulations to address the importance of properties and processes affecting the saltwater interface in Broward County along the southeastern coast of Florida.

On the southwestern coast of Florida, Klein (1954) studied saltwater intrusion in coastal areas near Naples. In the 1960's, field studies by McCoy (1962), Cooper (1964), Henry (1964), and Glover (1964) advanced the knowledge and understanding of ground-water movement near the saltwater interface in southern Florida. Sherwood and Klein (1963) mapped a salinity plume beneath the Caloosahatchee River, whose source was a leaky well with connection to the deeper, more saline, and higher pressure Floridan aquifer system. Kohout (1979) used remote sensing to map a geothermal submarine ground-water spring off the coast of Bonita Springs, informally known as the "mudhole" by local fisherman. Stewart and others (1982) used direct-current (DC) resistivity soundings to map the saltwater interface near Belle Meade south of the study area.

Acknowledgments

Technical support for this project was provided by Chris Langevin and Keith Halford of the USGS, Mark Stewart of the University of South Florida Department of Geology, and Akin Owosina and Terry Bengtsson of the SFWMD. Terry Bengtsson and Lee Worst from the SFWMD helped delineate areas near Bonita Springs where unmonitored ground-water pumpage is likely occurring. Pamela Telis helped design, distribute, and compile results from a survey designed to estimate unmonitored ground-water pumpage. Several colleagues reviewed the initial drafts of this report, including Terry Bengtsson and Rama Rani, and the following USGS employees: Barbara Howie, Eric Swain, Chris Langevin, Melinda Wolfert, Richard Krulikas, Ward Sanford, Gary Mahon, Eve Kuniansky, Michael Deacon, Roy Sonenshein and David Schmerge. Fernando Miralles-Wilhelm of the University of Miami and Eric Swain of the USGS provided useful insight into the sensitivity behavior of saltwater intrusion simulations. Rhonda Howard and Barbara Howie provided many suggestions that significantly improved the clarity and content of the report. Kimberly Swidarski prepared the illustrations. USGS employee Haymeli Castillo, is recognized for her constant support, patience, and guidance.

HYDROGEOLOGY OF SOUTHWESTERN FLORIDA

Southern Florida is underlain by rocks of Cenozoic age to a depth of about 1,525 m. These rocks principally are carbonates (limestone and dolostone), with minor amounts of evaporites (gypsum and anhydrite) in the lower part of the section and clastics (sand and clay) in the upper part. The movement of ground water from inland areas to the ocean (and the reverse) occurs primarily through the carbonate rocks (Meyer, 1989, p. G5). This section of the report describes the hydrogeologic framework of the study area including the lithology, stratigraphy, hydrogeologic units, and hydraulic characteristics. Also discussed are the water-budget components, which used in conjunction with the hydrogeologic framework, are necessary to understand the processes that affect ground-water flow. Finally, water-quality and geochemical data collected from the lower Tamiami aquifer near Bonita Springs are used to examine salinity. The locations of monitoring stations for data used in the study are presented in the appendix.

Lithology and Stratigraphy

Geologic units in southwestern Florida consist, in ascending order, of the Suwannee Limestone of Oligocene age, Hawthorn Group of Oligocene to Pliocene age, Tamiami Formation of Pliocene age, and undifferentiated sediments of Holocene to Pleistocene age (fig. 3). The Suwannee Limestone is composed of fossiliferous, calcarenitic limestone with minor amounts of quartz sand. The thickness of the limestone varies widely, but commonly is greater than 100 m in Lee and Collier Counties. The basal Suwannee Limestone generally contains fine-grained, phosphatic, clastic material with interbeds of micrite and clay (Reese, 2000).

The Hawthorn Group is divided into the Arcadia Formation and the Peace River Formation (fig. 3). The Arcadia Formation, which unconformably overlies the Suwannee Limestone, consists of fine-grained carbonate sediments as well as sandy limestone, shell beds, dolomite, phosphatic sand and carbonate, sand, silt, and clay. The predominantly clastic Peace River Formation has a highly irregular erosional, and karstic surface. The contact with the overlying Tamiami Formation appears to be unconformable in some areas,

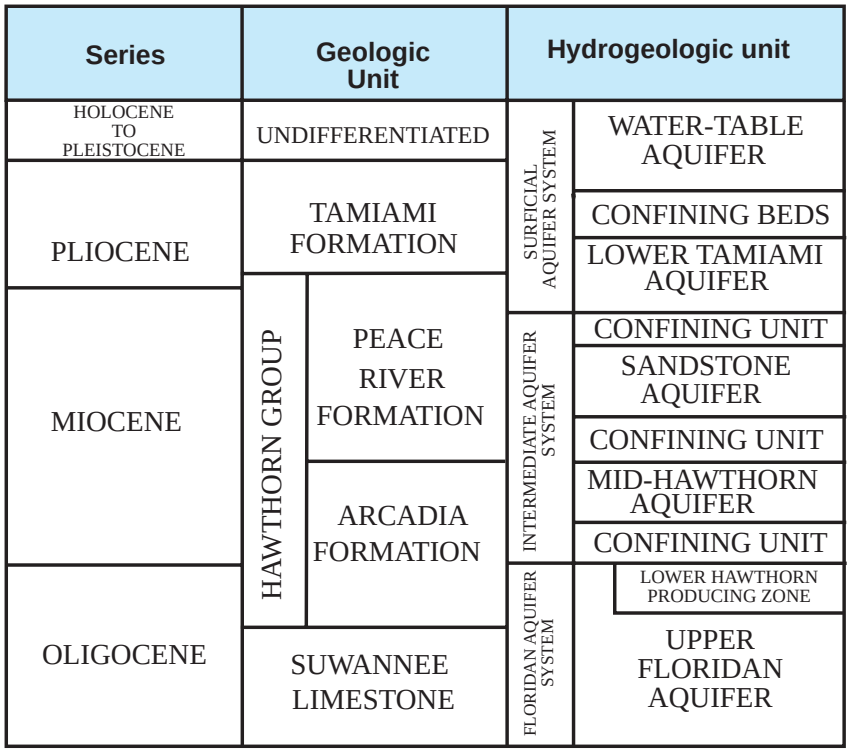

Figure 3. Generalized geologic and hydrogeologic units in the study area. Modified from Reese (2000).

but indistinct in other areas. The siliciclastic sediments of the Peace River Formation consist of interbedded, fine- to coarse-grained quartz sand, quartz silt, gravel, clay, carbonate, and phosphatic sand (Reese, 2000).

The Tamiami Formation overlies the Peace River Formation and consists of varying amounts of silt, sandy clay, micritic limestone, sandy and shelly limestone, calcareous sandstone, and quartz sand. The lithology of the Tamiami Formation varies greatly because of the complex nature of the depositional environment. The limestone is well indurated to unindurated, slightly phosphatic, variably sandy, and fossiliferous. The sand facies varies from well sorted, clean sand with abundant shells and traces of silt-size phosphate, to clayey sand with sand-size phosphate, clay-size carbonate in the matrix, and abundant well-preserved mollusk shells (Knapp and others, 1986; Reese, 2000).

The undifferentiated sediments of Holocene to Pleistocene age overlie the Tamiami Formation at land surface (Reese, 2000). These deposits mainly consist of quartz sand with minor amounts of shell and clay, and contain interfingering limestones, sandstones, and shell beds. With increasing elevation inland, the sand becomes thicker and less calcareous. The sand facies varies from fine to coarse grained, nonindurated to poorly indurated, and nonclayey to slightly clayey. Included in this group are marine terrace sediments, aeolian sand dunes, fluvial deposits, freshwater carbonates, peats, and clay beds.

Hydrogeologic Units and Hydraulic Characteristics

The principal aquifer systems in southwestern Florida are, in descending order, the surficial, intermediate, and Floridan aquifer systems (fig. 3). The focus of this report is the water-table and lower Tamiami aquifers of the surficial aquifer system and the sandstone aquifer of the upper part of the intermediate aquifer system. The confining beds of the Tamiami Formation and the upper confining unit of the Peace River Formation also are considered because they vertically "straddle" the lower Tamiami aquifer. For simplicity, these semiconfining units are called the Tamiami confining beds and the upper Hawthorn confining unit (Wedderburn and others, 1982) in this report. More detailed information on the water-bearing and confining units in southwestern Florida is presented in Reese (2000).

Maps are used in this section to show estimated hydraulic conductivities and depict the lines of equal thickness of the rock units that comprise the water-table, lower Tamiami, and sandstone aquifers. Maps showing lines of equal thicknesses were constructed by the South Florida Water Management District (1994). Histograms (fig. 4) and maps showing estimated hydraulic conductivities were developed using well construction reports and previous aquifer performance test data (Knapp and others, 1986; Montgomery, 1988). Many previously conducted aquifer performance tests were reanalyzed to assess reliability and to "fill in data gaps" (K.M. Edwards, U.S. Geological Survey, written commun., 2000). Horizontal hydraulic conductivity values (in meters per day) were computed by dividing transmissivity estimates by the thickness of the aquifer at the location of the aquifer performance test. Numerous estimates of hydraulic characteristics were compiled from various sources. Hydraulic conductivity was assumed to be log-normally distributed when computing permeability averages and standard deviations (fig. 4).

In southwestern Florida, the water-table aquifer is present in the undifferentiated deposits of Holocene to Pleistocene age and the upper part of the Tamiami Formation (fig. 3). The lines of equal thickness of the rock units that comprise the water-table aquifer range from 6 m (about 20 ft) in Hendry County south of the Caloosahatchee River to 30 m (about 100 ft) in northern Collier County along the border with Lee and Hendry Counties (fig. 5). The spatial distribution of estimated horizontal hydraulic conductivity in the water-table aquifer (fig. 6) reflects the complex heterogeneity of this characteristic in the study area. In log space (fig. 4A), the mean and standard deviation of 244 log estimates of horizontal hydraulic conductivity in the water-table aquifer were 2.16 and 0.6, respectively. In parameter space, this translates to a range of about 40 to 600 m/d, which is one standard deviation from the mean.

The water-table aquifer is underlain by rocks and sediments that form the confining beds of the Tamiami Formation (fig. 3). The thickness of these Tamiami confining beds ranges from 0 to about 15 m (about 0 to 50 ft) in Lee, Collier, and Hendry Counties (South Florida Water Management District, 1994). The beds, which pinch out in the central and northern parts of Lee County and northwestern Hendry County, are thickest in localized areas near Bonita Springs in northern and eastern Collier County, and in central and

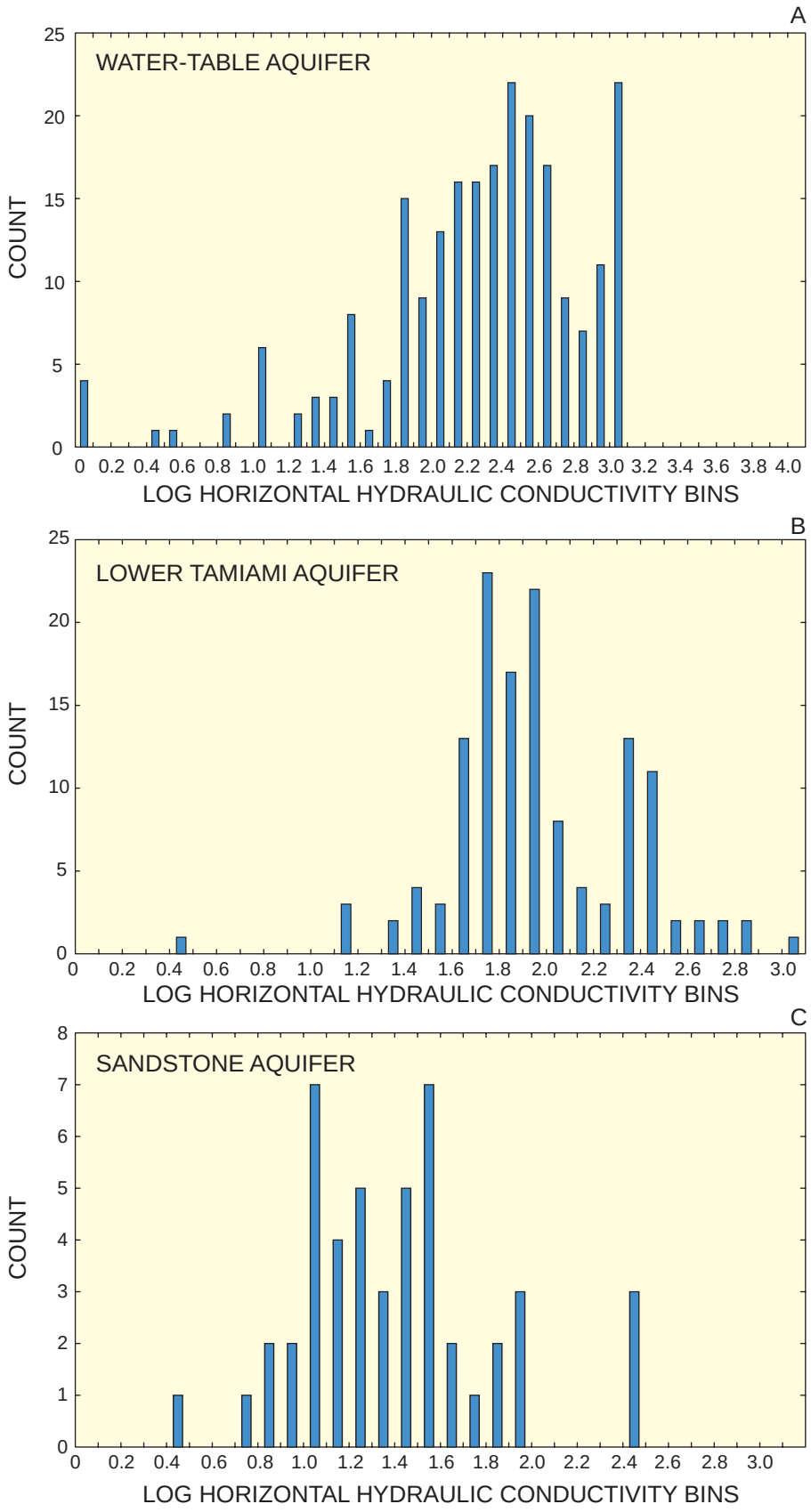

Figure 4. Estimated horizontal hydraulic conductivity values of the (A) water-table, (B) lower Tamiami, and (C) sandstone aquifers. The values of hydraulic conductivity are in meters per day.

southern Hendry County. Sparse data are available to describe the distribution of vertical hydraulic conductivity in the Tamiami confining beds. Montgomery (1988) reports a value of 0.004 m/d for vertical hydraulic conductivity based on aquifer performance tests. In a reanalysis of aquifer performance tests (K.M. Edwards, U.S. Geological Survey, written commun., 2000), four reliable values of the vertical hydraulic conductivity of the Tamiami confining beds each equaled about 0.004 m/d.

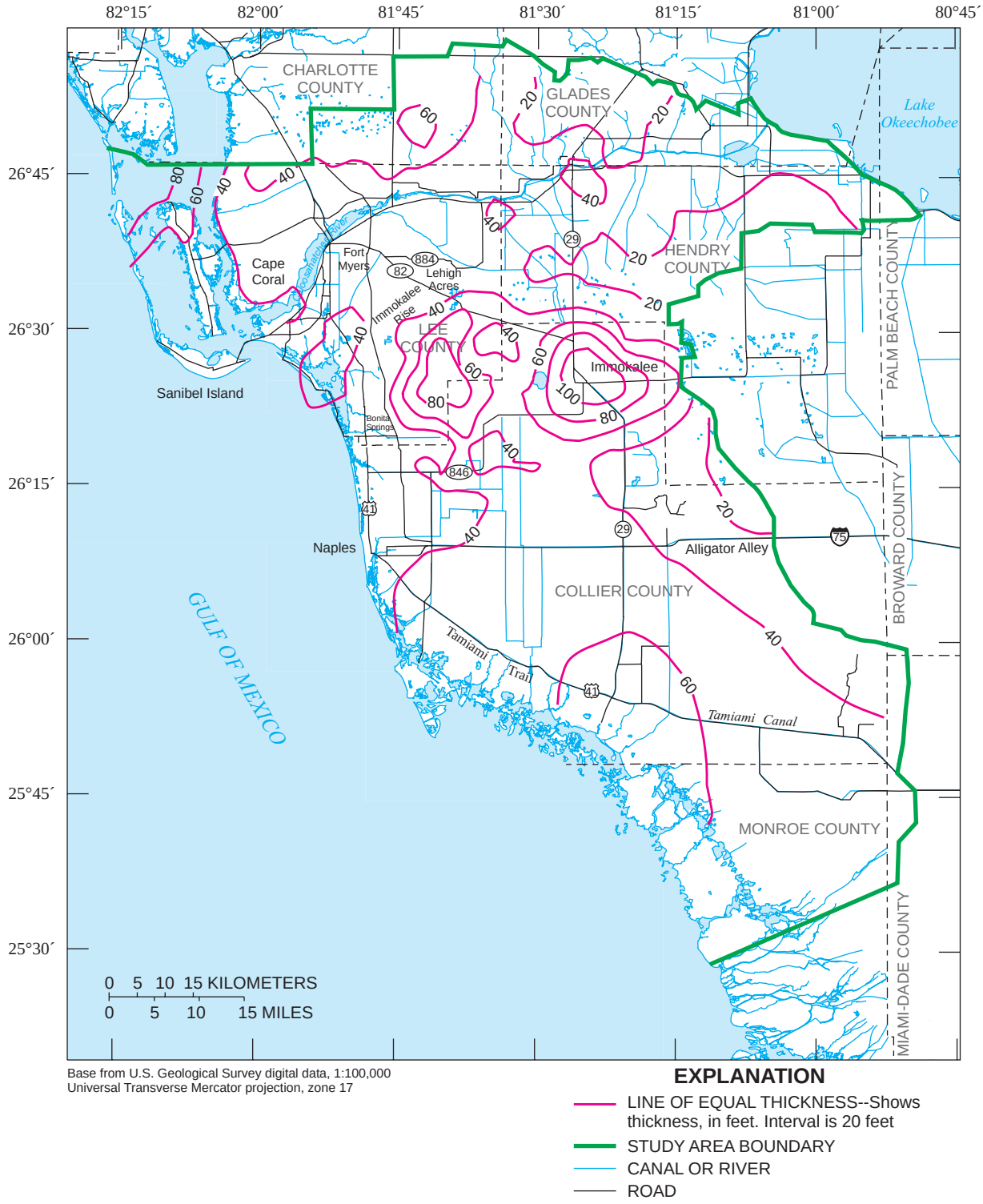

Figure 5. Lines of equal thickness of the rock units that comprise the water-table aquifer. From the South Florida Water Management District (1994).

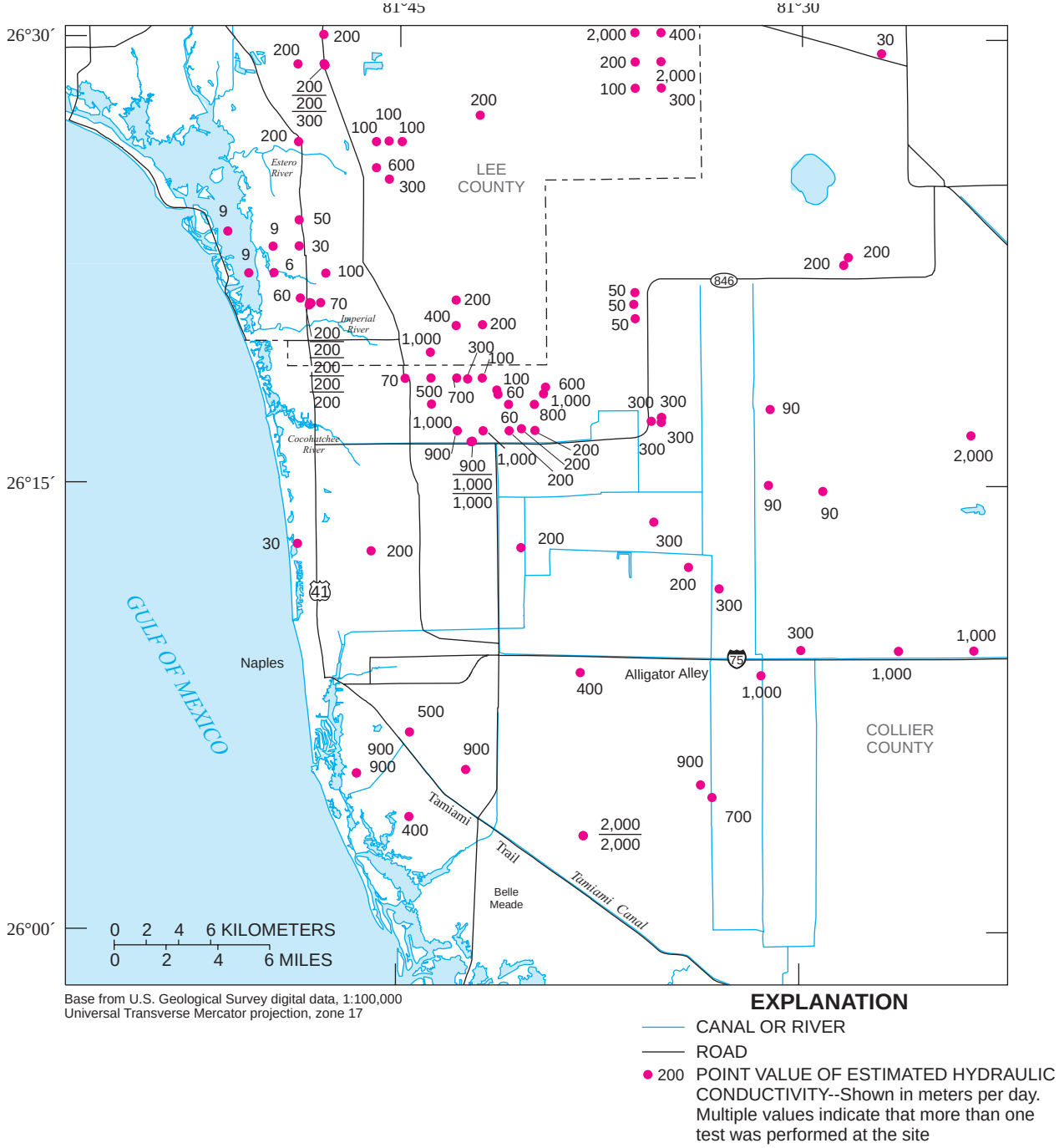

Figure 6. Spatial distribution of horizontal hydraulic conductivity in the water-table aquifer estimated from analyses of aquifer performance tests.

Underlying the confining beds, the lower Tamiami aquifer, a major water-producing unit within much of the study area, generally lies within the lower part of the Tamiami Formation of Pliocene age (fig. 3). In some places, the lower Tamiami aquifer includes unconsolidated quartz sand of late Miocene age (Knapp and others, 1986; Weedman and others, 1997; Edwards and others, 1998). The lines of equal thickness of the rock units that comprise the lower Tamiami aquifer ranges from 0 to 55 m (about 0 to 180 ft) in Lee, Henry, and Collier Counties (fig. 7). The aquifer, which is not present in the central and northern parts of Lee County and in northwestern Hendry County, is thickest in localized areas southeast of Bonita Springs (fig. 7).

Estimates of horizontal hydraulic conductivity in the lower Tamiami aquifer seem to have a bimodal log K distribution (fig. 4B). Results from this and previous research (Meeder, 1979) suggest that the lower Tamiami aquifer is highly permeable where coral reef facies are present (fig. 8). In the coral reef facies mapped by Meeder (1979), the mean and standard deviation of eight log estimates of horizontal hydraulic conductivity (fig 4B) were 2.11 and 0.4, respectively. In parameter space, this translates to a range of about 50 to 300 m/d, which is one standard deviation from the mean. In places within the lower Tamiami aquifer

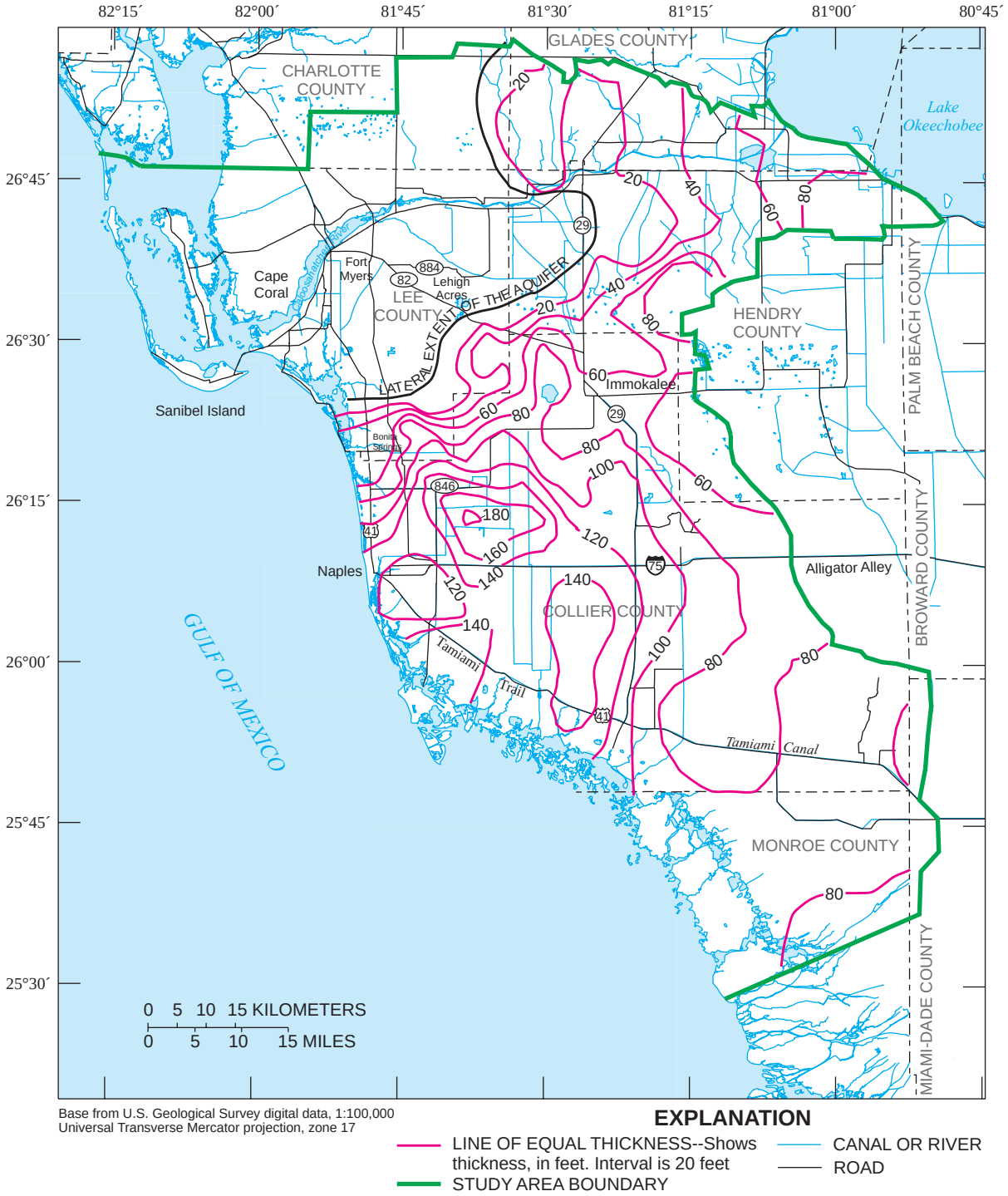

Figure 7. Lines of equal thickness of the rock units that comprise the lower Tamiami aquifer. From the South Florida Water Management District (1994).

where coral reef facies are not present, the mean and standard deviation of 136 log estimates of horizontal hydraulic conductivity (fig. 4B) were 1.8 and 0.4, respectively. In parameter space, this translates to a range of about 30 to 200 m/d, which is one standard deviation from the mean.

The lower Tamiami aquifer is underlain by rocks and sediments that form the upper confining unit of the Hawthorn Group (fig. 3). This unit, called the upper Hawthorn confining unit in this report, thins and may be absent near Bonita Springs (Wedderburn and others, 1982). Limited data are available to describe the

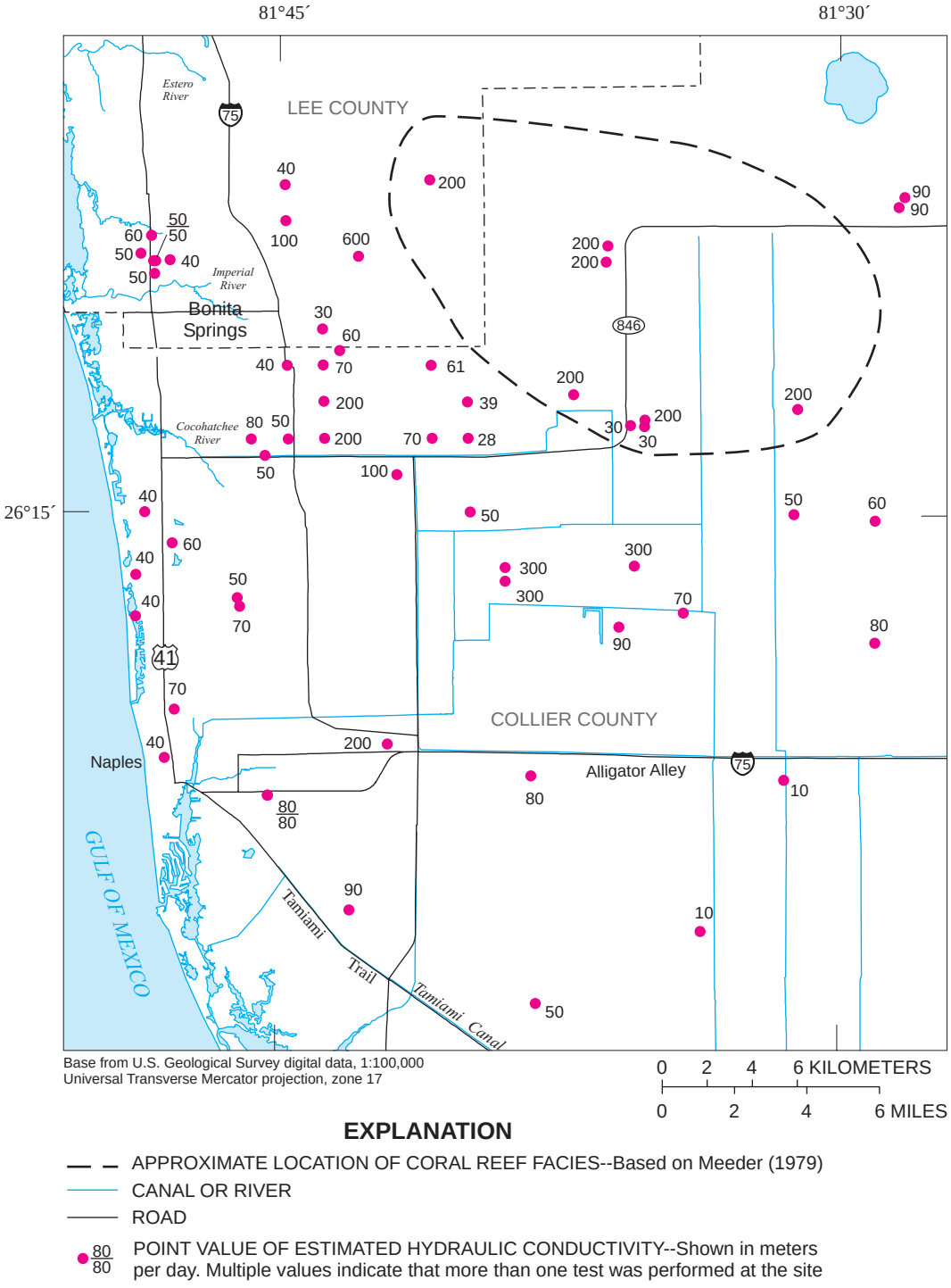

Figure 8. Spatial distribution of horizontal hydraulic conductivity in the lower Tamiami aquifer estimated from analyses of aquifer performance tests.

distribution of vertical hydraulic conductivity in the upper Hawthorn confining unit. Montgomery (1988) reports a value of 0.003 m/d for vertical hydraulic conductivity based on aquifer performance tests. This value was used by Bower and others (1990) and Bennett (1992) in numerical models for parts of the study area.

The sandstone aquifer underlies the upper Hawthorn confining unit in the intermediate aquifer system (fig. 3). The lines of equal thickness of the rock units that comprise the sandstone aquifer range from 0 to 33 m (0 to about 110 ft) in Lee, Henry, and Collier Counties (fig. 9). The sandstone aquifer seems to be

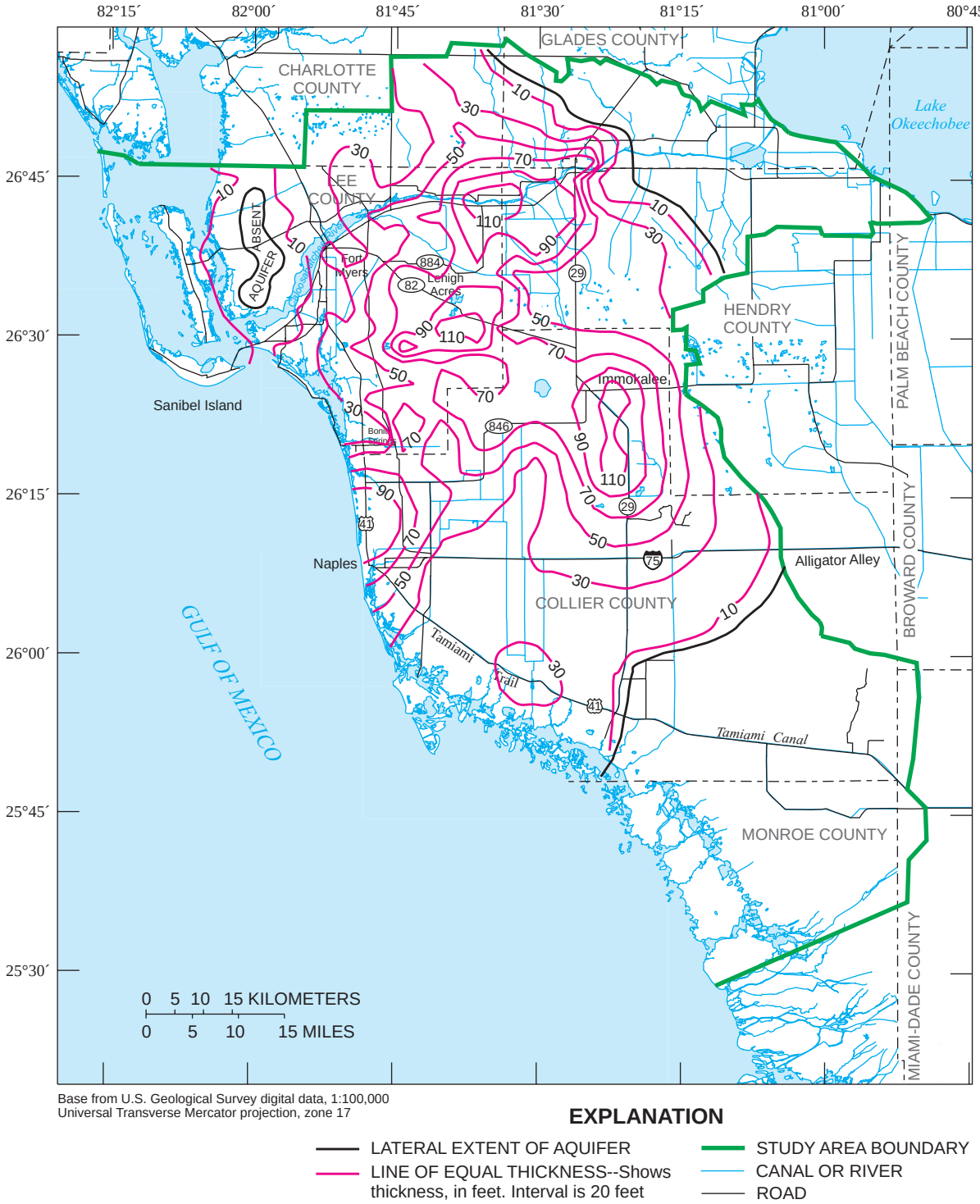

Figure 9. Lines of equal thickness of the rock units that comprise the sandstone aquifer. From the South Florida Water Management District (1994).

thickest in localized areas in northern Collier County, southeastern Lee County, and northeastern Lee County and is absent in southeastern Collier County, northeastern Hendry County, and in parts of northwestern Lee County (fig. 9). The spatial distribution of estimated horizontal hydraulic conductivity in the sandstone aquifer (fig. 10) reflects the complex heterogeneity of this characteristic in the study area. In log space (fig. 4C), the mean and standard deviation of 25 log estimates of horizontal hydraulic conductivity in the sandstone aquifer were 1.26 and 0.4, respectively. In parameter space, this translates to a range of about 10 to 50 m/d, which is one standard deviation from the mean.

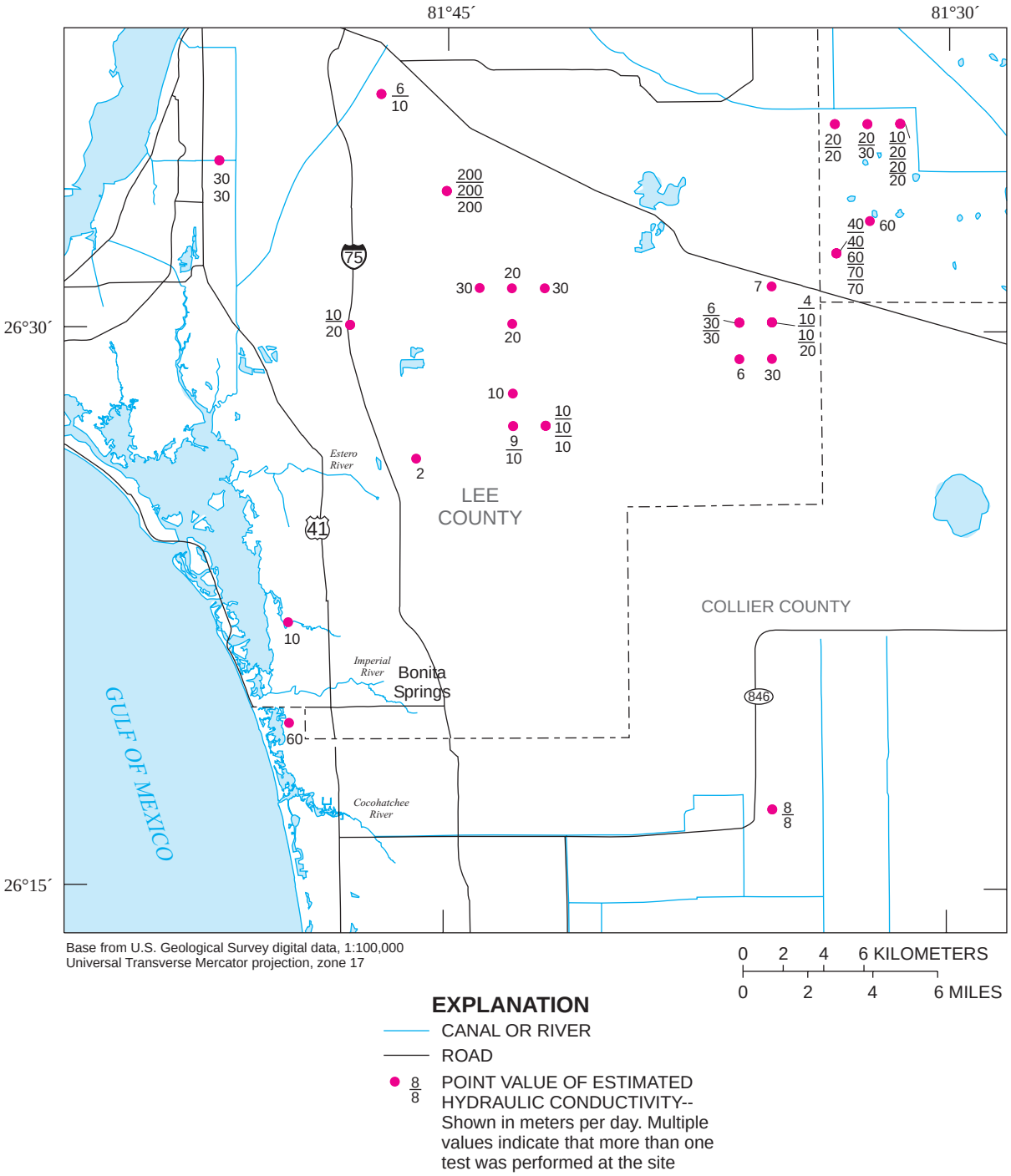

Figure 10. Spatial distribution of estimated horizontal hydraulic conductivity in the sandstone aquifer.

Water Budget

This section describes components of the water budget that may be affecting saltwater movement in the water-table and lower Tamiami aquifers near Bonita Springs (fig. 11). Equation 1 provides a qualitative understanding of how these components interact. The terms are not summed together in this analysis; therefore, the units of each component are sometimes reported differently depending upon the source of information.

$$P + I - ET - D - Q_S - Q_P - Q - Q_{uk} = \Delta S \cong 0, \quad (1)$$

where

P is precipitation;

I is irrigation;

ET is evapotranspiration;

D is net deep leakage between the sandstone aquifer and the lower Tamiami aquifer;

Q_S is submarine ground-water discharge to the Gulf of Mexico,

Q_P is pumpage from the water-table and lower Tamiami aquifers;

Q is stream discharge, which is composed of surface runoff, Q_{ro}, and baseflow, Q_B;

Q_{uk} is other or unknown components of the water budget that may be affecting saltwater movement; and

ΔS is change in storage, which is assumed to be negligible over the long term.

Precipitation (P) and irrigation (I) that exceed evapotranspiration (ET) and runoff (Q_{ro}) can recharge the water table if it infiltrates land surface and overcomes capillary forces in the unsaturated zone. This recharge is generally called net recharge. Krulikas and Giese (1995) estimate net recharge in the study area to range from 1.5 to 22.9 cm/yr, using chloride concentration ratios and flow-tube analysis methods. They further indicate that net recharge rates greater than 22.9 cm/yr could be induced by lowering the water table through ground-water withdrawals or seepage to canals.

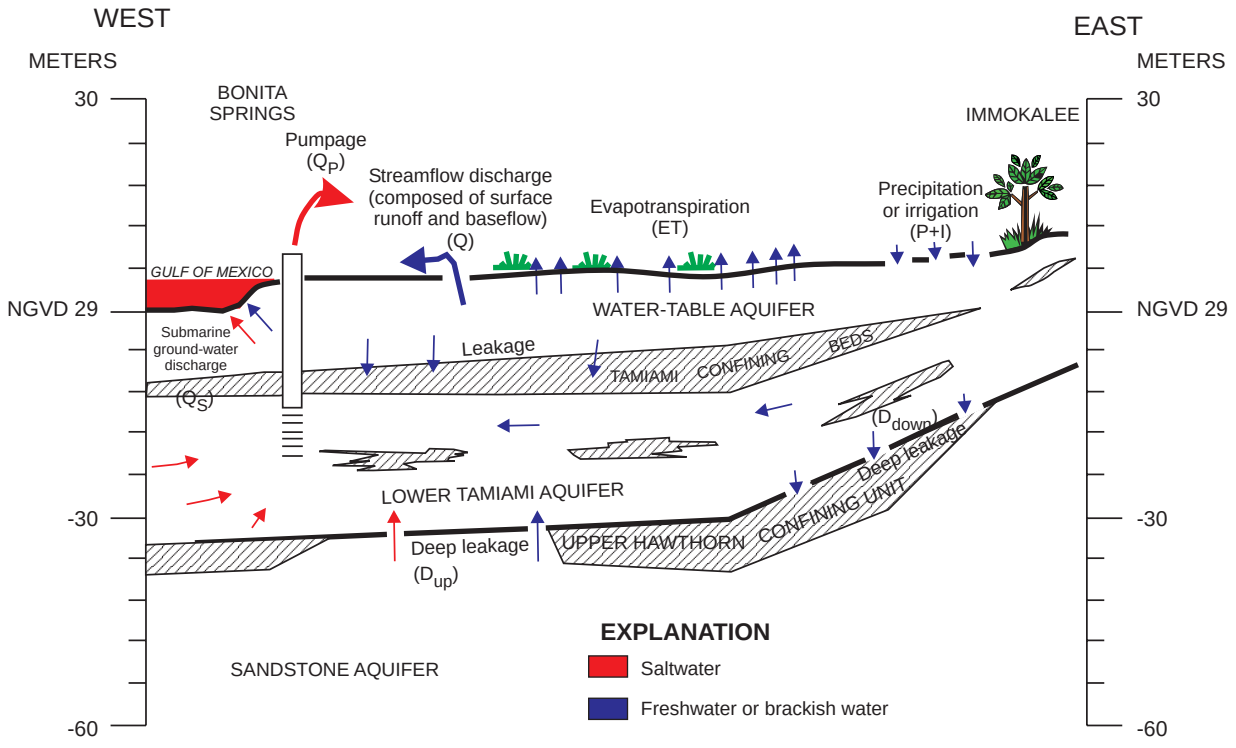

Figure 11. Hypothetical control volume and selected water-budget components within the study area. D_{up} is deep upward leakage and D_{down} is deep downward leakage. NGVD 29 is National Geodetic Vertical Datum of 1929.

Net deep leakage, D, represents the difference between upward, $D_{up,}$ and downward leakage, D_{down}, that occurs naturally between the lower Tamiami and sandstone aquifers. This leakage results from the semiconfining nature of the upper Hawthorn confining unit and the difference in head between the aquifers (fig. 11). Deep leakage was inferred between the lower Tamiami and sandstone aquifers using a map of the head difference between these two units. Average 1996 water levels were computed from water levels measured in 45 USGS monitoring wells in the lower Tamiami aquifer, and from 30 USGS monitoring wells in the sandstone aquifer (table 1). Average water levels were plotted and contoured and spatially interpolated to a common grid. The difference in interpolated head between the lower Tamiami and sandstone aquifers was then computed. This approach has many assumptions including: (1) water-level contours in the lower Tamiami aquifer are vertical; (2) water-level contours in the sandstone aquifer are vertical; and (3) the head difference, as calculated from the water-level contours, occurs directly within the upper Hawthorn confining unit.

In 1996, head differences between the lower Tamiami and sandstone aquifers ranged from -2.0 to 2.6 m (fig. 12). A negative sign suggests leakage is upward into the lower Tamiami aquifer, whereas a positive sign suggests leakage is downward into the sandstone aquifer. Areas where relatively large amounts of deep leakage occur are indicated by large positive or negative head-difference values. For example, Bonita Springs may have the largest amount of deep leakage occurring into the lower Tamiami aquifer because this area has the largest negative head-difference values (about -2.0 to -0.5 m). The assumption is that the upper Hawthorn confining unit is continuous with a constant vertical hydraulic conductivity.

Submarine ground-water discharge to the Gulf of Mexico, Q_S, occurs as ground water flowing toward the Gulf of Mexico moves upward and over more saline ground water. Fresher ground water discharges to the bottom of the Gulf of Mexico or Estero Bay. Estimates of submarine ground-water discharge are difficult to find in the study area. However, a recent study of submarine ground-water discharge from the Biscayne aquifer to Biscayne Bay in coastal southeastern Florida was completed by Langevin (2001). The average rate of submarine ground-water discharge to Biscayne Bay over a 10-year period was 200,000 m^3/d along 100 km of coastline. The Biscayne aquifer is more permeable and receives more recharge than the water-table aquifer near Bonita Springs, which suggests submarine ground-water discharge near this area would be less than that in Biscayne Bay.

Ground-water pumpage, Q_P, from the water-table and lower Tamiami aquifers in the study area (fig. 11) is monitored by the SFWMD. According to R.L. Marella (U.S. Geological Survey, written commun., 1999), ground-water withdrawals by municipal supply facilities in Lee and Collier Counties nearly doubled from 1985 to 1998 (fig. 13). Withdrawals generally are greater during the dry season (October to May) when rainfall is scarce than during the wet season (June to September) when rainfall is abundant (fig. 14). A water-use survey suggests a large volume of unmonitored ground-water pumpage from the lower Tamiami aquifer occurred for irrigation and agricultural uses (P.A. Telis, U.S. Geological Survey, written communication, 2000). This survey, however, was restricted to a small sample size with an even smaller number of responses. Unmonitored ground-water pumpage could exceed monitored ground-water pumpage in the lower Tamiami aquifer because the deepest areas of potentiometric drawdown exist at locations where no monitored ground-water pumpage is occurring (K.J. Halford, U.S. Geological Survey, written communication, 1999).

Streamflow discharge, Q, is composed of surface runoff, Q_{ro}, and baseflow, Q_B (fig. 11). In 1996, the average annual streamflow (including runoff and baseflow) at four gaging stations was about 2 m^3/s (fig. 1, Spring Creek, Imperial River, and northern and southern branches of Estero River). The area of the Imperial River basin is about 2.2 x 10^8 m^2 (Johnson Engineering, Inc., and others, 1999). By dividing the average annual streamflow by the area of the Imperial River basin, the average rate of streamflow in the basin equates to about 29 cm/yr in 1996. The rainfall rate in the Imperial River basin was about 1.3 m/yr in 1996, as estimated from a rainfall monitoring station near Bonita Springs. Land use in the Imperial River basin is predominantly nonurban where runoff coefficients averaged from Bennett (1992) are about 0.1. Using this runoff coefficient to assume a 13-cm/yr average runoff rate from the 1.3-m/yr rainfall rate, the average rate of baseflow, B_f, in the basin equates to about 16 cm/yr. Higher (wet season) water levels from the water-table aquifer can force more baseflow to surface-water features, creating rates greater than 16 cm/yr. Conversely, lower (dry season) water levels can induce baseflow rates less than 16 cm/yr.

Table 1. Average 1996 water levels computed from selected monitoring wells in the lower Tamiami and sandstone aquifers

[USGS, U.S. Geological Survey; Aquifer: SS, sandstone; LT, lower Tamiami; QWDATA, Water-Quality Database; ADAPS, Automated Data Processing System]

Site identification	Latitude	Longitude	Average 1996 head (meters)	Aquifer	USGS data source	Site identification	Latitude	Longitude	Average 1996 head (meters)	Aquifer	USGS data source
C-130	260903	814803	0.76	LT	QWDATA	C-1083	261856	814719	0.77	LT	ADAPS
C-304	261636	813612	2.19	LT	QWDATA	L-738	262023	814640	.40	LT	ADAPS
C-363	262556	812424	7.89	LT	QWDATA	L-1625	263330	813942	5.17	LT	QWDATA
C-391	261124	814730	1.24	LT	ADAPS	L-1691	262043	814549	.80	LT	QWDATA
C-458	261402	814613	1.52	LT	QWDATA	L-5723	262103	814643	-.03	LT	QWDATA
C-460	261406	814654	1.33	LT	QWDATA	L-5725	261947	814902	.47	LT	QWDATA
C-460	261408	814706	1.78	LT	ADAPS	L-5745	261925	814536	.52	LT	QWDATA
C-462	262725	812606	8.73	LT	QWDATA	L-5747	262259	814716	-.20	LT	QWDATA
C-472A	260926	814751	1.05	LT	QWDATA	C-298	262508	812351	6.25	SS	QWDATA
C-474A	261115	814822	.47	LT	QWDATA	C-303	261622	814122	1.71	SS	QWDATA
C-490	261244	814802	1.25	LT	QWDATA	C-687	262555	812837	6.66	SS	QWDATA
C-492	262228	813619	5.09	LT	ADAPS	C-688	261803	813547	3.30	SS	QWDATA
C-516	261157	814757	1.54	LT	QWDATA	C-689	261741	812353	3.52	SS	QWDATA
C-525	261003	814836	.83	LT	QWDATA	C-989	261734	812854	2.61	SS	QWDATA
C-526	261019	814840	.80	LT	QWDATA	C-1077	262823	812131	7.88	SS	QWDATA
C-528	261201	814829	.68	LT	QWDATA	L-727	263851	813653	4.10	SS	QWDATA
C-600	260550	814418	.91	LT	QWDATA	L-741	262553	814585	2.61	SS	QWDATA
C-951	261349	813513	1.54	LT	ADAPS	L-1853	262707	814353	2.30	SS	QWDATA
C-956	261344	813847	1.24	LT	QWDATA	L-1907	264309	814059	2.71	SS	QWDATA
C-973	260844	813241	1.72	LT	QWDATA	L-1963	263345	813616	4.47	SS	QWDATA
C-975	260305	813913	2.08	LT	QWDATA	L-1965	263354	813357	4.83	SS	QWDATA
C-977	260916	813858	1.92	LT	QWDATA	L-1974	263719	814849	4.91	SS	QWDATA
C-979	262122	813554	4.46	LT	QWDATA	L-1975	264400	814246	4.83	SS	QWDATA
C-982	262159	812833	2.77	LT	QWDATA	L-1977	264321	813656	2.80	SS	QWDATA
C-985	261734	812854	3.02	LT	QWDATA	L-2186	263345	813616	4.99	SS	QWDATA
C-988	261447	812849	3.73	LT	ADAPS	L-2187	263951	813553	4.15	SS	QWDATA
C-998	261621	814501	.71	LT	QWDATA	L-2192	262700	813824	5.08	SS	QWDATA
C-1003	261437	814802	1.78	LT	QWDATA	L-2194	262022	814321	1.93	SS	ADAPS
C-1004	261622	814644	.92	LT	ADAPS	L-2200	264330	813403	2.91	SS	QWDATA
C-1058	261538	814611	.22	LT	QWDATA	L-2215	263128	813515	5.63	SS	QWDATA
C-1064	260138	813758	.58	LT	QWDATA	L-2216	264609	814540	5.46	SS	QWDATA
C-1066	255638	812813	-.04	LT	QWDATA	L-5648	263250	814743	4.61	SS	QWDATA
C-1068	260315	813230	1.02	LT	QWDATA	L-5649	262935	814957	3.73	SS	QWDATA
C-1070	260814	812142	3.85	LT	QWDATA	L-5664	262515	81933	2.81	SS	QWDATA
C-1073	261741	812353	4.22	LT	QWDATA	L-5666	262514	814328	1.63	SS	QWDATA
C-1074	262520	811620	7.16	LT	QWDATA	L-5668	262514	814717	2.57	SS	QWDATA
C-1076	262823	812131	8.40	LT	QWDATA	L-5672	262332	813831	4.25	SS	QWDATA
						L-5673	262332	813831	1.90	SS	QWDATA

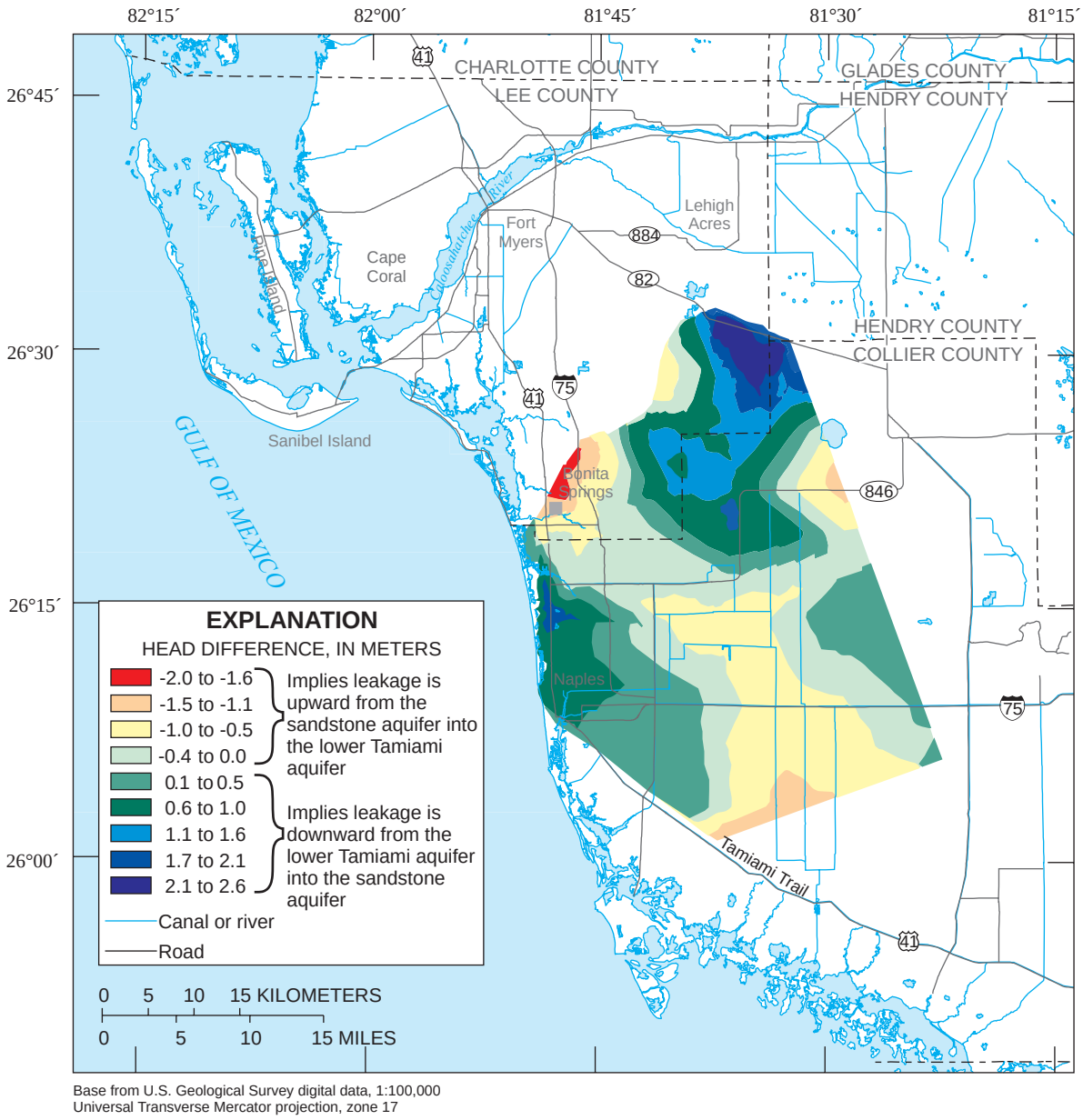

Figure 12. Average annual head difference between the lower Tamiami and sandstone aquifers in 1996.

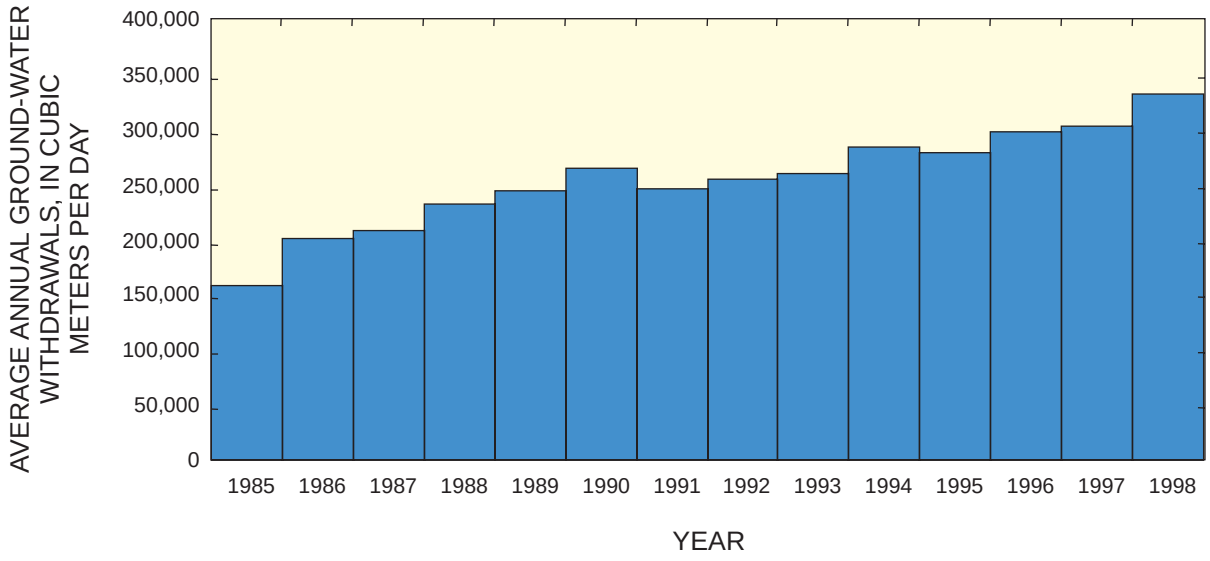

Figure 13. Average annual ground-water withdrawals from municipal supply facilities in Lee and Collier Counties, 1985-98. From R.L Marella (U.S. Geological Survey, written commun. 1999).

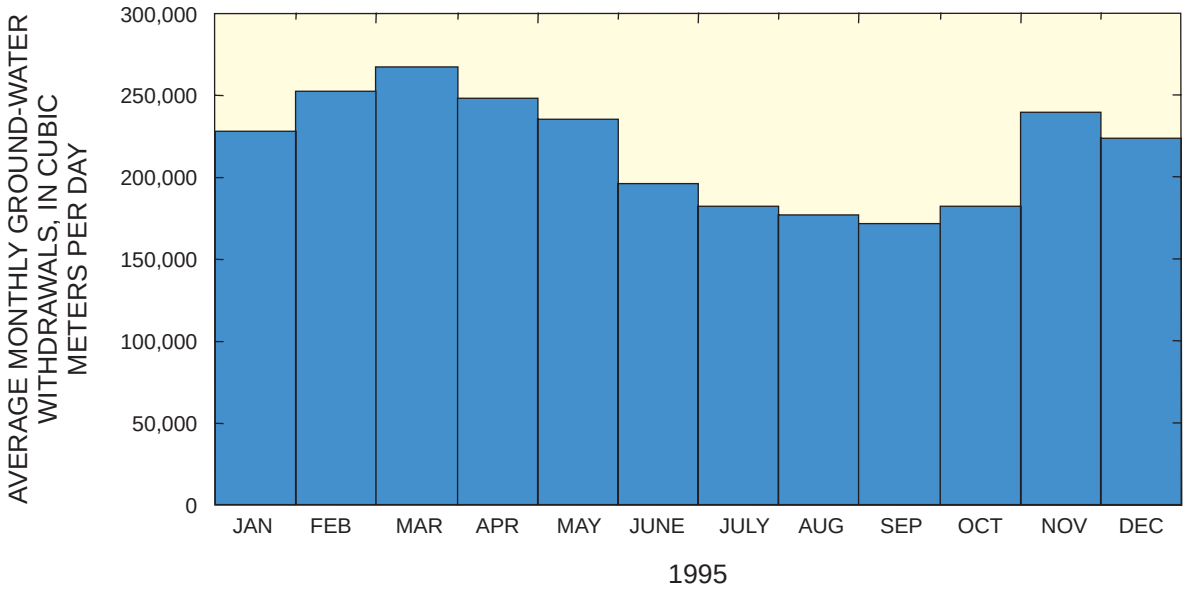

Figure 14. Average monthly ground-water withdrawals from municipal supply facilities in Lee and Collier Counties, 1995.

Water Quality and Geochemistry

Water-quality and geochemical data collected from the lower Tamiami aquifer near Bonita Springs were used to examine historical trends in salinity and to identify potential sources of saltwater. Numerous water samples were collected and analyzed for chloride concentration and strontium isotopes (Schmerge, 2001). Chloride concentration is a common surrogate for salinity, and strontium isotopes have proven to be a useful tracer for determining ground-water movement and the origin of salinity (Clark and Fritz, 1997). Further explanation of methods and data analysis of strontium isotopes can be found in Schmerge (2001).

Historical trends in salinity were examined for nine USGS monitoring wells open to the lower Tamiami aquifer near Bonita Springs; chloride concentrations ranged from about 10 to 1,300 mg/L (fig. 15). Monitoring well L-738 is the only well examined with a record that pre-dates 1985. Chloride concentrations in well L-738 have increased steadily from about 100 mg/L in 1968 to about 350 mg/L in 1998. A statistical analysis conducted by Prinos and others (2002) detected a significant upward trend in chloride concentration at monitoring well L-738. Chloride concentrations in this well have increased at a rate of about 6.6 mg/L annually from 1974 through 1998 (Prinos and others, 2002). Several possible explanations for this increasing chloride concentration are presented later in the discussion of ground-water flow and mechanisms of saltwater intrusion. In the other eight wells, chloride concentrations remained relatively stable or decreased over time.

Salinity also was examined historically by comparing areal maps of chloride concentration in the lower Tamiami aquifer. In a study by Knapp and others (1986), lines of equal chloride concentration reached a maximum value of 500 mg/L near Bonita Springs (fig. 16A). In a study by Schmerge (2001), lines of equal chloride concentration reached a maximum value of 1,000 mg/L near Bonita Springs (fig. 16B). Additionally, the 300-mg/L line of equal chloride concentration extended farther inland in the latter study. This comparison suggests saltwater occurs farther eastward than in 1986 in the lower Tamiami aquifer near Bonita Springs. Differences in the locations of lines of equal chloride concentrations, however, could be explained by differences in the amount and location of data available for contouring in Knapp and others (1986) and Schmerge (2001). With this in mind, the historical comparison of lines of equal chloride concentration does not conclusively determine if saltwater has moved since 1986.

Water samples were collected from the lower Tamiami aquifer near Bonita Springs for strontium isotope analyses (Schmerge, 2001). Strontium isotope data can be used in conjunction with the hydrogeologic framework to provide evidence of the source of strontium in ground water (Sacks and Tihansky, 1996). Results suggest that the source of strontium in ground water sampled in the lower Tamiami aquifer near Bonita Springs is the underlying Floridan aquifer system (Schmerge, 2001).

GROUND-WATER FLOW AND MECHANISMS OF SALTWATER INTRUSION

Ground-water flow patterns and potential mechanisms of saltwater intrusion in the study area are described in this section. Lateral ground-water flow in the lower Tamiami aquifer occurs in a southwesterly direction and becomes radially convergent near Bonita Springs. Vertical ground-water flow can be inferred from a map of the head difference between the lower Tamiami and sandstone aquifers (fig. 12). This map suggests that the greatest rates of vertical ground-water flow from the sandstone aquifer to the lower Tamiami aquifer are occurring beneath Bonita Springs, assuming that the upper Hawthorn confining unit is continuous and uniform in thickness and hydraulic conductivity. Approaching the saltwater interface, fresher ground water flowing toward the Gulf of Mexico moves upward and over more saline ground water that is flowing toward inland areas in lower parts of the lower Tamiami aquifer. This circulation process in the saltwater interface was observed in the Biscayne aquifer by Kohout (1964) and can only be inferred from the current monitoring well network established near Bonita Springs.

The distribution of saltwater in the lower Tamiami aquifer is likely not at equilibrium with current hydrologic conditions near Bonita Springs because of rapidly increasing rates of ground-water pumpage, rising sea level, and the lag in response time for saltwater to move to equilibrium when hydrologic conditions change. In fact, four potential mechanisms could move saltwater into zones of the lower Tamiami aquifer previously occupied by fresher waters. These mechanisms are: (1) lateral movement of the

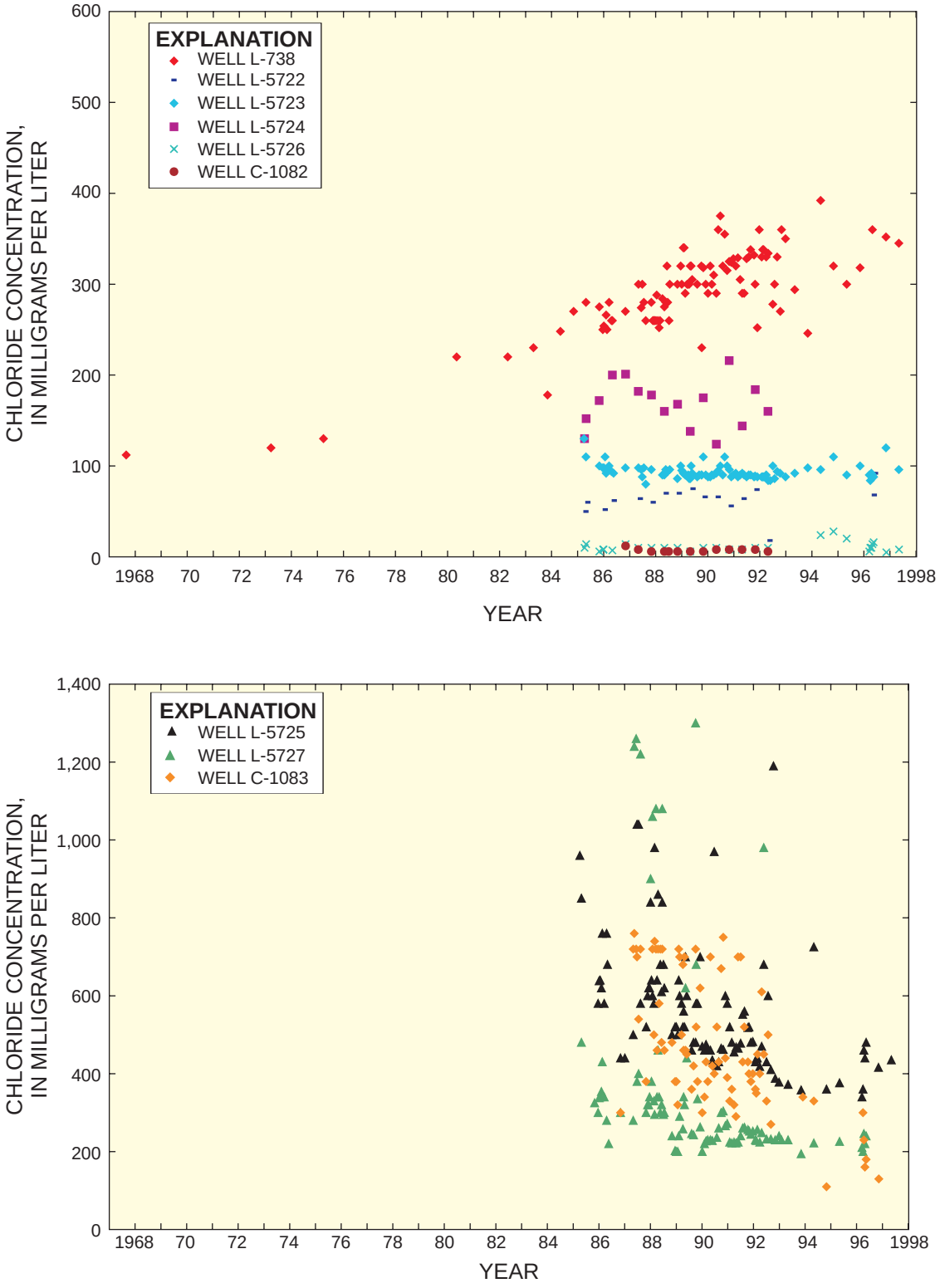

Figure 15. Historical trends in chloride concentration for selected monitoring wells near Bonita Springs, 1968-98. Well locations are shown in figure 1.

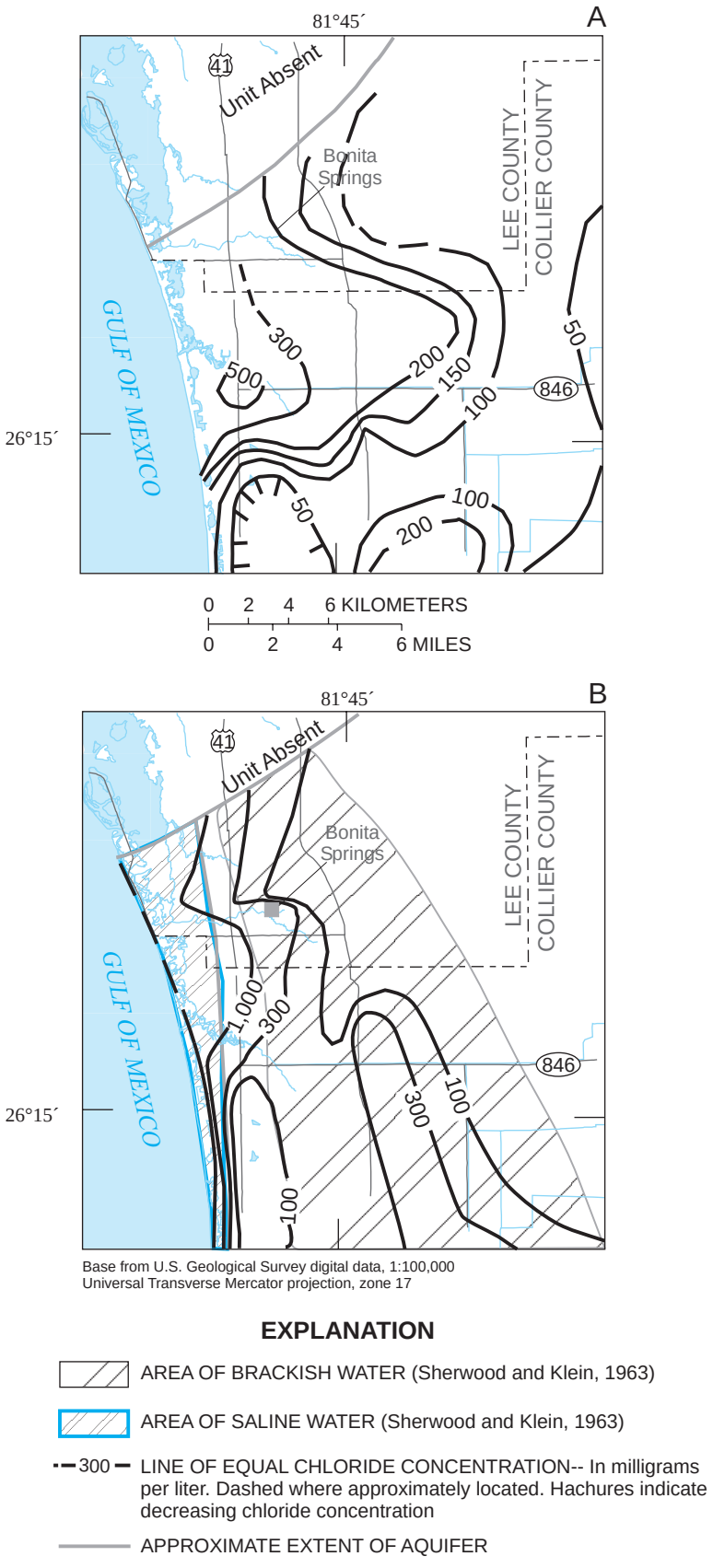

Figure 16. Lines of equal chloride concentration in the lower Tamiami aquifer near Bonita Springs over time. Map A modified from Knapp and others (1986), and map B modified from Schmerge (2001).

freshwater-saltwater interface inland from the southwestern coast of Florida; (2) upward leakage from deeper, saline water-bearing zones through natural upwelling and upconing; (3) downward leakage of saltwater from surface-water channels; and (4) movement of unflushed pockets of relict seawater in the lower Tamiami and water-table aquifers (fig. 17).

Lateral Encroachment

Lateral encroachment of recent seawater into the lower Tamiami aquifer may be possible in southwestern Florida. Saline ground water beneath the Gulf of Mexico could move through the permeable rock comprising the lower Tamiami aquifer to come into equilibrium with modern natural and anthropogenic stresses, such as withdrawals, sea level, and drought (fig. 17). Some evidence indirectly suggests the occurrence of lateral encroachment in the lower Tamiami aquifer near Bonita Springs. For instance, the average annual potentiometric surface of the lower Tamiami aquifer in 1996 is below sea level in some areas beneath Bonita Springs adjacent to the Gulf of Mexico; however, the predominance of lateral encroachment is uncertain.

Upward Leakage

A plausible mechanism for the movement of saline ground water into the freshwater zones of the lower Tamiami aquifer near Bonita Springs is upward leakage (fig. 17) either through natural upwelling or upconing. Natural upwelling is defined here as the upward movement of ground water within or into the lower Tamiami aquifer due to head differences caused by natural stress-producing processes. Natural upwelling can cause saltwater intrusion where salinity is higher in deeper locations of higher head. Upconing is defined here as the upward movement of saline ground water within or into the lower Tamiami aquifer due to head differences caused by anthropogenic stress. The primary difference between these two processes is the source of stress, either natural or anthropogenic.

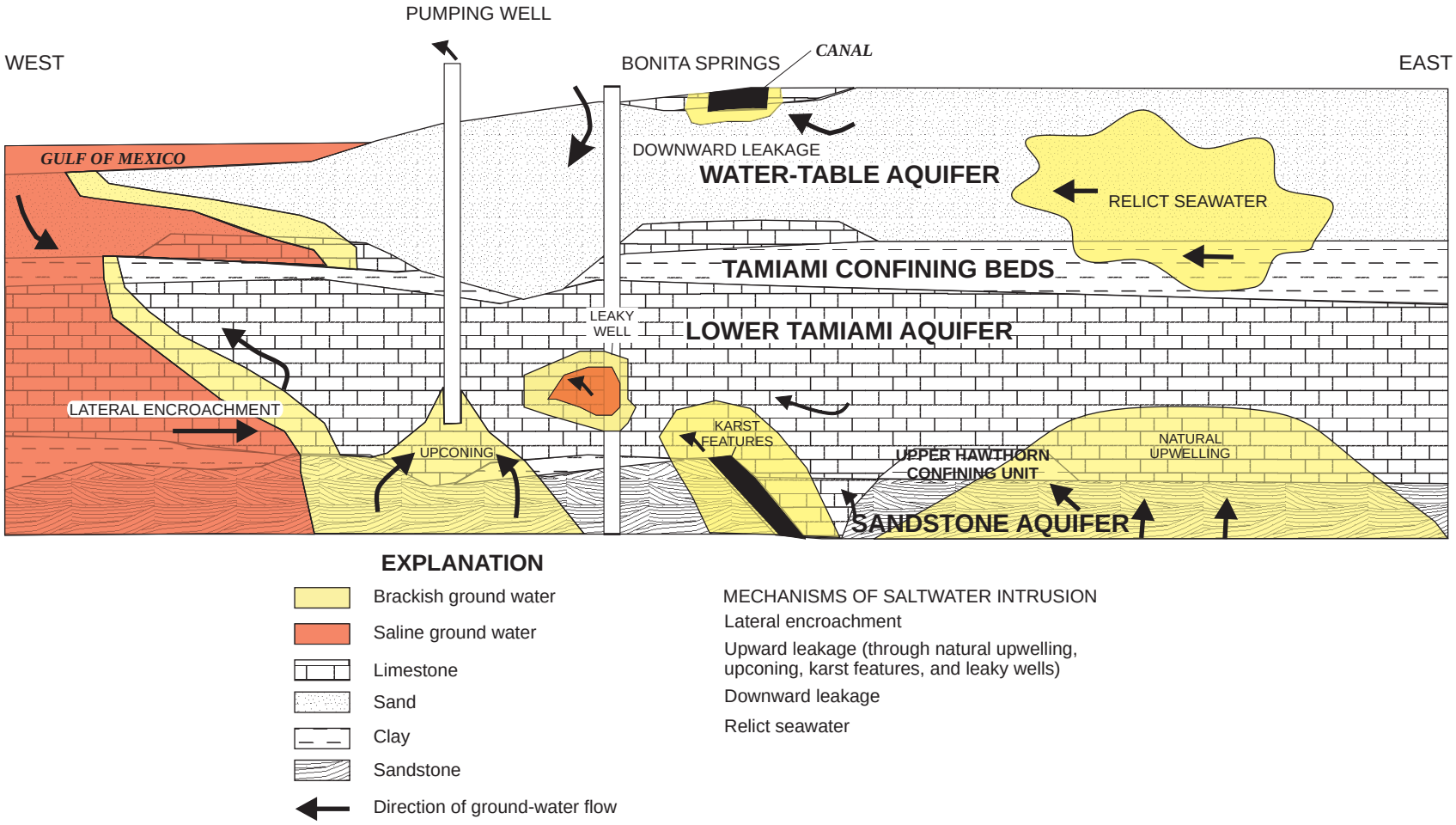

Figure 17. Potential mechanisms of saltwater intrusion in the lower Tamiami aquifer near Bonita Springs.

Diffuse natural upwelling of brackish ground water from the sandstone aquifer to the lower Tamiami aquifer probably is occurring in some parts of the study area. There is evidence of upward leakage to the base of the lower Tamiami aquifer in southwestern Collier County several kilometers north and south of I-75 and north of U.S. Highway 41 (fig. 12). These areas can be isolated as natural upwelling rather than upconing because they are characterized by sloughs, swamps, cypress domes, pine and/or oak islands, and mangrove estuaries where little anthropogenic stress, such as ground-water withdrawal, occurs. Upward leakage through natural upwelling is not apparent in the lower Tamiami aquifer beneath Bonita Springs because the potentiometric surface of the aquifer has been drawn down as a result of ground-water pumpage. This drawdown means natural upwelling probably is secondary to upconing.

Upconing of saltwater probably can be considered of utmost concern in the lower Tamiami aquifer beneath Bonita Springs. Upward leakage to the base of the lower Tamiami aquifer was inferred to be occurring at maximum rates beneath Bonita Springs in 1996 (fig. 12), assuming the upper Hawthorn confining unit is continuous and uniform. However, Wedderburn and others (1982) report that the upper confining unit thins and is absent in southernmost Lee County near Bonita Springs. Thus, saltwater upconing can occur more easily in this area because of less resistance to vertical flow. Other evidence shows that water in this area of the lower Tamiami aquifer was less saline in the past (Prinos and others, 2002) and originated from deeper discharging aquifers (Schmerge, 2001). This latter evidence also suggests that upconing may be occurring in the lower Tamiami aquifer beneath Bonita Springs.

As previously discussed, diffuse natural upwelling probably is not important in the lower Tamiami aquifer near Bonita Springs. Earlier studies had suggested that non-diffuse natural upwelling and upconing of saltwater through karst features could be occurring. Kohout (1979) identified the “mudhole” (fig. 1) discharging warm water to the Gulf of Mexico about 26 km northwest of Bonita Springs. Additionally, heads in the Floridan aquifer system are about 10 m higher than heads in the lower Tamiami aquifer near Bonita Springs. Thus, ground water would naturally tend to flow from deeper, more saline, and more pressurized aquifer systems to the lower Tamiami aquifer along preferential karstic flow paths. Although karst features exist in the study area, this mechanism of saltwater intrusion probably is not predominant in the lower Tamiami aquifer near Bonita Springs based on historical chloride concentration trends (Prinos and others, 2002). Water in the lower Tamiami aquifer would have chloride concentrations similar to the Floridan aquifer system (about 1,200 to 1,600 mg/L) if karst features were naturally transporting large quantities of saltwater from deeper aquifers for thousands of years.

According to previous investigators (Sherwood and Klein, 1963; Burns, 1983; Schmerge, 2001), natural upwelling and upconing of saltwater through leaky wells could be occurring in the lower Tamiami aquifer near Bonita Springs. Additionally, a poorly sealed annulus of well L-2310 (not shown) was hypothesized as the source of saltwater intrusion in well L-738 (fig. 15) by Schmerge (2001). Well L-2310 tapped the Upper Floridan aquifer and may have provided a pathway for upward leakage to the lower Tamiami aquifer near well L-738. The existence of other leaky wells (or potential leaky wells) is unknown; therefore, the predominance of leaky wells as a mechanism of saltwater intrusion in the lower Tamiami aquifer near Bonita Springs remains uncertain.

Downward Leakage

Downward leakage could occur as saline water from surface-water channels moves through the water-table aquifer and underlying Tamiami confining beds to come into equilibrium with modern natural and anthropogenic stresses. Downward leakage of saltwater from rivers and canals has been documented in the water-table aquifer near Naples (McCoy, 1962) and near boat basins in Naples (Klein, 1954). Downward leakage, however, seems an unlikely mechanism of saltwater intrusion in the lower Tamiami aquifer near Bonita Springs. Gaging stations on the northern and southern branches of the Estero River, Spring Creek, and the Imperial River record flow during the dry season, suggesting ground water flows from the water-table aquifer to these rivers and creeks even in times of drought. Additionally, flow from the water-table aquifer to the base of the Imperial River was observed during field reconnaissance in July 2000. Given these observations, it seems unlikely that saltwater moving upstream along Spring Creek and the Estero, Imperial, and Cocohatchee Rivers (fig. 1) would infiltrate through the water-table aquifer and underlying Tamiami confining beds and result in the distribution of saltwater mapped by Knapp and others (1986) and Schmerge (2001).

Relict Seawater

Relict seawater from former high sea-level stands could move through the permeable rock comprising the lower Tamiami aquifer to come into equilibrium with modern natural and anthropogenic stresses (fig. 17). The presence of unflushed relict seawater has been hypothesized as a source of brackish ground water in the shallow surficial aquifer system in parts of southwestern Florida (Sherwood and Klein, 1963; Schmerge, 2001). Evidence suggests, however, that relict seawater is not present in the lower Tamiami aquifer near Bonita Springs. For example, strontium isotope data indicate ground water in the area is from deeper discharging aquifers (Schmerge, 2001). Additionally, McCoy (1962) reports that flushing of most seawater in the shallow aquifers would have occurred since the Pleistocene based on ambient ground-water flow and recharge rates. According to Knapp and others (1986), the regional presence of unflushed water from sea inundations during Pleistocene interglacial stages is minimal.

SIMULATION OF SALTWATER INTRUSION NEAR BONITA SPRINGS

Numerical simulation is used to quantify modern and seasonal stresses, help identify mechanisms of saltwater intrusion, and estimate the potential extent of saltwater intrusion in the lower Tamiami aquifer near Bonita Springs. Numerical codes were selected to (1) solve the constant-density ground-water flow equation, (2) solve the variable-density ground-water flow and solute transport equations, and (3) facilitate model calibration and sensitivity analysis in three dimensions (table 2). Model discretization, assignment of aquifer properties, and assignment of boundary conditions provided the spatial and temporal framework necessary for solving the finite-difference equations. A predevelopment distribution of saltwater was simulated, and the model was calibrated to typical and modern stresses. The potential movement of saltwater from predevelopment distribution to dynamic equilibrium with calibrated typical, modern, and seasonal stresses was then simulated. Modern stresses are represented as stresses with the desired characteristics.

Table 2. Description and primary use of modeling tasks

Task	Spatial discretization	Temporal discretization	Code[1]	Initial conditions	Primary use
1	105 rows, 80 columns, 17 layers[2]	One steady-state flow stress period, representing predevelopment (1930) conditions. Transient transport time steps	SEAWAT	Freshwater equivalent heads equal to zero, a wall of saltwater at coast	Estimate predevelopment salinity conditions and establish initial head and salinity conditions for predictive simulations of saltwater movement
2	Same as above	Two steady-state flow stress periods, representing March and September 1996 conditions. Transient transport time steps	MODFLOW-88	Heads at land surface	Obtain an accurate representation of March and September 1996 head and flow conditions
3	Same as above	1,200 alternating steady-state flow stress periods, representing March and September 1996.[3] Transient transport time steps.	SEAWAT	Final predevelopment distribution of freshwater equivalent head and salinity	Help identify mechanisms of saltwater intrusion and estimate the extent of saltwater intrusion in the lower Tamiami aquifer beneath Bonita Springs

[1]SEAWAT (Guo and Langevin, 2002); MODFLOW-88 (McDonald and Harbaugh, 1988).
[2]Aquifer properties as described in this report.
[3]Ran for a total of 600 years.

Modeling Approach

The modeling approach for this study can be summarized by three tasks (table 2):

1. Variable-density simulation of predevelopment conditions,
2. Calibration of a constant-density flow model to typical, modern and seasonal stresses, and
3. Variable-density predictive simulations of saltwater movement to equilibrium with the typical, modern, and seasonal stresses.

The rationale and limitations for each modeling task, and solely simulating advective solute transport while neglecting the effects of dispersion, were considered.

The first task of simulating a predevelopment distribution of saltwater was performed so a comparison could be made between the distribution of saltwater under predevelopment conditions and the distribution of saltwater at equilibrium with typical, modern, and seasonal stresses. This comparison was made to determine the potential occurrence of saltwater intrusion. Additionally, the predevelopment simulation provided a no-flow boundary condition at the saltwater interface for model calibration in task 2. Another reason for simulating a predevelopment distribution of saltwater was to develop initial conditions of freshwater equivalent head and ground-water salinity that were internally self-consistent for predictive simulations of saltwater movement (task 3). While performing variable-density flow simulations, consistent initial conditions of equivalent freshwater head and salinity will result in a model that responds to the imposed hydrologic stresses rather than to disequilibrium of the initial conditions.

The second task in the modeling approach is model calibration. A constant-density ground-water flow simulator was chosen for this task for two reasons:

1. Matching observed heads and flows in the study area was not highly dependent upon simulating saltwater movement. Chloride concentrations in observation wells were about 100 to 1,300 mg/L (fig. 15), suggesting the bulk of the saltwater transition zone remains either offshore, between the monitoring wells and the coastline, or within deeper hydrogeologic units. Thus, the difference between hydraulic-head observations and their simulated equivalents (when modeling) was more likely attributable to uncertainties in aquifer properties and boundary conditions, rather than saltwater or saltwater movement.
2. Computer run times for constant-density ground-water flow simulations are much shorter than computer run times for variable-density flow simulations. Therefore, more time is available to test different conceptual models and parameter estimates while calibrating with a constant-density flow simulator. A limitation of this approach, however, was that the information contained in salinity observation could not be used to better estimate values of transport parameters, such as effective porosity and dispersivity. These parameters are important to solute transport, and thus saltwater movement.

The model was calibrated to typical, modern, and seasonal stresses with certain attributes. A year with "typical" stresses was selected to prevent approximations of saltwater movement from being biased toward wet or dry years. A year with "modern" stresses was selected to determine whether natural and anthropogenic stresses such as recharge, ground-water withdrawal, canal drainage, and sea level would move saltwater to areas previously occupied by fresher waters. "Seasonal" stresses were represented to test theories that alternating wet- and dry-season water levels move saltwater into and out of the lower Tamiami aquifer, respectively, but result in no net saltwater intrusion over a typical water year.

Typical, modern, and seasonal stresses were observed during 1996, so this year was chosen for model calibration. The year 1996 (which had about 1.3 m of rainfall) was selected as "typical" after plotting average annual rainfall values at Bonita Springs Utility rainfall monitoring station (fig. 18). The rainfall data indicate that 1995 represents a wet year (with about 2.1 m of rainfall) and 1950 represents a dry year (with about 1.1 m of rainfall). The average of annual rainfall values in figure 18 is about 1.4 m. The 1996 year also was selected because: (1) pumpage data obtained from the SFWMD began that year, and (2) numerous water-level and flow measurements were taken near Bonita Springs that year relative to other years. Perhaps the flooding of Bonita Springs during the heavy rains of 1995 (Johnson Engineering, Inc., and others, 1999) prompted increased awareness about the importance of data collection during 1996.

During model calibration, seasonal fluctuations in water levels were approximated by designing two steady-state flow stress periods, representing time periods in 1996 when water levels were high (wet

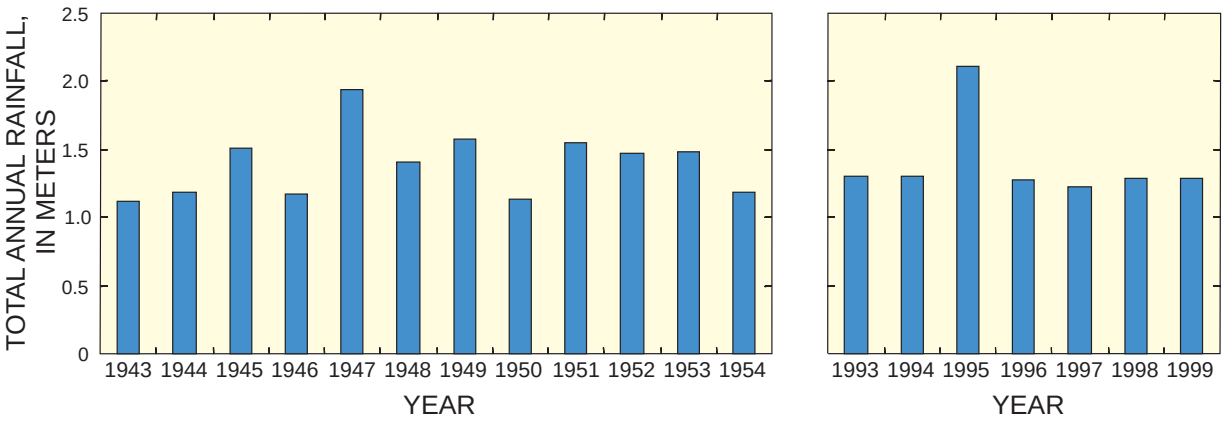

Figure 18. Historical record of annual rainfall at Bonita Springs Utility rainfall monitoring station, 1943-54 and 1993-99.

season) and low (dry season) (table 2). By simulating periods with high and low water levels, the seasonal movement of the saltwater interface can be approximated. Additionally, a steady-state approach can be employed when the selected time periods show relatively stable water levels, suggesting the ground-water flow system is as close to steady state as realistically possible. There are two advantages to using the steady-state approach. First, a steady-state model does not require aquifer storage values. This eliminates the need to specify an additional parameter, which may be highly uncertain. Second, steady-state models tend to run faster than transient models because there are fewer input requirements and fewer solutions to the flow equation. Shorter computer run times allow more time for calibration and sensitivity analysis. A disadvantage of the steady-state approach is the possibility of developing a model that may fail to represent transient particularities important to the true nature of ground-water flow and saltwater movement near Bonita Springs.

March and September 1996 were selected to represent typical, modern, and seasonal stresses because ground-water levels in the water table and lower Tamiami aquifers generally were at or near seasonal lows and highs and also were relatively stable (fig. 19), justifying the steady-state assumption. Given these data and the above considerations, developing a model with two steady-state stress periods calibrated to average March and September 1996 conditions seemed to be a reasonable representation of typical, modern, and seasonal stresses.

Most ground-water models are calibrated by adjusting hydraulic conductivity until simulation results match with observed field conditions. The model documented here was calibrated by assuming hydraulic conductivity parameters were accurate, and estimating unmonitored ground-water pumpage and pan evaporation multipliers using UCODE. Unmonitored ground-water pumpage was estimated because unknown pumpage parameters caused the largest discrepancies between observed and simulated heads near the coast in the lower Tamiami aquifer beneath Bonita Springs. Accurately simulated heads in this location are most important for accurately simulating saltwater movement in this location, which was a primary objective of this study. Pan evaporation multipliers were estimated simultaneously with unmonitored pumpage because pan evaporation parameters were the most sensitive model parameters that were not correlated with unknown pumpage. Correlated parameter values cannot be simultaneously estimated by parameter estimation codes, such as UCODE. This is because coordinated linear changes in correlated parameter values produce the same simulated heads and flows at observation locations (Poeter and Hill, 1997).

The third task in the modeling approach was to simulate the movement of saltwater to equilibrium with the typical, modern, and seasonal stresses. This task was accomplished using the predevelopment distribution of saltwater and calibrated March and September 1996 steady-state flow stress periods. The calibrated steady-state flow stress periods were run in continual succession with a variable density ground-water flow simulator until the total salt mass in the simulation approached “dynamic equilibrium.” At dynamic equilibrium, the average annual total salt mass in the simulation is a constant value, even though some seasonal fluctuation in total salt mass may occur between stress periods.

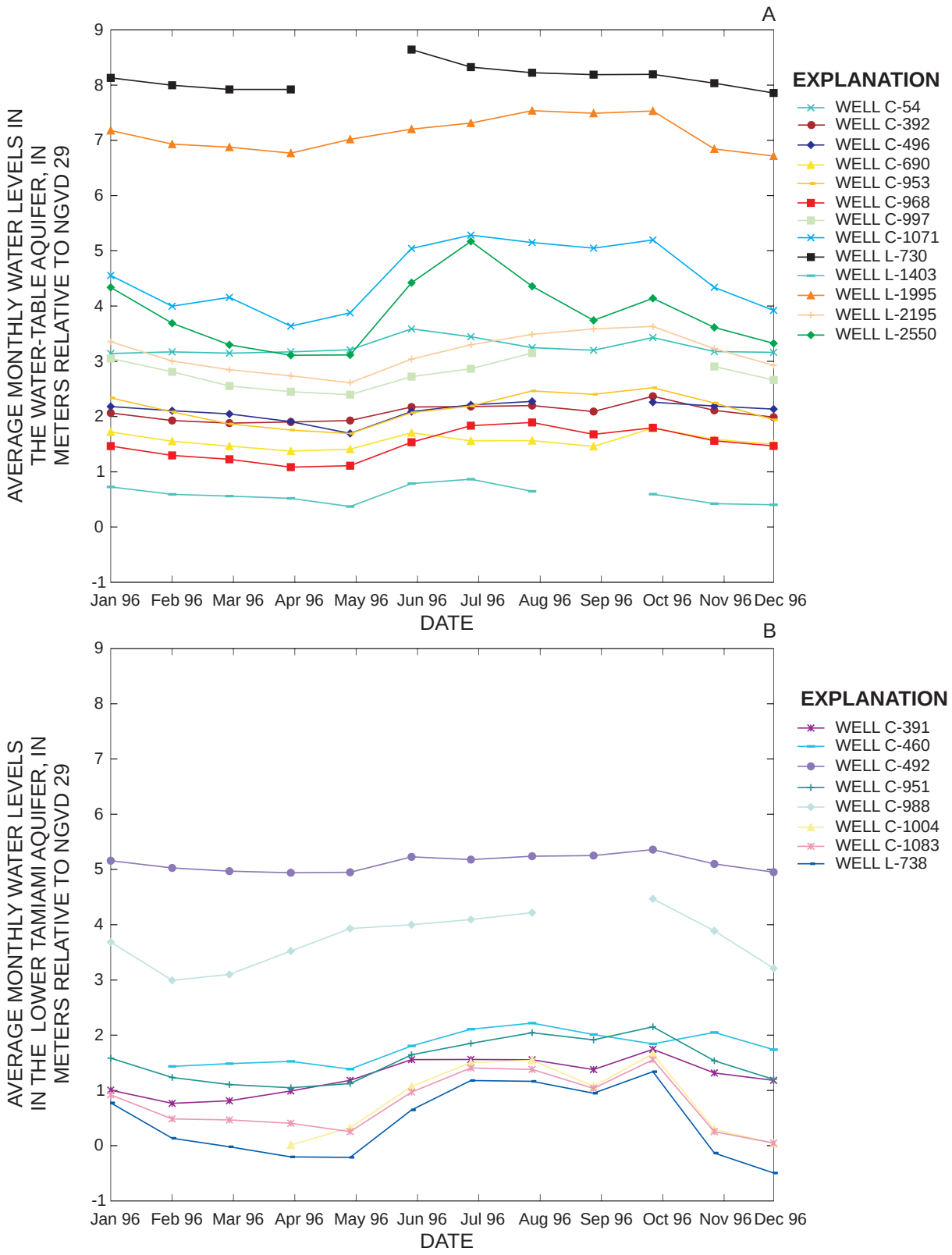

Figure 19. Average monthly water levels from selected monitoring wells in the (A) water-table and (B) lower Tamiami aquifers near Bonita Springs. Well locations are shown in figure 1. NGVD 29 is National Geodetic Vertical Datum of 1929.

Steady-state flow conditions were used for task 3 by assigning a small value (1×10^{-8}) for aquifer storage properties. This means that within each transport step, heads respond instantaneously (or nearly instantaneously) to changes in salinity. Thus, heads and flows for a particular transport step are always of steady state with salinity for that transport step. This approach is a simpler alternative than trying to determine appropriate storage values and run a fully transient model.

Advective solute transport was simulated while solving for the predevelopment distribution of saltwater and solving for the potential movement of saltwater from predevelopment distribution. Dispersive solute transport was not simulated. According to traditional advection-dispersion theory, hydrodynamic dispersion is the tendency for a solute to spread from the path it would be expected to follow according to advective hydraulics (Freeze and Cherry, 1979). Hydrodynamic dispersion results from molecular diffusion and mechanical dispersion. Molecular diffusion, the process by which a plume spreads due to concentration gradients, is small enough in magnitude to be ignored in ground-water flow systems with velocities as high as the system near Bonita Springs. Mechanical dispersion, another process by which a plume spreads, is caused by small-scale velocity variations.

Rather than assign dispersivity values, which would contain a high level of uncertainty, the numerical dispersion caused by the model was assumed to be similar in magnitude to the actual dispersion in the aquifer. Although there was no way to evaluate this assumption, it seemed justified by a lack of field data that could be used to calibrate dispersivity values and considerably long computer run times for simulations that directly represented dispersion. Neglecting dispersion may cause the potential extent of saltwater intrusion to be overestimated. This limitation is discussed in more detail in the model limitation section of the report. If field data are available, the effects of dispersion could be evaluated with future simulations of saltwater intrusion.

Code Selection

Two modular, three-dimensional, finite-difference models were used to simulate ground-water flow and salinity transport in this study (table 2). MODFLOW (McDonald and Harbaugh, 1988) was chosen as the constant-density ground-water flow simulator, and SEAWAT (Guo and Langevin, 2002) was chosen as the variable-density ground-water flow simulator.

Constant-Density Ground-Water Flow Simulator

MODFLOW (McDonald and Harbaugh, 1988), widely accepted by the modeling community as a reliable tool, was chosen as the constant-density ground-water flow simulator. This program was used to solve the following steady-state ground-water flow equation:

$$\frac{\partial}{\partial x}\left(K_{xx}\frac{\partial h}{\partial x}\right)+\frac{\partial}{\partial y}\left(K_{yy}\frac{\partial h}{\partial y}\right)+\frac{\partial}{\partial z}\left(K_{zz}\frac{\partial h}{\partial z}\right)-W=0\ , \quad (2)$$

where K_{xx}, K_{yy}, and K_{zz} are values of hydraulic conductivity along the x-, y-, and z-coordinate axes, which are assumed to be parallel to the major axes of hydraulic conductivity [LT^{-1}]; h is the potentiometric head [L], and W is a volumetric flux per unit volume and represents sources and/or sinks of water [T^{-1}].

Variable-Density Ground-Water Flow Simulator

SEAWAT (Guo and Langevin, 2002), capable of solving for variable-density ground-water flow patterns in three dimensions, was chosen as the variable-density ground-water flow simulator. The SEAWAT program explicitly or implicitly couples a variable-density form of the ground-water flow equation solved with MODFLOW-88 (McDonald and Harbaugh, 1988) to the solute transport equation solved with MT3Dms (Zheng and Wang, 1998). Because MT3Dms is used, solute concentrations or salinities are approximated with transient, three-dimensional, variable-density, ground-water flow patterns. Several methods are available to solve the advection and dispersion terms of the transport equation using MT3Dms (Zheng and Wang, 1998). Thus, the user can experiment to find a solution with acceptable levels of numerical dispersion and/or artificial oscillation while attempting to maintain a reasonable computer run time.

SEAWAT reformulates the ground-water flow equation to solve for freshwater equivalent head as follows:

$$\frac{\partial}{\partial x}\left(\rho K_{fx}\left[\frac{\partial h_f}{\partial x}+\frac{\rho-\rho_f}{\rho_f}\frac{\partial Z}{\partial x}\right]\right)+$$
$$\frac{\partial}{\partial y}\left(\rho K_{fy}\left[\frac{\partial h_f}{\partial y}+\frac{\rho-\rho_f}{\rho_f}\frac{\partial Z}{\partial y}\right]\right)+$$
$$\frac{\partial}{\partial z}\left(\rho K_{fz}\left[\frac{\partial h_f}{\partial z}+\frac{\rho-\rho_f}{\rho_f}\frac{\partial Z}{\partial z}\right]\right)=$$
$$\rho S_f\frac{\partial h_f}{\partial t}+\theta\frac{\partial \rho}{\partial C}\frac{\partial C}{\partial t}-\bar{\rho}q_s \quad , \quad (3)$$

where x, y, and z are the principal directions of permeability,

ρ is fluid density [M/L^3],

K_f is the freshwater hydraulic conductivity [L/T],

h_f is the freshwater equivalent head [L],

ρ_f is the density of freshwater [M/L^3],

Z is the vertical direction or elevation of the center of the model cell [L],

S_f is the freshwater equivalent storage coefficient [L^{-1}],

t is time [T],

θ is effective porosity [dimensionless],

C is the solute concentration [M/L^3],

$\bar{\rho}$ is the density of water from the source or sink [M/L^3], and

q_s is the volumetric flux of water representing sources and sinks per unit volume of aquifer [T^{-1}].

The reformulated ground-water flow equation is coupled to the following solute-transport equation:

$$\nabla(D\nabla C)-\nabla\bullet(\hat{v}C)-\frac{q_s}{\theta}C_s+\sum_{k=1}^{n}R_k=\frac{\partial C}{\partial t}, \quad (4)$$

where

D is the hydrodynamic dispersion coefficient [L^2/T],

∇ is the spatial gradient operator,

$\hat{v}$ is the fluid velocity vector [L/T],

C_s is the solute concentration of the source or sink [M/L^3], and

R_k is the rate of solute production or decay in reaction k of n different reactions [M/L^{3}T].

Equations 3 and 4 are sequentially solved by first solving the variable-density ground-water flow equation and then solving the solute-transport equation. After new concentrations are calculated, a linear equation of state is used to relate solute concentrations to fluid density. The linear equation of state is:

$$\rho = \rho_f + EC \quad , \quad (5)$$

where E is an empirical, dimensionless constant with an approximate value of 0.7143 for salts commonly found in seawater.

Spatial Discretization and Assignment of Aquifer Properties

Finite-difference methods require the discretization of space into a grid consisting of rows, columns, and layers of model cells. Additionally, ground-water flow is proportional to the horizontal and vertical permeability properties of the aquifer matrix, and advective and dispersive solute transport is dependent upon the effective porosity of the aquifer matrix. Thus, in a three-dimensional, finite-difference SEAWAT model using the robust layer type 3 option (LAYCON 3), information describing the grid discretization, horizontal hydraulic conductivity, vertical conductance (VCONT) (McDonald and Harbaugh, 1988), and effective porosity must be written to model input files. The aquifer property information must be assigned to model cells in a way that reflects the bulk occurrence of these properties within the entire volume of the model cell.

The study area was spatially discretized into a grid with 105 rows, 80 columns, and 17 layers of square cells. Seventeen layers were used to obtain sufficient vertical resolution of the saltwater interface. Each model cell is 600 by 600 m and 5 m thick, except for layer 1 where the cell top varies to match land surface, and the cell bottom is 5 m below National Geodetic Vertical Datum (NGVD) of 1929. Uniform cell volumes were used, except for layer 1, to minimize mass-balance errors that could occur if a mixed Eulerian-Lagrangian method was needed to solve the advection term of the transport equation. Examples of such a method with MT3Dms are the method of characteristics (MOC), modified method of characteristics (MMOC), or hybrid method of characteristics (HMOC). Eulerian-Lagrangian methods do not guarantee local mass conservation at a particular time step because of the discrete nature of particle tracking used in these techniques (Zheng and Wang, 1998).

Mass-balance errors can be exacerbated by nonuniform cell volumes.

Bulk values of horizontal hydraulic conductivity and VCONT were assigned to model cells using a three-dimensional conceptual permeability model, the configuration of the model grid, and weighted arithmetic or harmonic averaging. The three-dimensional conceptual permeability model was developed by assigning the values of horizontal and vertical hydraulic conductivity, shown in table 3, to the framework of the water-table aquifer, Tamiami confining beds, lower Tamiami aquifer, upper Hawthorn confining unit, and sandstone aquifer. Because hydraulic conductivity typically is considered to be log-normally distributed, permeability values were assigned (as described below) using the log K histograms of aquifer horizontal hydraulic conductivity (fig. 4) compiled from: (1) previous literature (Bower and others, 1990), and (2) reanalysis of previous aquifer performance tests (K.M. Edwards, U.S. Geological Survey, written commun., 2000).

Table 3. Hydraulic conductivities used in the conceptual permeability model

Hydrogeologic unit	Hydraulic conductivity (meters per day)	
	Horizontal	Vertical
Water-table aquifer	300	15
Tamiami confining beds	.04	.004
Lower Tamiami aquifer	70	3.5
Lower Tamiami aquifer, coral reef facies	130	6.5
Upper Hawthorn confining unit	.03	.003
Sandstone aquifer	20	2

The water-table aquifer was assigned a horizontal hydraulic conductivity of 300 m/d (table 3). The horizontal hydraulic conductivity was based on the inverse log of the midpoint of the first mode in the distribution of 244 measurements (fig. 4A). A vertical hydraulic conductivity of 15 m/d was assigned to the water-table aquifer (table 3) because reanalysis of aquifer performance tests in the study area by K.M. Edwards (U.S. Geological Survey, written commun., 2000) suggests that the anisotropy ratio of horizontal to vertical hydraulic conductivity is about 20:1 in the water-table aquifer.

The Tamiami confining beds and the upper Hawthorn confining unit were assigned horizontal hydraulic conductivities of 0.04 and 0.03 m/d, respectively, and vertical hydraulic conductivities of 0.004 and 0.003 m/d, respectively (table 3). The same vertical hydraulic conductivities (0.004 and 0.003 m/d) were measured by Montgomery (1988). Little published information was available to constrain values of horizontal hydraulic conductivity for both confining units. In modeling applications, the ratio of horizontal hydraulic conductivity to vertical hydraulic conductivity is often assumed to range from 1 to 1,000 (Anderson and Woessner, 1992). Thus, the horizontal hydraulic conductivities of the Tamiami confining beds and the upper Hawthorn confining unit were set to 0.04 and 0.03 m/d, respectively, or 10 times the measured vertical hydraulic conductivity found by Montgomery (1988). This may seem somewhat arbitrary, but the results of ground-water flow models typically are insensitive to values of horizontal hydraulic conductivity in confining units. Because of the low permeability of these units, horizontal flow within them is essentially negligible.

In the lower Tamiami aquifer, horizontal hydraulic conductivity appears to have a bimodal log K distribution (fig. 4B). Results from aquifer performance tests compiled for this study (figs. 4B and 8) and for previous research (Meeder, 1979) suggest that permeabilities in the lower Tamiami aquifer are much greater in areas where coral reef facies are present. The lower Tamiami aquifer was assigned a horizontal hydraulic conductivity value of 130 m/d in areas where the coral reef facies are known to exist (table 3). This value was the inverse log of the arithmetic average log K value computed from eight aquifer performance tests completed in coral reef facies (fig. 8). Elsewhere, the lower Tamiami aquifer was assigned a horizontal hydraulic conductivity of 70 m/d (table 3) –the inverse log of the arithmetic average log K value computed from 136 measurements (fig. 4B). A vertical hydraulic conductivity value of 6.5 m/d was assigned in areas of the lower Tamiami aquifer where coral reef facies are present and 3.5 m/d elsewhere because reanalysis of aquifer performance tests suggests the anisotropy ratio of horizontal to vertical hydraulic conductivity is about 20:1 in the aquifer.

The sandstone aquifer was assigned a horizontal hydraulic conductivity of 20 m/d and a vertical hydraulic conductivity of 2 m/d (table 3). The horizontal hydraulic conductivity was based on the inverse log of the arithmetic average log K value computed from the distribution of 25 measurements (fig. 4C). Little published information was available to constrain values of vertical hydraulic conductivity for the sandstone aquifer. The vertical hydraulic conductivity was based on the 1 to 1,000 range of vertical to horizontal conductivity ratios. Thus, the vertical hydraulic conductivity of the sandstone aquifer was set to 2 m/d, or one-tenth the horizontal hydraulic conductivity. Again, this may seem somewhat arbitrary, but model results are expected to be insensitive to the vertical hydraulic conductivity of the sandstone aquifer. Because the focus of this study is the lower Tamiami aquifer, flow into or out of the aquifer will be controlled more by the vertical hydraulic conductivity of the underlying upper Hawthorn confining unit than the vertical hydraulic conductivity of the sandstone aquifer.

Because the hydrogeologic units do not coincide with model layers, bulk values of horizontal hydraulic conductivity (fig. 20) were computed as the weighted arithmetic mean of the hydraulic conductivities (table 3) that lie within the model cell (fig. 21). The weighted arithmetic mean is expressed as:

$$Kxy_{i,\ j,\ k} = \sum_{u=1}^{n} W_u Kxy_u \quad , \qquad (6)$$

where $Kxy_{i,j,k}$ is the bulk horizontal hydraulic conductivity of the model cell i,j,k [L/T], u is a counter ranging from 1 to n, in which n is the number of hydrogeologic units within the model cell [dimensionless], W_u is weight representing the fraction of the model cell's thickness occupied by the hydrogeologic unit (the sum of the weights for each model cell must equal 1 [dimensionless]), and Kxy_u is the horizontal hydraulic conductivity of the hydrogeologic unit [L/T].

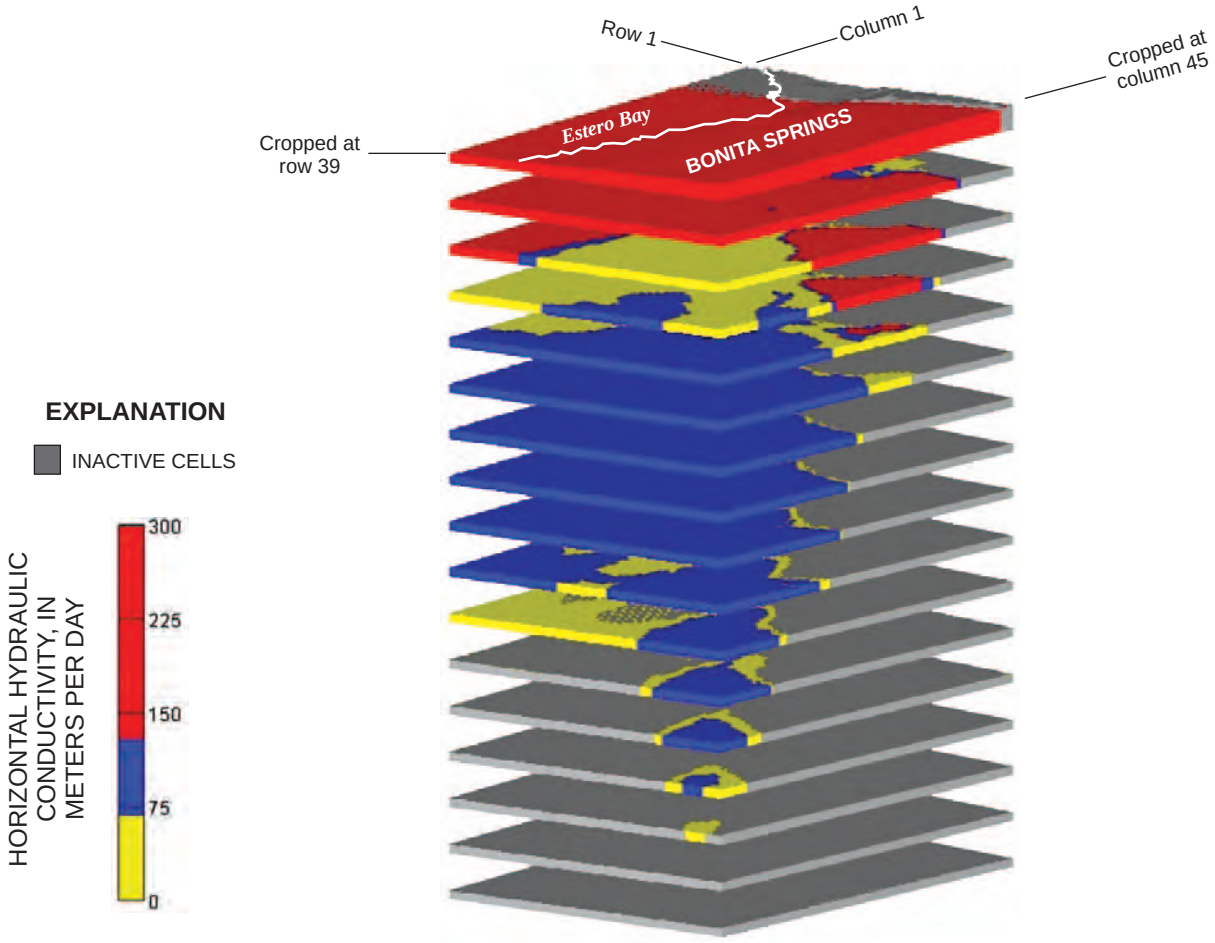

Figure 20. Distribution of bulk horizontal hydraulic conductivity in selected model cells.

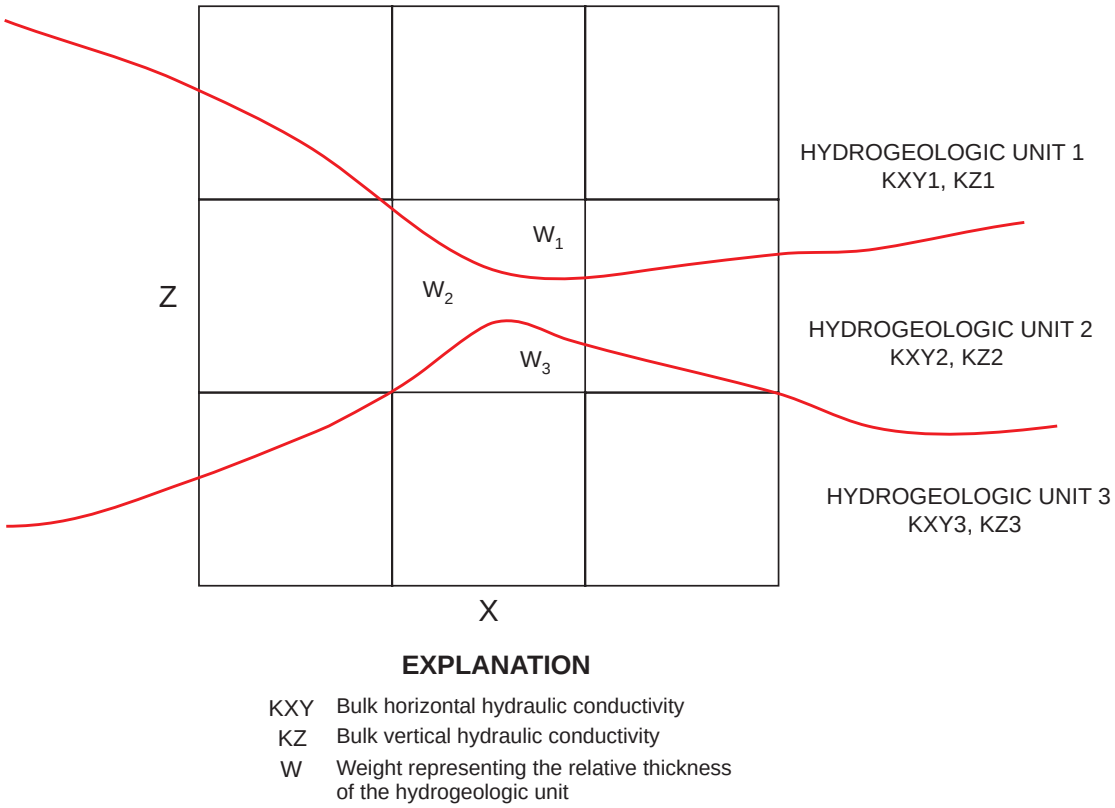

Figure 21. Approach used to compute bulk hydraulic conductivities for each model cell using weighted arithmetic and harmonic averaging.

Bulk values of vertical hydraulic conductivity for model cells were computed as the weighted harmonic mean of hydraulic conductivities (table 3) that lie within the model cell (fig. 21). A three-dimensional diagram of bulk values of vertical hydraulic conductivity would look similar to the three-dimensional diagram of bulk values of horizontal hydraulic conductivity (fig. 20), except values would range would from 15 to 0.003 m/d. The weighted harmonic mean is expressed as:

$$Kz_{i,\ j,\ k} = \frac{1}{\sum_{u=1}^{n} W_u \frac{1}{Kz_u}}, \qquad (7)$$

where $Kz_{i,j,k}$ is the bulk vertical hydraulic conductivity of the model cell [L/T], and Kz_u is the vertical hydraulic conductivity of the hydrogeologic unit [L/T].

Except for the bottom layer (layer 17), a VCONT term is required input for each model cell in a MODFLOW or SEAWAT simulation. Bulk values of VCONT were computed as:

$$VCONT_{i,\ j,\ k} = \frac{2(Kz_{i,\ j,\ k})(Kz_{i,\ j,\ k+1})}{\Delta b_{i,\ j,\ k}(Kz_{i,\ j,\ k}) + \Delta b_{i,\ j,\ k+1}(Kz_{i,\ j,\ k+1})}, \qquad (8)$$

where $VCONT_{i,j,k,}$ is the required VCONT term [1/T], and $\Delta b_{i,j,k}$ is the thickness of the model cell [L].

Estimates of effective porosity were needed for variable-density ground-water flow simulations. Effective porosity, the percentage of interconnected pore space within geologic material, was uniformly set to 30 percent. This percentage is based on analysis of exploratory cores collected from the gray limestone and lower Tamiami aquifers in the study area (Reese and Cunningham, 2000).

Simulation of Predevelopment Conditions

In the first modeling task, the SEAWAT program was used to simulate the location of the interface prior to development. The year 1930 was selected to represent predevelopment conditions primarily because the network of canals had not yet been constructed (Ananta Nath, Big Cypress Basin, oral commun., 2001), and ground-water pumpage probably was negligible. A single steady-state stress period was used to represent conditions in 1930. The spatial discretization and aquifer properties previously described were used for the simulation. Results from the predevelopment model consist of three-dimensional distributions of head and salinity. These model results are used to help define a coastal boundary condition for model calibration (task 2). Results from the predevelopment simulation also are used as initial conditions for predictive simulations of saltwater movement (task 3).

Boundary Conditions

Boundary conditions for simulating the predevelopment distribution of saltwater include rainfall, evapotranspiration, rivers, lateral conditions of no flows, and constant heads with constant concentrations (pl. 1). Rainfall and evapotranspiration boundary conditions were used to allow the simulation to calculate the net recharge to the top of active model cells located inland from the coastline. Because rainfall and evapotranspiration are assigned to active cells in layer 1, these boundary conditions are not shaded nor labeled on plate 1. River boundary conditions were used to represent Spring Creek, and the Imperial, Cocohatchee and Estero Rivers. No-flow boundary conditions were used to represent predevelopment hydrologic divides that were assumed to exist along modern ground-water flow lines. Because each cell in layers 16 and 17 is a no-flow boundary condition, only layers 1 to 15 are plotted on plate 1. Layers 16 and 17 were kept in the model, however, in case they are needed to represent deeper hydrogeologic units in future investigations. Constant-head and constant-concentration boundary conditions were used to represent the Gulf of Mexico. The salinity of inflow from each source boundary condition was set to zero, with exception to the boundary conditions representing the Gulf of Mexico, which were assigned a salinity of seawater.

Recharge

Limited data were available that describe recharge in 1930; therefore, recharge was simulated using the approach described by Motz (1996) and Stewart and Langevin (1999). Using this approach, both rainfall and evapotranspiration are included in the model, with the maximum potential ground-water evapotranspiration rate set equal to the rainfall rate. This creates an aquifer system where water levels are controlled by land-surface topography (Motz, 1996). Using this method to simulate recharge is advantageous because spatial distributions of net recharge are generated rather than discrete zones. Disadvantages include the potential for additional uncertainty in model simulations due to the lack of data to support estimates of rainfall, maximum potential evapotranspiration rates, extinction depths, and the evapotranspiration surface.

Rainfall was entered using the Recharge package (McDonald and Harbaugh, 1988). The Recharge package requires input of an areal flux [L/T] to the top grid layer, a specified vertical distribution of layers, or the highest active cell in a vertical column of layers. The areal recharge flux was added to the highest active cell in a vertical column of layers. Average annual rainfall rates were computed from historical rainfall recorded at the Bonita Springs monitoring station from 1943 to 1999 (fig. 18). Years with no average annual rainfall rate indicate missing or insufficient data (1955-92). No trends of annual average rainfall rates are evident, thus an extrapolation relation to compute the average annual rainfall rate in 1930 was not necessary. The average of annual average rainfall rates was about 1.3 m/yr and was written as the areal flux in the Recharge package.

Evapotranspiration was entered using the Evapotranspiration package (McDonald and Harbaugh, 1988) where evapotranspiration is approximated as a linearly varying rate that is greatest at the evapotranspiration surface and decreases to zero at the extinction depth. As required by the coupled aquifer approach, the maximum evapotranspiration rate of the evapotranspiration surface was set equal to the rainfall rate. The evapotranspiration surface was set to land surface, and extinction depths were set to 5 m below land surface.

Extinction depths are uncertain in the study area. Extinction depths at about 0.3 to 2.1 m were used in previous modeling studies of southwestern Florida (Bower and others, 1990; Bennett, 1992). These depths were related to land use and based upon estimated root depths for various types of vegetation. In addition to vegetation root depth, evapotranspiration is

dependent upon other processes and properties, such as climate and soil type. For example, fine-grained soils will have deeper extinction depths than coarse-grained soils because more energy is required to lift ground water through coarse-grained soils.

A network of evapotranspiration stations maintained in southern Florida by the USGS suggests extinction depths of at least 1 m over many types of land cover (S.L. Kinnaman, U.S. Geological Survey, written commun., 2001). Tibbals (1990) estimated evapotranspiration rates of about 76 cm/yr in areas where the water table was about 4 m below land surface in east-central Florida. Merritt (1996) used extinction depths up to 6 m below land surface in a coastal ridge area of southeastern Florida. Setting extinction depths to 5 m below land surface seemed to be a reasonable compromise, given the current understanding of evapotranspiration in Florida.

Rivers

Predevelopment river boundary conditions (pl. 1) were entered using the River package (McDonald and Harbaugh, 1988). The conceptual model for the River package is based on the vertical leakage of water across river bottom sediments. The cross section of the river is conceptualized in the model code as rectangular with impermeable vertical sides. Leakage into or out of the model cell is dependent on the stage in the river (h_{riv}), the value of head in the model cell ($h_{i,j,k}$), and a conductance term. The conductance term of the river is mathematically defined as:

$$COND_{riv} = \frac{LwK_{seds}}{b_{seds}}, \qquad (9)$$

where $COND_{riv}$ is the conductance of the river bed [L^2/T],

L is the length of the river segment in the model cell [L],

w is the bottom width of the river [L],

K_{seds} is the vertical hydraulic conductivity of the river bottom sediments [L/T], and

b_{seds} is the thickness of the river bottom sediments [L].

The elevation of the base of the river bottom sediments is specified as *RBOT*, an input parameter for the River package. When $h_{i,j,k}$ is greater than *RBOT*, leakage from the aquifer to the river, Q_{riv}, is calculated as:

$$Q_{riv} = COND_{riv}(h_{riv} - h_{i,\ j,\ k}) . \qquad (10)$$

When $h_{i,j,k}$ is less than *RBOT*, the leakage rate from the river to the aquifer is calculated as:

$$Q_{riv} = COND_{riv}(h_{riv} - RBOT) . \qquad (11)$$

The Estero River, Imperial River, Cocohatchee River, and Spring Creek (fig. 1) were simulated with the River package. These surface-water features were digitized from a USGS 1:100,000-scale topographic-bathymetric map. For predevelopment conditions, an attempt was made to digitize only parts of the river and creek channels that appeared to be unaltered. Input for the River package includes the layer, row, column, h_{riv}, $COND_{riv}$, and *RBOT*. The layer, row, and column of river cells were determined by overlying the digitized river features with the model grid. The river stage, h_{riv}, was estimated at 0.5 m below the land-surface elevation of the model cell because this value seems reasonable, and no quantitative data describing river stages in 1930 exist. For each river cell, $COND_{riv}$ was computed by multiplying the area of the river or creek channel within the model cell by K_{seds} . The value of K_{seds} is assumed to be 15 m/d, which is the vertical hydraulic conductivity used for the water-table aquifer (table 3); the value of b_{seds} was set to 1 m for lack of a better value, and the value of *RBOT* was estimated at 2 m less than h_{riv}.

There may be some reason for concern about the lack of predevelopment data for assigning river parameter values. It is likely, however, that these parameters have little effect on the goal of this simulation, which is to simulate a predevelopment distribution of saltwater. River parameters control a relatively small component of the water budget in this simulation; namely, flow between the aquifer and surface-water features. Parameters that control small components of the water budget typically are less sensitive than parameters that control large components of the water budget.

No Flow

Ground-water divides observed in the water-table and lower Tamiami aquifers during March and September 1996 (fig. 22) were represented as no-flow boundary conditions in the predevelopment simulation (pl. 1). Representing a ground-water divide as a no-flow boundary is conceptually consistent with the actual behavior of the divide; ground water on each side of the divide moves away, and no flow crosses the divide (Reilly, 2001).

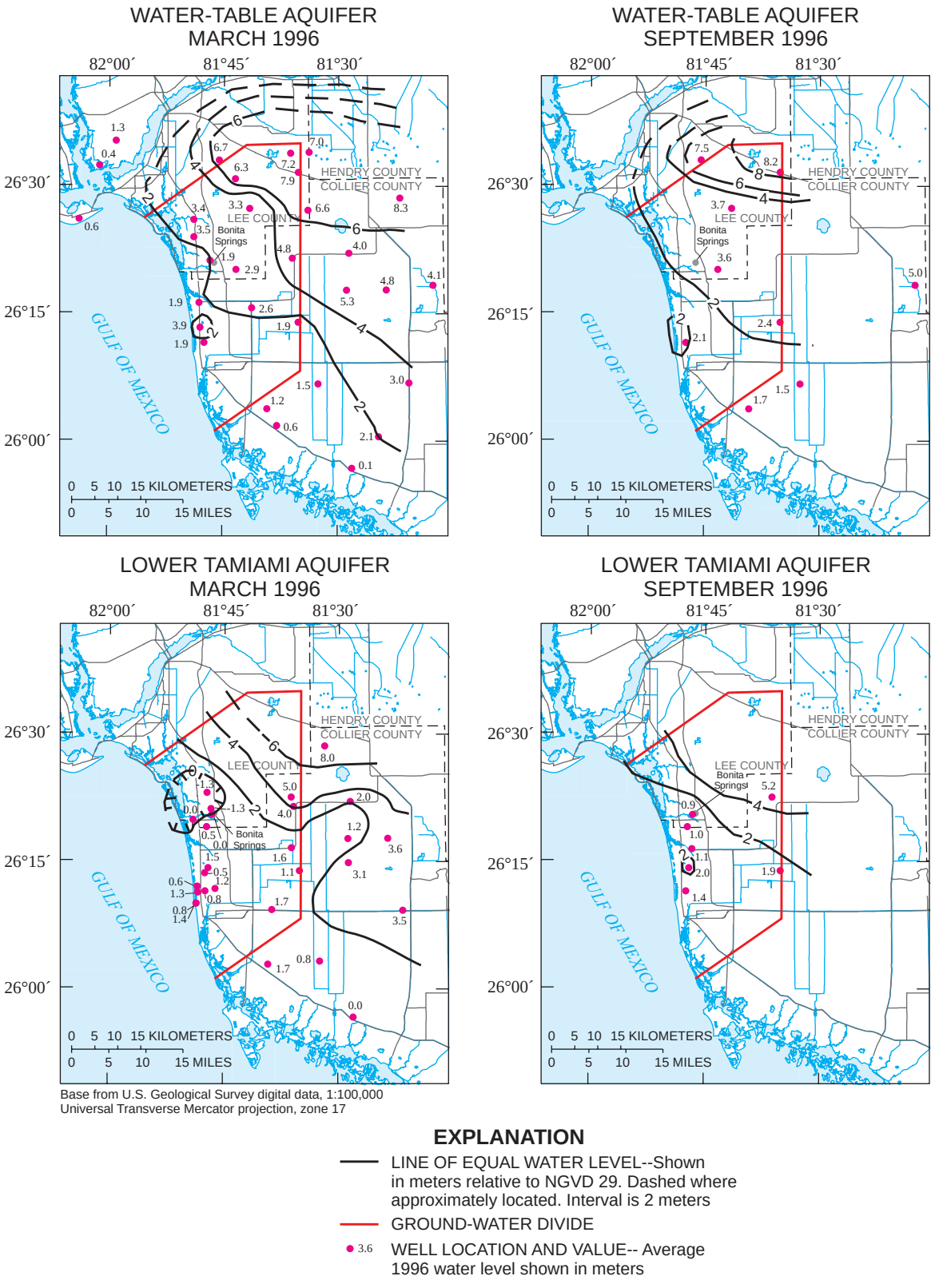

Figure 22. Average monthly water levels in the water-table and lower Tamiami aquifers during March and September 1996. NGVD 29 is National Geodetic Vertical Datum of 1929.

Ground-water divides observed in the water-table and lower Tamiami aquifers during March and September 1996 may or may not have been in the same location in 1930. It seems reasonable to expect that the northern and southern ground-water divides remain relatively stable. Recharge on the Florida Peninsula creates a mound of ground water in aquifers above sea level, resulting in flow from inland areas toward the coast. Additionally, contemporary ground-water withdrawal near these northern and southern divides is less prevalent, resulting in less opportunity for stress to move the location of these divides. The location of the eastern ground-water divide during 1930, however, is more uncertain; in fact, the divide may never have existed. This boundary condition probably is far enough away from the saltwater transition zone in the lower Tamiami aquifer to have little consequence on model results. Regardless, a better method for approximating the location of lateral predevelopment boundary conditions would reduce uncertainty in model results.

Constant Heads and Concentrations

Constant-head boundary conditions were entered into SEAWAT using the IBOUND and Shead arrays of the Basic package (McDonald and Harbaugh, 1988). An integer value less than zero in the IBOUND array of the Basic package indicates that the model cell has a constant-head throughout the simulation. The constant-head value will be equal to a real number entered in the same location of the Shead array of the Basic package. Constant-concentration boundary conditions were entered using the ICBUND array in the Basic Transport package and the Source Sink Mixing package (Zheng and Wang, 1998). An integer value less than zero in the ICBUND array of the Basic Transport package indicates the model cell has a constant concentration equal to a value specified for that model cell in the Source Sink Mixing package.

Constant-concentration boundary conditions were used for layer 1 and along the western boundary of the model in layers 2 to 15 to represent the Gulf of Mexico (pl. 1). The boundary conditions were assigned a constant salt concentration equal to 35 kg/m^3 (the salinity of seawater).

Constant-head boundary conditions were used in layer 1 and along the western boundary of the model in layers 2 to 15 to represent the Gulf of Mexico (pl. 1). Constant-head values representing the Gulf of Mexico in 1930 were assigned by: (1) computing the average value of sea level in 1996 using daily sea level measurements recorded at National Oceanic and Atmospheric Administration (NOAA) station 8725110 (not shown), (2) extrapolating sea level backward to 1930 using the average 1996 value and a 2-mm/yr rate of sea-level rise (National Research Council, 1987), and (3) converting the extrapolated 1930 sea level value to a hydrostatic freshwater equivalent sea level for input to the SEAWAT simulator. On average, sea level in 1996 was about 0.2 m above NGVD 1929. By extrapolating, sea level in 1930 was calculated to be about 0.07 m above NVGD 1929. Hydrostatic freshwater equivalent sea level (h_f) was computed using the following equation:

$$h_f = Z + \frac{\rho}{\rho_f}(h_s - Z) \quad . \tag{12}$$

Z was set to the elevation of the center of the model cell. Fluid density (ρ) was set to 1,025 kg/m^3 (density of saltwater). Extrapolated 1930 sea level (h_s) was computed as 0.07 m. Using the equation and data above, the freshwater equivalent sea level in 1930 was 0.12 m above NVGD 1929 for layer 1 and proportionately greater than 0.12 m at the western boundary of the model in layers 2 to 15 because the elevation of the center of these model cells, Z, is farther below NVGD 1929.

Simulation Results

The predevelopment simulation was run until heads and salinity reached steady state. An evaluation of simulated predevelopment heads (not shown) suggested that the model provides a reasonable representation of coastal ground-water flow. An estimate of the predevelopment distribution of saltwater is obtained by evaluating the solute concentrations simulated by the model.

A three-dimensional view of the predevelopment distribution of saltwater was prepared using Modelviewer, a visualization and animation program (Hsieh and Winston, 2002) (fig. 23). Although this view provides a more complete perspective of the predevelopment distribution of saltwater, it is difficult to visualize how ground-water salinity relates with other prominent features in the study area. Thus, a two-dimensional map showing the intersection of the predevelopment saltwater interface with the base of the lower Tamiami aquifer was prepared (fig. 24).

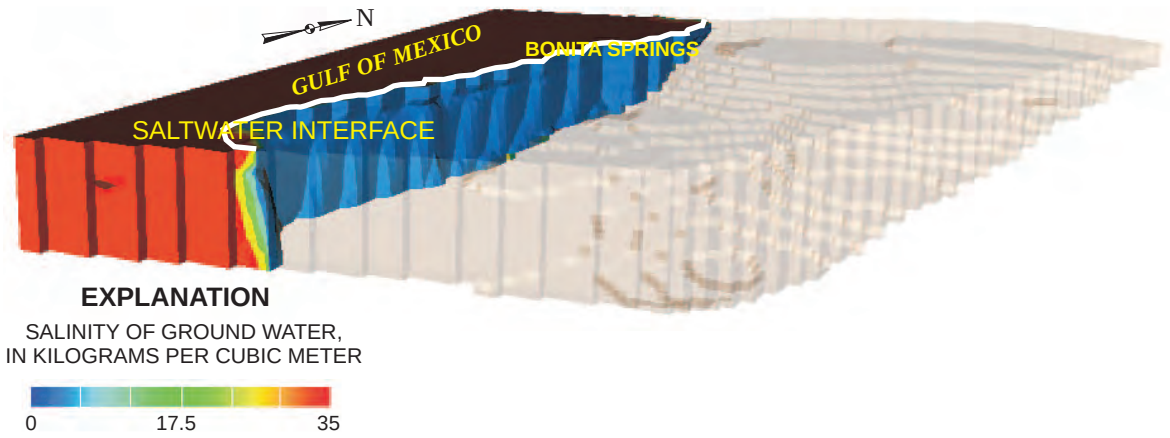

Figure 23. Three-dimensional view of the simulated predevelopment distribution of saltwater. All shaded areas represent active model cells. Blue and tan cells are equivalent in salinity; the tan shading is used to highlight the topography of the base of the lower Tamiami aquifer.

The predevelopment distribution of saltwater consists of a sharp, steep interface that roughly parallels the coast. Near Naples and central Estero Bay, the saltwater interface intersects with the base of the lower Tamiami aquifer directly beneath the coastline. In most other areas, the intersection is as much as 2 km offshore. Model results suggest the interface is directly beneath the coastline in locations where less ground water is discharging to the Gulf of Mexico. Conversely, the interface is farther from the coastline in locations where more ground water is discharging to the Gulf of Mexico. These results appear to be a reasonable estimate of salinity conditions in the water-table and lower Tamiami aquifers prior to modern stresses, such as ground-water development and canal drainage.

Model Calibration to Typical, Modern, and Seasonal Stresses

Model calibration was necessary to move the predevelopment distribution of saltwater to equilibrium with a reasonable representation of March and September 1996 conditions (table 2). The same spatial discretization and aquifer properties previously described were used for calibration. Two steady-state stress periods representing average March and September 1996 conditions were designed. The MODFLOW program was used to simulate ground-water flow.

The calibration objective of this study was to find the combination of model parameters or boundary conditions that best represent March and September 1996 conditions. Boundary conditions were assigned to closely resemble the time periods of interest. The parameter estimation routine, UCODE (Poeter and Hill, 1998), was used to "best fit" simulated heads and flows to their observed equivalents by solving for parameter estimates using a nonlinear least squares regression. The reliability or uncertainty in parameter estimates also was quantified with linear 95-percent confidence intervals.

Boundary Conditions

Boundary conditions for model calibration under March and September 1996 hydrologic conditions include no flow, constant heads, rivers, general heads, rainfall, evapotranspiration, and wells (pl. 2). No-flow boundary conditions were used to represent hydrologic divides and the saltwater interface. Layers 16 and 17 consist entirely of no-flow cells; therefore, these layers are not plotted on plate 2. Constant-head boundary conditions were used to represent the Gulf of Mexico. River boundary conditions were used to

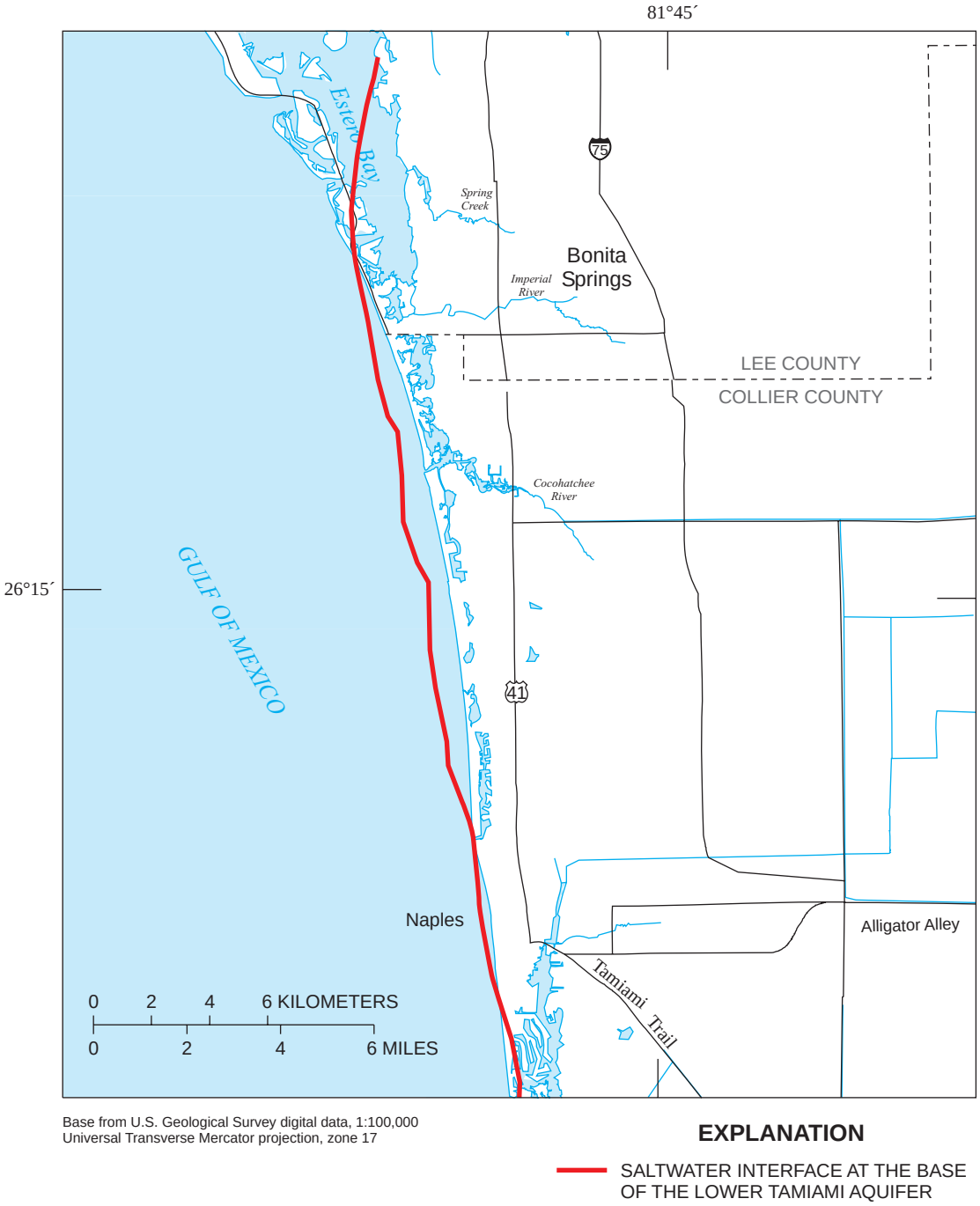

Figure 24. Approximate position of the simulated predevelopment saltwater interface at the base of the lower Tamiami aquifer.

represent local rivers and the system of canals in the southeastern part of the study area. General-head boundary conditions were used to represent deep leakage of ground water to and from the base of the lower Tamiami aquifer. Rainfall and evapotranspiration boundary conditions were used to represent net recharge; however, these boundary conditions are not plotted or labeled on plate 2 for the same reasons they are not plotted on plate 1 as previously mentioned. Well boundary conditions were used to represent ground-water pumpage from the water-table and lower Tamiami aquifers.

No Flow

The Basic package (McDonald and Harbaugh, 1988) was used to set no-flow boundary conditions that represent hydrologic divides and the saltwater interface (pl. 2). The input and mechanics of accomplishing this using the Basic package were previously described. No-flow boundary conditions representing hydrologic divides were assigned to model layers at the northern, eastern, and southern boundaries of the simulation for both steady-state stress periods. These boundary conditions were set using water-level contour maps of the water-table and lower Tamiami aquifers during March and September 1996 (fig. 22).

No-flow boundary conditions representing the saltwater interface in layers 2 to 15 beneath the Gulf of Mexico were set using the predevelopment distribution of saltwater. All model cells west of the 50-percent seawater zone in the predevelopment simulation were designated as no-flow cells in both steady-state stress periods. In systems where density changes abruptly between a freshwater zone and a more dense "salty" zone, the boundary between freshwater and saltwater can be conceptualized as a no-flow boundary condition when movement of the boundary is assumed to be of negligible importance to the problem (Reilly, 2001). Most water-level and flow observations for calibrating the model to March and September 1996 conditions are several kilometers inland with chloride concentrations less than 1,000 mg/L. This suggests the bulk of the saltwater interface has not moved through the vicinity of these observations, and the error in simulated heads and flows will more likely be attributable to uncertainty in rock properties and other boundary conditions, such as recharge, than from the position or movement of saltwater or brackish water with greater fluid density.

Constant Heads

The Constant Head Boundary (CHD) package (Leake and Prudic, 1991) was used to set constant-head boundary conditions that represent the average elevation of sea level in the Gulf of Mexico during March and September 1996. The IBOUND and Shead arrays in the Basic package could not be used because the average elevation of sea level in March 1996 (the first steady-state stress period) is different than the average elevation of sea level in September 1996 (the second steady-state stress period). The IBOUND and Shead arrays of the Basic package can apply only one constant head value entered in the Shead array for the entire length of a simulation.

The CHD package requires the input of the layer, row, column, starting head, and ending head values for the constant-head cell for each stress period. The ARC/INFO coverages of the Gulf of Mexico were overlain with ARC/INFO coverages of the model grid to identify rows and columns of model cells in layer 1 that needed to be constant heads. The starting and ending head values for the first steady-state stress period representing March 1996 were set equal to the average elevation of sea level in the Gulf of Mexico recorded at Naples station 8725110 (about 0.1 m). The starting and ending head values for the second steady-state stress period representing September 1996 were set equal to the average elevation of sea level in the Gulf of Mexico recorded by NOAA station 8725110 (about 0.3 m). By setting the starting and ending head values equal, a constant-head boundary condition was enforced with a different value for each steady-state stress period.

Rivers

The River package (McDonald and Harbaugh, 1988) was used to set river boundary conditions that represent leakage of water to and from the groundwater flow system through surface-water channels (pl. 2). The input and mechanics of the River package (McDonald and Harbaugh, 1988) were previously described. For calibrating the model to March and September 1996 conditions, the River package requires the layer, row, column, h_{riv}, $COND_{riv}$, and *RBOT* for both steady-state stress periods. The layer, row, and column of river cells were determined by overlying ARC/INFO coverages of contemporary surface-water features with the model grid. The USGS or SFWMD surface-water gaging stations, if available, were used to interpolate or extrapolate average March and September 1996 h_{riv} values for both steady-state stress periods. For each river cell, $COND_{riv}$ was computed using equation 9. The value of K_{seds} is assumed to be 15 m/d, which is the vertical hydraulic conductivity used for the water-table aquifer (table 3); the value of b_{seds} was given a reasonable value of 1 m, and the value of *RBOT* was about 2 m less than h_{riv}.

General Heads

The General-Head Boundary (GHB) package (McDonald and Harbaugh, 1988) was used to set general-head boundary conditions that represent the deep leakage of ground water to and from the base of the lower Tamiami aquifer and the sandstone aquifer during March and September 1996 (pl. 2). In MODFLOW-88, the GHB package is one of the most robust packages available for simulating a wide range of boundary conditions. General-head boundaries are head-dependent boundaries where the volumetric flux, Q_{GHB}, is proportional to the head difference between an assigned external head and the approximated head in the model cell. The form of Darcy's law used to characterize the flux is:

$$Q_{GHB} = COND_{GHB}(h_{GHB} - h_{i,\ j,\ k}) , \qquad (13)$$

where $COND_{GHB}$ is the conductance of the general-head boundary [L^2/T], and h_{GHB} is the assigned external head value of the general-head boundary [L].

The conductance value, $COND_{GHB}$, of the general-head boundary was mathematically defined as:

$$COND_{GHB} = \frac{LwK_{GHB}}{b_{GHB}} , \qquad (14)$$

where L is the length of the model cell [L], w is the width of the model cell [L], K_{GHB} is the vertical hydraulic conductivity of the upper Hawthorn confining unit [L/T], and b_{GHB} is the thickness of the upper Hawthorn confining unit [L].

Variables L and w of the model cells were assigned values of 600 m each, and a value of 0.003 m/d was used for K_{GHB} (Montgomery, 1988). A value of 9.14 m was used for b_{GHB}, the average thickness of the upper Hawthorn confining unit reported by Knapp and others (1986). The b_{GHB} could not be spatially variable because no published maps of the thickness of this unit could be found.

The h_{GHB} values were set using contour maps of the potentiometric surface of the sandstone aquifer. Sufficient water-level measurements were obtained for the March 1996 steady stress period, but not for the September 1996 period. To approximately define the potentiometric surface of the sandstone aquifer, water levels at 15 monitoring wells for March 1996 were averaged, plotted, contoured, and interpolated to the h_{GHB}. For the September 1996 period, average water levels at the same 15 monitoring wells were computed, plotted, and contoured to define the average potentiometric surface of the sandstone aquifer for the entire 1996 calendar year. This average surface then was interpolated to the h_{GHB} for the September 1996 steady-state stress period.

Recharge

The Recharge and Evapotranspiration packages (McDonald and Harbaugh, 1988) were used to represent net recharge, or the water applied to land surface through precipitation that exceeds evapotranspiration and runoff and infiltrates through the unsaturated zone to the water table. An areal flux [L/T] of rainfall minus runoff was applied to the highest active cell in a vertical column of layers using the Recharge package (McDonald and Harbaugh, 1988) for both steady-state stress periods. Average monthly rainfall rates were computed from daily rainfall totals collected in 1996 at a rainfall monitoring station near Bonita Springs. The average rainfall rate in March 1996 was about 0.3 cm/d, and the average rainfall rate in September 1996 was about 0.4 cm/d. Runoff was estimated using land-use coefficients developed during previous investigations of the study area (Bennett, 1992). These land-use coefficients suggest 10 to 30 percent of rainfall is converted to runoff during a storm event. The average of land-use coefficients (about 0.127) reported by Bennett (1992) was used to estimate the amount of rainfall lost to runoff during March and September 1996. A weighted average based on the individual area of each land-use type within the total area of the active model domain could not be computed because runoff coefficients for recent land-use maps were not available. As previously mentioned, runoff was subtracted from rainfall, and the resulting areal flux [L/T] was input for both steady-state stress periods in the Recharge package.

Evapotranspiration was simulated using the Evapotranspiration package (McDonald and Harbaugh, 1988), with the evapotranspiration surface set to land surface and an extinction depth set to 5 m at all active cells in the model domain. As previously defined, setting extinction depths to 5 m is a reasonable compromise given the current understanding of the evapotranspiration process in Florida. Maximum evapotranspiration rates were uniformly set across the model grid using free surface pan evaporation data (fig. 25) and a pan multiplier of 0.7 (Swancar and

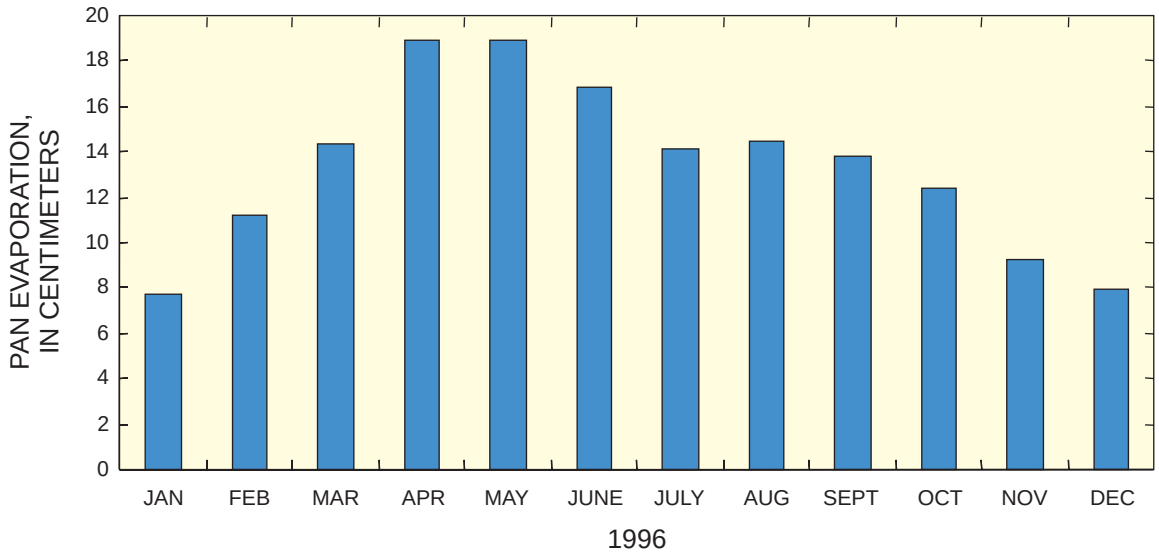

Figure 25. Total monthly pan evaporation from several monitoring stations near Bonita Springs.

others, 2000, p. 42). This means maximum ground-water evapotranspiration rates in the Evapotranspiration package were 70 percent of the average March 1996 pan evaporation rate for the first steady-state stress period and 70 percent of the average September 1996 pan evaporation rate for the second steady-state stress period.

Wells

The Well package (McDonald and Harbaugh, 1988) was used to represent the withdrawal of ground water from the water-table and lower Tamiami aquifers. Well boundaries may be used for injection or extraction wells. The layer, row, column, and injection or extraction volumetric rate are required input for the Well package. The location and volumetric rate of monitored ground-water pumpage were obtained from the SFWMD and translated to the appropriate layer, row, column, and stress period of the model simulation. Well construction information, such as depth to the top of casing and depth to the bottom of the open-hole interval, was used to determine the appropriate model layer in which to place the pumping well. Areas near Bonita Springs that are most likely to withdraw large quantities of unmonitored ground water from the lower Tamiami aquifer also were delineated (fig. 26) with the help of SFWMD personnel. Because this pumpage was unmonitored, volumetric rates and open-hole intervals were not known. The missing pumpage rates were set approximately equal to the monitored ground-water pumpage in March and September 1996. Although this may seem arbitrary, these missing pumpage rates were better estimated with UCODE during model calibration. The open-hole intervals of unmonitored pumping wells were assumed to be present at the center of the lower Tamiami aquifer (pl. 2).

Parameter Estimation

The model was calibrated with the UCODE parameter estimation routine (Poeter and Hill, 1998) to 41 average monthly head and 2 average monthly flow observations computed from USGS monitoring wells and gaging stations, respectively, in the study area (table 4). Each head observation is the average of all measurements made at the well during March or September 1996. Flow observations are the sum of the average of all flow measurements made at the northern and southern branches of the Estero River, Spring Creek, and Imperial River during March and September 1996.

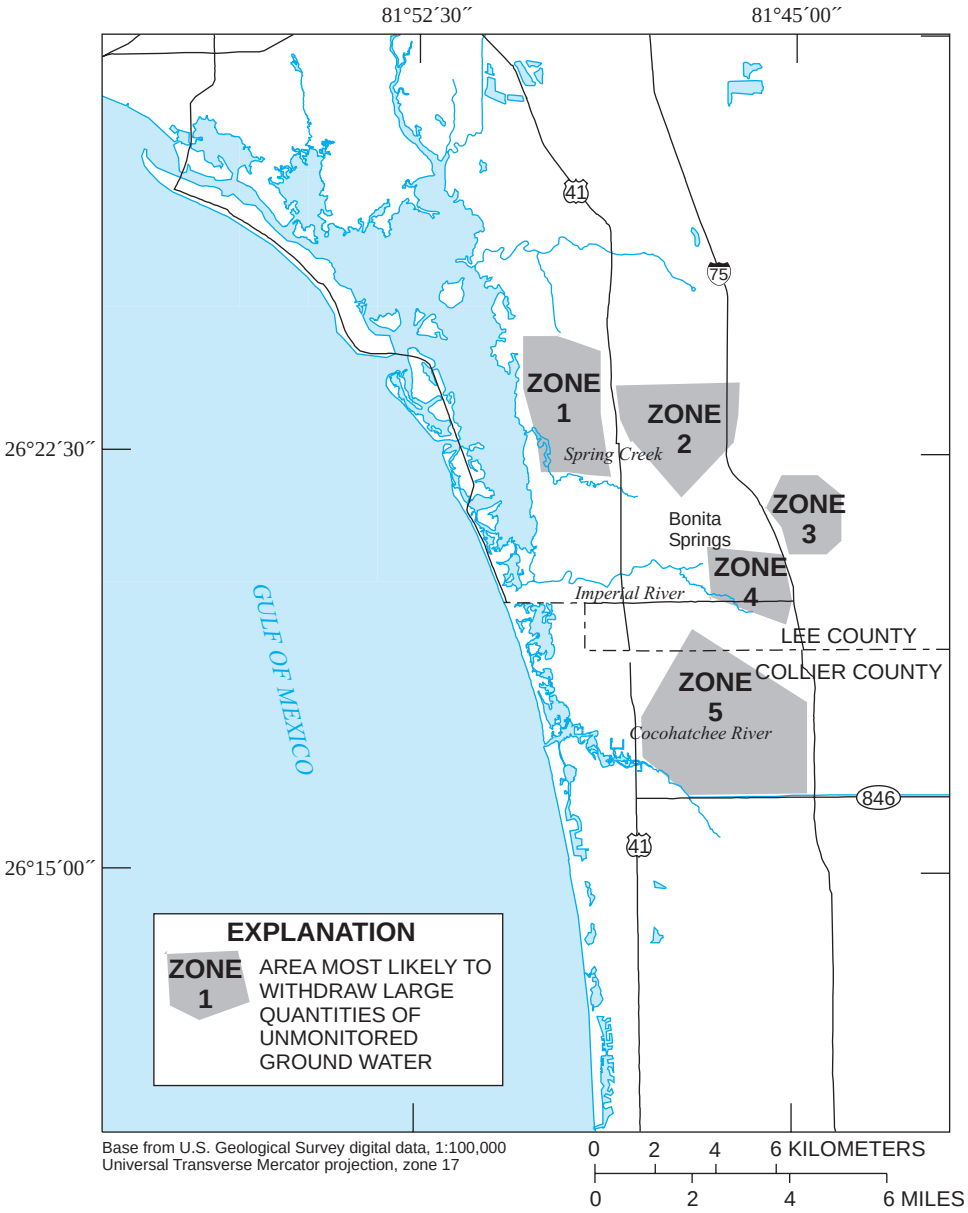

Figure 26. Areas with potentially large quantities of unmonitored ground-water pumpage.

With UCODE, head and flow observations were weighted and summed together with their simulated equivalents as the objective function, *S(b)*,

$$S(b) = \sum_{i=1}^{nh} w_i [h_i - h_i'(b)]^2 + \sum_{i=1}^{nq} w_i [q_i - q_i'(b)]^2 , \qquad (15)$$

where b is a vector containing values of each of the parameters being estimated, nh is the number of head observations, w_i is the weight for the ith observation, h_i is the ith observed water level, $h_i'(b)$ is the simulated equivalent of the ith observed water level (a function of b), nq is the number of flow observations, q_i is the ith observed flow, and $q_i'(b)$ is the simulated equivalent of the ith observed flow (a function of b). UCODE solved for parameter values, b, that minimize this objective function, *S(b)*, resulting in simulated heads and flows that most closely resemble their observed equivalents.

Table 4. Observations used during model calibration to March and September 1996 conditions

[Aquifer: LT, lower Tamiami aquifer; WT, water-table aquifer. USGS, U.S. Geological Survey; N/A, not applicable; QWDATA,Water Quality Database; ADAPS, Automated Data Processing System]

Site identification	Universal transverse mercator coordinates		Aquifer	Date	Average head (meters) or flow[1]	USGS data source
	x (meters)	y (meters)				
C-304	439677	2906341	LT	Mar. 96	1.6	QWDATA
C-391	420917	2897007	LT	Mar. 96	.8	ADAPS
C-391	420917	2897007	LT	Sept. 96	1.4	ADAPS
C-392	420945	2897038	WT	Mar. 96	1.9	ADAPS
C-392	420945	2897038	WT	Sept. 96	2.1	ADAPS
C-430	423141	2897516	LT	Mar. 96	1.2	QWDATA
C-460	421614	2902048	LT	Mar. 96	1.5	ADAPS
C-460	421614	2902048	LT	Sept. 96	2	ADAPS
C-489	420885	2900914	LT	Mar. 96	.5	QWDATA
C-492	439638	2917334	WT	Mar. 96	5	ADAPS
C-492	439638	2917334	WT	Sept. 96	5.3	ADAPS
C-516	419370	2896761	LT	Mar. 96	1.3	QWDATA
C-528	419240	2898054	LT	Mar. 96	.6	QWDATA
C-951	441394	2901359	LT	Mar. 96	1.1	ADAPS
C-951	441394	2901359	LT	Sept. 96	1.9	ADAPS
C-953	441394	2901359	WT	Mar. 96	1.9	ADAPS
C-953	441394	2901359	WT	Sept. 96	2.4	ADAPS
C-977	435395	2892948	LT	Mar. 96	1.7	QWDATA
C-978	440163	2915292	WT	Mar. 96	4.8	QWDATA
C-979	440163	2915292	LT	Mar. 96	4	QWDATA
C-997	431283	2904547	WT	Mar. 96	2.6	ADAPS
C-1004	422249	2906167	LT	Sept. 96	1.1	ADAPS
C-1059	419870	2905711	WT	Mar. 96	1.9	QWDATA
C-1061	420058	2900325	WT	Mar. 96	3.9	QWDATA
C-1083	421307	2910911	LT	Mar. 96	.5	ADAPS
C-1083	421307	2910911	LT	Sept. 96	1	ADAPS
FLOW1	N/A[2]	N/A[2]	N/A	Mar. 96	40,394	ADAPS
FLOW2	N/A[2]	N/A [2]	N/A	Sept. 96	271,820	ADAPS
L-738	422405	2913580	LT	Mar. 96	0	ADAPS
L-738	422405	2913580	LT	Sept. 96	.9	ADAPS
L-1964	439799	2938122	WT	Mar. 96	7.2	QWDATA
L-1999	427787	2932554	WT	Mar. 96	6.3	QWDATA
L-2195	427917	2912841	WT	Mar. 96	2.8	ADAPS
L-2195	427917	2912841	WT	Sept. 96	3.6	ADAPS
L-2308	418735	2923716	WT	Mar. 96	3.4	QWDATA
L-2550	430872	2926115	WT	Mar. 96	3.3	ADAPS
L-2550	430872	2926115	WT	Sept. 96	3.7	ADAPS
L-5722	422255	2914834	WT	Mar. 96	1.9	QWDATA
L-5723	422255	2914834	LT	Mar. 96	-1.3	QWDATA
L-5724	418350	2912528	WT	Mar. 96	2.6	QWDATA
L-5725	418332	2912489	LT	Mar. 96	0	QWDATA
L-5730	418739	2919993	WT	Mar. 96	3.4	QWDATA
L-5747	421417	2918346	LT	Mar. 96	-1.3	QWDATA

[1]Flow shown in meters per day.

[2]Flow observations are the sum of estimated flows at four different locations. These locations (northern and southern branches of the Estero River, Spring Creek, and Imperial River) are discussed in the text.

With UCODE, observations are weighted to: (1) maintain similar dimensions in the objective function so that head and flow residuals can be added together, and (2) emphasize observations that are more or less important to "best fit" with regression. For example, weights can be used to make an accurately measured observation more important to "best fit" and an inaccurately measured observation less important to "best fit." For this study, observations were weighted to: (1) account for the potential measurement error, such as the top-of-casing elevation, down-to-water distance, or instrumentation drift; and (2) account for the potential deviance from the true monthly average.

The variance statistic was used to compute observation weights. A variance was assigned to each observation well to account for the potential measurement errors described above. For convenience, the variance statistic was also used to account for the potential deviance from the true monthly average. This was accomplished by summing the squared differences of individual water-level measurements from the monthly average and dividing by one less than the total number of measurements. At monitoring wells where only one or two depth-to-water measurements were taken during March or September 1996, the average variance of water-level measurements at observation wells with continuous monitoring equipment was used. Using the variance statistic was convenient because variances are additive, and the final variance statistic used to calculate observation weights was the sum of the variance that accounts for measurement error and the variance that accounts for the potential deviance from the true monthly average.

A primary objective of this project was to accurately simulate saltwater movement in the lower Tamiami aquifer beneath Bonita Springs. To accomplish this objective, accurately simulated water levels in this area of the aquifer were necessary. Unmonitored ground-water pumpage created large cones of depression in the lower Tamiami aquifer beneath Bonita Springs. Large discrepancies between observed and simulated water levels initially were present in this area of the model because simulated water levels cannot be drawn down where pumpage data do not exist. For this reason, zones of unmonitored ground-water pumpage with "sufficient" sensitivity were estimated with UCODE, resulting in simulated water levels that closely match observed water levels in important areas near the coast.

Zones of unmonitored ground-water pumpage were determined to have "sufficient" sensitivity by examining composite-scaled sensitivities. Composite-scaled sensitivities (CSS) computed by UCODE are measures of the amount of information that all the observations provide for estimating a parameter (Poeter and Hill, 1998). If a parameter has large CSS, then the observations hold much information for estimating that parameter value. If a parameter has small CSS, then the observations hold little information for estimating that parameter value. Given this relation, the regression performed by UCODE can have difficulty converging on estimates of parameters with small CSS, because very little information is provided by the observations for estimating these parameter values. Thus, only parameters with large or "sufficient" CSS that are not correlated are successfully estimated with UCODE.

Parameter correlation is measured using correlation coefficients calculated as the covariance between two parameters divided by the product of their standard deviations (Hill, 1998). Correlation coefficients range from 1.0 to -1.0, with values close to 1.0 or -1.0 indicating parameters that are correlated or inversely correlated, but cannot be estimated uniquely with the observations used to calibrate a flow model. It is already well established that hydraulic conductivity parameters (K) and flow parameters (Q) representing, for example, recharge or ground-water pumpage are often highly correlated when calibrating a flow model using only hydraulic-head observations (Hill, 1998). Adding flow observations, such as streamflow gains and losses, can greatly reduce correlation of K and Q parameters and result in unique parameter estimates.

Unmonitored ground-water pumpage was correlated with the most sensitive model parameters (evapotranspiration extinction depth, canal conductance, and vertical hydraulic conductivities of the Tamiami confining beds and upper Hawthorn confining unit) as indicated by CSS (fig. 27) and correlation coefficients. This meant that while trying to estimate unmonitored ground-water pumpage with more sensitive model parameters, unique estimates could not be found. This is a disadvantage because: (1) a better regional model fit probably could be attained if the more sensitive model parameters could be estimated; and (2) some of the more sensitive model parameters, such as hydraulic conductivities and canal conductances, probably are more uncertain than the unmonitored ground-water pumpage. However, unique UCODE estimates of

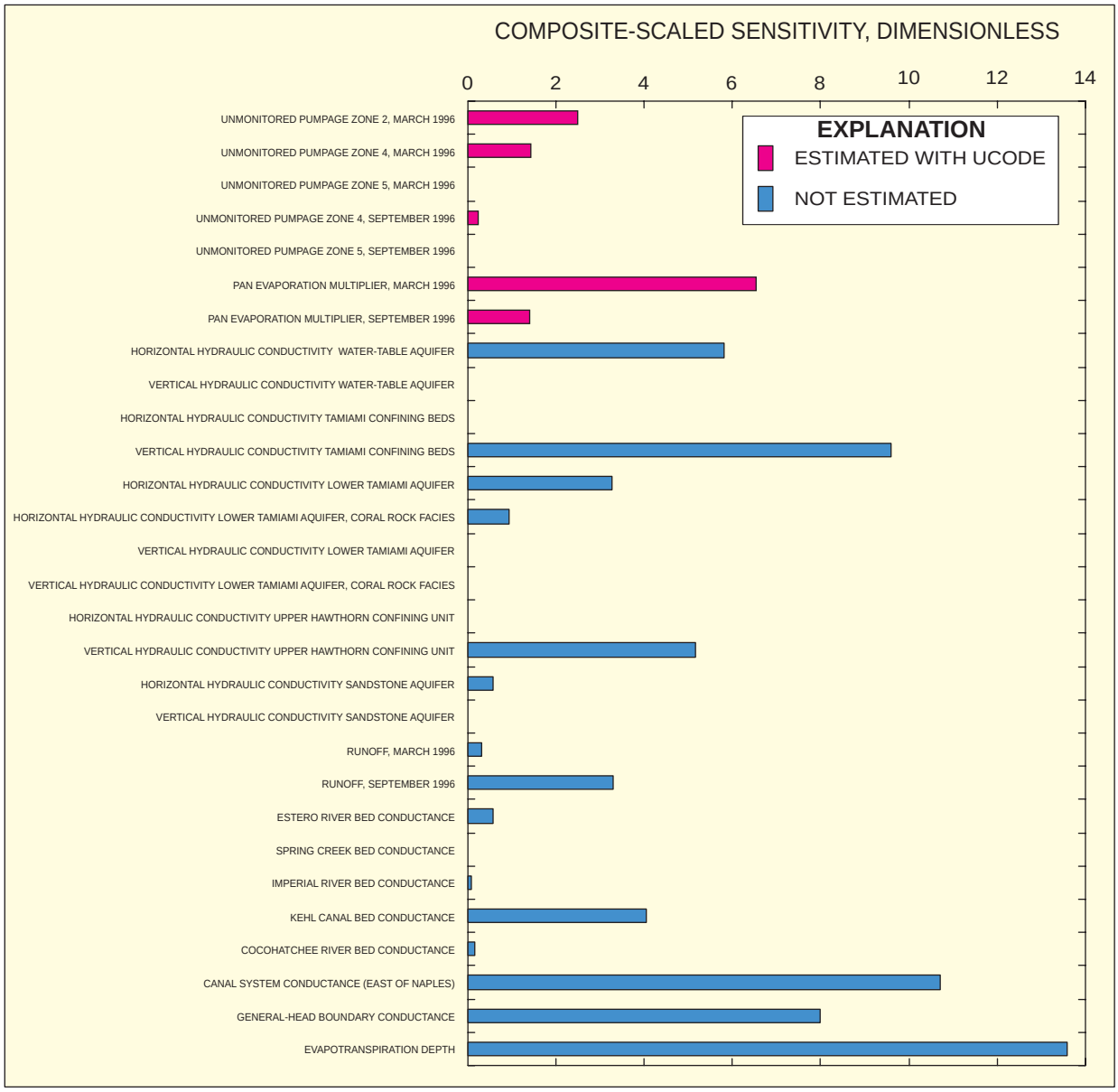

Figure 27. Composite-scaled sensitivities computed while calibrating the model to March and September 1996 conditions. Parameters with no visible bar have very small or zero sensitivity.

unmonitored ground-water pumpage zones with sufficient sensitivity and pan evaporation multipliers were found (table 5). The uniqueness is indicated by UCODE correlation coefficients (table 6) and the fact that final UCODE estimates of these parameters were not sensitive to the parameter starting values.

In the stress period representing September 1996, UCODE estimated a pan evaporation multiplier of 1.13, which means the maximum evapotranspiration rate is about 13 percent larger than the pan evaporation rate. This parameter estimate probably is unreasonable because maximum evapotranspiration rates likely are less than pan evaporation rates in most circumstances. Unreasonable parameter estimates are valuable because they suggest that either the model may not accurately represent some aspect of the physical system (most likely), or there may be an error in the observations used to calibrate the model (Poeter and Hill, 1997).

Table 5. Estimates of unmonitored ground-water pumpage and evapotranspiration multipliers with confidence intervals computed by UCODE

[Parameters are in cubic meters per day, except for evaporation multipliers, which are dimensionless]

Parameter	Parameter estimate	Linear 95-percent confidence interval
Unmonitored pumpage zone 1, March 1996	-1,080	275; -2,440
Unmonitored pumpage zone 4, March 1996	-1,180	1,650; -4,010
Unmonitored pumpage zone 5, March 1996	-6.1	4,450; -4,750
Unmonitored pumpage zone 4, September 1996	-352	4,610; -5,310
Unmonitored pumpage zone 5, September 1996	11	8.26; -30
Pan evaporation multiplier, March 1996	.64	0.78; 0.53
Pan evaporation multiplier, September 1996	1.13	1.46; 0.87

Table 6. UCODE estimated parameter correlation coefficients

Parameter	Unmonitored ground-water pumpage					Pan evaporation multiplier	
	Zone 1 (March 1996)	Zone 4, (March 1996)	Zone 5 (March 1996)	Zone 4, (September 1996)	Zone 5, (September 1996)	March 1996	September 1996
Unmonitored pumpage zone 1, March 1996	1.00						
Unmonitored pumpage zone 4, March 1996	-.15	1.00					
Unmonitored pumpage zone 5, March 1996	.03	-.38	1.00				
Unmonitored pumpage zone 4, September 1996	.00	.00	.00	1.00			
Unmonitored pumpage zone 5, September 1996	.00	.00	.00	.00	1.00		
Pan evaporation multiplier, March 1996	.06	.09	.26	.00	.00	1.00	
Pan evaporation multiplier September 1996	.00	.00	.01	.20	.00	.01	1.00

In this model, rainfall may be overestimated, runoff may be underestimated, hydraulic conductivity may be underestimated, or a combination of these and other errors may exist. It is also possible that a process such as interception that prevents rainfall from reaching the water table is not represented in the model. In any of these circumstances, UCODE would estimate a larger maximum evapotranspiration to compensate for the model error, or the missing process that affects "net recharge." Because maps of "net recharge" looked reasonable and were consistent with field observations by Krulikas and Giese (1995), the model error was not resolved. Although undesirable, the unresolved error was justified because compensating errors in a model representing the various processes that affect "net recharge" can produce "net recharge" rates that are accurate.

When estimating zones of unmonitored ground-water pumpage with sufficient sensitivity and pan evaporation multipliers, the nonlinear least-squares regression performed by UCODE converged by satisfying the sum of the squares residual criteria, which was set to zero difference between parameter estimation iterations. This means the difference in the weighted objective function changed by this amount over three parameter estimation or regression iterations (Poeter and Hill, 1998). A traditional statistic for reporting calibration results is the mean absolute error (MAE), which is calculated by taking the average of the absolute values of the differences between observed and simulated heads. The MAE of the calibration was 0.73 m for the 41 average monthly water-level observations in the water-table and lower Tamiami aquifers. Graphical representations of the model

calibration are made by comparing observed and simulated water levels (fig. 28) and comparing weighted residuals and weighted simulated values (fig. 29). The comparison of weighted residuals and weighted simulated values is presented because this plot may identify model bias or trends that are obscured by the traditional comparison of observed and simulated water levels (Mary Hill, U.S. Geological Survey, written commun., 1999). No bias or trends are obvious on the plot in figure 29. The calibration plots and MAE statistic suggest that the model adequately represents the ground-water flow system in the water-table and lower Tamiami aquifers near Bonita Springs.

A component of the water budget important to water managers is unmonitored ground-water pumpage. Estimates of unmonitored ground-water pumpage zone rates per cell with confidence intervals were computed by UCODE (table 5). By calibrating to March and September 1996 water-level and flow observations, the average 1996 rate of unmonitored ground-water pumpage is bracketed because the rate of unmonitored ground-water pumpage probably is greatest during March 1995 and lowest during September 1995, as evidenced by historical ground-water withdrawals. The average 1996 rate of unmonitored ground-water pumpage can be estimated by: (1) multiplying the UCODE-estimated unmonitored ground-water pumpage rate for each zone by the number of model cells in that zone, (2) summing the total rate of unmonitored ground-water pumpage in March 1996 and September 1996, and (3) computing a weighted average. The weight was based on a 7 to 5 ratio of dry- to wet-season months, a typical southwestern Florida water year (Virogroup, Inc., 1993). Using this method, the average estimated rate of unmonitored ground-water pumpage from the lower Tamiami aquifer was

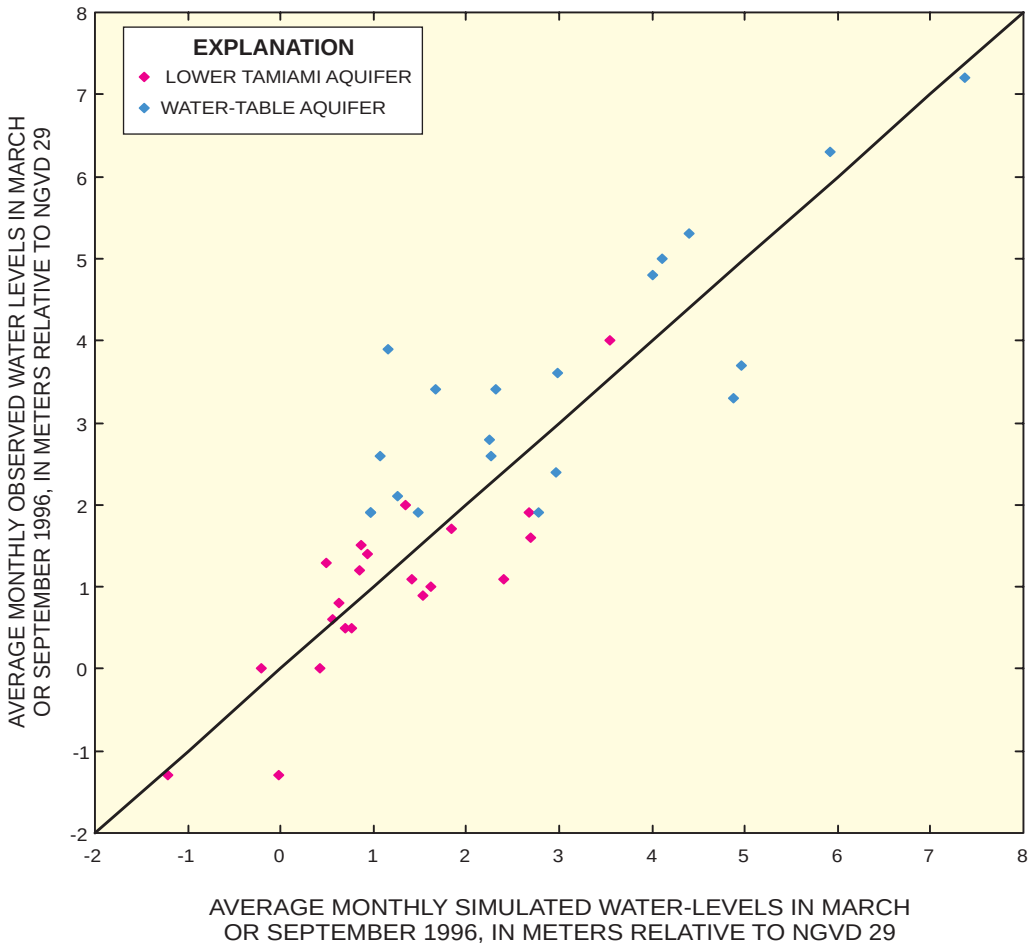

Figure 28. Comparison of observed and simulated water levels. NGVD 29 is National Geodetic Vertical Datum of 1929.

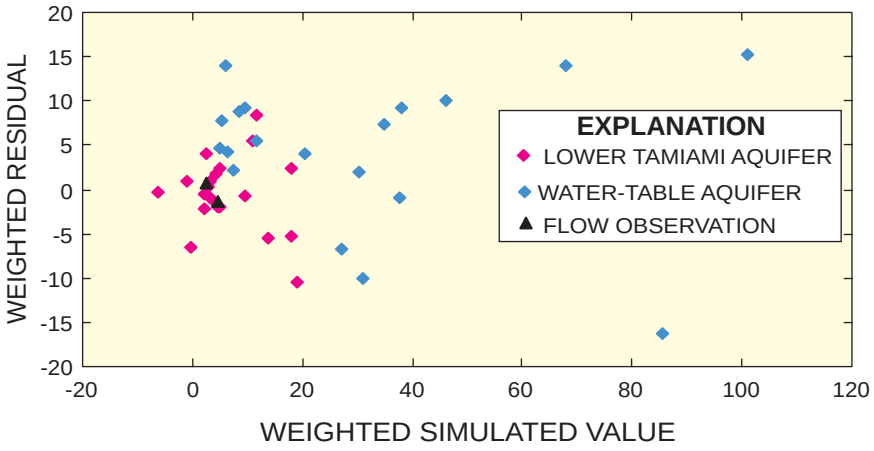

Figure 29. Comparison of weighted residuals and weighted simulated values.

about 52,000 m^3/d in 1996. The average estimated rate of monitored ground-water pumpage from the water-table and lower Tamiami aquifers in the active model domain (pl. 2) was about 59,000 m^3/d in 1996.

A good exercise to test a simulated water budget is to compare simulated net recharge with estimates of net recharge as computed by other methods. Krulikas and Giese (1995) used the chloride concentration ratio and flow-tube analysis methods to estimate net recharge, which ranged from 0 to 25 cm/yr in the study area in 1989. Net recharge maps were prepared for March and September 1996 using the cell-by-cell flow output from the MODFLOW simulations (figs. 30 and 31, respectively). Simulated values of net recharge generally ranged from 0 to 38 cm/yr. Net discharge occurred in small areas as indicated by the negative values shown in figures 30 and 31. One possible explanation for the difference in maximum net recharge rates (field-data computed compared to simulated) is that lowering the water table through pumping between 1989 and 1996 could have induced recharge rates in excess of 25 cm/yr (Krulikas and Giese, 1995).

Topography appears to influence the distribution of net recharge. In fact, simulation results suggest that there are localized areas in the water-table aquifer where net discharge occurs because of the close proximity of the water table to land surface and the effects of evapotranspiration (figs. 30 and 31). These net discharge areas constitute about 5 percent of the active model domain. Net recharge is greater in areas where land surface is relatively higher, such as Bonita Springs and areas south of the Caloosahatchee River along the Immokalee Rise (figs. 1 and 2), because the water table is deeper below land surface and the effects of evapotranspiration are less. The resulting net recharge maps (figs. 30 and 31) reflect the local topography.

Simulated water levels, streamflows, and net recharge rates adequately represent the empirical data describing these hydrologic processes in the study area. However, adequate representation of selected parameters does not ensure the accuracy of predictive simulations (Konikow and Bredehoft, 1992). Nevertheless, calibration or history matching is necessary to reduce errors in the conceptual model and to obtain more representative parameter values, given the scale of simulation.

Confidence Intervals

Linear 95-percent confidence intervals are one of the many useful statistics computed by UCODE during model calibration. Linear 95-percent confidence intervals were calculated for each UCODE estimated parameter, and represent a range that has a 95-percent probability of containing the true value if the model correctly represents the true ground-water flow system (Hill, 1998). The width of a confidence interval can be thought of as a measure of the likely precision of the parameter estimate. Wide intervals indicate less precision or more uncertainty, and narrow intervals indicate more precision or less uncertainty.

The linear 95-percent confidence intervals are wide for estimates of unmonitored ground-water pumpage and narrow for estimates of pan evapotranspiration multipliers (table 5). This suggests unmonitored ground-water pumpage rates are estimated with

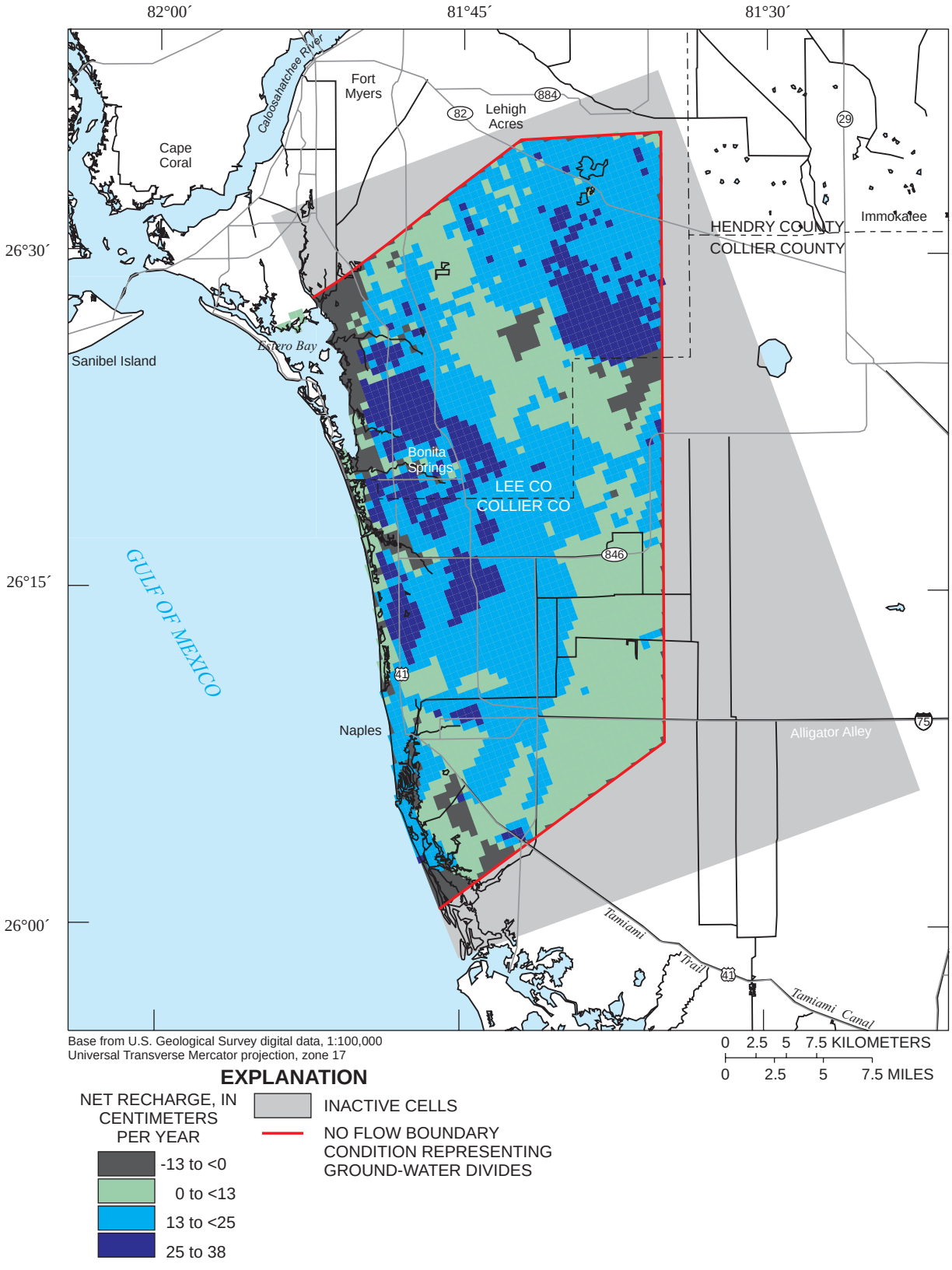

Figure 30. Simulated net recharge to the water-table aquifer during March 1996.

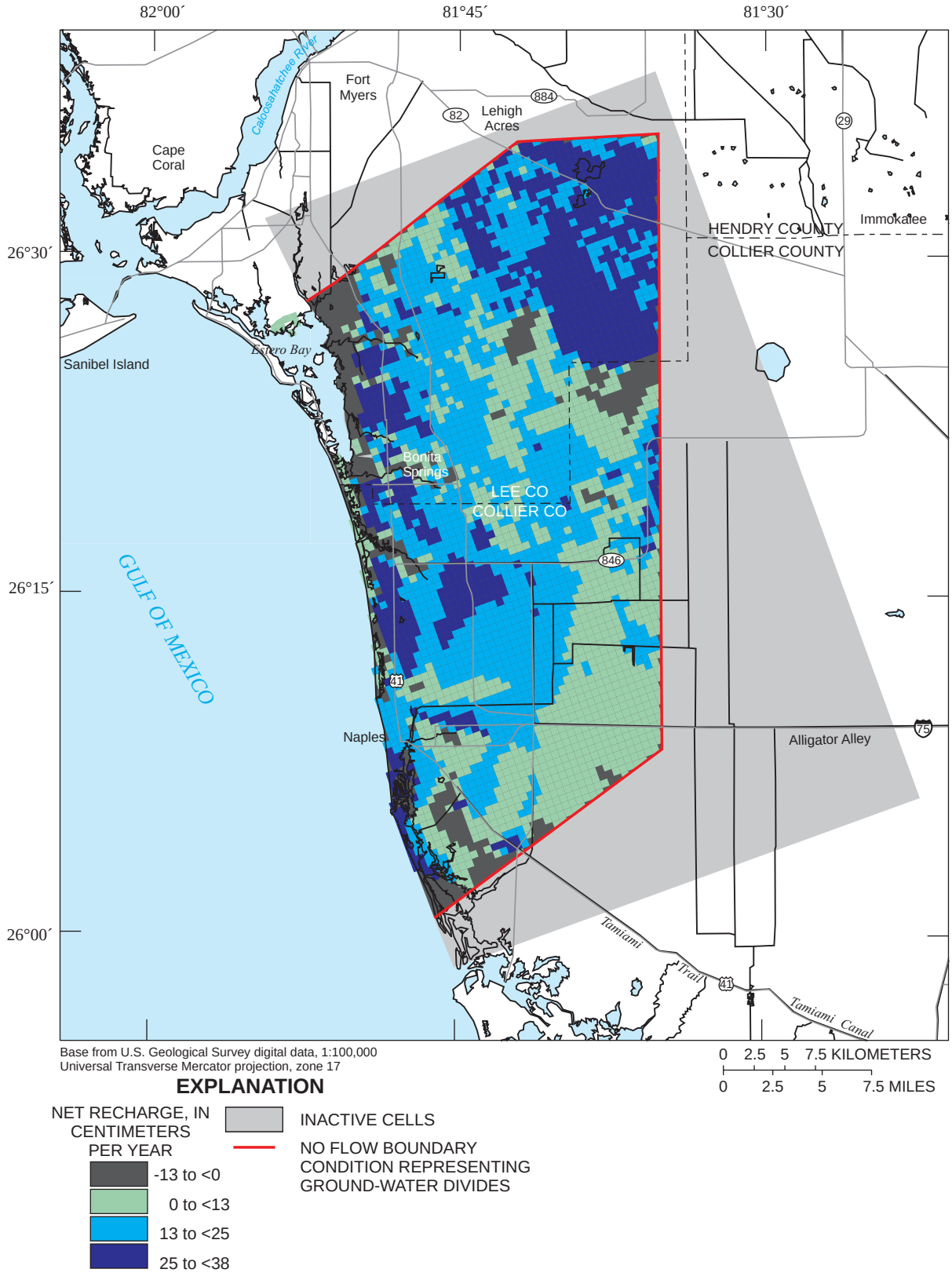

Figure 31. Simulated net recharge to the water-table aquifer during September 1996.

less precision or more uncertainty than pan evaporation multipliers. The design of the USGS network of monitoring wells and streamgaging stations in the study area apparently provides more information on estimating pan evaporation multipliers than estimating unmonitored ground-water pumpage rates. Conversely, one could also say that the pan evaporation parameters explain more of the water-level and discharge data monitored by the network than does the unmonitored ground-water pumpage.

Potential Movement of Saltwater to Equilibrium with Typical, Modern, and Seasonal Stresses

The predevelopment distribution of saltwater was moved to dynamic equilibrium with calibrated March and September 1996 steady-state stress periods (table 2). The same spatial discretization and aquifer properties previously described were used. Calibrated March and September 1996 steady-state stress periods were run successively until saltwater entering and leaving the simulation was about equal, which took about 600 years, or 1,200 steady-state stress periods. The SEAWAT program (Guo and Langevin, 2002) was used with initial conditions that consisted of the final distribution of freshwater equivalent head and salinity in the predevelopment simulation. The primary use of this simulation was to provide a baseline scenario to help identify potential mechanisms of saltwater intrusion and to estimate the potential extent of saltwater intrusion at dynamic equilibrium with modern stresses. Sensitivity analyses were performed for each of these primary objectives using the baseline scenario results.

In general, boundary conditions for this simulation are the same as boundary conditions used while calibrating the model to March and September 1996 conditions (pl. 2). The UCODE estimates of unmonitored ground-water pumpage and pan evaporation multipliers (table 5) were used. Some minor modifications to boundary conditions were necessary.

- Conversion of constant-head boundary conditions (pl. 2) to freshwater equivalent constant-head boundary conditions in the Gulf of Mexico, and conversion of the external heads of general-head boundary conditions (pl. 2) to freshwater equivalent external heads at the base of the lower Tamiami aquifer. These conversions were accomplished using chloride concentrations measured in the field, where data were available.
- Assignment of a constant concentration boundary equal to 35 kg/m^3 (salinity of seawater) in layer 1 at the Gulf of Mexico (pl. 2).
- Assignment of a constant-concentration boundary equal to 35 kg/m^3 (salinity of seawater) in layers 2 to 15 at the westernmost column (column 1) in and beneath the Gulf of Mexico (pl. 1).
- Removal of the no-flow boundary condition used in layers 2 to 15 to represent the saltwater interface (pl. 2).
- Assignment of a salinity value of 0.3 kg/m^3 to water entering the model from the general-head boundary condition at the base of the lower Tamiami aquifer. This was based on limited water-quality data from the sandstone aquifer (pl. 2).

Baseline Scenario

The final distribution of saltwater in the baseline scenario (fig. 32) supports two mechanisms of

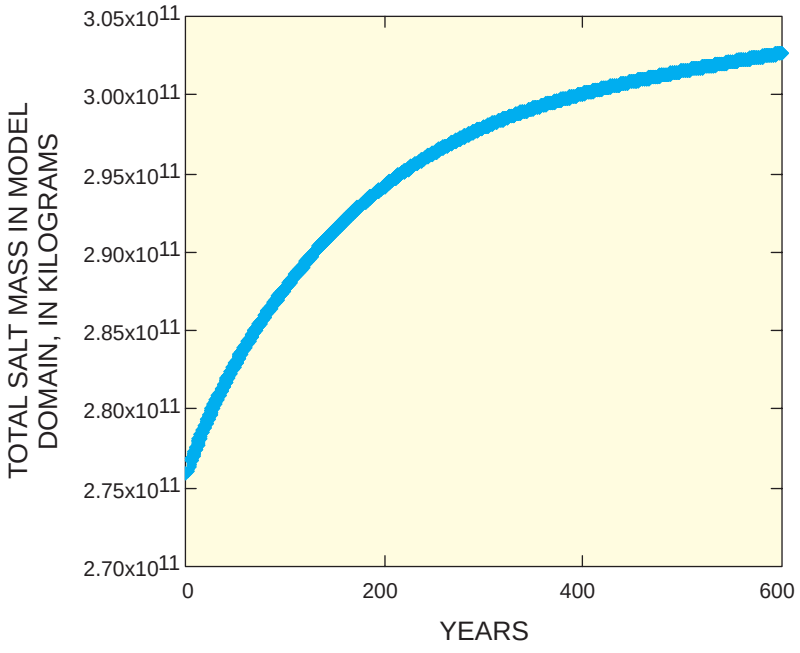

Figure 32. Total salt mass in the model while moving the simulated predevelopment distribution of saltwater to equilibrium with calibrated March and September 1996 conditions.

saltwater intrusion in the lower Tamiami aquifer near Bonita Springs—upconing and lateral saltwater intrusion. Results from the baseline scenario were used to estimate the potential extent of saltwater intrusion in the lower Tamiami aquifer beneath Bonita Springs.

Mechanisms of Saltwater Intrusion

The baseline scenario suggests that upconing of saltwater is the most predominant saltwater intrusion mechanism in the lower Tamiami aquifer beneath Bonita Springs (figs. 33 and 34). Predominance was

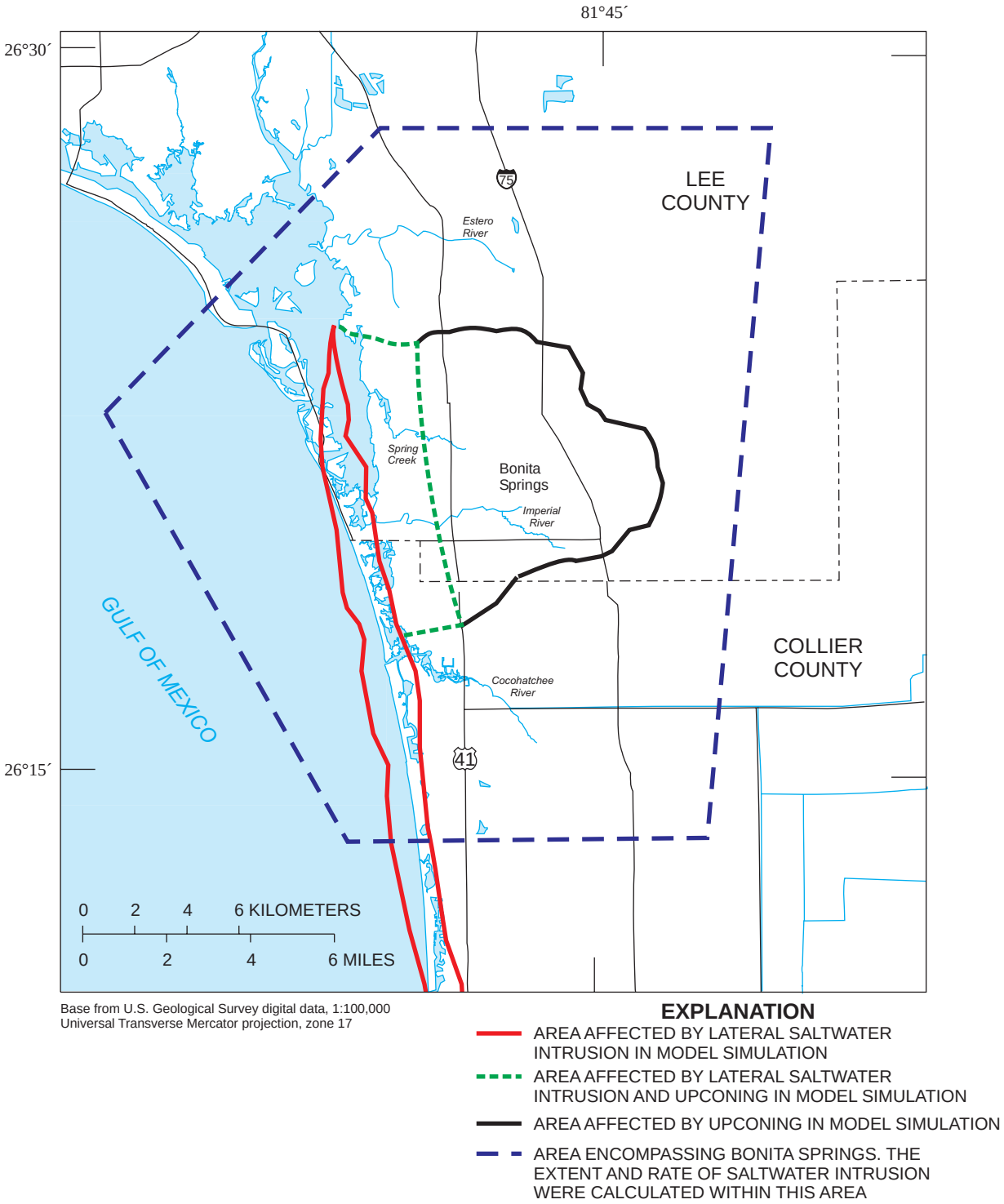

Figure 33. Simulated potential extent of saltwater intrusion in the lower Tamiami aquifer from the baseline scenario near Bonita Springs.

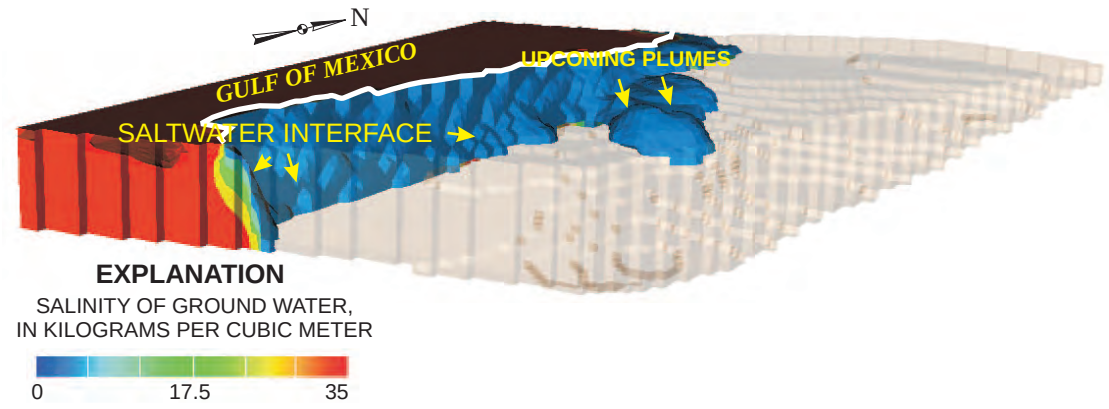

Figure 34. The saltwater interface and upconing plumes near equilibrium with calibrated March and September 1996 conditions in the water-table and lower Tamiami aquifers near Bonita Springs. The upconing plumes are directly beneath Bonita Springs. All shaded areas represent active model cells. Blue and tan cells are equivalent in salinity; the tan shading is used to highlight the topography of the base of the lower Tamiami aquifer.

established by identifying the saltwater intrusion mechanism that affected the largest inland area. A plume of higher salinity ground water (encompassing about 100 km^2 in area) developed in the lower Tamiami aquifer near Bonita Springs after 600 years of transport with calibrated March and September 1996 conditions. By animating model results, it was determined that this plume of higher salinity ground water developed from upconing of ground water in the underlying sandstone aquifer.

The baseline scenario suggests that lateral encroachment is the second most predominant mechanism of saltwater intrusion in the lower Tamiami aquifer near Bonita Springs (figs. 33 and 34). The saltwater interface in the lower Tamiami aquifer near Bonita Springs moved about 1.5 km inland from its predevelopment position after 600 years of transport with calibrated March and September 1996 conditions. As a result, the rate of lateral encroachment averaged about 2.5 m/yr, which is the total distance that the saltwater interface moved (1.5 km) divided by the time length of the baseline scenario (600 years). Additionally, the baseline scenario suggests that lateral encroachment into the potentiometric depression (fig. 22) of the lower Tamiami aquifer was hindered by the presence of a ground-water mound located between the saltwater interface and the potentiometric depression (fig. 35). This simulated ground-water mound seems to force freshwater toward the coast and prevents further lateral encroachment. No field data are available, however, to verify the presence of the simulated mound. If it were shown through the collection of additional field data that the mound does not exist, then the effects of lateral encroachment may be much more severe.

Extent of Saltwater Intrusion

The extent of saltwater intrusion is defined herein as the areal or volumetric movement of saltwater from the predevelopment distribution to equilibrium with calibrated March and September 1996 conditions. Because Bonita Springs was the main area of concern, the extent of saltwater intrusion was computed for a subarea centered on Bonita Springs (fig. 33). The baseline scenario suggests that the areal extent of saltwater intrusion at the base of the lower Tamiami aquifer is about 100 km^2, and the volumetric extent of saltwater intrusion is about 70,000 hectare-meters (fig. 34). The volumetric extent of saltwater intrusion was computed using the same subarea, vertically extended only through the active cells representing the lower Tamiami aquifer. Within this volume, the extent of saltwater intrusion was computed by: (1) summing the volume of cells in the lower Tamiami

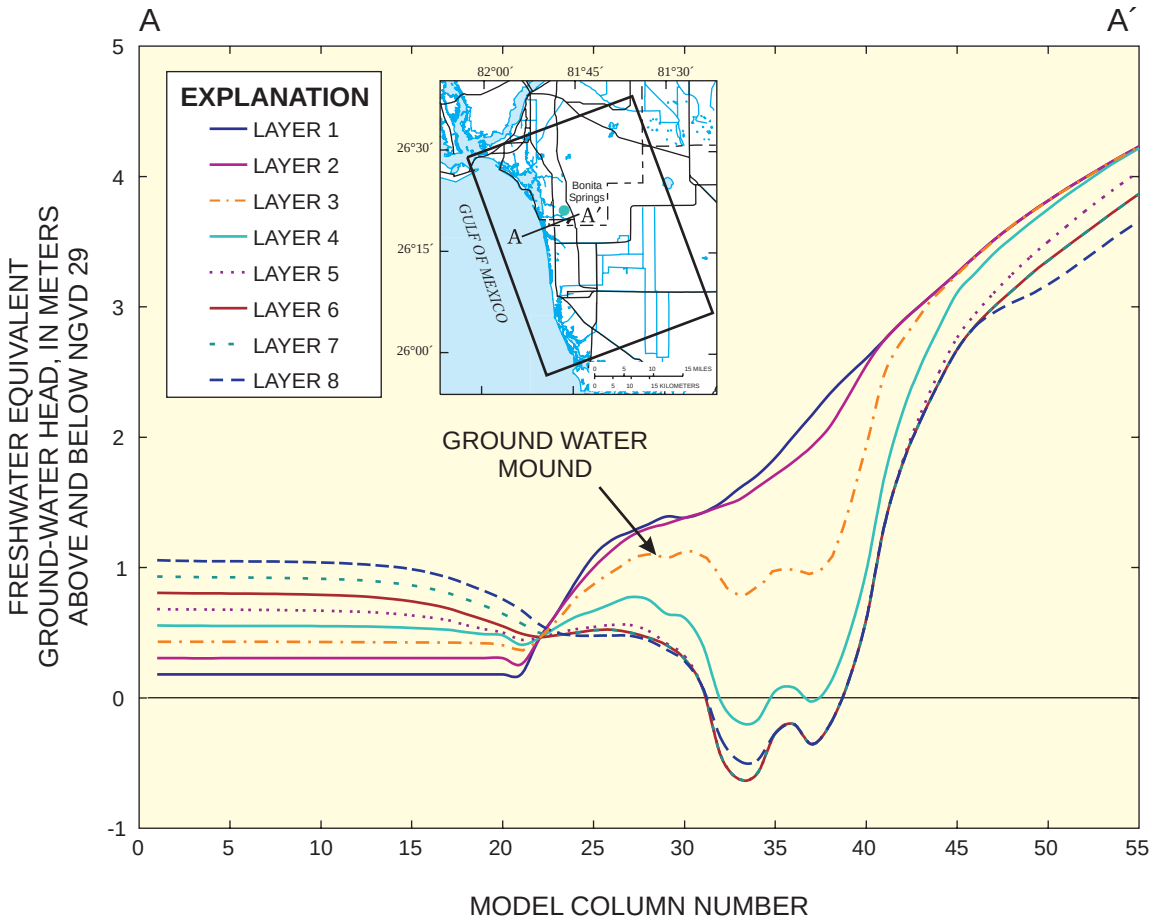

Figure 35. Cross section A-A' along row 40 of the model grid showing a mound of ground water between the cones of depression in the lower Tamiami aquifer and the saltwater interface.

aquifer with a salinity value less than the potable limit (a chloride concentration of about 250 mg/L) in the predevelopment distribution of saltwater, (2) summing the volume of cells in the lower Tamiami aquifer with salinity values less than the potable limit in the baseline scenario, and (3) subtracting the two volumes to isolate a volumetric extent of saltwater intrusion.

Areas affected by saltwater intrusion in the baseline scenario (fig. 33) coincide with areas that seem to be affected by saltwater intrusion as indicated in isochlor maps created by Schmerge (2001) and Knapp and others (1986) (fig. 16). There are discrepancies, however, between simulated salinities and salinities measured at the same location in the field. Possible causes of these discrepancies include that: (1) dispersive solute transport was not performed in the baseline scenario, and (2) the model was run for 600 years with 1996 conditions, so the results cannot be directly compared.

Sensitivity Analyses

The two goals of sensitivity analysis were to: (1) determine how uncertainty in the baseline scenario parameters and boundary conditions may affect solution results, and (2) determine which parameters and boundary conditions in the baseline scenario are most important to solution results. The phrase "important to solution results" is used rather than "influential on solution results" because *influence* has a specific statistical meaning related more to the occurrence and leverage characteristics of the observations used

during calibration. Solution results of primary interest for this study include mechanisms of saltwater intrusion and the potential extent of saltwater intrusion. Thus, sensitivity analyses were performed for both of these primary objectives. If the primary objective could be easily quantified, the two goals of sensitivity analyses (as stated above) were more completely accomplished. For example, the extent of saltwater intrusion was relatively easy to quantify in three dimensions; therefore, parameter values and parameter uncertainties most important to this primary objective were more easily determined.

Mechanisms of Saltwater Intrusion

The sensitivity analyses, described in this section, were used to help identify mechanisms of saltwater intrusion into the lower Tamiami aquifer near Bonita Springs. Identifying predominant mechanisms of saltwater intrusion was a difficult objective to quantify; therefore, sensitivity analysis scenarios were designed instead of using quantitative prediction-scaled sensitivities (PSS) as done by Poeter and Hill (1998). Two sensitivity analysis scenarios were designed to evaluate potential mechanisms of saltwater intrusion without changing simulated heads and flows from their calibrated values. It is important to maintain simulated heads and flows near observed values during sensitivity analyses so the model still resembles the system being studied (Poeter, 2001).

Sensitivity scenario 1 was designed to test the potential for downward leakage of saltwater from a tidal canal or river. This scenario was conducted by modifying the river boundary conditions in the baseline scenario. Unlike the baseline scenario, river cells (pl. 2) in sensitivity scenario 1 were assigned a salinity value of 35 kg/m^3 in an area about 8 to 16 km inland from the Gulf of Mexico along Spring Creek and the Estero, Imperial, and Cocohatchee Rivers (fig. 1). The MAE of water-level observations was 0.73 m using this modification to river-cell boundary conditions, which is the same as the MAE of water-level observations without this modification to river-cell boundary conditions. This suggests the modification did not substantially change heads from their calibrated values. Additionally, simulated baseflow was not substantially different from its calibrated value.

After 600 years of advective solute transport with the river modification noted above, the distribution of saltwater in the lower Tamiami aquifer is identical to the distribution of saltwater in the lower Tamiami aquifer in the baseline scenario (fig. 36). Ground-water flow vectors in sensitivity scenario 1 suggest baseflow from the aquifer to the river prevents salt in the river cells from leaking downward into the water-table aquifer and, subsequently, into the lower Tamiami aquifer. Field reconnaissance along the headwaters of the Imperial River during July 2000 confirmed the presence of baseflow from the aquifer to the Imperial River. Gaging stations on the northern and southern branches of the Estero River, Spring Creek, and Imperial River record flow during the dry season, suggesting ground water flows from the water-table aquifer to these rivers or creeks even in times of drought.

Sensitivity scenario 2 was designed to test a leaky artesian well as a mechanism of saltwater intrusion in the lower Tamiami aquifer near Bonita Springs. This scenario was conducted by modifying a general-head boundary condition at the base of the lower Tamiami aquifer in one model cell (layer 7, row 38, column 28). This single general-head boundary cell was modified to represent a hypothetical leaky artesian ground-water well with connection to the lower Hawthorn producing zone (fig. 3). The external head for the general-head boundary was set to the average of water levels measured in well L-2310 (fig. 36) (Prinos and others, 1996). This well has casing that is open to the lower Hawthorn producing zone. During March and September 1996, average water levels in well L-2310 were adjusted for freshwater equivalence using a salinity value of 1.3 kg/m^3, which is similar to salinity values measured in the lower Hawthorn producing zone by Reese (2000). The conductance term for the general-head boundary was computed using the area of a 0.1-m diameter well and a hydraulic conductivity of 1 x 10^6 m/d. The high value of hydraulic conductivity is considered large enough to transmit water (like a leaky well would transmit) from the lower Hawthorn producing zone to the base of the lower Tamiami aquifer. The salinity of the general-head boundary, representing the lower Hawthorn producing zone locally, was set to the salinity value used to adjust average measured water levels for freshwater equivalence (1.3 kg/m^3). The MAE of water-level observations was 0.71 m using this modification to represent a leaky well, which was slightly less than the MAE to water-level observations without this modification.

The distribution of saltwater at the base of the lower Tamiami aquifer, after 600 years of advective solute transport using the general-head boundary mod-

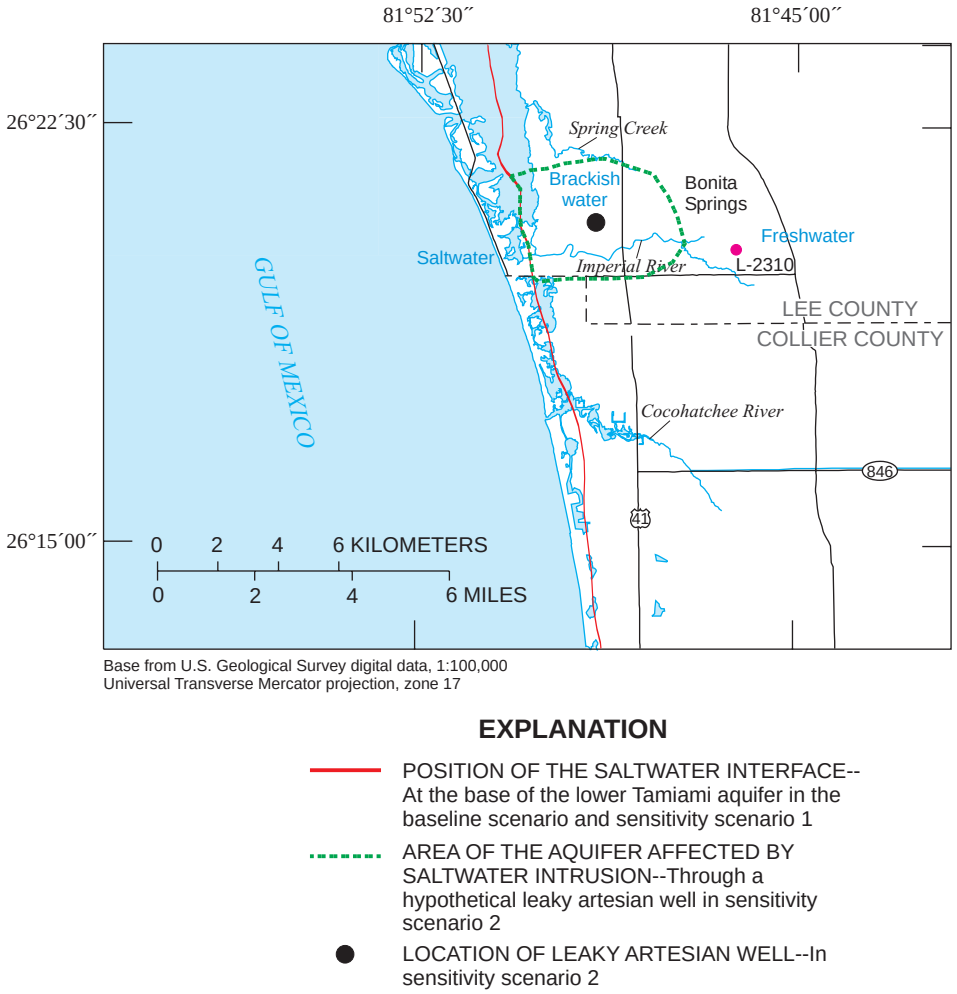

Figure 36. Distribution of saltwater at the base of the lower Tamiami aquifer at the end of the baseline scenario, and two sensitivity analysis scenarios.

ification noted above, is quite different than the distribution of saltwater at the base of the lower Tamiami producing zone in the baseline scenario (fig. 36). The different distribution of salinity suggests leaky wells with connection to the lower Hawthorn producing zone could transport large amounts of saltwater into areas of the lower Tamiami aquifer previously occupied by fresher ground water. These results probably have a physical basis because leaky artesian wells have often been identified as sources of saltwater intrusion in shallow aquifers in southwestern Florida (Burns, 1983; Schmerge, 2001).

Extent of Saltwater Intrusion

The sensitivity analyses, described in this section, were used to help identify the parameters and parameter uncertainties most important to estimating the extent of saltwater intrusion in the lower Tamiami aquifer near Bonita Springs (table 7). Estimating the extent of saltwater intrusion was an objective relatively easy to quantify; therefore, quantitative PSS (Hill, 1998) were computed instead of using sensitivity analysis scenarios. PSS allow parameters to be ranked by relative importance. Furthermore, the contribution of uncertainty in a given input parameter to the overall uncertainty in a model increases as sensitivity coefficients increase (Zheng and Bennett, 2002). As discussed, these sensitivity coefficients are analogous to the PSS that are computed and described herein. Thus, the main contributors of uncertainty to estimating the extent of saltwater intrusion in the lower Tamiami aquifer may be identified by the PSS presented herein.

Table 7. Changes made to baseline scenario parameters for a sensitivity analysis of the extent of saltwater intrusion in the lower Tamiami aquifer near Bonita Springs

Parameter	Change from baseline scenario
Sea level	Increased by 5 percent
Elevation of general-head boundary	Increased by 5 percent
River bottoms	Increased by 5 percent
Runoff for March 1996	Increased by 2.54 centimeters
Potentiometric surface of the sandstone aquifer	Increased by 0.5 meters
Ground-water pumpage	Increased by 10 percent
Horizontal hydraulic conductivity of water-table aquifer	Increased by 700 meters per day
Vertical hydraulic conductivity of Tamiami confining beds	Increased by 0.005 meter per day
Runoff September 1996	Increased by 2.54 centimeters
Horizontal hydraulic conductivity, zone 1, lower Tamiami aquifer	Increased by 130 meters per day
Salinity in sandstone aquifer	Increased by 0.3 kilogram per cubic meter
Horizontal hydraulic conductivity, zone 2, lower Tamiami aquifer (coral reef facies)	Increased by 170 meters per day
Vertical hydraulic conductivity of upper Hawthorn confining unit	Increased by 0.006 meter per day
Horizontal hydraulic conductivity of sandstone aquifer	Increased by 80 meters per day
River and canal stages	Increased both by 0.05 meter per day
River salinity	Increased by 0.3 kilogram per cubic meter
Pan evaporation multiplier for March 1996	Increased by 5 percent
Pan evaporation multiplier for September 1996	Increased by 5 percent
General-head boundary conductance	Increased by 100 percent
River conductance	Increased by 100 percent
Effective porosity	Decreased by 20 percent

The PSS were calculated using the volumetric estimate rather than the areal estimate of the extent of saltwater intrusion in the baseline scenario. The volumetric estimate is more representative of the extent of saltwater intrusion that would be observed in the real ground-water flow system near Bonita Springs (saltwater moves in three dimensions). The PSS were computed as:

$$PSS = (\Delta PD/\Delta B)(B/100)(100/PD), \qquad (16)$$

where ΔPD is the change in the volumetric extent of saltwater intrusion from the baseline scenario, ΔB is the perturbation of the parameter; B is the parameter value in the baseline scenario; and PD is the volumetric extent of saltwater intrusion in the baseline scenario. The resulting statistic is the ratio of the fractional change in the volumetric extent of saltwater intrusion after 600 years of transport to the fractional change in the parameter value.

Preliminary attempts to save time by shortening the time length of the baseline scenario (600 years) and, thus, the time length of PSS runs, resulted in zero sensitivity for many parameters because the change in the volumetric extent of saltwater intrusion (ΔPD) remained the same as the volumetric extent of saltwater intrusion in the baseline scenario (PD). Additionally, zero sensitivity was computed when parameter perturbations (ΔB) were too small. In theory, PSS should approach an exact value as the size of parameter perturbations (ΔB) decrease. However, Poeter and Hill (1998) explain that small parameter perturbations (ΔB) could result in zero sensitivity because, for instance, the volumetric extent of saltwater intrusion under small parameter perturbations (ΔB) could remain the same as the volumetric extent of saltwater

intrusion in the baseline scenario (*PD*) within the accuracy of the model output. Under this circumstance, ΔPD in equation 16 would be equal to zero, resulting in zero sensitivity. Conversely, parameter perturbations (ΔB) that are too large can result in inaccurate PSS because simulated heads and flows may no longer be near observed values, resulting in a model that no longer resembles the system being studied. Parameter perturbations listed in table 7 were determined based on this information.

Because the equations used to compute the extent of saltwater intrusion may be nonlinear with respect to some parameter values, the PSS can change with different perturbations in the parameter value (ΔB) (table 7). This change is described in more general terms by Zheng and Bennett (2002). Based on this description, it is also expected that if the equations used to estimate the extent of saltwater intrusion are linear with respect to a parameter value (B), then the different perturbations in the parameter value (ΔB) will result in the same PSS.

Apparently, runoff, pan evaporation multipliers, ground-water pumpage, sea level and salinity of the Gulf of Mexico, and the potentiometric surface of the sandstone aquifer (when ranked by PSS) are most important for estimating the extent of saltwater intrusion near Bonita Springs (fig. 37). Future efforts at estimating the extent of saltwater intrusion in this location would likely benefit from improved representation of these stresses and boundary conditions. For simplicity of reporting and communicating results, the sensitivity of evapotranspiration parameters and runoff can be grouped into net recharge, although it is notable that dry-season sensitivities for these two processes are higher than wet-season sensitivities (fig. 37). When trying to estimate the extent of saltwater intrusion in the lower Tamiami aquifer near Bonita Springs, determination of net recharge during the dry season apparently is more important than during the wet season. This may be because the dry season generally comprises more days of a total year than the wet season.

The CSS that were computed during calibration (fig. 27) were compared with the PSS that were computed during sensitivity analysis of the extent of saltwater intrusion at equilibrium in the lower Tamiami aquifer near Bonita Springs (fig. 37). The CSS of evapotranspiration parameters and runoff can be grouped together to emphasize that observed conditions near Bonita Springs provided the most information for estimating net recharge. Additionally,

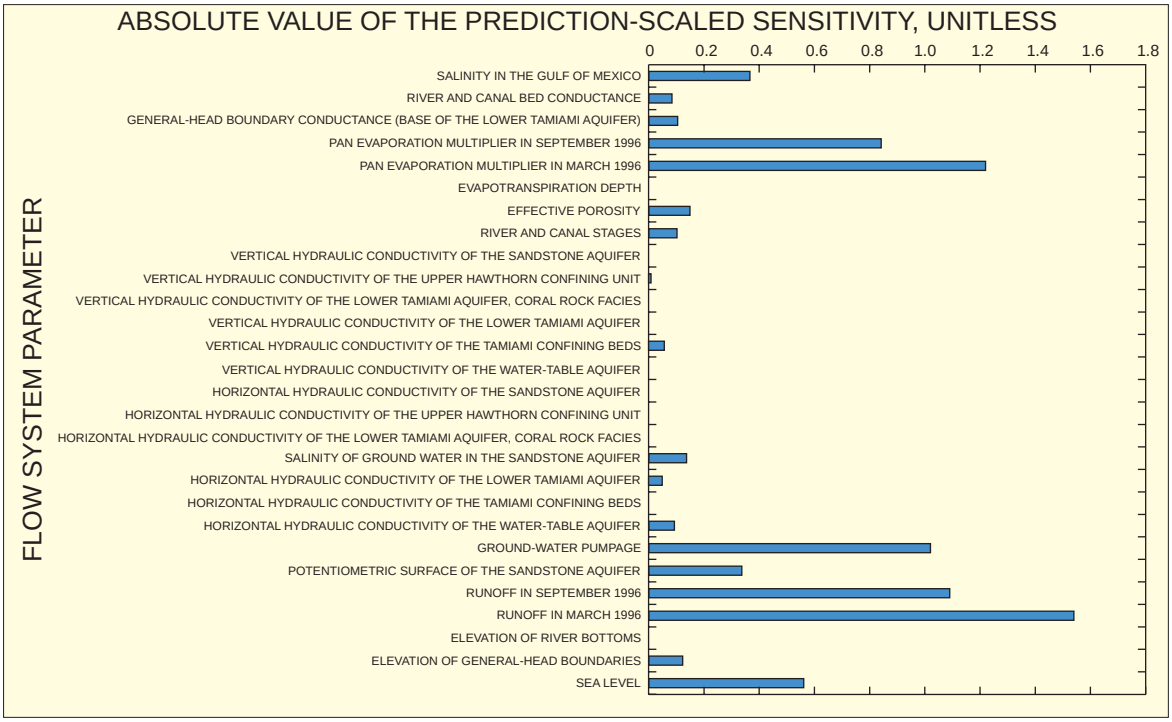

Figure 37. Sensitivity analysis of the extent of saltwater intrusion. Parameters with no visible bar have very small or zero sensitivity.

the PSS of evapotranspiration parameters and runoff (fig. 37) can be grouped together to emphasize net recharge as the most important parameter for estimating the extent of saltwater intrusion in the lower Tamiami aquifer near Bonita Springs. The fact that observed conditions provided the most information for estimating net recharge (the parameter most important for estimating the extent of saltwater intrusion in the lower Tamiami aquifer near Bonita Springs) is encouraging and supports the idea that calibrated ground-water flow models can adequately simulate saltwater movement.

The next most important parameter for estimating the extent of saltwater intrusion in the lower Tamiami aquifer near Bonita Springs is ground-water pumpage, as evidenced by the PSS (fig. 37). Water level and flow observations used while calibrating the model provided relatively little information for estimating unmonitored ground-water pumpage rates as evidenced by the CSS (fig. 27), and the width of the 95-percent confidence intervals on estimates of unmonitored ground-water pumpage rates (table 5). Future efforts to simulate saltwater movement would benefit by improving the representation and estimates of ground-water pumpage, because this parameter was second in relative importance to estimating the extent of saltwater intrusion, but was not precisely estimated with UCODE.

Model Limitations

The model results and interpretations described in this report are limited by: (1) assumptions inherent to MODFLOW-88 and SEAWAT that may or may not be satisfied; (2) difficulty in characterizing small-scale heterogeneity that may greatly influence regional ground-water flow and saltwater movement; (3) the modeling approach; and (4) the inability to quantitatively assess uncertainty in a rigorous fashion for the modeling objectives. The primary objectives were to identify the predominant mechanisms of saltwater intrusion and to estimate the extent of saltwater intrusion in the lower Tamiami aquifer near Bonita Springs.

The partial differential equations approximated by MODFLOW-88 and SEAWAT are based on many assumptions. Those assumptions relevant to simulating saltwater intrusion in the lower Tamiami aquifer near Bonita Springs are that: (1) ground water fully saturates the porous media in areas of ground-water flow, (2) ground-water flow is described by Darcy's law or a variable-density form of Darcy's law, (3) the fluid is incompressible, (4) the standard expression for specific storage in a confined aquifer is applicable, (5) isothermal conditions prevail, (7) fluid density is a linear function of ground-water salinity, and (8) the coordinate system is aligned with the principal axis of the permeability tensor so that this tensor is diagonal for anisotropic media. The natural system probably violates some of these assumptions, thus the relevance of model results and interpretations to the natural system are limited by the degree to which individual assumptions are violated.

The difficulty in characterizing small-scale heterogeneity limits model results, because this heterogeneity may greatly influence regional ground-water flow and saltwater movement in the study area. Complete and accurate characterization of heterogeneity in the lower Tamiami aquifer, including subsurface structural complexity, variations in hydraulic properties, and variations in stresses at multiple scales, was not attainable even with the numerous studies documented over the years. Thus, heterogeneity at multiple scales was averaged, interpolated, or zoned into finite-difference approximations that neglect small-scale particularities, which may be important in the true ground-water flow system in the lower Tamiami aquifer near Bonita Springs.

Clearly, the influence of heterogeneity in porosity at any one particular scale on movement of saltwater is not understood. Effective porosity was assigned a uniform value of 30 percent (Reese and Cunningham, 2000) in the baseline scenario. However, ground-water tracer tests suggest fractures and/or high permeability zones can give effective porosities of 2 to 4 percent (Langevin and others, 1998). Furthermore, some researchers have suggested decimeter-scale heterogeneities and preferential flow paths have the dominant effect on solute transport at the plume scale, with 15 percent of the aquifer involved in advective transport while 85 percent of the aquifer serves as a reservoir for essentially immobile solute (Zheng and Gorelick, 2001). Collectively, these investigations highlight the difficulty in characterizing small-scale heterogeneity and suggest the likelihood of a "dual porosity" system. Further research into this limitation would be useful.

Several assumptions and estimations were employed in the modeling approach that could limit the reliability of results. These include, but are not limited to: (1) the steady-state assumption, (2) estimating

stresses rather than hydraulic conductivities during model calibration, (3) the 7 to 5 ratio of dry- to wet-season months in a typical southwestern Florida water year, (4) neglecting the effects of dispersion on simulations of saltwater movement, and (5) initial conditions for simulating the movement of saltwater at equilibrium.

Steady-state flow occurs when at any point in the flow field, the magnitude and direction of the flow velocity are constant with time (Freeze and Cherry, 1979). Because longer term average values are being computed, a steady-state assumption was employed while computing the predevelopment distribution of saltwater, calibrating to March and September 1996 conditions, and moving saltwater at equilibrium. The steady-state assumption is limiting because transient particularities that could be important to saltwater movement in the lower Tamiami aquifer near Bonita Springs may not be considered. Additionally, using the steady-state assumption to calibrate to March and September 1996 conditions is limiting because it is possible the regional ground-water flow system is never at true steady state as defined by Freeze and Cherry (1979).

Most ground-water models are calibrated by adjusting hydraulic conductivity parameters until simulated results match observed field conditions. The model documented here was calibrated by estimating unmonitored ground-water pumpage and pan evaporation multipliers with UCODE. Unmonitored ground-water pumpage was estimated because accurately simulated water levels in the lower Tamiami aquifer beneath Bonita Springs was most important for accurately simulating saltwater movement—a primary objective of this study. Hydraulic conductivity was correlated with unmonitored ground-water pumpage and, therefore, could not be uniquely estimated together with UCODE. This was unfortunate because the model was more sensitive to hydraulic conductivity parameters, such as canal conductances and the vertical hydraulic conductivity of the Tamiami confining beds, than to pan evaporation multipliers. A better model fit may have resulted by estimating hydraulic conductivity parameters. Additional observations, particularly flow observations, could help obliterate the correlation between unknown pumpage and hydraulic conductivity parameters. Future modeling efforts would likely benefit from using additional flow observations while calibrating.

Previous studies have used a 7 to 5 ratio to represent the number of dry-season months to the number of wet-season months during a typical water year in southwestern Florida. The 7 to 5 ratio is potentially limiting because a plot of average monthly rainfall from 69 rainfall stations in southwestern Florida suggests the possibility that an 8 to 4 ratio may be more appropriate (fig. 38). The 7 to 5 ratio was used in this study to estimate annual average unmonitored ground-water pumpage rates, and also was used in the baseline scenario and during sensitivity of the baseline

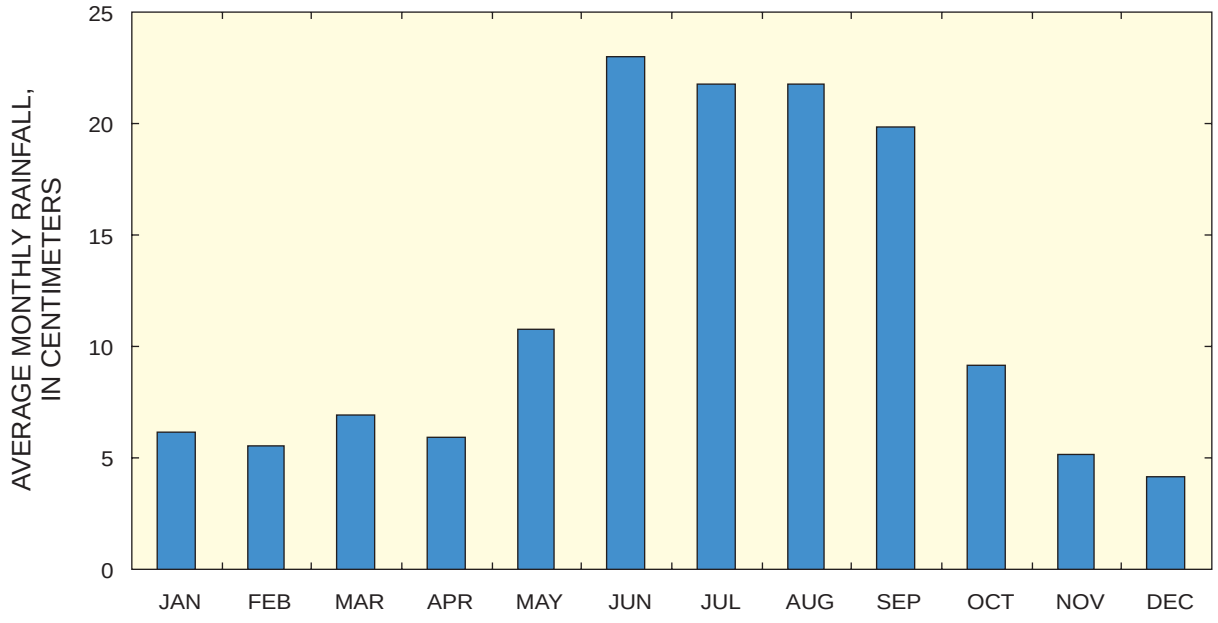

Figure 38. Average monthly rainfall from selected rainfall stations in southwestern Florida, 1909-99.

scenario. Using an 8 to 4 ratio would likely have little effect on identifying predominant mechanisms of saltwater intrusion and have little effect on sensitivity analysis of the baseline scenario. It is probable, however, that using an 8 to 4 ratio would increase estimates of unmonitored ground-water pumpage and increase estimates of the extent of saltwater intrusion.

Neglecting the effects of dispersion on simulations of saltwater movement limits the relevance of model results to the real nature of ground-water flow and saltwater movement in the study area. This is a limitation because: (1) the real nature of saltwater movement involves mixing, and (2) a dispersive solute-transport simulation suggests dispersion will reduce the extent of saltwater intrusion in the lower Tamiami aquifer near Bonita Springs.

In a hypothetical dispersive solute-transport simulation, dispersivity in three dimensions was estimated using the relation defined in Gelhar and others (1992) and Zheng and Bennett (1995). Longitudinal dispersivity was set to 60 m, or one-tenth the horizontal model cell dimension (Gelhar and others, 1992). Transverse and vertical dispersivities were set to 6 m, or one-tenth the longitudinal dispersivity (Zheng and Bennett, 1995). Six hundred years of dispersive and advective solute transport was simulated using the same modeling approach employed in the baseline scenario. In general, dispersion reduced the extent of saltwater intrusion. These results are consistent with historical studies (Cooper, 1964; Glover, 1964; Henry, 1964; Kohout, 1964) of the effects of dispersion on the saltwater interface, which suggest that including the effects of dispersion moves the interface seaward.

Dispersion was not simulated while solving for the predevelopment distribution of saltwater, during the baseline scenario, and during sensitivity analysis of the baseline scenario due to the length of computer run times and uncertainty in estimates of dispersivity. Field estimates of dispersivity in the lower Tamiami aquifer near Bonita Springs could be useful to constrain the potential effects of dispersion on saltwater movement. If computer run times are substantially diminished, and if field data can be obtained to set reasonable values of dispersivity at the scale of the model grid, then detailed three-dimensional studies of the position and behavior of the “toe” of the saltwater interface in the lower Tamiami aquifer could be more conclusively accomplished.

The lack of initial conditions is a well documented limitation for studies of solute transport in ground water. Although maps of salinity distribution are available (Knapp and others, 1986; Schmerge, 2001), these maps are based on field data collected over time. Only sparse amounts of salinity data are available to instantaneously capture the distribution of saltwater at any given time. If salinity is known only at a few points within the region to be modeled, and assumed initial values are assigned in between, the unrealistic flows probably will be calculated by the variable-density ground-water flow simulator (Voss, 1999). A practical solution to this problem was found by attempting to solve for initial conditions using predevelopment stresses and boundary conditions assumed or extrapolated from contemporary data. This approach has several advantages, as outlined in the modeling approach section of the report, but still is limiting because more accurate solutions to the primary objectives of this study could be obtained if the true distribution of freshwater equivalent head and ground-water salinity were known. Airborne electromagnetic survey techniques (Fitterman and Deszcz-Pan, 1998), if successfully applied to the water-table and lower Tamiami aquifers in southwestern Florida, could represent another useful solution to the lack of data on initial conditions for saltwater intrusion simulations near Bonita Springs.

Parameter and conceptual uncertainty limit the applicability of the modeling results presented here. When parameters are changed within reasonable ranges, or combinations of parameters are changed within reasonable ranges, mechanisms of saltwater intrusion become more or less predominant, saltwater moves to different extents, and saltwater moves at different rates. This problem is exacerbated by conceptual uncertainty because the ground-water flow system could be represented equally well by many different boundary conditions, regional distributions of aquifer properties, and initial conditions. The effects of this uncertainty on the primary study objectives were indirectly addressed through sensitivity analyses. Linear 95-percent confidence intervals, computed for each primary modeling objective, would probably be a practical and useful type of analysis to directly address parameter uncertainty. The effects of parameter and conceptual uncertainty could be directly addressed using a composite range of confidence intervals for a reasonable set of conceptual models (Poeter, 2001). However, these analyses were considered beyond the scope of this investigation.

SUMMARY

Saltwater intrusion is a concern near Bonita Springs in southwestern Florida where the average annual potentiometric surface in some areas of the lower Tamiami aquifer is below sea level. Field data were analyzed, and model simulations were performed to: (1) spatially quantify modern and seasonal stresses, (2) help identify potential mechanisms of saltwater intrusion, (3) and estimate the potential extent of saltwater intrusion in the lower Tamiami aquifer near Bonita Springs.

MODFLOW and the inverse modeling routine UCODE were used to spatially quantify modern and seasonal stresses in 1996 by calibrating a constant-density ground-water flow model. The model was calibrated by assuming hydraulic conductivity parameters were accurate and by estimating unmonitored ground-water pumpage and pan-evaporation multipliers with UCODE. Additionally, uncertainty in estimates of these parameters was quantified through 95-percent confidence intervals. These confidence intervals indicate more uncertainty or less reliability in the estimates of unmonitored ground-water pumpage than estimates of pan-evaporation multipliers due to the nature and distribution of observations used during calibration. Comparison of simulated water levels, streamflows, and net recharge with field data demonstrate the adequacy of the simulated water budget.

Net recharge and unmonitored ground-water pumpage are two components of the water budget of interest to water managers. Using modeling results for 1996, average net recharge to the water-table aquifer was estimated to range between 0 and 38 cm/yr, and unmonitored ground-water pumpage from the lower Tamiami aquifer was estimated to be 52,000 m^3/d. Net recharge less than zero occurred over less than 5 percent of the active model domain due to the close proximity of the water table to land surface. The average estimated rate of unmonitored ground-water pumpage in 1996 from the lower Tamiami aquifer (52,000 m^3/d) was almost as much as the monitored ground-water pumpage in 1996 from the water-table and lower Tamiami aquifers (59,000 m^3/d) in the active model domain.

Potential mechanisms of saltwater intrusion into the lower Tamiami aquifer near Bonita Springs include: (1) lateral inland movement of the freshwater-saltwater interface from the southwestern coast of Florida; (2) upward leakage from deeper, saline water-bearing zones through natural upwelling and upconing, both of which could occur as diffuse upward flow through semiconfining layers, conduit flow through karst features, or pipe flow through leaky artesian wells; (3) downward leakage of saltwater from surface-water channels; and (4) movement of unflushed pockets of relict seawater. Of the many potential mechanisms, field data and variable-density ground-water flow simulations suggest upconing is probably of utmost concern, and lateral encroachment is probably of second most concern in the lower Tamiami aquifer beneath Bonita Springs. This interpretation is uncertain, however, because the predominance of leaky wells with connection to deeper, more saline, and more pressurized aquifers was difficult to establish.

The potential extent of saltwater intrusion was estimated using a variable-density ground-water flow simulator and 1996 seasonal stresses. The potential extent of saltwater intrusion in the lower Tamiami aquifer beneath Bonita Springs is about 100 km^2 and 70,000 hectare-meters. The volumetric extent of saltwater intrusion was most sensitive to changes in recharge, ground-water pumpage, sea level, salinity of the Gulf of Mexico, and the potentiometric surface of the sandstone aquifer, respectively, as indicated by prediction-scaled sensitivities. Future efforts at estimating the extent of saltwater intrusion in this area would likely benefit from improved representation of these hydrologic stresses and boundary conditions.

Composite-scaled sensitivities that were computed while calibrating the model were compared with prediction-scaled sensitivities computed for the potential extent of saltwater intrusion predicted by the model. Composite-scaled sensitivities suggested observed conditions provided the most information for estimating net recharge. Prediction-scaled sensitivities suggested net recharge is the most important parameter for estimating the extent of saltwater intrusion in the lower Tamiami aquifer beneath Bonita Springs. This consistency was encouraging and supports the idea that calibrated ground-water flow models can be used to adequately simulate saltwater movement.

SELECTED REFERENCES

Albury, Carl, Langevin, C.D., and Stewart, M.T., 1998, Determining the feasibility for wetland rehydration: Simulation of application rates and transport of reclaimed water: Hydrogeology Laboratory, University of South Florida, Tampa, 11 p.

Anderson, M.P., and Woessner, W.W., 1992, Applied groundwater modeling: London, Academic Press, 381 p.

Badon-Ghyben, W., 1888, Nota in verband met de voorgenomen putboring nabij Amsterdam (Notes on the probable results of well drilling near Amsterdam): The Hague, Tijdschrift van het Koninklijk Instituut van Ingenieurs, p. 8-22.

Bear, Jacob, and others 1999, Seawater intrusion in coastal aquifers – concepts, methods, and practices: The Netherlands, Kluwer Academic Publishers, 625 p.

Bennett, W., 1992, Three dimensional finite difference ground-water flow model of western Collier County, Florida: West Palm Beach, South Florida Water Management District Technical Publication 92-04, 358 p.

Boggess, D.H., Missimer, T.M., and O'Donnell, T.H., 1981, Hydrogeologic sections through Lee County and adjacent areas of Hendry and Collier Counties, Florida: U.S. Geological Survey Open-File Report 81-638, 1 sheet.

Bower, R.F., Adams, K.M., and Restrepo, J.I., 1990, Three dimensional finite difference ground-water flow model of Lee County, Florida: West Palm Beach, South Florida Water Management District Technical Publication 90-01, 283 p.

Burns, W.S., 1983, Well plugging applications to the inter-aquifer migration of saline groundwater in Lee County, Florida: West Palm Beach, South Florida Water Management District Technical Publication 83-8, 77 p.

Clark, I.D., and Fritz, Peter, 1997, Environmental isotopes in hydrogeology: Boca Raton, Fla., Lewis Publishers, 328 p.

Cooper, H.H., 1964, Sea water in coastal aquifers: U.S. Geological Survey Water-Supply Paper 1613-C, 84 p.

Edwards, L.E., Weedman, S.D., Simmons, K.B., and others, 1998, Lithostratigraphy, petrostratigraphy, biostratigraphy, and strontium isotope stratigraphy of the surficial aquifer system of western Collier County, Florida: U.S. Geological Survey Open-File Report 98-205, 79 p.

Fernald, E.A., and Purdum, E.D., eds., 1998, Water resources atlas of Florida: Gainesville, University Press of Florida, 312 p.

Fitterman D.V., and Deszcz-Pan, M., 1998, Helicopter EM mapping of saltwater intrusion in Everglades National Park: Florida Exploration Geophysics, v. 29, p. 240-243.

Freeze, A.R., and Cherry, J.A., 1979, Groundwater: Englewood Cliffs, N.J., Prentice Hall, 604 p.

Gee and Jenson, Inc., 1980, Regional water resources study in the Big Cypress Basin: 106 p.

Gelhar L.W., Welty, C., and Rehfeldt, K.R., 1992, A critical review of data on field-scale dispersion in aquifers: Water Resources Research, v. 28, no. 7, p. 1955-1974.

Glover, R.E., 1964, The pattern of freshwater flow in a coastal aquifer in sea water in coastal aquifers: U.S. Geological Survey Water-Supply Paper 1613-C, 84 p.

Guo, Weixing, and Bennett, G.D., 1998, SEAWAT –A computer program for simulations of ground-water flow of variable density: Fort Myers, Fla., Report prepared by Missimer International, Inc., 51 p.

Guo, Weixing, and Langevin, C.D., 2002, User's guide to SEAWAT: A computer program for simulation of three-dimensional variable-density ground-water flow: U.S. Geological Survey Techniques of Water-Resources Investigations, book 6, chap. A7, 77 p.

Henry, H.R., 1964, Interfaces between salt water and fresh water in coastal aquifers in sea water in coastal aquifers: U.S. Geological Survey Water-Supply Paper 1613–C, 84 p.

Herzberg, A., 1901, DieWasserversorgung einiger Nordseeber (The water supply of parts of the North Sea coast in Germany): Z. Gasbeleucht Wasserversorg, 844 p.

Hill, M.C., 1998, Methods and guidelines for effective model calibration: U.S. Geological Survey Water-Resources Investigations Report 98-4005, 90 p.

Hite, L.R., 1997, Aquifer delineation in southwest Florida using time-domain electromagnetics: Dayton, Ohio, MS Thesis, Wright State University, 77 p.

Hsieh, P., and Winston, R.B., 2002, User's guide to model viewer: A program for three dimensional visualization of ground-water model results: U.S. Geological Survey Open-File Report 02-106, 18 p.

Hull, J.E., and Meyer, F.W., 1973, Salinity studies in East Glades agricultural area, southeastern Dade County, Florida: Tallahassee Florida Bureau of Geology Report of Investigations 66, 39 p.

Johnson Engineering, Inc.; Agnoli, Barber and Brundage, Inc.; and Boylan Environmental Consultants, Inc., 1999, South Lee County watershed plan: Report Prepared for the South Florida Water Management District, West Palm Beach,12 chapters and appendix.

Jones, B.F., Vengosh, A., Rosenthal, E., and Yechiele, Y., 1999, Geochemical investigations; *in* Bear, Jacob, and others, eds., Seawater intrusion in coastal aquifers–Concepts, methods, and practices: The Netherlands, Kluwer Academic Publishers, p. 51-71.

Klein, Howard, 1954, Ground-water resources of the Naples area, Collier County, Florida: Tallahassee Florida Geological Survey Report of Investigations 11, 63 p.

Klein, Howard, and Ratzlaff, K.W., 1989, Changes in saltwater intrusion in the Biscayne aquifer, Hialeah-Miami Springs area, Dade County, Florida: U.S. Geological Survey Water-Resources Investigations Report 87-4249, 1 sheet.

Klein, Howard, and Waller, B.G., 1985, Synopsis of saltwater intrusion in Dade County, Florida, through 1984: U.S. Geological Survey Water-Resources Investigations Report 85-4101, 1 sheet.

Knapp, M.S., Burns, W.S., and Sharp, T.S., 1986, Preliminary assessment of the ground-water resources of western Collier County, Florida: West Palm Beach, South Florida Water Management District Technical Publication 86-1, 142 p.

Kohout, F.A., 1964, The flow of fresh water and salt water in the Biscayne aquifer of the Miami area, Florida; *in* Cooper, H.H., and others, eds., Sea water in coastal aquifers: U.S. Geological Survey Water–Supply Paper 1613-C, p. C-12-C-32.

——— 1979, Satellite observations of a geothermal submarine spring off the Florida west coast: Satellite Hydrology: American Water Resources Association, June, p. 570-577.

Konikow, L.F., and Bredehoft, J.D., 1992, Ground-water models cannot be validated: Advances in Water Resources, v. 15, p. 75-83.

Konikow, L.F., and Reilly, T.E., 1999, Seawater intrusion in the United States; *in* Bear, Jacob, and others, eds., Seawater intrusion in coastal aquifers-Concepts, methods and practices: The Netherlands, Kluwer Academic Publishers, p. 463-506.

Krulikas, R.K., and Giese, G.L., 1995, Recharge to the surficial aquifer system in Lee and Hendry Counties, Florida: U.S. Geological Survey Water-Resources Investigations Report 95-0003, 21 p.

Langevin, C.D., 2001, Simulation of ground-water discharge to Biscayne Bay, southeastern Florida: U.S. Geological Survey Water-Resources Investigations Report 00-4251, 127 p.

Langevin, C.D., and Guo, Weixing, 1999, Improvements to SEAWAT, a variable-density modeling code: EOS Transactions, v. 80, no. 46, p. F-373.

Langevin, C.D., Thompson, D., LaRoche, J., and others,1998, Development of a conceptual hydrogeologic model from field and laboratory data, phase II results, North Lakes wetland Hillsborough County, Florida: Hydrogeology Laboratory, Geology Department, University of South Florida, Tampa, 63 p.

Leake, S.A., and Prudic, D.E., 1991, Documentation of a computer program to simulate aquifer-system compaction using the finite-difference ground-water flow model: U.S. Geological Survey Techniques of Water Resources Investigations, book 6, chap. A2, 68 p.

McCoy, H.J., 1962, Ground-water resources of Collier County, Florida: Tallahassee Florida Geological Survey Report of Investigations 31, 79 p.

McDonald, M.G., and Harbaugh, A.W., 1988, A modular three-dimensional finite-difference ground-water flow model: U.S. Geological Survey Techniques of Water Resources Investigations, book 6, chap. A1, 586 p.

Meeder, J.F., 1979, The Pliocene fossil reef of southwest Florida: Miami Geological Society 1979 Field Trip Guidebook, 18 p.

Merritt, M.L., 1996, Assessment of saltwater intrusion in southern coastal Broward County, Florida: U.S. Geological Survey Water-Resources Investigations Report 96-4221, 133 p.

Meyer, F.W., 1989, Hydrogeology, ground-water movement, and subsurface storage in the Floridan aquifer system in southern Florida: U.S. Geological Survey Professional Paper 1403-G, 59 p.

Montgomery, James, M., Consulting Engineers Inc., 1988, Lee County Water Resources Management Project.

Motz, L.H., 1996, Nonsteady-state drawdowns in two coupled aquifers: Journal of Irrigation and Drainage Engineering, v. 122, no. 1, p. 19-23.

National Research Council, 1987, Responding to changes in sea level change: Engineering implications: Washington D.C., National Academy Press, 148 p.

Parker, G.G., Ferguson, G.E., Love, S.K., and others, 1955, Water resources of southeastern Florida: U.S. Geological Survey Water-Supply Paper 1255, 965 p.

Poeter, E.P., 2001, Initial conditions, sensitivities and other reflections on the modeling odyssey; *in* Proceedings of MODFLOW 2001 and other Modeling Odysseys, September 11-14, 2001: Golden, Colo., International Ground-Water Modeling Center (IGWMC), Colorado School of Mines, v. 1, p. 14.

Poeter, E.P., and Hill, M.C., 1997, Inverse models: A necessary next step in ground-water modeling: Ground Water, v. 35, no. 2, p. 250-260.

——— 1998, Documentation of UCODE, a computer code for universal inverse modeling: U.S. Geological Survey Water-Resources Investigations Report 98-4080, 116 p.

Prinos, S.T., Lietz, A.C., and Irvin, Bruce, 2002, Design of a real-time ground-water level monitoring network and portrayal of hydrologic conditions in southern Florida: U.S. Geological Survey Water-Resources Investigations Report 01-4275.

Prinos, S.T., Richards, Tom, and Krulikas, Richard, 1996, Water-resources data – south Florida, Volume 2B, ground water: U.S. Geological Survey Water-Data Report FL-96-2B, 610 p.

Reese, R.S., 2000, Hydrogeology and distribution of salinity in the Floridan aquifer system, southwestern Florida: U.S. Geological Survey Water-Resources Investigations Report 98-4253, 86 p.

Reese, R.S., and Cunningham, K.J., 2000, Hydrogeology of the gray limestone aquifer in southern Florida: U.S. Geological Survey Water-Resources Investigations Report 99-4213, 244 p.

Reilly, T.E., 2001, System and boundary conceptualization in ground-water flow simulation: U.S. Geological Survey Techniques of Water Resources Investigations, book 3, chap. B8, 30 p.

Sacks, L.A., and Tihansky, A.B., 1996, Geochemical and isotopic composition of ground water with emphasis on sources of sulfate in the Upper Floridan aquifer and intermediate aquifer system in southwest Florida: U.S. Geological Survey Water-Resources Investigations Report 96-4146, 55 p.

Sanford, W.E., and others, 1998, Numerical analysis of seawater circulation in carbonate platforms: Part I. Geothermal convection: American Journal of Science, v. 298, no. 12, p. 801-828.

Schmerge, D.L., 2001, Distribution and origin of saline water in the surficial and intermediate aquifer systems in southwestern Florida: U.S Geological Survey Water-Resources Investigations Report 01-4159, 41 p.

Sherwood, C.B., and Klein, Howard, 1963, Saline ground-water in southern Florida: Ground Water, v. 1, no. 2, 6 p.

Shoemaker, W.B., 1998, Geophysical delineation of hydrostratigraphy in the Big Cypress National Preserve, Florida: Tampa MS Thesis, University of South Florida, 119 p.

Sonenshein, R.S., 1997, Delineation and extent of saltwater intrusion in the Biscayne aquifer, eastern Dade County, Florida, 1995: U.S. Geological Survey Water Resources Investigations Report 96-4285, 1 sheet.

Sonenshein, R.S., and Koszalka, E.J., 1996, Trends in water-table altitude (1984-93) and saltwater intrusion (1974-93) in the Biscayne aquifer, Dade County, Florida: U.S. Geological Survey Open-File Report 95-705, 2 sheets.

South Florida Water Management District, 1989, ARC information coverage of south Florida watershed basins: West Palm Beach, originally created by Jim Lane.

——— 1994, The lower west coast water supply plan, appendices: West Palm Beach, South Florida Water Management District Publication, 12 sections.

Stewart, M.T., 1999, Geophysical investigations; *in* Bear, Jacob, and others, eds., Seawater intrusion in coastal aquifers–Concepts, methods and practices: The Netherlands, Kluwer Academic Publishers, p. 9-50.

Stewart, M.T., and Langevin, C.D., 1999, Post audit of a numerical prediction of wellfield drawdown in a semiconfined aquifer system: Ground Water, v. 37, no. 2, p. 245-250.

Stewart, M.T., Lizanec, T., and Layton, M., 1982, Application of DC resistivity surveys to regional hydrogeologic investigation, Collier County, Florida: West Palm Beach, South Florida Water Management District Technical Publication 82-6, 95 p.

Swancar, A., Lee, T.M., and O'Hare, T.M., 2000, Hydrogeologic setting, water budget, and preliminary analysis of ground-water exchange at Lake Starr, a seepage lake in Polk County, Florida: U.S. Geological Survey Water-Resources Investigations Report 00-4030, 72 p.

Tibbals, C.H., 1990, Hydrology of the Floridan aquifer system in east-central Florida: U.S. Geological Survey Professional Paper 1403-E, 98 p.

Virogroup, Inc., 1993, Lee County regional water supply master plan, ground-water hydrology and computer impact modeling of potential future withdrawals: Report prepared for the South Florida Water Management District, West Palm Beach, 174 p.

Voss, C.I., 1999, USGS SUTRA code –History, practical use, and application in Hawaii, *in* Bear, Jacob, and others, eds., Seawater intrusion in coastal aquifers–Concepts, methods and practices: The Netherlands, Kluwer Academic Publishers, p. 249-313.

Wedderburn, L.A., Knapp, M.S., Waltz, D.P., and Burns, W.S., 1982, Hydrogeologic reconnaissance of Lee County, Florida, West Palm Beach, South Florida Water Management District Technical Publication 82-1, 192 p.

Weedman, S.D., 1999, Lithostratigraphy, geophysics, biostratigraphy, and strontium isotope stratigraphy of the surficial aquifer system of eastern Collier County and northern Monroe County, Florida: U.S. Geological Survey Open-File Report 99-432, 125 p.

Weedman, S.D., Paillet, F.L., Means, G.H., and Scott, T.M., 1997, Lithology and geophysics of the surficial aquifer system in western Collier County, Florida: U.S. Geological Survey Open-File Report 97-436, 167 p.

Zheng, Chunmiao, and Bennett, G.D., 1995, Applied contaminant transport modeling: New York, N.Y., Van Nostrand Reinhold, A Division of International Thomson Publishing, Inc., 440 p.

——— 2002, Applied contaminant transport modeling (2d ed.): New York, John Wiley and Sons, Inc., 621 p.

Zheng, Chunmiao, and Gorelick, S.M., 2001, Analysis of solute transport and remediation in flow fields influenced by decimeter-scale preferential flow path, *in* Proceedings of MODFLOW 2001 and other Modeling Odysseys, September 11-14, 2001, Golden, Colo., International Ground-water Modeling Center (IGWMC), Colorado School of Mines, v. 1, p. 11.

Zheng, Chunmiao, and Wang, P.P., 1998, MT3Dms–A modular three-dimensional multispecies transport model for simulation of advection, dispersion and chemical reactions of contaminants in ground-water systems: Tuscaloosa, University of Alabama Department of Geology and Mathematics, 7 chapters.

Appendix

Monitoring Stations Used for this Study

[Station type: C, chloride; E, pan-evapotranspiration; R, rainfall; WL, water level. Data source: DBHYDRO, South Florida Water Management District hydrometorologic database; NWIS, U.S. Geological Survey National Water Information System]

Appendix. Monitoring stations used in this study

Station identification	Station type	Latitude	Longi-tude	Data source
951EXT_R	R	261809	814118	DBHYDRO
ALVA FAR_R	R	264245	813747	DBHYDRO
ASGROW	R	261616	814229	DBHYDRO
BARRON_R	R	255801	812059	DBHYDRO
BAY WEST_R	R	261630	814208	DBHYDRO
BCBNAPLE_R	R	261331	814829	DBHYDRO
BONITA S_R	R	262001	814459	DBHYDRO
C-39	C	254859	812315	NWIS
C-54	WL	261019	805301	NWIS
C-54	C	261019	805301	NWIS
C-54_R	R	261019	805301	DBHYDRO
C-123	C	261004	814757	NWIS
C-130	C	260903	814803	NWIS
C-131	WL	262522	811618	NWIS
C-131	C	262522	811618	NWIS
C-161	C	261024	814706	NWIS
C-175	C	260913	814345	NWIS
C-258	C	262505	812458	NWIS
C-269	C	255701	812744	NWIS
C-296	C	260641	812042	NWIS
C-296_R	R	260641	812042	DBHYDRO
C-298	C	262508	812351	NWIS
C-303	C	261622	814122	NWIS
C-304	C	261636	813612	NWIS
C-308	C	260920	811558	NWIS
C-311	C	255431	812209	NWIS
C-321	C	261436	814724	NWIS
C-363	C	262556	812424	NWIS
C-384	C	261621	814506	NWIS
C-391	WL	261125	814702	NWIS
C-392	WL	261125	814700	NWIS
C-392	C	261125	814700	NWIS
C-409	C	261025	814800	NWIS
C-409A	WL	261025	814800	NWIS
C-409A	C	261025	814800	NWIS
C-424	C	261525	814803	NWIS
C-430	C	261147	814606	NWIS
C-445	C	255135	812305	NWIS
C-446	C	260449	814115	NWIS
C-458	C	261402	814613	NWIS
C-459	C	261404	814706	NWIS
C-460	WL	261406	814654	NWIS
C-460	C	261406	814654	NWIS
C-462	WL	262725	812606	NWIS
C-462	C	262725	812606	NWIS
C-472A	C	260926	814751	NWIS
C-474	C	261115	814822	NWIS
C-474A	C	261115	814822	NWIS
C-489	C	261303	814738	NWIS
C-490	C	261244	814802	NWIS
C-491	C	261118	814800	NWIS
C-492	WL	262229	813618	NWIS
C-492	C	262229	813618	NWIS
C-495	C	255749	811817	NWIS
C-496	WL	260112	812438	NWIS
C-496	C	260112	812438	NWIS
C-503	C	261742	812353	NWIS
C-506A	WL	261234	814801	NWIS
C-506A	C	261234	814801	NWIS
C-515	C	261347	814801	NWIS
C-516	C	261157	814757	NWIS
C-524	C	260949	814832	NWIS
C-525	C	261003	814836	NWIS
C-526	C	261019	814840	NWIS
C-527	C	261049	814847	NWIS
C-528	C	261201	814829	NWIS
C-531	WL	262900	812729	NWIS
C-531	C	262900	812729	NWIS
C-532	C	262900	812729	NWIS
C-575	C	261318	814804	NWIS
C-598	WL	261418	813053	NWIS
C-598	C	261418	813053	NWIS
C-599	C	260631	814113	NWIS
C-600	WL	260550	814418	NWIS
C-600	C	260550	814418	NWIS
C-684	C	261741	812353	NWIS
C-687	C	262555	812837	NWIS
C-688	C	261803	813547	NWIS
C-689	C	261741	812353	NWIS
C-690	WL	260630	813234	NWIS
C-690	C	260630	813234	NWIS
C-948	C	261348	813516	NWIS
C-951	WL	261348	813511	NWIS
C-951	C	261348	813511	NWIS
C-953	WL	261348	813511	NWIS
C-953	C	261348	813511	NWIS
C-955	C	261722	813512	NWIS
C-956	C	261344	813847	NWIS
C-963	C	262122	813554	NWIS
C-965	C	262137	812041	NWIS
C-966	C	262137	812041	NWIS
C-967	C	260541	814305	NWIS
C-968	WL	260335	813915	NWIS
C-968	C	260335	813915	NWIS
C-969	WL	260231	814013	NWIS
C-969	C	260238	814014	NWIS
C-970	C	261722	813512	NWIS
C-971	C	261722	813512	NWIS
C-972	C	260844	813241	NWIS
C-973	C	260844	813241	NWIS
C-974	C	260942	813241	NWIS
C-975	C	260305	813913	NWIS
C-976	C	260916	813858	NWIS
C-977	C	260916	813858	NWIS
C-978	C	262122	813554	NWIS
C-979	C	262122	813554	NWIS
C-980	C	261344	813847	NWIS
C-981	C	262159	812833	NWIS

Appendix. Monitoring stations used in this study (Continued)

Station identification	Station type	Latitude	Longi-tude	Data source	Station identification	Station type	Latitude	Longi-tude	Data source
C-982	C	262159	812833	NWIS	C-1079	C	262159	812823	NWIS
C-983	C	262159	812833	NWIS	C-1080	C	262229	813618	NWIS
C-984	C	261734	812854	NWIS	C-1081	C	260248	814121	NWIS
C-985	C	261734	812854	NWIS	C-1082	C	261805	814733	NWIS
C-986	C	261201	812048	NWIS	C-1083	WL	261856	814719	NWIS
C-987	C	260310	812725	NWIS	CAPECOR1_R	R	263524	820054	DBHYDRO
C-988	WL	261445	812848	NWIS	CAPECOR2_R	R	263445	815748	DBHYDRO
C-988	C	261445	812848	NWIS	CAPTIVA_R	R	263201	821059	DBHYDRO
C-989	WL	261734	812854	NWIS	CARIBBEA_E	E	261001	814659	DBHYDRO
C-989	C	261734	812854	NWIS	CCWTP_R	R	261601	814659	DBHYDRO
C-995	C	255704	812137	NWIS	CCWWTP_R	R	261606	814712	DBHYDRO
C-996	C	260909	814111	NWIS	CCWWTP2_R	R	261431	814029	DBHYDRO
C-997	WL	252751	802833	NWIS	COCO1_R	R	261622	814647	DBHYDRO
C-997	C	261530	814120	NWIS	COCOH.WB_R	R	261622	814550	DBHYDRO
C-998	C	261621	814501	NWIS	COLGOV_R	R	260747	814545	DBHYDRO
C-999	C	261509	814848	NWIS	COLLICTY	R	261011	814116	DBHYDRO
C-1000	C	261104	814748	NWIS	COLLIER_R	R	260924	813929	DBHYDRO
C-1001	C	261117	814802	NWIS	COLLISEM	R	255926	813529	DBHYDRO
C-1002	C	261242	814653	NWIS	COPELAND_R	R	255701	812136	DBHYDRO
C-1003	C	261437	814802	NWIS	CORK.CP_R	R	262427	813658	DBHYDRO
C-1004	WL	261621	814643	NWIS	CORK.HQ_E	R	262301	813459	DBHYDRO
C-1004	C	261621	814643	NWIS	CORK.HQ_R	R	262301	813459	DBHYDRO
C-1026	C	261234	814801	NWIS	CORK.LCI_R	R	262431	813417	DBHYDRO
C-1051	C	261025	814637	NWIS	CORK.SD_R	R	262147	813826	DBHYDRO
C-1052	C	260920	814604	NWIS	CORK.TOW_R	R	263123	813459	DBHYDRO
C-1053	C	260920	814604	NWIS	CORK_R	R	262520	813443	DBHYDRO
C-1054	C	261128	814609	NWIS	CORKISL	R	262152	813531	DBHYDRO
C-1055	C	261212	814412	NWIS	DANHP_R	R	255843	812851	DBHYDRO
C-1056	C	261458	814608	NWIS	DUDA.NAP_R	R	260151	813911	DBHYDRO
C-1057	C	261538	814611	NWIS	EAGLECRK	R	260307	814224	DBHYDRO
C-1058	C	261538	814611	NWIS	ESTERO T_R	R	262826	815017	DBHYDRO
C-1059	C	261605	814808	NWIS	EVERGL 2_R	R	255043	812313	DBHYDRO
C-1060	C	261500	814803	NWIS	FAKA_R	R	255738	813034	DBHYDRO
C-1061	C	261312	814800	NWIS	FAKAHAT_R	R	255845	812429	DBHYDRO
C-1062	C	260926	814750	NWIS	FAKAHATC_R	R	261002	812140	DBHYDRO
C-1063	C	260138	813758	NWIS	FORT MEY_R	R	263501	815159	DBHYDRO
C-1064	WL	260138	813758	NWIS	FPWX	R	262557	814324	DBHYDRO
C-1064	C	260138	813758	NWIS	FT MEYER_R	R	263451	815151	DBHYDRO
C-1065	C	255638	812813	NWIS	GOLD.FS_R	R	261058	814216	DBHYDRO
C-1066	C	255638	812813	NWIS	GOLD.W1_R	R	261004	814604	DBHYDRO
C-1067	C	260315	813230	NWIS	GOLD.WP_R	R	261101	814159	DBHYDRO
C-1068	C	260315	813230	NWIS	GOLD.WP2_R	R	261001	814214	DBHYDRO
C-1069	C	260814	812142	NWIS	GOLD.WP3_E	E	261001	814159	DBHYDRO
C-1070	C	260814	812142	NWIS	GOLD75	R	260929	813114	DBHYDRO
C-1071	WL	261824	811718	NWIS	GOLDFS2	R	261342	813755	DBHYDRO
C-1071	C	261824	811718	NWIS	GORDON_R	R	261022	814705	DBHYDRO
C-1072	WL	261824	811718	NWIS	HENDER_R	R	260559	814112	DBHYDRO
C-1072	C	261824	811718	NWIS	IMMOKA 2_R	R	262426	812459	DBHYDRO
C-1073	C	261741	812353	NWIS	IMMOKA 3_R	R	262741	812614	DBHYDRO
C-1074	WL	262520	811620	NWIS	IMMOKALE_R	R	262335	812425	DBHYDRO
C-1074	C	262520	811620	NWIS	JUNGLE L_R	R	261005	814723	DBHYDRO
C-1075	C	262823	812131	NWIS	KANTORS_R	R	261129	814141	DBHYDRO
C-1076	C	262823	812131	NWIS	L TRAFFO_R	R	262601	812859	DBHYDRO
C-1077	C	262823	812131	NWIS	L.B.MINO_R	R	264436	813557	DBHYDRO
C-1078	C	262559	812704	NWIS	L-246	C	263803	814934	NWIS

Appendix. Monitoring stations used in this study (Continued)

Station identification	Station type	Latitude	Longi-tude	Data source	Station identification	Station type	Latitude	Longi-tude	Data source
L-331	C	263126	815117	NWIS	L-1156	C	263316	815241	NWIS
L-345	C	262035	814647	NWIS	L-1403	WL	262550	820352	NWIS
L-346	C	262035	814646	NWIS	L-1403	C	262550	820352	NWIS
L-351	C	262911	820035	NWIS	L-1418	WL	263631	813752	NWIS
L-352	C	262909	820037	NWIS	L-1418	C	263631	813752	NWIS
L-357	C	263059	815607	NWIS	L-1456	C	262623	820219	NWIS
L-581	WL	263533	815921	NWIS	L-1457	C	262623	820219	NWIS
L-581	C	263533	815921	NWIS	L-1598	C	263234	815502	NWIS
L-585	C	262709	820053	NWIS	L-1625	C	263330	813942	NWIS
L-588	C	262539	820456	NWIS	L-1634	C	262436	815350	NWIS
L-590	C	262549	820509	NWIS	L-1635	C	262436	815349	NWIS
L-652	C	264102	814429	NWIS	L-1691	WL	262043	814549	NWIS
L-721	C	264154	820222	NWIS	L-1691	C	262043	814549	NWIS
L-726	C	264426	814539	NWIS	L-1853	C	262707	814353	NWIS
L-727	WL	263851	813653	NWIS	L-1907	C	264309	814059	NWIS
L-727	C	263851	813653	NWIS	L-1963	C	263345	813616	NWIS
L-728	C	263713	814611	NWIS	L-1964	C	263345	813616	NWIS
L-729	WL	263336	813942	NWIS	L-1965	C	263354	813357	NWIS
L-729	C	263336	813942	NWIS	L-1968	C	263808	814302	NWIS
L-730	C	263138	815458	NWIS	L-1973	C	263719	814849	NWIS
L-730	WL	263138	815458	NWIS	L-1974	C	263719	814849	NWIS
L-731	WL	262704	813401	NWIS	L-1975	C	264400	814246	NWIS
L-731	C	262704	813401	NWIS	L-1976	C	264400	814246	NWIS
L-735	C	262840	815030	NWIS	L-1977	C	264321	813656	NWIS
L-738	C	262023	814641	NWIS	L-1978	C	264321	813656	NWIS
L-739	C	262658	814434	NWIS	L-1983	C	263042	814330	NWIS
L-741	C	262553	814856	NWIS	L-1984	C	262714	814145	NWIS
L-742	WL	263324	815223	NWIS	L-1985	C	262714	814146	NWIS
L-742	C	263324	815223	NWIS	L-1992	C	263354	813357	NWIS
L-781	WL	263835	820052	NWIS	L-1993	WL	263252	814527	NWIS
L-781	C	263835	820052	NWIS	L-1993	C	263252	814527	NWIS
L-954	WL	263904	815503	NWIS	L-1994	WL	263252	814527	NWIS
L-954	C	263904	815503	NWIS	L-1994	C	263252	814527	NWIS
L-1058	C	263815	820206	NWIS	L-1995	WL	263252	814527	NWIS
L-1059	C	264518	820220	NWIS	L-1995	C	263252	814527	NWIS
L-1089	C	263125	815213	NWIS	L-1996	WL	261955	814100	NWIS
L-1099	C	264054	815631	NWIS	L-1996	C	261955	814100	NWIS
L-1106	C	264055	815925	NWIS	L-1997	WL	261955	814100	NWIS
L-1107	C	264147	815922	NWIS	L-1997	C	261955	814100	NWIS
L-1108	C	264145	815825	NWIS	L-1998	WL	263042	814330	NWIS
L-1109	C	264056	815830	NWIS	L-1998	C	263042	814330	NWIS
L-1110	C	264242	815823	NWIS	L-1999	C	263042	814330	NWIS
L-1111	C	264148	815626	NWIS	L-2186	WL	263345	813616	NWIS
L-1113	C	264121	820220	NWIS	L-2186	C	263345	813616	NWIS
L-1114	C	263721	815730	NWIS	L-2187	C	263951	813553	NWIS
L-1115	C	263906	815727	NWIS	L-2190	C	264145	815202	NWIS
L-1116	C	263634	820026	NWIS	L-2191	C	264145	815202	NWIS
L-1117	C	263439	815631	NWIS	L-2192	C	262700	813824	NWIS
L-1121	C	263328	815119	NWIS	L-2194	WL	261958	814321	NWIS
L-1124	C	263247	815314	NWIS	L-2194	C	261958	814321	NWIS
L-1129	C	263324	815352	NWIS	L-2195	WL	261958	814321	NWIS
L-1136	C	263533	815921	NWIS	L-2195	C	261958	814321	NWIS
L-1137	WL	263951	813553	NWIS	L-2198	C	261955	814321	NWIS
L-1137	C	263951	813553	NWIS	L-2200	C	264330	813403	NWIS
L-1138	C	262704	813401	NWIS	L-2202	C	264330	813403	NWIS

Appendix. Monitoring stations used in this study (Continued)

Station identification	Station type	Latitude	Longi-tude	Data source	Station identification	Station type	Latitude	Longi-tude	Data source
L-2204	C	263330	813942	NWIS	L-3213	C	263358	815755	NWIS
L-2212	C	262832	815758	NWIS	L-3214	C	263956	820830	NWIS
L-2215	C	263128	813515	NWIS	L-3215	C	263118	820509	NWIS
L-2216	C	264609	814540	NWIS	L-4820	C	264054	815724	NWIS
L-2217	C	264609	814540	NWIS	L-5648	C	263250	814743	NWIS
L-2244	C	263243	815720	NWIS	L-5649	WL	262935	814957	NWIS
L-2292	C	263719	814849	NWIS	L-5649	C	262935	814957	NWIS
L-2295	C	262553	814856	NWIS	L-5664	C	262515	813933	NWIS
L-2308	C	262553	814856	NWIS	L-5665	C	262515	813933	NWIS
L-2310	C	262023	814641	NWIS	L-5666	C	262514	814328	NWIS
L-2311	C	263345	813616	NWIS	L-5667	C	262514	814325	NWIS
L-2313	C	262704	813401	NWIS	L-5668	C	262514	814717	NWIS
L-2315	C	263005	821116	NWIS	L-5669	C	262512	814717	NWIS
L-2328	C	264609	814540	NWIS	L-5672	C	262332	813831	NWIS
L-2341	C	264518	815131	NWIS	L-5673	C	262332	813831	NWIS
L-2434	WL	263527	820101	NWIS	L-5707	C	263853	815147	NWIS
L-2434	C	263527	820101	NWIS	L-5720	C	263250	814743	NWIS
L-2435	C	263407	815559	NWIS	L-5721	C	262935	814957	NWIS
L-2524	C	262623	820743	NWIS	L-5722	C	262103	814643	NWIS
L-2525	C	263118	820509	NWIS	L-5723	C	262103	814643	NWIS
L-2526	C	264518	820220	NWIS	L-5724	C	261947	814902	NWIS
L-2527	C	263956	820830	NWIS	L-5725	C	261947	814902	NWIS
L-2528	C	263908	815926	NWIS	L-5726	C	261900	814818	NWIS
L-2529	C	262914	815624	NWIS	L-5727	C	261900	814818	NWIS
L-2530	C	264309	814053	NWIS	LEHIGH 1_R	R	263625	813859	DBHYDRO
L-2531	C	264428	813625	NWIS	LEHIGH 2_R	R	263907	813935	DBHYDRO
L-2549	C	263956	820830	NWIS	LEHIGH 3_R	R	263726	813403	DBHYDRO
L-2550	WL	262712	814137	NWIS	LEHIGH 4_R	R	263325	813623	DBHYDRO
L-2640	C	263814	815527	NWIS	LEHIGH 5_R	R	263616	814218	DBHYDRO
L-2641	C	263534	815733	NWIS	LEHIGH 6_R	R	263701	814359	DBHYDRO
L-2642	C	263258	815856	NWIS	LEHIGH E_R	R	263301	814259	DBHYDRO
L-2643	C	263254	820141	NWIS	LEHIGH W_R	R	263626	813859	DBHYDRO
L-2644	WL	263441	820219	NWIS	LEHIGH_R	R	263625	813859	DBHYDRO
L-2644	C	263441	820219	NWIS	MARCO FI_R	R	255548	814201	DBHYDRO
L-2645	C	263744	820411	NWIS	MARCO TO_R	R	260001	813459	DBHYDRO
L-2646	C	264538	815521	NWIS	MILES 2_R	R	261145	812045	DBHYDRO
L-2700	C	264003	820127	NWIS	MILES 3_E	E	261100	812600	DBHYDRO
L-2701	WL	263820	815857	NWIS	MILES CI_R	R	261104	812047	DBHYDRO
L-2701	C	263820	815857	NWIS	MONROE T_R	R	255131	810624	DBHYDRO
L-2702	WL	263622	815636	NWIS	NAPLES C_R	R	260738	814459	DBHYDRO
L-2702	C	263622	815636	NWIS	NAPLES T_R	R	260914	814532	DBHYDRO
L-2703	WL	263358	815755	NWIS	NAPLES_R	R	261005	814723	DBHYDRO
L-2703	C	263358	815755	NWIS	NNAPFS42	R	261620	814332	DBHYDRO
L-2820	C	263956	820830	NWIS	NP-EVC	R	255112	812249	DBHYDRO
L-2821	C	263118	820509	NWIS	NP-OAS	R	255127	810205	DBHYDRO
L-3203	C	263814	815527	NWIS	OASIS	R	255101	810159	DBHYDRO
L-3204	C	263534	815733	NWIS	RACOON PT	R	255801	811859	DBHYDRO
L-3205	C	263258	815856	NWIS	ROYAL HA_R	R	255926	813529	DBHYDRO
L-3206	C	263254	820141	NWIS	S79_R	R	264326	814154	DBHYDRO
L-3207	C	263441	820219	NWIS	SDS_R	R	261630	814208	DBHYDRO
L-3208	C	263744	820411	NWIS	SILVER S_R	R	261749	812618	DBHYDRO
L-3209	C	264538	815521	NWIS	SITE #1_R	R	260900	814100	DBHYDRO
L-3210	C	264003	820127	NWIS	SITE #2_R	R	255300	811800	DBHYDRO
L-3211	C	263820	815857	NWIS	SITE1_R	R	261643	813341	DBHYDRO
L-3212	C	263622	815636	NWIS	SITE2_R	R	261149	814016	DBHYDRO

Appendix. Monitoring stations used in this study (Continued)

Station identification	Station type	Latitude	Longi-tude	Data source	Station identification	Station type	Latitude	Longi-tude	Data source
SITE3_R	R	260343	813124	DBHYDRO	SR_R	R	263501	815159	DBHYDRO
SITE4 2_R	R	261616	813144	DBHYDRO	STEPHAN	R	261011	814116	DBHYDRO
SIX L.7_R	R	260114	813723	DBHYDRO	TAMIAMI_R	R	255311	811529	DBHYDRO
SLEE_R	R	264145	814637	DBHYDRO	USDA IMM_R	R	262741	812614	DBHYDRO
					VICTORIA_R	R	261541	814614	DBHYDRO

Solute Transport Modeling
Technical Memorandum No. STM-3

Predictive Modeling Results for the City of St. Petersburg's Deep Injection Well Systems

Prepared for

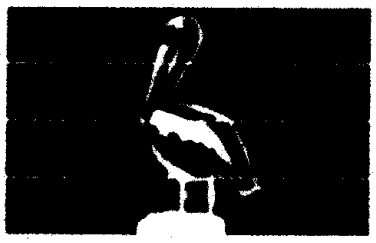

THE CITY OF ST. PETERSBURG
St. Petersburg, Florida

Prepared by

CH2MHILL

Tampa, Florida
November 1996
103855.C0

Predictive Modeling Results for the City of St. Petersburg's Deep Injection Well Systems

PREPARED FOR:	City of St. Petersburg
PREPARED BY:	CH2M HILL
DATE:	November 13, 1996
CITY TASK ORDER:	03-CH
CITY PROJECT:	94420-147
CH2M HILL PROJECT NUMBER:	103855.C0.06

Introduction

The City of St. Petersburg is pursuing injection well operating permits for 10 deep injection wells at its four Water Reclamation Facilities (WRFs). Solute transport modeling is being used as a tool to develop a better understanding of historical and projected water quality changes at the City's four injection sites. The City has negotiated consent orders with the Florida Department of Environmental Protection (FDEP) to continue operation of the deep injection wells while outstanding permitting issues are addressed. As part of the consent order process, the City is developing technical data in support of the injection well operating permits. Technical Memorandum No. STM-3 is the third in a series of technical memoranda related to solute transport modeling conducted in support of the re-permitting process. Technical Memorandum No. STM-1, *Development of the Solute Transport Conceptual Model*, was submitted to the FDEP Technical Advisory Committee (TAC) in February 1995. Background information and the conceptual approach to the modeling was described in STM-1. Technical Memorandum No. STM-2, *Solute Transport Model Calibration for the City of St. Petersburg's Deep Injection Well Systems*, was presented to the FDEP TAC in October 1995. In STM-2, the numerical representation of the conceptual model was presented, and simulated and observed water quality and water level trends were compared at each of the four WRFs.

In this Technical Memorandum (STM-3), *Predictive Modeling Results for the City of St. Petersburg's Deep Injection Well Systems*, the calibrated model simulations presented in STM-2 are extended into the future to evaluate possible changes in water quality in selected hydrogeologic zones. The results of this effort are intended to provide insight to the City and the FDEP TAC to aid in development of an appropriate permitting strategy for each WRF.

Predictive Modeling Approach

Predictive models for each WRF use the same properties and setup developed during model calibration. The purpose of the calibration was to establish the degree to which the

idealized flow system of the conceptual model approached the observed overlying aquifer response to reclaimed water injection. The calibration process involved comparing model-derived water quality and water level distributions with the observed historical data. Based on the relative comparison, selected model input was systematically revised to improve correlation between the simulated and observed aquifer response. The conceptual model layout and the model input properties of the final calibrated model for each WRF are provided in Appendix A. STM-1 and STM-2 document the development of the conceptual model and the calibration process in great detail.

Each calibrated model has been modified to simulate injection of reclaimed water through the year 2005. This 10-year period represents two FDEP permitting cycles, which provides FDEP an opportunity to re-visit the modeling twice during this time period. With the exception of the Albert Whitted WRF model, the 10-year period extrapolates out less than the historical period of record, increasing confidence in the model simulation results. The calibrated models, completed in October 1995, were updated to reflect the actual annual average daily injection rates for 1994 and 1995, and continued injection at an assumed annual average daily injection rate through the year 2005. Forecasts of future reclaimed water injection are not available; Demand for reuse water, however, is expected to rise at a rate greater than the rate of expansion of wastewater service, further reducing the volume injected at the City's facilities.

The City is studying reclaimed water Aquifer Storage Recovery (ASR) as a mechanism to provide seasonal storage of reclaimed water, resulting in the ability to add new reuse customers to the reuse system. The City has been somewhat limited to date in its ability to add new customers because of the need to maintain a reliable dry season supply of reclaimed water to its existing customers. Additional conservation efforts under way by the City are also expected to result in less excess reclaimed water disposal via deep well injection. Finally, inflow and infiltration improvements are underway which should further reduce future wet weather disposal by deep well injection. It is reasonable, therefore, to assume that the average annual daily injection rate for the next 10 years will be less than or equal to the lowest observed annual average daily injection rate for each WRF. In fact, the City's long-term goal is to be able to maximize the use of its valuable freshwater resources, further minimizing flows to the injection wells. For each simulation, the assumed future injection rate was specified as the minimum average annual daily injection rate on record. Table 1 lists the average annual daily injection rate and associated operational period.

Using the calibrated models, simulated TDS concentration output data were compiled for locations in the model grid corresponding to actual observation wells. This provides a comparison with the actual observed values at each observation well. For the predictive models, TDS concentration data were compiled for locations in the model chosen to provide the greatest insight for evaluating various re-permitting options. These locations were chosen to make predictions of the TDS concentration in the zones corresponding to permitting considerations. The average across Zone A of each model was selected because this was the only zone yielding significant quantities and qualities of water to be potentially economically viable for future development in southern Pinellas County (through membrane processes, for example). The base of the Underground Source of Drinking Water (USDW [i.e., the depth at which the pre-injection TDS concentration equaled 10,000 ppm]) was also selected because many permitting options available to the City involve regulations restricting fluid movement and water quality degradation above this point.

Table 1
Injection Rates Used For Solute Transport Model Predictions

Southwest WRF Model:

Injection Period			Time (Days)	Time since 9/10/79 (days)	Average Injection Rate Over Period (MGD)	Q (million gallons)
9/10/79	to	5/10/82	973	973	4.4	4301
5/11/82	to	7/1/83	417	1390	15.0	6255
7/2/83	to	12/31/83	183	1573	14.9	2727
1/1/84	to	12/31/84	366	1939	13.3	4868
1/1/85	to	12/31/85	365	2304	10.0	3650
1/1/86	to	12/31/86	365	2669	6.5	2373
1/1/87	to	12/31/87	365	3034	11.5	4198
1/1/88	to	12/31/88	366	3400	12.8	4685
1/1/89	to	12/31/89	365	3765	6.9	2519
1/1/90	to	12/31/90	365	4130	6.7	2446
1/1/91	to	12/31/91	365	4495	3.9	1424
1/1/92	to	12/31/92	366	4861	3.0	1098
1/1/93	to	12/31/93	365	5226	4.8	1752
1/1/94	to	12/31/94	365	5591	3.8	1376
1/1/95	to	12/31/95	365	5956	5.2	1913
1/1/96	to	12/31/05	3653	9609	3.0	10959

Total Volume Injected = 56,540 million gallons

Average Overall Inj. Rate = 5.88 MGD

Northeast WRF Model:

Injection Period			Time (Days)	Time since 6/9/80 (days)	Average Injection Rate Over Period (MGD)	Q (million gallons)
6/9/80	to	12/31/85	2031	2031	6.1	12389
1/1/86	to	12/31/86	365	2396	3.8	1387
1/1/87	to	12/31/87	365	2761	6.7	2446
1/1/88	to	12/31/88	366	3127	7.5	2745
1/1/89	to	12/31/89	365	3492	6.6	2409
1/1/90	to	12/31/90	365	3857	5.9	2154
1/1/91	to	12/31/91	365	4222	5.5	2008
1/1/92	to	12/31/92	366	4588	3.8	1391
1/1/93	to	12/31/93	365	4953	4.1	1497
1/1/94	to	12/31/94	365	5318	3.9	1420
1/1/95	to	12/31/95	365	5683	3.4	1226
1/1/96	to	12/31/05	3653	9336	3.4	12274

Total Volume Injected = 43,344 million gallons

Average Overall Inj. Rate = 4.64 MGD

Table1 (continued)
Injection Rates Used For Solute Transport Model Calibration

Northwest WRF Model:

Injection Period			Time (Days)	Time since 1/1/85 (days)	Average Injection Rate Over Period (MGD)	Q (million gallons)
1/1/85	to	12/31/85	364	364	4.7	1711
1/1/86	to	12/31/86	365	729	10.0	3650
1/1/87	to	12/31/87	365	1094	8.1	2957
1/1/88	to	12/31/88	366	1460	9.2	3367
1/1/89	to	12/31/89	365	1825	5.6	2044
1/1/90	to	12/31/90	365	2190	3.4	1241
1/1/91	to	12/31/91	365	2555	10.1	3687
1/1/92	to	12/31/92	366	2921	8.8	3221
1/1/93	to	12/31/93	365	3286	7.1	2592
1/1/94	to	12/31/94	365	3651	7.2	2621
1/1/95	to	12/31/95	365	4016	11.2	4081
1/1/96	to	12/31/05	3653	7669	3.4	12420

Total Volume Injected = 43,590 million gallons

Average Overall Inj. Rate = 5.68 MGD

Albert Whitted WRF Model:

Injection Period			Time (Days)	Time since 1/1/89 (days)	Average Injection Rate Over Period (MGD)	Q (million gallons)
1/1/89	to	12/31/89	364	364	4.6	1674
1/1/90	to	12/31/90	365	729	3.7	1351
1/1/91	to	12/31/91	365	1094	2.2	803
1/1/92	to	12/31/92	366	1460	3.1	1135
1/1/93	to	12/31/93	365	1825	5.0	1825
1/1/94	to	12/31/94	365	2190	6.2	2256
1/1/95	to	12/31/95	365	2555	7.7	2818
1/1/96	to	12/31/05	3653	6208	2.2	8037

Total Volume Injected = 19,898 million gallons

Average Overall Inj. Rate = 3.21 MGD

Distances of 0.25, 0.5, 1, 2, and 3 miles from each WRF were selected to evaluate potential water quality changes at various distances under the injection scenarios modeled. The simulated TDS concentrations were plotted with respect to time, and are discussed in the following section.

Results of Predictive Modeling

Results from each of the four predictive models are presented graphically. The first figure for each model shows a radial cross-section with injection at the site represented as a single injection well on the left side of the model. The simulated TDS distribution from the last time step of each model (December 31, 2005) is contoured using the TDS values from each model node. To gauge the extent of water quality changes, the pre-injection TDS distribution is also shown (shaded) on the figure. Because multiple injection wells are simulated as a single well, these cross-sections are more representative of the TDS distribution in the aquifer system at distance (i.e., greater than approximately 2,000 feet from the injection wells). Closer in, water quality may respond more closely to individual injection well operations. It should be noted that the models simulate changes in the TDS concentration, and not the extent of reclaimed water migration. Justification for modeling TDS changes in lieu of the reclaimed water fraction was discussed in STM-1 (CH2M HILL, February 1995).

Two data plots are presented for each predictive model. The "Predicted Average TDS in Zone A" represents hypothetical observation wells at 0.25, 0.5, 1, 2, and 3 miles from each WRF. The hypothetical observation wells are assumed to be completed through the entire thickness of Zone A of the upper Floridan aquifer. The average TDS value is computed as the mean of the TDS concentration from model nodes in Zone A at the appropriate radial distance from the injection well.

In contrast with the simple averaging of node values of TDS discussed previously, the TDS at the base of the USDW is taken as a weighted average of the two nodes whose initial pre-injection TDS values straddle the 10,000 ppm concentration. The TDS value reported in the plots is weighted such that the initial TDS equals 10,000 ppm.

Southwest WRF

Figure 1 shows the cross-section of the model at the Southwest WRF with the TDS distribution at the end of year 2005 contoured. The model indicates increases in TDS in Zone A, but the increases are slight and limited to approximately a 1-mile radius from the site. Decreases in TDS concentration in the zones underlying Zone A indicate the presence of reclaimed water.

Figure 2 illustrates the simulated TDS concentration in Zone A from hypothetical wells located 0.25, 0.5, 1, 2, and 3 miles from the center of injection at the Southwest WRF. Model results indicate that at a distance of 0.25 miles from the site, the TDS concentration is predicted to increase from approximately 5,600 ppm to 6,700 ppm. At 1 mile from the site, the model predicts only a slight increase, from approximately 5,600 ppm to 6,100 ppm. This is considered to be within the range of discernible water quality changes, and the slight

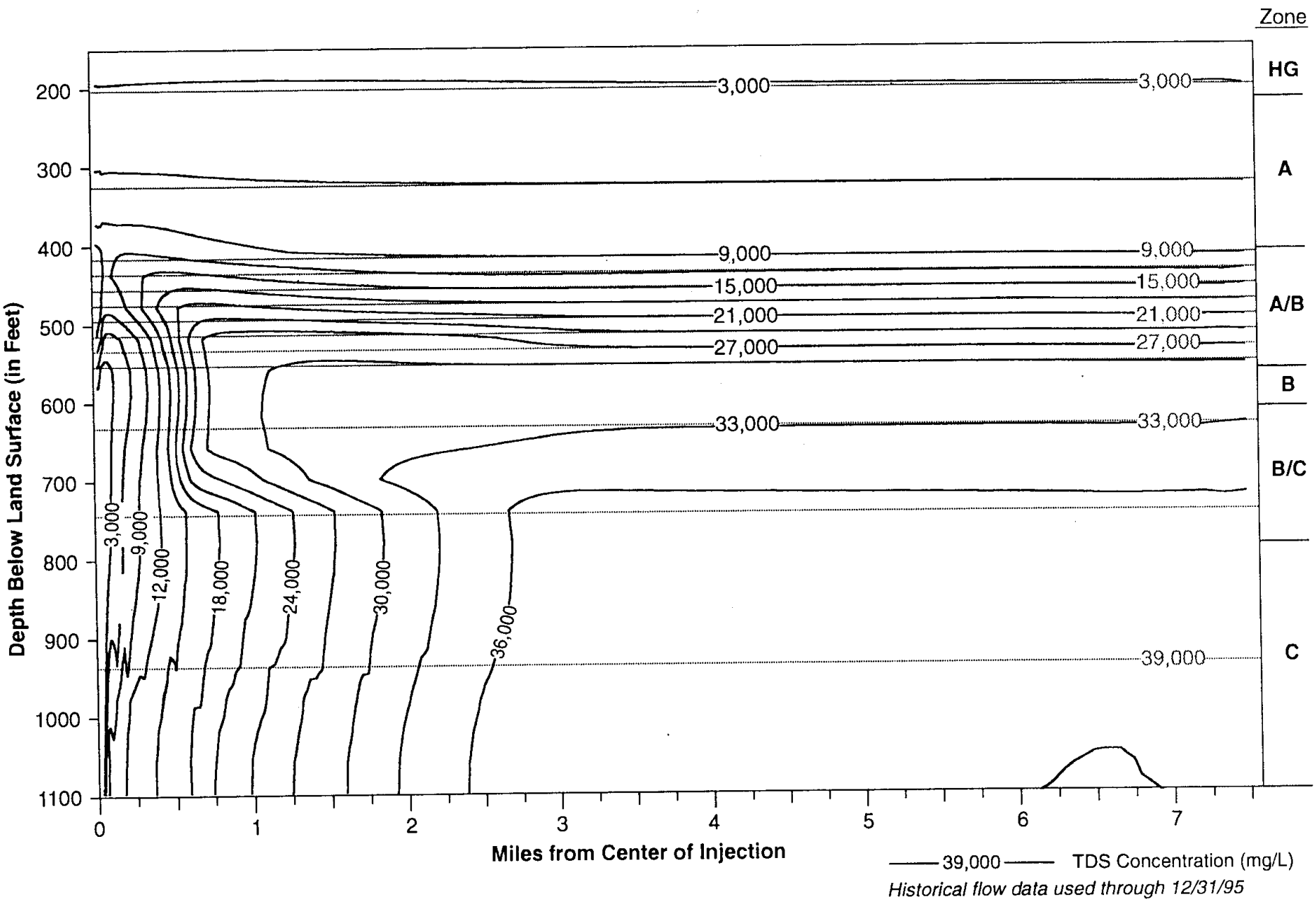

FIGURE 1
Solute Transport Model (Run SWPR-1)
Southwest WRF 9/10/79 - 12/31/05

CH2MHILL

Southwest WRF Predictive Model; Average TDS in Zone A

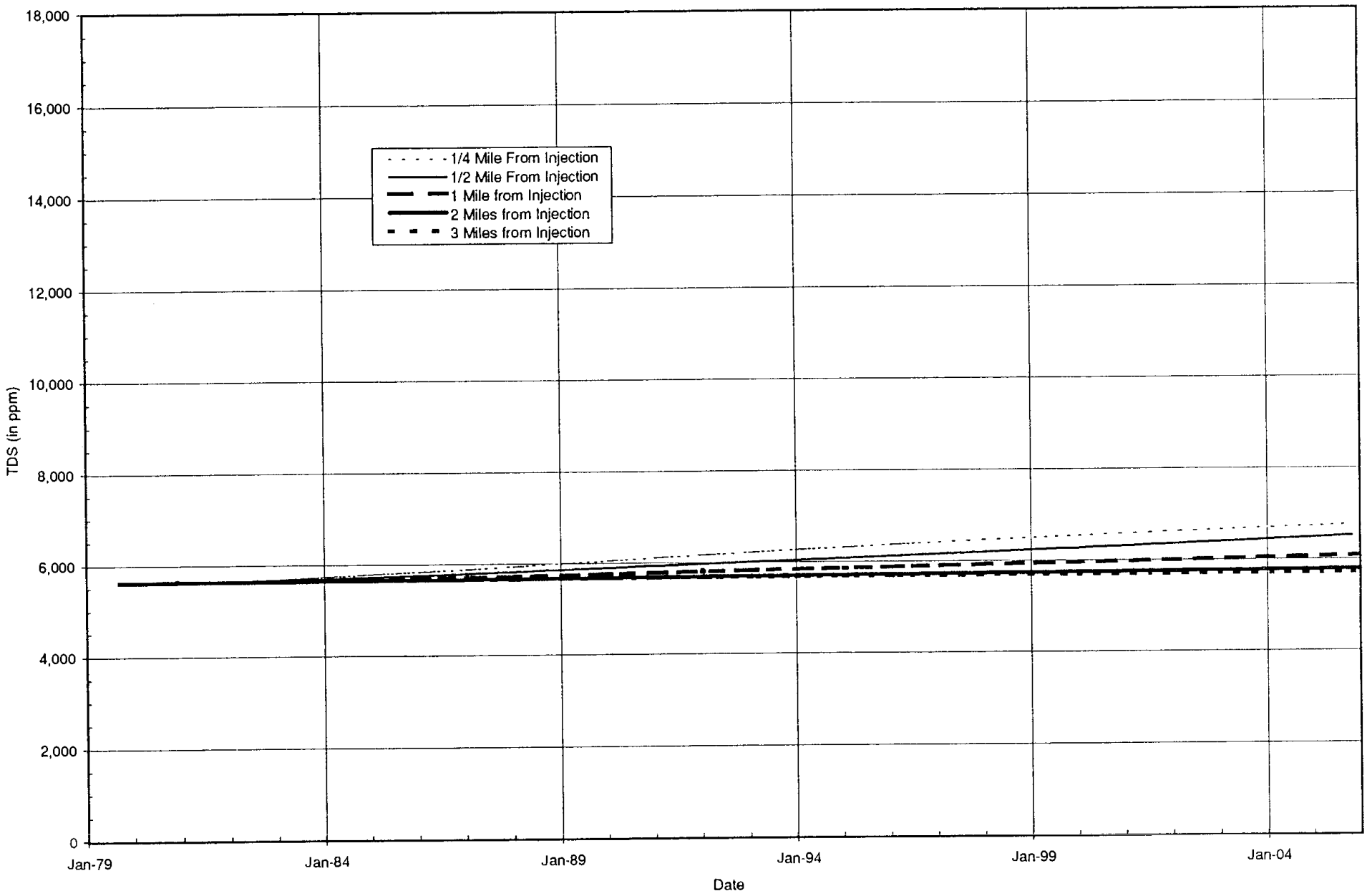

Figure 2

Southwest Chart 1 11/13/96

increase would not likely change the usability of this groundwater resource from previously available applications.

Figure 3 illustrates the simulated TDS concentration at the base of the USDW from hypothetical wells located 0.25, 0.5, 1, 2, and 3 miles from the center of injection. For the Southwest model, the bottom of the USDW occurs in the semi-confining unit below Zone A (semi-confining unit A/B) at an approximate depth of 420 feet below land surface. At a distance of 0.25 miles from the site, the simulated TDS concentration is predicted to increase from 10,000 ppm to a maximum value of approximately 13,000 ppm before dropping slightly after the year 2001. At a 1-mile distance from the center of injection, TDS concentrations at the base of the USDW are predicted to increase to approximately 11,700 ppm. At distances of 2 and 3 miles from the site, the model predicts a negligible TDS change at the base of the USDW.

Northwest WRF

Figure 4 shows the cross-section of the model at the Northwest WRF with the TDS distribution at the end of year 2005 contoured. Simulated water quality changes in Zone A are indicated within approximately 4000 feet of the injection well. Some freshening has occurred in Zone A, although at distances between 1,000 and 4,000 feet of the well, TDS concentrations increased only modestly. Freshening in the zones underlying Zone A in the vicinity of the injection well indicates the presence of reclaimed water.

Figure 5 illustrates the simulated TDS concentration in Zone A from hypothetical wells located 0.25, 0.5, 1, 2, and 3 miles from the site. The model predicts that at a distance of 0.25 miles from the site, the TDS concentration will increase from approximately 5,100 ppm to a maximum of 7,500 ppm in the year 2002, before freshening slightly following the arrival of reclaimed water. Beyond 1 mile, little discernible change in TDS is predicted in Zone A.

Figure 6 illustrates the simulated TDS concentration at the base of the USDW from hypothetical wells located 0.25, 0.5, 1, 2, and 3 miles from the site. For the Northwest model, the bottom of the USDW occurs in the semi-confining unit below zone A (semi-confining unit A/B) at an approximate depth of 360 feet below land surface. At a distance of 0.25 miles from the site, the simulated TDS concentration increased from 10,000 ppm to a maximum value of approximately 13,000 ppm in late 1994. By the end of the simulation, the TDS concentration 0.25 miles from the site is predicted to decrease to approximately 9,200 ppm. Beyond 1 mile from the site, the model predicts a slight increase in TDS at the base of the USDW. This increase would most likely be indiscernible beyond 2 miles from the injection well.

Albert Whitted WRF

Figure 7 shows the cross-section of the model for the Albert Whitted WRF with the TDS distribution at the end of the year 2005 contoured. Within 500 feet of the injection well, some freshening is predicted to occur in Zone A. Conversely, between 500 and 5,000 feet of the well, TDS concentrations are predicted to increase modestly. Model results indicate that freshening in zones above the injection zone will be restricted to an area within 1,000 feet of each injection well.

Southwest WRF Predictive Model; TDS at the Bottom of USDW

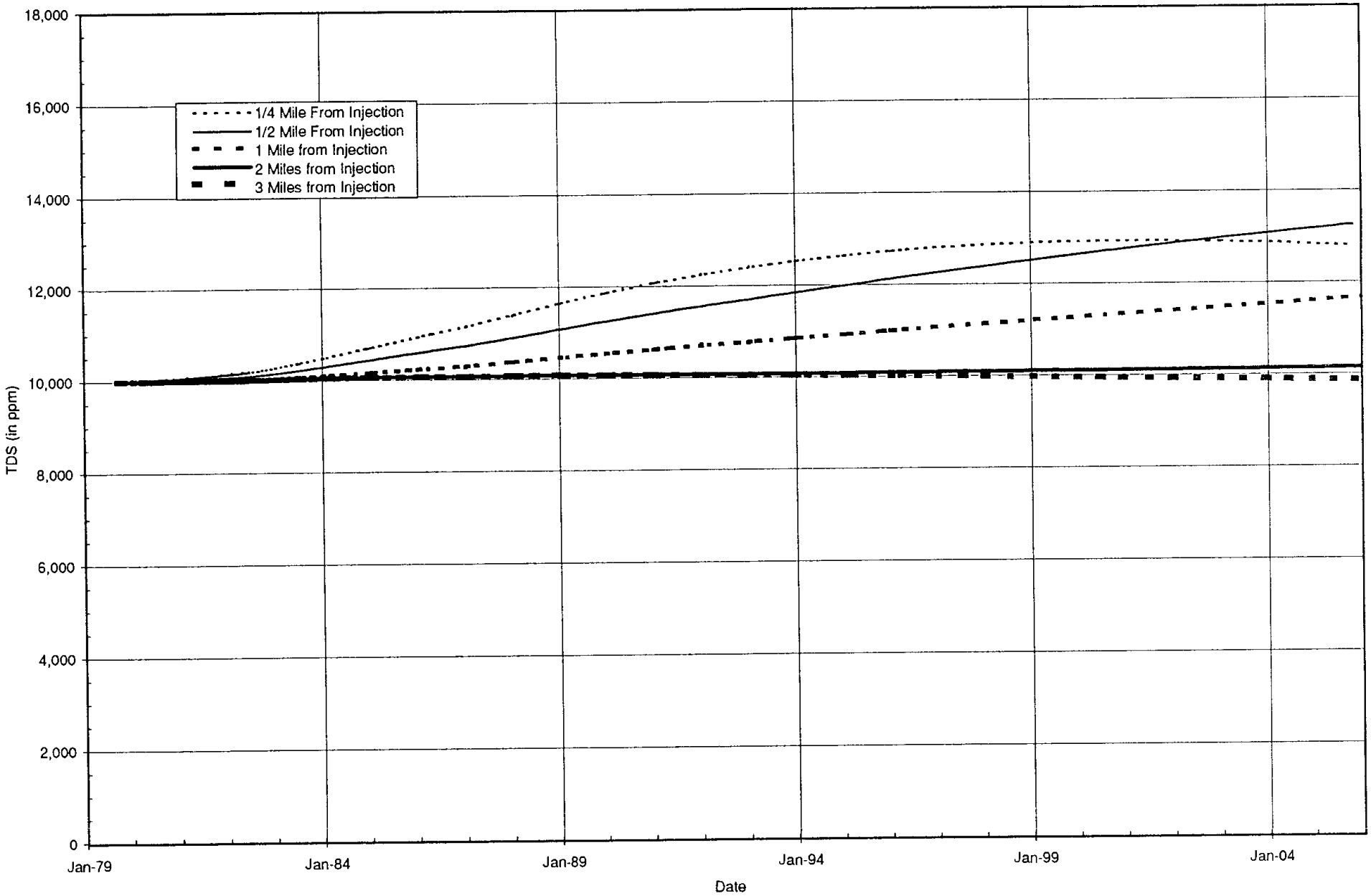

Figure 3

Southwest Chart 2 11/13/96

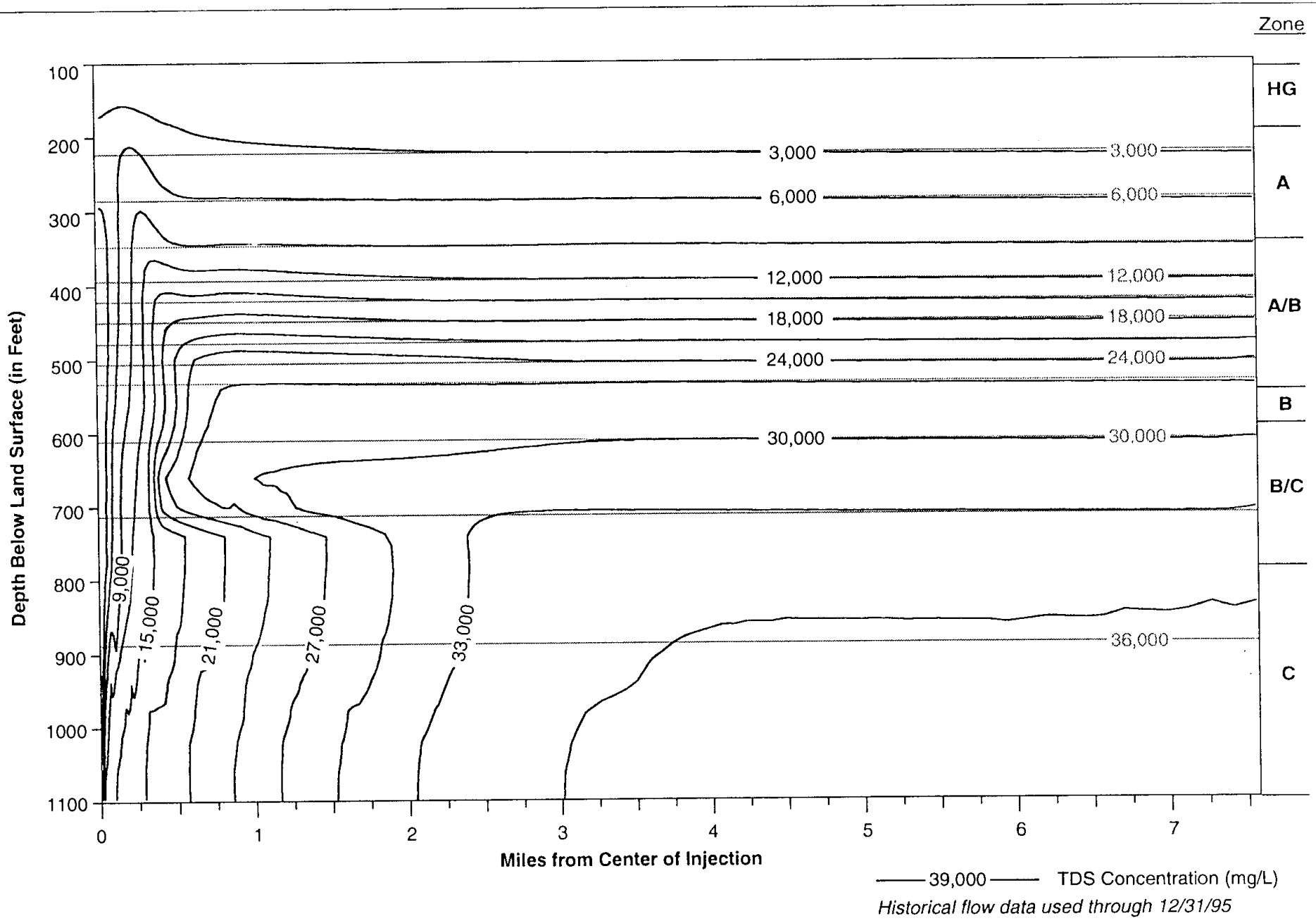

FIGURE 4
Solute Transport Model (Run NWPR-1)
Northwest WRF 1/1/85 - 12/31/05

CH2MHILL

Northwest WRF Predictive Model; Average TDS in Zone A

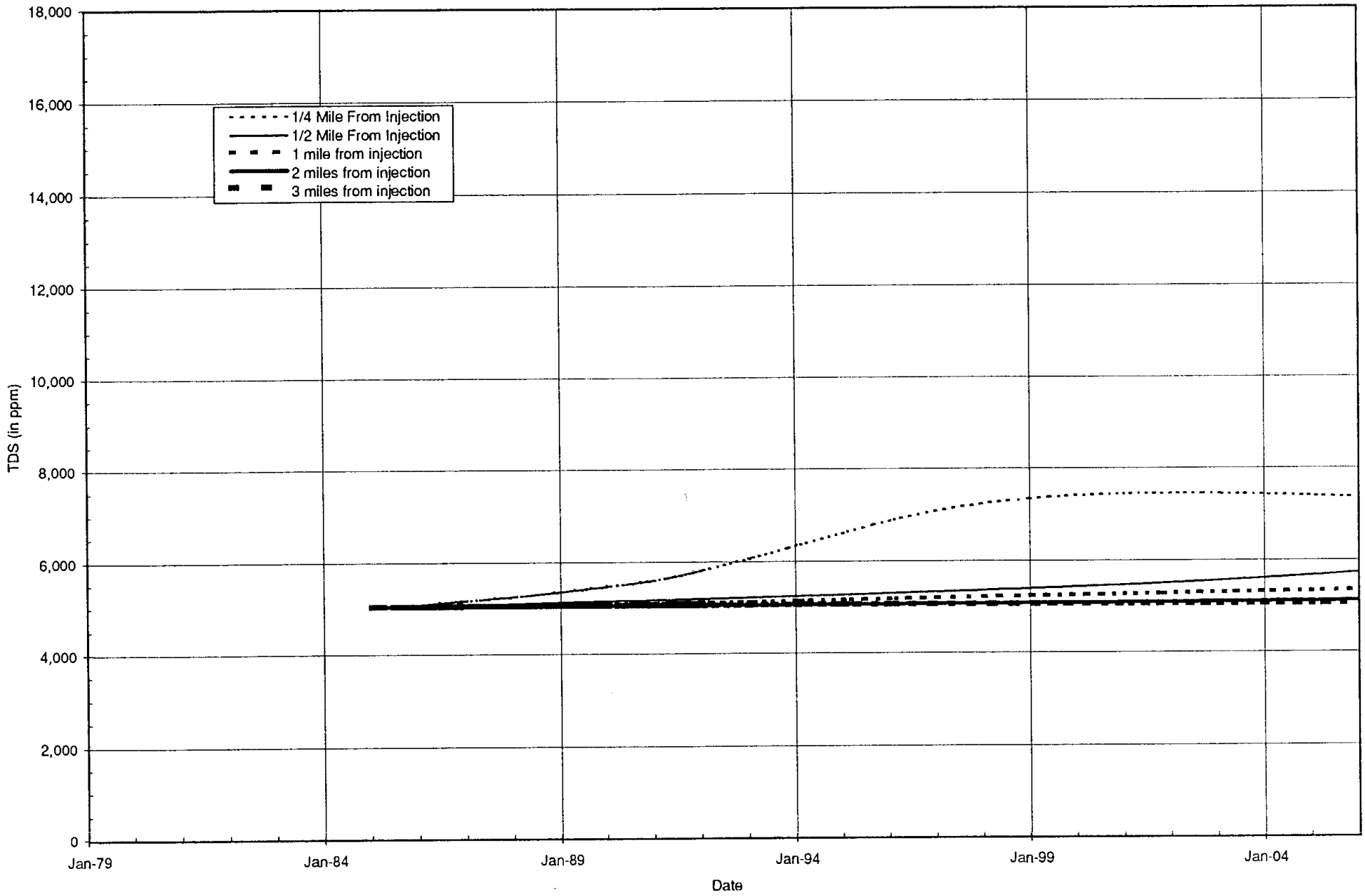

Figure 5

Northwest Chart 1 11/13/96

Northwest WRF Predictive Model; TDS at the Bottom of USDW

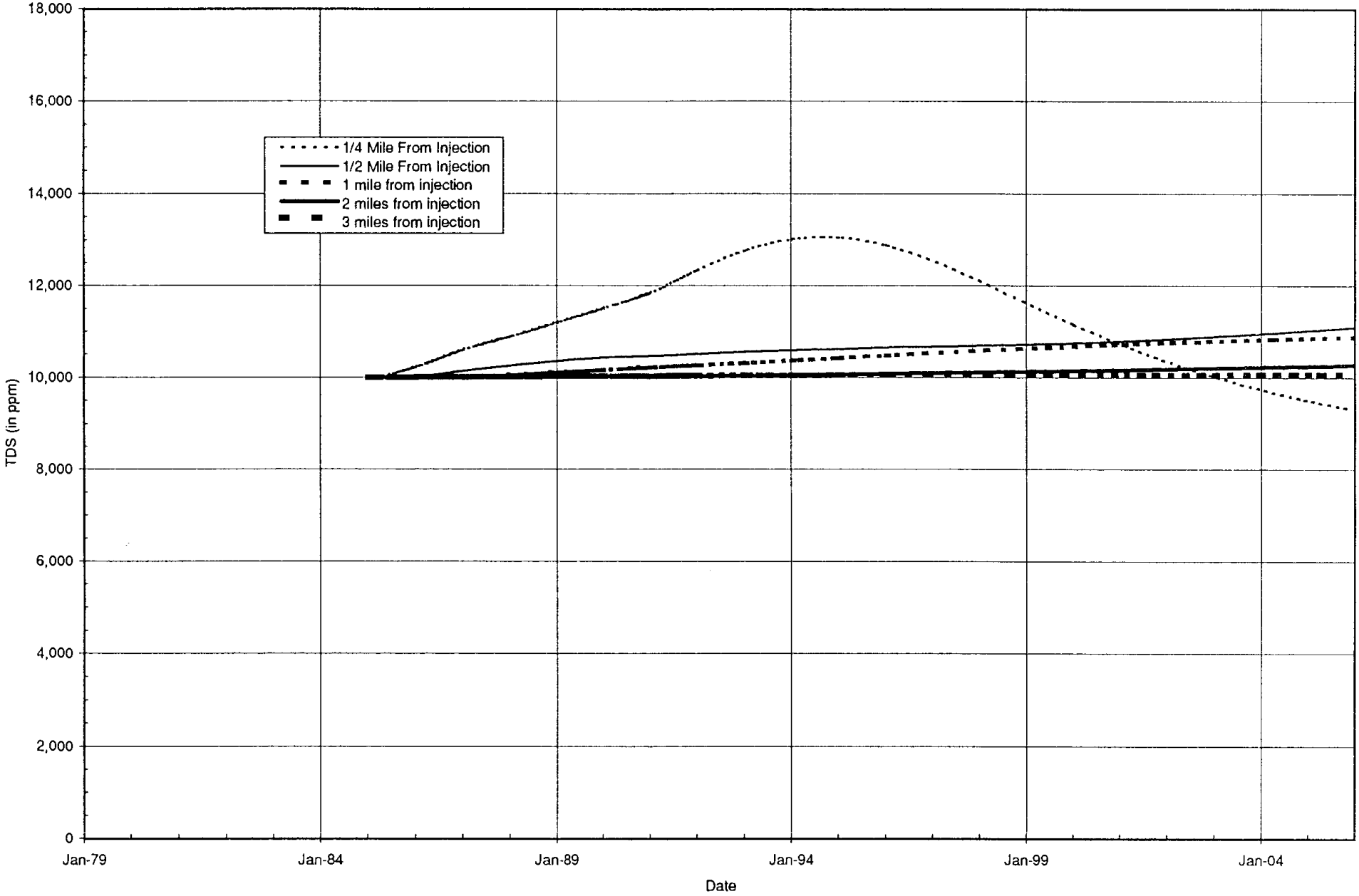

Northwest Chart 2 11/13/96

Figure 6

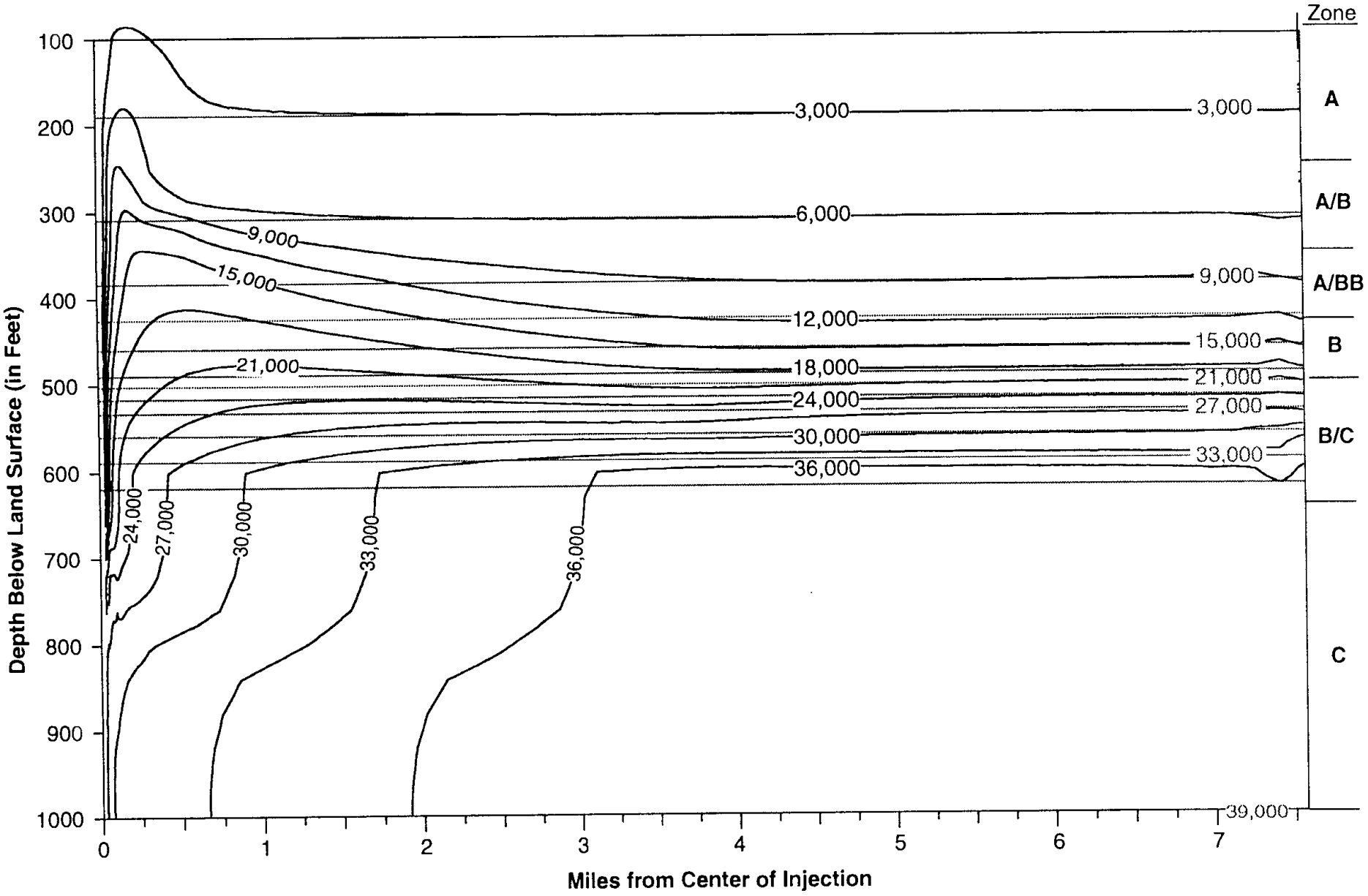

FIGURE 7
Solute Transport Model (Run AWPR-1)
Albert Whitted WRF 1/1/89 - 12/31/05

Historical flow data used through 12/31/95

CH2MHILL

Figure 8 illustrates the simulated TDS concentration in Zone A from hypothetical wells located 0.25, 0.5, 1, 2, and 3 miles from the site. As with the other models, the most significant changes in water quality are predicted to occur within 0.25 miles of the injection well. The model predicts that at a distance of 0.25 miles from the site, the TDS concentration will increase from approximately 3,000 ppm to approximately 6,000 ppm over the simulation period. At a distance of 0.5 miles from the site, however, only a modest increase in TDS concentration (to approximately 3,500 ppm) is predicted. At distances greater than 1 mile, no change is discernible at the end of year 2005.

Figure 9 illustrates the simulated TDS concentration at the base of the USDW from hypothetical wells located 0.25, 0.5, 1, 2, and 3 miles from the site. For the Albert Whitted model, the bottom of the USDW occurs in the permeable unit A/BB at an approximate depth of 400 feet below land surface. Significant increases in TDS concentration occur out to about 2 miles from the site. At a distance of 3 miles from the modeled injection well, a relatively modest increase in TDS concentration is predicted, from 10,000 ppm to approximately 11,200 ppm.

Northeast WRF

Figure 10 shows the cross-section of the model at the Northeast WRF with the TDS distribution at the end of year 2005 contoured. Water quality changes are primarily limited to zones below the USDW, as relatively low permeability semi-confining units at the site restrict vertical migration of injected fluids.

Competent confinement at the Northeast WRF is further demonstrated in Figure 11, which illustrates the simulated TDS concentration in Zone A from hypothetical wells located 0.25, 0.5, 1, 2, and 3 miles from the site. The model predicts only insignificant increases in TDS concentration, even at a distance of 0.25 miles from the site.

Figure 12 illustrates the simulated TDS concentration at the base of the USDW from hypothetical wells located 0.25, 0.5, 1, 2, and 3 miles from the site. For the Northeast WRF model, the bottom of the USDW is located in the middle of Zone A at a depth of approximately 200 feet below land surface. Because the base of the USDW occurs in Zone A, Figure 12 resembles Figure 11 very closely, showing only relatively insignificant increases in TDS concentrations even at a distance of 0.25 miles from the site.

Summary

Solute transport modeling is being used to evaluate historical and potential future water quality changes that may occur in the vicinity of each of the City of St. Petersburg's WRFs as a result of operation of the City's deep injection well systems. This modeling is being used as technical support for the City's pending Class V injection well operating permits, to provide the City and the regulatory agencies responsible for permitting the deep injection system with an understanding of the estimated water quality changes that may occur. Model conceptualization and calibration have been presented in previous technical memoranda submitted to the FDEP (STM-1 and STM-2). This technical memorandum presents the results of the initial predictive modeling conducted at each of the four injection sites.

Albert Whitted WRF Predictive Model; Average TDS in Zone A

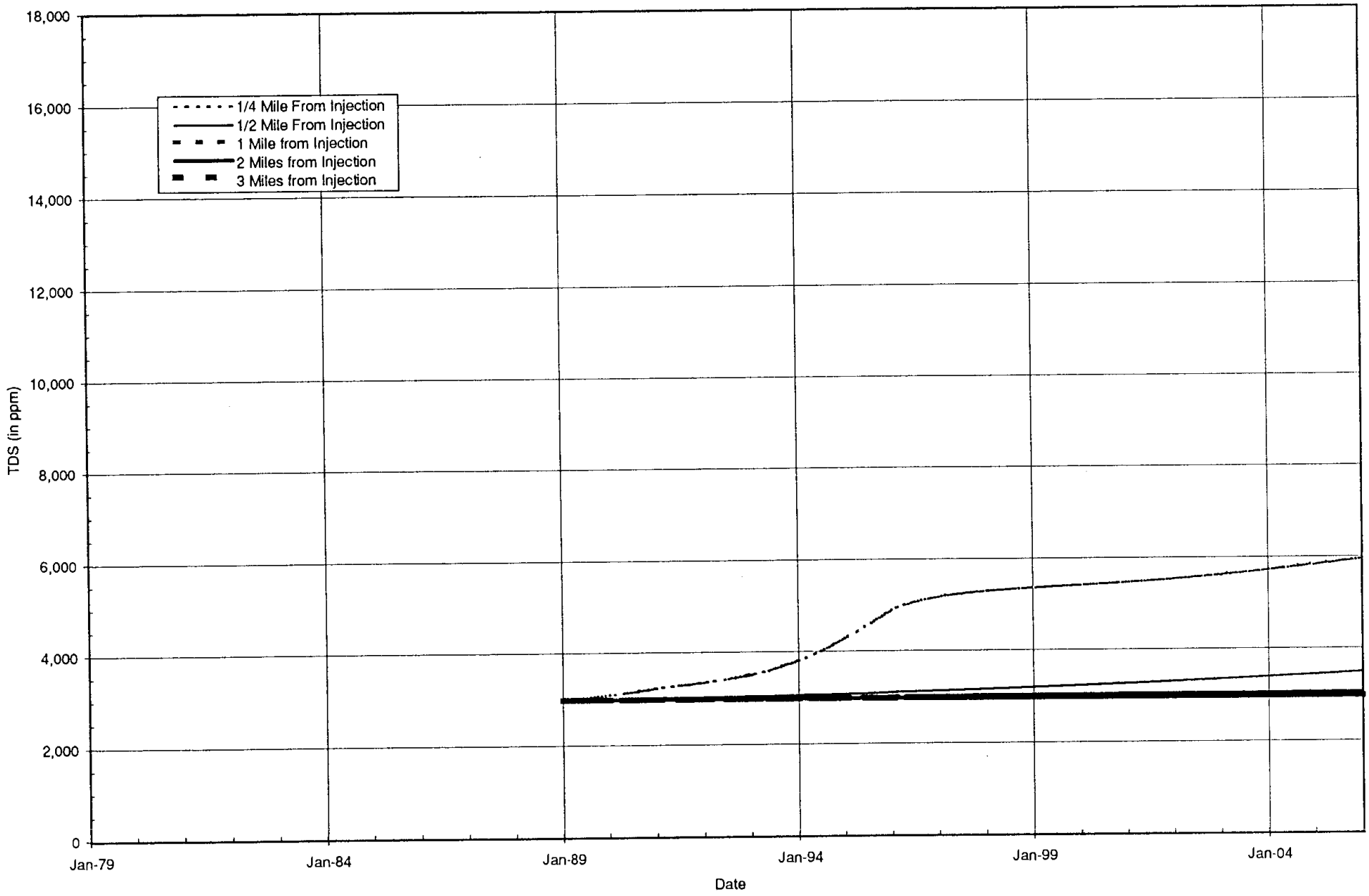

Figure 8

Albert Whitted Chart 1 11/13/96

Albert Whitted WRF Predictive Model; TDS at the Bottom of USDW

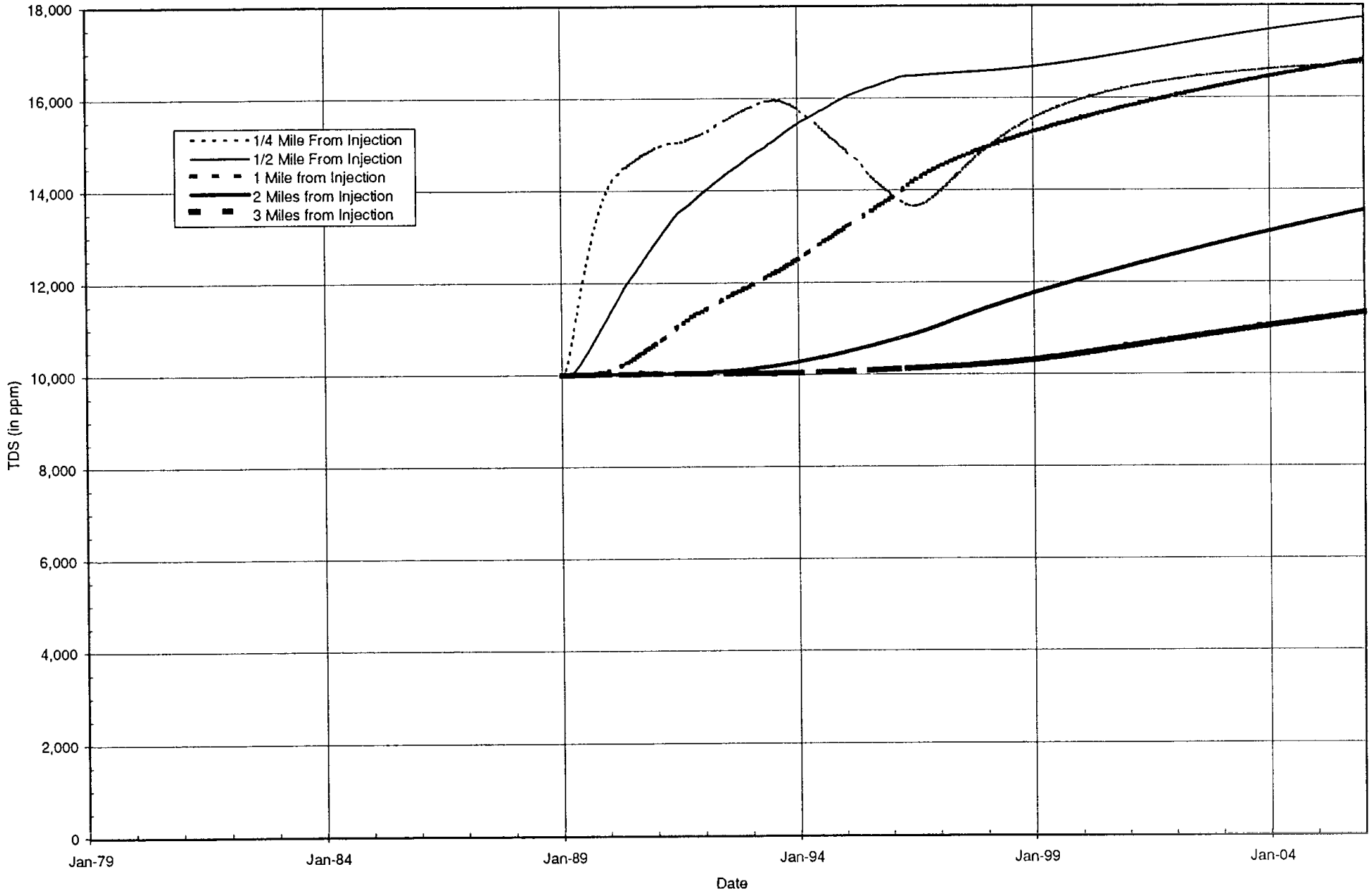

Figure 9

Albert Whitted Chart 2 11/13/96

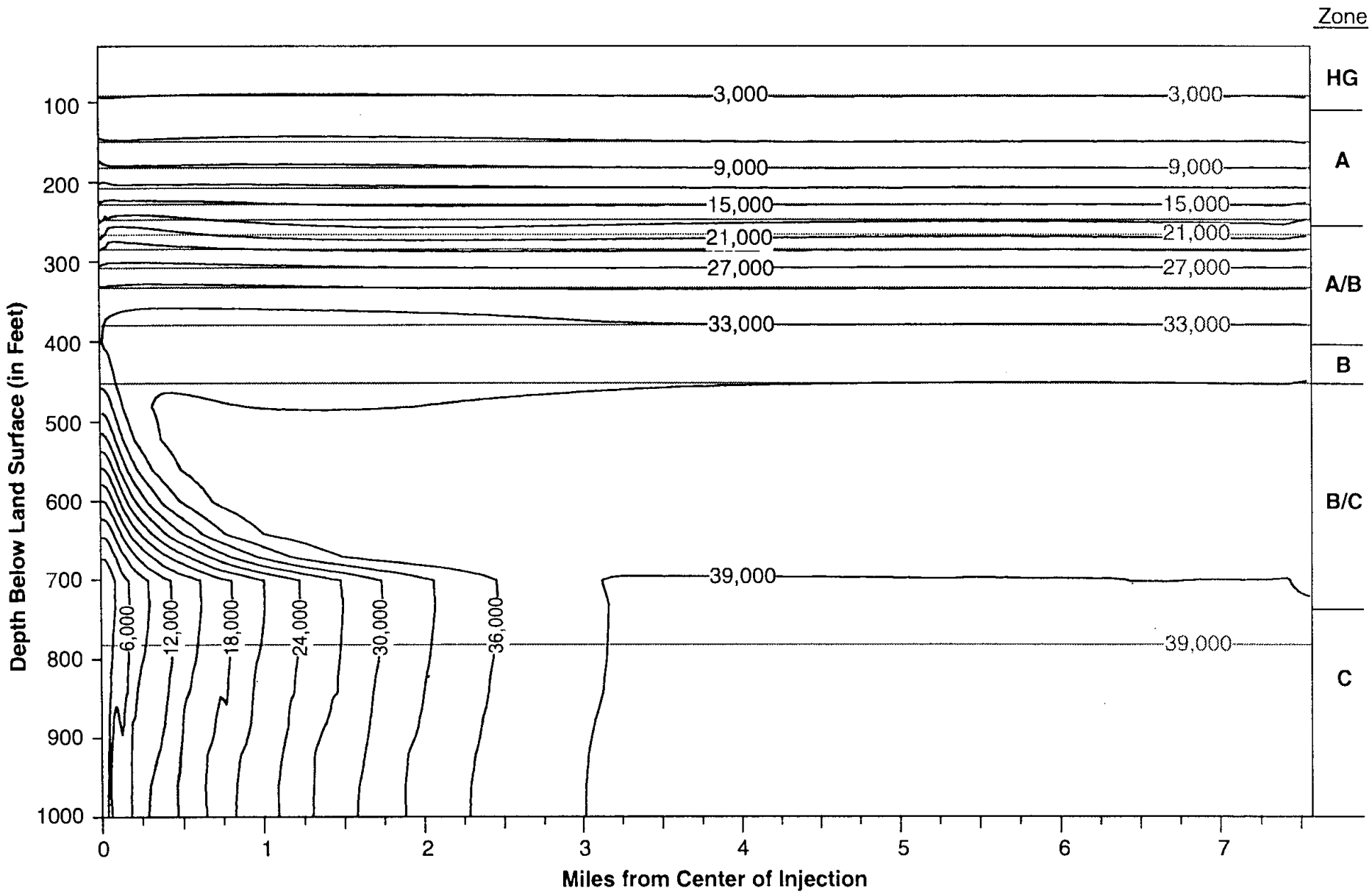

FIGURE 10
Solute Transport Model (Run NEPR-1)
Northeast WRF 6/9/80 - 12/31/05

CH2MHILL

Northeast WRF Predictive Model; Average TDS in Zone A

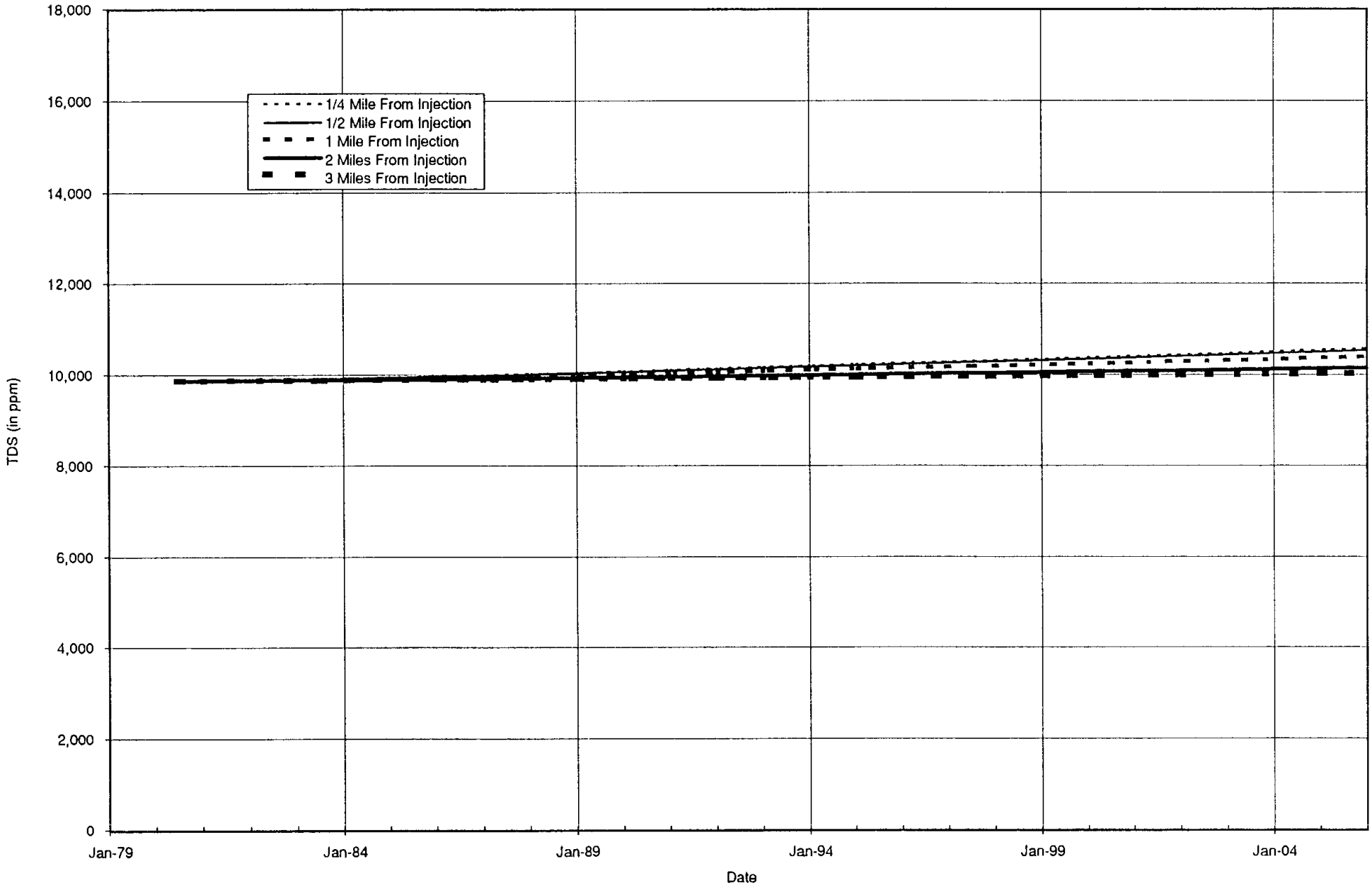

Northeast Chart 2 11/13/96

Figure 11

Northeast WRF Predictive Model; TDS at the Bottom of USDW

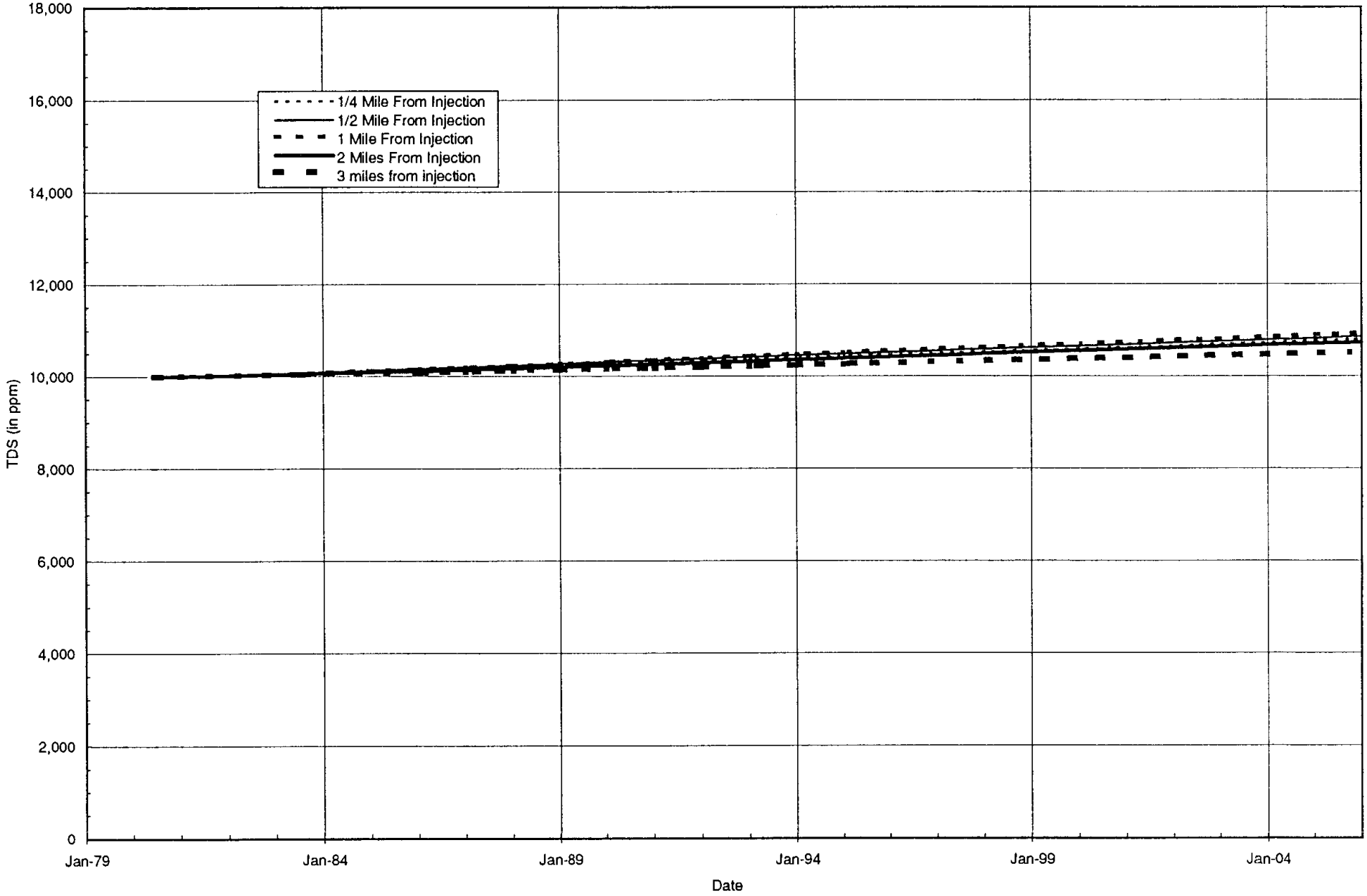

Northeast Chart 1 11/13/96

Figure 12

The predictive modeling used historical flow data through December 1995. An additional 10 years of projected flow data were used to estimate and evaluate the possibility of future water quality changes within the USDW at each site. The 10-year period represents two FDEP permitting cycles. Projected injection rates were estimated as minimum historical flows in response to conditions presented in this technical memorandum.

Discernible water quality changes at the base of the USDW can be expected to occur within the following approximate radial distances from each injection site:

- Albert Whitted WRF -- Up to 3 miles
- Northeast WRF -- 0.25 miles or less
- Northwest WRF -- 2 miles or less
- Southwest WRF -- 1 mile or less

In addition, discernible water quality changes in Zone A can be expected to occur within the following approximate radial distances from each injection facility:

- Albert Whitted WRF -- 0.5 miles or less
- Northeast WRF -- 0.25 miles or less
- Northwest WRF -- 0.5 miles or less
- Southwest WRF -- 0.25 miles or less

The predictive models suggest that outside of these radial distances, water quality changes—although they may occur—are expected to be indiscernible and insignificant, and should not restrict the potential to develop future groundwater resources relative to previously available uses.

The extent of predicted water quality changes at the base of the USDW at the Albert Whitted WRF is most likely an over-statement of what is actually occurring in the area. The model was calibrated to best-fit onsite monitoring data and assumes homogeneous conditions exist for approximately 7 miles surrounding this injection site. Conditions encountered at the other three injection sites, however, suggest that the Albert Whitted WRF hydrogeologic conditions are anomalous and indicate that a localized fracture most likely exists in the area. To assume that this degree of leakance exists beyond a very short distance from the wells is to be overly conservative in estimating water quality changes that may be occurring at distance.

The results of the predictive modeling are reasonable and largely consistent with historical observed data, except for the monitoring data available from the Northeast WRF injection system. Reasons for the difference between observed and modeled water quality changes at the Northeast WRF are primarily a result of integrity problems associated with the cluster well, as discussed in detail in STM-2, which have been repaired. The modeled results are supported by the minimal amount of reclaimed water which has arrived at the lowermost monitoring interval (M-2) at the Northeast WRF.

Recommendations

Based on the results of the initial predictive modeling, CH2M HILL offers the following recommendations:

1. Continue to operate the injection wells on an as-needed basis as a backup to the reclaimed water reuse program. The solute transport modeling conducted to date suggests that water quality changes observed with the deep injection well program are localized and will not adversely impact future water resource availability in southern Pinellas County.

2. Continue pursuing the reclassification of the existing Class I deep injection wells to Class V. Solute transport modeling suggests that salinity increases are predicted to continue at the base of the USDW and in Zone A within a short distance of each WRF. Class V injection system regulations are not as stringent in restricting fluid movement across the base of the USDW. The deep injection system currently functions more as a Class V injection system than as a typical Florida Class I domestic injection well.

3. Continue to develop additional reuse customers, as available, to further decrease the amount of future injection to the deep injection wells. Investigate reclaimed water ASR as a method to seasonally store and re-use excess available reclaimed water during the wet periods.

4. Meet with FDEP to discuss the results of the solute transport modeling used to support issuance of Class V operating permits for the City's deep injection well program.

APPENDIX A

Conceptual Model Layout and Input Properties

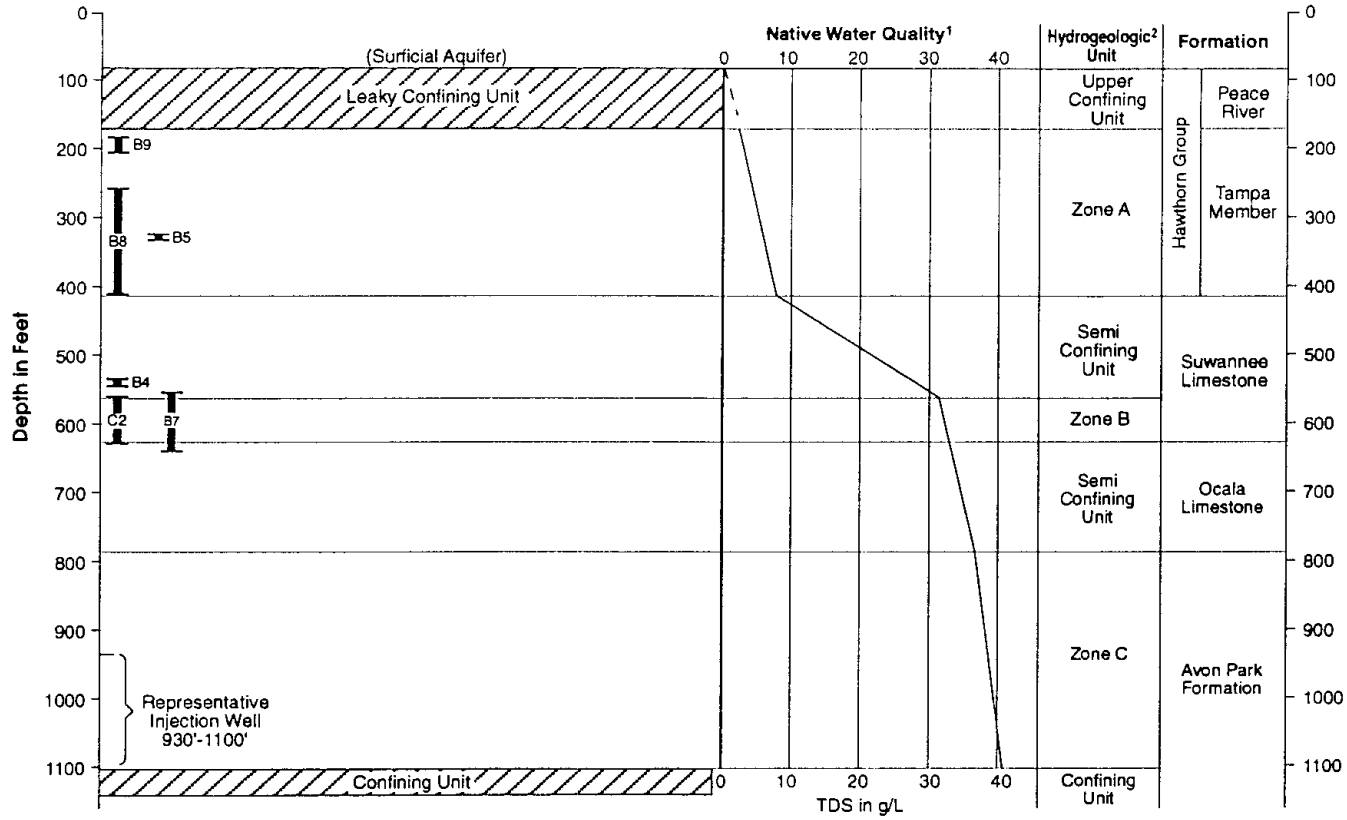

1 Water Quality Adapted from Hickey (1979) and CH2M HILL (Aug. 1982)
2 Hydrologic Unit Depths from Hickey (1982)
Monitoring Zones

Note: No Horizontal Scale

FIGURE A-3
Southwest WRF Conceptual Model Layout

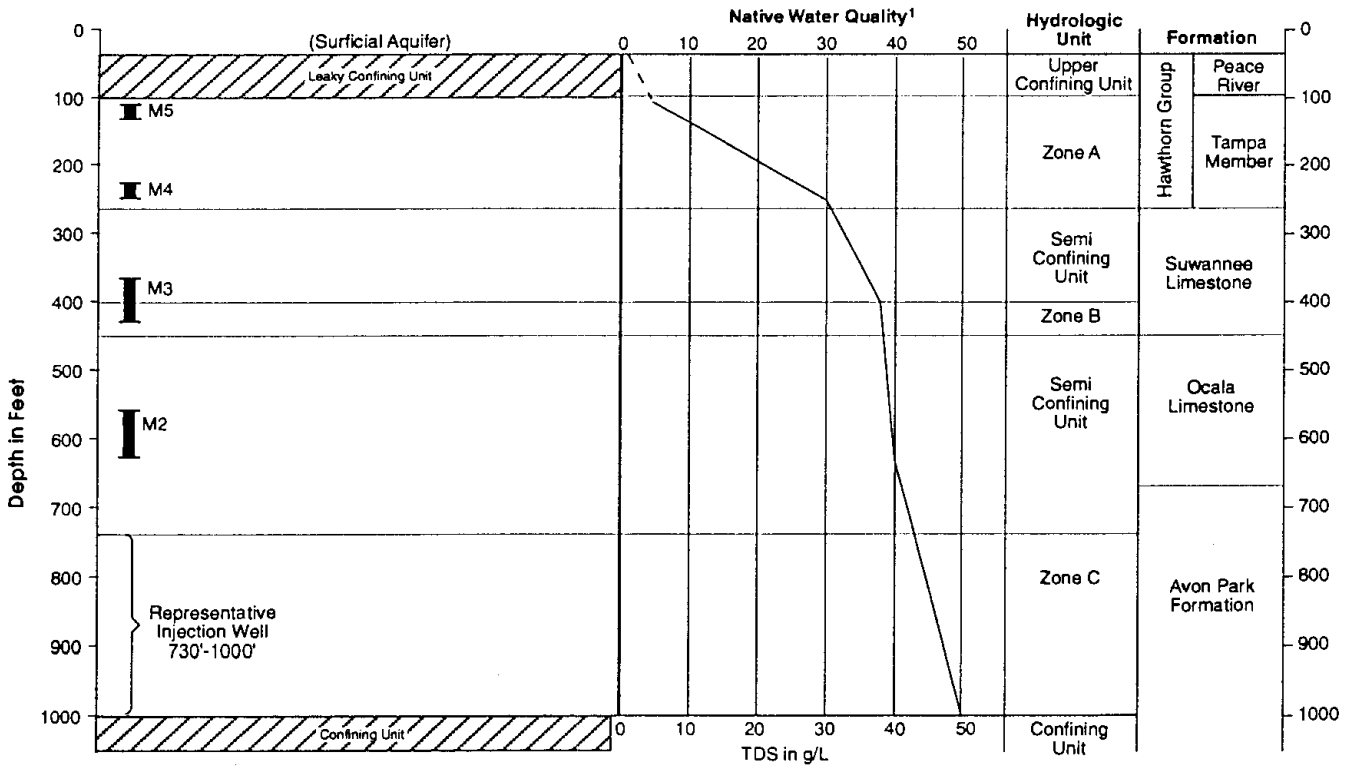

1 Water quality data from background samples at monitoring wells and reverse-air samples during drilling

Monitoring Zones

Note: No Horizontal Scale

FIGURE A-4
Northeast WRF Conceptual Model Layout

Table A-1
Constants Used For Solute Transport Model Calibration

Fluid and Solute Properties:

Fluid Compressibility	3.03×10^{-6}	psi^{-1}	
Fluid Temperature	82	° F	(constant throughout simulation)
Fluid Viscosity	0.8418	cp	(Viscosity is constant w/ TDS)
Molecular Diffusivity	9.0×10^{-7}	ft^2/day	
Fluid Density (at atmospheric pressure and 82° F)			(density varies with depth according
At 0.0 ppm TDS	62.17	lb/ft^3	to fluid compressibility)
At 50,000 ppm TDS	64.45	lb/ft^3	(Density is extrapolated linearly)
TDS of Injected Fluid:			
For Southwest Model	600	ppm	
For Northeast Model	900	ppm	
For Northwest Model	1000	ppm	
For Albert Whitted Model	400	ppm	

Table A-2 - City of St. Petersburg Solute Transport Model Calibration

Porous Media Zone	Parameter	Model Calibration Properties				Reported Regional Range	
		AW WRF	NE WRF	NW WRF	SW WRF	Max	Min
Hawthorn Group	Horiz. Cond. (fpd)	0.07	0.07	0.07	0.07	0.07	0.0008
	Vert. Cond. (fpd)	0.007	0.007	0.007	0.007	0.007	0.007
	Porosity (%)	35	35	35	35	35	30
	Specific Storage (ft^{-1})	3.1×10^{-5}	3.1×10^{-5}	3.1×10^{-5}	3.1×10^{-5}	3.1×10^{-5}	3.1×10^{-5}
	Long. Dispersivity (ft)	50	50	50	50	50	12.5
	Trans. Dispersivity (ft)	10	10	10	10	10	2.5
	Depth Interval (feet bls)	40 - 115	30 - 105	40 - 190	150 - 210	N/D	N/D
Zone A	Horiz. Cond. (fpd)	126	63	10	126	167	125
	Vert. Cond. (fpd)	12.6	6.3	0.5	12.6	12.5	12.5
	Porosity (%)	25	25	30	25	30	10
	Specific Storage (ft^{-1})	1.5×10^{-6}	1.5×10^{-6}	1.5×10^{-6}	1.5×10^{-6}	1.6×10^{-6}	1.6×10^{-6}
	Long. Dispersivity (ft)	50	50	50	50	50	12.5
	Trans. Dispersivity (ft)	10	10	10	10	10	2.5
	Depth Interval (feet bls)	115 - 250	105 - 260	190 - 340	210 - 410	N/D	N/D
Semi-Confining Unit A/B	Horiz. Cond. (fpd)	5	0.1	5	0.1	5	0.1
	Vert. Cond. (fpd)	2	0.01	2	0.01	2	0.0013
	Porosity (%)	10	15	15	15	35	25
	Specific Storage (ft^{-1})	1.0×10^{-6}	1.1×10^{-6}	1.1×10^{-6}	1.1×10^{-6}	1.2×10^{-6}	1.2×10^{-6}
	Long. Dispersivity (ft)	50	50	50	50	50	12.5
	Trans. Dispersivity (ft)	10	10	10	10	10	2.5
	Depth Interval (feet bls)	250 - 350	260 - 400	340 - 540	410 - 560	N/D	N/D
Permeable Unit A/BB	Horiz. Cond. (fpd)	40	N/M	N/M	N/M	N/M	N/M
	Vert. Cond. (fpd)	10	N/M	N/M	N/M	N/M	N/M
	Porosity (%)	5	N/M	N/M	N/M	N/M	N/M
	Specific Storage (ft^{-1})	9.4×10^{-7}	N/M	N/M	N/M	N/M	N/M
	Long. Dispersivity (ft)	50	N/M	N/M	N/M	N/M	N/M
	Trans. Dispersivity (ft)	10	N/M	N/M	N/M	N/M	N/M
	Depth Interval (feet bls)	350 - 430	N/M	N/M	N/M	N/M	N/M
Zone B	Horiz. Cond. (fpd)	59	59	59	59	60	60
	Vert. Cond. (fpd)	20	5.9	5.9	5.9	6	6
	Porosity (%)	5	15	15	15	25	10
	Specific Storage (ft^{-1})	9.4×10^{-7}	1.1×10^{-6}	1.1×10^{-6}	1.1×10^{-6}	1.2×10^{-6}	1.2×10^{-6}
	Long. Dispersivity (ft)	50	50	50	50	50	12.5
	Trans. Dispersivity (ft)	10	10	10	10	10	2.5
	Depth Interval (feet bls)	430 - 480	400 - 450	540 - 590	560 - 620	N/D	N/D
Semi-Confining Unit B/C	Horiz. Cond. (fpd)	50	1	5	5	5	0.5
	Vert. Cond. (fpd)	20	0.1	4	1	2	0.0014
	Porosity (%)	5	15	15	15	35	15
	Specific Storage (ft^{-1})	9.5×10^{-7}	1.1×10^{-6}	1.1×10^{-6}	1.1×10^{-6}	1.2×10^{-6}	1.2×10^{-6}
	Long. Dispersivity (ft)	50	50	50	50	50	12.5
	Trans. Dispersivity (ft)	10	10	10	10	10	2.5
	Depth Interval (feet bls)	480 - 630	450 - 730	590 - 780	620 - 780	N/D	N/D
Zone C	Horiz. Cond. (fpd)	8100	4274	4274	2500	8100	2500
	Vert. Cond. (fpd)	810	855	855	500	855	500
	Porosity (%)	10	10	10	10	20	10
	Specific Storage (ft^{-1})	1.0×10^{-6}	1.0×10^{-6}	1.0×10^{-6}	1.0×10^{-6}	1.0×10^{-6}	1.0×10^{-6}
	Long. Dispersivity (ft)	100	100	100	100	50	12.5
	Trans. Dispersivity (ft)	20	20	20	20	10	2.5
	Depth Interval (feet bls)	630 - 1000	730 - 1000	780 - 1100	780 - 1100	N/D	N/D

Legend

N/M: Not modeled
N/D: Not determined

Preliminary Assessment of Injection, Storage, and Recovery of Freshwater in the Lower Hawthorn Aquifer, Cape Coral, Florida

By Vicente Quiñones-Aponte *and* Eliezer J. Wexler

U.S. Geological Survey

Water-Resources Investigations Report 94-4121

Prepared in cooperation with the

City of Cape Coral and the
South Florida Water Management District

Tallahassee, Florida
1995

U.S. DEPARTMENT OF THE INTERIOR
BRUCE BABBITT, Secretary

U.S. GEOLOGICAL SURVEY
Gordon P. Eaton, Director

For additional information
write to:

District Chief
U.S. Geological Survey
Suite 3015
227 N. Bronough Street
Tallahassee, FL 32301

Copies of this report can be
purchased from:

U.S. Geological Survey
Earth Science Information Center
Open-File Reports Section
Box 25286, MS 517
Denver Federal Center
Denver, CO 80225

CONTENTS

FIGURES

TABLES

CONVERSION FACTORS, VERTICAL DATUM, AND ADDITIONAL ABBREVIATIONS

Multiply	By	To obtain
millimeter (mm)	0.03937	inch
millimeter per year (mm/yr)	0.03937	inch per year
meter (m)	3.281	foot
meter per second (m/s)	3.281	foot per second
meter per day (m/d)	3.281	foot per day
kilometer (km)	0.6214	mile
square meter (m^2)	10.76	square foot
meter squared per second (m^2/s)	10.76	foot squared per second
meter squared per day (m^2/d)	10.76	foot squared per day
square kilometer (km^2)	0.3861	square mile
cubic meter (m^3)	35.31	cubic foot
cubic meter (m^3)	264.2	gallon
cubic meter per second (m^3/s)	264.2	gallon per second
cubic meter per day (m^3/d)	264.2	gallon per day
liter per second per meter (L/s/m)	4.831	gallon per minute per foot
kilogram per meter per second (kg/m/s)	0.6716	pound mass per foot per second
kilogram per meter per second squared ($kg/m/s^2$)	0.6716	pound mass per foot per second squared
kilogram per cubic meter (km/m^3)	0.0624	pound per cubic foot

Sea level: In this report, “sea level” refers to the National Geodetic Vertical Datum of 1929 (NGVD of 1929)—a geodetic datum derived from a general adjustment of the first-order level nets of both the United States and Canada, formerly called Sea Level Datum of 1929.

The standard unit for transmissivity (T) is cubic meter per day per square meter times meter of aquifer thickness. This mathematical expression reduces to meter squared per day.

Temperature in degrees Celsius (°C) can be converted to degrees Fahrenheit (°F) as follows:
°F = 1.8(°C) + 32

Additional Abbreviations

RO = reverse osmosis
SISRF = subsurface injection, storage, and recovery of freshwater
SUTRA = **S**aturated-**U**nsaturated **TRA**nsport
mg/L = milligrams per liter

Preliminary Assessment of Injection, Storage, and Recovery of Freshwater in the Lower Hawthorn Aquifer, Cape Coral, Florida

By Vicente Quiñones-Aponte *and* Eliezer J. Wexler

Abstract

A preliminary assessment of subsurface injection, storage and recovery of fresh canal water was made in the naturally brackish lower Hawthorn aquifer in Cape Coral, southwestern Florida. A digital modeling approach was used for this preliminary assessment, incorporating available data on hydrologic conditions, aquifer properties, and water quality to simulate density-dependent ground-water flow and advective-dispersive transport of a conservative ground-water solute (chloride ion).

A baseline simulation was used as reference to compare the effects of changing various operational factors on the recovery efficiency. A recovery efficiency of 64 percent was estimated for the baseline simulation. Based on the model, the recovery efficiency increases if the injection rate and recovery rates are increased and if the ratio of recovery rate to injection rate is increased. Recovery efficiency decreases if the amount of water injected is increased; slightly decreases if the storage time is increased; is not changed significantly if the water is injected to a specific flow zone; increases with successive cycles of injection, storage, and recovery; and decreases if the chloride concentrations in either the injection water or native aquifer water are increased. In everal hypothetical tests, the recovery efficiency fluctuated between 22 and about 100 percent.

Two successive cycles could bring the recovery efficiency from 60 to about 80 percent. Interlayer solute mass movement across the upper and lower boundaries seems to be the most important factor affecting the recovery efficiency. A sensitivity analysis was performed applying a technique in which the change in the various factors and the corresponding model responses are normalized so that meaningful comparisons among the responses could be made. The general results from the sensitivity analysis indicated that the permeabilities of the upper and lower flow zones were the most important factors that produced the greatest changes in the relative sensitivity of the recovery efficiency. Almost equally significant changes occurred in the relative sensitivity of the recovery efficiency when all porosity values of the upper and lower flow zones and the leaky confining units and the vertical anisotropy ratio were changed.

The advective factors are the most important in the Cape Coral area according to the sensitivity analysis. However, the dispersivity values used in the model were extrapolated from studies conducted at the nearby Lee County Water Treatment Plant, and these values might not be representative of the actual dispersive characteristics of the lower Hawthorn aquifer in the Cape Coral area.

INTRODUCTION

Cape Coral, a coastal suburban community in western Lee County (fig. 1), is a fast growing city in southwestern Florida, with the population increasing at a rate of 8.5 percent during the year ending in April 1989 (City of Cape Coral, Planning Division, written commun., 1989). The city had less than 500 residents in 1960, but became the largest city in Lee County by 1983. The number of permanent residents in 1990 was estimated at more than 73,600. Temporary residents from the northern United States and Canada typically increase the population by about 20 percent during the winter months (City of Cape Coral, Planning Division, 1988).

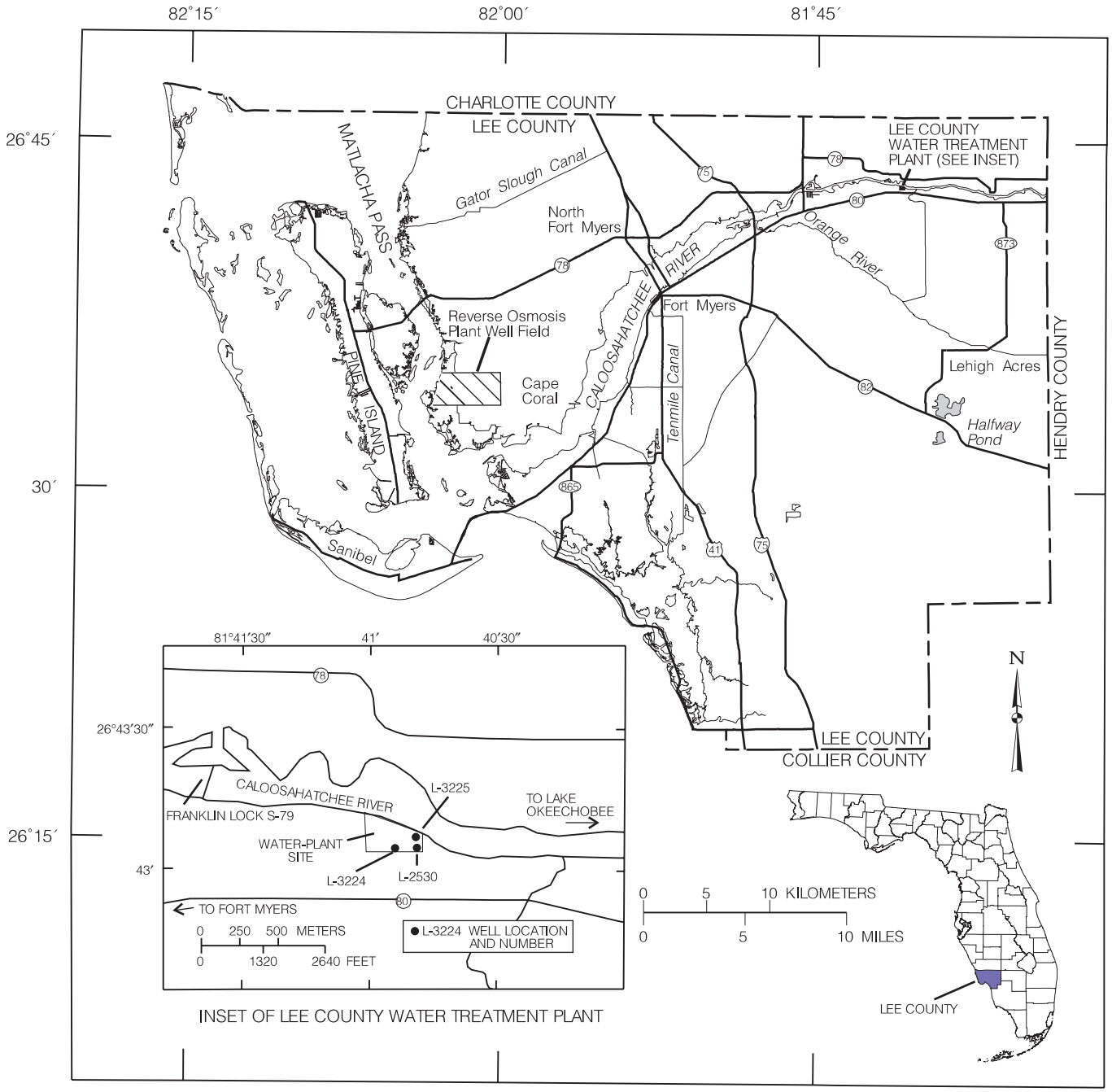

Figure 1. Location of the Cape Coral study area, wells, and the Lee County Water Treatment Plant site.

The rapidly increasing population has placed a stress on the potable water supply for Lee County. The upper Hawthorn aquifer (also referred to as the mid-Hawthorn aquifer) is the principal source of fresh ground water in Cape Coral. This aquifer is moderately permeable and has been subjected to severe drawdowns, particularly during a recent 3-year drought period (1989-91). At present (1994), the most reliable municipal water supply to Cape Coral (and nearby Pine Island) is brackish water from the lower Hawthorn aquifer that is treated at a 52,990 m^3/d reverse-osmosis (RO) plant. Drawdowns in this moderately permeable aquifer have also been substantial. Increased population and water demands in Charlotte County to the north and upgradient of Cape Coral could have an effect on the amount of water available in the two aquifers.

Demand for water is seasonal with peak use occurring during the dry season (November-April) when monthly precipitation averages less than 51 mm (National Oceanic and Atmospheric Administration,

1944-88). Lawn, golf course, agricultural irrigation, and public-supply demands are highest during this period. Temporary water-use restrictions have been implemented occasionally during recent years because of drought conditions and could become permanent as the demand for water becomes more acute.

Alternative water supplies or a means of augmenting existing supplies is a major concern to water-management officials. For this reason, the U.S. Geological Survey, in cooperation with the City of Cape Coral and the South Florida Water Management District, began a study in October 1986 to assess the feasibility of subsurface injection, storage, and recovery of freshwater (SISRF) in Cape Coral. The objectives of the study were to: (1) define the runoff pattern of the freshwater canal system, (2) assess quantities of excess runoff occurring during the wet season, and (3) assess the feasibility of conserving the excess runoff through subsurface storage. This report involves the development and testing of a digital model for assessing hypothetical SISRF tests in Cape Coral.

Although a site seems favorable for SISRF, the recovery efficiency at a particular site can only be determined by establishing a full-scale test facility and conducting full cycle testing under various conditions. Pilot tests are generally too expensive for preliminary assessments, such as this study. However, recent SISRF tests conducted by the U.S. Geological Survey at the Lee County Water Treatment Plant (Fitzpatrick, 1986a) can provide information, which when supplemented with less expensive computer-modeling techniques, yield usable preliminary information on recovery efficiency for an SISRF operation in Cape Coral.

Purpose and Scope

This report presents the results of a preliminary assessment of the subsurface injection, storage, and recovery operation in the lower Hawthorn aquifer in Cape Coral, Fla., using a digital modeling technique. Model simulations were made to assess: (1) recovery efficiencies for injected water; (2) the effect of repeated cycles, length of storage period, injection rates, and volumes of injected water on recovery efficiency; and (3) the relation between recovery efficiencies and the uncertainty in values for hydrogeologic properties. Hydrogeologic data from boreholes in Cape Coral and at the Lee County Water Treatment Plant were used to estimate hydraulic characteristics of the lower Hawthorn aquifer.

A modified SUTRA (**S**aturated-**U**nsaturated **TRA**nsport) ground-water flow and solute-transport digital model was used for the simulations. Data from an earlier study at the Lee County Water Treatment Plant were used to calibrate and test the model, and the model was then applied to simulate a hypothetical injection and recovery operation in Cape Coral. Nearly 30 simulations calculated recovery efficiencies for various changes in injection and recovery rates, volumes of water injected, storage time, and solute concentrations.

Description of Study Area

The city of Cape Coral occupies an area of 259 km^2 in Lee County, southwestern Florida (fig. 1). The development of the area, originally a low-lying pineland subject to frequent flooding, began in 1958 and continued to the early 1960's with the construction of a 724-km drainage canal system that interlaces the entire area (Knapp and others, 1984).

The Cape Coral watershed is similar to most southern Florida watersheds in that it is characterized by sheetflow runoff conditions and swamp type vegetation. Surface-water runoff in these watersheds is exclusively derived from rainfall. Rainfall is subdivided into surface-water runoff, evapotranspiration, and natural recharge to the shallow surficial aquifer. Some of the recharge to shallow aquifers returns to the drainage canals in Cape Coral. Many of the canals (totaling about 193 km in length) convey saltwater because they are affected by tidal reaches of the Caloosahatchee River and bays in the Gulf of Mexico. The remaining canals on higher lands convey surface-water runoff collected from the watershed. Although canals that convey fresh surface-water runoff and those that contain saltwater are connected, the movement of saltwater into the freshwater canals is impeded by a series of weir structures with crests that are above sea level.

The freshwater canal system contains two different systems, the north Cape Coral canal system and the south Cape Coral canal system. The canal systems are separated by U.S. Highway 78 with the northern system bounded by Gator Slough. Dredge spoil obtained during canal construction was used to raise land surface as much as 0.62 m in some areas (Fitzpatrick, 1986b). H.R. La Rose indicates that flow through the canals responds to seasonal patterns (U.S. Geological Survey, written commun., 1994). Records for the north Cape Coral canal system indicate that canal flow (not including flood peaks) ranges from 0.85 to 2.83 m^3/s during wet seasons and can be as low as 0.003 m^3/s during dry seasons.

Cape Coral has a subtropical climate with temperatures that are moderated by the Gulf of Mexico. The average annual temperature is 23°C with monthly averages ranging between 28°C in August and 18°C in January. Annual precipitation averages 1,372 mm. Hurricanes have caused damage in the past with high-velocity winds, rainfall, and tidal surges in Lee County. Additional data on local climate are available in a summary report by the Lee County Planning Department (1977).

Subsurface Injection, Storage, and Recovery of Freshwater Concept

Subsurface injection, storage, and recovery of freshwater in saline aquifers underlying southern Florida is a method of water-supply augmentation that has received increased attention in recent years. The SISRF concept is particularly suited for southern Florida where there is: (1) a surplus of freshwater during the wet season; (2) lack of suitable surface storage reservoirs because of the high cost of land, low relief, and high rates of evapotranspiration; and (3) availability of moderately permeable aquifers near the surface which contain brackish water (defined in the table below).

The average monthly rainfall in Cape Coral is more than 178 mm during the wet season (May-October). Most of this water ultimately discharges to the tidal reach of the Caloosahatchee River or Matlacha Pass through an extensive network of drainage canals totaling about 483 km. In the SISRF concept, part of the surface freshwater discharge is intercepted, treated for removal of suspended solids, chlorinated, and then injected through wells into the lower Hawthorn aquifer or deeper aquifers. Water is stored in the aquifers for 3 to 6 months and recovered during the dry season (November-April) to augment supply or meet peak demand. This cyclic procedure of injection, storage, and recovery is repeated on an annual basis.

Success of an SISRF cycle is measured by the recovery efficiency—defined as the volume of mixed injected and native aquifer waters recovered that meets a prescribed chemical standard, expressed as a percentage of the volume of water initially injected (Meyer, 1989). Most recent studies of SISRF, including this study, have assumed the Florida Department of Environmental Protection (1993) recommended level of 250 mg/L (milligrams per liter) for chloride ion as the standard which is equivalent to about 500 to 600 mg/L total dissolved solids. Generally, the degree of water is expressed as a percent of seawater in terms of total dissolved solids. The U.S. Geological Survey has adopted the following classification:

Classification	Total dissolved solids concentration (milligrams per liter)	Percent seawater
Freshwater	<1,000	<2.9
Slightly saline (brackish water)	1,000 - 3,000	2.9 - 8.6
Moderately saline (brackish water)	3,000 - 10,000	8.6 - 29
Very saline (saltwater)	10,000 - 35,000	29 - 100
Brine	>35,000	>100

Factors Affecting Recovery Efficiency

Merritt (1985) and Merritt and others (1983) studied the potential for SISRF in southern Florida and described a number of physical mechanisms that control the recoverability of freshwater and determine the suitability of the receiving aquifer for SISRF. The three dominant processes are buoyancy stratification, mixing due to hydrodynamic dispersion, and downgradient displacement of the injected freshwater.

Buoyancy stratification describes the tendency for the lighter freshwater to rise through the aquifer as it moves outward from the injection well and overrides the denser, native saltwater. Native saltwater in the lower part of the injection zone is drawn into the well during recovery, whereas potable water remains in the upper part of the zone. Buoyancy stratification is controlled by several factors, including: (1) the density contrast between native and injected waters, (2) permeability of the injection zone, and (3) the thickness of the injection zone (Merritt, 1985). These studies indicate that the effect of buoyancy stratification is smaller in relatively thin aquifers of moderate permeability and containing native water of low total dissolved solids concentration. These type of aquifers, therefore, are suitable for SISRF. Confinement of the injection zone by low-permeability materials can also aid in limiting the upward movement of freshwater.

Hydrodynamic dispersion is the mixing of solutes between zones of high and low solute concentrations as a result of molecular diffusion and mechanical dispersion. Molecular diffusion is caused by the flux of solute particles from areas of high solute concentration to areas of low solute concentration. The effect of molecular diffusion is independent of the fluid velocity. Mechanical dispersion is caused by mixing of solutes due to variations in fluid velocities at the microscopic scale. Enhanced mechanical dispersion or macrodispersion is caused by fluid velocity variations resulting from local differences in hydraulic conductivity.

Mechanical dispersion is dependent on the fluid velocity. At the relatively large fluid velocities during injection and recovery cycles, the effects of mechanical dispersion are generally greater than those of molecular diffusion.

Dispersive mixing causes the formation of a transition zone between the native and injected waters. The size of this zone depends on the rate of injection, length of injection period, and the solute-concentration difference between native and injected waters. Because fluid velocities are highest near the well, most of the mixing occurs at the beginning of the injection process. As injection continues, the transition zone moves outward at continually decreasing fluid velocities, leading to decreasing dispersive mixing. Merritt (1985) reported that the growth of the transition zone did not keep pace with the growth of the freshwater zone for long injection periods, thus providing for enhancement of the recovery by injecting larger volumes of water.

The effect of downgradient movement of the freshwater zone on recovery efficiency depends on the length of the cycle and the regional ground-water flow velocities. It is possible to design multiple-well injection systems in situations where flow velocities are high and storage periods are long, similar to those described by Merritt (1985) or Kimbler and others (1975). These multiple well systems can be used to offset the effects of downgradient movement.

The lower Hawthorn aquifer beneath Cape Coral seems to meet most of the criteria for consideration in an SISRF scheme. The aquifer has moderate permeability with mean values representing the vertical distribution of hydraulic conductivity that ranges from 21.3 to 41.4 m/d (estimated using data from Missimer and Associates, Inc., 1985). The aquifer, confined by low-permeability leaky units on the top and bottom, has a thickness of about 60 m. The native water is brackish with chloride concentrations (500-600 mg/L), total dissolved solids concentrations (greater than 1,000 mg/L), and densities (1,001 kg/m^3) not much different from the treated surface water that is proposed to be injected. Rates of regional movement of ground water are generally lower in the northern part of Cape Coral and are higher in the vicinity of the RO wells to the south (fig. 1). Other factors in favor of SISRF are: (1) the artesian heads to be overcome by forced pumping are relatively low; (2) the aquifer is moderately permeable, allowing reasonable rates of pumping be maintained; and (3) well-construction costs would probably not be much higher than for typical water-supply wells in the area.

Another factor that can affect SISRF efficiency is clogging of the aquifer around the injection wellbore. This clogging can be caused by bacterial growth, suspended sediments in the injected water, and chemical precipitation of solutes caused by chemical reactions between the injected fluid and the aquifer material or native water. Removal of sediments and disinfection of the water would likely be required before injecting surface waters. Geochemical models can be used to predict the reactions likely to occur during rock-water interaction and mixing of injected and native waters; additional treatment requirements for the injected water could then be determined. However, the analysis of the well-clogging potential was beyond the scope of this study.

GENERAL HYDROGEOLOGIC SETTING

The geology of Lee County and the Cape Coral area has been described by previous investigators, including Wedderburn and others (1982), Knapp and others (1984), and Missimer and Associates, Inc. (1984). The upper 228 m of sediments in the Cape Coral area are composed of the upper part of the Suwannee Limestone of Oligocene age, the Tampa Limestone and the Hawthorn Formation of Miocene age, the Tamiami Formation of Pliocene age, and undifferentiated deposits chiefly of Pleistocene and Holocene age (fig. 2).

The Suwannee Limestone underlying Cape Coral is predominantly a very pale orange to tan medium-grained limestone, but tends to be sandy and slightly phosphatic (Knapp and others, 1984). The top of the unit generally dips to the south-southeast and ranges from 183 m below sea level at the northern border of Cape Coral to about 229 m below sea level at the southeastern end (Missimer and Associates, Inc., 1984). The base of the unit lies between 274 and 366 m below sea level although few wells in the area penetrate beyond the upper part of the Suwannee Limestone.

Earlier reports by the U.S. Geological Survey divide the Miocene age sediments into two units, the Tampa Limestone and Hawthorn Formation. Recent studies (Wedderburn and others, 1982; Missimer and Associates, Inc., 1984) refer to the Tampa Limestone as the Tampa Formation and, although lithologically distinctive, include these sediments within the Hawthorn Formation.

The Tampa Limestone is present from about 150 to 200 m below land surface and is described by Wedderburn and others (1982) as a very light orange to white,

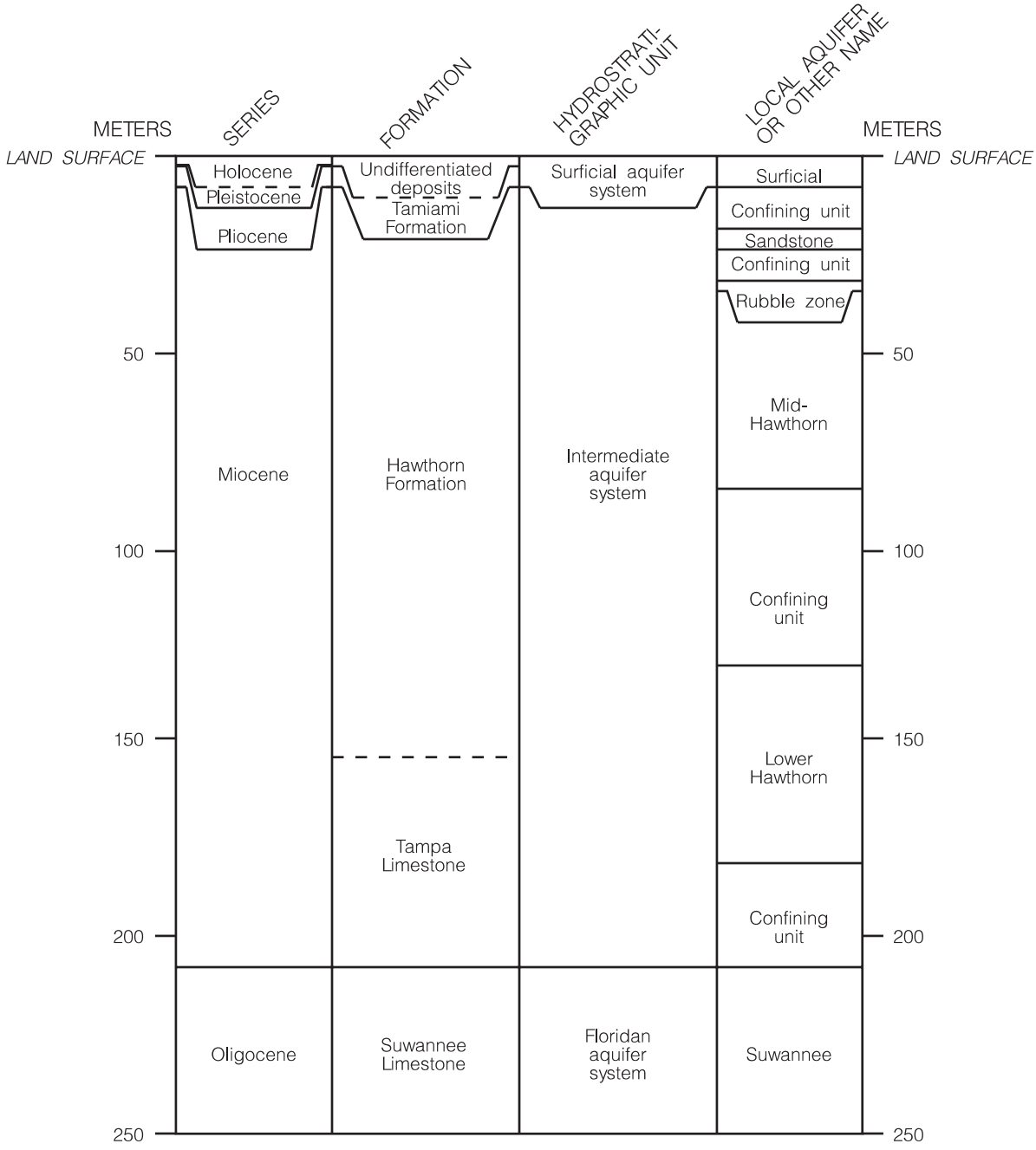

Figure 2. Profile showing geologic formations, hydrostratigraphic units, and local aquifers underlying Cape Coral (modified from La Rose, 1990).

biogenic, micritic, very fine grained limestone with up to 10 percent quartz sand. The Hawthorn Formation is a predominantly clastic unit. The thickness of the formation is about 150 m (Wedderburn and others, 1982). The Hawthorn Formation consists of a series of highly heterogeneous, interbedded clayey phosphatic dolosilts and phosphatic sandy dolomites and limestones (Wedderburn and others, 1982). The upper part of the Hawthorn Formation is a slightly sandy, dolomitic, phosphatic limestone with a maximum thickness of 46 m (Wedderburn and others, 1982). The top of this bed is about 30 m below sea level beneath Cape Coral and dips primarily to the southeast reaching 53 m below sea level in the southeastern corner of Cape Coral. Local names for zones within the upper part of the Hawthorn Formation have been listed by Missimer and Associates, Inc. (1984) and include the Cape Coral clay, Lehigh Acres sandstone, and Fort Myers clay.

Pliocene and Pleistocene age sediments range from 6.1 to 12.2 m thick in the study area (Missimer and Associates, Inc., 1984). Locally, four geologic formations occur within these undifferentiated sediments: (1) the Pamlico sand, (2) the Fort Thompson formation, (3) the Caloosahatchee formation, and (4) the Pinecrest member of the Tamiami Formation. Detailed stratigraphic descriptions are given by Missimer and Associates, Inc. (1984).

Hydrogeology of the Lower Hawthorn Aquifer

The lower Hawthorn aquifer occurs in the lower part of the Hawthorn Formation and the upper part of the Tampa Limestone (fig. 2). The lower Hawthorn aquifer in Cape Coral occurs from about 128 to 188 m below land surface, having an average thickness of 60 m. However, the thickness of its water-yielding zone is less than 30 m (La Rose, 1990). The lower Hawthorn aquifer is confined by thick, leaky clay sequences above and below. Because of this confinement and the higher heads in the upgradient recharge area, this aquifer is considered to be an artesian system with a producing capacity ranging from 0.019 to 0.032 m^3/s in large-diameter wells under natural flow conditions.

Although abundant water is available from the lower Hawthorn aquifer, high chloride concentrations (greater than 500 mg/L) preclude its direct use for public-water supply. Water from the lower Hawthorn aquifer is used to feed RO desalination plants in Cape Coral. According to an interpretation of the hydrogeologic system by La Rose (1990), recharge to the lower Hawthorn aquifer comes from the mid-Hawthorn aquifer north of the study area where the upper confining unit pinches out in Hillsborough, Polk, Manatee, and Hardee Counties.

Hydraulic Characteristics of the Lower Hawthorn Aquifer

Three individual flow zones in the lower Hawthorn aquifer at the Lee County Water Treatment Plant are identified by Fitzpatrick (1986a) using data from geophysical logs (caliper, flow velocity, fluid resistivity, and fluid temperature) during pumping and injection conditions (table 1).

The percentages of flow from the individual zones at the Lee County Water Treatment Plant (table 1) are estimated from caliper/velocity borehole studies conducted by Fitzpatrick (1986a). The aquifer is characteristic of a leaky confined aquifer with hydraulic characteristics as follows (Fitzpatrick, 1986a):

$$T = 7.526 \times 10^{-4}\ m^2/s \text{ to } 8.601 \times 10^{-4}\ m^2/s,$$

$$S = 1 \times 10^{-4}, \text{ and}$$

$$K_v'/b' = 0.01 \text{ per day} = 864 \text{ per second}$$

where,

T is transmissivity;
S is storage coefficient;
K_v' is vertical hydraulic conductivity of the confining beds; and
b' is thickness of the confining beds.

The hydraulic characteristics of the individual flow zones at the Lee County Water Treatment Plant are estimated using the following procedure:

$$Q_T = Q_1 + Q_2 + Q_3 \quad (1)$$

where,

Q_T is the total flow rate through the well; and
Q_i (i = 1,2,3) represents the flow components from the different flow zones.

Table 1. General hydrogeologic characteristics of flow zones and confining units in the lower Hawthorn aquifer at the Lee County Water Treatment Plant and Cape Coral

Location	Flow zones and leaky confining units (meters below land surface)	Thickness (meters)	Percent of flow from this zone	Hydraulic conductivity (meters per second)	Intrinsic permeability (square meters)
Lee County Water Treatment Plant	153.9–160.0	6.1	30	3.775×10^{-5}	3.846×10^{-12}
	160.0–167.6	7.6	5	5.044×10^{-6}	5.140×10^{-13}
	167.6–176.8	9.2	65	5.468×10^{-5}	5.572×10^{-12}
Cape Coral	198.0–213.3	15.3	34	1.065×10^{-4}	1.085×10^{-11}
	213.3–222.5	9.2	2	1.041×10^{-5}	1.061×10^{-12}
	222.5–231.6	9.1	64	3.370×10^{-4}	3.435×10^{-11}

For each flow zone:

$$Q_i = 2\pi r T_i \frac{dh_i}{dr} \quad (2)$$

where,

r is radial distance from pumping well;
dh_i is the head change in the different flow zones; and
dr is the change in distance from the pumping well.

Assuming no head gradient among the flow zones, $dh_i/dr = dh/dr$, and uniform head in the wellbore:

$$Q_T = 2\pi r(T_1 + T_2 + T_3)\frac{dh}{dr} = 2\pi r T \frac{dh}{dr} \quad (3)$$

and

$$T = T_1 + T_2 + T_3 = K_1 b_1 + K_2 b_2 + K_3 b_3 . \quad (4)$$

For example, if T is the composite transmissivity estimated from an aquifer test, assuming that equation 4 can be applied, $Q_i/Q_T = T_i/T$ and $T_i = K_i b_i$ gives the hydraulic conductivity of each zone. If $T = 7.68 \times 10^{-4}$ m^2/s (aquifer test), 30 percent of the total flow (Q_T) comes from zone 1 (flowmeter survey), and this zone has a thickness of 6.1 m:

$$T_1 = \frac{Q_i}{Q_T} T = 0.30 \times 7.68 \times 10^{-4} (m^2/s) = 2.30 \times 10^{-4} (m^2/s),$$

and

$$K_1 = \frac{T_1}{b_1} = \frac{2.30 \times 10^{-4} (m^2/s)}{6.1 \text{ m}} = 3.775 \times 10^{-5} \text{ (m/s)},$$

The hydraulic conductivity (K_i) values for the different flow zones are given in table 1. Aquifer matrix permeability (k_i, intrinsic permeability) values from table 1 are then computed using:

$$k_i = \frac{\mu}{\rho} \frac{K_i}{g} \quad (5)$$

where,

μ is dynamic viscosity of the fluid [M/LT];
ρ is fluid density [M/L^3]; and
g is gravitational acceleration [L/T^2].

Although the general hydrogeologic framework of the lower Hawthorn aquifer at the two sites (Cape Coral and the Lee County Water Treatment Plant) is similar, the magnitude of the hydraulic characteristics is somewhat different. Analysis of flow velocity and caliper borehole logs (fig. 3) in Cape Coral indicated a similar flow zoning, occurring at different depths below land surface and with different thicknesses and hydraulic coefficients (table 1). The upper flow zone and the low permeability unit seem to be thicker in Cape Coral, but the distribution of flow across these hydrogeologic units is almost the same (table 1).

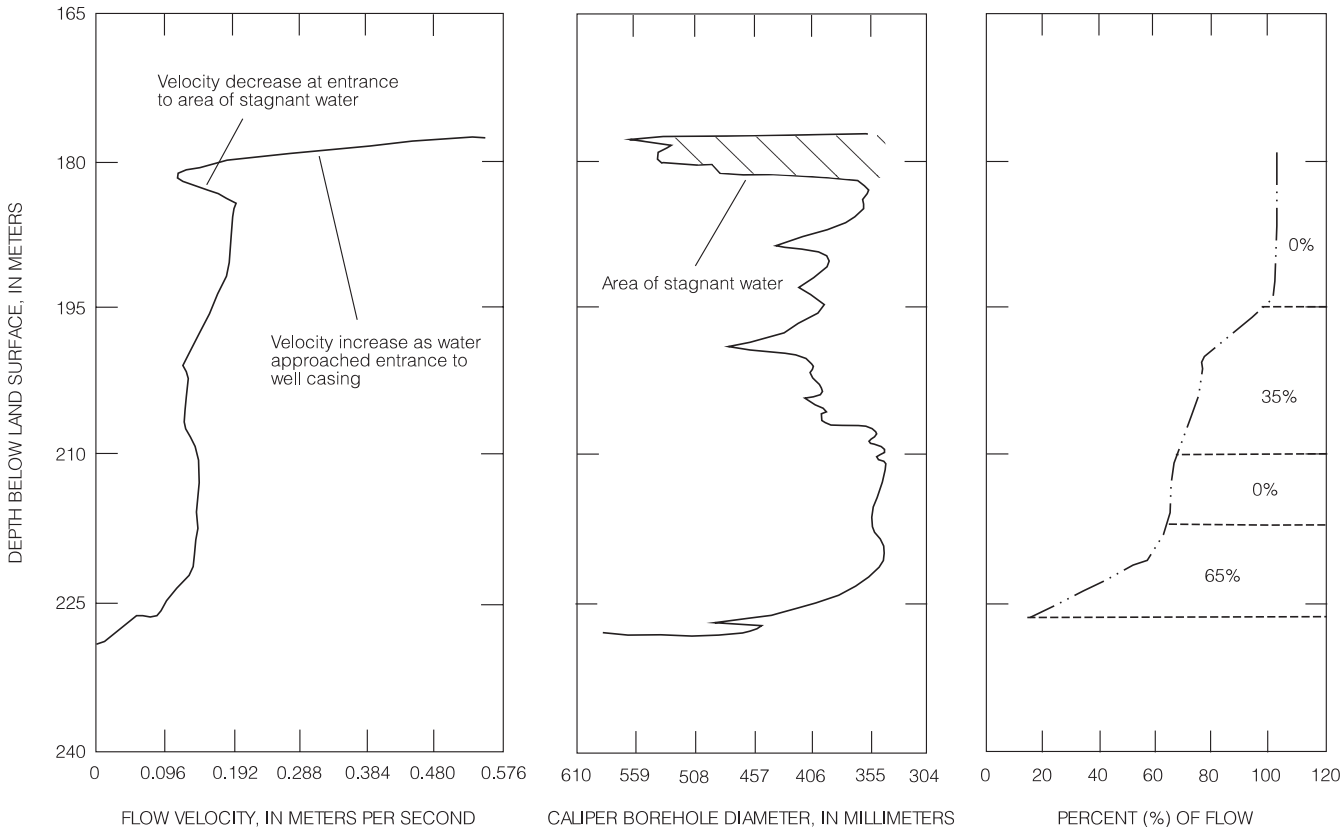

Figure 3. Percent of total flow estimated using velocity and caliper borehole logs for well L-M-2426 at Cape Coral.

Apparent transmissivity values are estimated for several wells in Cape Coral (table 2), using specific capacity values from step-drawdown tests conducted by Missimer and Associates, Inc. (1985), and the empirical equation by Brown (1963). Estimated transmissivity values range from 149 to about 807 m^2/d (fig. 4 and table 2) with a geometric mean value of about 414 m^2/d. Values of hydraulic conductivity and intrinsic permeability are estimated for the lower Hawthorn aquifer in Cape Coral (table 1), using the geometric mean of the transmissivity values and equations 1 to 5.

Table 2. Specific capacity and apparent transmissivity values for wells completed in the lower Hawthorn aquifer at Cape Coral

[Specific capacity values from Missimer and Associates, Inc. (1985); apparent transmissivity values estimated using the empirical equation by Brown (1963)]

Well identification number	Specific capacity (liters per second per meter)	Apparent transmissivity (meters squared per day)
L-M-2417	4.74	496.7
L-M-2418	5.20	546.4
L-M-2419	3.97	409.8
L-M-2420	5.55	583.6
L-M-2421	3.35	347.7
L-M-2422	4.57	496.7
L-M-2423	1.74	149.0
L-M-2424	2.24	223.5
L-M-2425	2.84	273.2
L-M-2426	7.64	807.2
L-M-2427	7.27	782.3
L-M-2428	4.14	397.4
Geometric mean		414.3
Standard deviation		203.7

THEORETICAL BACKGROUND

The ability to assess whether SISRF could be an economical water-supply alternative is enhanced by the capability to predict the movement of water and solutes under the conditions of injection, storage, and recovery. Digital models have been developed by the U.S. Geological Survey and others to simulate the density-dependent flow of ground water and the transport of solutes in ground-water systems. These models can utilize data on fluid and aquifer properties to estimate recovery efficiencies under conditions expected at a particular study area.

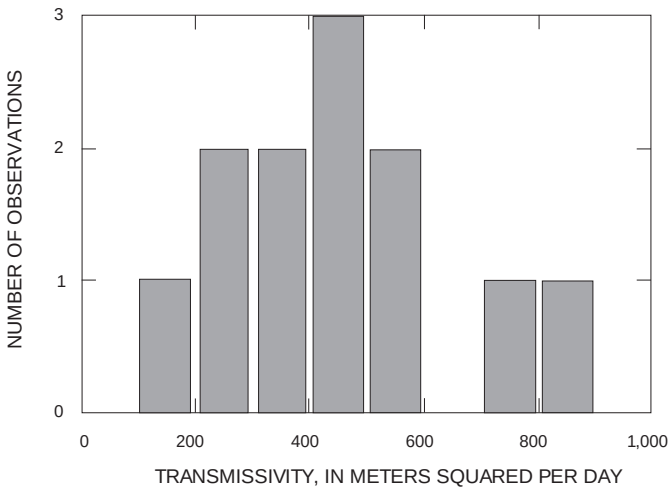

Figure 4. Histogram of apparent transmissivity values estimated from wells tapping the lower Hawthorn aquifer at Cape Coral.

Simulation of density-dependent ground-water flow and solute transport requires the solution of two governing partial differential equations subject to appropriate boundary and initial conditions. The first equation describes transient ground-water flow under conditions where density differences due to solute concentrations can affect flow. The second equation describes the movement and spread of solutes within the flowing ground water using data on the distribution of ground-water velocities obtained by solving the first equation. The two equations are solved iteratively, as the distribution of solute concentrations needed to solve the first equation is initially estimated and updated after solving the second equation. The theoretical background of the governing equations is discussed in the next section.

Density-Dependent Ground-Water Flow Equation

The rate of ground-water flow is assumed to be governed by Darcy's law, which when written in terms of fluid pressure (rather than piezometric head), is:

$$q = -k(\nabla\rho - \rho g z)/\mu \qquad (6)$$

where,

q is specific discharge (flow rate per unit cross-sectional area) [L/T];
k is the intrinsic permeability of the aquifer materials [L^2];
∇ is the gradient operator [1/L];
p is the fluid pressure [M/LT^2];
ρ is the fluid density [M/L^3];
g is the gravitational acceleration vector [L/T^2];
z is the elevation above a reference datum [L]; and
μ is the dynamic viscosity of the fluid [M/LT].

Using Darcy's law and the principle of conservation of fluid mass, a mass-balance equation can be written as:

$$\frac{\partial(n\rho)}{\partial t} = -\nabla \bullet (\rho q) \pm Q_p \qquad (7)$$

where,

n is aquifer porosity [dimensionless], and

Q_p is mass of fluid injected (+) or withdrawn (-) per unit time per unit volume of aquifer [M/L^3T].

The dependence of fluid density on solute concentration has an important effect on the mass-balance equation, which can be seen by expanding the first term in equation 7:

$$\frac{\partial(n\rho)}{\partial t} = \frac{\rho\partial n\partial p}{\partial p\partial t} + \frac{n\partial\rho\partial p}{\partial p\partial t} + \frac{n\partial\rho\partial c}{\partial c\partial t} \ , \qquad (8)$$

or

$$\frac{\partial(n\rho)}{\partial t} = \frac{S_s\partial p}{\partial t} + \frac{n\partial\rho\partial c}{\partial c\partial t} \qquad (9)$$

where,

c is solute concentration (mass of solute/mass of water) [dimensionless]; and

S_s is specific pressure storativity of the aquifer

given by $S_s = [(1\text{-}n)\,\alpha + n\,\beta]$ for an unconsolidating aquifer [LT^2/M] where,

α is compressibility of the aquifer solid matrix [LT^2/M], and

β is compressibility of water [LT^2/M].

The determination of fluid pressures at any given time, which affects the rates of fluid movement, requires the prior or simultaneous determination of the rate of change in fluid concentration over time. The specific discharge, as determined by Darcy's law, is also dependent on solute concentration through the density and viscosity terms (eq. 6), which is only slightly dependent on solute concentration.

A system of equations, such as equation 7, can be simultaneously solved for a given set of boundary conditions, aquifer properties, fluid densities, and rates of recharge or withdrawals from the aquifer. The solution will be in terms of the pressure at all points in the aquifer. The average pore velocity, v, can then be determined from the distribution of hydraulic head by Darcy's law:

$$v = -\frac{q}{n} \qquad (10)$$

where,

n is the effective porosity of the aquifer [dimensionless].

Advection and Hydrodynamic Dispersion

Movement of solutes through a porous medium is controlled by advection and hydrodynamic dispersion. Advective transport describes the movement of solute particles along the mean direction of fluid flow at a rate equal to the average pore-water velocity. Hydrodynamic dispersion describes the spread of solute particles along and transverse to the direction of average fluid flow in response to molecular diffusion and mechanical dispersion.

Molecular diffusion produces a flux of solute particles from areas of high to low solute concentrations; its effect is independent of the fluid velocity. Mechanical dispersion is the mixing of solutes caused by variations in fluid velocities at the microscopic scale. Velocity variations are caused by several factors, including: (1) velocity distributions within the pore space, (2) variations in pore size, (3) differences in path lengths for different solute particles, and (4) the effect of converging and diverging flow paths (Bear, 1979). Mechanical dispersion is dependent on fluid velocity, and at the relatively large pore-water velocities expected during injection and recovery phases, the effects are greater than those of molecular diffusion. Fluid movement during the storage phase is mainly from buoyancy forces, and at these low velocities, molecular diffusion can have a more significant role in solute movement.

Dispersive flux, J, can be described by Fick's first law as:

$$J = -D_m \nabla c \qquad (11)$$

where,

c is the volumetric concentration of solute [M/L^3]; and

D_m is the second rank tensor containing the coefficients of mechanical dispersion [L^2/T].

Mechanical dispersion coefficients are related to the average pore velocity by the dispersivity of the medium (Scheidegger, 1961). The coefficients of dispersivity are dependent on properties of the medium including permeability, length of a characteristic flow path, and tortuosity. In an isotropic medium (with respect to dispersion), the coefficients of mechanical dispersion can be expressed in terms of two components: (1) longitudinal dispersivity (α_L), which represents dispersion in the direction of the flow path; and (2) transverse dispersivity (α_T), which represents dispersion in the direction perpendicular to the flow path. Transverse dispersivities are usually smaller than longitudinal dispersivities by a factor of 5 to 20 (Freeze and Cherry, 1979).

The nine components of the symmetric mechanical dispersion tensor can be expressed in terms of v (the average pore-water velocity vector) and the velocity components v_x, v_y, and v_z (Bear, 1979). In a system where ground-water flow is horizontal (v_z=0), the components of the mechanical dispersion tensor are:

$$\begin{aligned} D_{xx} &= (\alpha_L v_x^2 + \alpha_T v_y^2) / |v| \\ D_{xy} &= D_{yx} = (\alpha_L - \alpha_T) v_x v_y / |v| \\ D_{yy} &= (\alpha_L v_y^2 + \alpha_T v_x^2) / |v| \\ D_{xz} &= D_{zx} = D_{yz} = D_{zy} = 0 \\ D_{zz} &= \alpha_T |v|. \end{aligned} \quad (12)$$

For radially symmetric irrational flow (v_Θ=0) systems, subscripts x and y are replaced by r and z, respectively.

The hydrodynamic dispersion tensor can be written as:

$$D_h = D_m + D_d \underline{I} \quad (13)$$

where,

D_h is the second order hydrodynamic dispersion tensor [L^2/T];
D_m is the mechanical dispersion tensor [L^2/T];
D_d is the coefficient of molecular diffusion [L^2/T]; and
$\underline{I}$ is the identity tensor.

Macrodispersion

Longitudinal dispersivities typically range from 0.100 to 10.00 mm in laboratory experiments with homogeneous materials and have been estimated as much as 90 m from field studies of contaminant plumes (Freeze and Cherry, 1979). The larger values in field studies are related to increased mixing (on a macroscopic scale) because of local variations in aquifer hydraulic and dispersive characteristics.

Most studies of radial injection have assumed that macrodispersive fluxes can be represented by Fick's law with a constant dispersion coefficient. However, recent studies of transport in porous media have indicated that dispersion can increase away from the source and reach an asymptotic value after travel distances of hundreds or thousands of feet (Gelhar and Axness, 1983). Dispersivities are scale dependent at short distances with values increasing away from the contaminant source as larger scale heterogeneities occur (Gelhar and others, 1979). Recent developments in the macrodispersion theory are discussed by Anderson (1984).

In this study, aquifer dispersivity values were estimated from the analysis of field test data from a previous study (Fitzpatrick, 1986a). Values of aquifer dispersivity used in the different simulations and sensitivity analyses are discussed in later sections. Limitations of the advective-dispersive model must be recognized along with the other limitations introduced because of uncertainties in aquifer properties.

Advective-Dispersive Solute-Transport Equation

A version of the variable-density advective-dispersive solute-transport equation modified for saturated flow and conservative solute species presented by Voss (1984) is:

$$\frac{\partial(n\rho c)}{\partial t} = -\nabla\cdot(n\rho v c) + \nabla\cdot[ns(Dd\,\underline{I} + Dm)\cdot\nabla C] + Q' c^* \quad (14)$$

where,

Q' is the volumetric injection rate per unit area of aquifer [L/T]; and

c^* is volumetric solute concentration in the injected fluid [M/L^3].

When applying equation 14 to freshwater injection in an aquifer, flow can be assumed to be either: (1) radially symmetric about the injection well (regional flow is negligible), or (2) horizontal and the solute concentration and fluid density are vertically uniform (regional flow is considered). In the latter case, the term c represents the vertically averaged concentration at a point in the aquifer. For this study, the first option was used.

The term $Q' c^*$ represents only sources of solute mass. Withdrawals of fluid from the aquifer do not need to be considered in the transport equation because the concentration of solute in the fluid withdrawn from the aquifer c^* is identical to the solute concentration c. The source term from equation 14 is incorporated as part of the boundary conditions.

PRELIMINARY ASSESSMENT OF INJECTION, STORAGE AND RECOVERY OF FRESHWATER

Solution of the two governing partial-differential equations generally requires sophisticated digital models. These models use numerical approximation techniques that determine aquifer pressure and solute concentrations at a finite number of points and at specified time intervals. SUTRA (**S**aturated-**U**nsaturated **TRA**nsport), a computer code based on the Galerkin finite element technique (Voss, 1984), was applied in this study. Modifications were made to the code to compute the solution in terms of a regular rectangular grid with the intention of minimizing computer storage and time (apps. 1 and 2). Appendix 1 contains the hierarchic levels of subprograms in the original SUTRA version and in the modified SUTRA version, hereafter referred to as QSUTRA.

Subprograms PLOT, CONNEC, BANWID, NCHECK, and PINCHB were not included. All of these subprograms, except for PLOT, were used in the original SUTRA version to process information related to the irregularity of element shapes forming the mesh or grid. A new subprogram (FOPEN) was added to open files and assign unit numbers (apps. 1 and 2) (C.I. Voss, U.S. Geological Survey, written commun., 1994). Subprogram SOLVEB, which includes the algorithms to solve the system of equations (eqs. 7 and 15), was substituted by subprograms SOLVEC and LSORA (apps. 1 and 3). SOLVEC uses the incomplete Cholesky-conjugate gradient method (Kuiper, 1987) to solve a system of ground-water flow equations (eq. 7). LSORA uses the line successive overrelaxation method (Young, 1954) to solve a system of solute-transport equations (eq. 15). Some other changes to the code are highlighted in the program listing (app. 2).

QSUTRA was tested by applying it to Henry's (1964) density-dependent flow problem described in Voss (1984, p. 196-203). This problem was selected because it provides a good opportunity to test the capabilities of QSUTRA in solving nonlinearities occurring in variable density flow problems. Comparison of results from QSUTRA and SUTRA for Henry's (1964) problem are presented in appendix 4. As shown in appendix 4, concentration profiles from QSUTRA and SUTRA are identical. Also, QSUTRA and SUTRA estimates of flux across one model boundary compare very well.

Simulations of freshwater injection, storage, and recovery in the lower Hawthorn aquifer were made using the QSUTRA code with a radial coordinates grid. The following assumptions are made: (1) the effect of the background hydraulic gradient is negligible, (2) the aquifer is divided into vertically adjacent layers characterized in the model as homogeneous with respect to the hydraulic and transport characteristics, (3) the hydraulic and transport characteristics are homogeneous along the radial direction of flow, and (4) the aquifer characteristics are isotropic along the horizontal (radial) direction. Assumptions 2 and 3 are made because of the lack of information on the spatial variability of the hydraulic and transport characteristics. Estimates of the transport characteristics of the lower Hawthorn aquifer were made using data from previous freshwater injection tests (Fitzpatrick, 1986a) conducted at the Lee County Water Treatment Plant (fig. 1).

Grid Design

Although the configuration of the lower Hawthorn aquifer at the Lee County Water Treatment Plant and Cape Coral are similar, differences on the thickness of the flow zones and on the magnitude of the hydraulic properties precluded the use of the same model grid for both sites. Two finite-element grids were required. The first grid was used for calibrating and testing the model with data from field tests conducted at the Lee County Water Treatment Plant and documented (Fitzpatrick, 1986a). The second grid was used to represent the hydrogeologic conditions at the Cape Coral site. Transport characteristics obtained from simulating Fitzpatrick's tests were extrapolated to the Cape Coral area.

The Lee County Water Treatment Plant site grid consists of 1,400 elements and 1,491 nodes (fig. 5A), and the Cape Coral grid consists of 2,100 elements and 2,201 nodes (fig. 6A). Both grids extend out radially to 10,384 m (figs. 5A and 6A). The Cape Coral grid was used to conduct hypothetical tests of freshwater injection, storage, and recovery in the lower Hawthorn aquifer in the study area (fig. 1). The grids are very fine (2 m) in the vicinity of the injection well so as to avoid errors associated with numerical dispersion (artificial dispersion introduced by inappropriate spatial discretization) and high aspect ratios (large difference between sides of an element). At a distance of 100 m, element lengths increased to 4 and 8 m at 120 m from the well. Beyond 160 m, element lengths were successively doubled until a maximum length of 4,096 m was reached. The thickness of elements remained constant (2 m). The part of the finite-element grids extending to a distance of 160 m from the injection well is shown in figures 5B and 6B, and the entire finite-element grids are shown in figures 5A and 6A.

Boundary and Initial Conditions

Boundary conditions were set at r=0, r=10,384 m, z=144.8 m below land surface, and z=184.8 m below land surface for the Lee County Water Treatment Plant model, and set at r=0, r=10,384 m, z=186 m below land surface, and z=246 m below land surface for the Cape Coral model—the limits of the finite-element grids (figs. 5 and 6). Boundaries at the top and bottom of the aquifer (upper and lower limits of the modeled zone) were set constant for pressure and concentration. The solute concentration was set equal to the solute concentration of the native water at these boundaries, and the pressures were set equal to the hydrostatic pressures at the specific depths where the boundaries were located.

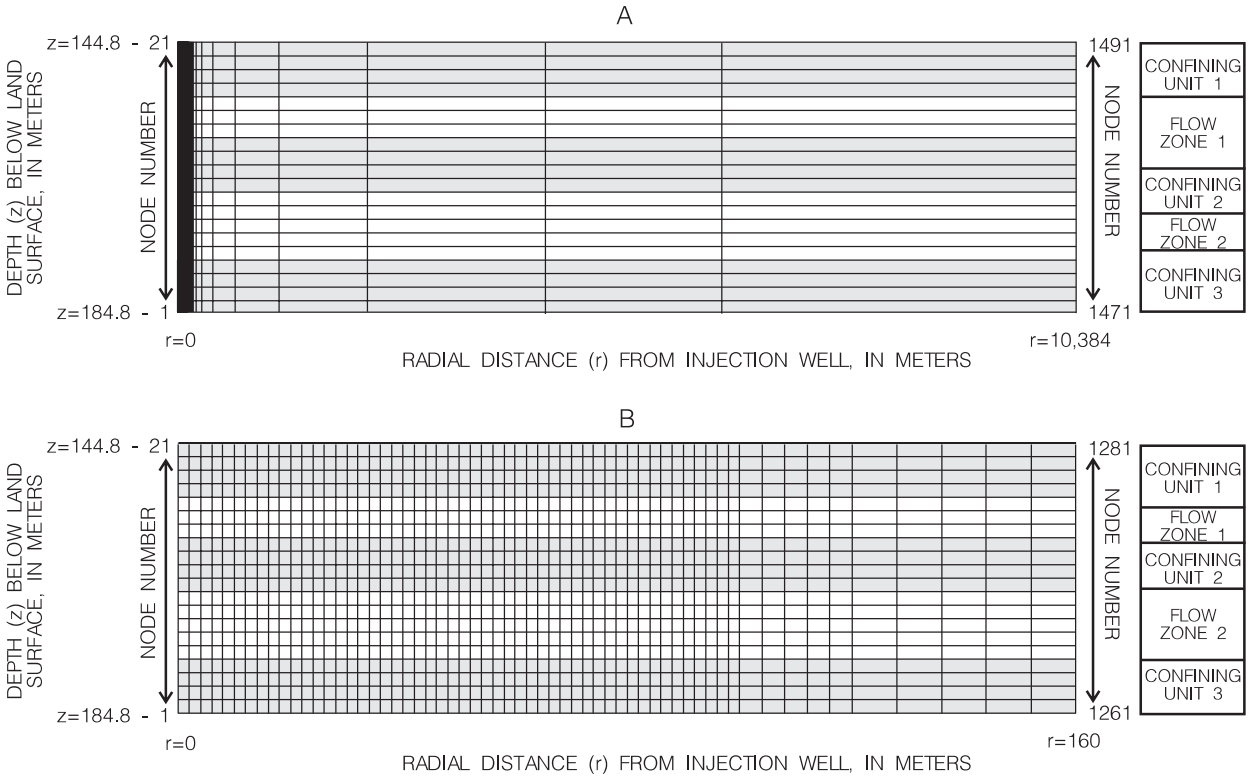

Figure 5. Sectional views of the cylindrical coordinate finite-element grid used to study previous subsurface injection, storage, and recovery of freshwater in the lower Hawthorn aquifer at the Lee County Water Treatment Plant.

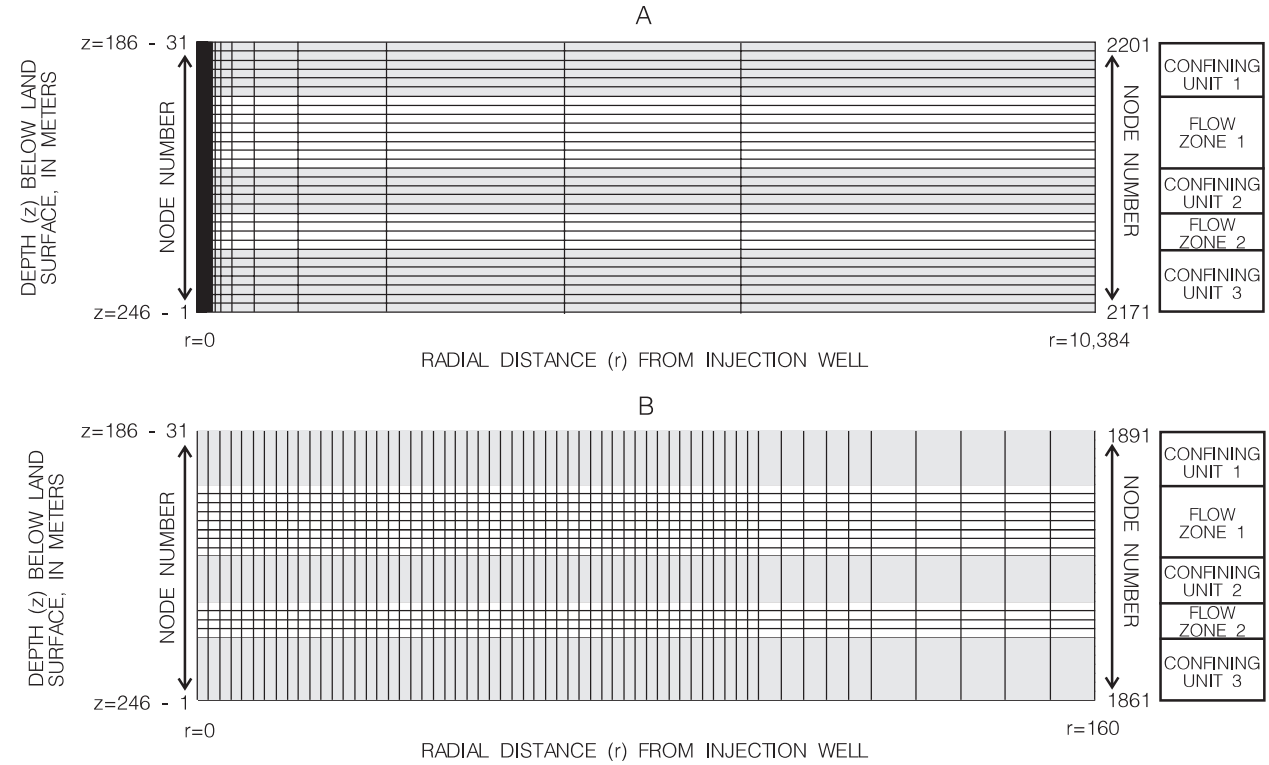

Figure 6. Sectional views of the cylindrical coordinate finite-element grid used to study hypothetical subsurface injection, storage, and recovery of freshwater in the lower Hawthorn aquifer at Cape Coral.

One limitation setting of these types of boundary conditions (constant pressure and concentration on top and bottom) is that if injected or mixed water passes across these boundaries, the model would be unable to consider it during the recovery pumping because the concentrations along these boundaries are assumed to represent a constant value. However, for the present study, these boundary conditions yielded the best representation of the actual aquifer in terms of approximating measured pressure and concentration changes in observation wells and in the injection well during recovery. Also, these boundary conditions would yield more conservative estimates of recovery efficiency. The lack of detailed hydrogeologic information beyond these boundaries precluded the location of the boundaries farther from flow zones receiving the injection water. An attempt was made to locate the boundaries farther from the injection source by extrapolating the hydrogeologic information, but the results were discouraging in terms of matching field measured pressure and concentration changes.

At r=10,384 m, no-flow/no-transport boundary conditions were specified. This boundary was intentionally located far from the injection source to prevent any effect that it might have on the determination of pressures and concentrations in the aquifer segment affected by the injection. Boundary conditions at the well (r=0) were set by specifying a mass flux equal to the injection rate. The flux was proportionally distributed among the boundary nodes along the length of the injection zone using the aquifer hydraulic characteristics (K) as a weighting factor. The solute concentration in the injected water during injection was specified at the well boundary (r=0). A flux average concentration for water withdrawn during recovery was calculated from concentration values at boundary nodes representing the well.

The hydraulic conductivity value of the upper and lower confining zones was modified using the model to replicate the effect of these leaky units on pressure and concentration changes in the main flow zones (discussed later). Although more sophisticated boundary types are currently available, they are not available in QSUTRA, and this study lacks the field data to justify their application. For large volumes of water injected (larger than those used in this study), the vertical and horizontal boundaries can become invalid yielding unrealistic model results.

Initial pressures were assumed to be hydrostatic and set equal to an equivalent freshwater head of 10.49 m above sea level for the Lee County Water Treatment Plant model and 7.62 m for the Cape Coral area model. Initial solute concentration was set equal to solute concentration in the native water. For this study, fluid density was assumed to depend only on solute concentration. Fluid density was calculated by the model based on initial solute concentrations and the following functional relation between density and solute concentration:

$$\rho = \rho_i + (\rho_n - \rho_i)\,[(C-C_i)/(C_n-C_i)] \qquad (15)$$

where,

ρ_i is density of injected water [M/L^3];

ρ_n is density of native water [M/L^3]l;

C is solute concentration in the mixed water [M/L^3];

C_i is solute concentration in the injected water [M/L^3]; and

C_n is solute concentration in the native water [M/L^3].

Solute Source

Chloride ion, the dominant conservative anion in the native aquifer water and the injected surface water, was selected as the solute to be modeled. Chloride concentrations in water samples from the lower Hawthorn aquifer ranged from 500 to 550 mg/L at the Lee County Water Treatment Plant and from 350 to 750 mg/L in Cape Coral (Missimer and Associates, Inc., 1985). The model computes relative or normalized concentrations that range from 0.1 to 1, where 0.1 represents concentration in the injected water and 1 represents concentration in the native water.

Time Steps

Initial time-step sizes were kept equal or smaller than 400 seconds to avoid numerical dispersion associated with a large time-step size. The time-step size was increased during the injection phase in such a way that the injected water front (neglecting dispersion) moved a constant distance during each successive time step. The final time-step size from the injection phase was used and kept constant for the entire simulation of the storage period. During the recovery phase, the time-step size was gradually reduced from its maximum value as the injected water front moved closer to the well. Generally, except for the first time step in each run, only two iterations per time step were needed to resolve the nonlinearities of the density-dependent flow equation (eq. 7).

Model Simulation Results for the Lee County Water Treatment Plant—Calibration and Testing

Data from a study by Fitzpatrick (1986a) were used in this study to define the hydrogeologic system and to provide a basis for estimating the hydraulic and transport characteristics for the lower Hawthorn aquifer in Cape Coral. The conceptual model for the Lee County Water Treatment Plant site was developed on the basis of interpretation of velocity, caliper, fluid resistivity, and fluid temperature borehole logs and interpretation of aquifer-test data (Fitzpatrick, 1986a). The conceptual model consists of two main flow zones and three leaky confining units (fig. 5). Aquifer hydraulic characteristics, boundary conditions, and nodes subject to them were previously described.

Two injection, storage, and recovery tests and results (table 3) from the study by Fitzpatrick (1986a) were useful in calibrating the model (tests 2 and 3). Test 3 was used for model calibration and test 2 for model testing. Data for test 3 were obtained for the injection well (L-3225) and two observation wells (L-2530 and L-3224), about 43 and 102 m, respectively, from the injection well. The calibration of the model was performed using the classical interactive process in which the model variables were changed within realistic limits, until a satisfactory match to the measured data was obtained. Initial model variables were set according to data presented in table 1 and information previously described in this report.

Increases in hydraulic head at observation wells L-2530 and L-3224 were used to calibrate the hydraulic variables. The permeability of the flow zones is assumed to be isotropic, and no attempt was made to change it. However, the permeability of the leaky confining units was decreased from an estimated value of 1.89×10^{-13} to 1.67×10^{-13} m^2 to obtain a satisfactory match between observed and modeled head change data (fig. 7A). The permeability is assumed to be isotropic in the vertical and horizontal directions. Following the hydraulic calibration, data on chloride concentration changes in the two observation wells (L-2530 and L-3224) were used to calibrate the transport model for effective porosity and longitudinal and transverse dispersivities. The model yielded better results when using an effective porosity of 0.12, a longitudinal dispersivity (α_L) of 3.0 m, and a transverse dispersivity (α_T) of 0.3 m for a ratio of $\alpha_T/\alpha_L = 0.1$ (fig. 7B). However, the model did not fit the field test data for the early arrival times of the injected water front at well L-2530 (fig. 7B). Several simulations were made varying the effective porosity, dispersivity values (α_L and α_T), and the aquifer permeability without obtaining a good match to the field data from well L-2530, while simultaneously matching the field data from well L-3224. This is probably because of the nature of flow in a part of the aquifer, which according to the borehole velocity logs (fig. 3), seems to have cavernous porosity, whereas the model is based on equations that are developed for a porous media system.

Table 3. Results of two injection, storage, and recovery of freshwater tests conducted from a previous study in the lower Hawthorn aquifer at the Lee County Water Treatment Plant

[Tests conducted by Fitzpatrick (1986a). Recovery time indicates time since the beginning of recovery when chloride concentration of recovered water approached background concentration of native aquifer water]

Test number	Average injection rate (cubic meters per day)	Average recovery rate (cubic meters per day)	Total volume injected (cubic meters)	Injection time (days)	Storage time (days)	Recovery time (days)	Average chloride concentration of injected water (milligrams per liter)
2	1,635	899	26,160	16	47	50	171
3	1,423	818	109,571	77	98	150	69

Model results for test 3 were compared with field data at the injection well (L-3225) for the recovery phase. Although a satisfactory match was obtained for breakthrough at observation wells L-2530 and L-3224, model predicted values for recovery chloride concentrations at the injection well (L-3225) were low compared to field measured values. Different porosity values were assigned to the main flow zones and the leaky confining units in an attempt to improve the model predictions at the injection well while keeping a good match at the two observation wells. A combination of porosity values of 0.15 for the main flow zones and 0.05 for the leaky confining units yielded satisfactory results (fig. 8). The characteristics used in the calibrated model and the fluid, solute, and rock matrix properties used in the simulations are listed in tables 4 and 5, respectively.

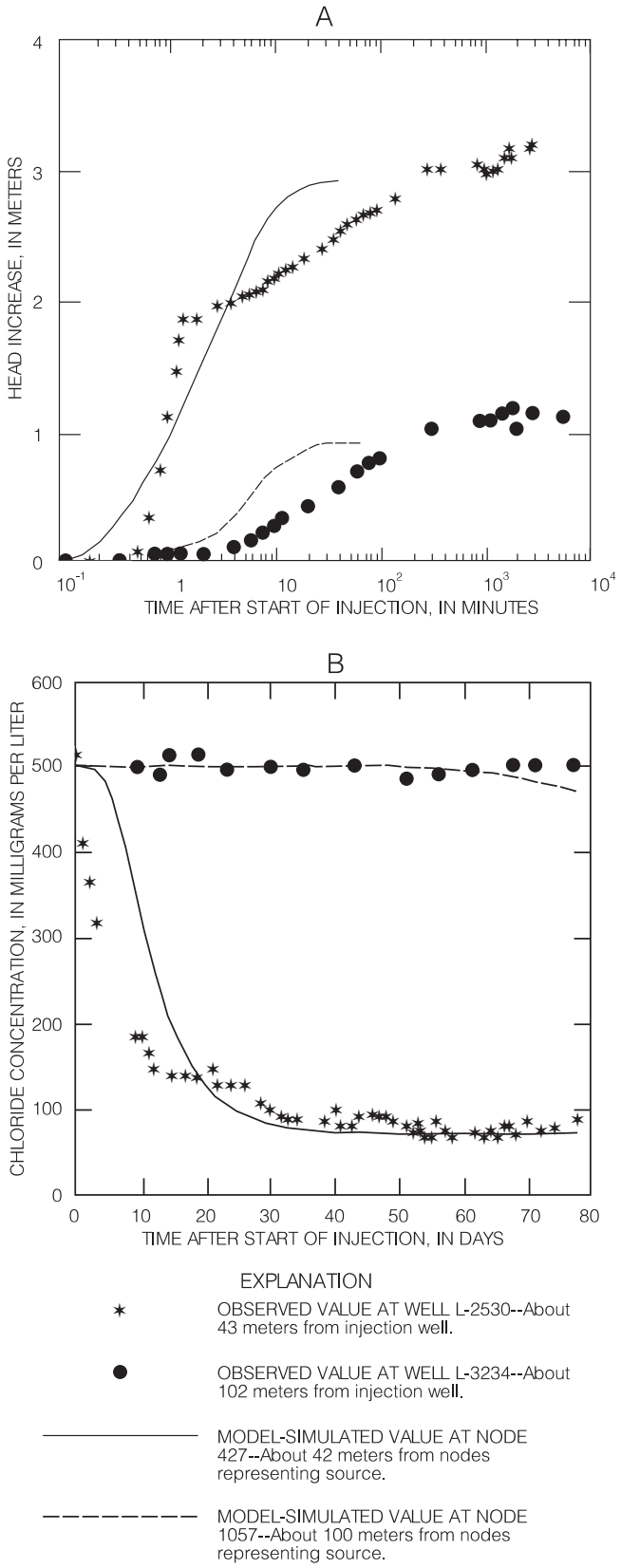

Figure 7. Observed and model simulated head increase during the first 7 days of injection and chloride concentration breakthrough curves at observation wells L-2530 and L-3224 during the injection phase of test 3 at the Lee County Water Treatment Plant.

The model was tested using chloride concentration data at the injection well (L-3225) during the recovery phase of test 2 (Fitzpatrick, 1986a). The test simulation was made using the same hydraulic and transport characteristics from the calibration run for test 3. The resulting chloride concentration breakthrough curve produced by the model was low compared to the field data (fig. 9). In an attempt to provide a closer match of the field data, the longitudinal and transverse dispersivity values were increased from 3.0 and 0.3 m to 5.0 and 0.5 m, respectively. This change resulted in a good match of the field measured data by the model-generated data (fig. 9). According to the present knowledge on the scale dependency of the dispersion coefficient (Gelhar and others, 1979; Gelhar and Axness, 1983; and Mercado, 1984), the value used to effectively simulate test 2 was expected to be smaller than its counterpart for test 3. However, the dispersivity value from test 2 was larger than that from test 3, but the difference between the values was small (α_L = 3.0 m and α_T = 0.3 m for test 3; α_L = 5.0 m and α_T = 0.5 m for test 2). No further attempt was made in this study to explain the differences in the dispersivity values between the two tests because detailed field information was unavailable.

Model Simulation Results for Cape Coral—Effects of Operational Factors on Recovery Efficiency

A series of hypothetical SISRF tests were made for the lower Hawthorn aquifer in Cape Coral using the digital modeling technique. Estimates of the hydrologic and transport characteristics from the analysis of previous test data (Fitzpatrick, 1986a) were used in a baseline simulation with other factors represented by values from studies in similar geologic units. The baseline simulation was used as a reference to study the effects of changing a series of SISRF operational factors on the recovery efficiency. The hydrologic and transport characteristics used in the baseline simulation were selected as the best possible representation of the actual field values in Cape Coral. These characteristic values might not necessarily represent the entire spatial spectrum of possible values in the lower Hawthorn aquifer. Therefore, the characteristic values used in the simulations are subject to some uncertainty. The effects on the recovery efficiency of the rates of injection and recovery; volume of water injected; storage time; injection into selected flow zones; successive cycles of injection, storage, and recovery; and chloride concentrations of injected and native waters were also studied using the digital model.

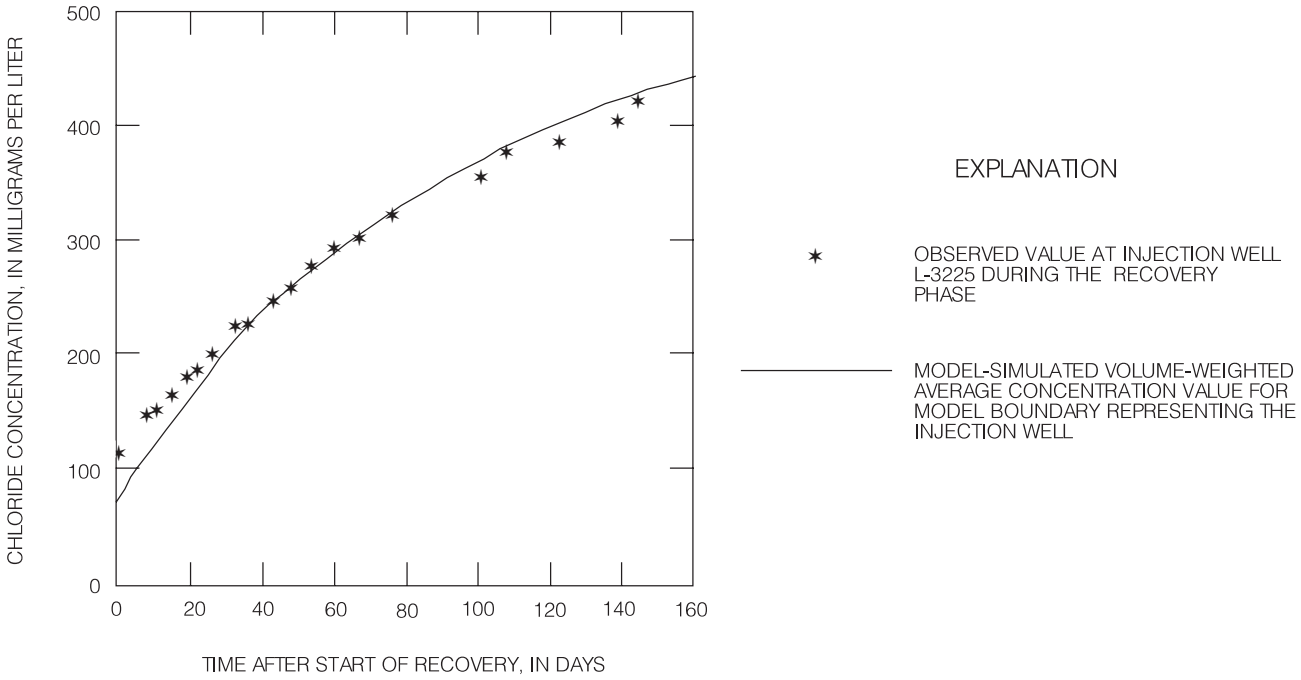

Figure 8. Observed and model-simulated chloride concentration in water recovered from injection well L-3225 during the recovery phase of test 3 at the Lee County Water Treatment Plant (data from Fitzpatrick, 1986a).

Table 4. Characteristics of flow zones and confining units used to model the lower Hawthorn aquifer at the Lee County Water Treatment Plant

Flow zones and leaky confining units (meters below land surface)	Permeability (square meters)	Effective porosity (percent)	Specific pressure storativity (kilograms per meter per second squared)$^{-1}$	Longitudinal dispersivity (meters)	Transverse dispersivity (meters)
144.8–152.8	1.670×10^{-13}	5	1.36×10^{-10}	3.0	0.3
152.8–158.8	3.846×10^{-12}	15	1.68×10^{-10}	3.0	.3
158.8–166.8	5.140×10^{-13}	5	1.36×10^{-10}	3.0	.3
166.8–176.8	5.572×10^{-12}	15	1.68×10^{-10}	3.0	.3
176.8–184.8	1.670×10^{-13}	5	1.36×10^{-10}	3.0	.3

Table 5. Fluid, solute, and rock matrix properties used in the simulations

Property	Value
Dynamic viscosity of native water, in kilograms per meter per second	0.001
Dynamic viscosity of injected water, in kilograms per meter per second	0.001
Density of native water, in kilograms per cubic meter	1,001.0
Density of injected water, in kilograms per cubic meter	1,000.1
Coefficient of molecular diffusion, in meters squared per second	5.0×10^{-10}
Fluid compressibility, in (kilograms per meter per second squared)$^{-1}$	4.4×10^{-10}
Rock matrix compressibility, in (kilograms per meter per second squared)$^{-1}$	1.2×10^{-10}

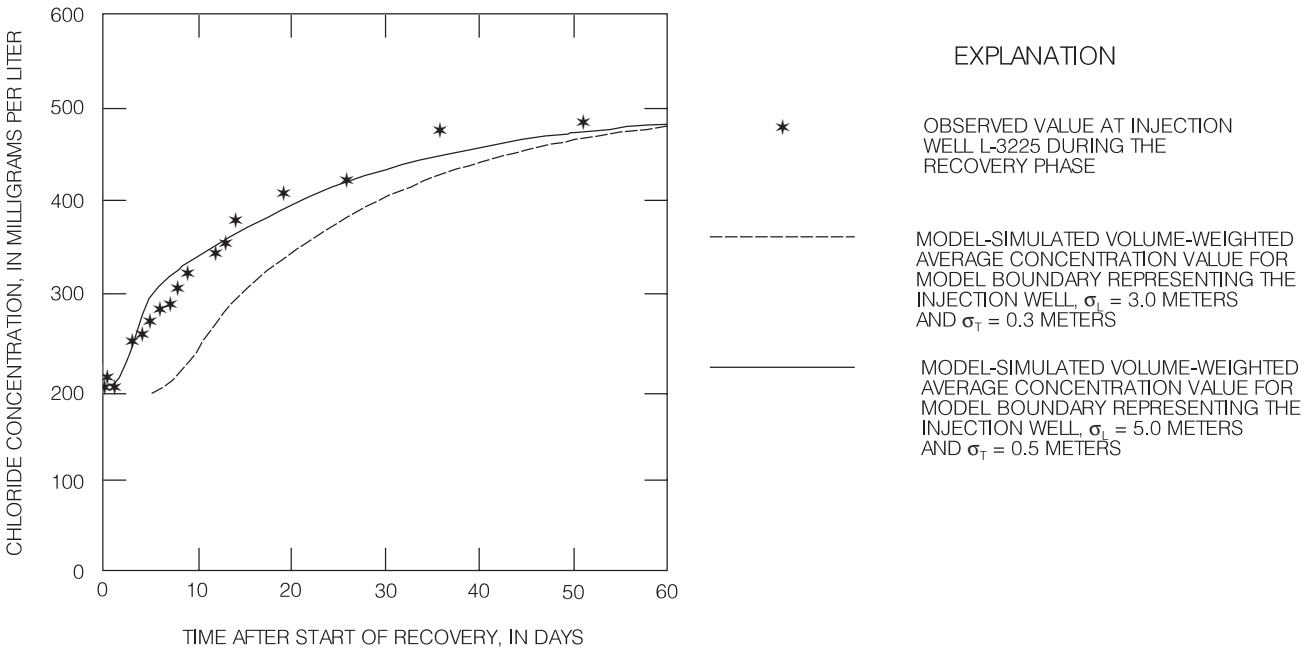

Figure 9. Observed and model-simulated chloride concentration in water recovered from injection well L-3225 during the recovery phase of test 2 at the Lee County Water Treatment Plant (observed data from Fitzpatrick, 1986a).

Baseline Simulation

A baseline simulation was made using the previously described model grid (fig. 6), estimated hydraulic and transport characteristics (tables 1, 5, and 6), and the conditions presented in table 7. The growth of the injected water body and the chloride distribution profiles (mixing zone) during the injection phase of the baseline simulation are depicted in figure 10. Although the injected water body in the lower main flow zone has twice the radial extent of its counterpart in the upper main flow zone, the difference between the chloride distribution profiles of the two flow zones was not significant (fig. 10). The injected water front was about 50 m from the injection well in the lower main flow zone and 25 m from the injection well in the upper main flow zone at the end of the injection phase (fig. 10D). A vector representation of the pore-water velocity field was generated by the model (fig. 11). This velocity vector shows that the injected water, in general, is moving: (1) horizontally outward along the two main flow zones, (2) vertically upward from the upper main flow zone into the upper confining zone, (3) vertically downward from the lower main flow zone into the lower confining zone, and (4) vertically upward from the lower main flow zone through the middle confining zone into the upper main flow zone (fig. 11). A similar vector representation was generated by the model during the recovery phase, but the vectors point in the opposite direction (fig. 12).

Table 6. Characteristics of flow zones and confining units used to model the lower Hawthorn aquifer at Cape Coral

Flow zones and leaky confining units (meters below land surface)	Permeability (square meters)	Effective porosity (percent)	Specific pressure storativity (kilograms per meter per second squared)$^{-1}$	Longitudinal dispersivity (meters)	Transverse dispersivity (meters)
186.0–198.0	1.061×10^{-12}	5	1.36×10^{-10}	3.0	0.3
198.0–214.0	1.085×10^{-11}	15	1.68×10^{-10}	3.0	.3
214.0–224.0	1.061×10^{-12}	5	1.36×10^{-10}	3.0	.3
224.0–232.0	3.435×10^{-11}	15	1.68×10^{-10}	3.0	.3
232.0–246.0	1.061×10^{-12}	5	1.36×10^{-10}	3.0	.3

Table 7. Conditions and results for recovery times and efficiencies for the baseline simulation and other simulations of subsurface freshwater injection, storage, and recovery for the lower Hawthorn aquifer at Cape Coral

[Recovery time is when the preestablished chloride concentration limit of 250 milligrams per liter is reached]

Simulation number	Injection rate (cubic meters per day)	Recovery rate (cubic meters per day)	Recovery rate/ injection rate (dimension-less)	Volume of injected water (cubic meters)	Injection time (days)	Storage time (days)	Chloride concentrations, milligrams per liter		Recovery time (days)	Recovery efficiency (percent)
							Injection water	Native aquifer water		
Baseline Simulation										
1	1,635.2	1,635.2	1.00	49,055	30	0	50	500	19.2	64
Changes in Rates of Injection and Recovery										
2	408.8	408.8	1.00	49,055	120.0	0	50	500	76.1	63
3	817.6	817.6	1.00	49,055	60.0	0	50	500	37.5	63
4	3,270.3	3,270.3	1.00	49,055	15.0	0	50	500	10.2	68
5	6,540.7	6,540.7	1.00	49,055	7.5	0	50	500	6.9	92
Changes in Recovery Rate/Injection Rate Ratio										
6	1,635.2	408.8	.25	49,055	120.0	0	50	500	74.3	62
7	1,635.2	817.6	.50	49,055	60.0	0	50	500	37.5	63
8	1,635.2	3,270.3	2.00	49,055	15.0	0	50	500	10.2	68
9	1,635.2	6,540.7	4.00	49,055	7.5	0	50	500	7.0	93
Changes in Volume of Water Injected										
10	1,635.2	1,635.2	1.00	12,264	7.5	0	50	500	7.6	100
11	1,635.2	1,635.2	1.00	24,528	15.0	0	50	500	12.1	81
12	1,635.2	1,635.2	1.00	98,110	60.0	0	50	500	33.5	56
13	1,635.2	1,635.2	1.00	196,221	120.0	0	50	500	51.8	43
Changes in Storage Time										
14	1,635.2	1,635.2	1.00	49,055	30	5	50	500	19.2	64
15	1,635.2	1,635.2	1.00	49,055	30	30	50	500	19.0	63
16	1,635.2	1,635.2	1.00	49,055	30	90	50	500	18.6	62
17	1,635.2	1,635.2	1.00	49,055	30	180	50	500	18.1	60
Injection into Upper Flow Zone (198–214 meters)										
18	1,635.2	1,635.2	1.00	49,055	30	0	50	500	18.3	61
Injection into Lower Flow Zone (224–232 meters)										
19	1,635.2	1,635.2	1.00	49,055	30	0	50	500	18.6	62
Five Successive Cycles										
20	1,635.2	1,635.2	1.00	49,055	30	180	50	500	18.3	61
21	1,635.2	1,635.2	1.00	49,055	30	180	50	500	23.4	78
22	1,635.2	1,635.2	1.00	49,055	30	180	50	500	25.0	83
23	1,635.2	1,635.2	1.00	49,055	30	180	50	500	25.8	86
24	1,635.2	1,635.2	1.00	49,055	30	180	50	500	26.6	89
Different Injected and Native Water Chloride Concentrations										
25	1,635.2	1,635.2	1.00	49,055	30	0	100	500	16.6	55
26	1,635.2	1,635.2	1.00	49,055	30	0	200	500	9.0	30
27	1,635.2	1,635.2	1.00	49,055	30	0	50	1,000	10.7	36
28	1,635.2	1,635.2	1.00	49,055	30	0	50	2,000	6.5	22

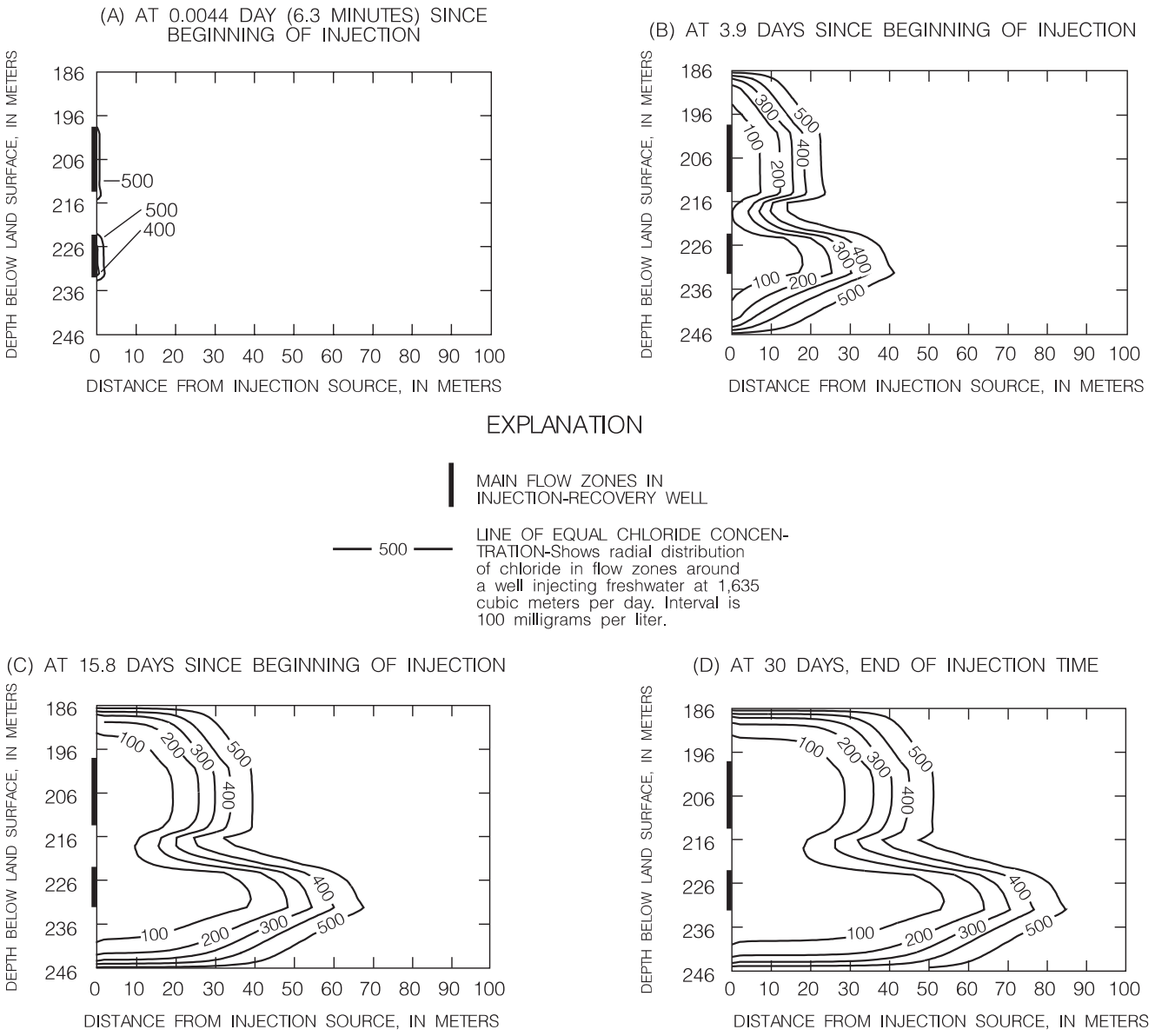

Figure 10. Chloride distribution profiles at different times during the injection phase of the baseline simulation.

A 64 percent recovery efficiency value was obtained for the baseline simulation for the preselected 250-mg/L chloride concentration limit. The thickness of the mixing zone at the end of the recovery phase grew from 1.5 to 2 times compared to its thickness at the end of the injection phase (figs. 13 and 10D). Some residual injected water was still inside the injection zones at the end of recovery (fig. 13). A subsequent injection phase would result in a wider mixing zone and a higher recovery efficiency.

A simulation was made with the same parameters that were used in the baseline simulation but using no-flow/no-transport boundaries at the top and bottom limits of the model. This simulation was conducted to test the effect on the recovery efficiency of using a constant pressure/constant concentration boundary condition to represent interlayer solute mass movement across these boundaries. The simulation yielded a recovery efficiency of 83 percentage points, which is 19 percentage points higher than the value estimated from the baseline simulation (64 percentage points). This indicates that the constant pressure/constant concentration boundaries are important in the determination of the recovery efficiency and that this type of boundary would yield more conservative estimates of the recovery efficiency.

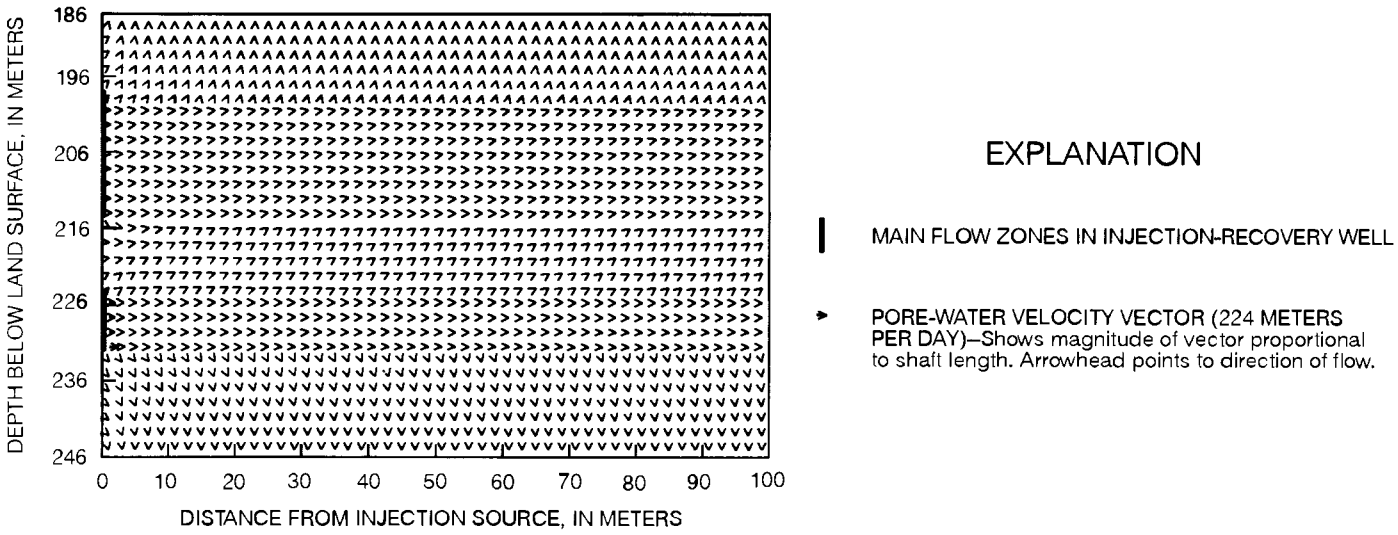

Figure 11. Vector field representing pore-water velocities in a radial section of the flow zones at the end of the injection phase of the baseline simulation.

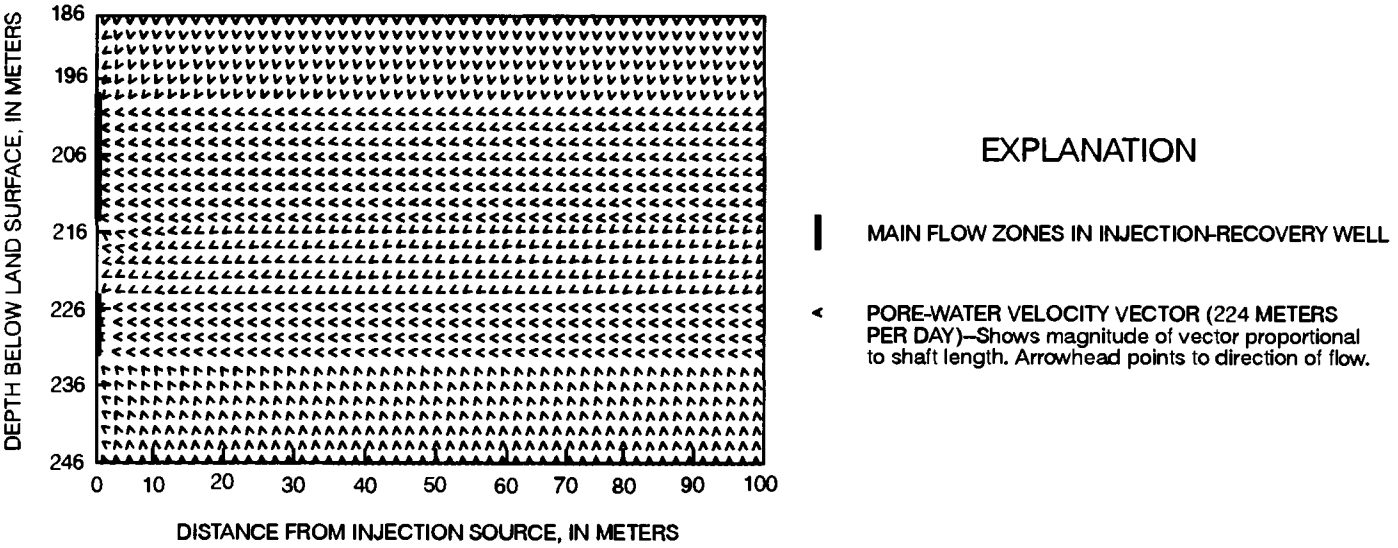

Figure 12. Vector field representing pore-water velocities in a radial section of the flow zones at the end of the recovery phase of the baseline simulation.

Rates of Injection and Recovery

The effect of the rates of injection and recovery on the recovery efficiency was studied with eight simulations using different injection and recovery rates and injection rate/recovery rate ratios (simulations 2-9 in table 7). In simulations 2 to 5, the injection rate (Q_I) and the recovery rate (Q_R) were each changed by 25, 50, 200, and 400 percent from the value used in the baseline simulation. In simulations 6 to 9, the ratio of Q_R/Q_I was changed by 25, 50, 200, and 400 percent from the baseline simulation ratio ($Q_R/Q_I = 1$).

The results of the simulations indicated that when the injection rate was decreased by 25 and 50 percent while keeping Q_R/Q_I equal to 1, an insignificant decrease in the recovery efficiency occurred (fig. 14 and table 7). However, when the injection and recovery rates were increased by 200 and 400 percent, the recovery efficiency increased from 64 percent (for the baseline simulation) to 68 and 92 percent, respectively (fig. 14 and table 7). Although in a previous hypothetical study (Merritt, 1985) no relation was reported between the rates of injection and recovery and the

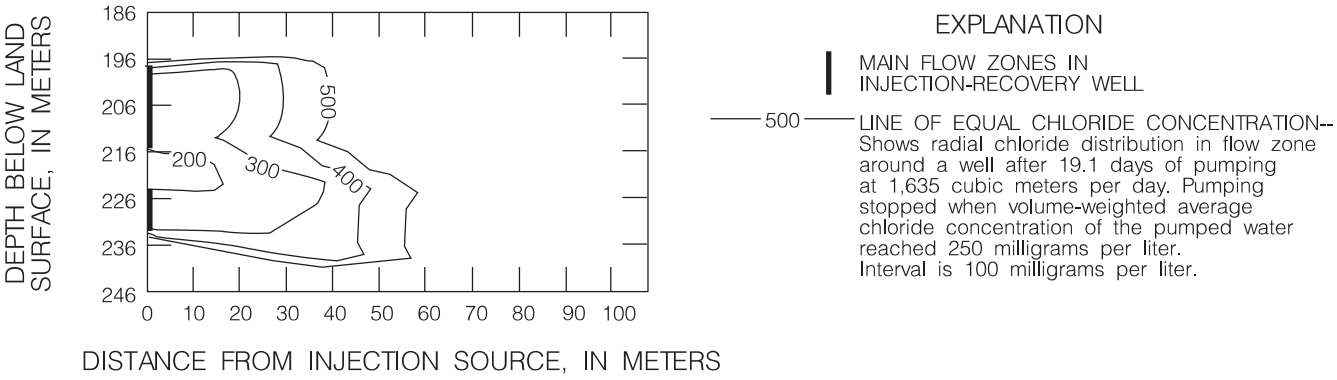

Figure 13. Chloride distribution profile at the end of the recovery phase of the baseline simulation.

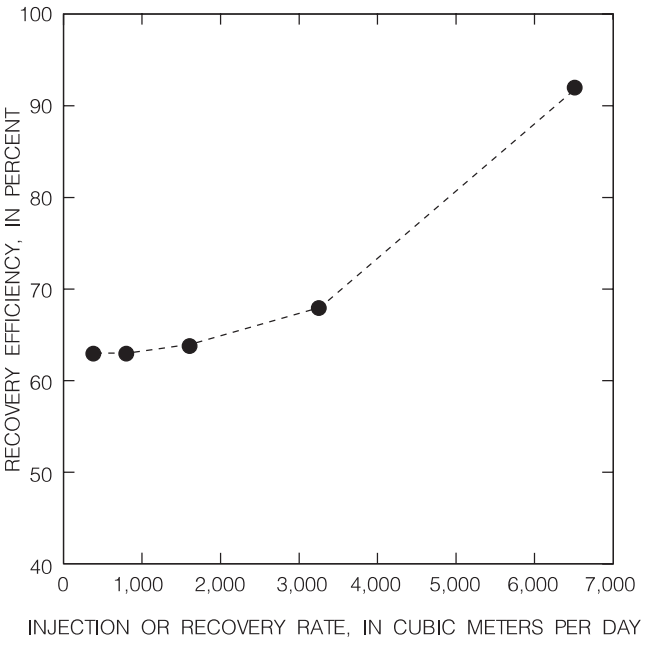

Figure 14. Relation between recovery efficiency and injection or recovery rate in the lower Hawthorn aquifer for $Q_R/Q_I = 1$.

recovery efficiency, the injected solute mass was confined by the upper and lower boundaries, keeping the injected mass near the well region and precluding mass migration across the upper and lower model boundaries. Because the mass of injected water was confined, no vertical movement occurred, and therefore, the duration and rate of injection and recovery were not important. Leakance occurs in most confined aquifers, and interlayer solute mass movement provides mechanics for mass migration, thereby affecting the recovery efficiency.

For the recovery rate/injection rate (Q_R/Q_I) ratios of 25 and 50 percent, the recovery efficiency decreased slightly (fig. 15 and table 7). For Q_R/Q_I ratios of 200 and 400 percent, the recovery efficiency increased from 64 percent (for the baseline simulation value) to 68 and 93 percent, respectively (fig. 15 and table 7). This relation can be explained by the fact that vertical mass transfer in leaky aquifers can be significant. For fast recovery rates, the vertical migration of mass would be smaller, providing for higher recoverability.

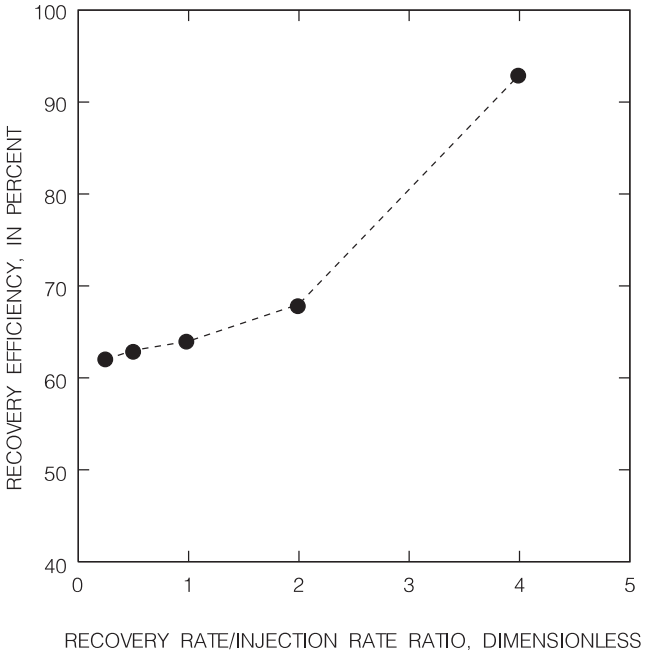

Figure 15. Relation between recovery efficiency and recovery rate/injection rate ratio in the lower Hawthorn aquifer.

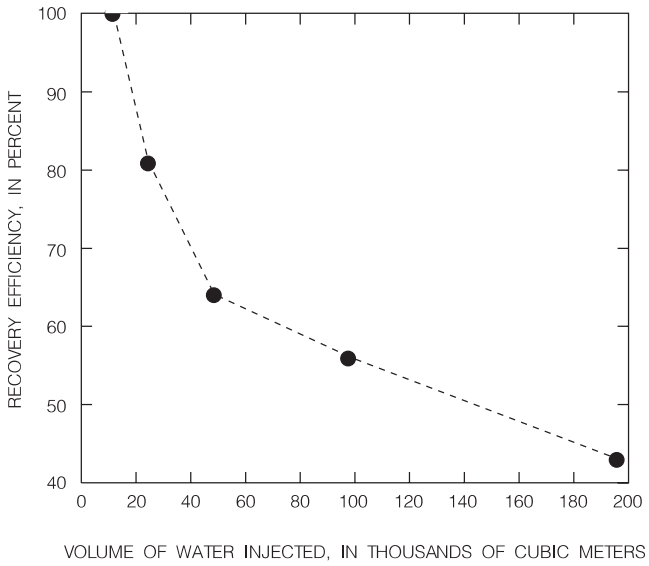

Figure 16. Relation between recovery efficiency and volume of water injected in the lower Hawthorn aquifer.

Volume of Water Injected

The effect of injecting different size volumes was studied using four simulations in which the injected volume was changed by 25, 50, 200, and 400 percent from the baseline simulation value (simulations 10-13 in table 7). This was accomplished by decreasing or increasing the injection time, while keeping the same injection rate used in the baseline simulation. Results from these simulations show that for the range of injected volumes tested in this study the recovery efficiency decreases as the volume of water injected increases (fig. 16 and table 7). Initially, the recovery efficiency decreases at a great rate as the volume of water injected is increased, but an asymptote is approached at a recovery efficiency value of about 40 percent (fig. 16); however, this result cannot be generalized. Some investigators (Merritt, 1985; Quiñones-Aponte and others, 1989) reported that the relation between the volume of water injected and the recovery efficiency can change direction for different ranges of volumes of water injected. For instance, the recovery efficiency for a range of small volumes of water injected can increase as the volume of water injected increases, and the recovery efficiency for a range of large volumes of water injected can decrease as the volume of injected water increases. The type of aquifer (confined or leaky) and boundary conditions can also affect the relation between volume of water injected and recovery efficiency. The leaky nature of the aquifer represented in this study model provides for transfer of injected water into low-permeability units. For longer injection times, larger volumes of water would migrate into and across the low-permeability units, thus reducing the potential for freshwater recovery.

Storage Time

The effect of storage time duration was assessed by increasing the duration of the storage time from the baseline simulation value of 0 days. Four simulations were made using storage times of 5, 30, 90, and 180 days (simulations 14-17 in table 7). Results from the simulations indicated that the storage time did not greatly affect the recovery efficiency, showing only a 4 percentage point decrease in recovery efficiency when the storage time was increased from 0 to 180 days (fig. 17 and table 7). However, the present model does not consider the regional background flow, which, combined with the storage time, could significantly reduce the recovery efficiency. Quiñones-Aponte and others (1989) interpreted actual SISRF tests and suggested that the recovery efficiency generally decreases as the storage time increases, but the rate of decrease in recovery efficiency would also depend on the volume of water injected. When small volumes of water are injected, the storage time has a stronger effect on reducing the recovery efficiency than when large volumes are injected (Quiñones-Aponte and others, 1989). The effect of storage time on the recovery efficiency would become overshadowed by the effect of the volume of water injected when the volume injected is large.

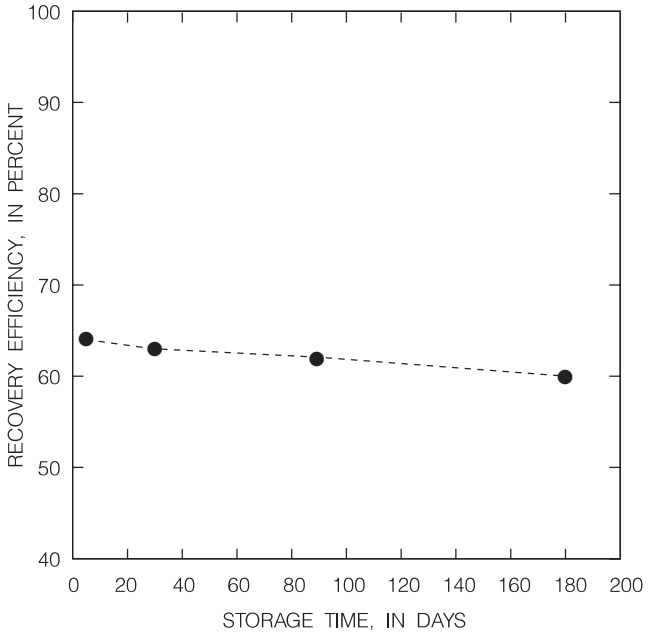

Figure 17. Relation between recovery efficiency and storage time in the lower Hawthorn aquifer.

Water Injected into Selected Flow Zones

The effect of injection into selected flow zones on recovery efficiency was studied by individually injecting the same volume of water at the same rate (volume and rate used for the baseline simulation) to each of the two more permeable flow zones. Two simulations were made—injection into the upper flow zone (198-213.3 m) and injection into the lower flow zone (222.5-231.6 m). The recovery efficiency did not change significantly; however, the configuration of the lines of equal chloride concentration at the end of the injection phase for both simulation cases revealed a sharp contrast between cases (fig. 18) and compared to their counterpart for the baseline simulation (figs. 18 and 10D). Model results indicated that the recovery efficiency in both cases decreased by a very small amount (simulations 18 and 19 in table 7) compared with the baseline simulation, which is not significant if the errors associated with the numerical method are taken into consideration. Merritt (1985) reported similar results; however, to generalize these results, a more-detailed study focusing on this aspect (injection into different flow zones) is needed.

When the injection well is open to all of the flow zones, a potential problem is the occurrence of interflow from higher to lower permeability zones through the wellbore during storage time. Water from flow zones under higher hydraulic pressure flows through the wellbore into flow zones under lower hydraulic pressure. This potential problem was not assessed by the model presented in this report; however, it should be considered for the design of actual injection wells.

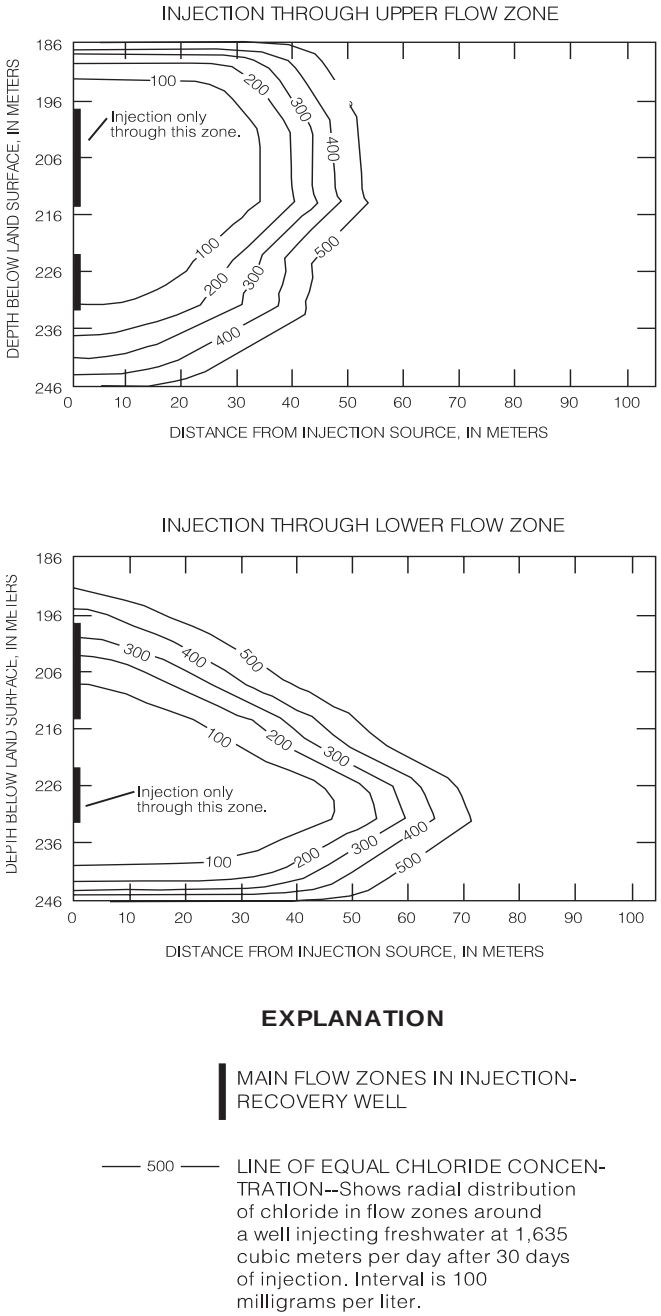

Figure 18. Chloride distribution profiles at the end of a 30-day injection period for the cases of injection into the upper and lower flow zones.

Successive Cycles of Injection, Storage, and Recovery

Five consecutive simulations were made to study the effect of successive cycles of injection, storage, and recovery on the recovery efficiency. The different factors were not changed from the baseline simulation values; however, a storage time of 180 days was used for each cycle (simulations 20-24 in table 7). Results from the preceding cycle were used as initial values for simulating the following cycle. Model results were similar to those reported by Merritt (1985). The rate of improvement on recovery efficiency with successive SISRF cycles was higher during the early cycles, increasing from about 60 to 84 percent during the first three cycles (fig. 19). Recovery efficiency increased from about 84 to 88 percent for cycles 3, 4, and 5 (fig. 19). It can be inferred from Merritt (1985, fig. 12) that the relation between recovery efficiency and the number of SISRF cycles approaches an asymptote after a certain number of cycles, where for practical purposes, no improvement of recovery efficiency occurs. The asymptote is reached at earlier cycle numbers for aquifers having small longitudinal dispersivity values (Merritt, 1985).

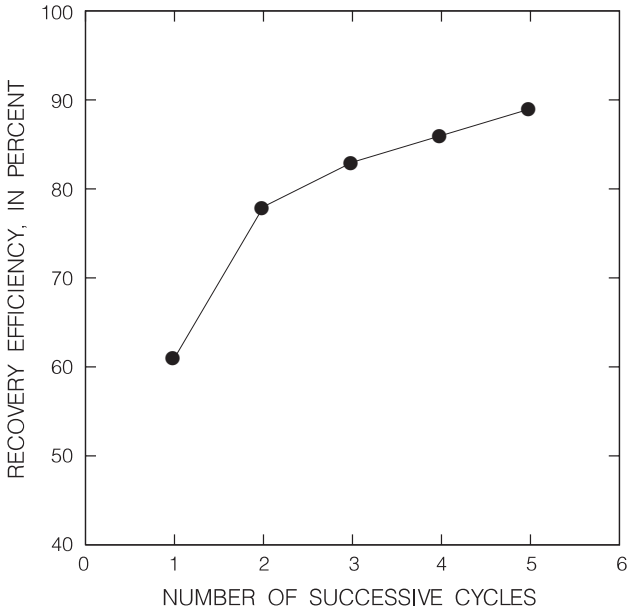

Figure 19. Relation between recovery efficiency and successive subsurface injection, storage, and recovery of freshwater cycles in the lower Hawthorn aquifer.

Chloride Concentrations in Injected and Native Waters

Four simulations were made to study the effects of different chloride concentrations in the injected and native waters. The chloride concentration in the injected water was changed in two simulations by increasing the value used in the baseline simulation by 200 and 400 percent. The chloride concentration in the native water in the remaining two simulations was changed in the same manner. The recovery efficiency in all of the simulations indicated reductions ranging from 9 percentage points (from the baseline simulation value) for 100 mg/L of chloride concentration in injected water to 42 percentage points (from the baseline simulation value) for 2,000 mg/L of chloride concentration in native water (simulations 25-28 in table 7). The analysis indicates: (1) the changes in the quality of injected water could result in reduction of the recovery efficiency; and (2) increases in the chloride concentration in native water because of saltwater intrusion, upconing, or other factors can decrease the recovery efficiency (table 7).

Sensitivity Analysis

Simulations were made to determine the sensitivity of the model-predicted recovery efficiency to variation in modeled aquifer characteristics, including permeability, ratios of anisotropy, longitudinal and transverse dispersivities, molecular diffusion, and effective porosity. The sensitivity analysis was conducted to assess the uncertainty of estimating the aquifer hydraulic and transport properties. A sensitivity analysis provides the means to identify the most important aquifer characteristics.

The relative sensitivity approach developed by Simon (1988) was applied in this sensitivity study. In the relative sensitivity approach, modeled aquifer characteristics are varied from an optimum or calibrated value by different arbitrarily selected percentages. An objective function is used to represent the overall changes in model results because of a change in the optimum aquifer characteristic value.

For this sensitivity analysis, the recovery efficiency was used as an objective function. Relative changes in the objective function values (recovery efficiency values) were related to relative changes in the different aquifer characteristics. Each of the selected aquifer characteristic values was changed individually while keeping the other values unchanged. According to Simon (1988), the first relative change in the recovery efficiency value from the baseline simulation value can be defined by:

$$REFFREL_i = \frac{ACV_b(REFF_i - REFF_b)}{REFF_b(ACV_i - ACV_b)} \qquad (16)$$

where,

$REFFREL_i$ is the relative change in the recovery efficiency;
$REFF_i$ is the recovery efficiency for a given change in an aquifer characteristic value;
$REFF_b$ is the recovery efficiency for the baseline simulation;
ACV_i is the changed or modified aquifer characteristic value; and
ACV_b is the aquifer characteristic value used in the baseline simulation.

Subsequent relative changes can be defined by:

$$REFFREL_i = \frac{ACV_b(REFF_i - REFF_{i-1})}{REFF_b(ACV_i - ACV_{i-1})} . \qquad (17)$$

For this sensitivity analysis, the parameters were divided into two categories—hydraulic and transport. The general results from the two categories, which are described in the following sections, indicated that the permeability values of the upper and lower flow zones were the most important factors and produced the greatest changes in the relative sensitivity of the recovery efficiency (fig. 20A-C). In second place of importance,

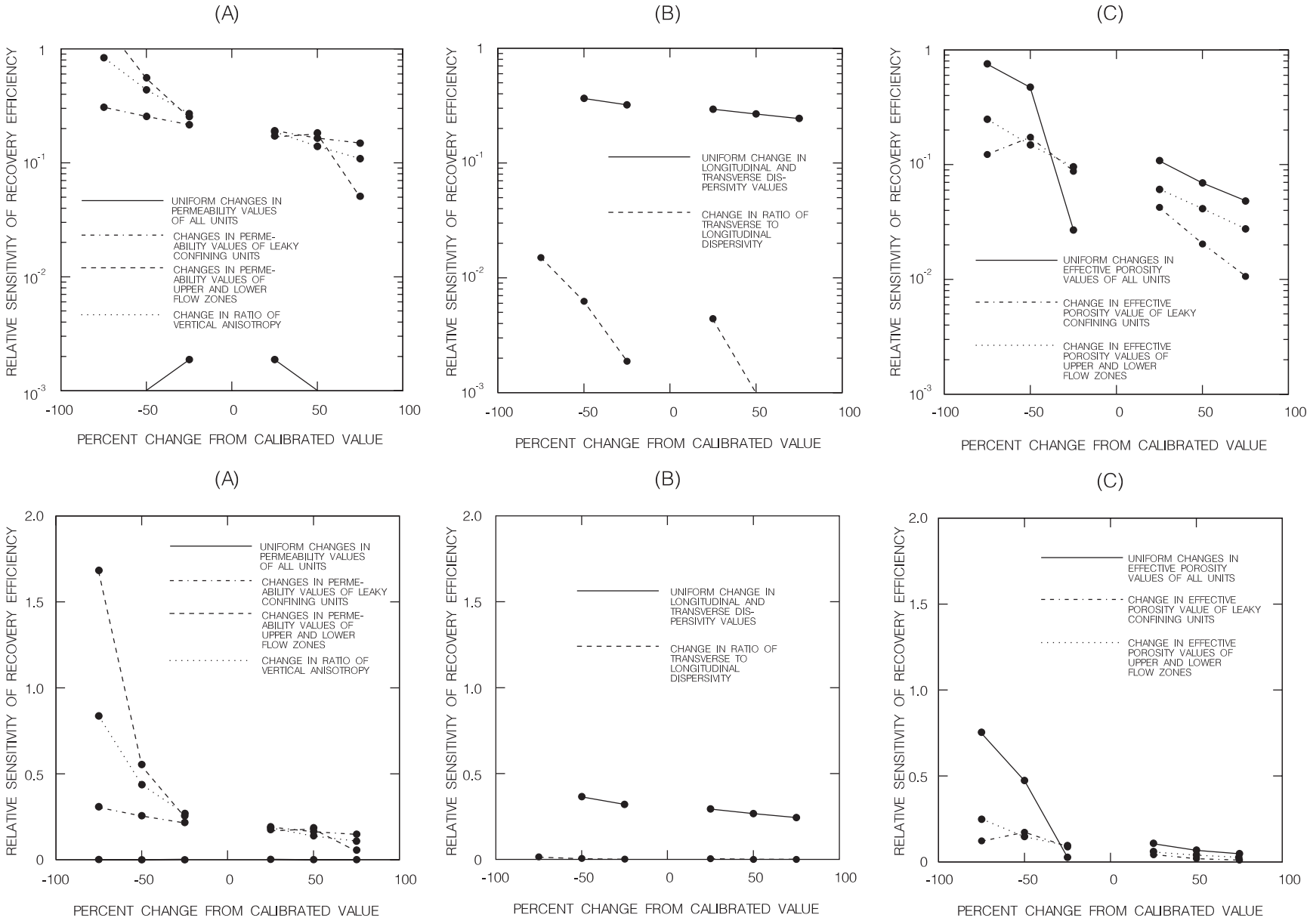

Figure 20. Relative sensitivity of recovery efficiency to variations in (A) permeability values and vertical anisotropy ratio, (B) longitudinal and transverse dispersivities and the ratio of transverse to longitudinal dispersivities, and (C) effective porosity.

but of about equal significance between them, are changes in the relative sensitivity of the recovery efficiency, produced by changing all the porosity values (porosity values of the upper and lower flow zones and the leaky confining units) and those produced by changing the vertical anisotropy ratio (fig. 20C). The fact that permeability, vertical anisotropy, and porosity are the most important factors indicates that the advection process is the most important transport process for this study. Another general observation is that the effect of changing the characteristic values on the relative sensitivity of the recovery efficiency increases when the values are decreased and decreases when the values are increased for all cases (figs. 20A-C).

Permeability and Vertical Anisotropy

The aquifer permeability determines the specific discharge or Darcy's velocity (eq. 6), which in turn, is combined with the effective aquifer porosity to determine the average pore-water velocity (eq. 10). The average pore-water velocity is directly used in the advective term of the transport equation (eq. 14) and indirectly used through the hydrodynamic dispersion tensor (eq. 12) in the dispersive term of the transport equation (eq. 14). Uncertainty in the permeability value would, therefore, affect the advective and dispersive components of the transport computations. The sensitivity of the model to the permeability value was limited to changing the magnitude of the permeability tensor and the vertical anisotropy. Other factors having potential effects on the permeability, such as horizontal anisotropy and heterogeneity, were not considered in this analysis because of the lack of available information.

The magnitude of the permeability was changed in three different ways: (1) uniform changes in all permeability values, (2) changes in permeability values of the leaky confining units, and (3) changes in permeability values of the upper and lower flow zones. The permeability values of the upper and lower flow zones (seemingly the most important in the permeability category) produced the greater changes in the relative sensitivity of the recovery efficiency when the calibrated value was decreased or increased, but showed greater effects when the permeability values were decreased (fig. 20A). Changes in the permeability value of the leaky confining units indicated some sensitivity when the value was increased or decreased by 25 percent, but for greater changes the relative sensitivity was not significantly affected (fig. 20A). It can be inferred from figure 20A that a uniform change in the permeabilities of model layers representing all flow zones and leaky confining units produced an insignificant effect on the recovery efficiency.

Vertical anisotropy, the ratio of vertical to horizontal permeability, was also studied. Changes in the ratio of horizontal to vertical permeability produced the second greatest changes in the relative sensitivity of the recovery efficiency in the permeability category (fig. 20A).

Hydrodynamic Dispersion and Effective Porosity

The hydrodynamic dispersion tensor describes the combined effects of the flow field, aquifer matrix, and molecular diffusion on the transport of solute particles (eq. 13). Flow field and aquifer matrix effects are represented by mechanical dispersion (eq. 12), whereas molecular diffusion is described by Fick's law. The effect of hydrodynamic dispersion on the relative sensitivity of recovery efficiency was studied through the different components of the hydrodynamic dispersion coefficient. The longitudinal and transverse dispersivities represent the dispersive mechanisms of the process. Although molecular diffusion is also a component of the hydrodynamic dispersion coefficient, it is widely recognized among scientists that the effect of molecular diffusion is negligible when compared to longitudinal and transverse dispersivities. Therefore, no attempt was made to study the effects of changing the coefficient of molecular diffusion in this study.

Two different tests were made for the longitudinal and transverse dispersivity values. Both dispersivity values were simultaneously changed by the same percentage in the first test, keeping the ratio of transverse to longitudinal dispersivity equal to 1/10. The ratio of transverse to longitudinal dispersivity was changed in the second test, keeping the longitudinal dispersivity value constant while changing the transverse dispersivity value. The results from the analysis indicated that the uniform change in both transverse and longitudinal dispersivity values produced more significant changes in the relative sensitivity of the recovery efficiency than when the ratio of transverse to longitudinal dispersivities was changed (fig. 20B). In both cases, the relative sensitivity of the recovery efficiency decreased as the dispersivity values or ratio of transverse to longitudinal dispersivity were increased (fig. 20B).

Effective porosity is a factor in the ground-water hydraulic equation (eq. 7) and the advective-dispersive solute-transport equation (eq. 14) in the storage term. However, this porosity has a double effect on the

advective dispersive solute-transport equation (eq. 14). In addition to the effect on the storage term for the transport equation, the effective porosity value is combined with the specific discharge (obtained from the ground-water flow equation) to determine the average pore-water velocities, which are used to represent the advection term in the transport equation (eq. 14).

The effective porosity values were changed in three different ways: (1) the porosity values of all the different layers representing the hydrogeologic units were changed by the same percentage from their calibrated values, (2) changes were made to porosity values of the upper and lower flow zones, and (3) changes were made to porosity values of the leaky confining units. Results from the analysis indicated that the most significant changes in the relative sensitivity of the recovery efficiency (and seemingly the most important in the hydrodynamic dispersion category) were produced by changing the porosity values of all layers using the same percentage (figs. 20B and 20C). The second most significant changes to the relative sensitivity of the recovery efficiency were produced by changing the porosity of the upper and lower flow zones (fig. 20C). Smaller changes in the relative sensitivity of the recovery efficiency were produced when porosity values of the leaky confining units were changed (fig. 20C). These results suggest that a specific combination of porosity values of the flow zones and the leaky confining units is needed to provide an adequate representation of the transport system.

LIMITATIONS

Confidence in the model and in the resulting simulations is limited by a number of factors. These factors can be segregated into two categories—the hydrogeologic information and the aspects of the model code. Among the hydrogeologic information, the most important limiting factors in this study were lack of:

- Complete understanding about the spatial variability of the hydraulic conductivity or permeability values (heterogeneity),
- Field information on changes in the magnitude of the hydraulic conductivity or permeability in the horizontal and vertical directions (horizontal and vertical anisotropies),
- Field information on the porosity values,
- Knowledge about the potential effect of fractures or solution cavities on the flow and transport processes (result of effective secondary porosity),
- Real SISRF tests in the Cape Coral area, and
- Assumptions made to represent the top and bottom boundary conditions as having constant solute concentration and pressure.

The computer code (QSUTRA) used in this study has some intrinsic limitations:

- The fact that the code provides only for two-dimensional simulations precluded the study of the effect of background regional flow on the displacement of the injected water when the cylindrical (radial) coordinate option was used;
- When the Cartesian coordinate option is used, the assumption of vertical homogeneity and isotropy must be made, and such an assumption would be unrealistic for the Cape Coral site; and
- In QSUTRA, the solute-transport equation for transient compressible fluid flow is represented by an analogous numerical expression where porosity, thickness, and fluid density are kept constant by producing a mass-balance error. This affects the determination of velocities and dispersion coefficients (Goode, 1990; 1992). However, this intrinsic error is not expected to greatly affect the simulation of field-scale problems in which the uncertainty and variability of the modeled aquifer characteristics overshadow the potential effects from the intrinsic mass-balance error.

SUMMARY AND CONCLUSIONS

A preliminary assessment of subsurface injection, storage, and recovery of freshwater (SISRF) was made as a potential alternative to the growing water-supply problems of Cape Coral in Lee County, southwestern Florida. A digital modeling approach was used for this preliminary assessment to research the actual potential of SISRF without having to spend the large amounts of money required for real field testing of this technique.

The hydrogeologic framework used for this study was modified or developed from the interpretation of data from previous studies. Aquifer characteristics were estimated from interpretation of data from previous studies. A combination of caliper and flow-velocity borehole geophysical logs was used to estimate the percentages of flow entering different flow zones. These percentages of flow and information on the aquifer transmissivity were used to estimate permeability values for the different flow zones.

A general presentation was made of the density-dependent ground-water flow and advective dispersive solute-transport equations. A modified version of the computer code SUTRA (QSUTRA) and a cylindrical coordinates grid were used for this preliminary assessment because of the lack of information required to represent the real three-dimensional ground-water flow and transport system.

Dispersive characteristics were estimated on the basis of data from a previous study at the Lee County Water Treatment Plant. This was accomplished by calibrating a model for the Lee County Water Treatment Plant site and testing this model using field data from a previous study. A second model was made for the Cape Coral area using local hydraulic characteristics and adopting the dispersive characteristics estimated for the Lee County Water Treatment Plant site model.

A series of 28 hypothetical tests of subsurface injection, storage, and recovery of freshwater were made for the lower Hawthorn aquifer in Cape Coral using the digital modeling technique to assess the efficiency of this operation in the subject aquifer. A baseline simulation was used as reference to compare the effects of changing some operational factors on the recovery efficiency. A recovery efficiency of 64 percent was estimated for the baseline simulation. This recovery efficiency represents the total amount of water pumped during the recovery phase before the 250-milligrams per liter chloride limit is reached divided by the total amount of injected water. The effects of the following operational factors were assessed using the model: rates of injection and recovery; volume of water injected; storage time; injection into selected flow zones; successive cycles of injection, storage, and recovery; and chloride concentrations in injected and native aquifer waters.

A summary of the simulation results from the model, which is based on the limited knowledge of the aquifer, indicates that the recovery efficiency increased when the injection rate and recovery rates were increased, and when the ratio of recovery rate to injection rate was increased. Recovery efficiency decreased when the amount of water injected was increased; decreased slightly when the storage time was increased; was not changed significantly when the water was injected to a specific flow zone; increased with successive cycles of injection, storage, and recovery; and decreased when the chloride concentrations in either the injected water or native aquifer water were increased. The different simulation results for storage time might be unrealistic because the cylindrical coordinates used in the model did not consider the regional background flow, which was an important factor in previous studies.

The higher recovery efficiencies were obtained for three simulation tests for which the duration of injection and recovery phases was shorter. This is expected because of the nature of the conceptual system in which migration of the solute particles to areas beyond the vertical boundaries will reduce the recoverability for tests of longer duration. The recovery efficiency fluctuated from its baseline value of 64 percent to an upper value of about 100 percent and to a lower value of 22 percent in all of the simulations.

Interlayer solute mass movement across the upper and lower boundaries seems to be the most important factor affecting the recovery efficiency. A simulation that was conducted with the same parameters used for the baseline simulation, but representing the top and bottom boundaries as impermeable (no flow and no solute transport), yielded a recovery efficiency value of 83 percentage points. This value is 19 percentage points higher than the estimated value from the baseline simulation showing that this boundary is important in determining the recovery efficiency, and that using constant pressure and constant solute concentration, boundaries will yield more conservative estimates of the recovery efficiency.

The sensitivity analysis was performed applying the relative sensitivity technique in which changes in the different factors and model responses are normalized to make a meaningful comparison of the model responses due to changes in the different factors. Two categories of factors were recognized for the sensitivity analysis—aquifer permeability and hydrodynamic dispersion. Several combinations of changes were made for factors of the two categories. For instance, a factor was changed only for a specific flow zone. The general results from the sensitivity analysis indicated that the permeability values of the upper and lower flow zones are the most important factors, producing the overall greater changes in the relative sensitivity of the recovery efficiency. In second place of importance, but of about equal significance between them, are changes in the relative sensitivity of the recovery efficiency, produced by changing all the porosity values (porosity values of the upper and lower flow zones and the confining beds) and those produced by changing the vertical anisotropy ratio.

Model results indicate that high recovery efficiencies (from 64 to about 100 percent) can be achieved for different SISRF operational schemes. Two successive injection, storage, and recovery cycles can increase the recovery efficiency from 60 to about 80 percent. Combinations of different operational factors also can be used to maintain high recovery efficiencies. The advective factors (pore-water velocities derived from permeability and porosity values) were apparently the most

important to the model sensitivity in the Cape Coral area. However, the dispersivity values used for the lower Hawthorn aquifer in the Cape Coral area model were not field values, but values that were extrapolated from the model of the lower Hawthorn aquifer at the Lee County Water Treatment Plant site. These dispersivity values might not be representative of the actual dispersive characteristics of the lower Hawthorn aquifer in the Cape Coral area. The model presented in this report is a generalized version of the actual hydrogeologic system and could be refined if additional information on the advective and dispersive characteristics of the aquifer is made available.

REFERENCES CITED

Anderson, M.P., 1984, Movement of contaminants in groundwater: Groundwater transport-advection and dispersion, *in* Groundwater Contamination: Washington, D.C., National Academy Press, p. 37-45.

Bear, J., 1979, Hydraulics of Groundwater: New York, McGraw-Hill, 569 p.

Brown, R.H., 1963, Estimating the transmissivity of an artesian aquifer from the specific capacity of a well, *in* Methods of Determining Permeability, Transmissivity, and Drawdown: U.S. Geological Survey Water-Supply Paper 1536-I, p. 336-338.

City of Cape Coral Planning Division, 1988, Comprehensive plan—future land use element—Volume 1. Population and Demographics, 31 p.

Fitzpatrick, D.J., 1986a, Tests for injecting, storing, and recovering freshwater in a saline artesian aquifer, Lee County, Florida: U.S. Geological Survey Water-Resources Investigations Report 85-4249, 53 p.

——— 1986b, Hydrogeologic conditions and saline-water intrusion, Cape Coral, Florida, 1978-81: U.S. Geological Survey Water-Resources Investigations Report 85-4231, 31 p.

Florida Department of Environmental Protection, 1993, Drinking water standards, monitoring and reporting: Chapter 17-550, Florida Administrative Code, 38 p.

Freeze and Cherry, 1979, Groundwater: Englewood Cliffs, N.J., Prentice-Hall, 604 p.

Gelhar, L.W., and Axness, C.L., 1983, Three-dimensional stochastic analysis of macrodispersion in aquifers, Water Resources Research, v. 19, no. 1, p. 161-180.

Gelhar, L.W., Gutjahr, A.L., and Naff, R.L., 1979, Stochastic analysis of macrodispersion in a stratified aquifer: Water Resources Research, v. 15, no. 6, p. 1387-1397.

Goode, D.J., 1990, Governing equations and model approximation errors associated with the effects of fluid-storage transients on solute transport in aquifers: U.S. Geological Survey Water-Resources Investigations Report 90-4156, 20 p.

——— 1992, Modeling transport in transient ground-water flow: An unacknowledged approximation: Ground Water, v. 30, no. 2, p. 257-261.

Kimbler, O.K., Kazmann, R.G., and Whitehead, W.R., 1975, Cyclic storage of fresh water in saline aquifers: Louisiana Water Resources Research Institute Bulletin 10, Baton Rouge, Louisiana State University, 78 p.

Knapp, M.S., Burns, W.S., Sharp, T.S., and Shih, George, 1984, Preliminary water resources assessment of the mid and lower Hawthorn aquifers in western Lee County, Florida: South Florida Water Management District Technical Report 84-10, 106 p.

Kuiper, L.K., 1987, Computer program for solving groundwater flow equations by the preconditioned conjugate gradient method: U.S. Geological Survey Water-Resources Investigations Report 87-4091, 34 p.

La Rose, H.R., 1990, Geohydrologic framework and an analysis of a well-plugging program, Lee County, Florida: U.S. Geological Survey Water-Resources Investigations Report 90-4063, 26 p., 1 pl.

Lee County Planning Department, 1977, Climate of Lee County: Lee County Planning Department report, 62 p.

Mercado, A., 1984, A note on micro and macrodispersion: Ground Water, v. 22, no. 6, p. 790-791.

Merritt, M.L., 1985, Subsurface storage of freshwater in south Florida: A digital model analysis of recoverability: U.S. Geological Survey Water Supply Paper 2261, 44 p.

Merritt, M.L., Meyer, F.W., Sonntag, W.H., and Fitzpatrick, D.J., 1983, Subsurface storage of freshwater in south Florida: A prospectus: U.S. Geological Survey Water-Resources Investigations Report 83-4214, 69 p.

Meyer, F.W., 1989, Subsurface storage of liquids in the Floridan aquifer system in south Florida: U.S. Geological Survey Open-File Report 88-477, 25 p.

Missimer and Associates, Inc., 1984, Hydrogeology of the lower part of the Hawthorn aquifer system, Cape Coral Florida: Consultant's Report, 84 p.

——— 1985, Cape Coral reverse osmosis wellfield final construction report and operational and maintenance recommendations: v. 1, 58 p.

National Oceanic and Atmospheric Administration, 1944-88, Climatological data, Florida: Monthly summaries for 1984 to 1988.

Quiñones-Aponte, Vicente, Whiteside, D.V., and Zack, Allen, 1989, Single well injection and recovery of freshwater from an aquifer containing saline water in Arecibo, Puerto Rico: U.S. Geological Survey Water-Resources Investigations Report 88-4037, 19 p.

Scheidegger, A.E., 1961, General theory of dispersion in porous media: Journal of Geophysical Research, v. 66, p. 3273-3278.

Simon, E., 1988, Parameter sensitivity analysis for hydrologic simulation models: Water International, v. 13, p. 46-56.

Voss, C.I., 1984, A finite-element simulation model for saturated-unsaturated, fluid density-dependent groundwater flow with energy transport or chemically reactive single species solute transport: U.S. Geological Survey Water-Resources Investigations Report 84-4369, 409 p.

Wedderburn, L.A., Knapp, M.S., Waltz, D.P., and Burns, W.S., 1982, Hydrogeologic reconnaissance of Lee County, Florida—Part 1: South Florida Water Management District Technical Report 82-1, 192 p.

Young, D.M., 1954, Iterative method for solving partial differential equations of the elliptic type: Transactions American Mathematical Society, v. 76, p. 92-111.

Appendix I

Appendix II

QSUTRA Program Listing (Model Version 1284-2DICG Modified for Regular Grid)

[MODIFIED, Changes as per updated version of SUTRA, version V06902D; NEW, Changes made as part of QSUTRA implementation, version 1284-2DICG]

```
C     SUTRA            M A I N   P R O G R A M   SUTRA-VERSION 1284-2D A10.....
C_____________________________________________________________________A20.....
C|                                                                    |A30.....
C|                                                                    |A40.....
C|                 UNITED STATES GEOLOGICAL SURVEY                    |A50.....
C|   GROUND-WATER FLOW AND ENERGY OR SOLUTE TRANSPORT SIMULATION MODEL |A60.....
C|                                                                    |A70.....
C|                                                                    |A80.....
C|                                                                    |A90.....
C|                                                                    |A100....
C|                     _____________________                          |A110....
C|                    |                     |                         |A120....
C|                    |   S   U   T   R   A |                         |A130....
C|                    |_____________________|                         |A140....
C|                                                                    |A150....
C|                                                                    |A160....
C|                Saturated    Unsaturated    TRAnsport               |A170....
C|                =            =              ===                     |A180....
C|                                                                    |A190....
C|                                                                    |A200....
C|                                                                    |A210....
C|     * * * * * * * * * * * * * * * * * * * * * * * * * * * * * *    |A220....
C|     * ->saturated and/or unsaturated groundwater flow         *    |A230....
C|     * ->either single species reactive solute transport       *    |A240....
C|     *    or thermal energy transport                          *    |A250....
C|     * ->two-dimensional areal or cross-sectional simulation   *    |A260....
C|     * ->either cartesian or radial/cylindrical coordinates    *    |A270....
C|     * ->hybrid galerkin-finite-element method and             *    |A280....
C|     *    integrated-finite-difference method                  *    |A290....
C|     *    with two-dimensional quadrilateral finite elements   *    |A300....
C|     * ->finite-difference time discretization                 *    |A310....
C|     * ->non-linear iterative, sequential or steady-state      *    |A320....
C|     *    solution modes                                       *    |A330....
C|     * ->optional fluid velocity calculation                   *    |A340....
C|     * ->optional observation well output                      *    |A350....
C|     * ->modified for regular grid only  - to minimize storage *    |NEW
C|     * ->optional fluid mass and solute mass or energy budget  *    |A370....
C|     * * * * * * * * * * * * * * * * * * * * * * * * * * * * *    |A380....
C|                                                                    |A390....
C|                                                                    |A400....
C|                                                                    |A410....
C|       Complete explanation of function and use of this code        |A420....
C|       is given in :                                                |A430....
C|                                                                    |A440....
C|       Voss, Clifford I., 1984, SUTRA: A Finite-Element             |A450....
C|            Simulation Model for Saturated-Unsaturated              |A460....
C|            Fluid-Density-Dependent Ground-Water Flow               |A470....
C|            with Energy Transport or Chemically-Reactive            |A480....
C|            Single-Species Solute Transport, U.S. Geological        |A490....
C|            Survey Water-Resources Investigations Report            |A500....
C|            84-4369.                                               |A510....
C|                                                                    |A520....
C|                                                                    |A530....
C|                                                                    |A540....
C|       Users who wish to be notified of updates of the SUTRA        |A550....
C|       code and documentation may be added to the mailing           |A560....
C|       by sending a request to :                                    |A570....
C|                                                                    |A580....
C|                      Chief Hydrologist - SUTRA                     |A590....
C|                       U.S. Geological Survey                       |A600....
C|                        431 National Center                         |A610....
C|                       Reston, Virginia 22092                       |A620....
C|                                USA                                 |A630....
C|                                                                    |A640....
```

```
C|     * * * * * * * * * * * * * * * * * * * * * * * * * * * * * *     |A650....
C|     * The SUTRA code and documentation were prepared under a  *     |A660....
C|     * joint research project of the U.S. Geological Survey,   *     |A670....
C|     * Department of the Interior, Reston, Virginia, and the   *     |A680....
C|     * Engineering and Services Laboratory,  U.S. Air Force    *     |A690....
C|     * Engineering and Services Center, Tyndall A.F.B.,        *     |A700....
C|     * Florida.  The SUTRA code and documentation are          *     |A710....
C|     * available for unlimited distribution.                   *     |A720....
C|     * * * * * * * * * * * * * * * * * * * * * * * * * * * * * *     |A730....
C|                                                                     |A740....
C|                                                                     |A750....
C|                                                                     |A760....
C|_____________________________________________________________________|A770....
C                                                                       A780....
C                                                                       A790....
C                                                                       A800....
      IMPLICIT DOUBLE PRECISION (A-H,O-Z)                               A810....
      COMMON/FUNITS/ K00,K0,K1,K2,K3,K4,K5,K6,K7,K8                     MODIFIED
      COMMON/LGE/ RM,RV,IMV                                             A820....
C     COMMON/LGEV/ RV                                                   A830....
C     COMMON/LGEMV/ IMV                                                 A840....
      COMMON/DIMS/ NN,NE,NIN,IS,JT,NBIP,NBIS,NPT(9),NPBC,NUBC,          NEW
     1   NSOP,NSOU,NBCN
      COMMON/CNTRL1/ GNU,UP,DTMULT,DTMAX,ME,ISSFLO,ISSTRA,ITCYC,        NEW
     1   NPCYC,NUCYC,NPRINT,IREAD,ISTORE,NOUMAT,IUNSAT,ITIME            NEW
      COMMON/OBS/ NOBSN,NTOBSN,NOBCYC,ITCNT                             A890....
      CHARACTER*1 TITLE1(80),TITLE2(80)                                 A900....
      CHARACTER*6 SIMULA(2)                                             A910....
      CHARACTER*80 UNAME,ENAME,FNAME                                    MODIFIED
        INTEGER RMDIM,RVDIM,IMVDIM,RMDIMA,RVDIMA,IMVDMA                 NEW
      DIMENSION KRV(100),FNAME(8),IUNIT(8)                              MODIFIED
C                                                                       A930....
C                                                                       A940....
C_______________________________________________________________________A950....
C|* * * * * * * * * * * * * * * * * * * * * * * * * * * * * * * * * *|A960....
C|* ***************************************************************** *|A970....
C|* *                                                               * *|A980....
C|* *   The three arrays that need be dimensioned                   * *|A990....
C|* *    are dimensioned as follows:                                * *|A1000...
C|* *                                                               * *|A1010...
C|* *   DIMENSION  RM( RMDIM), RV( RVDIM), IMV(IMVDIM)              * *|A1020...
C|* *                                                               * *|A1030...
C|* *   RMDIM >= NN*(NBIP + NBIS + 9)                                  NEW
C|* *                                                               * *|A1050...
C|* *   RVDIM >= (( NNV*NN + (NEV+8)*NE + NBCN*3                    * *|A1060...
C|* *              + (NOBS+1)*(NTOBS+2)*2 + NTOBS + 5 ))            * *|A1070...
C|* *                                                               * *|A1080...
C|* *   IMVDIM >= (( NE*8 + NN +  NSOP + NSOU                       * *|  NEW
C|* *              + NBCN*2 + NOBS + NTOBS + 12 ))                  * *|A1100...
C|* *                                                               * *|A1110...
C|* *   where:                                                      * *|A1120...
C|* *                                                               * *|A1130...
C|* *    NNV = 30                                                   * *|A1140...
C|* *    NEV = 10                                                   * *|A1150...
C|* *    NBCN = NPBC + NUBC                                         * *|A1160...
C|* *                                                               * *|A1170...
C|* *    NBIP = 5   for a regular grid                              * *|  NEW
C|* *    NBIS = 9   for a regular grid                              * *|  NEW
C|* *    NBIA = 13  for a regular grid                              * *|  NEW
C|* *                                                               * *|
C|* *   and:                                                        * *|A1180...
```

```
C|* *                                                              * *|  A1190...
C|* *    NN = number of nodes in finite element mesh               * *|  A1200...
C|* *    NE = number of elements in finite element mesh            * *|  A1210...
C|* *    NOBS = number of observation nodes in mesh                * *|  A1220...
C|* *    NTOBS = maximum number of time steps with observations    * *|  A1230...
C|* *    NSOP = number of fluid mass source nodes in mesh          * *|  A1250...
C|* *    NSOU = number of energy or solute mass source nodes       * *|  A1260...
C|* *    NPBC = number of specified pressure nodes in mesh         * *|  A1270...
C|* *    NUBC = number of specified concentration or temperature   * *|  A1280...
C|* *           nodes in mesh                                      * *|  A1290...
C|* *                                                              * *|  A1300...
C|* *                                                              * *|  A1310...
C|* *   The three arrays must be given dimensions just below.      * *|  A1320...
C|* *                                                              * *|  A1330...
C|* *                                                              * *|  A1330...
C|* *   REMEMBER also to change the dimension values,              * *|  A1330.1MODIFIED
C|* *    RMDIM, RVDIM and IMVDIM in the three assignment           * *|  A1330.2MODIFIED
C|*.*    statements below the DIMENSION statement!                 * *|  A1330.3MODIFIED
C|* *                                                              * *|  A1330.4MODIFIED
C|* *   AND ALSO :                                                 * *|  A1330.5MODIFIED
C|* *    Two files must be permanently assigned just below for     * *|  A1330.6MODIFIED
C|* *    your computer installation.  One file captures error      * *|  A1330.7MODIFIED
C|* *    output written during subsequient file opening.  The      * *|  A1330.8MODIFIED
C|* *    other file contains the unit numbers and file names       * *|  A1330.9MODIFIED
C|* *    to be assigned as SUTRA input and output files            * *|  A1331.0MODIFIED
C|* *    for each simulation.                                      * *|  A1331.1MODIFIED
C|* *                                                              * *|  A1331.2MODIFIED
C|* *    STANDARD ASSIGNMENTS TO BE MADE:                          * *|  A1331.3MODIFIED
C|* *    for Error Output:                                         * *|  A1331.4MODIFIED
C|* *        Filename is contained in ENAME                        * *|  A1331.5MODIFIED
C|* *        Unit Number is contained in K00                       * *|  A1331.6MODIFIED
C|* *    for Simulation Units and Files:                           * *|  A1331.7MODIFIED
C|* *        Filename is contained in UNAME                        * *|  A1331.8MODIFIED
C|* *        Unit Number is contained in K0                        * *|  A1332.9MODIFIED
C|* *                                                              * *|  A1333.0MODIFIED
C|* ********************  D I M E N S I O N S  ********************* *|  A1341..MODIFIED
C|* ************************************************************** *|  A1340...
      DIMENSION   RM(1100000), RV(2250000), IMV(500000)                  A1350...
        RMDIMA=1100000                                                   MODIFIED
        RVDIMA=2250000                                                   MODIFIED
        IMVDMA= 500000                                                   MODIFIED
C
C|* *****  S T A N D A R D   F I L E   A S S I G N M E N T S  ***** *|  A1346..MODIFIED
C|*   E R R O R   O U T P U T                                     * *|  A1347..MODIFIED
      ENAME = 'SUTRA.ERR'                                                A1348..MODIFIED
      K00 = 1                                                            A1349..MODIFIED
C|*   S I M U L A T I O N   U N I T S   A N D   F I L E S         * *|  A1350..MODIFIED
      UNAME = 'SUTRA.FIL'                                                A1351..MODIFIED
CDJGOODE      K0 = 100                                                   A1352..MODIFIED
      K0 = 99
C|*                                                                  * *|  A1352.1MODIFIED
C|*   -------> Required Format of Unit K0 :                          * *|  A1352.2MODIFIED
C|*                                                                  * *|  A1352.3MODIFIED
C|*              V A R I A B L E          F O R M A T               * *|  A1352.4MODIFIED
C|*                                                                  * *|  A1352.5MODIFIED
C|*              Unit Number for K1         (free format)           * *|  A1352.6MODIFIED
C|*               File Name for K1           (A80)                  * *|  A1352.7MODIFIED
C|*              Unit Number for K2         (free format)           * *|  A1352.8MODIFIED
C|*               File Name for K2           (A80)                  * *|  A1352.9MODIFIED
C|*              Unit Number for K3         (free format)           * *|  A1353..MODIFIED
C|*               File Name for K3           (A80)                  * *|  A1353.5MODIFIED
```

```
C|*              Unit Number for K4         (free format)         * *|  A1354..MODIFIED
C|*               File Name for K4           (A80)                * *|  A1355..MODIFIED
C|*                                                               * *|  A1356..MODIFIED
C|*                                                               * *|  A1357..MODIFIED
C|*   The last two lines need not be included if UNIT-K4 will not * *|  A1358..MODIFIED
C|*   be used.  This file has six or eight lines.                 * *|  A1359..MODIFIED
C|* ************************************************************* *|  A1360...
C|* * * * * * * * * * * * * * * * * * * * * * * * * * * * * * * * *|  A1370...
C|_____________________________________________________________________|  A1380...
C                                                                        A1390...
C                                                                        A1400...
C ---> Programmers making code changes that affect dimensions must      A1401..MODIFIED
C --->  check and change the following assignments for NNV and NEV:     A1402..MODIFIED
C                                                                        A1403..MODIFIED
C                                                                        A1408..MODIFIED
C                                                                        A1409..MODIFIED
C                                                                        A1410...
C.....ASSIGN UNIT NUMBERS AND OPEN FILE UNITS FOR THIS SIMULATION        A1412..MODIFIED
      CALL FOPEN(UNAME,ENAME,FNAME,IUNIT,NFILE)                          A1414..MODIFIED
C                                                                        A1416..MODIFIED
C                                                                        A1410...
C.....INPUT DATASET 1:  INPUT DATA HEADING                               A1420...
C.....( SET ME=-1 FOR SOLUTE TRANSPORT, ME=+1 FOR ENERGY TRANSPORT )     A1430...
      READ(K1,100) SIMULA                                                A1440...
  100 FORMAT(2A6)                                                        A1450...
      WRITE(K3,110)                                                      A1460...
  110 FORMAT(1H1,131(1H*)////3(132(1H*)////)////                         A1470...
     1   47X,' SSSS   UU  UU  TTTTTT  RRRRR     AA  '/                  A1480...
     2   47X,'SS   S  UU  UU  T TT T  RR  RR   AAAA '/                  A1490...
     3   47X,'SSSS    UU  UU    TT    RRRRR   AA  AA'/                  A1500...
     4   47X,'    SS  UU  UU    TT    RR R    AAAAAA'/                  A1510...
     5   47X,'SS  SS  UU  UU    TT    RR RR   AA  AA'/                  A1520...
     6   47X,' SSSS    UUUU     TT    RR  RR  AA  AA'/                  A1530...
     7   7(/),37X,'U N I T E D   S T A T E S   ',                        A1540...
     8   'G E O L O G I C A L   S U R V E Y'////                         A1550...
     9   45X,'SUBSURFACE FLOW AND TRANSPORT SIMULATION MODEL'/           A1560...
     *   //59X,'-VERSION 1284-2DICG MODIFIED FOR A REGULAR GRID-'///    A1570NEW
     A   36X,'*  SATURATED-UNSATURATED FLOW AND SOLUTE OR ENERGY',      A1580...
     B   ' TRANSPORT  *'////4(////1X,132(1H*)))                         A1590...
C                                                                        A1600...
      IF(SIMULA(1).NE.'SUTRA ') GOTO 115                                 A1610...
      IF(SIMULA(2).EQ.'SOLUTE') GOTO 120                                 A1620...
      IF(SIMULA(2).EQ.'ENERGY') GOTO 140                                 A1630...
  115 WRITE(K3,116)                                                      A1640...
  116 FORMAT(1H1/////20X,'* * * * *   ERROR IN FIRST DATA CARD--',       A1650...
     1   '------DATA INPUT HALTED FOR CORRECTIONS   * * * * *')          A1660...
      ENDFILE(K3)                                                        A1661...
      STOP                                                               A1670...
  120 ME=-1                                                              A1680...
      WRITE(K3,130)                                                      A1690...
  130 FORMAT(1H1//132(1H*)///20X,'* * * * *   S U T R A   S O L U ',    A1700...
     1   'T E   T R A N S P O R T   S I M U L A T I O N   * * * * *'//   A1710...
     2   /132(1H*)/)                                                    A1720...
      GOTO 160                                                           A1730...
  140 ME=+1                                                              A1740...
      WRITE(K3,150)                                                      A1750...
  150 FORMAT(1H1//132(1H*)///20X,'* * * * *   S U T R A   E N E R ',    A1760...
     1   'G Y   T R A N S P O R T   S I M U L A T I O N   * * * * *'//   A1770...
     2   /132(1H*)/)                                                    A1780...
  160 CONTINUE                                                           A1790...
C                                                                        A1800...
```

```
C.....INPUT DATASET 2:  OUTPUT HEADING                                  A1810...
      READ(K1,170) TITLE1,TITLE2                                        A1820...
  170 FORMAT(80A1/80A1)                                                 A1830...
      WRITE(K3,180) TITLE1,TITLE2                                       A1840...
  180 FORMAT(////1X,131(1H-)//26X,80A1//26X,80A1//1X,131(1H-))          A1850...
C.....OUTPUT FILE UNIT ASSIGNMENTS                                      A1850.5MODIFIED
      WRITE(K3,202) (IUNIT(NF),FNAME(NF),NF=1,3)                        A1851..MODIFIED
  202 FORMAT(/////11X,'F I L E   U N I T   A S S I G N M E N T S'//     A1852..MODIFIED
     1   13X,'INPUT UNITS:'/                                            A1853..MODIFIED
     2   13X,' SIMULATION DATA    ',I3,4X,'ASSIGNED TO ',A80/           A1854..MODIFIED
     3   13X,' INITIAL CONDITIONS ',I3,4X,'ASSIGNED TO ',A80//          A1855..MODIFIED
     4   13X,'OUTPUT UNITS:'/                                           A1856..MODIFIED
     5   13X,' SIMULATION RESULTS ',I3,4X,'ASSIGNED TO ',A80)           A1857..MODIFIED
      IF(NFILE.EQ.4) WRITE(K3,203) IUNIT(4),FNAME(4)                    A1858..MODIFIED
  203 FORMAT(13X,' RESTART DATA       ',I3,4X,'ASSIGNED TO ',A80)       A1859..MODIFIED
C.....INPUT AND OUTPUT DATASET 4:  SIMULATION MODE OPTIONS              A1865..MODIFIED
      READ(K1,200) IS,JT,NBI,NPINCH,NPBC,NUBC,NSOP,NSOU,NOBS,NTOBS      A1860NEW
        NN=IS*JT                                                        NEW
        NE=(IS-1)*(JT-1)                                                NEW
      READ(K1,200) IUNSAT,ISSFLO,ISSTRA,IREAD,ISTORE,ITIME              A1870NEW
  200 FORMAT(16I5)                                                      A1880...
      WRITE(K3,205)                                                     A1890...
  205 FORMAT(/////11X,'S I M U L A T I O N   M O D E   ',               A1900...
     1   'O P T I O N S'/)                                              A1910...
      IF(ISSTRA.EQ.1.AND.ISSFLO.NE.1) THEN                              A1920...
       WRITE(K3,210)                                                    A1930...
  210  FORMAT(////11X,'STEADY-STATE TRANSPORT ALSO REQUIRES THAT ',      A1940...
     1    'FLOW IS AT STEADY STATE.'//11X,'PLEASE CORRECT ISSFLO ',     A1950...
     2    'AND ISSTRA IN THE INPUT DATA, AND RERUN.'////////            A1960...
     3    45X,'S I M U L A T I O N   H A L T E D   DUE TO INPUT ERROR') A1970...
       ENDFILE(K3)                                                      A1980...
       STOP                                                             A1990...
      ENDIF                                                             A2000...
      IF(IUNSAT.EQ.+1) WRITE(K3,215)                                    A2010...
      IF(IUNSAT.EQ.0) WRITE(K3,216)                                     A2020...
  215 FORMAT(11X,'- ALLOW UNSATURATED AND SATURATED FLOW:  UNSATURATED',A2030...
     1   ' PROPERTIES ARE USER-PROGRAMMED IN SUBROUTINE   U N S A T')   A2040...
  216 FORMAT(11X,'- ASSUME SATURATED FLOW ONLY')                        A2050...
      IF(ISSFLO.EQ.+1.AND.ME.EQ.-1) WRITE(K3,219)                       A2060...
      IF(ISSFLO.EQ.+1.AND.ME.EQ.+1) WRITE(K3,220)                       A2070...
      IF(ISSFLO.EQ.0) WRITE(K3,221)                                     A2080...
  219 FORMAT(11X,'- ASSUME STEADY-STATE FLOW FIELD CONSISTENT WITH ',   A2090...
     1   'INITIAL CONCENTRATION CONDITIONS')                            A2100...
  220 FORMAT(11X,'- ASSUME STEADY-STATE FLOW FIELD CONSISTENT WITH ',   A2110...
     1   'INITIAL TEMPERATURE CONDITIONS')                              A2120...
  221 FORMAT(11X,'- ALLOW TIME-DEPENDENT FLOW FIELD')                   A2130...
      IF(ISSTRA.EQ.+1) WRITE(K3,225)                                    A2140...
      IF(ISSTRA.EQ.0) WRITE(K3,226)                                     A2150...
  225 FORMAT(11X,'- ASSUME STEADY-STATE TRANSPORT')                     A2160...
  226 FORMAT(11X,'- ALLOW TIME-DEPENDENT TRANSPORT')                    A2170...
      IF(IREAD.EQ.-1) WRITE(K3,230)                                     A2180...
      IF(IREAD.EQ.+1) WRITE(K3,231)                                     A2190...
  230 FORMAT(11X,'- WARM START - SIMULATION IS TO BE ',                 A2200...
     1   'CONTINUED FROM PREVIOUSLY-STORED DATA')                       A2210...
  231 FORMAT(11X,'- COLD START - BEGIN NEW SIMULATION')                 A2220...
      IF(ISTORE.EQ.+1) WRITE(K3,240)                                    A2230...
      IF(ISTORE.EQ.0) WRITE(K3,241)                                     A2240...
  240 FORMAT(11X,'- STORE RESULTS AFTER EACH TIME STEP ON UNIT-66',     A2250...
     1   ' AS BACK-UP AND FOR USE IN A SIMULATION RE-START')            A2260...
  241 FORMAT(11X,'- DO NOT STORE RESULTS FOR USE IN A ',                A2270...
     1   'RE-START OF SIMULATION')                                      A2280...
```

```
C                                                                       A2290...
      IF(ME.EQ.-1)                                                      A2300...
     1   WRITE(K3,245) NN,NE,NPBC,NUBC,NSOP,NSOU,NOBS,NTOBS             A2310NEW
  245 FORMAT(////11X,'S I M U L A T I O N   C O N T R O L   ',          A2320...
     1   'N U M B E R S'//11X,I6,5X,'NUMBER OF NODES IN FINITE-',       A2330...
     2   'ELEMENT MESH'/11X,I6,5X,'NUMBER OF ELEMENTS IN MESH'/         A2340...
     5   11X,I6,5X,'EXACT NUMBER OF NODES IN MESH AT WHICH ',           A2370...
     6   'PRESSURE IS A SPECIFIED CONSTANT OR FUNCTION OF TIME'/        A2380...
     7   11X,I6,5X,'EXACT NUMBER OF NODES IN MESH AT WHICH ',           A2390...
     8   'SOLUTE CONCENTRATION IS A SPECIFIED CONSTANT OR ',            A2400...
     9   'FUNCTION OF TIME'//11X,I6,5X,'EXACT NUMBER OF NODES AT',      A2410...
     *   ' WHICH FLUID INFLOW OR OUTFLOW IS A SPECIFIED CONSTANT',      A2420...
     A   ' OR FUNCTION OF TIME'/11X,I6,5X,'EXACT NUMBER OF NODES AT',   A2430...
     B   ' WHICH A SOURCE OR SINK OF SOLUTE MASS IS A SPECIFIED ',      A2440...
     C   'CONSTANT OR FUNCTION OF TIME'//11X,I6,5X,'EXACT NUMBER OF ',  A2450...
     D   'NODES AT WHICH PRESSURE AND CONCENTRATION WILL BE OBSERVED',  A2460...
     E   /11X,I6,5X,'MAXIMUM NUMBER OF TIME STEPS ON WHICH ',           A2470...
     F   'OBSERVATIONS WILL BE MADE')                                   A2480...
C                                                                       A2490...
      IF(ME.EQ.+1)                                                      A2500...
     1    WRITE(K3,255) NN,NE,NPBC,NUBC,NSOP,NSOU,NOBS,NTOBS            A2510NEW
  255 FORMAT(////11X,'S I M U L A T I O N   C O N T R O L   ',          A2520...
     1   'N U M B E R S'//11X,I6,5X,'NUMBER OF NODES IN FINITE-',       A2530...
     2   'ELEMENT MESH'/11X,I6,5X,'NUMBER OF ELEMENTS IN MESH'/         A2540...
     5   11X,I6,5X,'EXACT NUMBER OF NODES IN MESH AT WHICH ',           A2570...
     6   'PRESSURE IS A SPECIFIED CONSTANT OR FUNCTION OF TIME'/        A2580...
     7   11X,I6,5X,'EXACT NUMBER OF NODES IN MESH AT WHICH ',           A2590...
     8   'TEMPERATURE IS A SPECIFIED CONSTANT OR ',                     A2600...
     9   'FUNCTION OF TIME'//11X,I6,5X,'EXACT NUMBER OF NODES AT',      A2610...
     *   ' WHICH FLUID INFLOW OR OUTFLOW IS A SPECIFIED CONSTANT',      A2620...
     A   ' OR FUNCTION OF TIME'/11X,I6,5X,'EXACT NUMBER OF NODES AT',   A2630...
     B   ' WHICH A SOURCE OR SINK OF ENERGY IS A SPECIFIED CONSTANT',   A2640...
     C   ' OR FUNCTION OF TIME'//11X,I6,5X,'EXACT NUMBER OF NODES ',    A2650...
     D   'AT WHICH PRESSURE AND TEMPERATURE WILL BE OBSERVED'           A2660...
     E   /11X,I6,5X,'MAXIMUM NUMBER OF TIME STEPS ON WHICH ',           A2670...
     F   'OBSERVATIONS WILL BE MADE')                                   A2680...
C                                                                       A2690...
C                                                                       A2700...
C.....CALCULATE DIMENSIONS FOR POINTERS                                 A2710...
C                                                                       A2720...
      NBCN=NPBC+NUBC+1                                                  A2730...
      NSOP=NSOP+1                                                       A2740...
      NSOU=NSOU+1                                                       A2750...
      NPINCH=1                                                          A2760NEW
      NBIP=5                                                            NEW
      NBIS=9                                                            NEW
      MATDMP=NN*NBIP                                                    A2770NEW
      MATDMS=NN*NBIS                                                    A2770NEW
      NIN=NE*8                                                          A2780...
      NOBSN=NOBS+1                                                      A2790...
      NTOBSN=NTOBS+2                                                    A2800...
      MATOBS=NOBSN*NTOBSN                                               A2810...
      NE4=NE*4                                                          A2820...
C                                                                       A2830...
C                                                                       A2840...
C.....SET UP POINTERS FOR REAL MATRICES                                 A2850...
C                                                                       A2860...
      KRM1=1                                                            A2870...
      KRM2=KRM1+   MATDMP                                               A2880NEW
      KRM3=KRM2+   MATDMS                                               A2890NEW
      KRM4=KRM3+NN                                                      NEW
```

```
      KRM5=KRM4+NN                                                          NEW
      KRM6=KRM5+NN                                                          NEW
      KRM7=KRM6+NN                                                          NEW
C     KRM8=KRM7+NN*9                                                        NEW
C     NOTE: THE LAST POINTER IN THE ABOVE LIST, CURRENTLY, KRM8,            A2900...
C           MAY  N E V E R  BE PASSED TO SUTRA.  IT POINTS TO THE           A2910...
C           STARTING ELEMENT OF THE NEXT NEW MATRIX TO BE ADDED.            A2920...
C           PRESENTLY, SPACE IS ALLOCATED FOR (7) MATRICES.                 A2930...
C                                                                           A2940...
C                                                                           A2950...
C.....SET UP POINTERS FOR REAL VECTORS                                      A2960...
C                                                                           A2970...
C     NNV IS NUMBER OF REAL VECTORS THAT ARE NN LONG                        A2980...
      NNV=30                                                                A2990...
C     NEV IS NUMBER OF REAL VECTORS THAT ARE NE LONG                        A3000...
      NEV=10                                                                A3010...
C                                                                           A3020...
      M2=1                                                                  A3030...
      KRV(1)=1                                                              A3040...
      M1=M2+1                                                               A3050...
      M2=M2+       ( NNV )                                                  A3060...
      DO 400 J=M1,M2                                                        A3070...
  400 KRV(J)=KRV(J-1)+  NN                                                  A3080...
      M1=M2+1                                                               A3090...
      M2=M2+       ( NEV )                                                  A3100...
      DO 410 J=M1,M2                                                        A3110...
  410 KRV(J)=KRV(J-1)+  NE                                                  A3120...
      M1=M2+1                                                               A3130...
      M2=M2+       ( 3 )                                                    A3140...
      DO 420 J=M1,M2                                                        A3150...
  420 KRV(J)=KRV(J-1)+  NBCN                                                A3160...
      M1=M2+1                                                               A3170...
      M2=M2+       ( 2 )                                                    A3180...
      DO 430 J=M1,M2                                                        A3190...
  430 KRV(J)=KRV(J-1)+  MATOBS                                              A3200...
      M2=M2+       ( 1 )                                                    A3210...
      KRV(M2)=KRV(M2-1)+NTOBSN                                              A3220...
      M1=M2+1                                                               A3230...
      M2=M2+       ( 2 )                                                    A3240...
      DO 440 J=M1,M2                                                        A3250...
  440 KRV(J)=KRV(J-1)+  NE4                                                 A3260...
C     NOTE: THE LAST POINTER IN THE ABOVE LIST, CURRENTLY, KRV(J=49),       A3270...
C           MAY  N E V E R  BE PASSED TO SUTRA.  IT POINTS TO THE           A3280...
C           STARTING ELEMENT OF THE NEXT NEW REAL VECTOR TO BE ADDED.       A3290...
C           PRESENTLY, SPACE IS ALLOCATED FOR (48) VECTORS.                 A3300...
C                                                                           A3310...
C                                                                           A3320...
C.....SET UP POINTERS FOR INTEGER VECTORS                                   A3330...
C                                                                           A3340...
      KIMV1=1                                                               A3350...
      KIMV2=KIMV1+    NIN                                                   A3360...
      KIMV3=KIMV2+    NPINCH*3                                              A3370...
      KIMV4=KIMV3+    NSOP                                                  A3380...
      KIMV5=KIMV4+    NSOU                                                  A3390...
      KIMV6=KIMV5+    NBCN                                                  A3400...
      KIMV7=KIMV6+    NBCN                                                  A3410...
      KIMV8=KIMV7+    NN                                                    A3420...
      KIMV9=KIMV8+    NOBSN                                                 A3430...
C     KIMV10=KIMV9+    NTOBSN                                               A3440...
C     NOTE: THE LAST POINTER IN THE ABOVE LIST, CURRENTLY, KIMV10,          A3450...
C           MAY  N E V E R  BE PASSED TO SUTRA.  IT POINTS TO THE           A3460...
```

```
C           STARTING ELEMENT OF THE NEXT NEW INTEGER VECTOR TO BE ADDED.A3470...
C           PRESENTLY, SPACE IS ALLOCATED FOR (8) INTEGER VECTORS.      A3480...
C                                                                       A3490...
C                                                                       NEW
C               CHECK FOR CORRECT DIMENSIONS                            NEW
        RMDIM = NN*(NBIP+NBIS+9)                                        NEW
        RVDIM = (( NNV*NN + (NEV+8)*NE + NBCN*3                         NEW
     1             + (NOBS+1)*(NTOBS+2)*2 + NTOBS + 5 ))               NEW
        IMVDIM = (( NE*8 + NN + NPINCH*3 + NSOP + NSOU                  NEW
     1             + NBCN*2 + NOBS + NTOBS + 12 ))                     NEW
       IF(RMDIM.GT.RMDIMA.OR.RVDIM.GT.RVDIMA.OR.IMVDIM.GT.IMVDMA) THEN  NEW
         WRITE(*,*) 'MAXIMUM DIMENSIONS EXCEEDED, PLEASE CORRECT'       NEW
         STOP 101                                                       NEW
       END IF                                                           NEW
C                                                                       A3500...
C.....PASS POINTERS TO MAIN CONTROL ROUTINE, SUTRA                      A3510...
       CALL SUTRA(RM(KRM1),RM(KRM2),RM(KRM3),RM(KRM4),RM(KRM5),
     1   RM(KRM6),RM(KRM7),                                           A3520NEW
     1   RV(KRV(1)),RV(KRV(2)),RV(KRV(3)),RV(KRV(4)),RV(KRV(5)),      A3530...
     2   RV(KRV(6)),RV(KRV(7)),RV(KRV(8)),RV(KRV(9)),RV(KRV(10)),     A3540...
     3   RV(KRV(11)),RV(KRV(12)),RV(KRV(13)),RV(KRV(14)),RV(KRV(15)), A3550...
     4   RV(KRV(16)),RV(KRV(17)),RV(KRV(18)),RV(KRV(19)),RV(KRV(20)), A3560...
     5   RV(KRV(21)),RV(KRV(22)),RV(KRV(23)),RV(KRV(24)),RV(KRV(25)), A3570...
     6   RV(KRV(26)),RV(KRV(27)),RV(KRV(28)),RV(KRV(29)),RV(KRV(30)), A3580...
     7   RV(KRV(31)),RV(KRV(32)),RV(KRV(33)),RV(KRV(34)),RV(KRV(35)), A3590...
     8   RV(KRV(36)),RV(KRV(37)),RV(KRV(38)),RV(KRV(39)),RV(KRV(40)), A3600...
     9   RV(KRV(41)),RV(KRV(42)),RV(KRV(43)),RV(KRV(44)),RV(KRV(45)), A3610...
     *   RV(KRV(46)),RV(KRV(47)),RV(KRV(48)),                         A3620...
     1   IMV(KIMV1),IMV(KIMV2),IMV(KIMV3),IMV(KIMV4),IMV(KIMV5),      A3630...
     2   IMV(KIMV6),IMV(KIMV7),IMV(KIMV8),IMV(KIMV9) )                A3640...
C                                                                       A3650...
C                                                                       A3660...
       ENDFILE(K3)                                                      A3670...
       STOP                                                             A3680...
       END                                                              A3690...
C      SUBROUTINE        S  U  T  R  A          SUTRA - VERSION 1284-2D B10.....
C                                                                       B20.....
C *** PURPOSE :                                                         B30.....
C ***  MAIN CONTROL ROUTINE FOR SUTRA SIMULATION.                       B40.....
C ***  ORGANIZES DATA INPUT, INITIALIZATION, CALCULATIONS FOR           B50.....
C ***  EACH TIME STEP AND ITERATION, AND VARIOUS OUTPUTS.               B60.....
C ***  CALLS MOST OTHER SUBROUTINES.                                    B70.....
C                                                                       B80.....
       SUBROUTINE SUTRA( PMAT,UMAT,CWRK,CWRK2,CWRK3,CWRK4,CWRK5,        B90NEW
     1   PITER,UITER,PM1,UM1,UM2,PVEL,SL,SR,                          B100....
     2   X,Y,THICK,VOL,POR,CS1,CS2,CS3,SW,DSWDP,RHO,SOP,              B110....
     3   QIN,UIN,QUIN,PVEC,UVEC,RCIT,RCITM1,CC,XX,YY,                 B120....
     4   ALMAX,ALMIN,ATAVG,VMAG,VANG,                                 B130....
     5   PERMXX,PERMXY,PERMYX,PERMYY,PANGLE,                          B140....
     6   PBC,UBC,QPLITR,POBS,UOBS,OBSTIM,GXSI,GETA,                   B150....
     7   IN,IPINCH,IQSOP,IQSOU,IPBC,IUBC,INDEX,IOBS,ITOBS )           B160....
       IMPLICIT DOUBLE PRECISION (A-H,O-Z)                            B170....
       CHARACTER*10 ADSMOD                                            B180....
       COMMON/FUNITS/ K00,K0,K1,K2,K3,K4,K5,K6                       MODIFIED
       COMMON/MODSOR/ ADSMOD                                          B190....
       COMMON/DIMS/ NN,NE,NIN,IS,JT,NBIP,NBIS,NPT(9),NPBC,NUBC,      B200NEW
     1   NSOP,NSOU,NBCN                                               B210
       COMMON/TIME/ DELT,TSEC,TMIN,THOUR,TDAY,TWEEK,TMONTH,TYEAR,     B220....
     1   TMAX,DELTP,DELTU,DLTPM1,DLTUM1,IT,ITMAX                      B230....
       COMMON/CNTRL1/ GNU,UP,DTMULT,DTMAX,ME,ISSFLO,ISSTRA,ITCYC,     B240....
     1   NPCYC,NUCYC,NPRINT,IREAD,ISTORE,NOUMAT,IUNSAT,ITIME          B250NEW
```

```
      COMMON/PARAMS/ COMPFL,COMPMA,DRWDU,CW,CS,RHOS,DECAY,SIGMAW,SIGMAS,B260....
     1   RHOW0,URHOW0,VISC0,PRODF1,PRODS1,PRODF0,PRODS0,CHI1,CHI2       B270....
      COMMON/ITERAT/ RPM,RPMAX,RUM,RUMAX,ITER,ITRMAX,IPWORS,IUWORS,     B280....
     1               ICON,ITRMX2,OMEGA,RPMX2,RUMX2                      NEW
      COMMON/KPRINT/ KNODAL,KELMNT,KINCID,KPLOTP,KPLOTU,KVEL,KBUDG      B290....
      COMMON/OBS/ NOBSN,NTOBSN,NOBCYC,ITCNT                             B300....
      DIMENSION QIN(NN),UIN(NN),IQSOP(NSOP),QUIN(NN),IQSOU(NSOU)        B310....
      DIMENSION IPBC(NBCN),PBC(NBCN),IUBC(NBCN),UBC(NBCN),QPLITR(NBCN)  B320....
      DIMENSION IN(NIN),IPINCH(1,3)                                     B330NEW
      DIMENSION X(NN),Y(NN),THICK(NN),SW(NN),DSWDP(NN),RHO(NN),SOP(NN), B340....
     1   POR(NN),PVEL(NN)                                               B350....
      DIMENSION PERMXX(NE),PERMXY(NE),PERMYX(NE),PERMYY(NE),PANGLE(NE), B360....
     1   ALMAX(NE),ALMIN(NE),ATAVG(NE),VMAG(NE),VANG(NE),               B370....
     2   GXSI(NE,4),GETA(NE,4)                                          B380....
      DIMENSION VOL(NN),PMAT(NN,NBIP),PVEC(NN),UMAT(NN,NBIS),UVEC(NN)   B390NEW
      DIMENSION CWRK(NN),CWRK2(NN),CWRK3(NN),CWRK4(NN),CWRK5(NN,5)      AQUI
      DIMENSION PM1(NN),UM1(NN),UM2(NN),PITER(NN),UITER(NN),            B400....
     1   RCIT(NN),RCITM1(NN),CS1(NN),CS2(NN),CS3(NN)                    B410....
      DIMENSION CC(NN),INDEX(NN),XX(NN),YY(NN)                          B420....
      DIMENSION POBS(NOBSN,NTOBSN),UOBS(NOBSN,NTOBSN),OBSTIM(NTOBSN),   B430....
     1   IOBS(NOBSN),ITOBS(NTOBSN)                                      B440....
      DATA IT/0/                                                        B450....
C                                                                       B460....
C                                                                       B470....
C                                                                       B480....
C.....INPUT SIMULATION DATA FROM UNIT-5 (DATASETS 3 THROUGH 15B)        B490....
      CALL INDAT1(X,Y,THICK,POR,ALMAX,ALMIN,ATAVG,PERMXX,PERMXY,        B500....
     1   PERMYX,PERMYY,PANGLE,SOP,IN)                                   B510NEW
C                                                                       B550....
C.....INPUT FLUID MASS, AND ENERGY OR SOLUTE MASS SOURCES               B560....
C        (DATASETS 17 AND 18)                                           B570....
      CALL ZERO(QIN,NN,0.0D0)                                           B580....
      CALL ZERO(UIN,NN,0.0D0)                                           B590....
      CALL ZERO(QUIN,NN,0.0D0)                                          B600....
      IF(NSOP-1.GT.0.OR.NSOU-1.GT.0)                                    B610....
     1    CALL SOURCE(QIN,UIN,IQSOP,QUIN,IQSOU,IQSOPT,IQSOUT)           B620....
C                                                                       B630....
C.....INPUT SPECIFIED P AND U BOUNDARY CONDITIONS (DATASETS 19 AND 20)  B640....
      IF(NBCN-1.GT.0) CALL BOUND(IPBC,PBC,IUBC,UBC,IPBCT,IUBCT)         B650....
C                                                                       B660....
C.....SET FLAG FOR TIME-DEPENDENT SOURCES OR BOUNDARY CONDITIONS.       B670....
C     WHEN IBCT=+4, THERE ARE NO TIME-DEPENDENT SPECIFICATIONS.         B680....
      IBCT=IQSOPT+IQSOUT+IPBCT+IUBCT                                    B690....
C                                                                       B700....
C.....INPUT OBSERVATION NODE DATA (DATASET 21)                          B710....
      IF(NOBSN-1.GT.0) CALL OBSERV(0,IOBS,ITOBS,POBS,UOBS,OBSTIM,       B720....
     1   PVEC,UVEC,ISTOP)                                               B730....
      WRITE(K3,4000)                                                    NEW
 4000 FORMAT(////////1X,132(1H-)///42X,'E N D   O F   I N P U T   ',    NEW
     1  'F R O M  U N I T - 5'//132(1H-))                 NEW C
B830....
C.....INPUT INITIAL OR RESTART CONDITIONS AND INITIALIZE PARAMETERS     B840....
C        (READ UNIT-55 DATA)                                            B850....
      CALL INDAT2(PVEC,UVEC,PM1,UM1,UM2,CS1,CS2,CS3,SL,SR,RCIT,SW,DSWDP,B860....
     1   PBC,IPBC,IPBCT)                                                B870....
C                                                                       B880....
C.....SET STARTING TIME OF SIMULATION CLOCK                             B890....
C     TSEC=TSTART                                                       B900....
      TSECP0=TSEC                                                       B910....
      TSECU0=TSEC                                                       B920....
      TMIN=TSEC/60.D0                                                   B930....
```

```
      THOUR=TMIN/60.D0                                                  B940....
      TDAY=THOUR/24.D0                                                  B950....
      TWEEK=TDAY/7.D0                                                   B960....
      TMONTH=TDAY/30.4375D0                                             B970....
      TYEAR=TDAY/365.25D0                                               B980....
      DELT0=DELT                                                        NEW
C                                                                       B990....
C.....OUTPUT INITIAL CONDITIONS OR STARTING CONDITIONS                  B1000...
      IF(ISSTRA.NE.1) CALL PRISOL(0,0,0,PVEC,UVEC,VMAG,VANG,SW)         B1010...
C                                                                       B1020...
C.....SET SWITCHES AND PARAMETERS FOR SOLUTION WITH STEADY-STATE FLOW   B1030...
      IF(ISSFLO.NE.1) GOTO 1000                                         B1040...
      ML=1                                                              B1050...
      NOUMAT=0                                                          B1060...
      ISSFLO=2                                                          B1070...
      ITER=0                                                            B1080...
      DLTPM1=DELTP                                                      B1090...
      DLTUM1=DELTU                                                      B1100...
      BDELP=0.0D0                                                       B1110...
      BDELU=0.0D0                                                       B1120...
      GOTO 1100                                                         B1130...
C                                                                       B1140...
C                                                                       B1150...
C ***********************************************************************B1160...
C.....BEGIN TIME STEP *************************************************B1170...
C ***********************************************************************B1180...
 1000 IT=IT+1                                                           B1190...
      ITER=0                                                            B1200...
      ML=0                                                              B1210...
      NOUMAT=0                                                          B1220...
C.....SET NOUMAT TO OBTAIN U SOLUTION WITHOUT REFORMULATING THE MATRIX  B1230NEW
C        BEGINNING ON SECOND TIME STEP AFTER A PRESSURE SOLUTION        B1240...
C        IF THE SOLUTION IS NON-ITERATIVE (ITRMAX=1)                    B1250...
C     IF(MOD(IT-1,NPCYC).NE.0.AND.MOD(IT,NPCYC).NE.0.AND.IT.GT.2        B1260...
C    1   .AND.ITRMAX.EQ.1) NOUMAT=1                                     B1270...
C.....CHOOSE SOLUTION VARIABLE ON THIS TIME STEP:                       B1280...
C        ML=0 FOR P AND U, ML=1 FOR P ONLY, AND ML=2 FOR U ONLY.        B1290...
      IF(IT.EQ.1.AND.ISSFLO.NE.2) GOTO 1005                             B1300...
      IF(MOD(IT,NPCYC).NE.0) ML=2                                       B1310...
      IF(MOD(IT,NUCYC).NE.0) ML=1                                       B1320...
C.....MULTIPLY TIME STEP SIZE BY DTMULT EACH ITCYC TIME STEPS           B1330...
C.....THE FOLLOWING CARDS WERE ADDED TO ALLOW FOR THE TIME STEP         NEW
C.....TO YIELD A CONSTANT DISTANCE INCREMENT IN A RADIAL FLOW SYSTEM     NEW
      IF(ITIME.EQ.0) THEN                                               NEW
        IF(MOD(IT,ITCYC).EQ.0.AND.IT.GT.1) DELT=DELT*DTMULT             B1340...
      END IF                                                            NEW
      IF(ITIME.EQ.1 .AND. IT.GT.1) THEN                                 NEW
C       DELT0 = THE INITIAL TIME INCREMENT                              NEW
C       ITCYC = A FLAG -- FOR ITCYC>0, TIME STEP SIZE IS INCREASED      NEW
C       FOR ITCYC<0, TIME STEP SIZE IS DECREASED, WHERE -ITCYC =        NEW
C                    MAXIMUM NUMBER OF TIME STEPS IN PREVIOUS RUN       NEW
C       FOR ITCYC=0, TIME STEP SIZE IS HELD CONSTANT                    NEW
        IF(ITCYC.GT.0) DELT=DELT0*(2.0*IT-1)                            NEW
        IF(ITCYC.LT.0) DELT=DELT0*(2.*(-ITCYC-IT+1)-1)                  NEW
      END IF                                                            NEW
C.....SET TIME STEP SIZE TO MAXIMUM ALLOWED SIZE, DTMAX                 B1350...
      IF(DELT.GT.DTMAX) DELT=DTMAX                                      B1360...
C.....INCREMENT SIMULATION CLOCK, TSEC, TO END OF NEW TIME STEP         B1370...
 1005 TSEC=TSEC+DELT                                                    B1380...
      TMIN=TSEC/60.D0                                                   B1390...
      THOUR=TMIN/60.D0                                                  B1400...
```

```
      TDAY=THOUR/24.D0                                                  B1410...
      TWEEK=TDAY/7.D0                                                   B1420...
      TMONTH=TDAY/30.4375D0                                             B1430...
      TYEAR=TDAY/365.25D0                                               B1440...
C                                                                       B1450...
C.....SET TIME STEP FOR P AND/OR U, WHICHEVER ARE SOLVED FOR            B1460...
C        ON THIS TIME STEP                                              B1470...
      IF(ML-1) 1010,1020,1030                                           B1480...
 1010 DLTUM1=DELTU                                                      B1490...
      DLTPM1=DELTP                                                      B1500...
      GOTO 1040                                                         B1510...
 1020 DLTPM1=DELTP                                                      B1520...
      GOTO 1040                                                         B1530...
 1030 DLTUM1=DELTU                                                      B1540...
 1040 CONTINUE                                                          B1550...
      DELTP=TSEC-TSECP0                                                 B1560...
      DELTU=TSEC-TSECU0                                                 B1570...
C.....SET PROJECTION FACTORS USED ON FIRST ITERATION TO EXTRAPOLATE     B1580...
C        AHEAD ONE-HALF TIME STEP                                       B1590...
      BDELP=(DELTP/DLTPM1)*0.50D0                                       B1600...
      BDELU=(DELTU/DLTUM1)*0.50D0                                       B1610...
      BDELP1=BDELP+1.0D0                                                B1620...
      BDELU1=BDELU+1.0D0                                                B1630...
C.....INCREMENT CLOCK FOR WHICHEVER OF P AND U WILL BE SOLVED FOR       B1640...
C        ON THIS TIME STEP                                              B1650...
      IF(ML-1) 1060,1070,1080                                           B1660...
 1060 TSECP0=TSEC                                                       B1670...
      TSECU0=TSEC                                                       B1680...
      GOTO 1090                                                         B1690...
 1070 TSECP0=TSEC                                                       B1700...
      GOTO 1090                                                         B1710...
 1080 TSECU0=TSEC                                                       B1720...
 1090 CONTINUE                                                          B1730...
C                                                                       B1740...
C - - - - - - - - - - - - - - - - - - - - - - - - - - - - - - - - - - - B1750...
C.....BEGIN ITERATION - - - - - - - - - - - - - - - - - - - - - - - - - B1760...
C - - - - - - - - - - - - - - - - - - - - - - - - - - - - - - - - - - - B1770...
 1100 ITER=ITER+1                                                       B1780...
C                                                                       B1790...
      IF(ML-1) 2000,2200,2400                                           B1800...
C.....SHIFT AND SET VECTORS FOR TIME STEP WITH BOTH P AND U SOLUTIONS   B1810...
 2000 DO 2025 I=1,NN                                                    B1820...
      PITER(I)=PVEC(I)                                                  B1830...
      PVEL(I)=PVEC(I)                                                   B1840...
      UITER(I)=UVEC(I)                                                  B1850...
      RCITM1(I)=RCIT(I)                                                 B1860...
 2025 RCIT(I)=RHOW0+DRWDU*(UITER(I)-URHOW0)                             B1870...
      DO 2050 IP=1,NPBC                                                 B1880...
      I=IABS(IPBC(IP))                                                  B1890...
      QPLITR(IP)=GNU*(PBC(IP)-PITER(I))                                 B1900...
 2050 CONTINUE                                                          B1910...
      IF(ITER.GT.1) GOTO 2600                                           B1920...
      DO 2075 I=1,NN                                                    B1930...
      PITER(I)=BDELP1*PVEC(I)-BDELP*PM1(I)                              B1940...
      UITER(I)=BDELU1*UVEC(I)-BDELU*UM1(I)                              B1950...
      PM1(I)=PVEC(I)                                                    B1960...
      UM2(I)=UM1(I)                                                     B1970...
 2075 UM1(I)=UVEC(I)                                                    B1980...
      GOTO 2600                                                         B1990...
C.....SHIFT AND SET VECTORS FOR TIME STEP WITH P SOLUTION ONLY          B2000...
 2200 DO 2225 I=1,NN                                                    B2010...
```

```
      PVEL(I)=PVEC(I)                                                   B2020...
 2225 PITER(I)=PVEC(I)                                                  B2030...
      IF(ITER.GT.1) GOTO 2600                                           B2040...
      DO 2250 I=1,NN                                                    B2050...
      PITER(I)=BDELP1*PVEC(I)-BDELP*PM1(I)                              B2060...
      UITER(I)=UVEC(I)                                                  B2070...
      RCITM1(I)=RCIT(I)                                                 B2080...
      RCIT(I)=RHOW0+DRWDU*(UITER(I)-URHOW0)                             B2090...
 2250 PM1(I)=PVEC(I)                                                    B2100...
      GOTO 2600                                                         B2110...
C.....SHIFT AND SET VECTORS FOR TIME STEP WITH U SOLUTION ONLY          B2120...
 2400 IF(NOUMAT.EQ.1) GOTO 2480                                         B2130...
      DO 2425 I=1,NN                                                    B2140...
 2425 UITER(I)=UVEC(I)                                                  B2150...
      IF(ITER.GT.1) GOTO 2600                                           B2160...
      DO 2450 I=1,NN                                                    B2170...
      PITER(I)=PVEC(I)                                                  B2180...
      PVEL(I)=PVEC(I)                                                   B2190...
      UITER(I)=BDELU1*UVEC(I)-BDELU*UM1(I)                              B2200...
 2450 RCITM1(I)=RCIT(I)                                                 B2210...
      DO 2475 IP=1,NPBC                                                 B2220...
      I=IABS(IPBC(IP))                                                  B2230...
      QPLITR(IP)=GNU*(PBC(IP)-PITER(I))                                 B2240...
 2475 CONTINUE                                                          B2250...
 2480 DO 2500 I=1,NN                                                    B2260...
      UM2(I)=UM1(I)                                                     B2270...
 2500 UM1(I)=UVEC(I)                                                    B2280...
 2600 CONTINUE                                                          B2290...
C                                                                       B2300...
C.....INITIALIZE ARRAYS WITH VALUE OF ZERO                              B2310...
      MATDMP=NN*NBIP                                                    B2320...
      MATDMS=NN*NBIS                                                    B2320...
      IF(ML-1) 3000,3000,3300                                           B2330...
 3000 CALL ZERO(PMAT,MATDMP,0.0D0)                                      B2340...
      CALL ZERO(PVEC,NN,0.0D0)                                          B2350...
      CALL ZERO(VOL,NN,0.0D0)                                           B2360...
      IF(ML-1) 3300,3400,3300                                           B2370...
 3300 IF(NOUMAT) 3350,3350,3375                                         B2380...
 3350 CALL ZERO(UMAT,MATDMS,0.0D0)                                      B2390...
 3375 CALL ZERO(UVEC,NN,0.0D0)                                          B2400...
 3400 CONTINUE                                                          B2410...
C                                                                       B2420...
C.....SET TIME-DEPENDENT BOUNDARY CONDITIONS, SOURCES AND SINKS         B2430...
C        FOR THIS TIME STEP                                             B2440...
      IF(ITER.EQ.1.AND.IBCT.NE.4)                                       B2450...
     1   CALL BCTIME(IPBC,PBC,IUBC,UBC,QIN,UIN,QUIN,IQSOP,IQSOU,        B2460...
     2   IPBCT,IUBCT,IQSOPT,IQSOUT,UM1)                                 B2470NEW
C                                                                       B2480...
C.....SET SORPTION PARAMETERS FOR THIS TIME STEP                        B2490...
      IF(ML.NE.1.AND.ME.EQ.-1.AND.NOUMAT.EQ.0.AND.                      B2500...
     1   ADSMOD.NE.'NONE      ') CALL ADSORB(CS1,CS2,CS3,SL,SR,UITER)   B2510...
C                                                                       B2520...
C.....DO ELEMENTWISE CALCULATIONS IN MATRIX EQUATION FOR P AND/OR U     B2530...
      IF(NOUMAT.EQ.0)                                                   B2540...
     1 CALL ELEMEN(ML,IN,X,Y,THICK,PITER,UITER,RCIT,RCITM1,POR,         B2550...
     2   ALMAX,ALMIN,ATAVG,PERMXX,PERMXY,PERMYX,PERMYY,PANGLE,          B2560...
     3   VMAG,VANG,VOL,PMAT,PVEC,UMAT,UVEC,GXSI,GETA,PVEL,CWRK)         B2570NEW
C                                                                       B2580...
C.....DO NODEWISE CALCULATIONS IN MATRIX EQUATION FOR P AND/OR U        B2590...
      CALL NODALB(ML,VOL,PMAT,PVEC,UMAT,UVEC,PITER,UITER,PM1,UM1,UM2,   B2600...
     1   POR,QIN,UIN,QUIN,CS1,CS2,CS3,SL,SR,SW,DSWDP,RHO,SOP)           B2610...
```

```
C.....SET SPECIFIED P AND U CONDITIONS IN MATRIX EQUATION FOR P AND/OR UB2630...
      CALL BCB(ML,PMAT,PVEC,UMAT,UVEC,IPBC,PBC,IUBC,UBC,QPLITR)         B2640...
 4200 CONTINUE                                                          B2690...
C                                                                       B2700...
C.....MATRIX EQUATION FOR P AND/OR U ARE COMPLETE,  SOLVE EQUATIONS:    B2710...
      IF(ML-1) 5000,5000,5500                                           B2750...
C.....SOLVE FOR P                                                       B2760...
 5000 IPS=0                                                             B2770NEW
      CALL SOLVEC(NBIP,PMAT,PM1,PVEC,CWRK,CWRK2,CWRK3,CWRK4,CWRK5)      NEW
C.....P SOLUTION NOW IN PVEC                                            B2790...
      IF(ML-1) 5500,6000,5500                                           B2800...
C.....SOLVE FOR U                                                       B2810...
 5500 IPS=1                                                             B2820NEW
 5700  CALL LSORA(NBIS,UMAT,UVEC,UITER,CWRK,CWRK2,CWRK5)                NEW
C.....U SOLUTION NOW IN UVEC                                            B2860...
 6000 CONTINUE                                                          B2870...
C                                                                       B2880...
C.....CHECK PROGRESS AND CONVERGENCE OF ITERATIONS                      B2890...
C        AND SET STOP AND GO FLAGS:                                     B2900...
C           ISTOP = -1   NOT CONVERGED - STOP SIMULATION                B2910...
C           ISTOP =  0   ITERATIONS LEFT OR CONVERGED - KEEP SIMULATING B2920...
C           ISTOP =  1   LAST TIME STEP REACHED - STOP SIMULATION       B2930...
C           ISTOP =  2   MAXIMUM TIME REACHED - STOP SIMULATION         B2940...
C           IGOI = 0   P AND U CONVERGED, OR NO ITERATIONS DONE         B2950...
C           IGOI = 1   ONLY P HAS NOT YET CONVERGED TO CRITERION        B2960...
C           IGOI = 2   ONLY U HAS NOT YET CONVERGED TO CRITERION        B2970...
C           IGOI = 3   BOTH P AND U HAVE NOT YET CONVERGED TO CRITERIA  B2980...
      ISTOP=0                                                           B2990...
      IGOI=0                                                            B3000...
      IF(ITRMAX-1) 7500,7500,7000                                       B3010...
 7000 RPM=0.D0                                                          B3020...
      RUM=0.D0                                                          B3030...
      IPWORS=0                                                          B3040...
      IUWORS=0                                                          B3050...
      IF(ML-1) 7050,7050,7150                                           B3060...
 7050 DO 7100 I=1,NN                                                    B3070...
      RP=DABS(PVEC(I)-PITER(I))                                         B3080...
      IF(RP-RPM) 7100,7060,7060                                         B3090...
 7060 RPM=RP                                                            B3100...
      IPWORS=I                                                          B3110...
 7100 CONTINUE                                                          B3120...
      IF(RPM.GT.RPMAX) IGOI=IGOI+1                                      B3130...
 7150 IF(ML-1) 7200,7350,7200                                           B3140...
 7200 DO 7300 I=1,NN                                                    B3150...
      RU=DABS(UVEC(I)-UITER(I))                                         B3160...
      IF(RU-RUM) 7300,7260,7260                                         B3170...
 7260 RUM=RU                                                            B3180...
      IUWORS=I                                                          B3190...
 7300 CONTINUE                                                          B3200...
      IF(RUM.GT.RUMAX) IGOI=IGOI+2                                      B3210...
 7350 CONTINUE                                                          B3220...
      IF(IGOI.GT.0.AND.ITER.EQ.ITRMAX) ISTOP=-1                         B3230...
      IF(IGOI.GT.0.AND.ISTOP.EQ.0) GOTO 1100                            B3240...
C - - - - - - - - - - - - - - - - - - - - - - - - - - - - - - - - - - - B3250...
C.....END ITERATION - - - - - - - - - - - - - - - - - - - - - - - - - - B3260...
C - - - - - - - - - - - - - - - - - - - - - - - - - - - - - - - - - - - B3270...
C                                                                       B3280...
 7500 CONTINUE                                                          B3290...
      IF(ISTOP.NE.-1.AND.IT.EQ.ITMAX) ISTOP=1                           B3300...
      IF(ISTOP.NE.-1.AND.TSEC.GE.TMAX) ISTOP=2                          B3310...
C                                                                       B3320...
```

```
C.....OUTPUT RESULTS FOR TIME STEP EACH NPRINT TIME STEPS               B3330...
      IF(IT.GT.1.AND.MOD(IT,NPRINT).NE.0.AND.ISTOP.EQ.0) GOTO 8000      B3340...
C.....PRINT P AND/OR U, AND MAYBE SW AND/OR V                           B3350...
      CALL PRISOL(ML,ISTOP,IGOI,PVEC,UVEC,VMAG,VANG,SW)                 B3360...
C.....CALCULATE AND PRINT FLUID MASS AND/OR ENERGY OR SOLUTE MASS BUDGETB3370...
      IF(KBUDG.EQ.1)                                                    B3380...
     1   CALL BUDGET(ML,IBCT,VOL,SW,DSWDP,RHO,SOP,QIN,PVEC,PM1,         B3390...
     2   PBC,QPLITR,IPBC,IQSOP,POR,UVEC,UM1,UM2,UIN,QUIN,IQSOU,UBC,     B3400...
     3   CS1,CS2,CS3,SL,SR)                                             B3410...
 8000 CONTINUE                                                          B3500...
C                                                                       B3510...
C.....MAKE OBSERVATIONS AT OBSERVATION NODES EACH NOBCYC TIME STEPS     B3520...
      IF(NOBSN-1.GT.0) CALL OBSERV(1,IOBS,ITOBS,POBS,UOBS,OBSTIM,       B3530...
     1                  PVEC,UVEC,ISTOP)                                B3540...
C                                                                       B3550...
C.....STORE RESULTS FOR POSSIBLE RESTART OF SIMULATION EACH TIME STEP   B3560...
      IF(ISTORE.NE.1) GOTO 8150                                         B3570...
      CALL STORE(PVEC,UVEC,PM1,UM1,CS1,RCIT,SW,PBC)                     B3580...
C                                                                       B3590...
 8150 IF(ISTOP.EQ.0) GOTO 1000                                          B3600...
C ***********************************************************************B3610...
C.....END TIME STEP *************************************************B3620...
C ***********************************************************************B3630...
C                                                                       B3640...
C                                                                       B3650...
C.....COMPLETE OUTPUT AND TERMINATE SIMULATION                          B3660...
      IF(ISTORE.EQ.1) WRITE(K3,8100)                                    B3670...
 8100 FORMAT(//////11X,'*** LAST SOLUTION HAS BEEN STORED ',            B3680...
     1   'ON UNIT 66 ***')                                              B3690...
C                                                                       B3700...
C.....OUTPUT RESULTS OF OBSERVATIONS                                    B3710...
 8200 IF(NOBSN-1.GT.0) CALL OBSERV(2,IOBS,ITOBS,POBS,UOBS,OBSTIM,       B3720...
     1                    PVEC,UVEC,ISTOP)                              B3730...
C                                                                       B3740...
C.....OUTPUT END OF SIMULATION MESSAGE AND RETURN TO MAIN FOR STOP      B3750...
      IF(ISTOP.GT.0) GOTO 8400                                          B3760...
      IF(IGOI-2) 8230,8260,8290                                         B3770...
 8230 WRITE(K3,8235)                                                    B3780...
 8235 FORMAT(////////11X,'SIMULATION TERMINATED DUE TO ',               B3790...
     1   'NON-CONVERGENT PRESSURE',                                     B3800...
     2             /11X,'********** ********** *** ** ',               B3810...
     3   '************** ********')                                     B3820...
      RETURN                                                            B3830...
 8260 IF(ME) 8262,8262,8266                                             B3840...
 8262 WRITE(K3,8264)                                                    B3850...
 8264 FORMAT(////////11X,'SIMULATION TERMINATED DUE TO ',               B3860...
     1   'NON-CONVERGENT CONCENTRATION',                                B3870...
     2             /11X,'********** ********** *** ** ',               B3880...
     3   '************** *************')                                B3890...
      RETURN                                                            B3900...
 8266 WRITE(K3,8268)                                                    B3910...
 8268 FORMAT(////////11X,'SIMULATION TERMINATED DUE TO ',               B3920...
     1   'NON-CONVERGENT TEMPERATURE',                                  B3930...
     2             /11X,'********** ********** *** ** ',               B3940...
     3   '************** ***********')                                 B3950...
      RETURN                                                            B3960...
 8290 IF(ME) 8292,8292,8296                                             B3970...
 8292 WRITE(K3,8294)                                                    B3980...
 8294 FORMAT(////////11X,'SIMULATION TERMINATED DUE TO ',               B3990...
     1   'NON-CONVERGENT PRESSURE AND CONCENTRATION',                   B4000...
     2             /11X,'********** ********** *** ** ',               B4010...
```

```
     3   '************** ******** *** *************')                  B4020...
      RETURN                                                           B4030...
 8296 WRITE(K3,8298)                                                   B4040...
 8298 FORMAT(////////11X,'SIMULATION TERMINATED DUE TO ',               B4050...
     1   'NON-CONVERGENT PRESSURE AND TEMPERATURE',                    B4060...
     2             /11X,'********** ********** *** ** ',               B4070...
     3   '************** ******** *** ************')                   B4080...
      RETURN                                                           B4090...
C                                                                      B4100...
 8400 IF(ISTOP.EQ.2) GOTO 8500                                         B4110...
      WRITE(K3,8450)                                                   B4120...
 8450 FORMAT(////////11X,'SUTRA SIMULATION TERMINATED AT COMPLETION ',  B4130...
     1   'OF TIME STEPS'/                                              B4140...
     2              11X,'***** ********** ********** ** ********** ',  B4150...
     3   '** **** *****')                                              B4160...
      RETURN                                                           B4170...
 8500 WRITE(K3,8550)                                                   B4180...
 8550 FORMAT(////////11X,'SUTRA SIMULATION TERMINATED AT COMPLETION ',  B4190...
     1   'OF TIME PERIOD'/                                             B4200...
     2              11X,'***** ********** ********** ** ********** ',  B4210...
     3   '** **** ******')                                             B4220...
      RETURN                                                           B4230...
C                                                                      B4240...
      END                                                              B4250...
C     SUBROUTINE        I  N  D  A  T  1        SUTRA - VERSION 1284-2D C10.....
C                                                                      C20.....
C *** PURPOSE :                                                        C30.....
C ***  TO INPUT ,OUTPUT, AND ORGANIZE A MAJOR PORTION OF               C40.....
C ***  UNIT-5 INPUT DATA (DATASET 5 THROUGH DATASET 15B)               C50.....
C                                                                      C60.....
      SUBROUTINE INDAT1(X,Y,THICK,POR,ALMAX,ALMIN,ATAVG,PERMXX,PERMXY, C70.....
     1   PERMYX,PERMYY,PANGLE,SOP,IN)                                  C80.....
      IMPLICIT DOUBLE PRECISION (A-H,O-Z)                              C90.....
      CHARACTER*10 ADSMOD                                              C100....
      CHARACTER*14 UTYPE(2)                                            C110....
      CHARACTER*6 STYPE(2)                                             C120....
      COMMON/FUNITS/ K00,K0,K1,K2,K3,K4,K5,K6                          MODIFIED
      COMMON/MODSOR/ ADSMOD                                            C130....
      COMMON/DIMS/ NN,NE,NIN,IS,JT,NBIP,NBIS,NPT(9),NPBC,NUBC,         C140NEW
     1   NSOP,NSOU,NBCN                                                C150....
      COMMON/TIME/ DELT,TSEC,TMIN,THOUR,TDAY,TWEEK,TMONTH,TYEAR,       C160....
     1   TMAX,DELTP,DELTU,DLTPM1,DLTUM1,IT,ITMAX                       C170....
      COMMON/CNTRL1/ GNU,UP,DTMULT,DTMAX,ME,ISSFLO,ISSTRA,ITCYC,       C180....
     1   NPCYC,NUCYC,NPRINT,IREAD,ISTORE,NOUMAT,IUNSAT,ITIME           C190NEW
      COMMON/ITERAT/ RPM,RPMAX,RUM,RUMAX,ITER,ITRMAX,IPWORS,IUWORS,    C200....
     1              ICON,ITRMX2,OMEGA,RPMX2,RUMX2                      NEW
      COMMON/TENSOR/ GRAVX,GRAVY                                       C210....
      COMMON/PARAMS/ COMPFL,COMPMA,DRWDU,CW,CS,RHOS,DECAY,SIGMAW,SIGMAS,C220....
     1   RHOW0,URHOW0,VISC0,PRODF1,PRODS1,PRODF0,PRODS0,CHI1,CHI2       C230....
      COMMON/SATPAR/ PCENT,SWRES,PCRES,SSLOPE,SINCPT                   C240....
      COMMON/KPRINT/ KNODAL,KELMNT,KINCID,KPLOTP,KPLOTU,KVEL,KBUDG     C250....
      DIMENSION X(NN),Y(NN),THICK(NN),POR(NN),SOP(NN),IN(NIN)          C260NEW
      DIMENSION PERMXX(NE),PERMXY(NE),PERMYX(NE),PERMYY(NE),PANGLE(NE), C270....
     1   ALMAX(NE),ALMIN(NE),ATAVG(NE)                                 C280....
      DIMENSION IIN(4)                                                 NEW
      DATA UTYPE(1)/' TEMPERATURES '/,UTYPE(2)/'CONCENTRATIONS'/       C290....
      DATA STYPE(1)/'ENERGY'/,STYPE(2)/'SOLUTE'/                       C300....
C                                                                      C310....
      INSTOP=0                                                         C320....
C                                                                      C330....
C.....INPUT DATASET 5: NUMERICAL CONTROL PARAMETERS                    C340....
```

```
      READ(K1,50) UP,GNU                                                C350....
   50 FORMAT(G10.0,G15.0)                                               C360....
      WRITE(K3,70) UP,GNU                                               C370....
   70 FORMAT(////11X,'N U M E R I C A L   C O N T R O L   D A T A'//    C380....
     1   11X,F15.5,5X,'"UPSTREAM WEIGHTING" FACTOR'/                    C390....
     2   11X,1PD15.4,5X,'SPECIFIED PRESSURE BOUNDARY CONDITION FACTOR') C400....
C                                                                       C410....
C.....INPUT DATASET 6: TEMPORAL CONTROL AND SOLUTION CYCLING DATA       C420....
      READ(K1,100) ITMAX,DELT,TMAX,ITCYC,DTMULT,DTMAX,NPCYC,NUCYC       C430....
  100 FORMAT(I5,2G15.0,I10,G10.0,G15.0,2I5)                             C440....
      WRITE(K3,120) ITMAX,DELT,TMAX,ITCYC,DTMULT,DTMAX,NPCYC,NUCYC      C450....
  120 FORMAT(1H1////11X,'T E M P O R A L   C O N T R O L   A N D   ',   C460....
     1   'S O L U T I O N   C Y C L I N G   D A T A',                   C470....
     2   //11X,I15,5X,'MAXIMUM ALLOWED NUMBER OF TIME STEPS'           C480....
     3   /11X,1PD15.4,5X,'INITIAL TIME STEP (IN SECONDS)'             C490....
     4   /11X,1PD15.4,5X,'MAXIMUM ALLOWED SIMULATION TIME (IN SECONDS)' C500....
     5   //11X,I15,5X,'TIME STEP MULTIPLIER CYCLE (IN TIME STEPS)'     C510....
     6   /11X,0PF15.5,5X,'MULTIPLICATION FACTOR FOR TIME STEP CHANGE'  C520....
     7   /11X,1PD15.4,5X,'MAXIMUM ALLOWED TIME STEP (IN SECONDS)'      C530....
     8   //11X,I15,5X,'FLOW SOLUTION CYCLE (IN TIME STEPS)'           C540....
     9   /11X,I15,5X,'TRANSPORT SOLUTION CYCLE (IN TIME STEPS)')      C550....
      IF(NPCYC.GE.1.AND.NUCYC.GE.1) GOTO 140                            C560....
      WRITE(K3,130)                                                     C570....
  130 FORMAT(//11X,'* * * * ERROR DETECTED :  BOTH NPCYC AND ',        C580....
     1   'NUCYC MUST BE SET GREATER THAN OR EQUAL TO 1.')               C590....
      INSTOP=INSTOP-1                                                   C600....
  140 IF(NPCYC.EQ.1.OR.NUCYC.EQ.1) GOTO 160                             C610....
      WRITE(K3,150)                                                     C620....
  150 FORMAT(//11X,'* * * * ERROR DETECTED :  EITHER NPCYC OR ',       C630....
     1   'NUCYC MUST BE SET TO 1.')                                     C640....
      INSTOP=INSTOP-1                                                   C650....
  160 CONTINUE                                                          C660....
C.....SET MAXIMUM ALLOWED TIME STEPS IN SIMULATION FOR                  C670....
C        STEADY-STATE FLOW AND STEADY-STATE TRANSPORT SOLUTION MODES    C680....
      IF(ISSFLO.EQ.1) THEN                                              C690....
       NPCYC=ITMAX+1                                                    C700....
       NUCYC=1                                                          C710....
       ENDIF                                                            C720....
      IF(ISSTRA.EQ.1) ITMAX=1                                           C730....
C                                                                       C740....
C.....INPUT DATASET 7: OUTPUT CONTROLS AND OPTIONS                      C750....
      READ(K1,170) NPRINT,KNODAL,KELMNT,KINCID,KPLOTP,KPLOTU,KVEL,KBUDG C760....
  170 FORMAT(16I5)                                                      C770....
      WRITE(K3,172) NPRINT                                              C780....
  172 FORMAT(////11X,'O U T P U T   C O N T R O L S   A N D   ',        C790....
     1   'O P T I O N S'//11X,I6,5X,'PRINTED OUTPUT CYCLE ',            C800....
     2   '(IN TIME STEPS)')                                             C810....
      IF(KNODAL.EQ.+1) WRITE(K3,174)                                    C820....
      IF(KNODAL.EQ.0) WRITE(K3,175)                                     C830....
  174 FORMAT(/11X,'- PRINT NODE COORDINATES, THICKNESSES AND',          C840....
     1   ' POROSITIES')                                                 C850....
  175 FORMAT(/11X,'- CANCEL PRINT OF NODE COORDINATES, THICKNESSES AND',C860....
     1   ' POROSITIES')                                                 C870....
      IF(KELMNT.EQ.+1) WRITE(K3,176)                                    C880....
      IF(KELMNT.EQ.0) WRITE(K3,177)                                     C890....
  176 FORMAT(11X,'- PRINT ELEMENT PERMEABILITIES AND DISPERSIVITIES')   C900....
  177 FORMAT(11X,'- CANCEL PRINT OF ELEMENT PERMEABILITIES AND ',       C910....
     1   'DISPERSIVITIES')                                              C920....
      IF(KINCID.EQ.+1) WRITE(K3,178)                                    C930....
      IF(KINCID.EQ.0) WRITE(K3,179)                                     C940....
  178 FORMAT(11X,'- PRINT NODE INCIDENCES IN EACH ELEMENT')             C950NEW
```

```
  179 FORMAT(11X,'- CANCEL PRINT OF NODE INCIDENCES IN EACH ELEMENT')   C970NEW
      IME=2                                                            C1030...
      IF(ME.EQ.+1) IME=1                                               C1040...
      IF(KVEL.EQ.+1) WRITE(K3,184)                                     C1090...
      IF(KVEL.EQ.0) WRITE(K3,185)                                      C1100...
  184 FORMAT(/11X,'- CALCULATE AND PRINT VELOCITIES AT ELEMENT ',      C1110...
     1   'CENTROIDS ON EACH TIME STEP WITH OUTPUT')                    C1120...
  185 FORMAT(/11X,'- CANCEL PRINT OF VELOCITIES')                      C1130...
      IF(KBUDG.EQ.+1) WRITE(K3,186) STYPE(IME)                         C1140...
      IF(KBUDG.EQ.0) WRITE(K3,187)                                     C1150...
  186 FORMAT(/11X,'- CALCULATE AND PRINT FLUID AND ',A6,' BUDGETS ',   C1160...
     1   'ON EACH TIME STEP WITH OUTPUT')                              C1170...
  187 FORMAT(/11X,'- CANCEL PRINT OF BUDGETS')                         C1180...
C                                                                      C1190...
C.....INPUT DATASET 8: ITERATION CONTROLS                              C1200...
      READ(K1,190) ITRMAX,RPMAX,RUMAX,ICON,ITRMX2,OMEGA,RPMX2,RUMX2    C1210NEW
  190 FORMAT(I10,2G10.0,2I10,3G10.0)                                   C1220NEW
      IF(ITRMAX.EQ.1) WRITE(K3,193)                                    C1230NEW
  193 FORMAT(////11X,'I T E R A T I O N   C O N T R O L   D A T A',    C1250...
     1   //11X,'  NO ITERATION FOR NON-LINEARITIES')                   C1260...
      WRITE(K3,195) ITRMAX,RPMAX,RUMAX                                 C1280...
  195 FORMAT(////11X,'I T E R A T I O N   C O N T R O L   D A T A',    C1290...
     1   //11X,I15,5X,'MAXIMUM NUMBER OF ITERATIONS PER TIME STEP',    C1300...
     2   /11X,1PD15.4,5X,'ABSOLUTE CONVERGENCE CRITERION FOR FLOW',    C1310...
     3   ' SOLUTION'/11X,1PD15.4,5X,'ABSOLUTE CONVERGENCE CRITERION',  C1320...
     4   ' FOR TRANSPORT SOLUTION')                                    C1330...
      WRITE(K3,1951) ICON,ITRMX2,OMEGA,RPMX2,RUMX2                     NEW
 1951 FORMAT(////11X,'I T E R A T I V E   S O L V E R   D A T A',      NEW
     4   //11X,I15,5X,'OPTION NUMBER FOR PRECONDITIONED CONJUGATE ',   NEW
     5   ' GRADIENT SOLVER'/11X,I15,5X,                               NEW
     6   'MAXIMUM NUMBER OF ITERATIONS FOR ITERATIVE SOLVERS'/11X,     NEW
     7   1P1E15.4,5X,'ACCELERATION FACTOR FOR LSOR SOLUTION',         NEW
     2   /11X,1PD15.4,5X,'ABSOLUTE CONVERGENCE CRITERION FOR FLOW',   NEW
     3   ' SOLUTION'/11X,1PD15.4,5X,'ABSOLUTE CONVERGENCE CRITERION', NEW
     4   ' FOR TRANSPORT SOLUTION')                                   NEW
      CONTINUE                                                         C1340...
C                                                                      C1350...
C.....INPUT DATASET 9: FLUID PROPERTIES                                C1360...
      READ(K1,200) COMPFL,CW,SIGMAW,RHOW0,URHOW0,DRWDU,VISC0           C1370...
C.....INPUT DATASET 10: SOLID MATRIX PROPERTIES                        C1380...
      READ(K1,200) COMPMA,CS,SIGMAS,RHOS                               C1390...
  200 FORMAT(8G10.0)                                                   C1400...
      IF(ME.EQ.+1)                                                     C1410...
     1   WRITE(K3,210)COMPFL,COMPMA,CW,CS,VISC0,RHOS,RHOW0,DRWDU,URHOW0,C1420...
     2               SIGMAW,SIGMAS                                     C1430...
  210 FORMAT(1H1///11X,'C O N S T A N T   P R O P E R T I E S   O F',  C1440...
     1   '   F L U I D   A N D   S O L I D   M A T R I X'              C1450...
     2   //11X,1PD15.4,5X,'COMPRESSIBILITY OF FLUID'/11X,1PD15.4,5X,  C1460...
     3   'COMPRESSIBILITY OF POROUS MATRIX'//11X,1PD15.4,5X,           C1470...
     4   'SPECIFIC HEAT CAPACITY OF FLUID',/11X,1PD15.4,5X,            C1480...
     5   'SPECIFIC HEAT CAPACITY OF SOLID GRAIN'//13X,'FLUID VISCOSITY',C1490...
     6   ' IS CALCULATED BY SUTRA AS A FUNCTION OF TEMPERATURE IN ',   C1500...
     7   'UNITS OF [kg/(m*s)]'//11X,1PD15.4,5X,'VISC0, CONVERSION ',   C1510...
     8   'FACTOR FOR VISCOSITY UNITS,  [desired units] = VISC0*',      C1520...
     9   '[kg/(m*s)]'//11X,1PD15.4,5X,'DENSITY OF A SOLID GRAIN'       C1530...
     *   //13X,'FLUID DENSITY, RHOW'/13X,'CALCULATED BY ',            C1540...
     1   'SUTRA IN TERMS OF TEMPERATURE, U, AS:'/13X,'RHOW = RHOW0 + ', C1550...
     2   'DRWDU*(U-URHOW0)'//11X,1PD15.4,5X,'FLUID BASE DENSITY, RHOW0' C1560...
     3   /11X,1PD15.4,5X,'COEFFICIENT OF DENSITY CHANGE WITH ',        C1570...
     4   'TEMPERATURE, DRWDU'/11X,1PD15.4,5X,'TEMPERATURE, URHOW0, ',  C1580...
     5   'AT WHICH FLUID DENSITY IS AT BASE VALUE, RHOW0'              C1590...
```

```
     6   //11X,1PD15.4,5X,'THERMAL CONDUCTIVITY OF FLUID'                C1600...
     7   /11X,1PD15.4,5X,'THERMAL CONDUCTIVITY OF SOLID GRAIN')          C1610...
      IF(ME.EQ.-1)                                                       C1620...
     1   WRITE(K3,220)COMPFL,COMPMA,VISC0,RHOS,RHOW0,DRWDU,URHOW0,SIGMAWC1630...
  220 FORMAT(1H1////11X,'C O N S T A N T   P R O P E R T I E S   O F',  C1640...
     1   '   F L U I D   A N D   S O L I D   M A T R I X'               C1650...
     2   //11X,1PD15.4,5X,'COMPRESSIBILITY OF FLUID'/11X,1PD15.4,5X,    C1660...
     3   'COMPRESSIBILITY OF POROUS MATRIX'                             C1670...
     4   //11X,1PD15.4,5X,'FLUID VISCOSITY'                             C1680...
     4   //11X,1PD15.4,5X,'DENSITY OF A SOLID GRAIN'                    C1690...
     5   //13X,'FLUID DENSITY, RHOW'/13X,'CALCULATED BY ',              C1700...
     6   'SUTRA IN TERMS OF SOLUTE CONCENTRATION, U, AS:',              C1710...
     7   /13X,'RHOW = RHOW0 + DRWDU*(U-URHOW0)'                         C1720...
     8   //11X,1PD15.4,5X,'FLUID BASE DENSITY, RHOW0'                   C1730...
     9   /11X,1PD15.4,5X,'COEFFICIENT OF DENSITY CHANGE WITH ',         C1740...
     *   'SOLUTE CONCENTRATION, DRWDU'                                  C1750...
     1   /11X,1PD15.4,5X,'SOLUTE CONCENTRATION, URHOW0, ',              C1760...
     4   'AT WHICH FLUID DENSITY IS AT BASE VALUE, RHOW0'               C1770...
     5   //11X,1PD15.4,5X,'MOLECULAR DIFFUSIVITY OF SOLUTE IN FLUID')   C1780...
C                                                                       C1790...
C.....INPUT DATASET 11: ADSORPTION PARAMETERS                           C1800...
      READ(K1,230) ADSMOD,CHI1,CHI2                                     C1810...
  230 FORMAT(A10,2G10.0)                                                C1820...
      IF(ME.EQ.+1) GOTO 248                                             C1830...
      IF(ADSMOD.EQ.'NONE      ') GOTO 234                               C1840...
      WRITE(K3,232) ADSMOD                                              C1850...
  232 FORMAT(////11X,'A D S O R P T I O N   P A R A M E T E R S'        C1860...
     1   //16X,A10,5X,'EQUILIBRIUM SORPTION ISOTHERM')                  C1870...
      GOTO 236                                                          C1880...
  234 WRITE(K3,235)                                                     C1890...
  235 FORMAT(////11X,'A D S O R P T I O N   P A R A M E T E R S'        C1900...
     1   //16X,'NON-SORBING SOLUTE')                                    C1910...
  236 IF((ADSMOD.EQ.'NONE ').OR.(ADSMOD.EQ.'LINEAR    ').OR.            C1920...
     1   (ADSMOD.EQ.'FREUNDLICH').OR.(ADSMOD.EQ.'LANGMUIR  ')) GOTO 238 C1930...
      WRITE(K3,237)                                                     C1940...
  237 FORMAT(//11X,'* * * * ERROR DETECTED :  TYPE OF SORPTION MODEL ', C1950...
     1   'IS NOT SPECIFIED CORRECTLY.'/11X,'CHECK FOR TYPE AND ',       C1960...
     2   'SPELLING, AND THAT TYPE IS LEFT-JUSTIFIED IN INPUT FIELD')    C1970...
      INSTOP=INSTOP-1                                                   C1980...
  238 IF(ADSMOD.EQ.'LINEAR    ') WRITE(K3,242) CHI1                     C1990...
  242 FORMAT(11X,1PD15.4,5X,'LINEAR DISTRIBUTION COEFFICIENT')          C2000...
      IF(ADSMOD.EQ.'FREUNDLICH') WRITE(K3,244) CHI1,CHI2                C2010...
  244 FORMAT(11X,1PD15.4,5X,'FREUNDLICH DISTRIBUTION COEFFICIENT'       C2020...
     1   /11X,1PD15.4,5X,'SECOND FREUNDLICH COEFFICIENT')               C2030...
      IF(ADSMOD.EQ.'FREUNDLICH'.AND.CHI2.LE.0.D0) THEN                  C2040...
       WRITE(K3,245)                                                    C2050...
  245  FORMAT(11X,'* * * * ERROR DETECTED :  SECOND COEFFICIENT ',      C2060...
     1    'MUST BE GREATER THAN ZERO')                                  C2070...
       INSTOP=INSTOP-1                                                  C2080...
       ENDIF                                                            C2090...
      IF(ADSMOD.EQ.'LANGMUIR  ') WRITE(K3,246) CHI1,CHI2                C2100...
  246 FORMAT(11X,1PD15.4,5X,'LANGMUIR DISTRIBUTION COEFFICIENT'         C2110...
     1   /11X,1PD15.4,5X,'SECOND LANGMUIR COEFFICIENT')                 C2120...
C                                                                       C2130...
C.....INPUT DATASET 12: PRODUCTION OF ENERGY OR SOLUTE MASS             C2140...
  248 READ(K1,200) PRODF0,PRODS0,PRODF1,PRODS1                          C2150...
      IF(ME.EQ.-1) WRITE(K3,250) PRODF0,PRODS0,PRODF1,PRODS1            C2160...
  250 FORMAT(////11X,'P R O D U C T I O N   A N D   D E C A Y   O F   ',C2170...
     1   'S P E C I E S   M A S S'//13X,'PRODUCTION RATE (+)'/13X,      C2180...
     2   'DECAY RATE (-)'//11X,1PD15.4,5X,'ZERO-ORDER RATE OF SOLUTE ', C2190...
     3   'MASS PRODUCTION/DECAY IN FLUID'/11X,1PD15.4,5X,               C2200...
```

```
     4   'ZERO-ORDER RATE OF ADSORBATE MASS PRODUCTION/DECAY IN ',      C2210...
     5   'IMMOBILE PHASE'/11X,1PD15.4,5X,'FIRST-ORDER RATE OF SOLUTE ', C2220...
     3   'MASS PRODUCTION/DECAY IN FLUID'/11X,1PD15.4,5X,               C2230...
     4   'FIRST-ORDER RATE OF ADSORBATE MASS PRODUCTION/DECAY IN ',     C2240...
     5   'IMMOBILE PHASE')                                             C2250...
      IF(ME.EQ.+1) WRITE(K3,260) PRODF0,PRODS0                         C2260...
  260 FORMAT(////11X,'P R O D U C T I O N   A N D   L O S S   O F   ',  C2270...
     1   'E N E R G Y'//13X,'PRODUCTION RATE (+)'/13X,                  C2280...
     2   'LOSS RATE (-)'//11X,1PD15.4,5X,'ZERO-ORDER RATE OF ENERGY ',  C2290...
     3   'PRODUCTION/LOSS IN FLUID'/11X,1PD15.4,5X,                     C2300...
     4   'ZERO-ORDER RATE OF ENERGY PRODUCTION/LOSS IN ',               C2310...
     5   'SOLID GRAINS')                                               C2320...
C.....SET PARAMETER SWITCHES FOR EITHER ENERGY OR SOLUTE TRANSPORT      C2330...
      IF(ME) 272,272,274                                               C2340...
C     FOR SOLUTE TRANSPORT:                                            C2350...
  272 CS=0.0D0                                                         C2360...
      CW=1.D00                                                         C2370...
      SIGMAS=0.0D0                                                     C2380...
      GOTO 278                                                         C2390...
C     FOR ENERGY TRANSPORT:                                            C2400...
  274 ADSMOD='NONE      '                                              C2410...
      CHI1=0.0D0                                                       C2420...
      CHI2=0.0D0                                                       C2430...
      PRODF1=0.0D0                                                     C2440...
      PRODS1=0.0D0                                                     C2450...
C     DIVIDE SIGMA TO CANCEL MULTIPLICATION BY RHOW*CW                 C2460...
C        IN SUBROUTINE ELEMEN.                                         C2470...
      RC0=RHOW0*CW                                                     C2480...
      SIGMAW=SIGMAW/RC0                                                C2490...
      SIGMAS=SIGMAS/RC0                                                C2500...
  278 CONTINUE                                                         C2510...
C                                                                      C2520...
C.....INPUT DATASET 13: ORIENTATION OF COORDINATES TO GRAVITY          C2530...
      READ(K1,200) GRAVX,GRAVY                                         C2540...
      WRITE(K3,320) GRAVX,GRAVY                                        C2550...
  320 FORMAT(////11X,'C O O R D I N A T E   O R I E N T A T I O N   ',  C2560...
     1   'T O   G R A V I T Y'//13X,'COMPONENT OF GRAVITY VECTOR',      C2570...
     2   /13X,'IN +X DIRECTION, GRAVX'/11X,1PD15.4,5X,                  C2580...
     3   'GRAVX = -GRAV * D(ELEVATION)/DX'//13X,'COMPONENT OF GRAVITY', C2590...
     4   ' VECTOR'/13X,'IN +Y DIRECTION, GRAVY'/11X,1PD15.4,5X,         C2600...
     5   'GRAVY = -GRAV * D(ELEVATION)/DY')                            C2610...
C                                                                      C2620...
C.....INPUT DATASETS 14A AND 14B: NODEWISE DATA                        C2630...
      READ(K1,330) SCALX,SCALY,SCALTH,PORFAC                           C2640...
  330 FORMAT(10X,4G10.0)                                               C2650...
      DO 450 I=1,NN                                                    C2660...
      READ(K1,400) II,X(II),Y(II),THICK(II),POR(II)                    C2670...
  400 FORMAT(I5,5X,4G10.0)                                             C2680NEW
      X(II)=X(II)*SCALX                                                C2690...
      Y(II)=Y(II)*SCALY                                                C2700...
      THICK(II)=THICK(II)*SCALTH                                       C2710...
      POR(II)=POR(II)*PORFAC                                           C2720...
C     SET SPECIFIC PRESSURE STORATIVITY, SOP.                          C2730...
  450 SOP(II)=(1.D0-POR(II))*COMPMA+POR(II)*COMPFL                     C2740...
  460 IF(KNODAL.EQ.0) WRITE(K3,469) SCALX,SCALY,SCALTH,PORFAC          C2750...
  469 FORMAT(1H1////11X,'N O D E   I N F O R M A T I O N'//16X,        C2760...
     1   'PRINTOUT OF NODE COORDINATES, THICKNESSES AND POROSITIES ',  C2770...
     2   'CANCELLED.'//16X,'SCALE FACTORS :'/33X,1PD15.4,5X,'X-SCALE'/ C2780...
     1   33X,1PD15.4,5X,'Y-SCALE'/33X,1PD15.4,5X,'THICKNESS FACTOR'/   C2790...
     2   33X,1PD15.4,5X,'POROSITY FACTOR')                             C2800...
      IF(KNODAL.EQ.+1)WRITE(K3,470)(I,X(I),Y(I),THICK(I),POR(I),I=1,NN) C2810...
```

```
  470 FORMAT(1H1//11X,'N O D E   I N F O R M A T I O N'//13X,          C2820...
     1   'NODE',7X,'X',16X,'Y',17X,'THICKNESS',6X,'POROSITY'//         C2830...
     2   (11X,I6,3(3X,1PD14.5),6X,0PF8.5))                             C2840...
C                                                                      C2850...
C.....INPUT DATASETS 15A AND 15B: ELEMENTWISE DATA                     C2860...
      READ(K1,490) PMAXFA,PMINFA,ANGFAC,ALMAXF,ALMINF,ATAVGF           C2870...
  490 FORMAT(10X,6G10.0)                                               C2880...
      IF(KELMNT.EQ.+1) WRITE(K3,500)                                   C2890...
  500 FORMAT(1H1//11X,'E L E M E N T   I N F O R M A T I O N'//        C2900...
     1   11X,'ELEMENT',4X,'MAXIMUM',9X,'MINIMUM',12X,                  C2910...
     2   'ANGLE BETWEEN',3X,'     MAXIMUM',5X,'   MINIMUM',5X,          C2920...
     3   '   AVERAGE'/22X,'PERMEABILITY',4X,'PERMEABILITY',4X,          C2930...
     4   '+X-DIRECTION AND',3X,'LONGITUDINAL',3X,'LONGITUDINAL'3X,     C2940...
     5   '  TRANSVERSE'/50X,'MAXIMUM PERMEABILITY',3X,'DISPERSIVITY',  C2950...
     6   3X,'DISPERSIVITY',3X,'DISPERSIVITY'/58X,'(IN DEGREES)'//)     C2960...
      DO 550 LL=1,NE                                                   C2970...
      READ(K1,510) L,PMAX,PMIN,ANGLEX,ALMAX(L),ALMIN(L),ATAVG(L)       C2980...
  510 FORMAT(I5,5X,6G10.0)                                             C2990NEW
      PMAX=PMAX*PMAXFA                                                 C3000...
      PMIN=PMIN*PMINFA                                                 C3010...
      ANGLEX=ANGLEX*ANGFAC                                             C3020...
      ALMAX(L)=ALMAX(L)*ALMAXF                                         C3030...
      ALMIN(L)=ALMIN(L)*ALMINF                                         C3040...
      ATAVG(L)=ATAVG(L)*ATAVGF                                         C3050...
      IF(KELMNT.EQ.+1) WRITE(K3,520) L,PMAX,PMIN,ANGLEX,               C3060...
     1   ALMAX(L),ALMIN(L),ATAVG(L)                                    C3070...
  520 FORMAT(11X,I7,2X,2(1PD14.5,2X),8X,4(0PF10.3,5X))                 C3080...
C                                                                      C3090...
C.....ROTATE PERMEABILITY FROM MAXIMUM/MINIMUM TO X/Y DIRECTIONS       C3100...
      RADIAX=1.745329D-02*ANGLEX                                       C3110...
      SINA=DSIN(RADIAX)                                                C3120...
      COSA=DCOS(RADIAX)                                                C3130...
      SINA2=SINA*SINA                                                  C3140...
      COSA2=COSA*COSA                                                  C3150...
      PERMXX(L)=PMAX*COSA2+PMIN*SINA2                                  C3160...
      PERMYY(L)=PMAX*SINA2+PMIN*COSA2                                  C3170...
      PERMXY(L)=(PMAX-PMIN)*SINA*COSA                                  C3180...
      PERMYX(L)=PERMXY(L)                                              C3190...
      PANGLE(L)=RADIAX                                                 C3200...
  550 CONTINUE                                                         C3210...
      IF(KELMNT.EQ.0)                                                  C3220...
     1   WRITE(K3,569) PMAXFA,PMINFA,ANGFAC,ALMAXF,ALMINF,ATAVGF       C3230...
  569 FORMAT(////11X,'E L E M E N T   I N F O R M A T I O N'//         C3240...
     1   16X,'PRINTOUT OF ELEMENT PERMEABILITIES AND DISPERSIVITIES ',  C3250...
     2   'CANCELLED.'//16X,'SCALE FACTORS :'/33X,1PD15.4,5X,'MAXIMUM ', C3260...
     1   'PERMEABILITY FACTOR'/33X,1PD15.4,5X,'MINIMUM PERMEABILITY ',  C3270...
     2   'FACTOR'/33X,1PD15.4,5X,'ANGLE FROM +X TO MAXIMUM DIRECTION',  C3280...
     3   ' FACTOR'/33X,1PD15.4,5X,'MAXIMUM LONGITUDINAL DISPERSIVITY',  C3290...
     4   ' FACTOR'/33X,1PD15.4,5X,'MINIMUM LONGITUDINAL DISPERSIVITY',  C3300...
     5   ' FACTOR'/33X,1PD15.4,5X,'TRANSVERSE DISPERSIVITY FACTOR')     C3310...
C                                                                      C3320...
C.....END SIMULATION FOR CORRECTIONS TO UNIT-5 DATA IF NECESSARY       C3330...
      IF(INSTOP.EQ.0) GOTO 1000                                        C3340...
      WRITE(K3,999)                                                    C3350...
  999 FORMAT(////////11X,'PLEASE CORRECT INPUT DATA AND RERUN.',       C3360...
     1   ///22X,'S I M U L A T I O N   H A L T E D',                   C3370...
     2     /22X,'******************   ***********')                   C3380...
      ENDFILE(K3)                                                      C3390...
      STOP                                                             C3400...
C                                                                      C3410...
C                                                                      C3420...
```

```
1000  IF(KINCID.EQ.0) WRITE(K3,1)                                        NEW
    1 FORMAT(1H1////11X,'M E S H   C O N N E C T I O N   D A T A'//      NEW
     1   16X,'PRINTOUT OF NODAL INCIDENCES CANCELLED.')                   NEW
      IF(KINCID.EQ.+1) WRITE(K3,2)                                       NEW
    2 FORMAT(1H1////11X,'M E S H   C O N N E C T I O N   D A T A',       NEW
     1   ///11X,'**** NODAL INCIDENCES ****'///)                         NEW
C                                                                        NEW
C.....CALCULATE INCIDENCES FOR REGULAR GRID                              NEW
      NEX=IS-1                                                           NEW
      NEY=JT-1                                                           NEW
      NELEMN=0                                                           NEW
      DO 560 IE2=1,NEX                                                   NEW
      DO 560 IE1=1,NEY                                                   NEW
      NELEMN=NELEMN+1                                                    NEW
      N0=IE1+(IE2-1)*JT                                                  NEW
      IIN(1)=N0                                                          NEW
      IIN(2)=N0+JT                                                       NEW
      IIN(3)=N0+JT+1                                                     NEW
      IIN(4)=N0+1                                                        NEW
C                                                                        NEW
C.....PREPARE NODE INCIDENCE LIST FOR MESH, IN.                          NEW
      DO 570 II=1,4                                                      NEW
      III=II+(NELEMN-1)*4                                                NEW
  570 IN(III)=IIN(II)                                                    NEW
C                                                                        NEW
      IF(KINCID.EQ.0) GOTO 560                                           NEW
      WRITE(K3,650) NELEMN,(IIN(M),M=1,4)                                NEW
  650 FORMAT(11X,'ELEMENT',I6,5X,' NODES AT : ',6X,'CORNERS ',           NEW
     1   5(1H*),4I6,1X,5(1H*))                                           NEW
C                                                                        NEW
  560 CONTINUE                                                           NEW
C                                                                        NEW
C ***       NOTE: BANDWIDTH FOR A REGULAR GRID IS FIXED                  NEW
      WRITE(K3,2500) NBIP,NBIS                                           NEW
 2500 FORMAT(////13X,'BANDWIDTH FOR PRESSURE MATRIX, ',I4/               NEW
     1 13X,'BANDWIDTH FOR TRANSPORT MATRIX, ',I4)                        NEW
C                                                                        NEW
C     SET UP POINTER ARRAYS FOR MATRICES                                 NEW
      NPT(1)=-JT                                                         NEW
      NPT(2)=1-JT                                                        NEW
      NPT(3)=2-JT                                                        NEW
      NPT(4)=0                                                           NEW
      NPT(5)=1                                                           NEW
      NPT(6)=2                                                           NEW
      NPT(7)=JT                                                          NEW
      NPT(8)=1+JT                                                        NEW
      NPT(9)=JT+2                                                        NEW
C                                                                        NEW
      RETURN                                                             NEW
      END                                                                C3440...
C     SUBROUTINE        S  O  U  R  C  E        SUTRA - VERSION 1284-2D  E10.....
C                                                                        E20.....
C *** PURPOSE :                                                          E30.....
C ***  TO READ AND ORGANIZE FLUID MASS SOURCE DATA AND ENERGY OR         E40.....
C ***  SOLUTE MASS SOURCE DATA.                                          E50.....
C                                                                        E60.....
      SUBROUTINE SOURCE(QIN,UIN,IQSOP,QUIN,IQSOU,IQSOPT,IQSOUT)         E70.....
      IMPLICIT DOUBLE PRECISION (A-H,O-Z)                                E80.....
      COMMON/FUNITS/ K00,K0,K1,K2,K3,K4,K5,K6                            MODIFIED
      COMMON/DIMS/ NN,NE,NIN,IS,JT,NBIP,NBIS,NPT(9),NPBC,NUBC,           E90NEW
     1   NSOP,NSOU,NBCN                                                  E100....
```

```
      COMMON/CNTRL1/ GNU,UP,DTMULT,DTMAX,ME,ISSFLO,ISSTRA,ITCYC,        E110NEW
     1   NPCYC,NUCYC,NPRINT,IREAD,ISTORE,NOUMAT,IUNSAT,ITIME            E120NEW
      DIMENSION QIN(NN),UIN(NN),IQSOP(NSOP),QUIN(NN),IQSOU(NSOU)        E130....
C                                                                       E140....
C.....NSOPI IS ACTUAL NUMBER OF FLUID SOURCE NODES                      E150....
C.....NSOUI IS ACTUAL NUMBER OF SOLUTE MASS OR ENERGY SOURCE NODES      E160....
      NSOPI=NSOP-1                                                      E170....
      NSOUI=NSOU-1                                                      E180....
      IQSOPT=1                                                          E190....
      IQSOUT=1                                                          E200....
      NIQP=0                                                            E210....
      NIQU=0                                                            E220....
      IF(NSOPI.EQ.0) GOTO 1000                                          E230....
      IF(ME) 50,50,150                                                  E240....
   50 WRITE(K3,100)                                                     E250....
  100 FORMAT(1H1////11X,'F L U I D   S O U R C E   D A T A'             E260....
     1   ////11X,'**** NODES AT WHICH FLUID INFLOWS OR OUTFLOWS ARE ',  E270....
     2   'SPECIFIED ****'//11X,'NODE NUMBER',10X,                      E280....
     3   'FLUID INFLOW(+)/OUTFLOW(-)',5X,'SOLUTE CONCENTRATION OF'     E290....
     4   /11X,'(MINUS INDICATES',5X,'(FLUID MASS/SECOND)',             E300....
     5   12X,'INFLOWING FLUID'/12X,'TIME-VARYING',39X,                 E310....
     6   '(MASS SOLUTE/MASS WATER)'/12X,'FLOW RATE OR'/12X,            E320....
     7   'CONCENTRATION)'//)                                           E330....
      GOTO 300                                                          E340....
  150 WRITE(K3,200)                                                     E350....
  200 FORMAT(1H1////11X,'F L U I D   S O U R C E   D A T A'             E360....
     1   ////11X,'**** NODES AT WHICH FLUID INFLOWS OR OUTFLOWS ARE ',  E370....
     2   'SPECIFIED ****'//11X,'NODE NUMBER',10X,                      E380....
     3   'FLUID INFLOW(+)/OUTFLOW(-)',5X,'TEMPERATURE [DEGREES CELCIUS]'E390....
     4   /11X,'(MINUS INDICATES',5X,'(FLUID MASS/SECOND)',12X,         E400....
     5   'OF INFLOWING FLUID'/12X,'TIME-VARYING'/12X,'FLOW OR'/12X,    E410....
     6   'TEMPERATURE)'//)                                             E420....
C                                                                       E430....
C.....INPUT DATASET 17                                                  E440....
  300 CONTINUE                                                          E450....
      READ(K1,400) IQCP,QINC,UINC                                       E460....
  400 FORMAT(I10,2G15.0)                                                E470....
      IF(IQCP.EQ.0) GOTO 700                                            E480....
      NIQP=NIQP+1                                                       E490....
      IQSOP(NIQP)=IQCP                                                  E500....
      IF(IQCP.LT.0) IQSOPT=-1                                           E510....
      IQP=IABS(IQCP)                                                    E520....
      QIN(IQP)=QINC                                                     E530....
      UIN(IQP)=UINC                                                     E540....
      IF(IQCP.GT.0) GOTO 450                                            E550....
      WRITE(K3,500) IQCP                                                E560....
      GOTO 600                                                          E570....
  450 IF(QINC.GT.0) GOTO 460                                            E580....
      WRITE(K3,500) IQCP,QINC                                           E590....
      GOTO 600                                                          E600....
  460 WRITE(K3,500) IQCP,QINC,UINC                                      E610....
  500 FORMAT(11X,I10,13X,1PE14.7,16X,1PE14.7)                           E620....
  600 GOTO 300                                                          E630....
  700 IF(NIQP.EQ.NSOPI) GOTO 890                                        E640....
C.....END SIMULATION IF THERE NEED BE CORRECTIONS TO DATASET 17         E650....
      WRITE(K3,750) NIQP,NSOPI                                          E660....
  750 FORMAT(////11X,'THE NUMBER OF FLUID SOURCE NODES READ, ',I5,      E670....
     1   ' IS NOT EQUAL TO THE NUMBER SPECIFIED, ',I5////              E680....
     2   11X,'PLEASE CORRECT DATA AND RERUN'////////                    E690....
     3   22X,'S I M U L A T I O N   H A L T E D'/                      E700....
     4   22X,'_____________________________________')                  E710....
```

```
      ENDFILE(K3)                                                       E720....
      STOP                                                              E730....
  890 IF(IQSOPT.EQ.-1) WRITE(K3,900)                                    E740....
  900 FORMAT(////11X,'THE SPECIFIED TIME VARIATIONS ARE ',              E750....
     1   'USER-PROGRAMMED IN SUBROUTINE  B C T I M E .')                E760....
C                                                                       E770....
C                                                                       E780....
 1000 IF(NSOUI.EQ.0) GOTO 9000                                          E790....
      IF(ME) 1050,1050,1150                                             E800....
 1050 WRITE(K3,1100)                                                    E810....
 1100 FORMAT(////////11X,'S O L U T E   S O U R C E   D A T A'          E820....
     1   ////11X,'**** NODES AT WHICH SOURCES OR SINKS OF SOLUTE ',     E830....
     2   'MASS ARE SPECIFIED ****'//11X,'NODE NUMBER',10X,              E840....
     3   'SOLUTE SOURCE(+)/SINK(-)'/11X,'(MINUS INDICATES',5X,          E850....
     4   '(SOLUTE MASS/SECOND)'/12X,'TIME-VARYING'/12X,                 E860....
     5   'SOURCE OR SINK)'//)                                           E870....
      GOTO 1300                                                         E880....
 1150 WRITE(K3,1200)                                                    E890....
 1200 FORMAT(////////11X,'E N E R G Y   S O U R C E   D A T A'          E900....
     1   ////11X,'**** NODES AT WHICH SOURCES OR SINKS OF ',            E910....
     2   'ENERGY ARE SPECIFIED ****'//11X,'NODE NUMBER',10X,            E920....
     3   'ENERGY SOURCE(+)/SINK(-)'/11X,'(MINUS INDICATES',5X,          E930....
     4   '(ENERGY/SECOND)'/12X,'TIME-VARYING'/12X,                      E940....
     5   'SOURCE OR SINK)'//)                                           E950....
C                                                                       E960....
C.....INPUT DATASET 18                                                  E970....
 1300 CONTINUE                                                          E980....
      READ(K1,400) IQCU,QUINC                                           E990....
      IF(IQCU.EQ.0) GOTO 1700                                           E1000...
      NIQU=NIQU+1                                                       E1010...
      IQSOU(NIQU)=IQCU                                                  E1020...
      IF(IQCU.LT.0) IQSOUT=-1                                           E1030...
      IQU=IABS(IQCU)                                                    E1040...
      QUIN(IQU)=QUINC                                                   E1050...
      IF(IQCU.GT.0) GOTO 1450                                           E1060...
      WRITE(K3,1500) IQCU                                               E1070...
      GOTO 1600                                                         E1080...
 1450 WRITE(K3,1500) IQCU,QUINC                                         E1090...
 1500 FORMAT(11X,I10,13X,1PE14.7)                                       E1100...
 1600 GOTO 1300                                                         E1110...
 1700 IF(NIQU.EQ.NSOUI) GOTO 1890                                       E1120...
C.....END SIMULATION IF THERE NEED BE CORRECTIONS TO DATASET 18         E1130...
      IF(ME) 1740,1740,1760                                             E1140...
 1740 WRITE(K3,1750) NIQU,NSOUI                                         E1150...
 1750 FORMAT(////11X,'THE NUMBER OF SOLUTE SOURCE NODES READ, ',I5,     E1160...
     1   ' IS NOT EQUAL TO THE NUMBER SPECIFIED, ',I5////               E1170...
     2   11X,'PLEASE CORRECT DATA AND RERUN'////////                    E1180...
     3   22X,'S I M U L A T I O N   H A L T E D'/                       E1190...
     4   22X,'_____________________________________')                   E1200...
      ENDFILE(K3)                                                       E1210...
      STOP                                                              E1220...
 1760 WRITE(K3,1770) NIQU,NSOUI                                         E1230...
 1770 FORMAT(////11X,'THE NUMBER OF ENERGY SOURCE NODES READ, ',I5,     E1240...
     1     ' IS NOT EQUAL TO THE NUMBER SPECIFIED, ',I5////           E1250...
     2   11X,'PLEASE CORRECT DATA AND RERUN'////////                    E1260...
     3   22X,'S I M U L A T I O N   H A L T E D'/                       E1270...
     4   22X,'_____________________________________')                   E1280...
      ENDFILE(K3)                                                       E1290...
      STOP                                                              E1300...
 1890 IF(IQSOUT.EQ.-1) WRITE(K3,900)                                    E1310...
C                                                                       E1320...
```

```
 9000 RETURN                                                            E1330...
C                                                                       E1340...
      END                                                               E1350...
C     SUBROUTINE        B  O  U  N  D           SUTRA - VERSION 1284-2D F10.....
C                                                                       F20.....
C *** PURPOSE :                                                         F30.....
C ***  TO READ AND ORGANIZE SPECIFIED PRESSURE DATA AND                 F40.....
C ***  SPECIFIED TEMPERATURE OR CONCENTRATION DATA.                     F50.....
C                                                                       F60.....
      SUBROUTINE BOUND(IPBC,PBC,IUBC,UBC,IPBCT,IUBCT)                   F70.....
      IMPLICIT DOUBLE PRECISION (A-H,O-Z)                               F80.....
      COMMON/FUNITS/ K00,K0,K1,K2,K3,K4,K5,K6                           MODIFIED
      COMMON/DIMS/ NN,NE,NIN,IS,JT,NBIP,NBIS,NPT(9),NPBC,NUBC,          F90NEW
     1   NSOP,NSOU,NBCN                                                 F100
      COMMON/CNTRL1/ GNU,UP,DTMULT,DTMAX,ME,ISSFLO,ISSTRA,ITCYC,        F110....
     1   NPCYC,NUCYC,NPRINT,IREAD,ISTORE,NOUMAT,IUNSAT,ITIME            F120NEW
      DIMENSION IPBC(NBCN),PBC(NBCN),IUBC(NBCN),UBC(NBCN)               F130....
C                                                                       F140....
C                                                                       F150....
      IPBCT=1                                                           F160....
      IUBCT=1                                                           F170....
      ISTOPP=0                                                          F180....
      ISTOPU=0                                                          F190....
      IPU=0                                                             F200....
      WRITE(K3,50)                                                      F210....
   50 FORMAT(1H1////11X,'B O U N D A R Y   C O N D I T I O N S')        F220....
      IF(NPBC.EQ.0) GOTO 400                                            F230....
      WRITE(K3,100)                                                     F240....
  100 FORMAT(//11X,'**** NODES AT WHICH PRESSURES ARE',                 F250....
     1   ' SPECIFIED ****'/)                                            F260....
      IF(ME) 107,107,114                                                F270....
  107 WRITE(K3,108)                                                     F280....
  108 FORMAT(11X,'     (AS WELL AS SOLUTE CONCENTRATION OF ANY'         F290....
     1   /16X,' FLUID INFLOW WHICH MAY OCCUR AT THE POINT'              F300....
     2   /16X,' OF SPECIFIED PRESSURE)'//12X,'NODE',18X,'PRESSURE',     F310....
     3   13X,'CONCENTRATION'//)                                         F320....
      GOTO 120                                                          F330....
  114 WRITE(K3,115)                                                     F340....
  115 FORMAT(11X,'     (AS WELL AS TEMPERATURE [DEGREES CELCIUS] OF ANY'F350....
     1   /16X,' FLUID INFLOW WHICH MAY OCCUR AT THE POINT'              F360....
     2   /16X,' OF SPECIFIED PRESSURE)'//12X,'NODE',18X,                F370....
     2   'PRESSURE',13X,'  TEMPERATURE'//)                             F380....
C                                                                       F390....
C.....INPUT DATASET 14                                                  F400....
  120 IPU=IPU+1                                                         F410....
      READ(K1,150) IPBC(IPU),PBC(IPU),UBC(IPU)                          F420....
  150 FORMAT(I5,2G20.0)                                                 F430....
      IF(IPBC(IPU).LT.0) IPBCT=-1                                       F440....
      IF(IPBC(IPU).EQ.0) GOTO 180                                       F450....
      IF(IPBC(IPU).GT.0) WRITE(K3,160) IPBC(IPU),PBC(IPU),UBC(IPU)      F460....
      IF(IPBC(IPU).LT.0) WRITE(K3,160) IPBC(IPU)                        F470....
  160 FORMAT(11X,I5,6X,1PD20.13,6X,1PD20.13)                            F480....
      GOTO 120                                                          F490....
  180 IPU=IPU-1                                                         F500....
      IP=IPU                                                            F510....
      IF(IP.EQ.NPBC) GOTO 200                                           F520....
      ISTOPP=1                                                          F530....
  200 IF(IPBCT.NE.-1) GOTO 400                                          F540....
      IF(ME) 205,205,215                                                F550....
  205 WRITE(K3,206)                                                     F560....
  206 FORMAT(//12X,'TIME-DEPENDENT SPECIFIED PRESSURE'/12X,'OR INFLOW ',F570....
```

```
     1   'CONCENTRATION INDICATED'/12X,'BY NEGATIVE NODE NUMBER')      F580....
      GOTO 400                                                         F590....
  215 WRITE(K3,216)                                                    F600....
  216 FORMAT(//11X,'TIME-DEPENDENT SPECIFIED PRESSURE'/12X,'OR INFLOW ',F610....
     1   'TEMPERATURE INDICATED'/12X,'BY NEGATIVE NODE NUMBER')        F620....
  400 IF(NUBC.EQ.0) GOTO 2000                                          F630....
C                                                                      F640....
      IF(ME) 500,500,550                                               F650....
  500 WRITE(K3,1000)                                                   F660....
 1000 FORMAT(////11X,'**** NODES AT WHICH SOLUTE CONCENTRATIONS ARE ',  F670....
     1   'SPECIFIED TO BE INDEPENDENT OF LOCAL FLOWS AND FLUID SOURCES',F680....
     2   ' ****'//12X,'NODE',13X,'CONCENTRATION'//)                    F690....
      GOTO 1120                                                        F700....
  550 WRITE(K3,1001)                                                   F710....
 1001 FORMAT(////11X,'**** NODES AT WHICH TEMPERATURES ARE ',          F720....
     1   'SPECIFIED TO BE INDEPENDENT OF LOCAL FLOWS AND FLUID SOURCES',F730....
     2   ' ****'//12X,'NODE',15X,'TEMPERATURE'//)                      F740....
C                                                                      F750....
C.....INPUT DATASET 20                                                 F760....
 1120 IPU=IPU+1                                                        F770....
      READ(K1,150) IUBC(IPU),UBC(IPU)                                  F780....
      IF(IUBC(IPU).LT.0) IUBCT=-1                                      F790....
      IF(IUBC(IPU).EQ.0) GOTO 1180                                     F800....
      IF(IUBC(IPU).GT.0) WRITE(K3,1150) IUBC(IPU),UBC(IPU)             F810....
      IF(IUBC(IPU).LT.0) WRITE(K3,1150) IUBC(IPU)                      F820....
 1150 FORMAT(11X,I5,6X,1PD20.13)                                       F830....
      GOTO 1120                                                        F840....
 1180 IPU=IPU-1                                                        F850....
      IU=IPU-IP                                                        F860....
      IF(IU.EQ.NUBC) GOTO 1200                                         F870....
      ISTOPU=1                                                         F880....
 1200 IF(IUBCT.NE.-1) GOTO 2000                                        F890....
      IF(ME) 1205,1205,1215                                            F900....
 1205 WRITE(K3,1206)                                                   F910....
 1206 FORMAT(//12X,'TIME-DEPENDENT SPECIFIED CONCENTRATION'/12X,'IS ',  F920....
     1   'INDICATED BY NEGATIVE NODE NUMBER')                          F930....
      GOTO 2000                                                        F940....
 1215 WRITE(K3,1216)                                                   F950....
 1216 FORMAT(//11X,'TIME-DEPENDENT SPECIFIED TEMPERATURE'/12X,'IS ',    F960....
     1   'INDICATED BY NEGATIVE NODE NUMBER')                          F970....
C                                                                      F980....
C.....END SIMULATION IF THERE NEED BE CORRECTIONS TO DATASET 19 OR 20   F990....
 2000 IF(ISTOPP.EQ.0.AND.ISTOPU.EQ.0) GOTO 6000                        F1000...
      IF(ISTOPP.EQ.1) WRITE(K3,3000) IP,NPBC                           F1010...
 3000 FORMAT(////11X,'ACTUAL NUMBER OF SPECIFIED PRESSURE NODES',      F1020...
     1   ' READ, ',I5,', IS NOT EQUAL TO NUMBER SPECIFIED IN',         F1030...
     2   ' INPUT, ',I5)                                               F1040...
      IF(ME) 3500,3500,4600                                            F1050...
 3500 IF(ISTOPU.EQ.1) WRITE(K3,4000) IU,NUBC                           F1060...
 4000 FORMAT(////11X,'ACTUAL NUMBER OF SPECIFIED CONCENTRATION NODES',  F1070...
     1   ' READ, ',I5,', IS NOT EQUAL TO NUMBER SPECIFIED IN',         F1080...
     2   ' INPUT, ',I5)                                               F1090...
      GOTO 4800                                                        F1100...
 4600 IF(ISTOPU.EQ.1) WRITE(K3,4700) IU,NUBC                           F1110...
 4700 FORMAT(////11X,'ACTUAL NUMBER OF SPECIFIED TEMPERATURE NODES',    F1120...
     1   ' READ, ',I5,', IS NOT EQUAL TO NUMBER SPECIFIED IN',         F1130...
     2   ' INPUT, ',I5)                                               F1140...
 4800 WRITE(K3,5000)                                                   F1150...
 5000 FORMAT(////11X,'PLEASE CORRECT DATA AND RERUN.'////////          F1160...
     1   22X,'S I M U L A T I O N   H A L T E D'/                      F1170...
     2   22X,'_____________________________________')                  F1180...
```

```
      ENDFILE(K3)                                                          F1190...
      STOP                                                                 F1200...
C                                                                          F1210...
 6000 IF(IPBCT.EQ.-1.OR.IUBCT.EQ.-1) WRITE(K3,7000)                        F1220...
 7000 FORMAT(////11X,'THE SPECIFIED TIME VARIATIONS ARE ',                 F1230...
     1   'USER-PROGRAMMED IN SUBROUTINE  B C T I M E .')                   F1240...
C                                                                          F1250...
C                                                                          F1260...
      RETURN                                                               F1270...
      END                                                                  F1280...
C     SUBROUTINE        O  B  S  E  R  V        SUTRA - VERSION 1284-2D  G10.....
C                                                                          G20.....
C *** PURPOSE :                                                            G30.....
C ***  (1) TO READ AND ORGANIZE OBSERVATION NODE DATA                      G40.....
C ***  (2) TO MAKE OBSERVATIONS ON PARTICULAR TIME STEPS                   G50.....
C ***  (3) TO OUTPUT OBSERVATIONS AFTER COMPLETION OF SIMULATION           G60.....
C                                                                          G70.....
      SUBROUTINE OBSERV(ICALL,IOBS,ITOBS,POBS,UOBS,OBSTIM,PVEC,UVEC,       G80.....
     1   ISTOP)                                                            G90.....
      IMPLICIT DOUBLE PRECISION (A-H,O-Z)                                  G100....
      CHARACTER*13 UNAME(2)                                                G110....
      CHARACTER*10 UNDERS                                                  G120....
      COMMON/FUNITS/ K00,K0,K1,K2,K3,K4,K5,K6                              MODIFIED
      COMMON/DIMS/ NN,NE,NIN,IS,JT,NBIP,NBIS,NPT(9),NPBC,NUBC,             G130NEW
     1   NSOP,NSOU,NBCN                                                    G140....
      COMMON/CNTRL1/ GNU,UP,DTMULT,DTMAX,ME,ISSFLO,ISSTRA,ITCYC,           G150NEW
     1   NPCYC,NUCYC,NPRINT,IREAD,ISTORE,NOUMAT,IUNSAT,ITIME               G160NEW
      COMMON/TIME/ DELT,TSEC,TMIN,THOUR,TDAY,TWEEK,TMONTH,TYEAR,           G170....
     1   TMAX,DELTP,DELTU,DLTPM1,DLTUM1,IT,ITMAX                           G180....
      COMMON/OBS/ NOBSN,NTOBSN,NOBCYC,ITCNT                                G190....
      DIMENSION INOB(66)                                                   G200....
      DIMENSION IOBS(NOBSN),POBS(NOBSN,NTOBSN),UOBS(NOBSN,NTOBSN),         G210....
     1   OBSTIM(NTOBSN),ITOBS(NTOBSN),PVEC(NN),UVEC(NN)                    G220....
      DATA UNAME(1)/'CONCENTRATION',UNAME(2)/'  TEMPERATURE',/,             G230....
     1   UNDERS/'__________'/,                                             G240....
     1   ITCNT/0000/                                                       G250....
C                                                                          G260....
C.....NOBS IS ACTUAL NUMBER OF OBSERVATION NODES                           G270....
C.....NTOBS IS MAXIMUM NUMBER OF TIME STEPS WITH OBSERVATIONS              G280....
      NOBS=NOBSN-1                                                         G290....
      NTOBS=NTOBSN-2                                                       G300....
      IOB=0                                                                G530NEW
      IF(ICALL-1) 50,500,5000                                              G310....
C                                                                          G320....
C.....INITIALIZATION CALL                                                  G330....
C.....INPUT DATASET 21                                                     G340....
   50 CONTINUE                                                             G350....
      JSTOP=0                                                              G360....
      WRITE(K3,60)                                                         G370....
   60 FORMAT(////11X,'O B S E R V A T I O N   N O D E S')                   G380....
      READ(K1,65) NOBCYC                                                   G390....
   65 FORMAT(I10)                                                          G400....
      WRITE(K3,70) NOBCYC                                                  G410....
   70 FORMAT(//11X,'**** NODES AT WHICH OBSERVATIONS WILL BE MADE',        G420....
     1   ' EVERY',I5,' TIME STEPS ****'//)                                 G430....
      NTOBSP=ITMAX/NOBCYC                                                  G440....
      IF(NTOBSP.GT.NTOBS) WRITE(K3,80) NTOBS,NTOBSP,ITMAX                  G450....
   80 FORMAT(//11X,'-  W  A  R  N  I  N  G  -'/11X,                        G460....
     1   'NUMBER OF OBSERVATION STEPS SPECIFIED ',I5,                      G470....
     2   ', IS LESS THAN THE NUMBER POSSIBLE ',I5,','/                     G480....
     3   11X,'WITHIN THE MAXIMUM NUMBER OF ALLOWED TIME STEPS, ',I5,'.'/G490....
```

```
     4   11X,'PLEASE RECONFIRM THAT OBSERVATION COUNTS ARE CORRECT.'//) G500....
  100 READ(K1,150) INOB                                                 G510....
  150 FORMAT(16I5)                                                      G520....
      DO 200 JJ=1,16                                                    G540....
      IF(INOB(JJ).EQ.0) GOTO 250                                        G550....
      IOB=IOB+1                                                         G560....
      IOBS(IOB)=INOB(JJ)                                                G570....
  200 CONTINUE                                                          G580....
      IF(IOB.LT.NOBS) GOTO 100                                          G590....
  250 IF(IOB.NE.NOBS) JSTOP=1                                           G600....
      WRITE(K3,300) (IOBS(JJ),JJ=1,NOBS)                                G610....
  300 FORMAT((11X,16(3X,I6)))                                           G620....
      IF(JSTOP.EQ.0) GOTO 400                                           G630....
C.....END SIMULATION IF CORRECTIONS ARE NECESSARY IN DATASET 21         G640....
      WRITE(K3,350) IOB,NOBS                                            G650....
  350 FORMAT(////11X,'ACTUAL NUMBER OF OBSERVATION NODES',              G660....
     1   ' READ, ',I5,', IS NOT EQUAL TO NUMBER SPECIFIED IN',          G670....
     2   ' INPUT, ',I5////11X,'PLEASE CORRECT DATA AND RERUN.',         G680....
     3   ////////22X,'S I M U L A T I O N   H A L T E D'/               G690....
     4   22X,        '_____________________________________')           G700....
      STOP                                                              G710....
  400 RETURN                                                            G720....
C                                                                       G730....
C.....MAKE OBSERVATIONS EACH NOBCYC TIME STEPS                          G740....
  500 CONTINUE                                                          G750....
      IF(MOD(IT,NOBCYC).NE.0.AND.IT.GT.1.AND.ISTOP.EQ.0) RETURN         G760....
      IF(IT.EQ.0) RETURN                                                G770....
      ITCNT=ITCNT+1                                                     G780....
      ITOBS(ITCNT)=IT                                                   G790....
      OBSTIM(ITCNT)=TSEC                                                G800....
      DO 1000 JJ=1,NOBS                                                 G810....
      I=IOBS(JJ)                                                        G820....
      POBS(JJ,ITCNT)=PVEC(I)                                            G830....
      UOBS(JJ,ITCNT)=UVEC(I)                                            G840....
 1000 CONTINUE                                                          G850....
      RETURN                                                            G860....
C                                                                       G870....
C.....OUTPUT OBSERVATIONS                                               G880....
 5000 CONTINUE                                                          G890....
      MN=2                                                              G900....
      IF(ME.EQ.-1) MN=1                                                 G910....
      JJ2=0                                                             G920....
      MLOOP=(NOBS+3)/4                                                  G930....
      DO 7000 LOOP=1,MLOOP                                              G940....
      JJ1=JJ2+1                                                         G950....
      JJ2=JJ2+4                                                         G960....
      IF(LOOP.EQ.MLOOP) JJ2=NOBS                                        G970....
      WRITE(K3,5999) (IOBS(JJ),JJ=JJ1,JJ2)                              G980....
 5999 FORMAT(1H1///5X,'O  B  S  E  R  V  A  T  I  O  N     ',           G990....
     1   'N  O  D  E     D  A  T  A'///23X,4(:8X,'NODE ',I5,8X))        G1000...
      WRITE(K3,6000) (UNDERS,JJ=JJ1,JJ2)                                G1010...
 6000 FORMAT(                        23X,4(:8X,  A10   ,  8X))         G1020...
      WRITE(K3,6001) (UNAME(MN),JJ=JJ1,JJ2)                             G1030...
 6001 FORMAT(/1X,'TIME STEP',4X,'TIME(SEC)',4(:2X,'PRESSURE',3X,A13))   G1040...
      DO 6500 ITT=1,ITCNT                                               G1050...
      WRITE(K3,6100) ITOBS(ITT),OBSTIM(ITT),                            G1060...
     1   (POBS(JJ,ITT),UOBS(JJ,ITT),JJ=JJ1,JJ2)                         G1070...
 6100 FORMAT(5X,I5,1X,1PD12.5,8(1X,1PD12.5))                            G1080...
 6500 CONTINUE                                                          G1090...
 7000 CONTINUE                                                          G1100...
      RETURN                                                            G1110...
```

```
C                                                                       G1120...
C                                                                       G1130...
      END                                                               G1140...
C     SUBROUTINE        I  N  D  A  T  2        SUTRA - VERSION 1284-2D K10.....
C                                                                       K20.....
C *** PURPOSE :                                                         K30.....
C ***  TO READ INITIAL CONDITIONS FROM UNIT-55, AND TO                  K40.....
C ***  INITIALIZE DATA FOR EITHER WARM OR COLD START OF                 K50.....
C ***  THE SIMULATION.                                                  K60.....
C                                                                       K70.....
      SUBROUTINE INDAT2(PVEC,UVEC,PM1,UM1,UM2,CS1,CS2,CS3,SL,SR,RCIT,   K80.....
     1   SW,DSWDP,PBC,IPBC,IPBCT)                                       K90.....
      IMPLICIT DOUBLE PRECISION (A-H,O-Z)                               K100....
      COMMON/FUNITS/ K00,K0,K1,K2,K3,K4,K5,K6                           MODIFIED
      COMMON/DIMS/ NN,NE,NIN,IS,JT,NBIP,NBIS,NPT(9),NPBC,NUBC,          K110NEW
     1   NSOP,NSOU,NBCN                                                 K120....
      COMMON/CNTRL1/ GNU,UP,DTMULT,DTMAX,ME,ISSFLO,ISSTRA,ITCYC,        K130NEW
     1   NPCYC,NUCYC,NPRINT,IREAD,ISTORE,NOUMAT,IUNSAT,ITIME            K140NEW
      COMMON/TIME/ DELT,TSEC,TMIN,THOUR,TDAY,TWEEK,TMONTH,TYEAR,        K150....
     1   TMAX,DELTP,DELTU,DLTPM1,DLTUM1,IT,ITMAX                        K160....
      COMMON/PARAMS/ COMPFL,COMPMA,DRWDU,CW,CS,RHOS,DECAY,SIGMAW,SIGMAS,K170....
     1   RHOW0,URHOW0,VISC0,PRODF1,PRODS1,PRODF0,PRODS0,CHI1,CHI2       K180....
      DIMENSION PVEC(NN),UVEC(NN),PM1(NN),UM1(NN),UM2(NN),SL(NN),SR(NN),K190....
     1   CS1(NN),CS2(NN),CS3(NN),RCIT(NN),SW(NN),DSWDP(NN),             K200....
     2   PBC(NBCN),IPBC(NBCN)                                           K210....
C                                                                       K220....
C                                                                       K230....
      IF(IREAD) 500,500,620                                             K240....
C.....INPUT INITIAL CONDITIONS FOR WARM START (UNIT-55 DATA)            K250....
  500 READ(K2,510) TSTART,DELTP,DELTU                                   K260....
  510 FORMAT(4G20.10)                                                   K270....
      READ(K2,510) (PVEC(I),I=1,NN)                                     K280....
      READ(K2,510) (UVEC(I),I=1,NN)                                     K290....
      READ(K2,510) (PM1(I),I=1,NN)                                      K300....
      READ(K2,510) (UM1(I),I=1,NN)                                      K310....
      READ(K2,510) (CS1(I),I=1,NN)                                      K320....
      READ(K2,510) (RCIT(I),I=1,NN)                                     K330....
      READ(K2,510) (SW(I),I=1,NN)                                       K340....
      READ(K2,510) (PBC(IPU),IPU=1,NBCN)                                K350....
C     CALL ZERO(CS2,NN,0.0D0)                                           K360....
C     CALL ZERO(CS3,NN,0.0D0)                                           K370....
      CALL ZERO(SL,NN,0.0D0)                                            K380....
      CALL ZERO(SR,NN,0.0D0)                                            K390....
      CALL ZERO(DSWDP,NN,0.0D0)                                         K400....
      DO 550 I=1,NN                                                     K410....
  550 UM2(I)=UM1(I)                                                     K420....
      GOTO 1000                                                         K430....
C                                                                       K440....
C.....INPUT INITIAL CONDITIONS FOR COLD START (UNIT-55 DATA)            K450....
  620 READ(K2,510) TSTART                                               K460....
      READ(K2,510) (PVEC(I),I=1,NN)                                     K470....
      READ(K2,510) (UVEC(I),I=1,NN)                                     K480....
C.....START-UP WITH NO PROJECTIONS BY SETTING BDELP=BDELU=1.D-16        K490....
C     IN PROJECTION FORMULAE FOUND IN SUBROUTINE SUTRA.                 K500....
      DELTP=DELT*1.D-16                                                 K510....
      DELTU=DELT*1.D-16                                                 K520....
C.....INITIALIZE SPECIFIED TIME-VARYING PRESSURES TO INITIAL PRESSURE   K530....
C     VALUES FOR START-UP CALCULATION OF INFLOWS OR OUTFLOWS            K540....
C     (SET QPLITR=0)                                                   K550....
      IF(IPBCT) 680,740,740                                             K560....
  680 DO 730 IP=1,NPBC                                                  K570....
```

```
      I=IPBC(IP)                                                        K580....
      IF(I) 700,700,730                                                 K590....
  700 PBC(IP)=PVEC(-I)                                                  K600....
  730 CONTINUE                                                          K610....
C.....INITIALIZE P, U, AND CONSISTENT DENSITY                           K620....
  740 DO 800 I=1,NN                                                     K630....
      PM1(I)=PVEC(I)                                                    K640....
      UM1(I)=UVEC(I)                                                    K650....
      UM2(I)=UVEC(I)                                                    K660....
      RCIT(I)=RHOW0+DRWDU*(UVEC(I)-URHOW0)                              K670....
  800 CONTINUE                                                          K680....
C.....INITIALIZE SATURATION, SW(I)                                      K690....
      CALL ZERO(SW,NN,1.0D0)                                            K700....
      CALL ZERO(DSWDP,NN,0.0D0)                                         K710....
      IF(IUNSAT.NE.1) GOTO 990                                          K720....
      IUNSAT=3                                                          K730....
      DO 900 I=1,NN                                                     K740....
  900 IF(PVEC(I).LT.0) CALL UNSAT(SW(I),DSWDP(I),RELK,PVEC(I))          K750....
  990 CONTINUE                                                          K760....
      CALL ZERO(CS1,NN,CS)                                              K770....
C     CALL ZERO(CS2,NN,0.0D0)                                           K780....
C     CALL ZERO(CS3,NN,0.0D0)                                           K790....
      CALL ZERO(SL,NN,0.0D0)                                            K800....
      CALL ZERO(SR,NN,0.0D0)                                            K810....
 1000 CONTINUE                                                          K820....
C                                                                       K830....
C.....SET STARTING TIME OF SIMULATION CLOCK, TSEC                       K840....
      TSEC=TSTART                                                       K850....
C                                                                       K860....
C                                                                       K870....
      RETURN                                                            K880....
      END                                                               K890....
C     SUBROUTINE        P  R  I  S  O  L        SUTRA - VERSION 1284-2D L10.....
C                                                                       L20.....
C *** PURPOSE :                                                         L30.....
C ***  TO PRINT PRESSURE AND TEMPERATURE OR CONCENTRATION               L40.....
C ***  SOLUTIONS AND TO OUTPUT INFORMATION ON TIME STEP, ITERATIONS,    L50.....
C ***  SATURATIONS, AND FLUID VELOCITIES.                               L60.....
C                                                                       L70.....
      SUBROUTINE PRISOL(ML,ISTOP,IGOI,PVEC,UVEC,VMAG,VANG,SW)           L80.....
      IMPLICIT DOUBLE PRECISION (A-H,O-Z)                               L90.....
      COMMON/FUNITS/ K00,K0,K1,K2,K3,K4,K5,K6,K7,K8                     MODIFIED
      COMMON/DIMS/ NN,NE,NIN,IS,JT,NBIP,NBIS,NPT(9),NPBC,NUBC,          L100NEW
     1   NSOP,NSOU,NBCN                                                 L110....
      COMMON/CNTRL1/ GNU,UP,DTMULT,DTMAX,ME,ISSFLO,ISSTRA,ITCYC,        L120NEW
     1   NPCYC,NUCYC,NPRINT,IREAD,ISTORE,NOUMAT,IUNSAT,ITIME            L130NEW
      COMMON/TIME/ DELT,TSEC,TMIN,THOUR,TDAY,TWEEK,TMONTH,TYEAR,        L140....
     1   TMAX,DELTP,DELTU,DLTPM1,DLTUM1,IT,ITMAX                        L150....
      COMMON/ITERAT/ RPM,RPMAX,RUM,RUMAX,ITER,ITRMAX,IPWORS,IUWORS,     L160....
     1              ICON,ITRMX2,OMEGA,RPMX2,RUMX2                       NEW
      COMMON/KPRINT/ KCOORD,KELINF,KINCID,KPLOTP,KPLOTU,KVEL,KBUDG      L170....
      DIMENSION PVEC(NN),UVEC(NN),VMAG(NE),VANG(NE),SW(NN)              L180....
C                                                                       L190....
C.....OUTPUT MAJOR HEADINGS FOR CURRENT TIME STEP                       L200....
      IF(IT.GT.0.OR.ISSFLO.EQ.2.OR.ISSTRA.EQ.1) GOTO 100                L210....
      WRITE(K3,60)                                                      L220....
   60 FORMAT(1H1///11X,'I N I T I A L   C O N D I T I O N S',           L230....
     1            /11X,'_____________________________________')         L240....
      IF(IREAD.EQ.-1) WRITE(K3,65)                                      L250....
   65 FORMAT(//11X,'INITIAL CONDITIONS RETRIEVED FROM STORAGE ',        L260....
     1   'ON UNIT 55.')                                                 L270....
```

```
      GOTO 500                                                          L280....
C                                                                       L290....
  100 IF(IGOI.NE.0.AND.ISTOP.EQ.0) WRITE(K3,150) ITER,IT                L300....
  150 FORMAT(////////11X,'ITERATION ',I3,' SOLUTION FOR TIME STEP ',I4) L310....
C                                                                       L320....
      IF(ISTOP.EQ.-1) WRITE(K3,250) IT,ITER                             L330....
  250 FORMAT(1H1//11X,'SOLUTION FOR TIME STEP ',I4,                     L340....
     1   ' NOT CONVERGED AFTER ',I3,' ITERATIONS.')                     L350....
C                                                                       L360....
      IF(ISTOP.GE.0) WRITE(K3,350) IT                                   L370....
  350 FORMAT(1H1//11X,'RESULTS FOR TIME STEP ',I4/                      L380....
     1   11X,'_______ ___ ____ ____ ____')                              L390....
      IF(ITRMAX.EQ.1) GOTO 500                                          L400....
      IF(ISTOP.GE.0.AND.IT.GT.0) WRITE(K3,355) ITER                     L410....
      IF(IT.EQ.0.AND.ISTOP.GE.0.AND.ISSFLO.EQ.2) WRITE(K3,355) ITER     L420....
  355 FORMAT(11X,'(AFTER ',I3,' ITERATIONS) :')                         L430....
      WRITE(K3,450) RPM,IPWORS,RUM,IUWORS                               L440....
  450 FORMAT(//11X,'MAXIMUM P CHANGE FROM PREVIOUS ITERATION ',         L450....
     1   1PD14.5,' AT NODE ',I5/11X,'MAXIMUM U CHANGE FROM PREVIOUS ',  L460....
     2   'ITERATION ',1PD14.5,' AT NODE ',I5)                           L470....
C                                                                       L480....
  500 IF(IT.EQ.0.AND.ISSFLO.EQ.2) GOTO 680                              L490....
      IF(ISSTRA.EQ.1) GOTO 800                                          L500....
      WRITE(K3,550) DELT,TSEC,TMIN,THOUR,TDAY,TWEEK,                    L510....
     1   TMONTH,TYEAR                                                   L520....
  550 FORMAT(///11X,'TIME INCREMENT :',T27,1PD15.4,' SECONDS'//11X,     L530....
     1   'ELAPSED TIME :',T27,1PD15.4,' SECONDS',/T27,1PD15.4,' MINUTES'L540....
     2   /T27,1PD15.4,' HOURS'/T27,1PD15.4,' DAYS'/T27,1PD15.4,' WEEKS'/L550....
     3   T27,1PD15.4,' MONTHS'/T27,1PD15.4,' YEARS')                    L560....
C                                                                       L570....
C.....OUTPUT PRESSURES FOR TRANSIENT FLOW SOLUTION (AND POSSIBLY,       L580....
C        SATURATION AND VELOCITY)                                       L590....
      IF(ML.EQ.2.AND.ISTOP.GE.0) GOTO 700                               L600....
      IF(ISSFLO.GT.0) GOTO 700                                          L610....
      WRITE(K3,650) (I,PVEC(I),I=1,NN)                                  L620....
  650 FORMAT(///11X,'P  R  E  S  S  U  R  E'//8X,6('NODE',17X)/         L630....
     1   (7X,6(1X,I4,1X,1PD15.8)))                                      L640....
      IF(IUNSAT.NE.0) WRITE(K3,651) (I,SW(I),I=1,NN)                    L650....
  651 FORMAT(///11X,'S  A  T  U  R  A  T  I  O  N'//8X,6('NODE',17X)/   L660....
     1   (7X,6(1X,I4,1X,1PD15.8)))                                      L670....
      IF(KVEL.EQ.1.AND.IT.GT.0) WRITE(K3,655) (L,VMAG(L),L=1,NE)        L680....
      IF(KVEL.EQ.1.AND.IT.GT.0) WRITE(K3,656) (L,VANG(L),L=1,NE)        L690....
  655 FORMAT(///11X,'F  L  U  I  D     V  E  L  O  C  I  T  Y'//        L700....
     1   11X,'M A G N I T U D E   AT CENTROID OF ELEMENT'//             L710....
     2   5X,6('ELEMENT',14X)/(7X,6(1X,I4,1X,1PD15.8)))                  L720....
  656 FORMAT(///11X,'F  L  U  I  D     V  E  L  O  C  I  T  Y'//        L730....
     1   11X,'A N G L E   IN DEGREES FROM +X-AXIS TO FLOW DIRECTION ',  L740....
     2   'AT CENTROID OF ELEMENT'//                                     L750....
     3   5X,6('ELEMENT',14X)/(7X,6(1X,I4,1X,1PD15.8)))                  L760....
      GOTO 700                                                          L770....
C                                                                       L780....
C.....OUTPUT PRESSURES FOR STEADY-STATE FLOW SOLUTION                   L790....
  680 WRITE(K3,690) (I,PVEC(I),I=1,NN)                                  L800....
  690 FORMAT(///11X,'S  T  E  A  D  Y  -  S  T  A  T  E     P  R  E  S',L810....
     1   '  S  U  R  E'//8X,6('NODE',17X)/(7X,6(1X,I4,1X,1PD15.8)))     L820....
      IF(IUNSAT.NE.0) WRITE(K3,651) (I,SW(I),I=1,NN)                    L830....
      GOTO 1000                                                         L840....
C                                                                       L850....
C.....OUTPUT CONCENTRATIONS OR TEMPERATURES FOR                         L860....
C        TRANSIENT TRANSPORT SOLUTION                                   L870....
  700 IF(ML.EQ.1.AND.ISTOP.GE.0) GOTO 1000                              L880....
```

```
      IF(ME) 720,720,730                                                L890....
  720 WRITE(K3,725) (I,UVEC(I),I=1,NN)                                  L900....
  725 FORMAT(///11X,'C  O  N  C  E  N  T  R  A  T  I  O  N'//8X,        L910....
     1   6('NODE',17X)/(7X,6(1X,I4,1X,1PD15.8)))                       L920....
      GOTO 900                                                          L930....
  730 WRITE(K3,735) (I,UVEC(I),I=1,NN)                                  L940....
  735 FORMAT(///11X,'T  E  M  P  E  R  A  T  U  R  E'//8X,6('NODE',17X)/L950....
     1   (7X,6(1X,I4,1X,F15.9)))                                        L960....
      GOTO 900                                                          L970....
C                                                                       L980....
C.....OUTPUT CONCENTRATIONS OR TEMPERATURES FOR                         L990....
C        STEADY-STATE TRANSPORT SOLUTION                                L1000...
  800 IF(ME) 820,820,830                                                L1010...
  820 WRITE(K3,825) (I,UVEC(I),I=1,NN)                                  L1020...
  825 FORMAT(///11X,'S  T  E  A  D  Y  -  S  T  A  T  E    C  O  N  C', L1030...
     1   '  E  N  T  R  A  T  I  O  N'//8X,6('NODE',17X)/               L1040...
     2   (7X,6(1X,I4,1X,1PD15.8)))                                      L1050...
      GOTO 900                                                          L1060...
  830 WRITE(K3,835) (I,UVEC(I),I=1,NN)                                  L1070...
  835 FORMAT(///11X,'S  T  E  A  D  Y  -  S  T  A  T  E    T  E  M  P', L1080...
     1   '  E  R  A  T  U  R  E'//8X,6('NODE',17X)/                     L1090...
     2   (7X,6(1X,I4,1X,F15.9)))                                        L1100...
C                                                                       L1110...
C.....OUTPUT VELOCITIES FOR STEADY-STATE FLOW SOLUTION                  L1120...
  900 IF(ISSFLO.NE.2.OR.IT.NE.1.OR.KVEL.NE.1) GOTO 1000                 L1130...
      WRITE(K3,925) (L,VMAG(L),L=1,NE)                                  L1140...
      WRITE(K3,950) (L,VANG(L),L=1,NE)                                  L1150...
  925 FORMAT(///11X,'S  T  E  A  D  Y  -  S  T  A  T  E     ',         L1160...
     1   'F  L  U  I  D     V  E  L  O  C  I  T  Y'//                   L1170...
     2   11X,'M A G N I T U D E   AT CENTROID OF ELEMENT'//             L1180...
     3   5X,6('ELEMENT',14X)/(7X,6(1X,I4,1X,1PD15.8)))                  L1190...
  950 FORMAT(///11X,'S  T  E  A  D  Y  -  S  T  A  T  E     ',         L1200...
     1   'F  L  U  I  D     V  E  L  O  C  I  T  Y'//                   L1210...
     2   11X,'A N G L E   IN DEGREES FROM +X-AXIS TO FLOW DIRECTION ',  L1220...
     3   'AT CENTROID OF ELEMENT'//                                     L1230...
     4   5X,6('ELEMENT',14X)/(7X,6(1X,I4,1X,1PD15.8)))                  L1240...
C                                                                       L1250...
 1000 RETURN                                                            L1260...
C                                                                       L1270...
      END                                                               L1280...
C     SUBROUTINE        Z  E  R  O             SUTRA - VERSION 1284-2D M10.....
C                                                                       M20.....
C *** PURPOSE :                                                         M30.....
C ***  TO FILL AN ARRAY WITH A CONSTANT VALUE.                          M40.....
C                                                                       M50.....
      SUBROUTINE ZERO(A,IADIM,FILL)                                     M60.....
      IMPLICIT DOUBLE PRECISION (A-H,O-Z)                               M70.....
      DIMENSION A(IADIM)                                                M80.....
C                                                                       M90.....
C.....FILL ARRAY A WITH VALUE IN VARIABLE 'FILL'                        M100....
      DO 10 I=1,IADIM                                                   M110....
   10 A(I)=FILL                                                         M120....
C                                                                       M130....
C                                                                       M140....
      RETURN                                                            M150....
      END                                                               M160....
C     SUBROUTINE        B  C  T  I  M  E       SUTRA - VERSION 1284-2D N10.....
C                                                                       N20.....
C *** PURPOSE :                                                         N30.....
C ***  USER-PROGRAMMED SUBROUTINE WHICH ALLOWS THE USER TO SPECIFY:     N40.....
C ***   (1) TIME-DEPENDENT SPECIFIED PRESSURES AND TIME-DEPENDENT       N50.....
```

```
C ***       CONCENTRATIONS OR TEMPERATURES OF INFLOWS AT THESE POINTS   N60.....
C ***   (2) TIME-DEPENDENT SPECIFIED CONCENTRATIONS OR TEMPERATURES     N70.....
C ***   (3) TIME-DEPENDENT FLUID SOURCES AND CONCENTRATIONS             N80.....
C ***       OR TEMPERATURES OF INFLOWS AT THESE POINTS                  N90.....
C ***   (4) TIME-DEPENDENT ENERGY OR SOLUTE MASS SOURCES                N100....
C                                                                       N110....
      SUBROUTINE BCTIME(IPBC,PBC,IUBC,UBC,QIN,UIN,QUIN,IQSOP,IQSOU,     N120....
     1   IPBCT,IUBCT,IQSOPT,IQSOUT,UVEC)                                N130NEW
      IMPLICIT DOUBLE PRECISION (A-H,O-Z)                               N140....
      COMMON/FUNITS/ K00,K0,K1,K2,K3,K4,K5,K6,K7,K8                     MODIFIED
      COMMON/CNTRL1/ GNU,UP,DTMULT,DTMAX,ME,ISSFLO,ISSTRA,ITCYC,        NEW
     1   NPCYC,NUCYC,NPRINT,IREAD,ISTORE,NOUMAT,IUNSAT,ITIME            NEW
      COMMON/DIMS/ NN,NE,NIN,IS,JT,NBIP,NBIS,NPT(9),NPBC,NUBC,          N150NEW
     1   NSOP,NSOU,NBCN                                                 N160....
      COMMON/TIME/ DELT,TSEC,TMIN,THOUR,TDAY,TWEEK,TMONTH,TYEAR,        N170....
     1   TMAX,DELTP,DELTU,DLTPM1,DLTUM1,IT,ITMAX                        N180....
      DIMENSION IPBC(NBCN),PBC(NBCN),IUBC(NBCN),UBC(NBCN),              N190....
     1   QIN(NN),UIN(NN),QUIN(NN),IQSOP(NSOP),IQSOU(NSOU)               N200....
       DIMENSION UVEC(NN)                                               NEW
C                                                                       N210....
C.....DEFINITION OF REQUIRED VARIABLES                                  N220....
C . . . . . . . . . . . . . . . . . . . . . . . . . . . . . . . . . . . N230....
C     NN = EXACT NUMBER OF NODES IN MESH                                N240....
C     NPBC = EXACT NUMBER OF SPECIFIED PRESSURE NODES                   N250....
C     NUBC = EXACT NUMBER OF SPECIFIED CONCENTRATION                    N260....
C            OR TEMPERATURE NODES                                       N270....
C . . . . . . . . . . . . . . . . . . . . . . . . . . . . . . . . . . . N280....
C     IT = NUMBER OF CURRENT TIME STEP                                  N290....
C . . . . . . . . . . . . . . . . . . . . . . . . . . . . . . . . . . . N300....
C     TSEC = TIME AT END OF CURRENT TIME STEP IN SECONDS                N310....
C     TMIN = TIME AT END OF CURRENT TIME STEP IN MINUTES                N320....
C     THOUR = TIME AT END OF CURRENT TIME STEP IN HOURS                 N330....
C     TDAY = TIME AT END OF CURRENT TIME STEP IN DAYS                   N340....
C     TWEEK = TIME AT END OF CURRENT TIME STEP IN WEEKS                 N350....
C     TMONTH = TIME AT END OF CURRENT TIME STEP IN MONTHS               N360....
C     TYEAR = TIME AT END OF CURRENT TIME STEP IN YEARS                 N370....
C . . . . . . . . . . . . . . . . . . . . . . . . . . . . . . . . . . . N380....
C     PBC(IP) = SPECIFIED PRESSURE VALUE AT IP(TH) SPECIFIED            N390....
C               PRESSURE NODE                                           N400....
C     UBC(IP) = SPECIFIED CONCENTRATION OR TEMPERATURE VALUE OF ANY     N410....
C               INFLOW OCCURRING AT IP(TH) SPECIFIED PRESSURE NODE      N420....
C     IPBC(IP) = ACTUAL NODE NUMBER OF IP(TH) SPECIFIED PRESSURE NODE   N430....
C                [WHEN NODE NUMBER I=IPBC(IP) IS NEGATIVE (I<0),        N440....
C                VALUES MUST BE SPECIFIED FOR PBC AND UBC.]             N450....
C . . . . . . . . . . . . . . . . . . . . . . . . . . . . . . . . . . . N460....
C     UBC(IUP) = SPECIFIED CONCENTRATION OR TEMPERATURE VALUE AT        N470....
C                IU(TH) SPECIFIED CONCENTRATION OR TEMPERATURE NODE     N480....
C                (WHERE IUP=IU+NPBC)                                    N490....
C     IUBC(IUP) = ACTUAL NODE NUMBER OF IU(TH) SPECIFIED CONCENTRATION  N500....
C                 OR TEMPERATURE NODE (WHERE IUP=IU+NPBC)               N510....
C                 [WHEN NODE NUMBER I=IUBC(IU) IS NEGATIVE (I<0),       N520....
C                 A VALUE MUST BE SPECIFIED FOR UBC.]                   N530....
C . . . . . . . . . . . . . . . . . . . . . . . . . . . . . . . . . . . N540....
C     IQSOP(IQP) = NODE NUMBER OF IQP(TH) FLUID SOURCE NODE.            N550....
C                  [WHEN NODE NUMBER I=IQSOP(IQP) IS NEGATIVE (I<0),    N560....
C                  VALUES MUST BE SPECIFIED FOR QIN AND UIN.]           N570....
C     QIN(-I) = SPECIFIED FLUID SOURCE VALUE AT NODE (-I)               N580....
C     UIN(-I) = SPECIFIED CONCENTRATION OR TEMPERATURE VALUE OF ANY     N590....
C               INFLOW OCCURRING AT FLUID SOURCE NODE (-I)              N600....
C . . . . . . . . . . . . . . . . . . . . . . . . . . . . . . . . . . . N610....
C     IQSOU(IQU) = NODE NUMBER OF IQU(TH) ENERGY OR                     N620....
```

```
C                  SOLUTE MASS SOURCE NODE                                N630....
C                  [WHEN NODE NUMBER I=IQSOU(IQU) IS NEGATIVE (I<0),      N640....
C                  A VALUE MUST BE SPECIFIED FOR QUIN.]                   N650....
C     QUIN(-I) = SPECIFIED ENERGY OR SOLUTE MASS SOURCE VALUE             N660....
C                AT NODE (-I)                                             N670....
C . . . . . . . . . . . . . . . . . . . . . . . . . . . . . . . . . . . . N680....
C                                                                        N690....
C                                                                        N700....
C.....NSOPI IS ACTUAL NUMBER OF FLUID SOURCE NODES                       N710....
      NSOPI=NSOP-1                                                       N720....
C.....NSOUI IS ACTUAL NUMBER OF ENERGY OR SOLUTE MASS SOURCE NODES       N730....
      NSOUI=NSOU-1                                                       N740....
C                                                                        N750....
C                                                                        N760....
C                                                                        N770....
C                                                                        N780....
C                                                                        N790....
C                                                                        N800....
      IF(IPBCT) 50,240,240                                               N810....
C - - - - - - - - - - - - - - - - - - - - - - - - - - - - - - - - - - - - N820....
C - - - - - - - - - - - - - - - - - - - - - - - - - - - - - - - - - - - - N830....
C.....SECTION (1):  SET TIME-DEPENDENT SPECIFIED PRESSURES OR             N840....
C     CONCENTRATIONS (TEMPERATURES) OF INFLOWS AT SPECIFIED              N850....
C     PRESSURE NODES                                                     N860....
C                                                                        N870....
   50 CONTINUE                                                           N880....
      DO 200 IP=1,NPBC                                                   N890....
      I=IPBC(IP)                                                         N900....
      IF(I) 100,200,200                                                  N910....
  100 CONTINUE                                                           N920....
C     NOTE : A FLOW AND TRANSPORT SOLUTION MUST OCCUR FOR ANY            N930....
C            TIME STEP IN WHICH PBC( ) CHANGES.                          N940....
C     PBC(IP) =  ((          ))                                          N950....
C     UBC(IP) =  ((          ))                                          N960....
  200 CONTINUE                                                           N970....
C - - - - - - - - - - - - - - - - - - - - - - - - - - - - - - - - - - - - N980....
C - - - - - - - - - - - - - - - - - - - - - - - - - - - - - - - - - - - - N990....
C                                                                        N1000...
C                                                                        N1010...
C                                                                        N1020...
C                                                                        N1030...
C                                                                        N1040...
C                                                                        N1050...
  240 IF(IUBCT) 250,440,440                                              N1060...
C - - - - - - - - - - - - - - - - - - - - - - - - - - - - - - - - - - - - N1070...
C - - - - - - - - - - - - - - - - - - - - - - - - - - - - - - - - - - - - N1080...
C.....SECTION (2):  SET TIME-DEPENDENT SPECIFIED                         N1090...
C     CONCENTRATIONS (TEMPERATURES)                                      N1100...
C                                                                        N1110...
  250 CONTINUE                                                           N1120...
      DO 400 IU=1,NUBC                                                   N1130...
      IUP=IU+NPBC                                                        N1140...
      I=IUBC(IUP)                                                        N1150...
      IF(I) 300,400,400                                                  N1160...
  300 CONTINUE                                                           N1170...
C     NOTE : A TRANSPORT SOLUTION MUST OCCUR FOR ANY TIME STEP           N1180...
C            IN WHICH UBC( ) CHANGES.  IN ADDITION, IF FLUID PROPERTIES N1190...
C            ARE SENSITIVE TO 'U' THEN A FLOW SOLUTION MUST OCCUR AS WELN1200...
C     UBC(IUP) =   ((          ))                                        N1210...
  400 CONTINUE                                                           N1220...
C - - - - - - - - - - - - - - - - - - - - - - - - - - - - - - - - - - - - N1230...
```

```
C - - - - - - - - - - - - - - - - - - - - - - - - - - - - - - - - - - - - - - - N1240...
C                                                                             N1250...
C                                                                             N1260...
C                                                                             N1270...
C                                                                             N1280...
C                                                                             N1290...
C                                                                             N1300...
  440 IF(IQSOPT) 450,640,640                                                  N1310...
C - - - - - - - - - - - - - - - - - - - - - - - - - - - - - - - - - - - - - - - N1320...
C - - - - - - - - - - - - - - - - - - - - - - - - - - - - - - - - - - - - - - - N1330...
C.....SECTION (3):  SET TIME-DEPENDENT FLUID SOURCES/SINKS,                   N1340...
C      OR CONCENTRATIONS (TEMPERATURES) OF SOURCE FLUID                       N1350...
C                                                                             N1360...
  450 CONTINUE                                                                N1370...
C                                                                             NEW
C                *** THE FOLLOWING MODIFICATION IS MADE TO                    NEW
C                    TURN OF WITHDRAWL WELLS WHEN AVERAGE                     NEW
C                    FLUID CONCENTRATION IS GREATER THAN CMAX                 NEW
C                                                                             NEW
C                                                                             NEW
C                   FIRST CALCULATE VOLUME AVERAGED CONCENTRATION             NEW
      CMAX=0.9980                                                             NEW
      CBAR=0.0D0                                                              NEW
      QTOT=0.0D0                                                              NEW
      DO 605 IQP=1,NSOPI                                                      NEW
      I=IQSOP(IQP)                                                            NEW
      I=IABS(I)                                                               NEW
      CBAR=CBAR+UVEC(I)*QIN(I)                                                NEW
      QTOT=QTOT+QIN(I)                                                        NEW
  605 CONTINUE                                                                NEW
      CBAR=CBAR/QTOT                                                          NEW
      WRITE (K6,606) TDAY,CBAR                                                NEW
  606 FORMAT(1H0,10X,'VOLUME AVERAGED SOLUTE CONCENTRATION',                  NEW
     +' AT TIME STEP ',F10.2,' =',F10.4)                                      NEW
      IF (CBAR.LE.CMAX) GO TO 610                                             NEW
C                                                                             NEW
C               CBAR EXCEEDS CMAX, TURN OFF THE WELLS AND                     NEW
C               RESET IQSOPT SO PROGRAM DOES NOT RETURN HERE                  NEW
      IQSOPT=+1                                                               NEW
      WRITE(K3,608) DELT,TSEC,TMIN,THOUR,TDAY,TWEEK,TMONTH,TYEAR              NEW
  608 FORMAT(///11X,'TIME INCREMENT :',T27,1PD15.4,' SECONDS'//11X,           NEW
     1   'ELAPSED TIME :',T27,1PD15.4,' SECONDS',/T27,1PD15.4,' MINUTES'NEW
     2   /T27,1PD15.4,' HOURS'/T27,1PD15.4,' DAYS'/T27,1PD15.4,' WEEKS'/NEW
     3   T27,1PD15.4,' MONTHS'/T27,1PD15.4,' YEARS')                          NEW
      CALL RUNDAT(TDAY)                                                       NEW
  607 FORMAT(1H0,10X,'CONCENTRATION EXCEEDS MAXIMUM VALUE (',F10.4,           NEW
     1 ')'/1H ,10X,'WELLS AT R=0 ARE TURNED OFF '/)                           NEW
      DO 600 IQP=1,NSOPI                                                      N1380...
      I=IQSOP(IQP)                                                            N1390...
      I=IABS(I)                                                               NEW
      QIN(I) =   0.0D0                                                        N1440...
      UIN(I) =   0.0D0                                                        N1470...
  600 CONTINUE                                                                N1480...
C                                                                             NEW
C              RESET FLAG TO KEEP TIME STEP SIZE CONSTANT (MODIFIED           NEW
C              VERSION ONLY)                                                  NEW
      ITCYC=0                                                                 NEW
C                                                                             NEW
  610 CONTINUE                                                                NEW
C - - - - - - - - - - - - - - - - - - - - - - - - - - - - - - - - - - - - - - - N1490...
C - - - - - - - - - - - - - - - - - - - - - - - - - - - - - - - - - - - - - - - N1500...
```

```
C                                                                       N1510...
C                                                                       N1520...
C                                                                       N1530...
C                                                                       N1540...
C                                                                       N1550...
C                                                                       N1560...
  640 IF(IQSOUT) 650,840,840                                            N1570...
C - - - - - - - - - - - - - - - - - - - - - - - - - - - - - - - - - - - - N1580...
C - - - - - - - - - - - - - - - - - - - - - - - - - - - - - - - - - - - - N1590...
C.....SECTION (4):  SET TIME-DEPENDENT SOURCES/SINKS                    N1600...
C     OF SOLUTE MASS OR ENERGY                                          N1610...
C                                                                       N1620...
  650 CONTINUE                                                          N1630...
      DO 800 IQU=1,NSOUI                                                N1640...
      I=IQSOU(IQU)                                                      N1650...
      IF(I) 700,800,800                                                 N1660...
  700 CONTINUE                                                          N1670...
C     NOTE : A TRANSPORT SOLUTION MUST OCCUR FOR ANY                    N1680...
C            TIME STEP IN WHICH QUIN( ) CHANGES.                        N1690...
C     QUIN(-I) =   ((           ))                                      N1700...
  800 CONTINUE                                                          N1710...
C - - - - - - - - - - - - - - - - - - - - - - - - - - - - - - - - - - - - N1720...
C - - - - - - - - - - - - - - - - - - - - - - - - - - - - - - - - - - - - N1730...
C                                                                       N1740...
C                                                                       N1750...
C                                                                       N1760...
C                                                                       N1770...
C                                                                       N1780...
C                                                                       N1790...
  840 CONTINUE                                                          N1800...
C                                                                       N1810...
      RETURN                                                            N1820...
      END                                                               N1830...
C     SUBROUTINE        A  D  S  O  R  B        SUTRA - VERSION 1284-2D O10.....
C                                                                       O20.....
C *** PURPOSE :                                                         O30.....
C ***  TO CALCULATE VALUES OF EQUILIBRIUM SORPTION PARAMETERS FOR       O40.....
C ***  LINEAR, FREUNDLICH, AND LANGMUIR MODELS.                         O50.....
C                                                                       O60.....
      SUBROUTINE ADSORB(CS1,CS2,CS3,SL,SR,U)                            O70.....
      IMPLICIT DOUBLE PRECISION (A-H,O-Z)                               O80.....
      CHARACTER*10 ADSMOD                                               O90.....
      COMMON/MODSOR/ ADSMOD                                             O100....
      COMMON/DIMS/ NN,NE,NIN,IS,JT,NBIP,NBIS,NPT(9),NPBC,NUBC,          0110NEW
     1   NSOP,NSOU,NBCN                                                 0120....
      COMMON/PARAMS/ COMPFL,COMPMA,DRWDU,CW,CS,RHOS,DECAY,SIGMAW,SIGMAS,O130....
     1   RHOW0,URHOW0,VISC0,PRODF1,PRODS1,PRODF0,PRODS0,CHI1,CHI2       O140....
      DIMENSION CS1(NN),CS2(NN),CS3(NN),SL(NN),SR(NN),U(NN)             O150....
C                                                                       O160....
C.....NOTE THAT THE CONCENTRATION OF ADSORBATE, CS(I), IS GIVEN BY:     O170....
C     CS(I) = SL(I)*U(I) + SR(I)                                        O180....
C                                                                       O190....
C.....NO SORPTION                                                       O200....
      IF(ADSMOD.NE.'NONE      ') GOTO 450                               O210....
      DO 250 I=1,NN                                                     O220....
      CS1(I)=0.D0                                                       O230....
      CS2(I)=0.D0                                                       O240....
      CS3(I)=0.D0                                                       O250....
      SL(I)=0.D0                                                        O260....
      SR(I)=0.D0                                                        O270....
  250 CONTINUE                                                          O280....
```

```
      GOTO 2000                                                          O290....
C                                                                        O300....
C.....LINEAR SORPTION MODEL                                              O310....
  450 IF(ADSMOD.NE.'LINEAR    ') GOTO 700                                O320....
      DO 500 I=1,NN                                                      O330....
      CS1(I)=CHI1*RHOW0                                                  O340....
      CS2(I)=0.D0                                                        O350....
      CS3(I)=0.D0                                                        O360....
      SL(I)=CHI1*RHOW0                                                   O370....
      SR(I)=0.D0                                                         O380....
  500 CONTINUE                                                           O390....
      GOTO 2000                                                          O400....
C                                                                        O410....
C.....FREUNDLICH SORPTION MODEL                                          O420....
  700 IF(ADSMOD.NE.'FREUNDLICH') GOTO 950                                O430....
      CHCH=CHI1/CHI2                                                     O440....
      DCHI2=1.D0/CHI2                                                    O450....
      RH2=RHOW0**DCHI2                                                   O460....
      CHI2F=((1.D0-CHI2)/CHI2)                                           O470....
      CH12=CHI1**DCHI2                                                   O480....
      DO 750 I=1,NN                                                      O490....
      IF(U(I)) 720,720,730                                               O500....
  720 UCH=1.0D0                                                          O510....
      GOTO 740                                                           O520....
  730 UCH=U(I)**CHI2F                                                    O530....
  740 RU=RH2*UCH                                                         O540....
      CS1(I)=CHCH*RU                                                     O550....
      CS2(I)=0.D0                                                        O560....
      CS3(I)=0.D0                                                        O570....
      SL(I)=CH12*RU                                                      O580....
      SR(I)=0.D0                                                         O590....
  750 CONTINUE                                                           O600....
      GOTO 2000                                                          O610....
C                                                                        O620....
C.....LANGMUIR SORPTION MODEL                                            O630....
  950 IF(ADSMOD.NE.'LANGMUIR  ') GOTO 2000                               O640....
      DO 1000 I=1,NN                                                     O650....
      DD=1.D0+CHI2*RHOW0*U(I)                                            O660....
      CS1(I)=(CHI1*RHOW0)/(DD*DD)                                        O670....
      CS2(I)=0.D0                                                        O680....
      CS3(I)=0.D0                                                        O690....
      SL(I)=CS1(I)                                                       O700....
      SR(I)=CS1(I)*CHI2*RHOW0*U(I)*U(I)                                  O710....
 1000 CONTINUE                                                           O720....
C                                                                        O730....
 2000 RETURN                                                             O740....
      END                                                                O750....
C     SUBROUTINE        E  L  E  M  E  N        SUTRA - VERSION 1284-2D P10.....
C                                                                        P20.....
C *** PURPOSE :                                                          P30.....
C ***  TO CONTROL AND CARRY OUT ALL CALCULATIONS FOR EACH ELEMENT BY     P40.....
C ***  OBTAINING ELEMENT INFORMATION FROM THE BASIS FUNCTION ROUTINE,    P50.....
C ***  CARRYING OUT GAUSSIAN INTEGRATION OF FINITE ELEMENT INTEGRALS,    P60.....
C ***  AND SENDING RESULTS OF ELEMENT INTEGRATIONS TO GLOBAL ASSEMBLY    P70.....
C ***  ROUTINE.  ALSO CALCULATES VELOCITY AT EACH ELEMENT CENTROID FOR   P80.....
C ***  PRINTED OUTPUT.                                                   P90.....
C                                                                        P100....
      SUBROUTINE ELEMEN(ML,IN,X,Y,THICK,PITER,UITER,RCIT,RCITM1,POR,     P110....
     1   ALMAX,ALMIN,ATAVG,PERMXX,PERMXY,PERMYX,PERMYY,PANGLE,           P120....
     2   VMAG,VANG,VOL,PMAT,PVEC,UMAT,UVEC,GXSI,GETA,PVEL,CWRK)          P130NEW
      IMPLICIT DOUBLE PRECISION (A-H,O-Z)                                P140....
```

```
      COMMON/FUNITS/ K00,K0,K1,K2,K3,K4,K5,K6,K7,K8                      MODIFIED
      COMMON/DIMS/ NN,NE,NIN,IS,JT,NBIP,NBIS,NPT(9),NPBC,NUBC,           P150NEW
     1   NSOP,NSOU,NBCN                                                  P160....
      COMMON/TENSOR/ GRAVX,GRAVY                                         P170....
      COMMON/PARAMS/ COMPFL,COMPMA,DRWDU,CW,CS,RHOS,DECAY,SIGMAW,SIGMAS, P180....
     1   RHOW0,URHOW0,VISC0,PRODF1,PRODS1,PRODF0,PRODS0,CHI1,CHI2        P190....
      COMMON/TIME/ DELT,TSEC,TMIN,THOUR,TDAY,TWEEK,TMONTH,TYEAR,         P200....
     1   TMAX,DELTP,DELTU,DLTPM1,DLTUM1,IT,ITMAX                         P210....
      COMMON/CNTRL1/ GNU,UP,DTMULT,DTMAX,ME,ISSFLO,ISSTRA,ITCYC,         P220NEW
     1   NPCYC,NUCYC,NPRINT,IREAD,ISTORE,NOUMAT,IUNSAT,ITIME             P230NEW
      COMMON/KPRINT/ KNODAL,KELMNT,KINCID,KPLOTP,KPLOTU,KVEL,KBUDG       P240....
      DIMENSION IN(NIN),X(NN),Y(NN),THICK(NN),PITER(NN),                 P250....
     1   UITER(NN),RCIT(NN),RCITM1(NN),POR(NN),PVEL(NN)                  P260....
      DIMENSION PERMXX(NE),PERMXY(NE),PERMYX(NE),PERMYY(NE),PANGLE(NE),  P270....
     1   ALMAX(NE),ALMIN(NE),ATAVG(NE),VMAG(NE),VANG(NE),                P280....
     2   GXSI(NE,4),GETA(NE,4)                                           P290....
      DIMENSION VOL(NN),PMAT(NN,NBIP),PVEC(NN),UMAT(NN,NBIS),UVEC(NN)    P300NEW
      DIMENSION CWRK(NN)                                                 NEW
      DIMENSION BFLOWE(4,4),DFLOWE(4),BTRANE(4,4),DTRANE(4,4),VOLE(4)    P310....
      DIMENSION F(4,4),W(4,4),DET(4),DFDXG(4,4),DFDYG(4,4),              P320....
     1   DWDXG(4,4),DWDYG(4,4)                                           P330....
      DIMENSION SWG(4),RHOG(4),VISCG(4),PORG(4),VXG(4),VYG(4),           P340....
     1   RELKG(4),RGXG(4),RGYG(4),VGMAG(4),THICKG(4)                     P350....
      DIMENSION RXXG(4),RXYG(4),RYXG(4),RYYG(4)                          P360....
      DIMENSION BXXG(4),BXYG(4),BYXG(4),BYYG(4),                         P370....
     1   EXG(4),EYG(4)                                                   P380....
      DIMENSION GXLOC(4),GYLOC(4)                                        P390....
      DATA GLOC/0.577350269189626D0/                                     P400....
      DATA INTIM/0/,ISTOP/0/,GXLOC/-1.D0,1.D0,1.D0,-1.D0/,               P410....
     1   GYLOC/-1.D0,-1.D0,1.D0,1.D0/                                    P420....
C                                                                        P430....
C.....DECIDE WHETHER TO CALCULATE CENTROID VELOCITIES ON THIS CALL       P440....
      IVPRNT=0                                                           P450....
      IF(MOD(IT,NPRINT).EQ.0.AND.ML.NE.2.AND.IT.NE.0) IVPRNT=1           P460....
      IF(IT.EQ.1) IVPRNT=1                                               P470....
      KVPRNT=IVPRNT+KVEL                                                 P480....
C                                                                        P490....
C.....ON FIRST TIME STEP, PREPARE GRAVITY VECTOR COMPONENTS,             P500....
C        GXSI AND GETA, FOR CONSISTENT VELOCITIES,                       P510....
C        AND CHECK ELEMENT SHAPES                                        P520....
      IF(INTIM) 100,100,2000                                             P530....
  100 INTIM=1                                                            P540....
C.....LOOP THROUGH ALL ELEMENTS TO OBTAIN THE JACOBIAN                   P550....
C        AT EACH OF THE FOUR NODES IN EACH ELEMENT                       P560....
      DO 1000 L=1,NE                                                     P570....
       DO 500 IL=1,4                                                     P580....
        XLOC=GXLOC(IL)                                                   P590....
        YLOC=GYLOC(IL)                                                   P600....
        CALL BASIS2(0000,L,XLOC,YLOC,IN,X,Y,F(1,IL),W(1,IL),DET(IL),     P610....
     1     DFDXG(1,IL),DFDYG(1,IL),DWDXG(1,IL),DWDYG(1,IL),              P620....
     2     PITER,UITER,PVEL,POR,THICK,THICKG(IL),VXG(IL),VYG(IL),        P630....
     3     SWG(IL),RHOG(IL),VISCG(IL),PORG(IL),VGMAG(IL),RELKG(IL),      P640....
     4     PERMXX,PERMXY,PERMYX,PERMYY,CJ11,CJ12,CJ21,CJ22,              P650....
     5     GXSI,GETA,RCIT,RCITM1,RGXG(IL),RGYG(IL))                      P660....
        GXSI(L,IL)=CJ11*GRAVX+CJ12*GRAVY                                 P670....
        GETA(L,IL)=CJ21*GRAVX+CJ22*GRAVY                                 P680....
C.....CHECK FOR NEGATIVE- OR ZERO-AREA ERRORS IN ELEMENT SHAPES          P690....
        IF(DET(IL)) 200,200,500                                          P700....
  200   ISTOP=ISTOP+1                                                    P710....
        WRITE(K3,400) IN((L-1)*4+IL),L,DET(IL)                           P720....
  400   FORMAT(11X,'THE DETERMINANT OF THE JACOBIAN AT GAUSS POINT ',I4,P730....
```

```
     1     ' IN ELEMENT ',I4,' IS NEGATIVE OR ZERO, ',1PE15.7)          P740....
  500  CONTINUE                                                         P750....
 1000 CONTINUE                                                         P760....
C                                                                      P770....
      IF(ISTOP.EQ.0) GOTO 2000                                         P780....
      WRITE(K3,1500)                                                   P790....
 1500 FORMAT(//////11X,'SOME ELEMENTS HAVE INCORRECT GEOMETRY.'        P800....
     1   //11X,'PLEASE CHECK THE NODE COORDINATES AND ',               P810....
     2   'INCIDENCE LIST, MAKE CORRECTIONS, AND THEN RERUN.'////////   P820....
     3   11X,'S I M U L A T I O N   H A L T E D'/                      P830....
     4   11X,'_____________________   ___________')                    P840....
      ENDFILE(K3)                                                      P850....
      STOP                                                             P860....
C                                                                      P870....
C.....LOOP THROUGH ALL ELEMENTS TO CARRY OUT SPATIAL INTEGRATION       P880....
C        OF FLUX TERMS IN P AND/OR U EQUATIONS                         P890....
 2000 IF(IUNSAT.NE.0) IUNSAT=2                                         P900....
C - - - - - - - - - - - - - - - - - - - - - - - - - - - - - - - - - - - P910....
C - - - - - - - - - - - - - - - - - - - - - - - - - - - - - - - - - - - P920....
C - - - - - - - - - - - - - - - - - - - - - - - - - - - - - - - - - - - P930....
      DO 9999 L=1,NE                                                   P940....
       XIX=-1.D0                                                       P950....
       YIY=-1.D0                                                       P960....
       KG=0                                                            P970....
C.....OBTAIN BASIS FUNCTION AND RELATED INFORMATION AT EACH OF         P980....
C        FOUR GAUSS POINTS IN THE ELEMENT                              P990....
       DO 2200 IYL=1,2                                                 P1000...
        DO 2100 IXL=1,2                                                P1010...
         KG=KG+1                                                       P1020...
         XLOC=XIX*GLOC                                                 P1030...
         YLOC=YIY*GLOC                                                 P1040...
       CALL BASIS2(0001,L,XLOC,YLOC,IN,X,Y,F(1,KG),W(1,KG),DET(KG),    P1050...
     1      DFDXG(1,KG),DFDYG(1,KG),DWDXG(1,KG),DWDYG(1,KG),           P1060...
     2      PITER,UITER,PVEL,POR,THICK,THICKG(KG),VXG(KG),VYG(KG),     P1070...
     3      SWG(KG),RHOG(KG),VISCG(KG),PORG(KG),VGMAG(KG),RELKG(KG),   P1080...
     4      PERMXX,PERMXY,PERMYX,PERMYY,CJ11,CJ12,CJ21,CJ22,           P1090...
     5      GXSI,GETA,RCIT,RCITM1,RGXG(KG),RGYG(KG))                   P1100...
 2100    XIX=-XIX                                                      P1110...
 2200   YIY=-YIY                                                       P1120...
C                                                                      P1130...
C.....CALCULATE VELOCITY AT ELEMENT CENTROID WHEN REQUIRED             P1140...
       IF(KVPRNT-2) 3000,2300,3000                                     P1150...
 2300  AXSUM=0.0D0                                                     P1160...
       AYSUM=0.0D0                                                     P1170...
       DO 2400 KG=1,4                                                  P1180...
        AXSUM=AXSUM+VXG(KG)                                            P1190...
 2400   AYSUM=AYSUM+VYG(KG)                                            P1200...
       VMAG(L)=DSQRT(AXSUM*AXSUM+AYSUM*AYSUM)/4.0D0                    P1210...
       IF(AXSUM) 2500,2700,2800                                        P1220...
 2500  AYX=AYSUM/AXSUM                                                 P1230...
       VANG(L)=DATAN(AYX)/1.745329D-02                                 P1240...
       IF(AYSUM.LT.0.0D0) GOTO 2600                                    P1250...
       VANG(L)=VANG(L)+180.0D0                                         P1260...
       GOTO 3000                                                       P1270...
 2600  VANG(L)=VANG(L)-180.0D0                                         P1280...
       GOTO 3000                                                       P1290...
 2700  VANG(L)=90.0D0                                                  P1300...
       IF(AYSUM.LT.0.0D0) VANG(L)=-90.0D0                              P1310...
       GOTO 3000                                                       P1320...
 2800  AYX=AYSUM/AXSUM                                                 P1330...
       VANG(L)=DATAN(AYX)/1.745329D-02                                 P1340...
```

```
C                                                                       P1350...
C.....INCLUDE MESH THICKNESS IN NUMERICAL INTEGRATION                   P1360...
 3000  DO 3300 KG=1,4                                                   P1370...
 3300   DET(KG)=THICKG(KG)*DET(KG)                                      P1380...
C                                                                       P1390...
C.....CALCULATE PARAMETERS FOR FLUID MASS BALANCE AT GAUSS POINTS       P1400...
       IF(ML-1) 3400,3400,6100                                          P1410...
 3400  SWTEST=0.D0                                                      P1420...
       DO 4000 KG=1,4                                                   P1430...
        SWTEST=SWTEST+SWG(KG)                                           P1440...
        ROMG=RHOG(KG)*RELKG(KG)/VISCG(KG)                               P1450...
        RXXG(KG)=PERMXX(L)*ROMG                                         P1460...
        RXYG(KG)=PERMXY(L)*ROMG                                         P1470...
        RYXG(KG)=PERMYX(L)*ROMG                                         P1480...
        RYYG(KG)=PERMYY(L)*ROMG                                         P1490...
 4000   CONTINUE                                                        P1500...
C                                                                       P1510...
C.....INTEGRATE FLUID MASS BALANCE IN AN UNSATURATED ELEMENT            P1520...
C        USING ASYMMETRIC WEIGHTING FUNCTIONS                           P1530...
       IF(UP.LE.1.0D-06) GOTO 5200                                      P1540...
       IF(SWTEST-3.999D0) 4200,5200,5200                                P1550...
 4200  DO 5000 I=1,4                                                    P1560...
        DF=0.D0                                                         P1570...
        VO=0.D0                                                         P1580...
        DO 4400 KG=1,4                                                  P1590...
         VO=VO+F(I,KG)*DET(KG)                                          P1600...
 4400    DF=DF+((RXXG(KG)*RGXG(KG)+RXYG(KG)*RGYG(KG))                   P1610...
     1          *DWDXG(I,KG)                                            P1620...
     2        + (RYXG(KG)*RGXG(KG)+RYYG(KG)*RGYG(KG))                   P1630...
     3          *DWDYG(I,KG))*DET(KG)                                   P1640...
        DO 4800 J=1,4                                                   P1650...
         BF=0.D0                                                        P1660...
         DO 4600 KG=1,4                                                 P1670...
 4600     BF=BF+((RXXG(KG)*DFDXG(J,KG)+RXYG(KG)*DFDYG(J,KG))*DWDXG(I,KG)P1680...
     2         +(RYXG(KG)*DFDXG(J,KG)+RYYG(KG)*DFDYG(J,KG))*DWDYG(I,KG))P1690...
     3          *DET(KG)                                               P1700...
 4800    BFLOWE(I,J)=BF                                                 P1710...
        VOLE(I)=VO                                                      P1720...
 5000   DFLOWE(I)=DF                                                    P1730...
       GOTO 6200                                                        P1740...
C                                                                       P1750...
C.....INTEGRATE FLUID MASS BALANCE IN A SATURATED OR UNSATURATED        P1760...
C        ELEMENT USING SYMMETRIC WEIGHTING FUNCTIONS                    P1770...
 5200  DO 6000 I=1,4                                                    P1780...
        DF=0.D0                                                         P1790...
        VO=0.D0                                                         P1800...
        DO 5400 KG=1,4                                                  P1810...
         VO=VO+F(I,KG)*DET(KG)                                          P1820...
 5400    DF=DF+((RXXG(KG)*RGXG(KG)+RXYG(KG)*RGYG(KG))*DFDXG(I,KG)       P1830...
     2       + (RYXG(KG)*RGXG(KG)+RYYG(KG)*RGYG(KG))*DFDYG(I,KG))       P1840...
     3         *DET(KG)                                                 P1850...
        DO 5800 J=1,4                                                   P1860...
         BF=0.D0                                                        P1870...
         DO 5600 KG=1,4                                                 P1880...
 5600     BF=BF+((RXXG(KG)*DFDXG(J,KG)+RXYG(KG)*DFDYG(J,KG))*DFDXG(I,KG)P1890...
     1        + (RYXG(KG)*DFDXG(J,KG)+RYYG(KG)*DFDYG(J,KG))*DFDYG(I,KG))P1900...
     2          *DET(KG)                                               P1910...
 5800    BFLOWE(I,J)=BF                                                 P1920...
        VOLE(I)=VO                                                      P1930...
 6000   DFLOWE(I)=DF                                                    P1940...
 6200  CONTINUE                                                         P1950...
```

```
       IF(ML-1) 6100,9000,6100                                          P1960...
 6100  IF(NOUMAT.EQ.1) GOTO 9000                                        P1970...
C                                                                       P1980...
C                                                                       P1990...
C.....CALCULATE PARAMETERS FOR ENERGY BALANCE OR SOLUTE MASS BALANCE    P2000...
C        AT GAUSS POINTS                                                P2010...
       DO 7000 KG=1,4                                                   P2020...
        ESWG=PORG(KG)*SWG(KG)                                           P2030...
        RHOCWG=RHOG(KG)*CW                                              P2040...
        ESRCG=ESWG*RHOCWG                                               P2050...
        IF(VGMAG(KG)) 6300,6300,6600                                    P2060...
 6300   EXG(KG)=0.0D0                                                   P2070...
        EYG(KG)=0.0D0                                                   P2080...
        DXXG=0.0D0                                                      P2090...
        DXYG=0.0D0                                                      P2100...
        DYXG=0.0D0                                                      P2110...
        DYYG=0.0D0                                                      P2120...
        GOTO 6900                                                       P2130...
 6600   EXG(KG)=ESRCG*VXG(KG)                                           P2140...
        EYG(KG)=ESRCG*VYG(KG)                                           P2150...
C                                                                       P2160...
C.....DISPERSIVITY MODEL FOR ANISOTROPIC MEDIA                          P2170...
C        WITH PRINCIPAL DISPERSIVITIES:  ALMAX,ALMIN, AND ATAVG         P2180...
        VANGG=1.570796327D0                                             P2190...
        IF(VXG(KG)*VXG(KG).GT.0.D0) VANGG=DATAN(VYG(KG)/VXG(KG))        P2200...
        VKANGG=VANGG-PANGLE(L)                                          P2210...
        DCO=DCOS(VKANGG)                                                P2220...
        DSI=DSIN(VKANGG)                                                P2230...
C.....EFFECTIVE LONGITUDINAL DISPERSIVITY IN FLOW DIRECTION, ALEFF      P2240...
        ALEFF=0.0D0                                                     P2250...
        IF(ALMAX(L)+ALMIN(L)) 6800,6800,6700                            P2260...
 6700   ALEFF=ALMAX(L)*ALMIN(L)/(ALMIN(L)*DCO*DCO+ALMAX(L)*DSI*DSI)     P2270...
 6800   DLG=ALEFF*VGMAG(KG)                                             P2280...
        DTG=ATAVG(L)*VGMAG(KG)                                          P2290...
C                                                                       P2300...
        V2GMI=1.D0/(VGMAG(KG)*VGMAG(KG))                                P2310...
        V2ILTG=V2GMI*(DLG-DTG)                                          P2320...
        VX2G=VXG(KG)*VXG(KG)                                            P2330...
        VY2G=VYG(KG)*VYG(KG)                                            P2340...
C.....DISPERSION TENSOR                                                 P2350...
        DXXG=V2GMI*(DLG*VX2G+DTG*VY2G)                                  P2360...
        DYYG=V2GMI*(DTG*VX2G+DLG*VY2G)                                  P2370...
        DXYG=V2ILTG*VXG(KG)*VYG(KG)                                     P2380...
        DYXG=DXYG                                                       P2390...
C                                                                       P2400...
C.....IN-PARALLEL CONDUCTIVITIES (DIFFUSIVITIES) FORMULA                P2410...
 6900   ESE=ESRCG*SIGMAW+(1.D0-PORG(KG))*RHOCWG*SIGMAS                  P2420...
C.....ADD DIFFUSION AND DISPERSION TERMS TO TOTAL DISPERSION TENSOR     P2430...
        BXXG(KG)=ESRCG*DXXG+ESE                                         P2440...
        BXYG(KG)=ESRCG*DXYG                                             P2450...
        BYXG(KG)=ESRCG*DYXG                                             P2460...
 7000   BYYG(KG)=ESRCG*DYYG+ESE                                         P2470...
C                                                                       P2480...
C.....INTEGRATE SOLUTE MASS BALANCE OR ENERGY BALANCE                   P2490...
C        USING SYMMETRIC WEIGHTING FUNCTIONS FOR DISPERSION TERM AND    P2500...
C        USING EITHER SYMMETRIC OR ASYMMETRIC WEIGHTING FUNCTIONS       P2510...
C        FOR ADVECTION TERM                                             P2520...
        DO 8000 I=1,4                                                   P2530...
         DO 8000 J=1,4                                                  P2540...
         BT=0.D0                                                        P2550...
         DT=0.D0                                                        P2560...
```

```
         DO 7500 KG=1,4                                                 P2570...
          BT=BT+((BXXG(KG)*DFDXG(J,KG)+BXYG(KG)*DFDYG(J,KG))*DFDXG(I,KG)P2580...
     1         +(BYXG(KG)*DFDXG(J,KG)+BYYG(KG)*DFDYG(J,KG))*DFDYG(I,KG))P2590...
     2          *DET(KG)                                                P2600...
 7500     DT=DT+(EXG(KG)*DFDXG(J,KG)+EYG(KG)*DFDYG(J,KG))               P2610...
     1          *W(I,KG)*DET(KG)                                        P2620...
         BTRANE(I,J)=BT                                                 P2630...
 8000    DTRANE(I,J)=DT                                                 P2640...
 9000  CONTINUE                                                         P2650...
C                                                                       P2660...
C                                                                       P2670...
C.....SEND RESULTS OF INTEGRATIONS FOR THIS ELEMENT TO                  P2680...
C        GLOBAL ASSEMBLY ROUTINE                                        P2690...
 9999  CALL GLOBAN(L,ML,VOLE,BFLOWE,DFLOWE,BTRANE,DTRANE,               P2700...
     1    IN,VOL,PMAT,PVEC,UMAT,UVEC,CWRK)                             P2710NEW
C - - - - - - - - - - - - - - - - - - - - - - - - - - - - - - - - - - - P2720...
C - - - - - - - - - - - - - - - - - - - - - - - - - - - - - - - - - - - P2730...
C - - - - - - - - - - - - - - - - - - - - - - - - - - - - - - - - - - - P2740...
C                                                                       P2750...
C                                                                       P2760...
      RETURN                                                            P2770...
      END                                                               P2780...
C     SUBROUTINE        B  A  S  I  S  2        SUTRA - VERSION 1284-2D Q10.....
C                                                                       Q20.....
C *** PURPOSE :                                                         Q30.....
C ***  TO CALCULATE VALUES OF BASIS AND WEIGHTING FUNCTIONS AND THEIR   Q40.....
C ***  DERIVATIVES, TRANSFORMATION MATRICES BETWEEN LOCAL AND GLOBAL    Q50.....
C ***  COORDINATES AND PARAMETER VALUES AT A SPECIFIED POINT IN A       Q60.....
C ***  QUADRILATERAL FINITE ELEMENT.                                    Q70.....
C                                                                       Q80.....
      SUBROUTINE BASIS2(ICALL,L,XLOC,YLOC,IN,X,Y,F,W,DET,               Q90.....
     1   DFDXG,DFDYG,DWDXG,DWDYG,PITER,UITER,PVEL,POR,THICK,THICKG,     Q100....
     2   VXG,VYG,SWG,RHOG,VISCG,PORG,VGMAG,RELKG,                       Q110....
     3   PERMXX,PERMXY,PERMYX,PERMYY,CJ11,CJ12,CJ21,CJ22,               Q120....
     4   GXSI,GETA,RCIT,RCITM1,RGXG,RGYG)                               Q130....
      IMPLICIT DOUBLE PRECISION (A-H,O-Z)                               Q140....
      COMMON/DIMS/ NN,NE,NIN,IS,JT,NBIP,NBIS,NPT(9),NPBC,NUBC,          Q150NEW
     1   NSOP,NSOU,NBCN                                                 Q160....
      COMMON/CNTRL1/ GNU,UP,DTMULT,DTMAX,ME,ISSFLO,ISSTRA,ITCYC,        Q170NEW
     1   NPCYC,NUCYC,NPRINT,IREAD,ISTORE,NOUMAT,IUNSAT,ITIME            Q180NEW
      COMMON/SATPAR/ PCENT,SWRES,PCRES,SSLOPE,SINCPT                    Q190....
      COMMON/PARAMS/ COMPFL,COMPMA,DRWDU,CW,CS,RHOS,DECAY,SIGMAW,SIGMAS,Q200....
     1   RHOW0,URHOW0,VISC0,PRODF1,PRODS1,PRODF0,PRODS0,CHI1,CHI2       Q210....
      COMMON/TENSOR/ GRAVX,GRAVY                                        Q220....
      DOUBLE PRECISION XLOC,YLOC                                        Q230....
      DIMENSION IN(NIN),X(NN),Y(NN),UITER(NN),PITER(NN),PVEL(NN),       Q240....
     1   POR(NN),PERMXX(NE),PERMXY(NE),PERMYX(NE),PERMYY(NE),THICK(NN)  Q250....
      DIMENSION GXSI(NE,4),GETA(NE,4),RCIT(NN),RCITM1(NN)               Q260....
      DIMENSION F(4),W(4),DFDXG(4),DFDYG(4),DWDXG(4),DWDYG(4)           Q270....
      DIMENSION FX(4),FY(4),AFX(4),AFY(4),                              Q280....
     1   DFDXL(4),DFDYL(4),DWDXL(4),DWDYL(4),                           Q290....
     2   XDW(4),YDW(4),XIIX(4),YIIY(4)                                  Q300....
      DATA XIIX/-1.D0,+1.D0,+1.D0,-1.D0/,                               Q310....
     1   YIIY/-1.D0,-1.D0,+1.D0,+1.D0/                                  Q320....
C                                                                       Q330....
C                                                                       Q340....
C.....AT THIS LOCATION IN LOCAL COORDINATES, (XLOC,YLOC),               Q350....
C        CALCULATE SYMMETRIC WEIGHTING FUNCTIONS, F(I),                 Q360....
C        SPACE DERIVATIVES, DFDXG(I) AND DFDYG(I), AND                  Q370....
C        DETERMINANT OF JACOBIAN, DET.                                  Q380....
C                                                                       Q390....
```

```
      XF1=1.D0-XLOC                                                     Q400....
      XF2=1.D0+XLOC                                                     Q410....
      YF1=1.D0-YLOC                                                     Q420....
      YF2=1.D0+YLOC                                                     Q430....
C                                                                       Q440....
C.....CALCULATE BASIS FUNCTION, F.                                      Q450....
      FX(1)=XF1                                                         Q460....
      FX(2)=XF2                                                         Q470....
      FX(3)=XF2                                                         Q480....
      FX(4)=XF1                                                         Q490....
      FY(1)=YF1                                                         Q500....
      FY(2)=YF1                                                         Q510....
      FY(3)=YF2                                                         Q520....
      FY(4)=YF2                                                         Q530....
      DO 10 I=1,4                                                       Q540....
   10 F(I)=0.250D0*FX(I)*FY(I)                                          Q550....
C                                                                       Q560....
C.....CALCULATE DERIVATIVES WITH RESPECT TO LOCAL COORDINATES.          Q570....
      DO 20 I=1,4                                                       Q580....
      DFDXL(I)=XIIX(I)*0.250D0*FY(I)                                    Q590....
   20 DFDYL(I)=YIIY(I)*0.250D0*FX(I)                                    Q600....
C                                                                       Q610....
C.....CALCULATE ELEMENTS OF JACOBIAN MATRIX, CJ.                        Q620....
      CJ11=0.D0                                                         Q630....
      CJ12=0.D0                                                         Q640....
      CJ21=0.D0                                                         Q650....
      CJ22=0.D0                                                         Q660....
      DO 100 IL=1,4                                                     Q670....
      II=(L-1)*4+IL                                                     Q680....
      I=IN(II)                                                          Q690....
      CJ11=CJ11+DFDXL(IL)*X(I)                                          Q700....
      CJ12=CJ12+DFDXL(IL)*Y(I)                                          Q710....
      CJ21=CJ21+DFDYL(IL)*X(I)                                          Q720....
  100 CJ22=CJ22+DFDYL(IL)*Y(I)                                          Q730....
C                                                                       Q740....
C.....CALCULATE DETERMINANT OF JACOBIAN MATRIX.                         Q750....
      DET=CJ11*CJ22-CJ21*CJ12                                           Q760....
C                                                                       Q770....
C.....RETURN TO ELEMEN WITH JACOBIAN MATRIX ON FIRST TIME STEP.         Q780....
      IF(ICALL.EQ.0) RETURN                                             Q790....
C                                                                       Q800....
C.....CALCULATE ELEMENTS OF INVERSE JACOBIAN MATRIX, CIJ.               Q810....
      ODET=1.D0/DET                                                     Q820....
      CIJ11=+ODET*CJ22                                                  Q830....
      CIJ12=-ODET*CJ12                                                  Q840....
      CIJ21=-ODET*CJ21                                                  Q850....
      CIJ22=+ODET*CJ11                                                  Q860....
C                                                                       Q870....
C.....CALCULATE DERIVATIVES WITH RESPECT TO GLOBAL COORDINATES          Q880....
      DO 200 I=1,4                                                      Q890....
      DFDXG(I)=CIJ11*DFDXL(I)+CIJ12*DFDYL(I)                            Q900....
  200 DFDYG(I)=CIJ21*DFDXL(I)+CIJ22*DFDYL(I)                            Q910....
C                                                                       Q920....
C.....CALCULATE CONSISTENT COMPONENTS OF (RHO*GRAV) TERM IN LOCAL        Q930....
C        COORDINATES AT THIS LOCATION, (XLOC,YLOC)                      Q940....
      RGXL=0.D0                                                         Q950....
      RGYL=0.D0                                                         Q960....
      RGXLM1=0.D0                                                       Q970....
      RGYLM1=0.D0                                                       Q980....
      DO 800 IL=1,4                                                     Q990....
      II=(L-1)*4+IL                                                     Q1000...
```

```
      I=IN(II)                                                          Q1010...
      ADFDXL=DABS(DFDXL(IL))                                            Q1020...
      ADFDYL=DABS(DFDYL(IL))                                            Q1030...
      RGXL=RGXL+RCIT(I)*GXSI(L,IL)*ADFDXL                               Q1040...
      RGYL=RGYL+RCIT(I)*GETA(L,IL)*ADFDYL                               Q1050...
      RGXLM1=RGXLM1+RCITM1(I)*GXSI(L,IL)*ADFDXL                         Q1060...
      RGYLM1=RGYLM1+RCITM1(I)*GETA(L,IL)*ADFDYL                         Q1070...
  800 CONTINUE                                                          Q1080...
C                                                                       Q1090...
C.....TRANSFORM CONSISTENT COMPONENTS OF (RHO*GRAV) TERM TO             Q1100...
C        GLOBAL COORDINATES                                             Q1110...
      RGXG=CIJ11*RGXL+CIJ12*RGYL                                        Q1120...
      RGYG=CIJ21*RGXL+CIJ22*RGYL                                        Q1130...
      RGXGM1=CIJ11*RGXLM1+CIJ12*RGYLM1                                  Q1140...
      RGYGM1=CIJ21*RGXLM1+CIJ22*RGYLM1                                  Q1150...
C                                                                       Q1160...
C.....CALCULATE PARAMETER VALUES AT THIS LOCATION, (XLOC,YLOC)          Q1170...
C                                                                       Q1180...
      PITERG=0.D0                                                       Q1190...
      UITERG=0.D0                                                       Q1200...
      DPDXG=0.D0                                                        Q1210...
      DPDYG=0.D0                                                        Q1220...
      PORG=0.D0                                                         Q1230...
      THICKG=0.0D0                                                      Q1240...
      DO 1000 IL=1,4                                                    Q1250...
      II=(L-1)*4 +IL                                                    Q1260...
      I=IN(II)                                                          Q1270...
      DPDXG=DPDXG+PVEL(I)*DFDXG(IL)                                     Q1280...
      DPDYG=DPDYG+PVEL(I)*DFDYG(IL)                                     Q1290...
      PORG=PORG+POR(I)*F(IL)                                            Q1300...
      THICKG=THICKG+THICK(I)*F(IL)                                      Q1310...
      PITERG=PITERG+PITER(I)*F(IL)                                      Q1320...
      UITERG=UITERG+UITER(I)*F(IL)                                      Q1330...
 1000 CONTINUE                                                          Q1340...
C                                                                       Q1350...
C.....SET VALUES FOR DENSITY AND VISCOSITY                              Q1360...
C.....RHOG = FUNCTION(UITER)                                           Q1370...
      RHOG=RHOW0+DRWDU*(UITERG-URHOW0)                                  Q1380...
C.....VISCG = FUNCTION(UITER)                                          Q1390...
C        VISCOSITY IN UNITS OF VISC0*(KG/(M*SEC))                       Q1400...
      IF(ME) 1300,1300,1200                                             Q1410...
 1200 VISCG=VISC0*239.4D-07*(10.D0**(248.37D0/(UITERG+133.15D0)))       Q1420...
      GOTO 1400                                                         Q1430...
C.....FOR SOLUTE TRANSPORT... VISCG IS TAKEN TO BE CONSTANT             Q1440...
 1300 VISCG=VISC0                                                       Q1450...
 1400 CONTINUE                                                          Q1460...
C                                                                       Q1470...
C.....SET UNSATURATED FLOW PARAMETERS SWG AND RELKG                     Q1480...
      IF(IUNSAT-2) 1600,1500,1600                                       Q1490...
 1500 IF(PITERG) 1550,1600,1600                                         Q1500...
 1550 CALL UNSAT(SWG,DSWDPG,RELKG,PITERG)                               Q1510...
      GOTO 1700                                                         Q1520...
 1600 SWG=1.0D0                                                         Q1530...
      RELKG=1.0D0                                                       Q1540...
 1700 CONTINUE                                                          Q1550...
C                                                                       Q1560...
C.....CALCULATE CONSISTENT FLUID VELOCITIES WITH RESPECT TO GLOBAL      Q1570...
C        COORDINATES, VXG, VYG, AND VGMAG, AT THIS LOCATION, (XLOC,YLOC)Q1580...
      DENOM=1.D0/(PORG*SWG*VISCG)                                       Q1590...
      PGX=DPDXG-RGXGM1                                                  Q1600...
      PGY=DPDYG-RGYGM1                                                  Q1610...
```

```
C.....ZERO OUT RANDOM BOUYANT DRIVING FORCES DUE TO DIFFERENCING       Q1620...
C..... NUMBERS PAST PRECISION LIMIT                                   Q1630...
C..... MINIMUM DRIVING FORCE IS 1.D-10 OF PRESSURE GRADIENT           Q1640...
C..... (THIS VALUE MAY BE CHANGED DEPENDING ON MACHINE PRECISION)     Q1650...
      IF(DPDXG) 1720,1730,1720                                        Q1660...
 1720 IF(DABS(PGX/DPDXG)-1.0D-10) 1725,1725,1730                      Q1670...
 1725 PGX=0.0D0                                                       Q1680...
 1730 IF(DPDYG) 1750,1760,1750                                        Q1690...
 1750 IF(DABS(PGY/DPDYG)-1.0D-10) 1755,1755,1760                      Q1700...
 1755 PGY=0.0D0                                                       Q1710...
 1760 VXG=-DENOM*(PERMXX(L)*PGX+PERMXY(L)*PGY)*RELKG                  Q1720...
      VYG=-DENOM*(PERMYX(L)*PGX+PERMYY(L)*PGY)*RELKG                  Q1730...
      VXG2=VXG*VXG                                                    Q1740...
      VYG2=VYG*VYG                                                    Q1750...
      VGMAG=DSQRT(VXG2+VYG2)                                          Q1760...
C                                                                     Q1770...
C.....AT THIS POINT IN LOCAL COORDINATES, (XLOC,YLOC),                Q1780...
C        CALCULATE ASYMMETRIC WEIGHTING FUNCTIONS, W(I),              Q1790...
C        AND SPACE DERIVATIVES, DWDXG(I) AND DWDYG(I).                Q1800...
C                                                                     Q1810...
C.....ASYMMETRIC FUNCTIONS SIMPLIFY WHEN  UP=0.0                      Q1820...
      IF(UP.GT.1.0D-06.AND.NOUMAT.EQ.0) GOTO 1790                     Q1830...
      DO 1780 I=1,4                                                   Q1840...
      W(I)=F(I)                                                       Q1850...
      DWDXG(I)=DFDXG(I)                                               Q1860...
      DWDYG(I)=DFDYG(I)                                               Q1870...
 1780 CONTINUE                                                        Q1880...
C.....RETURN WHEN ONLY SYMMETRIC WEIGHTING FUNCTIONS ARE USED         Q1890...
      RETURN                                                          Q1900...
C                                                                     Q1910...
C.....CALCULATE FLUID VELOCITIES WITH RESPECT TO LOCAL COORDINATES,   Q1920...
C..... VXL, VYL, AND VLMAG, AT THIS LOCATION, (XLOC,YLOC).            Q1930...
 1790 VXL=CIJ11*VXG+CIJ21*VYG                                         Q1940...
      VYL=CIJ12*VXG+CIJ22*VYG                                         Q1950...
      VLMAG=DSQRT(VXL*VXL+VYL*VYL)                                    Q1960...
C                                                                     Q1970...
      AA=0.0D0                                                        Q1980...
      BB=0.0D0                                                        Q1990...
      IF(VLMAG) 1900,1900,1800                                        Q2000...
 1800 AA=UP*VXL/VLMAG                                                 Q2010...
      BB=UP*VYL/VLMAG                                                 Q2020...
C                                                                     Q2030...
 1900 XIXI=.750D0*AA*XF1*XF2                                          Q2040...
      YIYI=.750D0*BB*YF1*YF2                                          Q2050...
      DO 2000 I=1,4                                                   Q2060...
      AFX(I)=.50D0*FX(I)+XIIX(I)*XIXI                                 Q2070...
 2000 AFY(I)=.50D0*FY(I)+YIIY(I)*YIYI                                 Q2080...
C                                                                     Q2090...
C.....CALCULATE ASYMMETRIC WEIGHTING FUNCTION, W.                     Q2100...
      DO 3000 I=1,4                                                   Q2110...
 3000 W(I)=AFX(I)*AFY(I)                                              Q2120...
C                                                                     Q2130...
      THAAX=0.50D0-1.50D0*AA*XLOC                                     Q2140...
      THBBY=0.50D0-1.50D0*BB*YLOC                                     Q2150...
      DO 4000 I=1,4                                                   Q2160...
      XDW(I)=XIIX(I)*THAAX                                            Q2170...
 4000 YDW(I)=YIIY(I)*THBBY                                            Q2180...
C                                                                     Q2190...
C.....CALCULATE DERIVATIVES WITH RESPECT TO LOCAL COORDINATES.        Q2200...
      DO 5000 I=1,4                                                   Q2210...
      DWDXL(I)=XDW(I)*AFY(I)                                          Q2220...
```

```
 5000 DWDYL(I)=YDW(I)*AFX(I)                                                Q2230...
C                                                                           Q2240...
C.....CALCULATE DERIVATIVES WITH RESPECT TO GLOBAL COORDINATES.             Q2250...
      DO 6000 I=1,4                                                         Q2260...
      DWDXG(I)=CIJ11*DWDXL(I)+CIJ12*DWDYL(I)                               Q2270...
 6000 DWDYG(I)=CIJ21*DWDXL(I)+CIJ22*DWDYL(I)                               Q2280...
C                                                                           Q2290...
C                                                                           Q2300...
      RETURN                                                                Q2310...
      END                                                                   Q2320...
C     SUBROUTINE        U  N  S  A  T          SUTRA - VERSION 1284-2D     R10.....
C                                                                           R20.....
C *** PURPOSE :                                                             R30.....
C ***  USER-PROGRAMMED SUBROUTINE GIVING:                                   R40.....
C ***  (1)  SATURATION AS A FUNCTION OF PRESSURE ( SW(PRES) )               R50.....
C ***  (2)  DERIVATIVE OF SATURATION WITH RESPECT TO PRESSURE               R60.....
C ***       AS A FUNCTION OF EITHER PRESSURE OR SATURATION                  R70.....
C ***       ( DSWDP(PRES), OR DSWDP(SW) )                                   R80.....
C ***  (3)  RELATIVE PERMEABILITY AS A FUNCTION OF EITHER                   R90.....
C ***       PRESSURE OR SATURATION ( REL(PRES) OR RELK(SW) )                R100....
C ***                                                                       R110....
C ***  CODE BETWEEN DASHED LINES MUST BE REPLACED TO GIVE THE               R120....
C ***  PARTICULAR UNSATURATED RELATIONSHIPS DESIRED.                        R130....
C                                                                           R140....
      SUBROUTINE UNSAT(SW,DSWDP,RELK,PRES)                                  R150....
      IMPLICIT DOUBLE PRECISION (A-H,O-Z)                                   R160....
      COMMON/CNTRL1/ GNU,UP,DTMULT,DTMAX,ME,ISSFLO,ISSTRA,ITCYC,            R170NEW
     1   NPCYC,NUCYC,NPRINT,IREAD,ISTORE,NOUMAT,IUNSAT  ,ITIME             R180NEW
C                                                                           R190....
C - - - - - - - - - - - - - - - - - - - - - - - - - - - - - - - - - - - - --R200....
C     THREE PARAMETERS FOR UNSATURATED FLOW RELATIONSHIPS OF                R210....
C     VAN GENUCHTEN(1980)                                                   R220....
C        RESIDUAL SATURATION, SWRES, GIVEN IN UNITS [L**0]                  R230....
C        PARAMETER, AA, GIVEN IN INVERSE PRESSURE UNITS [m*(s**2)/kg]       R240....
C        PARAMETER, VN, GIVEN IN UNITS [L**0]                               R250....
      DATA   SWRES/0.30D0/,   AA/5.0D-05/,   VN/2.0D0/                      R260....
C - - - - - - - - - - - - - - - - - - - - - - - - - - - - - - - - - - - - --R270....
C                                                                           R280....
C                                                                           R290....
C                                                                           R300....
C                                                                           R310....
C                                                                           R320....
C                                                                           R330....
C***********************************************************************R340....
C***********************************************************************R350....
C.....SECTION (1):                                                          R360....
C     SW VS. PRES   (VALUE CALCULATED ON EACH CALL TO UNSAT)                R370....
C     CODING MUST GIVE A VALUE TO SATURATION, SW.                           R380....
C                                                                           R390....
C - - - - - - - - - - - - - - - - - - - - - - - - - - - - - - - - - - - - - R400....
C     THREE PARAMETER MODEL OF VAN GENUCHTEN(1980)                          R410....
      SWRM1=1.D0-SWRES                                                      R420....
      AAPVN=1.D0+(AA*(-PRES))**VN                                           R430....
      VNF=(VN-1.D0)/VN                                                      R440....
      AAPVNN=AAPVN**VNF                                                     R450....
      S W   =   SWRES+SWRM1/AAPVNN                                          R460....
C - - - - - - - - - - - - - - - - - - - - - - - - - - - - - - - - - - - - - R470....
C***********************************************************************R480....
C***********************************************************************R490....
C                                                                           R500....
C                                                                           R510....
```

```
C                                                                       R520....
C                                                                       R530....
C                                                                       R540....
C                                                                       R550....
      IF(IUNSAT-2) 600,1200,1800                                        R560....
C***********************************************************************R570....
C***********************************************************************R580....
C.....SECTION (2):                                                      R590....
C     DSWDP VS. PRES, OR DSWDP VS. SW   (CALCULATED ONLY WHEN IUNSAT=1) R600....
C     CODING MUST GIVE A VALUE TO DERIVATIVE OF SATURATION WITH         R610....
C     RESPECT TO PRESSURE, DSWDP.                                       R620....
C                                                                       R630....
  600 CONTINUE                                                          R640....
C - - - - - - - - - - - - - - - - - - - - - - - - - - - - - - - - - - - - R650....
      DNUM=AA*(VN-1.D0)*SWRM1*(AA*(-PRES))**(VN-1.D0)                   R660....
      DNOM=AAPVN*AAPVNN                                                 R670....
      D S W D P   =   DNUM/DNOM                                         R680....
C - - - - - - - - - - - - - - - - - - - - - - - - - - - - - - - - - - - - R690....
      GOTO 1800                                                         R700....
C***********************************************************************R710....
C***********************************************************************R720....
C                                                                       R730....
C                                                                       R740....
C                                                                       R750....
C                                                                       R760....
C                                                                       R770....
C                                                                       R780....
C***********************************************************************R790....
C***********************************************************************R800....
C.....SECTION (3):                                                      R810....
C     RELK VS. P, OR RELK VS. SW   (CALCULATED ONLY WHEN IUNSAT=2)      R820....
C     CODING MUST GIVE A VALUE TO RELATIVE PERMEABILITY, RELK.          R830....
C                                                                       R840....
 1200 CONTINUE                                                          R850....
C - - - - - - - - - - - - - - - - - - - - - - - - - - - - - - - - - - - - R860....
C     GENERAL RELATIVE PERMEABILITY MODEL FROM VAN GENUCHTEN(1980)      R870....
      SWSTAR=(SW-SWRES)/SWRM1                                           R880....
      R E L K   =   DSQRT(SWSTAR)*                                      R890....
     1                  (1.D0-(1.D0-SWSTAR**(1.D0/VNF))**(VNF))**2.D0  R900....
C - - - - - - - - - - - - - - - - - - - - - - - - - - - - - - - - - - - - R910....
C                                                                       R920....
C***********************************************************************R930....
C***********************************************************************R940....
C                                                                       R950....
C                                                                       R960....
C                                                                       R970....
C                                                                       R980....
C                                                                       R990....
C                                                                       R1000...
 1800 RETURN                                                            R1010...
C                                                                       R1020...
      END                                                               R1030...
C     SUBROUTINE        G  L  O  B  A  N        SUTRA - VERSION 1284-2D S10.....
C                                                                       S20.....
C *** PURPOSE :                                                         S30.....
C ***  TO ASSEMBLE RESULTS OF ELEMENTWISE INTEGRATIONS INTO             S40.....
C ***  A GLOBAL BANDED MATRIX AND GLOBAL VECTOR FOR BOTH                S50.....
C ***  FLOW AND TRANSPORT EQUATIONS.                                    S60.....
C                                                                       S70.....
      SUBROUTINE GLOBAN(L,ML,VOLE,BFLOWE,DFLOWE,BTRANE,DTRANE,          S80.....
     1   IN,VOL,PMAT,PVEC,UMAT,UVEC,CWRK)                               S90.....
```

```
      IMPLICIT DOUBLE PRECISION (A-H,O-Z)                                S100....
      COMMON/DIMS/ NN,NE,NIN,IS,JT,NBIP,NBIS,NPT(9),NPBC,NUBC,           S110NEW
     1   NSOP,NSOU,NBCN                                                  S120....
      COMMON/CNTRL1/ GNU,UP,DTMULT,DTMAX,ME,ISSFLO,ISSTRA,ITCYC,         S130NEW
     1   NPCYC,NUCYC,NPRINT,IREAD,ISTORE,NOUMAT,IUNSAT,ITIME             S140NEW
      DIMENSION BFLOWE(4,4),DFLOWE(4),BTRANE(4,4),DTRANE(4,4),VOLE(4)    S150....
      DIMENSION VOL(NN),PMAT(NN,NBIP),PVEC(NN),UMAT(NN,NBIS),UVEC(NN)    S160NEW
      DIMENSION CWRK(NN)                                                 NEW
      DIMENSION IN(NIN)                                                  S170....
C                                                                        S180....
      N1=(L-1)*4+1                                                       S190....
      N4=N1+3                                                            S200....
C                                                                        S210....
C.....ADD RESULTS OF INTEGRATIONS OVER ELEMENT L TO GLOBAL               S220....
C        P-MATRIX AND P-VECTOR                                           S230....
      IF(ML-1) 50,50,150                                                 S240....
   50 IE=0                                                               S250....
C       (NBHALF=1 FOR PRESSURE EQN)                                      NEW
        NBHALF=1                                                         NEW
        NBWR=JT+2                                                        NEW
      DO 100 II=N1,N4                                                    S260....
C       ZERO OUT WORK ARRAY                                              NEW
        DO 60 IR=1,NBWR                                                  NEW
   60   CWRK(IR)=0.0                                                     NEW
      IE=IE+1                                                            S270....
      IB=IN(II)                                                          S280....
      VOL(IB)=VOL(IB)+VOLE(IE)                                           S290....
      PVEC(IB)=PVEC(IB)+DFLOWE(IE)                                       S300....
      JE=0                                                               S310....
      DO 110 JJ=N1,N4                                                    S320....
      JE=JE+1                                                            S330....
C       SAVE ONLY SYMMETRIC HALF IN CONDENSED FORM                       NEW
      JB=IN(JJ)-IB+NBHALF                                                S340....
        IF(JB.LT.1) GO TO 110                                            NEW
      CWRK(JB)=CWRK(JB)+BFLOWE(IE,JE)                                    NEW
  110 CONTINUE                                                           NEW
C       ADD TERMS FROM WORK ARRAY TO GLOBAL MATRIX                       NEW
      DO 120 IR=1,NBIP                                                   NEW
      NR=NPT(IR+4)                                                       NEW
  120 PMAT(IB,IR)=PMAT(IB,IR)+CWRK(NR)                                   NEW
  100 CONTINUE                                                           NEW
      IF(ML-1) 150,300,150                                               S360....
C                                                                        S370....
C.....ADD RESULTS OF INTEGRATIONS OVER ELEMENT L TO GLOBAL               S380....
C        U-MATRIX                                                        S390....
  150 IF(NOUMAT.EQ.1) GOTO 300                                           S400....
      IE=0                                                               S410....
C       (NBHALF=JT+2 FOR TRANSPORT EQN)                                  NEW
        NBHALF=JT+2                                                      NEW
        NBWR=2*JT+3                                                      NEW
      DO 200 II=N1,N4                                                    S420....
C       ZERO OUT WORK ARRAY                                              NEW
        DO 70 IR=1,NBWR                                                  NEW
   70   CWRK(IR)=0.0                                                     NEW
      IE=IE+1                                                            S430....
      IB=IN(II)                                                          S440....
C.....POSITION FOR ADDITION TO U-VECTOR                                  S450....
C     UVEC(IB)=UVEC(IB)+ ((   ))                                         S460....
      JE=0                                                               S470....
      DO 210 JJ=N1,N4                                                    S480....
      JE=JE+1                                                            S490....
```

```
      JB=IN(JJ)-IB+NBHALF                                                S500....
C       SAVE FULL ROW IN CONDENSED FORM                                  NEW
      JB=IN(JJ)-IB+NBHALF                                                NEW
      CWRK(JB)=CWRK(JB)+DTRANE(IE,JE)+BTRANE(IE,JE)                      NEW
  210 CONTINUE                                                           NEW
C       ADD TERMS FROM WORK ARRAY TO GLOBAL MATRIX                       NEW
      DO 220 IR=1,NBIS                                                   NEW
      NR=NBHALF+NPT(IR)-1                                                NEW
  220 UMAT(IB,IR)=UMAT(IB,IR)+CWRK(NR)                                   NEW
  200 CONTINUE                                                           NEW
C                                                                        S520....
  300 CONTINUE                                                           S530....
C                                                                        S540....
C                                                                        S550....
      RETURN                                                             S560....
      END                                                                S570....
C     SUBROUTINE        N  O  D  A  L  B        SUTRA - VERSION 1284-2D  T10.....
C                                                                        T20.....
C *** PURPOSE :                                                          T30.....
C ***  (1) TO CARRY OUT ALL CELLWISE CALCULATIONS AND TO ADD CELLWISE    T40.....
C ***      TERMS TO THE GLOBAL BANDED MATRIX AND GLOBAL VECTOR FOR       T50.....
C ***      BOTH FLOW AND TRANSPORT EQUATIONS.                            T60.....
C ***  (2) TO ADD FLUID SOURCE AND SOLUTE MASS OR ENERGY SOURCE TERMS    T70.....
C ***      TO THE MATRIX EQUATIONS.                                      T80.....
C                                                                        T90.....
      SUBROUTINE NODALB(ML,VOL,PMAT,PVEC,UMAT,UVEC,PITER,UITER,PM1,UM1,  T100....
     1   UM2,POR,QIN,UIN,QUIN,CS1,CS2,CS3,SL,SR,SW,DSWDP,RHO,SOP)         T110....
      IMPLICIT DOUBLE PRECISION (A-H,O-Z)                                T120....
      COMMON/DIMS/ NN,NE,NIN,IS,JT,NBIP,NBIS,NPT(9),NPBC,NUBC,           T130NEW
     1   NSOP,NSOU,NBCN                                                  T140....
      COMMON/TIME/ DELT,TSEC,TMIN,THOUR,TDAY,TWEEK,TMONTH,TYEAR,         T150....
     1   TMAX,DELTP,DELTU,DLTPM1,DLTUM1,IT,ITMAX                         T160....
      COMMON/PARAMS/ COMPFL,COMPMA,DRWDU,CW,CS,RHOS,DECAY,SIGMAW,SIGMAS, T170....
     1   RHOW0,URHOW0,VISC0,PRODF1,PRODS1,PRODF0,PRODS0,CHI1,CHI2        T180....
      COMMON/SATPAR/ PCENT,SWRES,PCRES,SSLOPE,SINCPT                     T190....
      COMMON/CNTRL1/ GNU,UP,DTMULT,DTMAX,ME,ISSFLO,ISSTRA,ITCYC,         T200NEW
     1   NPCYC,NUCYC,NPRINT,IREAD,ISTORE,NOUMAT,IUNSAT,ITIME             T210NEW
      DIMENSION VOL(NN),PMAT(NN,NBIP),PVEC(NN),UMAT(NN,NBIS),UVEC(NN)    T220NEW
      DIMENSION PITER(NN),UITER(NN),PM1(NN),UM1(NN),UM2(NN),             T230....
     1   POR(NN),QIN(NN),UIN(NN),QUIN(NN),CS1(NN),CS2(NN),CS3(NN),       T240....
     2   SL(NN),SR(NN),SW(NN),RHO(NN),DSWDP(NN),SOP(NN)                  T250....
C                                                                        T260....
C                                                                        T270....
      IF(IUNSAT.NE.0) IUNSAT=1                                           T280....
C                                                                        T290....
C.....DO NOT UPDATE NODAL PARAMETERS ON A TIME STEP WHEN ONLY U IS       T300....
C     SOLVED FOR BY BACK SUBSTITUTION (IE: WHEN NOUMAT=1)                T310....
      IF(NOUMAT) 50,50,200                                               T320....
C.....SET UNSATURATED FLOW PARAMETERS AT NODES, SW(I) AND DSWDP(I)       T330....
   50 DO 120 I=1,NN                                                      T340....
      IF(IUNSAT-1) 120,100,120                                           T350....
  100 IF(PITER(I)) 110,120,120                                           T360....
  110 CALL UNSAT(SW(I),DSWDP(I),RELK,PITER(I))                           T370....
  120 CONTINUE                                                           T380....
C.....SET FLUID DENSITY AT NODES, RHO(I)                                 T390....
C     RHO = F (UITER(I))                                                 T400....
      DO 150 I=1,NN                                                      T410....
  150 RHO(I)=RHOW0+DRWDU*(UITER(I)-URHOW0)                               T420....
  200 CONTINUE                                                           T430....
C                                                                        T440....
      DO 1000 I=1,NN                                                     T450....
```

```
      SWRHON=SW(I)*RHO(I)                                                    T460....
C                                                                            T470....
      IF(ML-1) 220,220,230                                                   T480....
C                                                                            T490....
C.....CALCULATE CELLWISE TERMS FOR P EQUATION                                T500....
C.....FOR STEADY-STATE FLOW, ISSFLO=2; FOR TRANSIENT FLOW, ISSFLO=0          T510....
  220 AFLN=(1-ISSFLO/2)*                                                     T520....
     1   (SWRHON*SOP(I)+POR(I)*RHO(I)*DSWDP(I))*VOL(I)/DELTP                T530....
      CFLN=POR(I)*SW(I)*DRWDU*VOL(I)                                         T540....
      DUDT=(1-ISSFLO/2)*(UM1(I)-UM2(I))/DLTUM1                               T550....
      CFLN=CFLN*DUDT                                                         T560....
C.....ADD CELLWISE TERMS AND FLUID SOURCES OR FLUXES TO P EQUATION           T570....
C       LOAD TERMS ON DIAGONAL (NBHALF=1 FOR PRESSURE EQN)                   NEW
        NBHALF=1                                                             NEW
      PMAT(I,NBHALF) = PMAT(I,NBHALF) + AFLN                                 T580....
      PVEC(I) = PVEC(I) - CFLN + AFLN*PM1(I) + QIN(I)                        T590....
C                                                                            T600....
      IF(ML-1) 230,1000,230                                                  T610....
C                                                                            T620....
C.....CALCULATE CELLWISE TERMS FOR U-EQUATION                                T630....
  230 EPRS=(1.D0-POR(I))*RHOS                                                T640....
      ATRN=(1-ISSTRA)*(POR(I)*SWRHON*CW+EPRS*CS1(I))*VOL(I)/DELTU            T650....
      GTRN=POR(I)*SWRHON*PRODF1*VOL(I)                                       T660....
      GSV=EPRS*PRODS1*VOL(I)                                                 T670....
      GSLTRN=GSV*SL(I)                                                       T680....
      GSRTRN=GSV*SR(I)                                                       T690....
      ETRN=(POR(I)*SWRHON*PRODF0+EPRS*PRODS0)*VOL(I)                         T700....
C.....CALCULATE SOURCES OF SOLUTE OR ENERGY CONTAINED IN                     T710....
C     SOURCES OF FLUID (ZERO CONTRIBUTION FOR OUTFLOWING FLUID)              T720....
      QUR=0.0D0                                                              T730....
      QUL=0.0D0                                                              T740....
      IF(QIN(I)) 360,360,340                                                 T750....
  340 QUL=-CW*QIN(I)                                                         T760....
      QUR=-QUL*UIN(I)                                                        T770....
C.....ADD CELLWISE TERMS, SOURCES OF SOLUTE OR ENERGY IN FLUID INFLOWS,      T780....
C        AND PURE SOURCES OR FLUXES OF SOLUTE OR ENERGY TO U-EQUATION        T790....
  360 IF(NOUMAT) 370,370,380                                                 T800....
C       LOAD TERMS ON DIAGONAL (NBHALF=5 FOR TRANSPORT EQN)                  NEW
  370   NBHALF=5                                                             NEW
      UMAT(I,NBHALF) = UMAT(I,NBHALF) + ATRN - GTRN - GSLTRN - QUL           T810....
  380 UVEC(I) = UVEC(I) + ATRN*UM1(I) + ETRN + GSRTRN + QUR + QUIN(I)        T820....
C                                                                            T830....
 1000 CONTINUE                                                               T840....
C                                                                            T850....
      RETURN                                                                 T860....
      END                                                                    T870....
C     SUBROUTINE        B  C  B                SUTRA - VERSION 1284-2D     U10.....
C                                                                            U20.....
C *** PURPOSE :                                                              U30.....
C ***  TO IMPLEMENT SPECIFIED PRESSURE AND SPECIFIED TEMPERATURE OR          U40.....
C ***  CONCENTRATION CONDITIONS BY MODIFYING THE GLOBAL FLOW AND             U50.....
C ***  TRANSPORT MATRIX EQUATIONS.                                           U60.....
C                                                                            U70.....
      SUBROUTINE BCB(ML,PMAT,PVEC,UMAT,UVEC,IPBC,PBC,IUBC,UBC,QPLITR)        U80.....
      IMPLICIT DOUBLE PRECISION (A-H,O-Z)                                    U90.....
      COMMON/DIMS/ NN,NE,NIN,IS,JT,NBIP,NBIS,NPT(9),NPBC,NUBC,              U100NEW
     1   NSOP,NSOU,NBCN                                                      U110....
      COMMON/TIME/ DELT,TSEC,TMIN,THOUR,TDAY,TWEEK,TMONTH,TYEAR,             U120....
     1   TMAX,DELTP,DELTU,DLTPM1,DLTUM1,IT,ITMAX                             U130....
      COMMON/PARAMS/ COMPFL,COMPMA,DRWDU,CW,CS,RHOS,DECAY,SIGMAW,SIGMAS,     U140....
     1   RHOW0,URHOW0,VISC0,PRODF1,PRODS1,PRODF0,PRODS0,CHI1,CHI2            U150....
```

```
      COMMON/CNTRL1/ GNU,UP,DTMULT,DTMAX,ME,ISSFLO,ISSTRA,ITCYC,        U160NEW
     1   NPCYC,NUCYC,NPRINT,IREAD,ISTORE,NOUMAT,IUNSAT,ITIME            U170NEW
      DIMENSION PMAT(NN,NBIP),PVEC(NN),UMAT(NN,NBIS),UVEC(NN),         U180NEW
     1   IPBC(NBCN),PBC(NBCN),IUBC(NBCN),UBC(NBCN),QPLITR(NBCN)        U190....
C                                                                      U200....
C                                                                      U210....
      IF(NPBC.EQ.0) GOTO 1050                                          U220....
C.....SPECIFIED P BOUNDARY CONDITIONS                                  U230....
      DO 1000 IP=1,NPBC                                                U240....
      I=IABS(IPBC(IP))                                                 U250....
C                                                                      U260....
      IF(ML-1) 100,100,200                                             U270....
C.....MODIFY EQUATION FOR P BY ADDING FLUID SOURCE AT SPECIFIED        U280....
C        PRESSURE NODE                                                 U290....
  100 GINL=-GNU                                                        U300....
      GINR=GNU*PBC(IP)                                                 U310....
C       LOAD TERMS ON DIAGONAL (NBHALF=1 FOR PRESSURE EQN)             NEW
        NBHALF=1                                                       NEW
      PMAT(I,NBHALF)=PMAT(I,NBHALF)-GINL                               U320....
      PVEC(I)=PVEC(I)+GINR                                             U330....
C                                                                      U340....
      IF(ML-1) 200,1000,200                                            U350....
C.....MODIFY EQUATION FOR U BY ADDING U SOURCE WHEN FLUID FLOWS IN     U360....
C        AT SPECIFIED PRESSURE NODE                                    U370....
  200 GUR=0.0D0                                                        U380....
      GUL=0.0D0                                                        U390....
      IF(QPLITR(IP)) 360,360,340                                       U400....
  340 GUL=-CW*QPLITR(IP)                                               U410....
      GUR=-GUL*UBC(IP)                                                 U420....
  360 IF(NOUMAT) 370,370,380                                           U430....
C       LOAD TERMS ON DIAGONAL (NBHALF=5 FOR TRANSPORT EQN)            NEW
  370   NBHALF=5                                                       NEW
      UMAT(I,NBHALF)=UMAT(I,NBHALF)-GUL                                U440....
  380 UVEC(I)=UVEC(I)+GUR                                              U450....
 1000 CONTINUE                                                         U460....
C                                                                      U470....
C                                                                      U480....
 1050 IF(ML-1) 1100,3000,1100                                          U490....
C.....SPECIFIED U BOUNDARY CONDITIONS                                  U500....
C        MODIFY U EQUATION AT SPECIFIED U NODE TO READ: U = UBC        U510....
 1100 IF(NUBC.EQ.0) GOTO 3000                                          U520....
      DO 2000 IU=1,NUBC                                                U530....
      IUP=IU+NPBC                                                      U540....
      I=IABS(IUBC(IUP))                                                U550....
      IF(NOUMAT) 1200,1200,2000                                        U560....
 1200 DO 1500 JB=1,NBIS                                                U570....
 1500 UMAT(I,JB)=0.0D0                                                 U580....
C       LOAD TERMS ON DIAGONAL (NBHALF=5 FOR TRANSPORT EQN)            NEW
        NBHALF=5                                                       NEW
      UMAT(I,NBHALF)=1.0D0                                             U590....
 2000 UVEC(I)=UBC(IUP)                                                 U600....
C                                                                      U610....
 3000 CONTINUE                                                         U620....
C                                                                      U630....
C                                                                      U640....
      RETURN                                                           U650....
      END                                                              U660....
C     SUBROUTINE        B  U  D  G  E  T        SUTRA - VERSION 1284-2D X10.....
C                                                                      X20.....
C *** PURPOSE :                                                        X30.....
C ***  TO CALCULATE AND OUTPUT FLUID MASS AND SOLUTE MASS OR           X40.....
```

```
C ***  ENERGY BUDGETS.                                                  X50.....
C                                                                       X60.....
      SUBROUTINE BUDGET(ML,IBCT,VOL,SW,DSWDP,RHO,SOP,QIN,PVEC,PM1,      X70.....
     1   PBC,QPLITR,IPBC,IQSOP,POR,UVEC,UM1,UM2,UIN,QUIN,IQSOU,UBC,     X80.....
     2   CS1,CS2,CS3,SL,SR)                                             X90.....
      IMPLICIT DOUBLE PRECISION (A-H,O-Z)                               X100....
      CHARACTER*10 ADSMOD                                               X110....
      COMMON/FUNITS/ K00,K0,K1,K2,K3,K4,K5,K6,K7,K8                     MODIFIED
      COMMON/MODSOR/ ADSMOD                                             X120....
      COMMON/DIMS/ NN,NE,NIN,IS,JT,NBIP,NBIS,NPT(9),NPBC,NUBC,          X130NEW
     1   NSOP,NSOU,NBCN                                                 X140....
      COMMON/TIME/ DELT,TSEC,TMIN,THOUR,TDAY,TWEEK,TMONTH,TYEAR,        X150....
     1   TMAX,DELTP,DELTU,DLTPM1,DLTUM1,IT,ITMAX                        X160....
      COMMON/PARAMS/ COMPFL,COMPMA,DRWDU,CW,CS,RHOS,DECAY,SIGMAW,SIGMAS,X170....
     1   RHOW0,URHOW0,VISC0,PRODF1,PRODS1,PRODF0,PRODS0,CHI1,CHI2       X180....
      COMMON/CNTRL1/ GNU,UP,DTMULT,DTMAX,ME,ISSFLO,ISSTRA,ITCYC,        X190NEW
     1   NPCYC,NUCYC,NPRINT,IREAD,ISTORE,NOUMAT,IUNSAT  ,ITIME          X200NEW
      CHARACTER*13 UNAME(2)                                             X210....
      DIMENSION QIN(NN),UIN(NN),IQSOP(NSOP),QUIN(NN),IQSOU(NSOU)        X220....
      DIMENSION IPBC(NBCN),UBC(NBCN),QPLITR(NBCN),PBC(NBCN)             X230....
      DIMENSION POR(NN),VOL(NN),PVEC(NN),UVEC(NN),SW(NN),DSWDP(NN),     X240....
     1   RHO(NN),SOP(NN),PM1(NN),UM1(NN),UM2(NN),                       X250....
     2   CS1(NN),CS2(NN),CS3(NN),SL(NN),SR(NN)                          X260....
      DATA UNAME(1)/'CONCENTRATION'/,UNAME(2)/' TEMPERATURE '/          X270....
C                                                                       X280....
C                                                                       X290....
      MN=2                                                              X300....
      IF(IUNSAT.NE.0) IUNSAT=1                                          X310....
      IF(ME.EQ.-1) MN=1                                                 X320....
      WRITE(K3,10)                                                      X330....
   10 FORMAT(1H1)                                                       X340....
C.....SET UNSATURATED FLOW PARAMETERS, SW(I) AND DSWDP(I)               X350....
      IF(IUNSAT-1) 40,20,40                                             X360....
   20 DO 30 I=1,NN                                                      X370....
      IF(PVEC(I)) 25,27,27                                              X380....
   25 CALL UNSAT(SW(I),DSWDP(I),RELK,PVEC(I))                           X390....
      GOTO 30                                                           X400....
   27 SW(I)=1.0D0                                                       X410....
      DSWDP(I)=0.0D0                                                    X420....
   30 CONTINUE                                                          X430....
C                                                                       X440....
C.....CALCULATE COMPONENTS OF FLUID MASS BUDGET                         X450....
   40 IF(ML-1) 50,50,1000                                               X460....
   50 CONTINUE                                                          X470....
      STPTOT=0.D0                                                       X480....
      STUTOT=0.D0                                                       X490....
      QINTOT=0.D0                                                       X500....
      DO 100 I=1,NN                                                     X510....
      STPTOT=STPTOT+(1-ISSFLO/2)*RHO(I)*VOL(I)*                         X520....
     1   (SW(I)*SOP(I)+POR(I)*DSWDP(I))*(PVEC(I)-PM1(I))/DELTP          X530....
      STUTOT=STUTOT+(1-ISSFLO/2)*POR(I)*SW(I)*DRWDU*VOL(I)*             X540....
     1   (UM1(I)-UM2(I))/DLTUM1                                         X550....
      QINTOT=QINTOT+QIN(I)                                              X560....
  100 CONTINUE                                                          X570....
C                                                                       X580....
      QPLTOT=0.D0                                                       X590....
      DO 200 IP=1,NPBC                                                  X600....
      I=IABS(IPBC(IP))                                                  X610....
      QPLITR(IP)=GNU*(PBC(IP)-PVEC(I))                                  X620....
      QPLTOT=QPLTOT+QPLITR(IP)                                          X630....
  200 CONTINUE                                                          X640....
```

```
C                                                                       X650....
C.....OUTPUT FLUID MASS BUDGET                                          X660....
      WRITE(K3,300) IT,STPTOT,STUTOT,UNAME(MN),QINTOT,QPLTOT            X670....
  300 FORMAT(//11X,'F L U I D   M A S S   B U D G E T      AFTER TIME', X680....
     1   ' STEP ',I5,',     IN (MASS/SECOND)'///11X,1PD15.7,5X,         X690....
     2   'RATE OF CHANGE IN TOTAL STORED FLUID DUE TO PRESSURE CHANGE', X700....
     3   ', INCREASE(+)/DECREASE(-)',/11X,1PD15.7,5X,                   X710....
     2   'RATE OF CHANGE IN TOTAL STORED FLUID DUE TO ',A13,' CHANGE',  X720....
     3   ', INCREASE(+)/DECREASE(-)',                                   X730....
     3   /11X,1PD15.7,5X,'TOTAL OF FLUID SOURCES AND SINKS, ',          X740....
     4   'NET INFLOW(+)/NET OUTFLOW(-)'/11X,1PD15.7,5X,                 X750....
     5   'TOTAL OF FLUID FLOWS AT POINTS OF SPECIFIED PRESSURE, ',      X760....
     6   'NET INFLOW(+)/NET OUTFLOW(-)')                                X770....
C                                                                       X780....
      IF(IBCT.EQ.4) GOTO 600                                            X790....
      NSOPI=NSOP-1                                                      X800....
      INEGCT=0                                                          X810....
      DO 500 IQP=1,NSOPI                                                X820....
      I=IQSOP(IQP)                                                      X830....
      IF(I) 325,500,500                                                 X840....
  325 INEGCT=INEGCT+1                                                   X850....
      IF(INEGCT.EQ.1) WRITE(K3,350)                                     X860....
  350 FORMAT(///22X,'TIME-DEPENDENT FLUID SOURCES OR SINKS'//22X,       X870....
     1   ' NODE',5X,'INFLOW(+)/OUTFLOW(-)'/37X,'  (MASS/SECOND)'//)     X880....
      WRITE(K3,450) -I,QIN(-I)                                          X890....
  450 FORMAT(22X,I5,10X,1PD15.7)                                        X900....
  500 CONTINUE                                                          X910....
C                                                                       X920....
  600 IF(NPBC.EQ.0) GOTO 800                                            X930....
      WRITE(K3,650)                                                     X940....
  650 FORMAT(///22X,'FLUID SOURCES OR SINKS DUE TO SPECIFIED PRESSURES',X950....
     1   //22X,' NODE',5X,'INFLOW(+)/OUTFLOW(-)'/37X,'  (MASS/SECOND)'/)X960....
      DO 700 IP=1,NPBC                                                  X970....
      I=IABS(IPBC(IP))                                                  X980....
      WRITE(K3,450) I,QPLITR(IP)                                        X990....
  700 CONTINUE                                                          X1000...
C                                                                       X1010...
C.....CALCULATE COMPONENTS OF ENERGY OR SOLUTE MASS BUDGET              X1020...
  800 IF(ML-1) 1000,4500,1000                                           X1030...
 1000 CONTINUE                                                          X1040...
      FLDTOT=0.D0                                                       X1050...
      SLDTOT=0.D0                                                       X1060...
      P1FTOT=0.D0                                                       X1070...
      P1STOT=0.D0                                                       X1080...
      P0FTOT=0.D0                                                       X1090...
      P0STOT=0.D0                                                       X1100...
      QQUTOT=0.D0                                                       X1110...
      QIUTOT=0.D0                                                       X1120...
C.....SET ADSORPTION PARAMETERS                                         X1130...
      IF(ME.EQ.-1.AND.ADSMOD.NE.'NONE      ')                           X1140...
     1   CALL ADSORB(CS1,CS2,CS3,SL,SR,UVEC)                            X1150...
      DO 1300 I=1,NN                                                    X1160...
      ESRV=POR(I)*SW(I)*RHO(I)*VOL(I)                                   X1170...
      EPRSV=(1.D0-POR(I))*RHOS*VOL(I)                                   X1180...
      DUDT=(1-ISSTRA)*(UVEC(I)-UM1(I))/DELTU                            X1190...
      FLDTOT=FLDTOT+ESRV*CW*DUDT                                        X1200...
      SLDTOT=SLDTOT+EPRSV*CS1(I)*DUDT                                   X1210...
      P1FTOT=P1FTOT+ESRV*PRODF1                                         X1220...
      P1STOT=P1STOT+EPRSV*PRODS1*(SL(I)*UVEC(I)+SR(I))                  X1230...
      P0FTOT=P0FTOT+ESRV*PRODF0                                         X1240...
      P0STOT=P0STOT+EPRSV*PRODS0                                        X1250...
```

```
      QQUTOT=QQUTOT+QUIN(I)                                                 X1260...
      IF(QIN(I)) 1200,1200,1250                                             X1270...
 1200 QIUTOT=QIUTOT+QIN(I)*CW*UVEC(I)                                       X1280...
      GOTO 1300                                                             X1290...
 1250 QIUTOT=QIUTOT+QIN(I)*CW*UIN(I)                                        X1300...
 1300 CONTINUE                                                              X1310...
C                                                                           X1320...
      QPUTOT=0.D0                                                           X1330...
      DO 1500 IP=1,NPBC                                                     X1340...
      IF(QPLITR(IP)) 1400,1400,1450                                         X1350...
 1400 I=IABS(IPBC(IP))                                                      X1360...
      QPUTOT=QPUTOT+QPLITR(IP)*CW*UVEC(I)                                   X1370...
      GOTO 1500                                                             X1380...
 1450 QPUTOT=QPUTOT+QPLITR(IP)*CW*UBC(IP)                                   X1390...
 1500 CONTINUE                                                              X1400...
C                                                                           X1410...
      IF(ME) 1550,1550,1615                                                 X1420...
C                                                                           X1430...
C.....OUTPUT SOLUTE MASS BUDGET                                             X1440...
 1550 WRITE(K3,1600) IT,FLDTOT,SLDTOT,P1FTOT,P1STOT,P0FTOT,P0STOT,          X1450...
     1   QIUTOT,QPUTOT,QQUTOT                                               X1460...
 1600 FORMAT(//11X,'S O L U T E   B U D G E T      AFTER TIME STEP ',I5,X1470...
     1   ',   IN (SOLUTE MASS/SECOND)'///11X,1PD15.7,5X,'NET RATE OF ',     X1480...
     2   'INCREASE(+)/DECREASE(-) OF SOLUTE'/11X,1PD15.7,5X,                X1490...
     3   'NET RATE OF INCREASE(+)/DECREASE(-) OF ADSORBATE'/11X,1PD15.7,X1500...
     4   5X,'NET FIRST-ORDER PRODUCTION(+)/DECAY(-) OF SOLUTE'/11X,         X1510...
     5   1PD15.7,5X,'NET FIRST-ORDER PRODUCTION(+)/DECAY(-) OF ',           X1520...
     6   'ADSORBATE'/11X,1PD15.7,5X,'NET ZERO-ORDER PRODUCTION(+)/',        X1530...
     7   'DECAY(-) OF SOLUTE'/11X,1PD15.7,5X,'NET ZERO-ORDER ',             X1540...
     8   'PRODUCTION(+)/DECAY(-) OF ADSORBATE'/11X,1PD15.7,5X,              X1550...
     9   'NET GAIN(+)/LOSS(-) OF SOLUTE THROUGH FLUID SOURCES AND SINKS'X1560...
     *   /11X,1PD15.7,5X,'NET GAIN(+)/LOSS(-) OF SOLUTE THROUGH ',          X1570...
     1   'INFLOWS OR OUTFLOWS AT POINTS OF SPECIFIED PRESSURE'              X1580...
     2   /11X,1PD15.7,5X,'NET GAIN(+)/LOSS(-) OF SOLUTE THROUGH ',          X1590...
     3   'SOLUTE SOURCES AND SINKS')                                        X1600...
      GOTO 1645                                                             X1610...
C                                                                           X1620...
C.....OUTPUT ENERGY BUDGET                                                  X1630...
 1615 WRITE(K3,1635) IT,FLDTOT,SLDTOT,P0FTOT,P0STOT,QIUTOT,QPUTOT,QQUTOTX1640...
 1635 FORMAT(//11X,'E N E R G Y   B U D G E T      AFTER TIME STEP ',I5,X1650...
     1   ',   IN (ENERGY/SECOND)'///11X,1PD15.7,5X,'NET RATE OF ',           X1660...
     2   'INCREASE(+)/DECREASE(-) OF ENERGY IN FLUID'/11X,1PD15.7,5X,       X1670...
     3   'NET RATE OF INCREASE(+)/DECREASE(-) OF ENERGY IN SOLID GRAINS'X1680...
     4   /11X,1PD15.7,5X,'NET ZERO-ORDER PRODUCTION(+)/LOSS(-) OF ',        X1690...
     5   'ENERGY IN FLUID'/11X,1PD15.7,5X,'NET ZERO-ORDER ',                X1700...
     6   'PRODUCTION(+)/LOSS(-) OF ENERGY IN SOLID GRAINS'                  X1710...
     7   /11X,1PD15.7,5X,'NET GAIN(+)/LOSS(-) OF ENERGY THROUGH FLUID ',X1720...
     8   'SOURCES AND SINKS'/11X,1PD15.7,5X,'NET GAIN(+)/LOSS(-) OF ',      X1730...
     9   'ENERGY THROUGH INFLOWS OR OUTFLOWS AT POINTS OF SPECIFIED ',      X1740...
     *   'PRESSURE'/11X,1PD15.7,5X,'NET GAIN(+)/LOSS(-) OF ENERGY ',        X1750...
     1   'THROUGH ENERGY SOURCES AND SINKS')                                X1760...
C                                                                           X1770...
 1645 NSOPI=NSOP-1                                                          X1780...
      IF(NSOPI.EQ.0) GOTO 2000                                              X1790...
      IF(ME) 1649,1649,1659                                                 X1800...
 1649 WRITE(K3,1650)                                                        X1810...
 1650 FORMAT(///22X,'SOLUTE SOURCES OR SINKS AT FLUID SOURCES AND ',        X1820...
     1   'SINKS'//22X,' NODE',8X,'SOURCE(+)/SINK(-)'/32X,                   X1830...
     2   '(SOLUTE MASS/SECOND)'/)                                           X1840...
      GOTO 1680                                                             X1850...
 1659 WRITE(K3,1660)                                                        X1860...
```

```
 1660 FORMAT(///22X,'ENERGY SOURCES OR SINKS AT FLUID SOURCES AND ',    X1870...
     1   'SINKS'//22X,' NODE',8X,'SOURCE(+)/SINK(-)'/37X,               X1880...
     2   '(ENERGY/SECOND)'/)                                            X1890...
 1680 DO 1900 IQP=1,NSOPI                                              X1900...
      I=IABS(IQSOP(IQP))                                               X1910...
      IF(QIN(I)) 1700,1700,1750                                        X1920...
 1700 QU=QIN(I)*CW*UVEC(I)                                             X1930...
      GOTO 1800                                                        X1940...
 1750 QU=QIN(I)*CW*UIN(I)                                              X1950...
 1800 WRITE(K3,450) I,QU                                               X1960...
 1900 CONTINUE                                                         X1970...
C                                                                      X1980...
 2000 IF(NPBC.EQ.0) GOTO 4500                                          X1990...
      IF(ME) 2090,2090,2150                                            X2000...
 2090 WRITE(K3,2100)                                                   X2010...
 2100 FORMAT(///22X,'SOLUTE SOURCES OR SINKS DUE TO FLUID INFLOWS OR ', X2020...
     1   'OUTFLOWS AT POINTS OF SPECIFIED PRESSURE'//22X,' NODE',8X,    X2030...
     2   'SOURCE(+)/SINK(-)'/32X,'(SOLUTE MASS/SECOND)'/)               X2040...
      GOTO 2190                                                        X2050...
 2150 WRITE(K3,2160)                                                   X2060...
 2160 FORMAT(///22X,'ENERGY SOURCES OR SINKS DUE TO FLUID INFLOWS OR ', X2070...
     1   'OUTFLOWS AT POINTS OF SPECIFIED PRESSURE'//22X,' NODE',8X,    X2080...
     2   'SOURCE(+)/SINK(-)'/37X,'(ENERGY/SECOND)'/)                    X2090...
 2190 DO 2400 IP=1,NPBC                                                X2100...
      I=IABS(IPBC(IP))                                                 X2110...
      IF(QPLITR(IP)) 2200,2200,2250                                    X2120...
 2200 QPU=QPLITR(IP)*CW*UVEC(I)                                        X2130...
      GOTO 2300                                                        X2140...
 2250 QPU=QPLITR(IP)*CW*UBC(IP)                                        X2150...
 2300 WRITE(K3,450) I,QPU                                              X2160...
 2400 CONTINUE                                                         X2170...
C                                                                      X2180...
      IF(IBCT.EQ.4) GOTO 4500                                          X2190...
      NSOUI=NSOU-1                                                     X2200...
      INEGCT=0                                                         X2210...
      DO 3500 IQU=1,NSOUI                                              X2220...
      I=IQSOU(IQU)                                                     X2230...
      IF(I) 3400,3500,3500                                             X2240...
 3400 INEGCT=INEGCT+1                                                  X2250...
      IF(ME) 3450,3450,3460                                            X2260...
 3450 IF(INEGCT.EQ.1) WRITE(K3,3455)                                   X2270...
 3455 FORMAT(///22X,'TIME-DEPENDENT SOLUTE SOURCES AND SINKS'//22X,    X2280...
     1   ' NODE',10X,'GAIN(+)/LOSS(-)'/30X,'  (SOLUTE MASS/SECOND)'//) X2290...
      GOTO 3475                                                        X2300...
 3460 IF(INEGCT.EQ.1) WRITE(K3,3465)                                   X2310...
 3465 FORMAT(///22X,'TIME-DEPENDENT ENERGY SOURCES AND SINKS'//22X,    X2320...
     1   ' NODE',10X,'GAIN(+)/LOSS(-)'/35X,'  (ENERGY/SECOND)'//)      X2330...
 3475 CONTINUE                                                         X2340...
      WRITE(K3,3490) -I,QUIN(-I)                                       X2350...
 3490 FORMAT(22X,I5,10X,1PD15.7)                                       X2360...
 3500 CONTINUE                                                         X2370...
C                                                                      X2380...
C                                                                      X2390...
 4500 CONTINUE                                                         X2400...
C                                                                      X2410...
      RETURN                                                           X2420...
      END                                                              X2430...
C     SUBROUTINE        S  T  O  R  E          SUTRA - VERSION 1284-2D Y10.....
C                                                                      Y20.....
C *** PURPOSE :                                                        Y30.....
C ***  TO STORE RESULTS THAT MAY LATER BE USED TO RE-START             Y40.....
```

```
C ***  THE SIMULATION.                                                  Y50.....
C                                                                       Y60.....
      SUBROUTINE STORE(PVEC,UVEC,PM1,UM1,CS1,RCIT,SW,PBC)               Y70.....
      IMPLICIT DOUBLE PRECISION (A-H,O-Z)                               Y80.....
      COMMON/FUNITS/ K00,K0,K1,K2,K3,K4,K5,K6,K7,K8                     MODIFIED
      COMMON/DIMS/ NN,NE,NIN,IS,JT,NBIP,NBIS,NPT(9),NPBC,NUBC,          Y90NEW
     1   NSOP,NSOU,NBCN                                                 Y100....
      COMMON/TIME/ DELT,TSEC,TMIN,THOUR,TDAY,TWEEK,TMONTH,TYEAR,        Y110....
     1   TMAX,DELTP,DELTU,DLTPM1,DLTUM1,IT,ITMAX                        Y120....
      DIMENSION PVEC(NN),UVEC(NN),PM1(NN),UM1(NN),CS1(NN),RCIT(NN),     Y130....
     1   SW(NN),PBC(NBCN)                                               Y140....
C                                                                       Y150....
C.....REWIND UNIT-66 FOR WRITING RESULTS OF CURRENT TIME STEP           Y160....
      REWIND(66)                                                        Y170....
C                                                                       Y180....
C.....STORE TIME INFORMATION                                            Y190....
      WRITE(K4,100) TSEC,DELTP,DELTU                                    Y200....
  100 FORMAT(4D20.10)                                                   Y210....
C                                                                       Y220....
C.....STORE SOLUTION                                                    Y230....
      WRITE(K4,110) (PVEC(I),I=1,NN)                                    Y240....
      WRITE(K4,110) (UVEC(I),I=1,NN)                                    Y250....
      WRITE(K4,110) (PM1(I),I=1,NN)                                     Y260....
      WRITE(K4,110) (UM1(I),I=1,NN)                                     Y270....
      WRITE(K4,110) (CS1(I),I=1,NN)                                     Y280....
      WRITE(K4,110) (RCIT(I),I=1,NN)                                    Y290....
      WRITE(K4,110) (SW(I),I=1,NN)                                      Y300....
      WRITE(K4,110) (PBC(IP),IP=1,NBCN)                                 Y310....
  110 FORMAT(4(1PD20.13))                                               Y320....
C                                                                       Y330....
      ENDFILE(K4)                                                       Y340....
C                                                                       Y350....
      RETURN                                                            Y360....
      END                                                               Y370....
C     SUBROUTINE        F  O  P  E  N          SUTRA - VERSION 0690-2D Z10....MODIFIED
C                                                                       Z20....MODIFIED
C *** PURPOSE :                                                         Z30....MODIFIED
C ***  OPENS FILES FOR SUTRA SIMULATION.                                Z40....MODIFIED
C ***  OPENS ERROR OUTPUT FILE, READS FILE NUMBERS AND NAMES,           Z50....MODIFIED
C ***  CHECKS FOR EXISTENCE OF INPUT FILES, AND WRITES ERROR MESSAGES.  Z60....MODIFIED
C                                                                       Z70....MODIFIED
      SUBROUTINE FOPEN(UNAME,ENAME,FNAME,IUNIT,NFILE)                   Z90....MODIFIED
      CHARACTER*80 FN,UNAME,ENAME,FNAME                                 Z100...MODIFIED
      LOGICAL IS                                                        Z110...MODIFIED
      COMMON/FUNITS/ K00,K0,K1,K2,K3,K4,K5,K6,K7,K8                     Z120...MODIFIED
      DIMENSION FNAME(8),IUNIT(8)                                       Z130...MODIFIED
C                                                                       Z140...MODIFIED
C.....OPEN FILE UNIT CONTAINING UNIT NUMBERS AND FILE ASSIGNMENTS       Z150...MODIFIED
      IU=K0                                                             Z160...MODIFIED
      FN=UNAME                                                          Z170...MODIFIED
      INQUIRE(FILE=UNAME,EXIST=IS)                                      Z180...MODIFIED
      IF(IS) THEN                                                       Z190...MODIFIED
       OPEN(UNIT=IU,FILE=UNAME,STATUS='OLD',FORM='FORMATTED',           Z200...MODIFIED
     1   IOSTAT=KERR)                                                   Z210...MODIFIED
      ELSE                                                              Z220...MODIFIED
       GOTO 8000                                                        Z230...MODIFIED
      ENDIF                                                             Z240...MODIFIED
      IF(KERR.GT.0) GOTO 9000                                           Z250...MODIFIED
C                                                                       Z260...MODIFIED
C.....READ FILE CONTAINING UNIT NUMBERS AND FILE ASSIGNMENTS            Z270...MODIFIED
      NFILE=0                                                           Z280...MODIFIED
```

```
  100 READ(K0,*,END=200) IU                                              Z290...MODIFIED
      READ(K0,150,END=200) FN                                            Z300...MODIFIED
  150 FORMAT(A80)                                                        Z310...MODIFIED
      NFILE=NFILE+1                                                      Z320...MODIFIED
      IUNIT(NFILE)=IU                                                    Z330...MODIFIED
      FNAME(NFILE)=FN                                                    Z340...MODIFIED
      GOTO 100                                                           Z350...MODIFIED
  200 CONTINUE                                                           Z360...MODIFIED
C.....CHECK FOR EXISTENCE OF INPUT FILES                                 Z370...MODIFIED
C        AND OPEN BOTH INPUT AND OUTPUT FILES                            Z380...MODIFIED
      DO 300 NF=1,NFILE                                                  Z390...MODIFIED
      IU=IUNIT(NF)                                                       Z400...MODIFIED
      FN=FNAME(NF)                                                       Z410...MODIFIED
      IF(NF.LE.2) THEN                                                   Z420...MODIFIED
       INQUIRE(FILE=FN,EXIST=IS)                                         Z430...MODIFIED
       IF(IS) THEN                                                       Z440...MODIFIED
        OPEN(UNIT=IU,FILE=FN,STATUS='OLD',FORM='FORMATTED',IOSTAT=KERR)  Z450...MODIFIED
       ELSE                                                              Z460...MODIFIED
        GOTO 8000                                                        Z470...MODIFIED
       ENDIF                                                             Z480...MODIFIED
      ELSE                                                               Z490...MODIFIED
       OPEN(UNIT=IU,FILE=FN,STATUS='UNKNOWN',FORM='FORMATTED',           Z500...MODIFIED
     1    IOSTAT=KERR)                                                   Z510...MODIFIED
      ENDIF                                                              Z520...MODIFIED
      IF(KERR.GT.0) GOTO 9000                                            Z530...MODIFIED
  300 CONTINUE                                                           Z540...MODIFIED
      K1=IUNIT(1)                                                        Z550...MODIFIED
      K2=IUNIT(2)                                                        Z560...MODIFIED
      K3=IUNIT(3)                                                        Z570...MODIFIED
      K4=IUNIT(4)                                                        Z580...MODIFIED
      K5=IUNIT(5)                                                        Z581...MODIFIED
      K6=IUNIT(6)                                                        Z582...MODIFIED
      K7=IUNIT(7)                                                        Z583...MODIFIED
      K8=IUNIT(8)                                                        Z584...MODIFIED
      RETURN                                                             Z590...MODIFIED
C                                                                        Z600...MODIFIED
C.....OPEN FILE UNIT FOR ERROR MESSAGES                                  Z610...MODIFIED
 8000 OPEN(UNIT=K00,FILE=ENAME,STATUS='UNKNOWN',FORM='FORMATTED')        Z620...MODIFIED
C.....WRITE ERROR MESSAGE AND STOP                                       Z630...MODIFIED
      WRITE(K00,8888) FN                                                 Z640...MODIFIED
 8888 FORMAT('* E R R O R *'/'THE FILE:'/A80/'DOES NOT EXIST!')          Z650...MODIFIED
      ENDFILE(K00)                                                       Z660...MODIFIED
      STOP                                                               Z670...MODIFIED
C                                                                        Z680...MODIFIED
C.....OPEN FILE UNIT FOR ERROR MESSAGES                                  Z690...MODIFIED
 9000 OPEN(UNIT=K00,FILE=ENAME,STATUS='UNKNOWN',FORM='FORMATTED') Z700...MODIFIED
C.....WRITE ERROR MESSAGE AND STOP                                       Z710...MODIFIED
      WRITE(K00,9999) IU,FN                                              Z720...MODIFIED
 9999 FORMAT('* E R R O R *'/'UNIT ',I3/'ASSIGNED TO FILE:'/A80/         Z730...MODIFIED
     1   'CANNOT BE OPENED!')                                            Z740...MODIFIED
      ENDFILE(K00)                                                       Z750...MODIFIED
      STOP                                                               Z760...MODIFIED
C                                                                        Z770...MODIFIED
      END                                                                Z780...MODIFIED
```

Appendix III

Subprograms SOLVEC and LSORA Used to Solve System of Equations

```
C     SUBROUTINE   N E W   S O L V E
C.....SUBROUTINE   N E W   S O L V E
C
C.....PURPOSE: SOLVE FLOW EQUATIONS USING THE INCOMPLETE
C               CHOLESKY-CONJUGATE GRADIENT TECHNIQUE
C
C.....SOLVE SYSTEM OF EQUATIONS FOR FLOW
C
      SUBROUTINE SOLVEC(NBW,A,OLDH,RHS,P,R,AP,XK1,AB)
      IMPLICIT DOUBLE PRECISION (A-H,O-Z)
      COMMON/FUNITS/ K00,K0,K1,K2,K3,K4,K5,K6,K7,K8
      COMMON/DIMS/ NN,NE,NIN,IS,JT,NBIP,NBIS,NPT(9),NPBC,NUBC,
     1   NSOP,NSOU,NBCN
      COMMON/ITERAT/ RPM,RPMAX,RUM,RUMAX,ITER,ITRMAX,IPWORS,IUWORS,
     1               ICON,ITRMX2,OMEGA,RPMX2,RUMX2
      DIMENSION A(NN,NBW),OLDH(NN),RHS(NN)
      DIMENSION P(NN),R(NN),AP(NN),XK1(NN),AB(NN,5)
C
      EPS1=RPMX2
C
C.....INITIALIZE R1 AND P1, AND STORE OLDH IN RHS FOR ITERATIVE SOLUTION
      CALL MATMLP(A,OLDH,R,NBW)
      DO 20 I=1,NN
      R(I)=RHS(I)-R(I)
      RHS(I)=OLDH(I)
20    CONTINUE
        IDC=0
        CALL SDCOMP(A,AB,R,P,NBW,IDC)
        IDC=1
        CALL SDCOMP(A,AB,R,P,NBW,IDC)
C
C.....BEGIN ITERATIVE LOOP -- SOLUTION MUST CONVERGE IN NN ITERATIONS
      NN1=NN+1
      DO 30 ITR=1,NN1
      CALL MATMLP(A,P,AP,NBW)
C
C.....FORM DOT PRODUCT OF P AND AP AND STORE IT AS LAMDA
      XLAM=0.0
      DO 110 K=1,NN
110   XLAM=XLAM+P(K)*AP(K)
        IDC=1
        CALL SDCOMP(A,AB,R,XK1,NBW,IDC)
C
C.....FORM DOT PRODUCT OF R AND XK1 AND STORE IT AS RR1
      RR1=0.0
      DO 120 K=1,NN
120   RR1=RR1+R(K)*XK1(K)
C
C.....UPDATE H (BUT STORE IT IN RHS)
C.....UPDATE R AND XKI AND CHECK MAXIMUM ERROR
      ALPHA=RR1/XLAM
      RMAX=0.0
      DO 40 J=1,NN
      RHS(J)=RHS(J)+ALPHA*P(J)
```

```
      R(J)=R(J)-ALPHA*AP(J)
      RABS=DABS(R(J))
40    IF(RABS.GT.RMAX) RMAX=RABS
C
C.....CHECK IF METHOD HAS CONVERGED
      IF(RMAX.LT.EPS1) GOTO 70
C
C.....CHECK IF USER SPECIFIED ITERATION LIMIT IS EXCEEDED
      IF(ITR.GE.ITRMX2) GOTO 50
C
      IF(MOD(ITR,10).EQ.0) WRITE(6,533) ITR,RMAX
C
C.....UPDATE P AND GO ON TO NEXT ITERATION
        IDC=1
        CALL SDCOMP(A,AB,R,XK1,NBW,IDC)
C       FORM DOT PRODUCT OF R AND XK1 AND STORE IT AS RR2
      RR2=0.0
      DO 130 K=1,NN
130   RR2=RR2+R(K)*XK1(K)
      BETA= RR2/RR1
        DO 35 J=1,NN
35      P(J)=XK1(J)+BETA*P(J)
30    CONTINUE
70    CONTINUE
      WRITE(K3,99) ITR
99    FORMAT(/10X,'ICCG METHOD CONVERGED IN',I5,' ITERATIONS')
      GO TO 60
50    WRITE(K3,98) ITRMX2
98    FORMAT(//,5X,'FAILED TO CONVERGE AFTER ',I6,' ITERATIONS'/
     1       /,5X,'PROGRAM WILL STOP')
533   FORMAT(1H ,3X,'RMAX AT ITERATION',I5,' =',1P1E15.5)
      STOP 151
60    RETURN
      END

C
C     SUBROUTINE MATMLP-- WRITTEN BY E.J. WEXLER
C     PURPOSE: TO MULTIPLY A VECTOR B BY A NN X NN BANDED MATRIX
C     WITH ONLY THE UPPER NON-ZERO BANDS OF A STORED.
C
C       LOOP THROUGH ALL ROWS OF MATRIX A

      SUBROUTINE MATMLP (A,B,C,NBW)
      IMPLICIT DOUBLE PRECISION (A-H,O-Z)
      COMMON/DIMS/ NN,NE,NIN,IS,JT,NBIP,NBIS,NPT(9),NPBC,NUBC,
     1   NSOP,NSOU,NBCN
      DIMENSION A(NN,NBW),B(NN),C(NN)
      DO 100 K=1,NN
      SUM=0.0
      DO 300 J=1,NBW
      NPTJ=NPT(J+4)
      IC1=NPTJ+K-1
      IC2=K-NPTJ+1
```

```
      IF(IC1.LE.NN) SUM=SUM+A(K,J)*B(IC1)
      IF (J.LT.2) GOTO 300
      IF(IC2.GT.0) SUM=SUM+A(IC2,J)*B(IC2)
300   CONTINUE
      C(K)=SUM
100   CONTINUE
      RETURN
      END

C
C          SDCOMP--MODIFIED BY E.J. WEXLER TO DO AN INCOMPLETE
C     C         CHOLESKY DECOMPOSITION OF A SYMMETRIC BANDED MATRIX
C                 SSOLVE DOES THE FOWARD AND BACKWARDS SUBSTITUTION

      SUBROUTINE SDCOMP (A,AB,R,XK1,NBW,IDC)
      IMPLICIT DOUBLE PRECISION (A-H,O-Z)
      COMMON/FUNITS/ K00,K0,K1,K2,K3,K4,K5,K6,K7,K8
      COMMON/DIMS/ NN,NE,NIN,IS,JT,NBIP,NBIS,NPT(9),NPBC,NUBC,
     1   NSOP,NSOU,NBCN
      DIMENSION A(NN,NBW),AB(NN,5),R(NN),XK1(NN)
C
      IF(IDC.GT.0) GOTO 300
C
C.....DECOMPOSE SYM. MATRIX A AND STORE IN AB
      DO 100 K=1,NN
      DO 100 J=1,NBW
      NPTJ=NPT(J+4)
      IC1=NPTJ+K-1
      IF (IC1.GT.NN) GO TO 100
      SUM=A(K,J)
      DO 10 L=2,NBW
      NPTL=NPT(L+4)
      IC2=K-NPTL+1
      IF (IC2.LT.1) GO TO 10
      IC3=NPTJ+NPTL-1
      M=J+L-1
      IF (M.GT.NBW) GO TO 10
      NPTM=NPT(M+4)
      IF(NPTM.NE.IC3) GO TO 10
      SUM=SUM-AB(IC2,L)*AB(IC2,M)
   10 CONTINUE
      IF (NPTJ.EQ.1) THEN
C         STOP IF DIVIDING BY ZERO.
        IF (SUM.LE.0.0) THEN
C          WRITE (*,120) K,SUM
C          WRITE (K3,120) K,SUM
          STOP
        END IF
        ADIAGN=1./DSQRT(SUM)
        AB(K,J)=ADIAGN
      END IF
      IF (NPTJ.GT.1) AB(K,J)=SUM*ADIAGN
  100 CONTINUE
      RETURN
```

```
C
C     ************
C     ENTRY SSOLVE
C
C.....FORWARD SUBSTITUTE FOR LOWER TRIANGLE
300   DO 80 K=1,NN
      SUM=R(K)
      DO 60 J=2,NBW
      NPTJ=NPT(J+4)
      IC2=K-NPTJ+1
      IF (IC2.LT.1) GO TO 80
      SUM=SUM-AB(IC2,J)*XK1(IC2)
   60 CONTINUE
   80 XK1(K)=SUM*AB(K,1)
C
C.....BACKWARD SUBSTITUTE FOR UPPER TRIANGLE
      DO 110 K=1,NN
      IJ=NN-K+1
      SUM=XK1(IJ)
      DO 90 J=2,NBW
      NPTJ=NPT(J+4)
      IC1=NPTJ+IJ-1
      IF (IC1.GT.NN) GO TO 110
   90 SUM=SUM-AB(IJ,J)*XK1(IC1)
  110 XK1(IJ)=SUM*AB(IJ,1)
      RETURN
C
C
  120 FORMAT (1H1,5X,'**ERROR**',5X,'DIVIDE BY ZERO AT LINE ',I4,' IN DE
     1COMPOSITION ROUTINE',3X,'SUM =',1P1E13.5)
      END

C
C     SUBROUTINE LSORA
C
C     SOLVE SYSTEM OF EQUATIONS FOR TRANSPORT
C
C       LINE-SUCCESSIVE OVER-RELAXATION TECHNIQUE (LSOR)
C         A = FULL ASYMETRIC MATRIX
C         B = RHS (SOLUTION IS LOADED INTO B AT END)
C         X0 = INITIAL GUESS
C         X = SOLUTION VECTOR
C         AA = WORK ARRAYS FOR LSOR SOLUTION
C       LOAD X0 INTO X AS INITIAL GUESS
      SUBROUTINE LSORA (NBW,A,B,X0,X,XP,AA)
      IMPLICIT DOUBLE PRECISION (A-H,O-Z)
      COMMON/FUNITS/ K00,K0,K1,K2,K3,K4,K5,K6,K7,K8
      COMMON/DIMS/ NN,NE,NIN,IS,JT,NBIP,NBIS,NPT(9),NPBC,NUBC,
     1   NSOP,NSOU,NBCN
      COMMON/ITERAT/ RPM,RPMAX,RUM,RUMAX,ITER,ITRMAX,IPWORS,IUWORS,
     1               ICON,ITRMX2,OMEGA,RPMX2,RUMX2
      DIMENSION A(NN,NBW),B(NN),X0(NN),X(NN),AA(NN,5),XP(NN)
      EPS=RUMX2
```

```
      DO 5 I=1,NN
      XP(I)=X0(I)
5     X(I)=XP(I)
C
C.....BEGIN ITERATION LOOP
      ITER1 = 0
10    ITER1 = ITER1 + 1
C
C.....LOOP THROUGH ALL I
      DO 50 I=1,IS
      II=(I-1)*JT
C
C.....LOAD COEFFICIENTS FOR LINE INTO AA
      DO 20 J=1,JT
      JJ=II+J
      AA(J,1)=A(JJ,4)
      AA(J,2)=A(JJ,5)
      AA(J,3)=A(JJ,6)
      DD=B(JJ)
      DO 30 K=1,3
      NPTK=NPT(K+6)
      IC1=JJ+NPTK-1
      IF(IC1.LE.NN) DD=DD-A(JJ,K+6)*X(IC1)
      NPTK=NPT(K)
      IC2=JJ+NPTK-1
      IF(IC2.GE.1) DD=DD-A(JJ,K)*X(IC2)
30    CONTINUE
      AA(J,4)=DD
20    CONTINUE
C
C.....SOLVE ROW EQUATIONS USING THOMAS ALGORITHM
      CALL THOMAS (AA,JT,NN)
C
C.....LOAD NEW BLOCK VALUES INTO X ARRAY
      DO 45 J=1,JT
      JJ=II+J
      X(JJ)=XP(JJ) + OMEGA*(AA(J,5)-XP(JJ))
45    CONTINUE
50    CONTINUE
C
C.....FIND LARGEST CHANGE AND STORE NEW VALUE FOR X(I) IN XP(I)
      DIFMAX=0.0
      DO 40 I=1,NN
      DIF = DABS(X(I)-XP(I))
      IF(DIF.GT.DIFMAX) DIFMAX=DIF
      XP(I)=X(I)
40    CONTINUE
C
C.....CHECK FOR MAXIMUM NUMBER OF ITERATIONS
      IF (ITER1.GT.ITRMX2) THEN
        WRITE (K3,901)
901     FORMAT (5X,'MAXIMUM ITERATIONS EXCEEDED, PROGRAM WILL STOP')
        STOP
      END IF
```

```
C
C.....CHECK FOR CONVERGENCE
      IF (MOD(ITER1,10).EQ.0) WRITE (K3,105) ITER1,DIFMAX
105   FORMAT (5X,'MAXIMUM DIFFERENCE AT ITERATION NUMBER',I5,' = ',
     1 1P1E12.5)
      IF (DIFMAX.GT.EPS) GO TO 10
C
C.....CONVERGENCE ACHIEVED
      WRITE (K3,101) ITER1
101   FORMAT (10X,'LSOR METHOD CONVERGED IN',I5,' ITERATIONS'/)
C       LOAD SOLUTION INTO B
      DO 70 I=1,NN
70    B(I)=X(I)
      RETURN
      END
C
C      SUBROUTINE THOMAS ALGORITHIM
C
C       THOMAS ALGORITHIM FOR A TRIDIAGONAL MATRIX
C       A(I,1),A(I,2),A(I,3) ARE THE DIAGONALS OF THE MATRIX
C       A(I,4) IS THE RHS, A(I,5) IS THE SOLUTION VECTOR

      SUBROUTINE THOMAS (A,N,NN)
      IMPLICIT DOUBLE PRECISION (A-H,O-Z)
      DIMENSION A(NN,5)
      DO 10 I=2,N
      A(I,2) = A(I,2)-A(I,1)*A(I-1,3)/A(I-1,2)
      A(I,4) = A(I,4)-A(I,1)*A(I-1,4)/A(I-1,2)
10    CONTINUE
C
C.....BACK SUBSTITUTE
      A(N,5) = A(N,4)/A(N,2)
      N1=N-1
      DO 20 I=1,N1
      NI=N-I
      A(NI,5) = (A(NI,4)-A(NI,3)*A(NI+1,5))/A(NI,2)
20    CONTINUE
      RETURN
      END
```

Appendix IV

Comparison of Results from SUTRA and QSUTRA for Henry's (1964) Seawater Intrustion Problem [See Voss (1984, p. 196-203) for details on problem]

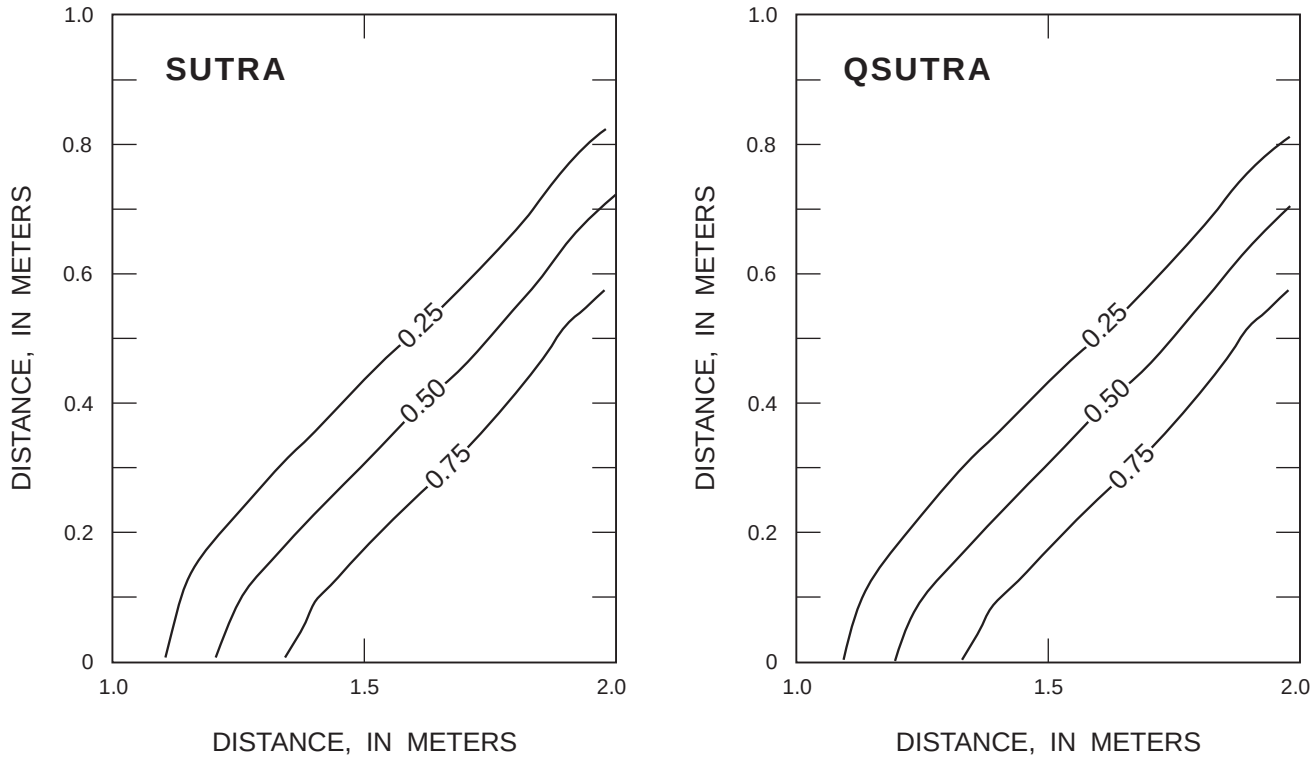

Comparison of concentration profiles for Henry's (1964) problem using QSUTRA and the original SUTRA codes.

Comparison of mass flux across the model boundary for Henry's (1964) problem using QSUTRA and the original SUTRA codes

[Fluid sources or sinks due to specified pressures]

QSUTRA		SUTRA	
Node	Inflow(+)/outflow(-) (mass per second)	Node	Inflow(+)/outflow(-) (mass per second)
221	2.0505180D-03	221	2.0445683D-03
222	3.9052976D-03	222	3.8945305D-03
223	3.6464678D-03	223	3.6372692D-03
224	3.1973050D-03	224	3.1903238D-03
225	2.4313601D-03	225	2.4270948D-03
226	1.0648645D-03	226	1.0642539D-03
227	-1.8302268D-03	227	-1.8264702D-03
228	-7.0298556D-03	228	-7.0211951D-03
229	-1.5196096D-02	229	-1.5180209D-02
230	-2.8955106D-02	230	-2.8933956D-02
231	-2.9209879D-02	231	-2.9197070D-02

ground water

Process-Based Interpretation of Tracer Tests in Carbonate Aquifers

by Steffen Birk[1,3], Tobias Geyer[2], Rudolf Liedl[1], and Martin Sauter[2]

Abstract

A tracer test in a carbonate aquifer is analyzed using the method of moments and two analytical advection-dispersion models (ADMs) as well as a numerical model. The numerical model is a coupled continuum-pipe flow and transport model that accounts for two different flow components in karstified carbonate aquifers, i.e., rapid and often turbulent conduit flow and Darcian flow in the fissured porous rock. All techniques employed provide reasonable fits to the tracer breakthrough curve (TBC) measured at a spring. The resulting parameter estimates are compared to investigate how each conceptual model of flow and transport processes that forms the basis of the analyses affects the interpretation of the tracer test. Numerical modeling results suggest that the method of moments and the analytical ADMs tend to overestimate the conduit volume because part of the water discharged at the spring is wrongly attributed to the conduit system if flow in the fissured porous rock is ignored. In addition, numerical modeling suggests that mixing of the two flow components accounts for part of the dispersion apparent in the measured TBC, while the remaining part can be attributed to Taylor dispersion. These processes, however, cannot reasonably explain the tail of the TBC. Instead, retention in immobile-fluid regions as included in a nonequilibrium ADM provides a possible explanation.

Introduction

Ground water flow in carbonate aquifers is often focused in solution conduits that comprise only a small percentage of total aquifer porosity. The majority of aquifer storage, however, is generally provided by the fissured porous rock. The permeability contrast between the highly conductive conduit system and the much less conductive fissured porous rock poses a great challenge to the hydrogeological characterization of carbonate aquifers, mainly because location and geometry of the conduit system are generally known inadequately. In particular, some standard investigation techniques, such as pumping tests, are often of limited value for aquifer characterization. Ground water tracing, which is the subject of this paper, appears to be a more promising method for the characterization of conduit-dominated carbonate aquifers.

A qualitative tracer detection can be sufficient in investigations that aim at identifying point-to-point connections, e.g., for the delineation of spring catchments. However, the information provided by such qualitative tracer tests is insufficient for making quantitative transport prediction in these aquifers. More detailed information can be obtained from quantitative ground water tracing. Brown et al. (1969), Brown and Ford (1971), and Atkinson et al. (1973) demonstrated that the type of conduit network can be inferred from ground water tracing if both tracer concentration and discharge are measured in a sinking stream (i.e., one that disappears underground) and at the resurgence. Smart (1988) inferred a more detailed structural model of a karst aquifer from a series of tracer tests. More recently, a method has been suggested that provides estimates for flow and transport parameters, such as mean flow velocity and longitudinal dispersion, as well as for geometric conduit parameters, such as conduit volume and diameter, from an evaluation of the tracer breakthrough curve (TBC) and the spring discharge (Field and Nash 1997; Field 1999). Any such quantitative interpretation, however, is likely to depend on the conceptual model of flow and transport processes that form the basis of the analysis. The purpose of this paper is to examine the role of model selection in the

[1]Center for Applied Geoscience, University of Tübingen, Sigwartstr. 10, D-72076 Tübingen, Germany.

[2]Geoscience Center Göttingen, University of Göttingen, Goldschmidtstr. 3, D-37077 Göttingen, Germany.

[3]Corresponding author: (49) 7071 2974691; fax: (49) 7071 5059; steffen.birk@uni-tuebingen.de

Received January 14, 2004; accepted August 1, 2004.

interpretation of tracer tests in carbonate aquifers. To this end, a tracer test conducted at a field site in southwest Germany is analyzed using several standard techniques, namely the method of moments and two types of one-dimensional advection-dispersion models (ADMs). In addition, a numerical flow and transport model is introduced and applied to the data. This numerical model accounts for both conduit flow and Darcian flow within the fissured porous rock and does not require the specification of dispersion coefficients, as these are directly determined from the conduit properties based on an approach introduced by Taylor (1954). Results from all of these analyses are compared to investigate how the different underlying conceptual models affect the interpretation of tracer-test results.

Modeling Techniques

ADMs are based on the transport equation

$$\frac{\partial c}{\partial t} = -v\frac{\partial c}{\partial x} + D\frac{\partial^2 c}{\partial x^2} \tag{1}$$

where c = concentration, t = time, v = velocity, x = distance along the direction of flow, and D = dispersion coefficient. The dispersion coefficient is commonly assumed to be proportional to the flow velocity, i.e., $D = \alpha v$, where the proportionality constant α is termed dispersivity. In this work, the program CXTFIT version 2.1 (Toride et al. 1999) is employed to calibrate an analytical solution of the ADM to a measured TBC.

In addition to the ADM given by Equation 1, CXTFIT provides analytical solutions to an ADM that is extended by a first-order mass transfer term and a supplementing equation accounting for retention in immobile-fluid regions. The parameters that must be adjusted in this nonequilibrium ADM include not only flow velocity and dispersion coefficient but also the mobile fraction of water as well as a mass transfer coefficient determining the rate of mass transfer between mobile and immobile water. Field and Pinsky (2000) provide a detailed description of both versions of the ADM and their application to tracer tests in carbonate aquifers.

The method of moments evaluates the first and second statistical moments of the TBC in order to obtain estimates for the flow velocity and the dispersivity, respectively. Field and Nash (1997) describe fundamentals of this method and its application for tracer-test analysis in carbonate aquifers. QTRACER software (Field 1999) was used to conduct the analysis.

Using the flow velocity v resulting from the ADM or the method of moments, an estimate for the phreatic conduit volume V can be obtained if the mean discharge $\bar{Q}$ is known:

$$V = \bar{Q}\frac{L}{v} \tag{2}$$

where L = flow distance. The conduit volume can easily be transformed into the corresponding diameter of a circular conduit (e.g., Field and Nash 1997).

The aforementioned standard techniques can be criticized from a process-based viewpoint for at least two reasons. First, the method of moments and the ADMs yield estimates for the dispersion coefficient by evaluating statistical moments or by model calibration, respectively, but the nature of the process creating such dispersion is undefined in either case. Second, one-dimensional transport between injection site and karst spring is assumed. This approach may be appropriate to describe tracer transport between a stream sink and its resurgence if tributaries and losses between sink and resurgence are negligible. In many karst catchments, however, drainage occurs mainly via the subsurface, and surface water is rare. Consequently, the tracer is injected, e.g., into a sinkhole and flushed with an amount of water that is very small compared to the water volume discharged at the spring. Thus, the injected tracer solution is diluted along the flowpath due to mixing with the regional flow component that feeds the spring. The method of moments and the one-dimensional ADMs do not explicitly account for this mixing process. A numerical modeling approach that includes these two mechanisms is introduced subsequently.

In principle, two different flow systems can be distinguished in karst aquifers, namely, rapid and often turbulent conduit flow and Darcian flow in the fissured porous rock (Shuster and White 1971). Thus, carbonate aquifers can be conceptualized as dual-flow systems consisting of a discrete conduit system embedded in a continuous fissured system. In order to transfer this conceptual model into a numerical flow model, a pipe-network model (Clemens et al. 1996; Liedl et al. 2003), representing the conduit system, was hydraulically coupled to the continuum flow model MODFLOW-96 (Harbaugh and McDonald 1996), representing the fissured system. Assuming a proportional exchange flow rate and head difference between conduit and fissured system, the two models are coupled by a linear exchange term (Barenblatt et al. 1960)

$$Q_{ex} = \gamma\left(h_f - h_c\right) \tag{3}$$

where Q_{ex} = exchange flow rate, h_f = head in the fissured system, h_c = head in the conduit system, and γ = proportionality constant termed exchange coefficient, which is considered here as a parameter that must be adjusted during model calibration.

Conduit flow is simulated using the Darcy-Weisbach equation

$$\Delta h_c = \frac{fL}{2ga}v^2 \tag{4}$$

where Δh_c = head difference along the distance L, a = conduit diameter, v = average flow velocity in the conduit, g = gravitational acceleration, and f = friction factor. Under the conditions considered in this work, conduit flow is always turbulent, and the friction factor is obtained by iteratively solving the implicit Colebrook-White formula

$$\frac{1}{\sqrt{f}} = -2\log\left(\frac{e}{3.71a} + \frac{2.51}{Re\sqrt{f}}\right) \tag{5}$$

where e is roughness height of the conduit wall and Re Reynolds number. This continuum-pipe flow model was initially designed for the simulation of conduit development in carbonate aquifers and thus termed CAVE (Carbonate Aquifer Void Evolution) (Birk et al. 2003; Liedl et al. 2003; Bauer et al. 2003).

In order to be able to simulate tracer transport in the conduit system, an explicit upwind finite-difference scheme solving the advection-dispersion equation (Equation 1) in the pipe network was implemented in CAVE. Solute concentrations in both flow from the fissured system and direct recharge into the conduit system are specified as boundary conditions for the transport simulation in the pipe network.

As mentioned previously, the dispersion coefficient can be calculated by $D = \alpha v$, where the dispersivity α must be adjusted during model calibration. A more process-based approach developed by Taylor (1953, 1954) attributes dispersion to mass transfer processes arising from velocity differences within the flow cross section. Under turbulent flow conditions, the dispersion coefficient is given by (Taylor 1954)

$$D = 10.1 a v_* \tag{6}$$

where a = conduit diameter and v_* = friction velocity. The friction velocity is given by (Clark 1996):

$$v_* = \sqrt{\frac{ag}{2}\frac{\Delta h}{L}} \tag{7}$$

The finite-difference scheme employed to solve the advection-dispersion equation generally creates numerical dispersion, i.e., an artificial dispersion term is added on the dispersion term in Equation 1. However, the magnitude of the numerical dispersion can be calculated for each pipe a priori (Kinzelbach 1992). Hence, the dispersion coefficient determined by one of the aforementioned methods is accordingly reduced to compensate for the effect of numerical dispersion.

Tracer Experiment

The Gallusquelle catchment situated in southwest Germany was selected for this investigation (Figure 1). This catchment has been characterized with hydrogeological investigations that included piezometric surface mapping, ground water tracing, borehole hydraulic tests, and analyses of spring hydrographs and physicochemical parameters of spring water (Sauter 1992).

The spring catchment covers an area of ~45 km^2 on the Swabian Alb, a northeast-southwest–striking low mountain range composed of Upper Jurassic carbonates. The landscape is characterized by dry valleys, which are interpreted as formerly active water courses that dried up with the advance of karstification. Today's drainage occurs mainly via the subsurface. Based on analyses of ground water level records and regional ground water potentials as well as on the knowledge of the former topographic elevations of the spring, which had been significantly below the present spring level at times during the Quarternary, Sauter (1995) concluded that a highly karstified zone is submerged within today's active aquifer. Thus, subsurface drainage is likely to occur through phreatic (i.e., water filled) karst conduits.

Recharge estimates amount to ~380 mm/a, yielding a total recharge within the spring catchment of ~0.54 m^3/s. The spring discharge varies from <0.1 to 2.5 m^3/s with an average of ~0.5 m^3/s. Part of the outflow from the catchment, however, is likely to occur via diffuse seepage into the river Lauchert southeast of the Gallusquelle catchment. Estimates for this flow component range from <0.05 to 0.2 m^3/s (Sauter 1992).

A tracer test was conducted to provide information about the conduit system of the Gallusquelle catchment. The tracer injection location was a sinkhole, assumed to be well connected to the conduit system, instead of a borehole, which may not be well connected. A sinkhole located 3000 m east-northeast of the spring was selected as injection site for the tracer test, as it was easily accessible and water supply for flushing was available on site. In the past, this sinkhole had been filled up with sediments to facilitate agricultural land use and to improve ground water protection. The sediment filling was excavated to the depth of bedrock, i.e., ~5 m below ground level, and the sinkhole was left open during the experiment.

1.5 kg of sodium fluorescein dissolved in ~1 m^3 of water was injected into the excavated sinkhole on April 29, 2003. The depth of the water table at the sinkhole is not known. Measurements in two boreholes 1.0 and 1.5 km north-northeast of the doline suggest that it might be ~100 m below ground level. It should be noted, however, that this value represents the water level in the fractured porous rock rather than that in the conduit system. In order to obtain temporarily saturated conditions within the thick vadose zone, the sinkhole was flushed with ~91 m^3 of water over a time period of ~5 h prior to tracer injection. Flushing was continued at the same rate for ~4 h after tracer injection, yielding an additional water injection of 73 m^3.

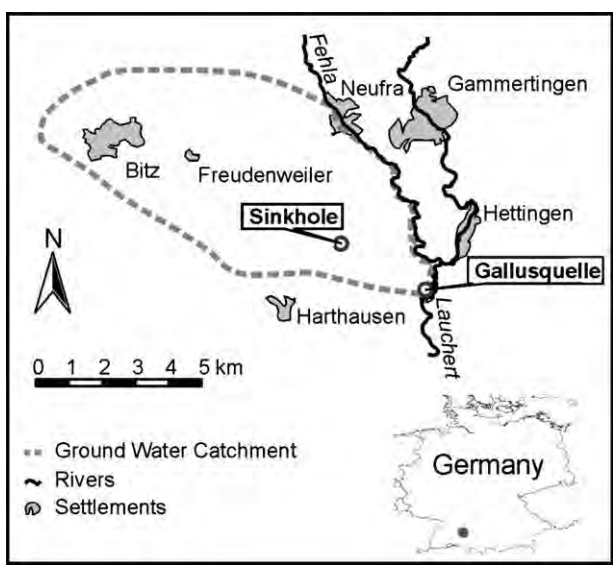

Figure 1. Location of the Gallusquelle catchment (delineation according to Sauter 1992).

The fluorescein concentration at the Gallusquelle was measured using a field spectrofluorometer (GGUN-FL30; Schnegg 2002). The measurement interval varied between 1 and 5 min. In addition, water samples were taken from nearby springs that could potentially drain some water from the injection site and analyzed in the laboratory using high-performance liquid chromatography with fluorescence detector. The Gallusquelle discharge was derived from stream-stage measurements using a stage-discharge relationship provided by the local water authority.

Results

The first arrival of the tracer was detected at the Gallusquelle ~35 h after tracer injection (Figure 2). Forty-two hours after tracer injection, the fluorescein concentration reached its maximum of 132 mg/m^3. After ~1 week, the concentration had returned to the background value. The spring discharge stayed at ~0.43 m^3/s during this time period.

Evaluation of the TBC with the method of moments yielded a mean tracer transit time of ~45 h. The corresponding mean tracer velocity as well as the resulting dispersion coefficient and dispersivity are given in Table 1. The analysis also reveals that ~94% of the injected tracer mass was recovered. While no tracer was detected at nearby springs, the observed mass loss could be caused by seepage into the river Lauchert or retention in the formation. Since the accuracy of the discharge is 5% or greater, the mass loss may be simply a result of discharge measurement errors.

The calibration of both the ADM given by Equation 1 and the nonequilibrium ADM was based on concentration values at regular time intervals of 30 min within a 5-d period after tracer injection in order to make the root mean square error (RMSE) of the resulting model solutions comparable to that obtained with the numerical model. The tracer injection was represented by a Dirac pulse, i.e., it has been assumed that the tracer mass penetrated instantaneously into the aquifer. Two scenarios have been considered for calibration of the ADMs, one with an injected mass equal to the actual injected tracer mass and the other with an injected mass equal to the recovered tracer mass, i.e., 94% of the actual injected tracer mass, thus accounting for the observed mass loss. As both scenarios yield very similar results, only those obtained with the actual injected mass are reported here.

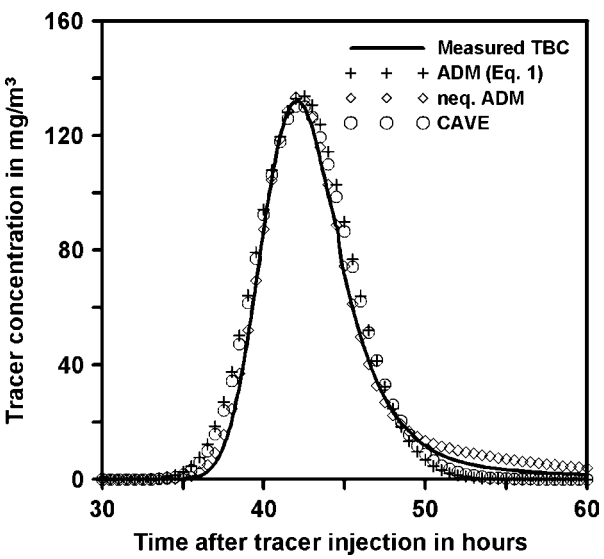

Figure 2. Measured TBC compared to results from the calibrated models (ADM (Eq. 1) = ADM given by Equation 1, neq. ADM = nonequilibrium ADM, CAVE = CAVE model).

In order to account for dilution of the tracer solution by mixing with regional flow, the transformation of the injection mass into a concentration, which is required as boundary condition for the ADM, was based on the measured spring discharge but not on the rate of injection. Thus, it has been implicitly assumed that dilution occurs instantaneously at the injection site.

Figure 2 compares the result from the ADMs to the measured TBC. All calibrated models match the measured TBC reasonably well. The ADM given by Equation 1 does not account for the tail of the measured TBC and therefore yields shorter travel times than the method of moments, which evaluates the whole TBC. Thus, the ADM yields slightly higher velocities than the method of moments (Table 1). Moreover, a higher dispersivity value has to be used in the ADM given by Equation 1 to improve the model fit in the tailing part of the TBC. Nevertheless, this model clearly fails to account for the skewness of the measured TBC, i.e., the tail of the curve is not adequately reproduced.

Field and Pinsky (2000) demonstrated that nonequilibrium ADMs are able to produce better fits of the tails of TBCs. This is also apparent in the modeled TBC (Figure 2) as well as in the residuals (observed minus fitted concentrations) plotted in Figure 3. The RMSE of this model fit is significantly lower than that resulting from the pure ADM given by Equation 1 (Table 1). Dispersion coefficient and dispersivity agree fairly well with the parameter estimates from the method of moments and thus are significantly lower than those resulting from the pure ADM. In contrast, the flow velocities resulting from both types of ADMs are nearly equal (Table 1). Inserting flow distance, spring discharge, and the calculated velocities in Equation 2 yielded estimates for the conduit volume, which were transformed to the corresponding diameter of a circular conduit (Table 1). Volume and diameter from the ADMs and the method of moments agree fairly well.

In addition to the parameters listed in Table 1, the calibration of the nonequilibrium ADM yields a mobile fraction of water of 0.95 as well as mass transfer coefficients of 1.9×10^{-6} 1/s. The mobile fraction of water is greater than and the mass transfer coefficient is less than the corresponding parameter values calculated by Field and Pinsky (2000) for each of five tracer tests in carbonate aquifers.

In order to verify the numerical implementation of Equation 1 in CAVE, transport was numerically simulated in a single conduit decoupled from the continuum using the parameter values identified with CXTFIT for the ADM given by Equation 1 (Table 1, ADM (Eq.1)), i.e., a conduit diameter of ~5.3 m and a dispersivity of 6.9 m.

Table 1
Parameter Estimates from Different Evaluation Techniques

Parameter	Method of Moments	ADM (Eq. 1)	Nonequilibrium ADM	CAVE
Velocity (m/s)	0.018	0.020	0.019	0.032–0.002
Dispersion coefficient (m^2/s)	0.082	0.14	0.086	0.14–0.010
Dispersivity (m)	4.4	6.9	4.6	4.4
Conduit volume (m^3)	7.0×10^4	6.6×10^4	6.9×10^4	4.2×10^4
Conduit diameter(m)	5.5	5.3	5.4	4.2
RMSE (mg/m^3)	—	3.9	1.4	3.1

ADM (Eq.1) = ADM given by Equation 1.

The 3000-m distance between injection site and spring was subdivided into 150 successive pipes of 20-m length each, and the flow rate was set to the spring discharge of 0.43 m^3/s. The result from the numerical simulation was in good agreement with that from the analytical solution provided by CXTFIT (RMSE = 0.6 mg/m^3).

In addition, the model was run in a mode where the dispersion coefficient is calculated using Taylor's approach given by Equations 6 and 7. The hydraulic gradient in Equation 7 is determined by the flow calculation and thus depends on the roughness height of the conduit wall as demonstrated by Equations 4 and 5. The roughness height was adjusted in a model calibration using the parameter optimizer PEST (Doherty 2002). A roughness height of ~0.25 m provided the best fit to the measured TBC. Both methods employed for the calculation of the dispersion coefficient perform equally well. Yet, calibration of the model that uses Taylor's approach yields the roughness height of the conduit wall instead of the physically less meaningful dispersivity. The roughness height is not only involved in the transport calculation but also in the flow calculation and thus could, in principle, be verified if both hydraulic gradient and flow rate were known accurately. Taylor's approach, therefore, provides a more process-based interpretation of dispersion as requested by one of the aforementioned criticisms of the standard techniques for tracer-test analysis.

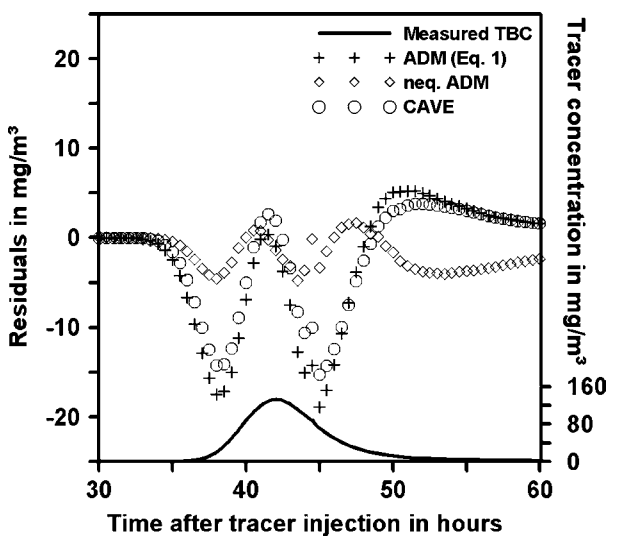

Figure 3. Residuals (observed minus fitted concentrations) from the calibrated models (ADM (Eq.1) = ADM given by Equation 1, neq. ADM = nonequilibrium ADM, CAVE = CAVE model).

The other criticism concerns the source of the large water volume discharged at the spring and its mixing with the injected, tracer-bearing water, which is not explicitly accounted for by the standard techniques. Since there are no stream sinks within the Gallusquelle catchment, the distributed recharge to the catchment area must provide the source of water discharged at the spring. Part of this water is most likely mixed with the injection water somewhere between injection site and spring rather than directly at the injection site. It was attempted to account for these processes in a highly simplified numerical model of the Gallusquelle catchment. To this end, the above conduit model, comprising 150 pipes that represent a karst conduit connection between injection site and spring, was coupled to the continuum model, which simulates regional flow in the catchment. For lack of better knowledge, the diameter was held constant along the length of the conduit.

The model domain is a rectangle of 11,000 m in length and 5500 m in width that is approximately aligned with the longitudinal axis of the actual catchment (Figure 4). Sauter (1992) provides estimates of hydraulic aquifer parameters in the area that vary depending on both investigation site and method (e.g., spring hydrograph analysis, slug tests, injection tests) employed. In order to keep the model simple, approximate average values of 10^{-4} m/s and 0.01 were uniformly assigned to hydraulic conductivity and storativity of the unconfined aquifer. The spring discharge measured during the tracer experiment amounts only to 86% of the average spring discharge. The estimated average recharge was correspondingly reduced and uniformly applied to the model domain. The model domain is drained across one of the narrow sides of the rectangle with a fixed head equal to the spring water level of 633 m a.s.l., while all other sides are no-flow boundaries. Note that the area covered by the model domain is larger than the actual catchment area because outflow from the continuum across the fixed-head boundary does not contribute to spring discharge. Conceptually, this outflow corresponds to the aforementioned diffuse seepage into the river Lauchert.

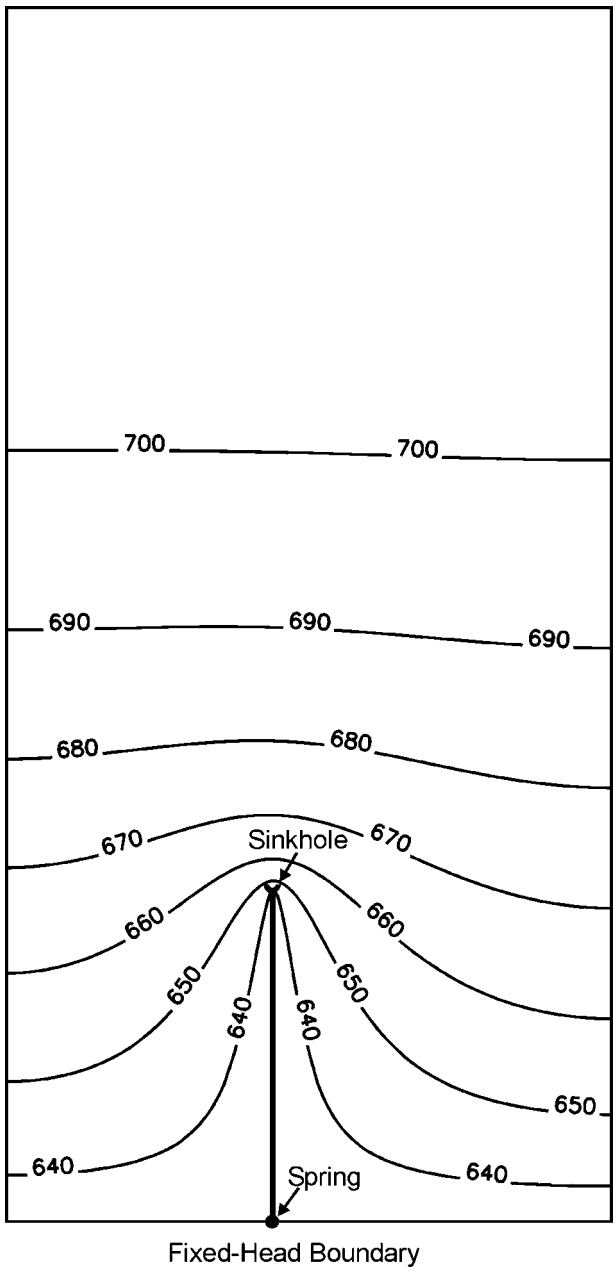

Figure 4. Model domain with a single conduit (thick line) linking the injection site (sinkhole) to the spring. Labeled thin lines represent the initial hydraulic-head distribution (values in m a.s.l.) of the calibrated model.

The steady-state flow field (Figure 4) determined by the aforementioned model parameters and boundary conditions as well as by the exchange coefficient γ and the conduit parameters a and e provided the starting heads for the transient tracer-test simulation. Initial concentrations were zero in the entire model domain. Flushing of the sinkhole was represented by a point injection of 5 L/s into the conduit over a time period of 9 h. After 5 h, a tracer mass of 1.5 kg was added to the injection water within 1 s. The tracer concentration in the injection water was zero at any other time. As before, the parameter optimizer PEST was employed to calibrate the model.

Exchange coefficient, conduit diameter, and roughness height were calibration parameters, while dispersion was quantified using Taylor's approach given by Equations 6 and 7. Changing the given calibration parameters affects both simulated spring discharge and TBC. Hence, as opposed to the standard techniques employed before, not only the measured TBC but also the measured spring discharge had to be matched by the model. The calibrated model yields a spring discharge of ~0.44 m^3/s, i.e., ~2% greater than the measured discharge and thus well within the range of the measurement error. The TBC resulting from the calibrated model is shown in Figure 2, the residuals (observed minus fitted concentrations) are plotted in Figure 3. The RMSE of 3.1 mg/m^3 (referring to the TBC only) is close to that of the ADM given by Equation 1 (Table 1). The calibration approximately yields a conduit diameter of 4.2 m, corresponding to a conduit volume of 4.2×10^4 m^3, a roughness height of 0.067 m, and an exchange coefficient of 5.8×10^{-3} m^2/s. Diameter and volume, thus, are significantly lower than predicted by the standard methods (Table 1). The roughness height in the calibrated dual-flow model is lower by almost a factor of four compared to the model without a coupled continuum.

In order to allow comparison with the dispersivities resulting from the standard techniques, the model was also run in a mode with $D = \alpha v$ (Table 1; CAVE). The dispersivity α was adjusted, while exchange coefficient, conduit diameter, and roughness height were kept constant, yielding a dispersivity of ~4.4 m. The dispersivity obtained is comparable to those resulting from the methods of moments and the nonequilibrium ADM but is significantly less than that from the ADM given by Equation 1.

Discussion

All models presented in the previous sections provide reasonable fits to the measured TBC. Yet, the nonequilibrium ADM is the only model that is capable of reproducing the weak tailing apparent in the measured TBC. In addition to velocity and dispersivity, which are the only calibration parameters in the pure ADM, this model type includes two other fitting parameters to account for first-order mass transfer into immobile-fluid regions. The physical nature of this process, however, is not entirely clear. Results from process-based numerical simulations of tracer transport in turbulent flow at meter-length scale suggest that the tailing of TBCs is caused by flow reversal due to turbulent eddies in pools (Hauns et al. 2001).

The flow velocity resulting from the nonequilibrium ADM is not much different from those obtained with the method of moments and the pure ADM given by Equation 1. Consequently, estimates for conduit diameter and volume are also nearly identical (Table 1). Together with the aforementioned parameter comparison among other carbonate aquifers (Field and Pinsky 2000) the results suggest that retention in immobile-fluid regions is relatively unimportant here. It should be noted, however, that the dispersivity required to match the measured TBC is significantly less for the nonequilibrium ADM than for the pure ADM (Table 1). Thus, part of the dispersion

apparent in the TBC can possibly be explained by retention in immobile-fluid regions.

The dispersion coefficient included in the advection-dispersion equation is commonly calculated by $D = \alpha v$, where the dispersivity a is determined by model calibration. With a more process-based approach, which quantifies the dispersion coefficient depending on flow conditions and geometric properties of the conduit (Taylor 1954), the model calibration yields the roughness height of the conduit wall instead of the dispersivity. In principle, the roughness height could be independently determined if both flow rate and hydraulic gradient were known. Thus, it provides a link between flow and transport modeling. In this work, a transport model based on the advection-dispersion equation is built on the flow model CAVE, which accounts for a dual-flow system in a carbonate aquifer. The calibration of this numerical flow and transport model is entirely based on an adjustment of flow and conduit parameters, which can be constrained by hydraulic field data, such as spring discharge and hydraulic heads.

In order to illustrate this process-based approach to tracer-test interpretation in carbonate aquifers, a highly simplified model of the Gallusquelle catchment has been presented in this work. Both spring discharge and TBC were simultaneously used as calibration targets that had to be matched by the model. Calibration results suggest that the conduit volume is smaller than that predicted by standard techniques because part of the water discharged at the spring is derived from regional flow through the fissured porous rock and thus wrongly attributed to the conduit system if the fissured system is ignored in the analysis. The dispersivity value corresponding to the calibrated flow and conduit parameters is also smaller than that resulting from an equivalent transport model neglecting the effect of the fissured system. Thus, part of the dispersion apparent in the TBC appears to be caused by mixing of regional flow and tracer-marked conduit water.

Conclusions

The techniques employed for tracer-test analysis in this work are based on different conceptual models of flow and transport in carbonate aquifers. With respect to the number of parameters involved in the calibration, the one-dimensional ADM represents the simplest model. It yields reasonable fits to the measured TBC and thus should be considered an adequate standard technique unless there is good reason to apply more complex approaches.

Such reason could be the demand for a better model fit, in particular, in the tailing part of the measured TBC. In principle, a nonequilibrium ADM appears to be suitable for this purpose. Another reason is the wish for a tracer-test interpretation consistent with the knowledge of the flow system. A process-based numerical flow and transport model, such as the CAVE model presented here, can be employed to accomplish this task.

The model application illustrating this approach to a process-based interpretation of tracer tests is based on a highly simplified conceptual aquifer model, which is found to be adequate for presenting the basic methodology. Quantitative results, however, should be interpreted with caution at the present stage of model development because the model calibration did not consider measured hydraulic heads. More reliable parameter estimates will be obtained if the model is built on detailed information gained from a thorough hydrogeological site investigation and if, in addition to spring discharge and tracer concentrations, measured hydraulic heads are used to calibrate the model. Design and calibration of such a model is subject of ongoing research.

Acknowledgments

This work is funded by the Deutsche Forschungsgemeinschaft (DFG; German Research Foundation) under grants no. LI 727/10 and SA 501/17. The reviews by Malcolm Field, Tim Scheibe, and Todd Halihan greatly helped improve the manuscript.

References

Atkinson, T.C., D.I. Smith, J.J. Lavis, and R.J. Whitaker. 1973. Experiments in tracing underground waters in limestones. *Journal of Hydrology* 19, no. 4: 323–349.

Barenblatt, G.I., I.P. Zheltov, and I.N. Kochina. 1960. Basic concepts in the theory of seepage of homogeneous liquids in fissured rocks. *Journal of Applied Mathematics and Mechanics* 24, no. 5: 1286–1303.

Bauer, S., R. Liedl, and M. Sauter. 2003. Modeling of karst aquifer genesis: Influence of exchange flow. *Water Resources Research* 39, no. 10: 1285, doi: 10.1029/2003WR002218.

Birk, S., R. Liedl, M. Sauter, and G. Teutsch. 2003. Hydraulic boundary conditions as a controlling factor in karst genesis: A numerical modeling study on artesian conduit development in gypsum. *Water Resources Research* 39, no. 1: 1004, doi: 10.1029/2002WR001308.

Brown, M.C., and D.C. Ford. 1971. Quantitative tracer methods for investigations of karst hydrology systems, with special reference to the Maligne Basin area, Canada. *Transactions of the Cave Research Group of Great Britain* 13, no. 1: 37–51.

Brown, M.C., D.C. Ford, and T.M.L. Wigley. 1969. Water budget studies in karst aquifers. *Journal of Hydrology* 9, no. 1: 113–116.

Clark, M.M. 1996. *Transport Modeling for Environmental Engineers and Scientists*. New York: John Wiley and Sons.

Clemens T., D. Hückinghaus, M. Sauter, R. Liedl, and G. Teutsch. 1996. A combined continuum and discrete network reactive transport model for simulation of karst development. In *Calibration and Reliability in Groundwater Modelling*, ed. K. Kovar and P. van der Heijde. Wallingford, UK: IAHS Publication 237: 309–318.

Doherty, J. 2002. PEST: Model-Independent Parameter Estimation, 4th ed. Brisbane: Watermark Numerical Computing.

Field, M.S. 1999. The QTRACER program for tracer-breakthrough curve analysis for karst and fractured-rock aquifers. Washington, DC: U.S. Environmental Protection Agency.

Field, M.S., and S.G. Nash. 1997. Risk assessment methodology for karst aquifers: (1) Estimating karst conduit-flow parameters. *Environmental Monitoring and Assessment* 47, no. 1: 1–21.

Field, M.S., and P.F. Pinsky. 2000. A two-region nonequilibrium model for solute transport in solution conduits in karstic aquifers. *Journal of Contaminant Hydrology* 44, no. 3–4: 329–351.

Harbaugh, A.W., and M.G. McDonald. 1996. *Programmer's documentation for MODFLOW-96—An update to the U.S.*

Geological Survey modular finite-difference groundwater model. Reston, Virginia: USGS Open-File Report 96–486.

Hauns, M., P.-Y. Jeannin, and O. Atteia. 2001. Dispersion, retardation and scale effect in tracer breakthrough curves in karst conduits. *Journal of Hydrology* 241, no. 3–4: 177–193.

Kinzelbach, W. 1992. *Numerische Methoden zur Modellierung des Transports von Schadstoffen im Grundwasser*, 2nd ed. Munich, Germany: Oldenbourg.

Liedl, R., M. Sauter, D. Hückinghaus, T. Clemens, and G. Teutsch. 2003. Simulation of the development of karst aquifers using a coupled continuum pipe flow model. *Water Resources Research* 39, no.1: 1057, doi: 10.1029/2001WR001206.

Sauter, M. 1995. Delineation of a karst aquifer using geological and hydrological data and information on landscape development. *Carbonates and Evaporites* 10, no. 2: 129–139.

Sauter, M. 1992. *Quantification and Forecasting of Regional Groundwater Flow and Transport in a Karst Aquifer (Gallusquelle, Malm, SW-Germany)*. Tübinger Geowissenschaftliche Arbeiten *C13*. Tübingen, Germany: Geological Institute of the University of Tübingen.

Schnegg, P.A. 2002. An inexpensive field fluorometer for hydrogeological tracer tests with three tracers and turbidity measurement. In *Groundwater and Human Development*, ed. E. Bocanegra, D. Martínez, and H. Massone, 1484–1488. Mar Del Plata, Argentina, October 2002.

Shuster, E.T., and W.B. White. 1971. Seasonal fluctuations in the chemistry of limestone springs: A possible means for characterizing carbonate aquifers. *Journal of Hydrology* 14, no. 2: 93–128.

Smart, C.C. 1988. Artificial tracer techniques for the determination of the structure of conduit aquifers. *Ground Water* 26, no. 4: 445–453.

Taylor, G.I. 1954. The dispersion of matter in turbulent flow through a pipe. *Proceedings of the Royal Society of London, Series A* 223, no. 1155: 446–468.

Taylor, G.I. 1953. Dispersion of soluble matter in solvent flowing slowly through a tube. *Proceedings of the Royal Society of London, Series A* 219, no. 1137: 186–203.

Toride, J.F.N. Leij, and M.T. van Genuchten. 1999. The CXTFIT code for estimating transport parameters from laboratory or field tracer experiments—version 2.1. Riverside, California: U.S. Salinity Laboratory Agricultural Research Service, U.S. Department of Agriculture, Research Report No. 137.

Recovering Fresh Water Stored in Saline Limestone Aquifers

by Michael L. Merritt[a]

ABSTRACT

Numerical modeling techniques are used to examine the hydrogeologic, design, and management factors governing the recovery efficiency of subsurface fresh-water storage. The modeling approach permitted many combinations of conditions to be studied. A sensitivity analysis was used that consisted of varying certain parameters while keeping constant as many other parameters or processes as possible. The results show that a loss of recovery efficiency resulted from: (1) processes causing mixing of injected fresh water with native saline water (hydrodynamic dispersion); (2) processes or conditions causing the irreversible displacement of the injected fresh water with respect to the well (buoyancy stratification and background hydraulic gradients); or (3) processes or procedures causing injection and withdrawal flow patterns to be dissimilar (dissimilar injection and withdrawal schedules in multiple-well systems). Other results indicated that recovery efficiency improved considerably during the first several successive cycles, provided that each recovery phase ended when the chloride concentration of withdrawn water exceeded established criteria for potability (usually 250 milligrams per liter). Other findings were that fresh water injected into highly permeable or highly saline aquifers would buoy rapidly with a deleterious effect on recovery efficiency.

INTRODUCTION

Injection of surplus fresh water into saline aquifers for later recovery and use during periods of water scarcity is a concept of particular significance for regions where the natural water supply tends to shift seasonally between surplus and deficit relative to public supply requirements. South Florida provides a typical example of such a hydrologic regime. The climate is characterized by a usually pronounced seasonal cycle of wet and dry periods. To prevent flooding during wet periods, large quantities of water are flushed through canals to the ocean. The waters exit through control structures that are closed during dry periods to maintain water levels sufficiently high to prevent salt-water intrusion in the vicinity of coastal well fields.

The flat topography of south Florida and high cost of land inhibit enlargement of the surface reservoir system, which includes Lake Okeechobee and the three water-conservation areas. However, subsurface reservoirs exist in the form of artesian aquifers that occur within 1,000 to 1,500 feet of land surface. Throughout most of the region shown in Figure 1, these aquifers contain water sufficiently saline to be considered nonpotable (more than 250

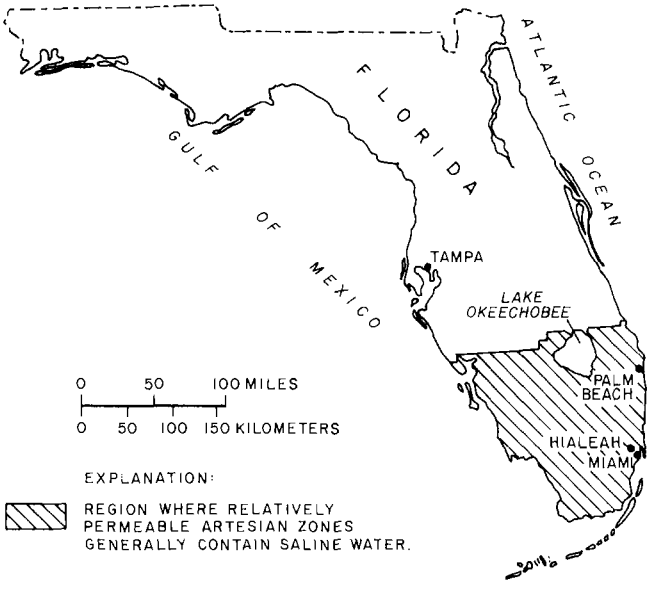

Fig. 1. Map showing region of Florida where relatively permeable artesian zones generally contain saline water.

[a]U.S. Geological Survey, Suite 106, 9100 N.W. 36th Street, P.O. Box 026052, Miami, Florida 33102.

Received July 1985, revised December 1985, accepted December 1985.

Discussion open until January 1, 1987.

mg/l chloride) according to published standards of the U.S. Environmental Protection Agency (1976). Where these aquifers contain water of low to moderate salinity (500 to 2,000 mg/l chloride), they would be suitable receptacles for the temporary storage of amounts of water equivalent to part of the fresh water that is presently released to the ocean during the wet season. Various aspects of this water-conservation technique related to south Florida are discussed by Merritt and others (1983). A statistical analysis of coastal and inland fresh-water discharge in the south Florida area, suggesting available amounts of seasonal surplus, is presented by Sonntag (1984).

Experimental fresh-water injection and recovery systems in saline aquifers at several locations in central and south Florida (Black, Crow, and Eidsness, Inc., 1974; Tibbals and Frazee, 1976; J. J. Plappert, Florida Department of Environmental Regulation, written commun., 1977; F. W. Meyer, U.S. Geological Survey, oral commun., 1980; and D. J. Fitzpatrick (1985) have demonstrated varying degrees of success, as summarized by Merritt and others (1983). An operational system to inject fresh water into a high sulfide/sulfate aquifer for later recovery was described by Reynolds and Pyne (1983) and CH_2M HILL (1984). Recovery efficiencies (the volume of potable water recovered expressed as a percentage of the volume of fresh water injected) have ranged from 0 to 75 percent in the saline aquifer tests. This variation has been attributed mainly to differences in the hydraulic characteristics of the receiving aquifers and in the chemical characteristics of their native water, and possibly to the technique or schedule of injection and withdrawal (length of storage period, volume, and rate of injection).

At substantial cost, the injection tests generally have indicated the nature of some of the factors governing the success of subsurface fresh-water storage. As part of a recent study by the U.S. Geological Survey in cooperation with the U.S. Army Corps of Engineers, digital modeling techniques were used to better explain the relation of recovery efficiency to various hydrogeologic, system design, and management parameters. The digital modeling approach permitted many combinations of conditions in a generalized prototype to be studied in a relatively inexpensive manner. There is a trade-off between cost and results, however. The simulation of the transport of solute in secondary-porosity limestone aquifers is a research problem with results subject to various qualifications, particularly when a porous media flow model is used. Operational test results, on the other hand, are direct field evidence, despite their substantially greater cost and the often challenging problem of interpreting them for an understanding of causal processes.

As presented in this paper and others (Merritt, 1982, 1983), the relations developed in the analyses are not all mutually independent, as various physical processes affect one another. Nevertheless, a sensitivity analysis approach was considered best, which was to study the effect of varying each parameter while keeping constant as many other parameters or processes as possible. The hypothetical prototype aquifer designed for the analyses was generally based upon the injection zone at the fresh-water injection test site at Hialeah, Florida (F. W. Meyer, U.S. Geological Survey, oral commun., 1980). This site is considered representative of potential limestone injection zones in Florida. Generally, such zones are permeable, confined limestone strata occurring within 2,000 feet of land surface that contain brackish water of less than 2,000 mg/l chloride. Deeper or more saline strata could be used, but less fresh-water recovery would be anticipated.

The present study follows earlier efforts to study subsurface fresh-water storage in a quantitative manner. Kimbler and others (1975) addressed many of the same problems with different modeling techniques. Grove and Konikow (1976) were the first to use the approach of the present study, and Khanal (1980) also studied the process with other methods. Results of a single small-volume injection test cycle in St. Lucie County, Florida (Wedderburn and Knapp, 1983) were extended to some degree by the author based on various hypothetical assumptions and using modeling techniques similar to those described in this paper.

The model-based study was broad in scope and of short duration. Results of the analyses were briefly summarized (Merritt, 1982) and presented in detail (Merritt, 1983). The purpose of this paper is to describe basic concepts related to the subsurface fresh-water storage alternative. A brief description of the simulator is followed by a discussion of the concept of hydrodynamic dispersion, its representation in the computer model, and its relation to the choice of a finite-difference solution algorithm. These topics are presented in some detail in order to help in evaluating results of the recovery efficiency analyses and to illustrate the conceptual development and selection of appropriate modeling techniques that were found necessary for accomplishment of the goals of the study.

MATHEMATICAL SOLUTION AND COMPUTATIONAL ASPECTS

Basic Equations and Computer Code

The generic digital simulator used in the study was developed under sponsorship of the U.S. Geological Survey (INTERCOMP Resource Development and Engineering, Inc., 1976; INTERA Environmental Consultants, Inc., 1979). The model solves equations in three spatial dimensions for the pressure (p, P/L^2) field [equation (1)] and for the transport of dissolved solute [equation (2)] represented as a constituent fraction (C), taking unitless values that represent the relative proportions of two fluids (represented by C = 0 and C = 1) in a mixture which varies spatially and temporally. A third equation may also be solved for temperature (T) to represent the transport of thermal energy. Solution of either the solute or thermal transport equations is optional. The equations pertinent to this study are:

$$\nabla \cdot \frac{\rho \underset{\sim}{k}}{\mu} (\nabla p - \rho \nabla z) = \frac{\partial}{\partial t} (\phi \rho) + q' \qquad (1)$$

$$\nabla \cdot \frac{\rho C \underset{\sim}{k}}{\mu} (\nabla p - \rho \nabla z)$$

$$+ \nabla \cdot (\rho \underset{\sim}{D} \cdot \nabla C) = \frac{\partial}{\partial t} (\phi \rho C) + Cq + \Sigma C_i q_i \qquad (2)$$

$$\phi = \phi_0 (1 + C_r [p - p_0]) \qquad (3)$$

$$\rho = \rho_0 (1 + C_w [p - p_0] + C_T [T - T_0] + \frac{\partial \rho}{\partial C} [C - C_0]) \qquad (4)$$

$$\mu = \mu (T, C) \qquad (5)$$

$$\underset{\sim}{D} = \underset{\sim}{D} (v, \alpha_\ell, \alpha_t, D_m) \qquad (6)$$

where

ρ is density (P/L^3);

$\underset{\sim}{k}$ is the intrinsic permeability tensor (L^2);

μ is dynamic viscosity (PT/L^2);

q' is the sum of sources and sinks of fluids, expressed as mass flux per unit volume (P/L^3T);

$\underset{\sim}{D}$ is the hydrodynamic dispersion tensor (L^2/T);

q is a sum of fluid sinks (P/L^3T);

q_i is a fluid source (P/L^3T) of constituent concentration C_i;

ϕ is porosity (unitless);

C_r is compressibility of the aquifer solid matrix (LT^2/P);

C_T is the coefficient of thermal expansion (reciprocal temperature units);

C_w is compressibility of water (LT^2/P);

α_ℓ, α_t are longitudinal and transverse dispersivity parameters (L);

D_m is molecular diffusivity (L/T^2); and

P, L, T indicate pound-force, length, and time units.

Equation (3) shows that porosity is considered to be a function of pressure depending upon the compressibility of the aquifer matrix. Equation (4) shows fluid density to be a function of pressure, temperature, and constituent fraction that depends upon the compressibility of water, the coefficient of thermal expansion, and upon its variation with constituent fraction ($\partial \rho / \partial C$). Reference values of porosity and density (ϕ_0, ρ_0) are model inputs corresponding to reference conditions of pressure, temperature, and constituent fraction (p_0, T_0, C_0). Equation (5) shows that dynamic viscosity is considered to depend upon temperature and solute fraction. Several types of functional dependence may be selected as a user option. Equation (6) indicates the assumed functional dependence of dispersion that will be discussed later.

Coordinate directions are assumed to be aligned with the principal axes of the permeability tensor ($\underset{\sim}{k}$) so that directional components of permeability may be specified. These components and the initial value of porosity (ϕ_0) may vary spatially as specified by the user. Values of fluid density are associated by the program user with the extreme values of constituent fraction (0 and 1). The code permits solution of the equations in Cartesian or cylindrical coordinates, depending upon the type of geometric symmetry (or lack of it) which characterize the application problem. Solution of each equation is by a three-dimensional, finite-difference method (INTERCOMP Resource Development and Engineering, Inc., 1976).

Hydrodynamic Dispersion and Its Representation

Flow from wells in secondary-porosity limestone aquifers probably does not occur as the spatially uniform displacement of native water by injected water. It is usually assumed that flow is through a network of solution channels that vary in size and tortuosity, and that the velocity of flow

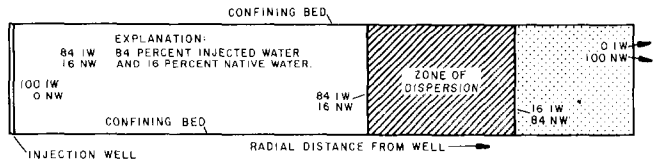

Fig. 2. Diagram showing conceptual model of mixing caused by mechanical dispersion.

may vary over the cross section of each channel. A well drilled near the outer limit of water moving outward from an injection well would penetrate many flow paths containing injected water, native water, or a mixture of the two waters. This situation is usually conceived as occurring within some radius beyond which little injected water has penetrated the aquifer and outward of some smaller radius within which virtually all native water has been flushed by injected water. The volume between the limiting radii, referred to as the "transition zone" or "zone of dispersion," is described mathematically as a spatially averaged concentration mix of the two waters that varies from nearly that of the injected water near the inner boundary to nearly that of the native water near the outer boundary. Figure 2 is a schematic of the "zone of dispersion." This cylindrical section arbitrarily depicts the zone as the region occurring between radii to the 84 and 16 percent concentrations of injected water. The concentration gradient is greatest in the center of this region. The process just described is referred to as "mechanical dispersion." If molecular diffusion effects are included, the term "hydrodynamic dispersion" is used.

The mathematical representation of dispersion [second term, equation (2)] is based upon a diffusion model that suggests the migration of solute from locations of higher to lower concentration at a rate dependent upon a set of dispersion coefficients (D) and the concentration gradient. The functional dependence of the dispersion coefficients is indicated by equation (6). The elements of the dispersion tensor are trigonometric projections of the parametric coefficients longitudinal and transverse dispersivity (α_ℓ and α_t), which relate to dispersion in the direction of flow (α_ℓ) and in the plane perpendicular to the direction of flow (α_t). The relative magnitude of the projections is a function of the net speed (v) and direction of flow. This characterization assumes that flow can be approximated as a spatially continuous process within an isotropic medium (Scheidegger, 1961), and that actual small-scale flow heterogeneities are represented by the dispersion terms. The directional components of dispersion are encoded in the finite-difference model as:

$$A_{i+1,i}\,C_{i+1} - A_{i+1,i}\,C_i - A_{i,i-1}\,C_i + A_{i,i-1}\,C_{i-1} \quad (7)$$

where the internodal mass-flux term $A_{i+1,i}$ contains the dependence upon the dispersivity coefficients, the velocity of flow, the concentration gradient, and molecular diffusion. C_i is the concentration value at node i. This writing suggests a conceptualization of the dispersion process as an interchange of equal amounts of fluid across the interface between two grid cells with the fluid received by each cell having the concentration fraction of the node center of the other cell. The cell with lower concentration receives the greater amount of constituent; thus, an alternative conceptualization is that of constituent moving in the direction of decreasing concentration. Molz and others (1983) describe the concept of "macrodispersion" in which a scale-dependent convective term dominates a term related to "local hydrodynamic dispersivity." The latter term is analogous to the model representation of dispersion by longitudinal and transverse dispersivity coefficients. The scale-dependent component is a result of vertical nonuniformities in the permeability of the aquifer and the resulting different rates of solute movement at various depths.

In the hypothetical perfectly stratified aquifer used as a prototype for this study, the effect of layering was explicitly represented in the spatial design of the model by discrete layers of uniform permeability. Local hydrodynamic dispersion occurred within each discrete layer to a degree determined by the dispersivity coefficients chosen by the model user. The concentration fraction of water arriving at a pumping well was computed as a weighted multizone composite of water from individual zones. This modeling approach as applied to field studies might not fully account for the effect of layering; representation of aquifers by layers of uniform hydraulic characteristics is only a generalization. Given any conceptual subdivision of an aquifer into discrete layers, the dispersion process in each layer might still be characterized by some degree of scale dependence.

The numerical techniques used to approximate the advective flow terms [first term, equation (2)] can affect the apparent degree of dispersion portrayed by the model. If the user specifies upstream weighting for the advective terms, then the concentration of the component of mass advective flux between nodes i and i + 1 ($C_{i+1,i}$)

takes the value of the upstream node. This backward difference method introduces "numerical dispersion" (Lantz, 1971), the degree of which is a function of the grid spacing. The effect is indistinguishable from the simulation of physical dispersion by the specification of dispersivity coefficients, so that the apparent degree of dispersion portrayed in the solute-transport computation can be much greater than is realistic if the grid spacing is too coarse. Backward differencing the time derivative has the same effect to a degree depending upon the time step size (Lantz, 1971).

If the user selects spatially centered differencing, $C_{i+1,i}$ is computed by linear interpolation to be the concentration value at the cell interface as a function of the values at nodes i + 1 and i. This scheme greatly reduces numerical dispersion, as does use of central differencing (Crank-Nicholson) in approximating the time derivative, so that the apparent degree of dispersion in model computations is primarily dependent upon local flow velocity, to a degree under user control through the specification of dispersivity coefficients.

The degree of dispersion as fresh water flowed from the well into the aquifer matrix during injection and subsequently back toward the well during recovery was of major importance in most analyses. Therefore, it was considered advantageous to minimize numerical dispersion by using space and time centered differences. The central difference approach, however, has a drawback in that the size of grid cells and the length of time steps must be controlled to prevent oscillatory behavior ("overshoot" and "undershoot") near the interface between the fluids (Price and others, 1966). The criteria to control oscillations (INTERCOMP Resource Development and Engineering, Inc., 1976) become more restrictive with lower specified degrees of mechanical dispersion (the dispersivity coefficients). However, for the 2- to 30-foot range of longitudinal dispersivity values used in this study, these criteria were satisfied to a sufficient degree that the oscillatory behavior that did occur did not hamper interpretation of results.

Few field studies have been performed to determine the degree of dispersion occurring in carbonate aquifers. In northwest Florida, Ehrlich and others (1979) estimated 30 feet for ("local") longitudinal dispersivity by measuring the increasing concentration of a conservative tracer at an observation well located about 1,000 feet from a waste injection well. Their computational method was based upon assumptions that the permeability and porosity of the injection zone were vertically

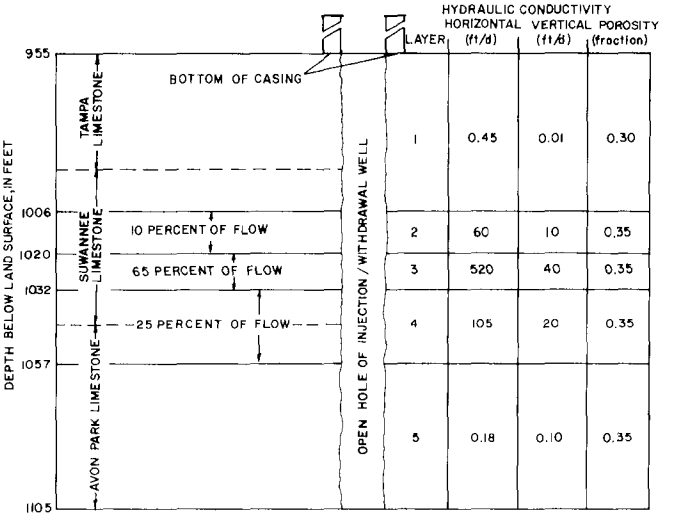

Fig. 3. Sketch of hypothetical aquifer resembling the Tertiary limestone injection zone at the Hialeah test site, Dade County.

uniform throughout a 60-foot aquifer thickness and that permeability was laterally isotropic (within the plane of flow). Implicit in these assumptions is the further assumption that the measured dispersivity would not be scale-dependent. Other carbonate injection zones at sites where detailed geophysical data have been obtained, the Hialeah, Florida site being such an example (F. W. Meyer, U.S. Geological Survey, oral commun., 1980), depart substantially from assumptions of permeability uniformity within such a large interval. The measured value could be considered an estimate of scale-dependent "macrodispersion" if it is understood to be valid only for the distance scale of the test.

The molecular diffusion component (D_m, L^2T) of the hydrodynamic dispersion tensor [equation (6)] is usually considered to be of negligible magnitude compared to mechanical dispersion in large-scale field situations of fluids moving at appreciable velocities (Ren Jen Sun, 1976). An estimate of 1×10^{-5} cm^2/s (0.13 ft^2/d) was used by Hoopes and Harleman (1967) in analyzing results of tests with their sand model.

DESIGN OF A HYPOTHETICAL AQUIFER FOR MODEL ANALYSES

A hypothetical aquifer was designed that was considered representative of a brackish artesian limestone aquifer. The hydraulic characteristics of this prototype (Figure 3) were based upon those estimated from aquifer tests and geophysical

logging of the injection zone at the U.S. Geological Survey fresh-water injection and recovery test site at Hialeah (Figure 1) in Dade County, Florida. The hydraulic conductivity estimates were based on the measured transmissivity of the injection interval and the contributions of flow from various depth intervals as indicated by flowmeter logs. Porosity estimates were based on a correlation of neutron, sonic, and caliper logs (F. W. Meyer, U.S. Geological Survey, oral commun., 1980). The 150-foot interval shown in Figure 3 is divided into five hydraulically distinct, vertically uniform layers. The outer layers are relatively impermeable and act as confining layers receiving very little flow from the injection wells. The 12-foot middle layer is the most permeable, receiving 65 percent of the injected water. As shown in Figure 3, the most permeable layer at the Hialeah site was about 12 feet thick and occurred within the Oligocene Suwannee Limestone from 1,020 to 1,032 feet below land surface. The permeable layer was surrounded by much less permeable limestone of the Suwannee Limestone, the overlying Miocene Tampa Formation, and the underlying Eocene Avon Park Limestone. The injection zone was found to have a static head of 42 feet above mean sea level, or 33 feet above land surface (F. W. Meyer, U.S. Geological Survey, oral commun., 1980). A more complete description of the Floridan aquifer system in south Florida is included in Merritt and others (1983).

The Hialeah site data seemed to show a vertical variation from 800 to 2,000 mg/l in chloride concentration, but native-water chloride concentration and density were considered vertically uniform at various values in the hypothetical aquifer because none of the results of the sensitivity analyses would have benefitted from a spatial density variation. The chloride concentration of injected water was considered to be 65 mg/l.

The hypothetical aquifer was simulated in various ways depending upon the requirements of the problems considered. Analyses in which the injection and recovery processes were characterized by radial symmetry were simulated with a cylindrical coordinates (r, z) model design with each layer represented as one or two layers in the model. Analyses in which radial symmetry did not apply (regional flow and multiple wells) required three-dimensional Cartesian-coordinate simulations. To reduce costs, and taking advantage of the vertical hydraulic uniformity of layers in the hypothetical aquifer, the 12-foot, most permeable layer was represented in Cartesian coordinates with a two-dimensional areal model design. The cylindrical coordinate models were discretized into 27 annuli, with the outer radius at 30,000 feet, where constant pressure and concentration boundary conditions could be specified without affecting the simulated flow of fresh water near the well. Annuli widths ranged from less than 2 feet near the well (and should have been larger for better stability) to 10,000 feet near the outer radius, but were less than 60 feet in the area containing the fresh-water mass. The areal grids were symmetric, and boundary edges were more than 20,000 feet from the center. Grid cells in the vicinity of fresh-water movement were less than 200 feet on a side.

In some analyses of buoyancy stratification, it was found advantageous to design an entirely different prototype 170 feet thick with uniform hydraulic characteristics similar to the five-layer model, except that nominal horizontal and vertical hydraulic conductivities were 100 and 10 ft/d. The model of this prototype was discretized into 17 10-foot layers in cylindrical coordinates.

As the Hialeah site data did not support any estimates of the degree of hydrodynamic dispersion, various dispersion models [choices of longitudinal (α_ℓ) and transverse (α_t) dispersivity coefficients] were used. The one most often used was: $\alpha_\ell = 4$ feet, $\alpha_t = 0$. Assigning a α_ℓ value of 4 feet assumes that the value from Ehrlich and others (1979) was scale-dependent, and that a reasonable estimate of "local" hydrodynamic dispersivity would be smaller. Longitudinal dispersivity was assigned other values in some analyses. Setting $\alpha_t = 0$ assumes no transverse dispersion ("interlayer dispersion" when flow is predominantly in the lateral direction). Transverse dispersivity was assigned nonzero values in some analyses discussed in Merritt (1983).

RELATION OF RECOVERY EFFICIENCY TO HYDROGEOLOGIC CHARACTERISTICS

Buoyancy Stratification

If a substantial amount of injected fresh water buoys upward about the well during injection, storage, or withdrawal, the amount which is recoverable will be reduced. Native salt water will tend to migrate inward toward the bottom of the well, and the injected fresh water will tend to migrate outward in upper intervals of the injection zone. During withdrawal, salt water will reach the bottom of the well and contaminate withdrawn water even while fresh water remains around the well bore in the upper part of the zone. One objective of the computer analyses was to deter-

Table 1. Relation of Recovery Efficiency to Permeability

K_r and K_z multiplied by	Recovery efficiency (percent) Native-water density 62.57 lb/ft^3	64.0 lb/ft^3
0.1	–	47.8
0.2	–	47.3
0.5	67.5	45.4
1.0	67.0	32.7
2.0	65.2	23.8
5.0	63.8	9.0
10.0	58.8	–
20.0	47.4	–
50.0	30.4	–
100.0	21.9	–

[K_r and K_z (feet per day) are radial and vertical hydraulic conductivity values.]

mine the degree to which the magnitude of this process was related to the density contrast between injected and native waters and to the permeability of the aquifer material.

Table 1 shows results of two series of runs with the five-layer cylindrical coordinates model in which both horizontal and vertical hydraulic conductivities varied from the Hialeah site prototype values by the same multiple. Values in the second column are for a native-water density of 62.57 lb/ft^3, similar to the Hialeah site injection zone, and values in the third column are for a native-water density of 64.0 lb/ft^3, about that of sea water. Simulated injection was for 53 days, followed immediately by withdrawal. The five-layer model was not considered to provide a detailed representation of buoyancy stratification but was used to establish general quantitative relations.

Where recovery efficiency changes little with successive multiples, little stratification is portrayed by the simulations. A comparison of results from the two sets of runs shows native-water density to be an important factor affecting the degree of buoyancy stratification. Results indicate that for a given native-water density there seems to be a certain range of permeability in which virtually no stratification occurs during time periods comparable to those of the simulation. This permeability range is lower for higher values of native-water density. As simulated permeability values increase beyond this range for each density value, an increasing degree of stratification occurs, apparently because of a decrease in the frictional retarding force opposing upward (buoyant) flow for the prevailing density contrast and outward flow in upper layers.

These observations were consistent with results of runs of the 17-layer model of the hypothetical prototype with spatially uniform hydraulic characteristics, which showed the stratification pattern in greater detail. Of particular interest is a run in which horizontal (radial) hydraulic conductivity was increased by a factor of 100 while vertical hydraulic conductivity was not increased. In this scenario, the aquifer initially contained water of sea-water density (64.0 lb/ft^3). At the end of injection (Figure 4A), considerably more fresh water is present in the top layer than in lower layers, and considerably less is present in the lowest layer. Intervening layers were relatively uniform in volumes of fresh water, and the model computed a relatively uniform vertical fluid particle velocity of 0.86 ft/d in the fresh-water region around the well bore. Withdrawal followed immediately, and Figure 4B shows fresh water remaining in the injection zone when sufficient saline water reached the well in lower layers to cause the mix of withdrawn water to exceed the 250-mg/l chloride concentration limit. Runs in which longitudinal

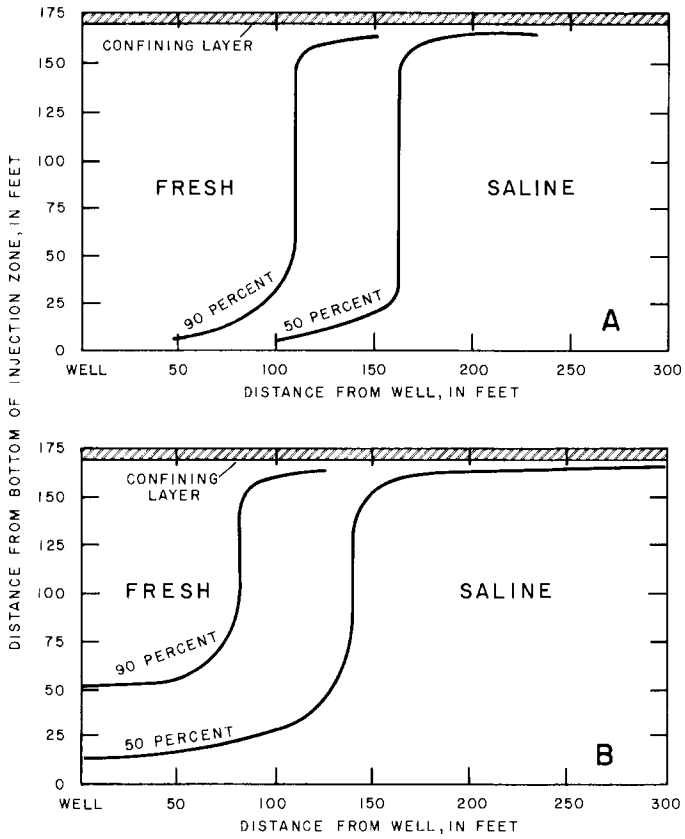

Fig. 4. Diagrams showing vertical and radial distribution of fresh water resulting from buoyancy stratification during injection and withdrawal.

dispersivity was increased show a decrease in buoyancy stratification, perhaps because waters of contrasting density are more widely separated by a broader zone of dispersion.

Evidently, aquifers of high permeability containing highly saline water are a worst case for successful recovery of injected fresh water. Because carbonate injection-zone hydraulic and chemical characteristics typically vary regionally and even locally, it is appropriate to evaluate the possibility that some degree of buoyancy might occur on a site-by-site basis.

Hydrodynamic Dispersion

When the upper limit of the concentration of some constituent considered acceptable in recovered water is less than half the average of the concentrations in the injected and native aquifer waters, hydrodynamic dispersion is a deleterious process that reduces recovery efficiency. If the upper limit is greater than the average, hydrodynamic dispersion works to the benefit of the injector, and recovery efficiencies greater than 100 percent can be realized. In the hypothetical test cases posed in this study, the acceptable limit for chloride (250 mg/l) was less than the average of the injected water (65 mg/l) and native aquifer water (2,000 to 19,000 mg/l) concentrations.

Although part of the water within the zone of dispersion may be potable, the total amount of recoverable water is lower when the volume of the zone of dispersion is larger relative to the volume injected, a result of a higher degree of hydrodynamic dispersion. In a series of tests with the five-layer model of the Hialeah prototype to observe the simulated effect upon recovery efficiency, longitudinal dispersivity was varied from 2 to 30 feet, while the volume injected was kept constant. Recovery efficiency decreased as the dispersivity value increased. Results are shown in Figure 5 for three different values of native-water density. Transverse dispersivity was assumed to be zero. When α_ℓ = 4 feet, the native-water chloride concentration was 2,000 mg/l, and the acceptable limit for chloride was raised to 1,300 mg/l, the computed recovery efficiency was 108 percent, demonstrating that dispersive mixing is a beneficial process when the native-water concentration does not greatly exceed the acceptable limit in recovered water.

Native-Water Salinity

The greater the salinity of the native water, the greater will be the range of salinity across the zone of dispersion, and the proportion of potable

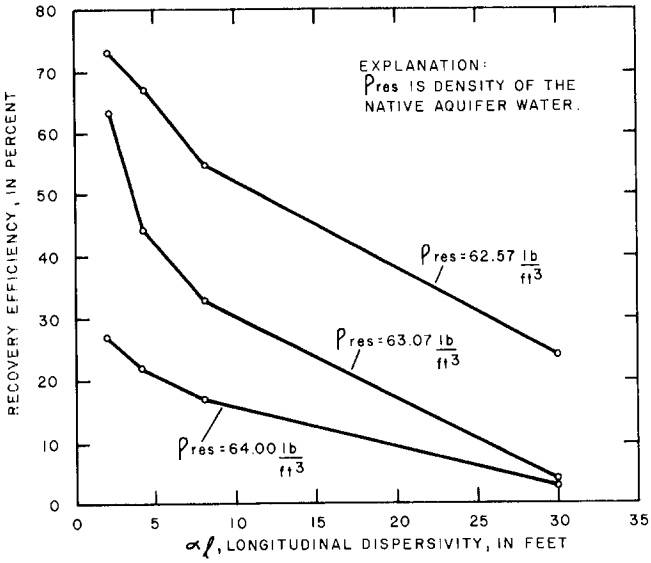

Fig. 5. Graph showing relation between recovery efficiency and the degree of dispersion.

water within the zone will be smaller. The inverse relationship between recovery efficiency and aquifer-water salinity, computed by the model as a recovery efficiency-density relation, is shown in Figure 6 for a range of longitudinal dispersivity coefficients (α_t). α_ℓ was zero in the analyses illustrated (no interlayer dispersion). No effort was made to isolate the deleterious effect of buoyancy stratification at higher values of native-water density.

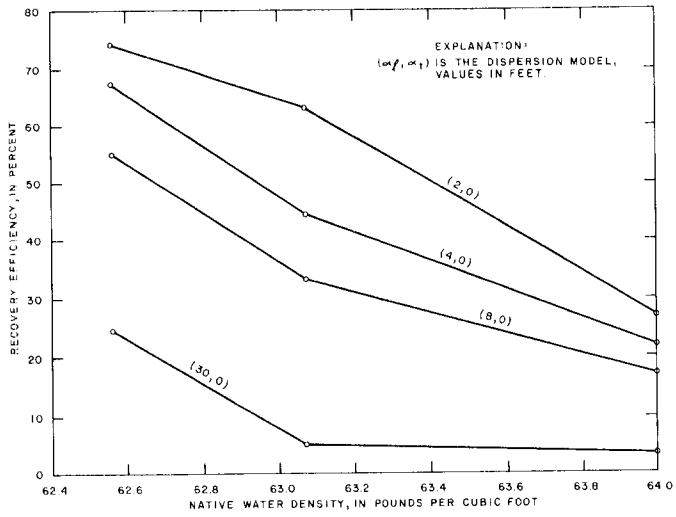

Fig. 6. Graph showing relation between recovery efficiency and native-water density.

Aquifer Storativity

The aquifer storage coefficient is modeled as an algebraic combination of values of porosity, native-water density, layer thickness, and compressibility of the aquifer material and of water (Lohman, 1979). Of the parameters other than density, porosity and layer thickness were considered to have the greatest possible range of variation in the class of aquifers with potential as receptacles for injected fresh water. Therefore, these two parameters were varied in model tests to determine the relation between recovery efficiency and aquifer storativity.

This relation is less obvious conceptually than others tested with the model. For a given volume of injected fresh water, a thicker receiving layer will have a zone of dispersion which is smaller in lateral dimension because of the reduced distance of radial outflow from the well but greater in vertical dimension because of the increased thickness of the receiving zone. Given greater porosity, the zone of dispersion will be reduced in lateral dimension but will contain a greater amount of water per unit volume. The question posed is whether the relative volumes of water within the unmixed fresh-water zone and mixed fresh and native saline water within the zone of dispersion would change if the layer thickness or porosity were different. If the relative volume of the zone of dispersion were to increase, which would mean a reduction in the volume of unmixed fresh water, recovery efficiency would be reduced because only part of the water in the zone of dispersion is potable.

Results of model runs (Figure 7) for a dispersion model in which α_ℓ = 4 feet and α_t = 0 (no interlayer dispersion) indicate that recovery efficiency is lower for larger values of layer thickness and porosity. Indicated recovery efficiency decreases with increasing porosity and layer thickness are not dramatic. An assumption underlying analyses with the model was that hydraulic conductivity and the degree of hydrodynamic dispersion are unrelated to changes in porosity.

Background Hydraulic Gradients and Length of Storage Period

Of major interest relative to the potential feasibility of fresh-water injection is the effect of delaying recovery of the injected fresh water until it is needed. The length of a storage period can be a significant factor if natural or man-made background hydraulic gradients move the injected fresh water downgradient from the injection well. If the shift is appreciable, the well will no longer be near the center of the fresh-water mass during recovery. After recovering part of the potable water, further pumping would then draw saline water from the upgradient direction while appreciable amounts of fresh water remain in the downgradient direction. When the saline contribution becomes substantial enough that the salinity of withdrawn water exceeds the limit established for potability, the remaining fresh water is lost as such unless downgradient wells are available for its recovery.

The degree to which a mass of injected water will shift during a given storage period with respect to the well used for injection will vary depending upon the diameter of the fresh-water mass and the rate of background flow. If the diameter of the fresh-water mass is relatively large, a relatively large amount of downgradient movement can occur before the degree of the shift is sufficient to appreciably affect recovery efficiency, because the injection and recovery well would be closer to the center of the larger fresh-water mass. The diameter of the fresh-water mass is a function of its volume and the thickness and porosity of the injection zone. This dependence upon diameter was not tested with the model, but the length of the storage period was varied in model tests assuming a given injection volume, aquifer dimensions and hydraulic characteristics, and rate of background flow.

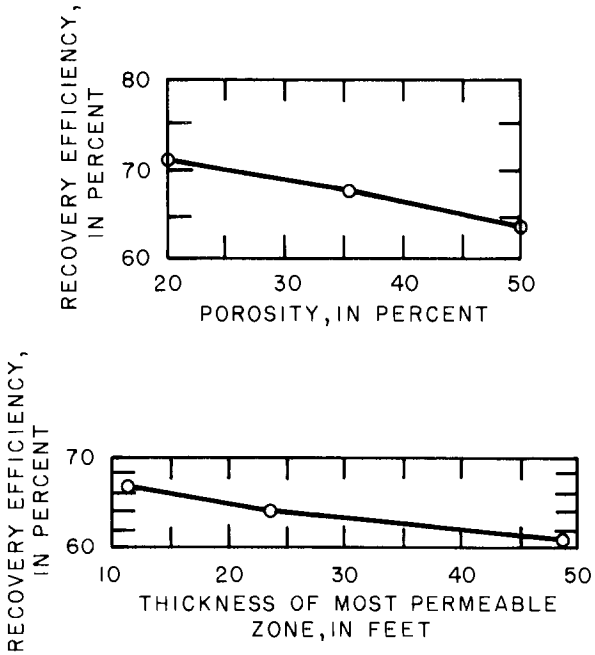

Fig. 7. Graph showing relation between recovery efficiency and aquifer storativity parameters.

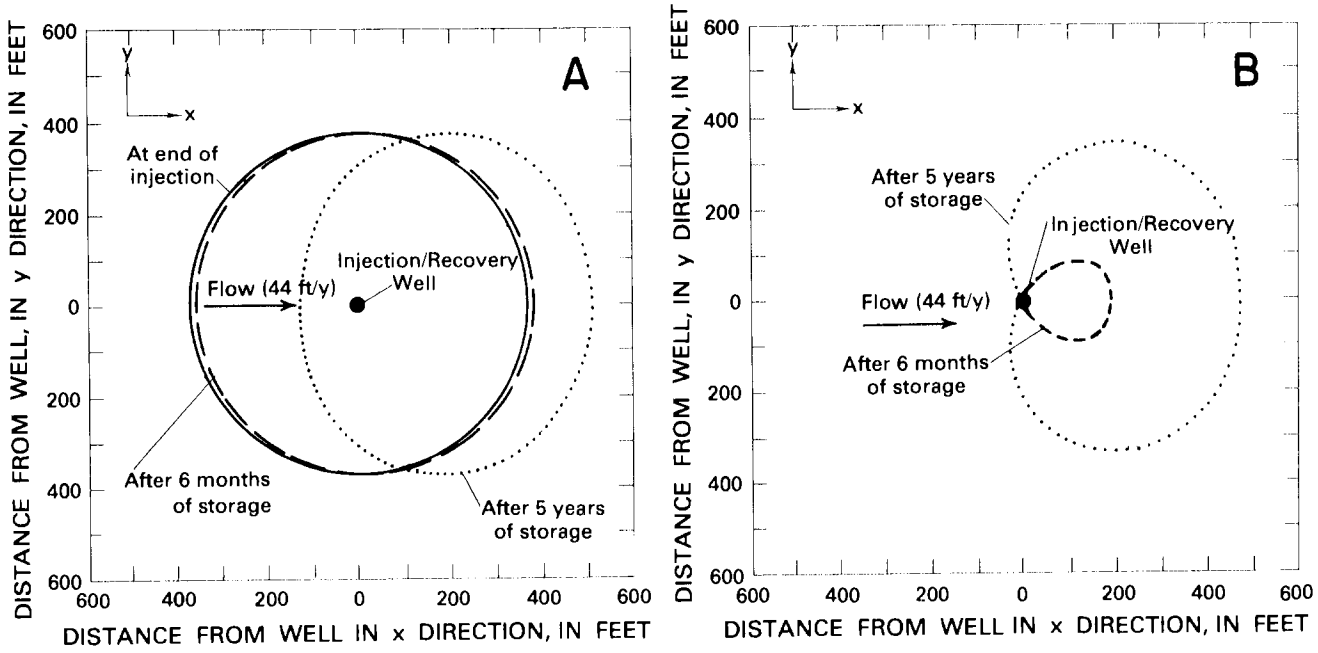

Fig. 8. Diagrams showing effect of regional flow upon the position and recoverability of potable water.

The single-layer Cartesian representation of the 12-foot, most permeable layer at Hialeah was used for the analysis. Background flow, caused by a natural hydraulic gradient in the aquifer, was assumed to be 44 ft/yr along the x-axis of the grid, and was simulated by compatible initial and boundary pressure specifications. The native-water salinity was insufficient to cause appreciable buoyancy stratification. Results (Figure 8A) show the nearly circular fresh-water mass at the end of the injection period (solid line) shifted slightly after six months of storage (dashed line) and shifted substantially after five years of storage (dotted line). In the latter case, appreciable movement downgradient has caused additional hydrodynamic dispersion which has compressed the 250-mg/l chloride profile. Recovery efficiencies when recovery began immediately following injection, after six months of storage, and after five years of storage, were 60.9, 59.9, and 21.8 percent. Figure 8B shows fresh water remaining when recovery ended because withdrawn water became saline following storage periods of six months (dashed line) and five years (dotted line).

As the specified hydraulic conductivity and rate of flow in a layer of high permeability are probably not atypical of potential limestone injection zones, the analysis indicates that the possible deleterious effects of background flow need assessment on a site-by-site basis, taking into consideration aquifer characteristics, the likely volumes to be injected, and the likely storage period prior to recovery.

RELATION OF RECOVERY EFFICIENCY TO DESIGN AND MANAGEMENT PARAMETERS

Rates of Injection and Recovery

It is of interest relative to the feasibility of recovering injected fresh water to ascertain whether certain ranges of injection and recovery rates will favor high recovery efficiencies. The five-layer model was used to simulate the injection and withdrawal of a fixed volume at various rates. In one series of tests, injection at different rates with the time period of injection adjusted to maintain the fixed volume was followed by withdrawal at a fixed rate. In the second series of tests, injection at a fixed rate for a fixed time period was followed by withdrawal at different rates until the concentration of withdrawn water reached 250 mg/l.

No variation in recovery efficiency was observed in the tests. The zone of dispersion at the end of injection was virtually unchanged when the injection rate varied, demonstrating that the model represents the dispersion process in radial flow from a well as a function of the extent of fluid movement to a new position and not of the rate of movement to that position, despite the functional dependence upon flow velocity. This is consistent with other analytical formulations describing the

concentration variation within the zone of dispersion (Hoopes and Harleman, 1967; Ren Jen Sun, 1976).

Volume of Water Injected

The five-layer model was used to show the relation of recovery efficiency to the volume of fresh water injected. From a theoretical standpoint, the problem actually considered is whether the volume of the zone of dispersion varies in proportion to the injection volume. If not, there would be a variation in recovery efficiency as the injection volume changes.

The rate of injection for a fixed time period was varied in model tests from 1,000 to 250,000 ft^3/d, as results of the previous analysis had shown that recovery efficiency was independent of rate in model simulations. The dispersion model (α_ℓ = 4 feet, α_t = 0) represented the assumption that no interlayer dispersion occurred. Results of this analysis (Figure 9) show that there is a large increase of recovery efficiency with increasing volume for small volumes, but that the rate of increase is small at large volumes. Zero recovery efficiency would occur for a sufficiently small injection volume because of the effect of hydrodynamic dispersion. Evidently, operational tests performed with small injection volumes cannot be expected to yield encouraging results. Results of this analysis apply to a single cycle of injection and recovery; whether the relation with volume continues in successive cycles was not established.

Well Not Open to Full Thickness of Injection Zone

For various reasons, operational injection wells might be constructed to be open only to part of a permeable receiving zone, instead of being open to an entire permeable zone and to sections of overlying and underlying confining layers, as was the case at the Hialeah test site used as a prototype in this study. To investigate this type of situation, the five-layer model was modified so that the well was open only to the lower 77 feet of the 150-foot Hialeah site interval; that is, to the lower 4 feet of the most permeable layer, to the next underlying relatively permeable layer, and to a section of the lower confining layer. Simulated conditions did not permit any appreciable buoyancy effect.

Virtually no change in recovery efficiency was observed. Injected fresh water flowed upward near the well to fill permeable zones, but there was virtually no vertical flow at radii greater than 300 feet. The concentration gradient of the zone of dispersion at the end of the injection phase was quite similar to that of the fully penetrating case, in which very little vertical flow occurred during either injection or withdrawal. Results are of significance relative to the design of operational injection systems in that they suggest that partial well penetration of a permeable unit might not affect the recoverability of potable water.

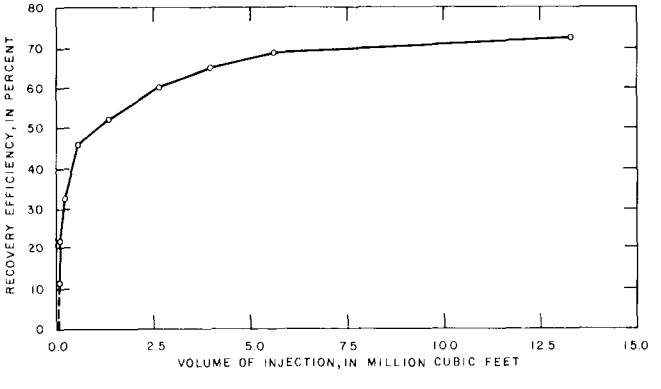

Fig. 9. Graph showing relation between recovery efficiency and volume of fresh water injected.

Successive Cycles of Injection and Recovery

If implemented as a water-conservation practice in regions with an annual wet- and dry-season climatic cycle, fresh-water injection and recovery would likely be done on a seasonal schedule. The recovery efficiency of the first cycle of injection and recovery is not a good indicator of the potential of the system, as recovery efficiency tends to improve in subsequent cycles. Such improvement was observed to some extent in several short-duration operational tests in south Florida (Tibbals and Frazee, 1976; J. J. Plappert, Florida Department of Environmental Regulation, written commun., 1977; and F. W. Meyer, U.S. Geological Survey, oral commun., 1980) though the tests were not specifically designed to measure it.

A conceptual explanation for the improvement of recovery efficiency is that it is caused by changes in the zone of dispersion. If withdrawal were to end when withdrawn water exceeded potability (250 mg/l chloride), the chloride distribution in the aquifer at that time would become the initial distribution for the next injection phase. This mix of injected fresh water and saline native water about the well would mix with additional fresh water during the next injection to form a new zone of dispersion. Thus, with each successive injection, the zone of dispersion would progressively increase

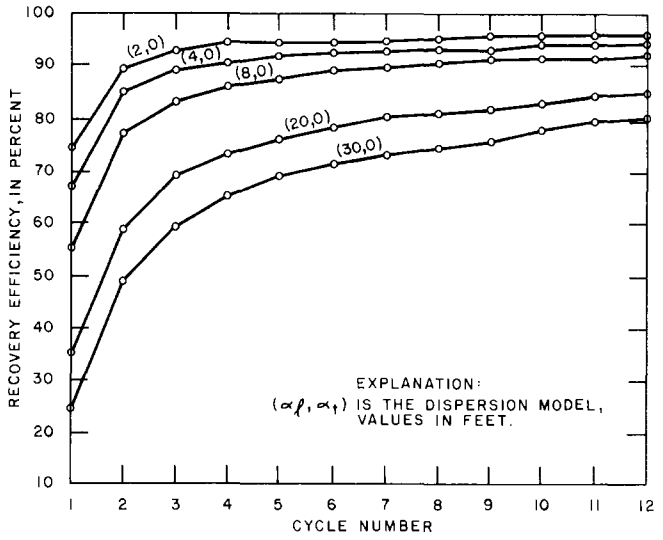

Fig. 10. Graph showing improvement of recovery efficiency with successive injection and recovery cycles.

in volume from accretion of residual fresh water from previous injections and contain greater quantities of mixed water that is potable. This would lead to a progressive increase in recovery efficiency even if the volumes of injected fresh water did not increase. Because the cost of the fresh-water storage alternative is most realistically based upon the recovery efficiency obtainable after initial cycles, and because operational tests have not clearly established what the degree of improvement will be, the model was used to assess the possible degree of improvement.

Twelve similar cycles of injection and recovery were simulated in the five-layer model, and each recovery was terminated when withdrawn water exceeded potability (250 mg/l chloride). Results for various dispersion models (Figure 10) indicate major improvement in the first several cycles. Improvement continues at a reduced rate in later cycles. It is of interest that even when recovery efficiency is 35 percent in the first cycle (α_ℓ = 20 feet, α_t = 0), the model indicates that it could improve to 70 percent in the third cycle and to 80 percent in the seventh cycle.

Multiple-Well Configurations

Operational fresh-water injection and recovery systems may require more than one well if the volumes to be injected and the required inflow rate exceed the capacity of a single well, or if the pressure must be distributed to avoid fracturing the aquifer or damaging the well. The recovery efficiency of a group of wells depends upon the extent and nature of their interaction. Model analyses were designed to compare the recovery efficiencies of groups of wells arranged in various geometries. A single-well simulation was also performed for further comparison.

As most of the simulated cases were not radially symmetric, the single-layer Cartesian representation of the most permeable layer of the Hialeah site prototype was used. The dispersion model was α_ℓ = 4 feet, α_t = 0. Analyses assumed approximately uniform flow in an isotropic aquifer with no background hydraulic gradient and insufficient density contrast to cause appreciable buoyancy. Wells were arranged so that adjacent wells were 500 feet apart. The total volume injected was the same in most of the runs and was apportioned equally among wells in operation at a particular time.

Centered configurations (a central well surrounded by peripheral wells at a 500-foot radius) of three, four, five, seven, and nine wells were tested. Noncentered configurations tested included a two-well arrangement and triangular and square arrangements. A simultaneous injection schedule (injection at equal rates at all wells for the entire time period of the injection) was tested in the noncentered configurations and in the five-well centered configuration. A sequential injection schedule (injection at the center well until fresh water reached peripheral wells, followed by injection at equal rates at all wells) was tested in centered configurations and in the two-well arrangement (with one well serving as the "center"). Generally, withdrawal schedules consisted of equal-rate withdrawals with various wells being shut down when pumped water exceeded a salinity limit corresponding to 250 mg/l chloride. In one test, a sequential injection schedule in a five-well centered configuration was followed by withdrawal solely from the center well.

There were no major variations in recovery efficiency in any configurations or for any schedules when the volume injected remained constant. Sequential injection schedules in the centered configurations followed by equal-rate withdrawals generally had the highest recovery efficiencies, nearly that of the single-well test. Simultaneous injection and equal-rate withdrawal in noncentered configurations produced recovery efficiencies less than the single-well simulation by factors of 3 to 4 percent. Variations in the volume showed the same type of relation to recovery efficiency, and variation in rate showed the same lack of relation, as in the single-well analyses.

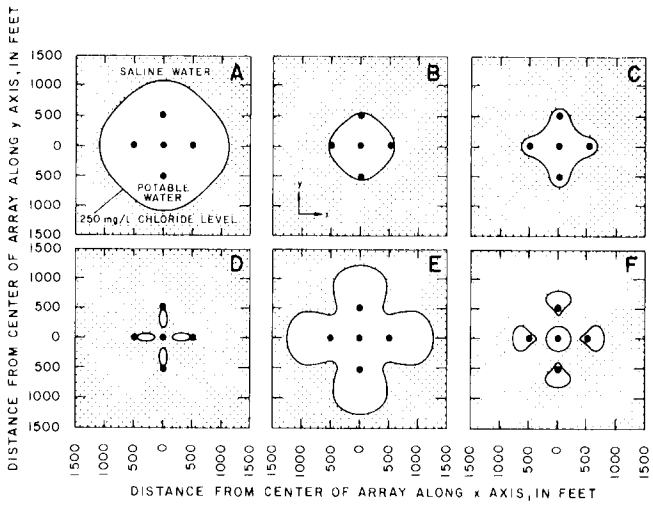

Fig. 11. Diagrams showing the distribution of potable water resulting from various schedules of injection and withdrawal in a centered configuration of five wells.

The five-well centered configuration serves as a useful test case for comparing various types of injection and withdrawal schedules. Figure 11A shows the fresh-water mass at the end of sequential injection in the five-well configuration, and Figure 11B shows the fresh-water mass at the point during recovery when saline water had just reached the peripheral wells. When the sequential injection was followed by withdrawal from only the central well, the fresh-water distribution (Figure 11C) after the same volume of recovery as in Figure 11B was different. When all wells became saline, some fresh water remained (Figure 11D), and recovery efficiency was less than the equal-rate withdrawal (Figure 11B) by a factor of 6 percent.

Simultaneous injection in the five-well centered configuration produced a cloverleaf distribution of fresh water (Figure 11E). The water remaining (Figure 11F) after the same volume of withdrawal (at equal rates) as the other examples is in five distinct masses. When recovery ended, small amounts of fresh water remained outside the peripheral wells, and recovery efficiency was less than the sequential injection and equal-rate withdrawal case (Figure 11A-B) by a factor of 10 percent.

The basic principle illustrated by the multiple-well analyses seemed to be that recovery efficiency is somewhat enhanced when flow patterns during injection and recovery are similar (though reversed), as in the sequential injection and equal-rate withdrawal case.

CONCLUSIONS

Generally, the study shows that a loss of recovery efficiency resulted from: (1) processes causing mixing of injected fresh water with native saline water (hydrodynamic dispersion); (2) processes or conditions causing the irreversible displacement of the injected fresh water with respect to the well (buoyancy stratification and background hydraulic gradients); and (3) processes or procedures causing injection and withdrawal flow patterns to be dissimilar (dissimilar injection and withdrawal schedules in multiple-well systems). A significant result is the theoretical demonstration that recovery efficiency should improve considerably in initial successive cycles, provided that each recovery phase ends when the chloride concentration of withdrawn water increases to some prescribed value less than that of the more-saline native water. Other results show that a high degree of aquifer permeability or high salinity of the native water, or a combination of these factors, would permit rapid buoyancy stratification and bring about a substantial loss of recovery efficiency.

ACKNOWLEDGMENTS

The author is indebted to his colleague Fred Meyer, now retired from the U.S. Geological Survey, Miami, Florida. Fred Meyer initially provided the author with technical guidance enabling the author to begin his study of fresh-water subsurface storage, and his suggestions as the author conducted the model study were very helpful. The author would also like to thank Howard Klein of the same office for his advice concerning the manuscripts of the various reports.

The author is grateful to Toney Lanier of the U.S. Army Corps of Engineers, whose patient support insured the success of the study.

REFERENCES CITED

Black, Crow, and Eidsness, Inc. 1974. Results of drilling and testing of the stormwater injection well for the City of St. Petersburg, Florida. Project no. 412-72-01(4), July 1974.

CH_2M HILL. 1984. Final report—Recharge-recovery at Lake Manatee: Phase II. FC16398.AO, March 1984.

Ehrlich, G. G., E. M. Godsy, C. A. Pascale, and John Vecchioli. 1979. Chemical changes in an industrial waste liquid during post-injection movement in a limestone aquifer, Pensacola, Florida. Ground Water. v. 17, no. 6, pp. 562-573.

Fitzpatrick, D. J. 1985. Tests for injecting, storing, and recovering freshwater in a saline artesian aquifer, Lee County, Florida. U.S. Geological Survey Water-Resources Investigations 85-4249. 53 pp.

Grove, D. B. and L. F. Konikow. 1976. Modeling cyclic storage of water in aquifers. Abstract, EOS, Transactions of the American Geophysical Union. v. 57, no. 12, pp. 916-917.

Hoopes, J. A. and D.R.F. Harleman. 1967. Dispersion in radial flow from a recharge well. Journal of Geophysical Research. v. 72, no. 14, pp. 3595-3607.

INTERA Environmental Consultants, Inc. 1979. Revision of the documentation for a model for calculating effects of liquid waste disposal in deep saline aquifers. U.S. Geological Survey Water-Resources Investigations 79-96. 73 pp.

INTERCOMP Resource Development and Engineering, Inc. 1976. A model for calculating effects of liquid waste disposal in deep saline aquifers, Part 1—Development, Part 2—Documentation. U.S. Geological Survey Water-Resources Investigations 76-61. 253 pp.

Khanal, N. N. 1980. Advanced water supply alternative for the Upper East Coast Planning Area; Part I—Feasibility of cyclic storage of freshwater in a brackish aquifer, and Part II—Desalinization alternative. South Florida Water Management District Technical Publication no. 80-6. 75 pp.

Kimbler, O. K., R. G. Kazmann, and W. R. Whitehead. 1975. Cyclic storage of freshwater in saline aquifers. Louisiana Water Resources Research Institute Bulletin 10. 78 pp.

Lantz, R. B. 1971. Quantitative evaluation of numerical diffusion (truncation error). Society of Petroleum Engineers Journal. September 1971. pp. 315-320.

Lohman, S. W. 1979. Ground-water hydraulics. U.S. Geological Survey Professional Paper 708. 70 pp.

Merritt, M. L. 1982. Subsurface storage of freshwater, south Florida. ASCE National Specialty Conference on Environmentally Sound Water and Soil Management, Orlando, Florida, 1982, Proceedings. pp. 242-250.

Merritt, M. L. 1983. Subsurface storage of freshwater in south Florida: A digital model analysis of recoverability. U.S. Geological Survey Water-Supply Paper 2261. 44 pp.

Merritt, M. L., F. W. Meyer, W. H. Sonntag, and D. J. Fitzpatrick. 1983. Subsurface storage of freshwater in south Florida: A prospectus. U.S. Geological Survey Water-Resources Investigations Report 83-4214. 69 pp.

Molz, F. J., Oktay Güven, and J. G. Melville. 1983. An examination of scale-dependent dispersion coefficients. Ground Water. v. 21, no. 6, pp. 715-725.

Price, H. S., R. S. Varga, and J. E. Warren. 1966. Application of oscillation matrices to diffusion-convection equations. Journal of Mathematics and Physics. v. 45, pp. 301-311.

Ren Jen Sun. 1976. Hydrodynamic dispersion and movement of injected water. In Reeder, H. O., and others, Artificial recharge through a well in fissured carbonate rock, West St. Paul, Minnesota. U.S. Geological Survey Water-Supply Paper 2004. pp. 52-75.

Reynolds, S. F. and R.D.G. Pyne. 1983. Recharge-recovery: A new alternative for municipal water supply expansion. Abstract, presented to the National Water Well Association Eastern Regional Conference on Ground Water Management in Orlando, Florida, October 1983.

Scheidegger, A. E. 1961. General theory of dispersion in porous media. Journal of Geophysical Research. v. 66, no. 10, pp. 3273-3278.

Sonntag, W. H. 1984. Subsurface storage of freshwater in south Florida: Evaluation of surface-water discharge data at selected sites. U.S. Geological Survey Water-Resources Investigations Report 84-4008. 75 pp.

Tibbals, C. H. and J. M. Frazee, Jr. 1976. Ground-water hydrology of the Cocoa well-field area, Orange County, Florida. U.S. Geological Survey Open-File Report 76-676. 67 pp.

Wedderburn, L. E. and M. S. Knapp. 1983. Field investigation into the feasibility of storing freshwater in saline portions of the Floridan aquifer system, St. Lucie County, Florida. South Florida Water Management District Technical Publication no. 83-7. 71 pp.

U.S. Environmental Protection Agency. 1976 [1977]. Quality Criteria for Water. U.S. Government Printing Office. 256 pp.

* * * * *

Michael L. Merritt graduated from the University of Notre Dame in 1963 with a B.S. in Physics. In 1970, he earned an M.S. in Mathematics at New Mexico State University. Following two years with the General Electric Co. in Bay St. Louis, Mississippi, he attended Florida State University in Tallahassee, earning an M.S. in Applied Mathematics in 1976. Joining the U.S. Geological Survey in 1974, he has specialized in applying digital modeling techniques to ground-water hydrology.

New Approaches Characterizing Groundwater Flow, Seiler & Wohnlich (eds),
© 2001 Swets & Zeitlinger Lisse, ISBN 902651 848 X

Results from a forced gradient tracer test in a fractured aquifer with simultaneous input of different tracers

A. Bender
Technologieberatung Grundwasser und Umwelt GmbH, 56070 Koblenz, Germany

G. Battermann
Technologieberatung Grundwasser und Umwelt GmbH, 56070 Koblenz, Germany

ABSTRACT: Interpretation of pumping test and tracer test data allowed for the evaluation of capture areas of discharge wells as well as important hydraulic parameters of a multi-layered aquifer system such as longitudinal dispersivity, hydraulic conductivity, effective porosity and leakage flow. Evaluation of the tracer breakthrough curves was realized using an analytical solution of the mass transport equation for radial symmetric flow patterns induced by the forced gradient tracer test. The results of the tracer test yielded important input parameters for subsequent calculations of pollution spreading with a numerical groundwater model to optimize the location and necessary pumping rates of future discharge wells as part of hydraulic remediation measures.

1 INTRODUCTION

In order to design future remediation measures on a contaminated site the hydraulic characteristics of the fractured aquifer were investigated using a forced gradient tracer test. In the focus of interest were the capture areas of future discharge wells, the quantification of groundwater flow from different directions as well as the quantification of vertical leakage into the underlying siltstone.

2 SITE HYDROGEOLOGY

The subsurface consists of fractured sedimentary rocks of the Middle Buntsandstein formation (Triassic Sandstone). The sequence of sand, clay- and siltstones forms a complex multi-layered aquifer system. The upper sandstones are partially weathered and form a hydraulic unit with the underlying sandstones, i.e. the interbedded thin clay- and siltstone band does not seem to act as a hydraulic barrier. The lower sandstones though are hydraulically separated from each other by layers of clay and siltstones. The groundwater table is about 3-4 m below surface level. The thickness of the upper aquifer is about 8-10 m. Hydraulic conductivities as derived from previous pumping tests are in the order of $1x10^{-4}$ m/s. The groundwater flow from the site in the upper aquifer is in the order of 8 m^3/h. The aquifer thickness of the underlying sandstone is about 10 m, due to a lower hydraulic conductivity of about $1x10^{-5}$ m/s, the groundwater flow from the site in the underlying aquifer is about 5 m^3/h. As a consequence of the higher hydraulic heads in the upper aquifer vertical leakage downwards the lower aquifer was assumed.

3 TRACER TEST

The hydraulic parameters were investigated by a long-term forced gradient tracer test which was subdivided in three main pumping phases.

3.1 *First pumping phase*

Groundwater was pumped from two wells screened in the first/second aquifer for a total time of 18 weeks. At a constant discharge rate of about 4 m^3/h a forced gradient towards the pumped wells was superimposed on the natural gradient of groundwater flow. During pumping five fluorescent and chemical tracers were injected simultaneously into different observation wells spread around the pumped wells.

Table 1. Tracers, tracer mass injected and distances from the injection well to the pumping well in the first /second aquifer

Tracer substance	Tracer mass	Distance
Na-Naphthionate	2.0 kg	64 m
Sulforhodamine B	0.5 kg	25 m
Uranine	0.2 kg	50 m
Strontium Chloride	3.0 kg	90 m
Lithium Chloride	2.0 kg	42 m

These injection wells are screened in the first/second aquifer too. At the same time a mass of 2,0 kg of Ammonium Bromide was injected into an observation well screened in the third aquifer, located about 16 m from the pumping wells.

3.2 *Second pumping phase*

With a duration of 5 weeks groundwater was pumped from a well screened in the third aquifer in addition to the ongoing extraction from the first/second aquifer. The discharge rate from the third aquifer was kept constant at about 6 m^3/h. Similar to the first pumping phase 4 fluorescent and chemical tracers were now injected into observation wells screened in the third aquifer.

Table 2. Tracers, tracer mass injected and distances from the injection wells to the pumping well in the third aquifer

Tracer substance	Tracer mass	Distance
Na-Naphthionate	3.0 kg	56 m
Sulforhodamine B	2.0 kg	110 m
Uranine	1.0 kg	80 m
Lithium Chloride	6.0 kg	47 m

To make sure that tracer concentrations in the third aquifer are not influenced by the previous injection in the first/second aquifer, tracer injection in the third aquifer was repeated 2 weeks later using identical tracer substances and masses at the same injection wells.

3.3 *Third pumping phase*

For another 3 weeks the groundwater abstraction from the third aquifer was continued whereas the extraction from the first/second aquifer was stopped. No additional tracers were injected in this pumping phase.

3.4 *Sampling*

Tracer concentrations were monitored by sampling the pumped groundwater from the discharge wells and from selected observation wells.

3.4.1 *Discharge wells*

Representative samples were taken from the extracted groundwater assuming constant tracer concentrations over the thickness of the aquifer. During the first week of pumping samples were taken at intervals of 4 hours. In the second week sampling was realized at intervals of 6 hours. Sampling at intervals of 12 hours started in the third week of groundwater extraction.

3.4.2 *Observation wells*

In order to control time depending tracer concentrations in the nearby surrounding, especially in observation wells located down gradient of the natural flow direction a number of 10 observation wells were sampled in weekly intervals during the tracer test. Water extraction and sampling was accomplished by pumping the observation wells with a rate of up to 5 m^3/h for 1 to 2 hours. Analogous to sampling the pumping wells, all samples were taken assuming constant tracer concentrations over the thickness of the aquifer.

3.5 *Trace analysis*

In order to protect the fluorescent tracers from UV-radiation all groundwater samples were filled in small bottles (250 mL) of brown glass. Except bromide ion, all tracers were simultaneously analyzed from one sample but with different analytical methods to enable cost-effective analysis of the tracers simultaneously injected (Käss 1993). The feasibility of this analytical procedure was tested with groundwater samples from the site, which additionally proved no substantial interference of the analytical methods by organic contaminants such as PAH or phenols in the water.

Table 3. Analytical methods and lowest tracer detection limits

Tracer substance	Method	Detection Limit
Na-Naphthionate	Fluorescence spectroscopy	0.1 µg/L
Sulforhodamine B		0.02 µg/L
Uranine		0.002 µg/L
Strontium Chloride	Atomic absorption	2.0 µg/L
Lithium Chloride		0.2 µg/L
Ammonium Bromide	Flame spectroscopy	100.00 µg/L

4 RESULTS

4.1 *First/second aquifer*

4.1.1 *Discharge wells*

The best results were received from Strontium Chloride which could be detected at the pumping well after a travel time of 16 days. The first concentration peak appeared about 18 days after injection with two smaller peaks following about 28 and 45 days later (see figure 1). The total recovery rate of Strontium Chloride was approximately 51 %. A good result as

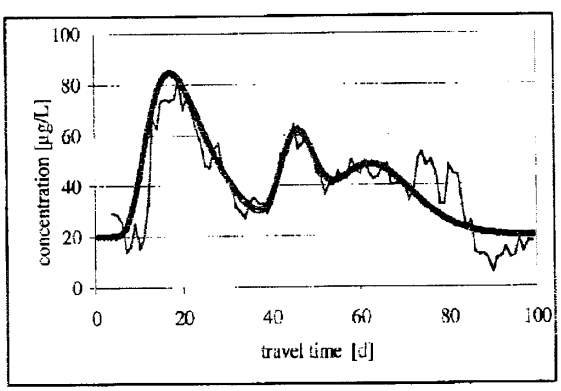

Figure 1. Strontium Chloride concentration during the tracer test, normal line = measured concentration, bold line = calculated concentration

well was received from Sulforhodamine B which was detected after a travel time of 59 days with the concentration peak 5 days later (see figure 2). The total recovery rate was 43 %. Uranine proved a travel time of 49 days and a total recovery rate of 9.5%. Concerning Uranine a concentration peak was not observed because tracer concentrations detected were still increasing until the end of the tracer test. In contrast to that, the tracers Na-Naphthionate and Lithium Chloride were impossible to detect throughout the complete tracer test.

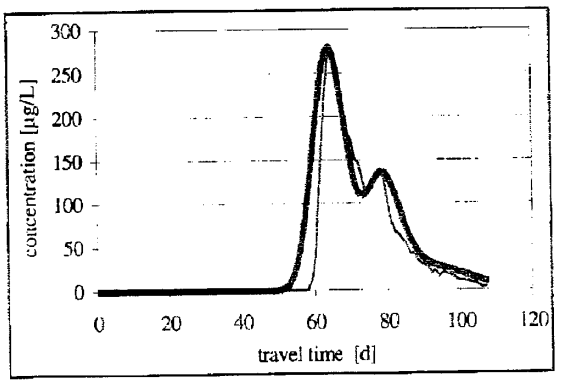

Figure 2. Sulforhodamine B concentration during the tracer test, normal line = measured concentration, bold line = calculated concentration

Bromide although injected into the third aquifer showed travel times of only 9 days with a long term peak concentration of about 20 days and a total recovery rate of more than 50 %.

4.1.2 *Observation wells*
Except Bromide all tracer substances injected were detected at least in one of the sampled down gradient observation wells with travel times between 7 days and up to 63 days. That means the tracers Na-Naphthionate and Lithium Chloride although not found in the pumping wells could be detected in some down gradient observation wells. The tracers registered at the pumping wells also drifted with the natural groundwater gradient to some extent, the concentrations found in the down gradient observation wells in most cases being much smaller than the concentrations detected at the pumping wells.

4.2 *Third aquifer*

4.2.1 *Discharge well*
Results received from the two identical tracer injections in an interval of two weeks nearly proved to be identical concerning travel times and recovery rates. Na-Naphthionate could be detected at the pumping well after a travel time of 1 day with a concentration peak 4 day after the injection (see figure 3). The total recovery rate of Na-Naphthionate was approximately 20 %. Uranine arrived at the pumping well 2

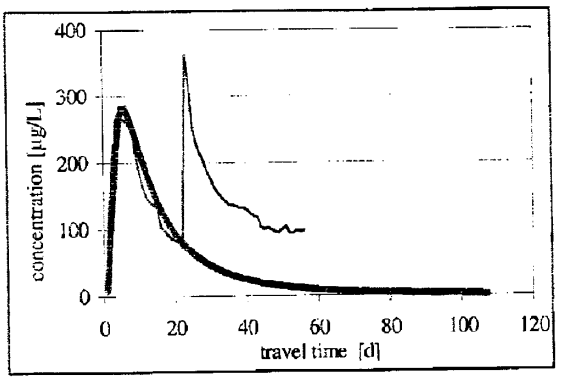

Figure 3. Na-Naphthionat concentration during the tracer test, normal line = measured concentration, bold line = calculated concentration (first injection)

days after the injection with a concentration peak another 2 days later. The recovery rate was 6 %. Lithium Chloride could be detected after a very short travel time of less than 1 day with the concentration peak 1 day after the injection and a total recovery rate of 16 %. Although providing an ideal breakthrough curve with a travel time of 2 days and the concentration peak 11 days later, the recovery rate of Sulforhodamine B was in the order of 1 %.

4.2.2 *Observation wells*
The concentration peak of Sulforhodamine B could be detected in one of the down gradient observation wells sampled approximately 7 days after the injection. The maximum concentration in this observation well exceeded the maximum concentration at the pumping well by a factor of 50. The other tracers injected could not be registered in the down gradient observation wells.

5 EVALUATION

The resulting concentrations of the tracer-substances previously injected into the observation wells allowed for the construction of corresponding breakthrough curves. Interpretation of the breakthrough curves in combination with the interpretation of different draw-down rates lead to the evaluation of the dominating fluid pathways within the multi-layered aquifer system. Assuming radial symmetric flow patterns induced by the constant groundwater extraction, the breakthrough curves at the pumping wells were calculated using Equation 1, which is an analytical solution of the mass transport equation published by Kinzelbach et al.:

$$c(r,t) = \frac{M}{2Q\sqrt{\pi a_L v_a t^3}} \exp\left(-\frac{(r - v_a t)^2}{4 D_L t}\right) \quad (1)$$

where M = injected tracer mass; Q = pumping rate; a_L = longitudinal aquifer dispersivity; v_a = average groundwater velocity; t = flow time; r = radial distance from injection to pumping well; D_L = longitudinal dispersion coefficient = $a_L * v_a$.

Fitting of measured and calculated breakthrough curves varying the input parameters allowed for the calculation of average groundwater velocity and aquifer dispersivity as well as an estimation of the effective porosity. Assuming breakthrough curves with more than one concentration peak to be a superimposition of tracer spreading on different flow paths, modeling of these breakthrough curves could be performed calculating a superimposition of up to three independent layers within one aquifer (see figures 1-3). Each layer is characterized by a specific dispersivity and a specific average groundwater velocity.

6 INTERPRETATION

6.1 *First/second aquifer*

The registered tracer signals from different injection wells located around the pumping well proved a clear anisotropy of the hydraulic characteristics. The results show a dominating groundwater flow direction towards the NE with an average groundwater velocity of 1.4 - 4 m/d and a longitudinal dispersivity in the range of 5 to 10 m. In contrast to that the average groundwater velocity calculated from tracer injections NNE of the pumping wells is less than 0.5 m/d and shows a longitudinal dispersivity in the order of 1 m. In addition no signals were registered from tracer substances injected into wells located N and NW at a distance of less than 30 m from the pumping wells. Due to a strong anisotropy of the hydraulic properties a well defined anisotropy of the capture area is obvious. The hydraulic anisotropy is also confirmed by the strong elliptical shape of the depression cone in the NE direction. The values calculated, especially longitudinal dispersivity and average groundwater velocity, hint at an aquifer with mixed properties. Fluid flow seems to occur through both the porous medium and through rock fractures.

Another important conclusion of the tracer test in the first/second aquifer is drawn from the observed travel times and recovery rates of Uranine and Sulforhodamine B compared to those of other tracers injected in analogous directions from the pumped wells. Whereas the average groundwater velocity from the other tracers is in the range of about 1–2 m/d, results of less than 0.4 m/d were calculated from Sulforhodamine B. Due to increasing tracer concentrations until the end of the test, the average groundwater velocity could not be calculated for Uranine. Both tracers are assumed not to be conservative but to some extent reactive tracers. That means both tracers are affected by significant reactions especially with organic contaminants found in the aquifer in residual concentrations. The travel times observed therefore are thought to be characterised by adsorption and chemical reactions with organic contaminants such as PAH and phenols. Though these substances did not significantly interfere the analytical methods of tracer detection, they are assumed to be responsible for a significant retardation of the fluorescent tracers Uranine and Sulforhodamine B. Travel times of these tracers in this case are not representative for the average groundwater velocity. As a consequence salt tracers are thought to be the best tracers to investigate aquifers with significant organic contamination.

6.2 *Third aquifer*

The average groundwater velocity calculated from all tracer substances injected is up to 10 m/d, the longitudinal dispersivity is in the order of 10 – 50 m. As regards the longitudinal dispersivity and the depression cone received from the pumping test a strong anisotropy of the hydraulic characteristics is also obvious. In the third aquifer, the depression cone also has an elliptical shape in the NE direction too. In contrast to that the calculated average ground water velocity received from the tracer substances injected does not depend on the flow direction.

Results obtained for the third aquifer are significantly different from the results of the first/second aquifer and allow for the identification of a distinct aquifer type. The high longitudinal dispersivity and average groundwater velocity calculated for this aquifer represent typical values for a fractured rock aquifer with an exclusively fluid flow within the fracture system. Though not proved by the tracer test in the third aquifer, the anisotropy of hydraulic characteristics observed in both aquifers indicates to a fracture system with a main direction towards the NE. This conclusion suits very well with the spreading of the contaminant plume previously observed.

6.3 *Vertical leakage*

Bromide tracer, injected into the third aquifer, and recovered in the pumped wells of the first/second aquifer is a clear proof of vertical ground water flow. As an important result of the tracer test, the layers of clay and siltstones, although representing an effective hydraulic separation of the two aquifers, do still allow for significant vertical leakage of contaminants.

7 SUMMARY

Interpretation of pumping test and tracer test data allowed for the evaluation of capture areas of discharge wells as well as important hydraulic parameters such as hydraulic dispersivity, hydraulic conductivity and anisotropy. In addition vertical ground water flow from the first/second aquifer to the third aquifer was identified. These parameters provided a basis for further groundwater modeling studies. With the numerical groundwater model calculations of pollution spreading were performed and the model calculations helped to optimize the location and necessary discharge rates of future discharge wells as part of hydraulic remediation measures. Due to the strong anisotropy of the capture area the total contaminated area is not contained by the pumping wells used for the tracer test, which was evident measuring tracer substances in down gradient observation wells too. As a result the remediation wells were placed at other sites than previously planned.

REFERENCES

Käss, W. 1992. Geohydrologische Markierungstechnik. In Matthess, G. (ed), Lehrbuch der Hydrogeologie, Band 9. Berlin, Stuttgart:Verlag Gebrüder Bornträger

Kinzelbach, W. et. al. 1996. Materialienband Berechnungsverfahren und Modelle. In Altlastenhandbuch des Landes Niedersachsen. Berlin, Heidelberg: Springer Verlag

Simulation of Subsurface Storage and Recovery of Effluent Using Multiple Wells, St. Petersburg, Florida

U.S. Geological Survey

Water-Resources Investigations Report 97-4024

Prepared in cooperation with the

City of St. Petersburg and the
Southwest Florida Water Management District

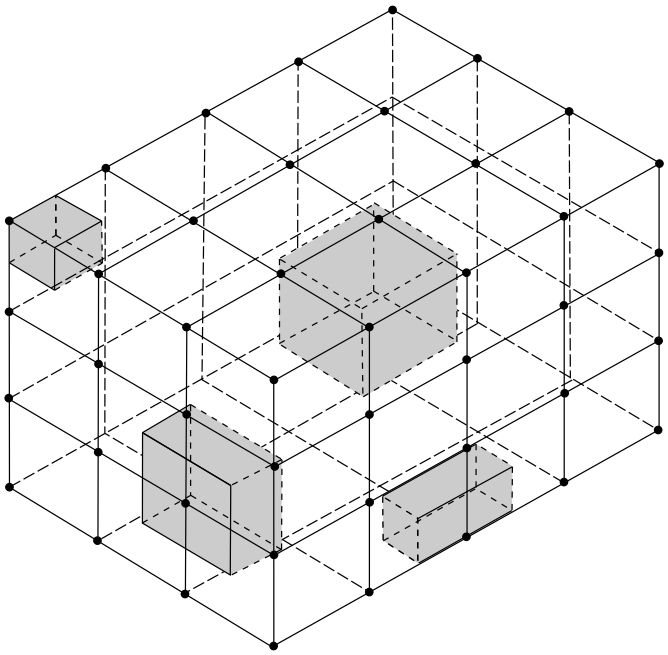

Cover: Sketch of finite-difference spatial discretization for a cartesian-coordinate system.

Simulation of Subsurface Storage and Recovery of Effluent Using Multiple Wells, St. Petersburg, Florida

By Dann K. Yobbi

U.S. GEOLOGICAL SURVEY

Water-Resources Investigations Report 97-4024

Prepared in cooperation with the

CITY OF ST. PETERSBURG and the
SOUTHWEST FLORIDA WATER MANAGEMENT DISTRICT

Tallahassee, Florida
1997

U.S. DEPARTMENT OF THE INTERIOR
BRUCE BABBITT, Secretary

U.S. GEOLOGICAL SURVEY
Gordon P. Eaton, Director

For additional information write to:

District Chief
U.S. Geological Survey
227 North Bronough Street, Suite 3015
Tallahassee, Florida 32301

Copies of this report can be purchased from:

U.S. Geological Survey
Branch of Information Center
Box 25286
Denver, CO 80225-0425

CONTENTS

FIGURES

TABLES

CONVERSION FACTORS AND ABBREVIATIONS

Multiply inch-pound unit	By	To obtain
foot (ft)	0.3048	meter
mile (mi)	1.6090	kilometer
foot squared (ft^2)	0.0920	meter squared
foot per day (ft/d)	0.3048	meter per day
foot per mile (ft/mi)	0.1894	meter per kilometer
foot squared per day (ft^2/d)	0.0920	square meter
gallon per minute (gal/min)	0.0631	liters per second
inch per year (in/yr)	25.4	millimeter per year
pounds per square inch (lb/in^2)	6.8950	kilopascal
pounds per cubic foot (lb/ft^3)	0.0160	grams per cubic centimeter
million gallons per day (Mgal/d)	0.4381	cubic meter per day

Equation for temperature conversion between degrees Celsius (^oC) and degrees Fahrenheit (^oF):

$$^oC = 5/9 \times (^oF-32)$$
$$^oF = (9/5\ ^oC) + 32$$

Milligrams per liter (mg/L) is a unit expressing the concentration of chemical constituents in solution as weight (milligrams) of solute per unit volume (liter) of water. For concentrations less than 7,000 mg/L, the numerical value is the same as for concentrations in parts per million.

Sea level: In this report, “sea level” refers to the National Geodetic Vertical Datum of 1929 (NGVD of 1929)---a geodetic datum derived from a general adjustment of the first-order level nets of the United States and Canada, formerly called “Sea Level Datum of 1929.”

ADDITIONAL ABBREVIATIONS

α_T	transverse dispersivity
α_L	longitudinal dispersivity
k_h	horizontal permeability
k_v	vertical permeability
C_r	rock compressibility
Q_r	recovery rate
Q	injection rate
S	storage coefficient

ACRONYMS USED IN THIS REPORT:

DS	dissolved solids
HST3D	U.S. Geological Survey Three Dimensional Heat- and Solute-Transport computer program
ICU	intermediate confining unit
SCU A/B	semiconfining unit between zones A and B
SSMF	scaled-solute mass fraction
SSR	subsurface storage and recovery
SWFWMD	Southwest Florida Water Management District
UFA	Upper Floridan aquifer
USGS	U.S. Geological Survey
WRF	water reclamation facilities

Simulation of Subsurface Storage and Recovery of Effluent Using Multiple Wells, St. Petersburg, Florida

By Dann K. Yobbi

Abstract

The potential for subsurface storage and recovery, otherwise called aquifer storage and recovery, of effluent in the uppermost producing zone of the Upper Floridan aquifer in St. Petersburg, Florida, was studied by the U.S. Geological Survey, in cooperation with the city of St. Petersburg and the Southwest Florida Water Management District. The success of subsurface storage and recovery depends on the recovery efficiency, or the quantity of water, relative to the quantity injected, that can be recovered before the water that is withdrawn fails to meet salinity limits. The viability of this practice will depend upon the ability of the injected zone to receive, store, and discharge the injected fluid.

A three-dimensional numerical model of ground-water flow and solute transport, incorporating available data on aquifer properties and water quality, was developed to evaluate the effects of changing various operational factors on recovery efficiency. The reference case for testing was a base model considered representative of the aquifer system underlying the Southwest St. Petersburg Water Treatment Facility. The base simulation used as a standard for comparison consisted of a single cycle of 90 days of simultaneous injection of effluent in three wells at a rate of 4.0 million gallons per day and then equal rate withdrawal of 4.0 million gallons per day until the pumped water in each well reached a dissolved-solids concentration of 1,500 milligrams per liter. A recovery efficiency of 14.8 percent was estimated for the base simulation. Ten successive injection and recovery cycles increased recovery efficiency to about 56 percent. Based on model simulations for hypothetical conditions, recovery efficiency (1) increased with successive injection and recovery cycles; (2) increased when the volume of injectant increased; (3) decreased when storage time increased; (4) did not change significantly when the injection rate or recovery rate increased, or when the ratio of recovery rate to injection rate increased, and (5) was not significantly affected by any particular geometric arrangement of wells or by the number of wells when the volume of water injected remained constant. Recovery efficiency from multiple wells was nearly the same as from a single well. Recovery efficiency ranged from about 7 to 56 percent, in several tests.

Sensitivity of recovery efficiency to variations in selected parameters such as dissolved-solids concentration of the injection zone, permeability, vertical anisotropy, longitudinal and transverse dispersivities, and effective porosity was tested. Changes in the dissolved-solids concentration of the injection zone produced the greatest change in recovery efficiency. Uniform changes in dispersivity values produced the second greatest change in recovery efficiency. Generally, recovery efficiency increased when the above parameter values were decreased and recovery efficiency decreased when these parameter values were increased.

Density difference between native and injected waters was the most important factor

affecting recovery efficiency in this study. For the base simulation, sensitivity tests indicated that recovery efficiency increased from about 15 to 78 percent when the dissolved-solids concentration of the native water decreased from about 7,800 to 500 milligrams per liter.

Dispersivity is another important factor affecting recovery efficiency. For the base simulation, sensitivity tests indicated that recovery efficiencies from about 9 to 24 percent can be obtained for different dispersivity values. A field determination of dispersivity was not made as part of this study, and values used may not be representative of the actual dispersive characteristics of the aquifer system at the study site. However, dispersivity values tested are within the range of values used in previous studies.

INTRODUCTION

The city of St. Petersburg owns and operates one of the largest urban reclaimed water reuse systems in the world. In 1995, approximately 21 Mgal/d of advanced secondary-treatment plant effluent was piped from the city's four water reclamation facilities (WRF's) through a 260-mi irrigation system to water residential, recreational, and commercial properties.

Demand for reclaimed water is seasonal. There is a deficiency of effluent for irrigation in the dry months (generally fall and spring) and an excess in the wet months (generally summer and winter). The excess is disposed of through deep underground injection wells into the lowermost zones of the Upper Floridan aquifer (a highly-fractured dolomite zone saturated with saltwater). The injected water from these deep permeable zones cannot be effectively recovered because of excess mixing occurring in the disposal zone (Hickey and Ehrlich, 1984).

Developing alternate methods for augmenting water supplies is a major priority for water managers. For this reason, the U.S. Geological Survey (USGS), in cooperation with the city of St. Petersburg and the Southwest Florida Water Management District (SWFWMD), began a study in 1994 to assess the feasibility of subsurface storage and recovery (SSR), otherwise known as aquifer storage and recovery, of effluent in a shallow, moderately transmissive limestone aquifer underlying St. Petersburg that is slightly to moderately saline.

The objective of this study was to provide an assessment of the potential for SSR in St. Petersburg. The study included two phases:

(1) development and testing of a prototype cylindrical numerical model to assess the recovery efficiency for injected water of a typical single well system in St. Petersburg; and,

(2) development and testing of a three-dimensional numerical model to assess the recovery efficiency for injected water using multiple wells at one of the four St. Petersburg's WRF's.

The phase 1 single-well cylindrical model was described by Yobbi (1996). That model was devised to evaluate recovery of injected water at a typical SSR well and to assess the relation between recovery efficiency and uncertainties in values of physical properties and operational variables. For practical ranges of hydraulic and fluid properties in the study area, the model analysis indicated that (1) the greater the density contrast between injected and resident formation water, the lower the recovery efficiency, (2) recovery efficiency decreased significantly as dispersion increased, (3) high permeability produced low recovery efficiencies, and (4) recovery efficiency increased as anisotropy increased and as porosity decreased. The recovery efficiency ranged from about 4 to 76 percent in several hypothetical tests performed with the single-well cylindrical model.

An implementation of SSR would probably require more than one well to handle the required inflow rates and wellhead pressures. Operational field tests of this size are generally too expensive for preliminary assessments. Modeling is a cost-effective approach for preliminary evaluation of the feasibility of SSR since many combinations of conditions can be investigated with relatively inexpensive computer simulations.

Purpose and Scope

This report presents the results of the development of the phase 2, three-dimensional numerical model and the results of an assessment of the potential for SSR using multiple wells at the Southwest St. Petersburg WRF. Specifically, the model was used as a simulation tool to assess: (1) recovery efficiencies for injected water for multiple-well configurations,

injection and recovery rates, volumes of injected water, injection/recovery ratios, length of storage times and background hydraulic gradients, and repeated cycles, and (2) the relation between recovery efficiency and the uncertainty in values for physical properties. This report also presents numerical analysis of hydraulic properties using the model. Data were obtained from published reports and from files of the USGS.

A finite-difference model, HST3D (Kipp, 1987, as modified), for simulating heat and solute transport in three dimensions was used for the simulations. The model is used to simulate a hypothetical injection and recovery operation at the Southwest St. Petersburg WRF. Approximately 75 simulations were run and recovery efficiencies were calculated for various SSR tests. Hydrologic properties of the aquifer system also were estimated using numerical simulation of data collected during a previous study at the Southwest St. Petersburg WRF.

Description of Study Site

The Southwest St. Petersburg WRF is located in southern Pinellas County, Florida (fig. 1). The study site is underlain by a thick sequence of honeycombed and fractured limestone and dolomite of Tertiary age overlain by a sequence of clastic deposits. Land altitudes range from about 6 to 10 ft above mean sea level.

Rainfall in the area averages about 53 in/yr, of which about 34 in. falls during the 5-month period May through September. August is the wettest month and April is the driest. The mean annual temperature

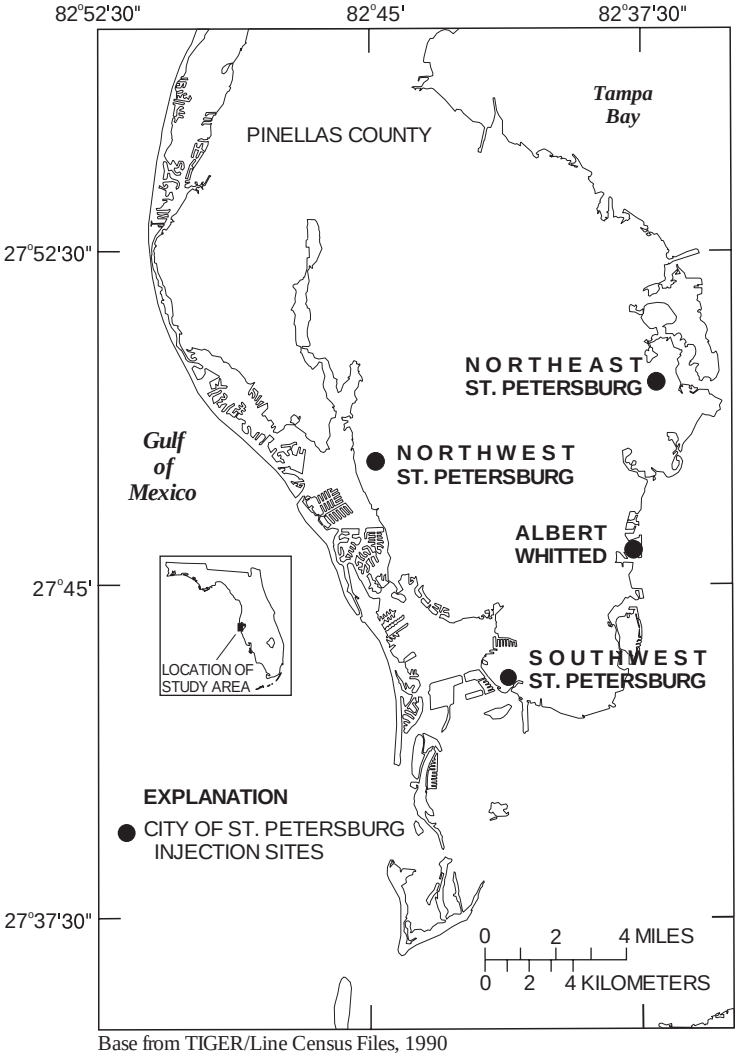

Base from TIGER/Line Census Files, 1990
Albers Equal-Area Conic projection
Standard parallels 29° 30' and 45° 30', central meridian -83° 00'

Figure 1. Location of study area and the city of St. Petersburg injection sites.

is about 74 °F, and monthly means range from about 83 °F in August to about 62 °F in January (National Oceanic and Atmospheric Administration, 1995).

Three deep injection wells comprise the injection system at the Southwest St. Petersburg WRF. The injection zone at the site is within the most productive of the identified permeable zones, with a transmissivity of about 1,200,000 ft^2/d, and about 1,000 ft below land surface. The injection wells were put into continuous operation in 1979 and were designed to accept about 15.2 Mgal/d each of highly treated wastewater. In 1995, the wells were permitted for 9 Mgal/d each.

Subsurface Storage and Recovery Concept

Subsurface storage and recovery is a strategy of water-supply augmentation by which effluent is injected underground, by one or more wells, for storage during wet periods when demand is low, and then recovered later for water use during dry periods when demand is high. SSR is especially appropriate for areas like St. Petersburg where there is (1) seasonal variation in reclaimed water and demand, and (2) a moderately permeable aquifer near land surface that contains water of low to moderate salinity.

The feasibility of a SSR system depends upon the ability of the injected zone to receive, store, and discharge the injected effluent. Recovery of the stored effluent is dependent upon the effective emplacement of a relatively stable, thick lens of low-density effluent during the injection phase. To form this lens, enough effluent must be injected to displace a large volume of saline water; the mixing of the effluent and native waters must not be significant; and confinement must be sufficiently tight to prevent rapid vertical migration of the less dense effluent (Rosenshein and Hickey, 1977). The lens of effluent formed must have sufficient aerial extent and thickness to be tapped by a system of recovery wells.

The success of a SSR system is measured by the quantity of water that can be recovered relative to the quantity injected, or the recovery efficiency. Recovery efficiency, usually expressed as a percentage per cycle of injection, storage, and recovery, is defined as the quantity of water, relative to the quantity injected, that can be recovered before the water that is withdrawn fails to meet some prescribed salinity standard. In this report, the standard is a dissolved-solids (DS) concentration of 1,500 mg/L (about 600 mg/L chloride).

Throughout this report, statements are made concerning the salinity of water. The terminology used to describe the salinity is modified slightly from a USGS-classification system of water based on dissolved solids (Heath, 1989, table 2, p. 65), as follows:

Classification	Dissolved-solids concentration (mg/L)	Percent seawater
Freshwater	<500	<1.5
Slightly saline (brackish water)	500 to 3,000	1.5 to 8.6
Moderately saline (brackish water)	3,000 to 10,000	8.6 to 29
Very saline (saltwater)	10,000 to 35,000	29 to 100
Briny	>35,000	>100

Freshwater meets the DS concentration limit for potable water. Slightly saline water is generally nonpotable, but it may be suitable for irrigation. Moderately saline water is suitable for desalinization plant feed, and very saline water and briny water are considered unusable.

Factors Affecting Recovery Efficiency

Two primary physical processes affect the recoverability of the injected water: (1) mixing by molecular diffusion and hydrodynamic dispersion, and (2) density stratification. Unfavorable physical and solute properties of the aquifer system also can reduce the recoverability of injected water.

When two fluids of different composition are in contact, a transfer of molecules occurs. As time passes, the random movement of molecules creates a mixed zone where the two fluids have diffused into one another (molecular diffusion). When one fluid miscibly displaces another fluid in a porous medium, the mixed zone will be greater than that formed due to molecular diffusion alone. The additional mixing, primarily dependent on pore geometry, results from variations in the velocity field and the constant intermingling of flow paths as displacement progresses. This additional mixing, known as mechanical dispersion, occurs both longitudinally (in the direction of gross fluid movement) and transversely (in the direction normal to the gross fluid movement). Mechanical dispersion is caused by mixing of solutes due to variations in fluid velocities

resulting from local differences in hydraulic conductivity (Skibitzke and Robinson, 1963, p. B3). At the relatively large fluid velocities during injection and recovery cycles, the effects of mechanical dispersion are generally greater than those of molecular diffusion.

Density stratification describes the tendency for a lighter fluid to rise above a denser fluid. When fluids of unequal densities are in contact in a porous medium, gravity causes the less dense fluid to rise relative to the more dense fluid. Density stratification is controlled by several factors, including: (1) the density contrast between native and injected waters, (2) permeability of the injection zone, and (3) the thickness of the injection zone (Merritt, 1985). Stratification in porous media can be separated into two cases, static and dynamic (Kimbler and others, 1975). The static case involves no bulk flow of fluids except that arising from convective currents attributable to gravity. Dynamic stratification occurs in the presence of bulk flow of fluids caused by the displacement of a native fluid by an injected fluid of different density.

HYDROGEOLOGIC FRAMEWORK

The hydrogeology of the St. Petersburg area has been described by Hickey (1982). The hydrogeologic units beneath St. Petersburg consist of a thick sequence of carbonate rock overlain by clastic deposits (fig. 2). The upper 1,100 ft includes the unconfined, surficial aquifer and the confined, Upper Floridan aquifer (UFA). The units are separated by the intermediate confining unit (ICU).

The surficial aquifer is the uppermost water-bearing formation and consists of sand and shell of Pleistocene age. The surficial aquifer underlying the study area is about 85 ft thick. The aquifer is a source of recharge to the Upper Floridan aquifer and is mainly used as a source of water for lawn irrigation in St. Petersburg.

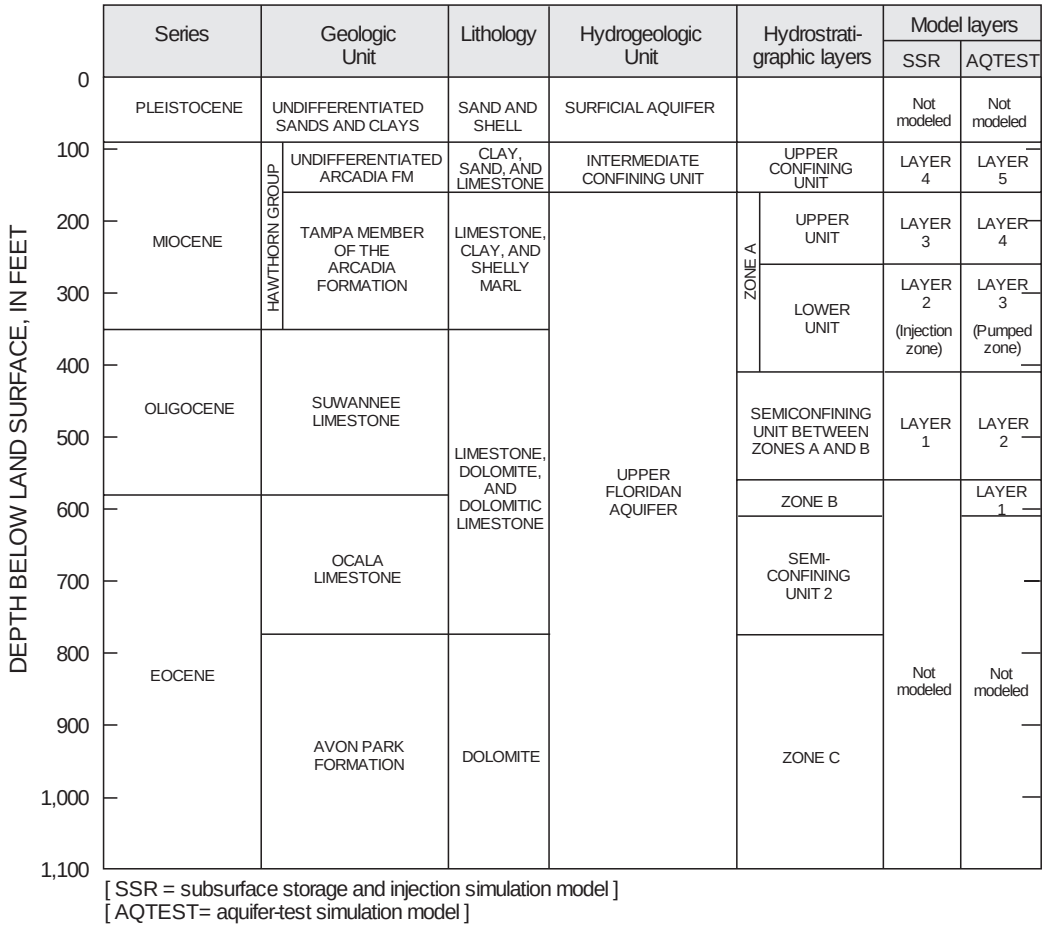

Figure 2. Generalized stratigraphic and hydrogeologic section, St. Petersburg, Florida. (Modified from Hickey, 1982.)

The low-permeable ICU lies between the surficial aquifer and the UFA. The unit coincides with the undifferentiated Arcadia Formation of the Hawthorn Group and at the study site consists of clay, sand, shell, and some limestone (Black, Crow and Eidsness, 1978). The ICU at the study site occurs at about 85 ft below land surface and is about 75 ft thick. Vertical hydraulic conductivities of the ICU range from about 3×10^{-3} to 7×10^{-5} ft/d, and average about 8×10^{-4} ft/d, as reported by Sinclair (1974). Vertical hydraulic conductivity of the ICU at the study site determined from laboratory tests is 6.9×10^{3} ft/d, as reported by Black, Crow and Eidsness (1978).

The UFA is a thick, regionally extensive sequence of limestone and dolomite. The upper part consists of, in ascending order, the Avon Park Formation, Ocala Limestone, Suwannee Limestone, and the Tampa Member of the Arcadia Formation of the Hawthorn Group. Identification of three permeable zones separated by two semiconfining beds within the UFA have been listed by Hickey (1982) and include permeable zones alphabetically labeled with increasing depth from A to C. The upper part of zone A is utilized on a limited basis for irrigation and municipal water supply and zone C is used as a repository for injected treated effluent. Zones B and C contain very saline water throughout southern Pinellas County and are not utilized for any supply purposes.

Zone A is the shallowest and freshest of the producing zones and is the most promising potential receiving zone for SSR in St. Petersburg. This zone comprises the Tampa Member of the Arcadia Formation of the Hawthorn Group and the upper part of the Suwannee Limestone. Zone A occurs at about 160 ft below land surface and is about 250 ft thick at the study site. Data collected during drilling, aquifer testing, and geophysical logging indicate that zone A contains two different permeability units. The upper 100 ft of zone A is a poorly-transmissive sequence of interbedded limestone, clay, and shelly marl. The lower 150 ft of zone A is a moderately-transmissive limestone (Black, Crow, and Eidsness, 1978). Transmissivity of zone A determined analytically from data collected from an aquifer test conducted at the study site is 29,000 ft^2/d (Hickey, 1982). The estimated storage coefficient of zone A (calculated from compressibility of cores and an estimated thickness of 250 ft) is 7.75×10^{-4} based on a specific storage value of 3.1×10^{-6}.

Underlying zone A is the first of a series of poorly transmissive carbonate rocks that act as semiconfining units that separate the permeable zones (Hickey, 1982). The semiconfining unit below zone A (SCU A/B) is part of the Suwannee Limestone. Thickness of the semiconfining unit at the study site is about 150 ft. The leakance coefficient of this semiconfining unit interpreted from the zone A aquifer test is 2.9×10^{-3} d^{-1} (Hickey, 1982).

Permeable zone B is composed of dolomite, dolomitic limestone, and limestone and includes the lower part of the Suwannee Limestone and the upper part of the Ocala Limestone. Zone B at the study site occurs at about 560 ft below sea level and is about 60 ft thick. The transmissivity, determined from specific capacity tests conducted on wells completed in zone B, is 5,000 ft^2/d (Hickey, 1982).

Underlying zone B is the Ocala Limestone that acts as a semiconfining unit. This semiconfining unit at the study site occurs at about 620 ft below sea level and is about 160 ft thick. Cores from this semiconfining unit indicate that the beds have closed fractures; consequently, the unit retards the vertical movement of water between zones B and C (Hickey, 1982). Calculated vertical hydraulic conductivities range from 0.1 to 1 ft/d (Hickey, 1982).

Permeable zone C is the present repository for injected effluent. The zone is composed of dolomite, dolomitic limestone, and limestone and includes the upper part of the Avon Park Formation (Hickey, 1982). Zone C is about 320 ft thick and occurs at about 780 ft below sea level. Zone C contains the most productive water-producing intervals within the Floridan aquifer in Pinellas County. The transmissivity of zone C, based on aquifer-test analysis, is 1,200,000 ft^2/d (Hickey, 1982). The storage coefficient, based on aquifer-test analysis, is 3.3×10^{-4} (Hickey, 1982). Effective porosity of zone C, determined from transport-model simulation, is 10 percent (Hickey, 1989).

NUMERICAL ANALYSIS OF HYDRAULIC PROPERTIES

A numerical ground-water flow and solute-transport model was developed to test and refine the conceptualization of the hydrogeologic system underlying the Southwest St. Petersburg WRF. Data from Hickey (1982) and interpretation of geophysical logs

and aquifer-test data were used to define the hydrostratigraphic units and to provide initial model input. The USGS computer code HST3D (Kipp, 1987, as modified) was applied using a cylindrical coordinate system. Backward-in-space and backward-in-time finite-difference equations were used in the numerical model. A brief discussion of the model is included in a subsequent section of this report.

Data were obtained from the aquifer test performed during the period of March 28 to April 1, 1977 (Hickey and Spechler, 1979) for three observation wells (B-9, B-5, and B-4, in fig. 3). A constant flow rate of 650 gal/min was maintained during the test. Results of the aquifer test indicate that water levels in well B-9 (zone A upper unit) began to decline 60 minutes after pumping of well B-8 began and the decline in water level after 3.45 days of pumping was 1.64 ft. Water levels in well B-5 (zone A lower unit) began to decline less than one minute after pumping began and drawdown in well B-5 after 3.45 days of pumping was 1.65 ft. Water levels in well B-4 (SCU A/B) began to decline 10 minutes after pumping began and the decline after 3.45 days was 1.04 ft. The delayed response in water-level drawdown in wells B-9 and B-4 and the presence of low permeable units in the depth intervals 95-250 ft and 396-520 ft indicate the existence of semiconfining beds between producing zones (Black, Crow and Eidsness, 1978).

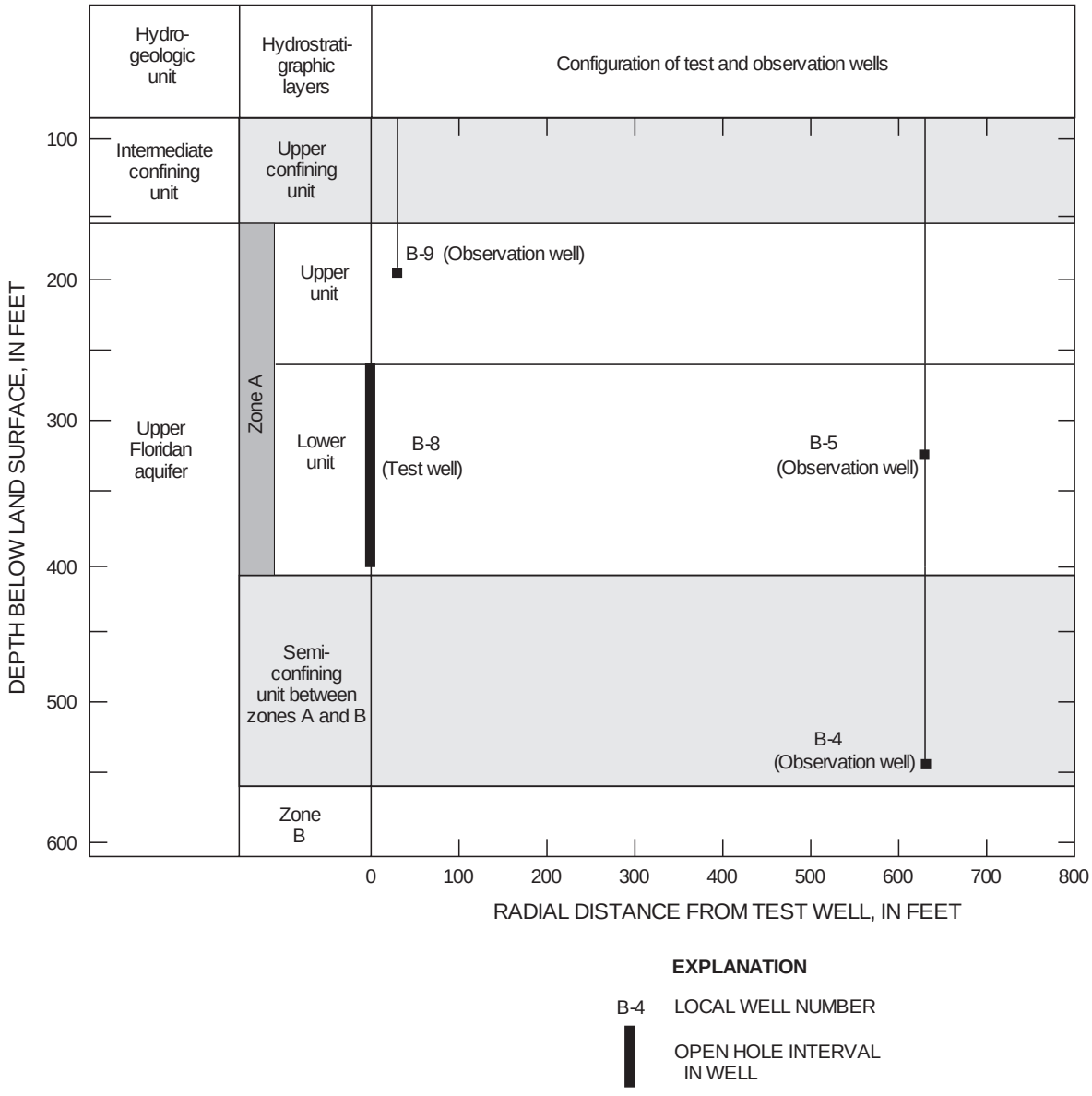

Figure 3. Generalized hydrogeologic section and configuration of test and observation wells.

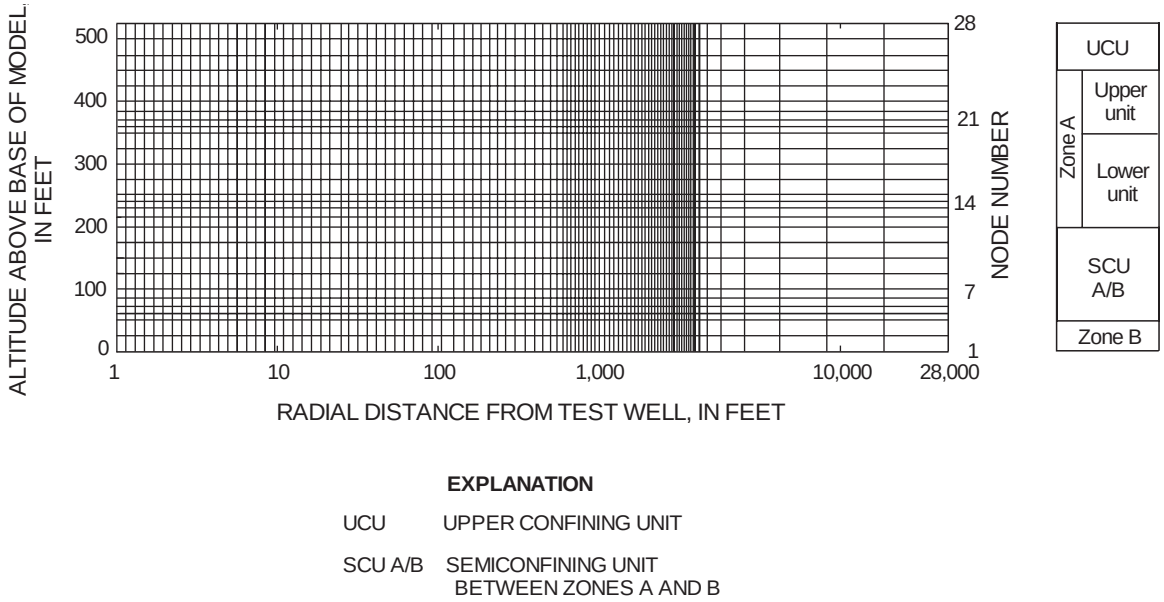

Figure 4. Cylindrical-model grid used for the simulation of hydraulic properties of the aquifer system at the Southwest St. Petersburg Water Reclamation Facility.

Model Grid and Boundary Conditions

The conceptual model consists of five layers including, from top to bottom, the upper confining unit, zone A upper unit, zone A lower unit, SCU A/B, and zone B. The model consists of 28 variable-width node spacings in the vertical direction and 97 variable-width node spacings in the radial direction (fig. 4). The model dimensions represent 28,000 ft horizontally and 675 ft vertically. The vertical spacing ranges from 10 to 25 ft. The radial grid spacings out to a distance of 105 ft present a very gradual logarithmic expansion from 0.14 ft at the well up to a maximum of 13.5 ft. With the exception of several radial grid spacings adjusted to fit the location of monitor wells, the radial dimensions of the grid from a distance of 105 ft to 2,500 ft show a constant spacing of 50 ft. The radial dimensions from a distance of 2,500 to the edge of the grid at 28,000 ft show an expansion from 100 ft to 12,800 ft.

A no-flow boundary condition was assumed at the top, bottom, outer radial edge, and the cased interval above and below the modeled withdrawal well. The no-flow boundary at the bottom of the model was deemed reasonable, because permeability is very low below the lower layer. The no-flow bounday at the top of the model was deemed reasonable, because of the distance from the withdrawal source and, because the intermediate confining bed has a hydraulic conductivity that is three orders of magnitude less than the overlying permeable zone. The outer radial edge boundary was intentionally located far from the withdrawal source to prevent any effect that it may have on determination of pressures in the aquifer segment affected by the withdrawal. One advantage of setting this type of boundary condition (no flow at the top, bottom, and outer edge) is that it restricts model computations to effects caused by withdrawal within a confined radially symmetrical cylinder and approximates the major flow processes during withdrawal. Both the pressure and concentration equations in the model were solved during the simulations, but only the pressure results were analyzed during calibration. Initial pressures were assumed to be hydrostatic and set on the basis of a column of water having dissolved-solids concentration specified as a function of depth. Initial solute concentrations were set equal to solute concentrations in the native water.

Calibration

Hydraulic properties of the hydrostratigraphic units were estimated from these drawdown data by using the numerical model to match simulated head changes to measured water-level changes in observation wells above, below, and within the pumped zone (zone A lower unit). The calibration focused on obtaining a satisfactory match between observed and

model-generated head change data. The model was calibrated by systematically adjusting:

(1) hydraulic conductivity of the various units.

(2) rock compressibility of the various units.

The time increments used to step through the model runs during calibration were gradually expanded from 1 minute to 0.54 days. A total of 16 time steps were used in the calibration. The total simulated time of pumping was 82.8 hours. The simulated well corresponds to an open hole interval from about 260 to 400 ft below land surface.

Measured drawdowns in observation wells B-4, B-5, and B-9 and the simulated drawdowns at the corresponding model nodes are shown in figure 5. Simulation results indicate that the model matched the measured responses reasonably well.

Late-time data were matched by varying hydraulic conductivity, specified in ft/d. Values of 0.0008, 0.01, 180, 0.04, and 150 ft/d for hydraulic conductivity for the upper confining unit, zone A upper unit, zone A lower unit, SCU A/B, and zone B provided the best match for late-time data.

Early-time data were matched by varying rock compressibility, specified in in^2/lb. This procedure is similar to varying storage coefficient in a hydraulic model because storage coefficient (S) is considered to be a linear function of rock compressibility (C_r) according to the following formulation (Merritt, 1994):

$$S = n\rho b(C_w + C_r) \qquad (1)$$

where: S is storage coefficient (dimensionless);
n is porosity (dimensionless);
ρ is fluid density (lb/ft^3);
b is layer thickness (ft);
C_w is water compressibility (3.03×10^{-6} in^2/lb); and
C_r is rock compressibility (in^2/lb).

Values of 5.5×10^{-5}, 3.4×10^{-5}, 3.4×10^{-6}, 3.4×10^{-6}, and 3.4×10^{-6} in^2/lb for rock compressibility of the intermediate confining unit, zone A upper unit, zone A lower unit, SCU A/B, and zone B, respectively, provide the best match for early-time data.

A vector representation of the flow field generated by the model is shown in figure 6. Flow was nearly lateral in the permeable zones and nearly vertical in the semiconfining units.

Sensitivity Analysis

A sensitivity analysis was done to evaluate the response of the model to changes in input parameters

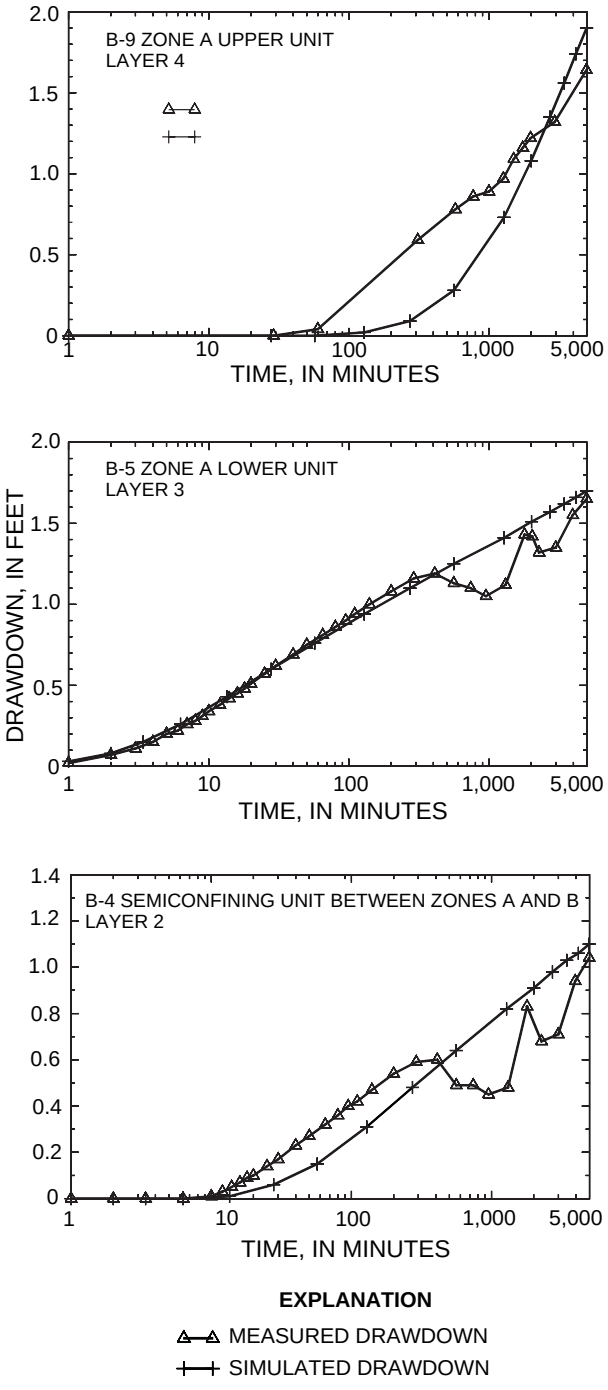

Figure 5. Simulated and observed drawdowns in wells B-9, B-5, and B-4.

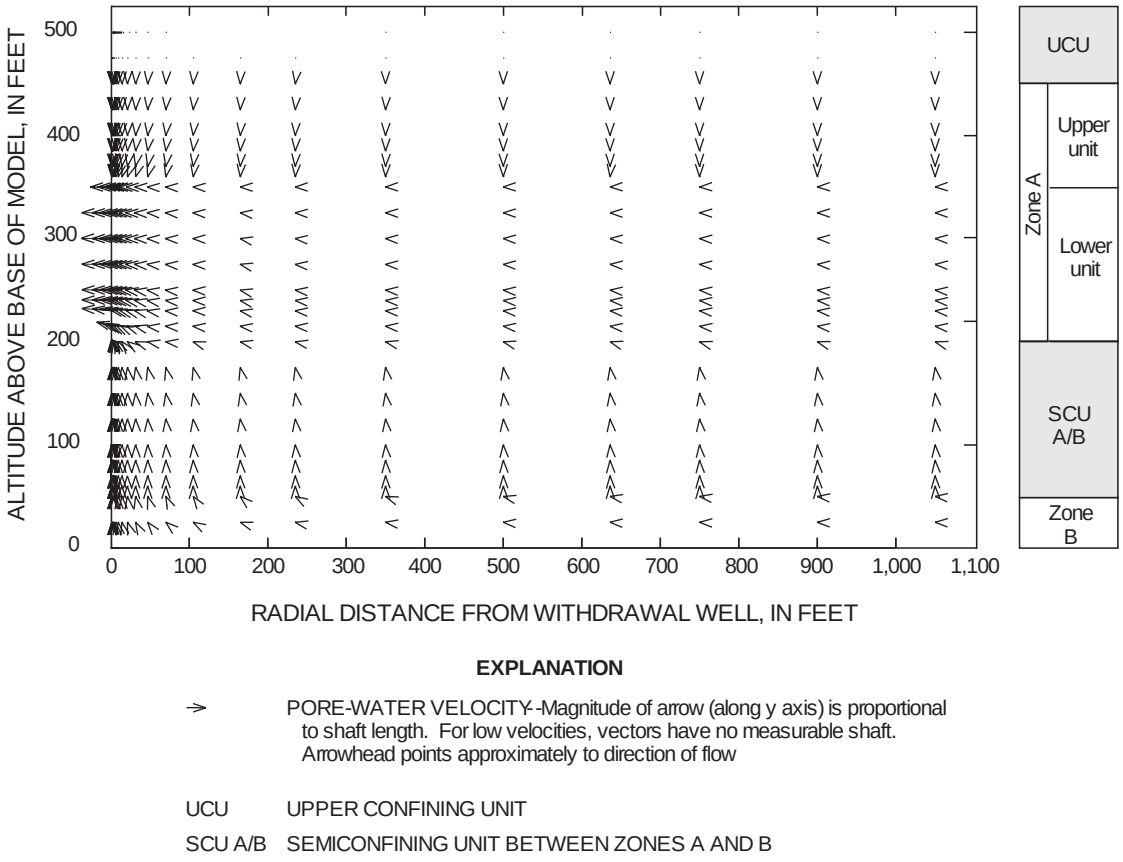

Figure 6. Simulated flow field at the end of the 3.45 day aquifer test.

and to gain an understanding of how much error could result by overestimating or underestimating the parameter values. The sensitivity analysis consisted of uniformly increasing or decreasing values of one model input parameter while others remained at calibration levels, then noting the change in drawdown as a result of the change. Hydraulic conductivity and compressibility of layers 2, 3, and 4 were increased and decreased by a factor of 10. The computed drawdowns are shown in figures 7 and 8. The tests show substantial variation from observed and simulated drawdowns at both early and late times for most of the changes.

Hydraulic Conductivity

Results of the sensitivity analysis indicate that changes in hydraulic conductivity of layer 3 (pumped zone) produced the greatest change in water levels. Generally, small changes in simulated drawdown occur when hydraulic conductivity values are increased while substantial changes in simulated drawdown occur when hydraulic conductivity values are decreased.

If layer 2 (SCU A/B) had a much higher hydraulic conductivity than the calibrated values, hydraulic response to pumping from layer 3 would be greater than otherwise would be observed in wells B-4 and B-5 and would be smaller than otherwise would be observed in well B-9. Maximum drawdown in wells B-4 and B-9 would be about 0.3 and 0.2 ft, respectively, more than observed drawdown, and maximum drawdown in well B-5 would be about 0.1 ft less than observed drawdown.

If layer 3 (zone A lower unit) had a much higher hydraulic conductivity, water-level changes would occur much slower than observed. Hydraulic response to pumping from layer 3 in each well would be considerably more sluggish compared to the observed response. Maximum drawdowns only would be about 0.3 ft in each well, compared to 1.10, 1.70, and 1.61 ft for wells B-4, B-5, and B-9, respectively, for the calibration.

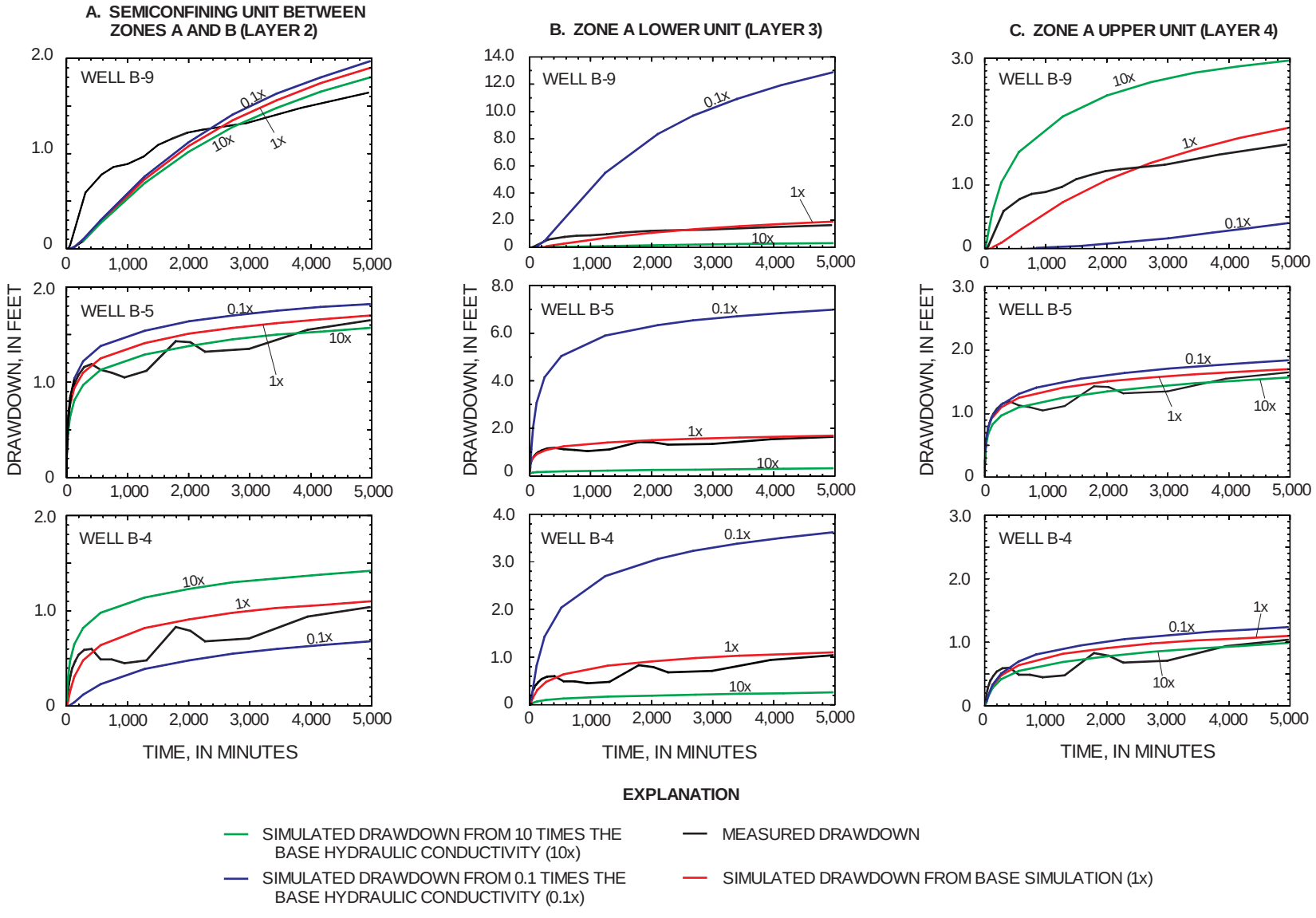

Figure 7. Effects of varying hydraulic conductivity on the simulated drawdowns in (A) semiconfining unit between zones A and B, (B) zone A lower unit, and (C) zone A upper unit.

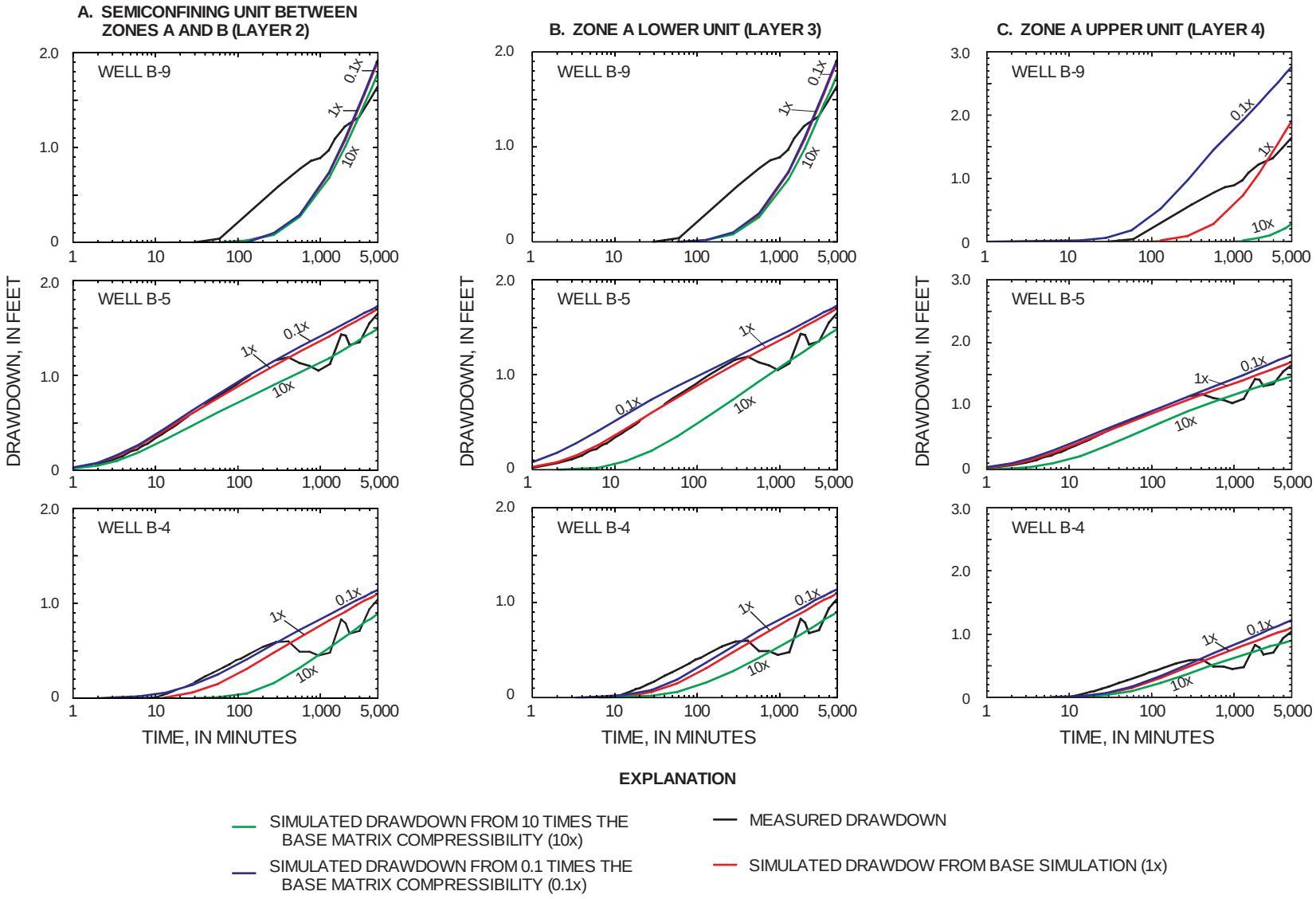

Figure 8. Effects of varying matrix compressibility on the simulated drawdowns in (A) semiconfining unit between zones A and B, (B) zone A lower unit, and (C) zone A upper unit.

If layer 4 (zone A upper unit) had a much higher hydraulic conductiviy, the hydraulic response to pumping from layer 3 would be slightly less than otherwise would be observed in well B-4 and B-5 and much greater than otherwise would be observed in well B-9. Maximum drawdowns in wells B-4 and B-5 would be about 0.1 ft less than observed drawdown in each well, and maximum drawdown in well B-9 would be about 1.3 ft greater than observed drawdown.

A contrasting hydraulic response is observed when much lower hydraulic conductivity values are simulated. A tenfold decrease in hydraulic conductivity of layer 2 would result in a more responsive hydrograph than was observed in wells B-5 and B-9 and a slightly less responsive hydrograph than was observed in well B-4. Maximum drawdowns in wells B-5 and B-9 would be about 0.2 ft higher than observed, and maximum drawdown in well B-9 would be about 0.4 ft lower than observed.

A much lower hydraulic conductivity of layer 3 would result in a considerably more responsive hydrograph than was observed in each well. Maximum drawdowns would be about 2.6, 5.3, and 11.2 ft, respectively, more than was observed in wells B-4, B-5, B-9 and water-level changes would occur much faster than observed.

If layer 4 had a much lower hydraulic conductivity, the hydraulic response to pumping layer 3 would result in a slightly more responsive hydrograph for wells B-4 and B-5, and a significantly less responsive hydrograph for well B-9. Maximum drawdowns in well B-4 and B-5 would be 0.1 ft more than was observed. Maximum drawdown in well B-9 would be about 1.2 ft lower than observed, and water-level changes would occur much slower than observed.

Matrix Compressibility

Compressibility of the limestone for each layer was increased and decreased by one order of magnitude. Substantial disagreement occurred in the early-time range when this value was increased while only slight disagreement occurred in the early-time range when this value was decreased. At later times, observed and simulated data are offset to a degree that seems to change only slightly with increasing time.

If layer 2 had a much higher matrix compressibility, water-level changes would occur much slower than observed in well B-4 and slightly slower in wells B-5 and B-9. If layer 2 had a much lower matrix compressibility, hydraulic response to pumping from layer 3 in each well would be slightly quicker compared to the simulated response.

If layer 3 had a much higher matrix compressibility, water-level changes would occur much slower than observed in wells B-4 and B-5 and only slightly slower in well B-9. If layer 3 had a much lower matrix compressibility, hydraulic response to pumping from layer 3 shows only slight discrepancies with observed data at early times.

If layer 4 had a much higher matrix compressibility, the hydraulic response to pumping layer 3 would result in a significantly less responsive hydrograph than would be observed in well B-9, and only a slightly lower response than would be observed in wells B-4 and B-5. If layer 4 had a much lower matrix compressibility, water-level changes in well B-9 would occur much faster than observed while water-level changes in well B-4 and B-5 would occur only slightly faster than observed.

SIMULATION OF SUBSURFACE STORAGE AND RECOVERY OF EFFLUENT USING MULTIPLE WELLS

A finite-difference three-dimensional variable-density ground-water flow and solute-transport model was used to simulate injection and recovery from a multiwell hypothetical SSR system open to a moderately transmissive, slightly to moderately saline aquifer, underlying the Southwest St. Petersburg WRF. The specific question to be answered is: In what quantitative fashion will operational and physical variables influence recovery efficiency from multiple wells? The recovery efficiency was defined as the volume of water recovered below a dissolved-solids concentration of 1,500 mg/L (about 600 mg/L chloride), divided by the volume injected, and expressed as a percentage.

To answer this question, the USGS model HST3D (Kipp, 1987, as modified) was used to simulate the hypothetical SSR system. The analysis implemented a conceptual modeling approach (Merritt, 1985), rather than a calibration and predictive approach (Merritt, 1994), because no injection and recovery data exist for comparison with model results. This type of analysis permitted many combinations of conditions to be studied. The input values are hydraulic and native chemical characteristics of the aquifer system underlying the Southwest St. Petersburg WRF.

The rate of ground-water flow is assumed to be governed by Darcy's law, which when written in terms of fluid pressure (rather than piezometric head) is:

$$q = -k (\nabla p + \rho g z) / \mu \quad (2)$$

where,

- q is specific discharge vector (flow rate per unit cross-sectional area) [L/T];
- k is the intrinsic permeability vector of the aquifer materials [L^2];
- ∇ is the gradient operator [1/L];
- p is the fluid pressure [M/LT^2];
- ρ is fluid density [M/L^3];
- g is gravitational acceleration vector [L/T^2];
- z is the unit vector in the vertical direction [dimensionless]; and
- μ is the dynamic viscosity of the fluid [M/LT].

Using Darcy's law and the principle of conservation of fluid mass, the transport of a conservative solute can be written as:

$$\partial (n\rho) / \partial t = -\nabla (\rho q) + Q_p \quad (3)$$

where,

- n is aquifer porosity (dimensionless);
- t is time (T);
- ∇ (ρq) denotes the divergence of the specific discharge mass flux [$M/(TL^3)$]; and
- Q_p is mass of fluid injected (+) or withdrawn (-) per unit time per unit volume of aquifer [$M/(TL^3)$].

Numerical Model

The HST3D model (Kipp, 1987, as modified) is a computer program written in FORTRAN-77 that simulates variable density fluid movement and transport of either dissolved substances or energy in the subsurface. The HST3D version used in this report (version 2.0) is a result of several modifications made after version 1.0. In addition to changes made at the programming level to facilitate the handling of data, the main technical modification that pertains to this study is the usage of a new iterative solver (Kenneth L. Kipp, written communication, 1995). The model, as used here, solves for two interdependent variables; pressure and mass-fractional concentration in Cartesian coordinates under isothermal conditions. Backward-in-space and backward-in-time finite-difference equations are used for solution of ground-water flow and the solute-transport equations in the numerical model. The reader is referred to Kipp's (1987) report for a complete discussion of the model code and numerical methods.

Two changes were made to the HST3D code (version 2.0). The first change was made to simulate the shutdown of the production well when the solute fraction of the withdrawn water reached 0.05769, corresponding to a DS concentration of 1,500 mg/L (about 600 mg/L chloride). The second change to the code was made to suppress the cross-derivative dispersive terms. This change was made to eliminate the nonradial spatial distribution of injectant caused by inaccuracies of the mathematical solution for radial flow in Cartesian coordinates.

Design of Base Model

The base model used as a standard for comparison for subsequent simulations was designed to be representative of the slightly to moderately saline aquifer system underlying the Southwest St. Petersburg WRF. The physical properties of the aquifer system were selected as the best possible representation of the actual field values at the study site. The chemical properties of the aquifer system were estimated values of the native formation waters prior to the start of deep well injection into zone C (about 1977). Initial pressures for the simulation were calculated by the solute-transport model on the basis of the boundaries and properties of the aquifer system.

Several simplifying assumptions are made in the conceptualization and simulation of the flow system:

1. The aquifer system is homogeneous and isotropic in all directions.
2. Hydrostatic conditions initially prevail.
3. A uniform native fluid density exists within each model layer.
4. The water-quality profile is laterally homogeneous throughout the model area.
5. The viscosity of the injected and native fluids is the same.
6. Dispersivity is constant throughout each model layer, and
7. Injection and recovery wells are 100 percent efficient.

Data from the numerical simulation discussed in the previous section were used to define the hydrogeologic system and to provide the basis for estimating the hydraulic characteristics for the aquifer system underlying the Southwest St. Petersburg WRF. The conceptual model consists of four layers representing,

from top to bottom, the upper confining unit, zone A upper unit, zone A lower unit, and the semiconfining unit between zones A and B (fig. 2).

Grid Design

To apply the HST3D model, the hydrologic and hydrogeologic characteristics of the aquifer system underlying the study site was discretized using a Cartesian coordinate system (fig. 9). The model area dimensions are 5,000 by 5,000 horizontal ft and 475 vertical ft. The horizontal grid consists of 31 rows by 31 columns. Grid dimensions range from 100 by 100 ft at the center of the grid to a maximum of 200 by 200 ft at the four corners of the grid. The vertical grid consists of 19 intervals each 25-ft thick (20 equally spaced nodes).

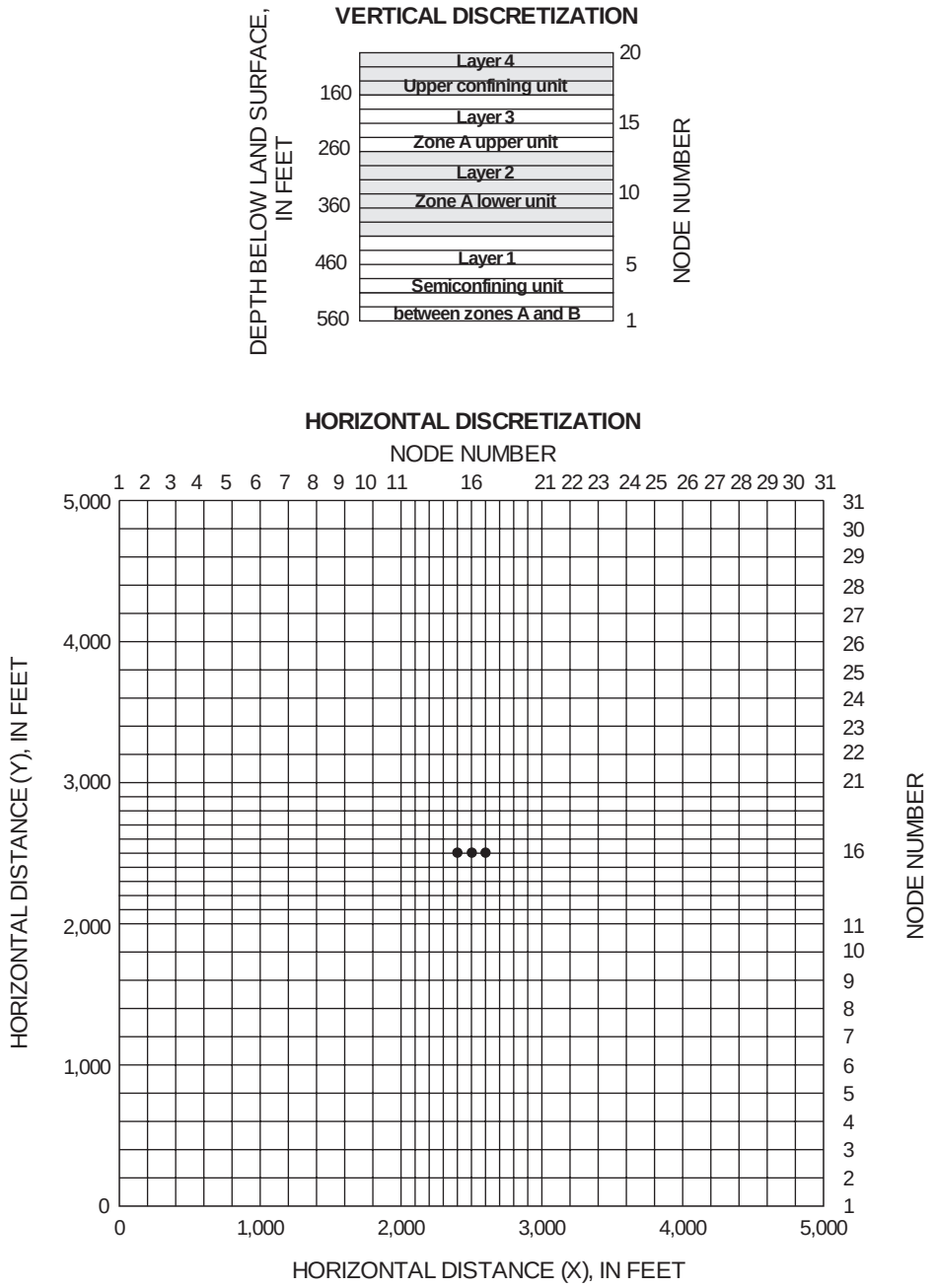

Figure 9. Vertical and horizontal discretization of the model grid used for the simulation of subsurface storage and recovery. (Position of injection/recovery wells used in the base simulation model is indicated by heavy dots.)

Boundary Conditions

Boundary conditions are used to constrain the lateral and vertical extent of the simulated flow system providing a simplified representation of the flow and transport processes at the model limits. The top and bottom boundaries of the model are specified pressure boundaries. The pressures were set equal to the hydrostatic pressures at the specific depths where the boundaries were located. Pressure on the upper boundary is set at 36.760 lb/in^2, equivalent to the pressure exerted from an overlying 85-ft column of freshwater presumed to exist in the overlying surficial aquifer. Pressure on the lower boundary is 243.465 lb/in^2, equivalent to the pressure exerted from a 560-ft column of freshwater and saline water presumed to exist in the overlying formations. One limitation of setting this type of boundary condition is that if injected or mixed water passes across these boundaries, the model would be unable to consider it during the recovery pumping. For this study, this boundary condition yielded the best representation of the actual aquifer and yielded more conservative estimates of recovery efficiency.

The lateral extent of the model is represented by leakage boundaries used to simulate flow into or out of the model at these locations. Representation of leakage-boundary conditions is based on the approach of Prickett and Lonnquist (1971, p. 30-35), which has been generalized to include variable-density and variable-viscosity flow (Kipp, 1987). The leakage-boundary employed in the HST3D code accounts for permeability and thickness of the confining unit, fluid density in the outer aquifer and at the simulation-region boundary, viscosity in the confining layer, and elevation of the simulation-region boundary and the elevation at the top of the confining layer. The reader is referred to Kipp's (1987) report for a complete discussion of this boundary condition.

Fluid Properties

The fluid properties of the native formation waters assumed for the simulations are listed in table 1 and include temperature, viscosity, fluid compressibility, molecular diffusivity, and DS concentration expressed as scaled-solute mass fraction (SSMF). Isothermal conditions at 75 ^oF were assumed to prevail. Fluid densities assigned to injected and native waters were based on the measured or estimated concentrations of DS concentrations in each fluid. Viscosity of the injected and native formation waters vary with temperature and solute fraction. Because isothermal conditions were assumed to prevail and because the viscosity of freshwater and saltwater differ by only 0.06 centipoise, a constant viscosity of 0.8904 centipoise (viscosity of pure water at 75 ^oF) was used. Compressibility of water was held constant at 3.03 x 10^{-6} $(lb/in^2)^{-1}$ (Freeze and Cherry, 1979, p. 52), and molecular diffusivity of the solute in the porous media was set at 9.30 x 10^{-5} ft^2/d (Kimbler and others, 1975). The model SSMF is a term ranging in value from 0 to 1. Any fluids present within or entering the aquifer system in simulation exercises are considered to be a mixture of the two fluids by the appropriate specification of SSMF values. SSMF = 0 was used to represent pure freshwater (0 mg/L), and SSMF = 1 represents the most saline native water (26,000 mg/L) residing within the aquifer system, than at the base of the model. The assigned densities of 62.2690 lb/ft^3 (SSMF = 0) and 63.4582 lb/ft^3 (SSMF = 1) at 75 ^oF and atmospheric pressure were obtained from a standard handbook (Chemical Rubber Company, 1982). The SSMF values of the injected effluent, the water of the aquifer system, and water in mixtures of effluent and native formation waters were assigned values based on their salinity relative to the two extremes. The model was simplified with the assumption of a vertically uniform initial DS concentration distribution assigned to each layer although a vertical salinity gradient has been documented (Hickey and Spechler, 1979; Hickey, 1982). SSMF values of 0.0192 (500 mg/L DS), 0.0769 (2,000 mg/L DS), 0.3005 (7,813 mg/L DS), and 0.6490 (16,874 mg/L DS) represent the composite background water quality in samples from wells at the Southwest St. Petersburg WRF injection site (Hickey and Spechler, 1979). These values were assigned to the upper confining unit, zone A upper unit, zone A lower unit and the SCU A/B, respectively. Measured injected-water DS concentration was about 700 mg/L and was assigned a SSMF value of 0.0269.

Table 1. Fluid properties assumed for simulation

[°F, degrees Fahrenheit; in^2/lb, inch squared per pound; ft^2/d, foot squared per day; mg/L, milligrams per liter; SSMF, solute scaled mass fraction; DS, dissolved-solids concentration]

Model unit	Hydrostratigraphic layer	Tem-peature (^{0}F)	Viscosity (centipoise)	Fluid compressibility (in^2/lb)	Molecular diffusivity (ft^2/d)	SSMF (unitless)	DS (mg/L)	Water classification
Layer 4	Upper confining unit	75	0.8904	3.03×10^{-6}	9.30×10^{-5}	0.0192	500	fresh water
Layer 3	Zone A upper unit	75	0.8904	3.03×10^{-6}	9.30×10^{-5}	0.0769	2,000	slightly saline
Layer 2	Zone A lower unit	75	0.8904	3.03×10^{-6}	9.30×10^{-5}	0.3005	7,813	moderately saline
Layer 1	Semiconfining unit between zones A and B	75	0.8904	3.03×10^{-6}	9.30×10^{-5}	0.6490	16,874	very saline

Matrix Properties

Matrix properties are defined for each of the four hydrogeologic layers of the model (fig. 2, table 2). The matrix properties are intrinsic permeability, matrix compressibility, effective porosity, longitudinal dispersivity, and transverse dispersivity.

Table 2. Matrix properties assumed for simulation

[ft/d, foot per day; ft^2 foot squared; α_L, longitudinal dispersivity; α_T, transverse dispersivity; in^2/lb, inch squared per pound]

Model unit	Hydrostratigraphic layer	Hydraulic conductivity (ft/d)	Intrinsic permeability (ft^2)	Effective porosity (unitless)	α_L (feet)	α_T (feet)	Matrix compressibility (in^2/lb)
Layer 4	Upper confining unit	0.0008	3.102×10^{-15}	0.3	25.0	2.5	5.5×10^{-5}
Layer 3	Zone A upper unit	0.01	3.878×10^{-14}	0.3	25.0	2.5	3.4×10^{-5}
Layer 2	Zone A lower unit	180	6.979×10^{-10}	0.3	25.0	2.5	3.4×10^{-6}
Layer 1	Semiconfining unit between zones A and B	0.04	1.551×10^{-12}	0.3	25.0	2.5	3.4×10^{-6}

Intrinsic permeability is defined as:

$$k = \mu K / \rho g$$

where,

- k is intrinsic permeability [L^2];
- μ is dynamic viscosity of the fluid [M/LT];
- K is hydraulic conductivity, [L/T];
- ρ is fluid density [M/L^3]; and
- g is gravitational acceleration [L/T^2].

Intrinsic permeability was calculated from hydraulic conductivity values given in table 2 and conversion factors obtained from Freeze and Cherry (1979, p. 29). Values of hydraulic conductivity and matrix compressibility were based on simulation of aquifer-test data as previously discussed. The ICU was assumed to be 75 ft thick, have a hydraulic conductivity of 0.008 ft/d, and a matrix compressibility of 5.5×10^{-5} $(lb/in^2)^{-1}$. Zone A upper unit was assumed to be 100 ft thick, have a hydraulic conductivity of 0.01 ft/d, and a matrix compressibility of 3.4×10^{-5} $(lb/in^2)^{-1}$. The injection zone (zone A lower unit) was assumed to be 140 ft thick, have a hydraulic conductivity value of 180 ft/d, and a matrix compressibility of 3.4×10^{-6} $(lb/in^2)^{-1}$. The SCU A/B was assumed to be 150 ft thick, have a hydraulic conductivity of 0.04 ft/d, and a matrix compressibily of 3.4 x 10-6 $(lb/in^2)^{-1}$.

The effective porosity of all layers was set at 30 percent, based on estimates from geophysical logs at the WRF injection sites in St. Petersburg (Hickey, 1982). The values of longitudinal (α_L) and transverse (α_T) dispersivity were not quantified as part of this study and were assumed to be 25 ft and 5 ft, respectively. These values meet gridding stability criteria recommended in Voss (1984, p. 232), where α_L and α_T are greater than one-fourth and one-tenth the spacings along and transverse to the flow direction.

Effects of Operational Factors on Recovery Efficiency

A series of hypothetical SSR tests were made for the aquifer system underlying the Southwest St. Petersburg WRF using the numerical modeling technique. A base simulation was used as the standard to study the effects of changing a series of SSR operational variables and physical properties on recovery efficiency. The effect on recovery efficiency from multiple-well configurations, rates of injection and recovery, volume of water injected, storage time and regional flow, and operational schedules were studied using the numerical model.

The general results from the analysis, which are described in the following sections, indicate that recovery efficiency improves as the volume of injectant increases and improves with successive injection and recovery cycles. Recovery efficiency decreases significantly as storage time increases due to advection and hydrodynamic dispersion. Recovery efficiency was not significantly affected by the rate of injection, by the rate of recovery, by the ratio of recovery to injection rate, by a particular multiple well geometric arrangement, or by the total number of wells used.

Base Simulation

The base simulation used as a standard for comparison consisted of a single cycle of 90 days of simultaneous injection of effluent in three wells at a total rate of 4.0 Mgal/d at a temperature of 75 ^{o}F, and then withdrawal of 4.0 Mgal/d from all wells until the pumped water in each well reached a salinity limit corresponding to 1,500 mg/L DS concentration, at which time the production well was shut off. The wells are centered in the middle of the grid and aligned 100 ft apart on the X-axis. For the base simulation, a DS concentration of 1,500 mg/L was reached in 12.4 days in the two peripheral wells and 15.1 days in the center well. The recovery efficiency calculated for the base simulation is 14.8 percent.

Two simulations were made with the same parameters that were used in the base simulation; one using no-flow/no-transport boundaries at the top and bottom limits of the model, and a second using no-flow/no-transport boundaries at the lateral limits of the model. These simulations were made to test the effect on recovery efficiency of using a constant pressure/constant concentration boundary condition at the top/bottom boundary and a leaky-aquifer boundary at the lateral boundaries to represent interlayer solute mass movement across these boundaries. The simulations yielded recovery efficiencies of 14.5 and 14.7 percent compared to 14.8 percent estimated from the base simulation. This indicates that constant pressure/constant concentration, and leaky-aquifer boundaries have a very small effect on recovery efficiency in the base simulation.

The simulated flow fields at the end of the 90-day injection simulation and at the end of the 12-day recovery phase are shown in figure 10. The general configuration of the flow field at the end of injection is typical of that of buoyant flow, where injectant mixes with and rides over the relatively denser native fluid. Flow of the injectant is along the upper part of the injection zone generally away from the center of the grid where it then is directed strongly downward beyond the leading edge of the injectant front. A similar, but opposite, flow field was generated by the model during the recovery phase.

The distribution of DS concentration associated with the flow field of figure 10 is shown in figure 11. The shape of the injectant mass is highlighted in figure 11, although vertically exaggerated, and provides an illustration of the lateral extent of the injectant mass at the end of injection and at the end of recovery. The DS concentration of the mixture increases outwardly in the transition zone between the injected effluent and native water. Figure 11A shows the upward movement of injectant above the injection wells and inward migration of more saline water in the lower part of the well. After 12 days of recovery (fig. 11B) injectant in the lower part of the wells has been depleted, although considerable injectant remains in the upper part of the wells.

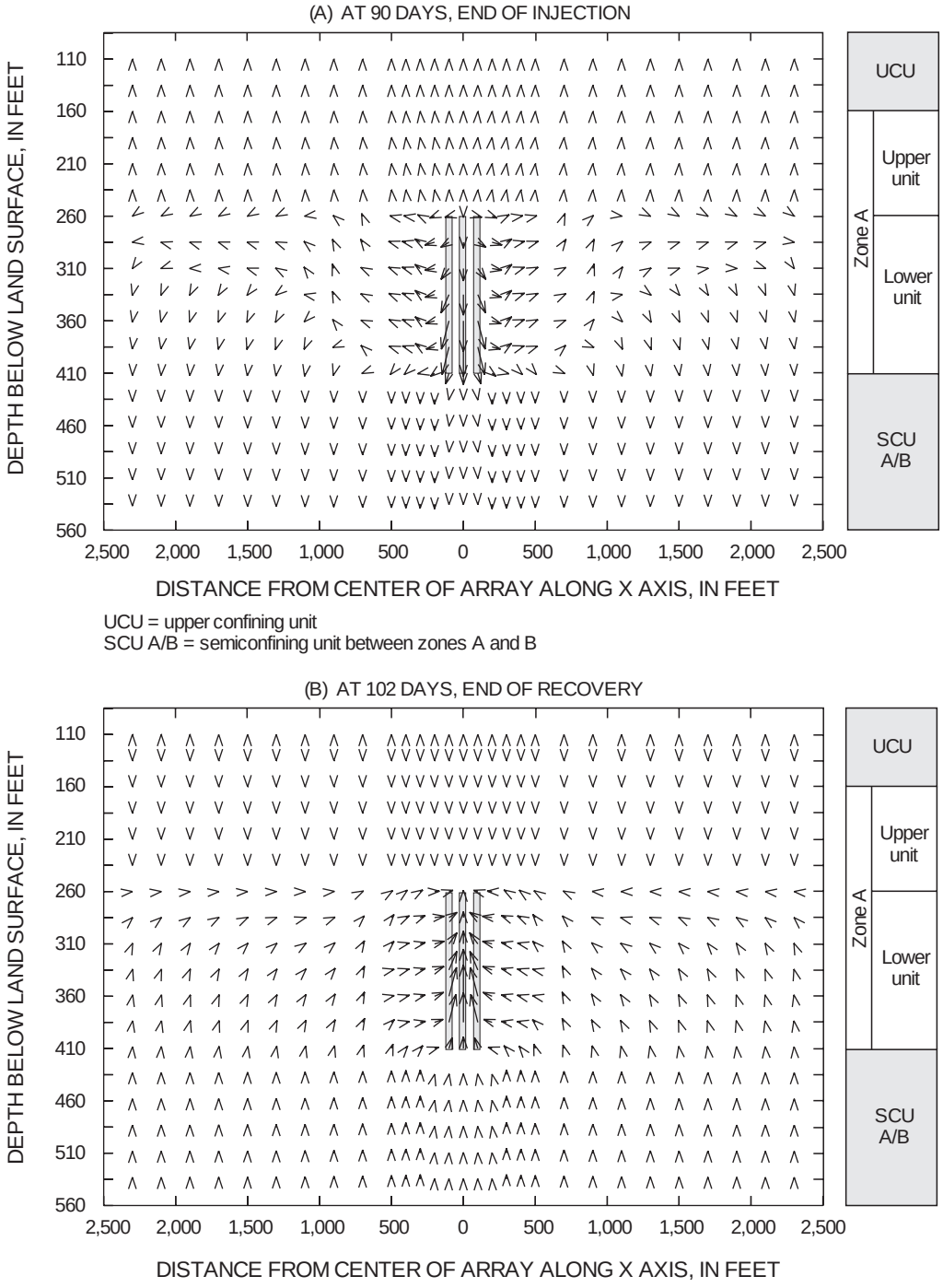

Figure 10. Simulated flow field along vertical plane 16 at the end of the injection and recovery phases of the base simulation.

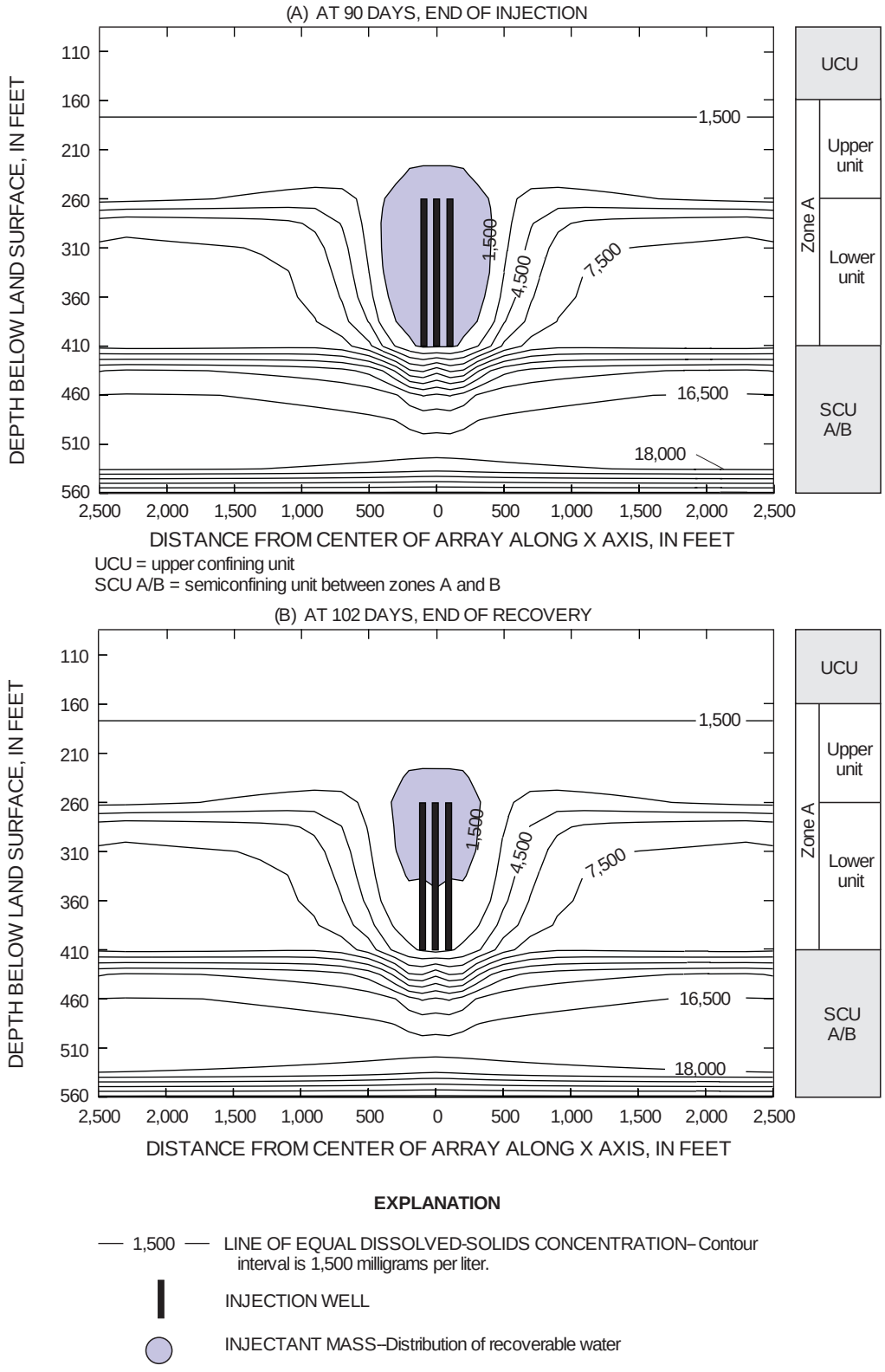

Figure 11. Simulated dissolved-solids concentration along vertical plane 16 at the end of the injection and recovery phases of the base simulation.

Multiple-Well Configurations

The effect of a group of wells on recovery efficiency was examined with ten simulations using different well configurations (fig. 12) and simultaneous equal rate injection of 4.0 Mgal/d for 90 days. Injection and recovery rates were divided equally among all wells operating at a particular time. Withdrawal was from all wells and wells were shut off when the water withdrawn reached 1,500 mg/L. All cases were compared with a control simulation from a single well, in which computed recovery efficiency was 14.7 percent. Results of the simulations are summarized below:

Number of wells	Well configuration	Recovery time (days)					Recovery efficiency (percent)
		Well number					
		1	2	3	4	5	
1	centered in grid	13.2					14.7
2	100 ft apart on x axis	13.1	13.1				14.6
3	100 ft apart on x axis (base)	12.4	15.1	12.4			14.8
3	triangle pattern	11.7	12.4	12.4			13.5
4	square array, 200 ft apart	10.9	10.9	10.9	10.9		12.1
4	square array, 100 ft apart	13.3	13.3	12.9	13.3		14.7
4	triangle array, well in center	11.9	16.1	12.2	12.2		14.6
5	square array, well in center	11.1	11.1	17.0	11.1	11.1	13.6
5	diamond array, well in center	13.4	13.4	15.5	13.4	13.4	15.4

Simultaneous injection and equal-rate withdrawals in the two-, three-, four-, and five-well systems led to no major variations upon recovery efficiency when the volume injected remained constant. Recovery efficiencies for these configurations was nearly the same as if injection and recovery had been from a single-well.

Injection and withdrawal in the square array with wells 200 ft apart produced recovery efficiency less than the base simulation by about one-fifth (from 14.8 to 12.1 percent). In the centered configurations, peripheral wells reached their salinity limit at virtually the same time, but earlier than the center well. Because of stratification and the leaky nature of the aquifer system, appreciable vertical flow of saline water into the injection zone occurred, and therefore, the geometric arrangement of the wells was not important. Model results were similar to those reported by Merritt (1985). Merritt (1985) reported that no major variations in recovery efficiency occurred in multiwell configurations when the volume injected remained constant. The number of wells varied from one to nine in Merritt's study; however, recovery efficiency was nearly the same as the single-well system.

Recovery efficiency from a particular arrangement of wells also may depend on the schedule of withdrawal at each well. Three simulations were used to study the effects of selected operational schedules on recovery efficiency. The base simulation (three-well center configuration) was the test case for comparing the withdrawal schedules. Each test consisted of four consecutive 90-day cycles of simultaneous injections and equal-rate withdrawals at all wells. Withdrawal was from selected wells until the solute fraction of the withdrawn water at any of the wells reached a DS concentration of 1,500 mg/L. Injection and withdrawal rates were the same in all tests (4.0 Mgal/d) and were divided equally among all wells operating at a particular time. The following withdrawal schedules were simulated:

Test 1-- Withdrawal at only the center well until the perimeter wells exceeds salinity limit.

Test 2-- Withdrawal at only the center well until withdrawn water exceeds salinity limit.

Test 3-- Equal rate withdrawal at all wells until the water in the perimeter wells exceeds salinity limit.

Results of the simulations were compared to the base simulation and are summarized below:

Cycle number	Base	Test 1	Test 2	Test 3
	Recovery Efficiency			
1	14.8	13.3	14.3	13.3
2	28.7	31.2	31.2	30.0
3	37.3	40.1	40.1	39.0
4	42.8	45.0	44.8	44.8

With the exception of the first cycle, recovery efficiency for the various schedules of withdrawal was only slightly higher than that of the base simulation. The recovery efficiency increased with each cycle because residual injectant accumulated in the aquifer from previous cycles.

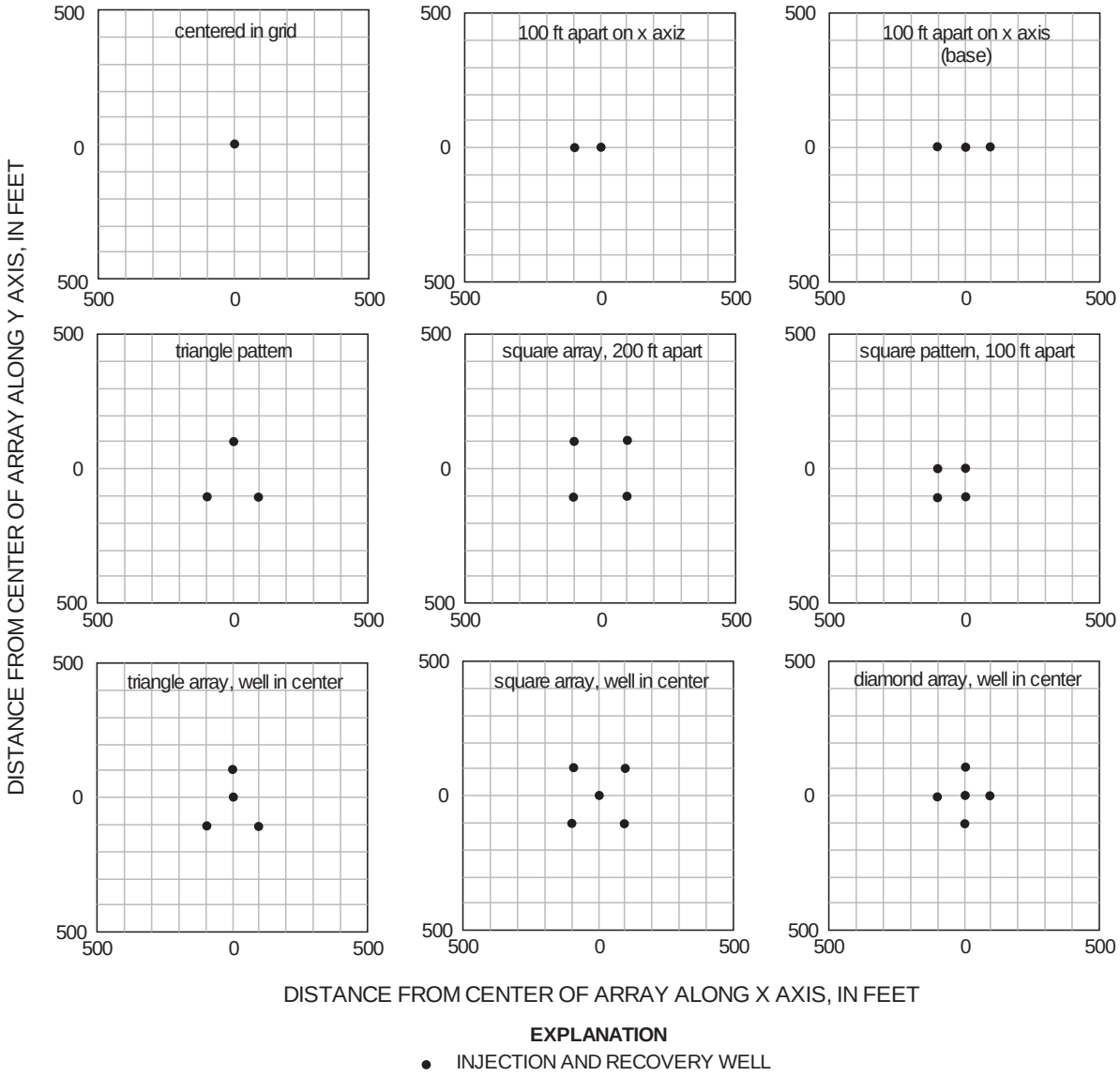

Figure 12. Geometric arrangement of injection and recovery wells.

Rates of Injection and Recovery

The base simulation model was used to simulate the injection and withdrawal of a fixed volume of water at various rates. The rate of injection and withdrawal for a fixed volume of water was varied by 0.25, 0.50, 2.0, and 4.0 times the base value. The duration of injection was adjusted so that the total volume injected remained constant at 360 Mgal. Durations of injection ranged from 22.5 days at 16.0 Mgal/d to 360 days at 1.0 Mgal/d. Results of the simulations are summarized below:

Injection/recovery rate (Mgal/d)	Volume of water injected (Mgal)	Injection time (days)	Recovery efficiency (percent)
16.0	360	22.5	15.0
8.0	360	45.0	13.9
4.0 base	360	90.0	14.8
2.0	360	180.0	14.8
1.0	360	360.0	13.6

Results of the simulations indicate no significant relation between the rate at which a given volume of water was injected or withdrawn and the amount of water that could be recovered. This implies that the

simulated dispersion process is most sensitive to the extent of fluid moment to a new position and not to the rate of movement to that position.

The effects of using different ratios of recovery to injection rates (Q_R/Q_I) also were studied and are summarized below:

Injection rate (Mgal/d)	Recovery rate (Mgal/d)	Q_R/Q_I	Recovery efficiency (percent)
4	1	1/4	14.0
4	2	1/2	14.4
4 (base)	4	1/1	14.8
4	8	2/1	14.9
4	16	4/1	15.1

When Q_R/Q_I ratios were decreased to 1/2 and 1/4, the recovery efficiency decreased slightly from 14.8 (base simulation) to 14.4 and 14.2 percent, respectively. When the Q_R/Q_I ratios were increased to 2/1 and 4/1, the recovery efficiency increased slightly from 14.8 percent (base simulation) to 14.9 and 15.4 percent, respectively. Because the mass of injected water buoys upward, native water generally remains near the bottom of the wells, and therefore, the duration and rate of injection and recovery are not important.

Volume of Water Injected

Various changes in the volume of water injected for a fixed time period were studied in the base simulation model using six simulations in which the injected volume was varied from 0.25 to 2.0 times the base value. This was accomplished by decreasing or increasing the injection rate, while keeping the same injection time (90 days) as used in the base simulation. Zero recovery efficiency would occur for a sufficiently small injection volume because of mixing. Results of the simulations are summarized below:

Volume of water injected (Mgal)	Injection rate (Mgal/d)	Recovery efficiency (percent)
720	8.0	16.9
540	6.0	16.3
450	5.0	15.7
360 (base)	4.0	14.8
270	3.0	13.6
180	2.0	11.4
90	1.0	6.9

Simulations suggest that recovery efficiency is proportional to the injected flow volume. Recovery efficiency increased as the volume of water increased, and conversely, decreased as the volume of water decreased. For injected volumes of 1.25, 1.50, and 2.0 times the base value, recovery efficiency increased from 14.8 percent (base simulation) to 15.7, 16.3, and 16.9 percent, respectively. For injection volumes of 0.75, 0.50, and 0.25, times the base value, recovery efficiency decreased from 14.8 percent (base simulation) to 13.6, 11.4, and 6.9 percent, respectively. Recovery efficiency increased at a greater rate at smaller volumes than at larger volumes, nearly doubling (from 6.9 to 13.6 percent) when the injection volume increased from 90 to 270 Mgal; while only increasing by about one-fifth (from 13.6 to 16.9) when the injection volume increased from 270 to 720 Mgal.

The effect of keeping the same injection rate (4.0 Mgal/d) while decreasing or increasing the injection time used in the base simulation also was tested. Results from these simulations are as follows:

Volume of water injected (Mgal)	Injection time (days)	Recovery efficiency (percent)
720	180.0	17.0
540	135.0	16.2
450	112.5	15.6
360 base	90.0	14.8
270	67.5	13.6
180	45.0	11.6
90	22.5	7.7

Results from these six simulations are similar to the previous six simulations. As discussed earlier, the dispersion process is simulated as a function of the extent of fluid movement to a new position and not the rate of movement to that position, despite the functional dependence upon flow velocity.

Storage Time and Regional Flow

Two series of model simulations were used to illustrate the effect of storage time and the effect of the regional flow in the Upper Floridan aquifer on recovery efficiency. The first series of tests consisted of five simulations using storage times of 0, 30, 90, 180, and 360 days and no regional flow. The second series of tests consisted of five simulations using storage times of 0, 30, 90, 180, 360 days and an assumed hydraulic gradient of 1 ft/mi observed at the study site. Regional flow was represented as occurring along the X-axis of the grid, and specified boundary pressure values were entered to maintain simulated flow. Results of the simulations follows:

Volume of water injected (Mgal)	Injection time (days)	Storage time (days)	Regional gradient 0 ft/mi	Regional gradient 1 ft/mi
			Recovery efficiency (percent)	Recovery efficiency (percent)
360	90	0	14.8 (base)	14.7
360	90	30	13.7	13.6
360	90	90	12.0	11.9
360	90	180	9.2	9.1
360	90	360	4.7	4.6

Simulations indicated that long storage time greatly affects recovery efficiency but shorter times do not. About a two-thirds decrease (from 14.8 to 4.7 percent) in recovery efficiency was simulated when storage time was increased from 0 to 360 days. But the difference between a storage of zero and 30 days was small. If the storage period were lengthened much beyond 360 days the remaining injectant would be nearly lost completely. Simulations also show that a regional gradient of 1 ft/mi had virtually no effect on the recoverability of the injected water, within the storage times simulated.

The simulated flow fields at the end of 30, 180, and 360 days of storage are shown in figure 13. After injection ceases, rapid stratification and upconing occurs. Oscillations of the flow field in the upper unit at 180 days of storage are due to temporal instabilities in pressure. The figures show circular convection throughout a large part of the injection zone, with counter flow of native water toward the injection well in the lower part of the injection zone. The native water then mixes with the injectant, and the mixture flows away from the injection wells in the upper part of the injection zone. Because of the leaky nature of the aquifer system represented in this model, appreciable vertical flow of saline water into the injection layer occurs from adjacent layers. The longer the withdrawal is delayed, the lower the recovery efficiency. This is a major limiting factor for SSR.

Successive Cycles of Injection and Recovery

A series of ten consecutive multicycle model simulations were used to illustrate the effects of successive cycles of injection and recovery on the recovery efficiency. As discussed earlier, the base simulation consisted of a single cycle of 90 days of simultaneous injection of effluent in three wells at a rate of 4.0 Mgal/d and then equal rate withdrawal of 4.0 Mgal/d until the pumped water in each well reached a DS concentration of 1,500 mg/L. Model results from the preceeding cycle were used as initial conditions for simulating the following cycle. Results of the simulations are shown in figure 14.

Model results are similar to those reported by Merritt, (1985), Quinones and Wexler (1995), and Yobbi (1996). Recovery efficiency per cycle increases with the total number of cycles. Recovery efficiency increases very rapidly in initial cycles, increasing from about 15 percent to about 47 percent during the first five cycles, and less rapidly in later cycles, increasing from about 49 percent to about 56 percent during the last five cycles. Results also indicate that recovery efficiency approaches an asymptote after several cycles, where little improvement of recovery efficiency occurs.

Two simulations were made with the same parameters that were used in the multicycle simulation; one using no-flow/no-transport boundaries at the top and bottom limits of the model, and a second using no-flow/no-transport boundaries at the lateral limits of the model. These simulations were made to test the effect on recovery efficiency of using a constant pressure/constant concentration boundary condition at the top/bottom boundary and a leaky-aquifer boundary at the lateral boundaries to represent interlayer solute mass movement across these boundaries for multicycle simulations. The simulations yielded recovery efficiencies of 74 and 58 percent compared to 56 percent estimated after ten cycles. This indicates that constant pressure/constant concentration boundaries are important in the determination of the recovery efficiency in multicyle simulations, while leaky-aquifer boundaries have a very small effect on recovery efficiency in multicyle simulations.

Sensitivity Analysis

A series of simulation runs that started with the base model were done to determine changes in recovery efficiency due to variations in model parameters, including DS concentration of injection zone water, permeability, anisotropy, longitudinal and transverse dispersivities, and effective porosity. The sensitivity

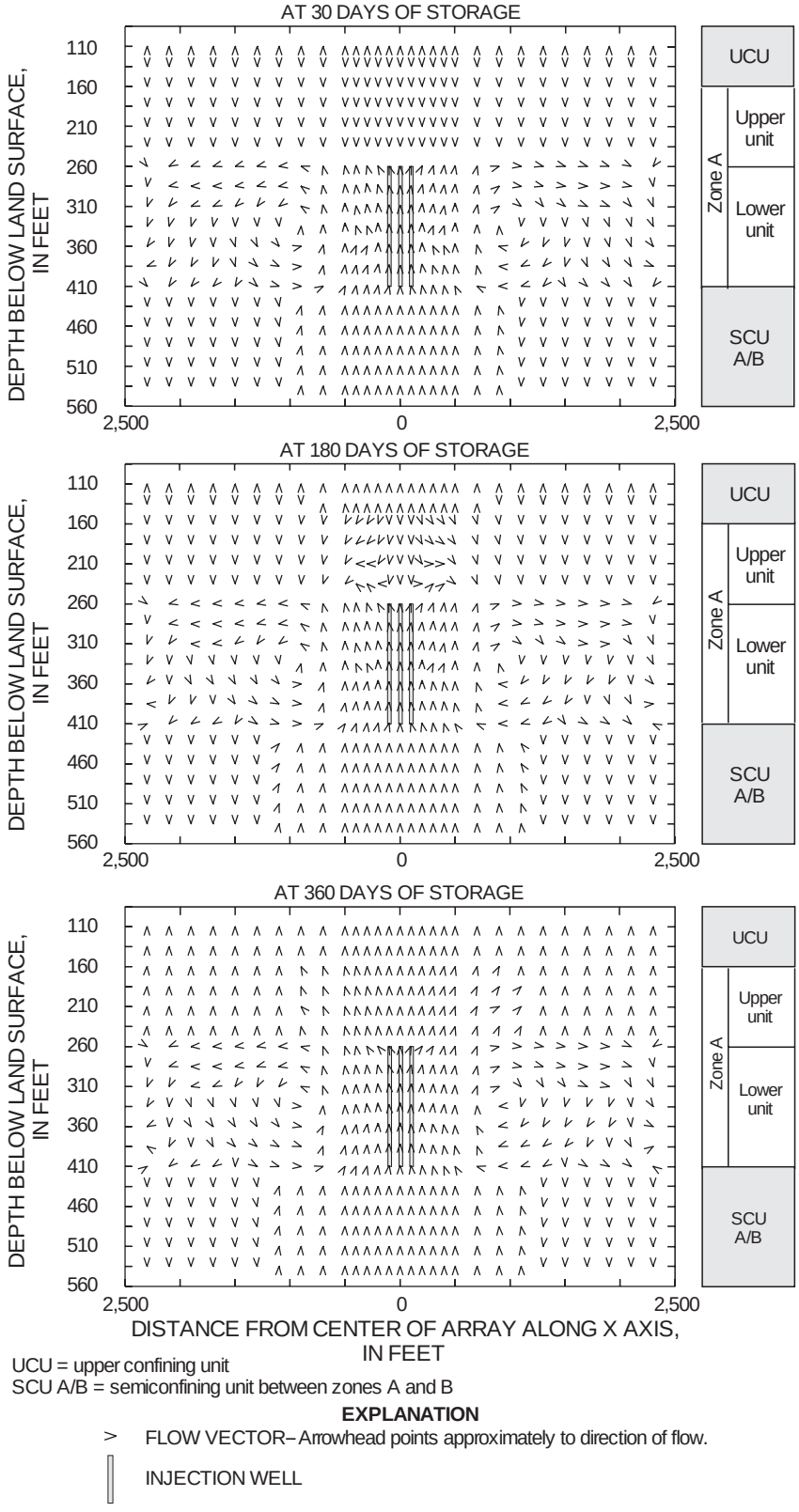

Figure 13. Simulated flow field along vertical plane 16 at the end of 30, 180, and 360 days of storage.

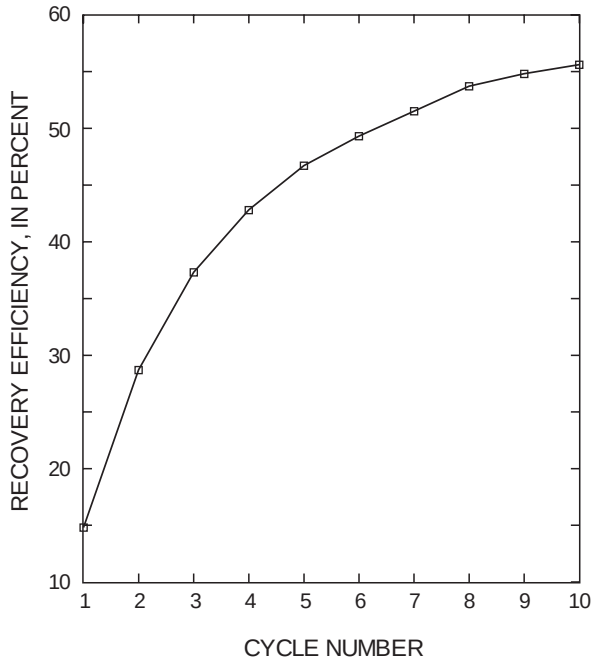

Figure 14. Recovery efficiency for ten successive injection/withdrawal cycles at 4.0 million gallons per day. (Withdrawal in each cycle ceases when the dissolved-solids concentration of water withdrawn reaches 1,500 milligrams per liter.)

analysis was conducted to assess the uncertainty of estimating selected matrix and fluid properties. For each simulation run, the value of an individual model parameter was changed by an amount that might reasonably be expected to vary from the value used in the base simulation, and noting the change in recovery efficiency as a result of the change. The simulation used as a base for comparison consisted of a single cycle of 90 days of simultaneous injection of effluent in three wells at a rate of 4.0 Mgal/d and then equal rate withdrawal of 4.0 Mgal/d until the pumped water in each well reached a DS concentration of 1,500 mg/L. A recovery efficiency of 14.8 percent was estimated for the base simulation.

The general results from the analysis, which are described in the following sections, indicate that the DS concentration of the injection zone is the most important factor, producing the greater change in recovery efficiency. The second most important factor producing significant changes in recovery efficiency is changes in longitudinal and transverse dispersivity values. Generally, recovery efficiency increased when parameter values decreased and recovery efficiency decreased when parameter values increased. The one exception is that recovery efficiency increased when there was an order of magnitude increase in the ratio of horizontal to vertical anisotropy.

Dissolved-Solids Concentration of the Injection Zone

Simulations were made to study the effects of different DS concentration of the injection zone (zone A lower unit) on recovery efficiency. The greater the salinity of the native water, the greater will be the range of salinity across the zone of dispersion; hence, density gradients will be greater causing bouyant movement and the proportion of recoverable water within the zone will be smaller. Six DS concentrations were selected for comparison: (1) 500 mg/L, representing the least saline layer of the model; (2) 1,000 mg/L, an arbitrary value representing water somewhat more saline than the base value of the injection zone; (3) 2,000 mg/L, an arbitrary value representing slightly saline water, (4) 3,400, mg/L, an arbitrary value representing a mix of the least saline layer of the model and that of the composite base value of the injection zone, (5) 7,800 mg/L, representing the composite base value of the injection zone, and (6) 16,900 mg/L, representing the most saline layer.

Results of the simulations indicate recovery efficiency is highly sensitive to changes in the DS concentration of the injection zone (fig. 15A). Recovery efficiency decreases at a great rate as low DS concentrations increase, decreasing from about 77.8 to 23.6 percent when DS concentrations increased from 500 to 3,400 mg/L; but the rate of decrease is small at higher DS concentrations, decreasing from about 23.6 to 6.1 percent when the DS concentration of the injection zone increased from 3,400 mg/L to 16,900 mg/L. This analysis indicates that: (1) increases in DS concentrations of the injection zone can decrease recovery efficiency significantly, and (2) SSR is most promising when the DS concentration of the injection zone is low and least promising when the DS concentration of the injection zone is high.

Permeability

Permeability and effective porosity control the velocity of injectant flow. Uncertainty in the permeability value will affect the advective and dispersive components of the transport computations and, hence, the rate of solute transport. Generally, low permeability optimizes recovery efficiency, assuming that injection wells remain practical at low permeabilities.

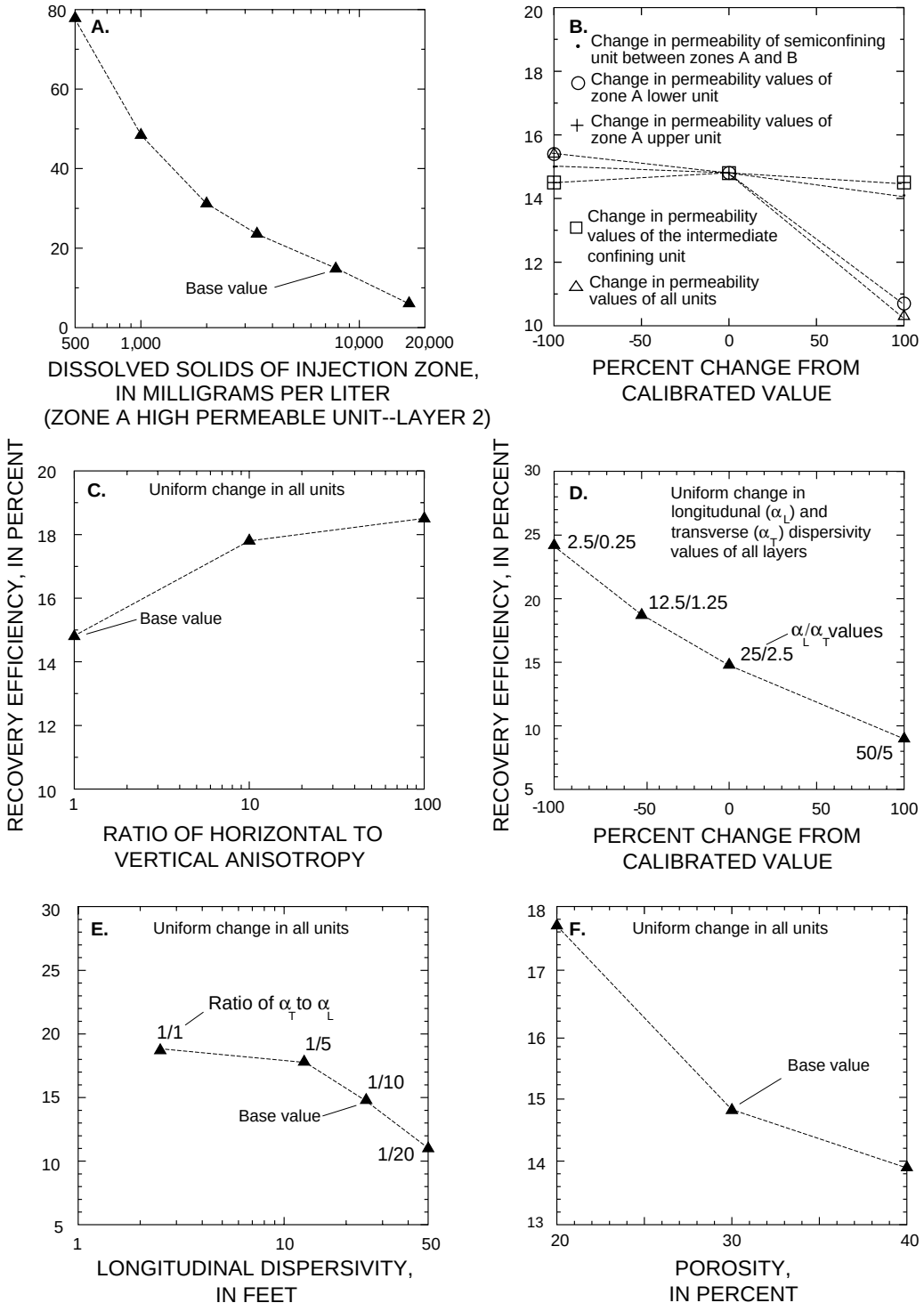

Figure 15. Relation between recovery efficiency and variations in selected model parameters.

The magnitude of permeability was changed in five different ways in the base simulation model: (1) uniform changes in all permeability values; (2) changes in permeability values of the intermediate confining unit; (3) changes in permeability values of zone A upper unit; (4) changes in permeability values of zone A lower unit; and (5) changes in permeability values of the semi-confining unit between zones A and B.

Figure 15B illustrates the variation of recovery efficiency due to permeability changes. Changes in the permeability values of all units produced the greatest change in recovery efficiency while changes in permeability values of zone A lower unit (injection zone) produced the second greatest change in recovery efficiency. Increasing permeability of the injection zone by a factor of 10 decreased recovery efficiency by about one-third (from 14.8 to 10.6 percent). The decrease in recovery efficiency is expected because of easier horizontal and vertical transport of the injected fluid, which results in greater stratification and buoyancy flow that prevents complete mixing of the injected and native waters. Also, figure 15B shows that when permeability of each layer was reduced by a factor of 0.1, recovery efficiency was not significantly affected. The major effect of the variation at lower permeability values is the increased wellhead pressure or drawdown required at the specified injection/withdrawal rate.

Anisotropy

If flow conditions vary with direction in a geologic formation, the formation is anisotropic and has differences in horizontal (k_h) and vertical (k_v) permeability. The greater the anisotropy ratio (k_h/k_v), the easier the injectant front moves along the axis of the larger permeability component. In the base simulation model, permeability is equal in all directions. To test for the effects of anisotropy, the ratio of k_h to k_v was varied from an isotropy base value ($k_h/k_v = 1$) to $k_h/k_v = 10$ and $k_h/k_v = 100$ (fig. 15C). Increasing k_h/k_v resulted in recovery efficiency increasing by about one-quarter (from 14.8 to 18.5 percent). Recovery efficiency increases because simulation of a larger k_h/k_v causes more lateral flow and inhibits upward movement of buoyant injectant.

Dispersivity

Dispersivity is a scale-dependent property of the porous medium that controls the mixing of injected and native formation fluids at their interface. When dispersivity is increased, more mixing occurs and a widening of the transition zone between the injectant and native formation waters occurs. Dispersion is a restrictive process that can severely limit recovery efficiency (Merritt, 1985).

Two different tests of the base model were made for the α_T and α_L values. In the first test, both dispersivity values were simultaneously changed by the same percentage, keeping the ratio of α_T to α_L equal to 1/10. In the second test, the ratio of α_T to α_L was changed by keeping the α_T value constant while changing the α_L value.

Figures 15D and 15E illustrate results of the simulations. The analysis indicates that uniform changes in both α_T and α_L values produced more significant changes in recovery efficiency than when the ratio of α_T to α_L was changed. Increasing α_T and α_L uniformly by 100 percent decreased recovery efficiency by about one-third (from 14.8 to 9.0 percent); while decreasing α_T and α_L uniformly by 100 percent increased recovery efficiency by about two-thirds, from 14.8 to 24.2 percent. When α_L was decreased from 25 to 2.5 ft (α_T to α_L =1/1) recovery efficiency increased by about one-quarter, from 14.8 to 18.7 percent. When α_L was increased from 25 to 50 ft (α_T to α_L = 1/20) recovery efficiency decreased by about one quarter, from 14.8 to 11.0 percent. In both cases, recovery efficiency decreases as dispersivity increases. A large rate of decrease in recovery efficiency is shown as the dispersivity value or ratio of α_T to α_L, increases from low values, but the rate of decrease is small at larger dispersivity values or ratios.

Effective Porosity

Effective porosity is part of the ground-water hydraulic equation and the advective-dispersive solute-transport equation. In addition to the effect on the storage term for the transport equation, the effective porosity value is combined with the specific discharge (obtained from the ground-water flow equation) to determine the average pore-water velocities, which are used to represent the advection term in the transport equation (Quinones and Wexler, 1995).

Effective porosity of the aquifer material was tested at 20 and 40 percent to bracket the base model value of 30 percent. Figure 15F illustrates the variation of recovery efficiency due to changes in porosity. Increasing porosity caused recovery efficiency to decrease slightly, from 14.8 to 13.9 percent, whereas decreasing porosity caused recovery efficiency to increase by about one-fifth, from 14.8 to 17.7 percent. The greater the porosity, the slower the solute front will move; thus, the longer the time it takes to replace the volume of native formation water in a given volume of the aquifer and the greater the dispersive mixing. Low porosity has the opposite effect.

SUMMARY AND CONCLUSIONS

A model-based study of subsurface storage and recovery (SSR) was made to assess the potential for SSR using multiple wells at the Southwest St. Petersburg WRF. SSR is a strategy of water conservation used to augment exiting water supplies. The study was specifically aimed toward applying a density-dependent, ground-water and solute-transport model to assess various operational variables and physical properties on recoverability of injected effluent.

The hydrogeologic framework used for this study was developed from interpretations of data from previous studies. The sediments underlying the study area form a sequence of two aquifers and one confining unit. The framework includes the unconfined surficial aquifer, and the confined Upper Floridan aquifer. The units are separated by the intermediate confining unit.

General aquifer characteristics were estimated from field and laboratory data including drillers logs, aquifer tests, and geophysical logs collected from previous studies. Hydraulic properties of the hydrostratigraphic units were estimated using numerical simulation of aquifer-test data. A cylindrical numerical model was calibrated by obtaining a satisfactory match between observed and model-generated head change data.

A three-dimensional numerical model of variable density ground-water flow and solute transport (HST3D) was used to evaluate the effects of changing various operational parameters on recovery efficiency of treated effluent stored in a saline aquifer underlying the study site using multiple wells. About 75 hypothetical tests of SSR were made to evaluate the efficiency of this operation in the study area. A base simulation of simultaneous injection of 4 Mgal/d in three wells for 90 days and then withdrawal of 4 Mgal/d from all wells until the pumped water exceeded a dissolved-solids concentration of 1,500 mg/L was used as a reference to compare the effects of changing selected operational factors on recovery efficiency. A recovery efficiency of 14.8 percent was estimated for the base simulation. The effects of the following operational factors were assessed using the model:

1. multiple-well configurations;
2. rates of injection and recovery;
3. volume of water injected;
4. storage time and regional flow, and
5. successive cycles of storage and recovery.

Simulation results for hypothetical conditions indicate that recovery efficiency increases when the volume of injectant increases; increases with successive injection and recovery cycles, and increases slightly when the ratio of recovery rate to injection rate increases. Recovery efficiency decreases significantly when the storage time increases significantly and decreases slightly when the ratio of recovery rate to injection rate decreases. Recovery does not change significantly when the rate of injection increases or decreases.

Model results show that recovery efficiencies of about 7 to 17 percent can be achieved for different SSR operational schemes. Ten successive injection and recovery cycles can increase the recovery efficiency to about 56 percent. Other results indicate that recovery efficiency does not improve significantly in particular geometric arrangement of wells or number of wells when the volume of water injected remains constant. Recovery efficiency for the various configurations tested was nearly the same as if injection and recovery had been from a single well.

Sensitivity analysis were performed to determine changes in recovery efficiency to variations in model parameters, including:

1. dissolved-solids concentration of the injection zone,
2. permeability,
3. anisotropy,
4. dispersivity, and
5. effective porosity.

The general results from the analysis indicate that changes in the dissolved-solids concentration of

the injection zone produced the greatest change in recovery efficiency. Uniform changes in dispersivity values produced the second most significant change in recovery efficiency. Generally, recovery efficiency increased when each parameter value decreased and recovery efficiency decreased when each parameter value increased.

Density differences between native and injected waters were the most important factor affecting recovery efficiency in this study. High salinity of native water at a given permeability level permits rapid buoyancy stratification and brings about a substantial loss of recovery efficiency. Simulation results indicated that recovery efficiency decreased rapidly when the dissolved-solids concentration increased, decreasing from about 77.8 to 23.6 percent when dissolved-solids concentration increased from 500 to 3,400 mg/L.

Dispersivity is an important factor to the model sensitivity and is a restrictive process that can severely limit recovery efficiency. However, the dispersivity values used for this model were not field tested and may not be representative of the actual dispersive characteristics of the aquifer system at the study site.

SELECTED REFERENCES

Black, Crow, and Eidsness, Inc., 1978, Drilling and testing of the monitoring and injection wells at Southwest Wastewater Treatment Plant for the city of St. Petersburg, Florida: Consultant's report in files of the city of St. Petersburg, Fla.

Chemical Rubber Company, 1982, CRC Handbook of chemistry and physics (63rd ed): Boca Raton, Fla., CRC Press.

Freeze, R.A., and Cherry, J.A., 1979, Groundwater: Englewood, N.J., Prentice-Hall, 604 p.

Heath, Ralph C., 1989, Basic ground-water hydrology: U.S. Geological Survey Water-Supply Paper 2220, 84 p.

Hickey, J.J., 1982, Hydrogeology and results of injection tests at waste-injection test sites in Pinellas County, Florida: U.S. Geological Survey Water-Supply Paper 2183, 42 p.

-----, 1989, Circular convection during subsurface injection of liquid waste, St. Petersburg, Florida: Water Resources Research, v. 25, no. 7, p. 1481-1494.

Hickey, J.J., and Ehrlich, G.G., 1984, Subsurface injection of treated sewage into a saline-water aquifer at St. Petersburg, Florida--Water quality changes and potential for recovery of injected sewage: Ground Water, v. 22, no. 4, p. 397-405.

Hickey, J.J., and Spechler, R.A., 1979, Hydrologic data for the southwest subsurface-injection test site, St. Petersburg, Florida: U.S. Geological Survey Open-File Report 78-852, 104 p.

Kimbler, O.K., Kazman, R.G., and Whitehead, W.R., 1975, Cyclic storage of freshwater in saline aquifers: Louisiana Water Resources Institute Bulletin 10, 78 p., with appendixes.

Kipp, K.L., 1987, HST: A computer code for simulation of heat and solute transport in three-dimensional groundwater flow systems: U.S. Geological Survey Water-Resources Investigations Report 86-4095, 519 p.

Merritt, M.L., 1985, Subsurface storage of freshwater in south Florida: A digital model analysis of recoverability: U.S. Geological Survey Water-Supply Paper 2261, 44 p.

----- 1994, Tests of subsurface storage of freshwater at Hialeah, Dade County, Florida, and digital simulation of the salinity of recovered water: U.S. Geological Survey Open-File Report 93-155, 112 p.

National Oceanic and Atmospheric Administration, Climatological data, Florida, monthly summaries, 1995.

Quinones-Aponte, Vicente, and Wexler, Eliezer J., 1995, Preliminary assessement of injection, storage, and recovery of freshwater in the lower Hawthorn aquifer, Cape Coral, Florida: U.S. Geological Survey Water-Resources Investigations Report 94-4121, 102 p.

Pricket, T.A., and Lonnquist, C.G., 1971, Selected digital computer techniques for groundwater resources evaluation: Urbana, State of Illinois, Department of Registration and Education, Illinois State Water Survey ISWS-71-BUL-55, 62 p.

Sinclair, W.C., 1974, Hydrogeologic characteristics of the surficial aquifer in northwest Hillsborough County, Florida: Florida Bureau of Geology Information Circular no. 86, 98 p.

Skibitzke, H.E. and Robinson, G.M., 1963, Dispersion in ground water flowing through heterogeneous materials: U.S. Geological Survey Professional Paper 386-B.

Rosenshein, J.S., and Hickey, J.J., 1977, Storage of treated sewage effluent and storm water in a saline aquifer, Pinellas Peninsula, Florida: Ground Water, v. 15, no. 4, p. 289-293.

Voss, C.I., 1984, A finite-element simulation model for saturated-unsaturated, fluid-density-dependent groundwater flow with energy transport or chemically-reactive single-species solute transport: U.S. Geological Survey Water-Resources Investigations Report 84-4369, p. 54-55.

Yobbi, D.K., 1996, Simulation of subsurface storage and recovery of treated effluent injected in a a saline aquifer, St. Petersburg, Florida: U.S. Geological Survey Water-Resources Investigations Report 95-4271, 29 p.

U.S. Department of the Interior
U.S. Geological Survey
227 N. Bronough St., Suite 3015
Tallahassee, Florida 32301

BOOK RATE

Simulation of Subsurface Storage and Recovery of Treated Effluent Injected in a Saline Aquifer, St. Petersburg, Florida

By Dann K. Yobbi

U.S. GEOLOGICAL SURVEY
Water-Resources investigations report 95-4271

Prepared in cooperation with the
CITY OF ST. PETERSBURG and the
SOUTHWEST FLORIDA WATER MANAGEMENT DISTRICT

Tallahassee, Florida
1996

U.S. DEPARTMENT OF THE INTERIOR
BRUCE BABBITT, Secretary

U.S. GEOLOGICAL SURVEY
Gordon P. Eaton, Director

For additional information write to:

District Chief
U.S. Geological Survey
Suite 3015
227 North Bronough Street
Tallahassee, Florida 32301

Copies of this report can be purchased from:

U.S. Geological Survey
Earth Science Information Center
Open-File Reports Section
P.O. Box 25286, MS 517
Denver, CO 80225-0425

CONTENTS

FIGURES

TABLES

CONVERSION FACTORS, VERTICAL DATUM, ABBREVIATIONS, AND ACRONYMS

Multiply inch-pound unit	By	To obtain
foot (ft)	0.3048	meter
mile (mi)	1.609	kilometer
foot squared (ft^2)	0.0929	meter squared
foot per day (ft/d)	0.3048	meter per day
foot squared per day (ft^2/d)	0.0920	square meter
foot squared per pound (ft^2/lb)	$1.007x10^{-6}$	square meter per Newton
inch squared per day (in^2/lb)	$1.45x10^{-4}$	square meter per Newton
pounds per square inch (lb/in^2)	6.895	kilopascal
pounds per cubic foot (lb/ft^3)	0.0160	gram per cubic centmeter
million gallons per day (Mgal/d)	0.4381	cubic meter per second

Equation for temperature conversion between degrees Celsius (oC) and degrees Fahrenheit (oF):

$^oC = 5/9 \times (^oF-32)$

$^oF = (9/5\ ^oC) + 32$

Sea level: In this report, "sea level" refers to the National Geodetic Vertical Datum of 1929 (NGVD of 1929)---a geodetic datum derived from a general adjustment of the first-order level nets of the United States and Canada, formerly called "Sea Level Datum of 1929."

ADDITIONAL ABBREVIATIONS

mg/L	milligrams per liter
α_T	transverse dispersivity
α_L	longitudinal dispersivity
k_h	horizontal permeability
k_v	vertical permeability

ACRONYMS:

AIF	aquifer influence function
DS	dissolved solids
HST3D	U.S. Geological Survey Three Dimensional Heat- and Solute-Transport computer program
PHREEQE	U.S. Geological Survey equilibrium speciation computer program for geochemical calculations
SSMF	scaled-solute mass fraction
SSR	subsurface storage and recovery
SWFWMD	Southwest Florida Water Management District
SI	saturation index
USGS	U.S. Geological Survey
WATEQF	U.S. Geological Survey equilibrium speciation computer program for natural waters
WRF	water reclamation facilities

Simulation of Subsurface Storage and Recovery of Treated Effluent Injected in a Saline Aquifer, St. Petersburg, Florida

By Dann K. Yobbi

Abstract

The potential for subsurface storage and recovery of treated effluent into the uppermost producing zone (zone A) of the Upper Floridan aquifer in St. Petersburg, Florida, is being studied by the U.S. Geological Survey, in cooperation with the city of St. Petersburg and the Southwest Florida Water Management District. A measure of the success of this practice is the recovery efficiency, or the quantity of water relative to the quantity injected, that can be recovered before the water that is withdrawn fails to meet water-quality standards. The feasibility of this practice will depend upon the ability of the injected zone to receive, store, and discharge the injected fluid.

A cylindrical model of ground-water flow and solute transport, incorporating available data on aquifer properties and water quality, was developed to determine the relation of recovery efficiency to various aquifer and fluid properties that could prevail in the study area. The reference case for testing was a base model considered representative of the saline aquifer underlying St. Petersburg. Parameter variations in the tests represent possible variations in aquifer conditions in the area. The model also was used to study the effect of various cyclic injection and withdrawal schemes on the recovery efficiency of the well and aquifer system.

A base simulation assuming 15 days of injection of effluent at a rate of 1.0 million gallons per day and 15 days of withdrawal at a rate of 1.0 million gallons per day was used as reference to compare changes in various hydraulic and chemical parameters on recovery efficiency. A recovery efficiency of 20 percent was estimated for the base simulation. For practical ranges of hydraulic and fluid properties that could prevail in the study area, the model analysis indicates that (1) the greater the density contrast between injected and resident formation water, the lower the recovery efficiency, (2) recovery efficiency decreases significantly as dispersion increases, (3) high formation permeability favors low recovery efficiencies, and (4) porosity and anisotropy have little effect on recovery efficiencies. In several hypothetical tests, the recovery efficiency fluctuated between about 4 and 76 percent.

The sensitivity of recovery efficiency to variations in the rate and duration of injection (0.25, 0.50, 1.0, and 2.0 million gallons per day) and withdrawal cycles (60, 180, and 365 days) was determined. For a given operational scheme, recovery efficiency increased as the injection and withdrawal rate is increased. Model results indicate that recovery efficiencies of between about 23 and 37 percent can be obtained for different subsurface storage and recovery schemes. Five successive injection, storage, and recovery cycles can increase the recovery efficiency to about 46 to 62 pecent. There is a larger rate of increase at smaller rates than at larger rates. Over the range of variables studied, recovery efficiency improved with successive cycles, increasing rapidly during initial cycles then more slowly at later cycles.

The operation of a single well used for subsurface storage and recovery appears to be technically feasible under moderately favorable conditions; however, the recovery efficiency is highly dependent upon local physical and operational parameters. A combination of hydraulic, chemical, and operational parameters that minimize dispersion and buoyancy flow, maximizes recovery efficiency. Recovery efficiency was optimal where resident formation water density and permeabilities were relatively similar and low.

INTRODUCTION

The city of St. Petersburg owns and operates one of the largest urban reclaimed-wastewater reuse systems in the world. Currently (1995), approximately 21 Mgal/d of advanced secondary-treated effluent is piped from the city's four water reclamation facilities (WRF) through a 260-mile irrigation system to water residential and commercial properties. Demand for reclaimed water is seasonal. There is a deficiency of effluent for irrigation in the dry months and an excess in the wet months, during which the excess is disposed of through deep underground injection wells. The injected water from these deep permeable zones cannot be effectively recovered because the disposal zone is in a highly fractured dolomite saturated with saltwater (Hickey and Ehrlich, 1984). One solution, known as subsurface storage and recovery (SSR), to this dilemma involves the injection of effluent into shallow, less transmissive formations of low or moderate salinity, by one or more wells, for storage during wet periods when demand is low. The injected water would be withdrawn later for irrgation use during dry periods when demand is high. SSR is especially appropriate for areas like St. Petersburg where there is: (1) seasonal variations in water supply and demand, and (2) availability of moderately permeable aquifers near the surface that contain brackish water.

The feasibility of a SSR system will depend upon the ability of the injected zone to receive, store, and discharge the injected effluent. A measure of the success of a SSR system is the quantity of water that can be recovered relative to the quantity injected, or recovery efficiency. Recovery efficiency, usually expressed as a percentage per cycle of injection, storage, and recovery, is defined as the volume of water recovered before the withdrawn water fails to meet some prescribed chemical standard. In this report, the standard has been taken to be when the water that is withdrawn exceeds a dissolved solids (DS) concentration of 1,500 mg/L.

Two primary physical processes limit the recoverability of the injected water: (1) mixing by advection and hydrodynamic dispersion, and (2) density stratification. Mixing and dispersion creates a diffused zone between the injected and formation waters as a result of molecular diffusion and mechanical dispersion. Density stratification describes the tendency for the lighter fluid to rise above the denser fluid. Unfavorable physical and solute properties of the aquifer system can strengthen these deleterious processes and reduce the recoverability of injected water.

An assessment of the potential recovey efficiency for the aquifer system underlying St. Petersburg needs to be made before a commitment of resources is made for operational testing at a specific site. This requires a semi-quantitative understanding of the dependence of recovery efficiencies on hydrogeologic and chemical characteristics of the aquifer system and on system designs and management parameters. A cost-effective alternative to field testing is simulation modeling, in which many combinations of conditions can be investigated with relatively inexpensive computer simulations.

In 1994, the U.S. Geological Survey (USGS), in cooperation with the city of St. Petersburg and the Southwest Florida Water Management District (SWFWMD), began a model-based investigation of the hydrogeologic and operational aspects of subsurface injection and storage of effluent, and possible future retrieval for nonpotable use. The study area is the city of St. Petersburg, located on the southern tip of Pinellas County (fig. 1).

Throughout this report, statements are made concerning the salinity of water. The terminology used to describe the salinity is modified slightly from a USGS classification system of water based on dissolved solids (Heath, 1989, table 2, p. 65), as follows:

Classification	Dissolved-solids concentration (milligrams per liter)	Percent seawater
Freshwater	<500	<1.5
Slightly saline (brackish water)	500 to 3,000	1.5 to 8.6
Moderately saline (brackish water)	3,000 to 10,000	8.6 to 29
Very saline (saltwater)	10,000 to 35,000	29 to 100
Brine	>35,000	>100

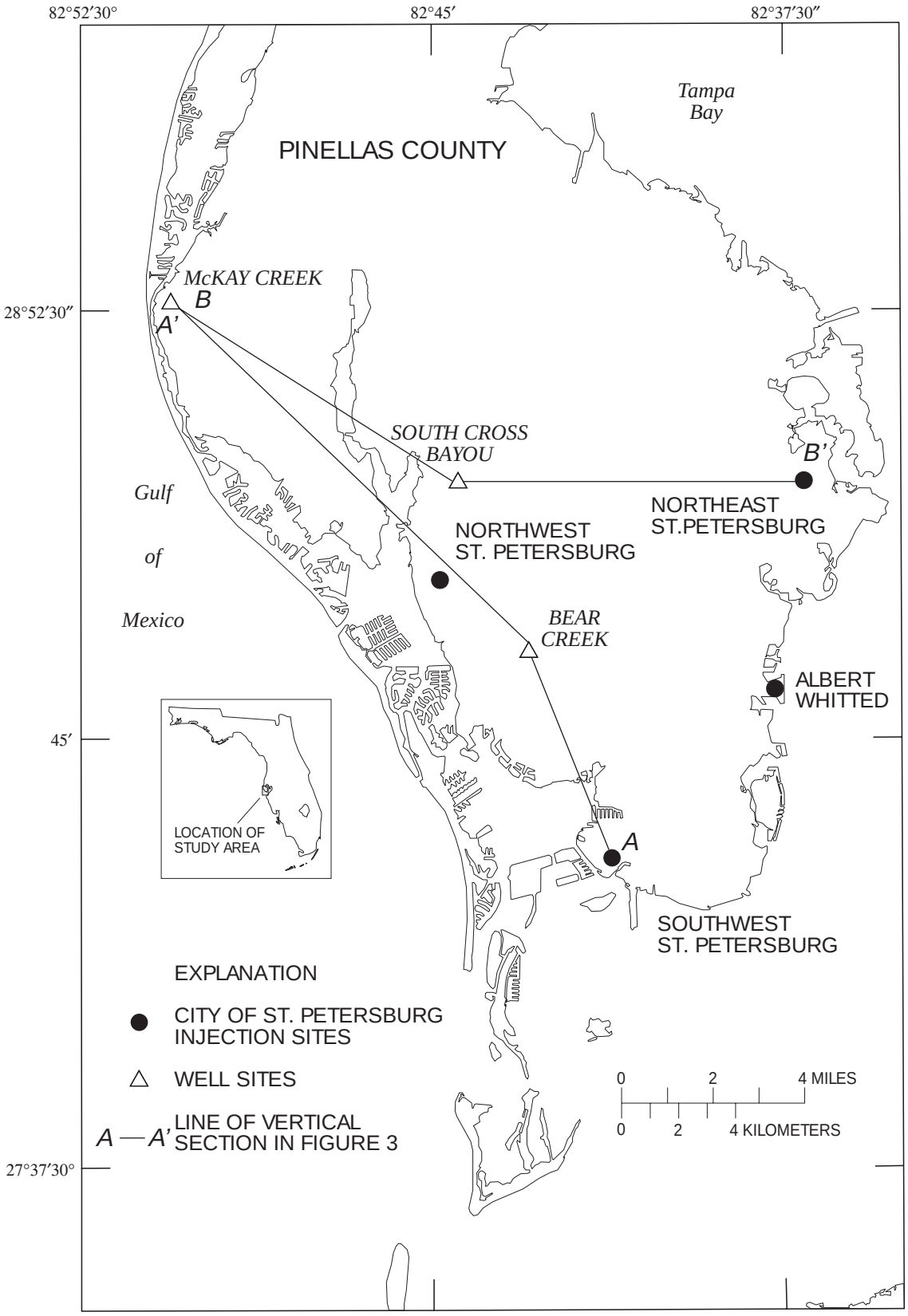

Figure 1. Location of study area, injection sites, and lines of vertical sections.

Freshwater meets the DS concentration limit for potable water. Slightly saline water is nonpotable, but it may be suitable for irrigation. Moderately saline water is suitable for desalinization, and very saline water and brine are considered unusable.

Purpose and Scope

This report presents the results of a study conducted to provide a better understanding of the potential for SSR in a moderately transmissive, slightly to moderately saline-water bearing, limestone aquifer underlying St. Petersburg. Specifically, the objectives are (1) define the hydrogeologic framework and quality of ground water, (2) determine the geochemical interactions associated with SSR, and (3) illustrate the application of a solute-transport model as a tool for understanding the relative importance of individual physical properties and operational variables on recovery efficiency. The scope of the study is limited to a preliminary analysis because no data exist for comparison with model results.

Information on the hydrogeologic framework, hydrologic properties, matrix properties, and water chemistry of the aquifer system was compiled from files of the USGS and from engineering reports of the city's four WRF injection well sites.

The possibilities for geochemical interactions between the injected and aquifer waters were evaluated using aqueous speciation (WATEQF) and chemical mass-balance (PHREEQE) models (Plummer and others, 1976; Parkhurst and others, 1980). The models were used to assess the potential for both precipitation and dissolution of certain carbonate minerals.

The three dimensional heat-and solute-transport model (HST3D), developed by Kipp (1987), was used to simulate a typical injection/recovery well system. Injection and withdrawal in a prototype aquifer were simulated and recovery efficiency was computed. The model was used to assess the relation of recovery efficiency to various aquifer and fluid properties and to simulate recovery efficiencies under selected hypothetical operational schemes.

HYDROGEOLOGIC FRAMEWORK

The hydrogeologic units beneath the study area consist of a thick sequence of carbonate rock overlain by clastic deposits. The sediments are subdivided into a sequence of discrete lithologic units that form a layered sequence of two aquifers and one confining unit. The framework includes the unconfined, surficial aquifer and the confined, Floridan aquifer system (fig. 2). The units are separated by the intermediate confining unit.

Surficial Aquifer

The surficial aquifer is the uppermost water bearing formation. It consists of undifferentiated sands and clays that vary in composition both laterally and vertically. The aquifer is a source of recharge to the Floridan aquifer system and is mainly used as a source of water for lawn irrigation. The surficial aquifer is generally less than 30 ft thick and is generally saturated to within 10 ft of land surface during dry weather. During wet weather, the water table in the surficial aquifer is generally close to land surface. The surficial aquifer has a horizontal hydraulic conductivity ranging from 13 to 33 ft/d and a vertical hydraulic conductivity ranging from 0.3 to 13 ft/d (Cherry and Brown; 1974; Sinclair, 1974; Hutchinson and Stewart, 1978).

Intermediate Confining Unit

The intermediate confining unit of low-permeability lies between the surficial aquifer and the Floridan aquifer system. The unit coincides with the undifferentiated Arcadia Formation of the Hawthorn Group and consists of a clastic and carbonate sequence. The carbonates in the sequence are generally underlain and overlained by clays and marls of relatively low permeability (Hickey, 1981). Thickness of the intermediate confining unit averages about 90 ft and ranges from about 50 to 140 ft. The confining unit is highly variable both spatially and vertically. A wide range of hydraulic characteristics occurs within the unit due to lithologic heterogeneity within the unit. Vertical hydraulic conductivity for the intermediate confining unit as reported by Sinclair (1974) and Black, Crow, and Eidsness, Inc. (1978) ranges from 1.3×10^{-4} to 6.9×10^{-3} ft/d.

Floridan Aquifer System

The Floridan aquifer system is a thick, regionally extensive sequence of Tertiary age carbonates. Miller (1986) defines the Floridan aquifer system to include the Upper Floridan aquifer, the middle confining unit, and the Lower Floridan aquifer. In the study area, the

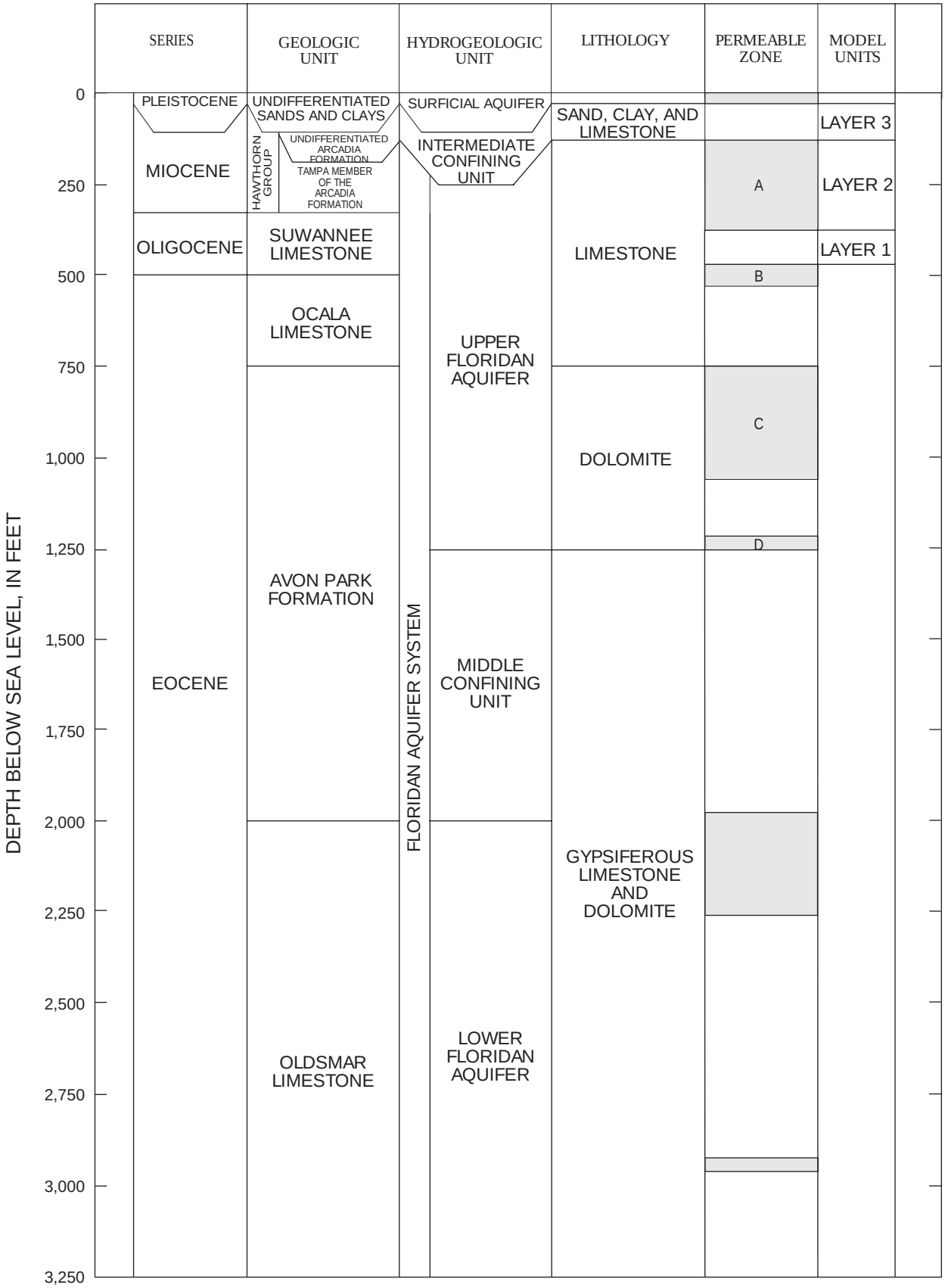

Figure 2. Generalized stratigraphic and hydrogeologic section, Pinellas County. (Modified from Hickey, 1982.)

middle confining unit and the Lower Floridan aquifer contain water comparable to seawater; the base of the freshwater flow system is limited to the Upper Floridan aquifer. The geologic formations that make up the Upper Floridan aquifer consists of limestone and dolomite rocks of, in ascending order, the Avon Park Formation, the Ocala and Suwannee Limestones, and the Tampa Member of the Arcadia Formation of the Hawthorn Group. The top of the Upper Floridan aquifer is defined as the first occurrence of a persistent carbonate sequence; the base of the Upper Floridan aquifer is defined as the first occurrence of interbedded gypsum in the carbonates below a dark-brown, microcrystalline dolomite in the Avon Park Formation (Hickey, 1982). In St. Petersburg, the Upper Floridan aquifer is subdivided into four permeable zones separated by semiconfining units (Hickey, 1982). The zones are alphabetically labeled with increasing depth from A to D (fig. 2). This study is concerned only with the uppermost producing zone of the Upper Floridan aquifer (zone A) , the overlying confining unit, and the underlying semiconfining unit between zone A and B, and further discussion will be restricted to these units.

Zone A

Zone A comprises the Tampa Member of the Arcadia Formation of the Hawthorn Group and the uppermost part of the Suwannee Limestone. Zone A is the shallowest and freshest of the producing zones and is the only potential receiving zone for SSR in St. Petersburg. Thickness of zone A averages about 180 ft and ranges from about 115 to 245 ft. Thickness varies from site to site, occurring with no regional pattern (Hickey, 1982). Geraghty and Miller, Inc. (1976), Robertson and Mallory (1977), Black, Crow, and Eidsness, Inc. (1978), Hickey (1982), and Brown and Associates (1986) reported values of transmissivity for zone A that ranged from 2.2×10^4 to 3.5×10^4 ft^2/d and values of storativity that range from 4×10^{-4} to 8×10^{-4}. Average values of porosity of zone A , estimated from geophysical logs, are 26, 32, and 41 percent (Hickey, 1982).

Semiconfining Unit Between Zones A and B

Underlying zone A (the uppermost permeable zone) is the first of a series of poorly transmissive carbonate rock that acts as semiconfining units that separate permeable zones. The existence of the semiconfining units was determined during previous studies by Hickey (1982). The semiconfining unit below zone A is in the limestone unit of the Suwannee Limestone. Thickness of the semiconfining unit averages about 150 ft and ranges from about 125 to about 170 ft. Average porosity of the semiconfining unit from geophysical logs is about 30 percent and ranges from 22 to 36 percent (Hickey, 1982). The semiconfining unit is considered a nonproducing zone in St. Petersburg.

Vertical hydraulic conductivity of the semiconfining unit between zones A and B, determined from laboratory and aquifer tests reported by Hickey (1982), ranges from 1.3×10^{-3} to 2.6 ft/d. The value of 1.3×10^{-3} ft/d was determined from a laboratory test of a limestone core from the northeast St. Petersburg WRF where a higher percentage of clay occurred in the limestone matrix than at other sites in St. Petersburg. Test results at southwest St. Petersburg WRF and South Cross Bayou indicate that a value of less than 0.1 ft/d probably is not representative of general conditions (Hickey, 1982). Comparison of aquifer and laboratory tests indicate that the plausible range of vertical hydraulic conductivity applicable to semiconfining units that do not contain clay would be in the range of 0.1 to 1.0 ft/d (Hickey, 1982). For the semiconfining beds that contain clay between zones A and B, the vertical hydraulic conductivity could be on the order of 10^{-2} to 10^{-3} ft/d.

Data from Black, Crow, and Eidsness (1978) collected at the southwest St. Petersburg WRF injection site, show little difference between vertical and horizontal hydraulic conductivity in the semiconfining units. This data agrees with Stewart's (1966) data from equivalent strata in Polk County, which also show little or no difference between vertical and horizontal conductivity.

WATER QUALITY

Freshwater, saltwater, and a mixture of the two occur in the rocks underlying St. Petersburg. Saline ground water predominates; freshwater typically occurs as a thin layer above the saltwater. Freshwater is maintained by recharge from rainfall that infiltrates the rocks underlying St. Petersburg. Sources of saline ground water are probably the Gulf of Mexico, Tampa Bay, and residual seawater from the geologic past (Hickey, 1982). Hydrodynamic dispersion or mechanical mixing is the dominant process associated with the spreading of the solute.

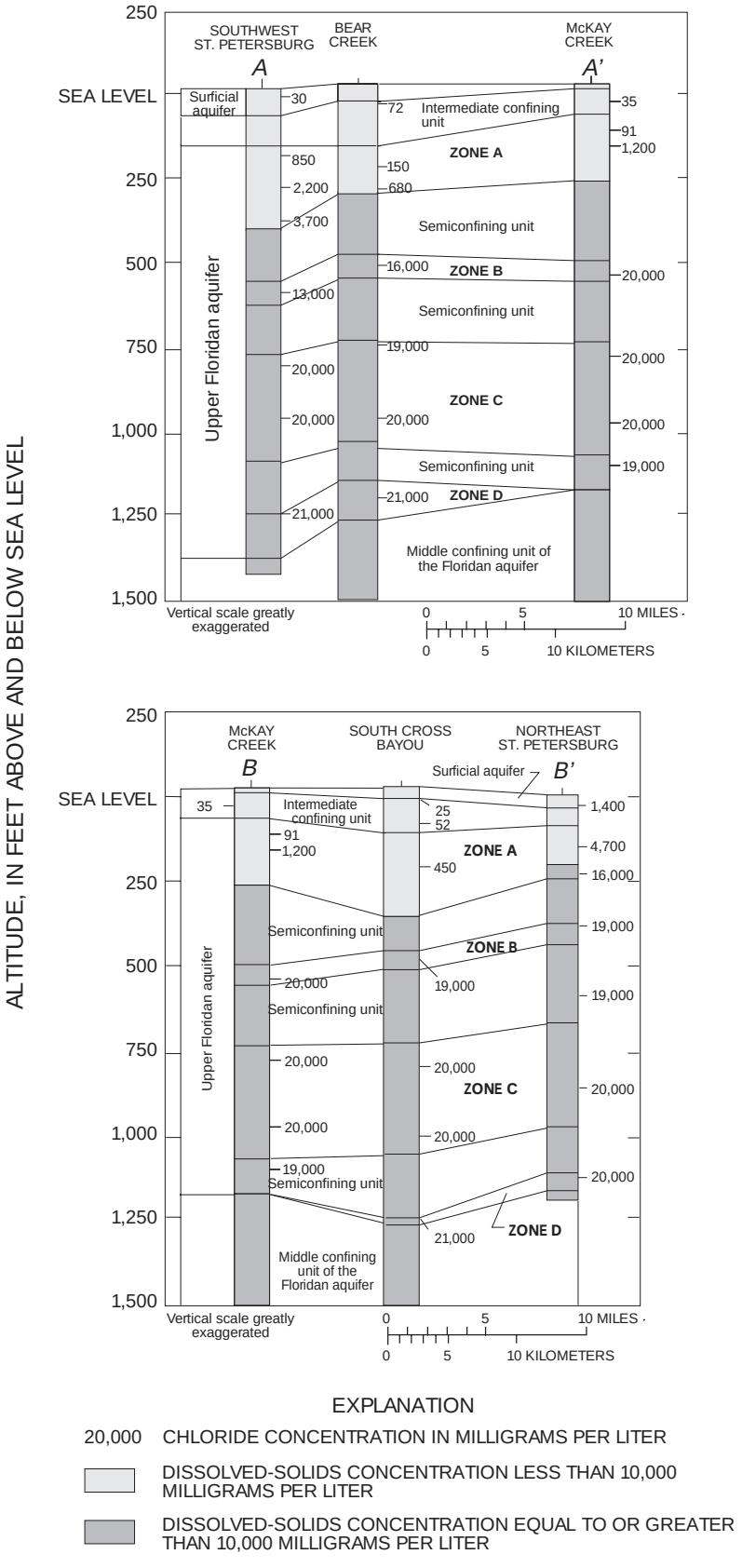

Figure 3. Vertical sections A-A' and B-B' showing chloride and dissolved-solids concentration in ground water. (Modified from Hickey, 1982.)

Native Ground Water

Water within the Upper Floridan aquifer is more mineralized than water from the surficial aquifer. Figure 3 shows vertical and lateral profiles of chloride and dissolved solid concentrations in ground water along lines A-A' and B-B'. Chloride concentrations in water from the surficial aquifer range from 30 to 1,400 mg/L. Chloride concentrations in water from zone A range from 91 to 16,000 mg/L and in water from zones B through D from 13,000 to 21,000 mg/L. Water in zones C and D is comparable to seawater.

The salinity of water within rocks comprising zone A varies both vertically and areally. Freshwater, where present, is typically in a thin lens at the top of the zone. Dissolved-solids concentrations increase with depth. Ground water near the coastal margins of St. Petersburg have higher concentrations in both the upper and lower parts of zone A. The vertical variation in water quality suggests that water in zone A is density stratified (Hickey, 1982).

Water-quality characteristics of zone A at each of the city's four WRF's are shown in table 1 (CH2M Hill, 1993). Most water in zone A is slightly to moderately saline with DS concentrations ranging from 2,520 to 32,900 mg/L. Waters of zone A generally are a sodium choride type (fig. 4).

Effluent

Effluent at each of the city's four WRF's is aerated, filtered, and chlorinated reclaimed wastewater. The water quality of the effluent is variable due to differences in the influent (incoming waste) and the treatment processes at each WRF (table 1). The average pH is about 7 and the effluent contains low concentrations of suspended solids (less than 3.0 mg/L). The DS and chloride concentrations range between about 400 to 900 mg/L and about 125 to 350 mg/L, respectively. All waters are a sodium chloride type (fig. 4).

A. WELLS OPEN TO ZONE A

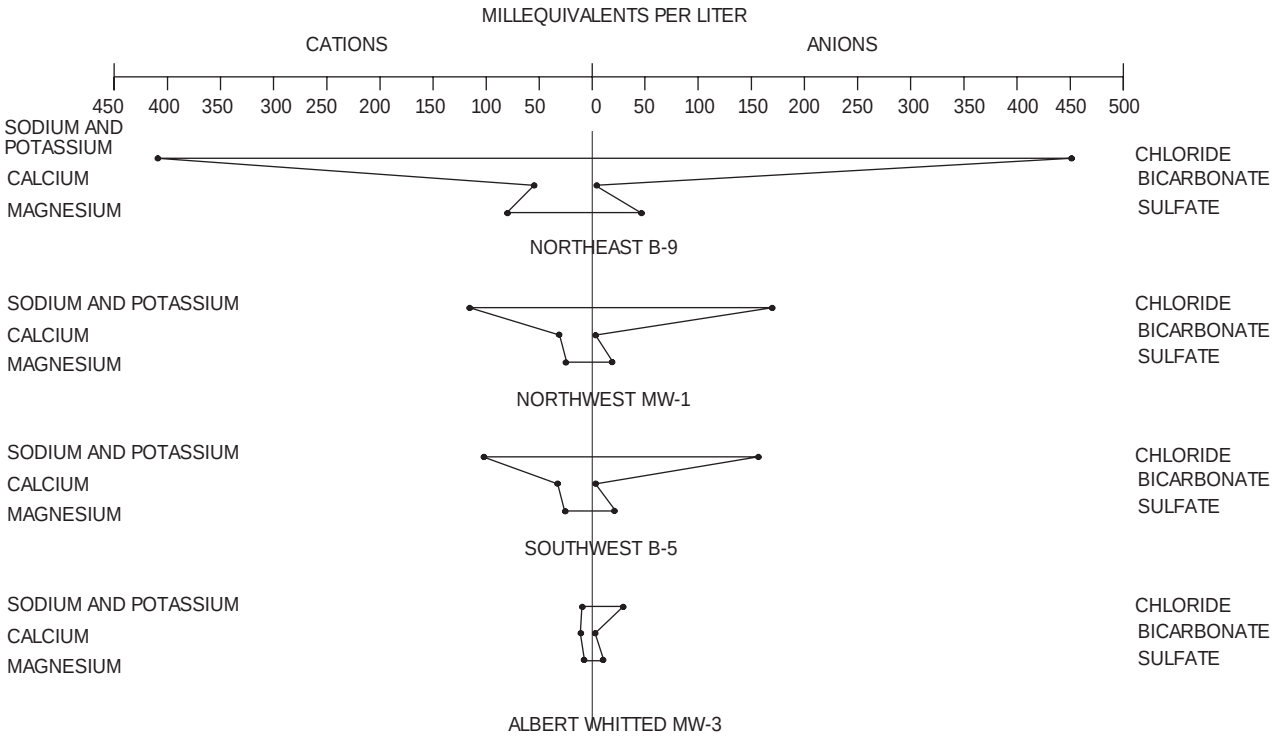

B. EFFLUENT

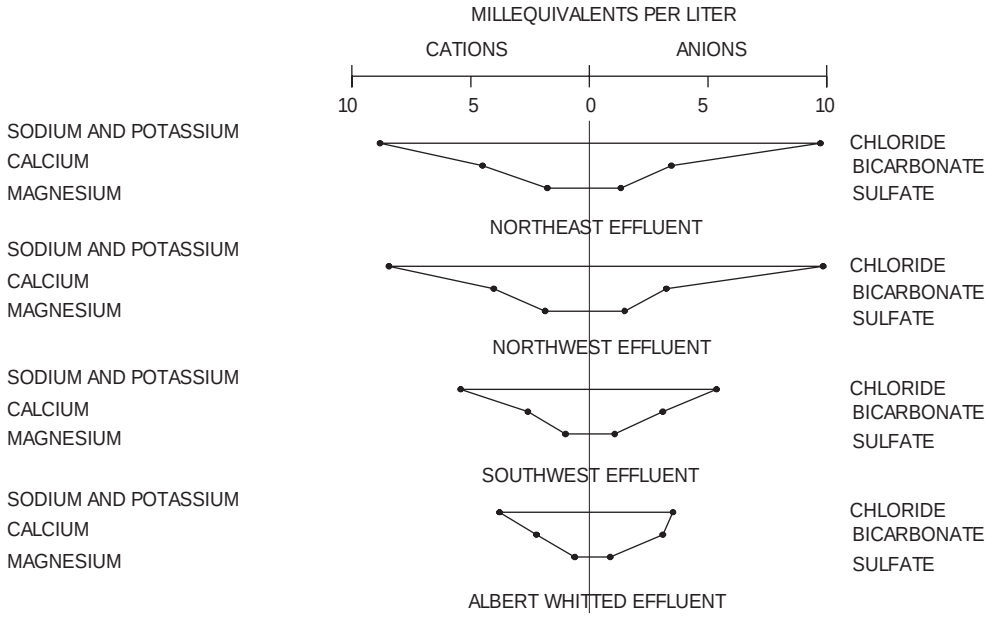

Figure 4. Chemical composition of water at the city of St. Petersburg's water reclamation facilities. (A) selected wells open to zone A, and (B) effluent.

Table 1. Chemical composition and saturation indices of ground water from zone A and effluent at the city of St.Petersburg water reclamation facilities

[<, less than, --, no data. Chemical analysis expressed in milligrams per liter except as noted; °C, degrees Celsius; µS/cm, microsiemens per centimeter]

	Ground water				Effluent[2]			
	Northeast well B-9[1]	Northwest well MW-1[2]	Southwest well B-5[2]	Albert Whitted well MW-3[3]	Northeast	Northwest	Southwest	Albert Whitted
Parameter								
Temperature (°C)	26.2	24.7	24.9	--	25.2	25.5	25.8	26.4
Specific conductance (µS/cm)	44,800	17,800	22,400	4,400	1,613	1,610	1,100	844
Dissolved solids	32,900	11,600	11,400	2,520	888	882	574	412
pH (units)	6.7	7.03	6.88	7.17	6.92	7.15	7.16	7.17
Calcium (Ca)	1,100	623	653	229	90.3	80.8	52.0	44.8
Magnesium (Mg)	980	296	318	84.8	21.6	22.7	12.3	7.62
Sodium (Na)	9,300	2,640	2,350	222	197	187	119	83.1
Potassium (K)	200	34	29	10.5	9.8	12	9.7	6.9
Chloride (Cl)	16,000	6,040	5,540	1,050	345	349	190	125
Sulfate (SO_4)	2,200	938	1,060	546	63.7	71.5	51.2	42.2
Bicarbonate (HCO_3)	160	202	188	161	211	198	189	189
Fluoride (F)	0.0	0.29	0.35	0.23	0.64	0.60	1.03	0.77
Total nitrogen (N)	0.61	3.3	3.4	--	12.9	11.6	8.2	19.4
Total phosphorous (P)	0.26	<0.04	<0.01	--	1.66	0.64	1.57	0.43
Saturation indices[4]								
Calcite	-0.258	0.154	-0.003	0.001	-0.351	-0.339	-0.192	0.360
Dolomite	-0.146	0.361	0.061	-0.063	-0.966	-0.942	-0.575	-1.121
Anhydrite	-0.441	-0.725	-0.647	-0.958	-2.005	-2.229	-1.993	2.325
Aragonite	-0.400	0.010	-0.147	-0.143	-0.495	-0.482	-0.336	-0.503
Gypsum	-0.251	-0.509	-0.432	-0.741	-1.789	-2.020	-1.780	2.121

[1]Chemical analyses from Hickey, 1982, table 5.
[2]Chemical analyses from CH2M Hill, 1993, table 5.2.
[3]Chemical analyses from Post, Buckley, Schuh & Jernigan, Inc., 1989, appendix 6.
[4]Log [ion activity proudct/equilibrium constant].

Geochemical Interactions

The injection of water into an aquifer having water of different quality than the injected water may change local conditions, resulting in geochemical interactions that lead to changes in water-quality and aquifer properties. Mixing of two waters of different chemical character may produce chemical reactions that could precipitate minerals, thus, reducing transmissivity and porosity; dissolve minerals, thus, increasing transmissivity and porosity, or the injected water may be in equilibrium with the aquifer minerals and native water, resulting in no chemical reactions.

The potential for a chemical reaction can be determined by calculating the chemical equilibrium of the injected and aquifer waters. The equilibrium state of the water with respect to a mineral phase can be determined by calculating a saturation index (SI) using analytical data. The SI is defined as the logarithm of the ratio of the ion activity product to the mineral equilibrium constant at a given temperature. If SI is equal to zero (0), the water is in equilibrium with the mineral; if it is less than 0, the water is undersaturated and if present, that mineral will dissolve; if the ratio is greater than 0, the water is supersaturated and mineral precipitation would be possible. Because of uncertainties in analytical and thermodynamic constants, a water with a SI value between 0.1 and -0.1 is assumed to represent saturation conditions or is in equilibrium with respect to the mineral phase (Swancar and Hutchinson, 1992).

The SI for the resident native waters and for the effluent, with respect to minerals commonly found in carbonate aquifers, was calculated using the computer program WATEQF (Plummer and others, 1976) and values are given in table 1. The values in table 1 show that most of the native ground water is saturated to supersaturated with respect to calcite and dolomite, and undersaturated with respect to the remaining minerals. The ground-water sample for the northeast WRF was undersaturated with respect to calcite and dolomite. This water has a very high concentration of DS and probably is residual seawater. The effluent is undersaturated with respect to all minerals; therefore, these waters apparently could dissolve minerals including calcite and dolomite, the principal minerals that compose carbonate aquifers.

The mass-balance model PHREEQE (Parkhurst and others, 1980) was used to simulate the geochemical reactions that may occur when effluent is mixed with native ground waters. PHREEQE is a generalized aqueous speciation, solubility, mass-transfer computer code that can simulate several types of reactions including the mixing of two waters of different chemical compositions. Modeled reactions were evaluated based on the equilibrium state of a 50 percent mix of the two water types with respect to selected mineral phases. Two simulations were made: The first model run simulated effluent from the Albert Whitted WRF entering the aquifer monitored by well MW-3. The second model run simulated effluent from the southwest WRF entering the aquifer monitored by well B-5. Results of the simulations indicate that the mixed effluent and ground water would be undersaturated with respect to all minerals (table 2). These data infer that the injected effluent, upon entering the aquifer and mixing with the aquifer waters, may dissolve calcite and dolomite. This process could produce a more porous limestone with increased transmissivity.

Table 2. Selected saturation indices from PHREEQE model results

Saturation indices	Model 1 [1]	Model 2 [2]
Calcite	-0.459	-0.122
Dolomite	-1.185	-0.068
Anhydrite	-2.324	-1.005
Aragonite	-0.645	-0.309
Gypsum	-2.116	-0.794

[1] Effluent at Albert Whitted facility entered the aquifer monitored by well MW-3.

[2] Effluent at Southwest facility entered the aquifer monitored by well B-5.

SIMULATION OF SUBSURFACE STORAGE AND RECOVERY OF TREATED EFFLUENT

A finite-difference cylindrical-flow model of ground-water movement and solute transport was used as a simulation tool to determine the recovery efficiency of a prototype SSR system for a moderately transmissive, slightly to moderately saline aquifer, underlying St. Petersburg. Specific questions to be answered are: (1) In what quantitative fashion will the physical and operational variables influence recovery efficiency?, and (2) Will recovery efficiency improve when SSR is conducted as a multiple-cycle operation?

To answer these questions, HST3D was used to simulate a well in a hypothetical hydrogeologic section representing St. Petersburg. The analysis implemented a conceptual modeling approach (Merritt, 1985), in comparison to a calibration and predictive approach (Merritt,1994), as no data exist for comparison with model results. This type of analysis permitted many combinations of conditions that could be investigated using parameters generally similar to those of the aquifer system underlying St. Petersburg. Sensitivity tests were used to examine the response of the model to a range of hydrogeologic and fluid properties and the effect of various injection/withdrawal schemes on the recovery efficiency of the SSR system.

Numerical Model

The HST3D model (Kipp, 1987) is a computer program written in FORTRAN-77 that simulates variable density fluid movement and transport of either dissolved substances or energy in the subsurface. The model, as used in this report, solves for two interdependent variables: pressure and mass-fractional concentration in cylindrically symetrical coordinates under isothermal conditions. Backward-in-space and backward-in-time finite-difference equations were used for solution of ground-water flow and the solute-transport equations in the numerical model. The reader is referred to Kipp's (1987) report for a complete discussion of the model code and numerical methods.

Design of Base Model

A base model used as a standard for comparisons for subsequent sensitivity analyses was designed to be representative of the slightly to moderately saline artesian limestone aquifer underlying St. Petersburg. Hydraulic and solute properties used in the model are representative of the city's four WRF injection sites and, as such, do not represent any specific location in St. Petersburg. Data were obtained from previous studies and laboratory values reported in text books.

To apply the HST3D model, the hydrologic and hydrogeologic characteristics of the aquifer system in St. Petersburg was simplified into the rectangular section in figure 5. The cylindrical-flow base model simulates the intermediate confining unit, permeable zone A, and the lower semiconfining unit. It consists of 26 variable-width node spacings in the vertical direction and 88 variable-width node spacings in the radial direction. The model dimensions are 2,500 horizontal ft and 420 vertical ft. The vertical spacing ranges from 10 to 50 ft. Radial spacing expands logarithmically from 0.14 ft at the well up to a maximum of 50 ft. The base model was used as the reference for sensitivity testing.

Several simplifying assumptions were made in the conceptualization and simulation of the flow system:

1. The aquifer system is homogeneous and isotropic in all directions,
2. Hydrostatic conditions initially prevail,
3. Regional horizontal and vertical flow is negligible,
4. A uniform native fluid density exists within each model layer,
5. The water-quality profile is laterally homogeneous throughout the model area,
6. The viscosities of the injected and native fluids are the same, and
7. Dispersivity is constant throughout each model layer.

Model Parameters

The strategy for the model analysis was to choose parameter values that, even though nonunique, would approximate conditions representative of the system so that the major processes affecting the mass fraction distribution during injection and withdrawal would be simulated. The parameters simulated in the model include boundary conditions, matrix properties, fluid properties, and well characteristics. A description of each model parameter follows:

1. Boundary conditions.--Boundary conditions are used to constrain the lateral and vertical extent of the simulated flow system providing a simplified representation of the flow and transport processes at the model limits. The top and bottom boundaries of the model are specified pressure boundaries because the producing zones are very permeable relative to the entire Floridan aquifer system (Knochenmus and Thompson, 1991). Pressure on the upper boundary is set at 12.967 lb/in^2, equivalent to the pressure exerted from an overlying 30 ft column of freshwater presumed to exist in the overlying hypothetical surficial aquifer. Pressure on the lower boundary is 195.719 lb/in^2, equivalent to the pressure exerted from a 450-ft column of freshwater and saline water presumed to exist in the overlying formations. The inner radial edge is defined by

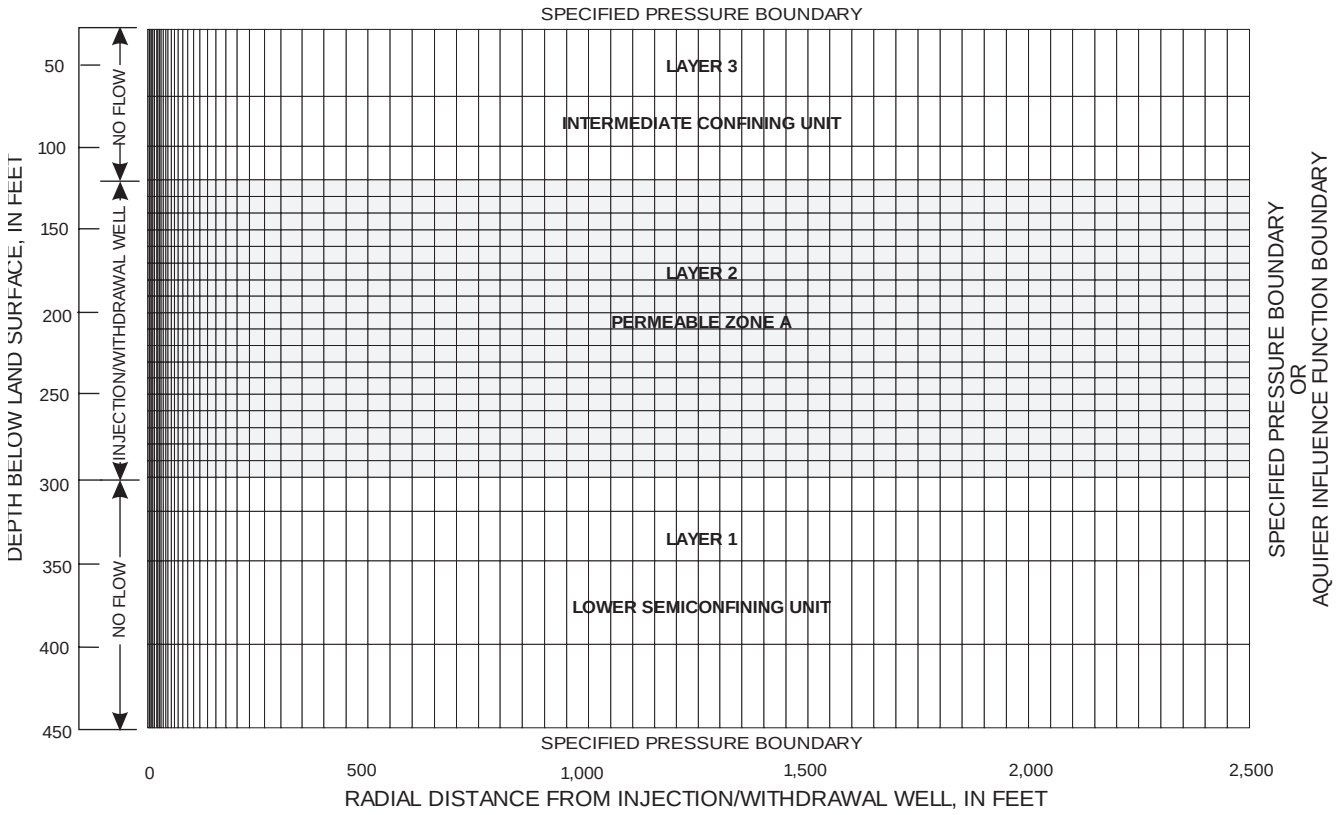

Figure 5. Radial-model grid, boundary conditions, and model layering.

the injection/production well in zone A and a no-flow boundary condition for the confining units above and below the well. The outer radial edge is specified pressure for the single 30-day test cycle and hydrostatic pressures at each node are based on a column of water having DS concentration specified as a function with depth. Water that enters the section at a given node as a result of a pressure gradient at the boundary is of specified concentration; water that exits at such a node is of ambient aquifer concentration. For the multiple-test cycles, the outer radial edge is defined by a transient flow, aquifer influence function (AIF). AIF utilizes the Carter-Tracy approximation (Kipp, 1987) to compute flow rates between the inner gridded aquifer region and an infinite homogeneous outer region where aquifer properties are known only in a general sense. The radius of the inner region was set at 2,500 ft and the outer region is modeled as an infinite cylinder with a height of 420 ft. Initial hydrostatic pressures throughout the model were set based on the boundary conditions.

2. Matrix properties.--Matrix properties are defined for each of the three hydrogeologic layers for the model in table 3. The porous media properties are intrinsic permeability, matrix compressibility, effective porosity, longitudinal dispersivity, and transverse dispersivity. Intrinsic permeability was calculated from hydraulic conductivity values reported by Hickey (1982), with conversion factors from Freeze and Cherry (1979, p. 29). Values of hydraulic conductivity and matrix compressibility were based on aquifer tests and laboratory tests of limestone samples collected during previous studies. The value of porosity used in this model, 0.3, is an estimate based on geophysical logs at the WRF injection sites in St. Petersburg. Longitudinal (α_L) and transverse (α_T) dispersivities of the system were set at 12.5 ft and 2.5 ft, respectively. Even though the spatial gridding stability rule-of-thumb criteria recommended in Voss (1984, p. 232), suggest that α_L and α_T be greater than one-fourth and one-tenth of the radial and vertical spacings, an acceptable solution was computed using an α_T value equal to 2.5 ft.

Table 3. Fluid and matrix properties assumed for simulation

[^{o}F, degrees Fahrenheit; lb/ft^3, pounds per cubic foot; in^2/lb, inch squared per pound; ft^2/d, foot squared per day; ft/d, foot per day; ft^2; foot squared]

Parameter	Lower semi-confining unit	Zone A	Intermediate confining unit
Fluid properties			
Temperature (^{o}F)	75.0	75.0	75.0
Specific weight (lb/ft^3)	63.177	62.468	62.241
Viscosity (centipoise)	0.8904	0.8904	0.8904
Fluid compressibility (in^2/lb)	3.03E^{-6}	3.03E^{-6}	3.03E^{-6}
Molecular diffusivity (ft^2/d)	9.30E^{-5}	9.30E^{-5}	9.30E^{-5}
Scaled mass fraction	1.0	0.25	0.025
Matrix properties			
Hydraulic conductivity (ft/d)	1.0	167.0	8.0E^{-4}
Intrinsic permeability (ft^2)	3.877E^{-12}	6.475E^{-10}	3.102E^{-15}
Porosity (unitless)	0.3	0.3	0.3
Longitudinal dispersivity (feet)	12.5	12.5	12.5
Transverse dispersivity (feet)	2.5	2.5	2.5
Matrix compressibility (in^2/lb)	6.2E^{-6}	6.2E^{-6}	6.2 E^{-6}

3. Fluid Properties.-- The fluid properties of the native formation water assumed for the simulations are listed in table 3 and include temperature, specific weight, viscosity, compressibility, molecular diffusivity, and DS expressed as scaled-solute mass fraction (SSMF). The model was simplified with the assumption of a vertically uniform initial DS concentration distribution assigned to each layer although a vertical salinity gradient has been documented. Isothermal conditions at 75^{o}F were assumed to prevail. Fluid densities assigned to injected and native waters were based on the measured or estimated concentration of DS in each fluid. Viscosity of the injected and native formation waters vary with temperature and solute fraction. Because isothermal conditions were assumed to prevail and because the viscosity of freshwater and saltwater differ by only 0.06 centipose, viscosity was assumed invariant in the simulations. The assigned value of viscosity was held constant at 0.8904 centipose (viscosity of pure water at 75^{o}F). Compressibility of water was held constant at 3.03x10^{-6} in^2/lb (Freeze and Cherry, 1979, p. 52), and molecular diffusivity of the solute in the porous media was set at 9.30x10^{-5} ft^2/d (Kimbler and others, 1975). The model SSMF is a dimensionless relative solute-concentration term ranging in value from 0 to 1. Any fluids present within the aquifer system, or entering it in simulation exercises, are considered to be a mixture of the two fluids by the appropriate specification of SSMF values. SSMF = 0 was used to represent pure freshwater, and SSMF = 1 represents the most saline water residing within the aquifer system, that in the lower confining unit. The assigned densities of 62.241 lb/ft^3 (SSMF = 0) and 63.177 lb/ft^3 (SSMF = 1) at 75^{o}F and atmospheric pressure were obtained from a standard handbook (Chemical Rubber Company, 1982). The SSMF values of the injected effluent, the water of the aquifer system, and water in mixtures of effluent and native formation waters are assigned based on their salinity relative to the two extremes. SSMF values of 0.025 (500 mg/L DS) and 0.25 (5,000 mg/L DS), representing the composite background water quality collected at the WRF injection sites, were assigned to the intermediate confining unit and zone A, respectively, based on the ratio of DS concentration to the estimate DS concentration of the lower confining unit. Measured injected-water DS concentration was about 700 mg/L and was assigned a SSMF value of 0.035.

4. Well information.--The well occurs at the first column of nodes and the open-hole interval of the well is defined by row numbers. Injection and withdrawal of effluent is through 18 nodes distributed vertically which, when combined, represent permeable zone A (180-ft interval). Injection and withdrawal flow at the well bore is allocated over rows 5 to 23 by mobility factors that are based on cell position, relative hydraulic conductivity, and an element completion factor. An element completion factor of 0 means the well is cased off from the aquifer in that element, whereas an element completion

factor of 1 means equivalent flow across the cell length.

Effects of Hydrologic Parameter Variations on Recovery Efficiency

When the results of a simulation study are largely based upon assumed estimates of data rather than measured data, as in this case, determining the effect of parameter variations on simulation results is of particular interest. To learn which properties and conditions substantially affect recovery efficiency, a series of simulation runs were made that started with the base model. For each simulation run, the value of an individual model parameter was changed by an amount that it might reasonably be expected to vary from the value used in the base simulation, then noting the change in recovery efficiency as a result of the change. The base simulation used as a standard for comparison consisted of a single cycle of 15 days of injection of effluent at a rate of 1.0 Mgal/d at a temperature of 75°F and a maximum of 15 days of withdrawal at a rate of 1.0 Mgal/d. Thus, one injection/withdrawal cycle is completed in 30 days. Withdrawal was assumed to end when the increasingly saline water exceeded the maximum DS concentration (1,500 mg/L) deemed acceptable for irrigation use. For the base model, a DS concentration of 1,500 mg/L was reached in 3 days. The recovery efficiency calculated for the base model single 30-day cycle simulation is 20.0 percent.

The effect of parameter changes on recovery efficiency is presented in the following sections. Discussion of individual parameters is ordered from most to least sensitive.

Resident Fluid Dissolved-Solids Concentration of Zone A

A series of sensitivity tests were used to show the relation between recovery efficiency and resident fluid DS concentration of the injection zone (zone A). Two resident fluid DS concentrations of zone A were selected for comparison with the 5,000 mg/L base value: (1) 2,300 mg/L, an arbitrary value representing water somewhat less saline than the composite base value, and (2) 20,000 mg/L, representing the most saline layer in the model. Relations were established for a range of α_L and α_T combinations. DS concentrations simulated for the base model were 500 mg/L for the intermediate confining unit, 5,000 mg/L for zone A, and 20,000 mg/L for the lower semiconfining unit.

Because of the lack of local field data to indicate the degree of dispersion in the carbonate system, three additional dispersion values (sets of longitudinal α_L and transverse α_T dispersivities representing some hypothetical degree of dispersion) were chosen to compare to the dispersion used in the base model. The additional dispersion values used for analysis are summarized below:

Dispersion value set	α_L (ft)	α_T (ft)
1	4.0	1.0
2	25.0	1.0
3	25.0	5.0

Dispersion value set 1 is a low degree of dispersion in the radial flow direction and a low degree of interlayer dispersion. Value set 2 introduces an appreciable degree of dispersion in the radial flow direction. Value set 3 represents appreciable degrees of dispersion in the radial flow direction and between layers.

Figure 6a shows the decline of recovery efficiencies with increasing resident fluid DS concentration for the various dispersivity combinations. The larger the DS difference between the injected water and resident formation water, the less efficient the SSR process. Recovery efficiency was shown by the model to be significantly less in aquifers of high salinity than in slightly saline aquifers. With higher resident fluid DS concentration, less water within the zone of mixing is acceptable for withdrawal. Higher DS concentrations also make density stratification of the fluids more likely to occur at a given permeability level, decreasing recovery efficiency. Recovery efficiency was shown to be greater when the level of dispersive mixing decreased, or such as when a smaller volume of injected fluid combines with more saline native formation water. Thus, recovery efficiency is most promising when resident fluid DS concentrations are low, and least promising when DS concentrations are high.

Dispersivity

Dispersivity is a scale-dependent property of the porous medium that controls the mixing of injected and resident formation fluids at their interface. When dispersivities are increased, there is more mixing that results in a widening of the transition zone between the injectant and native formation waters.

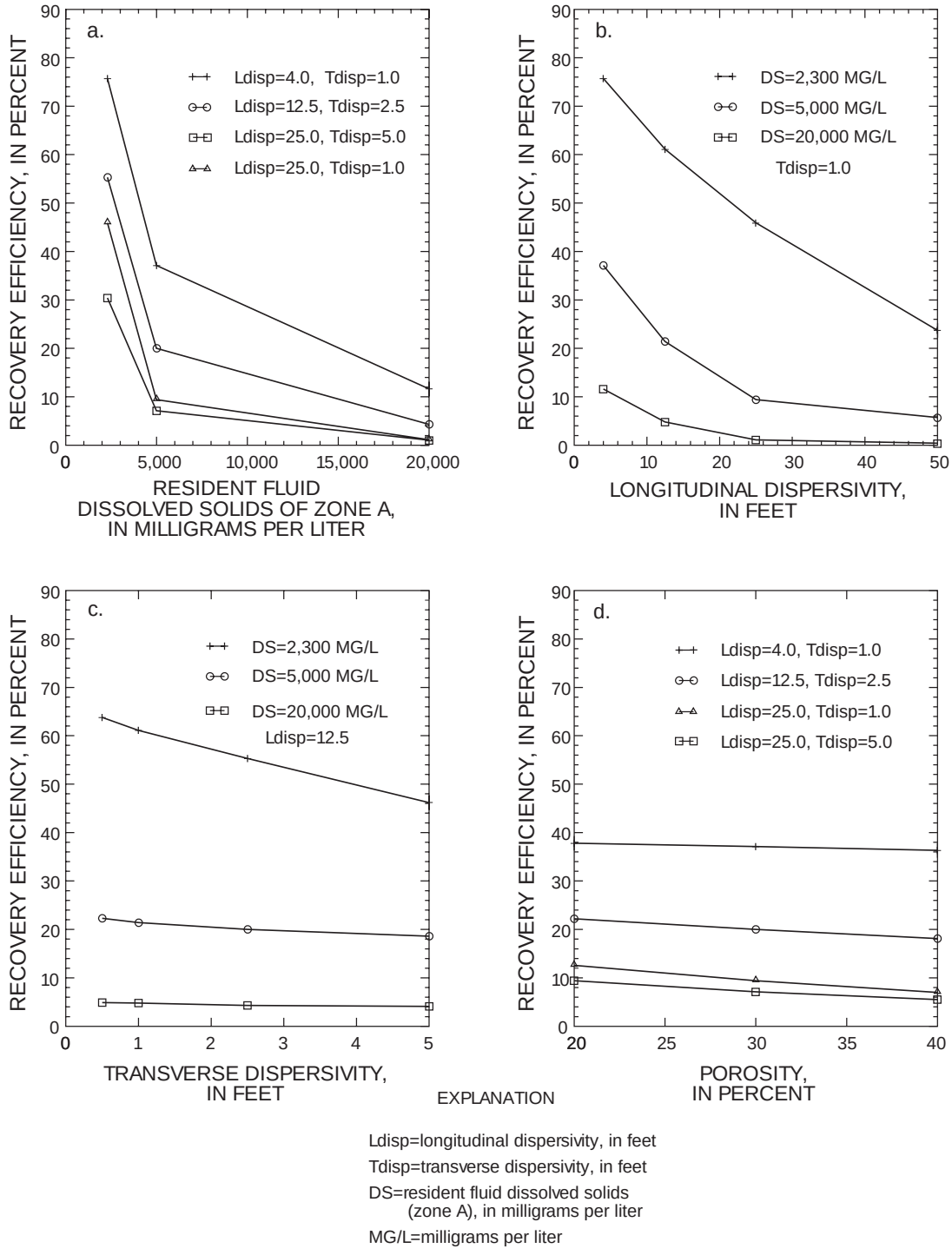

Figure 6. Relation between recovery efficiency and variations in selected model parameters.

Dispersion is a deleterious process that can severely limit recovery efficiency. Merritt (1985) reported that recovery efficiency is limited when the upper limit of the concentration of some constituent considered acceptable in recovered water is less than half of the average concentration of the injected and native formation waters. In the hypothetical test case posed in this analysis, the acceptable limit for DS concentration (1,500 mg/L) was equal to or less than the average of the injected water (700 mg/L) and the native water (2,300 to 20,000 mg/L).

Various values of dispersion in the direction of flow (longitudinal) and interlayer (transverse) were tested. Values of α_L were varied between 4 and 50 ft with respect to 12.5 ft in the base model, and values of α_T were varied between 0.5 and 5.0 ft with respect to 2.5 ft in the base model, when the rate and duration of injection and withdrawal was kept constant.

Figure 6b and c illustrates the results from the analysis for the three previously cited resident fluid DS concentrations (2,300, 5,000, and 20,000 mg/L). Results show the decline of recovery efficiency as the dispersivity value increases. A large decrease of recovery efficiency is shown as α_L increases from low values of α_L, but the rate of decrease is small at larger values of α_L. Recovery efficiency was slightly affected by changes in α_T at low ranges of the parameter but at higher ranges, recovery efficiency was relatively unaffected by its variation. Evidently, for every resident fluid TDS concentration, there are values of α_L and α_T above which recovery efficiency is significantly reduced

Porosity

Porosity of the injection zone (zone A) was tested at 0.2 and 0.4 to bracket the base model value of 0.3. Permeability and porosity control the velocity of injectant flow and, hence, the rate of solute transport. The greater the porosity, the slower the solute front will move; thus, the longer the time it takes to replace the volume of native formation water in a given volume of aquifer and the greater the dispersive mixing. Low porosity has the opposite effect.

Figure 6d illustrates the variation of recovery efficiency due to porosity changes in relation to the four previously cited dispersivity combinations. Increasing porosity caused recovery efficiency to decrease slightly for each dispersion model. Recovery efficiency decreased significantly, however, as the level of dispersive mixing increased.

Horizontal and Vertical Permeability of Zone A

The permeability of the aquifer material and the density contrast of the injected and native water determines whether an appreciable level of density stratification or buoyancy flow can occur. Density stratification refers to the physical process in which less dense injected fluid rises and flows over the more dense fluid. Generally, low permeability reduces stratification and optimizes recovery efficiency.

Values of horizontal (k_h) and vertical (k_v) permeability were changed simultaneously by the same factor that ranged from 0.1 to 10, with all other parameters remaining the same. The ratio of k_h to k_v was held to 1. Results of the simulations are as follows:

k_h and k_v (multiplier)	Recovery efficiency (percent)
0.5	19.8
1.0	20.0
2.0	19.5
5.0	15.7
10.0	7.7

When permeability was doubled or halved, recovery efficiency was not affected. The major effect of the variation at these permeability values was the wellhead pressure required at the specified injection/withdrawal rate. However, when permeability was made 10 times greater, recovery efficiency was reduced by 61.5 percent. This is because simulation of a larger permeability allowed for easier horizontal and vertical transport of the injected fluid, which resulted in greater stratification and buoyancy flow that prevented complete mixing of the injected water with the native water. Upon withdrawal, a greater percentage of native water was immediately available to the well.

Ratio of Horizontal to Vertical Permeability

If flow conditions vary with direction in a geologic formation, the formation is anisotropic and differences in horizontal (k_h) and vertical permeability (k_v) can influence fluid movement. The greater the anisotropy ratio (k_h/k_v), the easier the salt front moves along the axis with the larger permeability component which contains the injected water within the open interval of the injection well. In the base model, permeability is equal in all directions. Anisotropy in the model only can be simulated by varying the ratio of k_h to k_v. To test for the effects of anisotropy on model results the ratio of k_h to k_v was varied from an isotropic base condition ($k_h/k_v = 1$) to kh/kv equal to 100. Results of the simulations are as follows:

k_h/k_v	Recovery effciency
1	20.0 percent
10	21.9 percent
100	23.6 percent

Simulation of different values of k_h/k_v had a small affect on computed recovery efficiencies. Increasing k_h/k_v caused recovery efficiency to increase slightly. This is because simulation of a larger k_h/k_v causes more lateral flow and inhibits upward movement of buoyant injectant.

Effects of Operational Factors on Recovery Efficiency

The success of a SSR system is determined by the quantity of injected water that can be recovered from an aquifer. The sensitivity analyses indicated the physical and chemical parameters that substantially affect recovery efficiency. In addition to these parameters, operational factors also will affect the recovery efficiency of the SSR system. These factors include the duration and rate of injection and withdrawal, plus well construction. A series of model simulations was performed to evaluate the response of the model to changes in these factors. The base values of hydraulic and fluid properties were used in all simulations. Modifications were made to the HST3D model to simulate the shutdown of the production well when the solute fraction of the withdrawn water reached 0.0745, corresponding to a DS concentration of 1,500 mg/L. The production well was shutoff until the scheduled beginning of the next simulation.

Duration of Injection and Withdrawal Cycle

Two series of multicycle model simulation tests were used to illustrate the effects of variations in the duration of injection/withdrawal cycles on recovery efficiency. The first series of tests consisted of 3 simulations of five uniform successive cycles (60, 180, and 365 days) of injection and withdrawal of 1.0 Mgal/d. The following schedules were simulated:

1. 30 days of injection followed by a maximum of 30 days withdrawal
2. 90 days of injection followed by a maximum of 90 days of withdrawal
3. 183 days of injection followed by a maximum of 182 days of withdrawal

Figure 7 shows the results of the first series of testing cycles for five successive 60-, 180-, and 365-day cycles. The plot indicates that recovery efficiency improves with each successive cycle for the various operational schemes even if the volume of injectant

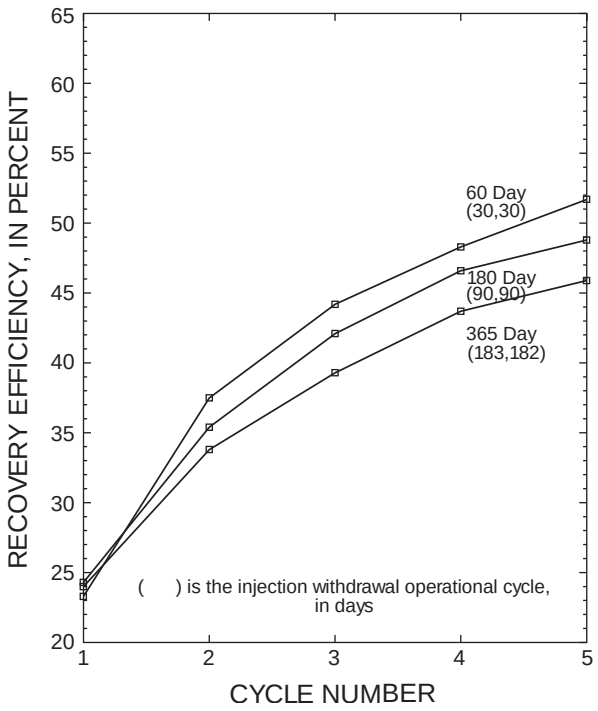

Figure 7. Recovery efficiencies for five successive 60-, 180-, and 365-day injection/withdrawal cycles at 1.0 million gallons per day. (Withdrawal in each cycle ceases when the dissolved-solids concentration of withdrawn water exceeds 1,500 milligrams per liter.)

does not increase. This is because of the continuous growth of the zone of dispersion (mixing zone) and the retarding effect of the zone of dispersion on the rate of gravitational segradation (Kumar and Klimbler, 1970). With each cycle, the zone of dispersion is greater due to mixing of the injectant with the residual water that was not completely recovered from the previous cycle. The graph also shows recovery efficiency increasing very rapidly in intitial cycles and then more slowly at later cycles for each operational schedule. After five cycles, recovery efficiencies ranged between 46 and 52 percent. Recovery efficiencies at the end of the first cycle had ranged between 23 and 24 percent.

Higher recovery efficienies were obtained for simulation tests when the duration of injection and recovery phases was shorter. This is expected because of the nature of the conceptual system in which migration of the solute particles across the low permeable units will reduce the recoverability for tests of longer duration (Quinones-Aponte and Wexler, 1995).

An operational SSR system would not function on uniform cycles but rather on irregular cycles based on seasonal surplus and demand. In the second series of tests, a hypothetical yearly schedule of injection and withdrawal was simulated. The schedule consisted of

five successive 1-year cycles of 4-months of injection, followed by a maximum of 3-months of withdrawal, followed by 3-months of injection, and finally followed by a maximum of 2 months of withdrawal. In St. Petersburg, the injection periods correspond to December through March and July through September (months when irrigation reuse is low), and the withdrawal periods might correspond to April through June and October through November (months when irrigation reuse is high).

Figure 8 shows the results of the second series of tests. The model conditions are similar to those previously described for the five successive 60-, 180-, and 365-day cycles. Recovery efficiencies range between 27 and 47 percent for the 0.5 Mgal/d simulations, 31 and 55 percent for the 1.0 Mgal/d simulations, and 37 and 62 percent for the 2.0 Mgal/d simulations. Results indicate that recovery efficiency approach an asymptote after several cycles, where for practical purposes, no improvement of recovey efficiency occurrs. For the 2.0 Mgal/d simulation the maximum recovery efficiency probably will be between 65 and 70 percent.

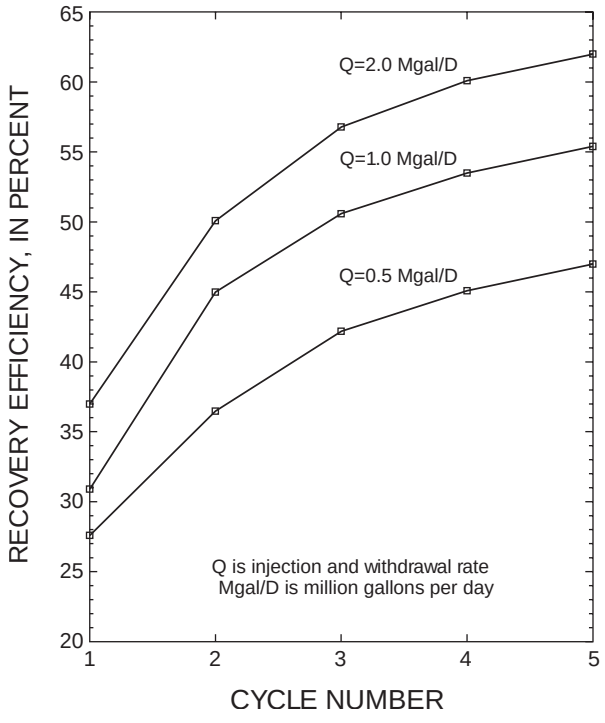

Figure 8. Recovery efficiencies for five successive 1-year cycles of 121 days of injection, 91 days of withdrawal, 92 days of injection, and 61 days of withdrawal at rates of 0.5, 1.0, and 2.0 million gallons per day. (Withdrawal in each cycle ceases when the dissolved-solids concentration of withdrawn water exceeds 1,500 milligrams per liter.)

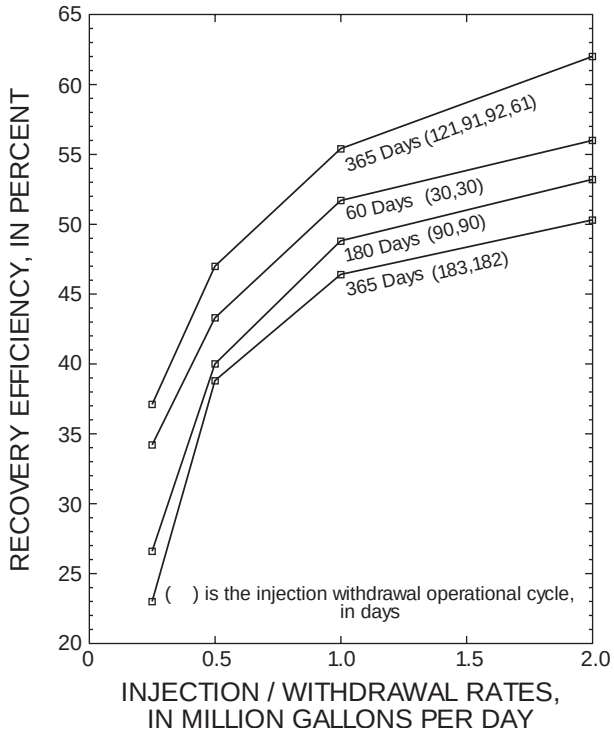

Figure 9. Recovery efficiencies after five cycles for various injection/withdrawal rates and operational schemes.

Rate of Injection and Withdrawal

The rate of injection and withdrawal for a fixed time period and for various operational schemes was varied from 0.25 and 2.0 Mgal/d to determine whether certain injection/withdrawal rates favor higher recovery efficiencies. Zero recovery efficiency would occur for a sufficiently small injection volume because of mixing. Results of the tests suggest that recovery efficiency is directly proportional to the injected flow volume. For a given operational scheme, recovery efficiency increases with higher volumes (fig. 9). There is a larger rate of increase of recovery efficiency at smaller volumes than at larger volumes. Recovery efficiencies after five cycles ranged between 50 and 62 percent for an injection/withdrawal rate of 2.0 Mgal/d and between 23 and 37 percent for an injection/withdrawal rate of 0.25 Mgal/d.

Partially Penetrating Well

Several well-completion designs were simulated to evaluate the effects of partial penetration. Operational wells may be open only to part of an aquifer; thus, it is of interest to compare the recovery

efficiency of a partially penetrating well with recovery efficiency of a well open to the full thickness. The recovery efficiency was expected to be higher in partially penetrating wells than for fully penetrating wells because a buffer zone of fresher water would exist between the pumped zone and the underlying water of poor quality. The simulated well penetrations ranged from 100 to 25 percent. The 25-percent penetration well is open to the upper 45 ft of layer 2. Results of the simulations are shown below:

Well penetration (percent)	Recovery efficiency (percent)
100	20.0
75	22.3
50	23.4
25	24.1

Simulations show a slight increase in recovery efficiency with a decrease in penetration depth. Merritt (1985) reported similiar results and suggests that recovery efficiencies in stratified aquifers may not be significantly affected if the well is open only to part of the aquifer. However, to generalize these results, a more-detailed study focusing on this aspect (injection into different flow zones) is needed.

SUMMARY AND CONCLUSIONS

A model-based study of the confined saline aquifer system underlying St. Petersburg is being conducted to analyze the hydrogeologic and operational aspects of underground injection, storage, and withdrawal of advanced secondary treated effluent in a single representative well. The study is specifically aimed toward (1) defining the hydrogeologic framework and ground-water quality in the study area, (2) assessing the geochemical interactions associated with the injection of effluent, and (3) applying a density-dependent, ground-water flow and solute-transport model to understand the relative importance of physical and chemical properties and operational variables on recoverability of injected effluent.

The sediments underlying the study area form a layered sequence of two aquifers and one confining unit. The framework includes the unconfined, surficial aquifer, and the confined Upper Floridan aquifer. The units are separated by the intermediate confining unit.

The surficial aquifer is composed of a layer of clastic deposits that is generally less than 30 ft thick. The aquifer is a source of recharge to the Floridan aquifer system and is primarily used as a source for lawn irrigation.

The intermediate confining unit is composed of clastic and carbonate sediments of Miocene and younger age. The carbonates are generally underlain and overlained by clays of relatively low permeability. Thickness of the unit averages about 90 ft and ranges from about 50 to 140 ft. The vertical hydraulic conductivity of the unit ranges from about 1.3×10^{-4} to 6.9×10^{-3} ft/d.

The Upper Floridan aquifer consists of a thick, regionally extensive sequence of Tertiary-aged carbonate rocks that comprise the following formations (in ascending order): Avon Park Formation, Ocala and Suwannee Limestones, and the Tampa Member of the Arcadia Formation which is part of the Hawthorn Group. The Upper Floridan aquifer underlying St. Petersburg contains four permeable zones separated by semconfining units. The zones are alphabetically labeled with increasing depth from A to D. The proposed receiving zone is within the uppermost part of the Upper Floridan aquifer (zone A) in the permeable limestone section of the Tampa Member of the Arcadia Formation of the Hawthorn Group and the Suwannee Limestone. Thickness of zone A averages about 180 ft and ranges from about 115 to 245 ft. Transmissivity of zone A ranges from 2.2×10^4 to 3.5×10^4 ft^2/d.

A semiconfining unit within the Suwannee Limestone is below the proposed injection zone and has a vertical hydraulic conductivity estimated to range from about 0.1 to 1.0 ft/d where the beds do not contain clay. Average thickness of this unit below the proposed injection zone is about 150 ft.

Limited fresh ground-water supplies exist in the Upper Floridan aquifer underlying St. Petersburg. Fresh ground water, where it is found, typically occurs as a thin layer within the uppermost permeable zone. Most water in the aquifer is saline with chloride concentration in the proposed injection zone ranging from 91 to 16,000 mg/L.

The chemical contrast between the injection and resident formation waters may lead to chemical reactions. The mix of the two water types would be understaturated with respect with calcite and dolomite. This might lead to dissolution of calcite and dolomite producing a more porous limestone with increased transmissivity.

A numerical model of variable density groundwater flow and solute transport (HST3D) was used to evaluate the importance of parameter variations affecting the recovery of effluent stored in a saline aquifer underlying the study area. The analyses consisted of a sensitivity testing approach, as opposed to the more familiar site-specfic calibration and prediction objective of modeling. Cyclic injection in a prototype aquifer was simulated and recovery efficiencies were calculated.

Sensitivity analyses were performed to determine changes in recovery efficiency when physical and chemical parameters of a base model are varied. The simulation cycle used as a standard for comparisons consisted of 15 days of injection of effluent at a rate of 1.0 Mgal/d and 15 days of withdrawal at a rate of 1.0 Mgal/d.

On the basis of computer simulations for hypothetical aquifer conditions, sensitivity tests for individual physical and chemical properties indicate:

1. The greater the density difference between the injected effluent and resident formation water, the lower the recovery efficiency during the first cycle. Higher salinity makes density stratification of the fluids more likely to occur at a given permeability level, thereby causing recovery efficiency to decrease.
2. Recovery efficiency decreases significantly as dispersivity increases. Dispersion is a deleterious process that can severely limit recovery efficiency.
3. Generally, high formation permeability causes poor recovery efficiencies. When the simulated permeability was increased by a factor of 10, recovery efficiency was reduced by 61.5 percent. This is because simulation of a larger permeability allowed for easier transport of the injected fluid, which resulted in greater stratification and buoyancy flow.
4. When the injection well was represented as open to only part of the aquifer, simulations show little difference as when the well was open to the entire aquifer.
5. For hypothetical conditions studied, porosity and anisotropy variations do not significantly alter recovery efficiencies.

The preliminary radial-flow and solute transport model also was used to examine the effects on recovery efficiency of hypothetical multicycle operations. Simulations consisted of five injection/withdrawal cycles of various duration and varying injection and withdrawal rates. Results of the simulations are:

1. Over the range of variables studied, the recovery efficiency per cycle increases with total number of cycles, provided that each recovery cycle phase ends when the DS concentration of withdrawn water reaches some prescribed value less than that of the more saline formation water. Thus, even though conditions may be such that recovery would be poor on the first cycle, the process should improve on subsequent cycles.
2. Recovery efficiencies increase rapidly during initial cycles and more slowly at later cycles. Recovery efficiencies may approach a maximum value after a number of cycles.
3. For a given operational scheme, recovery efficiencies increase with higher volumes of injected effluent. There is a larger rate of increase of recovery efficiency at small injection/withdrawal volumes than at larger injection/withdrawal volumes.

The operation of a single SSR well appears to be technically feasible under moderately favorable conditions. Model results indicate that recovery efficiencies from about 23 to 37 percent can be achieve for different SSR operational schemes. Five successive injection, storage, and recovery cycles and varying injection and recovery rates can increase the recovery efficiency to about 47 to 62 pecent. The recovery efficiency that will be attained, however, is highly dependent upon local physical and operational conditions. A combination of hydraulic, chemical, and operational parameters that minimize dispersion and buoyancy flow, maximizes recovery efficiency. The parameters that favor optimum recovery efficiencies are low aquifer water density and low to moderate permeabilities. SSR is most promising where native fluid density is low. The smaller the density contrast between resident formation water and injected water the better the recovery efficiency. A high injection rate and a small difference in density between the injected and resident formation waters should yield better results than a low injection rate and a large difference in density. Recoverability improves with successive cycles of injection, storage, and recovery even if initial recovery efficiency is low.

The results presented are preliminary and make up a part of the study in progress. Development of a fully three-dimensional variable density-ground-water flow and solute transport model is presently underway

to extend the analysis to multiwell systems for testing of large-scale injection. In a field application of the SSR process, a well field likely will be needed to handle the required inflow rates and wellhead pressures.

SELECTED REFERENCES

Black, Crow, and Eidsness, Inc., 1978, Drilling and testing of the monitoring and injection wells at Southwest Wastewater Treatment Plant for the city of St. Petersburg, Florida: Consultant's report in files of the city of St. Petersburg, Fla.

Brown, M.P., and Associates, 1986, Hydrological investigation for the development and management of the Floridan aquifer, city of Dunedin: Consultant's report in the files of the city of Dunedin, Fla.

Chemical Rubber Company, 1982, CRC Handbook of chemistry and physics (63rd ed): Boca Raton, Fla., CRC Press.

Cherry, R.N., and Brown, D.P., 1974, Hydrogeologic aspects of a proposed sanitary landfill near Old Tampa Bay, Florida: Florida Bureau of Geology Report of Investigations no. 68, 25 p.

CH2M Hill, 1993, Environmental risk and geochemical analysis related to the city of St. Petersburg's underground injection and monitoring system: Consultant's report in the files of the city of St. Petersburg, Fla.

Freeze, R.A., and Cherry, J.A., 1979, Groundwater: Englewood, N.J., Prentice-Hall, 604 p.

Geraghty and Miller, Inc, 1976, Management of the water resources of the Pinellas-Anclote and northwest Hillsborough basin, west-central Florida: Consultant's report in the files of the Southwest Florida Water Management District, Brooksville, Fla.

Heath, Ralph C., 1989, Basic ground-water hydrology: U.S. Geological Survey Water-Supply Paper 2220, 84 p.

Hickey, J.J., 1981, Hydrogeology, estimated impact, and regional well monitoring of effects of subsurface wastewater injection, Tampa Bay area, Florida: U.S. Geological Survey Water-Resources Investigations Report 80-118, 40 p.

———1982, Hydrogeology and results of injection tests at waste-injection test sites in Pinellas County, Florida: U.S. Geological Survey Water-Supply Paper 2183, 42 p.

Hickey,J.J., and Ehrlich, G.G., 1984, Subsurface injection of treated sewage into a saline-water aquifer at St. Petersburg, Florida--Water quality changes and potential for recovery of injected sewage: Ground Water, v. 22, no. 4, p. 397-405.

Hutchinson, C.B., and Stewart, J.W., 1978, Geohydrologic evaluation of a landfill in a coastal area, St. Petersburg, Florida: U.S. Geological Survey Water-Resources Investigations 77-78, 40 p.

Kimbler, O.K., Kazman, R.G., and Whitehead, W.R., 1975, Cyclic storage of freshwater in saline aquifers: Louisiana Water Resources Institute Bulletin 10, 78 p., with appendixes.

Kipp, K.L., 1987, HST: A computer code for simulation of heat and solute transport in three-dimensional ground-water flow systems: U.S. Geological Survey Water-Resources Investigations Report 86-4095, 519 p.

Knochenmus, L.A., and Thompson, T.H., 1991, Hydrogeology and simulated development of the brackish ground-water resources in Pinellas County, Florida: U.S. Geological Survey Water Resources Investigations Report 91-4026, 20 p.

Kumar, A., and Kimbler, O.K.,1970, Efffect of dispersion, gravitational segregation, and formation stratification on the recovery of freshwater stored in saline aquifers: Water Resources Research, vol. 6, no. 6., p. 1689-1700.

Merritt, M.L., 1985, Subsurface storage of freshwater in south Florida: A digital model analysis of recoverability: U.S. Geological Survey Water-Supply Paper 2261, 44 p.

———1994, Tests of subsurface storage of freshwater at Hialeah, Dade County, Florida, and digital simulation of the salinity of recovered water: U.S. Geological Survey Open-File Report 93-155, 150 p.

Miller, J.A., 1986, Hydrogeologic framework of the Floridan aquifer system in Florida and in parts of Georgia, Alabama, and South Carolina: U.S. Geological Survey Professional Paper 1403-B, 91 p., 33 pl.

Parkhurst, L.P., Thorstenson, D.C., and Plummer, L.N., 1980, PHREEQE - A computer program for geochemical calculations: U.S. Geologicial Water-Resources Investigations Report 80-96, 193 p.

Plummer, L.N., Jones, B.F.,and Truesdell, A.H., 1976, WATEQF--A FORTRAN IV version of WATEQ, a computer program for calculating chemical equilibrium of natural waters: U.S. Geological Survey Water-Resources Investigations Report 76-173, 70 p.

Post, Buckley, Schuh & Jernigan, Inc., 1989, Reverse osmosis pilot studies: Consultant's report in the files of the West Coast Regional Water Supply Authority, Clearwater, Fla.

Quinones-Aponte, Vicente, and Wexler, Eliezer J., 1995, Preliminary assessement of injection, storage, and recovery of freshwater in the lower Hawthorn aquifer, Cape Coral, Florida: U.S. Geoolgical Survey Water-Resources Investigations Report 94-4121, 102 p.

Robertson, A.F., and Mallory, M.J., 1977, A digital model of the Floridan aquifer north of Tampa, Florida: U.S. Geological Survey Water-Resources Investigations Report 77-64, 29 p.

Seaburn and Robertson, Inc., 1983, Results of hydrologic testing program for the city of Clearwater water supply investigation: Consultant's report in the files of the city of Clearwater, Fla.

Sinclair, W.C., 1974, Hydrogeologic characteristics of the surficial aquifer in northwest Hillsborough County, Florida: Florida Bureau of Geology Information Circular no. 86, 98 p.

Stewart, H.G., Jr., 1966, Ground-water resources of Polk County, Florida: Florida Geological Survey Report of Investigations 44, 170 p.

Swancar, A., and Hutchinson, C.B., 1992, Chemical and isotopic composition and potential for contamination of water in the Upper Floridan aquifer, west-central Florida: U.S. Geological Survey Open-File Report 92-47, 47 p.

Voss, C.I., 1984, A finite-element simulation model for saturated-unsaturated, fluid-density-dependent ground-water flow with energy transport or chemically-reactive single-species solute transport: U.S. Geological Survey Water-Resources Investigations Report 84-4369, p. 54-55.

APPENDIX

APPENDIX: LISTING OF MODEL INPUT FILE

A sample input-data listing is provide for the single cycle base simulation of 15 days of injection at 1.0 million gallons per day followed by 15 days of withdrawal at 1.0 million gallons per day. The listing contains 276 lines, of which 147 lines are comments that aid construction of the data file. Critical comments are keyed to input record descriptions of Kipp (1987). The following order generally is observed for data input: (1) fundamental and dimensioning information, (2) spatial geometry and mesh information, (3) fluid properties, (4) porous medium properties, (5) source information, (6) boundary condition information, (7) initial condition information, (8) calculation parameters, and (9) out specifications.

SAMPLE INPUT FILE: INJECT 1 MGAL/D FOR 15 DAYS FOLLOWED BY 15 DAYS

OF WITHDRAWAL AT 1 MGAL/D

```
C.....HST Data-Input Form

C.....UNRELEASE 2.0
C-------------------------------------------------------------------------------
C.....Start of the data file
C.....Specification and dimensioning data - READ1
C.1.1 .. TITLE LINE 1
Permeable Zone A simulation for St.Pete--1 Mgal/d injection followed by 1 Mgal/d
C.1.2 .. TITLE LINE 2
withdrawal--3 layers--initial mass fraction zone A = 0.25 (5000 TDS-2375 Cl)
C.1.3 .. RESTRT[T/F],TIMRST
F 0.0
C.1.4 .. HEAT[T/F],SOLUTE[T/F],EEUNIT[T/F],CYLIND[T/F],SCALMF[T/F]
F T T T T
C.1.5 .. TMUNIT[I]
4
C.1.6 .. NX,NY,NZ,NHCN
88,1,26,0
C.1.7 .. NSBC,NFBC,NAIFC,NLBC,NHCBC,NWEL
1 0 0 0 0 1
C.1.8 ..SLMETH[I]
1
C-------------------------------------------------------------------------------
C.....Static data - READ2
C.....Coordinate geometry information
C.....  Cylindrical coordinates
C.2.2B.1A .. R(1),R(NR),ARGRID[T/F];(O) - CYLIND [1.4]
1. 2500. F
C.2.2B.1B .. R(I);(O) - CYLIND [1.4] and NOT ARGRID [2.2B.1A]
   1.00   1.14   1.30   1.49   1.70   1.94   2.22   2.53    2.89    3.31
   3.78   4.31   4.92   5.62   6.42   7.33   8.38   9.57   10.93   12.48
  14.25  16.28  18.59  21.23  24.24  27.69  31.62  36.12   41.25   47.11
  53.80  61.44  70.17  80.14  91.52 104.53 119.38 136.34  155.71  177.83
 203.09 231.94 264.90 302.53 350.   400.   450.   500.    550.    600.
 650.   700.   750.   800.   850.   900.   950.  1000.   1050.   1100.
1150.  1200.  1250.  1300.  1350.  1400.  1450.  1500.   1550.   1600.
1650.  1700.  1750.  1800.  1850.  1900.  1950.  2000.   2050.   2100.
2150.  2200.  2250.  2300.  2350.  2400.  2450.  2500.
C.2.2B.2 .. UNIGRZ[T/F];(O) - CYLIND [1.4]
F
C.2.2B.3B .. Z(K);(O) - NOT UNIGRZ [2.2B.3A],CYLIND [1.4]
  0.  50. 100. 130. 150. 160. 170. 180. 190. 200. 210. 220. 230. 240. 250
260. 270. 280. 290. 300. 310. 320. 330. 350. 380. 420.
C-------------------------------------------------------------------------------
C.....Fluid property information
C.2.4.1 .. BP
3.03E-6
C.2.4.2 .. P0,T0,W0,DENF0
14.7 75.0 0 62.241
C.2.4.3 .. W1,DENF1;(O) - SOLUTE [1.4]
0.020 63.1772
C.2.5.1 .. VISFAC
-0.8904
C-------------------------------------------------------------------------------
C.....Reference condition information
C.2.6.1 .. PAATM
14.7
C.2.6.2 .. P0H,T0H
0,75.0
C-------------------------------------------------------------------------------
```

```
C.....Solute information
C.2.8 .. DM,DECLAM;(O) - SOLUTE [1.4]
9.30E-5,0
C-------------------------------------------------------------------------------
C.....Porous media zone information
C.2.9.1 .. IPMZ,X1Z(IPMZ),X2Z(IPMZ),Y1Z(IPMZ),Y2Z(IPMZ),Z1Z(IPMZ),Z2Z(IPMZ)
1 1 2500. 1 1 0. 150.
2 1 2500. 1 1 150. 330.
3 1 2500  1 1 330. 420.
END
C-------------------------------------------------------------------------------
C.....Porous media property information
C.2.10.1 .. KXX(IPMZ),KYY(IPMZ),KZZ(IPMZ),IPMZ=1 to NPMZ [1.7]
3.877E-12,,3.877E-12
6.475E-10,,6.475E-10
3.102E-15,,3.102E-15
C.2.10.2 .. POROS(IPMZ),IPMZ=1 to NPMZ [1.7]
.3 .3 .3
C.2.10.3 .. ABPM(IPMZ),IPMZ=1 to NPMZ [1.7]
6.2E-6 6.2E-6 6.2E-6
C-------------------------------------------------------------------------------
C.....Porous media solute and thermal dispersion information
C.2.12 .. ALPHL(IPMZ),ALPHT(IPMZ),IPMZ=1 to NPMZ [1.7];(O) - SOLUTE [1.4]
C..          and/or HEAT [1.4]
12.5 2.5
12.5 2.5
12.5 2.5
C-------------------------------------------------------------------------------
C.....Porous media solute property information
C.2.13 .. DBKD(IPMZ),IPMZ=1 to NPMZ [1.7];(O) - SOLUTE [1.4]
3*0.0
C-------------------------------------------------------------------------------
C.....Source-sink well information
C.2.14.1 .. IWEL,XW,YW,ZBW,ZTW,WBOD,WQMETH[I];(O) - NWEL [1.6] >0
C.2.14.2 .. WCF(L);L = 1 to NZ (EXCLUSIVE) by ELEMENT
C.2.14.3 .. WSF(L);L = 1 to NZ (EXCLUSIVE) by ELEMENT
1 1 1 150. 330. 2. 11
0,0,0,0,1,1,1,1,1,1,1,1,1,1,1,1,1,1,1,1,1,0,0,0
25*0
END
C-------------------------------------------------------------------------------
C.....Boundary condition information
C-------------------------------------------------------------------------------
C.....     Specified value b.c.
C.2.15 .. IBC by x,y,z range {0.1-0.3} with no IMOD parameter;(O) -
C..          NSBC [1.6] > 0
1. 2500. 1. 1. 420. 420.
101
1. 2500. 1. 1. 0. 0.
101
2500. 2500. 1 1 50. 150.
101
2500. 2500. 1 1 150. 330.
101
2500. 2500. 1 1 330. 380.
101
END
C-------------------------------------------------------------------------------
C.....Free surface b.c.
C.2.20 .. FRESUR[T/F],PRTCCM[T/F]
F F
C-------------------------------------------------------------------------------
C.....Initial condition information
C.2.21.1 .. ICHYDP,ICTPRO,ICCPRO; all [T/F]
T F F
C.2.21.3A .. ZPINIT,PINIT;(O) - ICHYDP [2.21.1] and NOT ICHWT [2.21.2]
```

```
450. 0.
C.2.21.6B .. C by x,y,z range {0.1-0.3};(O) - SOLUTE [1.4] and NOT ICCPRO
C..          [2.21.1]
1 2500. 1 1 0. 130.
1 1
1 2500. 1 1 150. 320.
0.25 1
1 2500. 1 1 330. 420.
0.0250 1
END
C-------------------------------------------------------------------------------
C.....Calculation information
C.2.22.1 .. FDSMTH,FDTMTH
0 1.
C.2.22.2 .. TOLDEN{.001},MAXITN{5}
.1 10
C.2.22.3 .. EPSFS;(O) - FRESUR [2.20]
C-------------------------------------------------------------------------------
C.....Output information
C.2.23.1 .. PRTPMP,PRTFP,PRTIC,PRTBC,PRTSLM,PRTWEL; all [T/F]
6*T
C.2.23.2 .. IPRPTC,PRTDV[T/F];(O) - PRTIC [2.23.1]
201 T
C.2.23.3 .. ORENPR[I];(O) - NOT CYLIND [1.4]
C.2.23.4 .. PLTZON[T/F];(O) - PRTPMP [2.23.1]
F
C.2.23.5 .. PLTTEM[T/F]
F
C-------------------------------------------------------------------------------
C..... TRANSIENT DATA - READ3
C.3.1 .. THRU[T/F]
F
C-------------------------------------------------------------------------------
C.....Source-sink well information
C.3.2.1 .. RDWTD[T/F];(O) - NWEL [1.6] > 0
T
C.3.2.2 .. IWEL,QWV,PWSUR,PWKT,TWSRKT,CWKT;(O) - RDWTD [3.2.1]
1 133690. 0 51.87 75.0 0.035
END
C-------------------------------------------------------------------------------
C.....Boundary condition information
C-------------------------------------------------------------------------------
C.....     Specified value b.c.
C.3.3.1 .. RDSPBC,RDSTBC,RDSCBC; all [T/F];(O) - NSBC [1.6] > 0
T F T
C.3.3.2 .. PNP B.C. by x,y,z range {0.1-0.3};(O) - RDSPBC [3.3.1]
1 2500. 1 1 420. 420.
12.967 1
1 2500. 1 1 0. 0.
195.719 1
2500. 2500. 1 1 50. 380.
3 5
50. 173.702 380. 30.256
END
C..          SOLUTE [1.4] ALWAYS NEED THIS IF SPEC PRESS BOUNDARY
END
C.3.3.6 .. CNP B.C. by x,y,z range {0.1-0.3};(O) - RDSCBC [3.3.1] and
C..          SOLUTE [1.4]
1 2500. 1 1 420. 420.
0.0250 1
1 2500. 1 1 0. 0.
1 1
2500. 2500. 1 1 50. 50.
1 1
2500. 2500. 1 1 100. 100.
```

```
1 1
2500. 2500. 1 1 130. 130.
1 1
2500. 2500. 1 1 150. 150.
0.25 1
2500. 2500. 1 1 150. 320.
0.25 1
2500. 2500. 1 1 330. 380.
0.0250 1
END
C-------------------------------------------------------------------------------
C.....Calculation information
C.3.7.1 .. RDCALC[T/F]
T
C.3.7.2 .. AUTOTS[T/F];(O) - RDCALC [3.7.1]
f
C.3.7.3.A .. DELTIM;(O) - RDCALC [3.7.1] and NOT AUTOTS [3.7.2]
0.5
C.3.7.3.B .. DPTAS{5E4},DTTAS{5.},DCTAS{.25},DTIMMN{1.E4},DTIMMX{1.E7};
C..          (O) - RDCALC [3.7.1] and AUTOTS [3.7.2]
C.3.7.4 .. TIMCHG
15.
C-------------------------------------------------------------------------------
C.....Output information
C.3.8.1 .. PRISLM,PRIKD,PRIPTC,PRIDV,PRIVEL,PRIGFB,PRIBCF,PRIWEL; all [I]
0 0 -15. 0 0 0 0 -15.
C.3.8.2 .. IPRPTC;(O) - IF PRIPTC [3.8.1] NOT = 0
201
C.3.8.3 .. CHKPTD[T/F],PRICPD,SAVLDO[T/F]
F /
C-------------------------------------------------------------------------------
C.....Contour and vector map information
C.3.9.1 .. CNTMAP[T/F],VECMAP[T/F],PRIMAP[I]
T T -15.0
C-------------------------------------------------------------------------------
C.....END OF FIRST SET OF TRANSIENT INFORMATION
C.....TRANSIENT DATA -READ3
C.....SECOND STAGE WITHDRAW 1MGAL/D FOR 15 DAYS.....................
C-------------------------------------------------------------------------------
C.3.1 .. THRU[T/F]
F
C-------------------------------------------------------------------------------
C.....Source-sink well information
C.3.2.1 .. RDWTD[T/F];(O) - NWEL [1.6] > 0
T
C.3.2.2 .. IWEL,QWV,PWSUR,PWKT,TWSRKT,CWKT;(O) - RDWTD [3.2.1]
1 -133690. 0 51.87 75.0 0.035
END
C-------------------------------------------------------------------------------
C.....Boundary condition information
C-------------------------------------------------------------------------------
C.....     Specified value b.c.
C.3.3.1 .. RDSPBC,RDSTBC,RDSCBC; all [T/F];(O) - NSBC [1.6] > 0
T F T
C-------------------------------------------------------------------------------
C.....Calculation information
C.3.7.1 .. RDCALC[T/F]
T
C.3.7.2 .. AUTOTS[T/F];(O) - RDCALC [3.7.1]
f
C.3.7.3.A .. DELTIM;(O) - RDCALC [3.7.1] and NOT AUTOTS [3.7.2]
0.25
C.3.7.4 .. TIMCHG
30.
C-------------------------------------------------------------------------------
C.....Output information
```

```
C.3.8.1 .. PRISLM,PRIKD,PRIPTC,PRIDV,PRIVEL,PRIGFB,PRIBCF,PRIWEL; all [I]
0 0 1 0 0 0 0 1
C.3.8.2 .. IPRPTC;(O) - IF PRIPTC [3.8.1] NOT = 0
201
C.3.8.3 .. CHKPTD[T/F],PRICPD,SAVLDO[T/F]
F /
C-------------------------------------------------------------------------------
C.....Contour and vector map information
C.3.9.1 .. CNTMAP[T/F],VECMAP[T/F],PRIMAP[I]
T T -30.
C-------------------------------------------------------------------------------
C.....End of second set of transient information
C.....End of simulation line follows, THRU=.TRUE.
C.3.99.1 .. THRU
T
C......End of the data file
```

Tests of Subsurface Storage of Freshwater at Hialeah, Dade County, Florida, and Numerical Simulation of the Salinity of Recovered Water

United States Geological Survey Water-Supply Paper 2431

Prepared in cooperation with the South Florida Water Management District and the Miami-Dade Water and Sewer Authority Department

AVAILABILITY OF BOOKS AND MAPS OF THE U.S. GEOLOGICAL SURVEY

Instructions on ordering publications of the U.S. Geological Survey, along with prices of the last offerings, are given in the current-year issues of the monthly catalog "New Publications of the U.S. Geological Survey." Prices of available U.S. Geological Survey publications released prior to the current year are listed in the most recent annual "Price and Availability List." Publications that may be listed in various U.S. Geological Survey catalogs (**see back inside cover**) but not listed in the most recent annual "Price and Availability List" may be no longer available.

Reports released through the NTIS may be obtained by writing to the National Technical Information Service, U.S. Department of Commerce, Springfield, VA 22161; please include NTIS report number with inquiry.

Order U.S. Geological Survey publications **by mail** or **over the counter** from the offices given below.

BY MAIL

Books

Professional Papers, Bulletins, Water-Supply Papers, Techniques of Water-Resources Investigations, Circulars, publications of general interest (such as leaflets, pamphlets, booklets), single copies of Earthquakes & Volcanoes, Preliminary Determination of Epicenters, and some miscellaneous reports, including some of the foregoing series that have gone out of print at the Superintendent of Documents, are obtainable by mail from

U.S. Geological Survey, Map Distribution
Box 25286, MS 306, Federal Center
Denver, CO 80225

Subscriptions to periodicals (Earthquakes & Volcanoes and Preliminary Determination of Epicenters) can be obtained ONLY from the

Superintendent of Documents
Government Printing Office
Washington, DC 20402

(Check or money order must be payable to Superintendent of Documents.)

Maps

For maps, address mail orders to

U.S. Geological Survey, Map Distribution
Box 25286, Bldg. 810, Federal Center
Denver, CO 80225

Residents of Alaska may order maps from

U.S. Geological Survey, Earth Science Information Center
101 Twelfth Ave. - Box 12
Fairbanks, AK 99701

OVER THE COUNTER

Books and Maps

Books and maps of the U.S. Geological Survey are available over the counter at the following U.S. Geological Survey offices, all of which are authorized agents of the Superintendent of Documents:

- **ANCHORAGE, Alaska**—Rm. 101, 4230 University Dr.
- **LAKEOOD, Colorado**—Federal Center, Bldg. 810
- **MENLO PARK, California**—Bldg. 3, Rm. 3128, 345 Middlefield Rd.
- **RESTON, Virginia**—USGS National Center, Rm. 1C402, 12201 Sunrise Valley Dr.
- **SALT LAKE CITY, Utah**—Federal Bldg., Rm. 8105, 125 South State St.
- **SPOKANE, Washington**—U.S. Post Office Bldg., Rm. 135, West 904 Riverside Ave.
- **WASHINGTON, D.C.**—Main Interior Bldg., Rm. 2650, 18th and C Sts., NW.

Maps Only

Maps may be purchased over the counter at the following U.S. Geological Survey offices:

- **FAIRBANKS, Alaska**—New Federal Bldg., 101 Twelfth Ave.
- **ROLLA, Missouri**—1400 Independence Rd.
- **STENNIS SPACE CENTER, Mississippi**—Bldg. 3101

Tests of Subsurface Storage of Freshwater at Hialeah, Dade County, Florida, and Numerical Simulation of the Salinity of Recovered Water

By MICHAEL L. MERRITT

Prepared in cooperation with the South Florida Water Management District and the Miami-Dade Water and Sewer Authority Department

U.S. GEOLOGICAL SURVEY WATER-SUPPLY PAPER 2431

U.S. DEPARTMENT OF THE INTERIOR
BRUCE BABBITT, Secretary

U.S. GEOLOGICAL SURVEY
Gordon P. Eaton, Director

Printed in the Eastern Region, Reston, Va.

UNITED STATES GOVERNMENT PRINTING OFFICE, WASHINGTON : 1997

For sale by the
U.S. Geological Survey, Branch of Information Services
Box 25286
Denver, CO 80225-0286

Library of Congress Cataloging in Publication Data

Merritt, Michael L.
Tests of Subsurface Storage of Freshwater at Hialeah, Dade County, Florida, and Digital Simulation of the Salinity of Recovered Water / by Michael L. Merritt.
p. cm.—(U.S. Geological Survey water supply paper ; 2431)
"Prepared in cooperation with the South Florida Water Management District and the Miami-Dade Water and Sewer Authority Department."
Includes bibliographical references.
1. Groundwater—Florida—Hialeah Region. 2. Aquifer storage recovery—Florida—Hialeah Region. 3. Water conservation—Florida—Hialeah Region. 4. Water salinization—Florida—Hialeah Region—Computer simulation. 5. Florida Aquifer. 6. South Florida Water Management District. I. South Florida Water Management District. II. Miami-Dade Water and Sewer Authority Dept. (Fla.) III. Title. IV. Series
TD224.F6M39 1996 94–21806
628. 1'3—DC20 CIP

ISBN 0–607–86594–6

CONTENTS

PLATES

[Plates are in pocket]

FIGURES

TABLES

CONVERSION FACTORS, VERTICAL DATUM, AND ACRONYMS

Multiply	By	To obtain
inch (in.)	25.4	millimeter
foot (ft)	0.3048	meter
mile (mi)	1.609	kilometer
foot per day (ft/d)	0.3048	meter per day
foot per mile (ft/mi)	0.1894	meter per kilometer
foot per year (ft/yr)	0.3048	meter per year
square foot per day (ft^2/d)	0.09290	meter squared per day
cubic foot (ft^3)	0.02832	cubic meter
cubic foot per day (ft^3/d)	0.02832	cubic meter per day
gallon (gal)	3.785	liter
gallon per minute (gal/min)	0.06309	liter per second
pound per cubic foot (lb/ft^3)	16.02	kilogram per cubic meter
pound per square inch (lb/in^2)	6.895	kilopascal
inverse pound per square inch ($(lb/in^2)^{-1}$)	0.1450	$(kilopascal)^{-1}$

Temperature, given in degrees Fahrenheit (°F), can be converted to degrees Celsius (°C) by the following equation:

$$°C = 5/9\ (°F - 32)$$

Temperature, given in degrees Celsius (°C), can be converted to degrees Fahrenheit (°F) by the following equation:

$$°F = 9/5\ (°C) + 32$$

Milligrams per liter (mg/L) is a unit expressing the concentration of chemical constituents in solution as weight (milligrams) of solute per unit volume (liter) of water. For concentrations less than 7,000 mg/L, the numerical value is the same as for concentrations in parts per million.

Sea level: In this report, "sea level" refers to the National Geodetic Vertical Datum of 1929 —a geodetic datum derived from a general adjustment of the first-order level nets of both the United States and Canada, formerly called Sea Level Datum of 1929.

ACRONYMS USED IN REPORT

ASR	aquifer storage and recovery
FGS	Florida Geological Survey
ID	inside diameter
MDWSA	Miami-Dade Water and Sewer Authority
OD	outside diameter
PVC	polyvinyl chloride
SFWMD	South Florida Water Management District
SWIP	Subsurface Waste Injection Program
USGS	U.S. Geological Survey

Tests of Subsurface Storage of Freshwater at Hialeah, Dade County, Florida, and Numerical Simulation of the Salinity of Recovered Water

By Michael L. Merritt

Abstract

Injection and observation wells were drilled in late 1974 for the purpose of conducting tests of storage and recovery of potable water in the brackish Upper Floridan aquifer. Three tests, involving storage and recovery cycles of varying volumes and storage period lengths, were performed between July 1975 and January 1980. Recovery was by natural artesian flow, and recovery efficiencies were 32.9, 47.8, and 38.5 percent. Wellbore plugging occurred during the injection stages, but injectivity was restored by periodic 2- to 3-hour backflushes at the natural artesian flow rate.

An interval of shelly limestone between 1,015 and 1,050 feet below land surface contained the flow zone. Data from an analysis of 18 spinner flowmeter logs indicated that the principal part of the flow zone extended from 1,024 to 1,036 feet below land surface and that minor amounts of flow occurred to a depth of about 1,047 feet. A neutron porosity log indicated the bulk porosity of both the flow zone and confining layers to be 35 percent. Chloride and dissolved-solids concentrations of water in the flow zone were 1,200 and 2,700 milligrams per liter, respectively.

A three-dimensional, finite-difference flow and solute-transport code was used to simulate pressure data measured during an aquifer test and observed salinity increases in recovered water during storage and recovery cycles. The aquifer test conducted in February 1975 was simulated by using a hydraulic conductivity estimate of 800 feet per day and a rock compressibility estimate of 0.0000400 (pound per square inch)$^{-1}$. The equivalent transmissivity and storage coefficients were 9,600 cubic feet per day per square foot times foot of aquifer thickness and 7.8×10^{-5}, respectively. Simulation of observed salinity increases during the three recoveries required dispersivities of 65 feet, a molecular diffusivity of 0.0002 foot squared per day, and a regional pore velocity of 260 feet per year. Central differencing in space and time was used for the solute-transport computations as well as an experimental method of computing vertical dispersion that used a scaling factor of 0.013.

Additional simulations of the aquifer-test data and recovery salinities were obtained based on assumptions that (1) the flow zone was 21 feet thick, (2) flow-zone effective porosity was 20 percent, and (3) flow-zone hydraulic conductivity was bipolar anisotropic by a ratio of 10:1. The four sets of simulation values were used in model runs in which 10 years of annual injection, storage, and recovery cycles were simulated. Computed recovery efficiencies increased from 40 percent in the first year to 68 percent in later cycles. The high regional pore velocity required for model calibration substantially limited the recovery efficiency achieved in later cycles.

INTRODUCTION

The subtropical climate of southern Florida has attracted a large and rapidly expanding population in recent decades, a trend likely to continue. As a result

of the population increase, the need for potable water has increased dramatically. Large quantities of potable water are available from the surficial Biscayne aquifer of Dade, Broward, and Palm Beach Counties, and smaller quantities are available from surficial or shallow artesian aquifers on the west coast, on the upper east coast (Martin and St. Lucie Counties), and in the interior of the southern peninsula (fig. 1).

The population growth of southern Florida has raised concerns about the adequacy of current sources of water supply to meet future demands. Since the early 1970's, water-management agencies have sponsored investigations into ways of augmenting these sources, particularly during the seasonal dry period (November–May) that is characteristic of the subtropical climate of southern Florida. Potable water normally is available in considerable surplus during the annual wet season (June–October), when the regional canal system is used to lower the water table throughout much of the area.

In 1974 the U.S. Geological Survey (USGS), in cooperation with the Central and Southern Florida Flood Control District, now the South Florida Water Management District (SFWMD), and the Miami-Dade Water and Sewer Authority (MDWSA) Department, began a pilot study to test the feasibility of injecting surplus potable water into the Floridan aquifer system for later retrieval when the supply of potable water became deficient. This water conservation strategy is particularly suited for the region because of its seasonal cycle of surplus and deficit of water supply. Because permeable zones in the Ocala Limestone and the upper part of the Avon Park Limestone of the Floridan aquifer system were known to contain brackish water, they were the injection zones selected for study.

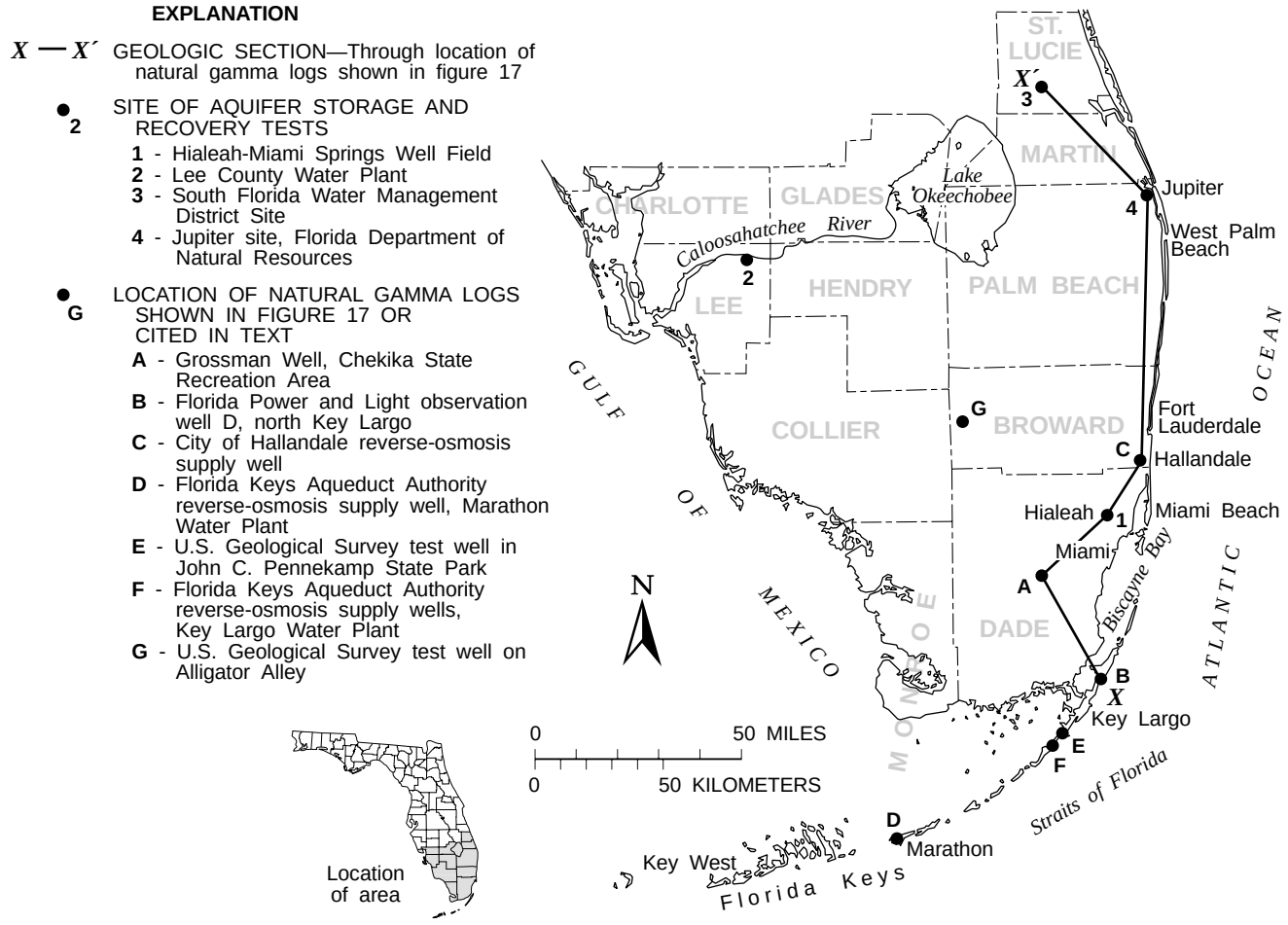

Figure 1. Location of Upper Floridan aquifer wells in southern Florida cited in this report.

The proposed study originally envisaged successive deepenings of an aquifer storage and recovery (ASR) well and two observation wells after performing ASR cycles in higher zones of interest. However, the funding provided limited activity to the testing of the uppermost permeable zone and the drilling of one observation well. The Hialeah-Miami Springs Well Field in Dade County, which at that time was the primary source of potable water for domestic consumption in the Miami area, was the site selected for the tests (fig. 1, site 1).

The injection and observation wells were constructed in October, November, and December 1974. Three ASR tests were performed, beginning in July 1975. The recovery phase of the third and last test continued until January 1980. During well construction and the subsequent ASR tests, a variety of data were collected, including pressure data, water-quality data, and volumetric measurements of quantities of inflow and outflow as a function of time. The present study interprets this data set to gain insight into the hydrogeologic processes occurring at the test site during the ASR cycles and to better define the potential feasibility of this technology in southern Florida.

In 1980–81, data from the tests at Hialeah were used by the USGS in an areal assessment of the feasibility of ASR as a water-conservation alternative for southern Florida which was conducted in cooperation with the U.S. Army Corps of Engineers. The ASR process and operational experience acquired by that time were summarized in the report presenting the results of the assessment (Merritt and others, 1983), and their relation to water-management needs in specific areas was considered. Data describing conditions at the Hialeah site were used to design a generalized aquifer prototype to be used for digital modeling to determine relations between hydrogeologic and operational conditions and the recoverability of injected water (Merritt, 1985). The modeling consisted of sensitivity analyses in which a simulation of injection, storage, and recovery in the aquifer prototype was repeated as various parameters were altered to represent changes in hydrogeologic conditions or operational management.

As useful as the results of the sensitivity analyses were, the more challenging problem remained of actually simulating the injection, storage, and recovery of water at Hialeah. The additional difficulty of simulation modeling compared to using a model of a hypothetical prototype to test relations and concepts arises from the need for realistic identification of parameters describing the processes of flow and transport in the aquifer, usually given inadequate data that require experience and intuition to interpret. In the present study, such a simulation model was constructed and used for predictive analyses to indicate the quantity of potable water that could be made available by an operational ASR program.

Opportunities for the application of computer simulation have increased as a result of recent advances in computer technology that make possible the more efficient use of three-dimensional solute-transport models and that facilitate their application to data sets such as that from Hialeah. The techniques for computer simulation of the transport of fresh water and brackish water during injection and recovery operations presented in this report can be used by water managers to estimate the amount of injected water that can be recovered at sites where data to support simulation are available and, also, to test various design and management alternatives.

Purpose and Scope

The complete data set acquired at the Hialeah ASR site is presented in this report to describe hydrogeologic conditions in the Upper Floridan aquifer, to describe hydrogeologic processes occurring during the injection and recovery tests, and to support the approach used for the simulation analysis. Selected data from other locations on the East Coast are included to augment the description of Upper Floridan aquifer conditions and for a tentative delineation of an areally extensive flow zone used for ASR at some locations and for reverse-osmosis plant supply at other locations. The remainder of the report describes the use of solute-transport modeling techniques to further interpret data from the field study by simulating the transport of fresh water and brackish water during the injection and recovery cycles, and describes the use of the calibrated simulation for predictions of recovery efficiency under hypothetical operational conditions.

Acknowledgments

The USGS expresses its appreciation to the SFWMD for providing funding for this study and to the late William B. Storch, former Executive Director, for his interest and encouragement. The USGS also expresses its gratitude to Garrett M. Sloan, former Director of the MDWSA, for the provision of various equipment and a water supply for conducting the tests. The author

benefited greatly from the help of Frederick W. Meyer (USGS, retired), who directed the subsurface storage and recovery tests at Hialeah over a period of many years and provided substantial guidance that helped the author to interpret data from the tests. Many of Fred Meyer's suggestions were incorporated into the analyses that follow in the remainder of this report.

SUMMARY DESCRIPTION OF INJECTION AND RECOVERY TESTS

The following pages present a brief description of the activities at the field site of the injection and recovery tests. This is followed by a summary of test results and a description of data collected at the site. Evidence indicating plugging of the wellbore during injection is also discussed.

Well Construction and Preliminary Data Collection

The sequence of stages in the construction and testing of the injection and observation wells is shown in figure 2. Drilling was principally by mud rotary. Casing extended to a depth of 955 feet (ft) in the completed injection well and to 953 ft in the observation well. The injection-well borehole was drilled to a depth of 1,105 ft, and the observation-well borehole was drilled to a depth of 1,064 ft. The deepest part of the injection well (below 960 ft) was drilled by reverse air, using a closed circulation system with discharge to a storm sewer. A supply well that tapped the Biscayne aquifer (Preston No. 7) provided a water supply for the injection tests. Drilled in June 1972, this well was 106 ft deep and was cased with 42-inch (in.) pipe to 65 ft. A suction line extended from the supply well to the injection wellhead.

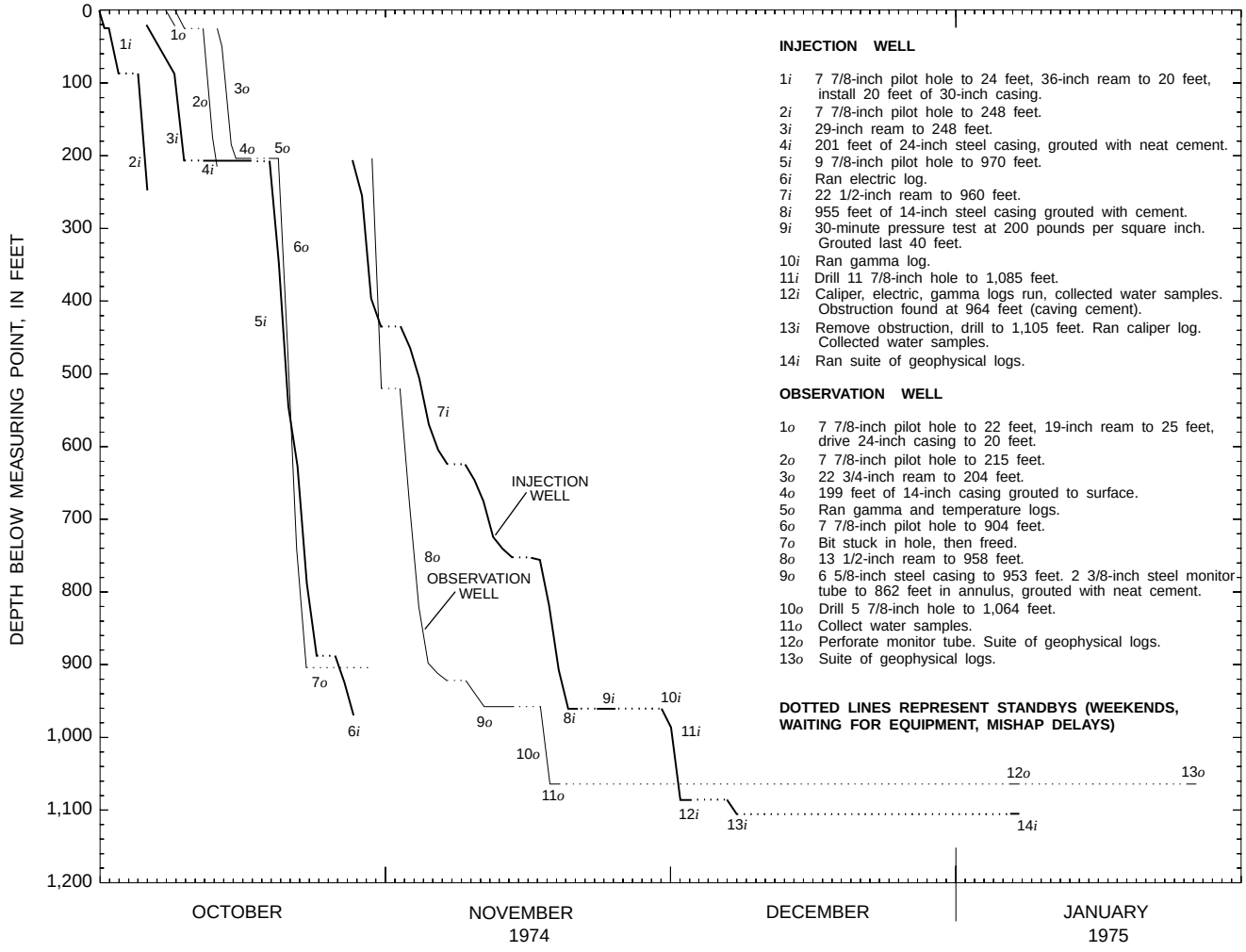

Figure 2. Details of the construction and testing of injection and observation wells at the Hialeah site.

During drilling, a 2-in. inside diameter (ID) steel tube was embedded in the cement annulus surrounding the 6 5/8-in. (OD) casing of the observation well to a depth of 862 ft. All casings in the injection and observation wells had a wall thickness of 3/8 in. except the 5 7/8-in. (ID) inner casing of the observation well, which had a wall thickness of 1/2 in. The 14-in. inner casing of the injection well was pressure tested at 200 pounds per square inch (lb/in^2) for 30 minutes (F.W. Meyer, USGS, written commun., 1974). USGS and Florida Geological Survey (FGS) identifiers for the wells, land-surface datums, and USGS datum measuring points at the injection and observation wells (selected as the tops of the concrete floors) are

Type of well	USGS local well number	FGS number	USGS site identifier	Datum, in feet above sea level	
				Land surface	Measuring point
Injection	G-3061	W-12997	254941080171701	8.39	9.44
Observation	G-3062	W-12998	254944080171801	5.43	5.93
Supply	S-3000	—	254943080172001	—	—

The injection and observation wells were located in Township 53 South, Range 41 East, Section 18, NW$^{1/4}$, SW$^{1/4}$ (near the junction of Okeechobee Road and West Third Avenue in Hialeah). The site was in the Hialeah-Preston Well Field near the north bank of the Miami Canal, on property adjacent to the Hialeah Water Treatment Plant. The observation well is about 289 ft north-northwest of the injection well. The wells and surrounding features present when construction was completed in 1974 are shown in figure 3. On June 4, 1980, the observation well was plugged with neat cement. The observation-well site now is covered by an MDWSA warehouse.

A comprehensive suite of data was obtained during and immediately after well construction. Geophysical logs made during this period are included in table 1, which is a complete and annotated summary of geophysical logging performed during the project. A driller's log of lithology recorded by the USGS at both the injection and observation wells is included as Appendix A. An analysis of cuttings from the two wells was made by the FGS, and descriptions of the lithology are included as Appendix B. The first two water samples collected for chemical and biological

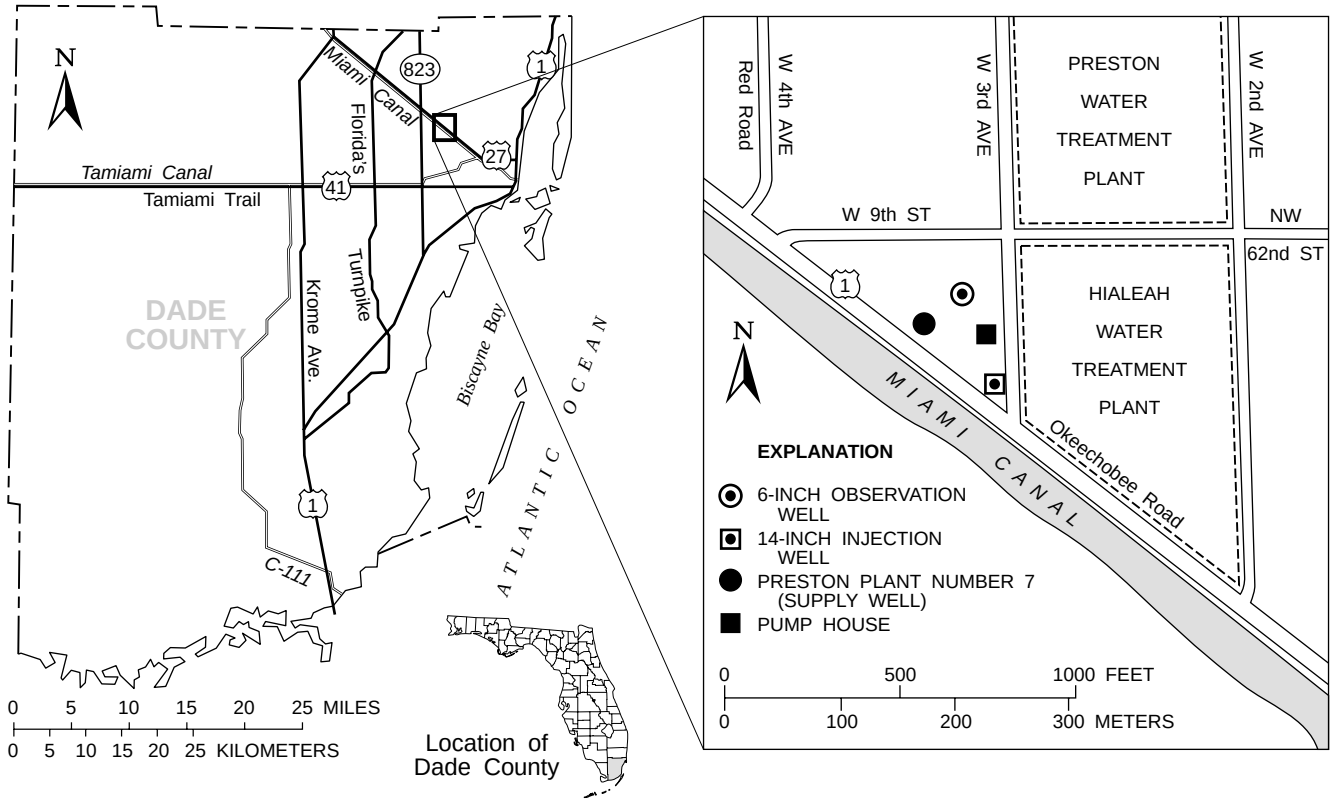

Figure 3. Location of wells and surrounding features at the Hialeah site at the time of well construction in 1974.

Table 1. Geophysical logging data obtained during construction and testing of the injection and observation wells and during subsequent storage and recovery tests at Hialeah, 1974–79

[All logs run by the U.S. Geological Survey, except where noted. OW, observation well; IW, injection well]

Date acquired	Type of log or data	Depth (feet)	Well	Remarks
		Construction		
10/21/74	Natural gamma	0–150	OW	Three days after cementing 14-inch casing.
	Temperature	0–125	OW	Same as above.
10/30/74	Electric	0–970	IW	Single-point resistivity and spontaneous potential. In a 9 7/8-in. pilot hole filled with aquagel. Shows correlation with layering of limestone and clay. Done in 14-in. casing with plug.
12/02/74	Natural gamma	0–970	IW	Poor log.
12/04/74	Electric	900–1, 085	IW	Single-point resistivity and spontaneous potential. Three runs.
	Natural gamma	0–1,085	IW	Three runs. Poor reproducibility.
	Caliper	865–1,080	IW	Showed obstruction at 964 ft.
12/09/74	Caliper	869–1,105	IW	Open hole to total depth.
		Postconstruction Testing		
01/07/75	Cement bond and natural gamma	0–960	OW	Schlumberger log.
01/08/75	Oriented perforation	840–844	OW	A 2-inch monitor tube perforated at 840 feet. Schlumberger log.
	Caliper	0–1,061	OW	Open hole to total depth.
	Borehole compensated sonic	955–1,088	IW	Schlumberger log.
	Cement bond	0–964	IW	Poor bond, except in isolated intervals and bottom of well. Schlumberger log.
	Compensated neutron-formation density and natural gamma	0–1,096	IW	Used for porosity estimates. Schlumberger log.
	Induction-electrical log	950–1,088	IW	Correlated with hard layers, 975–985 ft. and 1,030–1,040 ft. Schlumberger log.
01/27/75	Caliper	918–1,053	OW	
	Temperature	7–1,057	OW	Well flowing about 288 gal/min (1.36 gal/min in 6-inch casing). Temperature decreases with depth.
	Natural gamma	3–1,056	OW	
	Temperature	940–1,085	OW	Inverse of previous temperature log. Well flowing. Three flowmeter stations—tool would not go below 984 ft.
	Neutron porosity	3–1,056	OW	
	Gamma-gamma density	4–1,056	OW	
	Standard electric	943–1,053	OW	Spontaneous potential, long and short normal formation resistivity.
	Fluid resistivity	800–1,056	OW	

Table 1. Geophysical logging data obtained during construction and testing of the injection and observation wells and during subsequent storage and recovery tests at Hialeah, 1974-79--Continued

Date acquired	Type of log or data	Depth (feet)	Well	Remarks
During First Recovery				
10/10/75	Caliper	930 - 1,093	IW	
	Temperature	0 - 1,104	IW	Shows warmer water below 1,047 feet. Temperature increases with depth.
	Natural gamma	0 - 1,100	IW	High counts 950 to 1,040 feet.
	Fluid resistivity	0 - 1,102	IW	Shows fresher water below 1,047 feet.
	Neutron porosity	0 - 1,099	IW	
	Gamma-gamma density	0 - 1,100	IW	
	Standard electric	953 - 1,103	IW	Spontaneous potential, long and short normal formation resistivity. Two runs.
	Spinner flowmeter	612 - 1,097	IW	Three runs.
Last Day of First Recovery				
10/20/75	Standard electric	0 - 1,105	IW	Spontaneous potential, long and short normal formation resistivity. Warmer water below 1,047 feet.
	Fluid resistivity	0 - 1,103	IW	No good.
	Spinner flowmeter	0 - 1,105	IW	Up and down runs. Flowing at 835 gallons per minute.
During Second Recovery				
05/25/76	Standard electric	946 - 1,098	IW	Spontaneous potential, long and short normal formation resistivity.
	Caliper, spinner flowmeter	930 - 1,100	IW	Up and down runs of flowmeter.
	Fluid resistivity	920 - 1,102	IW	Shows water freshening below 1,020 feet.
During Third Injection				
08/27/76	Spinner flowmeter	920 - 1,100	IW	Up and down runs before, during, and after backflush.
During Third Recovery				
04/20/78	Acoustic televiewer	950 - 1,096	IW	Only parts in U.S. Geological Survey files.
	Temperature	60 - 1,100	IW	Shows warmer water below 1,040 feet.
	Fluid resistivity	900 - 1,100	IW	Shows fresher water below 1,040 feet.
	Spinner flowmeter	800 - 1,087	IW	Up and down runs.
07/17/79	Acoustic televiewer	950 - 1,096	IW	Only some duplicates in U.S. Geological Survey files.
	Spinner flowmeter	930 - 1,092	IW	Two runs up, one run down.
	Fluid resistivity	40 - 1,098	IW	Water below 1,040 feet is slightly saltier.
	Temperature	20 - 1,100	IW	Decreases with depth to 1,040 feet. Warmer water below 1,040 feet. Cooler water below 1,060 feet.
	Caliper	800 - 1,098	IW	

analysis (from injection and observation wells) are measurements of the preinjection quality of native water in the injection zone immediately after well construction. A complete list of the results of chemical and biological analyses of water samples collected from the injection and observation wells during the testing program is presented in Appendix D. The chemical and biological analyses normally consisted of major inorganic ions, bacteria, chemical oxygen demand, biochemical oxygen demand, nutrients, total organic carbon, metals, field pH, alkalinity, and specific conductance.

Additional data were collected during the period between well completion and the beginning of freshwater injection in July 1975. The 2-in. monitor tube in the observation well was perforated at 840 ft on January 8, 1975, by Schlumberger, Inc., as they ran a suite of logs on the injection and observation wells, and water samples began to be collected from this depth. On January 27, 1975, the USGS obtained static and flowing geophysical logs at the observation well (table 1). On February 6, 1975, prior to the aquifer test of February 10, 1975, flow and shut-in artesian heads were measured in the observation well and the 2-in. monitor tube, and shut-in pressure was also measured in the injection well. The heads measured in the injection and observation wells should be regarded as the same within measurement error. Flow from the observation well was measured at a 5-in. discharge orifice at an elevation of about 8 ft above sea level. Flow from the monitor tube was measured at an elevation of 6.23 ft above sea level. A flow estimate from the injection well had previously been obtained on December 10, 1974, as the well was being completed to total depth. The elevation of the point of discharge is unknown. During drilling of the injection well, the first flow 10–20 gallons per minute (gal/min) was reported when the well reached 985 ft in depth. The measured head and flow values are given below:

Type of well or tube	Shut-in head (feet above sea level)	Flow (gallons per minute)
Injection well	42.24	600
Observation well	42.13	280
Two-inch monitor tube	20.33	.5

Test Parameters and Observed Recovery Efficiencies

Three test cycles of injection, storage, and recovery were conducted between July 1975 and January 1980. Specific details of the test schedules are indicated in the annotation column of Appendix C, which also lists periodic measurements of the volume of injection and recovery. Injection was by forced pumping, and recovery was by natural artesian flow. The cycles differed considerably in the total volume injected and length of storage period. The recovery phase of the third cycle continued for 2.5 years, until recovered water approached the quality of background aquifer water. Results of the three cycles have been previously cited by Merritt and others (1983) and Meyer (1989b) and are summarized below:

Test parameters	Cycle 1 (July 17–Oct. 20, 1975)	Cycle 2 (Jan. 5 –July 20, 1976)	Cycle 3 (July 23, 1976–Jan. 30, 1980)
Quantity injected (gallons $\times 10^6$)	41.9	85.0	208.0
Storage period (days)	2	54	181
Quantity of potable water recovered (gallons $\times 10^6$)	13.8	40.7	80.1
Recovery efficiency	32.9	47.8	38.5

Recovery efficiency, in the above table, refers to the customary measure of the productivity of an ASR cycle. Recovery efficiency is defined as the volume of potable water recovered, expressed as a percent of the volume of water injected. The first attempt to do the second injection was terminated prematurely by a pump failure after 8.8×10^6 gal had been injected. This volume is included in the quantity injected for cycle 2 in the above table. Injection resumed 19 days after the pump failure.

Types and Methods of Data Acquisition During the Tests

An intensive and comprehensive data-collection program was designed for the program of injection and recovery testing. Types of data acquired were pressure, volumetric, water-quality, and geophysical data. The methods of data collection are described in the following sections. Most of the data are shown in illustrations or are listed in appendixes at the end of this report.

Pressure Data

Pressure gages with readouts in feet of head were placed on the injection wellhead and at the sampling ports of two monitoring tubes used for water-sample collection in the observation well. The tubes, part of a system described later in more detail, were the red monitor extending to a depth of 957 ft, which is near the top of the open borehole and about 65 ft above the flow zone, and the white monitor, the 2-in. pipe cemented in the annulus and perforated at a depth of 840 ft. The perforations were separated from the flow zone by about 180 ft of clayey marl and dense limestone. The head data, converted to pressures and referenced to sea level, are plotted on plate 1.

Pressure data from the injection well and red monitor (pl. 1) clearly show the effects of injection, storage, and recovery and the effect of backflushing operations. The pressure increase during the aborted second injection in December 1975 is readily apparent. The decrease of pressure during backflushes was usually not measured or only partly measured, and dashed lines are used on plate 1 to suggest the extent of the decrease when not recorded. During the third injection cycle, pressures generally were not recorded between backflushes, and upward trends due to wellbore clogging are not shown as they are for the first and second injection cycles. Pressure data from the 840-ft white monitor show no clear trends during the three ASR cycles, illustrating the degree of confinement provided by the marl and limestone beds separating the monitored zone from the receiving zone.

Volumetric Data

Injection-well inflow and outflow were directed through a single flowmeter by a pipe-and-valve arrangement. Meter readings were recorded frequently during injection and recovery. The cumulative volume of injected and recovered water during the three ASR cycles is shown on plate 1. Incremental volumes of recovered water were given a negative arithmetic value in compiling the volumetric curve, so that total volume in the figure decreases during recovery. Because the volume recovered during the third ASR cycle was quite large, the illustrated cumulative volume decreases below zero after November 1978.

A computed first difference of volumes recorded during injection and recovery was used to approximate the current rate (pl. 1). Like the pressure data, volumetric data were not collected often enough during the third injection phase to show the rate decrease between backflushes caused by wellbore clogging as they did in the first two injection phases. A tabulation of the volumetric data, calculated rates, and corresponding chloride concentration in recovered water is included in Appendix C.

Water-Quality Data

A considerable number of water samples were collected for field and laboratory analysis during the three ASR cycles. Most of the analytic results are stored in the computer files in the USGS office in Miami, Fla.

Before the first injection, a multiport sampling apparatus was installed in the injection horizon of the observation well. The apparatus consisted of a system of monitor tubes extending to various depths within the 6-in. open-hole part of the well. The tubes were attached to a 1/2-in. polyvinyl chloride (PVC) center pipe with a rosette attachment at each coupling of the center pipe (every 21 ft). Around the perimeter of the rosettes were five holes through which lengths of the 5/8-in. flexible plastic monitor tubing (polypipe) were inserted. The five polypipe tubes were color coded at the wellhead and extended to 957 ft (red monitor), 978 ft (green monitor), 999 ft (gold monitor), 1,020 ft (silver monitor), and 1,041 ft (black monitor). Depths are referenced to a flange about 4 ft above land surface, and about 3.5 ft above the measuring point used for referencing the geophysical logs; hence, the tube depths are shown slightly higher in subsequent illustrations. The center pipe extending to 1,062 ft was included in the automatic sampling system (blue monitor).

In the first few days of the first injection, daily samples were obtained manually from the monitor tubes and analyzed for specific conductance and chloride. After 5 days, an automatic sampler/recorder system was made operational. The sampler was pumped continuously at a rate of 5 gal/min. Every 30 minutes, the temperature, specific conductance, dissolved oxygen, and pH of the water were measured and recorded, and the sampler rotated to a different source tube. In this manner, each depth was sampled once every 3 hours. Of the automatically recorded data, only the silver monitor data (1,020 ft) were entered into the computer files. The 2-in. pipe extending to 840 ft (white monitor) was sampled separately.

Periodically, the automatic system was turned off, and samples were pumped from each of the six monitored depths and from the 2-in. pipe for field and laboratory measurements of temperature, specific conductance, and chloride. These data are shown on plate

1 for the three cycles. Automatic sampler-recorder data for the period of the first injection breakthrough (arrival of injected water at the observation well) are shown later in the report. The sampler/recorder was not used after the first cycle.

During the first injection, water from the supply well was sampled frequently for measurements of temperature, specific conductance, and chloride. Supply-well chloride data for all three cycles are shown on plate 1, and temperature data are shown later in the report. Five days into the first injection, a supply-well sample was obtained for chemical and biological analyses (App. D). Eighteen days into the first injection, a water sample was collected from the silver monitor for chemical and biological analyses.

The first injection was terminated at 1200 hours on September 8, 1975, in order to prepare for a short recovery test. About 1 hour later, the automatic sampler/recorder detected a significant freshening in the sample from the observation-well silver monitor (at 1,020 ft). After a few hours, as the other monitor tubes were sampled by the automatic sampling system, freshening was detected at all other monitoring depths except for the white monitor (at 840 ft) located in the overlying confining unit. Specific conductance data from the six injection-zone monitors during the period when freshening occurred are shown later in the report.

The first recovery began 2 days after the end of injection. Automatic sampler data continued to be recorded for the first 8 days of recovery. White-monitor data continued to be collected manually. After 8 days, weekly manual sampling of the six injection-zone monitor tubes was initiated for temperature, specific conductance, and chloride.

Water recovered from the injection well was also sampled and analyzed. During the initial 8 days of the first recovery, hourly measurements were made in the recovered water for temperature, specific conductance, dissolved oxygen, and pH. After 8 days, the measurement frequency was reduced to once per day. Temperature, specific conductance, and chloride were measured, and a flowmeter reading was recorded. Water samples collected 6, 13, 20, and 35 days into recovery received chemical and biological analysis (App. D).

During the second and third injections, sampling of the supply-well water for measurement of temperature, specific conductance, and chloride continued as before, but on a weekly schedule. One sample was collected for chemical and biological analyses during each injection (App. D).

During the second and third ASR cycles, samples were obtained from the seven monitor tubes in the observation well and analyzed for specific conductance, chloride, and sometimes temperature. The sampling was conducted weekly until the end of the third injection, bimonthly during the third storage, weekly for the first 6 months of the third recovery, monthly for another 10 months, and quarterly until January 1980. Water samples were collected from the seven monitoring tubes for chemical and biological analysis near the end of the second recovery (after 77 days of recovery); near the end of the third injection (after 181 days of injection), when water recovered from the monitor tubes consisted primarily of injected water; and near the end of the third recovery (after 729 days of recovery), when water in the monitoring zones virtually had returned to background quality (pl. 1).

During the second and third recovery cycles, measurements of the specific conductance and chloride concentration of the water recovered at the injection well were made frequently and tabulated with corresponding flowmeter readings. At the beginning of the second recovery, the measurement frequency was from one to five times each week, but was reduced to weekly near the end of the recovery. The measurement frequency was weekly during the first 6 months of the third recovery phase, but then was reduced to monthly and then quarterly, as at the observation well. Samples for chemical and biological analysis were obtained just prior to the second recovery, after 22 days of recovery, and near the end of the second recovery (after 77 days). Additional samples for chemical and biological analysis were collected just prior to the third recovery and near the end of the third recovery (after 729 days). Results of all chemical and biological analyses are listed in Appendix D.

Other water samples collected during the study were analyzed by university and private laboratories and by research laboratories of the USGS. Water samples were periodically sent to a private laboratory, Applied Research Laboratories of Florida, Inc., in Hialeah, for analysis of nitrate-reducing, sulfate-reducing, and iron-reducing bacteria. Results currently

available in USGS files are listed in Appendix D. Water samples were sent to the USGS research laboratory in Reston, Va., for dissolved-gas analyses. Results (D.H. Fisher, USGS, written commun., 1975, 1977) are also summarized in Appendix D. Three water samples (August 4, 1975, injection-supply water; September 23 and 30, 1975, backflowing water) were sent to Florida State University for uranium-isotope analysis (Meyer, 1989a).

Geophysical Data

Geophysical logging was performed by the USGS in the injection well on six occasions during the three ASR cycles. Five of these occasions were during recovery. The remaining logging was done before, during, and after a backflushing operation during the third injection. These six logging operations are depicted graphically on plate 1, and the logs obtained are listed in table 1.

The geophysical logging emphasis during the ASR cycles was on spinner flowmeter, temperature, and fluid-resistivity logs, which reveal the relative hydraulic characteristics of various strata within the injection interval (955–1,105 ft). However, caliper logs were obtained on three occasions and electric logs on two occasions. On October 10, 1975, natural gamma, gamma-gamma density, and neutron porosity logs were run in the injection well. Acoustic televiewer images were obtained in the open hole of the injection well on April 20, 1978, and July 17, 1979.

Wellbore Clogging

During injection, the wellhead pressure rose as the rate of injection dropped as a result of clogging of the wellbore. This is illustrated by pressure and rate data shown on plate 1 for the first and second ASR cycles. In the third cycle, measurements were made weekly at the time of backflushes, and pressure and rate changes in the intervening days were not measured. The 1-hour backflushes that began in the second cycle were effective in restoring injectivity, as shown by the general uniformity in peak pressures and injection rates. In the third ASR cycle, backflushes were by artesian flow for 2 to 3 hours at a rate of 500 to 600 gal/min. The well was not acidized.

According to F.W. Meyer (oral commun., 1986), air entrainment was not a problem after some initial difficulties with the pump were resolved. Furthermore, an X-ray diffraction analysis of the backflushed sediment revealed that it consisted mainly of very fine particles of calcite and an iron compound (not scale) that had precipitated (F.W. Meyer, oral commun., 1990).

Spinner flowmeter logs run before, during, and following a backflushing operation on August 27, 1976, during the third injection, were analyzed to detect any changes in the vertical distribution of permeability that occurred as a result of plugging. The data do not indicate that any such change occurred.

HYDROGEOLOGIC CONDITIONS IN AQUIFER USED FOR STORAGE OF FRESHWATER

A characterization of subsurface formations and the spatial variation of their properties is essential for an understanding of the design of the freshwater injection, storage, and recovery tests and their results. This characterization begins with a regional description of stratigraphy and hydrostratigraphy, which is followed by a detailed description of stratigraphy and properties of important formation sequences at the Hialeah site.

Regional Stratigraphy and Hydrostratigraphy

A generalized stratigraphic column showing the major formations and hydrologic units in southeastern Florida is presented in figure 4. Some authors (Miller, 1986; Scott, 1988) include the Tampa Limestone as part of the overlying Hawthorn Formation, but Meyer (1989a) treats it separately. The ASR wells in Hialeah and St. Lucie County tap permeable strata near the base of the Suwannee Limestone, as do wells used to supply brackish water for reverse-osmosis plants in the Florida Keys. The ASR well in St. Lucie County also taps permeable strata at the base of the Ocala Limestone that underlies the Suwannee Limestone. The Ocala Limestone is thin or absent in most of Monroe, Dade, and Broward Counties, and in south-central Palm Beach County, either never having been deposited or having been mostly eroded away (F.W. Meyer, USGS, oral commun., 1983). Chen (1965), however, infers the existence of a thin (less than 100 ft) layer of Ocala Limestone throughout the area on the basis of a few incomplete samples. Vertically adjacent limestone units of the lower part of the Suwannee Limestone and of the Ocala Limestone and upper part of the Avon Park Formation are considered the upper part of the Floridan aquifer system, referred to as the Upper Floridan aquifer, and contain thin, discrete zones of high permeability.

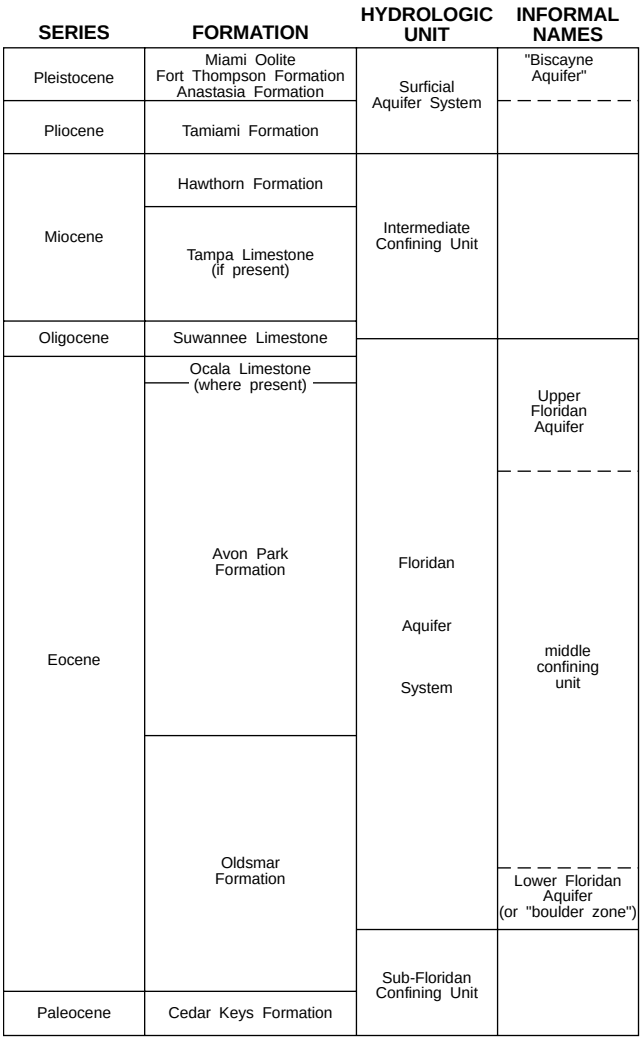

Figure 4. Generalized stratigraphic column for southeastern Florida showing major formations and hydrogeologic units.

Water quality in the Upper Floridan aquifer grades from brackish to saline with depth; hence, the permeable strata of the Upper Floridan aquifer is considered the most likely source of water in southeastern Florida for reverse-osmosis plant supply, or the most likely receptacle for temporary storage of freshwater. Where the aquifer contains water with less than 10,000 mg/L of dissolved solids, it is protected from contamination by Florida State law to ensure its continued availability for these and other uses. Water in the Upper Floridan aquifer originates as surface recharge in central Florida. Figure 5 shows estimated Upper Floridan hydraulic-head gradients and general direction of flows in the southern part of the Florida peninsula. Also shown is the region where water in the aquifer moving away from points of recharge retains a sufficient degree of freshwater recharge quality to be suitable for public consumption.

Stratigraphic and hydrostratigraphic units underlying the Upper Floridan aquifer generally are not suitable for freshwater storage because of their lack of permeability or the high salinity of the water contained within them. The lower part of the Avon Park Formation was formerly referred to as the Lake City Limestone, distinguished from overlying rocks primarily by its faunal composition, but Miller (1986) included it as part of the Avon Park Formation. The Lake City Limestone is no longer recognized as a formation by the USGS. The middle confining unit of the Floridan aquifer system contains discrete zones with solution porosity that generally are highly dolomitized and made up of very hard rock. No known aquifers match the high transmissivity of the cavernous, dolomitic Lower Floridan aquifer, better known by the drillers' term, boulder zone. This aquifer contains anomalously cold water of seawater-like composition. Meyer (1989a) presents data to support the thesis of Kohout (1965) that boulder-zone water originates as westerly flow through karst features or faults underneath the Straits of Florida near Fort Lauderdale. The boulder zone presently is used for the disposal of liquid wastes.

Stratigraphy and General Lithology at the Hialeah Site

A generalized sequence of predominant rock types at the Hialeah ASR site, based on a consideration of drillers' logs and sample descriptions from the injection and observation wells (Apps. A and B), is presented in figure 6. The upper 120 ft of limestone and sandstone at the site corresponds to the Pleistocene deposits that make up the upper part of the surficial aquifer system (the Biscayne aquifer and its overlying layer of compacted sands). Sandy, shelly, clayey marls interbedded with dense limestone or clay were found between a depth of 120 and about 975 ft. These beds correspond to the Tamiami Formation of Pliocene age, the Hawthorn Formation and Tampa Limestone of Miocene age, and the upper part of the Suwannee Limestone of Oligocene age. F.W. Meyer (USGS, written commun., 1975–80) picked 950 ft as the top of the Suwannee Limestone.

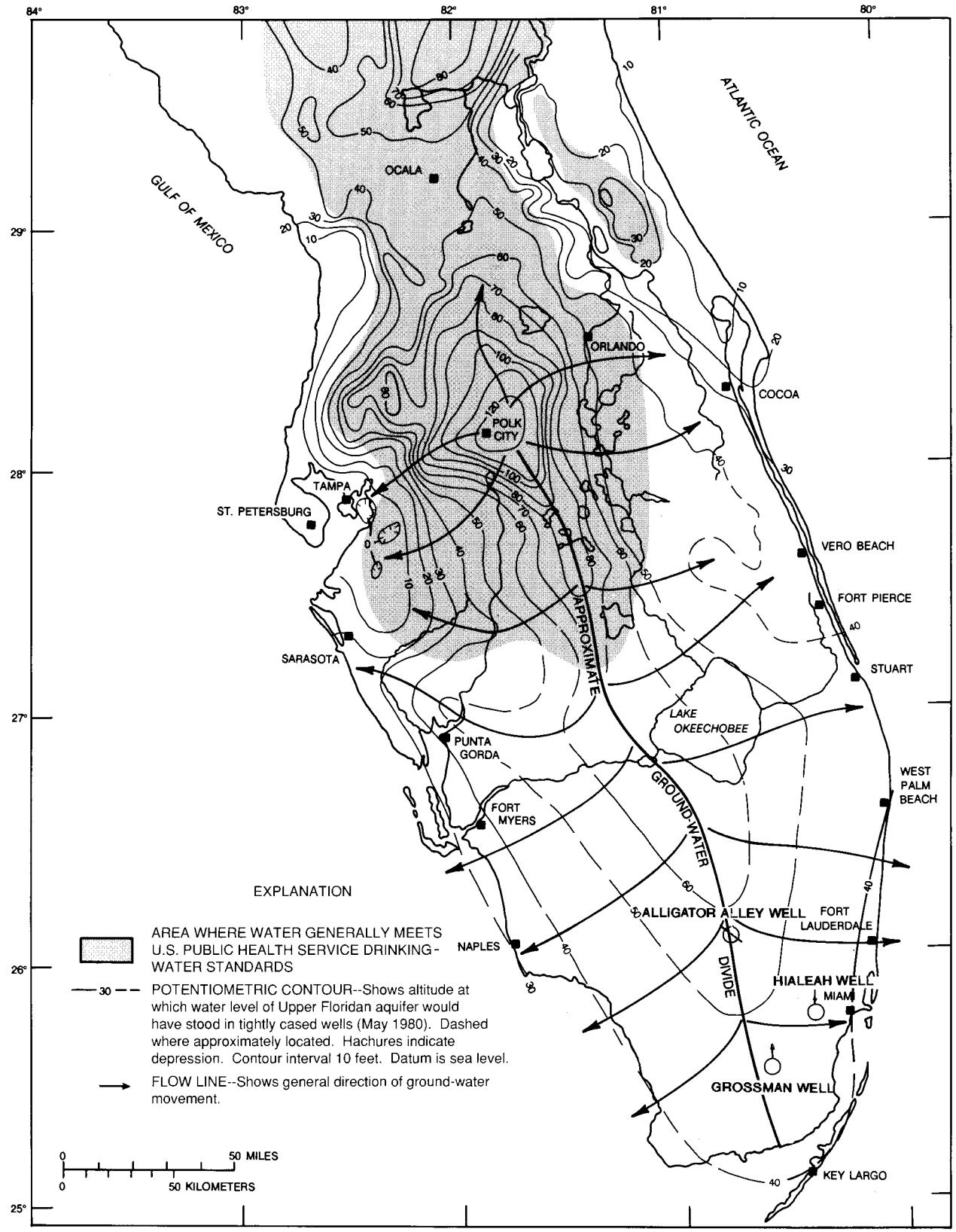

Figure 5. The potentiometric surface of the Upper Floridan aquifer in peninsular Florida in May 1980 and the area in which water in the aquifer is potable (from Meyer, 1989a).

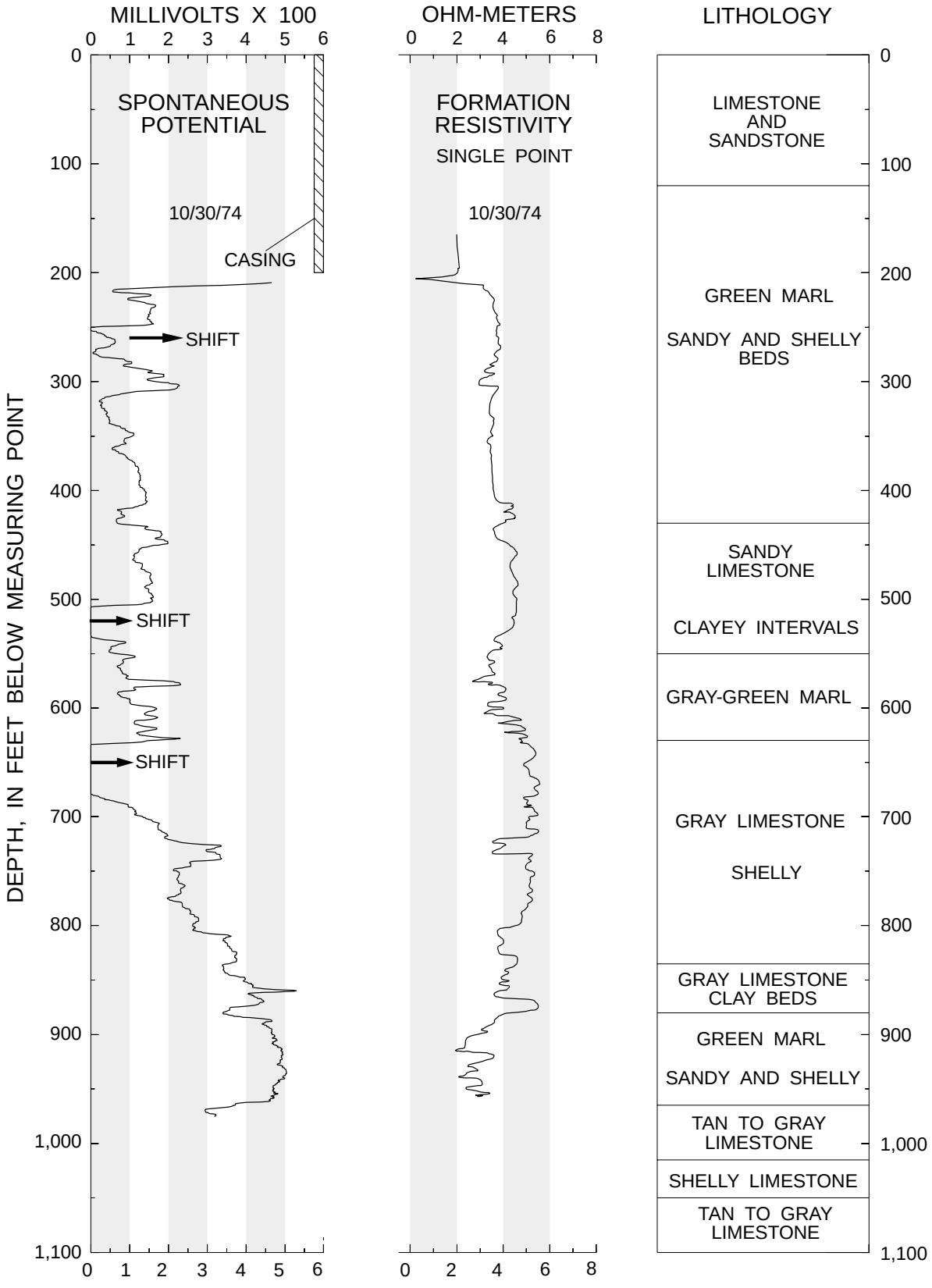

Figure 6. Electric logs of the Hialeah injection well (G-3061) and generalized lithology at the site.

Spontaneous-potential and single-point resistivity logs (fig. 6) were run to 975 ft in the nominal 10-in. injection-well pilot hole filled with aquagel on October 30, 1974. A correlation between the two log traces is evident. Increases in the spontaneous-potential readings that correlate with resistivity decreases indicate beds that predominantly are clay. The spontaneous-potential trace drifted, probably as a result of not grounding the borehole fluid, and was shifted three times to keep the pen on the left side of the chart. Inasmuch as the degree of the shifts is not indicated on the log, no attempt was made to compensate for them when the logs were digitized for report illustrations. The resistivity signal trace was highly oscillatory; thus, a trace of a line drawn through the center of the oscillating signal was digitized and provides the pertinent information. The single-point resistivity probe also commonly shows drift effects. The lower resistivity readings near the bottom of the hole probably indicate a more saline fluid.

The vertically contiguous, consolidated limestone beds of the Floridan aquifer system begin at a depth of about 975 ft and correspond to the lower part of the Suwannee Limestone of Oligocene age and the Avon Park Formation of Eocene age. The interval between depths of 1,015 and 1,050 ft is very shelly. Increases in flow were noted by the drillers as drilling progressed through this interval (App. A). The completed injection well was open to the depth interval between 955 and 1,105 ft, herein termed the injection zone. The receiving zone, or flow zone, is defined as the permeable interval between approximate depths of 1,024 and 1,036 ft that receives most of the inflowing freshwater.

Properties of the Injection Zone

Injection-zone properties needed to facilitate interpretation of the results of the injection and recovery tests are lithology, thickness of beds, hydraulic properties (hydraulic conductivity, porosity, and dispersivity), and the chemical quality of the water contained in the formation. These properties are described in the following sections.

Lithology

The generalized lithology of the depth interval 900–1,100 ft in the injection well (G-3061) is shown schematically in figure 7, which also depicts caliper, formation resistivity, natural gamma, and neutron porosity logs for correlation. The caliper log shows a decrease in diameter within the 14-in. casing below 940 ft from remains of the cement plug that was drilled through with a 12-in. bit. The log also shows part of the 22 1/2-in. reamed hole, just below the bottom of the casing, where cement washed out when drilling was resumed with a smaller bit. The caliper log does not show evidence of cavernous porosity or large solution features. In fact, the log gives no indication that any part of the injection zone has solution porosity. Thin hole enlargements at depths of 1,010, 1,050, 1,070, and 1,090 ft are probably the result of washouts occurring during successive stages of the drilling. Acoustic televiewer logs also failed to show evidence of solution porosity.

Other geophysical logs correlate with lithologic data. The large natural gamma counts from the bottom of the casing to 975 ft correlate with other wells regionally, as will be shown later in the report. The lithologic description for the injection well (App. B) notes phosphorite grains in the clay found in the depth interval from 900 to 975 ft. This mineral contains trace amounts of naturally radioactive material. The formation-resistivity logs (fig. 7) show high-resistivity zones centered at 986 and 1,032 ft, both apparently correlating with increases in natural gamma activity and a decrease of porosity on the neutron log. At the first depth, the drillers noted very hard streaks in the limestone. A hard dolomitic layer is found at the second depth, and the drillers log cites an increase in flow in this interval (App. A). Dolomite beds typically show higher resistivity because of their lower porosity and are sometimes found at the erosional surfaces of formations. The acoustic televiewer logs (not reproduced herein because of their generally poor quality) show what seem to be distinct bedding interfaces at 986 and 1,032 ft (F.W. Meyer, oral commun., 1975). A hypothesis consistent with these observations is that the hard beds mark upper and lower erosional surfaces of a thin section of the Ocala Formation. Verification of the existence of a thin bed of Ocala Formation rocks at this location, however, would require additional data acquisition and analysis.

A similar suite of geophysical logs (fig. 8) from the observation well (G-3062) helps to establish background conditions in the injection zone prior to the ASR cycles. The 16- and 64-in. normal-resistivity logs, the caliper log, and the natural gamma log have interpretations that are similar to those of logs from the injection well. The temperature and fluid-resistivity logs are discussed in the following sections. The schematic diagram (fig. 8) shows depths of the monitor tubes installed in the observation well.

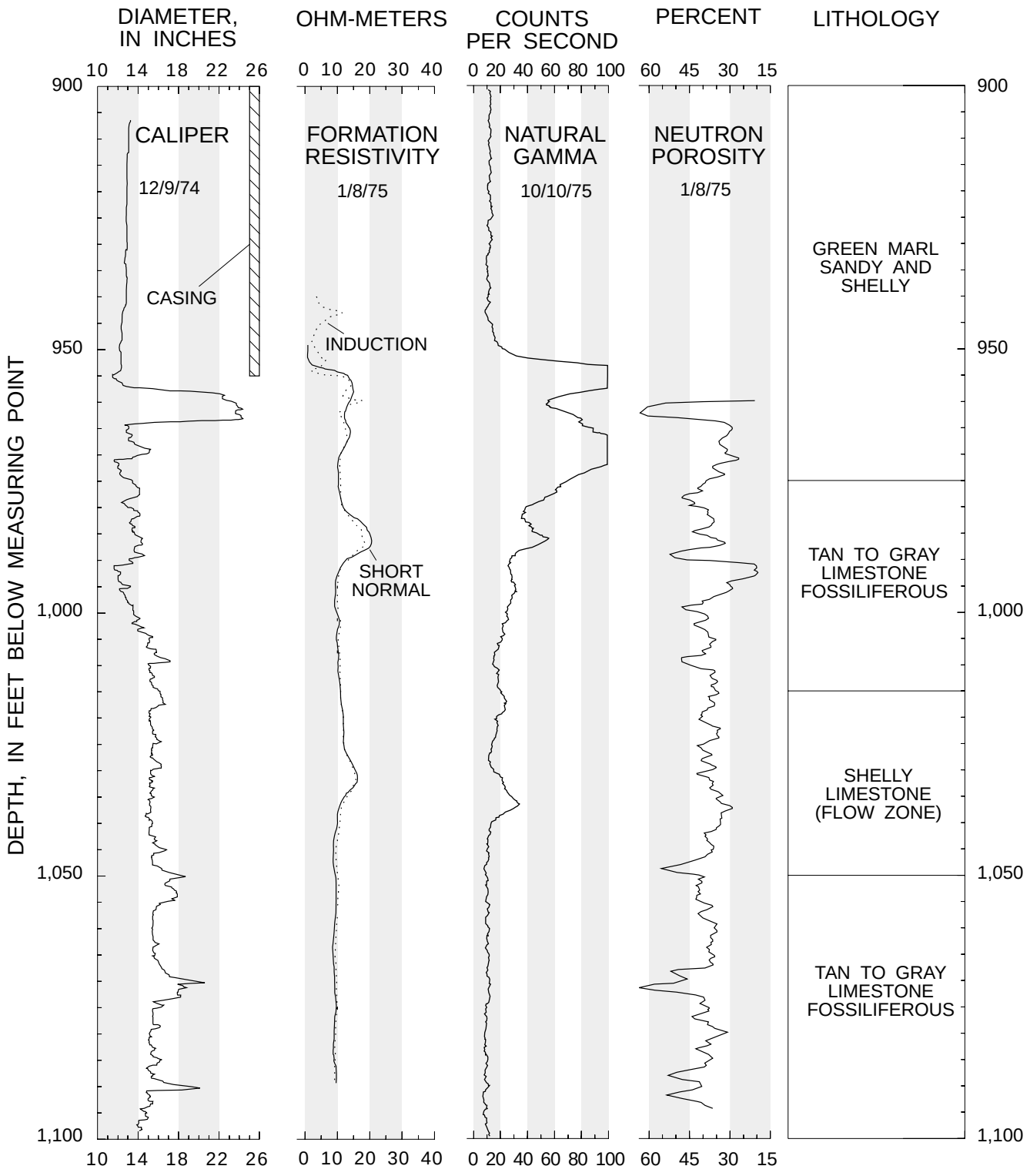

Figure 7. Geophysical logs of the Hialeah injection well (G-3061) and generalized lithology of the injection zone.

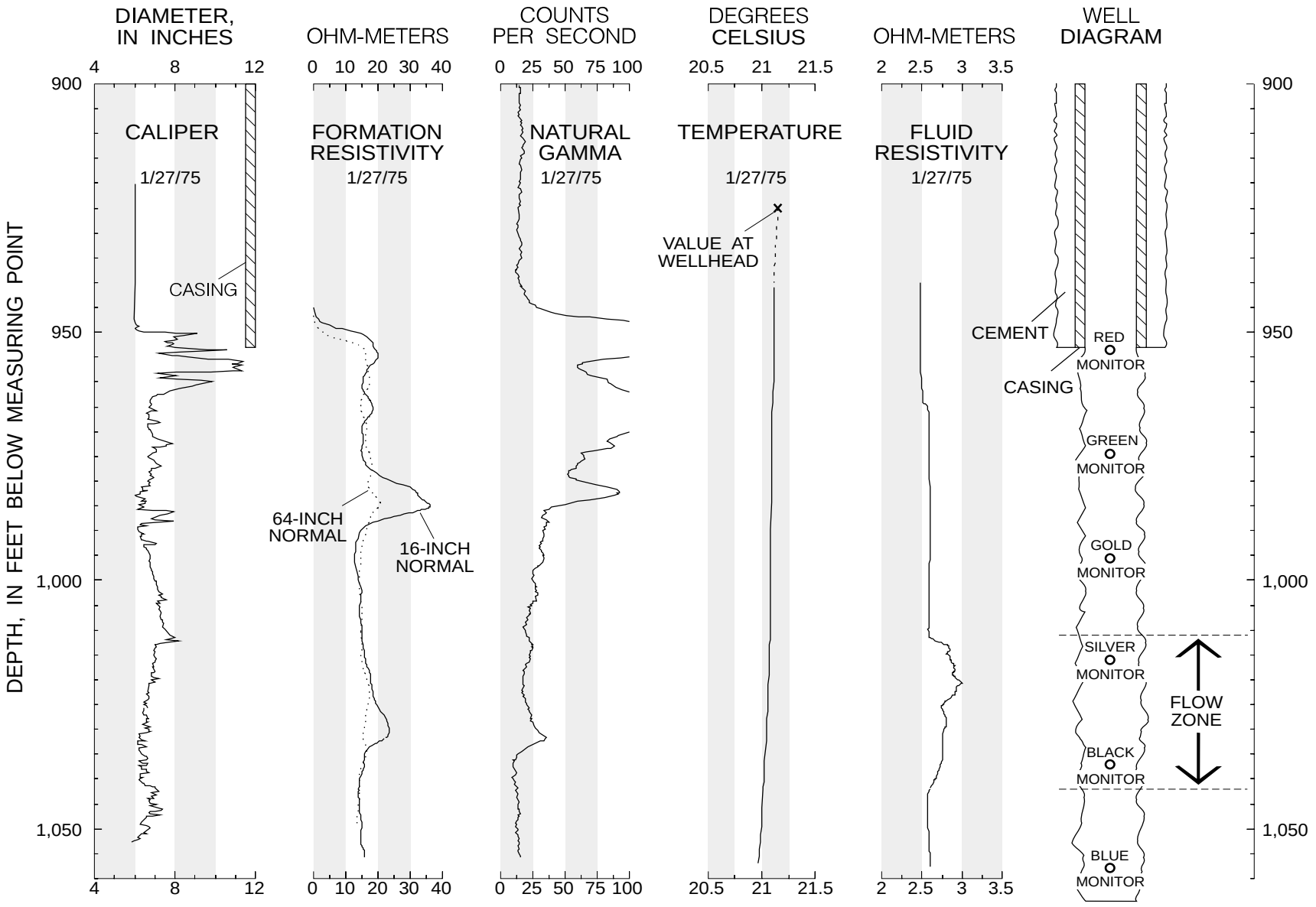

Figure 8. Geophysical logs of the Hialeah observation well (G-3062) and depths of monitor tubes.

Transmissivity

Aquifer tests were conducted to measure the composite transmissive capability of the 150-ft injection zone, known to be made up of strata of strongly contrasting permeability. When this information is combined with a knowledge of the thickness, distribution, and relative contribution of permeable flow zones obtained by geophysical logging under flowing conditions, a better understanding of the disposition of the water injected during the ASR process can be gained, and the transmissivity of each flow zone can be estimated. Estimates of hydraulic conductivity in individual zones can then be derived by dividing flow-zone transmissivities by their approximate thicknesses. The generic computer code used in this study requires input of estimates of hydraulic conductivity and the thickness and distribution of flow zones and confining layers for simulation of freshwater injection, storage, and recovery.

The first aquifer test was conducted on February 10, 1975, by allowing the 6-in. observation well at Hialeah to discharge for 100 minutes at 250 gallons per minute (gal/min) as pressures were measured in the injection well and in the 2-in. monitor tube open at 840 ft in the observation well. Discharge was measured using an orifice plate on the observation well. Two pressure gages, their readouts in feet of head, were used in the injection well. These gages had a display range of 0–60 ft of head at 0.2-ft scale divisions. The maximum drawdown at the injection well was 1.8 ft. Pressure changes during recovery were observed for 15 minutes immediately following the closing of the orifice. The following day, a second aquifer test, a constant-head discharge test, was performed.

During the first aquifer test, values of head from the two injection-well gages differed by about 2 ft and showed slightly different trends. Both drawdown data sets were analyzed for estimates of transmissivity (T) and storage coefficient (S) using the method of Jacob and Lohman (1952). Data from one gage, considered to be the more representative, were also analyzed using the Theis type-curve method. On the basis of the various analyses, transmissivity was estimated to be about 11,000 $[(ft^3/d)/ft^2]ft$ (Meyer, 1989b). The maximum drawdown in the 2-in. monitor tube was 0.2 ft (F.W. Meyer, written commun., February 1975), indicating that minor leakage occurred across the marly confining beds separating the injection zone from the perforations at 840 ft.

Flow-Zone Depth and Thickness

A delineation of the relative permeability of the various strata within the injection zone was partly based on a study of data collected during spinner flowmeter logging during injection and recovery. The quantitative analytic procedure developed for this study is described below. Also presented is a parallel description of the flow-zone depth and thickness based on an evaluation of fluid-resistivity and temperature logs.

Analysis of Data From Spinner Flowmeter Logs

Two sets of spinner flowmeter data were collected from the injection well on October 20, 1975, while the well backflowed under artesian pressure. These data are shown in figure 9, together with caliper log data, to illustrate a typical analysis for obtaining a vertical profile of the relative amount of flow in the wellbore. One set of data was recorded as the probe was lowered into the well, and the other as the tool was raised.

Spinner flowmeter probes contain a device that rotates in response to the relative speed of fluid movement past the probe. Measurements of the rotation speed are transmitted to the logger in counts per second. However, the probe does not indicate the direction of relative flow, only the rate of the spinner rotation. When the probe was lowered to the bottom of the well on October 20, 1975 (fig. 9), the direction of relative flow past the probe remained in the upward direction throughout the entire logged interval, including the stagnant zone between the flow zone and the bottom of the well. However, a different situation prevailed as the probe was raised from the bottom. The upward moving probe responded to apparent downward flow (relative to the changing position of the probe) in the stagnant zone. As the probe moved upward past the flow zone, relative flow through the probe reversed direction and was upward in the direction of discharge from the well. Therefore, as the relative flow direction changed, the spinner slowed, and a null reading was recorded, as shown at 1,028 ft in figure 9. Analysis of the recorded data to produce a vertical-flow profile requires reversing the arithmetic sign of the data at the depth where the null occurs.

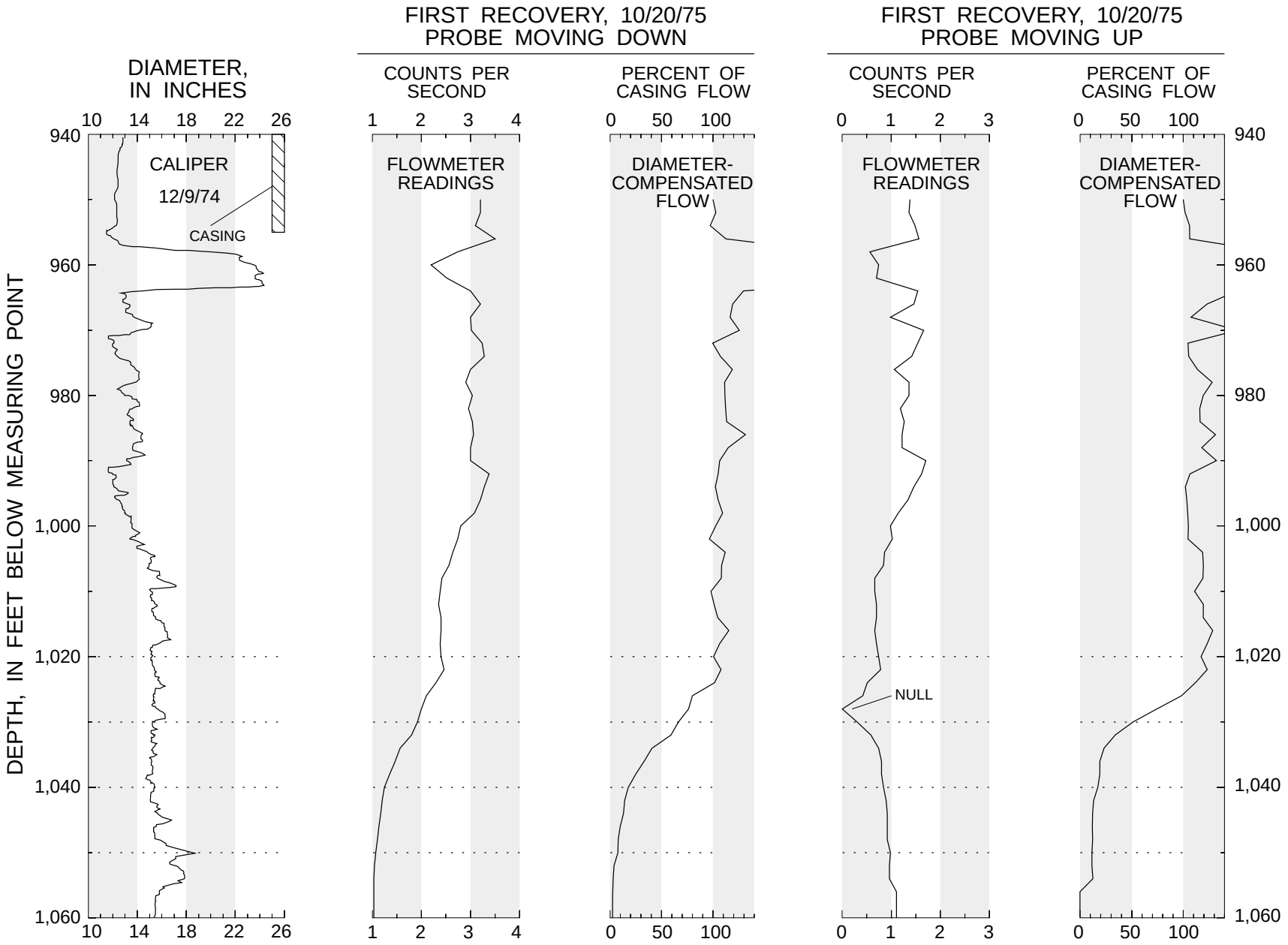

Figure 9. Conversion of a typical set of spinner flowmeter data to wellbore flow measurements.

Stationary spinner flowmeter measurements, in which the rotation speed is observed while the probe is hung at a fixed elevation, are more reliable than continuous readings that must be corrected for tool velocity, but often fail to clearly show the depths at which changes in flow occur. During the Hialeah tests, stationary flowmeter measurements were obtained during the logging sequences of May 25, 1976, and April 20, 1978 (fig. 10). On May 25, 1976, the stationary reading at 1,046 ft was only 7 percent of that measured in the casing, and a zero reading was obtained at 1,059 ft. On April 20, 1978, a zero reading was obtained at 1,040 ft. These measurements proved that flow in the bottom of the hole was negligible and aided in interpreting other geophysical logs.

Whether spinner flowmeter measurements are continuous or discrete, the measured velocity varies with the diameter of the borehole as well as with the quantity of flow produced. Therefore, in quantitative analyses, flowmeter data must be adjusted to compensate for borehole diameter. For example, the flowmeter data values recorded as the probe moved downward on October 20, 1975, show a decline below 992 ft. However, the borehole diameter increases, and the diameter-compensated flow values remain nearly uniform to a depth of 1,024 ft.

Quantitative analysis of flowmeter data consists of the diameter compensation and an adjustment for the velocity of the probe during descent or ascent. Flow at a given depth $Q(h)$ can be expressed as a percentage $\Delta Q(h)$ of flow within the lower part of the casing Q_0 where the radius r_0 is considered to be locally uniform. The computation can be written as

$$\Delta Q(h) = 100\frac{Q(h)}{Q_0} = 100\ \frac{\pi r(h)^2}{\pi {r_0}^2}\left(\frac{C(h)\beta - V_t(h)}{C_0\beta - V_0}\right) \qquad (1)$$

where: $r(h)$ is the borehole radius at depth h,
$C(h)$ is the measured counts per second at depth h,
C_0 is the measured counts per second in the casing,
β is a conversion factor relating counts per second to velocity,
$V_t(h)$ is the velocity of the tool at depth h, and
V_0 is the velocity of the tool at the depth where C_0 is measured in the casing.

In flowmeter logging in long boreholes, the probe velocity can vary appreciably, and a record usually is made of the tool velocity at regular depth intervals. In the flowmeter logging conducted during the Hialeah ASR tests, however, the logged interval was short (generally 940–1,100 ft), and at best, a single value for probe velocity is noted on the logs. Therefore, the assumption was made in the analysis that the probe velocity was uniform throughout; that is,

$$V_t(h) = V_t = V_0 \qquad (2)$$

Furthermore, because stagnant water is present in the bottom of the borehole, the probe velocity is related to counts recorded in the bottom of the hole C_b; that is

$$V_t = \beta C_b \qquad (3)$$

Equation 1 now reduces to

$$\Delta Q = 100\frac{r(h)^2}{{r_0}^2}\frac{[C(h) - C_b]}{(C_0 - C_b)} = 100\frac{r(h)^2}{{r_0}^2}\frac{\Delta C(h)}{\Delta C_0} \qquad (4)$$

In this formulation, counts at depth h, $C(h)$, are referenced to counts in the bottom of the hole (C_b) and adjusted by the ratio of the squares of the radii. This provides a simple formula for digital computation.

Many problems are associated with the quantitative analysis of spinner flowmeter logs. When the probe passes through thin zones of larger diameter, the moving fluid often apparently does not develop a uniform velocity throughout the enlarged borehole; thus, the diameter compensation can lead to error. When the probe moves in the direction of well discharge and the spinner reverses direction, the counts do not always read zero, or null, on the chart; thus, errors can occur in computing the degree of flow augmentation in this interval. Depth errors can occur as a result of cable stretch or errors in depth orientation. Such errors can be critical in making diameter compensations and in precise evaluation of the depths at which significant flow augmentation occurs. Errors can be introduced related to the physical operation of the spinner device; the device may be more sensitive to flow from one direction than the other, and a time lag can occur in the response of the device to changes in borehole flow, depending on the probe velocity.

Each of the 18 spinner flowmeter logs run during the ASR cycles was digitized at 2-ft depth increments and converted to relative volumes of flow using equation 4. Nulls were identified and assigned $C(h)$ values of zero, while data from lower depths were considered to be negative values and data from higher depths were considered to be positive values. Depth errors due to cable stretch or calibration error were identified by comparing low count intervals with the large-diameter interval centered at 960 ft in the injection well, and depth adjustments ranging from 0 to 6 ft were made to all recorded depths in the logged interval. Results of the analyses are shown in figure 10.

Examination of the computed flows indicates a depth of 1,024 ft to be the top of the flow zone. Evidence identifying the bottom of the flow zone is less clear, but the bottom is most likely at 1,036 ft, indicating a flow-zone thickness of only 12 ft. On the basis of some logs, the zone might extend to a depth of 1,040, 1,044, or 1,050 ft, indicating possible flow-zone thicknesses of 16, 20, or 26 ft.

A slight amount of flow between depths of 955 and 965 ft was noted during drilling (App. A), but the flowmeter log analyses show no evidence of it; thus, the amount of flow from this depth interval apparently is negligible compared with that from the principal flow zone (1,024–1,036 ft). No appreciable contribution to flow seemed to originate from the indicated bedding interface at 986 ft. Any slight contribution would have been masked by the effect of irregularities in the borehole diameter.

Spinner flowmeter logs in the observation well could have been used to verify that the narrow flow zone in the injection well was similar in character at the location of the observation well, and in supporting the hypothesis that the zone was similar throughout the region of injected freshwater flows. A flowmeter log was attempted in the observation well on January 27, 1975, but the probe would not pass below a depth of 983 ft. The installation of multidepth samplers in the observation well at the beginning of the ASR cycles rendered subsequent flowmeter logging of this well infeasible.

The flowmeter logs of August 27, 1976, as previously noted, are useful in assessing the degree to which the vertical permeability distribution may be affected by borehole plugging during injection. The spinner was raised and lowered during (1) injection before a backflush, when plugging had substantially reduced injectivity; (2) the backflush; and (3) injection immediately following the backflush, after most of the natural injectivity had been restored. An examination of the converted logs (fig. 10) shows more apparent difference between the up and down logs of each set than between any sets of logs. All tend to confirm the previously accepted hypothesis that the flow zone lies between depths of 1,024 and 1,036 ft, and there is no indication that any change in the vertical distribution of injectivity has occurred.

The flowmeter logs shown in figure 10 cover a period of injection, storage, and recovery lasting nearly 4 years. The similarity of the results throughout this time period indicates that no long-term changes in the vertical distribution of injectivity have occurred.

Interpretation of Data From Temperature and Fluid-Resistivity Logs

Logs of temperature and fluid resistivity run before and during the ASR cycles are used as additional means to corroborate the delineation of the flow zone. These logs are also used to aid interpretation of interesting facets of the injection and recovery process and the effect of the process upon water quality.

Temperature and fluid-resistivity logs run in the observation well on January 27, 1975 (fig. 8) were for the purpose of establishing background conditions prior to ASR cycles. The fluid-resistivity log, probably run during artesian flow, shows inflows of increasing resistivity (fresher water) between 1,011 and 1,042 ft, an interval which corresponds to 1,015 and 1,046 ft in the injection well because of the different elevations of the measuring points. The interval also correlates with the interval of shelly limestone (fig. 7) that contains the flow zone.

One possible interpretation of a zone of fresher water surrounded above and below by more saline water is that the zone is sufficiently permeable to be partly flushed by flow from upgradient areas of freshwater recharge. The Floridan aquifer system crops out in central Florida, where it receives atmospheric recharge and contains potable water (fig. 5). The peak resistivity in the log of January 27, 1975, is at a depth of 1,020 ft (1,024 ft in the injection well, the probable top of the permeable flow zone). The temperature log, run as the well flowed under artesian pressure, shows temperature to be nearly uniform from land surface to about 1,010 ft, below which the temperature decreases about 0.2 °C in 50 ft, an indication that inflow occurs in this interval.

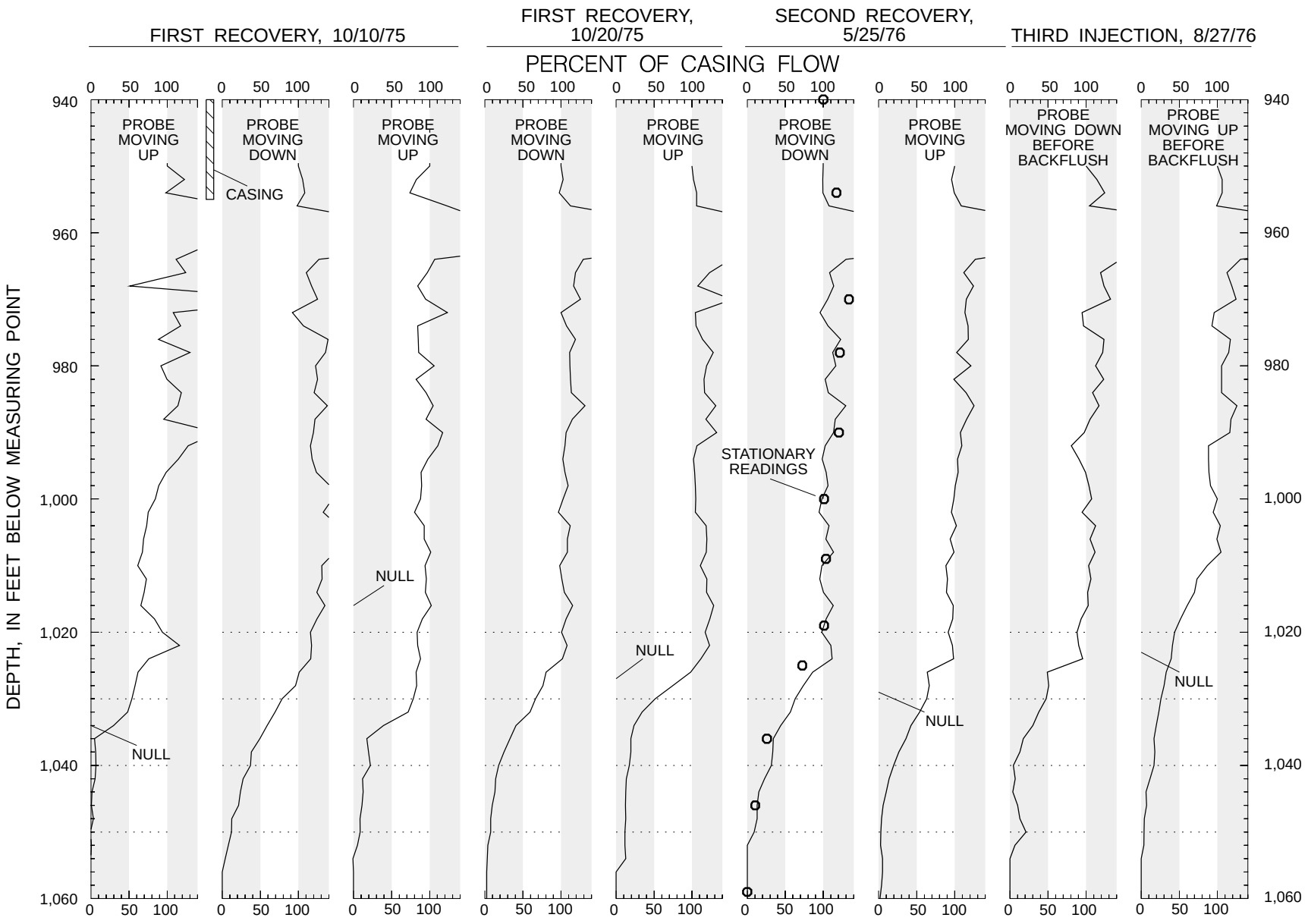

Figure 10. Wellbore flow measurements from conversion of spinner flowmeter logs of the injection well (G-3061) during three injection and recovery cycles (1975-79).

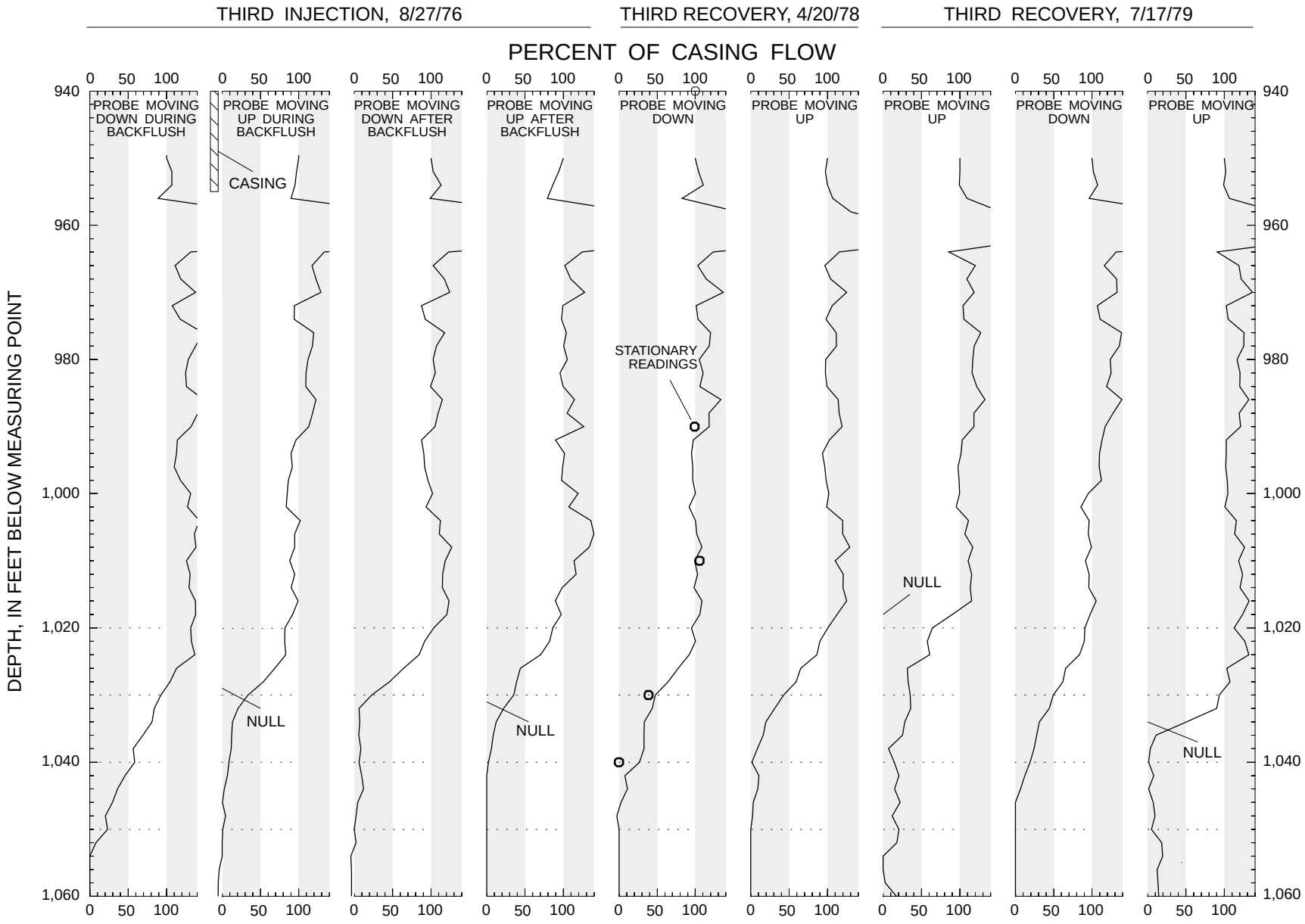

Figure 10. Wellbore flow measurements from conversion of spinner flowmeter logs of the injection well (G-3061) during three injection and recovery cycles (1975-79)--Continued.

Selected logs of temperature and fluid resistivity in the injection zone obtained as water backflowed during the three recovery phases are shown in figure 11. For comparison purposes, the temperature log run on October 10, 1975, 30 days into the first recovery, when the chloride concentration of recovered water had reached 300 milligrams per liter (mg/L), is shown together with the observation-well temperature log of January 27, 1975, which depicts preinjection conditions. Measurements of the temperature of water from the supply well during the three injection phases are shown in figure 12. The temperature of injected water in the first ASR cycle averaged 25.55 °C, in contrast with the preinjection temperature in the injection zone of about 21.2 °C. The temperature of recovered water on October 10, 1975, was about 24 °C, but the temperature increased rapidly to about 25 °C below 1,047 ft (fig. 11). Fluid resistivity on the same date also increased markedly below 1,047 ft. Below 1,047 ft, therefore, is a zone of warmer, fresher water that is likely stagnant injected water either forced into the zone of relatively low permeability underlying the flow zone during the previous injection or forced downhole by turbulent convection. At 300 mg/L of chloride concentration, recovered water contains about 22 percent native water. The temperature decrease from 25.5 °C to 24 °C probably is caused by mixing and thermal diffusion.

A break in the fluid-resistivity trace of October 10, 1975, and a slight break in the temperature trace of the same date, occurs just below 1,025 ft, indicating a concentration of flow at this depth. That the water becomes relatively more saline and slightly cooler above this elevation also suggests more rapid recovery of injected water from cavities at this elevation.

The fluid-resistivity log run on May 25, 1976, 22 days into the second recovery phase, when the chloride concentration of recovered water had reached 124 mg/L (about 6.5 percent native water), shows a more gradual resistivity increase with depth, beginning at about 1,018 ft and becoming more pronounced after about 1,047 ft (fig. 11). No temperature log was obtained. Again, there seems to be stagnant freshwater in the bottom of the hole, particularly below 1,047 ft.

The temperature and fluid-resistivity logs of April 20, 1978, 276 days into the third recovery, when the chloride concentration of recovered water had reached about 600 mg/L (about 48 percent native water), again show stagnant, warmer freshwater in the bottom of the hole below 1,043 ft. The average temperature of the injected water in the third ASR cycle was 25.93 °C. On April 20, 1978, recovered water above 1,020 ft had a temperature of about 22.8 °C (fig. 11), close to the preinjection background of 21.2 °C, apparently a result of both mixing and at least 457 days of thermal diffusion (the storage period was 181 days). A slight break in the trace of the fluid-resistivity log at about 1,022 ft suggests a concentration of inflow, possibly correlating with similar indications at 1,025 ft during the first recovery and at 1,018 ft during the second recovery. The slight difference in elevations could easily be attributed to depth measurement error. The temperature log of July 17, 1979, 729 days into the third recovery, when the chloride concentration of recovered water was 1,060 mg/L (about 88 percent of that in the native water), shows the recovered water temperature to have dropped to about 22.0 °C, even closer to that of the native water before injection. The fluid-resistivity log of the same date shows slightly more saline water below 1,030 ft. Apparently, recovery has been of sufficient duration to have flushed the stagnant freshwater from the bottom of the hole and surrounding rocks, though some of the thermal energy remains.

All of the temperature logs show some cooling of the warmer water near the bottom of the hole. This could be due to the closer proximity of stagnant warm water in the bottom of the hole to the vast thermal sink below.

On the basis of temperature and fluid-resistivity logs and the preceding analysis of the spinner flowmeter logs, it seems that a depth of 1,024 ft approximately marks the top of the flow zone and may be a point source for much of the flow. The bottom of the flow zone now seems to be in the 1,043- to 1,047-ft range. However, the proportionate amount of flow that occurs below 1,036 ft may be insignificant.

Porosity

A review of data that leads to estimates of aquifer porosity is useful because the generic simulator used in this study implicitly represents aquifer storativity with input specifications of effective porosity, rock and water compressibility, and thicknesses of permeable flow zones. Effective porosity, which changes slightly as pressure varies and the aquifer pores expand or contract, is a direct measure of the amount of injected freshwater that can be accepted by a unit pore volume of the aquifer. Total porosity is a measure of the amount of water contained within a unit pore volume and may be greater than effective porosity if some of the water is contained in pores that are not connected to flow pathways.

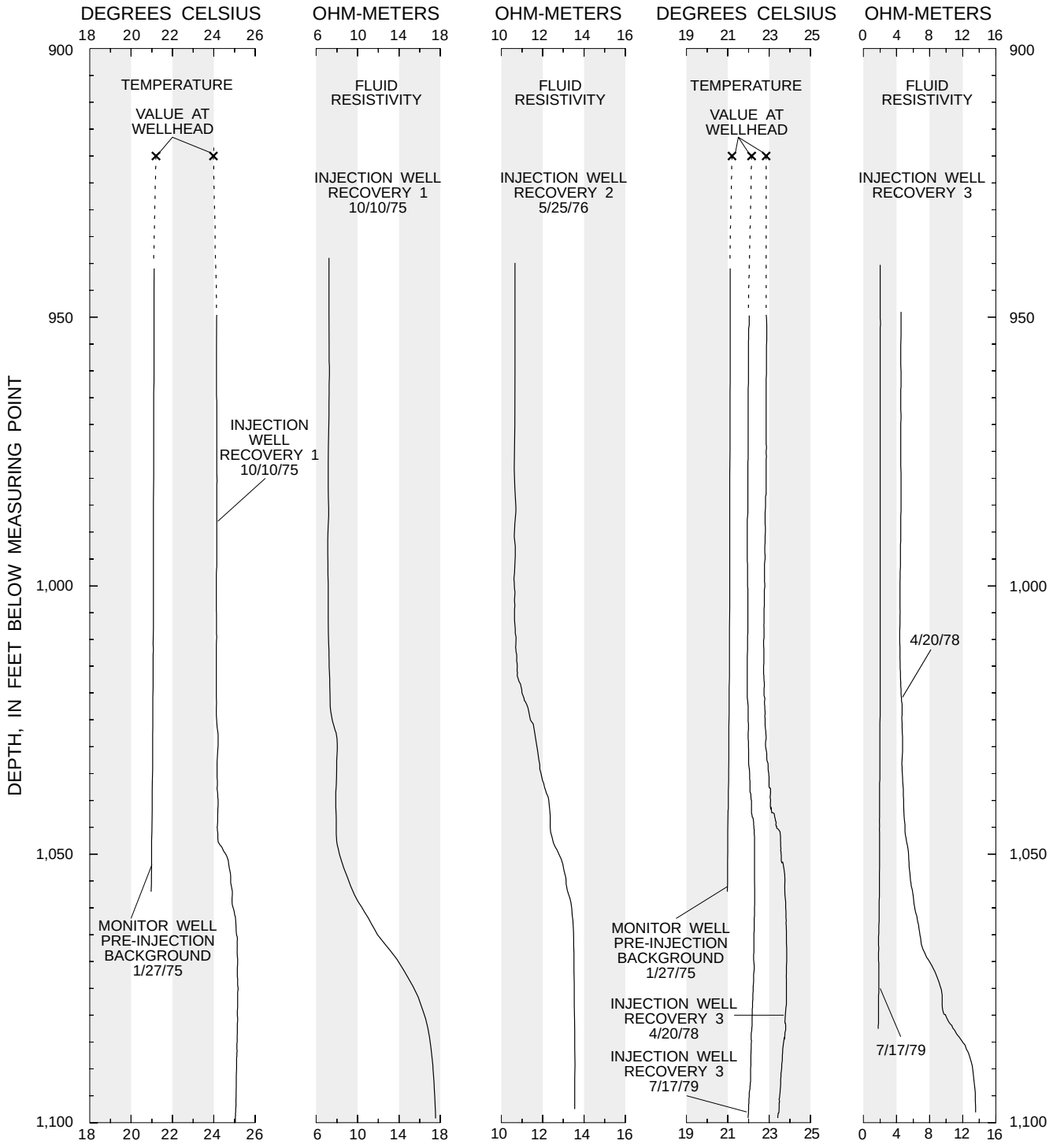

Figure 11. Temperature and fluid-resistivity logs of the injection well (G-3061) before and during aquifer storage and recovery cycles.

Direct measurements of injection-zone total porosity consist of the neutron porosity log run in the injection well by Schlumberger, Inc., on January 8, 1975, and neutron porosity logs run by the USGS in the injection and observation wells on October 10, 1975, and January 27, 1975, respectively. The Schlumberger log data, illustrated in figure 7, were stated by the contractor to have been compensated for borehole effects. Porosity seems to average about 35 percent throughout the injection zone. Large variations between extreme values of 20 and 65 percent occur within discrete intervals. Although no reason exists to

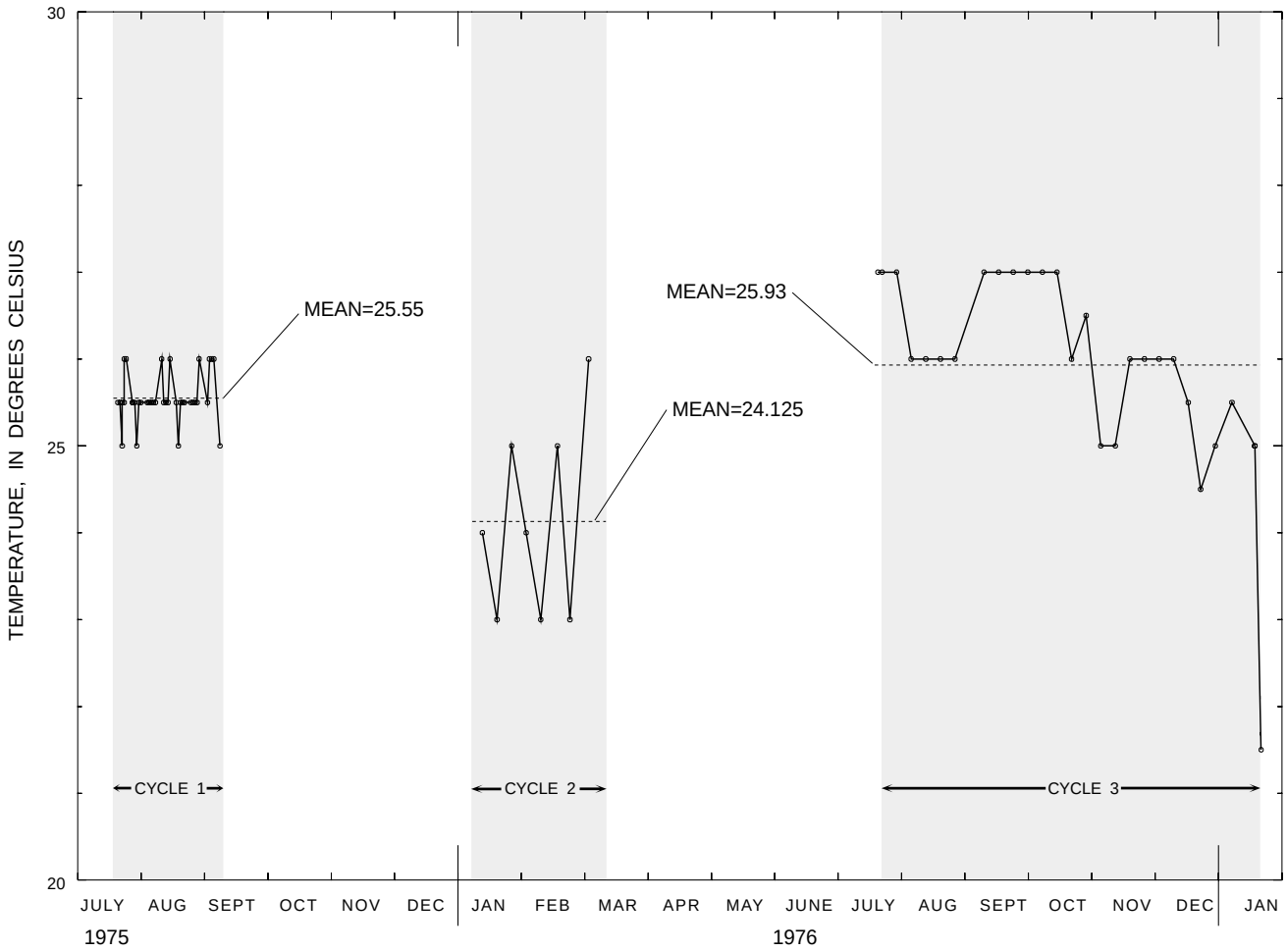

Figure 12. Temperature of water from the injection supply well during aquifer storage and recovery cycles.

question the validity of the lower values, the high-porosity spikes probably indicate where exceptional borehole irregularity has caused an overestimate of the amount of the compensation. The USGS logs were not compensated for borehole effects and were not used for porosity estimates.

Estimates of storage coefficient obtained from analyses of aquifer-test data can sometimes be used to check porosity data and corresponding estimates of rock compressibility and aquifer thickness. However, the disparity among the storage coefficients estimated from the Theis and Jacob-Lohman analyses of the February 10, 1975, aquifer test discouraged attempts to make such detailed comparisons.

The neutron porosity log measured the total water content of the formation, including that contained in either pores within the rock or in solution features. Of striking interest is the fact that the average value of 35 percent seems to be the water content not only of the solution-riddled flow zone, but also of overlying and underlying layers of negligible solution porosity. However, a 35 percent value for total porosity does seem to be consistent with the result of laboratory analyses of cores from the relatively impermeable confining layers that overlie the Lower Floridan aquifer (boulder zone). A cursory review of many core analyses performed by private laboratories for engineering consultants managing the construction of municipal waste-disposal wells indicates that porosities of 25–40 percent typically are measured on cores that are predominantly limestone. Porosities of dolomite cores, on the other hand, generally fall into a lower range of 1–15 percent.

Water Quality

A characterization of the quality of the native water is needed for an understanding of factors that affect flow processes, recoverability, wellbore plugging, and the quality of recovered water. Inclusion in

Appendix D of measurements of the chemical and biological constituents of native, injected, and recovered water provides the data to readers for many possible uses. One of the most interesting potential uses is to determine changes in the quality of the injected water after a period of residence in the aquifer. However, the interpretive scope of this report is limited to a discussion of water-quality characteristics affecting ASR flow processes and recoverability and the simulation of the ASR process with computer models. Therefore, the chemical characteristic of principal interest is density.

The degree of buoyancy stratification that occurs depends on the density contrast between injected and native water. Recoverability of injected water is reduced by buoyancy stratification (Merritt, 1985). Recoverability also is determined by the degree of dispersive mixing with the native water, another reason for accurately describing the salinity of the native water. The higher the salinity of the native water, the less the amount of mixed injected and native water that will be potable. Buoyancy stratification and dispersive mixing are processes that must be accurately represented to achieve the simulation objectives of this study.

Direct measurements of density usually lack sufficient accuracy for many purposes (Meyer, 1989a), and water density is more accurately estimated as a function of known salinity and temperature. Salinity is based herein on measurements of dissolved solids, which correlate well with chloride concentrations in brackish waters of the Upper Floridan aquifer.

A characterization of the salinity of native water in the injection zone is based on preinjection water-quality samples from the injection and observation wells, on water-quality data obtained from the observation-well monitor tubes early in the first ASR cycle, and from the preinjection fluid-resistivity log run in the observation well on January 27, 1975. The monitor-tube data obtained later in the ASR cycles help to corroborate this interpretation and also facilitate an understanding of flow processes during ASR cycles.

Preinjection Sampling and Geophysical Logging

The water-quality samples (App. D), obtained on November 20, 1974, from the observation well and on December 4, 1974, from the injection well represent a composite of water quality from all elevations within the 150-ft open borehole, dominated by the quality of water from elevations at which the formation has high permeability (the flow zone). The chloride concentration measured in each well was 1,200 mg/L, and the dissolved-solids concentration was about 2,700 mg/L.

A partial description of water-quality variation within the injection zone is obtained from a study of the preinjection temperature and fluid-resistivity logs from the observation well on January 27, 1975 (fig. 8). Before the logging, the observation well was allowed to flow on November 20, 1974, sampled, and then shut in. The well was logged on January 8, 1975, by Schlumberger, Inc. (caliper and cement bond), and the 2-in. monitor tube was perforated. The sequence of the logs run on January 27, 1975, is not known. Annotation on the temperature log indicates that the log was run under flowing conditions. The data show a temperature increase up the hole that is more rapid below about 1,015 ft than above 1,015 ft. This tends to indicate that most contributions of flow occur below about 1,015 ft. A fluid-velocity log was also attempted, but the probe would not pass below 983 ft. No annotation was found on the log to indicate that the well was flowing while the fluid-resistivity log was run. However, F.W. Meyer (written commun., 1980) has interpreted it as a production (flowing) log. The data depict an unusual description of resistivity variations within the wellbore that presents some interpretive difficulties. To describe these difficulties and their resolution, the usual method of interpreting flowing fluid-resistivity logs is briefly considered.

Generally, fluid-resistivity logs run during production (flow from the well) tend to show resistivity changes at elevations where the volume of flow from the well is augmented by appreciable amounts of water of different salinity from that of water flowing from lower zones in the well. At those elevations, the fluid resistivity changes to represent the new composite salinity of water from the new zone and from the lower zones. Often, in the Upper Floridan aquifer, salinity decreases upward, and the resistivity trace shows increases at permeable-zone elevations as the probe moves upward. The fluid-resistivity logs in figure 11 show a reverse pattern. In these logging runs, the probe was raised from a pool of stagnant freshwater at the bottom of the well and passed through permeable zones where a brackish mixture of native and injected waters flowed from the formation into the borehole under artesian pressure. As the probe passed through these zones, the measured resistivity decreased.

Because the trace of the January 27, 1975, flowing-resistivity log (fig. 8) shows both positive and negative deflections, the apparent conclusion is that water of lower salinity contributes to the flow at lower elevations and is then augmented by water of higher salinity at higher elevations. In fact, the log indicates water above 1,011 ft to be about equal in salinity to that at the bottom of the well, below 1,043 ft. Because the existence of a permeable zone containing water of higher salinity is unlikely, the data suggest that the instrument could have drifted out of calibration. The principal significance of these data is to show that a zone of low salinity at 1,020 ft (1,024 ft in the injection well) is surrounded above and below by more saline water. Possibly, water in the flow zone grades from lower salinity in the center of the flow zone to higher salinity at the upper and lower boundaries. The resistivity variation indicated by the log is not large. Water at the bottom of the well is stagnant and probably does not represent background conditions in the aquifer. This water may contain residual drilling fluid or may represent downward turbulent dispersion from the flow zone.

The resistivity values above 1,012 ft generally represent the salinity of the composite flow from the flow zone, and the actual salinity of water in the relatively impermeable rocks at those elevations might be greater. For purposes of this study, the native water in the confining zones is assumed to be more saline than water from the higher 840-ft white monitor, where the chloride concentration of samples was between 1,700 and 2,300 mg/L and the dissolved solids concentration varied from 3,900 to 5,000 mg/L. This assumption is based on the general trend of increasing salinity with depth that occurs within the Upper Floridan aquifer except in discrete flow zones flushed by fresher water.

The physical conceptual model accepted as a hypothesis for computer simulation was that of a flow zone within the interval 1,012–1,043 ft (1,016–1,047 ft in the injection well). Water is freshest in the center of the zone but may be more saline in the upper and lower parts of the zone because of greater permeability in the center and ionic diffusion or seepage of more saline water from overlying and underlying relatively impermeable rocks as flow in the zone moves downgradient from distant areas of freshwater recharge in central Florida (fig. 5). The composite chloride and dissolved-solids concentrations are about 1,200 and 2,700 mg/L, as measured in preinjection water samples. The contribution of flow from the lower part of the flow zone (above 1,043 ft) may be slight but would substantially change the salinity detected by the logger because water below is static. Therefore, this interpretation of the fluid-resistivity log generally is consistent with results of the flowmeter log analysis.

A preinjection fluid-resistivity log was run by the SFWMD at the St. Lucie County ASR site (Wedderburn and Knapp, 1983, p. 34). This log is strikingly similar to the Hialeah fluid-resistivity log of January 27, 1975 (fig. 8). A high-resistivity spike on the trace corresponds to the lower flow zone occurring at the contact between the Ocala Limestone and Avon Park Formation. Similar to the USGS log from Hialeah, no annotation is present on the log to indicate that the well was flowing; however, the log has been interpreted as a flowing log by Wedderburn and Knapp (1983, p. 32). Flowing water above the uppermost flow zone is lower in salinity (has higher resistivity) than stagnant water in the bottom of the well below the flow zones, as would be expected if the flow originates from a permeable zone containing fresher water. The fact that the lowest degree of salinity occurs near the center of the flow zone suggests a gradation of water quality within the flow zone, so that water flowing from the well will be more saline than the freshest water near the center of the flow zone.

Monitor-Tube Data From the Three Test Cycles

Interpretation of the fluid-resistivity log of January 27, 1975, is corroborated by water-quality data from the first ASR cycle taken from the monitor tubes in the observation well (pl. 1). The mean values of chloride concentration in water from tubes sampling the injection zone prior to detection of the injectant are listed in the following table:

Color code	Depth (feet)	Number of samples	Average chloride concentration (milligrams per liter)
Red	957	18	1,594
Green	978	19	1,574
Gold	999	18	1,500
Silver	1,020	18	1,211
Black	1,041	18	1,278
Blue	1,062	22	1,441

The 840-ft zone (white monitor) was sampled 41 times prior to injectant breakthrough at the observation well, and the average chloride concentration was 1,895 mg/L. This provides firm validation for the hypothesis that the flow zone is overlain by zones of more saline water.

The relation of the early chloride data from the monitor tubes to actual injection-zone water quality is better understood by considering data from the observation-well monitor tubes later in the ASR cycles. A very rapid change in water quality just after the end of the first injection on September 8, 1975, indicates the possibility that unmixed injected water has reached the observation-well borehole (pl. 1 and fig. 13). These changes are first apparent within the flow zone (fig. 8, silver and black monitors) but are detected hours later in the remaining monitors near sections of the borehole that are assumed to be relatively impermeable on the basis of the temperature and fluid-resistivity logs and the injection-well flow analysis. This indicates that the monitoring zones were not completely isolated by the rosettes holding the monitor tubes and that samples from each monitor are composites of water at that elevation and from other elevations within the borehole. Thus, water samples from the red, green, gold, and blue monitors acquired before arrival of the injected water at the observation well probably do not accurately represent the quality of water in the surrounding rocks, but partly contain lower-salinity water from the presumed flow zone. This supports the hypothesis that water in the relatively impermeable rocks overlying and underlying the flow zone is appreciably more saline than indicated by samples from the monitor tubes.

A sampling following the hiatus between the first recovery and second injection shows water in the red, green, gold, and blue monitors to have increased to concentrations of about 1,400 mg/L of chloride, unlike water from the silver and black flow-zone monitors. The increases may have been caused by ionic diffusion and are further evidence that relatively impermeable parts of the injection zone contain water of greater salinity than the flow zone.

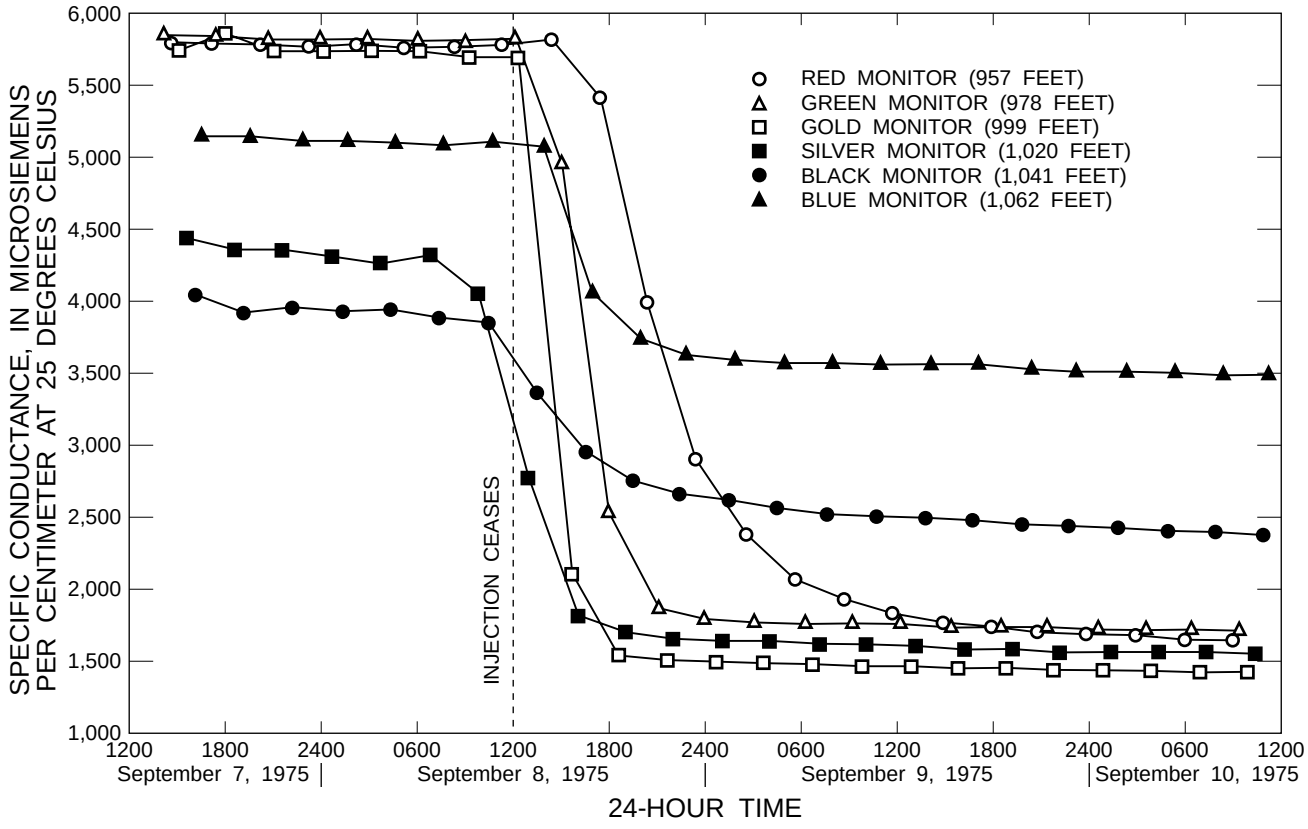

Figure 13. Automatic sampler-recorder data indicating freshening of water from monitor tubes after the first injection.

Later in the ASR cycles, the least saline water tended to be pumped from the silver and black monitors, which are the ones closest to the flow zone (pl. 1). Blue-monitor samples often were as fresh as samples from higher monitor tubes, apparently as the inflow of injected water and pumping of the monitor tube caused freshwater to move downhole. However, during storage and recovery periods, blue-monitor samples often became more saline, possibly as more saline water seeped into the well from surrounding rocks at the bottom of the well, displacing freshwater rising upward by buoyancy. This phenomenon was repeatedly reversed, possibly as a result of variation in the amount of pumping for water samples, and ceased to occur to any significant degree late in the third recovery, when water in the flow zone approached native-water salinity and the salinity contrast was reduced.

That water from all monitors late in the third recovery approached the flow-zone chloride concentration of 1,200 mg/L is further validation that water in the flow zone was appreciably less saline than that sampled from the 840-ft monitor tube. Although the salinity of water from the 840-ft zone (pl. 1) showed some irregularities that do not seem related to the ASR cycles, the salinity of water from this monitor zone remained consistently higher than that of water from all lower monitoring zones.

Dispersive Properties of Aquifer Material

The degree to which injected water mixes with the native brackish water is a key factor determining how much usable water can be recovered after subsurface storage. The mixing process is referred to as dispersion or dispersive mixing. Concepts related to dispersive mixing in radial flow from wells are developed by Hoopes and Harleman (1967). Dispersion concepts are discussed by Merritt (1985) in relation to modeling ASR cycles in the Upper Floridan aquifer.

Hydrodynamic dispersion is a term that represents the combined effects of molecular diffusion and mechanical dispersion. The concept of mechanical dispersion was formulated in the context of porous media and postulates that, because the myriad pathways through connected pores differ in size and tortuosity, radially oriented fluid movement in some will be retarded or accelerated in comparison with others. Therefore, in radial flow from an injection well, water particles will not have uniform outward speed, and in the vicinity of the interface separating injected and native water, some connected pore channels will have been flushed with the injectant, but others will still contain native water. Therefore, on a spatially averaged basis, there is a spreading, or dispersion, of the interface. Reeder and others (1976) use a simplified version of the formula derived by Hoopes and Harleman (1967) to represent the relative proportions of injected and native waters within the dispersed interface, written as

$$C/C_0 = 1/2 erfc\left[\frac{r-R}{(4/3\alpha_l R)^{1/2}}\right] \qquad (5)$$

where: erfc is the complementary error function,
α_l is longitudinal dispersivity (L),
C/C_0 is a unitless fraction having values ranging from 0 to 1 representing the relative concentration at radius r of some tracer present only in the injected water, and
R is defined by $V = \pi\theta h R^2$ (θ is aquifer porosity and h is the thickness of the injection zone).

R would be the precise radius of the injected water body if there were no dispersion. This approximation (eq. 5) is valid at large radii R and where $r \simeq R$ (in a relatively small interval surrounding the midpoint R) and assumes that molecular diffusivity is negligible in a vertically uniform aquifer. The width of the transition zone depends on the value of longitudinal dispersivity (α_l). Thus, fitting the formula to observed breakthrough data (concentration values showing the passage of a dispersed interface past an observation well) can be a method of deriving a dispersivity value from field measurements (Ehrlich and others, 1979).

Data from the very rapid apparent breakthrough at the observation-well silver monitor on September 8, 1975 (fig. 13), hours after the first injection ceased, were fitted to equation 5 for an estimate of α_l. Assuming isotropic flow in a 12-ft flow zone, an injection rate of about 80,000 cubic feet per day (ft^3/d) on September 8, 1975, and porosity of 35 percent, the rate of radial flow from the injection well would be 10.48 feet per day (ft/d) at a 289-ft radius, the distance to the observation well. The concentration of injected water within the silver-monitor sample was estimated to be 11 percent at 0955 hours and 50 percent at 1242 hours, during which time the front would have moved 1.22 ft. Setting

$$0.11 = 1/2\left(1 - erf\right)\left(\frac{1.22ft}{(4/3\alpha_l 289ft)^{1/2}}\right) \qquad (6)$$

α_l resolves to be 0.0072 ft. This value is about 3 or 4 orders of magnitude less than customary estimates of longitudinal dispersivity in large-scale tracer movement in aquifers and is, therefore, subject to considerable skepticism. In fact, it is highly unlikely for the breakthrough to have coincidentally occurred within hours after an arbitrary decision to halt injection had been implemented. Whether or not such a breakthrough could occur after injection stopped, given assumed hydrogeologic conditions, is another question subsequently considered as part of the modeling analysis.

Interpretation of Observation-Well Salinity Changes During the Three Test Cycles

Another curious aspect of the breakthrough data was the inconsistency of the apparent arrival time in the first cycle with the description of the flow zone based on evidence provided by the geophysical logs. Assuming planar isotropy, the hypothetical radius of the injected water body after 53 days of injection at an average rate of 105,661 ft^3/d (549 gal/min) can be estimated from the relation

$$V = \pi r^2 \theta h = Qt \qquad (7)$$

where: V is the volume injected (L^3);
r is the radius (L) of the injected water body at time t, ignoring dispersion;
θ is aquifer porosity (unitless);
h is aquifer thickness (L);
Q is the average injection rate (L^3/T); and
t is the time (53 days).

Assuming that q was 35 percent and aquifer thickness h was 12 ft, the radius of the injected water mass at 53 days should have been 651.5 ft. A 53-day radius of 289 ft could be achieved only by assuming a flow-zone thickness of 61 ft (35 percent porosity) or 32.8 ft (65 percent porosity). Both scenarios are very unlikely, given the evidence of the geophysical data. Assuming planar isotropy and nominal parameters of h = 12 ft and q = 35 percent, the theoretical volume injected when the freshwater radius reached 289 ft was 1,102,033 ft^3. As shown in the list of Appendix C, this volume was injected by day 8 of the first injection.

To better understand this anomaly and better visualize salinity changes in the observation well during the first and second injections, the manually collected samples shown in plate 1 are enlarged in figure 14 for the injection period and the period immediately following. Water samples collected from the silver and black monitors during the first injection show three periods of rapidly decreasing chloride concentrations before the end of the first injection. This raises the possibility that water in the observation well might have contained some injected water long before the end of the cycle. In fact, the first of the three periods of decreasing chloride concentrations falls between 6 and 12 days, close to the hypothetical arrival time of 8 days.

The salinity contrast showing breakthrough during the second and third injections was reduced because of the presence at the observation well of a residual amount of freshwater from the previous ASR cycle. Large salinity fluctuations in monitor-tube samples occurred during the second injection, as in the first. Immediately following the end of the second injection, there was a substantial lowering of chloride concentration in all monitor tubes (to 100 mg/L at the silver monitor) similar to that following the end of the first injection. However, assuming horizontal isotropy, the theoretical arrival time at the observation well (when 1,102,033 ft^3 has been injected) would have been January 12, 1976, after 7 days. Because the first observation-well sampling was on January 12, no data describing water quality in the observation well in the first 7 days of the second injection are available. Samples from the silver monitor tube showed a slight salinity decrease from 700 to 500 mg/L in chloride concentration almost immediately after the beginning of the third injection, between the second and ninth days, when samples were collected. The theoretical arrival time again should have been about 7 days, and the observed decrease may have indicated arrival of the injected water.

If the weak evidence of 7- or 8-day breakthrough times in the first and third cycles is rejected, at least two hypotheses can be postulated to explain inconsistencies between observed arrival times and the conceptual model formulated on the basis of geophysical logging. The first hypothesis is that the aquifer is horizontally anisotropic. The estimated direction of flow in the Upper Floridan aquifer at Hialeah is almost due east (fig. 5). The observation well is north-northwest of the injection well nearly at a right angle to the estimated regional flow direction. If solution porosity features have developed that favor aquifer flow in the direction of the regional gradient, horizontal anisotropy would exist, and the observation well would lie

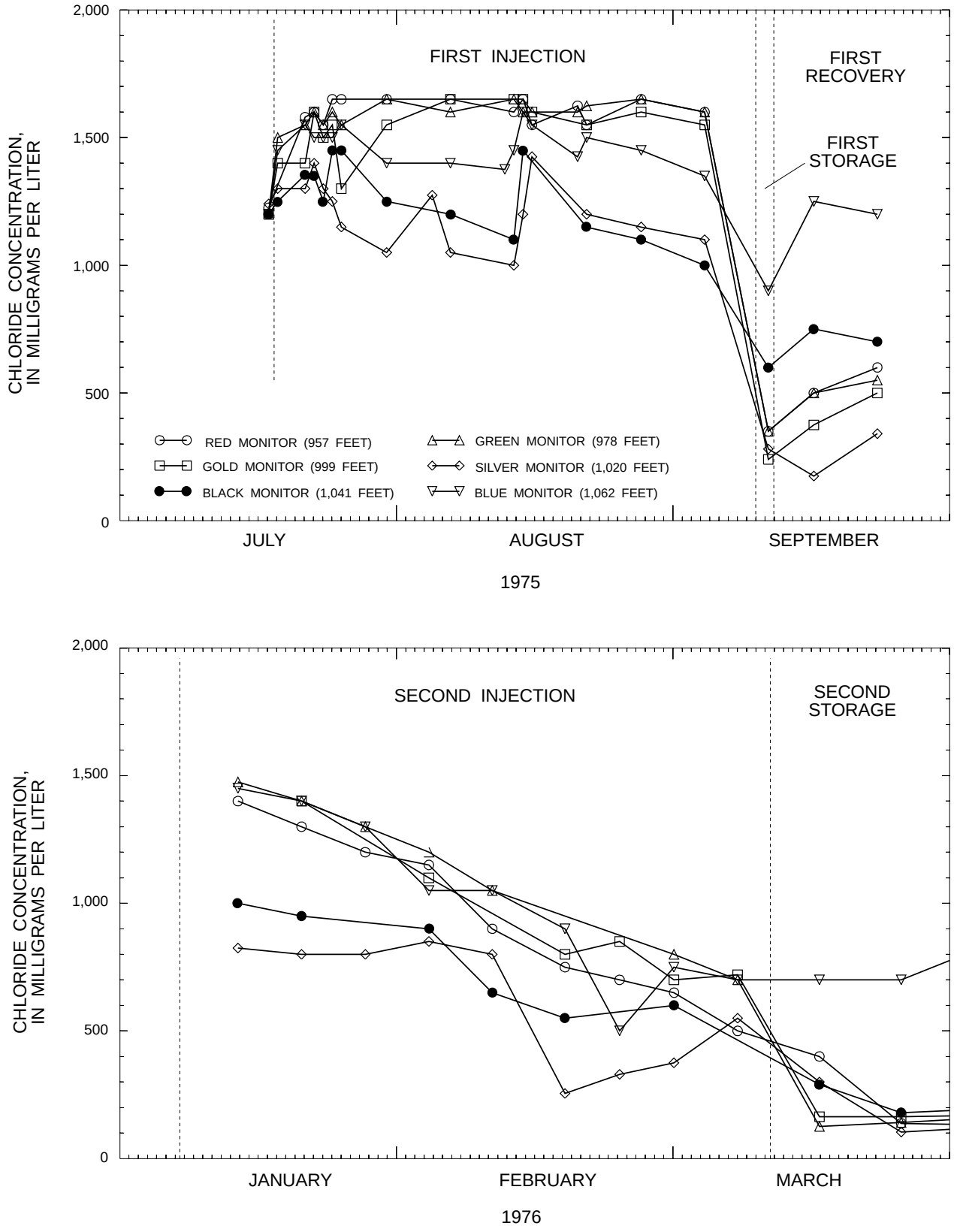

Figure 14. Chloride concentrations from observation-well monitor tubes during and after the first and second injections.

in a direction from the injection well in which the aquifer had less permeability than in the direction of the regional gradient. The flow of injected freshwater in the direction of the observation well would be slower than predicted by the isotropic conceptual model. The observed pressure at the observation well would be less than that at an equal distance in the preferred flow direction, leading to an erroneous interpretation of the aquifer-test data unless anisotropy was assumed in the analysis.

Another hypothesis is that the breakthrough data are misleading because of complex and poorly understood hydraulic properties of the aquifer in the vicinity of the observation well. The principal flow conduits might bypass the well, and complex solution features might permit the full interception of injected-water flow only after the injection pressure gradient ceases or after an extended period of time.

The latter hypothesis illustrates limitations that apply to the application of porous-media concepts of transmissivity and mechanical dispersion to secondary-porosity carbonate aquifers. The chloride concentration increases during the three recoveries were gradual, suggesting a dispersivity of many tens of feet. However, dispersivities of this magnitude may represent a more complex set of processes than considered in the development of the mechanical dispersion concept for porous media. Flow of injected water may be partly confined to an interconnected series of major and minor conduits, and mixing may occur, in part, as seepage of native water from the rock surrounding the conduits. The dispersion represented in the simulations of salinity increases during recovery, therefore, may be a representation of aquifer flow and mixing processes on a larger scale than implied by the uniform porous-media concept of solute transport. Hydraulic conductivity and dispersivity estimates may be inadequate to describe fluid movement and mixing at an isolated point, such as the location of the observation well at the Hialeah site.

Regional Flow at the Hialeah Site

An understanding of the velocity (speed and direction) of flow in the Upper Floridan aquifer in the vicinity of the Hialeah ASR site is helpful because background (regional or manmade) hydraulic gradients can substantially affect the recoverability of freshwater stored underground (Merritt, 1985). The regional gradient and the flow-zone hydraulic conductivity, thickness, and porosity determine the rate at which injected freshwater drifts downgradient, generally to the east. Thus, the influence of background gradients must be considered in the computer simulation of recovery salinity changes.

Figure 5 shows the estimated potentiometric surface and corresponding flow directions in the Upper Floridan aquifer in May 1980. The potentiometric surface in the southern part of the peninsula in the 1974–80 time period of the ASR cycles would be similar because the native water is not potable, and the only known manmade influences at that time were flowing wells located at some distance from the ASR site. Because these wells had been flowing for many years, a hydraulic equilibrium probably would have been established.

The potentiometric contours shown in southern Florida (fig. 5) are largely inferred on the basis of widely scattered data from wells containing waters of varying density. Subject to this qualification, it seems that flow in the Upper Floridan aquifer in the vicinity of Hialeah, a northwestern suburb of Miami, is maintained by an eastward hydraulic gradient of about 10 ft in 25 miles (mi), or about 0.4 ft/mi. Earlier estimates ranged from 0.1 to 0.22 ft/mi but were revised on the basis of new data and reinterpretation of data from wells in central Florida (Meyer, 1989a).

Hydrogeologic Conditions at Other Sites of Aquifer Storage and Recovery Tests

Some corroboration for the analysis of hydrogeologic conditions at the Hialeah ASR site can be obtained from a survey of data from other ASR sites where similar technical objectives dictated collection of similar types of data. The following sections present a partial evaluation of data from the town of Jupiter site and the St. Lucie County site.

Town of Jupiter Site

Tests of the subsurface storage and recovery of freshwater were performed from September 1973 to October 1976 for the Florida Department of Natural Resources at Jupiter in Palm Beach County (fig. 1, site 4). The data set collected at the Jupiter ASR site has been largely lost except for an unpublished executive summary report prepared for the Florida Department of Natural Resources by J.J. Plappert in February 1977, and suites of geophysical logs run at various times by the FGS and the USGS. The

geophysical data have not been previously published, and it was considered worthwhile to reproduce several logs for inclusion in this report.

The flow zone used for ASR cycles at the Jupiter site was found within the Avon Park Formation at about 1,220 ft. This conclusion was based on an analysis of caliper (January 30, 1975) and spinner flowmeter (July 25, 1974) logs run in the injection well by the FGS (fig. 15). Quantitative analysis of the flowmeter data was as previously described for the flowmeter data from the Hialeah site, but the diameter compensation was complicated in this case by the high rugosity of the borehole. The borehole flow, expressed as a percentage of that in the casing, is seen in figure 15 to have been generally uniform at 100 percent to a depth of 1,220 ft, below which it quickly diminishes to zero within another 10 ft.

Caliper and spinner flowmeter logs (fig. 16) were run in the observation well by the USGS on December 2, 1975. The borehole was smaller in diameter and less rugose. Results of the analysis suggest that borehole flow diminishes with depth between 1,207 and 1,228 ft, the most marked decrease occurring below a depth of 1,222 ft. Rock samples from the observation well examined by the Florida Bureau of Geology (written commun., 1975) indicate calcareous sandstone from 910 to 990 ft in depth and limestone (calcarenite) from 1,000 to about 1,250 ft in depth, except that the 1,140- to 1,200-ft depth interval is described as a foram-hash limestone. The interval from 1,200 to 1,240 ft is described as more porous than the other intervals.

The flow zone at Jupiter is, therefore, similar to the one at Hialeah in that it is also a thin, discrete zone of permeable limestone. The native water was also brackish in quality, having a chloride concentration of about 2,000 mg/L.

St. Lucie County Site

In 1981–83 the SFWMD conducted a single, low-volume ASR test in St. Lucie County (fig. 1, site 3). Results are documented by Wedderburn and Knapp (1983). Data gathered were static and flowing geophysical logs, pump tests of various depth intervals, pressure data at observation wells during ASR tests, and analysis of water-quality field parameters during recovery. The volume of injection was insufficient for the injected water to reach the observation well. Plans for further testing were canceled when analysis of results of the first test indicated that costs for recovered water were not competitive with current costs for domestic and irrigation water, and that available water for injection was of relatively poor quality because of its high dissolved-solids concentration.

Analysis of rock samples and spinner flowmeter data (Wedderburn and Knapp, 1983, p. 22) indicates appreciable quantities of flow originating from thin, discrete zones at formation contacts at depths of 650 ft (Suwannee-Ocala contact) and 740 ft (the Ocala-Avon Park contact), and small contributions of flow from four other discrete zones extending to a depth of 1,000 ft. The rock type generally was limestone (calcilutite) in elevations near the principal flow zones. However, the major flow zone at a depth of 750 ft approximately corresponded in elevation to a thin bed of dolomite. Coarse phosphate was present (about 15 percent) in an interval of high gamma counts above a depth of 650 ft. Below 800 ft are alternating beds of calcilutite, dolomite, and calcarenite. Water from the flow zones was brackish, with chloride concentrations ranging from 800 to 1,000 mg/L. The St. Lucie County data support the general conclusion that zones of significant permeability within the Upper Floridan aquifer, and potential zones for ASR, occur as discrete permeable zones often not much more than 10 ft thick.

Regional Extent of a Potential Aquifer Storage and Recovery Zone

In the present section, data from other ASR test sites and selected non-ASR site locations are considered for the more specific purpose of providing evidence for the existence of one areally extensive, brackish flow zone of moderate permeability. Besides its potential for ASR use, such a zone could also have potential for withdrawal of water to supply reverse-osmosis plants or to be used for blending with fresher water.

Some indication of the areal occurrence of a permeable zone containing brackish water in southeastern Florida can be gained by examination of natural gamma logs and related flow information from six locations (fig. 17) in southeastern Florida (section X-X' in fig. 1). These logs and others, shown later in the report, were digitized using a point cursor. At a certain depth, each log shows an interval of low natural gamma activity overlain by an interval of intense natural gamma activity.

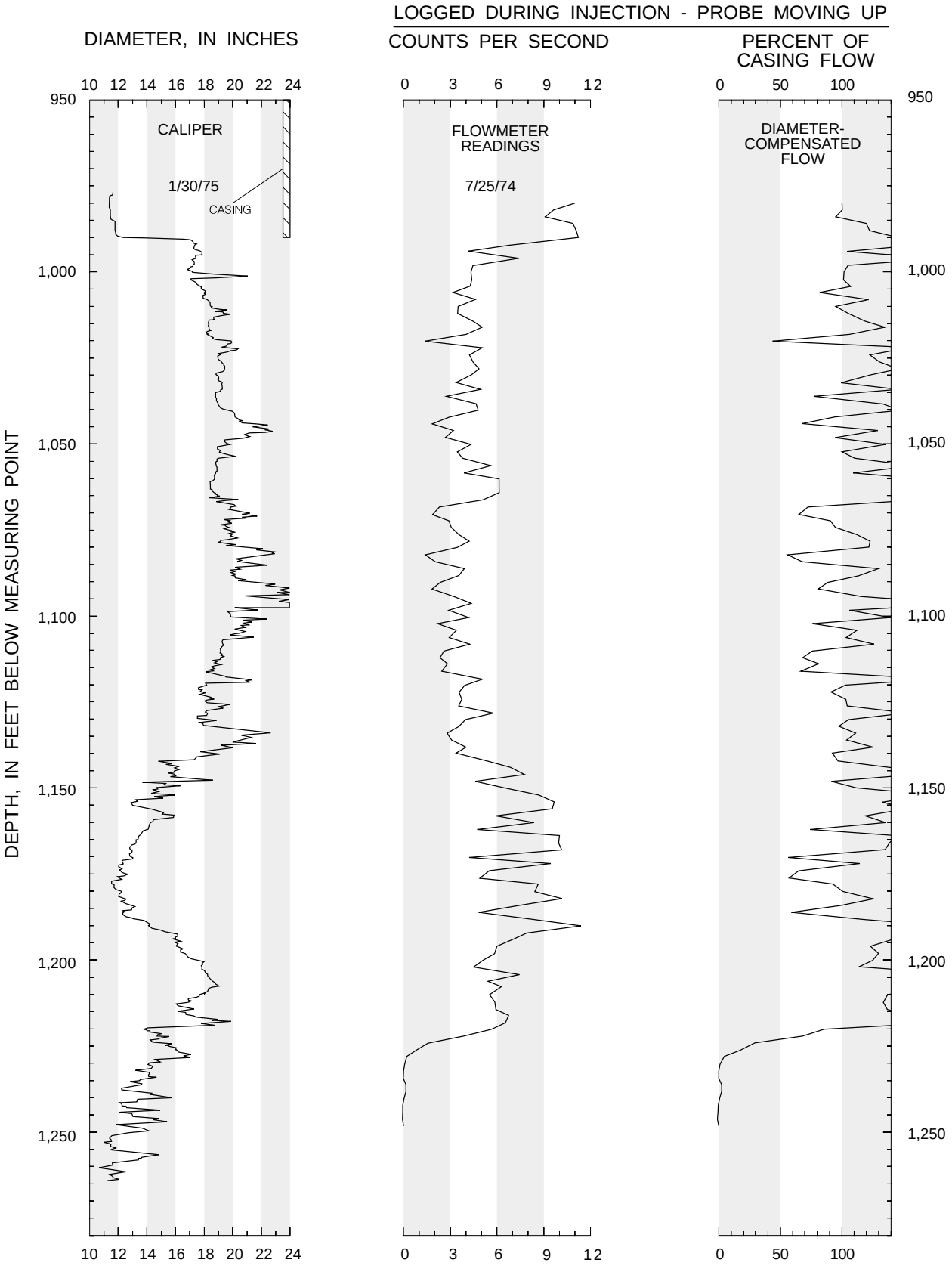

Figure 15. Results of analysis of data from spinner flowmeter logging of the injection well (PB-747) at the Town of Jupiter site.

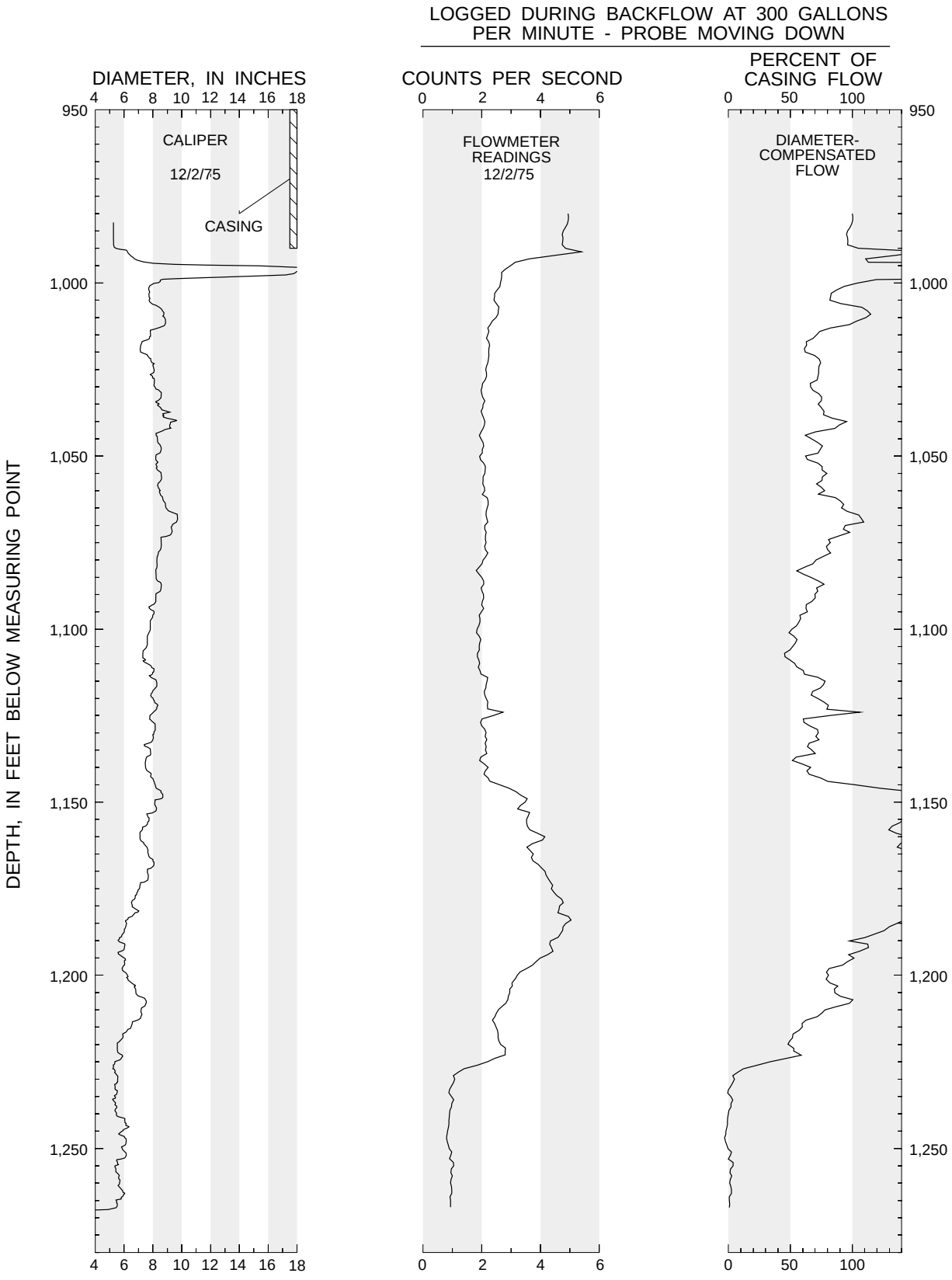

Figure 16. Results of analysis of data from spinner flowmeter logging of the observation well (PB-1145) at the Town of Jupiter site.

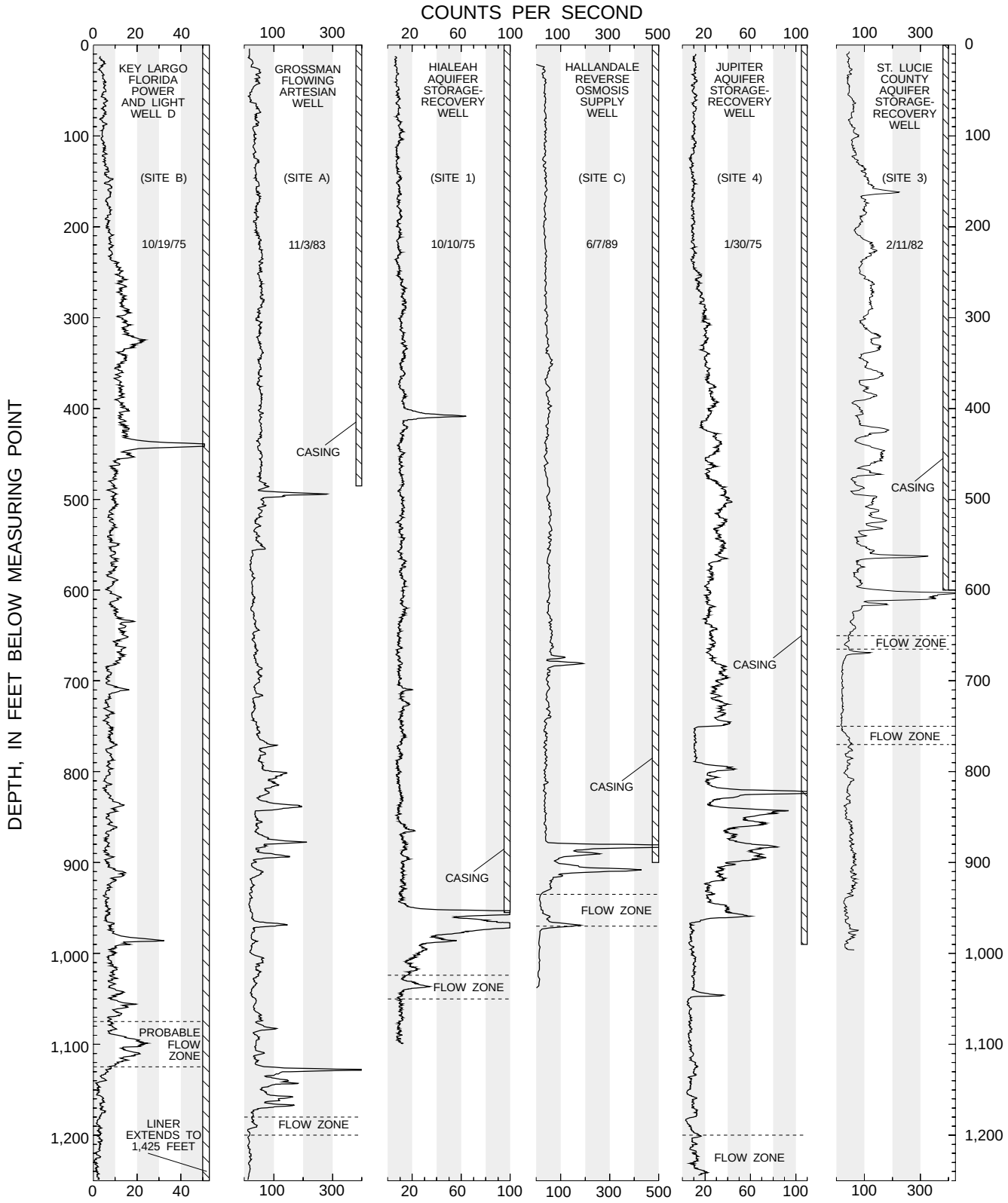

Figure 17. Natural gamma logs from selected Upper Floridan aquifer wells in southeastern Florida and elevations of known flow zones.

The high natural gamma activity usually is considered to be caused by the presence of phosphatic material containing traces of uranium. The underlying interval of low natural gamma activity is considered by some investigators to coincide with the top strata of Eocene age (the Ocala Limestone where present or the Avon Park Formation where the Ocala Limestone is absent). A clear example of this natural gamma contrast is presented by Meyer (1989a, p. 13), who correlates it with his determination of the Oligocene-Eocene contact in the Alligator Alley test well (Meyer, 1989a) near the Broward-Collier County line (fig. 1, site G).

At the site of the Florida Power and Light observation well D in undeveloped north Key Largo, Monroe County (fig. 1, site B), the interval of high natural gamma activity shown by the USGS log of October 19, 1975, is centered at a depth of 1,100 ft, and gamma activity decreases substantially with greater depth. A similar high-low activity contrast is found at a depth of 1,260 ft in the Florida Keys Aqueduct Authority reverse-osmosis supply well in Marathon (fig. 1, site D), as shown by the USGS natural gamma log of October 16, 1977. No flow information is available from well D, in which the casing extends to a depth of 1,425 ft. However, data from two reverse-osmosis plant supply wells a few miles to the southwest (fig. 1, site F) at the Florida Keys Aqueduct Authority Water Plant in the town of Key Largo (USGS natural gamma and flowmeter logs of October 16, 1975, and flowmeter log of June 14, 1978) and at a USGS test well in John C. Pennekamp State Park, just to the north of the town of Key Largo (USGS natural gamma log of October 16, 1975, and drillers log), show producing zones associated with intervals of high gamma activity centered at depths of 1,190 and 1,200 ft, respectively, that seem to correlate with the 1,100-ft depth interval in well D. However, the Florida Keys Aqueduct Authority and USGS wells were not sufficiently deep for the natural gamma logs to show an underlying interval of low gamma activity. A sample description (CH_2M HILL, Inc., written commun., 1974) picks a depth of 1,150 ft as the top of the Eocene in well D. Harbans Puri (FGS, written commun., 1965) picks a depth of 1,034 ft as the top of the Eocene in the USGS test well, which is at variance with the other finding. Water-quality data from the three wells indicate chloride concentrations ranging from 2,200 to 3,300 mg/L.

The recently plugged Grossman well was located in the Chekika State Recreation Area in central Dade County (fig. 1, site A). A sample description by L. Jordan (Sun Oil Company, written commun., November 1944) picks the top of the Eocene at a depth of about 1,150 ft; however, Jordan admits some uncertainty about the pick. Three series of readings from the stationary spinner flowmeter logs run by the FGS on June 11 and August 15, 1969, indicate a depth interval of 1,180–1,200 ft to be the sole flow-producing zone. The natural gamma log by the SFWMD shows the high-low gamma contrast at a depth of 1,170 ft.

At Hialeah the major receiving zone for injected freshwater was shown to be approximately between 1,024 and 1,036 ft in depth, and a depth of 1,045 ft was considered the approximate top of the Eocene. Thus, the flow zone at the three locations so far considered is approximately coincidental with the erosional surface of the Ocala Limestone or the Avon Park Formation as identified by several investigators. Both the Grossman well and the Hialeah ASR well produced water with a chloride concentration of about 1,200 mg/L.

A test well was recently drilled for the city of Hallandale in Broward County (fig. 1, site C) to determine whether a source of brackish water could be found for use by a reverse-osmosis plant. The plant is needed to augment supply from the municipal well field, which will soon be abandoned because of saltwater intrusion from the ocean. As in the other wells, a major flow zone was found just below the high-low gamma contrast at a depth of about 930 ft. Lithologic data are not presently available to verify that this elevation is coincidental with the top of the rocks of Eocene age. Other data indicate that most of the flow occurs at a depth of 935 ft, and an abrupt shift on a temperature log run during flow indicates that inflow at that elevation is anomalously warm compared with that from below. The chloride and dissolved-solids concentrations of water flowing from the well were 2,100 and 4,500 mg/L, respectively. These values are higher than those from the Grossman and Hialeah wells, possibly because the site is so close to the formation subcrop at the continental shelf about 3–4 mi east of the Atlantic coast.

At Jupiter, geologic sample descriptions provided by the FGS (written commun., 1974) pick the top of the Ocala Limestone at a depth of 1,060 ft in the injection well (no samples below 1,100 ft) and at a depth of 1,120 ft in the nearby observation well. A

pick of 970 ft in depth would correlate better with the top of the part of the natural gamma log run by the FGS on January 30, 1975 where low gamma activity occurred. However, the principal flow zone was found below a depth of 1,200 ft. Because the casing was set at a depth of 990 ft, if a flow zone existed near the elevation of the interval of contrasting gamma activity, it could have been cased off and remained undetected.

The top of the Ocala Limestone in the St. Lucie County ASR well was identified to be at a depth of 660 ft, and the top of the Avon Park Formation to be at a depth of 760 ft. The two depths correspond closely with the two principal flow zones identified with spinner flowmeter logging (Wedderburn and Knapp, 1983, p. 22), and the upper depth corresponds with a sharp reduction in gamma activity (fig. 17; Wedderburn and Knapp, 1983, p. 15). The well extended to a depth of 1,000 ft, but only minor amounts of flow occurred below 770 ft in depth. Water from the principal flow zone at a depth of 760 ft had a chloride concentration of about 900 mg/L.

On the basis of limited but relatively consistent evidence, it seems that formation contacts at the surface of rocks of Eocene age (the Ocala Limestone where present, or the Avon Park Formation) are the most probable depth intervals for the occurrence of permeable zones containing brackish water suitable for temporary storage of freshwater. A significant correlation exists between the elevation of the surface of rocks of Eocene age and the position of a sharp contrast in natural gamma activity (high above, low below) found in natural gamma logs at widely scattered locations along the southeast coast.

DIGITAL SIMULATION OF RECOVERED WATER QUALITY

The following sections begin with a description of the selection of a simulator and the selection of some parametric coefficients to represent aquifer characteristics based on data acquired at the Hialeah test site. A hydraulic calibration of the simulator is accomplished by a replication of data acquired during the aquifer test at the site. This is followed by a solute-transport simulation in which chloride increases during recovery are replicated by further calibration. Then various problems are considered that are related to the lack of accuracy with which aquifer characteristics are determined on the basis of field data and to the related problem of nonuniqueness of the calibration. Estimates of multiple-cycle recovery efficiency are then made. The report concludes with a comparison of model-computed solute concentrations with data collected from the observation well.

Simulation Code

The Subsurface Waste Injection Program (SWIP) code, the principal tool of investigation in this study, was developed by INTERCOMP Resource Development and Engineering, Inc. (1976), under sponsorship of the USGS. SWIP was later revised for the USGS by the same firm, renamed INTERA Environmental Consultants, Inc. (1979). Despite its intended use as a special package for waste injection problems, the SWIP code received wider use within the USGS as a general-purpose, three-dimensional simulator of solute and thermal-energy transport in ground water. The application of SWIP in USGS activities has been limited to a few users. A newer code developed by agency personnel, HST3D (Kipp, 1987), incorporated some parts of the SWIP code with adaptation. Outside the agency, the SWIP code has been adapted for special purposes by various public and private organizations.

Absolute pressure is the independent variable of the flow equation, and the model accounts for fluid density and viscosity dependence on temporal changes of pressure, temperature, and solute concentration. Solution of equations for flow and both solute and thermal transport is by standard finite-difference techniques, in which backward and central differencing in time and space are available as user options for solution of the solute- and thermal-transport equations. A Gaussian elimination technique is used to reduce the solution matrix size that results from coupling of the three equations. The aquifer simulated may be fully confined or have a free surface, and the equations may be solved in either Cartesian or cylindrical coordinates.

Fractional values (C) describe the relative concentrations of two miscible fluids ($C = 0$ and $C = 1$) in the aquifer. Any fluids present within the aquifer or entering it in simulation exercises are considered to be mixtures of these two fluids by the appropriate specification of C values. This approach works well for the problem of simulating the mixing of waters of different salinities that was a purpose of this study. $C = 0$ was used to represent pure freshwater, and $C = 1$ represented the most saline water residing within the aquifer or entering it as an influx. Injected water, the salinity of

water in some parts of the aquifer, and water in mixtures of injected and native waters were assigned or were computed to have C values that described their salinity relative to the two extreme salinities. Values of density are associated by SWIP with the extreme values of solute fraction ($C = 0$ and $C = 1$) and are used in calculations of flows driven by density gradients and in adjusting hydraulic parameters.

A more comprehensive description of the SWIP code, with reference to its application in ASR cycle modeling, has been provided by Merritt (1985). In 15 years of using the SWIP code, the author has made a number of modifications to adapt it to various applications. Most modifications have been nonmathematical in nature, and those that are revisions or extensions of the mathematical procedures of the 1979 version of SWIP have been coded as options to preserve the original solution methodology for use when needed. This study required the use of modifications affecting the computation of advective and dispersive fluxes of solute. A description of the original and experimental algorithms and their effect on computations is documented separately (Merritt, 1993), and a summary is presented later in this report.

Design of Hialeah Aquifer Storage and Recovery Simulator

The selection of parameter values and computational methods, the design of the grid, and the assignment of boundary conditions of pressure and solute fraction are described in the following sections. The rationale for design and value selections is explained, as is their basis in available data. The result of this process of selection is completion of the design of a simulator in which the process of injection, storage, and recovery of freshwater is represented, which can be used for a simulation of the salinity of the water recovered during the withdrawal stage. The substantial database acquired at the data site is used both in designing the simulator and in providing comparison data for the simulation of changes in the salinity of the recovered water.

Fluid Density and Viscosity Representation

The fluid densities assigned to injected and native waters were based on the measured or estimated concentration of dissolved solids in each fluid. Direct measurements of density were not considered to have adequate accuracy. The simulator required a density value to be associated with a solute fraction of $C = 0$, which was selected to represent pure water (zero dissolved solids). The assigned density of 62.3046 pounds per cubic foot (lb/ft^3) at 21 °C and atmospheric pressure were obtained from a standard handbook. Isothermal conditions at 70 °F (21.1°C) were assumed to prevail in all simulations on the basis of the preinjection temperature log in the observation well (fig. 8). Injected-water temperatures (fig. 12) ranged between 21.5 °C and 27 °C, but any effects of injecting somewhat warmer water were ignored. Values of density at 15 °C corresponding to various salinities were obtained from standard tables and were converted to 21 °C values by the factor 0.998892, the ratio of the densities of pure water at 15 °C and 21 °C. Measured injected-water dissolved-solids concentrations were about 400 mg/L, and the measured dissolved-solids concentrations of preinjection water samples from the injection zone were about 2,700 mg/L. As previously shown, water in the center of the flow zone may have been less saline, and water above and below more saline, than this composite value, but the composite value was assigned uniformly to the entire flow zone.

A solute-fraction value of $C = 1$ was associated with the most saline water in the aquifer, that in the relatively impermeable parts of the injection zone. The dissolved-solids concentration was estimated to be about 6,000 mg/L (about 20 percent greater than the average dissolved-solids concentration of samples from the 840-ft monitor tube). The corresponding density was 62.5414 lb/ft^3. Solute-fraction values of 0.0667 and 0.4500 were then assigned to the injected water and flow-zone water based on the ratio of dissolved solids to the estimated dissolved solids of the confining-zone water. The average chloride concentration of the injected water was 65 mg/L, and that of the flow-zone water was 1,200 mg/L. Computing the proportion of injected water in a mix of 250-mg/L chloride concentration to be 0.8370, the dissolved-solids concentration is estimated to be about 775 mg/L, using the injected- and native-water dissolved-solids values given in the previous paragraph. The corresponding solute fraction is 0.1292, and this was the maximum value of potability used in simulations in which recovery efficiency was computed. In similar fashion, chloride concentrations of recovered water were related to equivalent dissolved-solids concentrations and solute fraction for comparison with solute fraction of recovered water computed by the model.

The viscosity of injected and native waters is assumed by SWIP to vary with temperature and solute fraction. Because isothermal conditions at 21 °C were assumed to prevail, because the density contrast was low, and because viscosities of freshwater and seawater differ by only 0.06 centipoise, viscosity was assumed invariant in simulations. The assigned value of viscosity was 0.98 centipoise, the viscosity of pure water at 21 °C. The temperature of injected water ranged as high as 27 °C, at which the viscosity of injected water would have been 0.86 centipoise. Values of hydraulic conductivity in the freshwater bubble, inversely proportional to viscosity (INTERCOMP Resource Development and Engineering, Inc., 1976), would increase by as much as 14 percent. However, the simulated transport of injected freshwater was not affected by small variations in hydraulic conductivity, and simulation of viscosity variations would have been cumbersome and would have had little effect on the results.

Grid Design and Boundary Conditions

Because vertical flows caused by buoyancy stratification within the flow zone during storage might prove to have some influence on recovery efficiency, despite the low density contrast, the flow zone was discretized into six 2-ft-thick layers for calibration. Overlying and underlying relatively impermeable parts of the injection zone (the confining zones) were each represented as three layers. The layers immediately adjacent to the injection zone were thin (0.5 ft) in order to minimize the effect of the large ratio of flow-zone to confining-zone hydraulic conductivities on vertical advective flow approximations. The vertical grid discretization is shown in figure 18.

A selection of Cartesian or cylindrical coordinate systems needed to be made for the horizontal discretization in the horizontal plane. Cylindrical coordinates are well suited to problems of radial flow from wells, and solution of the equations is computationally more efficient than when using Cartesian coordinates. However, downgradient advection caused by a regional flow gradient was considered to be a likely factor explaining the quality of recovered water observed in the ASR cycles, and downgradient advection could not be represented in cylindrical coordinates. In addition, the possibility that aquifer flow was anisotropic in the horizontal plane was a hypothesis considered as an explanation of breakthrough data at the observation well and also could only be simulated in a Cartesian system. The Cartesian grid in the horizontal plane used for calibration is shown in figures 18 and 19.

The fine detail of the grid immediately surrounding the injection well cannot be shown clearly in the small-scale illustration of the 40,050-ft square horizontal grid mesh (fig. 18) but is shown in the middle-scale (7,050×5,050 ft) and large-scale (1,550-ft square) depictions of the inner mesh (fig. 19). The horizontal grid dimension of 43×31 is greater in the *x*-coordinate direction because regional flow is represented as occurring in this direction, taking advantage of special SWIP coding designed to represent regional flow. This coding provides for automatic modification of both initial pressures and specified pressure boundary conditions. Simulations of anisotropy assume the preferred flow direction to be along the *x*-coordinate axis; therefore, finer *x*-coordinate grid definition farther from the well is also needed for anisotropic simulations.

Placing the model boundaries at some distance from the region of freshwater movement confines solute movement to the center of the grid and enables constant-pressure boundary conditions to be used as an adequate approximation to actual conditions, in which a slight pressure change would occur at the boundaries during injection and withdrawal. A Theis equation calculation for an injection rate of 150,000 ft^3/d, a transmissivity of 9,600 $[(ft^3/d)/ft^2]ft$, and a storage coefficient of 2.75×10^{-4} indicates a hydraulic-head increase of 3.9 ft at the boundary after 100 days of injection. However, the known injection and withdrawal rates and estimated aquifer storage properties were the controlling factors on injected-freshwater movement, rather than transmissivity or boundary specifications.

Grid-cell dimensions in the region of freshwater movement ranged from 50 to 100 ft near the well to 250 ft farther from the well. The greatest distance in the positive *x*-coordinate direction reached by a 50 percent mix of injected and native waters in isotropic analyses was column 34 (*x*-dimension 250 ft). The injection- and observation-well nodes are both in column 22 and are five grid nodes apart (fig. 19, rows 12 and 17), providing sufficient discretization between the wells to accurately represent the hydraulic response at the injection well in simulations of the aquifer test of February 10, 1975. In some later analyses, where heads and solute fractions at the observation well were unimportant, the interwell grid definition was reduced so that the horizontal grid dimension of the model was 43×29. In special analyses designed to test various numerical approximation algorithms and value selections, the vertical discretization was enhanced, and the horizontal discretization (described in detail below) was in cylindrical coordinates.

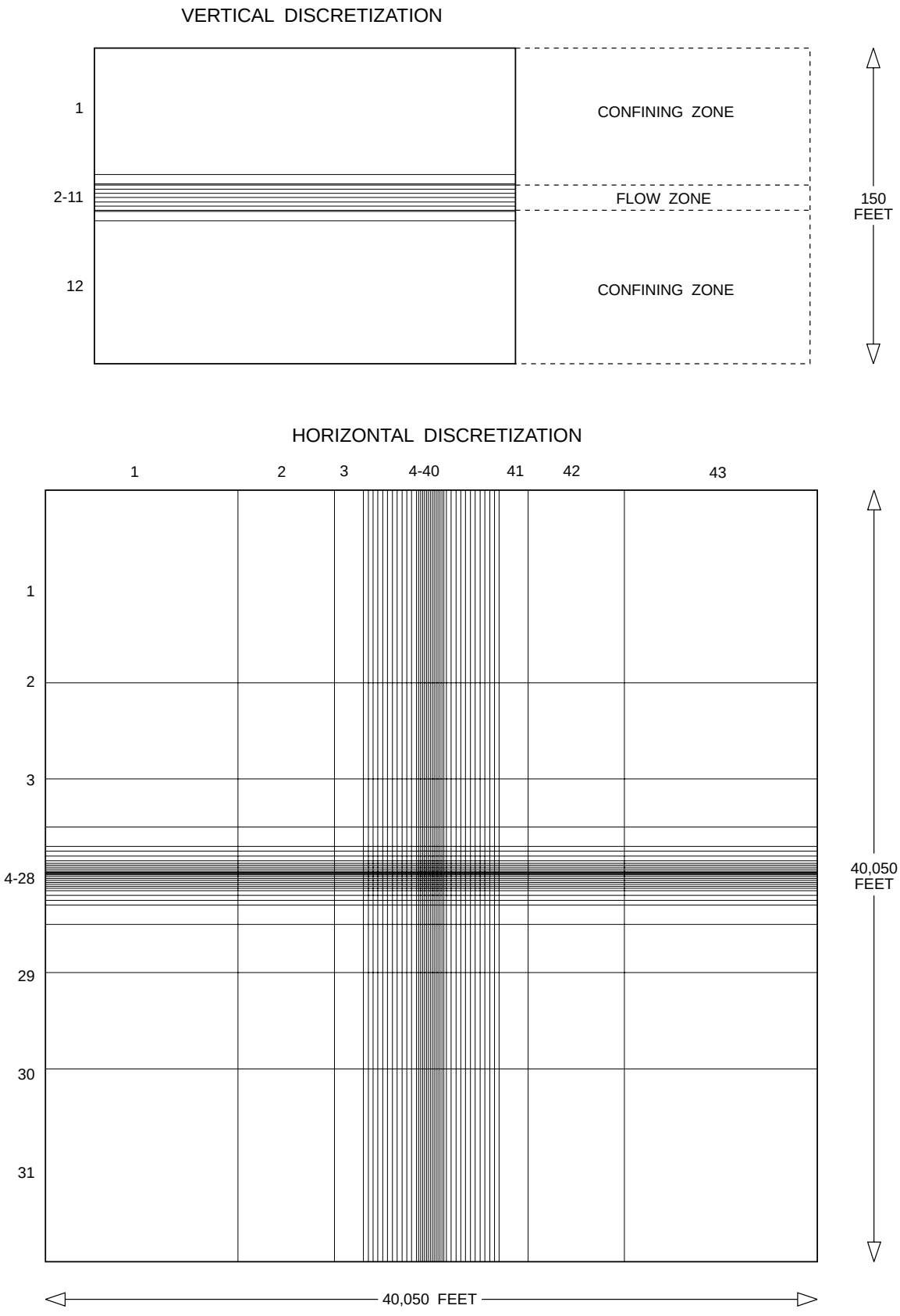

Figure 18. Vertical and horizontal discretization of the model grid used for the simulation of injection, storage, and recovery of freshwater at the Hialeah site.

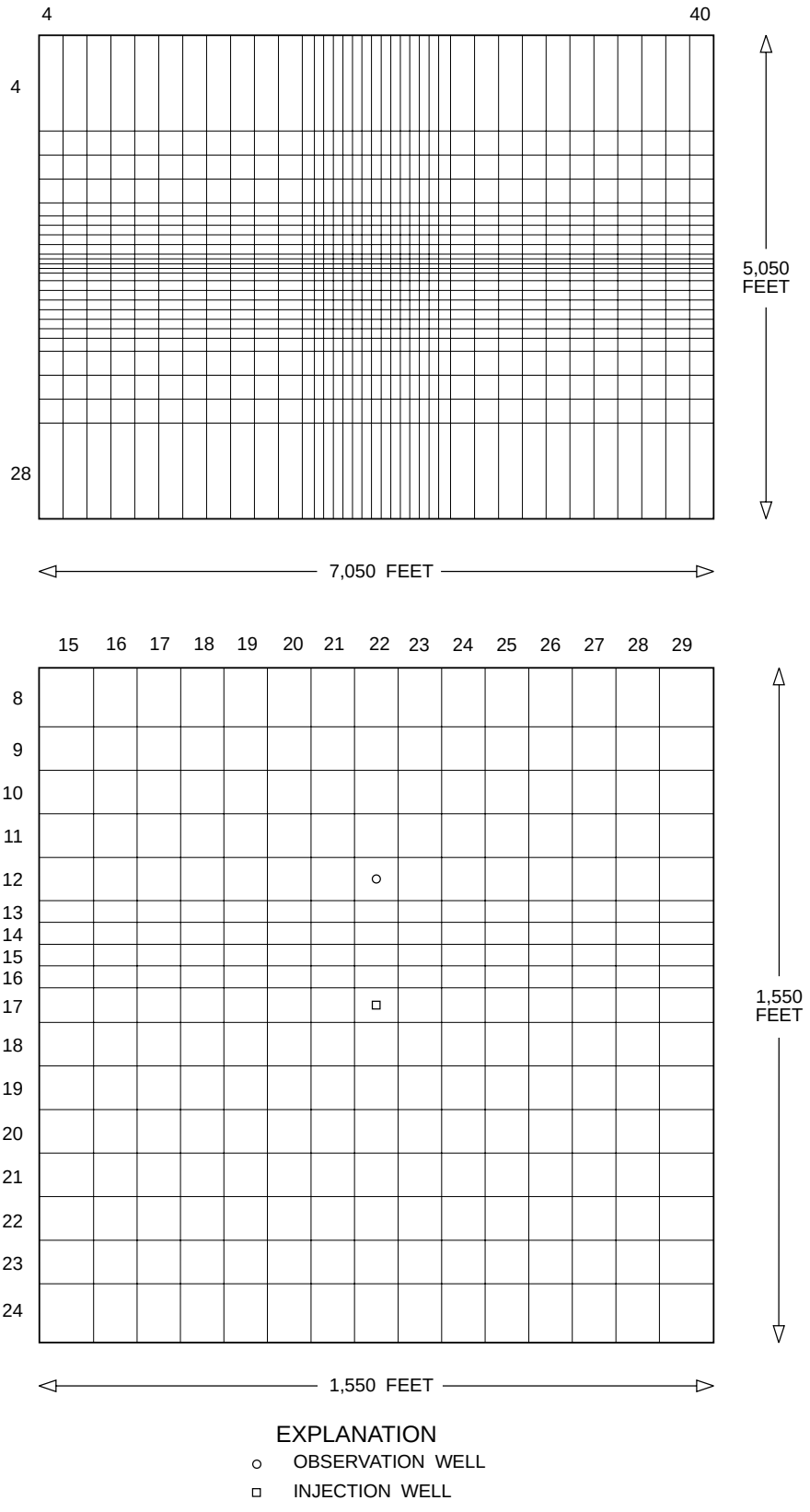

Figure 19. Horizontal discretization of larger and smaller areas surrounding the injection and observation wells within the model grid used for the simulation of injection, storage, and recovery of freshwater at the Hialeah site.

Selection of Numerical Computational Methods

Mechanical dispersion in the three coordinate directions at nodal locations is computed by the SWIP code as a function of the solute-concentration gradient, the total local fluid velocity (u), the angle of the velocity vector with respect to the coordinate directions, and longitudinal and transverse dispersivities (α_l and α_t, [L]) that specify the degree of dispersion both in the direction of flow (α_l) and perpendicular to the direction of flow (α_t). Molecular diffusion, computed as a function of the molecular diffusivity and the solute-concentration gradient, contributes additional dispersion, which in the direction of flow in large-scale grids is usually negligible in comparison with mechanical dispersion. The effect of both mechanical and molecular diffusion is termed hydrodynamic dispersion.

The numerical approximations used to represent the dispersion of solute and its relation to advective processes can, if improperly used, cause unrealistic solute-concentration values to be computed and can cause a misinterpretation of the hydrogeologic processes that are occurring. The selection of the best approximation method depends on the nature of the physical representation problem. For this reason, users of solute-transport models should consider the proposed selection of numerical algorithm methods and parameter values to determine whether the methods and values will lead to a representation that is physically realistic. Solute-transport simulation efforts often do not provide the resources for such an evaluation to be done, which is unfortunate in view of the critical nature of this aspect of the simulation problem.

The selection of the numerical approximation technique for evaluating the advective terms in the solute transport equation can be made from several optional selections, so these were tested in comparison with one another. Modifications made by the author to the model code include experimental algorithms for the computation of vertical advective and dispersive flux of solute. These new methods were tested in comparison with the original algorithms previously encoded in the 1979 version of the SWIP code.

A full description of the methods and results of the testing were documented by Merritt (1993). The following sections briefly summarize the results of this evaluation, which showed the interrelated effects of vertical mechanical dispersion and molecular diffusion from vertically adjacent confining layers to have a significant effect on the computation of recovery efficiency. This leads to a sophisticated calibration technique that accounts for molecular diffusion into the thin flow zone from overlying and underlying confining layers containing saline water.

Numerical Dispersion and Oscillatory Behavior

The SWIP code requires a user to select between backward and central methods of differencing the finite-difference approximations of the temporal and spatial derivatives in the transport equations. When backward spatial differencing is selected, a degree of first-order error is introduced into the solution that has the appearance of hydrodynamic dispersion. In one-dimensional computations the degree of numerical dispersion introduced into the solution has been shown (Lantz, 1971) to be $u\Delta x/2$, where α is the fluid velocity and Δx is the grid-cell dimension. The apparent dispersivity for the transport computation would be $(\alpha+\Delta x/2)$, where α is the dispersivity specified to represent the degree of physical dispersion that occurs. Lantz also shows in the one-dimensional case that backward differencing of the time derivative led to additional numerical dispersion of degree $u^2\Delta t/2\theta$, where Δt is the incremental time step and θ is the effective porosity. Thus, the actual degree of dispersion in the solute-transport solution would seem to be that which would be represented by a dispersivity of $(\alpha + u\Delta t/2\theta)$. In higher dimensions the numerical dispersion terms are more complex but continue to influence the apparent degree of dispersion in the solution.

When central differencing in time or space is the selected method, the corresponding finite-difference approximation is correct to the first order, and the first-order numerical dispersion terms are eliminated. Most of the degree of apparent dispersion in the transport solution depends on the dispersivities specified by the user, and is not determined by the local grid-cell size (given sufficiently fine discretization) or by a changing incremental time-step size. The different results obtained by use of the various techniques are illustrated with specific numerical examples in the aforementioned paper (Merritt, 1993). Central differencing techniques were selected for use in this study because it was desired to prevent the occurrence of numerical dispersion that would have been caused by the spatial discretization and time-step sequencing used in the simulations of injection and recovery if backward differencing techniques had been used.

The formulation of the dispersion terms in the SWIP code suggests an interpretation of the dispersion process as an interchange of equal amounts of fluid between adjacent grid nodes, with the fluid received by each having the solute concentration (or fluid mix) of the nodal center of the other cell. Intuitively, this representation may be understood to work best when a region of changing concentration is finely subdivided into many grid cells in the direction of fluid movement. Alternatively, the representation may work best in regions where the spatial variation of concentration is gradual relative to the grid spacing. Similar advisement on finely discretizing the zone of concentration change is offered by Kipp (1987, p. 116–117).

The dispersion representation does not function as effectively when concentration changes are abrupt relative to the grid spacing in the direction of flow. In this case, specification of a large longitudinal dispersivity can cause the computed concentration variation to be distributed over a larger spatial volume than is realistic. Specification of a small longitudinal dispersivity may allow spatial oscillations (caused by the tendency for the solution to overestimate the advective flux of solute between grid cells) to grow in the absence of the smoothing effect of dispersion (the overshoot and undershoot described by INTERCOMP Resource Development and Engineering, Inc.). Spatial oscillations, when using central differences, indicate an incompatibility between the selection of longitudinal dispersivity and the grid dimensions. In some models the range of values that can be assigned to longitudinal dispersivity may be restricted by a coarser than desired grid spacing mandated by the need for computational efficiency. Numerical oscillations at a grid node in sequential time steps indicate an incompatibility between the speed of solute movement and the computational time increment sequence used to simulate it.

Numerical criteria for avoiding oscillatory behavior were developed by Price and others (1966) and are cited in the SWIP code documentation (INTERCOMP Resource Development and Engineering, Inc., 1976) and in the HST3D code documentation (Kipp, 1987, p. 114). The ability to select grid-cell dimensions and dispersivities to realistically portray a zone of concentration change depends upon physical measurements or having some physical concept of the zone of dispersion based on real data, and on having adequate computational resources. In this study, data that explicitly describe the zone of dispersion are scanty, given the ambiguity of the freshwater breakthrough data at the observation well, and the spatial extent of the zone of dispersion can only be inferred on a spatially averaged basis from consideration of the chloride increases observed during recovery.

Experimental Algorithms for Dispersion and Advective Weighting

Transverse dispersivity describes the degree of dispersion in a plane perpendicular to the direction of flow without distinguishing between transverse dispersion within the plane of flow (the bedding plane) or perpendicular to it (dispersion in the crossbed or vertical direction), even though macroscopic hydraulic properties may be different or have different degrees of spatial continuity along the different directional components of fluid flow paths. In media with solution porosity, transverse dispersion may be partly related to the nonlongitudinal orientation of solution features along the flow path, but the extent to which this occurs may not be the same in the vertical direction as within the plane of flow.

When vertically adjacent layers are of different hydraulic conductivity, the more permeable layer may be partially flushed by water having a quality different from that of the other layer. This can occur as a result of flow in the more permeable layer from a recharge area or from an injection well that has not flushed the less permeable zone to a similar extent. Usually the flow direction is nearly parallel to the interface between layers. Because of common data limitations, the vertical transition of hydraulic properties and water quality usually is represented as a step function between adjacent layers of grid cells. In this case, use of central differencing for vertical advective flux of solute across the interface between layers would imply that water flowing across the interface would have a solute composition that is an average of that of the two waters. However, a more realistic conceptual model of seepage flux across the interface is as water having the quality of that in the originating layer. An upstream (backward) advective weighting scheme would seem to be more appropriate.

When vertically adjacent layers contain waters of different quality, the vertical component of dispersion implied by the dispersion algorithm may be inappropriate because the transition of water quality does not occur gradationally across the thicknesses of several grid cells and is nearly perpendicular to the direction of flow. Providing a finer vertical

discretization may not be computationally efficient, and there might not be any available data describing gradational hydraulic and water-quality variations.

Other problems can occur when there is a large difference in scale between the horizontal and vertical dimensions of grid cells. When transport processes occur over distances of several miles in aquifers a few tens of feet thick, computational economy may mandate that the ratio of average horizontal and vertical grid dimensions be as great as 1,000:1. A large longitudinal dispersivity may be required to match the coarse horizontal discretization. However, if small but still appreciable vertical flows occur, a large longitudinal dispersivity may lead to the simulation of a degree of vertical dispersion sufficient to obscure actual vertical variations in solute concentration.

Therefore, to provide the means for more physically realistic simulation of transport processes in the situation described, experimental algorithms for representing vertical advective and dispersive fluxes of solute were encoded as options in the SWIP simulator. The experimental algorithms implement the concepts described in the following statements:

- Mechanical dispersion in the vertical direction is identically zero between adjacent layers of different permeability [$K_x(k) \neq K_x(k-1)$, where K_x is the hydraulic conductivity in the x coordinate direction]. Molecular diffusion between layers occurs as before. Between layers of similar permeability [$K_x(k) = K_x(k-1)$], mechanical dispersion in the vertical direction is scaled by a user-specified factor S ($0 \leq S$).
- Vertical advective flux of solute receives upstream weighting (backward differencing) across the boundary between layers of different permeability [$K_x(k) \neq K_x(k-1)$], regardless of which weighting is used in the rest of the spatial domain of the model.

The experimental algorithms implement the conceptual view that solute flux across the boundaries between layers of different permeability occurs as molecular diffusion or as hydraulically driven seepage in which the water flux has the solute concentration of the source layer. The scaling factor is a user-specified parameter for use in application problems where bedding effects or the discretization may cause incompatibility in the description of horizontal and vertical dispersive processes within a hydraulically uniform layer.

A method of allowing longitudinal dispersivity to have a dependence on the flow direction is documented in the description of the two-dimensional SUTRA model by Voss (1984). Voss used a relatively fine vertical discretization to provide a cross-sectional depiction of a sharp freshwater-saltwater transition zone parallel to flow lines in a description of the simulation of saltwater intrusion on the island of Oahu, Hawaii (Voss and Souza, 1987). This has some generic similarities to the treatment of the problem described herein, in which the sharp transition in density occurs across flow lines parallel to a confining-zone interface. The use of the approach involving flow-dependent longitudinal dispersivity in a hypothetical cross-sectional model of saltwater intrusion is described in a paper by Reilly (1990).

Results of Testing Algorithms and Parameter Values

The tests of the original and experimental algorithms and parameter value selections consisted of a series of computer runs simulating the first injection of 53 days. A cylindrical coordinate system was used in which horizontal grid dimensions (grid annuli widths) in the region of injected-freshwater movement were less than 80 ft. The vertical discretization depicted in figure 18 was enhanced to illustrate the theoretical variation in the solute-concentration field near the boundary between the flow zone and confining layers. The assigned values of flow-zone hydraulic conductivity were 800 ft/d in the horizontal direction and 80 ft/d in the vertical direction. Confining layers were assigned values of 0.1 ft/d for horizontal and vertical hydraulic conductivity. Porosity was uniformly 35 percent. A longitudinal dispersivity (α_l) of 20 ft was assigned arbitrarily and was considered to be compatible with the horizontal discretization. Variables of the tests were (1) original versus experimental methods; (2) transverse dispersivities (α_t) of 20 ft and 0.1 ft; (3) scaling factors of 1 (no scaling), 0.1, 0.01, 0.001, 0.0001, and 0 (no vertical mechanical dispersion); and (4) molecular diffusivity (D_m) values of 0.001, 0.0001, and 0.00001 ft^2/d. In addition to a detailed description of the transition zone between fresh water and saline water at the end of injection, the effect on recovery of freshwater was assessed by simulations of withdrawal at a rate of 62,047 ft^3/d, the average rate of the first recovery at Hialeah. Results of the tests are described in detail by the author in a previous paper (Merritt, 1993).

The tests showed that when the experimental algorithm is used to eliminate vertical dispersion across flow-zone boundaries, the primary influence upon recovery efficiency and the salinization of water

at the boundaries of the freshwater mass is the degree of molecular diffusion from the more saline surrounding rocks. The magnitude of this influence depends on the degree of vertical dispersion occurring within the flow zone, and this is controlled by the transverse dispersivity (α_t) and by the size of the scaling factor specified by the user to compensate for bedding effects or for the incompatibility of horizontal and vertical discretization scales in the application problem. When the original algorithm is used and vertical dispersion across flow-zone boundaries is allowed to occur and a relatively low value of longitudinal dispersivity (α_l) is specified, the degree to which recovery efficiency is reduced depends on the size of the transverse dispersivity (α_t) specified by the user. Changing to upstream weighting for vertical advective flux had little effect in any of these tests because the amount of seepage across flow-zone boundaries was negligible in comparison with the amount of flux from molecular diffusion.

The tests of recovery efficiency revealed much about the effect of mechanical dispersion and molecular diffusion on computed recovery efficiencies without, however, leading directly to parameter estimates for the simulation model. Because a large degree of computed dispersion across flow-zone boundaries does not seem to represent any known physical process, it is probable that algorithms and parameter selections that minimize the degree of computed dispersion would lead to the most realistic simulation. Either the experimental algorithm and a scaling factor or the original method with a small transverse dispersivity should probably be used. The representation of molecular diffusion of solute from vertically adjacent confining layers into the body of injected freshwater within the flow zone is a more realistic simulation procedure than one that entirely disregards the transfer of solute between the injection zone and confining layers by treating the latter as impermeable no-flow boundaries.

Dispersion Tests in a Horizontal Plane

Additional insights into the dependence of model behavior upon dispersivity selections are gained by performing model tests with different sets of dispersivities in three-dimensional Cartesian coordinates. The 53-day first injection at the average rate of 105,661 ft^3/d was simulated in the Cartesian grid system illustrated in figures 18 and 19. The regional hydraulic gradient was set equal to zero. The experimental algorithms for computing vertical dispersion were used, and the longitudinal dispersivity (α_l) was set equal to 20 ft. The variables of the tests were the transverse dispersivity (α_t) and the vertical scaling factor (S). The aquifer was considered horizontally isotropic.

Two of the sets of values that were tested (α_l=α_t =20 ft, S=0.01 versus α_l=20 ft, α_t=0.1 ft, and S=1.0) illustrated a significant facet of model behavior. Because the mechanical dispersion term in the vertical direction resulting from the larger value of α_t was scaled by 0.01, vertical mechanical dispersion in the flow zone varied only by an approximate factor of 2 in the two cases, and the radial extent of freshwater flow was not affected by large simulated dispersive fluxes across upper and lower boundaries because the experimental algorithms were used. However, α_t also determined the degree of transverse dispersion in the horizontal plane, and between the two cases, the horizontal transverse dispersivity differed by a factor of 200. The comparison was, therefore, between relatively large and small degrees of transverse dispersion in the x-y plane.

The results of the tests are shown in figure 20 as planar views of freshwater distribution about the well (lines of 750 mg/L dissolved solids) in layer 6 (layer 3 of the flow zone). When α_t=20 ft and S=0.01, the line is virtually a perfect circle, as would be expected in radial flow from a well unaffected by a background hydraulic gradient. The line depicting the case in which α_t=0.1 ft and S=1.0, however, shows bulges of fresher water along the positive and negative x- and y-axes that have no physical meaning and are evidence of the inaccuracy of the mathematical solution for radial flow in Cartesian coordinates when horizontal transverse dispersion is small. Even when horizontal boundaries of the model grid were extended from 20,000 to more than 270,000 ft from the well to mitigate the possible effect of the nonuniform distance to the location of specified boundary pressures, there was no apparent effect upon the nonradial spatial distribution of freshwater. Requiring that at least two iterations of the solution to the solute-transport equation be performed and the use of subroutine CRSS for an alternate computation of nonaxial transport (INTERA Environmental Consultants, Inc., 1979) only resulted in a slight increase of solute movement in the positive x, positive y and negative x, negative y directions (fig. 20) without appreciably improving the depiction of radial flow.

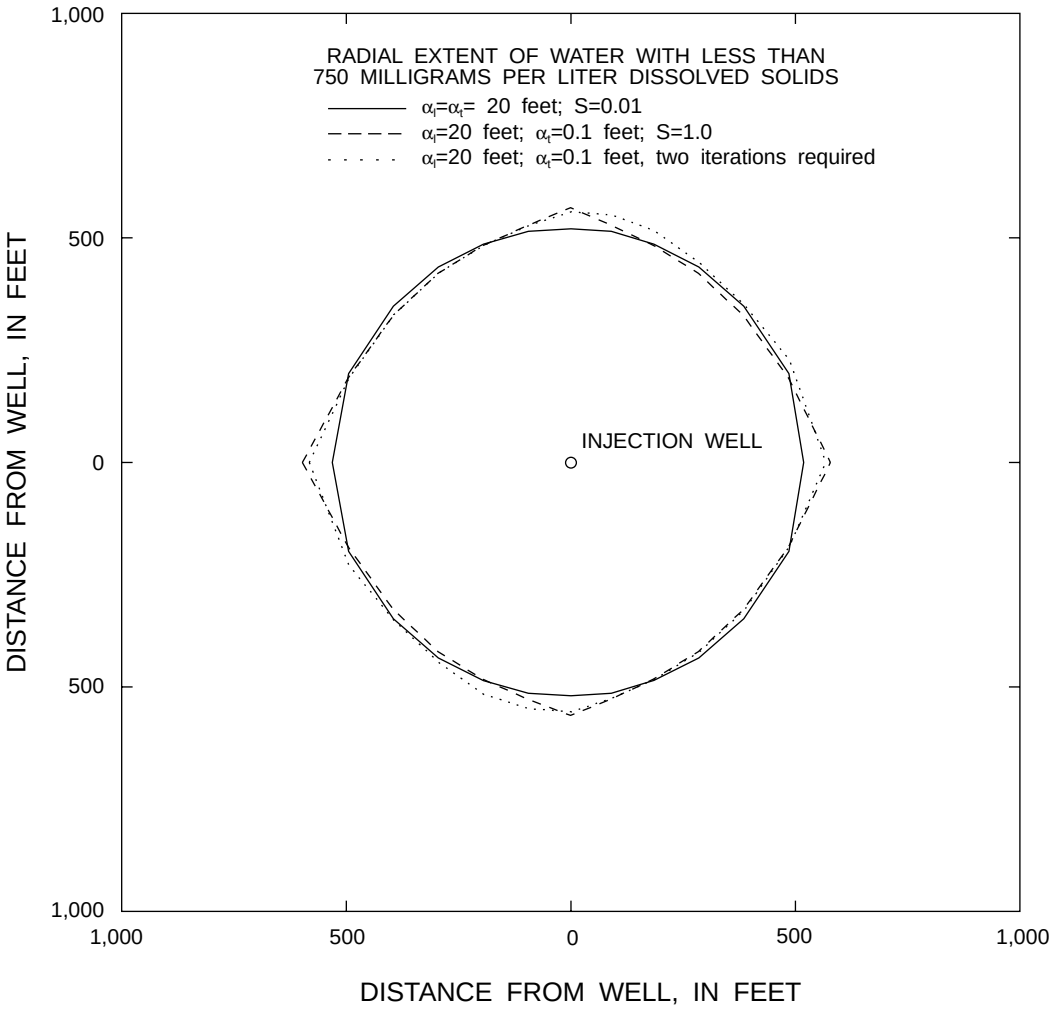

Figure 20. Plan view of the distribution of injected freshwater using two values of transverse dispersivity (α_t).

Simulations using the two sets of values were each followed by a simulation of recovery and computation of recovery efficiency. In case 1 (α_t=20 ft, *S*=0.01), recovery efficiency was 52.8 percent. In case 2 (α_t=0.1 ft, *S*=1.0), recovery efficiency was 53.1 percent. Thus, despite the apparent difference between computed freshwater distributions, the effect on computed recovery efficiency was slight. When case 2 with extended boundaries was followed by recovery, the computed recovery efficiency was 54.0 percent.

The result of these comparisons provides a basis for selecting the algorithms to be used for computing dispersion. Setting $\alpha_l=\alpha_t$, which produces the most realistic depiction of radial flow in Cartesian coordinates, is the preferred approach to the selection of values. This approach requires that some means be found to reduce the degree of vertical dispersion across flow-zone boundaries; therefore, the experimental dispersion algorithm was used for the simulations. A scaling factor of about 0.01 was used for vertical transverse dispersion within the flow zone. This selection was arbitrary but was partly based on the 100:1 ratio of horizontal to vertical grid-cell dimensions within the region of freshwater invasion of the flow zone. The value of molecular diffusivity was determined as part of the calibration process.

Hydraulic Parameter Estimation Methods

Hydraulic parameter estimates were based on data from the aquifer test of February 10, 1975. The estimates are subject to the usual reservations applying to aquifer testing in carbonate terranes, where local nonuniformities in hydraulic properties at the with-

drawal or observation points can yield estimates atypical of the average hydraulic properties of the aquifer. The results of Theis and Jacob-Lohman analyses (Lohman, 1979) were previously cited. In this section, a description of SWIP code simulations of the aquifer test is presented. The simulations were for the purposes of (1) deriving final estimates of hydraulic parameters for simulation, (2) sensitivity testing, and (3) testing alternative conceptual models of aquifer physical and hydraulic properties.

Simulation of Aquifer-Test Data and Sensitivity Analyses

The calibration of the aquifer test was based on the assumption that the flow zone was 12 ft thick and that the entire injection zone had a porosity of 35 percent. The confining-layer hydraulic conductivities were set equal to a small value (0.01 ft/d). This value was arbitrary, as no data were available upon which to base the estimate. The three-dimensional Cartesian grid design used for the calibration is shown in figures 18 and 19. Injection and observation wells were five grid nodes apart. Withdrawal from the observation well at the controlled rate of 250 gal/min was specified for a simulated period of 100 minutes. Nonvarying specified-pressure boundary conditions at a minimum of 20,000 ft from the wells were used and corresponded to uniform initial conditions within the aquifer. A Theis formula computation showed that the drawdown at 20,000 ft from 100 minutes of pumping at the cited rate was negligible.

A good match of observed and simulated drawdowns is shown as curve C in the various graphs of figure 21. Each pair of graphs shows the comparison and results of a sensitivity analysis for the entire 100-minute test period and for an early time period (first 3 minutes). The apparent stepping pattern of early time observations merely represents the limited resolution of the scale of the measuring instrument. Values of 800 ft/d for hydraulic conductivity in the horizontal (x-coordinate and y-coordinate) directions provided the best match for later time data, but the computed early time response was not highly sensitive to 25 percent changes (lines K1 and K2, fig. 21*A*) in horizontal hydraulic conductivity. The 25 percent variations caused unrepresentative later time drawdowns to be computed, the divergence increasing with time. Vertical hydraulic conductivity, for which data were not available to provide a basis for estimates, was arbitrarily considered to be 10 percent of the horizontal hydraulic conductivity in each sensitivity analysis.

The estimated values of horizontal hydraulic conductivity, integrated over the 12-ft thickness of the flow zone, give a transmissivity value of 9,600 $[(ft^3/d)/ft^2]ft$. The integration should include the confining-zone thicknesses, but because of their low estimated hydraulic conductivity, the transmissivity value would merely increase by 1.33 $[(ft^3/d)/ft^2]ft$.

Early time observations were matched by varying rock compressibility, specified in $(\text{pounds per square inch})^{-1}$. This procedure is similar to varying the storage coefficient in a two-dimensional areal hydraulic model because the storage coefficient (S) is considered (Lohman, 1979) to be a linear function of rock compressibility (C_r) according to the following formulation:

$$S = \theta\rho b(C_w + C_r) \qquad (8)$$

where: θ is porosity (unitless),
b is layer thickness (L),
ρ is fluid density ($P\,L^{-3}$), and
C_w is water compressibility ($P^{-1}\,L^2$).

Of the terms in the equation, all have been assigned values except for C_r. The value of C_w, 0.000003 $(\text{lb/in}^2)^{-1}$, is readily obtained from various handbooks. A C_r value of 0.0000400 $(\text{lb/in}^2)^{-1}$ was used to simulate the observed early-time drawdowns. Substantial disagreement occurred in the early time range when this value was increased and decreased by 25 percent (lines C1 and C2 in fig. 21*B*). The calibrated C_r value, together with the hydraulic conductivity value of 800 ft/d, also provided a good simulation of later drawdown data.

The compressibility and porosity estimates can be related to a storage coefficient value. Applying relation 10 to the flow zone (b=12 ft), an equivalent storage coefficient of 7.8×10^{-5} is obtained. Lohman (1979) states that equation 10 was derived (Jacob, 1940) by neglecting any release of water from confining beds. Because there is an assumed ratio of 80,000:1 for the horizontal permeability of the flow zone and that of the overlying 65 ft and underlying 68 ft of relatively impermeable strata, this approximation seems to be a good one. The hydraulic-head change at the observation well was 1.8 ft at the end of the 100-minute test. An inspection of the SWIP simulation shows a head change of 1.6 ft at an elevation 2.75 ft above the flow zone and a head change of 0.06 ft at an elevation 35 ft above the flow zone. Only a small part of the upper low-permeability layer has released an appreciable amount of water to the flow zone.

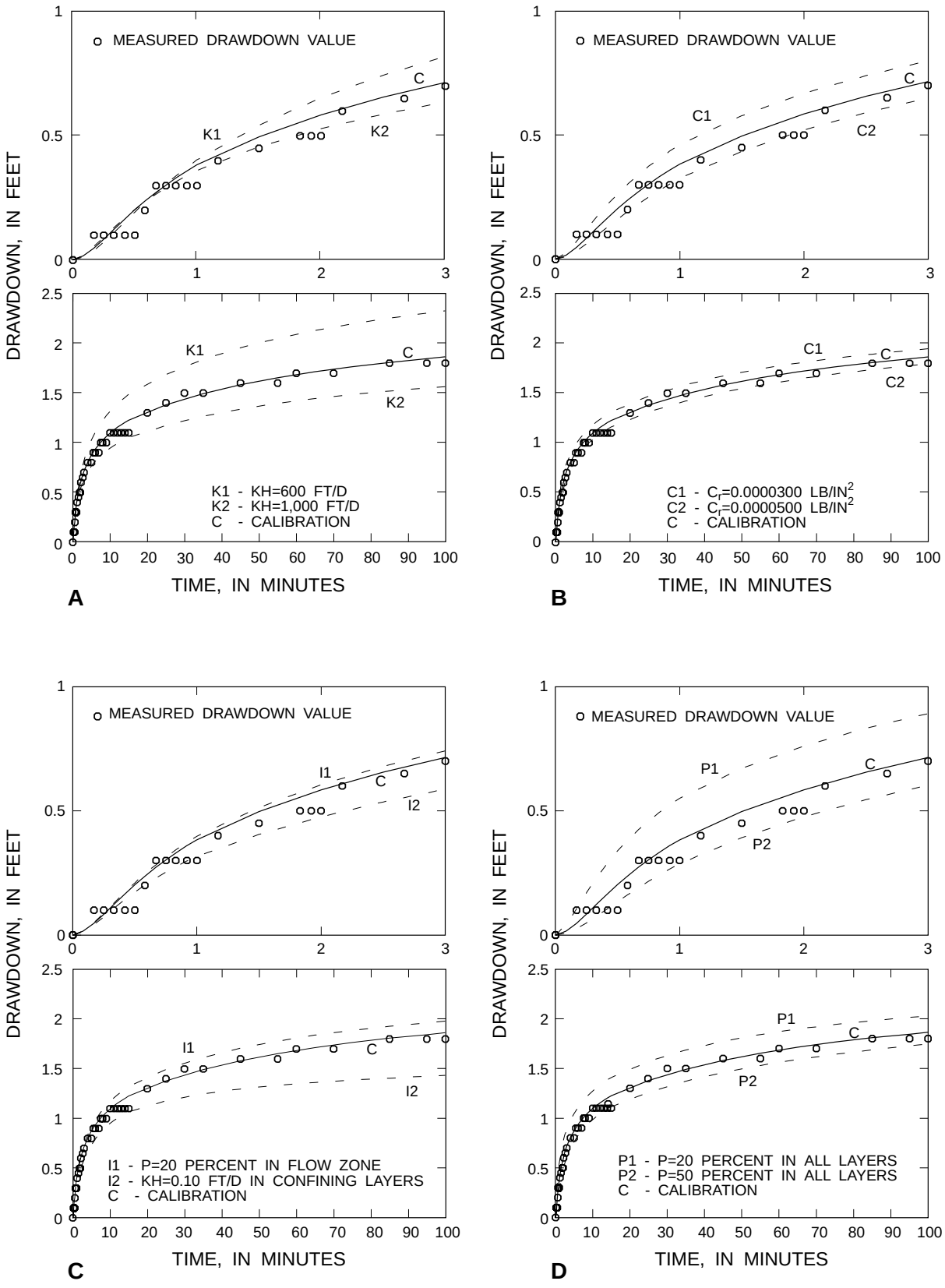

Figure 21. Simulation of the February 10, 1975, aquifer test data and sensitivity analyses. Results of sensitivity analyses are shown as dashed lines. KH, horizontal hydraulic conductivity, in feet per day (ft/d); P, porosity, in percent; CR, value of rock compressibility, in inverse pounds per square inch (lb/in^2).

As previously noted, the hydraulic-conductivity estimates for the confining layers were arbitrary, though permeability was known to be low. To gain an understanding of how much error could result by underestimating the value of this parameter, the model was run using a value of K_x=0.1 ft/d, 10 times greater than the value assigned for calibration of the aquifer test. The computed drawdowns are shown as curve I2 in figure 21*C*. Results of the test are relatively dramatic, showing a substantial underestimate of observed drawdowns at both early and late times. Thus, increasing by a factor of 10 the amount of injected water that can be accepted by 133 ft of relatively impermeable strata substantially lowers the hydraulic response of the flow zone. Other tests (not illustrated) indicated that the aquifer-test data could be simulated with flow-zone hydraulic-conductivity values of 750 ft/d and a rock compressibility value of 0.0000450 $(lb/in^2)^{-1}$ when the confining-layer hydraulic conductivity was considered to be 0.1 ft/d.

The solution dependence upon the specified porosity value of 35 percent for the entire injection zone was examined with sensitivity analyses that assumed that porosity in all zones was uniformly 20 and 50 percent. Results (curves P1 and P2 in fig. 21*D*) show significant discrepancies with observed data at early times. At later times, observed and computed data are offset to a degree that seems to change only slightly with increasing time.

Total porosity similarities between formations of dissimilar permeability, as indicated by the neutron porosity log of January 8, 1975, raise the issue of how total porosity relates to effective porosity, the pore or channel volume that is flushed by water moving in the aquifer. The SWIP code assumes that the specified pore volume of each layer receives flow from natural or user-specified sources, such as wells; thus, the specified SWIP porosity is considered to be effective porosity. Effective porosity is herein assumed to be equivalent to total porosity (35 percent) in the confining layers because the apparent lack of solution features implies that seepage through these rocks could occur at an equal rate in all pore spaces. The resistance to flow within the confining layers is accounted for by the specification of a low value for hydraulic conductivity rather than by considering porosity to be low. Specification of low values of effective porosity in the confining layers can lead to simulation error because inflow from the well is allocated to these layers on the basis of their low hydraulic conductivity, and the model would assume that even minor inflows into the confining beds were quickly distributed throughout an unrealistically large volume.

In the flow zone, a dual-porosity scenario might be more appropriate if water were contained partly within connected solution channels and partly within pores in rock surrounding the solution channels. Movement of water within pores isolated from solution channels would be insignificant relative to movement within the solution channels, and hydraulic conductivity and effective porosity would refer to the flow properties and relative volume of the latter. Effective porosity, therefore, might be less than the estimated 35 percent in the flow zone.

To test this possibility, an additional sensitivity analysis assumed that the flow-zone effective porosity was 20 percent. The result is shown in figure 21*C* as curve I1, which indicates that observed drawdowns are overestimated at late times. The later time result is similar to that when the entire injection-zone porosity is assumed to be 20 percent. The fact that some pores or solution channels admit flow and permit related solute-concentration change at a slower or faster rate than others, in either the confining layers or the flow zone, is accounted for by the mechanical dispersion concept.

Alternative Calibrations of Aquifer Test

Alternative calibrations of the aquifer test were performed to obtain separate sets of aquifer hydraulic parameters representing hypotheses that (1) the flow-zone thickness was 21 ft, (2) the effective porosity of the flow zone was 20 percent, and (3) the flow-zone permeability was horizontally anisotropic. In the third case, a 10:1 bipolar model of anisotropic hydraulic conductivity (K_x>K_y) was specified, where K_x and K_y are values of hydraulic conductivity in the two horizontal coordinate directions. These three test cases are the conceptual models of the aquifer that seem to represent the most likely errors in the accepted conceptual model or to have the greatest generic significance for model calibration. These alternative conceptual models are later used for separate calibrations of the recovery data. The accepted and alternative calibrations of the aquifer-test data are shown in figure 22 for 100- and 3-minute time periods as line C (calibration based on the accepted conceptual model of the aquifer), line C1 (21-ft flow-zone thickness), line C2 (20 percent effective porosity), and line C3 (anisotropic permeability).

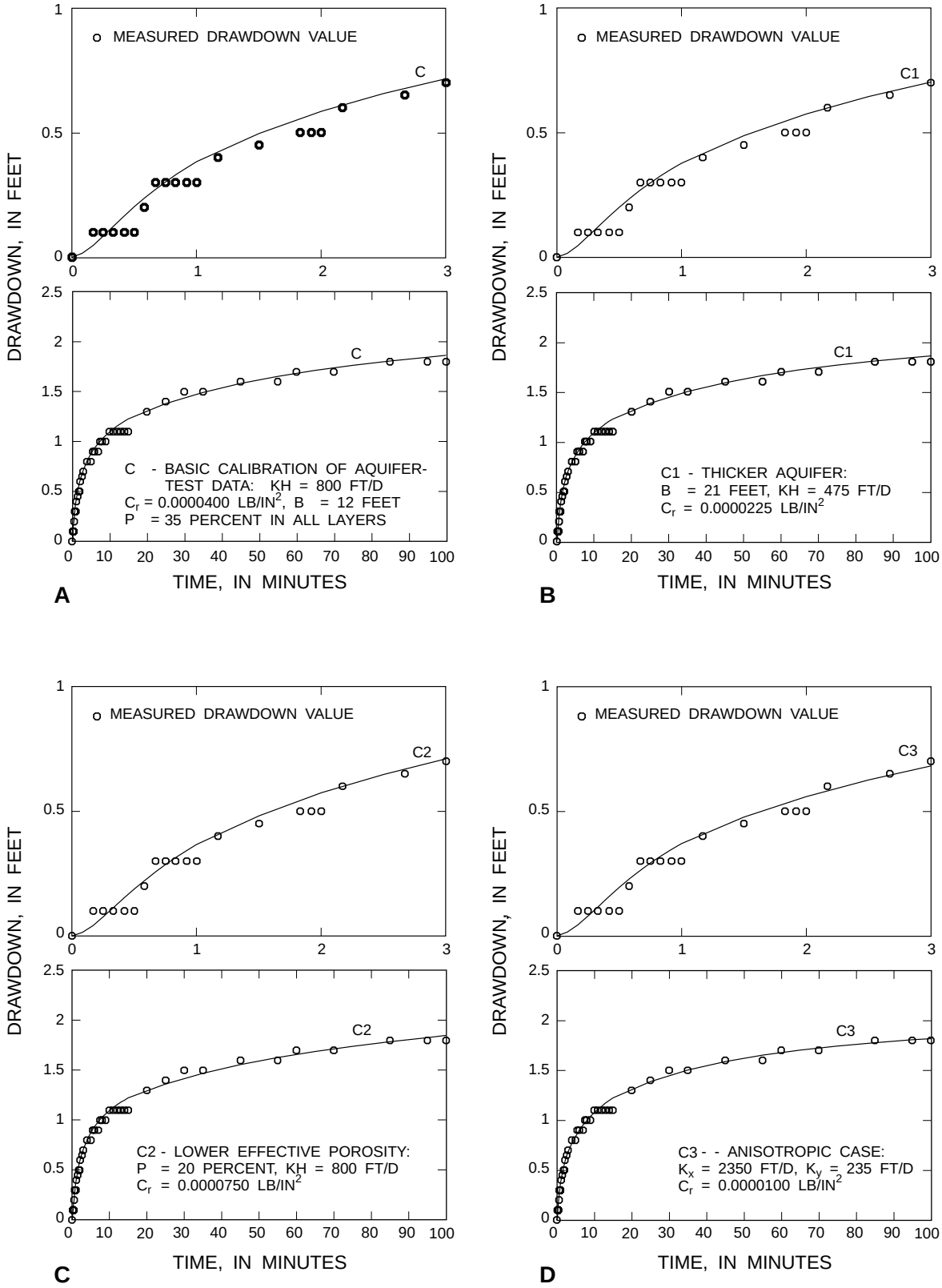

Figure 22. Alternative simulations of the February 10, 1975, aquifer-test data. KH, horizontal hydraulic conductivity, in feet per day (ft/d); K_X and K_Y, hydraulic conductivities in X and Y direction, in feet per day (ft/d); P, porosity, in percent; C_R, value of rock compressibility, in inverse pounds per square inch (lb/in^2); B, thickness of flow zone, in feet (ft).

The alternative calibrations match observed data as well as the calibration based on the accepted conceptual model. Estimating flow-zone effective porosity to be 20 percent (C2) requires that rock compressibility be increased to 0.0000750 $(lb/in^2)^{-1}$. Assuming that the flow-zone thickness is 21 ft (C1) requires that hydraulic conductivity be reduced to 475 ft/d and rock compressibility reduced to 0.0000225 $(lb/in^2)^{-1}$. Equivalent transmissivities (T) and storage coefficients (S) in the two cases are: (C2) T=9,600 $[(ft^3/d)/ft^2]ft$ and $S=7.8\times10^{-5}$, the same as for the primary calibration; and (C1) T=9,975 $[(ft^3/d)/ft^2]ft$ and $S = 7.2\times10^{-5}$.

When the flow zone was assumed to have a 10:1 bipolar anisotropy in the horizontal coordinate directions, and the observation well was assumed to be located in the direction of least permeability, calibration was achieved by setting K_x=2,350 ft/d and K_y=235 ft/d. The rock compressibility value (C_r) was 0.0000100 $(lb/in^2)^{-1}$. If expressed in bipolar components like hydraulic conductivity, then T_x=28,200 $[(ft^3/d)/ft^2]ft$ and T_y=2,820 $[(ft^3/d)/ft^2]ft$. The storage coefficient would be 1.8×10^{-5}.

Simulation of Recovery Salinity Data

Simulation of the increasing salinity (chloride or dissolved-solids concentrations) of recovered water implied a replication of the volume of withdrawal when withdrawn water reached the limiting chloride concentration used to calculate recovery efficiency and was, therefore, also a simulation of observed recovery efficiencies. The simulation required selection of values to represent aquifer hydraulic, chemical, and dispersive properties, representation of injection and recovery rates and volumes, and a method of relating simulated recovered volume to observed chloride data for matching purposes.

Parameter Value Selection and Comparison Techniques

For the initial calibration effort, parameter values were selected on the basis of an evaluation of data collected at the site, the simulation of the aquifer test, and a consideration of insights derived from the tests of dispersion models. On the basis of site data, the flow zone was assumed to be 12 ft thick, have an effective porosity of 35 percent, and contain water of 2,700 mg/L dissolved-solids concentration. The confining layers were assumed to have effective porosity of 35 percent and contain water of 6,000 mg/L dissolved-solids concentration. The hydraulic conductivity of the confining layers was set at an arbitrary low value, 0.01 ft/d. On the basis of the aquifer-test simulation, the flow-zone hydraulic conductivity was assigned a value of 800 ft/d, and rock compressibility was assigned a value of 0.0000400 $(lb/in^2)^{-1}$. On the basis of dispersion model tests, the experimental algorithm of vertical dispersion computation was selected to eliminate vertical dispersion across the boundaries between the flow zone and confining layers. Longitudinal and transverse dispersivities were assigned the same value to realistically represent radial flow from the well in the Cartesian grid shown in figures 18 and 19, and a scaling factor of 0.013 (ratio of average horizontal and vertical grid-cell dimensions) was used to reduce the degree of vertical dispersion occurring within the flow zone.

The values of longitudinal and transverse dispersivity and the molecular diffusivity could not be directly estimated on the basis of available data, but were found to be of primary importance in simulating the observed recovery salinity data. Therefore, they were determined by a process of trial-and-error adjustment and curve matching. The regional flow gradient was initially estimated to be 0.4 ft/mi on the basis of the regional potentiometric-surface map drawn by Meyer (1989a). This parameter also proved to be of major importance in matching observed data and needed considerable adjustment. Model calibration, therefore, consisted primarily of adjusting dispersivities, the molecular diffusivity, and the regional seepage velocity that depended on the regional hydraulic gradient and aquifer hydraulic parameters.

The time history of injection, storage, and recovery periods and hiatuses between cycles was represented approximately as listed in Appendix C. The time periods and corresponding rates of flow were encoded in the simulation as given in the table below, in which time 0 corresponds to the start of the first injection on July 17, 1975.

Stage	Time period (days)	Rate of flow (cubic feet per day)
Injection 1	0–53	105,661
Recovery 1	54–93	62,047
Hiatus	94–165	0
Injection 2	166–235	162,026
Storage 2	236–289	0
Recovery 2	290–367	95,333
Injection 3	368–554	147,442
Storage 3	555–729	0
Recovery 3	730–1,655	59,084

The 2-day storage period between the first injection and recovery was ignored, and the volume of the aborted second injection (App. C; pl. 1) was included in that of the subsequent successful second injection. Injection and recovery rates were represented as averages over each injection and recovery stage. Recovery efficiency and the distribution of injected water in the receiving zone were shown not to be related to injection or withdrawal rate in simulations with the SWIP code (Merritt, 1985), so use of average rates did not affect simulation of recovery salinity data. The estimated volumes of backflushes were subtracted from injection volumes (because only one flowmeter was used) before computing average rates.

Because average recovery rates were used, it was necessary to find a way to relate computed solute-fraction values of recovered water at given simulation times to the measured chloride concentrations of recovered water samples, which were recorded at various times as the actual recovery rate varied (App. C; pl. 1). This problem was resolved by using recovery volume rather than time as the common factor. The observed chloride concentrations were assigned artificial times equal to the actual recovered volume divided by the average rate. Thus, observed data times shown in subsequent illustrations differ slightly from the actual measurement times.

Chloride concentrations measured during recoveries were related to dissolved-solids concentrations by interpolation on the basis of chloride and dissolved-solids concentrations of injected-water samples and preinjection flow-zone water samples, as previously described. Based on the estimated dissolved-solids concentrations, recovered water samples were assigned values of solute fraction for comparison with the computed solute fraction of recovered water. (Solute-fraction values were 1.0 for 6,000 mg/L dissolved-solids concentration, 0.45 for native flow-zone water, and 0.0667 for injected water.) The SWIP code computes the solute fraction of withdrawn water as the weighted average of water withdrawn from each layer of the model. The weighting is a set of allocation factors that in these simulations was based on the relative thicknesses and hydraulic conductivities of the layers. Each of the six flow-zone layers had the same allocation factor, and allocation factors for the confining zone layers were so small as to make negligible their contribution to recovered volumes.

Basic Simulation

The process of calibrating the model to match observed recovery chloride data is illustrated in figure 23. An early simulation attempt (fig. 23A) was based on the supposition that the regional pore velocity had no influence on observed recovery data. The regional hydraulic gradient was set equal to zero. The dispersivity values were $\alpha_l=\alpha_t=65$ ft, and molecular diffusivity was $D_m=0.0002$ ft^2/d. A good match of the observed salinity increases was obtained in the first recovery and at the end of the third recovery, when recovered water salinity had returned nearly to the background level (the salinity of native flow-zone water). However, observed salinity exceeded computed values in the second recovery and during most of the third recovery, and the discrepancy was substantial.

To obtain a better match of observed and simulated data in the second and third cycles, the dispersivity values were increased to 100 ft (fig. 23B). The salinity increase is slightly faster in the third recovery, although computed values still are greatly exceeded by the observed data. However, computed salinity increases now substantially exceed observed increases in the first and second recoveries. It was evident that this simulation strategy could not be productive.

At this point, nonzero values of regional pore velocity were introduced, and the dispersivity values were reduced to the value of 65 ft that produced a good match in the first recovery. When pore velocity was set equal to 260 ft/yr, a good match was obtained in all three recoveries (fig. 23C). The computed salinity of recovered water in the brief first ASR cycle was unchanged by the use of a nonzero pore velocity. However, because recovery followed 54- and 181-day storage periods in the second and third ASR cycles and because the third recovery continued for 2.5 years, sufficient time elapsed for the simulation of a substantial downgradient shift of the injected freshwater mass. During the later part of the simulated second and third

recoveries, water entering the well from the upgradient direction was more saline than water coming from the downgradient direction. Thus, the computed recovery salinities increased relative to the earlier run with no regional flow and matched measured data.

This calibration (fig. 23C) will be referred to as the basic simulation to distinguish it from later simulations in which some of the parameter values not used as calibration adjustments were revised (alternative simulations). The downgradient shifts of injected freshwater caused by simulated regional flow are shown in figure 24, which shows planar views of lines of equal solute fraction in layer 6 (layer 3 of the flow zone) at selected times during the three ASR cycles. Other lines of equal computed solute fraction within the transition zone are also shown. The illustration helps to visualize the simulated distribution and movement of injected water within the flow zone during the ASR process, and also indicates the simulated degree of dispersion around the mass of potable water. Figure 24 was generated by selecting the locations of the solute value within each row of the model grid by linear interpolation between columns and then connecting the points successively. Small bulges along the *y*-axis are a consequence of using Cartesian coordinates to simulate radial flow from a well, as previously discussed, even when a large horizontal transverse dispersivity is specified. That this does not occur along the *x*-axis is due to the influence of regional flow.

Figure 24 shows the nearly circular injected water mass after the brief first injection and the injected water at the end of the second injection, when some downgradient drift is evident. The drift becomes progressively more pronounced after the second storage period of 54 days, at the end of the third injection, and at the end of the third storage period of 180 days. The transition zone is wider (more diffuse) downgradient of the injected well. After the end of the extended third recovery, water with a lower solute fraction than that of the native water (0.45) remains in the aquifer. This fresher water is a mixture of injected freshwater and native saline water. That small amounts of the fresh injected water remain in the aquifer at this time as a result of downgradient advection is especially remarkable because the volume of the third recovery was nearly twice that of the third injection and exceeded the volume of all three injections by 22 percent.

Using a pore velocity of 260 ft/yr for calibration requires a regional gradient of 1.6 ft/mi, given the hydraulic conductivity estimate of 800 ft/d and porosity estimate of 35 percent. However, this value is 4 times that estimated on the basis of published potentiometric-surface data (Meyer, 1989a). Errors of this magnitude in the published estimates are unlikely, raising questions about the accuracy of the hydraulic conductivity estimates determined from simulating the aquifer-test data. In fact, results of individual aquifer tests in carbonate terraces are known to be unreliable because local heterogeneities are common. Thus, average flow-zone hydraulic conductivity possibly could be larger than estimated, perhaps even 4 times larger, or could be anisotropic. The unusual trends previously cited in observation-well water-quality data during the three injections, which suggest a partial early breakthrough of injected water, also suggest the possibility of local heterogeneities in flow-zone solution features that might affect results of an aquifer test.

Near the end of the third recovery, computed recovery salinities were nearly the same as when the hydraulic gradient was specified to be zero, as would be expected if computed values are approaching the natural flow-zone salinity (1,200 and 2,700 mg/L concentrations of chloride and dissolved solids, respectively). The last chloride concentration measurement of recovered water, on January 28, 1980, was 1,120 mg/L. However, the magnitude of computed solute-fraction values near the end of the third recovery was highly sensitive to the molecular diffusivity value (D_m), which determined the rate at which solute ions from the more saline confining layers diffused into the injected water occupying the flow zone in the vicinity of the well. Figures 23D–E illustrate the dependence of the simulation result upon the value of D_m, as determined by additional simulation runs in which the dispersivities and regional pore velocities were the same as in the calibration (fig. 23C). D_m was increased to 0.001 ft^2/d (fig. 23D) and decreased to zero (fig. 23E). When D_m=0, no appreciable change in computed recovery salinities is observed in the first recovery, but computed salinities in the longer second and third recoveries are too small, and the salinities seem to converge to a value that is too low near the end of the third recovery. This illustrates results of the previously described algorithm tests showing that the observed recovery salinity data are highly influenced by the degree of molecular diffusion from overlying and underlying rocks

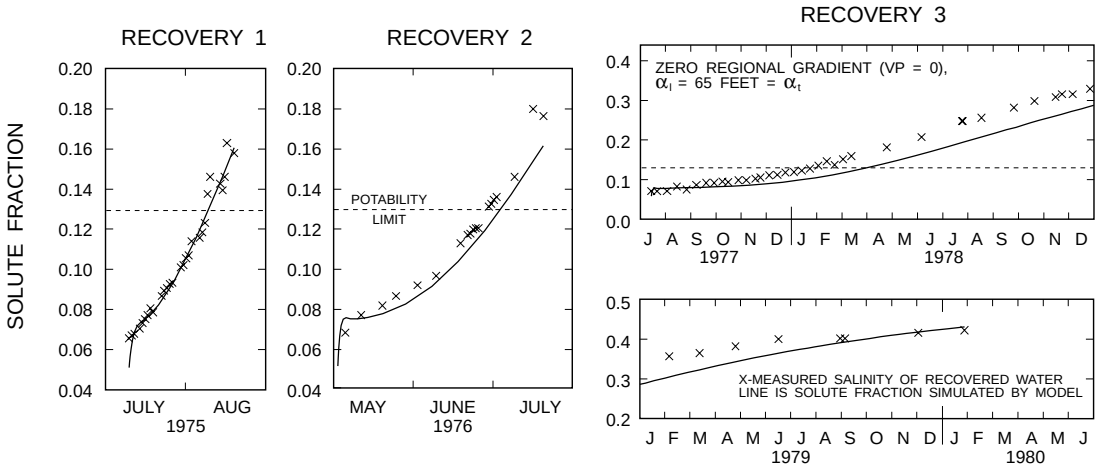

A. Unsuccessful attempt to simulate data using a zero regional gradient.

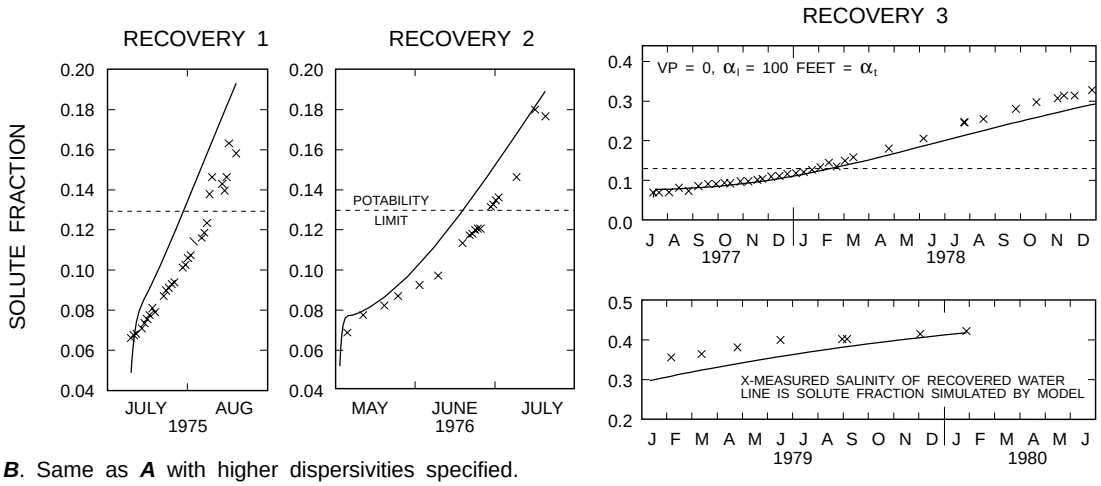

B. Same as ***A*** with higher dispersivities specified.

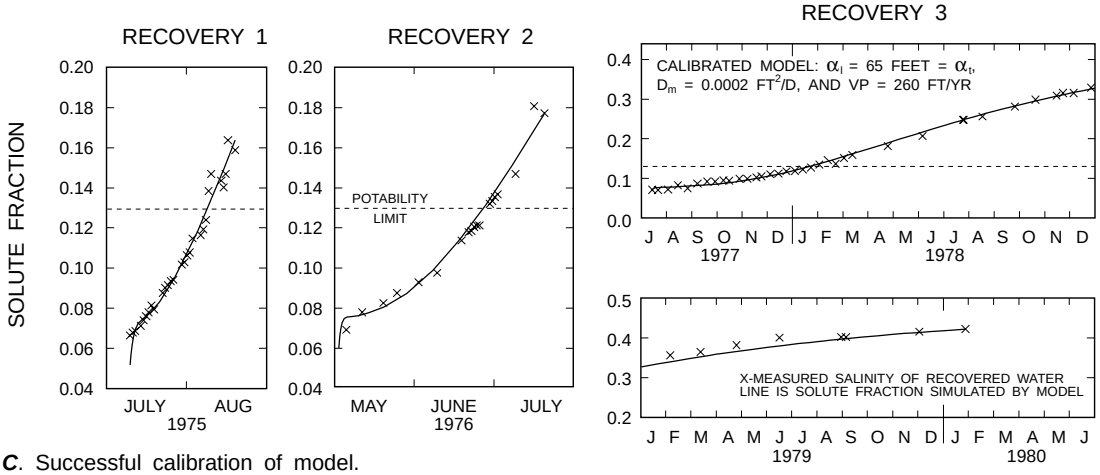

C. Successful calibration of model.

Figure 23. Results of the simulation of the salinity of recovered water and selected sensitivity analyses showing the calibration techniques. VP, aquifer pore velocity, in feet per year (ft/yr); α_l, α_t, longitudinal and transverse dispersivity, in feet; D_m, molecular diffusivity, in feet squared per day (ft^2/d).

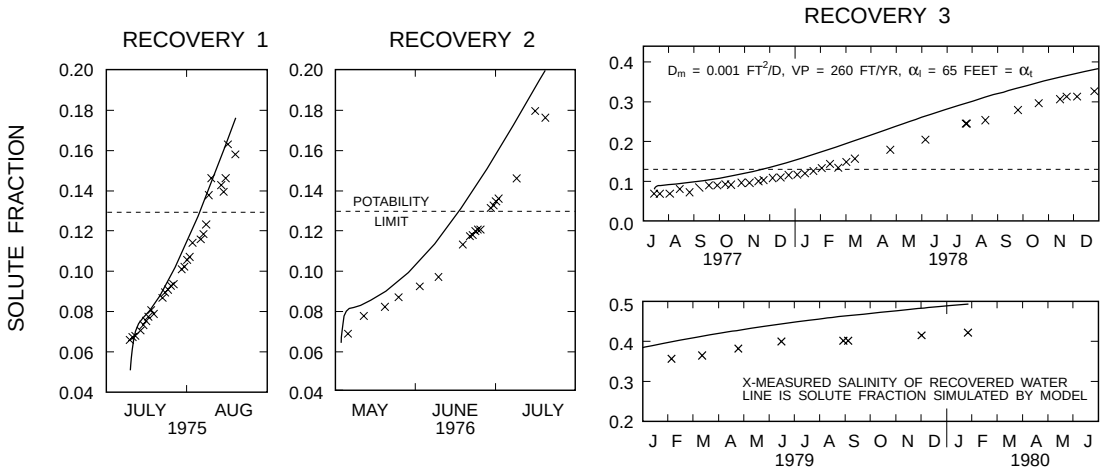

D. Sensitivity analysis: a higher value of molecular diffusivity is specified.

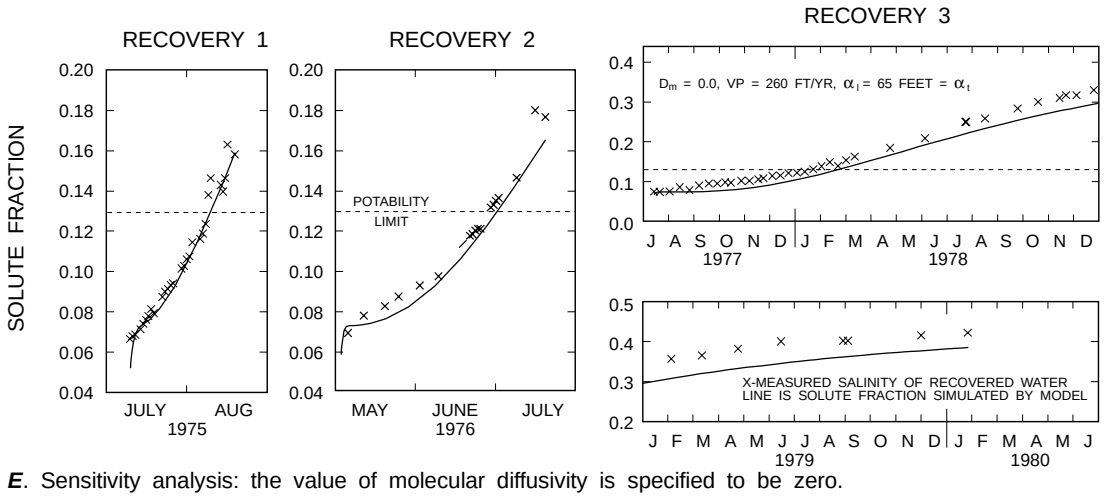

E. Sensitivity analysis: the value of molecular diffusivity is specified to be zero.

Figure 23. Results of the simulation of the salinity of recovered water and selected sensitivity analyses showing the calibration techniques--Continued.

containing more saline water. When D_m=0.001 ft^2/d, computed salinities are too large in all three recoveries and converge to a value that is too high near the end of the third recovery, indicating that the degree of molecular diffusion from adjacent layers has been overestimated.

On the basis of these observations, a convenient calibration strategy has evolved. The first recovery simulation is sensitive to the selection of dispersivities but insensitive to the selections of molecular diffusivity or regional pore velocity. The second and third recovery simulations are highly sensitive to regional pore velocity, and the computed salinity value near the end of the third recovery is especially sensitive to the specified value of molecular diffusivity, even when other calibration parameters are correct. Thus, these three parameters can be determined independently from comparison with separate parts of the observed data set. This set of conditions arises from the dissimilarity of the three ASR cycles and, particularly, from the fact that the third recovery was continued long enough to clearly show the effect of downgradient advection and the effect of molecular diffusion as the salinity of recovered water approached background levels.

Alternative Simulations

The simulation technique described in the preceding section was applied in additional calibration exercises in which flow-zone properties of the basic simulation were changed to investigate the implications of possible error in the interpretation of the field data. The same variations of the conceptual model of the flow zone that were the basis of alternative calibrations of the aquifer test, and one additional variation, were also used for alternative simulations of recovery salinity data. The objective was to determine if the

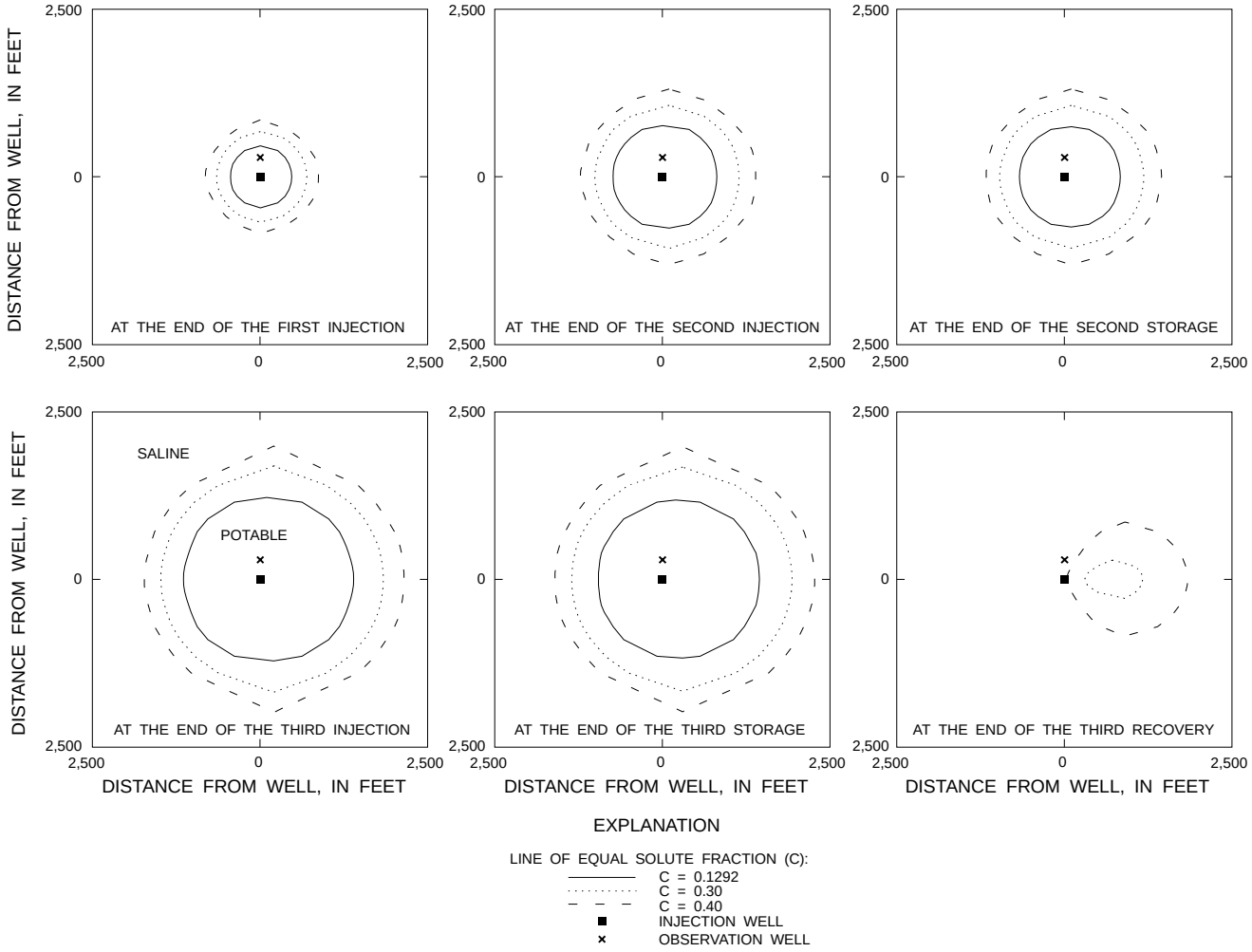

Figure 24. Horizontal distribution of injected freshwater at various stages of the aquifer storage and recovery cycles when permeability is horizontally isotropic. A solute fraction of 0.1292 corresponds to a chloride concentration of 250 milligrams per liter.

observed data could still be simulated, given the assumptions of the revised conceptual models. If so, results of subsequent predictive modeling could be strengthened by considering multiple cases that encompassed the possible range of variation of certain flow-zone properties determined from field data. This approach was the focus of a paper by Merritt (1991). The four cases considered and their significance are as follows:

- Flow-zone hydraulic conductivity was larger than that estimated from analysis of the aquifer-test data, resolving the discrepancy between calibrated model and literature estimates of hydraulic gradient;
- Flow-zone thickness was almost twice that estimated on the basis of some spinner flowmeter logs, as suggested by other flowmeter logs and some water-quality data;
- The effective porosity of the flow zone was lower than the total porosity of rock and pores measured by the neutron porosity log; and
- Flow-zone hydraulic conductivity might actually be anisotropic in the horizontal plane, the major flow direction being in the direction of the regional flow gradient and perpendicular to a line drawn between the injection and observation wells.

Excellent calibrations were achieved in all four cases and are illustrated, together with the basic calibration curve, in figure 25. Table 2 lists the assumed physical and hydraulic properties of the aquifer and parametric values used to calibrate each alternative simulation. In terms of the three parameters adjusted to calibrate the simulations, C-2 (increasing the flow-zone thickness to 21 ft) required doubling the molecular diffusivity, decreasing pore velocity by 15 percent, and decreasing the dispersivities by 23 percent; C-3

(decreasing the flow-zone porosity to 20 percent) required increasing the pore velocity by 40 percent, increasing the dispersivities by 23 percent, and decreasing the molecular diffusivity by 70 percent; and C-4 (anisotropic permeability having a 10 to 1 ratio of directional components) required increasing the pore velocity by 40 percent, decreasing the dispersivities by 23 percent, and leaving the molecular diffusivity unchanged.

In case C-1 the horizontal hydraulic conductivity value was increased to 3,200 ft/d, four times the original value determined from the aquifer-test simulation. This implied an injection-zone transmissivity increase to 38,400 [$(ft^3/d)/ft^2$]ft. The regional hydraulic gradient was decreased to 0.41 ft/mi, close to the value estimated from published literature and one-fourth the value used in the basic calibration (figs. 25A). Regional pore velocity remained the same at 260 ft/yr, and the dispersivity and molecular diffusion values were unchanged. The simulation curve (fig. 25B) is virtually identical to the previous one. This result indicates the absence of any significant degree of buoyancy stratification, which tends to increase with the value of hydraulic conductivity. However, at the prevailing density contrast, the degree of buoyancy stratification was still insignificant even when K_x=K_y=3,200 ft/d, though it did increase slightly.

That identical results were achieved with the two sets of hydraulic conductivities and regional gradient estimates meant that each simulation of alternate conceptual models could be considered to actually represent two test cases corresponding to the two regional gradient estimates. The consequent reduction in the number of simulation runs required to test all hypotheses was especially beneficial, considering the large amount of computer time required for each simulation. The basic simulation required 20.5 hours on the PRIME 9955. When K_x and K_y were increased to 3,200 ft/d in simulation C-1, oscillatory behavior occurred in the second and third recoveries. When the maximum time step was reduced to mitigate this undesirable behavior, the computer run time increased to 48.9 hours. Run times also depend on other work being processed by the computer concurrently, but the processing times per time step did not vary much in these simulation runs. Run times for the test cases are listed in table 2, as are the horizontal hydraulic conductivities that would have been used in simulations assuming that the regional gradient was 0.4 ft/mi.

The ellipsoidal planar distributions of injected freshwater at various stages of the ASR cycles in case C-4 are shown in figure 26. The views correspond to the same times and ASR cycle stages as in the isotropic case C (basic simulation) to facilitate comparison with figure 24. At the end of the first injection, potable freshwater has just reached the observation well along the axis of minimum permeability. This would be consistent with the rapid freshening observed in the observation well in the hours following the end of the first injection. Progressive downgradient advection is evident in the second and third cycles. As in the isotropic case, some injected freshwater remains in a mix with native saline water downgradient of the injection well at the end of the 2.5-year third recovery.

Estimates of Potential Recovery Efficiency After Several Cycles

The calibrated simulations were used for estimating the recovery efficiencies that would be achievable by operating a similar well at the Hialeah site for several annual cycles, as would be done if the ASR process were implemented by water utilities as an alternative for augmenting dry-season water supply. Merritt (1985) reported that, given favorable hydrogeologic conditions, recovery efficiency increases rapidly in early repetitions of the ASR cycle, particularly if each recovery is terminated just when withdrawn water exceeds salinity criteria for potability, leaving some injected freshwater in the flow zone in a nonpotable mix with native brackish water.

The SWIP code was used to simulate 10 successive ASR cycles, using the four sets of calibration values given in table 2 for cases C, C-2, C-3, and C-4. Each cycle consisted of 5 months of injection at 150,000 ft^3/d, 3 months of storage, and a maximum of 4 months of recovery at 150,000 ft^3/d. In southern Florida the injection period might correspond to June through October (when ground-water levels are highest), the storage period might correspond to November through January (the early months of the dry season), and the recovery period might correspond to February through May (the later months of the dry season when water shortages periodically occur in the region). The model was coded to stop recovery in each cycle when solute fraction approximately reached a value of 0.1292, corresponding to 250-mg/L chloride concentration. The pumping rate was then changed to zero until the scheduled beginning of the next simulated injection.

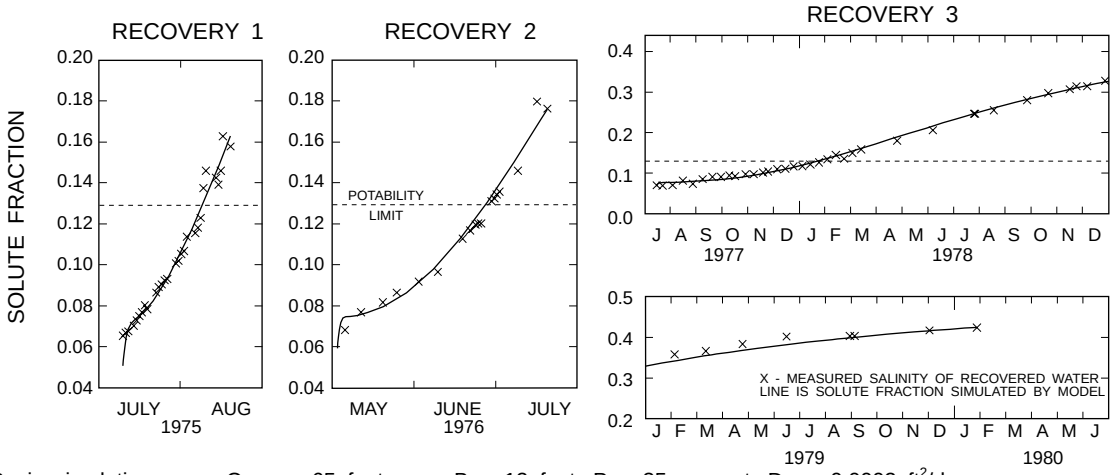

A. Basic simulation, case C: α_l = 65 feet = α_t, B = 12 feet, P = 35 percent, D_m = 0.0002 ft^2/d, VP = 260 ft/yr, K_x = K_y = 800 ft/d

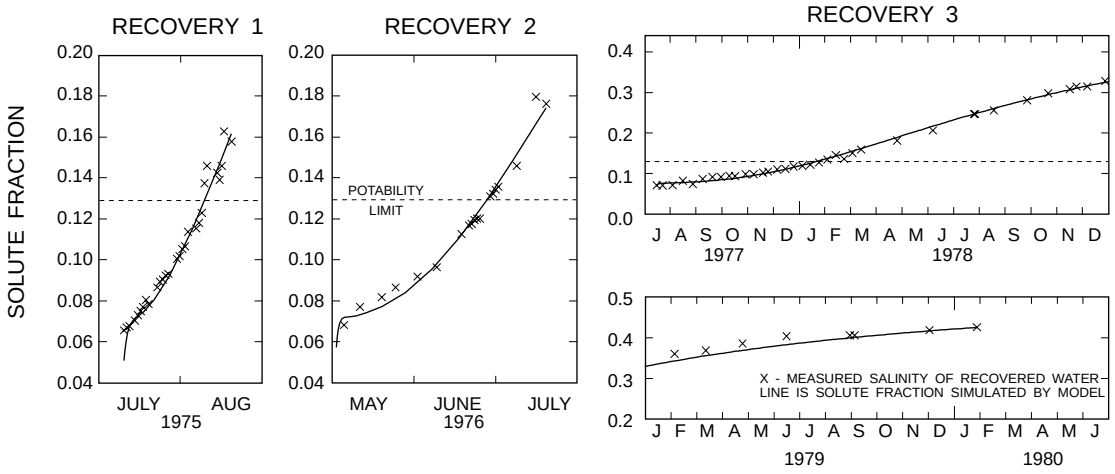

B. Higher hydraulic conductivities, lower regional gradient, case C1: K_x = K_y = 3,200 ft/d, VP = 260 ft/d, B = 12 feet, α_l = 65 feet = α_t, P = 35 percent, D_m = 0.0002 ft^2/d

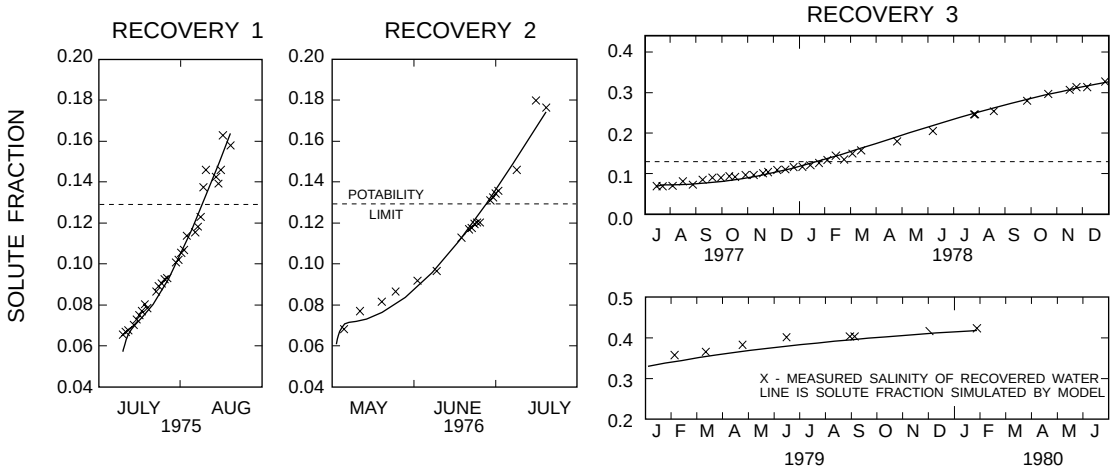

C. Increase flow-zone thickness, case C2: B = 21 feet, α_l = 50 feet = α_t, VP = 220 ft/yr, K_x = K_y = 475 ft/d, P = 35 percent, D_m = 0.0004 ft^2/d

Figure 25. Alternative simulations of the salinity of recovered water. P, flow-zone porosity, in percent; α_l, α_t, longitudinal and transverse dispersivities, in feet; B, flow-zone thickness, in feet; VP, aquifer pore velocity, in feet per year (ft/yr); D_m, molecular diffusivity, in feet squared per day (ft^2/d); K_X, K_Y, directional horizontal hydraulic conductivities, in feet per day (ft/d).

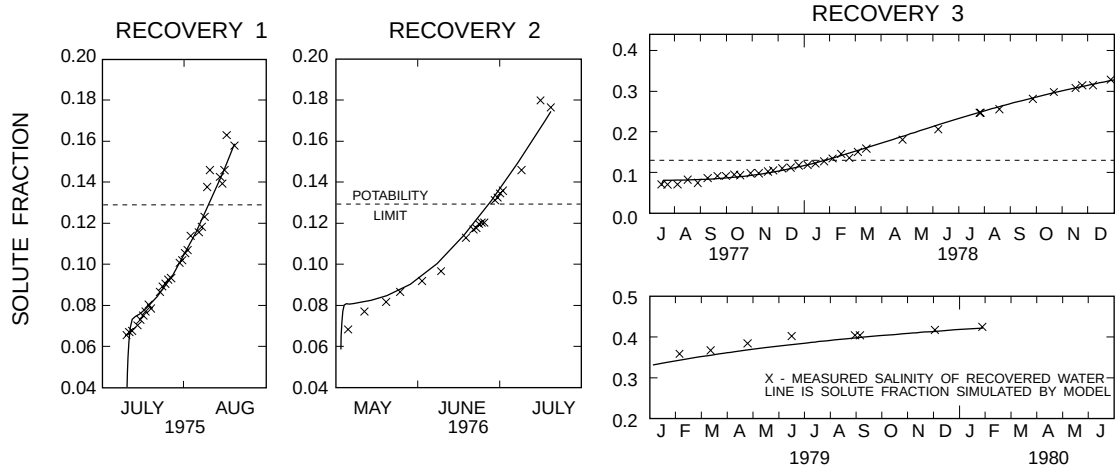

D. Lower flow-zone effective porosity, case C3: P = 20 percent, B = 12 feet, $K_X = K_Y$ = 750 ft/d, D_M = 0.0004 ft^2/d, VP = 364 ft/yr, α_l = 80 feet = α_t

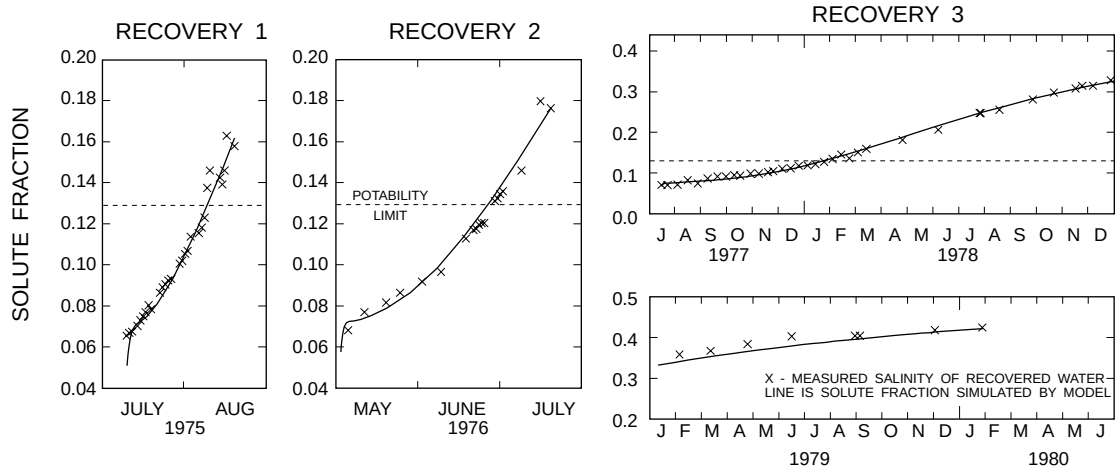

E. Anisotropic horizontal hydraulic conductivity, case C4: K_x = 2,350 ft/d, K_Y = 235 ft/d, B = 12 feet, VP = 364 ft/yr, α_l = 50 feet = α_t, P = 35 percent, D_M = 0.0002 ft^2/d

Figure 25. Alternative simulations of the salinity of recovered water--Continued.

Table 2. Physical and hydraulic properties and parameter values used to calibrate basic and alternative simulations of the freshwater injection, storage, and recovery tests

[Description: 1, basic simulation; 2, increase hydraulic conductivities, decrease regional gradient; 3, increase flow-zone thickness; 4, decrease flow-zone effective porosity; 5, anisotropic permeability. Abbreviations: ft/mi, feet per mile; ft/yr, feet per year; ft^2/d, square feet per day; in^2/lb, (pounds per square inch)$^{-1}$; K_x, K_y, hydraulic conductivities in the *x*- and *y*-coordinate directions, in ft/d; K_{xa}, and K_{ya}, adjusted hydraulic conductivities in the *x*- and *y*- coordinate directions, in ft/d]

Case	Description	Flow-zone thickness (feet)	Flow-zone porosity (percent)	Regional gradient (ft/mi)	Regional pore velocity (ft/yr)	Dispersivity value (feet)	Molecular diffusivity value (ft^2/d)	Rock compressibility (in^2/lb)	Hydraulic conductivity (ft/d)				Simulation run time (hours)
									Regional gradient				
									1.6 ft/mi		0.4 ft/mi		
									K_x	K_y	K_{xa}	K_{ya}	
C	**1**	12	35	1.6	260	65	0.0002	0.0000400	800	800	—	—	18.6–20.5
C-1	2	12	35	.4	260	65	.0002	.0000400	—	—	3,200	3,200	48.9
C-2	3	21	35	2.35	220	50	.0004	.0000225	475	475	2,780	2,780	13.3
C-3	4	12	20	1.4	364	80	.00006	.0000750	750	750	2,625	2,625	18.2
C-4	5	12	35	.8	364	50	.0002	.0000100	2,350	235	4,580	458	17.2–17.9

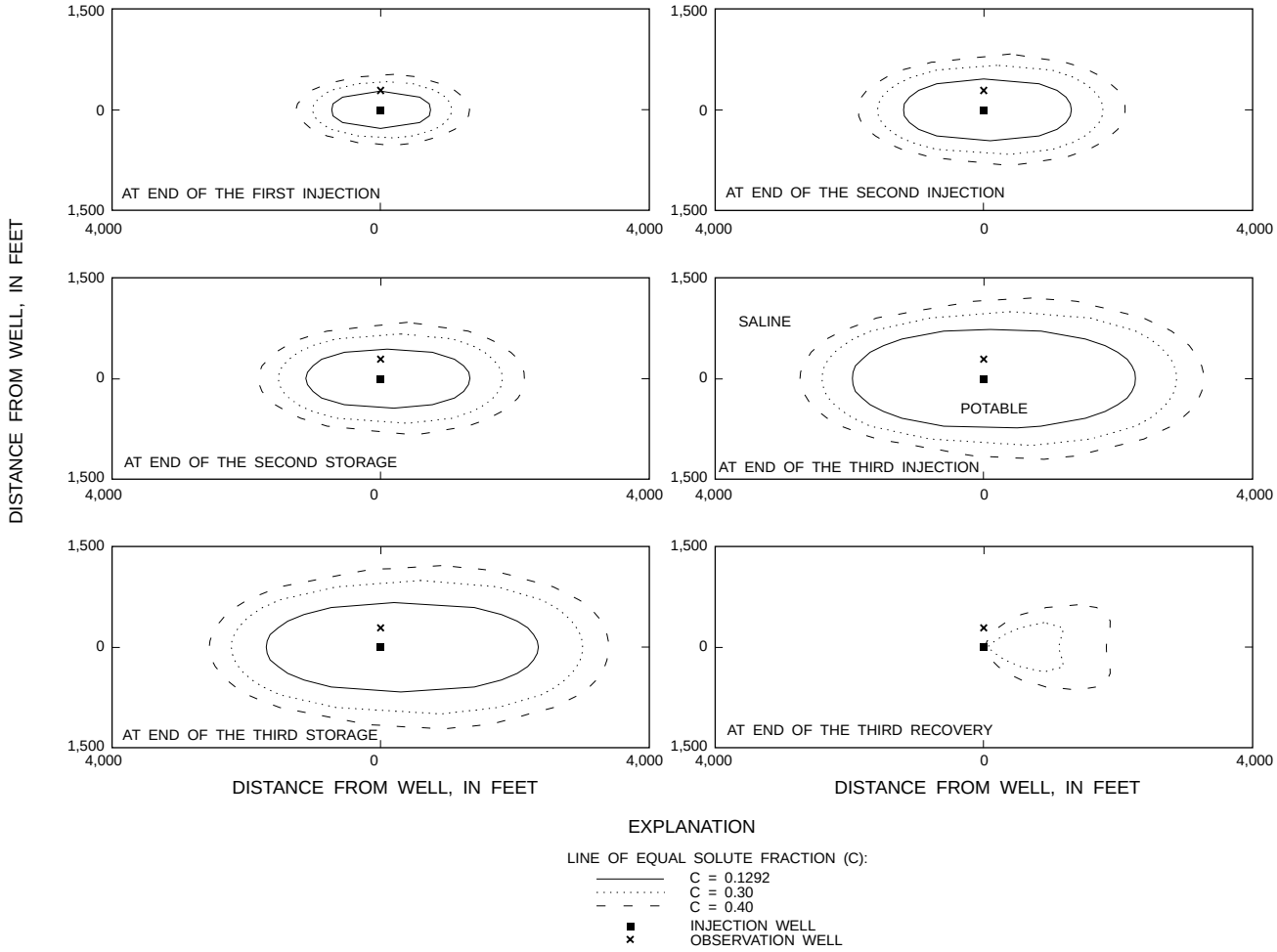

Figure 26. Horizontal distribution of injected freshwater at various stages of the aquifer storage and recovery cycles when permeability is anisotropic. A solute fraction of 0.1292 corresponds to a chloride concentration of 250 milligrams per liter.

Results of the 10 annual cycle simulations for the four cases and for an additional sensitivity analysis (case Ca) are given in the table below (values are recovery efficiency, in percent; dashes indicate not computed). Run C-2 was terminated by a power failure. As these computer runs required between 65 and 80 hours computing time on the PRIME 9955, and results of the run appeared definitive after six cycles, run C-2 was not repeated.

For each set of calibration values (C to C-4), virtually the same limiting recovery efficiency of 67–70 percent for the given schedule and rates was nearly realized after only four cycles. That the different simulations generally encompassed the likely range of possible values of true aquifer thickness, effective porosity, permeability, and permeability anisotropy enhances confidence in the result of the predictive simulations, which are shown to depend on the replication of observed changes in recovered water salinity in the three disparate ASR cycles rather than on the precise identification of aquifer parameters.

One of the principal limitations on recovery efficiency in these simulations was the high rate of regional flow, which was computed to be 260 ft/yr in

Case	Cycle 1	Cycle 2	Cycle 3	Cycle 4	Cycle 5	Cycle 6	Cycle 7	Cycle 8	Cycle 9	Cycle 10
C	40.6	58.4	63.9	66.3	67.4	68.0	68.3	68.4	68.5	68.55
C-2	41.8	58.4	63.2	65.1	65.9	66.3	—	—	—	—
C-3	42.0	58.1	62.5	64.6	65.7	66.4	66.8	67.0	67.2	67.2
C-4	40.1	58.9	65.1	67.8	69.1	69.7	70.1	70.2	70.3	70.3
Ca	45.1	67.9	76.3	>80.0	—	—	—	—	—	—

simulation C. The deleterious effect of downgradient advection is illustrated by simulation Ca, a sensitivity analysis in which the regional pore velocity was assumed to be much smaller (13 ft/yr). Substantially higher recovery efficiencies were realized, ranging from 45 percent in the first cycle to 76 percent in the third cycle. The maximum recovery efficiency possible in these simulations was 80 percent because injection was for 5 months, and recovery at the same rate was limited to 4 months. After 4 months of pumping potable water in the fourth cycle, the chloride concentration of the recovered water remained below the cutoff limit (250 mg/L), and indications were that recovery efficiency could have approached 90 percent in later cycles if a greater withdrawal rate had been specified.

Simulation of Observation-Well Data

Part of the data collected at the observation-well site during the injection and recovery cycles was considered earlier in describing the thickness and hydraulic properties of the injection zone. Generally, water-quality and pressure data from the observation well, though clearly showing qualitative changes caused by the injection and recovery process, fail to unambiguously support the conceptual model of flow and transport used as a basis for simulating water-quality changes during recovery.

A comparison of water-quality and pressure data measured at the observation well with solute fractions and pressures simulated at this location by the calibrated models described in the previous sections is helpful in (1) illustrating the similarities and dissimilarities between measurements and model computations, and (2) evaluating the accuracy of simulations of observed water-quality changes at specific locations in aquifers with solution porosity when the transport of fluids occurs near those locations.

Salinity Data

A simulation of salinity changes measured in the flow zone at the location of the observation well, 289 ft from the injection well, required a revision of the previously described simulation procedures. Because the injection rate varied as a result of wellbore clogging, there was an accompanying variation in the rate of freshwater movement toward the observation well that determined the water-quality changes occurring at the well. Therefore, valid synthetic times could not be assigned to observation-well samples, as was done for recovered water-quality data, and the transport of freshwater toward the observation well could not be accurately simulated using average rates. To provide the desired accuracy, the injection and recovery time periods were subdivided into shorter periods, during which rates remained approximately uniform. The three injection periods were subdivided into 9, 12, and 25 subperiods with corresponding average well rates. The aborted second injection was also explicitly simulated as a 7-day event. Because withdrawal rates varied less than the injection rates, the three recovery periods were subdivided into three, two, and nine subperiods for assignment of average rates.

The simulations were performed using the four sets of calibration values (C, C-2, C-3, and C-4) representing the basic calibration and three alternative calibrations. Chloride concentration values from the silver monitor (1,020 ft) were converted to solute-fraction values based on interpolated dissolved-solids estimates, as previously described, for comparison with the simulated solute-fraction values. The grid spacing that placed four nodes between the injection-well and observation-well nodes (fig. 19) used for aquifer-test simulations was employed again in these simulations.

Computed solute-fraction values and solute-fraction values based on measured data are shown on plate 2. Comparing the four computed curves, it seems that the 21-ft-thick aquifer simulation (C-2) and the horizontally bipolar anisotropic simulation (C-4), in which the observation well is in the direction of lowest permeability, each show a later arrival time of injected freshwater and a less rapid decrease in salinity at the observation well during the first injection, compared with the basic simulation (C, 12-ft thick horizontally isotropic aquifer, 35 percent flow-zone porosity). The observation-well salinity computed by C-2 and C-4 remains higher than that computed by C during the increase of the first recovery and the decreases of the second and third injections. In the simulation where porosity is decreased to 20 percent in the injection zone (C-3), the computed salinities are lower than when porosity is 35 percent (C), representing an earlier arrival and greater proportion of injected freshwater at the well. All simulations indicate a substantial decrease of computed solute fraction during the 7-day aborted second injection of December 1975. The approximate arrival time of freshwater at the observation well in the first cycle, assuming isotropy, was previously observed to be 7–8 days.

None of the four simulations of observation-well salinity matches the measured salinity data except when nearly 100 percent freshwater surrounded the

observation well. Because large dispersivities (65 ft in simulation C) were used to match chlorides measured during recovery at the injection well, the model portrays the observation-well salinity as beginning a rapid decrease at the start of each injection. Computed curves are smooth and monotonic during each injection. Generally, the measured salinity is higher, undergoes more abrupt changes, and occasionally fluctuates considerably, showing no clear trend, as in the first and second injections. The measured data show the changes predicted by the model in a qualitative sense, but do not validate the simulated salinity changes in a quantitatively precise way. As previously noted, salinity fluctuations between 6 and 8 days could indicate the arrival of part of the injected water at the observation-well location during the three cycles.

Pore-Velocity Computations

In an attempt to resolve previously cited difficulties in explaining observed water-quality changes at the observation well immediately following the first and second injections, the model was used for an analysis of aquifer flow rates immediately following the end of the first injection, after the injection pump had been turned off. The simulation addressed the possibility that a sharp interface existed between injected and native waters near the observation well, and that the interface had nearly reached the observation well when the first injection was stopped. If a slight hydraulic gradient prevailed within the flow zone for a short time thereafter, breakthrough of fresh injected water could occur even after the injection pump was turned off. In addition, continuous pumping of the observation well at 5 gal/min for the automatic sampler/recorder could have influenced a nearby sharp interface to approach the observation well by accentuating or maintaining a lingering hydraulic gradient.

Hydraulic-head values at the observation-well node (22, 12) and the immediately adjacent node (22, 13) on the axis toward the injection well (fig. 19) were used to compute approximate pore velocity at the observation-well location just before and following the end of the first injection. The computation was based on Darcy's equation and on assumptions of 800-ft/d horizontal hydraulic conductivity and 35 percent effective porosity. The hydraulic gradient was estimated as the difference in head between the two nodes, 75 ft apart. Darcian flow estimates are not strictly accurate in environments of varying density (Hickey, 1989) but were considered an adequate approximation for this analysis, given the low density contrast. When 5-gal/min pumping was specified, the nodal value representing a grid-block head average, and not a wellbore drawdown value, was used for the value of the well node head in the analysis. The subdivision of the first injection period into nine subperiods was used for the analysis to increase the accuracy of the computed flow rates in the aquifer near the observation well at the end of injection.

Assuming no pumping at the observation well, the computed pore velocity between the two nodes just before the end of the first injection was 14.08 ft/d. Fifteen minutes after injection pumping stopped, the simulated pore velocity dropped to 0.9 ft/d. After 24 hours, the pore velocity was 0.03 ft/d. The total distance traveled by water particles during the 24-hour period would have been about 0.05 ft. When the observation well was pumped at 5 gal/min in the simulation, the head simulated at node (22, 12) was about 0.1 ft lower during the first injection. The final injection pore velocity of 14.72 ft/d dropped to 1.55 ft/d 15 minutes after injection ceased, and to 0.67 ft/d after 24 hours. The total 24-hour travel distance was about 0.75 ft. Clearly, these simulations do not provide support for the hypothesis of substantial postinjection movement of a sharp interface between injected and native water. The movement of an interface in 24 hours under influence of the 260 ft/yr regional flow used in the basic calibration (C) would only be 0.71 ft. Furthermore, the direction of regional flow was approximately perpendicular to the radial-flow vector extending from the injection well to the observation well.

Pressure Data

Flow and transport processes between the two wells in the injection zone are further elucidated by comparing observation-well head changes during the ASR cycles with simulated head changes. Head changes at the observation well are determined by the injection-well inflow rate and aquifer characteristics, and are affected by injection-well borehole clogging only indirectly, through the effect on injection rate.

Observed and computed head changes at the observation-well location are shown on plate 2. Observed data are recorded pressures referenced to the preinjection value and converted to heads. The simulations shown are the basic calibration (C), the 21 ft-thick flow-zone calibration (C-2), the 20 percent flow-zone porosity calibration (C-3), and the

10:1 bipolar anisotropic calibration (C-4), each of which used a set of hydraulic parameters that replicated drawdowns observed at the injection well during the aquifer test of February 10, 1975. Hydrographs representing simulations C, C2, and C-3 depict similar head changes at the observation well. The C-2 head change is slightly less than that of simulation C, and the C-3 head change is slightly greater.

In harmony with theory, when anisotropy is assumed (curve C-4), computed head changes at the observation well located in the direction of least permeability are appreciably less than those computed by the isotropic basic calibration (C). The hydraulic response at the observation well is most rapid in the anisotropic case, in which the rock compressibility value was only one-fourth that of the isotropic case (C). A lower value of rock compressibility implies lower storativity and a more rapid transmission of hydraulic stresses through the aquifer.

Comparison of computed head changes with the observed data is difficult because the observed data seem to be affected by instrument calibration shifts and other errors occurring during the three ASR cycles. Unexplained pressure variations were recorded during the second storage period, and average heads during the four major inactive periods show variations of as much as 3 ft. Cessation of pumping water for the automatic sampler after the first cycle can only explain about 0.1 ft of the difference.

Arrival of warmer injected water at the observation well and consequent warming of water in the sampling tube in which pressure was monitored would have caused measured pressures to increase slightly at the wellhead. If the warmest injected water (27 °C) did not cool as it approached the observation well and entered the monitor tubes, the head increase at land surface could have been as much as 1.5 ft.

The observed hydraulic response to changes of stress is even more rapid at the observation well than predicted by the anisotropic model (C-4), lending some credence to the anisotropic hypothesis. Generally, the range of head variation in the second and third cycles is less than predicted by either isotropic or anisotropic models, though the difference is less with the anisotropic model. Possibly, a simulation with an even greater degree of anisotropy and using a smaller rock compressibility value would have better simulated the head data.

A comparison of injection and recovery hydraulic responses at the observation well in each cycle leads to an interesting result. Because the hydraulic response at a point within the aquifer is linearly related to the rate of inflow or outflow at the injection well, the ratio of inflow and outflow rates should be the same as the ratio of corresponding head changes at the observation well. Between August 28 and September 2, 1975, during the first injection, the inflow rate was approximately constant at 455 gal/min, and the head at the observation well was about 4.1 ft higher than the preinjection value. In the initial 14 days of the first recovery, the withdrawal rate averaged 335 gal/min, and the head at the observation well was about 4.8 ft lower than the preinjection value. Measured heads did not vary appreciably during these periods. The ratio of the injection and recovery rates is 1.36, and the ratio of the corresponding head changes is 0.85. This analysis was repeated for selected time intervals in the second and third ASR cycles, when rates were relatively constant. Results are given in the table below. To offset the apparent calibration drift after the first cycle, a head higher by 1.9 ft was accepted as representing a static (non-stress) condition in the second and third cycles.

Cycle	Injection			Withdrawal			Rate ratio	Head ratio
	Time period	Average rate (gallions per minute)	Average head change (feet)	Time period	Average rate (gallions per minute)	Average head change (feet)		
1	Aug. 28, 1975–Sept. 02, 1975	455	4.1	Sept. 10, 1975–Sept. 24, 1975	335	4.8	1.35	0.85
2	Feb. 20, 1976–Feb. 23, 1976	820	6.2	July 01, 1976–July 19, 1976	485	5.5	1.69	1.13
3	Oct. 22, 1976–Oct. 29, 1976	785	7.2	Nov. 04, 1977–Dec. 09, 1977	435	4.6	1.81	1.57

Subject to the difficulty in compensating for calibration errors in the pressure data, the results do not support the description of head changes measured in the observation well as being proportional to the inflow or outflow rate at the injection well. In fact, the head increases during injection seem to be damped in comparison with those observed during withdrawal, suggesting that some process retards flow between well locations during injection, compared with that occurring during withdrawal.

Directionally biased wellbore plugging, in which pores in the less permeable flow direction in an anisotropic aquifer would be plugged to a greater relative extent than in more permeable flow directions, was considered as a possible explanation. However, model simulations designed to test the hypothesis tended to refute rather than confirm it.

The difficulty in simulating observation-well pressure and salinity data illustrates the generalizing nature of porous-media models as applied to problems in secondary-porosity terranes. Simulating the salinity of recovered water merely requires a general representation of the diverse mixing processes occurring within the entire volume of aquifer occupied by injected freshwater. However, simulation of salinity changes at the observation-well location requires the correct representation of flow and mixing processes at all points between the two wells. If these processes differ from the generalizing assumptions of the recovery salinity model, a highly accurate simulation of observation-well data will likely not be achieved. In secondary-porosity media, such local departures from any generalized scenario of flow and mixing processes might be the norm rather than the exception.

SUMMARY

To deal with increasing water demands in a region characterized by seasonal surplus and deficit of water supply and limited reservoir capacity, water-management officials and others in southern Florida have sponsored operational testing of ASR, a water-conservation method in which subsurface formations containing brackish water are used for temporary storage of potable water. As part of a study conducted in cooperation with the SFWMD and the MDWSA, the USGS performed operational ASR tests at the Hialeah Well Field in Dade County.

A well for injecting freshwater and a second well for observing the hydraulic response and water quality were drilled 289 ft apart in late 1974 to depths of 1,105 and 1,064 ft. The injection- and observation-well casings extended to depths of 955 and 953 ft, respectively, so that the uncased part of the injection well was open to consolidated limestone of the intermediate confining unit and the Upper Floridan aquifer assigned to the Tampa Limestone, Suwannee Limestone, Ocala Limestone (if present), and Avon Park Formation. During drilling, a substantial augmentation of flow occurred between 985 and 1,065 ft.

Between July 1975 and January 1980, three ASR cycles were performed. In the first cycle, 41.9×10^6 gal of freshwater were injected. Recovery began after a 2-day storage period, and a recovery efficiency (volume of potable water recovered, expressed as a percentage of the volume injected) of 32.9 percent was realized. In the second cycle, 85×10^6 gal were injected and stored for 54 days. Recovery efficiency was 47.8 percent. In the third cycle, 208×10^6 gal were injected and stored for 181 days. Recovery efficiency was 38.5 percent, less than that of the second cycle. Recovery in all three cycles was by natural artesian flow.

Data acquired during the three ASR cycles include pressure-gage readings at the injection wellhead and in two monitor tubes within the observation well. Volumetric data on quantity of inflow and outflow were regularly obtained during the three cycles. A system of sampling tubes extending to various depths was installed in the open part of the observation well, and water samples were obtained both manually and also, during the first cycle, by means of an automatic sampler/recorder. Before the ASR cycles and at several times during the cycles, water samples from injection and observation wells and from the shallow well used for injection supply were analyzed for major inorganic ions, bacteria, chemical oxygen demand, biochemical oxygen demand, nutrients, total organic carbon, metals, field pH, alkalinity, and specific conductance. The chloride concentration and specific conductance of recovered water were measured frequently. Volumetric readouts from the in-line flowmeter were also recorded at the same time to establish a relation between volume of flow and water quality. Special analyses were made for algal species, nitrate-reducing bacteria, sulfate-reducing bacteria, iron bacteria, dissolved gases, and uranium isotopes.

Plugging of the wellbore occurred during the injections, causing the wellhead pressure to increase and the inflow rate to decrease. Injectivity was

restored by 2- or 3-hour backflushes at the natural artesian flow rate. These backflushes were performed at weekly intervals during the third injection, and well-head pressure and inflow rate remained generally uniform. An X-ray diffraction analysis of the back-flushed sediment showed very fine particles of calcite and iron (not scale).

At Hialeah the top of vertically contiguous consolidated limestone of the Floridan aquifer system is about 975 ft below land surface within the Suwannee Limestone. A shelly interval within the interval from 1,015 to 1,050 ft contains the principal flow zones. Data from an aquifer test at the site were analyzed using various methods, providing transmissivity estimates that range from 8,825 to 12,600 ft^2/d. A slight drawdown was measured in the 840-ft monitor tube during the aquifer test, indicating minor leakage across the confining beds separating it from the injection zone.

Data from spinner flowmeter logs were analyzed to delineate the flow zone by identifying intervals within the injection zone yielding the larger proportions of flow from the well. One such zone was found after analysis of 18 flowmeter logs. The top of the flow zone seemed to be about 1,024 ft below land surface in the injection well. The bottom of the flow zone seemed to be about 1,036 ft below land surface on the basis of some flowmeter log analyses. Temperature and fluid-resistivity logs run during recovery of injected water suggested that minor quantities of freshwater could enter the formation to a depth of about 1,047 ft below land surface. A diameter-compensated neutron porosity log showed porosity to average about 35 percent, there being wide variation in thin, discrete intervals.

Because of its importance for ASR feasibility, injection-zone salinity was the water-quality characteristic of most significance for this study. The chloride and dissolved-solids concentrations of water in the principal flow zone were 1,200 and 2,700 mg/L, respectively. Water from the 840-ft monitor tube had chloride and dissolved-solids concentrations of 1,700–2,300 mg/L and 3,900–5,000 mg/L, respectively, considerably higher than those of the flow zone 180 ft below. The dissolved-solids concentration in relatively impermeable rocks overlying and underlying the flow zone was assumed to be about 6,000 mg/L, and the relatively low salinity of the flow zone was assumed to be the result of flushing from areas of recharge in central Florida, 150 to 200 mi upgradient.

Data from widely scattered locations indicate that permeable strata in the Upper Floridan aquifer are present near erosional surfaces at the tops of the Ocala Limestone, if present, and Avon Park Formation, both of Eocene age. The top strata of Eocene age seems to correspond to a marked contrast in natural gamma activity (high above, in beds containing phosphatic materials, and low below). The chloride concentration of water at this contact increases from less than 900 mg/L at the St. Lucie County ASR site, to 1,200 mg/L in central and northeastern Dade County, and to more than 2,200 mg/L on the island of Key Largo in Monroe County.

A solute-transport code was used for simulating the salinity of water recovered after injection of freshwater. The model is fully three-dimensional, and solution of the equations is by standard finite-difference techniques. Fractional values ranging between 0 and 1 describe the relative concentrations of two miscible fluids in the aquifer. Values of density are associated with the extreme values of solute fraction, and water density within the modeled domain is considered to be a time-varying linear function of solute fraction, temperature, and pressure.

A Cartesian coordinate system was selected for the simulations so that downgradient advection and anisotropy could be represented. Boundaries were 20,000 ft from the injection well at their nearest point, and time-invariant pressure values were specified at the boundaries as an approximation that did not affect simulated freshwater flows during the ASR cycles. Central differencing techniques were used to eliminate first-order numerical dispersion related in degree to grid-cell sizes and the length of time increments.

A series of numerical tests was devised to examine the importance of the vertical component of mechanical dispersion and of molecular diffusion from the confining zones and their effect on recovery efficiency. The original 1979 SWIP code algorithms for vertical dispersion and advective weighting were compared with experimental techniques, and various values were assigned to transverse dispersivity, molecular diffusivity, and a scaling factor for vertical dispersion. The tests showed that when the experimental methods were used to eliminate vertical dispersion across flow-zone boundaries, a significant influence on recovery efficiency is the degree of molecular diffusion from the more saline confining zones. The magnitude of this influence depends upon the degree of vertical dispersion occurring within the

flow zone, which is under user control by use of the scaling factor. When the 1979 methods were used, vertical dispersion across flow-zone boundaries reduced recovery efficiency.

Observed drawdown data from the aquifer test of February 10, 1975, were simulated to derive estimates of hydraulic parameters for use in simulations of recovery chloride increases. Based on the assumption derived from interpretation of geophysical and water-quality data that the flow zone was 12 ft thick, isotropic, and had an effective porosity of about 35 percent, the drawdown data were calibrated by setting values of horizontal hydraulic conductivity equal to 800 ft/d and the value of rock compressibility to 0.0000400 $(lb/in^2)^{-1}$. The calibrated hydraulic parameters were used to derive estimates of composite hydraulic parameters (transmissivity and storage coefficient) for the injection zone. The transmissivity was computed to be 9,600 $[(ft^3/d)/ft^2]ft$, and the equivalent storage coefficient was computed to be 7.8×10^{-5}.

Alternative calibrations of the aquifer-test data were obtained to give consideration to the possibility that assumptions concerning the aquifer physical properties were in error. Alternative assumptions were that (1) the flow zone was 21 ft thick; (2) flow-zone effective porosity was 20 percent; and (3) flow-zone hydraulic conductivity had a 10:1 horizontal anisotropy, the preferred flow direction being at a right angle from a vector pointing from the injection well to the observation well. Each aquifer-test calibration showed excellent agreement with observed data.

The hydraulic parameters determined from the aquifer-test calibration that assumed a 12-ft flow zone having a 35 percent effective porosity were used as part of a simulation of the chloride increases observed during the three recoveries. A simulation was completed by setting the longitudinal and transverse dispersivities equal to 65 ft, by setting the molecular diffusivity equal to 0.0002 ft^2/d, and by assuming a hydraulic gradient in the aquifer of 1.6 ft/mi, about 4 times as large as estimated from regional hydraulic-head measurements. The computed regional pore velocity was 260 ft/yr. When results of simulating the aquifer test were disregarded and hydraulic conductivity values were assumed to be 3,200 ft/d, the literature estimate of 0.4 ft/mi for the regional hydraulic gradient led to a virtually identical simulation. This result was possible because the higher estimate of hydraulic conductivity did not lead to buoyancy stratification in the simulations, given the prevailing low density contrast between injected and native aquifer water.

Sets of hydraulic parameters determined from the three aquifer conceptual models used for alternative calibrations of the aquifer-test data were again used for three additional, and equally accurate, simulations of the recovery salinity data. Each simulation used a unique set of calibration parameters different from the others. Because the conceptual models differed in parameters based on field data that could not be accurately measured, the solution dependence upon possible errors in the accepted estimates of these parameters was evaluated by this procedure.

Given the accuracy with which recovered water salinity was simulated in three disparate ASR cycles, predictive simulations were made with a fair degree of confidence. An arbitrary schedule of injection and withdrawal was specified: five wet-season months of injection at 150,000 ft^3/d, followed by three early dry-season months of storage, and then by a maximum of four late dry-season months of withdrawal at 150,000 ft^3/d. These runs showed recovery efficiency to improve from about 40 percent in the initial cycle to nearly 70 percent in later cycles. The cited figures depend on the specified rates and schedule. The predictive run was repeated with sets of calibration parameters that represented the alternative conceptual models previously described. Each case yielded results similar to those of the basic simulation, lending credence to the predictive application of the model and showing that predictive results depended on the simulation of recovered water salinities rather than on the precise identification of aquifer parameters. When regional pore velocity was substantially reduced, recovery efficiency exceeded 80 percent in the fourth cycle, demonstrating the adverse influence of the large degree of downgradient advection indicated by the calibrated models.

Additional model runs in which the temporal variation in well rates was discretized in greater detail attempted to simulate head and salinity changes at the observation well, given the same four aquifer descriptions used for the simulations of recovered water salinity and the predictive analyses. Although the general trends of the measured data and simulated values are similar, neither the observed head changes nor the salinity changes are accurately matched by the model computations. Most likely, unknown local heterogeneities in aquifer hydraulic properties in the neighborhood of the observation well rendered the generalized design of the model, developed to simulate recovery salinity changes, inappropriate for precise simulations of hydraulic or water-quality changes at an isolated point location, such as that of the observation well.

REFERENCES CITED

Chih Shan Chen, 1965, The regional lithostratigraphic analysis of Paleocene and Eocene rocks of Florida: Florida Geological Survey Bulletin 45, 105 p.

Ehrlich, G.G., Godsy, E.M., Pascale, C.A., and Vecchioli, John, 1979, Chemical changes in an industrial waste liquid during post-injection movement in a limestone aquifer, Pensacola, Florida: Ground Water, v. 17, no. 6, p. 562–573.

Hickey, J.J., 1989, An approach to the field study of hydraulic gradients in variable-salinity ground water: Ground Water, v. 27, no. 4, p. 531–539.

Hoopes, J.A., and Harleman, D.R.F., 1967, Dispersion in radial flow from a recharge well: Journal of Geophysical Research, v. 72, no. 14, p. 3595–3607.

INTERA Environmental Consultants, Inc., 1979, Revision of the documentation for a model for calculating effects of liquid waste disposal in deep saline aquifers: U.S. Geological Survey Water-Resources Investigations Report 79–96, 73 p.

INTERCOMP Resource Development and Engineering, Inc., 1976, A model for calculating effects of liquid waste disposal in deep saline aquifers; Part 1—Development, Part 2—Documentation: U.S. Geological Survey Water-Resources Investigations Report 76–61, 253 p.

Jacob, C.E., 1940, On the flow of water in an elastic artesian aquifer: American Geophysical Union Transactions, pt. 2, p. 574–586.

Jacob, C.E., and Lohman, S.W., 1952, Nonsteady flow to a well of constant drawdown in an extensive aquifer: American Geophysical Union Transactions, v. 33, p. 559–569.

Kipp, K.L., Jr., 1987, HST3D—A computer code for simulation of heat and solute transport in three-dimensional ground-water flow systems: U.S. Geological Survey Water-Resources Investigations Report 86–4095, 517 p.

Kohout, F.A., 1965, A hypothesis concerning cyclic flow of salt water related to geothermal heating in the Floridan aquifer: New York Academy of Sciences Transactions, ser. II, v. 28, no. 2, p. 249–271.

Lantz, R.B., 1971, Quantitative evaluation of numerical diffusion (truncation error): Society of Petroleum Engineers Journal, September 1971, p. 315–320.

Lohman, S.W., 1979, Ground-water hydraulics: U.S. Geological Survey Professional Paper 708, 70 p.

Merritt, M.L., 1985, Subsurface storage of freshwater in south Florida—A digital model analysis of recoverability: U.S. Geological Survey Water-Supply Paper 2261, 44 p.

———1991, Nonunique simulations of the quality of water recovered following injection of freshwater into a brackish aquifer, *in* Proceedings of the Fifth Biennial Symposium on Artificial Recharge of Groundwater—Challenges of the 1990's, Tucson, Ariz., May 29–31, 1991, p. 255–266.

———1993, Aspects of numerical and representational methods related to the finite-difference simulation of advective and dispersive transport of freshwater in a thin brackish aquifer: Journal of Hydrology, 148, p. 61–92.

Merritt, M.L., Meyer, F.W., Sonntag, W.H., and Fitzpatrick, D.J., 1983, Subsurface storage of freshwater in south Florida—a prospectus: U.S. Geological Survey Water-Resources Investigations Report 83–4214, 69 p.

Meyer, F.W., 1989a, Hydrogeology, ground-water movement, and subsurface storage in the Floridan aquifer system in southern Florida: U.S. Geological Survey Professional Paper 1403-G, 59 p.

———1989b, Subsurface storage of liquids in the Floridan aquifer system in southern Florida, 1943–83: U.S. Geological Survey Open-File Report 88–477, 25 p.

Miller, J.A., 1986, Hydrogeologic framework of the Floridan aquifer system in Florida and in parts of Georgia, Alabama, and South Carolina: U.S. Geological Survey Professional Paper 1403-B, 91 p.

Price, H.S., Varga, R.S., and Warren, J.E., 1966, Application of oscillation matrices to diffusion-convection equations: Journal of Mathematics and Physics, no. 45, p. 301–311.

Reeder, H.O., Wood, W.W., Ehrlich, G.G., and Ren Jen Sun, 1976, Artificial recharge through a well in fissured carbonate rock, West St. Paul, Minnesota—Hydrodynamic dispersion and movement of injected water by Ren Jen Sun: U.S. Geological Survey Water-Supply Paper 2004, p. 52–75.

Reilly, T.E., 1990, Simulation of dispersion in layered coastal systems: Journal of Hydrology, 114, p. 211–228.

Scott, T.M., 1988, The lithostratigraphy of the Hawthorn Group (Miocene) of Florida: Florida Geological Survey Bulletin 59, 148 p.

Voss, C.I., 1984, SUTRA—a finite-element simulation model for saturated-unsaturated fluid-density-dependent ground-water flow with energy transport or chemically reactive single-species solute transport: U.S. Geological Survey Water-Resources Investigations Report 84–4369, 409 p.

Voss, C.I., and Souza, W.R., 1987, Variable density flow and solute transport simulation of regional aquifers containing a narrow freshwater-saltwater transition zone: Water Resources Research, v. 23, no. 10, p. 1851–1866.

Wedderburn, L.A., and Knapp, M.S., 1983, Field investigation into the feasibility of storing freshwater in saline parts of the Floridan aquifer system, St. Lucie County, Florida: South Florida Water Management District Technical Publication 83–7, 135 p.

APPENDIXES

APPENDIX A—DRILLING LOG OF INJECTION WELL G-3061 AND OBSERVATION WELL G-3062

Drilling Log of Injection Well G-3061

[Lithology and remarks by W.L. Miller to 970 feet and by F.W. Meyer below 970 feet. S, soft; VS, very soft; M, medium; H, hard; VH, very hard; min/ft, minute per foot; –, no data]

Date in 1974	Depth interval (feet)	Relative drilling hardness	Drilling speed (min/ft)	Lithology and remarks
Oct. 3	0–8	S	0.375	Black top soil, tan, sandy subsoil, light-tan limestone, oolite at about 8 ft.
	12–15	S-M	3.33	Light-tan limestone, solution-riddled, shells, some dark-tan limestone.
	20–23	M	1.66	Limestone-sandstone contact about 19–20 ft, white to light-tan sandstone, fine to medium, limestone fragments. Surface casing (30 in.) set to 19.95 ft below land surface, 13 in. cut off, 25 in. above ground, original length 23.11 ft. Drove 30-in. surface casing down.
Oct. 4	25–30	S	—	Fine to very fine quartz sandstone, shell fragments.
	30–35	S	—	White to light-tan coloration.
	35–40	S	—	
	40–45	S-M	—	Fine sandstone and lenses of limestone, hard zone at 41 ft, shell fragments in limestone, 10 percent limestone in cuttings.
	45–50	S	—	Fine quartz sandstone, some large quartz sand, ream.
	50–55	—	1.0	Limestone at 54 ft, hard rock.
	56–58	H	—	Gray to white limestone, quartz sand, coarse grains.
	60–62	H	3.0	
	62–65	H	—	Limestone, concretions, little sand.
	60–65	H	2.0	Calcareous sandstone, limestone, shells, quartz sand.
	65–68	—	—	Secondary calcite, sandy limestone, a few shells.
	68–70	H	7.0	
	70–75	H	—	More calcite (secondary), hard limestone.
	75–80	H	7.1	Cavernous sandy limestone, fine-grained quartz sand.
	80–82	H	—	Large cavities, lost circulation, very sandy limestone.
	82–88	H	—	No circulation, lost mud, large cavities. Surface casing settled to 3 ft below land surface, 22.03 ft of casing in ground must seal formation and cement in additional surface casing.
Oct. 7	88–90	M	3.0	Calcareous sandstone to limestone, large percentage of quartz sand, medium- to fine-grained, white to tan, cavities.
	90–95	M	3.2	Very sandy limestone, gray to tan, some loss of circulation.
	95–100	M	—	Fort Thompson/Caloosahatchee Marl(?). Soft, dense calcareous sandstone, tan to gray.
	100–105	S	—	Same as above, fast drilling, shells.
	105–108	S	—	Same as above.
	108–110	S	—	Same.
	110–115	S	—	Some green marl in sample, coarse.
	115–120	S	—	Quartz sand.
	120–125	S	—	Green marl, barnacles, large quartz grains, shells.
	125–128	S	—	Same as above, phosphates, shells.
	128–130	S	—	Same as above.
	130–135	S	—	No sample.
	135–140	S	—	Same as above.
	140–145	S	—	Caloosahatchee Marl/Tamiami(?). Some presence of white–green clay, oyster shell, *Ostrea hytensi(?)*.
	145–148	S	—	Some quartz sand, increasing amount of green clay.
	148–150	S	—	No sample.
	150–155	S	—	Green marl, shell, green clay increasing.
	155–160	S	—	No sample.
	160–168	S	—	More green clay balls, phosphates, shells.
	168–170	S	—	No sample.
	170–175	S	—	Green marl, green clay, shells, phosphates.
	175–180	S	—	Hawthorn Formation, large quantity of green clay (first predominant clay).
	180–188	S	—	Eighty-five-percent green clay.
	188–190	M	—	Decrease in clay, green marl, little clay.
	190–195	M	—	Green marl, coarse quartz sand, shell, little clay.
	195–200	M	—	Green marl, little clay, coarse quartz sand.

APPENDIX A—DRILLING LOG OF INJECTION WELL G-3061 AND OBSERVATION WELL G-3062—Continued

Date in 1974	Depth interval (feet)	Relative drilling hardness	Drilling speed (min/ft)	Lithology and remarks
Oct . 7	200–208	M	—	Still little or no clay.
	208–210	M	—	No sample.
	210–215	M	0.6	Dense sandstone, green sandy marl, little clay, quartz, medium to coarse.
	215–220	M	—	No sample.
	220–225	M	—	Dense green shale and sandstone, shell fragments, no clay.
	225–228	M	—	Same as above.
	228–235	M	—	Green shale, fine grained to sandy, dense.
	235–240	—	—	Clayey marl, green shale, quartz sand.
	240–248	—	—	Same as above.
Oct. 8				Ream to 48 ft.
Oct . 9				Ream to 72 ft, lost some mud.
Oct. 10				Ream to 95 ft, lost circulation 82–95 ft.
Oct. 11				Ream to 167 ft.
Oct. 14				Ream to 206 ft, hole reamed to 29-in. diameter to depth of 206 ft, will set 200 ft of 24-in. OD casing.
Oct. 15				Back into hole to check depth, only 3 ft short of 206 ft.
Oct. 16				Ten yards cement used to seal casing to a depth of about 201 ft. Shut down for day to allow cement to harden.
Oct. 17				Prepared to resume drilling, opened casing, and drilled bird nest.
Oct. 18				Cemented casing to land surface, took 1 yard additional cement.
Oct. 21				Start 9 7/8-in. pilot hole.
	250–260	S	1.2	Green marl, large percent clay, fine-grained quartz sand.
	260–270	S	—	Same as above.
	270–280	S	—	Green marl, 75–80 percent clay.
	280–290	S	—	Green marl, fine-grained quartz sand, some fragments limestone.
	290–300	M	2.1	Same as above.
	300–310	M	—	Green marl, large amount of very fine sand.
	310–320	M	—	Same as above.
	320–330	M	—	Same.
	330–340	M	—	Same.
	340–347	M	—	Same.
Oct. 22	347–360	S	.46	Fine-grained sand, green clay, 90 percent sand.
	360–370	S	—	No sample has reached surface yet.
	370–380	S	—	Same as above.
	380–390	S	—	Marl, fine sand, marl breaking up and sand too fine to settle, little or no sample can be collected.
	390–400	S	—	No sample.
	400–410	S	—	Hit layer of limestone at 406 ft, sample is fine sand and green clay.
	410–420	M	1.1	Dense clayey sand, green, very fine quartz.
	420–430	M	—	Sandy limestone and green marl, very fine green quartz, increasing limestone.
	430–440	M	—	Limestone, some very fine quartz sand.
	440–450	M	—	Sandy limestone, some green clay.
	450–460	M	—	Same as above.
	460–470	M	—	Same.
	470–480	M	—	Same.
	480–490	M	—	Same.
	490–500	S-M	—	Fine, dense limestone, white, some fine quartz sand.
	500–510	S-M	—	Limestone, breaks into small fragments.
	510–520	S-M	.8	Relatively clean limestone, little sand.

APPENDIX A—DRILLING LOG OF INJECTION WELL G-3061 AND OBSERVATION WELL G-3062—Continued

Date in 1974	Depth interval (feet)	Relative drilling hardness	Drilling speed (min/ft)	Lithology and remarks
Oct. 22	520–530	S-M	—	Limestone, soft, fragments crush easily.
	530–540	S-M	—	Same as above.
	540–550	S-M	—	Same.
Oct. 23	550–560	S-M	1.4	Gray lime marl.
	560–570	M	—	Gray and green marl, large amount of gray clay, limestone.
	570–580	S	—	Gray and green marl.
	580–590	S	—	Gray marl (clay)
	590–600	S	—	Same as above.
	600–610	S	—	Same.
	610–620	M	2.1	Gray-green marl, increasing shells, limestone.
	620–630	M	—	Same as above.
Oct. 24	630–647	M	—	White limestone, mostly shells, quartz sand, fine to coarse.
	647–660	S	—	Gray limestone, shelly, some green fragments.
	660–670	S	—	Same as above.
	670–675	S	—	Gray limestone, shelly, probably Tampa Formation.
	675–680	S	—	Gray limestone, shell, tan quartz sand increasing.
	680–685	S	—	Gray limestone, fine quartz sand, clear.
	685–690	S	—	Limestone, shell, echinoid spines, sand (sample of last 40 ft).
	690–695	S	—	Mostly shell fragments, some sand.
	695–700	S	—	Same as above.
	700–705	S	—	Large shell fragments, some sand.
	705–707	S	—	Large shell fragments, echinoid spines, circulating.
	707–715	S	—	Limestone, shelly, clay increasing.
	715–720	S	—	Gray limestone, shell, some gray clay.
	720–725	S	—	Gray limestone, shell, some fine quartz sand.
	725–727	M	—	Gray limestone, gray-green clay increasing, circulating.
	727–735	M	—	Gray limestone, shell, gray clay.
	735–740	H	—	Shell, sand, green clay.
	740–745	H	—	Green limestone, gray limestone, green clay, shell decreasing.
	745–747	H	—	Same as above, circulating.
	747–755	H	—	Gray limestone, not much clay, little shell.
	755–760	H	—	Same as above.
	760–765	H	—	Gray limestone, dense, breaks into small fragments.
	765–767	H	—	Same as above, circulating.
	767–775	M	—	Softer gray limestone, some shell, little sand.
	775–780	S	—	Gray limestone, no shell or sand.
	780–785	S	—	Same as above.
	785–787	—	—	Same as above, circulating.
Oct. 25	787–795	M	—	Gray limestone, some shell.
	795–800	M	—	Same as above, some dark-green fragments.
	800–805	M	—	Same as above, large amount of mollusks.
	805–807	M	—	Same as above, circulating.
	807–815	M	—	Some green clay in gray limestone.
	815–820	M	—	Clay increasing in gray limestone.
	820–825	M	—	Large amount of gray clay in shell limestone.
	825–827	S	—	Gray-green clay, stringer of limestone at 826 ft, circulating.
	827–835	—	—	Gray clay and tan limestone.
	835–840	—	—	Tan limestone.
	840–845	—	—	Same as above.
	845–847	—	—	Same as above, circulating.
	847–855	S	—	Fine-grained tan limestone.
	855–860	S	—	Tan limestone, crushes easily.
	860–865	S	—	Same as above, some green clay.
	865–867	S	—	Large amount of light-green clay and tan limestone, circulating.
	867–875	M	—	Gray-green clay and large amount of gray limestone.
	875–880	M	—	Gray limestone, soft, crushes easily, little clay.
	880–885	M	—	Soft gray limestone.
	885–887	M	—	Same as above and gray clay, circulating.

APPENDIX A—DRILLING LOG OF INJECTION WELL G-3061 AND OBSERVATION WELL G-3062—Continued

Date in 1974	Depth interval (feet)	Relative drilling hardness	Drilling speed (min/ft)	Lithology and remarks
Oct. 28	887–895	M	—	Very sandy green marl, very fine quartz sand.
	895–900	M	9.0	Sandy green marl, little sample because most of green clay is breaking up in mud, drilling mud has changed from gray to green color, limestone fragments increasing.
	905–907	M	—	Same as above, circulating.
	907–915	M	—	Sandy green marl, phosphates in sample.
	915–920	M	—	Lime chips, green marl, forams, phosphate.
	920–925	M	—	Same as above.
	925–927	M	—	Same.
	927–930	M	—	Same.
Oct. 29	930–935	M	9.0	Green marl, forams, shell.
	935–940	M	—	Same as above, more green clay.
	940–945	M	—	Same as above.
	945–947	M	—	Lighter colored green clay, shell, phosphate, softer material.
	947–955	S	5.0	Green marl, limestone at 954 ft.
	955–960	S	3.0	Green clay, some lime, fine quartz sand.
	960–965	S	—	No sample.
	965–967	S	—	Green clay, mostly shell, mollusks, tan fossiliferous limestone.
	967–970	S	—	Tan to gray limestone, fossiliferous. Will set casing at about 970 ft (F.W. Meyer), removed all drill pipe from hole.
Oct. 30				Reaming hole to 22.5 in. at 258 ft.
Oct. 31				Reaming hole to 22.5 in. at 389 ft.
Nov. 4				Reaming hole at 436 ft.
Nov. 5				Reaming hole at 460 ft.
Nov. 22				Cemented 14-in. casing at 955.28 ft below top of 24-in. casing.
Dec. 2				Obtained gamma log from 0 to ±940 ft. On bottom with 11 7/8-in. bit, top of cement at 946 ft. First sign of returns, 25-minute lag in cuttings from cement plug.
	946–955	H	3.63	
	955–965	H-S	3.50	Slight flow. Hard to 957 ft; soft at 957 ft.
	965–970	H	1.80	Soft streaks.
	970–975	H	1.60	Limestone, gray, silty, tiny black specks, soft streaks.
	975–980	H	1.20	Same as above, *Miogypsina* sp., soft streaks.
	980–985	S	1.60	Limestone, gray-white, fossils *Operculinoides* sp. and papillate(?). Laps. Flow estimated at 10 gal/min, hard streaks.
Dec. 3				Collected 1 pint water sample, T=73.0 °F; slight H_2S. Hole filled back to about 970 ft.
	970–985	—	—	Drilling out filled-in hole. First sign of returns. 25-minute lag in cuttings. Water sample collected.
	985–990	H	10.4	Very hard streaks.
	990–995	M	3.4	Limestone, gray, sand as above, very hard streaks, 985–990 ft.
	995–1,000	S	1.4	
	1,000–1,005	S	1.4	Limestone, cream-tan, fossils of *Operculinoides* sp., and gray limestone as above.
	1,005–1,010	S	2.0	
	1,010–1,015	S	1.8	Same as above, more forams and some shell fragments.
	1,015–1,020	S	1.6	Permeability increases here.
	1,020–1,025	S	1.8	Limestone, tan-gray, some shell but many forams, barnacles.
	1,025–1,030	S	1.8	Noticeable increase in flow. Coarse fragments of echinoids and ribbed mollusks.
	1,030–1,035	S	3.4	Hard streaks, 1,032–1,035 ft. Limestone, tan-gray, coarse fragments of mollusks.
	1,035–1,040	S	1.2	Increase in flow.
	1,040–1,045	S	1.0	Limestone, cream, soft, porous, fossiliferous, miliolids.
	1,045–1,050	S	1.4	

APPENDIX A—DRILLING LOG OF INJECTION WELL G-3061 AND OBSERVATION WELL G-3062—Continued

Date in 1974	Depth interval (feet)	Relative drilling hardness	Drilling speed (min/ft)	Lithology and remarks
Dec. 3	1,050–1,055	VS	.6	Same as above, some gray shale.
	1,055–1,060	S	1.4	
	1,060–1,065	S	.6	Same as above, many *Dictyoconus* sp., Avon Park Formation.
	1,065–1,070	S	1.2	
	1,070–1,075	S	.8	
	1,075–1,080	—	.6	
	1,080–1,085	—	.4	Limestone, tan, many *Dictyoconus* sp. Terminated circulation, coming out of hole.
Nov. 4				Barbara Howie collected water samples for extended complete analysis (bacteria, standard complete, chemical oxygen demand, biochemical oxygen demand, nutrients, total organic carbon, metals, field pH, alkalinity, specific conductance, chloride). F.W. Meyer and W.A. Long logged hole (electric, caliper, gamma) and found obstruction (cement at 964 ft prevented flowmeter survey). Apparently, a piece of cement wall in overdrill below casing cracked off and lodged across the borehole. Cancel logging by Schlumberger. Jim Kern plans to return December 9 with drilling rig to drill out the cement. Estimated flow about 500–600 gal/min.
Dec. 9				Collected water sample. T=70.3 °F, moderate H_2S, flow about same. Going into hole, on top of cement slab at 964 ft.
	964–1,085	—	—	Drilled 964–1,085 ft, cement now at bottom. Decided to drill another 20 ft below cement, cuttings show greater than 50 percent cement.
	1,085–1,090	S	.6	
	1,090–1,095	S	.6	
	1,095–1,100.5	S	.8	
	1,100–1,105.5	S	1.0	Limestone, tan, microfossils, and much cement.
Dec. 10				Collected 1 L water sample. Flow about same, about 600 gal/min. Drillers cleaning up area.
Dec. 11				Construction forms for floor.
Dec. 13				Poured concrete floor.
Dec. 16				Drillers clean up site, remove equipment.
Dec. 17				Pressure measurement.

Drilling Log of Injection Well G-3062

[Lithology and remarks by W.L. Miller to 183 feet and by F.W. Meyer below 183 feet. S, soft; VS, very soft; M, medium; H, hard; VH, very hard; min/ft, minute per foot;. —, no data]

Date	Depth interval (feet)	Relative drilling hardness	Drilling speed (min/ft)	Lithology and remarks
Oct. 11, 1974	0–5	VH	0.21	Fine-grained, white Miami Oolite and gray consolidated sand.
	5–10	S	1.0	Brown limestone and gray consolidated sand; tan limestone, some fossils evident.
	10–15	S	.8	Lost circulation at 13 ft, back at 14 ft.
	15–20	S	.4	White sandstone cemented with calcium carbonate.
	20–25	S	—	Same as above. Adding drill stem. Drill stopped for day for repairs.
Oct. 14, 1974	25–30	S	—	Drilling with 7 7/8-in. bit for pilot hole. Limestone and sand grains cemented with limestone. Large fragments greater than 5 millimeters.
	30–35	S	—	Same as above. Mainly small fragments, 1–5 millimeters.
	35–40	S	—	Bit chatter at 39 ft. Limestone, not as much sand as above.

APPENDIX A—DRILLING LOG OF INJECTION WELL G-3061 AND OBSERVATION WELL G-3062—Continued

Date	Depth interval (feet)	Relative drilling hardness	Drilling speed (min/ft)	Lithology and remarks
	40–43	VH	10	Equal amounts of small and large fragments.
	43–45	VH	9.0	Small limestone fragments, more cemented sand than at 35–40 ft.
	45–50	VH	5.0	Small fragments of limestone. Larger fragments of cemented sand grains.
	50–55	S	.8	Same as above.
	55–60	S	2.0	Same.
	60–63	VS	.67	Same.
	63–65	S	1.5	Same.
	65–70	S	2.0	Same.
	70–75	S	1.6	Same as above. Lost circulation at 72 ft, back at 73 ft.
	75–80	S	2.0	Very hard at 80 ft, bit chattering.
	80–85	H	—	Lost circulation at 81 ft, mixing mud.
	85–90	—	1.4	Pumped drilling mud at a very slow rate. No circulation.
	90–95	S	1.0	
	95–100	S	.4	No sampling from 80 to 100 ft.
	100–105	—	—	Gray sand cemented with limestone, many shell fragments. Upon reaching 103 ft, pumped at a faster rate and achieved circulation.
	105–110	VS	.5	
	110–115	VS	.3	Same as at 100–105 ft.
	115–120	VS	.4	Lost circulation between 117–118 ft.
	120–123	VS	.33	Grayish-white marl, sand grains, limestone and shell fragments.
	125–130	VS	1.0	Same as above.
	130–135	VS	.4	Same as above, but grayer.
	135–140	VS	.2	
	140–145	VS	—	Lost circulation at 143 ft.
	145–150	VS	.2	
	150–155	VS	.2	
	155–160	VS	.2	
	160–163	VS	.33	No circulation from 143 to 163 ft.
	163–165	VS	—	
	165–170	VS	.2	
	170–175	VS	.3	
	175–180	VS	.1	
	180–183	VS	.17	No samples from 143 to 183 ft. Started to pick up circulation at 183 ft. Letting hole set overnight.
Oct. 15, 1974	183–185	—	2.5	Shell, dark-gray, very coarse quartz sand, some green clay. Much aquagel. Losing returns.
	185–190	—	1.0	Shell, dark-gray to white, fine to very coarse quartz sand, some gray sandstone, phosphorite, cf. barnacles.
	190–203	VS	2.6	Still losing returns; shell as above.
	203–208	VS	1.0	Some hard streaks. Added rod, lost returns. Sand, light-gray, fine.
	208–215	S	1.4	Hard streaks. No returns. Removed drill pipe to add reaming bits. Start reaming 7 7/8-in. hole to 22 3/4 in. No lag.
Oct. 16, 1974				7 7/8-in. pilot hole reamed to 187 ft (22 3/4-in. diameter), rain stopped drilling.

APPENDIX A—DRILLING LOG OF INJECTION WELL G-3061 AND OBSERVATION WELL G-3062—Continued

Date	Depth interval (feet)	Relative drilling hardness	Drilling speed (min/ft)	Lithology and remarks
Oct. 17, 1974				200-ft level reached. Preparing to set 14-in. casing. Total casing 200.52 ft.
Oct. 18, 1974				Cemented casing to 200 ft, used 390 bags (17 yards).
Oct. 21, 1974				Temperature log of 150 ft of cased, cemented hole. Gamma log to 150 ft.
Oct. 22, 1974				Drilled 7 7/8-in. pilot hole to 460 ft. Caught own samples, no log kept.
Oct. 23, 1974				Pilot hole to 740 ft. No log kept.
Oct. 24, 1974				Began to go back into hole. Bridged at ±240 ft. On bottom at 740 ft. Circulating new mud.
	740–764	S	0.416	Shell, white to gray, cf. mollusks, white sticky clay, little hard dark-green sandy clay.
	764–769	S	.6	Shell, white to gray, cf. mollusks, white sticky clay, little hard, dark-green, sandy clay.
	769–774	S	1.4	Same as above.
	774–779	S	1.8	Same as above. Shell is bluish.
	779–784	S	.4	Limestone, white to gray, soft, shelly, sticky white clay and hard dark-green sandy clay concretions resembling casts of worm burrows.
	784–789	S	.6	Same as above; casts of small snails.
	789–794	S	.8	Same as above; snail casts, shark teeth, and light-green clay.
	794–799	S	1.25	Same as above; light-green sandy clay.
	799–804	S	1.0	Same as above.
	804–809	S	1.8	Limestone, white, soft, shelly, white calcareous clay and dark-green sandy clay concretions.
	809–814	S	1.8	Same as above.
	814–817	S	3.8	Clay, white, sticky, shelly, and limestone as above.
	819–824	S	3.0	Clay, white, some shell, and stringers of limestone. Some flat branching Bryozoa.
	824–829	S	.8	Limestone, tan to white, soft, some shell.
	829–834	S	.4	Same as above.
	834–839	S	.6	Same.
	839–844	S	2.0	Limestone, tan to white, soft, clayey, some shell (less than at 824 ft).
	844–849	S	1.0	Limestone, tan, soft, porous, clayey, some shell.
	849–854	S	.6	Same as above.
	854–859	S	1.4	Same as above; some hard streaks.
	859–864	S	2.6	Limestone, tan, soft, clayey, and some green clay.
	864–869	S	1.25	Same as above; shell.
	869–874	S	.6	Same as above; light-green “slipperly” clay.
	874–879	S	1.25	Shell, mollusks, and soft light-green to tan clay.
	879–884	S	1.4	Clay, light-green, “slippery,” and pieces of hard dark-green calcareous clay or limestone, some shell as at 804 ft.
	884–889	S	3.0	Clay, light-green, sticky, and tan shelly limestone.
	889–894	S	3.6	Same as above.
	894–899	S	2.4	Same as above.
	899–904	S	3.4	Clay, dark-green, slightly sandy (very fine quartz) and large mollusks.
Oct. 25, 1974				Driller has bit stuck at 884 ft.
Oct. 29, 1974				Driller retrieved 7 7/8-in. bit.
Oct. 30, 1974				Driller repairing equipment.
Oct. 31, 1974				Driller reaming 7 7/8-in. hole to 13.5 in.
Nov. 14, 1974				6 5/8-in. OD steel casing on bottom, free and clear, 953 ft deep.

APPENDIX A—DRILLING LOG OF INJECTION WELL G-3061 AND OBSERVATION WELL G-3062—Continued

Date	Depth interval (feet)	Relative drilling hardness	Drilling speed (min/ft)	Lithology and remarks
Nov. 19, 1974				5 7/8-in. bit on bottom and circulating. On float shoe, soft cement.
	953–958	—	1.8	Drilling out cement plug.
	958–961	—	3.3	Pieces of cement and the float shoe. Well is flowing from drill pipe.
	961–966	—	1.6	
	966–971	S	1.0	
	971–976	S	.8	
	976–984	S	.8	Tan to gray shell, sand, and dark-green shale. Duplicate sample shows tan fossiliferous limestone.
	984–989	S	.6	(?) Suwannee Limestone; *Miogypsina* sp. cf.
	989–994	S	1.6	Hard streak at 989 ft. Limestone, tan, many forams cf. *Miogypsina*.
	994–999	S	.4	Soft with hard streaks.
	999–1,004	VS	.6	Same as above.
	1,004–1,009	VS	.8	
	1,009–1,014	VS	.4	Same as above.
	1,014–1,019	VS	.2	
	1,019–1,024	VS	.2	Same as above; some blue-gray limestone.
	1,024–1,029	VS	.2	
	1,029–1,034	VS	1.0	
	1,034–1,044	VS	3.3	Medium to hard at 1,039 ft.
	1,044–1,049	S	.2	Flow about 200 gal/min estimated. Slight H_2S odor.
	1,049–1,054	S	.2	Tan limestone, fossiliferous, Avon Park fauna noted.
	1,054–1,059	S	.4	
	1,059–1,064	VS	.4	Limestone, tan, fossiliferous. Many *Dictyconus* and *Coskinolinus*, few *Lepidocyclinus* and *Operculinoides* sp. Water sample analyzed by Miami Water Department. Decided to terminate drilling at 1,064 ft. All drill pipe and collars out of hole. Flow increased to estimated 250 gal/min.
Nov. 20, 1974				Water samples collected by D.J. McKenzie for complete analysis. Q=240 gal/min.
Nov. 17, 1974				Pressure gage measurement.
Feb. 6, 1975				Measured flow with 4- and 5-in. orifices.
Feb. 10, 1975				Flow tests. Monitoring well Q=250 gal/min for 100 minutes.
Feb. 24, 1975				Obstruction at 983.7 ft. Original total depth is 1,064 ft. Filled into $\pm$1,054 ft. "Clean out" needed. Rig in place and drill stems stacked. No apparent obstruction at 983.7 ft. Bottomed at 1,058 ft. Clean out to 1,064.83 ft (total depth). Pulled off well and capped. Let run overnight. Rig will leave tomorrow.

APPENDIX B—LITHOLOGIC DESCRIPTION OF ROCK SAMPLES FROM INJECTION WELL G-3061 AND OBSERVATION WELL G-3062

Lithologic Description of Rock Samples from Injection Well G-3061

[Description is by R.T. Mooney, Florida Geological Survey]

Depth interval (feet)	Description
0–5	Sand; unconsolidated quartz; pale-yellowish-brown (10 YR 6/2); grains are primarily subangular to subrounded, clear, clean quartz; very fine to fine sand size, fair sorting; above 25 percent brown-black organic-looking materials (peat?); traces (1 percent) of limestone; small gastropod shell.
8–11	Limestone, very pale orange (10 YR 8/2); evidence of solution activity; some very fine quartz grains in the limestone; trace of white clay; few shell fragments and shell molds.
12–15	Primarily limestone as above; beginning of an unconsolidated sand layer; clear, very fine sand, moderately sorted, subangular to subrounded quartz grains; also much fine sand size, limestone pieces.
20–25	Sand; unconsolidated quartz; white (N 9); very clean, clear, subangular to subrounded; very fine to fine sand grains with fair sorting; some pieces of limestone as above; piece of crab claw; few abraded shell fragments.
25–50	Same as above.
51–53	Sandstone; pinkish-gray (5 YR 8/1); calcareous cement; sand grains are primarily quartz, subangular to subrounded, fine to very fine sand size; some calcite grains are present; some pieces of limestone with evidence of solution activity is also present; few shell fragments.
55–105	Same as above; varying from a calcareous sandstone to a sandy limestone in different sample intervals, increasing shell fragments.
105–110	Same as above, increasing shell fragments.
110–115	Shell bed; pinkish-gray (5 YR 8/1) to medium-gray (N 5); many warm, abraded, gray and white shell fragments; also pieces of limestone and sand with sandstone from above; few rounded sand-size phosphorite grains.
115–145	Same as above; traces of a white clay.
150–155	Shell bed as above; beginning of a very light olive-gray (5 Y 7/1) clay.
160–175	Same as above.
175–180	Clay, yellowish-gray (5 Y 7/2); fine sand-size, rounded, quartz grains in the clay; calcareous; some large quartz and phosphorite grains, rounded; many shell fragments, bryozoan; trace of limestone.
180–188	Same as above; less shell fragments.
188–190	Mixture of shell bed, worn abraded pelecypod shells, and clear quartz sandstone with a calcareous clay matrix.
190–195	Sandstone as above, yellowish-gray (5 Y 7/2); trace of shell fragments and limestone.
195–200	Same as above.
200–208	Much sandstone as above; beginning of a yellow-gray, slightly calcareous clay; trace of shell fragments.
208–215	Clay as above; some sandstone as above; trace of shell fragments.
220–225	Clay as above; decreasing sandstone and shell fragments.
225–228	Clay as above; same sandstone and sandy limestone.

APPENDIX B—LITHOLOGIC DESCRIPTION OF ROCKS SAMPLES FROM INJECTION WELL G-3061 AND OBSERVATION WELL G-3062—Continued

Depth interval (feet)	Description
228–235	Clay, pale-olive (10 Y 6/2); marly when wet, calcareous; trace of sandstone and limestone; few shell fragments; bryozoan, echinoid spine.
235–240	Same as above.
240–248	Clay, medium-olive (10 Y 5/2); very sandy, calcareous; some shell fragments and limestone pieces; bryozoan.
250–260	Same as above.
260–270	Clay, medium-olive (10 Y 5/2); very sandy, calcareous; trace of sandy limestone.
270–280	Same as above; trace of shell fragments.
280–290	Same as above; some phosphate.
290–300	Same as above; decreasing in sand.
300–310	Same as 260–270 ft; some phosphate.
310–327	Same as 300–310 ft.
330–347	Same as above; much quartz sand (fine to medium).
347–360	Sand, unconsolidated, clear quartz and phosphorite, fine to medium, moderately sorted, subrounded.
360–390	Same as above; trace of clay, some zircon(?) present, *Globigerina ruber.*
390–410	Unconsolidated sand as above, yellowish-gray (5 Y 7/2), change of color may be due to an increase of clay.
410–420	Same as 390–410 ft; slight increase in clay and larger grains phosphorite.
420–430	Same as above; beginning of a white limestone.
430–440	Same as above.
440–450	Same as above; increase in clay content.
450–460	Clay, yellowish-gray (5 Y 8/1), very sandy, phosphorite, trace of limestone, *Rubulus.*
460–470	Limestone, yellowish-gray (5 Y 8/1); much sand and clay, phosphorite, echinoid spine.
470–480	Same as above; slightly less clay, trace of sand and phosphorite.
480–490	Same as above.
490–500	Primarily limestone as above; increase in clay and sand (very fine) content, trace of very fine phosphorite.
500–510	Limestone, yellowish-gray (5 Y 8/1); yellowish-gray clay; phosphorite; some shell fragments.
510–550	Same as above.
550–560	Limestone as above; about 50 percent, except broken into larger granule-size fragments; about 40 percent clean quartz sand, subangular to subrounded, fine to medium sand size; some polished phosphorite grains; rest of sample is composed of traces of shell fragments, dolomite, and chert(?).
560–570	Limestone, yellowish-gray (5 Y 8/1); granule-size fragments covered with a yellowish-gray calcareous clay; some quartz sand, pieces of “proto” sandstone composed of quart sand grains with a clay matrix; traces of chert; unknown hard black material (possibly phosphorite), some of it in a honeycomb pattern.
570–580	Clay, yellowish-gray (5 Y 8/1); calcareous; pieces of limestone, shell fragments, dolomite, phosphorite from above.
580–630	Clay as above.

APPENDIX B—LITHOLOGIC DESCRIPTION OF ROCKS SAMPLES FROM INJECTION WELL G-3061 AND OBSERVATION WELL G-3062—Continued

Depth interval (feet)	Description
630–647	Limestone, white (N 9) to yellowish-gray (5 Y 8/1); covered with white clay; many shell fragments; some calcite crystals, fine.
647–705	Limestone as above; decreasing clay; many shell fragments.
705–725	Same as above.
725–727	Clay, yellowish-gray (5 Y 8/1); calcareous; silt to very fine sand size phosphorite (few coarse-size grains); many limestone and shell fragments; some quartz sand.
727–747	Same as above; trace of a light-olive gray (5 Y 6/1) clay; gradually turning into a limestone with high amount of clay.
747–755	Limestone; very light yellowish-gray (5 Y 9/1); seems to be a calcilutite to a very fine calcarenite; white clay; very fine calcite crystals; few shell fragments.
755–760	Same as above.
760–787	Same as above.
787–795	Primarily as above; beginning of a clay, light-olive-gray (5 Y 6/1); clay has a high percentage of quartz sand within it; in some cases it seems to be a “proto” sandstone composed of fine sand grains in a clay matrix.
795–820	Largely as above with an increasing clay covering on the limestone.
820–825	Limestone, yellowish-gray (5 Y 8/1); soft; much yellowish-gray calcareous clay; shell fragments; traces of quartz sand grains weakly cemented with clay matrix.
825–827	Clay, yellow-gray (5 Y 8/1); calcareous; many white limestone fragments, soft; shell fragments.
827–835	Clay as above.
835–875	Same as above.
875–880	Primarily clay as above; increasing limestone and shell fragments.
880–885	Shell hash; pinkish-gray (5 YR 8/1) to yellowish-gray (5 Y 8/1); many shell fragments, primarily pelecypod; limestone fragments with very fine phosphorite grains within it; trace of white clay.
885–887	Shell bed as above, but with much more clay; covers everything.
887–895	Sand, unconsolidated, yellowish-gray (5 Y 8/1); composed of calcite, quartz and phosphorite grains; silt to fine sand size; some clay material; forams, *Rubulus*(?), *Amphistegina*(?) (very small).
895–900	Same as above.
900–905	Sand, very light olive-gray (5 Y 7/1); primarily sand-size limestone fragments and silt to very fine quartz and phosphorite grains; much clay; traces of light-olive-gray (5 Y 6/1) clay; shell fragments.
905–907	Same as above.
907–915	Sand, yellowish-gray (5 Y 8/1); primarily fine sand-size quartz and calcite grains; many pieces of light-olive-gray (5 Y 6/1) clay; silt-size phosphorite(?) grains within the clay; shell fragments.
915–920	Same as above; much light-olive-gray (5 Y 6/1) clay; 50 percent of sample.
920–927	Sand as in sample 907–915 ft; traces of light-olive-gray (5 Y 6/1) clay.

APPENDIX B—LITHOLOGIC DESCRIPTION OF ROCKS SAMPLES FROM INJECTION WELL G-3061 AND OBSERVATION WELL G-3062—Continued

Depth interval (feet)	Description
927–930	Clay, light-gray (N 7) and yellowish-gray (5 Y 8/1); much quartz and calcite sand; shell fragments; traces of phosphorite and dolomite(?).
930–945	Same as above.
945–947	Primarily as above; pieces of chert.
947–955	Sand, white to a light-olive-gray (5 Y 6/1); composed of rounded phosphorite, quartz and calcite grains, fine to medium sand size, much light-gray (N 7) clay; chert and dolomite; shell fragments.
955–960	Clay, light-olive-gray (5 Y 6/1); sample contains much quartz, phosphorite, and calcite sand; chert; shell fragments.
960–965	Clay, white (N 9); very fine black specks (possibly phosphorite) in the clay; much unknown gray material (drilling contamination?); much limonite rust from drill stem.
965–975	White clay as above; less unknown gray material.
965–967	Light-olive-gray clay as in sample 955–960 feet; many shell fragments.
967–970	Same as above; pieces of white limestone.
975–985	Limestone, white (N 9); also pieces of buff white limestone and clay; everything is covered with clay; shell fragments; forams *Operculinoides*(?), abraded *Heterostegina*(?), *Miogypsina* sp.
985–995	White limestone as above; no clay; abraded *Heterostegina*; few shell fragments.
995–1,005	Limestone, pinkish-gray (5 YR 8/1); seems to be a calcarenite, possibly bioclastic; *Operculinoides* sp., *Lepidocyclinus*(?).
1,005–1,015	Same as above.
1,015–1,025	Limestone, light-gray (N 7) and pinkish-gray (5 YR 8/1); many pieces from calcarenite above; many worn and abraded shell fragments and forams; pieces of gray dolomite and rounded phosphorite; echinoid spines; also some white limestone with black specks from above.
1,025–1,035	Same as above, but larger fragments.
1,035–1,045	Limestone, pinkish-gray (5 YR 8/1); bioclastic calcarenite; pieces of gray dolomite(?); few shell fragments; pelecypod, gastropod.
1,045–1,055	Lithology as above, but small fragments; *Dictyoconus cookei*, *Textularia*.
1,055–1,065	Same as above; *Dictyoconus cookei*(?).
1,065–1,085	Limestone; white (N 9) to pinkish-gray (5 YR 8/1); seems to be a bioclastic calcarenite; some evidence of recrystallization; *Dictyoconus cookei*.
1,085–1,105	Same as above.

APPENDIX B—LITHOLOGIC DESCRIPTION OF ROCKS SAMPLES FROM INJECTION WELL G-3061 AND OBSERVATION WELL G-3062—Continued

Lithologic Description of Rock Samples from Injection Well G-3062

[Description is by R.T. Mooney, Florida Geological Survey]

Depth interval (feet)	Description
0–5	Limestone, pinkish-gray (5 YR 8/1); about 1 percent quartz sand grains in the limestone; evidence of solution activity.
5–55	Limestone as above; slightly higher percentage of quartz.
55–60	Sandstone, pinkish-gray (5 YR 8/1); calcareous matrix (almost a very sandy limestone); sandy grains are very fine to fine, subangular to subrounded, primarily quartz with some heavy minerals (darker, honey-colored grains); trace of shell fragments.
60–63	Largely sandstone as above; also pieces of a sandy limestone; traces of a white clay; traces of shell fragments.
63–65	Same as above; slightly increasing limestone.
65–70	Limestone, very light gray (N 8); quartz sand in the limestone (varying percentages); much sandstone as above; traces of shell fragments and white clay.
70–75	Same as above.
75–80	Same as above.
80–100	No sample.
100–105	Shell bed, white (N 9) and medium-gray (N 5); many broken, worn, and abraded pelecypod and gastropod shells; medium to coarse, rounded, polished quartz and phosphorite sand grains; pieces of limestone and sandstone as above.
110–115	Same as above.
120–123	Same as above.
125–130	Primarily as above; white clay on the cuttings; some fine sand-size limestone grains.
130–135	Same as above.
135–183	No sample.
183–190	Clay, light-olive-gray (5 Y 6/1); many very fine to fine quartz and calcite sand grains; some shell fragments from above; few medium sand-size, polished quartz and phosphorite grains as above.
190–203	Limestone, white (N 9) to greenish-gray (5 GY 6/1); large amount of calcareous clay and very fine quartz sand; shell fragments; phosphorite; traces of a calcareous sandstone.
203–208	Sand, unconsolidated; light-gray (N 7); primarily very fine to fine, clear quartz grains, angular to subrounded, some polished phosphorite and heavy mineral grains; some greenish-gray-clay from above; shell fragments and traces of limestone.
220–225	Clay; many pieces of limestone, shell fragments, and drill pipe rust all covered with a gray-greenish clay.
225–230	Same as above.
230–235	Clay, light-olive-gray (5 Y 6/1); calcareous; pieces of limestone, shell fragments, etc., from above; traces of fine quartz sand.
235–240	Same as above; minor phosphorite.

APPENDIX B—LITHOLOGIC DESCRIPTION OF ROCKS SAMPLES FROM INJECTION WELL G-3061 AND OBSERVATION WELL G-3062—Continued

Depth interval (feet)	Description
240–245	Clay, olive-gray (5 Y 4/1) (slightly marly when wet); minor very fine quartz sand in the clay, minor phosphorite, limestone fragments from above.
245–270	Clay as above; increasing very fine quartz sand.
270–275	Clay as above; slight color change to about medium-olive-gray (5 Y 5/1).
275–290	Same as above.
290–295	Clay (5 GY 6/1), greenish-gray, very fine clear quartz, sandy; minor phosphate, traces of limestone and shell fragments.
295–300	Same as above.
300–305	Same as above.
305–310	Same as above.
310–315	Same as above.
315–320	Same as above; peat; *Amphistegina*(?).
320–325	Primarily as above; increasing limestone.
325–330	Same as above.
330–405	No samples.
405–410	Limestone, yellowish-gray (5 Y 8/1); covered with a grayish clay; soft limestone; trace of shell fragments; phosphorite.
410–415	Same as above; echinoid spine.
415–420	Same as above.
420–425	Same as above; increasing clay.
425–430	Limestone, yellowish-gray (5 Y 8/1); clay covering the limestone; minor phosphorite; shell fragments.
430–435	Same as above.
435–440	Limestone as above; increasing clay (about 40 percent clay).
440–445	Primarily clay-covered limestone as above; minor phosphorite; beginning of a white limestone bed.
445–450	Same as above.
450–455	White limestone as above; increasing clay; minor quartz in the limestone.
455–460	Same as above; decrease in clay.
460–465	Same as above; increasing quartz and phosphorite; shell fragments; echinoid spine.
465–470	Same as above; less quartz.
470–475	Same as above; increasing quartz (same as 460–465 ft).
475–480	Same as above; less quartz.

APPENDIX B—LITHOLOGIC DESCRIPTION OF ROCKS SAMPLES FROM INJECTION WELL G-3061 AND OBSERVATION WELL G-3062—Continued

Depth interval (feet)	Description
480–485	Same as above.
485–490	Limestone, white (N 9); seems to be a calcilutite; minor phosphate in limestone; trace of clay; some shell fragments.
490–495	Same as above.
495–500	Same as above.
500–505	Same as above.
505–510	Same as above.
510–515	Same as above.
515–520	Same as above; some shell molds in the limestone.
520–525	Same as above.
525–530	Same as above.
530–535	Same as above; slight increase in clay.
535–540	Same as above; trace of peat.
540–545	Clay, yellowish-gray (5 Y 8/1); calcareous; phosphorite in clay; about 40 percent limestone as above; trace of shell fragments.
545–550	Limestone as in 530–535 ft; about 20 percent clay (micrite?).
555–560	Micrite limestone as above; minor phosphorite.
560–565	Same as above.
565–570	Same as above.
570–575	Same as above.
575–580	Same as above.
580–585	Same as above.
585–590	Same as above; echinoid spine; decrease in phosphorite.
590–595	Same as above.
595–600	Same as above; trace of shell fragments.
600–605	Same as above; increase in shell fragments.
605–610	Same as above.
610–615	Same as above.
615–620	Same as above.
620–625	Same as above.
625–630	Same as above.

APPENDIX B—LITHOLOGIC DESCRIPTION OF ROCKS SAMPLES FROM INJECTION WELL G-3061 AND OBSERVATION WELL G-3062—Continued

Depth interval (feet)	Description
630–635	Same as above.
635–640	Same as above.
640–645	Primarily as above; beginning of a consolidated, hard, white limestone, fossiliferous.
645–650	Same as above with increase of the fossiliferous hard limestone.
650–655	Same as above; shell fragments.
655–660	Same as above.
660–665	Same as above.
665–670	Limestone, white (N 9); fossiliferous, some of the micritic limestone; shell fragments.
670–675	Same as above; evidence of secondary calcite; echinoid spines.
675–680	Same as above.
680–685	Same as above.
685–690	Same as above.
690–695	Same as above.
695–700	Same as above.
700–705	Same as above.
705–710	Same as above.
710–715	Same as above.
715–720	Same as above.
720–725	Clay, yellowish-gray (5 Y 8/1); calcareous; silt-size phosphorite; about 40 percent limestone as above; shell fragments; trace of sand-size quartz.
725–730	Same as above.
730–735	Same as above; slightly decreasing clay.
735–740	Same as above.
744–764	Primarily as above; much quartz sand within clay (25 percent); beginning of a light-brown dolomitic limestone(?); shark tooth, shell fragments.
764–769	Limestone, white (N 9); much quartzitic clay as above; some dolomitic(?) limestone as above.
769–774	Same as above; white seems to be fossiliferous.
774–779	Same as above; phosphorite.
779–784	Same as above.
784–789	Same as above.

APPENDIX B—LITHOLOGIC DESCRIPTION OF ROCKS SAMPLES FROM INJECTION WELL G-3061 AND OBSERVATION WELL G-3062—Continued

Depth interval (feet)	Description
789–794	Same as above; less clay.
794–799	Same as above.
799–804	Limestone, white (N 9); fossiliferous, some quartzitic clay as above; minor phosphorite.
804–809	Same as above; increase in calcareous, white clay (micrite?).
809–814	Same as above.
814–819	Micrite, yellowish-gray (5 Y 8/1); trace of quartzitic clay as above.
819–824	Same as above; increase in micrite clay.
824–829	Same as above; phosphorite.
829–834	Same as above.
834–839	Same as above; trace of quartz (some granules).
839–844	Same as above; increase in sand-size quartz.
844–849	Same as above; trace of phosphorite.
849–854	Same as above.
854–859	Same as above; beginning of a white fossiliferous limestone.
859–864	Limestone, white (N 9) covered with a calcareous white clay; shell fragments.
864–869	Same as above; increase in calcareous clay gives slight color change to yellowish-gray (5 Y 8/1).
869–874	Same as above; trace of quartz sand, echinoid spine.
874–879	Same as above.
879–884	Same as above.
884–889	Same as above; increasing shell fragments; trace of phosphorite, very fine.
889–894	Same as above; beginning of a gray phosphatic clay; increase in shell fragments.
894–899	Clay, white-olive-gray (5 Y 6/1), very fine phosphorite in clay, shell fragments, coarse sand-size quartz grains; some limestone as above.
899–904	Clay as above.
953–984	Limestone, yellowish-gray (5 Y 8/1); covered with a light clay, seems to be fossiliferous (forams); *Miogypsin*a, *Camerina*(?).
961–984	*Operculinoides*, *Heterostegina.*
984–994	Limestone, pinkish-gray (5 YR 8/1); covered with calcareous clay-size particles; minor phosphate; shell fragments; *Miogypsina*, *Camerina.*
994–1,004	Same as above; *Miogypsina*, *Camerina*.
1,004–1,014	Same as above.

APPENDIX B—LITHOLOGIC DESCRIPTION OF ROCKS SAMPLES FROM INJECTION WELL G-3061 AND OBSERVATION WELL G-3062—Continued

Depth interval (feet)	Description
1,014–1,024	Same as above.
1,024–1,034	Dolomite, light-gray (N 7); moldic; microcrystalline; limestone as above (but bigger cuttings); less clay; quartz in limestone; minor phosphorite.
1,034–1,044	Same as above; limestone seems to be bioclastic in part.
1,044–1,054	Limestone, pinkish-gray (5 YR 8/1); fossiliferous; 35 percent dolomite as above; phosphorite; *Cermina*.
1,054–1,064	Limestone as above; less dolomite; more forams *Camerina*, *Amphistegina*.

APPENDIX C—VOLUME AND RATE DATA FROM INJECTION AND RECOVERY CYCLES AND QUALITY OF RECOVERED WATER

Time of measurement		Days from beginning of data	Cumulative volume readout on flowmeter (gallons)	Flow rate (gallons per minute)	Chemical concentrations in recovered water		Change of activity
Date	Hour				Chloride (milligrams per liter)	Specific conductance (microsiemens per centimeter)	
Aug. 1975							
17	1500		14,463				Begin injection 1
17	1610		16,110	-176			
18	803	1	115,795	-782			
18	1630	1	168,400	-776			
19	1435	2	302,440	-757			
21	706	4	543,540	-742			
21	1600	4	596,300	-739			
22	920	5	706,920	-796			
22	1535	5	736,510	-590			
23	1040	6	838,400	-666			
23	1610	6	875,590	-843			
24	755	7	964,650	-705			
24	1613	7	1,010,850	-694			
25	849	8	1,102,650	-689			
25	1456	8	1,136,245	-685			
28	738	11	1,470,180	-643			
28	1437	11	1,515,390	-807			
28	1618	11	1,524,900	-704			
29	747	12	1,602,050	-621			
30	742	13	1,722,930	-630			
31	725	14	1,841,560	-624			
Aug. 1975							
01	734	15	1,956,440	-593			
04	735	18	2,279,790	-560			
05	739	19	2,387,740	-559			
06	734	20	2,493,900	-553			
07	727	21	2,599,140	-549			
08	734	22	2,707,300	-559			
11	733	25	3,011,430	-527			
12	730	26	3,111,680	-522			
13	740	27	3,210,995	-512			
14	740	28	3,307,820	-503			
15	734	29	3,407,640	-521			
18	736	32	3,704,050	-513			
19	1600	33	3,834,570	-502			
20	741	34	3,895,860	-487			
21	749	35	3,994,380	-509			
22	748	36	4,088,880	-491			
25	735	39	4,366,030	-481			
26	814	40	4,450,440	-427			
27	811	41	4,550,850	-523			
28	756	42	4,638,030	-458			
29	740	43	4,726,000	-462			

APPENDIX C—VOLUME AND RATE DATA FROM INJECTION AND RECOVERY CYCLES AND QUALITY OF RECOVERED WATER—Continued

Time of measurement		Days from beginning of data	Cumulative volume readout on flowmeter (gallons)	Flow rate (gallons per minute)	Chemical concentrations in recovered water		Change of activity
Date	Hour				Chloride (milligrams per liter)	Specific conductance (microsiemens per centimeter)	
Sept. 1975							
02	800	47	5,074,400	-451			
03	759	48	5,150,450	-395			
04	744	49	5,245,300	-498			
05	750	50	5,332,120	-449			
08	746	53	5,585,730	-440			
08	1145	53	5,599,050	-417			
08	1157	53	5,600,032	-612			
10	1318	55	5,600,033				Begin backflow I
11	1253	56	5,664,050	338	66	650	
12	1241	57	5,728,500	338	68	650	
14	1020	59	5,851,400	336	76	680	
15	1100	60	5,918,500	339	84	720	
16	1030	61	5,981,700	335	90	760	
17	730	62	6,038,100	335	96	760	
18	820	63	6,105,400	338	106	800	
19	715	64	6,166,500	332	100	800	
22	825	67	6,362,460	334	124	870	
23	750	68	6,425,800	337	132	920	
24	815	69	6,491,500	335	136	900	
25	825	70	6,554,640	326	142	930	
26	855	71	6,619,000	328	144	950	
29	615	74	6,816,700	356	166	1,035	
30	820	75	6,873,600	272	270	1,040	
Oct. 1975							
01	830	76	6,938,000	332	180	1,075	
02	820	77	7,000,700	328	184	1,100	
03	840	78	7,065,200	330	205	1,150	
06	910	81	7,256,200	328	210	1,230	
07	900	82	7,319,200	330	218	1,215	
08	825	83	7,381,200	330	232	1,250	
09	840	84	7,443,480	320	275	1,280	
10	750	85	7,504,500	328	300	1,310	
10	1350	85	7,526,100	449			
10	1730	85	7,536,900	367			
14	815	89	7,738,500	290	290	1,435	
15	830	90	7,794,900	290	280	1,450	
16	900	91	7,840,200	231	300	1,450	
17	755	92	7,892,700	286	350	1,580	
20	755	95	8,068,100	304	335	1,620	
20	930	95	8,072,100	315			
24	1048	99	8,072,100				Pump test
24	1055	99	8,072,900	-855			
24	1130	99	8,077,100	-898			Meter burned out

APPENDIX C—VOLUME AND RATE DATA FROM INJECTION AND RECOVERY CYCLES AND QUALITY OF RECOVERED WATER—Continued

Time of measurement		Days from beginning of data	Cumulative volume readout on flowmeter (gallons)	Flow rate (gallons per minute)	Chemical concentrations in recovered water		Change of activity
Date	Hour				Chloride (milligrams per liter)	Specific conductance (microsiemens per centimeter)	
Nov. 1975							
07	900	113	8,082,396	-2			
Dec. 1975							
08	730	114	8,082,400				Pump test
08	917	144	8,085,542	-220			
10	1034	146	8,085,542				Injection
10	1108	146	8,090,960	-1,192			
11	931	147	8,239,930	-830			
16	1154	152	9,091,650	-868			
17	1100	153	9,270,200	-964			Pump failure
Jan. 1976							
05	1400	172	9,270,200				Begin injection II
06	900	173	9,419,450	-979			
07	920	174	9,606,920	-961			
08	730	175	9,771,860	-928			
12	800	179	10,448,360	-874			
13	830	180	10,615,100	-849			
14	830	181	10,777,270	-842			
15	830	182	10,936,960	-830			
16	830	183	11,089,260	-791			
16	1330	183	11,120,700	-784			
19	830	186	11,541,830	-784			
20	715	187	11,685,000	-785			
21	715	188	11,831,560	-761			
22	700	189	11,975,900	-758			
23	800	190	12,131,900	-778			
26	800	193	12,552,400	-728			
27	830	194	12,700,800	-755			
28	700	195	12,831,100	-722			
29	800	196	12,961,550	-651			
30	800	197	13,109,820	-770			
Feb. 1976							
02	815	200	13,497,200	-668			
02	849	200	13,500,470	-719			
02	904	200	13,502,465	995			End backflush
03	734	201	13,661,600	-882			
04	730	202	13,826,700	-860			
05	800	203	14,005,300	-909			
06	830	204	14,168,600	-831			
09	700	207	14,628,100	-813			
10	800	208	14,785,400	-784			
11	815	209	14,936,100	-775			
12	815	210	15,084,100	-769			
13	750	211	15,227,100	-756			
13	839	211	15,233,568	-987			End backflush
13	1203	211	15,250,920	-636			

APPENDIX C—VOLUME AND RATE DATA FROM INJECTION AND RECOVERY CYCLES AND QUALITY OF RECOVERED WATER—Continued

Time of measurement		Days from beginning of data	Cumulative volume readout on flowmeter (gallons)	Flow rate (gallons per minute)	Chemical concentrations in recovered water		Change of activity
Date	Hour				Chloride (milligrams per liter)	Specific conductance (microsiemens per centimeter)	
Feb. 1976							
17	800	215	16,906,200	-888			
18	800	216	16,072,200	-862			
19	800	217	16,231,100	-825			
20	830	218	16,392,200	-820			
23	830	221	16,865,600	-820			
24	900	222	17,021,400	-793			
25	800	223	17,172,900	-821			
26	800	224	17,318,700	-757			
27	935	225	17,472,200	-748			
27	1025	225	17,478,800	987			End backflush
Mar. 1976							
01	800	228	17,976,100	-891			
02	1015	229	18,153,600	-843			
03	800	230	18,305,500	-871			
04	830	231	18,468,300	-828			
05	800	232	18,623,500	-823			
08	800	235	19,090,100	-808			
08	900	235	19,098,020	987			End backflush
10	830	237	19,436,600	-889			
10	850	237	19,436,900	-112			
May 1976							
03	1312	291	19,436,900				Begin backflow II
06	800	294	19,709,100	508	70	670	
12	800	300	20,281,200	495	96	760	
19	955	307	20,946,900	488			
20	1150	308	21,046,900	481	110	810	
25	845	313	21,537,500	523	124	860	
25	1240	313	21,551,900	458			
June 1976							
02	1000	321	22,294,800	489	140	940	
09	900	328	22,969,900	504	154	990	
15	730	334	23,541,900	500			
18	1330	337	23,854,700	497	202	1,170	
21	745	340	24,115,500	495	214	1,200	
22	800	341	24,212,300	498	216	1,220	
23	800	342	24,308,600	500	222	1,240	
24	800	343	24,402,500	488	224	1,200	
25	800	344	24/496,300	487	224		
28	800	347	24,780,200	492			
29	800	348	24,874,200	488	256	1,450	
30	800	349	24,968,900	492	260	1,450	

APPENDIX C—VOLUME AND RATE DATA FROM INJECTION AND RECOVERY CYCLES AND QUALITY OF RECOVERED WATER—Continued

Time of measurement		Days from beginning of data	Cumulative volume readout on flowmeter (gallons)	Flow rate (gallons per minute)	Chemical concentrations in recovered water		Change of activity
Date	Hour				Chloride (milligrams per liter)	Specific conductance (microsiemens per centimeter)	
July 1976							
01	640	350	25,058,200	491	266	1,400	
02	800	351	25,157,300	488	270	1,350	
09	735	358	25,810,000	486	300	1,550	
16	1145	365	26,483,200	488	400	1,850	
19	1050	368	26,760,400	486			
20	958	369	26,850,100	483	390	1,860	
21	1015	370	26,850,100				Injection test
21	1035	370	26,852,700	-972			
23	800	372	27,160,200	-844			Begin injection III
30	1100	379	28,191,400	-752			
Aug. 1976							
06	930	386	29,117,000	-693			
06	1230	386	29,117,600	25			End backflush
13	830	393	30,162,100	-794			
13	935	393	30,179,200	-1,968			
13	1135	393	30,191,200	748			End backflush
20	700	400	31,274,500	-826			
20	800	400	31,285,300	-1,346			
20	1000	400	31,297,300	748			End backflush
27	830	407	32,748,500	-1,087			
27	900	407	32,760,500	2,992			End backflush
Sept. 1976							
02	1130	413	33,713,100	-811			
03	1400	414	33,898,600	-873			
03	1705	414	33,906,600	323			End backflush
10	800	421	34,983,600	-845			
10	1000	421	34,995,600	748			End backflush
17	900	428	36,122,500	-841			
17	1010	428	36,131,100	-919			
17	1210	428	36,143,100	748			End backflush
24	900	435	37,229,600	-822			
24	1015	435	37,234,400	-479			
24	1215	435	37,246,400	748			End backflush
Oct. 1976							
01	1300	442	38,358,650	-822			
01	1500	442	38,370,650	748			End backflush
08	1000	499	39,353,000	-751			
08	1300	449	39,365,000	499			End backflush
15	700	456	40,314,700	-731			
15	1000	456	40,326,700	499			End backflush
22	800	463	41,359,250	-776			
22	1100	463	41,371,250	499			End backflush
29	1000	470	42,425,860	-787			
29	1300	470	42,437,860	499			End backflush

APPENDIX C—VOLUME AND RATE DATA FROM INJECTION AND RECOVERY CYCLES AND QUALITY OF RECOVERED WATER—Continued

Time of measurement		Days from beginning of data	Cumulative volume readout on flowmeter (gallons)	Flow rate (gallons per minute)	Chemical concentrations in recovered water		Change of activity
Date	Hour				Chloride (milligrams per liter)	Specific conductance (microsiemens per centimeter)	
Nov. 1976							
05	845	477	43,478,970	-793			
05	1145	477	43,490,970	499			End backflush
12	900	484	44,509,900	-769			
12	1200	484	44,521,900	499			End backflush
19	845	491	45,548,870	-777			
19	1145	491	45,560,870	499			End backflush
26	700	498	46,579,800	-778			
26	1000	498	46,591,800	499			End backflush
Dec. 1976							
03	720	505	47,605,300	-764			
10	800	512	48,694,700	-805			
10	1100	512	48,706,700	499			End backflush
17	700	519	50,197,560	-1,133			
17	1000	519	50,209,560	499			End backflush
23	730	525	51,108,225	-792			
23	1030	525	51,120,225	499			End backflush
30	645	532	52,148,800	-781			
Jan. 1977							
07	1157	540	53,184,700	-655			
07	1500	540	53,196,700	491			End backflush
14	650	547	54,126,700	-725			
18	1230	551	54,661,017	-655			
24	1016	557	54,661,020				
Feb. 1977							
18	911	732	54,661,020				Begin backflow III
22	1034	736	55,071,210	525	78	700	
29	820	743	55,768,230	525	80	730	
Aug. 1977							
05	845	750	56,482,350	529	113	780	
12	1000	757	57,173,970	509	90	830	
19	1030	764	57,862,000	509	125	860	
26	900	771	58,552,870	517	140	885	
Sept. 1977							
02	1200	778	59,135,200	425	140	895	
09	730	785	59,722,900	448	150	935	
14	723	790	60,122,700	416	146	940	
23	1500	799	60,842,250	401	160	950	
Oct. 1977							
01	1600	807	61,420,780	374	160	1,000	
07	1500	813	62,059,150	557	172	1,080	
03	827	819	62,417,200	325	180	1,090	
21	911	827	63,055,100	413	196	1,080	
28	1300	834	63,628,550	416	200	1,200	

APPENDIX C—VOLUME AND RATE DATA FROM INJECTION AND RECOVERY CYCLES AND QUALITY OF RECOVERED WATER—Continued

Time of measurement		Days from beginning of data	Cumulative volume readout on flowmeter (gallons)	Flow rate (gallons per minute)	Chemical concentrations in recovered water		Change of activity
Date	Hour				Chloride (milligrams per liter)	Specific conductance (microsiemens per centimeter)	
Nov. 1977							
04	1300	841	64,206,250	429	217	1,200	
11	1400	848	64,803,950	441	220	1,340	
18	1100	855	65,364,850	424	230	1,250	
25	1000	862	65,953,570	440	246	1,320	
Dec. 1977							
02	1200	869	66,640,150	430	268		
09	1400	876	67,142,750	442	300	1,300	
16	1200	883	67,713,650	429	272		
23	1200	890	68,305,850	439	315	1,400	
30	1200	897	68,894,250	437	340	1,450	
Jan. 1978							
30	1000	928	71,412,025	423	405	1,825	
Mar. 1978							
03	1450	960	73,875,850	397	480	2,160	
Apr. 1978							
13	1307	1,001	76,762,950	366	600	2,450	
14	1200	1,002	76,823,500	330	600	2,450	
May 1978							
05	1045	1,023	78,135,800	325	625	2,550	
June 1978							
12	1050	1,061	80,460,400	318	700	3,000	
July 1978							
07	841	1,086	81,920,860	305	750	3,100	
Aug. 1978							
02	1045	1,112	83,429,220	300	780	3,300	
10	1030	1,120	83,888,600	299	800	3,240	
24	800	1,134	84,649,770	285	800	3,300	
Sept. 1978							
16	1300	1,157	85,878,700	275	840	3,400	
Oct. 1978							
31	1215	1,202	88,244,700	273	925	3,625	
Dec. 1978							
14	1050	1,246	90,398,500	255	950	3,800	
Feb. 1979							
27	1100	1,321	92,972,300	178	1,000	4,050	
Apr. 1979							
12	1230	1,365	96,029,400	360	1,055	4,120	
18	1300	1,371	96,308,800	241			
July 1979							
17	835	1,461	100,433,500	239	1,060		
18	835	1,462	100,479,700	240			
24	1215	1,468	100,769,500	245	1,060	4,260	
Nov. 1979							
15	1330	1,582	105,941,600	236			
16	1030	1,583	105,980,300	230	1,100	4,350	
Jan. 1980							
28	1051	1,656	109,283,100	235	1,120	4,290	
30	1000	1,658	109,373,100	238			

APPENDIX D—WATER-QUALITY DATA OBTAINED DURING WELL CONSTRUCTION AND THE SUBSEQUENT INJECTION AND RECOVERY CYCLES AT THE HIALEAH SITE

Bacteriological Analyses for Nitrogen-, Sulfate-, and Iron-Reducing Bacteria

[Nitrate, nitrate agar (14 days); sulfate, sulfate API media (14 weeks); iron, sphaerotilus agar; OW, observation well; SW, supply well; IW, injection well; —, no data]

Source	Date	Activity	Nitrate-reducing bacteria[1]	Sulfate-reducing bacteria[1]	Iron-reducing bacteria[2]	Microscopic iron bacteria[2]
OW	April 16, 1975	Preinjection background in injection zone	90	70	—	—
SW	July 22, 1975	Supply water for first injection	70	<30	—	—
OW	Aug. 04, 1975	Monitor zone, after 18 days of first injection	40	150	—	—
IW	Sept. 16, 1975	Recovered water, 6 days into first recovery	40	<30	—	—
	Sept. 23, 1975	13 days into first recovery	210	200	—	—
	Sept. 30, 1975	20 days into first recovery	110	200	—	—
	Oct. 15, 1975	35 days into first recovery				
	Mar. 04, 1976	Sampling supply water at injection wellhead during second injection	150	<30	—	—
	May 25, 1976	Recovered water, 22 days into second recovery	280	200	—	—
	July 18, 1977	Recovered water, first day of third backflow	<30	<30	<30	[2]

[1]MPN (most probable number) per 100 milliliters; MPN is based on multiple counts of bacteria colonies.
[2]Negative; considerable iron rust present.

APPENDIX D—WATER-QUALITY DATA OBTAINED DURING WELL CONSTRUCTION AND THE SUBSEQUENT INJECTION AND RECOVERY CYCLES AT THE HIALEAH SITE—Continued

Dissolved-Gas Analyses

[Analyses by D.H. Fisher, U.S. Geological Survey, written commun. (1975, 1977). ASR, aquifer storage and recovery; IW, injection well; OW, observation well;. —, no data]

Source	Date	Nitrogen	Oxygen	Argon	Methane	Carbon dioxide	Test status
			Pressures, in atmospheres, of Dissolved Gases at Sampling Temperature				
IW	Aug. 04, 1975	5.34	0.34	0.036	0.019	0.021	After 18 days of first injection (supply well water)[1]
	Sept. 16, 1975	.87	<.0001	.0104	.022	.0124	6 days into first recovery
	Sept. 30, 1975	.89	<.0005	—	.019	.0103	20 days into first recovery[2]
	Oct. 15, 1975	.99	<.0004	—	.017	.0088	35 days into first recovery[2]
OW	Apr. 24, 1975	1.05	<.001	.013	.0005	.0010	Background conditions in injection zone prior to ASR cycles
	Aug. 04, 1975	4.96	.61	.036	.007	.0047	After 18 days of first injection[1]
	Jan. 18, 1977	.89	<.002	—	.033	.019	Near end (after 181 days) of third injection
			Concentrations, in milligrams per liter				
IW	Aug. 04, 1975	99	14	2.1	.40	31	After 18 days of first injection (supply well water)
	Sept. 16, 1975	16	<.005	.61	.47	18	6 days into first recovery
	Sept. 30, 1975	17	<.02	—	.40	15	20 days into first recovery
	Oct. 15, 1975	19	<.02	—	.36	13	35 days into first recovery
OW	Apr. 24, 1975	21.4	<.05	.82	.012	1.7	Background conditions in injection zone prior to ASR cycles
	Aug. 04, 1975	96	26	2.17	.15	7.3	After 18 days of first injection
	Jan. 18, 1977	17	<.05	—	.72	29	Near end (after 181 days) of third injection

[1]High nitrogen pressures indicate atmospheric contamination (leaky stopcock or faulty sampling;, methane and carbon dioxide analyses should be relatively accurate; H_2S will have been oxidized.

[2]Argon added to the inner tube of the sampler.

APPENDIX D—WATER-QUALITY DATA OBTAINED DURING WELL CONSTRUCTION AND THE SUBSEQUENT INJECTION AND RECOVERY CYCLES AT THE HIALEAH SITE—Continued

Chemical Analyses of Water Samples

[mg/L, milligrams per liter; JTU, Jackson turbidity units; NTU, nephelometric turbidity units; Pt-Co, platinum cobalt units; µS/cm, microsiemens per centimeter; µg/L, micrograms per liter; mL, milliliter; g/mL, grams per milliliter, tons/acre-ft, tons per acre-feet; NO_2+NO_3, nitrate plus nitrite; ND, not detected; —, no data]

Well	Date	Time	Sampling depth (feet)	Temperature (degrees Celsius)	Agency analyzing sample (code number)	Turbidity (JTU)	Turbidity (NTU)	Color (Pt-Co)	Specific conductance (µS/cm)	Dissolved oxygen (mg/L)	Biochemical oxygen demand, 5 day (mg/L)
					During Construction						
G-3062	Nov. 20, 1974	0730	1,060	21.5	—	2	—	4	4,200	—	—
G-3061	Dec. 04, 1974	0900	1,090	21.5	—	1	—	5	4,750	—	0.9
					During First Injection						
G-3061	July 22, 1975	1000	1,110	25.5	—	6	—	55	665	—	.2
S-3000	July 22, 1975	1000	106	25.5	—	6	—	55	665	—	.2
G-3062	Aug. 04, 1975	1230	1,020	24.0	—	3	—	0	5,600	0.8	—
					During First Recovery						
G-3061	Sept. 16, 1975	0900	1,110	26.0	—	10	—	43	760	1.0	.9
	Sept. 23, 1975	0900	1,110	26.0	—	8	—	40	907	—	.5
	Sept. 30, 1975	0900	1,110	25.0	—	10	—	65	1,020	.4	.6
	Oct. 15, 1975	0930	1,110	25.0	—	10	—	10	1,460	.7	.6
					During Second Injection						
G-3061	Mar. 04, 1976	0900	1,110	26.0	—	3	—	50	657	—	—
S-3000	Mar. 04, 1976	0900	106	26.0	—	3	—	50	657	—	—
					During Second Recovery						
G-3061	May 30, 1976	1530	1,110	25.0	—	7	—	70	645	—	—
	May 25, 1976	1030	1,110	24.5	—	8	—	60	860	—	.7
	July 19, 1976	1200	1,110	24.0	—	10	—	20	1,860	—	1.3
G-3062	July 19, 1976	1210	840	26.5	—	—	—	0	8,200	—	—
	July 19, 1976	1215	957	24.5	—	—	—	0	3,110	—	—
	July 19, 1976	1220	978	25.0	—	—	—	0	3,100	—	—
	July 19, 1976	1225	999	25.0	—	—	—	0	2,860	—	—
	July 19, 1976	1230	1,020	25.0	—	—	—	0	2,630	—	—
	July 19, 1976	1235	1,040	25.0	—	—	—	0	2,960	—	—
	July 19, 1976	1240	1,060	25.5	—	—	—	5	3,370	—	—
					During Third Injection						
G-3061	Jan. 18, 1977	0800	1,110	25.0	—	2	—	40	660	—	—
S-3000	Jan. 18, 1977	0800	106	25.0	—	2	—	40	660	—	—
G-3062	Jan. 18, 1977	0830	1,060	23.5	—	30	—	0	1,060	—	—
	Jan. 18, 1977	0900	1,040	23.5	—	2	—	0	720	—	—
	Jan. 18, 1977	0930	1,020	23.5	—	2	—	0	700	—	—
	Jan. 18, 1977	0945	999	23.5	—	2	—	0	960	—	—
	Jan. 18, 1977	1000	978	23.5	—	2	—	0	1,100	—	—
	Jan. 18, 1977	1045	957	23.5	—	3	—	0	1,300	—	—
	Jan. 18, 1977	1115	840	23.0	—	4	—	0	6,020	—	—

APPENDIX D—WATER-QUALITY DATA OBTAINED DURING WELL CONSTRUCTION AND THE SUBSEQUENT INJECTION AND RECOVERY CYCLES AT THE HIALEAH SITE—Continued

Well	Date	Time	Sampling depth (feet)	Temperature (degrees Celsius)	Agency analyzing sample (code number)	Turbidity (JTU)	Turbidity (NTU)	Color (Pt-Co)	Specific conductance (μS/cm)	Dissolved oxygen (mg/L)	Biochemical oxygen demand, 5 day (mg/L)
					During Third Recovery						
G-3061	July 18, 1977	0930	1,110	26.0	—	5	—	90	708	—	—
	July 17, 1979	0930	—	22.5	80,010	—	2.0	5	3,900	—	—
G-3062	July 17, 1979	1005	957	24.0	80,010	—	1.0	5	4,260	—	—
	July 17, 1979	1025	978	24.0	80,010	—	1.0	0	4,020	—	—
	July 17, 1979	1040	1,020	24.0	80,010	—	1.0	3	4,020	—	—
	July 17, 1979	1055	999	24.0	80,010	—	1.0	1	4,070	—	—
	July 17, 1979	1108	1,040	—	80,010	—	1.0	0	4,180	—	—
	July 17, 1979	1130	1,060	24.0	80,010	—	1.0	0	4,180	—	—
	July 18, 1979	0830	840	26.5	80,010	—	1.0	2	7,300	—	—

Well	Date	Chemical oxygen demand (mg/L)	pH, field (units)	Dissolved carbon dioxide (mg/L as CO_2)	Alkalinity, field (mg/L as $CaCO_3$)	Acidity (mg/L as $CaCO_3$)	Bicarbonate, field (mg/L as HCO_3)	Carbonate, field (mg/L as CO_3)	Solids, residue at 105 degrees Celsius, total (mg/L)	Solids, volatile ignition, total (mg/L)	Oil and grease (mg/L)	Total nitrogen (mg/L as N)	Total organic nitrogen (mg/L as N)
						During Construction							
G-3062	Nov. 20, 1974	30	7.7	5.1	131	—	160	—	—	—	—	0.42	0.0
G-3061	Dec. 04, 1974	59	7.9	3.1	125	—	150	0	—	—	—	.45	.0
						During First Injection							
G-3061	July 22, 1975	—	7.2	29	240	—	290	0	—	—	0	1.3	.71
S-3000	July 22, 1975	—	7.2	29	240	—	290	0	—	—	0	1.3	.71
G-3062	Aug. 04, 1975	42	7.8	5.5	177	5	220	0	—	—	10	.70	.21
						During First Recovery							
G-3061	Sept. 16, 1975	22	7.1	46	288	29	350	0	—	—	0	1.2	.72
	Sept. 23, 1975	24	7.3	23	237	50	290	0	556	—	0	1.1	.60
	Sept. 30, 1975	37	7.1	42	262	40	320	0	651	—	0	1.1	.64
	Oct. 15, 1975	31	7.3	25	249	40	300	0	935	—	0	1.0	.47
						During Second Injection							
G-3061	Mar. 04, 1976	46	6.8	76	246	142	300	0	398	136	0	1.5	.87
S-3000	Mar. 04, 1976	46	6.8	76	246	142	300	0	398	136	0	1.5	.87
						During Second Recovery							
G-3061	May 03, 1976	—	7.4	18	237	—	290	0	—	—	—	1.4	.86
	May 25, 1976	26	7.1	43	269	55	330	0	522	143	0	1.5	1.0
	July 19, 1976	28	7.2	31	256	—	310	0	—	—	0	.80	.24
G-3062	July 19, 1976	—	6.8	38	125	—	150	0	—	—	—	—	—
	July 19, 1976	—	7.3	20	207	—	250	0	—	—	—	—	—
	July 19, 1976	—	7.2	29	239	—	290	0	—	—	—	—	—
	July 19, 1976	—	7.5	13	203	—	250	0	—	—	—	—	—
	July 19, 1976	—	6.8	71	233	—	280	0	—	—	—	—	—
	July 19, 1976	—	7.4	18	230	—	280	0	—	—	—	—	—
	July 19, 1976	—	7.6	11	223	—	270	0	—	—	—	—	—

APPENDIX D—WATER-QUALITY DATA OBTAINED DURING WELL CONSTRUCTION AND THE SUBSEQUENT INJECTION AND RECOVERY CYCLES AT THE HIALEAH SITE—Continued

Well	Date	Chemical oxygen demand (mg/L)	pH, field (units)	Dissolved carbon dioxide (mg/L as CO_2)	Alkalinity, field (mg/L as $CaCO_3$)	Acidity (mg/L as $CaCO_3$)	Bicarbonate, field (mg/L as HCO_3)	Carbonate, field (mg/L as CO_3)	Solids, residue at 105 degrees Celsius, total (mg/L)	Solids, volatile ignition, total (mg/L)	Oil and grease (mg/L)	Total nitrogen (mg/L as N)	Total organic nitrogen (mg/L as N)
					During Third Injection								
G-3061	Jan. 18, 1977	—	7.2	28	227	—	280	0	—	—	—	1.2	.60
S-3000	Jan. 18, 1977	—	7.2	28	227	—	280	0	—	—	—	1.2	.60
G-3062	Jan. 18, 1977	—	7.2	36	295	—	360	0	—	—	—	.79	.30
	Jan. 18, 1977	—	7.2	36	289	—	350	0	—	—	—	.82	.30
	Jan. 18, 1977	—	7.2	36	262	—	360	0	—	—	—	.97	.37
	Jan. 18, 1977	—	7.2	40	325	—	400	0	—	—	—	.97	.43
	Jan. 18, 1977	—	7.2	39	315	—	380	0	—	—	—	.97	.47
	Jan. 18, 1977	—	7.2	32	259	—	320	0	—	—	—	.72	.34
	Jan. 18, 1977	—	8.5	1.1	174	—	190	12	—	—	—	.81	.15
					During Third Recovery								
G-3061	July 18, 1977	40	7.2	28	230	—	280	0	—	—	—	1.4	.74
	July 17, 1979	—	7.7	5.6	140	—	180	0	—	—	—	1.1	.72
G-3062	July 17, 1979	—	7.7	5.6	140	—	180	0	—	—	—	1.1	.66
	July 17, 1979	—	7.7	5.4	140	—	170	0	—	—	—	1.1	.72
	July 17, 1979	—	7.7	5.1	130	—	160	0	—	—	—	.86	.50
	July 17, 1979	—	7.6	6.4	130	—	160	0	—	—	—	.87	.48
	July 17, 1979	—	7.8	4.1	130	—	160	0	—	—	—	.96	.57
	July 17, 1979	—	8.1	2.0	130	—	160	0	—	—	—	.96	.55
	July 18, 1979	—	8.6	.9	180	—	180	20	—	—	—	1.9	1.0

Well	Date	Dissolved organic nitrogen (mg/L as N)	Dissolved ammonia nitrogen (mg/L as N)	Total ammonia nitrogen (mg/L as N)	Dissolved nitrite nitrogen (mg/L as N)	Total nitrite nitrogen (mg/L as N)	Dissolved nitrate nitrogen (mg/L as N)	Total nitrate nitrogen (mg/L as N)	Dissolved ammonia + organic nitrogen (mg/L as N)	Total ammonia + organic nitrogen (mg/L as N)	Total NO_2+NO_3 nitrogen (mg/L as N)	Dissolved NO_2+NO_3 nitrogen (mg/L as N)
						During Construction						
G-3062	Nov. 20, 1974	—	—	0.42	—	<0.01	—	0.00	—	0.42	<0.10	—
G-3061	Dec. 04, 1974	—	—	.45	—	<.01	—	.00	—	.45	<.10	—
						During First Injection						
G-3061	July 22, 1975	—	—	.50	—	<.01	—	.14	—	1.2	.14	—
S-3000	July 22, 1975	—	—	.50	—	<.01	—	.14	—	1.2	.14	—
G-3062	Aug. 04, 1975	—	—	.47	—	.01	—	.01	—	.68	.02	—
						During First Recovery						
G-3061	Sept. 16, 1975	—	—	.49	—	<.01	—	.00	—	1.2	<.10	—
	Sept. 23, 1975	—	—	.51	—	<.01	—	.00	—	1.1	<.10	—
	Sept. 30, 1975	—	—	.48	—	<.01	—	.03	—	1.1	.03	—
	Oct. 15, 1975	—	—	.55	—	<.01	—	.03	—	1.0	.03	—
						During Second Injection						
G-3061	Mar. 04, 1976	0.78	0.57	.58	0.01	.01	0.00	.01	1.3	1.5	.02	0.01
S-3000	Mar. 04, 1976	.78	.57	.58	.01	.01	.00	.01	1.3	1.5	.02	.01

APPENDIX D—WATER-QUALITY DATA OBTAINED DURING WELL CONSTRUCTION AND THE SUBSEQUENT INJECTION AND RECOVERY CYCLES AT THE HIALEAH SITE—Continued

Well	Date	Dissolved organic nitrogen (mg/L as N)	Dissolved ammonia nitrogen (mg/L as N)	Total ammonia nitrogen (mg/L as N)	Dissolved nitrite nitrogen (mg/L as N)	Total nitrite nitrogen (mg/L as N)	Dissolved nitrate nitrogen (mg/L as N)	Total nitrate nitrogen (mg/L as N)	Dissolved ammonia + organic nitrogen (mg/L as N)	Total ammonia + organic nitrogen (mg/L as N)	Total NO_2+NO_3 nitrogen (mg/L as N)	Dissolved NO_2+NO_3 nitrogen (mg/L as N)
					During Second Recovery							
G-3061	May 03, 1976	—	—	.54	—	<.01	—	.01	—	1.4	.01	—
	May 25, 1976	1.0	.50	.50	.01	<.01	.01	.01	1.5	1.5	.01	.10
	July 19, 1976	—	—	.56	—	<.01	—	.00	—	.80	<.10	—
G-3062	July 19, 1976	—	—	—	—	—	—	—	—	—	—	—
	July 19, 1976	—	—	—	—	—	—	—	—	—	—	—
	July 19, 1976	—	—	—	—	—	—	—	—	—	—	—
	July 19, 1976	—	—	—	—	—	—	—	—	—	—	—
	July 19, 1976	—	—	—	—	—	—	—	—	—	—	—
	July 19, 1976	—	—	—	—	—	—	—	—	—	—	—
	July 19, 1976	—	—	—	—	—	—	—	—	—	—	—
					During Third Injection							
G-3061	Jan. 18, 1977	—	—	.60	—	<.01	—	.05	—	1.2	.05	—
S-3000	Jan. 18, 1977	—	—	.60	—	<.01	—	.05	—	1.2	.05	—
G-3062	Jan. 18, 1977	—	—	.48	—	.01	—	.00	—	.78	.01	—
	Jan. 18, 1977	—	—	.52	—	<.01	—	.00	—	.82	<.10	—
	Jan. 18, 1977	—	—	.60	—	<.01	—	.00	—	.97	<.10	—
	Jan. 18, 1977	—	—	.54	—	<.01	—	.00	—	.97	<.10	—
	Jan. 18, 1977	—	—	.50	—	<.01	—	.00	—	.97	<.10	—
	Jan. 18, 1977	—	—	.38	—	<.01	—	.00	—	.72	<.10	—
	Jan. 18, 1977	—	—	.66	—	<.01	—	.00	—	.81	<.10	—
					During Third Recovery							
G-3061	July 18, 1977	—	—	.68	—	<.01	—	.00	—	1.4	<.10	—
	July 17, 1979	—	—	.38	—	<.01	—	.00	—	1.1	<.10	—
G-3062	July 17, 1979	—	—	.45	—	<.01	—	.01	—	1.1	.01	—
	July 17, 1979	—	—	.39	—	<.01	—	.01	—	1.1	.01	—
	July 17, 1979	—	—	.35	—	<.01	—	.01	—	.85	.01	—
	July 17, 1979	—	—	.38	—	<.01	—	.01	—	.86	.01	—
	July 17, 1979	—	—	.38	—	<.01	—	.01	—	.95	.01	—
	July 17, 1979	—	—	.40	—	<.01	—	.01	—	.95	.01	—
	July 18, 1979	—	—	.86	—	<.01	—	.01	—	1.9	.01	—

Well	Date	Dissolved ortho phosphate (mg/L as PO_4)	Total phosphorus (mg/L as P)	Dissolved phosphorus (mg/L as P)	Dissolved ortho phosphorus (mg/L as P)	Total organic carbon (mg/L as C)	Dissolved organic carbon (mg/L as C)	Total cyanide (mg/L as Cn)	Total hardness (mg/L as $CaCO_3$)	Total noncarbonate hardness, field (mg/L as $CaCO_3$)	Dissolved calcium (mg/L as Ca)	Dissolved magnesium (mg/L as Mg)
						During Construction						
G-3062	Nov. 20, 1974	—	0.01	—	—	3	—	—	660	530	100	100
G-3061	Dec. 04, 1974	—	.01	—	—	5	—	—	740	620	100	120
						During First Injection						
G-3061	July 22, 1975	—	.03	—	—	12	—	0.01	260	18	89	8.4
S-3000	July 22, 1975	—	.03	—	—	12	—	.01	260	18	89	8.4
G-3062	Aug. 04, 1975	—	.01	—	—	2	—	.00	580	440	84	88

APPENDIX D—WATER-QUALITY DATA OBTAINED DURING WELL CONSTRUCTION AND THE SUBSEQUENT INJECTION AND RECOVERY CYCLES AT THE HIALEAH SITE—Continued

Well	Date	Dissolved ortho phosphate (mg/L as PO_4)	Total phosphorus (mg/L as P)	Dissolved phosphorus (mg/L as P)	Dissolved ortho phosphorus (mg/L as P)	Total organic carbon (mg/L as C)	Dissolved organic carbon (mg/L as C)	Total cyanide (mg/L as Cn)	Total hardness (mg/L as $CaCO_3$)	Total noncarbonate hardness, field (mg/L as $CaCO_3$)	Dissolved calcium (mg/L as Ca)	Dissolved magnesium (mg/L as Mg)
					During First Recovery							
G-3061	Sept. 16, 1975	—	.03	—	—	8	7	.00	280	40	92	12
	Sept. 23, 1975	—	.01	—	—	8	8	.00	300	66	91	18
	Sept. 30, 1975	—	.02	—	—	9	8	.00	310	70	88	21
	Oct. 15, 1975	—	.01	—	—	13	8	.00	360	130	89	32
					During Second Injection							
G-3061	Mar. 04/, 1976	0.09	.03	0.03	0.03	15	14	.00	260	30	90	8.4
S-3000	Mar. 04, 1976	.09	.03	.03	.03	15	14	.00	260	30	90	8.4
					During Second Recovery							
G-3061	May 03, 1976	—	.03	—	—	11	9	—	250	3	84	8.4
	May 25, 1976	.00	.01	.01	<.01	11	11	.00	280	58	84	17
	July 19, 1976	—	.01	—	—	7	7	.00	400	0	87	42
G-3062	July 19, 1976	—	—	—	—	—	—	—	520	390	40	100
	July 19, 1976	—	—	—	—	—	—	—	540	330	81	79
	July 19, 1976	—	—	—	—	—	—	—	540	300	81	80
	July 19, 1976	—	—	—	—	—	—	—	510	310	78	74
	July 19, 1976	—	—	—	—	—	—	—	490	260	78	70
	July 19, 1976	—	—	—	—	—	—	—	530	300	76	80
	July 19, 1976	—	—	—	—	—	—	—	550	330	77	86
					During Third Injection							
G-3061	Jan. 18, 1977	—	.02	—	—	16	—	—	250	26	87	8.4
S-3000	Jan. 18, 1977	—	.02	—	—	16	—	—	250	26	87	8.4
G-3061	Jan. 18, 1977	—	.01	—	—	7	—	—	320	25	73	31
	Jan. 18, 1977	—	.01	—	—	7	—	—	270	0	73	19
	Jan. 18, 1977	—	.01	—	—	11	—	—	260	0	79	15
	Jan. 18, 1977	—	.01	—	—	10	—	—	280	0	78	21
	Jan. 18, 1977	—	.01	—	—	8	—	—	340	25	69	40
	Jan. 18, 1977	—	.01	—	—	6	—	—	300	41	77	25
	Jan. 18, 1977	—	.01	—	—	3	—	—	630	460	51	120
					During Third Recovery							
G-3061	July 18, 1977	—	.02	—	—	27	—	—	250	22	86	8.8
	July 17, 1979	—	.01	—	—	14	—	—	630	490	83	100
G-3062	July 17, 1979	—	.01	—	—	3	—	—	670	520	82	110
	July 17, 1979	—	.01	—	—	11	—	—	640	500	88	100
	July 17, 1979	—	.01	—	—	10	—	—	640	510	88	100
	July 17, 1979	—	.01	—	—	8	—	—	630	500	84	100
	July 17, 1979	—	.01	—	—	17	—	—	680	550	88	110
	July 17, 1979	—	.01	—	—	12	—	—	680	550	87	110
	July 18, 1979	—	.01	—	—	5	—	—	680	500	71	120

APPENDIX D—WATER-QUALITY DATA OBTAINED DURING WELL CONSTRUCTION AND THE SUBSEQUENT INJECTION AND RECOVERY CYCLES AT THE HIALEAH SITE—Continued

Well	Date	Dissolved sodium (mg/L as Na)	Sodium adsorption ratio	Sodium percentage	Dissolved sodium + potassium (mg/L as Na)	Dissolved potassium (mg/L as K)	Dissolved chloride (mg/L as Cl)	Dissolved sulfate (mg/L as SO_4)	Dissolved fluoride (mg/L as F)	Dissolved silica (mg/L as SiO_2)	Dissolved arsenic (µg/L as As)	Total suspended arsenic (µg/L as As)
					During Construction							
G-3062	Nov. 20, 1974	700	12	68	—	32	1,200	480	1.2	14	—	—
G-3061	Dec. 04, 1974	700	11	66	—	35	1,200	500	1.1	14	—	—
					During First Injection							
G-3061	July 22, 1975	43	1	26	—	2.2	68	10	.3	7.2	2	<1
S-3000	July 22, 1975	43	1	26	—	2.2	68	10	.3	7.2	2	<1
G-3062	Aug. 04, 1975	640	12	69	—	34	1,300	410	1.3	16	<1	<1
					During First Recovery							
G-3061	Sept. 16, 1975	54	1	29	—	2.4	89	20	.4	7.6	1	<1
	Sept. 23, 1975	76	2	35	—	3.3	120	35	.7	8.0	1	<1
	Sept. 30, 1975	100	2	41	—	3.8	170	46	.5	8.5	<1	<1
	Oct. 15, 1975	180	4	52	—	7.0	280	100	.9	9.2	<1	1
					During Second Injection							
G-3061	Mar. 04, 1976	40	1	25	—	1.7	65	7.1	.4	7.3	2	<1
S-3000	Mar. 04, 1976	40	1	25	—	1.7	65	7.1	.4	7.3	2	<1
					During Second Recovery							
G-3061	May 03, 1976	41	1	27	—	2.0	65	8.0	.3	6.9	—	—
	May 25, 1976	70	2	35	—	2.9	120	27	.5	7.9	<1	<1
	July 19, 1976	230	5	55	—	10	390	140	.8	10	<1	1
G-3062	July 19, 1976	1,600	31	87	—	11	2,300	760	1.7	5.4	—	—
	July 19, 1976	430	8	62	—	27	720	310	1.3	13	—	—
	July 19, 1976	430	8	63	—	22	720	320	1.3	13	—	—
	July 19, 1976	380	7	61	—	20	650	270	1.2	12	—	—
	July 19, 1976	350	7	60	—	19	580	250	1.2	12	—	—
	July 19, 1976	410	8	62	—	22	690	310	1.2	13	—	—
	July 19, 1976	480	9	64	—	27	790	360	1.3	15	—	—
					During Third Injection							
G-3061	Jan. 18, 1977	46	1	28	—	2.1	79	11	.3	7.1	—	—
S-3000	Jan. 18, 1977	46	1	28	—	2.1	79	11	.3	7.1	—	—
G-3062	Jan. 18, 1977	110	3	43	—	6.6	170	80	.9	9.0	—	—
	Jan. 18, 1977	50	1	29	—	3.0	79	21	.9	7.6	—	—
	Jan. 18, 1977	46	1	28	—	2.5	76	13	.7	7.2	—	—
	Jan. 18, 1977	76	2	37	—	4.7	130	46	.8	8.1	—	—
	Jan. 18, 1977	140	3	47	—	4.8	200	140	1.0	11	—	—
	Jan. 18, 1977	100	3	42	—	6.6	170	69	.8	8.6	—	—
	Jan. 18, 1977	1,200	21	79	—	70	1,700	600	2.4	14	—	—
					During Third Recovery							
G-3061	July 18, 1977	48	1	29	—	2.2	79	6.6	.2	7.6	—	—
	July 17, 1979	630	11	68	—	26	990	430	1.0	12	—	—
G-3062	July 17, 1979	700	12	69	—	31	1,100	460	1.2	15	—	—
	July 17, 1979	650	11	68	680	28	1,100	440	1.2	13	—	—
	July 17, 1979	640	11	68	—	27	1,000	440	1.2	13	—	—
	July 17, 1979	640	11	68	—	26	1,000	440	1.2	13	—	—
	July 17, 1979	680	11	68	—	28	1,100	460	1.2	13	—	—
	July 17, 1979	680	11	68	—	28	1,100	460	1.2	13	—	—
	July 18, 1979	1,700	29	83	—	64	2,100	780	1.9	23	—	—

APPENDIX D—WATER-QUALITY DATA OBTAINED DURING WELL CONSTRUCTION AND THE SUBSEQUENT INJECTION AND RECOVERY CYCLES AT THE HIALEAH SITE—Continued

Well	Date	Total arsenic (µg/L as As)	Dissolved barium (µg/L as Ba)	Total recoverable barium (µg/L as Ba)	Dissolved boron (µg/L as B)	Total recoverable boron (µg/L as B)	Dissolved cadmium (µg/L as Cd)	Suspended recoverable cadmium (µg/L as Cd)	Total recoverable cadmium (µg/L as Cd)	Dissolved chromium (µg/L as Cr)	Suspended recoverable chromium (µg/L as Cr)	Dissolved hexavalent chromium (µg/L as Cr)
						During Construction						
G-3062	Nov. 20, 1974	<1	—	—	—	—	—	—	5	—	—	0
G-3061	Dec. 04, 1974	<1	—	—	—	—	—	—	5	—	—	0
						During First Injection						
G-3061	July 22, 1975	2	<100	—	70	—	ND	0	ND	ND	<10	—
S-3000	July 22, 1975	2	<100	—	70	—	ND	0	ND	ND	<10	—
G-3062	Aug. 04, 1975	<1	<100	—	480	—	<2.0	0	<2	ND	<10	—
						During First Recovery						
G-3061	Sept. 16, 1975	1	<100	—	70	—	ND	0	ND	ND	<10	—
	Sept. 23, 1975	1	<100	—	90	—	ND	0	ND	ND	10	—
	Sept. 30, 1975	<1	10	—	110	—	ND	0	ND	ND	10	—
	Oct. 15, 1975	1	<100	—	170	—	ND	0	ND	ND	<10	—
						During Second Injection						
G-3061	Mar. 04, 1976	2	<100	—	80	—	ND	2	2	<20	10	—
S-3000	Mar. 04, 1976	2	<100	—	80	—	ND	2	2	<20	10	—
						During Second Recovery						
G-3061	May 03, 1976	—	—	—	—	—	—	—	—	—	—	—
	May 25, 1976	<1	<100	—	110	—	<2.0	0	<2	ND	<10	—
	July 19, 1976	1	<100	<100	190	410	ND	1	<2	ND	20	—
G-3062	July 19, 1976	—	—	—	—	—	—	—	—	—	—	—
	July 19, 1976	—	—	—	—	—	—	—	—	—	—	—
	July 19, 1976	—	—	—	—	—	—	—	—	—	—	—
	July 19, 1976	—	—	—	—	—	—	—	—	—	—	—
	July 19, 1976	—	—	—	—	—	—	—	—	—	—	—
	July 19, 1976	—	—	—	—	—	—	—	—	—	—	—
	July 19, 1976	—	—	—	—	—	—	—	—	—	—	—
						During Third Injection						
G-3061	Jan. 18, 1977	—	—	<100	—	—	—	—	—	—	—	—
S-3000	Jan. 18, 1977	—	—	<100	—	—	—	—	—	—	—	—
G-3062	Jan. 18, 1977	—	—	—	—	—	—	—	—	—	—	—
	Jan. 18, 1977	—	—	—	—	—	—	—	—	—	—	—
	Jan. 18, 1977	—	—	—	—	—	—	—	—	—	—	—
	Jan. 18, 1977	—	—	—	—	—	—	—	—	—	—	—
	Jan. 18, 1977	—	—	—	—	—	—	—	—	—	—	—
	Jan. 18, 1977	—	—	—	—	—	—	—	—	—	—	—
	Jan. 18, 1977	—	—	—	—	—	—	—	—	—	—	—
						During Third Recovery						
G-3061	July 18, 1977	—	—	—	—	—	—	—	—	—	—	—
	July 17, 1979	—	—	—	—	—	—	—	—	—	—	—
G-3062	July 17, 1979	—	—	—	—	—	—	—	—	—	—	—
	July 17, 1979	—	—	—	—	—	—	—	—	—	—	—
	July 17, 1979	—	—	—	—	—	—	—	—	—	—	—
	July 17, 1979	—	—	—	—	—	—	—	—	—	—	—
	July 17, 1979	—	—	—	—	—	—	—	—	—	—	—
	July 17, 1979	—	—	—	—	—	—	—	—	—	—	—
	July 18, 1979	—	—	—	—	—	—	—	—	—	—	—

APPENDIX D—WATER-QUALITY DATA OBTAINED DURING WELL CONSTRUCTION AND THE SUBSEQUENT INJECTION AND RECOVERY CYCLES AT THE HIALEAH SITE—Continued

Well	Date	Total recoverable chromium (µg/L as Cr)	Dissolved copper (µg/L as Cu)	Suspended recoverable copper (µg/L as Cu)	Total recoverable copper (µg/L as Cu)	Suspended recoverable iron (µg/L as Fe)	Total recoverable iron (µg/L as Fe)	Dissolved iron (µg/L as Fe)	Dissolved lead (µg/L as Pb)	Suspended recoverable lead (µg/L as Pb)	Total recoverable lead (µg/L as Pb)	Suspended recoverable manganese (µg/L as Mn)
					During Construction							
G-3062	Nov. 20, 1974	<20	—	—	<2	—	—	—	—	—	3	—
G-3061	Dec. 04, 1974	20	—	—	ND	—	—	—	—	—	ND	—
					During First Injection							
G-3061	July 22, 1975	<20	<20	0	<20	—	810	760	ND	4	4	20
S-3000	July 22, 1975	<20	<20	0	<20	—	810	760	ND	4	4	20
G-3062	Aug. 04, 1975	<20	ND	1	<2	—	110	100	7	3	10	6
					During First Recovery							
G-3061	Sept. 16, 1975	<20	ND	1	<2	—	1,900	1,900	<2	3	4	10
	Sept. 23, 1975	<20	2	1	3	—	1,700	1,700	6	2	8	10
	Sept. 30, 1975	<20	2	2	4	—	1,700	1,600	2	4	6	20
	Oct. 15, 1975	<20	ND	5	5	—	1,600	1,600	11	0	11	0
					During Second Injection							
G-3061	Mar. 04, 1976	20	3	0	3	—	930	870	7	8	15	0
S-3000	Mar. 04, 1976	20	3	0	3	—	930	870	7	8	15	0
					During Second Recovery							
G-3061	May 03, 1976	—	—	—	—	—	—	—	—	—	—	—
	May 25, 1976	<20	ND	6	6	—	2,000	1,800	18	18	36	10
	July 19, 1976	20	ND	2	2	—	1,300	1,200	4	0	4	10
G-3062	July 19, 1976	—	—	—	—	—	—	—	—	—	—	—
	July 19, 1976	—	—	—	—	—	—	—	—	—	—	—
	July 19, 1976	—	—	—	—	—	—	—	—	—	—	—
	July 19, 1976	—	—	—	—	—	—	—	—	—	—	—
	July 19, 1976	—	—	—	—	—	—	—	—	—	—	—
	July 19, 1976	—	—	—	—	—	—	—	—	—	—	—
	July 19, 1976	—	—	—	—	—	—	—	—	—	—	—
					During Third Injection							
G-3061	Jan. 18, 1977	—	—	—	—	—	—	830	—	—	—	—
S-3000	Jan. 18, 1977	—	—	—	—	—	—	830	—	—	—	—
G-3062	Jan. 18, 1977	—	—	—	—	—	—	—	—	—	—	—
	Jan. 18, 1977	—	—	—	—	—	—	—	—	—	—	—
	Jan. 18, 1977	—	—	—	—	—	—	—	—	—	—	—
	Jan. 18, 1977	—	—	—	—	—	—	—	—	—	—	—
	Jan. 18, 1977	—	—	—	—	—	—	—	—	—	—	—
	Jan. 18, 1977	—	—	—	—	—	—	—	—	—	—	—
	Jan. 18, 1977	—	—	—	—	—	—	—	—	—	—	—
					During Third Recovery							
G-3061	July 18, 1977	—	—	—	—	—	2,200	—	—	—	—	—
	July 17, 1979	—	—	—	—	110	210	100	—	—	—	—
G-3062	July 17, 1979	—	—	—	—	110	150	40	—	—	—	—
	July 17, 1979	—	—	—	—	60	110	50	—	—	—	—
	July 17, 1979	—	—	—	—	70	110	40	—	—	—	—
	July 17, 1979	—	—	—	—	70	110	40	—	—	—	—
	July 17, 1979	—	—	—	—	40	80	40	—	—	—	—
	July 17, 1979	—	—	—	—	280	350	70	—	—	—	—
	July 18, 1979	—	—	—	—	80	150	70	—	—	—	—

APPENDIX D—WATER-QUALITY DATA OBTAINED DURING WELL CONSTRUCTION AND THE SUBSEQUENT INJECTION AND RECOVERY CYCLES AT THE HIALEAH SITE—Continued

Well	Date	Total recoverable manganese (µg/L as Mn)	Dissolved manganese (µg/L as Mn)	Dissolved molybdenum (µg/L as Mo)	Dissolved nickel (µg/L as Ni)	Suspended recoverable nickel (µg/L as Ni)	Total recoverable nickel (µg/L as Ni)	Dissolved silver (µg/L as Ag)	Total recoverable silver (µg/L as Ag)	Dissolved strontium (µg/L as Sr)	Dissolved zinc (µg/L as Zn)	Suspended recoverable zinc (µg/L as Zn)
					During Construction							
G-3062	Nov. 20, 1974	—	—	—	—	—	—	—	—	—	—	—
G-3061	Dec. 04, 1974	—	—	—	—	—	—	—	—	—	—	—
					During First Injection							
G-3061	July 22, 1975	20	<10	2	ND	4	4	ND	—	940	<20	0
S-3000	July 22, 1975	20	<10	2	ND	4	4	ND	—	940	<20	0
G-3062	Aug. 04, 1975	<10	4	<1	ND	—	ND	ND	—	7,800	<20	20
					During First Recovery							
G-3061	Sept. 16, 1975	30	20	<1	ND	0	ND	ND	—	1,000	4	20
	Sept. 23, 1975	30	20	<1	ND	0	ND	—	—	1,600	20	0
	Sept. 30, 1975	30	<10	<1	ND	3	3	—	—	2,000	40	30
	Oct. 15, 1975	30	30	<1	ND	5	5	—	—	4,500	20	0
					During Second Injection							
G-3061	Mar. 04, 1976	<10	<10	<1	2	0	2	—	—	780	<20	30
S-3000	Mar. 04, 1976	<10	<10	<1	2	0	2	—	—	780	<20	30
					During Second Recovery							
G-3061	May 03, 1976	—	—	—	—	—	—	—	—	960	—	—
	May 25, 1976	<10	<10	<1	ND	10	10	—	—	1,400	ND	30
	July 19, 1976	20	<10	<1	ND	4	4	ND	ND	4,400	<20	50
G-3062	July 19, 1976	—	—	—	—	—	—	—	—	3,700	—	—
	July 19, 1976	—	—	—	—	—	—	—	—	7,800	—	—
	July 19, 1976	—	—	—	—	—	—	—	—	8,300	—	—
	July 19, 1976	—	—	—	—	—	—	—	—	8,000	—	—
	July 19, 1976	—	—	—	—	—	—	—	—	8,200	—	—
	July 19, 1976	—	—	—	—	—	—	—	—	7,900	—	—
	July 19, 1976	—	—	—	—	—	—	—	—	7,200	—	—
					During Third Injection							
G-3061	Jan. 18, 1977	—	—	—	—	—	—	—	—	900	—	—
S-3000	Jan. 18, 1977	—	—	—	—	—	—	—	—	900	—	—
G-3062	Jan. 18, 1977	—	—	—	—	—	—	—	—	5,100	—	—
	Jan. 18, 1977	—	—	—	—	—	—	—	—	4,500	—	—
	Jan. 18, 1977	—	—	—	—	—	—	—	—	2,800	—	—
	Jan. 18, 1977	—	—	—	—	—	—	—	—	3,100	—	—
	Jan. 18, 1977	—	—	—	—	—	—	—	—	3,700	—	—
	Jan. 18, 1977	—	—	—	—	—	—	—	—	3,200	—	—
	Jan. 18, 1977	—	—	—	—	—	—	—	—	4,400	—	—
					During Third Recovery							
G-3061	July 18, 1977	—	—	—	—	—	—	—	—	1,000	—	—
	July 17, 1979	—	—	—	—	—	—	—	—	9,000	—	—
G-3062	July 17, 1979	—	—	—	—	—	—	—	—	9,000	—	—
	July 17, 1979	—	—	—	—	—	—	—	—	10,000	—	—
	July 17, 1979	—	—	—	—	—	—	—	—	10,000	—	—
	July 17, 1979	—	—	—	—	—	—	—	—	10,000	—	—
	July 17, 1979	—	—	—	—	—	—	—	—	10,000	—	—
	July 17, 1979	—	—	—	—	—	—	—	—	10,000	—	—
	July 18, 1979	—	—	—	—	—	—	—	—	8,000	—	—

APPENDIX D—WATER-QUALITY DATA OBTAINED DURING WELL CONSTRUCTION AND THE SUBSEQUENT INJECTION AND RECOVERY CYCLES AT THE HIALEAH SITE—Continued

Well	Date	Total recoverable zinc (µg/L as Zn)	Total recoverable aluminum (µg/L as Al)	Dissolved aluminum (µg/L as Al)	Suspended recoverable aluminum (µg/L as Al)	Dissolved selenium (µg/L as Se)	Total suspended selenium (µg/L as Se)	Total selenium (µg/L as Se)	Coliforms per 100 mL			Total phenols (µg/L)
									Total coliform	Fecal coliform	Fecal streptococci	
During Construction												
G-3062	Nov. 20, 1974	ND	--	--	--	--	--	--	<2	<2	<2	--
G-3061	Dec. 04, 1974	100	--	--	--	--	--	--	<2	<1	<1	--
During First Injection												
G-3061	July 22, 1975	<20	30	<100	30	<1	0	<1	<2	<1	<1	0
S-3000	July 22, 1975	<20	30	<100	30	<1	0	<1	<2	<1	<1	0
G-3062	Aug. 04, 1975	30	20	9	10	<1	0	<1	--	--	--	0
During First Recovery												
G-3061	Sept. 16, 1975	20	<100	<100	0	<1	0	<1	<1	<1	<2	2
	Sept. 23, 1975	20	60	30	30	<1	0	<1	<1	<1	<2	0
	Sept. 30, 1975	70	10	<100	10	<1	0	<1	--	--	--	1
	Oct. 15, 1975	20	50	20	30	<1	0	<1	--	--	--	1
During Second Injection												
G-3061	Mar. 04, 1976	40	10	10	0	<1	0	<1	--	--	--	1
S-3000	Mar. 04, 1976	40	10	10	0	<1	0	<1	--	--	--	1
During Second Recovery												
G-3061	May 03, 1976	--	--	--	--	--	--	--	--	--	--	--
	May 25, 1976	30	10	10	0	<1	--	2	--	--	--	1
	July 19, 1976	60	50	20	30	<1	0	<1	<1	<1	<1	4
G-3062	July 19, 1976	--	--	--	--	--	--	--	--	--	--	--
	July 19, 1976	--	--	--	--	--	--	--	--	--	--	--
	July 19, 1976	--	--	--	--	--	--	--	--	--	--	--
	July 19, 1976	--	--	--	--	--	--	--	--	--	--	--
	July 19, 1976	--	--	--	--	--	--	--	--	--	--	--
	July 19, 1976	--	--	--	--	--	--	--	--	--	--	--
	July 19, 1976	--	--	--	--	--	--	--	--	--	--	--
During Third Injection												
G-3061	Jan. 18, 1977	--	--	--	--	--	--	--	--	--	--	0
S-3000	Jan. 18, 1977	--	--	--	--	--	--	--	--	--	--	0
G-3062	Jan. 18, 1977	--	--	--	--	--	--	--	--	--	--	--
	Jan. 18, 1977	--	--	--	--	--	--	--	--	--	--	--
	Jan. 18, 1977	--	--	--	--	--	--	--	--	--	--	--
	Jan. 18, 1977	--	--	--	--	--	--	--	--	--	--	--
	Jan. 18, 1977	--	--	--	--	--	--	--	--	--	--	--
	Jan. 18, 1977	--	--	--	--	--	--	--	--	--	--	--
	Jan. 18, 1977	--	--	--	--	--	--	--	--	--	--	--
During Third Recovery												
G-3061	July 18, 1977	--	--	--	--	--	--	--	--	--	--	--
	July 17, 1979	--	--	--	--	--	--	--	--	--	--	--
G-3062	July 17, 1979	--	--	--	--	--	--	--	--	--	--	--
	July 17, 1979	--	--	--	--	--	--	--	--	--	--	--
	July 17, 1979	--	--	--	--	--	--	--	--	--	--	--
	July 17, 1979	--	--	--	--	--	--	--	--	--	--	--
	July 17, 1979	--	--	--	--	--	--	--	--	--	--	--
	July 17, 1979	--	--	--	--	--	--	--	--	--	--	--
	July 18, 1979	--	--	--	--	--	--	--	--	--	--	--

APPENDIX D—WATER-QUALITY DATA OBTAINED DURING WELL CONSTRUCTION AND THE SUBSEQUENT INJECTION AND RECOVERY CYCLES AT THE HIALEAH SITE—Continued

Well	Date	Methylene blue active substance (mg/L)	Total polychlorinated naphthalenes (µg/L)	Total aldrin (µg/L)	Total lindane (µg/L)	Total chlordane (µg/L)	Total DDD (µg/L)	Total DDE (µg/L)	Total DDT (µg/L)	Total dieldrin (µg/L)	Endrin water unfiltered (µg/L)	Total ethion (µg/L)
					During Construction							
G-3062	Nov. 20, 1974	—	—	—	—	—	—	—	—	—	—	—
G-3061	Dec. 04, 1974	—	—	—	—	—	—	—	—	—	—	—
					During First Injection							
G-3061	July 22, 1975	0.0	—	0.0	0.0	0	0.0	0.0	0.0	0.0	0.0	—
S-3000	July 22, 1975	.0	—	.0	.0	0	.0	.0	.0	.0	.0	—
G-3062	Aug. 04, 1975	.1	0.0	.0	.0	0	.0	.0	.0	.0	.0	—
					During First Recovery							
G-3061	Sept. 16, 1975	.0	—	—	—	—	—	—	—	—	—	—
	Sept. 23, 1975	.0	—	—	—	—	—	—	—	—	—	—
	Sept. 30, 1975	.2	—	—	—	—	—	—	—	—	—	—
	Oct. 15, 1975	.0	—	—	—	—	—	—	—	—	—	—
					During Second Injection							
G-3061	Mar. 04, 1976	.0	—	—	—	—	—	—	—	—	—	—
S-3000	Mar. 04, 1976	.0	—	—	—	—	—	—	—	—	—	—
					During Second Recovery							
G-3061	May 03, 1976	—	—	—	—	—	—	—	—	—	—	—
	May 25, 1976	.1	.0	.0	.0	0	.0	.0	.0	.0	.0	—
	July 19, 1976	.1	.0	.0	.0	0	.0	.0	.0	.0	.0	0.0
G-3062	July 19, 1976	—	—	—	—	—	—	—	—	—	—	—
	July 19, 1976	—	—	—	—	—	—	—	—	—	—	—
	July 19, 1976	—	—	—	—	—	—	—	—	—	—	—
	July 19, 1976	—	—	—	—	—	—	—	—	—	—	—
	July 19, 1976	—	—	—	—	—	—	—	—	—	—	—
	July 19, 1976	—	—	—	—	—	—	—	—	—	—	—
	July 19, 1976	—	—	—	—	—	—	—	—	—	—	—
					During Third Injection							
G-3061	Jan. 18, 1977	.1	—	—	—	—	—	—	—	—	—	—
S-3000	Jan. 18, 1977	.1	—	—	—	—	—	—	—	—	—	—
G-3062	Jan. 18, 1977	—	—	—	—	—	—	—	—	—	—	—
	Jan. 18, 1977	—	—	—	—	—	—	—	—	—	—	—
	Jan. 18, 1977	—	—	—	—	—	—	—	—	—	—	—
	Jan. 18, 1977	—	—	—	—	—	—	—	—	—	—	—
	Jan. 18, 1977	—	—	—	—	—	—	—	—	—	—	—
	Jan. 18, 1977	—	—	—	—	—	—	—	—	—	—	—
	Jan. 18, 1977	—	—	—	—	—	—	—	—	—	—	—
					During Third Recovery							
G-3061	July 18, 1977	—	—	—	—	—	—	—	—	—	—	—
	July 17, 1979	—	—	—	—	—	—	—	—	—	—	—
G-3062	July 17, 1979	—	—	—	—	—	—	—	—	—	—	—
	July 17, 1979	—	—	—	—	—	—	—	—	—	—	—
	July 17, 1979	—	—	—	—	—	—	—	—	—	—	—
	July 17, 1979	—	—	—	—	—	—	—	—	—	—	—
	July 17, 1979	—	—	—	—	—	—	—	—	—	—	—
	July 17, 1979	—	—	—	—	—	—	—	—	—	—	—
	July 18, 1979	—	—	—	—	—	—	—	—	—	—	—

APPENDIX D—WATER-QUALITY DATA OBTAINED DURING WELL CONSTRUCTION AND THE SUBSEQUENT INJECTION AND RECOVERY CYCLES AT THE HIALEAH SITE—Continued

Well	Date	Total toxaphene (µg/L)	Total heptachloride (µg/L)	Total heptachloride epoxide (µg/L)	Total polychloride biphenyls (µg/L)	Total malathion (µg/L)	Total parathion (µg/L)	Total diazinon (µg/L)	Total methyl parathion (µg/L)	Total 2,4-D (µg/L)	Total 2,4,5-T (µg/L)	Total silvex (µg/L)
					During Construction							
G-3062	Nov. 20, 1974	—	—	—	—	—	—	—	—	—	—	—
G-3061	Dec. 04, 1974	—	—	—	—	—	—	—	—	—	—	—
					During First Injection							
G-3061	July 22, 1975	0	0.0	0.0	0	—	—	—	—	0.0	0.0	0.0
S-3000	July 22, 1975	0	.0	.0	0	—	—	—	—	.0	.0	.0
G-3062	Aug. 04, 1975	0	.0	.0	0	—	—	—	—	.0	.0	.0
					During First Recovery							
G-3061	Sept. 16, 1975	—	—	—	—	—	—	—	—	—	—	—
	Sept. 23, 1975	—	—	—	—	—	—	—	—	—	—	—
	Sept. 30, 1975	—	—	—	—	—	—	—	—	—	—	—
	Oct. 15, 1975	—	—	—	—	—	—	—	—	—	—	—
					During Second Injection							
G-3061	Mar. 04, 1976	—	—	—	—	—	—	—	—	—	—	—
S-3000	Mar. 04, 1976	—	—	—	—	—	—	—	—	—	—	—
					During Second Recovery							
G-3061	May 03, 1976	—	—	—	—	—	—	—	—	—	—	—
	May 25, 1976	0	.0	.0	0	—	—	—	—	.0	.0	.0
	July 19, 1976	0	.0	.0	0	0.0	0.0	0.0	0.0	.0	.0	.0
G-3062	July 19, 1976	—	—	—	—	—	—	—	—	—	—	—
	July 19, 1976	—	—	—	—	—	—	—	—	—	—	—
	July 19, 1976	—	—	—	—	—	—	—	—	—	—	—
	July 19, 1976	—	—	—	—	—	—	—	—	—	—	—
	July 19, 1976	—	—	—	—	—	—	—	—	—	—	—
	July 19, 1976	—	—	—	—	—	—	—	—	—	—	—
	July 19, 1976	—	—	—	—	—	—	—	—	—	—	—
					During Third Injection							
G-3061	Jan. 18, 1977	—	—	—	—	—	—	—	—	—	—	—
S-3000	Jan. 18, 1977	—	—	—	—	—	—	—	—	—	—	—
G-3062	Jan. 18, 1977	—	—	—	—	—	—	—	—	—	—	—
	Jan. 18, 1977	—	—	—	—	—	—	—	—	—	—	—
	Jan. 18, 1977	—	—	—	—	—	—	—	—	—	—	—
	Jan. 18, 1977	—	—	—	—	—	—	—	—	—	—	—
	Jan. 18, 1977	—	—	—	—	—	—	—	—	—	—	—
	Jan. 18, 1977	—	—	—	—	—	—	—	—	—	—	—
	Jan. 18, 1977	—	—	—	—	—	—	—	—	—	—	—
					During Third Recovery							
G-3061	July 18, 1977	—	—	—	—	—	—	—	—	—	—	—
	July 17, 1979	—	—	—	—	—	—	—	—	—	—	—
G-3062	July 17, 1979	—	—	—	—	—	—	—	—	—	—	—
	July 17, 1979	—	—	—	—	—	—	—	—	—	—	—
	July 17, 1979	—	—	—	—	—	—	—	—	—	—	—
	July 17, 1979	—	—	—	—	—	—	—	—	—	—	—
	July 17, 1979	—	—	—	—	—	—	—	—	—	—	—
	July 17, 1979	—	—	—	—	—	—	—	—	—	—	—
	July 18, 1979	—	—	—	—	—	—	—	—	—	—	—

APPENDIX D—WATER-QUALITY DATA OBTAINED DURING WELL CONSTRUCTION AND THE SUBSEQUENT INJECTION AND RECOVERY CYCLES AT THE HIALEAH SITE—Continued

Well	Date	Total trithion (μg/L)	Total methyl trithion (μg/L)	Total suspended solids, residue at 110 degrees Celsius	Dissolved solids, residue at 180 degrees Celsius	Dissolved solids, sum of constituents (mg/L)	Dissolved solids (tons/acre-ft)	Total ortho phosphorus (mg/L as P)	Density (g/mL at 20 degrees Celsius)	Acidity (mg/L as H)	Dissolved ammonia nitrogen (mg/L as NH_4)	Dissolved nitrate nitrogen (mg/L as NO_3)
					During Construction							
G-3062	Nov. 20, 1974	—	—	0	2,830	2,710	3.85	0.01	—	—	—	—
G-3061	Dec. 04, 1974	—	—	0	2,920	2,740	3.97	0.01	—	—	—	—
					During First Injection							
G-3061	July 22, 1975	—	—	—	408	373	.55	.03	0.999	—	—	—
S-3000	July 22, 1975	—	—	—	408	373	.55	.03	.999	—	—	—
G-3062	Aug. 04, 1975	—	—	—	2,450	2,660	3.33	.01	—	0.1	—	—
					During First Recovery							
G-3061	Sept. 16, 1975	—	—	1	440	453	.60	.02	—	.6	—	—
	Sept. 23, 1975	—	—	—	540	498	.73	<.01	—	1.0	—	—
	Sept. 30, 1975	—	—	1	646	599	.88	.02	—	.8	—	—
	Oct. 15, 1975	—	—	2	892	854	1.21	.01	—	.8	—	—
					During Second Injection							
G-3061	Mar. 04, 1976	—	—	1	400	370	.54	.03	—	2.9	0.73	0.0
S-3000	Mar. 04, 1976	—	—	1	400	370	.54	.03	—	2.9	.73	.0
					During Second Recovery							
G-3061	May 03, 1976	—	—	—	399	359	.54	.02	—	—	—	—
	May 25, 1976	—	—	1	520	495	.71	.01	—	1.1	.64	.0
	July 19, 1976	0.0	0.0	—	1,080	1,070	1.47	.01	—	—	—	—
G-3062	July 19, 1976	—	—	—	4,880	4,900	6.64	—	—	—	—	—
	July 19, 1976	—	—	—	1,830	1,790	2.49	—	—	—	—	—
	July 19, 1976	—	—	—	1,830	1,820	2.49	—	—	—	—	—
	July 19, 1976	—	—	—	1,690	1,620	2.30	—	—	—	—	—
	July 19, 1976	—	—	—	1,560	1,510	2.12	—	—	—	—	—
	July 19, 1976	—	—	—	1,770	1,750	2.41	—	—	—	—	—
	July 19, 1976	—	—	—	2,010	1,980	2.73	—	—	—	—	—
					During Third Injection							
G-3061	Jan. 18, 1977	—	—	—	409	379	.56	.02	—	—	—	—
S-3000	Jan. 18, 1977	—	—	—	409	379	.56	.02	—	—	—	—
G-3062	Jan. 18, 1977	—	—	—	633	633	.86	<.01	—	—	—	—
	Jan. 18, 1977	—	—	—	410	431	.56	<.01	—	—	—	—
	Jan. 18, 1977	—	—	—	412	419	.56	<.01	—	—	—	—
	Jan. 18, 1977	—	—	—	518	562	.70	<.01	—	—	—	—
	Jan. 18, 1977	—	—	—	755	798	1.03	<.01	—	—	—	—
	Jan. 18, 1977	—	—	—	604	616	.82	<.01	—	—	—	—
	Jan. 18, 1977	—	—	—	3,780	3,870	5.14	<.01	—	—	—	—
					During Third Recovery							
G-3061	July 18, 1977	—	—	13	378	378	.51	.02	—	—	—	—
	July 17, 1979	—	—	—	2,640	2,370	3.59	.01	—	—	—	—
G-3062	July 17, 1979	—	—	—	2,900	2,590	3.94	.01	—	—	—	—
	July 17, 1979	—	—	—	2,680	2,510	3.64	.01	—	—	—	—
	July 17, 1979	—	—	—	2,670	2,400	3.63	.01	—	—	—	—
	July 17, 1979	—	—	—	2,550	2,390	3.47	.01	—	—	—	—
	July 17, 1979	—	—	—	2,760	2,570	3.75	.01	—	—	—	—
	July 17, 1979	—	—	—	2,750	2,570	3.74	<.01	—	—	—	—
	July 18, 1979	—	—	—	4,730	4,980	6.53	<.01	—	—	—	—

APPENDIX D—WATER-QUALITY DATA OBTAINED DURING WELL CONSTRUCTION AND THE SUBSEQUENT INJECTION AND RECOVERY CYCLES AT THE HIALEAH SITE—Continued

Well	Date	Dissolved nitrite nitrogen (mg/L as NO_2)	Total hydrogen sulfide (mg/L as H_2S)	Total nitrogen (mg/L as NO_3)	Dissolved mercury (µg/L as Hg)	Suspended recoverable mercury (µg/L as Hg)	Total recoverable mercury (µg/L as Hg)	Elevation of land surface datum (feet above sea level)	Total depth of well (feet)	Specific gravity	Depth to top of sample interval (feet)	Depth to bottom of sample interval (feet)
During Construction												
G-3062	Nov. 20, 1974	—	4.2	1.9	—	—	—	5.4	1,064	1.000	—	—
G-3061	Dec. 04, 1974	—	—	2.0	—	—	—	8.4	1,105	—	955	1,110
During First Injection												
G-3061	July 22, 1975	—	—	6.0	<0.5	0	<0.5	8.4	1,105	.999	—	—
S-3000	July 22, 1975	—	—	6.0	<.5	0	<.5	—	106	.999	—	—
G-3062	Aug. 04, 1975	—	4.0	3.1	<.5	0	<.5	5.4	1,064	1.002	—	—
During First Recovery												
G-3061	Sept. 16, 1975	—	3.0	5.4	<.5	0	<.5	8.4	1,105	1.001	—	—
	Sept. 23, 1975	—	3.2	4.9	<.5	.1	<.5	8.4	1,105	—	—	—
	Sept. 30, 1975	—	3.2	5.1	<.5	0	<.5	8.4	1,105	1.001	—	—
	Oct. 15, 1975	—	3.7	4.6	<.5	0	<.5	8.4	1,105	1.003	—	—
During Second Injection												
G-3061	Mar. 04, 1976	0.03	.0	6.5	<.5	0	<.5	8.4	1,105	1.000	—	—
S-3000	Mar. 04, 1976	.03	.0	6.5	<.5	0	<.5	—	106	1.000	—	—
During Second Recovery												
G-3061	May 03, 1976	—	—	6.2	—	—	—	8.4	1,105	—	—	—
	May 25, 1976	.00	7.7	6.7	<.5	0	<.5	8.4	1,105	1.001	—	—
	July 19, 1976	—	7.2	3.5	<.5	.5	.5	8.4	1,105	1.001	—	—
G-3062	July 19, 1976	—	—	—	—	—	—	5.4	1,064	—	—	—
	July 19, 1976	—	—	—	—	—	—	5.4	1,064	—	—	—
	July 19, 1976	—	—	—	—	—	—	5.4	1,064	—	—	—
	July 19, 1976	—	—	—	—	—	—	5.4	1,064	—	—	—
	July 19, 1976	—	—	—	—	—	—	5.4	1,064	—	—	—
	July 19, 1976	—	—	—	—	—	—	5.4	1,064	—	—	—
	July 19, 1976	—	—	—	—	—	—	5.4	1,064	—	—	—
During Third Injection												
G-3061	Jan. 18, 1977	—	0	5.5	—	—	—	8.4	1,105	—	—	—
S-3000	Jan. 18, 1977	—	0	5.5	—	—	—	8.4	106	—	—	—
G-3062	Jan. 18, 1977	—	5.4	3.5	—	—	—	5.4	1,064	—	—	—
	Jan. 18, 1977	—	6.4	3.6	—	—	—	5.4	1,064	—	—	—
	Jan. 18, 1977	—	3.5	4.3	—	—	—	5.4	1,064	—	—	—
	Jan. 18, 1977	—	4.2	4.3	—	—	—	5.4	1,064	—	—	—
	Jan. 18, 1977	—	4.8	4.3	—	—	—	5.4	1,064	—	—	—
	Jan. 18, 1977	—	1.6	3.2	—	—	—	5.4	1,064	—	—	—
	Jan. 18, 1977	—	2.2	3.6	—	—	—	5.4	1,064	—	—	—
During Third Recovery												
G-3061	July 18, 1977	—	—	6.3	—	—	—	8.4	1,105	1.000	—	—
	July 17, 1979	—	—	4.9	—	—	—	8.4	1,105	—	—	—
G-3062	July 17, 1979	—	—	5.0	—	—	—	5.4	1,064	—	—	—
	July 17, 1979	—	—	5.0	—	—	—	5.4	1,064	—	—	—
	July 17, 1979	—	—	3.8	—	—	—	5.4	1,064	—	—	—
	July 17, 1979	—	—	3.9	—	—	—	5.4	1,064	—	—	—
	July 17, 1979	—	—	4.2	—	—	—	5.4	1,064	—	—	—
	July 17, 1979	—	—	4.2	—	—	—	5.4	1,064	—	—	—
	July 18, 1979	—	—	8.3	—	—	—	5.4	1,064	—	—	—

WATER SUPPLY PAPER 2431
Pressure data and chloride concentrations--PLATE 1
Merritt, M.L., 1995, Tests of subsurface storage of freshwater at Hialeah, Dade County, Florida, and digital simulation of the salinity of recovered water

U.S. DEPARTMENT OF THE INTERIOR
U.S. GEOLOGICAL SURVEY

PREPARED IN COOPERATION WITH
SOUTH FLORIDA WATER MANAGEMENT DISTRICT AND THE
MIAMI-DADE WATER AND SEWER AUTHORITY DEPARTMENT

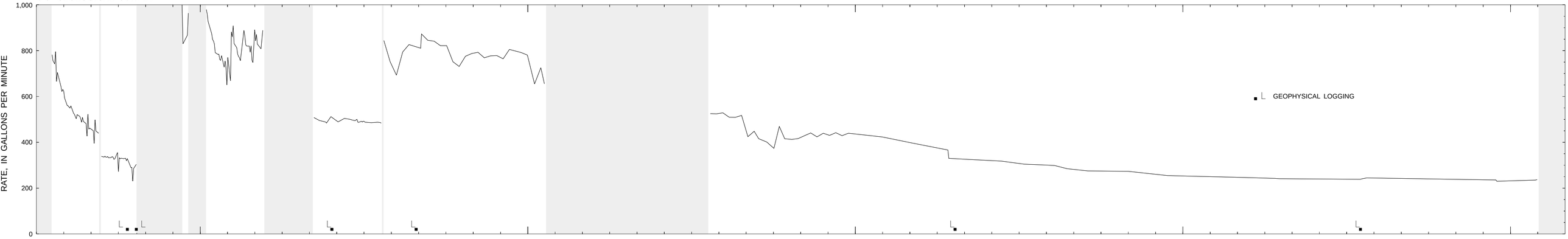

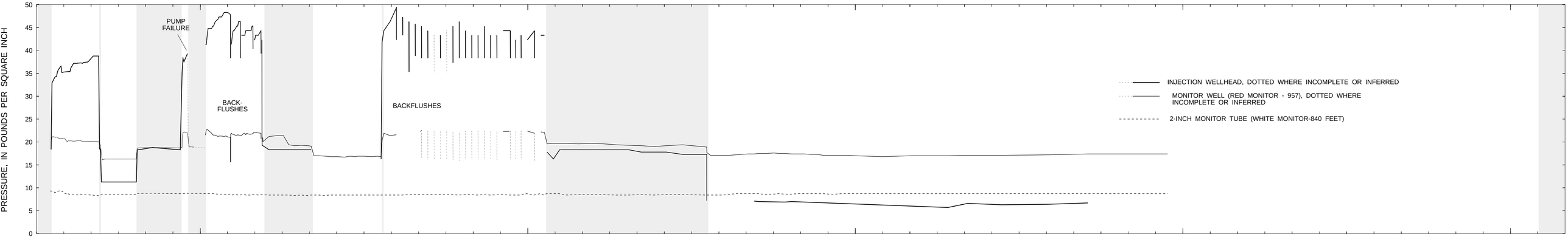

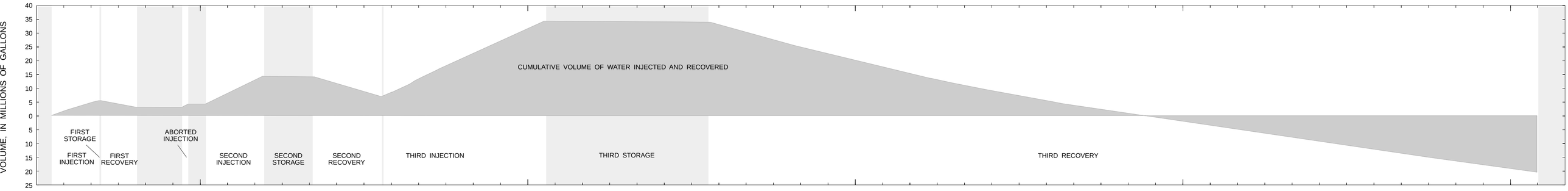

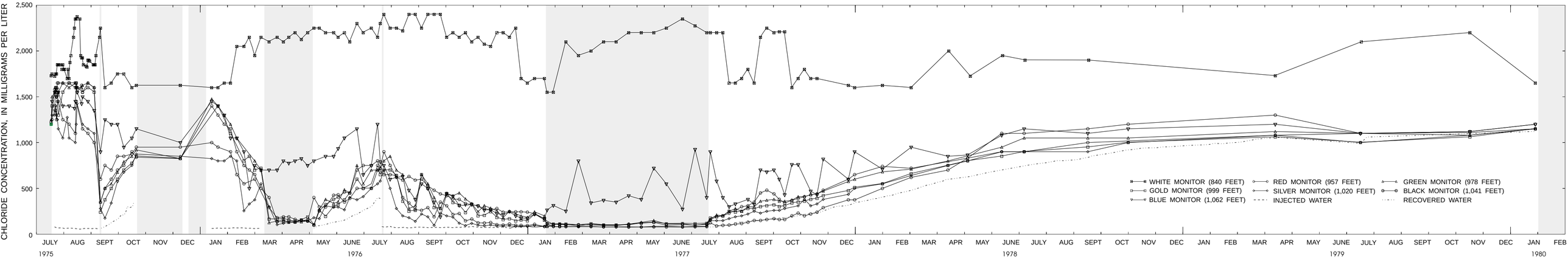

GRAPHS SHOWING PRESSURE DATA AND CHLORIDE CONCENTRATIONS FROM THE INJECTION AND OBSERVATION WELLS, INJECTION-WELL FLOW-RATE DATA, AND THE CUMULATIVE VOLUME OF WATER INJECTED AND RECOVERED DURING INJECTION, STORAGE, AND RECOVERY CYCLES

By
Michael L. Merritt
1995

U.S. DEPARTMENT OF THE INTERIOR
U.S. GEOLOGICAL SURVEY

PREPARED IN COOPERATION WITH
SOUTH FLORIDA WATER MANAGEMENT DISTRICT AND THE
MIAMI-DADE WATER AND SEWER AUTHORITY DEPARTMENT

WATER SUPPLY PAPER 2437
Head changes and salinities--PLATE 2
Merritt, M.L., 1995, Tests of subsurface storage of freshwater at Hialeah, Dade County, Florida, and digital simulation of the salinity of recovered water

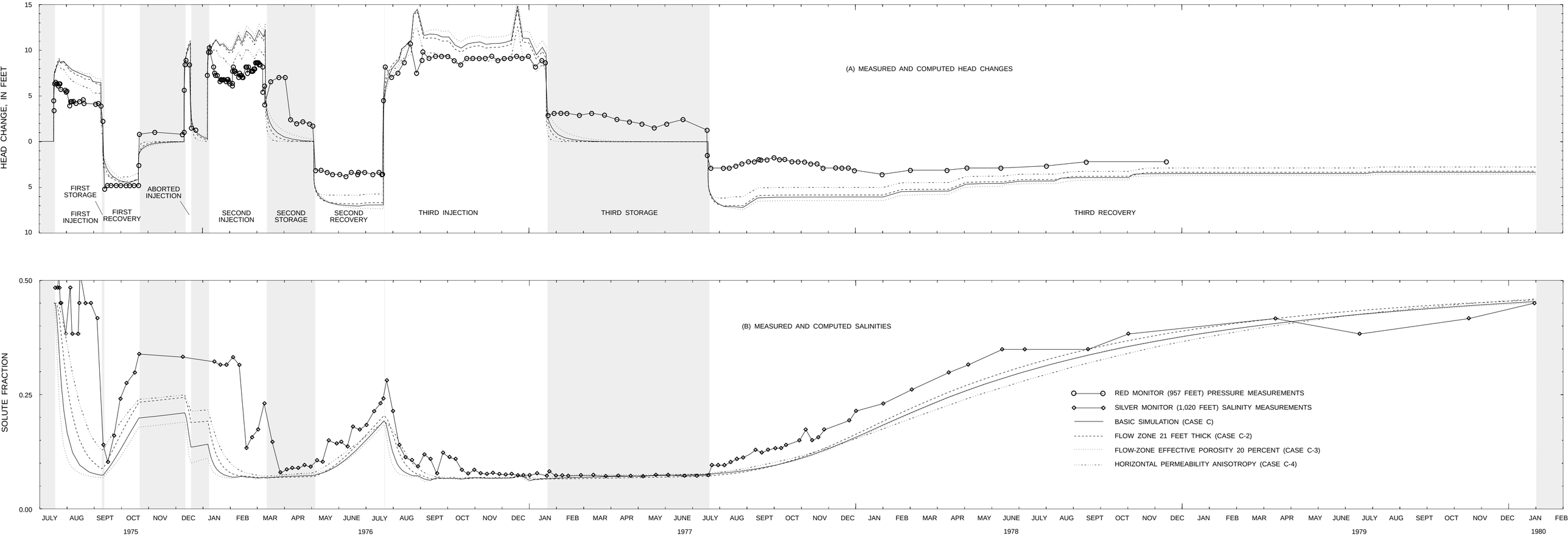

GRAPHS SHOWING MEASURED AND COMPUTED HYDRAULIC-HEAD CHANGES AND SALINITIES AT THE OBSERVATION-WELL LOCATION DURING AQUIFER STORAGE AND RECOVERY CYCLES

By
Michael L. Merritt
1994

SELECTED SERIES OF U.S. GEOLOGICAL SURVEY PUBLICATIONS

Periodicals

Earthquakes & Volcanoes (issued bimonthly).
Preliminary Determination of Epicenters (issued monthly).

Technical Books and Reports

Professional Papers are mainly comprehensive scientific reports of wide and lasting interest and importance to professional scientists and engineers. Included are reports on the results of resource studies and of topographic, hydrologic, and geologic investigations. They also include collections of related papers addressing different aspects of a single scientific topic.

Bulletins contain significant data and interpretations that are of lasting scientific interest but are generally more limited in scope or geographic coverage than Professional Papers. They include the results of resource studies and of geologic and topographic investigations, as well as collections of short papers related to a specific topic.

Water-Supply Papers are comprehensive reports that present significant interpretive results of hydrologic investigations of wide interest to professional geologists, hydrologists, and engineers. The series covers investigations in all phases of hydrology, including hydrogeology, availability of water, quality of water, and use of water.

Circulars present administrative information or important scientific information of wide popular interest in a format designed for distribution at no cost to the public. Information is usually of short-term interest.

Water-Resources Investigations Reports are papers of an interpretive nature made available to the public outside the formal USGS publications series. Copies are reproduced on request unlike formal USGS publications, and they are also available for public inspection at depositories indicated in USGS catalogs.

Open-File Reports include unpublished manuscript reports, maps, and other material that are made available for public consultation at depositories. They are a nonpermanent form of publication that may be cited in other publications as sources of information.

Maps

Geologic Quadrangle Maps are multicolor geologic maps on topographic bases in 7.5- or 15-minute quadrangle formats (scales mainly 1:24,000 or 1:62,500) showing bedrock, surficial, or engineering geology. Maps generally include brief texts; some maps include structure and columnar sections only.

Geophysical Investigations Maps are on topographic or planimetric bases at various scales; they show results of surveys using geophysical techniques, such as gravity, magnetic, seismic, or radioactivity, which reflect subsurface structures that are of economic or geologic significance. Many maps include correlations with the geology.

Miscellaneous Investigations Series Maps are on planimetric or topographic bases of regular and irregular areas at various scales; they present a wide variety of format and subject matter. The series also includes 7.5-minute quadrangle photogeologic maps on planimetric bases that show geology as interpreted from aerial photographs. Series also includes maps of Mars and the Moon.

Cost Investigations Maps are geologic maps on topographic or planimetric bases at various scales showing bedrock or surficial geology, stratigraphy, and structural relations in certain coal-resource areas.

Oil and Gas Investigations Charts show stratigraphic information for certain oil and gas fields and other areas having petroleum potential.

Miscellaneous Field Studies Maps are multicolor or black-and-white maps on topographic or planimetric bases for quadrangle or irregular areas at various scales. Pre-1971 maps show bedrock geology in relation to specific mining or mineral-deposit problems; post-1971 maps are primarily black-and-white maps on various subjects such as environmental studies or wilderness mineral investigations.

Hydrologic Investigations Atlases are multicolored or black-and-white maps on topographic or planimetric bases presenting a wide range of geohydrologic data of both regular and irregular areas; principal scale is 1:24,000, and regional studies are at 1:250,000 scale or smaller.

Catalogs

Permanent catalogs, as well as some others, giving comprehensive listings of U.S. Geological Survey publications are available under the conditions indicated below from the U.S. Geological Survey, Map Distribution, Box 25286, Bldg. 810, Federal Center, Denver, CO 80225. (See latest Price and Availability List.)

"Publications of the Geological Survey, 1879–1961" may be purchased by mail and over the counter in paperback book form and as a set of microfiche.

"Publications of the Geological Survey, 1962–1970" may be purchased by mail and over the counter in paperback book form and as a set of microfiche.

"Publications of the U.S. Geological Survey, 1971–1981" may be purchased by mail and over the counter in paperback book form (two volumes, publications listing and index) and as a set of microfiche.

Supplements for 1982, 1983, 1984, 1985, 1986, and for subsequent years since the last permanent catalog may be purchased by mail and over the counter in paperback book form.

State catalogs, "List of U.S. Geological Survey Geologic and Water-Supply Reports and Maps For (State)," may be purchased by mail and over the counter in paperback booklet form only.

"Price and Availability List of U.S. Geological Survey Publications," issued annually, is available free of charge in paperback booklet form only.

Selected copies of a monthly catalog "New Publications of the U.S. Geological Survey" are available free of charge by mail or may be obtained over the counter in paperback booklet form only. Those wishing a free subscription to the monthly catalog "New Publications of the U.S. Geological Survey" should write to the U.S. Geological Survey, 582 National Center, Reston, VA 22092.

Note.—Prices of Government publications listed in older catalogs, announcements, and publications may be incorrect. Therefore, the prices charged may differ from the prices in catalogs, announcements, and publications.

Make sure your browser allows pop-ups to receive PDF files	
ACN	930159281 - **PDF of article**
IND	LNN
ENT	931104
AUTHOR(S)	MUTCH R D JR;SCOTT J I;WILSON D J
TITLE	THE IMPACT OF MATRIX DIFFUSION ON THE CLEANUP OF FRACTURED IGNEOUS, METAMORPHIC, AND SEDIMENTARY ROCK AQUIFERS ISSUES (SEPTEMBER 27-29, 1993, RADISSON HOTEL BURLINGTON, BURLINGTON, VERMONT [GROUND WATER MANAGEMENT BOOK 16]); P77-90
SOURCE	PROCEEDINGS OF THE FOCUS CONFERENCE ON EASTERN REGIONAL GROUND WATER
ISSN	1047-9023
PUBLISHER	NGWA
REGION	SWEDEN;ONTARIO;CANADA;UNITED KINGDOM;WESTERN EUROPE;NORTH AMERICA
STATE	TN;NM
AQUIFER(S)	CONASAUGA SH;NOLICHUCKY SH;CULEBRA DOLOMITE;QUEENSTON SH
DATE OF PUB	00/1993
CLASS	GB1001.2.E271993
LAN	ENGLISH
LIB	NGWIC
NOTES	FIGURES;TABLES;REFERENCES
KEYWORD(S)	FRACTURES;IGNEOUS ROCK;METAMORPHIC ROCK;SEDIMENTARY ROCK;AQUIFER REHABILITATION;CONSOLIDATED ROCK;MATHEMATICAL MODELS;PUMPING AND TREATING;NUMERICAL MODELS;DISPERSION;SOLUTE TRANSPORT MODELS;STEADY STATE FLOW;POROSITY;SANDSTONE;SHALE;LIMESTONE;SILTSTONE;CONGLOMERATE; DOLOMITE;CHALK;MARBLE;SHALE;SLATE;GRANITE;GNEISS;SECONDARY POROSITY; PRIMARY POROSITY;ATTENUATION;WATER QUALITY
AFFILIATION	ECKENFELDER;VANDERBILT UNIV
ABSTRACT	IN ORDER TO EVALUATE THE IMPACT OF MATRIX DIFFUSION UPON THE CLEANUP OF FRACTURED ROCK AQUIFERS, A SIMPLE MATHEMATICAL MODEL HAS BEEN DEVELOPED WHICH PREDICTS CONTAMINANT LEVELS ALONG A REPRESENTATIVE FRACTURE IN THE ROCK AS A FUNCTION OF POSITION, TIME, AND PAST HISTORY OF CONTAMINANT LEVELS IN THE GROUND WATER. THE MODEL TAKES INTO ACCOUNT THE CHARACTERISTICS OF THE FRACTURED ROCK THROUGH WHICH THE GROUNDWATER IS MOVING, SPECIFICALLY FRACTURE POROSITY, MATRIX POROSITY, FRACTURE SPACING, MATRIX DIFFUSIVITY, GROUND WATER VELOCITY IN THE FRACTURES, LONGITUDINAL DISPERSION CONSTANT, AND LENGTH OF THE GROUND WATER FLOW PATH. THE MODEL IS EMPLOYED TO EVALUATE THE EFFECT OF MATRIX DIFFUSION ON THE CLEANUP OF TYPICAL SEDIMENTARY ROCK AQUIFERS AND TYPICAL METAMORPHIC OR IGNEOUS AQUIFERS. THROUGH SENSITIVITY ANALYSES, THE MODELING REVEALS THE PARAMETERS MOST STRONGLY GOVERNING THE PROCESS. THE MODELING ALSO LOOKS AT THE EFFECT OF PUMP AND TREAT SYSTEMS AND SPECIFICALLY THE "REBOUND EFFECT" THAT CAN RESULT FROM PREMATURE CESSATION OF PUMP AND TREAT SYSTEMS. THE FOLLOWING ARE MENTIONED: AVERAGE POROSITY VALUES FOR SANDSTONE, SHALE, AND LIMESTONE; RANGES OF VARIATION IN THE MATRIX POROSITY OF SANDSTONE, SILTSTONE, QUARTZITE, CHERT, CONGLOMERATE, LIMESTONE, DOLOMITE, CHALK, MARBLE, SHALE, CLAYSTONE, SLATE, GRANITE, AND GNEISS; RANGES OF FRACTURE POROSITY FOR SANDY SHALE PETROLEUM RESERVOIRS, "FISSURED RESERVOIRS," THE CONASAUGA SHALE, "SILICEOUS RESERVOIRS," THE NOLICHUCKY SHALE, THE CULEBRA DOLOMITE, AND IGNEOUS, SEDIMENTARY, AND METAMORPHIC ROCKS; AND RANGES OF MOLECULAR DIFFUSIVITY FOR A CLAYEY SOIL, THE QUEENSTON SHALE, U.K. GRANITE

	SAMPLES, SWEDISH GRANITE AND GNEISS SAMPLES, AND SOLUTES OF LOW MOLECULAR WEIGHT IN WATER AT AMBIENT TEMPERATURE.

Print This Some older browsers may not support this link.

dtSearch Engine Version 6.32 (Build 6429)

THE IMPACT OF MATRIX DIFFUSION ON THE CLEANUP OF FRACTURED IGNEOUS, METAMORPHIC, AND SEDIMENTARY ROCK AQUIFERS

Robert D. Mutch, Jr., P.Hg., P.E. and Joanna I. Scott, Ph.D.
ECKENFELDER, INC., Mahwah, NJ
David J. Wilson, Ph.D.,
Departments of Chemistry and Civil and Environmental Engineering,
Vanderbilt University, Nashville, TN

Abstract. Aquifer restoration has been recognized for many years to be an extremely difficult undertaking. For a variety of reasons, restoration of fractured rock aquifers appears to be especially difficult. One reason is the phenomenon of matrix diffusion. Matrix diffusion refers to the process by which contaminants diffuse into and out of the relatively immobile matrix pore water from the mobile fracture water.

In most (but not all) fractured rock, groundwater moves primarily through the interconnected network of fractures and the pore water within the matrix of the rock is relatively immobile. As contaminated groundwater moves through the fractures, the contamination is also subject to diffusion into the often stagnant matrix pore water of the rock. The diffusion of contaminants into the rock matrix is beneficial in one respect in that it retards the advance of a contaminant plume through a fractured rock aquifer. However, the diffusion-controlled release of contaminants from the rock matrix can substantially prolong aquifer cleanup efforts over what would be possible in a simple porous medium aquifer of equivalent hydraulic conductivity.

In order to evaluate the impact of matrix diffusion upon the cleanup of fractured rock aquifers, a simple mathematical model has been developed which predicts contaminant levels along a representative fracture in the rock as a function of position, time, and past history of contaminant levels in the groundwater. The model takes into account the characteristics of the fractured rock through which the groundwater is moving, specifically fracture porosity, matrix porosity, fracture spacing, matrix diffusivity, groundwater velocity in the fractures, longitudinal dispersion constant, and length of the groundwater flow path.

The model is employed to evaluate the effect of matrix diffusion on the cleanup of typical sedimentary rock aquifers and typical metamorphic or igneous aquifers. Through sensitivity analyses, the modeling reveals the parameters most strongly governing the process. The modeling also looks at the effect of pump and treat systems and specifically the "rebound effect" that can result from premature cessation of pump and treat systems.

INTRODUCTION

Much of the northeastern United States and New England, in particular, is characterized by a relatively thin, surficial mantle of glacial deposits underlain by fractured rock formations. In many areas, the fractured rock represents the only reliable source of groundwater and is heavily drawn upon for residential and municipal water supply. A number of fractured rock aquifers have been granted sole source aquifer status and have accordingly been granted special federal protection. At the same time, there has been an alarming increase in the incidence of contamination of these important aquifers as a result of improperly controlled waste disposal, leaking underground storage tanks, industrial spills, and other sources. Numerous groundwater extraction and treatment remedial

efforts have been initiated and still more are planned to control the spread of contamination and, in many cases, to clean up portions of contaminated bedrock aquifers.

Controlling the further spread of contamination plumes, while more complicated in fractured rock aquifers than in simple porous media, is not especially problematic. However, restoring aquifer water quality once the aquifer has become contaminated may be considerably more difficult. Not only are dense non-aqueous phase liquids (DNAPL) more difficult to purge from fractured rock (Mackay and Cherry, 1989), but the diffusion of contaminants from the mobile water in the fractures to the virtually stagnant water within the rock matrix can make aquifer restoration frustratingly slow at best, and, at worst, an exercise in futility. This phenomenon has become especially critical in recent years as mandated post-cleanup contaminant concentration levels have gravitated to the low parts per billion range. Since it is not unusual for initial concentration of some of the more soluble contaminants to exceed 100 or even 1,000 parts per million, expectations of 99.99 to 99.999 percent improvement in aquifer water quality are not uncommon. We here examine the parameters which govern matrix diffusion and discuss the implications of this process for aquifer restoration and groundwater protection.

As contaminated groundwater moves through the fractures of a bedrock aquifer, diffusion of contaminants will occur into the essentially stagnant matrix pore water of the rock, as illustrated in Figure 1. The extent of the diffusion and its hydrogeologic significance will depend upon the concentration gradient, the matrix diffusivity and porosity, the fracture spacing of the rock, and the duration of exposure. From one perspective, the diffusion of contaminants into the rock matrix is beneficial in that it retards the advance of a contaminant plume through the fractured rock. Lever and Bradbury (1985) reported that matrix diffusion can lead to effective retardation factors in excess of 100 and can reduce peak concentrations by three to four orders of magnitude, provided that the groundwater velocity is relatively small. However, when the objective is to purge contamination from an aquifer, the diffusion-controlled release of contaminants from the rock matrix can greatly prolong aquifer cleanup efforts over what would be possible in a simple porous medium of equivalent hydraulic conductivity.

MATHEMATICAL MODEL DEVELOPMENT

A mathematical model has been developed for the calculation of contaminant levels in groundwater as a function of the position, time, and past history of contaminant levels in the recharge water. The model includes the characteristics of the fractured porous rock in which the groundwater is moving--specifically, the fracture porosity, matrix porosity, fracture spacing, matrix diffusivity, groundwater velocity in the fractures, longitudinal dispersion constant, and flow path length. The model deals only with water movement in the zone of saturation, and assumes that advection of pore water within the porous medium itself can be neglected. In this initial study sorption was not considered.

The numerical model is for a single fracture in the zone of saturation, through which groundwater flows at a rate determined by the hydraulic conductivity and hydraulic gradient. A sketch of the system is given in Figure 2. Contaminants in the mobile fracture water are able to move into and out of the immobile pore water by molecular diffusion, and are carried in the direction of flow by advection and longitudinal dispersion. Contaminant concentrations in the recharge water can be varied to represent historical conditions and/or to simulate remedial efforts. The mathematical model's development is described in an earlier paper (Mutch, Scott, and Wilson, 1993).

PARAMETERS GOVERNING CONTAMINANT MIGRATION IN FRACTURED ROCK

The migration and ultimate fate of contaminants in fractured rock is governed by properties of both the geologic medium and the contaminant. The properties which have been incorporated into the model include advective flow rate and longitudinal dispersion in the fractures, matrix diffusivity, fracture porosity, matrix porosity, and fracture spacing. The model does not account for sorption or biological, chemical, or radioactive decay of contaminants, nor does it consider the fate of undissolved DNAPL chemicals. It also assumes steady-state water flow and no advection in the porous medium itself. The typical ranges of the hydrogeological parameters and the basic assumptions used in the modeling are discussed below.

Matrix Porosity

Virtually all consolidated rock possesses some matrix porosity, although in igneous and metamorphic rock the matrix porosity can be quite low. Sedimentary rocks tend to have fairly high porosity. Barrell (1914) reports that the average porosities of sandstone, shale, and limestone are 14.8, 8.2, and 5.3 percent, respectively. The variability of matrix porosity within different classes of rock can be quite high, however, depending upon degree of compaction, cementation, and sorting. A U.S. Geological Survey report by Manger (1963) on thousands of rock samples reveals that the matrix porosity of sandstone, siltstone, quartzite, chert, and conglomerate can vary from less than one percent to greater than 25 percent. The matrix porosity of limestone, dolomite, chalk, and marble is also reported by Manger to vary from 0.2 percent to nearly 20 percent. Shale, claystone, and slate are reported to range in porosity from 0.5 percent to 15 percent. Neretnieks (1985) studied the matrix porosity of 30 samples of granite and gneiss from Sweden and found that the porosity varied from 0.06 to 0.4 percent. In the subsequent modeling a matrix porosity of 7.5 percent was used for sedimentary rock and one of 0.1 percent for igneous and metamorphic rock.

Fracture Porosity

A review of the literature indicates that the typical range of the fracture porosity in sedimentary rocks is on the order of 1×10^{-3} to 5×10^{-3} (Streltsova, 1976a, 1976b; Walter and Thompson, 1982; Yurochko, 1982; Smith and Vaughan, 1985; Kelley et al., 1987). Streltsova (1976a) reported fracture porosities of 1×10^{-3} to 2×10^{-3} for sandy shale petroleum reservoirs and a range of 1×10^{-3} to 5×10^{-3} for "fissured reservoirs" in general (Streltsova, 1976b). Walter and Thompson (1982) noted a fracture porosity of 2×10^{-3} for the Conasauga Shale of Tennessee based upon field tracer studies. Yurochko (1982) reported a range in fracture porosity from 1×10^{-3} to 5×10^{-3} for "siliceous reservoirs". Based upon aquifer test analysis, Smith and Vaughan (1985) concluded that the fracture porosity of the Nolichucky Shale in Tennessee was on the order of 1×10^{-3}. Kelley et al. (1987) reported a fracture porosity of 2×10^{-3} for the Culebra Dolomite of New Mexico. Igneous and metamorphic rocks often have fracture porosities of approximately 1×10^{-4}, according to Freeze and Cherry (1979), who suggest a range of 10^{-2} to 10^{-5} for fracture porosities. In the subsequent calculations a fracture porosity of 2.5×10^{-3} is used for sedimentary rock and 1×10^{-4} for igneous and metamorphic rock.

Longitudinal Dispersion

Longitudinal dispersion refers to the process by which contaminants are spread in a direction parallel to groundwater flow by variations in flow velocity brought about by variations in fracture aperture and intrafracture velocity profiles. The longitudinal dispersion constant, D_L, is defined as the product of the longitudinal dispersivity, or characteristic length, α_L, and the mean groundwater velocity, V, as follows:

$$D_L = \alpha_L \cdot V$$

where D_L = longitudinal dispersion constant, m^2/sec; α_L = longitudinal dispersivity, m; and V = mean groundwater velocity, m/sec.

Dispersion has been shown to have a high degree of scale dependence; that is, the larger the scale of the transport situation studied, the larger the measured longitudinal dispersivity. Longitudinal dispersivity varies from as little as a few millimeters in laboratory column studies to more than 100 meters in large scale plumes (Anderson, 1979). In the subsequent modeling a longitudinal dispersivity of five meters is assumed.

Matrix Diffusivity

The molecular diffusivity of solutes of low molecular weight (M<500 gm/mole) in water at ambient temperatures is typically in the range of 1 to 5 x 10^{-9} m^2/sec (Rasmuson and Neretnieks, 1981). Barone et al. (1988) measured the matrix diffusivity, D_m, of a clayey soil as lying between 4.6 and 7.5 x 10^{-10} m^2/sec. Barone and his coworkers (1989) also found that the Queenston Shale of southern Ontario had a matrix diffusivity of 1.4 to 1.6 x 10^{-10} m^2/sec. In another study of the Queenston Shale of southern Ontario, Pankow et al. (1986) reported an average matrix diffusivity of 3.7 x 10^{-12} m^2/sec. These data indicate that sedimentary rocks tend to have matrix diffusivities lower than those for unconsolidated sediments. Igneous and metamorphic rocks have been shown to have even lower matrix diffusivities. Bradbury and Green (1985) measured the matrix diffusivity of granite samples from four regions of the United Kingdom and found that their matrix diffusivities varied from 2.3 x 10^{-14} to 1.6 x 10^{-12} m^2/sec. Neretnieks (1985) reported that the matrix diffusivity of 20 samples of Swedish granite and gneiss varied from 1 x 10^{-14} to 7 x 10^{-13} m^2/sec. In the subsequent modeling a matrix diffusivity of 3.1 x 10^{-11} m^2/sec is assumed for sedimentary rocks and 1 x 10^{-13} m^2/sec for igneous and metamorphic rocks.

Fracture Spacing

The mean spacing of fractures in rock can vary from a few centimeters in highly fractured rock to ten meters or more in granite and some other crystalline rocks. In the subsequent modeling a fracture spacing of one meter has been used.

MATHEMATICAL MODELING

Mathematical modeling was conducted to assess the role of matrix diffusion in retarding or attenuating the transport of groundwater contamination in fractured rock. Rock properties generally representative of a sedimentary rock such as shale were utilized in the

modeling with the exception of values of matrix diffusivity which were varied. The following properties were used in the modeling:

Mean Fracture Spacing	1 m
Fracture Porosity	0.0025
Matrix Porosity	0.75
Longitudinal Dispersivity	5 m
Hydraulic Conductivity	1×10^{-5} cm/sec

It was also assumed that the hydraulic gradient in the rock was 0.01. Combined with the above-listed hydraulic conductivity, this hydraulic gradient results in an average groundwater velocity of 0.035 m/d. Matrix diffusivity was varied from as low as 3.1×10^{-12} m^2/sec to 9.7×10^{-11} m^2/sec. These values are generally representative of those reported in the literature for sedimentary rock such as shale and fine-grained sandstone. For comparative purposes, the modeling was also conducted with matrix diffusivity set at zero. Figure 3 represents the results of the modeling, illustrating the advance of the plume of contamination through the rock after a time period of five years. Figure 3 illustrates the considerable importance of matrix diffusivity in dictating the rate of advance of a plume through fractured rock. With no matrix diffusion the plume has advanced an average (C_i/C_o = 0.5) of approximately 70 meters. By contrast, at a matrix diffusivity of 9.7×10^{-11} m^2/sec the plume has advanced an average of but seven meters. In each case, the matrix diffusivities used in this exercise resulted in some effective retardation. However, the effective retardation becomes less significant in the lower range of matrix diffusivities found to be characteristic of sedimentary rock.

It can be seen that the effect of matrix diffusion is to retard the advance of a plume of contamination through fractured rock. The extent of this retardation can be calculated by determining an effective retardation factor. The effective retardation factor can be thought of as the velocity of the contamination, represented by a particular value of C_i/C_o, with no matrix diffusion divided by the velocity of the contamination with varying levels of matrix diffusion. Table 1 presents effective retardation factors at C_i/C_o values of 0.8, 0.5, and 0.2.

TABLE 1
EFFECTIVE RETARDATION FACTORS

	Matrix Diffusivity - m^2/s			
C_i/C_o	3.1×10^{-12}	9.7×10^{-11}	3.1×10^{-11}	9.7×10^{-11}
0.8	2.2	6.2	13	20
0.5	1.3	2.5	5.2	9.7
0.2	1.1	1.6	2.9	4.7

It can be seen that the effective retardation factors vary considerably, ranging from as low as 1.1 to as high as 20. The effective retardation factor decreases with decreasing concentration ratios (C_i/C_o). This suggests that matrix diffusion is not as effective in retarding the advance of the leading edge of a plume as it is in retarding the higher concentration portions of the plume. As expected, effective retardation factors also decrease

with decreasing values of matrix diffusivity. It should be noted that the effective retardation factors are not a constant for a given fractured rock but rather vary significantly with the properties of the rock, the hydrogeologic system, and over time.

Further mathematical modeling was conducted to compare the effectiveness of a typical igneous and metamorphic rock versus a typical shale in retarding the advance of the contaminant plume. The hydrogeologic properties and physical properties of the rock were the same as in the previous modeling with the following exceptions. In modeling the behavior of a typical igneous and metamorphic rock, a matrix porosity of 0.001 was used and a matrix diffusivity of $1x10^{-13}$ m^2/sec. The typical shale was modeled using a matrix porosity of 0.075 and a matrix diffusivity of 3.1×10^{-11} m^2/sec. As depicted in Figure 4, there is a profound difference in the way the two rock types effectively retard the advance of a plume. The fractured rock with the properties of a typical shale significantly retards the plume. However, the typical igneous rock and metamorphic rock affords essentially no effective retardation as a result of matrix diffusion. The matrix diffusivity and porosity of this class of rock are simply too low to significantly retard the plume in the relatively high velocity, although not atypical, situation modeled herein.

In order to assess the impacts of matrix diffusion upon the cleanup of contaminated bedrock aquifers, the following two examples were modeled.

EXAMPLE 1

A fractured shale has been subject to groundwater contamination by a non-adsorbing, non-degradable contaminant at a concentration of 10000 units (the actual units are arbitrary, perhaps parts per billion) for a period of 20 years. During that time the contaminated water has moved in a fracture laterally a distance of 100 meters to a nearby sewer which has intercepted the plume and serves as a groundwater discharge point. The average groundwater velocity is 0.35 m/day (4.05×10^{-6} m/sec) and the shale has the following properties:

mean fracture spacing	1 m
fracture porosity	0.0025
matrix porosity	0.075
matrix diffusivity	3.1×10^{-11} m^2/sec
longitudinal dispersivity	5 m

If the source of the contaminant were removed, how long would it take the contaminants to be naturally flushed from this section of aquifer? One can apply the mathematical model to this situation to estimate the progressive flushing of contaminants from the representative fracture. The results of this modeling are presented in Figure 5. The plotted concentrations represent the highest concentration within the fracture, which, in this simple example, occurs during the cleanup at the downgradient side of the fracture, at the sewer. It is seen in Figure 5 that approximately 120 years is required to reduce the maximum fracture water concentration to 100 units, which represents a 99 percent improvement in water quality. It requires fully 650 years before the maximum fracture water concentration is reduced to one unit, representing a 99.99 percent improvement in water quality. The reason for this exceedingly lengthy cleanup time becomes clear as one examines what is occurring in the rock matrix as a result of diffusion from the flowing water into the fractures during the contamination process. Figure 6 presents a graphical history of contaminant levels in the rock fracture and in the rock matrix during the course

of the cleanup. Initially (i.e. at the end of the 20-year period of contamination) a substantial mass of contaminant has moved into the rock's matrix porosity as a result of diffusion. Actually, some 90 percent of the contaminant mass is held within the relatively immobile pore water, compared to only 10 percent in the flowing fracture water. The contaminant concentration at the midpoint of the block of porous matrix at this time is about 100 units. It is also evident that even as clean water begins to recharge the rock after the initial 20-year contamination period, diffusion continues to carry contamination farther into the rock matrix. This occurs even as contaminants closer to the fracture begin to diffuse back outward to the fracture. Contaminant continues to diffuse farther into the rock matrix for a period of approximately 50 years after the contaminant source has been cut off, ultimately reaching at that time a maximum concentration of approximately 1100 units at the block midpoint.

As seen in this case, diffusive movement of contaminant in rock often goes through three phases: an initial, or contamination phase, an intermediate phase, and a final phase. The latter two occur during aquifer restoration. In the contamination phase, contaminants are diffusing from the high concentrations in the mobile fracture water into the uncontaminated pore water in the rock matrix.

The intermediate phase begins once the contaminant source is removed and clean groundwater begins to enter the contaminated zone. The intermediate phase is characterized by simultaneous inward and outward diffusion. Contamination in the interior of the block continues to migrate inward toward the block's midpoint, while contaminant closer to the fractures begins to diffuse outward in response to the lower concentrations now occurring in the fracture water. In Figure 5 this phase is represented by the "initial" to 50 year (after source removal) curves.

The final phase occurs once the concentration at the midpoint of the block reaches a maximum (approximately 50 years in Figure 5) and the diffusive flux becomes universally outward to the fracture flow system. The final phase is characterized by concentrations in the fracture which decrease exponentially (linearly on a logarithmic scale) with time, as in Figure 5 after approximately 80 years. This means that in the final phase, each order of magnitude reduction in contaminant concentration requires the same length of time (approximately 260 years in this example).

If the matrix diffusivity is relatively high, the fracture spacing small, or the period of contamination long, contaminant can fully permeate the block, achieving a steady-state concentration equal to that in the mobile fracture water. In such cases, the intermediate phase does not occur; the contamination phase is directly followed by the final phase.

In order to assess the relative importance of the various parameters employed in the numerical modeling, a sensitivity analysis was performed using the parameters of Example 1 described above. This evaluated the effects of variations in matrix porosity, matrix diffusivity, fracture spacing, fracture porosity, longitudinal dispersivity, and the length of the antecedent period of contamination. The sensitivity analysis revealed that aquifer cleanup time is most sensitive to changes in matrix porosity, matrix diffusivity and fracture spacing. The sensitivity analysis is described in an earlier paper (Mutch, Scott, and Wilson, 1993).

EXAMPLE 2

Igneous and metamorphic rock aquifers often have low matrix diffusivities, low porosities, and wide fracture spacings. This combination of properties leads to hydrogeologic behavior which warrants special attention. Our second example therefore

addresses the cleanup of a representative rock aquifer of this type. A rock formation with the following properties was modeled:

fracture porosity	0.0005
matrix porosity	0.001
matrix diffusivity	1.0×10^{-13} m^2/sec

All other parameters are the same as in the previous example, with the exception of fracture spacing. Because the matrix diffusivity of igneous and metamorphic rock is so low (on the order of 1×10^{-13} m^2/sec), if fracture spacings are greater than approximately 0.4 m each fracture behaves essentially independently of the others over the time frames involved in this analysis. Therefore, in the simulation of igneous and metamorphic rock aquifers, the model was modified to divide the rock matrix of each volume element into 15 cells, each having a thickness of 0.01 m. The reasonableness of this approximation was tested by running the model for a simulated 1,000 year period and observing the buildup of contaminant in the innermost cell, representing the midpoint of the matrix block. In all cases the concentration developed in the innermost cell was negligibly small and insufficient to adversely affect the accuracy of the simulation.

The results of the igneous and metamorphic rock simulation are presented in Figure 7. As a result of the low matrix diffusivity and low porosity, improvement in water quality begins rapidly in igneous and metamorphic rock aquifers. In fact, a 99.99 percent improvement in water quality occurs in the first 35 years; this might be sufficient for many situations. However, higher degrees of aquifer quality restoration are more difficult to achieve because of the pronounced "tailing" effect evident in Figure 7. The very low matrix diffusivity of igneous and metamorphic rocks dictates that a correspondingly small diffusive flux out of the rock will occur for many centuries. Whether the resulting "tailing" effect is a problem will depend upon the nature of the contaminant and the cleanup objectives.

EFFECTIVENESS OF GROUNDWATER EXTRACTION SYSTEMS

A groundwater extraction and treatment system increases the rate of aquifer restoration by drawing groundwater through the contaminated zone more rapidly than would occur naturally, thus flushing contaminants more rapidly from the aquifer. We evaluated the effectiveness of groundwater extraction and treatment systems in restoration of water quality in the fracture system discussed above by means of our mathematical model. We used the parameters of our Example 1 (sedimentary rock) in simulating the effect of a groundwater extraction and treatment system; we increased the rate of groundwater flow through the 100 meter-long contaminated zone by a factor of five. This increase in flow is considered generally representative of what is achievable by a typical groundwater recovery system. The first simulation involved a 22-year period of groundwater extraction and treatment which, as indicated in Figure 8, improved groundwater quality during the active pumping period by 99 percent. However, upon cessation of pumping, contaminant concentration relatively quickly rebounded to levels nearly as high as would have occurred if no groundwater extraction had been undertaken. On comparing the cleanup curve for the 22-year period of remediation with the natural restoration curve, it becomes evident that the rebound effect negates most of the improvement in contaminant concentration attained during the active pumping period. In fact, after conclusion of the pumping, contaminant concentration is only 10 to 15 percent lower than would have been realized if no remedial action were taken.

A second simulation was performed to simulate a 100-year period of groundwater extraction; this is also shown in Figure 8. It is evident that in order to sustain a 99 percent improvement in water quality, given the rebound in contamination levels which occurs upon cessation of pumping, it would be necessary to pump the fracture for close to 100 years. The same degree of water quality improvement at this point in the fracture would be achievable by natural flushing in approximately 120 years.

The above analysis indicates that groundwater extraction and treatment programs in fractured rock aquifers are likely to meet with only limited success in restoring the quality of water in fractured bedrock aquifers in a reasonable period of time. In particular, overpumping to increase flow rates appreciably beyond those required to prevent further migration of the contaminant plume is not likely to result in significant benefits when one takes the rebound effect described above into account. In fractured rock aquifers, the rate of cleanup may well be controlled by the rate of contaminant diffusion from the rock matrix into the fractures--a process which cannot be very much enhanced by increasing groundwater velocities in the fractures, since increasing fracture flow velocity generally only marginally increases the concentration gradient between the rock matrix and the fracture flow system and has no effect on the low diffusivity of the contaminant in the porous medium. Thus, the rate of diffusion and the rate of cleanup are increased only marginally by pump and treat operations under these conditions.

CONCLUSIONS

1. Matrix diffusion can significantly retard the advance of a plume of contamination through a fractured rock, although the retardation is much less in low porosity igneous and metamorphic rock.

2. Cleanup of fractured rock aquifers, particularly more porous sedimentary rocks, can be exceedingly slow if the release of contaminants from the porous rock matrix is diffusion-controlled. This is especially true where an improvement in water quality of greater than 99 percent is necessary.

3. Igneous and metamorphic rocks, because of their typically low matrix porosity and matrix diffusivity, are capable of a more rapid initial restoration in water quality as compared to most sedimentary rocks. As much as a 99.99 percent improvement in water quality is achievable in relatively short periods of time. However, further improvements in water quality (above this level) may be quite time consuming, as the lower matrix diffusivity results in smaller but more persistent diffusion of contaminant out of the rock matrix into the mobile fracture water.

4. The analysis indicates that conventional groundwater extraction and treatment programs, while effective in preventing the further spread of a contaminant plume in an aquifer, are not likely to result in significantly more rapid rates of cleanup even if the wells are pumped at rates much faster than the minimum necessary to prevent further spread of the contaminant. Such overpumping improves aquifer water quality as long as it continues, but contaminant concentrations rebound relatively rapidly to nearly the no action levels upon cessation of pumping.

The persistence of contamination in fractures rock aquifers and the relative ineffectiveness of conventional extraction and treatment remedial programs which our

results indicate lead us to urge that greater emphasis should be placed upon the prevention of contamination in fractured rock aquifers.

REFERENCES

Anderson, M., 1979, "Using Models to Simulate the Movement of Contaminants through Groundwater Flow Systems", *CRC Critical Reviews in Environmental Control* **9** (2), pp. 97-156.

Barone, F.S. et al, 1988, "Effect of Multiple Contaminant Migration on Diffusion and Adsorption of Some Domestic Waste Contaminants in a Natural Clayey Soil", *Can. Geotech. J.* **26**, 189-198.

Barrell, J., 1914, "The Strength of the Earth's Crust", *J. Geol.* **22**.

Bradbury, M.H. and Green, A., 1985, "Measurement of Important Parameters Determining Aqueous Phase Diffusion Rates Through Crystalline Rock Matrices" *J. Hydrol.* **82**, 39-55.

Freeze, R. A. and Cherry, John A., 1979, *Groundwater*, Prentice-Hall, Inc. Englewood Cliffs, NJ

Kelley, V.A. et al" 1987, "Double-Porosity Tracer-Test Analysis for Interpretation of the Fracture Characteristics of a Dolomite Formation", *Proc. of Solving Ground Water Problems with Models Conf.*, NWWA, pp 147-169.

Lever, D.A. and Bradbury, M.H., 1985, "Rock-Matrix Diffusion and its Implication for Radionuclide Migration", *Mineral. Mag.* **49**, 245-254.

Mackay, D.M. and Cherry, J. A., 1989, "Groundwater Contamination: Pump-and-Treat Remediation", *Environ. Sci. Technol.* 23, pp. 630-636.

Manger, G.E., 1963, "Porosity and Bulk Density of Sedimentary Rocks", *U.S. Geological Survey Bull.* 1144-E.

Mutch, Robert D., Jr., Scott, Joanna I., and Wilson, David J., 1993, "Cleanup of Fractured Rock Aquifers: Implications of Matrix Diffusion", *Environ. Monit.and Assess.*, **24**, 45-70.

Neretnieks, I., 1985, "Transport in Fractured Rocks", *Intern. Assoc. of Hydrogeologists Memoirs* **XVII** (1), Proceedings, Hydrogeology of Rocks of Low Permeability, pp. 301-318.

Pankow, J.F. et al., 1986, "An Evaluation of Contaminant Migration Patterns at Two Waste Disposal Sites on Fractured Porous Media in Terms of the Equivalent Porous Medium (EPM) Model", *J. Contaminant Hydrol.* **1** 65-76.

Rasmuson, A. and Neretnieks, I., 1981, "Migration of Radionuclides in Fissured Rock: The Influence of Micropore Diffusion and Longitudinal Dispersion:, *J. Geophys. Res.* **86** (B5), 3749-3758.

Smith, E.D. and Vaughan, N.D., 1985, "Experience with Aquifer Testing and analysis in fractured Low-Permeability Sedimentary Rocks Exhibiting Non-Radial Pumping Response", *Hydrogeology of Rocks of Low Permeability,* Intern. Assoc. of Hydrogeologists, pp. 137-149.

Streltsova, T.D., 1976a, "Hydrodynamics of Groundwater Flow in a Fractured Formation", *Water Resour. Res.* **12**, 405-414.

Streltsova, T.D., 1976b, "Advances and Uncertainties in the Study of Groundwater Flow in Fissured Rocks", *Adv. Groundwater Hydrol.*, pp. 48-56.

Walter, G.R. and Thompson, G.M., 1982, "A Repeated Pulse Technique for Determining the Hydraulic Properties of Tight Formations", *Ground Water* **20**, 186-193.

Yurochko, A.I., 1982, in North, F.K., 1985, *Petroleum Geology,* Allen & Unwin, Boston, MA, 607 pp.

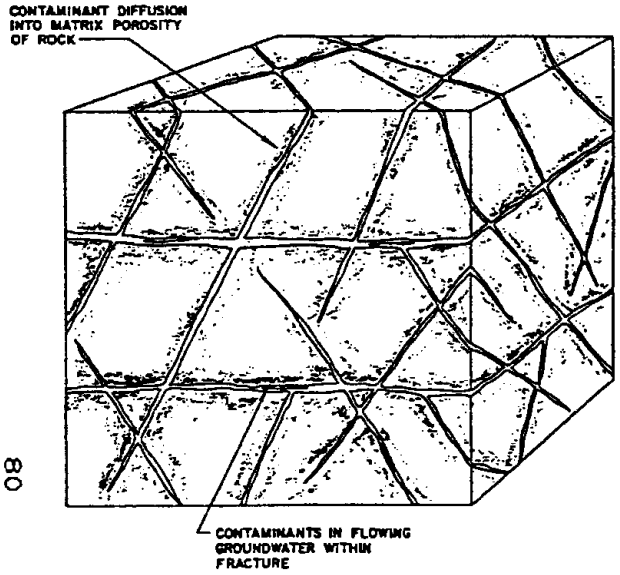

Figure 1
Matrix Diffusion in Fractured Rock Aquifers

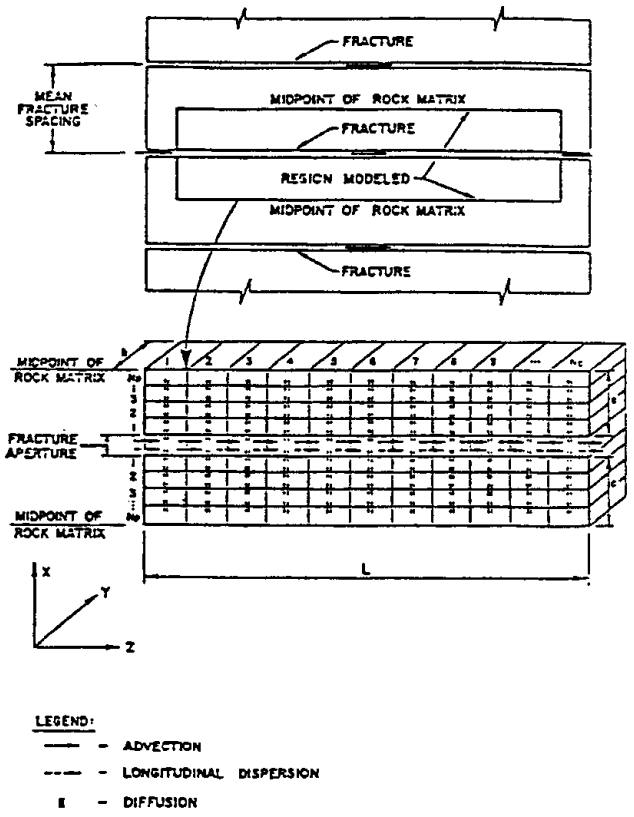

Figure 2
Sketch of the Physical Model and Notation

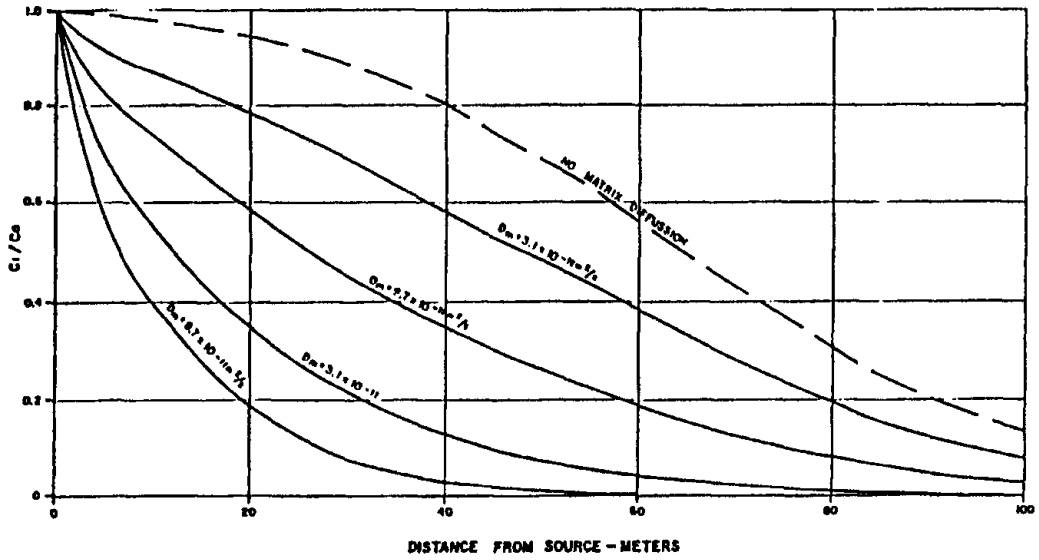

Figure 3
Graph of Relative Concentration Versus Distance From Source at Varying Matrix Diffusivities (T = 5.0 Years)

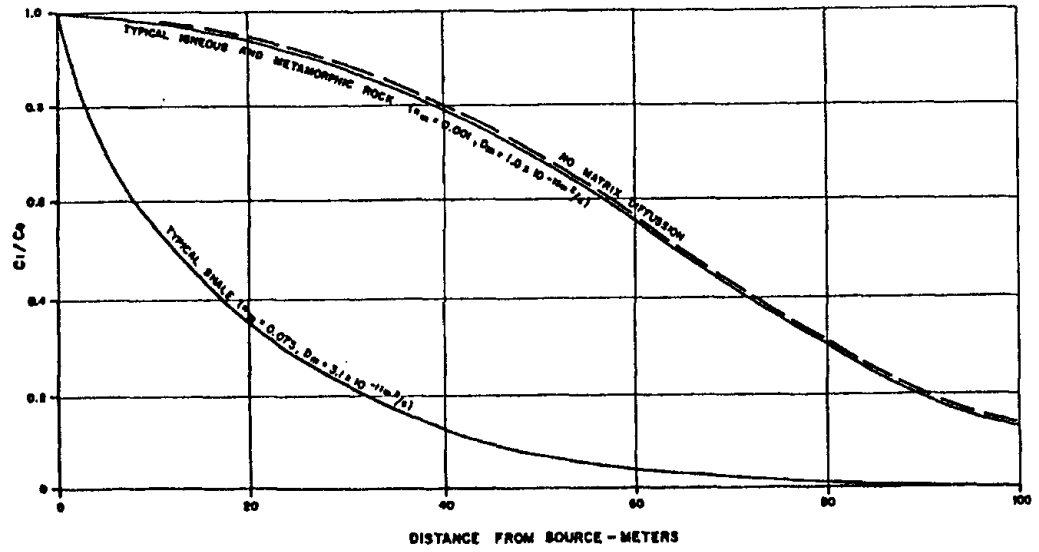

Figure 4
Comparison of the Effective Retardation Effect of Typical Shales and Granites

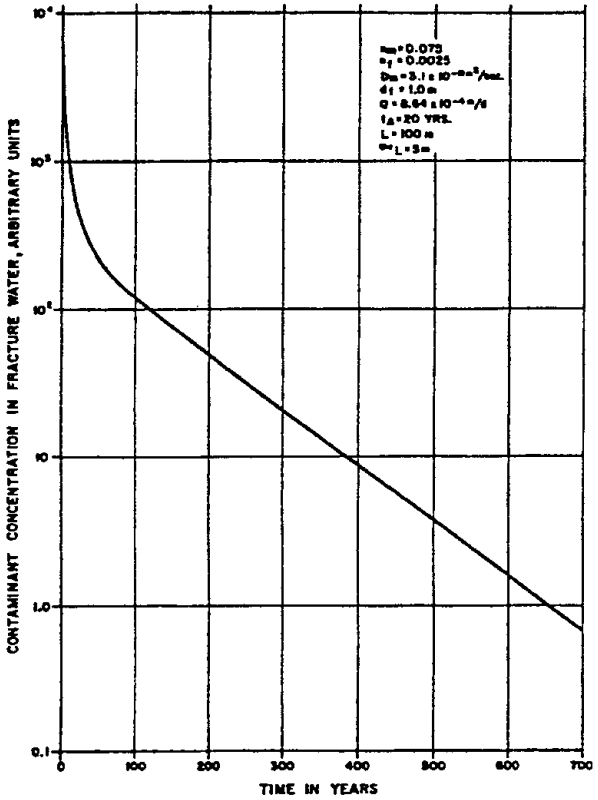

Figure 5
Graph of Aquifer Water Quality Over Time–
Natural Restoration

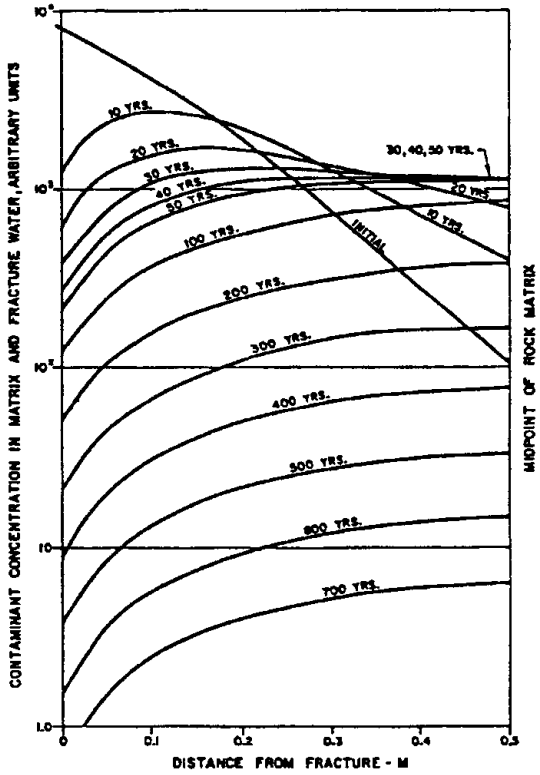

Figure 6
Graph of Matrix Water Quality Over Time

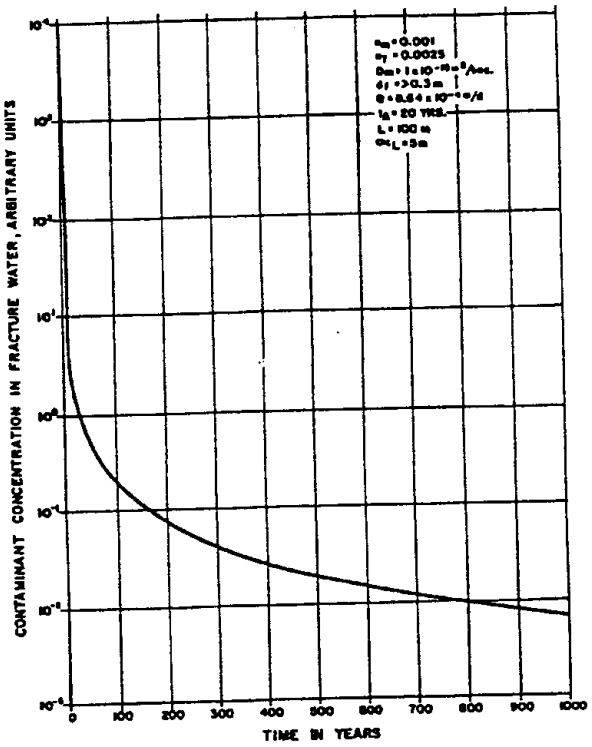

Figure 7
Graph of Aquifer Water Quality Over Time–
Natural Restoration

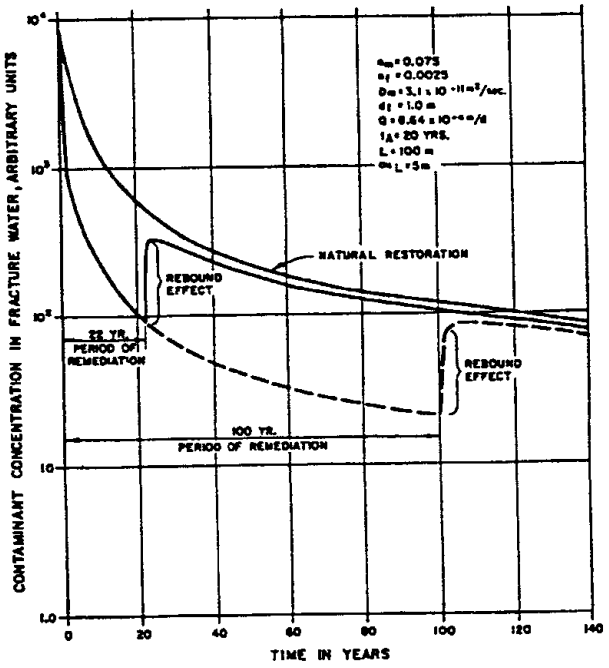

Figure 8
Comparison of Aquifer Clean-up Times for
Natural Restoration and Active Remediation

P085

THREE-DIMENSIONAL DENSITY-DEPENDENT FLOW AND TRANSPORT MODELING OF SALTWATER INTRUSION IN THE SOUTHERN WATER USE CAUTION AREA

Prepared for
Southwest Florida Water Management District
2379 Broad Street
Brooksville, FL 34604-6899

Prepared by
HydroGeoLogic, Inc.
1155 Herndon Parkway
Suite 900
Herndon, VA 20170

Professional Engineer
License No. PE 49883
Date: 7/5/2002

SEAL

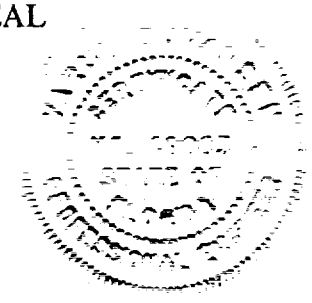

June 2002

04511

TABLE OF CONTENTS

TABLE OF CONTENTS (continued)

Page

LIST OF FIGURES

LIST OF FIGURES (continued)

LIST OF FIGURES (continued)

LIST OF TABLES

ACRONYMS AND ABBREVIATIONS

APT	Aquifer Performance Test
DSTRAM	Density-dependent Solute Transport Analysis
ETBWUCA	Eastern Tampa Bay Water Use Conservation Area
GHB	General Head Boundary
gpm	gallon/minute
LPZ	Lower Permeable Zone
mg/l	milligrams per liter
NGVD	National Geodetic Vertical Datum
ppm	parts per million
ROMP	Regional Observation and Monitor-well Program
SAS	Surficial aquifer system
SCU	Semi-Confining Unit
SWFWMD	Southwest Florida Water Management District
SWUCA	Southern Water Use Caution Area
TDS	total dissolved solids
UPZ	Upper Permeable Zone
USGS	U.S. Geological Survey
Waterstone	Waterstone Environmental Hydrology and Engineering, Inc.
WQMP	Water Quality and Monitoring Program
WUCA	Water Use Caution Area
WUP	Water Use Permit

1.0 INTRODUCTION

1.1 BACKGROUND

The Southwest Florida Water Management District (SWFWMD) is responsible for managing sensitive water resources within 16 counties in west-central Florida (Figure 1.1). Within this area, the SWFWMD is responsible for water supply, water quality, and the protection of natural systems related to water resources. The Floridan aquifer system is the primary source of potable groundwater within the southern portion of the SWFWMD. In this area, approximately 85% of groundwater supplies are derived from the Floridan aquifer system. Saltwater intrusion into the Floridan Aquifer along the coast of southern Hillsborough, Manatee, and Sarasota Counties is a principal constraint on the development of additional groundwater resources in the southern portion of the SWFWMD. Monitoring data collected by the SWFWMD indicates that saline water is slowly advancing further inland due to lowered water levels within the southern portion of the SWFWMD.

In response to this problem, the SWFWMD Governing Board designated the southern portion of the SWFWMD as the Southern Water Use Caution Area (SWUCA) (Figure 1.1). This area included all of the Eastern Tampa Bay and Lake Wales Ridge Water Use Caution Areas (WUCAs) and the areas within the SWFWMD that are south of Interstate 4. In total the SWUCA encompasses 5,100 square mile area including all of Manatee, Sarasota, Hardee, and DeSoto Counties and portions of Hillsborough, Charlotte, Polk, and Highlands Counties. In 1994, SWFWMD staff developed a resource management plan and a set of rules for water resources permitting aimed at limiting saltwater intrusion with the SWUCA. A principal objective of these rules was to protect freshwater resources within the Floridan aquifer system. For the past several years, the SWFWMD has revisited its options for managing groundwater within the SWUCA in an effort to develop additional sources of water for the growing population of the region while continuing to protect existing supplies. Physically based, numerical groundwater flow models of the region have provided an important component to the decision making process.

1.2 PROJECT OBJECTIVES

In October 2001, HydroGeoLogic, Inc. was retained by the SWFWMD to develop a density-dependent groundwater flow and solute transport numerical model to simulate the position and movement of saline water in the Upper Floridan aquifer along the coastal area of the SWUCA (Figure 1.2). The primary objective of this effort was to predict the long-term impact of proposed water use options on saltwater intrusion within the Upper Floridan aquifer. The saltwater intrusion model may be further used to establish minimum water levels or maximum pumping levels for groundwater extraction wells within the Upper Floridan aquifer or for developing a refined understanding of the stress response of chlorides to various regional management scenarios. The density-dependent model was constructed and calibrated to simulate conditions in the Upper Floridan aquifer that existed from the pre-development period (approximately 1900) to present conditions (through 2000). The model was then used to predict the long-term impacts associated with different usage rates for water within the area.

1.3 METHODOLOGY

The modeling investigation was completed in four phases including:

- Phase 1: Background literature review, conceptual model development, and model setup;
- Phase 2: Model calibration;
- Phase 3: Predictive scenarios; and
- Phase 4: Governing board meetings/presentations.

During Phase 1, historical reports and previous modeling investigations were reviewed to understand the hydrogeologic conceptual model, identify model calibration targets, and construct the framework for the saltwater intrusion model. Particular emphasis was placed on reviewing the Southern District Groundwater Flow model developed by the SWFWMD (2001) and an uncalibrated, saltwater intrusion model that was initiated by Waterstone Environmental Hydrology and Engineering, Inc. (Waterstone). These models will henceforth be referred to as the Southern District Model (SWFWMD, 2001) and the Waterstone Model (Waterstone 2001), respectively. Both of these models were provided to HydroGeoLogic in electronic form *via* Groundwater Vistas (Environmental Simulations, Inc.) project files. At the end of Phase 1, the framework for the saltwater intrusion model was established, and preliminary simulations were performed to ensure that all data was correctly entered into the density-dependent model, before proceeding to the Phase II calibration activities.

During Phase 2, the saltwater intrusion model was calibrated to simulate hydraulic heads and chloride concentrations in the Upper Floridan aquifer. The model was calibrated to steady-state pre-development (approximately 1900) conditions and transient conditions from approximately 1900 to 2000. A sensitivity analysis was also conducted, to identify the parameters that have the greatest impact on calibration and conclusions of the model.

Predictive simulations were completed as part of Phase 3 activities. The model was used to predict hydraulic heads and saltwater intrusion (i.e., saline water concentrations) for 20- to 50-year time periods. Four different water use scenarios proposed by the SWFWMD were evaluated. These comprise of withdrawing 400, 600, 800 and 1,000 million gallons per day (MGD) from the Southern District Model (SWFWMD, 2001) area. A predictive sensitivity analysis was also conducted to evaluate the uncertainty associated with the modeling results.

1.4 REPORT ORGANIZATION

This report documents the development of the conceptual and numerical model for saltwater intrusion in the SWUCA. Section 2 documents the hydrogeologic conceptual model, and Section 3 summarizes the previous modeling analyses that provide information and insights that will be utilized during the current modeling effort. Section 4 describes construction of the preliminary model, and Section 5 describes the model calibration effort and results. Section 6 details the sensitivity analysis that was conducted and Section 7 discusses the predictive analysis and predictive sensitivity studies. Finally, Section 8 provides a brief summary of the modeling activities and presents the major conclusions.

2.0 HYDROGEOLOGIC CONCEPTUAL MODEL

2.1 PHYSIOGRAPHY AND TOPOGRAPHY

The physiography of the Eastern Tampa Bay Water Use Caution Area (ETBWUCA) includes three provinces described by White (1970): Gulf Coastal Lowlands, the DeSoto Plain and the Polk Upland. These provinces reflect a series of marine sand terraces formed by the advance and retreat of shallow seas during ice age events. Elevations of these terraces correspond to changes in sea level. Additional physiographic features that lie within the SWUCA include a series of north-northwesterly trending sand ridges found along the eastern boundary of the SWFWMD. The elevation in the study area ranges from sea level along the coast to approximately 150 ft National Geodetic Vertical Datum (NGVD) along the ridges (SWFWMD 1993).

2.2 RAINFALL, EVAPOTRANSPIRATION AND RECHARGE

The climate in the southern SWFWMD is humid, subtropical and is characterized by warm, wet summers and mild, dry winters (SWFWMD, 1993). Based on records since 1911, the mean annual rainfall is about 54 inches per year at Bradenton in Manatee County. During the summer months of June through September, monthly rainfall averaging between 7 and 9 inches accounts for approximately 60 percent of the annual total. The mean evapotranspiration rate estimated for the ETBWUCA is 39 inches per year (Dohrenwend, 1977). According to SWFWMD (1993), nearly 60 percent of the annual evapotranspiration occurs between May and September with the greatest rates usually observed in May and June.

Recharge to the surficial aquifer occurs by infiltration of rainfall and irrigation water. Figure 2.1 depicts areas of recharge and discharge to the Upper Floridan aquifer for pre-development hydrologic conditions (Aucott, 1988).

2.3 HYDROGEOLOGY

Various geologic formations characterized by unconsolidated and consolidated sediments comprise the three principal aquifer systems that underlie the study area as shown in Table 2.1. These include: the surficial aquifer system; intermediate aquifer system; and the Floridan aquifer system. Undifferentiated near-surface deposits of sands, clayey sands and silts with some peat and shell comprise the surficial aquifer system. The intermediate aquifer system corresponds to the Hawthorn Group and generally consists of phosphatic clay and limestone. These near-surface materials in turn overlie the massive marine carbonates, limestones and dolomites of the Floridan aquifer system. Each of the three principal aquifer systems consists of higher permeability aquifer layers that are separated by lower permeability semi-confining layers, which restrict the vertical movement of groundwater between the aquifers.

Four major units comprise the Floridan aquifer system: the Upper Floridan aquifer, the middle confining unit, the Lower Floridan aquifer and the lower confining unit (Figure 2.2). Due to its large thickness and low permeability, the middle confining unit is generally considered as a barrier to flow. The Lower Floridan aquifer in the region is salty, and not a source of potable water.

Consequently, for the purposes of this study, the following discussion of the hydrogeology of the study area will focus on the surficial aquifer system, the intermediate aquifer system, the Upper Floridan aquifer and the middle confining units of the Floridan aquifer system.

2.3.1 Surficial Aquifer

The unconfined surficial aquifer system consists primarily of fine-to-medium grained quartz sands of the Holocene and Pleistocene epochs that range in thickness from 77 feet in south-central Hillsborough County to 19 feet in northern Sarasota County (Basso, 2001). The surficial aquifer generally produces only small quantities of water suitable for domestic purposes. The water table varies seasonally and has depths ranging from near land surface to depths of perhaps tens of feet beneath some sand ridges. Groundwater flow in the surficial aquifer system typically follows local topography and occurs in an east to west direction on a regional scale. Seasonal fluctuation of the water levels is generally less than 5 ft (SWFWMD, 1993). The base of the surficial aquifer system consists of Pliocene age clays and clayey sands that form the top of the intermediate aquifer system.

Basso (2001) cites various studies for the hydraulic properties of the surficial aquifer system. Two aquifer tests conducted in southeast Hillsborough County yielded hydraulic conductivity estimates of 6 and 18 ft/day. A hydraulic conductivity value of 9 ft/day was determined from a pumping test in Hardee County. An aquifer test in northeast Sarasota County resulted in an estimated hydraulic conductivity of 13 ft/day. The specific yield values from these tests ranged from 0.05 to 0.12.

2.3.2 Intermediate Aquifer System

The Peace River and Arcadia Formations of the Miocene age Hawthorn Group comprise the intermediate aquifer system. In general, the interbedded phosphatic clays, sands, gravels, dolomite and thin limestone beds of this system function as a confining unit that separates the surficial aquifer from the Upper Floridan aquifer; however, permeable units are found to exist within the clay matrix. In the ETBWUCA (Figure 1.1), the thickness of the intermediate aquifer system increases to the southwest (the direction of dip) from 230 to over 500 ft (Basso, 2001). While there is no clear pattern of decreasing vertical hydraulic conductivity southward, the increasing thickness acts to restrict vertical flow to the southwest (Waterstone, 2001a).

Three separate flow zones, identified as PZ1, PZ2 and PZ3 (in descending order), and three confining units, designated as UICU, MICU and LICU, occur within the intermediate aquifer system in Sarasota County (Barr, 1996). The lateral continuity of these zones is typically limited. The PZ1 zone is generally absent from the ETBWUCA. The PZ2 zone is more extensive than PZ1, but it is not very productive. The most productive aquifer unit is PZ3 which is mostly represented by the Tampa Member of the Hawthorn Group. In some areas, clays found at the base of the Tampa Member act as a confining unit between the intermediate aquifer system and the Upper Floridan aquifer; in others, the carbonate units of the Tampa Member appear to be in direct hydraulic communication with the Upper Floridan aquifer.

Basso (2001) presents a summary of hydraulic properties for the intermediate aquifer system. Based on the results of 10 falling-head tests conducted on core samples, the mean vertical hydraulic conductivity of the confining units in the system is $5x10^{-4}$ ft/day. The properties of the aquifer units in the system are available from pumping tests. For the PZ2 zone, the estimates of horizontal hydraulic conductivity from three tests showed large variability. Two of the tests yielded values of 0.01 ft/day while the other produced a value of 36 ft/day. Hydraulic conductivities determined from four tests conducted in the more productive PZ3 zone averaged 9 ft/day and varied from 0.3 to 19 ft/day. The groundwater flow direction is generally west to southwest. Seasonal fluctuations of the potentiometric surface may reach 30 ft (SWFWMD, 1993).

Figures 2.3, 2.4 and 2.5 show the leakance distributions of the various confining units of the intermediate aquifer system, as estimated during the calibration of the Southern District Model (SWFWMD, 2001). These leakance values are pertinent to development of the density-dependent, saltwater intrusion model (Section 4).

2.3.3 Upper Floridan Aquifer

Massive carbonates of the Suwannee Limestone, Ocala Limestone and part of the Avon Park Formation comprise the Upper Floridan aquifer in the study area. Each of these stratigraphic units corresponds to distinct hydrogeologic units. The Suwannee Limestone, a cream to tan, sandy, vuggy and fossiliferous limestone, functions as an aquifer unit designated as the upper permeable zone (UPZ). The Ocala Limestone is a white to tan, fine-grained calcavenitic limestone that behaves as a confining unit known as the semi-confining unit (SCU). The upper portion of the Avon Park Formation or lower permeable zone (LPZ) is a brown, sucrosic and fractured dolomite. The direction of groundwater flow in the Upper Floridan aquifer varies seasonally.

According to Basso (2001), the permeability of the UPZ is primarily intergranular. Secondary porosity such as fractures or solution conduits appear to be mostly absent from this unit. The top of the UPZ, which corresponds to the top of the Suwannee Limestone, ranges from about -250 to -450 ft NGVD in the Eastern Tampa Bay WUCA and exhibits a south to southwest dip direction. Figure 2.6 depicts the top of the Suwannee Limestone as assigned in the Waterstone Model (Waterstone, 2001b). The total thickness of this unit varies from 200 to 300 ft. Horizontal hydraulic conductivities estimated for this moderately permeable aquifer are generally uniform. Based on the results of 11 pumping tests, the mean horizontal hydraulic conductivity is 61 ft/day and ranges from 6 to 143 ft/day. Figure 2.7 provides the transmissivity distribution of the Suwannee Limestone over the study area, as assigned in the Southern District Model (SWFWMD, 2001). Transmissivities range from as high as 100,000 ft^2/d under Pinellas County to 16,250 ft^2/d in Sarasota County. Storativity values for this unit vary between $1.0x10^{-5}$ and $6.5x10^{-4}$.

The SCU of the Upper Floridan aquifer is characterized by a fine-grained calcarenitic limestone that typically corresponds to the Ocala Limestone (Basso, 2001). The base of this hydrogeologic unit is defined as the contact with highly permeable fractured dolomites that comprise the LPZ. Because the lower part of the Ocala Limestone may contain a sucrosic dolomitic limestone, the transition from the SCU to the LPZ may occur within the Ocala Limestone or the Avon Park

Formation. The top elevation of the SCU ranges from -500 to -800 ft NGVD in the Eastern Tampa Bay WUCA and dips to the southwest. Figure 2.8 depicts the top of the Semi-Confining Unit as provided by the Waterstone Model (Waterstone, 2001b). The total thickness of the unit is variable, ranging from 200 to 500 ft. The horizontal hydraulic conductivity of the SCU estimated from 16 packer tests ranges of 0.01 to 2.4 ft/day with a mean of 0.53 ft/day. Vertical hydraulic conductivities for this unit have been determined from field and laboratory tests. The vertical hydraulic conductivity estimated from aquifer performance test (APT) at the Region Observation and Monitor-Well (ROMP) TR9-2 site is 0.03 ft/day (Basso, 2001). Vertical hydraulic conductivities determined from 56 falling-head tests conducted on core samples obtained at different depths from 10 different sites within the Eastern Tampa Bay WUCA ranged from $1.0x10^{-7}$ to 2.5 ft/day with a mean of 0.19 ft/day and median of 0.023 ft/day. The APT value probably provides a more realistic estimate of the mean vertical hydraulic conductivity for the entire thickness of the SCU. The leakance distribution of the SCU is uniform with a value of 0.01 day^{-1} in the Southern District Model (SWFWMD, 2001).

The LPZ of the Upper Floridan aquifer is a regionally extensive, highly transmissive, sucrosic and fractured dolomite (Basso, 2001). Conceptually, the top of the LPZ corresponds to the top of the Avon Park Formation, but occasionally the lower portion of the Ocala Limestone also contributes to this unit. Within the Eastern Tampa Bay WUCA, the top of this unit occurs between -700 and -1400 ft NGVD. Figure 2.9 depicts the top of the LPZ as assigned in the Waterstone model (Waterstone, 2001b). The total thickness of this zone varies from 500 to 700 ft. According to Basso (2001), secondary porosity accounts for the permeability of the LPZ, the most productive unit in the Upper Floridan aquifer. Although multiple discrete flow zones are typical with perhaps 100 ft or more of relatively tight sections between individual flow zones, conceptual models of this unit tend to treat it as an equivalent porous medium. Based on eight APTs, the horizontal hydraulic conductivity of this unit varies from 96 to 475 ft/day with a mean of 308 ft/day. Figure 2.10 provides the transmissivity distribution of the Avon Park Formation over the study area, as used by the Southern District Model (SWFWMD, 2001). This transmissivity distribution is subsequently used for developing areal conductivity distributions for the Avon Park Formation in the density-dependent saltwater intrusion model.

2.3.4 Middle Confining Unit

The middle confining unit, composed of interbedded dolostones and evaporites, separates the Upper Floridan aquifer and Lower Floridan aquifer in the Floridan aquifer system (Basso, 2001). The top of this unit ranges from -1,200 to more than -1,700 ft NGVD in the Eastern Tampa Bay WUCA and forms the bottom of the model domain. Figure 2.11 depicts the top of the Middle Confining Unit as provided by the Waterstone Model (Waterstone, 2001). The horizontal hydraulic conductivity determined from five packer tests in the Middle Confining Unit ranges from 0.002 to 0.04 ft/day. No explicit vertical hydraulic conductivity measurements are available for this unit.

2.4 GROUNDWATER SOURCES AND SINKS

Over the past ten years (1989-1998), groundwater withdrawals from the SWUCA fluctuated between 562 MGD (1994) and 832 MGD (1989). Approximately 65 percent of this water is withdrawn for permitted agricultural use. The second largest demand is for public supply, approximately 21 percent. The surficial aquifer system produces only small quantities of water for lawn irrigation and domestic water supply. The intermediate aquifer system is primarily a source of domestic water supply, but occasionally supplements the Upper Floridan aquifer for both irrigation and public supply. Well yields in the intermediate aquifer system generally range from 20 to 200 gallons per minute (gpm). The Upper Floridan aquifer is the principal source of groundwater for water supply. Well yields in the UPZ range from 500 to 1,500 gpm. Wells completed in the highly transmissive LPZ can yield from 1,500 to 5,000 gpm (SWFWMD, 1993).

The Upper Floridan aquifer was once under artesian conditions along the coast, with at least 20 ft of pressure head at the coast. This implies that the Upper Floridan aquifer is well confined by the intermediate aquifer system, and that the intermediate aquifer system and Upper Floridan aquifer both extend a considerable distance offshore. The Upper Floridan aquifer likely subcrops about 120 miles offshore in the Gulf of Mexico where the sea bottom shelves abruptly. Offshore the Upper Floridan aquifer discharges into the Gulf of Mexico, probably mainly through diffuse leakage across the intermediate aquifer system. Potentiometric, water quality, and geologic data suggest that there is an enhanced discharge zone under Hillsborough Bay (Hutchinson, 1983).

In the coastal areas and southern portion of the basin, water levels in the Upper Floridan aquifer are usually higher than in the intermediate aquifer, creating areas of diffuse upward leakage. In these areas, groundwater discharge in the Floridan aquifer is on the order of zero to one inch per year (Barcelo and Basso, 1993).

2.5 GROUNDWATER FLOW DIRECTIONS

Pre-development groundwater flow patterns in the Upper Floridan aquifer are depicted in Figure 2.12 (Johnston, et. al, 1980). Regional groundwater flow is from the Green Swamp potentiometric high located near Polk City, Florida, toward the west/southwest. Major features of the potentiometric surface are the Green Swamp regional potentiometric high and the tendency for the potentiometric contours to wrap around the eastern portion of Tampa Bay, indicating discharge to the bay.

By the mid-1970s, pumping primarily for agricultural use, created a regionally extensive cone of depression at certain times of the year of over 40 feet in places in west-central Manatee County. Because all of the agricultural water use and a large portion of the public supply use are for supplemental irrigation, groundwater withdrawals are inversely correlated with rainfall. Consequently, maximum withdrawals occur near the end of the dry season, sometime in May or June. The potentiometric surface for May 2000 conditions is shown in Figure 2.13. The groundwater flow direction during this time is from the Gulf of Mexico inland. Since the transmissivity of the Upper Florida aquifer is high and the storativity low, most of the head recovery from pumping during the wet period occurs within a few months, resulting in groundwater flow resuming its coastward flow direction. However, recovery to pre-development

conditions does not occur. The potentiometric surface for September 2000 conditions is shown in Figure 2.14. The strong seasonal nature of demand causes considerable variability in the annual demand cycle and produces large fluctuations in groundwater levels during the year.

Barcelo and Basso (1993) provide a comparison of pre- and post-development potentiometric surface conditions. The major changes are that the 20- and 30-foot contours in Hillsborough and Manatee Counties have shifted significantly inland since pre-development, and the 50 to 100 foot potentiometric contours are closely spaced in the high-recharge region of northern Polk County.

2.6 GROUNDWATER QUALITY

2.6.1 General Water Quality Characteristics

The major threat to groundwater quality within the study area is considered to be the intrusion of saline waters, particularly seawater. Water quality in the area is generally good in all the aquifers above the middle confining unit ("evaporites") separating the Upper and Lower Floridan aquifers. In general, water quality degrades with depth and becomes more mineralized as the water flows from east to west along natural flow paths. The water quality also deteriorates from the north to the south as the thickness and depth of the Floridan and intermediate aquifer system increases (SWFWMD, 1993).

Water is generally considered fresh if it contains less than 1,000 mg/l (milligrams per liter) total dissolved solids (TDS), while brackish water ranges from 1,000 to 35,000 mg/l TDS (Clark and others, 1971). The SWFWMD defines saline water as water that is characterized by TDS concentration greater than 500 mg/l (SWFWMD, 1989). A concentration of 35,000 mg/l is considered equivalent to seawater. The State of Florida Drinking Water Standards requires that TDS concentrations for finished water be less than 500 mg/l (FDER, 1989).

There is considerable areal variation in the groundwater quality of the surficial aquifer system within the study area. Generally, the quality of the water in the surficial aquifer system is good except in the tidally influenced areas along the coast (Brown, 1983). Surficial aquifer system water along the coast and rivers is also influenced by lower quality water discharging from below (AGWQMP, 1991). AGWQMP (1991) also reports that chloride and sulfate concentrations in the study area are highest along the coastal reaches of the rivers.

The problem of assessing the water quality of the intermediate aquifer system is complicated by the hydrogeology of the aquifer. The existence of multiple, permeable zones, in poor hydraulic connection, complicates the analysis of water quality distributions (Ambient Ground-water Quality Monitoring Program [AGWQMP, 1990]). There is a lack of water quality data for this system, both spatially and temporally (SWFWMD, 1993). Overall water quality of the intermediate aquifer system is good (SWFWMD, 1993). Major ion concentrations in groundwater of the intermediate aquifer system are generally higher than ion concentrations observed in the surficial aquifer but lower than ion concentrations observed in the Floridan aquifer system (AGWQMP, 1990). The exception to this general observation is along the coast where chloride concentrations are frequently elevated (AGWQMP, 1990).

In the east and northeast areas of the study area, Upper Floridan aquifer water is principally of a calcium-magnesium-bicarbonate-sulfate type water of good quality (SWFWMD, 1993). Down gradient, to the west and southwest, the water changes to a sodium magnesium chloride type, similar to seawater. This down-gradient water of the Upper Floridan aquifer is of variable to poor quality (Steinkampf, 1982).

2.6.2 Saltwater Intrusion

In the coastal aquifers within the study area, lower density freshwater overlies denser seawater. The seawater and freshwater meet and blend in the aquifer to form a transition zone. The transition zone in the Upper Floridan aquifer ranges in thickness from about one hundred feet to several hundred feet (Beach and Kelley, 1998). The thickness depends on the conductivity of the subsurface matrix and the flow rate through the system. Chloride concentrations are the usual indicator of the transition zone existence. Chloride concentrations on the freshwater side (east) are often less the 50 mg/l and approach 19,000 mg/l on the seaward side (west) (Beach and Kelley, 1998). The ROMP wells located in Figure 2.15 provide the best quality information on chloride values at various depths within the study area. In general, the saltwater interface gets deeper from north to south. These depths generally coincide with a highly permeable zone within the Avon Park Formation. In addition, north of the Manatee River the transition zone is relatively sharp; while south of the river, the transition zone becomes more diffuse. This comparison is illustrated by the following discussion of water quality near Apollo Beach and Osprey, Florida (SWFWMD, 1993).

Near Apollo Beach an exploratory well (ROMP TR9-2) was cored to 819 feet and completed 1,254 feet below land surface (Figure 2.15). Based upon the observed relationship between chloride concentration and depth, the transition zone begins at a depth of 740 feet below land surface, and seawater is encountered at about 840 feet below land surface. The concentration of chloride is approximately 100 mg/l, or less, until the interface is contacted. This is slightly above the upper limit for ambient chlorides in Eastern Tampa Bay area from non-marine sources (Steinkampf, 1982). Above the interface, sulfate is the predominant anion. However, chloride replaces sulfate as the predominant anion below the transition zone.

Exploratory drilling near the city of Osprey began in 1991 (i.e., ROMP 20 site) (SWFWMD, 1993). Beginning at depths of 650 feet below land surface, the chloride concentrations began to increase above 100 mg/1. Chlorides increased gradually to a concentration of 2,230 mg/l at a depth of 1,439 feet below land surface where coring was discontinued. Subsequent thief sampling from the bottom of the well produced samples with chloride concentrations equivalent to seawater.

In 1991, AGWQMP conducted mapping exercises to delineate the chloride interface. More recently, Beach and Kelley (1998) projected the freshwater-seawater interface onto hydrogeologic cross sections at six locations along the coast (Figure 2.16). The cross section locations were selected where the SWFWMD has completed water quality explorations during drilling of ROMP wells (Figure 2.15). Detailed water quality data, often based on packer tests and thief samples, are available from these locations.

Based on exploratory drilling in the coastal regions of the SWUCA, the transition zone usually occurs in the upper portions of the Avon Park Formation within the Upper Florida aquifer. This represents the deepest production zone of the aquifer. In coastal Sarasota and Charlotte counties, the transition zone may occur within the Suwannee Limestone of the Upper Florida aquifer (Beach and Kelley, 1998). The transition zone may occur in the intermediate aquifer system when wells are drilled on the barrier islands or very near the coast. Exploratory wells completed in the surficial aquifer system (SAS) rarely encounter the transition zone although the transition zone may be present where such wells are adjacent to coastal surface water bodies (e.g., bays and estuaries) (Beach and Kelley, 1998).

The locations where multiple sites exist near the cross section were pivotal in this analysis. Multiple explorations along a transect permit estimates to be made as to the slope of the interface. Where a cross section had only one well to reference, the slope was interpolated from adjacent cross sections (Beach and Kelley, 1998). The interface line for each section was extended to the middle confining unit. The plane of the interface has a slight slope (0.5 to 3 degrees) downward as the interface dips landward (Beach and Kelley, 1998). The location where the interface intersects the bottom of an aquifer is known as the toe and defines the landward extent of seawater in the aquifer.

The distance along each cross section to the toe was superimposed onto a map. A smooth line through each toe was drawn delineating the 1,000 mg/l chloride concentration defining the areal extent of the interface between the freshwater and saltwater (Figure 2.16). This approach was later updated (Beach and Schultz, 2000) by delineating the top and bottom of the "highly permeable zone" within the Avon Park Formation from exploratory drilling data and adding this information to each cross section. Where exploratory drilling data was inadequate, the top of the "highly permeable zone" was derived from Miller (1986). The point on the cross sections where the interface exits the bottom of the "highly permeable" zone of the Avon Park was determined to be the toe of the interface.

Beach and Schultz (2000) determined that the current position of the interface toe in the Avon Park Formation is only two to three miles inland in south Hillsborough County. In Sarasota County, the interface toe in the Avon Park may be as much as ten miles inland. Beach and Schultz (2000) also provide estimates for future positions of the toe after 50 years of pumping at different levels (Figure 2.17). The estimates indicate that future movement will be greater in south Hillsborough County than in northern Sarasota County. Application of the Ghyben-Herzberg principal indicates that ultimately Sarasota County would be affected to a greater extent than Hillsborough or Manatee Counties (Beach and Schultz, 2000).

Appendix A shows the variation of chlorides with depth for various ROMP wells within the study area. Due to the high quality of spatial chloride distributions provided by this data, it is used for calibrating the density-dependent saltwater intrusion model.

2.6.3 Saltwater Intrusion Potential Risk

The risk of a well to saltwater intrusion is a function of at least four factors: (1) the completed depth of the well; (2) the proximity of the well to the coast; (3) the amount of water withdrawn

in the vicinity of the well; and (4) the local and regional properties of the aquifers and confining units (Beach and Kelley, 1998). Typically, deeper wells are closer to the transition zone and saline water. The closer a well is located to the coast, the thinner the freshwater zone. The greater the withdrawal quantity, the more likely wells are to induce local saltwater upconing from the transition zone. The distribution of hydraulic conductivity is the most important local and regional property of the aquifers and confining units, which affects the potential for saltwater intrusion. Sediments characterized by higher hydraulic conductivity values allow the interface to move more quickly under a given change in potential. Hydraulic conductivity heterogeneity is the variation in hydraulic conductivity that occurs from place to place in the aquifer and confining units. Frequently, hydraulic conductivity heterogeneity is caused by spatial or vertical variations in fracture density and/or distribution; lithologic properties; or distribution and magnitude of secondary dissolution features (i.e., karst conduits). Heterogeneity is the principal factor that accounts for multiple wells being affected to different extents by saltwater intrusion when all the wells are completed to the same depth, are located the same distance from the coast, and are located in similar withdrawal environments (Beach and Kelley, 1998).

Based on the four risk factors above, wells completed in the Avon Park Formation are generally at the greatest risk of experiencing saltwater intrusion. The Avon Park Formation of the Upper Floridan aquifer is a highly prolific water-producing unit due to its very high hydraulic conductivity. The high hydraulic conductivity results from a horizontal interval, about 100 to 400 feet thick, characterized by considerable fracturing and secondary porosity. This interval is frequently referred to as the "highly permeable" or "fractured" zone of the Avon Park Formation. Although this highly permeable zone comprises only 10 to 25 percent of the Avon Park thickness, as much as 95 percent of the Avon Park water production may be derived from this zone (Beach and Schultz, 2000). The remainder of the formation is characterized by relatively low permeability and limited groundwater production. For this reason, the Avon Park Formation wells are usually completed in the highly permeable zone.

Most exploratory drilling in coastal areas of Hillsborough, Manatee and Sarasota counties have located the seawater transition zone in the upper portions of the Avon Park. Increasing temporal trends in chloride concentration data from dedicated monitoring wells occur most frequently in wells completed in the Avon Park Formation. Based on that data, Beach and Kelley (1998) conclude that wells in Hillsborough and Manatee counties, completed in the Avon Park Formation and located within four to five miles to the coast, are most likely to experience saltwater intrusion in the near future. For the purposes of their discussion, the "near future" is considered to be within the next five or ten years (from 1998). On the other hand, wells completed above the toe of the interface would probably not experience saltwater intrusion within present long-term planning periods, generally out to 2025 (Beach and Kelley, 1998). These estimates assume no change in current withdrawal rates and patterns.

Avon Park Formation wells in Charlotte and DeSoto Counties already withdraw very poor quality water. The transition zone is more diffuse in these counties than in Hillsborough and Manatee Counties (Beach and Kelley, 1998). Data from exploratory wells in the area show the influence of seawater well into the Suwannee Limestone although chloride concentrations are somewhat less than 1,000 mg/l.

Based on the four risk factors, coastal Suwannee Limestone wells are at much less risk of saltwater intrusion than similarly located wells completed in the Avon Park Formation (Beach and Kelley, 1998). Generally, the lower hydraulic conductivity of the Suwannee Limestone is less susceptible to saltwater intrusion. Wells that appear to be a greatest risk are those located within several miles of the coast in Charlotte and southern Sarasota Counties (Beach and Kelley, 1998). Relatively high chloride concentrations, 570 to 1,800 mg/l were encountered in the Suwannee Limestone during exploratory drilling in those counties (i.e., ROMP 5, ROMP 9, and ROMP TR 4-1). In Hillsborough and Manatee Counties, there are a large number of Suwannee Limestone production wells located within several miles from the coast (Beach and Kelley, 1998). Based on water quality data from dedicated monitoring wells in the area, chloride concentrations range from 200 to 500 mg/l (ROMP TR 9-2, ROMP TR 9-3). However, there are no increasing trends in these data, unlike similar data from the Avon Park Formation dedicated monitoring wells at the same locations (Beach and Kelley, 1998). It has been demonstrated that such concentrated pumping from the Suwannee Limestone, as occurs in the area, could cause the interface to be pulled up into the Suwannee Limestone from the Avon Park Formation over the next 50 years (HydroGeoLogic, Inc, 1994a).

Regionally, the intermediate aquifer system and surficial aquifer system wells are at little risk of saltwater intrusion. However, there are local problems for intermediate aquifer system and surficial aquifer system wells in Manatee, Sarasota and Charlotte Counties that are located less than a mile from the coast or barrier islands (Beach and Kelley, 1998). The transition zone on the barrier islands is usually located in the intermediate aquifer system. The Water Use Permit (WUP) wells located on the barrier islands of northern Sarasota County are known to have experienced considerable degradation from saltwater intrusion for many years (Beach and Kelley, 1998). This is also true for many of the shallow intermediate and surficial aquifer system wells along the southwest coast of the area.

2.7 IMPLICATIONS OF CONCEPTUAL MODEL COMPONENTS AND UNCERTAINTY ON THE NUMERICAL MODEL

One primary goal of mathematical modeling is to synthesize the conceptual model into numerical terms from which flow and transport processes may be investigated under specified conditions. This process entails several discrete steps: (1) partitioning the conceptual model into units of time and space; (2) assignment of boundary conditions; and (3) specification of the parameter values. There are always uncertainties in predictions derived from modeling. These uncertainties are frequently divided into two main categories: 1) conceptual model uncertainty; and 2) parameter uncertainty. This section briefly describes these uncertainties and the approach that will be applied to address these uncertainties in the model calibration process.

The conceptual model is based on the modeler's experience and technical judgment and represents the modeler's understanding of the system framework and behavior, from all available data and information of a site. The conceptual model will naturally become more complex as more processes are identified and interrelationships of important components within the systems are considered. The transformation of the conceptual model into a mathematical model, is a further extrapolation of the basic understanding of the system, resulting in intrinsic simplifications of the system. For example, the mathematical model assumes that there is a direct scaling between the

model simulations and the scale at which the data are collected. The lack of knowledge about the system resulting from limited information also contributes to inevitable simplifications in the conceptual and mathematical models. Based upon the data and model review a number of conceptual model uncertainties have been identified and are presented in Table 2.2. This table also describes the methods that will be applied to address the primary uncertainties during the model calibration.

In addition to the conceptual model uncertainties, there are always uncertainties in the parameter values that are assigned in the model. As specified in the Work Order agreement between the SWFWMD and HydroGeoLogic, sensitivity analyses will be conducted to address parameter uncertainties during the model calibration. Sensitivity analyses will be conducted for key parameters (which may be performed on the pre-development or post-development model depending upon significance). Parameter sensitivities will be determined by varying a specific parameter and evaluating the change in hydraulic heads and/or chloride concentrations thus simulated. Depending upon the results of this initial sensitivity analyses, multiple parameters may be simultaneously perturbed during subsequent sensitivity analyses. Based on the results of the sensitivity analysis, the parameters will be categorized following the protocol developed by the American Society of Civil Engineers (ASCE) to determine the parameters of greatest concern. This approach will serve to provide recommendations for future data collection, as well as to design sensitivity simulations that will be conducted during the next phase of the project to evaluate prediction uncertainties.

3.0 SUMMARY OF PREVIOUS MODELING STUDIES

Over the last 15 years, a number of models have been constructed in the SWFWMD to address the problem of deteriorating groundwater quality due to lateral intrusion of seawater or the upconing of highly mineralized water from deeper stratigraphic units. One of the first documented studies is by Hutchinson (1983) in which a two-dimensional areal freshwater model was used to study the effects of the channelization in Tampa Bay and the effects of pumping in the vicinity. Wilson (1982) also used an areal freshwater model to predict the effect of pumping on the potentiometric surface in the west-central Florida area. Both investigators estimated the current location of the seawater-freshwater interface and estimated the rate of advancement using the freshwater flow velocity at the interface.

Mahon (1988) performed a cross-sectional analysis to evaluate the potential for saltwater intrusion in Hernando and Manatee Counties. Mahon conceptualized the Upper Floridan aquifer as having an upper permeable zone, semiconfining unit, and a lower permeable zone. Each hydrostratigraphic layer was divided into several computational layers for solute transport. The top of the middle confining unit was assumed to be impermeable, the intermediate aquifer system was explicitly simulated, and the surficial aquifer system was set as a constant pressure to provide a source for downward leakage to the intermediate aquifer system. The lateral freshwater flux on the landward model edge had to be lowered relative to the initial estimates in order to bring the approximate location of the interface to a reasonable location from its initial location somewhere in Tampa Bay.

HydroGeoLogic (1991a, b, and c) performed variable density flow and transport cross-sectional analyses (Figure 3.1) for three representative cross-sections in the Manatee-South Hillsborough Water Resources Assessment area where a large, groundwater depression was observed (Figure 2.9). The numerical code DSTRAM (Density-dependent Solute TRansport Analysis finite-element Model) was applied. For each cross-section, the model was first calibrated against steady-state pre-development conditions. Flow boundaries for the cross-sectional models were defined as a combination of flux and prescribed head boundaries based on the pre-development potentiometric surface map of the Upper Floridan aquifer. The middle confining unit at the bottom of the Avon Park were considered a no-flow boundary. Both Sinclair (1979) and Guyton and Associates 1976 report that highly mineralized water was found in this evaporites zone. Thus, along the bottom boundary, chloride concentrations were normalized to seawater (i.e., set equal to 1, which is representative of a chloride concentration of 18,000 mg/l). Hutchinson (1983) found that the water samples taken at Hillsborough Bay are slightly less saline than seawater (approximately, 14,400 mg/l). Therefore, the seaward boundary of the B-W cross-sectional model (HydroGeoLogic, 1991a) was assigned a concentration of 14,000 mg/l. Sensitivity analyses were subsequently performed to determine relative influences of changes in key parameters on system responses. Two post-development scenarios were simulated in a transient manner and are representative of the most pessimistic and optimistic conditions over a 100-year simulation period.

Model predicted chloride concentrations associated with pre-development conditions are shown on Figure 3.1 for the intermediate aquifer system. Modeling results along cross section B-W indicate that the length of the transition zone at the top of the Avon Park Formation is about 4

miles while at the bottom it is about 1 mile. The model predicted that chloride concentrations in wells constructed at the shoreline would range from 900 ppm to 17,000 mg/l over a depth of 250 feet in the Avon Park Formation. The vertical transition zone predicted by the model is more gradual than suggested by earlier field investigations. The authors note that the simulated transition zone can be made thinner by reducing the dispersivities and the element size further.

The second cross section, section M-S, passes through the city of Sarasota in Sarasota County, and terminates in the Gulf of Mexico (Figure 3.1). As shown in the figure, the pre-development 1,000 mg/l chloride isochlor in the Tampa/Suwannee layer is located somewhat west of the city of Sarasota. In the Avon Park, however, the 1,000 mg/l chloride is located approximately 6 miles east of Sarasota.

The third cross section, section H-M, is located along the Hillsborough-Manatee County border and lies in the middle of a large potentiometric depression during the dry season (Figure 2.9). Chloride concentration isochlors indicate that the chloride transition zone is very narrow which is consistent with field data indicating that wells located further inland and tapping the Tampa/ Suwannee and Avon Park Formations depict very small chloride concentrations values, as reported by Brown (1983).

During post-development simulations, the transition zones advanced landward in all three cross sections, however, with varying degrees. In the worst case scenarios the maximum advancement of 3 to 5 miles was observed in the southernmost section (S-M) while at most 2 miles of advancement was observed in the northernmost section (B-W).

In all three cross sections, the response of the saltwater-freshwater transition zone to the imposed conditions was more significant in the lower producing zone (the Avon Park Formation) of the Upper Floridan than in the upper producing zone (the Tampa/Suwannee Formation). Sensitivity analyses indicated that the results are very sensitive to vertical hydraulic conductivities of the confining units, particularly the Intermediate aquifer system.

Barcelo and Basso (1993) implemented a quasi-three dimensional MODFLOW modeling effort to assess regional groundwater flow in the eastern Tampa Bay WUCA. The flow model consisted of three layers to simulate groundwater flow within the Intermediate and Upper Floridan Aquifers and the vertical exchange of water between the surficial, intermediate and Upper Floridan Aquifers.

Although the Upper Floridan Aquifer has two major production zones (i.e., Suwannee Limestone, Avon Park Formation), the aquifer is conceptualized as a single hydrologic unit. Referring to the Upper Floridan Aquifer, Ryder (1982) noted that "despite the large permeability contrasts, aquifer-test results indicate that there is enough vertical interconnection between each formation to consider the Floridan Aquifer a single hydrologic unit." Menke (1961) noted that in Hillsborough County, the connection between the upper and lower production zones is such that "...when the time of interchange of water is great and the amount of water interchanged is small..." the system behaves as a single aquifer. The concept of treating the Upper Florida aquifer as a single hydrologic unit was further investigated by Guyton and Associates (1976). During an aquifer test of the Avon Park Formation that was performed in Manatee County, measured water

levels in two wells that were open to the different production zones were nearly identical. This conceptualization will be revisited for the saltwater intrusion model because it may not be adequate to investigate chloride intrusion.

Barcelo and Basso (1993) calibrated their model to steady-state, annual-average hydrologic conditions for calendar year 1989. Following the steady-state calibration, a transient calibration/ verification was performed to evaluate the response of the model to changes in hydrologic stress. The transient calibration was conducted for the period from October 1988 through September 1989.

As a means of evaluating the steady-state calibration effort during the calibration phase, the investigators periodically removed pumping from the model and the model was used to simulate pre-development hydrologic conditions. Because the original parameter estimates were based in part on a groundwater flow model that had been calibrated to pre-development conditions (Ryder, 1985), it was decided that emphasis should be placed on calibrating the model to more recent stressed conditions rather than calibrating to pre-development conditions. Calibration to pre-development conditions enables a determination of the areal distribution of the aquifer parameters without incurring the error associated with estimating water use; however, the authors believed that the pre-development target heads are not sufficiently well known. Although there is some degree of confidence in the pre-development potentiometric surface of the Upper Floridan aquifer (Johnston and others, 1980) there is no published map on the pre-development head distribution of the Intermediate Aquifer (Barcelo, and Basso, 1993).

In 1992, HydroGeoLogic developed a computer code called SIMLAS for the SWFWMD to simulate saltwater intrusion using a sharp-interface technique. The sharp interface technique assumes that the freshwater and the saltwater are immiscible and that the transition between the two liquids is abrupt. This assumption along with the Dupuit-Forchheimer approximation replaces the density-dependent flow and transport equations with a pair of flow equations for freshwater and saltwater. The two flow equations are still coupled, but are less prone to numerical difficulties than the variable density flow and transport equations for large scale simulations.

Two sharp-interface models were subsequently developed using SIMLAS (HydroGeoLogic, 1993; 1994b) to extend the work of Barcelo and Basso (1993) to include the dynamics of saltwater. One of HydroGeoLogic's objectives was to compare the sharp interface formulation in SIMLAS to the fully coupled density-dependent approach in DSTRAM. In order to make this comparison, the southernmost cross section (M-S) from HydroGeoLogic's 1991 study was selected. This southern cross-section was chosen, primarily because a well defined narrow transition zone exists in both lower and upper aquifer layers. Results indicated that the two numerical solutions are in good agreement when the effects of dispersion in the DSTRAM model are negligible. For zero dispersion, the only major difference between the two modeling approaches is the Dupuit-Forchheimer assumption employed in the sharp-interface formulation.

The saltwater-freshwater interface in the Upper Floridan aquifer was predicted by the SIMLAS model to occur over a large area. As shown in Figure 3.1, the predicted toe location is considerably further inland than in the Intermediate Aquifer System. The modeling results also indicted that when the leakance of the lower confining bed of the Intermediate System is reduced

(by a factor of 3), both the tip and the toe positions are pushed toward the coastline (west). However, the shift is much more pronounced for the tip than for the toe. Similar behavior was observed between the cross-sectional and areal simulations; the toe moved toward the coastline roughly five miles whereas the tip moved all the way to the offshore boundary.

Post-development simulations were also performed which concluded that after 500 years of pumping under post-development conditions, little change was observed on the position of the interface in the intermediate aquifer system. The toe of the interface in the Upper Floridan Aquifer, however, moved inland up to six miles in the northern half of the model domain. The tip of the interface hardly moved revealing the tightness of the overlying confining layer. The interface in the southern half of the model domain showed little change to the applied stress.

Major conclusions of these studies were that the Upper Floridan aquifer may need to be divided into major producing and confining zones, and that the leakance of the intermediate aquifer system should be adjusted to move the tip inland. In particular, the 1994 study showed that the MODFLOW-derived leakances offshore needed to be increased by a factor of 10 in order to avoid simulating the interface too far offshore.

In another variable density flow and transport analysis, HydroGeoLogic (1994c) performed two extensive cross sectional investigations of long-term pumping effects on chloride levels in the northern and southern regions of the ETBWUCA. The location of the toe of the pre-development interface at both cross sections is shown in Figure 3.1. With respect to the boundary conditions, Hillsborough Bay seawater was assigned a slightly lower (14,400 mg/l) chloride concentration than seawater (18,000 mg/l). The bottom of the model was placed at the top of the middle confining unit and assigned a concentration of seawater. However, no fluid flow was allowed along this bottom boundary. The system was found to be most sensitive to the vertical hydraulic conductivity of the evaporite zone and the horizontal hydraulic conductivity of the Avon Park formation. Recharge to the top of the Upper Floridan aquifer mainly affected heads with minor effects on chloride distributions, but both heads and chlorides were sensitive to the middle confining unit hydraulic conductivity.

All of the above models assumed that the fractured LPZ may be represented as an equivalent porous medium. Waterstone (Waterstone, 2001a), however, provides a discussion on alternative conceptualizations involving dual porosity, discrete fracture and dual permeability conceptualizations and their potential affects on groundwater flow and chloride migration. Waterstone concludes that an equivalent porous medium approach will adequately describe flow and transport through the LPZ.

4.0 NUMERICAL MODEL CONSTRUCTION

4.1 MODELING APPROACH

The following section describes the approach used to construct a density-dependent groundwater flow and solute transport model to simulate saltwater intrusion in coastal portions of the SWUCA. The framework for the saltwater intrusion model has been developed based on the conceptual model presented in Section 2.0. In addition, information derived from other modeling investigations has provided valuable information for the development of the current model. In particular, the regional groundwater flow model developed by the SWFWMD (2001) and an uncalibrated, local-scale, saltwater intrusion model developed by Waterstone (2001a, 2001b) have provided significant data that have been used for the preliminary construction of the current model.

As discussed in Section 3.3, the computer code MODFLOW (MacDonald and Harbaugh, 1988) has been applied by several models in the SWFWMD for simulating groundwater flow within the SWUCA. These models have culminated into the Southern District Groundwater Flow Model (SWFWMD, 2001), a regional MODFLOW model that integrates and updates previous models. This regional groundwater flow model, transmitted electronically (via Groundwater Vistas project files) to HydroGeoLogic, Inc. by the SWFWMD (SWFWMD, 2001), forms the basis for the current study. The primary objective of the Southern District Model was to provide a groundwater management tool to the SWFWMD. Currently, the SWFWMD is further updating the calibration of the regional groundwater flow model, but large changes to the model are not anticipated (Beach, pers. comm., 2001). Therefore, the Southern District Model of June 11, 2001 provided by the SWFWMD has been used to construct the current saltwater intrusion model. Since a report documenting the regional modeling effort is not completed, critical information related to the Southern District Model and its uncertainties have been acquired through numerous conversations with the SWFWMD and a thorough review of model input and output files.

Groundwater Vistas project files associated with an uncalibrated saltwater intrusion model developed by Waterstone (Waterstone, 2001b) have also been used to a certain extent in the current modeling effort. Specifically, the grid employed for their study, including hydrostratigraphic elevations and layering geometry, was also adopted for the current modeling investigation.

As will be discussed in greater detail in the sections that follow, both the Waterstone Model (Waterstone, 2001b) and the Southern District Model (SWFWMD, 2001) electronic data files were used to construct and initialize the density-dependent saltwater intrusion model. The regional MODFLOW model files were used primarily to assign hydraulic properties and boundary conditions, since the density-dependent model is conceptually based on the regional study. Alternatively, the Waterstone (Waterstone, 2001b) model files provided by the SWFWMD were used to assign the model domain, grid spacings and layer thicknesses to the density-dependent model, since these were acceptable to the SWFWMD for the previous study, and were reasonable for the goals and scale of the current study.

When the density-dependent model was constructed, it was first used to simulate groundwater flow only, to establish that the translation from regional to local grids was appropriate and that the simulated pre-development conditions for both models are the same. Once these "basecase" conditions were established (Section 5.1), the saltwater effects were incorporated into the density-dependent model. Parameter values (e.g., hydraulic conductivities) were, to a certain extent, adjusted from the basecase conditions during calibration of the density-dependent, saltwater intrusion model (Section 5.0), because the regional flow model does not include the affects of chloride concentration which affect groundwater flow.

4.2 COMPUTER CODE SELECTION AND OVERVIEW

The computer code MODHMS was selected for construction of the flow and solute transport model (HydroGeoLogic, 2000). MODHMS is a MODFLOW-based code developed by HydroGeoLogic for evaluating complex hydrologic and hydrogeologic settings. The density-dependent transport capabilities of MODHMS have been incorporated from DSTRAM, which is a well established and applied saltwater intrusion model developed by Huyakorn and Panday (1991). The MODFLOW structure of MODHMS provides several features that are attractive for use in this study. First, it makes the code fully compatible (in terms of numerical approximations, grid structure as well as input/output data structures) with the other MODFLOW- based models (regional as well as local) developed by the SWFWMD. Further, the MODFLOW framework of MODHMS allows for use of any of the pre- and post-processing tools developed for use with MODFLOW. Specifically, Groundwater Vistas (Environmental Simulations, Inc.) provides support to the additional modules of MODHMS used for density-dependent modeling. This is advantageous because the SWFWMD has developed the Southern District Model in Groundwater Vistas, and that model can be directly translated to MODHMS framework. In addition, all the MODFLOW features are available for use within MODHMS including a wide range of boundary conditions such as drains, streams, general-head conditions, and those involving water table conditions, infiltration, aquitard leakages, and pumping and injection wells. For contaminant transport simulation, MODHMS accounts for advection, anisotropic hydrodynamic dispersion (with separate areal and vertical components for the longitudinal and transverse dispersivities essential in such groundwater systems as encountered by the SWFWMD), linear equilibrium sorption, and first-order degradation.

The MODHMS code was selected for this study because of the following reasons:

- The code is fully documented and has been successfully applied to problems of similar complexity. For instance, the DSTRAM models for the Seminole County and East Orange County saltwater intrusion studies (Panday et al., 1994, HydroGeoLogic, 1998) were translated to MODHMS and transient as well as steady-state results were demonstrated to be accurate. MODHMS has also been verified against problems with known solutions.

- MODHMS employs the most advanced solution and matrix computation techniques available. The transport equation uses advanced flux-limiting Total Variation Diminishing (TVD) schemes to control unphysical oscillations and minimize numerical diffusion. The code has robust (Preconditioned Conjugate Gradient and Orthomin) matrix solvers unavailable in other standard codes which make it more efficient and versatile.

- MODHMS can quickly extend the Southern District Model developed by the SWFWMD under Groundwater Vistas, to include the density-dependent saltwater transport regime. Conversely, changes made within the calibrated saltwater intrusion model may be quickly and easily incorporated into the Southern District Model. Compatibility among all SWFWMD models allows for consistency and defensibility of results across models.

MODHMS is an extension to the USGS three-dimensional finite difference groundwater flow code, MODFLOW (McDonnald and Harbaugh, 1988), and is capable of simulating density-dependent, single-phase fluid flow and solute transport in saturated porous media. The code is applicable for complex situations where the flow of fluid (groundwater) is influenced significantly by variations in solute concentration. MODHMS can perform steady-state and transient simulations, and a wide range of boundary conditions can be accommodated. For contaminant transport simulation, MODHMS accounts for advection, hydrodynamic dispersion, linear equilibrium sorption, and first-order degradation. When MODHMS is used to simulate the combined processes of density-dependent groundwater flow and solute transport, the code solves two coupled partial differential equations: one for density-dependent fluid flow and one for the transport of dissolved solutes (e.g. chloride).

The governing equation for three-dimensional flow of a mixture fluid (i.e., water and salt) of a variable density in an aquifer system can be written in the form

$$\frac{\partial}{\partial x_i}\left[\rho\frac{k_{ij}}{\mu}\left(\frac{\partial p}{\partial x_i} + \rho g e_j\right)\right] = \frac{\partial}{\partial t}(\phi\rho), \qquad (4.1)$$

$$i,j = 1,2,3$$

where p is fluid pressure, k_{ij} is the intrinsic permeability tensor, ρ and μ are the fluid density and dynamic viscosity, respectively, g is the gravitational acceleration, e_j is the unit vector in the upward vertical direction, and Φ is the porosity of the porous medium. In working with the above flow equation, it is convenient to replace pressure by a reference hydraulic head defined as

$$h = \frac{p}{\rho_0 g} + z \qquad (4.2)$$

where ρ_0 is a reference (freshwater) density and z is the elevation above a reference datum plane. The reference hydraulic head is often referred to as the equivalent freshwater head. The reference hydraulic head is directly related to the true hydraulic head, H, by the relationship

$$H = \frac{h + z\eta c}{1 + \eta c} \qquad (4.3)$$

where H is defined as

$$H = \frac{p}{\rho g} + z \tag{4.4}$$

and

$$\eta = \frac{\rho_s - \rho_o}{\rho_o c_s} \tag{4.5}$$

where c_s is the solute concentration that corresponds to the maximum density, ρ_s. In practice, the term ηc is usually much less than 1 and thus equation (4.3) can be approximated by

$$H = h + \eta c z \tag{4.6}$$

In MODHMS, therefore, two types of boundary conditions must be entered: those that describe the reference (equivalent freshwater) head or fluid fluxes, and those that pertain to solute concentration or solute mass fluxes.

There is a third type of hydraulic head, referred to as environmental head (or potential head), which is defined as

$$\psi = h - \int_{z_1}^{z_2} \eta c \, dz \tag{4.7}$$

where z_1 is the elevation above datum at which the environmental head (ψ) is to be determined, and z_2 is the elevation above datum of the top of the model domain. The environmental head may be conceptualized as the head value that would be measured in a well that had open hole construction from the top of the aquifer system where solute concentrations are small or negligible (z_2) to a total depth of z_1.

The groundwater flow equation can be coupled with the solute transport equation, which may be written in the form

$$\frac{\partial}{\partial x_i}\left(D_{ij}\frac{\partial c}{\partial x_j}\right) - V_i\frac{\partial c}{\partial x_i} = \phi R\left(\frac{\partial c}{\partial t}\right) + \lambda\phi Rc, \qquad (4.8)$$

$$i,j = 1,2,3$$

where D_{ij} is the apparent hydrodynamic dispersion tensor, V_i is the Darcy velocity of fluid, R is the retardation coefficient, and λ is the decay or degradation constant of the solute. For a conservative solute species, such as chloride, there is no adsorption R = 1) and no decay (λ = 0). Equations (4.1) and (4.8) are coupled through the concentration variable and the Darcy velocity.

The hydrodynamic dispersion for three-dimensional anisotropic systems maybe computed from relations provided by Guvanasen (2002), as

$$D_{xx} = \alpha_{Lh}\frac{v_x^2}{|v|} + \alpha_{Th}\frac{v_y^2}{|v|} + \alpha_{Tv}\frac{v_z^2}{|v|} + \beta D_o \qquad (4.9a)$$

$$D_{yy} = \alpha_{Th}\frac{v_x^2}{|v|} + \alpha_{Lh}\frac{v_y^2}{|v|} + \alpha_{Tv}\frac{v_z^2}{|v|} + \beta D_o \qquad (4.9b)$$

$$D_{xz} = D_{zx} = \left(\frac{\alpha_{Lh} + \alpha_{Lv}}{2} - \alpha_{Tv}\right)\frac{v_x v_z}{|v|} \qquad (4.9c)$$

$$D_{zz} = \alpha_{Tv}\frac{v_x^2}{|v|} + \alpha_{Tv}\frac{v_y^2}{|v|} + \alpha_{Lv}\frac{v_z^2}{|v|} + \beta D_o \qquad (4.9d)$$

$$D_{xy} = D_{yx} = (\alpha_L - \alpha_T)\frac{v_x v_y}{|v|} \qquad (4.9e)$$

$$D_{yz} = D_{zy} = \left(\frac{\alpha_{Lh} + \alpha_{Lv}}{2} - \alpha_{Tv}\right)\frac{v_y v_z}{|v|} \qquad (4.9f)$$

where $|v|$ is the magnitude of the velocity vector, $|v| = (v_1^2 + v_2^2 + v_3^2)^{1/2}$, α_L and α_T are longitudinal and transverse dispersivities, respectively, δ_{ij} is the Kronecker delta, D^o is the free-water molecular diffusion coefficient, and β is the tortuosity given by the Millington-Quirk (1961) equation as $\beta = S_w^{10/3}\phi^{4/3}$. The subscripts *Lh*, *Th*, *Lv*, and *Tv* are indices for horizontal longitudinal, horizontal transverse, vertical longitudinal and vertical transverse directions respectively. Note that equations above collapse to equations for isotropic media when *Lv*=*Lh* and *Tv*=*Th*. The set of equations (4.9) is typically used to calculate dispersivities in a three dimensional system where vertical flow components are significant. In such cases, the vertical and horizontal components of dispersion can be an order of magnitude apart for their respective longitudinal and transverse components. For three-dimensional systems with mainly horizontal flows, the longitudinal dispersivities in vertical and horizontal directions may be treated as equal, to produce a 3-component dispersivity tensor. In such cases, the vertical transverse dispersivity is typically an order of magnitude less than the horizontal transverse dispersivity for areally extensive systems. Finally, for isotropic systems or two-dimensional analyses, the vertical and horizontal components of the transverse dispersivity may also be treated as equal, to produce the Scheidegger (1961) dispersivity equation.

The major assumptions and limitations incorporated into MODHMS that are relevant to this project are as follows:

- Fluid flow and salt transport occurs in a fully saturated porous medium. Flow and transport within individual fractures and solution cavities is not simulated explicitly.

- Flow of the fluid considered is isothermal and is governed by Darcy's Law.

- The fluid considered is slightly compressible and homogeneous.

- Dispersive transport in the porous medium system is governed by Fick's Law. The hydrodynamic dispersion is defined as the sum of the coefficients of mechanical dispersion and molecular diffusion. The medium dispersivity corresponds to that of an anisotropic porous medium and may be related to four constants, α_L and α_T, in the areal and vertical directions, which are the longitudinal and transverse dispersivities, respectively. This four component dispersivity tensor reduces to the two-component isotropic dispersivity tensor when the areal and vertical components for the dispersivities are equal.

One final comment is appropriate concerning the MODHMS code, and that is that it solves a mathematical problem that is "nonlinear". In the case of variable density flow, the nonlinearity of the system arises because the density of groundwater at some point depends upon the concentration of solute at that point, but the solute concentration is dependent upon the groundwater flow, which in turn depends upon the density, and so on. Nonlinear systems may be solved mathematically using iterative procedures. Iterative procedures require that some tolerance be specified for the dependent variables being solved for (in our case reference heads and concentrations at nodal points). When the differences between the dependent variable values calculated between successive iterations is less than the tolerance, the nonlinear solution is said to "converge" to within that tolerance. If the differences between the values calculated during successive iterates never become smaller than the tolerance, the solution is said to be

non-convergent. In many practical cases, one-step steady-state solutions may not converge, and transient time-marching or parameter stepping may be required to achieve a steady-state system.

The parameter stepping scheme uses a series of steady analysis starting from a mildly nonlinear problem that can be solved readily (see for example Herbert et al., 1988). Each successive problem, presumably more nonlinear, can be solved using the latest solution as the initial guess. The time-march approach starts from an initial condition, and the problem is solved by marching through a long period of time until a quasi-steady state is reached. The time-marching method is preferable, since the storage term provides greater stability to the linear matrix solver, which is not achieved by the parameter stepping scheme. To examine how close the final solution was to the true steady-state solution, the final solution was compared with earlier time solutions to detect movement. The mass-balance components were also examined and steady-state was assumed when the storage terms of the mass-balance for flow and transport are small in comparison to the other flux terms.

4.3 MODEL DOMAIN AND DISCRETIZATION

The domain of the Southern District Model (SWFWMD, 2001) includes all of the SWUCA as shown in Figure 4.1. The density-dependent saltwater intrusion model domain is identical to that of Waterstone Model (Waterstone, 2001b), and is also shown superimposed over the Southern District Model domain in Figure 4.1. The regional grid is uniform with nodal spacings of 5,000 by 5,000 feet (Figure 4.2). Such spacings are rather coarse when used to predict the transient movement of chlorides. In view of this, the density-dependent model grid was finer and consists of 103 columns and 123 rows with spacings that range from 2,500 to 5,000 feet (Figure 4.3). The 2,500 foot spacing within the density-dependent model is over the primary area of interest. The grid is deformed in the vertical direction to conform with formation geometries and topography.

As previously discussed in Section 2.0, groundwater flow occurs in three principal aquifers; the unconfined surficial aquifer, the intermediate aquifer, and the Upper Floridan aquifer. The Upper Floridan aquifer contains two productive zones, the upper productive zone (corresponding to the Suwannee Limestone) and the lower productive zone (corresponding to the Avon Park Formation), separated by the confining units of the Ocala Limestone. Two intermediate confining beds restrict vertical movement of groundwater between the overlying surficial and underlying Floridan Aquifers. The upper intermediate confining bed limits flow between the surficial and Intermediate Aquifers. The lower intermediate confining bed restricts flow between the Intermediate and Upper Floridan aquifers. The intermediate aquifer itself is divided vertically into two water producing zones separated by confining beds. The Southern District Model (2001), divides this hydrogeologic system into 5 model layers as shown in Figure 4.4, to represent the surficial, the two intermediate aquifer productive units, and the upper and lower productive zones of the Upper Floridan aquifer respectively.

To accurately simulate the migration of saltwater using MODHMS, the thickness of aquifers and aquitards must be explicitly assigned in the model, and hydraulic conductivity values must be assigned to each hydrostratigraphic unit. Because transmissivities (i.e., hydraulic conductivity multiplied by thickness), rather than hydraulic conductivities and thicknesses are assigned in the Southern District Model, the thicknesses of the aquifers and confining units could not be obtained

from the Southern District Model data files for input into the density-dependent model. The Waterstone Model (Waterstone, 2001b) includes generalized thicknesses and top/bottom elevations of the various hydrogeologic units. A comparison was made between the thicknesses provided in the Waterstone Model (Waterstone, 2001b) and several geologic cross sections constructed through the local model area. Barcelo and Basso (1993) present a series of cross sections and SWFWMD (1993) show similar cross sections. Basso (2001) also presents cross sections and isopach maps of the aquifers and confining units within the ETBWUCA. The hydrostratigraphy assigned in the Waterstone Model (Waterstone, 2001b) are consistent with the information provided in the cross sections and were used to construct the density-dependent model.

Vertical discretization of the density-dependent model is identical to that of the Waterstone Model (Waterstone, 2001b) and consists of 10 layers as shown in Figure 4.5. These layers conceptualize the Upper Floridan Aquifer system with explicit representation of the Suwannee Limestone, Ocala Limestone and Avon Park Formation, which are subdivided into 2, 3 and 5 finite-difference layers, respectively. The two upper units (i.e., Suwannee and Ocala) are equally divided and the Avon Park Formation has greater resolution in the uppermost layers (model layers 6 and 7) relative to the bottom model layers (8-10). The surficial aquifer system and intermediate confining units are incorporated into the density-dependent model via boundary conditions (Section 4.4).

The geometry of the hydrostratigraphic units assigned in the current model (i.e., top and bottom elevations) was adopted from the Waterstone Model (Waterstone, 2001b). During their modeling investigation, Waterstone estimated the top and bottom elevations for all of the hydrostratigraphic units based on lithologic data provided by the SWFWMD and information presented by Basso (2001). The uppermost formation in the current density-dependent model is the Suwannee Limestone. The Suwannee Limestone varies in thickness from less than 200 feet in central Hillsborough County to about 300 feet in northern Sarasota County (SWFWMD, 1993). The isopach map for the Suwannee Limestone as extracted from the Waterstone Model (Waterstone, 2001b) is shown in Figure 4.6. Figure 4.6 is essentially the difference between Figures 2.6 and 2.8. As shown in the figure, the Suwannee Limestone is thinnest in the east and thickens to approximately 465 feet along the western model boundary. Underlying the Suwannee Limestone are the Ocala Limestone and Avon Park Formation. Over the modeled area the Ocala thickens from approximately 200 feet in the northeast to approximately 800 feet thick in the southwest as shown in Figure 4.7. Figure 4.7 was created from the Waterstone Model (Waterstone, 2001b) files as a difference between Figures 2.8 and 2.9. Underlying the Ocala Formation is the soft to hard, chalky, cream to brown fossiliferous Avon Park Formation. The total thickness of the Avon Park Formation in the model area varies from approximately 400 to 710 feet as shown in Figure 4.8 which is the difference between the elevations of Figures 2.9 and 2.11. The evaporite zone within the Avon Park Formation is considered to be the bottom of the Upper Floridan aquifer, and the bottom of the model domain.

4.4 BOUNDARY CONDITIONS

4.4.1 Upper Boundary

As shown in Figure 4.4, the Southern District Model (SWFWMD, 2001) includes the unconfined surficial aquifer system (Layer 1) as well as two water-bearing zones in the intermediate aquifer

system (Layers 2 and 3). Instead of assigning precipitation recharge rates throughout the Southern District Model (SWFWMD, 2001) a constant head boundary condition, representing the water table was assigned in the uppermost layer (i.e., corresponding to the surficial aquifer system) of the model. Rather than explicitly incorporating the surficial and intermediate aquifers system into the density-dependent model, vertical flow through these aquifers is simulated by specifying a general head boundary (GHB) condition at the top of the UPZ (Layer 1 of the density-dependent local model). This approach is justified because the hydraulic conductivities of these intermediate aquifer system units are much smaller than those of the underlying Floridan aquifer system. Therefore, the hydraulic heads for the surficial aquifer system in the Southern District Model (SWFWMD, 2001) were used in conjunction with the leakance values assigned in the Southern District Model to represent the intermediate aquifer system (including confining units within the surficial aquifer system and two intermediate confining beds) to specify the general head boundaries. Figure 4.9 shows the head and conductance values of the general head boundary. The head values represent surficial aquifer system heads (extracted from the Southern District Model (SWFWMD, 2001), while the conductances were computed on a cell-by-cell basis as follows:

$$GHB_{cond} = 1/(1/L_1 + 1/L_2 + 1/L_3) * A_{Cell}$$

where

GHB_{cond} (ft^2/d)	=	The GHB conductance term between the Surficial Aquifer and Suwannee Limestone.
L_1 (1/d)	=	Leakance for Layer 1 (surficial aquifer) in the Southern District Model (Figure 2.3).
L_2 (1/d)	=	Leakance for Layer 2 (intermediate aquifer and confining unit) in the Southern District Model (Figure 2.4).
L_3 (1/d)	=	Leakance for Layer 3 (intermediate aquifer and confining unit) in the Southern District Model (Figure 2.5).
A_{Cell} (ft^2)	=	corresponding cell area in density-dependent model (Figure 4.3).

The exclusion of the surficial and intermediate aquifer systems facilitate the calibration of the density-dependent model (Section 5.0) by increasing the computational efficiency of the model. The justification for this approach is based upon the insensitivity of the water table to stresses within the lower artesian aquifers as evidenced by the fact that long-term and annual variations in water levels in the surficial aquifer are small compared to water level fluctuations in the Upper Floridan aquifer (Barcelo and Basso, 1993).

4.4.2 Lateral Boundaries

The pre-development heads simulated by the Southern District Model (SWFWMD, 2001) were used to provide prescribed head boundaries along the northern, southern and eastern faces of the density-dependent model. Prescribed heads along these boundaries were assigned to the Suwannee Limestone (Southern District Model Layer 2), and to the model layers that comprise the Avon Park Formation (Southern District Model Layers 6 though 10). The Ocala Limestone acts as a semi-confining unit within the modeled area and flow is predominantly vertical through this unit.

Therefore, prescribed head boundaries along the northern, southern and eastern faces of the Ocala Limestone were deemed unnecessary.

The western boundary conditions are also specified as constant heads (prescribed heads) and are in hydrostatic equilibrium with the Gulf of Mexico. These heads were adjusted during the model calibration process (Section 5.0). Theoretically, either hydraulic heads or water fluxes could have been applied along the lateral boundaries. The appropriateness of the constant head boundaries, particularly for the transient post-development simulations, was further evaluated during the model calibration process.

4.4.3 Lower Boundary

The lower boundary was chosen as the top of the middle confining unit of the Floridan Aquifer system. This is generally associated with the first occurrence of intergranular evaporites near the base of the Avon Park Formation (Barcelo and Basso, 1993). Because of the very low permeability in this part of the flow system, the bottom boundary was simulated as a no-flow boundary. This is consistent with all other modeling studies that have been conducted within the SWUCA.

4.5 PRELIMINARY MODEL PARAMETERIZATION

Hydraulic Conductivity

As discussed above, the modeling approach which was used by SWFWMD to perform the regional groundwater flow simulations requires transmissivity values as input for each of the aquifers and confining units. To accurately predict chloride transport through the aquifer, however, the two components of transmissivity (i.e., aquifer or confining unit thickness and hydraulic conductivity) must be explicitly defined using the following equation:

$$K_h = T/b$$

Where

K_h = aquifer layer horizontal hydraulic conductivity (ft/day)
T = aquifer layer transmissivity derived from the Southern District Model (ft^2/day)
b = aquifer layer thickness

Initial values for hydraulic conductivity of the aquifer layers and confining units were derived from calibrated transmissivity and leakance values that were assigned to the Southern District Model. These values may be slightly altered, however, during the future model calibration (Section 5.0), to honor the chloride transport physics and chloride data as well as the head data which alone were used to calibrate the regional groundwater flow model.

It was assumed that horizontal hydraulic conductivity is isotropic in all model layers. That is, horizontal hydraulic conductivity was assumed to be equal in the row and column directions. No regional-scale data on horizontal anisotropy exists within the model area, and the assumption of

isotropic conditions is consistent with previous models. A horizontal to vertical anisotropy of 100:1 is assumed for the aquifer units (i.e., the Suwannee Limestone and the Avon Park Formation). The vertical hydraulic conductivity of the Ocala Limestone was initially computed from the appropriate leakance of the Southern District Model, and Ocala Limestone thickness. However, since the leakance of the Southern District Model was a uniform value, its manipulation with non-uniform thickness provided spatially varying vertical hydraulic conductivities. This was deemed difficult to justify from sparse available measurements, therefore, a uniform vertical conductance of 0.2 ft/d was adopted early in the calibration process. It was noted that this conversion did not significantly affect simulated heads, flows or chlorides. A value of 2 ft/d was provided for the horizontal hydraulic conductivity of the Ocala Limestone. The horizontal conductance of the Ocala Limestone is much smaller than for the Avon Park Formation and the Suwannee Limestone with smaller total thickness, therefore the consequences of a uniform 2 ft/d horizontal hydraulic conductivity for the Ocala Limestone on horizontal flow through the system is minimal.

Suwannee Limestone

The transmissivity of the Suwannee Limestone assigned in the Southern District Model is shown in Figure 2.7. This transmissivity was divided by the thickness of the Suwannee Limestone (Figure 4.6) and input into the density-dependent model as horizontal hydraulic conductivity (Figure 4.10).

Ocala Limestone

In the Southern District Model the Ocala Limestone is treated in a quasi-three-dimensional manner, with leakance supplied across its thickness. A uniform leakance value of 10^{-2} ft/day was used throughout the domain. A uniform leakance value with varying thickness would produce a varying vertical conductivity for the Ocala Limestone, which would be difficult to justify based on available data. Therefore, a uniform value of hydraulic conductivity was used for the Ocala Limestone with horizontal conductivity of 2 ft/d and a vertical conductivity value of 0.2 ft/d. The vertical conductivity value is an average of available data. The horizontal conductivity value is not significant to the model because it is much smaller than the horizontal conductivity of the adjacent aquifer units of the Upper Floridan aquifer.

Avon Park Formation

The horizontal hydraulic conductivity of the Avon Park Formation (Figure 4.11) was derived by dividing the transmissivity of the Ocala Limestone/Avon Park Formation in the Southern District Model (Model Layer 5) (Figure 2.10) by the aquifer thickness of the Avon Park Formation in the Waterstone Model (Waterstone, 2001b) (Figure 4.8). This approach assumes that the Ocala Limestone does not contribute significantly to the transmissivity assigned to the Ocala Limestone/ Avon Park Limestone in the Southern District Model. Based upon the low hydraulic conductivity of the Ocala Limestone, this assumption is reasonable.

4.6 SOUTHERN DISTRICT MODEL TRANSLATION

The density-dependent saltwater intrusion study was initiated by first translating the regional model parameters and local model boundary conditions from the Southern District Model (SWFWMD,2001). A pre-development, steady-state groundwater flow simulation was then performed using MODHMS to evaluate the resultant hydraulic heads. This simulation was conducted in order to compare the hydraulic head distribution simulated using the local-scale MODHMS model to the hydraulic head distribution simulated using the regional MODFLOW model. The primary goals of this initial simulation were threefold: (1) to ensure that the input parameters and boundary conditions assigned in the local-scale model were consistent with the Southern District Model; (2) to detect errors in the model input files; and (3) develop the framework of the coupled flow and transport model, which will be calibrated to transient hydraulic heads and chloride distributions. For this simulation, pre-development steady-state conditions were evaluated by turning off all pumping and injection wells and the aquifer system was assumed to be free of saltwater. Parameter values and boundary conditions were derived from the regional groundwater flow model, of pre-development conditions. The pre-development modeling results (without saltwater) are shown for the Avon Park Formation (i.e., model layer 8) in Figure 4.12. The pre-development potentiometric surface for the Ocala Limestone/Avon Park Formation as predicted by the Southern District Model (SWFWMD, 2001) (i.e., model layer 5) is also presented in Figure 5.1. A comparison of the hydraulic heads simulated using both the regional and local-scale models indicates that the simulation results are in excellent overall agreement. The hydraulic head distributions calculated for the other model layers within the Upper Floridan aquifer also compare well with the Southern District Model.

4.7 SALTWATER TRANSPORT PROPERTIES

Since MODHMS simulates both freshwater and saltwater, additional data not contained in the Southern District Model files were required to complete simulations. The additional fluid and aquifer parameters required for this study are summarized in Table 4.1.

A key component in reliably evaluating density-dependent saltwater intrusion is the dispersivity of the various materials in the system. Due to large anisotropies between the horizontal and vertical directions, the dispersivities used in this system should reflect these anisotropies. The 4-component anisotropic dispersivity tensor of Guvanasen (2002) provides adequate control for such systems. The longitudinal and transverse dispersivities in the horizontal direction control dispersion due to horizontal flow in the longitudinal and horizontal transverse directions. The longitudinal and transverse dispersivities in the vertical direction control dispersion due to the vertical flow component, and vertical transverse dispersion due to horizontal flow, respectively. Typically, the vertical components of dispersivity are an order of magnitude lower than the corresponding horizontal components for three-dimensional anisotropic systems, since the mixing effects in the vertical direction are smaller than those of the horizontal direction. Using a 2- or 3-component dispersivity tensor for such systems tends to smear the transport species over the entire thickness of the modeled unit, and thus misrepresents the saltwater intrusion, causing further errors in the density-dependent flow term. Initial estimates of dispersivity coefficients for this study were taken from the Waterstone Model (Waterstone, 2001b) as shown in Table 4.2.

5.0 MODEL CALIBRATION

Model calibration is the process where model parameters and/or boundary conditions are adjusted to obtain a satisfactory match between observed and simulated conditions. Typically, the objective of model calibration is to develop a model that is capable of accurately predicting past, current, and/or future conditions. A model is calibrated by determining a set of parameters, boundary conditions, and hydraulic stresses that generate simulated potentiometric surfaces, fluxes and concentrations that match field-measured values to within an acceptable range of error. The end result of the process of model calibration is an optimal set of parameter values and boundary conditions that minimize the discrepancy between modeling results and the observed data.

The following sections detail the model calibration process that was completed as part of the current saltwater intrusion modeling investigation.

5.1 MODEL CALIBRATION STRATEGY

5.1.1 General Calibration Approach

At the beginning of the calibration process, model calibration goals were formulated in order to produce a model that accomplishes the project objectives outlined in Section 1.2, while recognizing the inherent uncertainties and limitations of the saltwater intrusion model. The primary limitations associated with the saltwater intrusion model are mainly caused by data uncertainties, resulting from the use of discrete borehole data to characterize subsurface conditions on a regional basis. Due to the size of the model domain and the spatial distribution of field data, hydraulic properties and boundary conditions are estimated over relatively large areas in the model, and small-scale heterogeneities cannot be represented. Therefore, the model is best suited to simulate groundwater flow patterns and chloride concentrations on a regional basis. This supports the primary objective of the model, which is to predict the large-scale impact of groundwater management options on saltwater intrusion.

The calibration strategy was designed to produce a model that is capable of simulating the general groundwater flow patterns and regional trends in chloride concentration. Consistent with this goal, model parameter values and boundary conditions were not adjusted beyond the limits of field measurements solely for the purpose of improving the calibration results. In addition, the principle of parameter parsimony was applied as a fundamental philosophy during the calibration. This rule dictates that the model should be calibrated with the fewest number of model parameters that are supported by field data or other supporting evidence. The use of excessive model parameters or parameter zones during model calibration creates a situation in which many combinations of model parameter values will produce equivalent calibration results. By following the principle of parameter parsimony, the goal is to reduce the degree of nonuniqueness and obtain a result which yields more reliable calibrated parameter values. The information gathered for the conceptual model guides any decision to add model parameters (e.g., zones of hydraulic conductivity) or change parameter values during the calibration process. Therefore, in the absence of hydrogeologic evidence that supports the inclusion of additional zones, the simpler model is preferred even at the expense of matching the calibration targets more closely. Although this approach may not result in the model that produces the best fit to the available data (i.e.,

calibration targets), it does, however, allow areas of greatest data uncertainty to be identified and targeted for future field work.

An iterative, two-phased approach was used to calibrate the local-scale, saltwater intrusion model. This involved the following:

- Pre-development Calibration (Phase 1): Calibration of the model to match hydraulic heads and chloride concentrations associated with pre-development conditions (i.e., year 1900); and

- Post-development Calibration (Phase 2): Transient calibration of the model to match hydraulic heads and chloride concentrations associated with post-development conditions (i.e., 1900 through 2000).

The first phase of the calibration process involved using MODHMS to simulate density-dependent groundwater flow and saltwater transport to reproduce pre-development conditions. During the calibration process, hydraulic parameters, transport parameters, and boundary conditions were adjusted, and the model results were compared to: (1) a map illustrating the development potentiometric surface in the Upper Floridan aquifer (Johnson et al., 1980); and (2) pre-development chloride concentrations simulated during previous saltwater intrusion modeling investigations (HydroGeoLogic, 1994a, 1994b, 1994c, 1993a, 1991a). Hydraulic head and chloride concentration data are not available for the pre-development period (i.e., approximately 1900); consequently, a rigorous, quantitative calibration was not performed during this phase of the calibration. However, estimates of the pre-development potentiometric surface was constructed by Johnston et al., (1980) and provided a qualitative means to check the pre-development calibration.

During the second phase of the calibration process, MODHMS was used to simulate transient, coupled groundwater flow and saltwater transport. These transient simulations were performed to simulate hydraulic heads and chloride concentrations from year 1900 (i.e., pre-development conditions) through December 2000. During the transient calibration, simulated hydraulic heads and chloride concentrations were compared to field data measured between 1993 and 2000. During the second phase, parameter values, model layering and boundary conditions were adjusted to allow the model to fit the calibration criterion discussed in detail in Section 5.1.2. The following sections describe the calibration process in greater detail.

5.1.2 Pre-Development Calibration

Prior to initiating the pre-development calibration, the local-scale model was revised to simulate coupled groundwater flow and saltwater transport. This involved the following:

- Assignment of constant chloride concentration boundary conditions along the lateral boundaries of the model:

- Specification of initial chloride concentrations throughout the model domain; and

- Assignment of transport properties within the model domain (e.g., porosity, dispersivities, fluid density, etc.).

The initial chloride concentrations that were assigned in the model were estimated based on observed chloride concentrations. Likewise, the preliminary chloride concentrations assigned to the constant concentration boundary conditions were also based on field data. These boundary conditions were adjusted along with transport properties, groundwater flow parameters, and constant head boundary conditions during the model calibration process described in Section 5.2.

Due to convergence problems that were encountered during preliminary simulations, the time-marching method described in Section 4.2 was applied during the pre-development simulations. To examine how close the final solution was to the true steady-state solution, chloride concentrations calculated for the last time step were compared to chloride concentrations calculated for earlier time steps. The solution was deemed to represent steady-state conditions when there were insignificant changes in chloride concentrations and when the storage terms of the mass-balance for flow and transport were small in comparison to the other flux terms.

The objective of the pre-development calibration was to simulate steady-state groundwater flow conditions and chloride concentrations for the period prior to the development of groundwater resources (i.e., approximately 1900). Because conditions that existed during this time are not known with certainty, a rigorous, quantitative calibration could not be completed. Instead, a qualitative calibration was completed, which involved the adjustment of model parameters and boundary conditions to match the following: 1) potentiometric surface contours estimated by Johnson et al., 1980; and 2) the lateral and vertical extent of chloride predicted for pre-development conditions during earlier investigations.

As discussed in Section 3.0, the distribution of chloride for pre-development conditions was estimated during several modeling investigations (HydroGeoLogic, 1994a,1993a,1991a). During the pre-development calibration, the chloride concentrations predicted by the current saltwater intrusion model were compared to the distribution of chloride presented in Figures 2.16 and 3.1. Because direct observations are not available for pre-development conditions, there is significant uncertainty in the distribution of chloride shown on these figures. Consequently, the goal of the pre-development calibration was to match the general pattern shown on the figures. A similar approach was adopted for calibrating the model to the inferred pre-development potentiometric surface contours developed by Johnson et al. (1980). The goal was simply to match the general shape of the contours.

5.1.3 Post-Development Calibration

During the second phase of the calibration process, the model was calibrated to post-development conditions (i.e., post-1900). To investigate the impact of groundwater withdrawals on the flow system, hydraulic heads and chloride concentrations were simulated for a period extending from approximately 1900 (i.e., pre-development conditions) to 2000. During these simulations, the hydraulic stresses associated with pumping were simulated by making two modifications to boundary conditions assigned in the model. First, the lateral boundaries of the model were modified to reflect the post-development hydraulic heads resulting from regional groundwater

production. The post-development hydraulic heads that were assigned as lateral boundary conditions in the density-dependent model were derived from hydraulic heads simulated using the Southern District Model (SWFWMD, 2001). Secondly, groundwater extraction rates associated with production wells were assigned throughout the model. The groundwater extraction rates assigned in the model were based on the estimated water use for the area, and derived from the pumping/ injection well data compiled by the SWFWMD and represented in the Southern District Model (SWFWMD, 2001).

To complete the simulations, landward lateral boundary heads and well pumping rates were varied every 5 years for the first 60 years, with yearly variations for the next 15 years, followed by variations every 4 months up to December 2000. Boundary heads were obtained using the hydraulic head fields developed by performing parallel transient simulations using the Southern District Model (SWFWMD, 2001) constructed by the SWFWMD. The location and model layer of the groundwater extraction/injection wells within the density-dependent model domain are shown in Figure 5.1. These wells were represented in the local-scale saltwater intrusion model using an analytic element boundary condition. This type of boundary condition allows the water, entering the well from multiple model layers, to be proportioned based upon the hydraulic properties of the respective model layers.

Both quantitative and qualitative methods were employed to calibrate the local-scale saltwater intrusion model to post-development conditions. As part of this effort, the following data were used as the primary calibration targets:

- Chloride data collected as part of the Regional Observation Monitoring Well Program (ROMP);
- Chloride data collected as part of the Water Quality Monitor-Well Program (WQMP); and
- Potentiometric surface maps prepared by the USGS (2001) for the Upper Floridan aquifer.

Chloride data collected as part of the Regional Observation Monitoring Well Program (ROMP) provided the primary data set that was used to calibrate the saltwater intrusion model to post-development conditions. The ROMP data differs from other sources of chloride data in that it characterizes both the spatial and vertical distribution of chloride through a large number of exploratory wells (Figure 2.15). This data generally characterizes the distribution of water quality with depth at a single location during a single sampling event. The ROMP data is collected using a variety of sampling methods including bailers, thief samplers, and packer tests. The locations of the ROMP wells that were used for determining model calibration statistics are shown in Figure 5.2. These wells lie in the central portion of the model domain within the primary areas of interest. Since the data quality at a number of the ROMP wells is questionable, only the ROMP data identified by the SWFWMD as being of high quality were used for this investigation. Chloride concentrations with depth for each of these ROMP wells are presented in the Appendix B.

Chloride data collected as part of the WQMP were used to augment the ROMP data during the model calibration. Under the WQMP, the SWFWMD routinely samples and analyzes

groundwater to monitor potential saltwater migration. This data is collected by the SWFWMD primarily from dedicated monitoring wells. The WQMP data is the best source of temporal chloride data within the coastal region of the SWUCA.

In addition to chloride data, the model was calibrated to hydraulic head data compiled by the USGS, which develops potentiometric surface maps for the Floridan Aquifer for September and May of each year. Typically, these represent the annual water-level low and high periods, respectively. During the post-development calibration, simulated hydraulic head distributions were compared to potentiometric surface maps developed for May and September 2000. This time period was selected, because it is the most recent time period in which hydraulic head data were available during this investigation.

Using the data described above, several measures were used to calibrate the saltwater intrusion model to post-development conditions including the following:

- Visual comparison of vertical profiles illustrating simulated chloride concentrations and chloride concentrations (using data from WQMP and ROMP wells);
- Statistical comparison of simulated chloride concentrations and chloride concentrations observed at the ROMP wells (using data from WQMP and ROMP wells);
- Plots illustrating the relationship between simulated chloride concentrations and chloride concentrations obtained from ROMP wells;
- Visual comparison of the predicted chloride distribution to maps illustrating the current extent of saltwater;
- Visual comparison of observed and temporal changes in chloride concentrations (using WQMP data); and
- Visual comparison of potentiometric surface maps developed using observed and simulated hydraulic head data (i.e., using potentiometric surface maps developed by the USGS for year 2000).

The vertical chloride profiles provided the most useful calibration measure to evaluate the model's ability to reproduce post-development conditions. The profiles that were used during the calibration are presented in Appendix A. The vertical profiles provided a mechanism to evaluate the slope, thickness, width, and depth of the saltwater interface. The ROMP wells provided the majority of the data that were used to develop the vertical profiles. However, the vertical profiles also included limited data that were collected as part of the WQMP.

A more quantitative assessment of the calibration was completed using statistical measures describing the relationship between simulated chloride concentrations and chloride concentrations observed at selected ROMP wells. The primary criterion for evaluating the calibration of a groundwater transport model is the difference between simulated and observed chloride concentrations at a set of calibration targets (typically monitoring wells). A residual or model

error, e_i, is defined as the difference between the observed and simulated chloride concentrations measured at a target location:

$$e_i = c_i - \hat{c}_i$$

where c_i is the measured value of chloride concentration and $\hat{c}_i$ is the simulated value at the ith target location (i.e., at an individual ROMP wells). A residual with a negative sign indicates over-prediction by the model (i.e., the simulated chloride concentration is higher than the measured value). Conversely, a positive residual indicates under-prediction.

Several statistical measures were used to gauge the success of the model calibration. During the calibration process, an objective was to minimize the residual sum of squares (RSS) while still honoring the field data:

$$RSS = \sum_{i=1}^{n} (e_i)^2$$

where n is the total number of calibration targets. The RSS is a primary measure of model fit. The root mean squared (RMS) error, which normalizes the RSS by the number of calibration targets, is defined as follows:

$$RMS = \sqrt{\frac{RSS}{n-1}}$$

Another calibration measure that was used to evaluate the calibration is the residual mean:

$$\bar{e} = \frac{1}{n} \sum_{i=1}^{n} e_i$$

A mean residual significantly different from zero indicates that the model produces biased results (i.e., over-predicts or under-predicts chloride concentrations).

The chloride concentrations observed at the ROMP wells represent a small, discrete vertical interval within a given hydrostratigraphic unit. The groundwater samples taken from the ROMP wells represent a much smaller interval than the thickness of the finite-difference cells in which chloride concentrations are calculated using the saltwater intrusion model. In fact, for each finite-difference cell containing a ROMP well, there are typically multiple observed chloride concentrations associated with different depth intervals. In order to compare the observed and calculated chloride concentrations, average observed chloride concentrations were calculated for each model layer associated with a ROMP well location, and the residuals were calculated by subtracting the simulated chloride concentration at each finite-difference cell from the average chloride concentrations obtained from the ROMP wells. This averaging, however, produced inherent errors within the statistical analysis which are accentuated due to the sharp increases in chloride concentrations over short intervals. A vertical refinement of the numerical grid would

probably result in better calibration statistics, although it would probably have little impact on the overall characteristics of the chloride distribution.

After a review of the existing data, and conversations with the SWFWMD regarding the quality of the well data, sixteen ROMP wells were selected for the statistical analysis. As shown in Figure 5.2, the majority of the wells are located over the primary area of interest, within the west central portion of the model domain within the chloride interface zone. Several of these wells are closely spaced, and aligned in an east-west orientation (e.g., TR AB-1, TR 9-2, TR AB-3). The data from these wells provided a means to evaluate the slope of the chloride interface during the model calibration.

In addition to the statistical evaluation of model residuals and the visual comparison of model results to vertical chloride profiles, maps were developed to evaluate the reliability of the calibration. A comparison between contour maps of measured and simulated values (i.e, hydraulic heads and chloride concentration) were prepared to provide a visual, qualitative measure of the similarity between patterns, thereby giving some idea of the spatial distribution of calibration errors. In addition, vertical and horizontal hydraulic heads and the fluid flux moving across the model boundaries were used as qualitative calibration criteria.

5.2 MODEL CALIBRATION IMPLEMENTATION

Section 4 describes in detail the approach used to construct the preliminary density-dependent groundwater flow and solute transport model to simulate saltwater intrusion in coastal portions of the SWUCA. The sections that follow primarily describe the changes and refinements that were made during the calibration process.

5.2.1 Evaluation of Alternative Conceptualizations and Uncertainty

One primary goal of mathematical modeling is to synthesize the conceptual model into numerical terms from which flow and transport processes may be investigated under specified conditions. This process entails several discrete steps: (1) partitioning the conceptual model into units of time and space; (2) assignment of boundary conditions; and (3) specification of the parameter values. There are always uncertainties in predictions derived from modeling. These uncertainties are frequently divided into two main categories: (1) conceptual model uncertainty; and (2) parameter uncertainty. This section briefly describes these uncertainties and the approach that was applied to address these uncertainties in the model calibration process.

The conceptual model is based on the modeler's knowledge, experience and technical judgment and represents the modeler's understanding of the system framework and behavior, from all available data and information at the site. The conceptual model will naturally become more complex as more processes are identified and interrelationships of important components within the system are considered. The transformation of the conceptual model into a mathematical model is a further extrapolation of the basic understanding of the system into a discretized numerical framework resulting in intrinsic simplifications of the system. The lack of knowledge about the system resulting from limited information also contributes to inevitable simplifications in the

conceptual and mathematical models, in the sense that spatial correlations or zoning of material properties may not represent existing conditions.

As part of the model calibration process, a series of hypotheses were developed and numerical experiments were performed to address aspects of the conceptualization or parameterization that could improve model performance during the model calibration. Table 5.1 provides several significant results of these analyses.

5.2.2 Calibrated Model Domain and Discretization

As described in Section 4.0, the initial local-scale model consisted of 10 layers of finite-difference cells. During the model calibration process, an additional model layer was added to the base of the model to allow chloride transport through the Middle Confining Unit (i.e., evaporites) to be explicitly simulated. The vertical discretization of the calibrated density-dependent model consists of 11 layers as shown in Figure 5.3. This additional layer provides the necessary mechanism to more adequately simulate chlorides entering the Avon Park Formation from the evaporites below.

5.2.3 Calibrated Boundary Conditions

Upper Boundary

As presented in Section 4.4, rather than explicitly incorporating the surficial and intermediate aquifer system into the density-dependent model, vertical flow through these aquifers is simulated by specifying a general head boundary condition at the top of the Suwannee Limestone (model layer 1). This conceptualization was maintained throughout the model calibration and the upper boundary and its values were unchanged from those presented in Figure 4.9. The exclusion of the surficial and intermediate aquifer system facilitated the density-dependent model calibration by increasing the computational efficiency of the model, and is justified based upon the insensitivity of the water table to stresses within the lower artesian aquifers as evidenced by the fact that long-term and annual variations in water levels in the surficial aquifer are small compared to water level fluctuations in the Upper Floridan aquifer (Barcelo and Basso, 1993).

Lateral Boundaries

The pre-development and post-development heads simulated using the Southern District Model (SWFWMD, 2001) were used to develop prescribed head boundaries along the northern, southern and eastern faces of the density-dependent model (Section 4.4). Prescribed heads were assigned along these boundaries in model layers representing the Suwannee Limestone (model layers 1&2) and Avon Park Formation (model layers 8,9 and 10). The Ocala Limestone acts as a confining unit within the modeled area and flow is predominantly vertical through this unit. Therefore, prescribed head boundaries along the northern, southern and eastern faces of the Ocala Limestone were deemed unnecessary. The northern, southern, and eastern lateral boundary heads presented in Section 4.4 were unchanged for the final calibration simulation. Figure 5.4 shows the boundary conditions that were applied to the lateral boundaries of the density-dependent model.

The western boundary conditions are also specified as constant heads (prescribed heads) and were originally derived from the heads calculated in the Southern District Model (SWFWMD, 2001). These heads are based on assumptions pertaining to the relationship between the pressure head within the aquifers and the hydrostatic head within the ocean. Therefore, in the calibrated model the heads along the western boundary are set to zero in the uppermost layer and increase with depth to account for chloride density.

During the post-development calibration, the hydraulic stresses associated with pumping were simulated by making two modifications to boundary conditions assigned in the predevelopment model. First, the landward lateral boundaries of the model were modified to reflect the post-development, transient hydraulic heads resulting from regional groundwater production. These boundaries were modified based on the results of transient simulations performed using the Southern District Model (SWFWMD, 2001). These transient effects on the head boundaries are obtained from parallel transient simulations made with the Southern District Model (SWFWMD, 2001) by the SWFWMD and representative variations in the north and southeast corners of the model domain as illustrated in Figure 5.5. Second, transient groundwater extraction rates associated with production wells were assigned throughout the model.

A relative chloride concentration of one was applied along the western lateral boundary and along seaward portions of the northern and southern lateral boundaries. These boundaries for concentrations are prescribed for all inflow nodes. The option in enabled in MODHMS to provide flux boundaries at outflow nodes along this boundary.

Lower Boundary

The lower boundary for the calibrated model is located between 200 and 400 feet below the top of the middle confining unit of the Floridan Aquifer system. A general head boundary (GHB) condition was applied along this boundary. A uniform environmental head of 40 feet and a vertical conductance of 0.001 ft/day was assigned to all general head boundary conditions. Concentrations assigned to the general head boundary conditions are variable and range from 5,700 mg/l along the eastern boundary to 19,000 mg/l at the ocean (Figure 5.6). This concentration distribution does not significantly affect results as compared with applying a uniform 19,000 mg/L concentration, however, the distributed concentration boundary was adopted in the calibrated model to honor available data.

5.2.4 Calibrated Model Parameters

Groundwater Flow Parameters

As discussed in Section 4, initial values for hydraulic conductivity of the aquifer layers and confining units were derived from calibrated transmissivity and leakance values that were assigned to the Southern District Model (SWFWMD, 2001). This approach was adhered to during the model calibration process.

A uniform vertical conductivity of 0.02 ft/d was applied to the Ocala Limestone to conform with average measurements. It is assumed that horizontal hydraulic conductivity is isotropic in all

model layers. That is, horizontal hydraulic conductivity was assumed to be equal in the row and column directions. Regional-scale data related to horizontal anisotropy was not available for the modeled area, and the assumption of isotropic conditions is consistent with previous models. A vertical to horizontal anisotropy ratio of 1:100 was applied to all units as discussed in Section 4.

Although the transmissivity assigned to the Avon Park Formation is the same in both the calibrated saltwater intrusion model and the Southern District Model (SWFWMD, 2001), the distribution of hydraulic conductivities among model layers within the Avon Park Formation was altered during model calibration. The Avon Park Formation is now conceptualized as having a highly permeable zone (in model layers 6 and 7) overlying the rest of the formation (model layers 8, 9 and 10). The hydraulic conductivities of these zones are presented in Figure 5.7 (for model layers 6 and 7) and Figure 5.8 (for model layers 8, 9, and 10). This hydraulic conductivity distribution provides an effective transmissivity for the Avon Park Formation that is identical to that used for the Southern District Model (SWFWMD, 2001), except for under Hillsborough Bay and Tampa Bay where the areal zones of transmissivity have been slightly modified by assigning a more gradational trend.

Saltwater Transport Properties

The values for effective porosity, dispersivity and storativity were adjusted during the model calibration in order to better match the measured field data. In general, lower effective porosities resulted in greater saltwater intrusion due to the increased velocities. Dispersivity values had a dominant effect on the spread and concentrations of the chlorides, with larger dispersivities causing a larger transition zone. The distribution of the post- development hydraulic heads are sensitive to the assigned storativity values. The transport properties that were assigned in the calibrated model are presented in Table 5.2.

5.3 MODEL CALIBRATION RESULTS

5.3.1 Pre-Development Calibration Analysis

As previously presented in Section 5.1.2, the calibration criteria for pre-development conditions are based primarily on the results of earlier modeling work that predicted the location of the saltwater interface shown in Figure 3.1. A comparison of the current modeling work with those earlier results is presented in Figure 5.9. As shown in that figure, the tip of the interface crisscrosses the tip location predicted by the HydroGeoLogic (1994) model. In the southwestern portion of the model the tip makes a sharp turn inland, due most likely to localized boundary effects. The toe of the plume follows the same general shape as that of the previous modeling investigations conducted by HydroGeoLogic, in 1993 and 1994. The most recent modeling, however, predicts greater saltwater intrusion in the northern part of the model domain than the other models and less intrusion from the center of the model southward. The toe location, in the cental portion of the model coincides reasonably well with the location predicted by the cross sectional model of HydroGeoLogic (1991).

Figure 5.10 presents calibrated pre-development potentiometric surface for the Suwannee Limestone (model layer 2) superimposed over the pre-development potentiometric surface

prepared by Johnston et. al. (1980). The model is in very good agreement with the estimated hydraulic heads and typically differ by less than 5 feet except in the northeastern region of the model. In a similar comparison, the potentiometric surface prepared by Johnston et. al. (1980) was superimposed over the surface predicted by the model for Avon Park Formation (model layer 7) (Figure 5.11). Again the heads compare favorably and generally there is less than a 5-foot head difference.

5.3.2 Post-Development Calibration Results

After satisfactory pre-development, steady-state chloride concentrations were simulated using the local-scale model, the model was calibrated to conditions observed between 1993 and 2000 by performing transient simulations. The local-scale model was used to simulate conditions from 1900 (i.e., pre-development conditions) through 2000.

Chloride Interface Characteristics

Chloride concentrations with depth have been measured for each of these ROMP wells and are presented in the Appendix B. As discussed in Section 5.1.2, the chloride concentrations predicted by the model were superimposed over the actual field data to visually inspect the ability of the model to simulate the observed vertical and spatial distribution of chloride. A more quantitative assessment of the calibration was performed by computing an average error and a root mean square error for chloride concentrations observed at selected ROMP wells. Since the data quality at a number of the ROMP wells is questionable only the ROMP wells where the data is known to be of high quality were used for this analysis and are shown in Figure 5.12 along with the areal distribution of calibration errors (i.e., residuals). These errors are depicted in three distinct model layers to present the distribution of errors within different aquifer units. It is noted that the model errors are generally unbiased in space. However, the model overestimates chloride concentrations in the deeper layers in the southern coastal regions of the domain and underestimates chloride concentrations in the deeper layers in coastal Hillsborough County.

The calibration statistics are also summarized in Table 5.3 and a scatterplot of measured vs. simulated chlorides is shown in Figure 5.13. The scatterplot presented in Figure 5.13 illustrates that there is not a systematic bias (i.e., underestimation or overestimation) of chloride concentrations within the model domain. This observation is supported by the part that the residual mean (-0.00439) is close to zero. It may be noted from the chloride profiles (Appendix B) that concentrations change over several orders of magnitude within a few hundred feet. As shown in the scatter plot and Table 5.3, the residuals are generally unbiased and tend to be over- and under-estimated with approximately the same degree of frequency. Other observations with respect to the model comparison with the ROMP well data includes the following:

1. A good fit was obtained to the low chloride concentrations inland at ROMP 61, 49, 39, 33, and 22.

2. The model predicted chloride concentrations satisfactorily match observed chloride concentrations in the Ocala Limestone in the north for coastal wells TR AB-1, TR 9-2, TR 9-1, TR AB-3, TR 8-1.

3. Model predictions are low for chloride in the Avon Park Formation in the north at TR AB-1, TR 9-2.

4. The model provides a good fit to chloride concentrations in the Avon Park Formation at coastal well TR 8-1 (northern well south of TR 9-2).

5. A good fit for chloride was obtained in the Ocala Limestone and Avon Park Formation at coastal wells TR 7-2 and TR 7-4 (south of TR 8-1).

6. Model predictions are high in the Ocala Limestone and low in the Avon Park Formation at coastal wells TR SA-1, TR SA-3 (south of TR 7-2).

7. Model predictions for chloride are high in the Ocala Limestone at coastal wells 20, TR 4-1 (south of TR SA-3).

8. The model provides a good fit to chloride concentrations in the Ocala Limestone at inland well 9 near the southern model boundary.

The slope of the chloride interface, that can be calculated from the exploratory data at TR-SA-1 and TR-SA-3 was also used as a calibration measure which was evaluated against ROMP wells TR AB-1, TR 9-2 and TR AB-3 in coastal Hillsborough County. These wells are aligned perpendicular to the coastline and provide a good cross-sectional representation of the interface slope since the interface lies within the sampled interval in all three wells. As shown in Appendix B, the model provides a good depiction of the chloride profiles for these wells, and, hence, of the interface slope.

Another metric applied to the calibration effort was the thickness of the transition zone. It is noted from available data (see Appendix A for chloride data in ROMP wells) that the transition zone is fairly thin with rapid degradation of water quality from fresh to saltwater across the interface. This feature was duplicated by the model in addition to providing a good fit on average chloride data and depth to interface.

As previously discussed in Section 2, Beach and Kelley (1998) projected the freshwater-seawater interface onto hydrogeologic cross sections at six locations along the coast (Figure 2.16). The distance along each cross section to the toe was superimposed onto a map. A smooth line through each toe was drawn delineating the 1,000 mg/l chloride concentration defining the areal extent of the interface between the freshwater and saltwater. This approach was later updated (Beach and Schultz, 2000) by delineating the top and bottom of the highly permeable zone from exploratory drilling data and adding this information to each cross section. Beach and Schultz (2000) determined that the current position of the interface toe in the Avon Park Formation is only two to three miles inland in south Hillsborough County. In Sarasota County, the interface toe in the Avon Park Formation may be as much as ten miles inland. These estimates have been superimposed on the calibrated model results and presented in Figure 5.14. This figure indicates that the model predicts a similar overall shape to the saltwater interface but predicts that the saltwater interface is less inland in the northern and southern portions of the model domain.

The chloride interface in the Suwannee Limestone is shown on Figure 5.15. The calibrated model indicates that there has been almost no saltwater intrusion within the Suwannee Limestone except in the southern portion of the model domain south of Sarasota. Chloride interface for the Avon Park Formation layers 6, 8, and 10 are shown in Figures 5.16 through 5.18, respectively. These figures indicate that chloride intrusion roughly follows the coastal profile and increases with depth in the Avon Park Formation.

To illustrate the changes of chloride concentrations with time, a series of plots have been constructed comparing the model predictions to the actual field data. Figures 5.19 through 24, show the model predicted chloride concentrations versus time, superimposed on field data measured at selected ROMP wells.

The trend of the chloride data in TR-9-3 is relatively stable in the Suwannee Limestone, and sharply increases in the Avon Park (Figure 5.19). The model underpredicts the chloride concentrations in both layers. The trend of the data in the Avon Park illustrates the difficulty in matching the sharp increases in concentrations over short time periods. Although the trend in the model is upward it is not nearly as steep as that observed in the measured data. Some of this difference can be attributed to the fact that the model averages chloride concentrations over grid blocks and cannot simulate the sharp fluctuations in the chloride concentrations, which occur over short intervals. Again, a similar effect is observed in ROMP TR 9-2 (Figure 5.20). TR 8-1 provides a very good match to the data in both chloride concentrations as well as temporal trends (Figure 5.21). Observed chloride concentrations in ROMP 50, however, are significantly overestimated by the model (Figure 5.21), although the tends are similar. ROMP 22 provides a reasonable match to the data, but the increasing trend predicted by the model is not replicated by the field data. The model overestimates the chloride data collected from ROMP 20 (Figure 5.22) and predicts an slightly increasing trend which the data suggests that the chloride concentrations may be decreasing. The model underestimates the observed concentrations in both in ROMP 33 and 39 (Figure 5.23), although at the low chloride concentrations in these wells the differences could represent only minor differences. Figure 5.24 indicates that indicates that the model is slightly over predicts the data from TR SA-1, and significantly over-predicts the data from ROMP TR SA-3.

Although the model did not fit the transient chloride data particularly well, in general, the model provided a much better fit to the static ROMP well data. The greatest source of error aside from the unknown heterogeneities within the aquifer property values, is probably associated with the vertical discretization of the model not being at the same scale as the collected data. Chloride concentrations in the model are averaged over several hundred feet as compared with tens of feet in the field. This inconsistency in scale makes it difficult to precisely match the field data, particularly at high chloride concentrations, without introducing too much chloride to the model. This problem is aggravated because the interface transition zone is relatively thin and concentrations change dramatically over short vertical distances. The model does, however, provides a very good representation of the chloride intrusion characteristics and should provide an adequate means to meet the project objectives of the SWFWMD.

Post-Development Hydraulic Heads

To evaluate the hydraulic response of the calibrated model, a comparison of the calibrated model hydraulic heads was made against the potentiometric surfaces from September 2000 and May 2000 prepared by the U.S. Geological Survey (USGS). Typically, these represent the annual high water level period and the annual low water period, respectively. A comparison between the USGS potentiometric surface for May 2000 and the corresponding model predicted head distribution for the Suwannee Limestone is shown in Figure 5.25. The potentiometric surface constructed by the USGS indicates that the measured head values are lower than the predicted head values by approximately 35 feet in the northeastern portion of the model to about zero feet within the southeastern portion of the model. The measured heads are approximately 5 to 20 feet lower than predicted values in the central portion of the model. The general shape of both contour sets, however, is very similar throughout the model domain.

A similar comparison of May 2000 heads for the Avon Park Formation is presented in Figure 5.26. Again the heads predicted by the model are higher than measured values. The greatest discrepancies between the measured and predicted heads are located in the central and northeast portions of the model domain. The general shape of the potentiometric surface contours for the model versus field data is very similar over the entire model domain, with contours closing around a depression in the potentiometric surface in the central portion of the region.

A comparison between the measured and predicted head values for September 2000 for the Suwannee Limestone and Avon Park Formation are shown in Figures 5.27 and 5.28, respectively. Of particular relevance is that the measured values for May and September vary by about 30 feet over much of the model domain. The predicted heads for the Suwannee Limestone are in reasonably good agreement with measured head contours over most of the model area. As shown in Figure 5.28, the predicted heads in the Avon Park Formation are not as close to the field data but still capture the general shape of the measured potentiometric surface.

The most probable reason for the differences between measured and predicted head values is that there are significant transient hydraulic stresses within the hydrogeologic system which are not captured by the flow model, which uses applying 4-month averaged pumping and boundary conditions. It should be noted that the head responses of the saltwater intrusion model are very similar to that of the transient Southern District Model (SWFWMD, 2001) run with similarly time-averaged pumping conditions.

Another calibration criterion is the head difference between the Suwannee Limestone and the Avon Park Formation for which there is not expected to be an appreciable difference. This assumption is based upon an aquifer test conducted in Manatee County within the Avon Park Formation. During the pumping test, measured water levels in two wells that were open to the different production zones (i.e., Suwannee Limestone and Avon Park Formation) were nearly identical (Guyton and Associates,1976). Figure 5.29 shows the difference between the heads predicted in the Suwannee Limestone verses those in the Avon Park Formation. Over most of the model domain the difference in heads is less than 5 feet. The exceptions to this are along the northeastern and southern boundaries which are local boundary effects.

Mass Balance

The reliability of the model was also assessed during the calibration process by evaluating the computed water balance. The water balance calculated for pre-development conditions using the calibrated model is shown in Figure 5.30 and Table 5.4. The locations of the eastern, southern and northern freshwater boundaries are shown in Figure 5.4 as a series of blue dots. These boundaries were set to prescribed heads as determined from the Southern District Model (SWFWMD, 2001). The lateral saltwater boundaries are designated in Figure 5.4 as green dashes along the northern and southern boundaries and as a solid red line along the western boundary. Information for the drains (i.e., location, depth, conductivity, heads) was derived directly from the Southern District Model (SWFWMD, 2001). The bottom boundary represents the amount of fluid exchange between the Avon Park Formation and the middle confining unit (i.e., evaporites) (Figure 5.3). The top boundary represents the interface between the Tampa and Suwannee Limestone members of the Upper Floridan aquifer (Figure 4.4).

The water balance indicates that during pre-development conditions large volumes of water enter from the eastern freshwater and lateral saltwater boundaries. Appreciable amounts of water also leave the model domain from the lateral, saltwater and top boundaries. Although considerable volumes of water enter the model through the top and bottom boundaries, a significant amount of water leaves the model through the top boundary due to upward gradients over much of the model, particularly in the western portions of the model domain. The total volume of water entering the model domain is essentially equal to that leaving the model.

The computed water balance for post-development conditions (i.e., December 2000) is shown in Figure 5.31 and Table 5.5. The greatest differences between the pre- and post- development water balances are the large volume of water removed by wells during the post development (current) period, although a small amount of water is introduced to the model via injection wells. The stress imposed on the system by the pumping wells considerably alters the head gradients which induces water to flow downward through the upper boundary and laterally from the eastern and saltwater boundaries. Greater amounts of water also enter the domain from the lower boundary during the post development simulations. Water entering the model from the top and bottom boundaries are almost equal. Furthermore, almost no water exits the bottom boundary. The total inflow and outflow for post-development conditions are also in excellent agreement.

6.0 SENSITIVITY ANALYSES

6.1 GENERAL SENSITIVITY APPROACH

The purpose of sensitivity analyses are to quantify the uncertainty in the calibrated model caused by uncertainty in the estimates of aquifer parameters, stresses, and boundary conditions (Anderson and Woosner, 1992). Their significance and use is aptly summarized by ASTM (1994) as:

1. To identify which model inputs have the most impact on the degree of calibration and on the conclusions of the modeling analysis.

2. To categorize the parameter sensitivities in a manner that identifies the predictive capability of the calibrated model for its intended conclusions.

The ASTM (1994) procedures were applied to perform the sensitivity analysis for this study. Where applicable, this process was enhanced to provide a further understanding of system behavior in the presence of uncertainties (ASTM, 1994).

The sensitivity analysis was performed in two parts. The first part was a parameter sensitivity performed by systematically changing the values of the calibrated model parameters or boundary conditions within pre-established reasonable limits. The second part investigated the effects of alternative conceptualizations on the calibrated model. The first step in both parts was to identify the parameters or model inputs that need to be varied during the sensitivity analysis. Then for each parameter, the specified range of variation was determined based on the expected range of observed values (i.e., field data) or conceptual validity. Simulations were subsequently performed over this range for each parameter or conceptualization, for steady-state pre-development and transient post-development conditions. For the current study, the 'most probable high and low' values associated with each parameter or boundary condition were used to perform the sensitivity analyses.

For the parameter sensitivities, the calibration residuals and the results of model predictions of chloride intrusion were graphed as a function of parameter input value for each of the parameters investigated. In this study, the model conclusions were defined as the percentage of pumping wells impacted by chlorides at concentrations exceeding 500 ppm, and the total chloride mass that is contained within the model domain. The first conclusion was selected as a specific model outcome of interest to the SWFWMD, the second being a general conclusion on the state of chlorides within the entire simulation domain. From this set of graphs, the model input parameters that have the most impact on the degree of calibration and on the conclusions, were identified. This set of graphs is also used to categorize parameter sensitivities into four types, which are described below.

Type I sensitive parameters are those which cause insignificant changes in calibration residuals as well as model predictions. Type I sensitivity on a parameter is of no concern, because regardless of the parameter input value (within the predetermined range), the model predictions remain the same. Type II sensitive parameters cause significant changes in the calibration residuals but insignificant changes in the model predictions. Type II sensitivity on a parameter

is of no concern because regardless of the value of the input, the model predictions remain the same. Type III sensitive parameters cause significant changes to both calibration residuals as well as the model predictions. Type III sensitivity on a parameter is of no concern because even though the model predictions change as a result of variation in input, the parameters used in those simulations cause the model to become uncalibrated with residuals increasing from the calibrated model that best represents the field conditions. Type IV sensitive parameters cause insignificant changes in calibration residuals but cause significant changes in the model predictions. Type IV sensitivities can have greater uncertainties because over the range of that parameter in which the model can be considered calibrated, the model predictions can change substantially. A Type IV sensitivity generally requires additional data collection to decrease the range of possible values of the parameter (ASTM, 1994).

For the conceptual sensitivities, the calibration residuals and model conclusions are noted along with a general description of notable or significant effects of the conceptual change, compared to the base case calibration simulation (Section 5.2.1). These conceptual changes from the base case correspond to uncertainties in the hydrogeologic system.

6.2 PARAMETER SENSITIVITY ANALYSIS AND RESULTS

A parameter sensitivity analysis was first conducted for the calibrated saltwater intrusion model to identify the model input groups that have the most impact on the model calibration and on the model predictions. The parameters and their range of variation were chosen in collaboration with SWFWMD staff, and are considered to be the important parameters that govern the behavior of saltwater intrusion in the domain. The parameter sensitivity study is summarized in Table 6.1. The first column of the table shows the parameters that were chosen for this sensitivity analysis followed by their selected variations in the second column. The remaining columns summarize calibration statistics and model predictions for the various parameters that were evaluated. The last column categorizes the various parameters into one of the four sensitivity analysis categories (i.e., Type I, II, III, or IV) as defined by ASTM (1994). The first row of Table 6.1 provides results for the calibrated model while subsequent rows discuss the various parameter sensitivities. Figure 6.1 provides significant calibration statistics and the results of model predictions of chloride intrusion for each of the parameter sensitivities. These calibration statistics include those that were evaluated during the model calibration process (i.e., residual mean error and root mean square error (RMS)).

Porosity (Parameter 1) is the most sensitive parameter in terms of the calibration statistics as well as on the conclusions of this study (Type III sensitivity). Since the effect of porosity is mainly to control the transient movement of chlorides, it is possible based on these statistics, to have an error in the pre-development location of chlorides with an associated error on porosity in the same region, to produce the same current conditions for chlorides. Therefore, the possibility of multiple solutions exists, to produce the same calibration, however, within the limits of the assumptions made in the model (uniform porosities of all materials), the calibrated model provides appropriate results for the noted transient behavior as discussed in Section 5.3.2. In fact, it may be noted that the multiplication factor of 2 (see Figure 6.1a) to the base-case porosity values provides a better "calibrated" model with a smaller average error and less spread in the results from observed chloride levels. However, these values are considered to be outside reasonable limits for

porosities in the region, and the transient behavior is inferior to that of the calibrated model in terms of depth to chlorides (also used as a calibration measure) and its movement. Finally, on Figure 6.1a, the mass of chlorides in the domain is an inappropriate surrogate measure for the general intrusion of chlorides into the domain, since the porosity value affects volume and hence mass of chlorides within the domain, for the same amount of intrusion.

The second most sensitive parameter is the landward lateral boundary head (Parameter 12) in terms of the calibration statistics and the model predictions (Type III sensitivity). Figure 6.11 shows that the model is well calibrated to this parameter, with an increase in the average error and RMS error for an increase or a decrease in the lateral landward boundary head value.

The bottom GHB head value (Parameter 9) is the next most sensitive parameter in terms of the calibration statistics and the conclusions of this study (Type III sensitivity). As may be noted from Figure 6.1i, a 10 ft drop in the heads assigned to the GHB boundaries gives a substantially smaller average error, with not much effect on the spread of the error (RMS). However, lowering the head assigned to the bottom GHBs by 10 feet, degrades the ability of the model to match vertical chloride profiles observed in many of the ROMP wells.

The other parameters with a high degree of sensitivity, in terms of the model calibration and predictions (Type III sensitivity), include:

- the hydraulic conductivity associated with the entire Avon Park Formation (model layers 6 through 10) (Parameter 2);

- the hydraulic conductivity associated with the "highly permeable zone" within the Avon Park Formation (model layers 6 and 7) (Parameter 3); and

- the head value applied to the GHB condition along the bottom model boundary (Parameter 8).

Parameter sensitivities 2 and 3 are similar (the former being on the entire Avon Park Formation, the other on the "high-flow-zone" only) with a multiplying factor of 2.0 providing significantly reduced average errors (Figure 6.1b) and only a slight increase in the error spread. In fact, as noted in Table 6.1, the average change in December 2000 heads from the base case is significantly positive indicating lower heads than the base case for December 2000 conditions. However, this was a less desirable option for the calibrated model because measured values are considered to be more reliable than a factor of 2, and because it produced less accurate depth to chlorides than shown in Appendix B. Similarly, the +10 ft sensitivity simulation of parameter sensitivity 8 has a smaller residual with less spread, however, 10 ft is added to all top GHB nodes including those in Tampa Bay and Gulf of Mexico, which would be conceptually questionable. This exhibited sensitivity suggests that the GHB heads could be refined if more data become available.

Parameter sensitivities 6, 10, and 11 (for top GHB conductance values, Bottom GHB conductance values and the coastal lateral boundary head respectively) show a Type II sensitivity whereby the parameters are sensitive to the residuals, but not to the conclusions or requested prediction. The calibration sensitivity is considerable for these parameters, with a large change in the average

chloride error for the range of parameters considered. Finally, parameter sensitivities 4, 5, 13, 14, and 15 (for vertical conductivity values of the modeled Ocala Limestone, hydraulic conductivity values of the modeled Suwannee Limestone, dispersion coefficients, diffusion coefficient, and Avon Park Formation's vertical anisotropy ratio, respectively) show Type I sensitivities whereby neither the residuals nor the conclusion are sensitive to changes in the parameter value. From Table 6.1, however, it may be noted that the Ocala Limestone's vertical conductivity value is most sensitive to the vertical head separation between the Suwannee Limestone and the Avon Park Formation. Conductivity values for the Avon Park Formation are the next most sensitive parameters for this head separation effect. Other parameters were not as sensitive.

Other model data that was evaluated during calibration included the overall bias of the model versus the data. It is noted in Table 6.1 that porosity, model layers 6 and 7 conductivity values, and bottom GHB head values can have the largest impact on chloride data fit among all the parameters. Fluxes through the top and bottom of the model were also evaluated during calibration and their sensitivity is also addressed. Flow in from the top GHB boundary was most sensitive (as much as 45% in volume) to top GHB conductance followed by top GHB heads (parameters 6 and 8 respectively). Flow out of the top GHB boundary was most sensitive (as much as 45% in volume) to top GHB conductance, top GHB heads and Coastal lateral boundary heads (6, 8, and 11 respectively) with a moderate sensitivity to the Avon Park conductivity values of sensitivities 2 and 3. Flow in and out of the bottom of the domain was most sensitive to bottom GHB head and bottom GHB conductance values. Aside from the porosity simulation, whereby chloride mass is not an indicator of intrusion into the domain as discussed earlier, the maximum chloride mass in the domain exists for the simulation with coastal lateral heads increased by +20 ft, and the minimum exists for the simulation with top GHB heads increased by +10 ft. In general, about two-thirds of the wells that are contaminated by chlorides greater than 500 ppm, also contain chlorides greater than 1,000 ppm. However, in general, the trends in parameter sensitivity of these conclusions are similar to those of the total chloride mass which may be used as an indicator here for the total chloride intrusion amount.

6.3 CONCEPTUAL SENSITIVITY ANALYSIS AND RESULTS

Conceptual uncertainties of the system, and their effect on saltwater intrusion have been investigated by the conceptual sensitivity analyses. Two primary conceptualizations are studied here, as an alternate to the calibrated model. First, it is unknown how the middle confining unit interacts with the overlying Upper Floridan aquifer, therefore, a sensitivity analysis was performed on this interaction. Second, the conceptualization of having a higher permeability zone within the Avon Park Formation was tested by performing a sensitivity simulation in which the higher permeable zone was removed from the model. Table 6.2 details these sensitivity analyses and provides calibration statistics and results.

For the first conceptual sensitivity simulation, the middle confining unit and its interaction with the Floridan Aquifer system under study exist only under the zone of high transmissivity in the Avon Park Formation under Pinellas County, Hillsborough Bay and Tampa Bay, to allow for saline water below the middle confining unit to interact with the Upper Floridan aquifer in this region only. The rest of the domain is unaffected by this interaction, as is the conceptualization

used throughout the Southern District Model (SWFWMD, 2001). Two simulations were performed for this sensitivity analysis, to understand the behavior of this boundary in a systematic manner. The first simulation is designed from the calibrated model by cutting off the bottom GHB condition from portions of the domain not underlying the highly permeable zone under Pinellas County, Hillsborough Bay, and Tampa Bay. The second simulation further increases the GHB conductance under the highly permeable zone by an order of magnitude to increase the interaction with the middle confining unit in this region (i.e., the intrusion of chlorides from the MCV can be larger due to its larger vertical conductivity). This conceptualization is motivated by the fact that modeled chlorides have the tendency to be excessive in the southern portions of the domain, while they are less in the north, specifically in the area of TR AB-1, TR 9-2 and TR AB-3.

The calibration statistics associated with these simulations show much improvement over those of the base-case calibrated model with lower average errors and a similar RMS error to the base-case. Final heads are higher than those of the base-case, which is also a desirable feature. Flow in and out of the top GHB boundary is similar to that of the base-case, however net flow in/out of the bottom GHB boundary changes. For the first simulation, net flow in the bottom is less because of the smaller area of interaction with the middle confining unit than the base-case. For the second simulation, the net flow in the bottom is higher because of the higher GHB conductances which increase the interaction. For this sensitivity, only around half the pumping wells extract greater than 500 mg/l chloride than for the base-case. This conceptualization therefore, has the possibility of improving calibration. Thus, if a data collection program can validate the possibility of this conceptualization, further tuning on the parameters may be performed with investigations of depth to chlorides, slope of the interface, and thickness of the transition zone - all features that were examined in calibrating the model. A general inspection of the results indicates that chlorides are not affected by this calibration in the southern regions of the domain, chlorides intrude less than the base case in the middle portion of the domain, and chloride intrusion can be greater in northern parts of the domain if the bottom GHB interaction there is increased.

For the second conceptual sensitivity simulation, the Avon Park Formation is treated as a single unit vertically. The hydraulic conductivity of this unit is applied in a manner that provides an equivalent transmissivity to the base-case simulation. This conceptualization is examined as an alternative, to investigate the results of this simplification (always made in flow models), on chloride transport behavior. The average error for this simulation shows an improved fit than for the base case, with a similar RMS error (Table 6.2). Other flow statistics and model conclusions are similar to that of the base case. The model is quite insensitive to this alternative conceptualization which may be used instead without significant loss of accuracy or predictive capability. However, the nature of the calibration of such a model should be first examined with respect to depth to chlorides, width of transition zone, and slope of interface to determine if it would be adequate. A general inspection of the results indicates that the chlorides moved seaward in the entire domain from the base-case, and the interface slant became more vertical (not desirable) for this simulation.

6.4 QUALITY ASSURANCE REVIEW RESULTS

After calibrating the density-dependent model, the SWFWMD reviewed the wells and well depths assigned in the Southern District Model (SWFWMD, 2001) and in the local-scale, density-dependent model. The review was undertaken to reconcile differences between previous assessments of wells at risk of saltwater intrusion prepared by the SWFWMD and the current, preliminary estimates made with the local scale density-dependent model.

The review examined the total depth and/or casing depth assigned to wells for which no value is reported in the SWFWMD Water Use Permit (WUP) data base. The review determined that procedures used to assign these values to model layers in the Southern District Model (SWFWMD, 2001), which does not use elevations or depths, had incorrectly assigned total depth and casing depth elevations to wells in the local scale density-dependent model. After assessing the situation, a revised process assigned corrected total depth and casing elevations to the wells of the transport model.

This resulted in 512 of the 2,681 wells being eliminated from the model when the total depth elevations were above the top of the UPZ as configured in the transport model. A review of these wells indicated that most of these wells were located along the southwest coast and are known to be completed in the IAS, which is not simulated by the transport model. Although the number of wells removed is nearly 20 percent of the total, the total withdrawal rate is only 5.7 percent of the original 223.38 mgal/day. The result of this change on the calibrated model is minor as illustrated by the relative chloride concentration contours for model Layers 2 and 6 (Figures 6.2 and 6.3). The results of the comparison of the environmental head potentiometric surfaces for Layers 2 and 6 also indicate minor changes (Figures 6.4 and 6.5).

The total withdrawal rate associated with each predictive scenario is unchanged. The reported number of wells at risk of saltwater intrusion under each scenario in Section 7.0 reflects the revised pumping data set.

7.0 PREDICTIVE SIMULATIONS

The calibrated density-dependent saltwater-intrusion model was used to predict potential changes to the groundwater flow system and associated chloride conditions, which would result from changes in groundwater withdrawals in the Upper Floridan aquifer. Projected pumping conditions include withdrawals of 400, 600, 800 and 1,000 MGD within the SWUCA. Based on these pumping projections, the saltwater intrusion model was used to predict the distribution of chloride after 20 years and 50 years of pumping. December 2000 conditions provided the initial conditions for the predictive simulations. Most boundary conditions for the predictive simulations were kept the same as those used for the pre-development to post-development simulation. The only differences in model input were groundwater withdrawals and the lateral landward freshwater boundary heads which were provided by the District for the saltwater intrusion model by performing parallel simulations with the Southern District Model (SWFWMD, 2001). Since the saltwater intrusion model includes only a portion of the SWUCA individual well pumping within the saltwater intrusion model was scaled according to the ratio of total pumping of the various scenarios (i.e., 400, 600, 800 or 1,000 MGD), to total pumping for December 2000 conditions. In addition, a predictive sensitivity analysis was conducted on each of the four scenarios. For these simulations, selected input parameters were changed in order to provide a range of potential impacts. The parameters included for the predictive sensitivity study were selected from those found to be most sensitive during the sensitive analysis discussed in Chapter 6.

For the predictive scenarios, an analysis was performed to determine the number of wells contaminated by chloride concentrations either exceeding 500 mg/l or 1,000 mg/l, at 20 and 50 years of simulation (i.e., year 2020 and 2050). For production wells that are completed across multiple hydrostratigraphic units, the chloride concentrations predicted by the model represent a homogeneous mixture of water that is contributed by each unit. This mixed concentration should approximate the actual concentration that is observed at the individual wells. The results of the predictive simulations are presented in Table 7.1. Also presented in the table is the 1995-1999 average annual usage from the contaminated wells and the associated 1999 permitted pumping from those wells. These columns of the table denote how much pumping (or permitted pumping) within the Upper Floridan aquifer would be at risk due to chloride intrusion, or moved to other locations. A total of 1,806 wells are included in the domain of the saltwater intrusion model. The saltwater intrusion model predicts that 154 of these wells (8.5%) are currently impacted by chloride at concentrations exceeding 500 mg/l. Furthermore, the model predicts that after 50 years of pumping, 224 of these wells (12.4%) will be impacted by chlorides at concentrations exceeding 500 mg/l. The model predicts that 63 wells (3.4%) are currently impacted by chlorides exceeding 1,000 mg/l, and chloride concentrations will exceed 1,000 mg/l in 147 wells (8.1%) after 50 years of continued pumping. Tables 7.2, 7.3 and 7.4 provide a detailed breakdown of this production well impact analysis for the Suwannee Limestone, the Ocala Limestone and the Avon Park Formation respectively. These tables illustrate that for the wells within the model domain, the wells completed in the Avon Park Formation are most likely to be impacted by saltwater.

Figure 7.1 shows the projected extraction well chloride concentration histogram for December 2000 of the post-development simulation. The histogram shows 1418 extraction wells with chloride concentration less than 100 mg/L and 1777 extraction wells with chloride concentration

less than 2000 mg/L. Notice that the 136 wells between 200 mg/L and 500 mg/L are decreasing from left to right and the 91 wells between 500 mg/L and 1,000 mg/L are approximately uniformly distributed. This suggests that for the predictive simulations, the number of wells above 500 mg/L will increase along a non-linear trend and number of wells above 1,000 mg/L will increase along a linear trend. Figure 7.1 also shows the average pumping rate for the wells in each histogram bar. Notice that the wells between 200 mg/L and 500 mg/L have a lower average pumping rate than the wells between 500 mg/L and 1,000 mg/L. All of the predictive simulations have more extraction wells passing the 1,000 mg/L threshold than pass the 500 mg/L threshold (Table 7.1). Column 7 of Table 7.1 shows that the number of wells above 500 mg/L increased along a non-linear trend and the number of wells above 1,000 mg/L increased along a linear trend. Columns 8 of Table 7.1 indicates that the extraction wells passing the 1,000 mg/L threshold have a higher average pumping rate than the wells passing the 500 mg/L threshold.

Figures 7.2, 7.3, 7.4 and 7.5 show the areal distribution of chlorides within the highly permeable zone of the Avon Park Formation after 50 years of pumping for each of the four scenarios respectively. The largest intrusion in the highly permeable zone of the Avon Park Formation was for model layer 7 for each of the four simulations, which is shown in these figures. Chlorides move inland by about 2.5 miles from the current position within 50 years of pumping 400 MGD, about 5 miles for a pumping of 600 MGD, about 7 miles for a pumping of 800 MGD and about 9 miles for a pumping of 1,000 MGD within the highly transmissive zone of the Avon Park Formation. Movement of chlorides is less in the northern portion of the domain where the aquifer is thinner.

Figure 7.5 shows the 1,000 mg/l chloride isochlor in the highly permeable zone of the Avon Park Formation, after 50 years of pumping for the various scenarios. A comparison of this figure with estimates of Beach and Schultz (2000) provided in Figure 2.17 shows a reasonable comparison of the modeled saltwater front with their estimates, for pumping of 400, 600, 800, and 1,000 MGD. The 50-year movement from current conditions is also similar for the various pumping cases. Chlorides are however, more landward in the southern regions of the model, and slightly more seaward in the northern portions of coastal Hillsborough County than the estimates of Beach and Schultz (2000).

7.1 PREDICTIVE SENSITIVITY ANALYSIS

The possible effects of projected pumping within the Floridan Aquifer System upon chloride intrusion to wells, is of particular concern within the SWUCA. Therefore, a sensitivity analysis was conducted to estimate the potential ranges of the predicted number of wells contaminated by greater than 500 mg/l and 1,000 mg/l of chlorides. This analysis is further broken up into estimating potential ranges for the predicted number of wells contaminated by greater than 500 mg/l and 1,000 mg/l of chlorides in each of the aquifer units (i.e., the Suwannee Limestone, the Ocala Limestone, and the Avon Park Formation).

Sensitivity parameters selected for this analysis include the porosity of the aquifer and aquitard materials, the landward lateral freshwater boundary head, and the GHB head value applied to the bottom of the model. In terms of the model predictions, these were determined to be the most sensitive parameters (Section 6). For each sensitivity simulation set, the parameter value was

raised and lowered by a predetermined amount that provides a reasonable range bounding that parameter value. This range of parameter sensitivity is identical to that used for the model sensitivity analysis in Chapter 6.

Table 7.5 shows the results of the predictive sensitivity study in the Floridan Aquifer system, and Tables 7.6, 7.7 and 7.8 provide a breakdown of these results for the Suwannee Limestone, the Ocala Limestone and the Avon Park Formation, respectively. The table presents the additional number of wells affected for each sensitivity study, from the respective base case scenario. It may be noted that multiplying the porosity value by 0.2 had greatest impact on the modeling results, in terms of increasing the number of wells that are affected by chlorides (both in the individual hydrostratigraphic units and within the entire Upper Floridan aquifer). The number of wells impacted by high chloride concentrations approximately double from the base case for this parameter perturbation, with wells completed in the Suwannee and Ocala Limestones being much more susceptible to contamination than wells completed in the Avon Park Formation. The decrease in the number of wells, affected by chlorides in the Suwannee Limestone and the Ocala Limestone, is most strongly influenced by the addition of 10 ft to the landward lateral boundary heads with the largest impact being in the Suwannee and Ocala Limestones. Alternatively, the most dominant factor for the decrease in the number of wells affected by chlorides in the Avon Park Formation is the lowering of the GHB boundary head value at the base of the model by 10 feet.

7.2 MODEL LIMITATIONS

The model described in this report is a numerical groundwater flow and solute transport model that uses the MODHMS computer code to approximate the groundwater flow and chloride transport system in the SWUCA. The model results are limited by the simplification of the conceptual model upon which the numerical model is based, by the grid scale, by the inaccuracies of measurement data and by incomplete knowledge of the spatial variability of input parameters.

The conceptual model used to construct the density-dependent saltwater intrusion model for the SWUCA is a simplified representation of the true groundwater flow and transport system. Due to its karstic nature, the Floridan aquifer system can be characterized as an extremely complex, heterogeneous aquifer system. These features may cause zones of preferential pathways caused by secondary porosity features and solution conduits. However, the secondary porosity features are believed to be so ubiquitous that the system behaves as an equivalent to a porous-medium at the scale of the modeled system.

The density-dependent saltwater intrusion model is based upon the Southern District Model (SWFWMD, 2001) for groundwater flow developed by the SWFWMD using the popular USGS MODFLOW code. Further, the calibrated saltwater intrusion model has almost the same conceptualization and parameter distribution as that of the Southern District Model (SWFWMD, 2001). Differences in conceptualizations are associated with the specifics of saltwater intrusion modeling. For instance, use of a transmissivity value for each aquifer unit is sufficient for groundwater flow modeling, however, saltwater intrusion simulations require the additional vertical resolution to capture the gradients in concentration resulting from saltwater intrusion

within each aquifer unit. To address these issues, the density-dependent model was more finely discretized than the Southern District Model.

Averaging of boundary conditions and well pumping over 4-month intervals for the latter part of the transient simulations should not have much impact on chloride intrusion levels, since intrusion is an extremely slow process with time-scales that are orders of magnitude larger than four months. However, this averaging has a significant impact on the simulated head field within the aquifers, which do not exhibit the seasonal extremes noted in the field since the time-scales for head response to pumping can be much smaller than four months.

The model simulates conditions represented by the static chloride data from the ROMP wells better than the subsequent field data collected over some ten years as shown in Figures 5.19 through 5.24. The primary reason for this discrepancy in the model predictions is that greater reliance was placed on establishing the chloride interface position and vertical concentration gradients rather than attempting to match the transients in the chloride data. The justification for this approach is that chloride interface changes very slowly with time and the chloride profiles provide a better overall description of the chloride distribution within the modeled area. Local chloride vs. time data were obtained from relatively short monitoring intervals within respective monitoring wells. These local concentration data are governed by small-scale heterogeneity. The model's inability to mimic the magnitudes of local-scale time dependent chloride data may be attributable to the finite-difference grid size that is larger than the local heterogeneity scale. In addition, local changes in chloride concentrations with time could be affected by ephemeral processes (e.g. changes in recharge rates). These processes may be either too localized to be captured adequately by the model, or are of such short duration that the quarterly averaging by the model is insufficient to duplicate the temporal changes in the field data.

Horizontal and vertical discretization into model grid cells requires the assumption of average values of hydrologic properties and stresses for each grid block. The larger the range of the true values of a property or stress within a grid cell area, the greater the difference between the average value and the true value at any particular location within a cell. This difference is probably greatest for confining unit leakances which can vary greatly due to local changes in thicknesses and vertical hydraulic conductivity not represented in the model. The location of stresses is also somewhat distorted by the grid scale since all pumping in the model is accumulated at a grid-block center. This error should be small for the current simulations due to the distributed nature of pumping throughout the model domain which is applied to a reasonably fine grid. Another error source is that the resolution of results cannot be made finer than that of the grid. This is significant for representing chloride values within the model, since chloride data from ROMP wells is at a much finer vertical scale than the model's vertical resolution. This problem is compounded by the fact that chlorides can change dramatically within the domain with an extremely narrow transition zone between freshwater and seawater.

Model results are limited by incomplete knowledge of the true spatial variability of input parameters. However, sensitivity analysis conducted on the input arrays of parameters and stresses used for this model have indicated that the model's calibration and predictive results are sensitive to certain input parameters and stresses and insensitive to others. Model calibration and predictions are most sensitive to the value of porosity used for the aquifer units, followed by value

of the lateral landward freshwater boundary head and the value of the bottom GHB head. Uncertainty of model results is therefore related primarily to the uncertainty in these input parameters. However, since the calibration is also sensitive to these parameters, a perturbation on the parameter value causes the model to be uncalibrated thereby restricting their values to those that provide a calibrated model. It may be noted that the model did not show a Type IV sensitivity to any parameter examined (A Type IV parameter is one which exhibits sensitivity to results but not to the calibration). Therefore, the reliability of the model is not compromised in this respect.

Results of the predictive sensitivity analyses indicate a range for the number of wells contaminated by 500 and 1,000 mg/l of chlorides after 50 years for the various scenarios examined. This range is greatest for the Avon Park Formation for all the cases examined, thereby providing a larger uncertainty of results for the Avon Park Formation than for the other units analyzed.

The density-dependent saltwater intrusion model was designed with grid-block scales of one-half mile. Material property zones were designed at a scale that is an order of magnitude larger. Temporal scales for varying pumping and boundary conditions for pre- to post-development simulations were initially large, reducing to an order of four months near the end of the simulation. Therefore, model results should be viewed at these space and time scales, and the model may be used to examine the general chloride intrusion trends for long-term average stress conditions.

8.0 SUMMARY AND CONCLUSIONS

HydroGeoLogic has completed the development of a numerical, coupled groundwater flow and density-dependent transport model for the coastal portions of the SWUCA. The primary objective of this effort was to predict the long-term impact of proposed water use options on saltwater intrusion within the Upper Floridan aquifer. The saltwater intrusion model may be further used to establish minimum water levels or maximum pumping levels for groundwater extraction wells within the Upper Floridan aquifer or for developing a refined understanding of the stress response of chlorides to various regional management scenarios.

Historical reports and previous modeling investigations were reviewed to understand the hydrogeologic conceptual model, identify model calibration targets, and construct the framework for the saltwater intrusion model. Once the density-dependent model was constructed, it was calibrated to simulate conditions in the Upper Floridan aquifer that existed from the pre-development period (approximately 1900) to present conditions (through 2000). The pre-development simulations were calibrated to the results of earlier modeling work that predicted the position of the tip and toe of the saltwater interface, and a historical reconstruction of pre-development hydraulic heads. The density-dependent model predicts greater saltwater intrusion in the northern part of the model domain than the earlier models, and less intrusion from the center of the model southward. Differences in the modeling results would be expected, however, since different approaches (e.g., two-vs. three-dimensional) and assumptions (e.g., sharp interface vs. fully coupled flow and transport) were made in the various models. A favorable comparison between the pre-development potentiometric surfaces predicted by the model and historical estimates were also obtained.

Following the calibration of the model to pre-development conditions, the hydraulic stresses associated with pumping were integrated into the model and the model was calibrated to post-development conditions (i.e., post-1900). During the post-development calibration process, the results of the model calibration were evaluated both qualitatively and quantitatively. In some instances, a comparison between contour maps of measured and simulated values (i.e, hydraulic heads and chloride concentration) was prepared to provide a visual, qualitative measure of the similarity between patterns, thereby giving qualification of the spatial distribution of calibration errors. In addition, vertical and horizontal hydraulic heads and the fluid flux moving across the model boundaries was used as qualitative calibration criteria. Quantitative statistical assessments were also performed on the model residuals to assess the reliability of the calibration.

A general observation, with respect to the model calibration, is that the model does not always provide a good match to the chloride data on a well-by-well basis. From a more regional perspective, however, the model does provide a reasonably good fit to chloride distribution maps that show the extent of the chloride interface. There are several explanations for this apparent discrepancy between the model predictions at the local and regional scales. One of the most significant of which is that the chloride interface is relatively thin vertically, and narrow in the east-west direction. This limited extent of the interface causes the chloride distribution to be controlled by heterogeneities at a scale that is considerably smaller than the horizontal discretization of the model elements (i.e., 2,500 feet). Similar issues arise with the vertical discretization of the model. Since the discretization is at a larger scale than the collected data,

chloride concentrations in the model are averaged over several hundred feet as compared with tens of feet in the field. In fact, for each finite-difference cell containing a ROMP well, there are typically multiple observed chloride concentrations associated with different depth intervals. This inconsistency in scale makes it difficult to precisely match the field data, particularly at high chloride concentrations. This problem is aggravated by the fact that the interface transition zone is relatively thin and concentrations change dramatically over short vertical distances. Furthermore, since all of the calibration wells are located within the chloride interface, the models inability to capture the effects of the localized heterogeneities on the chloride distribution give the impression that the model predictions are unreliable. As noted above, however, the model does perform well when compared to the regional chloride maps. Although the model could be more finely discretized in both the horizontal and vertical dimensions to improve the localized calibration, the simulations times (which currently are on the order of 16-18 hrs at a 2.0 Ghz processing speed) would become excessively long. Furthermore, as described in greater detail in Section 5, the principle of parameter parsimony was applied as a fundamental philosophy during the calibration. This principle favors the use of uniform parameter zones unless there is hydrogeologic evidence indicating the presence of localized heterogeneous properties. Therefore, rather than attempting to precisely match the localized borehole data, by increasing the discretization and/or heterogeneities, the model was calibrated to provide a very good representation of the chloride intrusion characteristics on a more regional scale and should provide an adequate means to meet the objectives of the SWFWMD.

A comparison of simulated potentiometric surfaces to potentiometric surface maps developed by the USGS indicates that the model predicted head distributions for the Suwannee Limestone and Avon Park Formation tend to be lower than actual field data. The general shape of the potentiometric contour developed for simulated heads is very similar to the potentiometric surface developed using field data. The most probable reason for the differences between measured and predicted head values is that the model does not exactly simulate the transients within the flow system, in which hydraulic heads vary by about 30 feet from May to September.

A sensitivity analysis was also conducted, to identify the model input parameters and boundary conditions that have the most impact on the model calibration and on the model predictions. Porosity was found to be the most sensitive parameter, followed by the landward lateral boundary heads and the bottom GHB heads. The hydraulic conductivity associated with the entire Avon Park Formation (model layers 6 through 10), and with the "high-flow-zone" within the Avon Park Formation (model layers 6 and 7) also exhibited a high degree of sensitivity, in terms of the model calibration and predictions.

Predictive simulations were completed to estimate hydraulic heads and saltwater intrusion (i.e., saline water concentrations) for 20- to 50-year time periods. The possible effects of projected Floridan aquifer system pumping upon chloride intrusion to wells is of particular concern within the SWUCA. Therefore, four different water use scenarios proposed by the SWFWMD were evaluated. These comprise of withdrawing 400, 600, 800 and 1,000 MGD within the SWUCA. For the predictive scenarios, an analysis was performed on the number of wells contaminated by average chloride concentrations either exceeding 500 mg/l or greater than 1,000 mg/l, at 20 and 50 years of simulation (years 2020 and 2050, respectively). A total of 1,806 wells are included in the domain of the saltwater intrusion model. The saltwater intrusion model predicts that 154

of these wells (8.5%) are currently impacted by chloride at concentrations exceeding 500 mg/l. Furthermore, the model predicts that after 50 years of pumping, 224 of these wells (12.4%) will be impacted by chlorides at concentrations exceeding 500 mg/l. The model predicts that 63 wells (3.4%) are currently impacted by chlorides exceeding 1,000 mg/l, and chloride concentrations will exceed 1,000 mg/l in 147 wells (8.1%) after 50 years of continued pumping.

A predictive sensitivity analysis was also conducted to provide confidence limits on the results. Sensitivity parameters selected for this analysis include the porosity of the aquifer and aquitard materials, the landward lateral freshwater boundary head, and the GHB head value applied to the bottom of the model. Results of the predictive sensitivity analyses indicate a range for the number of wells contaminated by 500 and 1,000 mg/l of chlorides after 50 years for the various scenarios examined. This range is greatest for the Avon Park Formation for all the cases examined, thereby providing a larger uncertainty of results for the Avon Park Formation than for the other units analyzed.

9.0 REFERENCES

Ambient Ground-Water Quality Monitoring Program, 1991, Coastal ground-water quality monitoring program report for the Southwest Florida Water Management District; 129 p.

Ambient Ground-Water Quality Monitoring Program, 1990, Ground- water quality of the Southwest Florida Water Management District, Southern Region, Section 2; Southwest Florida Water Management District in cooperation with the Florida Department of Environmental Regulation; 351 p.

Anderson, M.P., and W.W. Woessner, 1992. Applied Groundwater Modeling. Academic Press, San Diego, California.

ASTM, 1994. Standard Guide for Conducting Sensitivity Analysis for a Ground-Water Flow Model Application, American Society for Testing and Materials, Publication D5611-94, 1-5.

Aucott, W.R., 1988, Areal variation in recharge to and discharge from the Floridan Aquifer system in Florida, U.S. Geological Survey Open-File Report 88-4057.

Barcelo, M.D. and R. Basso, 1993, Computer model of ground-water flow in the Eastern Tampa Bay Water Use Caution Area: Southwest Florida Water Management District.

Barr, G.L., 1996, Hydrogeology of the Surficial and Intermediate Aquifer Systems in Sarasota and adjacent counties, Florida, U.S. Geological Survey Water Resources Investigations Report, 96-4063, 81 p.

Basso, R., 2001, Hydrostratigraphic Zones within the Eastern Tampa Bay Water Use Caution Area, Southwest Florida Water Management District, Draft Report, March 2001.

Beach, M.H. and G.M. Kelley, 1998, Location of freshwater to seawater transition zone in SWUCA; and risk of associated saltwater intrusion; SWFWMD Technical Memorandum, December 1, 1998.

Brown, David P., 1983, Water Resources of Manatee County, Florida, U.S. Geological Survey Water Resources Investigations 81-74, 112 p.

Dohrenwend, R.E., 1977, Evapotranspiration Patterns in Florida, Florida Scientist, v. 40, no. 2.

Florida Department of Environmental Regulation, 1989, State Drinking Water Standards Chapter 17-550 DER Rules F.A.C. 1989.

Guvanasen, V., 2002, A New Multiple-Dispersivity Model for Transversely Anisotropic Porous Media. In preparation for submission to Water Resources Research.

Guyton, W.F., and Associates, 1976. Hydraulics and Water Quality, Technical Report prepared for the Swift Agricultural Chemicals Corporation, Manatee Mine Site, Manatee County, Florida, 76 p.

Hutchinson, C.B., 1983, Assessment of the interconnection between Tampa Bay and the Florida Aquifer, Florida, USGS Water-Resources Investigation 82-54 Tallahassee, Florida.

Huyakorn, P.S., and S. Panday, 1991, DSTRAM: Density-dependent Solute Transport Analysis finite-element Model, User's Manual, Version 4.1.

HydroGeoLogic, Inc., 2000, MOD-HMS: A Comprehensive MODFLOW-based Hydrologic Modeling System. Version 1.1, Code Documentation and User's Guide, HydroGeoLogic, Inc., Herndon, VA.

HydroGeoLogic, Inc., 1998, Refinement of Groundwater Flow and Solute Transport Model for Eastern Orange County, Florida and Adjoining Regions, Prepared for St. Johns River Water Management District.

HydroGeoLogic, Inc., 1994a, Analysis of Chloride Intrusion in the Eastern Tampa Bay Water Use Caution Areas, Technical Report submitted to the Southwest Florida Water Management District, Brooksville, FL.

HydroGeoLogic, Inc., 1994b, Modeling Assessment of the Regional Freshwater-Saltwater Interface in the Northern Tampa Bay Groundwater Basin, Technical Report submitted to the Southwest Florida Water Management District, Brooksville, FL.

HydroGeoLogic, Inc., 1994c, DSTRAM-based cross-sectional modeling of saltwater intrusion in the Eastern Tampa Bay Water Use Caution Area (1994, September).

HydroGeoLogic, Inc., 1994d, Ground-water Flow and Solute Transport Modeling Study For Seminole County, Florida, and Adjoining Regions, Prepared for St. Johns River Water Management District.

HydroGeoLogic, Inc., 1993a, Application of SIMLAS for Saltwater Intrusion Problems in the Southern Groundwater Basin, Technical Report submitted to the Southwest Florida Water Management District, Brooksville, FL.

HydroGeoLogic, Inc., 1993b, SIMLAS: Saltwater Intrusion Model for Layered Aquifer Systems, Version 1.3, Code Documentation and User's Guide, HydroGeoLogic, Inc., Herndon, VA.

HydroGeoLogic, Inc., 1993c, Application of SIMLAS to saltwater intrusion problems in the Southern Ground-Water Basin, SWFWMD (May, 1993).

HydroGeoLogic, Inc., 1992, SIMLAS: Simulated Intrusion Model for Layered Aquifer Systems, Version 1.0., Documentation and Users Guide, Herndon, VA.

HydroGeoLogic, Inc., 1991a, Density-Dependent Cross-Sectional Flow and Solute Transport Modeling for Manatee-South Hillsborough Water Resources Assessment Project, Technical Report submitted to the Southwest Florida Water Management District, Brooksville, FL.

HydroGeoLogic, Inc., 1991b, DSTRAM: Density-Dependent Solute Transport Analysis Finite Element Model, User's Manual, Version 3.1, HydroGeoLogic, Inc., Herndon, VA.

Johnston, R. and R. Krause, F. Meyers, C. Tibbals, and J. Hunn, 1980, Estimated potentiometric surface for the tertiary limestone aquifer system, S.E. United States, prior to development, U.S. Geological Survey, Open-File Report 80-406, 1 p.

Mahon, G.L., 1988, Potential for Saltwater Intrusion into the Upper Floridan Aquifer, Hernando and Manatee Counties, Florida, U.S. Geological Survey Water-Resources Investigations Report 88-4171.

McDonnald, M.G., and A.W. Harbaugh, 1988, A modular three-dimensional finite-difference groundwater flow model, U.S. Geological Survey Techniques of Water Resources Investigations Book 6, Chapter A1.

Menke, C.G., and E.W. Meredith, and W.S. Wetterhall, 1961, Water resources of Hillsborough County, Florida: Florida Geological Survey Report of Investigation 25, 99 p.

Miller, J.A., 1986, HydroGeoLogic framework of the Floridan Aquifer system in Florida and parts of Georgia, Alabama, and South Carolina, U.S. Geological Survey Professional Paper, 1403-B.

Millington, R.J., and Quirk, J.M., 1961. Permeability of Porous Solids, Trans. Faraday Society, 57:1200-1207.

Ryder, P.D., 1982, Digital Model of Pre-development in the Tertiary Limestone (Floridan) Aquifer System in West-Central Florida, U.S. Geological Survey Water-Resources Investigations 81-54, 61 p.

Ryder, P.D., 1985, Hydrology of the Floridan Aquifer System in West-Central Florida, U.S. Geological Survey Professional Pater 1403-F.

Scheidegger, A.E., 1961, General theory of dispersion in porous media, Jour. of Geophysical Research, 66:3273-3278.

Sinclair, B.C., 1974, Hydrogeological Characteristics of the Surficial Aquifer in Northwest Assessment Project, Technical Report, Southwest Florida Water Management District, Brooksville, FL, 300 p.

Southwest Florida Water Management District, 2000, Groundwater Vistas Files for Southern District Model (June 11, 2001).

Southwest Florida Water Management District 2001, Draft Southern District Groundwater Flow Model.

Southwest Florida Water Management District, 1993, Eastern Tampa Bay Water Resource Assessment Project, March 1993.

Southwest Florida Water Management District, 1989, Water Use Permit Information Manual, Resource Regulation Department (October, 1989).

Steinkampf, W.C., 1982, Origins and distribution of saline ground waters in the Floridan Aquifer in coastal southwest Florida, U.S. Geological Survey Water-Resources Investigations 82-4052, 34 p.

Waterstone, Inc., 2001, Data and Conceptual Model Review, Conceptual Model Uncertainty Evaluation, and Simulation Approach.

Waterstone 2001b, Groundwater Vistas Files (an uncalibrated saltwater intrusion model for coastal Portions of the SWUCA), prepared for the SWFWMD.

White, William A., 1970, Geomorphology of the Florida Peninsula, Florida Bureau of Geology, Bulletin 51, 164 p.

Wilson, W.E., 1982, Estimated Effects of projected Ground-Water Withdrawals on Movement of the Saltwater Front in the Floridan Aquifer, 1976-2000, West-Central Florida, USGS Water Supply Paper; 2189.

FIGURES

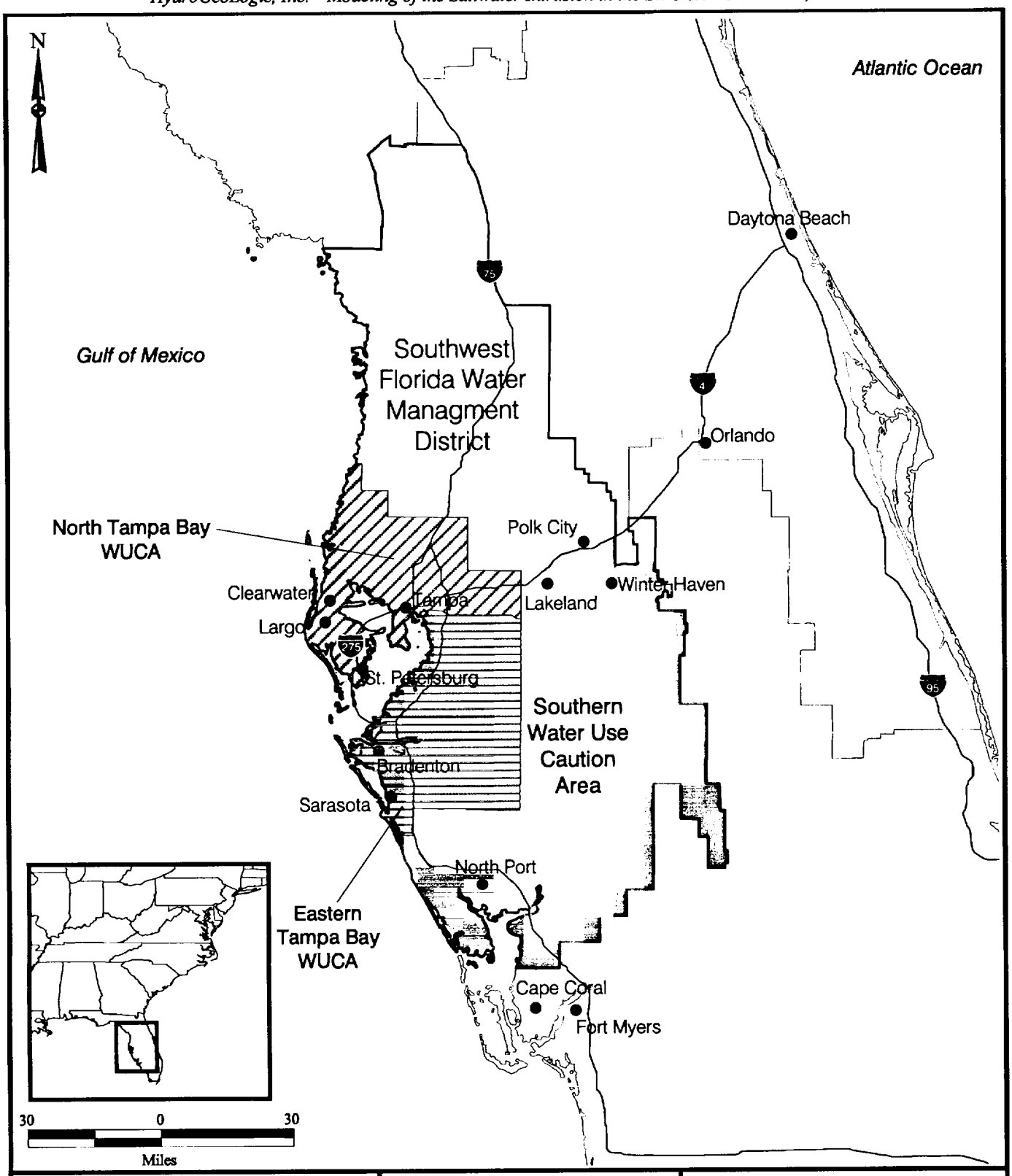

Filename: X:\SWF024\WO_01\saltwater_intrusion\fig1-1.apr
Project: SWF024-001-01
Created: 11/28/01 TB
Revised: 5/31/02 TB

HYDRO GeoLogic

Legend

- Southwest Florida Managment District Boundary
- Interstate
- Southern Water Use Caution Areas

Figure 1.1
Location of Southwest Florida Managment District and Southern Water Use Caution Area

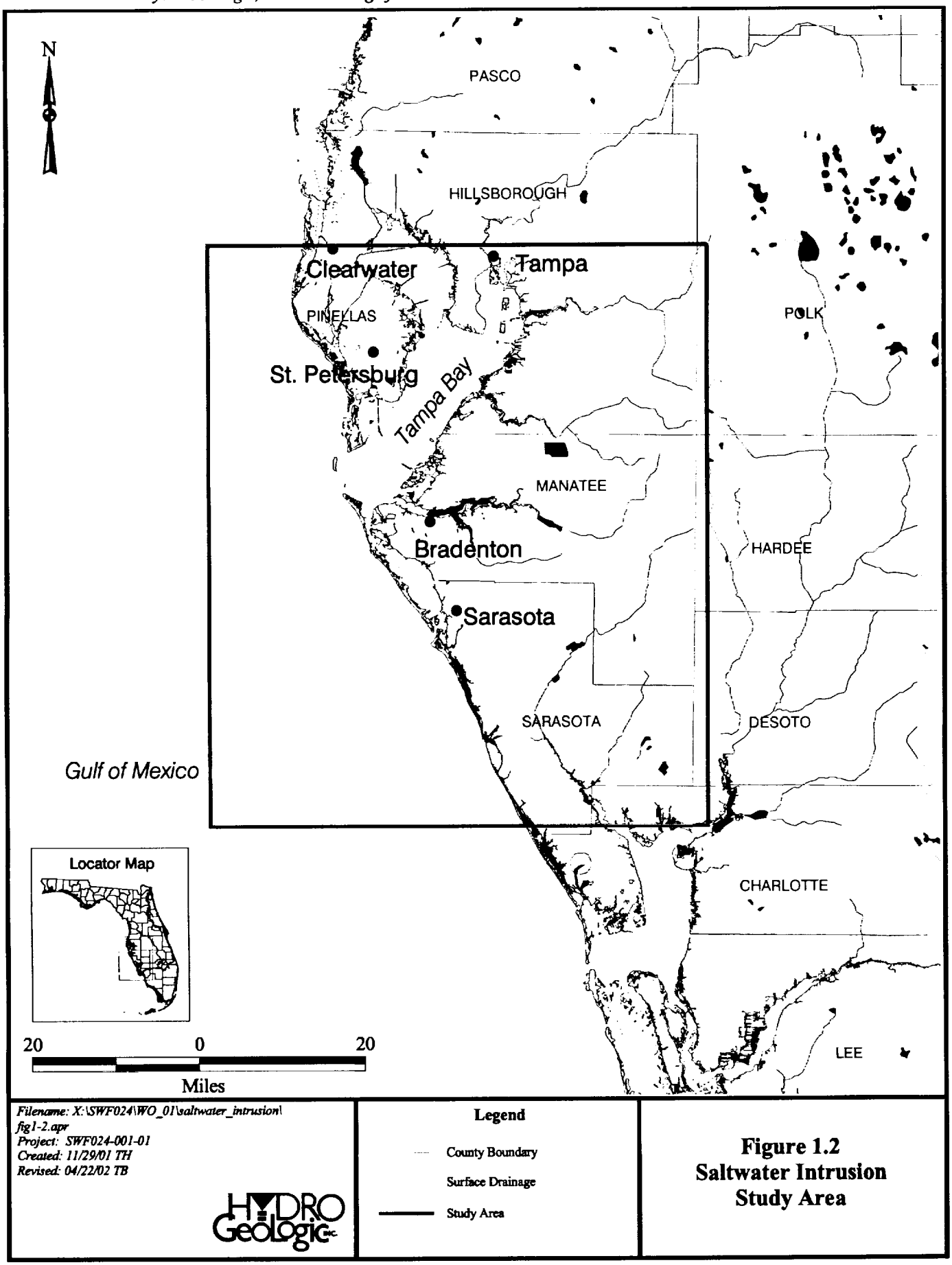
N
PASCO
HILLSBOROUGH
Clearwater
Tampa
PINELLAS
POLK
St. Petersburg
Tampa Bay
MANATEE
Bradenton
HARDEE
Sarasota
SARASOTA
DESOTO
Gulf of Mexico
CHARLOTTE
LEE
Locator Map
20
0
20
Miles
Filename: X:\SWF024\WO_01\saltwater_intrusion\fig1-2.apr
Project: SWF024-001-01
Created: 11/29/01 TH
Revised: 04/22/02 TB
HYDRO GeoLogic
Legend
County Boundary
Surface Drainage
Study Area
Figure 1.2
Saltwater Intrusion
Study Area

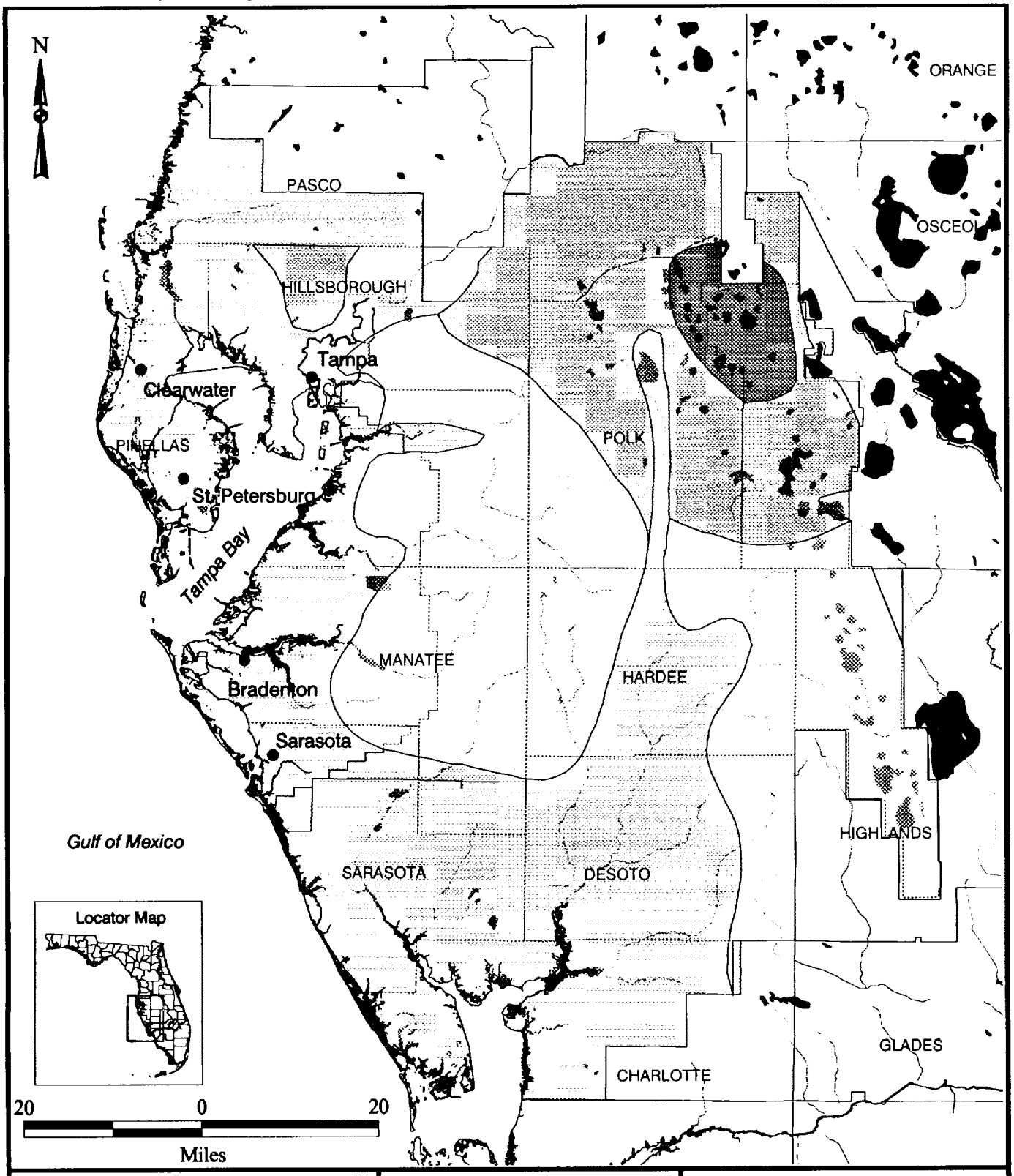

Filename: X:\SWF024\WO_01\saltwater_intrusion\fig2-1.apr
Project: SWF024-001-01
Created: 11/29/01 TH
Revised: 04/22/02 TB

HYDRO GeoLogic

Legend

County Boundary
Surface Drainage

Recharge (inches / year)
- Less than 1
- 1 to 10
- Greater than 10
- Discharge (less than 1)

Figure 2.1
Recharge / Discharge Zones of the Upper Floridan Aquifer for Pre-Development Conditions (Aucott, 1988)

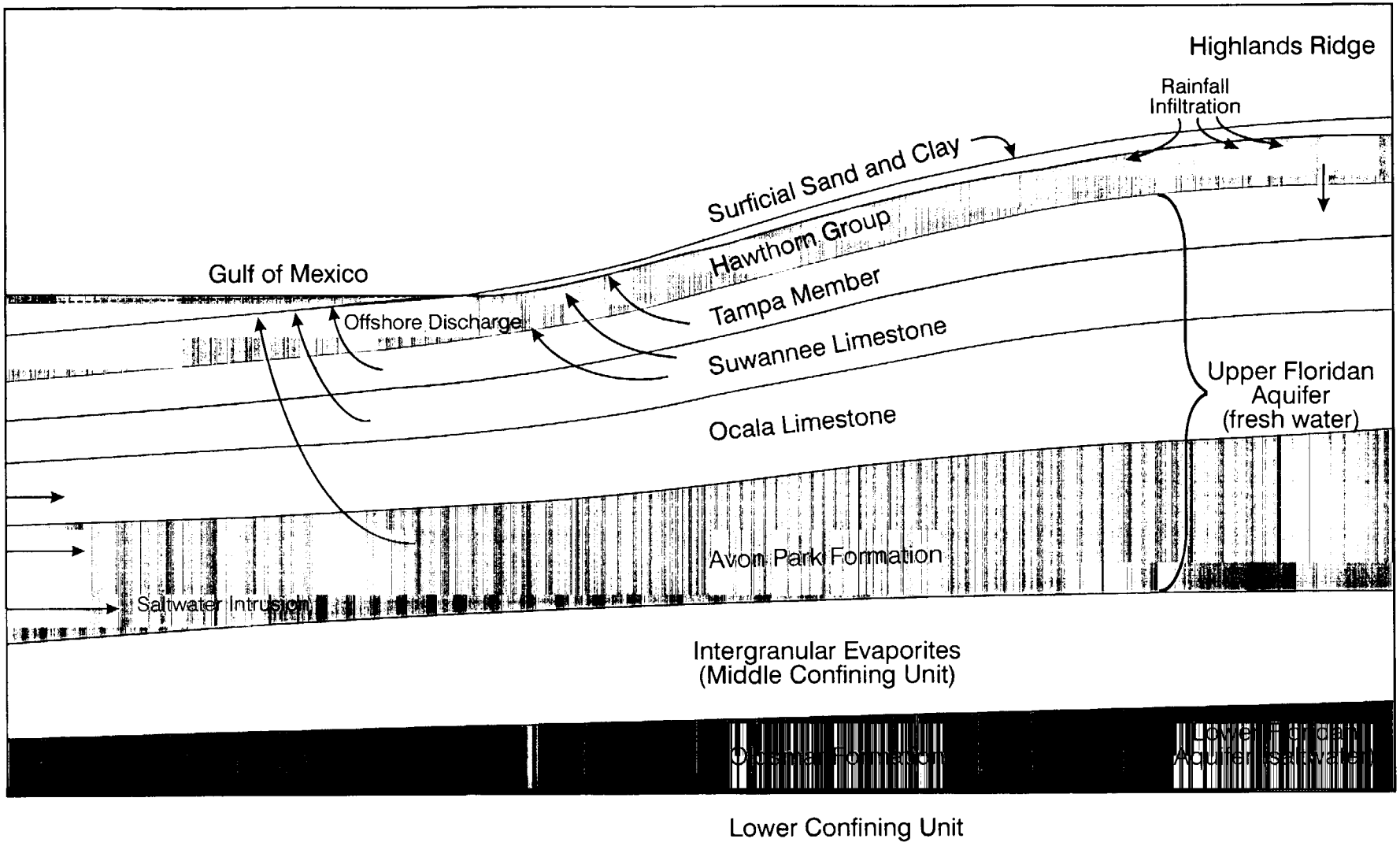

Filename: X:\SWF024\WO_01\conceptual_model_rev.cdr
Project: SWF024-001-03
Created by: cfarmer 12/14/01
Revised: 05/30/02 cf
Source: Waterstone (2000)

HYDRO GeoLogic INC.

Figure 2.2

Generalized Conceptual Model

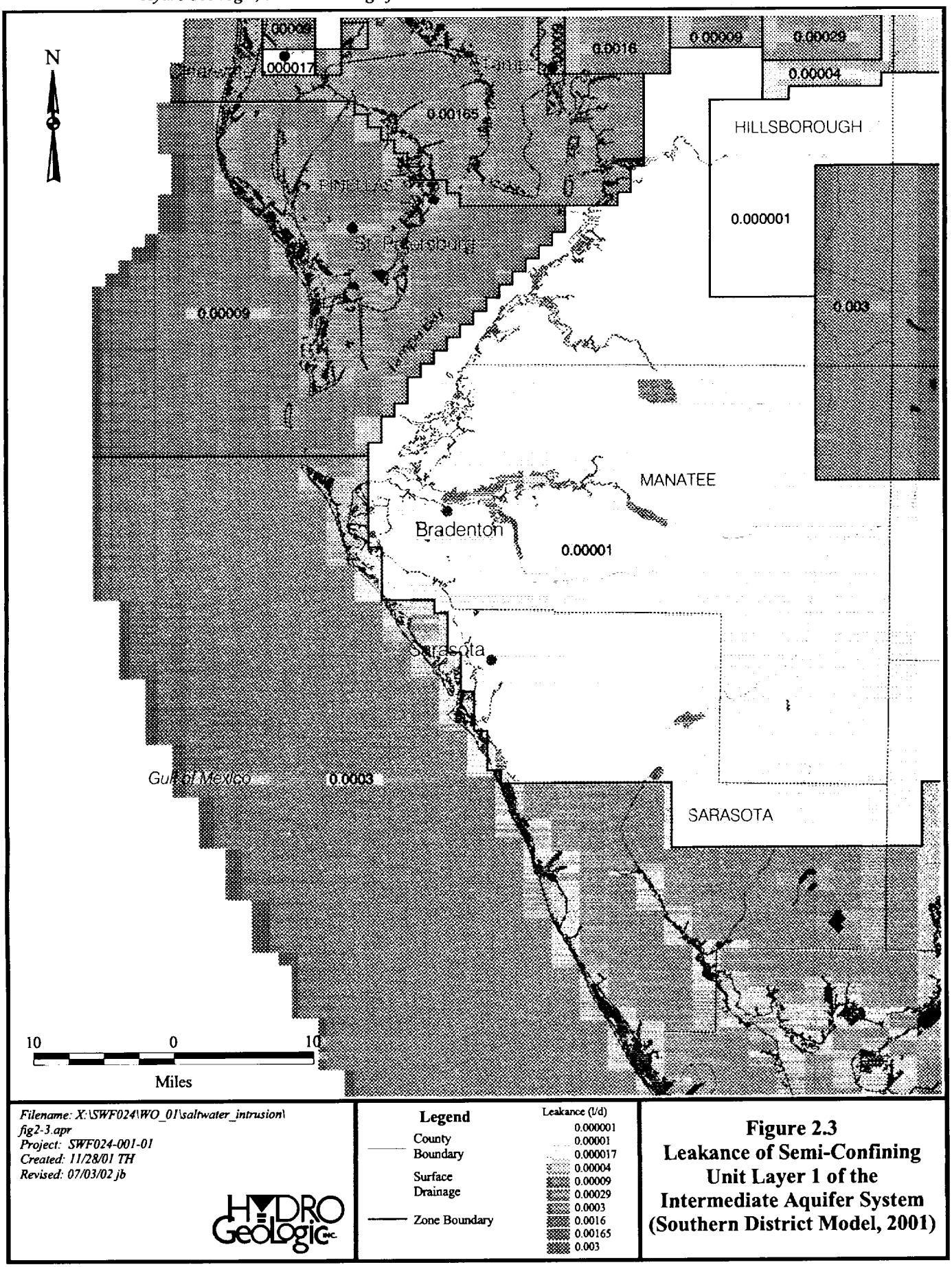

Figure 2.3
Leakance of Semi-Confining Unit Layer 1 of the Intermediate Aquifer System (Southern District Model, 2001)

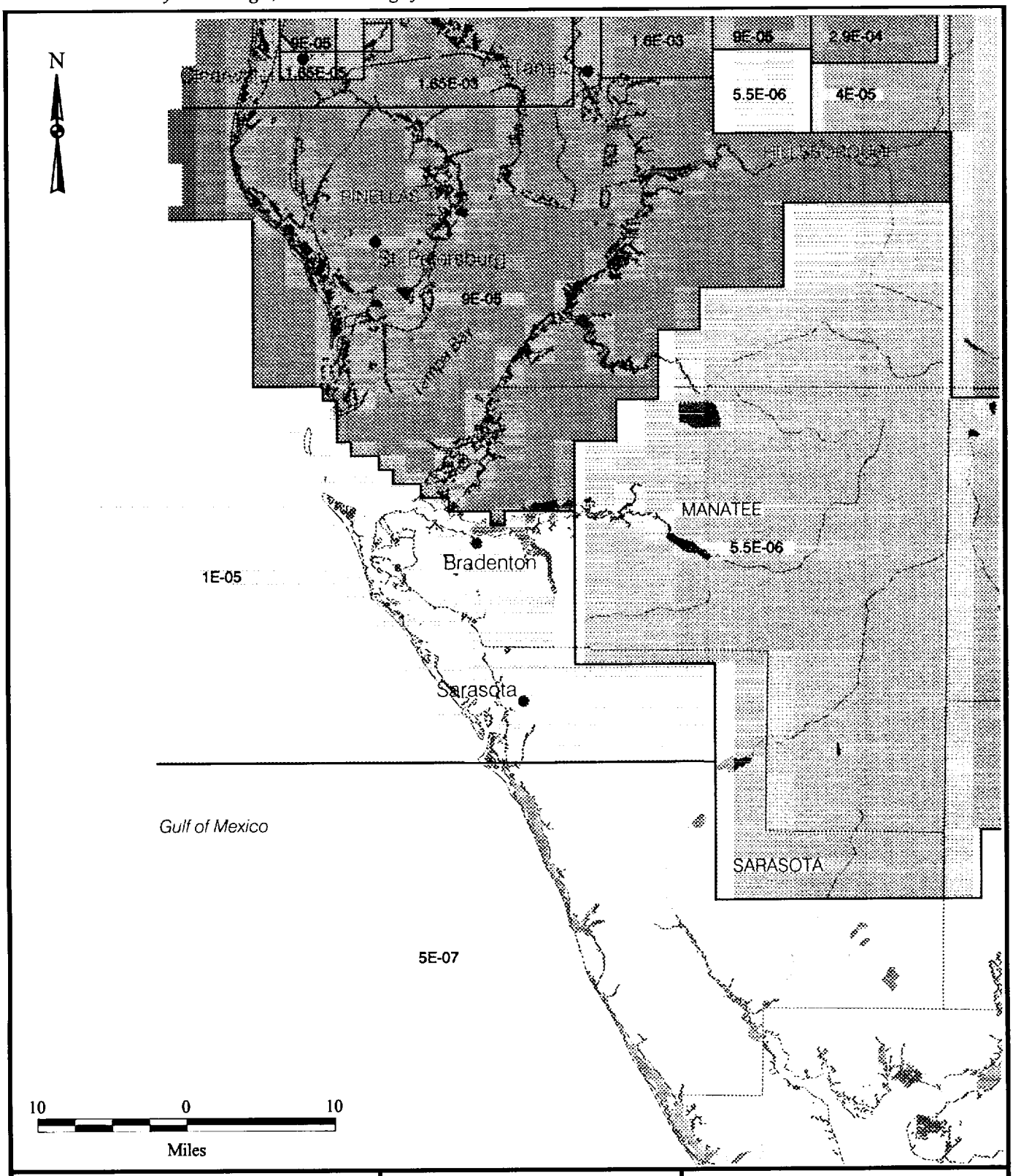

Filename: X:\SWF024\WO_01\saltwater_intrusion\fig2-4.apr
Project: SWF024-001-01
Created: 11/28/01 TH
Revised: 07/03/02 jb

HYDRO GeoLogic Inc

Legend

- County Boundary
- Surface Drainage
- Zone Boundary

Leakance (l/d)

- 5E-07
- 1E-05
- 5.5E-06
- 4E-05
- 9E-05
- 1.65E-05
- 2.9E-04
- 1.65E-03
- 1.6E-03

Figure 2.4
Leakance of Semi-Confining Unit Layer 2 of the Intermediate Aquifer System (Southern District Model, 2001)

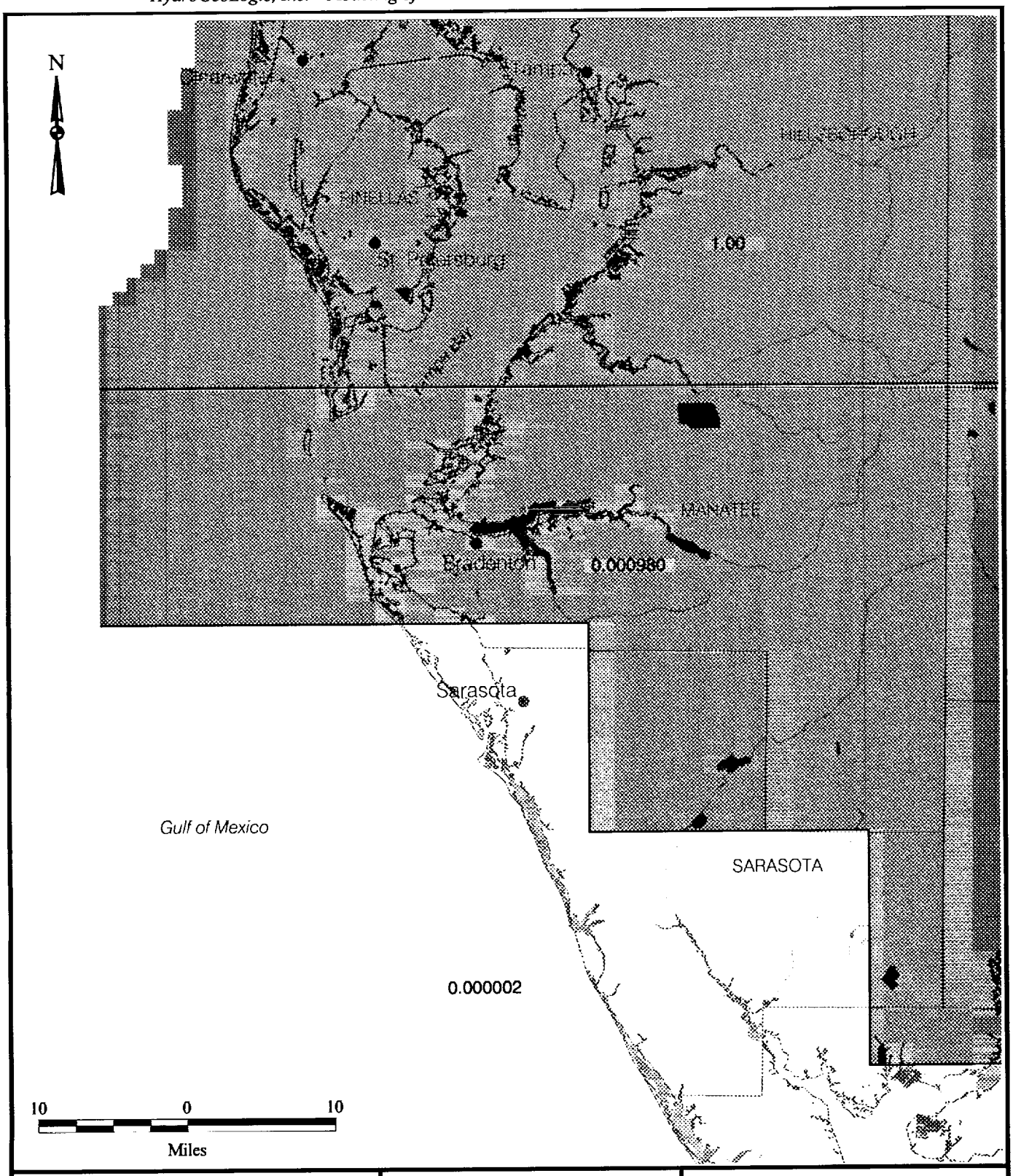

Filename: X:\SWF024\WO_01\saltwater_intrusion\fig2-5.apr
Project: SWF024-001-01
Created: 11/28/01 TH
Revised: 07/03/02 jb

HydroGeoLogic

Legend

- County Boundary
- Surface Drainage
- 1.00 Zone Boundary

Leakance (l/d)
- 0.000002
- 0.00098
- 1

Figure 2.5
Leakance of Semi-Confining Unit Layer 3 of the Intermediate Aquifer System (Southern District Model, 2001)

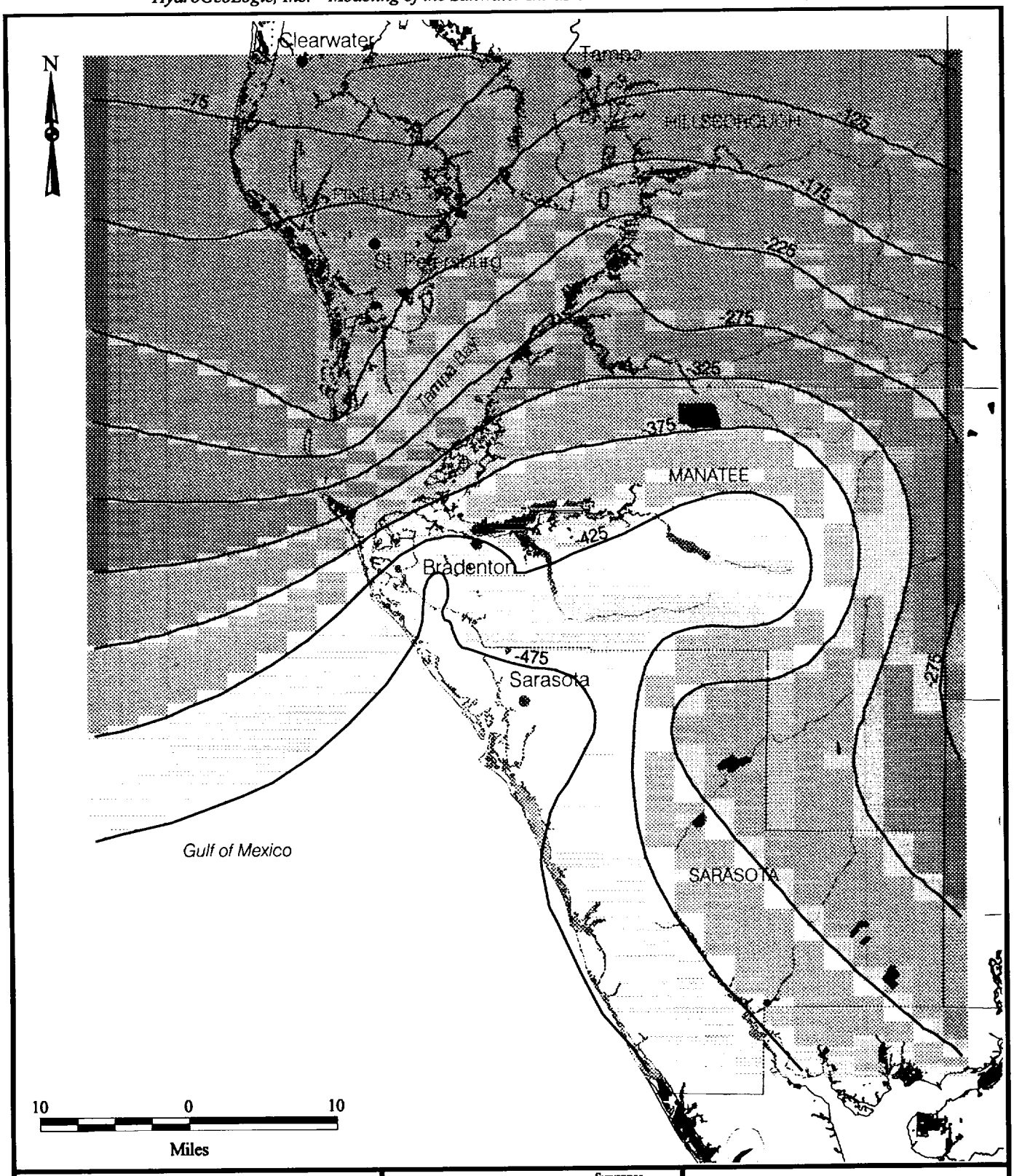

Filename: X:\SWF024\WO_01\saltwater_intrusion\fig2.6.apr
Project: SWF024-001-01
Created: 11/28/01 TH
Revised: 04/22/02 TB

HYDRO GeoLogic

Legend

County Boundary

Surface Drainage

-275 Suwannee Top Elevation Contour (ft)

Suwannee Elevation (ft)
-560 - -475
-475 - -425
-425 - -375
-375 - -325
-325 - -275
-275 - -225
-225 - -175
-175 - -125
-125 - -75
-75 - -25

Figure 2.6
Top Elevation of the Suwannee Limestone (Waterstone Model, 2001)

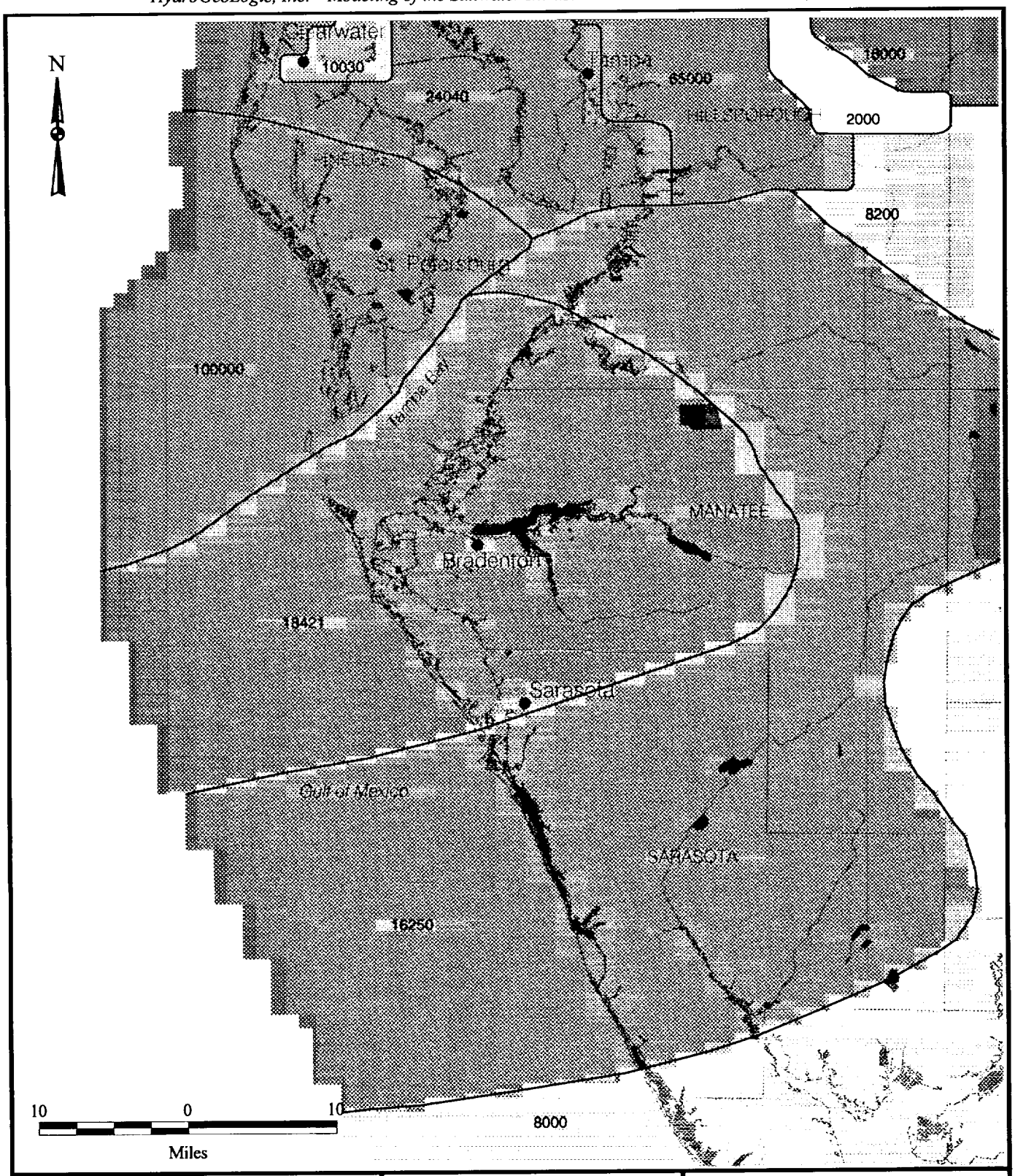

Filename: X:\SWF024\WO_01\saltwater_intrusion\fig2-7.apr
Project: SWF024-001-01
Created: 11/28/01 TH
Revised: 07/03/02 jb

HydroGeoLogic

Legend

County Boundary

Surface Drainage

Zone Boundary

Suwannee Transmissivity (ft^2/day)
2000
8000
8200
10030
16000
16250
18421
24040
65000
100000

Figure 2.7
Transmissivity of the Suwannee Limestone of the Southern District Model (SWFWMD, 2001)

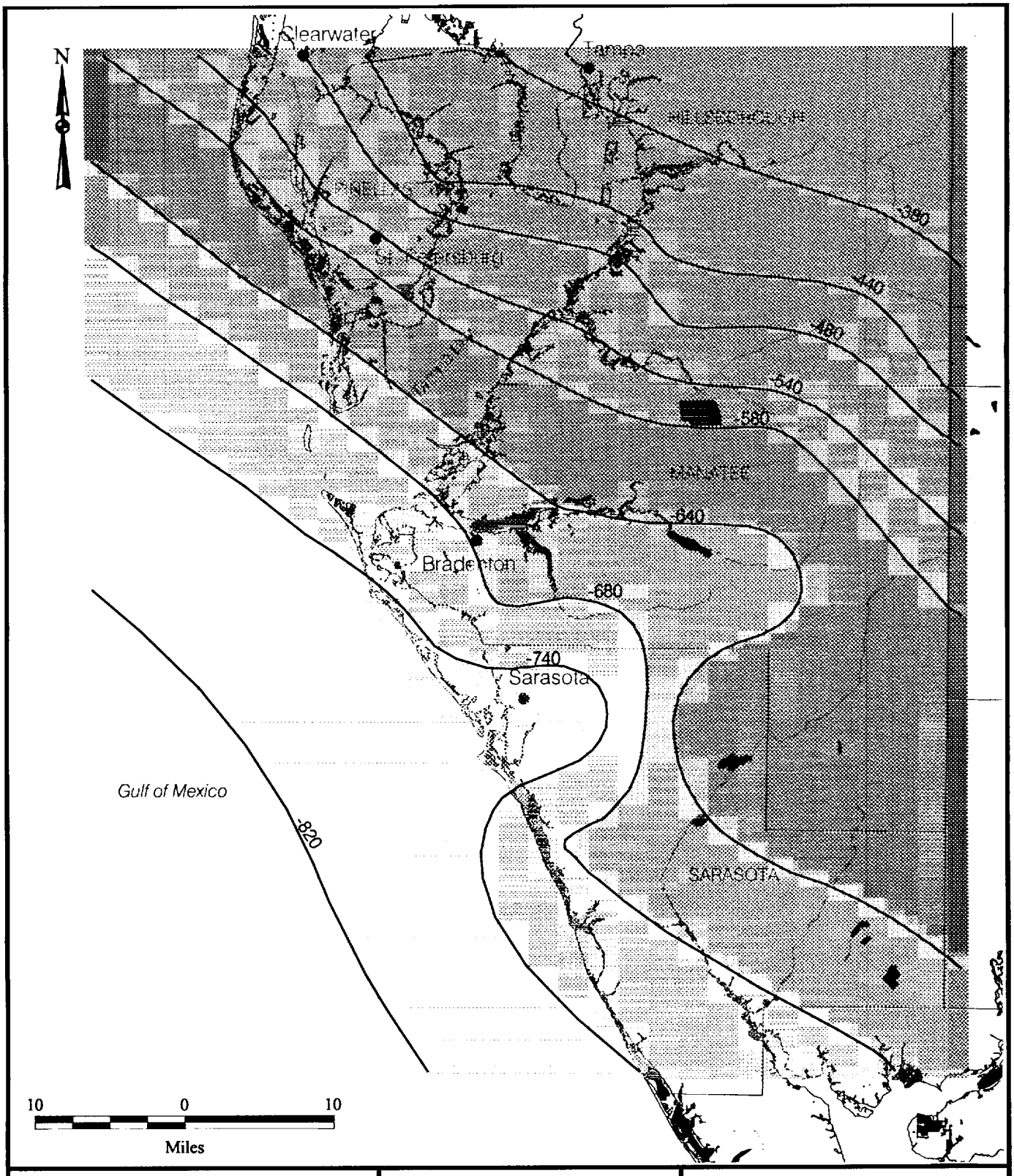

Filename: X:\SWF024\WO_01\saltwater_intrusion\fig2-8.apr
Project: SWF024-001-01
Created: 11/28/01 TH
Revised: 04/22/02 TB

HYDRO GeoLogic

Legend

County Boundary

Surface Drainage

-580 Ocala Top Elevation Contour (ft)

Ocala Elevation (ft)
-960 - -820
-820 - -740
-740 - -680
-680 - -640
-640 - -580
-580- -540
-540 - -480
-480 - -440
-440 - -380
-380 - -265

Figure 2.8
Top Elevation of the Ocala Limestone (Waterstone Model, 2001)

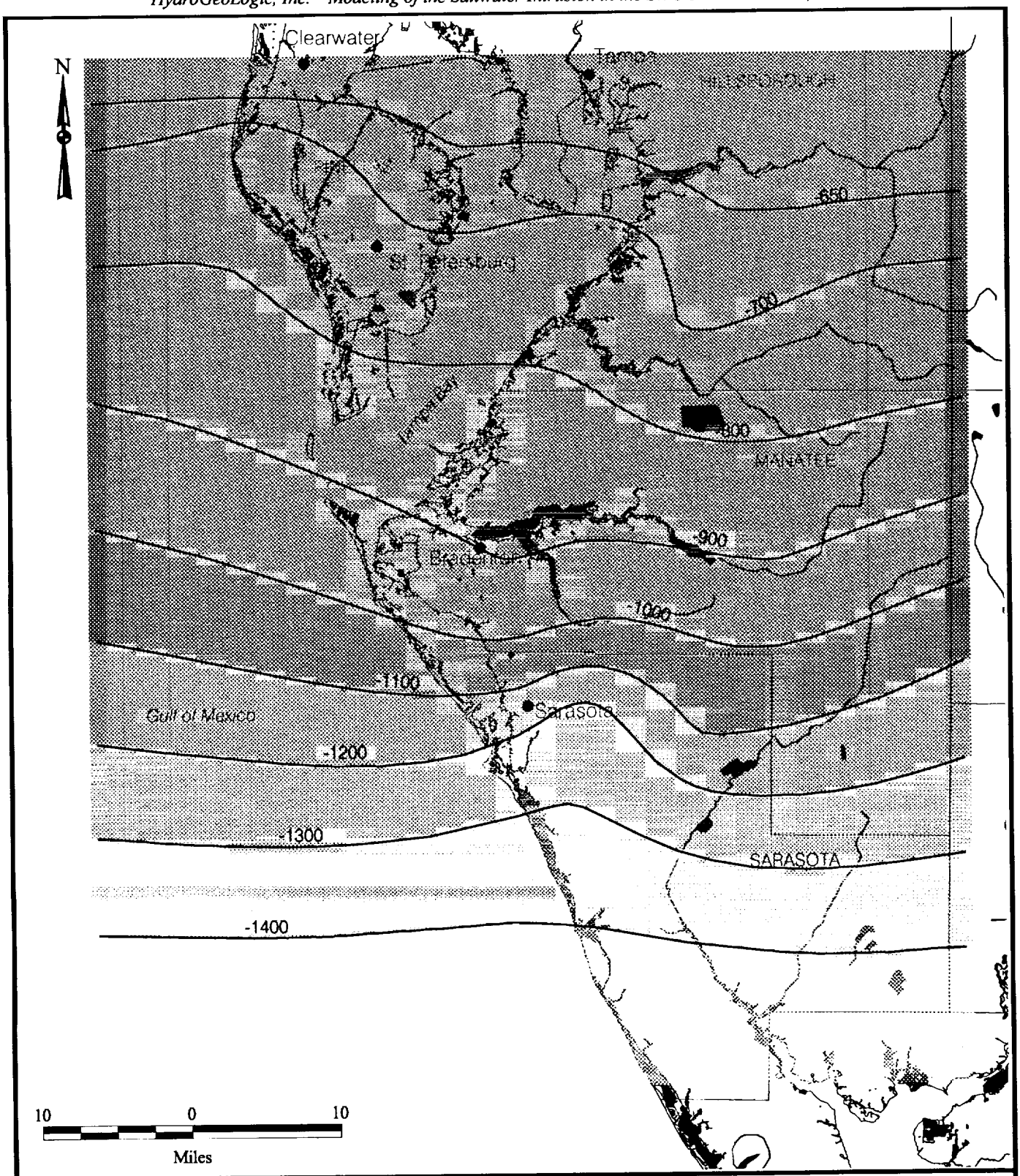

Filename: X:\SWF024\WO_01\saltwater_intrusion\fig2-9.apr
Project: SWF024-001-01
Created: 11/28/01 TH
Revised: 04/22/02 TB

HYDRO GeoLogic

Legend

County Boundary

Surface Drainage

-700 Avon Park Formation Top Elevation Contour (ft)

Avon Park Elevation (ft)
-1550 - -1400
-1400 - -1300
-1300 - -1200
-1200 - -1100
-1100 - -1000
-1000 - -900
-900 - -800
-800 - -700
-700 - -650
-650 - -550

Figure 2.9
Top Elevation of the Avon Park Formation (Waterstone Model, 2001)

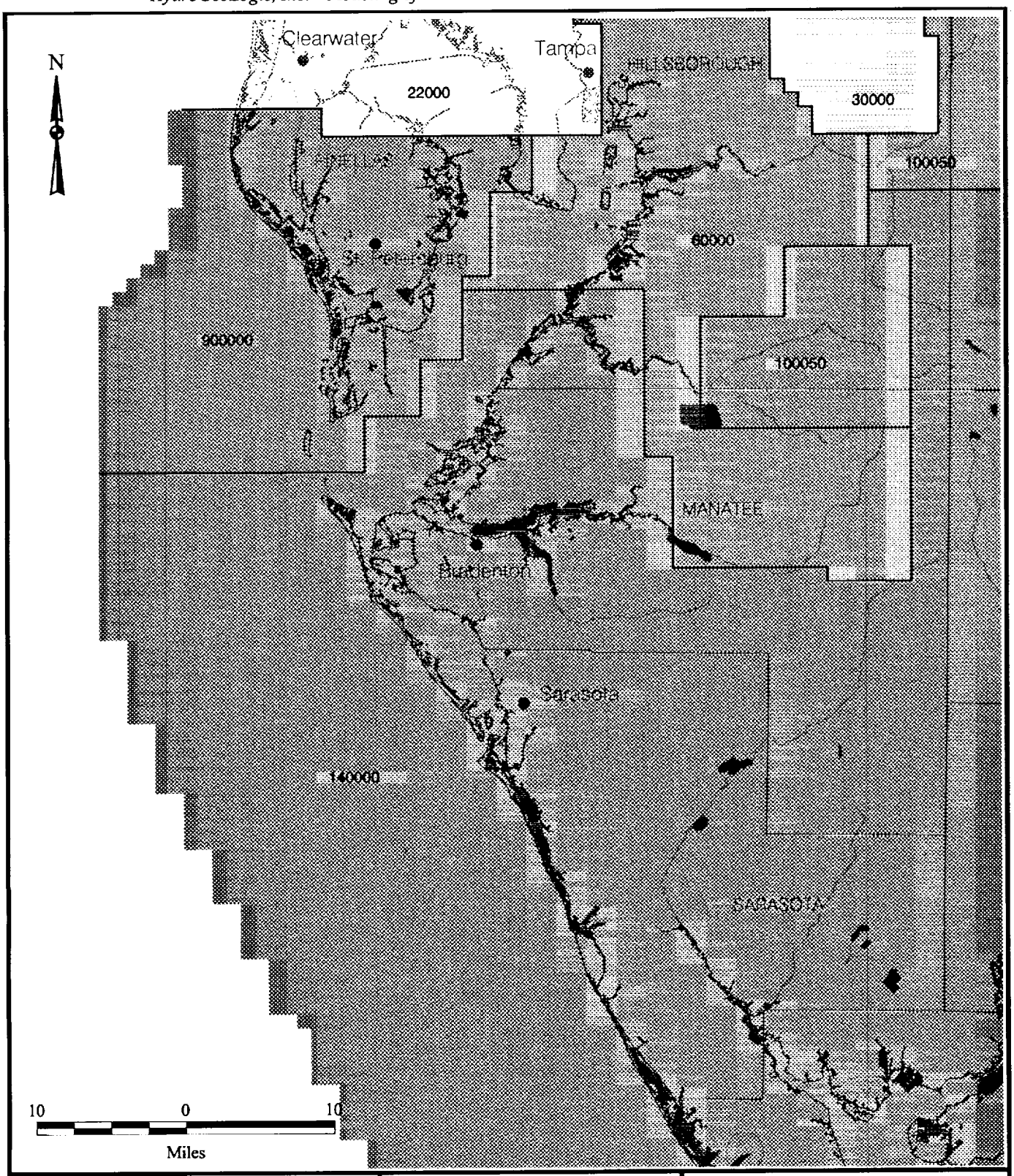

Filename: X:\SWF024\WO_01\saltwater_intrusion\fig2-10.apr
Project: SWF024-001-01
Created: 11/28/01 TH
Revised: 07/03/02 jb

HydroGeoLogic Inc.

Legend

- County Boundary
- Surface Drainage
- Zone Boundary

Ocala/Avon Park Transmissivity (ft^2/day)

- 22000
- 30000
- 60000
- 100050
- 140000
- 900000

Figure 2.10 Transmissivity of the Avon Park Formation of the Southern District Model (2001)

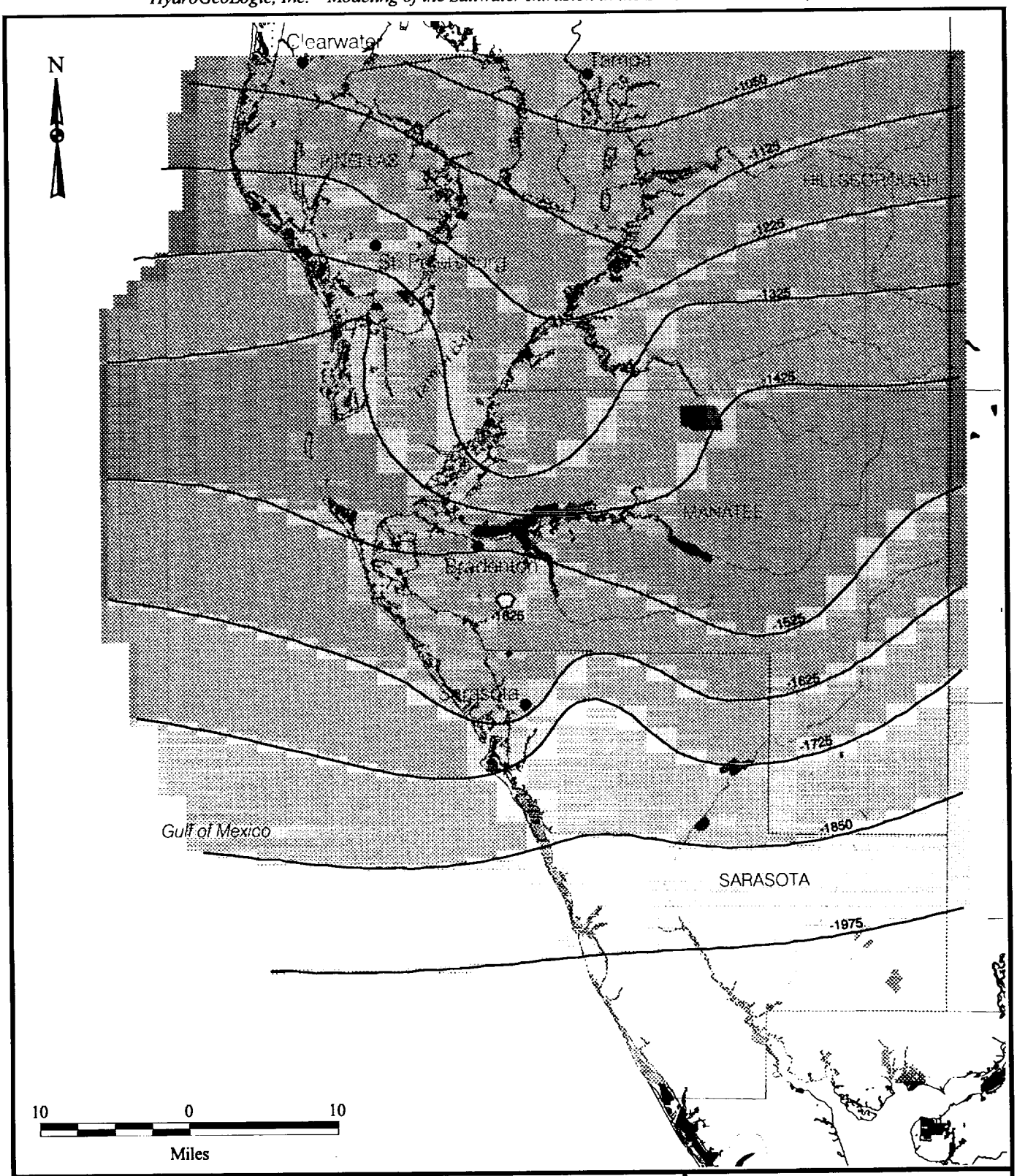

Filename: X:\SWF024\WO_01\saltwater_intrusion\fig2-11.apr
Project: SWF024-001-01
Created: 11/28/01 TH
Revised: 04/22/02 TB

HYDRO GeoLogic Inc.

Legend

County Boundary

Surface Drainage

-1425 Middle Confining Unit Elevation Contour (ft)

Middle Confining Unit Elevation (ft)
-2150 - -1975
-1975 - -1850
-1850 - -1725
-1725 - -1625
-1625 - -1525
-1525 - -1425
-1425 - -1325
-1325 - -1225
-1225 - -1125
-1125 - -1050
-1050 - -975

Figure 2.11
Top Elevation of the Middle Confining Unit (Waterstone Model, 2001)

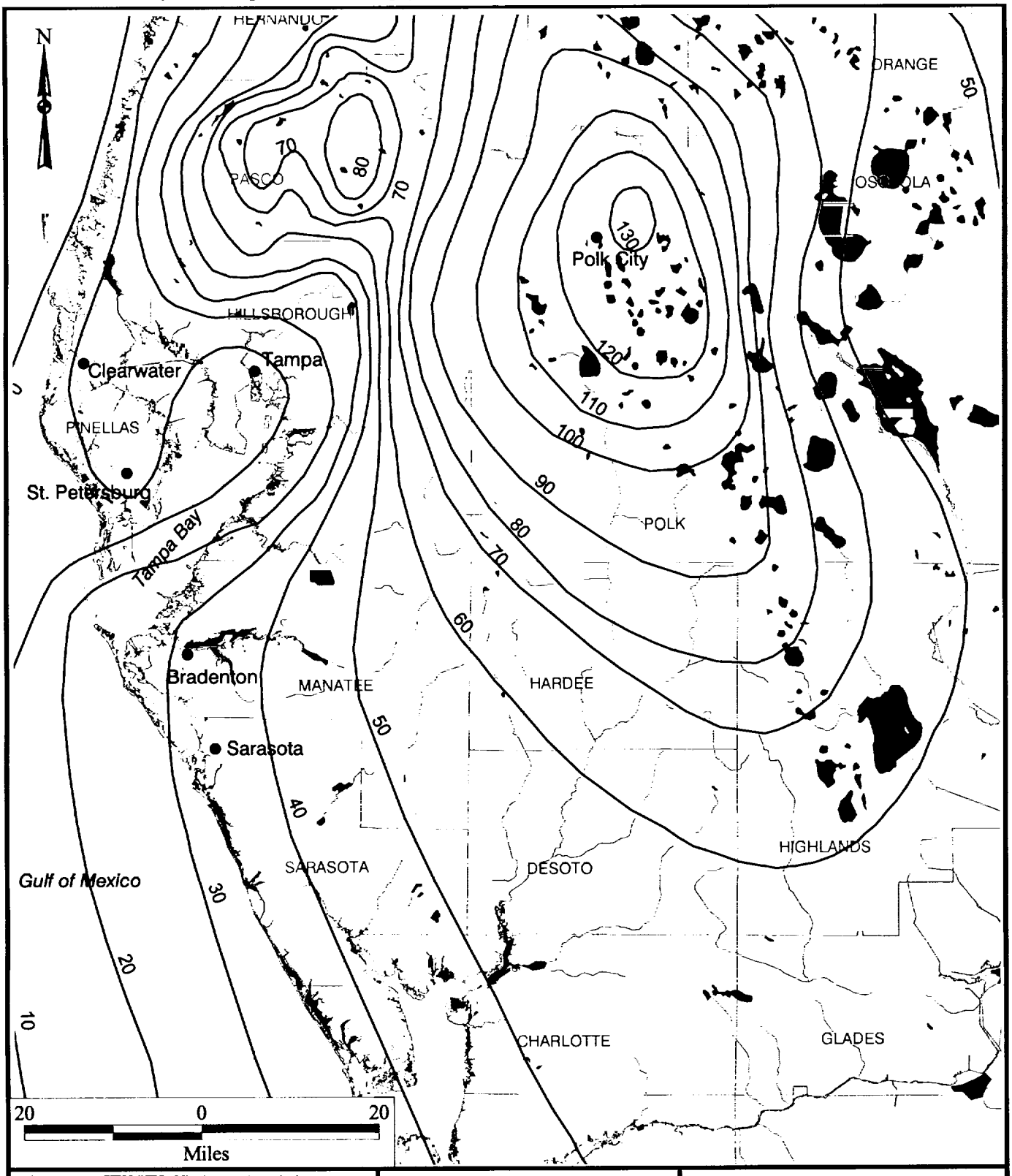

Filename: X:\SWF024\WO_01\saltwater_intrusion\fig2-12.apr
Project: SWF024-001-01
Created: 11/29/01 TH
Revised: 06/05/02 TB

HYDRO GeoLogic Inc.

Legend

County Boundary

Surface Drainage

30 Potentiometric Surface Elevation (ft)

Figure 2.12
Upper Floridan Aquifer Potentiometric Surface for Predevelopment Conditions (from Johnston et.al., 1980)

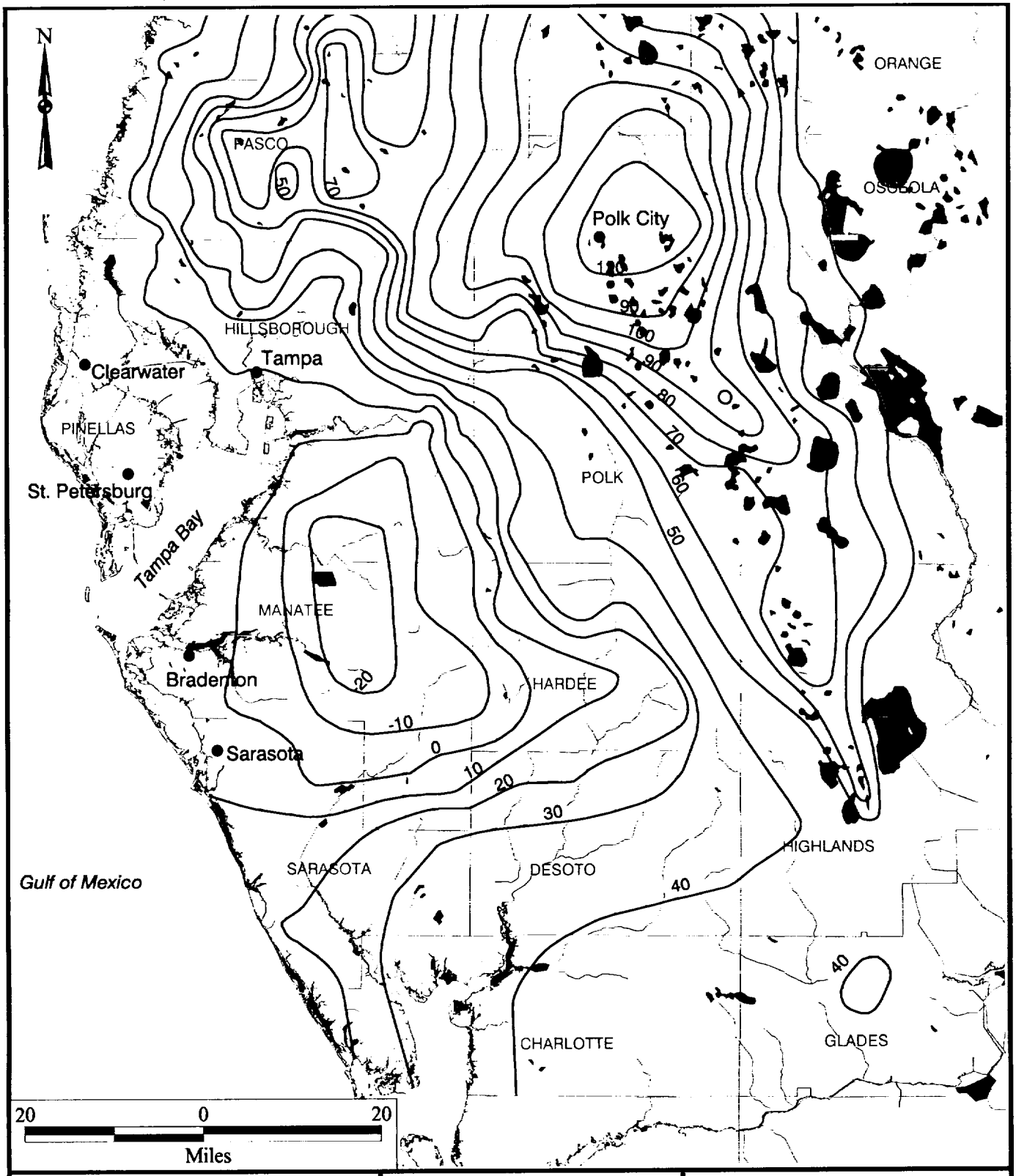

Filename: X:\SWF024\WO_01\saltwater_intrusion\fig2-13.apr
Project: SWF024-001-01
Created: 11/29/01 TH
Revised: 05/30/02 TB

HYDRO GeoLogic

Legend

County Boundary

Surface Drainage

30 Potentiometric Surface Elevation (ft)

Figure 2.13
Floridan Aquifer Potentiometric Surface for May 2000 (USGS, 2001)

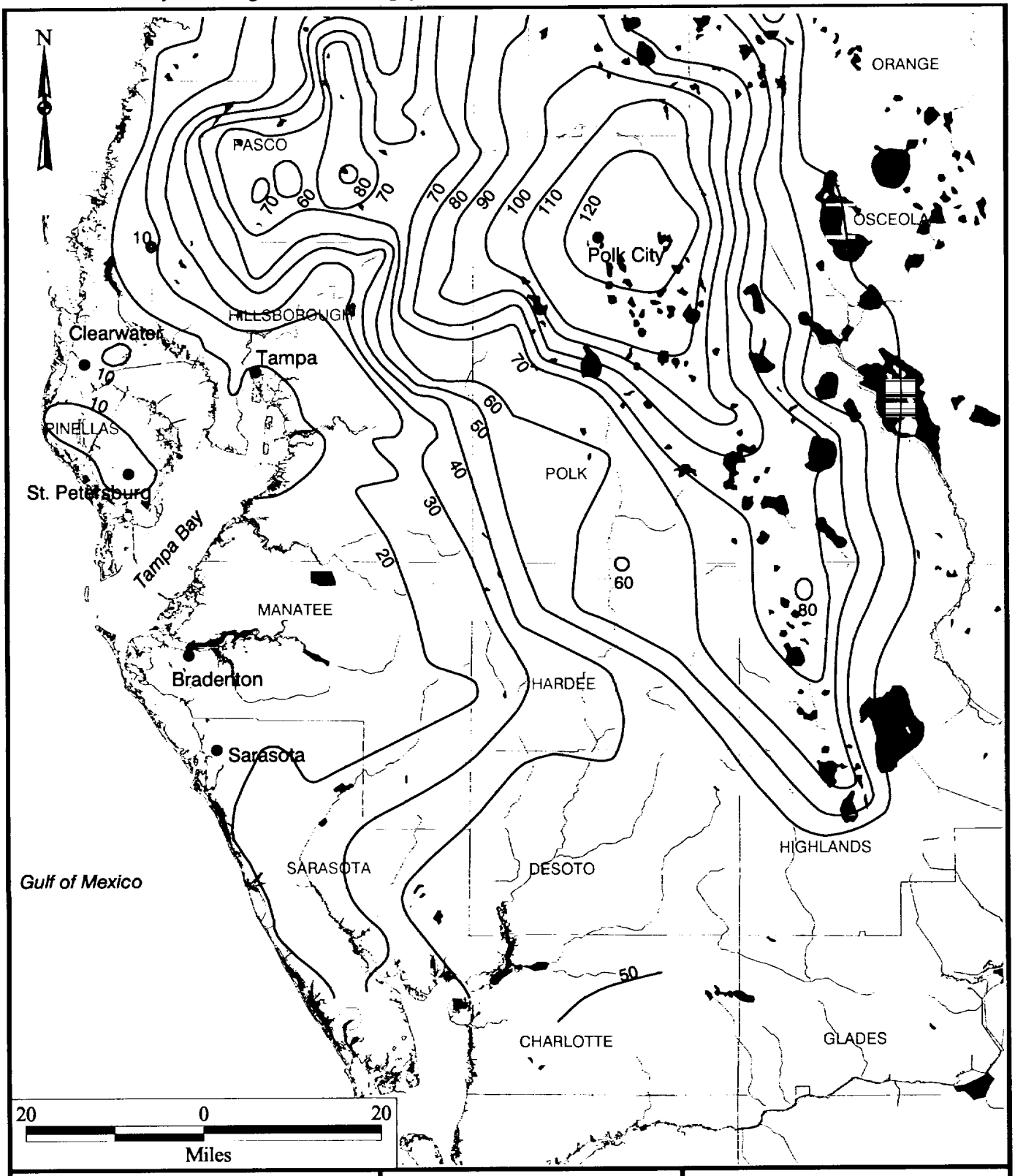

Filename: X:\SWF024\WO_01\saltwater_intrusion\fig2-14.apr
Project: SWF024-001-01
Created: 11/29/01 TH
Revised: 05/30/02 TB

HYDRO GeoLogic

Legend

County Boundary

Surface Drainage

30 Potentiometric Surface Elevation (ft)

Figure 2.14
Floridan Aquifer Potentiometric Surface for September 2000 (USGS, 2001)

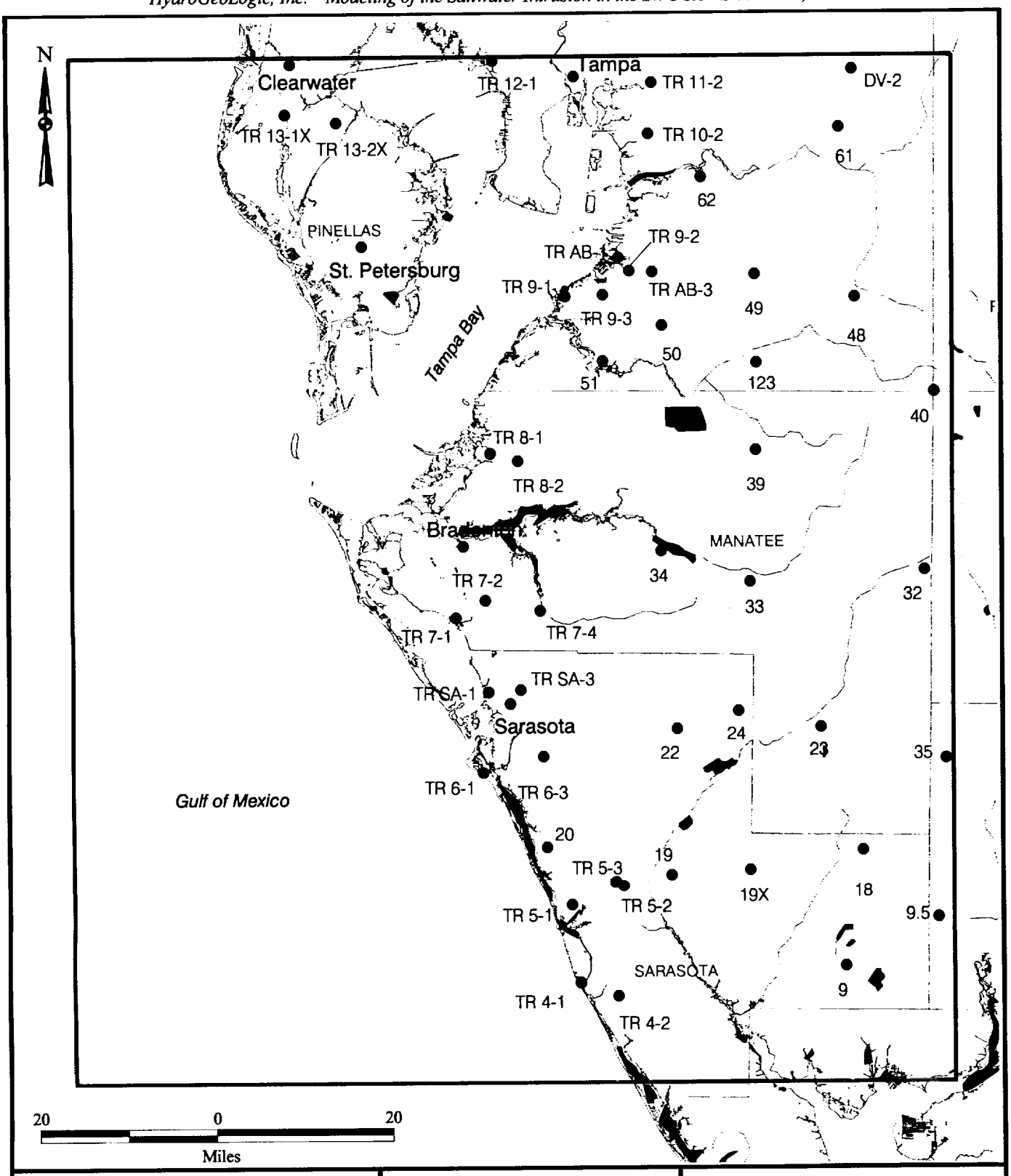

Filename: X:\SWF024\WO_01\saltwater_intrusion\fig2-15.apr
Project: SWF024-001-01
Created: 11/29/01 TH
Revised: 05/30/02 TB

HYDRO GeoLogic Inc

Legend

- County Boundary
- Surface Drainage
- Study Area
- 134 Well Location / ROMP ID

Figure 2.15
Location of ROMP Wells within the Study Area

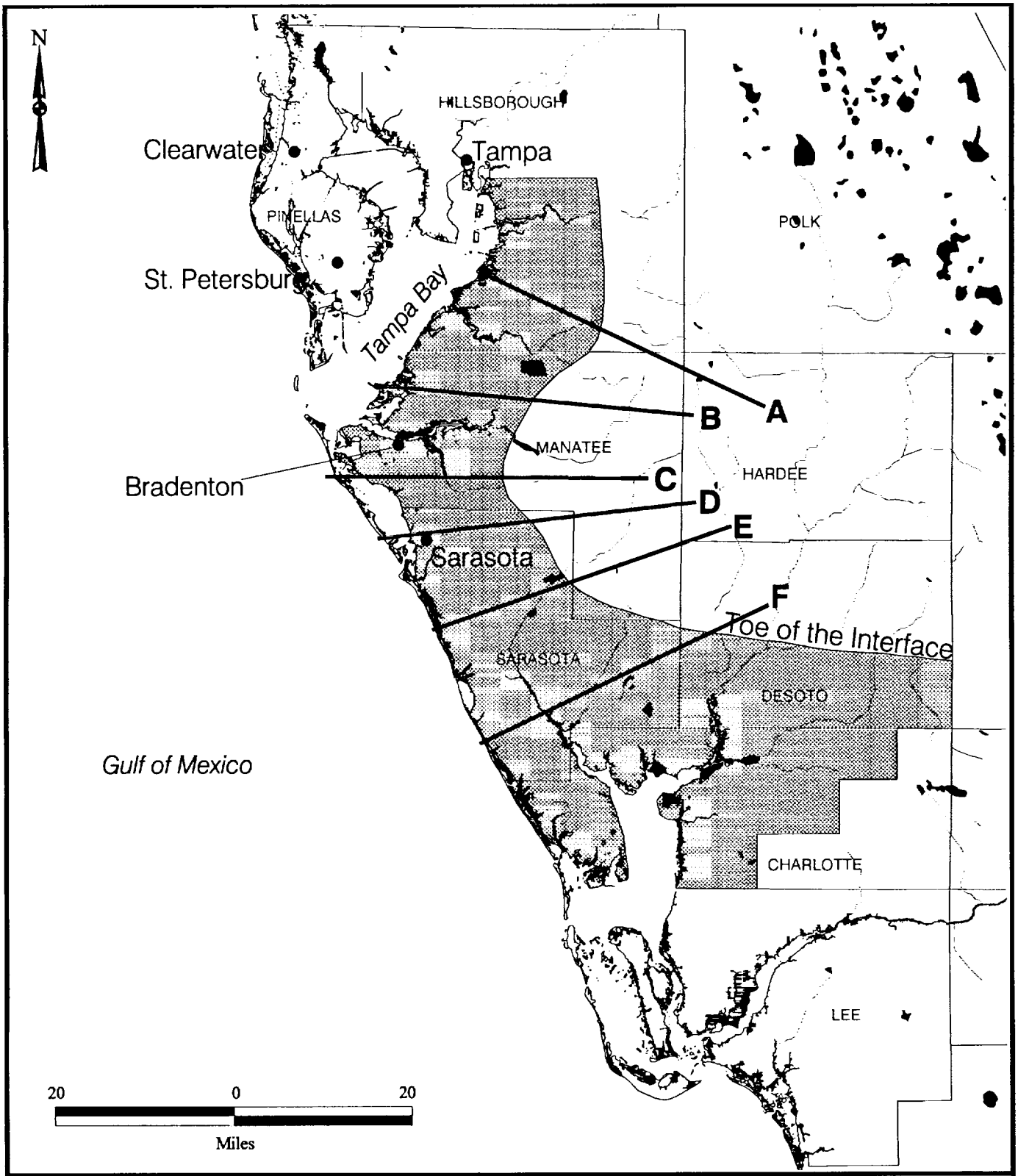

Filename: X:\SWF024\WO_01\saltwater_intrusion\fig2-16.apr
Project: SWF024-001-01
Created: 11/29/01 TH
Revised: 06/05/02 TB

HYDRO GeoLogic

Legend

- County Boundary
- Surface Drainage
- A — Cross-section Locations
- Chloride Transition Zone within the LPZ

Figure 2.16
Chloride Transition Zone within the Lower Permeable Zone of the Upper Floridan Aquifer (Beach and Kelley, 1998)

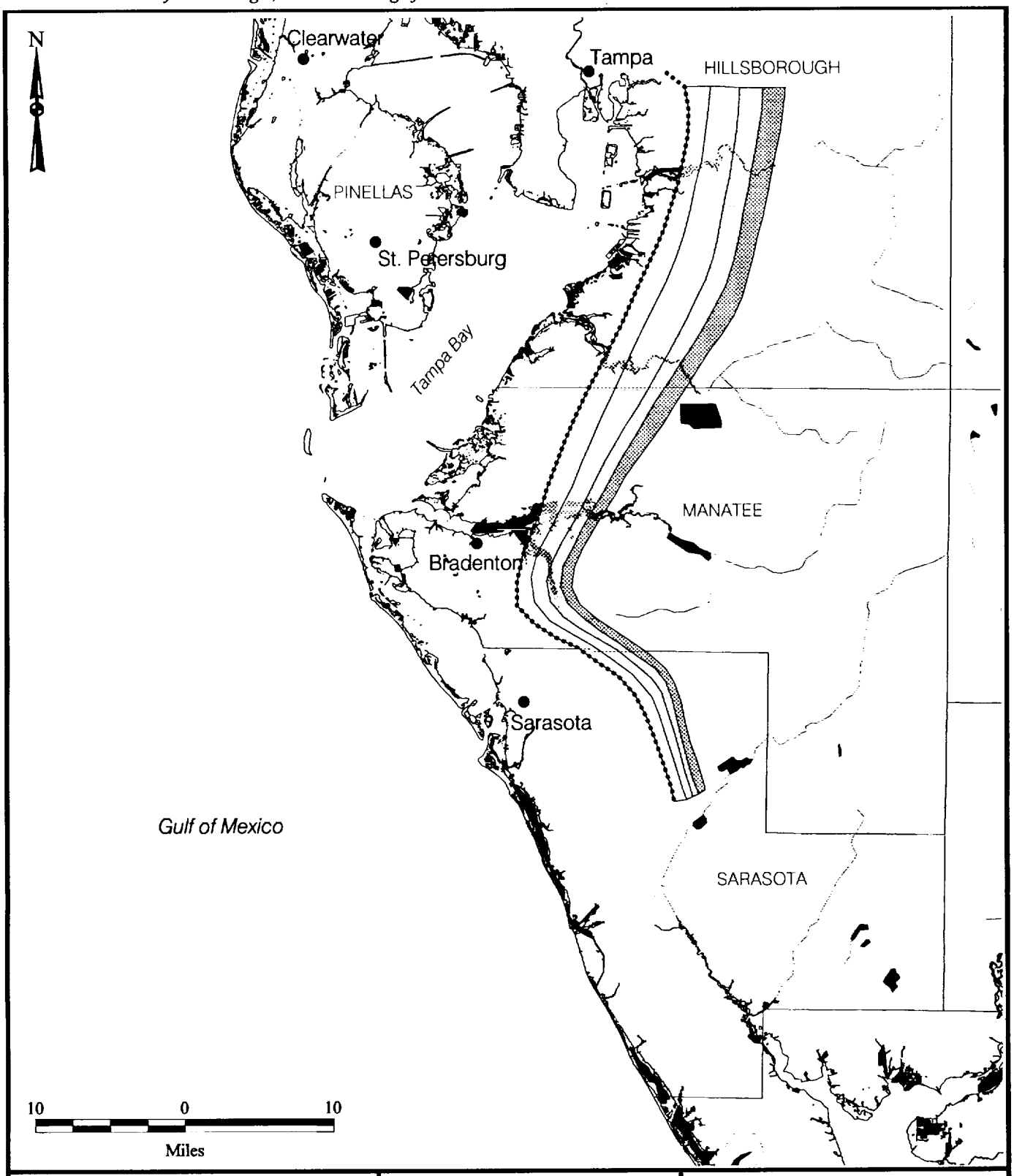

Filename: X:\SWF024\WO_01\saltwater_intrusion\fig2-17.apr
Project: SWF024-001-01
Created: 11/28/01 TH
Revised: 04/22/02 TB

HYDRO GeoLogic

Legend

- County Boundary
- Surface Drainage
- Present Postion (2000)
- 400 MGD
- 600 MGD
- 800 MGD
- 1000 MGD

Figure 2.17
Extent of the 1000 mg/l Chlorides in the Highly Permeable Zone of UFAS Fifty Year Position (Beach and Shultz, 2000)

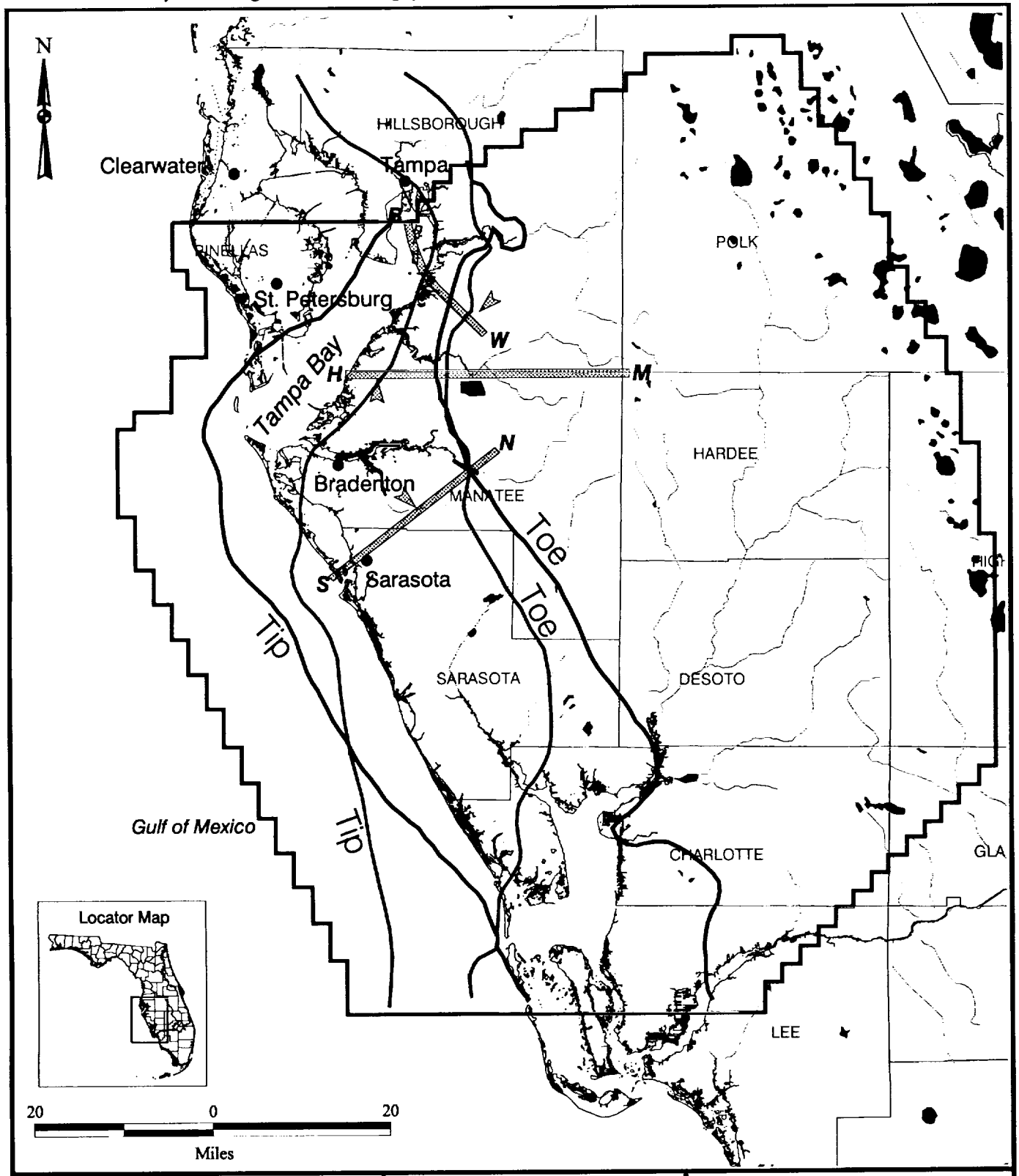

Filename: X:\SWF024\WO_01\saltwater_intrusion\fig3-1.apr
Project: SWF024-001-01
Created: 11/29/01 TH
Revised: 06/05/02 TB

HYDRO GeoLogic Inc.

Legend

- County Boundary
- Surface Drainage
- Eastern Tampa Bay Model Grid Boundary
- Cross-section Locations (HGL, 1991a)
- Prediction of Toe of the Plume (HGL, 1991a)
- Predevelopment Interface Position (HGL, 1994a)
- Predevelopment Interface Position (HGL, 1993a)

Figure 3.1
Previous Model Domain and Simulated Predevelopment Interface Position of the Upper Floridan System

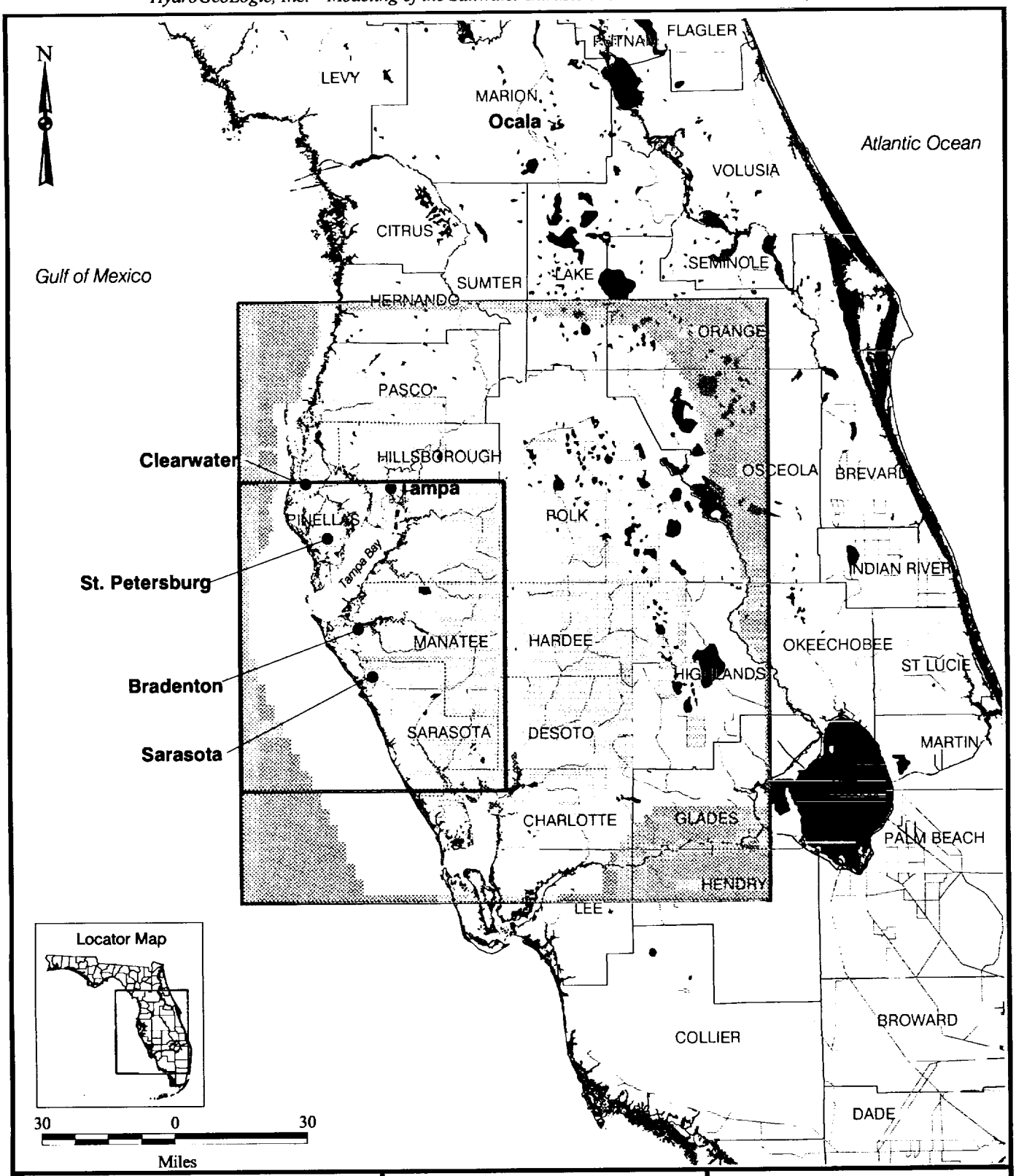

Filename: X:\SWF024\WO_01\saltwater_intrusion\fig4-1.apr
Project: SWF024-001-01
Created: 11/29/01 TH
Revised: 04/22/02 TB

HydroGeoLogic

Legend

- County Boundary
- Surface Drainage
- Regional Model Domain
- Local Density-Dependent Model Domain
- Inactive Model Cells
- Water Use Caution Areas

Figure 4.1
Regional and Density-Dependent Model Domains

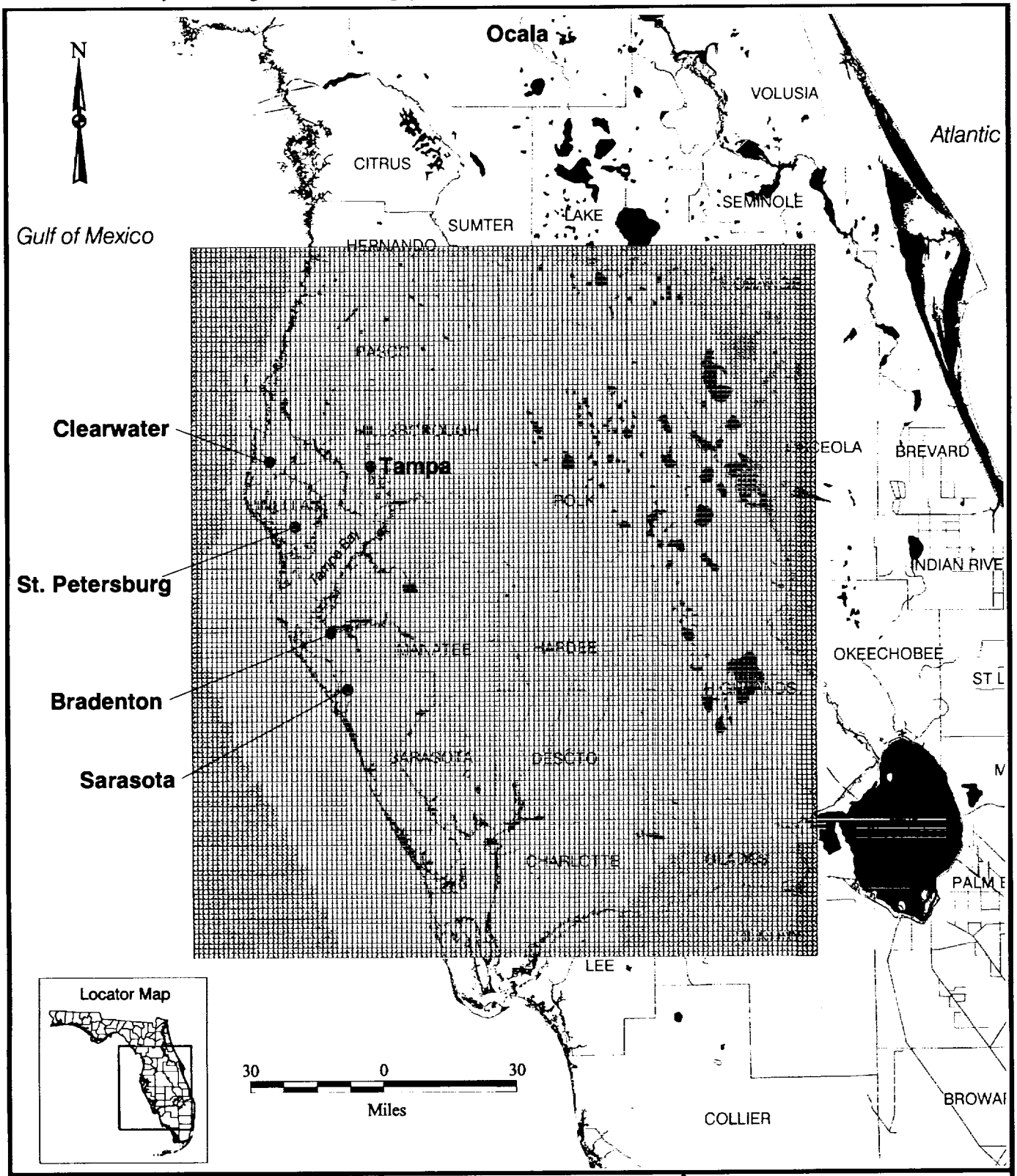

Filename: X:\SWF024\WO_01\saltwater_intrusion\fig4-2.apr
Project: SWF024-001-01
Created: 11/29/01 TH
Revised: 04/22/02 TB

HYDRO GeoLogic Inc.

Legend

- County Boundary
- Surface Drainage
- Active Grid Cell
- Inactive Grid Cell

Figure 4.2
Regional Flow Model
Finite-Difference Grid

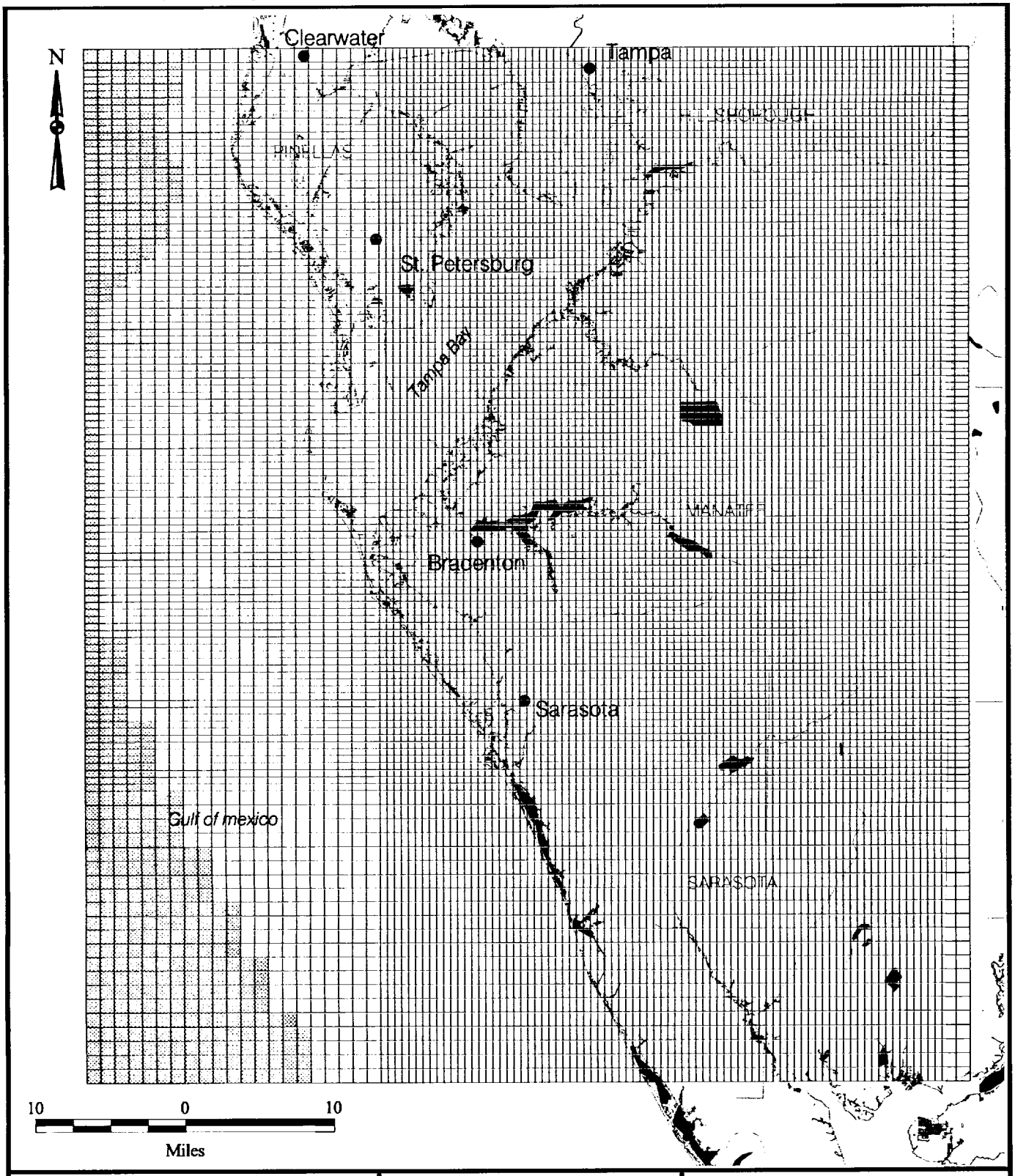

Filename: X:\SWF024\WO_01\saltwater_intrusion\fig4-3.apr
Project: SWF024-001-01
Created: 11/28/01 TH
Revised: 04/22/02 TB

HYDRO GeoLogic INC

Legend

- County Boundary
- Surface Drainage
- Active Grid Cell
- Inactive Grid Cell

Figure 4.3
Density-Dependent Model Finite-Difference Grid

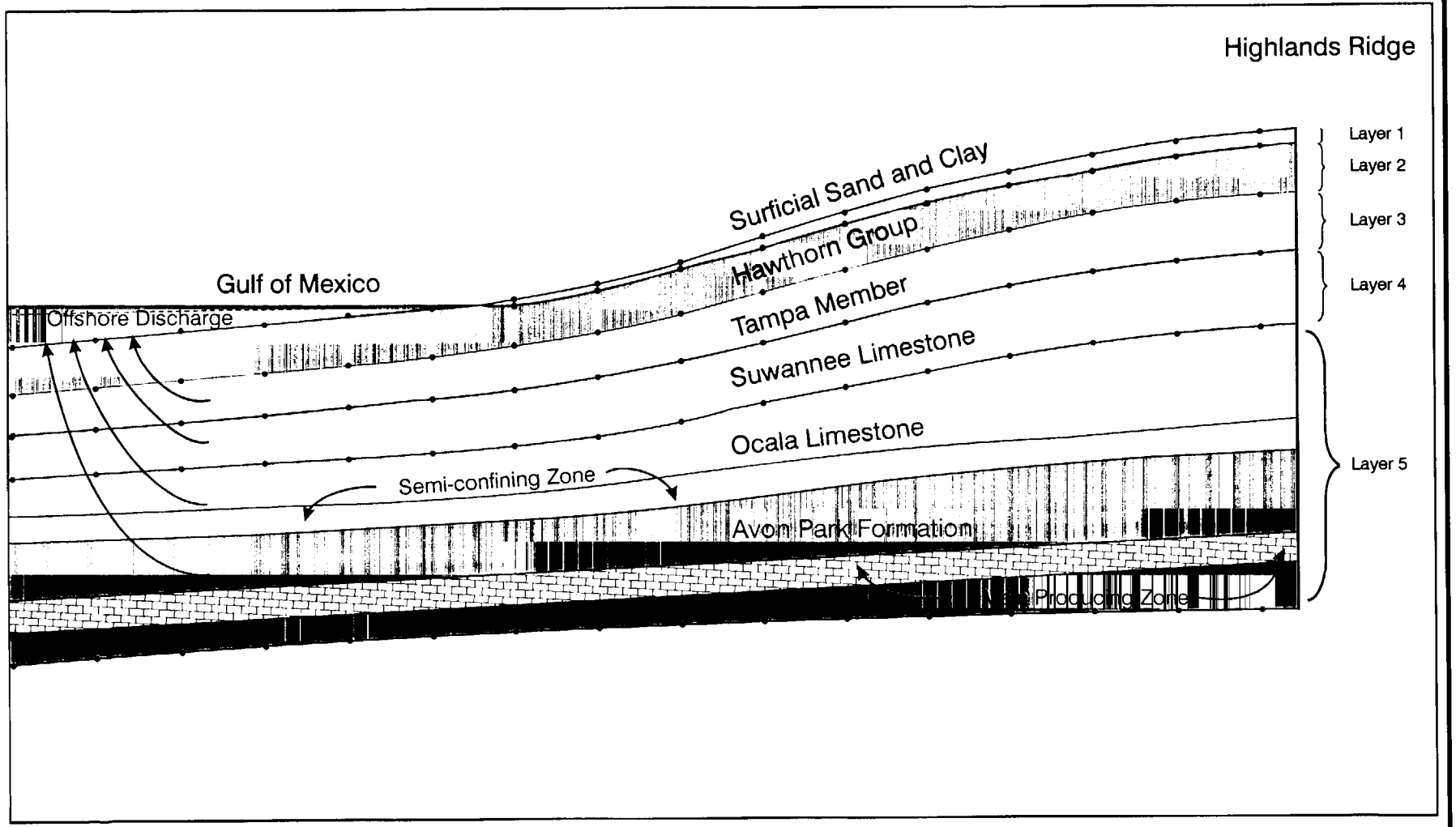

Filename: X:\SWF024\WO_01\saltwater_intrusion\vert_discret_regional.cdr
Project: SWF024-0101
Created by: cfarmer 12/14/01
Revised: 07/03/02 cf
Source: Waterstone (2000)

HYDRO GeoLogic INC

Figure 4.4

Vertical Discretization of Southern District Model

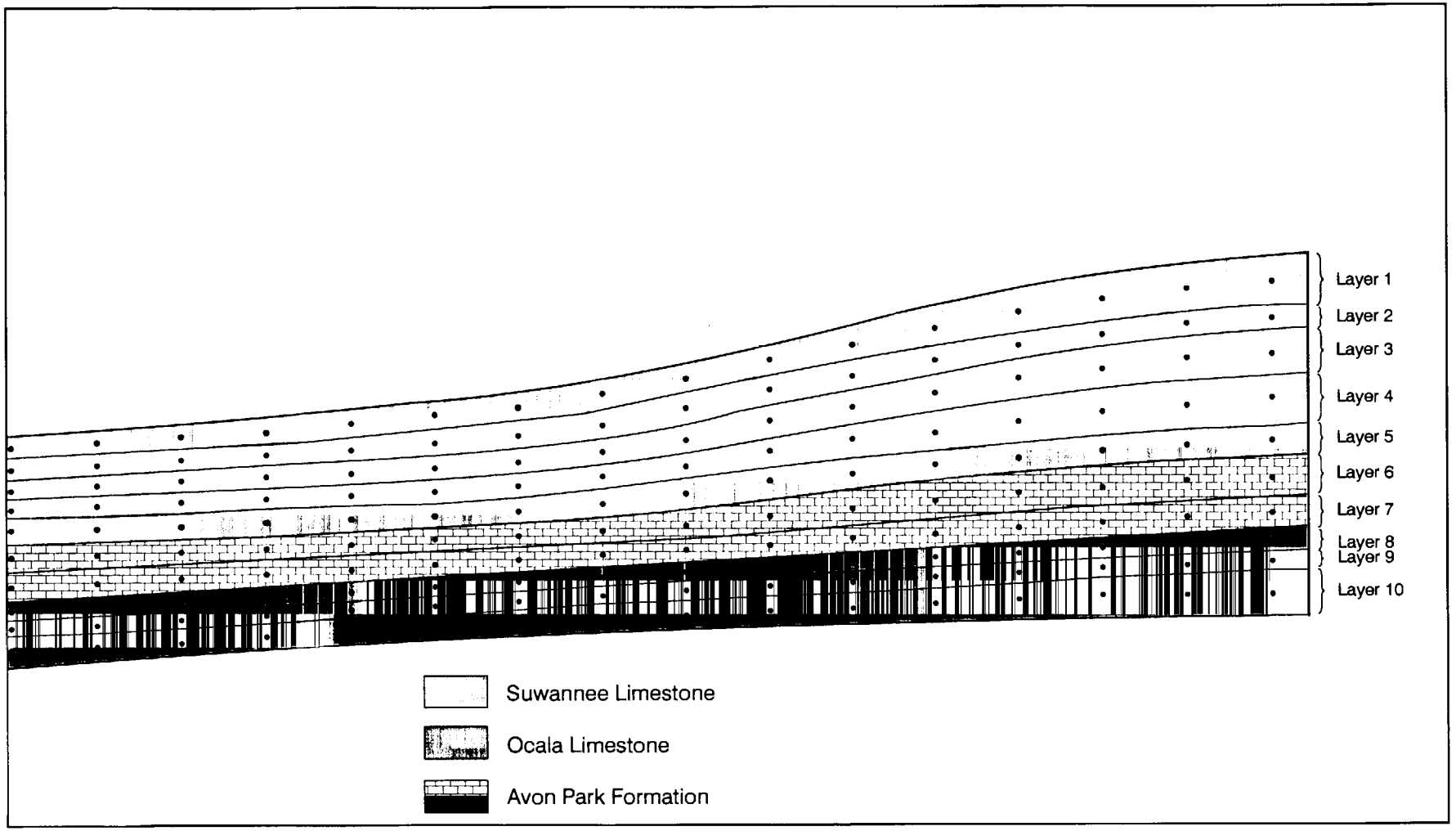

Filename: X:\SWF024\WO_01\vert_discret_local_rev.cdr
Project: SWF024-001-03
Created by: cfarmer 12/14/01
Revised: 05/30/02 cf
Source: Waterstone (2000)

HYDRO GeoLogic

Figure 4.5

Initial Vertical Discretization of the Density-Dependent Model

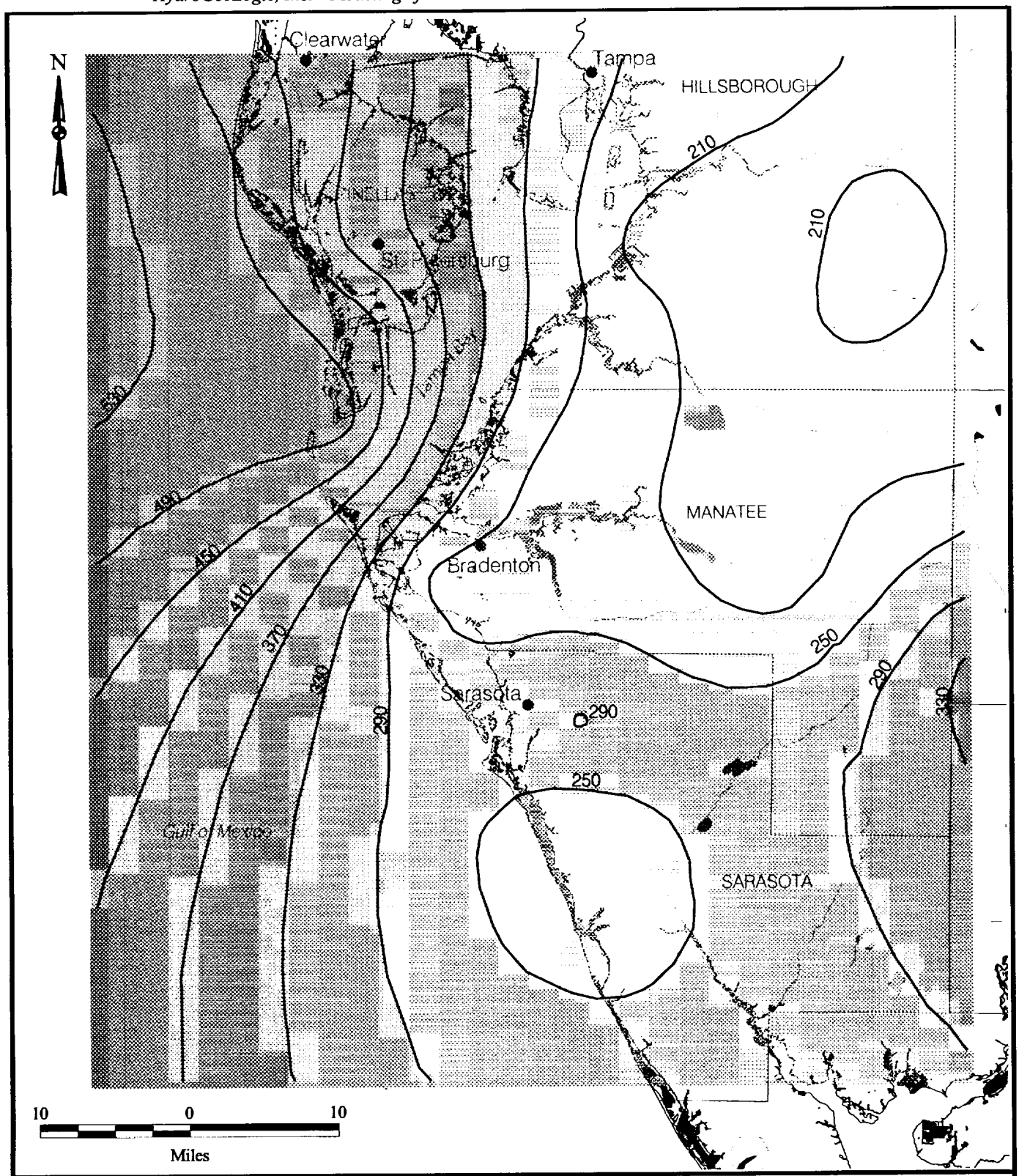

Filename: X:\SWF024\WO_01\saltwater_intrusion\fig4-6.apr
Project: SWF024-001-01
Created: 11/28/01 TH
Revised: 04/22/02 TB

HYDRO GeoLogic

Legend

County Boundary

Surface Drainage

250 Suwannee Thickness Contour (ft)

Suwannee Thickness (ft)
170 - 210
210 - 250
250 - 290
290 - 330
330 - 370
370 - 410
410 - 450
450 - 490
490 - 530
530 - 570

Figure 4.6
Thickness of the Suwannee Limestone (Model Layers 1 and 2)

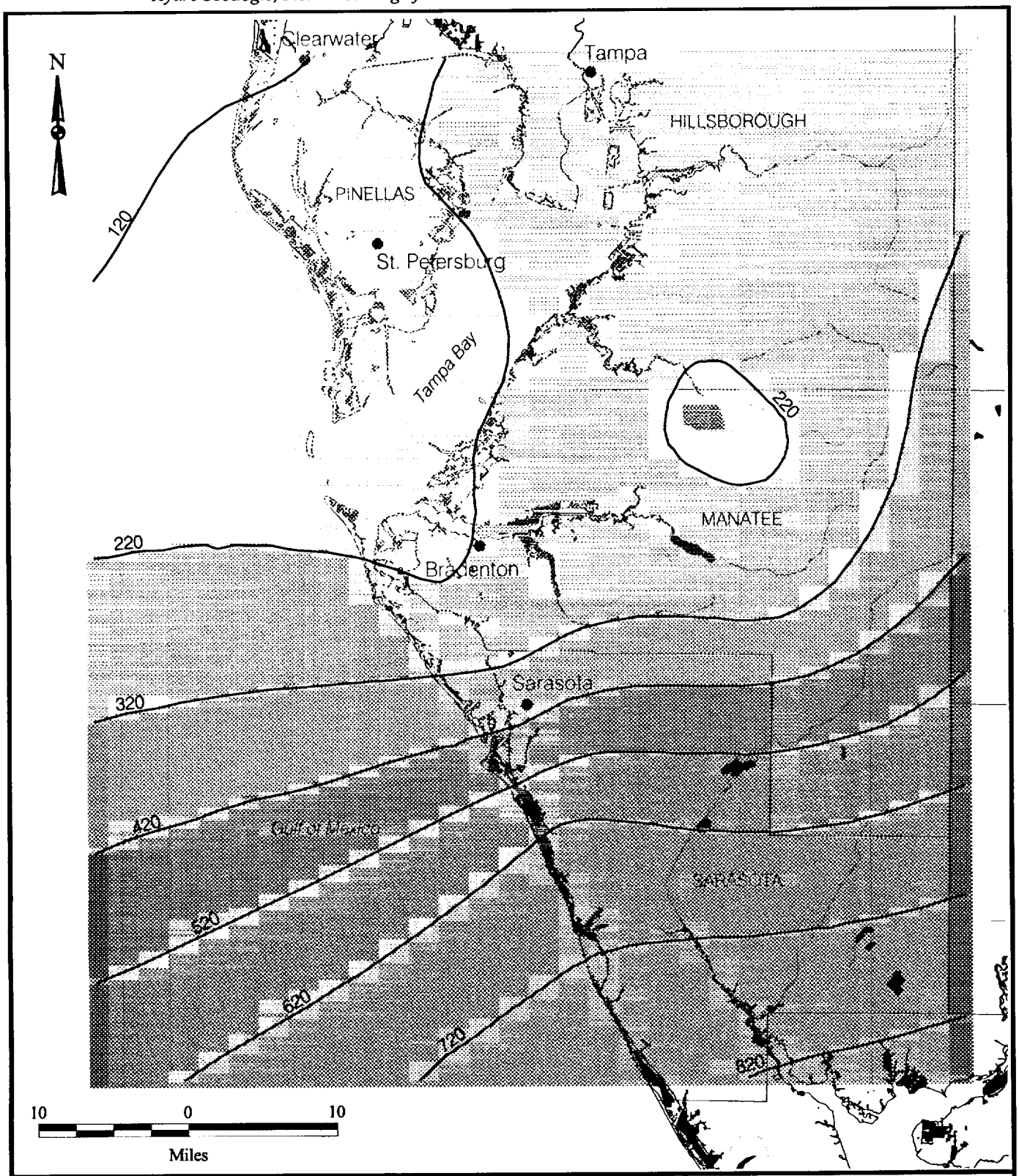

Filename: X:\SWF024\WO_01\saltwater_intrusion\fig4-7.apr
Project: SWF024-0001-01
Created: 11/28/01 TH
Revised: 04/22/02 TB

HYDRO GeoLogic

Legend

- County Boundary
- Surface Drainage
- 520 Ocala Thickness Contour (ft)

Ocala Thickness (ft)
1 - 120
120 - 220
220 - 320
320 - 420
420 - 520
520 - 620
620 - 720
720 - 820
820 - 920

Figure 4.7
Thickness of the Ocala Limestone (Model Layers 3, 4, and 5)

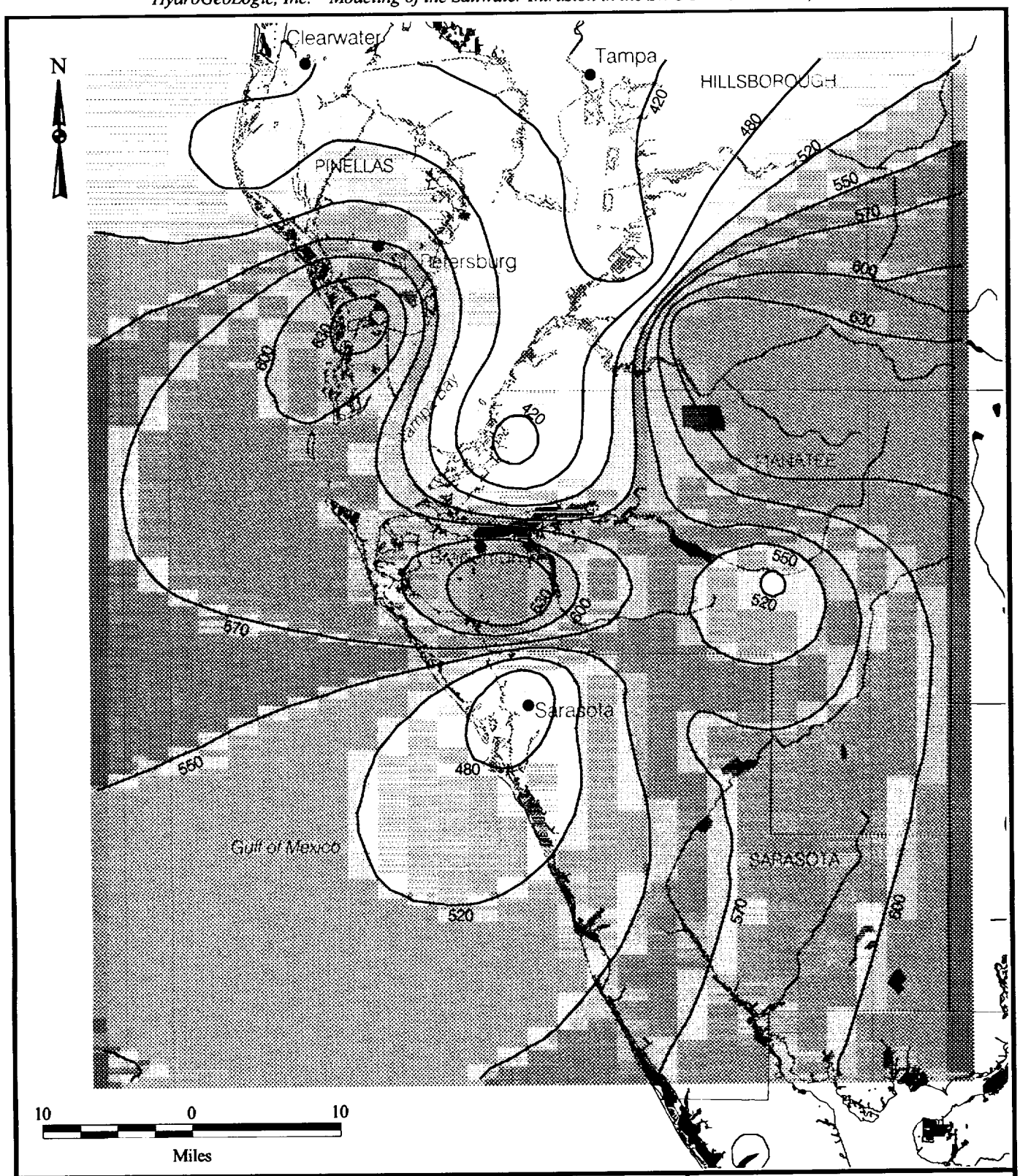

Filename: X:\SWF024\WO_01\saltwater_intrusion\fig4-8.apr
Project: SWF024-001-01
Created: 11/28/01 TH
Revised: 04/22/01 TB

HYDRO GeoLogic

Legend

- County Boundary
- Surface Drainage
- 570 Avon Park Thickness Contour (ft)

Avon Park Thickness (ft)
- 385 - 420
- 420 - 480
- 480 - 520
- 520 - 550
- 550 - 570
- 570 - 600
- 600 - 630
- 630 - 715

Figure 4.8
Thickness of the Avon Park Formation (Model Layers 6 through 10)

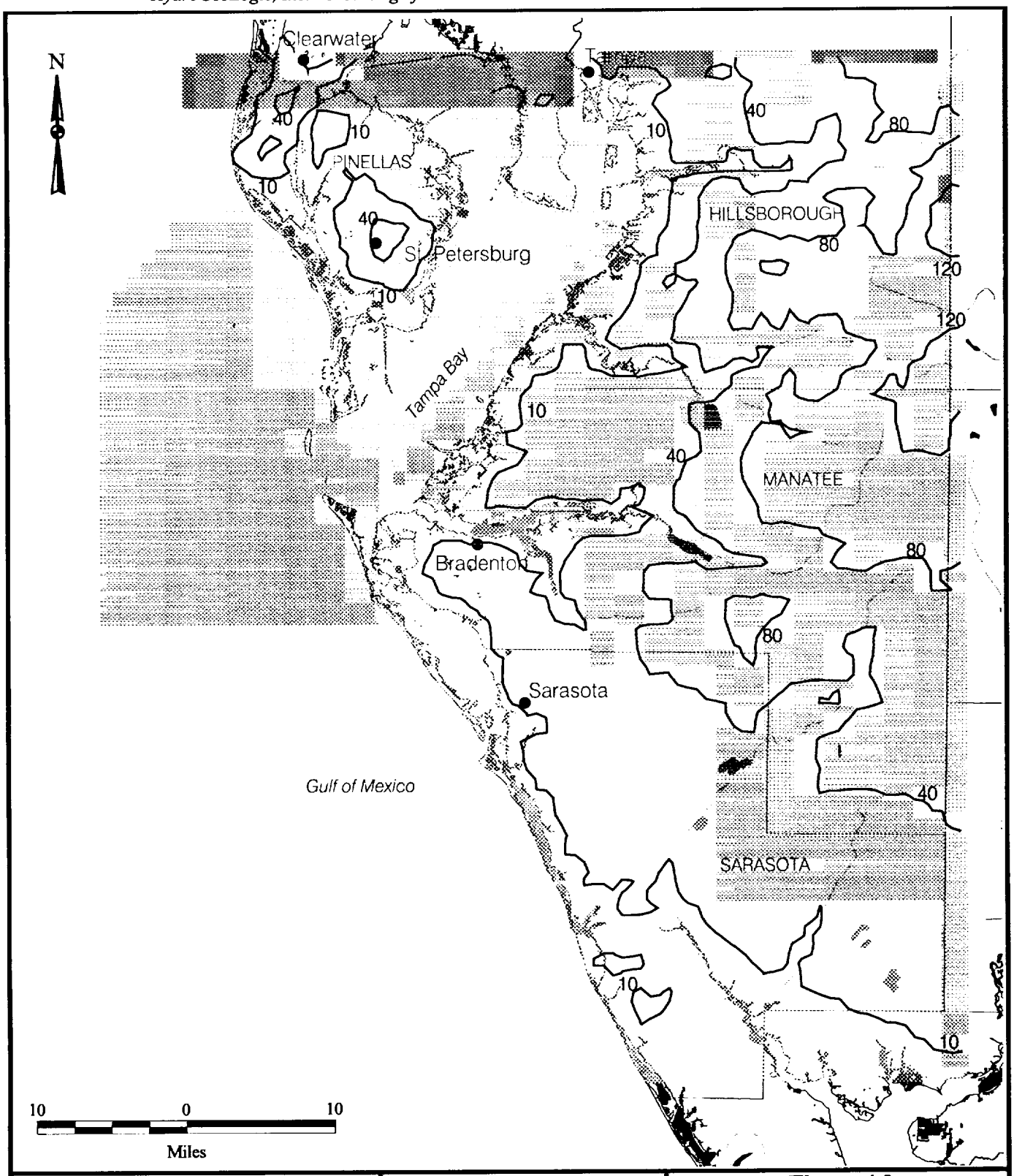

Filename: X:\SWF024\WO_01\saltwater_intrusion\fig 4-9.apr
Project: SWF024-001-01
Created: 11/28/01 TH
Revised: 04/22/02 TB

HYDRO GeoLogic

Legend

- County Boundary
- Surface Drainage
- 40 Hydraulic Head Assigned to General Head Boundaries (ft)

GHB Conductance - (1/Day)
- 1 - 10
- 10 - 100
- 100 - 1000
- 1000 - 10000
- 10000 - 100000

Figure 4.9
Head and Conductance Distribution of the General Head Boundaries Applied to the Top of the Suwannee Limestone (Model Layer 1)

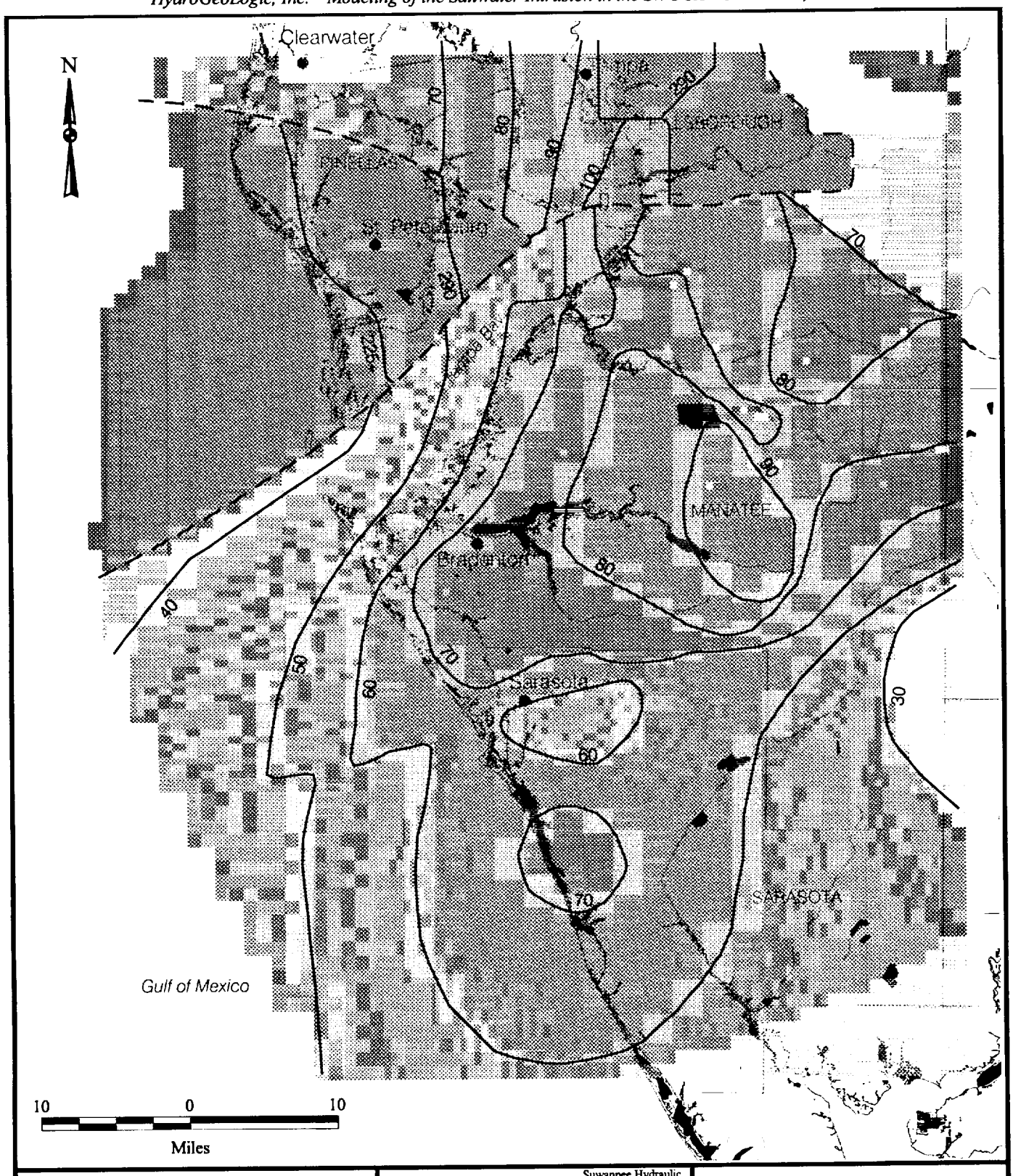

Filename: X:\SWF024\WO_01\saltwater_intrusion\fig4-10.apr
Project: SWF024-001-01
Created: 11/28/01 TH
Revised: 06/05/02 TB

HYDRO GeoLogic Inc

Legend

- County Boundary
- Surface Drainage
- 80 Suwannee Hydraulic Conductivity Contour (ft²/day)
- Zone Boundaries

Suwannee Hydraulic Conductivity (ft²/day)

0 - 10
10 - 20
20 - 30
30 - 40
40 - 50
50 - 60
60 - 70
70 - 80
80 - 90
90 - 100
100 - 225
225 - 290
290 - 420
420 - 600

Figure 4.10
Initial Hydraulic Conductivity of the Suwannee Limestone (Model Layers 1 and 2)

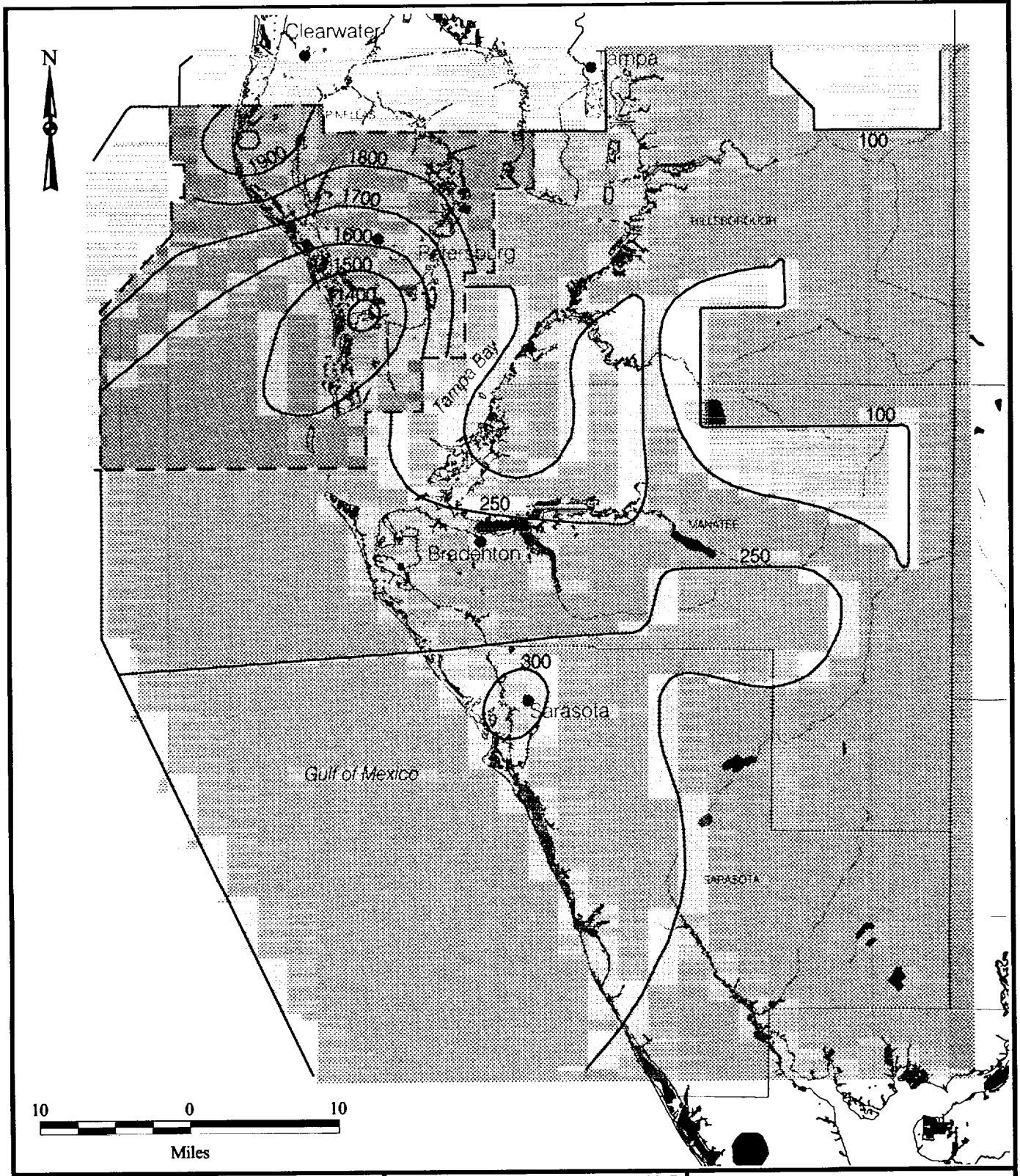

Filename: X:\SWF024\WO_01\saltwater_intrusion\fig4-11.apr
Project: SWF024-001-01
Created: 11/28/01 TH
Revised: 06/05/02 TB

HYDRO GeoLogic Inc

Legend

- County Boundary
- Surface Drainage
- 1600 Avon Park Hydraulic Conductivity Contour (ft/day)
- Zone Boundary

Avon Park Hydraulic Conductivity (ft/day)

0 - 1
1 - 10
10 - 100
100 - 1000
250 - 300
1000 - 1400
1400 - 1500
1500 - 1600
1600 - 1700
1700 - 1800
1800 - 1900
1900 - 2000
2000 - 10000

Figure 4.11
Initial Hydraulic Conductivity of the Avon Park Formation (Model Layers 6 through 10)

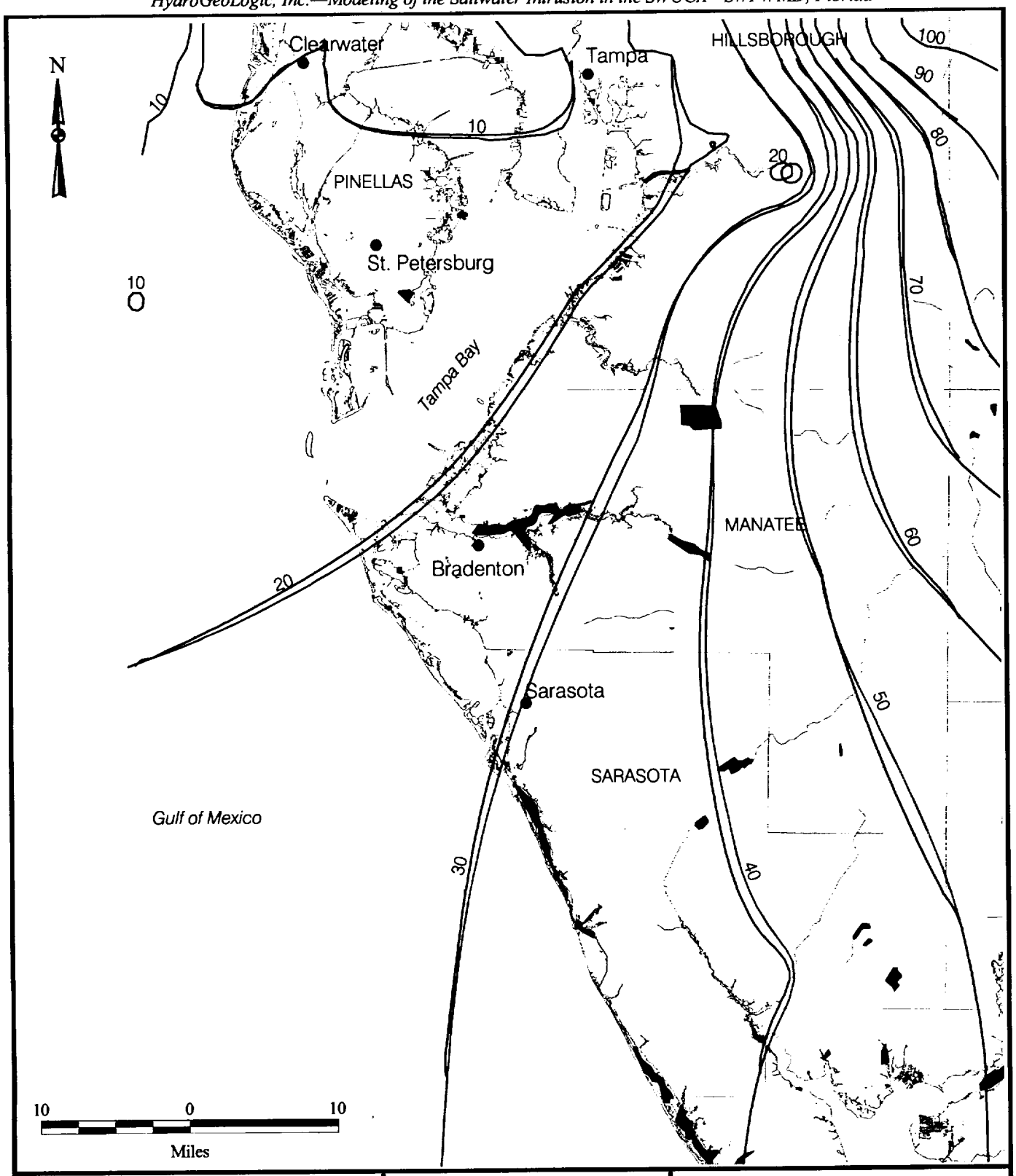

Filename: X:\SWF024\WO_01\saltwater_intrusion\fig5-1.apr
Project: SWF024-001-01
Created: 11/28/01 TB
Revised: 04/22/02 TB

HYDRO GeoLogic

Legend

County Boundary

Surface Drainage

10 Regional Model Contour Lines (ft)

10 Local Model Contour Lines (ft)

Figure 4.12
Comparison of Predevelopment Heads Predicted by the Regional Flow and Density Dependent Models

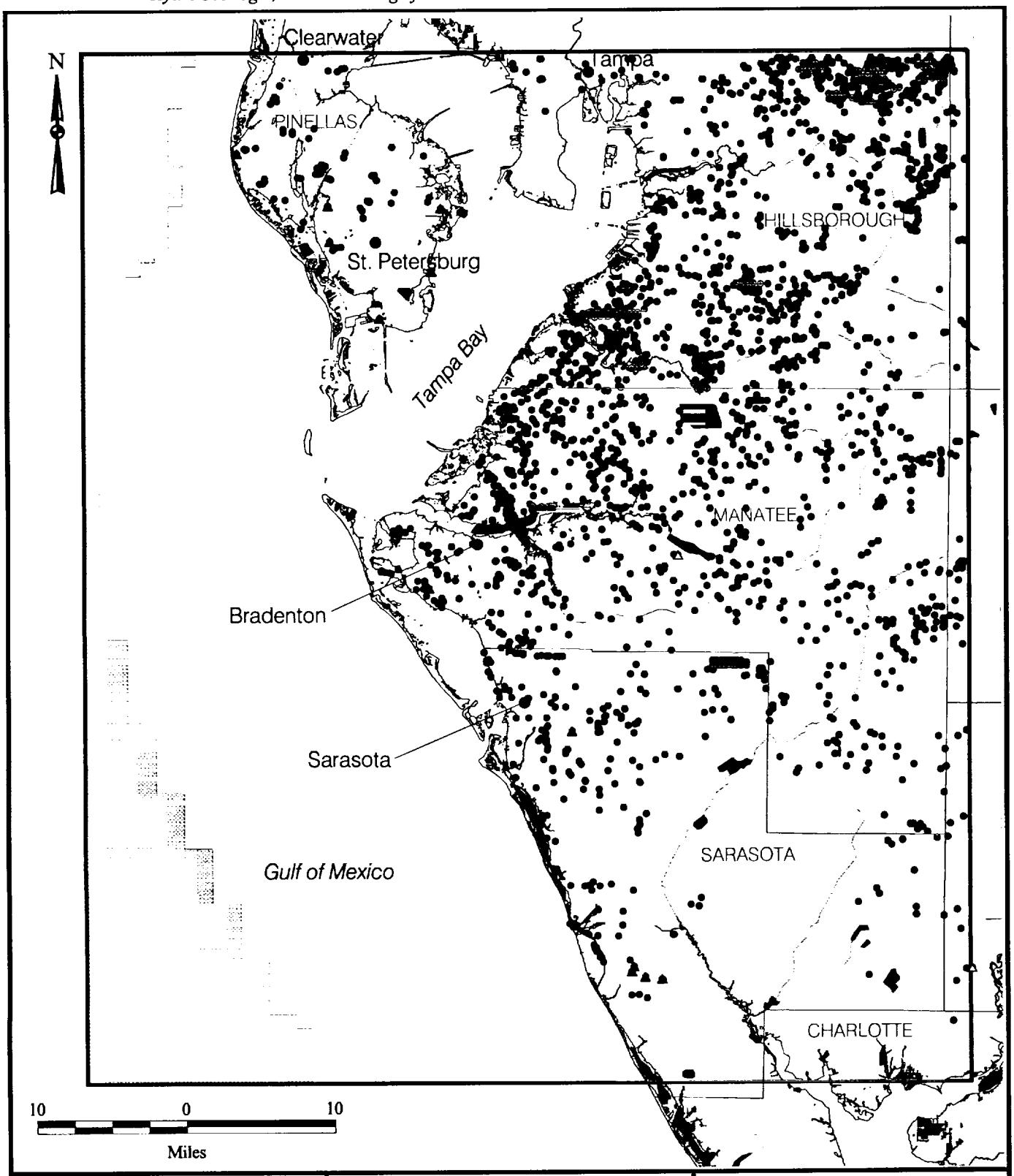

Filename: X:\SWF024\WO_01\saltwater_intrusion\well_loc_by_3area.apr
Project: SWF024-001-01
Created: 11/28/01 TH
Revised: 06/05/02 TB

HYDRO GeoLogic Inc.

Legend

- County Boundary
- Surface Drainage
- Model Domain
- Inactive Area
- Suwannee Well Locations
- Ocala Well Locations
- Avon Park Well Locations
- Avon Park Injection Well Locations
- Suwannee Injection Well Locations

Figure 5.1
Location of Groundwater Extraction/Injection Wells within the Study Area

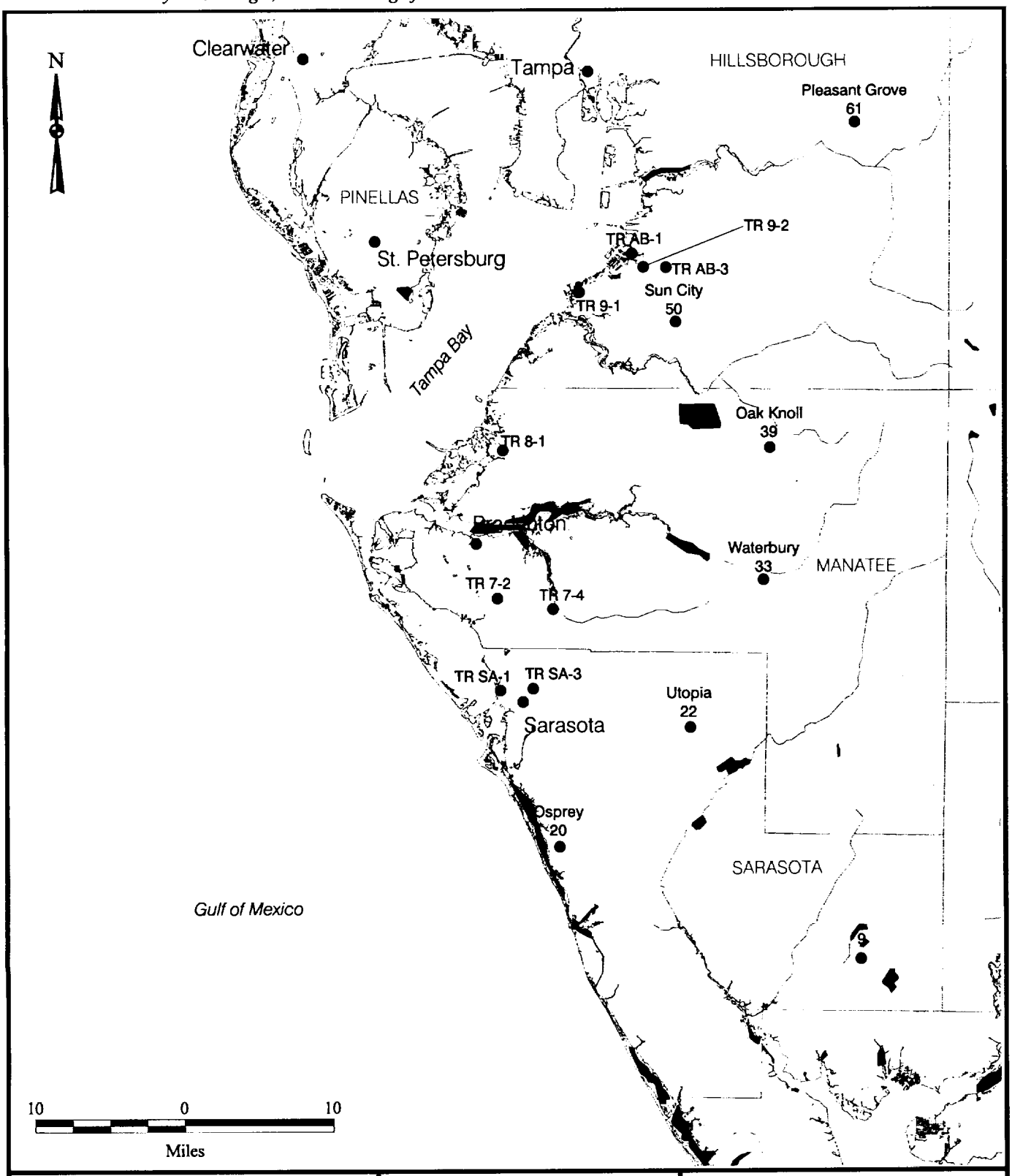

Filename: X:\SWF024\WO_01\saltwater_intrusion\reslay2-4-7.apr
Project: SWF024-001-01
Created: 11/28/01 TH
Revised: 06/07/02 TB

HYDRO GeoLogic Inc

Legend

County Boundary

Surface Drainage

TR 7-2 ROMP Well Name

ROMP Well Location

Figure 5.2
ROMP Wells Used for Determining Model Calibration Statistics

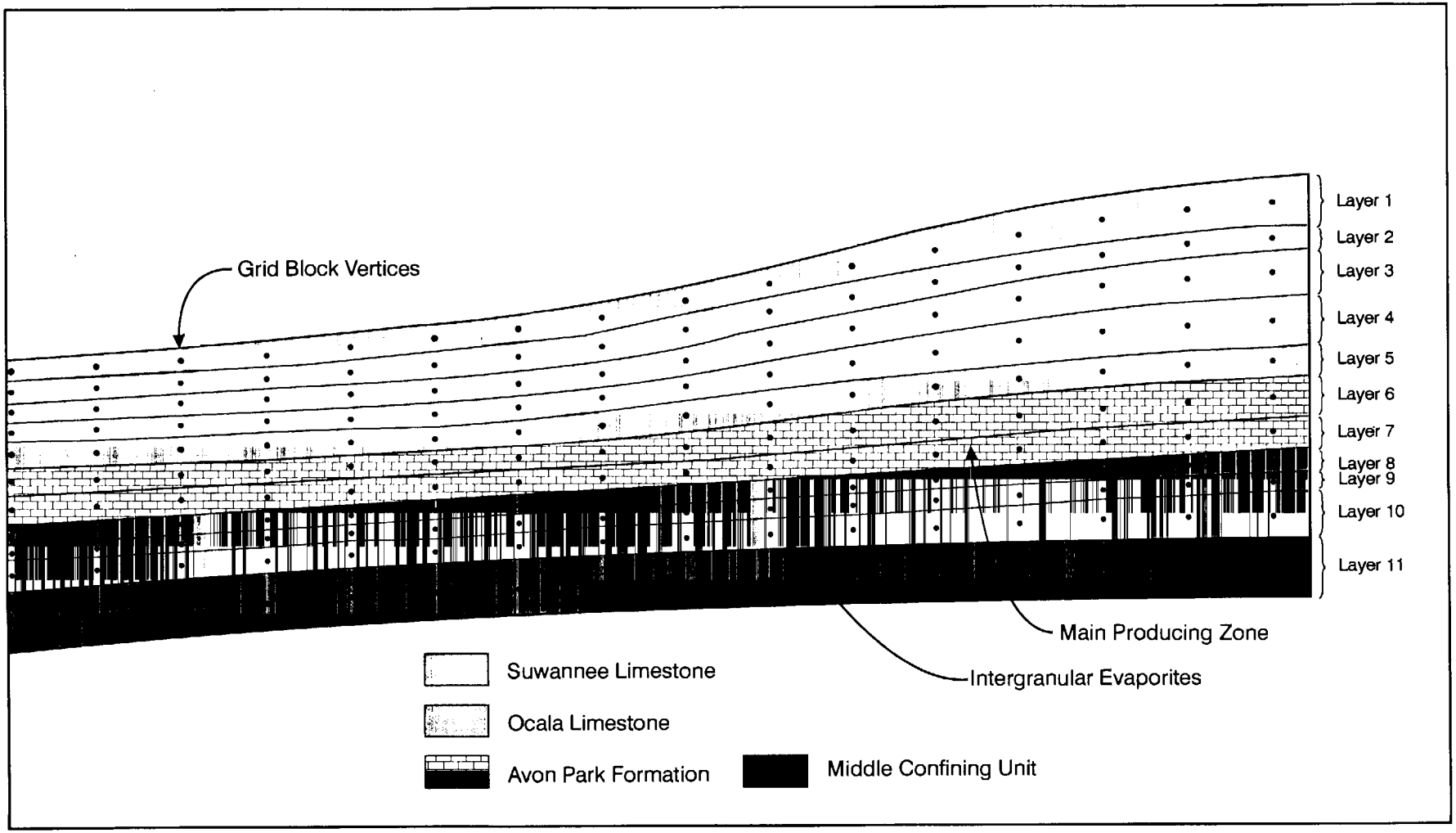

Filename: X:\SWF024\WO_01\vert_discret_calibrated_rev.cdr
Project: SWF024-001-03
Created by: cfarmer 04/03/02
Revised: 06/07/02 tbraswell
Source: Waterstone (2000)

HYDRO GeoLogic INC.

Figure 5.3

Vertical Discretization of the Calibrated Density-Dependent Model

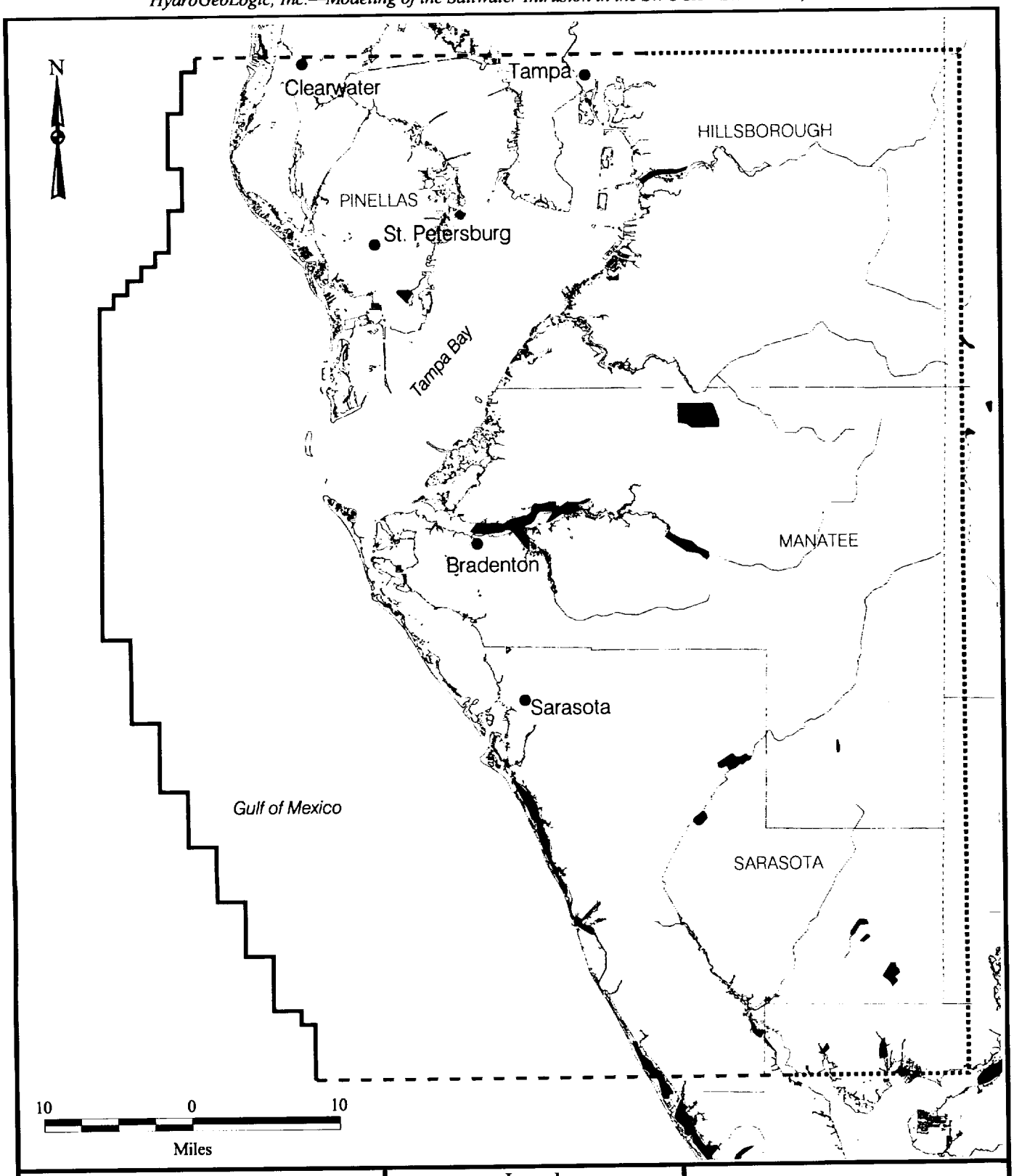

Filename: X:\SWF024\WO_01\saltwater_intrusion\bndry_cond.apr
Project: SWF024-001-01
Created: 11/28/01 TH
Revised: 06/07/02 TB

HYDRO GeoLogic Inc.

Legend

County Boundary
Surface Drainage
C = 1, h = 0
C = 0, h = prescribed from regional model (transient)
C = 1, h = constant, obtained from regional predevelopment model

Note: The Prescribed heads are converted to equivalent freshwater heads for use in the model.

Figure 5.4
Head and Chloride Lateral Boundary Conditions of the Density Dependent Model

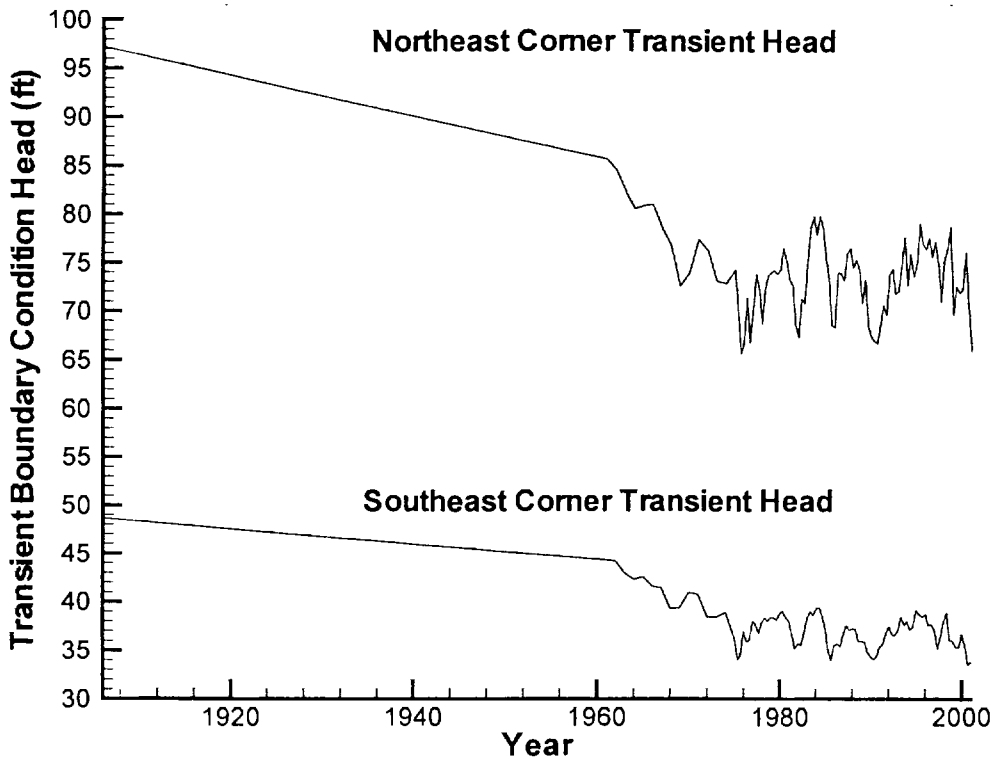

Figure 5.5 **Example of Transient Hydraulic Head Boundary Conditions Assigned to Cells Located in Northeast and Southeast Corners of Model Domain**

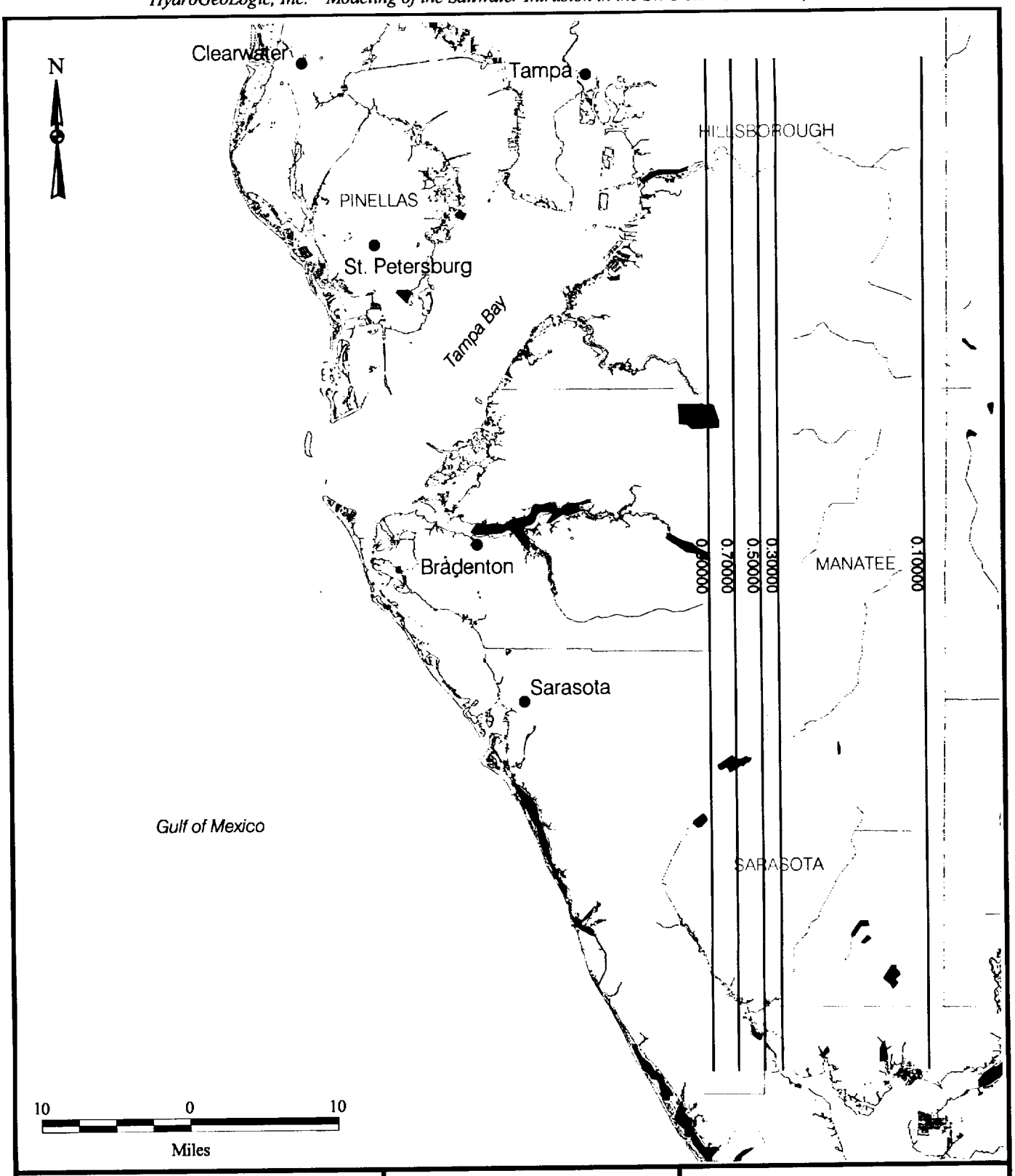

Filename: X:\SWF024\WO_01\saltwater_intrusion\bot_ghb_conc.apr
Project: SWF024-001-01
Created: 11/28/01 TH
Revised: 05/07/02 TB

HYDRO GeoLogic Inc.

Legend

County Boundary

Surface Drainage

0.5 Bottom General Head Boundary's Relative Concentration Contour

0.1 = 1,900 mg/l
0.3 = 5,700 mg/l
0.5 = 9,500 mg/l
0.7 = 13,300 mg/l
0.9 = 17,100 mg/l

Figure 5.6
Boundary Conditions at Base of Density Dependent Model

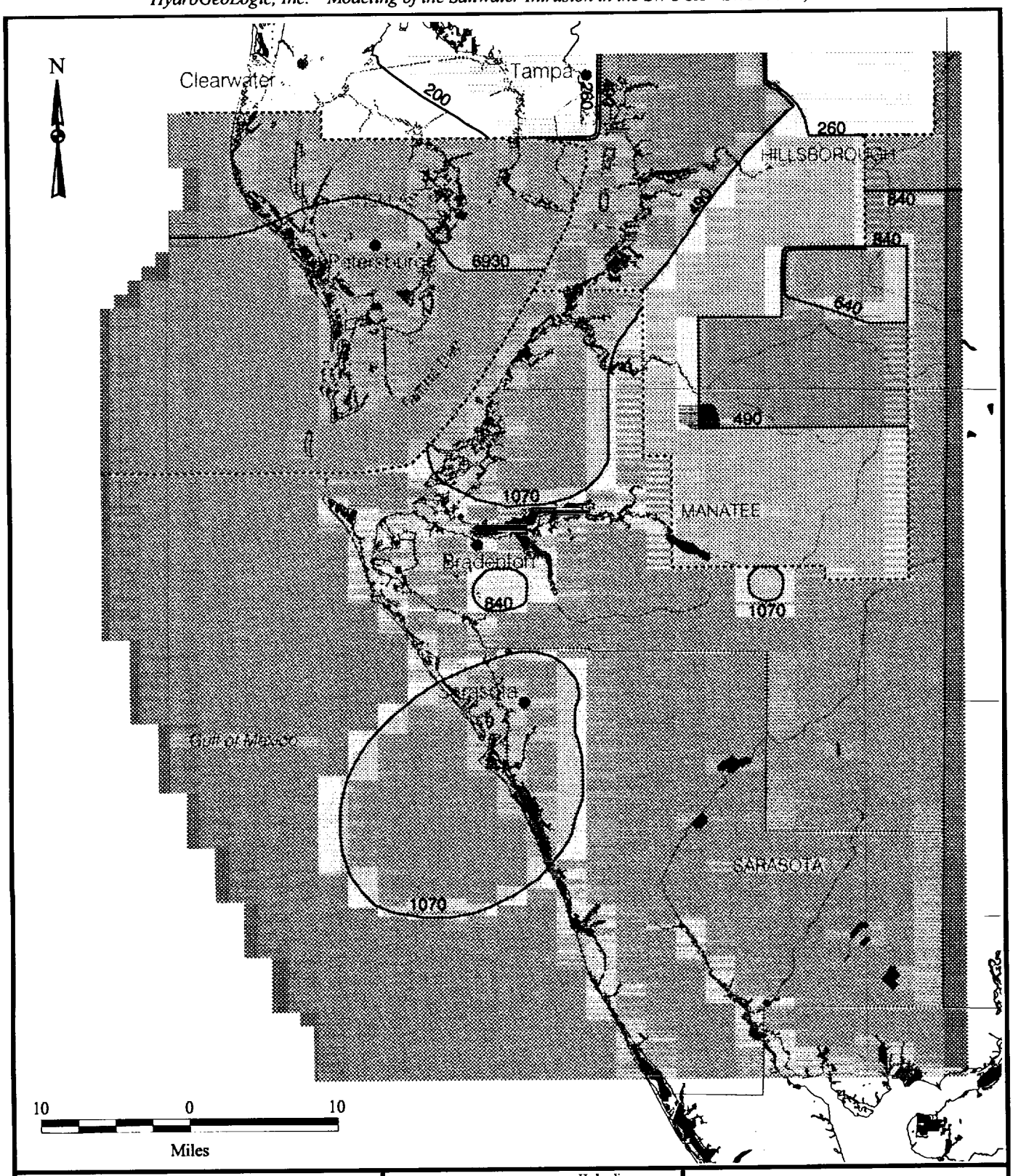

Filename: X:\SWF024\WO_01\saltwater_intrusion\conduct_highK.apr
Project: SWF024-001-01
Created: 11/28/01 TH
Revised: 06/07/02 tbraswell

HYDRO GeoLogic Inc

Legend

- County Boundary
- Surface Drainage
- Zone Boundary
- 840 Hydraulic Conductivity Contour (ft/d)

Hydraulic Conductivity (ft/d)

- 170 - 200
- 200 - 260
- 260 - 490
- 490 - 640
- 640 - 840
- 840 - 1070
- 1070 - 1430
- 1430 - 6930
- 6930 - 8480

Figure 5.7
Hydraulic Conductivity of the High K Zone in the Avon Park Formation (Model Layers 6 and 7)

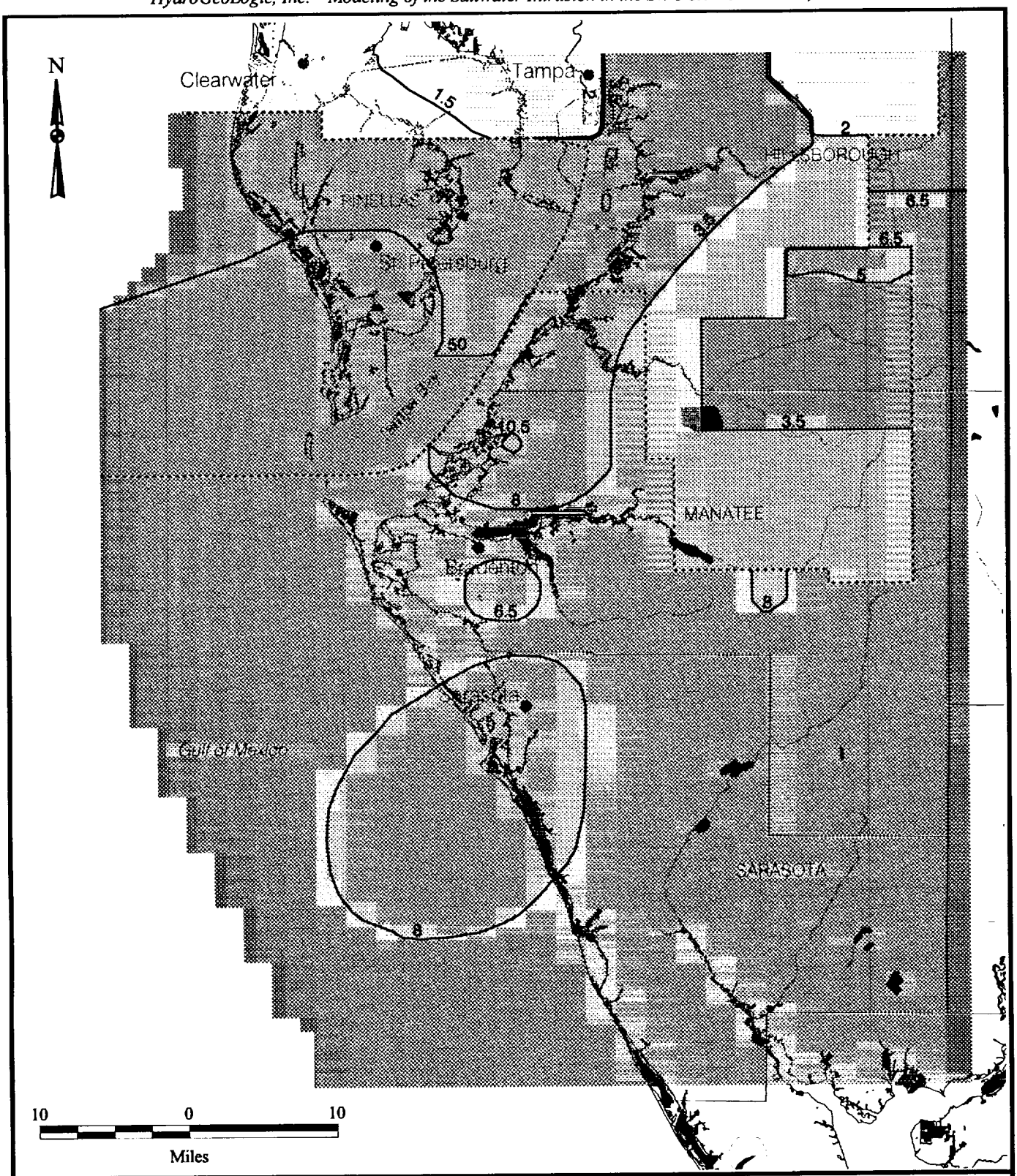

Filename: X:\SWF024\WO_01\saltwater_intrusion\conduct_lowK.apr
Project: SWF024-001-01
Created: 11/28/01 TH
Revised: 06/07/02 TB

HYDRO GeoLogic Inc.

Legend

- County Boundary
- Surface Drainage
- Zone Boundary
- 3.5 Hydraulic Conductivity Contour (ft/d)

Hydraulic Conductivity (ft/d)

- 1 - 1.5
- 1.5 - 2
- 2 - 3.5
- 3.5 - 5
- 5 - 6.5
- 6.5 - 8
- 8 - 10.5
- 10.5 - 50
- 50 - 64

Figure 5.8
Hydraulic Conductivity of the Lower K Zone in the Avon Park Formation (Model Layers 8, 9, and 10)

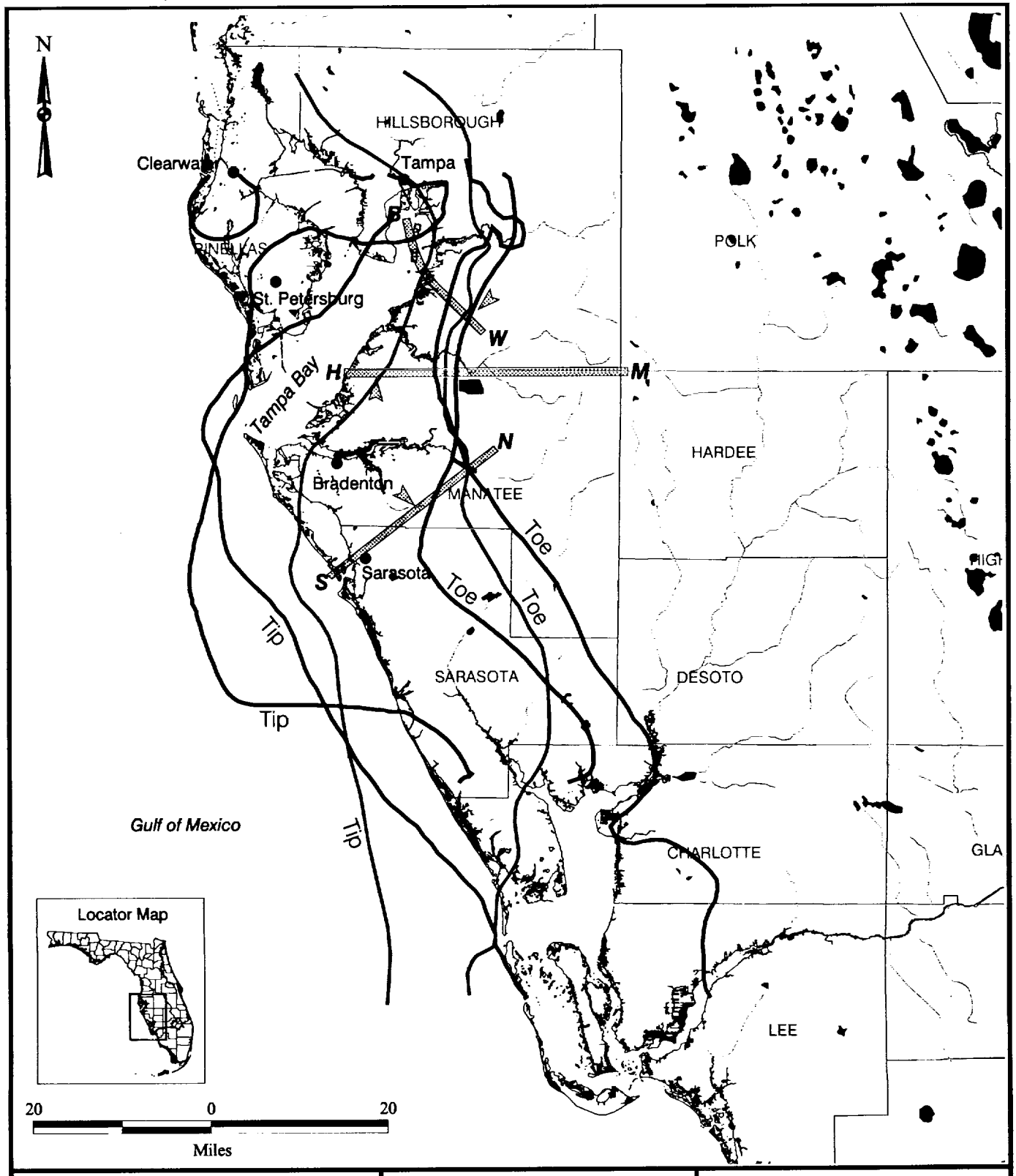

Filename: X:\SWF024\WO_01\saltwater_intrusion\tip-toe_dec2000-2.apr
Project: SWF024-001-01
Created: 11/29/01 TH
Revised: 06/07/02 TB

HYDRO GeoLogic

Legend

- County Boundary
- Surface Drainage
- Cross-section Locations (HGL, 1991a)
- Prediction of Toe of the Interface (HGL, 1991a)
- Predevelopment Interface Position (HGL, 1993a)
- Predevelopment Interface Position (HGL, 1994a)
- Predevelopment Interface Position (Present Study)

Figure 5.9
Comparison of Predicted Saltwater Interface Positions (Upper Floridan System)

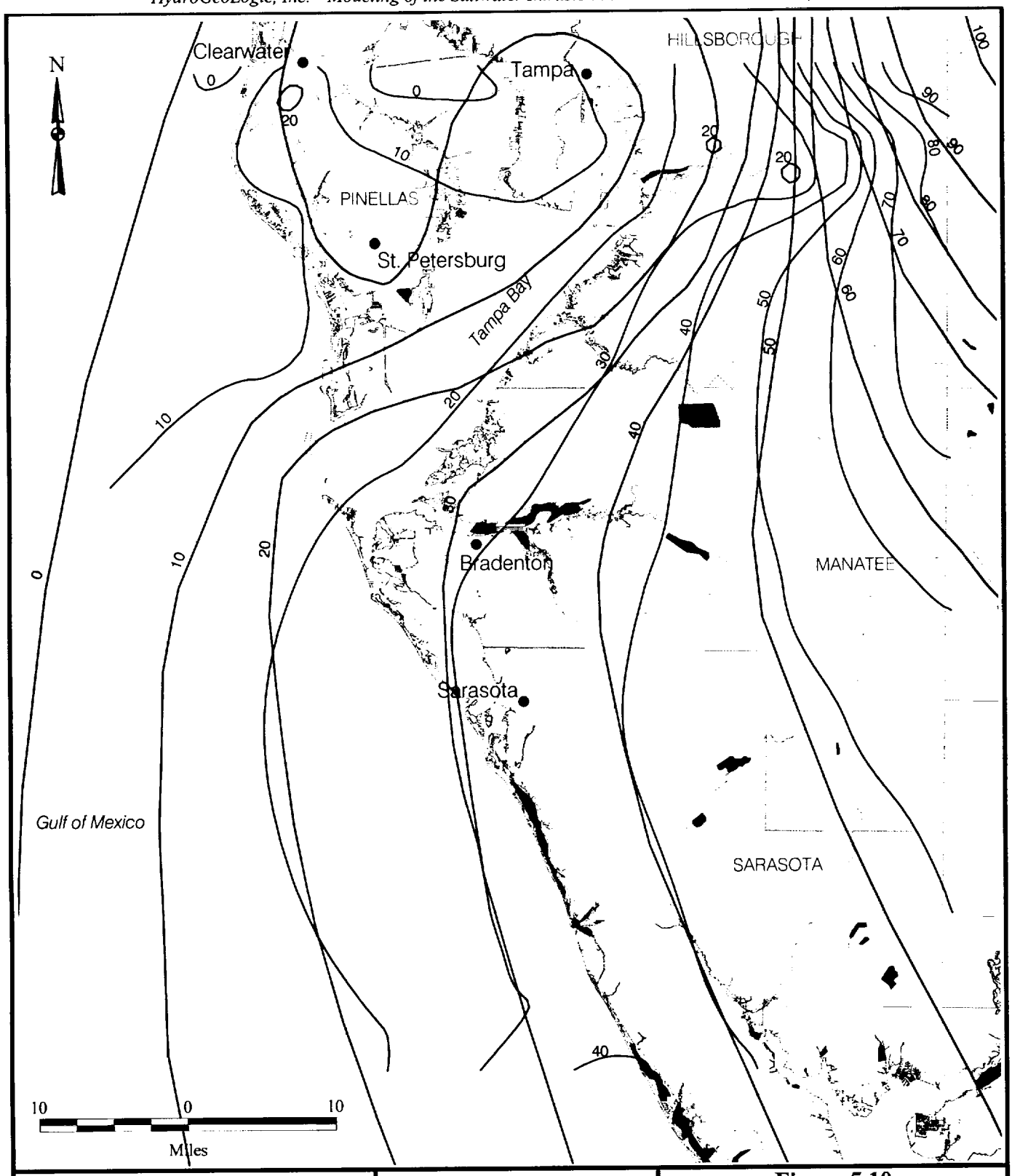

Filename: X:\SWF024\WO_01\saltwater_intrusion\head_dist_2_vs_PrePot.apr
Project: SWF024-001-01
Created: 11/28/01 TH
Revised: 06/07/02 TB

HYDRO GeoLogic Inc

Legend

County Boundary

Surface Drainage

60 Head Distribution Contour (ft, msl) Predicted using Local Scale Model

60 Predevelopment Potentiometric Surface Elevation (ft) - (Johnston, 1980)

Figure 5.10
Comparison of Calibrated Predevelopment Hydraulic Head Distribution in the Suwannee Limestone (Model Layer 2) to Johnston (1980)

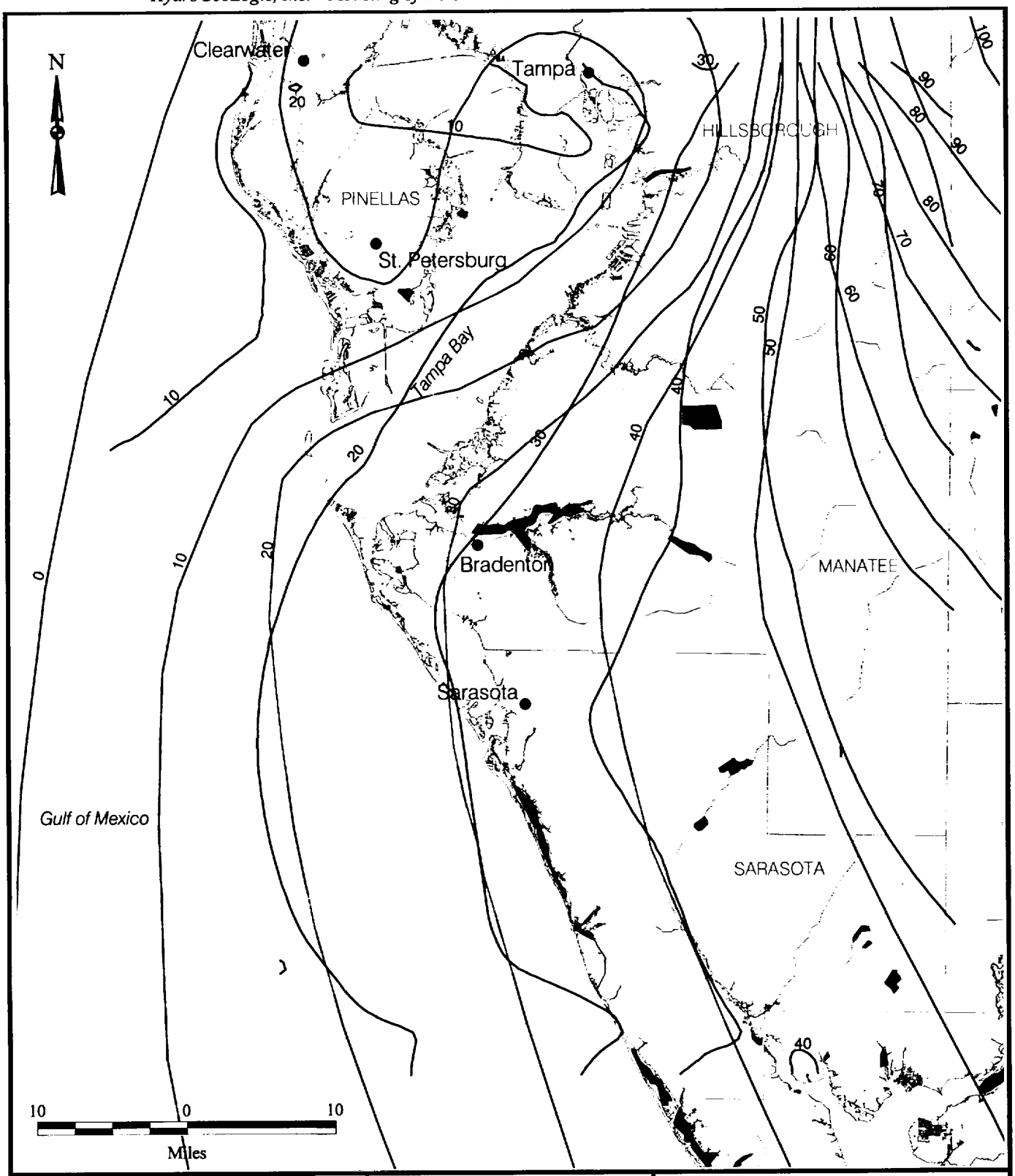

Filename: X:\SWF024\WO_01\saltwater_intrusion\head_dist_7_vs_PrePot.apr
Project: SWF024-001-01
Created: 11/28/01 TH
Revised: 06/07/02 TB

HYDRO GeoLogic Inc.

Legend

County Boundary

Surface Drainage

60 Head Distribution Contour (ft, msl) Predicted using Local Scale Model

60 Predevelopment Potentiometric Surface Elevation (ft) - (Johnston,1980)

Figure 5.11
Comparison of Calibrated Predevelopment Hydraulic Head Distribution in the Avon Park Formation (Model Layer 7) to Johnston (1980)

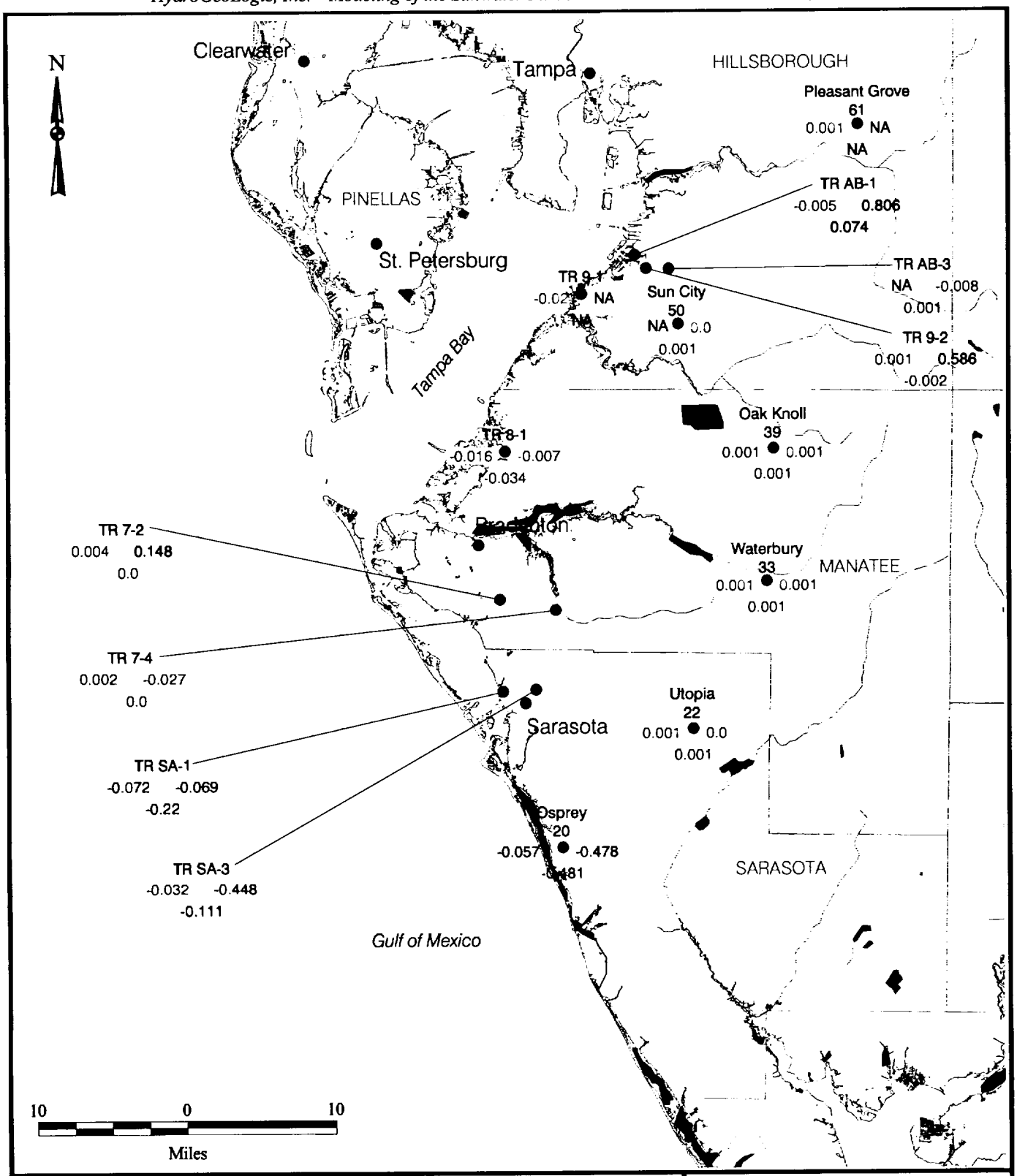

Filename: X:\SWF024\WO_01\saltwater_intrusion\reslay2-4-7.apr
Project: SWF024-001-01
Created: 11/28/01 TH
Revised: 04/22/02 TB

Legend

County Boundary — Surface Drainage

Well Name

Layer 2 ● Layer 7

Layer 4

-0.22 Residual Value < -0.05

0.001 Residual Value > -0.05 and < 0.05

0.148 Residual Value > 0.05

NA No Measurements Available

Figure 5.12
Relative Concentration Residuals Calculated at Selected ROMP Wells Layers 2, 4, and 7

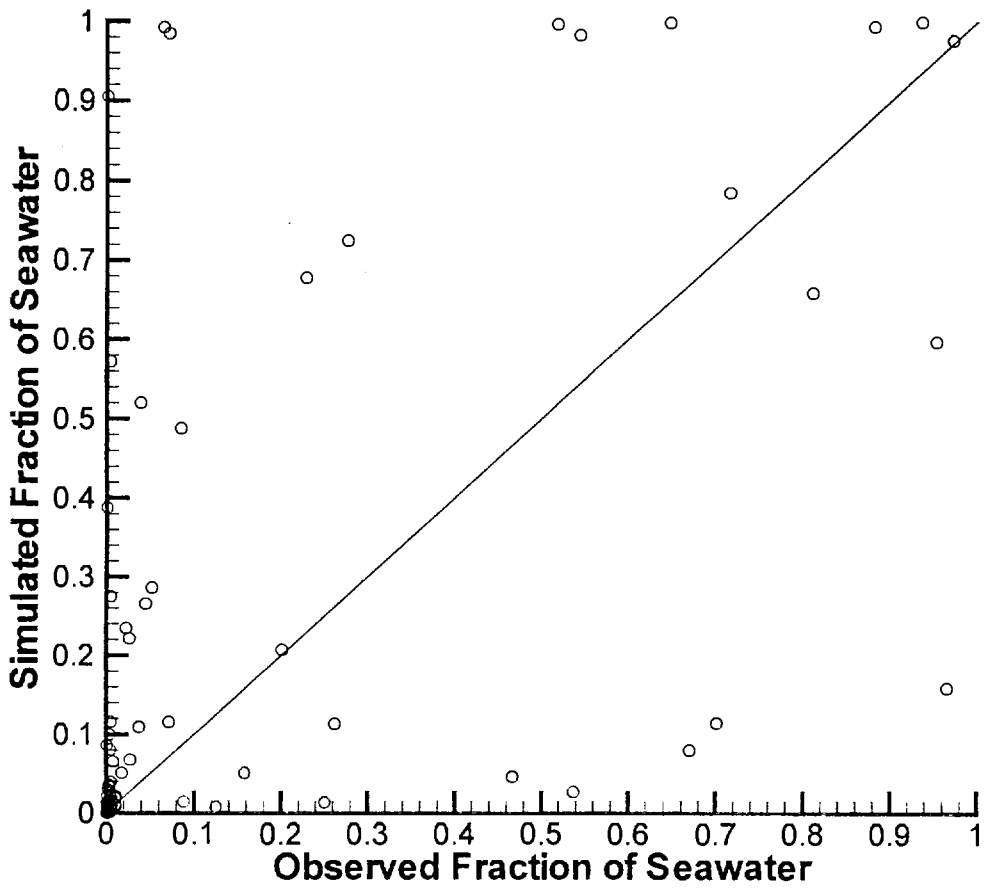

Figure 5.13 **Relationship between Simulated and Observed Relative Concentrations**

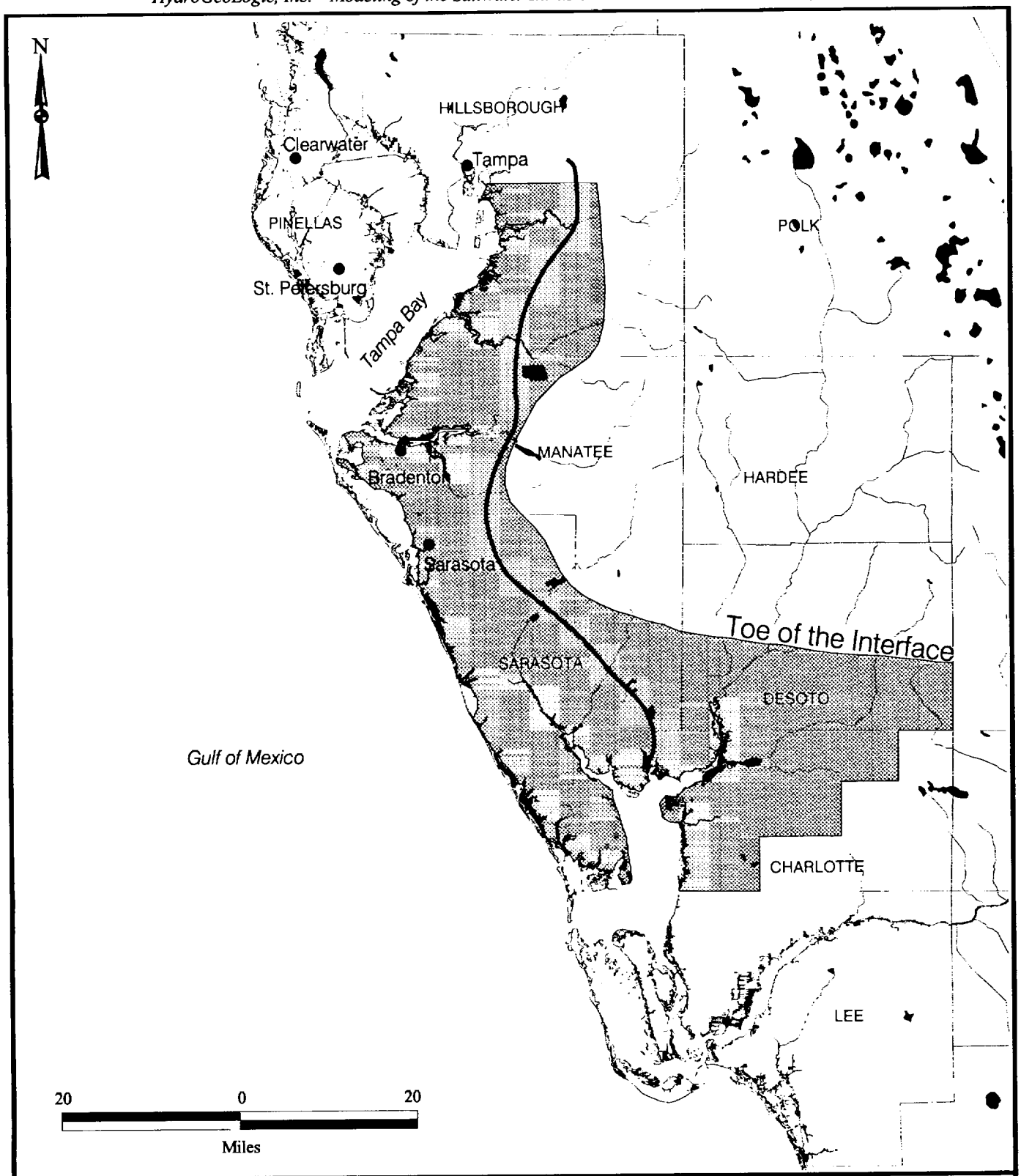

Filename: X:\SWF024\WO_01\saltwater_intrusion\chlor-extent-2.apr
Project: SWF024-001-01
Created: 11/29/01 TH
Revised: 06/05/02 TB

HYDRO GeoLogic Inc.

Legend

County Boundary

Surface Drainage

Extent of Chloride Concentration's exceeding 1000 mg/l (Calibrated Model)

Extent of Chloride Concentration's exceeding 1,000 mg/l (Beach and Shultz, 2000)

Figure 5.14
Comparison of Chloride Concentration in the LPZ Exceeding 1000 mg/l (Beach and Shultz) with Present Study for the Year 2000

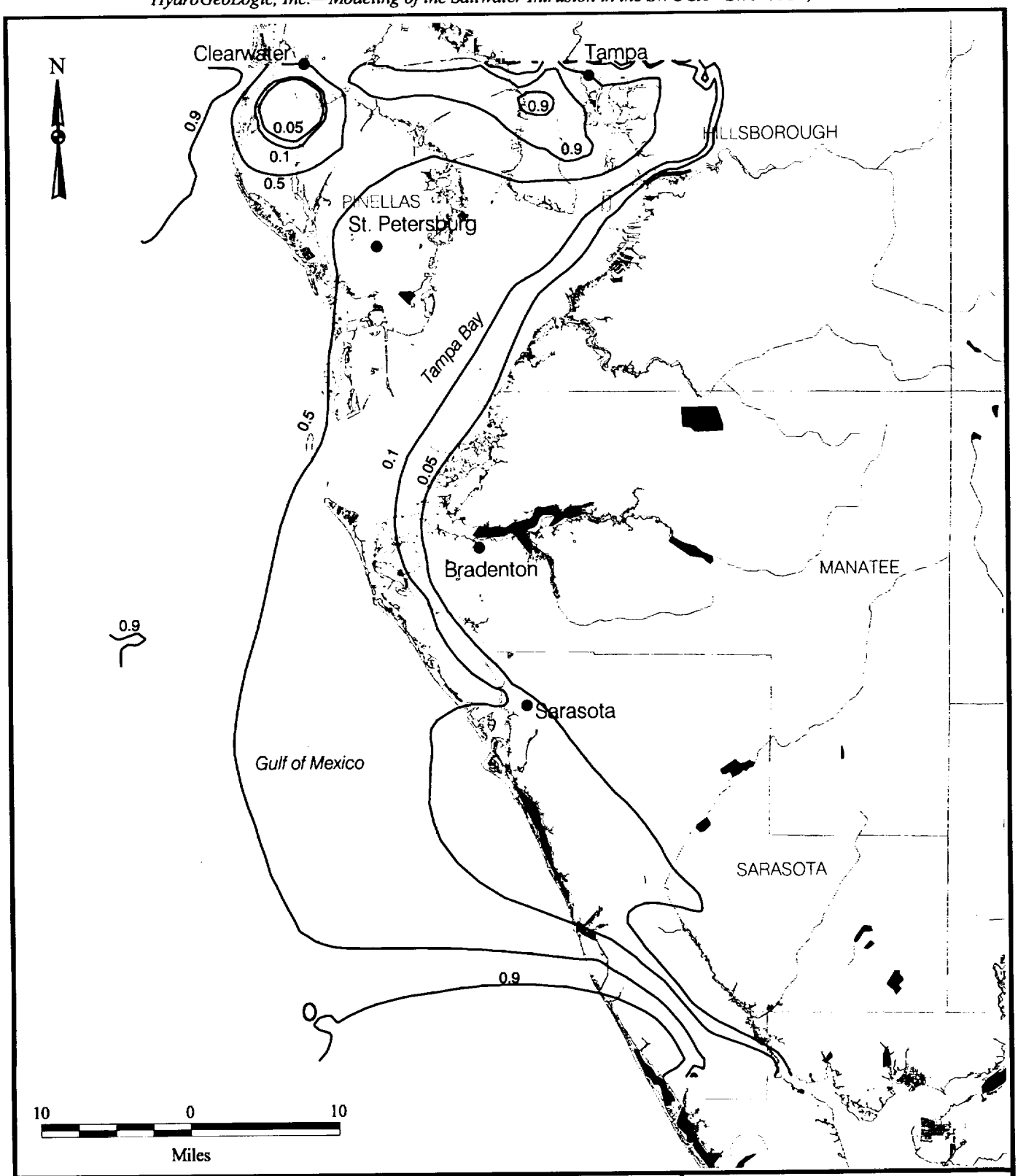

Filename: X:\SWF024\WO_01\saltwater_intrusion\r-chloride_dist_dec2000_2.apr
Project: SWF024-001-01
Created: 11/28/01 TH
Revised: 4/22/02 TB

HYDRO GeoLogic Inc.

Legend

County Boundary

Surface Drainage

0.05 Relative Chloride Concentration Contour
0.05 = 1000 mg/l

0.1 = 1,900 mg/l
0.3 = 5,700 mg/l
0.5 = 9,500 mg/l
0.7 = 13,300 mg/l
0.9 = 17,100 mg/l

Figure 5.15
Relative Chloride Concentrations Predicted Using the Calibrated Model for the Suwannee Limestone (Model Layer 2)

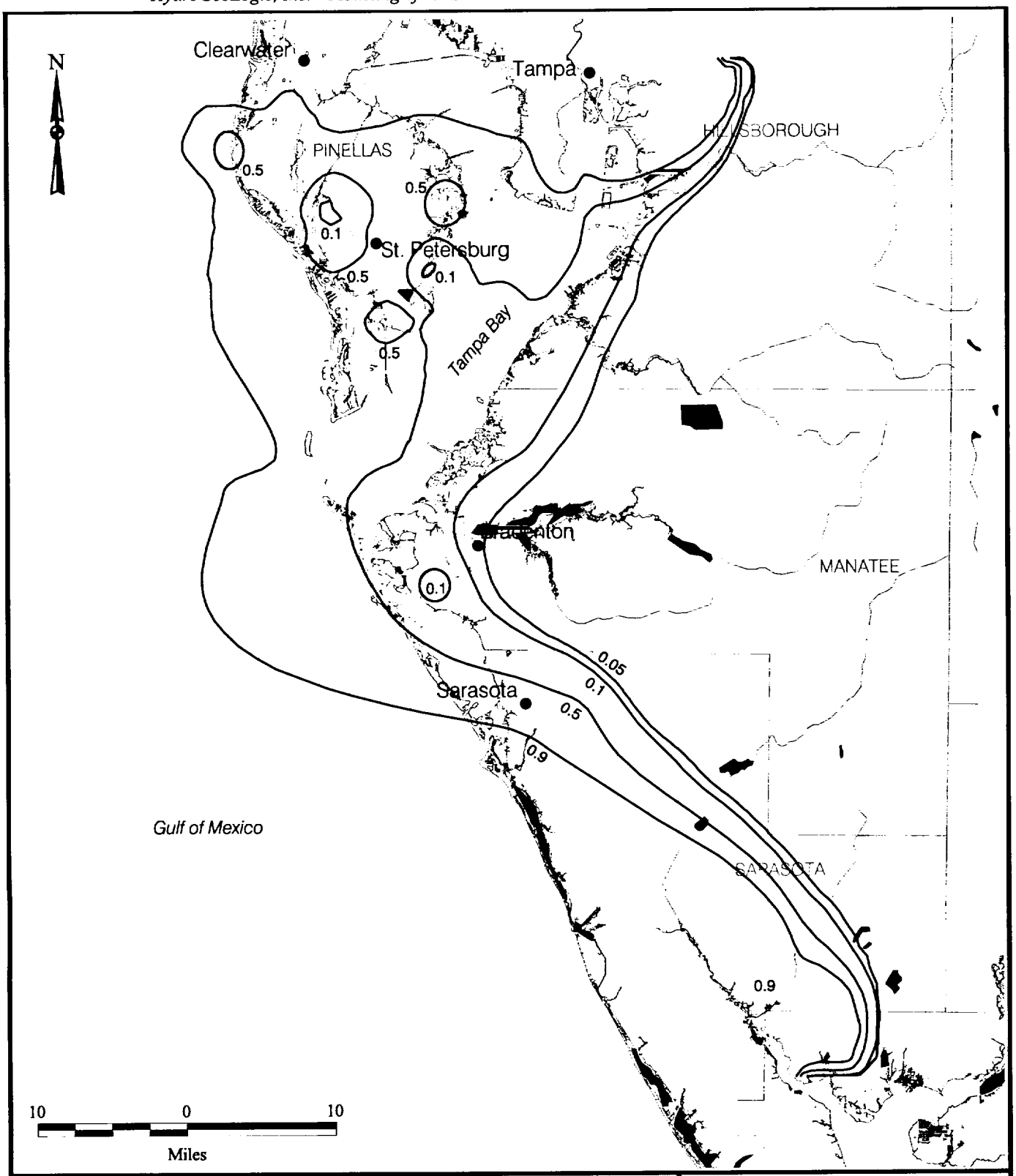

Filename: X:\SWF024\WO_01\saltwater_intrusion\r-chloride_dist_dec2000_6.apr
Project: SWF024-001-01
Created: 11/28/01 TH
Revised: 04/22/02 TB

HYDRO GeoLogic

Legend

County Boundary

Surface Drainage

0.05 Relative Chloride Concentration Contour
0.05 = 1000 mg/l

0.1 = 1,900 mg/l
0.3 = 5,700 mg/l
0.5 = 9,500 mg/l
0.7 = 13,300 mg/l
0.9 = 17,100 mg/l

Figure 5.16
Relative Chloride Concentrations Predicted Using the Calibrated Model for the Avon Park Formation (Model Layer 6)

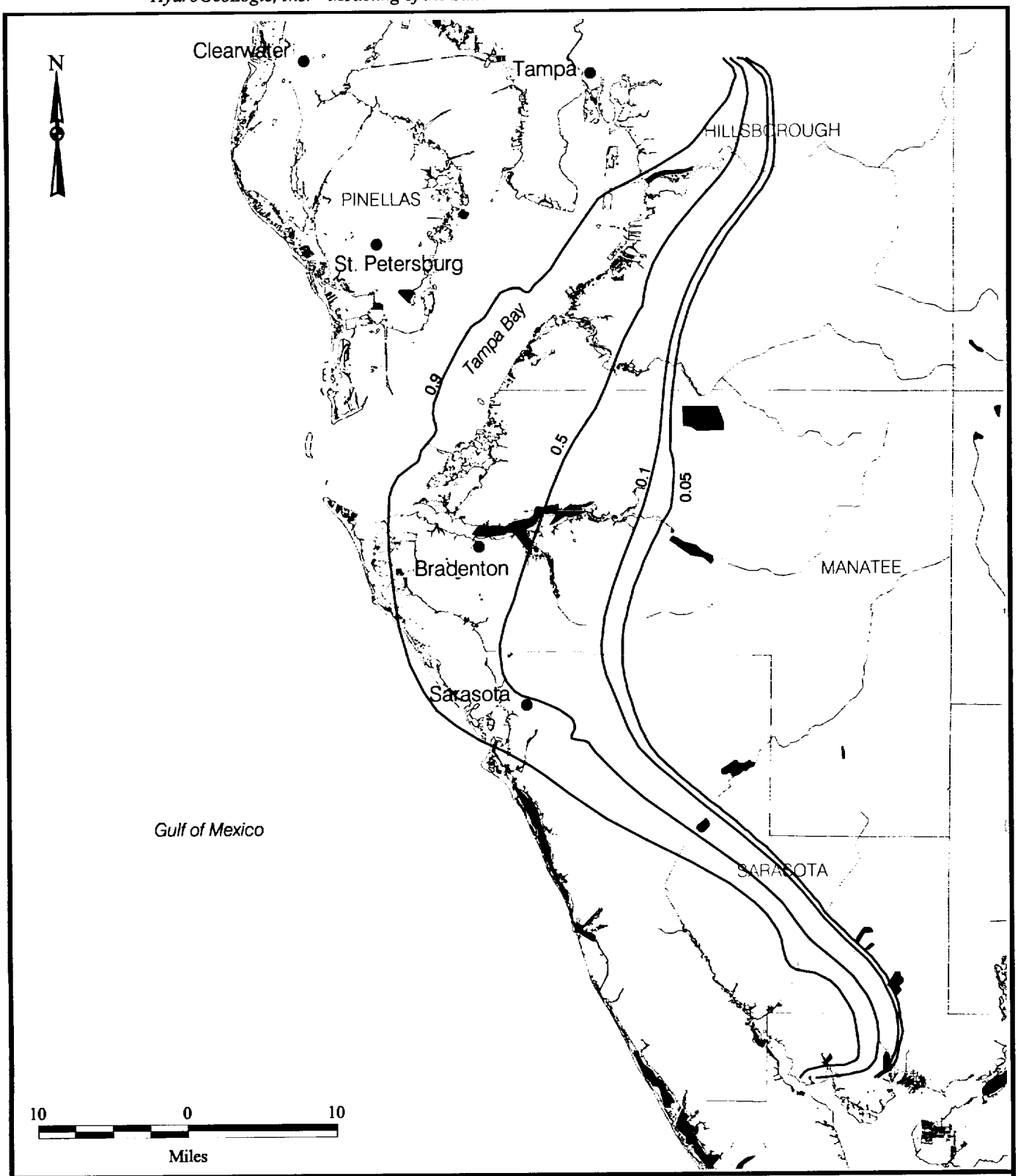

Filename: X:\SWF024\WO_01\saltwater_intrusion\r-chloride_dist_dec2000_8.apr
Project: SWF024-001-01
Created: 11/28/01 TH
Revised: 04/22/02 TB

HYDRO GeoLogic

Legend

County Boundary

Surface Drainage

0.05 Relative Chloride Concentration Contour
0.05 = 1000 mg/l

0.1 = 1,900 mg/l
0.3 = 5,700 mg/l
0.5 = 9,500 mg/l
0.7 = 13,300 mg/l
0.9 = 17,100 mg/l

Figure 5.17
Relative Chloride Concentrations Predicted Using the Calibrated Model for the Avon Park Formation (Model Layer 8)

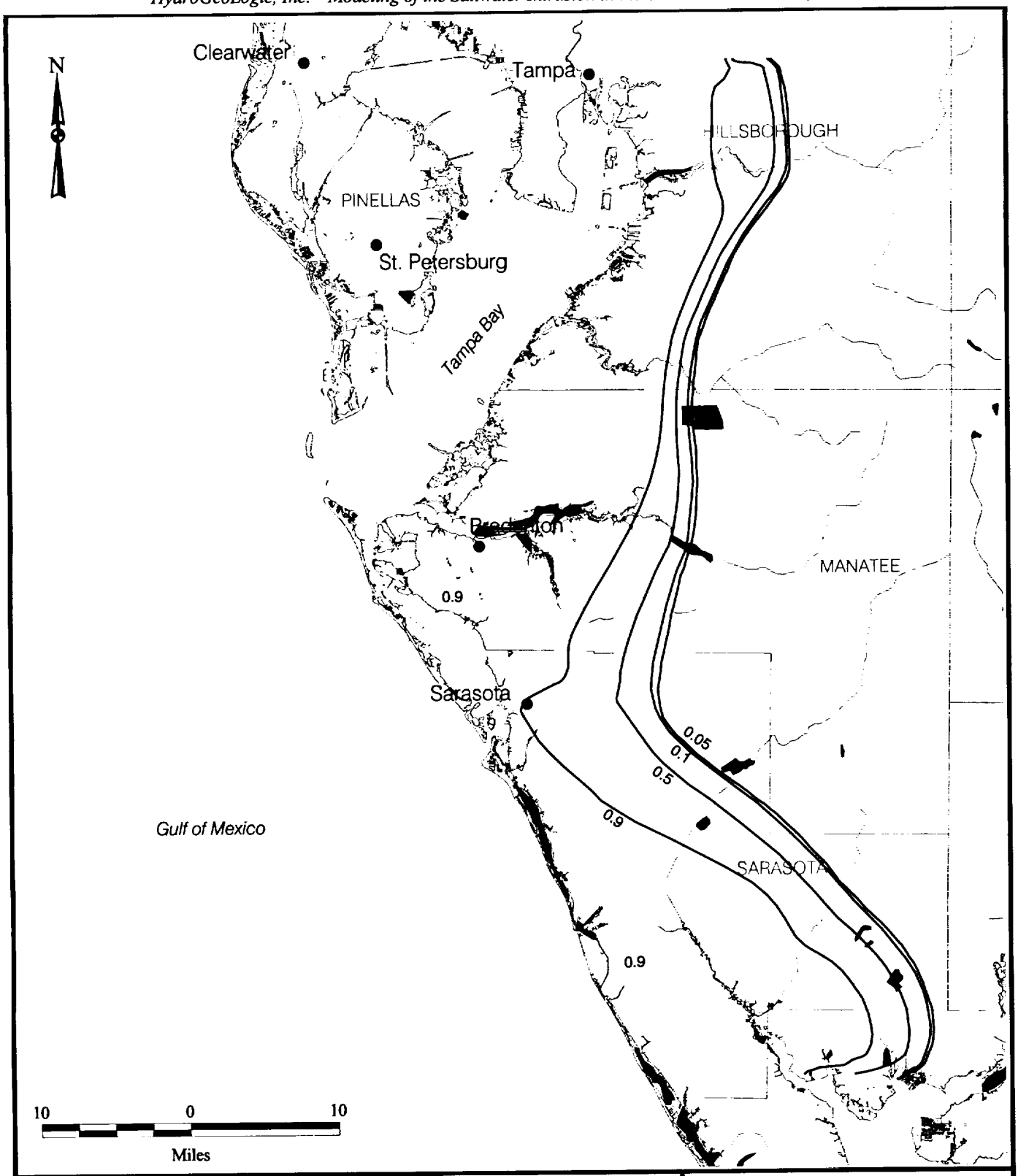

Filename: X:\SWF024\WO_01\saltwater_intrusion\r-chloride_dist_dec2000_10.apr
Project: SWF024-001-01
Created: 11/28/01 TH
Revised: 04/22/02 TB

Legend

County Boundary

Surface Drainage

0.05 Relative Chloride Concentration Contour
0.05 = 1000 mg/l

0.1 = 1,900 mg/l
0.3 = 5,700 mg/l
0.5 = 9,500 mg/l
0.7 = 13,300 mg/l
0.9 = 17,100 mg/l

Figure 5.18
Relative Chloride Concentrations Predicted Using the Calibrated Model for the Avon Park Formation (Model Layer 10)

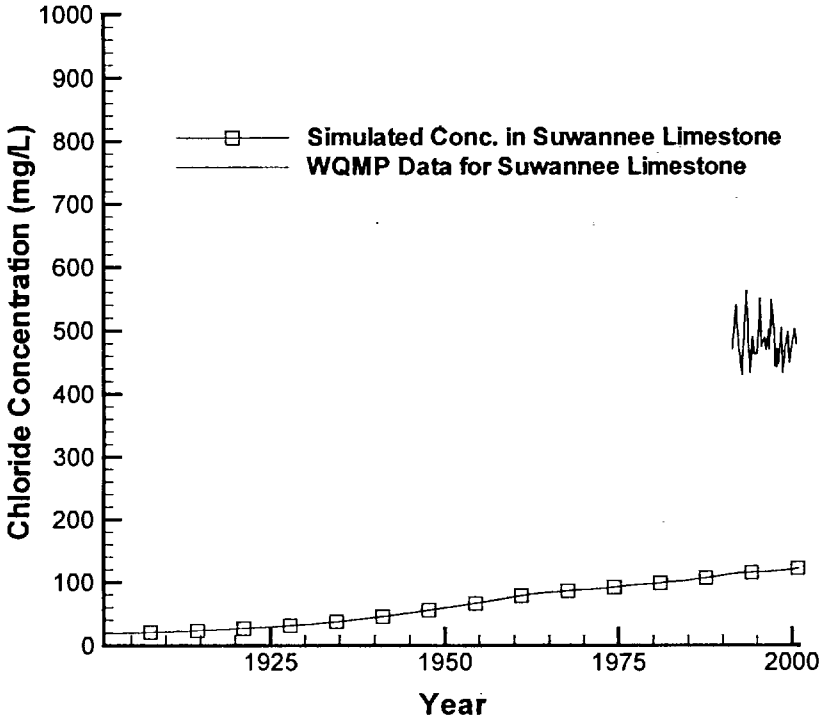

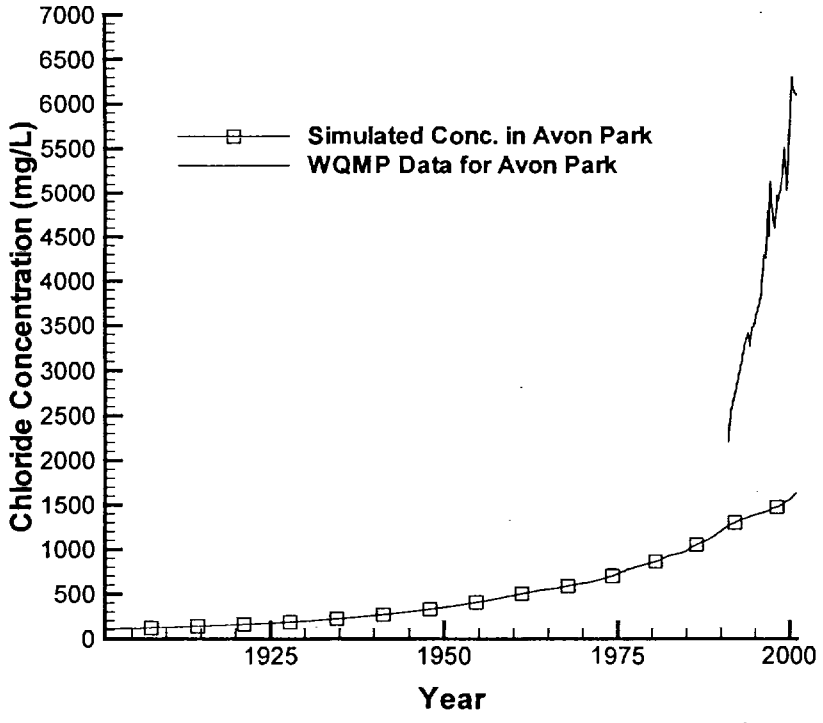

Figure 5.19 Model Predicted Verses Observed Chloride Concentrations with Time

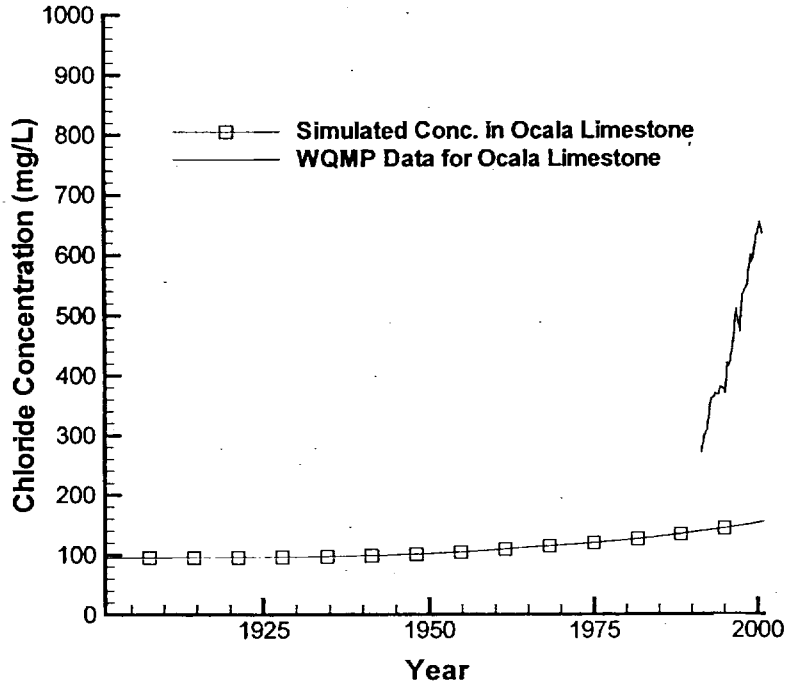

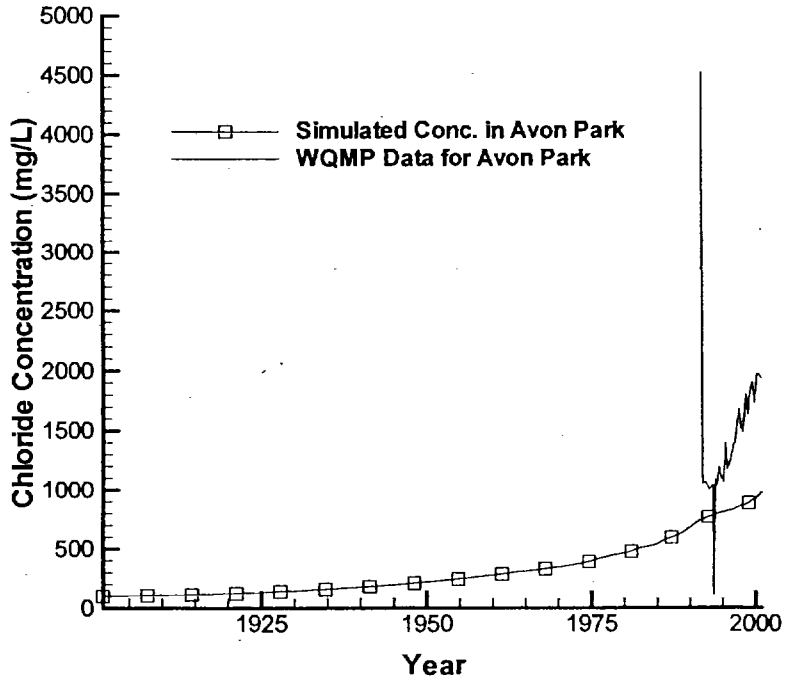

Figure 5.20 Model Predicted Verses Observed Chloride Concentrations with Time

ROMP TR 8-1

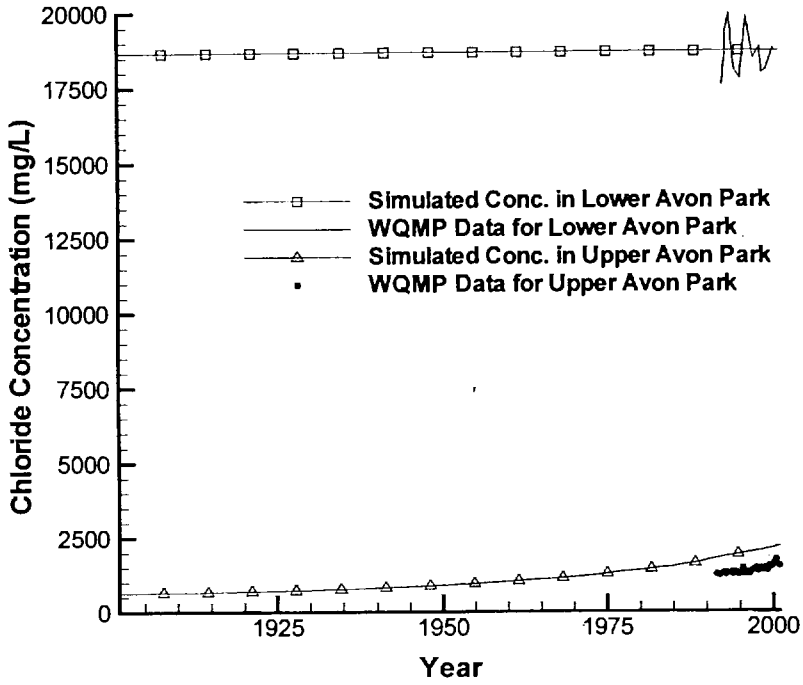

ROMP 50

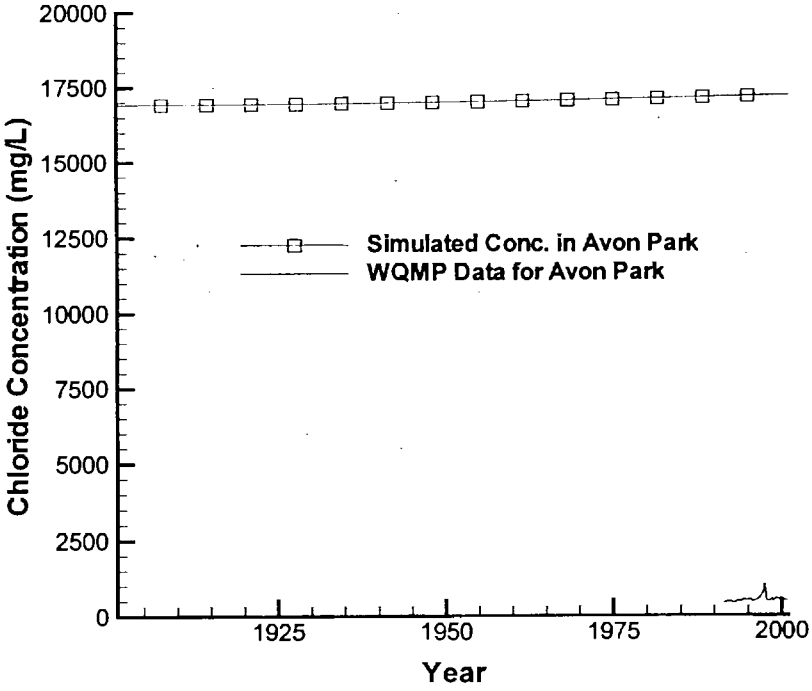

Figure 5.21 Model Predicted Verses Observed Chloride Concentrations with Time

ROMP 22

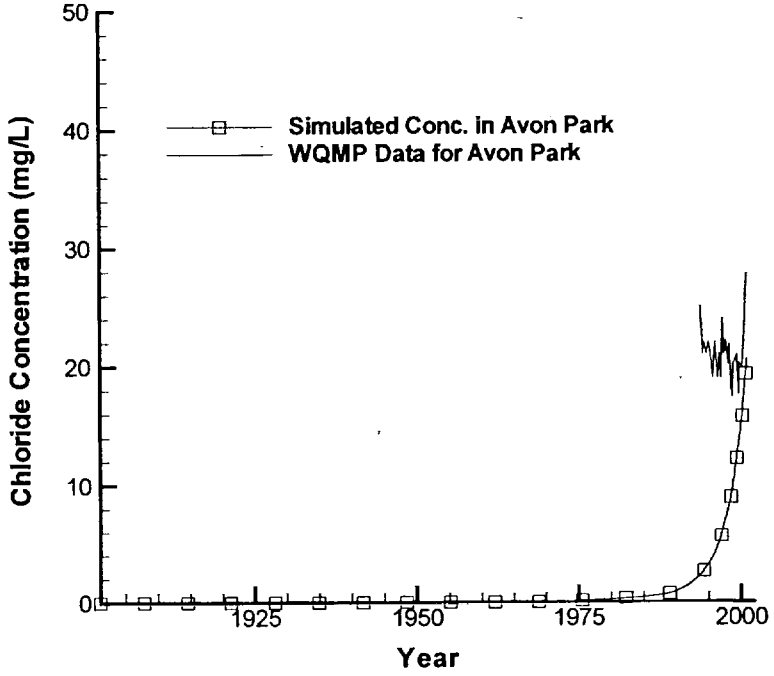

ROMP 20

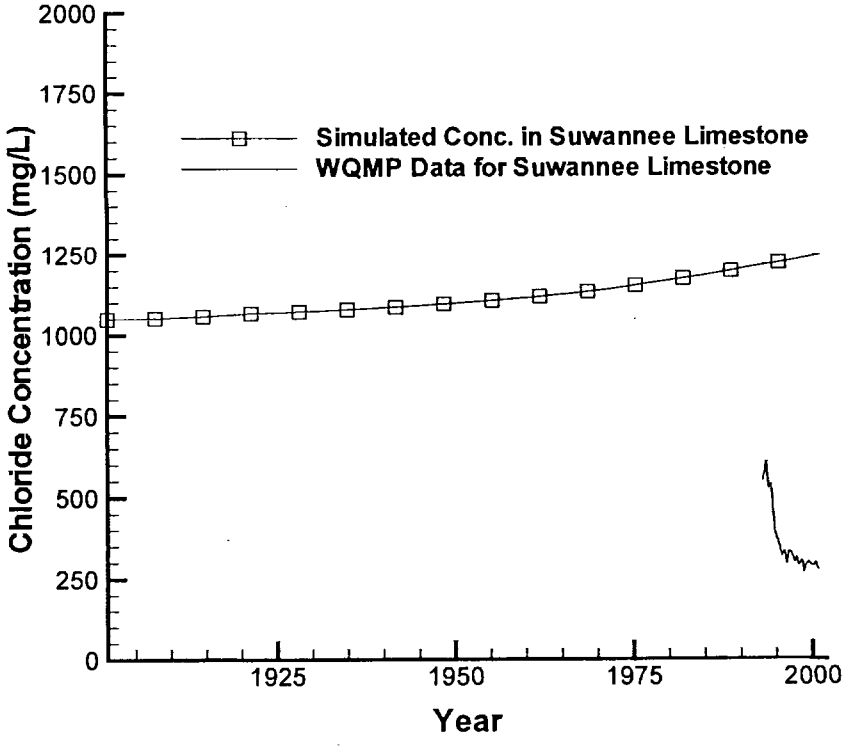

Figure 5.22 Model Predicted Verses Observed Chloride Concentrations with Time

ROMP 33

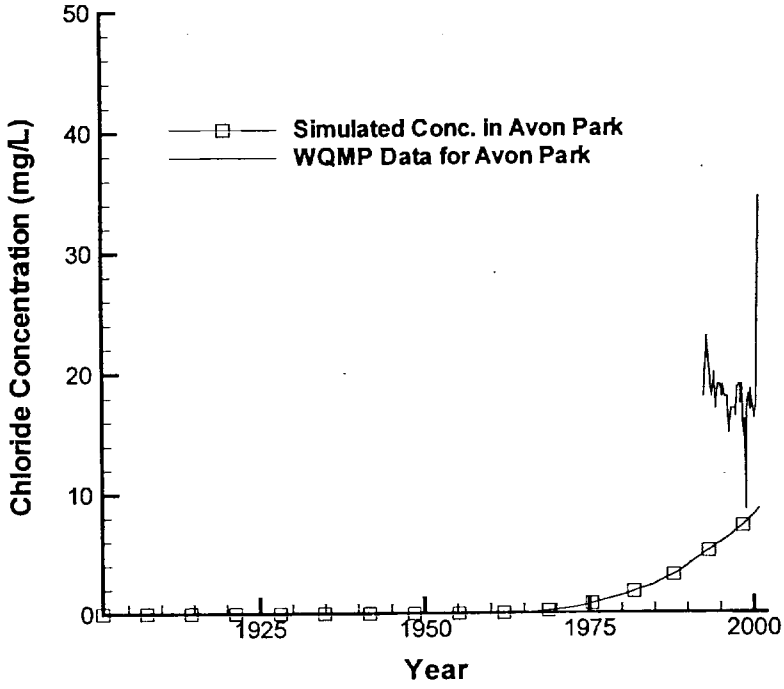

ROMP 39

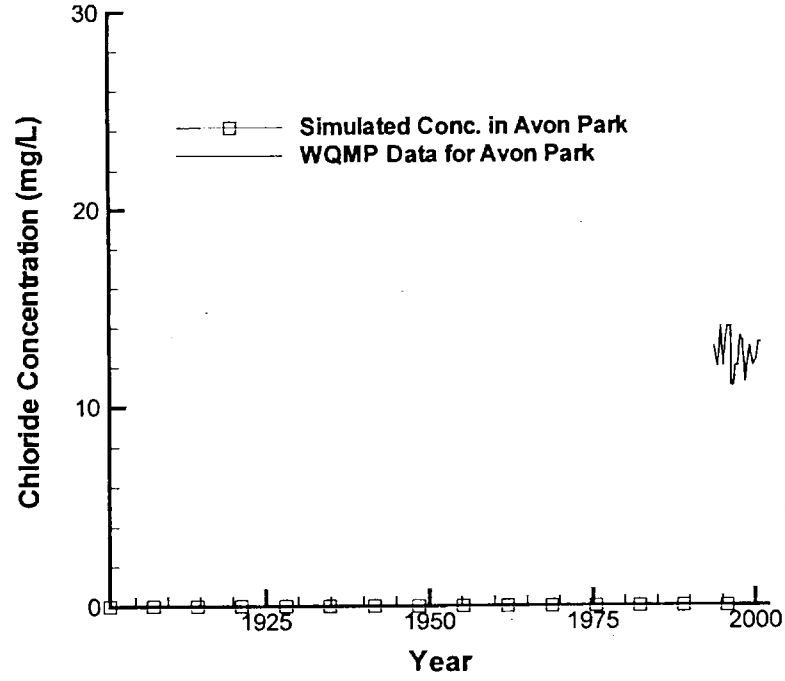

Figure 5.23 Model Predicted Verses Observed Chloride Concentrations with Time

ROMP TR SA-1

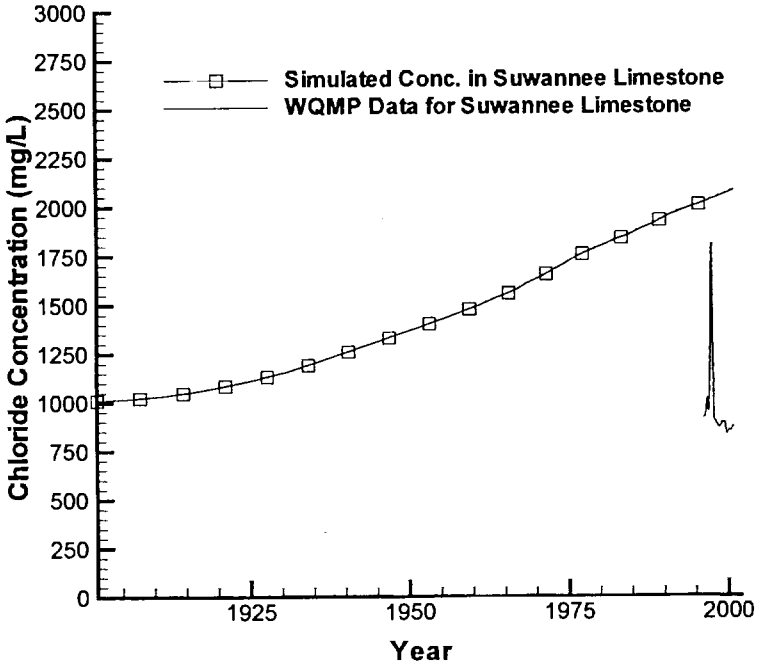

ROMP TR SA-3

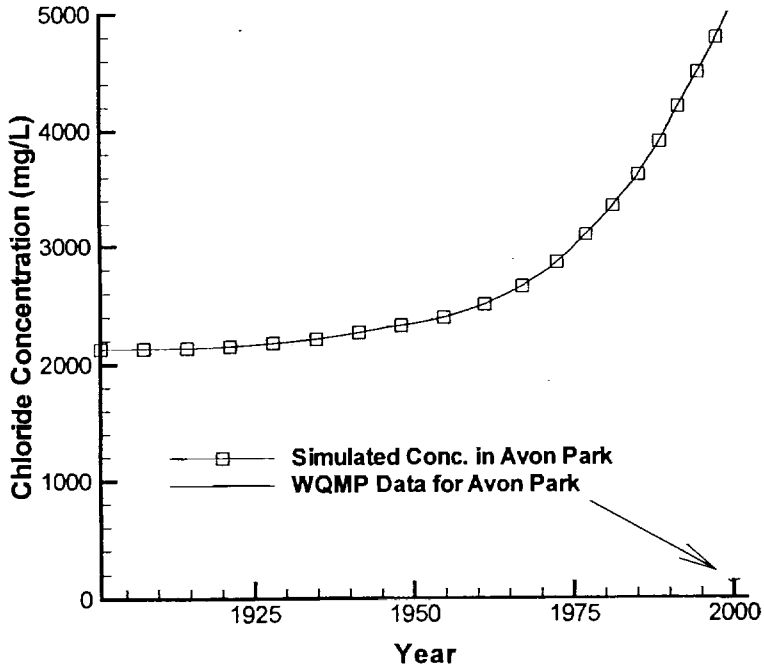

Figure 5.24 Model Predicted Verses Observed Chloride Concentrations with Time

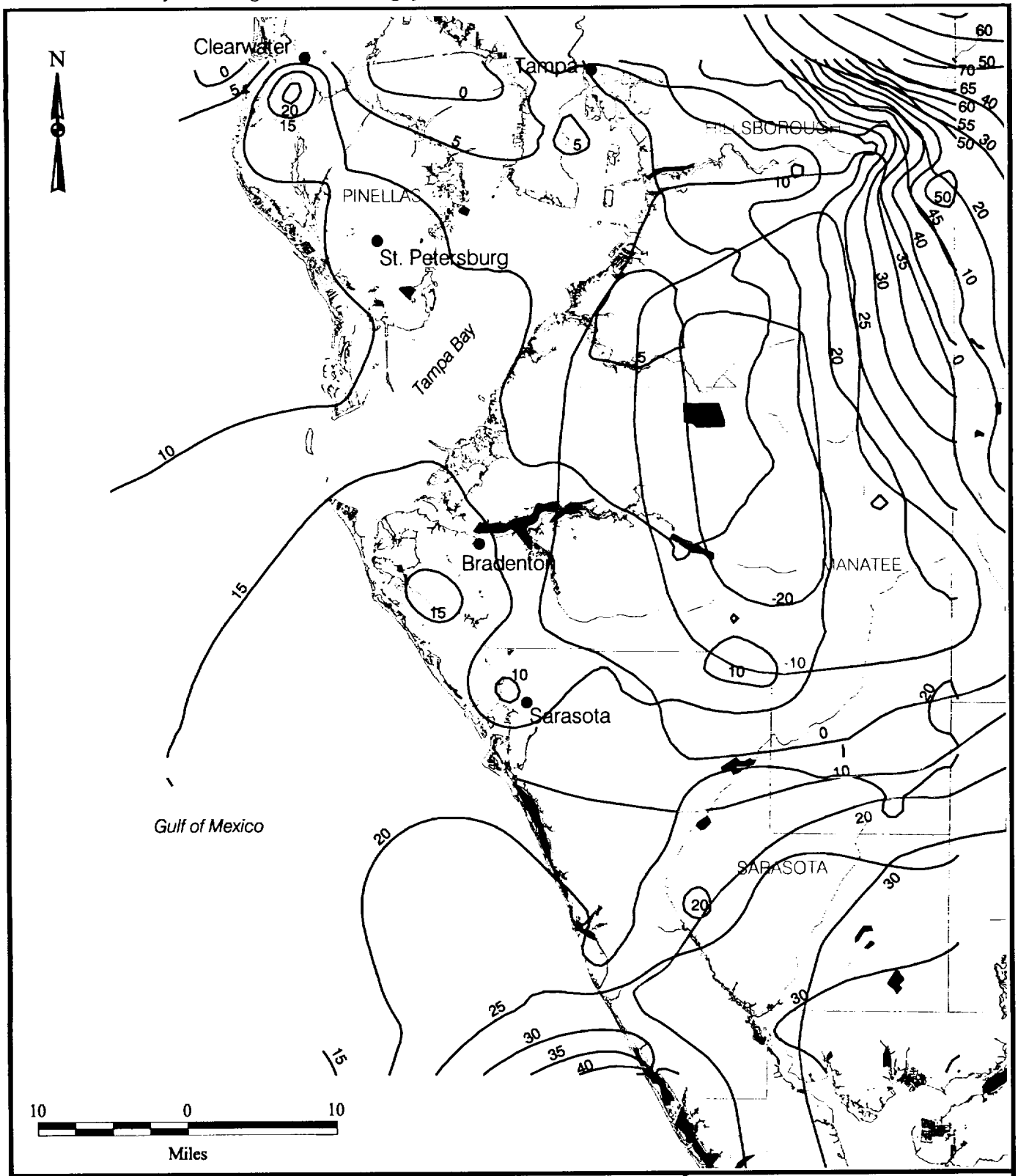

Filename: X:\SWF024\WO_01\saltwater_intrusion\head_dist_may2000_2.apr
Project: SWF024-001-01
Created: 11/28/01 TH
Revised: 06/07/02 TB

HYDRO GeoLogic

Legend

- County Boundary
- Surface Drainage
- 60 — Calibrated Model Potentiometric Surface Elevation Contour (ft, msl) (Model Layer 2)
- 60 — U.S.G.S. Potentiometric Surface Elevation (ft, msl)

Figure 5.25
Comparison of Observed and Predicted Potentiometric Surface - May 2000 (Suwannee Limestone, Model Layer 2)

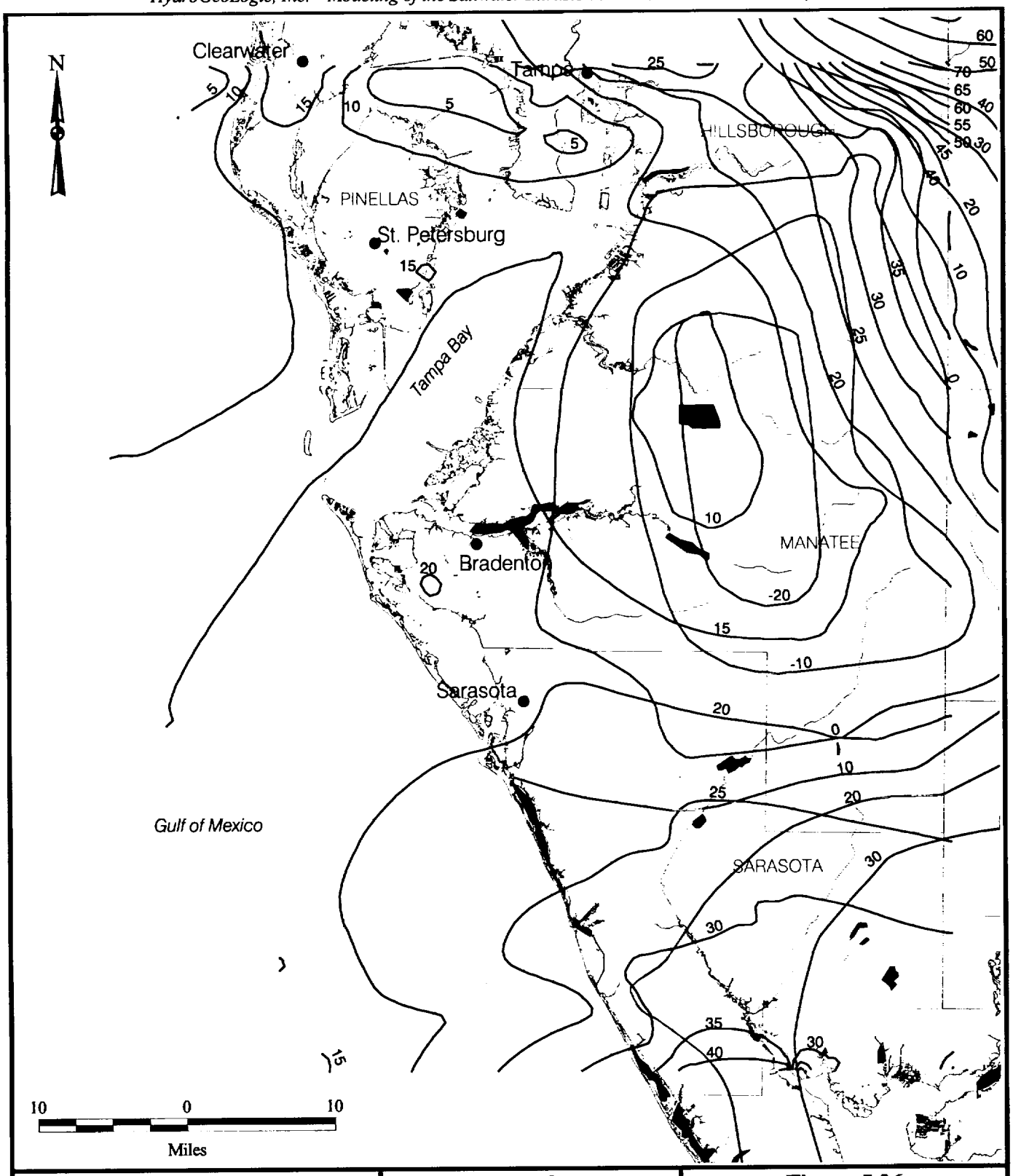

Filename: X:\SWF024\WO_01\saltwater_intrusion\head_dist_may2000_7.apr
Project: SWF024-001-01
Created: 11/28/01 TH
Revised: 06/07/02 TB

HYDRO GeoLogic Inc

Legend

- County Boundary
- Surface Drainage
- 60 — Calibrated Model Potentiometric Surface Elevation Contour (ft, msl) (Model Layer 7)
- 60 — U.S.G.S. Potentiometric Surface Elevation (ft, msl)

Figure 5.26
Comparison of Observed and Predicted Potentiometric Surface - May 2000 (Avon Park Formation, Model Layer 7)

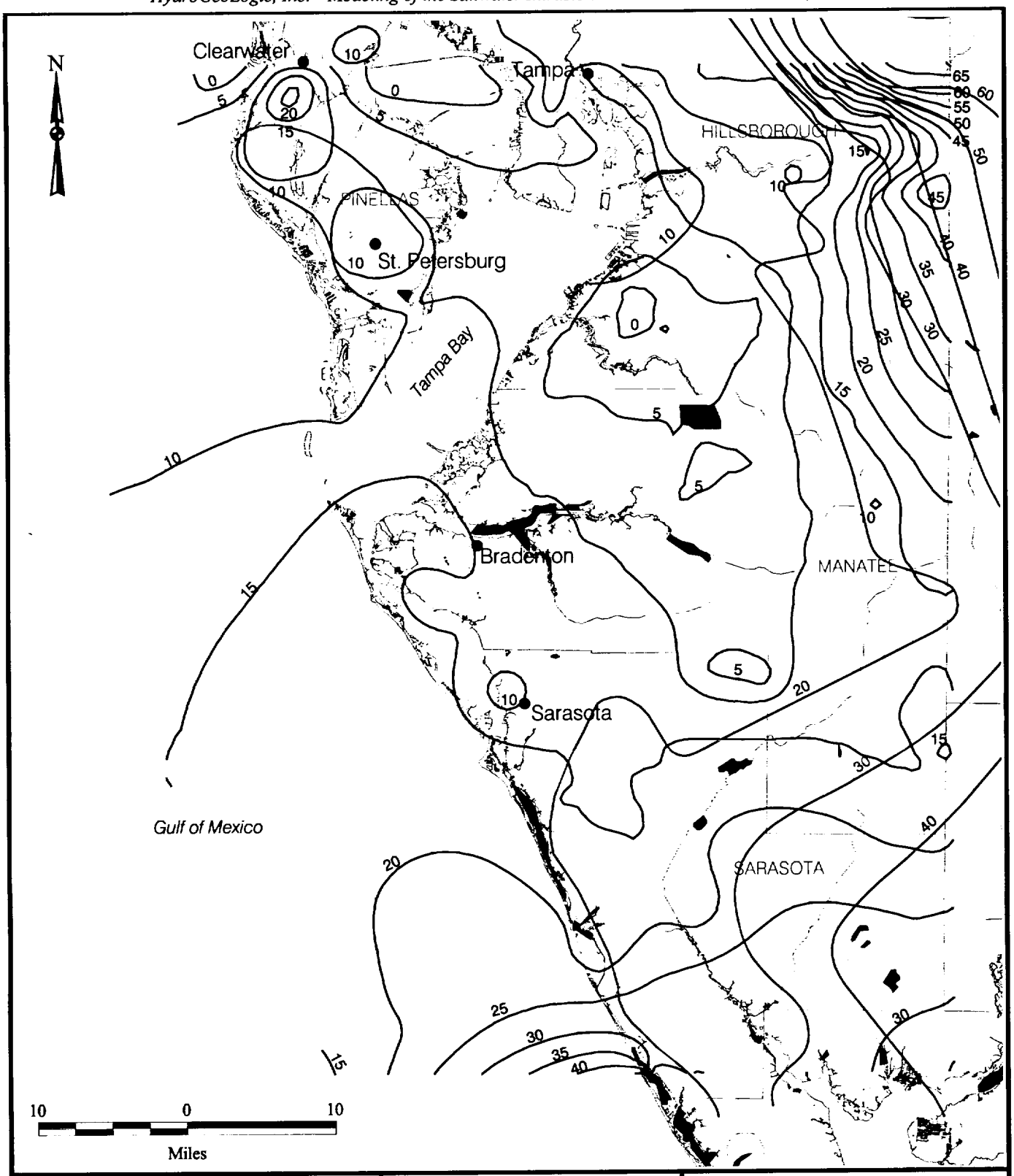

Filename: X:\SWF024\WO_01\saltwater_intrusion\head_dist_sept2000_2.apr
Project: SWF024-001-01
Created: 11/28/01 TH
Revised: 06/07/02 TB

HYDRO GeoLogic INC.

Legend

- County Boundary
- Surface Drainage
- 60 — Calibrated Model Potentiometric Surface Elevation Contour (ft, msl) (Model Layer 2)
- 60 — U.S.G.S. Potentiometric Surface Elevation (ft, msl)

Figure 5.27
Comparison of Observed and Predicted Potentiometric Surface - September 2000 (Suwannee Limestone, Model Layer 2)

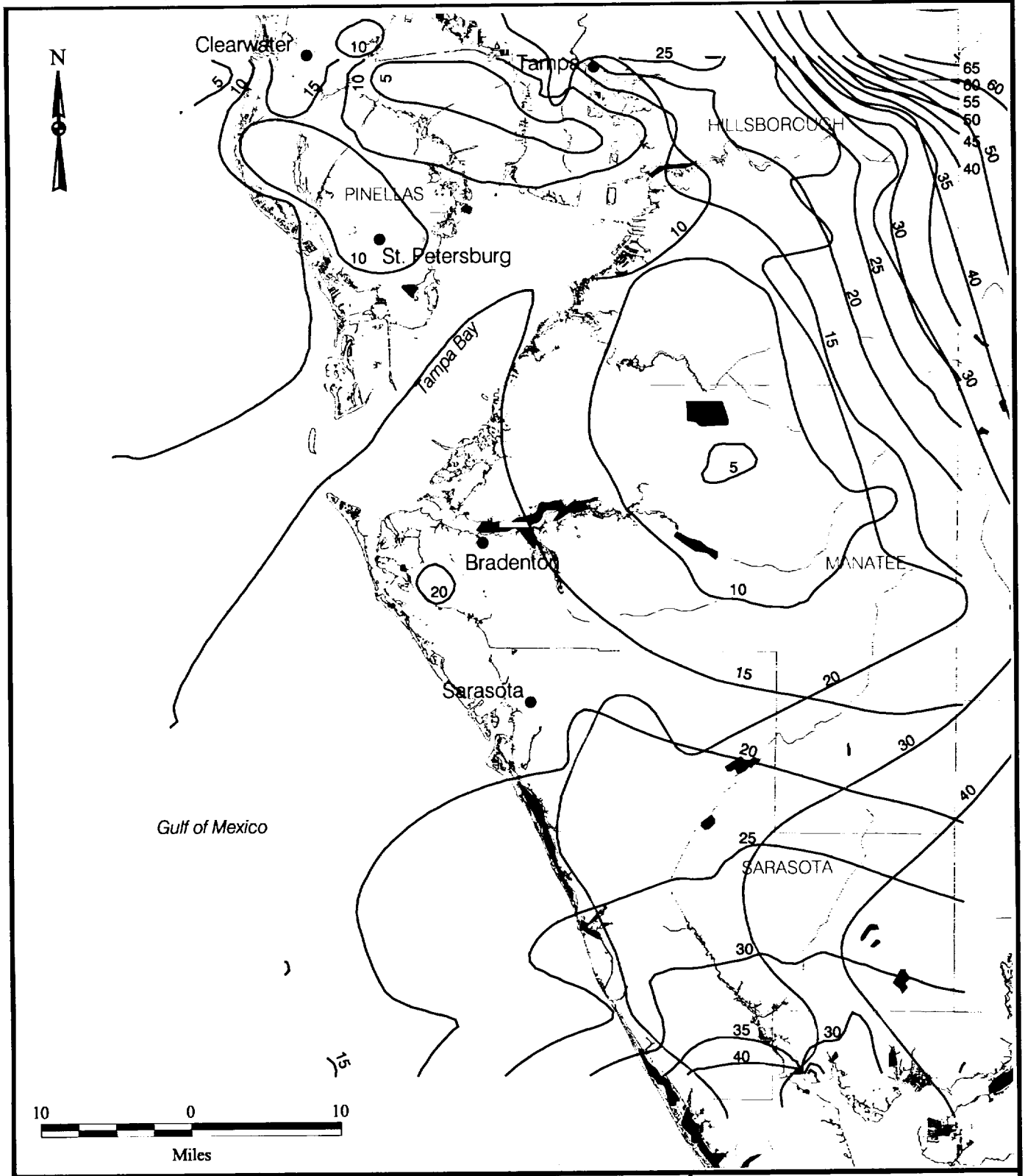

Filename: X:\SWF024\WO_01\saltwater_intrusion\head_dist_sept2000_7.apr
Project: SWF024-001-01
Created: 11/28/01 TH
Revised: 06/07/02 TB

HYDRO GeoLogic Inc.

Legend

- County Boundary
- Surface Drainage
- 60 — Calibrated Model Potentiometric Surface Elevation Contour (ft, msl) (Model Layer 7)
- 60 — U.S.G.S. Potentiometric Surface Elevation (ft, mls)

Figure 5.28
Comparison of Observed and Predicted Potentiometric Surface - September 2000 (Avon Park Formation, Model Layer 7)

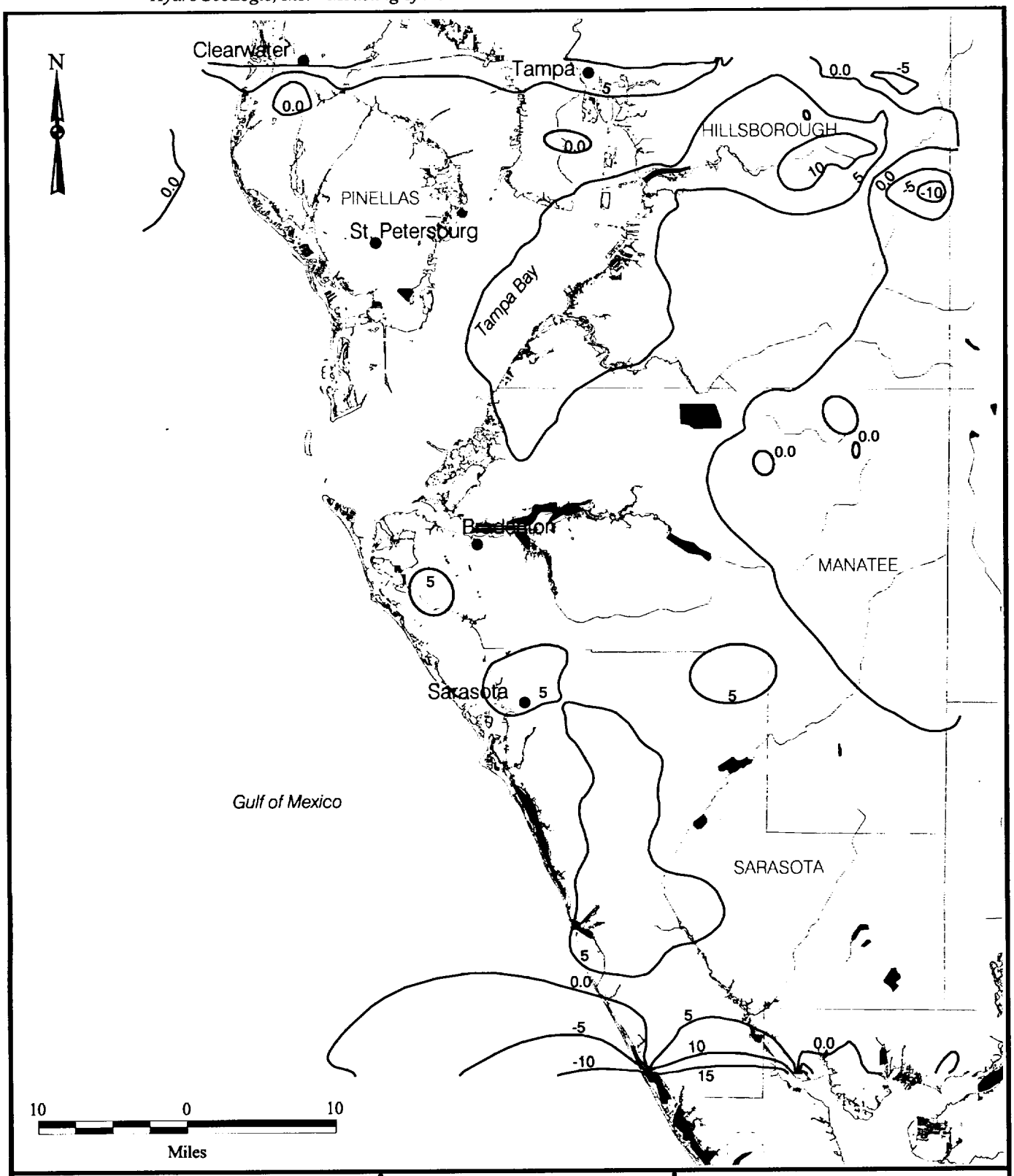

Filename: X:\SWF024\WO_01\saltwater_intrusion\head_diff.apr
Project: SWF024-001-01
Created: 11/28/01 TH
Revised: 06/07/02 TB

HYDRO GeoLogic

Legend

County Boundary

Surface Drainage

05 Head Difference Contour (ft, msl)

Figure 5.29
Simulated Head Difference Between the Suwannee Limestone and the Avon Park Formation for December 2000 Conditions

Figure 5.30. Global Mass/Water Budget for Pre-Development Conditions

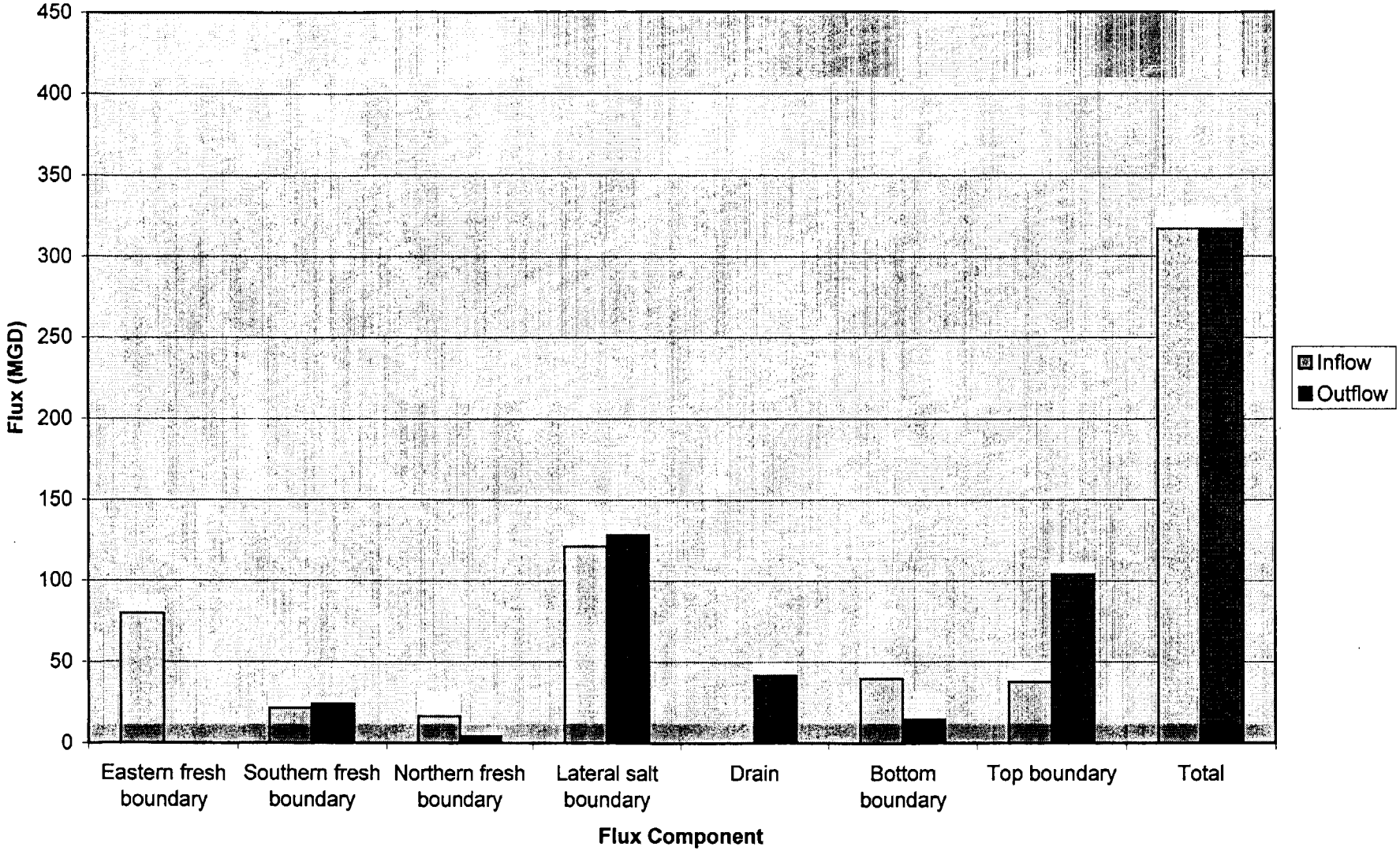

Figure 5.31. Global Mass/Water Budget For Post-Development (December 2000) Conditions

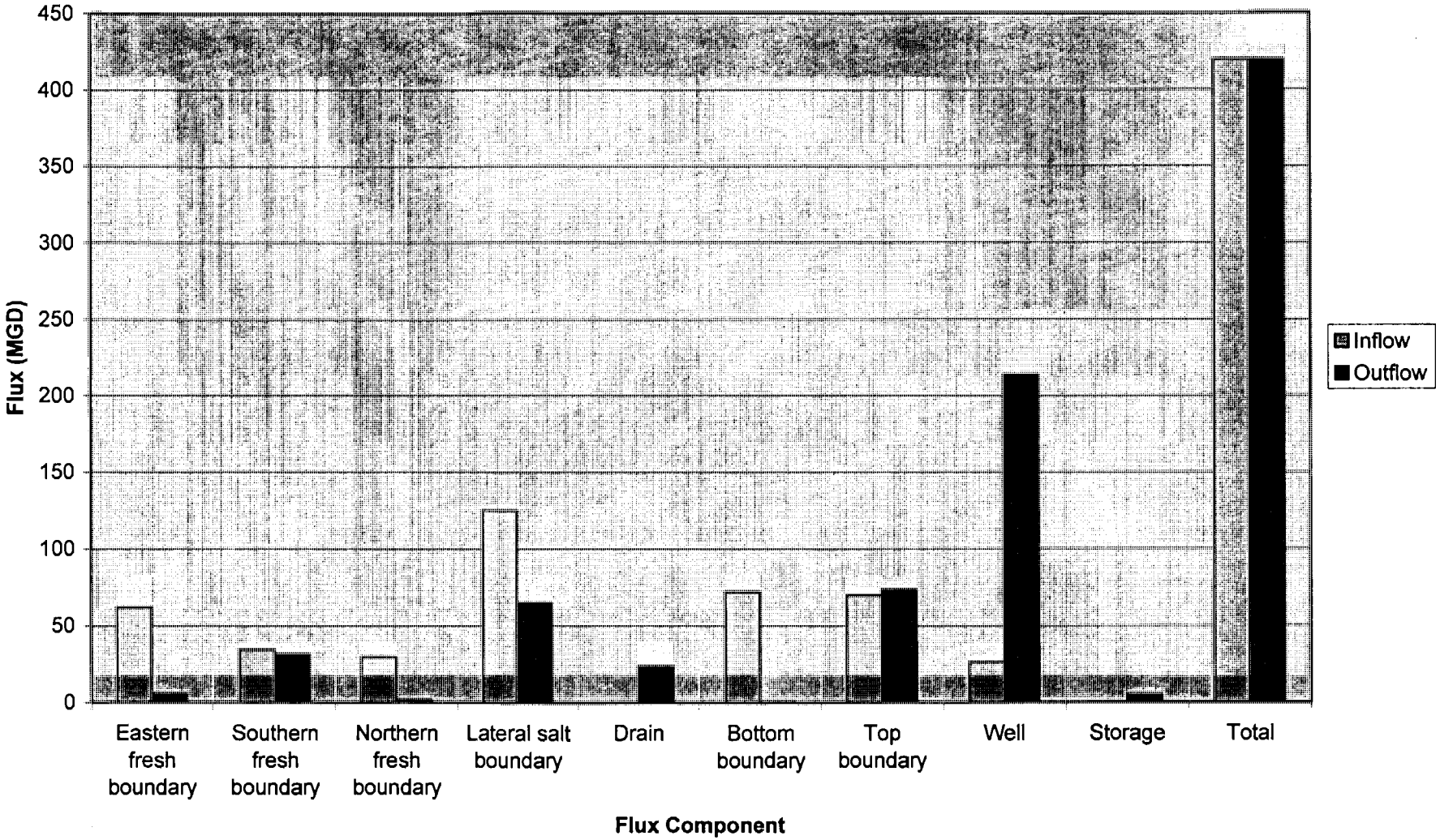

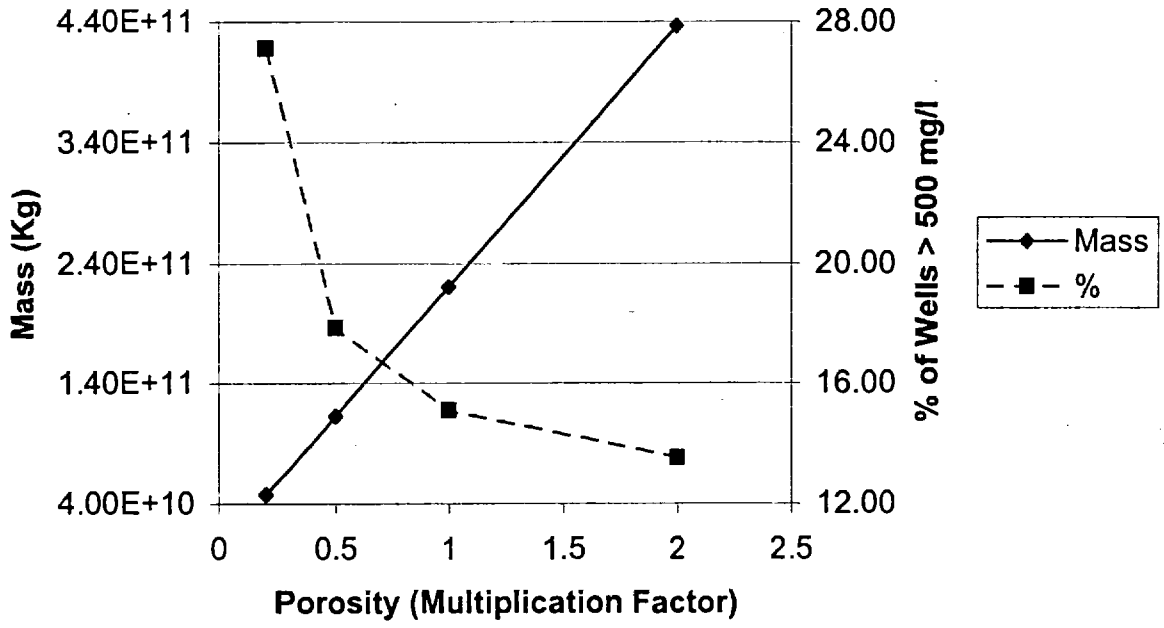

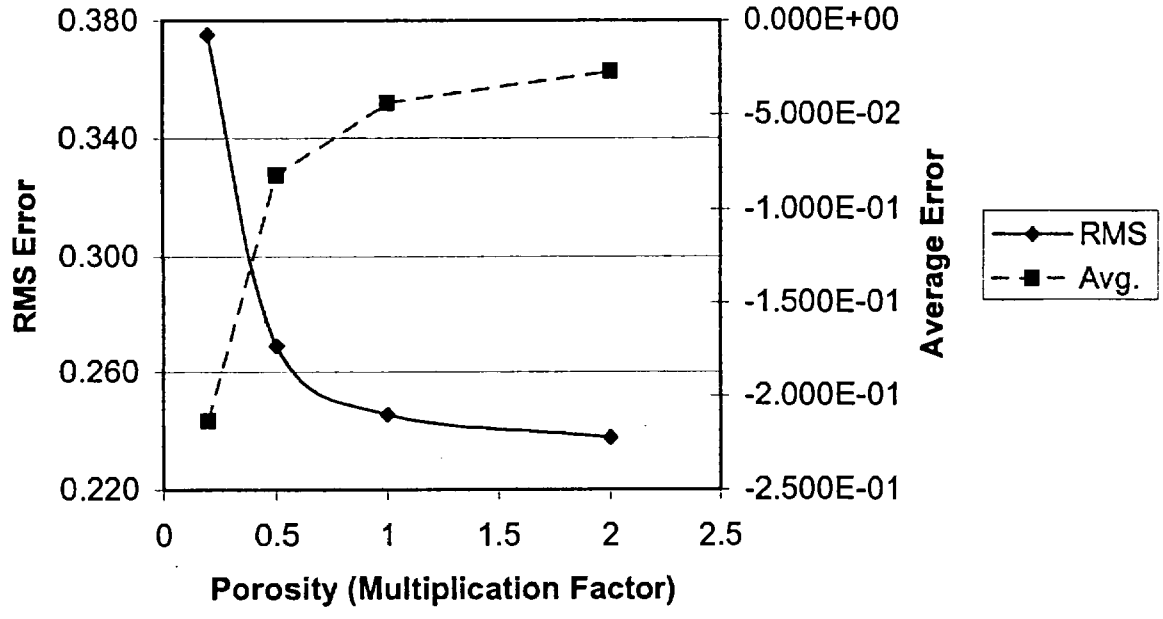

Figure 6.1 a. Sensitivity to Porosity

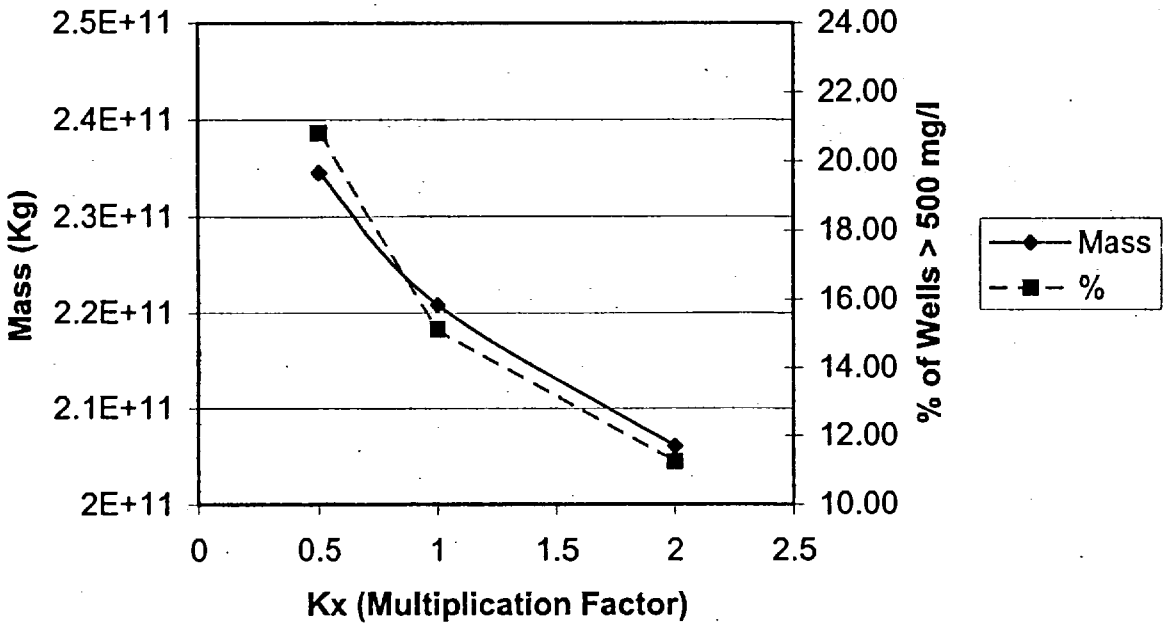

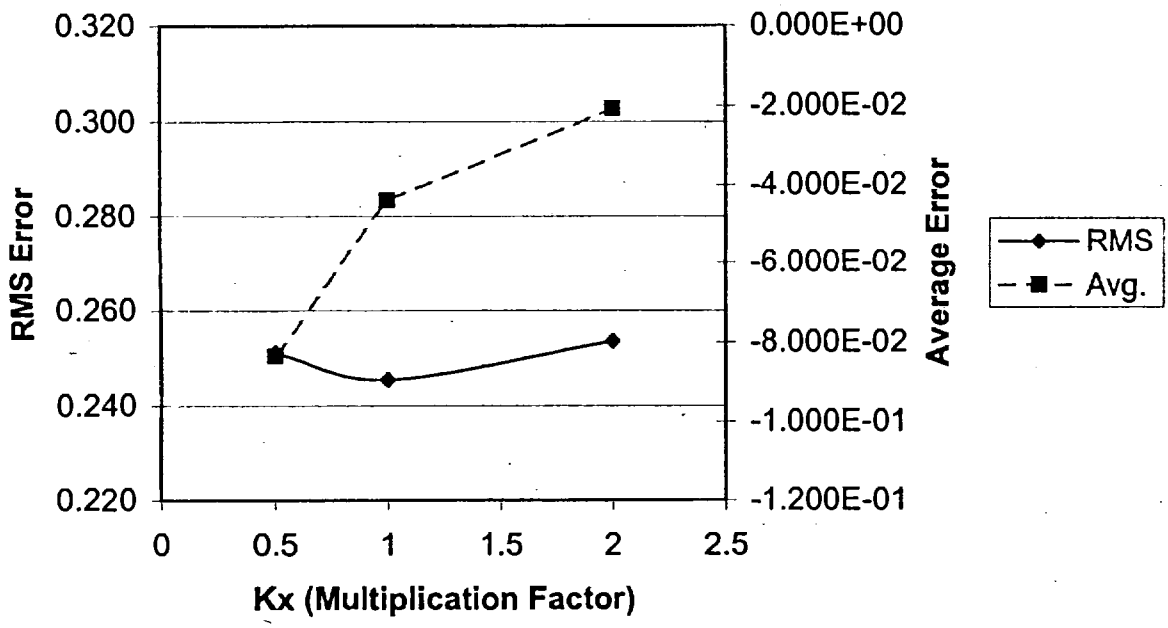

Figure 6.1b. Sensitivity to Avon Park Formation Hydraulic Conductivity Values (Model Layers 6 through 10)

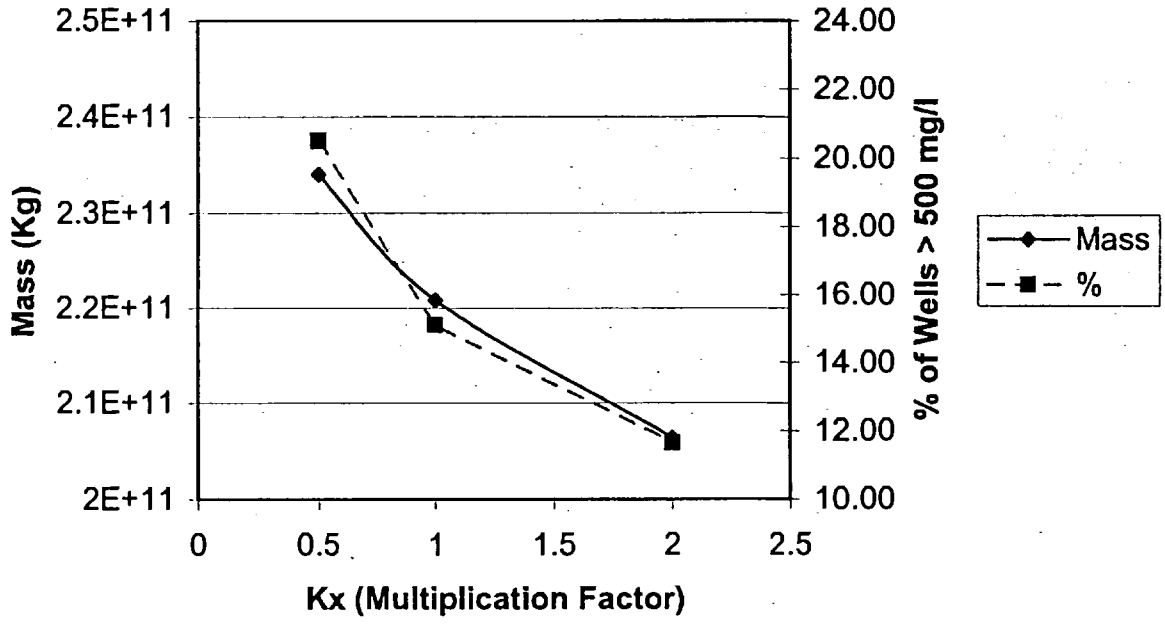

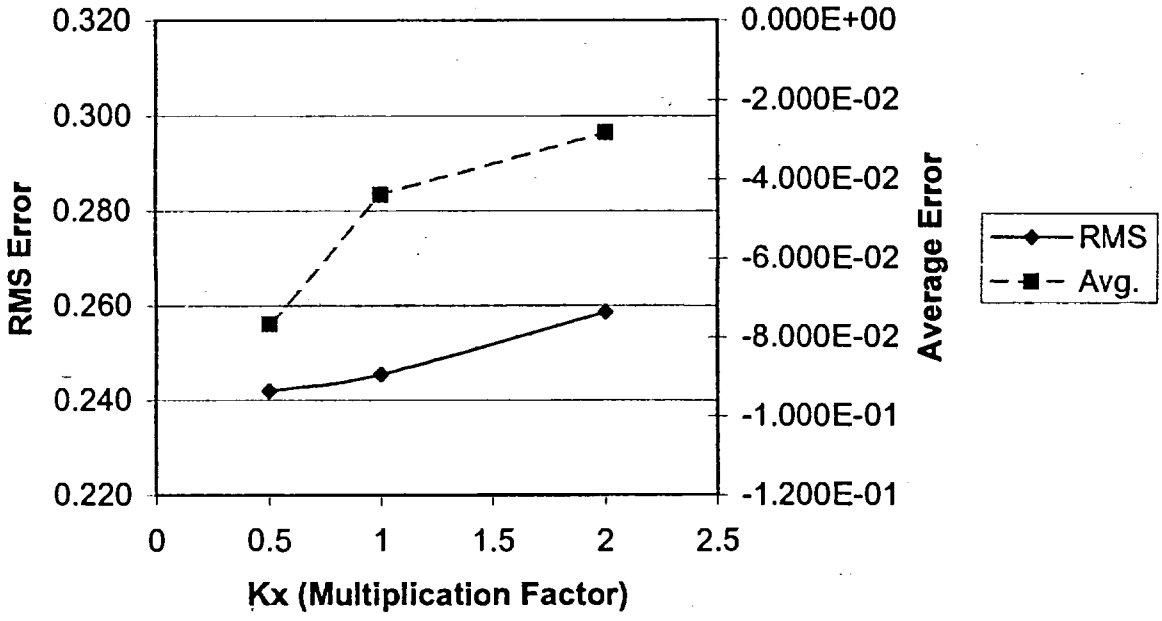

Figure 6.1c. Sensitivity to Conductivity Value of Highly Transmissive Zone in the Avon Park Formation (Model Layers 6 and 7)

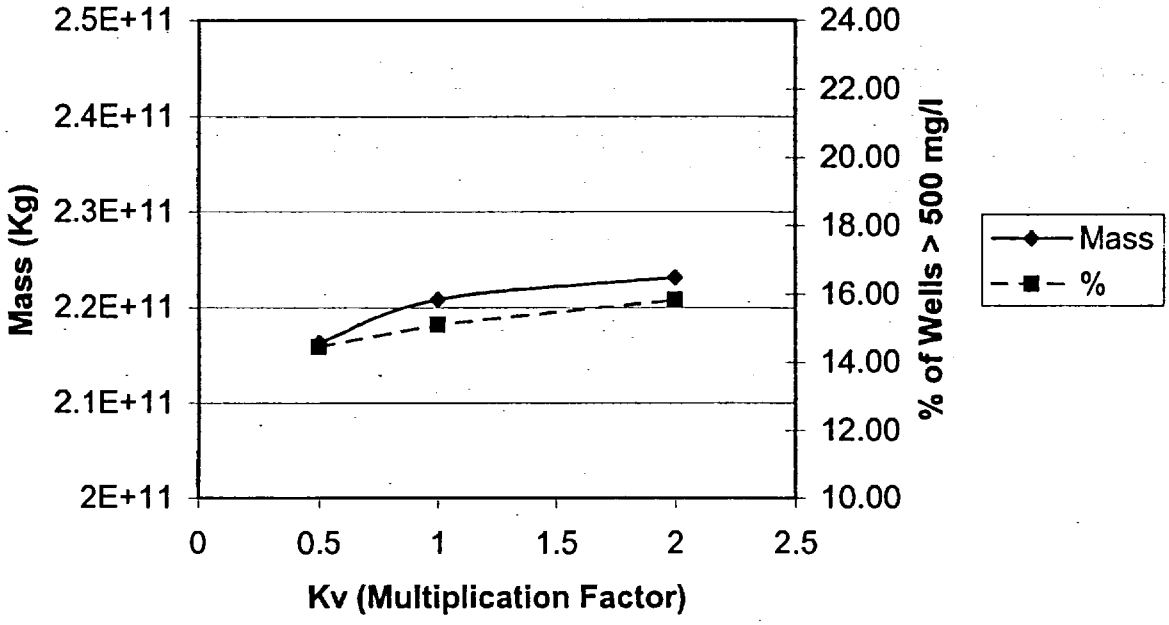

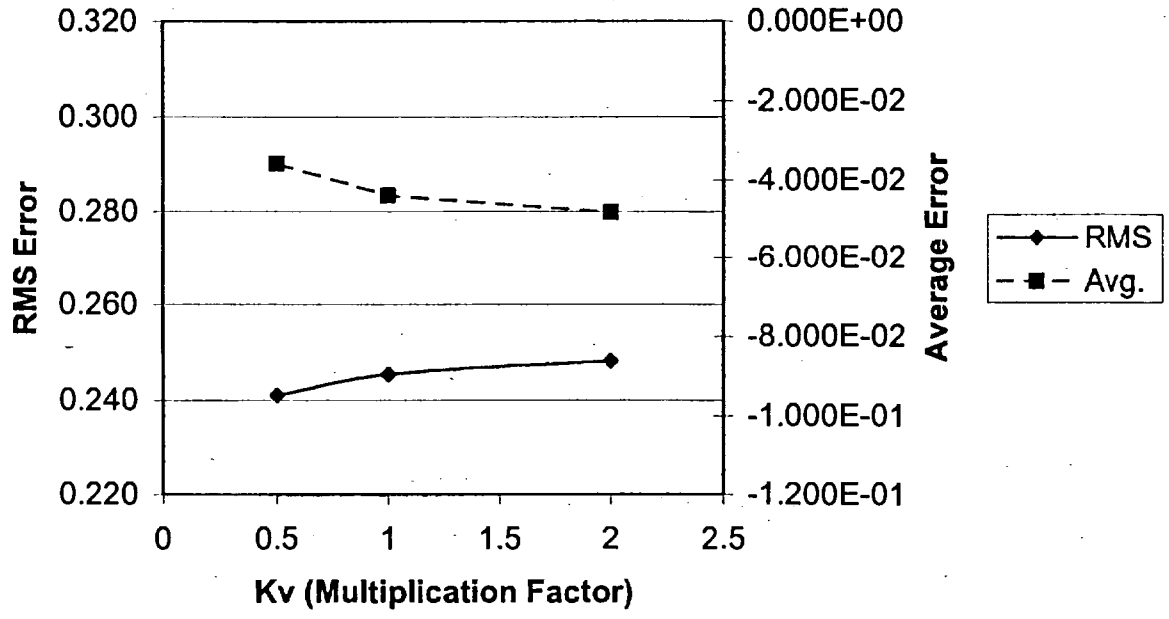

Figure 6.1 d. Sensitivity to Leakance in the Ocala Region (Model Layers 3 and 5)

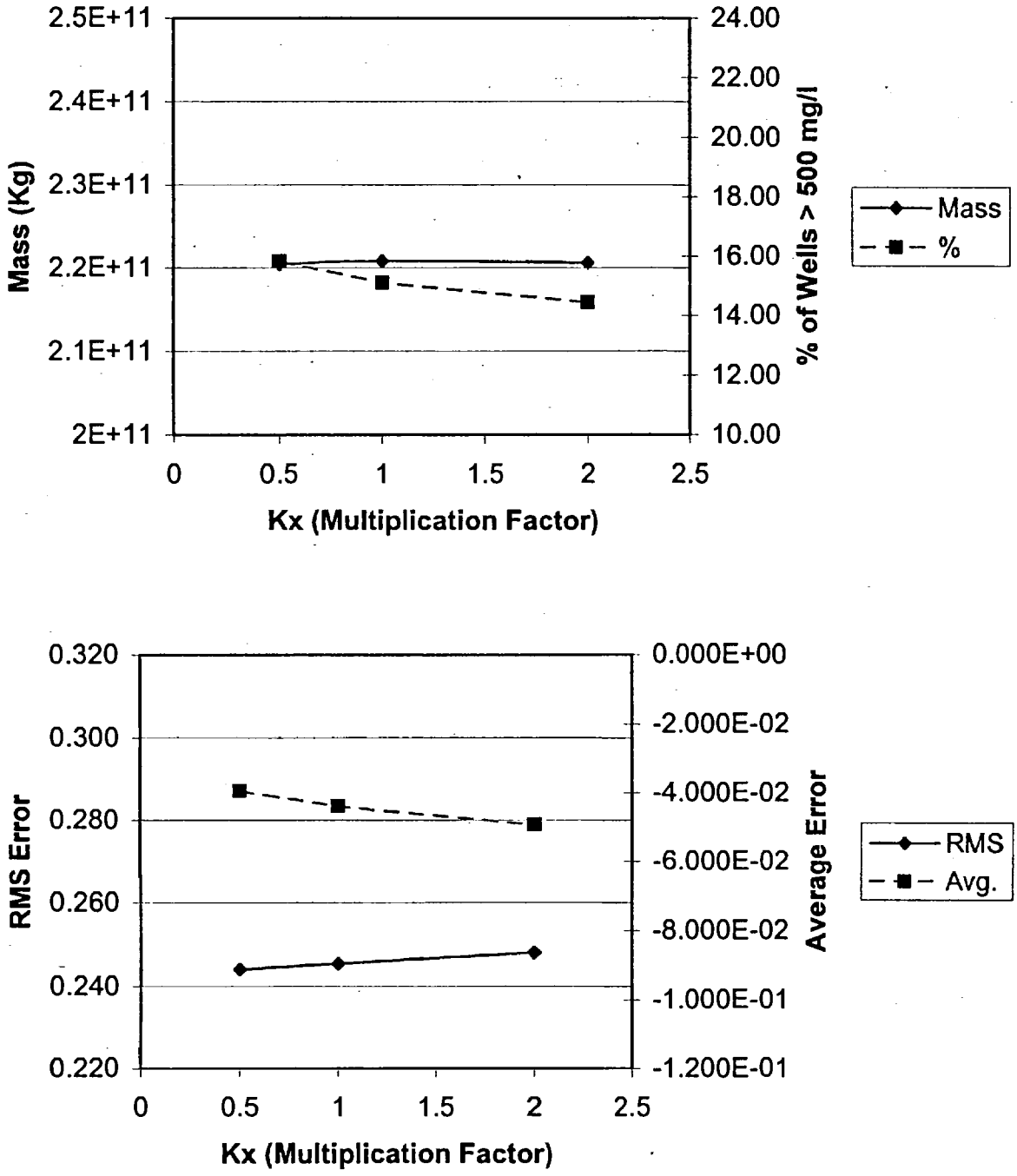

Figure 6.1 e. Sensitivity to Conductivity Value in the Suwannee Region (Model Layers 1 and 2)

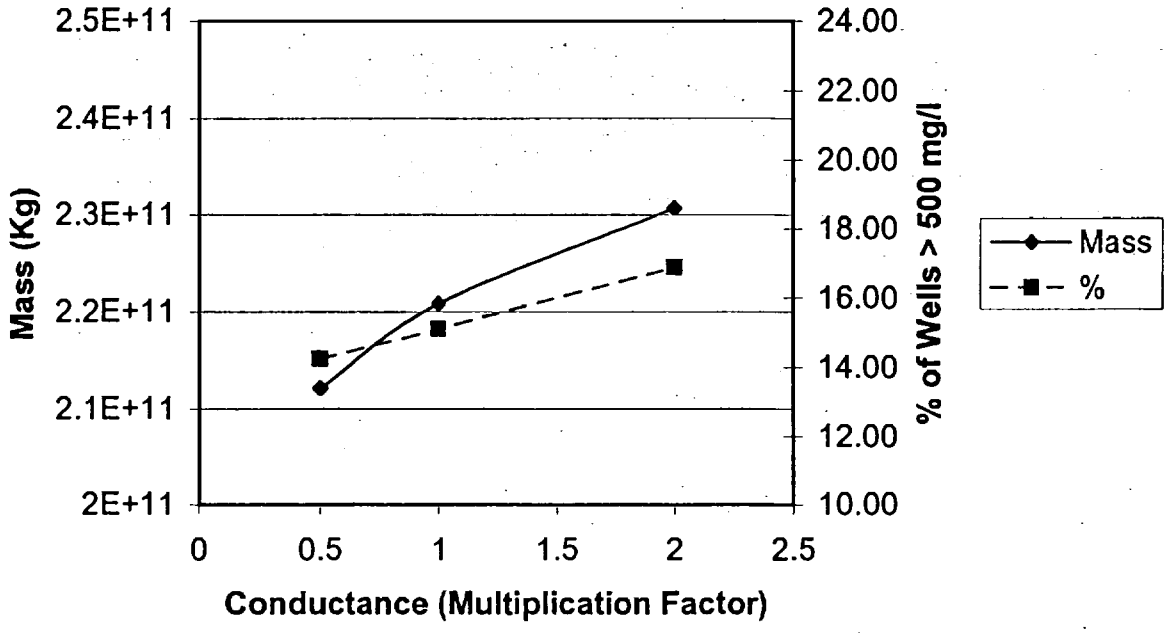

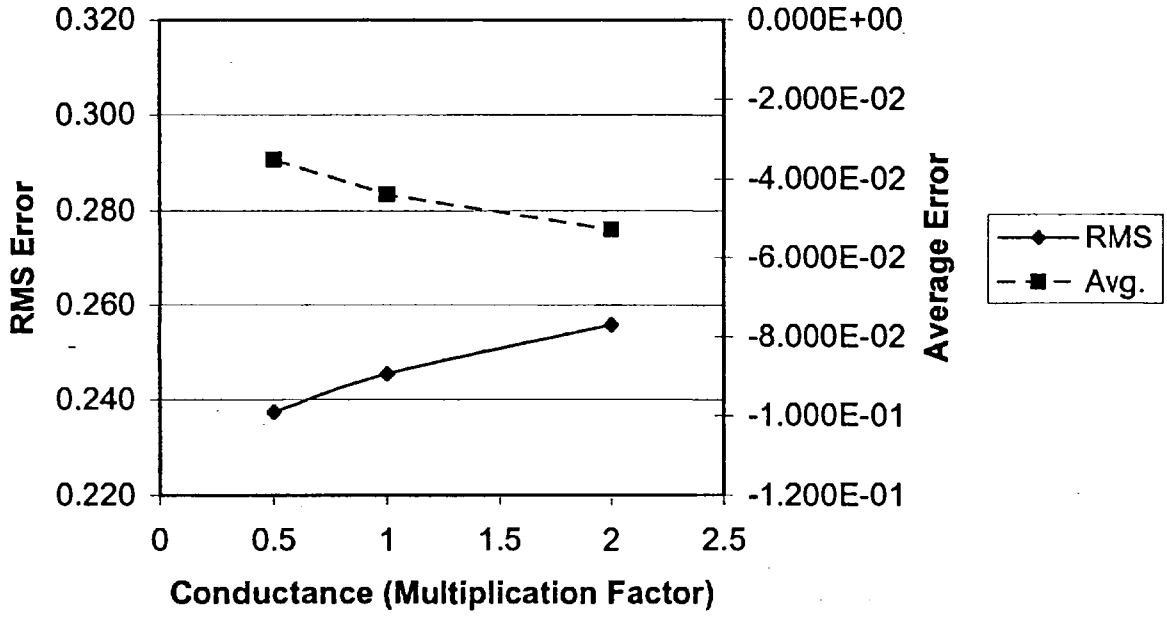

Figure 6.1 f. Sensitivity to GHB Conductance Values in the Top Layer

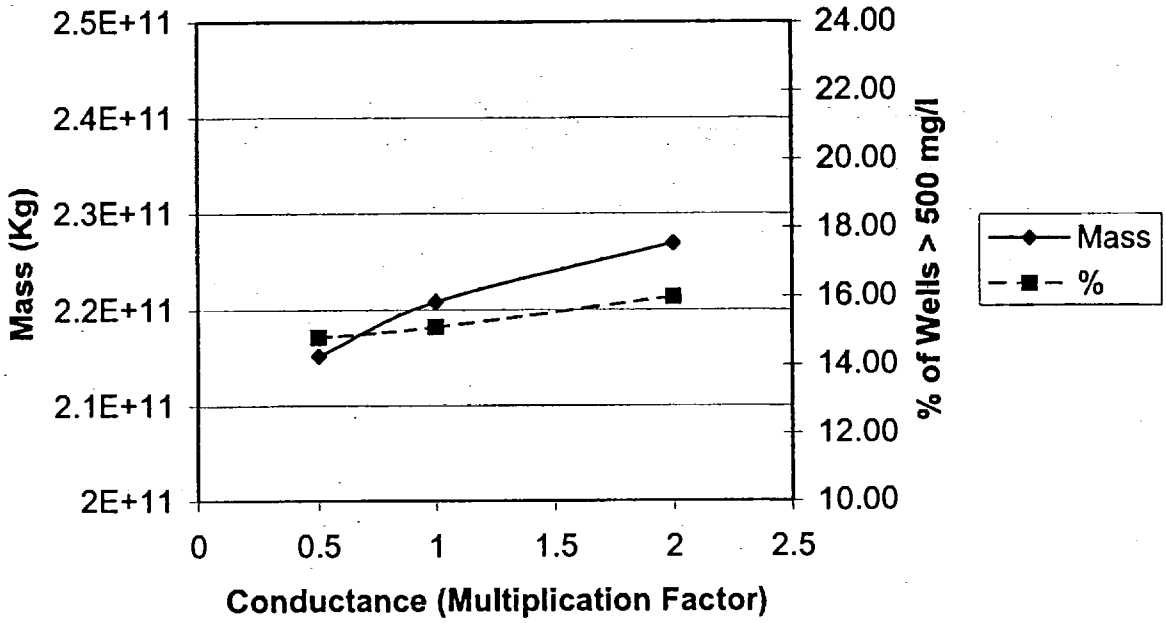

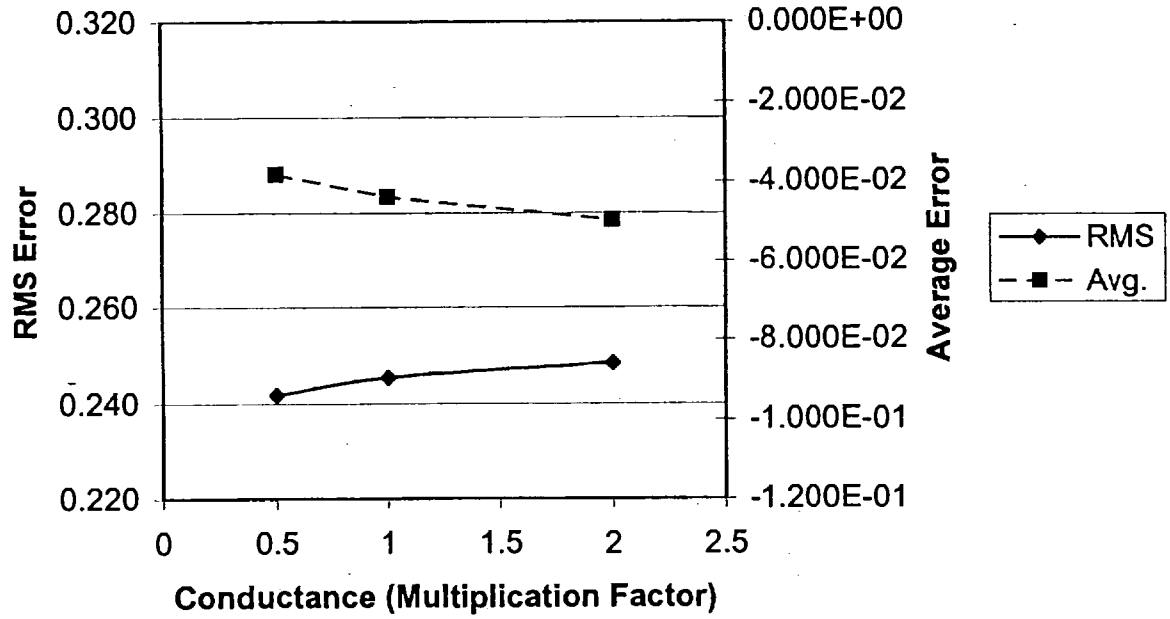

Figure 6.1 g. Sensitivity to GHB Conductance Values under Tampa Bay in the Top Layer

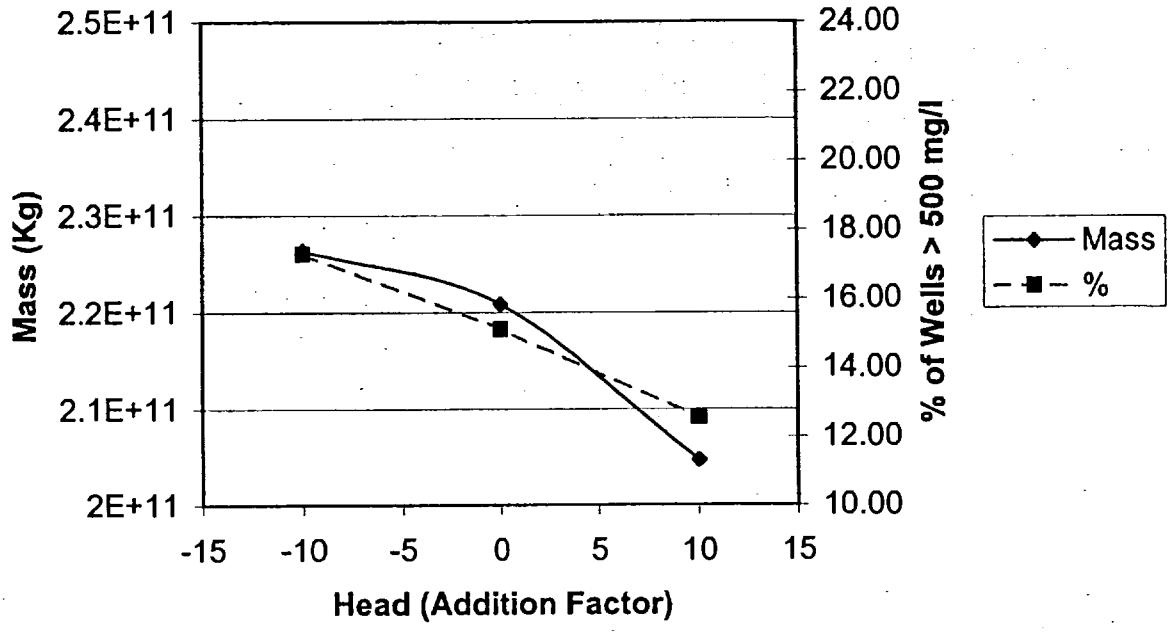

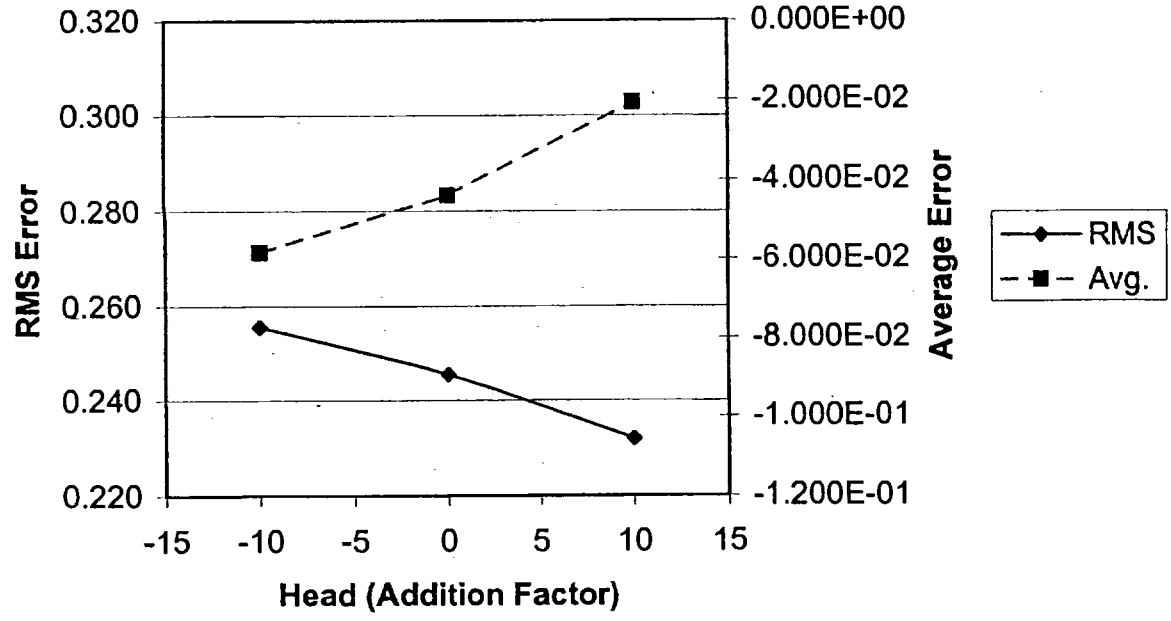

Figure 6.1 h. Sensitivity to GHB Head Values in the Top Layer

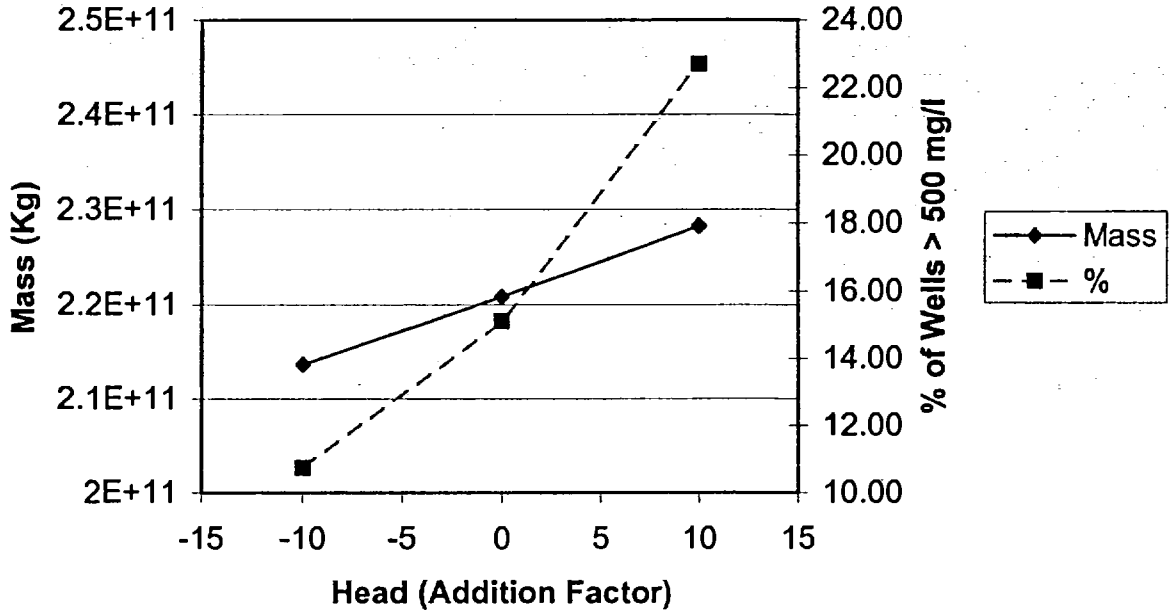

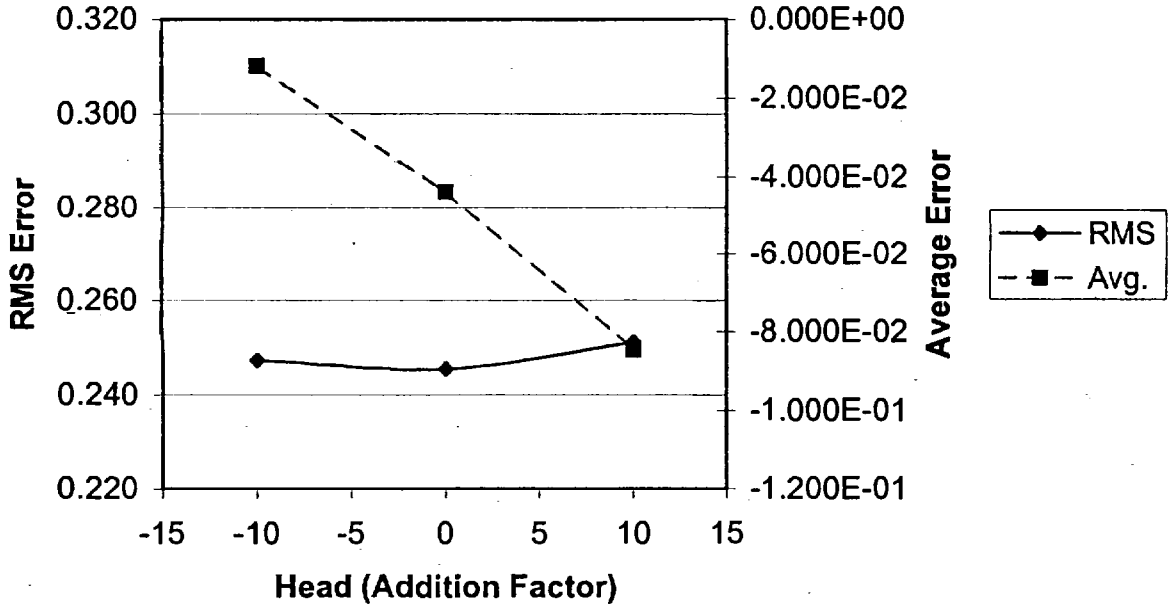

Figure 6.1 i. Sensitivity to GHB Head Values in the Bottom Layer

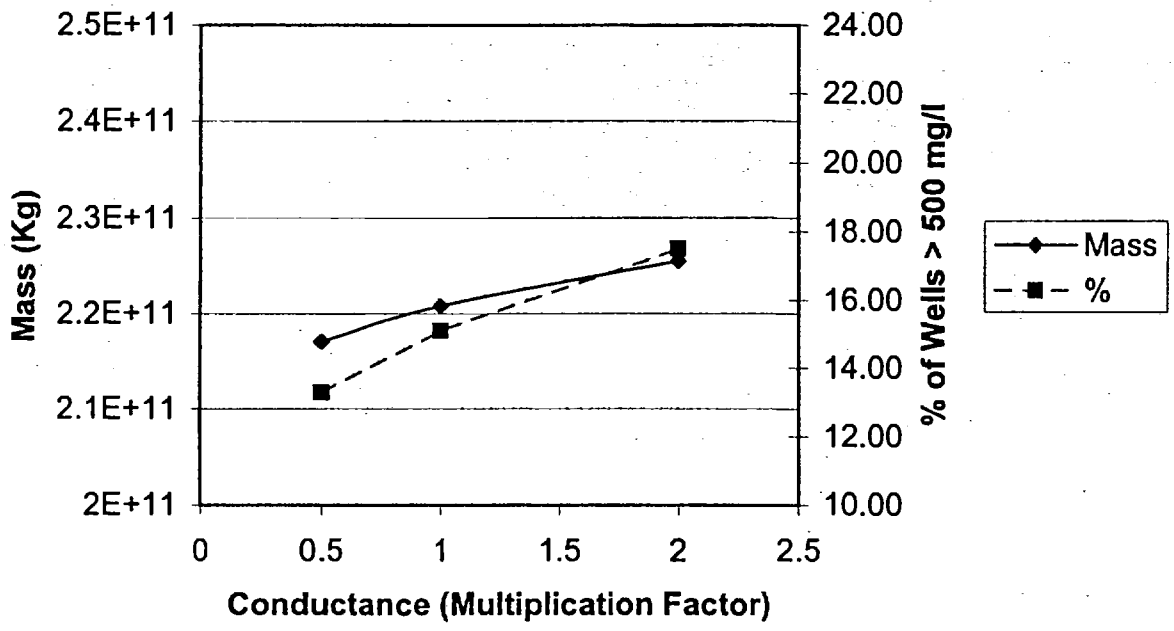

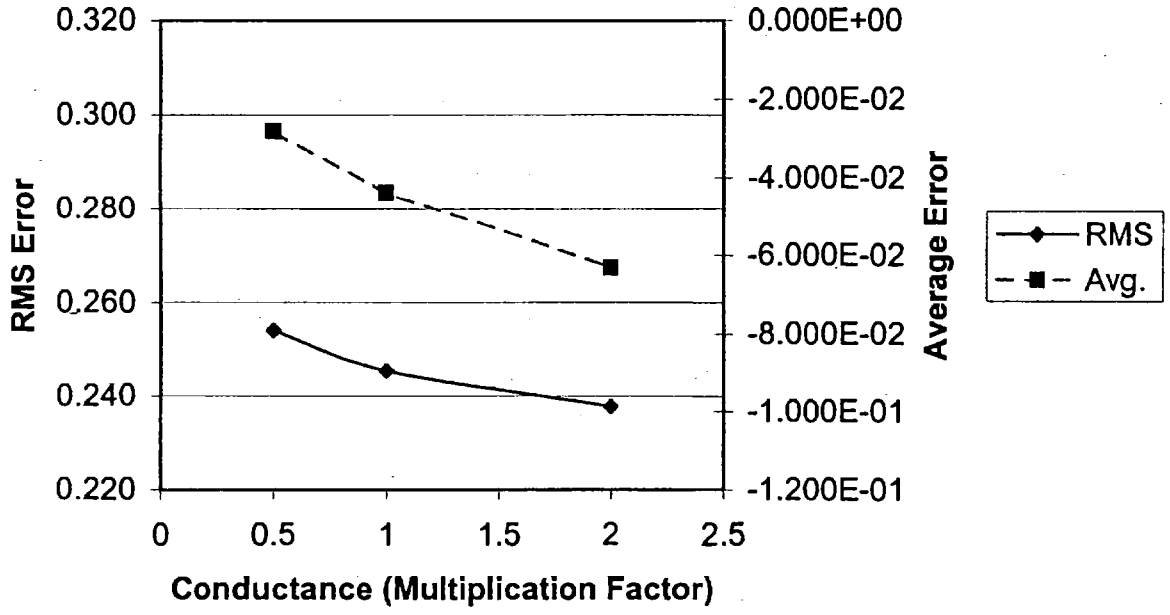

Figure 6.1 j. Sensitivity to GHB Conductance Values in the Bottom Layer

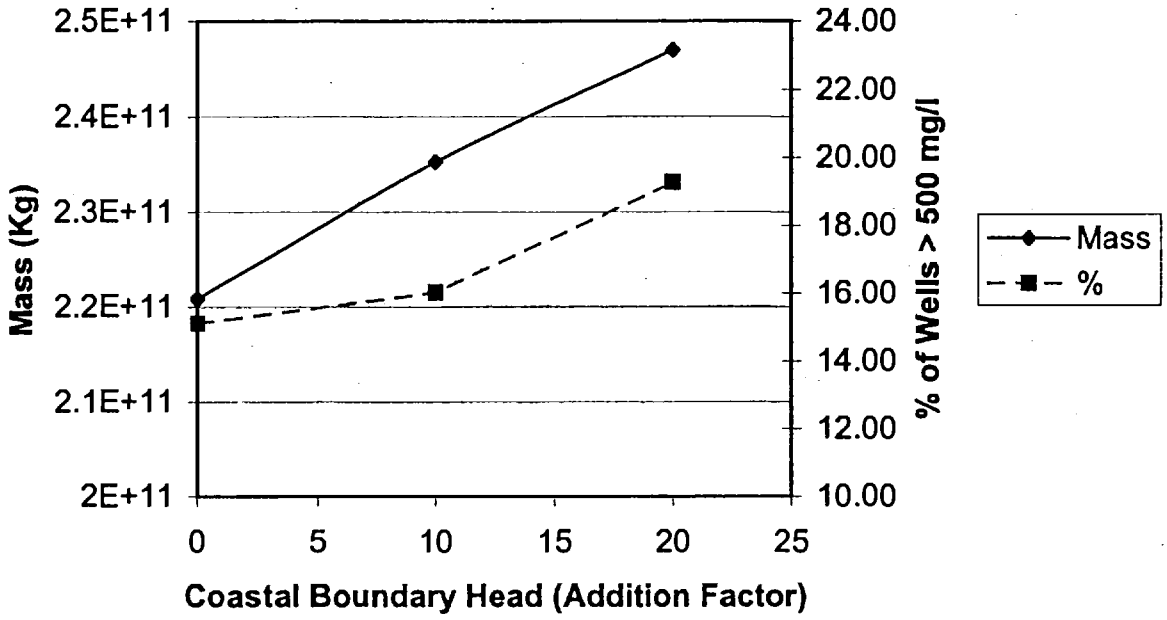

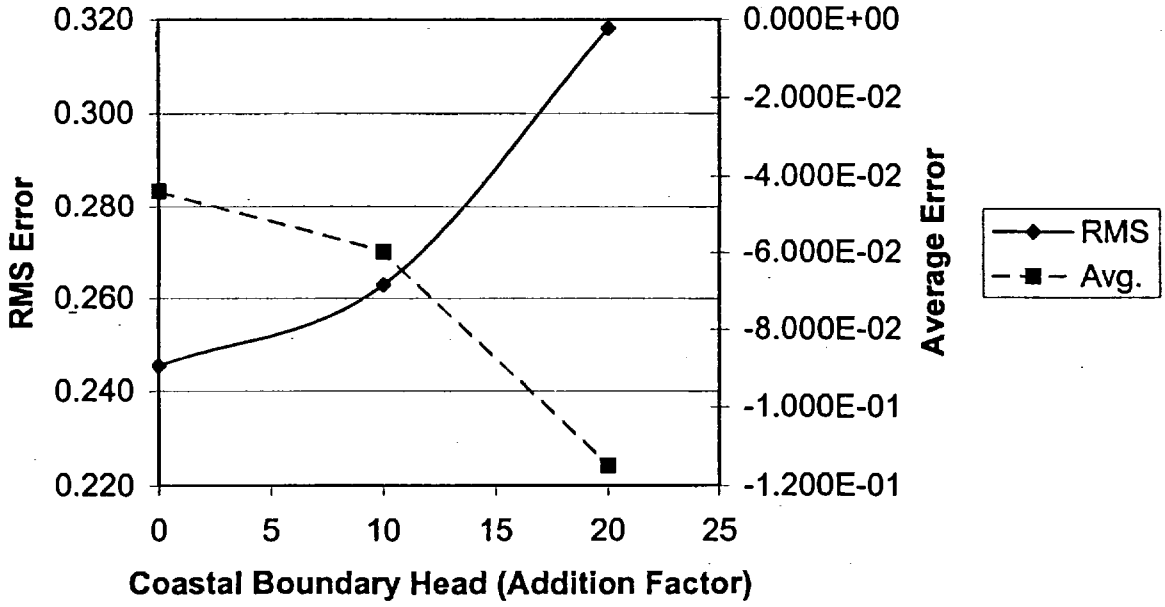

Figure 6.1 k. Sensitivity to Coastal Lateral Boundary Head

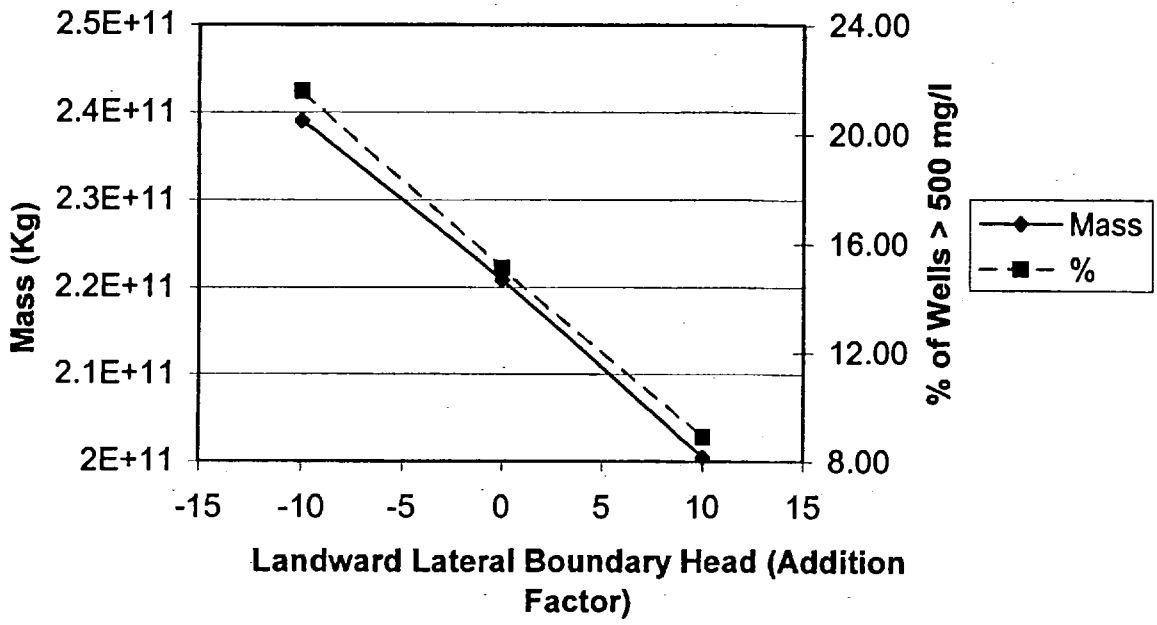

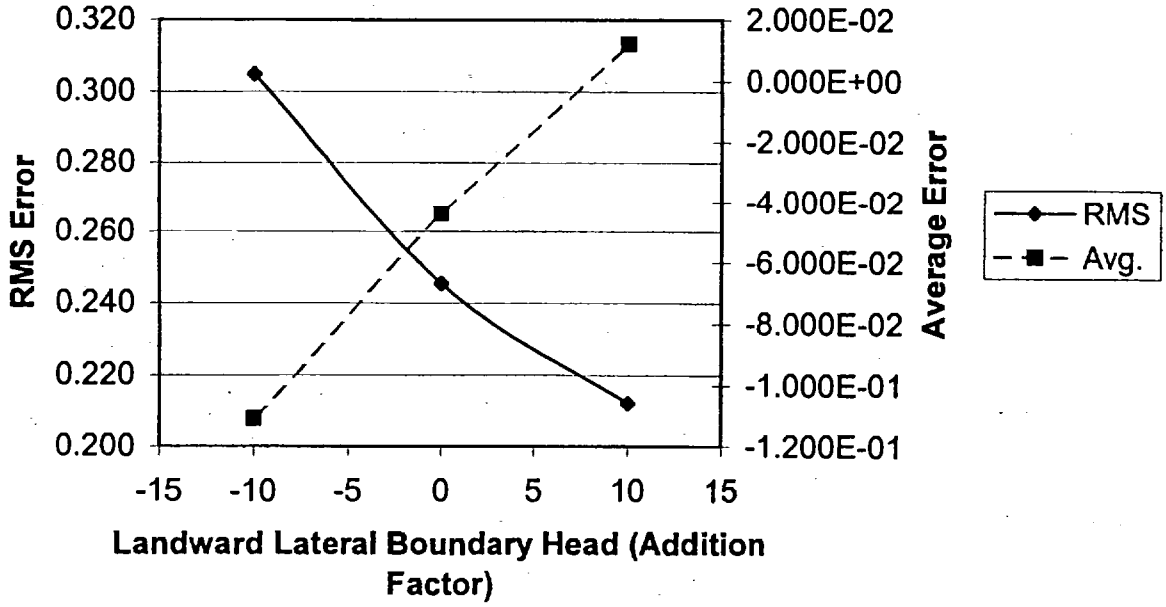

Figure 6.1 l. Sensitivity to Landward Lateral Boundary Head

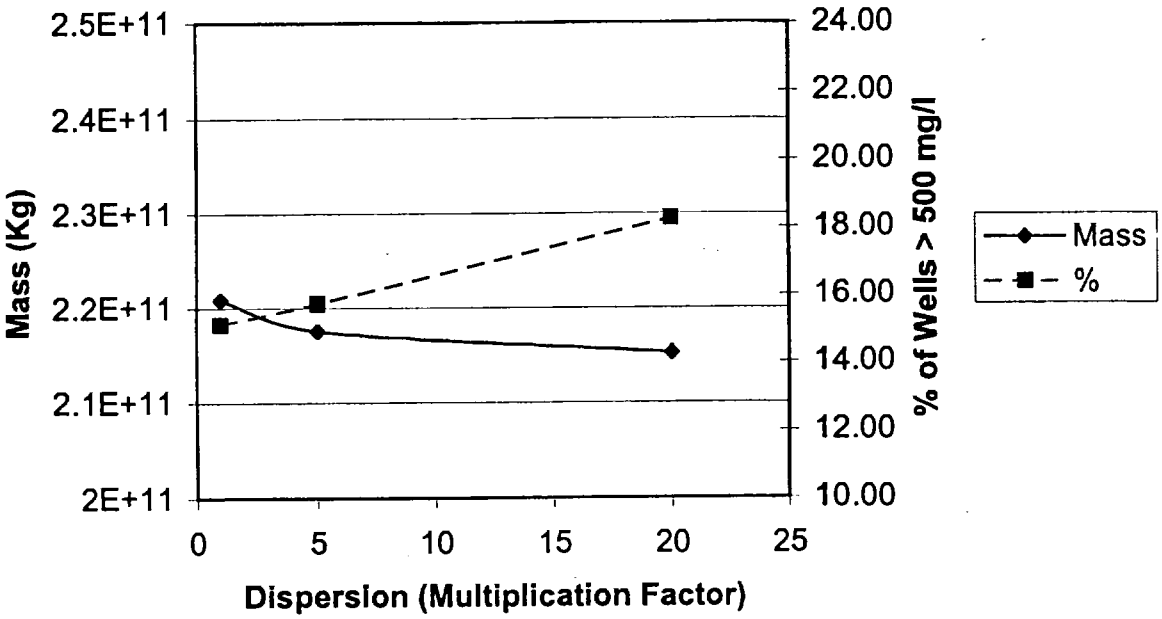

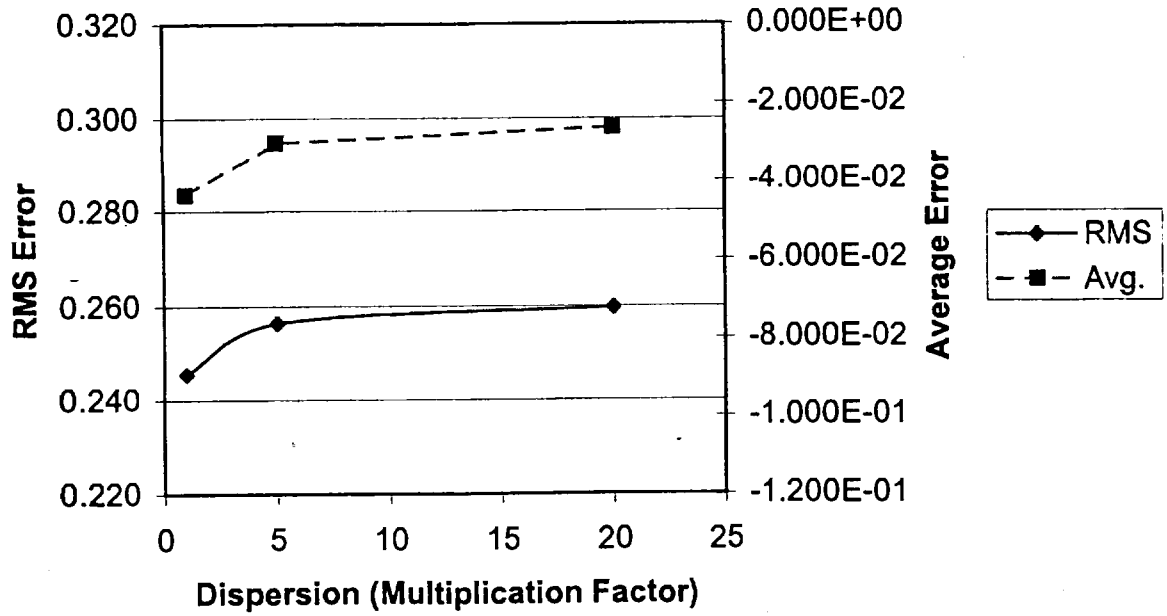

Figure 6.1 m. Sensitivity to Dispersion Coefficient

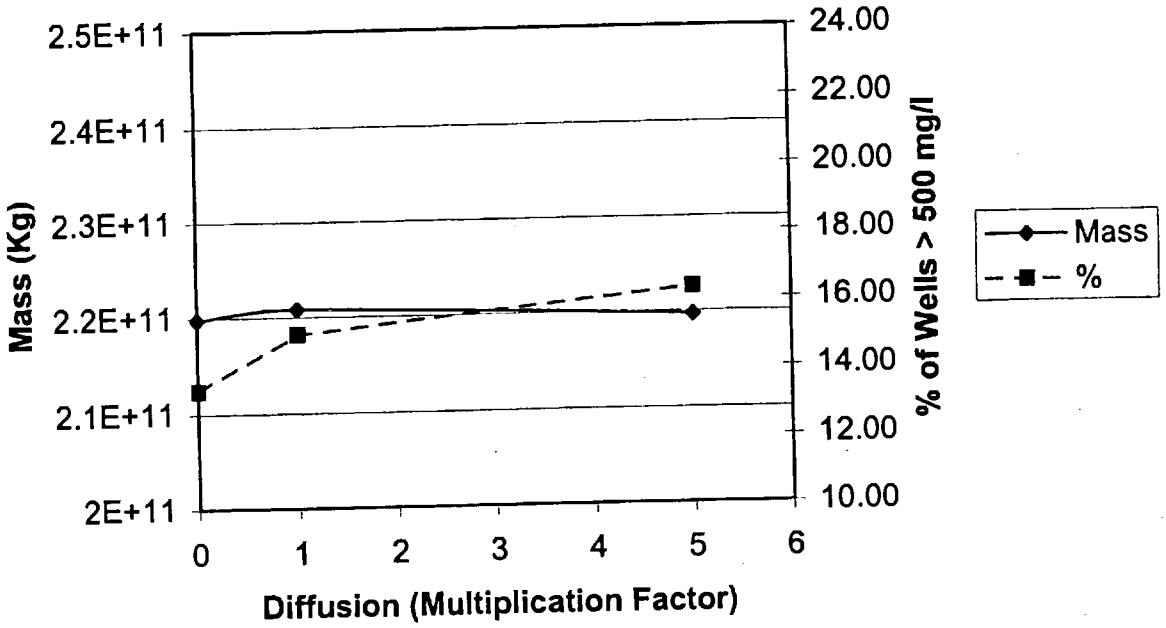

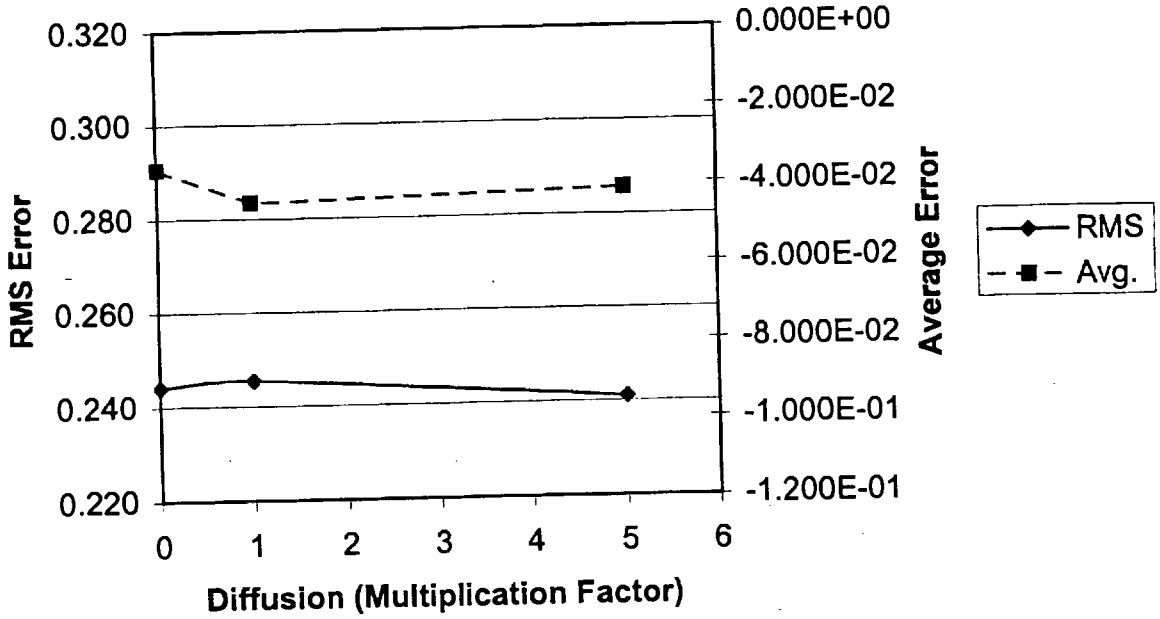

Figure 6.1 n. Sensitivity to Diffusion Coefficient

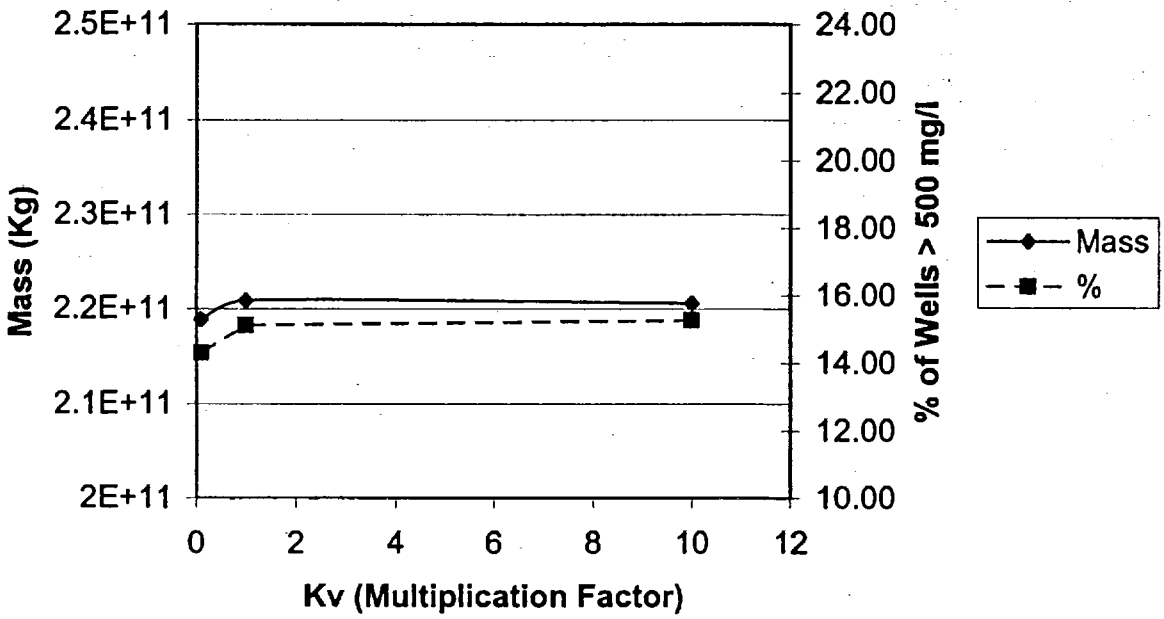

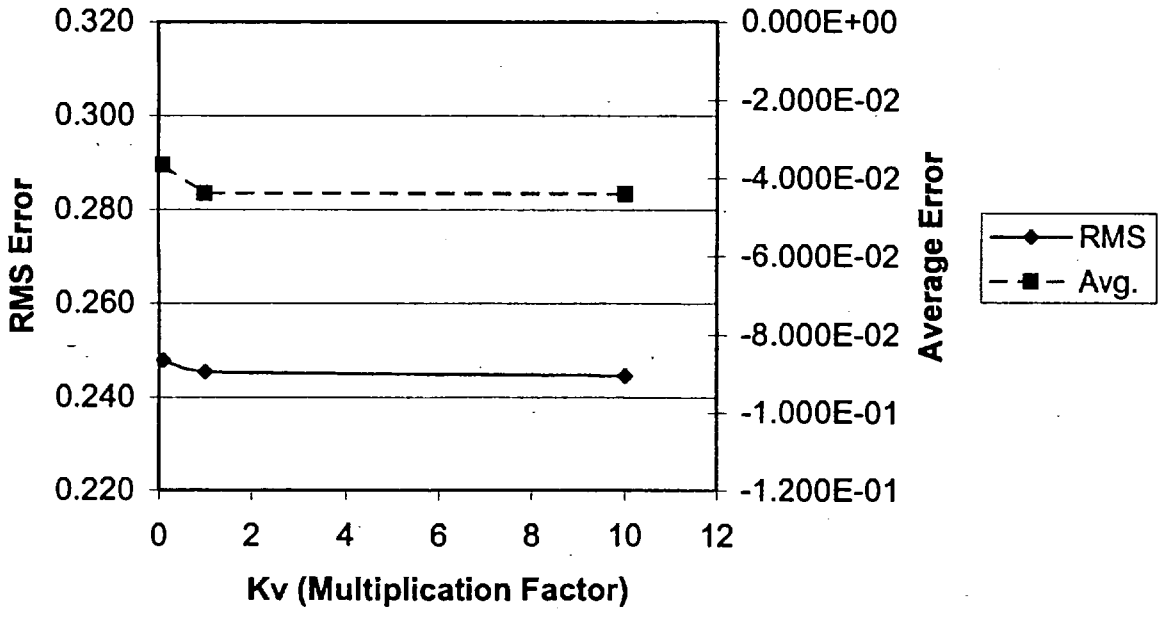

Figure 6.1 o. Sensitivity to Vertical Anisotropy in the Avon Park Formation

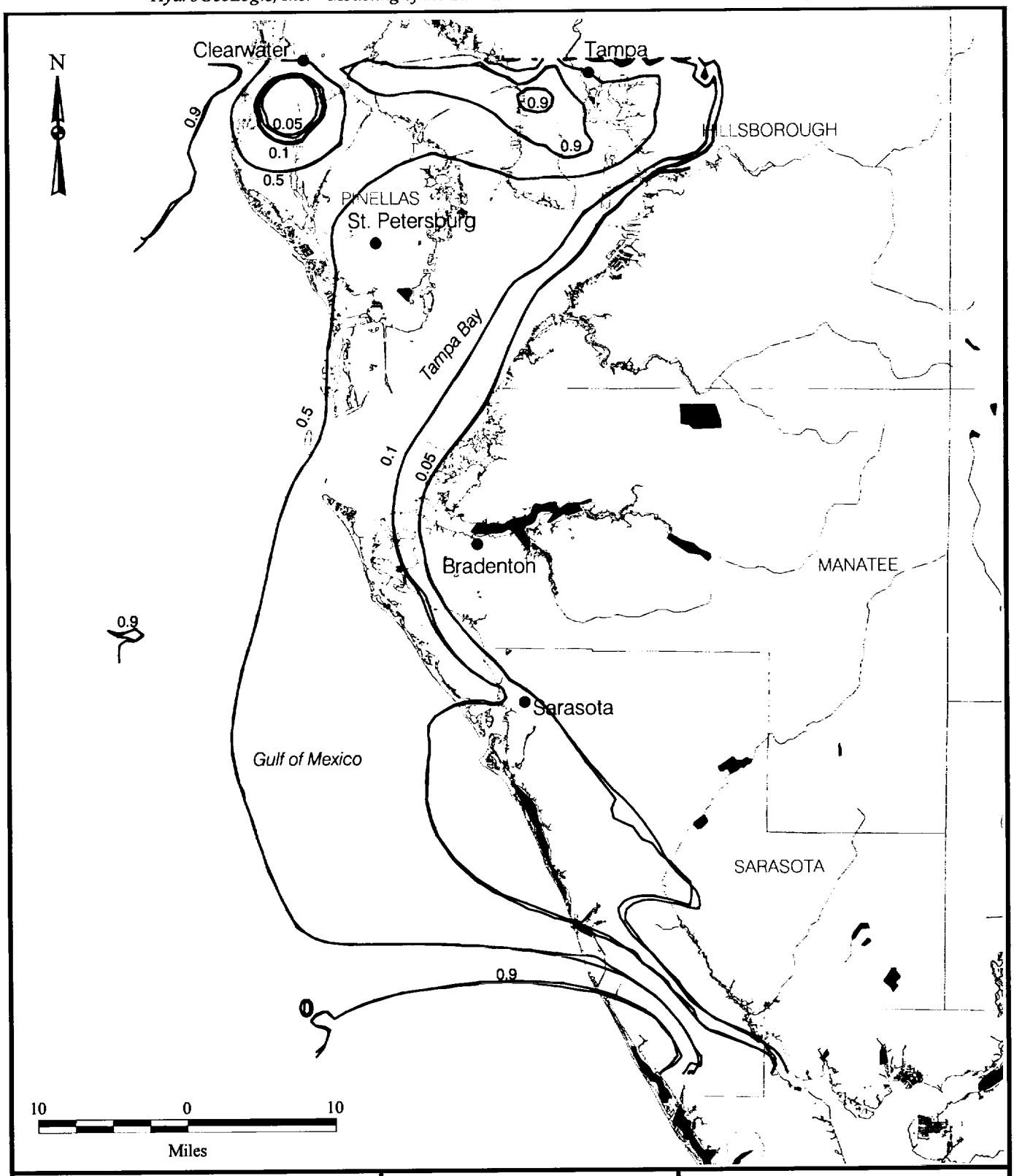

Filename: X:\SWF024\WO_01\saltwater_intrusion\r-chloride_dist_2_vs_L2c.apr
Project: SWF024-001-01
Created: 11/28/01 TH
Revised: 06/13/02 TB

HYDRO GeoLogic Inc.

Legend

County Boundary — Surface Drainage

0.05 — Relative Chloride Concentration Contour
0.05 = 1000 mg/l

0.05 — Relative Chloride Concentration Contour
0.05 = 1000 mg/l for Corrected Model

0.1 = 1,900 mg/l
0.3 = 5,700 mg/l
0.5 = 9,500 mg/l
0.7 = 13,300 mg/l
0.9 = 17,100 mg/l

Figure 6.2
Comparison of Calibrated Model Results to Corrected Well Depths for the Suwannee Limestone (Model Layer 2)

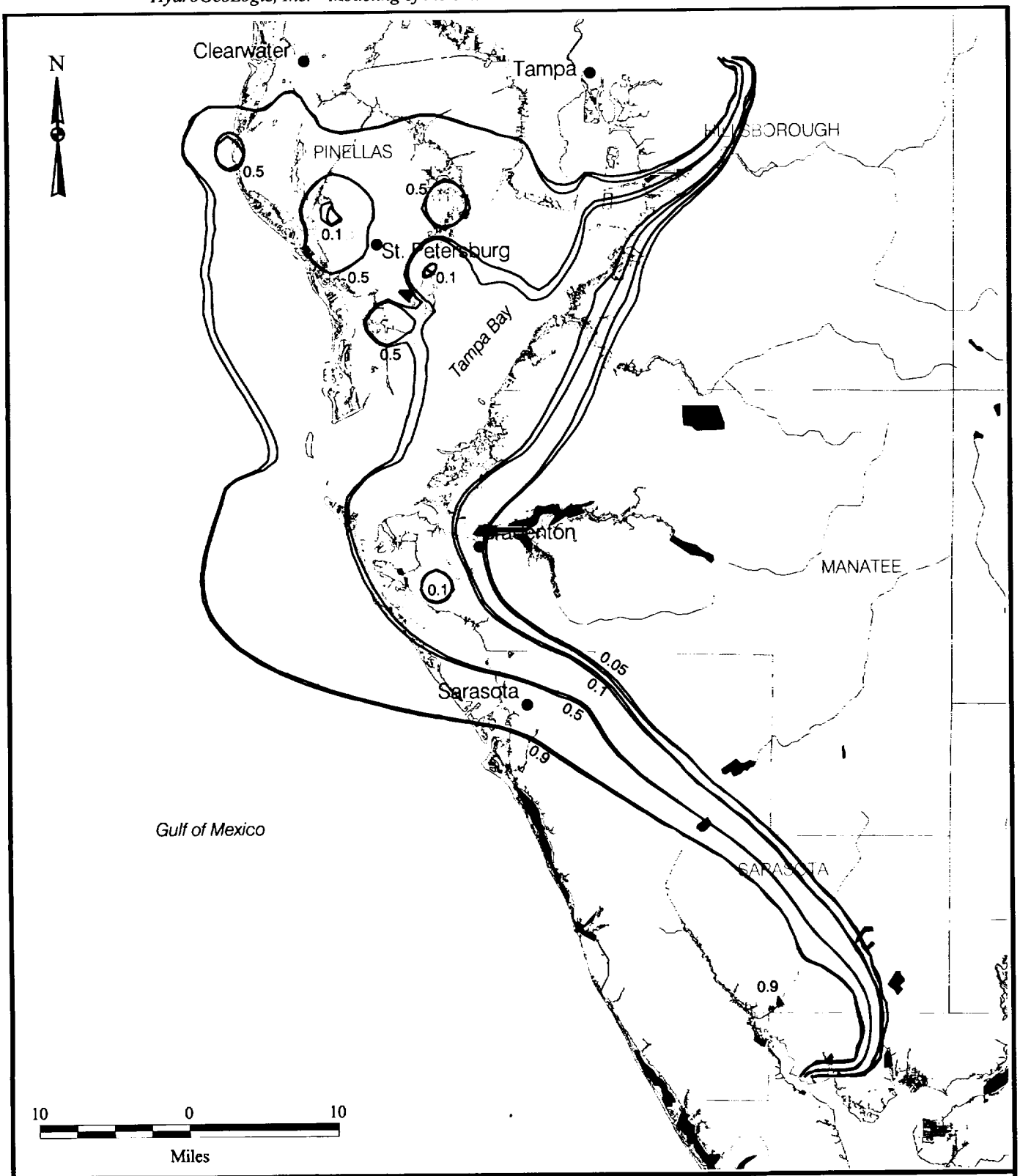

Filename: X:\SWF024\WO_01\saltwater_intrusion\r-chloride_dist_6_vs_L6c.apr
Project: SWF024-001-01
Created: 11/28/01 TH
Revised: 06/13/02 TB

HYDRO GeoLogic Inc

Legend

County Boundary — Surface Drainage

0.05 Relative Chloride Concentration Contour 0.05 = 1000 mg/l

0.05 Relative Chloride Concentration Contour 0.05 = 1000 mg/l for Corrected Model

0.1 = 1,900 mg/l
0.3 = 5,700 mg/l
0.5 = 9,500 mg/l
0.7 = 13,300 mg/l
0.9 = 17,100 mg/l

Figure 6.3 Comparison of Calibrated Model Results to Corrected Well Depths for the Avon Park Formation (Model Layer 6)

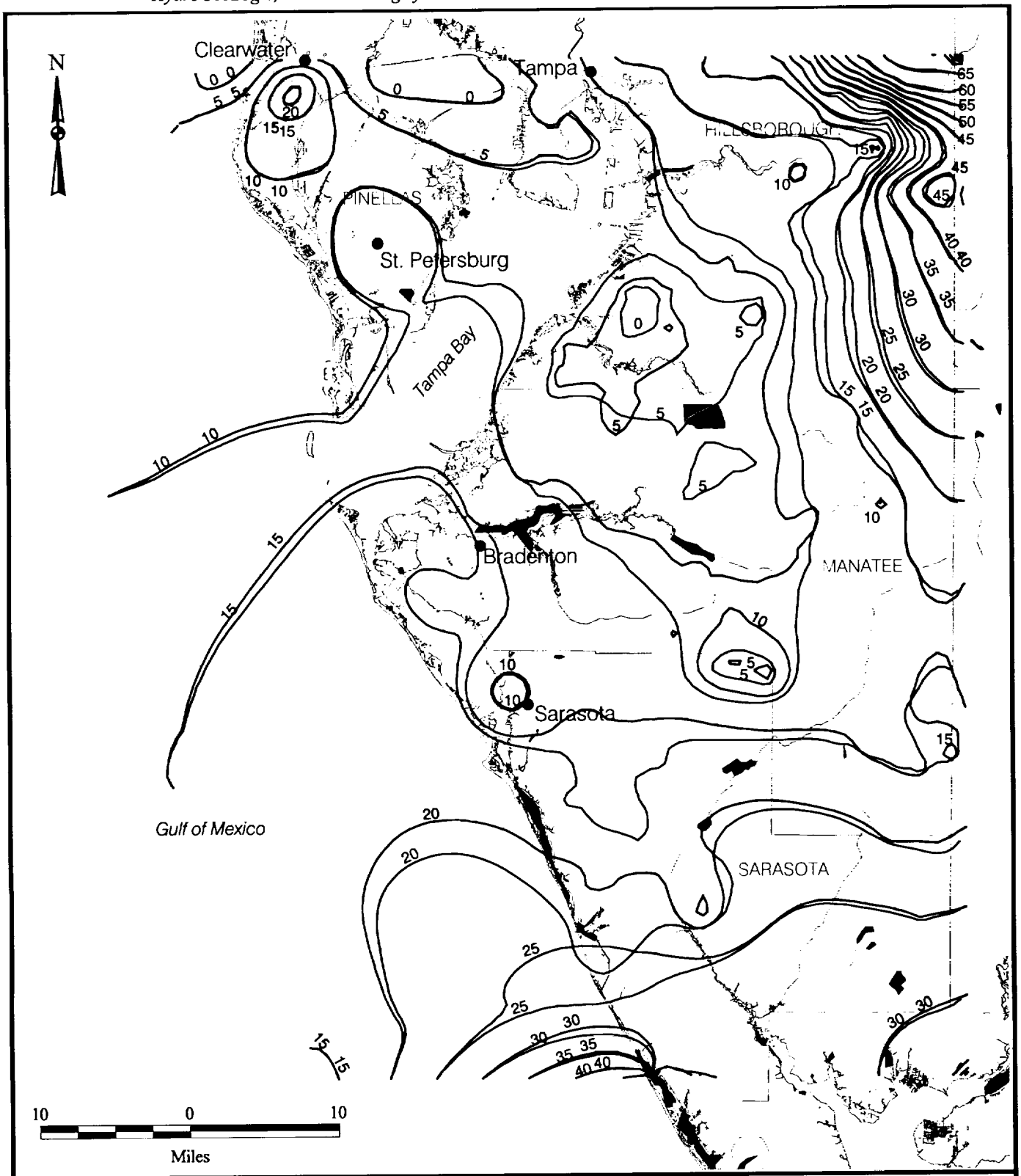

Filename: X:\SWF024\WO_01\saltwater_intrusion\head_dist_sept2000_2.apr
Project: SWF024-001-01
Created: 11/28/01 TH
Revised: 06/13/02 TB

HYDRO GeoLogic Inc

Legend

- County Boundary
- Surface Drainage
- 60 — Calibrated Model Potentiometric Surface Elevation Contour (ft, msl) (Model Layer 2)
- 60 — Corrected Potentiometric Surface Elevation (ft, msl)

Figure 6.4
Comparison of Calibrated and Corrected Potentiometric Surface - September 2000 (Suwannee Limestone, Model Layer 2)

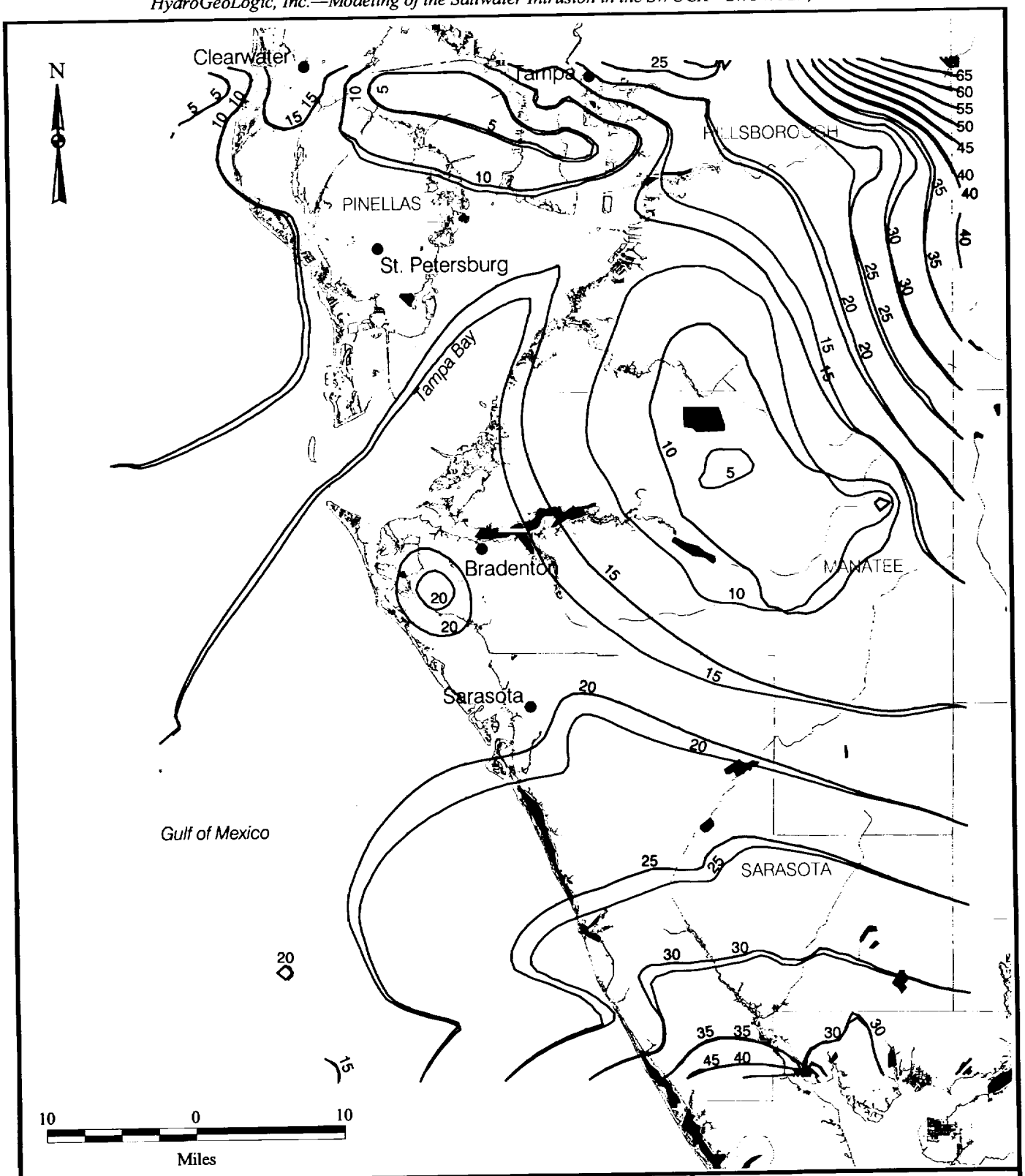

Filename: X:\SWF024\WO_01\saltwater_intrusion\head_dist_sept2000_7.apr
Project: SWF024-001-01
Created: 11/28/01 TH
Revised: 06/13/02 TB

HYDRO GeoLogic Inc.

Legend

- County Boundary
- Surface Drainage
- 60 — Calibrated Model Potentiometric Surface Elevation Contour (ft, msl) (Model Layer 7)
- 60 — Corrected Potentiometric Surface Elevation (ft, mls)

Figure 6.5
Comparison of Calibrated and Corrected Potentiometric Surface - September 2000 (Avon Park Formation, Model Layer 7)

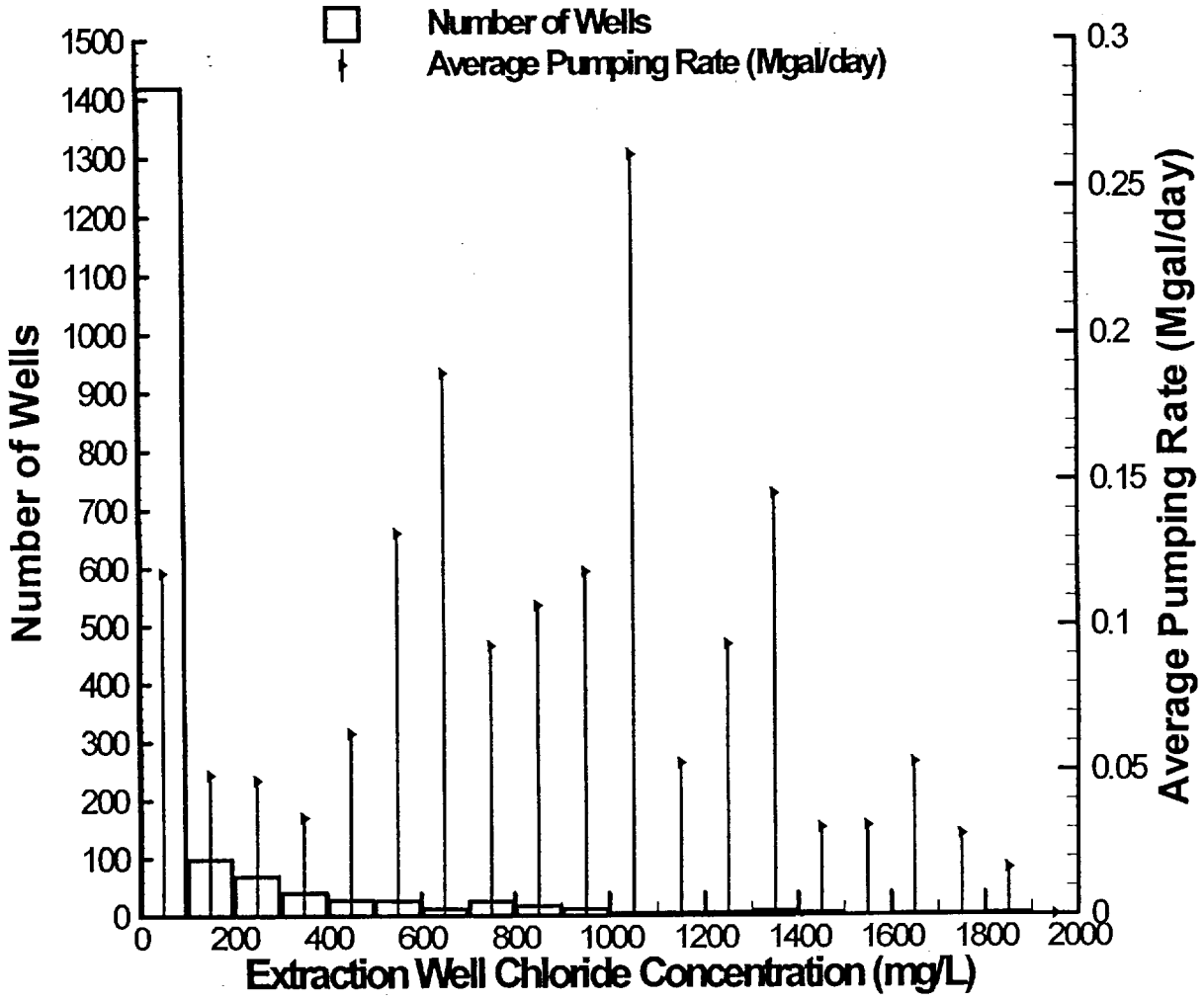

Figure 7.1 Extraction well chloride concentration histogram for December 2000

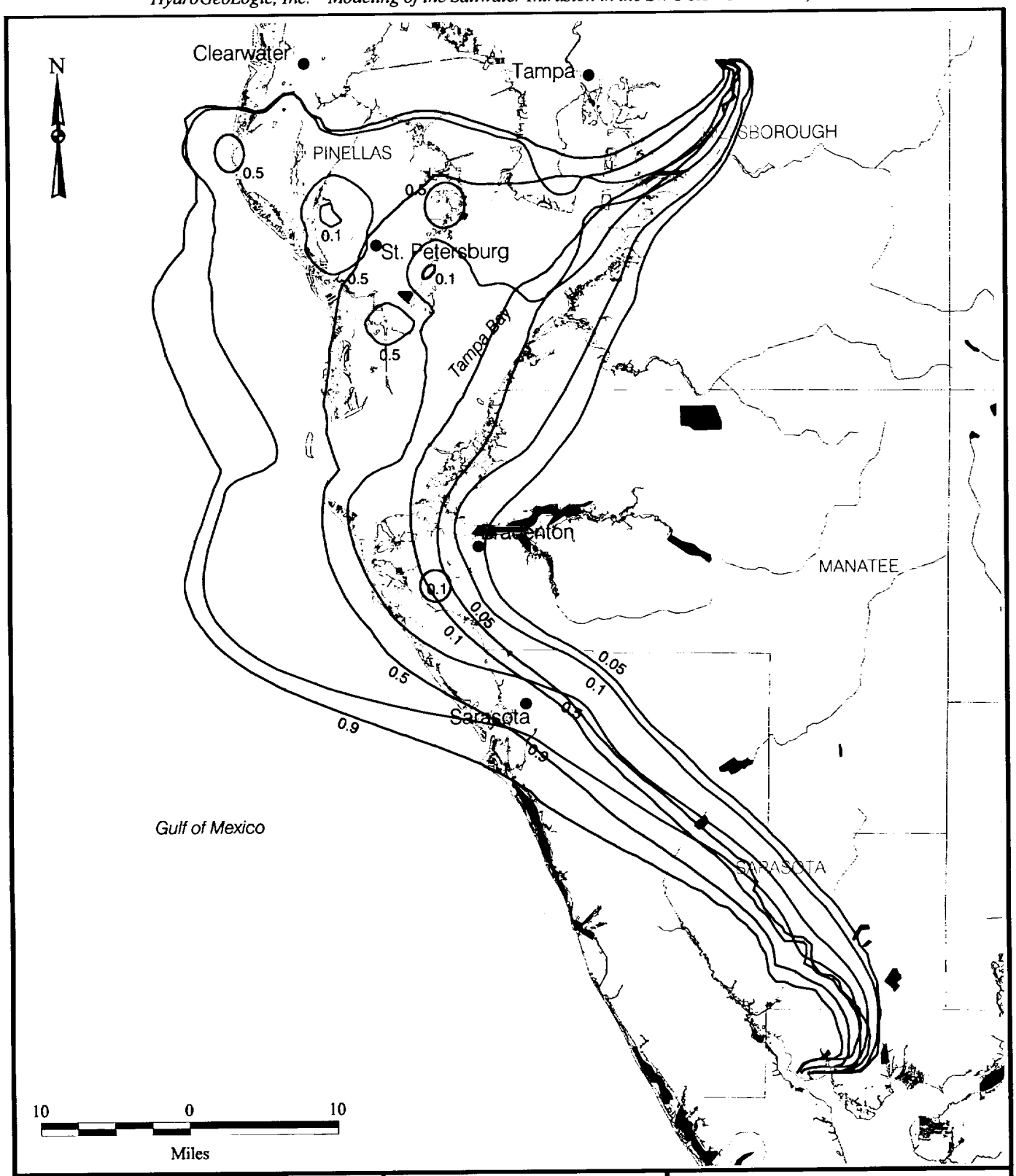

Filename: X:\SWF024\WO_01\saltwater_intrusion\r-chloride_dist_pre_post.apr
Project: SWF024-001-01
Created: 11/28/01 TH
Revised: 06/14/02 TB

HYDRO GeoLogic Inc.

Legend

County Boundary
Surface Drainage
0.05 Predevelopment Conditions
0.05 Relative Chloride Concentration Contour
0.05 = 1000 mg/l

0.1 = 1,900 mg/l	0.7 = 13,300 mg/l
0.3 = 5,700 mg/l	0.9 = 17,100 mg/l
0.5 = 9,500 mg/l	

Figure 7.2
Relative Chloride Concentrations Predicted Using the Calibrated Model for Pre and Post Development Conditions for the Avon Park Formation (Model Layer 6)

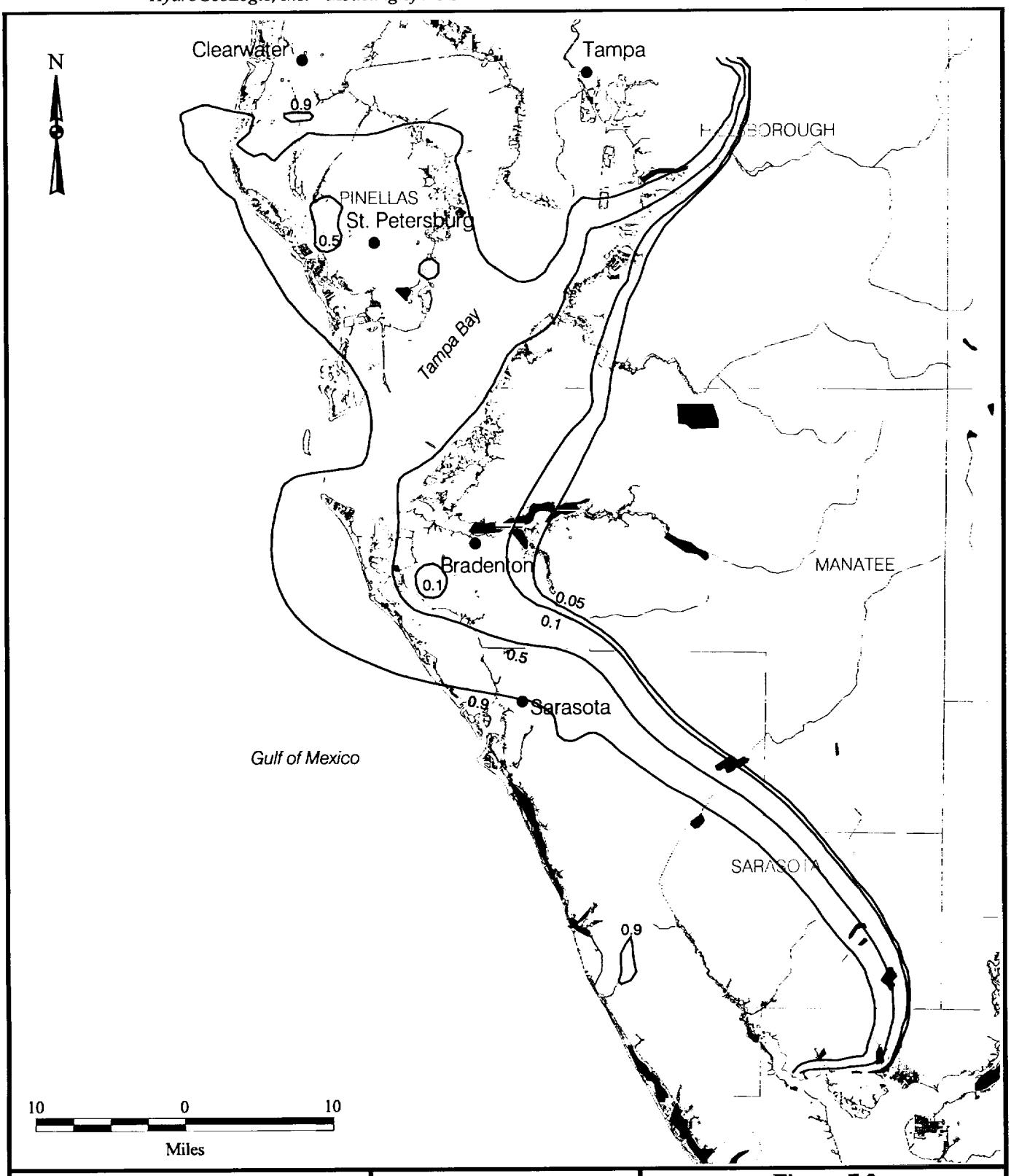

Filename: X:\SWF024\WO_01\saltwater_intrusion\chloride_dist_p400.apr
Project: SWF024-001-01
Created: 11/28/01 TH
Revised: 06/14/02 TB

HYDRO GeoLogic

Legend

County Boundary

Surface Drainage

0.05 Areal Distribution Concentration Contour
0.05 = 1000 mg/l

0.1 = 1,900 mg/l
0.3 = 5,700 mg/l
0.5 = 9,500 mg/l
0.7 = 13,300 mg/l
0.9 = 17,100 mg/l

Figure 7.3
Areal Distribution of Chlorides within the Highly Permeable Zone of the Avon Park Formation (Model Layer 7) after 50 years of Pumping 400 MGD

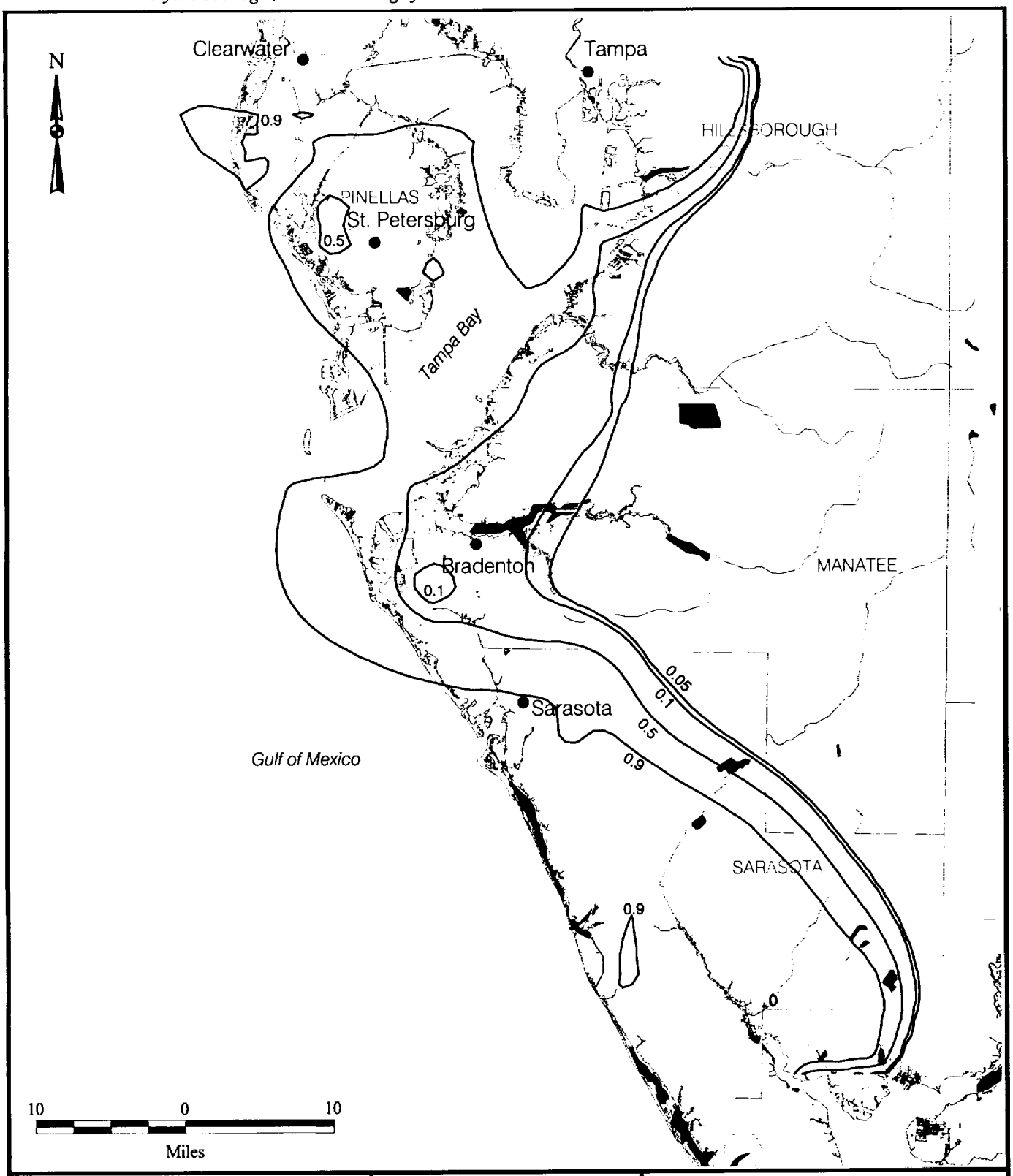

Filename: X:\SWF024\WO_01\saltwater_intrusion\chloride_dist_p600.apr
Project: SWF024-001-01
Created: 11/28/01 TH
Revised: 06/14/02 TB

HYDRO GeoLogic Inc.

Legend

County Boundary

Surface Drainage

0.05 Areal Distribution Concentration Contour
0.05 = 1000 mg/l

0.1 = 1,900 mg/l
0.3 = 5,700 mg/l
0.5 = 9,500 mg/l
0.7 = 13,300 mg/l
0.9 = 17,100 mg/l

Figure 7.4
Areal Distribution of Chlorides within the Highly Permeable Zone of the Avon Park Formation (Model Layer 7) after 50 years of Pumping 600 MGD

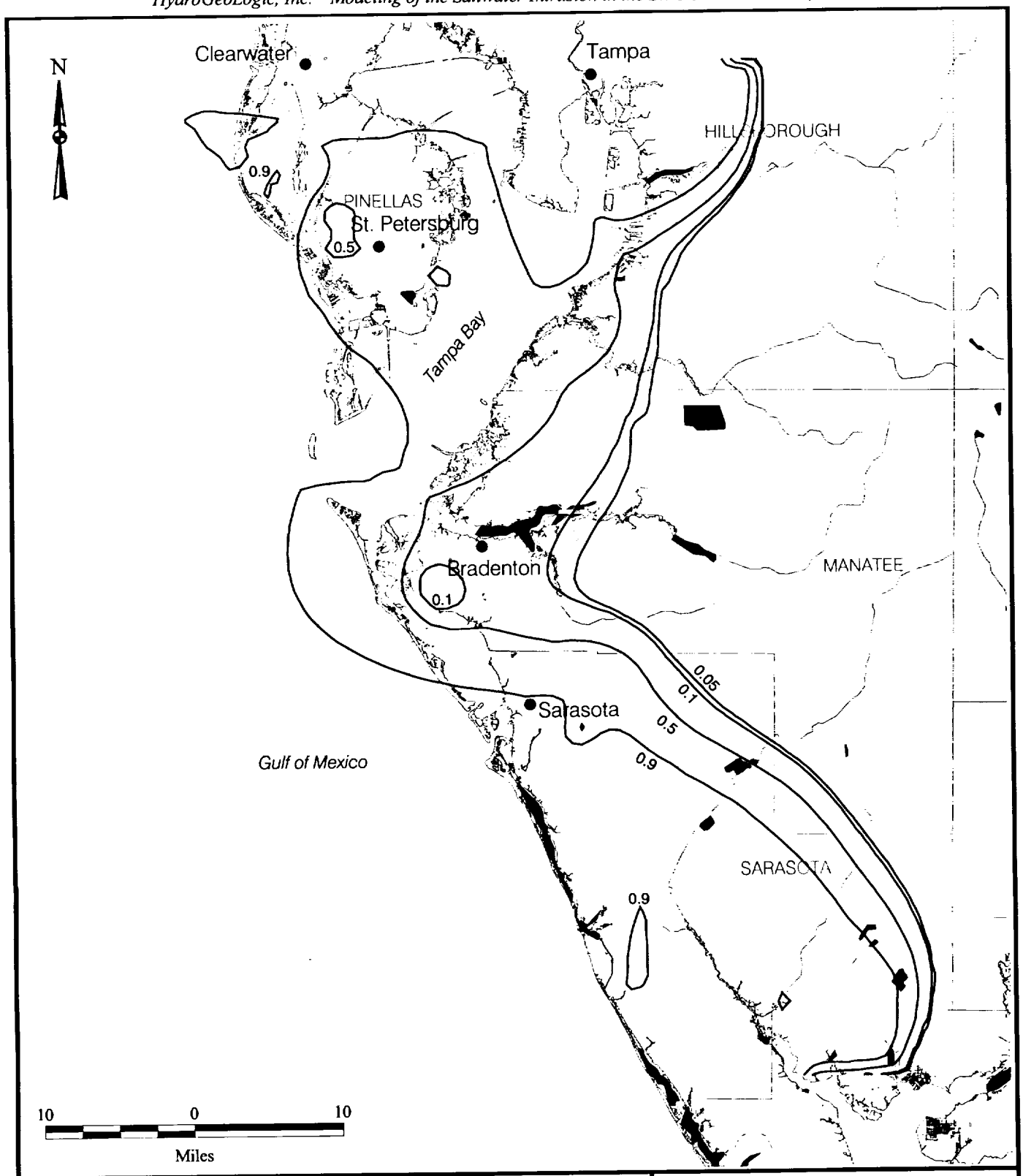

Filename: X:\SWF024\WO_01\saltwater_intrusion\chloride_dist_p800.apr
Project: SWF024-001-01
Created: 11/28/01 TH
Revised: 06/14/02 TB

HYDRO GeoLogic INC.

Legend

County Boundary

Surface Drainage

0.05 Areal Distribution Concentration Contour
0.05 = 1000 mg/l

0.1 = 1,900 mg/l
0.3 = 5,700 mg/l
0.5 = 9,500 mg/l
0.7 = 13,300 mg/l
0.9 = 17,100 mg/l

Figure 7.5
Areal Distribution of Chlorides within the Highly Permeable Zone of the Avon Park Formation (Model Layer 7) after 50 years of Pumping 800 MGD

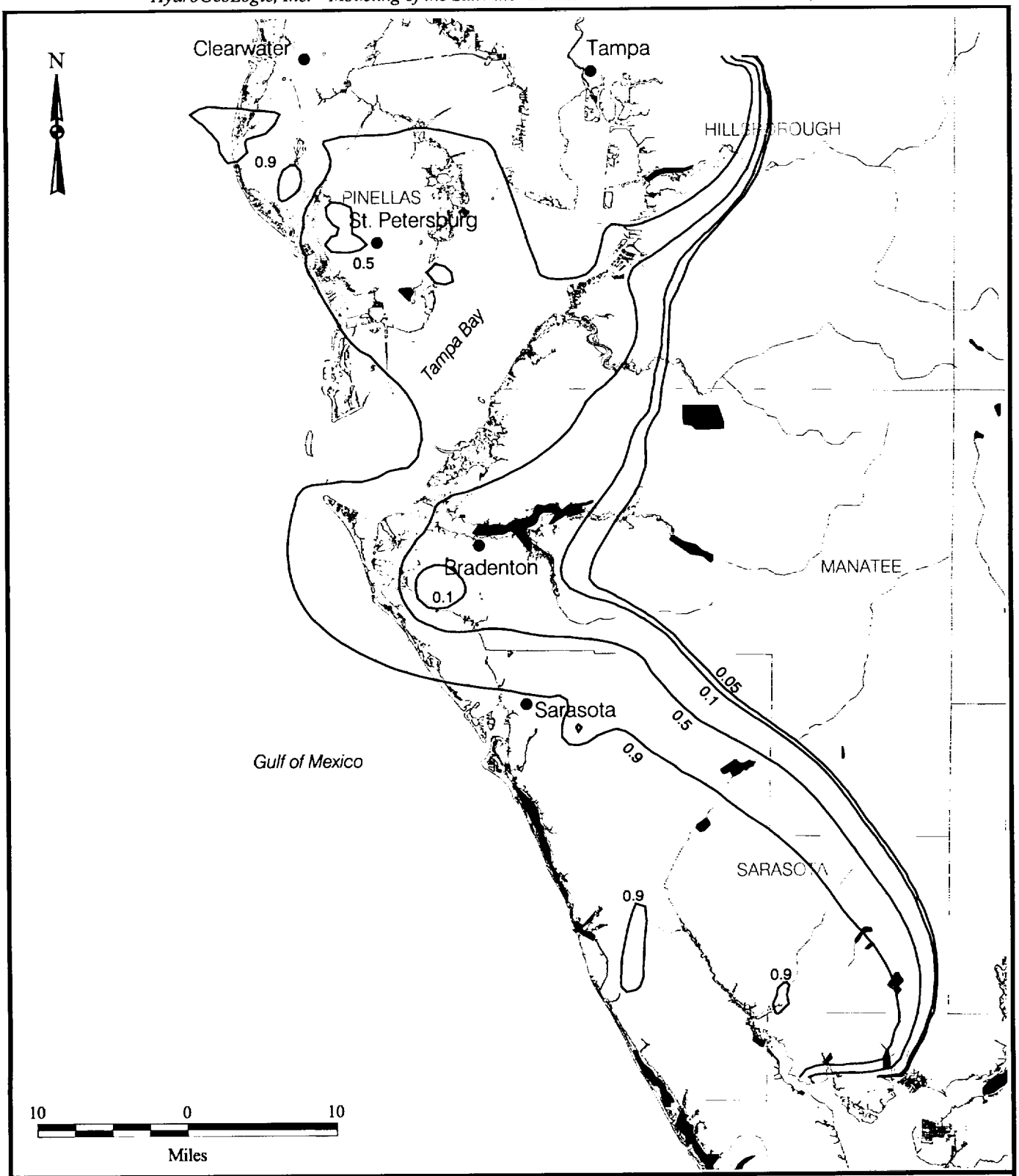

Filename: X:\SWF024\WO_01\saltwater_intrusion\chloride_dist_p1000.apr
Project: SWF024-001-01
Created: 11/28/01 TH
Revised: 06/14/02 TB

HYDRO GeoLogic INC.

Legend

County Boundary

Surface Drainage

0.05 Areal Distribution Concentration Contour
0.05 = 1000 mg/l

0.1 = 1,900 mg/l
0.3 = 5,700 mg/l
0.5 = 9,500 mg/l
0.7 = 13,300 mg/l
0.9 = 17,100 mg/l

Figure 7.6
Areal Distribution of Chlorides within the Highly Permeable Zone of the Avon Park Formation (Model Layer 7) after 50 years of Pumping 1000 MGD

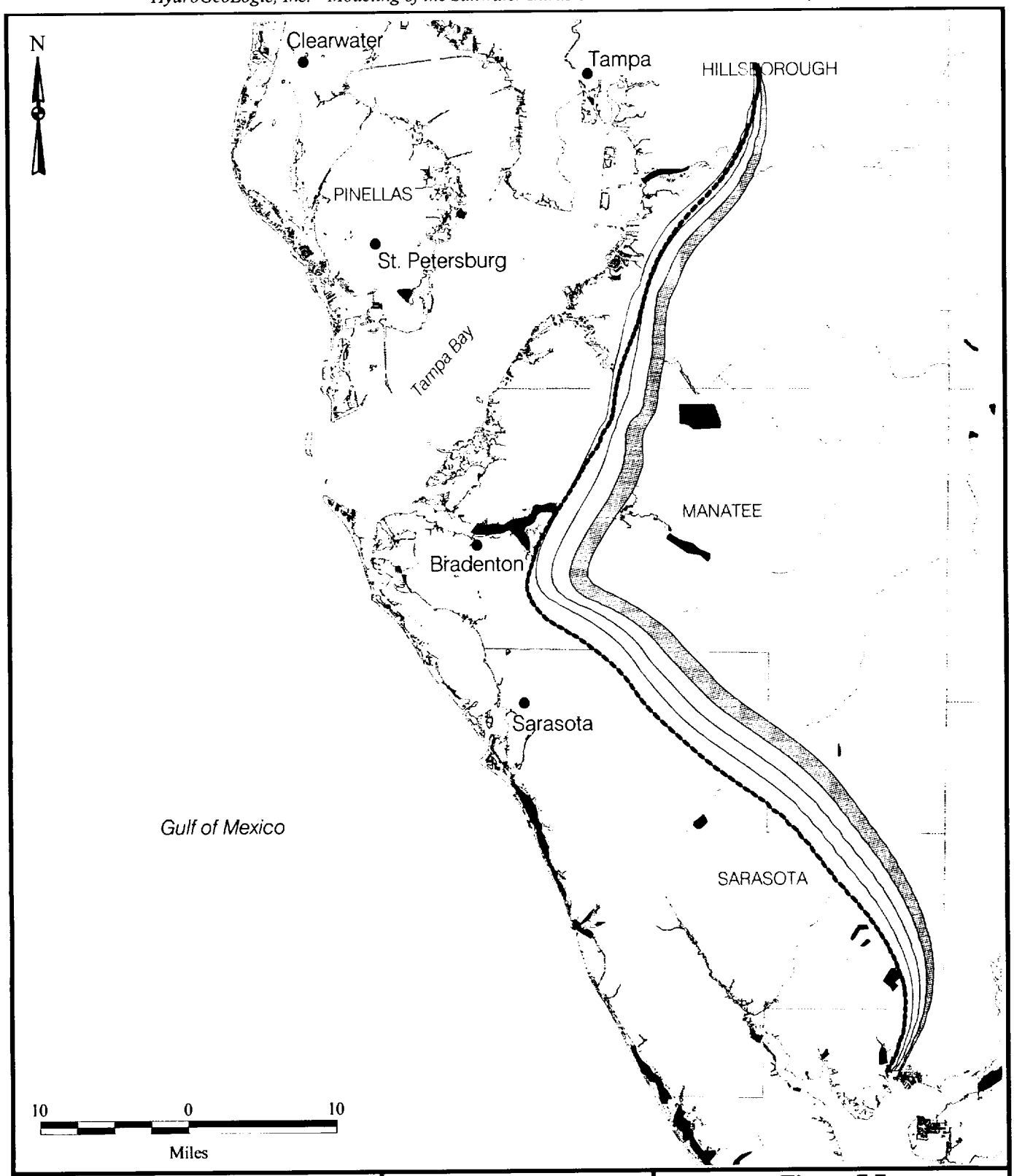

Filename: X:\SWF024\WO_01\saltwater_intrusion\chlor_extent.apr
Project: SWF024-001-01
Created: 11/28/01 TH
Revised: 06/14/02 TB

HYDRO GeoLogic

Legend

County Boundary
Surface Drainage
Present Postion
400 MGD
600 MGD
800 MGD
1000 MGD

Figure 7.7
Extent of the Simulated 1000 mg/L Chlorides in the Highly Permeable Zone of the UFAS - Fifty Year Position for the Various Pumping Cases

TABLES

Table 2.1
Geology and Hydrogeology of the Eastern Tampa Bay WUCA
(modified from Barr, 1996, Miller, 1986, and Basso, 2001)

Series	Stratigraphic Unit		Hydrogeologic Unit		Lithology
Holocene to Pliocene	Undifferentiated Surficial Deposits		Surficial Aquifer		Sand, silty sand, clayey sand, peat, and shell
Miocene	Hawthorn Group	Peace River Formation	UICU	Intermediate Aquifer System	Predominantly phosphatic clay, gray to green to brown, plastic, ductile, minor sand, residual limestone, and dolostone
			PZ2		
			MICU		
		Arcadia Formation			
		Tampa Member	PZ 3		Limestone, gray to tan, sandy, soft, clayey, minor stone, phosphatic. Chert found locally
			LICU		
Oligocene	Suwannee Limestone		UPZ	Upper Floridan Aquifer	Limestone, cream to tan, sandy, vuggy, fossiliferous
Eocene	Ocala Limestone		SCU		Limestone, white to tan, friable to micritic, fine-grained, soft, abundant foraminifera
	Avon Park Formation		LPZ		Limestone and dolomite. Limestone is tan, recrystallized. Dolomite is brown, fractured, sucrosic, hard. Peat found locally at top. Interstitial gypsum in lower part.
			Middle Confining Unit		

Table 2.2
Conceptual Model Components and Related Uncertainties

Conceptual Model Component	Integration into the Numerical Model	Conceptual Model Uncertainties and Possible Resolution
Physical Framework		
The Middle Confining Unit, because of the presence of evaporites, has a very low hydraulic conductivity.	The top of this unit may be assumed to be the base of the Upper Floridan Aquifer System (bottom of the model domain) and will be assigned no flow boundaries.	Hickey (1989) performed an assessment to evaluate the potential for groundwater from below the Middle Confining Unit to flow vertically upward into the permeable zone of the Avon Park. Hickey concluded that flow is upward and velocities vary by approximately 1 order of magnitude between pre and post-development conditions. Waterstone (2001) present calculations that show that the amount of vertical flow derived from below the Middle Confining Unit would have negligible impact on the water quality in the permeable portion of the Avon Park. This aspect of the conceptual model will probably not be tested during the model calibration. However, a sensitivity analysis could be performed in which the sensitivity of the effects of upward flow into the Avon Park on the water quality would be evaluated. This would also involve varying the chloride concentration derived from the anhydrites (see conceptual model components pertaining to lower boundary transport conditions).
The lower permeable zone (i.e., Avon Park Formation) of the Upper Floridan Aquifer may have discrete zones of high permeability.	The Avon Park will be discretized into multiple layers.	Aquifer tests of the Avon Park generally test the entire interval and are not at a resolution sufficient to differentiate individual zones in the Avon Park that may be laterally extensive. The implications of these zones are that they could create "fast paths" for chloride intrusion. The best means to investigate the potential existence of these high permeability zones is to calibrate the model to the high resolution chloride profiles available from the ROMP wells (Figure 2.10). This alternative conceptualization will also be evaluated during the sensitivity analysis if it is found to produce a reasonable calibration.

Table 2.2 (continued)
Conceptual Model Components and Related Uncertainties

Conceptual Model Component	Integration into the Numerical Model	Conceptual Model Uncertainties and Possible Resolution
The Ocala Formation behaves as a semi-confining unit.	The Ocala will be discretized separately from the Avon Park Formation.	Similar hydraulic responses were observed in the Suwannee and Avon Park during aquifer stress tests. This observation suggests that the Ocala is not fully confining and will not prevent water from moving upward. Therefore, upward coning from the Avon Park through the Ocala and into the Suwannee is a possibility. HydroGeoLogic (1994) evaluated a scenario in which the confining properties of the Ocala were decreased and found that the 1,000 mg/l isochlor rose over 200 feet in 50 years. Until more information becomes available from field tests of the Ocala vertical hydraulic conductivity, reliance will have to be placed on the model calibration and on the Southern District Model parameterization for estimating the actual conductivity of the Ocala.
Productive zones in the Intermediate Aquifer System are hydraulically isolated from the Upper Floridan Aquifer by clay units in the Hawthorn Group.	Units above the Suwannee Limestone do not have to be explicitly simulated, but can be treated as a general head boundary that considers the vertical conductance and overlying hydraulic heads, since these units are not of consequence to saltwater intrusion.	This aspect of the conceptual model could be tested by turning the wells on in the Suwannee and Ocala/Avon Park of the Southern District Model and observing head changes within the intermediate aquifer system in the Southern District Model.
All of the aquifer units behave as an equivalent porous media for both flow and transport.	The localized effects of fractures and molecular diffusion into matrix blocks is negligible.	There is evidence that suggest that flow and transport through the Avon Park may be controlled by dual porosity and/or dual permeability conceptualizations. The dual porosity conceptualization collapses to the equivalent porous medium representation for two extreme cases. When the fracture-matrix interaction is large, the equivalent porous medium representation allocates all pore spaces in the domain (fracture plus matrix) to transport. When this interaction is small, the equivalent porous medium representation allocates only the pore spaces within the fractures to transport approximate. Porosity values used in simulations will be adjusted to note the more appropriate representation.
Hydraulic conductivity does not show anisotropy in the horizontal direction within each respective confining unit and aquifer.	Horizontal hydraulic conductivities will be assumed to be isotropic within each respective unit.	Previous aquifer testing has not suggested that there are strong anisotropic components to flow. The validity of this assumption can be evaluated during sensitivity analyses to the regional model.

Table 2.2 (continued)
Conceptual Model Components and Related Uncertainties

Conceptual Model Component	Integration into the Numerical Model	Conceptual Model Uncertainties and Possible Resolution
Hydrologic Framework		
The majority of the water entering the study area from the north, east and south is of good quality.	The boundary conditions on these borders will all assume freshwater.	This component of the conceptual model is currently well supported by the existing field data, and will not be tested further.
Lateral encroachment of seawater and subsequent upconing in areas where wells are completed above the wedge is the primary source of high salinity water.	The boundary conditions on the western border (i.e., ocean) will be set at chloride concentrations measured in the bay.	This component of the conceptual model may be tested during model calibration by adjusting the chloride source concentrations.
Upconing of high salinity water derived from beneath the anhydrites in the Avon Park is not a significant source of chloride.	The lower boundary will be assumed to be impermeable to both water and chloride.	The effect of upconing of high salinity waters from the Middle Confining unit could be tested during the model calibration by placing a diffusion controlled chloride source at the base of the model (i.e., evaporites at the top of the Middle Confining Unit). As mentioned above, however, it is unlikely that the volume of chlorides derived from below the Middle Confining Unit would significantly affect the water quality.
The hydraulic heads along the ocean are probably not in hydrostatic equilibrium with the Gulf of Mexico, since the upper confining unit isolates the aquifer from the Gulf along this boundary, and the Upper Floridan aquifer outcrops into the Gulf probably more than a 100 miles offshore.	Prescribed equivalent freshwater heads will be used for the saltwater flow regime along the western lateral boundaries.	There is very little available data with respect to the equivalent freshwater heads along the western boundary. Consequently, these values will be adjusted during the model calibration.
The chloride concentrations in the Gulf of Mexico are approximately 14,500 mg/l.	The chloride concentrations along the western boundary will be assumed to be that of seawater (relative concentration equal to one). For inflow nodes, this chloride concentration is applied along the boundary. For outflow nodes, the concentration is not prescribed, and chloride levels will depend on the concentration of the outflowing water.	The information regarding chloride data for the post-development time period is relatively good. However, the chloride concentrations assumed for the pre-development time period, which are used to initialize the model, are relatively uncertain. This uncertainty will probably not be addressed during model calibration.

Table 2.2 (continued)
Conceptual Model Components and Related Uncertainties

Conceptual Model Component	Integration into the Numerical Model	Conceptual Model Uncertainties and Possible Resolution
Chloride Transport Characteristics		
The effects of elevated sulfate and constituents other than chloride can be neglected.	Fluid densities will be dependent solely upon chloride concentration values.	Different geochemical facies within the model area may impact the fluid densities. The effects, however, are expected to be small and will not be explicitly addressed during the model calibration.
The interface is relatively sharp and dispersion values are small.	As presented in Section 4.6, a four component dispersivity approach may be appropriate	Field tests typically do not provide reasonable estimates of dispersivity. Therefore, the dispersivity values will be based on calibration results. Based on earlier modeling activities it is expected that small dispersivity values will result in a better calibration.

Table 4.1
Transport Properties

Parameter	Value
Effective porosity	0.15
Freshwater density	1.0
Saltwater density	1.025
Storativity	$1x10^{-4}$
Dispersivity	(please see discussion below)

Table 4.2
Dispersivity Values Used to Initiate Calibration of the Density-dependent Model

Formation/Unit	Longitudinal dispersivity (ft)	Transverse dispersivity (ft)	Vertical transverse dispersivity (ft)
Suwannee Limestone	100	20	10
Ocala Limestone	10	5	5
Avon Park Formation	80	15	10

Table 5.1
Representative Calibration Simulations for the Saltwater Intrusion Model

Statement of the Problem	Hypotheses for the Cause	Experiments Designed to test the Hypotheses	Predicted Results	Observed Results	Conclusions from Results
1) Chloride intrusion from the Tampa Bay area to the east (landward) is too limited, particularly in the Avon Park Formation.	Resistance caused to landward movement of chlorides by the zone of high hydraulic conductivity extending under Tampa Bay abutting lower conductivity regions to the east.	The zone of high hydraulic conductivity under Pinellas county and Tampa Bay is extended to the Hillsborough County shoreline.	Chloride intrusion will accordingly move landward until the shoreline.	Chlorides move shoreward but not proportionately. More shoreward movement in upper layers of Avon Park Formation causes interface slant to become more vertical.	Experiment successful to a certain degree. However, this conceptualization was undesirable since the hydraulic conductivities are no longer representative of the District's conceptualization. A more vertical interface is also less desirable.
	Freshwater is not flowing out of the top of the model (i.e., Suwannee) at a sufficient rate to allow saltwater to intrude.	The general head boundary (GHB) conductance term of Layer 1 is increased by a factor of four.	Chloride intrusion will be greater.	In Tampa Bay area, chlorides intrude about 3 miles in layer 6 and about half a mile in layer 10 making the interface more vertical.	Desirable intrusion effects but undesirable effect on the slope of the interface.
	Saltwater is moving vertically up through the Ocala, rather than intruding further laterally.	The vertical hydraulic conductivity of the Ocala is lowered by an order of magnitude.	Chlorides should intrude more inland with less saltwater moving upwards.	In northern part of the model domain, chlorides move seaward. In south, chlorides remain the same.	The lower vertical (Kv) hydraulic conductivity of the Ocala also reduces upward freshwater flow pushing chlorides seawards in the North. In the South, the Ocala is thick, so the confining effect is not altered by reducing Kv further.

Table 5.1 (continued)
Representative Calibration Simulations for the Saltwater Intrusion Model

Statement of the Problem	Hypotheses for the Cause	Experiments Designed to test the Hypotheses	Predicted Results	Observed Results	Conclusions from Results
1) Chloride intrusion from the Tampa Bay area to the east (landward) is too limited, particularly in the Avon Park Formation. (continued)	From previous experiment described above, it was determined that freshwater needs to exit the Avon Park Formation faster than saltwater for further intrusion top layer of the model (i.e., Suwannee) to allow saltwater intrusion.	The vertical hydraulic conductivity of the Ocala is made four times higher throughout the model domain.	Chlorides should push more inland with more freshwater escaping upwards.	Chlorides move landward throughout domain. More movement is observed in layer 6 than in layer 8. Thus, the slope on the interface becomes more vertical.	Helps with front location but not with interface slope. Higher Kv reduces confining effect of thick Ocala in south. Experiments 12 and 13 suggest non-uniform (from east to west) changes in Ocala Kv may be needed.
	Intruding seawater follows path of least resistence upwards to Tampa Bay.	Use a 1,000:1 (Kh/Kv) anisotropy ratio for Avon Park Formation to reduce its vertical conductance.	Chloride front will move more landward.	Almost no change in front location, or in simulated heads.	Uniform anisotropy reduction slows down upward movement of both salt and freshwater. A non-uniform reduction in vertical hydraulic conductivity over Tampa Bay may be needed.
	Possible chloride intrusion from bottom of model (i.e., evaporites) is ignored.	Allow chloride intrusion from bottom using a GHB condition	More chlorides in domain due to intrusion from bottom.	Chloride landward intrusion is too far especially in southern portions of the model domain.	Chloride intrusion from the bottom could help solve the problem of chlorides being to far seaward.

Table 5.1 (continued)
Representative Calibration Simulations for the Saltwater Intrusion Model

Statement of the Problem	Hypotheses for the Cause	Experiments Designed to test the Hypotheses	Predicted Results	Observed Results	Conclusions from Results
1) Chloride intrusion from the Tampa Bay area to the east (landward) is too limited, particularly in the Avon Park Formation. (continued)	Too much freshwater is coming into the model domain from upstream (i.e., northen, southern and eastern) boundaries.	Reduce transmissivity of Avon Park Formation by 30% to allow less water to enter/flow through the domain	Less freshwater entering domain allows for the saltwater to intrude more.	Chlorides move landward in Avon Park Formation.	Reduced flows help saltwater intrusion, however smaller transmissivities are not justifiable based on the field data.
2) Chloride upconing from the base of model (i.e., evaporites) is too large, once this conceptualization is included.	Conductivity of GHB on the base of the model is too high allowing excessive brine to intrude from the bottom.	Reduce GHB conductance value at bottom.	Less saltwater entering the domain from bottom will push chlorides seaward.	Chlorides are more seawards in the south, but too far seawards in Tampa Bay area in the north.	Bottom boundary GHB of constant value either underpredicts chlorides in north or overpredicts them in south. It may be necessary to assign variable GHB boundaries and/or chloride concentrations on the GHB.
	Bottom GHB instantly supplies chlorides which results in chloride concentrations being too high.	Add one more layer representing the middle confining unit (i.e., evaporites) at bottom, through which chlorides move before reaching the Avon Park Formation.	Chlorides residing within middle confining unit should now move towards Avon Park Formation thereby reducing the intrusion rates.	Chlorides do not instantly upcone into Avon Park Formation.	An extra layer for MSU is needed at the bottom to appropriately represent the transients in the chloride migration.

Table 5.1 (continued)
Representative Calibration Simulations for the Saltwater Intrusion Model

Statement of the Problem	Hypotheses for the Cause	Experiments Designed to test the Hypotheses	Predicted Results	Observed Results	Conclusions from Results
3) Chlorides are too dispersed vertically, thereby limiting lateral intrusion.	Vertical dispersivity is too large.	Apply a 4-component dispersivity formulation and reduce longitudinal vertical dispersivity.	Chloride front will be less vertically diffuse causing more intrusion in lower layers of the model.	Areal chloride contours became more closely spaced in Suwannee Limestone but are still too dispersed vertically.	Reduction in vertical dispersivities results in greater saltwater intrusion inland.
	Diffusion is spreading the chlorides.	Diffusion coefficient is set to zero.	Chloride spread should be less due to no diffusion.	Very slight effect, although helpful.	Reducing diffusion helps but only marginally.
	Dispersion is spreading the chlorides.	All dispersion coefficients are reduced.	Chloride spread should be less due to lower dispersion coefficients.	Reduced the chloride spread considerably. The slope of the interface is also improved although more improvement is needed.	Low dispersivities are needed to reduce spread of chlorides and provide a slope to the interface.
4) Boundary conditions may not be appropriate	Western boundary heads are not representative of field conditions. These heads were taken from the Southern District Model which already account for average density effects.	Heads along western boundary set to zero (previously ranged from 10 - 20 ft), increasing with depth to account for chloride density.	Conceptualization is consistent. Chlorides will move seaward due to reduction of seaward heads.	Chlorides move seaward by about 1 mile. Environmental heads drop but still high as compared to Southern District Model.	Head field is satisfactory but chlorides need to move landward especially in Tampa Bay area. Effect of this on chlorides exists, but is not very prominent.

Table 5.1 (continued)
Representative Calibration Simulations for the Saltwater Intrusion Model

Statement of the Problem	Hypotheses for the Cause	Experiments Designed to test the Hypotheses	Predicted Results	Observed Results	Conclusions from Results
4) Boundary conditions may not be appropriate (continued)	Need to test the effect of northern lateral boundary heads on the area of interest.	Variation of heads along this boundary from west to east changed.	Unknown.	No change in chloride concentrations throughout the domain, or in heads in areas of interest.	Northern lateral boundary heads insensitive to intrusion and can be used from the Southern District Model.
5) Chloride front not sloped like observed under Tampa Bay.	A vertically consistent high K region under Tampa Bay makes the chlorides sit vertically abutting it.	Remove the high K region with K of a similar order as those landward.	Deeper seawater will flow further inland as compared to shallower regions without being controlled by a "wall effect".	Chlorides move seaward due to lower conductivities in the seawater region, but the interface slant is not affected.	For the current state being simulated, the high K region under Tampa Bay is not a controlling mechanism.
6) Avon Park Formation conceptualization does not account for vertical zones of higher conductivity.	All Avon Park Formation model layers have same conductivity value as calculated from Southern District Model.	Model layers 6 and 7 conductivities increased with associated decrease in conductivity of layers 8, 9 and 10 to produce the same transmissivity values as for the Southern District Model.	Conceptualization is consistent with observations. Chloride intrusion behavior will change due to the further vertical zonation.	Chlorides at about the same location in lower layers, but moves westward in upper layers. Therefore, the interface slope is less vertical in layers 6, 7 and 8 (as needed), but becomes more vertical in the lower layers.	Chlorides need to be further landward. Also, interface slope needs to be less vertical specifically in model layers 9 and 10.

Table 5.1 (continued)
Representative Calibration Simulations for the Saltwater Intrusion Model

Statement of the Problem	Hypotheses for the Cause	Experiments Designed to test the Hypotheses	Predicted Results	Observed Results	Conclusions from Results
7) Vertical zones of higher conductivity in AP do not have the hydraulic conductivity characterized. Interface needs to be less vertical.	Southern District Model does not include this conceptualization.	Model layers 6 and 7 conductivities increased by factor of 3 from the above experiment, with reduction of conductivity of layers 8, 9 and 10 for same effective transmissivity as that of Southern District Model.	Problem 6 above made the interface less vertical, so furthering the conductivity contrast of layers 6 and 7 with layers 8, 9 and 10 should make it even less vertical.	No change in chlorides.	Conductivity contrast of high K flow zones within AP is not significant beyond what is provided in experiment 6 above.
8) Post-development heads are higher than for Southern District Model or observed cases.	Water entering from bottom GHB in addition to Southern District Model conceptualization causes higher heads.	Reduce bottom GHB conductance to allow less water in.	Less water inflow will allow for larger drawdowns during pumping.	Drawdowns are greater, but salt intrusion is not sufficient in Tampa Bay area.	Need more water inflow from bottom to maintain salts. Note that pre-development heads are also higher, than the Southern District Model, so drawdowns are not that different.
	Excess freshwater entering domain from north and east supplies wells.	Lower northern and eastern boundary heads by 10 ft.	Less freshwater entering domain will cause for larger drawdowns with pumping as well as greater intrusion of saltwater.	Drawdowns are greater, and, as desired, saltwater intrusion is more extensive in the Avon Park Formation in the Tampa Bay area, but also greater in the south which is undesirable.	Allowing less freshwater into the system from lateral boundaries helps calibrate heads and chlorides in the north but worsens chloride behavior in the south.

Table 5.2
Calibrated Transport Properties

Parameter	Value
Effective porosity	0.15
Freshwater density	1.0
Saltwater density	1.025
Storativity	$1x10^{-4}$

Formation/Unit	Longitudinal dispersivity (ft)	Transverse dispersivity (ft)	Vertical transverse dispersivity (ft)
Suwannee Limestone	100	20	10
Ocala Limestone	10	5	5
Avon Park Formation	80	15	10

Table 5.3
Calibration Statistics for Observed ROMP Well Data

Well	Elevation (ft)	Average Fraction of Seawater at ROMP Well	Simulated Post-development Fraction of Seawater	Residual (data - model)	Residual Squared (data - model)^2
ROMP 22	-416.3	1.12E-03	9.88E-12	1.12E-03	1.25E-06
	-548.7	1.07E-03	4.19E-11	1.07E-03	1.15E-06
	-686.9	1.10E-03	2.43E-10	1.10E-03	1.21E-06
	-904.5	1.03E-03	2.65E-08	1.03E-03	1.05E-06
	-1073.9	9.47E-04	5.79E-06	9.42E-04	8.87E-07
	-1126.5	1.05E-03	4.40E-04	6.12E-04	3.75E-07
	-1197.6	1.16E-03	1.08E-03	7.65E-05	5.86E-09
	-1312.4	1.07E-03	2.32E-06	1.07E-03	1.13E-06
	-1455.9	1.42E-03	3.92E-06	1.42E-03	2.01E-06
	-1598.6	4.51E-03	9.36E-04	3.57E-03	1.28E-05
	-1837.0	5.37E-01	2.73E-02	5.10E-01	2.60E-01
ROMP AB-1	-314.4	1.65E-03	1.36E-03	2.85E-04	8.14E-08
	-413.2	1.64E-03	6.24E-03	-4.60E-03	2.11E-05
	-502.6	1.39E-03	9.69E-03	-8.29E-03	6.88E-05
	-623.0	8.84E-02	1.45E-02	7.39E-02	5.47E-03
	-716.7	4.67E-01	4.66E-02	4.20E-01	1.77E-01
	-750.2	6.70E-01	8.05E-02	5.89E-01	3.47E-01
	-800.5	9.65E-01	1.59E-01	8.06E-01	6.49E-01
ROMP 39	-439.5	8.42E-04	8.37E-28	8.42E-04	7.09E-07
	-541.5	9.82E-04	4.79E-25	9.82E-04	9.65E-07
	-624.4	1.05E-03	4.40E-22	1.05E-03	1.11E-06
	-720.6	9.87E-04	5.84E-19	9.87E-04	9.74E-07
	-839.6	9.37E-04	3.50E-14	9.37E-04	8.78E-07
	-922.4	9.58E-04	1.33E-12	9.58E-04	9.18E-07
	-1055.6	9.74E-04	5.55E-11	9.74E-04	9.48E-07
	-1222.0	1.18E-03	1.54E-07	1.18E-03	1.40E-06
	-1387.3	1.21E-03	2.04E-04	1.01E-03	1.01E-06
	-1617.0	1.25E-01	8.17E-03	1.16E-01	1.36E-02
ROMP TR SA-1	-552.5	2.75E-02	6.80E-02	-4.05E-02	1.64E-03
	-685.0	3.76E-02	1.09E-01	-7.18E-02	5.16E-03
	-803.8	2.66E-02	2.22E-01	-1.95E-01	3.80E-02
	-964.4	4.52E-02	2.66E-01	-2.20E-01	4.86E-02
	-1088.8	8.49E-02	4.88E-01	-4.03E-01	1.63E-01
	-1128.5	2.29E-01	6.78E-01	-4.49E-01	2.02E-01
	-1184.2	7.16E-01	7.86E-01	-6.95E-02	4.82E-03

Table 5.3 (continued)
Calibration Statistics for Observed ROMP Well Data

Well	Elevation (ft)	Average Fraction of Seawater at ROMP Well	Simulated Post-development Fraction of Seawater	Residual (data - model)	Residual Squared (data - model)^2
ROMP 20	-522.8	4.78E-03	2.27E-02	-1.79E-02	3.21E-04
	-630.0	8.25E-03	6.55E-02	-5.73E-02	3.28E-03
	-781.2	2.30E-02	2.34E-01	-2.12E-01	4.47E-02
	-1071.5	3.94E-02	5.20E-01	-4.81E-01	2.31E-01
	-1297.3	7.17E-02	9.84E-01	-9.13E-01	8.33E-01
	-1355.5	6.54E-02	9.92E-01	-9.27E-01	8.59E-01
	-1420.6	5.18E-01	9.96E-01	-4.78E-01	2.28E-01
	-1524.7	8.82E-01	9.94E-01	-1.12E-01	1.27E-02
ROMP TR 7-2	-491.6	2.99E-03	1.22E-03	1.77E-03	3.14E-06
	-611.0	8.59E-03	5.05E-03	3.54E-03	1.25E-05
	-709.8	1.13E-02	9.77E-03	1.50E-03	2.24E-06
	-825.9	1.09E-02	1.07E-02	1.50E-04	2.24E-08
	-915.9	1.11E-02	2.11E-02	-1.01E-02	1.02E-04
	-963.7	1.79E-02	5.12E-02	-3.33E-02	1.11E-03
	-1051.4	2.62E-01	1.14E-01	1.48E-01	2.20E-02
ROMP TR 8-1	-565.3	5.32E-03	2.12E-02	-1.59E-02	2.52E-04
	-667.7	4.32E-03	3.34E-02	-2.91E-02	8.44E-04
	-773.1	5.49E-03	3.93E-02	-3.39E-02	1.15E-03
	-854.0	4.95E-03	8.07E-02	-7.57E-02	5.73E-03
	-885.4	7.17E-02	1.16E-01	-4.39E-02	1.93E-03
	-937.0	2.01E-01	2.07E-01	-6.60E-03	4.35E-05
	-1018.7	8.11E-01	6.59E-01	1.52E-01	2.31E-02
ROMP 33	-517.5	7.76E-04	1.77E-25	7.76E-04	6.03E-07
	-610.0	8.16E-04	2.22E-22	8.16E-04	6.66E-07
	-695.0	7.89E-04	1.02E-19	7.89E-04	6.23E-07
	-813.6	7.47E-04	3.64E-17	7.47E-04	5.59E-07
	-905.3	7.37E-04	1.65E-14	7.37E-04	5.43E-07
	-944.1	7.37E-04	3.28E-13	7.37E-04	5.43E-07
	-1008.8	7.16E-04	4.17E-12	7.16E-04	5.12E-07
	-1111.0	6.84E-04	2.83E-10	6.84E-04	4.68E-07
	-1238.4	8.68E-04	6.58E-07	8.68E-04	7.53E-07
	-1367.2	8.60E-04	4.58E-04	4.01E-04	1.61E-07
	-1575.2	9.10E-04	1.35E-02	-1.26E-02	1.58E-04
ROMP TR 9-2	-311.8	2.37E-03	5.83E-04	1.79E-03	3.19E-06
	-410.1	3.86E-03	2.63E-03	1.24E-03	1.53E-06
	-500.2	5.33E-03	5.11E-03	2.19E-04	4.79E-08
	-622.2	6.18E-03	8.14E-03	-1.96E-03	3.83E-06

Table 5.3 (continued)
Calibration Statistics for Observed ROMP Well Data

Well	Elevation (ft)	Average Fraction of Seawater at ROMP Well	Simulated Post-development Fraction of Seawater	Residual (data - model)	Residual Squared (data - model)^2
ROMP TR 9-2 (cont.)	-717.0	4.95E-03	2.74E-02	-2.24E-02	5.03E-04
	-750.8	1.58E-01	5.13E-02	1.07E-01	1.14E-02
	-802.4	7.01E-01	1.15E-01	5.86E-01	3.44E-01
	-884.4	9.53E-01	5.97E-01	3.56E-01	1.27E-01
	-987.2	9.72E-01	9.76E-01	-4.13E-03	1.71E-05
	-1090.0	6.47E-01	9.98E-01	-3.51E-01	1.23E-01
	-1255.1	9.36E-01	1.00E+00	-6.40E-02	4.09E-03
ROMP TR AB-3	-594.5	1.78E-03	9.61E-04	8.15E-04	6.64E-07
	-680.8	1.65E-03	3.08E-03	-1.43E-03	2.05E-06
	-718.3	1.66E-03	6.09E-03	-4.43E-03	1.96E-05
	-781.2	1.09E-02	1.90E-02	-8.07E-03	6.52E-05
	-881.9	5.22E-02	2.86E-01	-2.34E-01	5.48E-02
ROMP 49	-1203.3	9.08E-04	3.94E-04	5.14E-04	2.65E-07
	-1406.0	2.51E-01	1.42E-02	2.36E-01	5.59E-02
ROMP TR 7-4	-500.4	2.56E-03	1.37E-04	2.42E-03	5.86E-06
	-621.2	2.28E-03	7.31E-04	1.55E-03	2.39E-06
	-724.0	2.65E-03	1.97E-03	6.82E-04	4.65E-07
	-853.1	2.27E-03	2.26E-03	3.21E-06	1.03E-11
	-953.7	2.00E-03	4.84E-03	-2.84E-03	8.08E-06
	-998.7	2.04E-03	1.20E-02	-9.94E-03	9.88E-05
	-1075.8	2.37E-03	2.99E-02	-2.75E-02	7.56E-04
ROMP TR SA-3	-689.4	3.16E-03	3.56E-02	-3.24E-02	1.05E-03
	-813.7	3.83E-03	1.00E-01	-9.61E-02	9.24E-03
	-984.6	5.32E-03	1.16E-01	-1.11E-01	1.23E-02
	-1117.8	5.30E-03	2.75E-01	-2.70E-01	7.27E-02
	-1159.4	5.05E-03	5.72E-01	-5.67E-01	3.22E-01
	-1216.1	2.77E-01	7.25E-01	-4.48E-01	2.01E-01
ROMP 61	-277.8	9.11E-04	1.41E-21	9.11E-04	8.29E-07
	-923.4	7.89E-04	1.20E-09	7.89E-04	6.23E-07
ROMP TR 9-1	-326.7	1.52E-03	7.63E-03	-6.11E-03	3.73E-05
	-452.4	1.47E-03	2.15E-02	-2.00E-02	4.02E-04
ROMP 50	-506.0	7.11E-04	1.41E-05	6.96E-04	4.85E-07
	-608.7	8.42E-04	5.17E-05	7.90E-04	6.25E-07
	-732.9	9.12E-04	2.30E-04	6.82E-04	4.65E-07
	-814.5	8.33E-04	1.24E-03	-4.07E-04	1.66E-07
	-945.8	8.90E-04	8.65E-02	-8.56E-02	7.33E-03
	-1110.2	9.34E-04	3.88E-01	-3.87E-01	1.50E-01

Table 5.3 (continued)
Calibration Statistics for Observed ROMP Well Data

Well	Elevation (ft)	Average Fraction of Seawater at ROMP Well	Simulated Post-development Fraction of Seawater	Residual (data - model)	Residual Squared (data - model)^2
ROMP 50 (cont.)	-1274.1	1.20E-03	9.05E-01	-9.04E-01	8.17E-01
	-1491.4	5.44E-01	9.82E-01	-4.39E-01	1.92E-01
				Average	RMS
				-4.39E-02	0.245498591

Table 5.4
Global Mass Budget for Pre-development Conditions

Budget Term	inflow (ft^3/d)	outflow (ft^3/d)	inflow (MGD)	outflow (MGD)
Eastern fresh boundary	10628115.2	16296.6	79.50	0.12
Southern fresh boundary	2778218	3212346	20.78	24.03
Northern fresh boundary	2239468	556303	16.75	4.16
lateral salt boundary	15783043.9	17658496	118.07	132.10
drain	0	5573737.8	0.00	41.69
bottom boundary	5318106.6	2226518	39.78	16.66
top boundary	6899861.6	14403115.9	51.61	107.74
Total	43646813.3	43646813.3	326.50	326.50

Table 5.5
Global Mass Budget for Post-development December 2000 Conditions

Budget Term	Inflow (ft^3/d)	Outflow (ft^3/d)	Inflow (mgal/day)	Outflow (mgal/day)
Eastern fresh boundary	8279517.2	739059	61.94	5.53
Southern fresh boundary	4420335.7	4336057.2	33.07	32.44
Northern fresh boundary	3927792.3	303590.3	29.38	2.27
lateral salt boundary	15234670	8991555	113.96	67.26
drain	0	3201738.9	0.00	23.95
bottom boundary	9743780.6	64614.9	72.89	0.48
top boundary	13128151.8	10080930.4	98.21	75.41
well	3571827.5	29861022	26.72	223.38
storage	70.6	727578	0.00	5.44
Total	58306145.7	58306145.7	436.16	436.16

Table 6.1
Scenarios and Results of Parameter Sensitivity Analysis

Sensitivity Parameter or Boundary Condition	Multiplication / Addition Factor	Chloride Data Fit			Hydraulic Head Data Fit			
		Percentage of Calibration Targets that are Overpredicted	Normalized Concentration		Change in final heads		Difference in head	
			Avg. Error (data-model)	RMS Error (data-model)	Avg. Error (base-final)	RMS Error (base-final)	Avg. Error (L6-L2)	RMS Error (L6-L2)
Sensitivity Parameter 0 : Base Case	n/a	45.9	-4.386E-02	0.245	0.0	0.0	2.3	3.7
Sensitivity Parameter 1 : Porosity	Multiply 0.5	56.8	-8.194E-02	0.269	0.2	0.4	2.2	3.6
	Multiply 0.2	70.3	-2.136E-01	0.375	0.8	1.3	2.1	3.4
	Multiply 2	42.3	-2.707E-02	0.238	-0.1	0.2	2.3	3.7
Sensitivity Parameter 2 : Avon Park Formation Conductivity (Layer 6-10)	Multiply 0.5	59.5	-8.342E-02	0.251	3.6	4.4	1.6	3.2
	Multiply 2	40.5	-2.065E-02	0.254	-3.0	3.5	2.9	4.3
Sensitivity Parameter 3 : Avon Park Formation Conductivity (Layer 6-7)	Multiply 0.5	60.4	-7.658E-02	0.242	3.5	4.2	1.7	3.2
	Multiply 2	39.6	-2.812E-02	0.259	-2.9	3.4	2.9	4.3
Sensitivity Parameter 4 : Ocala Region Leakance (Layer 3-5)	Multiply 0.5	44.1	-3.582E-02	0.241	-0.1	1.0	3.8	5.3
	Multiply 2	49.5	-4.808E-02	0.248	0.1	0.6	1.4	2.7
Sensitivity Parameter 5 : Suwannee Region Conductivity (Layer 1-2)	Multiply 0.5	45.0	-3.947E-02	0.244	0.1	0.5	2.3	3.8
	Multiply 2	50.5	-4.928E-02	0.248	-0.3	0.6	2.2	3.6
Sensitivity Parameter 6 : Top GHB conductance	Multiply 0.5	45.0	-3.513E-02	0.237	-0.2	1.3	2.5	3.6
	Multiply 2	50.5	-5.263E-02	0.256	-0.2	1.8	1.8	4.0
Sensitivity Parameter 7 : Top GHB conductance under Tampa bay	Multiply 0.5	44.1	-3.815E-02	0.242	-0.5	0.8	2.2	3.6
	Multiply 2	50.5	-4.965E-02	0.248	0.6	1.0	2.4	3.8
Sensitivity Parameter 8 : Top GHB head	Add -10	55.0	-5.826E-02	0.256	0.8	1.0	2.6	3.8
	Add +10	39.6	-2.070E-02	0.232	-2.0	2.7	1.7	3.3

Table 6.1 (continued)
Scenarios and Results of Parameter Sensitivity Analysis

Sensitivity Parameter or Boundary Condition	Multiplication / Addition Factor	Chloride Data Fit			Hydraulic Head Data Fit			
		Percentage of Calibration Targets that are Overpredicted	Normalized Concentration		Change in final heads		Difference in head	
			Avg. Error (data-model)	RMS Error (data-model)	Avg. Error (base-final)	RMS Error (base-final)	Avg. Error (L6-L2)	RMS Error (L6-L2)
Sensitivity Parameter 9 :	Add -10	33.3	-1.176E-02	0.247	0.7	0.8	2.2	3.6
Bottom GHB head	Add +10	63.1	-8.453E-02	0.251	-0.6	0.8	2.4	3.7
Sensitivity Parameter 10 :	Multiply 0.5	42.3	-2.816E-02	0.254	0.7	1.0	2.2	3.6
Bottom GHB conductance	Multiply 2	55.0	-6.308E-02	0.238	-1.2	1.6	2.4	3.8
Sensitivity Parameter 11 :	Add +10	47.7	-5.979E-02	0.263	-2.5	3.5	2.5	4.0
Coastal Lateral Boundary head	Add +20	50.5	-1.149E-01	0.318	-5.1	6.7	2.8	4.3
Sensitivity Parameter 12 :	Add -10	64.9	-1.107E-01	0.305	3.9	4.8	2.1	3.8
Landward Lateral Boundary head	Add +10	41.4	-5.341E-02	0.578	-2.9	4.3	2.3	3.7
Sensitivity Parameter 13 :	Multiply 5	52.3	-3.021E-02	0.256	0.0	0.3	2.3	3.7
Dispersion coefficients	Multiply 20	54.1	-2.634E-02	0.260	0.0	0.4	2.3	3.7
Sensitivity Parameter 14 :	Multiply 0	43.2	-3.531E-02	0.244	0.0	0.2	2.3	3.7
Diffusion coefficient	Multiply 5	52.3	-4.128E-02	0.241	0.0	0.1	2.3	3.7
Sensitivity Parameter 15 :	Multiply 0.1	43.2	-3.660E-02	0.248	-0.5	2.0	2.2	3.6
Avon Park Formation vertical anisotropy	Multiply 10	47.7	-4.390E-02	0.245	0.1	0.4	2.3	3.7

Table 6.1 (continued)
Scenarios and Results of Parameter Sensitivity Analysis

Sensitivity Parameter or Boundary Condition	Top Flux (MGD)		Bottom Flux (MGD)		Chloride Mass (kg)	Percent of Wells		Sensitivity Type
	Flow in	Flow out	Flow in	Flow out		>1,000 mg/l	>500 mg/l	
Sensitivity Parameter 0 : Base Case	9.82E+01	7.54E+01	7.29E+01	4.83E-01	2.20863E+11	10.74	15.11	
Sensitivity Parameter 1 :	9.84E+01	7.37E+01	7.22E+01	4.95E-01	1.12936E+11	14.05	17.86	III
Porosity	9.91E+01	6.94E+01	7.08E+01	5.33E-01	47826342636	21.42	27.12	
	9.81E+01	7.63E+01	7.32E+01	4.78E-01	4.36786E+11	9.11	13.54	
Sensitivity Parameter 2 :	1.05E+02	6.15E+01	8.12E+01	3.87E-01	2.34559E+11	14.66	20.81	III
Avon Park Formation Conductivity (Layer 6-10)	9.27E+01	9.31E+01	6.65E+01	7.90E-01	2.06053E+11	4.17	11.25	
Sensitivity Parameter 3 :	1.05E+02	6.17E+01	8.09E+01	3.89E-01	2.34095E+11	14.25	20.51	III
Avon Park Formation Conductivity (Layer 6-7)	9.28E+01	9.29E+01	6.66E+01	7.44E-01	2.06426E+11	4.83	11.65	
Sensitivity Parameter 4 :	9.90E+01	7.16E+01	7.21E+01	4.92E-01	2.16348E+11	9.52	14.45	I
Ocala Region Leakance (Layer 3-5)	9.79E+01	7.82E+01	7.34E+01	4.81E-01	2.23172E+11	11.60	15.83	
Sensitivity Parameter 5 :	9.36E+01	7.10E+01	7.34E+01	4.83E-01	2.2047E+11	11.40	15.83	I
Suwannee Region Conductivity (Layer 1-2)	1.02E+02	8.14E+01	7.21E+01	4.89E-01	2.20661E+11	10.99	14.45	
Sensitivity Parameter 6 :	5.23E+01	4.77E+01	7.40E+01	4.67E-01	2.12184E+11	10.08	14.25	II
Top GHB conductance	1.78E+02	1.15E+02	7.08E+01	5.22E-01	2.30721E+11	12.42	16.90	
Sensitivity Parameter 7 :	9.66E+01	6.63E+01	7.26E+01	4.85E-01	2.15242E+11	9.97	14.81	I
Top GHB conductance under Tampa bay	1.00E+02	8.63E+01	7.32E+01	4.84E-01	2.26944E+11	11.30	15.98	
Sensitivity Parameter 8 :	6.91E+01	9.73E+01	7.37E+01	4.79E-01	2.264E+11	12.52	17.30	III
Top GHB head	1.65E+02	2.77E+01	7.08E+01	4.93E-01	2.04739E+11	8.75	12.57	
Sensitivity Parameter 9 :	9.91E+01	7.40E+01	4.28E+01	2.90E+00	2.13647E+11	6.51	10.74	III
Bottom GHB head	9.74E+01	7.62E+01	1.05E+02	1.75E-01	2.28308E+11	15.17	22.70	
Sensitivity Parameter 10 :	9.92E+01	7.44E+01	3.87E+01	2.53E-01	2.17107E+11	7.94	13.28	II
Bottom GHB conductance	9.66E+01	7.71E+01	1.32E+02	9.26E-01	2.25564E+11	12.57	17.51	
Sensitivity Parameter 11 :	9.40E+01	9.84E+01	5.91E+01	5.13E-01	2.35311E+11	11.30	16.03	II
Coastal Lateral Boundary head	8.99E+01	1.29E+02	4.36E+01	8.41E-01	2.46999E+11	15.11	19.29	
Sensitivity Parameter 12 :	1.27E+02	5.76E+01	7.99E+01	1.88E-01	2.39063E+11	15.67	21.58	III
Landward Lateral Boundary head	7.72E+01	1.45E+02	2.16E+01	3.08E+00	2.13392E+11	2.44	5.60	

Table 6.1 (continued)
Scenarios and Results of Parameter Sensitivity Analysis

Sensitivity Parameter or Boundary Condition	Top Flux (MGD)		Bottom Flux (MGD)		Chloride Mass (kg)	Percent of Wells		Sensitivity Type
	Flow in	Flow out	Flow in	Flow out		>1,000 mg/l	>500 mg/l	
Sensitivity Parameter 13 :	9.81E+01	7.60E+01	7.39E+01	4.76E-01	2.17542E+11	9.26	15.73	I
Dispersion coefficients	9.81E+01	7.65E+01	7.48E+01	4.72E-01	2.15226E+11	9.97	18.27	
Sensitivity Parameter 14 :	9.82E+01	7.57E+01	7.30E+01	4.81E-01	2.19801E+11	9.26	13.49	I
Diffusion coefficient	9.82E+01	7.55E+01	7.32E+01	4.82E-01	2.19707E+11	11.35	16.34	
Sensitivity Parameter 15 :	9.88E+01	7.48E+01	5.95E+01	3.83E-01	2.18882E+11	9.77	14.30	I
Avon Park Formation vertical anisotropy	9.81E+01	7.56E+01	7.50E+01	5.23E-01	2.20614E+11	10.74	15.27	

Table 6.2
Scenarios and Results of Conceptual Sensitivity Analysis

Sensitivity Parameter or Boundary Condition	Percent of data points where model is high	Chloride Data fit: Normalized Concentration Error	
		Avg. (data-model)	RMS (data-model)
Sensitivity Parameter 0 : Base Case	45.946	-4.386E-02	0.245
Sensitivity Parameter 1 : Bottom GHB only in North-West	32.432	-7.534E-03	0.265
With higher GHB conductances	33.333	9.774E-03	0.246
Sensitivity Parameter 2 : Avon Park conductivity uniform vertically	44.144	1.641E-02	0.240

Sensitivity Parameter or Boundary Condition	Change in final heads (ft)		Difference in head (ft)		Top Flux (MGD)	
	Avg. (base-final)	RMS (base-final)	Avg. (L'6-L2)	RMS (L'6-L2)	Flow in	Flow out
Sensitivity Parameter 0 : Base Case	0.0	0.0	2.3	3.7	9.82E+01	7.54E+01
Sensitivity Parameter 1 : Bottom GHB only in North-West	1.4	1.9	2.1	3.5	1.00E+02	7.33E+01
With higher GHB conductances	1.3	3.0	2.6	4.0	1.03E+02	7.80E+01
Sensitivity Parameter 2 : Avon Park conductivity uniform vertically	-0.4	1.2	2.3	3.7	9.78E+01	7.20E+01

Sensitivity Parameter or Boundary Condition	Bottom Flux (MGD)		Chloride Mass (kg)	Percent of wells with Chloride	
	Flow in	Flow out		>1,000 mg/l	>500 mg/l
Sensitivity Parameter 0 : Base Case	7.29E+01	4.83E-01	2.20863E+11	10.74	15.11
Sensitivity Parameter 1 : Bottom GHB only in North-West	2.24E+01	0.00E+00	2.14566E+11	5.85	9.87
With higher GHB conductances	1.82E+02	0.00E+00	2.21148E+11	6.72	9.67
Sensitivity Parameter 2 : Avon Park conductivity uniform vertically	7.45E+01	5.31E-01	2.17959E+11	9.52	14.25

Table 7.1
Predicted Impacts of Changes in Regional Groundwater Pumpage of Chloride Concentrations in Wells Completed in the Suwannee Limestone, Ocala Limestone, and Avon Park Formation

Regional Pumping (mgal/day)	Year	Chloride Concentration Threshold (mg/L)	Number of Wells Impacted Above Threshold Concentration	1995-1999 Avg. Annual Use (mgal/day)	Change from Current Conditions			
					1999 Permitted Pumping (mgal/day)	# of Wells	1995-1999 Avg. Annual Use (mgal/day)	1999 Permitted Pumping (mgal/day)
Current	2000	500	154	15.84	22.20	0	0.00	0.00
400	2020	500	151	15.22	21.61	-3	-0.62	-0.59
600	2020	500	162	16.02	23.18	8	0.18	0.98
800	2020	500	169	16.47	23.85	15	0.63	1.65
1,000	2020	500	183	17.60	26.24	29	1.76	4.04
400	2050	500	159	15.27	21.49	5	-0.57	-0.71
600	2050	500	188	17.09	25.49	34	1.25	3.29
800	2050	500	204	18.34	27.52	50	2.5	5.32
1,000	2050	500	224	19.95	31.05	70	4.11	8.85
Current	2000	1,000	63	6.35	8.31	0	0.00	0.00
400	2020	1,000	71	7.72	10.13	8	1.37	1.82
600	2020	1,000	82	8.77	12.08	19	2.42	3.77
800	2020	1,000	91	10.14	13.98	28	3.79	5.67
1,000	2020	1,000	104	12.22	17.99	41	5.87	9.68
400	2050	1,000	79	9.18	11.83	16	2.83	3.52
600	2050	1,000	104	12.02	17.40	41	5.67	9.09
800	2050	1,000	126	14.00	20.90	63	7.65	12.59
1,000	2050	1,000	147	15.33	23.24	84	8.98	14.93

Table 7.2
Predicted Impacts of Changes in Regional Groundwater Pumpage of Chloride Concentrations in Wells Completed in the Suwannee Limestone

Regional Pumping (mgal/day)	Year	Chloride Concentration Threshold (mg/L)	Number of Wells Impacted Above Threshold Concentration	1995-1999 Avg. Annual Use (mgal/day)	Change from Current Conditions			
					1999 Permitted Pumping (mgal/day)	# of Wells	1995-1999 Avg. Annual Use (mgal/day)	1999 Permitted Pumping (mgal/day)
Current	2000	500	82	8.68	12.33	0	0.00	0.00
400	2020	500	82	8.75	12.40	0	0.07	0.07
600	2020	500	86	8.84	12.52	4	0.16	0.19
800	2020	500	88	8.94	12.58	6	0.26	0.25
1,000	2020	500	93	9.04	12.82	11	0.36	0.49
400	2050	500	90	8.99	12.62	8	0.31	0.29
600	2050	500	103	9.20	13.04	21	0.52	0.71
800	2050	500	107	9.41	13.38	25	0.73	1.05
1,000	2050	500	113	9.44	13.41	31	0.76	1.08
Current	2000	1,000	29	2.45	3.30	0	0.00	0.00
400	2020	1,000	32	3.32	4.48	3	0.87	1.18
600	2020	1,000	34	3.34	4.50	5	0.89	1.2
800	2020	1,000	35	3.36	4.77	6	0.91	1.47
1,000	2020	1,000	38	4.94	6.68	9	2.49	3.38
400	2050	1,000	36	4.76	6.14	7	2.31	2.84
600	2050	1,000	40	4.93	6.79	11	2.48	3.49
800	2050	1,000	50	6.32	8.84	21	3.87	5.54
1,000	2050	1,000	56	6.62	9.35	27	4.17	6.05

Table 7.3
Predicted Impacts of Changes in Regional Groundwater Pumpage of Chloride Concentrations in Wells Completed in the Ocala Limestone

Regional Pumping (mgal/day)	Year	Chloride Concentration Threshold (mg/L)	Number of Wells Impacted Above Threshold Concentration	1995-1999 Avg. Annual Use (mgal/day)	Change from Current Conditions			
					1999 Permitted Pumping (mgal/day)	# of Wells	1995-1999 Avg. Annual Use (mgal/day)	1999 Permitted Pumping (mgal/day)
Current	2000	500	35	1.35	2.60	0	0.00	0.00
400	2020	500	35	1.35	2.60	0	0	0
600	2020	500	35	1.35	2.60	0	0	0
800	2020	500	35	1.35	2.60	0	0	0
1,000	2020	500	35	1.35	2.60	0	0	0
400	2050	500	35	1.35	2.60	0	0	0
600	2050	500	35	1.35	2.60	0	0	0
800	2050	500	35	1.35	2.60	0	0	0
1,000	2050	500	37	1.46	3.38	2	0.11	0.78
Current	2000	1,000	15	0.57	1.54	0	0.00	0.00
400	2020	1,000	18	0.99	1.96	3	0.42	0.42
600	2020	1,000	18	0.99	1.96	3	0.42	0.42
800	2020	1,000	19	1.00	1.98	4	0.43	0.44
1,000	2020	1,000	21	1.00	1.98	6	0.43	0.44
400	2050	1,000	21	1.00	1.98	6	0.43	0.44
600	2050	1,000	24	1.06	2.13	9	0.49	0.59
800	2050	1,000	25	1.06	2.13	10	0.49	0.59
1,000	2050	1,000	29	1.12	2.22	14	0.55	0.68

Table 7.4
Predicted Impacts of Changes in Regional Groundwater Pumpage of Chloride Concentrations in Wells Completed Wells in the Avon Park Formation

Regional Pumping (mgal/day)	Year	Chloride Concentration Threshold (mg/L)	Number of Wells Impacted Above Threshold Concentration	Change from Current Conditions				
				1995-1999 Avg. Annual Use (mgal/day)	1999 Permitted Pumping (mgal/day)	# of Wells	1995-1999 Avg. Annual Use (mgal/day)	1999 Permitted Pumping (mgal/day)
Current	2000	500	37	5.81	7.26	0	0.00	0.00
400	2020	500	34	5.12	6.61	-3	-0.69	-0.65
600	2020	500	41	5.84	8.06	4	0.03	0.8
800	2020	500	46	6.18	8.67	9	0.37	1.41
1,000	2020	500	55	7.22	10.82	18	1.41	3.56
400	2050	500	34	4.94	6.26	-3	-0.87	-1
600	2050	500	50	6.55	9.85	13	0.74	2.59
800	2050	500	62	7.58	11.54	25	1.77	4.28
1,000	2050	500	74	9.05	14.26	37	3.24	7
Current	2000	1,000	19	3.33	3.47	0	0.00	0.00
400	2020	1,000	21	3.42	3.69	2	0.09	0.22
600	2020	1,000	30	4.45	5.62	11	1.12	2.15
800	2020	1,000	37	5.79	7.23	18	2.46	3.76
1,000	2020	1,000	45	6.29	9.33	26	2.96	5.86
400	2050	1,000	22	3.43	3.71	3	0.1	0.24
600	2050	1,000	40	6.03	8.49	21	2.7	5.02
800	2050	1,000	51	6.61	9.94	32	3.28	6.47
1,000	2050	1,000	62	7.59	11.67	43	4.26	8.2

Table 7.5
Impacts Predicted by Sensitivity Analysis of Wells Completed in the Suwannee Limestone, Ocala Limestone, and Avon Park Formation[1]

Regional Pumping (mgal/day)	Year	Chloride Concentration Threshold (mg/L)	Base Case Number of Wells Impacted	Sensitivity Change from Base Case (# of Wells)					
				#1 (Porosity)		#9 (Bottom GHB Head)		#12 (Landward Lateral Heads)	
				X 0.2	X 2.0	Add -10	Add 10	Add -10	Add 10
Current	2000	500	154	206	-20	-44	160	130	-108
400	2020	500	151	262	-19	-43	175	144	-104
600	2020	500	162	298	-24	-47	176	149	-113
800	2020	500	169	359	-26	-47	180	155	-113
1,000	2020	500	183	434	-39	-56	176	155	-115
400	2050	500	159	409	-27	-51	173	149	-111
600	2050	500	188	483	-43	-59	170	160	-126
800	2050	500	204	579	-51	-53	181	182	-123
1,000	2050	500	224	666	-58	-58	187	193	-128
Current	2000	1,000	63	194	-8	-17	93	98	-44
400	2020	1,000	71	228	-14	-25	89	101	-53
600	2020	1,000	82	273	-22	-31	94	97	-59
800	2020	1,000	91	333	-30	-31	92	101	-65
1,000	2020	1,000	104	406	-40	-43	90	101	-75
400	2050	1,000	79	404	-18	-31	91	106	-59
600	2050	1,000	104	487	-39	-39	92	103	-77
800	2050	1,000	126	555	-46	-46	89	114	-87
1,000	2050	1,000	147	674	-56	-49	89	110	-93

[1] Note: For each sensitivity simulation, the total number of wells that are predicted to be impacted by chlorides above the 500 or 1,000 mg/l thresholds is the sum of the wells that are affected during the basecase simulation and the increase/decrease in the number of affected wells caused by perturbing the model parameter during the sensitivity run.

Table 7.6
Impacts Predicted by Sensitivity Analysis of Wells Completed in the Suwannee Limestone[1]

Regional Pumping (mgal/day)	Year	Chloride Concentration Threshold (mg/L)	Base Case Number of Wells Impacted	Sensitivity Change from Base Case (# of Wells)					
				#1 (Porosity)		#9 (Bottom GHB Head)		#12 (Landward Lateral Heads)	
				X 0.2	X 2.0	Add 10	Add 10	Add 10	Add 10
Current	2000	500	82	102	-11	-20	111	90	-64
400	2020	500	82	141	-10	-20	123	96	-64
600	2020	500	86	150	-14	-24	120	101	-67
800	2020	500	88	177	-16	-24	124	103	-69
1,000	2020	500	93	203	-21	-28	126	105	-72
400	2050	500	90	256	-17	-27	119	99	-71
600	2050	500	103	283	-29	-36	117	102	-79
800	2050	500	107	316	-31	-31	120	115	-77
1,000	2050	500	113	347	-31	-37	120	120	-80
Current	2000	1,000	29	78	-4	-5	52	45	-26
400	2020	1,000	32	117	-6	-8	55	50	-29
600	2020	1,000	34	131	-7	-10	58	52	-31
800	2020	1,000	35	155	-9	-11	57	51	-32
1,000	2020	1,000	38	186	-11	-13	55	51	-34
400	2050	1,000	36	253	-8	-12	56	50	-32
600	2050	1,000	40	290	-11	-15	57	51	-36
800	2050	1,000	50	308	-18	-21	54	53	-46
1,000	2050	1,000	56	353	-22	-25	56	52	-51

[1] Note: For each sensitivity simulation, the total number of wells that are predicted to be impacted by chlorides above the 500 or 1,000 mg/l thresholds is the sum of the wells that are affected during the basecase simulation and the increase/decrease in the number of affected wells caused by perturbing the model parameter during the sensitivity run.

Table 7.7
Impacts Predicted by Sensitivity Analysis of Wells Completed in the Ocala Limestone[1]

Regional Pumping (Mgal/day)	Year	Chloride Concentration Threshold (mg/L)	Base Case Number of Wells Impacted	Sensitivity Change from Base Case (# of Wells)					
				#1 (Porosity)		#9 (Bottom GHB Head)		#12 (Landward Lateral Heads)	
				X 0.2	X 2.0	Add -10	Add 10	Add -10	Add 10
Current	2000	500	35	40	0	-1	25	19	-24
400	2020	500	35	67	0	-1	26	22	-24
600	2020	500	35	68	0	-1	28	23	-24
800	2020	500	35	75	0	-1	29	23	-24
1,000	2020	500	35	85	0	-1	29	24	-23
400	2050	500	35	94	0	-1	28	22	-24
600	2050	500	35	110	0	-1	31	24	-23
800	2050	500	35	124	0	-1	36	27	-23
1,000	2050	500	37	133	-2	-3	38	30	-24
Current	2000	1,000	15	41	0	-1	12	22	-11
400	2020	1,000	18	54	-3	-4	10	21	-14
600	2020	1,000	18	58	-3	-4	12	21	-13
800	2020	1,000	19	66	-3	-3	13	24	-14
1,000	2020	1,000	21	77	-5	-5	13	24	-16
400	2050	1,000	21	95	-5	-5	12	24	-16
600	2050	1,000	24	102	-8	-7	13	21	-19
800	2050	1,000	25	108	-7	-6	13	21	-19
1,000	2050	1,000	29	131	-11	-9	12	17	-21

[1] Note: For each sensitivity simulation, the total number of wells that are predicted to be impacted by chlorides above the 500 or 1,000 mg/l thresholds is the sum of the wells that are affected during the basecase simulation and the increase/decrease in the number of affected wells caused by perturbing the model parameter during the sensitivity run.

Table 7.8
Impacts Predicted by Sensitivity Analysis of Wells Completed in the Avon Park Formation[1]

Regional Pumping (mgal/day)	Year	Chloride Concentration Threshold (mg/L)	Base Case Number of Wells Impacted	Sensitivity Change from Base Case (# of Wells)					
				#1 (Porosity)		#9 (Bottom GHB Head)		#12 (Landward Lateral Heads)	
				X 0.2	X 2.0	Add -10	Add 10	Add -10	Add 10
Current	2000	500	37	64	-9	-23	24	21	-20
400	2020	500	34	54	-9	-22	26	26	-16
600	2020	500	41	80	-10	-22	28	25	-22
800	2020	500	46	107	-10	-22	27	29	-20
1,000	2020	500	55	146	-18	-27	21	26	-20
400	2050	500	34	59	-10	-23	26	28	-16
600	2050	500	50	90	-14	-22	22	34	-24
800	2050	500	62	139	-20	-21	25	40	-23
1,000	2050	500	74	186	-25	-18	29	43	-24
Current	2000	1,000	19	75	-4	-11	29	31	-7
400	2020	1,000	21	57	-5	-13	24	30	-10
600	2020	1,000	30	84	-12	-17	24	24	-15
800	2020	1,000	37	112	-18	-17	22	26	-19
1,000	2020	1,000	45	143	-24	-25	22	26	-25
400	2050	1,000	22	56	-5	-14	23	32	-11
600	2050	1,000	40	95	-20	-17	22	31	-22
800	2050	1,000	51	139	-21	-19	22	40	-22
1,000	2050	1,000	62	190	-23	-15	21	41	-21

[1] Note: For each sensitivity simulation, the total number of wells that are predicted to be impacted by chlorides above the 500 or 1,000 mg/l thresholds is the sum of the wells that are affected during the basecase simulation and the increase/decrease in the number of affected wells caused by perturbing the model parameter during the sensitivity run.

APPENDIX A

MEASURED VARIATION OF CHLORIDES WITH DEPTH FOR THE ROMP WELLS

ROMP TR AB-1

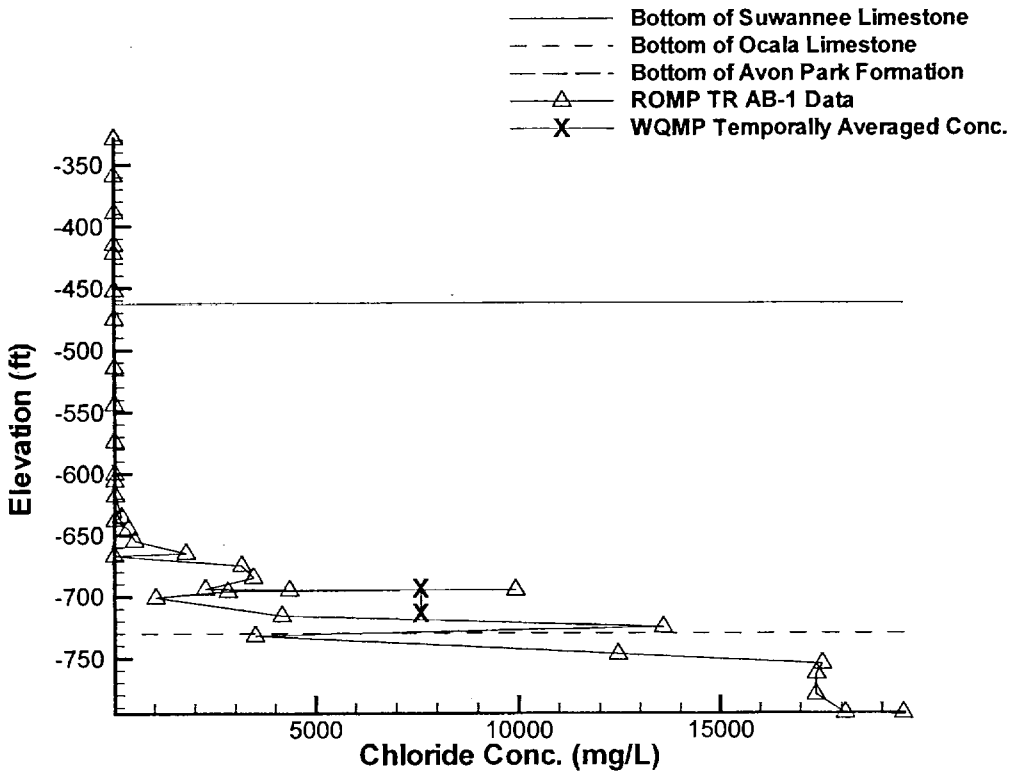

ROMP TR 9-2

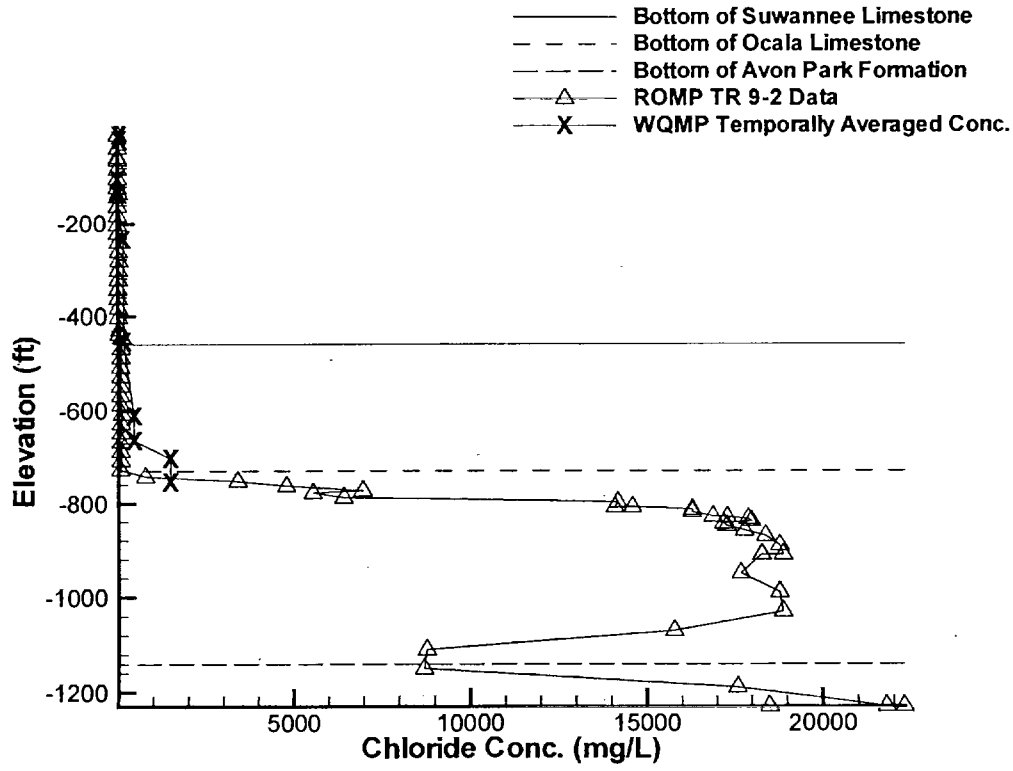

ROMP TR 9-1

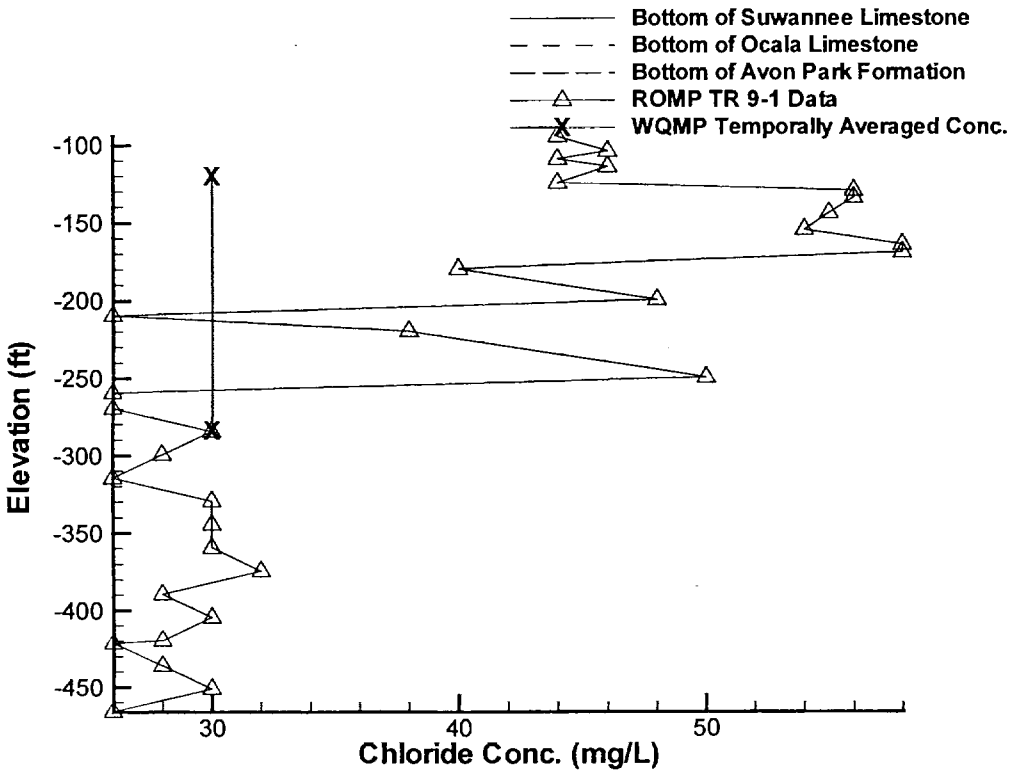

ROMP TR AB-3

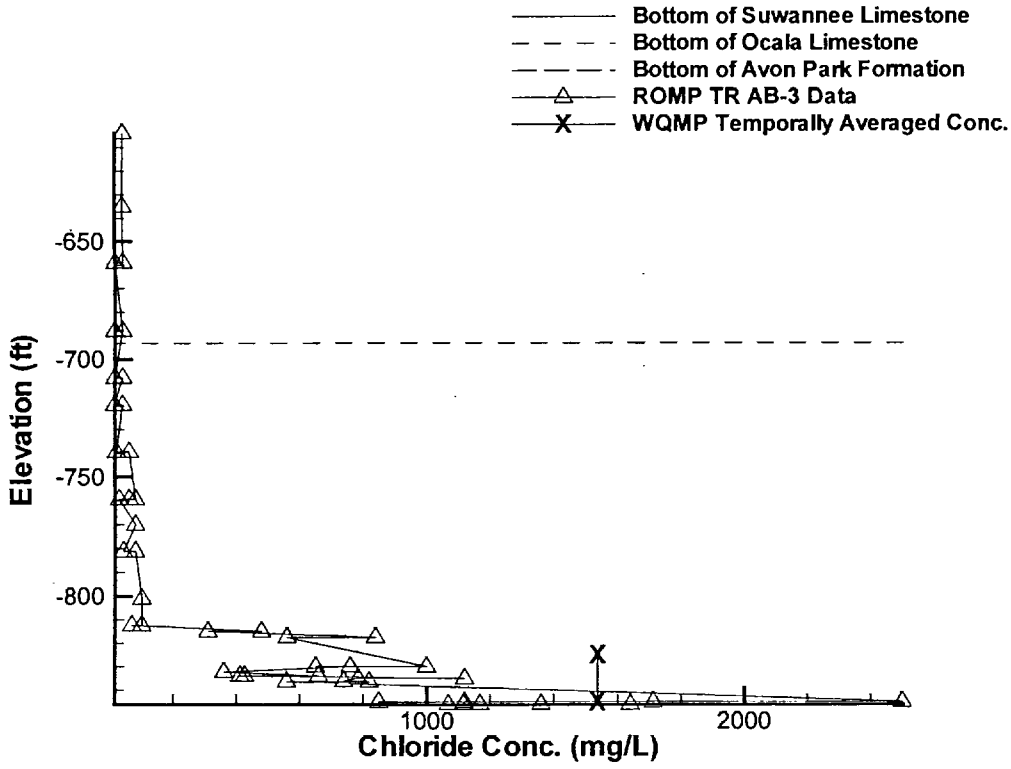

ROMP 50

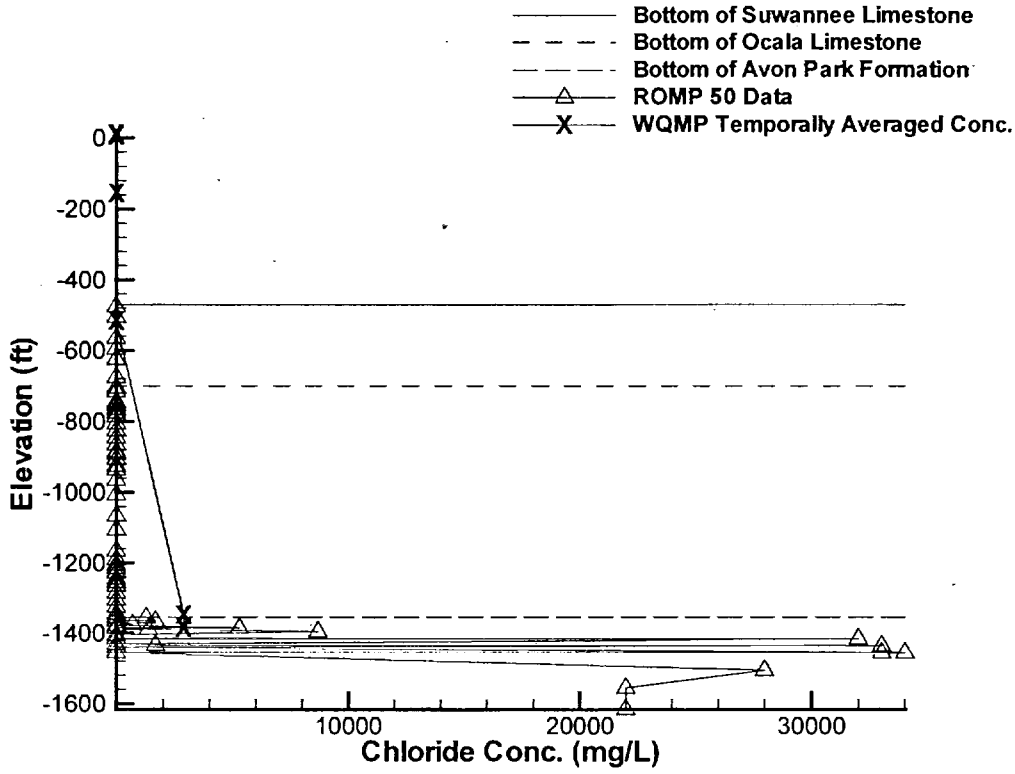

ROMP 39

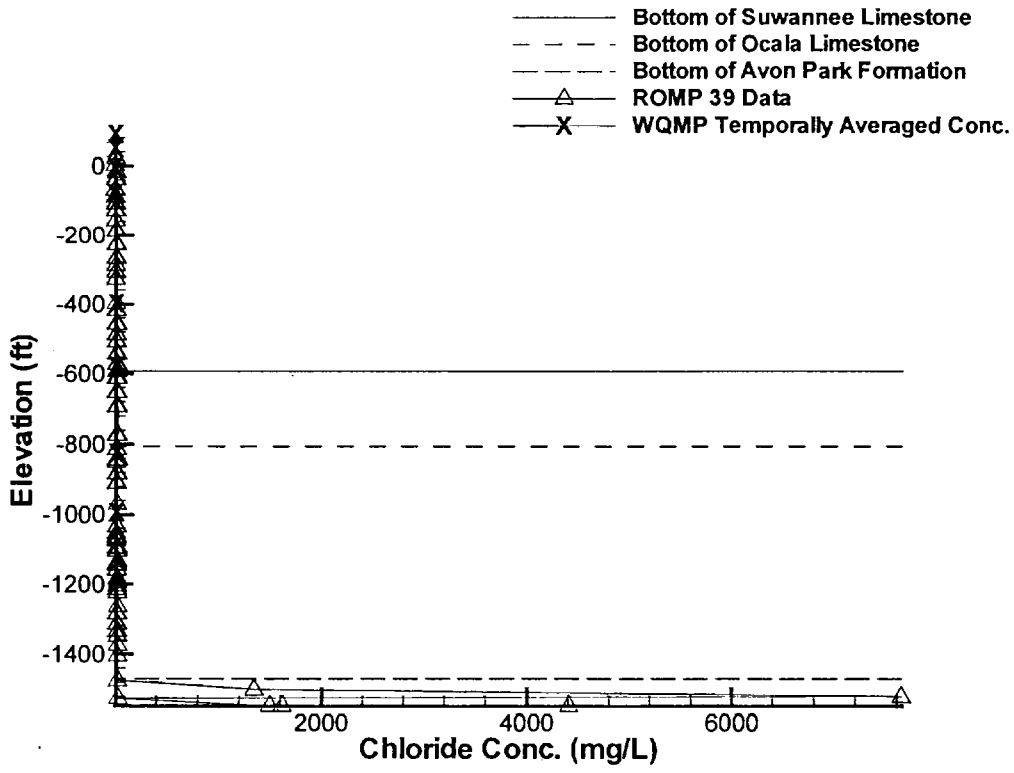

ROMP TR 8-1

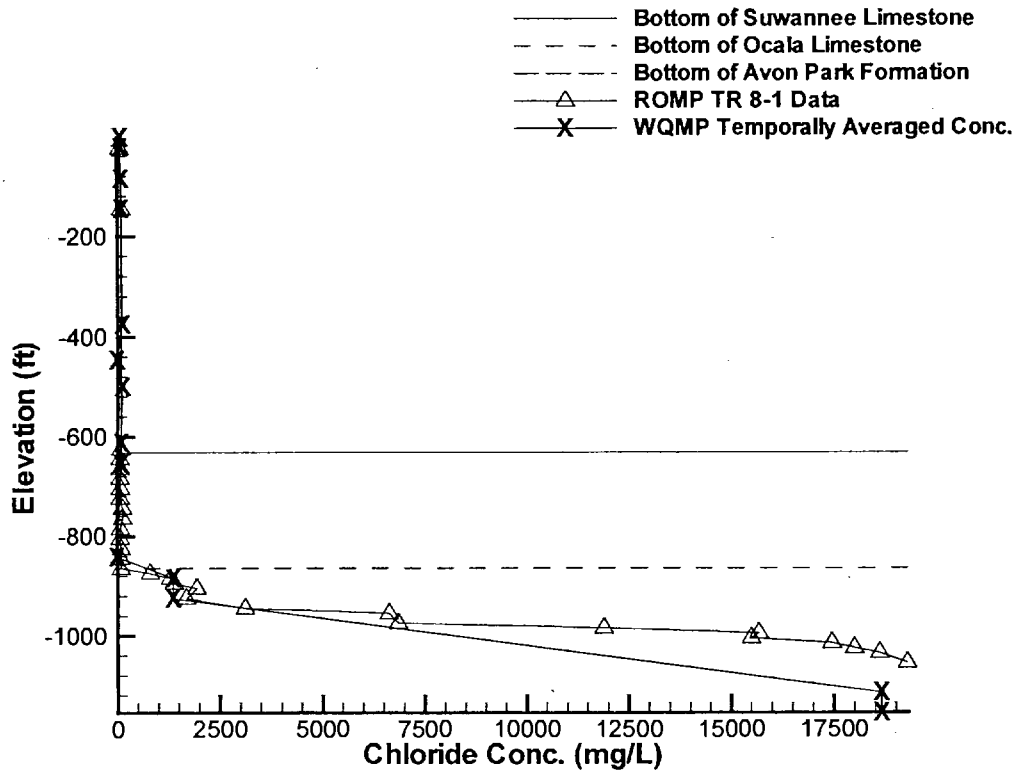

ROMP 33

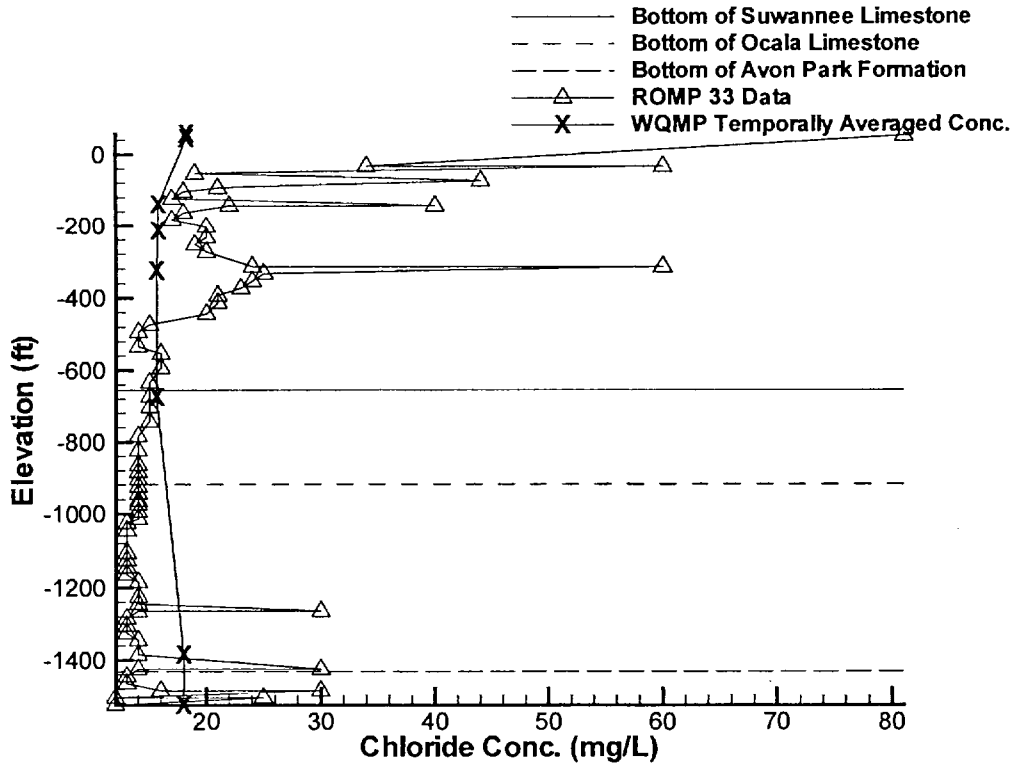

ROMP TR 7-2

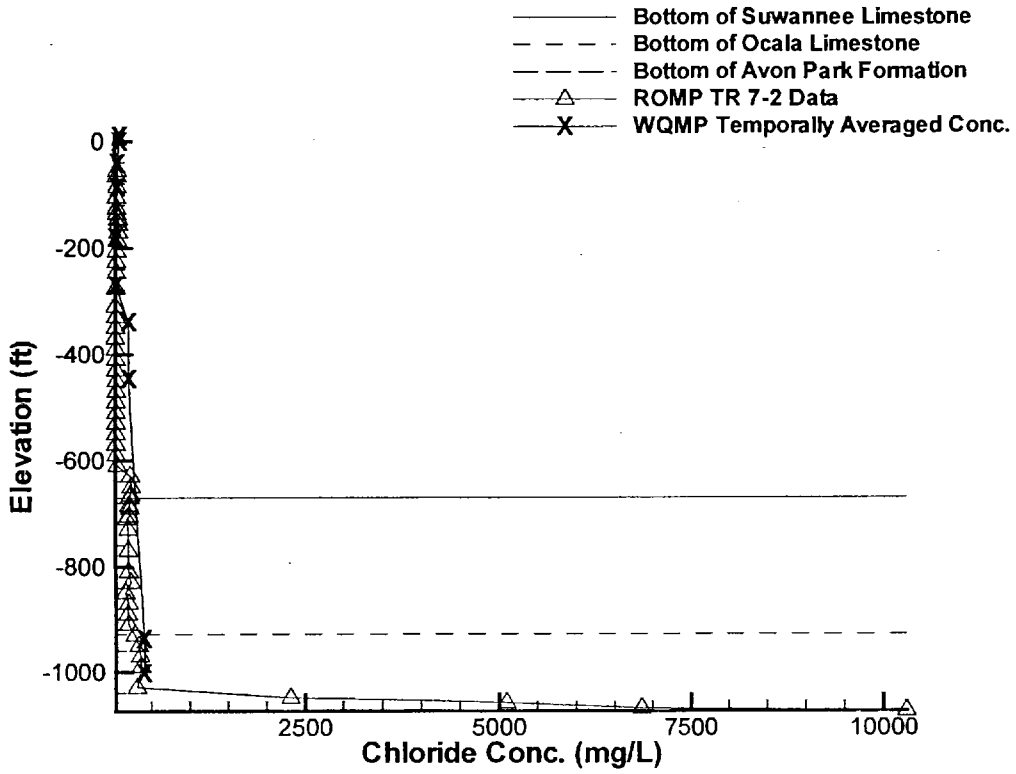

ROMP TR 7-4

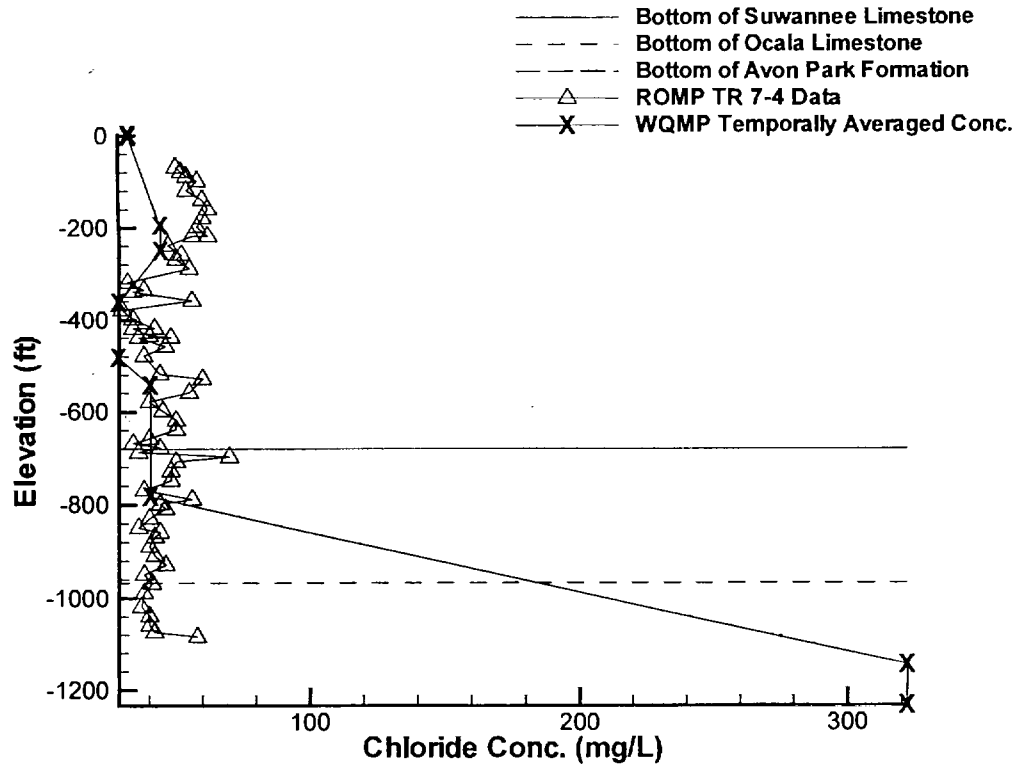

ROMP TR SA-1

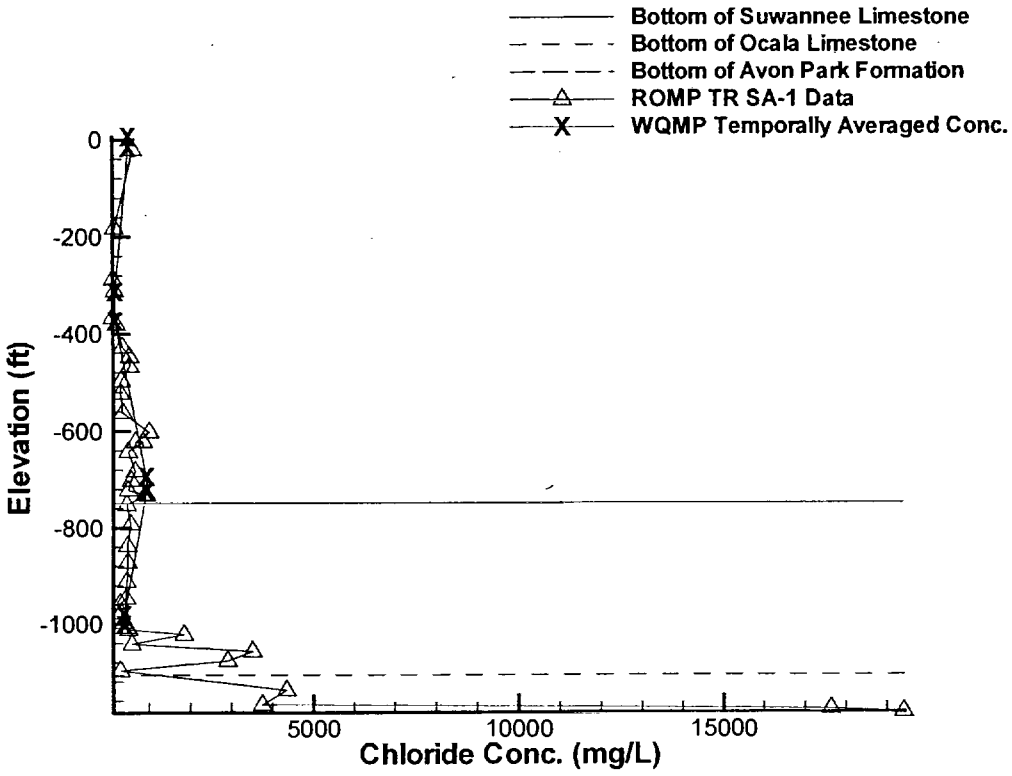

ROMP TR SA-3

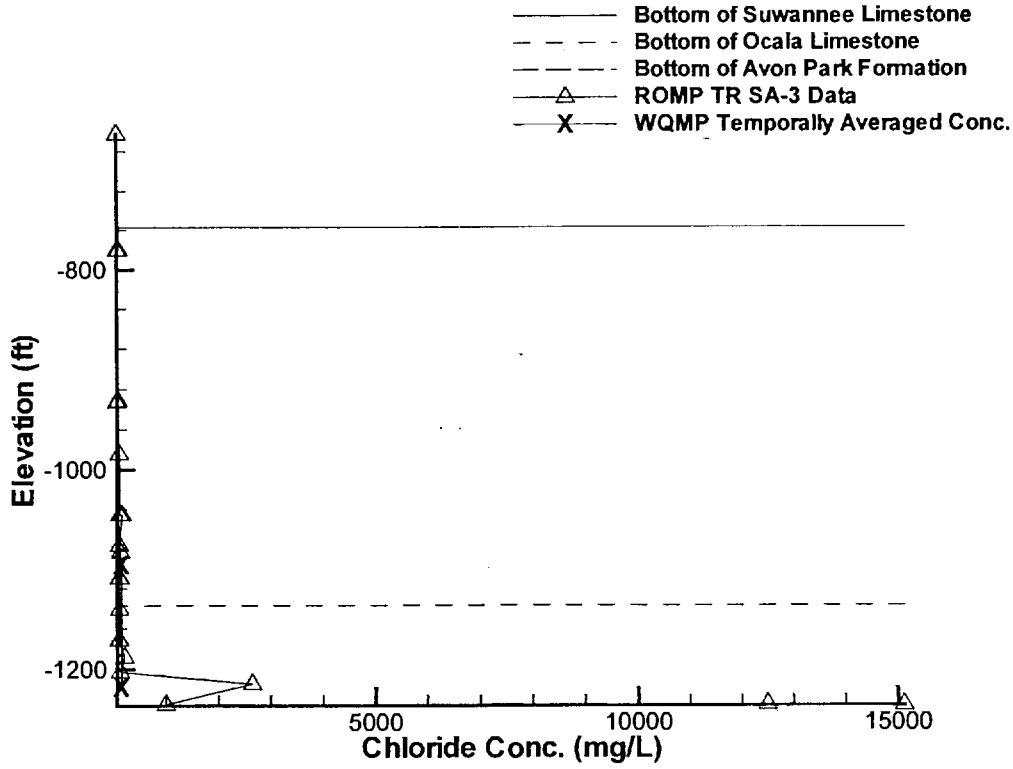

ROMP TR 6-1

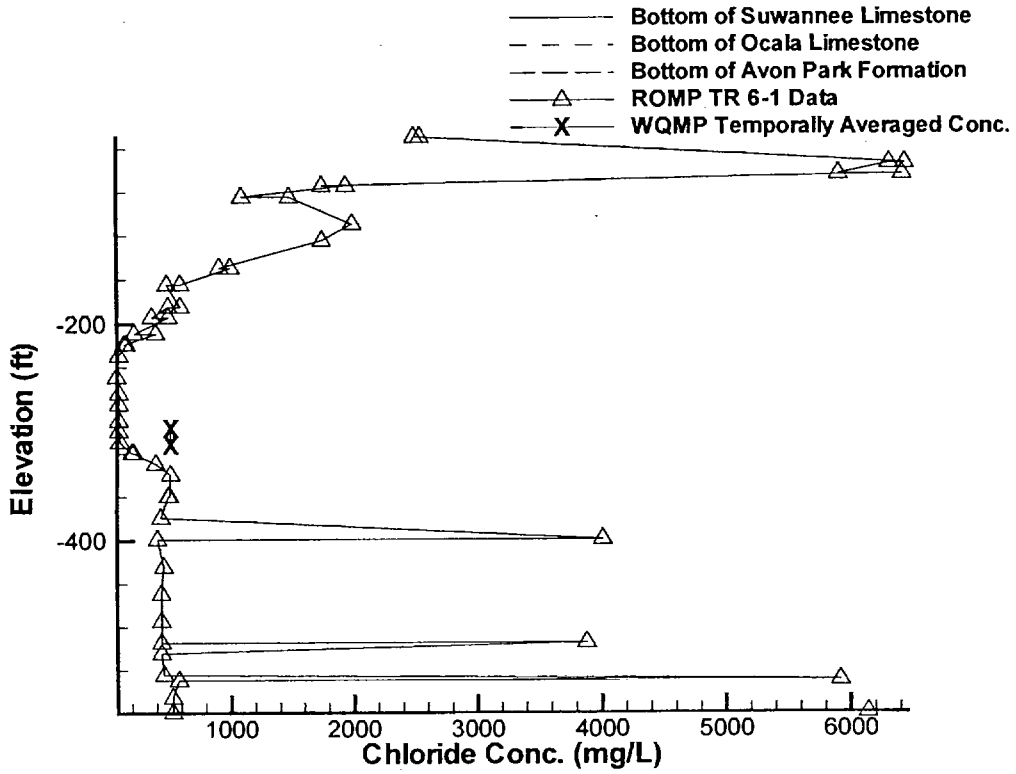

ROMP 22

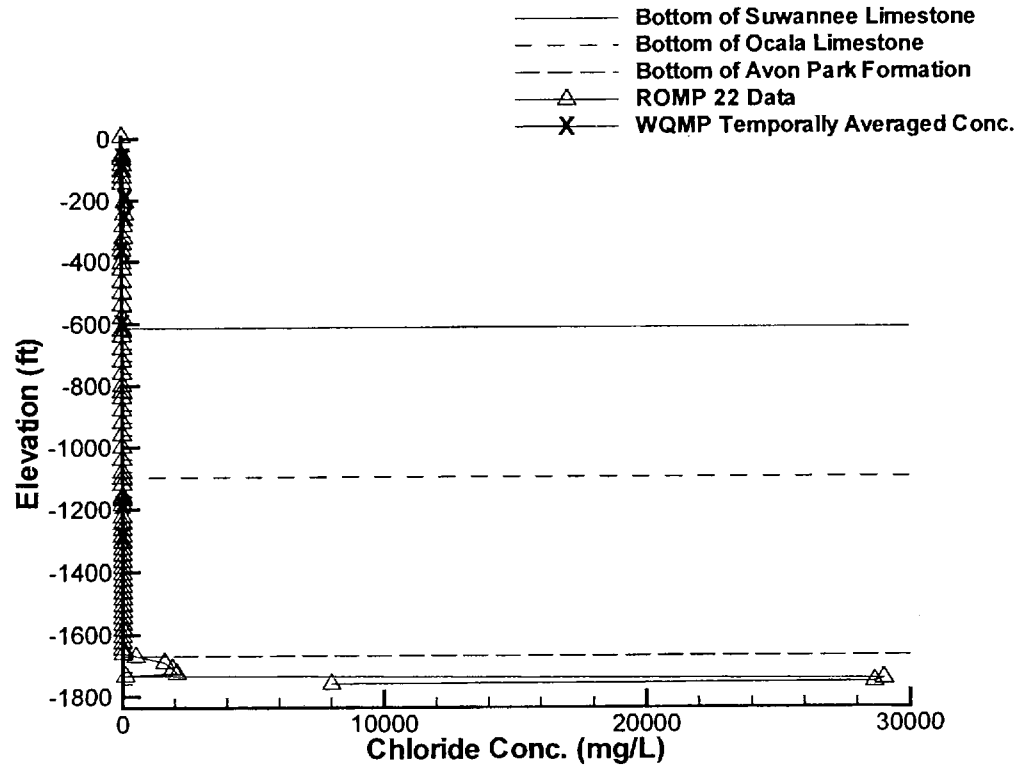

ROMP 20

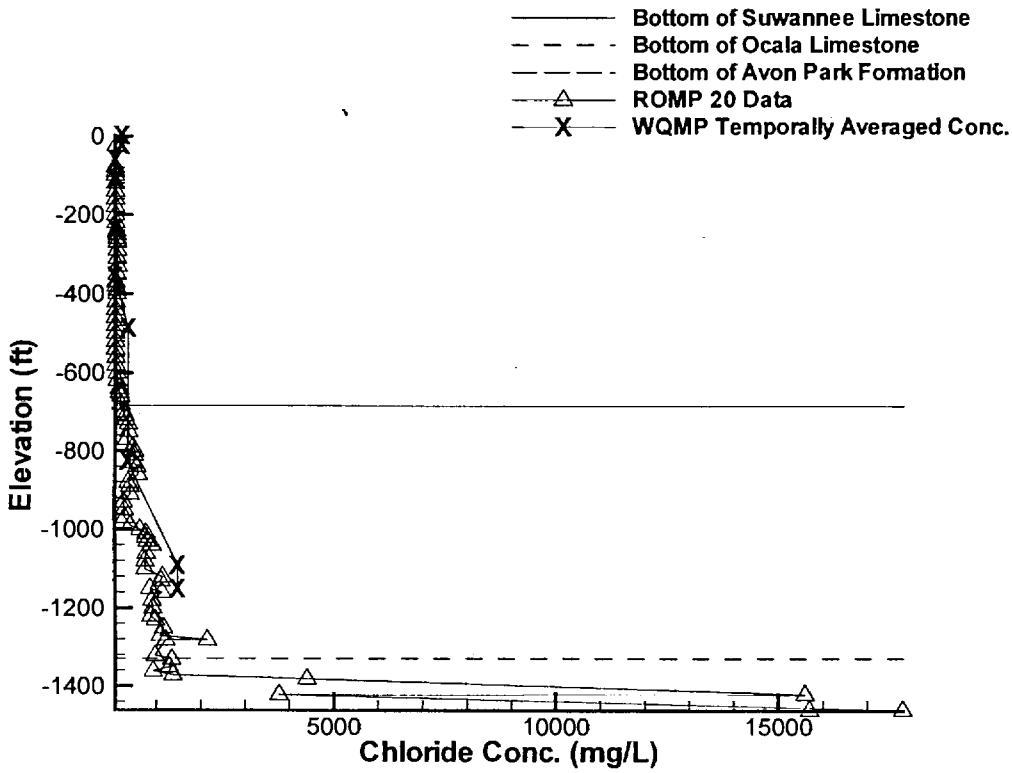

ROMP TR 4-1

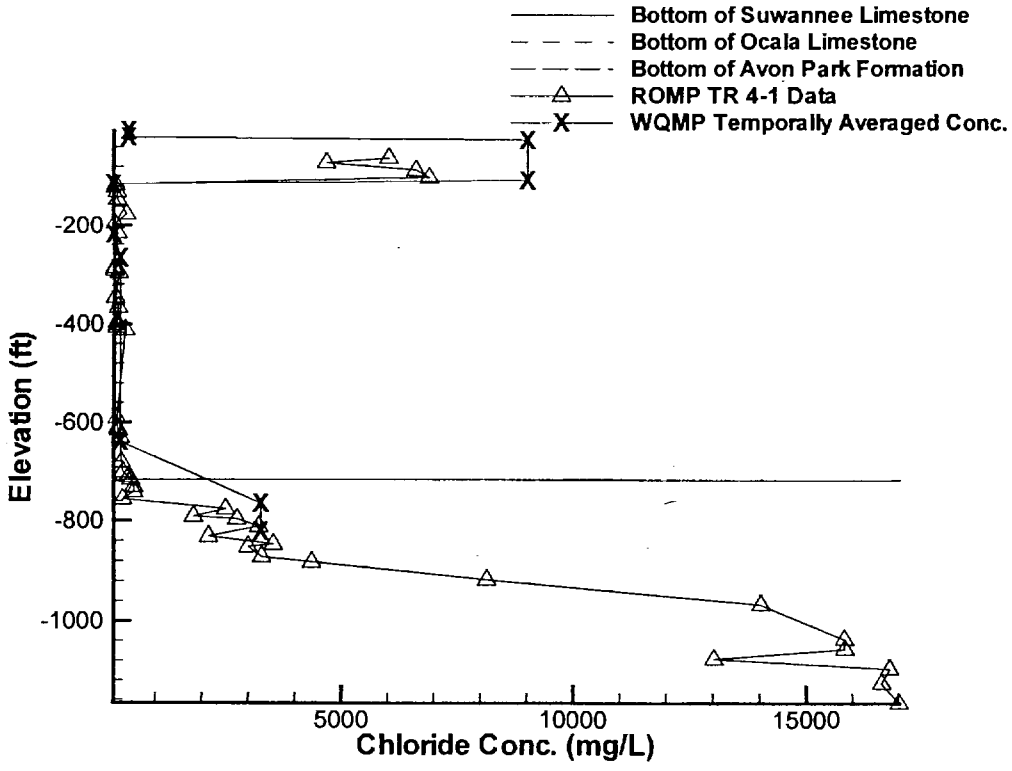

ROMP 9

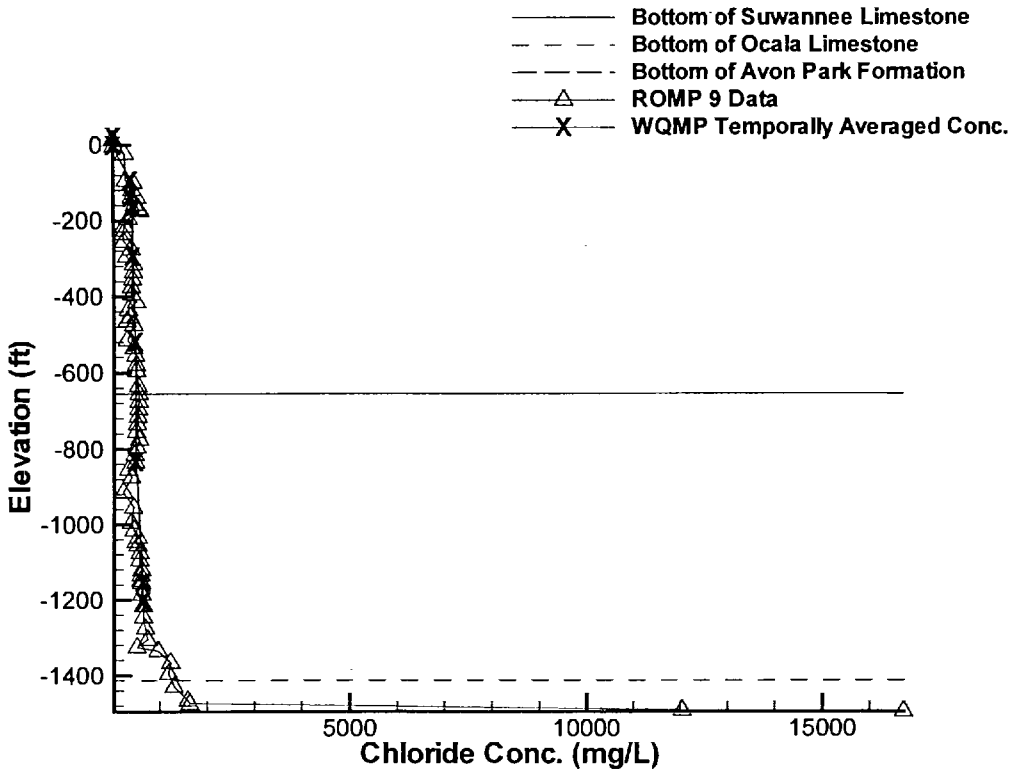
Bottom of Suwannee Limestone
Bottom of Ocala Limestone
Bottom of Avon Park Formation
ROMP 9 Data
WQMP Temporally Averaged Conc.
0
-200
-400
-600
-800
-1000
-1200
-1400
Elevation (ft)
5000
10000
15000
Chloride Conc. (mg/L)

APPENDIX B

SIMULATED VARIATION OF CHLORIDES WITH DEPTH COMPARED WITH MEASURED VALUES FOR THE ROMP WELLS

ROMP TR AB-1

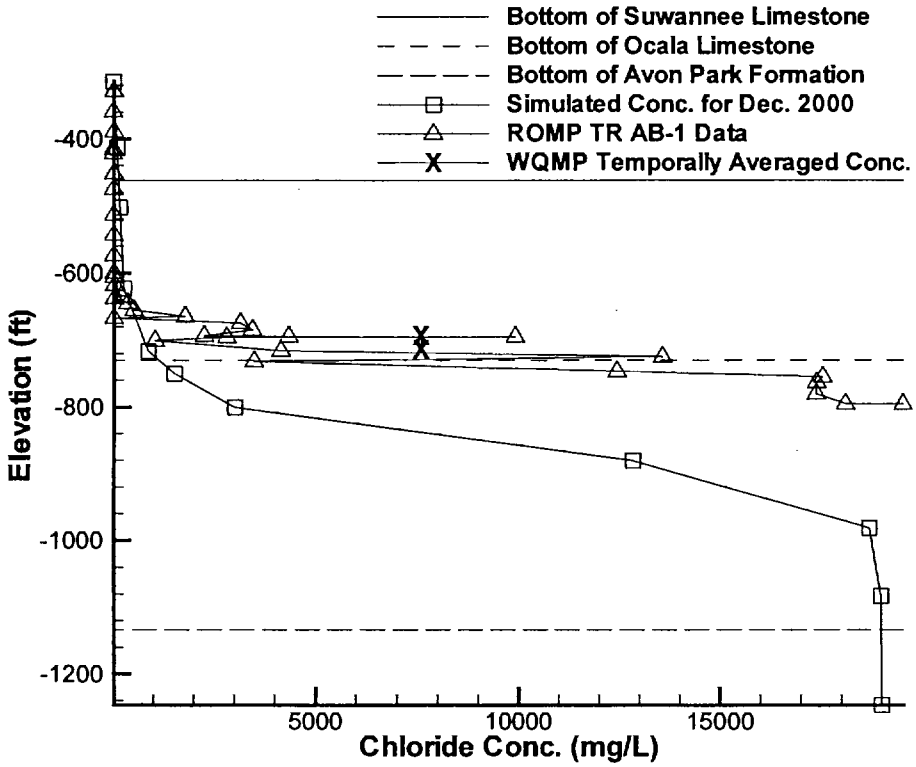

ROMP TR 9-2

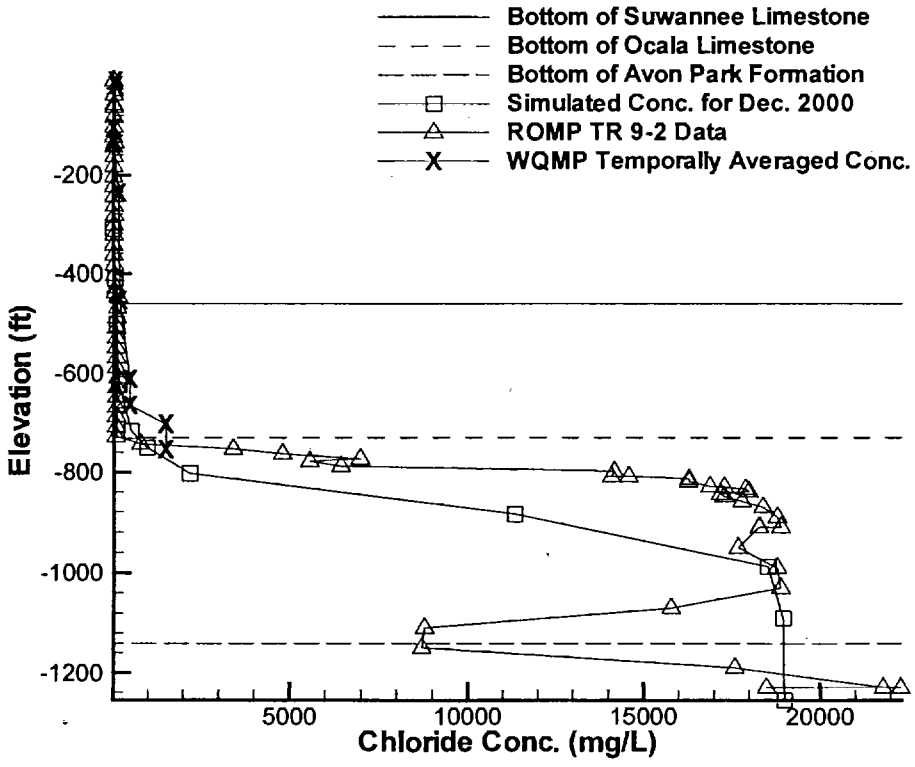

ROMP TR 9-1

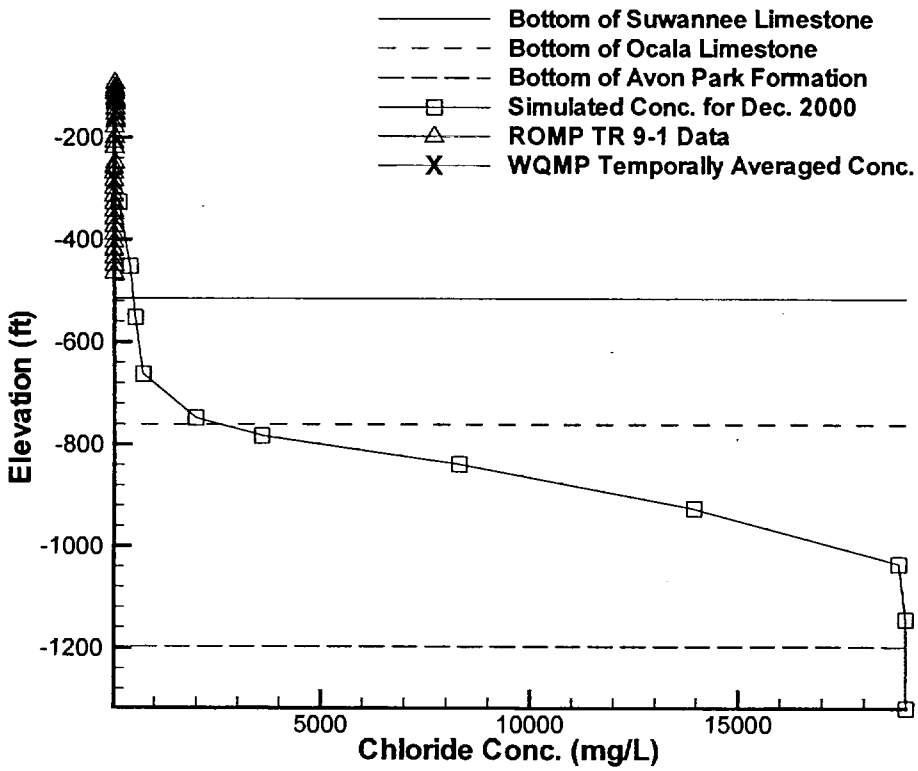

ROMP TR AB-3

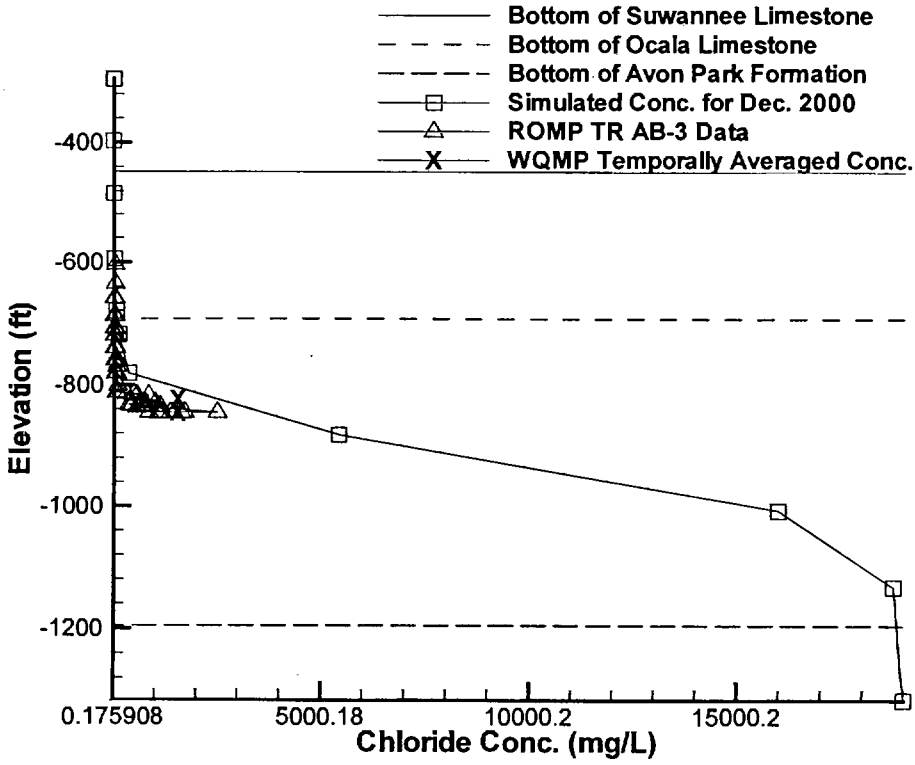

ROMP 50

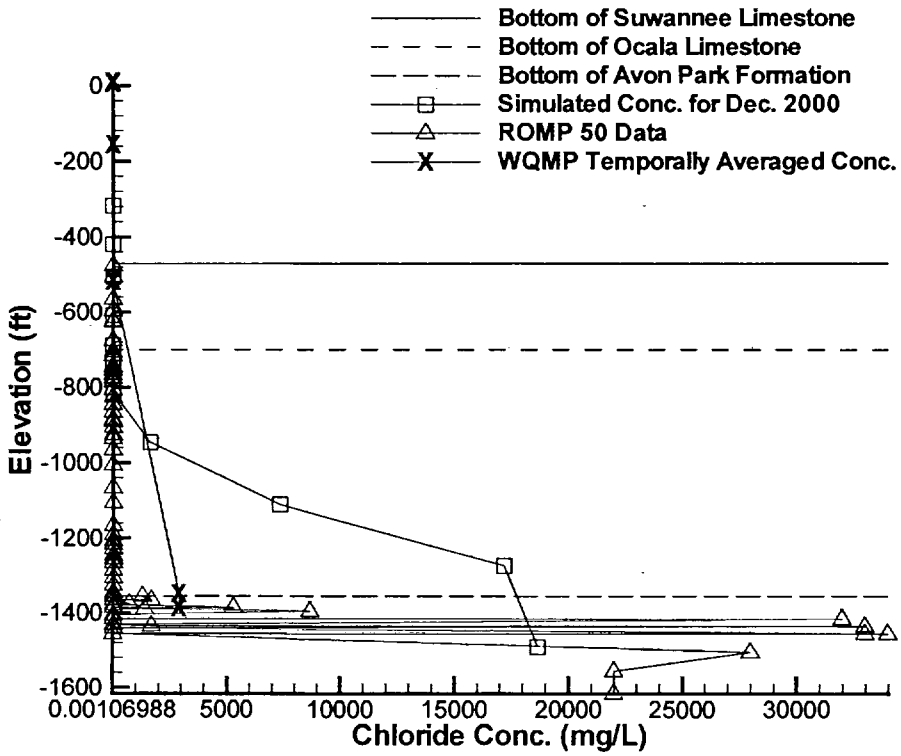

ROMP 39

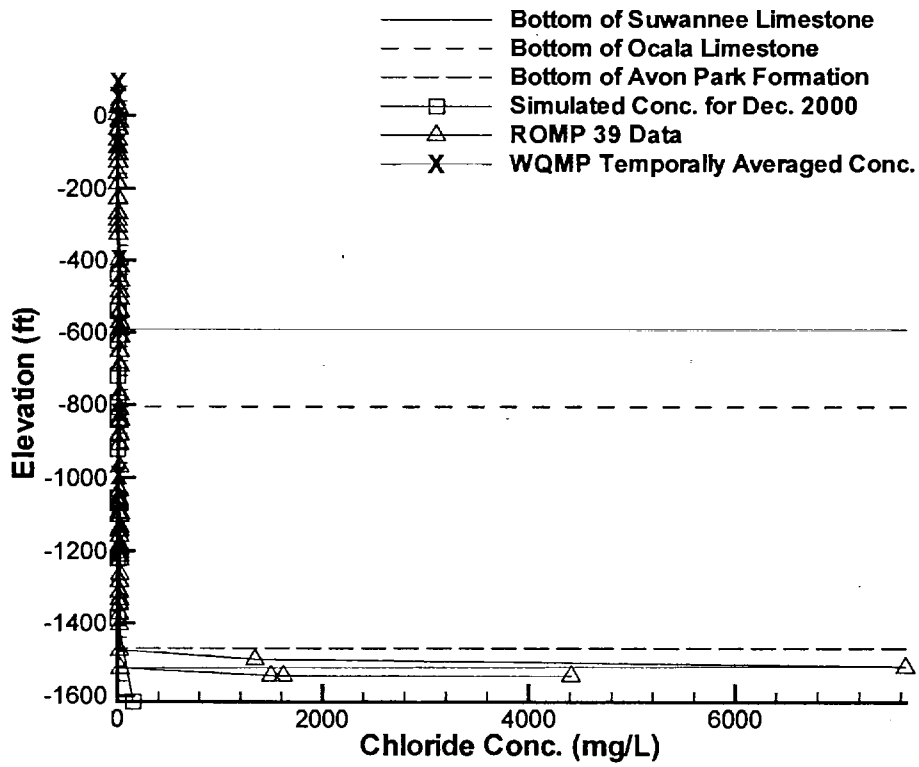

ROMP TR 8-1

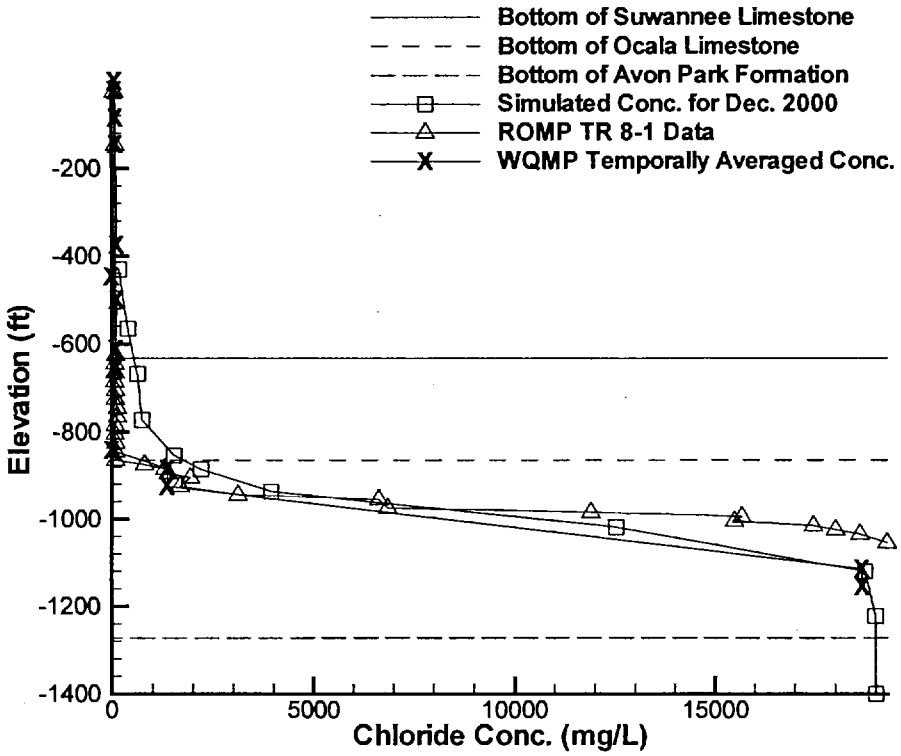

ROMP 33

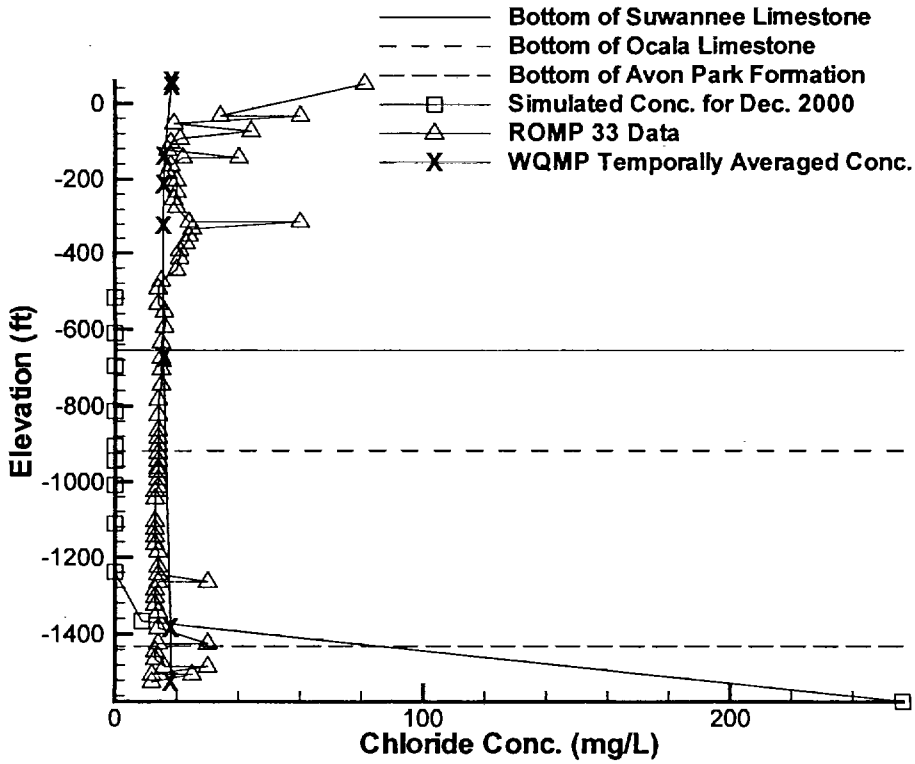

ROMP TR 7-2

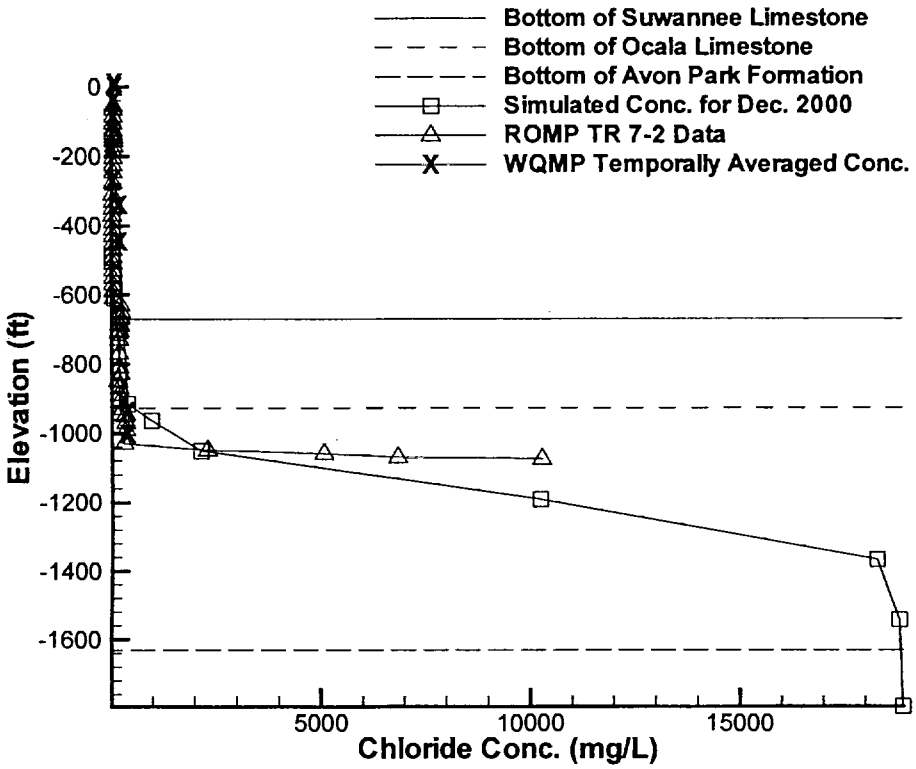

ROMP TR 7-4

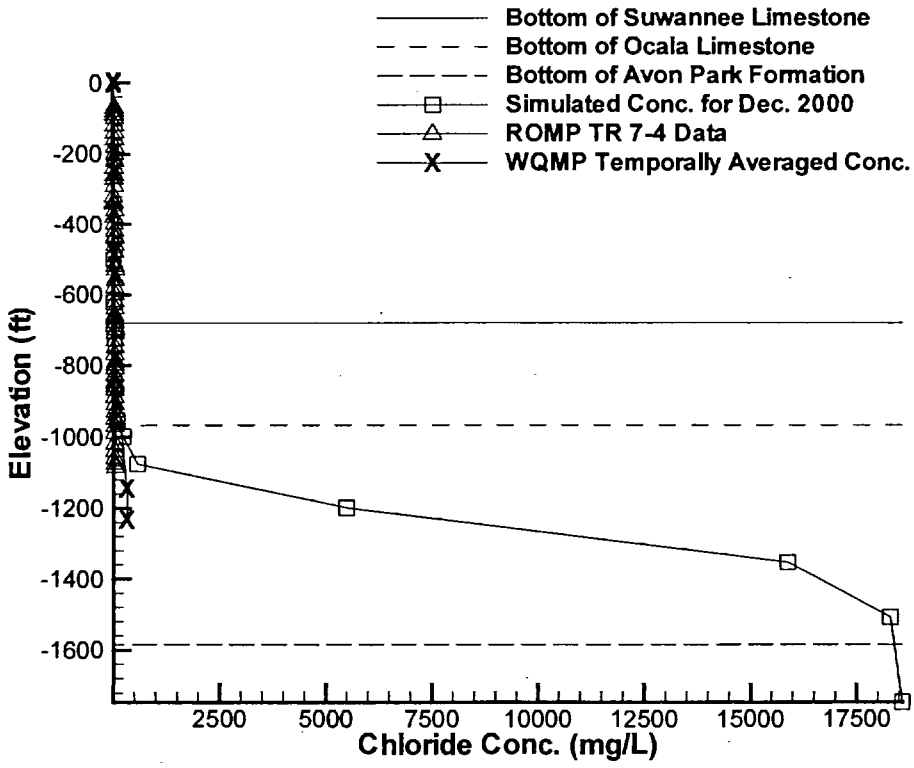

ROMP TR SA-1

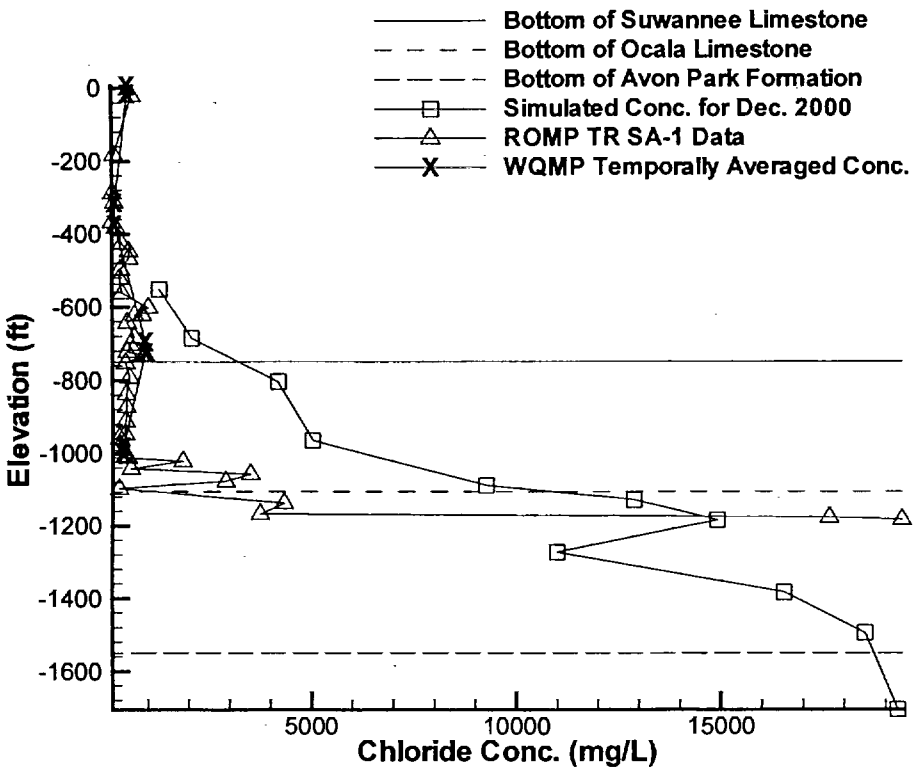

ROMP TR SA-3

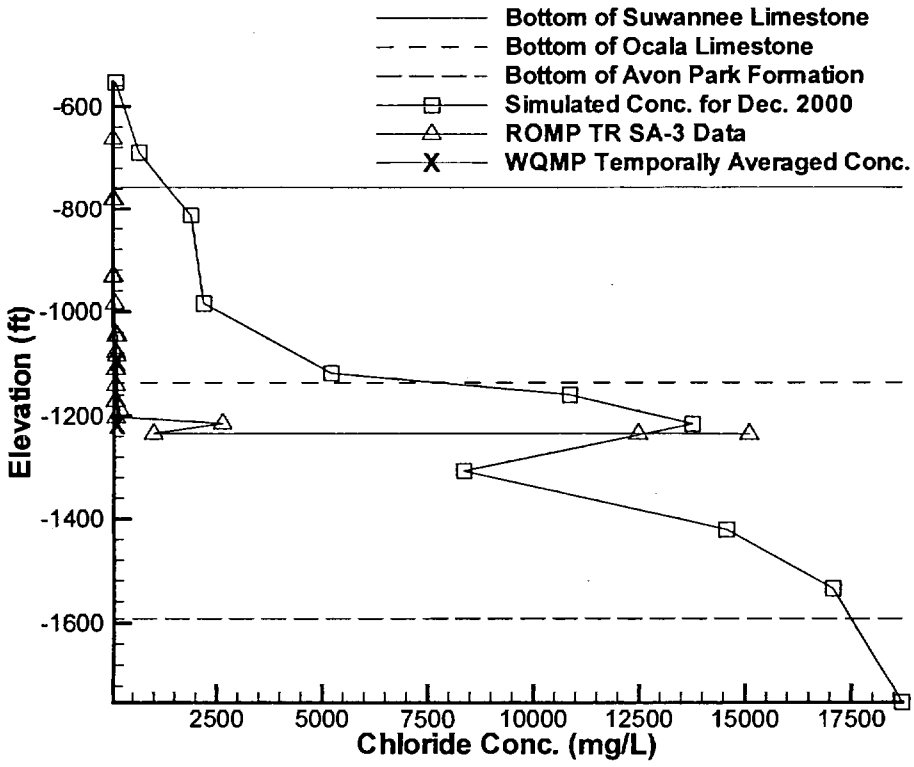

ROMP TR 6-1

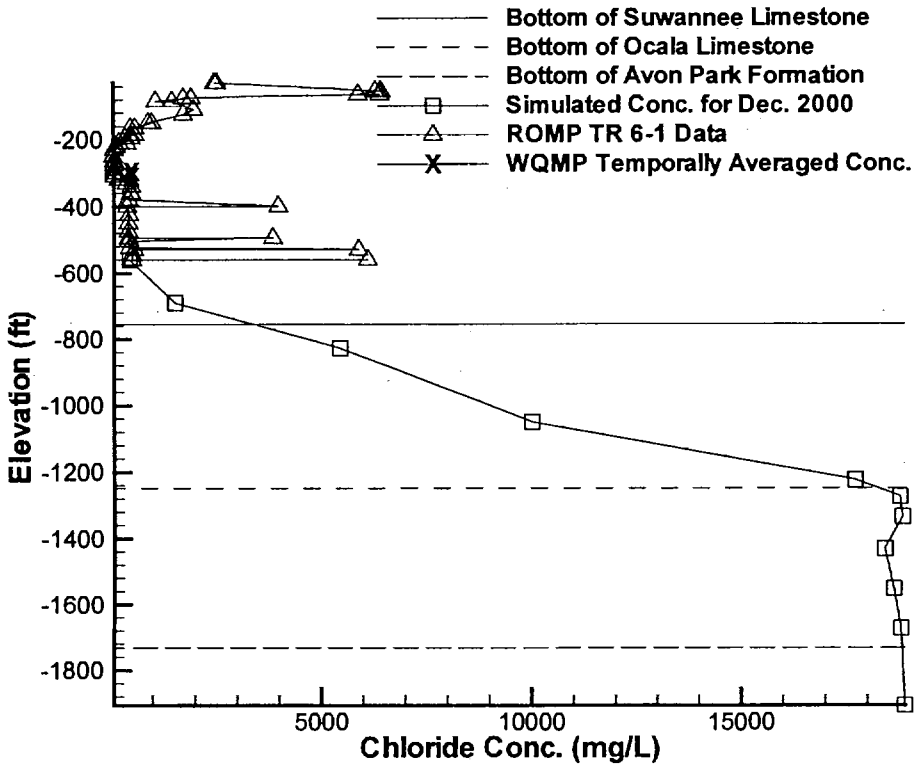

ROMP 22

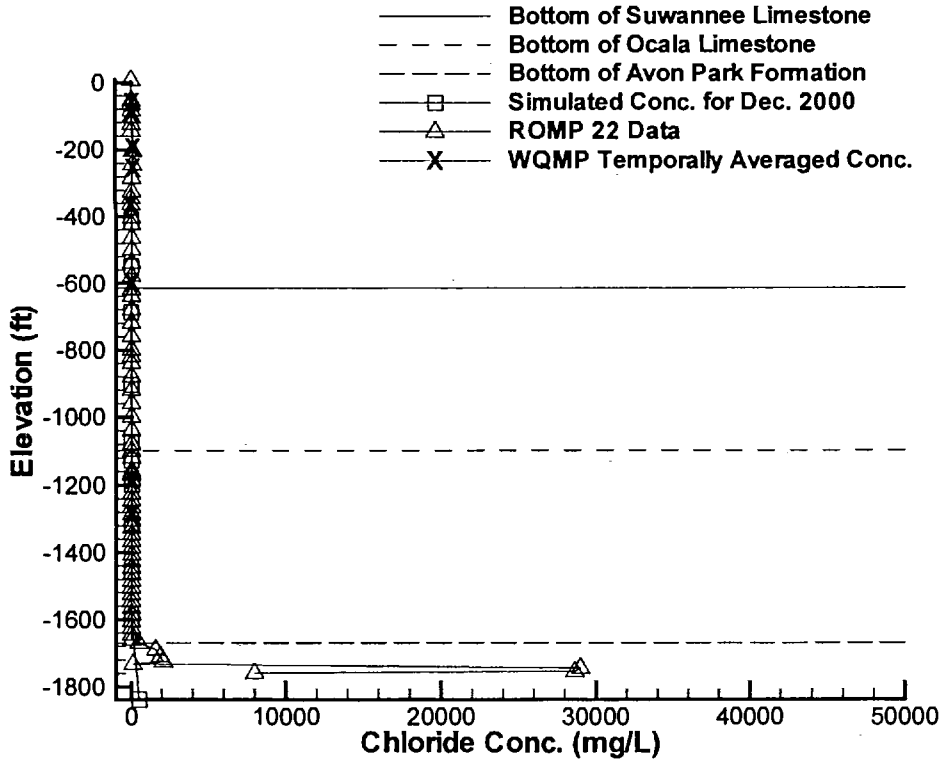

ROMP 20

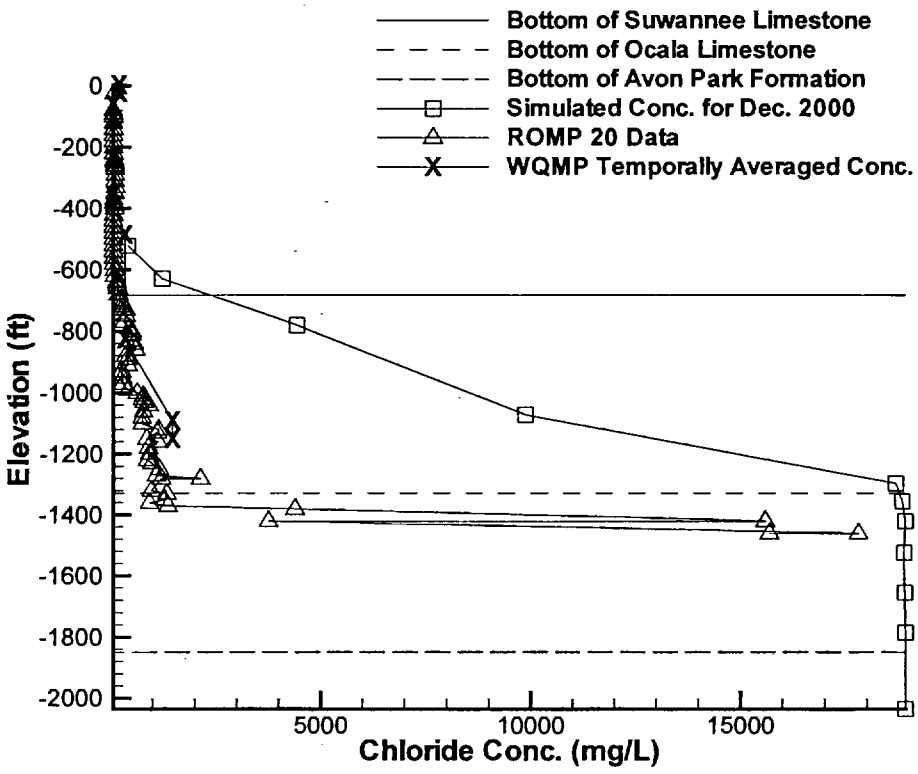

ROMP TR 4-1

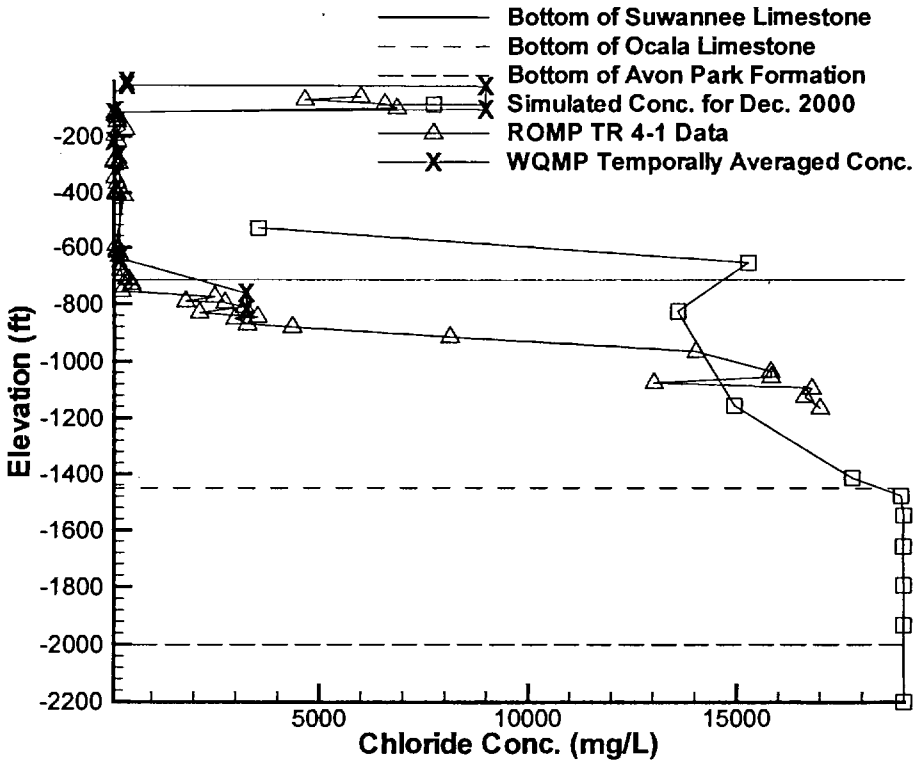

ROMP 9

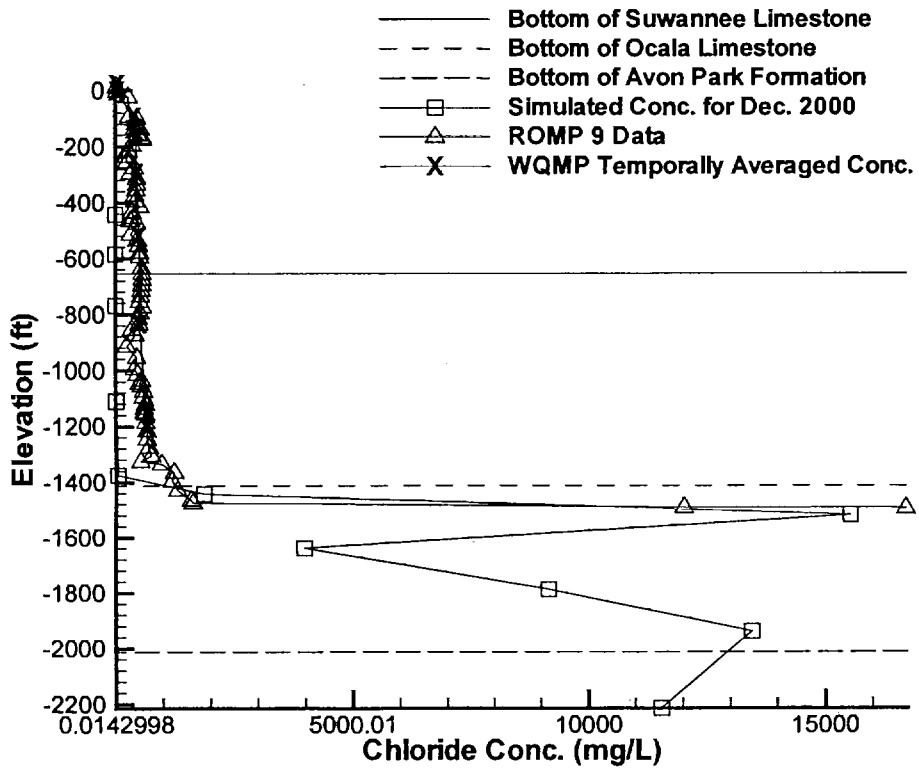
Bottom of Suwannee Limestone
Bottom of Ocala Limestone
Bottom of Avon Park Formation
Simulated Conc. for Dec. 2000
ROMP 9 Data
WQMP Temporally Averaged Conc.
Elevation (ft)
0
-200
-400
-600
-800
-1000
-1200
-1400
-1600
-1800
-2000
-2200
0.0142998
5000.01
10000
15000
Chloride Conc. (mg/L)

RP-04511

REPORT NAME:
THREE-DIMENSIONAL DENSITY-

AUTHOR & REPORT DATE:
HYDROGEOLOGIC, INC 06/01/2002

SUBJECT:
MODELING OF SALTWATER INTRUSIO

PAGES/CART #:
203 SS

215.1/REPORTS AND PUBLICATIONS

Water and Radioactive Tracer Flow in a Heterogeneous Field-Scale System

by Frank M. Dunnivant[a,b,c], Meredith E. Newman[a,b], Carolyn W. Bishop[a], Dave Burgess[a], John R. Giles[a], Brian D. Higgs[a], Joel M. Hubbell[a], Erick Neher[a] Greg T. Norrell[a], M. Cathy Pfiefer[a], Indrek Porro[a], Robert C. Starr[a], and Allan H. Wylie[a]

Abstract

A coupled field-scale aquifer pumping and water infiltration test was conducted at the Idaho National Engineering and Environmental Laboratory in order to evaluate subsurface water and contaminant transport processes in a heterogeneous flow system. The test included an aquifer pumping test to determine the storage properties of the aquifer and the state of confinement of the aquifer (~190 m below land surface), and a vadose zone infiltration test to determine vertical moisture and radioactive tracer migration rates. Pump test results indicated that the Snake River Plain Aquifer was locally unconfined with a transmissivity ranging from 5.57×10^5 to 9.29×10^4 m^2/day. Moisture monitoring with neutron probes indicated that infiltrating water was initially transported vertically through the upper basalt layer of the vadose zone, primarily through fractures and rubble zones, at an average rate of 5 m/day (based on vertical distance traveled and first arrival of water at the monitoring points). Analysis of breakthrough curves for a conservative tracer allowed estimation of the arrival of the peak concentration and yielded an average velocity of 1 m/day. The migration velocities from the neutron probe and tracer tests are in good agreement given the scale of the test and difference in analysis techniques. None of the data sets showed a correlation between migration velocity (arrival time) and distance from the point source, but they strongly indicate preferential flow through discrete fractures. Upon reaching the first continuous sedimentary interbed layer in the basalt formation, water flow was diverted laterally along the interbed surface where it spread outward in primarily three areas corresponding to topographic lows on the interbed surface, and slowly infiltrated into the interbed. The nonpredictable movement of water and tracer through specific fractures underlying the site suggests that a priori prediction of transmissive fractures in this media is not possible. Results do suggest that the continuous sedimentary interbed layers, in general, impede vertical water flow and contaminant migration.

Introduction

A difficult waste management problem facing developed countries today is the safe, long-term disposal and maintenance of nuclear waste. Considerable effort is currently being expended to locate one or more permanent storage facilities within the United States, as well as to understand the transport and fate of radioactive contaminants in existing burial sites. One of the largest subsurface disposal facilities of this type in the United States is located at the Idaho National Engineering and Environmental Laboratory (INEEL) and contains approximately one-third of the U.S. Department of Energy's (DOE) total inventory of plutonium-contaminated waste. Waste at the INEEL resides in the 144,100 m^2 (88-acre) Subsurface Disposal Area (SDA) within the Radioactive Waste Management Complex (RWMC) and was placed in unlined shallow pits, soil vaults, and trenches in surficial sediments. The waste, disposed during a 32-year period beginning in 1952, contains 31 radioactive contaminants (Arrenholz and Knight 1991; Loehr et al. 1994; EG&G Idaho Inc. 1994) as well as heavy metals, depleted uranium, asbestos, volatile and nonvolatile organics, and inorganic acids (Loehr et al. 1994). The SDA has been flooded on three separate occasions, in 1962, 1969, and 1982, by local snow melt water during Chinook-type conditions and infiltrating water may have contacted buried waste and promoted subsurface migration. Flood control and diking projects in the 1980s have, thus far, successfully avoided additional large-scale flooding events, although localized flooding may still occur during rapid snow melt and/or intense, short-term precipitation events. Thus, flow responsible for contaminant transport from the RWMC may be described as local intermittently saturated (during periods of high snow melt and flooding events), while the majority of the time the subsurface between land surface and the aquifer (at ~168 m) is unsaturated.

The INEEL burial site is unique in that it is underlain by undulating basaltic lava flows containing interbedded fluvial, lacustrine, and eolian deposits of clay, silt, sand, and gravel. The majority of the upper 168 m, the primary subject of this investigation, is unsaturated. One of the most important questions concerning the transport of radionuclide contaminants at the site is whether sedimentary interbeds in the vadose zone act as hydrologic barriers to water infiltrating to the eastern Snake River Plain Aquifer. The aquifer has been estimated to contain approximately 2.5×10^{11} m^3 of recoverable water (Hackett et al. 1986) and thus constitutes a major resource to the state of Idaho. Large-scale field investigations conducted in saturated, fractured media emphasize the complex

[a]Lockheed Martin Idaho Technologies Co., Idaho National Engineering and Environmental Laboratory, Integrated Earth Sciences, P.O. Box 1625, M.S. 2107, Idaho Falls, ID 83415-2107.

[b]Current address: Department of Chemistry, Hartwick College, Oneonta, NY 13820.

[c]Author for correspondence.

Received July 1997, accepted March 1998.

processes involved in the transport of contaminants in fractured media (Neretnieks 1987; Frick et al. 1992). The purpose of the Large-Scale Aquifer Pumping and Infiltration Test (LPIT) was to mimic the intermittent saturated flow events (flooding) potentially responsible for the migration of buried contaminants at the INEEL. The purpose of this article is to summarize and contrast the main elements of the test in one publication and inform the scientific community of the extensive data sets available through the cited Department of Energy publications. These diverse and complementary data sets will be useful to scientists studying flow through similar heterogeneous systems.

The LPIT consisted of several different, but complementary, experiments. Complementary methods were used to reduce data gaps and to provide moisture information in regions between monitoring wells. Results from four of these experiments are summarized in this paper and include: (1) the aquifer pumping test which determined characteristics of the aquifer such as transmissivity, specific yield, and state of confinement, and which also supplied water for the infiltration test; (2) the neutron probe monitoring of primarily vertical water movement in the vadose zone above a sedimentary interbed (located 55 m below land surface and ~113 m above the aquifer); (3) the surface direct-current resistivity monitoring of primarily lateral moisture movement, including spatial location and accumulation of perched water on the 55 m sedimentary interbed; and (4) the water sampling and analyses used to monitor the movement of radioactive tracers through the first 55 m of the vadose zone.

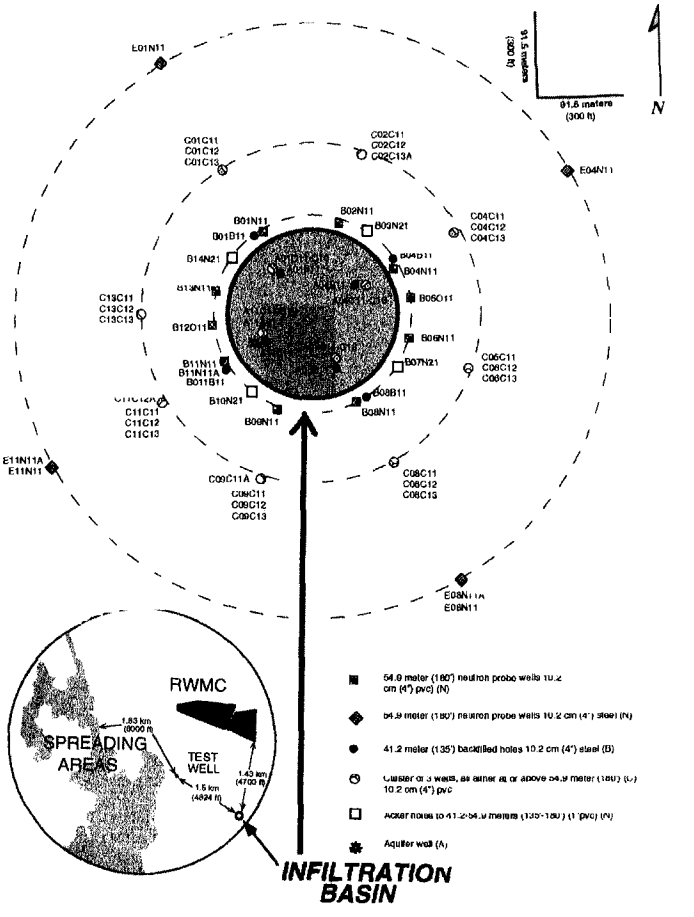

Figure 1. Map showing names and locations of wells, and general layout of the infiltration basin. Inset shows relative location of the RWMC, test well, spreading area for the diverted water, and the infiltration basin (shaded inner circle).

Methodology

General Test Design

Small- or intermediate-scale experiments are of limited value for hydrologic and geologic characterization in a highly heterogeneous environment such as the subsurface beneath the eastern Snake River Plain. In an effort to mimic the physical scale of the subsurface disposal area (144,100 m^2) while keeping the experiment to a manageable and economical size, a basin size of 26,300 m^2 (183 m diameter circular basin containing 32 million liters of water delivered from the test well) was selected. A subsurface monitoring network was set up that contained the basin and the area surrounding the basin, extending down to the 55 m interbed (contained a total monitoring volume of 17,660,000 m^3). Diagrams showing the locations of the RWMC, the test well, the infiltration basin (shaded inner circle), monitoring wells in and around the infiltration basin, and the spreading areas for water diverted from the test well are shown in Figure 1. The infiltration basin was located approximately 1400 m south of the RWMC. The circular basin (shaded area in Figure 1) was constructed by removing surface soil that was used to build an earthen berm (1.5 m high) around the area of interest. The floor of the basin was highly uneven. Approximately 80% of the basin floor consisted of a thin layer of soil overlying basalt while the remaining 20% consisted of exposed and elevated basalt. The water depth in the basin ranged from 0.3 to 2 m. The basin was approximately 1.5 km east of the test well, which was both the source of the water to the infiltration basin and the site for the aquifer pumping test (conducted simultaneously with the infiltration test). This distance of separation between the test well and the infiltration basin was based on the estimated region of influence of the test well and was selected to avoid interference between data collection for the aquifer pumping test and water reaching the aquifer from the infiltration test. Water was pumped from the test well at a rate of approximately 11,000 L/min. Because the infiltration basin could not accept the entire volume of water produced, a diversion pipe was installed to transport excess water to a spreading area approximately 1.8 km west of the test well (Figure 1; the lines and arrows indicate the location of the diversion pipe and the release point of water to the spreading area). The water level in the basin was maintained at a constant "pool-level" (32 million L) except during the addition of tracers to the subsurface. A complete summary of the water management system and water balance during the infiltration test is given in Starr and Rohe (1995).

A total of 70 wells were installed primarily along four axes extending radially from the infiltration basin with a few wells located between these axes (Figure 1). The primary monitoring area of interest was from land surface to the first continuous sedimentary interbed located at a depth of 55 m. Well depths ranged from 15 to 55 m (ground water beneath the basin was at approximately 190 m). Only well A11A31 penetrated the 55-m interbed and terminated in the aquifer at 207 m. Well A11A31 was screened from 165 to 207 m for collection of water samples. Wells in and around the infiltration basin were installed using an air rotary rig with a downhole percussion hammer, and were completed using PVC casing (five wells, for use in the DC resistivity system, were completed with carbon-steel casing). The annular space between the well casing and the borehole was completed using alternating layers of granular bentonite (10 to 20 mesh) and silica sand (6 to 10 mesh).

This type of well completion allowed water to pass freely through fractures or rubble zones, while impeding water movement along the annular space between the well casing and subsurface media in areas dominated by dense basalt. Fractures and dense basalt areas were located by reviewing caliper and video logs of the boreholes. Thus, sand was installed in the annular space when fractures or rubble zones were present, while bentonite was used to seal dense basalt areas between sand completion intervals. Wells were screened only at the bottom, which was usually located at the top of the interbed, to allow collection of water samples. The exact placement of the screen depended upon the presence of fractures, rubble zones, or voids in the area immediately above the interbed. In general, screened intervals ranged from 1 to 3 m immediately above the interbed down to the interbed (refer to Newman [1994] for completion diagrams and the location of all screened intervals). Nested lysimeters, for the collection of water samples, were installed in a similar manner using silica flour and silica sand filling materials immediately adjacent to the lysimeter and sealing between individual lysimeters, and between the lysimeters and land surface, using bentonite (refer to Newman [1994] for completion diagrams and the location of all lysimeters). Five wells and three lysimeter sets inside the basin were evaluated with respect to leakage of water (and ^{75}Se tracer) around the annular bentonite seals over the entire depth of the well. Results from this evaluation are reported in Dunnivant et al. (1997) and show that no leakage occurred; thus, the well installation methods used here appear to be adequate and allow the collection of water from individual fractures. This type of installation also allowed in situ moisture monitoring (with neutron probes) in discrete fractured intervals or rubble zones as well as in dense basalt formations over the entire depth of the wells, and collection of water samples from standing water at the bottom of the well as well as lysimeters located in fracture and rubble zones. Wells were clustered at the intersection of the four axes and four concentric circles moving outward from the basin (shaded area in Figure 1). The first ring of wells (A wells) were located within the basin at approximately 46 m from the basin center. The B, C, and E rings were located at 107, 183, and 320 m, respectively, from the basin center. All of these wells were used in moisture (neutron probe) monitoring and water sampling efforts. Piers were built from the berm out into the basin to provide access to the A-ring wells within the basin.

Water was first pumped into the basin July 25, 1994, at a rate of 11,000 L/min. The basin reached pool level, approximately 31.65×10^6 L (with water depth ranging from 0.3 to 2 m across the uneven surface of the basin), in two days. Tracers (selenium-75, ~2.0 Ci total; $t_{1/2}$ = 119.77 d, strontium-85, ~0.63 Ci total; $t_{1/2}$ = 64.84 d, and terbium-160, ~3.7 Ci total; $t_{1/2}$ = 70.3 d) were added July 31, 1994, as an 11-day finite-pulse input. Background tracer concentrations in the water from the test well were below the detection limit, which would be expected given the short half-lives of the tracers. Tracer addition was accomplished by adding the tracers as a spike to the full basin (approximately 31.65×10^6 L) and mixing the basin using three 7600 Lpm irrigation pumps. During this 11-day period, all water from the test well was diverted to the spreading areas. After the 11-day period, tracer-free water from the test well was again added to the basin and the basin was maintained at pool level through August 30, 1994. This last addition of tracer-free water provided approximately 86×10^6 L of water (or 2.72 times the volume of tracer-containing water) to move the tracers through the subsurface. The net result of this type of tracer addition was a potential broadening of the breakthrough curves and an increase in observed dispersion coefficients, but this was unavoidable given the scale of the experiment. Laboratory experiments confirmed the conservative (not reactive and adsorbed) nature of selenate for basalt and bentonite systems. Selenium-75 was selected because it should be present as the conservative (not reactive or adsorbed) selenate anion (SeO_4^{-2}) under the conditions of Snake River Plain Aquifer ground water (pH = 8.3, and E_H = + 0.24V). Analysis of basin and well water samples did not show a significant change in pH values, and since the water remained oxygenated during the infiltration experiment, ^{75}Se most likely remained present as the selenate anion. Strontium-85 was considered to be present as the free aquated cation and was selected because strontium is a fission product of concern at the RWMC. Terbium-160 was selected as a surrogate for lanthanides that have been disposed at the RWMC, and was expected to be strongly sorbed by INEEL subsurface materials. Laboratory studies indicated strontium had a K_d of 2.0 to 3.0 mL/g and was not expected to be observed at any of the monitoring sites under local equilibrium conditions. However, ^{85}Sr and ^{160}Tb were included to evaluate the presence of preferential flow and nonequilibrium transport in the system.

Aquifer Stress Test

The aquifer stress test was conducted by pumping the test well at an average rate of approximately 11,000 Lpm for 36 days. The test well was drilled to a total depth of 261 m with a cable tool rig and cased to 134 m. The remainder of the well was left as an open borehole with no casing or screen. Two observation wells were installed for this portion of the test; observation well 1 (OW1) was located 33.5 m N30E of the test well, and observation well 2 (OW2) was located 115 m S30E of the test well. The two observation wells were drilled to 304 m and cased to 183 m with a forward rotary drill equipped with a downhole hammer. The remainder of the boreholes were uncased. The water table was located at approximately 190 m below land surface and the presumed base of the aquifer is approximately 427 m below land surface. Drawdown of the aquifer during the pumping test was observed in three wells, OW1, OW2, and well 120 (229 m deep) located 36.6 m west of the test well (refer to the inset in Figure 2). Drawdown was measured in the observation wells using PTX-161D and PXD-260 transducers connected to a HERMIT 1000B and C data logger (In Situ Inc., Laramie, Wyoming). Observed drawdowns were corrected for fluctuations from barometric pressure changes, fluctuations associated with diurnal temperature/barometric pressure changes, and interruptions in pumping due to pump maintenance prior to data analysis. Data from the times when the pump was down for maintenance were deleted; these were short breaks in an otherwise long test.

Neutron Probe Measurements

Water movement and moisture changes in the vadose zone were monitored using 503DR HYDROPROBES (Boart Longyear CPN Co., Martinez, California). Several neutron probes of the same model were used during the test to provide increased coverage of the monitoring wells. Readings from the different probes were correlated to one another using calibration pits with different moisture conditions. This allowed readings made with one probe in a given well to be compared to readings made with other probes in the same well. All measurements during the experiment were made as 16-second counts at 0.30 m increments. All neutron probe wells at the test site were monitored at least once during the month just prior to the experiment to determine background moisture levels.

In most cases, wells were logged several times with several different probes. Sampling frequency of each well varied, and was intensive (approximately every four hours) during the initial portion of the test, but the frequency was reduced (approximately twice a day) as the changes in moisture decreased with time. Measurements made during the test were compared to the appropriate background log measurements to determine if moisture changes were occurring. Raw neutron probe counts were used in the analyses and no attempt was made to calibrate probe counts to water content. At each depth of measurement, a higher number of counts compared to the background level was taken as an increase in moisture. The positive difference between a given reading and the background was considered a real increase in moisture and not just the result of natural variation in readings if the difference continued to increase in subsequent logs. A more detailed description of the neutron probe monitoring can be found in Porro and Bishop (1995).

Direct Current Resistivity

The design for direct current (DC) resistivity monitoring of water infiltration was a bipole-bipole array using a fixed source bipole and a receiver array consisting of 2700 receiver bipoles (Pfeifer and Anderson 1995). The receiver bipole array consisted of a common remote electrode located near the center of the basin and a circular array of 2700 electrodes positioned in the areas between the monitoring wells outside the basin (Figure 1). The potential differences between each of the electrodes outside the basin and the common electrode within the basin were measured resulting in a maximum of 2700 potential difference measurements recorded during each monitoring session.

Water Sampling and Analyses

Water samples were collected on a regular basis from the infiltration basin, monitoring wells, and lysimeters in order to monitor the concentration of tracers in the basin and observe the breakthrough of tracers in the monitoring wells. A detailed account of the sampling methodology is given in Newman (1994) and Newman and Dunnivant (1995) and is only briefly summarized here. Eight locations within the infiltration basin were sampled using plastic containers. Well samples were collected using bottom-loading polyethylene bailers. Lysimeters were sampled by applying a vacuum of 65 to 70 kPa and allowing the lysimeter to collect water for 24 hours or until the tension in the lysimeter was approximately 35 kPa. The lysimeters were pressurized with bottled nitrogen or helium to evacuate the sample to land surface. Samples were analyzed on site in a mobile laboratory. Sample analyses included pH, specific conductivity, and radioactive tracers (^{75}Se, ^{85}Sr, and ^{160}Tb). Gamma spectroscopy for ^{75}Se, ^{85}Sr, and ^{160}Tb was performed using a high purity germanium system. Energy-line, full-width, half-maximum calibrations and background verifications were run each day prior to sample analysis. Specific conductivity and pH were analyzed using standard meters, cells, and electrodes. Instruments were calibrated once every two hours or prior to use.

Results and Discussion

Aquifer Stress Test

The aquifer pumping test was conducted to determine transmissivity, specific yield, and the state of confinement of the aquifer, as well as to supply water for the infiltration test. First, we will discuss the barometric "efficiency" of the well, which relates to the effectiveness of the pressure transmittal and is dependent upon the rigidity of the geologic media and the overall permeability of the rock. Typically the potentiometric surface of a confined aquifer is not affected directly by barometric pressure changes, so barometric pressure changes have a direct, measurable impact only on water levels in wells. However, the potentiometric surface of an unconfined aquifer is usually in direct contact with the atmosphere; hence, barometric pressure changes have a negligible impact on water levels in wells. Prior to the LPIT the barometric efficiency for well 120 in the Snake River Plain Aquifer was found to be approximately 90% for short-term fluctuations and 60% for long-term fluctuations, suggesting that the aquifer is confined (Wylie et al. 1995). However, data from the large-scale pumping test indicate that the aquifer is unconfined (Figure 2). One possible explanation for this observation is that those geologic units isolating the aquifer from barometric pressure fluctuations are above the potentiometric surface of the aquifer and do not act as aquitards. Our conceptual model is that aquifer permeability is largely controlled by the distribution of basalt flow contacts with some additional permeability contributed by fractures, vesicles, and intergranular pore spaces (Mundorff et al. 1964). Individual basalt flows within the Snake River Plain Aquifer consist of four elements: an upper vesicular element, a central nonvesicular element, a bottom vesicular element, and a substratum. The observed median thicknesses of the three upper elements are 1.8, 2.3, and 0.46 m, respectively (Knutson et al. 1989). On the scale of the aquifer test (hundreds of meters), dense basalt flow interiors act as "grains" while the "intergranular porosity" is reflected in the interflow zones between the dense interior (Whitehead 1992). These "grains" are formed as basalt flow sequences are deposited in an overlapping and coalescing manner, where younger flows build on the complex undulating topography of previous flows. Flow through the aquifer follows a tortuous path, around, through, and between these large particles in the general direction of the regional hydraulic gradient. If a well is open below the water table, or if the potentiometric surface is within a section of dense basalt, and the potentiometric surface is insulated

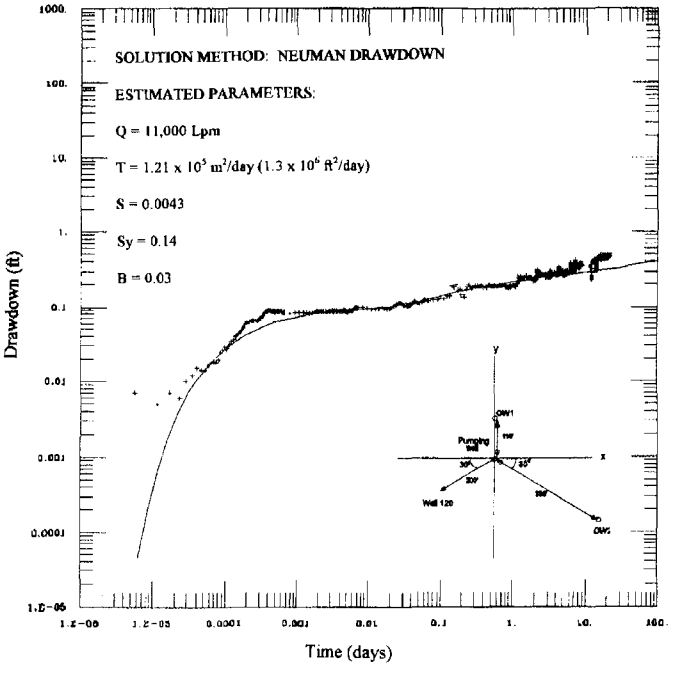

Figure 2. Neuman analysis of time-drawdown plot of well 120 data. The solid line represents the fitted curve. T = transmissivity, S_y = specific yield, S = storativity, and Q = pumping rate.

Table 1
Calculated Aquifer Coefficients

Observation Well	Transmissivity (m^2/day)	Storage	Kh/Kv Ratio	Analytical Method
OW1 upper	1.39×10^5	1.3×10^{-1}	1×10^2	Neuman
r = 33.5 m	5.48×10^5	5.3×10^{-2}		drawdown
				Theis recovery
OW1 lower	5.11×10^5	1.8×10^{-1}		Neuman
r = 33.5 m	3.25×10^5	2.3×10^{-2}		drawdown
				Theis recovery
Well 120	1.21×10^5	1.4×10^{-1}	6×10^1	Neuman
r = 60.96 m	1.11×10^5	5.0×10^{-2}		drawdown
				Theis recovery
OW2 upper	1.39×10^5	1.4×10^{-1}	3×10^1	Neuman
r = 115.2 m	7.25×10^5	4.2×10^{-2}		drawdown
				Theis recovery
All wells	1.30×10^5	9.0×10^{-2}		Distance drawdown

from barometric pressure changes, a barometric pressure change will result in a pressure difference between the well and aquifer, causing the water in the well to either rise or fall in response to the pressure difference.

The water level change is inverse to the barometric pressure change; if barometric pressure decreases, the water level will increase. Analytical results (Newman and Theis methods) for the pump test data presented in Figure 2 are summarized in Table 1. The Newman method was used to obtain estimates from the drawdown portion of the curve and the Theis method was used for the recovery portion of the curve. Estimates of transmissivity vary from 9.29×10^4 m^2/d to 5.57×10^5 m^2/d (1×10^6 ft^2/d to 6×10^6 ft^2/d) and the storage coefficient varies from 1×10^{-1} to 2×10^{-2}. The observed drawdown in the test well was 2.90 m, while the predicted drawdown using calculated aquifer coefficients from this test is 0.17 m. The well efficiency is 6%, yet the test well is completed as an open hole. An open hole is the most efficient well design possible. Perhaps the well efficiency is low because permeability is not evenly distributed throughout the length of the well. Aquifer permeability may be isolated in the basalt flow contacts, resulting in converging and turbulent flow within and adjacent to the well. Attempts to match the data with the Moench (1984) double porosity model yielded higher permeabilities within the matrix blocks than within the fractures. Perhaps the data are adequately described by the Neuman model because the matrix material is sufficiently low and the interflow zones are distributed evenly enough that fluid flow can be approximated with an equivalent porous granular media analytical model.

Neutron Probe Moisture Monitoring

Water movement in the fractured basalt vadose zone beneath and adjacent to the infiltration basin was monitored using neutron probes during the LPIT. Wetting fronts and wetted zones were readily distinguished using these probes. Moisture changes in the sand and bentonite used to fill the annular space between casing and basalt in the monitoring wells could also be detected during equilibration with antecedent vadose zone moisture. These changes occurred during the first few months after well completion and prior

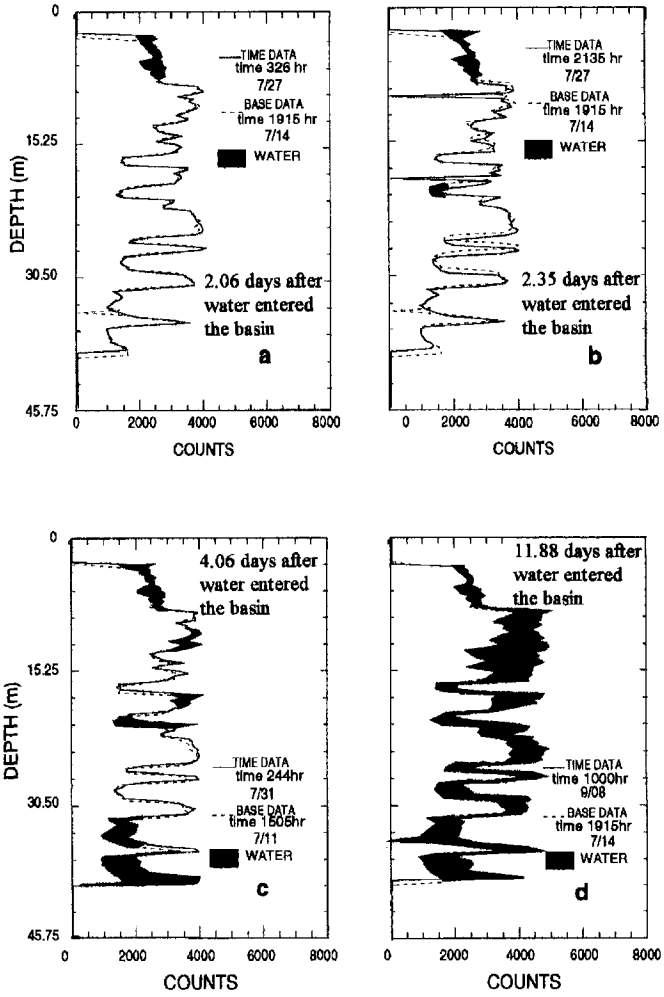

Figure 3. CPN (moisture monitoring) results from well A11C12 (inside the infiltration basin) illustrating the wetting progression from (a) 2.06 days after the addition of water to (b) 2.35 days after the addition of water to (c) 4.06 days after the addition of water to (d) 11.88 days after the addition of water to the basin. The dashed line in each plot represents the background neutron log while the solid line represents data collected on the specified day. Deviations between the two data sets are indicated by shaded areas.

to the LPIT so equilibrium was reached before infiltration was initiated. These observations indicate that vadose zone wells constructed in this manner and used in this type of subsurface environment should be installed and allowed to equilibrate sufficiently before they are used for moisture measurements.

In general terms, vertical water flow in the vadose zone during the infiltration test was confined within a cylinder directly beneath the infiltration basin. The rate of the wetting front advance averaged about 5.0 m/day (n = 38, ranging from 1.4 to 17.7 m/day, s.d. = 2.90). Although vertical water movement appeared to occur within a cylinder defined by the basin, wetting did not progress as a front uniformly distributed across this area. This is shown in neutron logs given in Figure 3. Figure 3 illustrates the general pattern of wetting observed in the infiltration basin monitoring wells. The shaded areas indicate where moisture levels have increased above background levels due to infiltration from the basin. Initial wetting was observed immediately underneath the infiltration basin to a depth of about 9 m (Figure 3a). Subsequently, a wetted zone appeared at the 19.8 to 21.4 m depths, while measurements between the 9 to 19.8 m depths remained unchanged from background levels (Figure 3b). Clearly, the water must have moved through preferential pathways to

reach the 19.8 to 21.4 m depths without wetting the zone from 9 to 19.8 m; it did not migrate downward uniformly through the geologic material surrounding the well. Figure 3c shows that water reached the 30.0 to 39.7 m depths while bypassing the 25.9 to 32.0 m depths, further illustrating preferential flow. A new wetted zone also appeared around the 12 m depth. Figures 3a to 3c illustrate water moving through the faster flowpaths. Figure 3d shows that 11 days after pumping entered the basin, wetting was evident throughout the entire length of the monitoring well. Water has obviously made its way more slowly through other pathways to wet those zones that were bypassed previously. While there was evidence of preferential and lateral flow within the cylinder beneath the basin, lateral flow did not extend to the B-ring wells just outside the basin, except in the region immediately above the 55 m sedimentary interbed. Moisture level changes were not observed at depths between land surface and the sedimentary interbed in any of the B-, C-, and E-ring wells, except in the media immediately above the interbed where water flowed along topographical lows.

Water movement through a few preferred pathways is suggested by the wetted porosity (0.02%). The wetted porosity was calculated by dividing the average infiltration rate (approximately 11 cm/day) by the wetting front travel rate (approximately 5 m/day). This compares to an average effective porosity of 0.23, which was averaged from 71, 5.6 cm long vesicular basalt cores taken from this area (Bishop 1991). This value was determined for a vesicular matrix without obvious fractures, and the presence of fractures and rubble zones in the field test should cause the porosity to increase. Thus, less than 10% of the total porosity actually conducted water. Bishop (1991) also found an average saturated hydraulic conductivity of 1.6 $\times$ 10^{-8} m/s for a 50 cm $\times$ 20 cm $\times$ 20 cm block of unfractured vesicular basalt. The much faster advance of the wetting front in the large-scale field test indicates that the basalt matrix played a minimal role in conveying water through the vadose zone and that fractures and rubble zones constituted the primary pathways.

Direct Current Resistivity

DC resistivity arrays are commonly used to map changes in the electrical properties of the subsurface due either to geological spatial changes or to changes in physical properties over time. The electrical properties measured are related to the moisture content of the medium so that changes in the DC resistivity measured over time can be used to monitor wetting or drying fronts (Pfeifer 1987; Ash and Morrison 1989; Truskowski 1994). Using this concept, a DC resistivity array was used to monitor the lateral movement of water outward from the infiltration basin. The array was designed to augment well data and to provide real-time coverage of the areas between the sampling wells. The areal extents needed to be covered in real time were large, and to expedite this process, only real-time lateral migration information could be obtained using the DC resistivity array configuration. However, well data were used to determine the depth of the lateral migration of water.

Real-time interpretation of the data was performed in the field and consisted of comparing the data collected during the test with background data collected prior to filling the basin with water. Interpretation consisted of two steps. The first step was to detect anomalous regions in the subsurface geology and the second step was to monitor changes in the potential electric field that could be related to the lateral spreading of water from the basin. First, a map of anomalous areas was generated using the data from each of the electrodes. The geology of the area was modeled using a layered

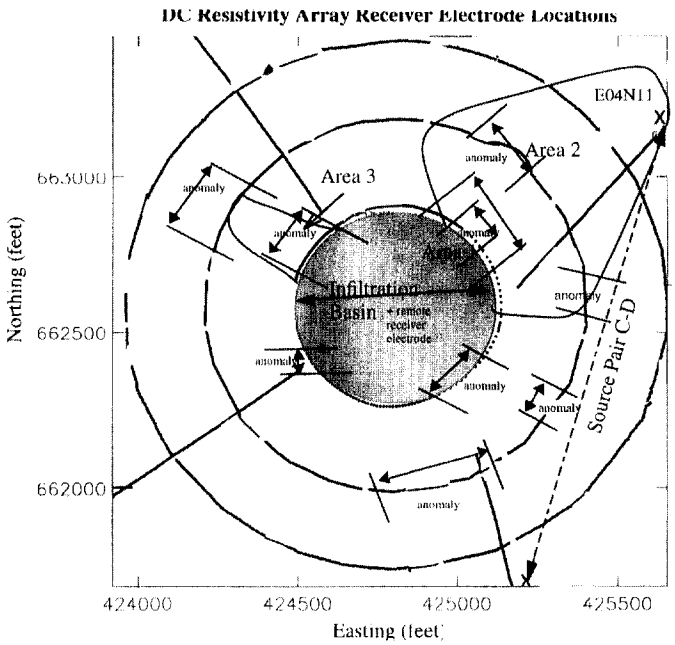

Figure 4. Map of anomalies detected by DC resistivity array superimposed on receiver array positions. Areas 1, 2, and 3 are areas corresponding to changes in the potential field due to lateral water migration. Note that the orientation of this figure is identical to Figure 1.

earth model; anomalous areas are those regions where the data diverged from the layered earth model indicating the presence of three-dimensional geologic structures such as rubble zones, depressions in the top of the interbed, and similar structures. Figure 4 is an areal summation of the geologic anomalies superimposed on the receiver array positions. The anomalous areas were postulated to be areas where lateral movement of water would occur. After mapping the geologically anomalous areas, the array was monitored over the course of the test to detect the lateral movement of water. As expected, the ring of electrodes directly adjacent to the infiltration basin showed the first changes in the anomalous areas. One anomalous area adjacent to the northeastern edge of the basin berm and well BO4N11 (designated Area 1 on Figure 4) showed a marked decrease in the potential electric field over time after the addition of water to the basin and prior to the arrival of water in well B04N11. This area was interpreted to be an area of lateral movement of water and the interpretation was confirmed by recovery of water from well BO4N11. Monitoring the array farther from the basin showed two areas where changes in the potential were measured. Area 2 (Figure 4) on the northeastern side of the basin coincides with a geologic anomaly and several wells from which water was recovered and was interpreted as a broad area of lateral water movement along the top of the interbed. The second area (Area 3 on Figure 4) is located on the western side of the basin near well B01N11 and is interpreted as a narrower zone of lateral water migration along the top of the interbed. Confirmation of perched water by water sampling could not be made in this area because wells could not be completed to the top of the interbed due to the presence of a large, subsurface rubble zone. Well B01N11 was the only well on the western side of the basin where water was recovered; however, the array data shows the migration of water in this area. In summary, water appeared to move laterally across the interbed surface and outward from the basin primarily in three areas coinciding with areas of geologic anomalies.

Water Sampling and Analyses

Each of the monitoring wells and lysimeters was frequently sampled in an effort to collect infiltrating water containing tracers. Wells were sampled at least once every 12 hours after the first detection of water. Lysimeters were sampled every 24 hours or when the tension fell below 35kPa. Of the 101 possible water sampling locations, water was recovered from only 30 and ^{75}Se-labeled selenate was detected in 26 of these 30. Nineteen of the 26 wells and lysimeters found to contain tracer produced sufficient data to construct breakthrough curves (BTCs). Neither ^{85}Sr nor ^{160}Tb were detected in any well or lysimeter water sample. However, in situ monitoring with a downhole HPGe detector suggested the presence of ^{85}Sr in a few selected zones (Dunnivant et al. 1994, 1997). Lack of detection of ^{85}Sr and ^{160}Tb in water samples indicated that, for most sampling locations, sufficient contact between the tracers and subsurface materials occurred to retard their transport. However, as previously mentioned, preferential flow may have occurred at a limited number of locations.

Representative BTCs from B-ring wells are shown in Figure 5. Although the BTCs obtained were all for the same tracer (^{75}Se labeled selenate), the shapes of the BTCs varied significantly between different wells and lysimeters. This dissimilarity between breakthrough curve shapes indicated that a variety of different flowpaths ranging from individual fractures to interconnecting flowpaths were present beneath the basin. Figures 5a and 5b show the more classical shaped BTCs represented by the Gaussian or bell shape. Figures 5c and 5d show two BTCs (or one bimodal curve) at one location and can be explained by the presence of two separate flow channels between the basin and monitoring point. It is interesting to note the difference in shapes for each of the bimodal BTCs, specifically the width, which is related to dispersion. Specific conductivities of the sampled water are also shown in Figure 5 and confirm the different source (with respect to flowpath) of each water.

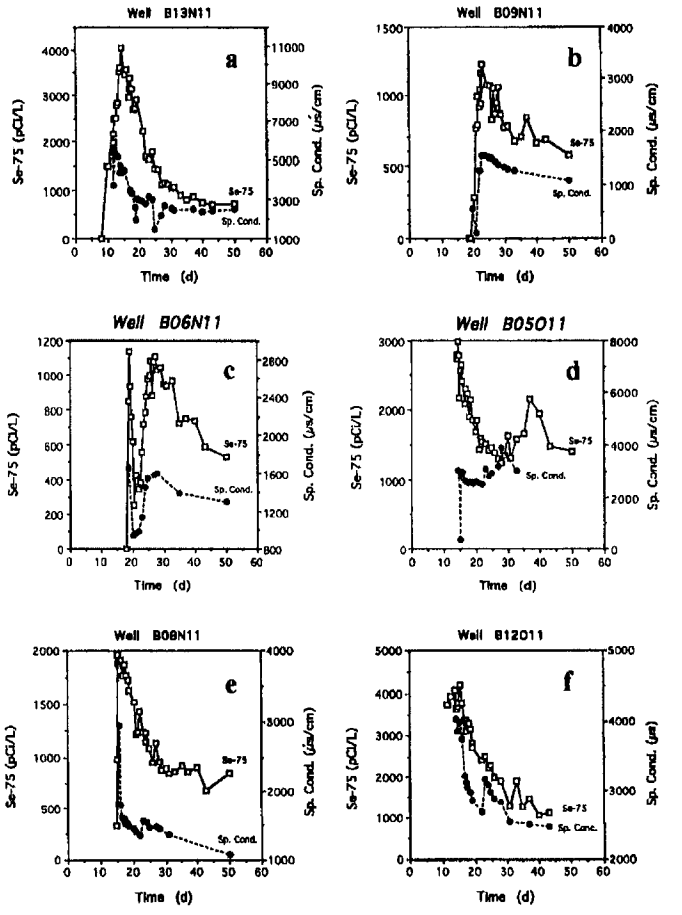

Figure 5. Examples of BTCs for Se-75 labeled selenate and electric conductivity measurements from B-ring wells. Note that time zero in these plots corresponds to the date of tracer addition (July 31, 1994) and not to initial water input to the basin. Figures a and b represent symmetrical or nearly symmetrical BTCs for ^{75}Se. Figures c and d represent bimodel BTCs for ^{75}Se. Figures e and f represent "unexpected" BTCs for ^{75}Se where the first water arriving at the monitoring site contained the highest concentration of ^{75}Se.

A common feature of the BTCs was tailing during the washout phase of the test. Tailing could have been caused by (1) transport in multiple fractures or rubble zones, (2) matrix diffusion, or diffusion from dead-end pores, (3) wall effects in fractures or rubble zones, (4) channeling, (5) mixing in the wells or lysimeters, and (6) the type of tracer input pulse used. Although mixing in the wells and lysimeters was possible, it is doubtful that it was the primary cause of the observed tailing because the degree of tailing varied considerably from well to well and from lysimeter to lysimeter with no apparent relationship between depth of standing water in the wells and degree of tailing observed. It is not possible from the current data set to isolate with certainty which of the first six possible causes was primarily responsible for the observed tailing. It is possible that the observed tailing resulted from a combination of all of these causes.

Several aspects of the data collected confirm the highly complex nature of the system under study. For example, tracer-free water was added to the infiltration basin for six days prior to the addition of tracers; however, the first water observed in several wells contained tracer (Figure 5e and f). Also, tracer-free water was observed in several lysimeters throughout the course of the test. Intervals containing insufficient water for the collection of samples were observed between water bearing zones. In addition, little correlation was observed between distance from the tracer source and tracer arrival time. Arrival times observed for B-ring wells, which were all the same distance from the tracer source, varied from 14.5 to 36.4 days. Results from nested lysimeters showed early arrival of ^{75}Se-labeled selenate at a given location while shallower and deeper lysimeters in the same installation showed significantly later arrival times.

One explanation for the diversity of BTCs and the lack of selenate at some monitoring points is the presence of dead-end fractures and fractures or dense basalt zones not directly or continuously connected to the flow of water. It is possible that some dead-end fractures intercepting the sampling points filled with tracer-free water early in the test, causing subsequent water flow at the origin of the flowpath to be diverted to an adjacent fracture or flowpath. The concomitant arrival of water and selenate at a monitoring point may be due to this diversion of water from these "filled" dead-end flowpaths or short circuiting in the system. These proposed flowpaths are illustrated in Figure 6.

Ten ^{75}Se breakthrough curves were analyzed using a modification of the one-dimensional advective-dispersive transport model (CXTFIT) of Parker and van Genuchten (1984). The nonreactive, one-dimensional model was selected since the flow regime between land surface and the 55 m interbed is best represented by channel flow through fractures and rubble zones. Basically, this program fits the one-dimensional model to the data set and estimates the most probable water velocity and dispersion coefficient. Results from this modeling effort are summarized in Table 2, while a detailed summary of this approach may be found in Dunnivant and Newman

Table 2
Parameter Estimates for ^{75}Se Breakthrough Curves

Location	Vertical Distance (m) from Land Surface	V (m/d) (Estimates from CXTFIT)	Dispersion (m^2/d) Coefficient (Estimates from CXTFIT)	r^2 (Regression Coefficient)	Calculated Dispersivity (m) (Dispersion Coefficient Times Velocity)
Lysimeters					
A01B11	6.38	0.45	0.079	0.8317	0.18
A08B11	7.60	0.80	0.55	0.9067	0.69
A08B11	11.55	0.57	0.68	0.9287	1.19
A11B11	14.63	0.71	1.01	0.9432	1.43
A11B11	21.34	0.90	3.52	0.9018	3.92
A11B11	31.62	2.63	4.15	0.9219	1.58
Average		**1.01**			
Wells					
B04N11	68.67	4.56	209.0	0.8850	45.80
B06N11	68.67	7.52	0.75	0.8862	0.10
B06N11	68.67	2.48	11.1	0.7064	4.48
B13N11	68.67	5.51	79.1	0.8491	14.40
Average		**5.02**			

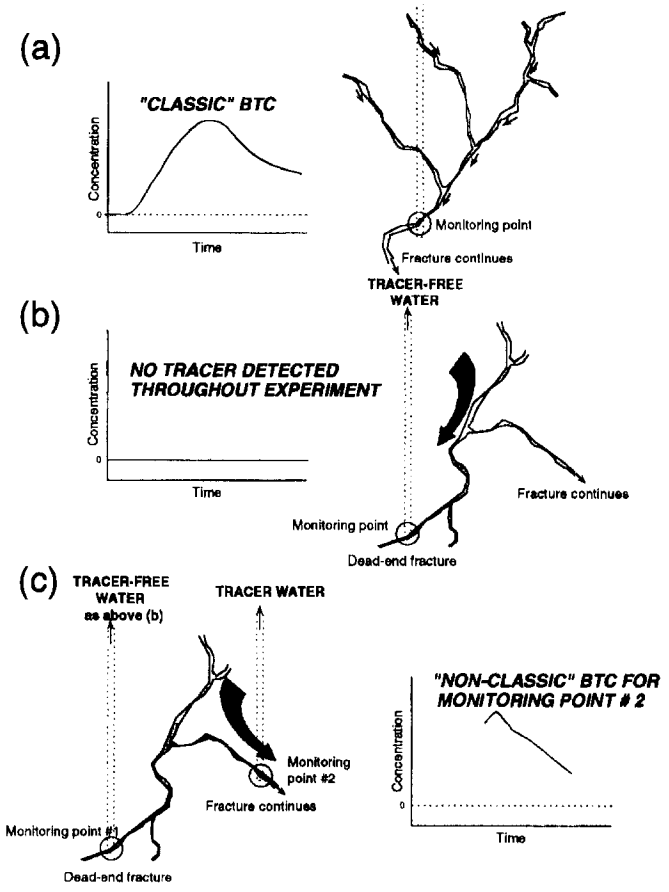

Figure 6. Conceptualization of the subsurface fractures and water flow beneath the basin.

(1996). The model estimated that dispersion coefficients for the fractured basalt regions above the interbed range from 0.079 to 4.15 m^2/d (mean = 1.66 m^2/d, s.d. = 1.72, n = 6), which correspond to longitudinal dispersivity values ranging from 0.176 to 3.92 m (mean = 1.5 m, s.d. = 1.29, n = 6). Water migration velocity (V in Table 2) estimates range from 0.45 to 2.63 m/d (mean = 1.01 m/d, s.d. = 0.81, n = 6). These predicted water velocities are in reasonable agreement with the rate of wetting front advance estimated from neutron probe measurements, especially considering that the velocity estimated from neutron probe measurements is for initial wetting while water samples could not be collected until near saturation conditions were reached, and therefore provide estimates of saturated interstitial velocity.

Results for water flow along the interbed are more difficult to interpret since water first flows through one or more fractured basalt regimes, and upon reaching the interbed flows along topographical lows. Under these conditions, the system is no longer one-dimensional and the flowpath length is the sum of the vertical and horizontal distance from the basin floor to the monitoring point. Water velocities to the B-ring wells range from 2.48 to 7.52 m/d (mean = 5.02 m/d, s.d. = 2.09, n = 4) . Dispersion coefficients range from 0.75 to 209 m^2/d (mean = 27.7 m^2/d, s.d. = 35.12, n = 4) and correspond to dispersivity values ranging from 0.10 to 45.8 m (mean = 16.2 m, s.d. = 20.6, n = 4).

Conclusions

The large-scale aquifer pumping and infiltration test provides the INEEL with a valuable data set for evaluating fate and transport of buried wastes at the RWMC, and also provides a unique data set for researchers interested in migration of water through intermittently saturated heterogeneous systems. Data from the pumping test indicate that the Snake River Plain Aquifer is highly transmissive (1.2×10^5 m^2/d), although water primarily flows from a few highly productive fractures, and is locally unconfined. Data from moisture and tracer monitoring in the vadose zone are summarized in the conceptualization shown in Figure 7. Water appeared to migrate downward through isolated fractures within a cylinder defined by the infiltration basin and did not spread horizontally outside the basin until reaching the 55 m interbed. The average rate of vertical water transport to the 55 m interbed was 5.0 m/day based on neutron probe results and was 1.0 m/d based on analysis of ^{75}Se BTCs. The difference in these two values is probably due to the use of the first arrival of water in the neutron probe technique, while the ^{75}Se-based technique used the mid-point of the BTC to estimate water velocity. These BTCs indicate that a variety of subsurface flowpaths exist, ranging from individual fractures to a complex series of intercon-

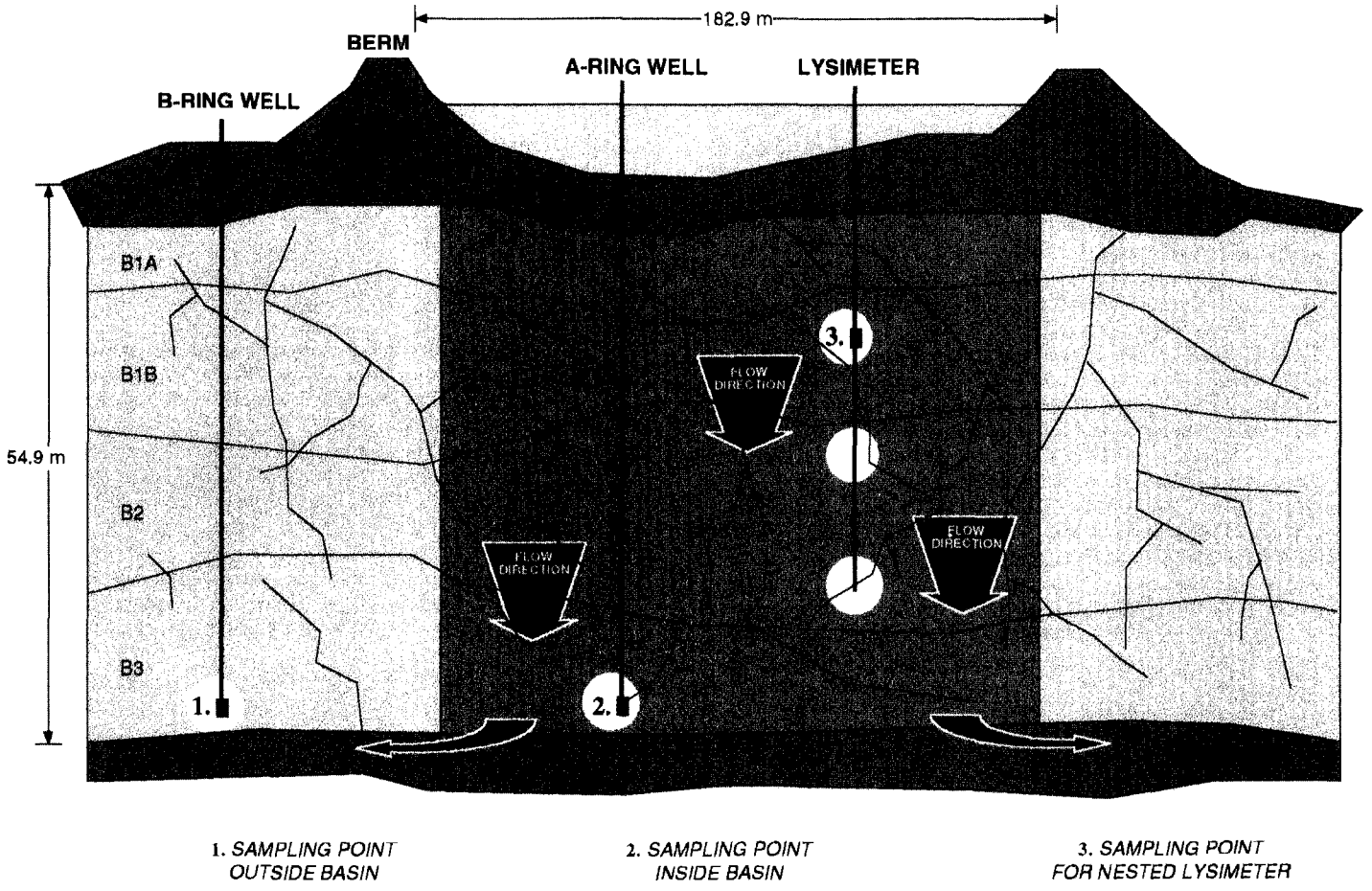

Figure 7. Conceptualization of the overall water flow beneath the basin. B1A, B1B, B2, and B3 represent individual basalt flow units.

nected flowpaths. Not all fractures intercepting monitoring wells or lysimeters produced water or tracer.

As the infiltration test progressed, water reached the 55 m interbed and formed a perched water body that was characterized by DC resistivity measurements and confirmed by recovery of water from monitoring wells. Water moved outward from the basin primarily in three areas coinciding with geological anomalies and with topographic lows on the interbed surface as determined from well logs. In addition, the 55 m interbed appears to impede the migration of water (and tracers). The presence of two similar interbeds below the RWMC suggests that buried waste in the SDA has probably not migrated to the aquifer.

Additional efforts, using an inverse modeling approach, to predict the spatial movement of moisture and estimate the range of dispersivity coefficients in these fractures are summarized in Magnuson (1995) and will be the subject of a subsequent publication. One clear result from this investigation is that a priori prediction of discrete water movement and tracer concentrations is difficult, if not impossible, in the fractured system underlying the INEEL.

Acknowledgments

A test of this magnitude required the efforts of a large number of people. We would like to acknowledge the U.S. DOE-ID, especially Patti Kroupa; program management by Kirk Dooley and Gary Mecham; water sampling by Steve Ugaki, Scott Barrie, and Hollie Gilbert; day-to-day oversight in the field by Pat Boyd, Joe Cook, and Tom Wood; DC resistivity assistance by Denise Psesser and Andy Anderson; numerous tasks performed by 30 dedicated summer students; and Jackie Brower for drafting of figures. This work was supported by the U. S. Department of Energy, Assistant Secretary for Environmental Management, under DOE Idaho Operations Office Contract DE-AC07-94ID13223.

References

Arrenholz, D.A., and J.L. Knight. 1991. A brief analysis and description of transuranic wastes in the subsurface disposal area of the radioactive waste management complex at the INEEL. Report no. EGG-WTD-9438. Idaho Falls, Idaho: U.S. Department of Energy, Idaho Operations Office.

Ash, T., and H.F. Morrison. 1989. Mapping and monitoring electrical resistivity with surface and subsurface electrode arrays. *Geophysics* 54, 235–244.

Bishop, C.W., 1991. Hydraulic properties of vesicular basalt. M.S. thesis, Dept. of Hydrology and Water Resources, University of Arizona, Tucson, Arizona.

Dunnivant, F.M., and M.E. Newman. 1996. Migration of radionuclide tracers through fractured media: Preliminary modeling results of breakthrough curves obtained during the large-scale aquifer pumping and infiltration tests. Engineering Design File ER-WAG7-84, INEEL Report no. INEEL-96/0288. Idaho Falls, Idaho: Idaho National Engineering Laboratory.

Dunnivant, F.M., I. Porro, C.W. Bishop, J. Hubbell, J.R. Giles, and M.E. Newman. 1997. Verifying the integrity of annular and back-filling seals for monitoring wells. *Ground Water* 35, no. 1: 140–148.

Dunnivant, F.M., G.D. Mecham, and J. Giles. 1994. Results from the large scale aquifer pumping and infiltration test: Down-hole gamma spectroscopy monitoring. Engineering Design File ER-WAG7-54, Report no. INEEL-94/064. Idaho Falls, Idaho: Idaho National Engineering Laboratory.

EG&G Idaho Inc. 1994. A comprehensive inventory of radiological and nonradiological contaminants in waste buried in the subsurface disposal area of the INEEL RWMC during the years 1952–1983. Report no. EGG-WM-10903. Idaho Falls, Idaho: U.S. Department of Energy, Idaho Operations Office.

Frick, U., W.R. Alexander, B. Baeyens, P. Bossart, M.H. Bradbury, C. Buhler, J. Eikenberg, T. Fierz, W. Heer, E. Hoehn, I.H. McKinley, and P.A. Smith. 1992. Grimsel test site, the radionuclide migration experiment—Overview of investigations 1985-1990. Paul Scherrer Institute, Wurenlinger and Villigen, CH-5232 Switzerland Villigen PSI, PSI-Report no. 120.

Hackett, B., J. Pelton, and C. Brockway. 1986. Geohydrologic study of the Eastern Snake River Plain and the Idaho National Laboratory. Idaho Falls, Idaho: US-DOE, Idaho Operations Office.

Loehr, C.A., B.H. Becker, D.E. Burns, R.M. Huntly, S.M. Rood, P. Sinton, and T.H. Smith. 1994. Preliminary scoping risk assessment for waste pits, trenches, and soil vaults at the subsurface disposal area, INEEL. Report no. EGG-WM-11181. Idaho Falls, Idaho: U.S. Department of Energy, Idaho Operations Office.

Knutson, C.F., K.A. McCormic, R.P. Smith, W.R. Hackett, J.P. O'Brien, and J.C. Crocker. 1989. RWMC vadose zone basalt characterization. EGG-WM-8949. Idaho Falls, Idaho: Idaho National Engineering & Environmental Lab.

Magnuson, S.M. 1995. Inverse modeling for field-scale hydrologic and transport parameters of fractured basalt. Report no. INEEL-95/0637. Idaho Falls, Idaho: U.S. Department of Energy, Idaho Operations Office.

Moench, A.F. 1984. Double-porosity model for a fissured groundwater reservoir with fracture skin. *Water Resources Research* 20, no. 7: 831–846.

Mundorff, M.J., E.G. Crosthwaite, and C. Kilburn. 1964. Groundwater for irrigation in the Snake River Basin in Idaho. Water Supply Paper 1654, 224. Reston, Virginia: U.S. Geological Survey.

Neretnieks, I. 1987. Channeling effects in flow and transport in fractured rocks—Some recent observations and models. In *Proceedings of GEOVAL-87 International Symposium.* Stockholm: Swed. Nucl. Inst.

Newman, M.E. 1994. Integrated large-scale aquifer pumping and infiltration tests—Water sampling and analysis test plan. Report no. EFF-ER-11367. Idaho Falls, Idaho: U.S. Department of Energy, Idaho Operations Office.

Newman, M.E., and F.M. Dunnivant. 1995. Results from the large-scale aquifer pumping and infiltration test: Transport of tracers through fractured media. Report no. INEL-95/146. Idaho Falls, Idaho: Idaho National Engineering Laboratory.

Parker, J.C., and M. Th. van Genuchten. 1984. Determining transport parameters from laboratory and field tracer experiments. Agricultural Experiment Station, Bull-Agric. Exp. Stat. No. 84-3, 1-97. Blacksburg, Virginia: Virginia Polytechnic Institute and State University.

Pfeifer, M.C. 1987. Multi-component underground DC resistivity study at the Waste Isolation Pilot Plant. M.S. thesis T3372, Dept. of Geophysics, Colorado School of Mines, Golden, Colorado.

Pfeifer, M.C., and H.T. Anderson. 1995. Electrical resistivity monitoring during the aquifer pumping and infiltration test. Report no. INEEL-95/010. Idaho Falls, Idaho: Idaho National Engineering Laboratory.

Porro, I., and C.W. Bishop. 1995. Large-scale infiltration test CPN data analysis. Report no. INEEL-95/040. Idaho Falls, Idaho: National Engineering Laboratory.

Starr, R.C., and M.J. Rohe. 1995. Large-scale aquifer stress test and infiltration test: Water management system operation and results. Report no. INEEL-95/059. Idaho Falls, Idaho: Idaho National Engineering Laboratory.

Truskowski, M.G. 1994. Detecting material property changes and fluid flow using a stationary DC resistivity grid. M.S. thesis T4490, Dept. of Geophysics, Colorado School of Mines, Golden, Colorado.

Whitehead, R.L. 1992. Geohydrologic framework of the Snake River Plain regional aquifer system, Idaho and Eastern Oregon. U.S. Geological Survey Professional Paper 1408-B.

Wylie, A.H., J.M. McCarthy, E. Neher, and B.D. Higgs. 1995. Large-scale aquifer pumping test results. Report no. INEEL-95/012. Idaho Falls, Idaho: Idaho National Engineering Laboratory.

ASR Regional Study – Benchscale Modeling

Final Report
July 2006
Prepared by:

Christopher J. Brown, Ph.D., P.E. – USACE
Steve England, P.E. – USACE
Glendon T. Stevens, P.E. - USACE
Hwai-Ping Cheng, Ph.D. – USACE ERDC
Emily Richardson, P.G. - SFWMD

Introduction:

The CERP recommends approximately 333 ASR wells to help with the supply, storage and distribution of water within the South Florida Region. The wells are dual purpose, since they are intended to store excess water during summer wet periods and recover the water during dry winter periods. It is hoped that the technology will provide a dependable water storage mechanism that can supplement surface storage reservoirs and provide water supply to the Lake Okeechobee ecosystem, Everglades ecosystem, agricultural irrigation, urban interests and others. The proposed injection and recovery pumping rate is approximately 1.65 billion gallons per day which is unprecedented in terms of other past or present ASR applications. Currently, only desktop spreadsheet evaluations or analytical solutions can provide an estimate of the aquifer response (e.g., piezometric head increases, fracturing pressures, increased flow) to such a large volume of injected water. A numerical model (or family of models), designed to simulate the regional groundwater system, will serve to make further evaluations of the plan. Porous media models and a discrete fracture network models have been considered but due to the lack of discrete fracture data related to the hydrogeology of south Florida, a porous media model has been pursued.

The CERP blue-print has been presented in a massive regional-scale plan that lacks engineering detail sufficient to construct the project. A large number of the construction features contained in the CERP were designed at various levels of detail based on information that was available during the plan formulation and evaluation phase. Many of the design assumptions for the components were based solely on output from the South Florida Water Management Model (SFWMM), which averages hydrologic conditions across a model comprised of grid cells with lengths and widths of 2 miles by 2 miles. Consequently, the engineering details of the construction features,

including the size and locations are conceptual and require additional studies. In addition, the SFWMM only simulates the Surficial Aquifer System explicitly. The Floridan Aquifer System where the proposed ASR wells would be located is not included. In general, the CERP proposed 200 ASR wells to be sited in the vicinity of Lake Okeechobee with the remaining wells located adjacent to the C-43 reservoir and in the Lower East Coast (specifically, Palm Beach and Broward Counties, Florida). A later effort, the Water Preserve Area (WPA) Feasibility Study, proposed adding additional wells in this area. The exact location and distribution of the proposed CERP ASR wells was never determined as part of the original CERP effort, however, the proposed wells were generally concentrated adjacent to reservoirs or Lake Okeechobee. The WPA Feasibility efforts proposed ASR wells at the C-9 impoundment.

Together with the ASR Pilot Projects and the ASR Contingency Plan, the ASR Regional Study will endeavor to reduce technical uncertainties associated with the proposed CERP ASR plan - a plan that is unprecedented in scale anywhere in the world. A Project Management Plan (PMP) was prepared for the ASR Regional Study in 2003. The center-piece of the ASR Regional Study is the preparation of a series of numerical simulation models. A multitude of issues need to be evaluated using the family of numerical models. The issues include local, sub-regional, and regional-scale concerns counting the following:

1. Regional changes in aquifer heads and flows
2. Regional changes in aquifer water quality TDS, sulfate, and chloride
3. Increased potential for salt-water intrusion caused by ASR pumping
4. Regional impacts to existing well users of the FAS
5. ASR well cluster site selection
6. ASR well cluster design and layout
7. ASR well cluster performance including estimating recovery efficiency
8. ASR well site evaluation of pressure induced changes
9. Localized transport of contaminants including heavy metals or pathogens
10. Localized ASR well pump design (dependent upon the appropriate model resolution)

Initially, a large, peninsula-wide numerical model will be developed. It is envisioned that this model will encompass an area of the Florida peninsula from Polk County south to Florida Bay. This model is intended for use as a planning tool to evaluate potential changes (e.g., head/flow and water quality) within the confined Floridan Aquifer System (FAS), aid in the site selection of ASR well clusters in the vicinity of Lake Okeechobee, adjacent to the C-43 reservoir and in the Lower East Coast area of South Florida, and aid ASR well cluster design and layout. In support of the main model development task, a number of smaller tasks will also be completed prior to or in parallel with the screening model development (e.g., literature search, data compilation, model selection, etc.). Once the Regional Screening Model is completed, more detailed sub-regional and/or local scale models will be developed to evaluate the ASR program in a higher level of detail. Depending upon model code selection and model domain design, all ten of the issues noted above could be evaluated. Table 1 displays the model scale required to address each of the identified issues. Both the sub-regional and regional scale

models should be designed to address as many of the issues listed as possible. In essence, the sooner the issue can be evaluated, the better. Obviously, one possible strategy would be to address the issue in two tiers. First, the regional model could provide planning-level information to address the specific issues. Then, an improved understanding of the issue could be obtained through the development of finer-resolution sub-regional models. For the three local-scale issues identified, only small models with fine horizontal and vertical resolution, will be sufficient to adequately address them.

Table 1. Model scale requirements.

Model Scale Required to Address Specific Issue	**Issues to be addressed as listed above**
Local Scale fine-resolution model	7, 9, 10
Sub-regional moderate-resolution model	1, 2, 3, 4, 6, 8
Regional Scale moderate to coarse resolution model	1, 2, 3, 4, 5, 6, 8

It is anticipated that the model development process will require approximately 1.75 to 2-years to finish and will involve numerous meetings, workshops, and conference calls. A team of model developers will work collaboratively over the internet and through video-conferences. It is expected that the model development effort will involve numerous technical challenges including addressing seawater boundary conditions; determining an appropriate number of model layers and grid/mesh spacing; developing manageable model computer run-times; evaluating vertical aquifer system connections/leakage; testing alternate locations for ASR clusters; developing reasonable ASR recharge and recovery scenarios; and determining whether or not steady state modeling is applicable.

Due to the large scale of the model, computer run-times are expected to be quite long. Therefore, the selection of an appropriate model code is of paramount importance. Consideration will be given to utilizing a fully density-dependent model code if performance tests confirm that such a code would be practical to use at the scale envisioned. Otherwise, consideration will be given to simulating density effects at the seawater boundaries and along the bottom of the model as necessary.

Model Code Bench-scale Testing Scope of Work:

The scope of work for the model development effort presented in the ASR Regional Study PMP recognized that a fully density-dependent code would be ultimately be required to simulate regional changes in aquifer pressure and water quality. This is due to a number of technical considerations including:

- Water exchange between various portions of the FAS
- Water flow and velocity issues near coastal portions of the model
- ASR recovery efficiency is partially dependent upon density stratification effects
- Density directly affects the regional heads and flow within the FAS
- Density is a function of water quality of the aquifer (e.g., function of TDS)

The PMP also considered alternate modeling approaches employing density-dependent boundaries to grossly simulate density affects. Therefore, the development of sub-regional models that possessed the requisite density-dependent capabilities were specified as part of the PMP to ensure the most realistic model simulations could be developed. Alternate modeling approaches may allow some flexibility in the development of a regional model, ensuring that the following constraints are managed:

- Limitations of existing density-dependent model codes
- Concerns about model run times
- Schedule constraints
- Resources available

Ideally, both the Regional Screening Model and the sub-regional models would be fully density-dependent models. Subsequent to completion of the PMP, advances in model codes have made the use of a density-dependent code more feasible as part of the Regional Screening Model development effort. There is concern, however, that the size of the model might limit the feasibility of the fully density-dependent approach due to the constraints listed above, especially model run times. In order to balance the needs of the project with the current technical capabilities of software and hardware, the model development team recommended the development of a bench-scale model to evaluate various model codes and approaches in order to aid the model code selection task.

The primary objectives of the bench-scale modeling effort are:

- Provide an improved estimate of model run times for 36-year simulations
- Provide a preliminary understanding of model development issues relating to resolution requirements, boundary types, and starting conditions
- Uncover model limitations and short comings

An appropriate code for the Regional Screening Model is to be selected on the basis of bench testing of various model codes at a sub-regional or county-wide scale. Although the proposed domain size is still considerably smaller than the anticipated regional model domain, it does provide a firm basis for the extrapolation of model performance to the larger domain. Bench testing of several model codes will provide a solid basis to make an informed decision on model code selection. This course of action will provide the following benefits:

- Aid in determining what class of model (constant density standard flow and transport, uncoupled density-dependent flow and transport, fully density-dependent flow and transport) is required to address CERP ASR issues
- Provide comparison performance metrics for various bench marked codes including relative accuracy, and model stability and run-times
- Aid in the evaluation of hardware needs & pre/post processing requirements

It was envisioned that the benchmark modeling effort would develop several identical (constant density standard flow and transport, uncoupled density-dependent flow and transport, fully density-dependent flow and transport) models covering a much smaller model region than projected for the Regional Screening Model. It was anticipated that a 40 mile X 40 mile area would provide a model domain of sufficient size and complexity to provide a valid test of each proposed model code and allow extrapolation of results to larger regional scales. The scale and design would be similar in size to Palm Beach County, Florida, where many ASR wells are proposed for installation. As part of the ASR Pilot Project Design Report (PPDR), a numerical model of the Palm Beach County area was available. In order to maximize the use of previously developed model tools as suggested by the Interagency Modeling Center (IMC), the USACE provided the Palm Beach County model as the "base" MODFLOW/MT3D model. Using the base model as a guide, four similar "box models" were prepared using four different model codes/approaches. The model was provided "as is" and was not optimized for any particular application.

The four codes were selected in a collaborative fashion among members of the modeling sub-team of the PDT. With the exception of the MODFLOW SWI package, the sub-team members had significant experience with the rest of the models selected. In addition, each of the codes selected was paired with a well-known pre/post-processor software package that simplified the model development process. Lastly, budget considerations limited the task scope to no more than four model codes. If time and budget had allowed, several other established codes would also have been considered, including FEFLOW and SUTRA, for example. The four model codes utilized for the bench-scale study are:

- MODFLOW and MT3DMS using equivalent freshwater heads to represent saltwater boundaries (e.g., constant density flow and transport model)
- SWI (Sea-Water Intrusion) Package for MODFLOW (density dependent vertically integrated flow with interface tracking)
- SEAWAT (fully coupled or uncoupled density-dependent flow and transport)
- WASH123 (fully coupled or uncoupled density-dependent flow and transport)

MODFLOW is a computer program that numerically solves the three-dimensional groundwater flow equation for a porous medium using a finite-difference method (McDonald and Harbaugh, 1988). MT3DMS is a computer program for modeling multi-species solute transport in three-dimensional ground-water systems using multiple solution techniques, including the finite-difference method, the method of characteristics (MOC), and the total-variation-diminishing (TVD) method (Zheng and Wang, 1999). MODFLOW is considered to be the most widely used program for constant-density groundwater flow problems. Key factors in MODFLOW's popularity in the modeling community are its thorough documentation, modular structure, which makes it easy to modify and enhance, and the public availability of the software and source code.

The Sea Water Intrusion (SWI) package is intended for the modeling of regional seawater intrusion with MODFLOW2000 (Bakker and Schaars, 2002). The SWI package utilizes

the Dupuit approximation that neglects vertical resistance to flow in the vertical direction. The vertical pressure distribution is hydrostatic in each aquifer. The advantage of using the Dupuit approximation is it allows multiple aquifer systems with one layer of cells. The vertical pressure distribution is hydrostatic in each aquifer, but this does not mean that there is no vertical flow; the vertical component of flow is computed from the three-dimensional continuity of flow. Variable-density flow may be simulated, through Darcy's Law, as stratified flow or as continuously varying density flow. The basic principle behind the formulation is to solve, during each time step, for the freshwater-head by considering continuity of flow in the entire aquifer, and to solve for the elevations of the interfaces by considering continuity of flow below each surface. Is should also be noted that the effects of dispersion and diffusion are not taken into account. Inversion, saltier (heavier) water above fresher (lighter) water, is also not allowed.

The SEAWAT program (Guo and Langevin, 2002) is a combination of MODFLOW and MT3DMS (Zheng and Wang, 1999) designed to simulate three-dimensional, variable-density, groundwater flow and solute-transport. The program was developed by modifying MODLOW subroutines to solve a variable-density form of the groundwater flow equation and by combining MODFLOW and MT3DMS into a single program. SEAWAT reads and write standard MODFLOW and MT3DMS input and output files, allowing most of the existing pre- and post-processors to facilitate application of the program to a wide range of practical problems. One advantage of SEAWAT is that because it uses MT3DMS to represent solute-transport, the program contains several diverse methods (Eulerian, Langrangian, or mixed) for solving the transport equation including the MOC, an explicit third order total-variation-diminishing (TVD) scheme, and a standard finite-difference method with central-in-space or upstream weighting.

WASH123D (Yeh et al. 1998) is a finite element numerical model designed to simulate variably saturated, variable-density water flow and reactive chemical and sediment transport in watershed systems. It is capable of conceptualizing a watershed system as a combination of 1D river/stream, 2D overland, and 3D subsurface sub-domains. A modified Richards' equation is used to solve for 3D flow when density effect is taken into account. The equation is solved with the Galerkin finite element method. The groundwater flow portion of the code utilizes an adaptation of the FEMWATER code (Lin et al. 1997). WASH123D uses the Lagrangian-Eulerian (LE) method to solve the transport equations. Particle tracking is used in the Lagrangian step to handle the advection term. Other terms (such as sources, sinks, diffusion, and dispersion) are calculated in the Eulerian step, where element matrices are assembled into a global matrix, and matrix solvers are used to solve for the spatial concentration distribution at the end of each time step. A predictor-corrector numerical technique, combined with an adaptive explicit-implicit numerical scheme, is employed to compute reactive transport efficiently and robustly. The use of this methodology allows the numerical stability of WASH123D not to be restricted by the Mesh Courant number. In addition, the Mesh Peclet number is restricted only by computational accuracy, not numerical stability. More detailed discussion on various types of numerical dispersion and how the LE method deals with these types of numerical dispersion are discussed in the referenced papers.

As described previously, each model would include a model boundary consisting of a 40-mile by 40-mile square box. Each model would contain 7 to 20 vertical layers representing the Surficial Aquifer System (SAS), Hawthorn Group confining unit, and the FAS. The four models each adopted the same hydrogeologic conceptual model, utilizing the same aquifers and confining units. Also, all of the model layers were assigned with identical hydraulic parameters (e.g., hydraulic conductivity and storage coefficient) in order to eliminate differences in these properties due to contouring algorithm chosen for each model. The exact number of layers was initially intended to be consistent for the different codes, however, model stability and accuracy requirements required refinement in some cases. Each box model would have identical boundary conditions, starting conditions (head and TDS concentration), influent TDS concentrations (150 mg/l), and aquifer/confining unit parameters. In addition, a common convergence criteria was agreed upon for both flow and transport portions of the models. Five separate cases were developed by the PDT to evaluate relevant ASR modeling issues including mixing, hydrodynamic dispersion, density stratification, upconing, and changes in salinity distribution as a result of ASR injection and/or recovery. The five cases are summarized in Table 2. Additional specific information summarizing each case is available following the table.

Table 2. Bench-scale case summary.

Case Number	**Purpose and basic setup**
IA	One ASR well recharge and recovery 5 MGD from FAS storage zone with TDS of 4,000 mg/l. Minimal upconing or leakage from below. No dispersivity assigned.
IB	One ASR well recharge and recovery 5 MGD from FAS storage zone with TDS of seawater (35,000 mg/l). Minimal upconing or leakage from below. No dispersivity assigned.
IC	One ASR well recharge and recovery 5 MGD from FAS storage zone with TDS of 4,000 mg/l. Major upconing or leakage from below encouraged through confining layer vertical conductivity assignment. No dispersivity assigned.
ID	One ASR well recharge and recovery 5 MGD from FAS storage zone with TDS of 4,000 mg/l. Minimal upconing or leakage from below. Dispersivity assigned with value of 25 feet.
IIA	One ASR well recovering for 5 years continuous to evaluate movement of salt-water interface from coast.

Case IA: Transient Model Simulation - One ASR well injecting 5 MGD into FAS in center of box for 30 days, followed by 305 day storage period, followed by 30 days of recovery at 5 MGD. The starting TDS of the FAS storage zone was assigned to be 4,000 mg/l, the TDS of the Middle FAS Confining Unit will be 35,000 mg/l, and the Middle FAS flow zone was assigned 35,000 mg/l. The Middle FAS Confining Unit was assigned a vertical conductivity of 0.001 feet per day to ensure minimal leakage between aquifer units. The Surficial Aquifer System (SAS) was assigned a constant head of 20 feet. The Hawthorn Group Clay (Intermediate Confining Unit) was assigned a vertical conductivity of 0.001 feet per day to ensure minimal leakage between the SAS and the Upper FAS. Prior to simulation start up, the model was run with the regional gradient to steady state conditions. The regional gradient was assigned from west to east at 0.0001 and is considered representative of the Upper FAS. The steady state gradient of 0.0001 was used to assign the starting heads of the Upper FAS for the one year simulation. The dispersivity tensor was assigned a value of zero in order to evaluate the degree of numerical dispersion produced from each code.
The purpose of Case 1A was to evaluate model code ability to simulate aquifer pressure changes, salinity changes due to conservative mixing, salinity changes due to hydrodynamic dispersion, and relative degree of numerical dispersion introduced. Since there was no known ASR case studies that have evaluated this issue, the comparison of numerical dispersion was relative in nature and assumed that the TVD solution was the most accurate as determined from previous publications. The flows between layers and to and from boundaries were also of interest. Landscape Figure 1 below (at the end of the report after the report appendices) depicts the assigned model parameters in detail for both the MODFLOW based models as well as the WASH123 model.

Case IB: Transient Model Simulation - One ASR well injecting 5 MGD into FAS in center of box for 30 days, followed by 305 day storage period, followed by 30 days of recovery at 5 MGD. The starting TDS of the FAS storage zone was assigned to be 35,000 mg/l, the TDS of the Middle FAS Confining Unit will be 35,000 mg/l, and the Middle FAS flow zone was assigned 35,000 mg/l. The Middle FAS Confining Unit was assigned a vertical conductivity of 0.001 feet per day to ensure minimal leakage between aquifer units. The Surficial Aquifer System (SAS) was assigned a constant head of 20 feet. The Hawthorn Group Clay (Intermediate Confining Unit) was assigned a vertical conductivity of 0.001 feet per day to ensure minimal leakage between the SAS and the Upper FAS. Prior to simulation start up, the model was run with the regional gradient to steady state conditions. The regional gradient was assigned from west to east at 0.0001 and is considered representative of the Upper FAS. The steady state gradient of 0.0001 was used to assign the starting heads of the Upper FAS for the one year simulation. The dispersivity tensor was assigned a value of zero in order to evaluate the degree of numerical dispersion produced from each code.

The purpose of Case 1B was to evaluate model code ability to simulate aquifer pressure changes, salinity changes due to conservative mixing, salinity changes due to hydrodynamic dispersion, and degree of buoyancy stratification that occurs during the storage period. The flows between layers and to and from boundaries were also of

interest. Landscape Figure 2 below depicts the assigned model parameters in detail for both the MODFLOW based models as well as the WASH123 model.

Case IC: Transient Model Simulation – One ASR well injecting 5 MGD into FAS in center of box for 30 days, followed by 305 day storage period, followed by 30 days of recovery at 5 MGD. The starting TDS of the FAS storage zone was assigned to be 4,000 mg/l, the TDS of the Middle FAS Confining Unit will be 35,000 mg/l, and the Middle FAS flow zone was assigned 35,000 mg/l. The Middle FAS Confining Unit was assigned a vertical conductivity of 1 feet per day to ensure leakage between the aquifer units. The Surficial Aquifer System (SAS) was assigned a constant head of 20 feet. The Hawthorn Group Clay (Intermediate Confining Unit) was assigned a vertical conductivity of 0.001 feet per day to ensure minimal leakage between the SAS and the Upper FAS. Prior to simulation start up, the model was run with the regional gradient to steady state conditions. The regional gradient was assigned from west to east at 0.0001 and is considered representative of the Upper FAS. The steady state gradient of 0.0001 was used to assign the starting heads of the Upper FAS for the one year simulation. The dispersivity tensor was assigned a value of zero in order to evaluate the degree of numerical dispersion produced from each code.

The purpose of Case 1C was to evaluate model code ability to simulate aquifer pressure changes, salinity changes due to conservative mixing, salinity changes due to hydrodynamic dispersion, and degree of density-driven upconing. The flows between layers and to and from boundaries were also of interest. Landscape Figure 3 below depicts the assigned model parameters in detail for both the MODFLOW based models as well as the WASH123 model.

Case ID: Transient Model Simulation - One ASR well injecting 5 MGD into FAS in center of box for 30 days, followed by 305 day storage period, followed by 30 days of recovery at 5 MGD. The starting TDS of the FAS storage zone was assigned to be 4,000 mg/l, the TDS of the Middle FAS Confining Unit will be 35,000 mg/l, and the Middle FAS flow zone was assigned 35,000 mg/l. The Middle FAS Confining Unit was assigned a vertical conductivity of 0.001 feet per day to ensure minimal leakage between aquifer units. The Surficial Aquifer System (SAS) was assigned a constant head of 20 feet. The Hawthorn Group Clay (Intermediate Confining Unit) was assigned a vertical conductivity of 0.001 feet per day to ensure minimal leakage between the SAS and the Upper FAS. Prior to simulation start up, the model was run with the regional gradient to steady state conditions. The regional gradient was assigned from west to east at 0.0001 and is considered representative of the Upper FAS. The steady state gradient of 0.0001 was used to assign the starting heads of the Upper FAS for the one year simulation. The dispersivity tensor was assigned a value of 25 feet in order to evaluate the model run times using a realistic amount of hydrodynamic dispersion.

The purpose of Case 1D was to evaluate model code ability to simulate aquifer pressure changes, salinity changes due to conservative mixing, salinity changes due to hydrodynamic dispersion, and degree of hydrodynamic dispersion introduced. The flows between layers and to and from boundaries were also of interest. Landscape Figure 4

below depicts the assigned model parameters in detail for both the MODFLOW based models as well as the WASH123 model.

Case IIA: Transient Model Simulation – Transient Model Simulation - One ASR well withdrawing 5 MGD from the Upper FAS in center of box for five years. The starting TDS of the FAS storage zone was assigned to be 4,000 mg/l, the TDS of the Middle FAS Confining Unit will be 35,000 mg/l, and the Middle FAS flow zone was assigned 35,000 mg/l. All units at the eastern boundary of the model were assigned a starting head of zero. The starting concentration of TDS in all model layers was based upon an approximation of the Ghyben-Herzberg relationship to define the 35,000 mg/l isochlor. The Middle FAS Confining Unit was assigned a vertical conductivity of 0.001 feet per day to ensure minimal leakage between aquifer units. The Surficial Aquifer System (SAS) was assigned a constant head of 20 feet. The Hawthorn Group Clay (Intermediate Confining Unit) was assigned a vertical conductivity of 0.001 feet per day to ensure minimal leakage between the SAS and the Upper FAS.

The purpose of Case IIA was to evaluate model code ability to simulate pumping induced regional changes in the three-dimensional salinity distribution.

Groundwater Model Testing and Comparison Protocols

Groundwater model testing has been the subject of multiple past studies and papers. Testing of groundwater simulation codes may take several forms including:

- Benchmarking against known analytical solutions
- Intra-code comparisons using different code functions and same stresses to emulate the same system response
- Inter-code comparisons simulating same stresses and systems
- Comparisons with field or laboratory data

One thing sorely lacking amongst the published literature is an approved or recommended protocol to perform the various comparisons. One such study was prepared by van der Heijde and Danzer (1997) for the United States EPA. This paper proposes a systematic evaluation and testing methodology or protocol that could be applicable to the bench-scale modeling effort. Although the bench-scale modeling effort was designed to test and compare model codes, it was not meant to be a full-scale code-testing and evaluation protocol; therefore, some of the evaluations recommended by van der Heijde and Danzer were not completed. Van der Heijde and Danzer recommend including an evaluation of code functionality and performance. Code functionality is defined as the set of functions and features which the code offers the user in terms of model framework geometry, simulated processes, boundary conditions, and analytical and operational capacities (van der Heijde and Danzer, page 2). Performance evaluations are aimed at determining the characteristics of the model code in terms of:

- Computational accuracy
- Reliability (convergence and stability of solution algorithms)

- Sensitivity for grid orientation, grid resolution, or time discretization
- Efficiency of coded algorithms (code execution time and memory/storage requirements)
- Resources required for model setup and analysis

First, all of the codes were evaluated for their overall functionality to address specific ASR issues discussed above. The overall code functionality was addressed based upon existing information available for each code, PDT experience, and published papers or case studies. Each issue requires a basic set of model development and analysis functions. These various functions are outlined in Table 3 along with qualitative scoring of each model code.

In reviewing Table 3, all codes could provide some of the functionality required to evaluate all relevant ASR issues to be studied. SEAWAT and WASH123 provide the highest overall functionality for the questions to be answered with the model. Table 4 provides a list of other general functions that are required of each model along with a qualitative score for each. In general all of the codes can provide much of the basic functionality required for the ASR Regional Study, however, SEAWAT and WASH123 provide the best overall functionality desired for the study.

Table 3. Required model functionality

Specific ASR Project Issue	**Desired Functionality**	**Modflow/MT3D**	**SEAWAT**	**WASH123**	**SWI**
Regional changes in aquifer heads and flows	1. Simulate head changes in region around proposed ASR well clusters	X	X	X	X
	2. Simulate flows from ASR wells, existing FAS user wells, boundaries, and between aquifers	X	X	X	X
Regional changes in aquifer water quality	1. Simulate water quality changes in region around proposed ASR wells, existing FAS user wells, boundaries, and between aquifers	X	X	X	
	2. Simulate density changes as a result		X	X	X
Increased potential for salt-water intrusion caused by ASR pumping	1. Simulate potential movement of salt-water wedge due to ASR recovery activities		X	X	X
	2. Simulate potential movement of salt-water wedge due to ASR recharge activities		X	X	X
Regional impacts to	1. Evaluate increases or decreases in head or water quality at existing well users	X	X	X	X

existing well users of the FAS	caused by ASR activity				
ASR well cluster site selection	1. Simulate superposition effects caused by multiple ASR wells recharging or recovering. Site ASR well clusters in order to minimize superposition effects and potential impacts on users. 2. Site selection is heavily influenced by all proposed well fields operating at same time (e.g., boundary effects are important in this instance).	X X	X X	X X	X X
ASR well cluster design and layout	1. Evaluate design and layout issues at one ASR cluster. 2. Varying horizontal resolution probably required.	X X	X X	X X	X X
ASR well cluster performance including estimating recovery efficiency	1. Evaluate ASR well cluster recovery efficiency and performance. 2. Evaluate upconing potential at each cluster site. 3. Evaluate density stratification at each cluster site.	X	X X X	X X X	 X
ASR well site evaluation of pressure induced changes	1. Evaluate aquifer pressure at each proposed ASR well, 1 mile distant from ASR well cluster, and at other FAS user wells. 2. Evaluate pressure changes within the Hawthorn Group at ASR well cluster.	X X	X X	X X	X
Localized transport of contaminants including heavy metals or pathogens	1. Evaluate transport of potential “bad actors” including heavy metals such as arsenic, nickel, and fluoride. 2. Evaluate conservative transport and reactive transport of pathogens.	X X	X X	X X	
Localized ASR well pump design	1. Evaluate aquifer pressure at each well and in entire well cluster.	X	X	X	X

Table 4. Additional model functionalities required.

Desired Functionality	Modflow/MT3D	SEAWAT	WASH123	SWI
Incorporate irregular geometry	X	X	X	X
Incorporate varying vertical model resolution and multiple layers	X	X	X	
Incorporate varying aquifer properties	X	X	X	X
Incorporate rainfall and recharge	X	X	X	X
Incorporate leakage between layers	X	X	X	X
Incorporate Dirichlet and Cauchy boundary types	X	X	X	X**
Incorporate constant and transient boundary conditions	X	X	X	X
Incorporate injection and recovery wells	X	X	X	X
Simulate advection, dispersion, and mixing	X	X	X	
Simulate contaminant decay or natural attenuation	X	X	X	
Simulate density-dependent flow		X	X	X

** - is capable for flow but not transport

An important consideration in any of model code is its overall credibility and suitability (van der Heijde and Kanzer, 1997). Therefore, the level at which the code has been tested is an important component in the decision-making process. Given the issues to be addressed with the ASR regional model, it is clear that groundwater hydraulics, conventional contaminant transport, and density-dependent flow concerns will all require critical contemplation. To aid in this determination, the PDT reviewed existing publications and past benchmarking cases in order to compile a list of tested problems. In addition, the PDT performed additional benchmarking against published analytical solutions. The PDT prepared several simple benchmarking tests to evaluate groundwater hydraulics and conventional contaminant transport. Both the finite-difference (MODFLOW/MT3DMS) and finite-element models (WASH123) were first tested using a series of groundwater hydraulics cases including pumping from a confined aquifer (Theis, 1935) and pumping from a leaky-confined aquifer (Hantush and Jacob, 1953). Since the ASR regional model will be simulating changes in head and flow caused by well pumping, the PDT felt this was a valuable test to evaluate. Then both predominant model types were tested using a conventional contaminant transport case (Ogata, 1970). The results of the Theis and Ogata benchmarking tests are available in figures 1 and 2. Each figure compares the numerical model results versus exact analytical solutions. Both the MODFLOW/MT3DMS and WASH123 numerical model results compare very favorably to the analytical solutions. The WASH123 code was further tested against both the “Elder problem” and the “Henry problem” with results available in Appendix A. All of these tests indicate that all of the codes tested appear to solve the governing equations accurately.

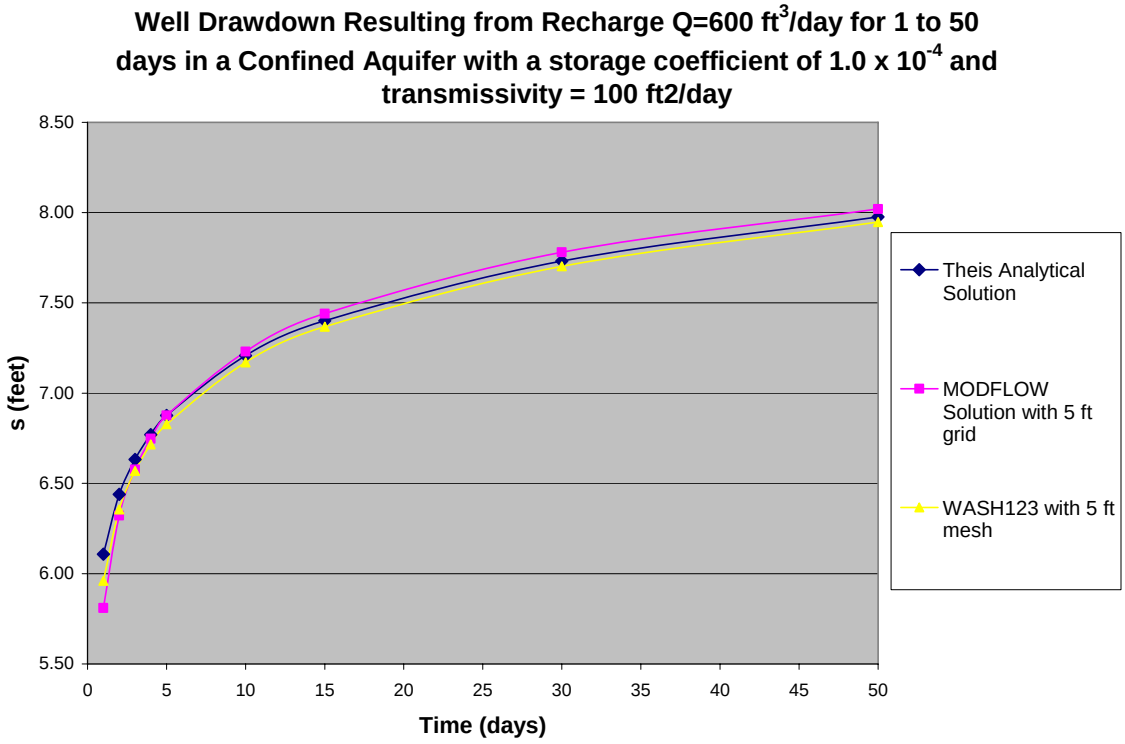

Figure 1. Theis confined aquifer benchmarking case comparing numerical model results to exact solution.

For variable-density groundwater flow, there are a suite of benchmark problems that have been designed to test the ability of a numerical code to accurately simulate the complex flow and transport dynamics associated with density dependent flow. Table 5 lists these commonly used benchmark problems and shows which codes have been tested to date. It should be noted that neither the SWI or the WASH123 codes have been tested as thoroughly as the SEAWAT code mainly due to their relatively young age. It is anticipated that both SWI and WASH123 will be tested against many of the remaining variable-density benchmark problems in the future as the codes become utilized by more users. Appendix A provides additional information on the variable-density test cases completed using WASH123.

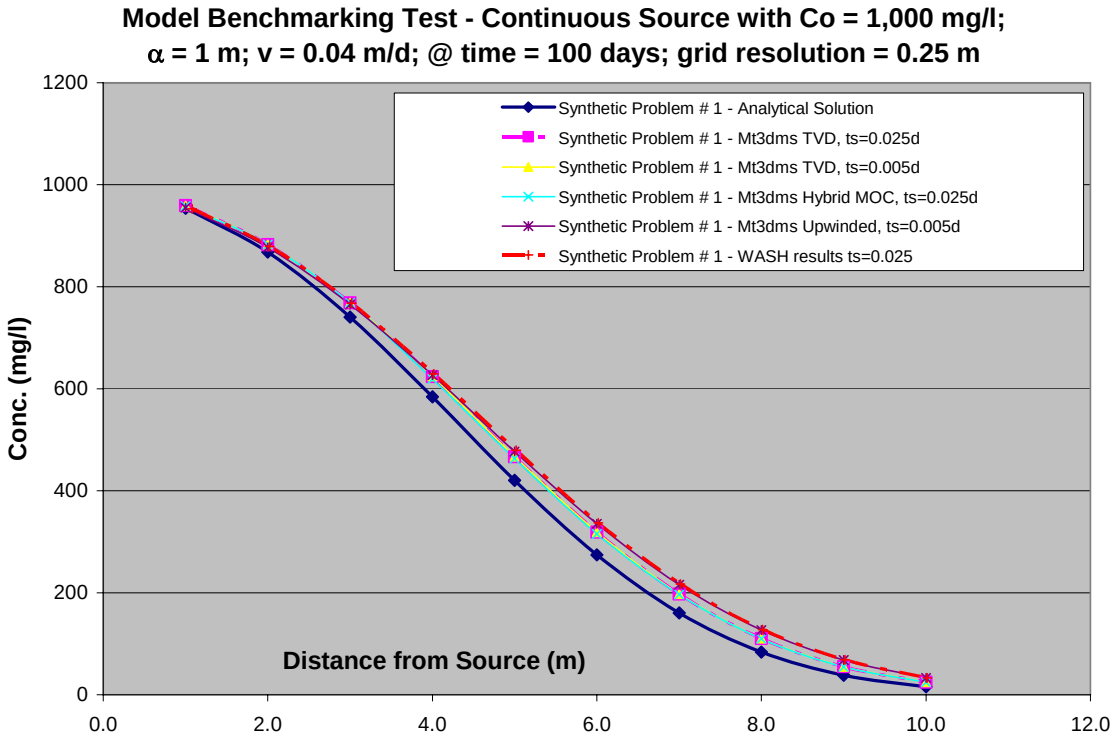

Figure 2. Ogata continuous source benchmarking case comparing numerical model results to exact solution.

Table 5. Variable-density benchmark problems.

Benchmark Problem	**SWI**	**SEAWAT**	**WASH123**
Box Problems		X	
Henry Case 1	NA	X	X
Henry Case 2	NA	X	X
Elder	NA	X	X
HYDROCOIN	NA	X	
Immiscible Fluid Rotation	X	X	
Rotating Interface	X		
Rotating Brackish Zone		X	
Upconing Beneath a Pumping Well	X		
Salt Pool 1	NA	X	
Salt Pool 10	NA	X	

NA – not applicable since SWI cannot simulate hydrodynamic dispersion

The overall performance assessment was measured through application of the various bench-scale cases completed as well as previous benchmarking work completed in support of each code. The performance assessment was measured against metrics listed previously including:

- Computational accuracy
- Reliability (convergence and stability of solution algorithms)
- Sensitivity for grid orientation, grid resolution, or time discretization
- Efficiency of coded algorithms (code execution time and memory/storage requirements)
  - Model run times were computed for all 5 ASR cases
  - Storage requirements were evaluated for all 5 ASR cases
- Resources required for model setup and analysis including
  - Pre and post processing effort
  - Computer type or hardware required
  - General ease of use for new modelers

Model Code Bench-scale Testing Results:

The four model codes were tested extensively using the five case studies outlined previously in this memorandum. Multiple contaminant transport algorithms were tested using both the existing MODFLOW/MT3DMS model and the SEAWAT model (e.g., central-difference solution and the TVD solution). WASH123 and SWI only provide one contaminant transport algorithm. Each of the codes revealed significant advantages and disadvantages. A comparison of performance metrics for each code is provided in the following sections of this memorandum. Appendix A and B of this memorandum contains additional information concerning the WASH123 results and the SEAWAT/SWI results.

Resources Required for Model Setup and Analysis

General Ease of Use

All of the model codes evaluated required significant user knowledge and experience in order to successfully utilize the model. The MODFLOW/MT3DMS, SEAWAT, and WASH123 models are all somewhat difficult to master but all three can link with readily available pre and post processors. The exception to this is the SWI code. The SWI model can be run independently but the results must be imported into a post-processor. The importation of the data requires some re-working of output files and required companion files. In general, table 6 lists the qualitative "ease of use" for each code along with pre/post processor tools utilized. In general, all of the codes rank similarly for this category.

Table 6. Model Code Ease of use.

Model Code	**Ease of Use (Easy, Moderate, or Difficult)**	**Compatible Pre and Post Processor**
MODFLOW/MT3DMS	Moderate	Groundwater Modeling System (GMS) ® Groundwater Vistas Argus Visual MODFLOW PMWIN, Modelviewer
SEAWAT	Moderate	Groundwater Vistas Argus Visual MODFLOW PMWIN, Modelviewer
WASH123	Moderate	GMS
SWI	Moderate	Argus, MATLAB

Required Time for Pre and Post Processing

All of the model codes required time for both pre and post processing of simulation results. The MODFLOW/MT3DMS, SEAWAT, and WASH123 models all link directly to relevant pre and post processing software packages. As discussed previously, the GMS and Groundwater Vistas software packages were utilized. Each software package provides an intuitive graphical user interface (GUI) that allows rapid data manipulation, formatting, and output preparation. Both software packages are widely used in the groundwater modeling community of practice. One advantage of the GMS is that it is freely available to the Corps of Engineers, its partners and its sponsors. Although the overall expense may be minor, the Groundwater Vistas, Argus, and Visual Modflow software must be purchased separately for team members to utilize effectively.

The required time for pre and post processing is probably least for the MODFLOW/MT3DMS code and greatest for the SWI code due to reformatting issues already discussed. Table 7 lists a qualitative assessment of the pre and post processing time for each code considered.

Table 7. Time for pre and post processing.

Model Code	**Pre and Post Processing Time (Low is less than 4 hours, Moderate is 4 to 8 hours, High is greater than 8 hours)**	**Pre and Post Processing Software Used**
MODFLOW/MT3DMS	Low	Groundwater Modeling System (GMS) ® Groundwater Vistas

		Argus Visual MODFLOW PMWIN
SEAWAT	Low	Groundwater Vistas Argus Visual MODFLOW PMWIN
WASH123	Moderate	GMS
SWI	Moderate	None can be used directly

Computer Type or Hardware Required

All of the model codes considered could be run on personal computer, however, when consideration is given to the proposed application (e.g., a large regional scale model), all of the models would likely require workstations to ensure computational efficiency. Since SWI does not calculate contaminant transport equations, it probably requires the least hardware demands. Obviously, for coarse resolution models, a regional model may be able to be run on a newer personal computer (2 years old or less with 2.6 GHz or faster processor and at least 1 GB of resident memory) also. Table 8 provides a comparison of required hardware.

Table 8. Computer Type/Hardware Requirements.

Model Code	**Hardware Required for small model**	**Hardware Required for regional model**
MODFLOW/MT3DMS	Personal computer	Workstation
SEAWAT	Personal computer	Workstation
WASH123	Personal computer	Workstation
SWI	Personal computer	Personal computer

Efficiency of coded algorithms (code execution time and memory/storage requirements)

Model Run Times and Storage Requirements

As part of the performance assessment of the model codes, model simulation times were measured for the various case studies. Since the models were run on different workstations with divergent processing architecture, an effort was undertaken to "normalize" the simulation times through standardized computer industry comparisons. Several independent information technology forums provide processor performance comparisons for different software applications. One of these provides the information for free at the internet site www.spec.org. Information provided at the site includes both base and peak processor speeds for different tasks. Table 9 provides a comparison of both metrics for the computer workstations utilized for the study. The exact workstation

utilized to run the SEAWAT and SWI simulations was not listed at spec.org site so an average of three similar computers was selected to be representative. Then the base processor speeds were normalized against 1,000 to provide simulation run time "factors" to be applied to the actual raw simulation times for each case.

Table 9. Workstation performance metrics from www.spec.org.

Computer	Base Floating Point Speed	Peak Floating Point Speed
Optiplex Computer, 2.66 GHz, 1GB Ram	919	927
Dell GX280 Computer, 3.60 GHz P4, 2GB Ram	1905	1916
Dell WS Computer, 3.06 GHz P4, 2GB Ram	1092	1103
Intel 3.46 GHz P4, 3GB Ram	1719	1724
AVG 3 Computers	1572	1581
XI Computer, AMD 148 Opteron Chip	1393	1490

The factors applied were 0.919 for the MODFLOW/MT3DMS models, 1.572 for the SEAWAT and SWI models, and 1.393 for the WASH123 models. In essence, the normalized run times would be reduced for the MODFLOW/MT3DMS models and increased for all of the other models. Based upon information contained on this site and an inventory of workstation hardware utilized for the ASR Benchmark study, a set of normalized simulation times were developed. Table 10 lists all of the normalized model run times for the study as well as the runtime per model calculation point. The fastest and slowest runtime per calculation point is highlighted in the table. The fastest times are highlighted in pink while the slowest times are shown in yellow. The normalized model run times were also formulated from model runs that had identical convergence criteria and similar time-step sizes. The time-step size required to ensure stability was code dependent but efforts were made to ensure the final time-step size was similar for all codes. Given the complexity of the models and domain size (County size), model run times were generally long.

Table 10. Normalized model simulation run times.

RUN 1A	Run Times (min)	Normalized Run Times	Normalized Run Time per Calculation Point
MODFLOW/MT3DMS - Upwind	217	199	1.3E-03
MODFLOW/MT3DMS - TVD	463	425	2.8E-03
SEAWAT - Upwind	55.84	88	5.8E-04
SEAWAT - TVD	3838.5	6034	4.0E-02
WASH123	330	460	4.1E-03
SWI	18.75	29	3.1E-04
RUN 1B	**Run Times (min)**	**Normalized Run Times**	**Normalized Run Time per Calculation Point**
MODFLOW/MT3DMS - Upwind	217	199	1.3E-03
MODFLOW/MT3DMS - TVD	466	428	2.8E-03
SEAWAT - Upwind	56.19	88	5.8E-04
SEAWAT - TVD	3864.95	6076	4.0E-02
WASH123	420	585	5.2E-03
SWI	15.27	24	2.5E-04
RUN 1C	**Run Times (min)**	**Normalized Run Times**	**Normalized Run Time per Calculation Point**
MODFLOW/MT3DMS - Upwind	217	199	1.3E-03
MODFLOW/MT3DMS - TVD	467	429	2.8E-03
SEAWAT - Upwind	57	90	5.9E-04
SEAWAT - TVD	3878.2	6097	4.0E-02
WASH123	330	460	4.1E-03
SWI	19.71	31	3.2E-04
RUN 1D	**Run Times (min)**	**Normalized Run Times**	**Normalized Run Time per Calculation Point**
MODFLOW/MT3DMS - Upwind	2157	1982	1.3E-02
MODFLOW/MT3DMS - TVD	4320	3970	2.6E-02
SEAWAT - Upwind	58.96	93	6.1E-04
SEAWAT - TVD	3929	6176	4.1E-02
WASH123	329	458	4.1E-03
RUN 2A	**Run Times (min)**	**Normalized Run Times**	**Normalized Run Time per Calculation Point**
SEAWAT - Upwind	767	1206	8.0E-03
SEAWAT - TVD	11171	17561	1.2E-01
WASH123	522	727	6.5E-03
SWI	11	15	1.6E-04

Generally, the SEAWAT TVD solution resulted in the longest normalized simulation times while the SWI resulted in the shortest. The TVD solution scheme in MT3D (and thus SEAWAT) required unreasonably short transport time step lengths for an accurate solution. Due to project time constraints, no attempt was made to resolve the issue, but it is possible that the issue could be fixed, in which case, the runtimes could reduced. Since both finite-difference models (MODFLOW/MT3DMS, SEAWAT, and SWI) and finite-element (WASH123) models were utilized in the study, further examination of the run time per calculation point is important. The WASH123 model had 112,716 calculation points versus 151,000 for the other models tested. A key difference to be noted is that the WASH123 model provided greater vertical resolution (30 layers) but varying horizontal resolution as compared to the other finite-difference models (16 vertical layers). When considering the horizontal resolution of the two model types, the WASH123 model resulted in fewer computational points than the comparable finite-difference model due to the flexible mesh design advantage that is inherent in finite-element formulations. This may be an important consideration in the design of the regional model. Figure 3 depicts the finite-difference model vertical resolution while Figure 4 depicts the comparable finite-element model vertical resolution.

Figure 3. Finite-difference model vertical resolution.

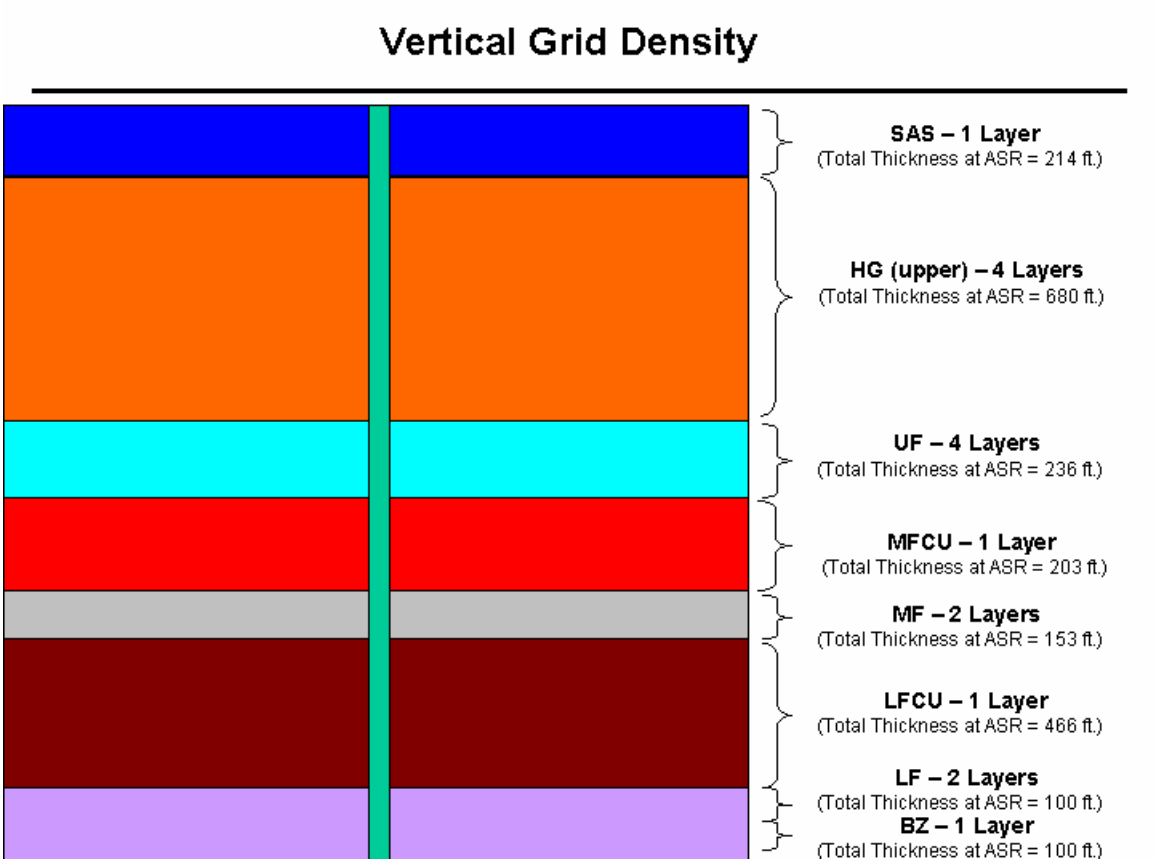

For all of the models, storage requirements were moderate and highly dependent upon model resolution, time-step size, and outputs designated. In general, large capacity hard

drives available on personal computers and work stations should be sufficient to handle requirements of the regional model development.

Figure 4. Finite-element model vertical resolution.

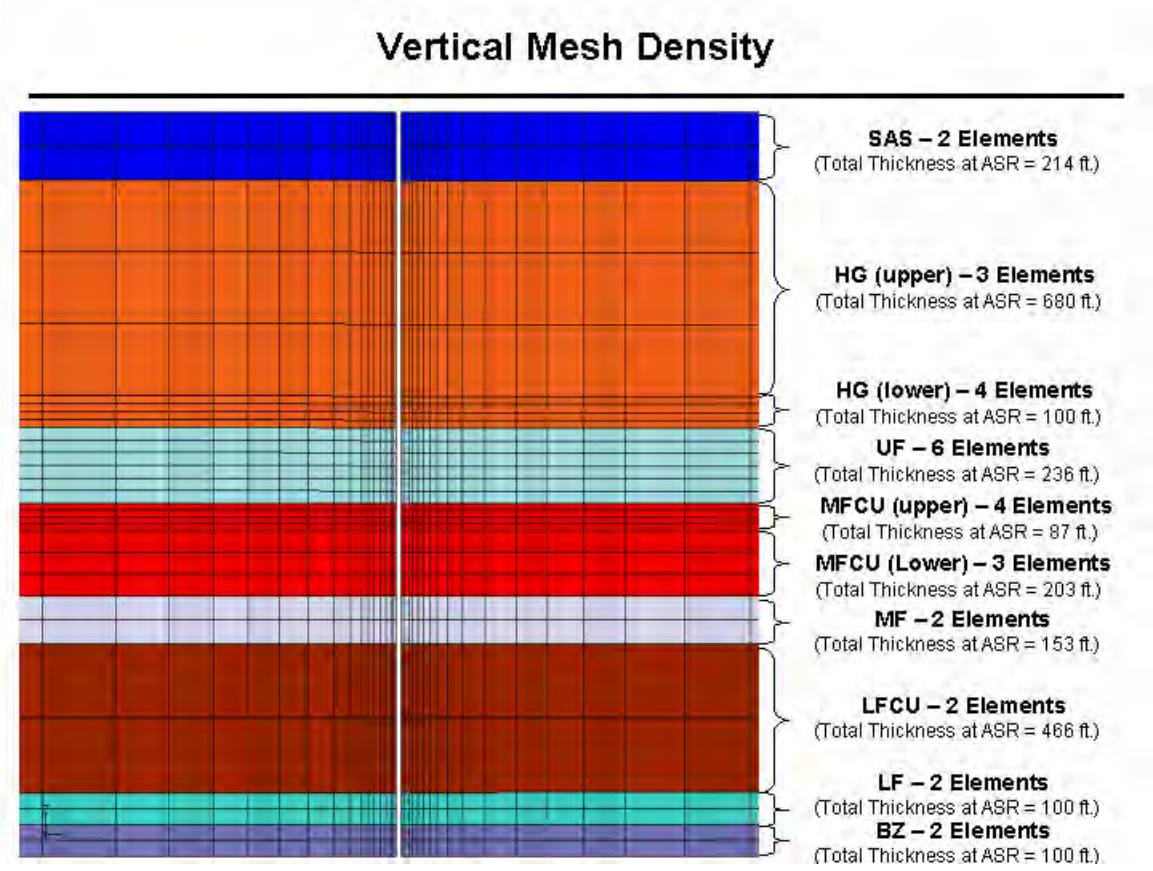

Time and resource constraints did not allow a systematic evaluation of each code's dependence upon grid resolution or time discretization to ensure accuracy. The time discretization was evaluated in a gross sense in order to minimize model run times, however, only minimal checks were completed to determine the effect on model accuracy. As the various case studies were completed, it was also determined that the vertical discretization of the model was very important for both the model stability and accuracy. This was especially true around the ASR wells where steep velocity gradients led to model oscillations and instability in some instances. Future ASR modeling efforts should carefully consider vertical discretization-related accuracy and stability issues.

Comparison of Simulation Results for Computational Accuracy and Reliability

Model simulation output from the four model codes was then compared to determine differences in numerical error, relative accuracy, stability, and flexibility. As the ASR cases were hypothetical, an examination of the actual accuracy of each model code was

not possible. However, an assumption was made that the SEAWAT TVD solution was the most accurate based upon past analysis and publications noted in the literature. Limited accuracy assessments as compared to known analytical solutions were also completed and discussed earlier in this report. Table 11 lists a qualitative assessment of the stability of each model code based upon all model results. None of the codes experienced major convergence problems but three of the model codes did experience some minor oscillations. It should be noted that the oscillations were most likely attributed to insufficient horizontal and vertical model resolution. Therefore, it is expected that the oscillations could be minimized or eliminated through more judicious model design.

Table 11. Stability Assessment.

Model Code	**Stability Assessment** Score A – No stability issues Score B – Minor Oscillations Score C – Did not converge
MODFLOW/MT3DMS – Upwinded	A
MODFLOW/TM3DMS – TVD	B
SEAWAT – Upwinded	A
SEAWAT – TVD	B
WASH123	A
SWI	B

The overall relative accuracy assessment is presented for each case and discussed in turn.

For Case 1A, comparisons were made at the ASR well and at different radii from the ASR well. Figure 5 depicts results from the different codes for concentrations versus time estimates during the 30-day ASR recovery period. It should be noted that the recovery curves represent average concentrations at the ASR well location.

For all of the ensuing figures, a naming convention is employed for each of the various model runs, model codes, and contaminant transport solution algorithms. The primary names are listed as follows:

- CenDiff-FW is a MODFLOW/MT3DMS simulation using the Central difference weighting algorithm
- TVD is a MODFLOW/MT3DMS simulation using the total variation diminishing scheme
- EQFW or FW are simulations using “equivalent freshwater heads” on the model boundaries rather than simulating true density-dependent flow
- SEAWAT-TVD are simulations using SEAWAT with the TVD scheme
- SEAWAT-Upwind are simulations using SEAWAT with the upwinded backward difference weighting algorithm
- WASH-Aq Node Ave are simulations using WASH123 and averaging the concentrations of the model aquifer nodes

- WASH-deep4000 are simulations using WASH123 and modifying the confining unit initial condition concentrations to mimic calculations performed by MT3DMS

Figure 5. Model simulation results for Case 1A at the ASR well.

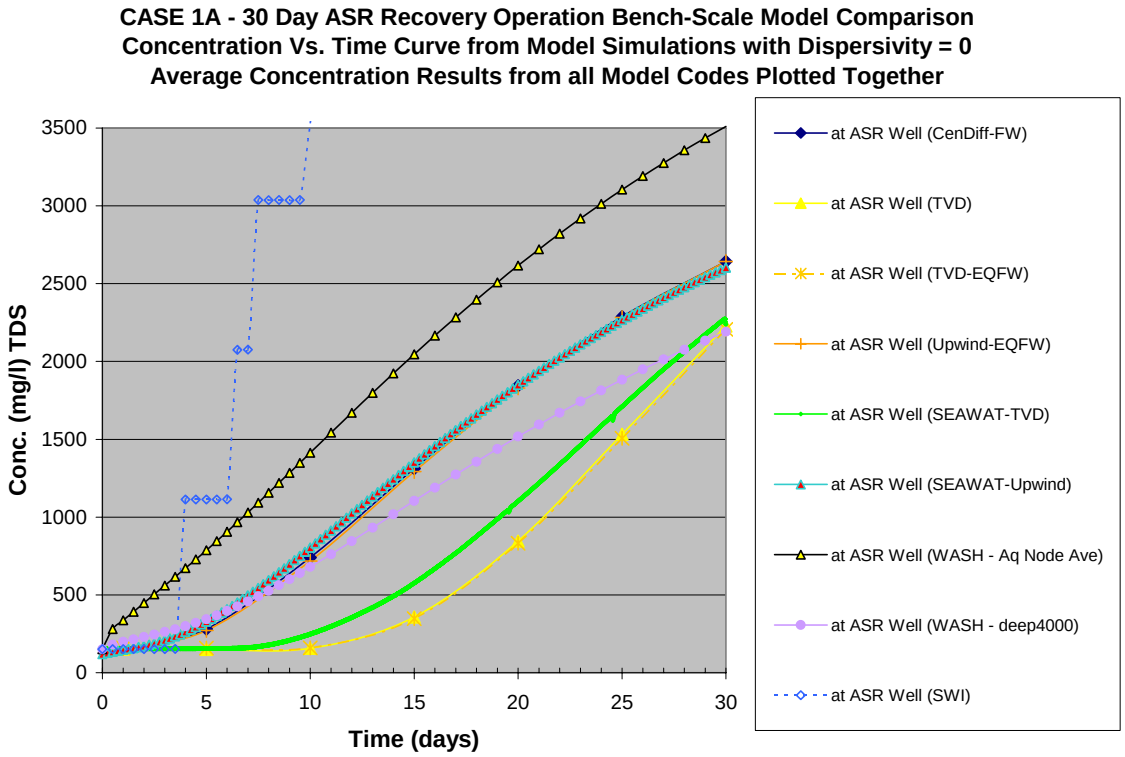

In examining the simulation results at the ASR well, it is apparent that the model codes, along with the various contaminant transport algorithms, result in a wide variation of concentration versus time predictions. During a real ASR recovery event, the recovery would be ceased once the TDS concentration exceeded a threshold value of 500 mg/l. In reviewing the simulation results, the number of days of recovery before exceeding 500 mg/l can be readily observed.

For the MODFLOW/MT3DMS solutions, two general results are observed. First, solutions using the TVD algorithm (using either uncorrected heads or density corrected/EQFW heads) predict that 500 mg/l level would be exceeded after 17 days. Using the central-difference or upwinding algorithms result in exceedance after 7 days. Since a dispersivity value of zero was utilized for Case 1A, the main difference between the TVD solution and the other finite-difference solutions is suspected to result from truncation error or so-called “numerical dispersion”. This finding is consistent with previous work completed by Merritt (1986; 1993). Merritt found that the predicted amount of freshwater recovered from an ASR well is sensitive to the contaminant transport solution selected for the simulation. In addition, Merrit (1993) noted that the

estimate of freshwater recovered is somewhat sensitive to vertical model resolution and the algorithm utilized to simulate vertical flow and dispersion. For ASR simulations involving large concentrated injection and recovery rates, the apparent degree of dispersion would also be greatly dependent upon local flow velocities.

For the two SEAWAT solutions, a similar pattern emerged. The TVD solution predicted that the 500 mg/l water quality threshold would be exceeded after approximately 14 days, whereas the upwinded solution predicted exceedance after 7 days. Since SEAWAT is a finite-difference model with the same geometry as the MODFLOW/MT3DMS model, the differences between the two solutions are also caused by numerical error. Another interesting finding is that the comparable upwinded solutions between non-density model and the density-dependent SEAWAT model are almost identical, suggesting that the numerical dispersion issues mask the density related differences. When a similar comparison is completed for the constant-density TVD solution versus the density-dependent SEAWAT TVD solution, there is a notable difference of 3 less days of ASR recovery for the SEAWAT TVD solution probably due to buoyancy stratification effects. This finding reveals that density stratification during the 305 day ASR storage period does marginally affect the predicted results. It would be expected that longer storage periods would result in additional stratification effects that would further reduce the amount of freshwater that would be recovered.

The WASH123 results also show variation between two different model simulations. The first simulation (WASH – Aq node avg) predicts that the water quality threshold of 500 mg/l would be exceeded after 2.5 days. The second simulation (WASH- deep4000) predicts an exceedance of the threshold after approximately 8 days. The only difference between these solutions is the assignment of the starting concentrations within the Middle Floridan Confining Unit (MFCU). The first simulation includes an assignment of 35,000 for all nodes within the MFCU, while the second simulation includes an assignment of 4,000 mg/l for upper nodes and 35,000 mg/l for lower nodes. The second simulation is thought to be equivalent to the finite-difference runs since the starting concentration for those runs is assigned at the cell center rather than at the cell edge. Further review of the second simulation (WASH – deep4000) still reveals that the concentration versus time curve is generally between the finite-difference upwinded and TVD solutions. It is likely that the WASH123 results are also subject to numerical dispersion. Woods (2004) noted similar numerical dispersion problems with the finite-element model SUTRA (Voss and Provost, 2002). Future improvements to WASH123 will utilize the “local zooming and peak-valley capturing algorithm as outlined by Cheng et al. (1998). These improvements should further minimize numerical errors.

The SWI result shows major differences as compared to the other model simulation results. The SWI simulation predicts that the water quality threshold of 500 mg/l would be exceeded after 4 days. Also, the slope of the concentration versus time curve is much steeper than any other simulation result. Since the SWI code was originally designed for regional sea water intrusion issues, this result is not surprising. Since the SWI code was designed based upon an interface approach, it was not designed to simulate dispersion.

Therefore, it is unclear if the SWI results are the "most accurate" or if the Dupuit approach implemented in SWI is resulting in unrealistic concentration increases.

Since no known ASR analytical solutions were available, a full accuracy assessment of the Case 1A results is not possible. The results clearly do show that the four codes predict a wide range of concentration estimates. It is theorized that the code results would converge and be more similar if the following improvements were incorporated:

- Additional horizontal resolution around the ASR well
- Additional vertical resolution within the storage zone and below the storage zone
- Lower well pumping rates would reduce the steep vertical gradients at the ASR well minimizing errors associated with the velocity field

Similar data plots were produced for a theoretical monitoring well approximately 120 feet distant from the ASR well. Figure 6 displays the simulation results from the various model codes and contaminant transport solutions during the 30-day ASR recovery period. At this radius (near the edge of the freshwater bubble), the effects of buoyancy stratification are probably more pronounced such that the differences among the various codes is likely due to a combination of numerical dispersion and the degree of buoyancy stratification predicted by the code.

Figure 6. Model simulation results for Case 1A at monitoring well 120 feet away.

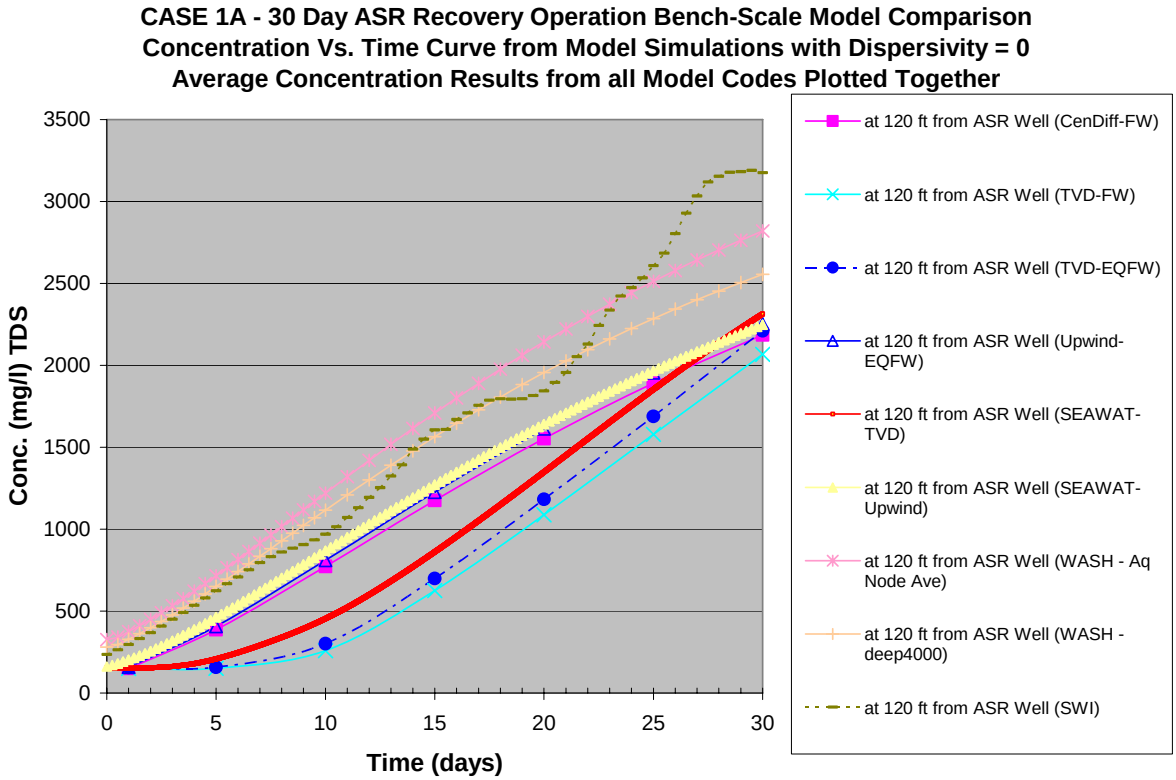

Generally, the simulation results can be subdivided into three groups. The TVD results from the MODFLOW/MT3DMS and SEAWAT models predict lower TDS concentrations over the first 15 days of ASR recovery as compared to the other model simulations. The WASH123 and the SWI model codes predict the highest TDS concentrations over the first 15 days of ASR recovery. The central-difference and upwinded solutions fall between the TVD and WASH123/SWI results. The "spread" of model results is less pronounced than at the ASR well as presented in figure 5. This also suggests that errors associated with the velocity field and the model resolution are larger at the pumping well location than 120 feet distant. Since dispersivities were assigned a value of zero, model stability was also an important issue. Some oscillations were seen in the results of all model codes with the exception of the WASH123 code and finite-difference upwinded solutions as discussed previously. Some of these are evident in the SWI results.

For Case 1B, comparisons were made at the ASR well and at different radii from the ASR well. Since Case 1B assigns a seawater TDS concentration in the ASR storage zone, more significant density effects were noted. Figure 7 depicts results from the different codes for concentrations versus time estimates during the entire 30-day ASR recovery period. Figure 8 depicts results from the different codes for concentrations versus time estimates during the entire 365-day ASR simulation period, including recharge for 30 days, storage for 305 days, and recovery for 30 days. It should be noted that the concentration curves represent average concentrations at the ASR well location for Figure 7, while discrete model layers are depicted in Figure 8.

Figure 7. Model simulation results at ASR well for Case 1B during ASR recovery period.

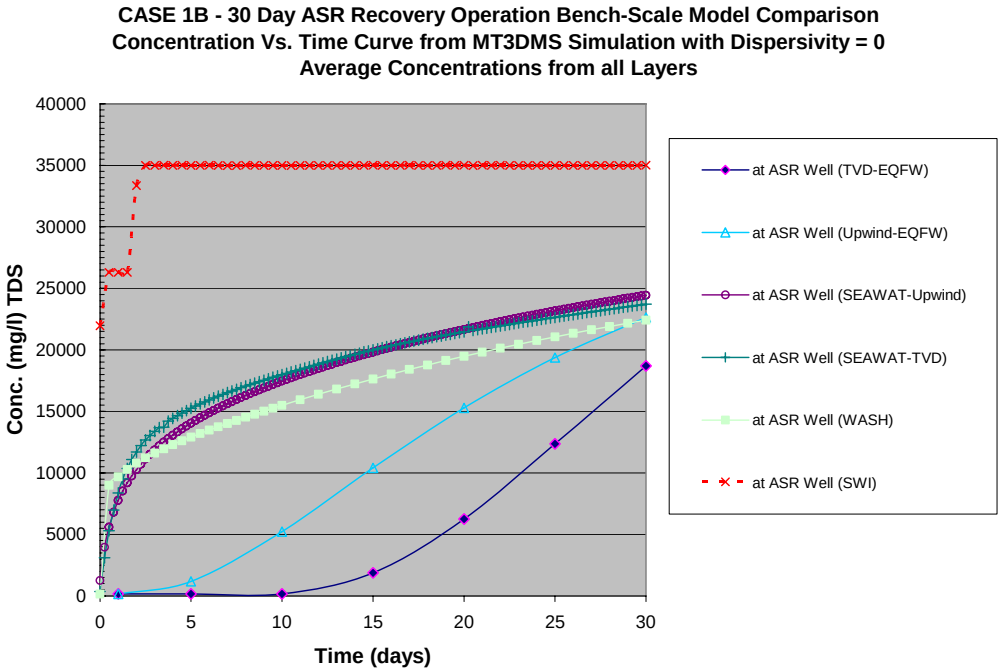

Figure 8. Model simulation results at ASR well for Case 1B during entire simulation period.

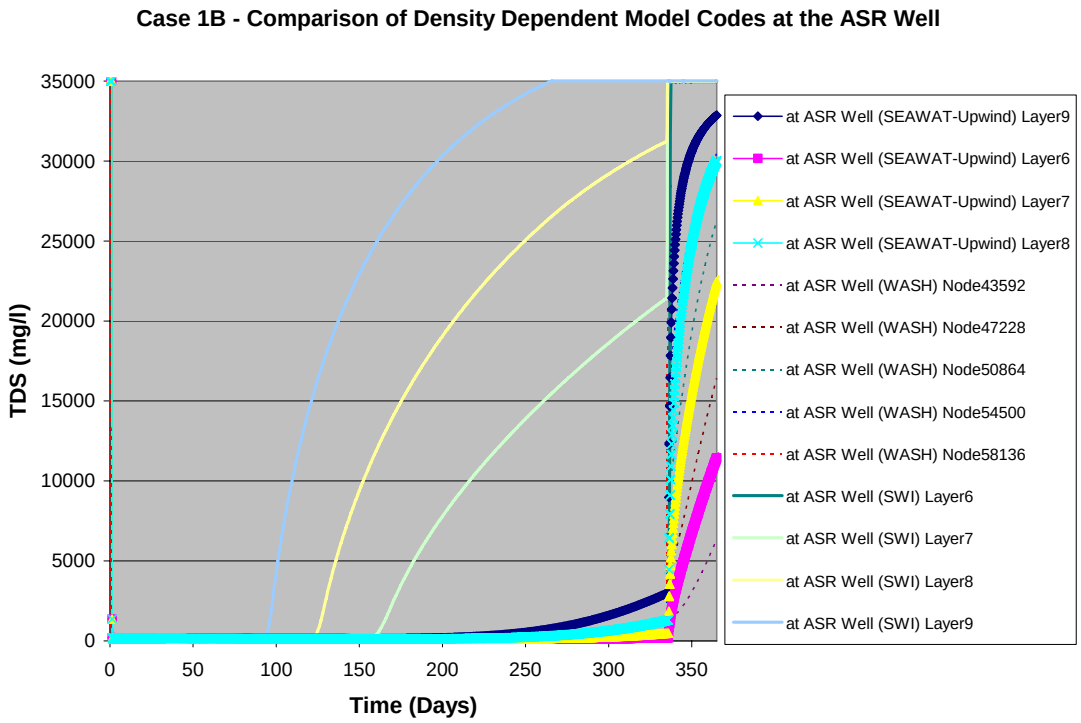

In reviewing Figure 7, it is evident that the results vary widely between the different codes. First, the non-density dependent simulations greatly underestimate the TDS concentration at the ASR well as compared to the other model codes. Both of the SEAWAT solutions and the WASH123 solution exhibit similar concentration versus time curves. The SWI results seem to overestimate the TDS concentrations at the ASR well location. The SWI code was originally designed for implementation at coastal boundaries, therefore the results may be misleading. Since the SWI code was not designed to model concentration changes around active pumping wells, it may not be the best tool for evaluating changes around the ASR well.

For Figure 8, only the density dependent capable model codes were investigated. Figure 8 clearly depicts large differences between the SEAWAT/WASH123 results versus the SWI results. Both SEAWAT and WASH123 predict moderate buoyancy stratification during the 305-day storage period as compared to the major buoyancy stratification predicted by SWI. In general, at the ASR well, the results predicted by SEAWAT and WASH123 are very similar. Both codes clearly demonstrate the capability to evaluate changes in water quality due to density stratification effects. Figure 9 depicts the results at a theoretical monitoring well located approximately 120 feet distant from the ASR well.

Figure 9. Model simulation results at 120 feet distant from the ASR well for Case 1B during entire simulation period.

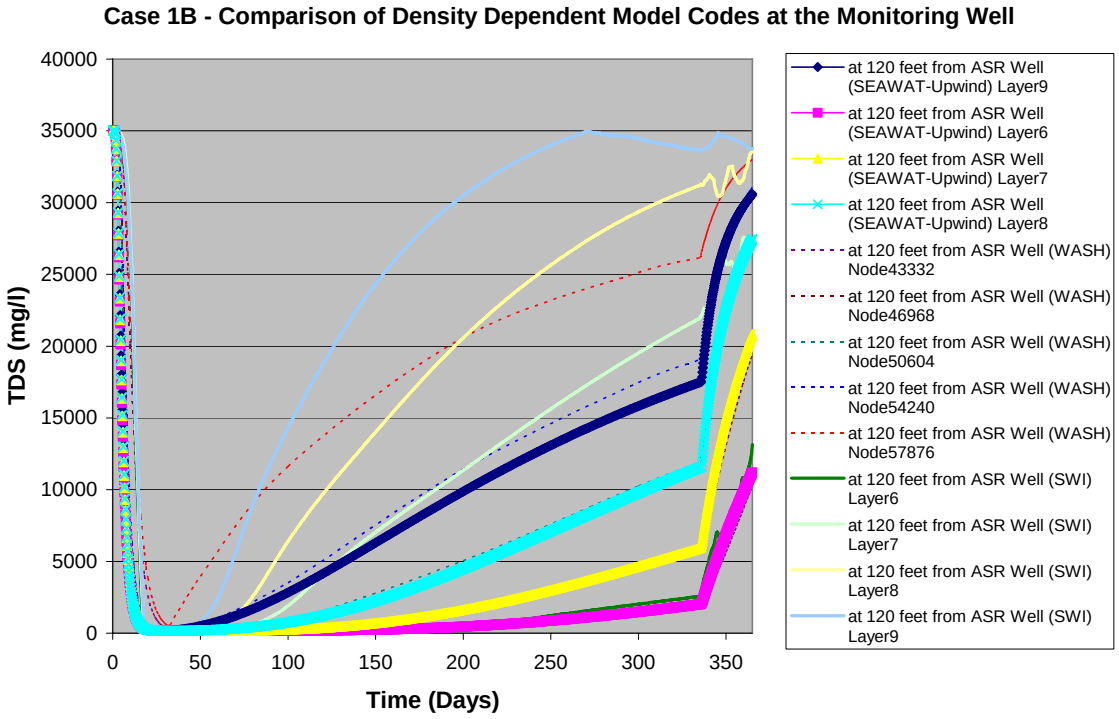

Figure 9 reveals that at the monitoring well located 120 feet from the ASR well, the SWI simulation predicts a higher degree of density stratification than the comparable SEAWAT TVD solution. The WASH123 results tend to fall in the middle of the SWI and SEAWAT results. During the 30-day recovery period, both the SEAWAT and WASH123 results exhibit similar shaped recovery curves as compared to the SWI simulation that appears to have some minor oscillations during the recovery duration. Figures 10 to 16 depict spatial concentration differences between the SEAWAT and WASH123 results for selected time steps during the one-year simulation period. The contour maps were developed from three sets of model output for the center of the aquifer storage zone. Each set of model output data was then contoured to a new two-dimensional mesh using an "inverse distance weighted" algorithm. The contouring resulted in minor oscillations in each dataset but did not inhibit the overall comparison of the results. The contour maps compare the spatial concentration differences at the middle of the ASR storage zone. The figures clearly show that both the finite-difference (upwinded or central difference) and WASH123 solutions are subject to moderate to high numerical dispersion and possibly more significant density stratification. WASH123 appears to have the highest numerical error with the upwinded solution exhibiting moderate to high error while the TVD solution had the smallest error. The SWI code was not included in this comparison since it does not have the capability to model hydrodynamic dispersion. It should also be noted that the finite-difference and WASH123 solutions are similar at day 365 as shown on Figures 15 and 16. The finite-difference and WASH123 results at day 365 both have a similar concentration gradient or

radius where seawater concentrations have been lowered at least 500 mg/l. The comparable radius for the TVD solution is much smaller. One notable difference is that the WASH123 solution displays more concentric contours, although curiously the circles are not centered on the ASR well, while the finite-difference results are heavily influenced by the grid resolution and bias. However, the WASH123 results also appear to be heavily influenced by mesh effects. As was mentioned previously, each of the models could have been improved through the incorporation of additional horizontal and vertical resolution around the ASR well.

Figure 10. Comparison of simulation results for Day 15.

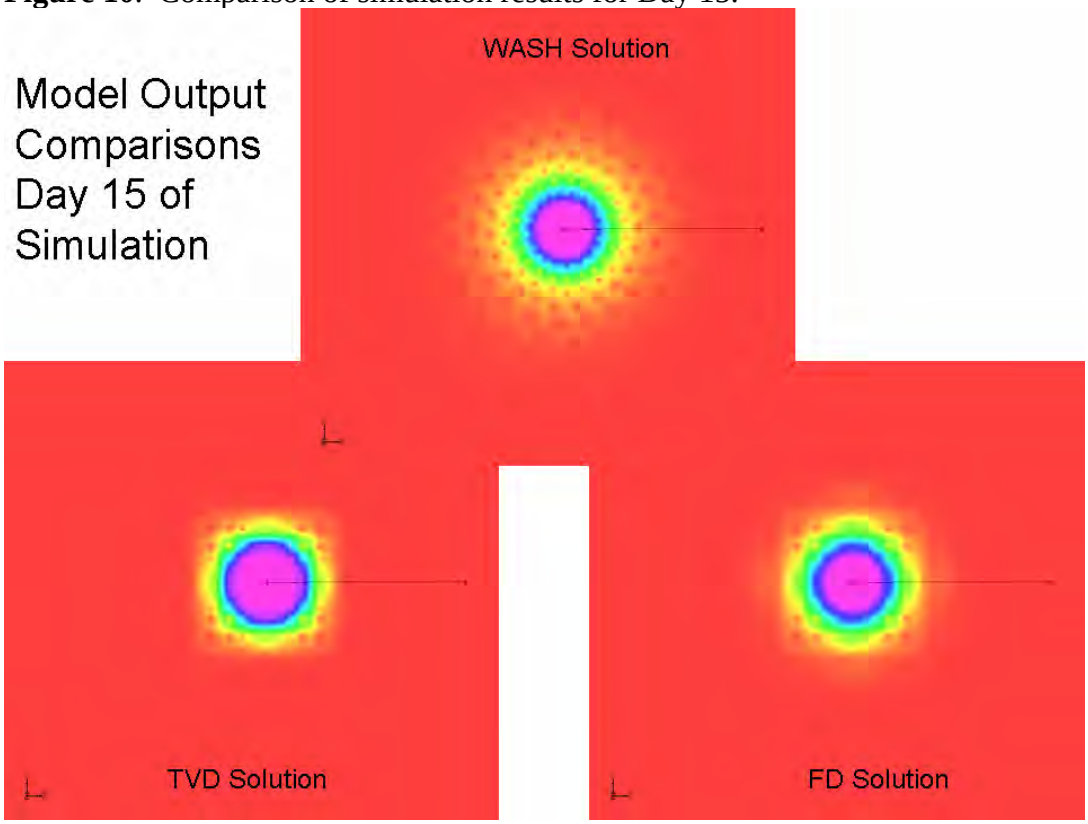

Figure 11. Comparison of simulation results for Day 30.

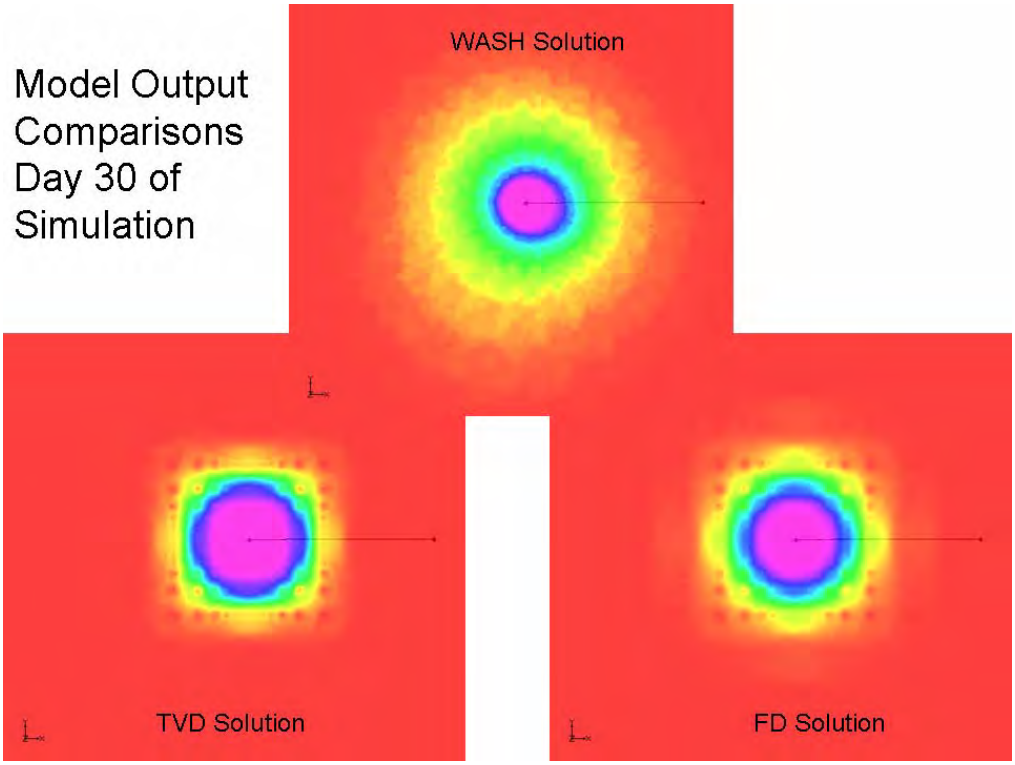

Figure 12. Comparison of simulation results for Day 105.

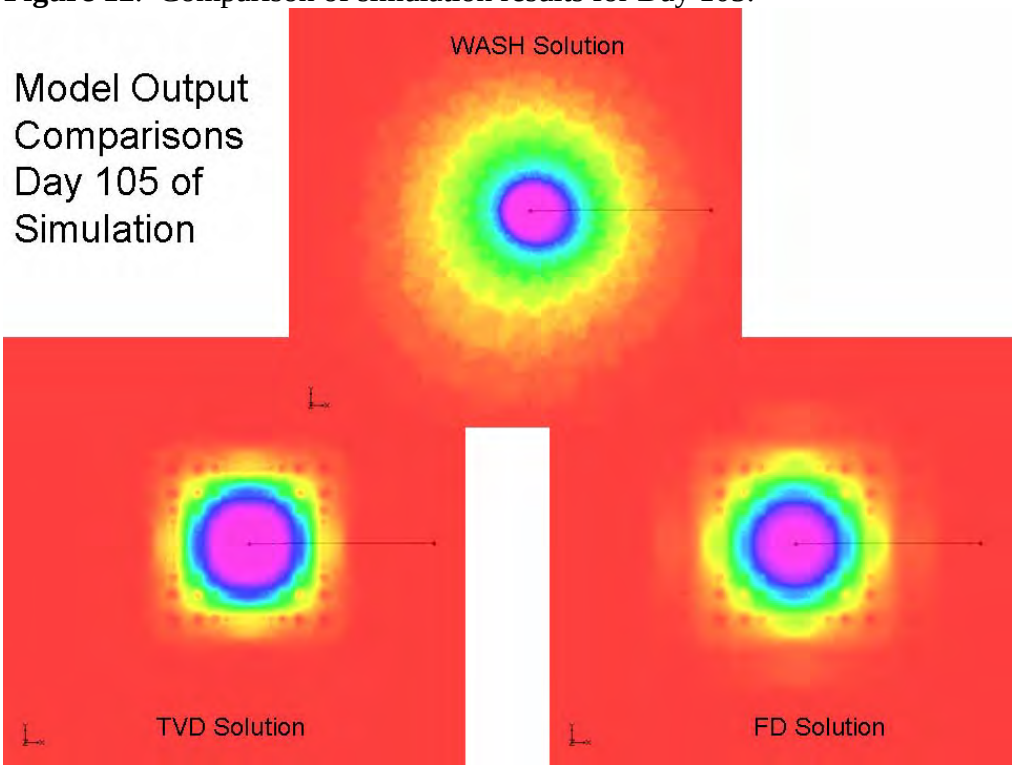

Figure 13. Comparison of simulation results for Day 335.

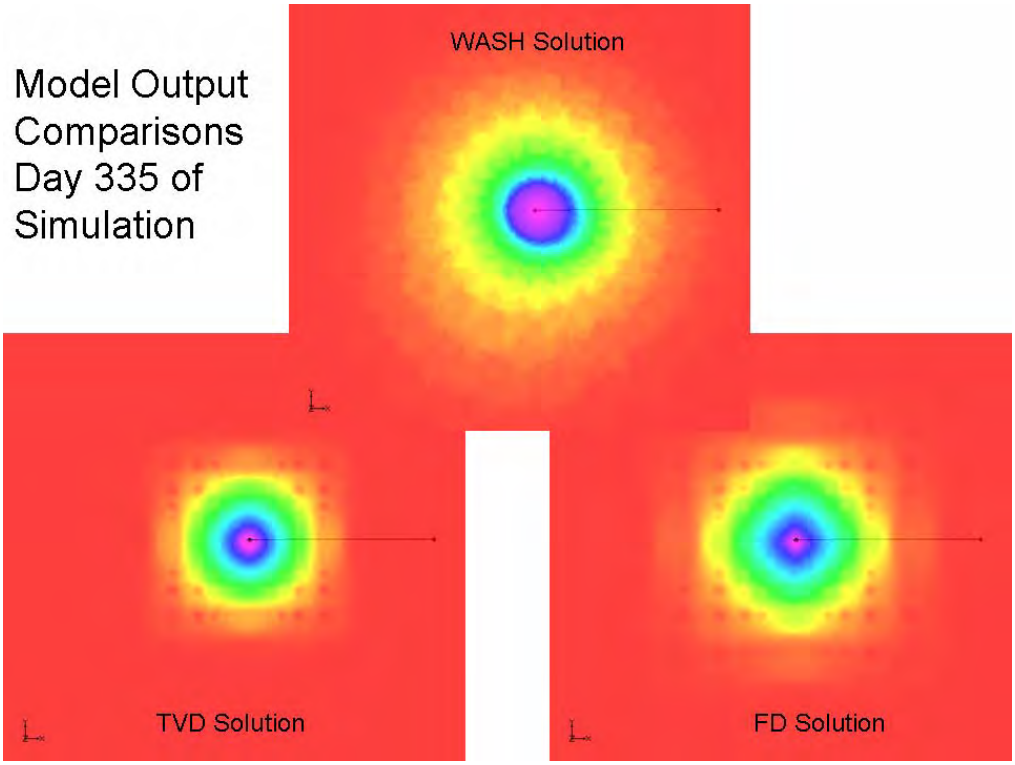

Figure 14. Comparison of simulation results for Day 350.

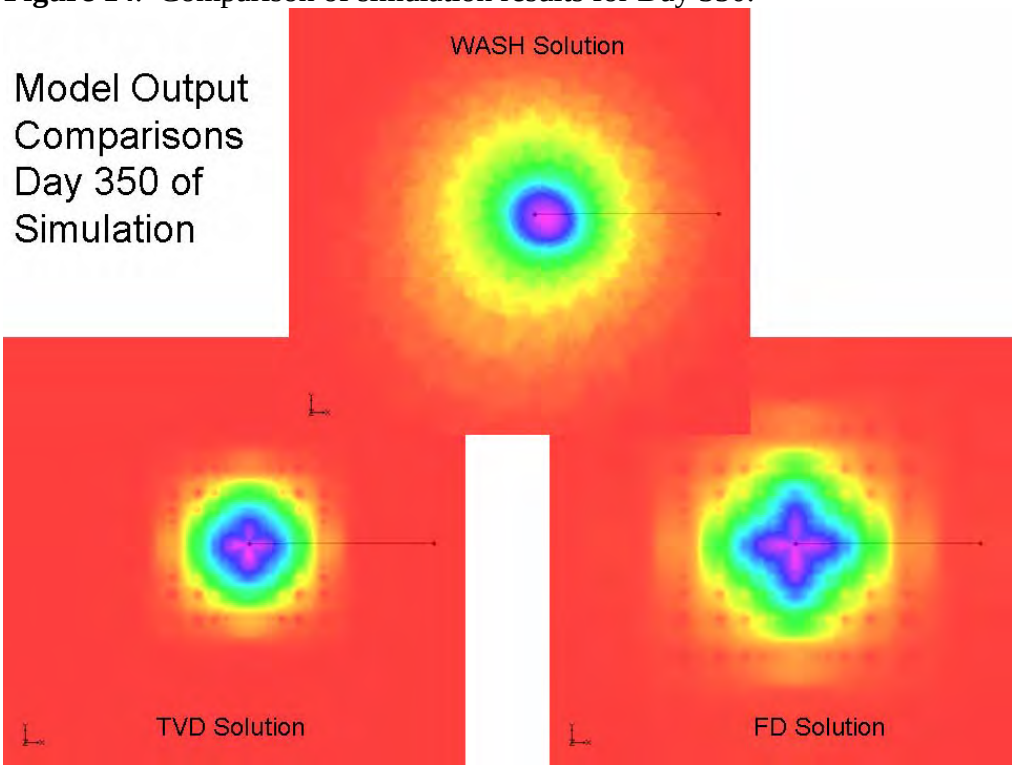

Figure 15. Comparison of simulation results for Day 365.

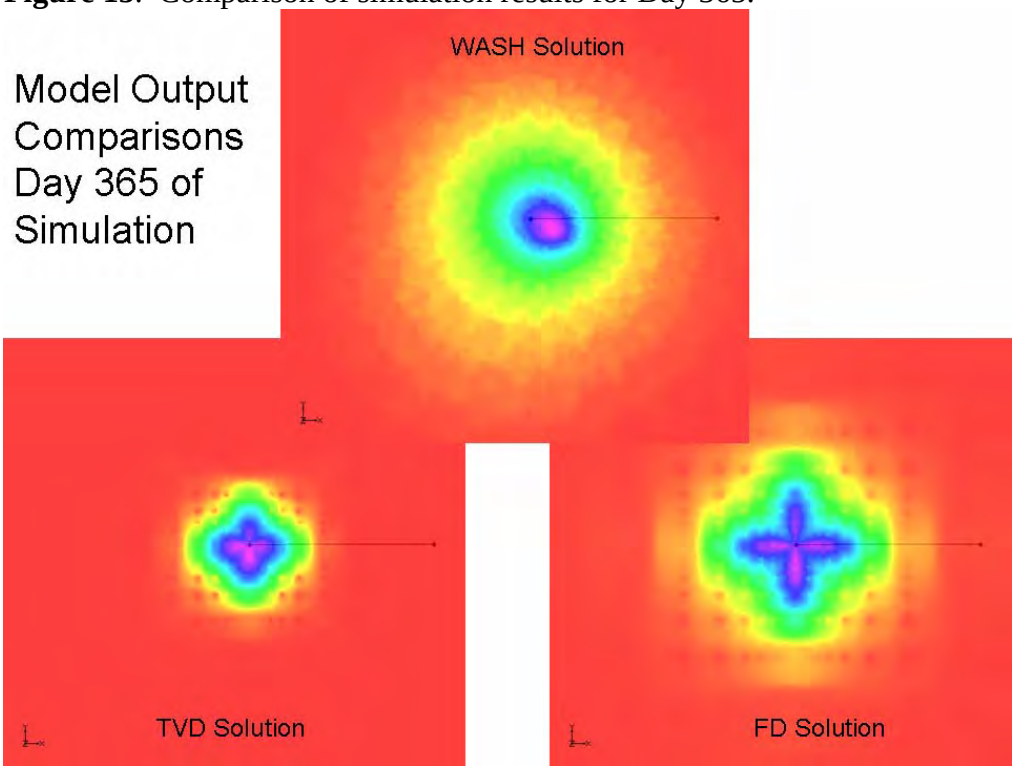

Figure 16. Comparison of simulation results for Day 365 with radius marker.

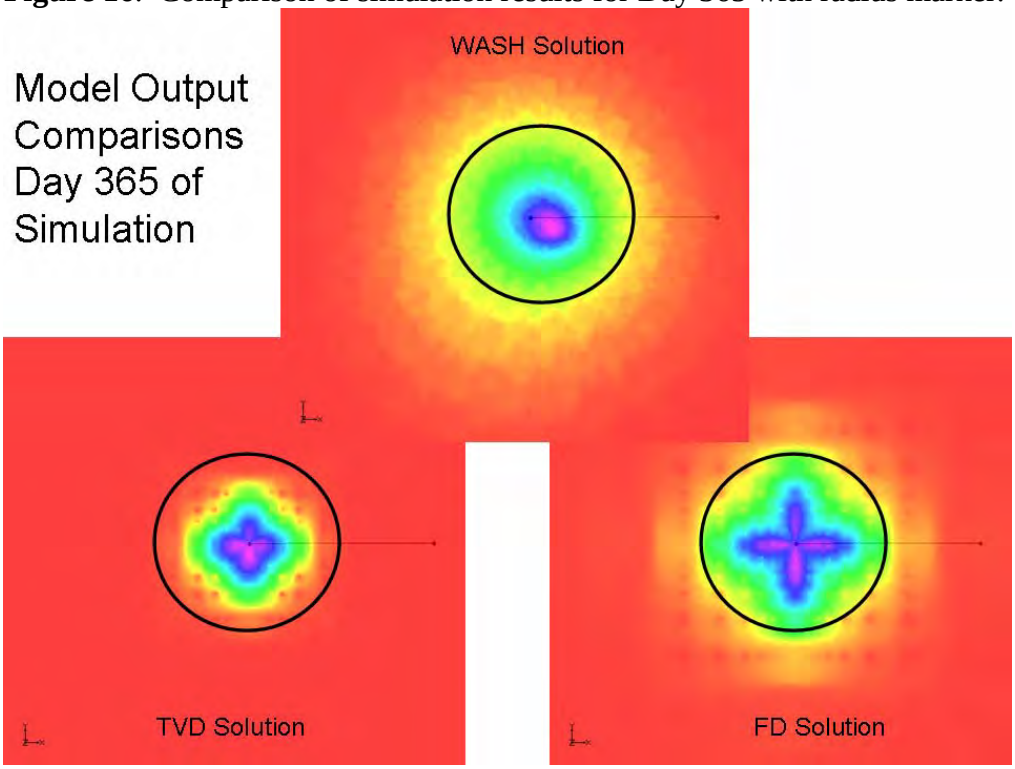

For Case 1C, the model simulation results were similar to those of Case 1A except that density-dependent upconing was encouraged to occur within the models due to assignment of much higher hydraulic conductivity within the MFCU as compared to the assignment for Case 1A. Figure 17 depicts the simulation results for the various model codes and contaminant transport solutions for Case 1C at the ASR well during the 30-day recovery period.

Figure 17. Simulation results for Case 1C at the ASR well during the recovery period.

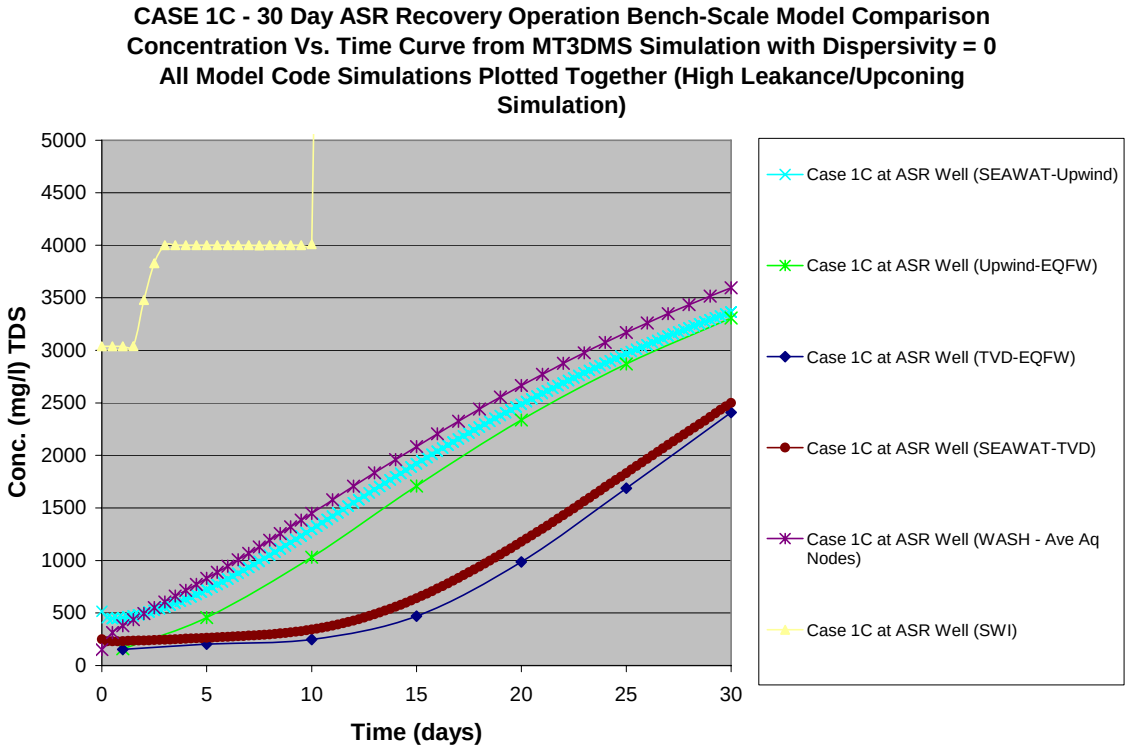

The results reveal three distinct groups of data. The SWI results clearly show predicted TDS concentrations that are considerably higher than the other codes. The TVD results from both the MODFLOW/MT3DMS and SEAWAT models predict the lowest TDS concentrations. The MODFLOW/MT3DMS and SEAWAT upwinded results and the WASH123 results fall between the TVD and the SWI results. It should be noted that the WASH123 results depict saltwater upconing more clearly than the other codes. The WASH123 results for Case 1C are shown on Figure 18.

Figure 18. Simulation results from Case 1C for WASH123 base run.

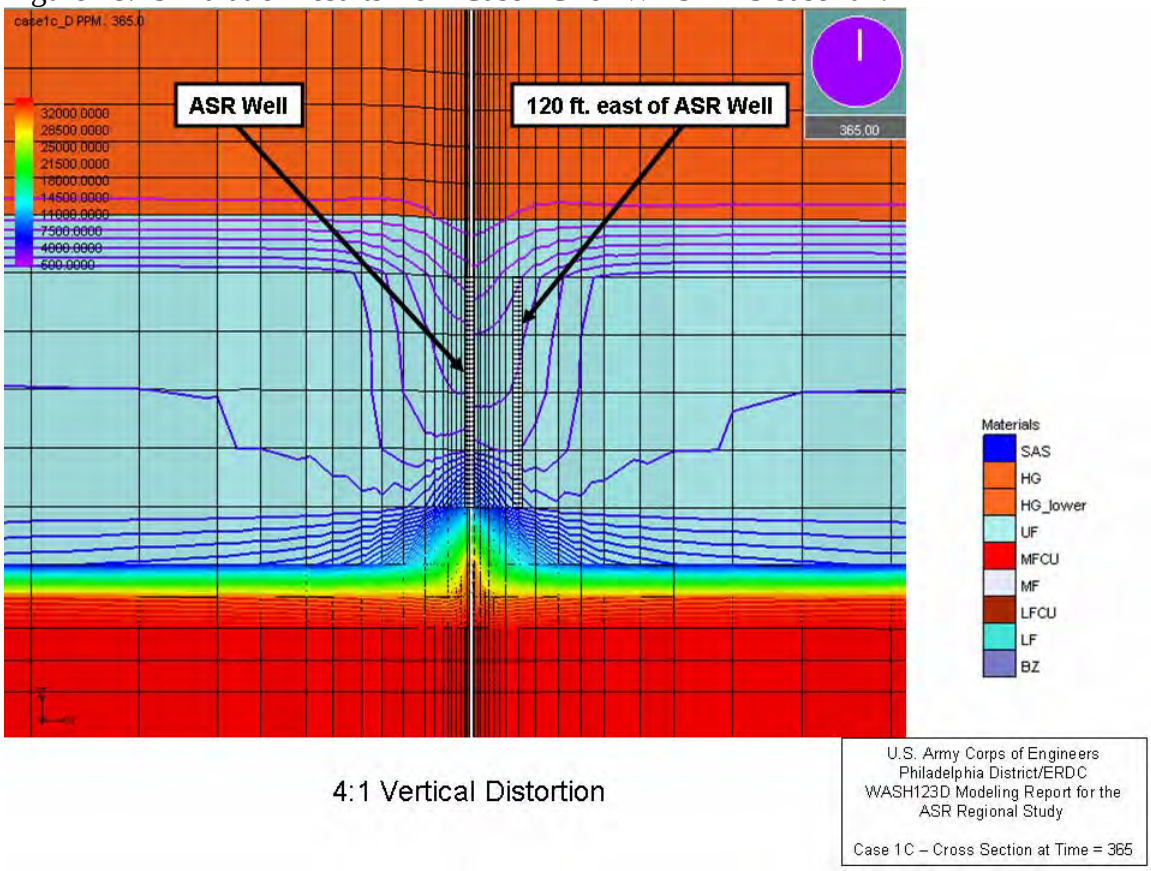

Although not completed for the study, an additional WASH123 run optimizing the boundary assignment of the MFCU (similar to WASH deep4000 for Case 1A) may have resulted in lower predicted TDS concentrations and less severe upconing. Figure 19 depicts similar model simulation comparisons for a theoretical monitoring well located 120 feet distant from the ASR well. The same three distinct data groups are visible.

Figure 19. Simulation results for Case 1C at 120 feet from the ASR well during the recovery period.

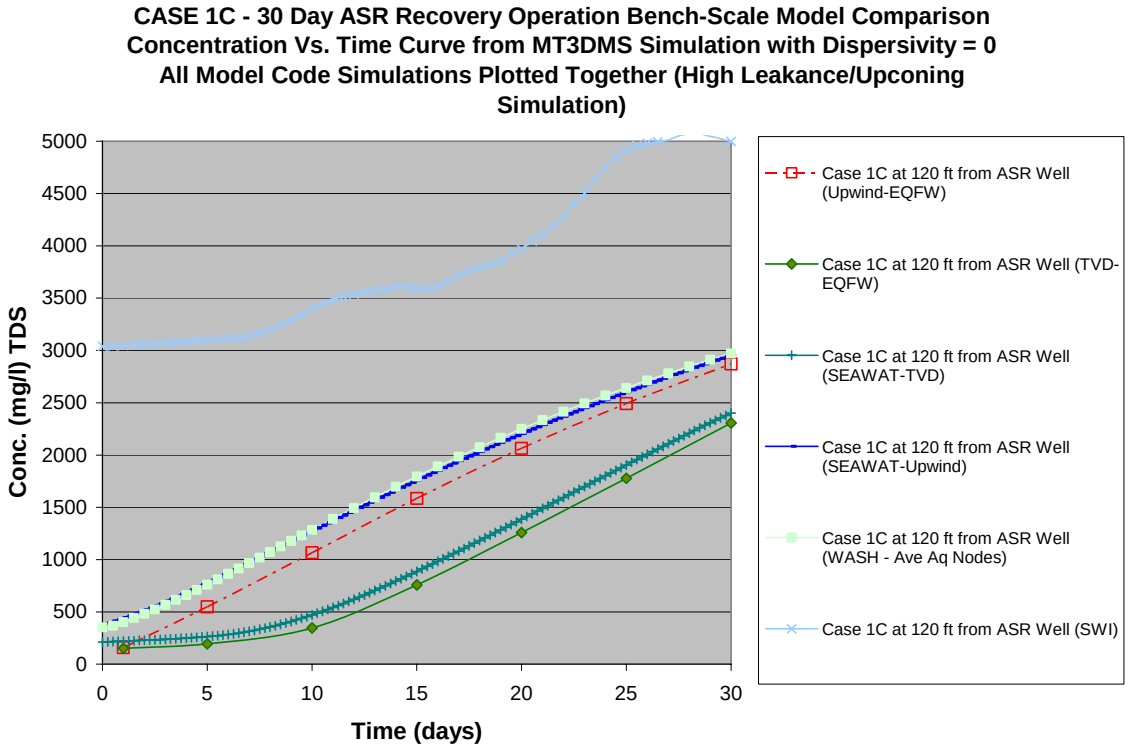

For Case 1D, the results were similar to Case 1A except that real dispersion was simulated through the assignment of 25 feet for the longitudinal dispersivity and transverse dispersivity. For Case 1D only the MODFLOW/MT3DMS, SEAWAT and WASH123 codes were compared since SWI does simulate hydrodynamic dispersion. Figure 19 depicts the results of the three comparisons. The MODFLOW/MT3DMS and SEAWAT results are very similar and predict higher TDS concentrations than the WASH123 simulation results. All three model codes predict TDS concentrations to quickly elapse the 500 mg/l regulatory limit following the long 305 day storage period. The MODFLOW/MT3DMS and SEAWAT results also predict concentrations at the ASR well in excess of 4,000 mg/l suggesting either upconing or significant numerical error.

Figure 19. Simulation results for Case 1D at the ASR well during the recovery period.

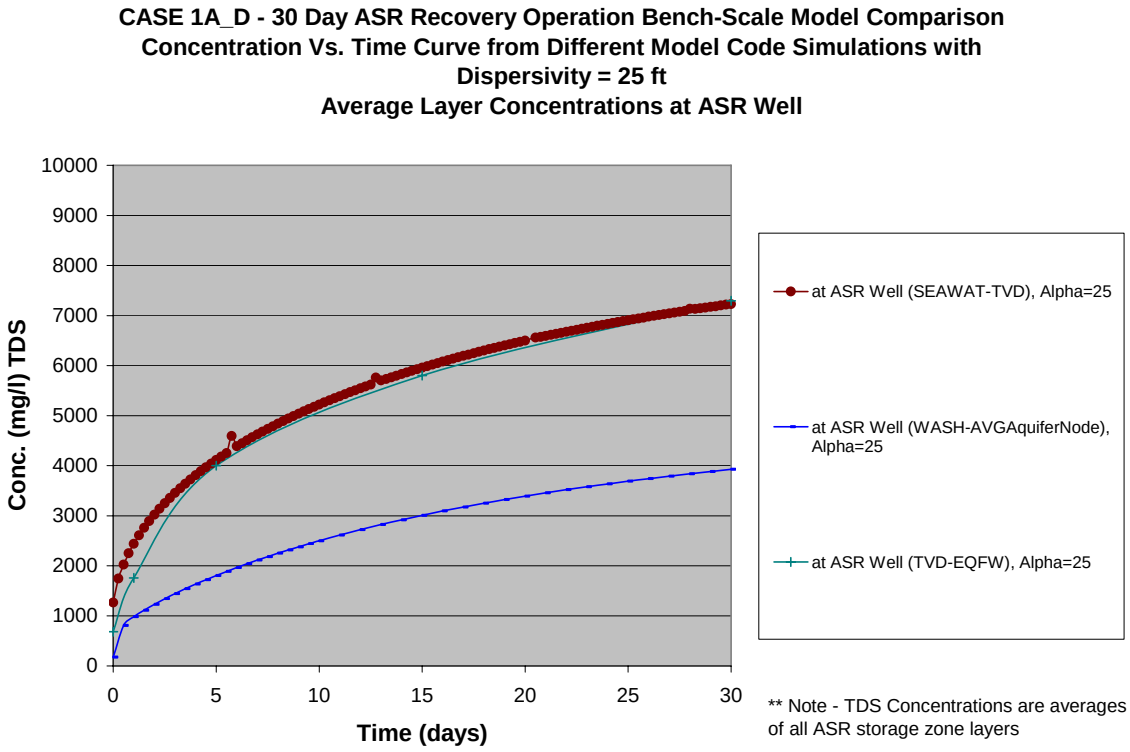

For Case 2A, the results for the SEAWAT, SWI, and WASH123 codes are all very similar. All three codes appear capable of handling any salt-water intrusion issues that may need to be simulated in the future as part of the ASR Regional Model.

Conclusions and Recommendations:

This benchscale study was developed to evaluate the potential for various model codes to provide answers to issues confronting the ASR Regional Study team. The benchscale study was developed and carried out by an interagency PDT. During the conduct of the study, problems and difficulties were encountered that limited the value of the study to address all goals outlined in the original plan. In general, the main problem was that the test models should have contained more horizontal and vertical model resolution to adequately simulate the cases selected. In addition, one or more benchmark problems with known solutions should have been thoroughly evaluated as part of this study to better ascertain the accuracy limitations of the various codes. An unfortunate consequence of the present work is that there really is no way to tell which code or solution mechanism provides the most accurate result. These shortcomings have been acknowledged and discussed in this report. However, even with the shortcomings identified, the study is valuable. The study also clearly indicated that the important issues

to be addressed for the ASR Regional Study represent three different scales of problem. Therefore, ultimately, three different model scales will be required to address them.

This benchscale study was useful in comparing four different model codes under consideration for use in development of a regional ASR model. The four codes tested represented a reasonable range of code options available and were selected based upon PDT members overall familiarity with the codes. Other codes such as SUTRA and FEFLOW were also considered but rejected. SUTRA has been used for past ASR simulation studies so that some of its advantages and disadvantages were already known. FEFLOW is a proprietary code from Europe that would have been difficult to procure for U.S. Government work efforts. Each code exhibited both strengths and weaknesses. All of the codes provide much of the model functionality desired for the ASR Regional Study team with the SEAWAT and WASH123 codes providing the best overall functionality. All of the codes were determined to be easy to moderately difficult to use, while all codes with the exception of SWI probably require workstation class computers to efficiently develop and calibrate a large regional model. Effective pre and post-processors can be utilized directly by all model codes with the exception of SWI.

A few notable lessons learned can be gleaned from the completed work efforts including the following:

- Where ASR wells with large injection or recovery rates are to be modeled, additional horizontal and vertical model resolution is necessary
- The combination of steep head gradients and sharp concentration fronts present very challenging model simulations
- Comparing code results to known published solutions is recommended even though no “ASR solutions” are currently available
- The initial goal to compare four identical models was a worthy one but ultimately difficult due to different stability requirements for the four codes

Overall the SWI code had the shortest run times while the SEAWAT (with TVD solution) had the longest run times. The SEAWAT (with upwinded finite-difference solution) and WASH123 fell in between. In general, based upon the results of the benchscale studies, the SEAWAT TVD code is approximately 7 times slower than the WASH123 code and the WASH123 code is approximately 10 times slower than the SEAWAT Upwind code. Due to geometry advantages inherent in finite-element codes, a model designed with WASH123 could have less calculation points than a comparable finite-difference code. Therefore, the run time difference between the SEAWAT Upwind and WASH123 would be reduced considerably. Based upon the results of the benchscale modeling, model run times were extrapolated for identical hypothetical models with 100,000 calculation points using either SEAWAT or WASH123. Run time estimates were calculated for 1 year transient simulations and 36 year transient simulations (similar to CERP modeling period). These are presented in Table 12. It should be noted that the predicted run-times for the SEAWAT TVD solution could be reduced if time step size could be increased. A code improvement of the TVD solution, allowing for larger step sizes, may be feasible in the future.

Table 12. Hypothetical Model Run Times for the ASR Regional Study.

Model Code	Projected Run Time for 1 Year Simulation (Days)	Projected Run Time for 36 Year Simulation (Days)
SEAWAT TVD	2.84	102
WASH123	0.41	14
SEAWAT Upwind	0.04	1.4

The SWI code is approximately twice as fast as the SEAWAT Upwind code but the SWI code does not have a capability to simulate hydrodynamic dispersion, a key ASR performance consideration for the CERP. The SWI code does appear useful for quick evaluations of possible salt-water intrusion episodes caused by ASR recovery. It may also be useful as a screening model tool. If the SWI code is eliminated from consideration, the WASH123 or SEAWAT codes would be the best candidates for use in the ASR Regional Model study. Based upon the results of the benchscale tests completed, a further analysis of potential run times for the ASR Regional Model were prepared assuming the domain would cover approximately 34,000 square miles and the model would contain 20 vertical layers with varying degree of horizontal resolution. Figure 20 depicts projected model run times for the SEAWAT code (TVD and Upwinded Finite Difference Solutions) and the WASH123 code. Also, it was assumed that the full CERP 36-year period of record would be run for each code. Scale up from the benchscale model domain size (County size) to the regional domain is generally straight forward using a simple domain size ratio and assuming additional vertical model resolution.

Figure 20. Estimated Model Run Times for the ASR Regional Model

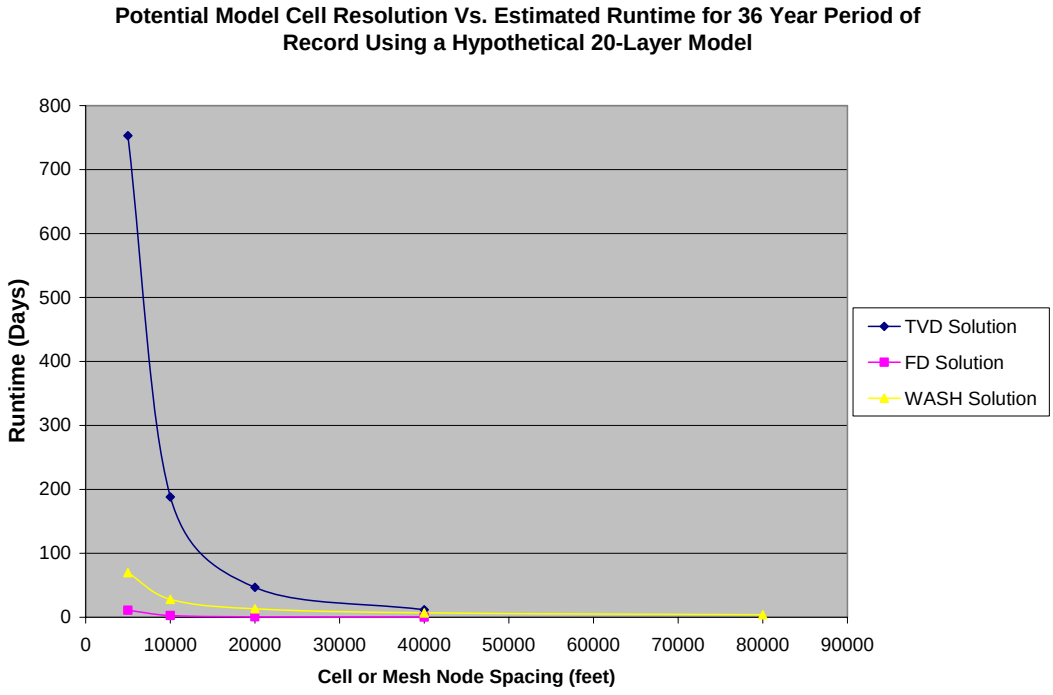

The SEAWAT (with upwinded finite-difference solution) and WASH123 codes appear to be subjected to the highest amount of numerical dispersion of the codes considered. A portion of the numerical dispersion most likely could be eliminated through better model grid or mesh design allowing for additional resolution in the vertical direction. In addition, accuracy could be further improved for these codes through improved horizontal grid or mesh resolution. It appears that the concentration changes around the ASR well are focused within 250 feet of the ASR well. Therefore, it may be appropriate to maintain a constant horizontal grid or mesh resolution within that radius, increasing grid or mesh size at a reasonable bias beyond 250 feet.

All codes seem capable of simulating density-stratification as evidenced in Case 1B. The accuracy of the codes for this case is unknown however, since no known analytical solution is available to provide a comparison or check. Qualitatively, the SEAWAT (TVD solution) and the WASH123 results appear very similar to each other so it is surmised they probably have a similar accuracy for this case. For Case 1C, the WASH123 code revealed more clear density upconing as compared to the other codes. Since no analytical solution was available for comparison, it is unknown if the simulation results are more representative than the other codes tested.

For Case 1D, the MT3DMS and SEAWAT codes predicted much higher concentrations at the ASR wellhead than the WASH123 code. It is unclear why the differences are so large for this case. Again, the vertical grid resolution may have been insufficient to ensure the highest accuracies of the velocity field around the ASR well. Inaccuracies in the vertical velocity field may have resulted in more significant contaminant transport errors for the model codes. For Case 2A, all the codes tested produced reasonable results and seem capable of simulating cases of salt-water intrusion.

Weighing all of the factors and considering improvements that could be made to the model grid or mesh for future models, it appears that either the SEAWAT (Upwinded finite-different Solution) or the WASH123 codes would be appropriate to utilize for the ASR Regional Study model development effort. Both codes appear to solve the requisite flow and transport equations adequately as well as providing a back stop of published comparisons against density-dependent case studies. SEAWAT appears to be the most widely tested code of the two but recent efforts conducted at the ERDC aim to lessen the gap here. Each of the codes also have inherent disadvantages including long model run times due to small time-step requirements for contaminant transport models. One strategy that was considered valuable was the employment of both model codes to study the same ASR problems thus ensuring a higher degree of reliability in overall conclusions and future recommendations. Using both codes to “bracket” the most likely issues and solutions would go a long way towards better overall decision making for the ASR program. For smaller domain models, the SEAWAT (TVD Solution) code could be utilized to minimize numerical errors and provide the best estimate of ASR recovery efficiency. The SWI code should not be utilized unless hydrodynamic dispersion can be ignored for the particular problem under consideration.

In order to address the maximum number of ASR questions as rapidly as possible, it is recommended that two models be developed simultaneously for the ASR Regional Study. As discussed above, the two codes would enable the PDT to bracket the cogent issues related to potential ASR system impacts and expected benefits. The two codes would provide a much needed measure of decision making reliability. First, a coarse resolution regional model should be developed with horizontal model resolution of 5,000 to 10,000 feet. The coarse model would be developed using the SEAWAT upwinded code and would be utilized to evaluate system groundwater exchange/flows and the movement of the salt-water interface. This model would be calibrated using existing water level and water quality information within the study area along with contour maps showing the depth to the salt-water interface. Long-term simulations of the salt-water interface would be required to simulate current steady-state conditions and concentrations. Therefore, this model needs to run rapidly in order to complete the numerous simulations required. A key advantage of this approach would be the large number of sensitivity tests that could be completed. This would result in a more reliable model calibration of heads and concentrations at the Florida coastline.

Second, a variable resolution regional model should be developed with horizontal model resolution of 100 to 250 feet around the proposed ASR wells increasing to 10,000 feet in the far reaches of the study area. This model would be developed using the WASH123 code and would take advantage of the geometry advantages of a finite-element code such that the model mesh would have varying resolution across the model domain. In essence, finer resolution could be employed at the areas of interest while far-field areas would be modeled with coarse resolution. This model would build upon calibration results achieved for the SEAWAT model by calibrating against seasonal water levels and water quality as well as utilizing transient calibration at existing ASR and well sites where aquifer test or ASR cycle testing data is available. It is believed that at least ten to fifteen such sites would have the necessary data to support this more rigorous calibration effort.

Based upon the model domain of 34,000 square miles, an estimate was made of the number of computational points for each model versus resolution. The SEAWAT grid would be a minimum of 5,000 feet horizontal resolution while the WASH123 mesh would be the same coarse resolution at the model exterior but with 1,000 feet resolution around Lake Okeechobee (key area of interest for the CERP). Table 13 lists the number of computational points for a 1 layer model at different horizontal resolutions. Based upon the benchscale study, the PDT has determined that the regional model should be limited to less than 500,000 computational points to ensure more reasonable run times. In reviewing Table 13, it is important to note that at 5,000 feet of horizontal resolution, both model codes would be similar but WASH123 would have finer resolution around the Lake Okeechobee study area. As resolutions become coarser, SEAWAT clearly results in less computational time. In order to stay within the prescribed number of computational points, the overall ASR regional study model resolution should be limited to minimum of 7,500 to 10,000 feet.

Table 13. Model resolution vs. # of computational points for a one layer model

Horizontal Resolution (feet)	# Grid Points	# Mesh Nodes
5,000	37,704	34,443
10,000	9,426	13,935
20,000	2,356	6,207

Both models would be developed by the same team and would utilize all of the same model input data sets (e.g., water levels, starting conditions, hydrogeology, water quality, and boundary conditions) in order to maximize synergy between the two development efforts. Both models would be combined into a single modeling report for review by an external ITR team. Ultimately, these two models and a very fine-resolution model would represent a "family" of models that could help the ASR Regional PDT address all of the outstanding technical issues identified previously. In addition, this family of models would be utilized to optimize the final design of the entire CERP system of wells.

References:

Cheng, Hwai-Ping, Jing-Ru Cheng and Gour-Tsyh Yeh, 1998. A Lagrangian-Eulerian Method with Adaptively Local Zooming Approach to Solve Three-Dimensional Advection-Diffusion Transport Equations. *International Journal for Numerical Methods in Engineering* 41(4):587-615.

Chiang, Wen-Hsing and Kinzelbach, Wolfgang, 2001. 3D-Groundwater Modeling with PMWIN, A Simulation System for Modeling Groundwater Flow and Pollution. Berlin, Germany, Springer Inc., 341 p.

Guo, W., and C.D. Langevin. 2002. User's Guide to SEAWAT: a Computer Program for Simulation of Three-Dimensional Variable-Density Ground-Water Flow. Open-File Report 01-434. U.S. Geological Survey, Tallahassee, Fla.

Hantush, M.S. & Jacob, C.E., 1954. "Plane potential flow of gound-water with linear leakage". *Transactions, American Geophysical Union*, Vol 35, pp. 917-936.

Lin, H.C., D. R. Richards, G. T. Yeh, J. R. Cheng, H. P. Cheng, and N. L. Jones, FEMWATER: A three-dimensional finite element computer model for simulating density-dependent flow and transport in variably saturated media, Report CHL-97-12, U.S. Army Corps of Engineer, 3909 Halls Ferry Road, Vicksburg, MS 39180-6199, September, 1997.

McDonald, M. G., and Harbaugh, A. W., 1988. A modular three-dimensional finite-difference ground water flow model: Techniques of Water-Resources Investigation Report, v. 06-A1.

Merritt, Michael L., 1986. Recovering Fresh Water Stored in Saline Limestone Aquifers. *Ground Water* 24(4):516-529.

Merritt, Michael L., 1993. Aspects of Numerical and Representational Methods Related to the Finite-Difference Simulation of Advective and Dispersive Transport of Freshwater in a Thin Brackish Aquifer. *Journal of Hydrology* 148:61-92.

Ogata, A., 1970. Theory of dispersion in a granular medium. U.S. Geological Survey Professional Paper 411-I.

Theis, C.V., 1935. "The relation between the lowering of the piezometric surface and the rate and duration of discharge of a well using ground-water storage", *American Geophysical Union Transactions*, Vol 16, pages 519 – 524.

Woods, Juliette, 2004. Numerical Accuracy of Variable-Density Groundwater Flow and Solute Transport Simulations. Ph.D. dissertation, University of Adelaide, Adelaide, Australia.

Voss, C. I., and A.M. Provost. 2002. A Model for Saturated-Unsaturated, Variable-Density Ground-Water Flow with Solute or Energy Transport. Water-Resources Investigations Report 02-4231. 409 p. Reston, Va.: U.S. Geological Survey.

Yeh, G.T., H. P. Cheng, J. R. Cheng, and H. C. Lin, A numerical model to simulate water flow and contaminant and sediment transport in WAterSHed systems of 1-D stream-river network, 2-D overland regime, and 3-D subsurface media (WASH123D: Version 2.0), Report CHL-98-19, Waterway Experimental Station, U. S. Army Corps of Engineers, 3909 Halls Ferry Road, Vicksburg, MS 39180-6199, July, 1998.

Van der Heijde, P.K.M., and D.A. Kanzer, 1997. Project Summary, Ground-Water Model Testing: Systematic Evaluation and Testing of Code Functionality and Performance, EPA Report # 600/SR-97/007, National Risk Management Research laboratory, Ada, OK, February 1997.

Zheng, C. and P. P. Wang, 1999, MT3DMS: A Modular Three-Dimensional Multi-Species Model for Simulation of Advection, Dispersion and Chemical Reactions of Contaminants in Groundwater Systems: Documentation and User's guide,SERDP-99-1: U.S. Army Engineer Research and Development Center, Vicksburg, MS.

Appendix A

MODELING BRACKISH AQUIFER STORAGE RECOVERY WITH THE WASH123D NUMERICAL MODEL

H.-P. Cheng[1], S. M. England[2], G. T. Stevens[2], E. V. Edris[1], C. J. Brown[3]
[1]Coastal & Hydraulics Laboratory, US Army Engineer Research & Development Center, 3909 Halls Ferry Road, Vicksburg, MS 39180-6199
[2]US Army Corps of Engineers, Philadelphia District, Wanamaker Building, 100 Penn Square East, Philadelphia, PA 19107-3390
[3]US Army Corps of Engineers, Jacksonville District, 400 W. Bay Street, Jacksonville, FL 32202

Abstract Aquifer Storage and Recovery (ASR) is the storage of fresh water in an aquifer via injection during times when water is available, and recovery of the water from the same aquifer via pumping during times when it is needed. ASR is expected to provide a cost-effective solution to many of the world's water management needs: storing water during times of flood or when water quality is good, and recovering it later during emergencies or times of water shortage, or when water quality from the source may be poor. ASR systems can usually meet water management needs at less than half the capital cost of other water supply alternatives. When compared to other alternatives that require construction of water treatment plants and surface reservoirs to meet increasing peak demands, potential cost savings have been anticipated. Besides, ASR has been recognized to have less impact on the environment, aquatic and terrestrial ecosystems. When water is stored deep underground in brackish aquifers, however, the mixing of the saline water that is originally in the brackish aquifer and the fresh water that is injected into the aquifer may degrade the water quality of the stored water and reduce the volume of the available fresh water in the following recovery periods of time. The mixing can be modeled by both the diffusion and the dispersion transport processes. Although both the diffusive and the dispersive fluxes are proportional to concentration gradient, the dispersion coefficients are highly dependent on the flow velocity, whereas the diffusion coefficients are independent of the flow velocity. Therefore in the evaluation of brackish aquifer storage recovery (BASR), whatever factor that would significantly affect the flow velocity in the brackish aquifer during both the injection and withdrawal periods should be accounted for in the associated evaluation models. In this paper, we will demonstrate how BASR can be modeled with the WASH123D numerical model that computes saline transport and density-dependent flow in a watershed system which can be conceptualized as a combination of 1D channel network, 2D overland regimes, and 3D subsurface media. A hypothetical example that includes various model parameters, *e.g.*, pumping rate, hydraulic conductivities, porosity, and

dispersivities will be employed to detail the model setup and conduct a sensitivity analysis.

INTRODUCTION

Aquifer Storage and Recovery (ASR) is one of the proposed alternatives recommended by the Comprehensive Everglades Restoration Plan (CERP). The goal of ASR in the South Florida Region is to help with water supply, storage, and distribution. The ASR Regional Study will include numerical groundwater models in order to evaluate the effectiveness of ASR. For this phase of the project, four box models (~ 40 miles x 40 miles x 2340 ft) were developed using the WASH123D finite element code. Each of the four "cases" is intended to evaluate modeling code performance under different hydraulic conditions. The following paper details the WASH123D model construction and summarizes the simulation results for one of the CERP box models.

WASH123D CODE

WASH123D is a finite element numerical model designed to simulate variably saturated, variable-density water flow and reactive chemical and sediment transport in watershed systems. It is capable of conceptualizing a watershed system as a combination of 1D river/stream, 2D overland, and 3D subsurface sub-domains. A modified Richards' equation is used to solve for 3D flow when density effect is taken into account. The equation is solved with the Galerkin finite element method. WASH123D uses the Lagrangian-Eulerian (LE) method to solve the transport equations. Particle tracking is used in the Lagrangian step to handle the advection term. Other terms (such as sources, sinks, diffusion, and dispersion) are calculated in the Eulerian step, where element matrices are assembled into a global matrix, and matrix solvers are used to solve for the spatial concentration distribution at the end of each time step. A predictor-corrector numerical technique, combined with an adaptive explicit-implicit numerical scheme, is employed to compute reactive transport efficiently and robustly. The use of this methodology allows the numerical stability of WASH123D not to be restricted by the Mesh Courant number. In addition, the Mesh Peclet number is restricted only by computational accuracy, not numerical stability. More detailed discussion on various types of numerical dispersion and how the LE method deals with these types of numerical dispersion are discussed in the referenced papers.

Since computational accuracy is dependent on the time step size used in the simulation, a sensitivity analysis was performed to evaluate the variations in the time-step size on model results. For this sensitivity analysis the time step of the injection and extraction cycles were varied between 0.05 and 5 days. The results of this analysis, presented in Figure A1, indicate that the change of the computational result becomes insignificant as the time step size is reduced to

below 0.5 days. Therefore, a time step size of 0.5 days was used during the injection and extraction cycles for all simulations in this study.

MESH DEVELOPMENT

WASH123D uses an unstructured three-dimensional (3D) finite element mesh to solve the flow and transport equations in variably-saturated media. Because flow and concentration gradients may be high in the vicinity of an ASR well, the vertical and horizontal resolution of the 3D mesh in the vicinity of the ASR well is important. Meshes that do not have sufficient resolution in the area of interest may not accurately simulate observed conditions in these high gradient areas. On the other hand, meshes that contain too much resolution will require more computational resources, resulting in extended simulation times. The mesh used for this study was based on conceptual geology developed by the Jacksonville District. The horizontal resolution of the mesh at the ASR well is 10 feet. The elements at the ASR well were deleted to allow Cauchy flux boundary conditions to be assigned directly to the interior faces of the mesh, representing the well screen. The mesh resolution expands to 5000 feet along the model perimeter. Vertical mesh resolution varied among the different conceptual geologic units. Increased resolution was used in the confining units directly above and below the ASR injection aquifer (Upper Floridian). This increased resolution allowed the WASH123D model to depict the large head and concentration gradient at the interfaces of these confining units. The final 3D mesh was composed of 112,716 nodes and 212,940 triangular-prism elements. Figures A2a and A2b illustrate the mesh resolution and conceptual geology used for the ASR simulations. The DoD Groundwater Modeling System (GMS) v.5.1 was used to generate the WASH123D mesh.

BOUNDARY CONDITIONS

Boundary conditions were assigned to the finite element model to simulate ASR pumping into the Upper Floridian aquifer. At the ASR well, Cauchy flux boundary conditions were used to simulate injection and extraction flow rates of 5 MGD. These boundary conditions were applied to the element faces representing the well screen within the Upper Floridian Unit (approximate elevation –1,014 to –1,171 ft). The saline concentration of the injected fluid was 150 mg/L. The saline concentration of the fluid at the ASR well during storage and extraction varies with depth and time depending on the relative saline concentration in the surrounding nodes, the extraction rate, and the mixing process in the ASR well. Dirichlet boundary conditions were used to assign the total head along the eastern and western model boundaries. WASH123D converts these assigned heads to equivalent fresh water heads based on the concentration and depth of each node. No-flow boundary conditions were used along the northern and southern model boundaries. Dirichlet boundary conditions were also used to assign the concentration along the model perimeter. Tables A1 and A2 show the

hydraulic and transport properties,respectively, for each geologic unit in the WASH123D model.

Table A1 Hydraulic Properties and Boundary Conditions

Geologic Unit	Head BC West Tot Head (ft)	Head BC East Tot Head (ft)	Head BC North Tot Head (ft)	Head BC South Tot Head (ft)	Conductivity Horiz (ft/day)	Conductivity Vert. (ft/day)	Mod. Compress of Matrix (1/ft)	Specific Storage (1/ft)	Effective Porosity
SAS	20	20	No Flow	No Flow	100	10	1.70E-03	1.70E-03	0.25
HG	No Flow	No Flow	No Flow	No Flow	0.01	0.001	7.00E-07	1.19E-06	0.4
UF	50	30	No Flow	No Flow	100	10	7.00E-07	1.01E-06	0.25
MFCU	No Flow	No Flow	No Flow	No Flow	0.01	0.001	7.00E-07	1.07E-06	0.3
MF	40	20	No Flow	No Flow	500	50	7.00E-07	1.01E-06	0.25
LFCU	No Flow	No Flow	No Flow	No Flow	0.01	0.001	7.00E-07	1.07E-06	0.3
LF	0	0	No Flow	No Flow	5000	500	7.00E-07	1.01E-06	0.25
BZ	0	0	No Flow	No Flow	10000	1000	7.00E-07	1.01E-06	0.25

Table A2 Transport Properties and Boundary Conditions

Geologic Unit	Con. BC West (mg/L)	Con. BC East (mg/L)	Con. BC North (mg/L)	Con. BC South (mg/L)	Tortuosity	Bulk Density (slug/ft^3)	Dispersivity Long. (ft)	Dispersivity Trans. (ft)	Flow IC Tot Head (ft)	Con. IC (mg/L)
SAS	150	150	N/A	N/A	1	3.784	0	0	Based on Steady State Simulation with no pumping	150
HG	150	150	N/A	N/A	1	2.969	0	0		150
UF	35000	35000	N/A	N/A	1	3.784	0	0		35000
MFCU	35000	35000	N/A	N/A	1	3.531	0	0		35000
MF	35000	35000	N/A	N/A	1	3.784	0	0		35000
LFCU	35000	35000	N/A	N/A	1	3.531	0	0		35000
LF	35000	35000	N/A	N/A	1	3.784	0	0		35000
BZ	35000	35000	N/A	N/A	1	3.784	0	0		35000

EVALUATION OF RESULTS

The WASH123D model simulated a 30-day injection period, followed by a 305-day storage period, and a 30-day recovery period. Prior to performing the transient simulation WASH123D calculates steady state initial hydraulic conditions based on the specified input parameters. The following discusses the results of the WASH123D model during each phase of the simulation.

Initial Condition

Since the WASH123D model is a coupled density dependent code, the initial hydraulic head boundary conditions were converted to equivalent freshwater heads based on the depth and saline concentration at each node. For this simulation, the nodes in the geologic units above the Upper Floridian aquifer were assigned a saline concentration of fresh water (150 mg/L), while the nodes in and below the Upper Floridian aquifer were assigned a saline concentration of seawater (35,000 mg/L). The specified boundary conditions result in a west to east hydraulic gradient. Figure A3a shows a cross sectional view of the concentration profile in the vicinity of the ASR well. The contours on this figure reflect the constant concentration profile used as the initial condition prior to pumping.

Injection Period

Once the initial steady state flow field is generated, the ASR pumping well injects fresh water into the Upper Floridian aquifer at 5 MGD for 30 days. During this injection cycle the hydraulic head at and immediately surrounding the ASR well increases substantially, nearly doubling in magnitude. Figure A3b shows a cross sectional view of the concentration profile in the vicinity of the ASR well at the end of the injection cycle. This figures show that the injected fresh water has displaced the ambient saline water forming a spheroid of lower concentration water in the vicinity of the ASR well. This lower concentration water permeates into the confining units above and below the Upper Floridian aquifer.

Storage Period

After the 30-day injection cycle, the ASR well is turned off for 305 days. During this storage period, the hydraulic conditions stabilize to near steady state conditions. Figure A3c shows a cross sectional view of the concentration profile in the vicinity of the ASR well at the end of the storage period. Although the concentration at the ASR well remains relatively constant, the effects of buoyancy stratification are noticeable. During the storage period, the density effect is the dominate factor in the flow fields simulated by WASH123D. Consequently, the concentrations at the nodes in the lower portion of the Upper Floridian aquifer increase substantially faster than the nodes at the top of the aquifer.

Extraction Period

After the storage period the ASR well extracts at 5 MGD for 30 days. During this extraction cycle the hydraulic head at and immediately surrounding the ASR well decreases substantially. Figure A3d shows a cross sectional view of the concentration profile in the vicinity of the ASR well at the end of the storage period. Up-coning of the higher concentration saline water below the ASR well was observed during extraction. It must be noted that the well screen of injection and extraction in the Upper Floridian aquifer covers the center four vertical elements, rather than all the six vertical elements in the aquifer. This setup allows the mesh to compute for convergent flow fields around the well at the interfaces of the Upper Floridian aquifer and the two aquitards above and below without using high resolution meshes and small time steps when the density effect is strong. Because of this, the salt concentration of nodes in the lower portion of the aquifer in the vicinity of the ASR well increase in concentration faster than the nodes above during the period of extraction due to both diffusion and up-coning.

FUTURE MODEL DEVELOPMENT

During the development of the WASH 123D model, meshes of various vertical and horizontal resolutions were tested. The WASH123D simulations became more computationally stable as the vertical resolution was increased in the geologic units above, below, and containing the ASR well. Additional studies are anticipated that evaluate the effect of various mesh resolutions on computational speed and accuracy.

In addition to the mesh sensitivity simulations, additional modifications to the WASH123D code are anticipated. One modification will be to the algorithm used to calculate the equivalent freshwater head in variable density flow systems. In simulations where higher density fluid is overlain by fluid of a lower density, the current algorithm tends to overestimate the equivalent freshwater head in the higher density solutions. Additional upgrades to address temperature variations on thermal transport will also be incorporated to the WASH123D code. These upgrades in conjunction with WASH123D's current ability to model variably saturated groundwater flow and surface/subsurface flow interactions will enhance WASH123D's ability to model the dynamic flow and transport issues inherent in the ASR program.

REFERENCES

Cheng, H.-P., Cheng, J.-R., and Yeh, G.-T. (1998). A Lagrangian-Eulerian method with adaptively local zooming and peak/valley capturing approach to solve three-dimensional advection-diffusion transport equations. International Journal for Numerical Methods in Engineering, 41(4), 587-615.

Cheng, J. R., Cheng, H. P., and Yeh, G. T. (1996). A Lagrangian-Eulerian method with adaptively local zooming and peak/valley capturing approach to solve two-dimensional advection-diffusion transport equations. International Journal for Numerical Methods in Engineering, 39(6), 987-1016.

Yeh, G. T., Chang, J. R., Cheng, H. P., and Sung, C. H. (1995). An adaptive local grid refinement based on the exact peak capturing and oscillation-free scheme to solve transport equations. Computers and Fluids, 24(3), 293-332.

Yeh, G.-T., Cheng, H.-P., Cheng, J.-R., and Lin, H.-C. (1998). A Numerical Model Simulating Water Flow and Contaminant and Sediment Transport in WAterSHed Systems of 1-D Stream-River Network, 2-D Overland Regime, and 3-D Subsurface Media (WASH123D: Version 1.0). Report CHL-98-19, U. S. Army Corps of Engineers, 3909 halls Ferry Road, Vicksburg, MS 39180-6199, July 1998.

Yeh, G.-T., Cheng, H.-P., Huang, G., Zhang, F., Lin, H.-C., Cheng, J.-R., Edris, E., and Richards, D. (2003). A Numerical Model Simulating Water Flow and Contaminant and Sediment Transport in WAterSHed Systems of 1-D Stream-River Network, 2-D Overland Regime, and 3-D Subsurface Media (WASH123D: Version 2.0). Draft Report, U. S. Army Corps of Engineers, 3909 halls Ferry Road, Vicksburg, MS 39180-6199, November 2003.

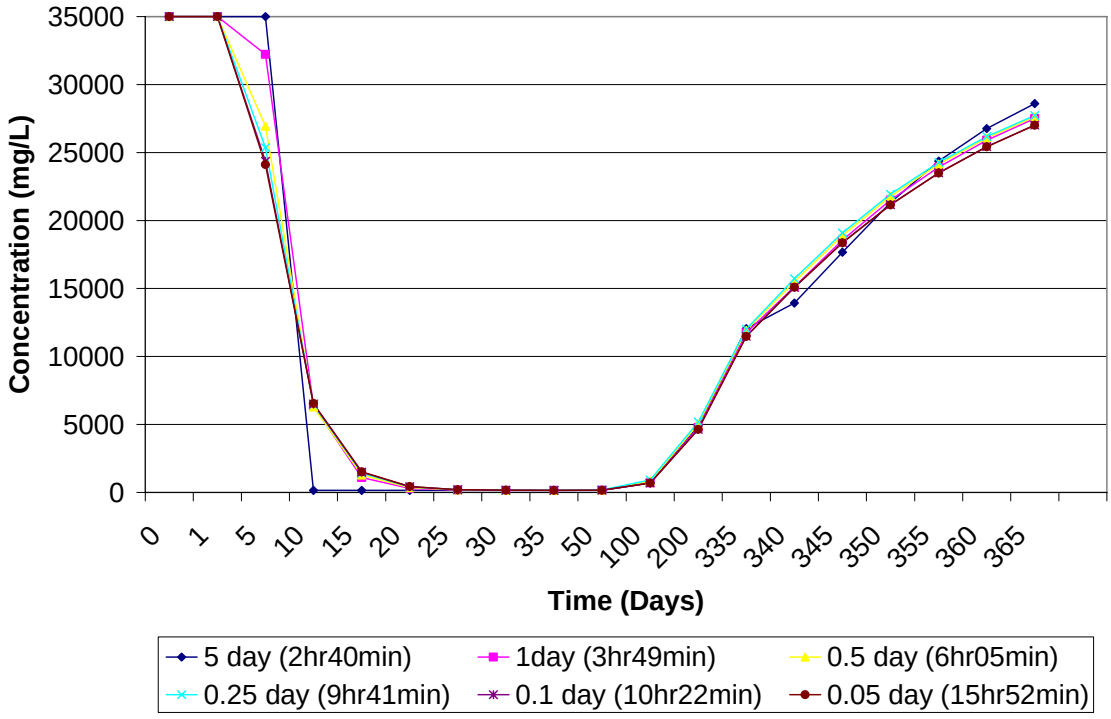

Note: Legend identifies the time step size of the injection and extraction cycles with the associated simulation time in parentheses

Figure A1 – Time Step Sensitivity Analysis

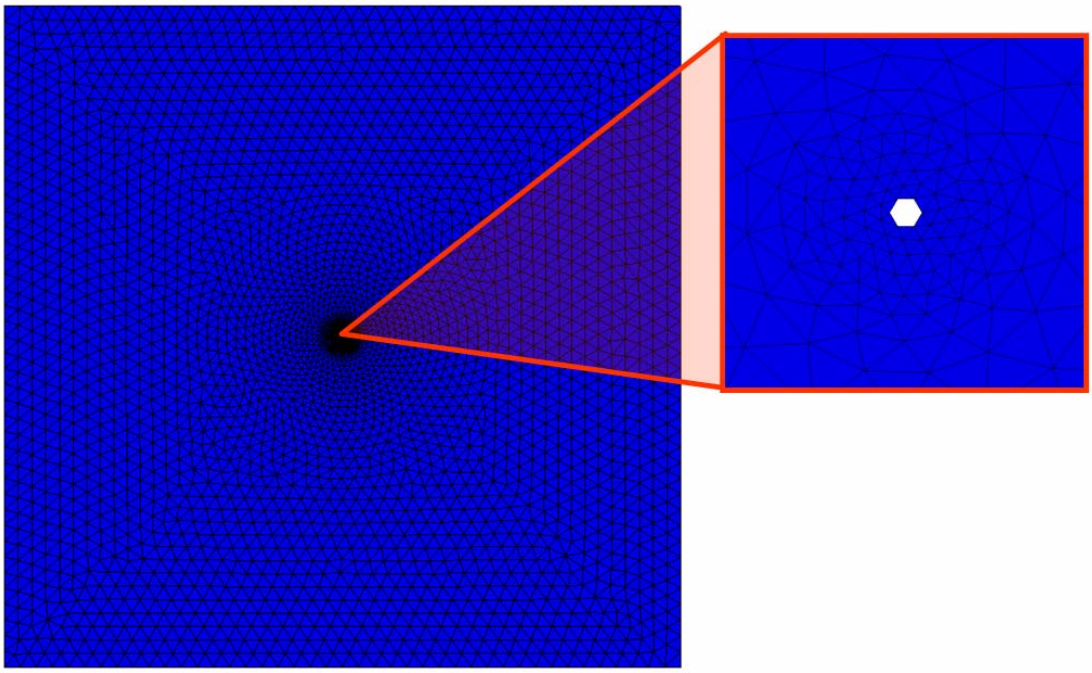

Figure A2a – Horizontal Mesh Resolution

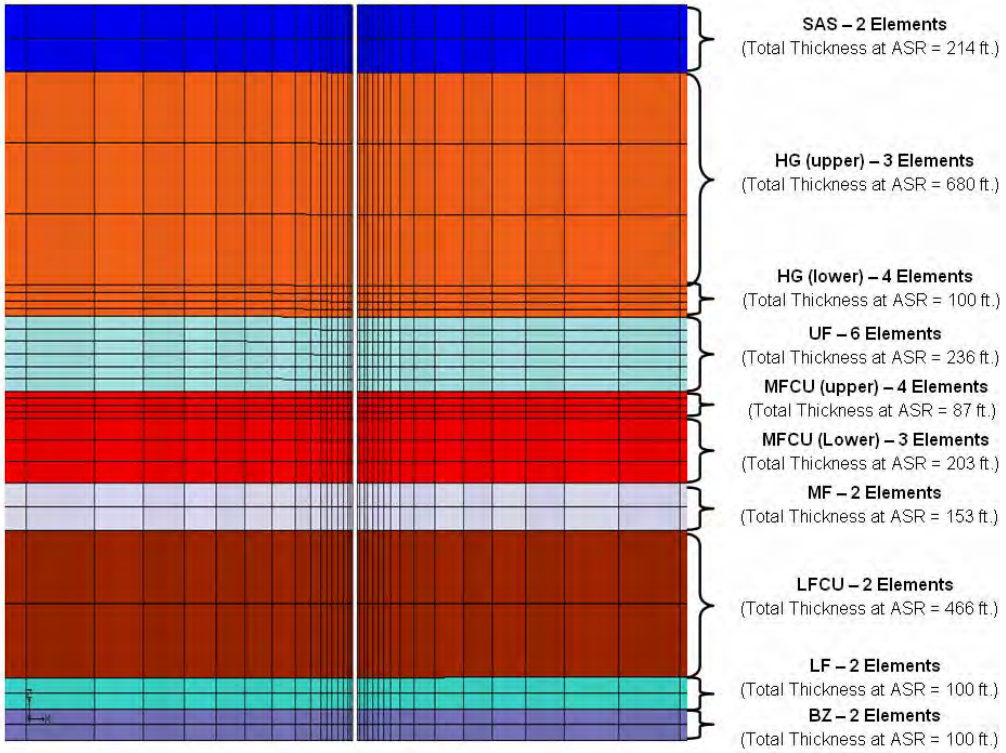

Figure A2b – Conceptual Geology and Vertical Mesh Resolution

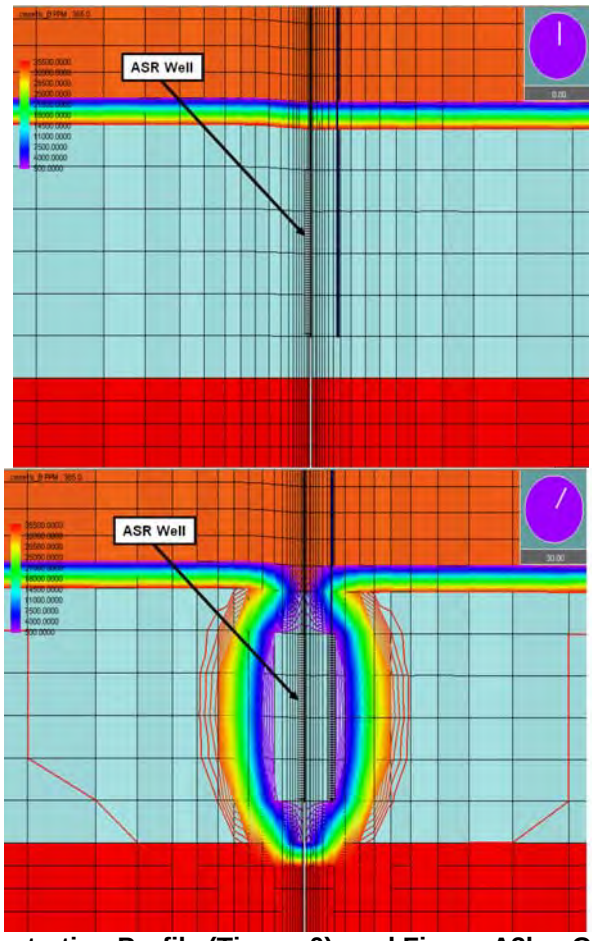

Figure A3a – Concentration Profile (Time = 0) and Figure A3b – Concentration Profile (Time = 30)

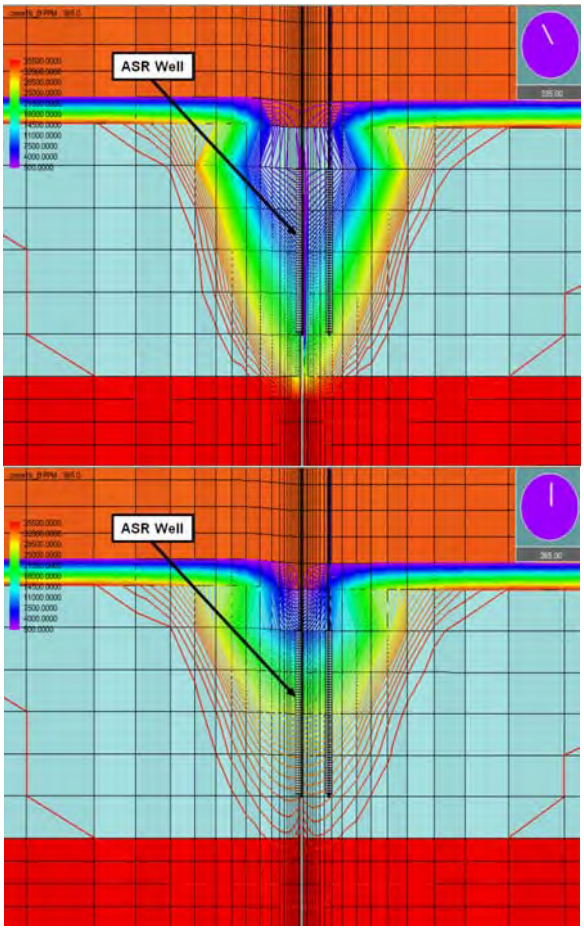

Figure A3c – Concentration Profile (Time = 335) and Figure A3d – Concentration Profile (Time = 365)

WASH123 Variable-Density Modeling Tests

Elder Model

Parameter	SEAWAT Value	SEAWAT Units	WASH123D (DB2) Value	WASH123D (DB2) Units	Remarks	File Location In WASH123D
Density of Fresh Water (p0)	1000	kg/m^3	1000	kg/m^3		UN1 (3) in *.glb
Density of Salt Water (p)	1200	kg/m^3	N/A	kg/m^3	Density of salt water is not a direct WASH input. It is calculated based on the "a" parameter calculated by the equation [p/p0 = 1 + aC] where p = density of H2O at saline concentration C and p0 is the density of water at a saline concentration of 0.	N/A
Alpha (a)	N/A	m^3/kg	0.2	m^3/kg	These values were revised for the DB2 run based on conversation with Pearce Cheng on 3/9/05. See runlog	UN2 (2) in *.glb
Salt Concentration Upper Boundary (Cs)	285.7	kg/m^3	1	molarity		XYS referenced by RS2 in *.3tp
Salt Concentration Lower Boundary (C)	0	kg/m^3	0	kg/m^3		XYS referenced by RS2 in *.3tp
Viscosity of Fresh Water	N/A		126.82	kg/(m*day)	SEAWAT report does not provide viscosity. Wash value converted from 2.65 slugs/(ft*day)	UN1 (4) in *.glb
Hydraulic Conductivity (Kf)	0.411	m/day	0.411	m/day	Assumed homogeneous	MP2 (2,3,4) in *.3bc
Modified Compressibility	N/A		0	(m*day^2)/kg	SEAWAT report does not provide. Assume incompressible	MP2 (8) in *.3bc
Porosity	0.1		0.1			MP2 (9) in *.3bc; MP5 (6) in *.3tp
Molecular Difusion	0.308	m^2/day	0.308	m^2/day		DF1 (2) in *.che
First Order Decay Constant for Salt	N/A		0	1/day	SEAWAT report does not provide. Assume 0.	DY1 (2) in *.che
Bulk Density	N/A		1500	kg/m^3	SEAWAT report does not provide. Assume material is sand with a bulk density of 1.5 kg/l or 1500 kg/m^3	MP5 (2) in *.3tp
Longitudinal Dispersivity	0	m	0	m		MP5 (3) in *.3tp
Transverse Dispersivity	0	m	0	m/m	In WASH this parameter is calcualted through a ratio (Tran/Long)	MP5 (4) in *.3tp
Tortuosity	N/A		1		SEAWAT report does not provide. Assume 1.	MP5 (5) in *.3tp

BASELINE ELDER INPUT PARAMETER COMPARISON

- March 2005 version of Wash Code
- PCG-1 Flow Solver
- Nodal/Gaussian Flow Quadrature
- PCG-2 Transport Solver
- Nodal/Gaussian Transport Quadrature
- Backwards Difference Non-linear Weighting

PREVIOUS ELDER MODEL RESULTS FOR COMPARISON

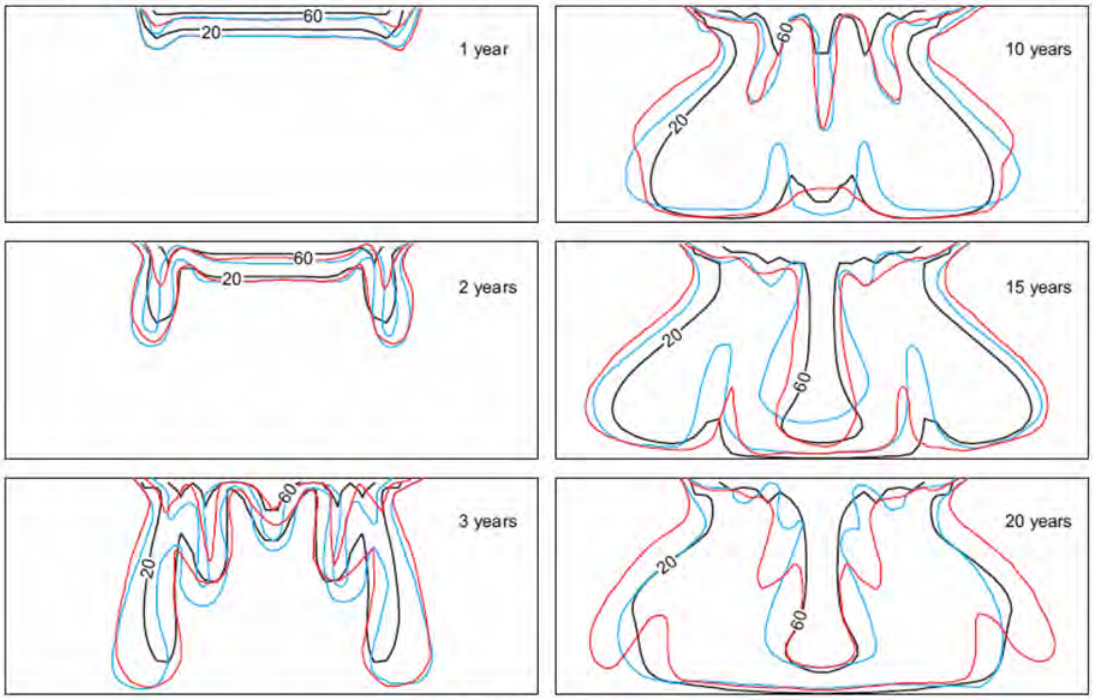

EXPLANATION

—20— SEAWAT line of relative salinity concentration, in percent

—20— SUTRA line of relative salinity concentration, in percent (Voss and Souza, 1987)

—20— Elder line of relative salinity concentration, in percent (Voss and Souza, 1987)

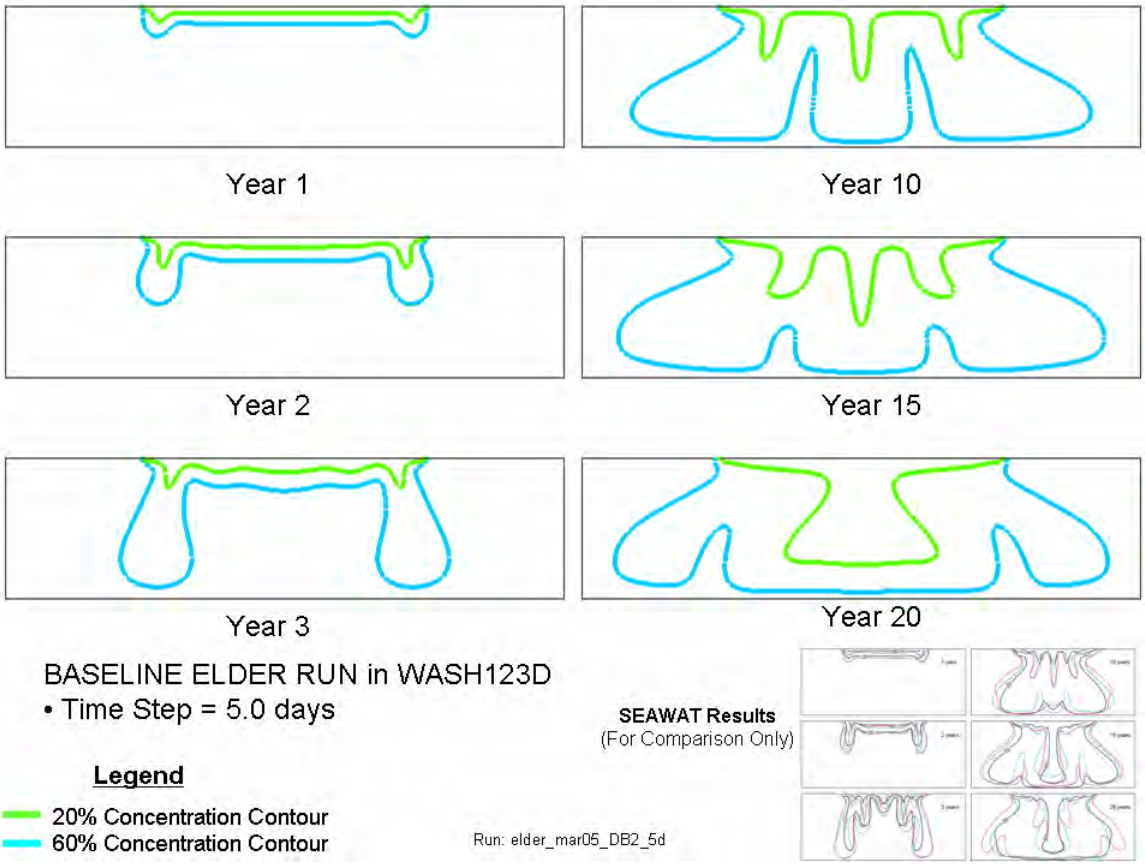
Year 1
Year 10
Year 2
Year 15
Year 3
Year 20
BASELINE ELDER RUN in WASH123D
• Time Step = 5.0 days
SEAWAT Results
(For Comparison Only)
Legend
20% Concentration Contour
60% Concentration Contour
Run: elder_mar05_DB2_5d

Henry Model

Results (at steady state)

Simulation run using WASH123D version January 2006

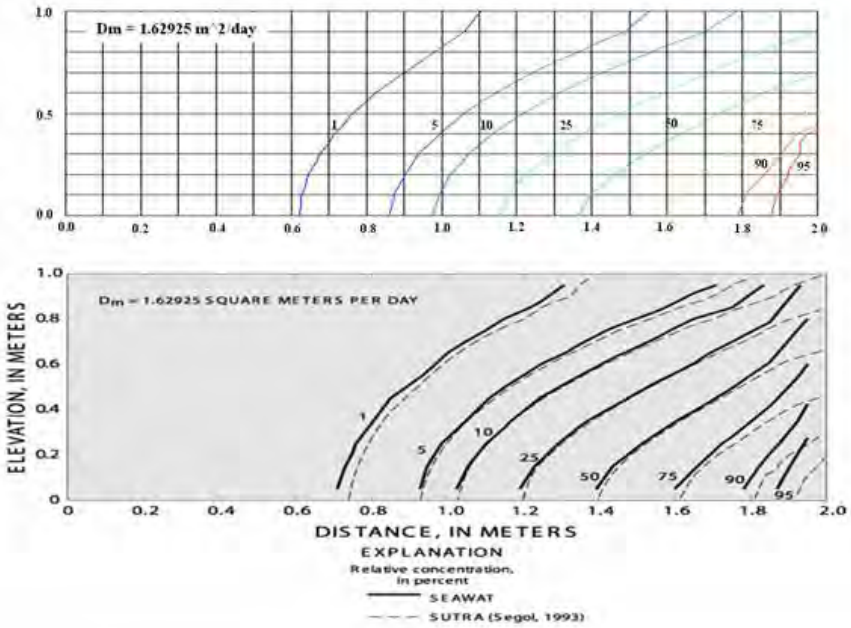

Appendix B

Journal Article to be Submitted by USGS – to be published under a separate cover

Landscape Figures for Main Report

Flow Initial Condition based on Head BC's defined below (no density effect/no pumping)
Concentration Initial Condition based on concentration BC's defined for each layer (constant for each layer)

					Flow Parameters									Density/Transport Parameters								Initial Conditions	
MODFLOW Cell Layer	WASH Element Layer	WASH Node Layer	WASH Material	Geologic Unit	Head BC West Tot Head (ft)	Head BC East Tot Head (ft)	Head BC North Tot Head (ft)	Head BC South Tot Head (ft)	Conductivity Horiz (ft/day)	Conductivity Vert. (ft/day)	Mod. Compress of Matrix (1/ft)	Specific Storage (1/ft)	Effective Porosity	Con. BC West (mg/L)	Con. BC East (mg/L)	Con. BC North (mg/L)	Con. BC South (mg/L)	Tortuosity	Bulk Density (slug/ft^3)	Dispersivity Long. (ft)	Dispersivity Trans. (ft)	Flow IC Tot Head (ft)	Con. IC (mg/L)
		1			20	20	No Flow	No Flow						150	150	N/A	N/A						150
1	1	2	1	SAS	20	20	No Flow	No Flow	100	10	1.70E-03	1.70E-03	0.25	150	150	N/A	N/A	1	3.784	0	0		150
	2	3	1	SAS	20	20	No Flow	No Flow	100	10	1.70E-03	1.70E-03	0.25	150	150	N/A	N/A	1	3.784	0	0		150
	3	4	2	HG	No Flow	No Flow	No Flow	No Flow	0.01	0.001	7.00E-07	1.19E-06	0.4	150	150	N/A	N/A	1	2.969	0	0		150
2,3,4,5	4	5	3	HG	No Flow	No Flow	No Flow	No Flow	0.01	0.001	7.00E-07	1.19E-06	0.4	250	250	N/A	N/A	1	2.969	0	0		250
	5	6	3	HG	50	30	No Flow	No Flow	0.01	0.001	7.00E-07	1.19E-06	0.4	500	500	N/A	N/A	1	2.969	0	0		500
	6	7	4	UF	50	30	No Flow	No Flow	100	10	7.00E-07	1.01E-06	0.25	4000	4000	N/A	N/A	1	3.784	0	0		4000
	7	8	4	UF	50	30	No Flow	No Flow	100	10	7.00E-07	1.01E-06	0.25	4000	4000	N/A	N/A	1	3.784	0	0		4000
6,7,8,9	8	9	4	UF	50	30	No Flow	No Flow	100	10	7.00E-07	1.01E-06	0.25	4000	4000	N/A	N/A	1	3.784	0	0		4000
	9	10	4	UF	50	30	No Flow	No Flow	100	10	7.00E-07	1.01E-06	0.25	4000	4000	N/A	N/A	1	3.784	0	0		4000
	10	11	4	UF	50	30	No Flow	No Flow	100	10	7.00E-07	1.01E-06	0.25	4000	4000	N/A	N/A	1	3.784	0	0		4000
	11	12	4	UF	50	30	No Flow	No Flow	100	10	7.00E-07	1.01E-06	0.25	4000	4000	N/A	N/A	1	3.784	0	0		4000
		13	5	MFCU	No Flow	No Flow	No Flow	No Flow	0.01	0.001	7.00E-07	1.07E-06	0.3	35000	35000	N/A	N/A	1	3.531	0	0		35000
10	12	14	5	MFCU	No Flow	No Flow	No Flow	No Flow	0.01	0.001	7.00E-07	1.07E-06	0.3	35000	35000	N/A	N/A	1	3.531	0	0		35000
	13	15	5	MFCU	40	20	No Flow	No Flow	0.01	0.001	7.00E-07	1.07E-06	0.3	35000	35000	N/A	N/A	1	3.531	0	0		35000
	14	16	6	MF	40	20	No Flow	No Flow	500	50	7.00E-07	1.01E-06	0.25	35000	35000	N/A	N/A	1	3.784	0	0		35000
11,12	15	17	6	MF	40	20	No Flow	No Flow	500	50	7.00E-07	1.01E-06	0.25	35000	35000	N/A	N/A	1	3.784	0	0		35000
	16	18	6	MF	40	20	No Flow	No Flow	500	50	7.00E-07	1.01E-06	0.25	35000	35000	N/A	N/A	1	3.784	0	0		35000
	17	19	7	LFCU	No Flow	No Flow	No Flow	No Flow	0.01	0.001	7.00E-07	1.07E-06	0.3	35000	35000	N/A	N/A	1	3.531	0	0		35000
13	18	20	7	LFCU	No Flow	No Flow	No Flow	No Flow	0.01	0.001	7.00E-07	1.07E-06	0.3	35000	35000	N/A	N/A	1	3.531	0	0		35000
		21			0	0	No Flow	No Flow						35000	35000	N/A	N/A						35000
	19	22	8	LF	0	0	No Flow	No Flow	5000	500	7.00E-07	1.01E-06	0.25	35000	35000	N/A	N/A	1	3.784	0	0		35000
14,15	20	23	8	LF	0	0	No Flow	No Flow	5000	500	7.00E-07	1.01E-06	0.25	35000	35000	N/A	N/A	1	3.784	0	0		35000
		24			0	0	No Flow	No Flow						35000	35000	N/A	N/A						35000
	21	25	9	BZ	0	0	No Flow	No Flow	10000	1000	7.00E-07	1.01E-06	0.25	35000	35000	N/A	N/A	1	3.784	0	0		35000
16	22	26	9	BZ	0	0	No Flow	No Flow	10000	1000	7.00E-07	1.01E-06	0.25	35000	35000	N/A	N/A	1	3.784	0	0		35000
		27			0	0	No Flow	No Flow						35000	35000	N/A	N/A						35000
				Model Top	Over Land = 20/Over Ocean = 20																			
				Model Bottom	No Flow																			

Based on Steady State Simulation with no pumping

Figure 1. Model Parameters for Case 1A.

Flow Initial Condition based on Head BC's defined below (no density effect/no pumping)
Concentration Initial Condition based on concentration BC's defined for each layer (constant for each layer)

					Flow Parameters									Density/Transport Parameters								Initial Conditions	
MODFLOW Cell Layer	WASH Element Layer	WASH Node Layer	WASH Material	Geologic Unit	Head BC West Tot Head (ft)	Head BC East Tot Head (ft)	Head BC North Tot Head (ft)	Head BC South Tot Head (ft)	Conductivity Horiz (ft/day)	Conductivity Vert. (ft/day)	Mod. Compress of Matrix (1/ft)	Specific Storage (1/ft)	Effective Porosity	Con. BC West (mg/L)	Con. BC East (mg/L)	Con. BC North (mg/L)	Con. BC South (mg/L)	Tortuosity	Bulk Density (slug/ft^3)	Dispersivity Long. (ft)	Dispersivity Trans. (ft)	Flow IC Tot Head (ft)	Con. IC (mg/L)
		1			20	20	No Flow	No Flow						150	150	N/A	N/A						150
1	1	2	1	SAS	20	20	No Flow	No Flow	100	10	1.70E-03	1.70E-03	0.25	150	150	N/A	N/A	1	3.784	0	0		150
	2	3	1	SAS	20	20	No Flow	No Flow	100	10	1.70E-03	1.70E-03	0.25	150	150	N/A	N/A	1	3.784	0	0		150
	3	4	2	HG	No Flow	No Flow	No Flow	No Flow	0.01	0.001	7.00E-07	1.19E-06	0.4	150	150	N/A	N/A	1	2.969	0	0		150
2,3,4,5	4	5	3	HG	No Flow	No Flow	No Flow	No Flow	0.01	0.001	7.00E-07	1.19E-06	0.4	250	250	N/A	N/A	1	2.969	0	0		250
	5	6	3	HG	50	30	No Flow	No Flow	0.01	0.001	7.00E-07	1.19E-06	0.4	35000	35000	N/A	N/A	1	2.969	0	0		35000
	6	7	4	UF	50	30	No Flow	No Flow	100	10	7.00E-07	1.01E-06	0.25	35000	35000	N/A	N/A	1	3.784	0	0		35000
	7	8	4	UF	50	30	No Flow	No Flow	100	10	7.00E-07	1.01E-06	0.25	35000	35000	N/A	N/A	1	3.784	0	0		35000
6,7,8,9	8	9	4	UF	50	30	No Flow	No Flow	100	10	7.00E-07	1.01E-06	0.25	35000	35000	N/A	N/A	1	3.784	0	0		35000
	9	10	4	UF	50	30	No Flow	No Flow	100	10	7.00E-07	1.01E-06	0.25	35000	35000	N/A	N/A	1	3.784	0	0		35000
	10	11	4	UF	50	30	No Flow	No Flow	100	10	7.00E-07	1.01E-06	0.25	35000	35000	N/A	N/A	1	3.784	0	0		35000
	11	12	4	UF	50	30	No Flow	No Flow	100	10	7.00E-07	1.01E-06	0.25	35000	35000	N/A	N/A	1	3.784	0	0		35000
	12	13	5	MFCU	No Flow	No Flow	No Flow	No Flow	0.01	0.001	7.00E-07	1.07E-06	0.3	35000	35000	N/A	N/A	1	3.531	0	0		35000
10	13	14	5	MFCU	No Flow	No Flow	No Flow	No Flow	0.01	0.001	7.00E-07	1.07E-06	0.3	35000	35000	N/A	N/A	1	3.531	0	0		35000
	14	15	5	MFCU	40	20	No Flow	No Flow	0.01	0.001	7.00E-07	1.07E-06	0.3	35000	35000	N/A	N/A	1	3.531	0	0		35000
	15	16	6	MF	40	20	No Flow	No Flow	500	50	7.00E-07	1.01E-06	0.25	35000	35000	N/A	N/A	1	3.784	0	0		35000
11,12	16	17	6	MF	40	20	No Flow	No Flow	500	50	7.00E-07	1.01E-06	0.25	35000	35000	N/A	N/A	1	3.784	0	0		35000
	17	18	7	LFCU	No Flow	No Flow	No Flow	No Flow	0.01	0.001	7.00E-07	1.07E-06	0.3	35000	35000	N/A	N/A	1	3.531	0	0		35000
13	18	19	7	LFCU	0	0	No Flow	No Flow	0.01	0.001	7.00E-07	1.07E-06	0.3	35000	35000	N/A	N/A	1	3.531	0	0		35000
	19	20	8	LF	0	0	No Flow	No Flow	5000	500	7.00E-07	1.01E-06	0.25	35000	35000	N/A	N/A	1	3.784	0	0		35000
14,15	20	21	8	LF	0	0	No Flow	No Flow	5000	500	7.00E-07	1.01E-06	0.25	35000	35000	N/A	N/A	1	3.784	0	0		35000
	21	22	9	BZ	0	0	No Flow	No Flow	10000	1000	7.00E-07	1.01E-06	0.25	35000	35000	N/A	N/A	1	3.784	0	0		35000
16	22	23	9	BZ	0	0	No Flow	No Flow	10000	1000	7.00E-07	1.01E-06	0.25	35000	35000	N/A	N/A	1	3.784	0	0		35000
				Model Top	Over Land = 20/Over Ocean = 20																		
				Model Bottom	No Flow																		

Based on Steady State Simulation with no pumping

Figure 2. Model Parameters for Case 1B.

Flow Initial Condition based on Head BC's defined below (no density effect/no pumping)
Concentration Initial Condition based on concentration BC's defined for each layer (constant for each layer)

					Flow Parameters									Density/Transport Parameters								Initial Conditions	
MODFLOW Cell Layer	WASH Element Layer	WASH Node Layer	WASH Material	Geologic Unit	Head BC West Tot Head (ft)	Head BC East Tot Head (ft)	Head BC North Tot Head (ft)	Head BC South Tot Head (ft)	Conductivity Horiz (ft/day)	Conductivity Vert. (ft/day)	Mod. Compress of Matrix (1/ft)	Specific Storage (1/ft)	Effective Porosity	Con. BC West (mg/L)	Con. BC East (mg/L)	Con. BC North (mg/L)	Con. BC South (mg/L)	Tortuosity	Bulk Density (slug/ft^3)	Dispersivity Long. (ft)	Dispersivity Trans. (ft)	Flow IC Tot Head (ft)	Con. IC (mg/L)
		1			20	20	No Flow	No Flow						150	150	N/A	N/A						150
1	1	2	1	SAS	20	20	No Flow	No Flow	100	10	1.70E-03	1.70E-03	0.25	150	150	N/A	N/A	1	3.784	0	0		150
	2		1	SAS					100	10	1.70E-03	1.70E-03	0.25					1	3.784	0	0		
		3			20	20	No Flow	No Flow						150	150	N/A	N/A						150
	3	4	2	HG	No Flow	No Flow	No Flow	No Flow	0.01	0.001	7.00E-07	1.19E-06	0.4	150	150	N/A	N/A	1	2.969	0	0		150
2,3,4,5	4		3	HG					0.01	0.001	7.00E-07	1.19E-06	0.4					1	2.969	0	0		
	5	5	3	HG	No Flow	No Flow	No Flow	No Flow	0.01	0.001	7.00E-07	1.19E-06	0.4	250	250	N/A	N/A	1	2.969	0	0		250
		6			50	30	No Flow	No Flow						500	500	N/A	N/A						500
	6	7	4	UF	50	30	No Flow	No Flow	100	10	7.00E-07	1.01E-06	0.25	4000	4000	N/A	N/A	1	3.784	0	0		4000
	7	8	4	UF	50	30	No Flow	No Flow	100	10	7.00E-07	1.01E-06	0.25	4000	4000	N/A	N/A	1	3.784	0	0		4000
	8	9	4	UF	50	30	No Flow	No Flow	100	10	7.00E-07	1.01E-06	0.25	4000	4000	N/A	N/A	1	3.784	0	0		4000
6,7,8,9	9	10	4	UF	50	30	No Flow	No Flow	100	10	7.00E-07	1.01E-06	0.25	4000	4000	N/A	N/A	1	3.784	0	0		4000
	10	11	4	UF	50	30	No Flow	No Flow	100	10	7.00E-07	1.01E-06	0.25	4000	4000	N/A	N/A	1	3.784	0	0		4000
	11		4	UF					100	10	7.00E-07	1.01E-06	0.25					1	3.784	0	0		
		12			50	30	No Flow	No Flow						4000	4000	N/A	N/A						4000
	12	13	5	MFCU	No Flow	No Flow	No Flow	No Flow	1	1	7.00E-07	1.07E-06	0.3	35000	35000	N/A	N/A	1	3.531	0	0		35000
10	13	14	5	MFCU	No Flow	No Flow	No Flow	No Flow	1	1	7.00E-07	1.07E-06	0.3	35000	35000	N/A	N/A	1	3.531	0	0		35000
	14		5	MFCU					1	1	7.00E-07	1.07E-06	0.3					1	3.531	0	0		
		15			40	20	No Flow	No Flow						35000	35000	N/A	N/A						35000
	15	16	6	MF	40	20	No Flow	No Flow	500	50	7.00E-07	1.01E-06	0.25	35000	35000	N/A	N/A	1	3.784	0	0		35000
11,12	16		6	MF					500	50	7.00E-07	1.01E-06	0.25					1	3.784	0	0		
		17			40	20	No Flow	No Flow						35000	35000	N/A	N/A						35000
	17	18	7	LFCU	No Flow	No Flow	No Flow	No Flow	0.01	0.001	7.00E-07	1.07E-06	0.3	35000	35000	N/A	N/A	1	3.531	0	0		35000
13	18		7	LFCU					0.01	0.001	7.00E-07	1.07E-06	0.3					1	3.531	0	0		
		19			0	0	No Flow	No Flow						35000	35000	N/A	N/A						35000
	19	20	8	LF	0	0	No Flow	No Flow	5000	500	7.00E-07	1.01E-06	0.25	35000	35000	N/A	N/A	1	3.784	0	0		35000
14,15	20		8	LF					5000	500	7.00E-07	1.01E-06	0.25					1	3.784	0	0		
		21			0	0	No Flow	No Flow						35000	35000	N/A	N/A						35000
	21	22	9	BZ	0	0	No Flow	No Flow	10000	1000	7.00E-07	1.01E-06	0.25	35000	35000	N/A	N/A	1	3.784	0	0		35000
16	22		9	BZ					10000	1000	7.00E-07	1.01E-06	0.25					1	3.784	0	0		
		23			0	0	No Flow	No Flow						35000	35000	N/A	N/A						35000
				Model Top	Over Land = 20/Over Ocean = 20																			
				Model Bottom	No Flow																			

Based on Steady State Simulation with no pumping

Figure 3. Model Parameters for Case 1C.

Flow Initial Condition based on Head BC's defined below (no density effect/no pumping)
Concentration Initial Condition based on concentration BC's defined for each layer (constant for each layer)

					Flow Parameters									Density/Transport Parameters								Initial Conditions	
MODFLOW Cell Layer	WASH Element Layer	WASH Node Layer	WASH Material	Geologic Unit	Head BC West Tot Head (ft)	Head BC East Tot Head (ft)	Head BC North Tot Head (ft)	Head BC South Tot Head (ft)	Conductivity Horiz (ft/day)	Conductivity Vert. (ft/day)	Mod. Compress of Matrix (1/ft)	Specific Storage (1/ft)	Effective Porosity	Con. BC West (mg/L)	Con. BC East (mg/L)	Con. BC North (mg/L)	Con. BC South (mg/L)	Tortuosity	Bulk Density (slug/ft^3)	Dispersivity Long. (ft)	Dispersivity Trans. (ft)	Flow IC Tot Head (ft)	Con. IC (mg/L)
		1			20	20	No Flow	No Flow						150	150	N/A	N/A						150
1	1	2	1	SAS	20	20	No Flow	No Flow	100	10	1.70E-03	1.70E-03	0.25	150	150	N/A	N/A	1	3.784	25	25		150
	2	3	1	SAS	20	20	No Flow	No Flow	100	10	1.70E-03	1.70E-03	0.25	150	150	N/A	N/A	1	3.784	25	25		150
	3	4	2	HG	No Flow	No Flow	No Flow	No Flow	0.01	0.001	7.00E-07	1.19E-06	0.4	150	150	N/A	N/A	1	2.969	25	25		150
2,3,4,5	4	5	3	HG	No Flow	No Flow	No Flow	No Flow	0.01	0.001	7.00E-07	1.19E-06	0.4	250	250	N/A	N/A	1	2.969	25	25		250
	5	6	3	HG	50	30	No Flow	No Flow	0.01	0.001	7.00E-07	1.19E-06	0.4	500	500	N/A	N/A	1	2.969	25	25		500
	6	7	4	UF	50	30	No Flow	No Flow	100	10	7.00E-07	1.01E-06	0.25	4000	4000	N/A	N/A	1	3.784	25	25		4000
	7	8	4	UF	50	30	No Flow	No Flow	100	10	7.00E-07	1.01E-06	0.25	4000	4000	N/A	N/A	1	3.784	25	25		4000
	8	9	4	UF	50	30	No Flow	No Flow	100	10	7.00E-07	1.01E-06	0.25	4000	4000	N/A	N/A	1	3.784	25	25		4000
6,7,8,9	9	10	4	UF	50	30	No Flow	No Flow	100	10	7.00E-07	1.01E-06	0.25	4000	4000	N/A	N/A	1	3.784	25	25		4000
	10	11	4	UF	50	30	No Flow	No Flow	100	10	7.00E-07	1.01E-06	0.25	4000	4000	N/A	N/A	1	3.784	25	25		4000
	11	12	4	UF	50	30	No Flow	No Flow	100	10	7.00E-07	1.01E-06	0.25	4000	4000	N/A	N/A	1	3.784	25	25		4000
																						Based on Steady State Simulation with no pumping	
	12	13	5	MFCU	No Flow	No Flow	No Flow	No Flow	0.01	0.001	7.00E-07	1.07E-06	0.3	35000	35000	N/A	N/A	1	3.531	25	25		35000
10	13	14	5	MFCU	No Flow	No Flow	No Flow	No Flow	0.01	0.001	7.00E-07	1.07E-06	0.3	35000	35000	N/A	N/A	1	3.531	25	25		35000
	14	15	5	MFCU	40	20	No Flow	No Flow	0.01	0.001	7.00E-07	1.07E-06	0.3	35000	35000	N/A	N/A	1	3.531	25	25		35000
	15	16	6	MF	40	20	No Flow	No Flow	500	50	7.00E-07	1.01E-06	0.25	35000	35000	N/A	N/A	1	3.784	25	25		35000
11,12	16	17	6	MF	40	20	No Flow	No Flow	500	50	7.00E-07	1.01E-06	0.25	35000	35000	N/A	N/A	1	3.784	25	25		35000
	17	18	7	LFCU	No Flow	No Flow	No Flow	No Flow	0.01	0.001	7.00E-07	1.07E-06	0.3	35000	35000	N/A	N/A	1	3.531	25	25		35000
13	18	19	7	LFCU	0	0	No Flow	No Flow	0.01	0.001	7.00E-07	1.07E-06	0.3	35000	35000	N/A	N/A	1	3.531	25	25		35000
	19	20	8	LF	0	0	No Flow	No Flow	5000	500	7.00E-07	1.01E-06	0.25	35000	35000	N/A	N/A	1	3.784	25	25		35000
14,15	20	21	8	LF	0	0	No Flow	No Flow	5000	500	7.00E-07	1.01E-06	0.25	35000	35000	N/A	N/A	1	3.784	25	25		35000
	21	22	9	BZ	0	0	No Flow	No Flow	10000	1000	7.00E-07	1.01E-06	0.25	35000	35000	N/A	N/A	1	3.784	25	25		35000
16	22	23	9	BZ	0	0	No Flow	No Flow	10000	1000	7.00E-07	1.01E-06	0.25	35000	35000	N/A	N/A	1	3.784	25	25		35000
				Model Top	Over Land = 20/Over Ocean = 20																		
				Model Bottom	No Flow																		

Figure 4. Model Parameters for Case 1D.

ASR Regional Study – Benchscale Modeling

Final Report
July 2006
Prepared by:

Christopher J. Brown, Ph.D., P.E. – USACE
Steve England, P.E. – USACE
Glendon T. Stevens, P.E. - USACE
Hwai-Ping Cheng, Ph.D. – USACE ERDC
Emily Richardson, P.G. - SFWMD

Introduction:

The CERP recommends approximately 333 ASR wells to help with the supply, storage and distribution of water within the South Florida Region. The wells are dual purpose, since they are intended to store excess water during summer wet periods and recover the water during dry winter periods. It is hoped that the technology will provide a dependable water storage mechanism that can supplement surface storage reservoirs and provide water supply to the Lake Okeechobee ecosystem, Everglades ecosystem, agricultural irrigation, urban interests and others. The proposed injection and recovery pumping rate is approximately 1.65 billion gallons per day which is unprecedented in terms of other past or present ASR applications. Currently, only desktop spreadsheet evaluations or analytical solutions can provide an estimate of the aquifer response (e.g., piezometric head increases, fracturing pressures, increased flow) to such a large volume of injected water. A numerical model (or family of models), designed to simulate the regional groundwater system, will serve to make further evaluations of the plan. Porous media models and a discrete fracture network models have been considered but due to the lack of discrete fracture data related to the hydrogeology of south Florida, a porous media model has been pursued.

The CERP blue-print has been presented in a massive regional-scale plan that lacks engineering detail sufficient to construct the project. A large number of the construction features contained in the CERP were designed at various levels of detail based on information that was available during the plan formulation and evaluation phase. Many of the design assumptions for the components were based solely on output from the South Florida Water Management Model (SFWMM), which averages hydrologic conditions across a model comprised of grid cells with lengths and widths of 2 miles by 2 miles. Consequently, the engineering details of the construction features,

including the size and locations are conceptual and require additional studies. In addition, the SFWMM only simulates the Surficial Aquifer System explicitly. The Floridan Aquifer System where the proposed ASR wells would be located is not included. In general, the CERP proposed 200 ASR wells to be sited in the vicinity of Lake Okeechobee with the remaining wells located adjacent to the C-43 reservoir and in the Lower East Coast (specifically, Palm Beach and Broward Counties, Florida). A later effort, the Water Preserve Area (WPA) Feasibility Study, proposed adding additional wells in this area. The exact location and distribution of the proposed CERP ASR wells was never determined as part of the original CERP effort, however, the proposed wells were generally concentrated adjacent to reservoirs or Lake Okeechobee. The WPA Feasibility efforts proposed ASR wells at the C-9 impoundment.

Together with the ASR Pilot Projects and the ASR Contingency Plan, the ASR Regional Study will endeavor to reduce technical uncertainties associated with the proposed CERP ASR plan - a plan that is unprecedented in scale anywhere in the world. A Project Management Plan (PMP) was prepared for the ASR Regional Study in 2003. The center-piece of the ASR Regional Study is the preparation of a series of numerical simulation models. A multitude of issues need to be evaluated using the family of numerical models. The issues include local, sub-regional, and regional-scale concerns counting the following:

1. Regional changes in aquifer heads and flows
2. Regional changes in aquifer water quality TDS, sulfate, and chloride
3. Increased potential for salt-water intrusion caused by ASR pumping
4. Regional impacts to existing well users of the FAS
5. ASR well cluster site selection
6. ASR well cluster design and layout
7. ASR well cluster performance including estimating recovery efficiency
8. ASR well site evaluation of pressure induced changes
9. Localized transport of contaminants including heavy metals or pathogens
10. Localized ASR well pump design (dependent upon the appropriate model resolution)

Initially, a large, peninsula-wide numerical model will be developed. It is envisioned that this model will encompass an area of the Florida peninsula from Polk County south to Florida Bay. This model is intended for use as a planning tool to evaluate potential changes (e.g., head/flow and water quality) within the confined Floridan Aquifer System (FAS), aid in the site selection of ASR well clusters in the vicinity of Lake Okeechobee, adjacent to the C-43 reservoir and in the Lower East Coast area of South Florida, and aid ASR well cluster design and layout. In support of the main model development task, a number of smaller tasks will also be completed prior to or in parallel with the screening model development (e.g., literature search, data compilation, model selection, etc.). Once the Regional Screening Model is completed, more detailed sub-regional and/or local scale models will be developed to evaluate the ASR program in a higher level of detail. Depending upon model code selection and model domain design, all ten of the issues noted above could be evaluated. Table 1 displays the model scale required to address each of the identified issues. Both the sub-regional and regional scale

models should be designed to address as many of the issues listed as possible. In essence, the sooner the issue can be evaluated, the better. Obviously, one possible strategy would be to address the issue in two tiers. First, the regional model could provide planning-level information to address the specific issues. Then, an improved understanding of the issue could be obtained through the development of finer-resolution sub-regional models. For the three local-scale issues identified, only small models with fine horizontal and vertical resolution, will be sufficient to adequately address them.

Table 1. Model scale requirements.

Model Scale Required to Address Specific Issue	**Issues to be addressed as listed above**
Local Scale fine-resolution model	7, 9, 10
Sub-regional moderate-resolution model	1, 2, 3, 4, 6, 8
Regional Scale moderate to coarse resolution model	1, 2, 3, 4, 5, 6, 8

It is anticipated that the model development process will require approximately 1.75 to 2-years to finish and will involve numerous meetings, workshops, and conference calls. A team of model developers will work collaboratively over the internet and through video-conferences. It is expected that the model development effort will involve numerous technical challenges including addressing seawater boundary conditions; determining an appropriate number of model layers and grid/mesh spacing; developing manageable model computer run-times; evaluating vertical aquifer system connections/leakage; testing alternate locations for ASR clusters; developing reasonable ASR recharge and recovery scenarios; and determining whether or not steady state modeling is applicable.

Due to the large scale of the model, computer run-times are expected to be quite long. Therefore, the selection of an appropriate model code is of paramount importance. Consideration will be given to utilizing a fully density-dependent model code if performance tests confirm that such a code would be practical to use at the scale envisioned. Otherwise, consideration will be given to simulating density effects at the seawater boundaries and along the bottom of the model as necessary.

Model Code Bench-scale Testing Scope of Work:

The scope of work for the model development effort presented in the ASR Regional Study PMP recognized that a fully density-dependent code would be ultimately be required to simulate regional changes in aquifer pressure and water quality. This is due to a number of technical considerations including:

- Water exchange between various portions of the FAS
- Water flow and velocity issues near coastal portions of the model
- ASR recovery efficiency is partially dependent upon density stratification effects
- Density directly affects the regional heads and flow within the FAS
- Density is a function of water quality of the aquifer (e.g., function of TDS)

The PMP also considered alternate modeling approaches employing density-dependent boundaries to grossly simulate density affects. Therefore, the development of sub-regional models that possessed the requisite density-dependent capabilities were specified as part of the PMP to ensure the most realistic model simulations could be developed. Alternate modeling approaches may allow some flexibility in the development of a regional model, ensuring that the following constraints are managed:

- Limitations of existing density-dependent model codes
- Concerns about model run times
- Schedule constraints
- Resources available

Ideally, both the Regional Screening Model and the sub-regional models would be fully density-dependent models. Subsequent to completion of the PMP, advances in model codes have made the use of a density-dependent code more feasible as part of the Regional Screening Model development effort. There is concern, however, that the size of the model might limit the feasibility of the fully density-dependent approach due to the constraints listed above, especially model run times. In order to balance the needs of the project with the current technical capabilities of software and hardware, the model development team recommended the development of a bench-scale model to evaluate various model codes and approaches in order to aid the model code selection task.

The primary objectives of the bench-scale modeling effort are:

- Provide an improved estimate of model run times for 36-year simulations
- Provide a preliminary understanding of model development issues relating to resolution requirements, boundary types, and starting conditions
- Uncover model limitations and short comings

An appropriate code for the Regional Screening Model is to be selected on the basis of bench testing of various model codes at a sub-regional or county-wide scale. Although the proposed domain size is still considerably smaller than the anticipated regional model domain, it does provide a firm basis for the extrapolation of model performance to the larger domain. Bench testing of several model codes will provide a solid basis to make an informed decision on model code selection. This course of action will provide the following benefits:

- Aid in determining what class of model (constant density standard flow and transport, uncoupled density-dependent flow and transport, fully density-dependent flow and transport) is required to address CERP ASR issues
- Provide comparison performance metrics for various bench marked codes including relative accuracy, and model stability and run-times
- Aid in the evaluation of hardware needs & pre/post processing requirements

It was envisioned that the benchmark modeling effort would develop several identical (constant density standard flow and transport, uncoupled density-dependent flow and transport, fully density-dependent flow and transport) models covering a much smaller model region than projected for the Regional Screening Model. It was anticipated that a 40 mile X 40 mile area would provide a model domain of sufficient size and complexity to provide a valid test of each proposed model code and allow extrapolation of results to larger regional scales. The scale and design would be similar in size to Palm Beach County, Florida, where many ASR wells are proposed for installation. As part of the ASR Pilot Project Design Report (PPDR), a numerical model of the Palm Beach County area was available. In order to maximize the use of previously developed model tools as suggested by the Interagency Modeling Center (IMC), the USACE provided the Palm Beach County model as the "base" MODFLOW/MT3D model. Using the base model as a guide, four similar "box models" were prepared using four different model codes/approaches. The model was provided "as is" and was not optimized for any particular application.

The four codes were selected in a collaborative fashion among members of the modeling sub-team of the PDT. With the exception of the MODFLOW SWI package, the sub-team members had significant experience with the rest of the models selected. In addition, each of the codes selected was paired with a well-known pre/post-processor software package that simplified the model development process. Lastly, budget considerations limited the task scope to no more than four model codes. If time and budget had allowed, several other established codes would also have been considered, including FEFLOW and SUTRA, for example. The four model codes utilized for the bench-scale study are:

- MODFLOW and MT3DMS using equivalent freshwater heads to represent saltwater boundaries (e.g., constant density flow and transport model)
- SWI (Sea-Water Intrusion) Package for MODFLOW (density dependent vertically integrated flow with interface tracking)
- SEAWAT (fully coupled or uncoupled density-dependent flow and transport)
- WASH123 (fully coupled or uncoupled density-dependent flow and transport)

MODFLOW is a computer program that numerically solves the three-dimensional groundwater flow equation for a porous medium using a finite-difference method (McDonald and Harbaugh, 1988). MT3DMS is a computer program for modeling multi-species solute transport in three-dimensional ground-water systems using multiple solution techniques, including the finite-difference method, the method of characteristics (MOC), and the total-variation-diminishing (TVD) method (Zheng and Wang, 1999). MODFLOW is considered to be the most widely used program for constant-density groundwater flow problems. Key factors in MODFLOW's popularity in the modeling community are its thorough documentation, modular structure, which makes it easy to modify and enhance, and the public availability of the software and source code.

The Sea Water Intrusion (SWI) package is intended for the modeling of regional seawater intrusion with MODFLOW2000 (Bakker and Schaars, 2002). The SWI package utilizes

the Dupuit approximation that neglects vertical resistance to flow in the vertical direction. The vertical pressure distribution is hydrostatic in each aquifer. The advantage of using the Dupuit approximation is it allows multiple aquifer systems with one layer of cells. The vertical pressure distribution is hydrostatic in each aquifer, but this does not mean that there is no vertical flow; the vertical component of flow is computed from the three-dimensional continuity of flow. Variable-density flow may be simulated, through Darcy's Law, as stratified flow or as continuously varying density flow. The basic principle behind the formulation is to solve, during each time step, for the freshwater-head by considering continuity of flow in the entire aquifer, and to solve for the elevations of the interfaces by considering continuity of flow below each surface. Is should also be noted that the effects of dispersion and diffusion are not taken into account. Inversion, saltier (heavier) water above fresher (lighter) water, is also not allowed.

The SEAWAT program (Guo and Langevin, 2002) is a combination of MODFLOW and MT3DMS (Zheng and Wang, 1999) designed to simulate three-dimensional, variable-density, groundwater flow and solute-transport. The program was developed by modifying MODLOW subroutines to solve a variable-density form of the groundwater flow equation and by combining MODFLOW and MT3DMS into a single program. SEAWAT reads and write standard MODFLOW and MT3DMS input and output files, allowing most of the existing pre- and post-processors to facilitate application of the program to a wide range of practical problems. One advantage of SEAWAT is that because it uses MT3DMS to represent solute-transport, the program contains several diverse methods (Eulerian, Langrangian, or mixed) for solving the transport equation including the MOC, an explicit third order total-variation-diminishing (TVD) scheme, and a standard finite-difference method with central-in-space or upstream weighting.

WASH123D (Yeh et al. 1998) is a finite element numerical model designed to simulate variably saturated, variable-density water flow and reactive chemical and sediment transport in watershed systems. It is capable of conceptualizing a watershed system as a combination of 1D river/stream, 2D overland, and 3D subsurface sub-domains. A modified Richards' equation is used to solve for 3D flow when density effect is taken into account. The equation is solved with the Galerkin finite element method. The groundwater flow portion of the code utilizes an adaptation of the FEMWATER code (Lin et al. 1997). WASH123D uses the Lagrangian-Eulerian (LE) method to solve the transport equations. Particle tracking is used in the Lagrangian step to handle the advection term. Other terms (such as sources, sinks, diffusion, and dispersion) are calculated in the Eulerian step, where element matrices are assembled into a global matrix, and matrix solvers are used to solve for the spatial concentration distribution at the end of each time step. A predictor-corrector numerical technique, combined with an adaptive explicit-implicit numerical scheme, is employed to compute reactive transport efficiently and robustly. The use of this methodology allows the numerical stability of WASH123D not to be restricted by the Mesh Courant number. In addition, the Mesh Peclet number is restricted only by computational accuracy, not numerical stability. More detailed discussion on various types of numerical dispersion and how the LE method deals with these types of numerical dispersion are discussed in the referenced papers.

As described previously, each model would include a model boundary consisting of a 40-mile by 40-mile square box. Each model would contain 7 to 20 vertical layers representing the Surficial Aquifer System (SAS), Hawthorn Group confining unit, and the FAS. The four models each adopted the same hydrogeologic conceptual model, utilizing the same aquifers and confining units. Also, all of the model layers were assigned with identical hydraulic parameters (e.g., hydraulic conductivity and storage coefficient) in order to eliminate differences in these properties due to contouring algorithm chosen for each model. The exact number of layers was initially intended to be consistent for the different codes, however, model stability and accuracy requirements required refinement in some cases. Each box model would have identical boundary conditions, starting conditions (head and TDS concentration), influent TDS concentrations (150 mg/l), and aquifer/confining unit parameters. In addition, a common convergence criteria was agreed upon for both flow and transport portions of the models. Five separate cases were developed by the PDT to evaluate relevant ASR modeling issues including mixing, hydrodynamic dispersion, density stratification, upconing, and changes in salinity distribution as a result of ASR injection and/or recovery. The five cases are summarized in Table 2. Additional specific information summarizing each case is available following the table.

Table 2. Bench-scale case summary.

Case Number	**Purpose and basic setup**
IA	One ASR well recharge and recovery 5 MGD from FAS storage zone with TDS of 4,000 mg/l. Minimal upconing or leakage from below. No dispersivity assigned.
IB	One ASR well recharge and recovery 5 MGD from FAS storage zone with TDS of seawater (35,000 mg/l). Minimal upconing or leakage from below. No dispersivity assigned.
IC	One ASR well recharge and recovery 5 MGD from FAS storage zone with TDS of 4,000 mg/l. Major upconing or leakage from below encouraged through confining layer vertical conductivity assignment. No dispersivity assigned.
ID	One ASR well recharge and recovery 5 MGD from FAS storage zone with TDS of 4,000 mg/l. Minimal upconing or leakage from below. Dispersivity assigned with value of 25 feet.
IIA	One ASR well recovering for 5 years continuous to evaluate movement of salt-water interface from coast.

Case IA: Transient Model Simulation - One ASR well injecting 5 MGD into FAS in center of box for 30 days, followed by 305 day storage period, followed by 30 days of recovery at 5 MGD. The starting TDS of the FAS storage zone was assigned to be 4,000 mg/l, the TDS of the Middle FAS Confining Unit will be 35,000 mg/l, and the Middle FAS flow zone was assigned 35,000 mg/l. The Middle FAS Confining Unit was assigned a vertical conductivity of 0.001 feet per day to ensure minimal leakage between aquifer units. The Surficial Aquifer System (SAS) was assigned a constant head of 20 feet. The Hawthorn Group Clay (Intermediate Confining Unit) was assigned a vertical conductivity of 0.001 feet per day to ensure minimal leakage between the SAS and the Upper FAS. Prior to simulation start up, the model was run with the regional gradient to steady state conditions. The regional gradient was assigned from west to east at 0.0001 and is considered representative of the Upper FAS. The steady state gradient of 0.0001 was used to assign the starting heads of the Upper FAS for the one year simulation. The dispersivity tensor was assigned a value of zero in order to evaluate the degree of numerical dispersion produced from each code.
The purpose of Case 1A was to evaluate model code ability to simulate aquifer pressure changes, salinity changes due to conservative mixing, salinity changes due to hydrodynamic dispersion, and relative degree of numerical dispersion introduced. Since there was no known ASR case studies that have evaluated this issue, the comparison of numerical dispersion was relative in nature and assumed that the TVD solution was the most accurate as determined from previous publications. The flows between layers and to and from boundaries were also of interest. Landscape Figure 1 below (at the end of the report after the report appendices) depicts the assigned model parameters in detail for both the MODFLOW based models as well as the WASH123 model.

Case IB: Transient Model Simulation - One ASR well injecting 5 MGD into FAS in center of box for 30 days, followed by 305 day storage period, followed by 30 days of recovery at 5 MGD. The starting TDS of the FAS storage zone was assigned to be 35,000 mg/l, the TDS of the Middle FAS Confining Unit will be 35,000 mg/l, and the Middle FAS flow zone was assigned 35,000 mg/l. The Middle FAS Confining Unit was assigned a vertical conductivity of 0.001 feet per day to ensure minimal leakage between aquifer units. The Surficial Aquifer System (SAS) was assigned a constant head of 20 feet. The Hawthorn Group Clay (Intermediate Confining Unit) was assigned a vertical conductivity of 0.001 feet per day to ensure minimal leakage between the SAS and the Upper FAS. Prior to simulation start up, the model was run with the regional gradient to steady state conditions. The regional gradient was assigned from west to east at 0.0001 and is considered representative of the Upper FAS. The steady state gradient of 0.0001 was used to assign the starting heads of the Upper FAS for the one year simulation. The dispersivity tensor was assigned a value of zero in order to evaluate the degree of numerical dispersion produced from each code.

The purpose of Case 1B was to evaluate model code ability to simulate aquifer pressure changes, salinity changes due to conservative mixing, salinity changes due to hydrodynamic dispersion, and degree of buoyancy stratification that occurs during the storage period. The flows between layers and to and from boundaries were also of

interest. Landscape Figure 2 below depicts the assigned model parameters in detail for both the MODFLOW based models as well as the WASH123 model.

Case IC: Transient Model Simulation – One ASR well injecting 5 MGD into FAS in center of box for 30 days, followed by 305 day storage period, followed by 30 days of recovery at 5 MGD. The starting TDS of the FAS storage zone was assigned to be 4,000 mg/l, the TDS of the Middle FAS Confining Unit will be 35,000 mg/l, and the Middle FAS flow zone was assigned 35,000 mg/l. The Middle FAS Confining Unit was assigned a vertical conductivity of 1 feet per day to ensure leakage between the aquifer units. The Surficial Aquifer System (SAS) was assigned a constant head of 20 feet. The Hawthorn Group Clay (Intermediate Confining Unit) was assigned a vertical conductivity of 0.001 feet per day to ensure minimal leakage between the SAS and the Upper FAS. Prior to simulation start up, the model was run with the regional gradient to steady state conditions. The regional gradient was assigned from west to east at 0.0001 and is considered representative of the Upper FAS. The steady state gradient of 0.0001 was used to assign the starting heads of the Upper FAS for the one year simulation. The dispersivity tensor was assigned a value of zero in order to evaluate the degree of numerical dispersion produced from each code.

The purpose of Case 1C was to evaluate model code ability to simulate aquifer pressure changes, salinity changes due to conservative mixing, salinity changes due to hydrodynamic dispersion, and degree of density-driven upconing. The flows between layers and to and from boundaries were also of interest. Landscape Figure 3 below depicts the assigned model parameters in detail for both the MODFLOW based models as well as the WASH123 model.

Case ID: Transient Model Simulation - One ASR well injecting 5 MGD into FAS in center of box for 30 days, followed by 305 day storage period, followed by 30 days of recovery at 5 MGD. The starting TDS of the FAS storage zone was assigned to be 4,000 mg/l, the TDS of the Middle FAS Confining Unit will be 35,000 mg/l, and the Middle FAS flow zone was assigned 35,000 mg/l. The Middle FAS Confining Unit was assigned a vertical conductivity of 0.001 feet per day to ensure minimal leakage between aquifer units. The Surficial Aquifer System (SAS) was assigned a constant head of 20 feet. The Hawthorn Group Clay (Intermediate Confining Unit) was assigned a vertical conductivity of 0.001 feet per day to ensure minimal leakage between the SAS and the Upper FAS. Prior to simulation start up, the model was run with the regional gradient to steady state conditions. The regional gradient was assigned from west to east at 0.0001 and is considered representative of the Upper FAS. The steady state gradient of 0.0001 was used to assign the starting heads of the Upper FAS for the one year simulation. The dispersivity tensor was assigned a value of 25 feet in order to evaluate the model run times using a realistic amount of hydrodynamic dispersion.

The purpose of Case 1D was to evaluate model code ability to simulate aquifer pressure changes, salinity changes due to conservative mixing, salinity changes due to hydrodynamic dispersion, and degree of hydrodynamic dispersion introduced. The flows between layers and to and from boundaries were also of interest. Landscape Figure 4

below depicts the assigned model parameters in detail for both the MODFLOW based models as well as the WASH123 model.

Case IIA: Transient Model Simulation – Transient Model Simulation - One ASR well withdrawing 5 MGD from the Upper FAS in center of box for five years. The starting TDS of the FAS storage zone was assigned to be 4,000 mg/l, the TDS of the Middle FAS Confining Unit will be 35,000 mg/l, and the Middle FAS flow zone was assigned 35,000 mg/l. All units at the eastern boundary of the model were assigned a starting head of zero. The starting concentration of TDS in all model layers was based upon an approximation of the Ghyben-Herzberg relationship to define the 35,000 mg/l isochlor. The Middle FAS Confining Unit was assigned a vertical conductivity of 0.001 feet per day to ensure minimal leakage between aquifer units. The Surficial Aquifer System (SAS) was assigned a constant head of 20 feet. The Hawthorn Group Clay (Intermediate Confining Unit) was assigned a vertical conductivity of 0.001 feet per day to ensure minimal leakage between the SAS and the Upper FAS.

The purpose of Case IIA was to evaluate model code ability to simulate pumping induced regional changes in the three-dimensional salinity distribution.

Groundwater Model Testing and Comparison Protocols

Groundwater model testing has been the subject of multiple past studies and papers. Testing of groundwater simulation codes may take several forms including:

- Benchmarking against known analytical solutions
- Intra-code comparisons using different code functions and same stresses to emulate the same system response
- Inter-code comparisons simulating same stresses and systems
- Comparisons with field or laboratory data

One thing sorely lacking amongst the published literature is an approved or recommended protocol to perform the various comparisons. One such study was prepared by van der Heijde and Danzer (1997) for the United States EPA. This paper proposes a systematic evaluation and testing methodology or protocol that could be applicable to the bench-scale modeling effort. Although the bench-scale modeling effort was designed to test and compare model codes, it was not meant to be a full-scale code-testing and evaluation protocol; therefore, some of the evaluations recommended by van der Heijde and Danzer were not completed. Van der Heijde and Danzer recommend including an evaluation of code functionality and performance. Code functionality is defined as the set of functions and features which the code offers the user in terms of model framework geometry, simulated processes, boundary conditions, and analytical and operational capacities (van der Heijde and Danzer, page 2). Performance evaluations are aimed at determining the characteristics of the model code in terms of:

- Computational accuracy
- Reliability (convergence and stability of solution algorithms)

- Sensitivity for grid orientation, grid resolution, or time discretization
- Efficiency of coded algorithms (code execution time and memory/storage requirements)
- Resources required for model setup and analysis

First, all of the codes were evaluated for their overall functionality to address specific ASR issues discussed above. The overall code functionality was addressed based upon existing information available for each code, PDT experience, and published papers or case studies. Each issue requires a basic set of model development and analysis functions. These various functions are outlined in Table 3 along with qualitative scoring of each model code.

In reviewing Table 3, all codes could provide some of the functionality required to evaluate all relevant ASR issues to be studied. SEAWAT and WASH123 provide the highest overall functionality for the questions to be answered with the model. Table 4 provides a list of other general functions that are required of each model along with a qualitative score for each. In general all of the codes can provide much of the basic functionality required for the ASR Regional Study, however, SEAWAT and WASH123 provide the best overall functionality desired for the study.

Table 3. Required model functionality

Specific ASR Project Issue	**Desired Functionality**	**Modflow/MT3D**	**SEAWAT**	**WASH123**	**SWI**
Regional changes in aquifer heads and flows	1. Simulate head changes in region around proposed ASR well clusters	X	X	X	X
	2. Simulate flows from ASR wells, existing FAS user wells, boundaries, and between aquifers	X	X	X	X
Regional changes in aquifer water quality	1. Simulate water quality changes in region around proposed ASR wells, existing FAS user wells, boundaries, and between aquifers	X	X	X	
	2. Simulate density changes as a result		X	X	X
Increased potential for salt-water intrusion caused by ASR pumping	1. Simulate potential movement of salt-water wedge due to ASR recovery activities		X	X	X
	2. Simulate potential movement of salt-water wedge due to ASR recharge activities		X	X	X
Regional impacts to	1. Evaluate increases or decreases in head or water quality at existing well users	X	X	X	X

existing well users of the FAS	caused by ASR activity				
ASR well cluster site selection	1. Simulate superposition effects caused by multiple ASR wells recharging or recovering. Site ASR well clusters in order to minimize superposition effects and potential impacts on users. 2. Site selection is heavily influenced by all proposed well fields operating at same time (e.g., boundary effects are important in this instance).	X X	X X	X X	X X
ASR well cluster design and layout	1. Evaluate design and layout issues at one ASR cluster. 2. Varying horizontal resolution probably required.	X X	X X	X X	X X
ASR well cluster performance including estimating recovery efficiency	1. Evaluate ASR well cluster recovery efficiency and performance. 2. Evaluate upconing potential at each cluster site. 3. Evaluate density stratification at each cluster site.	X	X X X	X X X	 X
ASR well site evaluation of pressure induced changes	1. Evaluate aquifer pressure at each proposed ASR well, 1 mile distant from ASR well cluster, and at other FAS user wells. 2. Evaluate pressure changes within the Hawthorn Group at ASR well cluster.	X X	X X	X X	X
Localized transport of contaminants including heavy metals or pathogens	1. Evaluate transport of potential “bad actors” including heavy metals such as arsenic, nickel, and fluoride. 2. Evaluate conservative transport and reactive transport of pathogens.	X X	X X	X X	
Localized ASR well pump design	1. Evaluate aquifer pressure at each well and in entire well cluster.	X	X	X	X

Table 4. Additional model functionalities required.

Desired Functionality	Modflow/MT3D	SEAWAT	WASH123	SWI
Incorporate irregular geometry	X	X	X	X
Incorporate varying vertical model resolution and multiple layers	X	X	X	
Incorporate varying aquifer properties	X	X	X	X
Incorporate rainfall and recharge	X	X	X	X
Incorporate leakage between layers	X	X	X	X
Incorporate Dirichlet and Cauchy boundary types	X	X	X	X**
Incorporate constant and transient boundary conditions	X	X	X	X
Incorporate injection and recovery wells	X	X	X	X
Simulate advection, dispersion, and mixing	X	X	X	
Simulate contaminant decay or natural attenuation	X	X	X	
Simulate density-dependent flow		X	X	X

** - is capable for flow but not transport

An important consideration in any of model code is its overall credibility and suitability (van der Heijde and Kanzer, 1997). Therefore, the level at which the code has been tested is an important component in the decision-making process. Given the issues to be addressed with the ASR regional model, it is clear that groundwater hydraulics, conventional contaminant transport, and density-dependent flow concerns will all require critical contemplation. To aid in this determination, the PDT reviewed existing publications and past benchmarking cases in order to compile a list of tested problems. In addition, the PDT performed additional benchmarking against published analytical solutions. The PDT prepared several simple benchmarking tests to evaluate groundwater hydraulics and conventional contaminant transport. Both the finite-difference (MODFLOW/MT3DMS) and finite-element models (WASH123) were first tested using a series of groundwater hydraulics cases including pumping from a confined aquifer (Theis, 1935) and pumping from a leaky-confined aquifer (Hantush and Jacob, 1953). Since the ASR regional model will be simulating changes in head and flow caused by well pumping, the PDT felt this was a valuable test to evaluate. Then both predominant model types were tested using a conventional contaminant transport case (Ogata, 1970). The results of the Theis and Ogata benchmarking tests are available in figures 1 and 2. Each figure compares the numerical model results versus exact analytical solutions. Both the MODFLOW/MT3DMS and WASH123 numerical model results compare very favorably to the analytical solutions. The WASH123 code was further tested against both the “Elder problem” and the “Henry problem” with results available in Appendix A. All of these tests indicate that all of the codes tested appear to solve the governing equations accurately.

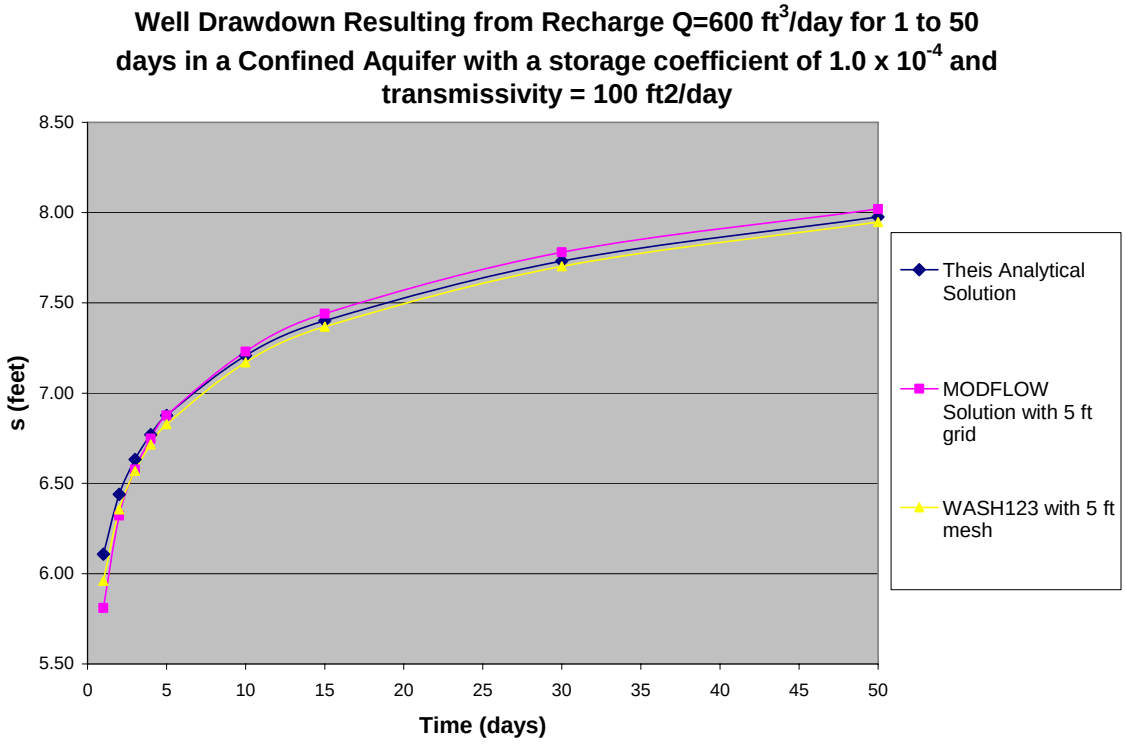

Figure 1. Theis confined aquifer benchmarking case comparing numerical model results to exact solution.

For variable-density groundwater flow, there are a suite of benchmark problems that have been designed to test the ability of a numerical code to accurately simulate the complex flow and transport dynamics associated with density dependent flow. Table 5 lists these commonly used benchmark problems and shows which codes have been tested to date. It should be noted that neither the SWI or the WASH123 codes have been tested as thoroughly as the SEAWAT code mainly due to their relatively young age. It is anticipated that both SWI and WASH123 will be tested against many of the remaining variable-density benchmark problems in the future as the codes become utilized by more users. Appendix A provides additional information on the variable-density test cases completed using WASH123.

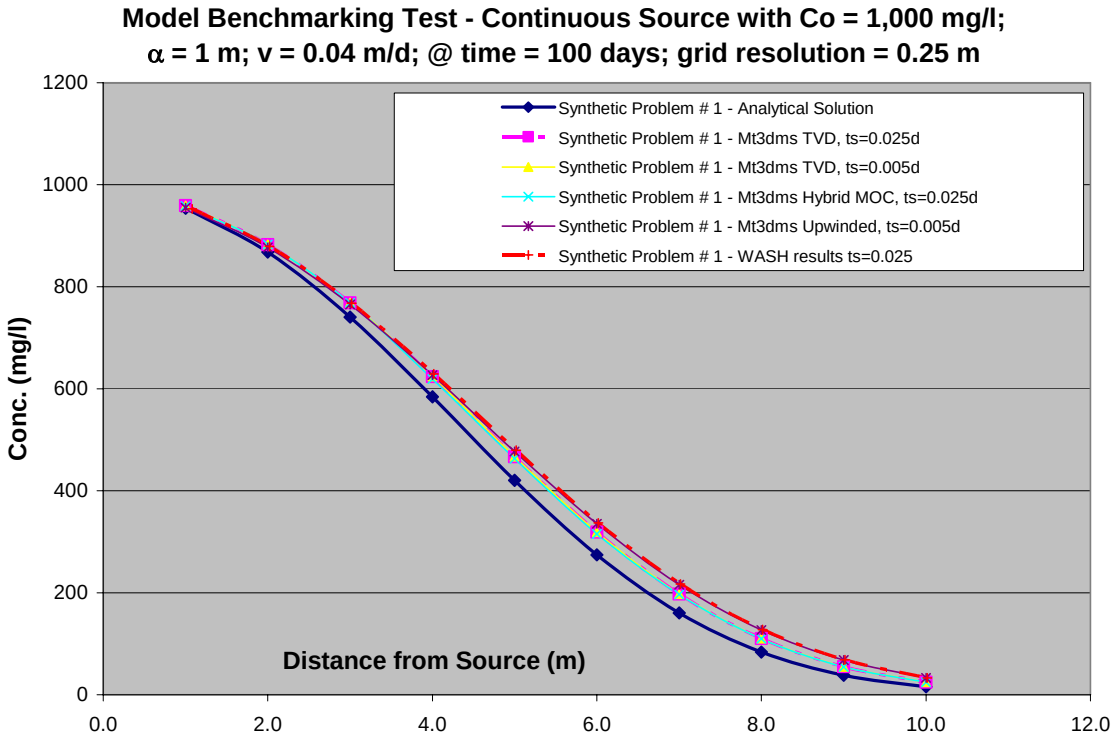

Figure 2. Ogata continuous source benchmarking case comparing numerical model results to exact solution.

Table 5. Variable-density benchmark problems.

Benchmark Problem	**SWI**	**SEAWAT**	**WASH123**
Box Problems		X	
Henry Case 1	NA	X	X
Henry Case 2	NA	X	X
Elder	NA	X	X
HYDROCOIN	NA	X	
Immiscible Fluid Rotation	X	X	
Rotating Interface	X		
Rotating Brackish Zone		X	
Upconing Beneath a Pumping Well	X		
Salt Pool 1	NA	X	
Salt Pool 10	NA	X	

NA – not applicable since SWI cannot simulate hydrodynamic dispersion

The overall performance assessment was measured through application of the various bench-scale cases completed as well as previous benchmarking work completed in support of each code. The performance assessment was measured against metrics listed previously including:

- Computational accuracy
- Reliability (convergence and stability of solution algorithms)
- Sensitivity for grid orientation, grid resolution, or time discretization
- Efficiency of coded algorithms (code execution time and memory/storage requirements)
  - Model run times were computed for all 5 ASR cases
  - Storage requirements were evaluated for all 5 ASR cases
- Resources required for model setup and analysis including
  - Pre and post processing effort
  - Computer type or hardware required
  - General ease of use for new modelers

Model Code Bench-scale Testing Results:

The four model codes were tested extensively using the five case studies outlined previously in this memorandum. Multiple contaminant transport algorithms were tested using both the existing MODFLOW/MT3DMS model and the SEAWAT model (e.g., central-difference solution and the TVD solution). WASH123 and SWI only provide one contaminant transport algorithm. Each of the codes revealed significant advantages and disadvantages. A comparison of performance metrics for each code is provided in the following sections of this memorandum. Appendix A and B of this memorandum contains additional information concerning the WASH123 results and the SEAWAT/SWI results.

Resources Required for Model Setup and Analysis

General Ease of Use

All of the model codes evaluated required significant user knowledge and experience in order to successfully utilize the model. The MODFLOW/MT3DMS, SEAWAT, and WASH123 models are all somewhat difficult to master but all three can link with readily available pre and post processors. The exception to this is the SWI code. The SWI model can be run independently but the results must be imported into a post-processor. The importation of the data requires some re-working of output files and required companion files. In general, table 6 lists the qualitative "ease of use" for each code along with pre/post processor tools utilized. In general, all of the codes rank similarly for this category.

Table 6. Model Code Ease of use.

Model Code	**Ease of Use (Easy, Moderate, or Difficult)**	**Compatible Pre and Post Processor**
MODFLOW/MT3DMS	Moderate	Groundwater Modeling System (GMS) ® Groundwater Vistas Argus Visual MODFLOW PMWIN, Modelviewer
SEAWAT	Moderate	Groundwater Vistas Argus Visual MODFLOW PMWIN, Modelviewer
WASH123	Moderate	GMS
SWI	Moderate	Argus, MATLAB

Required Time for Pre and Post Processing

All of the model codes required time for both pre and post processing of simulation results. The MODFLOW/MT3DMS, SEAWAT, and WASH123 models all link directly to relevant pre and post processing software packages. As discussed previously, the GMS and Groundwater Vistas software packages were utilized. Each software package provides an intuitive graphical user interface (GUI) that allows rapid data manipulation, formatting, and output preparation. Both software packages are widely used in the groundwater modeling community of practice. One advantage of the GMS is that it is freely available to the Corps of Engineers, its partners and its sponsors. Although the overall expense may be minor, the Groundwater Vistas, Argus, and Visual Modflow software must be purchased separately for team members to utilize effectively.

The required time for pre and post processing is probably least for the MODFLOW/MT3DMS code and greatest for the SWI code due to reformatting issues already discussed. Table 7 lists a qualitative assessment of the pre and post processing time for each code considered.

Table 7. Time for pre and post processing.

Model Code	**Pre and Post Processing Time (Low is less than 4 hours, Moderate is 4 to 8 hours, High is greater than 8 hours)**	**Pre and Post Processing Software Used**
MODFLOW/MT3DMS	Low	Groundwater Modeling System (GMS) ® Groundwater Vistas

		Argus Visual MODFLOW PMWIN
SEAWAT	Low	Groundwater Vistas Argus Visual MODFLOW PMWIN
WASH123	Moderate	GMS
SWI	Moderate	None can be used directly

Computer Type or Hardware Required

All of the model codes considered could be run on personal computer, however, when consideration is given to the proposed application (e.g., a large regional scale model), all of the models would likely require workstations to ensure computational efficiency. Since SWI does not calculate contaminant transport equations, it probably requires the least hardware demands. Obviously, for coarse resolution models, a regional model may be able to be run on a newer personal computer (2 years old or less with 2.6 GHz or faster processor and at least 1 GB of resident memory) also. Table 8 provides a comparison of required hardware.

Table 8. Computer Type/Hardware Requirements.

Model Code	**Hardware Required for small model**	**Hardware Required for regional model**
MODFLOW/MT3DMS	Personal computer	Workstation
SEAWAT	Personal computer	Workstation
WASH123	Personal computer	Workstation
SWI	Personal computer	Personal computer

Efficiency of coded algorithms (code execution time and memory/storage requirements)

Model Run Times and Storage Requirements

As part of the performance assessment of the model codes, model simulation times were measured for the various case studies. Since the models were run on different workstations with divergent processing architecture, an effort was undertaken to "normalize" the simulation times through standardized computer industry comparisons. Several independent information technology forums provide processor performance comparisons for different software applications. One of these provides the information for free at the internet site www.spec.org. Information provided at the site includes both base and peak processor speeds for different tasks. Table 9 provides a comparison of both metrics for the computer workstations utilized for the study. The exact workstation

utilized to run the SEAWAT and SWI simulations was not listed at spec.org site so an average of three similar computers was selected to be representative. Then the base processor speeds were normalized against 1,000 to provide simulation run time "factors" to be applied to the actual raw simulation times for each case.

Table 9. Workstation performance metrics from www.spec.org.

Computer	Base Floating Point Speed	Peak Floating Point Speed
Optiplex Computer, 2.66 GHz, 1GB Ram	919	927
Dell GX280 Computer, 3.60 GHz P4, 2GB Ram	1905	1916
Dell WS Computer, 3.06 GHz P4, 2GB Ram	1092	1103
Intel 3.46 GHz P4, 3GB Ram	1719	1724
AVG 3 Computers	1572	1581
XI Computer, AMD 148 Opteron Chip	1393	1490

The factors applied were 0.919 for the MODFLOW/MT3DMS models, 1.572 for the SEAWAT and SWI models, and 1.393 for the WASH123 models. In essence, the normalized run times would be reduced for the MODFLOW/MT3DMS models and increased for all of the other models. Based upon information contained on this site and an inventory of workstation hardware utilized for the ASR Benchmark study, a set of normalized simulation times were developed. Table 10 lists all of the normalized model run times for the study as well as the runtime per model calculation point. The fastest and slowest runtime per calculation point is highlighted in the table. The fastest times are highlighted in pink while the slowest times are shown in yellow. The normalized model run times were also formulated from model runs that had identical convergence criteria and similar time-step sizes. The time-step size required to ensure stability was code dependent but efforts were made to ensure the final time-step size was similar for all codes. Given the complexity of the models and domain size (County size), model run times were generally long.

Table 10. Normalized model simulation run times.

RUN 1A	Run Times (min)	Normalized Run Times	Normalized Run Time per Calculation Point
MODFLOW/MT3DMS - Upwind	217	199	1.3E-03
MODFLOW/MT3DMS - TVD	463	425	2.8E-03
SEAWAT - Upwind	55.84	88	5.8E-04
SEAWAT - TVD	3838.5	6034	4.0E-02
WASH123	330	460	4.1E-03
SWI	18.75	29	3.1E-04
RUN 1B	**Run Times (min)**	**Normalized Run Times**	**Normalized Run Time per Calculation Point**
MODFLOW/MT3DMS - Upwind	217	199	1.3E-03
MODFLOW/MT3DMS - TVD	466	428	2.8E-03
SEAWAT - Upwind	56.19	88	5.8E-04
SEAWAT - TVD	3864.95	6076	4.0E-02
WASH123	420	585	5.2E-03
SWI	15.27	24	2.5E-04
RUN 1C	**Run Times (min)**	**Normalized Run Times**	**Normalized Run Time per Calculation Point**
MODFLOW/MT3DMS - Upwind	217	199	1.3E-03
MODFLOW/MT3DMS - TVD	467	429	2.8E-03
SEAWAT - Upwind	57	90	5.9E-04
SEAWAT - TVD	3878.2	6097	4.0E-02
WASH123	330	460	4.1E-03
SWI	19.71	31	3.2E-04
RUN 1D	**Run Times (min)**	**Normalized Run Times**	**Normalized Run Time per Calculation Point**
MODFLOW/MT3DMS - Upwind	2157	1982	1.3E-02
MODFLOW/MT3DMS - TVD	4320	3970	2.6E-02
SEAWAT - Upwind	58.96	93	6.1E-04
SEAWAT - TVD	3929	6176	4.1E-02
WASH123	329	458	4.1E-03
RUN 2A	**Run Times (min)**	**Normalized Run Times**	**Normalized Run Time per Calculation Point**
SEAWAT - Upwind	767	1206	8.0E-03
SEAWAT - TVD	11171	17561	1.2E-01
WASH123	522	727	6.5E-03
SWI	11	15	1.6E-04

Generally, the SEAWAT TVD solution resulted in the longest normalized simulation times while the SWI resulted in the shortest. The TVD solution scheme in MT3D (and thus SEAWAT) required unreasonably short transport time step lengths for an accurate solution. Due to project time constraints, no attempt was made to resolve the issue, but it is possible that the issue could be fixed, in which case, the runtimes could reduced. Since both finite-difference models (MODFLOW/MT3DMS, SEAWAT, and SWI) and finite-element (WASH123) models were utilized in the study, further examination of the run time per calculation point is important. The WASH123 model had 112,716 calculation points versus 151,000 for the other models tested. A key difference to be noted is that the WASH123 model provided greater vertical resolution (30 layers) but varying horizontal resolution as compared to the other finite-difference models (16 vertical layers). When considering the horizontal resolution of the two model types, the WASH123 model resulted in fewer computational points than the comparable finite-difference model due to the flexible mesh design advantage that is inherent in finite-element formulations. This may be an important consideration in the design of the regional model. Figure 3 depicts the finite-difference model vertical resolution while Figure 4 depicts the comparable finite-element model vertical resolution.

Figure 3. Finite-difference model vertical resolution.

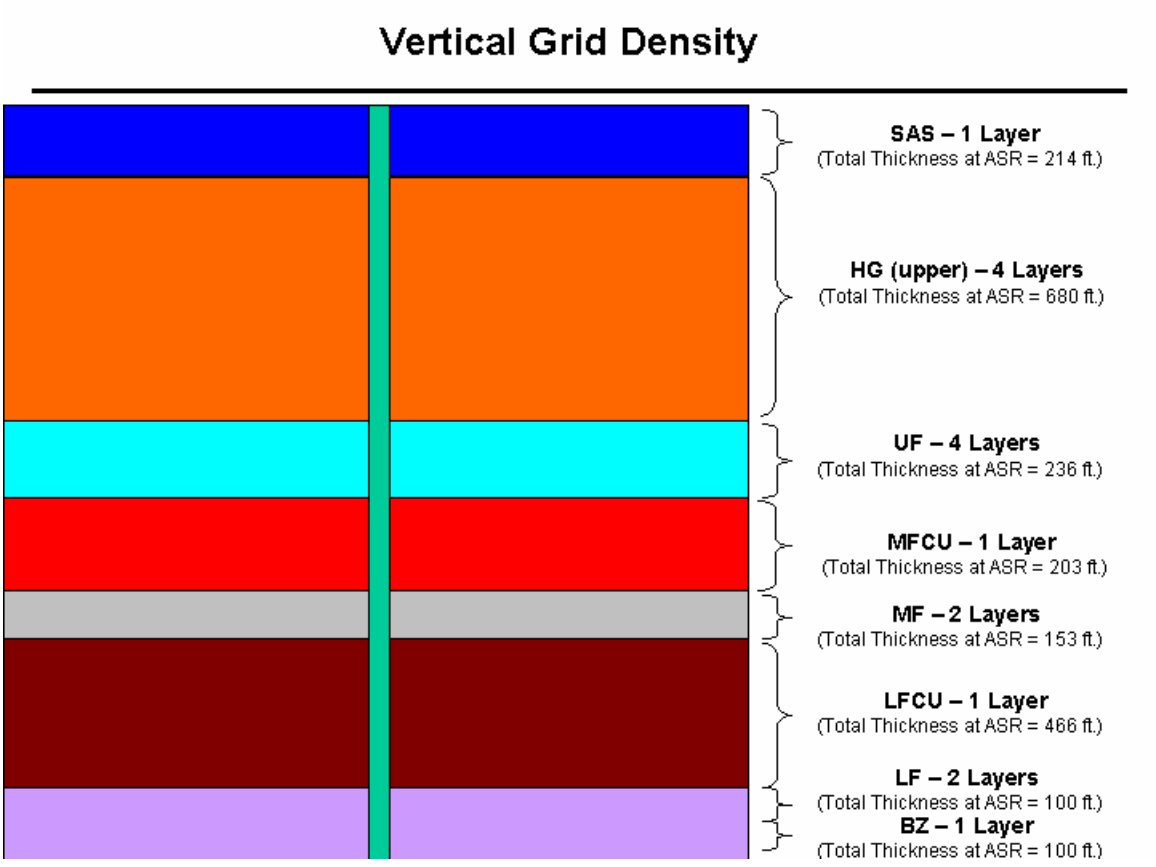

For all of the models, storage requirements were moderate and highly dependent upon model resolution, time-step size, and outputs designated. In general, large capacity hard

drives available on personal computers and work stations should be sufficient to handle requirements of the regional model development.

Figure 4. Finite-element model vertical resolution.

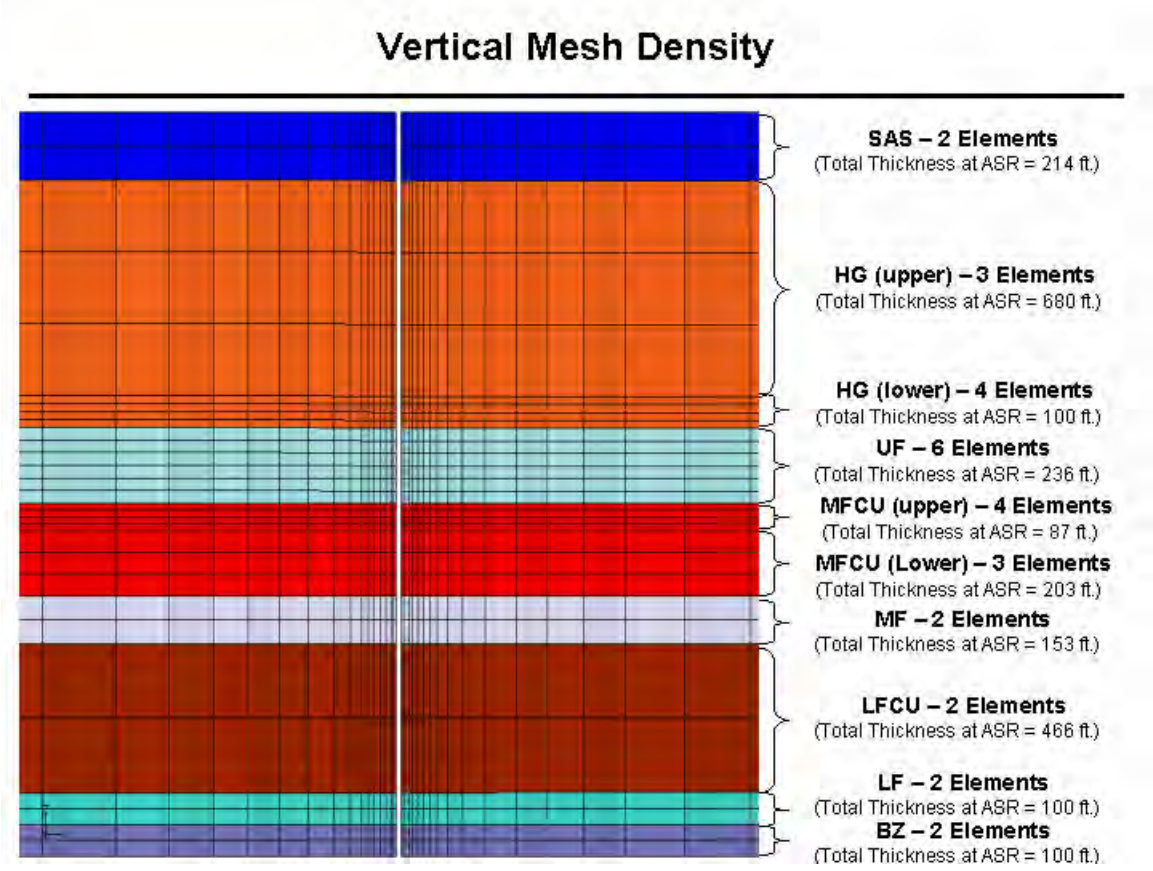

Time and resource constraints did not allow a systematic evaluation of each code's dependence upon grid resolution or time discretization to ensure accuracy. The time discretization was evaluated in a gross sense in order to minimize model run times, however, only minimal checks were completed to determine the effect on model accuracy. As the various case studies were completed, it was also determined that the vertical discretization of the model was very important for both the model stability and accuracy. This was especially true around the ASR wells where steep velocity gradients led to model oscillations and instability in some instances. Future ASR modeling efforts should carefully consider vertical discretization-related accuracy and stability issues.

Comparison of Simulation Results for Computational Accuracy and Reliability

Model simulation output from the four model codes was then compared to determine differences in numerical error, relative accuracy, stability, and flexibility. As the ASR cases were hypothetical, an examination of the actual accuracy of each model code was

not possible. However, an assumption was made that the SEAWAT TVD solution was the most accurate based upon past analysis and publications noted in the literature. Limited accuracy assessments as compared to known analytical solutions were also completed and discussed earlier in this report. Table 11 lists a qualitative assessment of the stability of each model code based upon all model results. None of the codes experienced major convergence problems but three of the model codes did experience some minor oscillations. It should be noted that the oscillations were most likely attributed to insufficient horizontal and vertical model resolution. Therefore, it is expected that the oscillations could be minimized or eliminated through more judicious model design.

Table 11. Stability Assessment.

Model Code	**Stability Assessment** Score A – No stability issues Score B – Minor Oscillations Score C – Did not converge
MODFLOW/MT3DMS – Upwinded	A
MODFLOW/TM3DMS – TVD	B
SEAWAT – Upwinded	A
SEAWAT – TVD	B
WASH123	A
SWI	B

The overall relative accuracy assessment is presented for each case and discussed in turn.

For Case 1A, comparisons were made at the ASR well and at different radii from the ASR well. Figure 5 depicts results from the different codes for concentrations versus time estimates during the 30-day ASR recovery period. It should be noted that the recovery curves represent average concentrations at the ASR well location.

For all of the ensuing figures, a naming convention is employed for each of the various model runs, model codes, and contaminant transport solution algorithms. The primary names are listed as follows:

- CenDiff-FW is a MODFLOW/MT3DMS simulation using the Central difference weighting algorithm
- TVD is a MODFLOW/MT3DMS simulation using the total variation diminishing scheme
- EQFW or FW are simulations using “equivalent freshwater heads” on the model boundaries rather than simulating true density-dependent flow
- SEAWAT-TVD are simulations using SEAWAT with the TVD scheme
- SEAWAT-Upwind are simulations using SEAWAT with the upwinded backward difference weighting algorithm
- WASH-Aq Node Ave are simulations using WASH123 and averaging the concentrations of the model aquifer nodes

- WASH-deep4000 are simulations using WASH123 and modifying the confining unit initial condition concentrations to mimic calculations performed by MT3DMS

Figure 5. Model simulation results for Case 1A at the ASR well.

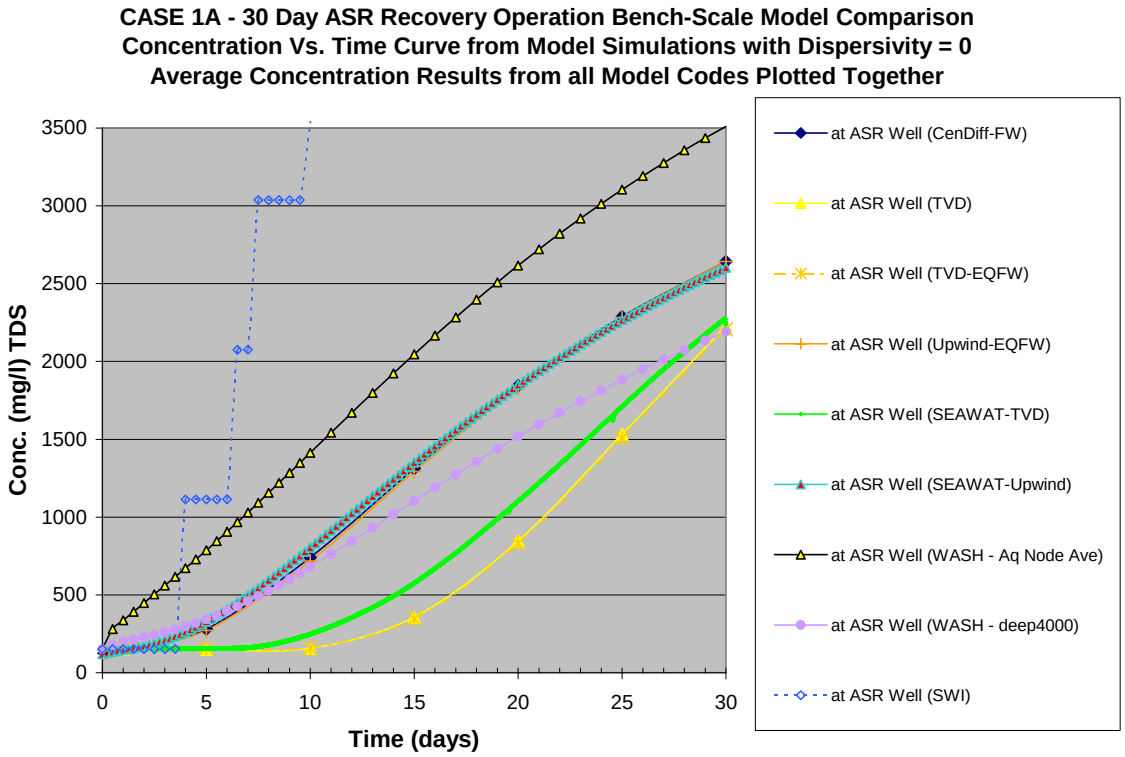

In examining the simulation results at the ASR well, it is apparent that the model codes, along with the various contaminant transport algorithms, result in a wide variation of concentration versus time predictions. During a real ASR recovery event, the recovery would be ceased once the TDS concentration exceeded a threshold value of 500 mg/l. In reviewing the simulation results, the number of days of recovery before exceeding 500 mg/l can be readily observed.

For the MODFLOW/MT3DMS solutions, two general results are observed. First, solutions using the TVD algorithm (using either uncorrected heads or density corrected/EQFW heads) predict that 500 mg/l level would be exceeded after 17 days. Using the central-difference or upwinding algorithms result in exceedance after 7 days. Since a dispersivity value of zero was utilized for Case 1A, the main difference between the TVD solution and the other finite-difference solutions is suspected to result from truncation error or so-called “numerical dispersion”. This finding is consistent with previous work completed by Merritt (1986; 1993). Merritt found that the predicted amount of freshwater recovered from an ASR well is sensitive to the contaminant transport solution selected for the simulation. In addition, Merrit (1993) noted that the

estimate of freshwater recovered is somewhat sensitive to vertical model resolution and the algorithm utilized to simulate vertical flow and dispersion. For ASR simulations involving large concentrated injection and recovery rates, the apparent degree of dispersion would also be greatly dependent upon local flow velocities.

For the two SEAWAT solutions, a similar pattern emerged. The TVD solution predicted that the 500 mg/l water quality threshold would be exceeded after approximately 14 days, whereas the upwinded solution predicted exceedance after 7 days. Since SEAWAT is a finite-difference model with the same geometry as the MODFLOW/MT3DMS model, the differences between the two solutions are also caused by numerical error. Another interesting finding is that the comparable upwinded solutions between non-density model and the density-dependent SEAWAT model are almost identical, suggesting that the numerical dispersion issues mask the density related differences. When a similar comparison is completed for the constant-density TVD solution versus the density-dependent SEAWAT TVD solution, there is a notable difference of 3 less days of ASR recovery for the SEAWAT TVD solution probably due to buoyancy stratification effects. This finding reveals that density stratification during the 305 day ASR storage period does marginally affect the predicted results. It would be expected that longer storage periods would result in additional stratification effects that would further reduce the amount of freshwater that would be recovered.

The WASH123 results also show variation between two different model simulations. The first simulation (WASH – Aq node avg) predicts that the water quality threshold of 500 mg/l would be exceeded after 2.5 days. The second simulation (WASH- deep4000) predicts an exceedance of the threshold after approximately 8 days. The only difference between these solutions is the assignment of the starting concentrations within the Middle Floridan Confining Unit (MFCU). The first simulation includes an assignment of 35,000 for all nodes within the MFCU, while the second simulation includes an assignment of 4,000 mg/l for upper nodes and 35,000 mg/l for lower nodes. The second simulation is thought to be equivalent to the finite-difference runs since the starting concentration for those runs is assigned at the cell center rather than at the cell edge. Further review of the second simulation (WASH – deep4000) still reveals that the concentration versus time curve is generally between the finite-difference upwinded and TVD solutions. It is likely that the WASH123 results are also subject to numerical dispersion. Woods (2004) noted similar numerical dispersion problems with the finite-element model SUTRA (Voss and Provost, 2002). Future improvements to WASH123 will utilize the “local zooming and peak-valley capturing algorithm as outlined by Cheng et al. (1998). These improvements should further minimize numerical errors.

The SWI result shows major differences as compared to the other model simulation results. The SWI simulation predicts that the water quality threshold of 500 mg/l would be exceeded after 4 days. Also, the slope of the concentration versus time curve is much steeper than any other simulation result. Since the SWI code was originally designed for regional sea water intrusion issues, this result is not surprising. Since the SWI code was designed based upon an interface approach, it was not designed to simulate dispersion.

Therefore, it is unclear if the SWI results are the "most accurate" or if the Dupuit approach implemented in SWI is resulting in unrealistic concentration increases.

Since no known ASR analytical solutions were available, a full accuracy assessment of the Case 1A results is not possible. The results clearly do show that the four codes predict a wide range of concentration estimates. It is theorized that the code results would converge and be more similar if the following improvements were incorporated:

- Additional horizontal resolution around the ASR well
- Additional vertical resolution within the storage zone and below the storage zone
- Lower well pumping rates would reduce the steep vertical gradients at the ASR well minimizing errors associated with the velocity field

Similar data plots were produced for a theoretical monitoring well approximately 120 feet distant from the ASR well. Figure 6 displays the simulation results from the various model codes and contaminant transport solutions during the 30-day ASR recovery period. At this radius (near the edge of the freshwater bubble), the effects of buoyancy stratification are probably more pronounced such that the differences among the various codes is likely due to a combination of numerical dispersion and the degree of buoyancy stratification predicted by the code.

Figure 6. Model simulation results for Case 1A at monitoring well 120 feet away.

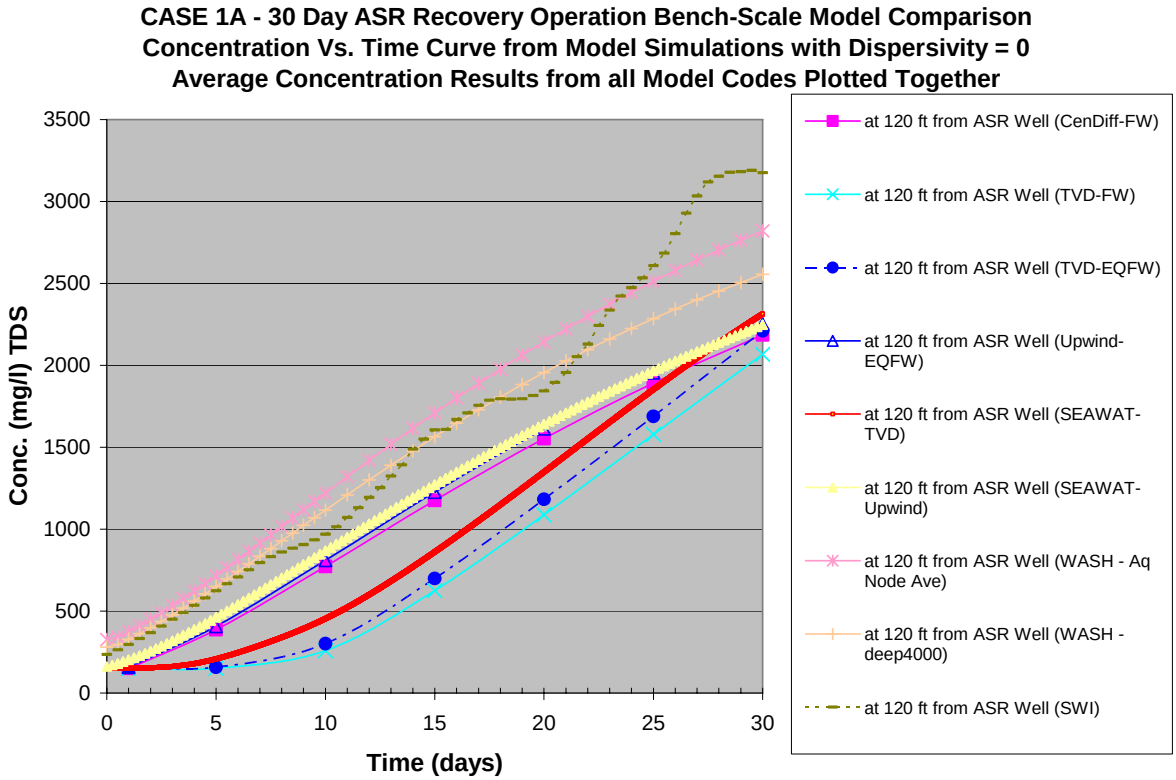

Generally, the simulation results can be subdivided into three groups. The TVD results from the MODFLOW/MT3DMS and SEAWAT models predict lower TDS concentrations over the first 15 days of ASR recovery as compared to the other model simulations. The WASH123 and the SWI model codes predict the highest TDS concentrations over the first 15 days of ASR recovery. The central-difference and upwinded solutions fall between the TVD and WASH123/SWI results. The "spread" of model results is less pronounced than at the ASR well as presented in figure 5. This also suggests that errors associated with the velocity field and the model resolution are larger at the pumping well location than 120 feet distant. Since dispersivities were assigned a value of zero, model stability was also an important issue. Some oscillations were seen in the results of all model codes with the exception of the WASH123 code and finite-difference upwinded solutions as discussed previously. Some of these are evident in the SWI results.

For Case 1B, comparisons were made at the ASR well and at different radii from the ASR well. Since Case 1B assigns a seawater TDS concentration in the ASR storage zone, more significant density effects were noted. Figure 7 depicts results from the different codes for concentrations versus time estimates during the entire 30-day ASR recovery period. Figure 8 depicts results from the different codes for concentrations versus time estimates during the entire 365-day ASR simulation period, including recharge for 30 days, storage for 305 days, and recovery for 30 days. It should be noted that the concentration curves represent average concentrations at the ASR well location for Figure 7, while discrete model layers are depicted in Figure 8.

Figure 7. Model simulation results at ASR well for Case 1B during ASR recovery period.

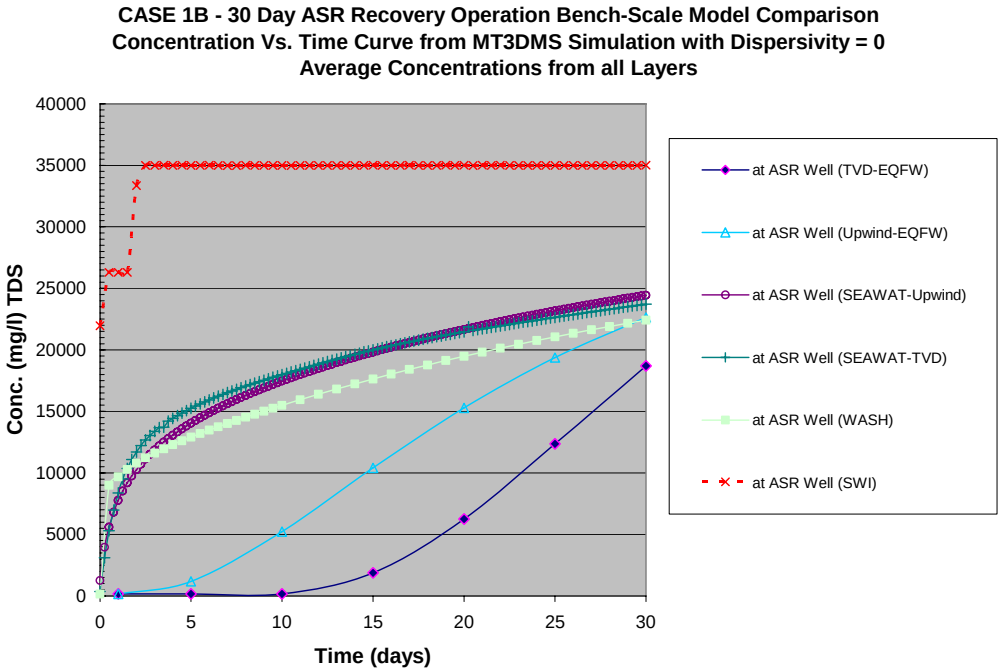

Figure 8. Model simulation results at ASR well for Case 1B during entire simulation period.

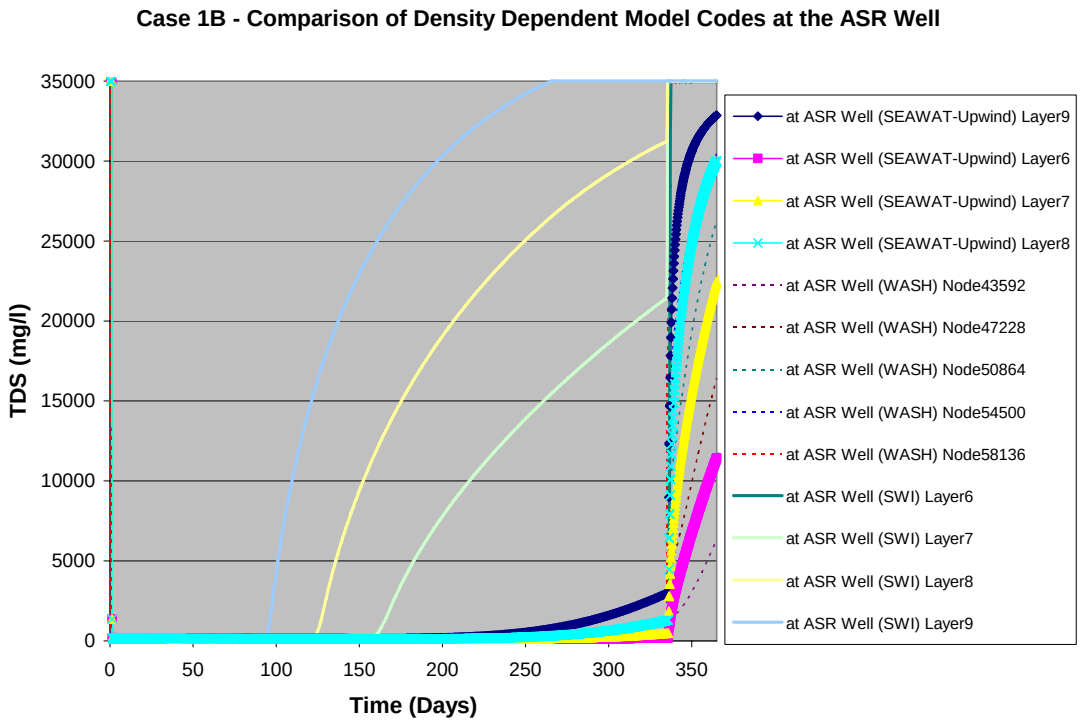

In reviewing Figure 7, it is evident that the results vary widely between the different codes. First, the non-density dependent simulations greatly underestimate the TDS concentration at the ASR well as compared to the other model codes. Both of the SEAWAT solutions and the WASH123 solution exhibit similar concentration versus time curves. The SWI results seem to overestimate the TDS concentrations at the ASR well location. The SWI code was originally designed for implementation at coastal boundaries, therefore the results may be misleading. Since the SWI code was not designed to model concentration changes around active pumping wells, it may not be the best tool for evaluating changes around the ASR well.

For Figure 8, only the density dependent capable model codes were investigated. Figure 8 clearly depicts large differences between the SEAWAT/WASH123 results versus the SWI results. Both SEAWAT and WASH123 predict moderate buoyancy stratification during the 305-day storage period as compared to the major buoyancy stratification predicted by SWI. In general, at the ASR well, the results predicted by SEAWAT and WASH123 are very similar. Both codes clearly demonstrate the capability to evaluate changes in water quality due to density stratification effects. Figure 9 depicts the results at a theoretical monitoring well located approximately 120 feet distant from the ASR well.

Figure 9. Model simulation results at 120 feet distant from the ASR well for Case 1B during entire simulation period.

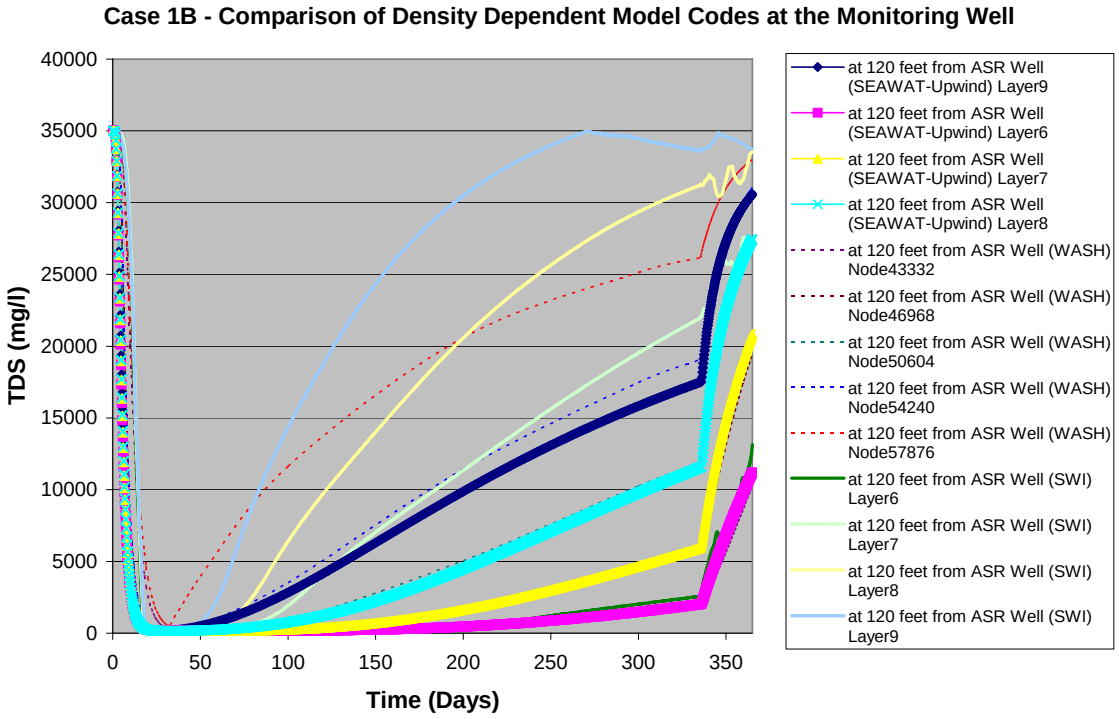

Figure 9 reveals that at the monitoring well located 120 feet from the ASR well, the SWI simulation predicts a higher degree of density stratification than the comparable SEAWAT TVD solution. The WASH123 results tend to fall in the middle of the SWI and SEAWAT results. During the 30-day recovery period, both the SEAWAT and WASH123 results exhibit similar shaped recovery curves as compared to the SWI simulation that appears to have some minor oscillations during the recovery duration. Figures 10 to 16 depict spatial concentration differences between the SEAWAT and WASH123 results for selected time steps during the one-year simulation period. The contour maps were developed from three sets of model output for the center of the aquifer storage zone. Each set of model output data was then contoured to a new two-dimensional mesh using an "inverse distance weighted" algorithm. The contouring resulted in minor oscillations in each dataset but did not inhibit the overall comparison of the results. The contour maps compare the spatial concentration differences at the middle of the ASR storage zone. The figures clearly show that both the finite-difference (upwinded or central difference) and WASH123 solutions are subject to moderate to high numerical dispersion and possibly more significant density stratification. WASH123 appears to have the highest numerical error with the upwinded solution exhibiting moderate to high error while the TVD solution had the smallest error. The SWI code was not included in this comparison since it does not have the capability to model hydrodynamic dispersion. It should also be noted that the finite-difference and WASH123 solutions are similar at day 365 as shown on Figures 15 and 16. The finite-difference and WASH123 results at day 365 both have a similar concentration gradient or

radius where seawater concentrations have been lowered at least 500 mg/l. The comparable radius for the TVD solution is much smaller. One notable difference is that the WASH123 solution displays more concentric contours, although curiously the circles are not centered on the ASR well, while the finite-difference results are heavily influenced by the grid resolution and bias. However, the WASH123 results also appear to be heavily influenced by mesh effects. As was mentioned previously, each of the models could have been improved through the incorporation of additional horizontal and vertical resolution around the ASR well.

Figure 10. Comparison of simulation results for Day 15.

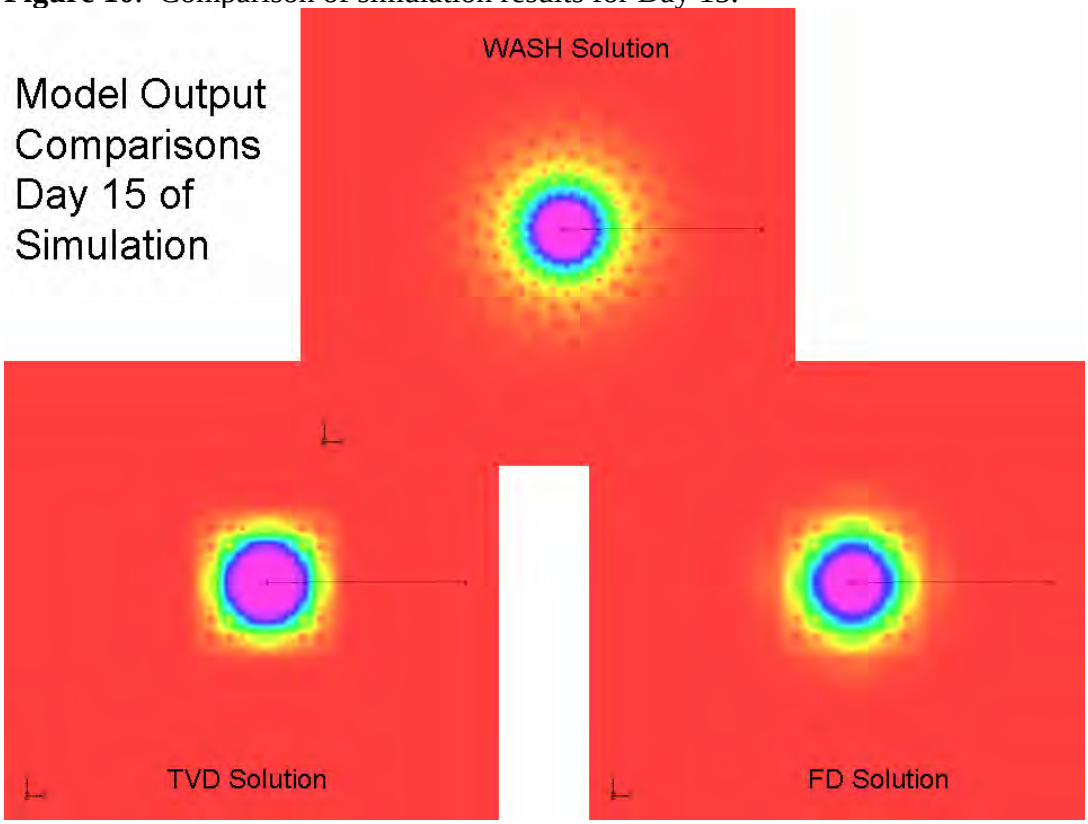

Figure 11. Comparison of simulation results for Day 30.

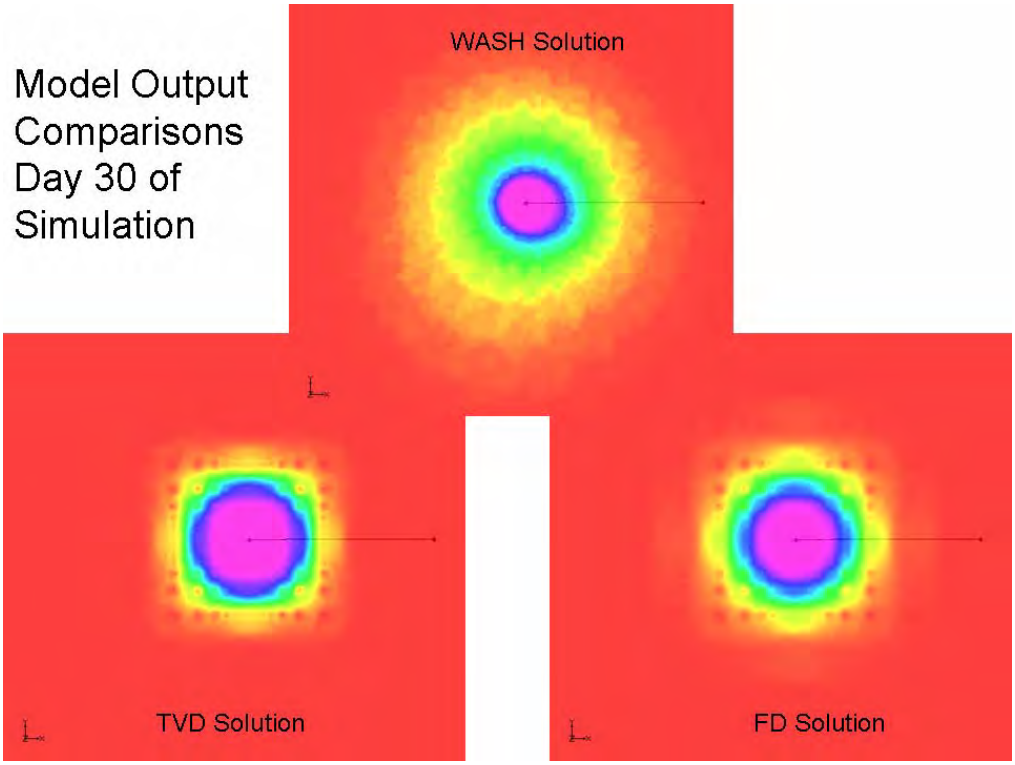

Figure 12. Comparison of simulation results for Day 105.

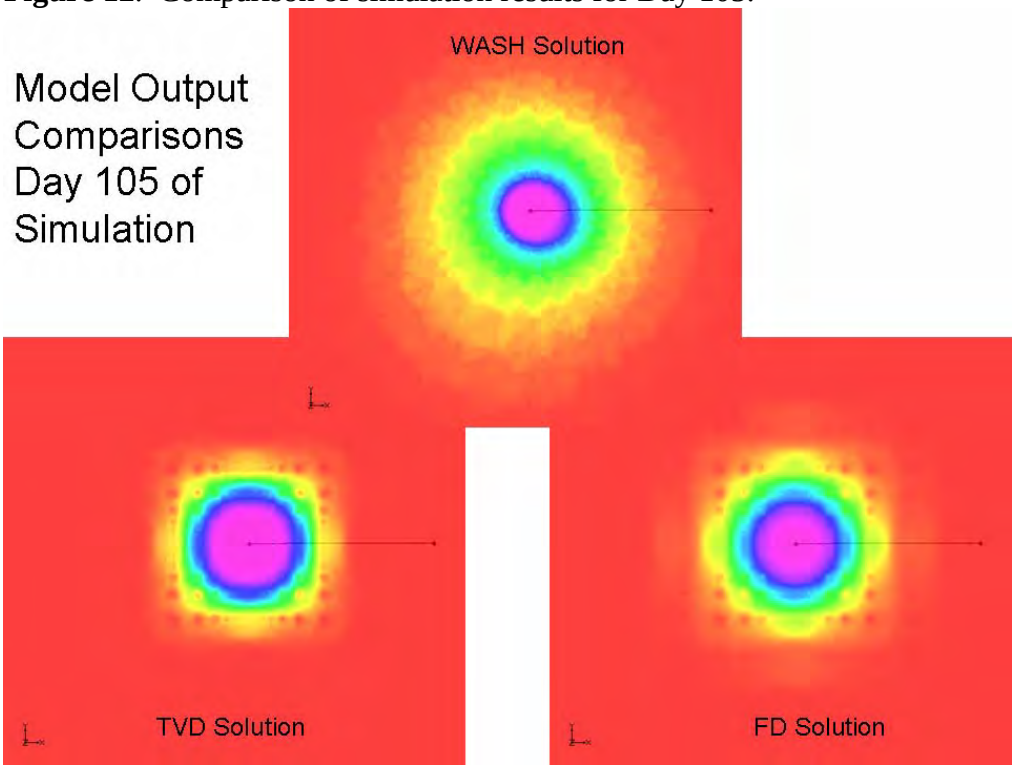

Figure 13. Comparison of simulation results for Day 335.

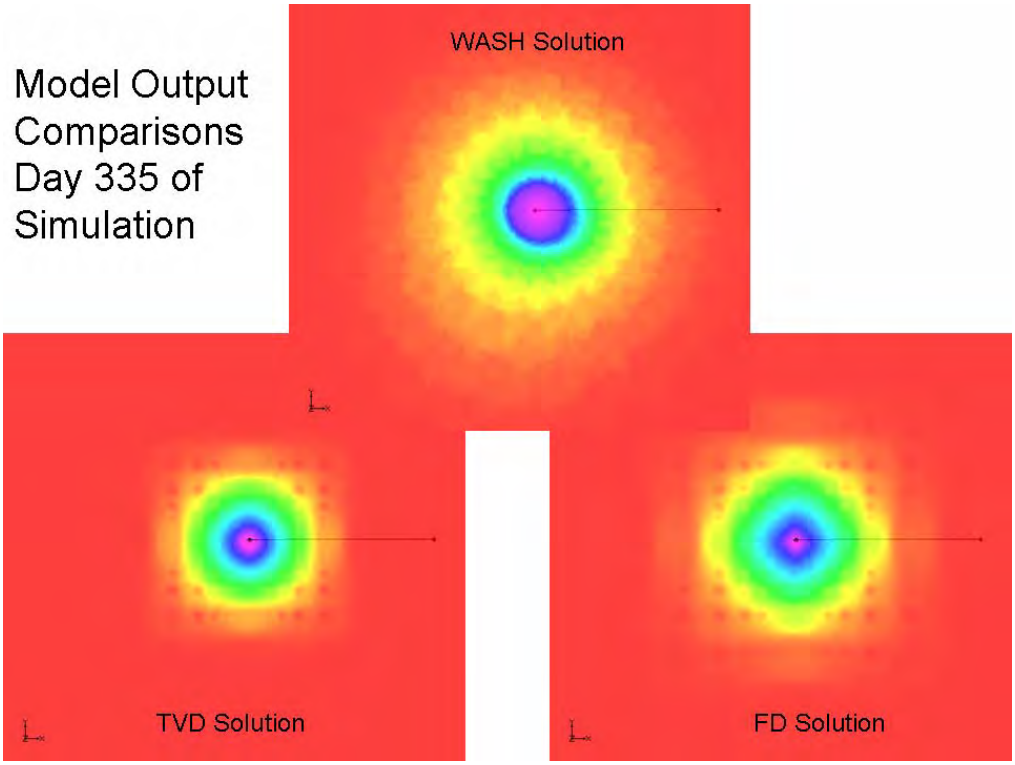

Figure 14. Comparison of simulation results for Day 350.

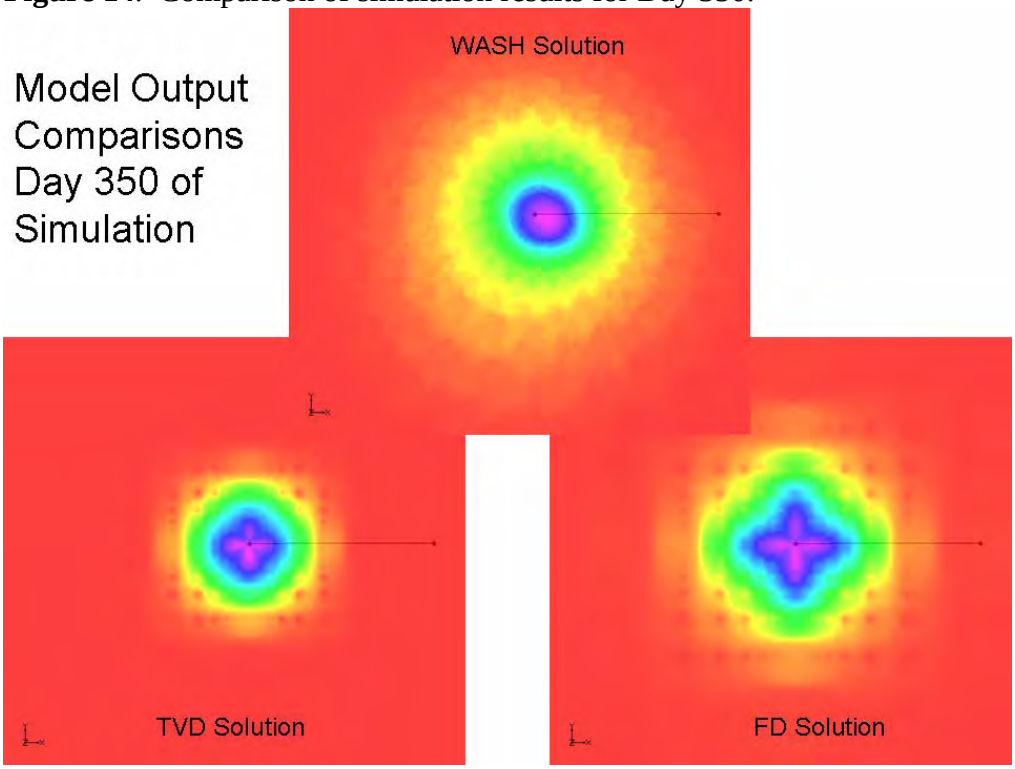

Figure 15. Comparison of simulation results for Day 365.

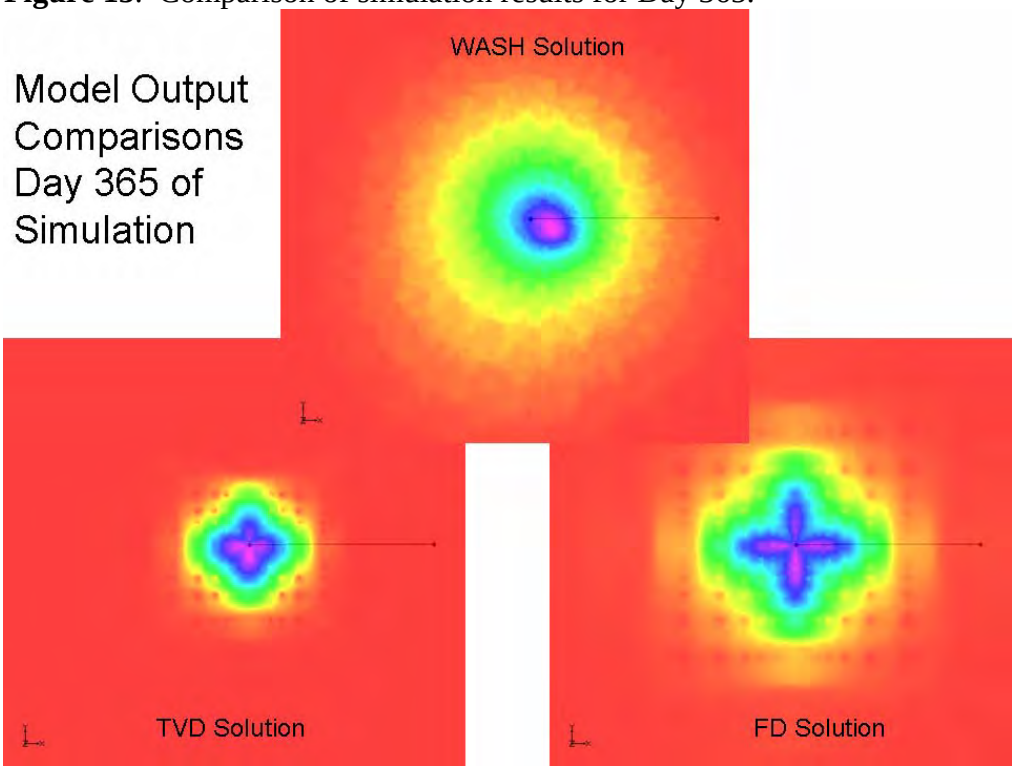

Figure 16. Comparison of simulation results for Day 365 with radius marker.

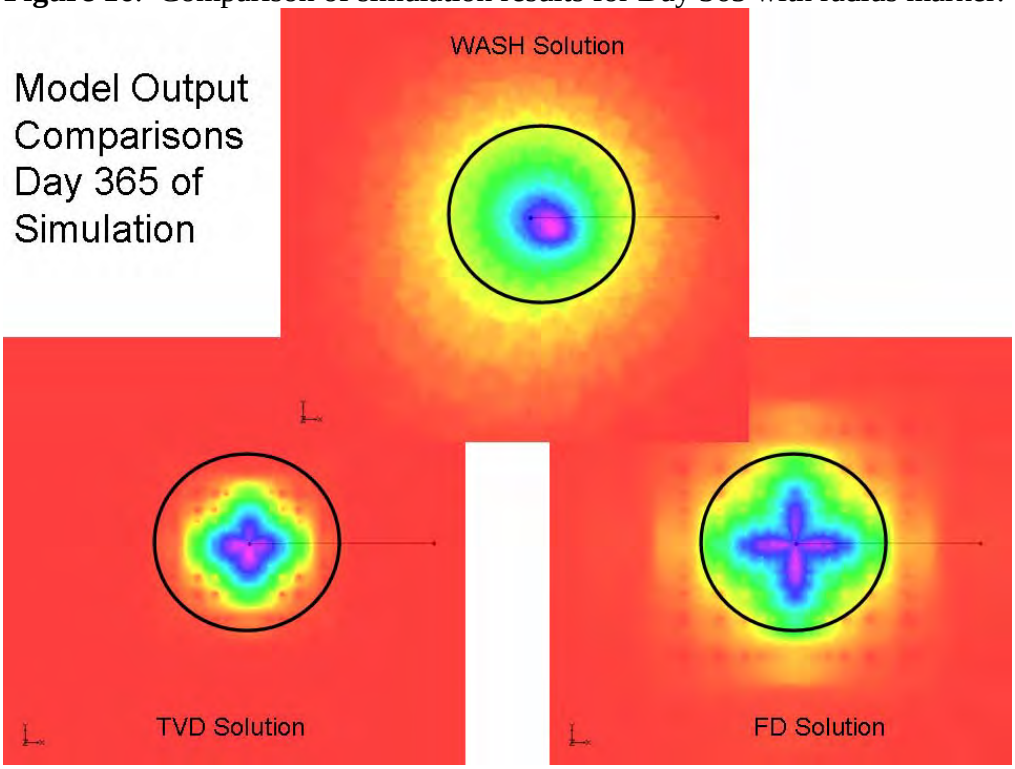

For Case 1C, the model simulation results were similar to those of Case 1A except that density-dependent upconing was encouraged to occur within the models due to assignment of much higher hydraulic conductivity within the MFCU as compared to the assignment for Case 1A. Figure 17 depicts the simulation results for the various model codes and contaminant transport solutions for Case 1C at the ASR well during the 30-day recovery period.

Figure 17. Simulation results for Case 1C at the ASR well during the recovery period.

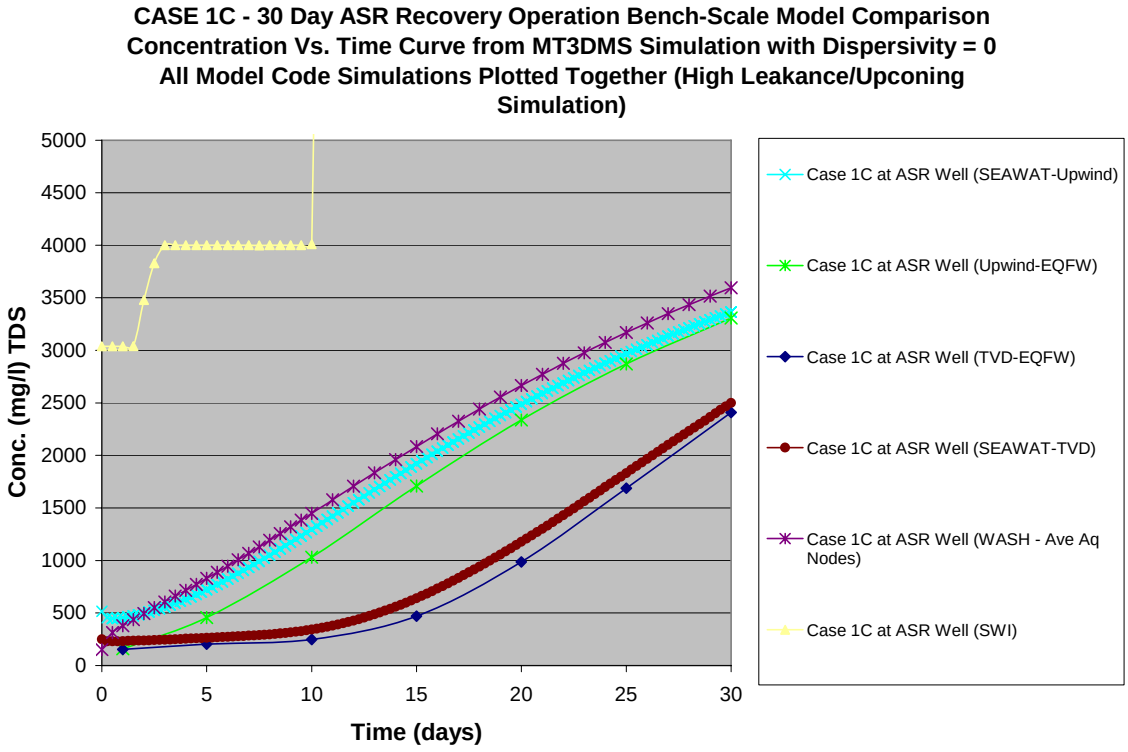

The results reveal three distinct groups of data. The SWI results clearly show predicted TDS concentrations that are considerably higher than the other codes. The TVD results from both the MODFLOW/MT3DMS and SEAWAT models predict the lowest TDS concentrations. The MODFLOW/MT3DMS and SEAWAT upwinded results and the WASH123 results fall between the TVD and the SWI results. It should be noted that the WASH123 results depict saltwater upconing more clearly than the other codes. The WASH123 results for Case 1C are shown on Figure 18.

Figure 18. Simulation results from Case 1C for WASH123 base run.

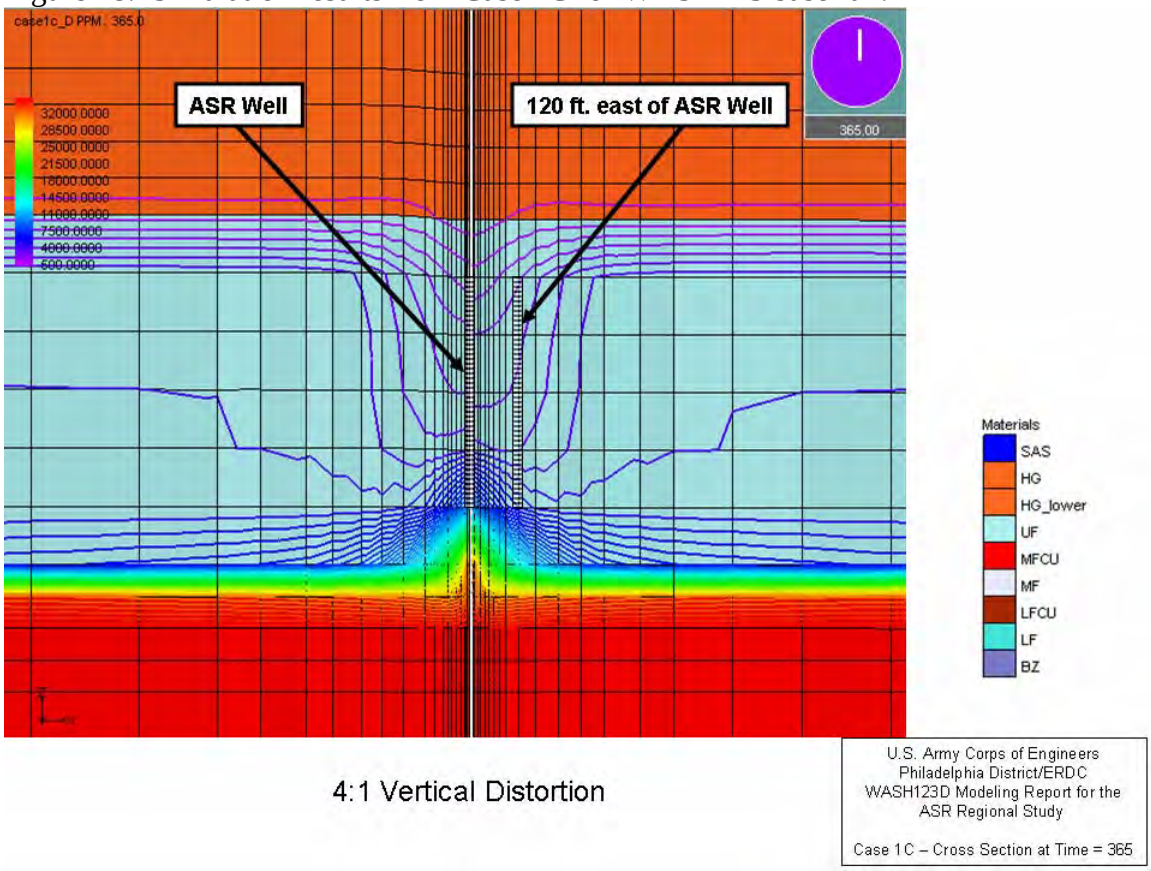

Although not completed for the study, an additional WASH123 run optimizing the boundary assignment of the MFCU (similar to WASH deep4000 for Case 1A) may have resulted in lower predicted TDS concentrations and less severe upconing. Figure 19 depicts similar model simulation comparisons for a theoretical monitoring well located 120 feet distant from the ASR well. The same three distinct data groups are visible.

Figure 19. Simulation results for Case 1C at 120 feet from the ASR well during the recovery period.

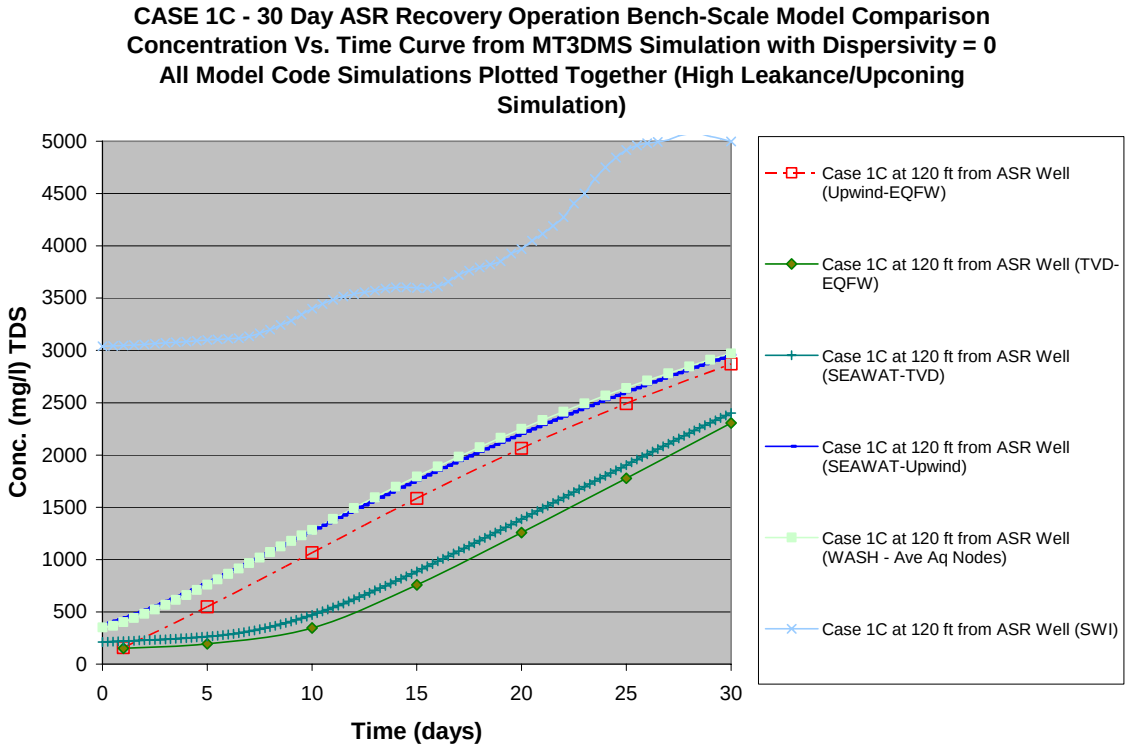

For Case 1D, the results were similar to Case 1A except that real dispersion was simulated through the assignment of 25 feet for the longitudinal dispersivity and transverse dispersivity. For Case 1D only the MODFLOW/MT3DMS, SEAWAT and WASH123 codes were compared since SWI does simulate hydrodynamic dispersion. Figure 19 depicts the results of the three comparisons. The MODFLOW/MT3DMS and SEAWAT results are very similar and predict higher TDS concentrations than the WASH123 simulation results. All three model codes predict TDS concentrations to quickly elapse the 500 mg/l regulatory limit following the long 305 day storage period. The MODFLOW/MT3DMS and SEAWAT results also predict concentrations at the ASR well in excess of 4,000 mg/l suggesting either upconing or significant numerical error.

Figure 19. Simulation results for Case 1D at the ASR well during the recovery period.

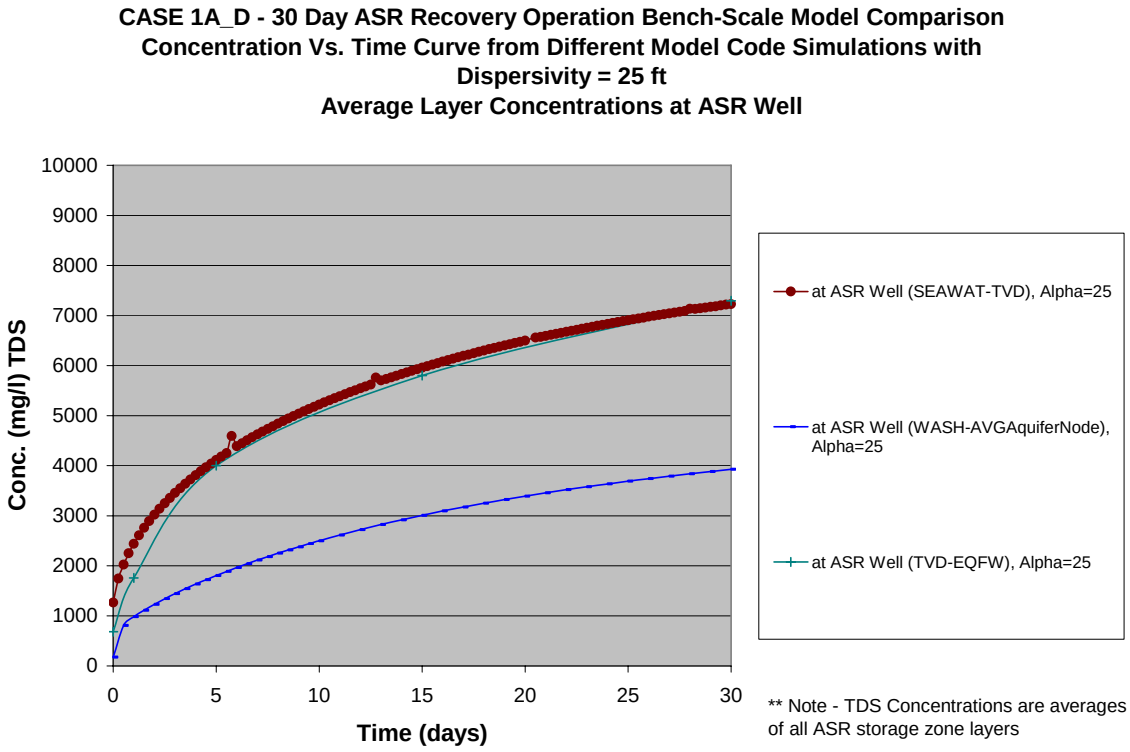

For Case 2A, the results for the SEAWAT, SWI, and WASH123 codes are all very similar. All three codes appear capable of handling any salt-water intrusion issues that may need to be simulated in the future as part of the ASR Regional Model.

Conclusions and Recommendations:

This benchscale study was developed to evaluate the potential for various model codes to provide answers to issues confronting the ASR Regional Study team. The benchscale study was developed and carried out by an interagency PDT. During the conduct of the study, problems and difficulties were encountered that limited the value of the study to address all goals outlined in the original plan. In general, the main problem was that the test models should have contained more horizontal and vertical model resolution to adequately simulate the cases selected. In addition, one or more benchmark problems with known solutions should have been thoroughly evaluated as part of this study to better ascertain the accuracy limitations of the various codes. An unfortunate consequence of the present work is that there really is no way to tell which code or solution mechanism provides the most accurate result. These shortcomings have been acknowledged and discussed in this report. However, even with the shortcomings identified, the study is valuable. The study also clearly indicated that the important issues

to be addressed for the ASR Regional Study represent three different scales of problem. Therefore, ultimately, three different model scales will be required to address them.

This benchscale study was useful in comparing four different model codes under consideration for use in development of a regional ASR model. The four codes tested represented a reasonable range of code options available and were selected based upon PDT members overall familiarity with the codes. Other codes such as SUTRA and FEFLOW were also considered but rejected. SUTRA has been used for past ASR simulation studies so that some of its advantages and disadvantages were already known. FEFLOW is a proprietary code from Europe that would have been difficult to procure for U.S. Government work efforts. Each code exhibited both strengths and weaknesses. All of the codes provide much of the model functionality desired for the ASR Regional Study team with the SEAWAT and WASH123 codes providing the best overall functionality. All of the codes were determined to be easy to moderately difficult to use, while all codes with the exception of SWI probably require workstation class computers to efficiently develop and calibrate a large regional model. Effective pre and post-processors can be utilized directly by all model codes with the exception of SWI.

A few notable lessons learned can be gleaned from the completed work efforts including the following:

- Where ASR wells with large injection or recovery rates are to be modeled, additional horizontal and vertical model resolution is necessary
- The combination of steep head gradients and sharp concentration fronts present very challenging model simulations
- Comparing code results to known published solutions is recommended even though no “ASR solutions” are currently available
- The initial goal to compare four identical models was a worthy one but ultimately difficult due to different stability requirements for the four codes

Overall the SWI code had the shortest run times while the SEAWAT (with TVD solution) had the longest run times. The SEAWAT (with upwinded finite-difference solution) and WASH123 fell in between. In general, based upon the results of the benchscale studies, the SEAWAT TVD code is approximately 7 times slower than the WASH123 code and the WASH123 code is approximately 10 times slower than the SEAWAT Upwind code. Due to geometry advantages inherent in finite-element codes, a model designed with WASH123 could have less calculation points than a comparable finite-difference code. Therefore, the run time difference between the SEAWAT Upwind and WASH123 would be reduced considerably. Based upon the results of the benchscale modeling, model run times were extrapolated for identical hypothetical models with 100,000 calculation points using either SEAWAT or WASH123. Run time estimates were calculated for 1 year transient simulations and 36 year transient simulations (similar to CERP modeling period). These are presented in Table 12. It should be noted that the predicted run-times for the SEAWAT TVD solution could be reduced if time step size could be increased. A code improvement of the TVD solution, allowing for larger step sizes, may be feasible in the future.

Table 12. Hypothetical Model Run Times for the ASR Regional Study.

Model Code	Projected Run Time for 1 Year Simulation (Days)	Projected Run Time for 36 Year Simulation (Days)
SEAWAT TVD	2.84	102
WASH123	0.41	14
SEAWAT Upwind	0.04	1.4

The SWI code is approximately twice as fast as the SEAWAT Upwind code but the SWI code does not have a capability to simulate hydrodynamic dispersion, a key ASR performance consideration for the CERP. The SWI code does appear useful for quick evaluations of possible salt-water intrusion episodes caused by ASR recovery. It may also be useful as a screening model tool. If the SWI code is eliminated from consideration, the WASH123 or SEAWAT codes would be the best candidates for use in the ASR Regional Model study. Based upon the results of the benchscale tests completed, a further analysis of potential run times for the ASR Regional Model were prepared assuming the domain would cover approximately 34,000 square miles and the model would contain 20 vertical layers with varying degree of horizontal resolution. Figure 20 depicts projected model run times for the SEAWAT code (TVD and Upwinded Finite Difference Solutions) and the WASH123 code. Also, it was assumed that the full CERP 36-year period of record would be run for each code. Scale up from the benchscale model domain size (County size) to the regional domain is generally straight forward using a simple domain size ratio and assuming additional vertical model resolution.

Figure 20. Estimated Model Run Times for the ASR Regional Model

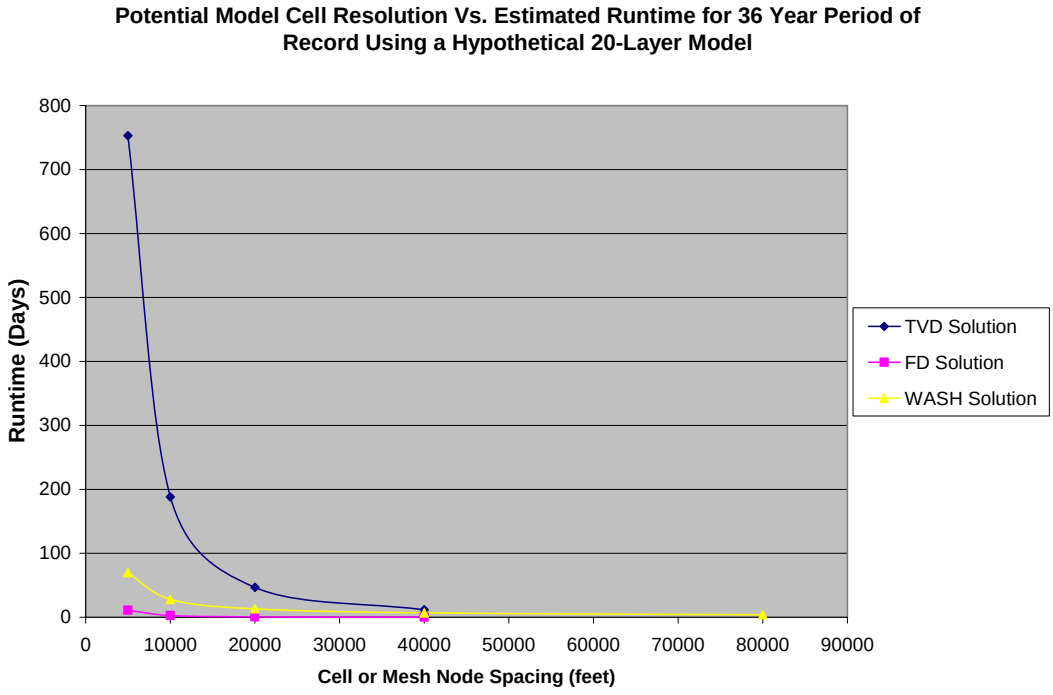

The SEAWAT (with upwinded finite-difference solution) and WASH123 codes appear to be subjected to the highest amount of numerical dispersion of the codes considered. A portion of the numerical dispersion most likely could be eliminated through better model grid or mesh design allowing for additional resolution in the vertical direction. In addition, accuracy could be further improved for these codes through improved horizontal grid or mesh resolution. It appears that the concentration changes around the ASR well are focused within 250 feet of the ASR well. Therefore, it may be appropriate to maintain a constant horizontal grid or mesh resolution within that radius, increasing grid or mesh size at a reasonable bias beyond 250 feet.

All codes seem capable of simulating density-stratification as evidenced in Case 1B. The accuracy of the codes for this case is unknown however, since no known analytical solution is available to provide a comparison or check. Qualitatively, the SEAWAT (TVD solution) and the WASH123 results appear very similar to each other so it is surmised they probably have a similar accuracy for this case. For Case 1C, the WASH123 code revealed more clear density upconing as compared to the other codes. Since no analytical solution was available for comparison, it is unknown if the simulation results are more representative than the other codes tested.

For Case 1D, the MT3DMS and SEAWAT codes predicted much higher concentrations at the ASR wellhead than the WASH123 code. It is unclear why the differences are so large for this case. Again, the vertical grid resolution may have been insufficient to ensure the highest accuracies of the velocity field around the ASR well. Inaccuracies in the vertical velocity field may have resulted in more significant contaminant transport errors for the model codes. For Case 2A, all the codes tested produced reasonable results and seem capable of simulating cases of salt-water intrusion.

Weighing all of the factors and considering improvements that could be made to the model grid or mesh for future models, it appears that either the SEAWAT (Upwinded finite-different Solution) or the WASH123 codes would be appropriate to utilize for the ASR Regional Study model development effort. Both codes appear to solve the requisite flow and transport equations adequately as well as providing a back stop of published comparisons against density-dependent case studies. SEAWAT appears to be the most widely tested code of the two but recent efforts conducted at the ERDC aim to lessen the gap here. Each of the codes also have inherent disadvantages including long model run times due to small time-step requirements for contaminant transport models. One strategy that was considered valuable was the employment of both model codes to study the same ASR problems thus ensuring a higher degree of reliability in overall conclusions and future recommendations. Using both codes to “bracket” the most likely issues and solutions would go a long way towards better overall decision making for the ASR program. For smaller domain models, the SEAWAT (TVD Solution) code could be utilized to minimize numerical errors and provide the best estimate of ASR recovery efficiency. The SWI code should not be utilized unless hydrodynamic dispersion can be ignored for the particular problem under consideration.

In order to address the maximum number of ASR questions as rapidly as possible, it is recommended that two models be developed simultaneously for the ASR Regional Study. As discussed above, the two codes would enable the PDT to bracket the cogent issues related to potential ASR system impacts and expected benefits. The two codes would provide a much needed measure of decision making reliability. First, a coarse resolution regional model should be developed with horizontal model resolution of 5,000 to 10,000 feet. The coarse model would be developed using the SEAWAT upwinded code and would be utilized to evaluate system groundwater exchange/flows and the movement of the salt-water interface. This model would be calibrated using existing water level and water quality information within the study area along with contour maps showing the depth to the salt-water interface. Long-term simulations of the salt-water interface would be required to simulate current steady-state conditions and concentrations. Therefore, this model needs to run rapidly in order to complete the numerous simulations required. A key advantage of this approach would be the large number of sensitivity tests that could be completed. This would result in a more reliable model calibration of heads and concentrations at the Florida coastline.

Second, a variable resolution regional model should be developed with horizontal model resolution of 100 to 250 feet around the proposed ASR wells increasing to 10,000 feet in the far reaches of the study area. This model would be developed using the WASH123 code and would take advantage of the geometry advantages of a finite-element code such that the model mesh would have varying resolution across the model domain. In essence, finer resolution could be employed at the areas of interest while far-field areas would be modeled with coarse resolution. This model would build upon calibration results achieved for the SEAWAT model by calibrating against seasonal water levels and water quality as well as utilizing transient calibration at existing ASR and well sites where aquifer test or ASR cycle testing data is available. It is believed that at least ten to fifteen such sites would have the necessary data to support this more rigorous calibration effort.

Based upon the model domain of 34,000 square miles, an estimate was made of the number of computational points for each model versus resolution. The SEAWAT grid would be a minimum of 5,000 feet horizontal resolution while the WASH123 mesh would be the same coarse resolution at the model exterior but with 1,000 feet resolution around Lake Okeechobee (key area of interest for the CERP). Table 13 lists the number of computational points for a 1 layer model at different horizontal resolutions. Based upon the benchscale study, the PDT has determined that the regional model should be limited to less than 500,000 computational points to ensure more reasonable run times. In reviewing Table 13, it is important to note that at 5,000 feet of horizontal resolution, both model codes would be similar but WASH123 would have finer resolution around the Lake Okeechobee study area. As resolutions become coarser, SEAWAT clearly results in less computational time. In order to stay within the prescribed number of computational points, the overall ASR regional study model resolution should be limited to minimum of 7,500 to 10,000 feet.

Table 13. Model resolution vs. # of computational points for a one layer model

Horizontal Resolution (feet)	# Grid Points	# Mesh Nodes
5,000	37,704	34,443
10,000	9,426	13,935
20,000	2,356	6,207

Both models would be developed by the same team and would utilize all of the same model input data sets (e.g., water levels, starting conditions, hydrogeology, water quality, and boundary conditions) in order to maximize synergy between the two development efforts. Both models would be combined into a single modeling report for review by an external ITR team. Ultimately, these two models and a very fine-resolution model would represent a "family" of models that could help the ASR Regional PDT address all of the outstanding technical issues identified previously. In addition, this family of models would be utilized to optimize the final design of the entire CERP system of wells.

References:

Cheng, Hwai-Ping, Jing-Ru Cheng and Gour-Tsyh Yeh, 1998. A Lagrangian-Eulerian Method with Adaptively Local Zooming Approach to Solve Three-Dimensional Advection-Diffusion Transport Equations. *International Journal for Numerical Methods in Engineering* 41(4):587-615.

Chiang, Wen-Hsing and Kinzelbach, Wolfgang, 2001. 3D-Groundwater Modeling with PMWIN, A Simulation System for Modeling Groundwater Flow and Pollution. Berlin, Germany, Springer Inc., 341 p.

Guo, W., and C.D. Langevin. 2002. User's Guide to SEAWAT: a Computer Program for Simulation of Three-Dimensional Variable-Density Ground-Water Flow. Open-File Report 01-434. U.S. Geological Survey, Tallahassee, Fla.

Hantush, M.S. & Jacob, C.E., 1954. "Plane potential flow of gound-water with linear leakage". *Transactions, American Geophysical Union*, Vol 35, pp. 917-936.

Lin, H.C., D. R. Richards, G. T. Yeh, J. R. Cheng, H. P. Cheng, and N. L. Jones, FEMWATER: A three-dimensional finite element computer model for simulating density-dependent flow and transport in variably saturated media, Report CHL-97-12, U.S. Army Corps of Engineer, 3909 Halls Ferry Road, Vicksburg, MS 39180-6199, September, 1997.

McDonald, M. G., and Harbaugh, A. W., 1988. A modular three-dimensional finite-difference ground water flow model: Techniques of Water-Resources Investigation Report, v. 06-A1.

Merritt, Michael L., 1986. Recovering Fresh Water Stored in Saline Limestone Aquifers. *Ground Water* 24(4):516-529.

Merritt, Michael L., 1993. Aspects of Numerical and Representational Methods Related to the Finite-Difference Simulation of Advective and Dispersive Transport of Freshwater in a Thin Brackish Aquifer. *Journal of Hydrology* 148:61-92.

Ogata, A., 1970. Theory of dispersion in a granular medium. U.S. Geological Survey Professional Paper 411-I.

Theis, C.V., 1935. "The relation between the lowering of the piezometric surface and the rate and duration of discharge of a well using ground-water storage", *American Geophysical Union Transactions*, Vol 16, pages 519 – 524.

Woods, Juliette, 2004. Numerical Accuracy of Variable-Density Groundwater Flow and Solute Transport Simulations. Ph.D. dissertation, University of Adelaide, Adelaide, Australia.

Voss, C. I., and A.M. Provost. 2002. A Model for Saturated-Unsaturated, Variable-Density Ground-Water Flow with Solute or Energy Transport. Water-Resources Investigations Report 02-4231. 409 p. Reston, Va.: U.S. Geological Survey.

Yeh, G.T., H. P. Cheng, J. R. Cheng, and H. C. Lin, A numerical model to simulate water flow and contaminant and sediment transport in WAterSHed systems of 1-D stream-river network, 2-D overland regime, and 3-D subsurface media (WASH123D: Version 2.0), Report CHL-98-19, Waterway Experimental Station, U. S. Army Corps of Engineers, 3909 Halls Ferry Road, Vicksburg, MS 39180-6199, July, 1998.

Van der Heijde, P.K.M., and D.A. Kanzer, 1997. Project Summary, Ground-Water Model Testing: Systematic Evaluation and Testing of Code Functionality and Performance, EPA Report # 600/SR-97/007, National Risk Management Research laboratory, Ada, OK, February 1997.

Zheng, C. and P. P. Wang, 1999, MT3DMS: A Modular Three-Dimensional Multi-Species Model for Simulation of Advection, Dispersion and Chemical Reactions of Contaminants in Groundwater Systems: Documentation and User's guide,SERDP-99-1: U.S. Army Engineer Research and Development Center, Vicksburg, MS.

Appendix A

MODELING BRACKISH AQUIFER STORAGE RECOVERY WITH THE WASH123D NUMERICAL MODEL

H.-P. Cheng[1], S. M. England[2], G. T. Stevens[2], E. V. Edris[1], C. J. Brown[3]
[1]Coastal & Hydraulics Laboratory, US Army Engineer Research & Development Center, 3909 Halls Ferry Road, Vicksburg, MS 39180-6199
[2]US Army Corps of Engineers, Philadelphia District, Wanamaker Building, 100 Penn Square East, Philadelphia, PA 19107-3390
[3]US Army Corps of Engineers, Jacksonville District, 400 W. Bay Street, Jacksonville, FL 32202

Abstract Aquifer Storage and Recovery (ASR) is the storage of fresh water in an aquifer via injection during times when water is available, and recovery of the water from the same aquifer via pumping during times when it is needed. ASR is expected to provide a cost-effective solution to many of the world's water management needs: storing water during times of flood or when water quality is good, and recovering it later during emergencies or times of water shortage, or when water quality from the source may be poor. ASR systems can usually meet water management needs at less than half the capital cost of other water supply alternatives. When compared to other alternatives that require construction of water treatment plants and surface reservoirs to meet increasing peak demands, potential cost savings have been anticipated. Besides, ASR has been recognized to have less impact on the environment, aquatic and terrestrial ecosystems. When water is stored deep underground in brackish aquifers, however, the mixing of the saline water that is originally in the brackish aquifer and the fresh water that is injected into the aquifer may degrade the water quality of the stored water and reduce the volume of the available fresh water in the following recovery periods of time. The mixing can be modeled by both the diffusion and the dispersion transport processes. Although both the diffusive and the dispersive fluxes are proportional to concentration gradient, the dispersion coefficients are highly dependent on the flow velocity, whereas the diffusion coefficients are independent of the flow velocity. Therefore in the evaluation of brackish aquifer storage recovery (BASR), whatever factor that would significantly affect the flow velocity in the brackish aquifer during both the injection and withdrawal periods should be accounted for in the associated evaluation models. In this paper, we will demonstrate how BASR can be modeled with the WASH123D numerical model that computes saline transport and density-dependent flow in a watershed system which can be conceptualized as a combination of 1D channel network, 2D overland regimes, and 3D subsurface media. A hypothetical example that includes various model parameters, *e.g.*, pumping rate, hydraulic conductivities, porosity, and

dispersivities will be employed to detail the model setup and conduct a sensitivity analysis.

INTRODUCTION

Aquifer Storage and Recovery (ASR) is one of the proposed alternatives recommended by the Comprehensive Everglades Restoration Plan (CERP). The goal of ASR in the South Florida Region is to help with water supply, storage, and distribution. The ASR Regional Study will include numerical groundwater models in order to evaluate the effectiveness of ASR. For this phase of the project, four box models (~ 40 miles x 40 miles x 2340 ft) were developed using the WASH123D finite element code. Each of the four "cases" is intended to evaluate modeling code performance under different hydraulic conditions. The following paper details the WASH123D model construction and summarizes the simulation results for one of the CERP box models.

WASH123D CODE

WASH123D is a finite element numerical model designed to simulate variably saturated, variable-density water flow and reactive chemical and sediment transport in watershed systems. It is capable of conceptualizing a watershed system as a combination of 1D river/stream, 2D overland, and 3D subsurface sub-domains. A modified Richards' equation is used to solve for 3D flow when density effect is taken into account. The equation is solved with the Galerkin finite element method. WASH123D uses the Lagrangian-Eulerian (LE) method to solve the transport equations. Particle tracking is used in the Lagrangian step to handle the advection term. Other terms (such as sources, sinks, diffusion, and dispersion) are calculated in the Eulerian step, where element matrices are assembled into a global matrix, and matrix solvers are used to solve for the spatial concentration distribution at the end of each time step. A predictor-corrector numerical technique, combined with an adaptive explicit-implicit numerical scheme, is employed to compute reactive transport efficiently and robustly. The use of this methodology allows the numerical stability of WASH123D not to be restricted by the Mesh Courant number. In addition, the Mesh Peclet number is restricted only by computational accuracy, not numerical stability. More detailed discussion on various types of numerical dispersion and how the LE method deals with these types of numerical dispersion are discussed in the referenced papers.

Since computational accuracy is dependent on the time step size used in the simulation, a sensitivity analysis was performed to evaluate the variations in the time-step size on model results. For this sensitivity analysis the time step of the injection and extraction cycles were varied between 0.05 and 5 days. The results of this analysis, presented in Figure A1, indicate that the change of the computational result becomes insignificant as the time step size is reduced to

below 0.5 days. Therefore, a time step size of 0.5 days was used during the injection and extraction cycles for all simulations in this study.

MESH DEVELOPMENT

WASH123D uses an unstructured three-dimensional (3D) finite element mesh to solve the flow and transport equations in variably-saturated media. Because flow and concentration gradients may be high in the vicinity of an ASR well, the vertical and horizontal resolution of the 3D mesh in the vicinity of the ASR well is important. Meshes that do not have sufficient resolution in the area of interest may not accurately simulate observed conditions in these high gradient areas. On the other hand, meshes that contain too much resolution will require more computational resources, resulting in extended simulation times. The mesh used for this study was based on conceptual geology developed by the Jacksonville District. The horizontal resolution of the mesh at the ASR well is 10 feet. The elements at the ASR well were deleted to allow Cauchy flux boundary conditions to be assigned directly to the interior faces of the mesh, representing the well screen. The mesh resolution expands to 5000 feet along the model perimeter. Vertical mesh resolution varied among the different conceptual geologic units. Increased resolution was used in the confining units directly above and below the ASR injection aquifer (Upper Floridian). This increased resolution allowed the WASH123D model to depict the large head and concentration gradient at the interfaces of these confining units. The final 3D mesh was composed of 112,716 nodes and 212,940 triangular-prism elements. Figures A2a and A2b illustrate the mesh resolution and conceptual geology used for the ASR simulations. The DoD Groundwater Modeling System (GMS) v.5.1 was used to generate the WASH123D mesh.

BOUNDARY CONDITIONS

Boundary conditions were assigned to the finite element model to simulate ASR pumping into the Upper Floridian aquifer. At the ASR well, Cauchy flux boundary conditions were used to simulate injection and extraction flow rates of 5 MGD. These boundary conditions were applied to the element faces representing the well screen within the Upper Floridian Unit (approximate elevation –1,014 to –1,171 ft). The saline concentration of the injected fluid was 150 mg/L. The saline concentration of the fluid at the ASR well during storage and extraction varies with depth and time depending on the relative saline concentration in the surrounding nodes, the extraction rate, and the mixing process in the ASR well. Dirichlet boundary conditions were used to assign the total head along the eastern and western model boundaries. WASH123D converts these assigned heads to equivalent fresh water heads based on the concentration and depth of each node. No-flow boundary conditions were used along the northern and southern model boundaries. Dirichlet boundary conditions were also used to assign the concentration along the model perimeter. Tables A1 and A2 show the

hydraulic and transport properties,respectively, for each geologic unit in the WASH123D model.

Table A1 Hydraulic Properties and Boundary Conditions

Geologic Unit	Head BC West Tot Head (ft)	Head BC East Tot Head (ft)	Head BC North Tot Head (ft)	Head BC South Tot Head (ft)	Conductivity Horiz (ft/day)	Conductivity Vert. (ft/day)	Mod. Compress of Matrix (1/ft)	Specific Storage (1/ft)	Effective Porosity
SAS	20	20	No Flow	No Flow	100	10	1.70E-03	1.70E-03	0.25
HG	No Flow	No Flow	No Flow	No Flow	0.01	0.001	7.00E-07	1.19E-06	0.4
UF	50	30	No Flow	No Flow	100	10	7.00E-07	1.01E-06	0.25
MFCU	No Flow	No Flow	No Flow	No Flow	0.01	0.001	7.00E-07	1.07E-06	0.3
MF	40	20	No Flow	No Flow	500	50	7.00E-07	1.01E-06	0.25
LFCU	No Flow	No Flow	No Flow	No Flow	0.01	0.001	7.00E-07	1.07E-06	0.3
LF	0	0	No Flow	No Flow	5000	500	7.00E-07	1.01E-06	0.25
BZ	0	0	No Flow	No Flow	10000	1000	7.00E-07	1.01E-06	0.25

Table A2 Transport Properties and Boundary Conditions

Geologic Unit	Con. BC West (mg/L)	Con. BC East (mg/L)	Con. BC North (mg/L)	Con. BC South (mg/L)	Tortuosity	Bulk Density (slug/ft^3)	Dispersivity Long. (ft)	Dispersivity Trans. (ft)	Flow IC Tot Head (ft)	Con. IC (mg/L)
SAS	150	150	N/A	N/A	1	3.784	0	0	Based on Steady State Simulation with no pumping	150
HG	150	150	N/A	N/A	1	2.969	0	0		150
UF	35000	35000	N/A	N/A	1	3.784	0	0		35000
MFCU	35000	35000	N/A	N/A	1	3.531	0	0		35000
MF	35000	35000	N/A	N/A	1	3.784	0	0		35000
LFCU	35000	35000	N/A	N/A	1	3.531	0	0		35000
LF	35000	35000	N/A	N/A	1	3.784	0	0		35000
BZ	35000	35000	N/A	N/A	1	3.784	0	0		35000

EVALUATION OF RESULTS

The WASH123D model simulated a 30-day injection period, followed by a 305-day storage period, and a 30-day recovery period. Prior to performing the transient simulation WASH123D calculates steady state initial hydraulic conditions based on the specified input parameters. The following discusses the results of the WASH123D model during each phase of the simulation.

Initial Condition

Since the WASH123D model is a coupled density dependent code, the initial hydraulic head boundary conditions were converted to equivalent freshwater heads based on the depth and saline concentration at each node. For this simulation, the nodes in the geologic units above the Upper Floridian aquifer were assigned a saline concentration of fresh water (150 mg/L), while the nodes in and below the Upper Floridian aquifer were assigned a saline concentration of seawater (35,000 mg/L). The specified boundary conditions result in a west to east hydraulic gradient. Figure A3a shows a cross sectional view of the concentration profile in the vicinity of the ASR well. The contours on this figure reflect the constant concentration profile used as the initial condition prior to pumping.

Injection Period

Once the initial steady state flow field is generated, the ASR pumping well injects fresh water into the Upper Floridian aquifer at 5 MGD for 30 days. During this injection cycle the hydraulic head at and immediately surrounding the ASR well increases substantially, nearly doubling in magnitude. Figure A3b shows a cross sectional view of the concentration profile in the vicinity of the ASR well at the end of the injection cycle. This figures show that the injected fresh water has displaced the ambient saline water forming a spheroid of lower concentration water in the vicinity of the ASR well. This lower concentration water permeates into the confining units above and below the Upper Floridian aquifer.

Storage Period

After the 30-day injection cycle, the ASR well is turned off for 305 days. During this storage period, the hydraulic conditions stabilize to near steady state conditions. Figure A3c shows a cross sectional view of the concentration profile in the vicinity of the ASR well at the end of the storage period. Although the concentration at the ASR well remains relatively constant, the effects of buoyancy stratification are noticeable. During the storage period, the density effect is the dominate factor in the flow fields simulated by WASH123D. Consequently, the concentrations at the nodes in the lower portion of the Upper Floridian aquifer increase substantially faster than the nodes at the top of the aquifer.

Extraction Period

After the storage period the ASR well extracts at 5 MGD for 30 days. During this extraction cycle the hydraulic head at and immediately surrounding the ASR well decreases substantially. Figure A3d shows a cross sectional view of the concentration profile in the vicinity of the ASR well at the end of the storage period. Up-coning of the higher concentration saline water below the ASR well was observed during extraction. It must be noted that the well screen of injection and extraction in the Upper Floridian aquifer covers the center four vertical elements, rather than all the six vertical elements in the aquifer. This setup allows the mesh to compute for convergent flow fields around the well at the interfaces of the Upper Floridian aquifer and the two aquitards above and below without using high resolution meshes and small time steps when the density effect is strong. Because of this, the salt concentration of nodes in the lower portion of the aquifer in the vicinity of the ASR well increase in concentration faster than the nodes above during the period of extraction due to both diffusion and up-coning.

FUTURE MODEL DEVELOPMENT

During the development of the WASH 123D model, meshes of various vertical and horizontal resolutions were tested. The WASH123D simulations became more computationally stable as the vertical resolution was increased in the geologic units above, below, and containing the ASR well. Additional studies are anticipated that evaluate the effect of various mesh resolutions on computational speed and accuracy.

In addition to the mesh sensitivity simulations, additional modifications to the WASH123D code are anticipated. One modification will be to the algorithm used to calculate the equivalent freshwater head in variable density flow systems. In simulations where higher density fluid is overlain by fluid of a lower density, the current algorithm tends to overestimate the equivalent freshwater head in the higher density solutions. Additional upgrades to address temperature variations on thermal transport will also be incorporated to the WASH123D code. These upgrades in conjunction with WASH123D's current ability to model variably saturated groundwater flow and surface/subsurface flow interactions will enhance WASH123D's ability to model the dynamic flow and transport issues inherent in the ASR program.

REFERENCES

Cheng, H.-P., Cheng, J.-R., and Yeh, G.-T. (1998). A Lagrangian-Eulerian method with adaptively local zooming and peak/valley capturing approach to solve three-dimensional advection-diffusion transport equations. International Journal for Numerical Methods in Engineering, 41(4), 587-615.

Cheng, J. R., Cheng, H. P., and Yeh, G. T. (1996). A Lagrangian-Eulerian method with adaptively local zooming and peak/valley capturing approach to solve two-dimensional advection-diffusion transport equations. International Journal for Numerical Methods in Engineering, 39(6), 987-1016.

Yeh, G. T., Chang, J. R., Cheng, H. P., and Sung, C. H. (1995). An adaptive local grid refinement based on the exact peak capturing and oscillation-free scheme to solve transport equations. Computers and Fluids, 24(3), 293-332.

Yeh, G.-T., Cheng, H.-P., Cheng, J.-R., and Lin, H.-C. (1998). A Numerical Model Simulating Water Flow and Contaminant and Sediment Transport in WAterSHed Systems of 1-D Stream-River Network, 2-D Overland Regime, and 3-D Subsurface Media (WASH123D: Version 1.0). Report CHL-98-19, U. S. Army Corps of Engineers, 3909 halls Ferry Road, Vicksburg, MS 39180-6199, July 1998.

Yeh, G.-T., Cheng, H.-P., Huang, G., Zhang, F., Lin, H.-C., Cheng, J.-R., Edris, E., and Richards, D. (2003). A Numerical Model Simulating Water Flow and Contaminant and Sediment Transport in WAterSHed Systems of 1-D Stream-River Network, 2-D Overland Regime, and 3-D Subsurface Media (WASH123D: Version 2.0). Draft Report, U. S. Army Corps of Engineers, 3909 halls Ferry Road, Vicksburg, MS 39180-6199, November 2003.

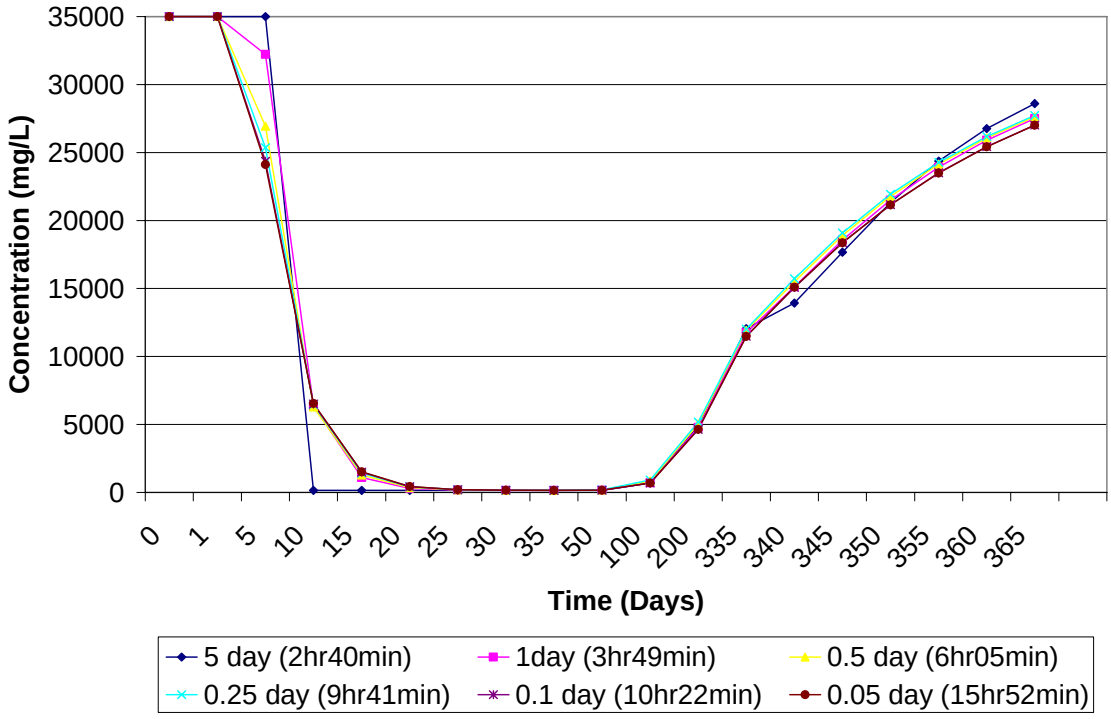

Note: Legend identifies the time step size of the injection and extraction cycles with the associated simulation time in parentheses

Figure A1 – Time Step Sensitivity Analysis

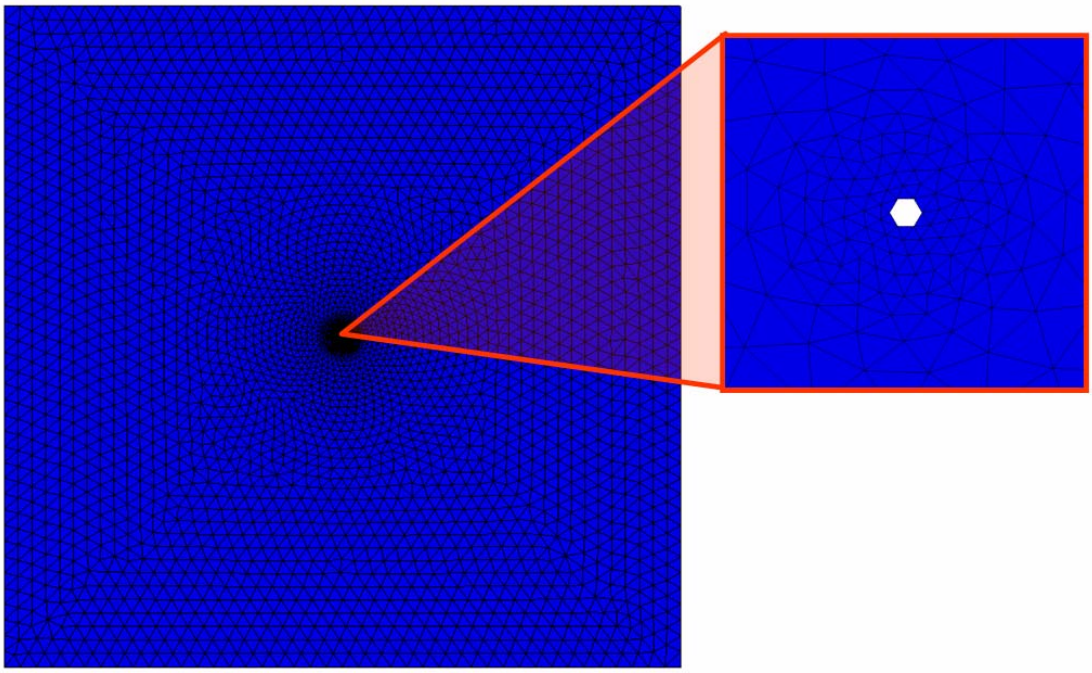

Figure A2a – Horizontal Mesh Resolution

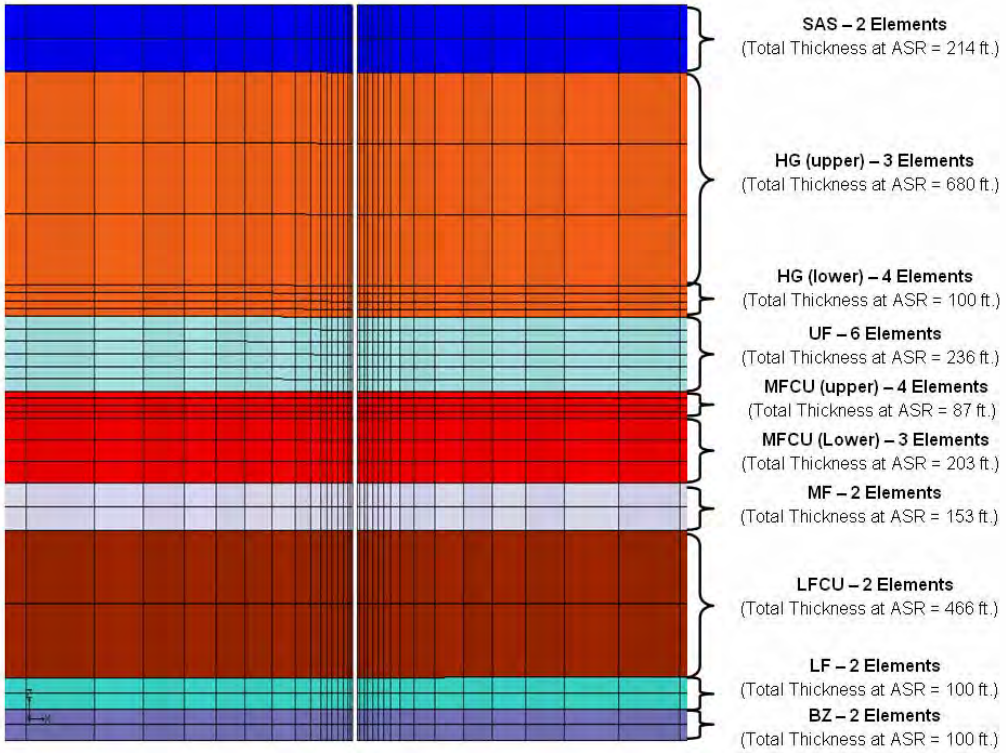

Figure A2b – Conceptual Geology and Vertical Mesh Resolution

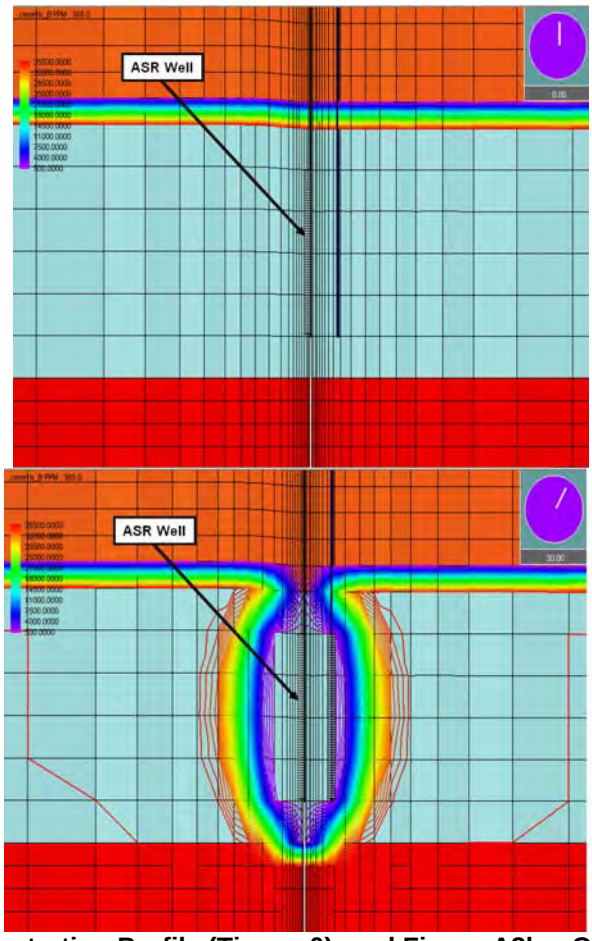

Figure A3a – Concentration Profile (Time = 0) and Figure A3b – Concentration Profile (Time = 30)

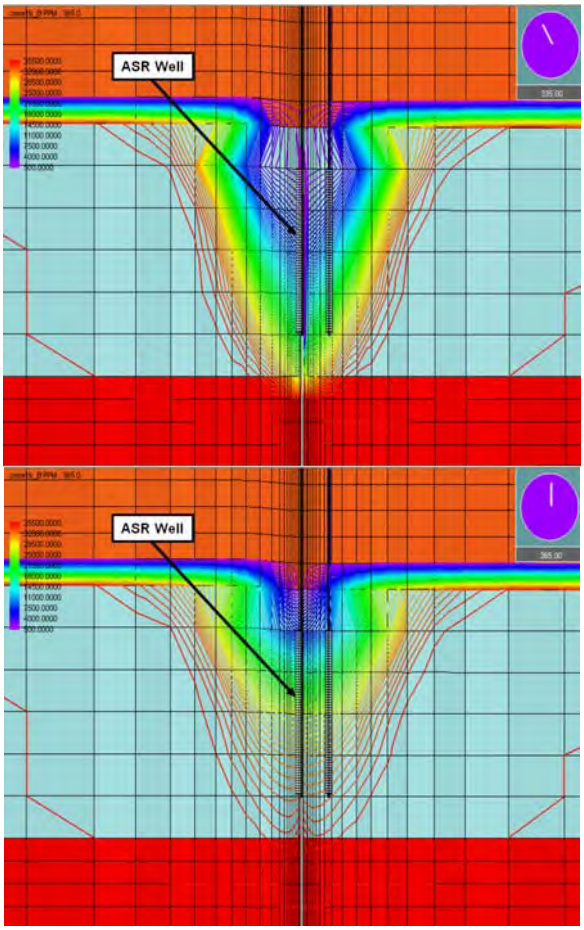

Figure A3c – Concentration Profile (Time = 335) and Figure A3d – Concentration Profile (Time = 365)

WASH123 Variable-Density Modeling Tests

Elder Model

Parameter	SEAWAT Value	SEAWAT Units	WASH123D (DB2) Value	WASH123D (DB2) Units	Remarks	File Location In WASH123D
Density of Fresh Water (p0)	1000	kg/m^3	1000	kg/m^3		UN1 (3) in *.glb
Density of Salt Water (p)	1200	kg/m^3	N/A	kg/m^3	Density of salt water is not a direct WASH input. It is calculated based on the "a" parameter calculated by the equation [p/p0 = 1 + aC] where p = density of H2O at saline concentration C and p0 is the density of water at a saline concentration of 0.	N/A
Alpha (a)	N/A	m^3/kg	0.2	m^3/kg	These values were revised for the DB2 run based on conversation with Pearce Cheng on 3/9/05. See runlog	UN2 (2) in *.glb
Salt Concentration Upper Boundary (Cs)	285.7	kg/m^3	1	molarity		XYS referenced by RS2 in *.3tp
Salt Concentration Lower Boundary (C)	0	kg/m^3	0	kg/m^3		XYS referenced by RS2 in *.3tp
Viscosity of Fresh Water	N/A		126.82	kg/(m*day)	SEAWAT report does not provide viscosity. Wash value converted from 2.65 slugs/(ft*day)	UN1 (4) in *.glb
Hydraulic Conductivity (Kf)	0.411	m/day	0.411	m/day	Assumed homogeneous	MP2 (2,3,4) in *.3bc
Modified Compressibility	N/A		0	(m*day^2)/kg	SEAWAT report does not provide. Assume incompressible	MP2 (8) in *.3bc
Porosity	0.1		0.1			MP2 (9) in *.3bc; MP5 (6) in *.3tp
Molecular Difusion	0.308	m^2/day	0.308	m^2/day		DF1 (2) in *.che
First Order Decay Constant for Salt	N/A		0	1/day	SEAWAT report does not provide. Assume 0.	DY1 (2) in *.che
Bulk Density	N/A		1500	kg/m^3	SEAWAT report does not provide. Assume material is sand with a bulk density of 1.5 kg/l or 1500 kg/m^3	MP5 (2) in *.3tp
Longitudinal Dispersivity	0	m	0	m		MP5 (3) in *.3tp
Transverse Dispersivity	0	m	0	m/m	In WASH this parameter is calcualted through a ratio (Tran/Long)	MP5 (4) in *.3tp
Tortuosity	N/A		1		SEAWAT report does not provide. Assume 1.	MP5 (5) in *.3tp

BASELINE ELDER INPUT PARAMETER COMPARISON

- March 2005 version of Wash Code
- PCG-1 Flow Solver
- Nodal/Gaussian Flow Quadrature
- PCG-2 Transport Solver
- Nodal/Gaussian Transport Quadrature
- Backwards Difference Non-linear Weighting

PREVIOUS ELDER MODEL RESULTS FOR COMPARISON

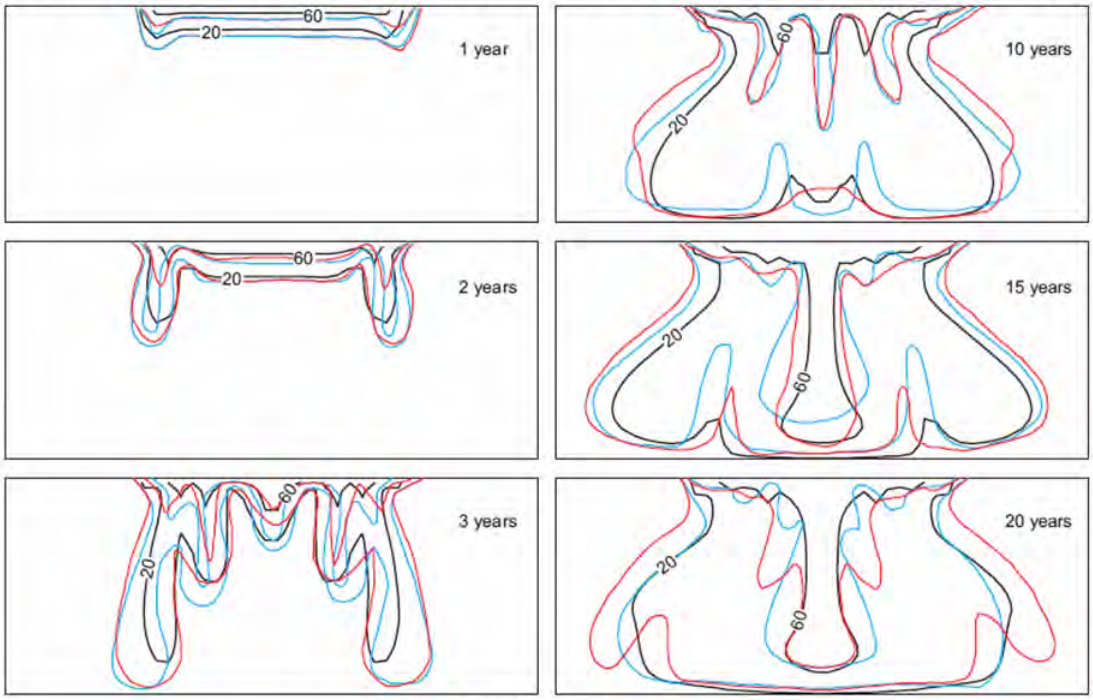

EXPLANATION

—20— SEAWAT line of relative salinity concentration, in percent

—20— SUTRA line of relative salinity concentration, in percent (Voss and Souza, 1987)

—20— Elder line of relative salinity concentration, in percent (Voss and Souza, 1987)

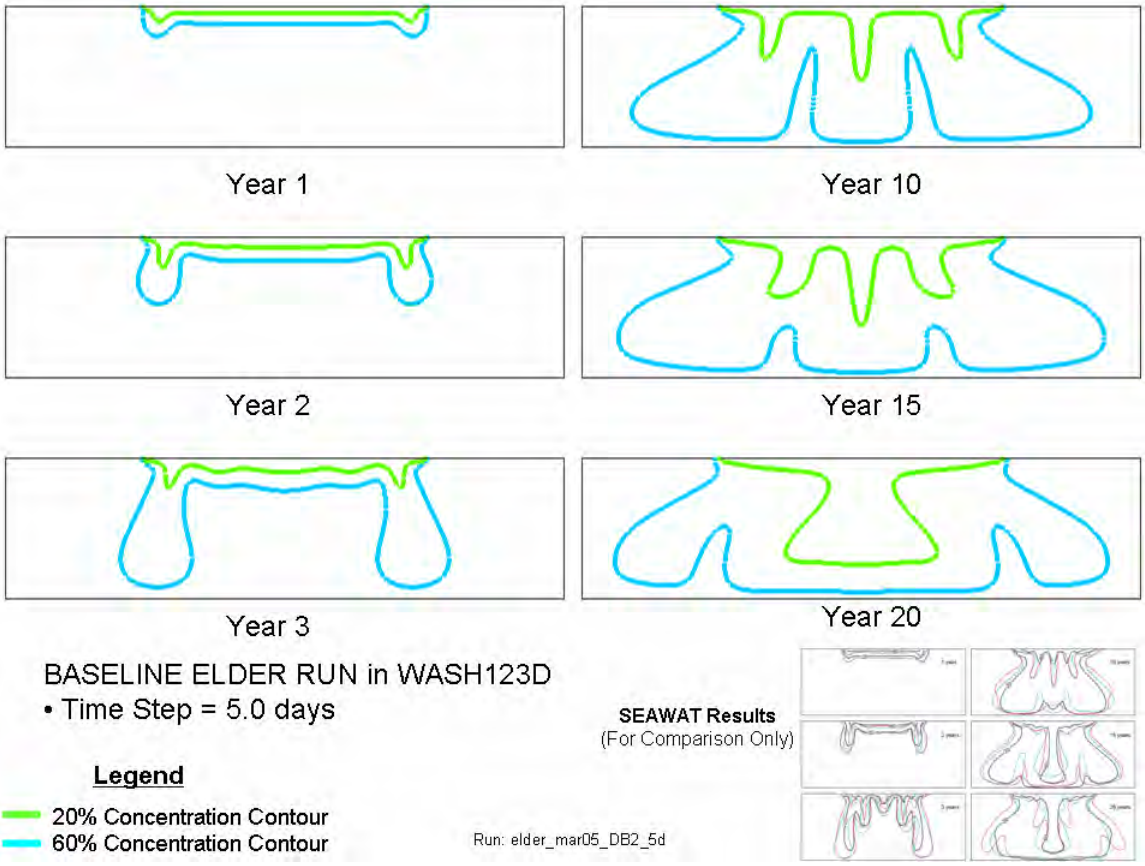
Year 1
Year 10
Year 2
Year 15
Year 3
Year 20
BASELINE ELDER RUN in WASH123D
• Time Step = 5.0 days
SEAWAT Results
(For Comparison Only)
Legend
20% Concentration Contour
60% Concentration Contour
Run: elder_mar05_DB2_5d

Henry Model

Results (at steady state)

Simulation run using WASH123D version January 2006

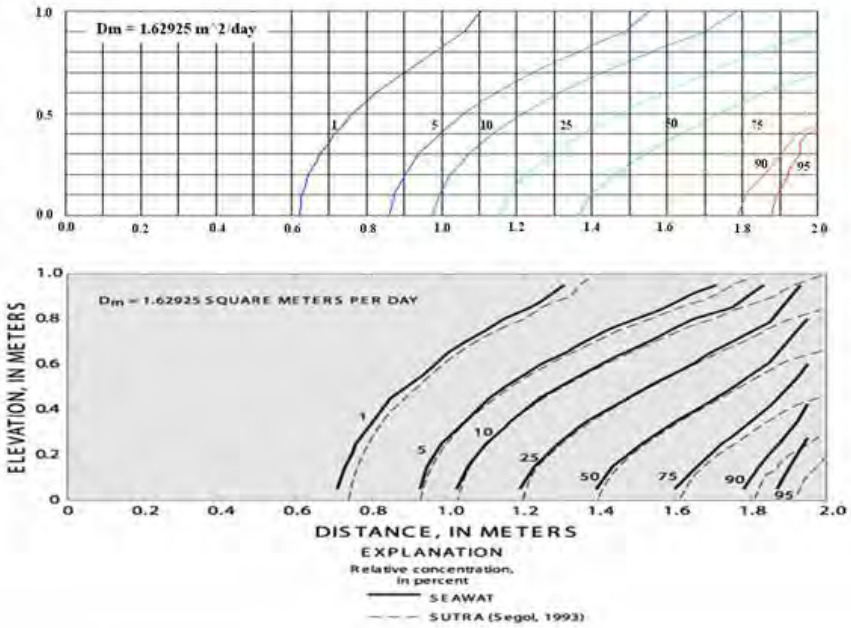

Appendix B

Journal Article to be Submitted by USGS – to be published under a separate cover

Landscape Figures for Main Report

Flow Initial Condition based on Head BC's defined below (no density effect/no pumping)
Concentration Initial Condition based on concentration BC's defined for each layer (constant for each layer)

					Flow Parameters									Density/Transport Parameters								Initial Conditions	
MODFLOW Cell Layer	WASH Element Layer	WASH Node Layer	WASH Material	Geologic Unit	Head BC West Tot Head (ft)	Head BC East Tot Head (ft)	Head BC North Tot Head (ft)	Head BC South Tot Head (ft)	Conductivity Horiz (ft/day)	Conductivity Vert. (ft/day)	Mod. Compress of Matrix (1/ft)	Specific Storage (1/ft)	Effective Porosity	Con. BC West (mg/L)	Con. BC East (mg/L)	Con. BC North (mg/L)	Con. BC South (mg/L)	Tortuosity	Bulk Density (slug/ft^3)	Dispersivity Long. (ft)	Dispersivity Trans. (ft)	Flow IC Tot Head (ft)	Con. IC (mg/L)
		1			20	20	No Flow	No Flow						150	150	N/A	N/A						150
1	1	2	1	SAS	20	20	No Flow	No Flow	100	10	1.70E-03	1.70E-03	0.25	150	150	N/A	N/A	1	3.784	0	0		150
	2	3	1	SAS	20	20	No Flow	No Flow	100	10	1.70E-03	1.70E-03	0.25	150	150	N/A	N/A	1	3.784	0	0		150
	3	4	2	HG	No Flow	No Flow	No Flow	No Flow	0.01	0.001	7.00E-07	1.19E-06	0.4	150	150	N/A	N/A	1	2.969	0	0		150
2,3,4,5	4	5	3	HG	No Flow	No Flow	No Flow	No Flow	0.01	0.001	7.00E-07	1.19E-06	0.4	250	250	N/A	N/A	1	2.969	0	0		250
	5	6	3	HG	50	30	No Flow	No Flow	0.01	0.001	7.00E-07	1.19E-06	0.4	500	500	N/A	N/A	1	2.969	0	0		500
	6	7	4	UF	50	30	No Flow	No Flow	100	10	7.00E-07	1.01E-06	0.25	4000	4000	N/A	N/A	1	3.784	0	0		4000
	7	8	4	UF	50	30	No Flow	No Flow	100	10	7.00E-07	1.01E-06	0.25	4000	4000	N/A	N/A	1	3.784	0	0		4000
6,7,8,9	8	9	4	UF	50	30	No Flow	No Flow	100	10	7.00E-07	1.01E-06	0.25	4000	4000	N/A	N/A	1	3.784	0	0		4000
	9	10	4	UF	50	30	No Flow	No Flow	100	10	7.00E-07	1.01E-06	0.25	4000	4000	N/A	N/A	1	3.784	0	0		4000
	10	11	4	UF	50	30	No Flow	No Flow	100	10	7.00E-07	1.01E-06	0.25	4000	4000	N/A	N/A	1	3.784	0	0		4000
	11	12	4	UF	50	30	No Flow	No Flow	100	10	7.00E-07	1.01E-06	0.25	4000	4000	N/A	N/A	1	3.784	0	0		4000
		13	5	MFCU	No Flow	No Flow	No Flow	No Flow	0.01	0.001	7.00E-07	1.07E-06	0.3	35000	35000	N/A	N/A	1	3.531	0	0		35000
10	12	14	5	MFCU	No Flow	No Flow	No Flow	No Flow	0.01	0.001	7.00E-07	1.07E-06	0.3	35000	35000	N/A	N/A	1	3.531	0	0		35000
	13	15	5	MFCU	40	20	No Flow	No Flow	0.01	0.001	7.00E-07	1.07E-06	0.3	35000	35000	N/A	N/A	1	3.531	0	0		35000
	14	16	6	MF	40	20	No Flow	No Flow	500	50	7.00E-07	1.01E-06	0.25	35000	35000	N/A	N/A	1	3.784	0	0		35000
11,12	15	17	6	MF	40	20	No Flow	No Flow	500	50	7.00E-07	1.01E-06	0.25	35000	35000	N/A	N/A	1	3.784	0	0		35000
	16	18	6	MF	40	20	No Flow	No Flow	500	50	7.00E-07	1.01E-06	0.25	35000	35000	N/A	N/A	1	3.784	0	0		35000
	17	19	7	LFCU	No Flow	No Flow	No Flow	No Flow	0.01	0.001	7.00E-07	1.07E-06	0.3	35000	35000	N/A	N/A	1	3.531	0	0		35000
13	18	20	7	LFCU	No Flow	No Flow	No Flow	No Flow	0.01	0.001	7.00E-07	1.07E-06	0.3	35000	35000	N/A	N/A	1	3.531	0	0		35000
		21			0	0	No Flow	No Flow						35000	35000	N/A	N/A						35000
	19	22	8	LF	0	0	No Flow	No Flow	5000	500	7.00E-07	1.01E-06	0.25	35000	35000	N/A	N/A	1	3.784	0	0		35000
14,15	20	23	8	LF	0	0	No Flow	No Flow	5000	500	7.00E-07	1.01E-06	0.25	35000	35000	N/A	N/A	1	3.784	0	0		35000
		24			0	0	No Flow	No Flow						35000	35000	N/A	N/A						35000
	21	25	9	BZ	0	0	No Flow	No Flow	10000	1000	7.00E-07	1.01E-06	0.25	35000	35000	N/A	N/A	1	3.784	0	0		35000
16	22	26	9	BZ	0	0	No Flow	No Flow	10000	1000	7.00E-07	1.01E-06	0.25	35000	35000	N/A	N/A	1	3.784	0	0		35000
		27			0	0	No Flow	No Flow						35000	35000	N/A	N/A						35000
				Model Top	Over Land = 20/Over Ocean = 20																			
				Model Bottom	No Flow																			

Based on Steady State Simulation with no pumping

Figure 1. Model Parameters for Case 1A.

Flow Initial Condition based on Head BC's defined below (no density effect/no pumping)
Concentration Initial Condition based on concentration BC's defined for each layer (constant for each layer)

					Flow Parameters									Density/Transport Parameters								Initial Conditions	
MODFLOW Cell Layer	WASH Element Layer	WASH Node Layer	WASH Material	Geologic Unit	Head BC West Tot Head (ft)	Head BC East Tot Head (ft)	Head BC North Tot Head (ft)	Head BC South Tot Head (ft)	Conductivity Horiz (ft/day)	Conductivity Vert. (ft/day)	Mod. Compress of Matrix (1/ft)	Specific Storage (1/ft)	Effective Porosity	Con. BC West (mg/L)	Con. BC East (mg/L)	Con. BC North (mg/L)	Con. BC South (mg/L)	Tortuosity	Bulk Density (slug/ft^3)	Dispersivity Long. (ft)	Dispersivity Trans. (ft)	Flow IC Tot Head (ft)	Con. IC (mg/L)
		1			20	20	No Flow	No Flow						150	150	N/A	N/A						150
1	1	2	1	SAS	20	20	No Flow	No Flow	100	10	1.70E-03	1.70E-03	0.25	150	150	N/A	N/A	1	3.784	0	0		150
	2	3	1	SAS	20	20	No Flow	No Flow	100	10	1.70E-03	1.70E-03	0.25	150	150	N/A	N/A	1	3.784	0	0		150
	3	4	2	HG	No Flow	No Flow	No Flow	No Flow	0.01	0.001	7.00E-07	1.19E-06	0.4	150	150	N/A	N/A	1	2.969	0	0		150
2,3,4,5	4	5	3	HG	No Flow	No Flow	No Flow	No Flow	0.01	0.001	7.00E-07	1.19E-06	0.4	250	250	N/A	N/A	1	2.969	0	0		250
	5	6	3	HG	50	30	No Flow	No Flow	0.01	0.001	7.00E-07	1.19E-06	0.4	35000	35000	N/A	N/A	1	2.969	0	0		35000
	6	7	4	UF	50	30	No Flow	No Flow	100	10	7.00E-07	1.01E-06	0.25	35000	35000	N/A	N/A	1	3.784	0	0		35000
	7	8	4	UF	50	30	No Flow	No Flow	100	10	7.00E-07	1.01E-06	0.25	35000	35000	N/A	N/A	1	3.784	0	0		35000
6,7,8,9	8	9	4	UF	50	30	No Flow	No Flow	100	10	7.00E-07	1.01E-06	0.25	35000	35000	N/A	N/A	1	3.784	0	0		35000
	9	10	4	UF	50	30	No Flow	No Flow	100	10	7.00E-07	1.01E-06	0.25	35000	35000	N/A	N/A	1	3.784	0	0		35000
	10	11	4	UF	50	30	No Flow	No Flow	100	10	7.00E-07	1.01E-06	0.25	35000	35000	N/A	N/A	1	3.784	0	0		35000
	11	12	4	UF	50	30	No Flow	No Flow	100	10	7.00E-07	1.01E-06	0.25	35000	35000	N/A	N/A	1	3.784	0	0		35000
	12	13	5	MFCU	No Flow	No Flow	No Flow	No Flow	0.01	0.001	7.00E-07	1.07E-06	0.3	35000	35000	N/A	N/A	1	3.531	0	0		35000
10	13	14	5	MFCU	No Flow	No Flow	No Flow	No Flow	0.01	0.001	7.00E-07	1.07E-06	0.3	35000	35000	N/A	N/A	1	3.531	0	0		35000
	14	15	5	MFCU	40	20	No Flow	No Flow	0.01	0.001	7.00E-07	1.07E-06	0.3	35000	35000	N/A	N/A	1	3.531	0	0		35000
	15	16	6	MF	40	20	No Flow	No Flow	500	50	7.00E-07	1.01E-06	0.25	35000	35000	N/A	N/A	1	3.784	0	0		35000
11,12	16	17	6	MF	40	20	No Flow	No Flow	500	50	7.00E-07	1.01E-06	0.25	35000	35000	N/A	N/A	1	3.784	0	0		35000
	17	18	7	LFCU	No Flow	No Flow	No Flow	No Flow	0.01	0.001	7.00E-07	1.07E-06	0.3	35000	35000	N/A	N/A	1	3.531	0	0		35000
13	18	19	7	LFCU	0	0	No Flow	No Flow	0.01	0.001	7.00E-07	1.07E-06	0.3	35000	35000	N/A	N/A	1	3.531	0	0		35000
	19	20	8	LF	0	0	No Flow	No Flow	5000	500	7.00E-07	1.01E-06	0.25	35000	35000	N/A	N/A	1	3.784	0	0		35000
14,15	20	21	8	LF	0	0	No Flow	No Flow	5000	500	7.00E-07	1.01E-06	0.25	35000	35000	N/A	N/A	1	3.784	0	0		35000
	21	22	9	BZ	0	0	No Flow	No Flow	10000	1000	7.00E-07	1.01E-06	0.25	35000	35000	N/A	N/A	1	3.784	0	0		35000
16	22	23	9	BZ	0	0	No Flow	No Flow	10000	1000	7.00E-07	1.01E-06	0.25	35000	35000	N/A	N/A	1	3.784	0	0		35000
				Model Top	Over Land = 20/Over Ocean = 20																		
				Model Bottom	No Flow																		

Based on Steady State Simulation with no pumping

Figure 2. Model Parameters for Case 1B.

Flow Initial Condition based on Head BC's defined below (no density effect/no pumping)
Concentration Initial Condition based on concentration BC's defined for each layer (constant for each layer)

					Flow Parameters									Density/Transport Parameters								Initial Conditions	
MODFLOW Cell Layer	WASH Element Layer	WASH Node Layer	WASH Material	Geologic Unit	Head BC West Tot Head (ft)	Head BC East Tot Head (ft)	Head BC North Tot Head (ft)	Head BC South Tot Head (ft)	Conductivity Horiz (ft/day)	Conductivity Vert. (ft/day)	Mod. Compress of Matrix (1/ft)	Specific Storage (1/ft)	Effective Porosity	Con. BC West (mg/L)	Con. BC East (mg/L)	Con. BC North (mg/L)	Con. BC South (mg/L)	Tortuosity	Bulk Density (slug/ft^3)	Dispersivity Long. (ft)	Dispersivity Trans. (ft)	Flow IC Tot Head (ft)	Con. IC (mg/L)
		1			20	20	No Flow	No Flow						150	150	N/A	N/A						150
1	1	2	1	SAS	20	20	No Flow	No Flow	100	10	1.70E-03	1.70E-03	0.25	150	150	N/A	N/A	1	3.784	0	0		150
	2		1	SAS					100	10	1.70E-03	1.70E-03	0.25					1	3.784	0	0		
		3			20	20	No Flow	No Flow						150	150	N/A	N/A						150
	3	4	2	HG	No Flow	No Flow	No Flow	No Flow	0.01	0.001	7.00E-07	1.19E-06	0.4	150	150	N/A	N/A	1	2.969	0	0		150
2,3,4,5	4		3	HG					0.01	0.001	7.00E-07	1.19E-06	0.4					1	2.969	0	0		
	5	5	3	HG	No Flow	No Flow	No Flow	No Flow	0.01	0.001	7.00E-07	1.19E-06	0.4	250	250	N/A	N/A	1	2.969	0	0		250
		6			50	30	No Flow	No Flow						500	500	N/A	N/A						500
	6	7	4	UF	50	30	No Flow	No Flow	100	10	7.00E-07	1.01E-06	0.25	4000	4000	N/A	N/A	1	3.784	0	0		4000
	7	8	4	UF	50	30	No Flow	No Flow	100	10	7.00E-07	1.01E-06	0.25	4000	4000	N/A	N/A	1	3.784	0	0		4000
	8	9	4	UF	50	30	No Flow	No Flow	100	10	7.00E-07	1.01E-06	0.25	4000	4000	N/A	N/A	1	3.784	0	0		4000
6,7,8,9	9	10	4	UF	50	30	No Flow	No Flow	100	10	7.00E-07	1.01E-06	0.25	4000	4000	N/A	N/A	1	3.784	0	0		4000
	10	11	4	UF	50	30	No Flow	No Flow	100	10	7.00E-07	1.01E-06	0.25	4000	4000	N/A	N/A	1	3.784	0	0		4000
	11		4	UF					100	10	7.00E-07	1.01E-06	0.25					1	3.784	0	0		
		12			50	30	No Flow	No Flow						4000	4000	N/A	N/A						4000
	12	13	5	MFCU	No Flow	No Flow	No Flow	No Flow	1	1	7.00E-07	1.07E-06	0.3	35000	35000	N/A	N/A	1	3.531	0	0		35000
10	13	14	5	MFCU	No Flow	No Flow	No Flow	No Flow	1	1	7.00E-07	1.07E-06	0.3	35000	35000	N/A	N/A	1	3.531	0	0		35000
	14		5	MFCU					1	1	7.00E-07	1.07E-06	0.3					1	3.531	0	0		
		15			40	20	No Flow	No Flow						35000	35000	N/A	N/A						35000
	15	16	6	MF	40	20	No Flow	No Flow	500	50	7.00E-07	1.01E-06	0.25	35000	35000	N/A	N/A	1	3.784	0	0		35000
11,12	16		6	MF					500	50	7.00E-07	1.01E-06	0.25					1	3.784	0	0		
		17			40	20	No Flow	No Flow						35000	35000	N/A	N/A						35000
	17	18	7	LFCU	No Flow	No Flow	No Flow	No Flow	0.01	0.001	7.00E-07	1.07E-06	0.3	35000	35000	N/A	N/A	1	3.531	0	0		35000
13	18		7	LFCU					0.01	0.001	7.00E-07	1.07E-06	0.3					1	3.531	0	0		
		19			0	0	No Flow	No Flow						35000	35000	N/A	N/A						35000
	19	20	8	LF	0	0	No Flow	No Flow	5000	500	7.00E-07	1.01E-06	0.25	35000	35000	N/A	N/A	1	3.784	0	0		35000
14,15	20		8	LF					5000	500	7.00E-07	1.01E-06	0.25					1	3.784	0	0		
		21			0	0	No Flow	No Flow						35000	35000	N/A	N/A						35000
	21	22	9	BZ	0	0	No Flow	No Flow	10000	1000	7.00E-07	1.01E-06	0.25	35000	35000	N/A	N/A	1	3.784	0	0		35000
16	22		9	BZ					10000	1000	7.00E-07	1.01E-06	0.25					1	3.784	0	0		
		23			0	0	No Flow	No Flow						35000	35000	N/A	N/A						35000
				Model Top	Over Land = 20/Over Ocean = 20																			
				Model Bottom	No Flow																			

Based on Steady State Simulation with no pumping

Figure 3. Model Parameters for Case 1C.

Flow Initial Condition based on Head BC's defined below (no density effect/no pumping)
Concentration Initial Condition based on concentration BC's defined for each layer (constant for each layer)

					Flow Parameters									Density/Transport Parameters								Initial Conditions	
MODFLOW Cell Layer	WASH Element Layer	WASH Node Layer	WASH Material	Geologic Unit	Head BC West Tot Head (ft)	Head BC East Tot Head (ft)	Head BC North Tot Head (ft)	Head BC South Tot Head (ft)	Conductivity Horiz (ft/day)	Conductivity Vert. (ft/day)	Mod. Compress of Matrix (1/ft)	Specific Storage (1/ft)	Effective Porosity	Con. BC West (mg/L)	Con. BC East (mg/L)	Con. BC North (mg/L)	Con. BC South (mg/L)	Tortuosity	Bulk Density (slug/ft^3)	Dispersivity Long. (ft)	Dispersivity Trans. (ft)	Flow IC Tot Head (ft)	Con. IC (mg/L)
		1			20	20	No Flow	No Flow						150	150	N/A	N/A						150
1	1	2	1	SAS	20	20	No Flow	No Flow	100	10	1.70E-03	1.70E-03	0.25	150	150	N/A	N/A	1	3.784	25	25		150
	2	3	1	SAS	20	20	No Flow	No Flow	100	10	1.70E-03	1.70E-03	0.25	150	150	N/A	N/A	1	3.784	25	25		150
	3	4	2	HG	No Flow	No Flow	No Flow	No Flow	0.01	0.001	7.00E-07	1.19E-06	0.4	150	150	N/A	N/A	1	2.969	25	25		150
2,3,4,5	4	5	3	HG	No Flow	No Flow	No Flow	No Flow	0.01	0.001	7.00E-07	1.19E-06	0.4	250	250	N/A	N/A	1	2.969	25	25		250
	5	6	3	HG	50	30	No Flow	No Flow	0.01	0.001	7.00E-07	1.19E-06	0.4	500	500	N/A	N/A	1	2.969	25	25		500
	6	7	4	UF	50	30	No Flow	No Flow	100	10	7.00E-07	1.01E-06	0.25	4000	4000	N/A	N/A	1	3.784	25	25		4000
	7	8	4	UF	50	30	No Flow	No Flow	100	10	7.00E-07	1.01E-06	0.25	4000	4000	N/A	N/A	1	3.784	25	25		4000
	8	9	4	UF	50	30	No Flow	No Flow	100	10	7.00E-07	1.01E-06	0.25	4000	4000	N/A	N/A	1	3.784	25	25		4000
6,7,8,9	9	10	4	UF	50	30	No Flow	No Flow	100	10	7.00E-07	1.01E-06	0.25	4000	4000	N/A	N/A	1	3.784	25	25		4000
	10	11	4	UF	50	30	No Flow	No Flow	100	10	7.00E-07	1.01E-06	0.25	4000	4000	N/A	N/A	1	3.784	25	25		4000
	11	12	4	UF	50	30	No Flow	No Flow	100	10	7.00E-07	1.01E-06	0.25	4000	4000	N/A	N/A	1	3.784	25	25		4000
																						Based on Steady State Simulation with no pumping	
	12	13	5	MFCU	No Flow	No Flow	No Flow	No Flow	0.01	0.001	7.00E-07	1.07E-06	0.3	35000	35000	N/A	N/A	1	3.531	25	25		35000
10	13	14	5	MFCU	No Flow	No Flow	No Flow	No Flow	0.01	0.001	7.00E-07	1.07E-06	0.3	35000	35000	N/A	N/A	1	3.531	25	25		35000
	14	15	5	MFCU	40	20	No Flow	No Flow	0.01	0.001	7.00E-07	1.07E-06	0.3	35000	35000	N/A	N/A	1	3.531	25	25		35000
	15	16	6	MF	40	20	No Flow	No Flow	500	50	7.00E-07	1.01E-06	0.25	35000	35000	N/A	N/A	1	3.784	25	25		35000
11,12	16	17	6	MF	40	20	No Flow	No Flow	500	50	7.00E-07	1.01E-06	0.25	35000	35000	N/A	N/A	1	3.784	25	25		35000
	17	18	7	LFCU	No Flow	No Flow	No Flow	No Flow	0.01	0.001	7.00E-07	1.07E-06	0.3	35000	35000	N/A	N/A	1	3.531	25	25		35000
13	18	19	7	LFCU	0	0	No Flow	No Flow	0.01	0.001	7.00E-07	1.07E-06	0.3	35000	35000	N/A	N/A	1	3.531	25	25		35000
	19	20	8	LF	0	0	No Flow	No Flow	5000	500	7.00E-07	1.01E-06	0.25	35000	35000	N/A	N/A	1	3.784	25	25		35000
14,15	20	21	8	LF	0	0	No Flow	No Flow	5000	500	7.00E-07	1.01E-06	0.25	35000	35000	N/A	N/A	1	3.784	25	25		35000
	21	22	9	BZ	0	0	No Flow	No Flow	10000	1000	7.00E-07	1.01E-06	0.25	35000	35000	N/A	N/A	1	3.784	25	25		35000
16	22	23	9	BZ	0	0	No Flow	No Flow	10000	1000	7.00E-07	1.01E-06	0.25	35000	35000	N/A	N/A	1	3.784	25	25		35000
				Model Top	Over Land = 20/Over Ocean = 20																		
				Model Bottom	No Flow																		

Figure 4. Model Parameters for Case 1D.

Draft

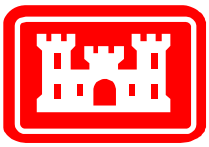

U.S. Army Corps of Engineers
Philadelphia District

Draft ASR Regional Study
Phase I - Groundwater Modeling

Prepared for
U.S. Army Corps of Engineers
Jacksonville District

and

South Florida Water Management District

Prepared by
U.S. Army Corps of Engineers
Philadelphia District

December 2006

Draft ASR Regional Study
Phase I – Groundwater Modeling
December 2006

Table of Contents

List of Figures

1.0 INTRODUCTION

The U.S. Army Corps of Engineers (USACE), Philadelphia District, has prepared this report for the USACE, Jacksonville District, and the South Florida Water Management District (SFWMD) in support of the Comprehensive Everglades Restoration Plan (CERP). Aquifer Storage and Recovery (ASR) is one of the proposed alternatives recommended by the CERP to help with water supply, storage, and distribution in South Florida. The CERP recommends approximately 333 ASR wells distributed over a large region with well field clusters proposed within the Floridan Aquifer System (FAS) near Lake Okeechobee, near the proposed C-43 reservoir in Hendry County, and at several locations along the Lower East Coast in Palm Beach and Broward Counties. The proposed plan, with an injection and recovery pumping rate of approximately 1.65 billion gallons per day, is larger than any currently operating ASR project. To evaluate the numerous design considerations and the variation in aquifer response on regional, sub-regional, and local scales, density-dependent numerical modeling of the FAS is required as discussed in the ASR Regional Study Project Management Plan developed in 2003.

The ASR Regional Study – Benchscale Modeling report (Brown et al, 2006) evaluated several density-dependent flow and transport modeling codes. Two codes were selected for use in the ASR Regional Modeling application: the finite element code, WASH123D (Yeh et al., 1998) and the finite difference code, SEAWAT (Langevin et al, 2003, and Guo and Langevin, 2002). The two models were selected as the best of those evaluated to address the maximum number of questions regarding the ASR Regional Study and to reduce technical uncertainties that might arise from the proposed CERP ASR plan. Some of the issues to be addressed by the two models include potential regional changes in aquifers heads, flows, and water quality, the potential for salt water intrusion caused by ASR pumping, regional impacts to wells completed in the FAS, and ASR design, siting, layout, and performance considerations. The WASH123D and SEAWAT models, under development simultaneously, encompass a peninsula-wide area of approximately 39,000 square miles extending from Polk County to Florida Bay (Figure 1).

The regional modeling effort was divided into 2 Phases because of its extent and complexity. The Phase I model is a coarse test bed for the more refined Phase II model. Specific goals of the Phase I and Phase II models are:

Phase I

- Identify model boundaries and test model boundary parameters
- Identify regional flow and salt migration pathways
- Identify the timing of salt water intrusion
- Evaluate model run times and model sensitivity to time step sizes
- Test hydraulic and transport parameter sensitivity
- Compare WASH123D and SEAWAT results

Phase II

- Identify areas of the Phase I model for refinement
- Incorporate regional-scale transient groundwater withdrawal

- Calibrate density-dependent flow and transport results to observed measurements in major geologic units
- Select sites and determine refinement locations to incorporate ASR well field clusters
- Evaluate proposed ASR project alternatives effects on aquifer heads, flows, and water quality; for pressure-induced changes; for increased potential for salt-water intrusion; and on withdrawals for existing well users

The focus of this report is the Phase I Regional Modeling. This Phase I effort includes regional conceptualization, estimates of hydraulic and transport parameters, density-dependent 3-D groundwater model construction, gross comparisons to head and concentration data, evaluation of flow and transport patterns, and sensitivity analyses to several model parameters. Each of these tasks and analyses provide a greater understanding of the flow and transport system that makes up the majority of the Florida subsurface. This increased understanding provides a platform on which to build in the additional complexities of the Phase II model.

2.0 PHASE I REGIONAL MODELING APPROACH AND ASSUMPTIONS

The primary objective of the Phase I model is to identify the parameters and issues that will be most important when building the more-detailed Phase II model. The Phase I model is a coarse resolution regional-scale model constructed based on several simplifying assumptions. The simplifying assumptions are intended to maintain the model ability to represent the regional flow and transport patterns while facilitating model construction and reducing model run times. This section introduces the most significant model assumptions. Model conceptual and construction details are presented in Sections 3 and 4.

For the Phase I modeling effort, it was assumed that porous media models adequately and accurately represent the system modeled for both flow and transport. The impact of lineament and/or fracture flow was not included in the Phase I model, but may be significant as discussed in Section 5.

The boundary used for the Phase I model was approximately twenty miles offshore to reduce the effects of boundary conditions on model results and to attempt to simplify boundary condition assignments. The horizontal model resolution was coarse to decrease the model run times and to allow long-term simulations to be investigated.

Geologic interpretations were based on previous ASR Regional Study reports discussed in Section 3. The model focuses on the FAS, the geologic units where the ASR wells are proposed. Geologic units that are shallower and deeper than the FAS are incorporated to the Phase I model with geologic information that is greatly simplified and functions only to provide flow and salinity interaction with the FAS. Unsaturated flow in the surface aquifers is omitted as it is not pertinent to the model objectives. Therefore the top of the model is assumed to be the water table surface rather than ground topography.

Pumping wells are omitted from the Phase I model. The coarse resolution of the model makes incorporating pumping wells difficult. Also, model parameter assignments can be simplified without the inclusion of pumping wells. The omission of pumping has a significant effect on the results; however, these "pre-development" results can provide an overall picture of flow and transport patterns.

Flow boundary conditions around the model perimeter are specified as constant heads that do not vary in time. This simplification was made to reduce the amount of data collection required for the Phase I model. The heads specified at the boundaries are considered as "pre-development" heads because there is no pumping in the model. Pre-development boundary heads were assembled based on pre-development head contours generated by USGS (Bush and Johnston, 1988) and by selecting the highest consistent values at selected wells from online databases. Although the boundary heads were based on available data, some interpretation was required for boundaries that either did not have adequate water level data or that did not intersect the ocean, where head values are known. As discussed later in this report, the heads assigned to these boundaries were extensively tested until reasonable regional flow patterns were developed. The head data in the surface aquifer were utilized to specify the model surface head boundary instead of estimating recharge based on precipitation and evapo-transpiration. This assumption is reasonable since only the surface aquifer flow interaction with the Floridan aquifers is necessary to meet the ASR model objectives. No flow is assumed to enter or exit the model from the bottom.

Boundary conditions for salt concentrations also were set around the perimeter of the model. Water quality data from SFWMD and online databases were used to estimate the salt concentration around the boundary. Much less water quality data were available than head data so considerable interpolation and extrapolation was necessary to determine the boundary concentrations. Due to this uncertainty, sensitivities were performed on the type of boundary condition used, fixed or variable, as well as on concentrations specified. These sensitivities were completed for both the aquifer perimeter and model bottom. The concentration boundary conditions on the model surface were fixed as fresh water over land and seawater over the ocean. These estimates of boundary concentrations are sufficient to generate and test transport patterns for this investigation. Further discussion of these sensitivity analyses is presented in Sections 5 and 6.

The effect of heat transfer was not considered for the Phase I model and is not currently within the scope of the ASR Regional Study effort. Heat transfer may be important as a primary mechanism for salt intrusion based on the convectional cell theory (Kohout 1965). The convectional cell theory states that salt water upwells from deep geologic units based on the geothermal reduction of water density. For the Phase I model, it is assumed that the temperature variation does not have a significant impact on the water density. Although heat transfer is not considered, limited temperature effects within the deepest model aquifer are examined as part of the sensitivity analyses (Section 5).

Variable density models must be run under transient conditions to allow the system to equilibrate over time and because solute transport calculations always are performed under transient conditions. The duration of the simulations was dictated by recent

groundwater age research as discussed in Section 3.4 and 4.4. Steady state runs were done first to provide initial conditions for the transient simulations to help the solution converge on an answer more quickly. Once steady state results compared reasonably with monitoring data, long-term transient simulations were completed. The transient results were used as a basis for several sensitivity tests.

The Phase I modeling was performed using both WASH123D and SEAWAT codes. The model parameters used to produce results comparable with monitoring well data were determined using the WASH123D model runs. Subsequently, the WASH123D model configuration and parameters were used, with conversion to the proper format, to complete a comparable model run in SEAWAT. The differences in the results from the two codes are compared and evaluated. In addition, sensitivities were performed for both models to evaluate the effects of several parameters. This approach helped evaluate the sensitivity of each model to variations in input data, as well as similarities and differences between the two codes.

3.0 CONCEPTUAL MODEL

A conceptual model was developed for the system to identify all known hydrologic and hydrogeologic factors that influence flow and transport. The factors include sources/sinks, the boundary of the model domain, and stratigraphy. The conceptual model provides an understanding of observed groundwater flow directions and transport pathways and helps determine the dimensions and important features of the numerical model.

A wealth of geologic and hydrogeologic data exists across the region. As part of previous ASR Regional Study tasks, certain information was collected and evaluated for use in the Phase I model. Reese and Richardson (2004) compiled The Draft-Final Report – Task 3.0 Define Preliminary Hydrogeologic Framework, (referred to herein as the Preliminary Hydrogeologic Framework), which presents an evaluation of regionally significant works and new data to generate a consistent hydrostratigraphic and hydrogeologic visualization of the Florida peninsula subsurface from Orlando to Key West. A further assessment of geologic and hydrogeologic data is presented by CH2MHill (2006) in Groundwater Numerical Model Development Support and Data Collection Report, (referred to herein as the Data Collection Report). The Data Collection Report provides a review of the Preliminary Hydrogeologic Framework together with geologic and hydrogeologic data used for eight existing numerical models of various scales and resolutions across the peninsula (Figure 2). Also included in the Data Collection Report is a dispersion research study that gathered and tabulated dispersion data from technical reports of similar geologic environments around the world. Additional information for the Phase I conceptual model was collected from other sources listed in the References section and from online databases including SFWMD's DBHYDRO, USGS's South Florida Information Access (SOFIA), and the National Park Service's South Florida Natural Resources Center (SFNRC).

All geographic information associated with geologic and hydrogeologic data was converted to the following coordinates:

- Horizontal geographic data – Florida East State Plane 1983 (FESP 83)
- Vertical geographic data – National Geodetic Vertical Datum 1929 (NGVD)

3.1 CONCEPTUAL GEOLOGIC FRAMEWORK

The conceptual geology is based predominantly on the findings documented in the Preliminary Hydrogeologic Framework. For that report, key wells were reviewed to correlate major aquifers and confining units of the FAS. Figure 3, taken from Table 1 of the Preliminary Hydrogeologic Framework, shows the resulting Regional Study schematic cross section representing the geologic units that are defined for the numerical models. The Preliminary Hydrogeologic Framework also defined hydrostratigraphic surfaces for the geologic units and hydraulic parameters for the FAS units. Hydrostratigraphic surfaces define the depth and thickness of the geologic units over the study area. (Figure 4). Hydraulic parameters were generated for the Upper Floridan (UF), Middle Floridan (MF), Lower Floridan (LF), Upper Middle Confining Unit (MC1), Lower Middle Confining Unit (MC2), and the Lower Confining Unit (LC) (Figures 5, 6, 7, 8, 9 and 10, respectively). The transmissivity of the Boulder Zone (BZ) was estimated to be on the order of 10^6 to 10^7 ft^2/d. Details regarding the correlation of the geologic units and the definition of the hydrostratigraphic surfaces and hydrogeologic parameters for the FAS can be found in the Preliminary Hydrogeologic Framework.

The Preliminary Hydrogeologic Framework defines the hydrostratigraphic surface between the Intermediate Confining Unit/Intermediate Aquifer System (IC/IA) and the Surficial Aquifer System (SAS) but does not define hydraulic parameters for those units. These two units are both complex systems of alternating aquifers and confining units. Part of the conceptualization of the IC/IA and SAS is to greatly simplify these units because they are not the focus of this modeling effort. The primary function of these two units in the Regional Model is to permit water to enter the FAS, where the ASR wells are proposed.

Hydraulic parameters for the IC/IA were composited from information in the Data Collection Report. All of the eight numerical models reviewed for the Data Collection report provide ranges and distributions of hydraulic parameters for portions of the IC/IA. The IC is represented as a thick semi-confining and confining unit that retards flow between the SAS and IA or between the SAS and UF, where the IA is not present. The IA is found only in west-central and southwest Florida. The lateral extent of the IA is shown in Randazzo and Jones (1997), Figure 6.23.

The hydraulic conductivities for the SAS were based on a figure generated by SFWMD (Figure 11). The lateral extent of the SAS is shown in Randazzo and Jones (1997), Figure 6.6. In the northwest corner of the model area, the SAS pinches out and the IC/IA is present at the surface. For this Phase I model, this simplified SAS layer acts primarily as a boundary condition providing the driving flow into and out of the FAS.

3.2 DISCHARGE AND RECHARGE

Discharge from the system is mainly to the Atlantic Ocean or Gulf of Mexico and also to surface water features, such as rivers, lakes, streams, canals. Although the numerous agricultural and municipal pumping wells are a significant discharge from the system, no pumping is included in the Phase I model. Without pumping, all heads generated by the Phase I model are considered to be "predevelopment heads". Regional pumping information, including locations, open hole depths, and transient pumping rates, will be assembled and assessed for model input to the Phase II model.

Recharge to the system is mainly attributed to infiltration to ground water from precipitation. Infiltration can be difficult to quantify, especially over such a large region, as it depends on obtaining transient precipitation gage information and estimating evapo-transpiration rates and land-use information. Correctly quantifying infiltration would facilitate computing correct heads within the SAS that make up the driving head through the IC/IA to the FAS. Because the SAS heads are important mainly as a surface boundary condition, the head data in the SAS was set based on observations rather than estimating several parameters to compute head data in the SAS layer. This simplifying assumption facilitates model construction and should not have an adverse effect on the computed results in the FAS, the primary area of concern for the Regional Study.

Head data from SAS monitoring wells was gathered and used to specify the heads over the surface of the model domain. SAS monitoring well head data was gathered from a number of sources, including online databases, a depth-to-water grid from the Florida Geological Survey (FGS), Reese and Cunningham (2000), and model results from Sepulveda, 2002. Not all SAS monitoring well head data available in online databases were used. SAS wells that form well clusters with wells screened in lower geologic units were favored. Additional SAS wells were selected to obtain an adequate coverage over the model area. Also notable is that transient data sets available for SAS monitoring wells were condensed into a constant head value that represents the highest consistent value over the period of record. The highest consistent value for the period of record of each well was chosen as a representation of the predevelopment condition for the Phase I model. The highest consistent value for the SAS was selected from all the aquifers present in a particular region, including artesian aquifers that exist in the SAS. As a result, some of the SAS heads selected are actually above ground surface, such as those beneath the Caloosahatchee River Basin west of Lake Okeechobee.

Figure 12 shows the surface head distribution and values over the peninsula. The FGS depth-to-water grid data is not shown in the figure because the data density is too large for clarity. The FGS data compares favorably with the data shown in Figure 12 except where artesian values were selected.

Figure 12 shows the highest head values and the area of most significant recharge are in the Polk County area with values as high as 175 ft NGVD. Much lower heads are found across the large area south of Lake Okeechobee, where head values range from 0 to 20 feet NGVD.

3.3 ANALYSIS OF MONITORING WELL DATA

Visualization of regional groundwater elevation and water quality data provides an understanding of groundwater flow patterns and the location and movement of the salt water concentrations over time. The visualization was performed using the Department of Defense's Groundwater Modeling System (GMS) version 6.0. Head monitoring data for numerous wells across South Florida is contained within online databases, but not all wells were used. Wells clusters were chosen to see the relative changes in different geologic units, and additional wells were selected to allow for adequate coverage across the unit. From the transient head data set available at a particular well, only the highest consistent value was chosen to represent predevelopment conditions. These datasets were also used to compare with the computed results of the Phase I model.

Figure 13 shows the predevelopment head distribution and values for the UF as collected from selected wells in online databases, model results from Sepulveda (2002), and from Development of a Density-Dependent Saltwater Intrusion Model for the Lower East Coast Project Area, prepared by HydroGeoLogic, Inc., April 2006. Also shown in the figure are contours of UF predevelopment heads generated by USGS (Bush and Johnston, 1988). This data gives the overall flow pattern of UF predevelopment heads. The primary inflow to the UF is in the Polk County area. Groundwater flows radially from the high point in Polk County toward the eastern and western coasts and to the south from the central ridge of higher heads.

Figure 14 shows that less head information was evaluated in the MF. The data were collected from online databases and HydroGeoLogic, Inc., April 2006. Generally the MF heads seem similar to the UF heads with the highest heads in the Polk County area. Lower heads are found in all directions surrounding the highest head in Polk County.

Head information for the LF was gathered from HydroGeoLogic, Inc., April 2006, from online databases and from Hydrogeology and Water-Quality Characteristics of the Lower Floridan Aquifer in East-Central Florida (O'Reilly et al., 2002) as shown in Figure 15. These head values are generally lower than the UF and MF heads. Much lower heads in the LF are found in the southern counties. In the northern counties, especially Polk County, the heads are somewhat lower but more similar to those observed in the UF and MF. A similar pattern appears to exist for each of the units with the highest heads in central part of the Florida peninsula and lower heads to the south.

Similar visualizations were performed for selected water quality data. For this study, total dissolved solids (TDS) are used as a measure of salinity. Seawater salinity is assumed if TDS values are 35,000 mg/l or larger (Parker et al, 1955). An overall depiction of the water quality pattern in South Florida is shown in Figure 16 which shows elevation contours where the TDS concentrations are 10,000 mg/l as developed by SFWMD. Fresh-to-brackish groundwater is present at greater depths below Polk County than at the coasts. There is a secondary area of fresh-to-brackish groundwater south of Lake Okeechobee. Visualizations of water quality data in the UF, MF and LF taken from online databases and HydroGeoLogic, Inc., April 2006 (Figures 17, 18 and 19), show that the majority of the UF has TDS values lower than 5,000 mg/l while MF concentrations

are slightly higher and LF concentrations are much higher. These values are generally consistent with the elevation of 10,000 mg/l TDS data depicted in Figure 16. However, in some areas on the west coast, the selected data evaluated for Phase I shows fresher water at greater depths than shown in Figure 16. Judgment was used in determining the value used for model input.

3.4 GROUNDWATER AGE ANALYSIS

To better understand the timing of water flow through the FAS, additional investigations related to groundwater age data for the UF and MF were reviewed. These investigations included Kaufmann and Bennett (2005) and Mirecki (unpublished) (Figures 20 and 21). The contours in these figures indicate the age of groundwater in "years before present" and were computed based on the Pearson correction method. The general trend shows that the groundwater age is younger near Polk County where rainfall infiltration is believed to occur and along the central portion of the peninsula extending southward just west of Lake Okeechobee. Groundwater becomes increasingly older as it moves to the south and as it moves east and west of the central peninsula ridge. An area near the east coast indicates some mixing with ocean water because the groundwater ages are younger than those upgradient. Also, the MF groundwater ages are younger than the UF groundwater ages indicating that groundwater moves faster in the MF. The maximum age of groundwater in both aquifers is about 35,000 years.

3.5 CONCEPTUAL MODEL SUMMARY

The final conceptual model for Phase I was formed with the information and data gathered, and provided the basis upon which the numerical models were developed. Recharge through infiltration to the SAS provides driving heads that supply water to the FAS through the IC/IA. The primary area of recharge to the FAS appears to be in the Polk County area where flow infiltrates through the confining units to recharge the UF, MF and the LF. This statement is supported by the fact that the highest observed heads for the UF, MF and LF monitoring wells compiled for this study occur in Polk County and lower salinity is found in the deeper units in the Polk County area. Based on the data used for the Phase I model, flow appears to move through the aquifers in all directions from Polk County. In the UF, fresh-to-brackish water exists through much of the aquifer until it reaches an outcrop to ocean water on the east coast where some mixing occurs. The MF has similar heads and slightly higher concentrations compared to the UF. In the MF, a salinity mixing zone is also present on the east coast. Water flow is expected to move faster through the MF as hydraulic conductivities are larger and groundwater ages are younger than the UF. The LF appears to be influenced in the north by recharge from the Polk County region with water elevations that are much higher than those observed in the south. The southern LF water levels and salt concentrations are more consistent with ocean water. Mixing is expected in areas of the LF where the less-saline infiltrated water mixes with the ocean water. Discharge from the system is mainly to the Atlantic Ocean or Gulf of Mexico and also to surface water features.

The conceptual model was translated into the two numerical models, but the process is an iterative one. Numerical model results will be used to refine and revise the conceptual model with an updated understanding of flow and salt transport processes for Phase II.

4.0 MODEL CONSTRUCTION

Two density-dependent flow and transport codes, WASH123D and SEAWAT, were used in the Phase I modeling. The following sections chronicle model development from mesh/grid development to model input selection. Mesh/grid development and model input was completed for both models using GMS, version 6.0.

4.1 MODEL CODES

The WASH123D model code (Yeh et al., 2003), compiled in September 2006, was one of the codes used for model construction. WASH123D is an unstructured finite element code that simulates variable-density flow and reactive chemical and sediment transport in 1-D channel networks, 2-D overland regimes and 3-D subsurface media. For the Phase I model, the capability of computing density-dependent coupled subsurface flow and transport using WASH123D was utilized. With WASH123D, the variably saturated, density-dependent water flow is described by the modified Richards' equation and solved with the Galerkin finite element method. The Lagrangian-Eulerian (LE) method is employed to solve the subsurface transport equation, where particle tracking is used in the Lagragian step to handle the advection term, and the other terms (such as sources, sinks, diffusion, and dispersion) are calculated in the Eulerian step to determine the spatial concentration distribution at the end of each time step. The use of this methodology allows the numerical stability of WASH123D not to be restricted by the Mesh Courant number. In addition, the Mesh Peclet number is restricted only by computational accuracy, not numerical stability. Therefore, a sensitivity to time step sizing was performed to ensure the numerical accuracy was adequate for the scale and stated goals of the Phase I modeling effort. More detailed discussion on various types of numerical dispersion and how the LE method deals with these types of numerical dispersion are found elsewhere. (Cheng et al., 1996; Cheng et al., 1998; Yeh et al., 2006).

The SEAWAT model code (Langevin, et al, 2003, and Guo and Langevin, 2002) also was chosen for the Phase I modeling effort. SEAWAT is a finite difference code that simulates variable-density flow in three dimensions by combining a version of MODFLOW–2000 (Harbaugh et al, 2000) and MT3DMS (Zheng and Wang, 1999) in a single program to solve the coupled flow and solute transport equations necessary to model variable-density flow. MODFLOW—2000 is used to solve the flow part of the variable-density flow equations and MT3DMS is used to solve the solute transport equations. SEAWAT runs in one of four simulation modes: Constant-density flow without solute transport; constant-density flow with solute transport; variable-density flow without solute transport; and variable-density flow with solute transport. SEAWAT uses a finite difference approximation for the variable-density form of Darcy's law for groundwater flow and simulates dispersive transport using Fick's law. The program contains several methods for solving the solute transport equation including an implicit finite difference method with either upwinded or central-in-space weighting, the method of characteristics, and a third order total-variation-diminishing (TVD) scheme. For the Phase I study, SEAWAT modeling was performed with the variable-density flow with solute transport mode to simulate the system.

4.2 THREE DIMENSIONAL MESH/GRID DEVELOPMENT

The 3-D nature of the study area must be considered during mesh/grid development. As such, the 3-D mesh/grid must balance accurate depiction of topography, geology, and groundwater sources/sinks with model goals and computational resources.

Horizontally, the ideal model boundary alignment would be around the Florida peninsula boundary, where all the geologic units outcrop to the ocean (Figure 22). This would ensure that boundary effects in the interior of the model would be limited because boundary condition assignments would be greatly simplified: all of the boundary heads in each geologic unit would be equal to sea level and all of the boundary concentrations 100% salt water. However, since the Florida peninsula extends 150 miles westward into the Gulf of Mexico, modeling the entire peninsula was not feasible within the scope of this study. The model boundary chosen for the Phase I model generally follows a path just north of Polk County and extends around the peninsula approximately 20 miles seaward from the coast (Figure 23). The northern boundary was chosen to ensure that the entire recharge area, the driving force of the model, was incorporated. The remainder of the model boundary was selected a distance offshore to reduce boundary effects, but close enough to the coast to maintain a model size that would not result in unreasonable computation times and to have some information on which to base the head and concentration boundary condition assignments. The model encompasses an area of approximately 39,000 square miles.

Vertically, the mesh/grid was based on the geologic interpretations discussed in the Conceptual Geologic Framework section of this report. The 3-D mesh/grid represents geology between the low water table and the Sub-Floridan Confining Unit. The top of the model is the low water table rather than the land surface. The low water table was generated by selecting the lowest value from the transient data set of SAS monitoring well heads in online databases and interpolating over the model area. Low water table was chosen for the top of model to eliminate computations within the unsaturated zone. Computations within the unsaturated zone are not needed to reach the model goals and would slow model run times. From the low water table, the model extends down to a constant elevation of approximately -3250 feet NGVD. Figure 24 shows a cross section of the geologic units as classified in the 3-D mesh and grid. The cross section shows the distribution of the model's 23 layers of nodes for the WASH123D model and 22 layers of cells for the SEAWAT model. Each geologic unit is represented by a number of layers depending on its importance to the model goals. The SAS is only represented by 1 layer because variation in the SAS is not expected to impact the ASR plan objectives. The UF and MF are each represented by three layers of elements as the results within these layers will affect several ASR plan decisions. Between the LC and BZ is a transition layer that represents a combination of non-continuous permeable layers and confining units. This transition layer also allows for a transition of hydraulic parameters between the low magnitude values assigned for the LC and the extremely high values for the BZ. The cross section also shows that the shallower layers, SAS and IC/IA, are very thin in the recharge area in the northern part of the model and become thicker toward the south. Additional horizontal resolution in the recharge area, an area with large flow gradients, may be necessary for stability because the vertical resolution is fine.

The WASH123D mesh and the SEAWAT grid were developed in GMS using triangular irregular network (TIN) surfaces based on the hydrostratigraphic surfaces from the Preliminary Hydrogeologic Framework. The same TIN surfaces were used to create the mesh and the grid. For both models, a relatively coarse resolution is used for the Phase I study to allow the long-term simulations to run quickly to test many model parameters. Figure 25 shows the resolution and horizontal extent of the mesh and grid.

The WASH123D mesh used element sizes of approximately 25,000 feet along the model perimeter and no additional refinement within the model boundary. The mesh is comprised of 49,151 nodes and 90,376 elements.

The SEAWAT grid is comprised of 41 cells in the x-direction, 56 cells in the y-direction and 22 vertical layers. The model contains 50,512 cells and 55,062 nodes with a cell size of 25,000 feet by 25,000 feet across the entire model domain. The grid developed for the SEAWAT model is oriented along the major direction of flow, 18 degrees southeast, according to the predevelopment flow patterns in the region. The SEAWAT grid is created with the Layer-Property Flow (LPF) package, a MODFLOW package that allows for dipping beds.

4.3 MODEL INPUT PARAMETERS

WASH123D and SEAWAT groundwater flow and transport models are made up of three basic input file types: a 3-D mesh or grid, head and concentration boundary conditions, and initial total head and concentration files. For WASH123D, the 3-D mesh is comprised of unstructured prismatic elements that represent the low water table and geology of the study area. Computational nodes are located at the corner of each element. WASH123D solves for flow and transport parameters, such as head, velocity, and concentration at each node. For SEAWAT, a 3-D grid comprised of cells represents the study area low water table and geology. Computational points for the grid are cell-entered and represent the point at which flow and transport parameters are calculated. For both codes, model boundary conditions are used by the model to define flow and transport parameters within the system that are known with a reasonable degree of certainty. Boundary conditions are generally defined for parameters such as heads along the ocean or lakes and known concentrations such as salinity within the ocean. The initial total head conditions and initial salt concentrations must be defined at every node or grid cell within the model. The initial condition files are used as a starting point in the iterative solution process. The important considerations for each of these input files are described in the following sub-sections.

Both WASH123D and SEAWAT support the input of head data to the model as observed heads rather than equivalent freshwater heads. Equivalent freshwater head is the head of a column of water if the entire column's density is that of fresh water. Observed head is subject to the effects of the variation in density of the water column. During a simulation, the observed heads are applied as boundary conditions and converted to equivalent freshwater heads for the numerical model computations. Both model codes use the equivalent freshwater heads to compute the flow fields and velocities. Once the

head results are computed, the WASH123D code outputs both equivalent freshwater heads and observed heads, and the SEAWAT code outputs observed heads.

4.3.1 TRANSMISSIVITY AND HYDRAULIC CONDUCTIVITY

The transmissivity (T) and hydraulic conductivity (K) are both measures of the capability of an aquifer to transmit water where T is the product of K and the saturated thickness of the aquifer. Because WASH123D utilizes K rather than T as an input parameter, K values were estimated from each aquifer unit using the range of T values from the sources cited in the Conceptual Model. The saturated thickness of the aquifers was estimated from the distance between the hydrostratigraphic surfaces. For the aquifers, it is assumed that the vertical hydraulic conductivity (Kv) is 10 times less than the horizontal hydraulic conductivity (Kh).

For the confining units, MC1, MC2, and LC, Kv values published in the Preliminary Hydrogeologic Framework were input to the model. For the ICU, leakance and Kv values published in the Data Collection Report were used to estimate Kv. Values for Kh are assumed to be 2 times the Kv values.

Figures 26 through 37 present the Kh values and their distribution within each model geologic unit for the WASH123D mesh and SEAWAT grid. Kh values of 1.0 ft/d or less within an aquifer represents an area where the aquifer is not believed to be present based on the Preliminary Hydrogeologic Framework. In the case of the SAS, the IC outcrops to the surface in northwest corner of the model domain so the IC hydraulic conductivities are used within the upper layer of the model. Any element that was found to be completely within the ocean when compared to the bathymetry was assigned with an ocean material type (Figure 38) and a high hydraulic conductivity of 10,000 ft/d. Where the ocean abuts a confining unit hydraulic conductivity, a buffer hydraulic conductivity of 100 ft/d was defined to make the simulation more computationally stable.

4.3.2 STORAGE TERMS

Transient simulations require storage parameters to make the transient calculations. For WASH123D, the storage coefficient is made up of several terms including the porosity, moisture content and modified compressibility of the soil matrix for each geologic unit and the modified compressibility of water. For SEAWAT, the specific yield or specific storage for each geologic unit is defined. The values for the storage terms were obtained from the ASR Benchscale Modeling study (Brown et al, 2006).

4.3.3 WATER TABLE HEAD (RECHARGE)

To simplify the model input, recharge based on precipitation is not used. A specified constant head is assigned to the top of the model that represents the predevelopment water table, created as described in Section 3.2. This provides a constant source of water and the driving force of the model. Figure 39 shows the heads assigned to the SAS layer of the mesh and grid.

4.3.4 PERIMETER BOUNDARY CONDITIONS

The head boundary condition values are specified along the entire model perimeter for

each aquifer. The head data depicted in Figures 12, 13, 14, and 15 are used to help define the specified heads. Along the northern model boundary, the data coverage is good for the SAS and UF; however assumptions are required for the MF, LF, and BZ head boundaries. For the remainder of the model boundary, the head is known for the SAS, i.e. sea level, but the heads for the UF, MF, LF and BZ must be estimated. The UF specified heads are extrapolated from the predevelopment head contours generated by SFWMD in areas beyond the data shown in Figure 13. The MF specified heads along the entire model perimeter are assumed to be equal to the UF specified heads. The LF specified head boundary values are extrapolated from the data shown in Figure 15 along the northern boundary and are assumed to be 0.0 feet on the remainder of the boundary. Specified heads in the BZ are assumed to be 0.0 feet. For aquifer elements on the boundary that are completely within the ocean, a head value of 0.0 feet is assigned. Because many assumptions were made in assigning the specified boundary heads, these values were varied until they compared favorable with the head data. The distribution of assigned observed heads is shown in Figure 40. Figure 41 shows the same view after the observed heads are converted to equivalent freshwater heads.

Boundary conditions for salt concentration were assigned around the entire model perimeter using a variable concentration condition. A variable concentration is equal to the concentration specified in the input file if the direction of flow is into the model. If the direction of flow is out of the model, the concentration on the boundary is computed by the model. For both WASH123D and SEAWAT codes, salinity values along the SAS perimeter boundary are known and are specified as fresh water along the land boundary in the north and 100% salt water along the ocean boundary. Concentrations are also assigned for the SAS on the model top with fresh water specified over land and salt water specified over the ocean. For the UF, an extrapolation of concentrations shown in Figure 17 is used to assign the variable boundary concentrations. Boundary concentrations in the MF are assumed to be the same as for the UF. Figures 16 and 19 are used to help define variable boundary concentrations in the LF. The BZ boundaries are assumed to be fully salt water except for a small area along the northern boundary which is less than 10,000 mg/l based on Figure 16. For aquifer elements that are completely within the ocean, a 100% salinity value of 35,000 mg/l is assigned. Salt concentrations are specified as 35,000 mg/l on the model bottom. The distribution of assigned salt boundary concentrations is shown in Figure 42.

4.3.5 DISPERSIVITY

Dispersion refers to the spreading of salt, or any solute, caused by variations in fluid velocity about the mean velocity. Dispersion is taken into account in the model by defining the longitudinal and transverse dispersivity coefficients that represent mixing. As part of the Data Collection Report, a database of dispersion data for sandstone and carbonate aquifers around the world was created. Few of the values are based on physical test data and most values are based on estimates or groundwater model calibrations. Longitudinal dispersivities range from 0.002 feet to 13,100 feet. Transverse dispersivities are between 1% and 100% of the longitudinal values. Dispersivities are found to be scale-dependent, i.e. for large models, like the Phase I model, the dispersivities are typically higher than for well tracer tests. An analysis of the data

indicates that dispersivity is more of a model calibration parameter rather than a property of an aquifer. While the dispersivity values do depend on the nature of the aquifer materials, they also depend on the size of the flow field and model discretization. A range of dispersivity values were tested for use in the Phase I model as discussed in the sensitivity analyses. A value of 2.5 feet was chosen for use in all the geologic units while a value of 25.0 feet was used for elements within the ocean. For simplicity, the longitudinal and transverse coefficients used are equal. Further study of dispersivity will be performed for the Phase II model including calibration to field values as discussed in Section 8.0.

4.3.6 UNSATURATED PARAMETERS

Because the top of the model is the water table, no unsaturated zones occur within the model. Although they are not used, the WASH123D model requires unsaturated parameters in order to run, so simplified curves were adopted. For SEAWAT rewetting of the cells was allowed in the model, however, none of the cells went dry, so rewetting was not needed.

4.3.7 INITIAL CONDITIONS HEADS

The initial condition potentiometric heads were specified at every computational point in the model. The initial condition is used as a starting point in the iterative solution process. A constant total head was specified as elevation for the steady state model simulation. The resulting heads from the steady state simulation are used to begin the transient simulation. Initial head assumptions have no impact on final results because the convergence criteria used for the steady state results is very small, $1x10^{-6}$ feet.

4.3.8 INITIAL CONDITIONS CONCENTRATIONS

The initial condition salinity concentrations were specified at every computational point in the model based on the visualizations of monitoring well data in aquifers in Section 3.3. In addition, it is assumed that the SAS is 100% salt water in the ocean and 100% fresh water over land. The BZ is 100% salt water except under a small portion of the Polk County recharge area where Figure 16 shows that a value of 10,000 mg/l extends into the BZ. The salt concentrations in the confining units were interpolated based on the aquifer values. The initial condition is used as a starting point in the solution process. The distribution of initial concentrations is shown in the fence diagram in Figure 43 for the WASH123D model, but applies to SEAWAT as well.

4.4 SIMULATION DURATION SELECTION

Because the mesh and grid are coarse and simulations can run fairly quickly, geologic time-scale simulations are possible. Initial simulations were performed starting from 120,000 years ago, the last time that the peninsula was partially inundated by ocean water, and marching through time to the present. Initial concentrations for the simulations were 100% salinity throughout the entire model with fresh water infiltrating through the Polk County recharge area. These simulations were very unstable due to sharp salt fronts moving through the thin vertical elements in that area of the model. A shorter duration model with more variation in initial concentrations was chosen.

As shown in the groundwater age data for the UF and MF in Figures 20 and 21, the oldest groundwater within the aquifers is about 35,000 years old. A total simulation time of 35,000 years was estimated to provide enough time for groundwater to move completely through the system. The boundary heads and concentrations set as described throughout Sections 3 and 4 do not vary over the 35,000 years. The assumption is that the boundaries are in equilibrium over the course of the simulation time.

A time step of 10 years was used. This is the largest time step tested that provided results as accurate as any smaller time step. Time step sensitivities are presented in Sections 5 and 6.

5.0 WASH123D PHASE 1 MODEL RESULTS

The Phase I Regional WASH123D model was developed to meet specific objectives associated with the ASR Regional Study. Few density-dependent models of this size have been completed so the main goal of the Phase I model is to construct a test to determine what problems need to be addressed to build a successful Phase II model. Using the Phase I model, several parameters were tested including code computation parameters, site-specific flow and transport parameters, and code and platform run times. The model results provide insight into how the WASH123D model represents the behavior of the FAS, the impacts of changes in specific model parameters on that behavior, potential missing elements from the conceptual model, and the importance of collecting and understanding all available existing data for formulation of the Phase II model.

When viewing the model results, it is essential to remember that many significant factors are excluded from the Phase I model. The most notable omission is that of pumping stresses. Without pumping, the resulting heads are higher than measured monitoring well heads, the hydraulic conductivity values may not be reliable values and do not have as great an impact on the model results, and computed transport patterns may have a lesser variation. It is not advised that pumping be added to the Phase I model as it exists. The resolution of the Phase I model is not sufficient to capture the behavior of pumping stresses for any pump, let alone the numerous pumping wells that will need to be incorporated to completely assess pumping effects in the FAS.

Another important caveat regarding the Phase I model is related to the model time period. Although the model time period extends over 35,000 years, the model is not necessarily representative of the Florida subsurface changes over that period. Over the last 35,000 years, sea level has varied by 100 feet or more. Wet and dry rainfall periods have impacted the surface heads and recharge. Hydraulic conductivities have varied due to dissolution and diagenesis. The model boundary conditions have not been fixed in time as assumed in the model and salt concentrations 35,000 year ago did not have the pattern used as the initial conditions. This type of data is sparsely, if at all, available. These assumptions and simplifications were used to determine model behavior over a long time period rather than to reconstruct an accurate history of flow and transport in the Florida peninsula.

5.1 WASH123D COARSE MODEL RESULTS

To assess the WASH123D coarse model results, model input parameters were varied within a reasonable range in order to match simulated output to observed conditions within some acceptable error criteria. This comparison was completed for both steady-state or transient conditions. Steady-state model simulations provide a snap-shot of the hydraulic conditions in a stable aquifer system. Steady-state simulations were performed and results compared to observed data to improve model input parameters without waiting for longer transient simulations to complete. However, a transient comparison is a more reliable means of ensuring that a large scale regional model is accurately responding to a variety of stresses. Once model input parameters were relatively close to observed values, transient comparisons were performed. Comparisons of the computed head data were made to the UF predevelopment head contours shown in Figure 13 and to selected monitoring well head data in the IAS, UF, MF, and LF. Comparison to the elevation of 10,000 mg/l TDS map is used to compare salt transport patterns. More important than the actual comparisons of the computed values and monitoring data, this analysis is concerned with reproducing observed flow and transport patterns to generate starting parameters for the Phase II model. This section presents separate results for heads, velocities, and transport leading to a summary of how these results represent the entire system.

Because the monitoring head data are affected by pumping, the best comparison to the simulated heads is the UF predevelopment head contours (Bush and Johnston, 1988). Figure 44 shows the comparison for the steady state condition. Generally the contours agree with the highest heads in the Polk County area and the lowest heads at the coasts. The highest computed head is approximately 115 feet. The highest predevelopment head contour, 120 feet, is in the same area. Agreement between the computed and predevelopment head contours is very good down to the 70-foot contour. There is also fair agreement between the computed and predevelopment contours from the 40-foot contour down to the 10-foot contour. Between the 40-foot and 70-foot contours, the computed heads are much lower than the predevelopment heads. The predevelopment head contours show much higher head values into the southern part of the state.

Comparing the UF predevelopment heads to the UF computed heads after 35,000 years shows that the computed heads in the southern part of the state continue to decrease over time (Figure 45). The heads in the northern half of the model stay nearly the same as those shown in the steady state conditions with some increase in the 50-foot contour toward the west coast. A cross section showing flow vectors through the northern part of the model shows water entering the model in the Polk County area and moving down through the geologic units toward the coasts (Figure 46). Conversely, the flow vectors in a cross section (Figure 47) just south Lake Okeechobee shows that water in the central part of the UF moves vertically upward from the lower aquifers. The flow vectors show this pattern of upward movement throughout the southern part of the state.

In order to see the spatial variation of heads based on monitoring well data, computed water elevations were contoured along with calibration targets. The calibration targets show the location of each monitoring well water level and the relative error between

computed and monitoring well heads. Each target is color coded. Green means that the computed head is within 10 foot of the observed head, yellow means that the computed head is within 15 feet of the monitoring well head, and red means that the computed head is more than 15 feet different than the monitoring well head. If the target is colored above its centerline, the computed head is greater than the monitoring well head. If the target is colored below its centerline, the computed head is less than the monitoring well head.

Figures 48, 49, 50 and 51 show the computed heads and velocity vectors for the four major aquifer units under steady state conditions. In all of the aquifers, the highest computed heads are located in the Polk County and Highlands County areas with computed head values decreasing and the velocity vector pointing out toward the east and west coasts. The calibration targets comparing the computed heads to monitoring well heads are also shown in the figures.

For the IA, most of the wells show green calibration targets meaning the computed heads are within 10 feet of the monitoring wells heads. A few of the computed values are too high. Some of these discrepancies are due to small variations that cannot be reproduced with the coarse mesh resolution. For example, on the Sarasota and Charlotte County border there are two monitoring wells near each other where the heads differ by 13 feet. It is not possible to match both of these values with coarse resolution of this model. Other discrepancies between the computed and monitoring well heads result from the omission of pumping effects. At ROMP-49 near Tampa, the head at the well is largely affected by pumping (Figure 52) so it would be difficult to simulate the heads in this well with the Phase I model. In fact, because the Phase I model does not include pumping, the computed head values are expected to be higher than the monitoring well head values. Velocity vectors within the IA show flow from the Polk and Highlands County areas to the Gulf of Mexico. Outside the limits of the IA, the vectors point more vertically upward or downward transferring flow through the IC toward either the SAS or UF.

The computed head results compared to the monitoring data in the UF and MF show similar patterns to each other. In the Polk County area, where flow enters the two aquifers, the computed head values are generally higher than the monitoring data results. In the southern half of the state, the computed values are lower than the monitoring data results. The plots also show that the velocities are higher in the Polk County area for the UF and MF than in other areas of those aquifers. In the south, the velocities are low, except in the area along the east coast where the proximity to the ocean allows mixing of salt water with the brackish water in the aquifers.

The computed head contours for the LF match reasonably with several monitoring data points in the southern portion of the model; however velocity vectors for the LF appear to show chaotic patterns. To understand these patterns and some of the results in the UF and MF, it is necessary to review the initial salt concentrations and changes to those concentrations over time. Transport of salt is the mechanism that acts to change the model heads over time through solution of the variable density flow equations. Without salt transport, there is no transient stress in the model. Consequently the heads in the IA unit, which is close to the surface and mostly present in the northern part of the model

where water is freshest, do not vary greatly over the course of 35,000 years. Figures 53, 54, and 55 depict the change in salt concentrations from steady state conditions (Time 0.0 years) to the end of the 35,000 year simulation for the UF, MF, and LF, respectively. In the northern part of the model, salt concentrations in the UF and MF change very little since these areas start as fresh water and are constantly recharged by fresh water. In the southern part of the model, salt concentrations increase significantly in the UF and MF as flow from the coast and lower geologic units carry the salt upward and inward from the model boundary through time. The LF starts with concentrations that are much higher than the aquifers above it. In the Polk County area, the LF becomes fresher over time as fresh water infiltrates downward from the UF and MF. Salt concentrations in the LF start high in the south and remain high during the simulation as salt migrates with the upward flow from the bottom of the model.

Another view of the change in concentrations over time is shown in Figure 56. The left and right sides of the figure show elevation contours where salinity concentrations are 10,000 mg/l at time 0.0 years and time 35,000 years, respectively. At time 0.0 years, the elevation contours appear very similar to those shown in Figure 16 in the northern portion of the model, where fresher water is deepest. In the southwest at time 0.0 years, 10,000 mg/l salt concentrations are deeper in Figure 56 than in Figure 16 because the model initial conditions are based on monitoring well data used for Phase I that show that fresher water is located at greater depths. As time progresses to 35,000 years, the area where fresher water is deepest shrinks and moves from Polk County to just northwest of Lake Okeechobee. Also, the depth to fresher water decreases significantly in the south half of the model, especially on the southwest coast where the elevation of 10,000 mg/l TDS changes from -1,800 feet to -600 feet.

To summarize these results, water entering the model in the Polk County area moves downward to provide a source of fresh water to all of the aquifers. The highest heads and lowest salt concentrations occur in this area in all the aquifers. From Polk County, water moves out in all directions. As the water moves south, there is a point in the vicinity of Lake Okeechobee where the heads within the SAS are not high enough to maintain a downward gradient. In this area and south, the gradients of all of the confining units are upward. Freshwater in the UF moves to the surface. Saltier water from below and from the continental shelf on the east infiltrates the MF and UF and acts to reduce the heads in these units over time. As the heads in these units decrease in the southern part of the model, the gradient between the higher heads in the north and lowering heads in the south increases, resulting in a southern shift in the area where fresher water is deepest. The LF is an area where significant mixing takes place between fresher water infiltrating from above and the high salinity water that exists across most of the unit. The chaotic flow patterns seen in the LF are indicative of this mixing.

Numerous model simulations have been conducted to determine if the model is an accurate representation of the flow system or if something is missing in the conceptual model that leads to the significant increase in saltwater in the south. When salt concentrations are low, the southern part of the model is dominated by the boundary conditions. Looking at the UF steady state head results, Figure 48, the computed boundary heads all compare favorably with the monitoring well heads. The boundary

condition values could be revised to match these boundary wells more closely. However, during the transient simulation when salt water begins to enter the UF, the heads decrease significantly across the entire southern portion of the model. Based on data presented in the Conceptual Model section, these heads in the UF and MF are higher than the computed results at the end of the simulation and likewise the actual salt concentrations are lower.

The main problem is to identify the mechanism to allow more freshwater into the south part of the UF and MF aquifers. Freshwater can only come from the surface or from the upgradient Polk County area. Unless there is a shallow artesian aquifer south of Lake Okeechobee that has higher heads than the UF, the gradient will be upward preventing any surface freshwater from entering the UF. While artesian SAS aquifers do exist and have heads higher than the UF heads in some locations (i.e. beneath the Caloosahatchee River Basin), in areas further south their heads are not higher than the UF heads. If the hydraulic conductivity in the UF or MF is higher than that selected in the conceptual model, it is possible that more freshwater will travel to the south. Trials of several hydraulic conductivities in these aquifers improve the model results only slightly. If the hydraulic conductivity of the MC2 confining unit is lower or the IC is tighter, it is possible that more freshwater will travel to the south part of the UF and MF aquifers. Trials of several hydraulic conductivities in these confining units also showed only small improvements in the model results. Decreasing the hydraulic conductivity in the MC2 also acts to reduce the amount of water that enters the UF and MF because the gradient is upward. The hydraulic conductivity of the IC in the south is very small even in the conceptual model and reductions do not cause significant model changes. Another potential mechanism for freshwater flow south of Lake Okeechobee is preferential flowpaths or fractures. The USGS predevelopment head contours and the monitoring data indicate that the higher heads observed in the UF fall along a fairly narrow axis along the center of the peninsula. It is possible that a preferential pathway exists that leads flow from north to south along that axis. In fact, a recent unpublished study by the USACE, Jacksonville District identifies several northeast trending surface lineaments on the northwest side of Lake Okeechobee. Surface lineaments indicate possible fractures or fault zones which could act as conduits for groundwater flow.

Other possible explanations for the discrepancy in model results and observed values are related to model construction and assumptions. Many of the model parameters are dependent on mesh resolution. It is possible that with the more refined mesh that will be used for Phase II, some of the discrepancies in the results will be resolved. Also, a major assumption in conceptualizing the Phase I model is that the boundary conditions do not change over time and that the initial salt conditions, which represent salt conditions today, are representative of salt conditions 35,000 years ago. Over the last 35,000 years, there have been several major changes that are not coded into the model including changes in sea level which lead to changes in head and salt levels, changes in precipitation amounts, and changes to hydraulic conductivity in the geologic units due to dissolution and diagenesis.

A complete explanation of the salt migration processes over 35,000 years may be beyond the scope of the ASR Regional Model effort. To meet the Regional Study goals, the

Phase II model has to adequately capture the migration patterns over the calibration and validation periods and over the selected duration of the predictive simulations. For the calibration and validation periods, the simulation duration will be approximately 1 year. For the predictive simulations, the duration will be on the order of 1 to 50 years. Using the Phase I model run times as a guide, a simulation with a 5-day time step and a duration of 50 years shows a salt concentration change of less than 1 percent inland from the boundaries in the FAS. It may be that for the Phase II model runs, regional salt migration will not have a significant impact on the computed results relating to the specific ASR-related goals for the study.

5.2 WASH123D SENSITIVITY ANALYSIS RESULTS

Sensitivity analyses were performed to determine how changes in input values affected the model results compared to the base run results described in Section 5.1. Several parameters were varied as part of the Phase I model to determine what variables have the greatest impact. Those parameters include hydraulic conductivity, initial concentrations, concentration boundary conditions, dispersivity, time step size and temperature effects on boundary conditions in the BZ. The sensitivity analysis duration was chosen at 10,000 years to provide enough simulation time for significant changes in results to be observed without unnecessarily extending run times. The results of the Phase I sensitivity analysis provide some basis for how Phase II model parameters will behave however, most of these parameters are heavily dependent on mesh resolution. Additional sensitivity analyses will be performed as part of the Phase II modeling.

5.2.1 HYDRAULIC CONDUCTIVITY – AQUIFERS

Hydraulic conductivity was varied in all of the aquifers in the model by doubling and halving the values used for the base run. Head and concentration results compared in the Upper Floridan are typical of the results shown in the Middle and Lower Floridan. The base run head and concentration results at time 10,000 years across the model are shown in Figure 57 for the UF. Figure 58 presents the head and contour results for the UF for doubling the hydraulic conductivities in all the aquifers. When the aquifer K values are doubled, the resulting heads in the UF are lower than the base run along the central ridge of the peninsula. Between the central ridge and the coasts, the UF head values are higher than the base run head values except near the area where the UF abuts the ocean. The largest head differences are in the Polk County area with a maximum of approximately 6 feet. The concentrations decrease across the model when the aquifer K values are doubled except near the east coast where the UF abuts the ocean. In other words, in the Polk County region, fresh water enters the aquifer and the higher K values allow the fresh water to move quickly through the region resulting in lower heads and concentrations. The higher conductivities also allow fresh water to move more quickly out from the central ridge extending the area of fresher water and lowering concentrations. The increase in heads between the central ridge and the coast for the higher K run is a combination of the decrease in concentrations and the milder gradient between the lower maximum heads in Polk County and the constant boundary conditions. Near the ocean, the higher hydraulic conductivities allow salt intrusion to occur more quickly increasing the concentrations and decreasing the heads. Figure 59 shows the UF head and concentration results when the aquifer hydraulic conductivities are halved compared to

the base run. With the aquifer conductivities halved, the results are the opposite of doubling the conductivities.

Neither doubling nor halving the hydraulic conductivities in the aquifers has a significant impact on the flow or concentration patterns for the Phase I model.

5.2.2 HYDRAULIC CONDUCTIVITY – CONFINING UNITS

Hydraulic conductivity was varied in all the confining units in the model by doubling and halving the values used for the base run. Head and concentration results compared in the Upper Floridan are typical of the results shown in the Middle and Lower Floridan. The base run head and concentration results at time 10,000 years across the model are shown in Figure 57 for the UF. Figure 60 presents the head and contour results for the UF for doubling the hydraulic conductivities in all the confining units. When the confining units are more permeable, the resulting UF heads are higher than the base run along the central ridge of the peninsula because more fresh water is able to infiltrate from the surface. The UF heads are lower near the coasts and in the southern part of the peninsula when the confining units are more permeable compared to the base run due to saltwater intrusion from the coasts and from deeper units. Figure 61 shows the UF head and salt concentration results when the confining unit hydraulic conductivities are half as permeable. The results of halving the confining unit hydraulic conductivities are the opposite of doubling the conductivities.

Doubling the K values in the confining units has a larger impact on the model results than halving the confining unit K values, especially in the southern part of the model. For example, at the location where Dade, Broward and Collier Counties meet, the head value is 6 feet lower when the confining unit K values are doubled than the head values for the base run. When the K values are halved, the UF head at that location is only approximately 2 feet higher than the UF head for the base run. This result is directly related to the upward direction of the velocity vectors in the southern part of the model. When the confining units are more permeable, more salt water upwells to shallow aquifers. When the confining units are less permeable, the upwelling occurs but at a slower rate.

5.2.3 INITIAL CONCENTRATIONS

Initial concentrations were increased and decreased by 25% compared to the base run. The minimum and maximum concentrations were maintained at 0 mg/l and 35,000 mg/l, respectively. Head and concentration results compared in the Upper Floridan are typical of the results shown in the Middle and Lower Floridan. The base run head and concentration results at time 10,000 years across the model are shown in Figure 57 for the UF. Figures 62 and 63 show the heads and concentrations within the UF after 10,000 years when the initial concentrations are increased and decreased by 25%, respectively. The UF heads and concentrations along the central ridge of the model after 10,000 years are almost exactly the same for the three different initial conditions as shown in Figures 57, 62, and 63. The UF initial concentrations in the base run are very low in that area so varying them by +- 25% does not change the values significantly. In addition, fresh water enters the model in that area keeping the concentrations low. Beyond the central

ridge area, the UF heads are lower and concentration are higher where the initial concentrations were increased by 25% and the UF heads are higher and concentrations are lower where the initial concentrations were decreased by 25% compared to the base run. Note that the concentrations at 10,000 years are significantly impacted by the initial concentrations. When the concentrations start higher they remain higher for the duration of the simulation and vice versa.

5.2.4 CONCENTRATION BOUNDARY CONDITIONS

For the base run, the boundary salt concentrations are assigned as a variable boundary condition. This boundary condition allows the concentrations to be calculated by the model when the flow direction is out of the model. When the flow direction is into the model, the concentrations are defined based on a specified concentration that varies within each aquifer. A sensitivity analysis was performed to observe the results if the salt concentrations on the boundary were held constant using the observed data for each aquifer. The resulting heads and concentrations for the UF and LF are not very different compared to the base run. Generally, the UF heads are slightly lower and the LF heads are slightly higher than the base run. The opposite is true for the salt concentrations. In the MF, the head results can vary up to 5 feet. Also, the MF salt concentrations near the boundary increase as a result of salt intrusion from below. This creates a strange pattern where the concentration on the boundary is fixed at a lower value but just inside the boundary the concentrations are 20,000 mg/l higher (Figure 64). Therefore, it appears that the specified concentration boundary conditions do not provide an accurate picture of flow and transport patterns. Although the variable concentration boundary condition appears to provide the model more freedom to compute accurate flow and transport patterns, some oscillation occurs on the boundary which may result in propagation of error through the model. This is discussed further in Section 7.0.

5.2.5 DISPERSIVITY

Several values of dispersivity, 0.0, 25.0 and 250.0 feet, were tested and the results were compared to the base run results. The dispersivity of the base run is 2.5 feet for all materials except the ocean and the ocean buffer material types where dispersivities of 25.0 feet and 10 feet, respectively, were used. The dispersivities of the ocean and ocean buffer materials for the base run were the lower limits used for those material types in the sensitivity runs. As dispersivity increases, the rate of mixing of higher salinity water with lower salinity water increases. Through the upper part of the model, from the surface down to the MF, the salt concentrations are initially low, so a higher dispersivity acts to increase the concentrations and lower the heads in those areas over time. In some areas of the LF and deeper units where salt concentrations are initially high, large dispersivities cause a salt concentration reduction and an increase in head.

A further investigation was completed to determine the impact of dispersivity variation on head and concentration at specific wells within the UF. ROMP-45 is located in Polk County where water enters the UF from the surface geologic units. ENP-100 is located in Dade County where water enters the UF from the deeper geologic units. Locations for both wells are shown in Figure 57. Figure 65 shows the head and concentrations results over time for dispersivities of 0.0, 2.5, 25.0, and 250.0 feet. Note that for a dispersivity

of 0.0 feet, the code was unable to converge after 4,000 years as small instabilities can not be smoothed out without any mixing coefficient. At ROMP-45, the resulting concentrations vary through time from the initial concentration until a particular time when the concentration becomes constant until the end of the run. For a dispersivity of 250.0 feet, the concentration increases to a constant value of almost 6,000 mg/l. This result is unlikely to be correct since ROMP-45 is within the Polk County area where concentrations are expected to be low. The results from the runs with dispersivity values of 2.5 feet and 25.0 feet seem more reasonable as the concentrations are less than 1,000 mg/l. The same pattern is true for the head results at ROMP-45 where the heads for a dispersivity of 250.0 feet are much less than the values for both 2.5 feet and 25.0 feet. Also notable at ROMP-45 is that the heads decrease initially and then increase until approximately 4,000 years when a constant value is reached. This dip in the graph indicates an initial period of instability until the model reaches an equilibrium. In the case where dispersivity is 250.0 feet, the instability is so large that the long-term results are impacted.

In the southern part of the model at ENP-100 (Figure 65), the salt concentrations for the variety of dispersivities increase through the simulation as salt water intrusion occurs from the east coast and from the deeper geologic units. No constant value is reached as the salt continues to increase, and therefore the heads decrease, through time. The largest magnitude of increase in salt concentrations and decrease in head is shown for the dispersivity of 250.0 feet. The smallest changes in concentration and head are shown for dispersivities of 0.0 and 2.5 feet.

Based on these results, it is reasonable to remove a dispersivity of 250.0 feet from consideration as it results in too much mixing. However, it is difficult to determine which is better between a value in the magnitude of 2.5 or 25.0 feet. For the Phase I base run, a dispersivity of 2.5 feet was chosen in an attempt to limit the mixing and salt intrusion in the southern part of the model. For the Phase II model, additional sensitivity analysis will be completed to provide more insight in selection of this parameter. In Phase II, the spatial and temporal discretizations of the model will be more refined which will have a significant impact on dispersivity. In addition, whereas the Phase I model has a constant dispersivity across all the geologic units, the Phase II model will take account potential variation of dispersivity through and between geologic units. Calibration of the Phase II dispersivities will be dependent on data, where it's available, as discussed in Section 8.0.

5.2.6 TIME STEP SIZE

Several time steps were evaluated to determine the largest time step (i.e. shortest run time) that provides accurate results. These values include 0.2 year, 1 year, 5 years, 10 years and 100 years. Plots were created depicting the head and concentration variation over time at two specific wells within the UF (Figure 66). Locations for the two wells are shown in Figure 57. ROMP-45 is located in Polk County where water enters the UF from the surface geologic units. ENP-100 is located in Dade County where water enters the UF from the deeper geologic units. At ROMP-45, the heads are almost identical for each of the simulations tested except for the 100 year time step. Even for the 100-year

time step, the resulting heads are only approximately 0.5 foot higher than the head results using the other time steps. The concentration results at ROMP-45 using the different time steps are all very similar and decrease to a constant value of almost 0.0 mg/l at 5,000 years. Note that only 1,000 years are plotted in Figure 66 for ROMP-45 so the variation between the simulations is visible. At ENP-100, the head values decrease and concentrations increase throughout the simulation time for all the different time steps evaluated. The 100-year time step yields results that have the largest deviation from the results of the other time step simulations. The 100-year time step results are only plotted out to 3,000 years on Figure 66 because the simulation failed to converge due to boundary instabilities. The 0.2-year time step results are only plotted out to 1,000 years for the same reason.

Based on the results of this sensitivity, the 10-year time step was selected as the most computational efficient time step size because it provides the shortest run time and results that are very similar to those produced by the smaller time steps.

5.2.7 LIMITED TEMPERATURE EFFECTS IN THE BOULDER ZONE

The effect of temperature variation in the Boulder Zone was coded into the head boundary condition of the model for that geologic unit to observe any impact it may have on the aquifers above. Figure 67 shows the head used for the BZ boundary that incorporates the temperature effect on density added to the assumed head for the BZ boundary condition of 0.0 feet around the perimeter of the model. Note that heat transfer, temperature effects on salt concentrations on the boundary of the BZ, and temperature effects on head and salt concentrations within the model boundary and on other geologic units are not considered. Revising the boundary heads in the BZ does have an effect on the heads in the geologic units above the BZ as shown in Figure 68. The figure shows two maps of change in heads resulting from the revised BZ boundary condition as compared to the base run for Time 0.0 years. The impact on the heads in the overlying units is largest at Time 0.0 years and decreases as the model simulation proceeds. The left map shows the head change in the UF and MF layers where the magnitude varies from -1.0 foot on the southeast coast to 5.0 feet on the southwest coast. The map on the right shows the head change in the LF where the magnitude varies from -2.0 feet on the southeast coast to 18 feet beyond the southwest coast.

These results show that the temperature effects can have a significant impact on the computed model results. Consideration should be given to including temperature effects in the Phase II model boundary conditions or the possibility of including full heat transfer computations, if feasible.

5.3 WASH123D SALTWATER INTRUSION RESULTS

Where the model boundary extends to the Atlantic Ocean, it is possible to observe how the model behaves due to the effects of saltwater intrusion. Figure 69 shows the salt fronts at three time steps over the 35,000 year simulation at a cross section through the mixing zone. Comparing the three snap shots reveals the salt fronts in the UF, MF and LF moving westward from the coast. For the UF, the concentrations increase from a range up to 3,500 mg/l to a range up to 10,500 mg/l with the 10,500 mg/l contour moving

westward by approximately 30 miles over 35,000 years. In the MF, the concentrations increase from a range up to 7,000 mg/l to a range up to 14,000 mg/l with the 14,000 mg/l contour moving westward by more than 40 miles over 35,000 years. The concentrations in the LF increase from a range up to 28,000 mg/l to up to 31,500 mg/l and the 31,500 mg/l contours moves westward by approximately 15 miles. Even at the coarse resolution of the Phase I mesh, the wedge shape of the salt water front in each aquifer is clearly visible with the denser, saltier water extending further westward along the bottom of the aquifer and the less dense, less salty water extending further eastward along the top of the aquifer. This demonstrates that WASH123D is capturing the processes that occur in the saltwater intrusion mixing zone which will be important for the Phase II model.

6.0 SEAWAT PHASE I MODEL RESULTS

As stated previously, the Phase I modeling effort included the construction of a fully density-dependent SEAWAT model. This model had essentially the same grid resolution and utilized the same hydraulic parameters developed for the Phase I WASH123D model. The purpose of this SEAWAT model was to provide a comparison of the WASH123D model results, identify similarities and differences in the flow and concentration fields computed by the two models, and help identify issues to be addressed in the Phase II modeling effort.

Using the Phase I SEAWAT model, several parameters were tested including code computation parameters, site-specific flow and transport parameters, and code and platform run times. The model results provide insight into how the SEAWAT model represents the behavior of the FAS, the impacts of changes in specific model parameters on that behavior, potential missing elements from the conceptual model, and the importance of collecting and understanding all available existing data for formulation of the Phase II model.

Since the SEAWAT model was constructed in a manner consistent with the WASH123D model, this SEAWAT model will have the same abilities and limitations discussed for the WASH123D model. Another potential limitation of the Phase I model is the relatively coarse vertical discretization. The model contains 22 vertical layers. The UF and the MF are represented by three layers each; the LF has two model layers. Guo and Langevin (2002) discuss the importance of grid resolution for variable density flow models in particular vertical resolution. In areas of complex flow patterns and high concentration gradients, additional vertical discretization often is needed to adequately represent the flow system. These authors have found that vertical grid resolution often needs to be much finer than horizontal resolution and recommend up to 10 model layers per aquifer. The grid will be refined in Phase II of the ASR modeling study.

6.1 COMPARISON OF WASH123D AND SEAWAT RESULTS

The SEAWAT model was run as a base case to 35,000 years with two stress periods starting with a steady state stress period for one day. Those steady state results were used as the starting point for the transient stress period. Most parameters were kept the same between the WASH123D and SEAWAT models; however, minor variations were required due to the inherent differences between the model codes. The SEAWAT model

was not compared to monitoring well data to determine input parameters, but rather used the input parameters generated from the WASH123D results for the same period. When the results of the WASH123D and SEAWAT models were compared, several interesting similarities and differences were observed.

The steady state results computed for both the SEAWAT and WASH123D models were similar. Figures 70, 71, 72, 73 and 74 show the computed heads in both models for the SAS, UF, MF, LF, and BZ, respectively. The computed SEAWAT heads are shown as dashed lines while the computed WASH123D heads are shown as solid lines. Although some minor discrepancies exist, the regional steady state flow patterns simulated for both models are reasonably consistent.

The results of the transient simulations revealed that several differences exist between the WASH123D and SEAWAT model results. The magnitude of these differences increased with time. One of the most notable differences occurs in the BZ in the Polk County area. Figure 75 shows that after 35,000 years the WASH123D simulation computes heads in Polk County of between 30 and 40 feet, while SEAWAT computes higher heads of approximately 60 to 70 feet in the same area. The differences in heads between the two models are directly related to the way in which salt concentrations are computed in each model. In both models the salt concentrations in the northern portion of the BZ start at 10,000 mg/L TDS. However, in the WASH123D model, the concentration quickly increases to a fully saline concentration of 35,000 mg/L TDS. Conversely, the concentrations computed in the SEAWAT model gradually decrease during the simulation to a concentration of less than 100 mg/L TDS at 35,000 years. Figure 76 shows a cross sectional view of the concentration distribution in each model after 35,000 years. The primary reason for this discrepancy is due to differences in the boundary conditions applied to the bottom of each model. In the WASH123D model, the BZ is represented by one element layer with computational nodes above and below this layer. The conceptual model for the BZ assumed that the bottom of the BZ is a no-flow boundary with a constant saline concentration. As such, a constant salt concentration boundary condition of 35,000 mg/L was applied to the bottom layer of nodes in the WASH123D model. In the SEAWAT model, one element/cell was again used to simulate the BZ. However, since the computations are cell centered in SEAWAT, a constant concentration boundary condition could not be reasonably applied without overly constraining the salt transport in the bottom layer of the model. Instead a variable boundary condition was applied that allowed the model to compute the concentration in the BZ based on the flow and concentration of the surrounding cells, unless flow was into the model from the boundary. Along the model boundary, if the flow was into the model, the assigned salt concentration of the fluid entering the model was assumed to be 35,000 mg/L TDS. After comparing the computed results in both models, the WASH123D model was modified to simulate a variable boundary condition similar to that used in the SEAWAT model. Figure 77 shows the computed heads in the BZ at 20,000 years in the SEAWAT model and the revised WASH123D model. This figure illustrates that once the WASH123D boundary condition was revised to a variable concentration type boundary, the computed results are similar in WASH123D and SEAWAT. Figure 78 shows that this revision also improved the correlation between the two models in the Polk County area in the LF.

In addition to the differences noted in the heads of the BZ and LF, the heads in the southern portion of the UF and MF (Figures 79 and 80, respectively) appear to be lower in the SEAWAT model. This again is a direct result of the salt migration patterns. In these areas of lower head, the SEAWAT model computed higher salt concentrations than those in the WASH123D model. Figure 81 shows a cross section view of the concentration distribution in each model after 35,000 years. These differences in computed salt migration may be caused by the resolution of the mesh and grid used in the models and how each model calculates hydraulic conductivity for a particular element or cell. Figure 82 shows a simplified representation of the way in which vertical hydraulic conductivities are treated in each model. For the numerical computations, WASH123D determines the inter-nodal conductivity based on the conductivity assigned to each of the elements in the model. This inter-nodal conductivity is used in the matrix equations to resolve the flow fields and corresponding heads at each finite element node. SEAWAT treats the conductivity slightly differently. The vertical conductivity between each cell is described as the equivalent conductance between the cells, when a fully three dimensional approach is used. This difference in the treatment of vertical hydraulic conductivity is compounded by the configuration of the finite element computational nodes and the finite difference computational cells. As shown in Figure 82, the finite element nodes are not located at the same horizontal and vertical location as the center of the finite difference cells. Some of the issues with vertical conductance may be resolved by adding increased vertical discretization in the Phase II SEAWAT model.

The differences in computational methodologies and treatment of hydraulic parameters between WASH12D and SEAWAT may require actual calibration to observed heads and salt concentrations for both models in Phase II of the project. The WASH123D model parameters were determined as discussed in previous sections of this report; however, the SEAWAT model used hydraulic and transport parameters from the WASH123D model and the best parameters for the SEAWAT model were not developed independently. Hydraulic parameters used to calibrate the finite difference based model may be slightly different than those required to calibrate the finite element model. A detailed examination of this phenomenon was not within the scope of the Phase I ASR work.

6.2 SEAWAT SENSITIVITY ANALYSIS RESULTS

In addition to the comparisons between the SEAWAT and WASH123D results, several sensitivity analyses were performed on the SEAWAT simulation. These sensitivity analyses varied parameters such as time step size, flow and transport solvers, dispersivity and initial salt concentrations. The results of these sensitivity simulations were then compared to the base run described in the previous section. As discussed for the WASH123D model, the results of the Phase I sensitivity analysis provide some basis for how Phase II model parameters will behave. However, since most of these parameters are heavily dependent on mesh resolution, additional sensitivity analyses will be performed as part of the Phase II modeling.

6.2.1 TIME STEP SIZE

Time step size sensitivity SEAWAT model runs were made using the Strongly Implicit

Procedure (SIP) flow solver and the implicit finite-difference solver with upwinded weighting to solve the solute transport equations. This transport solver allows the user to select the length of the transport time step, however long transport time steps with this method can lead to problems with numerical dispersion that can result in sharp concentration fronts and large concentration gradients.

Model simulations using a 0.1 year, 1 year, 10 years and 100 years time step sizes were evaluated to determine the largest time step (i.e. shortest run time) that provides accurate results. Plots showing head and concentration variation over time at two specific wells within the UF (ROMP-45 and ENP-100) are shown in Figure 83. At both wells, the base run time step size of 10 years, shows oscillations in the computed heads for the first 100 year period. These oscillations are substantially greater in the ROMP-45 well. After this first 100 year period, the computed heads using the 10 year time step are in relatively synchronous agreement with the heads computed using the 0.1 and 1 year time step sizes. Results at both wells also show noticeable deviations in the computed heads when the time step size is increased to 100 years.

6.2.2 SOLVER

SEAWAT uses one set of solvers for the flow portion of the variable density flow equation and another set of solvers for the solute transport portion of the equations. Osiensky and Williams (1996) discuss the accuracies and problems associated with different flow solvers. The solvers that had the best results were the Strongly Implicit Procedure (SIP) and Preconditioned Conjugate-Gradient (PCG2) solvers. The main flow solver used for the Phase I modeling was the SIP solver, although the base run was tested with the PCG solver as a test of solver sensitivity. An advantage of the PCG2 solver is that one of its convergence criteria depends on the water budget, so errors related to water budget are reduced. In addition to the PCG2 solver, a sensitivity simulation was also performed using the Geometric Multigrid Solver (GMG), based on recommendations from the USGS. The computed heads using each of these flow solvers at groundwater wells, ENP-100 and ROMP-45, are shown in Figure 84. The heads computed using each of these flow solvers are reasonably correlated. All SEAWAT runs had solutions that converged, except where noted, and mass balance errors that were less than 1.0%.

In addition to flow solvers, different numerical methods and corresponding solvers exist to solve the advection-dispersion-reaction equations. Details of the transport solvers are described by Zheng and Wang, 1999. One solution method is the Eulerian approach which uses a fixed grid, in this case a finite difference grid, to solve the transport equation. The Eulerian approach is better in advection-dominated groundwater systems, but may be subject to numerical dispersion and/or artificial oscillation in the results. Two options within the Eulerian approach finite difference solution are available to calculate advection; upwinded weighting and central-in-space weighting. Upwinded weighting can result in fewer oscillations, but numerical dispersion can be increased because upwinding provides only a first order solution. Central-in-space weighting solves the advection term with an accuracy to the second order and problems related to numerical dispersion are minimized. However, if the transport in the system is advection-dominated, this scheme can cause excessive oscillation in the model results. Because of this oscillation issue,

Phase I simulations using the central-in-space weighting methodology were very unstable and consequently are not evaluated as part of this sensitivity analysis. The standard finite difference method is somewhat limited in systems that are advection-dominated, however, when the grid Peclet number is smaller than four (Zheng and Bennett, 1995), this method is thought to be reasonably accurate. Another advantage of the finite difference method is faster run times.

Another class of transport solution techniques for advection are the total-variation-diminishing (TVD) methods. MT3DMS contains a third-order TVD solver with a universal flux limiter called the third-order ULTIMATE scheme (Zheng and Wang, 1999). This scheme conserves mass, has little numerical dispersion, and is fairly free of numerical oscillation. TVD solutions are generally more accurate for advection-dominated flow, but have much longer run times than the finite difference methods.

The SEAWAT model for Phase I was run initially with the finite-difference solution for the transport equations with upwinded weighting. Sensitivity runs were made to test the central-in-space weighting, and also the third-order TVD solver. The TVD runs were slow in comparison to the standard finite difference solver simulations. The TVD solver selects the best time step that meets convergence criteria. For SEAWAT runs with the TVD solver, the Courant number was specified to be 0.75. For these SEAWAT TVD runs, the time step size was on the order of 0.2 days. By comparison, the upwinded simulations used time step sizes of 10 years. This resulted in significantly longer model run times for the TVD simulations, as shown in Section 8.2 of this report. The computed heads for each of the transport solver simulations at the ENP-100 and ROMP-45 groundwater wells are shown in Figure 84. This figure shows that although more oscillation occurred in the finite difference solver simulations, the results of the TVD solver are higher than those computed using the upwinded methodology. This slightly higher head in the UF, is the result of slower vertical salt migration in the TVD solution. However, it is important to note that because of the extended run times for the TVD solution, only 1,000 years of each simulation is shown on Figure 84. Since the ASR injection and extraction is expected to be advection-dominant, the computed differences between the two transport solvers are expected to be significant once pumping stresses are incorporated into the model. Additional methodologies for increasing the speed of the simulations using the TVD solver are being examined. The goal of this effort is to be able to decrease the run time of the TVD simulations, without compromising numerical accuracy in the Phase II modeling effort.

6.2.3 DISPERSIVITY

The dispersivity sensitivity analysis performed for the SEAWAT simulation was similar to that performed for WASH123D. The baseline SEAWAT simulation used a dispersivity value of 2.5 feet for longitudinal and transverse dispersivity for the aquifer and confining unit materials, which was the same as used in the baseline WASH123D simulation. The ocean and the ocean buffer used dispersivities of 25.0 feet and 10 feet, respectively. For the SEAWAT sensitivity analysis, dispersivity values of 0.0, 25.0 and 250.0 feet were simulated and compared to the base run. The dispersivities of the ocean and ocean buffer materials for the base run were the lower limits used for those materials in the sensitivity runs.

As seen in the WASH123D dispersivity sensitivity analysis, increases in dispersivity generally resulted in higher concentrations with time. This increase in concentration resulted in a corresponding decrease in heads, especially in the southern portion of the model. An example of this can be seen in the vicinity of ENP-100. Figure 85 shows the head and concentration profiles for the dispersivity simulations at ENP-100 and ROMP-45. The charts for ENP-100 show an increase in concentration and decrease in head as dispersivity is increased. This indicates that as dispersivity increases, the rate of mixing of higher salinity water with lower salinity water also increases.

A similar trend, but with a smaller magnitude, is observed in the Polk County area. In this area of the model, the concentration generally drops with time. However, increases in dispersivity tend to keep the concentrations higher for a slightly longer period of time. This results in slightly lower computed heads in the high dispersivity simulations, as shown ROMP-45 charts in Figure 85. Since dispersivity is scale dependent parameter, further evaluations of its affect on computed heads will be performed for the more refined Phase II model.

7.0 SOURCES OF ERROR

Many potential sources of error exist for the Phase I model. For such a large model, it is impossible not to condense available data and make several simplifying assumptions. In addition, the Phase I model is a test bed model so some simplifications are built-in to the conceptual model with the knowledge that more details will be incorporated and more data will be available for Phase II.

Model Resolution

The horizontal distance between computational points for the WASH123D and SEAWAT models is 5 miles. The vertical distance between computational points varies, with some computational points only a few feet from each other as found in the northern part of the SAS and others up to 500 feet apart as found in parts of the MC2. This resolution contributes to several potential sources of error. The surface heads are set as fixed boundary conditions across the top of the model. Because the computation points are 5 miles apart, the driving head of the model is very dependent on the interpolation of the data applied to the surface. For example, if the computational points fall on either side of the central ridge through Polk and Highlands Counties, the highest value of head that forces water into the top of the model may be missed therefore underestimating the head in geologic units below. Also the location where the majority of water enters the model from the top is the same area where the model elements are very thin vertically compared to their large horizontal scale. Large gradients occurring through these horizontally coarse and large aspect ratio elements/cells may result in increased instabilities which can propagate through the model. Generally, the large distances between the computational points leads to the inability to resolve small variations that may be important to fully understand the flow and transport results.

Boundary heads and salt concentrations

An exhaustive data search was not completed for the Phase I model. Particular data that was considered representative was selected for use in determining head and concentration boundary conditions. No attempt was made to collect data to vary the head and

concentration boundaries through time. This strategy was implemented in order to shorten the time needed for data collection and model construction so that boundary conditions and other parameters could be tested. Additional data collection for Phase II will provide more information on which to base boundary conditions, allow transient boundary condition assignments, and therefore reduce the error associated with estimating the boundary values.

It will not be possible to completely eliminate the error regarding the boundary conditions. One problem is the availability of data for use along the boundaries. For the UF, a large number of monitoring wells exist to provide head and water quality data over time. In the LF and BZ, this is not the case and some estimation will still be required and potential errors will exist. In addition, because the model boundaries are set 20 miles into the ocean, the head and concentration boundary conditions for the UF, MF, and LF are extrapolated from the selected data at the Florida coast. This extrapolation introduces uncertainties that are a potential source of error for the model. This is especially true in the southern portion of the model where boundary conditions have a greater impact on the head and concentration results. As discussed in Section 8.2, the Phase II model boundary may be moved inland along the western coast of Florida to minimize the amount of extrapolation necessary to generate the boundary condition values.

The model boundaries were set out from the coast to reduce boundary effects in the areas of the proposed ASR wells. Because a variable concentration boundary condition is used, oscillations of concentrations and heads are possible due to minor changes in flow direction at computational points on the model boundary. If the direction of flow varies over consecutive time steps such that flow is into the model for one time step but out of the model for the next time step, then the salt concentration is computed differently for the two time steps. Also, when heads are specified, it is the effective freshwater head that is specified rather than the observed head. Therefore a change in concentration over two consecutive time steps results in a change in observed heads when the constant equivalent freshwater head is converted to observed head. Figure 86 shows a graph of head and salt concentration computed using the WASH123D model over the simulation duration for a node on the boundary in the MF. The observed head specified at the node is 35 feet and the concentration is variable with a value of 5,200 mg/l specified when flow is moving into the model. The observed head oscillates around the specified value of 35 feet and the salt concentration oscillates around the model computed value of approximately 11,000 mg/l. The southern boundary of the MF is the model location where the oscillations are the most pronounced. A plan view of the south boundary of the MF (Figure 87) shows that the oscillating head and concentrations do not propagate to the interior of the model and so do not have a critical impact on the results. However, for this reason, it is appropriate to maintain the model boundaries far away from the areas of interest.

More investigation of this boundary oscillation issue will be conducted for the Phase II model. For the Phase II model, maintaining the boundaries at 20 miles offshore with a finer spatial discretization may result in too many model computational points. With a finer spatial and temporal discretization and shorter simulation duration that will be used for Phase II, the oscillations observed in the Phase I model may not occur.

Pumping

As mentioned several times through this report, pumping is not included in the Phase I model which constitutes a significant source of error for the head and concentration results and the determination of other parameters such as hydraulic conductivity. Pumping was excluded to shorten the data collection and model set-up time and because the model resolution was not sufficient to support pumping. Pumping will be included in the Phase II model and will also be considered a source of error for that model. Errors associated with the availability and accuracy of transient pumping data and the likelihood that several pumps will need to be combined on a computational point will result in sources of error for Phase II.

Dispersivity

For this study, the value of dispersivity used in the model is an estimate. From the sensitivity results, it appears that the value is in the range of 1 to 50 feet, however no site specific data has been reviewed at this time. Site specific data will be reviewed in conjunction with the Phase II model (Section 8.2) to attempt to obtain values that are more representative. However, because dispersivity is difficult to measure and depends on mesh/grid resolution as well as geologic material, some variation in this parameter will remain to be a potential source of error for Phase II.

Time Step and Duration

The use of such a large time step, 10 years, creates some error in the model results. However the time step sensitivity plots indicate that this error is small enough to be acceptable for this Phase I test model. Use of smaller time steps does produce less instability on the boundaries. For Phase II, a much smaller time step will be required because the spatial resolution will be refined. A time step sensitivity will also be performed for all Phase II models.

The Phase I model duration is 35,000 years. Data is not available for this time period to determine the accuracy of the initial condition concentrations or to understand how the head and concentration values have varied over that period. The Phase I model is not an accurate representation of actual changes in head and concentration over 35,000 years as discussed in Section 5.0. For the Phase II model calibration, simulation durations will not exceed 1 years which will allow for a better comparison of model result variation with variation observed in monitoring wells.

Despite all the assumptions and potential sources of error, the model fulfills its intended purpose. That is, to test several parameters to determine their relative importance to the numerical model, to determine starting parameters for the Phase II model, and to identify some of the problems that may develop during the Phase II model.

8.0 PHASE I SUMMARY AND PHASE II RECOMMENDATIONS

A regional groundwater model was developed for southern Florida using both the WASH123D and SEAWAT density-dependent codes. This coarse-resolution model was developed to test model boundaries, hydraulic and transport parameters and run times; to generate preliminary flow and transport results to compare against monitoring well data;

and to compare the WASH123D and SEAWAT results as Phase I of the ASR Regional Modeling Study. Lessons learned in the Phase I study will be incorporated into the development of the more-detailed Phase II regional model.

8.1 PHASE I MODEL SUMMARY

The Phase I model conceptualization was completed using information from existing ASR Regional Study task reports and limited review of existing monitoring well data. Based on the information, the primary area of freshwater recharge for the FAS is the highland ridge area of Polk County. In this area, groundwater elevations are highest and salt concentrations lowest in all of the Floridan aquifers. As groundwater moves out in all directions from this area towards the locations where the geologic units outcrop to the ocean, heads decrease and salinity increases. Groundwater in the UF is fresh-to-brackish through most of the unit with an increase in salinity near the southeast coast adjacent to the ocean. The MF has slightly higher salt concentration and the LF has significantly higher salt concentrations.

Using WASH123D and SEAWAT, the Phase I model was constructed to include the Surficial Aquifer System, the Intermediate Aquifer System, the Floridan Aquifer System and the Boulder Zone but the focus of the model is the Floridan Aquifer System. Three vertical layers of elements were used to define the most important units for the ASR study, the UF and MF, with most of the other units represented with two or less vertical layers. The horizontal model boundaries were defined just north of the recharge area and 20 mile beyond the coast with 5 miles between computational points. The model was run for 35,000 years assuming that the oldest age of groundwater found in recent groundwater age research is the length of time for water to traverse the system. The major assumptions used in construction of the Phase I model are:

- Coarse resolution is able to resolve flow and transport behavior
- No pumping stresses
- Top of the model is the water table (no unsaturated zones)
- Bottom of the model is a no-flow boundary
- Recharge from precipitation is represented using fixed surface heads generated from existing surface aquifer monitoring well data
- Head boundary conditions do not vary over time
- Dispersivity is constant throughout the model for all materials
- No temperature effects on groundwater density

The results of the model replicate flow and transport behavior in the Polk County recharge area. Model heads are highest and salt concentrations are lowest in that area for all the aquifers. Model heads are too low and salt concentrations too high compared to monitoring well data in the southern part of the model. In that area, the direction of flow is vertically upward so salt intrudes from the model bottom as well as the ocean in the southeast resulting in an over-estimation of the salinity. The timing of this upward salt migration is faster in the SEAWAT simulations than in the WASH123D simulations. This results in significantly lower computed heads in the UF and MF in the SEAWAT model at the end of the 35,000 year simulation. Despite varying several parameters including surface heads, hydraulic conductivities, and boundary heads and

concentrations, the mechanism for allowing more fresh water into the southern part of the model is unclear. It is possible that the mechanism is missing from the conceptual model, such as a preferential flowpath or lineament/fracture zone, or that the Phase I model construction assumptions limit the ability to reproduce the long-term flow and transport patterns. Additional work will be completed for the Phase II model to determine if higher spatial and temporal resolution and a shorter transient duration exhibit similar results.

Sensitivity analysis results show that the Phase I model is very sensitive to the concentration boundary condition method selected and the effect of temperature on density. The trials for confining unit hydraulic conductivity, initial concentration conditions and dispersivity show the model is somewhat sensitive to those parameters. The smallest effects were demonstrated by changes in aquifer hydraulic conductivity. These results provide some basis for how Phase II model parameters will behave however, most of these parameters are heavily dependent on mesh resolution. Additional sensitivity analyses will be required for the Phase II model.

8.2 RECOMMENDATIONS FOR PHASE II

Construction and execution of the Phase I model provide valuable information to aid in the approach and construction of the Phase II model. The Phase II model will consist of several parts. First, a comprehensive data review will be completed to ensure that all available head, concentration, and groundwater withdrawal data is incorporated. Phase II model construction will accompany the data review since the model construction will depend heavily on data availability and data requirements. Once the Phase II model is constructed, a flow only calibration will be performed. For the flow-only transient calibration, concentration values and transport parameters will be held constant. Flow parameters will be adjusted until the computed heads reasonably match observed data. Once a satisfactory flow-only calibration is obtained, full transient calibrations, with variable flow and concentration data, will be completed. In conjunction with the regional model, smaller scale transient stress-test “inset” models will be developed in the vicinity of operational ASR wells. Data collected during the on-going operations or cycle testing will be used to facilitate the calibration of transport parameters for the regional model. Regional model calibration data will encompass flow and water quality data in approximately 200 monitoring wells in multiple geologic units. Regional model calibration will be performed where computed and observed data are correlated over a duration of approximately 1 year. Flow and water quality data for a different 1-year time period, representing a different hydraulic condition (e.g. drier or wetter year), will be used for model validation. The goal of this effort is a fully-calibrated Phase II Regional Model. The calibrated Phase II model will ultimately be used in the evaluation of proposed ASR project alternatives.

During the data review and model construction portion of Phase II, several decisions will be required. The location of the model boundary is a trade-off between keeping the boundary conditions as far away from the areas of interest as possible and limiting the number of computational points required. The areas of interest for this modeling study are the proposed locations of the ASR wells. Most of the ASR wells are proposed near Lake Okeechobee and on the east coast (e.g. Hillsborough and Palm Beach County).

Only one proposed ASR location, near proposed reservoir C-43, is a west of Lake Okeechobee. It is located approximately 40 miles away from the western coast so moving the model boundary closer to the western coast should not impact it. It is recommended that the model boundary on the west and south side of the state be moved in to the Florida coastline as shown in Figure 88. In addition to reducing the amount of model computational points, moving the model boundary to the western coast has the benefit of eliminating uncertainties associated with extrapolating head and concentration boundary condition values along a portion of the model perimeter. As discussed in Section 7.0, testing will be required to determine if potential oscillations on the boundary will limit how close to the coast the boundary can be moved.

Once the model boundary is defined, the resolution will be selected. The Phase II model resolution will depend on how many calibration wells are chosen, how many pumping wells are incorporated for the time period selected, the potential for combining several pumping wells in the model and how the proposed ASR locations are simulated. This selection is critical because the number of computational points selected will dictate the model run times. The Phase I model contains approximately 50,000 computational points for both WASH123D and SEAWAT. To run 50,000 points with a 10-year time step for 35,000 years takes approximately 110 hours for WASH123D, 3.25 hours for SEAWAT (upwinded) and 1,247 hours (estimated) for SEAWAT (TVD). For Phase II, the mesh size will increase by approximately 10-fold yielding 500,000 computational points. Because the mesh resolution will be finer, the time step size will be smaller. Even though, more computations will be made at more frequent intervals, the run times are still expected to be reasonable because the total simulation duration will decrease to approximately 1 year for the separate calibration and validation runs. Table 1 shows the estimated run times for a 1 year simulation for a 500,000 node discretization with a 0.5-day, 1-day and 5-day time step size, assuming a direct relationship between the variables. This estimate indicates that run times should be reasonable as long as the mesh resolution does not increase beyond 500,000 computational points. Note that the additional model stresses resulting from incorporating pumping into the Phase II model could alter these calculations.

Table 1. Phase II Run Time Estimate

WASH123D			
Nodes	Time step	Duration (yrs)	Run time (hrs)
Phase I – 50,000	10 year	35,000	110
Phase II – 500,000	5 day	1	23
Phase II – 500,000	1 day	1	115
Phase II – 500,000	0.5 day	1	230

Table 1. Phase II Run Time Estimate (cont'd)

SEAWAT			
Cells	Time step	Duration (yrs)	Run time (hrs)
Phase I (upwinded) – 50,000	10 year	35,000	3.25
Phase II (upwinded) – 500,000	5 day	1	0.7
Phase II (upwinded) – 500,000	1 day	1	3.4
Phase II (upwinded) – 500,000	0.5 day	1	6.8
Phase I (TVD) – 50,000	10 year	35,000	1,247 (est.)
Phase II (TVD)– 500,000	5 day	1	260
Phase II (TVD) – 500,000	1 day	1	1,300
Phase II (TVD) – 500,000	0.5 day	1	2,600

Another model construction decision that will impact the resolution and run time is the vertical discretization. Near the ASR wells, complex flow patterns and high concentration gradients will exist that may not be adequately resolved with the three layers defined in both the UF and MF for Phase I. ASR wells will be located in the both UF and MF so these layers will require additional vertical discretization.

Additional vertical discretization may also be necessary in the confining units. As part of Phase II, several test models will be constructed to further examine the differences between WASH123D and SEAWAT noted in Section 6.1. Mesh/grid resolution issues, differences in treatment of vertical hydraulic conductivity and the configuration of the finite element computational nodes and the finite difference computational cells may affect the computed rate of vertical salt migration. A better understanding of these differences is required to ensure that the proper vertical salt migration is simulated in both the SEAWAT and WASH123D models.

Boundary heads will be set in all aquifers for Phase II based on transient data collected for the stress periods selected. The head and salt concentration within the surface aquifer will also be set based on transient data collected for the stress period. Variable concentration boundary conditions will be used in both models for the salinity boundaries in all aquifers. When the flow direction on the boundary is into the model, the concentration will be based on transient data collected for the stress period selected. When the flow direction is out of the model, the concentration will be model-computed.

For the flow-only calibration, a good concentration initial condition dataset will be selected based on available data. The initial condition concentrations will be smoothed by running the model for a few time steps and using the resulting concentration variation as the initial conditions for the calibration runs. This method should reduce any sharp fronts or "blockiness" in the concentration initial condition from data interpolation.

Based on the results of the sensitivity to temperature effects for Phase I, it is also recommended that temperature be included in some capacity in the Phase II model. At a minimum, the boundary head for the BZ should incorporate temperature effects. Additional Phase II sensitivity runs may determine whether temperature effects should be coded to other head boundaries or if full heat transfer computations are warranted.

9.0 FIGURES

Report Figures are submitted in a separate file “ASRDraftReportFigures.pdf

10.0 REFERENCES

Brown, C.J, England, Steve, Stevens, G.L. Cheng, H-P, and Richardson, Emily, (2006), ASR Regional Study—Benchscale Modeling, Final Report.

Bush, P.W., and R.H. Johnston, (1988), "Groundwater Hydraulics, Regional Flow and Groundwater Development of the Floridan Aquifer System in Florida and in Parts of Georgia, South Carolina, and Alabama", U.S. Geological Survey Professional Paper 1403-C Plate 4.

CH2M Hill, "Groundwater Numerical Model Development Support and Data Collection Report", CH2M Hill, Tampa, FL for U.S. Army Corps of Engineers, Jacksonville, FL, July 2006.

Cheng, H.-P., J.-R. Cheng, and G.-T. Yeh, 1998. "A Lagrangian-Eulerian method with adaptively local zooming and peak/valley capturing approach to solve three-dimensional advection-diffusion transport equations." *International Journal for Numerical Methods in Engineering*, *41*(4), 587-615.

Cheng, J.-R., H.-P. Cheng, and G.-T. Yeh, 1996. "A Lagrangian-Eulerian method with adaptively local zooming and peak/valley capturing approach to solve two-dimensional advection-diffusion transport equations." *International Journal for Numerical Methods in Engineering*, *39*(6), 987-1016.

Fies, Michael W., unpublished. Lineament Analysis South Florida Region, Aquifer Storage and Recovery Regional Study.

Guo, W., and C.D. Langevin. 2002. User's Guide to SEAWAT: a Computer Program for Simulation of Three-Dimensional Variable-Density Ground-Water Flow. Open-File Report 01-434. U.S. Geological Survey, Tallahassee, Fla.

Harbaugh, A.W., Banta, E.R, Hill, M.C., and McDonald, M.G., 2000, MODFLOW—2000, the U.S. Geological Survey modular ground-water model—User guide to the modularization concepts and the ground-water flow process. U.S. Geological Survey Open File Report 00-92, 121 p.

HydroGeoLogic, Inc., 2006. Development of a Density-Dependent Saltwater Intrusion Model for the Lower East Coast Project Area

Kaufmann and Bennett. 2005. Lower West Coast Water Supply Plan, Southwest Florida Water Management District.

Kohout, F.A., 1965, A hypothesis concerning cyclic flow of salt water related to geothermal heating in the Floridan aquifer: New York Academy of Sciences Transactions, ser. 2, v. 28, no. 2, p. 249-271.

Langevin, C.D., Shoemaker, W.B., and Guo, W., 2003, MODFLOW-2000, the U.S. Geological Survey Modular Ground-Water Model—Documentation of the SEAWAT-2000 Version with the Variable-Density Flow Process (VDF) and the Integrated MT3DMS Transport Process (IMT), U.S. Geological Survey Open-File Report 03-426, 43 p.

Miller, J.A. 1986. *Hydrogeologic Framework of the Floridan Aquifer System in Florida and Parts of Georgia, Alabama and South Carolina.* Professional Paper 1403-B. Washington, D.C.: U.S. Geological Survey.

Mirecki (unpublished) Groundwater age data research

O'Reilly, A.M., R.M. Spechler, and B.E. McGurk. 2002. Hydrogeology and Water-Quality Characteristics of the Lower Floridan Aquifer in East-Central Florida. U.S. Geological Survey Water-Resources Investigations Report 02-4193.

Osiensky, J.L., and Williams, R.E., 1996, Potential Inaccuracies in MODFLOW simulations involving the SIP and SSOR methods for matrix solution, Ground Water 35 (2), p. 229-232.

Parker, G.G., Ferguson, G.E., Love, S.K., and others, 1955, Water resources of southeastern Florida: Geological Survey Water-Supply Paper 1255, 965 p.

Randazzo, A.F., and D.S. Jones. 1997. The Geology of Florida, University Press of Florida.

Reese, R.S., and K.J. Cunningham. 2000. Hydrogeology of the Gray Limestone Aquifer in Southern Florida. U.S. Geological Survey Water-Resources Investigations Report 99-4213.

Reese, Ron and Emily Richardson, Task 3.0 Define Preliminary Hydrogeologic Framework, ASR Regional Study, October 4, 2004.

Sepulveda, 2002. Simulation of Groundwater Flow in the Intermediate and Floridan Aquifer Systems in Peninsular Florida, U.S. Geological Survey Water Resources Investigations Report 02-4009.

South Florida Water Management District's environmental database (DBHYDRO), http://www.sfwmd.gov/site/index.php?id=38.

Yeh, G.-T., G. Huang, H.-P. Cheng, F. Zhang, H.-C. Lin, E. Edris, and D. Richards, 2006. "A First-Principle, Physics-Based Watershed Model: WASH123D, Chapter 9, Watershed Models", 653 pp., Edited by V. P. Singh and D. K. Frevert, CRC Press, Taylor & Francis Group.

Yeh, G.-T., H.-P. Cheng, G. Huang, F. Zhang, H.-C. Lin, J.-R. Cheng, E. Edris, and D. Richards, 2003. "A Numerical Model Simulating Water Flow and Contaminant and Sediment Transport in WAterSHed Systems of 1-D Stream-River Network, 2-D Overland Regime, and 3-D Subsurface Media (WASH123D: Version 2.0)".

Zheng, C. and G.D. Bennett. 1995. Applied Contaminant Transport Modeling: Theory and Practice, John Wiley & Sons, New York, 440 pp.

Zheng, C. and P.P. Wang, 1999, MT3DMS: A Modular Three-Dimensional Multi-Species Model for Simulation of Advection, Dispersion and Chemical Reaction of Contaminants in Groundwater Systems: Documentation and User's guide, SERDP-99-1: U.S. Army Engineer Research and Development Center, Vicksburg, MS.

Figure 1
Model Area
ASR Regional Model – Phase I
December 2006

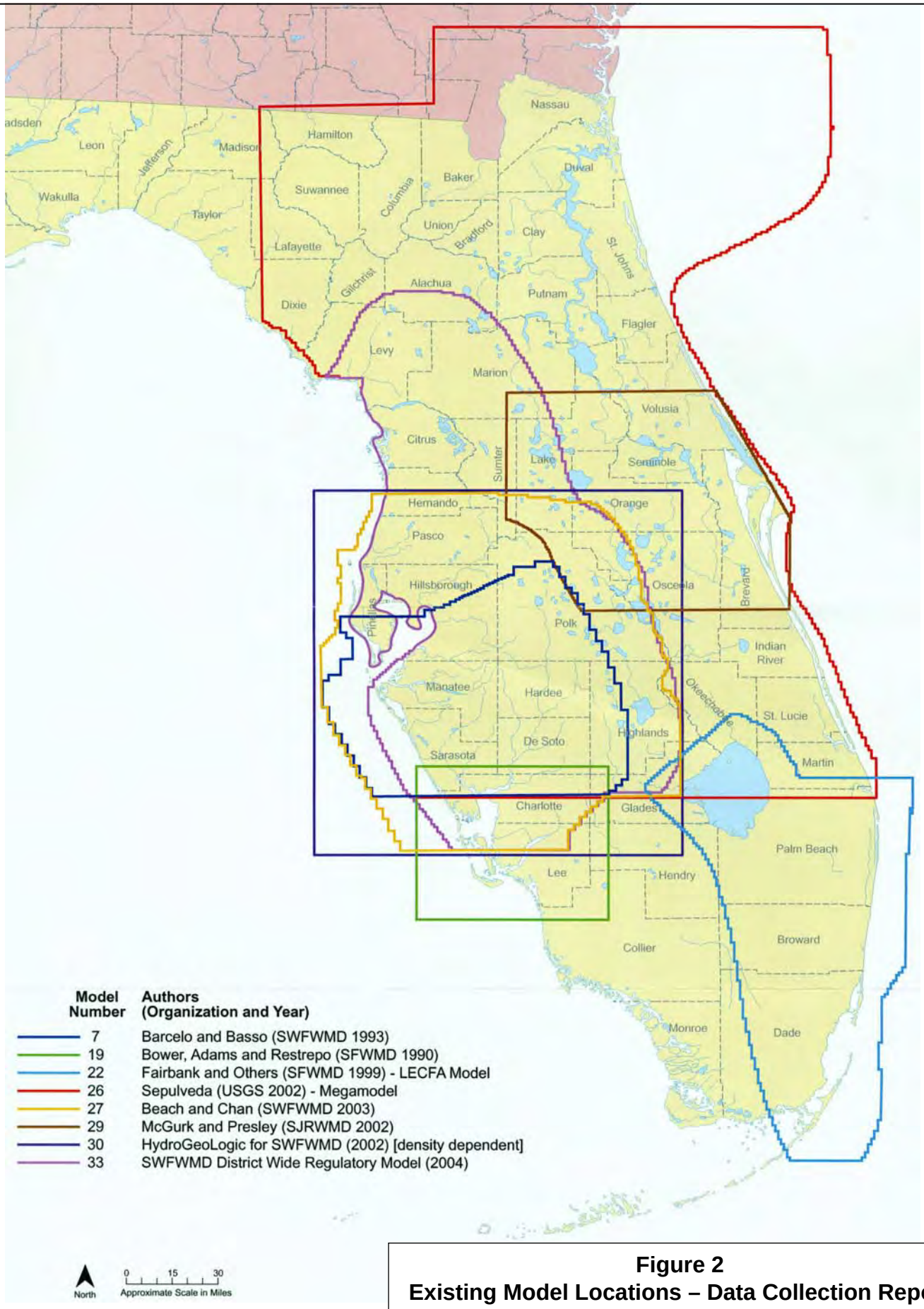

From CH2MHill (2006)

Figure 2
Existing Model Locations – Data Collection Report
ASR Regional Model – Phase I
December 2006

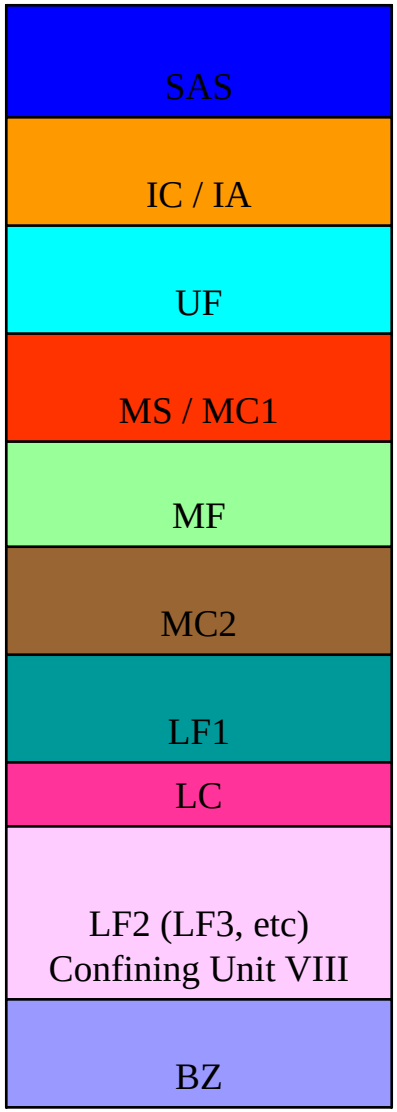

Surficial Aquifer System

Intermediate Confining and/or Intermediate Aquifer System

Upper Floridan Aquifer

Upper middle semi and/or confining unit

Middle Floridan aquifer

Lower middle confining unit (SFCU is sub Floridan confining unit)

Lower Floridan Aquifer - first permeable zone.

Lower confining unit

Confining Units from Miller, 1986 - not always continuous within region. LF2, LF3, etc. are deeper permeable zones within the Lower Floridan Aquifer.

Boulder Zone - not continuous across study area

From Reese and Richardson (2004)

Figure 3
Schematic Geologic Cross Section
ASR Regional Model – Phase I
December 2006

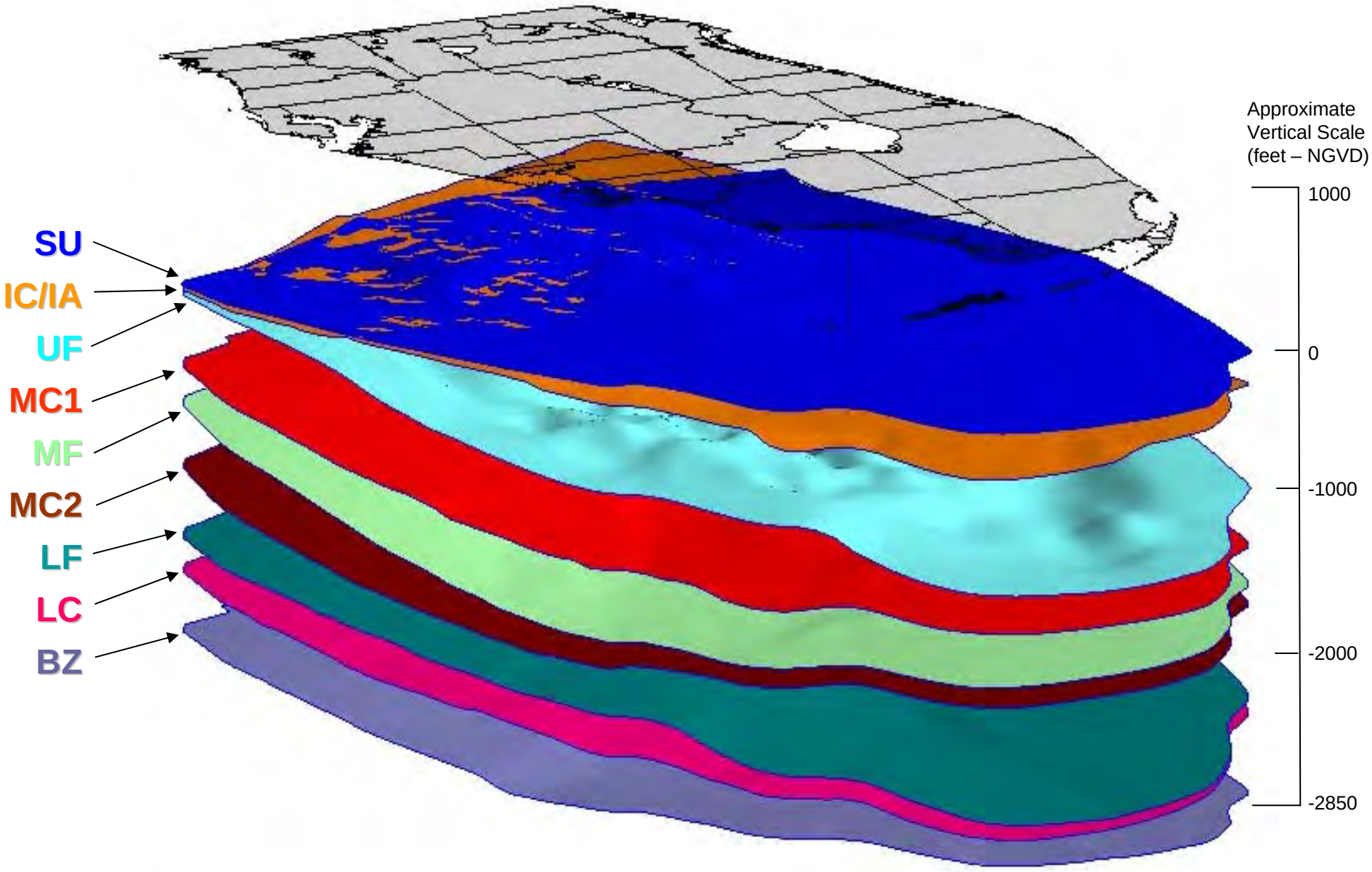

Vertical scale exaggerated by 200:1
Graphic of Florida at elevation 1000' for reference

Figure 4
Hydrostratigraphic Surfaces
ASR Regional Model – Phase I
December 2006

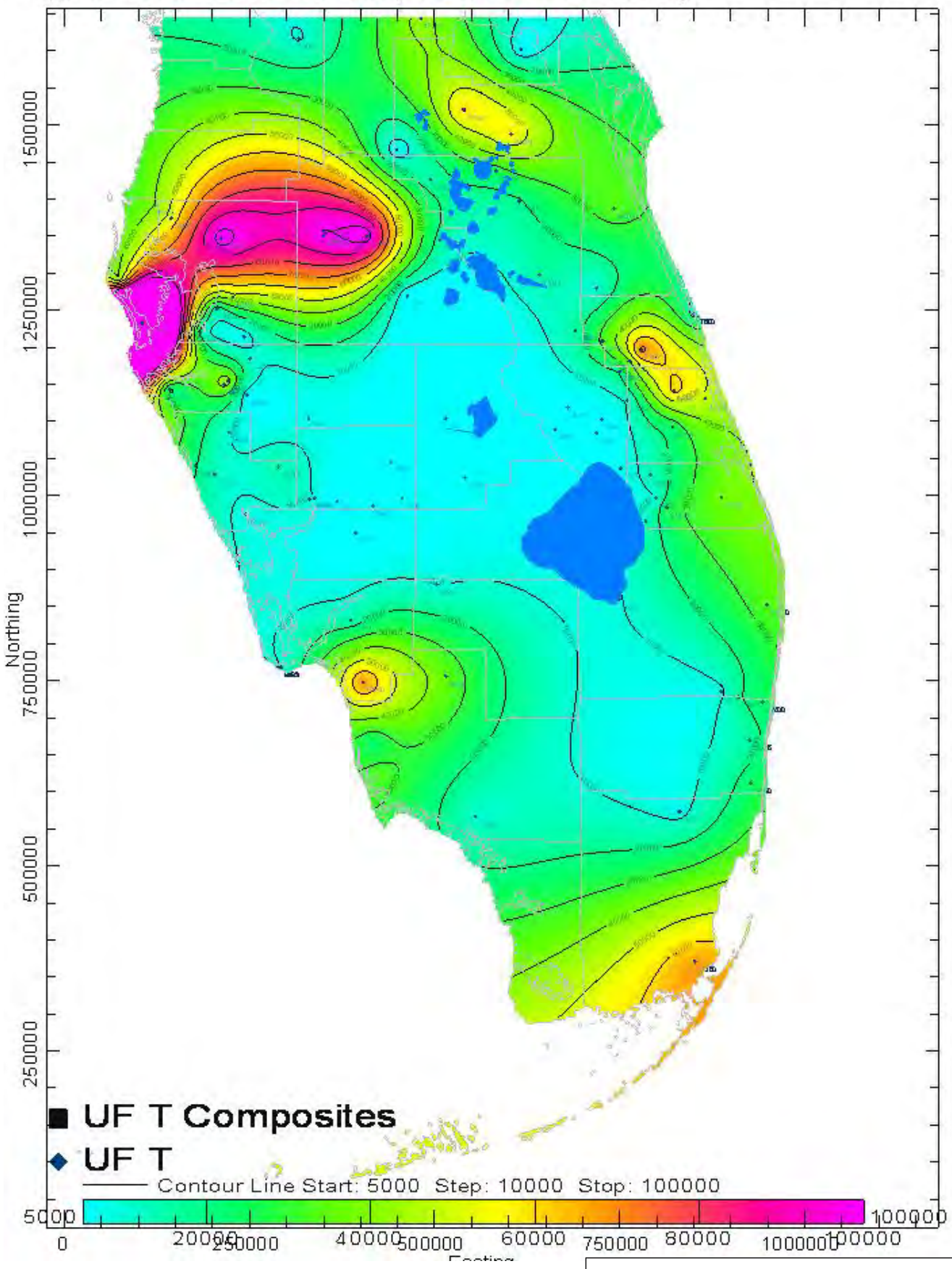

From Reese and Richardson (2004)

Figure 5
UF - Transmissivity
ASR Regional Model – Phase I
December 2006

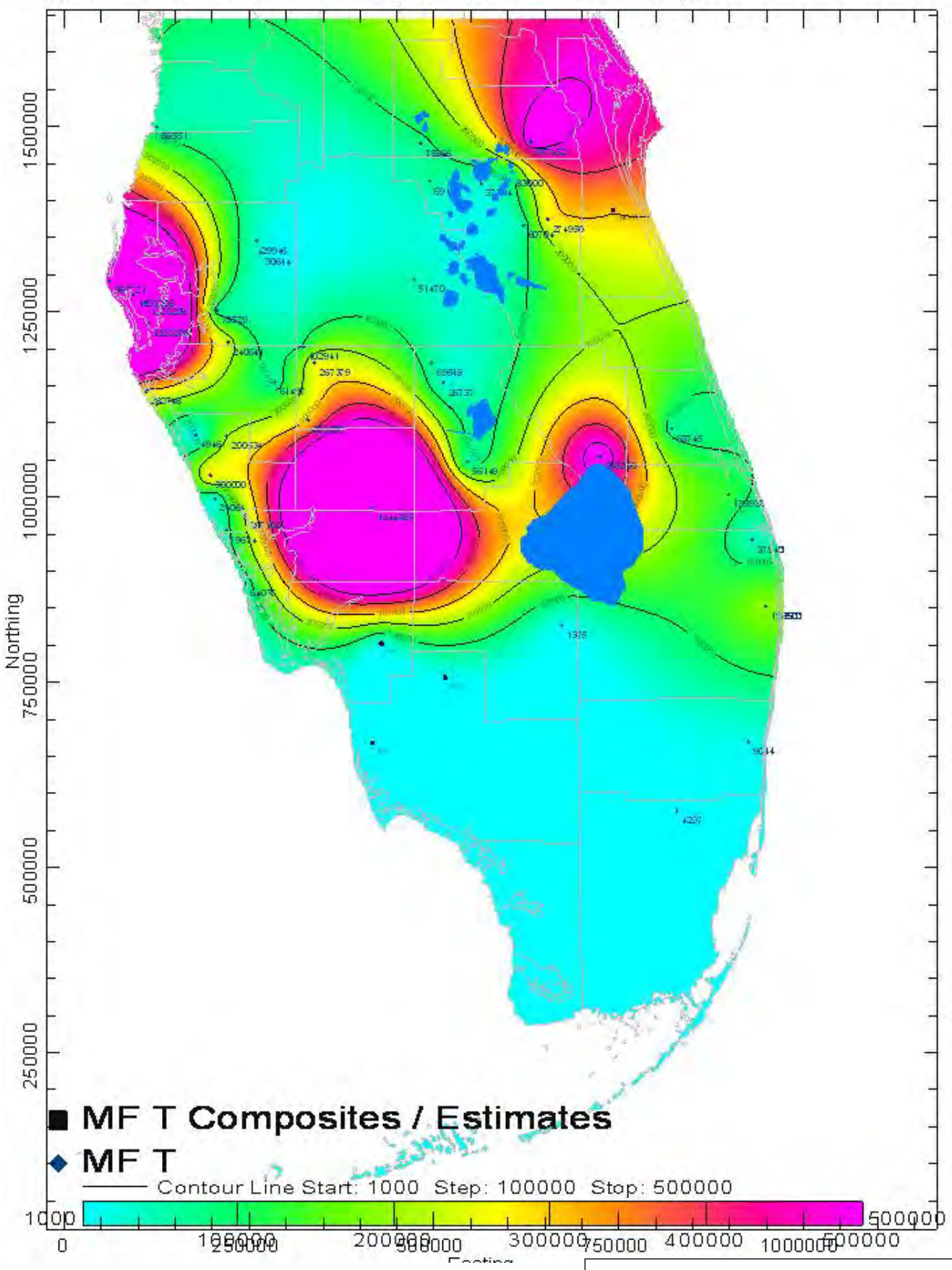

From Reese and Richardson (2004)

Figure 6
MF - Transmissivity
ASR Regional Model – Phase I
December 2006

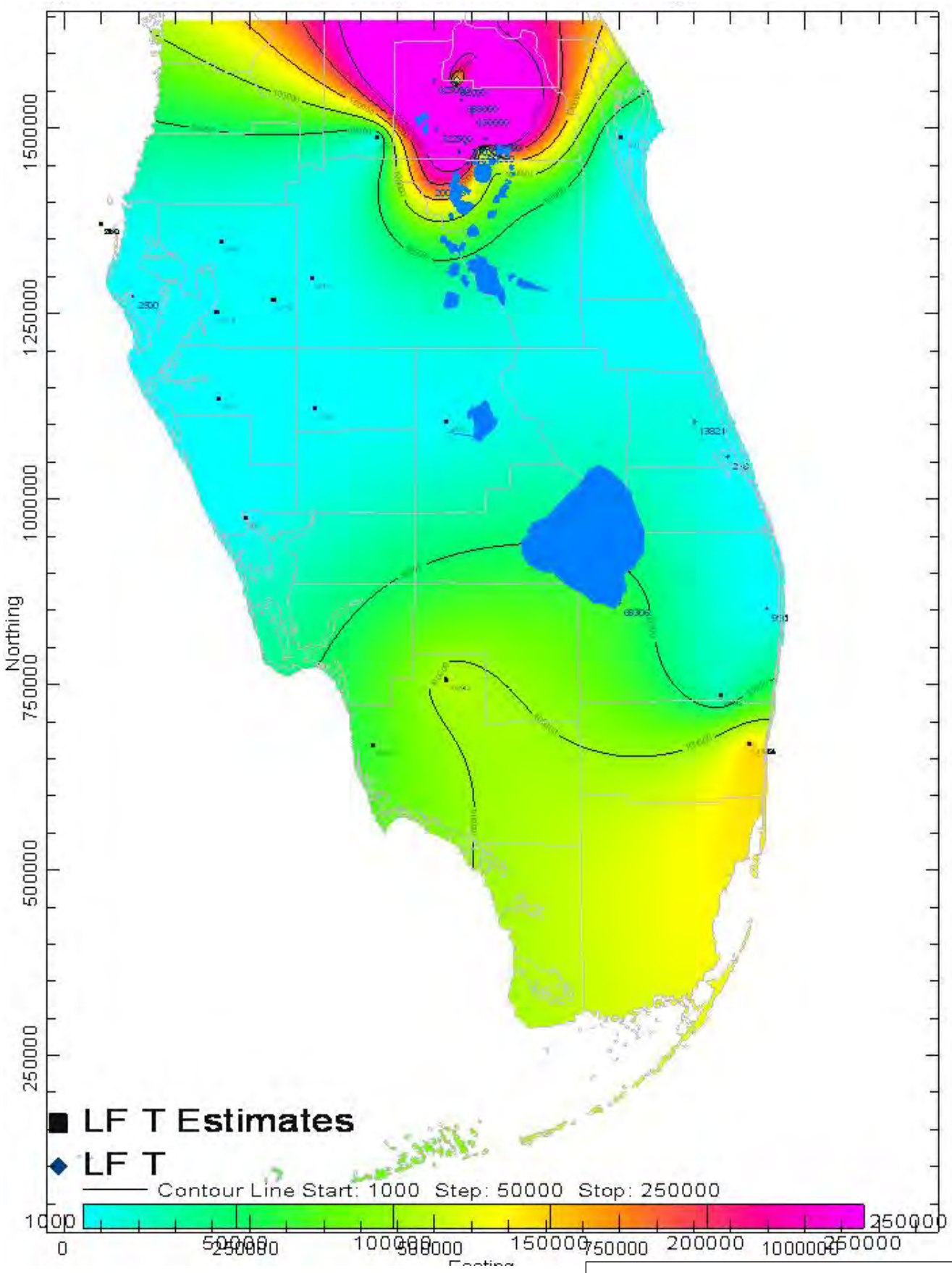

From Reese and Richardson (2004)

Figure 7
LF - Transmissivity
ASR Regional Model – Phase I
December 2006

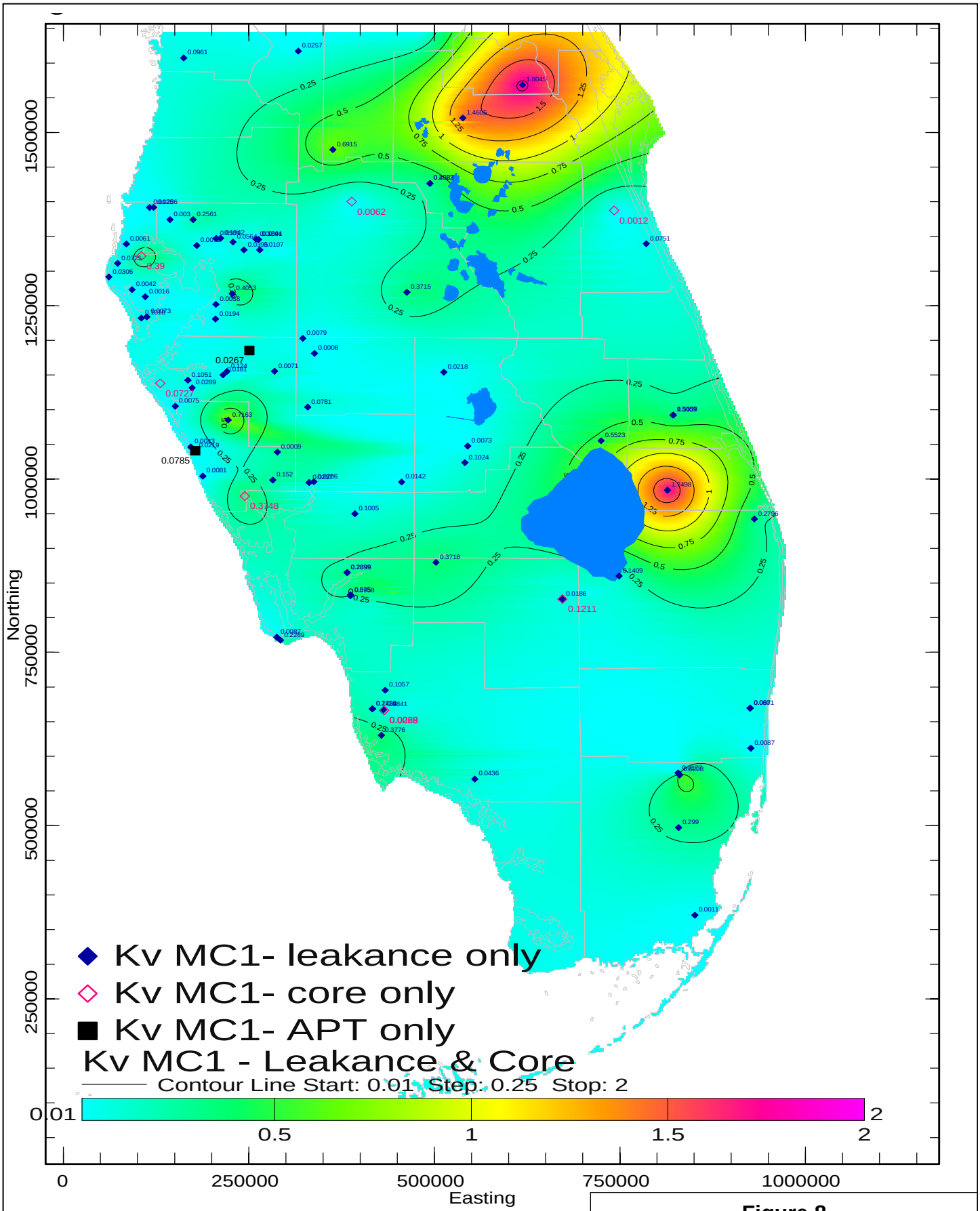

From Reese and Richardson (2004)

Figure 8
MC1 - Hydraulic Conductivity
ASR Regional Model – Phase I
December 2006

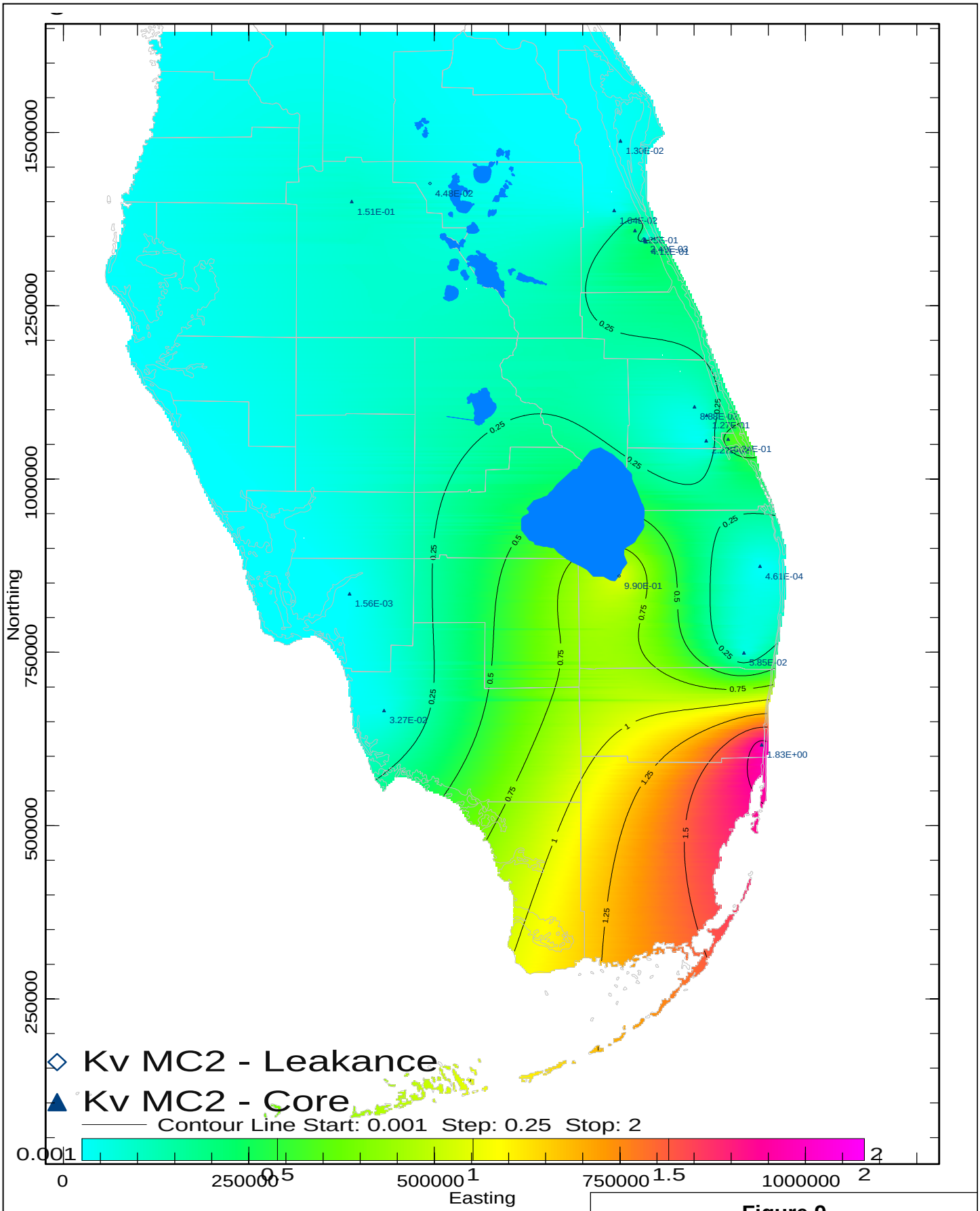

From Reese and Richardson (2004)

Figure 9
MC2 - Hydraulic Conductivity
ASR Regional Model – Phase I
December 2006

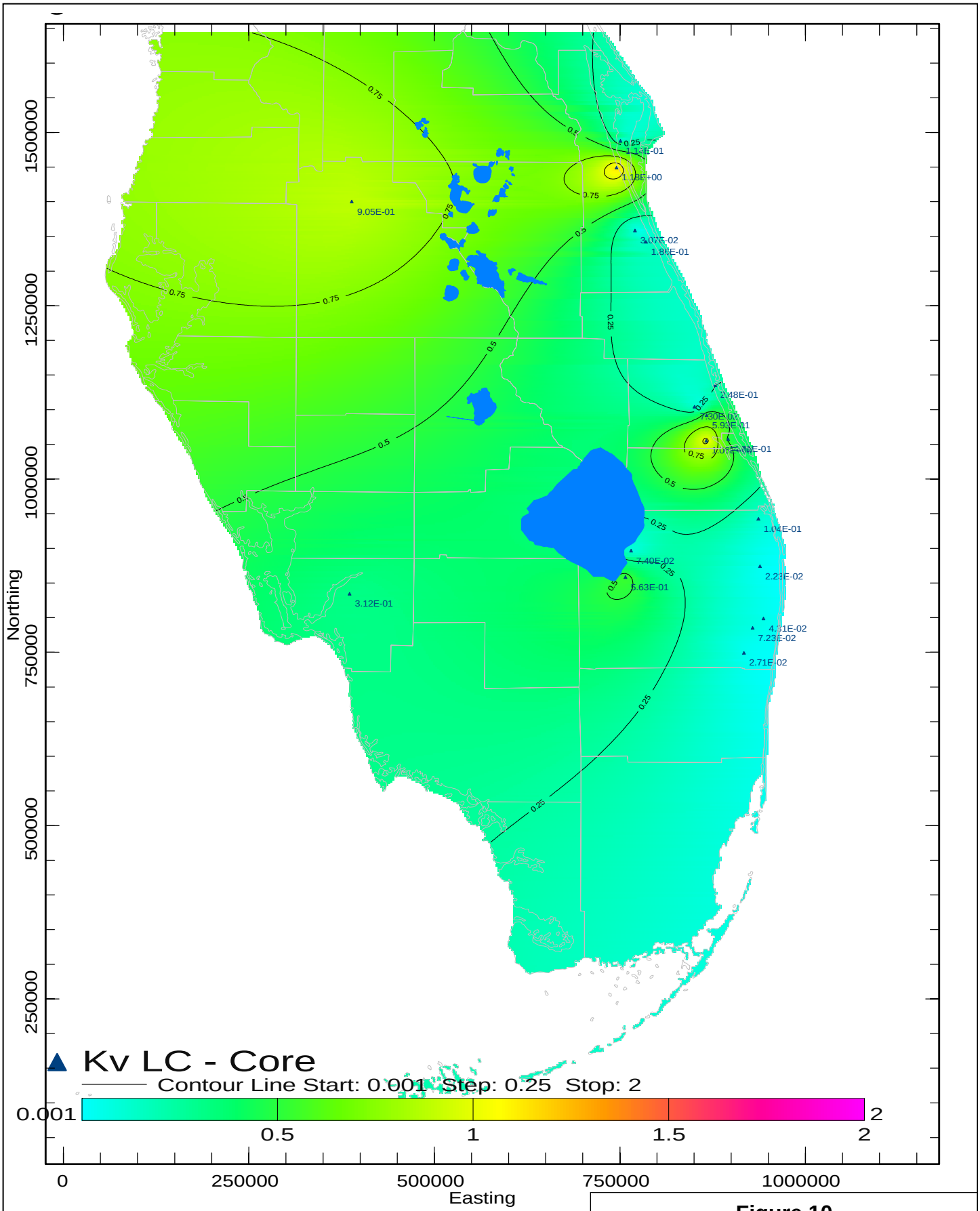

From Reese and Richardson (2004)

Figure 10
LC - Hydraulic Conductivity
ASR Regional Model – Phase I
December 2006

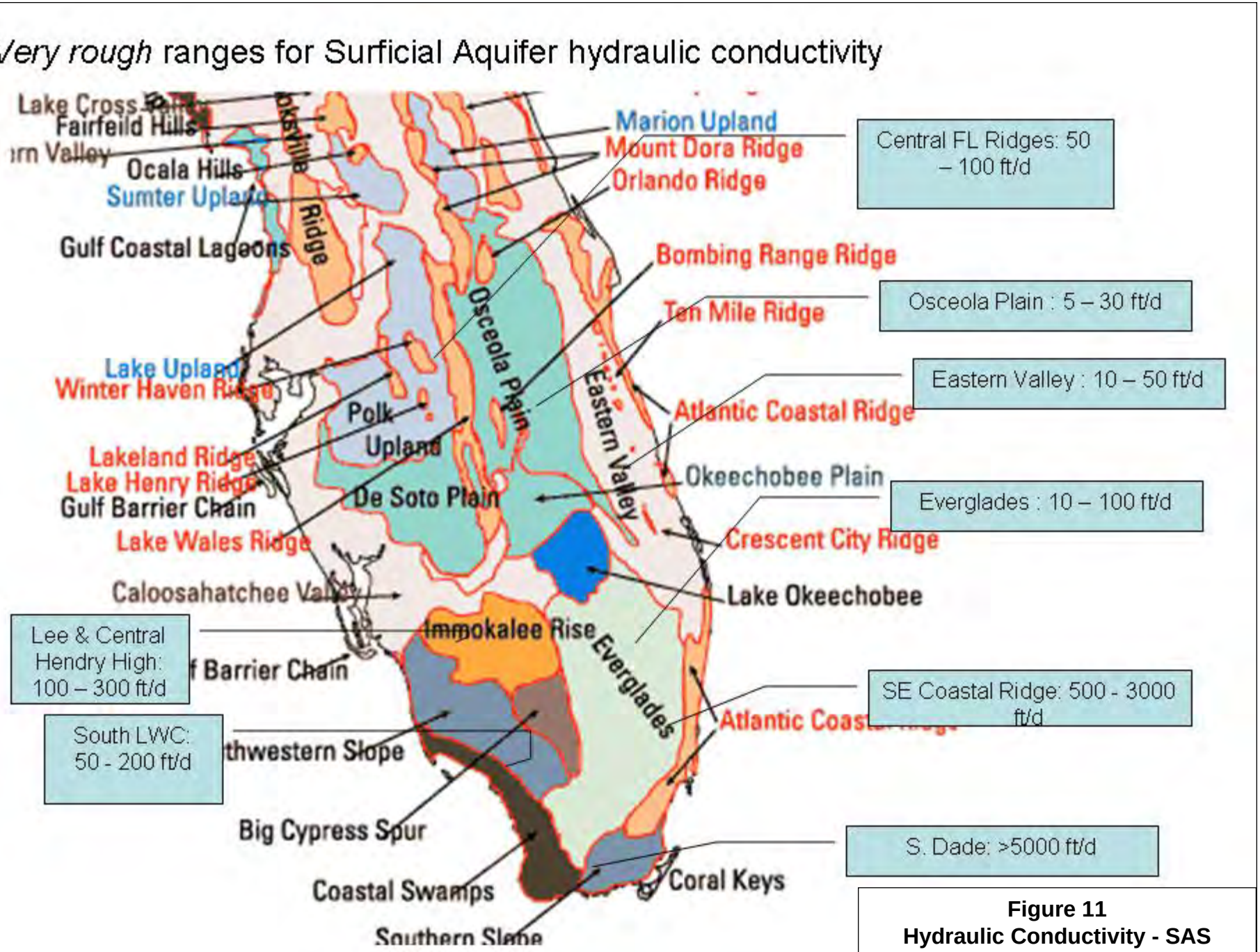

Figure 11
Hydraulic Conductivity - SAS
ASR Regional Model – Phase I
December 2006

From SFWMD

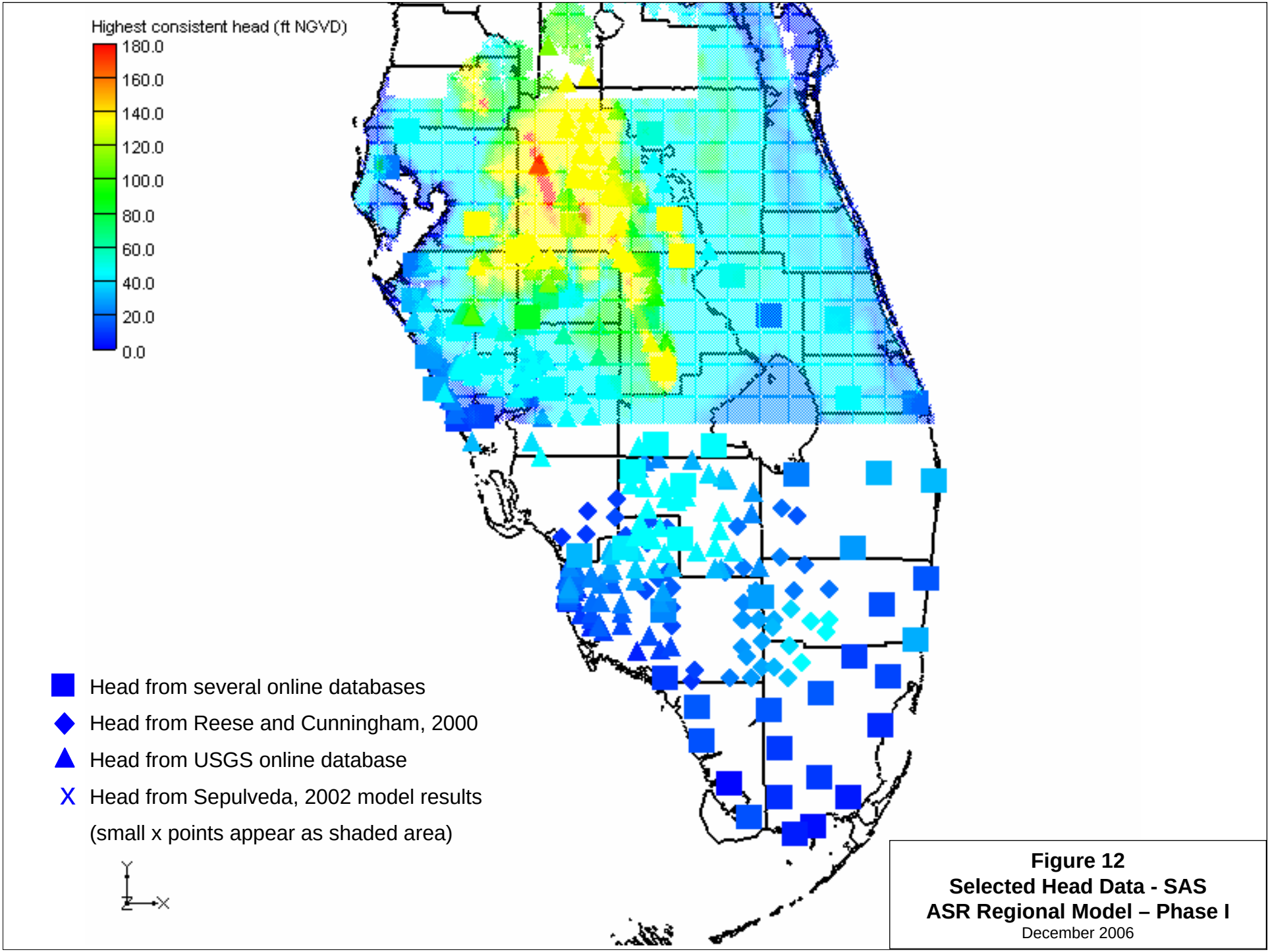

Figure 12
Selected Head Data - SAS
ASR Regional Model – Phase I
December 2006

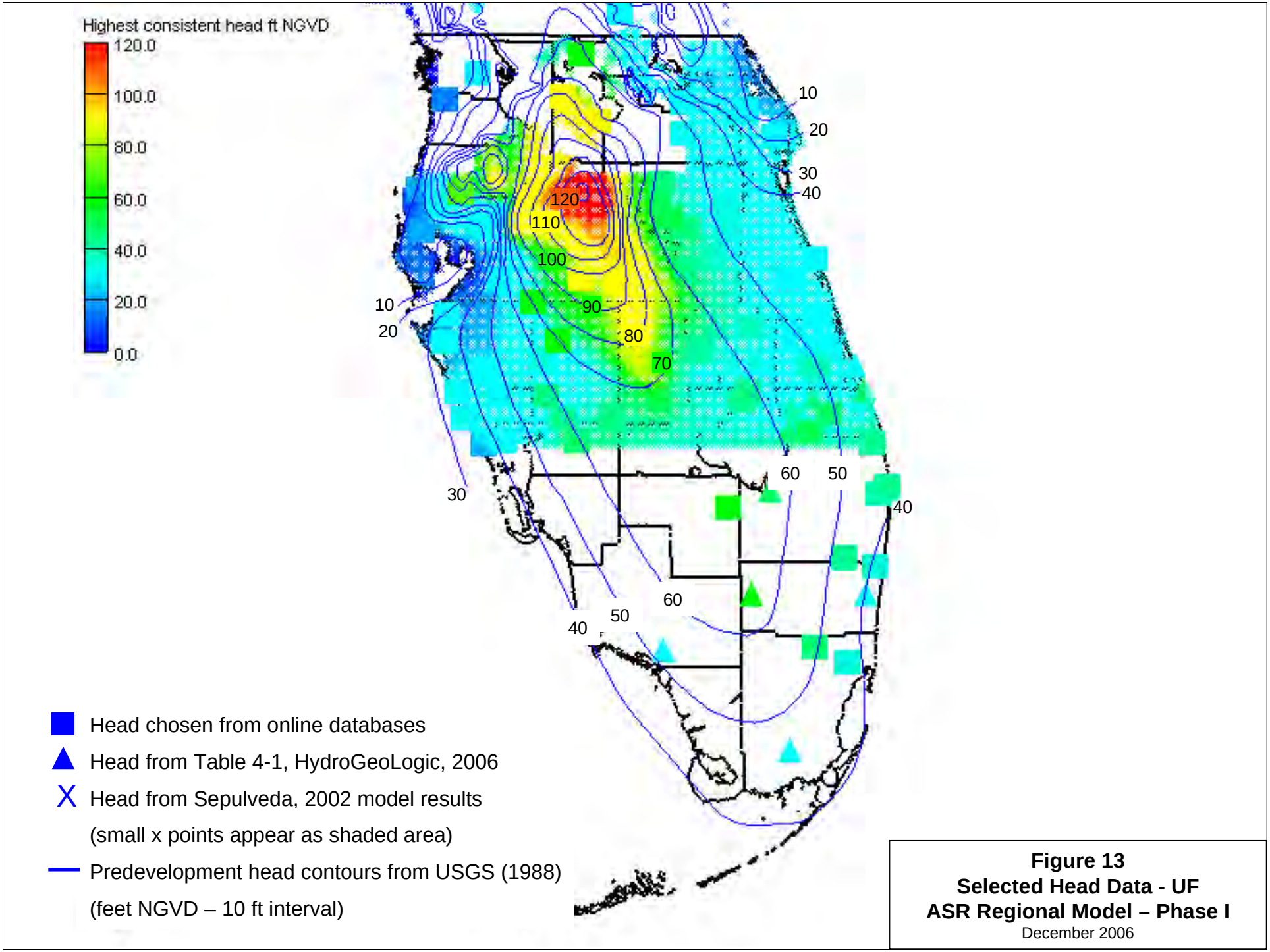

Figure 13
Selected Head Data - UF
ASR Regional Model – Phase I
December 2006

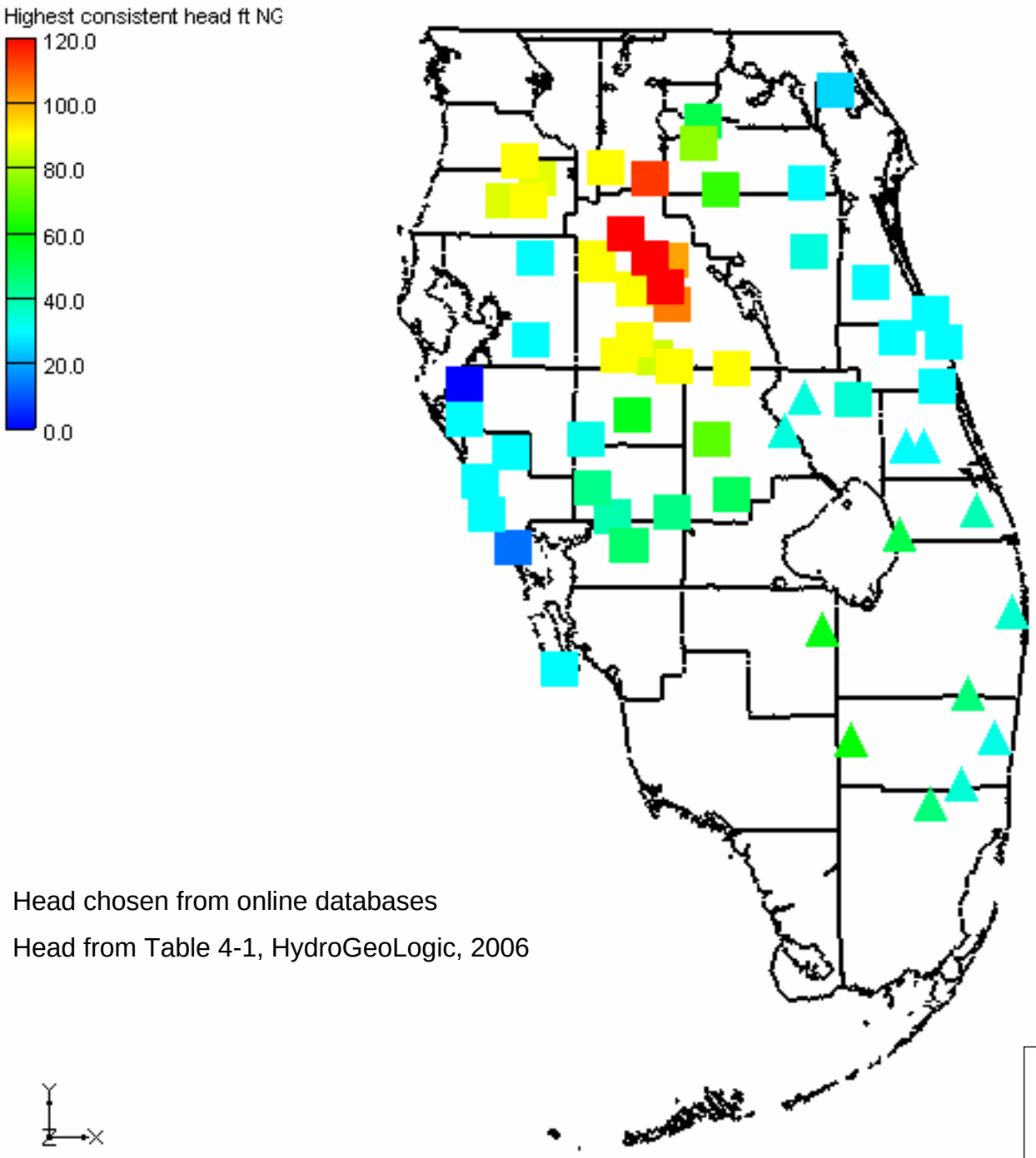

Figure 14
Selected Head Data - MF
ASR Regional Model – Phase I
December 2006

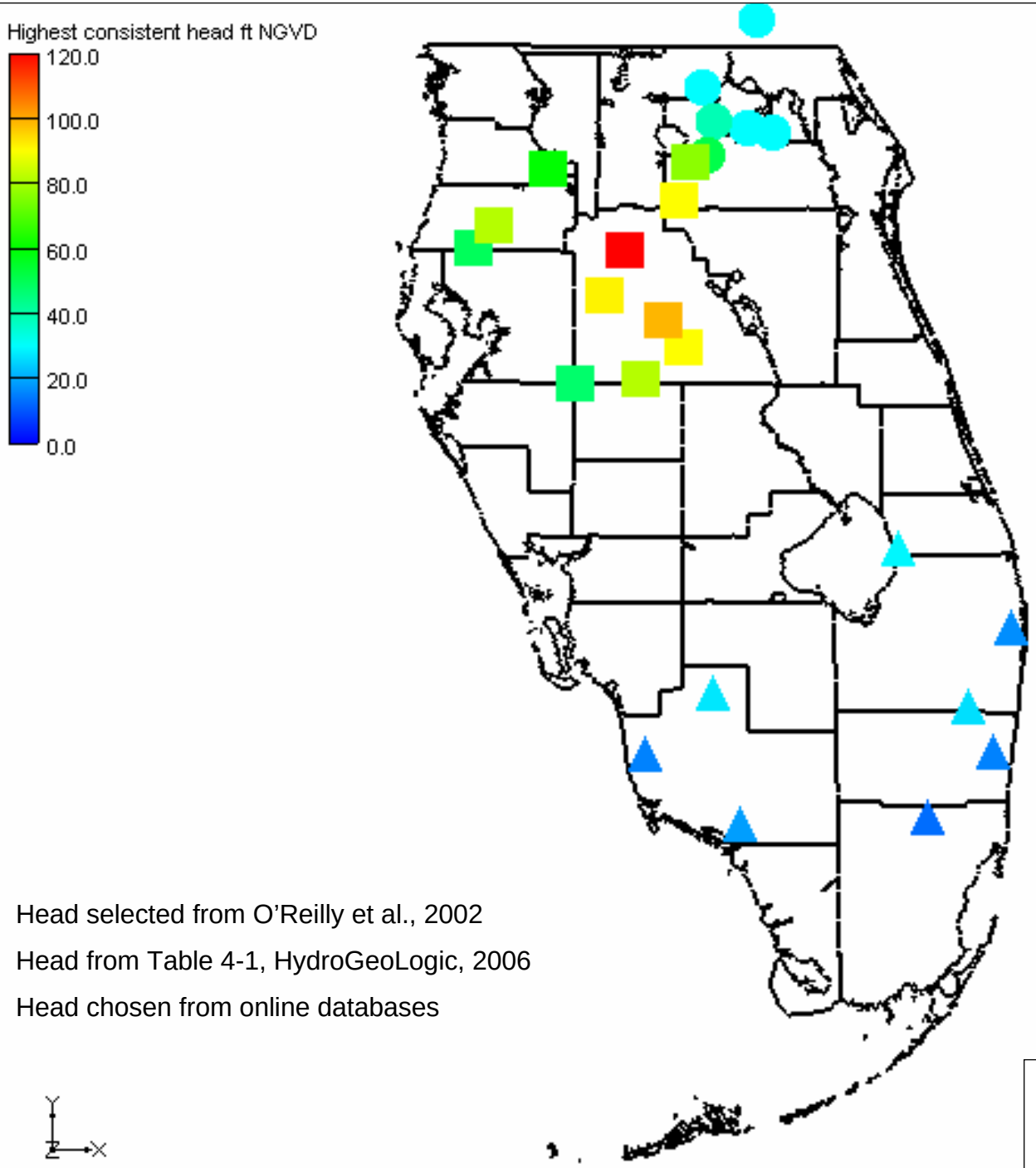

Figure 15
Selected Head Data - LF
ASR Regional Model – Phase I
December 2006

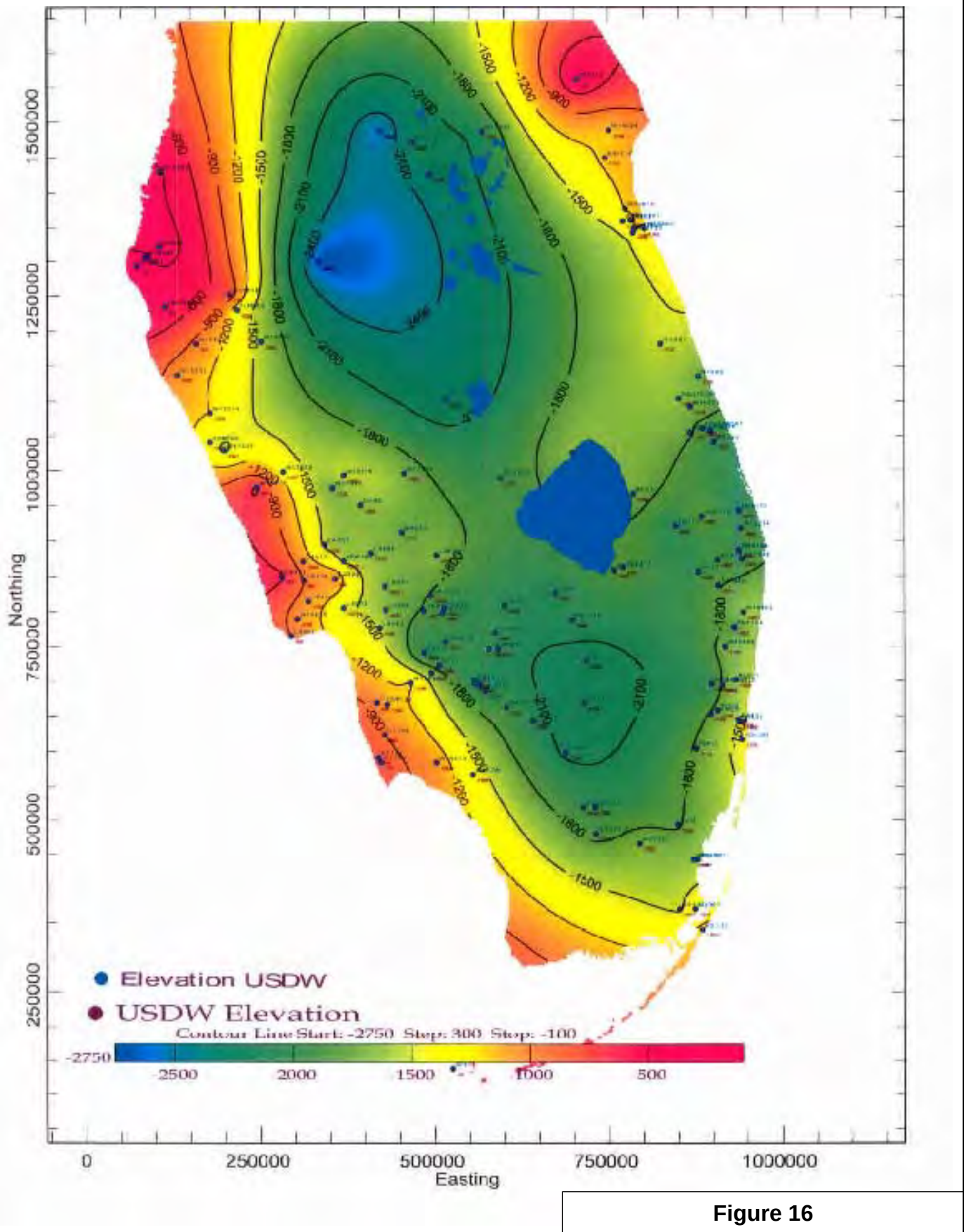

Figure 16
Elevation of 10,000 mg/l TDS
ASR Regional Model – Phase I
December 2006

Prepared by SFWMD

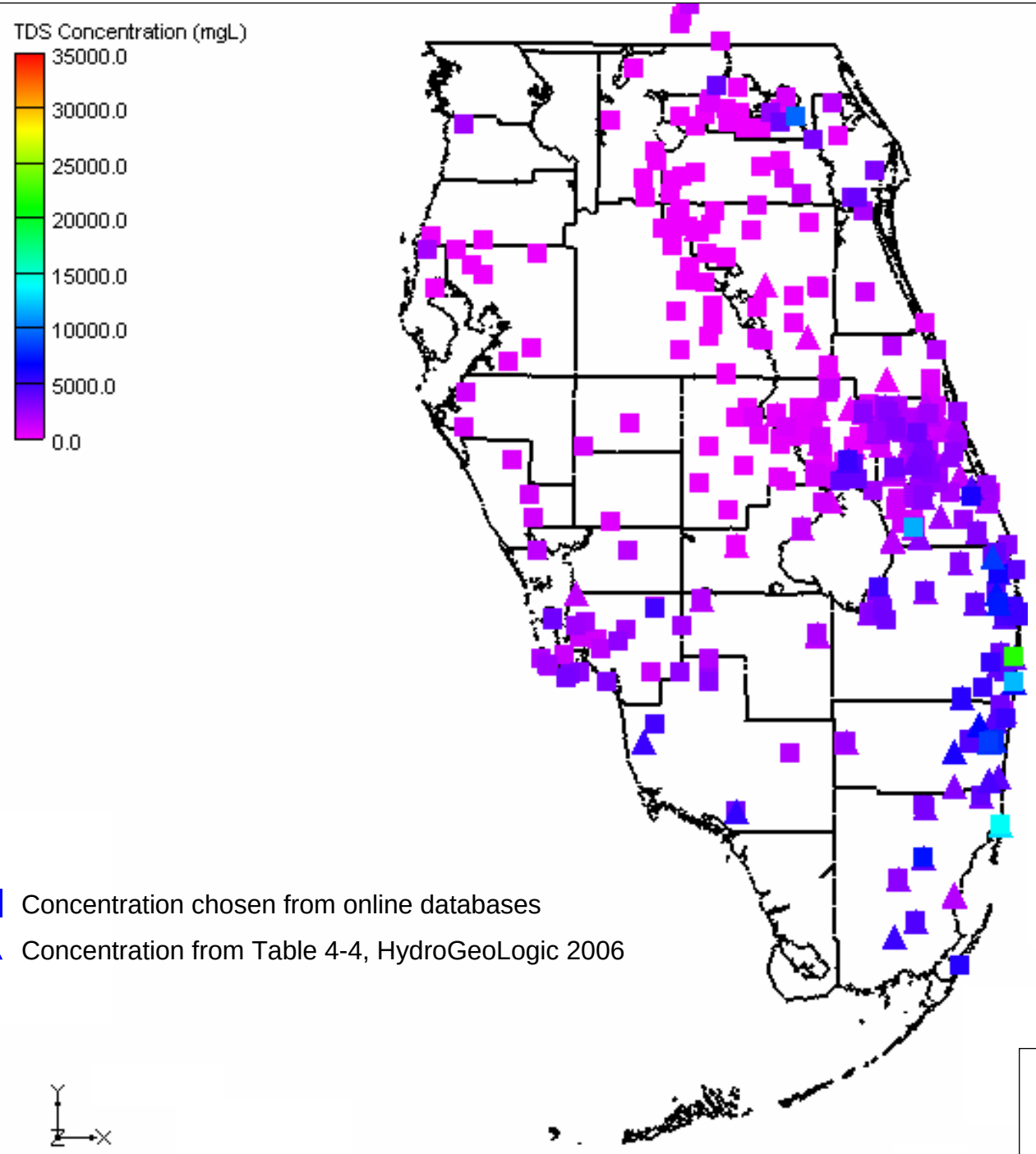

Figure 17
Water Quality Data - UF
ASR Regional Model – Phase I
December 2006

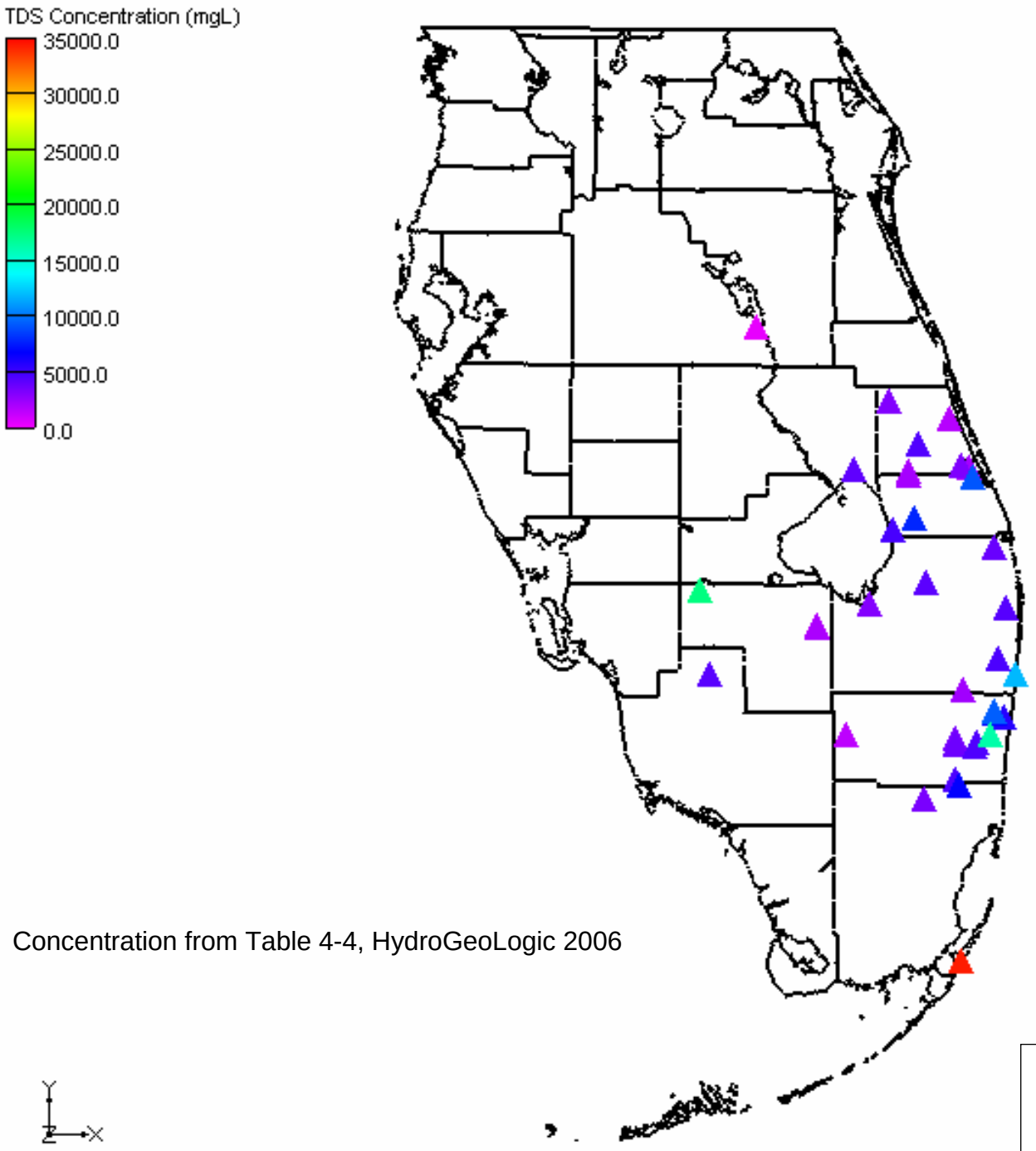

Figure 18
Water Quality Data - MF
ASR Regional Model – Phase I
December 2006

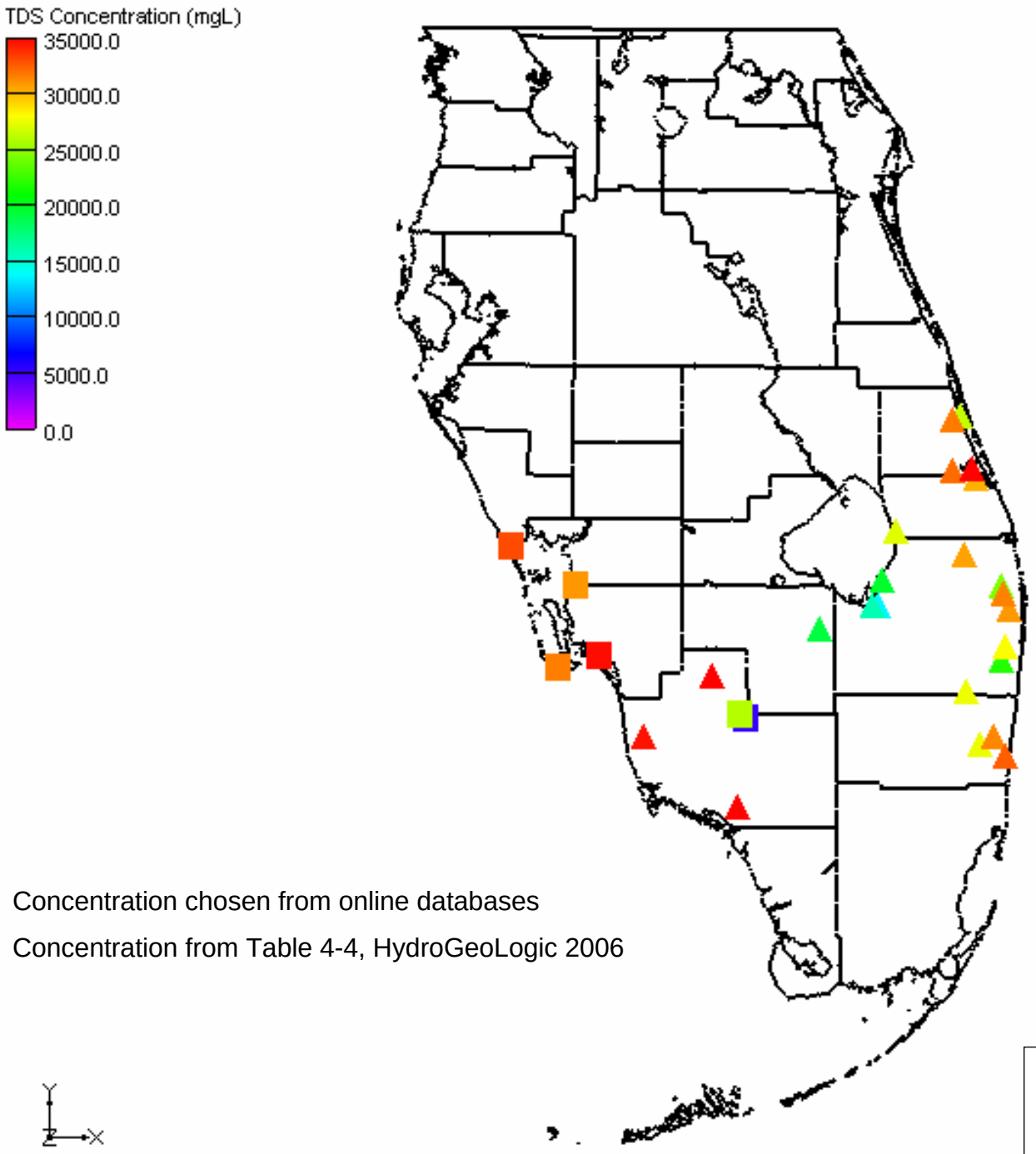

Figure 19
Water Quality Data - LF
ASR Regional Model – Phase I
December 2006

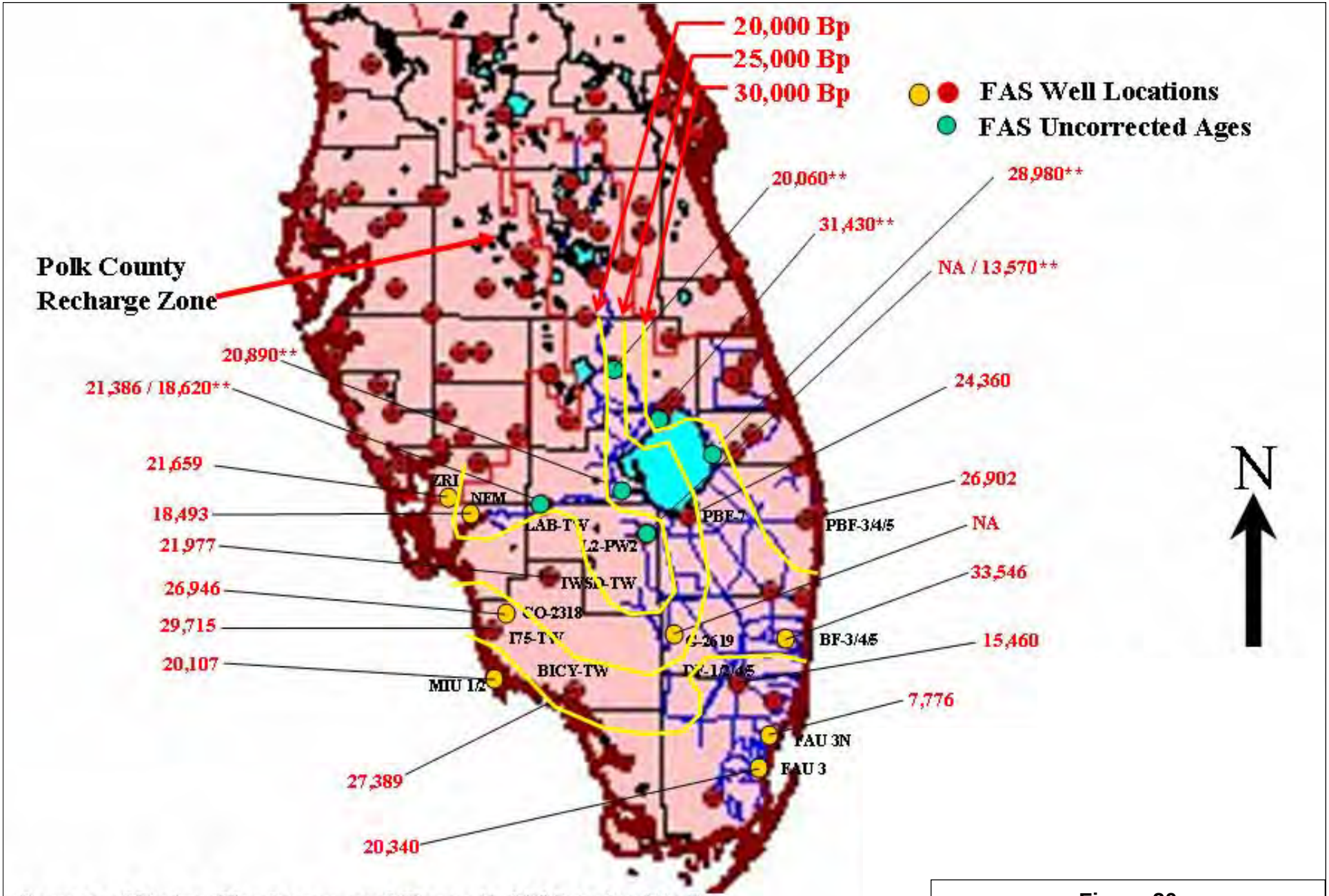

Source of Data: Kaufmann and Bennett, 2005 (submitted);
Years before present based upon Pearson correction method.
Mirecki – Uncorrected Data

Figure 20
Age of Groundwater - UF
ASR Regional Model – Phase I
December 2006

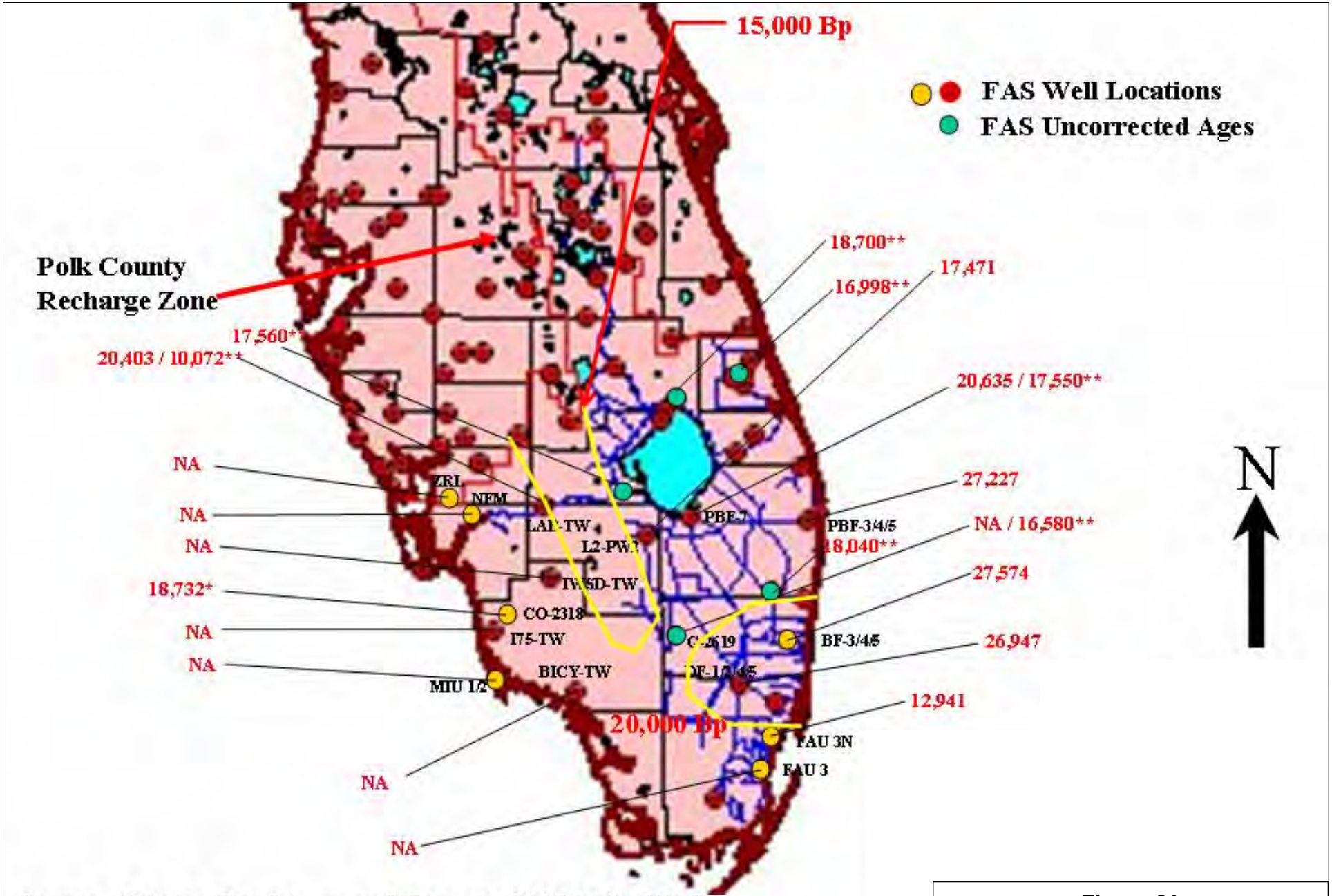

Figure 21
Age of Groundwater - MF
ASR Regional Model – Phase I
December 2006

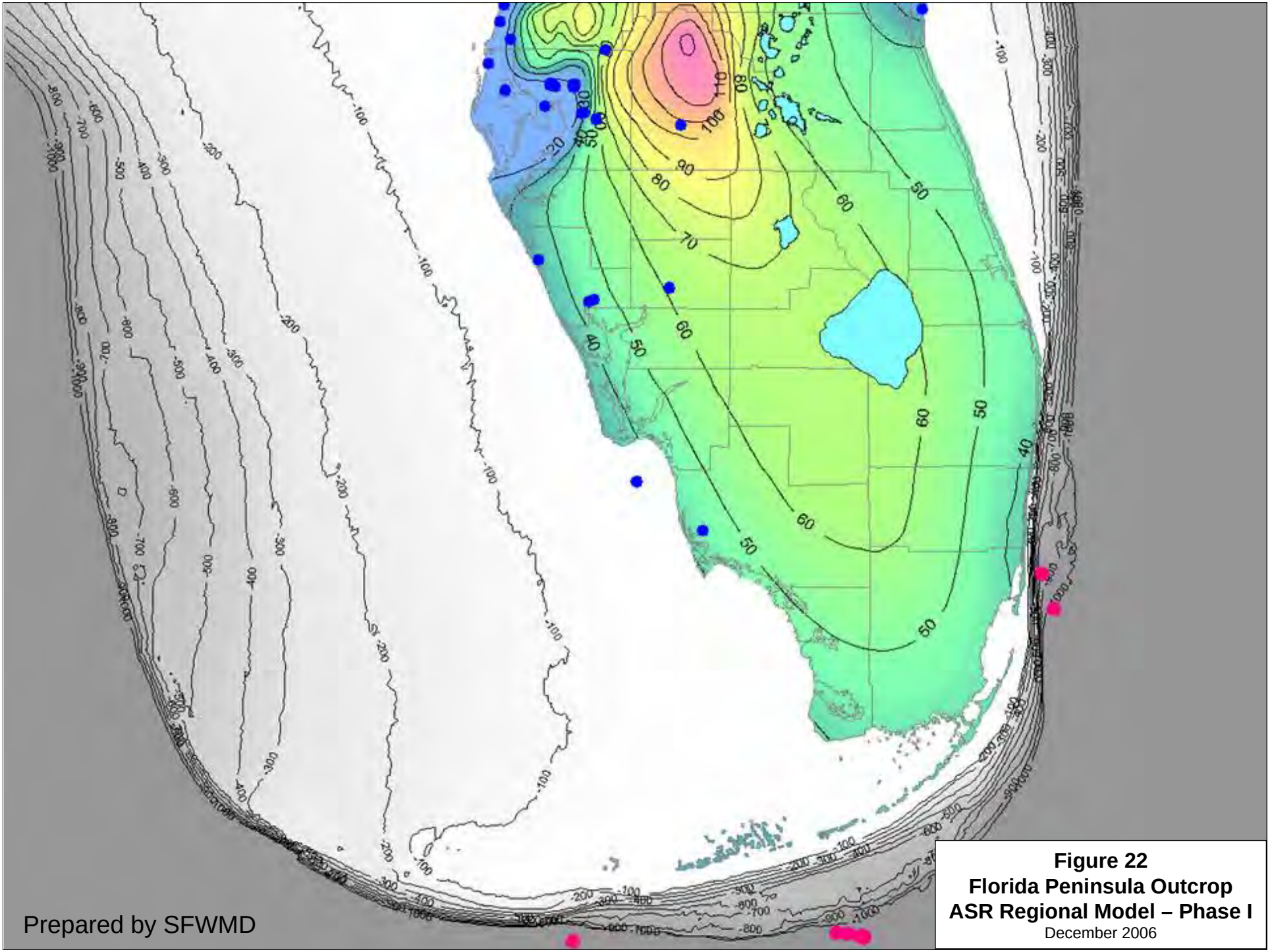

Figure 22
Florida Peninsula Outcrop
ASR Regional Model – Phase I
December 2006

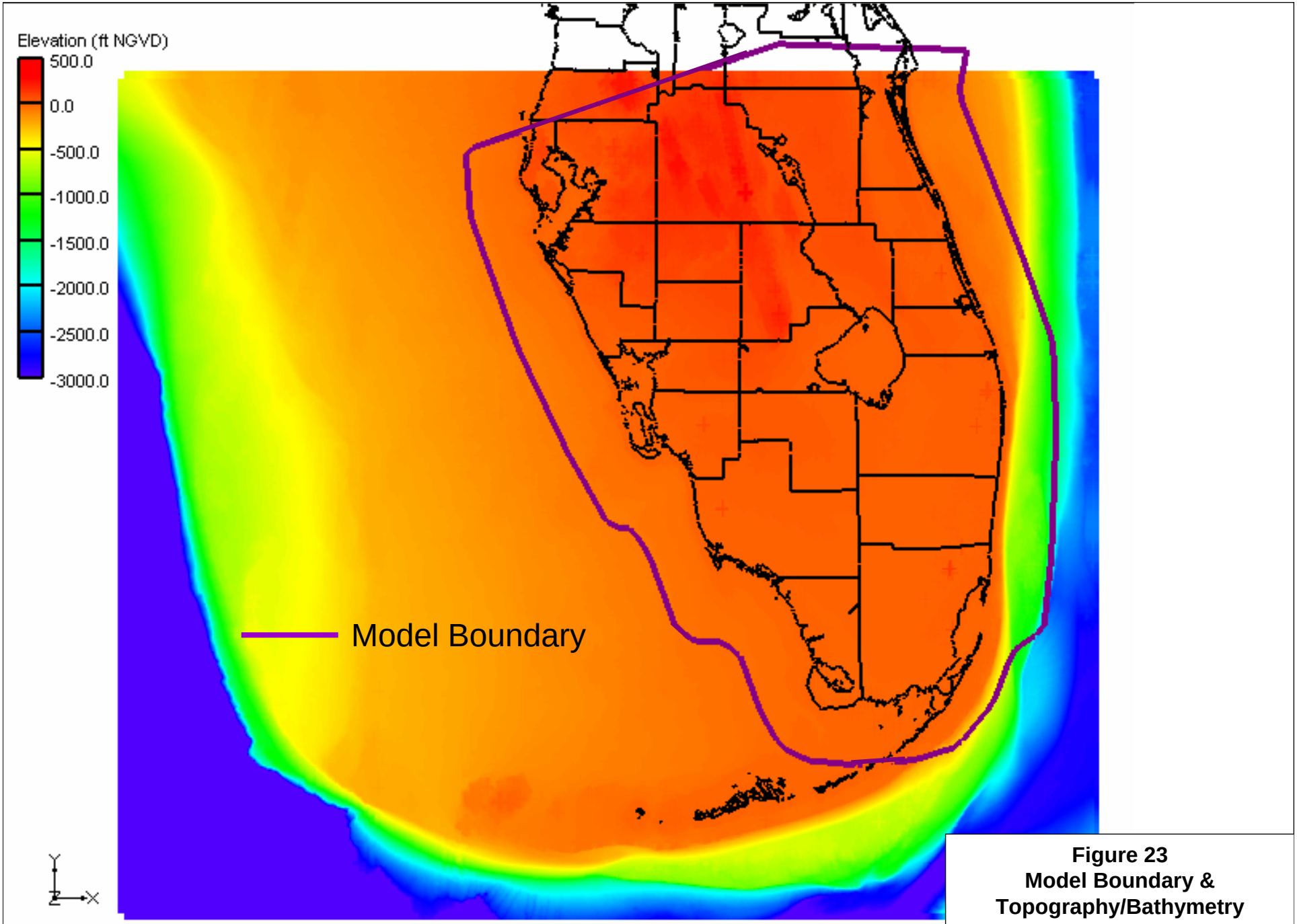

Topography/Bathymetry prepared by Jacksonville District

Figure 23
Model Boundary & Topography/Bathymetry
ASR Regional Model – Phase I
December 2006

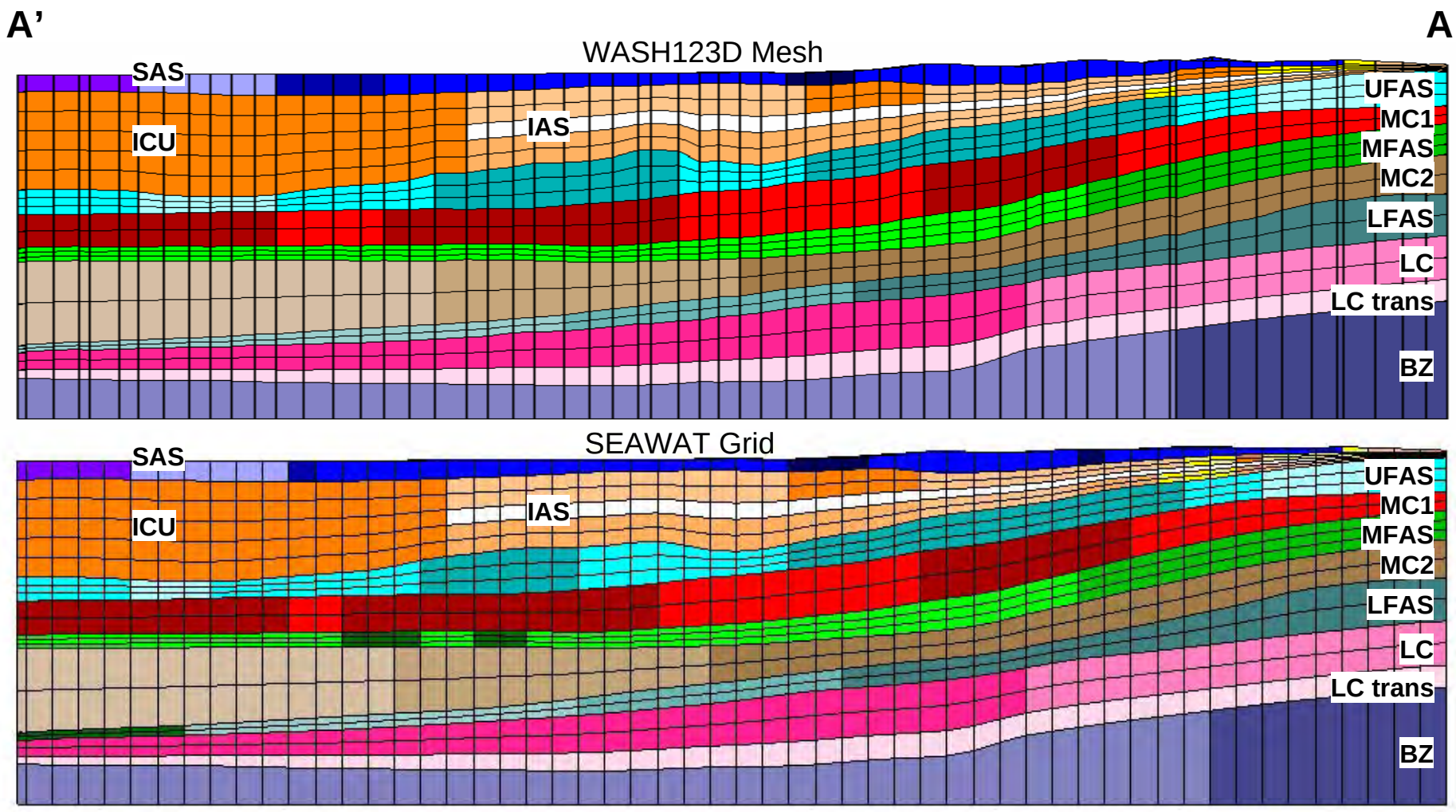

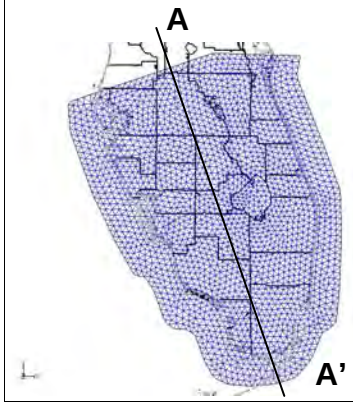

23 layers of WASH123D nodes and 22 layers of SEAWAT cells
1 Surficial Aquifer System (SAS)
5 Hawthorne Group or Intermediate Confining Unit (HG or ICU)
Middle layer of 5 contains Intermediate Aquifer System (IAS)
3 Upper Floridan Aquifer (UFAS)
2 Middle Confining Unit 1 (MC1)
3 Middle Floridan Aquifer (MFAS)
2 Middle Confining Unit 2 (MC2)
2 Lower Floridan Aquifer (LFAS)
2 Lower Confining Unit (LC)
1 Lower Confining Unit transition zone (LC Transition)
1 Boulder Zone (BZ)

Figure 24
Model Cross Section
ASR Regional Model – Phase I
December 2006

WASH123D Mesh

SEAWAT Grid

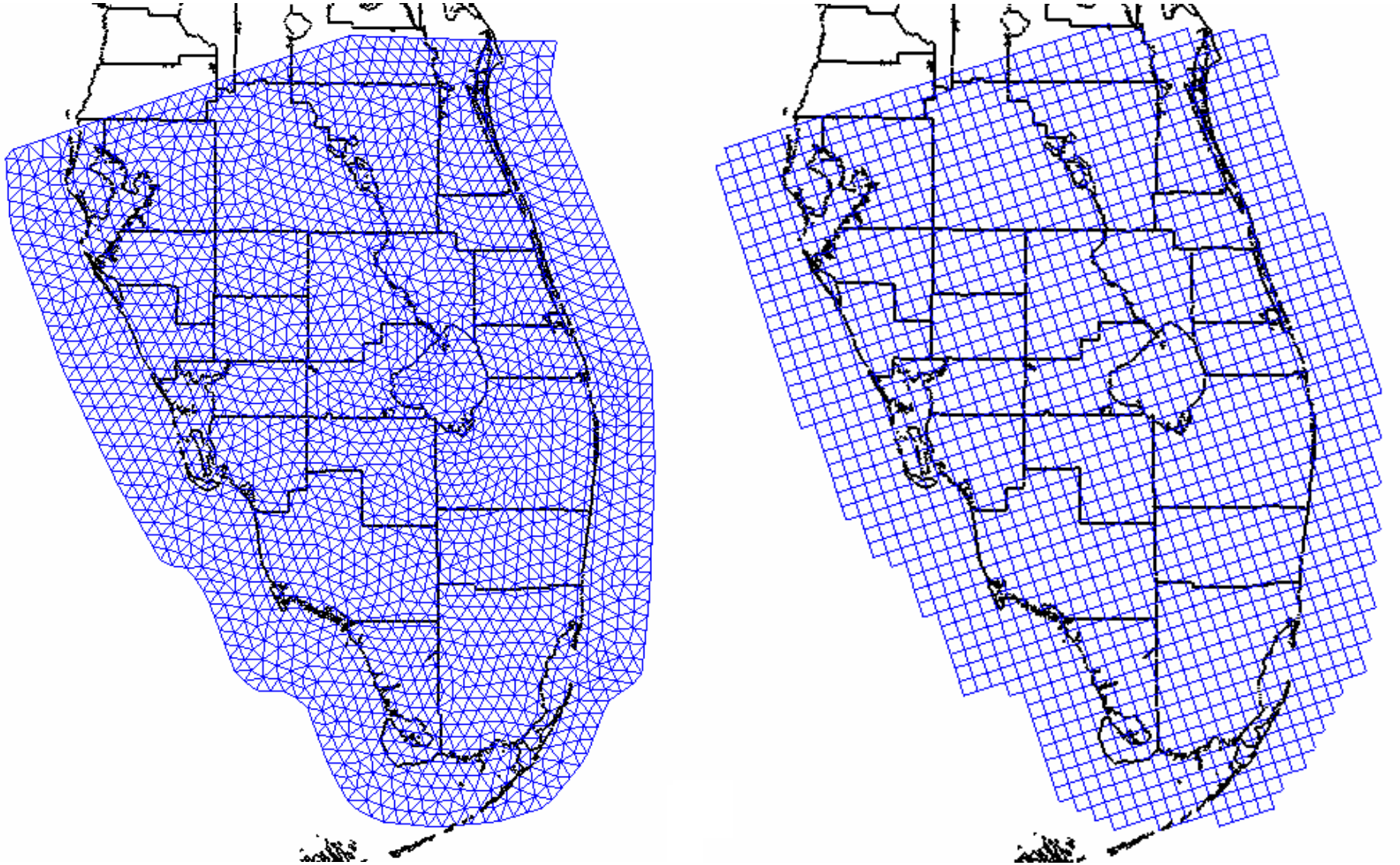

Figure 25
Horizontal Mesh & Grid Resolution
ASR Regional Model – Phase I
December 2006

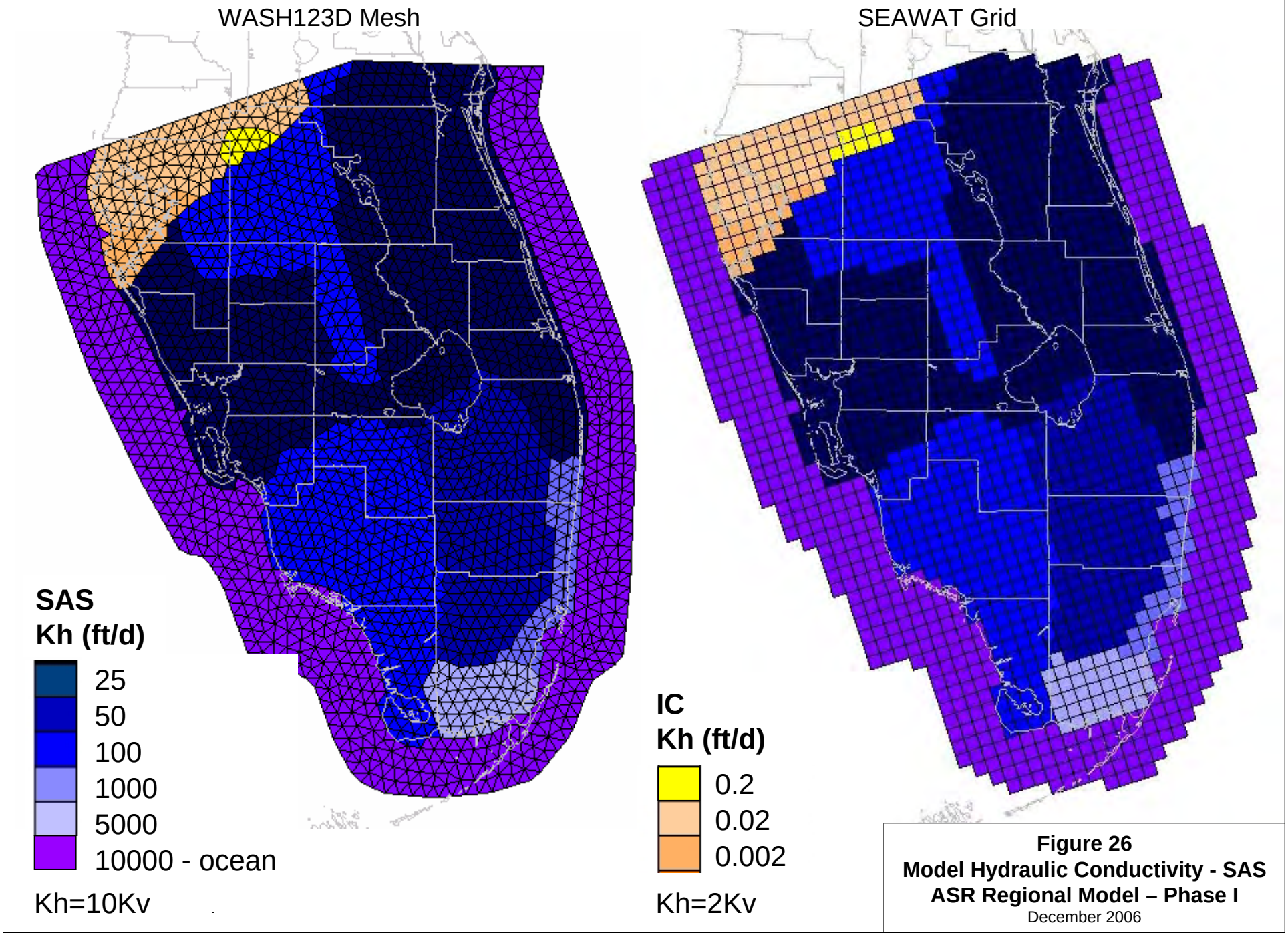

Figure 26
Model Hydraulic Conductivity - SAS
ASR Regional Model – Phase I
December 2006

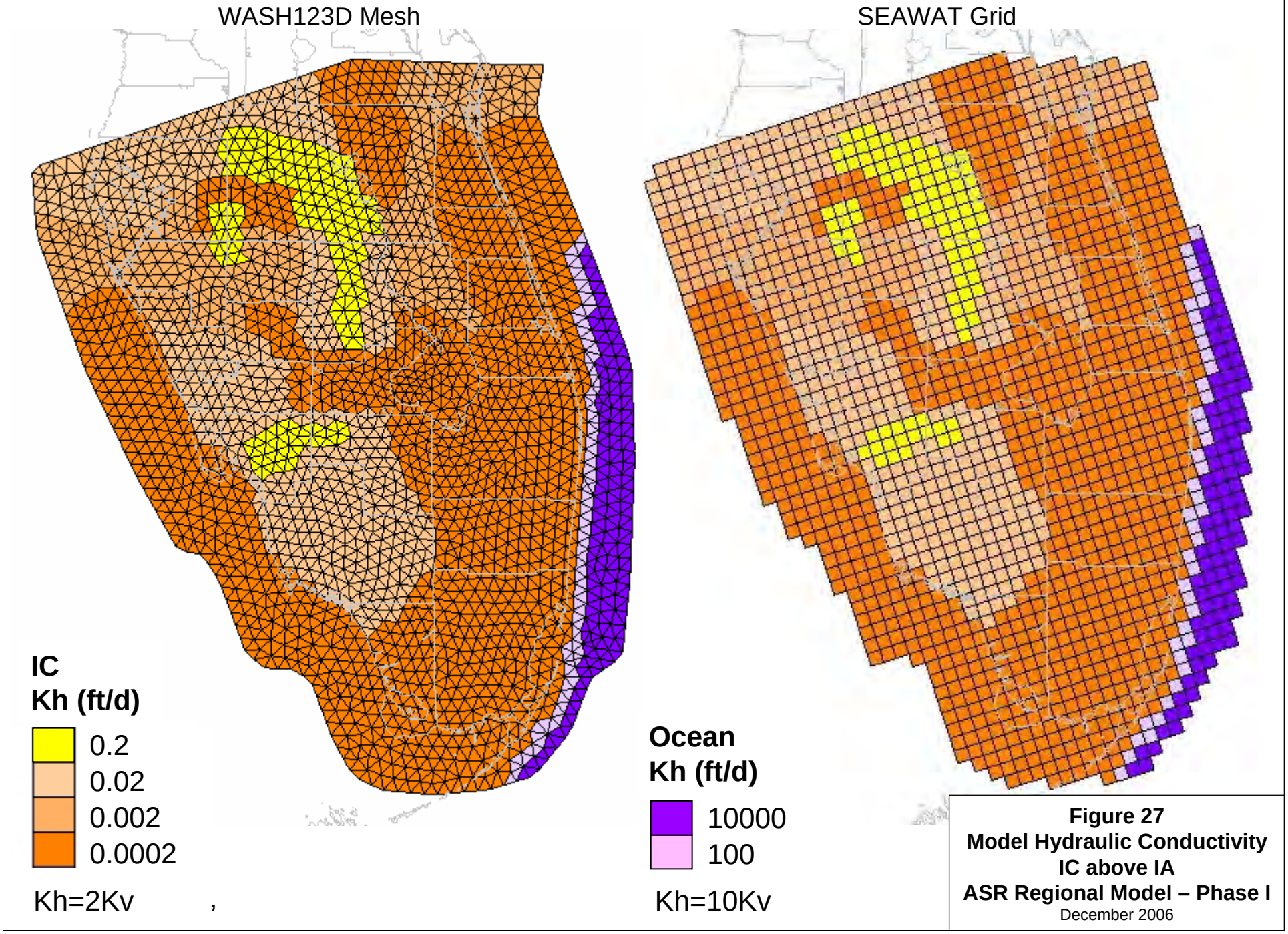

Figure 27
Model Hydraulic Conductivity
IC above IA
ASR Regional Model – Phase I
December 2006

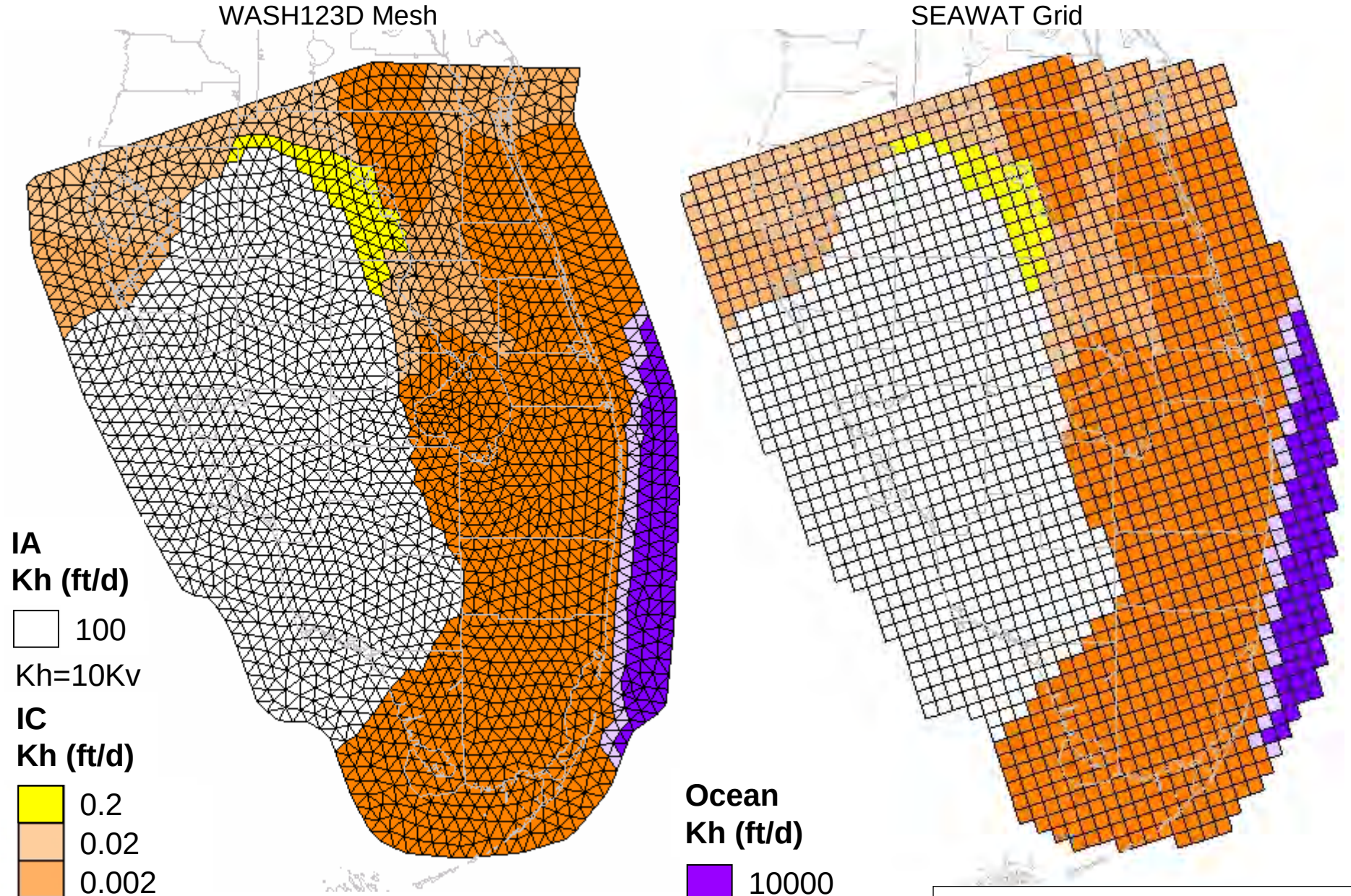

Figure 28
Model Hydraulic Conductivity – IC/IA
ASR Regional Model – Phase I
December 2006

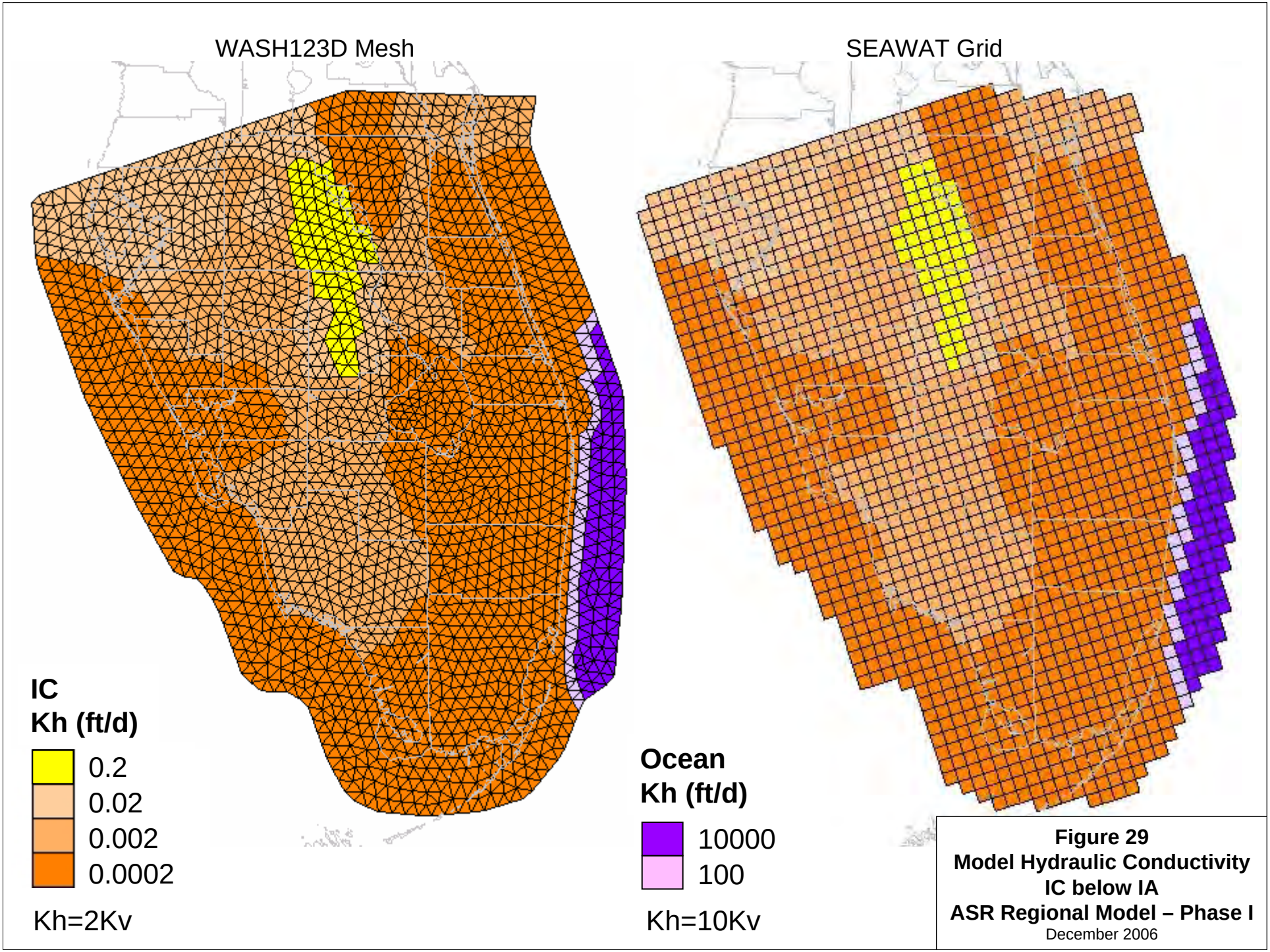

Figure 29
Model Hydraulic Conductivity
IC below IA
ASR Regional Model – Phase I
December 2006

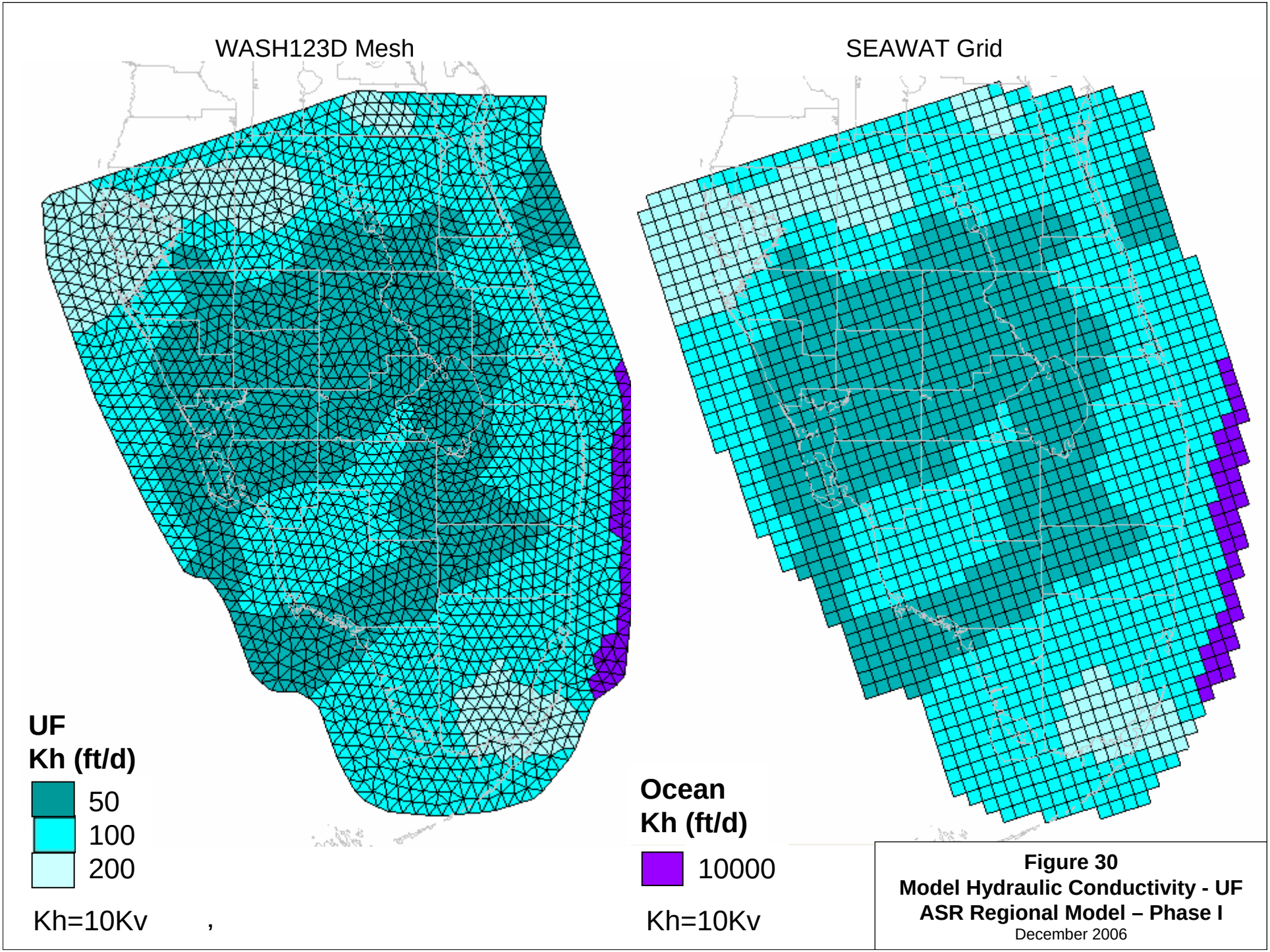

Figure 30
Model Hydraulic Conductivity - UF
ASR Regional Model – Phase I
December 2006

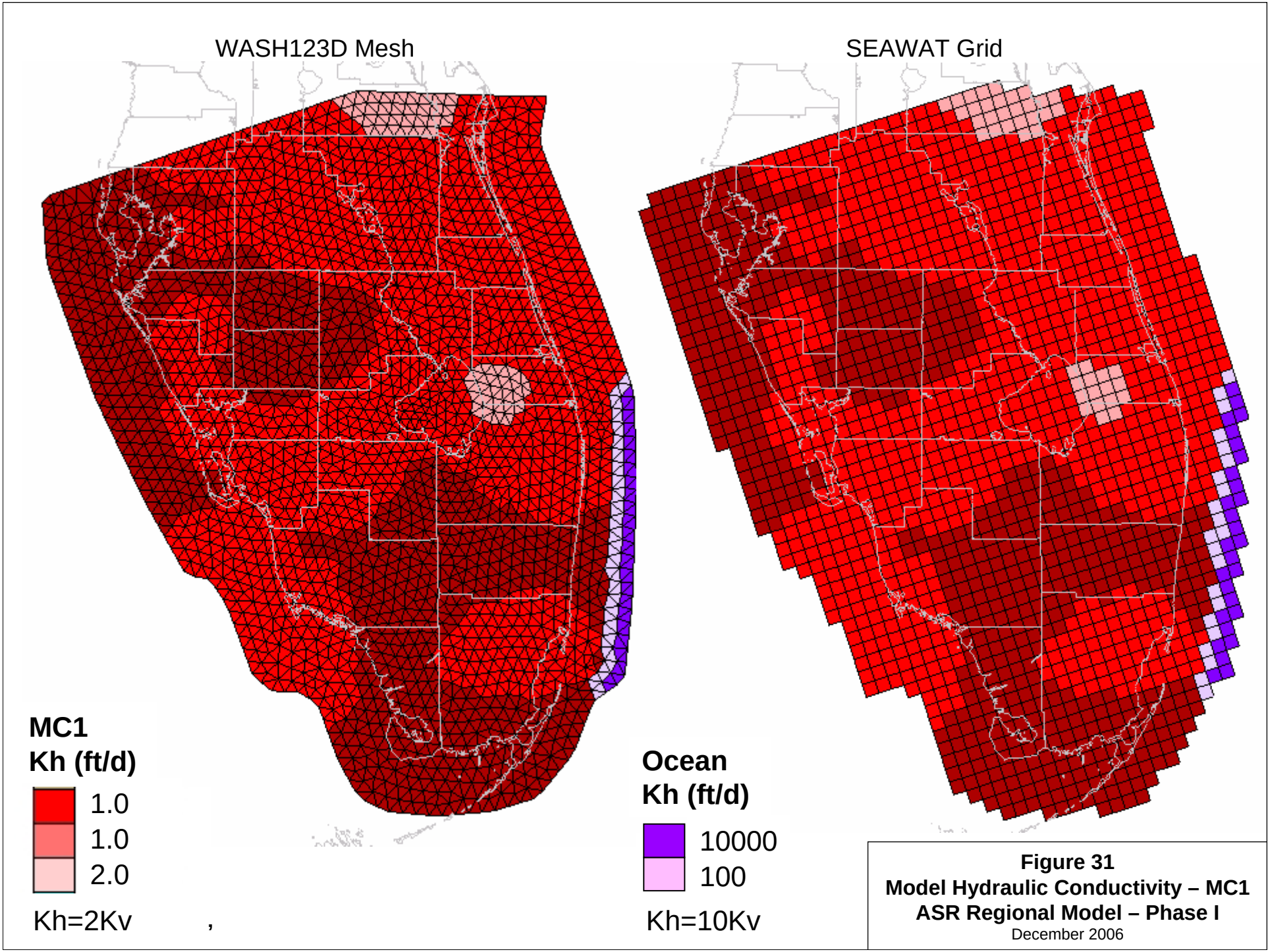

Figure 31
Model Hydraulic Conductivity – MC1
ASR Regional Model – Phase I
December 2006

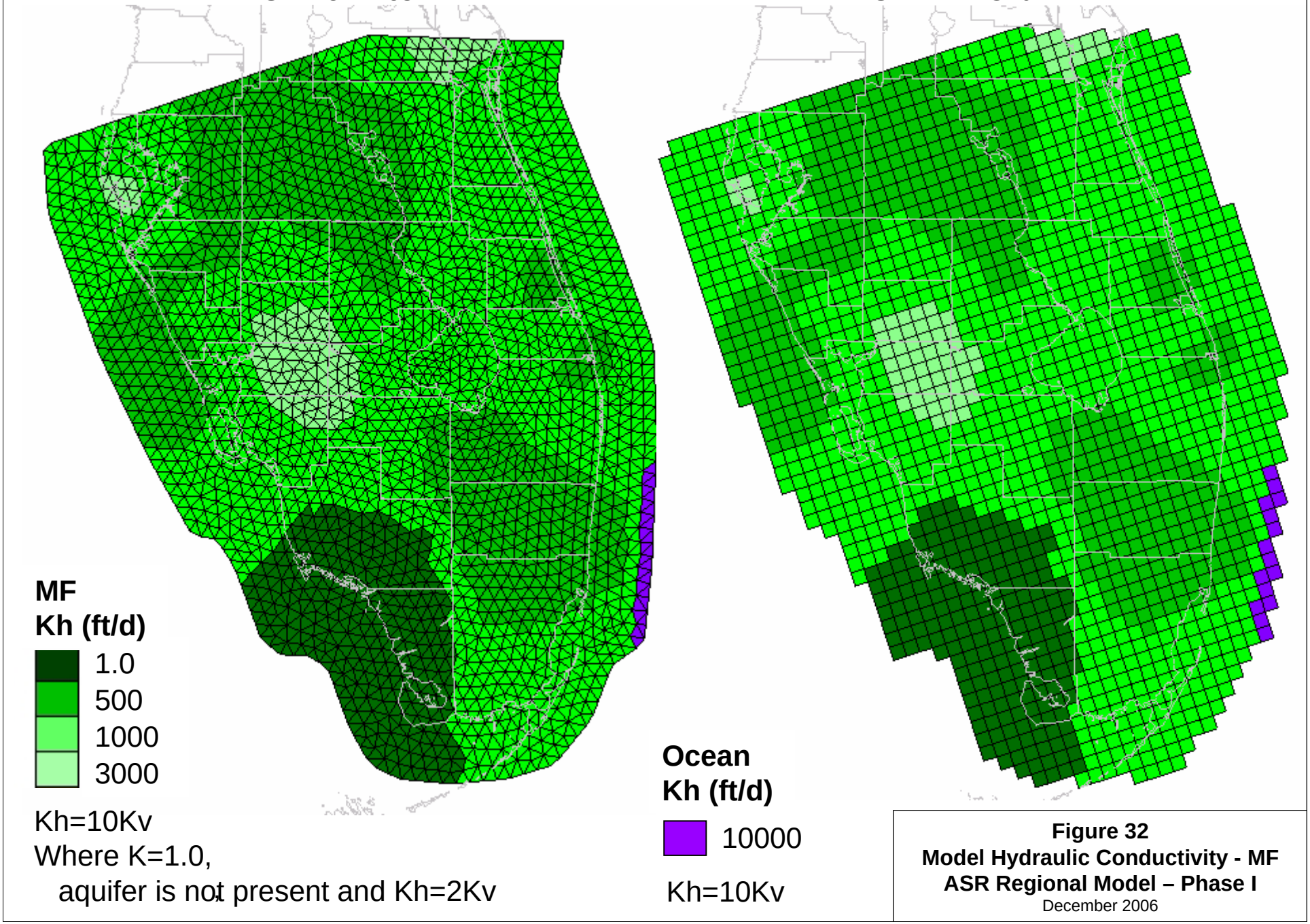

Figure 32
Model Hydraulic Conductivity - MF
ASR Regional Model – Phase I
December 2006

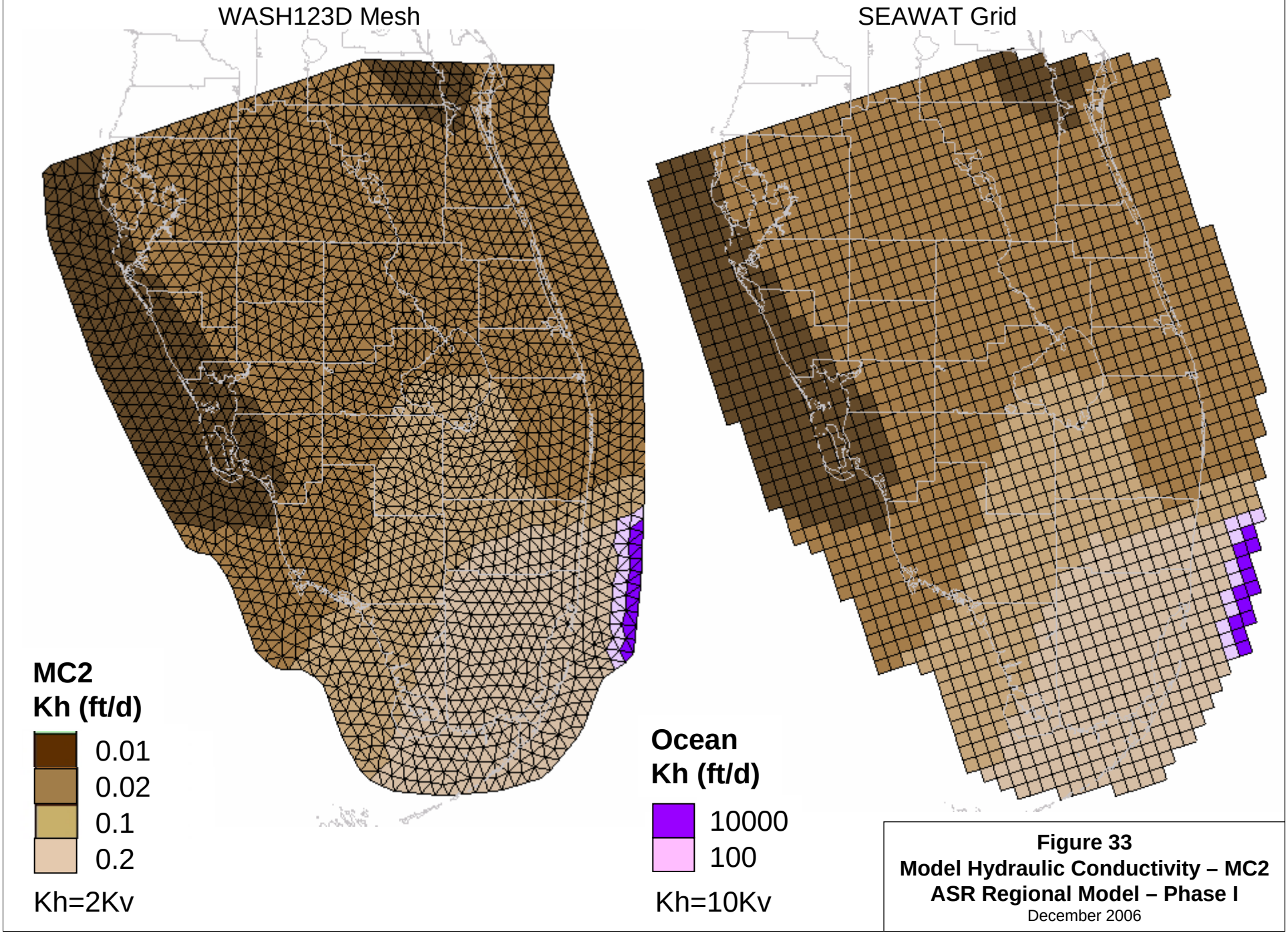

Figure 33
Model Hydraulic Conductivity – MC2
ASR Regional Model – Phase I
December 2006

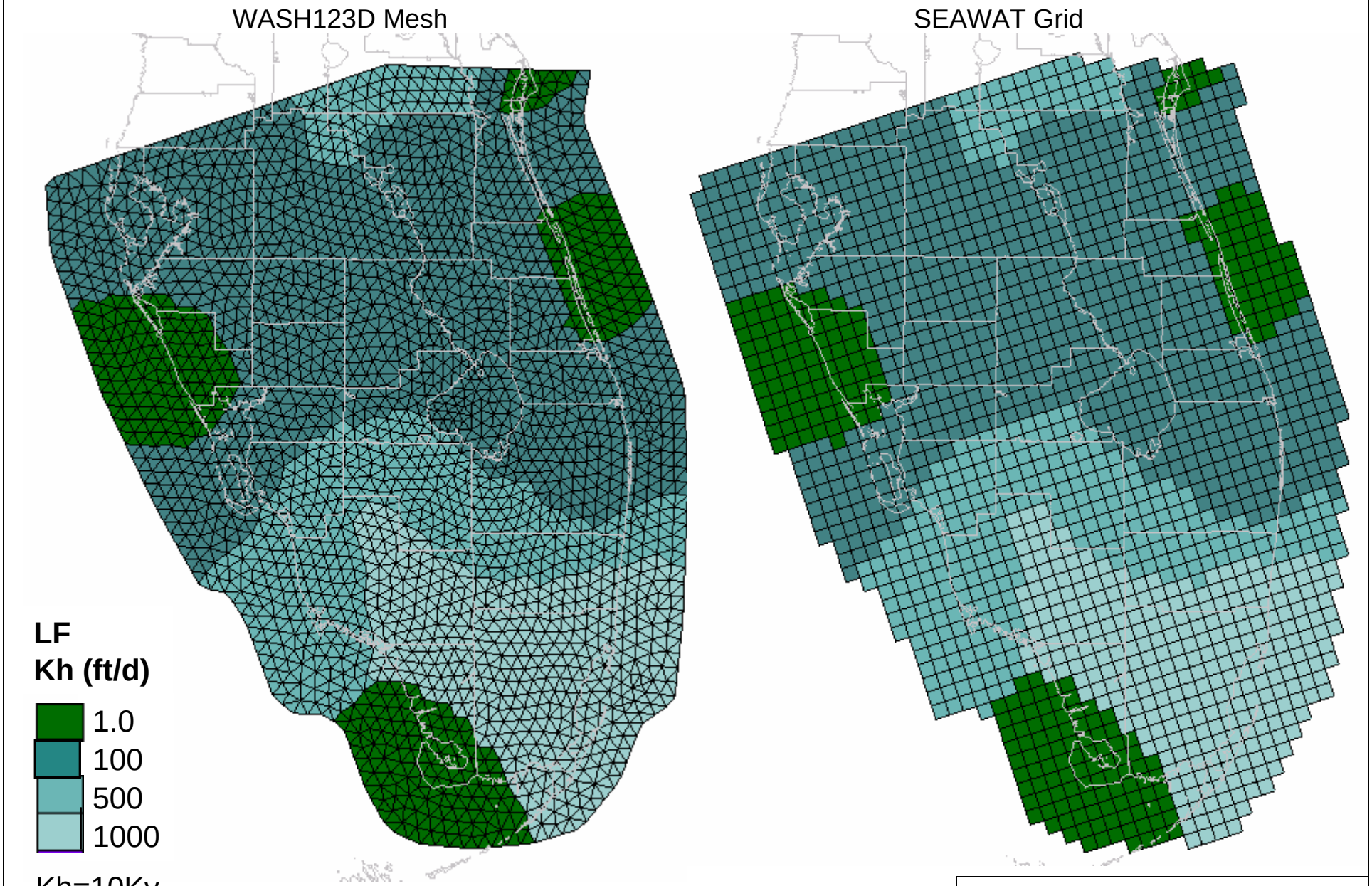

Figure 34
Model Hydraulic Conductivity - LF
ASR Regional Model – Phase I
December 2006

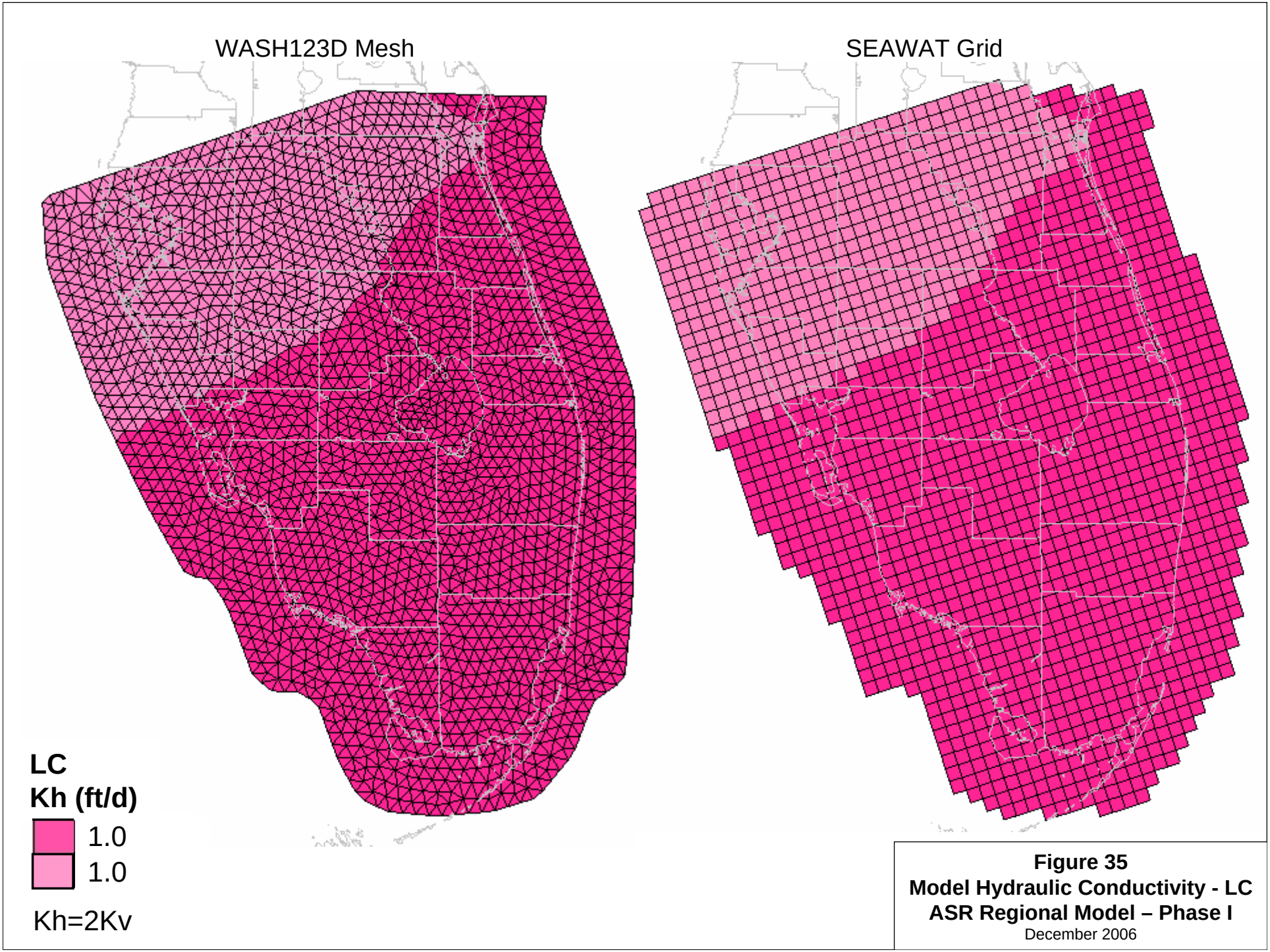

Figure 35
Model Hydraulic Conductivity - LC
ASR Regional Model – Phase I
December 2006

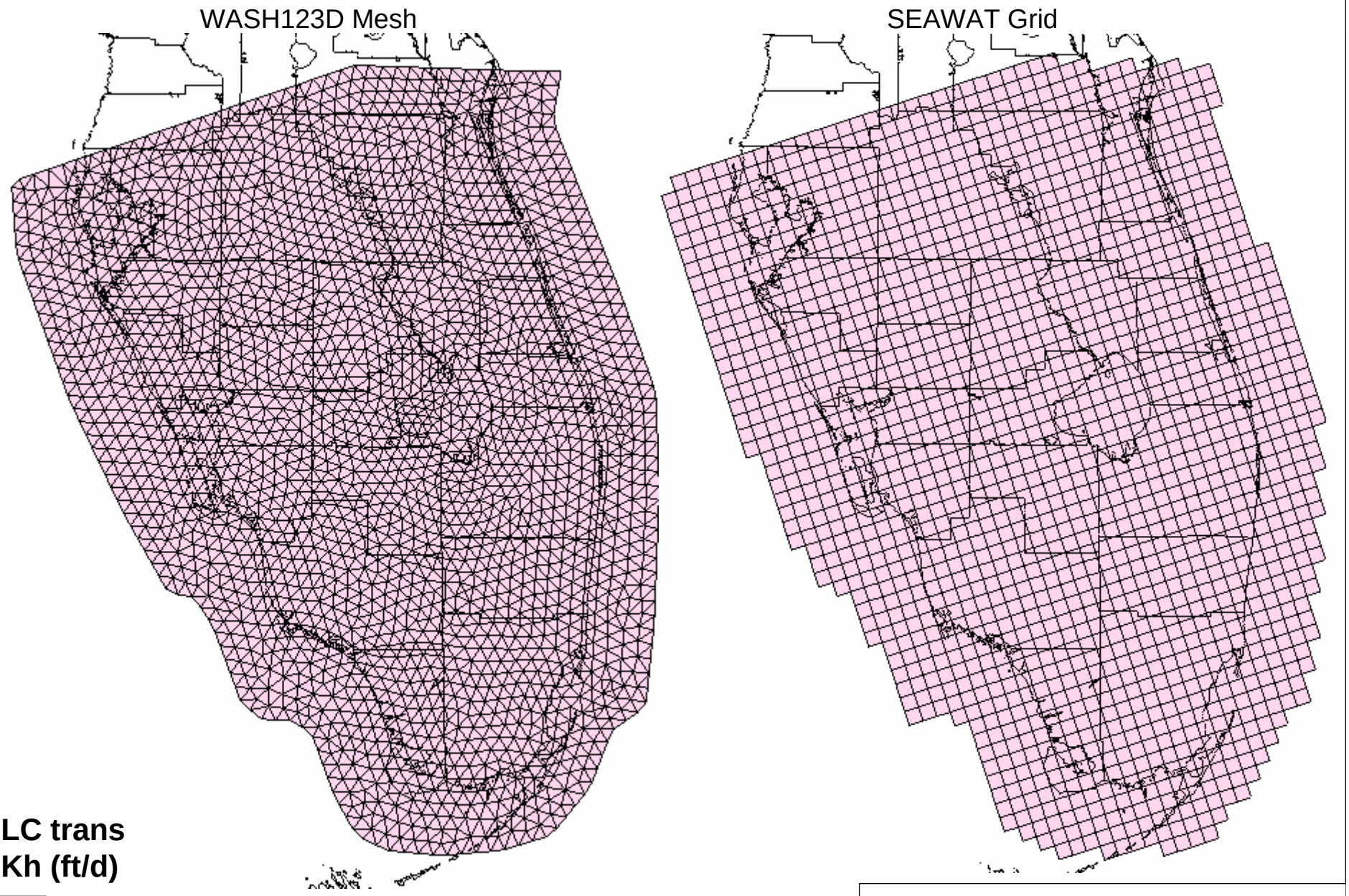

Figure 36
Model Hydraulic Conductivity – LC trans
ASR Regional Model – Phase I
December 2006

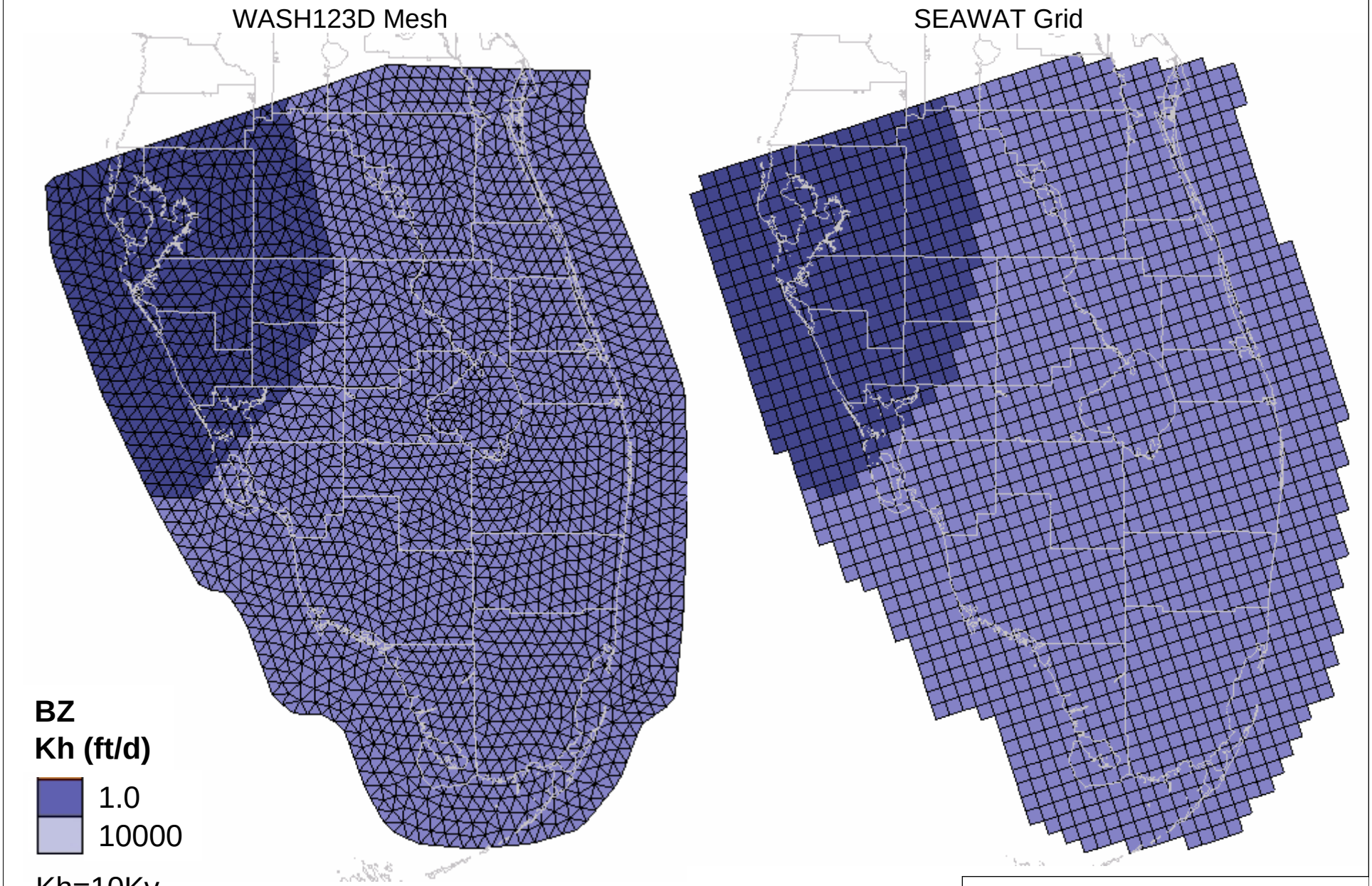

Figure 37
Model Hydraulic Conductivity - BZ
ASR Regional Model – Phase I
December 2006

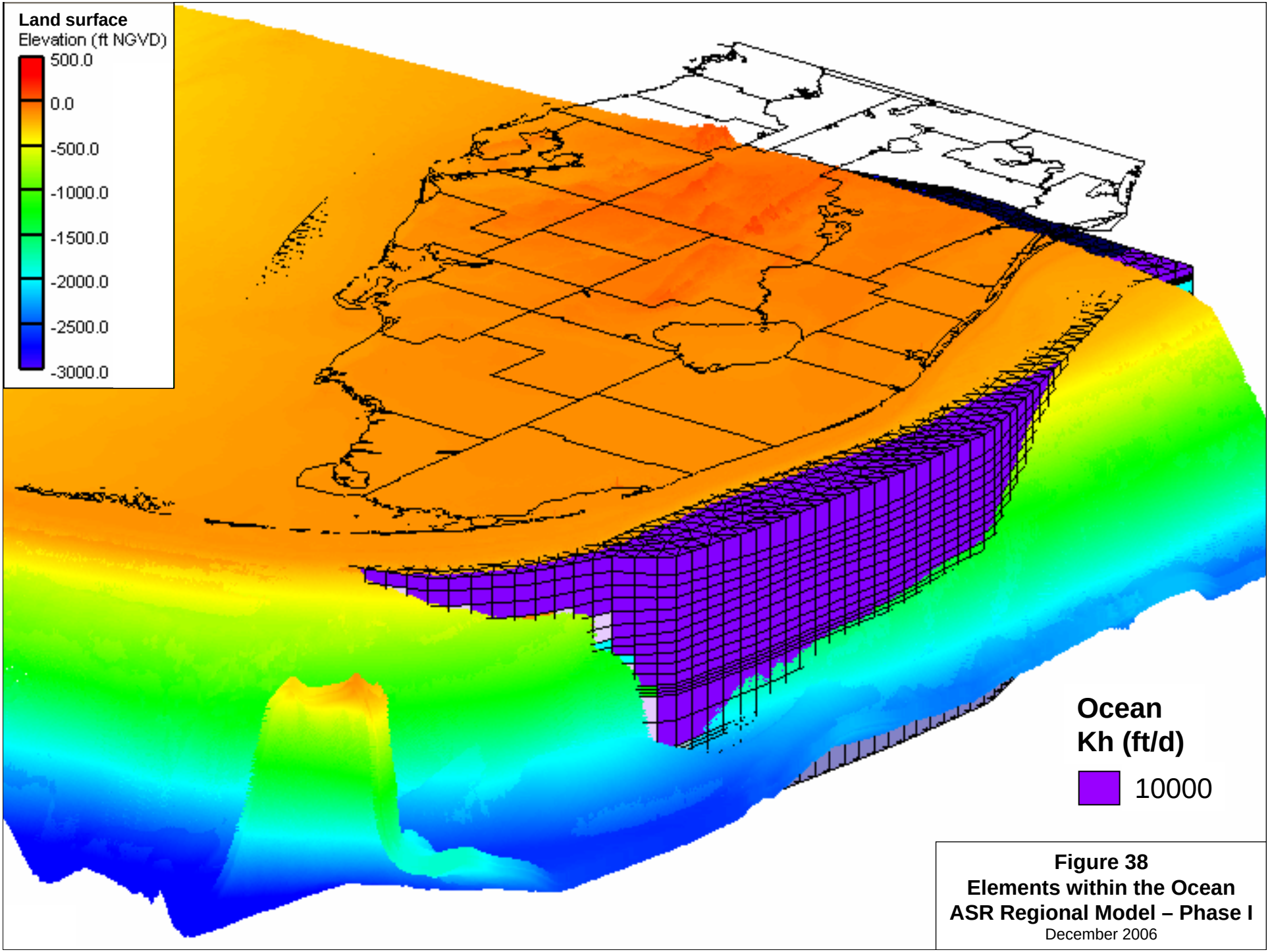

Figure 38
Elements within the Ocean
ASR Regional Model – Phase I
December 2006

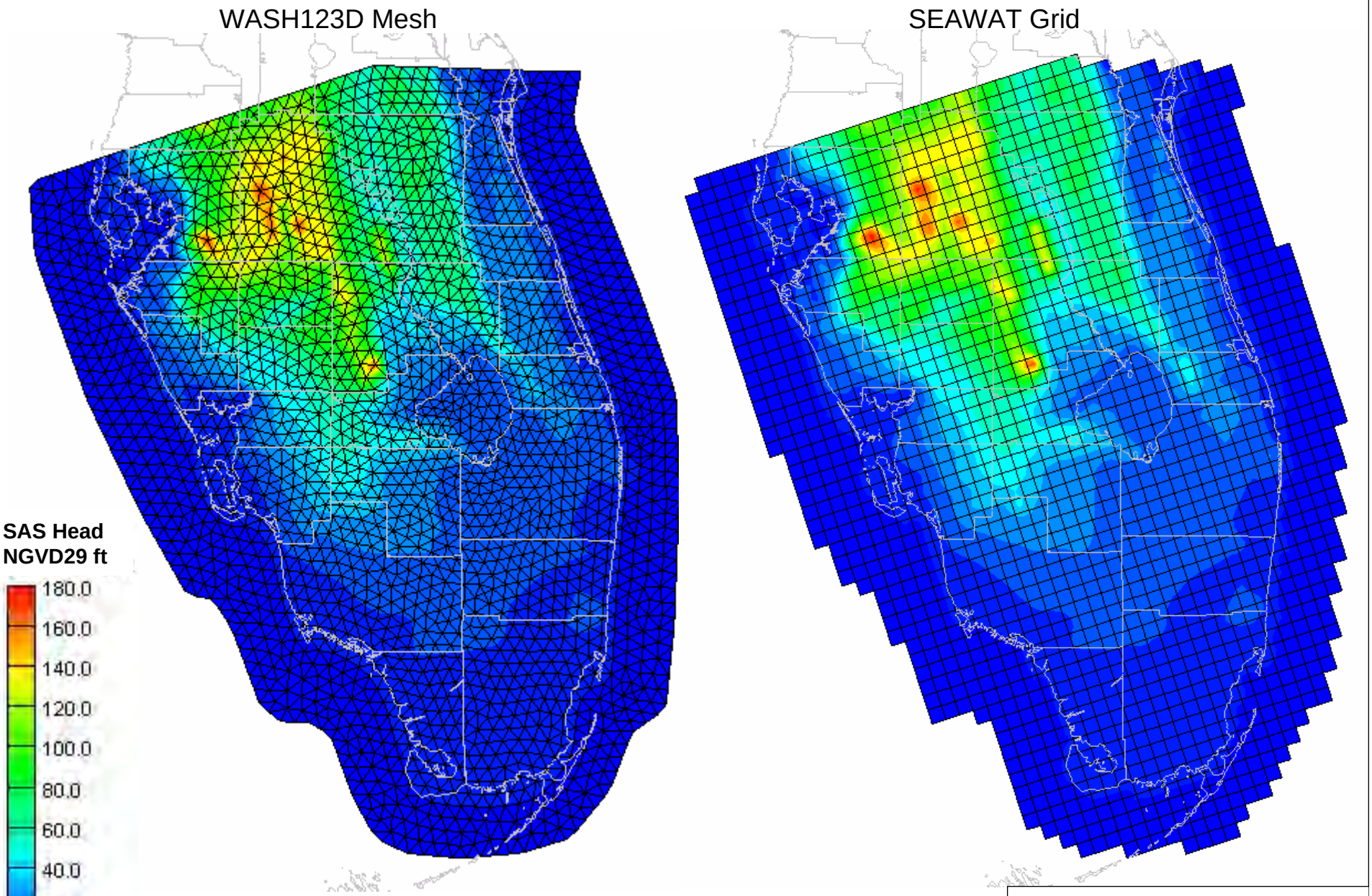

Figure 39
Specified Surface Heads
ASR Regional Model – Phase I
December 2006

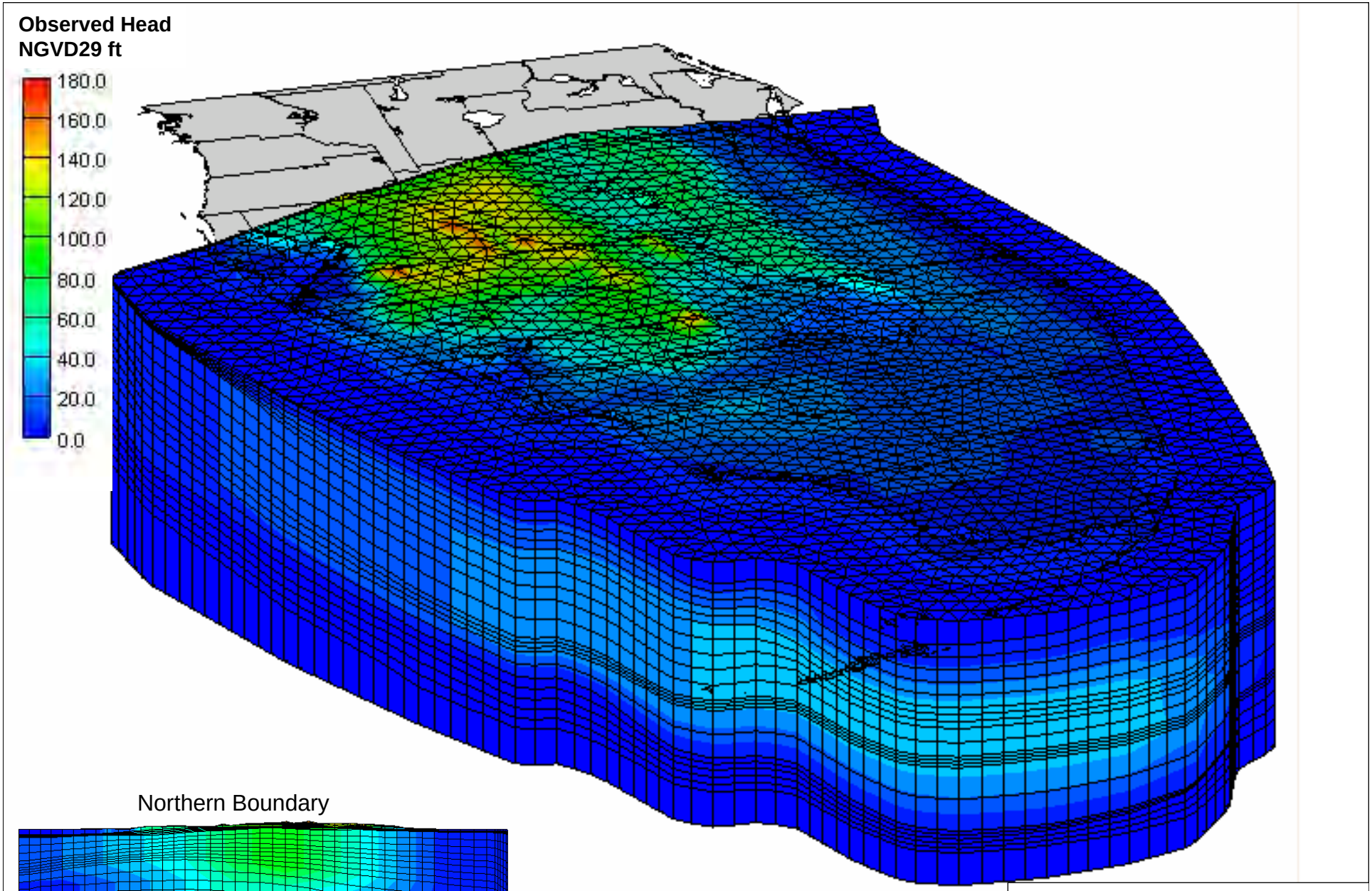

Figure 40
Specified Observed Heads
Boundary Conditions
ASR Regional Model – Phase I
December 2006

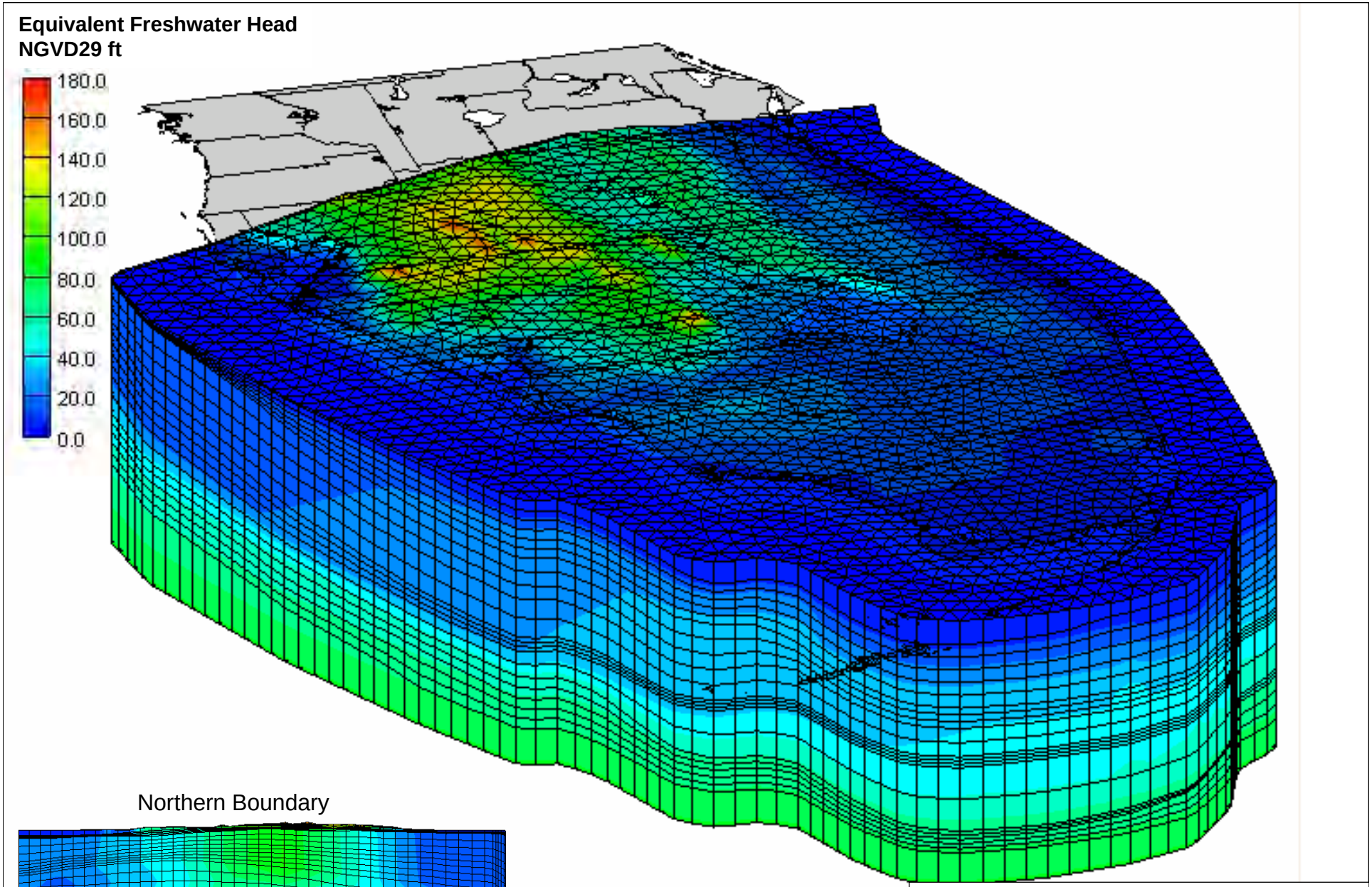

Figure 41
Specified Equivalent Freshwater Heads
Boundary Conditions
ASR Regional Model – Phase I
December 2006

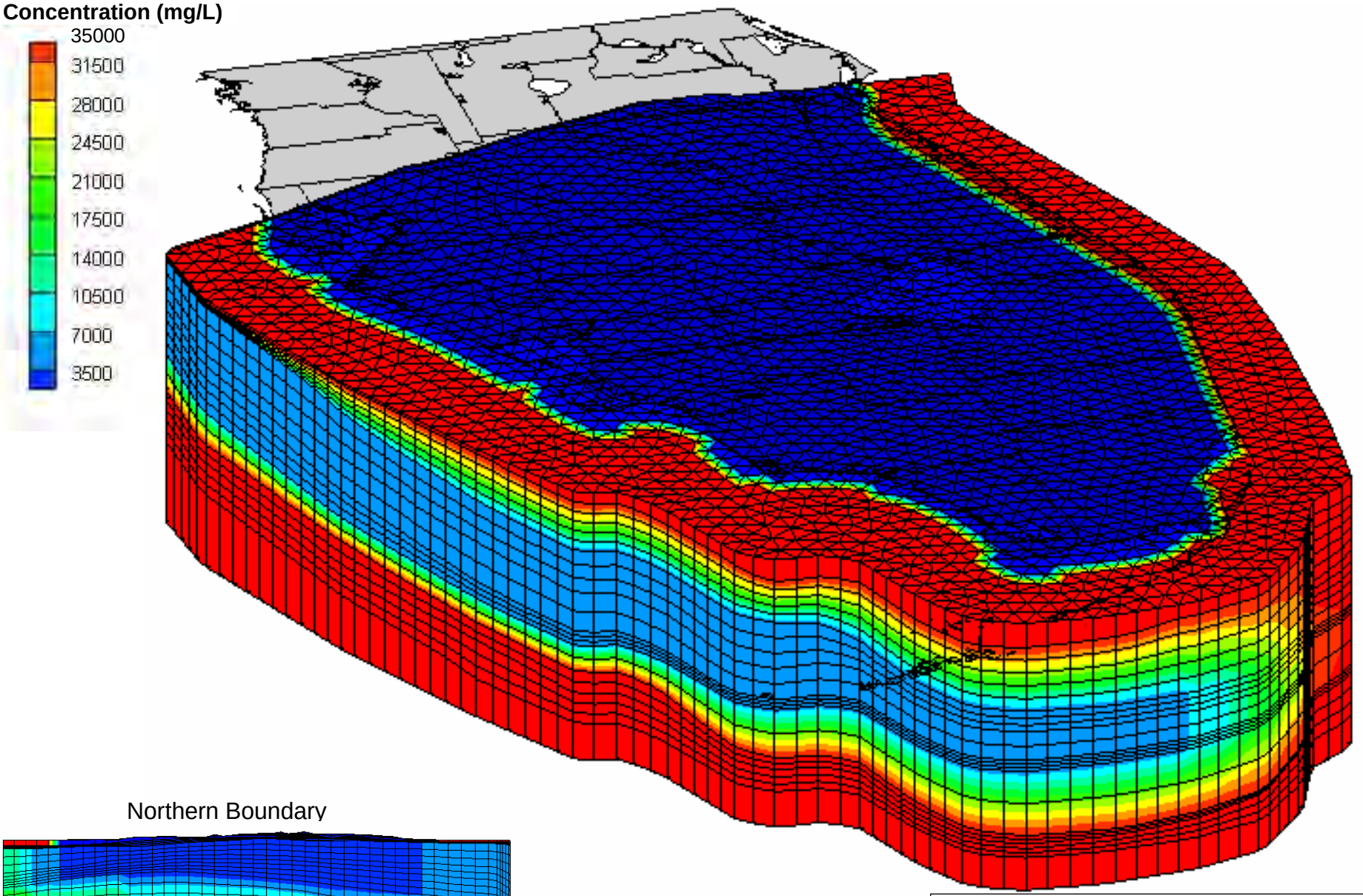

Figure 42
Salt Concentrations in mg/l TDS
Boundary Conditions
ASR Regional Model – Phase I
December 2006

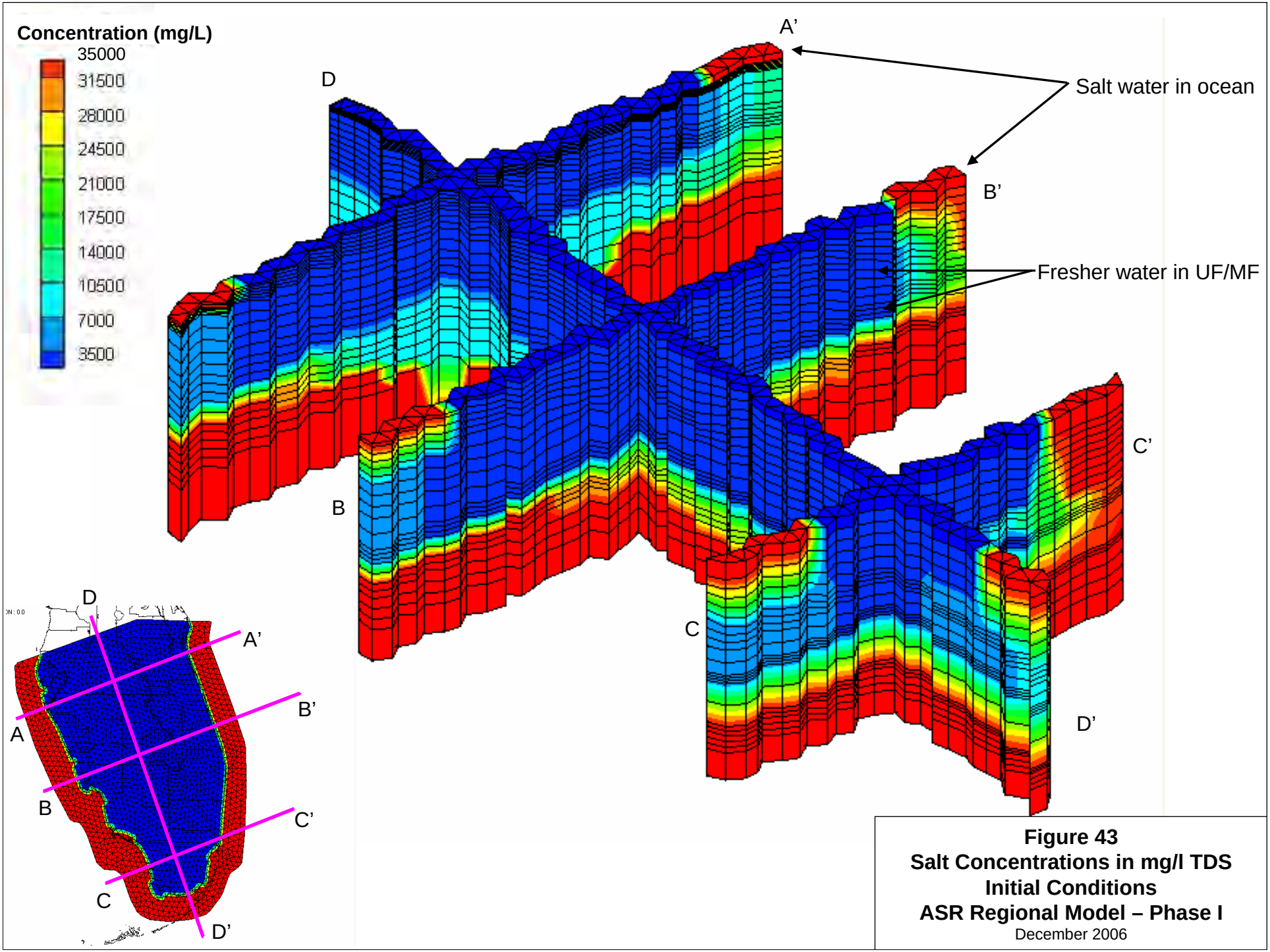

Figure 43
Salt Concentrations in mg/l TDS
Initial Conditions
ASR Regional Model – Phase I
December 2006

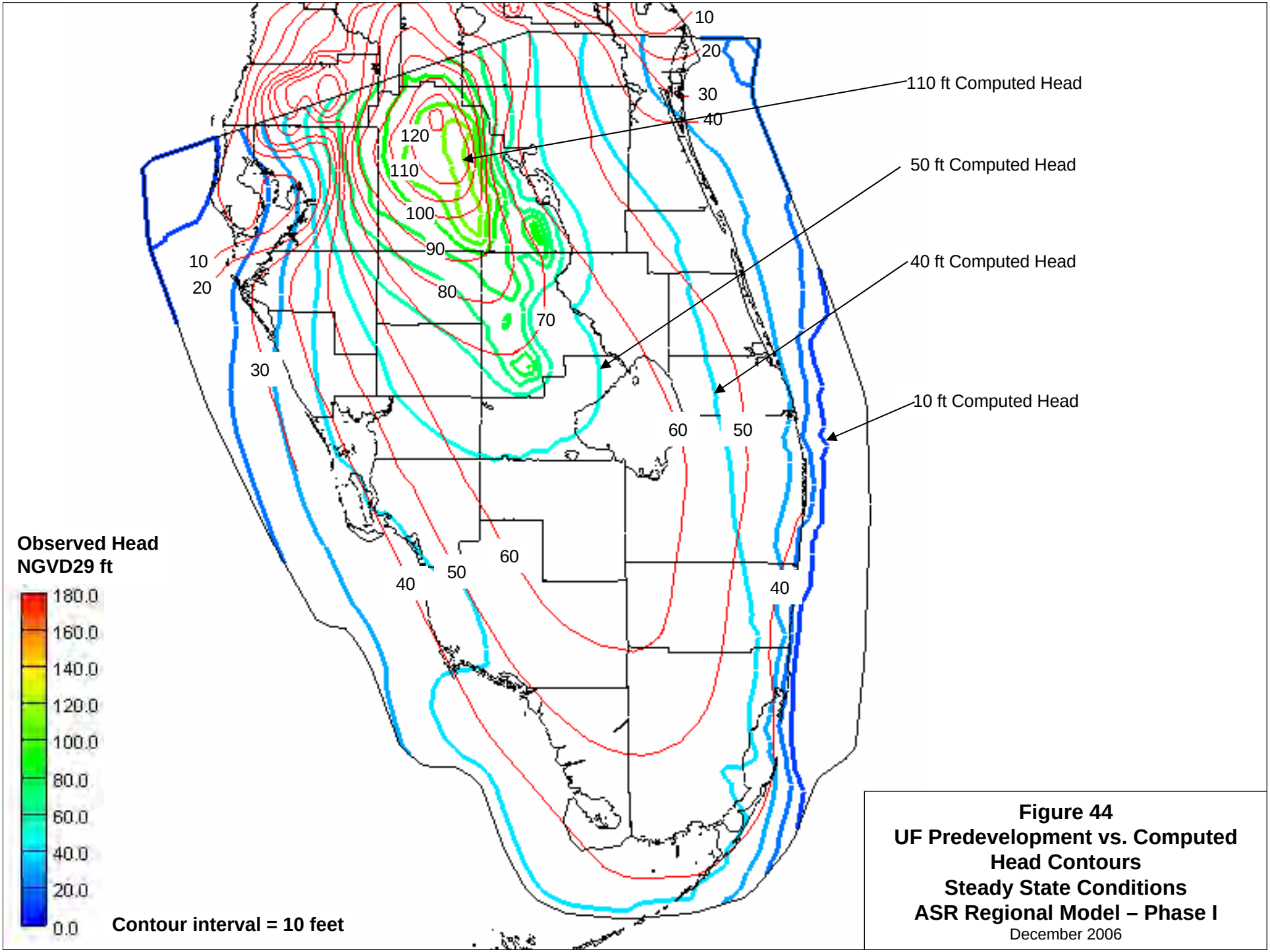

Figure 44
UF Predevelopment vs. Computed Head Contours
Steady State Conditions
ASR Regional Model – Phase I
December 2006

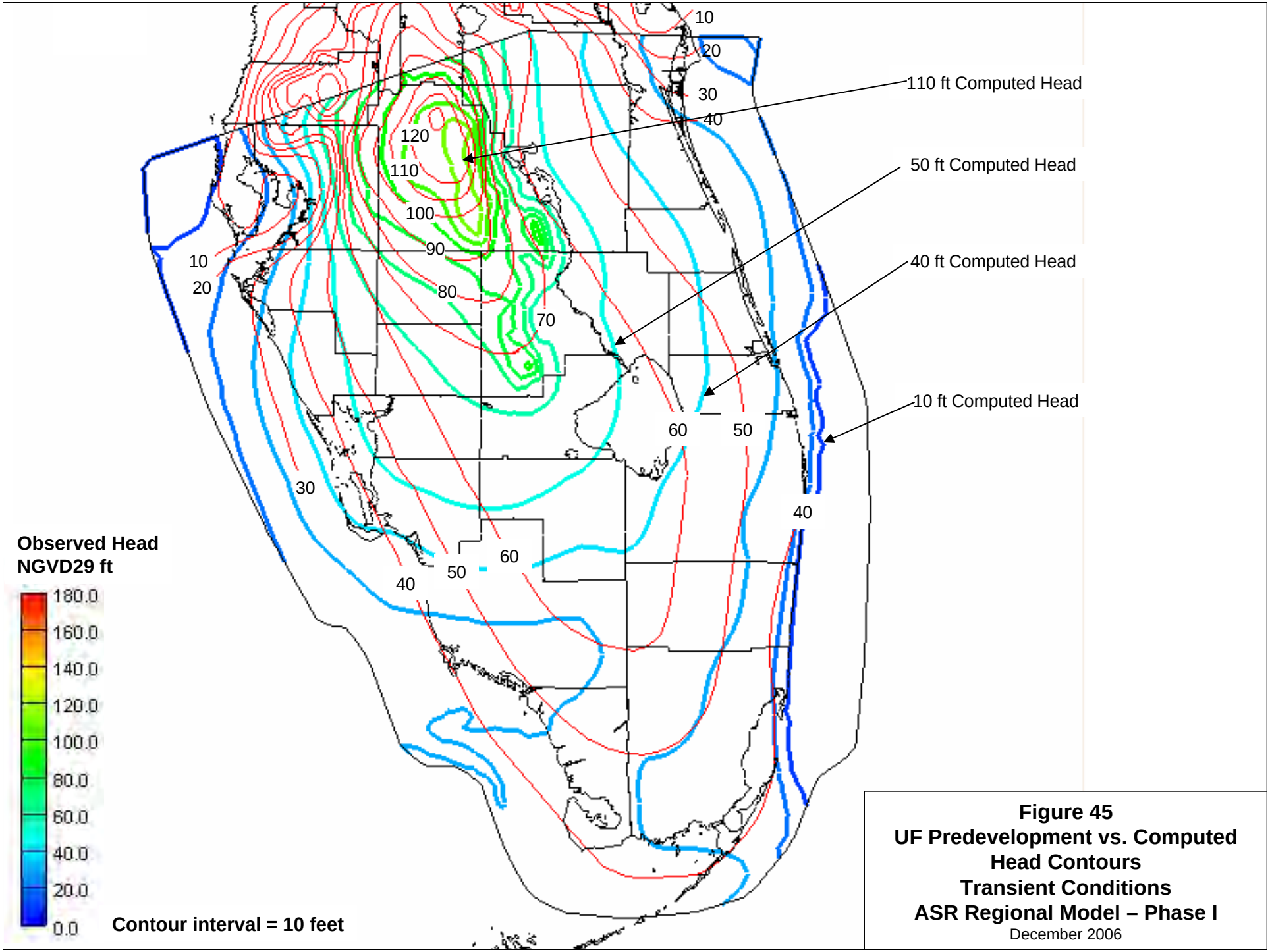

Figure 45
UF Predevelopment vs. Computed Head Contours
Transient Conditions
ASR Regional Model – Phase I
December 2006

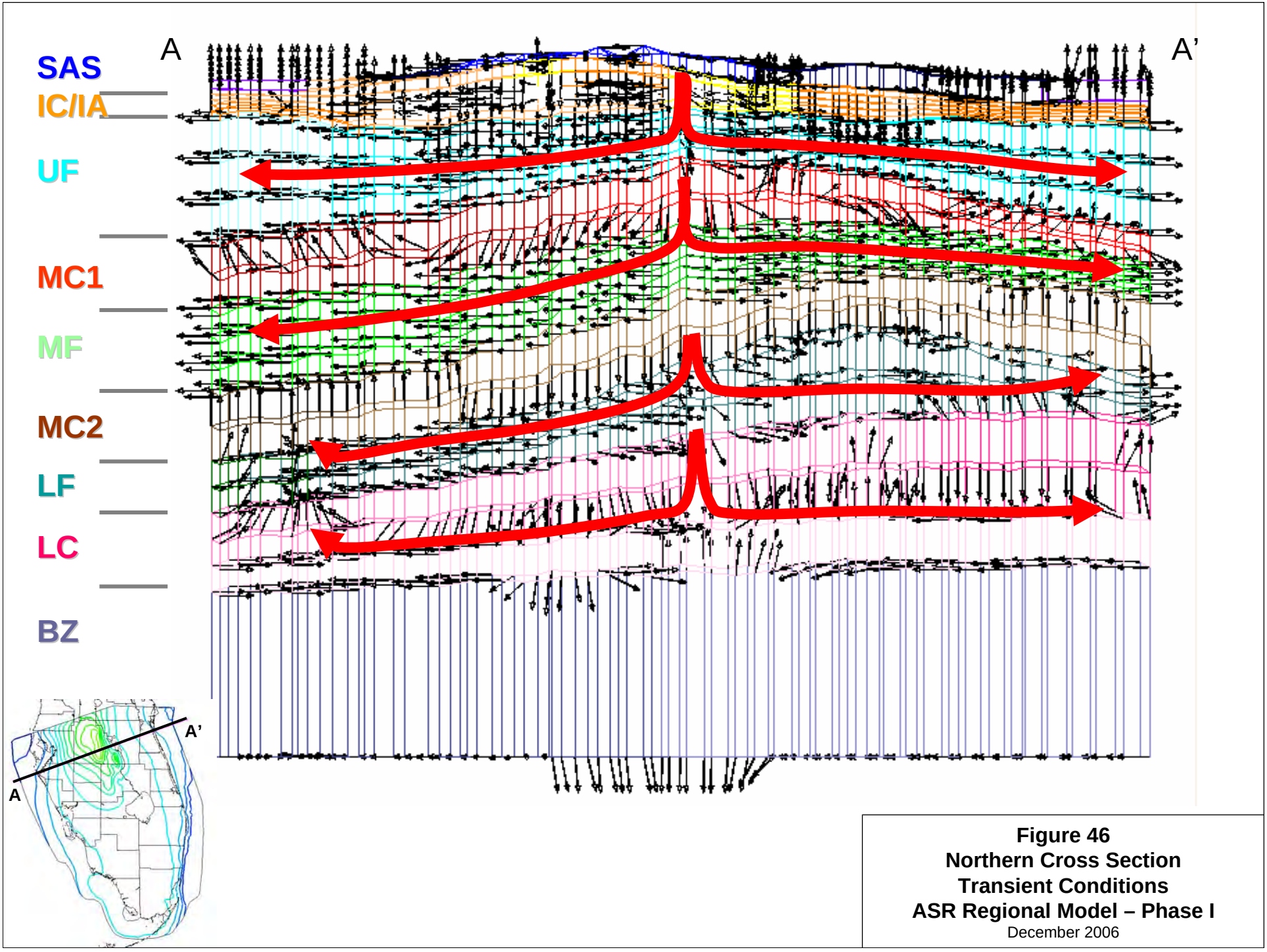

Figure 46
Northern Cross Section
Transient Conditions
ASR Regional Model – Phase I
December 2006

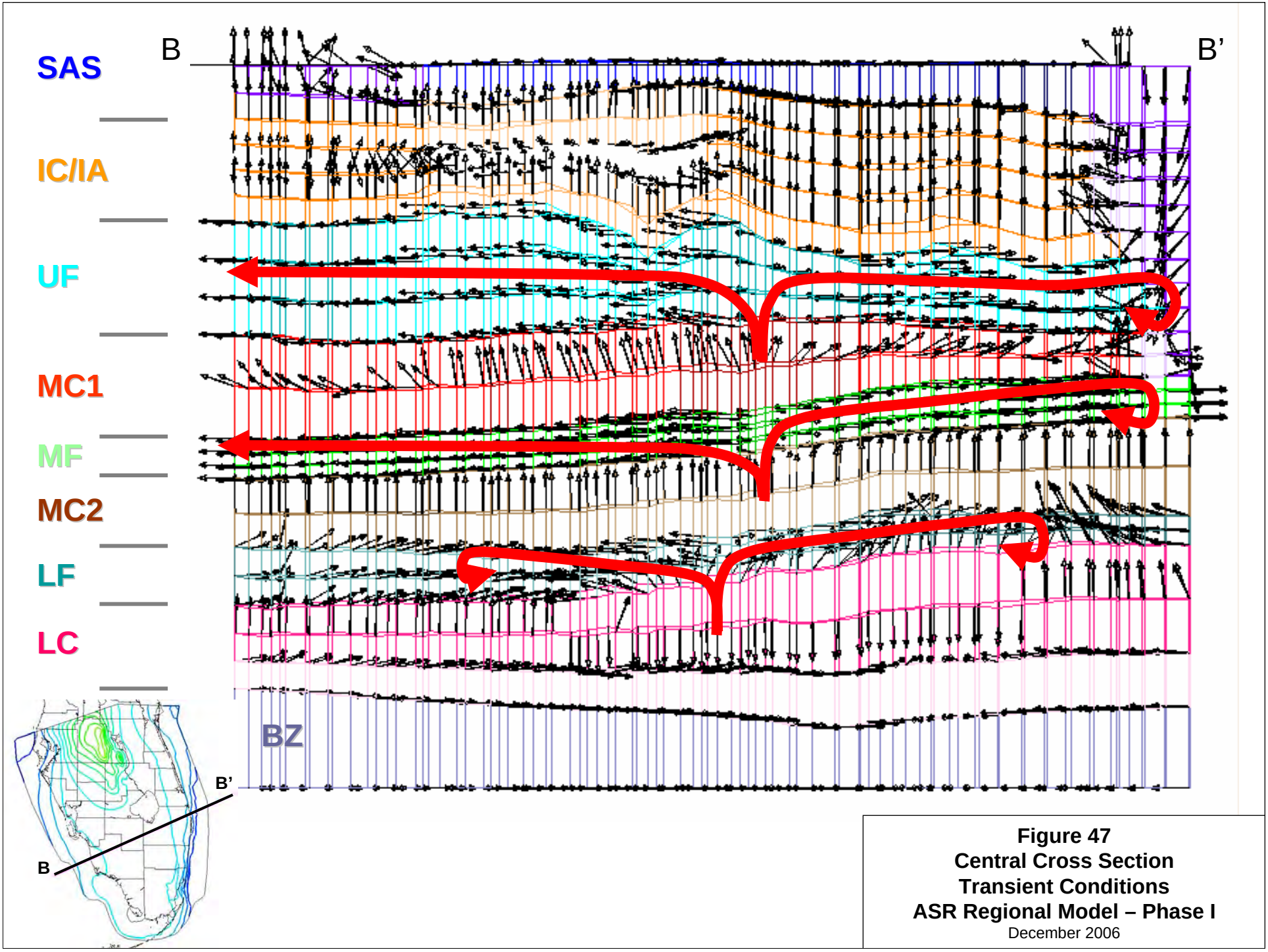

Figure 47
Central Cross Section
Transient Conditions
ASR Regional Model – Phase I
December 2006

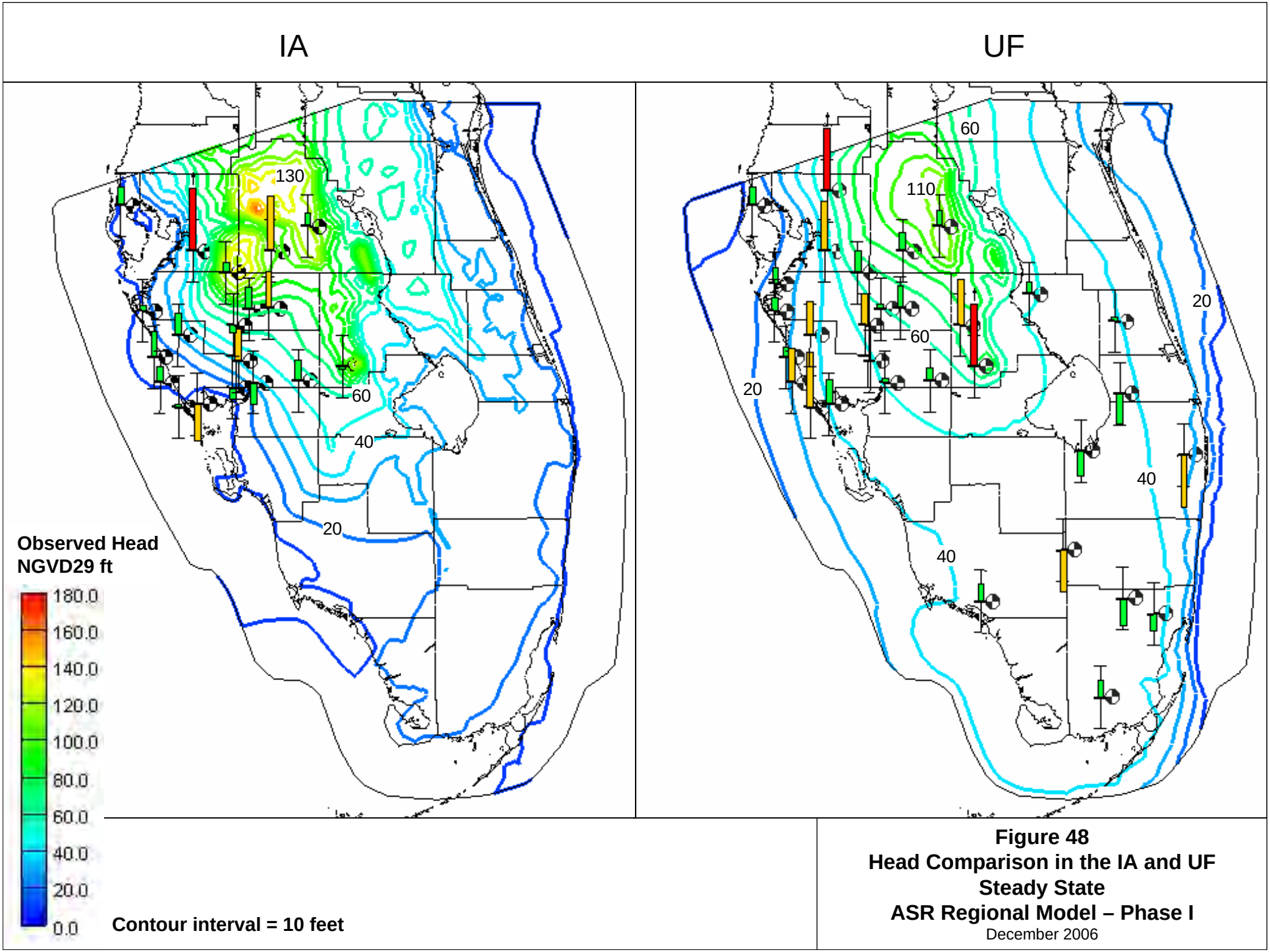

Figure 48
Head Comparison in the IA and UF
Steady State
ASR Regional Model – Phase I
December 2006

IA

UF

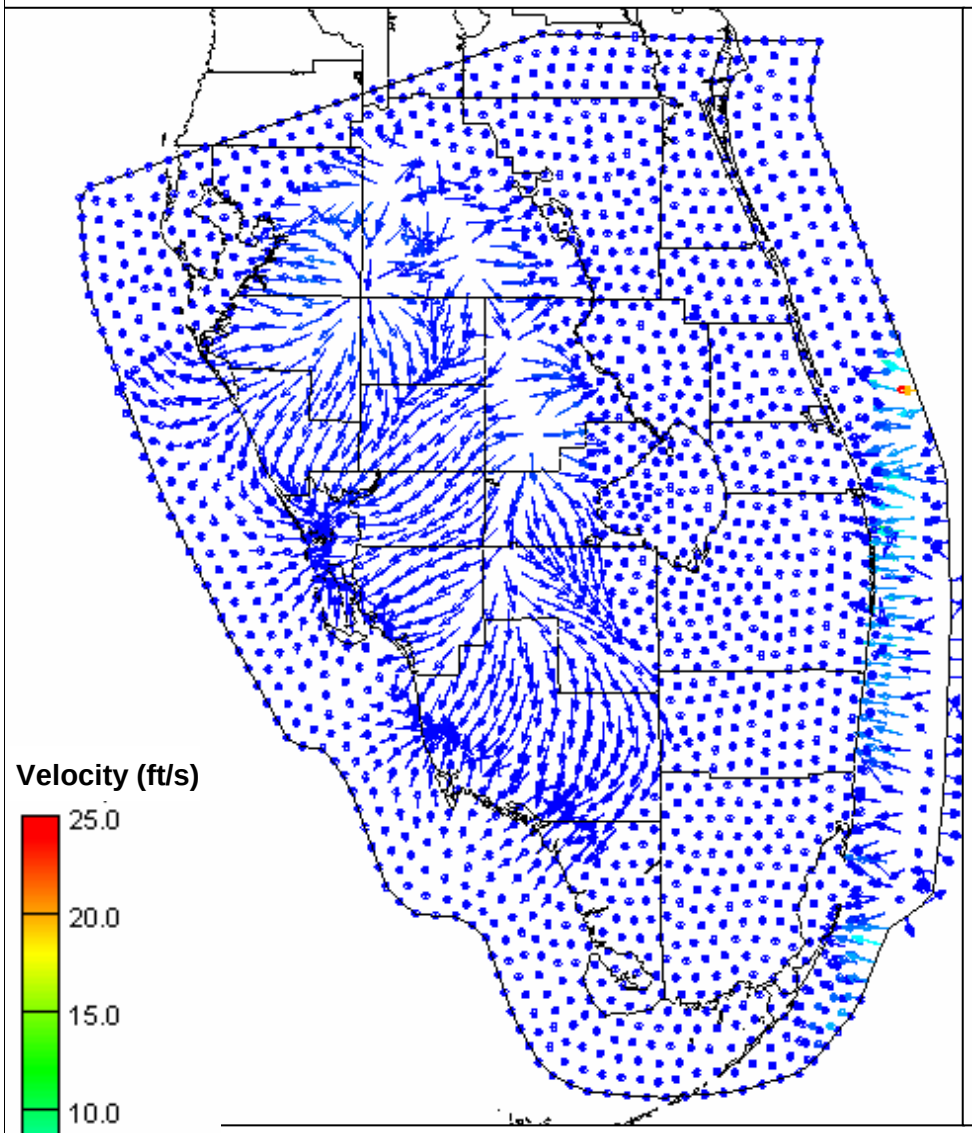

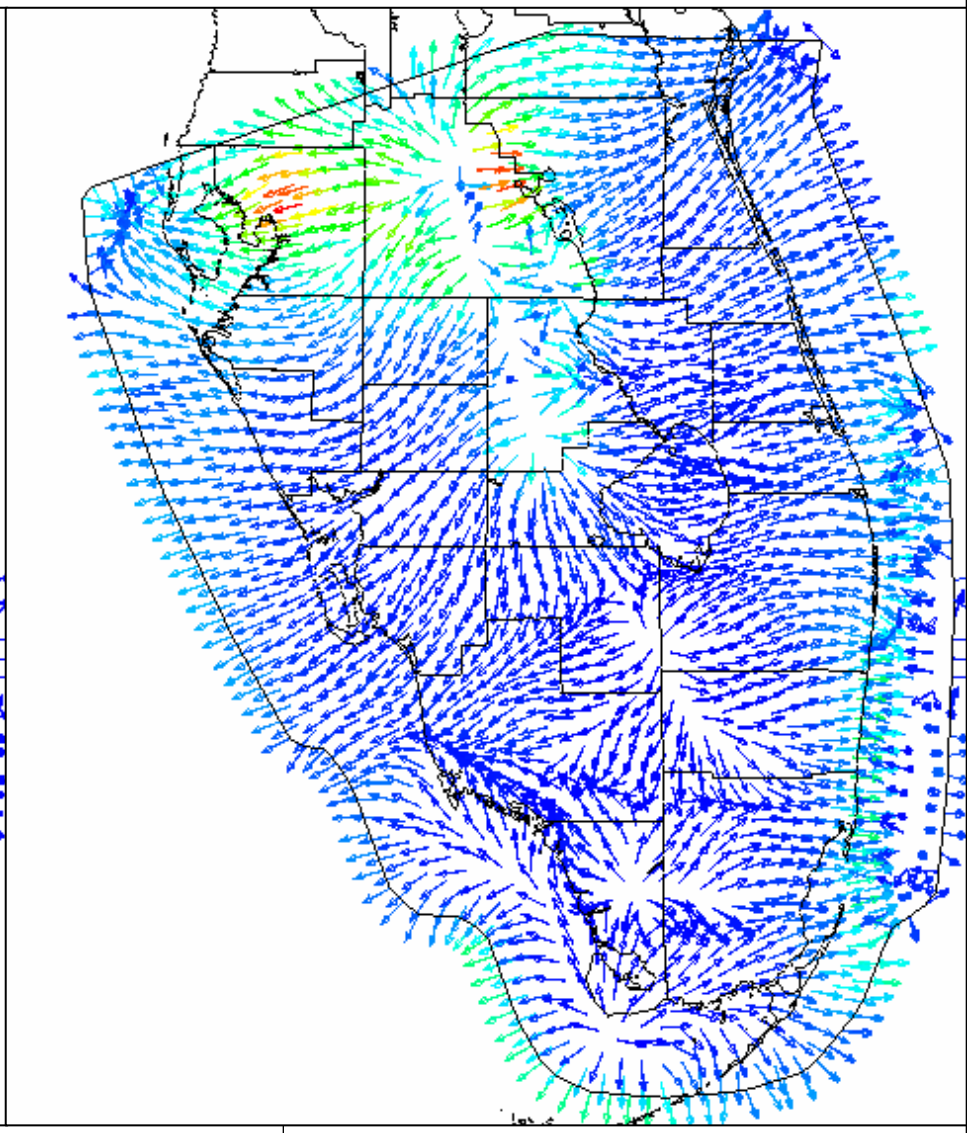

Figure 49
Velocity Vectors in the IA and UF
Steady State
ASR Regional Model – Phase I
December 2006

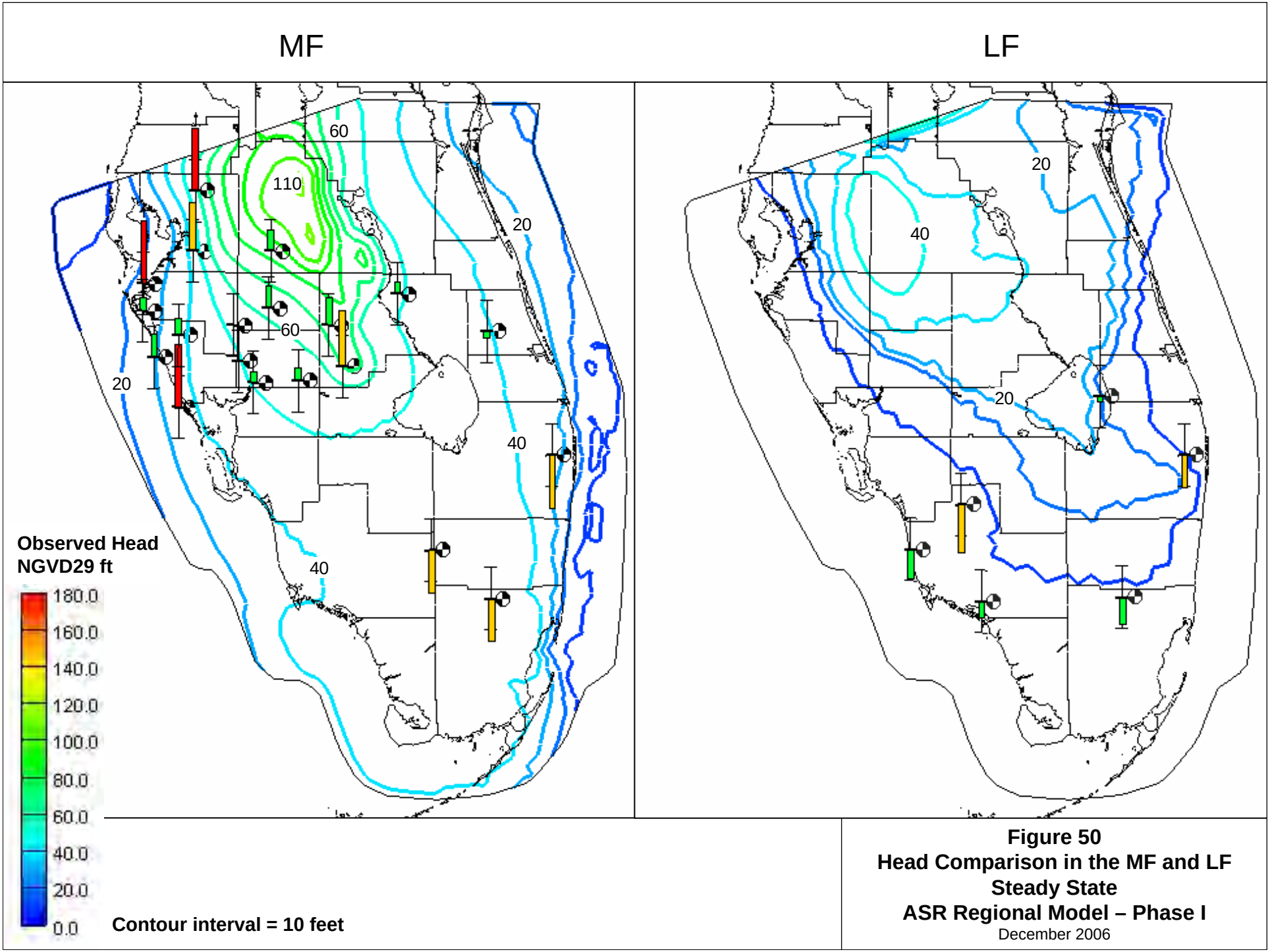

Figure 50
Head Comparison in the MF and LF
Steady State
ASR Regional Model – Phase I
December 2006

MF

LF

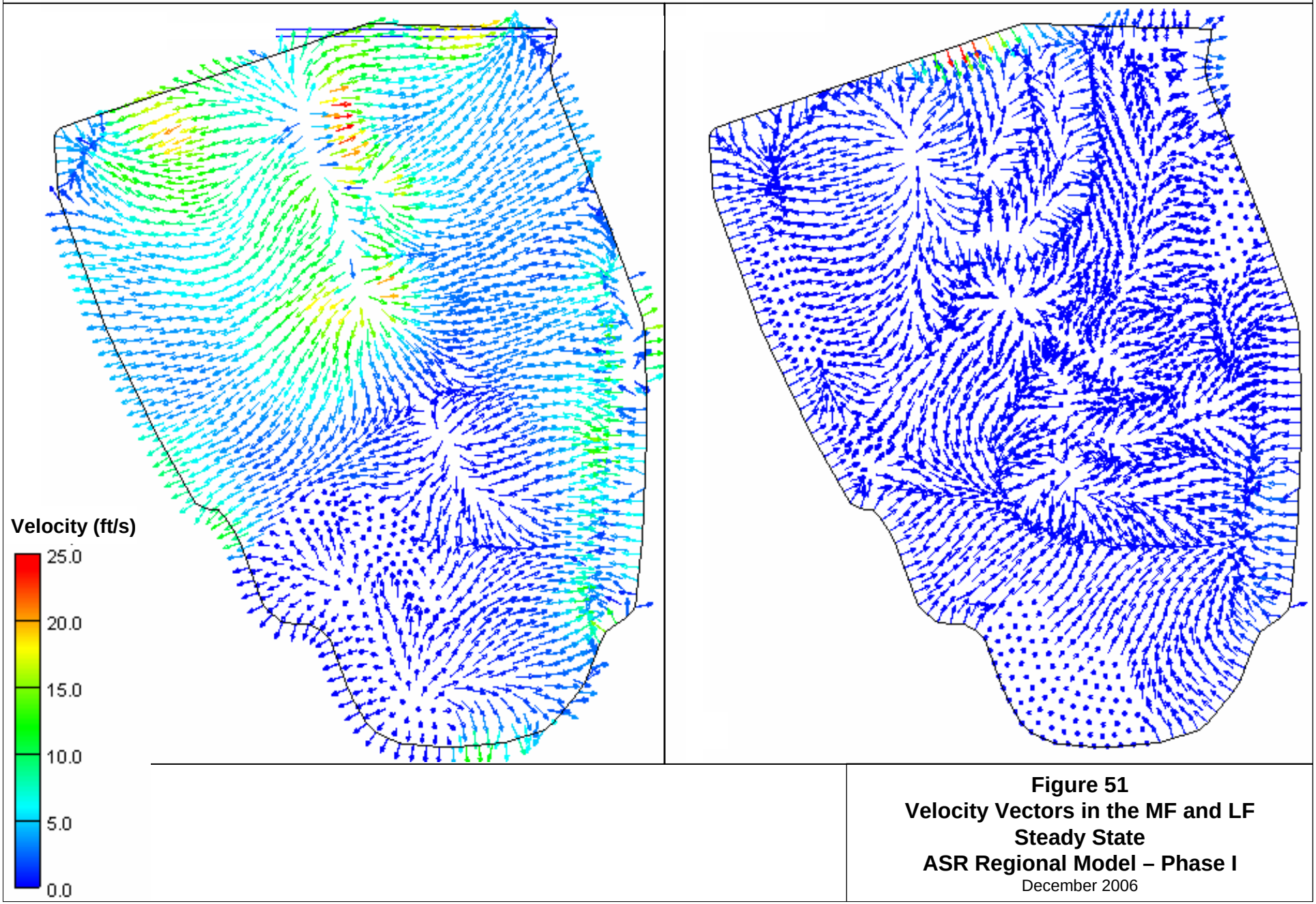

Figure 51
Velocity Vectors in the MF and LF
Steady State
ASR Regional Model – Phase I
December 2006

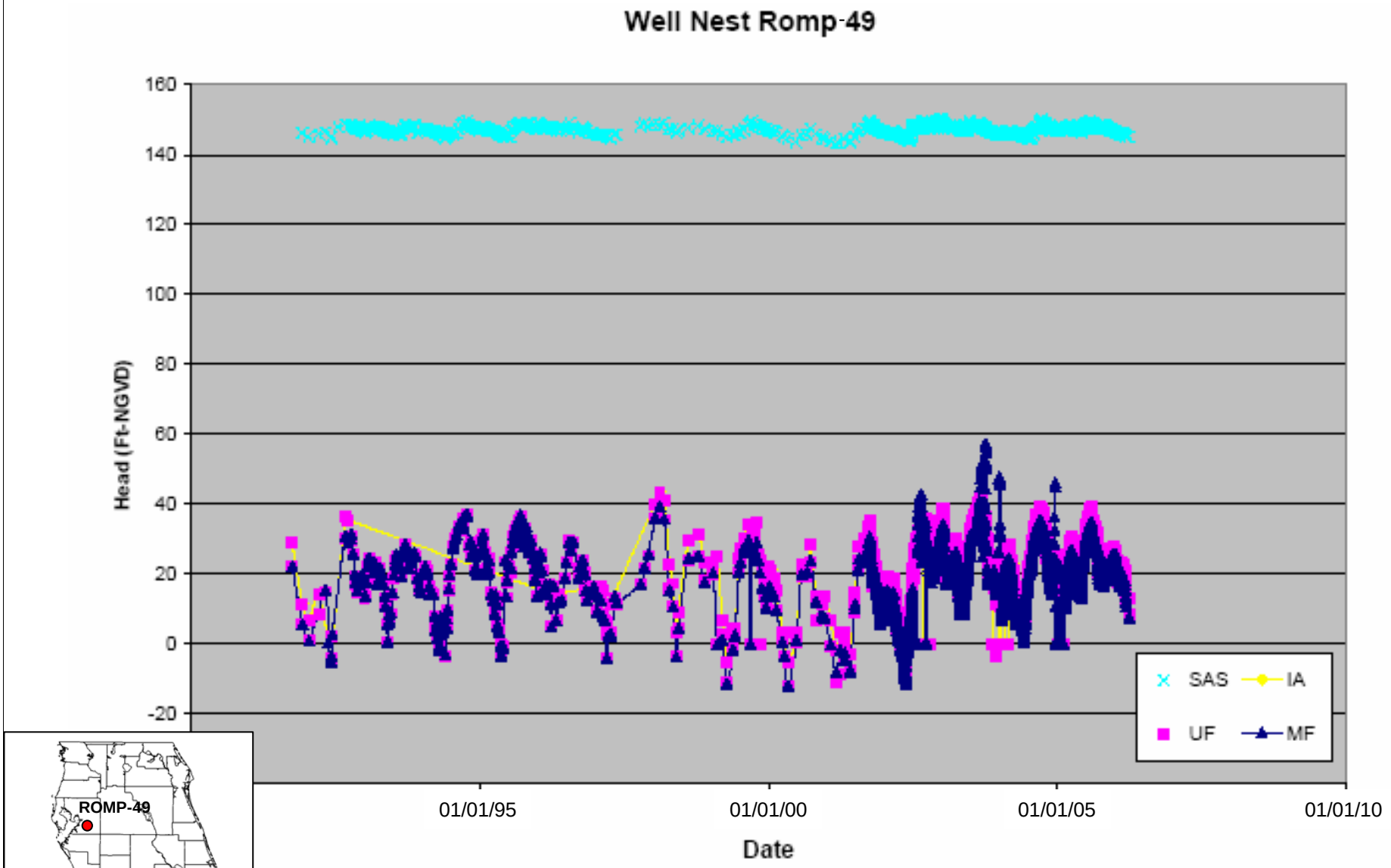

Figure 52
ROMP-49 Head Data
ASR Regional Model – Phase I
December 2006

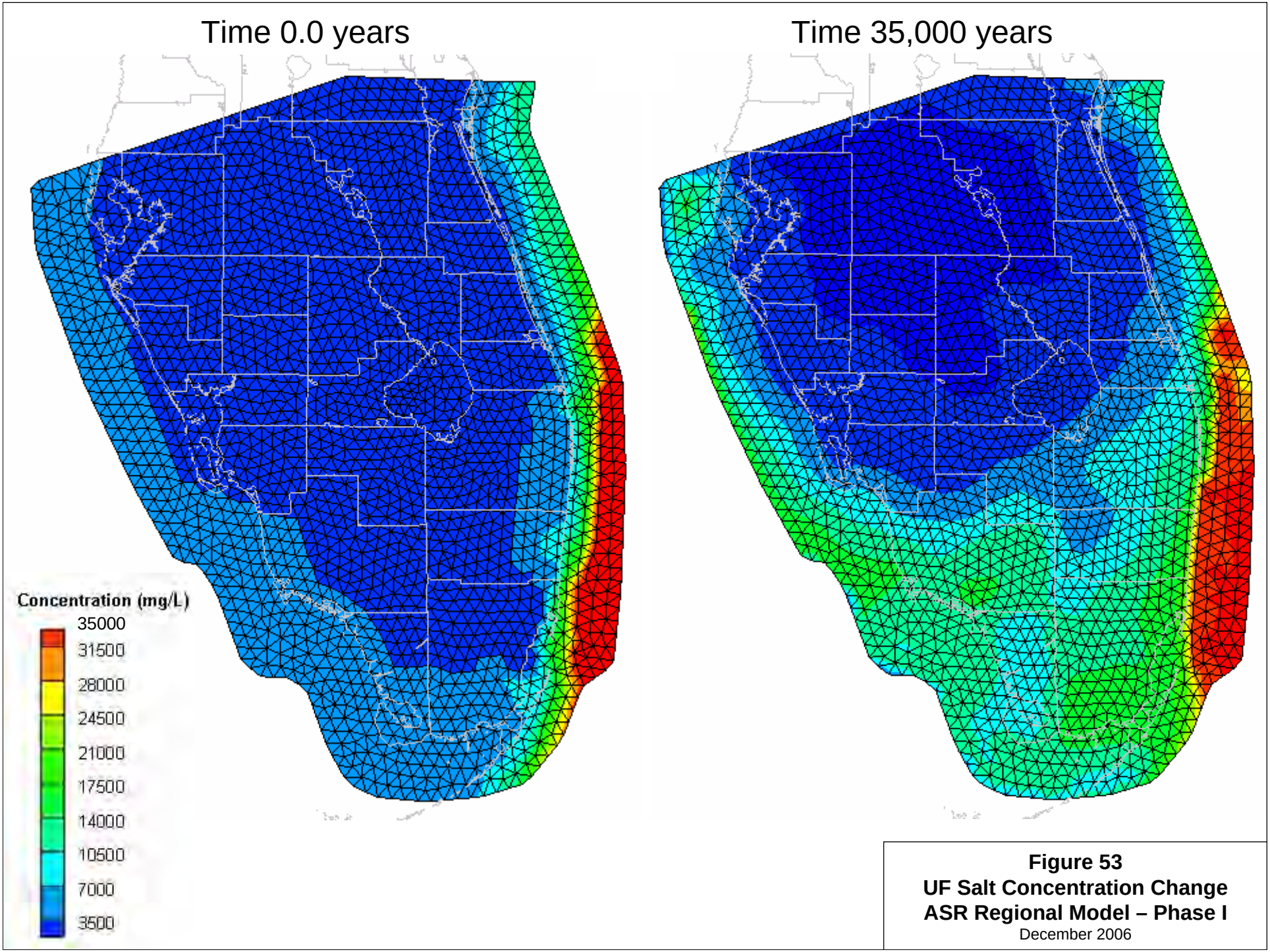

Figure 53
UF Salt Concentration Change
ASR Regional Model – Phase I
December 2006

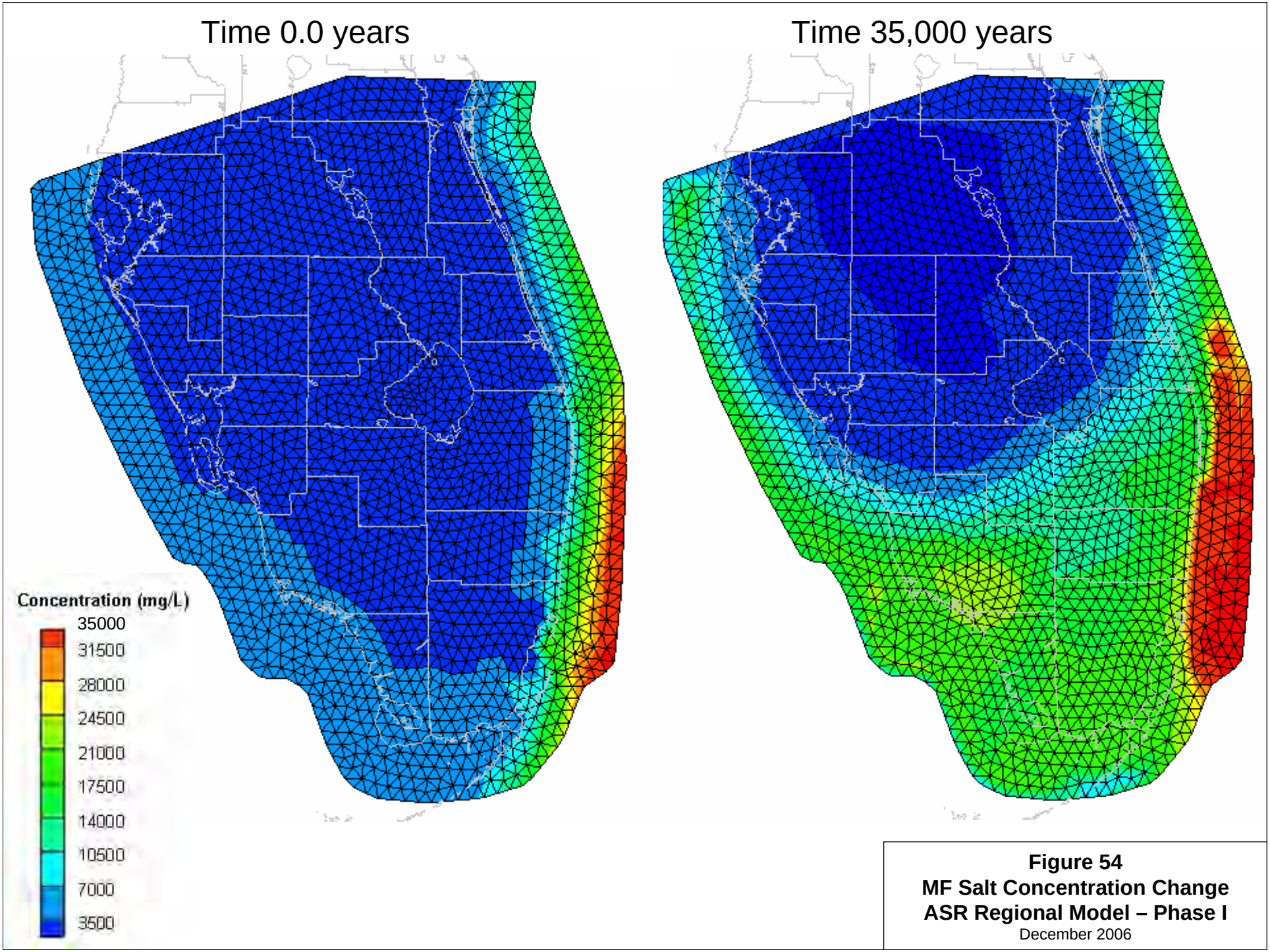

Figure 54
MF Salt Concentration Change
ASR Regional Model – Phase I
December 2006

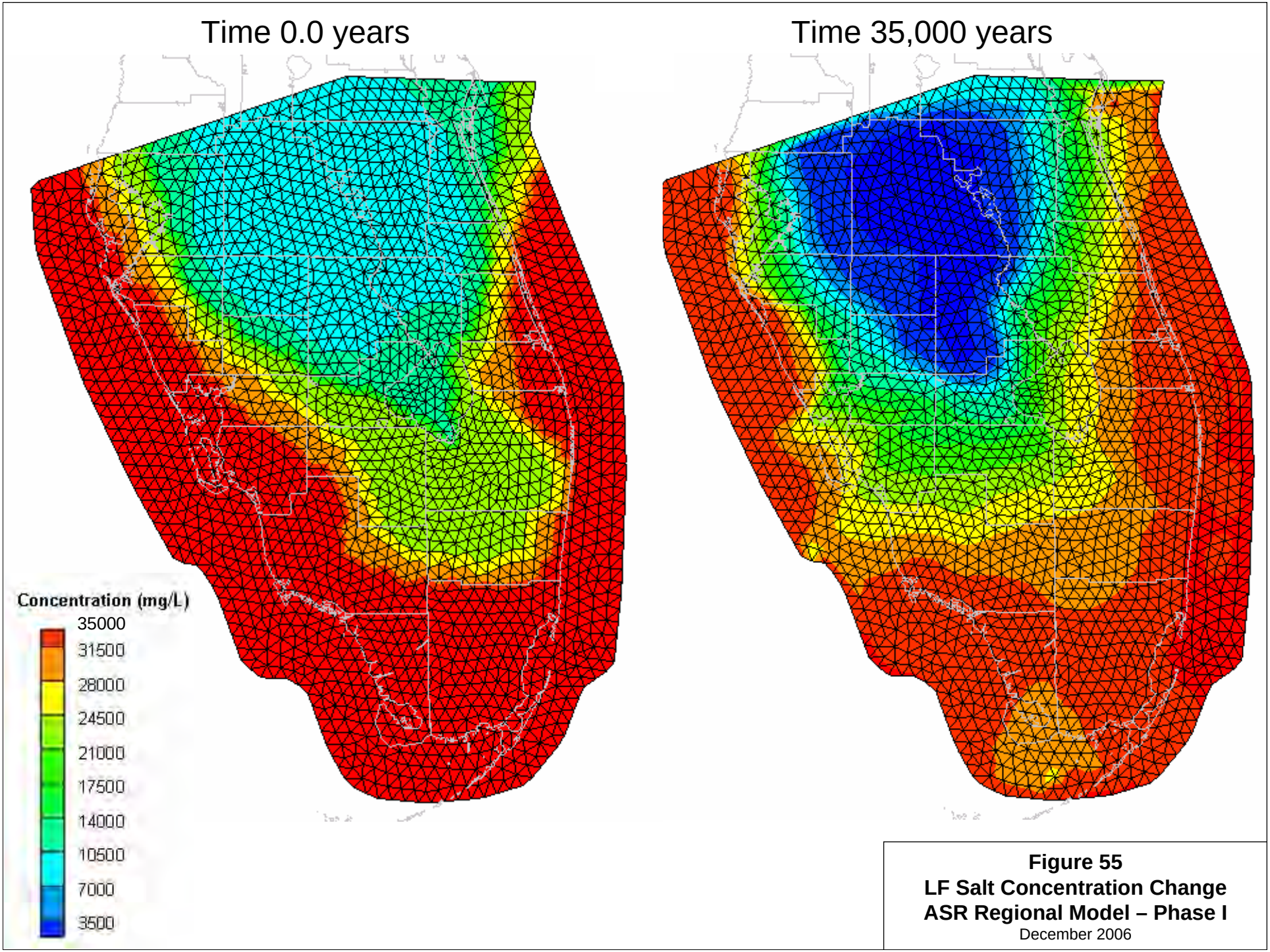

Figure 55
LF Salt Concentration Change
ASR Regional Model – Phase I
December 2006

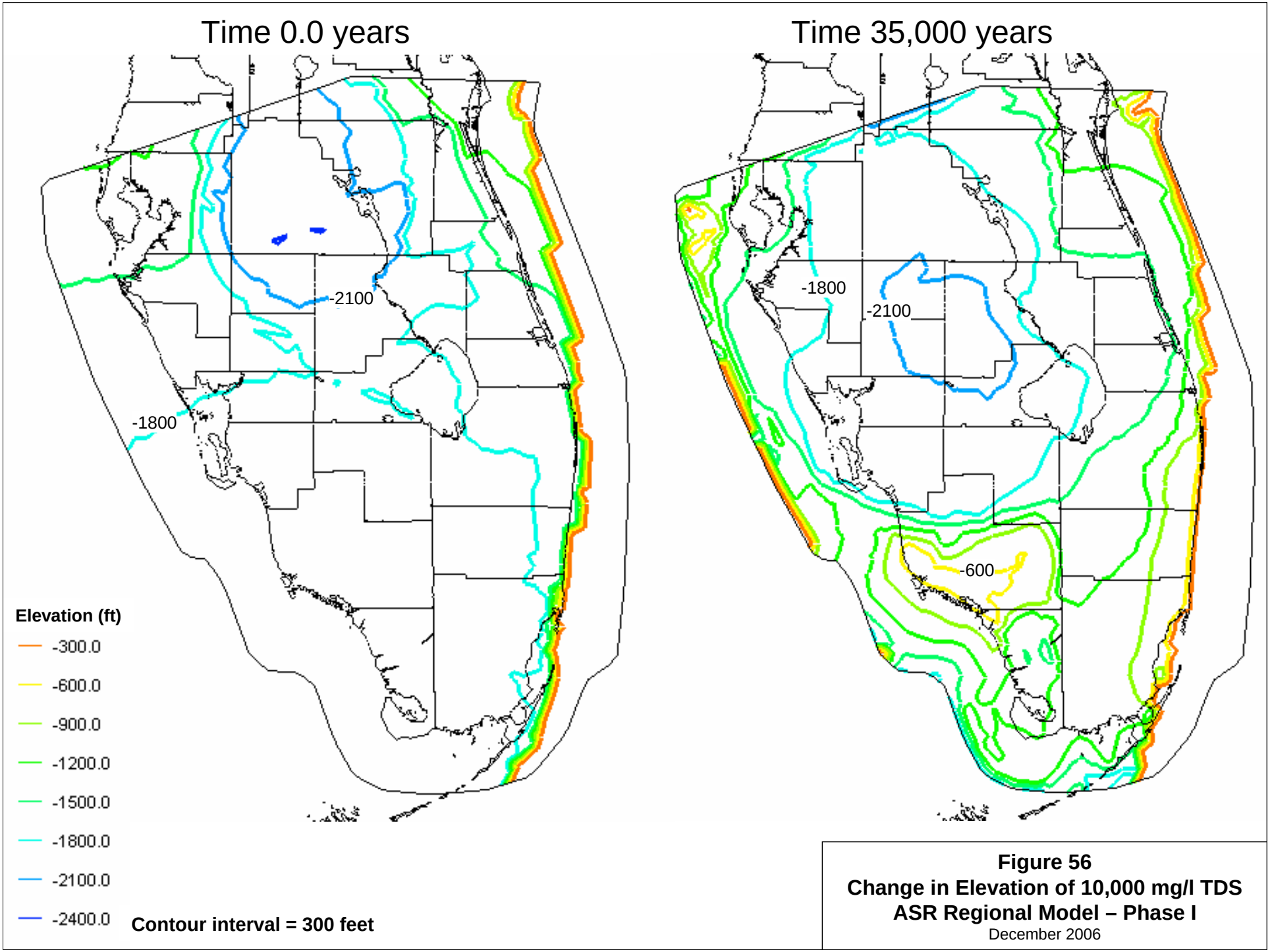

Figure 56
Change in Elevation of 10,000 mg/l TDS
ASR Regional Model – Phase I
December 2006

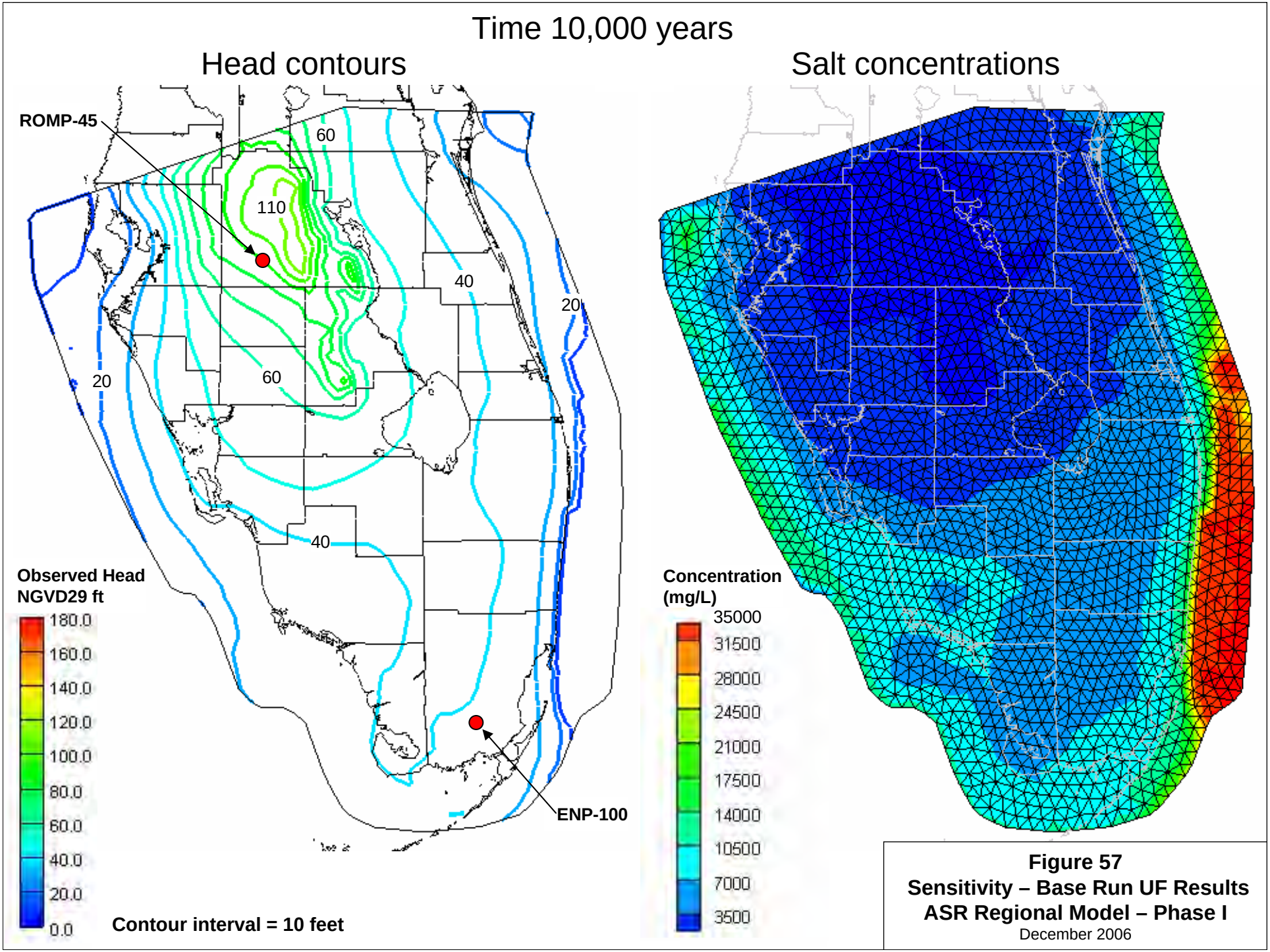

Figure 57
Sensitivity – Base Run UF Results
ASR Regional Model – Phase I
December 2006

Time 10,000 years

Head contours

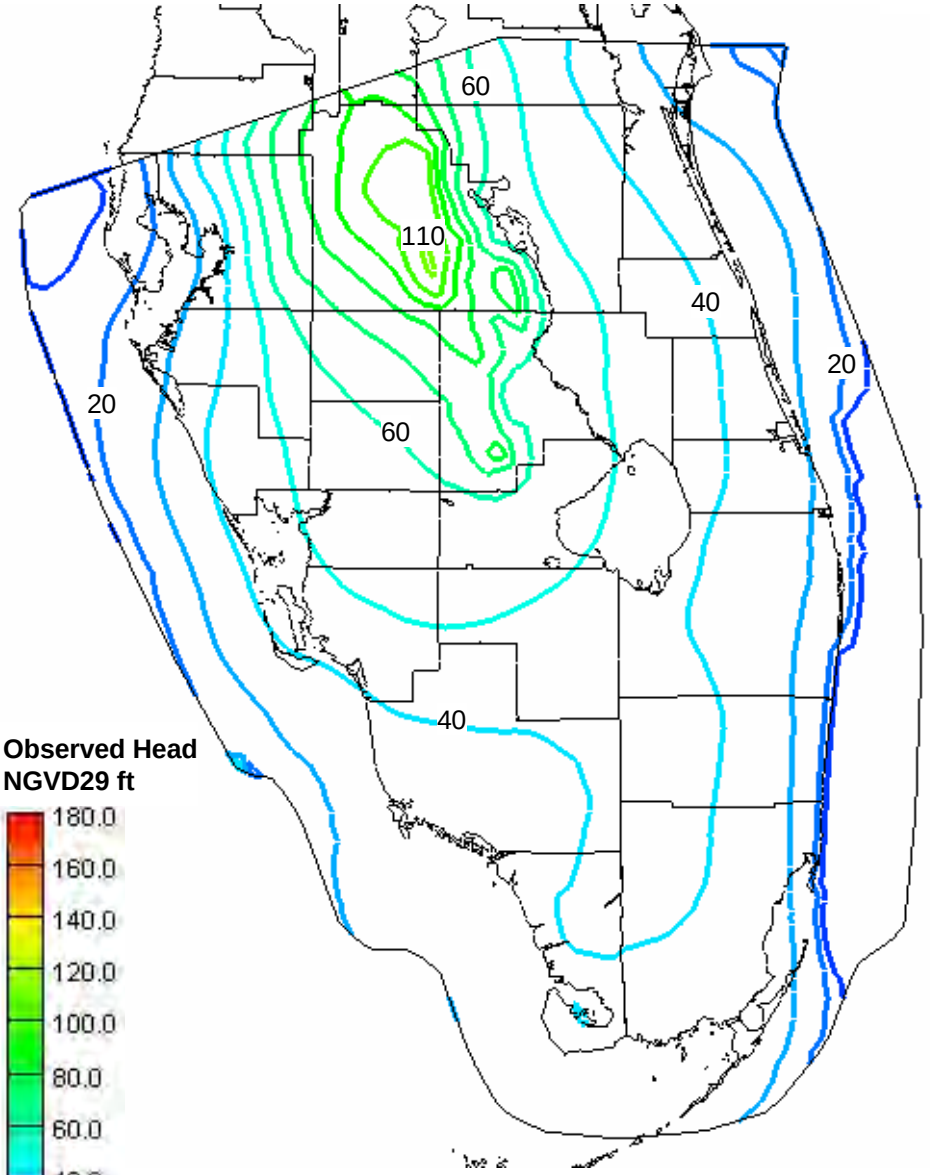

Observed Head
NGVD29 ft

180.0
160.0
140.0
120.0
100.0
80.0
60.0
40.0
20.0
0.0

Contour interval = 10 feet

Salt concentrations

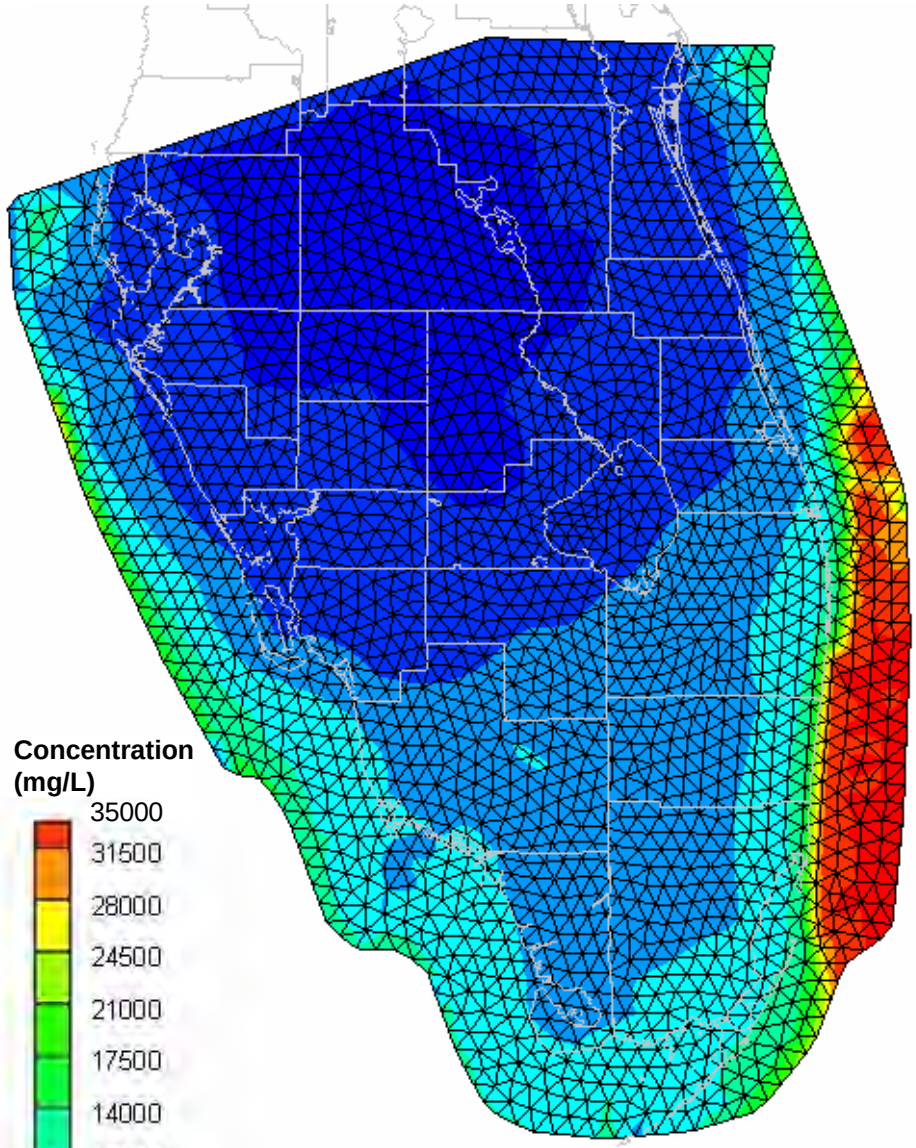

Concentration
(mg/L)

35000
31500
28000
24500
21000
17500
14000
10500
7000
3500

Figure 58
Sensitivity – 2 x K(Aquifer) UF Results
ASR Regional Model – Phase I
December 2006

Time 10,000 years

Head contours

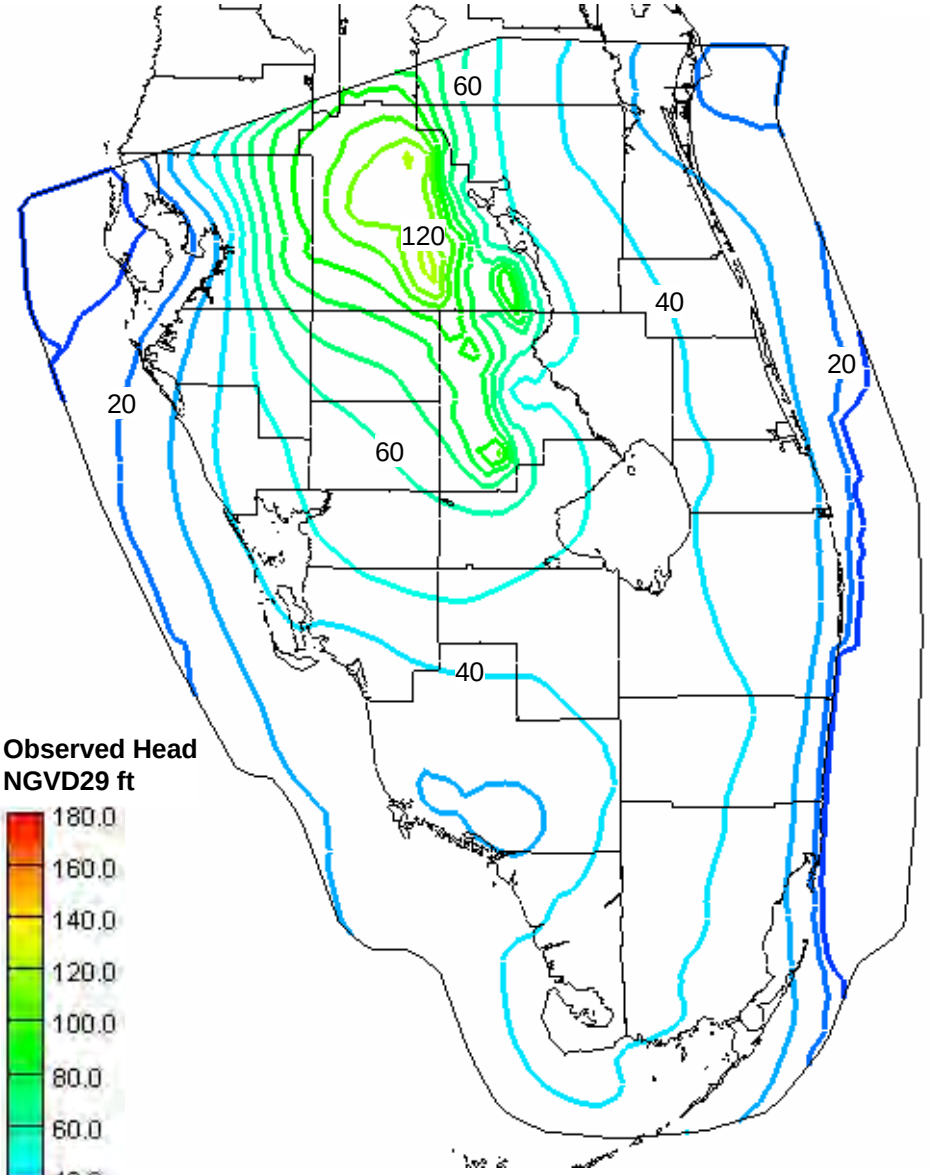

Observed Head
NGVD29 ft

Contour interval = 10 feet

Salt concentrations

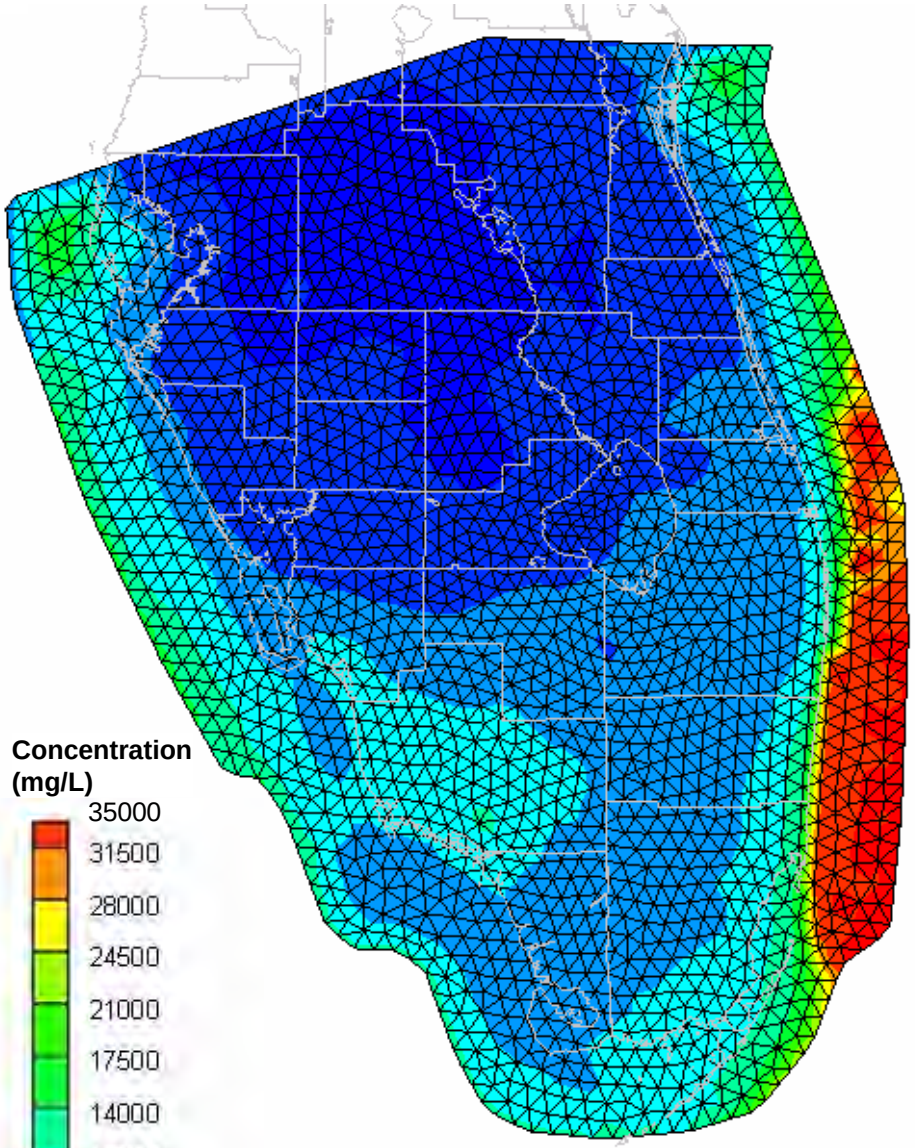

Concentration
(mg/L)

Figure 59
Sensitivity – Half K(Aquifer) UF Results
ASR Regional Model – Phase I
December 2006

Time 10,000 years

Head contours

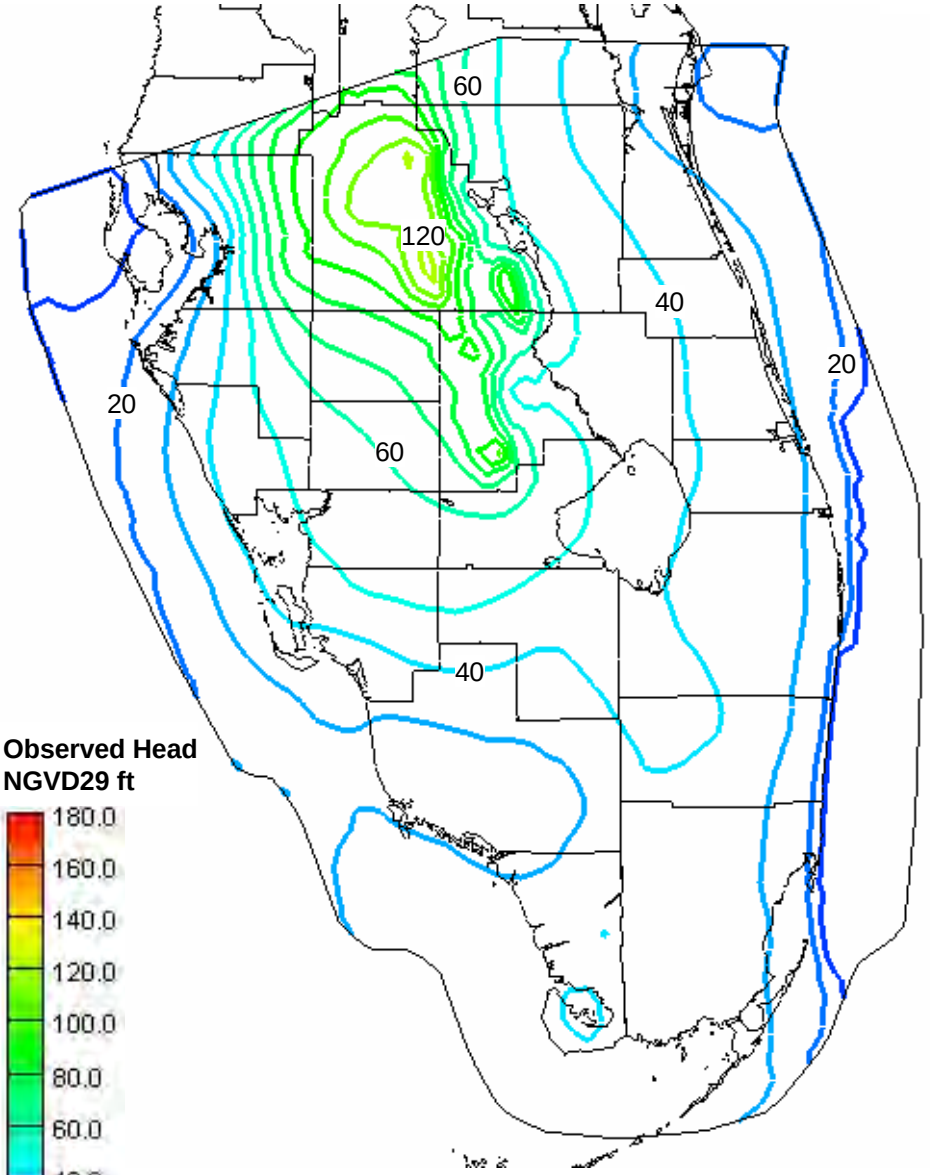

Observed Head
NGVD29 ft

Contour interval = 10 feet

Salt concentrations

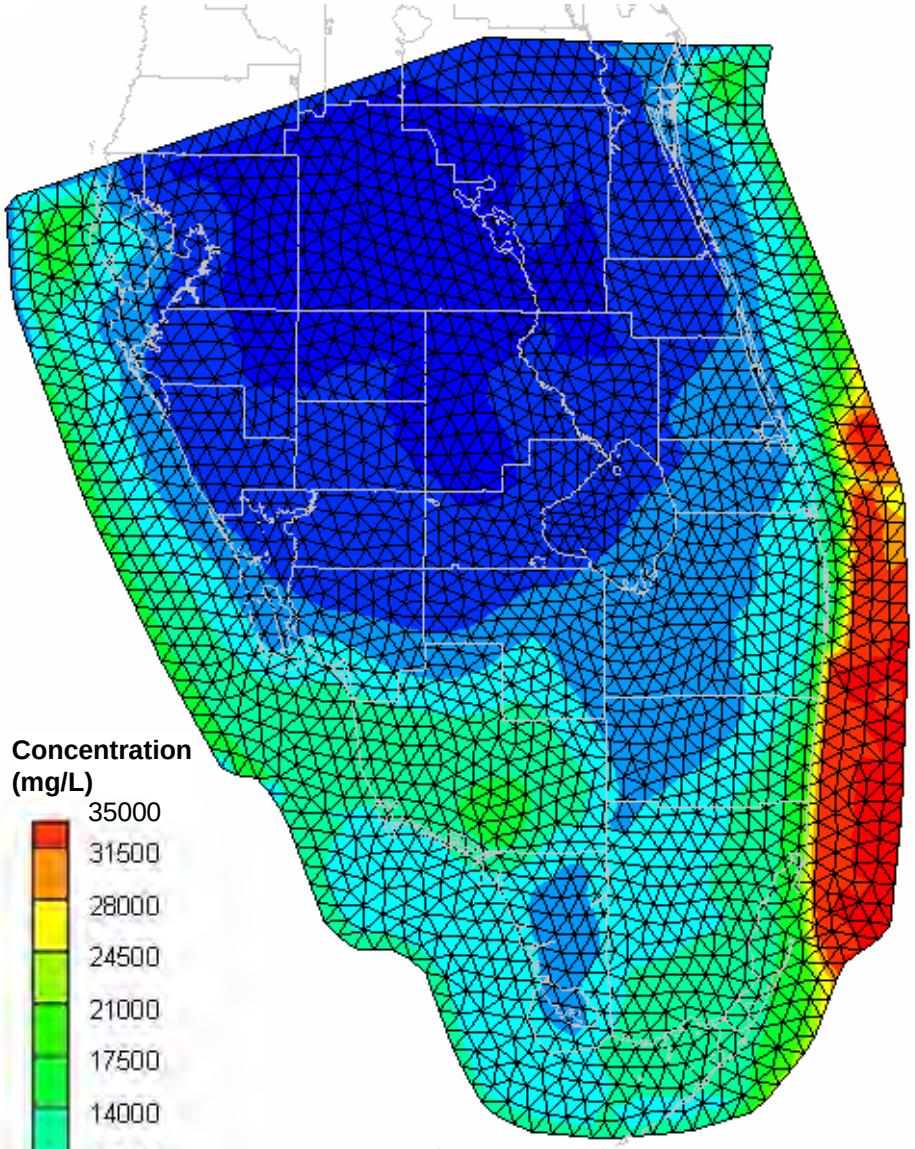

Concentration
(mg/L)

Figure 60
Sensitivity – 2 x K(Confining Unit) UF Results
ASR Regional Model – Phase I
December 2006

Time 10,000 years

Head contours

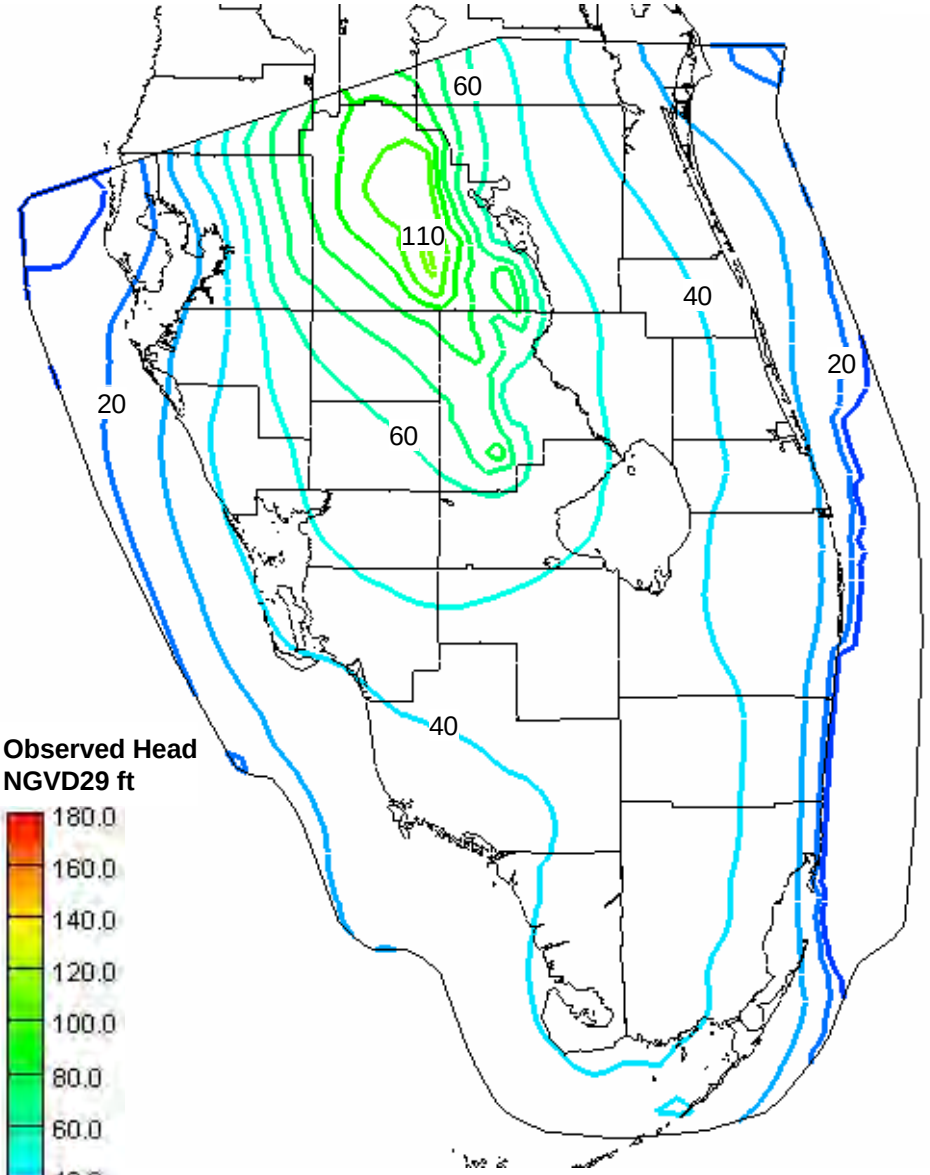

Observed Head
NGVD29 ft

180.0
160.0
140.0
120.0
100.0
80.0
60.0
40.0
20.0
0.0

Contour interval = 10 feet

Salt concentrations

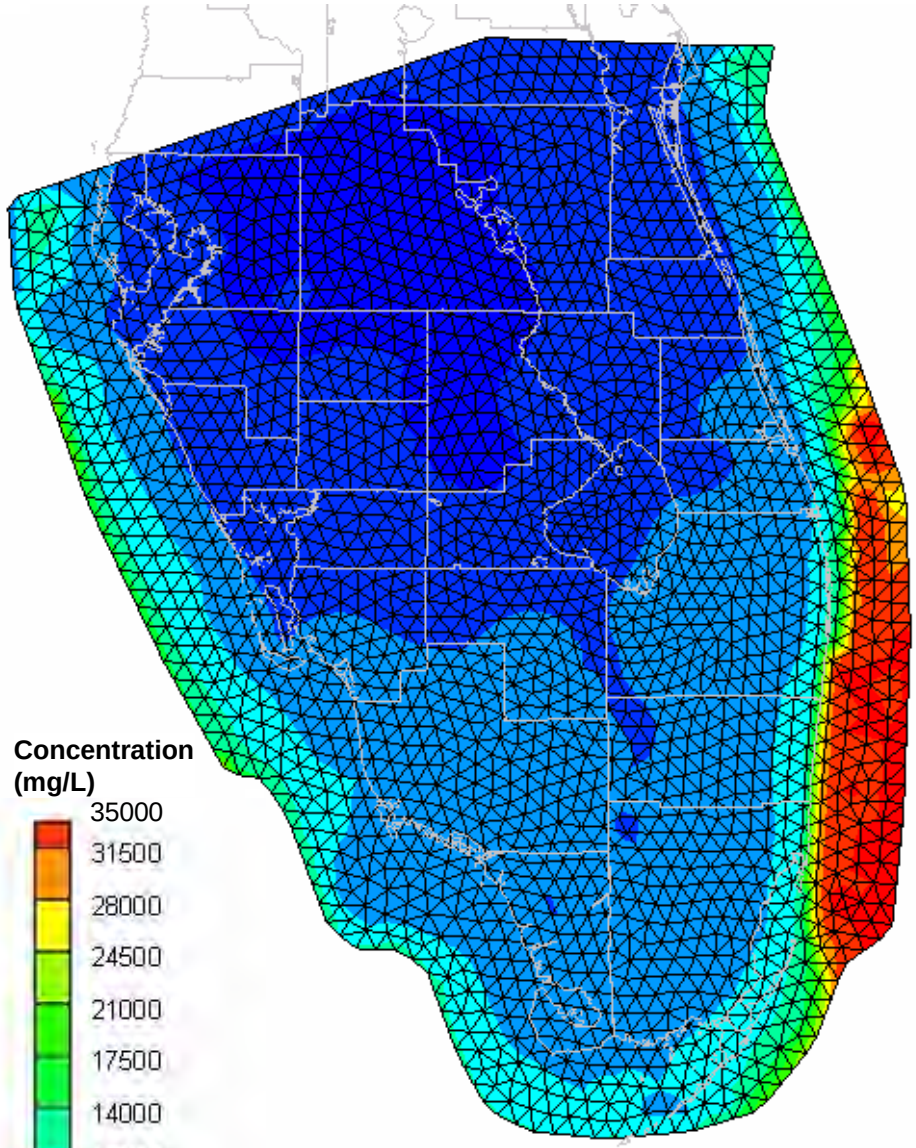

Concentration
(mg/L)

35000
31500
28000
24500
21000
17500
14000
10500
7000
3500

Figure 61
Sensitivity – Half K(Confining Unit) UF Results
ASR Regional Model – Phase I
December 2006

Time 10,000 years

Head contours

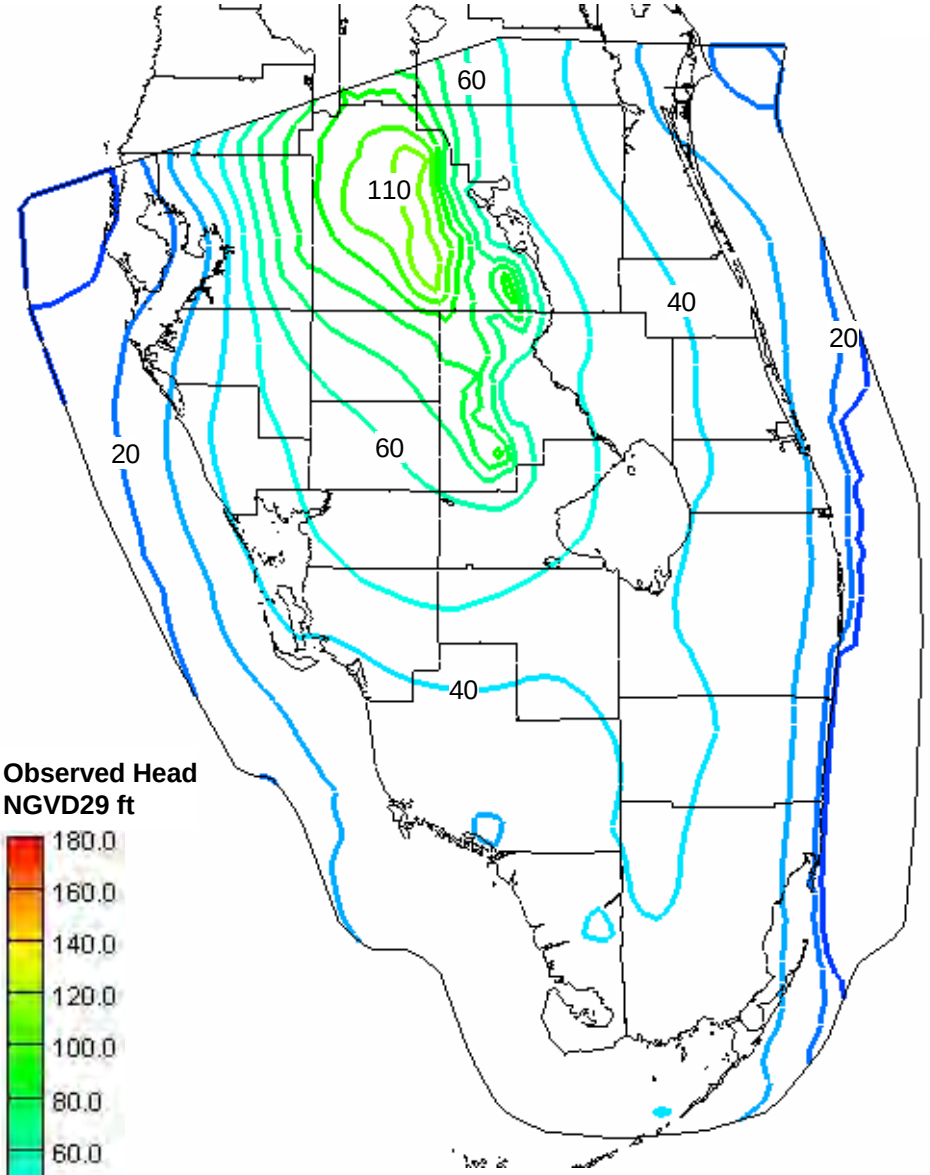

Observed Head
NGVD29 ft

180.0
160.0
140.0
120.0
100.0
80.0
60.0
40.0
20.0
0.0

Contour interval = 10 feet

Salt concentrations

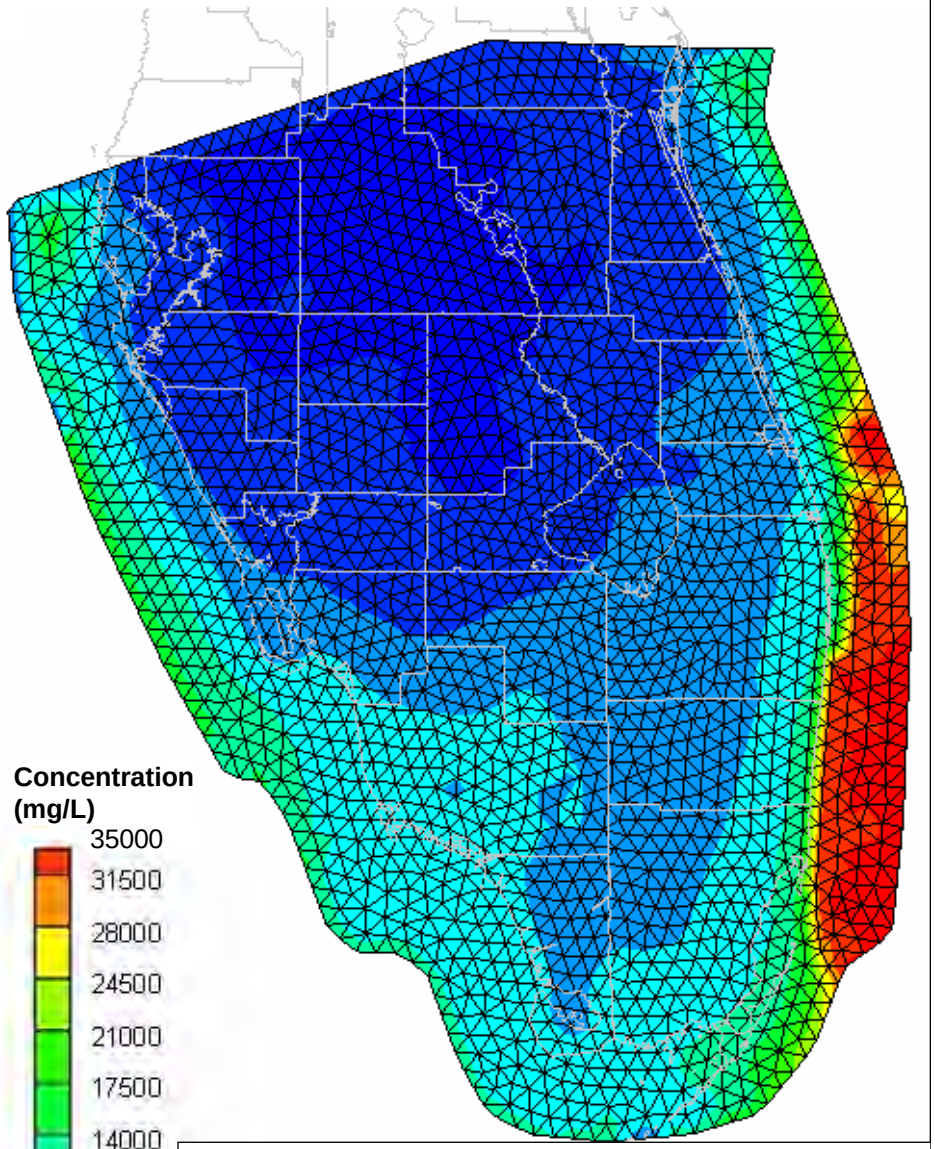

Concentration
(mg/L)

35000
31500
28000
24500
21000
17500
14000
10500
7000
3500

Figure 62
Sensitivity – Increase Initial Concentrations 25%
UF Results
ASR Regional Model – Phase I
December 2006

Time 10,000 years

Head contours

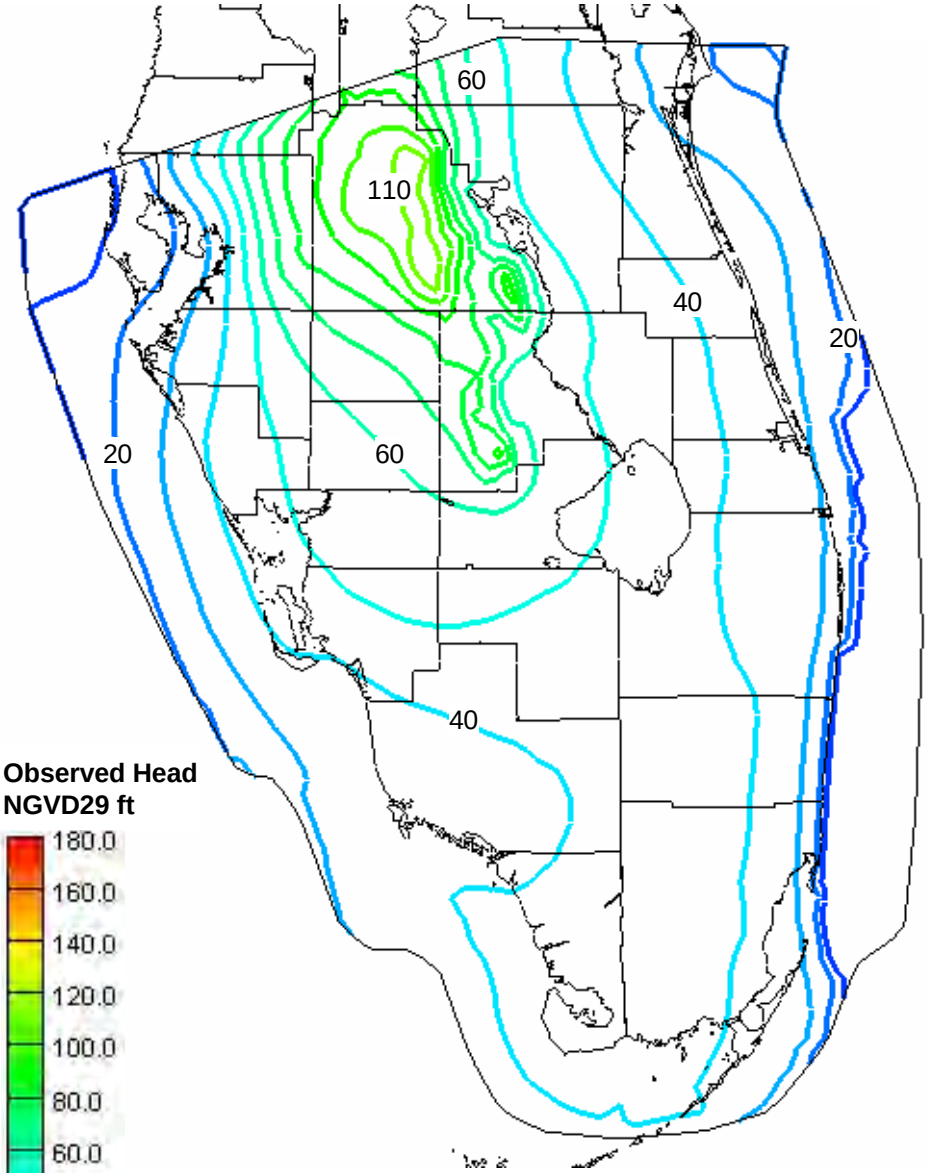

Observed Head
NGVD29 ft

180.0
160.0
140.0
120.0
100.0
80.0
60.0
40.0
20.0
0.0

Contour interval = 10 feet

Salt concentrations

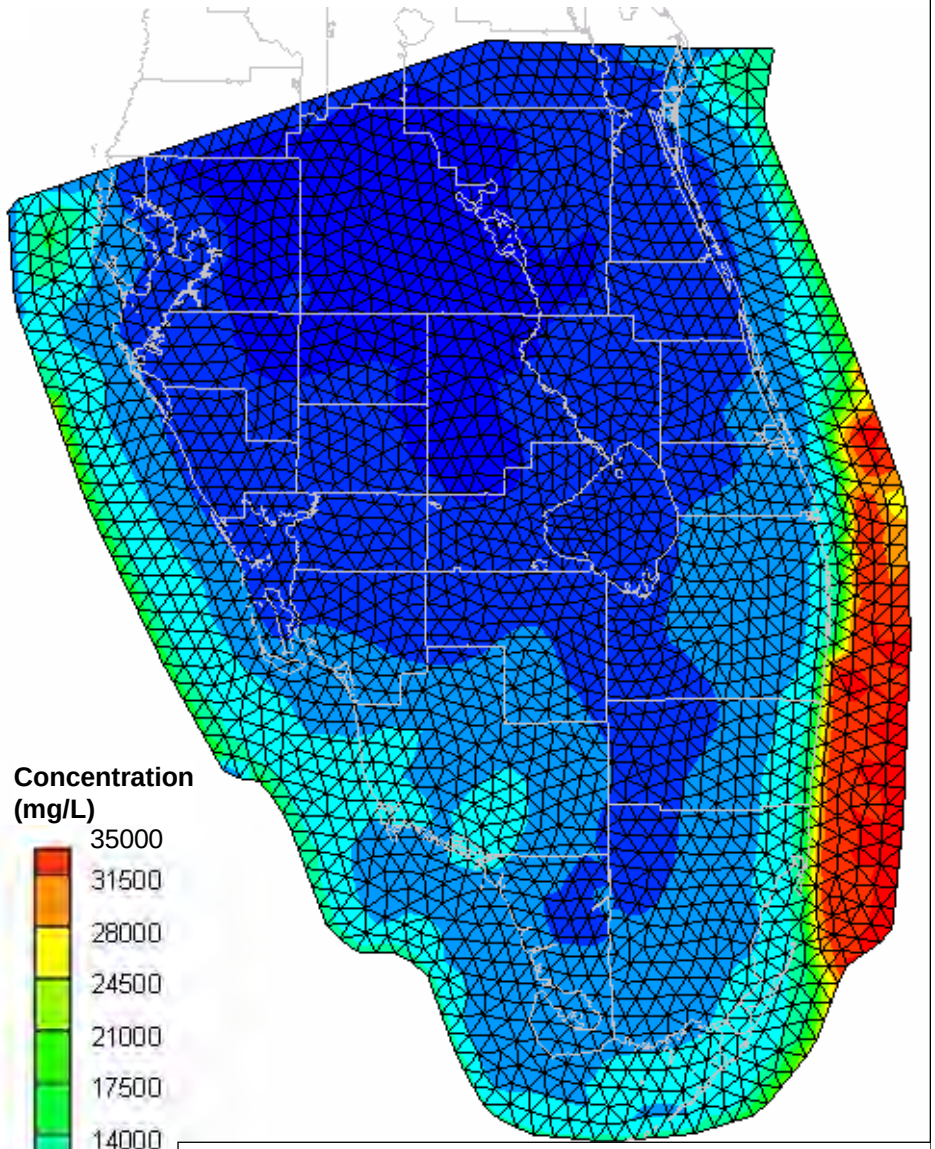

Concentration
(mg/L)

35000
31500
28000
24500
21000
17500
14000
10500
7000
3500

Figure 63
Sensitivity – Decrease Initial Concentrations 25%
UF Results
ASR Regional Model – Phase I
December 2006

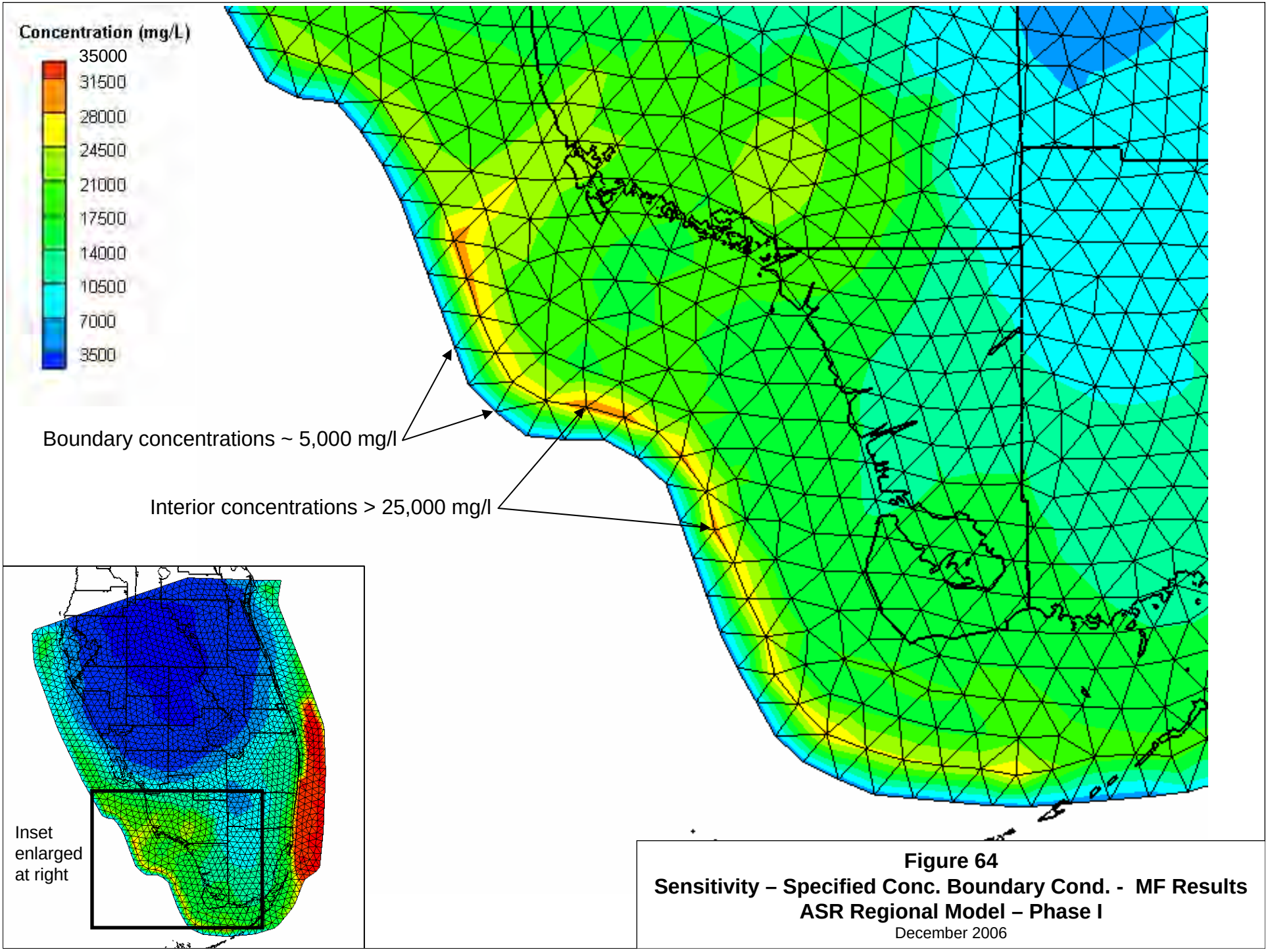

Figure 64
Sensitivity – Specified Conc. Boundary Cond. - MF Results
ASR Regional Model – Phase I
December 2006

ROMP-45

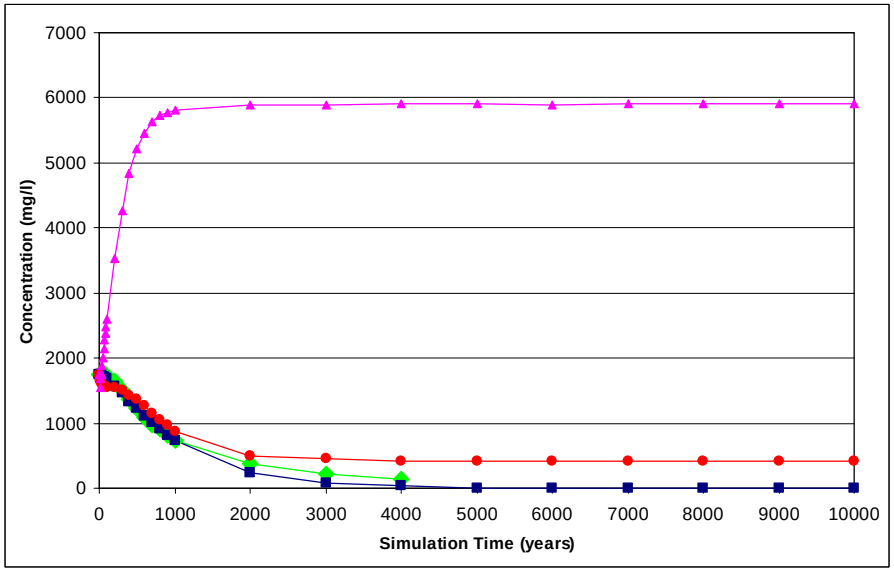

ENP-100

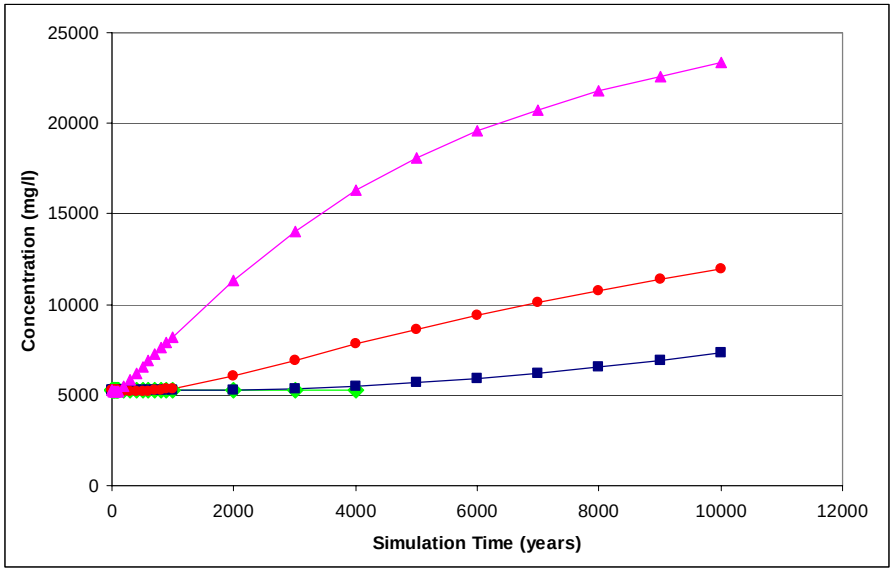

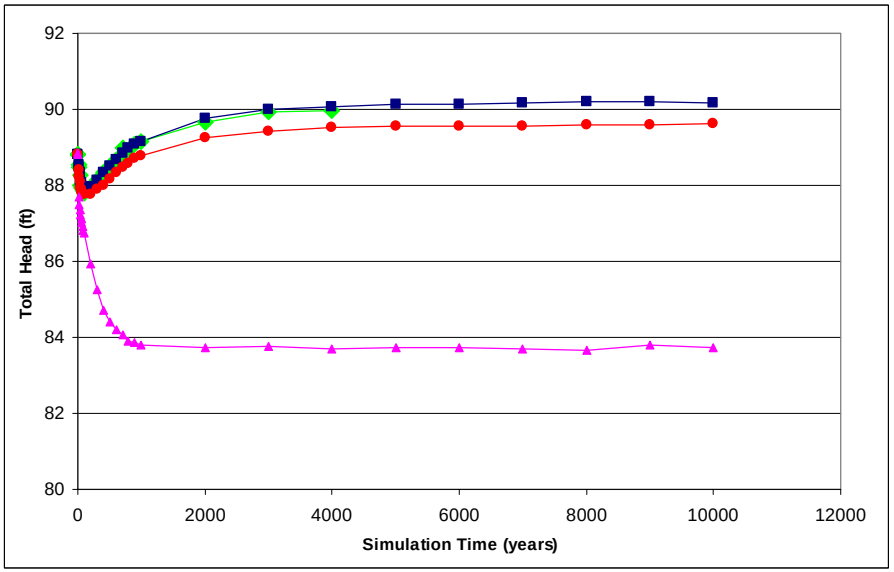

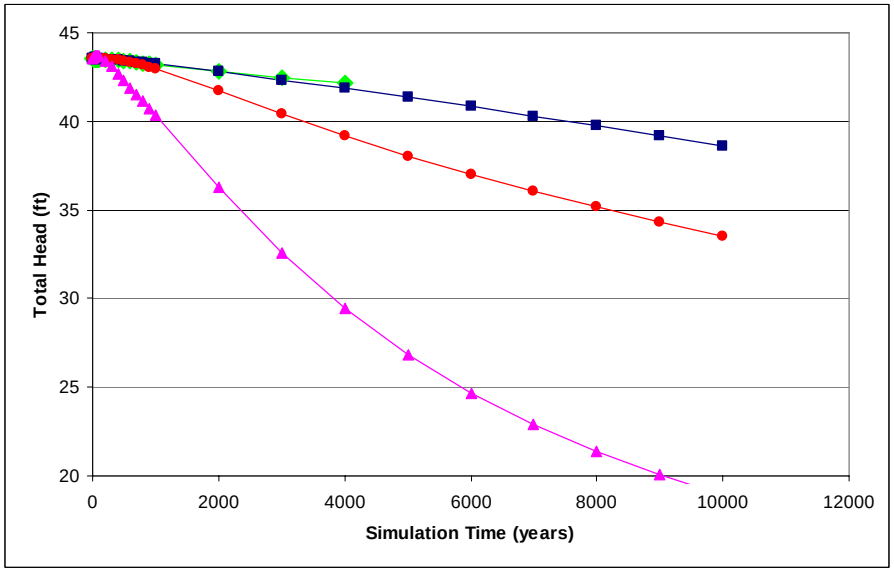

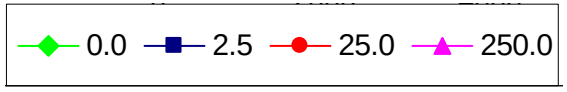

Figure 65
Sensitivity – Dispersivity Effects at Selected Wells
ASR Regional Model – Phase I
December 2006

ROMP-45

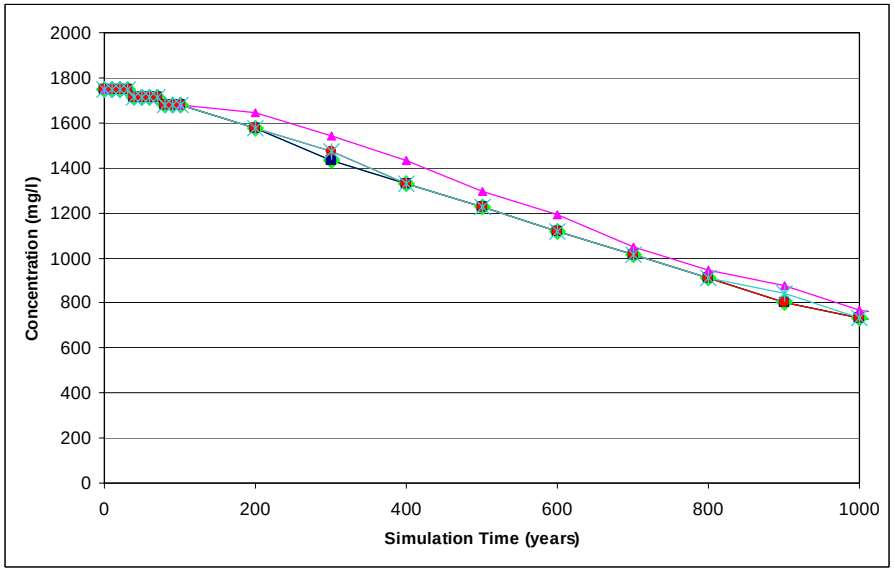

ENP-100

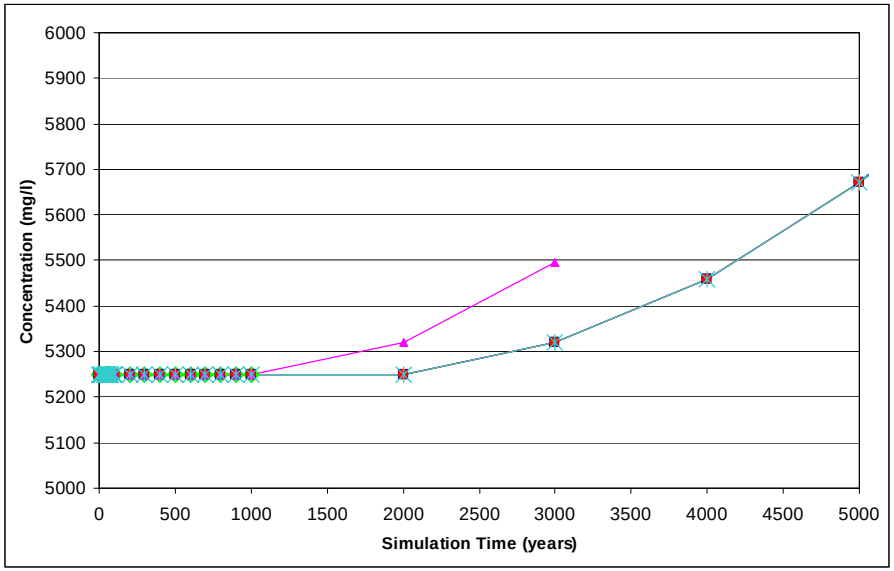

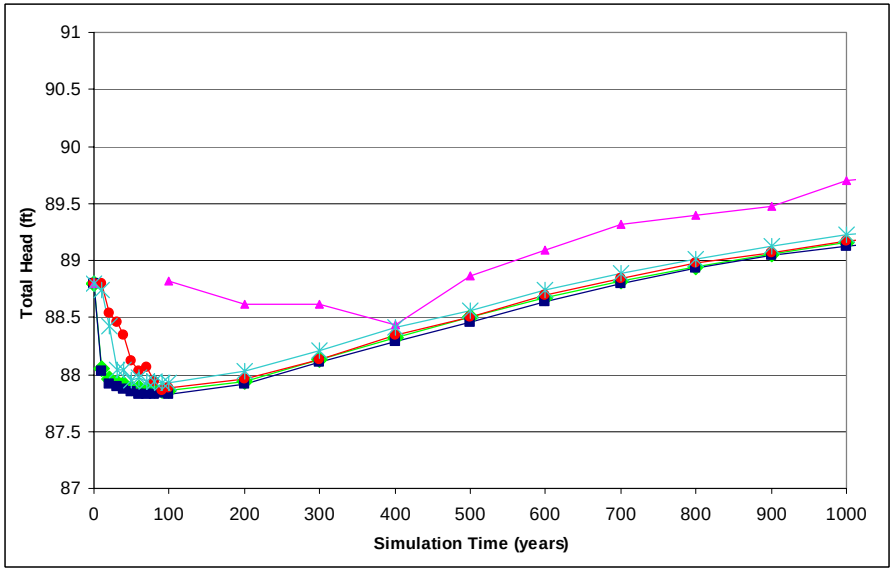

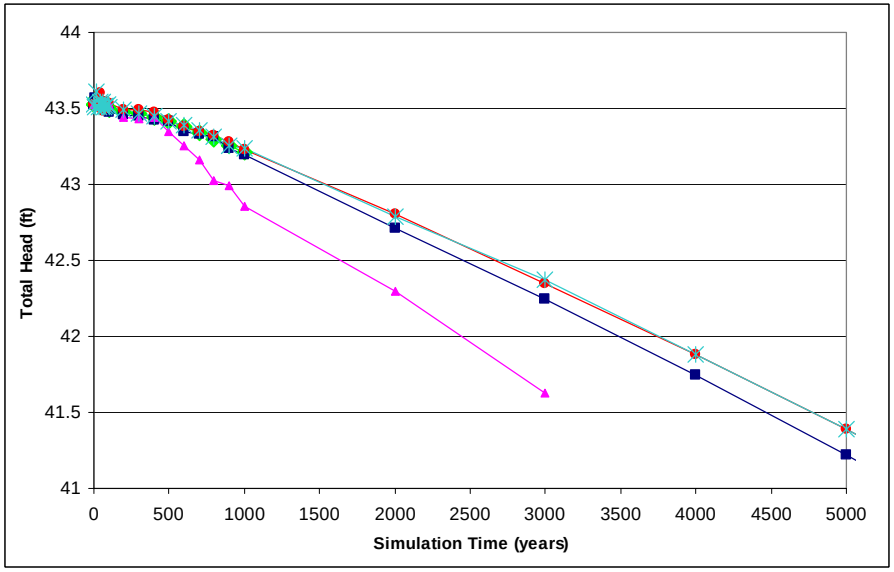

Figure 66
Sensitivity – Time Step Effects at Selected Wells
ASR Regional Model – Phase I
December 2006

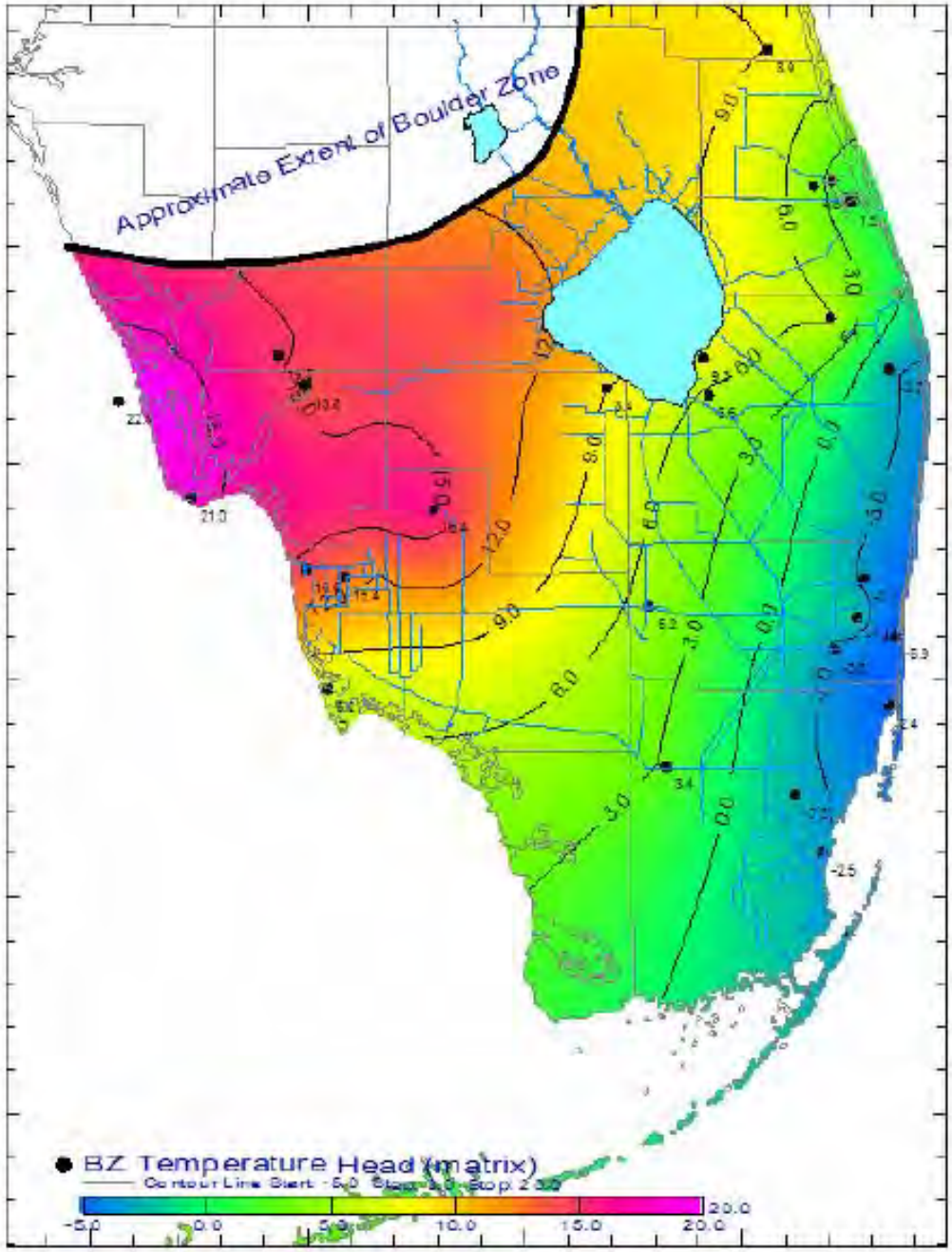

Estimated Boulder Zone Head [Ft NGVD] as a result of temperature induced density differential.

Assumptions:

- Constant TDS = 37,500 ppm
- In the absence of temperature effect, BZ head would be zero.
- Specific Weight at Standard Temperature (4 °C) = 64.07 lb/ft^3. {Baxter-Wallace Equation}.
- Reference Depth = Estimated top of the Boulder Zone.

Prepared by SFWMD

Figure 67
Sensitivity – Temperature Effects on BZ BC
ASR Regional Model – Phase I
December 2006

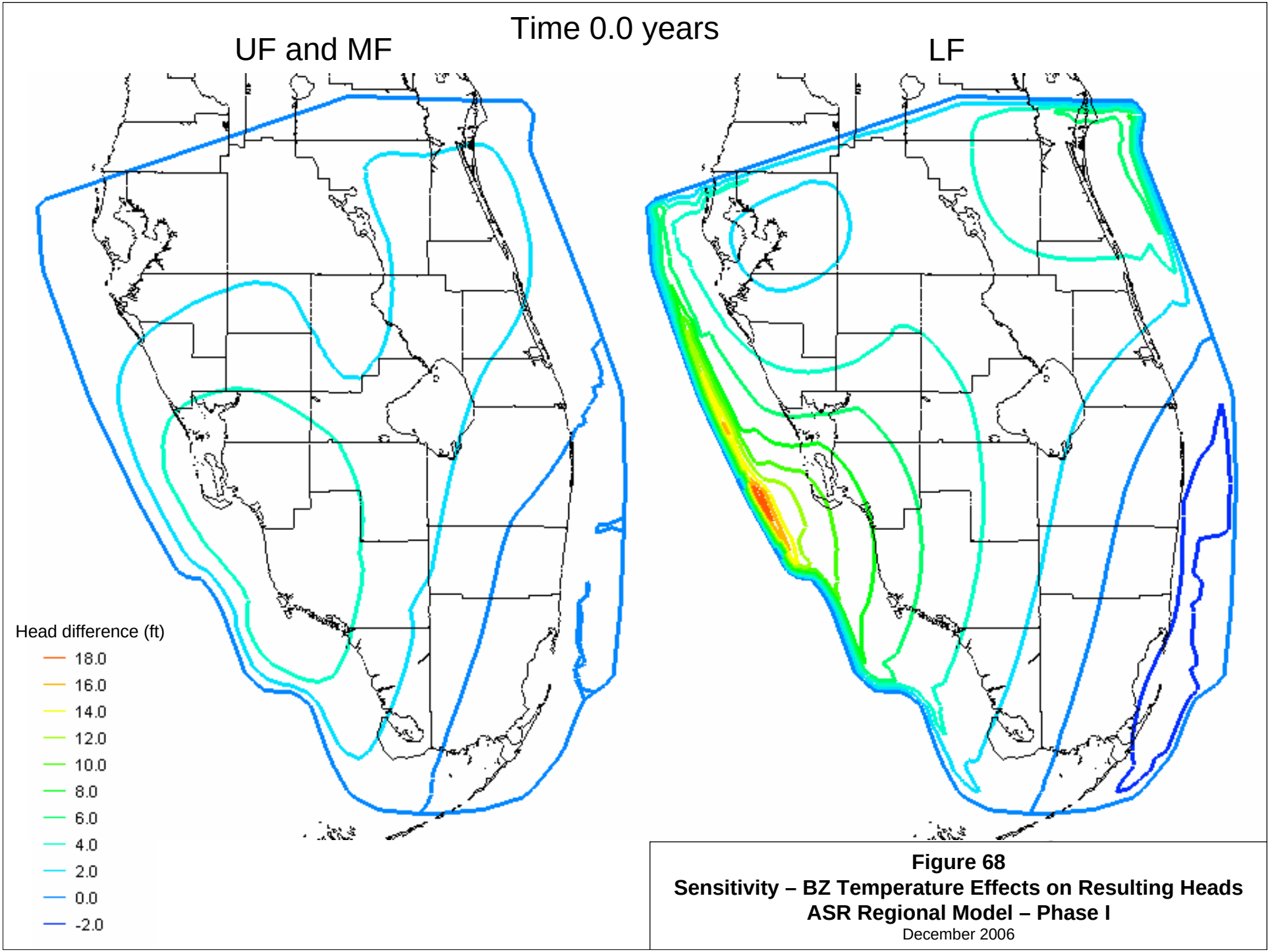

Figure 68
Sensitivity – BZ Temperature Effects on Resulting Heads
ASR Regional Model – Phase I
December 2006

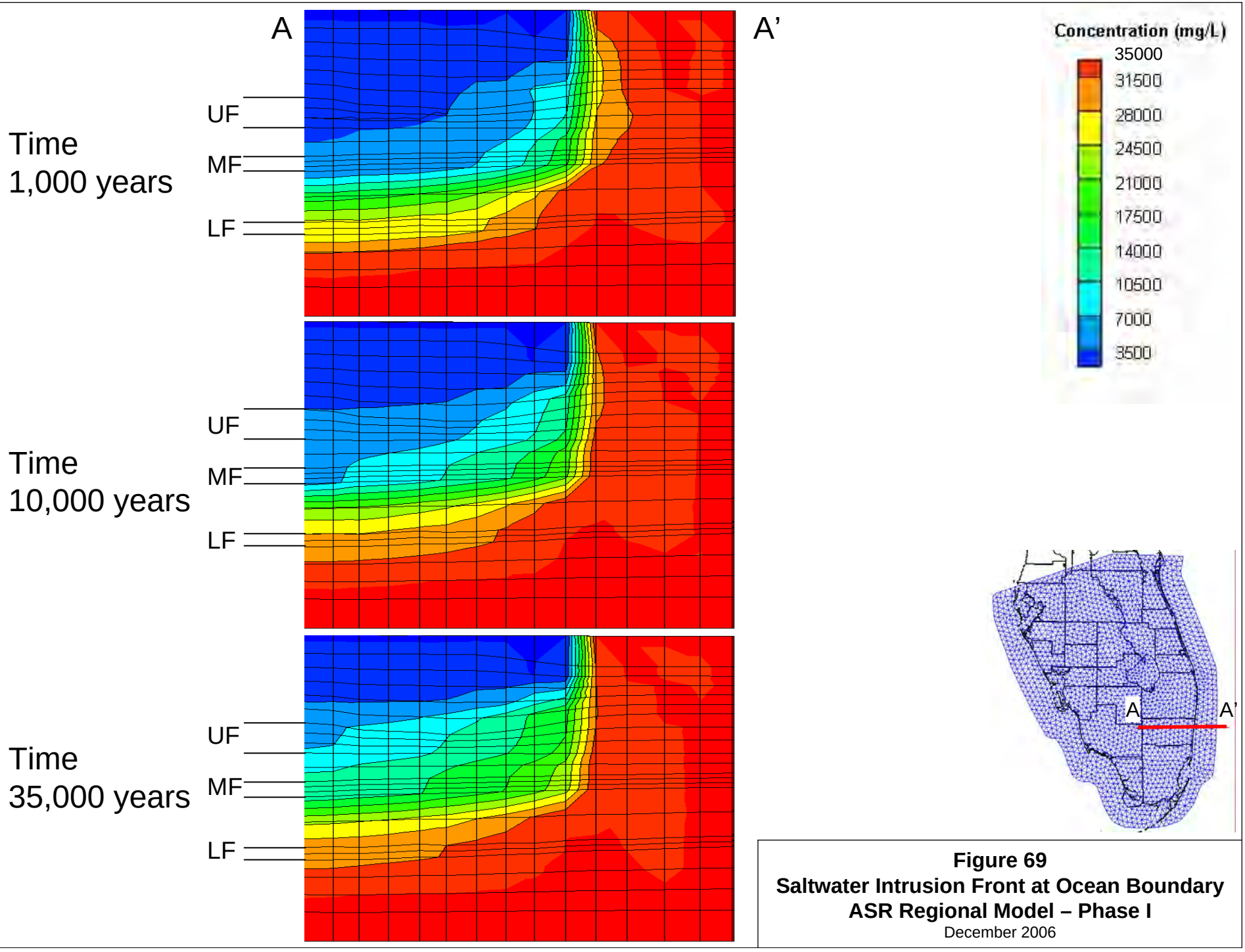

Figure 69
Saltwater Intrusion Front at Ocean Boundary
ASR Regional Model – Phase I
December 2006

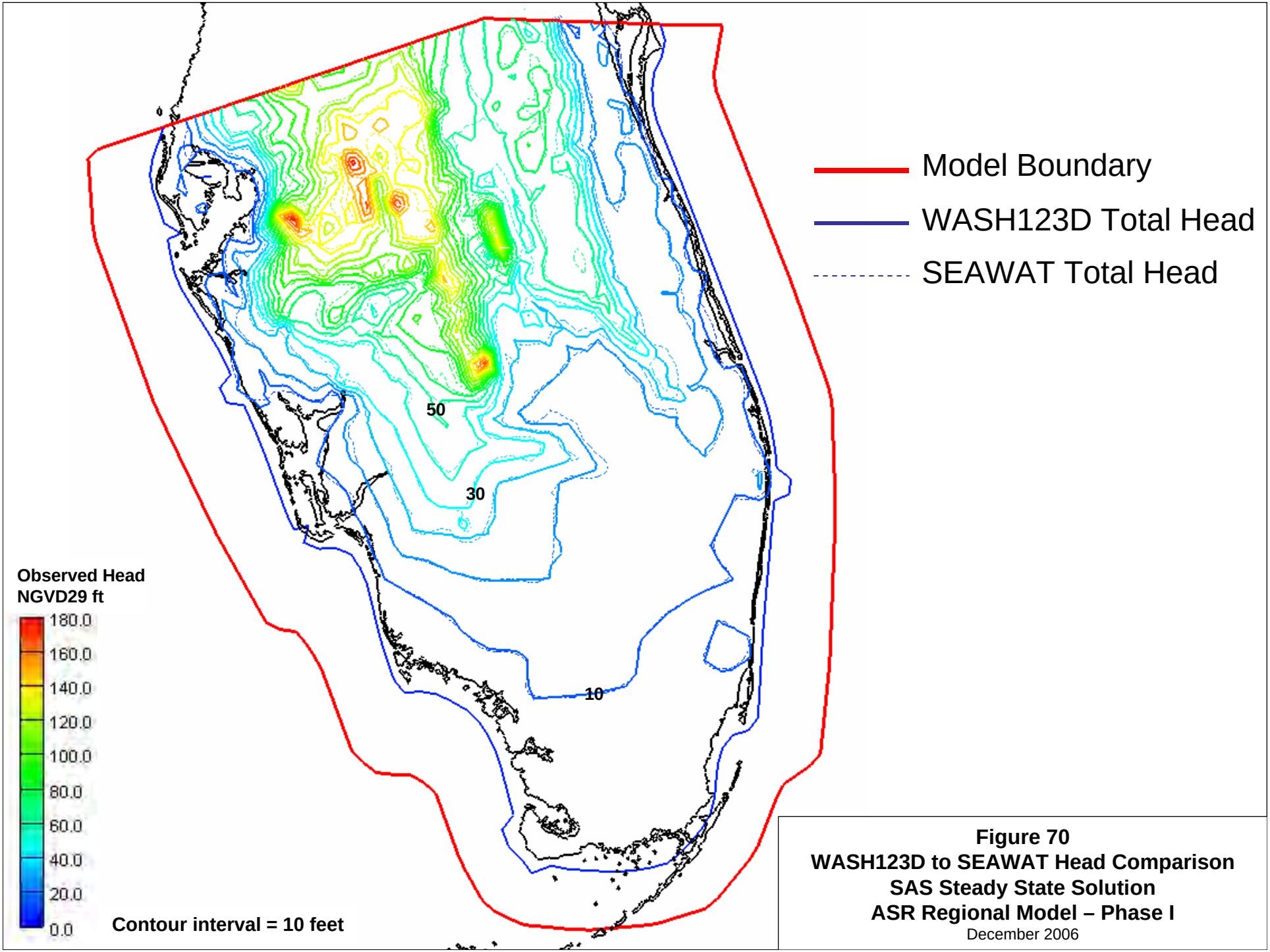

Figure 70
WASH123D to SEAWAT Head Comparison
SAS Steady State Solution
ASR Regional Model – Phase I
December 2006

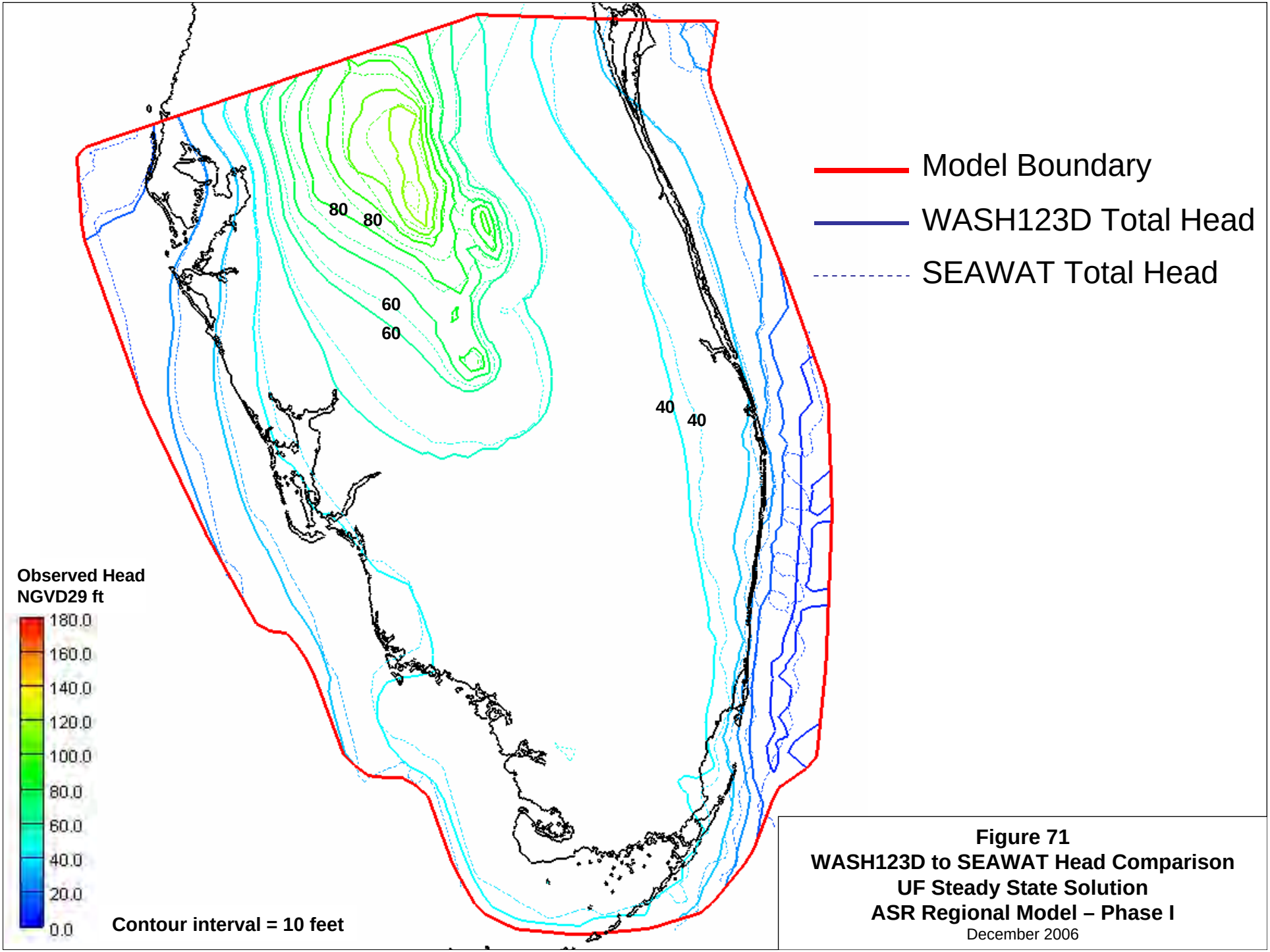

Figure 71
WASH123D to SEAWAT Head Comparison
UF Steady State Solution
ASR Regional Model – Phase I
December 2006

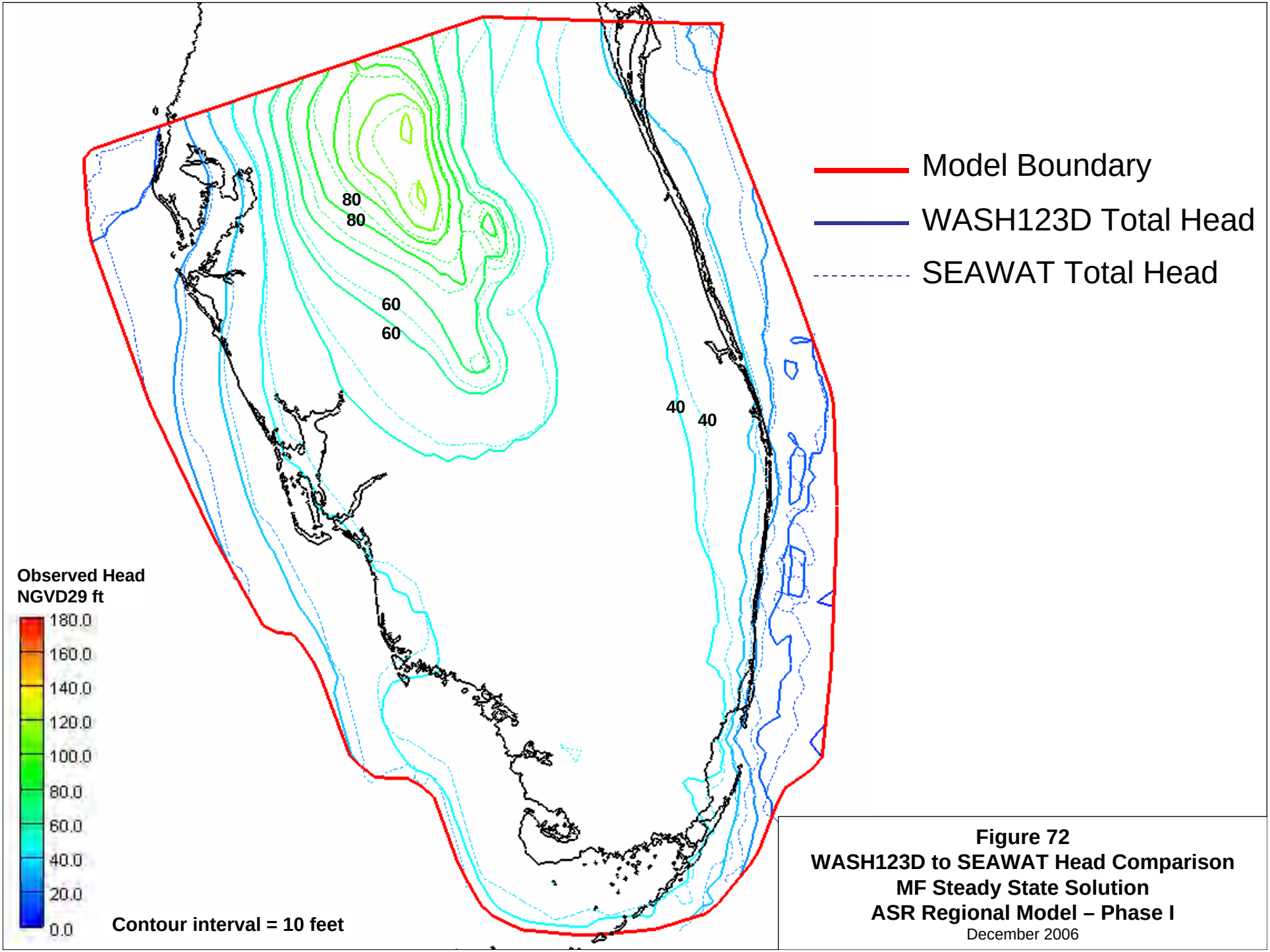

Figure 72
WASH123D to SEAWAT Head Comparison
MF Steady State Solution
ASR Regional Model – Phase I
December 2006

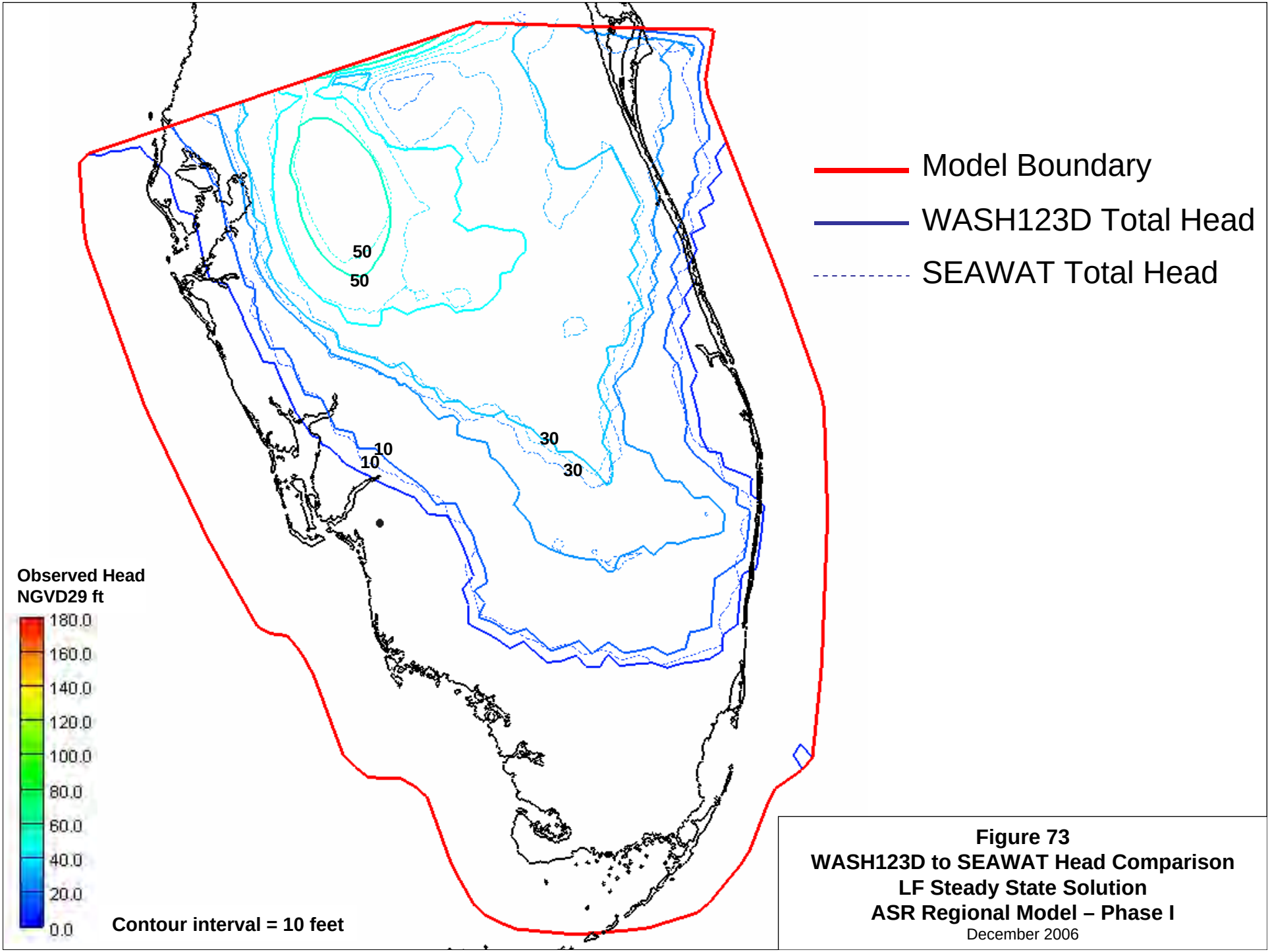

Figure 73
WASH123D to SEAWAT Head Comparison
LF Steady State Solution
ASR Regional Model – Phase I
December 2006

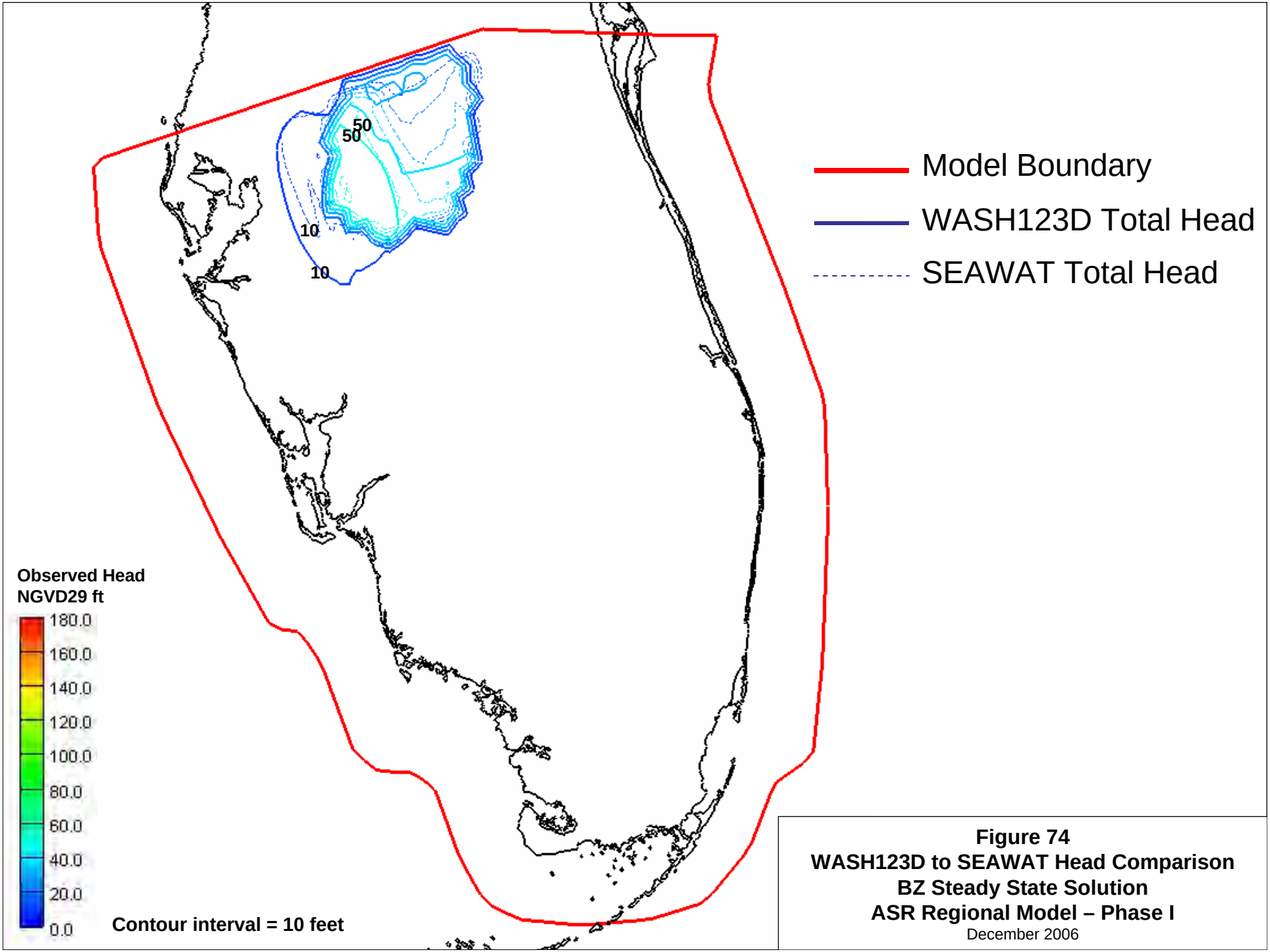

Figure 74
WASH123D to SEAWAT Head Comparison
BZ Steady State Solution
ASR Regional Model – Phase I
December 2006

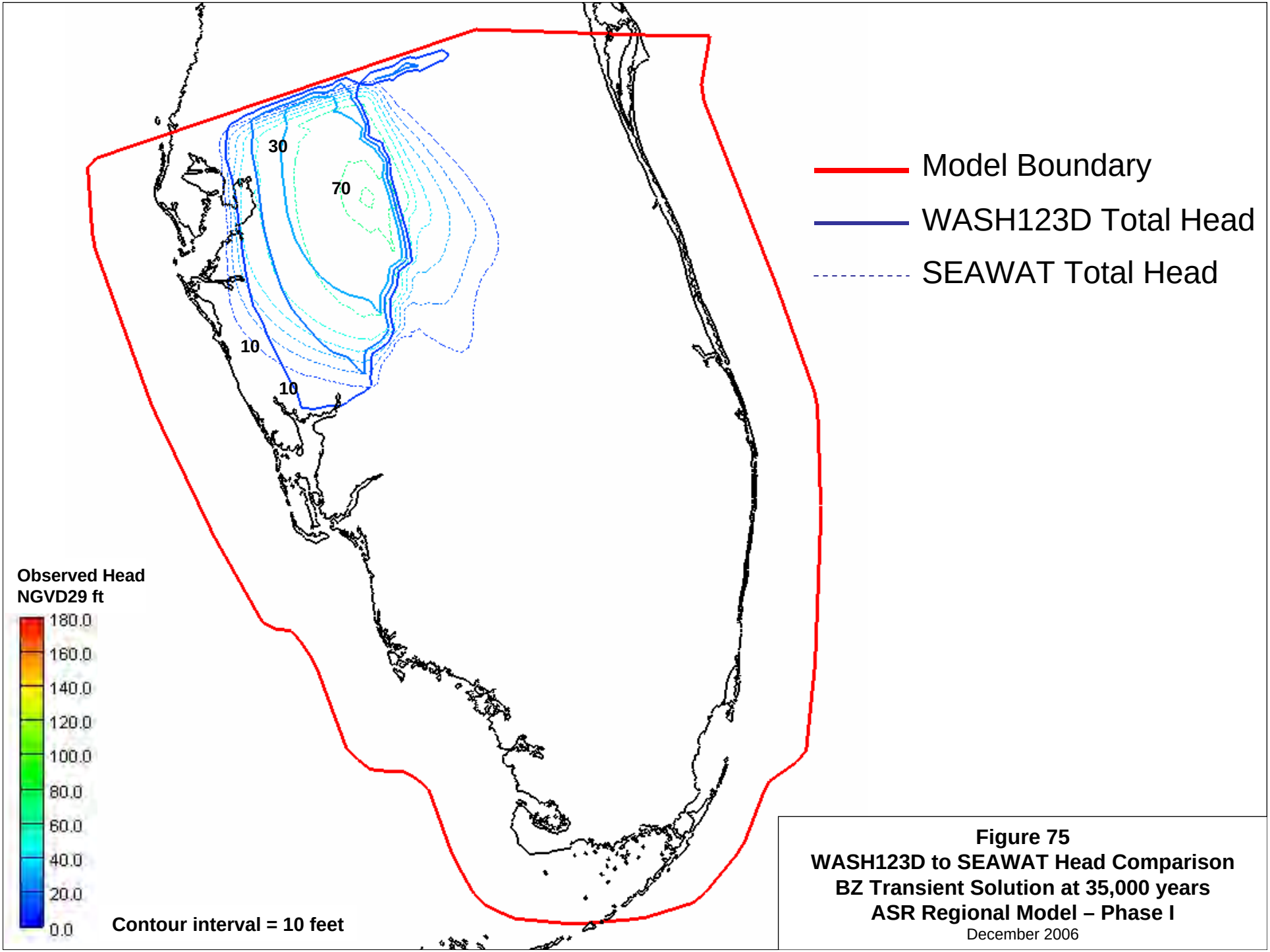

Figure 75
WASH123D to SEAWAT Head Comparison
BZ Transient Solution at 35,000 years
ASR Regional Model – Phase I
December 2006

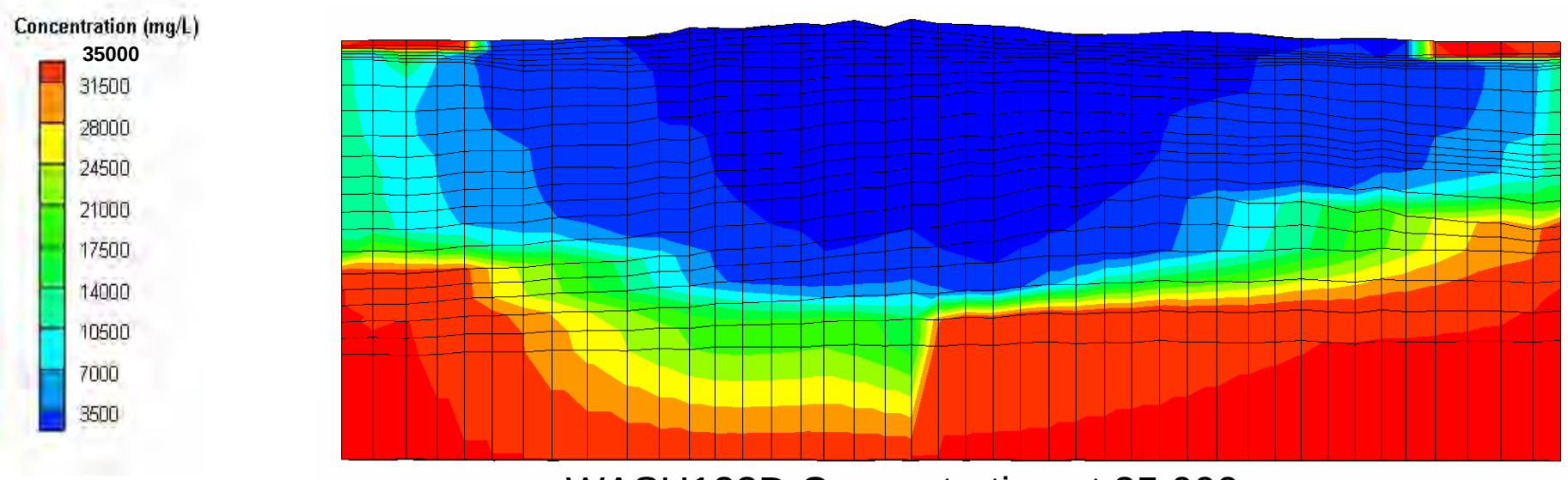

WASH123D Concentration at 35,000 years

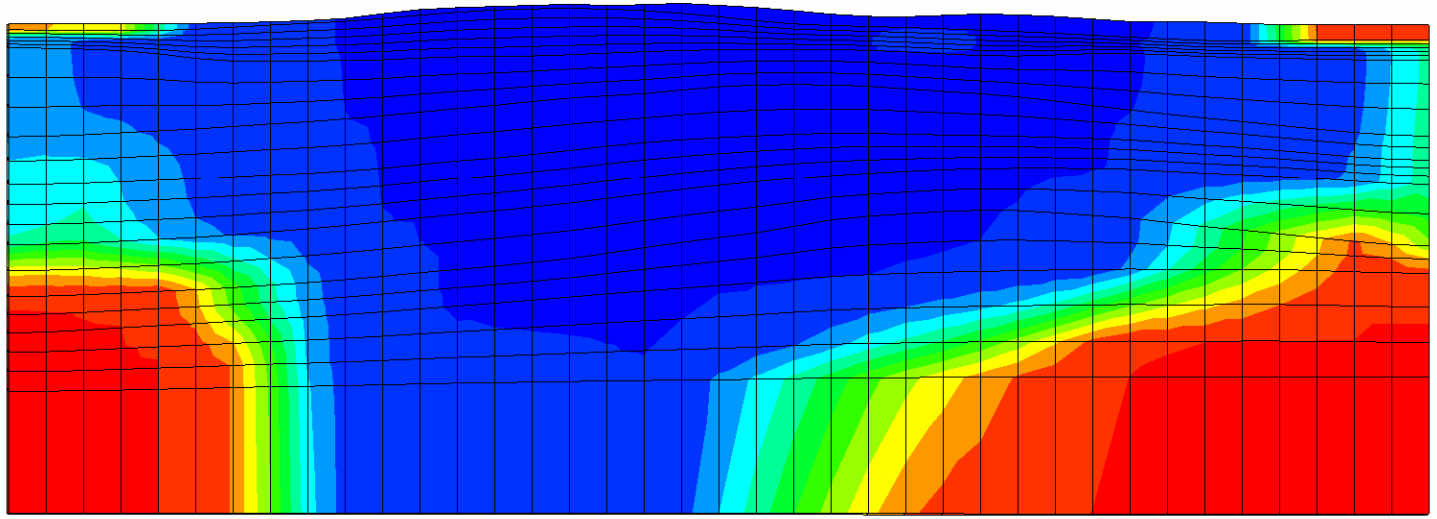

SEAWAT Concentration at 35,000 years

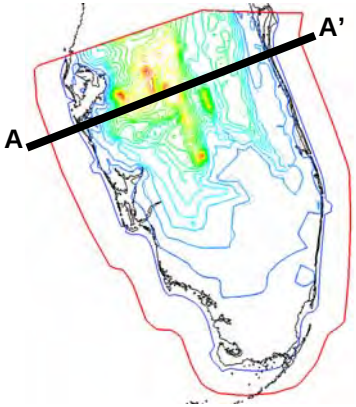

Figure 76
WASH123D to SEAWAT Concentration Comparison
Transient Solution at 35,000 years
ASR Regional Model – Phase I
December 2006

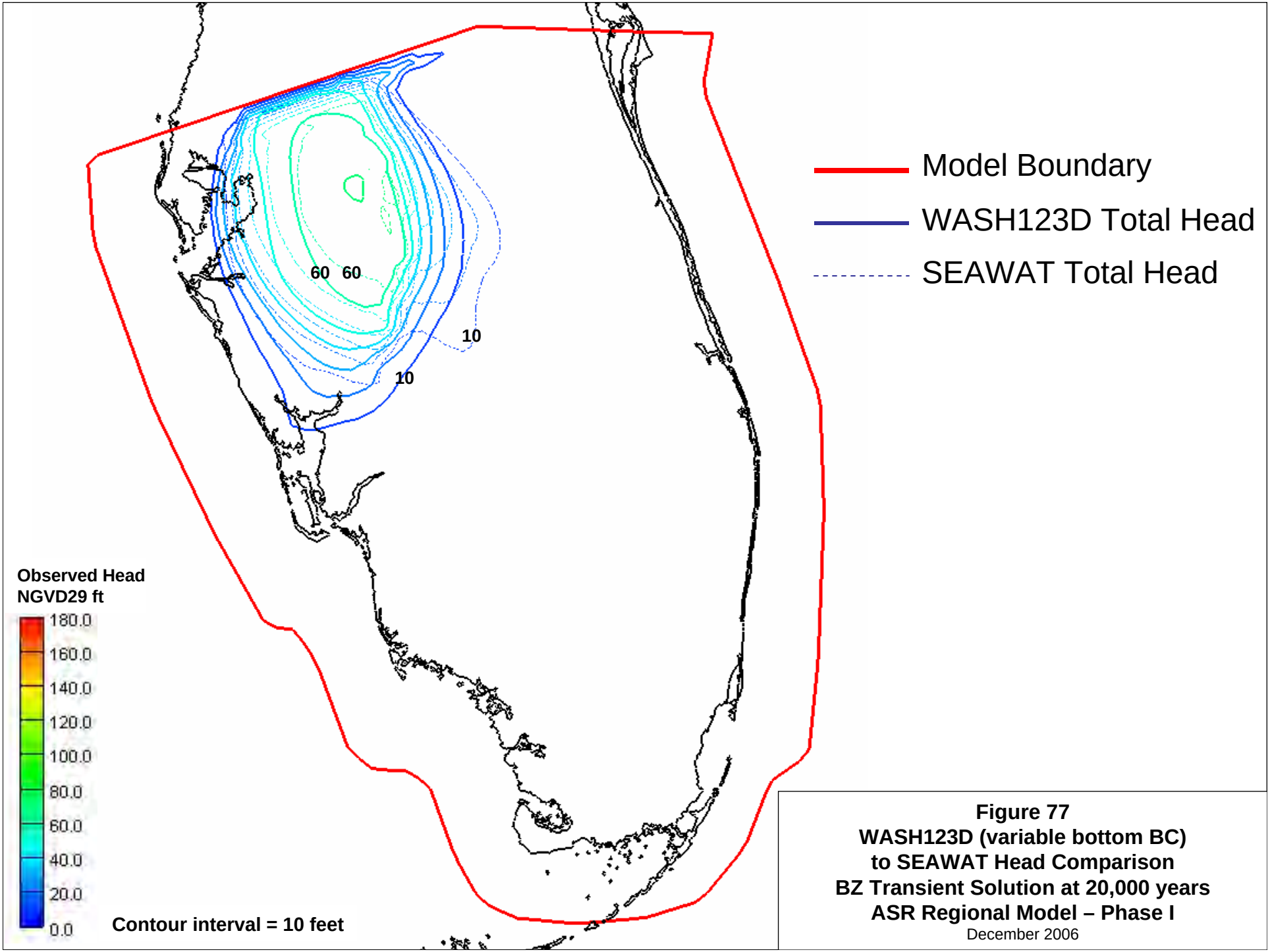

Figure 77
WASH123D (variable bottom BC)
to SEAWAT Head Comparison
BZ Transient Solution at 20,000 years
ASR Regional Model – Phase I
December 2006

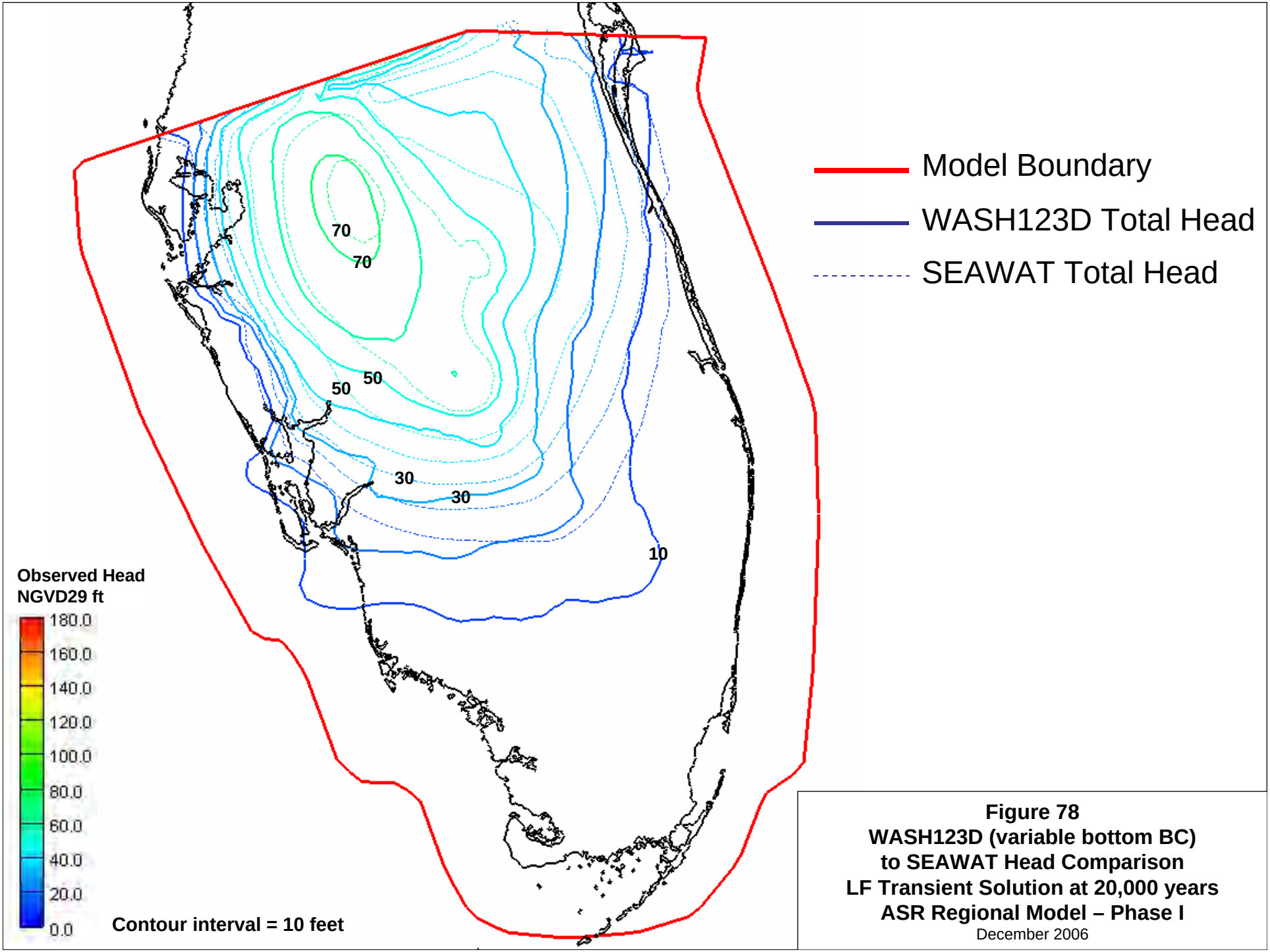

Figure 78
WASH123D (variable bottom BC)
to SEAWAT Head Comparison
LF Transient Solution at 20,000 years
ASR Regional Model – Phase I
December 2006

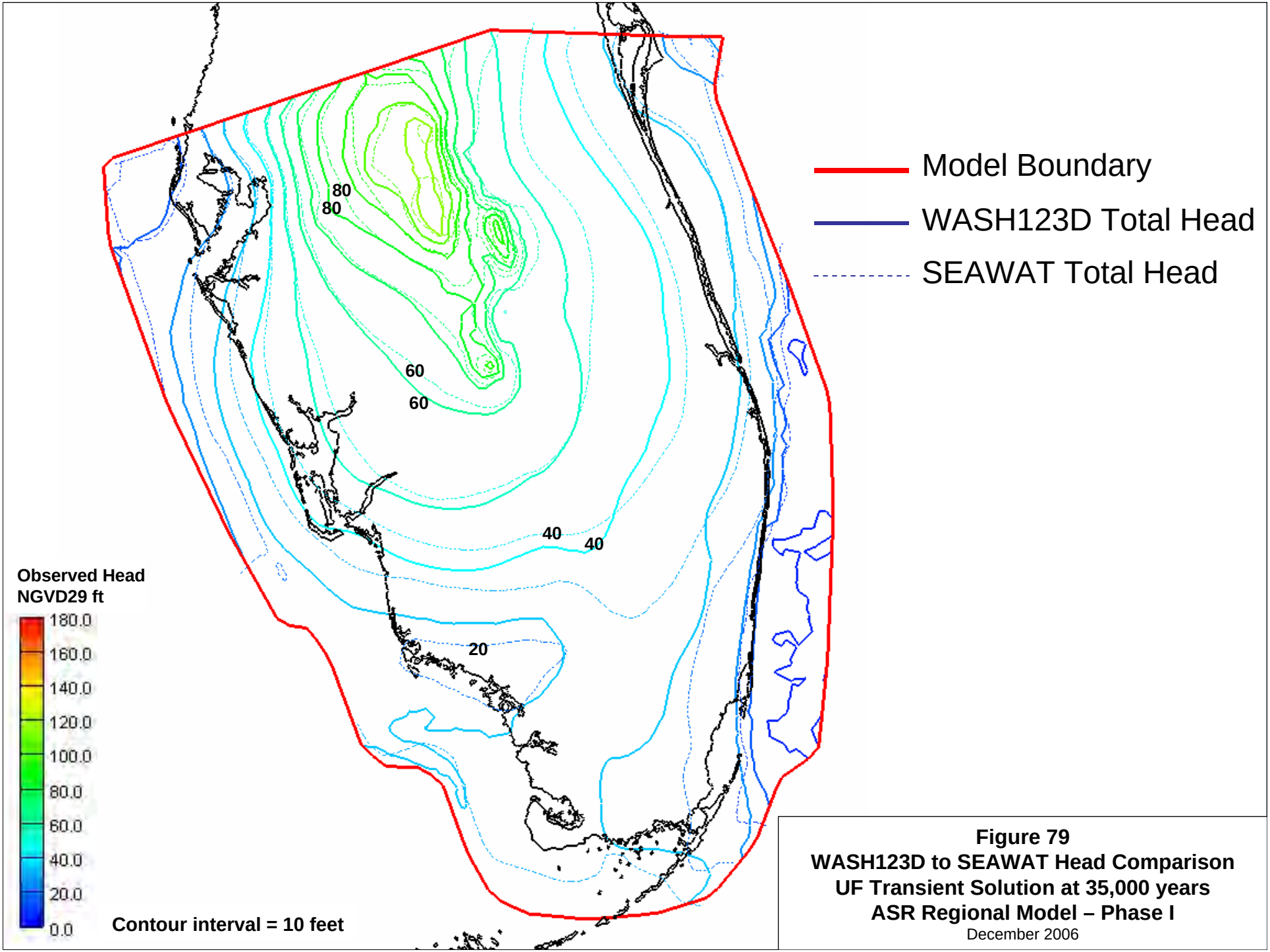

Figure 79
WASH123D to SEAWAT Head Comparison
UF Transient Solution at 35,000 years
ASR Regional Model – Phase I
December 2006

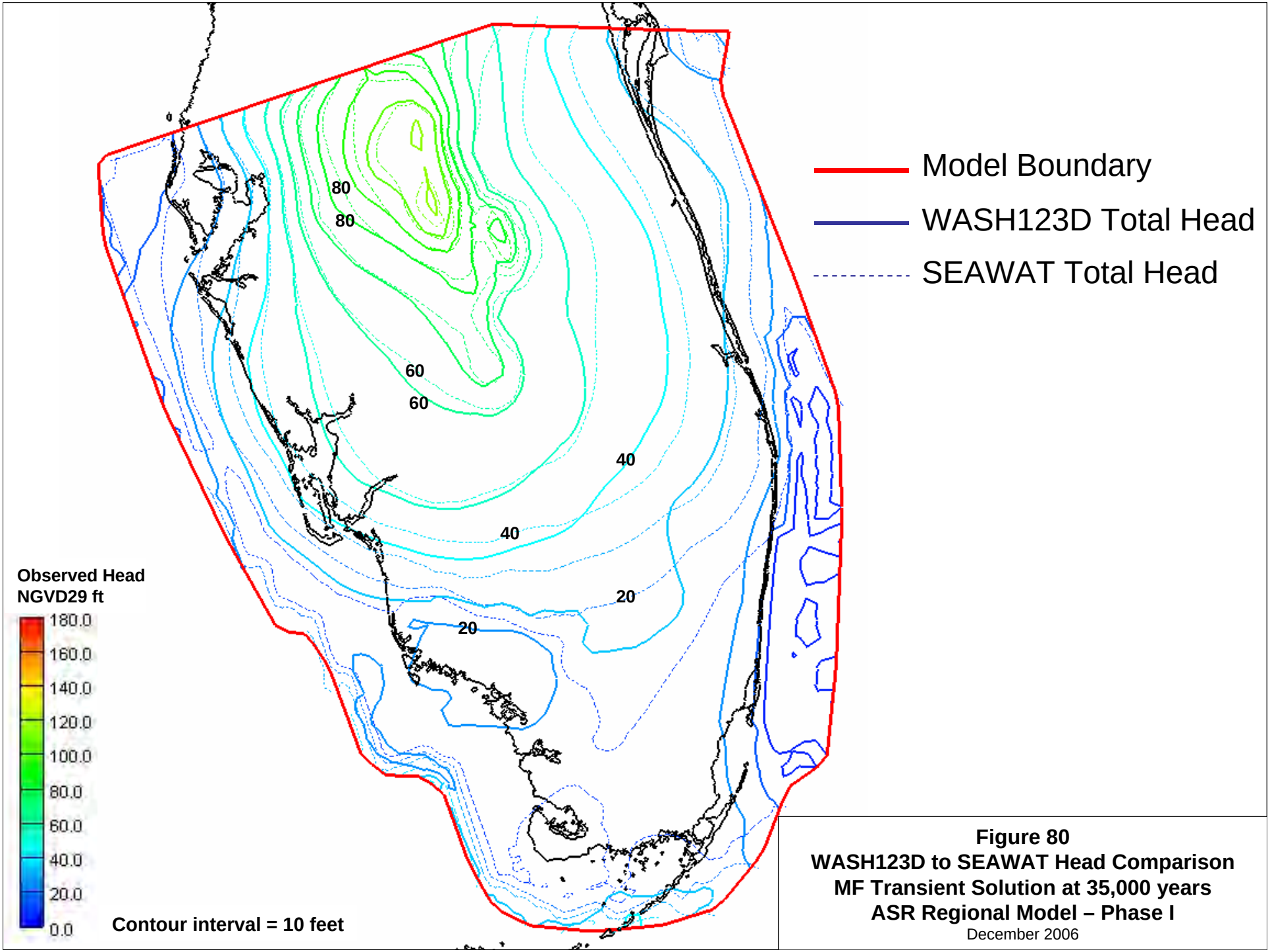

Figure 80
WASH123D to SEAWAT Head Comparison
MF Transient Solution at 35,000 years
ASR Regional Model – Phase I
December 2006

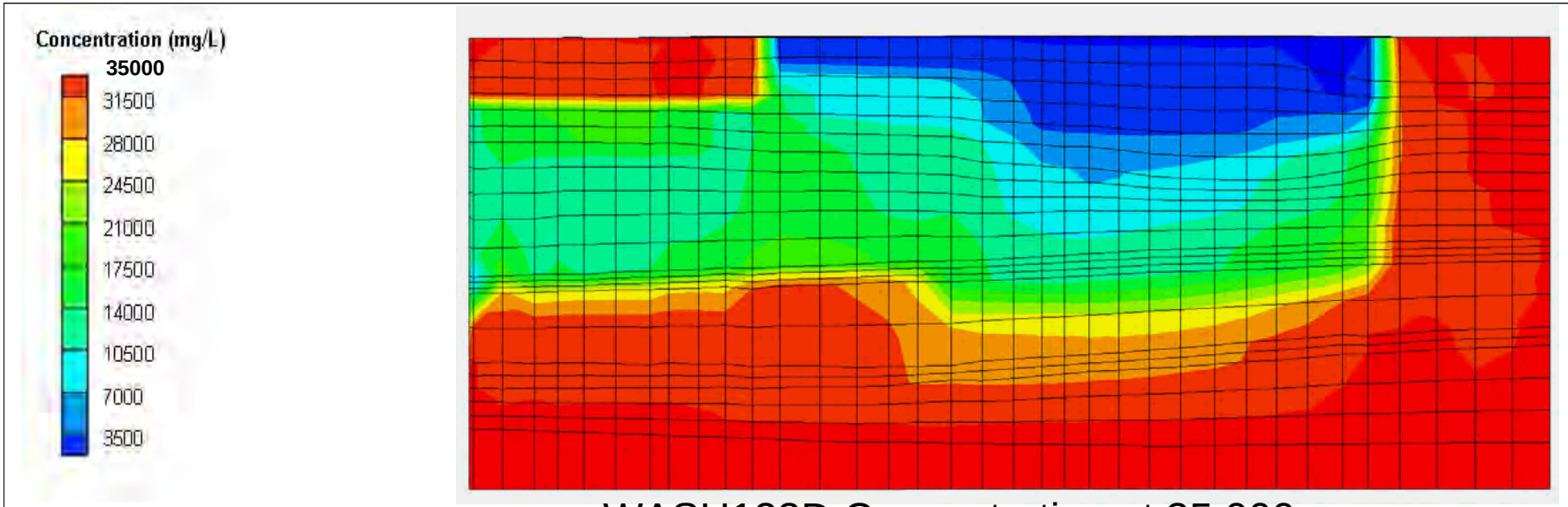

WASH123D Concentration at 35,000 years

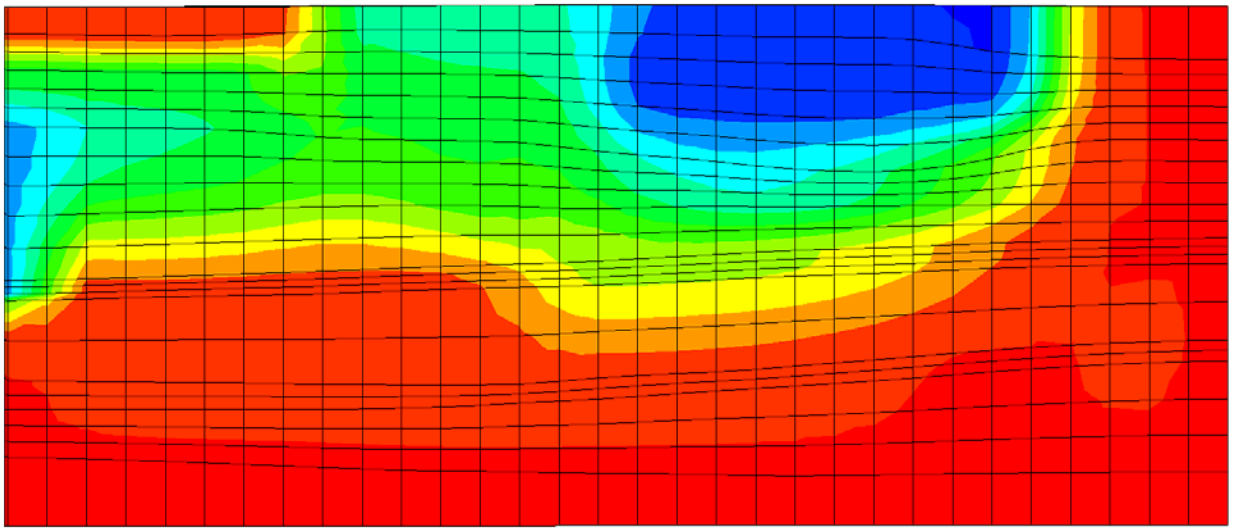

SEAWAT Concentration at 35,000 years

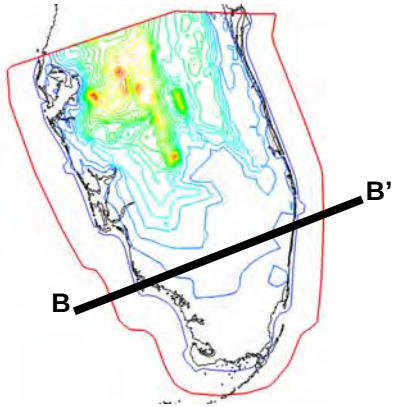

Figure 81
WASH123D to SEAWAT Concentration Comparison
Transient Solution at 35,000 years
ASR Regional Model – Phase I
December 2006

SEAWAT Hydraulic Conductivity

SEAWAT Layer	Cell Vertical K
1	100
2	1
3	1
4	100

WASH123D Hydraulic Conductivity

WASH123D Layer	Element Vertical K
1	100
2	1
3	1
4	100

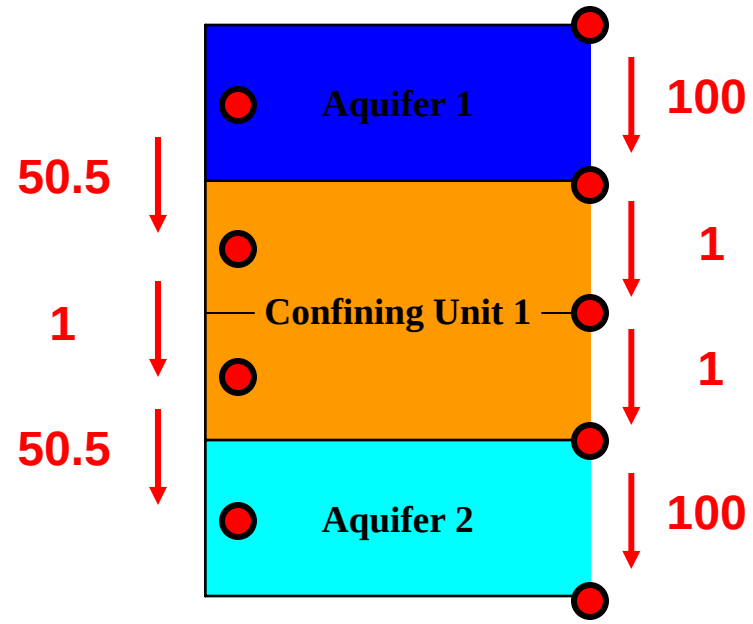

Computational Locations

Figure 82
Schematic Conductivity Distribution
ASR Regional Model – Phase I
December 2006

ROMP-45

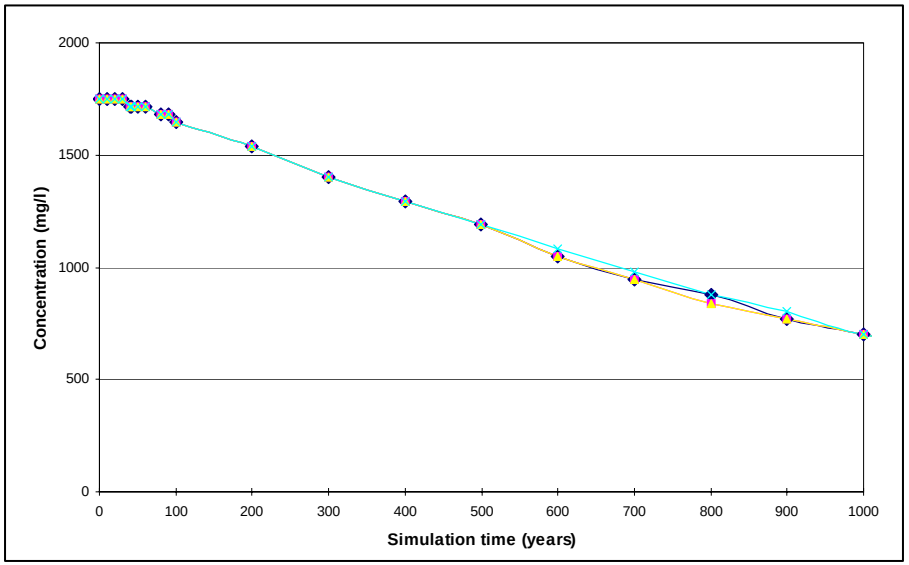

ENP-100

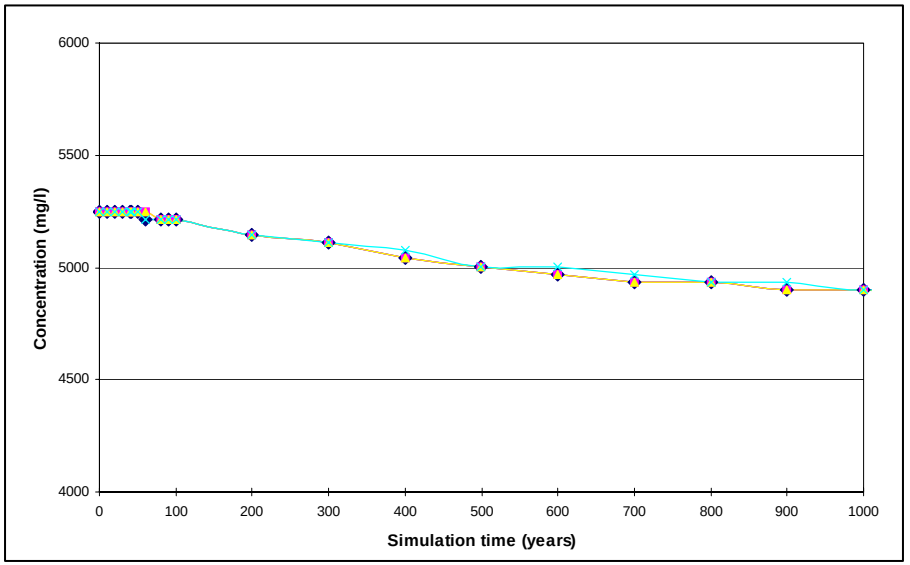

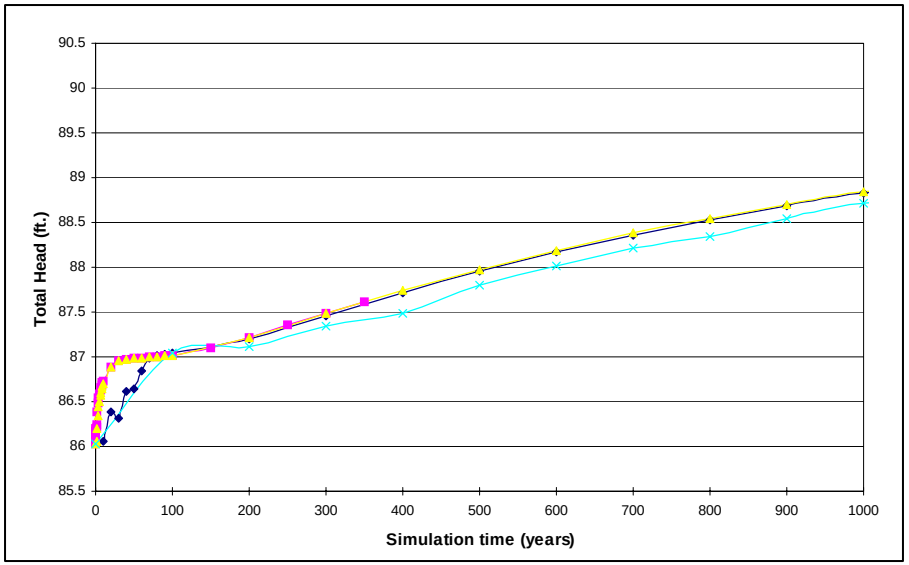

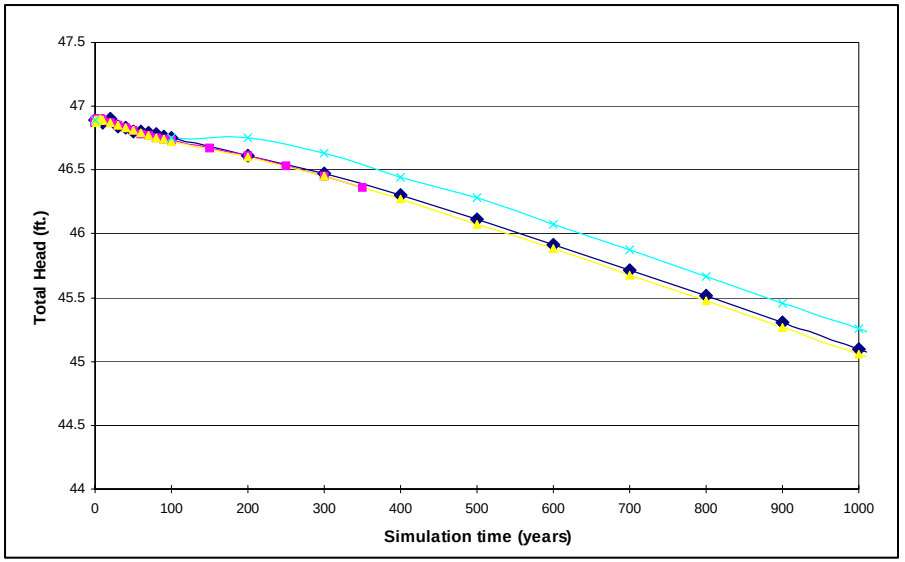

Figure 83
Sensitivity – Time Step Effects at Selected Wells
ASR Regional Model – Phase I
December 2006

ROMP-45

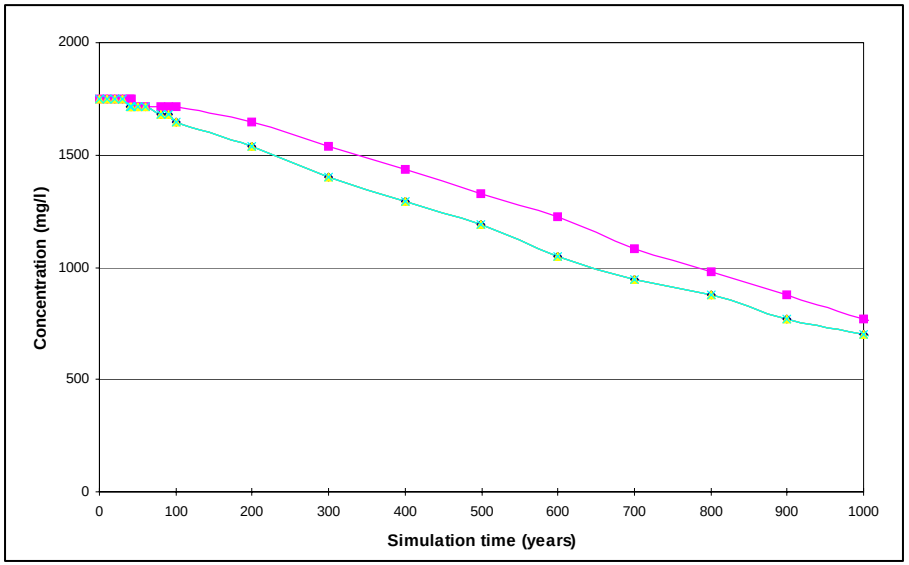

ENP-100

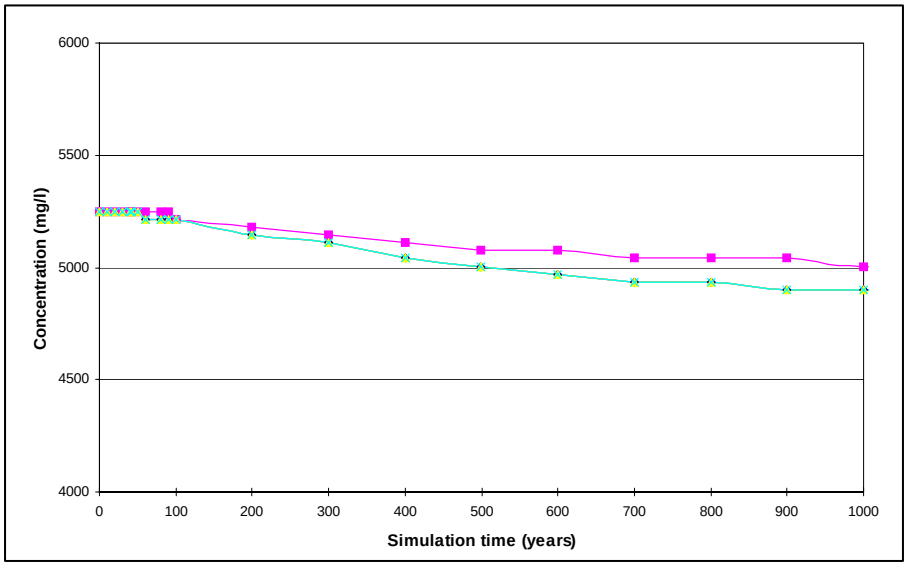

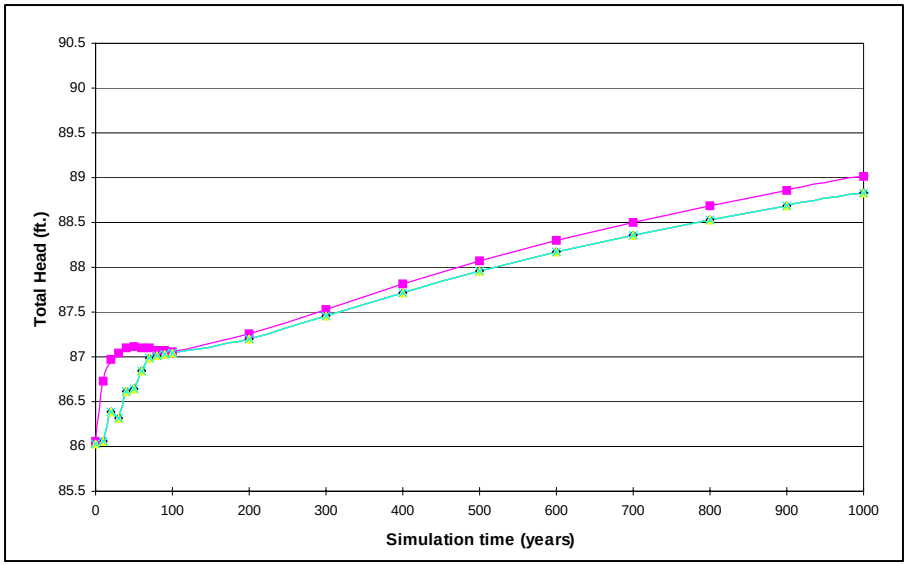

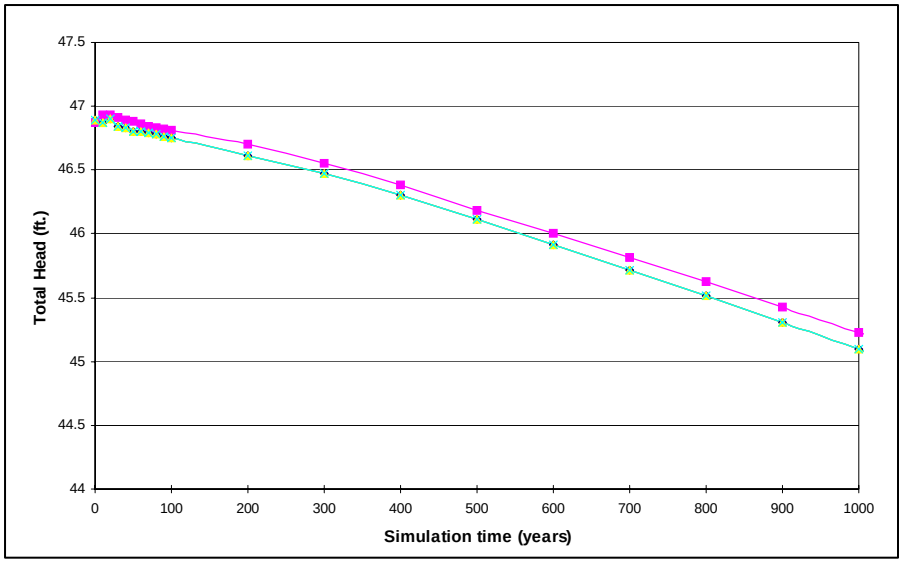

SIP Upwinded SIP TVD GMG Upwinded PCG Upwinded

Figure 84
Sensitivity – Solver Effects at Selected Wells
ASR Regional Model – Phase I
December 2006

ROMP-45

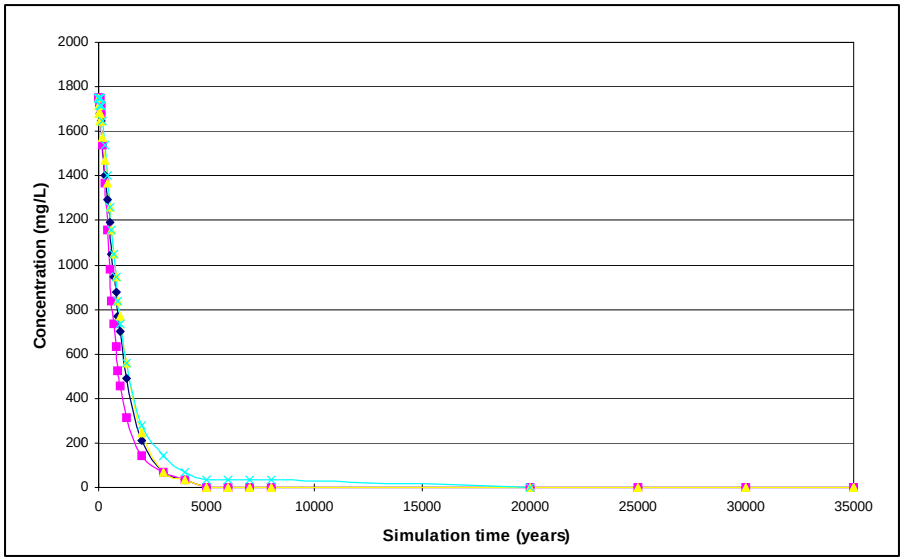

ENP-100

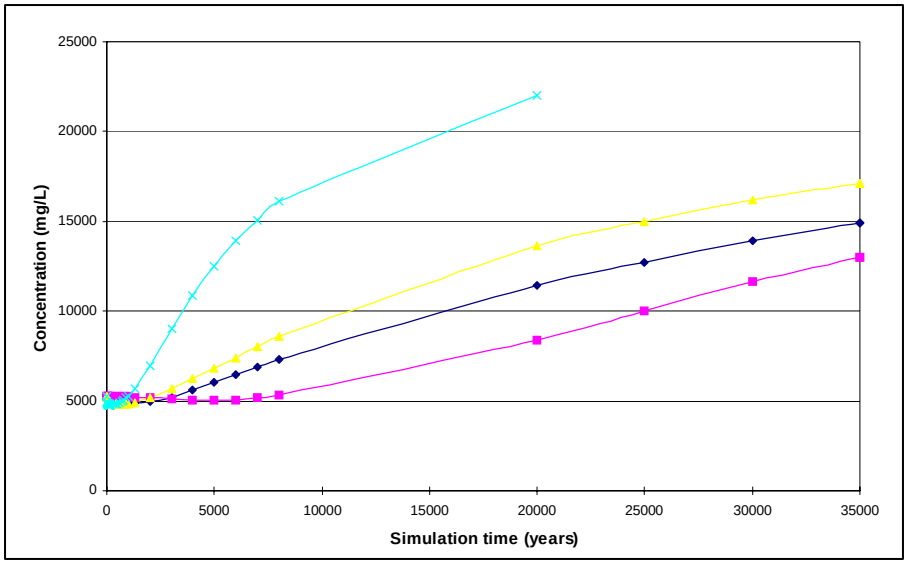

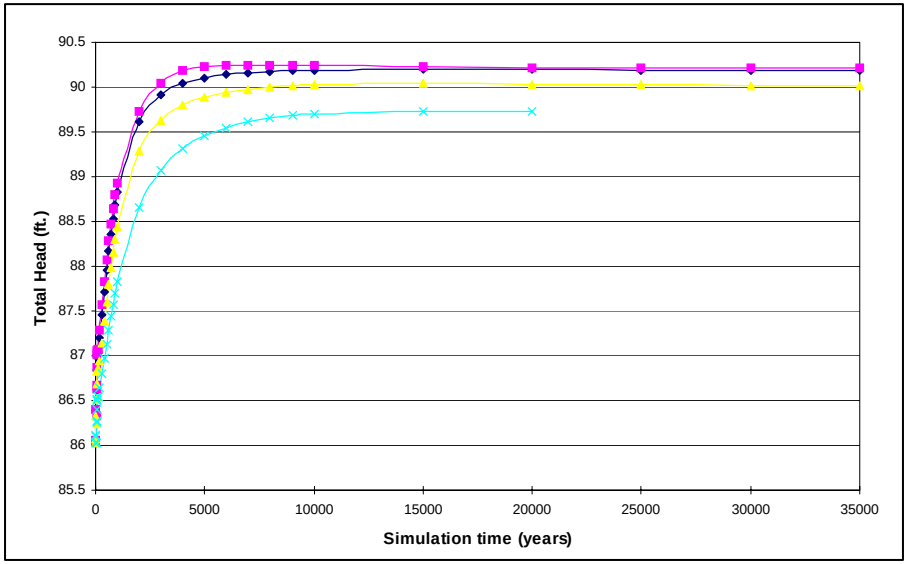

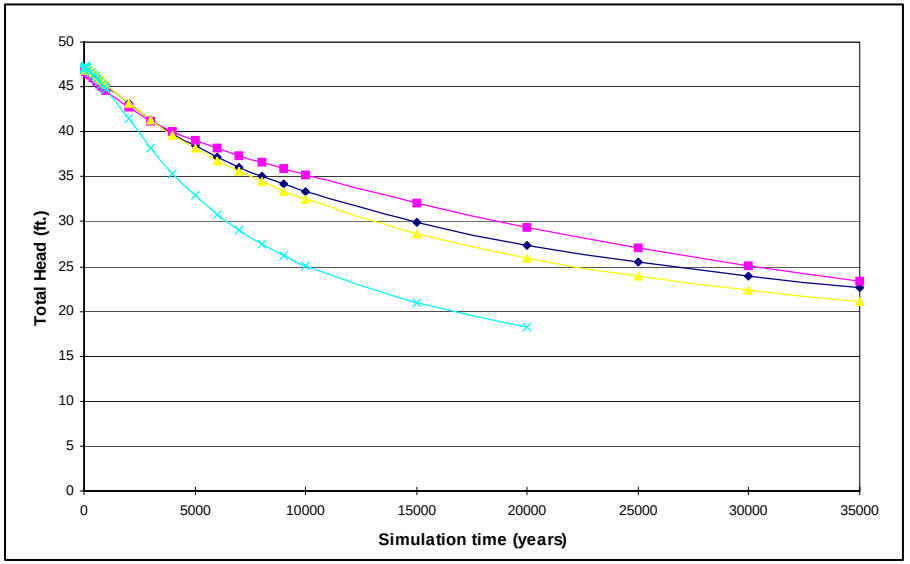

2.5 ft 0.0 ft 25.0 ft 250.0 ft

Figure 85
Sensitivity – Dispersivity Effects at Selected Wells
ASR Regional Model – Phase I
December 2006

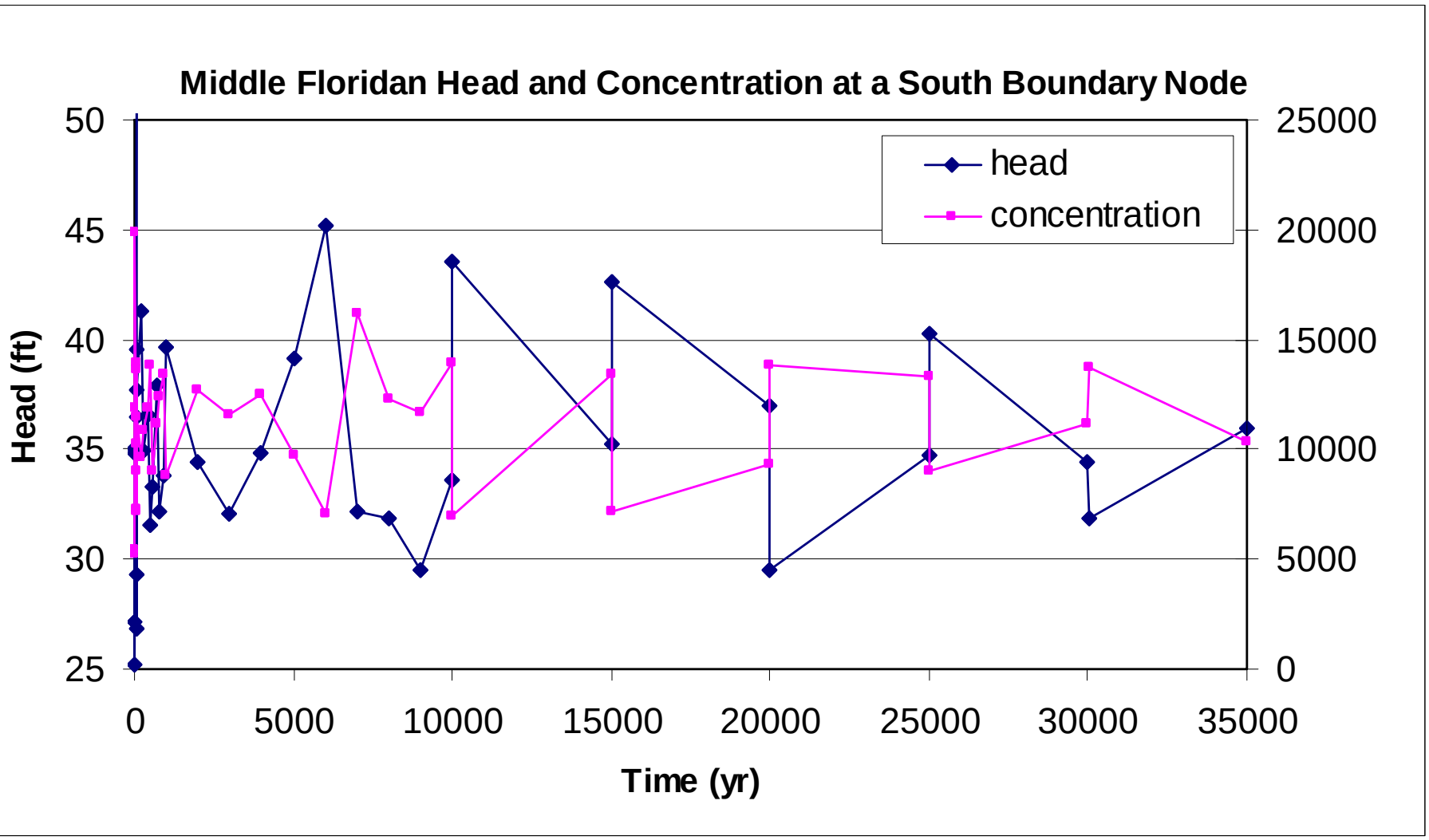

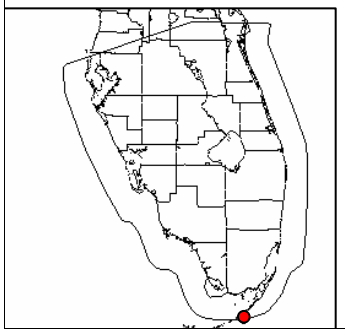

Figure 86
Head and Concentration Oscillations over Time
WASH123D Model
ASR Regional Model – Phase I
December 2006

Head contours

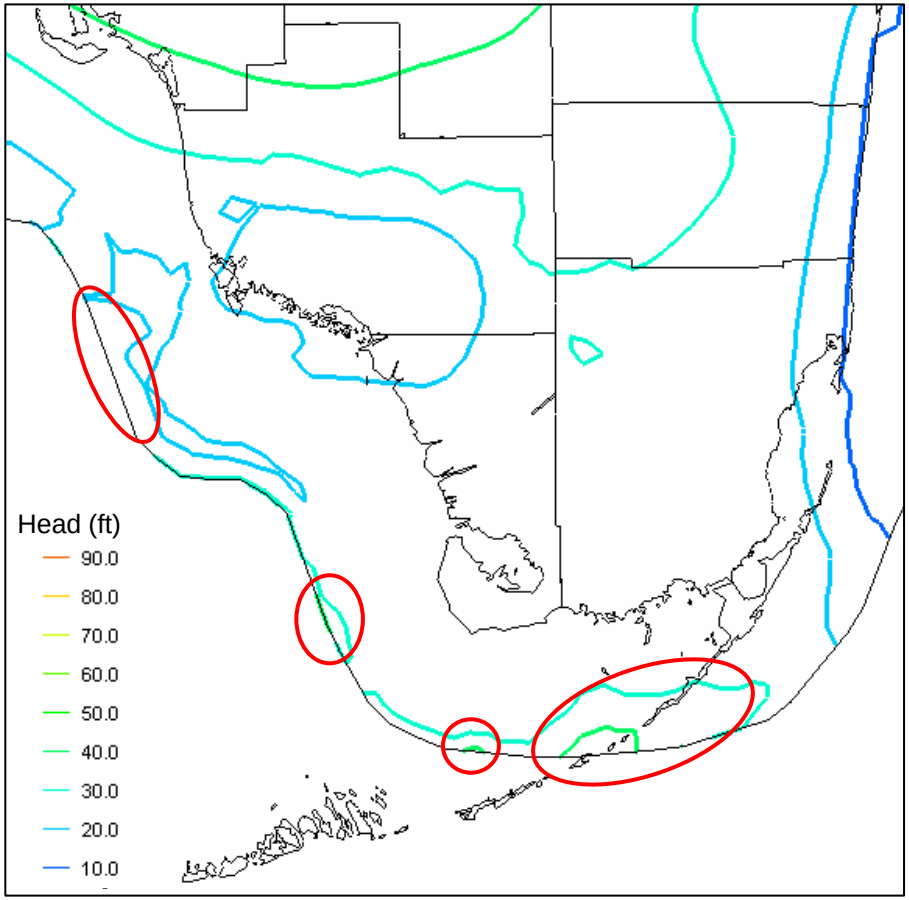

Salt concentrations

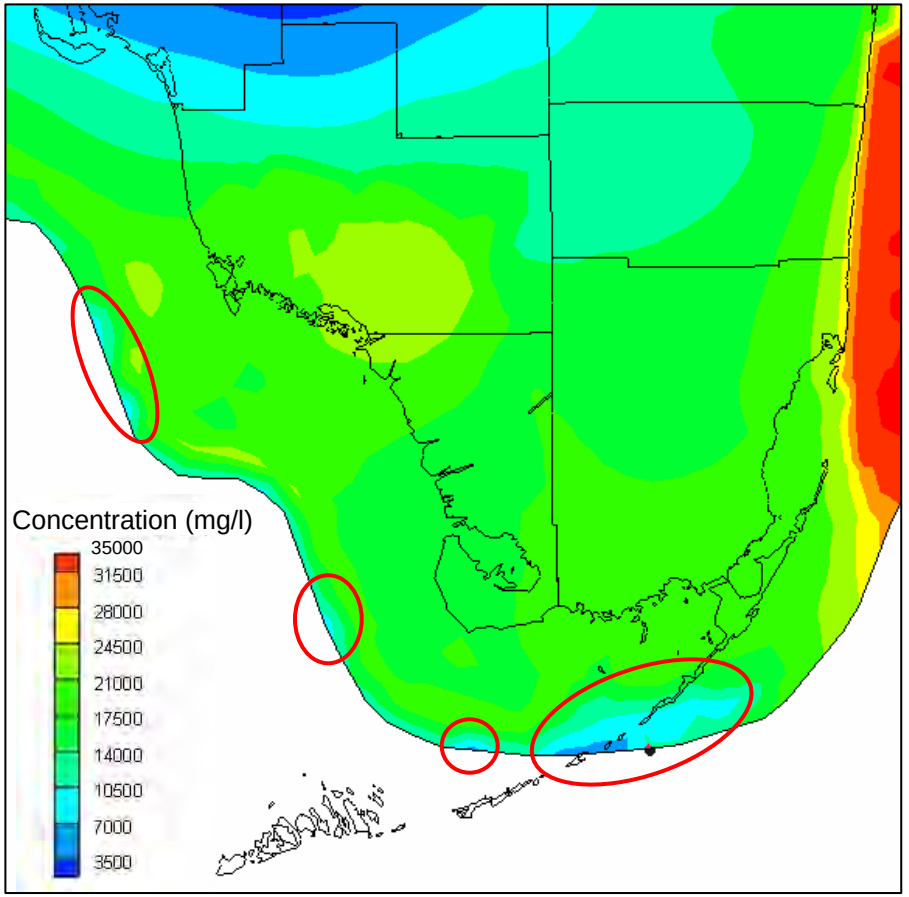

Oscillation locations

Figure 87
Head and Concentration Oscillations – Plan View
WASH123D Model
ASR Regional Model – Phase I
December 2006

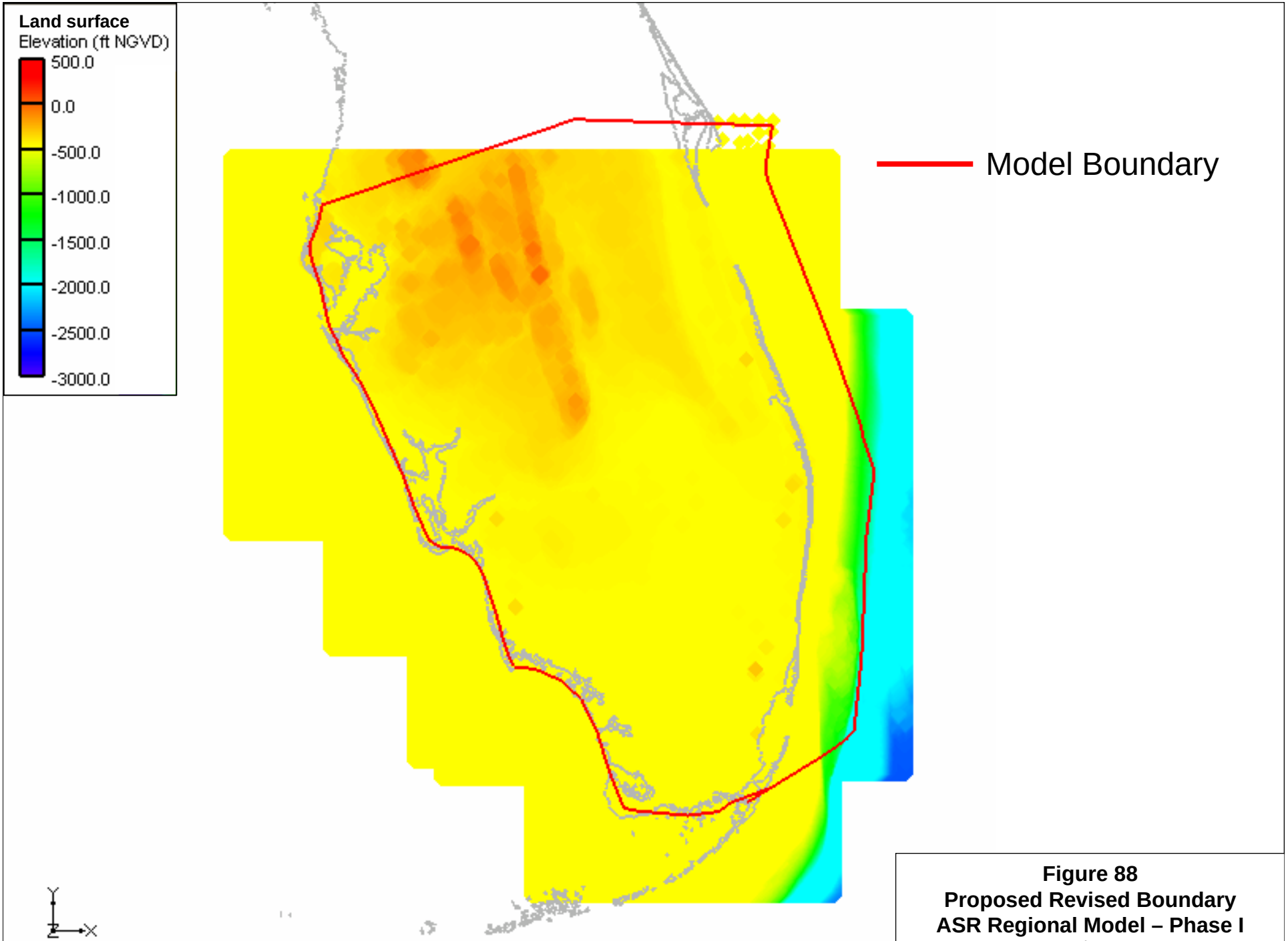

Figure 88
Proposed Revised Boundary
ASR Regional Model – Phase I
December 2006

U.S. Army Corps of Engineers

Philadelphia District

Final Groundwater Model Calibration Report

Aquifer Storage and Recovery

Regional Modeling Study

Prepared for

U.S. Army Corps of Engineers

Jacksonville District

Prepared by

U.S. Army Corps of Engineers

Philadelphia District

February 2011

Table of Contents

Acronyms

APPZ	Avon Park Permeable Zone
APT	Aquifer Pump Test
ASR	Aquifer Storage and Recovery
BTN	Basic Transport Package (MT3D)
BZ	Boulder Zone
CERP	Comprehensive Everglades Restoration Plan
CHD	Time-Variant Specified-Head Package (SEAWAT)
CRM	Coastal Relief Model
DB	Dirichlet Boundary
DEM	Digital Elevation Model
DOH	Department of Health
DSP	Dispersion Package (MT3D)
ERDC	Engineer Research and Development Center
FAS	Floridan Aquifer System
FDEP	Florida Department of Environmental Protection
FDM	Finite Difference Method
HOB	Head Observation Package (MODFLOW)
IA	Intermediate Aquifer
IAS	Intermediate Aquifer System
ICU	Intermediate Confining Unit
IMC	Interagency Modeling Center
KASR	Kissimmee Aquifer Storage and Recovery Pilot Test
LC	Lower Confining Unit

LE	Lagrangian-Eulerian
LF1	First Permeable Unit of the Lower Floridan Aquifer
LPF	Layer-Property Flow Package (MODFLOW)
MC1	Upper Middle Confining Unit
MC2	Lower Middle Confining Unit
MAE	Mean Absolute Error
ME	Mean Error
NAD	North American Datum
NAP	(North Atlantic Division) Philadelphia District
NED	National Elevation Data set
NGVD29	North Geodetic Vertical Datum of 1929
NOAA	National Oceanographic and Atmospheric Administration
PDT	Project Delivery Team
PEST	Parameter ESTimation
RMS	Root Mean Square Error
SAJ	(South Atlantic Division) Jacksonville District
SAS	Surficial Aquifer System
SFNRC	South Florida Natural Resources Center
SFWMD	South Florida Water Management District
SIR	(USGS) Scientific Investigation Report
SOFIA	South Florida Information Access
SSM	Source & Sink Mixing Package (SEAWAT)
SJRWMD	Saint Johns River Water Management District
SWFWMD	Southwest Florida Water Management District

TDR	Technical Data Report
TDS	Total Dissolved Solids
TEC	Topographic Engineering Center
TVD	Total-Variation-Diminishing
UF	Upper Floridan Aquifer
USACE	United States Army Corps of Engineers
USGS	United States Geologic Survey
VDF	Variable Density Flow Package (SEAWAT)
WRDA	Water Resources Development Act

Executive Summary

The primary objective of the Comprehensive Everglades Restoration Plan (CERP) is the "restoration, preservation, and protection of the South Florida Ecosystem while providing for other water-related needs of the region, including water supply and flood protection (WRDA, 2000)." Aquifer Storage and Recovery (ASR) is one of the alternatives proposed by the CERP to provide long-term storage of excess water, resulting in a more stable water supply in South Florida. The CERP recommends the construction of 333 ASR wells completed in the Floridan Aquifer System (FAS) and distributed over a large region surrounding Lake Okeechobee. This report is the third in a series of four documents describing the multi-phased groundwater modeling approach undertaken to evaluate the proposed CERP ASR system. The four documents are:

- ASR Regional Study – Benchscale Modeling (Brown, et al, 2006). This report evaluated several model code options and concluded with the selection of WASH123D and SEAWAT as the best-suited to the ASR regional evaluation.

- Draft ASR Regional Study Phase I – Groundwater Modeling (NAP, 2006). This report described the first phase of the model development, including identification of boundaries and regional flow and salt migration pathways; evaluation of model run times and sensitivity to timestep sizes; testing of boundary parameters and the sensitivity of hydraulic and transport parameters; and a comparison of results from WASH123D and SEAWAT.

- Final Groundwater Model Calibration Report, Aquifer Storage and Recovery Regional Modeling Study (this report). This document presents the model setup, boundary condition development and calibration for the regional model, which will be the basis of the model evaluation of the CERP ASR plan. It further analyzes the sensitivity of the regional model to a number of parameters and discusses possible sources of error to the regional model.

- A final report will describe the evaluation of the CERP ASR plan against performance objectives such as rock fracture potential, impacts to nearby wells, recovery efficiency and the effects of ASR on salt water intrusion. This evaluation will be performed by running the calibrated, regional model with the addition of the ASR wells as described in the D13R scenario of the SFWMM model (SFWMD and USACE, 1999) and by the use of inset models, with higher grid resolution, centered on the locations of the Kissimmee ASR Pilot Site and the Hillsboro ASR Pilot Site.

This calibration report begins with a review of the modeling codes selected for the model in the Benchscale Report (Brown, et al, 2006), the development of the computational grids as presented in the Phase I Study (NAP, 2006) and the conceptual model, much of which was presented in Reese and Richardson, 2004 and Reese and Richardson, 2008. Other sections of the report describe data analyses and model setup. The boundary conditions and initial conditions for the model were based, wherever possible, on available site data. In areas of sparse data, both were necessarily estimated using available research and local knowledge as described in this report.

The most important groundwater flow parameters (principally hydraulic conductivity and specific storage) were set during the calibration process. Calibration proceeded by varying these input parameters and noting their effects on the model output. Parameters were changed until the model results most closely matched field measurements. A combination of hand calibration and automated calibration (PEST) was employed to minimize the time required while still allowing the introduction of engineering judgment in the manipulation of input parameter values. The model was calibrated to two separate periods: October 2003 through December 2004 for calibration, and October 1993 through July 1994 for validation.

The final calibration is sufficient for the purpose of the regional model, which is to determine on a coarse, regional scale, the impact of the CERP ASR program on the groundwater system in South Florida. Chapter 4 of the report presents details of the calibration and describes the quality of calibration both qualitatively and quantitatively.

Uncertainty in the regional pumping is considered to be the most important source of error in the model. It is recommended that future efforts be directed at collecting better quality data on the rates of extraction at private wells.

The report finishes with a description of a number of sensitivity runs, which were made to test the importance of some of the most uncertain model parameters. The sensitivity analyses determined that most of the transport parameters (porosity, diffusion and dispersion) are relatively insensitive. Also insensitive on a regional scale are the advection solution method, timestep size and specified head boundary conditions.

The Interagency Modeling Center (IMC) has reviewed this study and their comments on the draft report are listed in Appendix G with responses from the modeling team. While the modeling team addressed most of their comments with additional analyses or text, there are some differences of opinion between the two groups. The IMC comments on the final report and the modeler responses are provided in Appendix H and illustrate the two sides of each issue.

The recommendations for the future of the regional modeling study are that the calibrated SEAWAT model be used for evaluation of the regional impacts of the CERP ASR program. SEAWAT should also be used in the development of a pair of local-scale models, which will be highly resolved and capable of evaluating more local effects of small groups of ASR wells, such as recovery efficiency and well-to-well interaction. It is also recommended that the production simulations be performed in a probabilistic manner (e.g. Monte Carlo method) to provide for a quantification of uncertainties inherent in the model and the data.

1.0 Introduction

The U.S. Army Corps of Engineers (USACE), Philadelphia District (NAP), has prepared this report for the USACE, Jacksonville District (SAJ), and the South Florida Water Management District (SFWMD) in support of the Comprehensive Everglades Restoration Plan (CERP). This report documents Phase II of the regional groundwater modeling calibration effort and is the third in a series of four documents describing the multi-phased modeling approach undertaken to evaluate the proposed CERP Aquifer Storage and Recovery (ASR) system. The previous two modeling documents include the "ASR Regional Study – Benchscale Modeling Report" (Brown et al, 2006) and the "Draft ASR Regional Study Phase I - Groundwater Modeling" (NAP, 2006). The final document in the series will summarize the local scale model development and evaluation of various CERP ASR alternatives using the regional model. In addition to these modeling reports, an evaluation of the effects of various hydrogeologic theories on groundwater flow in South Florida was presented in the conference paper "Using Density-Dependent Numerical Models to Evaluate Regional Groundwater Flow Patterns in South Florida" (Bittner et al, 2008). This study was also preceded and is supported by "Groundwater Numerical Model Development Support and Data Collection Report" (CH2MHill, 2005). This report reviews the hydrogeologic framework and a number of previous modeling projects within the current model domain.

ASR is one of the alternatives proposed by the CERP to provide fresh water storage in South Florida. The CERP recommends the installation of 333 ASR wells open in the Floridan Aquifer System (FAS) and distributed over a large region with well field clusters near Lake Okeechobee, along the Caloosahatchee River, and at several locations along existing canals in the Lower East Coast Region (Palm Beach and Broward Counties). Figure 1.1 shows the study area and Figure 1.2 shows the approximate location of the proposed ASR well clusters envisioned in the CERP. The proposed plan, with total injection and recovery pumping rates of approximately 1.65 billion gallons per day, is larger than any currently operating ASR project. To evaluate the numerous design considerations and the variation in aquifer response on regional, sub-regional, and local scales, density-dependent numerical modeling of the FAS is required as discussed in the ASR Regional Study Project Management Plan developed in 2003.

The focus of this report is the Phase II Regional Model calibration. This Phase II effort builds on the findings of the Benchscale and Phase I modeling efforts and includes refinements to the regional conceptualization of the FAS. In addition, the modeling was supported by an extensive data collection effort performed by SAJ to compile and evaluate all pumping, water level, and salinity data available for the model domain. SAJ provided a description of the data collection effort and their report is included as Appendix A to this document. The following sections of this report describe how the available data was incorporated into the regional models and the model calibration process.

1.1 Acknowledgements

This report is part of a study prepared for and in cooperation with the SAJ and SFWMD. Thanks are given to the USACE Engineering Research and Development Center (ERDC) and the United States Geological Survey (USGS) for their cooperation, modeling code development assistance, and technical guidance during this study. Thanks are also given to South West Florida Water Management District

(SWFWMD), St. Johns River Water Management District (SJRWMD), the Florida Department of Environmental Protection (FDEP) and the Florida Department of Health (DOH) for their assistance in the data collection effort. Special thanks are given to the IMC for their cooperation in the review of the various phases of this study.

2.0 Regional Modeling Approach

The first and most important step in the modeling process is to define clear, achievable goals and objectives for each stage of the process based on the desired end results. Both the modeling team and the end user must keep the end goal in mind and have a clear understanding of the capabilities and limitations of the model.

The primary objective of the Phase II ASR modeling effort is to evaluate the impacts of the proposed CERP ASR wells on the hydrogeologic conditions in the FAS. This evaluation will be performed by using both regional and local scale models. Each scale of model will be used to address different project objectives. The current report pertains to development and calibration of the regional scale models, which will provide planning level information to address large-scale issues, such as the regional effect of the ASR well clusters on salt water intrusion, water levels, groundwater flow patterns, groundwater quality, and the potential for rock fracturing. This scale of modeling is *not* appropriate for evaluating local issues, such as well-to-well interaction within an ASR well cluster or ASR well recovery efficiency. These issues will be addressed as part of the next report with local scale models that have significantly finer mesh/grid resolution.

Data gaps and constraints on time, resources and budgets necessitate the use of simplifying assumptions in the construction of models. Efforts were made to ensure that assumptions had little or no impact on the primary objectives and goals of the modeling project. Those assumptions which might have impacted the objectives were tested using sensitivity analyses. Table 2.1 is a detailed list of the assumptions made in the development of the regional model. Each assumption is listed with a section of the report where the basis for the assumption, sensitivity analysis or explanation is provided.

2.1 Concept of Equivalent Freshwater Head

Because of the close hydraulic relationship between the aquifers in South Florida and the Atlantic Ocean and Gulf of Mexico, there are significant variations in the salinity of the groundwater. Except for small areas in the north part of the model domain, deep aquifers are highly saline due to their close interaction with the ocean. Some areas have been measured with salinity values higher than ocean water due to mineral build up. Surface aquifers are fed more by rainfall, resulting in generally low salinity.

Total Dissolved Solids (TDS) was used as a proxy for salinity in the ASR regional model and the two terms are used interchangeably in this report. TDS data was normalized by dividing each measured value by 35,000 mg/L, a commonly accepted TDS value for seawater. This results in a unitless value of approximately 1.0 for seawater and 0.0 for freshwater.

Comments from reviewers early in the modeling process indicated that temperature variations might also play a significant role in flow conditions in the model. Deeper aquifers are generally warmer near the west coast, likely due to geothermal effects, and cooler on the east coast, similar to ocean waters at depth.

Variations in both temperature and salinity of the groundwater cause variations in density. In addition, due to the significant depths in the model, pressure variations can also impact density. The density in the model is calculated to vary from about 62.2 lb/ft^3 to about 64.2 lb/ft^3. Temperature does not have as great an effect on water density as salinity, but it is included in the model and treated as another constituent concentration. Pressure has the least impact of the three variables controlling density.

Both SEAWAT and WASH123D require the user to enter head boundary conditions and initial conditions as observed head based on local density, or the water level measured in a well. The models then use the temperature and salinity to calculate the *equivalent freshwater head*, which takes into account TDS, temperature, and pressure to determine the potential energy at a given location. The flow equations are solved based on equivalent freshwater heads and then the solutions are converted back to observed heads for viewing and analysis. The governing equations used by SEAWAT and WASH123D are described in more detail in Section 2.2.

Because model results are reported as observed heads, the solutions sometimes appear to show unusual flow patterns. When there are significant differences in salinity, groundwater flow may appear to be moving "uphill." Since the equivalent freshwater head is actually the potential energy of the water at a given point, fluid flow would be expected to occur from locations of high equivalent freshwater head to locations of lower equivalent freshwater head. If the salinity is markedly different between two points, high observed heads may not correspond to high equivalent freshwater heads.

Equivalent freshwater head is calculated from observed head by first calculating the observed density from the TDS, temperature, and pressure, using Equation 2.1:

$$\rho = \rho_f + m_{tds}\left(TDS - TDS_{ref}\right) + m_{tmp}\left(TMP - TMP_{ref}\right) + m_p(P - P_{ref}) \qquad \text{Equation 2.1}$$

where:

ρ	=	Observed density
ρ_f	=	Density of water at the reference TDS and temperature
m_{tds}	=	Slope of the assumed linear relationship between density and TDS
TDS	=	Total dissolved solids in the water (proxy for salinity) normalized by dividing by 35,000 mg/L
TDS_{ref}	=	Reference TDS, normalized by dividing by 35,000
m_{tmp}	=	Slope of the assumed linear relationship between density and temperature
TMP	=	Temperature in the water (°C)
TMP_{ref}	=	Reference temperature
m_p	=	Slope of the assumed linear relationship between density and pressure
P	=	Pressure of the water calculated in terms of head
P_{ref}	=	Reference pressure calculated in terms of head

Once the observed density has been calculated, the equivalent freshwater head can be directly calculated by using Equation 2.2 (Guo and Langevin, 2002):

$$h_f = \left(\frac{\rho}{\rho_f}\right)h - \left(\frac{\rho - \rho_f}{\rho_f}\right)Z \qquad \text{Equation 2.2}$$

where:

h_f = Equivalent freshwater head
h = Observed head
Z = Elevation of point (using NGVD29 as a datum)

Table 2.2 lists the physical constants used in the flow equations.

2.2 Modeling Codes

The Benchscale and Phase I modeling efforts concluded that both the SEAWAT (finite-difference solution) and the WASH123D (finite-element solution) modeling codes would be used for the Phase II regional model. Since each code has inherent advantages and disadvantages, the use of both codes ensures a higher degree of reliability in the overall calibration, conclusions, and future recommendations.

2.2.1 SEAWAT

The SEAWAT (version 4) model (Langevin, et al, 2008, Langevin, et al, 2003, Guo and Langevin, 2002, Guo and Bennett, 1998) was chosen as one of the codes for the Phase II modeling effort. SEAWAT is a finite difference code that simulates variable-density flow in three dimensions by combining the flow equations in MODFLOW–2000 (Harbaugh et al, 2000) with the solute transport equations in MT3DMS (Zheng and Wang, 1999) into a single program coupling the flow and solute transport solutions.

SEAWAT uses a finite difference approximation for Equation 2.3, the governing equation for variable-density flow in terms of freshwater head and Equation 2.4, the governing equation for fate and transport of a contaminant in a three-dimensional, transient groundwater flow system (Guo and Langevin, 2002). (The reaction term has been removed from Equation 2.4 since the chemical reaction package was not used in this model.)

$$\frac{\partial}{\partial\alpha}\left[\rho K_{f\alpha}\left(\frac{\partial h_f}{\partial\alpha}+\frac{\rho-\rho_f}{\rho_f}\frac{\partial Z}{\partial\alpha}\right)\right]+\frac{\partial}{\partial\beta}\left[\rho K_{f\beta}\left(\frac{\partial h_f}{\partial\beta}+\frac{\rho-\rho_f}{\rho_f}\frac{\partial Z}{\partial\beta}\right)\right]$$
$$+\frac{\partial}{\partial\gamma}\left[\rho K_{f\gamma}\left(\frac{\partial h_f}{\partial\gamma}+\frac{\rho-\rho_f}{\rho_f}\frac{\partial Z}{\partial\gamma}\right)\right]=\rho S_f\frac{\partial h_f}{\partial t}+\theta\frac{\partial\rho}{\partial C}\frac{\partial C}{\partial t}-\rho_s q_s \qquad \text{Equation 2.3}$$

Where:

α,β,γ = Orthogonal coordinate axes, aligned with the principal directions of permeability
K_f = Equivalent freshwater hydraulic conductivity
S_f = Equivalent freshwater specific storage

t = Time
ϑ = Effective porosity
C = Solute concentration
ρ_s = Fluid density source or sink water
q_s = Volumetric flow rate of sources and sinks per unit volume of aquifer

$$\frac{\partial C}{\partial t} = \nabla \cdot (D \cdot \nabla C) - \nabla \cdot (vC) - \frac{q_s}{\theta} C_s \qquad \text{Equation 2.4}$$

Where
D = Hydrodynamic dispersion coefficient
v = Fluid velocity
q_s = Source/sink volumetric flow rate per unit volume of aquifer
C_S = Solute concentration of water entering from sources or sinks

The program contains several methods for solving the solute transport equation including an implicit finite difference method with either upwinded or central-in-space weighting, the method of characteristics, and a third order total-variation-diminishing (TVD) scheme. All simulations performed for Phase II model calibration and validation used the finite-difference upwinded solver; however, a final validation simulation was performed using the more robust TVD solver to confirm that any numerical dispersion in this solver was within acceptable tolerances. (See Section 5.1)

2.2.2 WASH123D

The October 2009 compile of WASH123D (Yeh et al., 2003) was also used to evaluate the regional effects of the proposed ASR wells. WASH123D is a finite element code that simulates variable-density flow and reactive chemical and sediment transport in 1-D channel networks, 2-D overland regimes and 3-D subsurface media on an unstructured mesh. For the Phase II model, only the 3-D subsurface variable-density flow options were enabled. With WASH123D, the variably saturated, density-dependent groundwater flow is described by the modified Richards' equation (Equation 2.5 and 2.6) and solved with the Galerkin finite element method.

$$\frac{\rho}{\rho_f} F \frac{\partial ph}{\partial t} = \nabla \cdot \left[\mathbf{K} \cdot \left(\nabla ph + \frac{\rho}{\rho_o} \nabla Z \right) \right] + \frac{\rho_s}{\rho_f} q_s \qquad \text{Equation 2.5}$$

Where:
ph = Referenced pressure head
$\mathbf{K}$ = Hydraulic conductivity tensor
F = Water capacity (see Equation 2.6)

$$F = a' \frac{\theta_e}{n_e} + \beta' \theta_e + n_e \frac{dS}{dh} \qquad \text{Equation 2.6}$$

Where:

α'	=	Modified compressibility of the medium
θ_e	=	Effective moisture content
n_e	=	Effective porosity
B'	=	Modified compressibility of water
S	=	Degree of saturation

The Lagrangian-Eulerian (LE) method is employed to solve the subsurface transport equation (Equation 2.4), where particle tracking is used in the Lagragian step to handle the advection term, and the other terms (such as sources, sinks, diffusion, and dispersion) are calculated in the Eulerian step to determine the spatial concentration distribution at the end of each timestep. The use of this methodology provides numerical stability without a Courant number restriction. In addition, the mesh's Peclet number is limited only by computational accuracy, not numerical stability. A sensitivity analysis of timestep sizing was performed to ensure the numerical accuracy was adequate for the scale and stated goals of the Phase II modeling effort (see Appendix F). More detailed discussion on various types of numerical dispersion and how the LE method deals with these types of numerical dispersion are found elsewhere. (Cheng et al., 1996; Cheng et al., 1998; Yeh et al., 2006).

2.3 Model Extent and Spatial Discretization

Both WASH123D and SEAWAT report numerical solutions to partial differential equations governing flow and transport at a set of discrete points. SEAWAT arranges these points as the centers of cube-shaped cells arranged in rows, columns and layers of a structured grid. WASH123D solves its equations at nodes on an unstructured 3-D mesh made up of prism-shaped elements. In each case, the grid or mesh was built to cover the area of interest (the proposed locations of the 333 CERP ASR wells) both horizontally and vertically. The sides of the grid or mesh were placed to coincide with convenient locations for assigning boundary conditions. Both the grid cells and mesh nodes were arranged in layers corresponding to the geologic layering of south Florida.

The Phase II model boundaries were established based on conclusions from the Benchscale and Phase I modeling efforts. The side boundaries of the model were generally established along geologic outcrops to the ocean or aligned near observation wells with available data during the calibration and validation periods. Figure 2.1 shows the horizontal extent of the model domain, which covers just over 23,000 square miles of the Floridan peninsula. The eastern boundary of the top model layer is located along the coast of the Atlantic Ocean. Subterranean geologic units extend eastward to their outcrop on the ocean floor, resulting in an additional 7,000 square miles of the model located offshore beneath the Atlantic Ocean. The northern model boundary for all geologic units cuts across the Florida peninsula, through Orlando and slightly to the south of Lake Apopka. The western model boundary closely follows the gulf coast of Florida, beginning at the model's northwest corner, just west of Tampa. South of Sanibel Island, the model boundary moves inland, crossing the Everglades to intersect the eastern boundary at the south end of Biscayne Bay. (All place names from this section are labeled on Figure 1.1.)

The computational grid/mesh resolution was selected to balance the purpose of the model with the constraints of time and computer resources. Higher resolution on the grid or mesh can provide greater accuracy and detail, but can also tax project budgets and computer resources due to the additional time required to compute the solution. The model purpose, as described in the introduction to Section 2.0, is to reasonably replicate the regional groundwater flow fields and effects of the proposed ASR well clusters.

Figure 2.1 shows the horizontal resolution of the WASH123D computational mesh and the SEAWAT computational grid. The smallest resolution (1,000 ft. in the WASH123D mesh and 2,000 ft. for the SEAWAT grid) is found at the proposed ASR well cluster locations where accuracy and detail are necessary. In the WASH123D, even finer resolution (100 ft.) is incorporated at the Kissimmee and Hillsboro ASR pilot sites to facilitate future local scale model construction. The size of both the grid cells and the mesh elements increases to 10,000 ft along the model boundary.

Vertically, the models extend from near the ground surface to the bottom of the confined Boulder Zone (BZ) member of the Lower Floridan (LF1) aquifer. Although the top layer of the SEAWAT grid is set to coincide with the Surficial Aquifer System (SAS), no calculations were made in this layer. To achieve the same effect in the WASH123D model, the top of the mesh is set at the bottom of the Surficial Aquifer system. This is explained in more detail in Appendix C. Although the depth of the model varies, the topographic high is near elevation 250 ft NGVD29 and the deepest point in the model is about -3,600 ft. NGVD29.

As shown in Figure 2.2, the models include five confined aquifers and four confining units. The SEAWAT grid also includes the Surficial Aquifer System (SAS), although no calculations are made here. The colors in Figures 2.3 and 2.4 are used to illustrate the arrangement of broadly-defined hydrogeologic material layers used in the model. Heterogeneity within the model layers was incorporated using zonal modifications to hydrogeologic properties of each geologic unit, or pilot point interpolation of hydrogeologic properties to individual cells of the model.

The 3-D grid contains 22 vertical cell layers and the 3-D mesh is made up of 23 vertical element layers. Figure 2.3 shows the geologic units associated with each layer in the SEAWAT model, while Figure 2.4 shows the geologic units associated with each layer in the WASH123D model. The 3-D mesh for this model is comprised of 391,228 nodes and 740,637 elements. The 3-D grid for this model is comprised of 1,092,256 cells, 823,038 of which are active. (The organized arrangement of the grid cells requires a rectangular shape to the grid. The desired shape of the model is incorporated by inactivating unnecessary cells.) Additional details concerning the model set up are discussed in Section 3.

Due to the dipping nature of the geologic layers some concerns were raised about the model resolution and aspect ratio and their possible contribution to model instability and inaccuracy. To respond to these concerns, a sensitivity analysis was performed to evaluate how the model discretization would affect the computed results of the regional models. The results of this analysis indicated that the errors resulting from model discretization were within the model's error tolerance for the majority of the model domain, including the area of interest for the proposed CERP ASR wells. Grid resolution was shown to

have a more significant effect in a small area in the northwest portion of the model near Tampa (where the geologic units thin significantly). However, since this area is north of the Polk County recharge area and does not appear to be influenced by the proposed ASR wells, the inaccuracies introduced by model resolution issues were considered acceptable for the scale and purpose of this modeling effort. Appendix B provides additional details on this sensitivity analysis.

2.4 Model Time Discretization

The calibration period selected for the transient calibration of the regional model was October 31, 2003 through December 31, 2004. The SEAWAT model was set up with 15 stress periods – one for each month of the period. Most boundary conditions and source/sink options in SEAWAT require constant values during each stress period. Thus, for head data, the average measured head during each month was applied to the entire month. For pumping data, the total pumped volume was divided by the number of days in the month and applied as a constant flux during the entire month. This simplification can result in some differences between observed and calculated data, but was necessary due to the paucity of reliable pumping data available at many locations in the model domain. Although the WASH123D model does not use stress periods, the same monthly averages were used to allow for direct comparisons between the two models and to minimize additional data collection.

The validation period of August 1993 through July 1994 was originally selected to be consistent with the calibration period of the USGS model by Sepulveda (2002). Analysis of the head data indicated that October 1993 was a better starting point for the model since the heads were generally relatively constant during the period leading up to October 1993. The validation period was, therefore, shortened to October 1993 through July 1994. The same process of assigning month-long stress periods to the model period was followed as explained above.

In each case, the first stress period was one day long and was solved as a steady state model to provide a starting condition for the rest of the modeled time periods. Timesteps (times at which the model computed and reported a solution) for both the flow and transport models were spaced evenly through the remaining stress periods. Each month was given 6 equally-sized timesteps, except for February 2004 and 1994, which only had 5 timesteps. Depending on the length of the month, this provided timesteps that were approximately 5 days long. Head results at the observation points are available at each timestep (approximately every 5 days). Head results on the grid as a whole were output about every 10 days to save on file sizes.

For the SEAWAT model, acceptable Courant numbers require a timestep about 8 hours long on average because of some of the thin cells located in the northwest section of the model. The approximately 5-day timesteps used for the calibration simulations were selected to provide a faster run time during calibration. At the end of calibration, additional model runs were made using a model-selected timestep to ensure accuracy of the final result (see Section 5.1). These final simulations used the TVD solution scheme, which used timestep sizes that were less than 1 day.

Additional details on the testing used to select the regional model time discretization are given in Appendix B.

2.5 Model Datum

Numerous data sources were compiled to generate the model input parameters, boundary conditions, and calibration/validation data sets. All data sets were converted to a common horizontal and vertical datum. The horizontal datum used for this model is feet North American Datum 1983 (NAD83), State Plane Florida East. The vertical datum used is feet North Geodetic Vertical Datum 1929 (NGVD29). Any data in a different coordinate system was converted using the coordinate conversion software, Corpscon, version 6.0 (December 2004 release), developed by the Topographic Engineering Center (TEC) of the U.S. Army Corps of Engineers.

All elevation data presented in this report are in NGVD29. Water levels (head) are presented as total head elevation, also in NGVD29.

3.0 Conceptual Model

Prior to construction of any numerical groundwater model, it is important to properly conceptualize the flow system in question. A conceptual model is a detailed description of the groundwater flow system to be modeled and should identify the hydrologic and hydrogeologic conditions and all important features and drivers of the groundwater system, including sources, sinks, boundary conditions, geophysical features that convey water or interrupt flow, recharge, site stratigraphy, material properties, etc. The conceptual model is generally developed through extensive literature research and data analysis. Most of the conceptualization for the Phase II ASR Regional Model had already been completed during the earlier phases of the project and is presented in previous reports (Brown et al, 2006 and NAP, 2006). However, additional conceptualizations were required for parameters that affect the density of the groundwater: temperature and salinity (represented by Total Dissolved Solids [TDS]). These analyses are presented in Appendix E.

The conceptual model should start with the basic components that are expected to have the greatest effect on groundwater flow. The preliminary conceptual model can be used to construct the model grid or mesh and develop the required simulations. Complexity can then be added to the conceptual and computational models as model outputs are compared to known conditions at the site and as the understanding of the flow system is refined. This often is an iterative process where interim numerical model results are used to help direct the research process and improve the conceptual model.

When evaluating the results of the WASH123D and SEAWAT models, it is important that the reader have an adequate understanding of the conceptual model so that potential model limitations are fully understood. The following subsections provide a brief description of the features included in the Phase II conceptual model and detail how these features were incorporated into the WASH123D and SEAWAT numerical models.

3.1 Topography

The topographic data was provided by SAJ and included bathymetric data for the offshore portion of the models. This data was a compilation of the SFTOPO-RC5 Topography/Bathymetry, National Elevation Data set (NED), and the National Oceanographic and Atmospheric Administration (NOAA) Coastal Relief

Model (CRM) bathymetry. The data was smoothed by SAJ to produce a topographic data set with uniform 1,000-foot grid spacing. Additional Digital Elevation Model (DEM) data was merged with this data set to ensure coverage across the entire model domain. The vertical datum of the final topographic data is NGVD29.

Traditionally, topographic information is often used to define the surface of the 3-D computational mesh or grid of a groundwater model with recharge and evapotranspiration applied to the surface as a flux boundary condition. However, since the purpose of the Phase II regional models is to evaluate flow in the FAS, the model was simplified by assigning specified heads in the Surficial Aquifer System (SAS) as explained in Section 3.3.1. Because there are no calculations made in the SAS, the top elevation becomes unimportant to the model calculations. The topographic data was useful for visualization of the SEAWAT results, development of regression correlations used to apply surface boundary heads, and for determining the layer outcrop locations in the Atlantic Ocean for both models.

This topographic data was also used to determine open intervals for monitoring wells and pumping wells. Usually, surface elevations at wells were not provided and the pumping and/or sampling intervals were reported as depths below ground surface. To estimate the elevations of pumping and sampling intervals at wells, the topographic data set was linearly interpolated to the well points and the depths were subtracted from the interpolated surface elevations. Well interval elevations were then compared to geologic layer elevations to determine the hydrogeologic unit tapped by the well's open interval. Any error introduced by using these interpolated well surface elevations is small compared to the accuracy of the geologic layer elevations.

3.2 Geology

A wealth of geologic and hydrogeologic data is available for the regional model domain. Geologic interpretations were based primarily on the USGS Scientific Investigations Report (SIR) 2007-5207 (Reese and Richardson, 2008) and a Draft report developed by Reese and Richardson (2004) entitled "The Draft-Final Report – Task 3.0 Define Preliminary Hydrogeologic Framework" (referred to herein as the Preliminary Hydrogeologic Framework). The following subsections describe the hydrostratographic layering and hydrogeologic data for the regional model.

3.2.1 Regional Geology

SFWMD used SIR2007-5207 and the Preliminary Hydrogeologic Framework to define the surfaces of the hydrostratigraphic units in the Phase II models and provided grids of the elevations (NGVD29) of the tops of the major geologic units. These gridded surfaces were used to develop the computational grid and mesh. Figures 2.2 to 2.4 show a gross conceptualization of all the geologic units used in the Phase II modeling and defined by SFWMD.

For the Phase II models, the FAS is divided into 4 producing units: the Upper Floridan (UF), Avon Park Permeable Zone (APPZ), Lower Floridan (LF1), and Boulder Zone (BZ); and three confining units: Upper Middle Confining Unit (MC1), Lower Middle Confining Unit (MC2), and the Lower Confining Unit (LC). The Framework documents divide the LF into LF1, LF2 and LF3, which are not all found at every location.

However, the LF, as simulated in this model, represents the first permeable zone of the Lower Floridan Aquifer (LF1). The LC is a composite of any remaining units (permeable or confining) between the first permeable zone and the BZ. The cited studies did not report the precise location of the base of the BZ, but estimated its thickness to be between 200 and 700 feet. The model was built with a uniform thickness of 500 feet for the BZ layer and a sensitivity analysis of the thickness was performed (see Section 5.4).

The thickness of each hydrogeologic unit (UF through LC) as defined in the model is presented in Figures 3.1 through 3.6. Although these figures were created from the SEAWAT computational grid, the same thicknesses were applied to the layering of the WASH123D computational mesh.

It is also important to note that the term 'confining unit' is somewhat relative. The MC1, MC2 and LC are confining units only by comparison to the producing units of the Floridan system. Anderson and Woesner (1992) define a confining bed as a 'unit of porous material that retards the movement of water.' The hydraulic conductivities of the MC1, MC2 and LC do not seem very low when compared to those found in other systems. (Materials such as glacial till, clay, unfractured shale or unfractured basalt can have hydraulic conductivities less than 10^{-6} ft/d, which is several orders of magnitude lower than most of the conductivity values used in the model for the confining units.) Because the conductivities in the MC1, MC2 and LC are a few orders of magnitude lower than those in the UF, APPZ, LF1 and BZ, they impede groundwater movement and are designated as confining units.

As indicated in Figure 2.3, the hydrogeologic layering was subdivided for the layers of the SEAWAT computational grid. The confining units (MC1, MC2, and LC) were each equally divided into two model layers. The aquifers were also equally subdivided into a number of layers based on the expected importance of each aquifer to the planned ASR production runs. Initial plans indicate that all of the CERP ASR wells will be open in the UF, so this layer was equally subdivided into 6 layers. The APPZ was equally subdivided into 3 layers because of the slight possibility that the ASR wells in the UF might impact the heads in the APPZ. Some members of the PDT have expressed an interest in testing ASR wells in the APPZ layer, so the additional layer may become important in the future. The LF1 and BZ layers are not expected to be impacted by the CERP ASR pumping, so they were given 2 layers and 1 layer, respectively, in the SEAWAT model.

The FAS is overlain by a complex system of alternating aquifers and confining units often referred to as the Surficial Aquifer System (SAS) and the Intermediate Aquifer System (IAS). Since they are not the focus of this modeling effort, these systems are greatly simplified for the model conceptualization. In the model, the SAS is simplified to a vertically homogeneous unit between the topographic surface to the top of the IAS, as defined in SIR2007-5207. The IAS consists of everything between the SAS and UF and is conceptualized in two components: the Intermediate Aquifer (IA) and the Intermediate Confining Unit (ICU). The IA exists only in west-central and southwest Florida (Miller, 1997), but non-continuous layers (pinch-outs) are difficult to simulate in either the computational grid or mesh. The IA was modeled by assigning IA aquifer parameters to the west-central and southwest third of layer 3 of the SEAWAT model. The ICU was modeled in layer 2, 4 and the non-IAS section of layer 3. Thus, layer 3 has two distinct sections with starkly different aquifer parameters (see Figure 2.3). These simplifications are

acceptable since the primary function of the SAS and the IAS in the model is to conduct water from the surface to the FAS.

Similarly, the Hydrogeologic Framework (Reese and Richardson, 2008) indicates that the APPZ does not exist in the southwest section of the model (most of Collier and Monroe Counties). This pinchout was approximated by making these layers extremely thin in this area. Each of the three layers thins to a minimum of 2 feet, resulting in a 6-foot thickness for the entire layer (see Figure 3.3). Since this is also the limestone section of the APPZ, the hydraulic conductivity is very low and the APPZ does not conduct much flow in this area.

As previously mentioned, the BZ thickness is assumed to be universally 500 feet across the model domain. However, Reese and Richardson (2008) report that the BZ does not occur in west-central Florida. To model the non-existence of the BZ, the hydraulic conductivity for layer 22 in west-central Florida is set to values similar to that of the LF1. Since the LF1 conductivity is much smaller than the generally present BZ conductivities, this approach results in greatly diminished BZ flow. (Because of the assumed constant thickness of the BZ, a figure similar to Figures 3.1 through 3.6 is not provided for the BZ.)

The layering of the WASH123D model was similar to the SEAWAT model as can be seen by a comparison of Figures 2.3 and 2.4. Most of the hydrogeologic unit layers were defined by the same number of model layers. The MC1, MC2 and LC confining units were all divided equally into two model layers. The UF, APPZ and LF1 aquifers were divided into 6, 3 and 2 layers, respectively, just as in the SEAWAT model. However, because of computational differences between the two models, the BZ was divided into two layers and the IAS was divided into four.

The additional layer is added to the IA to account for differences between finite difference (SEAWAT) and finite element (WASH123D) computational points and the application of hydraulic conductivity to those points. In SEAWAT, the hydraulic conductivity is assigned to a cell and the center of the cell is the computational point. In WASH123D, the conductivity is assigned to an element and the computational points are at the nodes on the element faces. Figure 3.7 is a diagram that shows the comparison between the SEAWAT and WASH123D computational points in the area where the IA is present. The WASH123D computational point 3 in Figure 3.7 uses the aquifer conductivity from Layers 2 and 3 to compute the heads in the aquifer in a similar way to computational point 2 for SEAWAT Layer 3. The WASH123D computational points 2 and 4 use an average conductivity from the confining unit and the aquifer. Splitting the IA into two layers in the WASH123D model provides a layer of nodes that are assigned the aquifer conductivity and ensures an accurate representation of the recharge entering and moving through the IA. Similarly, the BZ is divided into two layers to provide the model with at least one layer of nodes assigned a BZ hydraulic conductivity value.

Pinchouts in the APPZ and BZ in the WASH123D model are handled in the same way as the SEAWAT model. Since the mesh is layered, it is difficult to remove the elements from the mesh. Instead, the elements were made thin and the hydraulic conductivity was used to approximate the condition. As mentioned above, the model simulated APPZ in Collier and Monroe Counties is very thin with a low

hydraulic conductivity. The absence of the BZ in the northwest part of the model is simulated by setting the hydraulic conductivity to values similar to the LF1.

The SAS was not defined as a WASH123D model layer because no flow calculations were made in the SAS. The SAS heads (interpolated from available data) were assigned to the top nodes of Layer 1 of the IAS, as described in Section 3.3.1 and Appendix C.

3.2.2 Hydrogeologic Properties

Hydrogeologic properties such as hydraulic conductivity and specific storage were estimated for each model layer based on the available data. Then, during the calibration process (see Section 4), the property values were adjusted until an adequate calibration to available data was achieved. During calibration, the parameter values were required to remain within reasonable ranges as defined in the Preliminary Hydrogeologic Framework, SIR2007-5207 and APT (Aquifer Pump Test) data provided by SFWMD. Additional information for the Phase II conceptual model was collected from other sources and from online databases including SFWMD's DBHYDRO, USGS's South Florida Information Access (SOFIA), the National Park Service's South Florida Natural Resources Center (SFNRC), CH2MHill's Groundwater Numerical Model Development Support and Data Collection Report, and a number of published reports and papers (see Section 8).

The available field data used to guide the calibration process is presented in Figures 3.8 through 3.15. This field data includes horizontal hydraulic conductivity data for the aquifers (Figures 3.8 through 3.10), vertical hydraulic conductivity data for the confining units (Figures 3.11 through 3.13) and specific storage for the UF and APPZ (Figures 3.14 and 3.15). (Specific storage was converted from storage coefficient by dividing by the aquifer thickness.) The final calibrated hydraulic conductivity and specific storage distribution for each model layer will be presented later in Section 4 (See Sections 4.1.2 and 4.2.4 along with Figures 4.31 through 4. 40 and 4.111 through 4.118). Differences between WASH123D and SEAWAT resulted in slight differences in the material parameters used in the calibration model.

Additional properties such as porosity, dispersivity and molecular diffusion coefficient, were found to have little effect on the calibration of the model. Sensitivity analyses of these parameters are presented in Section 5.2 and 5.3.

3.2.3 Regional Anisotropy

During the Phase I modeling, the SEAWAT grid angle was set at 18 degrees west of north to align with the axis of the Floridan peninsula. Bittner, et al. (2008) analyzed a number of options for improving the agreement between the initial model results and the estimates of pre-development heads in the UF from Meyer (1989). This paper concluded that both the inclusion of anisotropy in the aquifers and the inclusion of temperature effects on density could improve the calibration of the model.

A lineament study (Fies, 2004) and preliminary results from some image log fracture analysis work at SFWMD indicated that the dominant fracture orientation was NW to SE at an angle of about 38 degrees west of north. For this reason, the regional grid for Phase II modeling was designed with a 38 degree angle, in place of the 18 degree angle used in earlier reports. However, additional analysis by SFWMD

indicated that the NW to SE orientation was based on a lumped view of all the UF fractures from all the wells. When the data was split out to look at the dominant orientations from individual wells, it became clear that the dominant orientations varied geographically. The lumped view gave additional weight to a large volume of fractures in the UF at the Kissimmee River pilot location. This led to the conclusion that there is currently no conclusive evidence of regionally dominant orientation for fractures in the UF. The anisotropy option was, therefore, not used in this regional model (although the grid angle of 38 degrees remained). Greater detail will be available on this study when the final report on the lineament study is completed in time for inclusion in the final Technical Data Report (TDR) for the regional study.

3.3 Boundary Conditions

Specified head boundary conditions were applied to the sides and top of both Phase II regional models. In SEAWAT, the time-variant specified-head boundary (CHD) package was used to specify the heads in the cells on the top and sides of the model. Similarly, in WASH123D, a DB card (Dirichlet boundary condition) was listed in the input file for each node on the sides and top of the mesh. No boundary condition was applied to nodes on the bottom of either model. By default, unassigned nodes on the boundary of the mesh and unassigned boundary cells of the grid are considered to be no-flow nodes. The use of the no-flow boundary on the bottom of the model is appropriate because of the much lower conductivity of the Sub-Floridan confining unit, which underlies the Boulder Zone. Preferential flow in the Boulder Zone is expected to be horizontal with only insignificant flows in or out of the bottom of the model.

The following subsections provide a brief summary of the methodology used to set the specified head boundary conditions on the Phase II regional models. Additional details are provided in Appendix C.

3.3.1 Surficial Head Boundary Conditions

The heads assigned to the top boundary of the models simulate recharge (precipitation less evaporation, transpiration and runoff) and provide one of the primary sources of water to the models. Generally, groundwater models use a flux-type boundary condition at the surface to simulate recharge. The flux is often calculated using a flow budget, subtracting such sinks as evapotranspiration and runoff from precipitation to determine the volume of water seeping through surface soils into the model. Runoff and evapotranspiration are usually approximated using empirical equations with estimated parameters based on sparse data. Because of the inherent uncertainty in these calculations, recharge is often used as a calibration parameter and is varied along with hydrogeologic material properties until the model result matches measured aquifer conditions.

For these regional ASR models, a specified head was assigned to the top surface of the models, based on an interpolation of available head data from monitoring wells open in the SAS. This approach avoids the difficulties and inaccuracies inherent in calculation of recharge values and seepage rates and makes possible the direct usage of the abundance of SAS head data. The purpose of the Phase II regional models is to evaluate regional flow characteristics in the FAS and estimate the aquifer effects from the proposed CERP ASR wells. Since the ASR pumping is not expected to affect the heads in the SAS, the use of specified heads is considered valid.

In the SEAWAT model, the SAS was modeled as the top layer of cells with the top of each cell corresponding to ground surface and the bottom of each cell set at the elevation of the bottom of the SAS. Each cell was assigned a specified head as described above and SEAWAT made no horizontal flow calculations in the top layer. The specified head was calculated based on an interpolation of the average head data at all available wells for each month of the calibration and validation period as described in Appendix C.

The same interpolation process was used to assign specified heads to the top layer of nodes in the WASH123D model. The elevations of these nodes correspond to the elevation of the bottom of the SAS layer. Thus, the SAS was not included in the computational mesh. This makes the two models comparable since neither one made horizontal flow calculations in the SAS. See Appendix C for additional details

3.3.2 Simulation of Ocean Boundary

Along the eastern boundary, each modeled hydrogeologic layer extends to its projected outcrop in the Atlantic Ocean. The outcrop location was defined by cutting each layer when the geologic unit surface grids provided by SFWMD (see Section 3.2.1) intersected the bathymetry data (see Section 3.1) for the floor of the Atlantic Ocean. The assigned boundary head simulated the level of the ocean and was based on the monthly mean sea level measured at two NOAA tide gauges – one at Virginia Key, near Miami, and the other at Naples, on the west coast of the Florida peninsula. The tide gauge locations are marked on Figure 1.1 and the monthly average water levels for each gauge, plus the average value used in the model are plotted in Figure 3.16. There is some monthly variation in the ocean level, with slightly higher levels in the fall and lower levels in the spring and summer. The annual variation of monthly mean sea levels is less than 1 foot, which is much smaller than the variation in monthly average heads at most observation wells in the model domain. Note that with the coarse time discretization, this model does not attempt to reproduce daily tidal cycles.

3.3.3 Aquifer Head Boundary Conditions

Ideally, the west and south boundaries would also extend out to the locations of the outcrops for each layer in the Gulf of Mexico. However, these outcrops occur nearly 150 miles from the Florida coastline. Extension of the model boundary to these outcrops would add significantly to the model size, computational requirements, and the time required to reach a converged solution. This would also add a large area to the model which has not been extensively studied and for which there is no significant data regarding heads, water quality or aquifer characteristics. Instead, the north, west and south boundaries coincide with available water level data points. For each aquifer (IAS, UF, APPZ, LF1, and BZ), heads assigned are based on monthly averaged measured values from wells located near the boundary. Figure 3.17 shows the areas where specified head boundary conditions were applied to the models as well as the location of the available data points. The process used to assign specified heads to the sides of the aquifer layers of the model accounted for all available data and incorporated the conceptual model for the site. It is described in detail in Appendix C.

Some concerns have been raised that the use of specified head boundary conditions at these coastal and inland locations might cause inaccuracies since there are numerous pumping wells located very close to the boundary. However, these errors are mitigated by basing the boundary heads on measured heads, which already include the drawdown effects of regional pumping. Near-field effects of pumping would likely not be captured, but they are beyond the scope of this model and not important to the goals of the regional model (See Section 2.0).

3.3.4 Confining Unit Head Boundary Conditions

No-flow boundaries were used at nodes (WASH123D) and cells (SEAWAT) along the side boundaries of the confining units, except where they outcropped to the ocean. The horizontal flow through the model boundary in these confining units is not believed to be a significant source or sink when compared to flow through the aquifers. A sensitivity analysis confirmed this assumption and is presented in Section 5.5.3.

3.3.5 TDS and Temperature at the Boundaries

SEAWAT and WASH123D both allow the user to define the water quality of the flows entering the model at any boundary condition. In SEAWAT, the SSM package (Source & Sink Mixing) was used to assign the TDS and temperature to each cell with a CHD boundary condition and all injection wells. WASH123D has a similar requirement in the form of an RS2 and RS6 card (variable boundary TDS concentration and temperature, respectively) corresponding to each of the specified head nodes and a PS2 and PS6 card (point source TDS concentration and temperature, respectively) for each of the injection wells.

For the boundary cells and nodes, the water quality of the incoming water was set based on the initial conditions at that location (see Section 3.4). For injection wells, the TDS values were assigned using available data (see Appendix E). At injection wells where no data was available, it was assumed that TDS values would be similar to nearby injection wells of the same type. The two types of injection wells were deep injection wells (typically have high TDS values) and existing ASR wells (typically have low TDS values). Injected temperature values were assumed to be consistent with the temperature initial conditions for the SAS (see Section 3.4.2).

3.4 Initial Conditions

The initial conditions applied to the model included initial head, salinity and temperature. The initial head condition was based on early test runs of the model. It is important to note that while the initial head condition affects the speed at which the steady state solution is reached, it has no effect on the model results. For the transient model, the first stress period was solved in steady state mode to give the starting head condition for the subsequent transient simulation. The initial salinity and temperature conditions were used by the models in the initial calculation of groundwater density. Studies have shown that regional groundwater flow patterns in the FAS can be significantly affected by variations in the groundwater fluid density [Hughes, Vacher, and Sanford (2007), Meyer (1989), Sanford et al (1998), Kohout (1965), Kohout et al (1977)]. The ability of SEAWAT and WASH123D to model density-dependent flow was the main criteria in selection of these models. The following subsections describe the data and methodology used to create these initial condition distributions.

3.4.1 Salinity (TDS) Distribution

For this study, reported measurements of total dissolved solids (TDS) are used as proxy for salinity. The terms 'TDS' and 'salinity' are used interchangeably in this report. The model requires that initial salinity concentrations be specified at every computational point in the model domain. In order to meet this requirement, an extensive data collection effort was undertaken to identify representative water quality data from the SAS to the BZ. Where possible, water quality data from the beginning of the calibration period (October 2003) was used; however, in areas where data was sparse, reported measurements from other time periods were used to fill data gaps. Since the regional water quality does not normally change drastically over a period of a few years, this method of filling data gaps was considered to be adequate. It is important to note that data at or near injection wells was not used if the samples appeared to reflect the quality of the injected water instead of the native water quality. A variety of data sources were used to collect the available TDS data, including USGS, DOH, SFWMD, SJRWMD, and SWFWMD. Additional details on the data collection effort are summarized in Appendix A.

Once the TDS data was collected, it was carefully evaluated by the modeling team to ensure that it reflected the known regional water quality. Several recording errors (e.g. data transposed between zones, significant fluctuation in water quality readings, etc.) were identified and corrected. The TDS at the ocean outcrops was set to 35,000 mg/l to reflect the salinity of seawater. Since the quantity and quality of the TDS data in the confining units was limited, the interpolation results in these layers were compared to the overlying and underlying aquifer water quality to ensure consistency. The validated data for each aquifer was then interpolated to the corresponding model layer. Figures 3.18 to 3.24 show the final TDS initial condition distribution by layer. The quantity of data used in the interpolation and assumptions specific to each layer are explained on each figure. Figure 3.25 shows the same data as a 3-dimensional fence diagram.

For the SEAWAT model, the TDS initial condition values for the FAS (Layers 5 through 22) were specified based on the corresponding aquifer and confining unit values shown in Figures 3.18 through 3.24. The SAS (Layer 1) was given a uniform TDS concentration of 100 mg/l in the land areas and 35,000 mg/l at the ocean. The TDS values for the ICU (Layers 2 and 4 and a portion of Layer 3) were determined by taking the average of the SAS and UF layers. Available data in the IA was interpolated to determine the initial conditions for the aquifer portion of Layer 3.

In the WASH123D model, the assignment of the initial conditions were somewhat different than for the SEAWAT model as a result of the differences between finite difference (SEAWAT) and finite element (WASH123D) computational points. For the SEAWAT grid, the computational points are located at the centers of the grid cells, so the initial conditions are required at each grid cell center. The WASH123D computational points and initial condition assignments are located at the nodes on the element interfaces. Figure 3.26 is an illustration that shows the comparison of the SEAWAT and WASH123D computational point locations and the differences in the assignment of TDS initial condition for the two models. In this example of a vertical column of grid cells and mesh elements, there are two confining units and two aquifers, each with a different TDS concentration. For SEAWAT, the assignment of initial conditions for each aquifer and confining unit was straightforward and based on the interpolation of

available data as explained previously. However, for the WASH123D assignment, the aquifer TDS values (from the interpolation of the available data) were assigned to any computational point within or at the top or bottom of the aquifer. For confining units, the TDS values from interpolation were only assigned to nodes that were completely surrounded by a single hydrogeologic unit. So, points 2, 3 and 4 were given the interpolated aquifer TDS value of 2000 mg/L, but only point 5 had the interpolated TDS value of 5000 mg/L which was associated with that confining unit.

Although the SAS was not explicitly modeled in the WASH123D model, the SAS initial TDS values used in the SEAWAT model were assigned to the top layer of nodes in the WASH123D model, top of Layer 1. The initial TDS values in the remaining layers of nodes representing the IAS, nodes on the interfaces of Layers 2 and 3, were the average of the values for the SAS and UF layers.

In general, fresher zones in the deeper geologic units are seen in the northern portion of the model beneath the Polk County recharge area and south of Orlando. The TDS concentration increases to the south and near the geologic outcrops at the ocean. Additional details concerning the procedure used to develop the TDS data sets and initial conditions are presented in Appendix E.

Because of the short calibration period (14 months) and validation period (10 months), no appreciable change in the TDS distribution was noted in the model results. Final TDS distributions are quite similar to initial TDS distributions, except in the immediate vicinity of injection wells. Because of the coarseness of the model grid, the model-calculated TDS close to an injection well cannot be expected to be accurate, and is not important to the regional goals of this study. For this reason, model results of water quality data are not presented in this report. Water quality will be of greater import during the production runs on the local-scale models, which will look at ASR efficiencies and near-well effects.

3.4.2 Temperature Distribution

The models also required the definition of the initial groundwater temperature at every computational point in the model domain. Temperature data was collected to construct a data set of values from the IAS to the BZ throughout the horizontal extent of the model domain. For the SAS, an average temperature value of 24°C can be assumed for the entire unit because shallow density variations have little impact on model results. Where possible, temperature data from the calibration period was used; however, in areas where data was sparse, reported measurements from other time periods were used to fill data gaps. This approach is based on the assumption that regional water temperature does not vary significantly over a period of a few years. As noted for the TDS data analysis, data at or near injection wells was not used if the samples appeared to reflect the temperature of the injected water and not the native water temperature. In some of these cases, well drilling reports containing native water temperature measurements were available and were used in place of more recent temperature measurements. Several data sources were used to collect the available temperature data, including USGS, SFWMD, SJRWMD, and SWFWMD. On the ocean boundary, temperature variation was estimated using a general temperature-depth of ocean water profile compiled by the University Corporation for Atmospheric Research (Figure 3.27).

The collected data was analyzed to determine the values that best represented the regional temperature in each aquifer and confining unit. The details of this analysis are included in Appendix E. Figures 3.28 to 3.35 show the initial condition temperature distribution for each hydrogeologic layer. The number of data points used in the interpolation and assumptions specific to each layer are described on each figure. The same data is displayed in a 3-dimensional fence diagram in Figure 3.36.

The temperature initial condition values were assigned to the SEAWAT and WASH123D models in a similar manner to the assignment of the TDS initial condition values. See Section 3.4.1 for a description of the differences in model assignments resulting from the differences in the location of their computational points.

In general, the temperature increases with depth on the western side of the peninsula and decreases with depth on the ocean boundary. This trend creates a very large temperature variation, from 5^{o}C to 44^{o}C, in the BZ where temperature effects on density have the largest impacts on model results. The warmer west coast temperatures also extend through the mid-section of the state toward Lake Okeechobee in most of the geologic units.

Because of the short calibration period (14 months) and validation period (10 months), no appreciable change in the temperature distribution was noted in the model results. Final temperature distributions are quite similar to initial temperature distributions, except in the immediate vicinity of injection wells. Because of the coarseness of the model grid, the model-calculated temperature close to an injection well cannot be expected to be accurate, and is not important to the regional goals of this study. For this reason, model results of water quality data are not presented in this report.

3.5 Sources and Sinks

In addition to the model boundaries, pumping wells constitute a significant source/sink for groundwater in South Florida. This pumping includes withdrawal wells (irrigation, water supply, etc.), existing ASR wells, and Class I injection wells. An extensive data collection effort was performed by SAJ to compile and evaluate detailed data sets of the pumping distribution within the model domain. Over 30,000 wells were identified as active during the calibration/validation periods within the model domain. However, many of the wells were missing specific location information such as horizontal coordinates or open interval depths. Also, monthly transient pumping rate records for many wells were often either unavailable or incomplete. As part of the data collection effort, estimates were made to fill these data gaps. Additional details on the data collection effort for the pumping wells and the methodology used to fill the data gaps are summarized in Appendix A.

Additional effort was required to appropriately assign the pumping to the grid and mesh. The depths of the top and bottom of the open interval for each pump were converted to elevations based on the approximate ground surface elevation at the point. These elevations were compared to the model-simplified geology to determine the aquifer (or aquifers) impacted by each well. The pumping elevations were adjusted to prevent the model from pumping in confining units. Pump rates for wells covering more than one aquifer were prorated based on the length of open interval and the estimated hydraulic conductivity of each aquifer. SEAWAT requires all pumping to be applied to the center of a

cell; WASH123D requires all pumping to be applied to a node. To accommodate these requirements, the wells were moved horizontally to nearest computational point. In SEAWAT, any well located within a grid cell, was automatically moved to the center of the cell and added to the pump rates of any other wells located in the same cell. Vertically, the pumping from each well was divided among the cells or nodes in the aquifer according to the vertical location of the open interval of the well. See Appendix D for more details. For a regional scale model, this methodology is sufficient, but it should be noted that near-field effects of individual pumping wells are not well-portrayed in this regional model, since cell and element sizes are as large as 10,000 feet on a side.

During of the early stages of calibration, the substantial influence of pumping on the FAS water levels was noted. A substantial portion of the pumping data had been estimated because monthly pumping rates were not available (see Appendix A). For the October 2003 to December 2004 period, there were 5,669 irrigation wells with reported data for all months, 4,206 irrigation wells with reported data in some of the months, and 6,628 wells with no data. A detailed evaluation of the pumping data and its correlation to observed water level and climatologic trends indicated that critical errors were present in this estimated pumping data. The methodology used to estimate missing transient pumping data was reevaluated to better correlate with observed pumping trends and the climatologic patterns that drive irrigation. Additional details on the methodology used to estimate missing transient pumping data are presented in Appendix D.

The pumps located in each aquifer are shown in Figures 3.37 to 3.41 and summarized in Table 3.1.

4.0 Calibration/Validation

Model calibration is the process of varying model input parameters within a reasonable range until the model output matches observed conditions within some acceptable error criteria. This calibration can be either to steady-state or transient conditions. Steady-state model simulations eliminate the time terms in the governing equations (see Equations 2.3 through 2.6) and provide a snap-shot of the hydraulic conditions in a stable aquifer system. An inherent assumption with this type of simulation is that the system has achieved an equilibrium condition. Steady state results are also commonly used as initial conditions for subsequent transient simulations. For models that are affected by a variety of constantly changing stresses, transient calibration is necessary to ensure that the model is providing a reliable representation of the system.

Once a model is considered calibrated, it is then validated against at least one different set of observed conditions using the hydraulic parameters established during calibration. A model is considered validated when the set of model parameters from the calibration process yields a similar satisfactory degree of agreement between field observations and computed model results for the independent validation period(s). If the validation results are not satisfactory, then the model calibration process resumes, continuing until a satisfactory agreement is obtained for the calibration and validation data sets.

For the Phase II ASR Regional model, a steady state calibration was first performed to the October 2003 and February 2004 observed water level data sets. Once the steady state model was calibrated, a

transient calibration was performed for the 15 month period from October 2003 to December 2004. Finally, a transient validation simulation was performed for a 10-month transient period from October 1993 to July 1994. Observation wells for calibration were selected from the monitoring well database provided by SAJ. Generally, observation wells were selected when at least 50% of their open section (between the cased and drilled depths) coincided with the model-simplified geology at that location. Additional wells were removed for a number of reasons: because their data indicated the effects of local pumping; their data was quite sparse; the data indicated a probe error; etc. Some wells located in the Hillsborough River valley north of the Polk County recharge area were removed because there were so many wells in this area that the calibration statistics were being skewed to an area far removed from the proposed CERP ASR sites. Table 4.1 lists all of the wells in the SAJ database and their use in the model (either for boundary conditions or calibration) or the reason for removal from the model.

The steady state and transient calibration/validation descriptions below are only for the final calibration of the SEAWAT model. After the draft regional model calibration was completed using both the SEAWAT and WASH123D codes, it was determined that the codes both provided a reasonable calibration of the steady state and transient flow fields. However, it was more difficult to incorporate the widespread heterogeneity of the hydrogeologic model parameters in the WASH123D model due to the zonal method of assigning these parameters in the WASH123D code. Appendix F provides details on the excessive number of WASH123D zones required to provide the necessary heterogeneity in hydrogeologic parameters. In addition, because SEAWAT provides several solver options, it is possible to make many model runs using a less accurate solver (standard finite difference method with upstream weighting) to get close to calibrated results. Once the solution is nearly calibrated, a more accurate but slower running solver (third-order TVD) can be used to take the last steps to reach the final calibrated solution. The WASH123D code is not equipped with a fast, less accurate solver. The combination of difficulty in assigning widespread heterogeneity and fewer solver options means that the WASH123D model requires more time for calibration. Because programmatic constraints have made it difficult to support the use of more than one code for the future of the project, a decision was made to proceed solely with the SEAWAT model. A comparison of the WASH123D and SEAWAT model results for the draft calibration are included in Appendix F. Although these results are from the draft calibration, the fact that the similarly-constructed WASH123D and SEAWAT models computed similar results provides reinforcement for the SEAWAT final calibration results.

4.1 Steady State Calibration

A steady state calibration was performed for October 2003 and February 2004 by varying the input parameters (principally hydraulic conductivity) until the model output (heads) matched the measured heads at non-pumping monitoring wells with data for either month. The model for each month was provided with a separate set of specified heads around the edges of the aquifers and at the surface, simulating different hydrologic conditions as reflected in the available data (see Section 3.3). The pumping data was also different for each month and based on the available reported pump rates and estimates as described in Section 3.5. Starting conditions (salinity and temperature), hydraulic conductivity, and all other input parameters were identical for the two steady state calibration models (see Section 3.4).

October 2003 was selected for steady state calibration to ensure a good starting condition for the transient calibration. However, analysis of the available head data indicated that water levels declined sharply in many wells during October 2003 as shown in Figure 4.1. This indicates that the aquifers were responding to pumping stresses and that the measured heads in October 2003 do not represent an equilibrium or steady state condition. For this reason, February 2004 was added as an additional steady state calibration period. This month was chosen because many of the monitoring wells have relatively constant heads for a period of a few months ending in February, indicating a more equilibrium condition and less variation in pumping. Calibration to October 2003 continued in order to provide a quality starting condition for the transient calibration, but the measured water levels from the end of October 2003 were used for calibration instead of the average head over the month, since the heads at the end of the month would be expected to be closer to the steady state level caused by the pumping from that month. During February, there was much less pumping and the model calculated heads were compared to the average measured heads for the month. The calibration for both months continued in tandem, with slightly more emphasis placed on the month of February. When head levels at a certain well could not be matched in both months using the same input data set, efforts were made to select parameter values that would calculate the head in one month a little higher than measured and the other a little lower. Table 4.2 lists the wells used for steady state calibration, the observed water levels during the calibration periods, and the modeled water level.

The quality of the steady state calibration was evaluated in several different ways, including error statistics, calibration target figures, gradient analysis of well clusters, and comparison to other published information, such as estimates of recharge to the UF and pre-development heads. The following paragraphs describe each of these evaluations of the steady state calibration. Details pertaining to each model's calibration will be presented in later sections.

A model's calibration is measured mathematically by the use of error statistics. The three criteria generally used are the mean error (ME), mean absolute error (MAE), and the root mean square (RMS) error, defined by Equation 4.1, 4.2 and 4.3.

$$ME = \frac{\sum_{i=1}^{n}(c_i - o_i)}{n} \qquad \text{Equation 4.1}$$

$$MAE = \frac{\sum_{i=1}^{n}|c_i - o_i|}{n} \qquad \text{Equation 4.2}$$

$$RMS = \sqrt{\frac{\sum_{i=1}^{n}(c_i - o_i)^2}{n}} \qquad \text{Equation 4.3}$$

Where:

c_i = Model calculated head at observation point *i*

o_i = Observed head at observation point *i*

n = Number of observation points

The mean error (Equation 4.1) is the average of the differences between the observed and calculated heads (or residuals) and can indicate the overall comparison between computed and observed data. Negative and positive residuals can cancel each other out, resulting in a mean error close to zero even when the calibration is not good. The sign of the mean error is an indication of the overall comparison of the model to the data (e.g. a positive mean error indicates the model is generally computing too high).

The mean absolute error (Equation 4.2) is the average of the absolute values of the residuals. The absolute value prevents positive and negative residuals from canceling each other, providing a clearer picture of the magnitude of errors across the model, without an indication of the direction (high or low) of the errors.

The root mean square (RMS) error (Equation 4.3) is the square root of the average of the squares of the residuals. The RMS adds additional weight to points where the residual is greatest. If the residuals at all points are very similar, the RMS will be close to the mean absolute error. Alternatively, a few points with high errors can add significantly to the RMS for an otherwise well-calibrated model. For all three of these criteria the optimal value is zero.

The spatial variation of the fit between model calculated heads and field measured heads is shown in the calibration target figures which are provided for each of the main aquifers in each model (Figure 4.2 through 4.11, with zooms to specific locations in Figures 4.12 through 4.17). The calibration figures show the head contours (interpolated from the model-calculated heads at each cell for a specific model layer) and a set of targets placed at the location of each measured head. The targets indicate the calibration quality at that point with its color and the direction of the colored bar. Green bars indicate computed results within 2 feet of the observed head; yellow bars indicate computed results within 4 feet of the observed head. Red bars are for locations where the difference between computed and observed heads is more than 4 feet. The bar in each target is drawn above the center line for points where the computed head is higher than the observed head (positive residual). Conversely, targets below the center line indicate computed heads lower than observed heads (negative residual). The details of the quality of the calibration as shown through these figures will be discussed in Section 4.1.3.

The quality of the calibration can be assessed using these figures by noting the color and direction of the target bars. Generally, a well-calibrated model will show a random field of small errors with no clustering of either positive or negative residuals. Often the reasons for poor calibration at an individual monitoring well can be assessed by noting the location of the point – perhaps it is in an area of steep slopes or close to a large pump. The steady state calibration figures also show a plot of computed vs. observed values with a point plotted for each observation point. In a perfect calibration, all points will lie along the line y=x (shown as a black line). For good calibration, all points should lie close to this line and points should not be clustered in any other part of the plot.

The quality of the steady state calibration was also assessed using a gradient analysis of a number of well clusters. This analysis ensures that minor head residuals are not compounded, resulting in

unrealistic gradients between aquifers. Figures 4.18 through 4.28 show the model-calculated head at the center of each cell in a vertical column compared with the heads measured in a number of wells located within this column but screened at different depths. The gradient analysis helps verify that both the direction of flow and the slope of the gradient are accurately reproduced in the model.

Finally, the model results were compared to a published estimate of recharge/discharge to the UF (Figure 4.29) and a published estimate of pre-development heads (Figure 4.30). Although this is not a comparison to actual measured data and therefore, cannot truly be termed calibration, this model's similarity to other independent, published analyses helps to strengthen its credibility.

As stated in Anderson, 1992, "The judgment of when the fit between model and reality is good enough is a subjective one. To date, there is no standard protocol for evaluating the calibration process…" A common rule of thumb is that in a well-calibrated model, the RMS should be less than 10% of the head difference across the domain. This rule is not especially applicable to the ASR Regional Model, where the head difference across the model domain is over 200 feet. Few would find 20 feet of error acceptable for this model.

In reality, the acceptable level of calibration varies across the area and depends on the conditions at each location. In the northern portion of the model, particularly in the Polk County recharge area, the hydraulic gradient is relatively steep. Many of the high residuals at observation wells in this area are due to grid resolution, which is too coarse to accurately portray every nuance of the highly variable hydrogeologic conditions. For example, the pumping wells had to be moved up to 5000 feet to the nearest cell center (see Section 3.5) but the observation points were not moved. Additionally, near well effects are not accurately modeled when the cells are this large. For these reasons, calibration errors up to a few feet might be acceptable in this area.

On the other hand, much less head variation is observed in the southern portion of the peninsula. Here, errors caused by grid resolution or the placement of monitoring and pumping wells are less likely to be significant. Thus, acceptable residuals at observation points in this area would be much smaller.

Acceptable calibration error also depends on what question the model is answering. This regional model is built specifically to predict the large-scale effects of the CERP ASR program on the heads and salinities in the groundwater. For this reason, greater residuals are often acceptable for observation wells far from the area of interest or for wells which are directly impacted by local pumping.

4.1.1 Calibration Process Description

For reasons described above, the steady state regional ASR model was calibrated to head data collected in both October 2003 and February 2004. The calibration process was a combination of "trial and error" calibration and automated calibration. The "trial and error" calibration involved making small changes to the input files, running SEAWAT and assessing the improvement made. This type of calibration is time consuming, but it also allows the modeler to inject his own knowledge and understanding of the hydrogeologic system into the calibration process. Further, through this tedious process, the modeler

develops an important understanding of the hydraulic stresses impacting the model and the sensitivities of both the input parameters and the calibration points.

The automated calibration technique employed for this model was an open source code called PEST (Parameter ESTimation), developed by Watermark Numerical Computing. PEST implements a variation of the Gauss-Marquardt-Levenberg method of nonlinear parameter estimation and can be strapped around a modeling code so that it calls the code numerous times with slightly different parameter values and analyzes the results (Watermark, 2004). In many cases, PEST can be very efficient, especially when running in parallel. During the course of this project we found it necessary to link up to 30 computers into a "pest nest." This allowed PEST to run 30 SEAWAT simulations simultaneously, resulting in a significant speed up in the calibration process. A drawback to automated calibration is that PEST only knows as much about the system as the modeler is able to tell it. Not all hydrogeologic knowledge is easily imparted in the PEST input files. Sometimes PEST can move too far from known data in an effort to closely match observed data.

During the course of the steady state calibration, it was found that the best calibration method was a combination of "trial and error" calibration with PEST calibration. The calibration results described in this section are the result of thousands of "trial and error" SEAWAT runs and tens of thousands of PEST-generated SEAWAT runs. The process also included numerous discussions with scientists from SFWMD to "truth-check" the calibration parameters against their superior local hydrogeologic knowledge and experience.

The main parameters varied for the steady state calibration were horizontal and vertical hydraulic conductivity for layers 2 through 22 (IAS through BZ). Although hydraulic conductivities were assigned to the SAS in the SEAWAT model, no calculations were made in this layer. The assigned hydraulic conductivities had a minor effect on the infiltration of recharge, but the effect was trivial enough that these conductivities were not varied during calibration.

The initial conductivity fields for all layers were designed by combining all the available information from the literature along with that provided by SFWMD or available in various online data repositories. The conductivity values were assigned in zones with constant values across each zone. The shapes of the zones were occasionally based on known structural changes, but more often were placed arbitrarily based on the locations of data points. As the calibration proceeded, many of these zones were split into smaller ones and some were combined or reshaped. A reasonable calibration was achieved using this method, although it often resulted in unrealistic sharp corners to head contour lines caused by sudden changes in conductivity between neighboring zones.

Eventually, the decision was made to convert the zonal hydraulic conductivity fields to a smooth, interpolated conductivity field. Although the placement of the interpolation points can be as arbitrary as the shape of the conductivity zones, this method allowed for a more credible conductivity field with few sudden changes in flow characteristics. The use of both the "trial and error" and automatic calibration using these interpolated conductivity fields achieved a much better calibration.

In PEST, the method for creating the smooth conductivity field is called the "pilot point method." Each aquifer or confining unit was given a set of "pilot points" placed somewhat randomly, but with a greater density in areas of expected heterogeneity. A hydraulic conductivity value was assigned to each point and a kriging algorithm (distributed with PEST for use with MODFLOW) was applied to assign a unique hydraulic conductivity value to each grid cell. This added an extra step to the calibration process. Each change to the input parameters was made by changing the conductivity of one or more pilot points, and then the kriging was repeated with the new points before SEAWAT was run with the new conductivity surface.

When running PEST for automated calibration, an option called "regularization" was employed to reduce the number of degrees of freedom and minimize the heterogeneity of the calibrated conductivity fields. The use of the pilot point method often leads to an under-constrained problem, where there are more pilot points than there are observation points. This can lead to non-uniqueness of the calibration solution. In other words, if there are too many pilot points, there will be numerous, possibly quite different, conductivity fields which will yield the same quality of calibration. Some of these sets of conductivity values can be eliminated because of known characteristics of the aquifers, but some cannot be eliminated without additional data. In the regularization method, PEST gives preference to solutions that minimize the variance of conductivity values assigned to neighboring pilot points. Thus, the result of a PEST regularization run is the smoothest set of conductivity fields which will yield a solution that matches the observed data within a user-defined tolerance.

4.1.2 Calibrated Hydraulic Conductivity Fields

Figures 4.31 through 4.40 show the final calibrated maps of hydraulic conductivity for all model layers. Aquifers are shown with horizontal hydraulic conductivities (vertical conductivities were always 1/10 of the horizontal value). Confining units are shown with vertical hydraulic conductivities (horizontal conductivities were always twice the vertical value).

The IAS layers are shown in Figures 4.31 through 4.33. In reality, this geologic layer is a complex combination of interbedded confining units and sub-regional aquifers. Because of the complexity of this system and because the ASR wells are not expected to impact this layer substantially, the IA and ICU were combined into layers 2 through 4 of the SEAWAT grid. The aquifer section was modeled in the northwestern portion of the model domain in layer 3 of the SEAWAT grid. The boundary between the aquifer and aquitard in this model layer is based on a figure in "The Hydrogeology of Florida" (Miller, 1997). All ICU layers have identical vertical hydraulic conductivities in the areas outside of this aquifer zone in both models. (Note that Figure 4.32 shows horizontal hydraulic conductivity, not vertical conductivity, so the colors are slightly different.) Variability was allowed between the ICU conductivities overlying (layer 2) and underlying (layer 4) the aquifer portion of the IAS to provide some variation in the source of pumped water in the IA. It is important to remember that the conductivity distributions for these layers are not expected to replicate reality. The model was not calibrated in the IAS and no attempt has been made to correctly simulate flow in this section. These layers act simply as a conduit for recharge water traveling to the UF and discharge water traveling to the surface. The objective was merely to correctly define these flows.

Figures 4.34 and 4.36 show the calibrated horizontal hydraulic conductivity values for the UF and APPZ. Small dots indicating measured conductivity values are overlain on the calibrated conductivity field in both figures for comparison between the model calibration and the field data. There was a significant amount of data available for both these layers; consequently, conductivities were not allowed to vary significantly from what has been measured during the calibration process. The UF (Figure 4.34) shows a zone of somewhat low conductivity along the Kissimmee River, with higher conductivities in the southern portion of the model. It is important to note that the lower conductivities found in the west portion of the model coincide with greater thickness, so the transmissivity does not drop as low as it may seem from this figure. This is also the area where the Hawthorn and Suwannee units are found. This model has combined both of these units into the UF, so the conductivities may vary somewhat from known measurements in either of these units. It is also interesting to note that the Kissimmee River ASR Pilot Project (KASR) is located in a small area of high conductivity. The drop in conductivity towards the east is documented, but the exact location and nature of this anomaly is unknown. The areas of lower conductivity which surround KASR may significantly impact the efficiency of the proposed CERP ASR wells in this area.

The conductivities in the APPZ (Figure 4.36) are low along the north-south ridges west of Kissimmee River and reach higher levels on the east side of the model, including an area of very high conductivity directly beneath the low conductivity area in the UF near KASR. The line between the northern dolomite rock and the southern limestone is one of the few sudden changes in conductivity in this model. The location of the interface between the two rocks is based on USGS Scientific Investigation Report 2007-5207 (Reese and Richardson, 2008) though its exact location may be unknown. Suggestions were made to try to soften the conversion from dolomite to limestone. Some early sensitivity analyses were run to determine the importance of the placement of that line, but the effects were minor and localized. Since the precise location of this line did not affect the regional calibration, the location of this interface was kept consistent with that depicted in USGS Scientific Investigation Report 2007-5207 (Reese and Richardson, 2008).

Figures 4.38 and 4.40 present the horizontal hydraulic conductivity fields for the LF1 and BZ layers of the model. Very little data was available for either layer. The final calibrated results show generally increasing conductivity to the southeastern portion of the model domain. This distribution is consistent with the current understanding of these deeper aquifers (Reese and Richardson, 2008). As mentioned previously, the northwest section of the BZ has been assigned conductivity values similar to those found in LF1 to account for the absence of the BZ in this area.

Finally, Figures 4.35, 4.37, and 4.39 show the vertical hydraulic conductivity values selected for the three confining units in the Floridan system. Although some data was available for these layers, it was used only as a loose constraint on the range of conductivities in each layer. The conductivity values in these layers were valuable tools in the calibration process since the model was highly sensitive to these parameters.

4.1.3 Description of the Steady State Calibration Quality

Figures 4.2 through 4.11 show the calibration target plots and the error statistics separated by layer and month. The UF steady state head solution and corresponding calibration targets in Figures 4.2 and 4.6 (February 2004 and October 2003, respectively) shows a good calibration. The RMS in both months is less than 2.2 feet with the mean error values very close to zero. The majority of the calibration targets are green, indicating a match within 2 feet of the measured head value. The exceptions are due to steep head gradients, near-well pumping effects or the inability to calibrate both months simultaneously (likely due to errors in the pumping estimates or lack of a local steady state condition). Some of these exceptions are described below:

- **ROMP 33 TMPA/SWNN in Manatee County and ROMP TR 5-2 SWNN and ROMP 22 SWNN in Sarasota County (See zoom on Figure 4.12)**: All three points calibrate well in one of the two steady state calibration months, but have a residual error of 2.0 to 2.5 feet in the other month. The inability to better calibrate these points for both October 2003 and February 2004 is likely due to pumping estimates or simplifications in the model in these counties. This error is considered acceptable for an area distant from the proposed ASR wells.

- **ROMP 32 SWNN and ROMP 25 SWNN near the boundary between Manatee and Hardee Counties (See zoom on Figure 4.12)**: The calibrated model calculates 2.5 and 3.2 feet low in October 2003 and about 3.0 and 1.5 feet high in February 2004 for ROMP 32 and ROMP 25, respectively. The inability to calibrate these points for both October 2003 and February 2004 is likely due to pumping estimates or simplifications in the model. In these situations, the aim was to model a state between the two months' data with a closer emphasis on February data.

- **L-2528 and L-2435, two wells in the Cape Coral area of Lee County (See zoom on Figure 4.13)**: These wells are greatly affected by large scale pumping. Because of the resolution of the grid, these near-field effects are not accurately simulated in the model. Additionally, the actual pumping locations had to be altered to coincide with cell centers, while observation well locations were not moved. Better calibration in this area cannot be expected on a model of this regional scale and is not necessary to evaluate the CERP ASR program. These wells are responsible for much of the RMS error of the UF. When these 2 wells are removed from the calculations, the RMS in February 2004 is 1.13 ft and in October 2003 is 1.26 ft.

- **ROMP DV-1 SWNN, CONE RANCH CM-10S UPL SUR, and Alston Deep FLDN in the northeast corner of Hillsborough County; and Lake Sawyer Well in the southwest corner of Orange County (see zoom in Figure 4.14)**: These wells are located in the steep gradient area around the recharge zone. Small changes to the horizontal locations of the substantial number of monitoring wells in these areas would result in improvements in the calibration. Since this area is not near the area of interest for the CERP ASR program, the resolution of the grid is coarse near these calibration points, preventing a better calibration. Further, the flow at these wells is from the recharge area towards the boundary and will not affect the CERP ASR sites, which are the main areas of emphasis for this model.

- **PBF-2 and PBF-3 in the central coastal area of Palm Beach County (see zoom in Figure 4.15)**: The calibrated heads for PBF-2 in October and February are both low by about 3 feet. A much better match is shown at PBF-3, approximately 3 miles away, where the calibrated heads for both months are only about 1 foot high. The model contours show that the computed heads drop off toward the coast along the length of Palm Beach County. Because the 2 wells are only 2 model cells apart and because the well closer to the coast (PBF-2) had a higher observed head, it would be very difficult for the model to calibrate both points. The calibration goal was to split the error between PBF-2 and PBF-3. Because PBF-3 is part of a UF, APPZ, LF1 well cluster, this well was favored in the calibration split.

The statistics and calibration targets for the APPZ steady state calibration are shown on Figures 4.3 and 4.7 (February 2004 and October 2003, respectively). These plots show slightly less error than the UF with the RMS less than 1.6 in both months. Most of the calibration points in this layer show a close similarity between calculated and measured heads. A few exceptions, described below, skew the statistics, but do not materially affect the usefulness of the model.

- **ROMP 86A AVPK located in Pasco County near the northwest boundary of the model (see zoom in Figure 4.16)**: This well is located at the edge of the recharge zone in an area of very steep gradient. A small change to the horizontal location of this well would result in improvement to the calibration at this point. Since this area is not near the area of interest for the CERP ASR program, the resolution of the grid is coarse near these calibration points, preventing a better calibration. Further, the flow at this well is from the recharge area towards the boundary and will not affect the CERP ASR sites, which are the main areas of emphasis for this model.

- **ROMP 30 AVPK and ROMP 25 AVPK in Hardee County and ROMP 28 AVPK in Hillsborough County (see zoom in Figure 4.17)**: The model calculates the October 2003 head 2.3, 1,4 and 2.2 feet low, respectively and the February 2004 head 1.4, 3.7 and 0.5 feet high, respectively. The inability to calibrate these points for both October 2003 and February 2004 is likely due to pumping estimates or simplifications in the model. In these situations, the aim was to model a state between the two months' data with a closer emphasis on February 2004 data.

- **ROMP 33 AVPK in Manatee County (see zoom in Figure 4.17)**: This well calibrates high by 2.2 feet in February 2004 and low in October 2003 by about 0.4 feet. Wells in this area are greatly affected by the Manatee County pumping, so the calibration error at this well is probably due to errors in pumping estimates or grid resolution.

Figures 4.4 and 4.8 show the head solution and calibration information for the LF1, while Figures 4.5 and 4.9 show the same data for the BZ. The unusual shapes in the head contours are due to the influence of density as caused by salinity and temperature and a great depth. At this depth, there is much less data for comparison, but the figure shows that all data has been matched very closely and the RMS values are impressive at less than 1 foot. Due to the small number of calibration points in the LF1 and BZ, an expanded calibration was performed in these layers.

Figures 4.10 and 4.11 show the head solution and a comparison of model results from the LF1 and BZ to data that has been collected for these units during a time period other than the calibration period. Since the water level data used for this expanded calibration was not from the modeled period, these figures use a confidence interval of 5 ft rather than the 2 ft interval used in the other calibration plots (i.e. green bars indicate agreement within 5 feet). The error statistics for this expanded calibration are consistent with that seen in the other layers of the model.

Another important aspect of the calibration is the comparison of gradients in the model to those measured in the field. Minor head differences in neighboring wells, if the residuals are of opposite signs, can impact flow rates significantly due to changes in gradient. This series of figures (4.18 through 4.28) presents the vertical gradients computed by the SEAWAT model (February 2004) as compared to gradients measured in the field.

Figure 4.18 presents the gradient comparison for the calibration model in February 2004 at the Alligator Alley well cluster in western Broward County. The model and the field data match very closely through the UF wells (G-2619 and G-2618) and the APPZ well (G-2617), showing almost no vertical gradient. Although there is no field data to verify the model-computed gradient changes in the confining unit, the overall gradient between the APPZ (G-2617) and the LF1 (G-2296) is nearly identical in the two plots.

Some readers may feel some concern about the shape of the head gradient plot presented at the left of Figure 4.18. Initially, it may seem that the plot indicates upward flow from the UF/APPZ to the surface and *downward* flow from the APPZ to the BZ. The reason for this seemingly anomalous result is that the heads presented here are observed heads, not equivalent fresh water heads. When the density effect is included by converting the observed head values to equivalent freshwater heads, the resulting gradient plot looks like that shown in the upper right corner of Figure 4.18. The deep layers with high levels of TDS actually exert a greater pressure on the water column resulting in an upward gradient in all layers. The remainder of the gradient plots will be shown with observed head values since this is the data measured in the field. However, the reader should be aware than these heads are not necessarily indicative of water flow direction. (See Section 2.1)

The majority of the well clusters shown in Figures 4.18 through 4.28 indicate a close agreement between model-calculated head gradients and field measured head gradients. All figures show February 2004 calibration results from the SEAWAT model. The following bullets will present a few comments on the plots of well clusters with poorer correlation in vertical gradient.

- **ROMP 86A in southwest Pasco County (Figure 4.19)**: This well is poorly calibrated with a head residual of about 5 feet in both the Suwannee and Avon Park zones. This well is located on the north side of the recharge area and so flow at this location has no effect on the ASR well locations to the south. However, it is encouraging to note that despite the head error (due likely to steep gradients and coarse grid resolution) the model is correctly calculating the gradient between the UF and APPZ layers of the model as shown by a nearly identical slope in the two lines.

- **ROMP 13 in the southeast corner of De Soto County (Figure 4.21) and ROMP TR 7-4 in Manatee County (Figure 4.23)**: Both the modeled gradient and the measured gradient at these wells are nearly flat between the UF and APPZ zones. The main differences in the plots are in the IAS layers and the SAS. As explained in Section 4.1.2, this model made no attempt to model either the SAS or the IAS section of the subsurface. The SAS was included only to simulate recharge and the IAS layers were intended only as a pass-through layer to regulate water reaching the UF or exiting at the surface. The small differences in gradient shown at these clusters are not important to the purposes of this ASR Regional Model.

- **Intercession City well cluster just west of the Kissimmee River in Osceola County (Figure 4.22)**: Here the gradient calculated by the model closely matches that measured in the field, with the exception of OSF-97. In this area, there is a very sudden, stark change in salinity which may not be replicated in the model because of lack of data and coarse vertical grid resolution. Because there is only one layer of cells in the BZ, the location of the salinity change in the model must be linear between the two bottom cells, making it difficult to precisely match the head at OSF-97. This area is deep and far from the ASR locations, so this minor error is not expected to be of great concern to the purposes of the model.

- **Hillsboro ASR well cluster in Palm Beach County (Figure 4.28)**: The model calculated gradient through the UF and APPZ layers closely matches the field measured data. Although the head variations in the MC2 layer cannot be verified because of a lack of field data, the overall gradient between the APPZ and the LF1 is nearly perfect at this well.

4.1.4 Comparison of Model Results to some Published Information

In an effort to further verify the model, the results were compared to the conclusions from two published reports. It is important to note that the conclusions in these reports were based on numerous assumptions, other models and sometimes minimal data. Minute differences between these published conclusions and the ASR regional model are not of concern. The purpose in this comparison was simply to show general agreement with other published work and analysis.

First, the model calculated recharge and discharge to the Upper Floridan layers was compared to the generalized recharge map published in USGS Water-Resources Investigations Report 88-4057 (Aucott, 1988). The recharge map presented in this USGS publication included data collection, analysis and some modeling. Figure 4.29 shows the comparison between the regional ASR model results and the USGS estimated recharge/discharge areas. Although there are minor differences, it is encouraging to note that the coastal areas and the southern half of the model domain are generally shown to be discharge areas by both analyses. Interestingly, the location of the model-calculated change from discharge to recharge north of Lake Okeechobee is very close to the estimated interface shown in the USGS figure. The northwest boundary area of the ASR regional model shows small areas of large discharge, interspersed with small areas of large recharge. These areas are likely caused by large changes in topography and coarse grid resolution in the ASR Regional Model. The fact that these areas of discharge are not shown in the USGS map is not cause for concern, especially since this area is separated from the ASR locations by the main recharge area.

The second comparison was made by rerunning the calibrated February 2004 SEAWAT model with all pumping removed (See Figure 4.30). The result of this "no-pumping" simulation was compared to the USGS (Bush and Johnston, 1988) published pre-development head contours for the UF. Because of the specified head boundary conditions along the south, west and north boundaries of the calibration model, it is impossible to completely remove pumping from the model. Drawdown caused by pumping would necessarily impact the measured heads in wells near the boundary, which were used to set the specified heads. However, despite this drawback, the correlation between the USGS estimated pre-development heads and the ASR no pumping heads is reasonable. The maximum head at the top of the recharge zone is nearly perfect, though the location is slightly different. The southern extent of the computed 70-foot contour is in good agreement with the USGS contour although along the eastern and western sides of the recharge area, the model underpredicts the USGS 70-foot contour by 5 to 10 feet. This discrepancy is the result of the discharge of the UF to low-lying river valleys where the surface heads are low. Another feature of the predevelopment heads captured in the model is that the 50-foot contour curves out along the eastern shore in Saint Lucie and Martin Counties more than the Bush and Johnston contour. Differences in the 40- and 50-foot contours along the west coast are mostly due to the implicit inclusion of pumping effects in the data used to determine the specified heads at the western boundary.

The most notable difference between the USGS predevelopment head contours and the computed head contours is the discontinuity of the computed 60-foot contour between the area of recharge from the surface and the southern 60-foot high southwest of Lake Okeechobee. Computed heads in this "trough area", in the vicinity of Lake Okeechobee and west along the Caloosahatchee River, are between 55 feet and 60 feet. While the difference is within the range of other differences observed between the predevelopment heads and computed heads, the trough indicates that Upper Floridan water south of Lake Okeechobee originates from a location other than the recharge area north of Lake Okeechobee. Bush and Johnston (1988) argued against this hypothesis. No data from the predevelopment time period exists to clarify whether the head trough existed. Head data from 2003-2004 at LaBelle and Kissimmee River Pilot site is less than 53 feet indicating a shallow trough similar to that shown in the model results exists under current "with-pumping" conditions. Geochemical data from a recently published study (Morrissey, S. K., et al, 2010) provides evidence that water found in the Upper Floridan aquifer in south Florida "is consistent with recharge from meteoric water during the last glacial period" rather than recent recharge from areas north of Lake Okeechobee. Considering this new evidence, it is entirely possible that a head trough such as that shown in the predevelopment model head results through the Caloosahatchee River/Lake Okeechobee area was present prior to development.

Although the match between the ASR regional model and these published conclusions cannot be considered to carry the same weight as comparisons to actual measured data, the close agreement helps to validate the model and shows concurrence with the conclusions being drawn by other scientists in South Florida.

4.2 Transient Calibration/Validation

In order to model the successive recharge, storage and recovery periods for the ASR wells, it was necessary that the ASR regional model be transient (i.e. include the time term in Equations 2.3 through 2.6). The addition of the time term necessitates a substantial increase in the number of parameters which can be varied during calibration. The hydraulic conductivity values had been tentatively set during the steady state calibration, though some iteration between the steady state and transient models occurred. Most of the transport parameters (porosity, dispersivity, and molecular diffusion coefficient) proved to be relatively insensitive on a regional scale due to the minimal TDS and temperature transport occurring on the small time scale of the model calibration and validation periods (15 months or less). Specific storage was found to be the most sensitive parameter during the transient calibration.

The convergence of the transient model was good in all timesteps for both flow and transport. Table 4.3 shows the mass balance and percent discrepancy for the flow portion of the model. The maximum percent discrepancy between flows in and out of the model is 0.0539%. Table 4.4 shows the percent discrepancy in the transport of the two modeled constituents: TDS and temperature (heat). All discrepancies are on the order of 10^{-8}% and 10^{-6}% for constituent transport.

The transient SEAWAT calibration proceeded in a manner similar to the steady state SEAWAT calibration. Initial specific storage values were assigned to polygonal zones and based on the available data. The storage data provided was divided by the aquifer thickness to derive the specific storage term used in the model. Storage data was much sparser than conductivity data. Calibration proceeded as a combination of "trial and error" calibration and automated calibration. PEST was again used as the code for automated calibration. Eventually, when significant progress had been made using the zonal specific storage fields, the pilot point method was again implemented to create smoothed fields of specific storage.

Figures 4.41 through 4.94 show the SEAWAT calibration at a number of observation wells which had significant data available. In each case, the observed and calculated heads are plotted during the 15 month calibration period (October 2003 through December 2004). Note that because of differing ranges of heads measured and calculated at each well, each plot has a different head scale on the y-axis. In order to facilitate the analysis of these plots, every graph has a horizontal grid line at every foot of head. In this way, the reader can tell, at a glance, whether the well has a large swing in heads (many grid lines) or has very little head variation (few grid lines).

4.2.1 Calibration Statistics

In addition to the visual inspection of the calibration at each observation point, a number of statistics were calculated at each point to aid in the calibration process. Each statistic compared the mean monthly heads in the observation dataset with the mean monthly heads from the model output. The first statistics were the mean residual error (ME), mean absolute error (MAE) and the RMS error. These equations were provided in Section 4 with the discussion of the steady state calibration (see Equations 4.1, 4.2 and 4.3). Additional statistics included the Coefficient of Determination (r^2) and the Nash-

Sutcliffe Model Efficiency Coefficient (E) as shown in Equations 4.4 and 4.5. The statistics for each point are listed in tables on Figures 4.41 through 4.94 and all are shown together on Figures 4.95 through 4.99.

$$r^2 = \frac{\left(\sum_{i=1}^{n}(c_i - \bar{c})(o_i - \bar{o})\right)^2}{\sum_{i=1}^{n}(c_i - \bar{c})^2 \sum_{i=1}^{n}(o_i - \bar{o})^2} \qquad \text{Equation 4.4}$$

where

r^2 = Coefficient of Determination

c_i = Average model calculated head during month *i*

$\bar{c}$ = Average calculated monthly head over all months

o_i = Average observed head during month *i*

$\bar{o}$ = Average observed monthly head over all months

$$E = 1 - \frac{\sum(o_i - c_i)^2}{\sum(o_i - \bar{o})^2} \qquad \text{Equation 4.5}$$

where

E = Nash-Sutcliffe Model Efficiency Coefficient (Nash and Sutcliffe, 1970)

None of these statistics alone can perfectly describe the calibration quality at every point. Each provides some information, but they all must be used together, coupled with a visual inspection of the model results. The mean error (Equation 4.1) shows the average residual between model calculations and observed data. Its optimum value is zero. The drawback to the use of this statistic is that positive and negative errors can cancel each other out, resulting in an unnaturally low mean error. An example of this effect is shown in the plot for Sarasota Well 9 (Figure 4.58). Here, the positive residual during the summer of 2004 cancels out the negative residual during the fall of 2004, resulting in a mean error of only 0.346. This low mean error overstates the calibration quality at this point.

This canceling effect can be best captured with a comparison between the mean error and the mean absolute error (Equation 4.2). In the calculation of the mean absolute error, the absolute value of the residual is taken before it is averaged. Again, the optimum value is zero. When the mean absolute error is very close to the mean error or when it is a similar value with the opposite sign, the cancelation effect is small. See OS0231 (Figure 4.52) where the mean error is -1.319 and the absolute error is 1.319 showing that there has been no cancelation of positive and negative residuals – all residuals in this case are negative. For Sarasota Well 9 (Figure 4.58), the mean absolute error is 1.991, much higher than the mean error, indicating significant cancelation of positive residuals with negative residuals.

The root mean square error (RMS) gives additional weight to large residuals and minimizes the impact of residuals less than 1.0 (Equation 4.3). Its optimum value is also zero. This result can help indicate the

variations in the residuals when it is compared to the mean absolute error. See, for example, PBF-2 (Figure 4.72). Here, the mean absolute residual is 2.997, while the RMS is only slightly higher at 3.036. The similarity of these two numbers indicates that every residual value was very close to -3 feet. Conversely, at ROMP 33 TMPA/SWNN (Figure 4.57), the mean absolute error is 3.691 while the RMS is larger, at 4.647. The difference in these two values is caused by a few months where the residual is large (November 2003, April 2004 and December 2004).

The mean error, mean absolute error and RMS do not take into account the ranges of observed heads at each well. All observation wells are held to the same standard whether they have wide swings in head values, or stay at a relatively constant head level. To account for this, the figures report each RMS value as a percentage of the range of observed heads at the well. Compare, for example, the Edgeville Deep Well 3 (Figure 4.60), with an RMS value of about 2.5, to BF-4S (Figure 4.74), which has an RMS value of about 1.5. A visual inspection of the two plots shows that, despite its higher RMS value, the Edgeville well calibration is much better than that at BF-4S. The variability at the Edgeville well is much larger – over 25 feet, compared to a range of only about 4 feet at BF-4S. The closer calibration at Edgeville is quantified by comparing the RMS values as percentages of the observed range – about 10% at Edgeville and 34% at BF-4S. Some modelers advocate a rule of thumb, requiring that the RMS of a calibrated model be less than 10% of the range of observations. The optimum value is, of course, zero.

The coefficient of determination (r^2) is a measure of the correlation of the observed vs. computed head values to a straight line (Equation 4.4). Its optimum value is 1.0. The importance of this statistic can be understood if one imagines a plot with the calculated heads on the y-axis and the observed heads on the x-axis. The model results and the observed dataset are used to place a point for each month in the calibration period. In a perfectly calibrated model, the computed head would equal the observed head, and all points would fall along the line y=x and the r^2 value would be 1.0. However, the r^2 value will also be 1.0 if the points fall along any straight line with any offset from the x axis or any slope. See, for example, TFRO-5 (Figure 4.84). The r^2 value at this well is 0.916, which is quite high compared to many of the other points. Although this point is fairly well calibrated, the model calculated head consistently falls about 1.8 feet higher than the observed head. The high r^2 value is an indication that the observed vs. computed heads would fall along a line with the equation $y = x + 1.8$. Some of the other statistics, such as the mean error and mean absolute error, alert us to the fact that the model is calculating slightly high. In this case, the high r^2 value when combined with an equivalent mean error and mean absolute error indicate that although the initial condition (based on a steady state run) is not perfectly calibrated, the heads at this well correctly respond to model stresses. The rise in head caused by the fall wet season closely matches that seen in the observed data.

ROMP 30 AVPK (Figure 4.80) is another example of a well where the high r^2 value (0.925) is deceiving. Here, the model is over-estimating the heads during the summer dry period and underestimating the heads during the fall of 2004 when the observed heads rise. The line that these points fall along is $y=mx + b$ where m is less than 1.0 and b is greater than zero. Despite these points, this well is not a particularly poorly calibrated point. The RMS is only 12% of the observed range of heads, but the quality of calibration is not as high as that indicated by the coefficient of determination.

The final statistic presented is the Nash-Sutcliffe Model Efficiency Coefficient (Equation 4.5). This equation was developed for quantifying the efficiency of a model for forecasting river flow and is seldom used for groundwater modeling studies. It is included at the request of IMC reviewers. When the Nash-Sutcliffe value is greater than zero, the model output is better than the observed data as a predictor of future conditions. When it is less than zero, the model is inefficient, i.e. the variation between calculated and observed values is greater than the variance in the observed data. The optimum value is 1.0. The comparison to the observed data variance takes into account the different head ranges at each well. In other words, points with smaller variations are held to higher standards than those with large variations.

When taken together, these statistics can help to quantify the calibration quality at any of the points. For example, OS0230 (Figure 4.52) has possibly the closest agreement between the observed and model calculated data. All of the statistical measures of the calibration at this point are very close to optimum values. Conversely, the worst calibration probably occurs at ROMP 17 SWNN (Figure 4.61) where all the statistical measures are far from optimum.

4.2.2 Transient Calibration Analysis - Heads

Because of the time discretization (constant boundary conditions and pumping for each month) it is impossible for the model to correctly calculate the head every single day. The goal of the calibration effort was to match gross seasonal variations in head, including the average head during the driest period (usually during the month of June 2004) and the average head during the wettest period (usually late fall 2004).

Because the model can only attempt a calculation of the average monthly heads, it is not surprising that the model will seldom match the lowest measured head (usually during the first few days of June 2004). Further, the time discretization often results in the lowest model-calculated head occurring several weeks after the lowest measured head. During June 2004, the head changes on nearly all observation wells indicate that significant pumping occurred during the first few days of the month and then abruptly stopped, causing a steep rise in water levels. Because of the ASR regional model's time discretization, this high pumping is averaged over the entire month, resulting in the lowest heads being calculated at the end of the month. See for example, the results at ROMP 9 SWNN in Sarasota County (Figure 4.62). The continued pumping during the month of June causes the model to calculate a lower head for the whole month of June, but the measured data shows a sudden, steep increase in head beginning in the first week of June.

It is significant that the pumping across the region exerts a much greater effect on the transient head data than the specific storage values. Section 3.5 and Appendix D detail some of the difficulties in collecting and using the pumping data. A huge percentage of the pumping data had to be estimated based on well type and seasonal averages.

These estimates of pumping caused additional problems during calibration. These are made clear by comparing the results at Edgeville Deep Well 3 in Manatee County (Figure 4.60) and BF-6 in Broward County (Figure 4.73). At Edgeville, the calibration is good until the last month of the model (December

2004). During December, the model results indicate a significant reduction in pumping which is not replicated in the measured data at this well. This implies that the pumping in the model in this area is incorrect – likely due to the failure of the assumptions made during the pumping estimated (described in Appendix D). There are a number of observation wells that show similar problems in the calibration during the month of December 2004.

Conversely, at BF-6, there is clearly a reduction in pumping during the months of November 2003 and January 2004, with a return to normal, seasonal pumping rates during December 2003 and after January 2004. In this case, the pumping data used in the model appear to closely match reality, as shown by the close similarity of the heads at this well.

Pumping estimation errors can also be the cause of the failure of the model to reproduce the low heads in the summer of 2004 or the high heads in the fall of 2004. As will be explained later in Section 6, the pumping data quality represents the single largest source of error to this model. The estimates made to fill in missing data are only sufficient to provide enough accuracy for gross, regional-scale estimates of the effects of the CERP ASR program. Because of pumping errors, the regional model cannot be used for near-scale problems or to answer questions requiring high accuracy.

The greatest effort during calibration was exerted to improve the agreement of the model to the observed heads near Lake Okeechobee and the other proposed ASR sites. For this reason, calibration near the north boundary is often poor. Especially near the Hillsborough River Valley, there are numerous wells and some are clearly reacting to stresses not included in the model. Many of the wells are located very close to the boundary, which was given a specified head boundary condition based on an average of the measured heads in nearby wells. Many wells near the model boundary can be recognized from their stair-step model results. See, for example, the Green Swamp Marsh well and the Eva Well Deep (Figure 4.45). Because these wells are so close to the boundary, they feel the effects of head changes immediately, and the computed head is nearly constant during each stress period. No changes to conductivity or storage would improve the calibration at the Eva Well. Only a change to the boundary condition could change this. However, the Eva well was determined to be too far from the boundary for use in the selection of boundary condition heads (See Appendix C).

Some wells (especially in the northwest) are very closely controlled by the specified heads in the SAS. See for example, the Alston Deep Well (Figure 4.46). Perhaps some improvement in the calibration at this point could be brought by reducing the hydraulic conductivity in the ICU layers, to reduce the impact of the SAS on the UF calibration point. However, this point is north of the Polk County recharge area and so the heads here will have little impact on the proposed CERP ASR sites.

The calibration in the northeast quadrant of the model (north of Lake Okeechobee and east of the Kissimmee River) is generally quite good. Most of the observation wells show a steep drop in head between February and May 2004, with a matching steep rise in head from June to October 2004. The model easily reproduces this effect. There are a few points with some possible data errors, which impact the statistics. For example, the observed data at SLF-74 (Figure 4.84) shows a sudden drop of about 1 foot during December 2003. The model more closely matches the data after this apparent

probe movement. The model is not able to perfectly reproduce the head rise during the late summer of 2004, but it does correctly time all major slope changes. SLF-76 (Figure 4.84) is at the same location in the APPZ and similarly does not perfectly match the rising head slope. This could be the result of slight errors in the regional pumping.

A similar probe error seems to have occurred at TCRK_GW2 (Figure 4.83) in June 2004. The model closely matches the observed heads before this time and follows the expected trend after this error. The statistics, which cannot account for the probe movement, are slightly worse than they would be if the error had not occurred.

The east coast calibration is fairly good between St. Lucie and Biscayne Bay. Generally, the steady state result used as the starting condition is within 1 or 2 feet of the observed value. However, because the variability in observed heads over the 15-month calibration period is so low, some of the statistics (notably the RMS as a percentage of observed range and the Nash-Sutcliffe value) are lower than could be hoped. Generally, the model is able to reproduce the effects of simulated stresses, despite the small errors in starting condition. For example, see PBF-2 and PBF-3 (Figure 4.72). PBF-2 is located closer to the coast, but its head is generally measured about 2 feet higher than PBF-3. This is caused by an unknown anomaly which is not included in the model. Therefore, the model computation sets the starting condition at PBF-2 about 2.5 feet too low while that at PBF-3 is about 1 foot too high. Because heads tend to drop close to the coastline towards the ocean outcrops, no acceptable changes to hydraulic conductivity can improve the steady state calibrations of these points. Since the error in starting condition is large compared to the range of measured heads, the statistics are far from optimum values. The Nash-Sutcliffe values are greatly negative in each case and the RMS values are large compared to the observed range of heads. The r^2 values are reasonable, which is an indication that the model is correctly reproducing the effects of seasonal stresses at these wells. The shape of both calibration plots is similar to that shown in the observed dataset, but the heads are shifted up or down. This calibration is as good as can be expected without a more detailed, more highly refined model. Without a better understanding of the local effects resulting in the reversal of heads in this area, no model can hope to reproduce these observations.

BF-4S (Figure 4.74) is an example of a problem with the pumping database. The model easily reproduces the sudden reduction in pumping which occurred in late January 2004, but does not hold the high heads long enough, nor does it reproduce the sudden resumption of pumping in June 2004. The model also shows the effects of a short stoppage in the pumping in October 2004 which is not shown in the observed water level dataset. The problems in collecting the pumping data and implementing it in the model are described in detail in Section 3.5 and Appendix D. This well shows an area where the assumptions used in that process did not hold true. No changes to either hydraulic conductivity or specific storage could improve the calibration at this point. Only better pumping data could improve the calibration in this area.

The calibration in the southern portion of the model (south of Lake Okeechobee and inland of the eastern coast) is generally quite good. At most points, the model calculated heads are within 1 or 2 feet of the observed heads and gross trends are correctly reproduced. As observed near the east coast,

some of these wells also suffer from poor statistics because of the small head variations seen in the observed datasets. While the mean error, RMS and r^2 values are generally quite good, the RMS as a percentage of the observed range and the Nash-Sutcliffe values are both poor. This is not especially worrisome since the model reproduces the trends seen in the observed datasets and the actual differences between observed and calculated heads are small.

The section of the model just south of Tampa Bay (Manatee and Sarasota Counties) is generally well calibrated. The statistics in this area are all near optimum values and the visual comparison between calculated and observed heads shows a close similarity. The largest head swings in the model occur in this area, resulting in an advantage in the statistics.

The area which caused the greatest problems during the transient calibration is the area surrounding Port Charlotte (DeSoto, Charlotte and Lee Counties). The statistics in these areas are generally poor and visual inspection of the results indicates that the heads at several wells are not acceptably reproduced by the model. During trial and error calibration, substantial heterogeneity was added to the storage in this area. Wells located near each other were found to have quite different storage requirements. It is believed that the calibration issues in this area are the result of a number of complications. Head variations in the IAS in this area exert a marked effect on the lower layers. There is a great deal of pumping in this area, including the Peace River ASR. The model has also been simplified in this area by combining the Suwannee and Hawthorn aquifers into the UF and by simplifying the IAS and ICU layers. Because this area is away from the proposed CERP ASR sites, the cell sizes are large. The main conclusion after extensive calibration efforts focused on this area was that this model is too coarse and over-simplified in this region to accurately reproduce the measured heads in all of the observation wells. This is not unexpected in a regional model of this scale and is not worrisome since most of the ASR locations are away from this area. The closest CERP ASR site to this area is located at Riverbend on the Caloosahatchee River, which is about 10 miles east of the problem area. LAB-MZ1 (located close to the Riverbend site; Figure 4.66) calibrates quite well.

The greatest effort in calibration was applied in the areas around Lake Okeechobee where most of the CERP ASR wells are proposed. Calibration at these points is generally good. See Figures 4.68, 4.70, and 4.71 for a visual analysis of the calibration in the UF. Statistics at these wells (L2-PW2, MF-37, PBF-7U, and OKF-100) are also quite good, with Nash-Sutcliffe values all above zero, r^2 values above 0.5, and RMS values less than 25% of the observed head ranges.

The calibration near the Hillsboro Pilot Site (and proposed site for 30 CERP ASR wells) is not as good as that around the Lake Okeechobee sites. See the calibration plot for PBF-10R in Figure 4.73. Although the steady state calibration resulted in a starting condition about 1 foot higher than the observed October 2003 head, the transient model reproduced relative head changes quite well until September 2004. During the last few months of the model, the head in this area seems to be heavily impacted by the cessation of pumping nearby. But this impact is not felt in the observed dataset. This is probably the result of an error in the pumping dataset or in the assumptions used to estimate missing data. These few months of poor calibration, in conjunction with the small range of heads measured at this well (just over 2 feet of variation), result in the poorer calibration statistics at this point.

4.2.3 Transient Calibration Analysis – Vertical Gradients

Figures 4.100 through 4.110 show the vertical gradient plots (similar to those in Figure 4.18 through 4.28 for the steady state calibration). In these plots, the model results are compared to measured data at the end of May 2004 and October 2004. May and June 2004 generally represent the lowest heads of the period, while the highest heads of the period are often measured in October 2004.

Generally the gradients do not change significantly during the year. The model tends to do a better job of predicting fall 2004 gradients and heads than it does for summer 2004. As explained above, this is generally due to coarse time and grid discretization and the likelihood of errors in the pumping data, especially where it was estimated.

4.2.4 Transient Calibration Analysis – Conclusion

In general, the model is a good representation of groundwater conditions on a regional scale. Although some measured data in a few areas could not be reproduced by the model, the areas nearest the proposed ASR sites have good calibrations. This meets the goal of the regional modeling effort, since it was never the intent to reproduce local anomalies or near field effects of pumping wells with this scale of model.

The specific storage terms used in the calibrated transient model are presented in Figures 4.111 through 4.118. Conductivity values were the same as those used for the steady state model (See Section 4.1). Table 4.5 presents the other transport parameters used in the transient model. These parameters were selected to be similar to generally accepted values. Their sensitivity will be discussed in Section 5.2 and 5.3.

In addition to the 2003/2004 calibration period, the final set of hydraulic conductivity and specific storage values were applied to the validation period from October 1993 to July 1994. These results are presented in Figures 4.119 through 4.150. Like the calibration model, the first timestep of the validation model (October 1993) was run in steady state mode to develop a starting condition for the model. There is less agreement between the field data and the model results in October 1993 than in October 2003 (start of the transient calibration model period). This causes an initial offset in the transient validation result plots. Some of the problem wells had no available data in the 2003/2004 calibration period, so they were not included in the steady state calibration process. Others are probably the result of errors in the assumptions made during the estimation of missing pumping data or in the estimation of missing head data for the boundary conditions. Still, despite these starting condition errors, the model was able to reproduce the general shape of the head plots in the majority of the observation wells.

ROMP 58 NRSD in Polk County (Figure 4.140) was measured with a nearly constant head around 120 feet for the last 8 months of the validation period. However, the model produced a widely varying head signature with the highest heads about 110 feet in the winter and fall seasons, and the lowest heads, about 100 feet, in the late spring. It is believed that the data for this well is faulty or a pump that was not operational during the validation period was wrongly incorporated into the model, resulting in modeled heads that are lower and have more variation than the observed data.

As with the calibration period, the statistics for the transient validation run are shown spatially on Figures 4.151 through 4.155.

The validation exercise indicates that this regional model can be used for answering broad, regional questions whenever the pumping and boundary heads are known to a reasonable degree. Use of this model to reproduce D13R periods or to predict future aquifer changes must be made only with the understanding that the results are only as good as the estimates for pumping and boundary conditions.

4.3 Model Analysis

An analysis of the model calculations of velocity, flow directions and boundary flux can be instructive. Figures 4.156 through 4.159 show the model results when converted to equivalent freshwater head using Equations 2.1 and 2.2. Unlike the observed type heads output from the model, equivalent freshwater heads (which include density effects) are a measure of potential energy, and groundwater flows perpendicular to these contours from areas of high to low head. Because of the shallow depths and low salinity levels, the UF equivalent freshwater heads are not significantly different from the model output observed heads (see Figure 4.156), with the exception of the Atlantic Ocean outcrop location (where salinities are high). Generally, recharge occurs in Polk County and water flows towards the ocean to the east, south and west. Significant pumping is clear at several points along the west coast, especially in the Pasco County Area and in Lee County. Both figures show an area of high heads southwest of Lake Okeechobee.

Differences between observed head and equivalent freshwater head are also minor in most areas of the APPZ (Figure 4.157). Most differences are at the coastline where salinities are higher. As with the UF, the main source of water is the recharge in Polk County. The bubble of high head in Hendry County is also visible

More significant disparity is observed when the model output is compared to equivalent freshwater heads in the LF1 layer (Figure 4.158). Here, the high salinity has caused a significant depression in measured heads in many areas of the model. Flow is still infiltrating from the surface in Polk County and significant flows still move east and west towards boundary sinks in Hillsborough and Brevard Counties. Additional flow seems to be moving northward from the Everglades area. Much of this flow moves upward into more shallow layers (APPZ, UF) in the center of the peninsula (Charlotte, Glades, and Palm Beach County) instead of continuing northward in the LF1 layer.

Because of its high salinity, great depth and large temperature variation, the calculation of equivalent freshwater head has the greatest impact on the BZ layer (Figure 4.159). Density effects cause huge changes in head values. The recharge from the surface in Polk County is still visible. But a large contingent of the flow comes in from the east and south coast, moving north and northwest to exit in Hillsborough or Orange Counties. The BZ provides a significant amount of pressure on the upper layers and is an important component of the groundwater system in south Florida.

Flow vectors are shown for a number of cross-sections of the model in Figures 4.160 and 4.161. Vectors in these plots are printed for every eighth cell, so closely spaced vectors occur where cell sizes are small

to provide additional resolution and accuracy (see Section 2.3). These figures make several important points clear:

- Flow is mostly horizontal in the aquifers and vertical in the confining units
- Recharge in Polk County causes downward flow all the way to the BZ.
- Inward flow in the BZ along the lower east coast is a significant source of water pressure throughout the model.
- Most flow is upward in the southern half of the model (south of Lake Okeechobee)

Figure 4.162 shows the discharge and recharge to the top of the IAS, UF, APPZ and LF1 layers. In this figure, recharge (green, yellow and red colors) indicate downward flow while discharge (blue colors) indicates upward flow. As expected the southern and eastern parts of the model show upward flow in every layer. The Polk County recharge area is clearly depicted with downward flow in every layer. As explained previously, the mottled red and blue sections at the northwest boundary of the model are caused by significant variability in the topography and the specified surface heads, combined with a course grid resolution.

Finally, Figure 4.163 tabulates the flow in and out of the boundaries of the model in each aquifer layer. Of note are the large flow into the model through the BZ Atlantic boundary and the larger flow out of the model through the UF Northern Boundary. Initially it appears that the majority (78%) of the BZ Atlantic inflow (589 mgd) is being lost through the western boundary (460 mgd). However, the BZ is also home to a number of large injection wells, which add a significant amount of flow to the model. Major injectors include 17 Miami-Dade South wells, 4 of the 5 G.T. Lohmeyer wells, 6 Broward County wells and 3 City of Sunrise wells. Together, these wells inject nearly 200 mgd during February 2004. Most of this flow exits through the western boundary in the BZ, accounting for over 40% of the outward flow through the western boundary.

When taken together these visualizations of the model results indicate that the major sources of flow to the model are the Boulder Zone along the southern and eastern boundaries of the model and the precipitation recharge in the highlands of Polk County. BZ flow continues north and west, eventually moving upward to meet other layers of the model. The effects of recharge in Polk County reach as deep as the BZ and result in radial flow vectors out to the south, east and west from the recharge area. An area of high freshwater head is also found southwest of Lake Okeechobee from which flow vectors move radially outward (See Section 4.1.4 for additional details).

5.0 Sensitivity Simulations

In order to evaluate the effect of various assumptions made in the modeling process, several sensitivity analyses were performed. The following subsections describe these analyses and the uncertainty inherent in the model.

5.1 Advection Solution

SEAWAT provides several solver options for the advection solution. The majority of the model runs made during calibration used the standard finite difference method with upstream weighting. The timesteps were set to about 5 days. (See Section 2.4) Using these settings, a steady state solution could be computed in less than 3 minutes and a transient solution in less than 1.5 hours, for most available computers. This method is known to be less accurate than the third-order TVD scheme, but it is also much faster. In order to ensure that the accuracy loss due to time constraints was not excessive, a sensitivity run was made for the transient calibrated model using the TVD scheme. Since the first timestep of the transient model computes a steady state solution, both model types were tested together in this way. When this solution method is used, the model selects the timestep size based on the user defined Courant number. The transient model was run with Courant number set to 1.0 and 0.5. With these settings, the transient models took between 12 and 15 hours to run to solution.

The transient TVD model results are compared to the transient FDM results at the timestep with the maximum differences in Figure 5.1. This timestep corresponds to December 10, 2004 which is Day 407 of the total of 428 days modeled. The head difference between the TVD and FDM solutions was over one foot at only a few isolated cells. None of the calibration points show changes significant enough to have affected the calibration. The maximum head change at any observation point during the first (steady state) timestep was less than 0.5 feet, with the average difference less than 0.2 feet. For the transient solutions at each timestep, the maximum head difference was 2.7 feet, but the average was less than 0.1 foot. Most of the differences are found during precipitous changes in head. At these times, the TVD solution has a slightly greater change (perhaps 0.5 feet) immediately after the change begins, but within 2 or 3 timesteps, it again matches the FDM solution. Only nine observation wells were impacted by more than 1.0 foot when the solution method was changed. All nine are located in Hillsborough, Manatee, De Soto or Sarasota County and have head variations of 20 to 45 feet over the calibration period, indicating significant impacts from pumping. Similarly, the head differences shown in Figure 5.1 across the model domain are most significant in this area.

Salinity and temperature results when the TVD advection scheme is activated are also nearly identical to the calibration run salinity and temperature results. A few, isolated cells where the initial salinity gradient between neighboring cells is large (especially near the ocean outcrop) were affected with differences up to about 1,050 mg/L TDS for the final timestep. The temperature differences in the Floridan aquifer at the final timestep vary from -1.3˚C to 0.6˚C in isolated cells near the model boundaries.

That the selection of a solver had little effect on the model results or the calibration supports the early decision to calibrate with the FDM solver, despite concerns about the accuracy of the results. The biggest impact occurred where pumping and head variations were largest. Because the ASR program will involve significant pumping and large head changes, final production runs of the CERP ASR program should be calculated using the TVD solver. However, because the differences are minor, intermediate runs will continue to be made using the FDM solver in order to take advantage of the significant time savings. The opportunity to achieve these time savings using the SEAWAT FDM solver is part of the

reason that the WASH123D model will not be used in the future phases of this project. WASH123D does not provide a faster solver alternative.

5.2 Porosity

Transport properties such as porosity were largely ignored during calibration. Because the model does not have a traditional "plume," with a sharp front, whose movement through the model domain is being estimated, porosity was not expected to be a significant factor in the model results. In the calibrated model, aquifers were given a porosity of 0.25, the IAS, a value of 0.4 and all other confining units, a value of 0.3. Three additional sensitivity runs were made to ensure that the results were not sensitive to porosity. The porosity values used are shown in Table 5.1.

These porosity changes made no discernible difference to any of the heads at the calibration points. Across the grid, the head differences were minor. When compared to the calibration run, the greatest difference in head occurred in the Boulder Zone in Porosity Sensitivity Run 1 during the last time step of the model. During this time step, there were 39 cells with a difference in head ranging from 1 foot to 14.5 feet. The areas that showed the greatest difference were isolated and coincident with the locations of deep injection wells along the coast in Indian River, Palm Beach, Broward, and Miami-Dade Counties. Porosity Sensitivity Run 3 resulted in smaller head differences when compared to the calibration run, with 25 cells having a difference between 1 foot and 6 feet in the Boulder Zone during the last time step. The differences were observed in the same locations as the differences in Run 1. Porosity Sensitivity Run 2 showed no differences in head greater than 1 foot when compared to the calibration run. Over the majority of the model domain, the difference was less than 0.1 feet for all the sensitivity runs. Regionally, the differences were small enough to eliminate the need for a figure.

Variations in porosity also caused only minor differences in calculated salinity and temperature. The greatest difference occurred in the Boulder Zone during the final time step of Sensitivity Run 1. A few isolated areas of the Boulder Zone in Broward County had differences of up to 5,500 mg/L TDS and 2˚C in this time step, but most differences were less than 10 mg/L TDS and 0.1˚C across the rest of the model.

These runs indicate that the sensitivity of the regional model is within the acceptable error of the calibration. The difference caused by changes to input porosity is negligible. It is anticipated that porosity will have a more marked effect on the local scale models which simulate the ASR pumping schedules in more detail.

5.3 Dispersion/Diffusion

Like porosity, dispersion and diffusion were expected to have minimal effects on the flow of temperature or salinity in the groundwater because the concentration and temperature gradients are usually not very sharp. During calibration, the longitudinal dispersivity was set at 2.5 feet with the ratios for horizontal to transverse and vertical to transverse dispersivity set to 1 (meaning dispersivity in every direction was 2.5 feet). In order to verify that this parameter is unimportant to the regional model, four additional model runs were made with varying dispersivity as shown in Table 5.2.

Figures 5.2 through 5.9 show the difference in head between the calibrated model and each sensitivity run. Runs 2 through 4 (Figures 5.4-5.9) had only minor effects on the calibration point heads. Run 1 (Figures 5.2 and 5.3), which increased longitudinal dispersivity from 2.5 feet to 25.0 feet, did have a marked effect on some of the calibration points. Most of the differences in head between the calibrated model and the sensitivity runs can be attributed to wells injecting fresh water into a comparatively more saline aquifer. Overall, there is little effect near the proposed ASR project sites.

Additional calibration of the dispersivity values will be performed with the local scale models using the ASR pilot study data at the Kissimmee and Hillsboro sites. Further, the results of this sensitivity run indicate that a range of dispersivity values should be used in the running of the production runs on the regional model.

Molecular diffusion was ignored for both salinity and temperature during calibration by setting the effective molecular diffusion coefficient to 0.0 ft^2/d. To test its sensitivity, an additional run was made using published information to estimate effective molecular diffusion coefficients for salinity and temperature.

Fetter (1999) provides a table of diffusion coefficients for common ions and recommends multiplying by ω, a coefficient related to tortuosity. The ions in Fetter's table have diffusion coefficients ranging from 5.5e-4 ft^2/d to 8.7e-3 ft^2/d. Fetter quotes Freeze and Cherry (1979) as giving a range for ω of 0.01 to 0.5. When this range is applied, the result is a range of effective molecular diffusion coefficients of 5.5e-6 ft^2/d to 4.3e-3 ft^3/d. 5.0e-4 was selected since it is close to the upper end of this range and is near the value for Na^+.

The source for the diffusion coefficient for heat was obtained from the 2007 SEAWAT manual (Langevin, et al). This report provides the following equation for molecular diffusion of heat:

$$D_{m\_temp} = \frac{k_{Tbulk}}{\theta \rho c_{Pfluid}} \qquad \text{Equation 5.1}$$

Where

k_{Tbulk} = Bulk thermal diffusivity
ϑ = Porosity
ρ = Fluid density
c_{Pfluid} = Specific heat capacity of fluid

Langevin, et al, suggests calculating the bulk thermal diffusivity using either an arithmetic mean or geometric mean (weighted by volume) of the water and solid. The accompanying table lists the bulk thermal diffusivity of freshwater at 0.58 W/mK and for limestone at 1.26 – 2.15 W/mK. However, this calculation (with a range of porosities from 0.25 to 0.4) yields a range of bulk thermal diffusivities of 0.92 to 1.61 W/mK. When applied to Equation 5.1 with the same range of porosities, a density of 2.7e3 kg/m^3 for limestone and specific heat capacity for freshwater of 4.186 (both from Table 2 in Langevin, et al), a range of effective diffusion for heat is 0.2 to 0.5 ft^2/d. The maximum value (0.5) was used in the sensitivity analysis. Clearly, this can only be an estimate since not all materials in the model are

limestone and not all the water is fresh. However, the variation is sufficient to indicate the sensitivity of the parameter.

As expected, molecular diffusion proved to be an insensitive parameter. At the calibration points, there was no discernible difference between the calibration run and the sensitivity run. When compared at each cell in the Floridan aquifer, a few cells (primarily in deep layers) had head differences up to about 2.5 feet, but the vast majority of the cells had head differences less than 0.1 feet. The highest head differences occurred at isolated locations in the Lower Confining Unit in Hardee County and on the border of Manatee and Sarasota Counties, well away from the proposed ASR locations. Differences in salinity caused by the diffusion coefficient changes were negligible, with a maximum difference of less than 100 mg/L TDS. Similarly, the diffusion coefficient changes caused no more than about 2° C change in the temperature calculated at the end of the 15 month simulation. As with porosity, the sensitivity of diffusion was not significant enough to warrant a figure.

5.4 Boulder Zone Thickness

As explained in Section 3.2.1, there was no specific data on the thickness of the Boulder Zone. Available estimates of the thickness were roughly averaged to 500 feet. This thickness was applied uniformly to the bottom layer of the model. However, because the flow in the Boulder Zone can have a large impact on flow and pressure conditions in all areas of the model, a number of sensitivity runs were made in an attempt to quantify the uncertainty introduced to the model by this assumption. The first two sensitivity runs simply changed the thickness of the layer across the domain. One doubled the thickness to 1000 feet and the other halved the thickness to 250 feet.

The next two sensitivity runs were made by changing both the thickness of the bottom layer and the assigned horizontal and vertical conductivity values for this layer. Data on the hydraulic material properties for this layer were nearly as sparse as thickness data. Although the thickness may be wrong, the calibrated conductivity value is based on this thickness and there may be a number of combinations of thicknesses and conductivity values which will lead to the same result. In the absence of local flow impacts such as wells, Darcy's law indicates that when the thickness of the aquifer is doubled, horizontal flow rates can be preserved by halving horizontal conductivity. Conversely, vertical flow can be retained by doubling vertical conductivity. Thus, two additional sensitivity runs were made to test this theory. The complete list of sensitivity runs testing the effect of the Boulder Zone thickness is shown in Table 5.3.

For the transient model, these changes had no effect on the rate of head change or the shape of the head vs. time plot. The Boulder Zone properties only affected the initial steady state stress period and thus, the starting condition of the plot. Each run was a nearly perfect copy of the calibration run with an offset which varied based on the location of the well and the particular sensitivity run. For this reason, the remainder of this section will deal only with the steady state solution comparisons.

As expected, Runs 1 and 2 resulted in rather large changes to the steady state head solution. The heads in the south and east portions of the model were significantly higher for Run 1 (with a thicker BZ layer) than for the calibration run and they were lower for Run 2 (which had a thinner BZ layer). This is

because the BZ provides a large portion of the water to the southern part of the model. The heads in the northwest section of the model were much less affected by Boulder Zone changes. Runs 3 and 4 were much less different from the Calibration results. The changes to the conductivity did not perfectly remove the effects of the thickness change due to complexities in the flow conditions.

The calibration statistics for the February 2004 steady state model are shown in Table 5.4. Notice that Run 2 and 4 often have statistics nearly as low as the calibration run, and in some cases, the statistics are lower than the calibration run. Figure 5.10 shows the Upper Floridan aquifer solution and the calibration targets as an example. Similar effects were seen in the deeper layers.

This study indicates that although the thickness of the Boulder Zone is an unknown and can cause marked effects on the results of the model, the effects of the zone thickness can be offset by the effects of the zone conductivity values, which are equally poorly known. The combination of Boulder Zone thickness and Boulder Zone conductivity have resulted in a calibrated model which can be used to estimate the effects of ASR wells on a gross, regional scale. When the production scenarios are built to evaluate the CERP ASR program, a range of BZ thicknesses and conductivity values will be used to ensure that uncertainty due to this data gap is considered in evaluating model predictions.

5.5 Specified Head Boundaries

As explained in Section 3.3, the use of specified head boundaries is not recommended where there is the possibility of impacts to boundary heads from interior hydraulic conditions. The reasons for selection of specified heads despite the drawbacks are outlined in Section 3.3 and Appendix C. There are two areas of the boundary where available head data was sparse and specified heads assigned are questionable: along the north boundary between Orlando and Tampa, and along the boundary as it passes through Everglades National Park. In order to ascertain the impacts of the assumption of specified heads at these areas, several additional sensitivity runs were made.

5.5.1 North Boundary

Between Orlando and Tampa, the north boundary of the model passes through some areas of increased head and low salinity, caused by high recharge. Some data is available in the upper layers of the model, especially the UF and APPZ. As explained in Appendix C, the gradient in this area was assumed to be downward, but not especially steep. Equivalent freshwater heads in the deeper layers were set just slightly below the values found in the upper layers.

Two sensitivity runs were made to verify that possible errors in the assumptions made in setting up the northern specified head boundaries are unimportant to the purposes of the model. A section of cells from Tampa to Orlando were selected. In one run, the specified heads in the LF1 were dropped by 5 feet and the heads in the BZ were dropped by 10 feet. This assumes a small but significant downward gradient. For the second run, the specified heads in the LF1 were decreased by 20 feet and the heads in the BZ were decreased by 40 feet. This assumes a large downward gradient. For simplicity's sake, the change in boundary conditions was not gradual near Tampa or Orlando, so the local flow conditions at

each end of the selected section of cells are expected to look unusual. However, this simple method is sufficient to determine the regional impact of possible errors in the head assigned at the boundary.

These changes to the north boundary had only a localized effect on the results of the model. The effect was only to the starting condition (initial steady state solution for October 31.) The transient solutions were parallel to the transient calibrated solution. Only a few observation wells displayed differences in head. The largest differences were at the Intercession City observation well in both the LF1 and the BZ. The first sensitivity run (which reduced the Boulder Zone specified head by 10 feet and the LF1 specified head by 5 feet) resulted in a reduction in head at the Intercession City well of about 1 foot in both aquifers. The second run (reducing the Boulder Zone head by 40 feet and the LF1 by 20 feet) caused a drop at Intercession city of about 4 feet in both aquifers. Smaller differences were also observed at two northern LF1 observations wells, OSF-82L and OS0025. The differences at these wells were 0.1 feet and 0.5 feet at OS0025 and 0.7 feet and 2.8 feet at OSF-82L for the first and second sensitivity runs, respectively.

Figure 5.11 shows the head changes caused by these alterations to the BZ and LF1 boundary conditions. As expected, the greatest changes are in the immediate vicinity of the northwest boundary. The effect of the boundary condition extends less than 50 miles from the boundary and does not affect the heads at the proposed ASR well locations. No discernible differences were observed in any of the other aquifer layers. Although there may be disagreement about the applied gradient at the northwest boundary of the model, it has no effect on the end purposes of the ASR Regional Model.

5.5.2 Southwest Boundary

Some concern has been raised about the specified head assigned through the Everglades because of the impression that there is very little data available in this area. As shown in Figure 3.17, there are actually several wells in this area which were used for assigning the specified heads at this boundary. However, in order to verify these values, two sensitivity runs were made to show that there is very little impact to the interior of the model. In one sensitivity run, all of the specified heads in the UF were removed from the counties of Collier, Monroe and the western half of Miami-Dade. This is equivalent to defining a no-flow boundary at this location. The second run removed all specified heads in same area for all layers.

Neither of these sensitivity runs had significant effects on the calibration of the steady state model as shown in Table 5.5 which compares the RMS of the calibration runs to the RMS from these two sensitivity runs. Cutting off flow through the UF boundary on the southwest edge of the model resulted in no change to the calibration statistics in the UF, APPZ, and BZ and a change of only 0.01 in the LF1. The change is greater when the flow in all aquifers is cut off, but it is still very small, with a maximum change in RMS of 0.4, occurring in both the APPZ and the LF1.

Figures 5.12 and 5.13 show the difference between the head calculated by the calibration model run and each of these sensitivity runs. When the outbound flow in the UF is blocked along the southwest boundary, the head in the UF rises in the area of the Everglades and decreases in the Naples area. However, the area of difference is small – about 25 miles from the boundary -- and the head change is less than 1 foot. This boundary change also impacted the APPZ in about the same area, though the

heads right at the boundary are fixed, so there is no change in the first line of cells. Some small changes occurred in the IAS, but there was no impact to either the LF1 or the BZ.

When the flow was blocked to all aquifers (Figure 5.13), the magnitude of the head changes are greater and the area of impact is greater – extending nearly 100 miles in from the boundary for the UF, APPZ, LF1 and BZ. The extent of the effects in the IAS is smaller – extending only 55 miles from the boundary. However, the highest magnitude changes in head occur in the IAS with a maximum drop of 73 feet. In the calibrated model, significant IAS pumping in Collier County pulls water into the model from the boundary. When this boundary inflow is blocked, pumping drawdown increases.

It is also interesting to note that the effects are less pronounced in the BZ. Initially, this appears to contradict the flow regime shown in Figure 4.163, which indicates a significant flow component exiting the model through the BZ in the Everglades region. However, because of the larger conductivities present in the BZ, the excess water is able to more easily move to a secondary exit location (the south end of the model in Miami-Dade county, just outside the Everglades boundary). Layers above the BZ (LF1 and APPZ) have a smaller flow component crossing this boundary in the calibration model, but the effects of the boundary condition change are greater because lower conductivity values make it harder for water to find other avenues to leave the model and the heads build up.

Although the results of the sensitivities show that some minor impacts would extend to areas near proposed ASR wells, the sensitivities represent an extreme condition. By assigning a no-flow boundary to all the layers along the southwest boundary, the heads respond in a way that is not supported by available data. Figure 3.17 shows there are several available data points along the southwest boundary in the IAS, UF, APPZ, and LF1 that were used to set a specified head. Thus a no-flow boundary is not reasonable in this region.

5.5.3 Confining Units Boundary

As explained in Section 3.3, the SEAWAT model uses time-variant specified-head boundary conditions for the aquifers and Atlantic Ocean outcrops of the confining units. No-flow boundaries were assigned to the confining units on the inland sides of the model (north, west, south) because horizontal flow in these cells is limited and not believed to be a significant source or sink of groundwater. IMC reviewers raised the concern that horizontal flow in these units might be important. To determine the effect of boundary condition choice on the computed model results, a new steady state SEAWAT simulation was created using data from October 2003 and changing the no-flow boundary conditions to specified heads along the north, west and south boundaries of the confining unit layers. Linear interpolation between the overlying and underlying aquifer heads was used to determine the head for each new specified head cell. A steady state simulation was run using the newly created specified head boundary conditions, and the results were compared to the October 2003 calibration.

Only minor differences in head were observed when comparing the two model runs, with none of the observed differences having an effect on the groundwater at the proposed CERP ASR sites. The greatest differences in head are located along the boundaries of the confining units. Figure 5.14 shows the difference in head in the confining unit layers between the October 2003 calibration and the sensitivity

run. The difference in head is mostly observed along the boundary or within one or two cells of the boundary. The exception to this is seen in layers 2, 3, and 4 in Collier County and is due to a minor oversight in assigning the original boundary conditions to the IA (layer 3). When the boundary conditions were initially set, the specified head boundary applied to layer 3 was terminated just north of the southern border of Collier County (see Figure 3.17) at the last point with available observation data. However, the aquifer portion of layer 3 extends slightly farther southeast into Monroe County, leaving a small section of the aquifer with no boundary condition assigned. This section of aquifer boundary without an applied specified head boundary condition resulted in the difference in head seen in Figure 5.14 in layers 2 through 4. Even with this omission, the effects do not extend to any of the proposed CERP ASR sites.

In the aquifers, the only notable difference in computed head was observed within one to two cells of the boundary in the vicinity of Cape Coral. These differences were also only seen in the UF and APPZ. The maximum head difference in the UF is less than 0.9 feet, and less than 100 cells were changed by more than 0.1 feet. In the APPZ, the maximum head difference is less than 0.6 feet, with less than 50 cells being changed by more than 0.1 feet. These results indicate that the use of a no-flow boundary condition on the land boundaries of the confining units is an acceptable simplification to the model.

5.6 Ratio of Horizontal to Vertical Hydraulic Conductivity

As explained in Section 4.1.2, the ratio between horizontal and vertical conductivity was set at 10:1 for aquifers and 2:1 for confining units. The exception to this rule was the third layer, whose western section represents the IA, while the remaining part is lumped with layers 2 and 4 to simulate the ICU. In layer 3, the horizontal to vertical conductivity ratio was set to 10:1. The ratios were set using MODFLOW's array multiplier option, so only a single multiplier could be used in any layer. These ratios were selected with little data based on the expectation that the majority of the flow would be horizontal in the aquifers and vertical in the confining units, so the calibration would be insensitive to the conductivity in the cross-flow direction. IMC comments indicated that this might not always be true, and recommended a sensitivity run to quantify this effect.

Four separate sensitivity runs were developed as follows:

1. Set the ratio of horizontal to vertical conductivity to 1:1 in all layers (2-22), keeping the horizontal conductivity in the aquifers and the vertical conductivity in the confining units at their calibrated values.

2. Set the ratio of horizontal to vertical conductivity to 1:10 in the aquifers (layers 3, 5-10, 13-15, 18-19,22) and 1:2 in the confining units (layers 2, 4, 11-12, 16-17, 20-21), keeping the horizontal conductivity in the aquifers and the vertical conductivity in the confining units at their calibrated values.

3. Repeat Run 1 in layers 5-22 only. Layers 2 through 4 keep their calibrated values and ratios.

4. Repeat Run 2 in layers 5-22 only. Layers 2 through 4 keep their calibrated values and ratios.

The reason for runs 3 and 4 is related to the use of MODFLOW's array multipliers to make these changes quickly and easily. No single multiplier could keep the horizontal conductivity in layer 3 constant in the west (IA), while keeping the vertical conductivity the same in the east (ICU). Although this effect could have been achieved by changing the arrays, the decision was made to check the sensitivity on the existing runs before expending the effort to redevelop the arrays.

The results generally support the original hypothesis – that the calibration is not sensitive to either horizontal conductivity in the confining units or vertical conductivity in the aquifers. The few exceptions include the recharge area and a few areas with heavy pumping, where one might expect significant vertical movement of water in the aquifers.

The effect of the changes on the calibration was minimal. For the runs with changes to layers 2 through 4, the maximum head change at any calibration point for the February 2004 run is less than 2 feet, with the average at about 0.2 feet. When layers 2 through 4 were left unchanged from the calibration values, the maximum head change at any calibration point was less than 0.5 feet and the average change was about 0.03 feet.

As expected, Runs 1 and 2 caused more significant and widespread effects on the February 2004 steady state run in layers 2 through 4. Figure 5.15 shows the differences in head in these layers for the first two sensitivity runs for these upper layers. These differences propagate down into deeper layers, but they diminish with depth and are largely undetectable in the LF, LC and BZ layers.

Figure 5.16 shows the comparison between the first two and last two runs in the UF and indicates the areas of greatest impact at the major pumping location in Lee County. Overall, the effects to proposed CERP ASR sites are minimal – even with Runs 1 and 2, which caused such large changes in the IAS. These results indicate that flow is generally horizontal in the aquifers and vertical in the confining units, except in areas of changes to the direction of flow or where there is significant recharge or pumping.

Because the CERP ASR plan calls for significant pumping in several areas, it is possible that the ratio of horizontal to vertical conductivity will affect the outcome of the production scenarios as flow directions change to provide water to the ASR wells. To quantify this uncertainty, the ratio will be the subject of some sensitivity and Monte Carlo simulations on the final selected CERP ASR regional model run.

6.0 Sources of Uncertainty

Overall, the model does a good job replicating observed field conditions. There is a high degree of confidence that it will provide valuable insights to the CERP ASR program. As with all models, uncertainty exists in the input data and in the simplifying assumptions. It is important to identify these areas of uncertainty and quantify them so that the model results can be used in an informed way. The following subsections describe the major sources of uncertainty, including some of these assumptions, and how they may affect model results and overall goals of the project.

6.1 Pumping Rate Data Limitations

Limitations in the pumping data constitute the principal source of error in this model. Figure 6.1 shows the drawdown occurring throughout the UF due to seasonal pumping in February 2004, which is a relatively low pumping period. Drawdown exceeds 30 feet in some areas of the northwest part of the model (Manatee, Hillsborough and Polk County) and in the Cape Coral area. A huge portion of the peninsula is impacted by pumping activities to a lesser, but significant degree. Head changes in numerous monitoring wells show swings in head greater than what can be caused by seasonal rainfall changes. The available data indicates head changes on the order of only 1 to 5 feet in the SAS within our model domain. (See Figures 4.41-4.94 for measured head changes during the calibration period.) Pumping rate errors are the likely reason for poor calibration at almost all the observation points described in Section 4.1.3. Clearly, it is important that the model correctly incorporate pumping.

As explained in Section 3.5 and Appendix D, the information on the pumping rates of permitted wells is sparse. SAJ made valiant efforts to gather as much available data as possible, but a large part of the data had to be estimated based on the well type, capacity/allocation information and other available pumping data. Figures 3.37 through 3.41 and Table 3.1 show how much of the pumping in the model is based on estimates. In each month of the calibration period, between 20% and 25% of the volume of pumped water is based on estimates. It is of special importance that the largest estimated pump rates occur at wells in the middle swath of the model – along the Caloosahatchee River, the southern reach of the Kissimmee River and into St. Lucie County. These areas caused the greatest problems in the calibration of the model and contain many of the proposed CERP ASR sites.

Figure 6.2 presents the results of a sensitivity analysis on the October 2003 steady state model to demonstrate the effect of the estimated pumping on the model calculation. All of the estimated pumping for this month was reduced by 50%. Reported (known) pump rates remained the same. Figure 6.2 shows the difference between the heads calculated by the calibrated model and this sensitivity run. Differences of one foot or more are found covering nearly half of the model domain. Smaller areas with much larger head differences are scattered across the region. It is clear that errors or poor assumptions in the estimation of missing pumping data can have a marked effect on the model results. Any pumping errors have a significant impact on the calibrated aquifer parameters and will influence predictions made by the model and recommendations based on model predictions. A variety of sensitivity analyses will be performed on the ASR production simulations. During the PDT evaluation of the CERP ASR program, the uncertainty due to pumping must be kept in mind and carefully evaluated.

6.2 Temporal Distribution of Pumping Data

Because of the difficulties associated with gathering pumping data for over 30,000 wells in the South Florida region, an early decision was made to average the pumping over each month of the model period. This resulted in a much simpler (though still arduous) data collection effort and likely had only minimal effects on the calibration. For consistency, the same process was applied to heads assigned as boundary conditions on the edges of the aquifers and on the surface of the model. The temporal distribution of the pumping data and boundary conditions meant that the transient calibration could not

be expected to match measured head data on a daily basis, but rather that it was calibrated until the general trends and average monthly heads were similar to measured data.

When the model is used to evaluate ASR well placement, pump rates and schedules, this coarse temporal distribution of the pumping data may have a minor effect on the results of the model. Although the time constraint may be lifted for ASR wells, boundary conditions and nearby pumping will still be on the monthly schedule and some daily effects might not be entirely accurate.

6.3 Salinity Distribution

The initial condition salinity distribution was developed as an interpolation of the available TDS data. Data is more plentiful in the shallower layers and becomes much sparser in the deep layers. Unfortunately, since the impact of density differences becomes greater with depth, the model is much more sensitive to the TDS in the deep layers than in the shallow layers. Early sensitivity runs showed that density changes (caused by TDS) can have a great effect on both the direction of flow and the impact of head changes. The results of these early tests led to the use of measured TDS data whenever possible. Further, a Monte Carlo analysis is planned for the production runs to determine the effect of variation in TDS on the ASR system predictions.

6.4 Temperature Distribution

The initial condition temperature distribution was developed as an interpolation of the available temperature data. Like TDS data, temperature data was sparser in deep layers of the model. Temperature exerts a much smaller impact on the density of water – even at deep elevations. Errors in the temperature data probably exert only a minor effect on the calibration or the future production runs of the ASR regional model.

6.5 Surficial Aquifer Boundary Assumption

The decision to apply a specified head boundary condition to the surface of the model was made to simplify both data collection and model implementation. As explained in Section 3.3.1, the application of a flux boundary condition at the surface to simulate recharge and discharge would have required additional data such as rainfall, evapotranspiration, seepage rates, etc. This data is available only sparsely and in most models, the inability to appropriately assign recharge/discharge rates at the surface leads to problems with the model. Many models include recharge as a calibration parameter.

By applying specified heads to the surface, many of these problems were alleviated and the heads used to interpolate the SAS head boundary had already been collected as part of the data gathering effort. The downside of this type of boundary condition is that ASR scenarios which impact the SAS will not be accurately simulated in the model. This is expected to be a minor problem since impacts to the SAS will most likely occur after other performance measures (rock fracturing potential, impacts to nearby wells) have already eliminated the scenario as a viable option.

6.6 Spatial Discretization

Due to time and computational constraints, the spatial discretization of the model is quite coarse. In the SEAWAT grid, the largest cells are 10,000 feet on a side (nearly 2 miles). Even at the ASR well locations, cell sizes only drop to 2,000 feet. At this discretization level, only regional effects of the ASR well scenarios can be simulated. Near-well effects for ASR wells or any other wells cannot be evaluated on this model.

In order to minimize the impact of the spatial discretization to the ASR program, the next study will utilize a number of telescopically refined models. These models will be smaller in regional extent and will have smaller grid cells. They will take their boundary conditions from the regional model. With smaller computational cells at the ASR wells, near well effects will be more easily simulated. The small regional extent will allow the models to reach converged solutions on available computers in a reasonable amount of time.

6.7 Variability in Transport Parameters

Very little attention was paid to the transport parameters inherent in the SEAWAT equation. These parameters include porosity, dispersivity and molecular diffusion. Because the calibration models were run for no more than 15 months, the salinity and temperature did not change significantly from the initial conditions (except near injection wells). Some sensitivity runs were made to verify their low sensitivity and are presented in Section 5.2 and 5.3.

The selection of transport parameters likely has little effect on either the calibration models or any short-term production runs. However, as the process moves forward and longer ASR runs are made to evaluate the freshwater bubble at the ASR wells or seawater intrusion, these transport parameters may become more important. Production simulations will be conducted for an extended time period time period (10 years or more). Variability in the transport parameters will be evaluated as part of this modeling effort as well as in the local scale modeling during the next study phase.

7.0 Conclusions/Recommendations

The goal of this modeling effort was to develop a tool to evaluate the regional impacts of the CERP ASR program on the hydrogeologic conditions in the FAS. An extensive data collection and multi-phase modeling effort has been undertaken to ensure that the models achieve this goal. This report presents the details of the construction, calibration and sensitivity analysis of the models that will be used to evaluate the regional effects of the CERP ASR program.

As with any numerical model, uncertainty in the input data and computational methodology are inherent in the ASR Regional Model. In order to address these issues, numerous sensitivity analyses have been performed to determine how the model reacts to various input stresses. Pumping (both into and out of the FAS) has a substantial impact on the water levels in the FAS. Unfortunately, the pumping data used for this regional modeling effort also has a high degree of uncertainty, primarily resulting from the lack of pumping records. On-going improvements in the recording of FAS pumping will be critical in protecting the long term water quality of the aquifer. In addition to pumping, various other model

inputs (including BZ parameters and density distributions) were determined to be sensitive in the regional model calibration. Given this uncertainty in the input data, the calibrated regional models do an excellent job reproducing the FAS flow system and will serve as a useful baseline against which the CERP ASR program can be evaluated. However, to appropriately assess the impacts of the CERP ASR program it is anticipated that additional sensitivity analyses will be performed on any production simulations that will be performed on this calibrated model.

The complex numerical methodology required to address the variable density flow system present in the FAS may also have inherent uncertainty. In order to address this issue, the ASR Regional Model was developed using two numerical codes: WASH123D and SEAWAT. The model inputs for these codes were nearly identical. As presented in Appendix F, both codes replicate the regional steady state and transient flow fields of the FAS. As such, it would be reasonable to perform subsequent model simulations (regional production and local scale modeling effort) using either code. However, due to programmatic constraints it will be more efficient to proceed with the ASR modeling effort using a single numerical code. Although the finite element distribution afforded in the WASH123D mesh provides an efficient framework for placing higher resolution in the areas of interest, the substantial complexity and heterogeneity of the FAS is difficult to incorporate. This is primarily due to zonal methodology used by WASH123D to incorporate hydrogeologic parameters. The hydrogeologic complexity of the local scale models is anticipated to be greater than that of the regional model in order to accurately replicate the formation, mixing and collapse of the ASR freshwater "bubble". In these local scale models, parameters such as dispersivity and porosity, which were relatively insensitive in the regional model, are expected to be more sensitive, requiring a greater degree of variation. Other hydrogeologic parameters, such as hydraulic conductivity and storage, are also anticipated to be highly heterogeneous in the local scale models. This hydrogeologic complexity can be more easily incorporated into SEAWAT. Therefore, it is anticipated that SEAWAT will be the primary model used in the local scale modeling effort.

It is also anticipated that refinements of the regional hydrogeologic properties based on the local scale model calibration will be incorporated into the calibrated regional model. This iterative process will ensure consistency between the models and provide the best numerical platform against which the CERP ASR program can be evaluated.

In conclusion, the models developed and calibrated in this Phase II modeling effort do an excellent job of replicating the regional flow system in the Floridan Aquifer System. A variety of previous modeling and scientific studies have been used to develop and evaluate this model. The hydrogeologic framework is consistent with numerous detailed studies of specific areas of the FAS. Improvements have been made to this framework during the course of the modeling study as various hydrogeologic theories have been evaluated using the physics in the models. The final calibrated model not only calibrates to steady state snap shots of the aquifers, but also reasonably replicates the effects of transient stresses in the FAS. As such, this model will be a useful tool in the evaluation of the proposed CERP ASR system.

8.0 References

Anderson, Mary P. and William W. Woessner, 1992. "Applied Groundwater Modeling: Simulation of Flow and Advective Transport", Academic Press, London.

ASR Contingenct Study Team, 2008. Central and Southern Florida Project Comprehensive Everglades Restoration Program Aquifer Storage and Recovery Contingency Study: A Reconnaissance Level Assessment and Proposed Path Forward Strategy Toward Development of and Aquifer Storage and Recovery Contingency Plan.

Aucott, Walter R., 1988. Areal Variation in Recharge to and Discharge from the Floridan Aquifer System in Florida, U.S. Geological Survey Water-Resources Investigations Report 88-4057.

Bittner, Laura D., Emily Richardson, Christian D. Langevin, Stephen M. England, and Glendon T. Stevens, 2008. Using Density-Dependent Numerical Models to Evaluate Regional Groundwater Flow Patterns in South Florida.

Brown, C.J, England, Steve, Stevens, G.L. Cheng, H-P, and Richardson, Emily, 2006. ASR Regional Study—Benchscale Modeling, Final Report.

Bush, P.W. and R.H. Johnson, 1988. Ground-Water Hydraulics, Regional Flow, and Ground-Water Development of the Floridan Aquifer System in Florida and in Parts of Georgia, South Carolina, and Alabama, U.S. Geological Survey Professional Paper 1403-C.

Cheng, H.-P., J.-R. Cheng, and G.-T. Yeh, 1998. "A Lagrangian-Eulerian method with adaptively local zooming and peak/valley capturing approach to solve three-dimensional advection-diffusion transport equations." *International Journal for Numerical Methods in Engineering*, *41*(4), 587-615.

Cheng, J.-R., H.-P. Cheng, and G.-T. Yeh, 1996. "A Lagrangian-Eulerian method with adaptively local zooming and peak/valley capturing approach to solve two-dimensional advection-diffusion transport equations." *International Journal for Numerical Methods in Engineering*, *39*(6), 987-1016.

CH2MHill, 2005. Sub-Task No. 3 – Groundwater Numerical Model Development Support and Data Collection Report.

Divins, D.L., and D. Metzger, NGDC Coastal Relief Model, http://www.ngdc.noaa.gov/mgg/coastal/coastal.html

Fetter, C.W., 1999. *Contaminant Hydrogeology.* New Jersey: Prentice-Hall.

Fies, Michael, 2004. *Comprehensive Everglades Restoration Plan, Lineament Analysis South Florida Region Aquifer Storage and Recovery Regional Study.* U.S. Army Corps of Engineers, Jacksonville, FL. Available from http://www.evergladesplan.org/pm/projects/project_docs/pdp_asr_combined/013007_asr_lineament_dtmt.pdf

Freeze, R. Allen, and John A. Cherry, 1979. *Groundwater*. New Jersey: Prentice-Hall.

Guo W., and Bennett, G.D., 1998. Simulation of saline/fresh water flows using MODFLOW. In: MODFLOW '98 Conference, Golden, Colorado. pp; 267-274.

Guo, W., and C.D. Langevin, 2002. User's Guide to SEAWAT: a Computer Program for Simulation of Three-Dimensional Variable-Density Ground-Water Flow. Open-File Report 01- 434. U.S. Geological Survey, Tallahassee, Fla.

Harbaugh, A.W., Banta, E.R, Hill, M.C., and McDonald, M.G., 2000. MODFLOW—2000, the U.S. Geological Survey modular ground-water model—User guide to the modularization concepts and the ground-water flow process. U.S. Geological Survey Open File Report 00-92, 121 p.

Huges, Joseph D., Vacher, H.L., Sanford, Ward E, 2007. Three-dimensional flow in the Florida platform: Theoretical analysis of Kohout convection at its type locality. Geology. Vol 35, Issue 7, pp663-666.

Kohout, F.A.,H.R. Henry, and J.E. Banks, 1977. Hydrogeology related to geothermal conditions of the Floridan Plateau. In The geothermal nature of the Floridan Plateau, edited by D.L. Smith and G.M. Griffin, 1-41. Florida Geological Survey Special Publication no. 21.

Kohout, F.A., 1965. A hypothesis concerning cyclic flow of salt water related to geothermal heating in the Floridan aquifer: New York Academy of Sciences Transactions, ser. 2, v. 28, no. 2, p. 249-271.

Langevin, C.D., Shoemaker, W.B., and Guo, W., 2003. MODFLOW-2000, the U.S. Geological Survey Modular Ground-Water Model—Documentation of the SEAWAT-2000 Version with the Variable-Density Flow Process (VDF) and the Integrated MT3DMS Transport Process (IMT), U.S. Geological Survey Open-File Report 03-426, 43 p.

Langervin, Christian D., Daniel T. Thorne, Jr., Alyssa M. Dausman, Michael C. Sukop, and Weixing Guo, 2008. SEAWAT Version 4: A Computer Program for Simulation of Multi-Species Solute and Heat Transport, U.S. Geological Survey Techniques and Methods Book 6, Chapter A22.

Meyer, Fredrick W., 1989. Hydrogeology, Ground-Water Movement, and Subsurface Storage in the Floridan Aquifer System in Southern Florida, U.S. Geological Survey Professional Paper 1403-G.

Miller, James A., 1997. The Hydrogeology of Florida. In The Geology of Florida, edited by Anthony F. Randazzo and Douglas S. Jones. p. 69-88.

Morrissey, Sheila K., Jordan F. Clark, Michael Bennett, Emily Richardson, and Martin Stute, 2010. Groundwater reorganization in the Floridan aquifer following Holocene sea-level rise. Nature Geoscience, doi:10.1038/NGEO956.

Nash, J.E. and Sutcliffe, J.V., 1970. *River Flow Forecasting Through Conceptual Models Part I – A Discussion of Principles.* Journal of Hydrology 10:282-290.

National Oceanic and Atmospheric Administration (NOAA), http://tidesandcurrents.noaa.gov/geo.shtml?location=8723214

National Oceanic and Atmospheric Administration (NOAA), http://tidesandcurrents.noaa.gov/geo.shtml?location=8725110

National Park Service's South Florida Natural Resources Center (SFNRC), http://www.nps.gov/ever/naturescience/sfnrc.htm

Reese, Ronald S., 2000. Hydrogeology and the Distribution of Salinity in the Floridan Aquifer System, Southwest Florida, U.S. Geological Survey Water-Resources Investigations Report 98-4253.

Reese, Ronald S., 2004. Hydrogeology, Water Quality, and Distribution and Sources of Salinity in the Floridan Aquifer System, Martin and St. Lucie Counties, Florida, U.S. Geological Survey Water Resources Investigations Report 03-4242.

Reese, Ronald S., 2002. Inventory and Review of Aquifer Storage and Recovery in Southern Florida, U.S. Geological Survey Water-Resources Investigations Report 02-4036.

Reese, Ron and Emily Richardson, 2008. Synthesis of the Hydrogeologic Framework of the Floridan Aquifer System and Delineation of a Major Avon Park Permeable Zone in Central and Southern Florida, U.S. Geological Survey Scientific Investigations Report 2007-5207.

Reese, Ron and Emily Richardson, 2004. Task 3.0 Define Preliminary Hydrogeologic Framework, ASR Regional Study.

Sanford, Ward E., Whitaker, Fiona F., Smart, Peter L., Jones, Gareth, 1998. Numerical analysis of seawater circulation in carbonate platforms: I. Geothermal convection. American Journal of Science. Vol 298, Issue 10, pp801-821.

Sepúlveda, Nicasio, 2002. Simulation of Ground-Water Flow in the Intermediate and Floridan Aquifer System in Peninsular Florida, U.S. Geological Survey Water-Resources Investigations Report 02-4009.

Sibson, R., 1981. A brief description of natural neighbor interpolations, In Interpreting Multivariate Data, Ed. V. Barnett, Chichester, 21-36, John Wiley.

South Florida Water Management District's environmental database (DBHYDRO), http://my.sfwmd.gov/dbhydroplsql/show_dbkey_info.main_menu

SFWMD and USACE, April 1999. The Central and Southern Florida Project Comprehensive Review Study.

Spechler, Rick M., and Sharon E. Kroening, 2007. Hydrology of Polk County, Florida, U.S. Geological Survey Scientific Investigations Report 2006-5320.

Torres, A.E., L.A. Sacks, D.K. Yobbi, L.A. Knochenmus, and B.G. Katz, 2001. Hydrogeologic Framework and Geochemistry of the Intermediate Aquifer System in Parts of Charlotte, De Soto, and Sarasota Counties, Florida, U.S. Geological Survey Water-Resources Investigations Report 01-4015.

U.S. Army Corps of Engineers Philadelphia District (NAP), 2006. Draft ASR Regional Study Phase I - Groundwater Modeling.

U.S. Geological Survey's Digital Elevation Model (DEM), http://seamless.usgs.gov/

U.S. Geological Survey's National Elevation Dataset (NED), http://ned.usgs.gov/

U.S. Geological Survey's South Florida Information Access (SOFIA), http://sofia.usgs.gov/

Ward, William C., Kevin J. Cunningham, Robert A. Renken, Michael A. Wacker, and Janine I. Carlson, 2003. Sequence-Stratigraphic Analysis of the Regional Observation Monitoring Program (ROMP) 29A Test Corehole and its Relation to Carbonate Porosity and Regional Transmissivity in the Floridan Aquifer System, Highlands County, Florida, U.S. Geological Survey Open-File Report 03-201.

Watermark Numerical Computing, 2004. *PEST Model-Independent Parameter Estimation User Manual: 5th Edition.*

WRDA, 2000, 33 CFR 385.

Yeh, G.-T., G. Huang, H.-P. Cheng, F. Zhang, H.-C. Lin, E. Edris, and D. Richards, 2006. "A First-Principle, Physics-Based Watershed Model: WASH123D, Chapter 9, Watershed Models", 653 pp., Edited by V. P. Singh and D. K. Frevert, CRC Press, Taylor & Francis Group.

Yeh, G.-T., H.-P. Cheng, G. Huang, F. Zhang, H.-C. Lin, J.-R. Cheng, E. Edris, and D. Richards, 2003. "A Numerical Model Simulating Water Flow and Contaminant and Sediment Transport in WAterSHed Systems of 1-D Stream-River Network, 2-D Overland Regime, and 3-D Subsurface Media (WASH123D: Version 2.0)".

Zheng, C. and P.P. Wang, 1999. MT3DMS: A Modular Three-Dimensional Multi-Species Model for Simulation of Advection, Dispersion and Chemical Reaction of Contaminants in Groundwater Systems: Documentation and User's guide, SERDP-99-1: U.S. Army Engineer Research and Development Center, Vicksburg, MS.

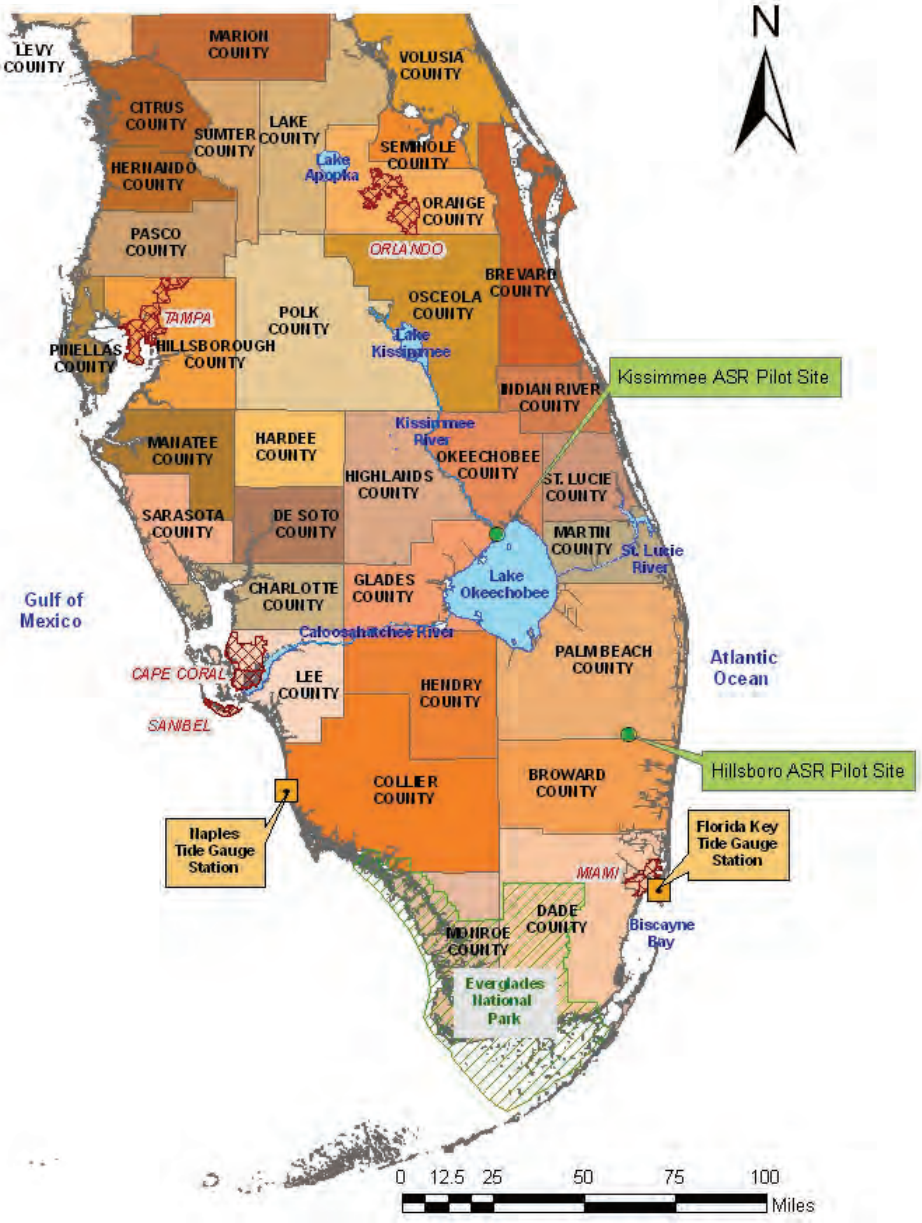

Notes:

Sources:

MJWATERBND – Major Waterbodies of Florida (ESRI) from www.fgdl.org

MJRIVP – FDEP Major Rivers – Polygons (FDEP) from www.fgdl.org

NHD100LINE_MAY06 – National Hydrography Data set – Linear Hydrographic Landmarks 1:100K (USGS) from www.fgdl.org

PAR_CITYLM_2008 – City Limits Derived from Parcel Data – 2007 (University of Florida GeoPlan Center) from www.fgdl.org

CNTSHR_2006 – Florida County Boundaries with Shorelines – 2006 (FDEP) from www.fgdl.org

ENP_boundary – Everglades National Park Boundary from fcelter.fiu.edu

Tide Gauge Stations – from tidesandcurrents.noaa.gov

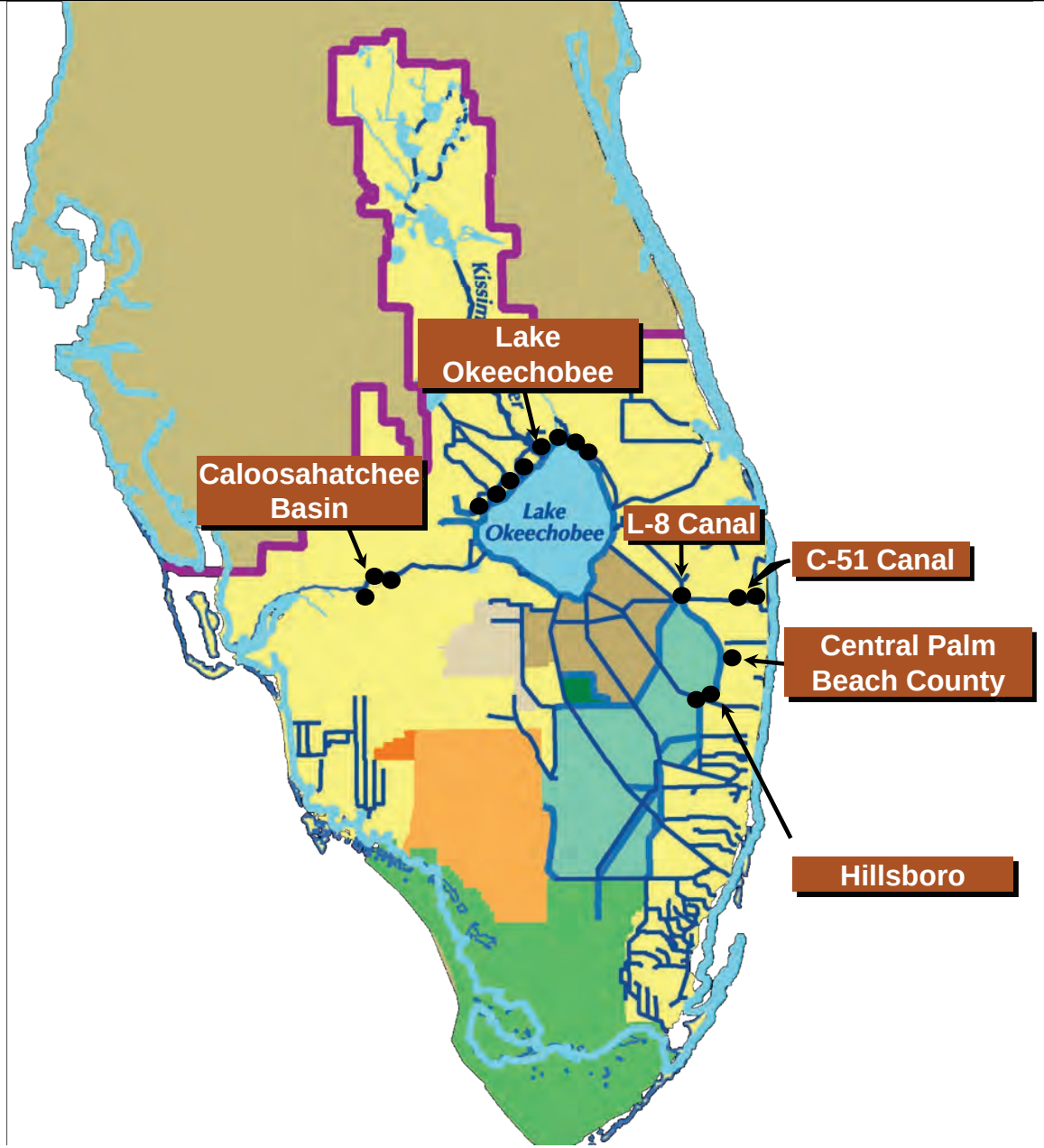

Notes:

Locations shown are approximate and based on the Comprehensive Everglades Restoration Plan (CERP)

Final locations of proposed ASR well clusters have been and continue to be adjusted based on findings of the ASR Regional Study

Site	# ASR Wells
Lake Okeechobee	200
Caloosahatchee	44
L-8 Basin	10
C-51 Basin	34
Central PBC	15
Hillsboro	30
TOTAL	333

Proposed CERP ASR Location Map

Figure 1.2

Final Groundwater Model Calibration Report

October 2010

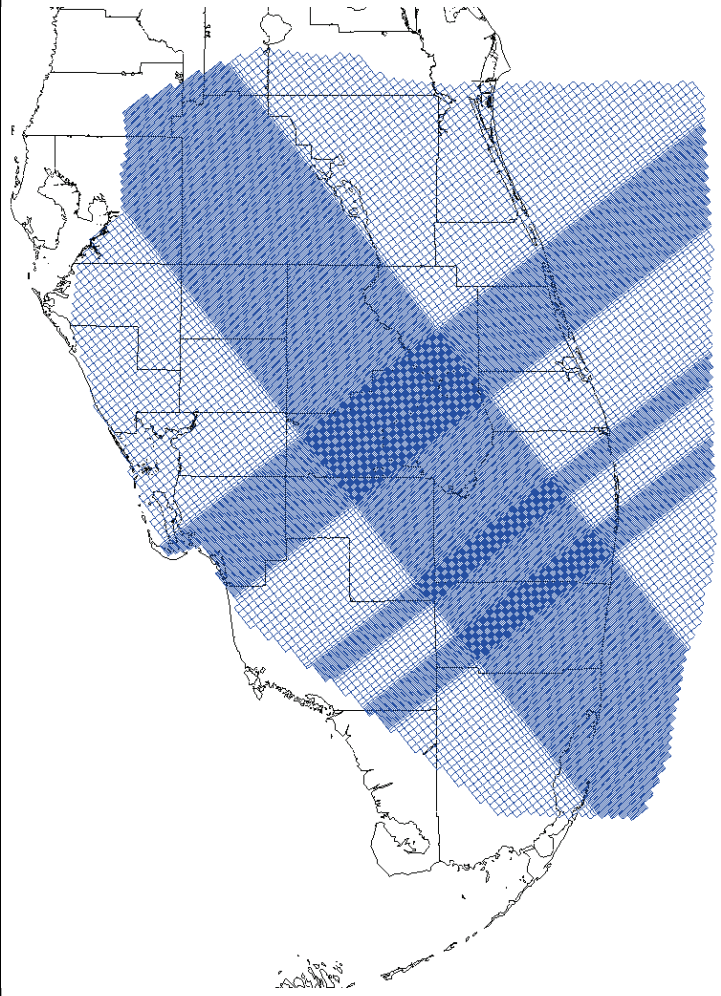

SEAWAT Computational Grid

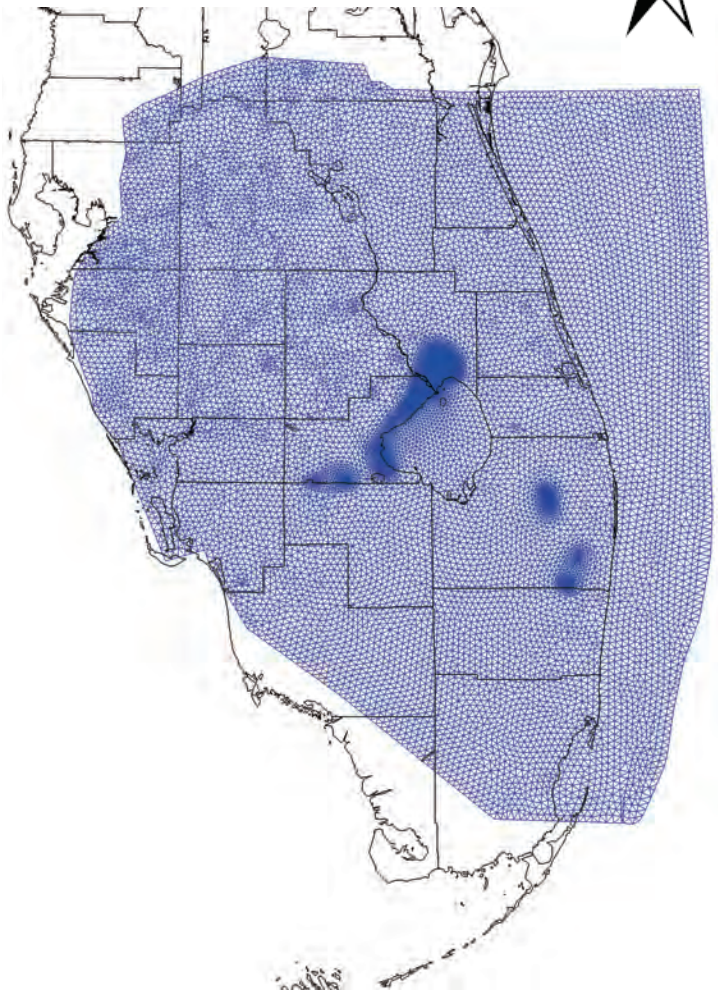

WASH123D Computational Mesh

N

Notes:

SEAWAT :

Min. Spacing – 2,000 ft.

Max. Spacing – 10,000 ft.

WASH123D :

Min. Spacing – 100 ft.

Max. Spacing – 10,000 ft.

Horizontal Model Extent

Figure 2.1

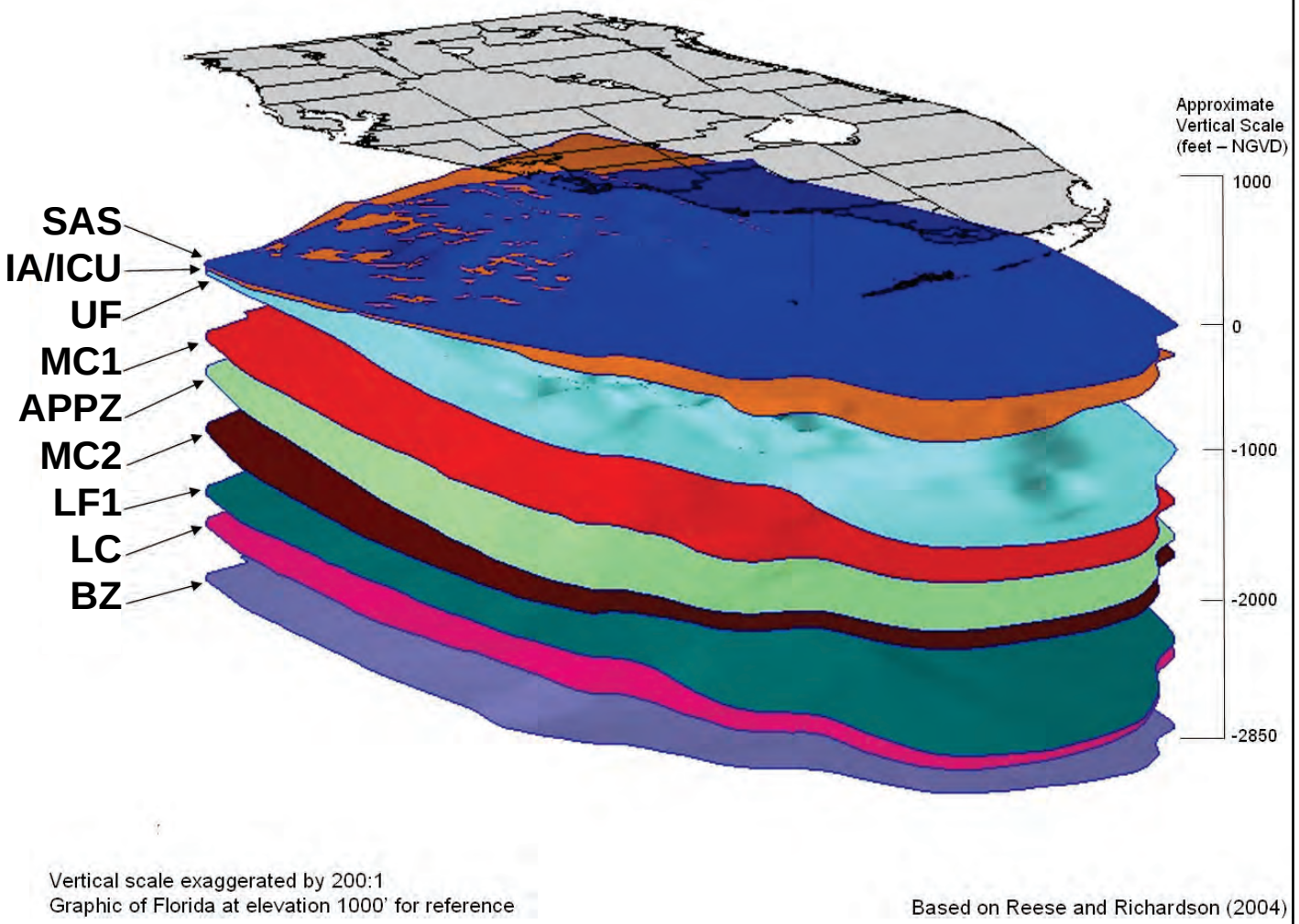

Notes:

Unconfined Aquifer :
Surficial Aquifer System (SAS)

Confined Aquifers :
Intermediate Aquifer (IA)
Upper Floridan (UF)
Avon Park Permeable Zone (APPZ)
Lower Floridan (LF1)
Boulder Zone (BZ)

Confining Units :
Intermediate Confining Unit (ICU)
Upper Middle Confining Unit 1 (MC1)
Lower Middle Confining Unit 2 (MC2)
Lower Confining Unit (LC)

Surfaces represent the top of each unit as defined in the model.

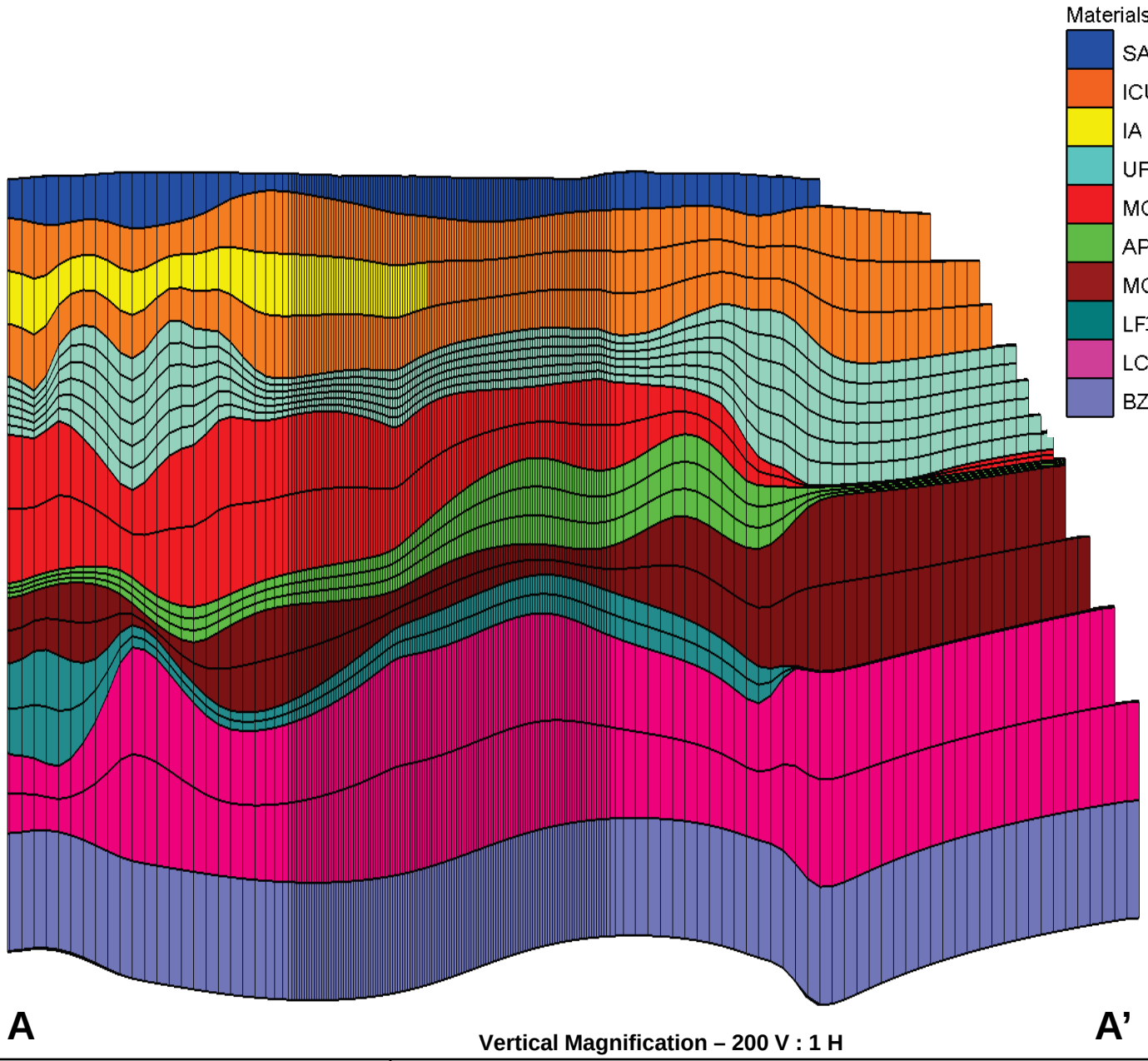

Vertical Magnification – 200 V : 1 H

Notes:

SEAWAT Layering :

- Layer 1 : SAS
- Layer 2 : ICU
- Layer 3 : IA/ICU
- Layer 4 : ICU
- Layers 5-10 : UF
- Layers 11-12 : MC1
- Layers 13-15 : APPZ
- Layers 16-17 : MC2
- Layers 18-19 : LF1
- Layers 20-21 : LC
- Layer 22 : BZ

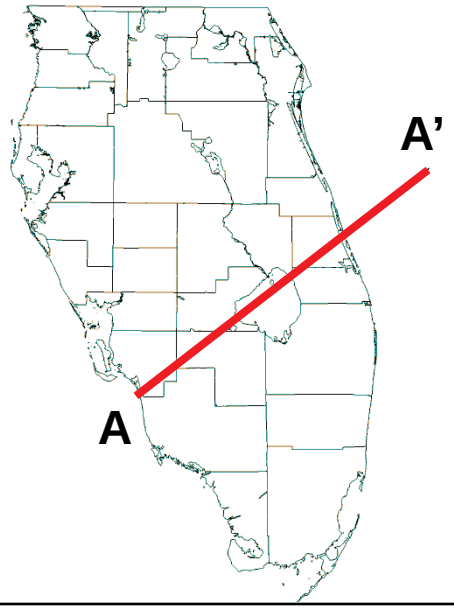

Vertical Model Layering (SEAWAT)

Figure 2.3

Final Groundwater Model Calibration Report

October 2010

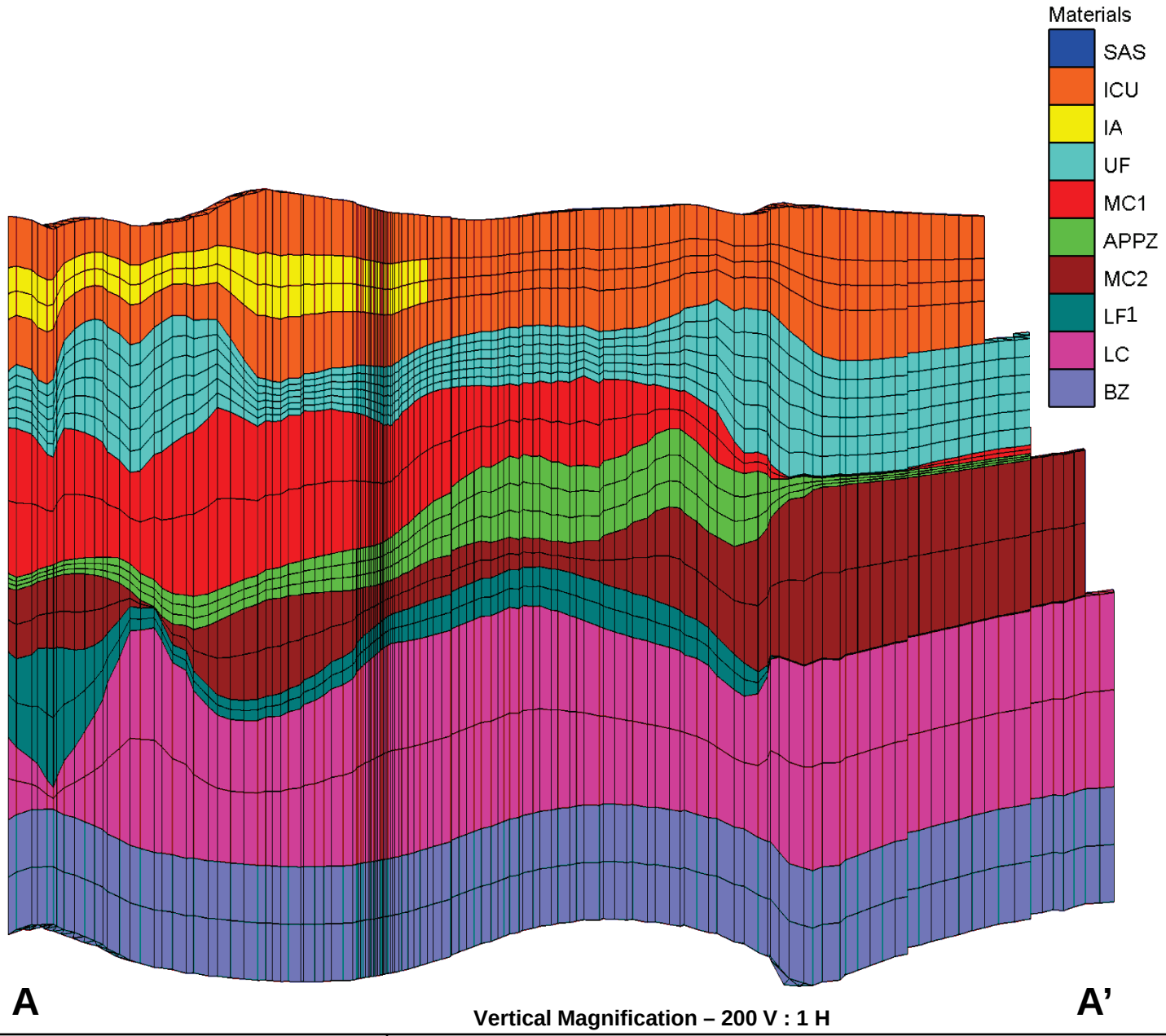

Vertical Magnification – 200 V : 1 H

Notes:

WASH123D Layering :

- Layer 1 : ICU
- Layers 2-4 : IA/ICU
- Layers 5-10 : UF
- Layers 11-12 : MC1
- Layers 13-15 : APPZ
- Layers 16-17 : MC2
- Layers 18-19 : LF1
- Layers 20-21 : LC
- Layers 22-23 : BZ

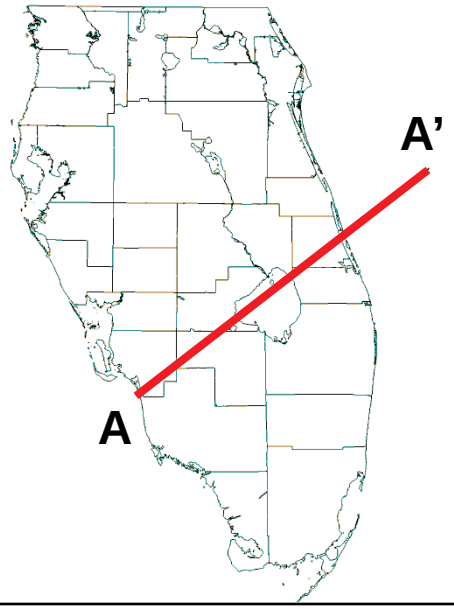

Vertical Model Layering (WASH123D)

Figure 2.4

Final Groundwater Model Calibration Report

October 2010

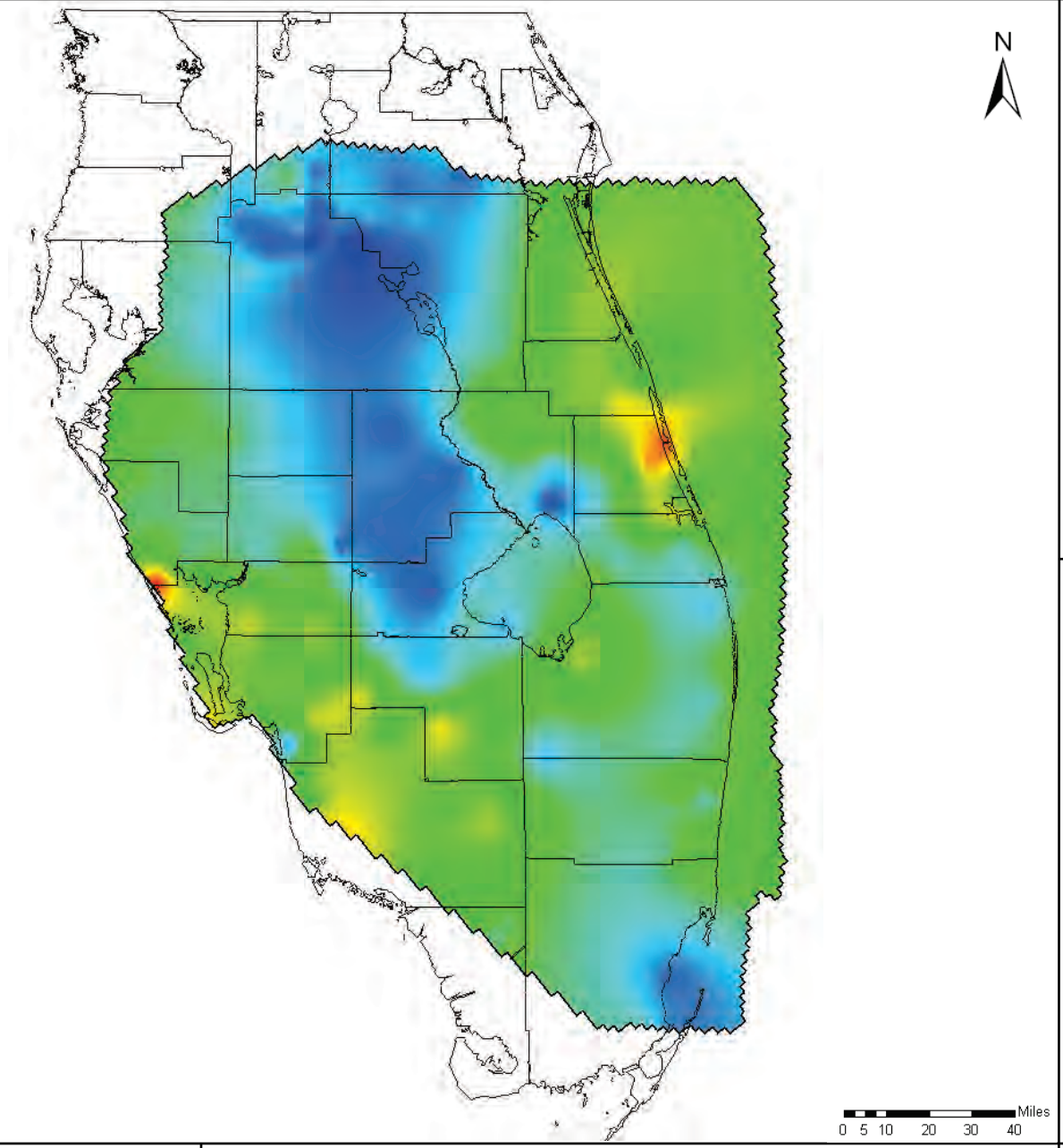

Aquifer Thickness (ft):

700
600
500
400
300
200
100

Notes:

Thickness of the Upper Floridan Aquifer as simulated in the regional models.

This thickness was evenly divided among SEAWAT cell layers 5 through 10 and WASH123D element layers 5 through 10.

Eastern boundary is the ocean outcrop location of layer 7.

Source: Reese and Richardson, 2008

Regional Phase II ASR Aquifer Thickness
Upper Floridan
Final Groundwater Model Calibration Report

Figure 3.1

October 2010

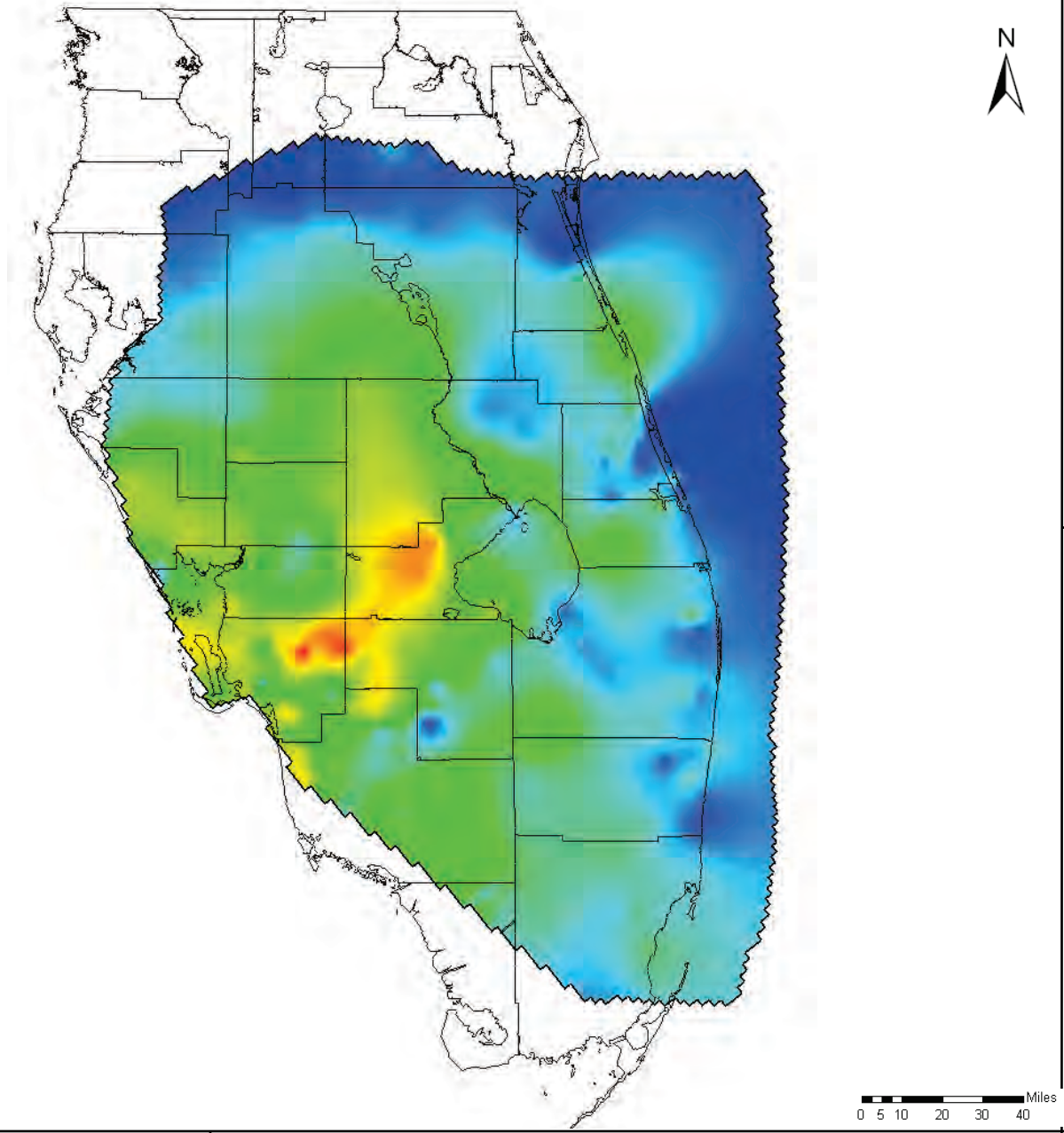

Confining Unit Thickness (ft):

- 900
- 800
- 700
- 600
- 500
- 400
- 300
- 200
- 100

Notes:

Thickness of the Upper Middle Confining Unit as simulated in the regional models.

This thickness was evenly divided between cell layers 11 and 12 for the SEAWAT grid and element layers 11 and 12 for the WASH123D mesh.

Eastern boundary is the ocean outcrop of layer 12.

Source: Reese and Richardson, 2008

Regional Phase II ASR Aquifer Thickness
Upper Middle Confining Unit (MC1)
Final Groundwater Model Calibration Report

Figure 3.2

October 2010

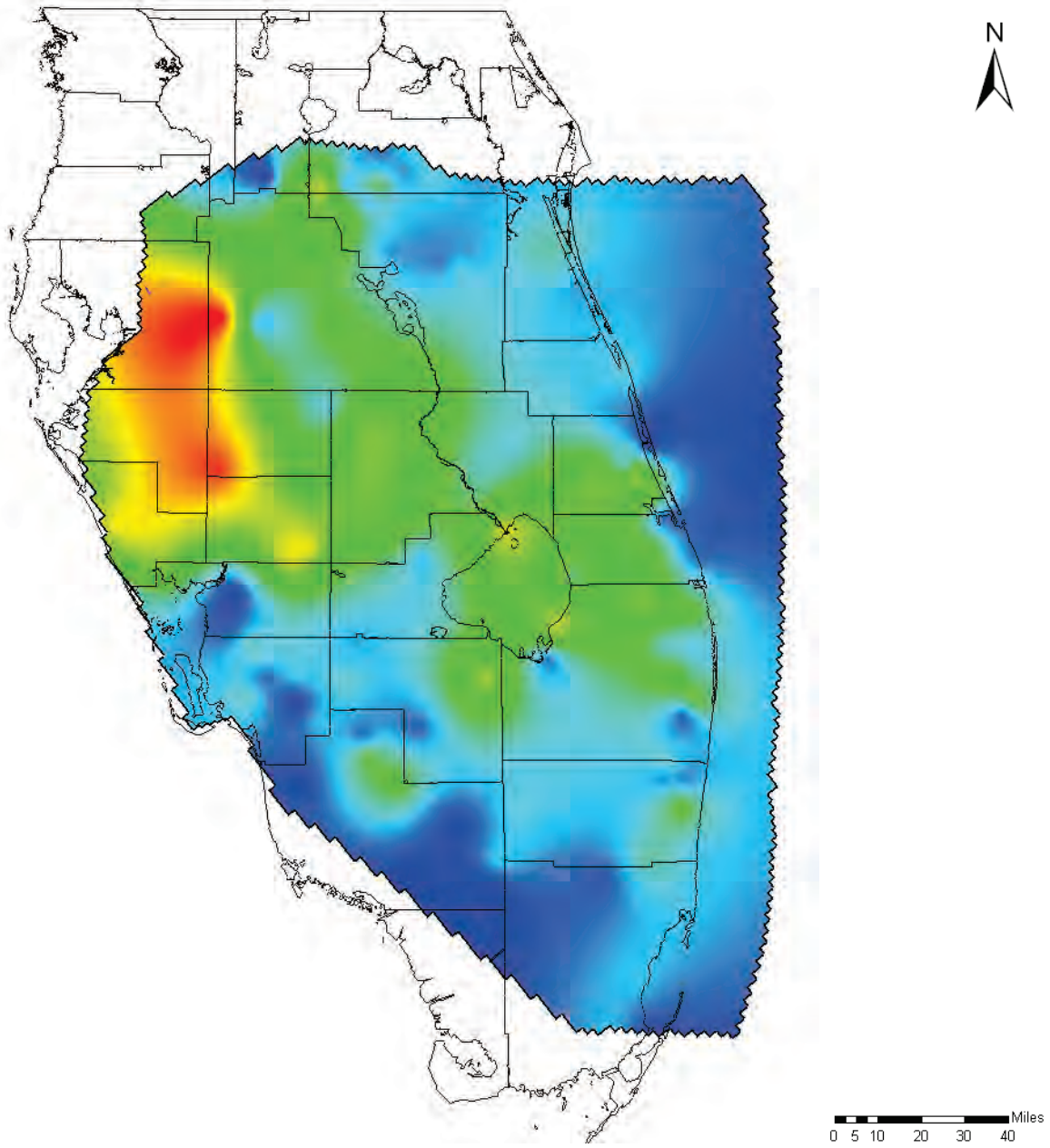

Aquifer Thickness (ft):

500
400
300
200
100

Notes:

Thickness of the Avon Park Permeable Zone as simulated in the regional models.

This thickness was evenly divided between cell layers 13 through 15 for the SEAWAT grid and element layers 13 through 15 for the WASH123D mesh.

Eastern boundary is the ocean outcrop of layer 14.

Thinning of layers in the southwest part of the model along with lower conductivity values accounts for the non-existence of the APPZ in most of Collier and Monroe Counties.

Source: Reese and Richardson, 2008

Regional Phase II ASR Aquifer Thickness
APPZ
Final Groundwater Model Calibration Report

Figure 3.3

October 2010

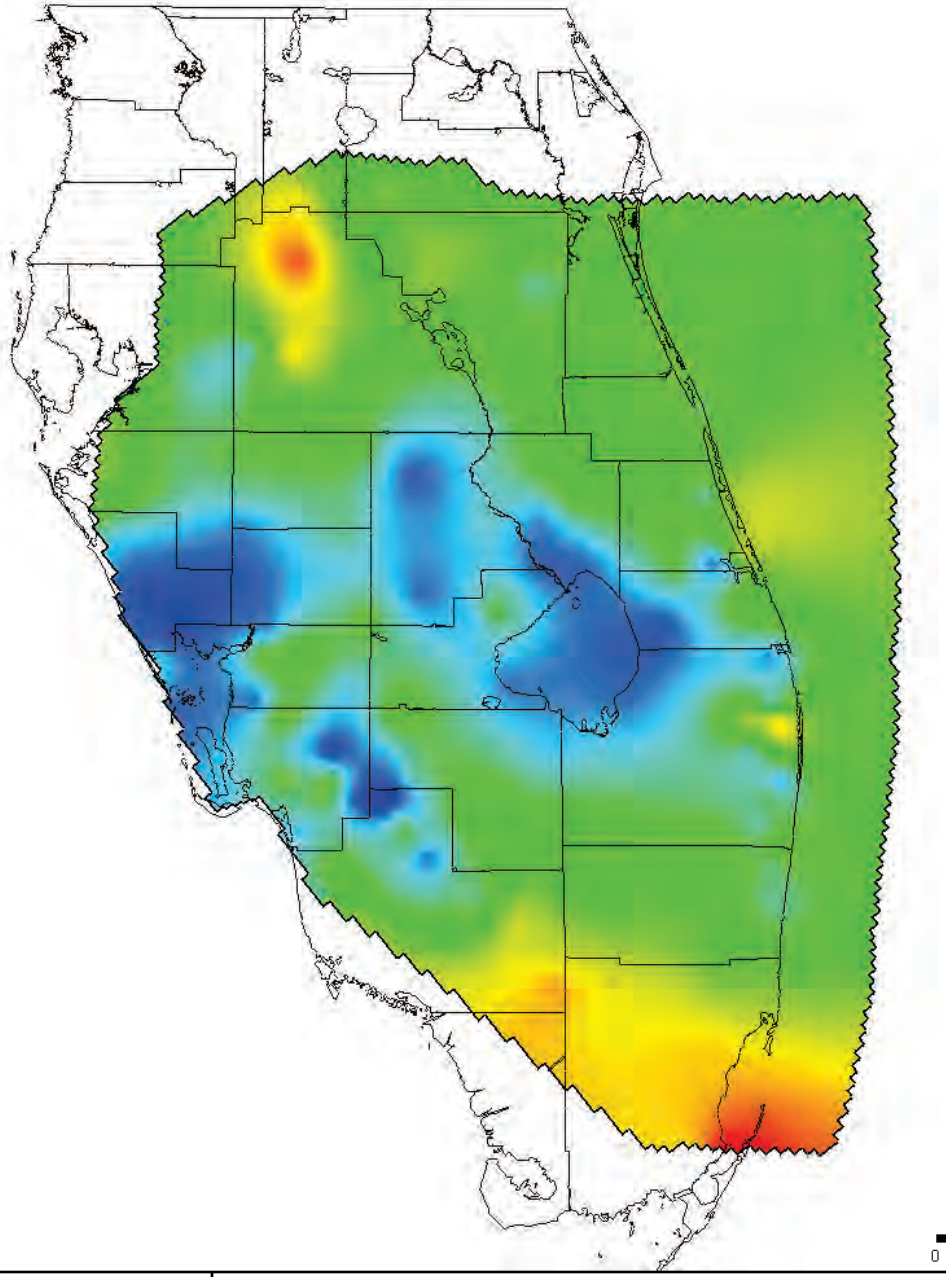

Confining Unit Thickness (ft):

- 1000
- 900
- 800
- 700
- 600
- 500
- 400
- 300
- 200
- 100

Notes:

Thickness of the Lower Middle Confining Unit as simulated in the regional models.

This thickness was evenly divided between cell layers 16 and 17 for the SEAWAT grid and element layers 16 and 17 for the WASH123D mesh.

Eastern boundary is the ocean outcrop of layer 17.

Source: Reese and Richardson, 2008

Regional Phase II ASR Aquifer Thickness
Lower Middle Confining Unit (MC2)
Final Groundwater Model Calibration Report

Figure 3.4

October 2010

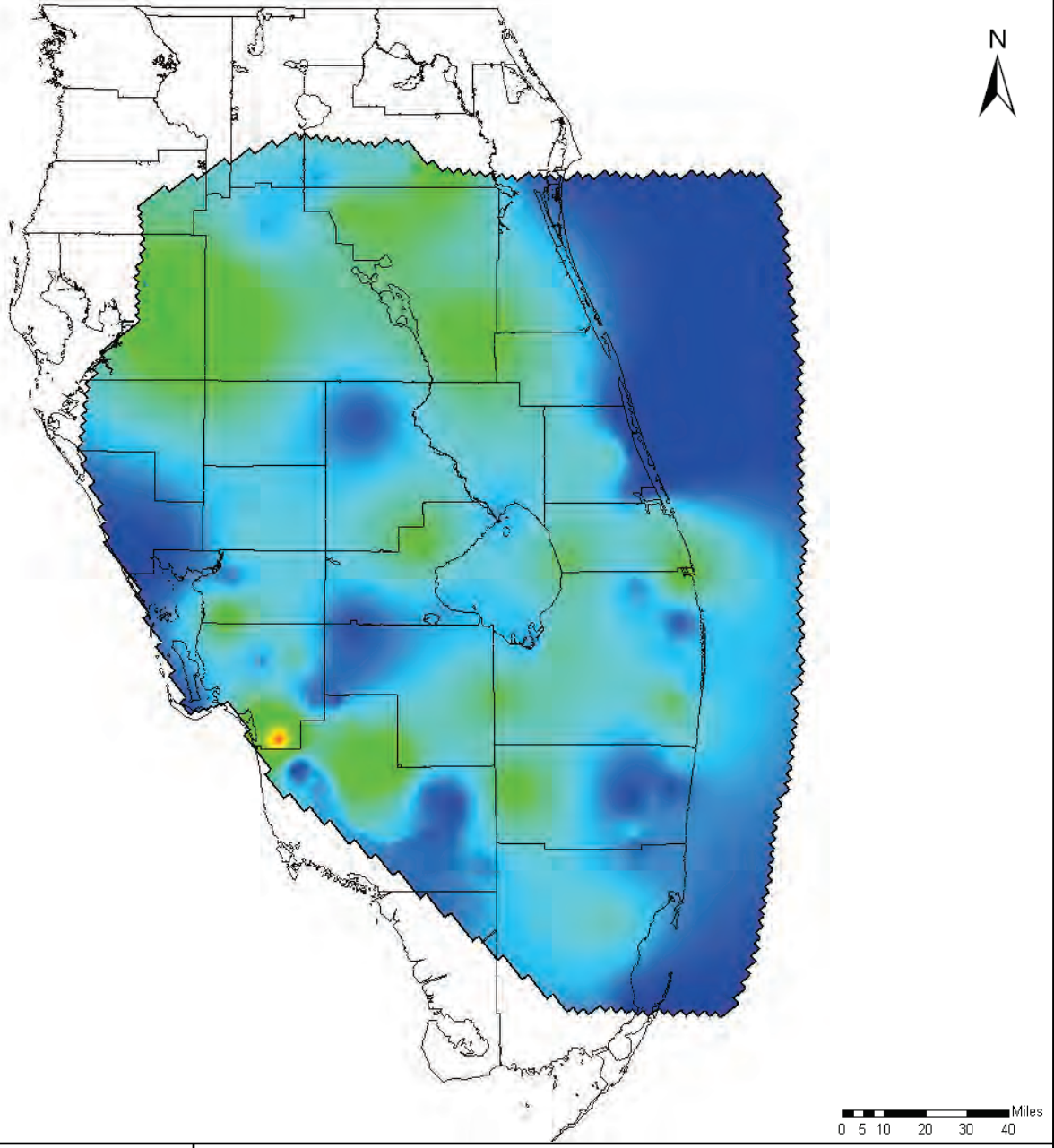

Aquifer Thickness (ft):

600
500
400
300
200
100

Notes:

Thickness of the Lower Floridan Aquifer as simulated in the regional models. This is the first permeable zone of the Lower Floridan (LF1) as defined in Reese and Richardson, 2008

This thickness was evenly divided between cell layers 18 and 19 for the SEAWAT grid and element layers 18 and 19 for the WASH123D mesh.

Eastern boundary is the ocean outcrop of layer 19.

Source: Reese and Richardson, 2008

Regional Phase II ASR Aquifer Thickness
Lower Floridan

Final Groundwater Model Calibration Report

Figure 3.5

October 2010

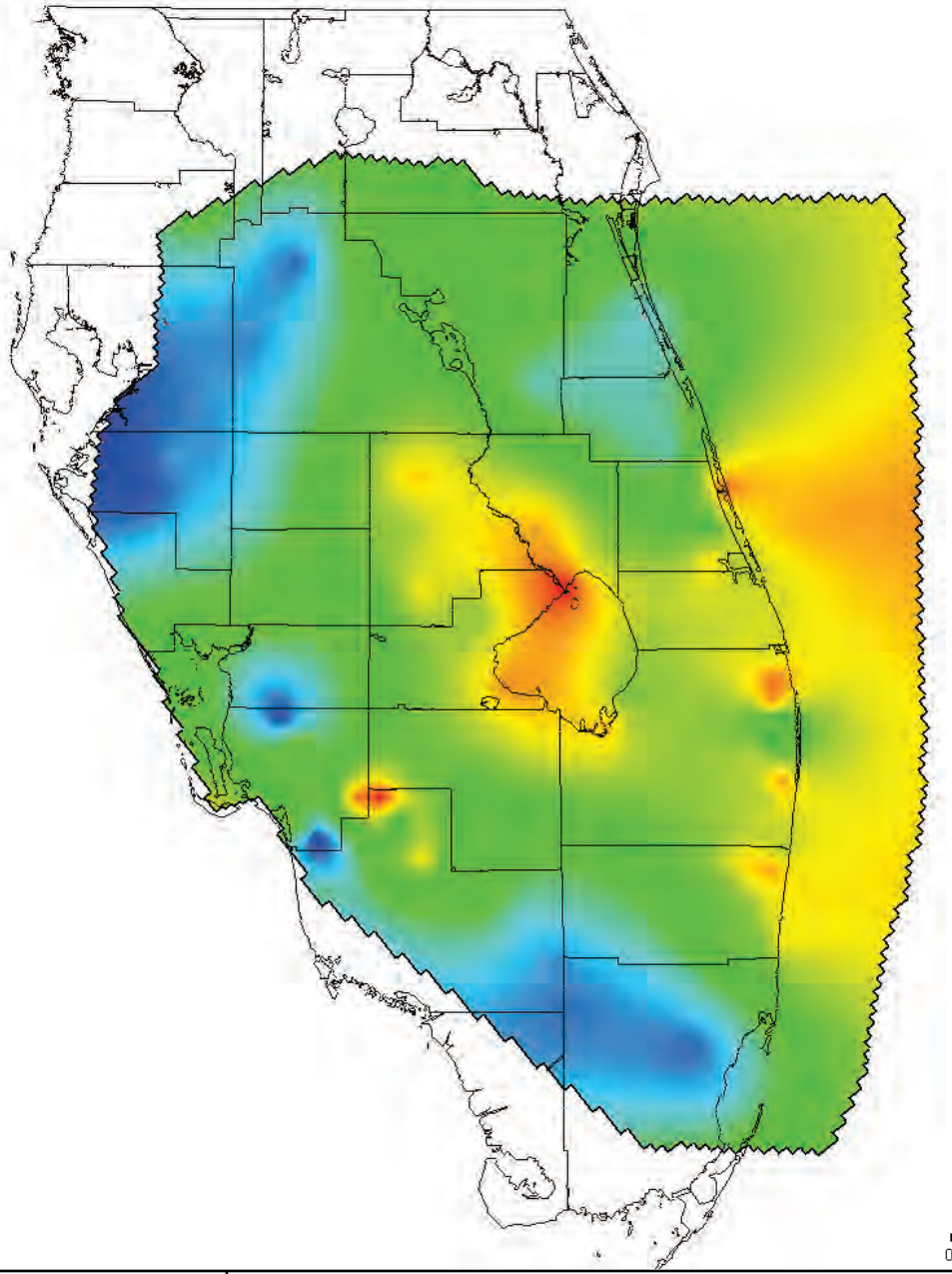

Confining Unit Thickness (ft):

- 1000
- 900
- 800
- 700
- 600
- 500
- 400
- 300
- 200
- 100

Notes:

Thickness of the Lower Confining Unit as simulated in the regional models. This comprises all units (confining and permeable) between LF1 and the BZ as defined in Reese and Richardson, 2008

This thickness was evenly divided between cell layers 20 and 21 for the SEAWAT grid and element layers 20 and 21 for the WASH123D mesh.

Eastern boundary is the ocean outcrop of layer 21.

Source: Reese and Richardson, 2008

Regional Phase II ASR Aquifer Thickness
Lower Confining Unit
Final Groundwater Model Calibration Report

Figure 3.6

October 2010

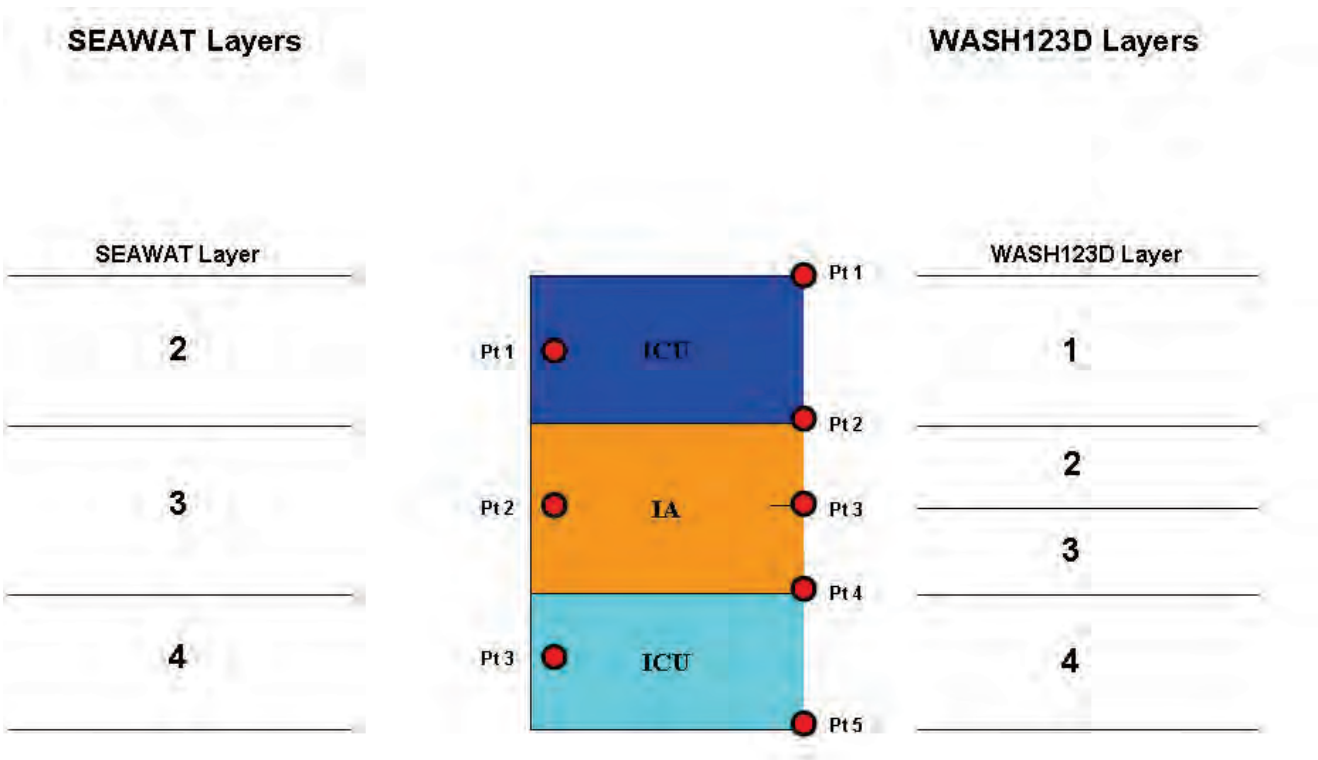

Legend:

Computational Locations.

Comparison of SEAWAT and WASH123D
Intermediate Aquifer System Conceptualization
Final Groundwater Model Calibration Report

Figure 3.7

October 2010

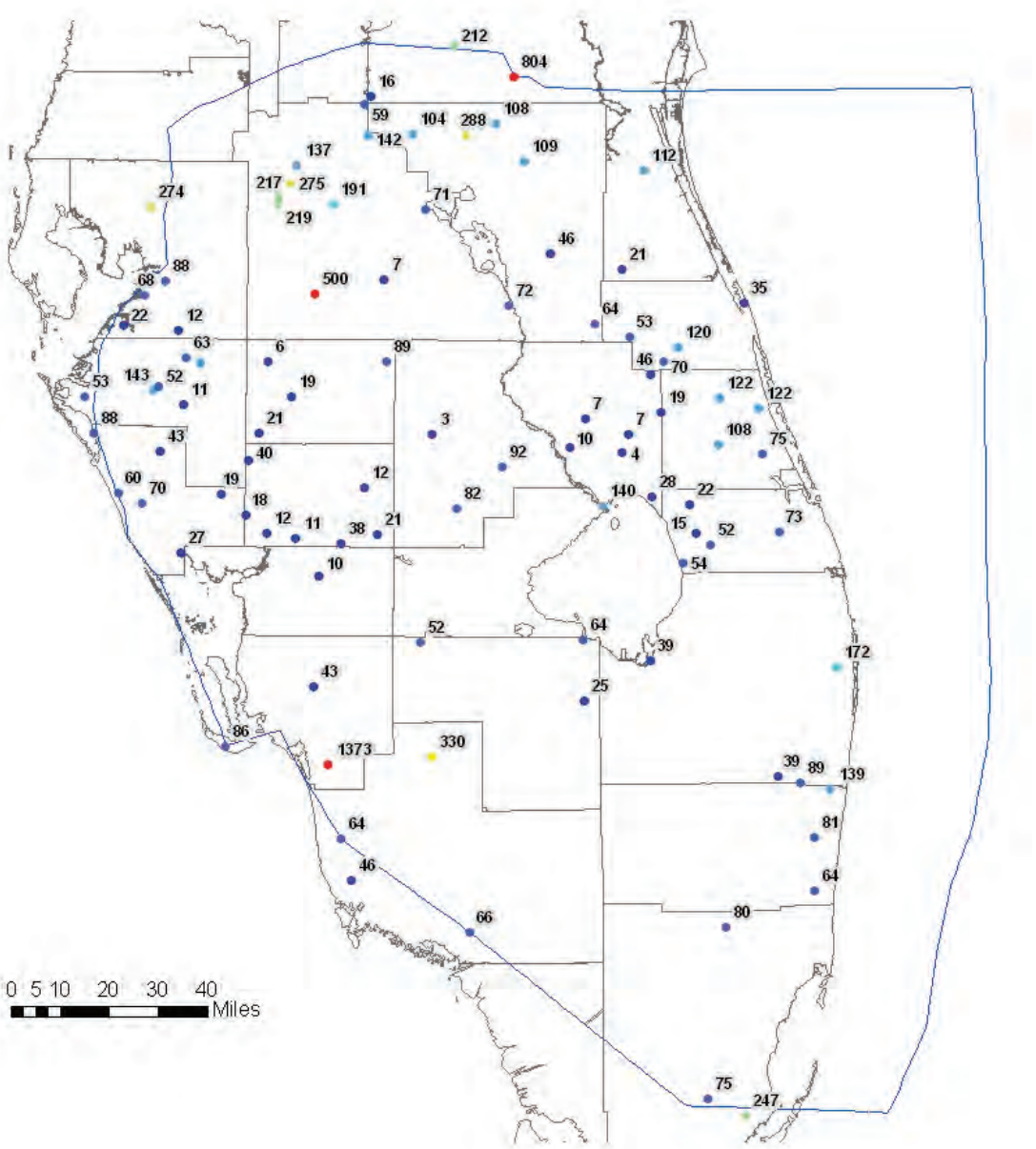

Horizontal Hydraulic Conductivity (ft/d)

- > 450.0
- 400.0 – 450.0
- 350.0 – 400.0
- 300.0 – 350.0
- 250.0 – 300.0
- 200.0 – 250.0
- 150.0 – 200.0
- 100.0 – 150.0
- 50.0 – 100.0
- < 50.0

Data Sources Include :

SIR2007-5207

Preliminary Hydrogeologic Framework

SFWMD's DBHYDRO

USGS's South Florida Information Access (SOFIA)

National Park Service's South Florida Natural Resources Center (SFNRC)

Previous Modeling Efforts

Observed Horizontal Hydraulic Conductivity
Upper Floridan Aquifer
Final Groundwater Model Calibration Report

Figure 3.8

October 2010

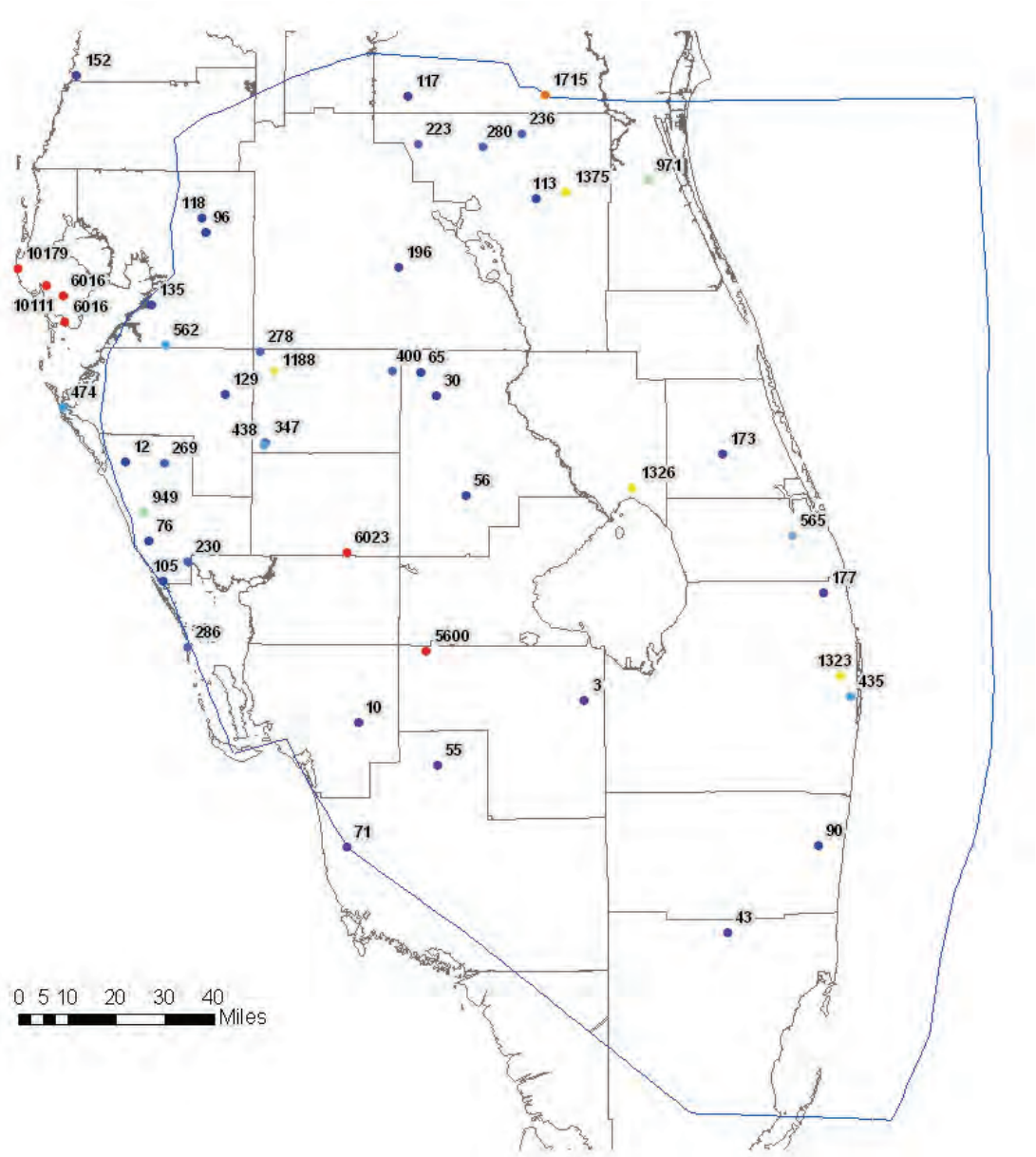

Horizontal Hydraulic Conductivity (ft/d)

- > 1800.0
- 1600.0 – 1800.0
- 1400.0 – 1600.0
- 1200.0 – 1400.0
- 1000.0 – 1200.0
- 800.0 – 1000.0
- 600.0 – 800.0
- 400.0 – 600.0
- 200.0 – 400.0
- < 200.0

Data Sources Include :

SIR2007-5207

Preliminary Hydrogeologic Framework

SFWMD's DBHYDRO

USGS's South Florida Information Access (SOFIA)

National Park Service's South Florida Natural Resources Center (SFNRC)

Previous Modeling Efforts

Communication with SFWMD

Observed Horizontal Hydraulic Conductivity Avon Park Permeable Zone

Final Groundwater Model Calibration Report

Figure 3.9

October 2010

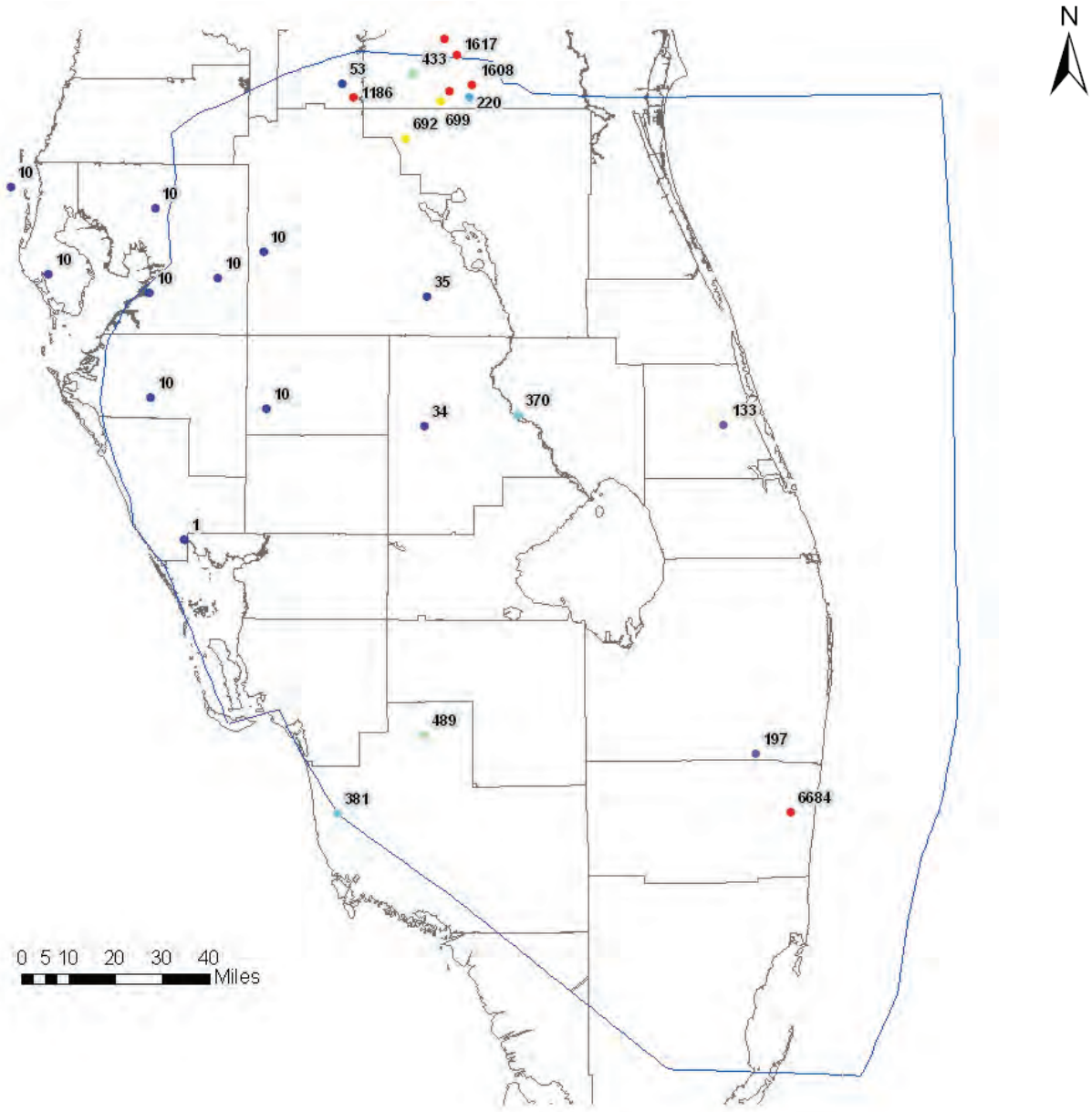

Horizontal Hydraulic Conductivity (ft/d)

- > 900.0
- 900.0 – 900.0
- 800.0 – 900.0
- 600.0 – 700.0
- 500.0 – 600.0
- 400.0 – 500.0
- 300.0 – 400.0
- 200.0 – 300.0
- 100.0 – 200.0
- < 100.0

Data Sources Include :

SIR2007-5207

Preliminary Hydrogeologic Framework

SFWMD's DBHYDRO

USGS's South Florida Information Access (SOFIA)

National Park Service's South Florida Natural Resources Center (SFNRC)

Previous Modeling Efforts

Communication with SFWMD

Observed Horizontal Hydraulic Conductivity Lower Floridan (LF1) Aquifer

Final Groundwater Model Calibration Report

Figure 3.10

October 2010

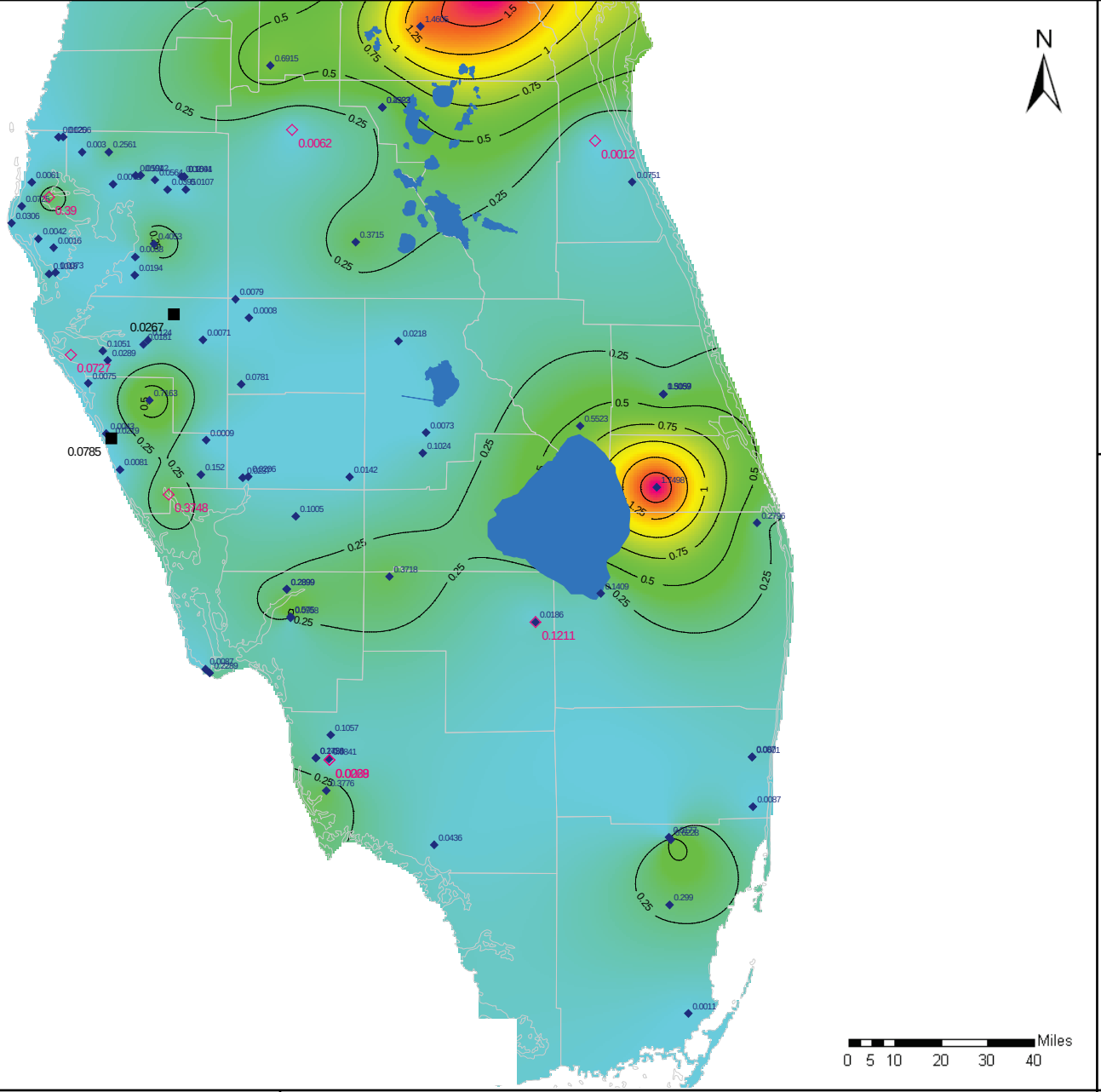

- K_v MC1 – leakance only
- K_v MC1 – core only
- K_v MC1 – APT only

Notes:

Data Source is the Preliminary Hydrogeologic Framework (Reese and Richardson, 2004)

Values for K_v are in ft/day

Interpolation and figure are from SFWMD.

Observed Vertical Hydraulic Conductivity Upper Middle Confining Unit (MC1)

Final Groundwater Model Calibration Report

Figure 3.11

October 2010

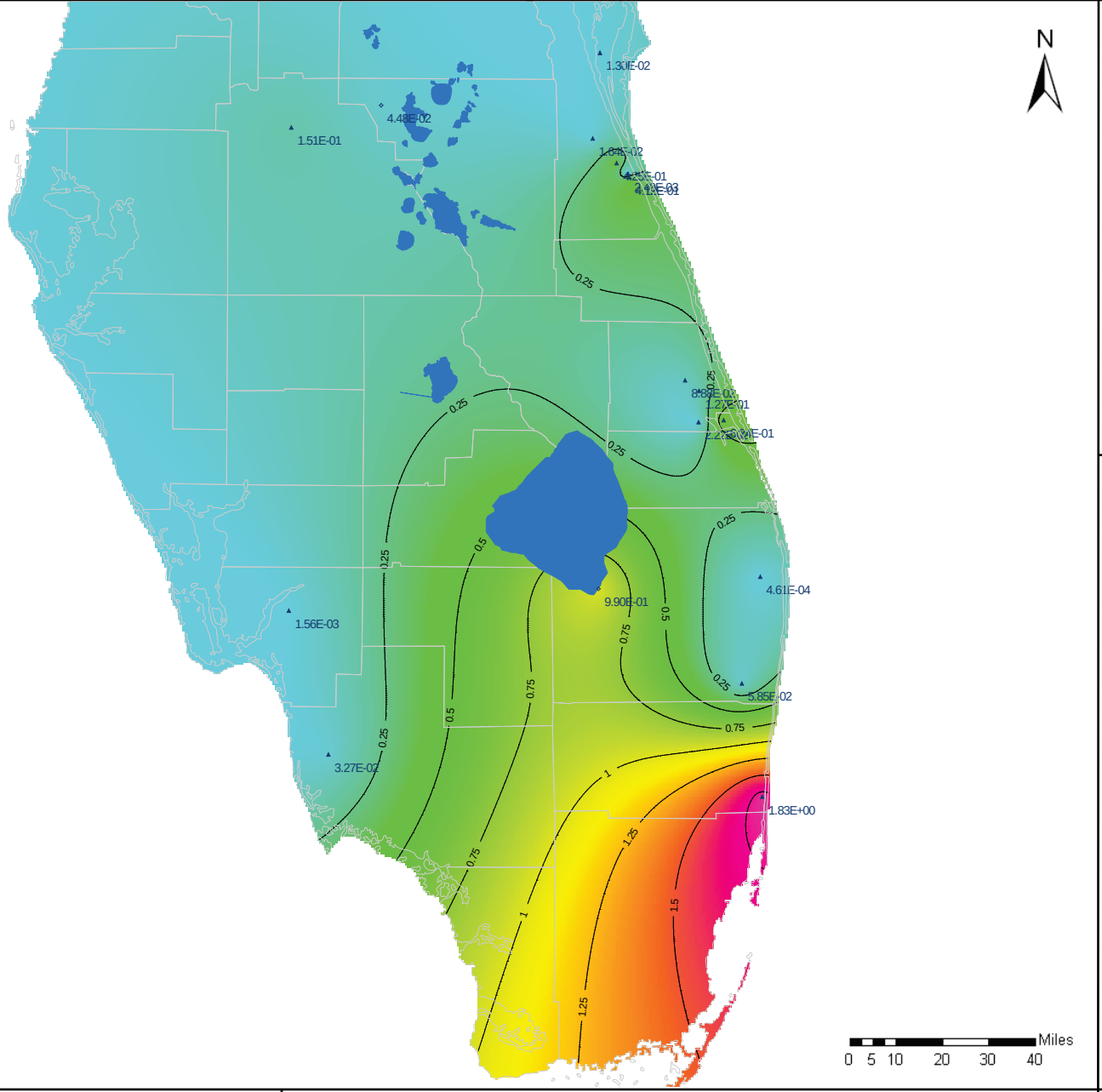

◇ K_v MC2 – leakance only

▲ K_v MC2 – core only

Notes:

Data Source is the Preliminary Hydrogeologic Framework (Reese and Richardson, 2004)

Values for K_v are in ft/day

Interpolation and figure are from SFWMD.

Observed Vertical Hydraulic Conductivity Lower Middle Confining Unit (MC2)

Final Groundwater Model Calibration Report

Figure 3.12

October 2010

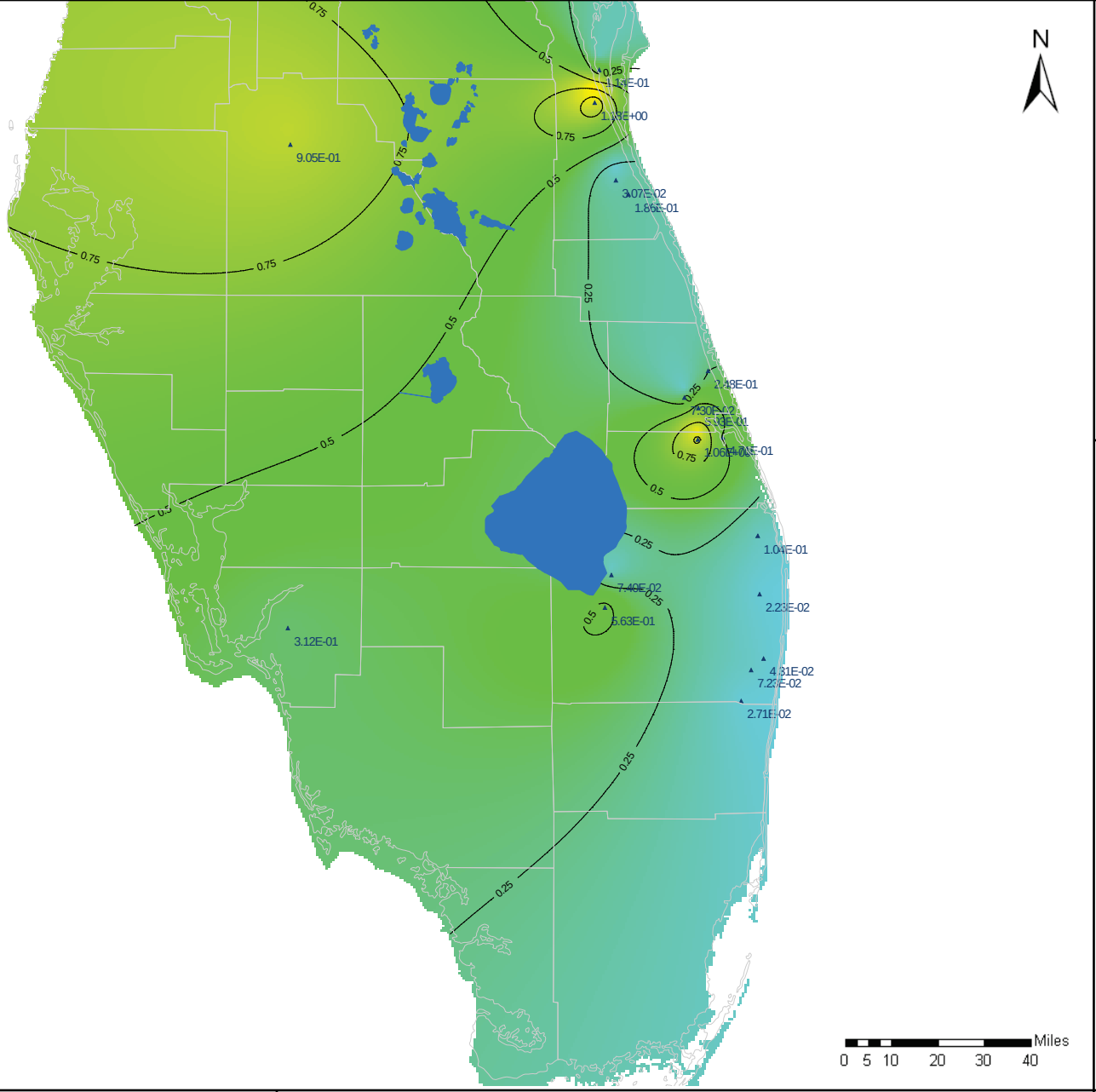

▲ K_v LC – core only

Notes:

Data Source is the Preliminary Hydrogeologic Framework (Reese and Richardson, 2004)

Values for K_v are in ft/day

Interpolation and figure are from SFWMD

Observed Vertical Hydraulic Conductivity Lower Confining Unit (LC)

Final Groundwater Model Calibration Report

Figure 3.13

October 2010

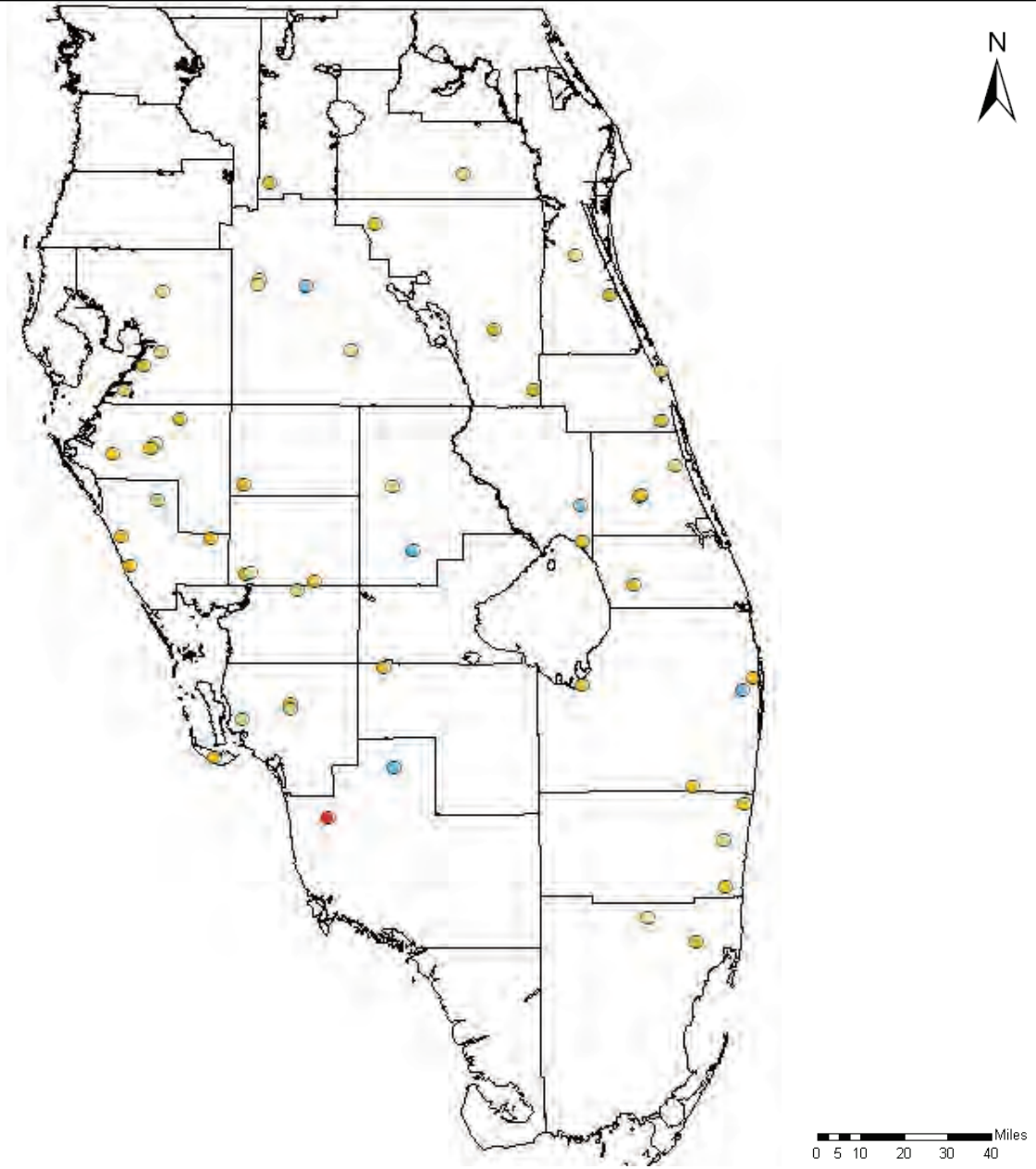

Specific Storage (ft^{-1})

- $1x10^{-4}$ - $1x10^{-3}$
- $1x10^{-5}$ - $1x10^{-4}$
- $1x10^{-6}$ - $1x10^{-5}$
- $1x10^{-7}$ - $1x10^{-6}$
- $1x10^{-8}$ - $1x10^{-7}$

Notes:

Values are for specific storage are ft^{-1}

These values are computed by dividing the field measured storage coefficient provided by SFWMD by the aquifer thickness at that location. Assumed aquifer thicknesses were based on the model-simplified geology.

Observed Specific Storage
Upper Floridan Aquifer
Final Groundwater Model Calibration Report

Figure 3.14

October 2010

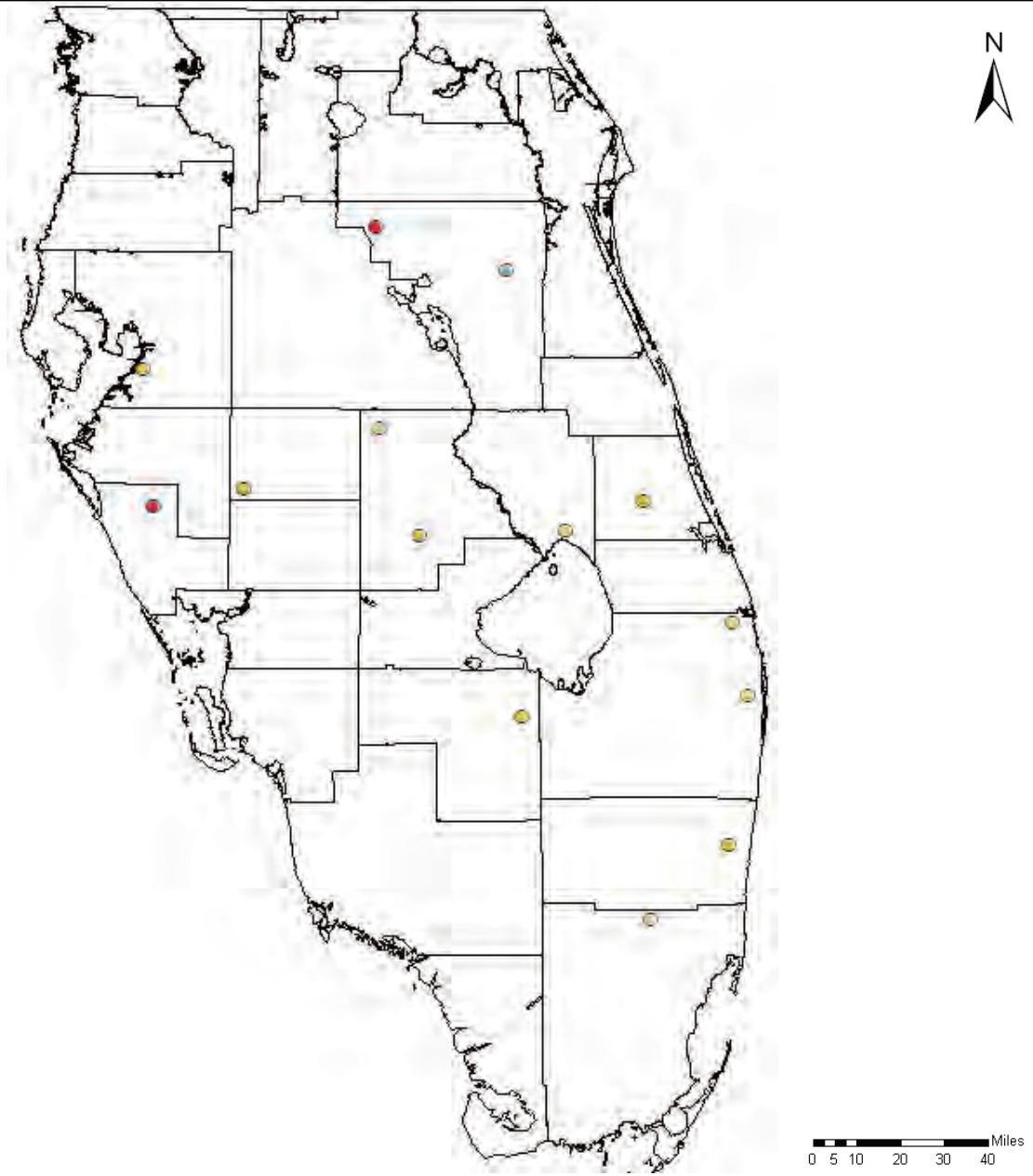

Specific Storage (ft^{-1})

- $1x10^{-4}$ - $1x10^{-3}$
- $1x10^{-5}$ - $1x10^{-4}$
- $1x10^{-6}$ - $1x10^{-5}$
- $1x10^{-7}$ - $1x10^{-6}$
- $1x10^{-8}$ - $1x10^{-7}$

Notes:

Values are for specific storage are ft^{-1}

These values are computed by dividing the field measured storage coefficient provided by SFWMD by the aquifer thickness at that location. Assumed aquifer thicknesses were based on the model-simplified geology.

Observed Specific Storage
Avon Park Permeable Zone
Final Groundwater Model Calibration Report

Figure 3.15

October 2010

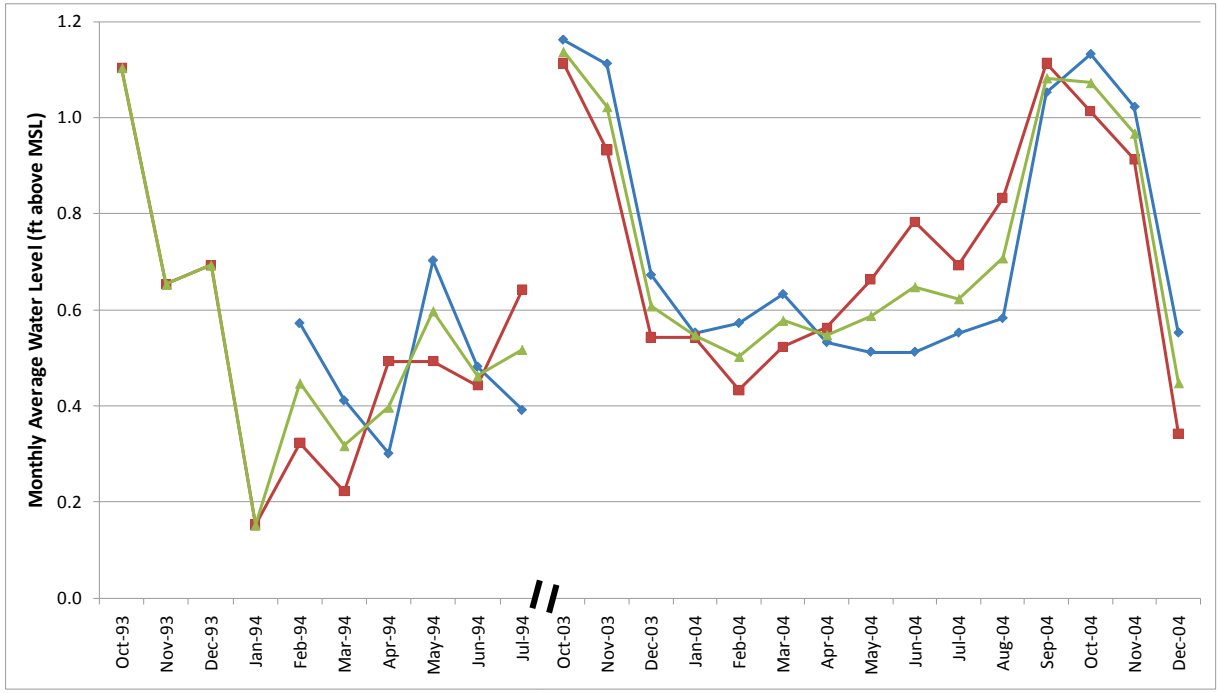

Naples Tide Gauge

Virginia Key Tide Gauge

Average

Notes:
Boundary conditions along the Atlantic coast were set based on the monthly average water levels reported at the Naples and Virginia Key Tide Gauges. The average of the two reported values (green line) was assigned to the model.

Locations of Naples and Virginia Key Tide Gauges are shown on Figure 1.1.

Monthly Average Water Levels - Ocean

Figure 3.16

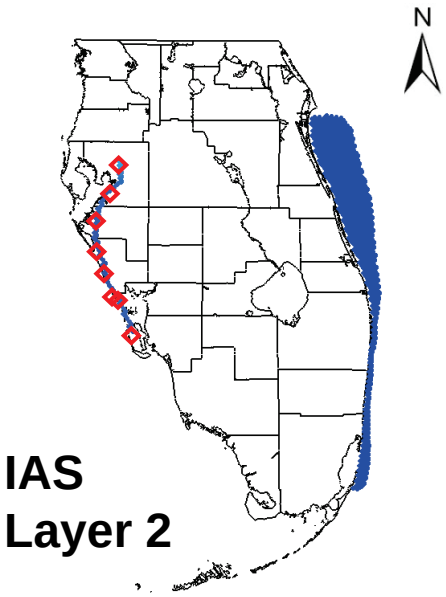

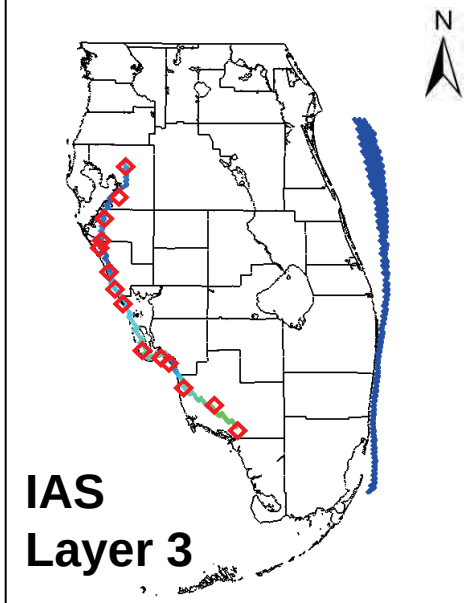

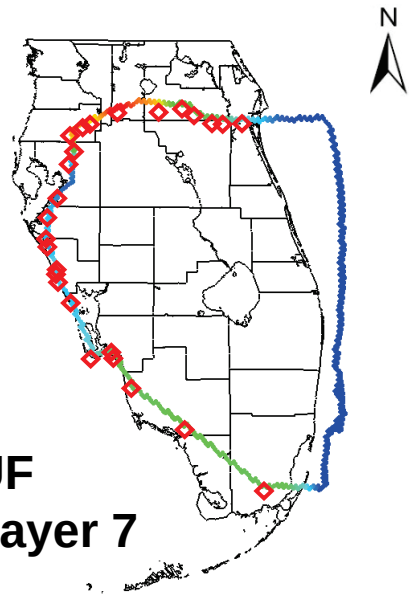

Legend

Applied Specified Head (ft)

100.0
80.0
60.0
40.0
20.0
0.0

◇ Available Water Level Data

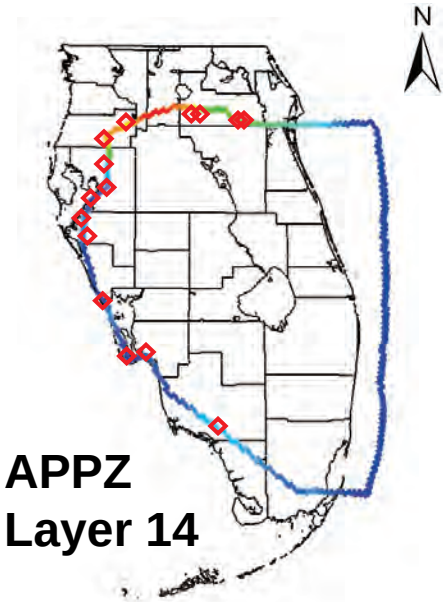

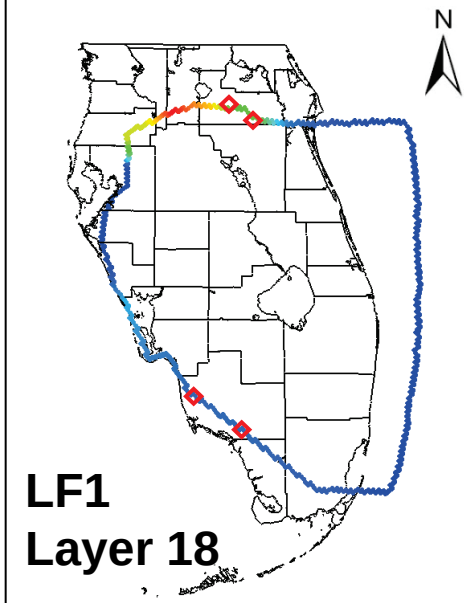

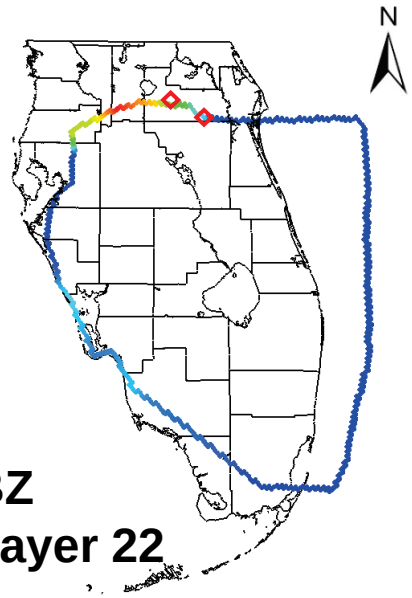

Notes:

The specified heads for each aquifer are the same, regardless of the layer. Thus, the heads shown for Layer 7 are the same as those applied to Layers 5, 6, 8, 9 and 10, since all are part of the UF.

Although only the data from October 2003 is shown here, similar boundary conditions were created for each month in the calibration and validation period.

Applied Specified Head Boundary Conditions

Figure 3.17

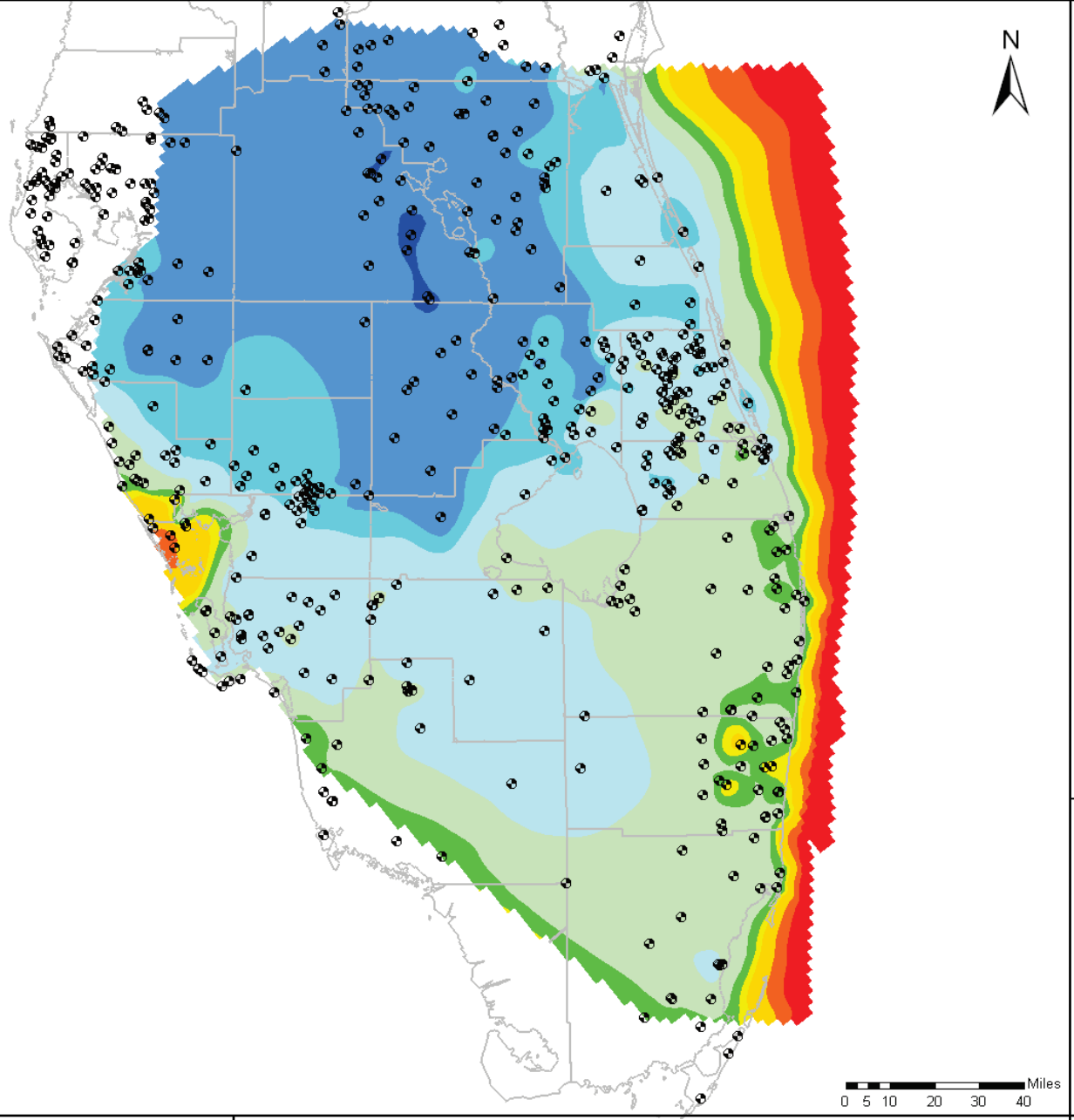

Legend

TDS (mg/L):

- 50-100
- 100-500
- 500-1000
- 1000-2500
- 2500-5000
- 5000-7500
- 7500-10000
- 10000-20000
- 20000-30000
- 30000-40000
- Wells With TDS Data

Notes:

535 wells used for interpolation

Natural Neighbor Interpolation scheme

Assumed 35,000 mg/l along the Atlantic Ocean outcrop

Total Dissolved Solids (TDS) Concentration Upper Floridan Aquifer

Final Groundwater Model Calibration Report

Figure 3.18

October 2010

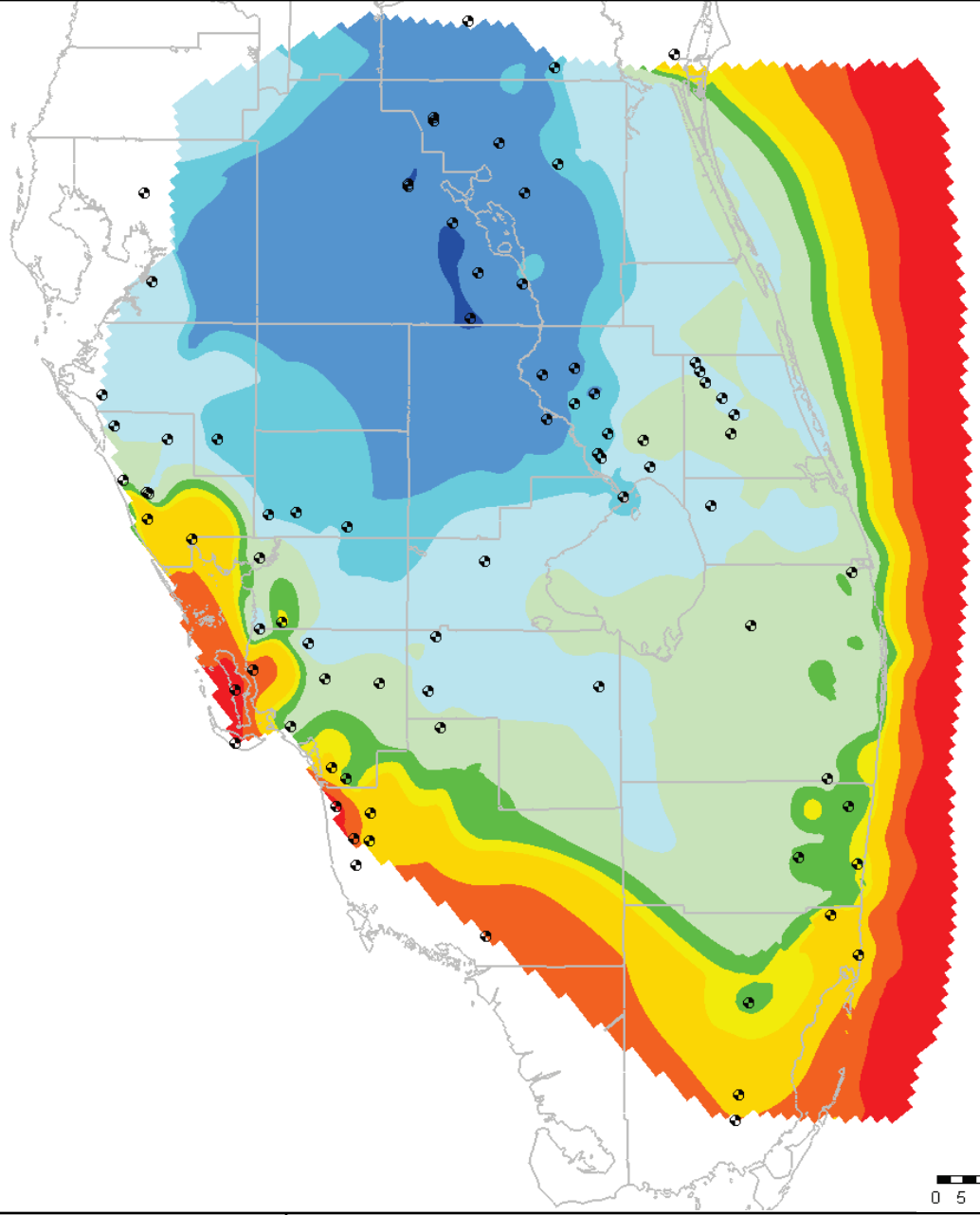

Legend

TDS (mg/L):

- 50-100
- 100-500
- 500-1000
- 1000-2500
- 2500-5000
- 5000-7500
- 7500-10000
- 10000-20000
- 20000-30000
- 30000-40000
- Wells With TDS Data

Notes:

83 wells used for interpolation/ verification

Confirmed MC1 interpolation between UF and APPZ TDS distributions

Assumed 35,000 mg/l along the Atlantic Ocean outcrop

Total Dissolved Solids (TDS) Concentration Middle Confining Unit 1

Final Groundwater Model Calibration Report

Figure 3.19

October 2010

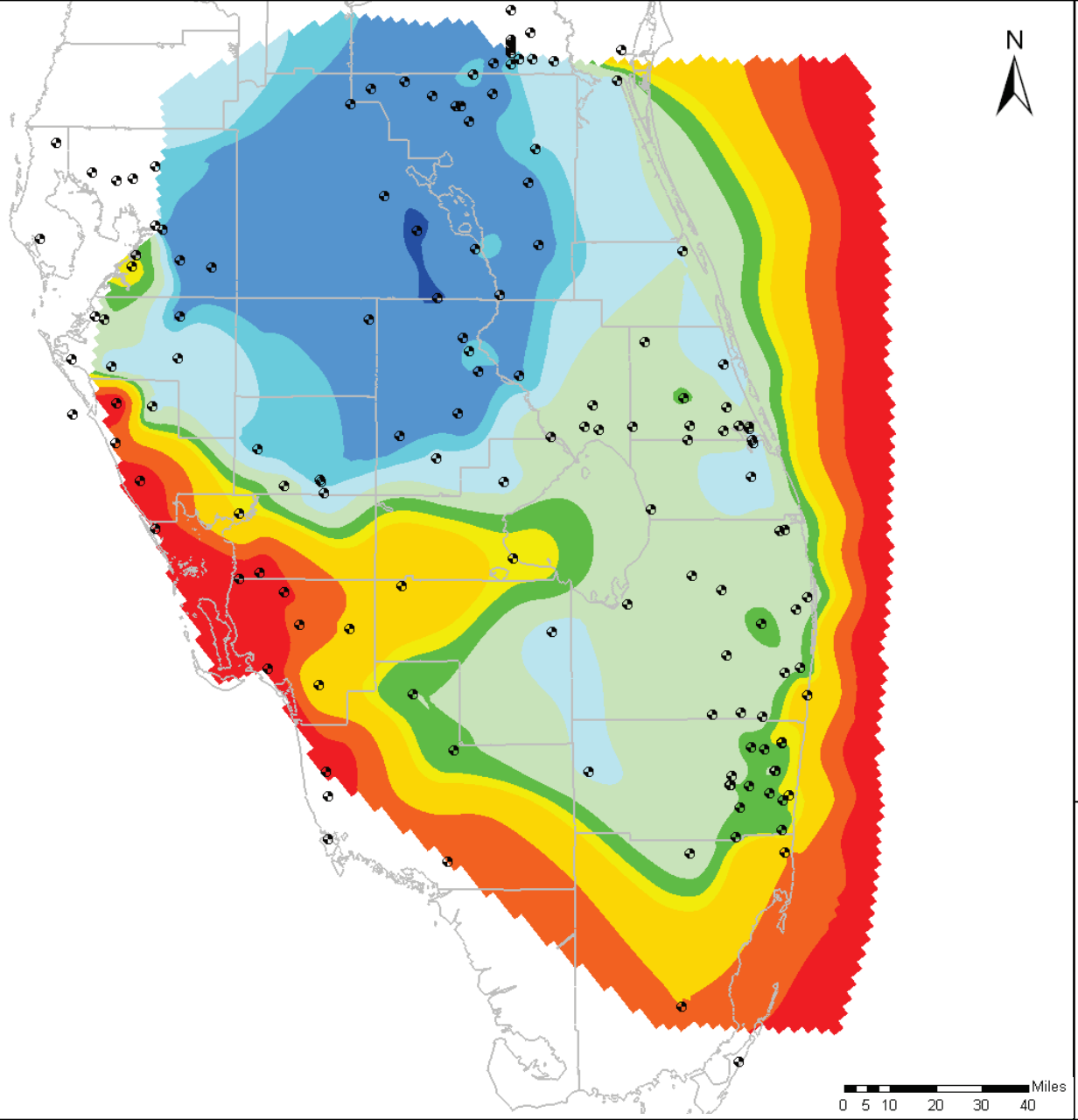

Legend

TDS (mg/L):

- 50-100
- 100-500
- 500-1000
- 1000-2500
- 2500-5000
- 5000-7500
- 7500-10000
- 10000-20000
- 20000-30000
- 30000-40000
- Wells With TDS Data

Notes:

141 wells used for interpolation

Natural Neighbor Interpolation scheme

Assumed 35,000 mg/l along the Atlantic Ocean outcrop

Total Dissolved Solids (TDS) Concentration
Avon Park Permeable Zone

Final Groundwater Model Calibration Report

Figure 3.20

October 2010

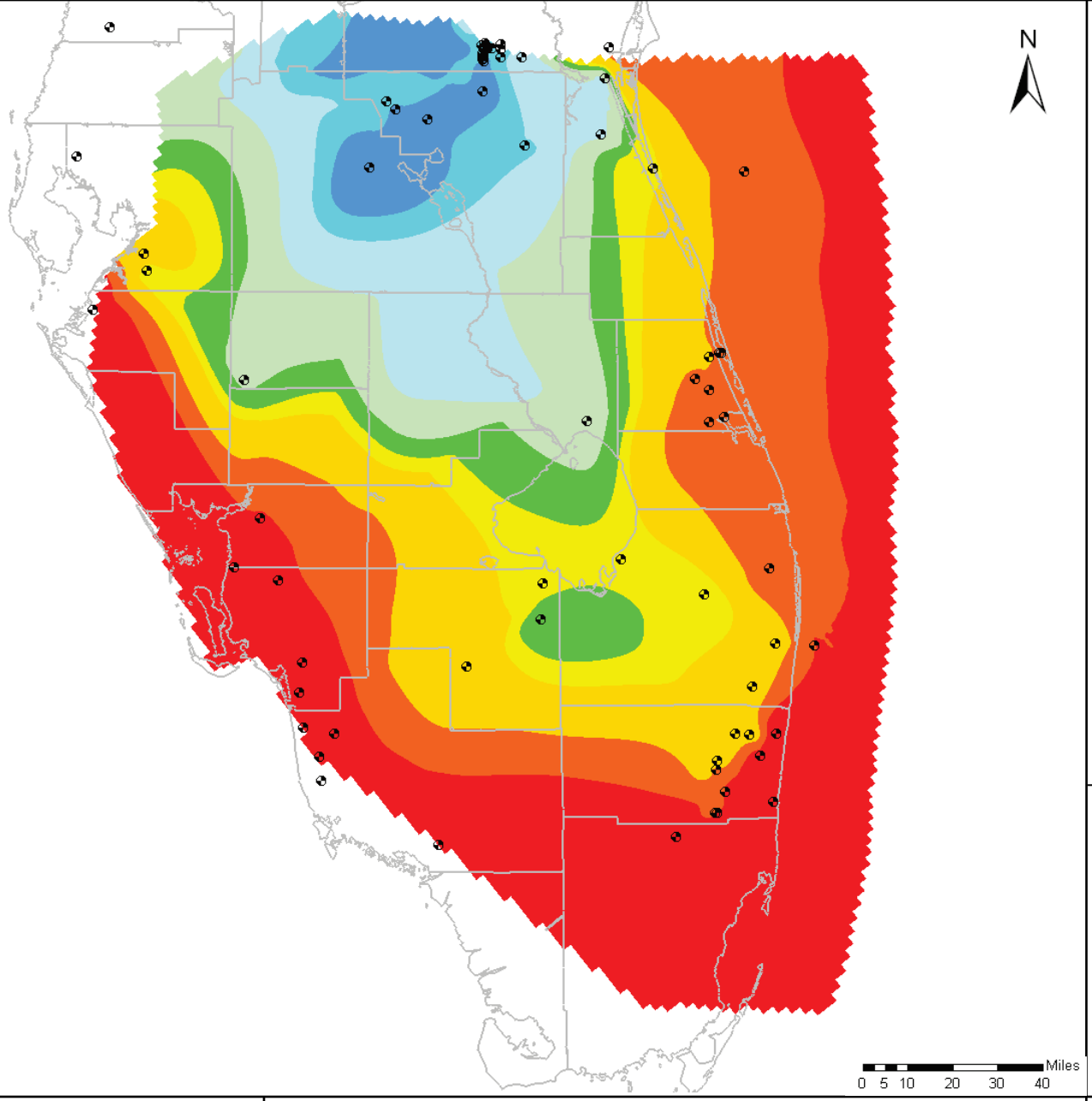

Legend

TDS (mg/L):

- 50-100
- 100-500
- 500-1000
- 1000-2500
- 2500-5000
- 5000-7500
- 7500-10000
- 10000-20000
- 20000-30000
- 30000-40000
- Wells With TDS Data

Notes:

75 wells used for interpolation

Natural Neighbor Interpolation scheme

Assumed 35,000 mg/l along the Atlantic Ocean outcrop

Not saltier than LF1 or fresher than APPZ

Total Dissolved Solids (TDS) Concentration Middle Confining Unit 2

Final Groundwater Model Calibration Report

Figure 3.21

October 2010

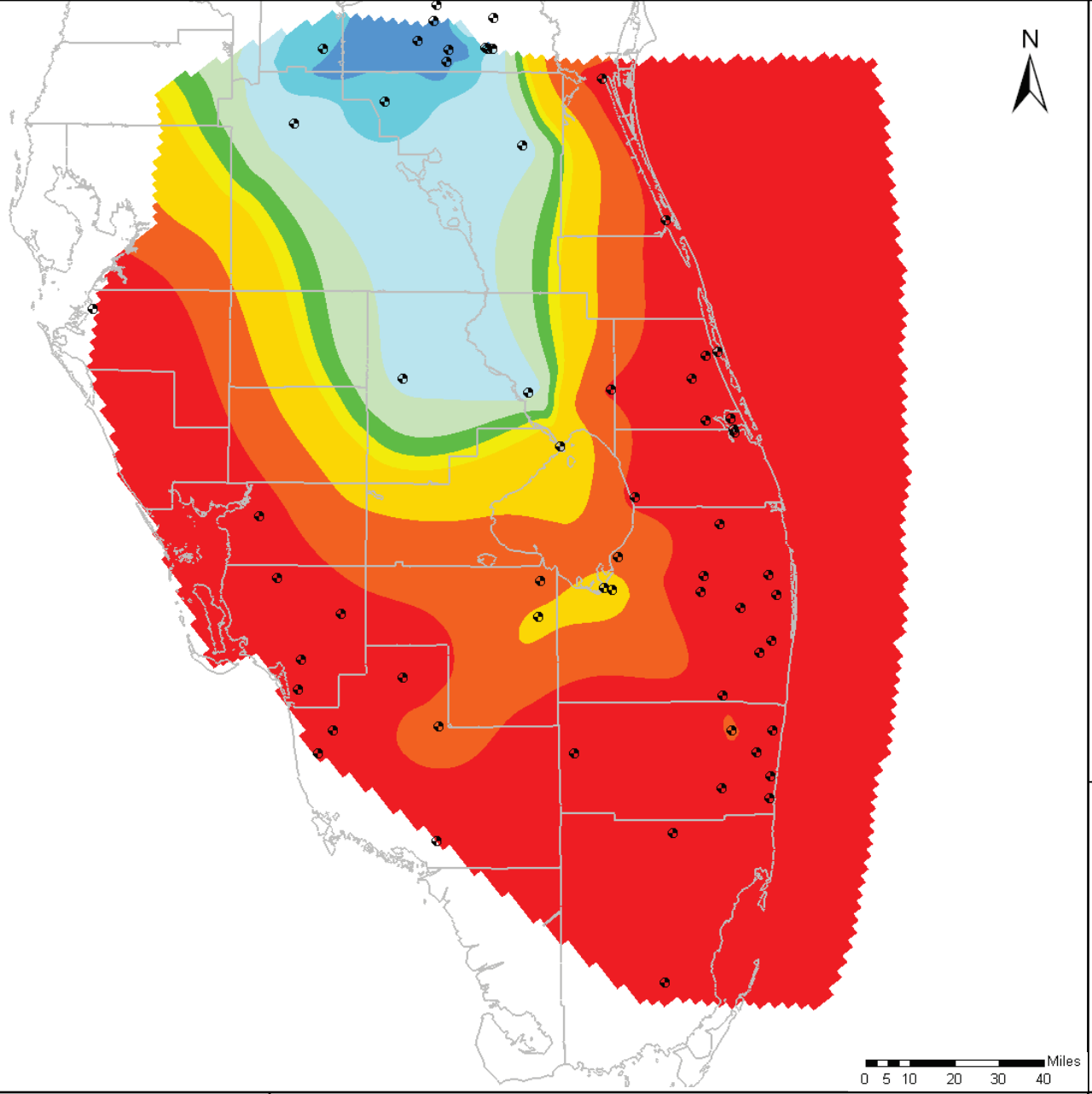

Legend

TDS (mg/L):

- 50-100
- 100-500
- 500-1000
- 1000-2500
- 2500-5000
- 5000-7500
- 7500-10000
- 10000-20000
- 20000-30000
- 30000-40000
- Wells With TDS Data

Notes:

57 wells used for interpolation

Natural Neighbor Interpolation scheme

Assumed 35,000 mg/l along the Atlantic Ocean outcrop

TDS data from wells in vicinity of injection wells was not used since it may not be indicative of native water quality

Total Dissolved Solids (TDS) Concentration Lower Floridan (LF1) Aquifer

Final Groundwater Model Calibration Report

Figure 3.22

October 2010

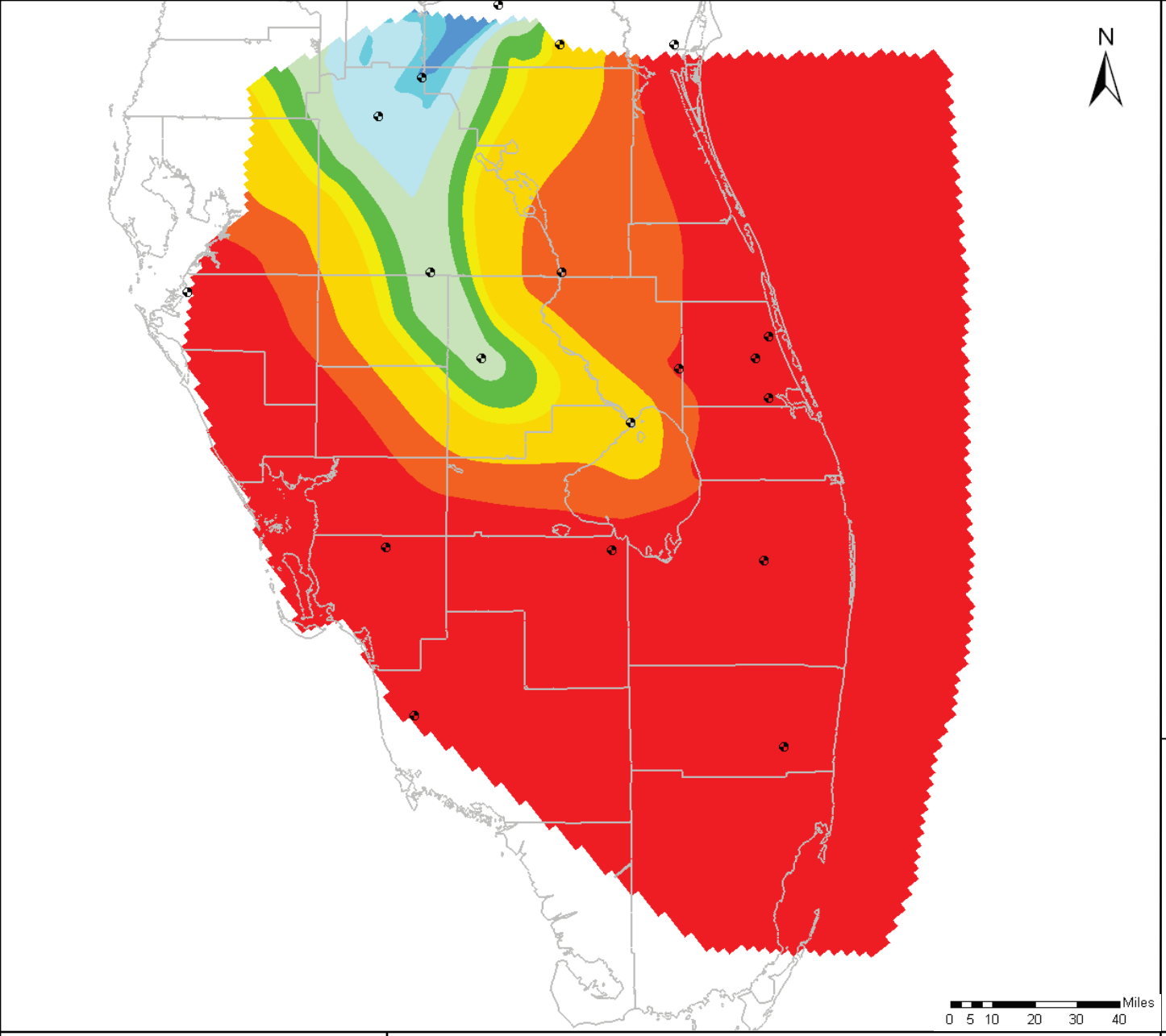

Legend

TDS (mg/L):

- 50-100
- 100-500
- 500-1000
- 1000-2500
- 2500-5000
- 5000-7500
- 7500-10000
- 10000-20000
- 20000-30000
- 30000-40000
- Wells With TDS Data

Notes:

14 wells used for interpolation

Natural Neighbor Interpolation scheme

Assumed 35,000 mg/l along the Atlantic Ocean outcrop

Not saltier than BZ or fresher than LF1

Total Dissolved Solids (TDS) Concentration Lower Confining Unit

Final Groundwater Model Calibration Report

Figure 3.23

October 2010

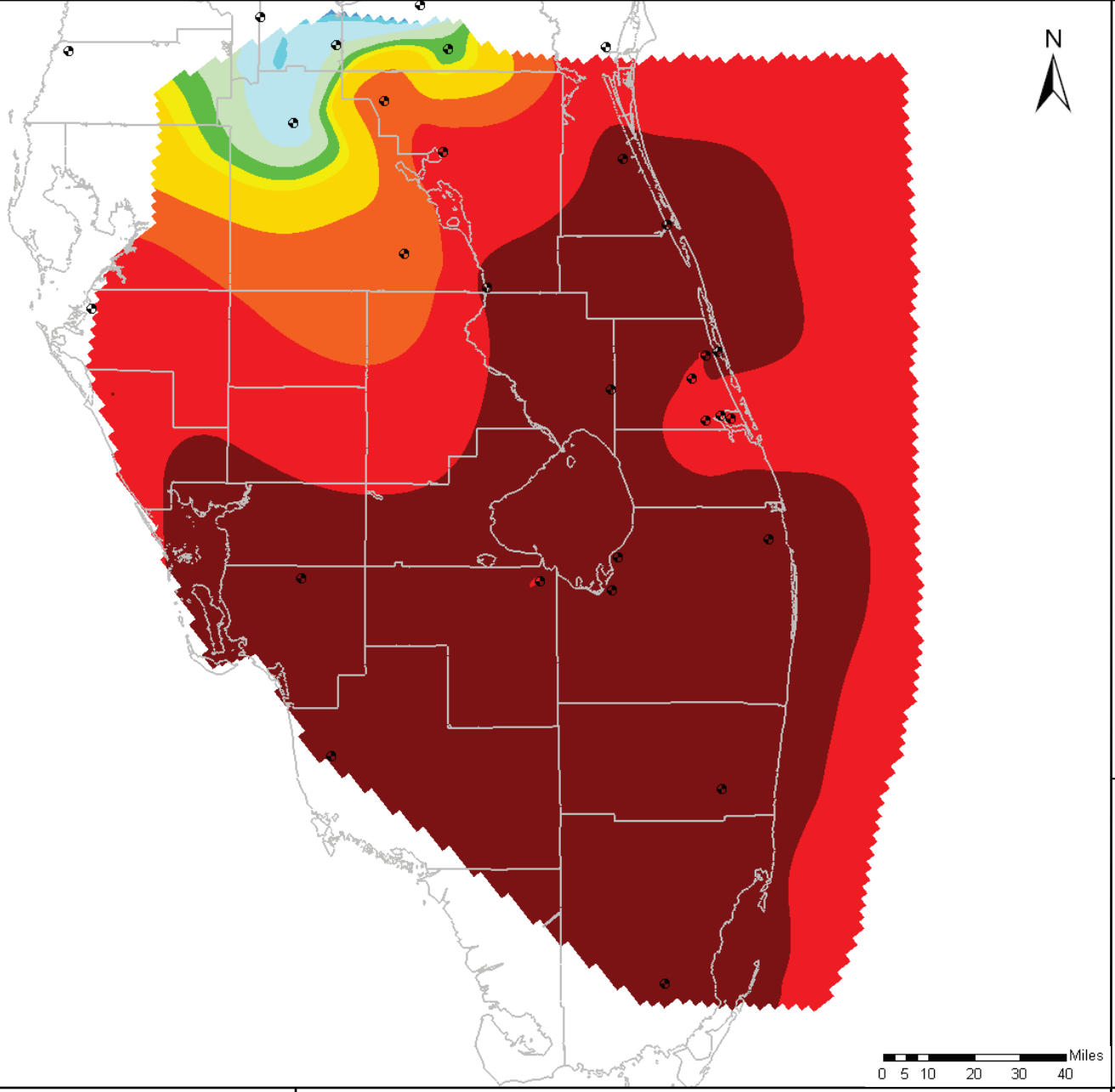

Legend

TDS (mg/L):

- 50-100
- 100-500
- 500-1000
- 1000-2500
- 2500-5000
- 5000-7500
- 7500-10000
- 10000-20000
- 20000-30000
- 30000-36000
- 36000-40000
- Wells With TDS Data

Notes:

26 wells used for interpolation

Natural Neighbor Interpolation scheme

Assumed 35,000 mg/l along the Atlantic Ocean outcrop

TDS data from wells in vicinity of injection wells were not used since it may not be indicative of native water quality

Total Dissolved Solids (TDS) Concentration Boulder Zone

Final Groundwater Model Calibration Report

Figure 3.24

October 2010

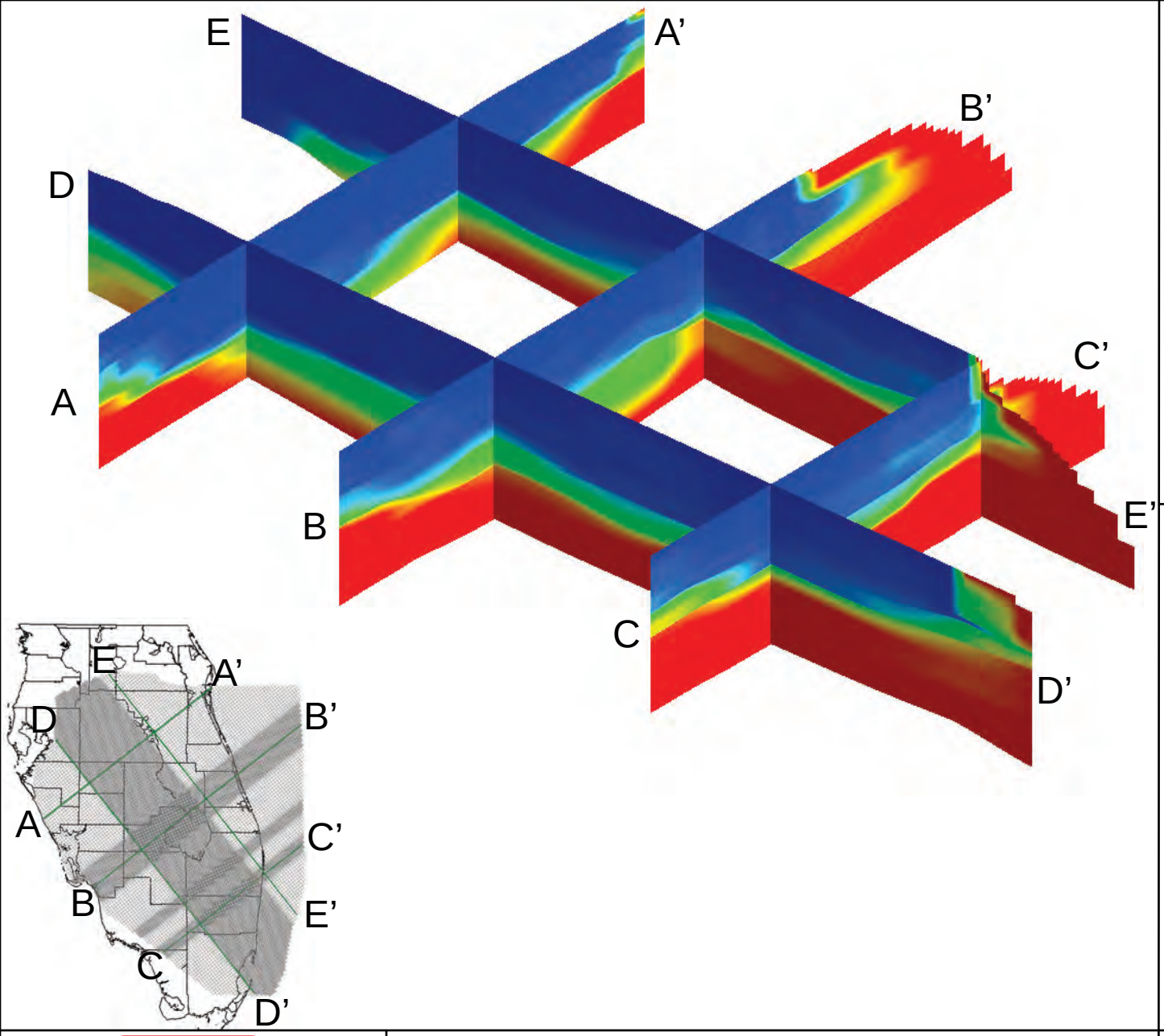

Initial TDS Concentration (mg/L):

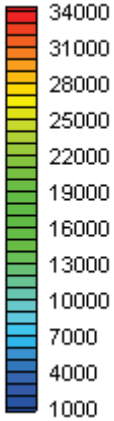

Notes:

TDS concentrations added to the SEAWAT model as initial conditions.

This figure shows the same data as Figures 3.18 through 3.24.

Initial Conditions
TDS Concentrations
Final Groundwater Model Calibration Report

Figure 3.25

October 2010

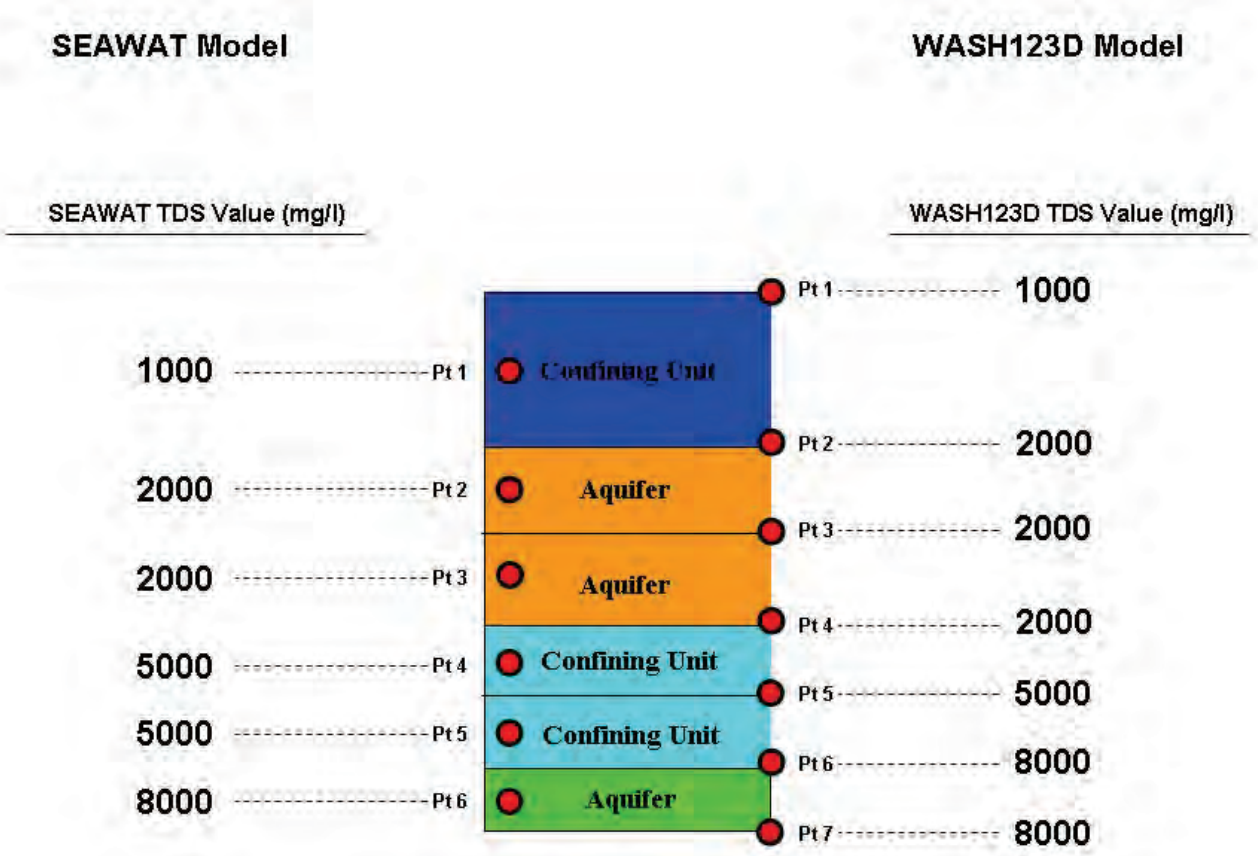

Legend:

Computational Locations.

Comparison of SEAWAT and WASH123D
TDS Initial Condition Assignment
Final Groundwater Model Calibration Report

Figure 3.26

October 2010

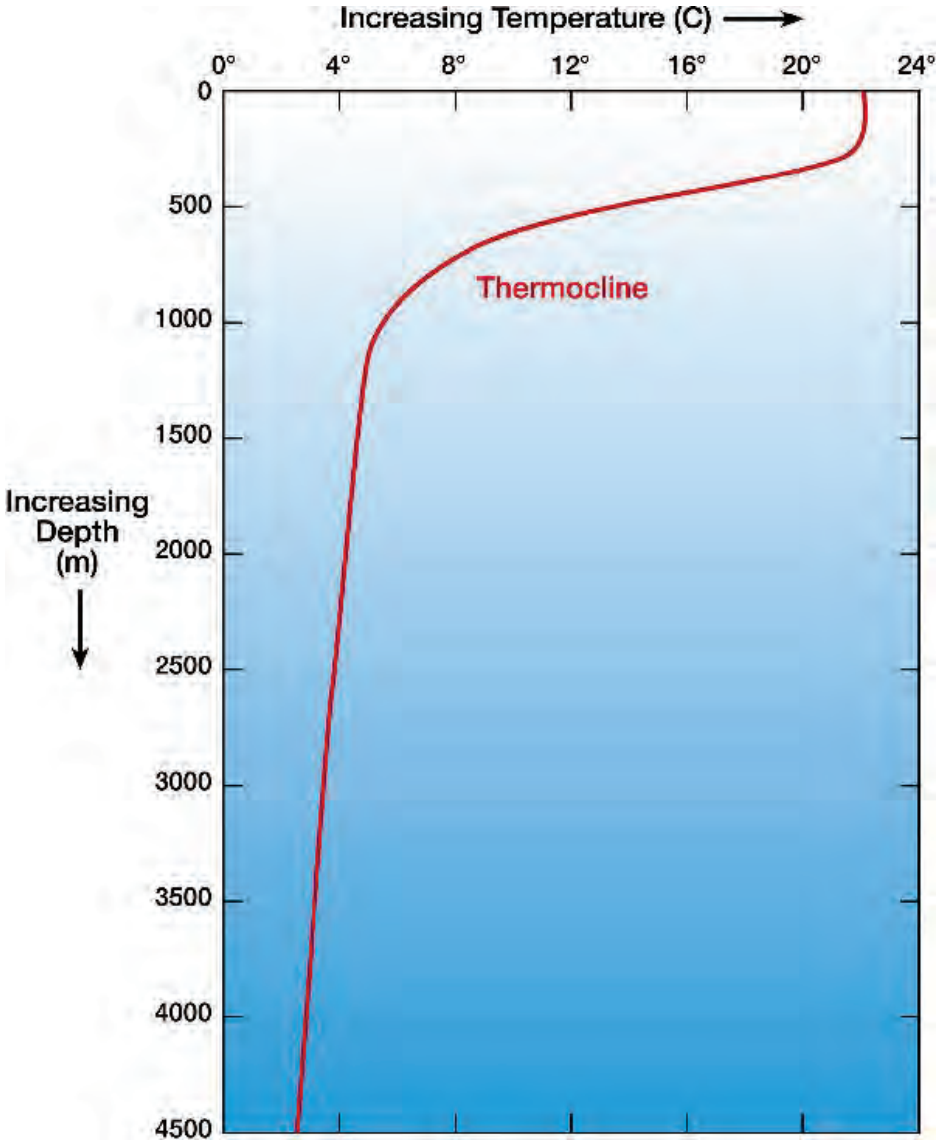

Source:

Windows to the Universe at the University Corporation for Atmospheric Research, nonprofit consortium of research universities. (http://www.windows.ucar.edu/tour/link=/earth/Water/temp.html&edu=high)

Depth where ocean intersects aquifer layers was used to determine ocean temperature (see Figures 3.28 to 3.35)

Ocean Thermocline not used to determine temperature within the SAS.

Temperature-Depth Ocean Profile
Middle Latitudes
Final Groundwater Model Calibration Report

Figure 3.27

October 2010

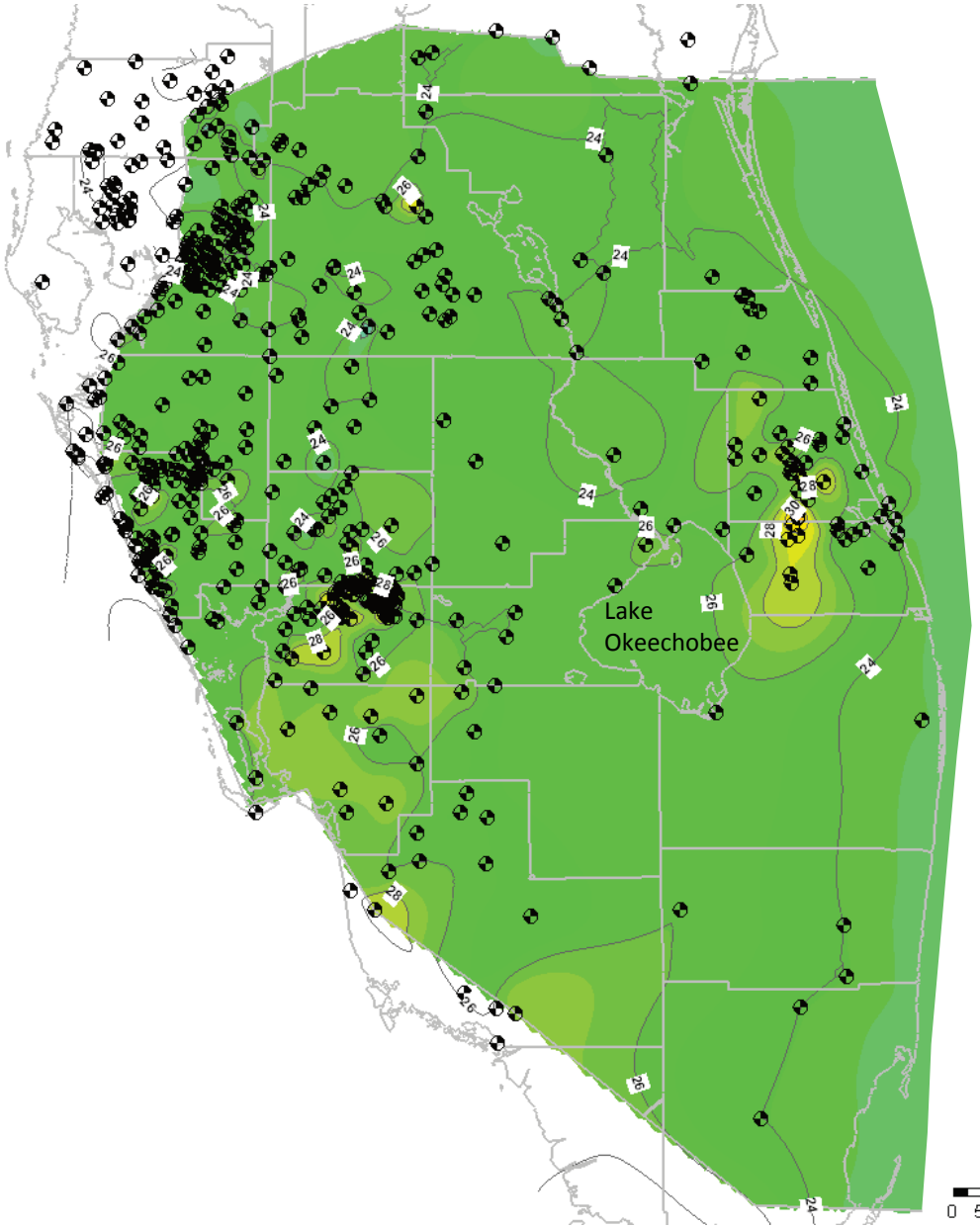

Temperature (°C)

34
32
30
28
26
24
22
20
18
16

Notes:

Data Points

Number of data points: 612

Data sources include SFWMD, SWFWMD, SJRWMD, and USGS.

Color fill depicting temperature variation is defined in the figure.

Linear contour interval is 2 °C.

Assumptions:

Data points used from wells that had open intervals completely or partly within the IAS

Temperature at ocean outcrop is based on Figure 3.27 for elevations varying from -125 to -350 feet.

Temperature Initial Condition Distribution Intermediate Aquifer System

Final Groundwater Model Calibration Report

Figure 3.28

October 2010

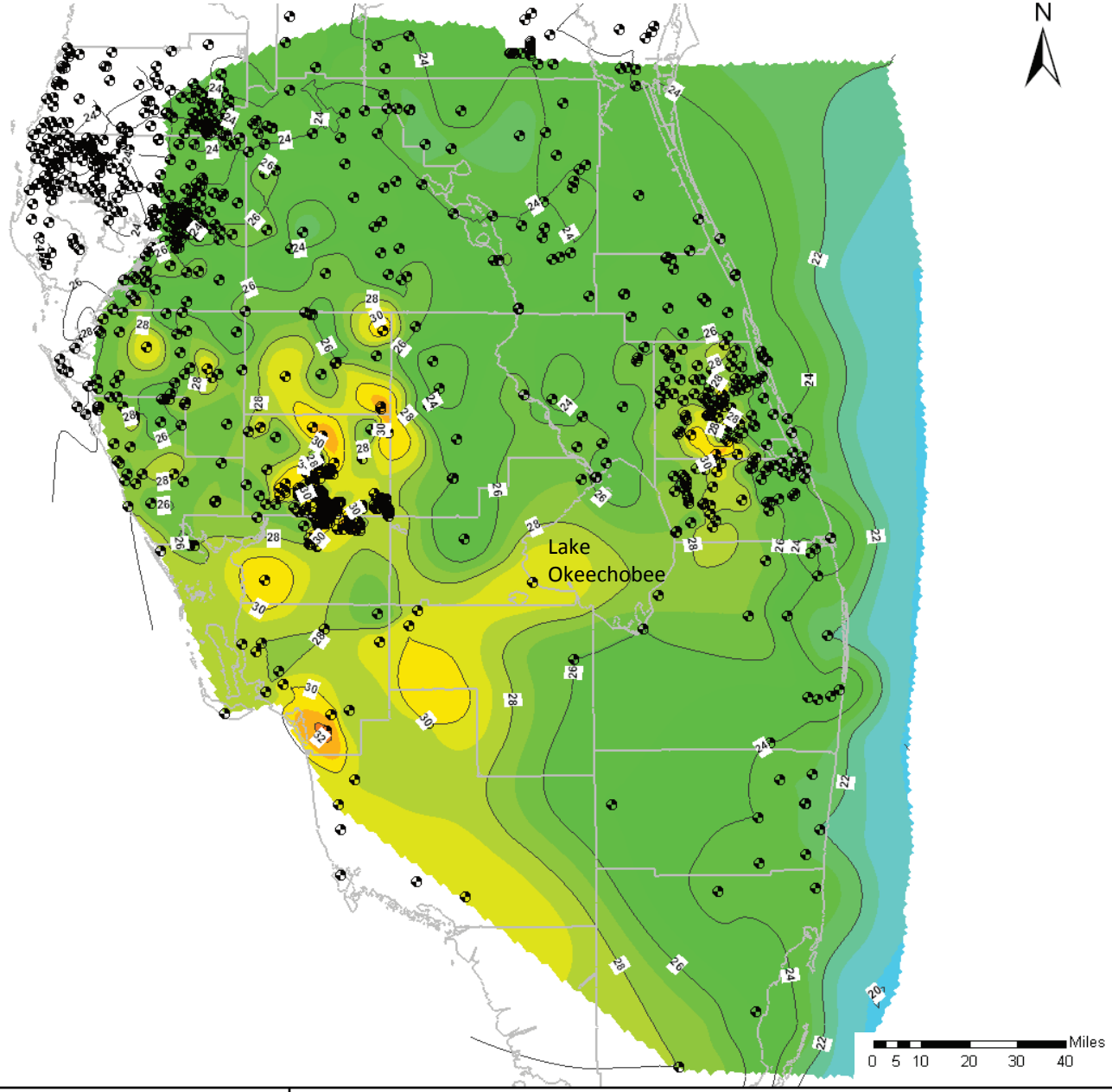

Temperature (°C)

34
32
30
28
26
24
22
20
18
16

Notes:

Data Points

Number of data points: 970

Data sources include SFWMD, SWFWMD, SJRWMD, and USGS.

Color fill depicting temperature variation is defined in the figure.

Linear contour interval is 2 °C.

Assumptions:

Data points used from wells that had open intervals completely or partly within the UF.

Temperature at ocean outcrop is based on Figure 3.27 for elevations varying from -800 to -1,150 feet.

Temperature Initial Condition Distribution
Upper Floridan Aquifer
Final Groundwater Model Calibration Report

Figure 3.29

October 2010

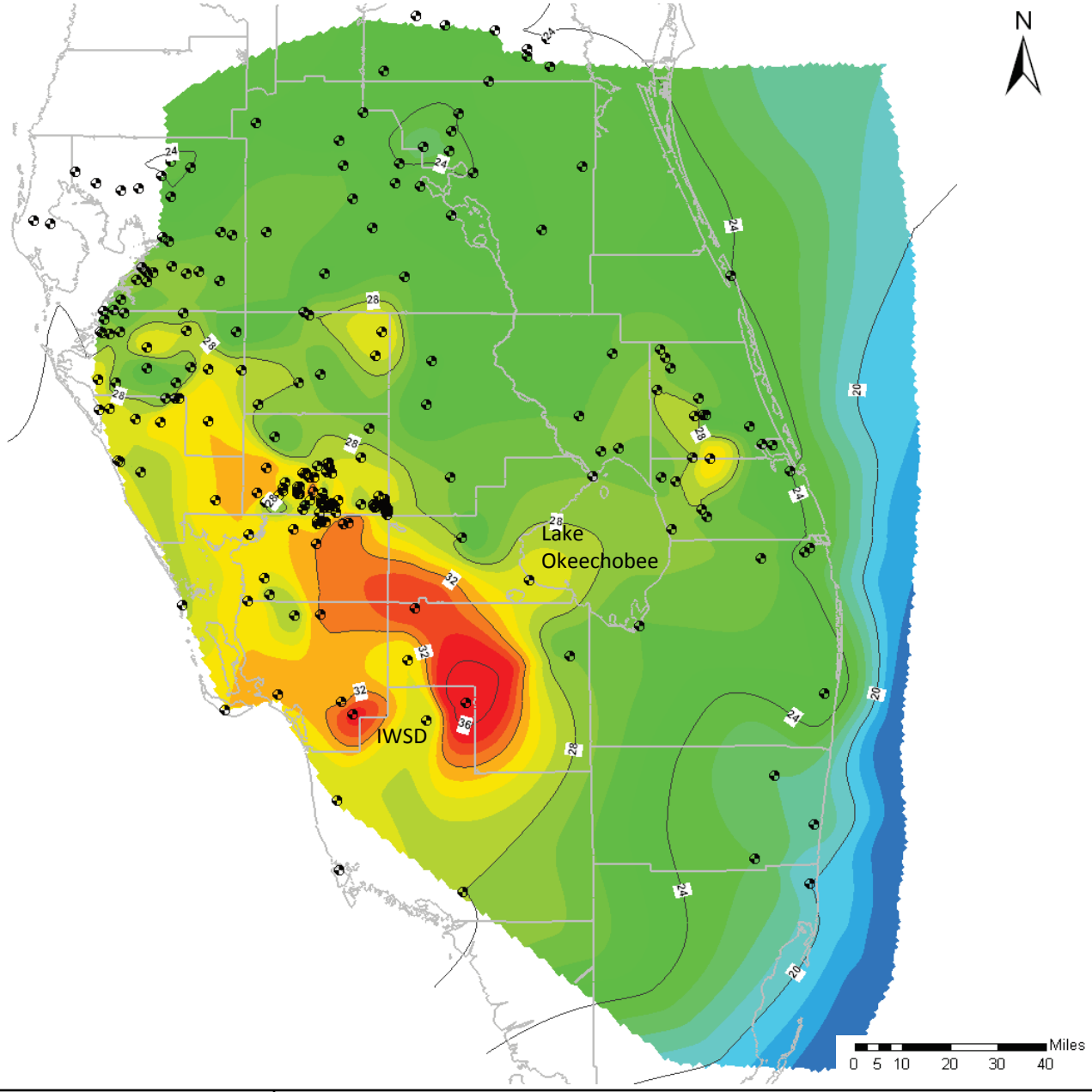

Temperature (°C)

34
32
30
28
26
24
22
20
18
16

Notes:

Data Points

Number of data points: 233

Data sources include SFWMD, SWFWMD, SJRWMD, and USGS.

Color fill depicting temperature variation is defined in the figure.

Linear contour interval is 4 °C.

Assumptions:

Data points used from wells that had open intervals completely or partly within the MC1.

Temperature at ocean outcrop is interpolated from estimates in the UF and APPZ.

Packer test value of 31°C was used at Immokalee Water and Sewer District well (IWSD) rather than the more recent value of 29°C to represent native water temperature.

Temperature Initial Condition Distribution
Upper Middle Confining Unit (MC1)

Final Groundwater Model Calibration Report

Figure 3.30

October 2010

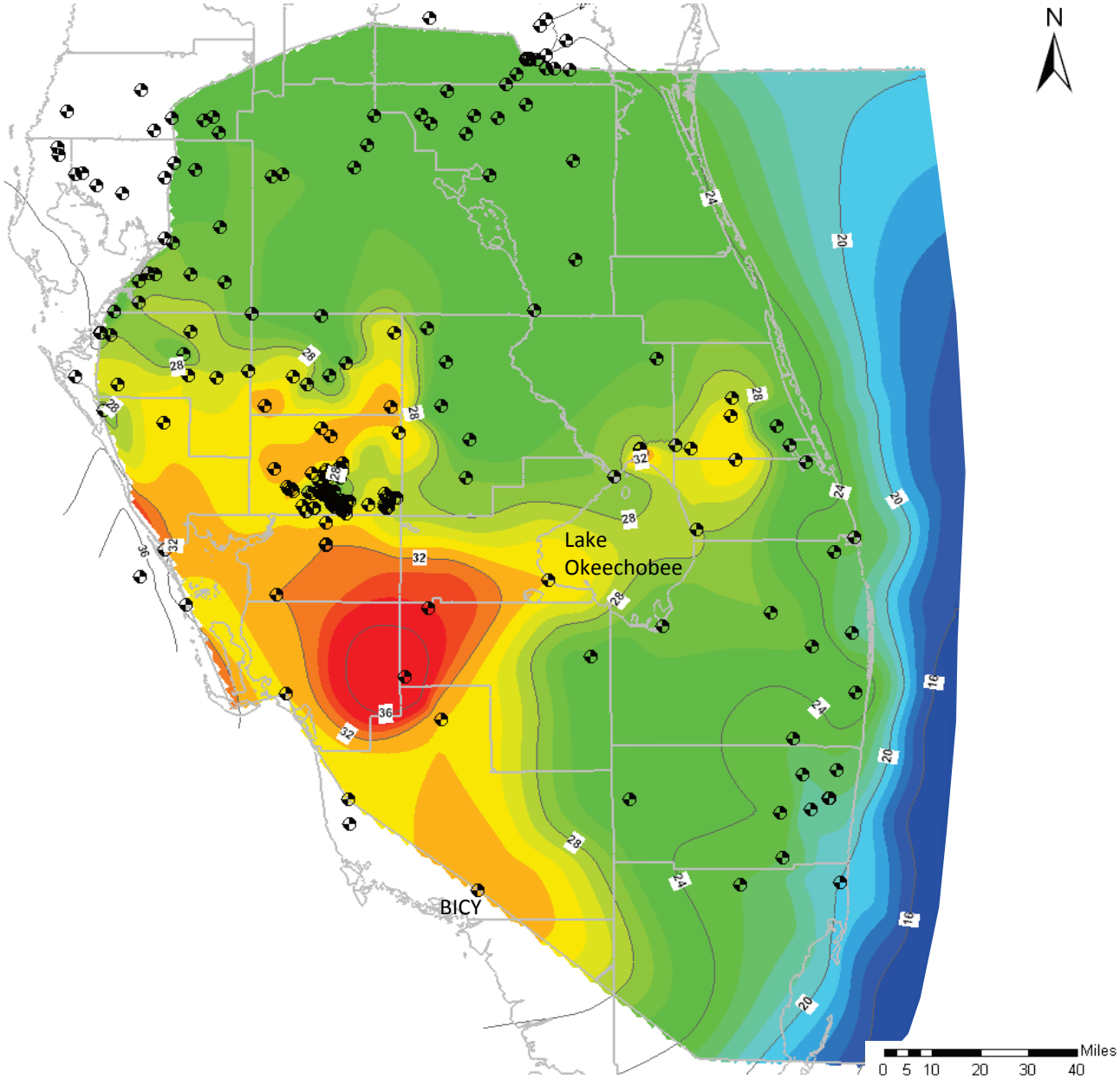

Temperature (°C)

34
32
30
28
26
24
22
20
18
16

Notes:

Data Points

Number of data points: 218

Data sources include SFWMD, SWFWMD, SJRWMD, and USGS.

Color fill depicting temperature variation is defined in the figure.

Linear contour interval is 4 °C.

Assumptions:

Data points used from wells that had open intervals completely or partly within the APPZ.

Temperature at ocean outcrop is based on Figure 3.27 for elevations varying from -950 to -1450 feet.

Packer test value of 32°C was used at Big Cypress Preserve well (BICY) rather than the more recent value of 28°C to represent native water temperature.

Temperature Initial Condition Distribution
Avon Park Permeable Zone
Final Groundwater Model Calibration Report

Figure 3.31

October 2010

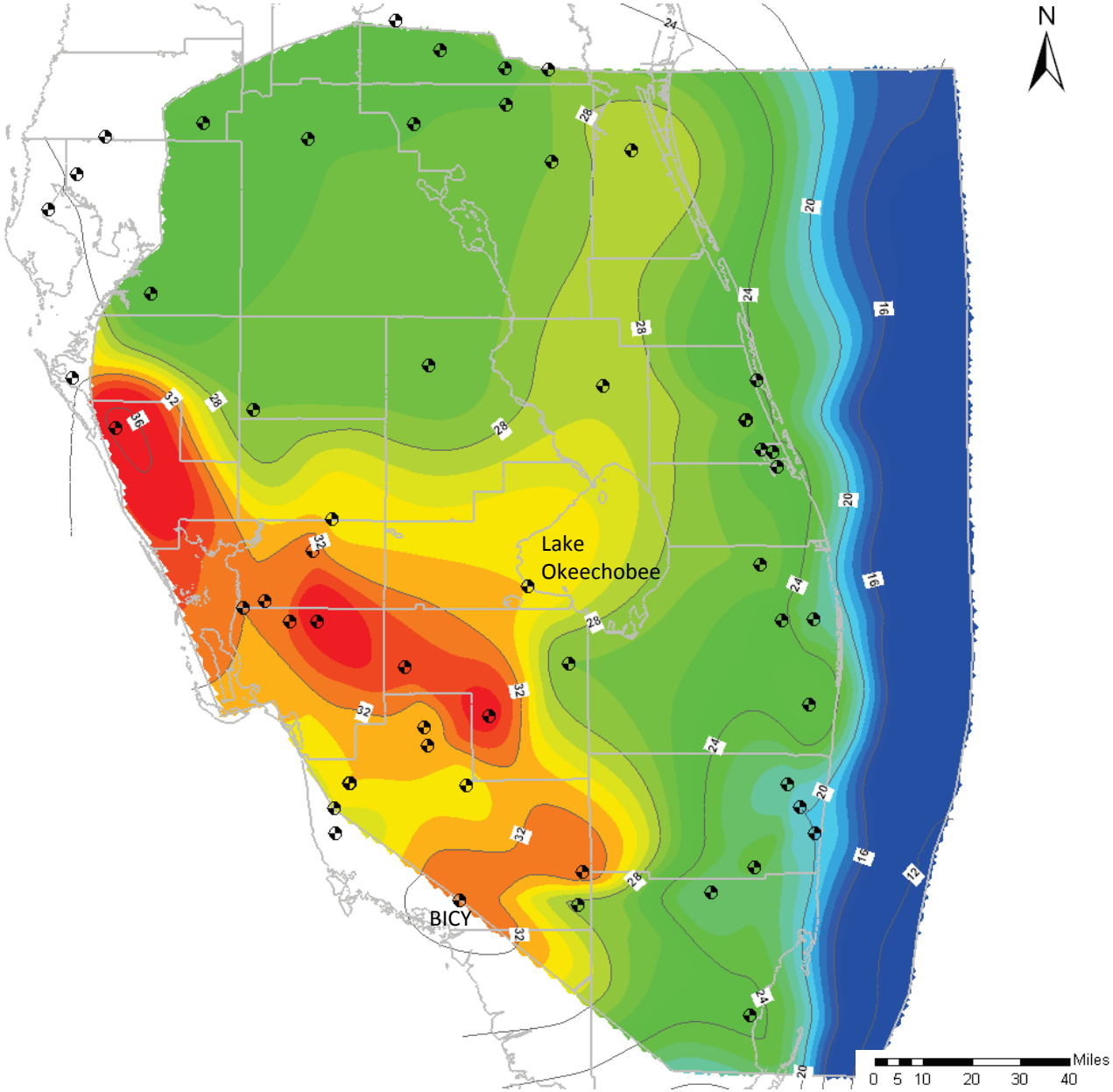

Temperature (°C)

34
32
30
28
26
24
22
20
18
16

Notes:

Data Points

Number of data points: 57

Data sources include SFWMD, SWFWMD, SJRWMD, and USGS.

Color fill depicting temperature variation is defined in the figure.

Linear contour interval is 4 °C.

Assumptions:

Data points used from wells that had open intervals completely or partly within the MC2.

Temperature at ocean outcrop is interpolated from estimates in the APPZ and LF1.

Packer test value of 33°C was used at Big Cypress Preserve well (BICY) rather than the more recent value of 28°C to represent native water temperature.

Temperature Initial Condition Distribution Lower Middle Confining Unit (MC2)

Final Groundwater Model Calibration Report

Figure 3.32

October 2010

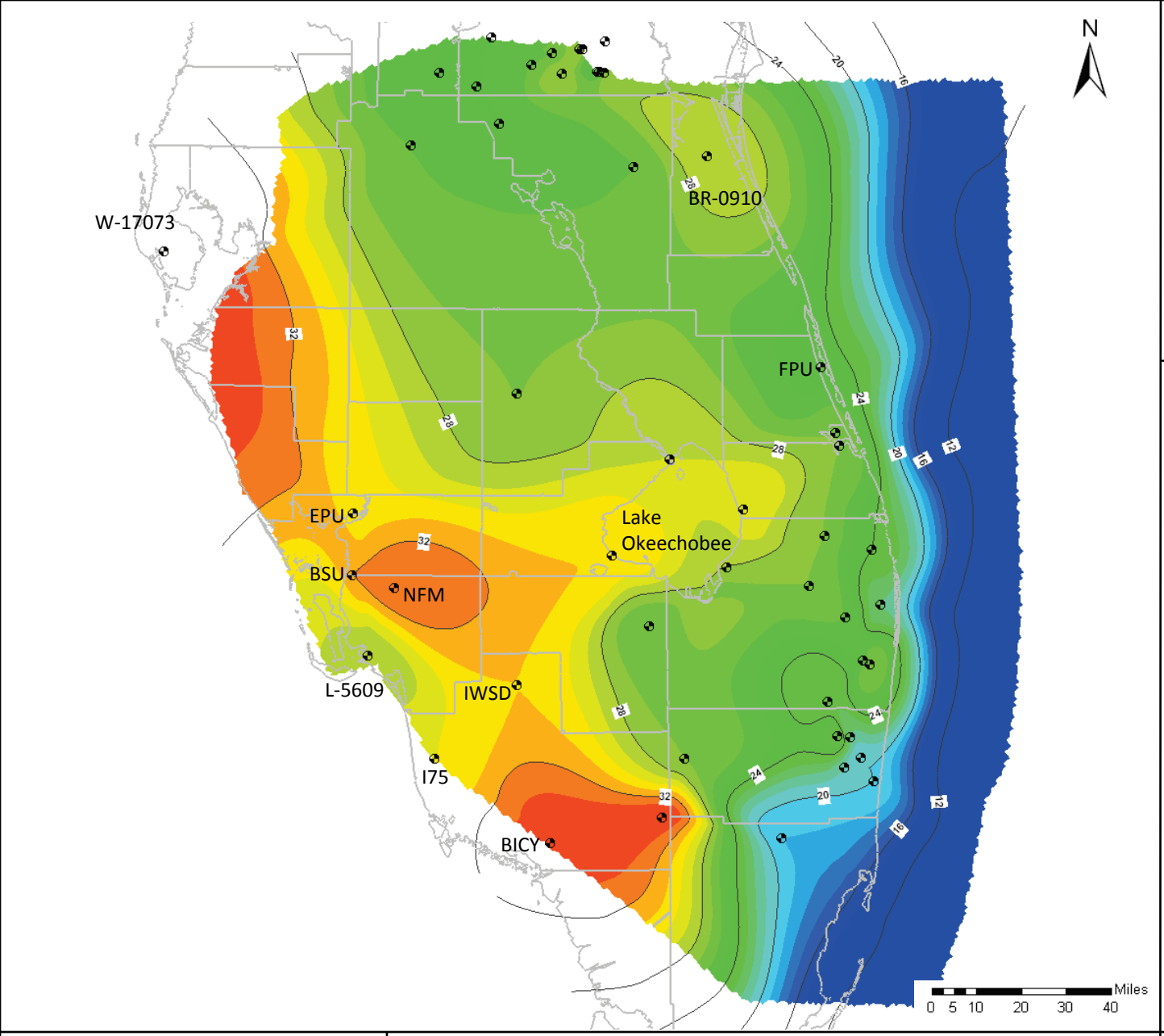

Temperature (°C)

34
32
30
28
26
24
22
20
18
16

Notes:

Data Points

Number of data points: 51

Data sources include SFWMD, SWFWMD, SJRWMD, and USGS.

Color fill depicting temperature variation is defined in the figure.

Linear contour interval is 4 °C.

Assumptions:

Data points used from wells that had open intervals completely or partly within the LF1.

Temperature at ocean outcrop is based on Figure 3.27 for elevations varying from -1,500 to -2,400 feet.

Packer test values of 34°C, 31°C, and 30°C were used at Big Cypress Preserve well (BICY), Immokalee Water and Sewer District (IWSD), and I-75 Canal (I75), respectively, rather than their more recent values of 28°C, 27°C and 28°C to represent native water temperature.

Some temperature data at wells open within the MC2 or LC were added to the LF1 data set to smooth the data between units. Those wells are NFM, BSU, BICY, FPU, BR-0910, and EPU.

Temperature Initial Condition Distribution
Lower Floridan (LF1) Aquifer
Final Groundwater Model Calibration Report

Figure 3.33

October 2010

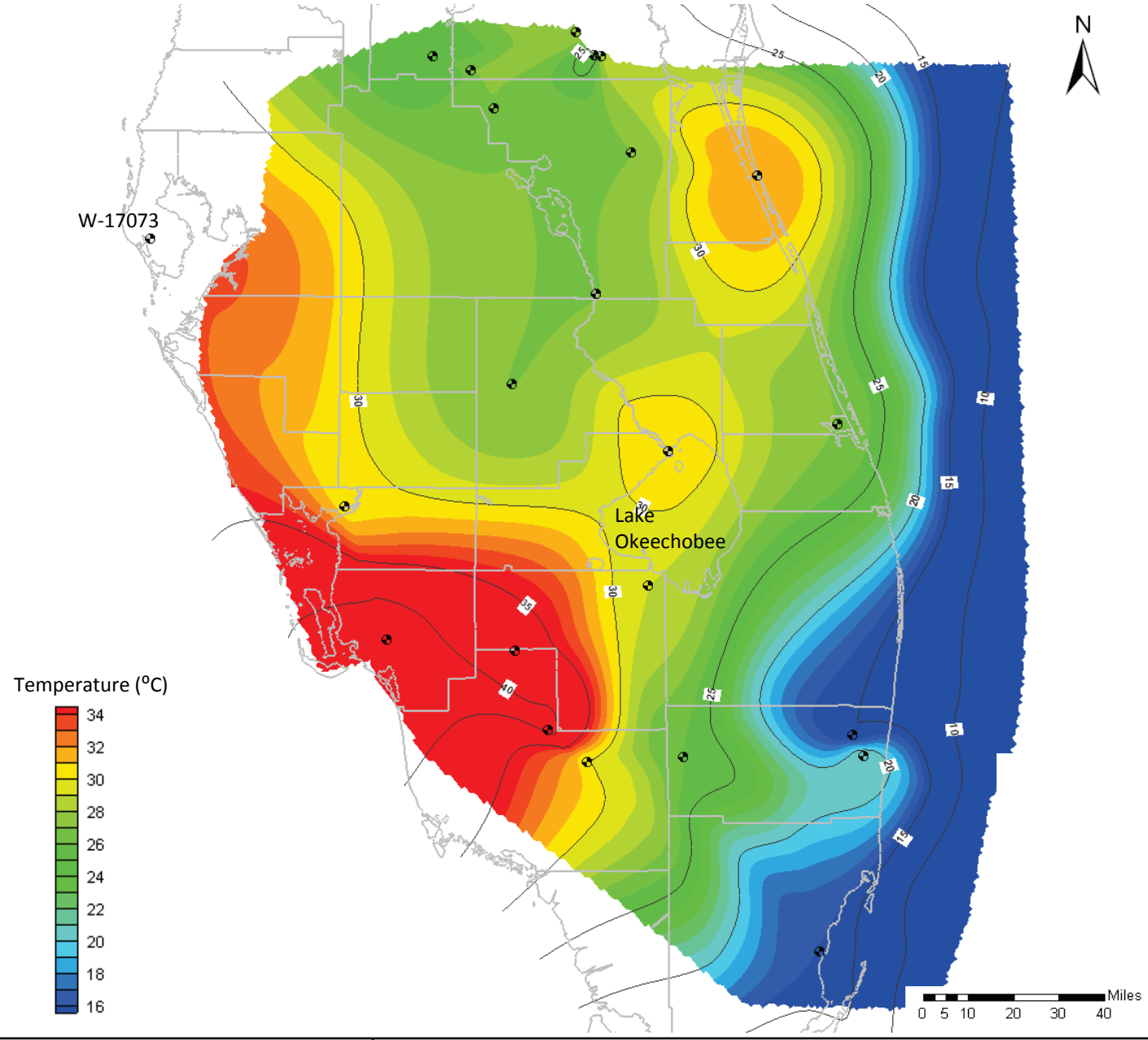

Notes:

Data Points

Number of data points: 23

Data sources include SFWMD, SJRWMD, and USGS.

Color fill depicting temperature variation is defined in the figure.

Linear contour interval is 5 °C.

Assumptions:

Data points used from wells that had open intervals completely or partly within the LC.

Temperature at ocean outcrop is interpolated from estimates in the LF1 and BZ.

Temperature data at well W-17073 open within the LF1 was added to the LC to smooth the data between the LF1 and the BZ.

Temperature Initial Condition Distribution
Lower Confining Unit
Final Groundwater Model Calibration Report

Figure 3.34

October 2010

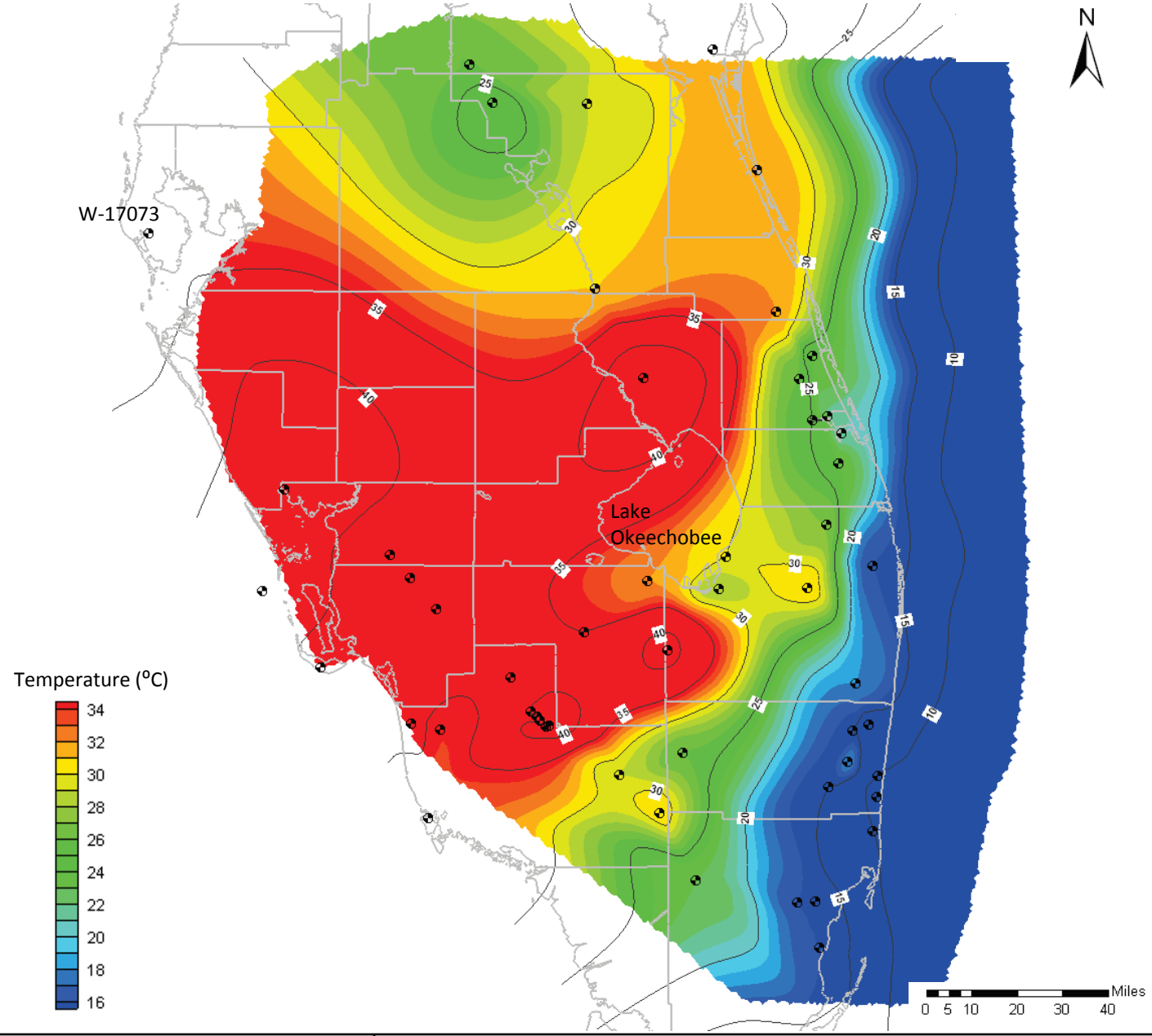

Notes:

Data Points

Number of data points: 55

Data sources include SFWMD, USGS, and well completion reports.

Color fill depicting temperature variation is defined in the figure.

Linear contour interval is 5 °C.

Assumptions:

Data points used from wells that had open intervals completely or partly within the BZ.

Temperature at ocean outcrop is based on Figure 3.27 for elevations varying from -2,600 to -3,000 feet.

Temperature data at well W-17073 open within the LF1 was added to the LC to smooth the data between the LF1 and the BZ.

Temperature Initial Condition Distribution
Boulder Zone

Final Groundwater Model Calibration Report

Figure 3.35

October 2010

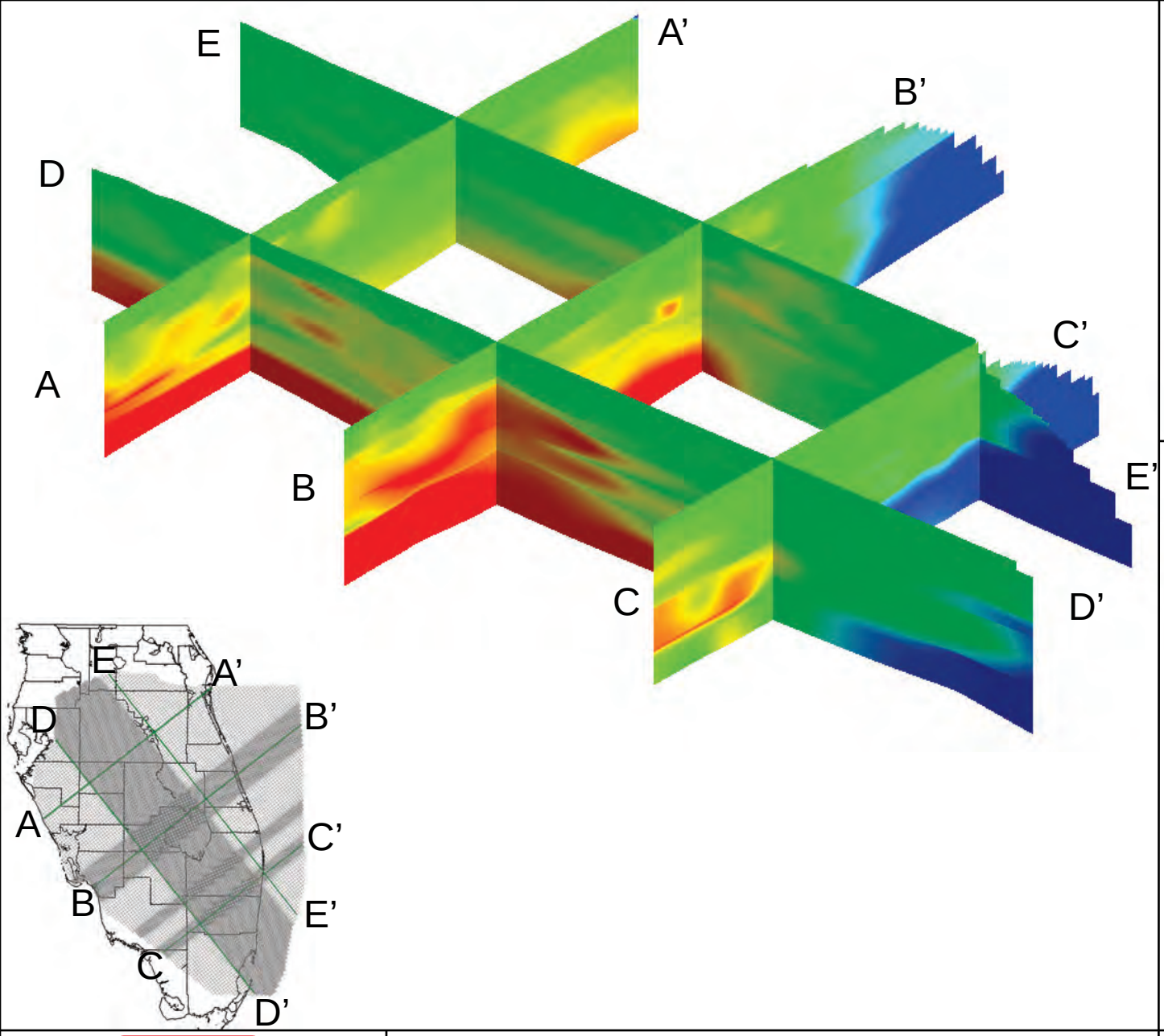

Initial Conditions
Temperature (°C):

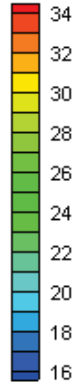

Notes:

TDS concentrations added to the SEAWAT model as initial conditions.

This figure shows the same data as Figures 3.28 through 3.35.

Temperature Initial Conditions

Figure 3.36

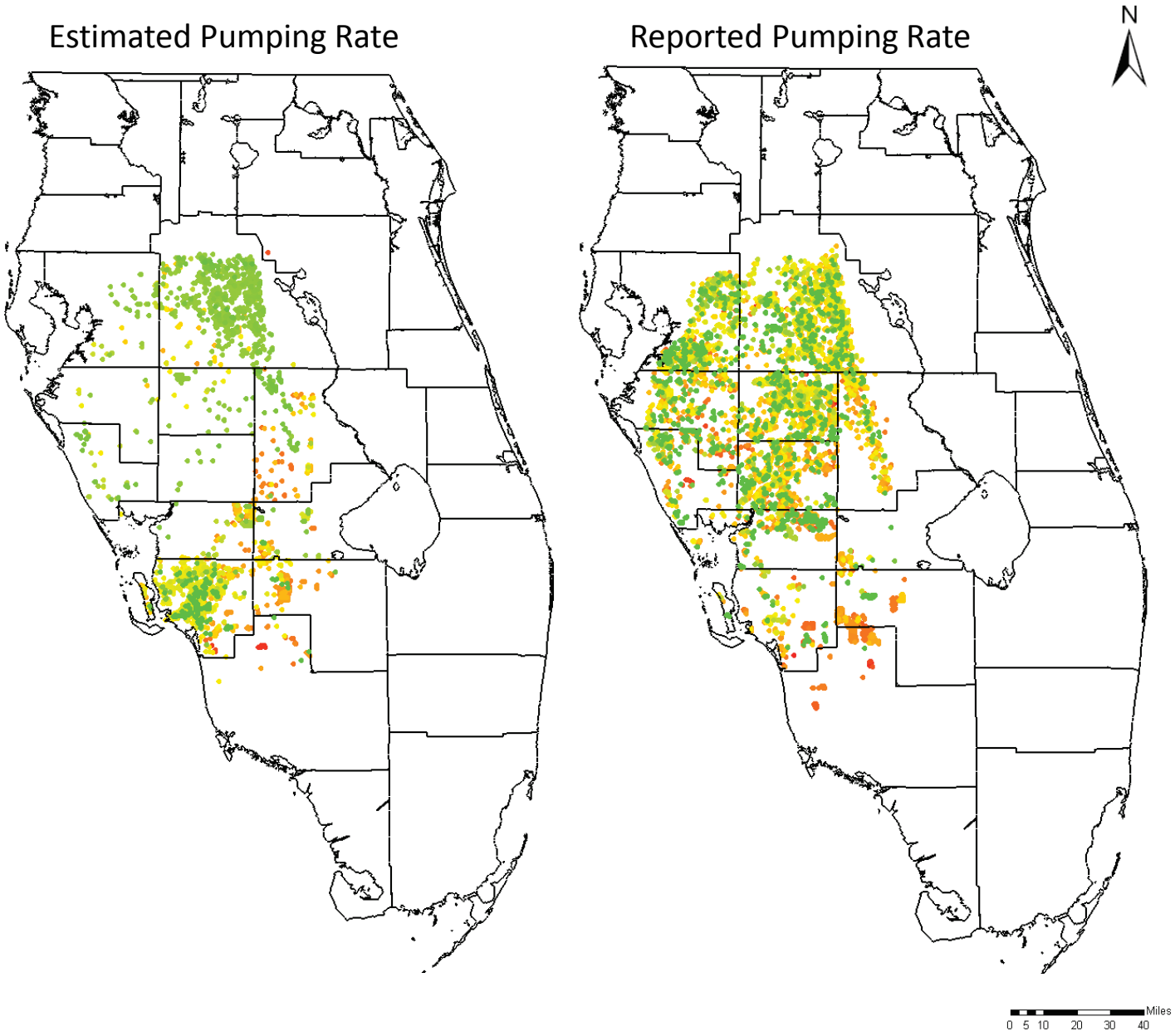

Pump Rate (MGD)

Injection

10

0.1

0.001

0

-0.001

-0.1

-10

Extraction

Notes:

Number of wells in layer :

6454 with Reported Data

3612 with Estimated Data

Wells shown are in layer 3 of the model. Pump rates assigned to the model are the sum of the actual and estimated data.

Pumping rates are from May 2004 (generally the highest rate of pumping).

Pumping Well Locations
Intermediate Aquifer

Final Groundwater Model Calibration Report

Figure 3.37

October 2010

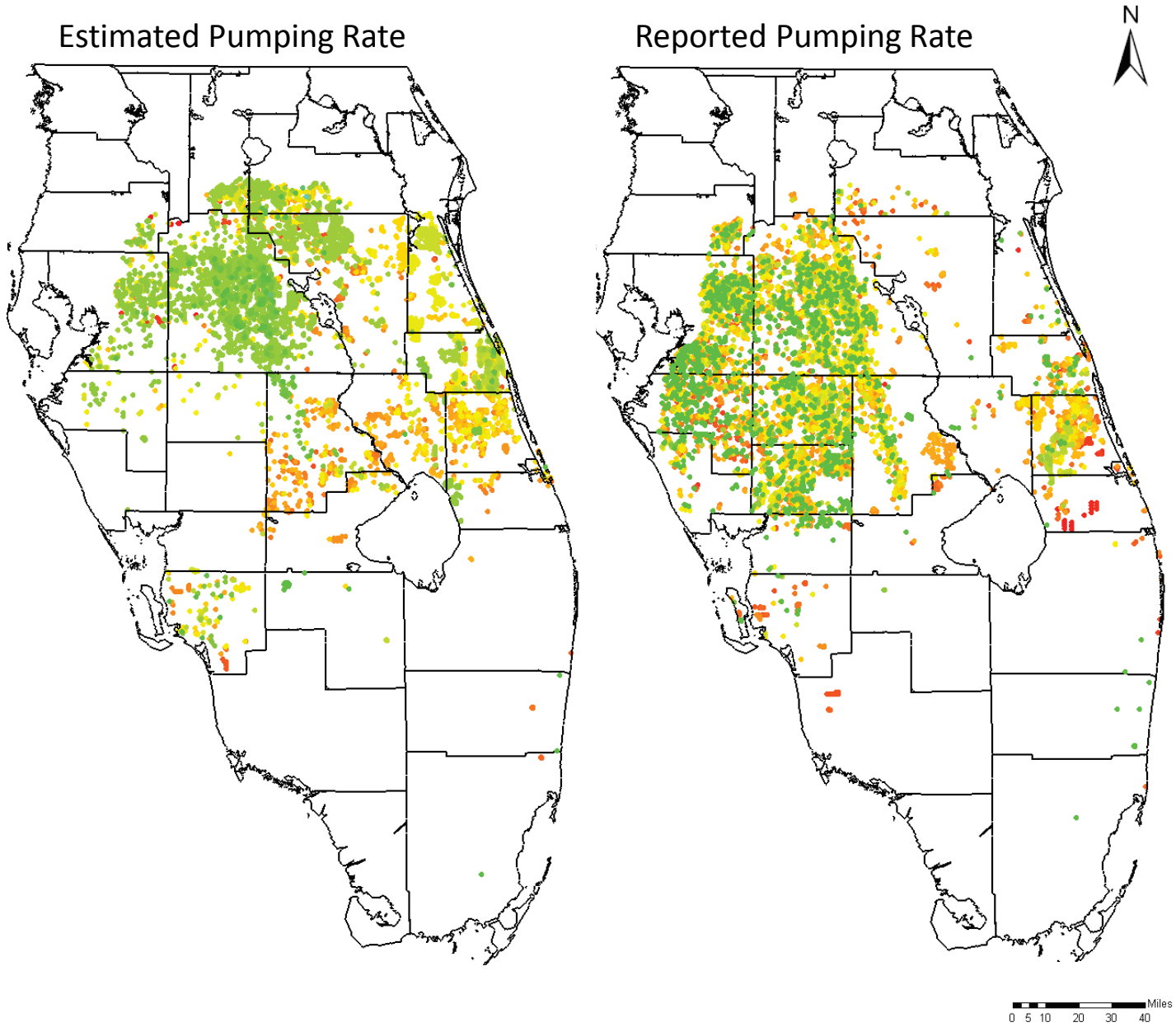

Pump Rate (MGD)

Injection

10
0.1
0.001
0
-0.001
-0.1
-10

Extraction

Notes:

Number of wells in layer :

10221 with Reported Data

12107 with Estimated Data

Wells shown are in layers 5-10 of the model. Pump rates assigned to the model are the sum of the actual and estimated data.

Pumping rates are from May 2004 (generally the highest rate of pumping).

Pumping Well Locations
Upper Floridan Aquifer

Final Groundwater Model Calibration Report

Figure 3.38

October 2010

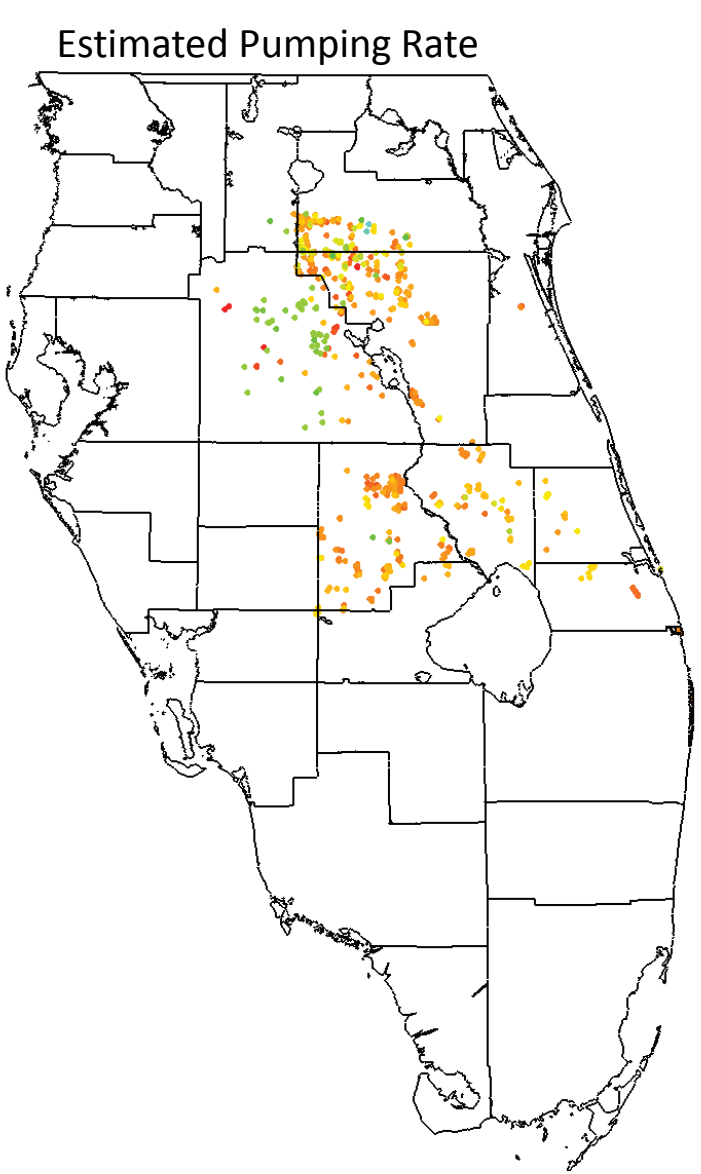

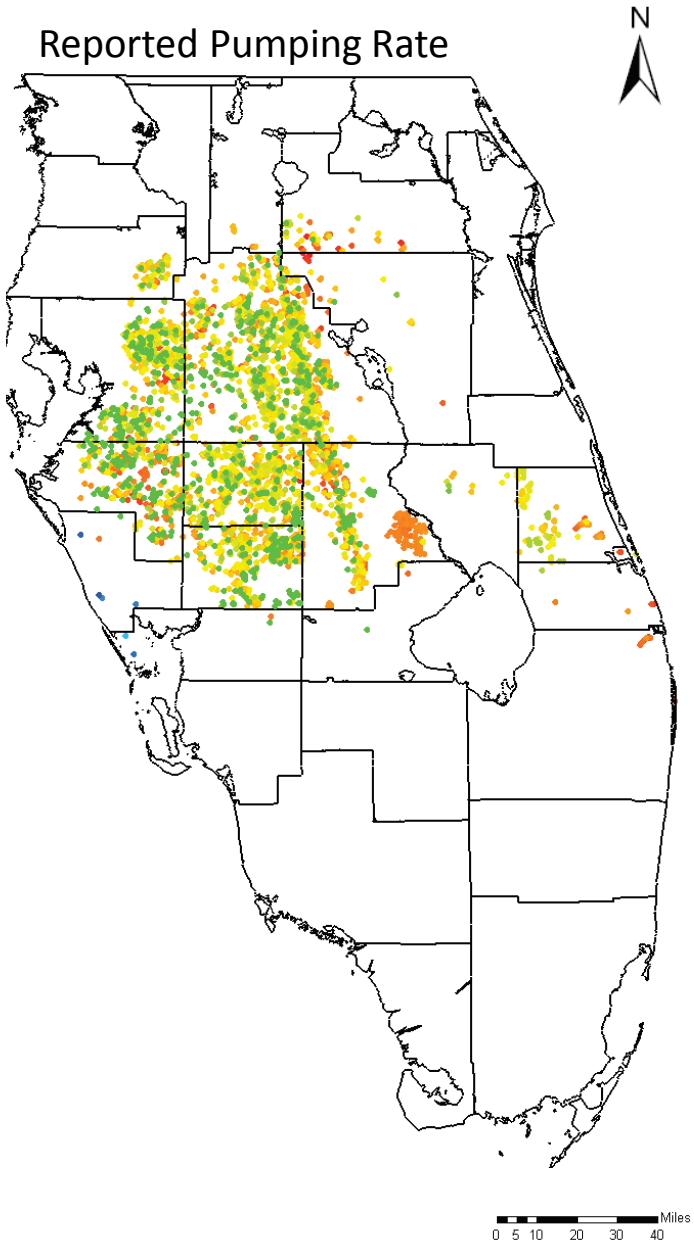

Pump Rate (MGD)

Injection

10
0.1
0.001
0
-0.001
-0.1
-10

Extraction

Notes:

Number of wells in layer :

4354 with Reported Data

674 with Estimated Data

Wells shown are in layers 13-15 of the model. Pump rates assigned to the model are the sum of the actual and estimated data.

Pumping rates are from May 2004 (generally the highest rate of pumping).

Pumping Well Locations
Avon Park Permeable Zone

Final Groundwater Model Calibration Report

Figure 3.39

October 2010

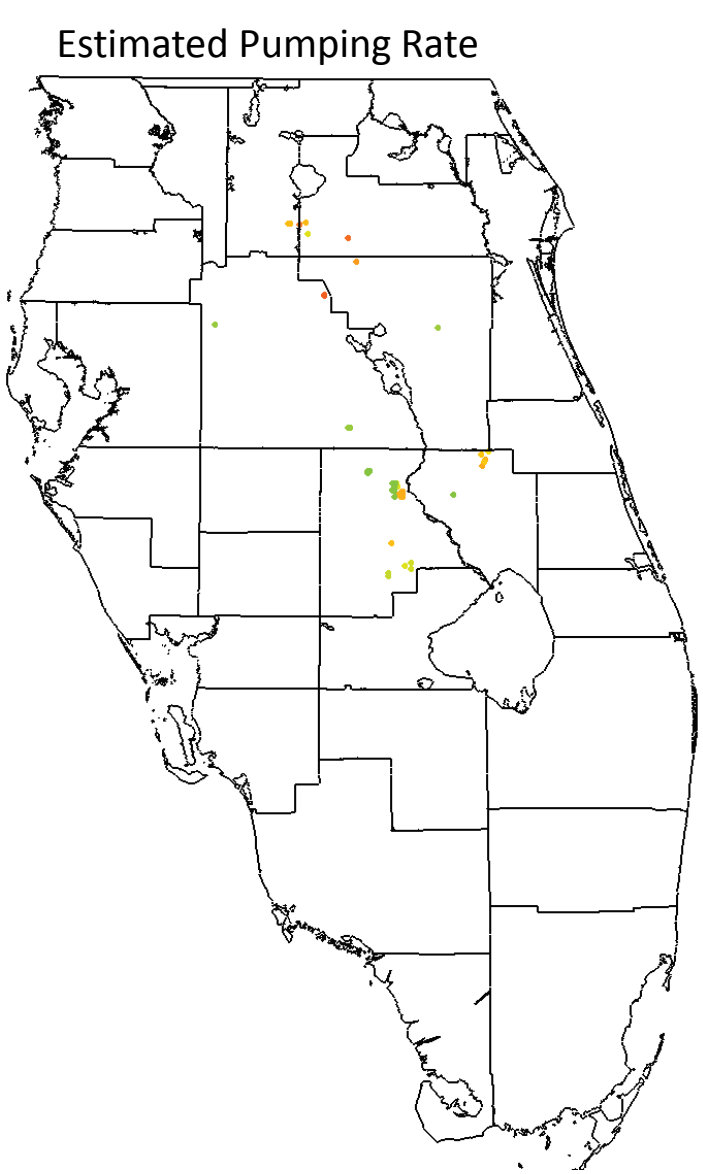

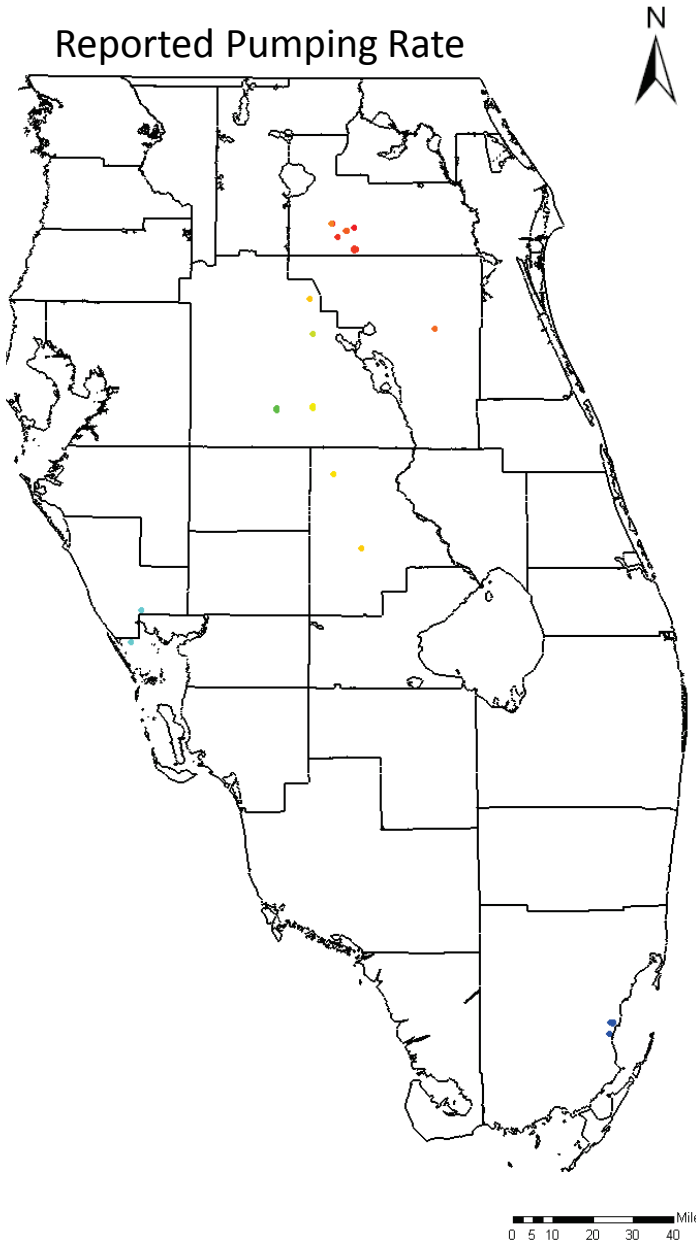

Pump Rate (MGD)

Injection

10

0.1

0.001

0

-0.001

-0.1

-10

Extraction

Notes:

Number of wells in layer :

38 with Reported Data

63 with Estimated Data

Wells shown are in layers 18 and 19 of the model. Pump rates assigned to the model are the sum of the actual and estimated data.

Pumping rates are from May 2004 (generally the highest rate of pumping).

Pumping Well Locations
Lower Floridan (LF1) Aquifer

Final Groundwater Model Calibration Report

Figure 3.40

October 2010

Reported Pumping Rate

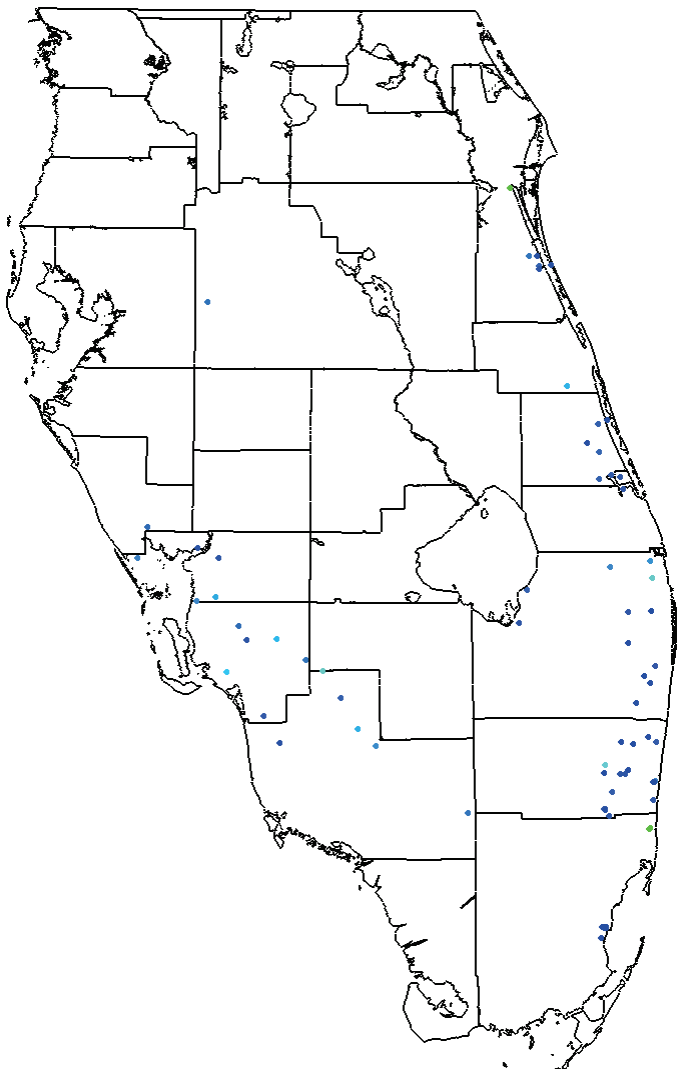

Pump Rate (MGD)

Injection

10

0.1

0.001

0

-0.001

-0.1

-10

Extraction

Notes:

Number of wells in layer :

111 with Reported Data

0 with Estimated Data

Wells shown are in layer 22 of the model. Pump rates assigned to the model are the sum of the actual and estimated data.

Pumping rates are from May 2004.

Pumping Well Locations
Boulder Zone
Final Groundwater Model Calibration Report

Figure 3.41

October 2010

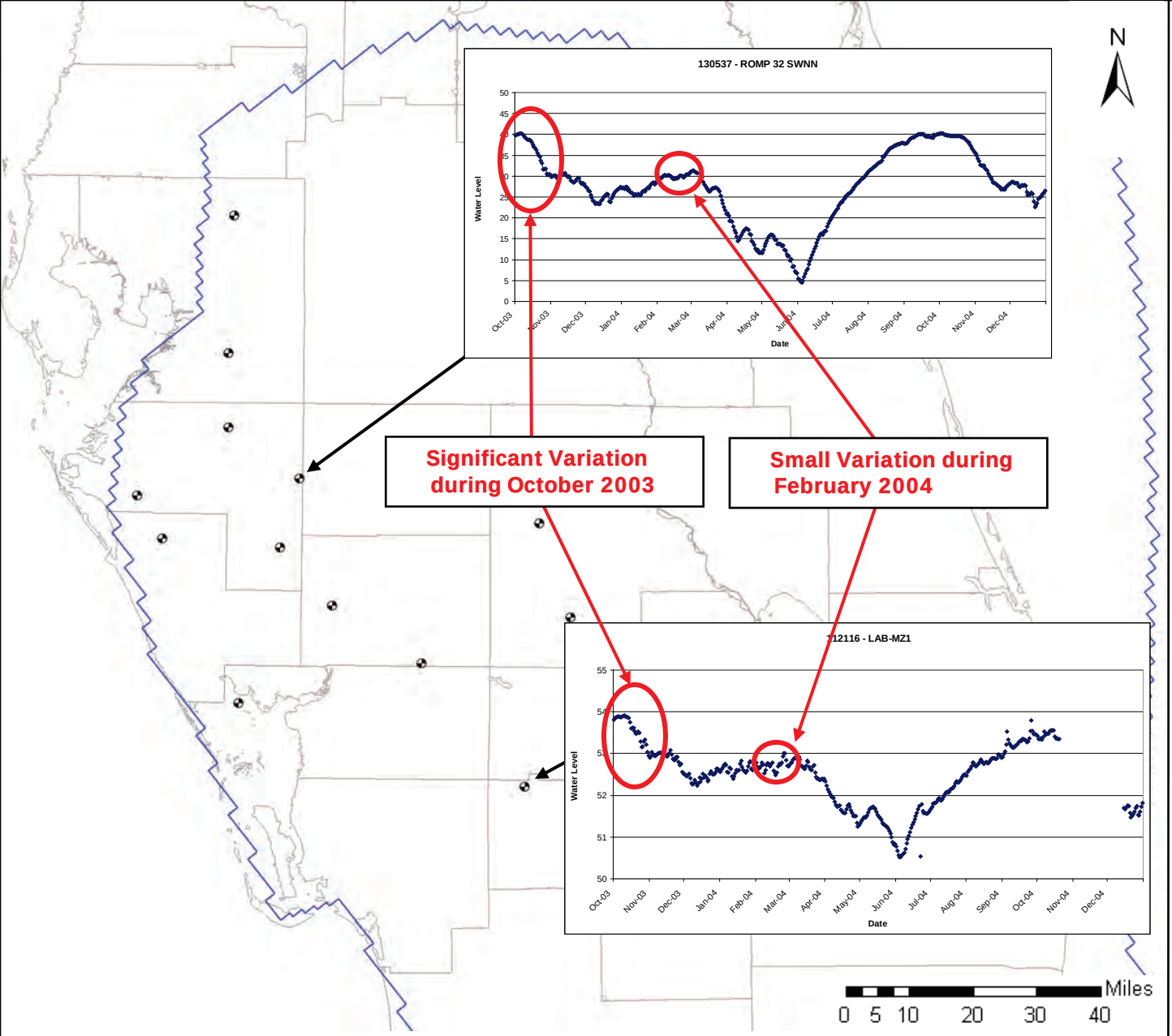

Legend

Wells showing significant decreasing trend in October 2003

Model Boundary

Example Of October 2003 Water Level Decline

Figure 4.1

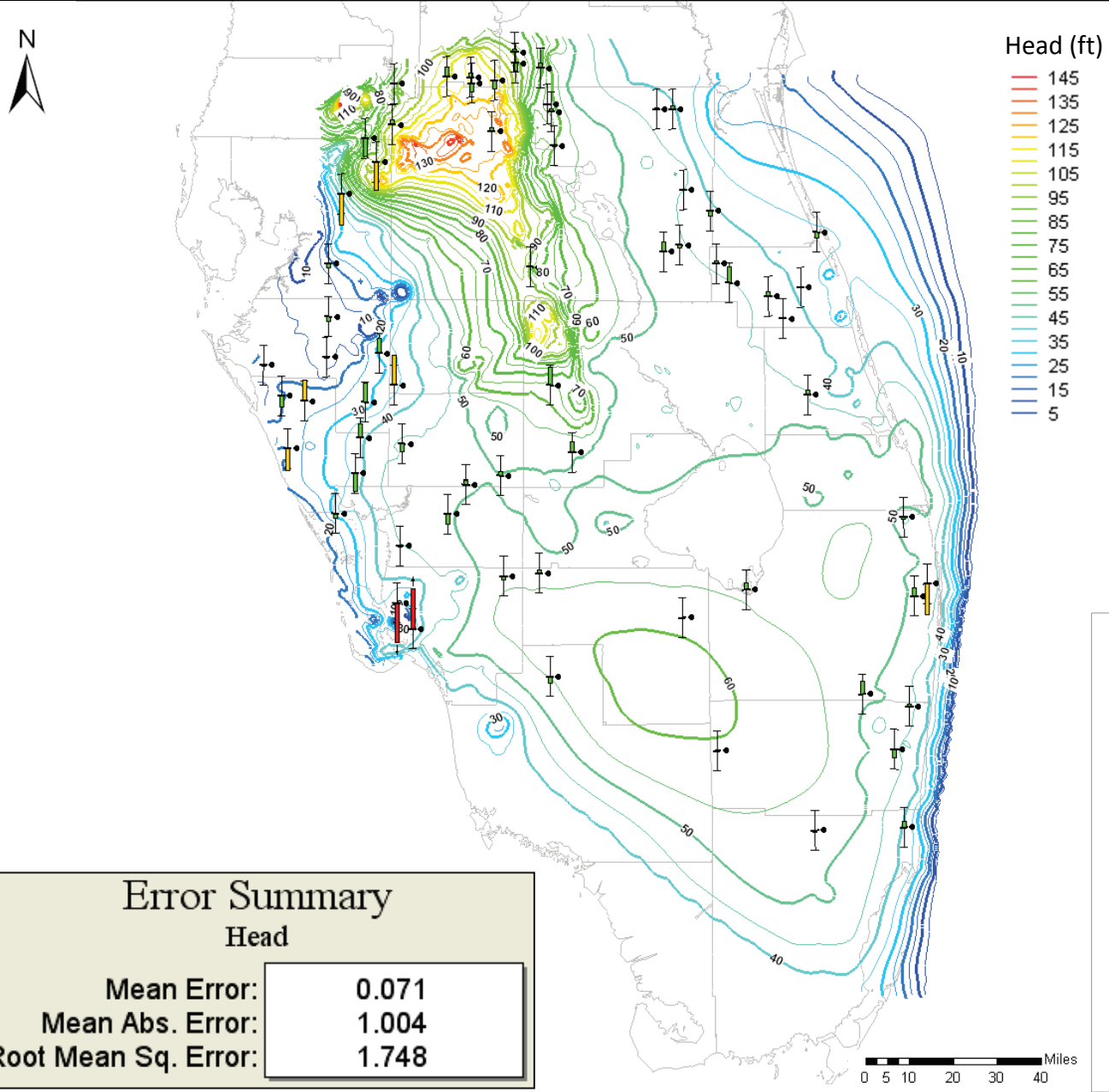

Notes:

Statistics (mean error, mean absolute error and root mean square error) are calculated based on equations presented in Section 4.1.

Calibration targets are green when the calculated value is within 2 feet of the measured head, yellow when within 4 feet and red when the model calculates a head more than 4 feet different from the measured value.

The direction of the colored bar on the calibration target indicates the sign on the residual: bars above the middle line indicate the model calculated higher heads than measured; bars below the middle line indicate negative residuals.

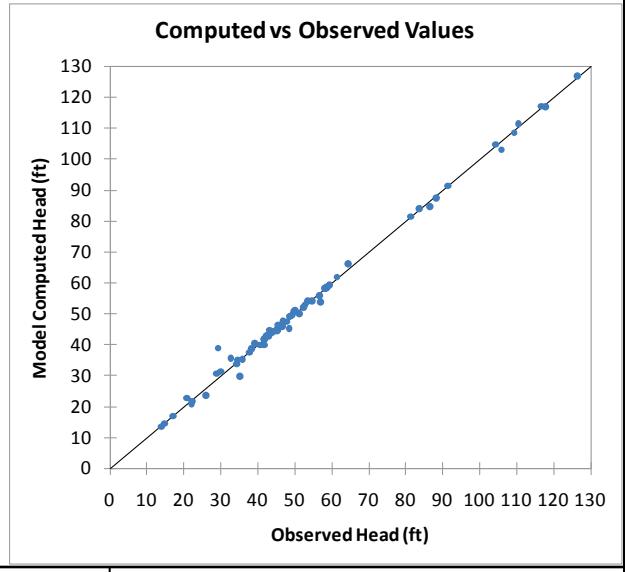

Error Summary

Head

Mean Error:	0.071
Mean Abs. Error:	1.004
Root Mean Sq. Error:	1.748

Regional SEAWAT Calibration
Upper Floridan Aquifer - February 2004
Final Groundwater Model Calibration Report

Figure 4.2

October 2010

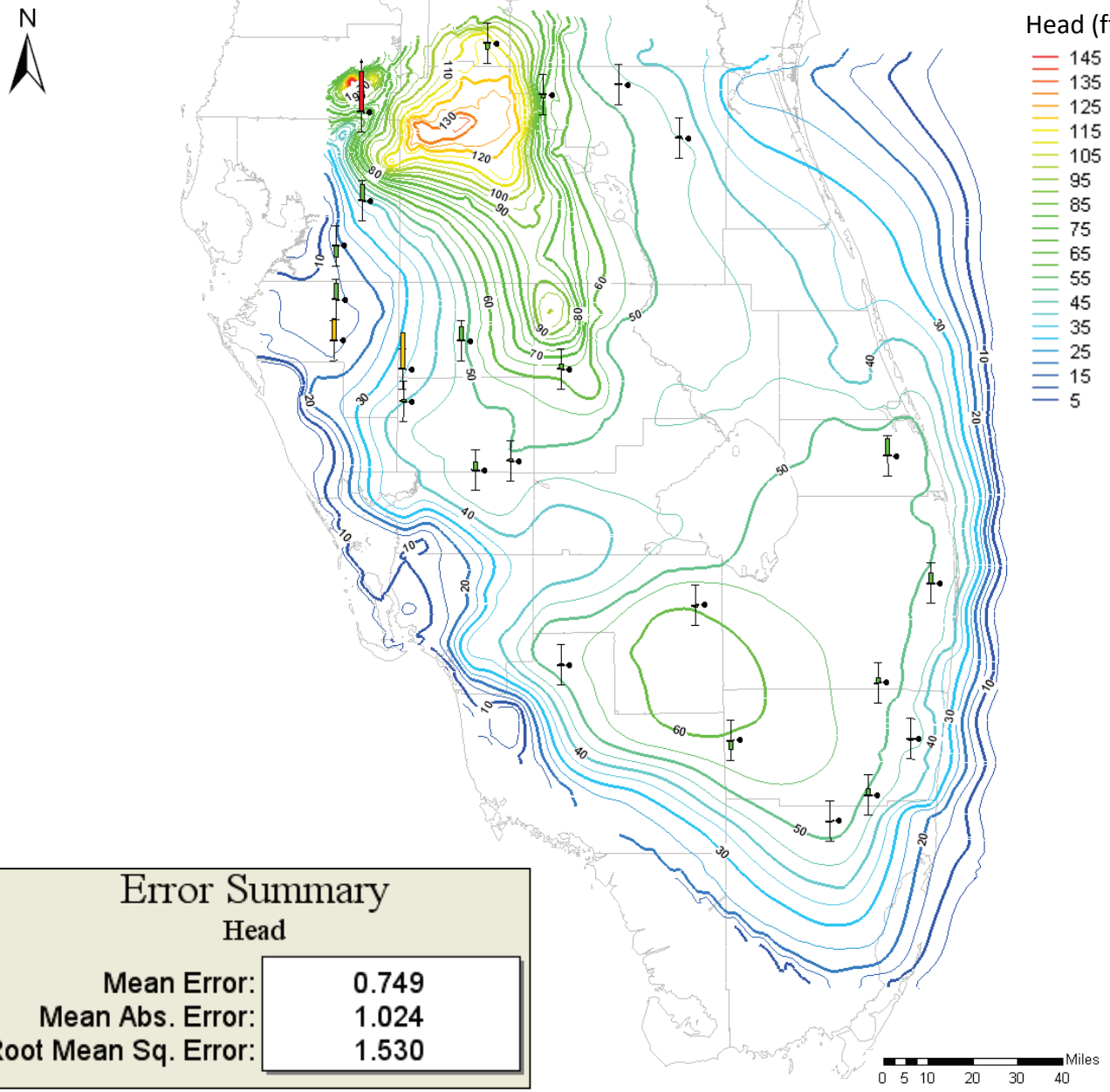

Notes:

Statistics (mean error, mean absolute error and root mean square error) are calculated based on equations presented in Section 4.1.

Calibration targets are green when the calculated value is within 2 feet of the measured head, yellow when within 4 feet and red when the model calculates a head more than 4 feet different from the measured value.

The direction of the colored bar on the calibration target indicates the sign on the residual: bars above the middle line indicate the model calculated higher heads than measured; bars below the middle line indicate negative residuals.

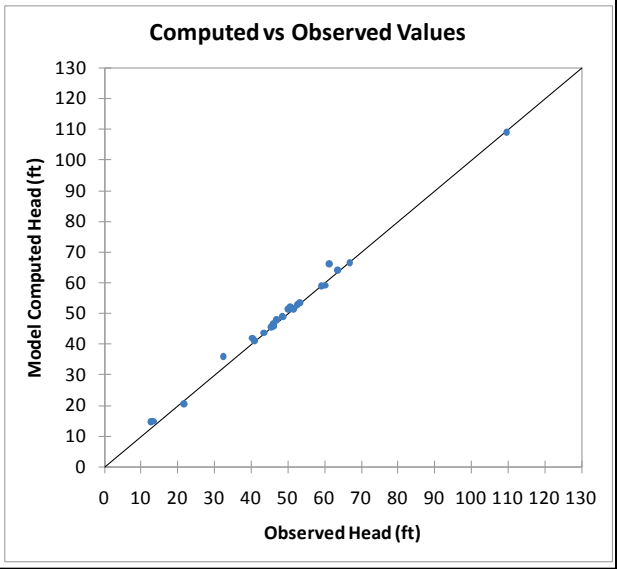

Error Summary

Head

Mean Error:	0.749
Mean Abs. Error:	1.024
Root Mean Sq. Error:	1.530

Regional SEAWAT Calibration
APPZ Aquifer - February 2004
Final Groundwater Model Calibration Report

Figure 4.3

October 2010

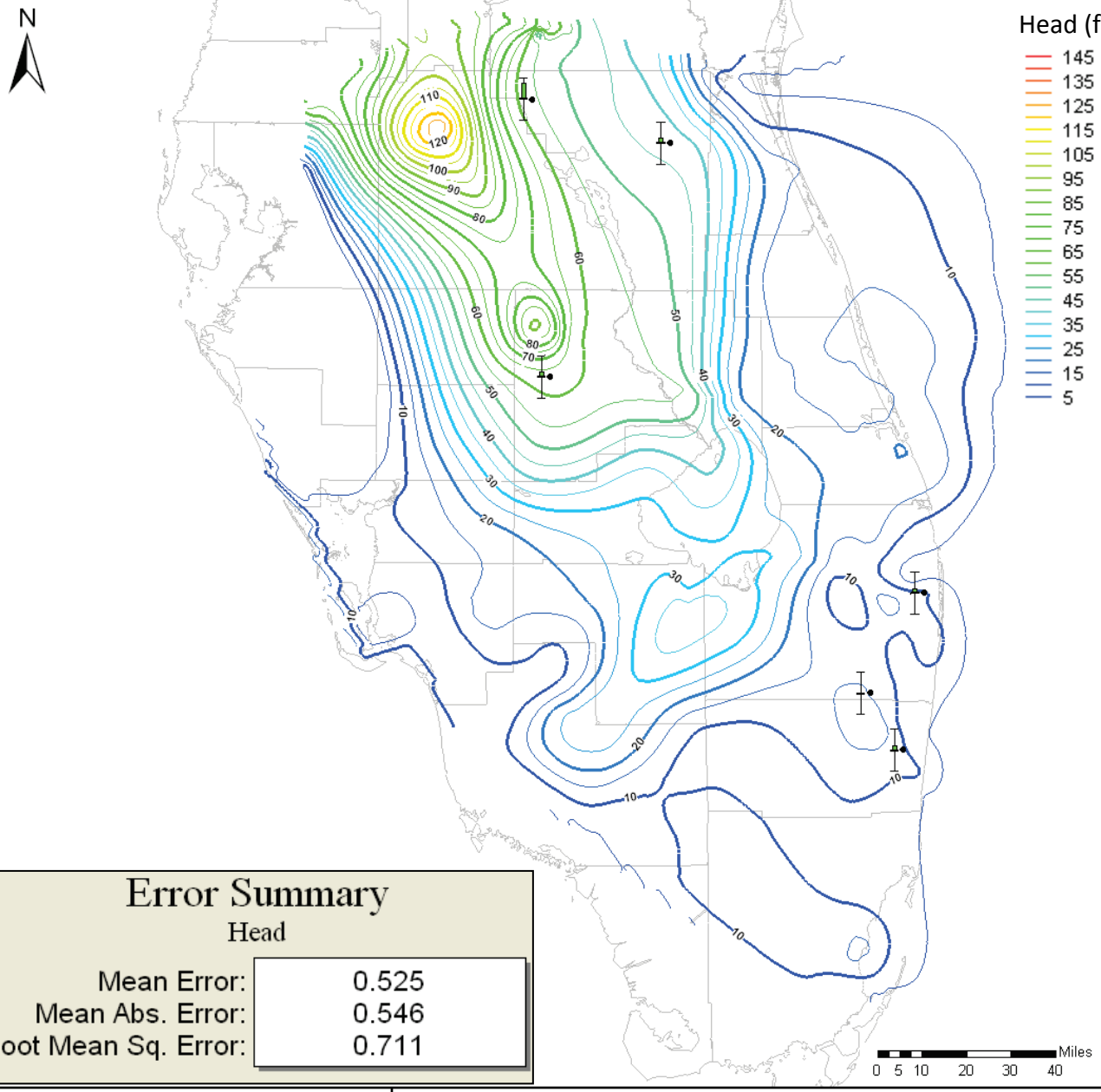

Notes:

Statistics (mean error, mean absolute error and root mean square error) are calculated based on equations presented in Section 4.1.

Calibration targets are green when the calculated value is within 2 feet of the measured head, yellow when within 4 feet and red when the model calculates a head more than 4 feet different from the measured value.

The direction of the colored bar on the calibration target indicates the sign on the residual: bars above the middle line indicate the model calculated higher heads than measured; bars below the middle line indicate negative residuals.

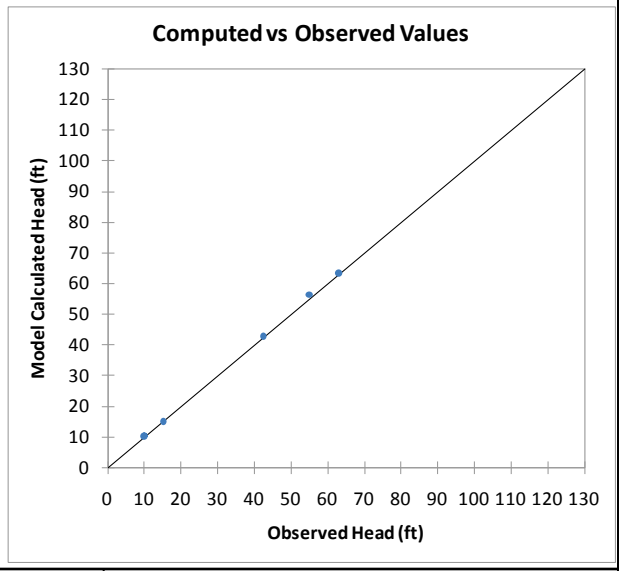

Error Summary

Head

Mean Error:	0.525
Mean Abs. Error:	0.546
Root Mean Sq. Error:	0.711

Regional SEAWAT Calibration
Lower Floridan (LF1) Aquifer - February 2004
Final Groundwater Model Calibration Report

Figure 4.4

October 2010

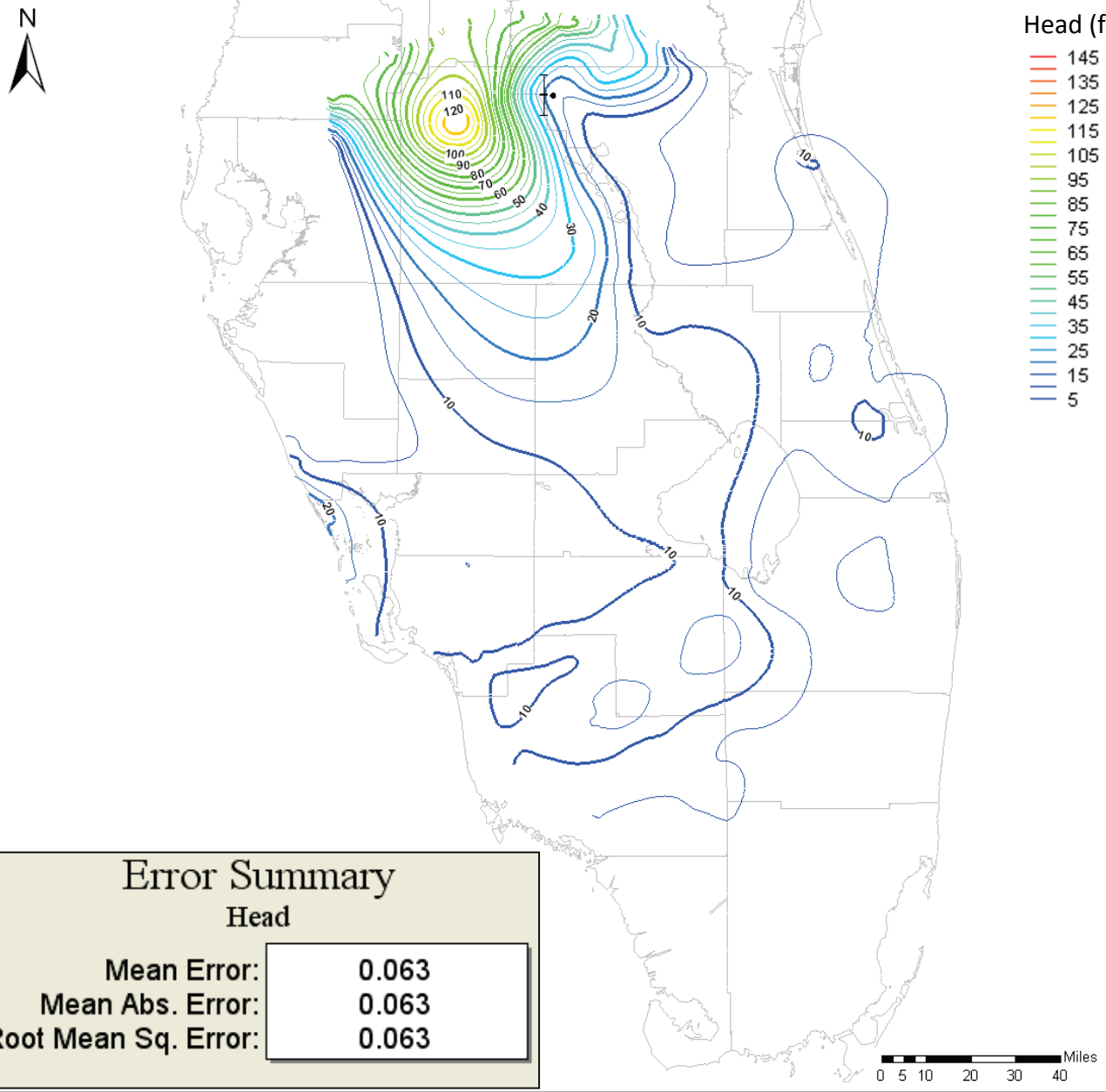

Notes:

Statistics (mean error, mean absolute error and root mean square error) are calculated based on equations presented in Section 4.1.

Calibration targets are green when the calculated value is within 2 feet of the measured head, yellow when within 4 feet and red when the model calculates a head more than 4 feet different from the measured value.

The direction of the colored bar on the calibration target indicates the sign on the residual: bars above the middle line indicate the model calculated higher heads than measured; bars below the middle line indicate negative residuals.

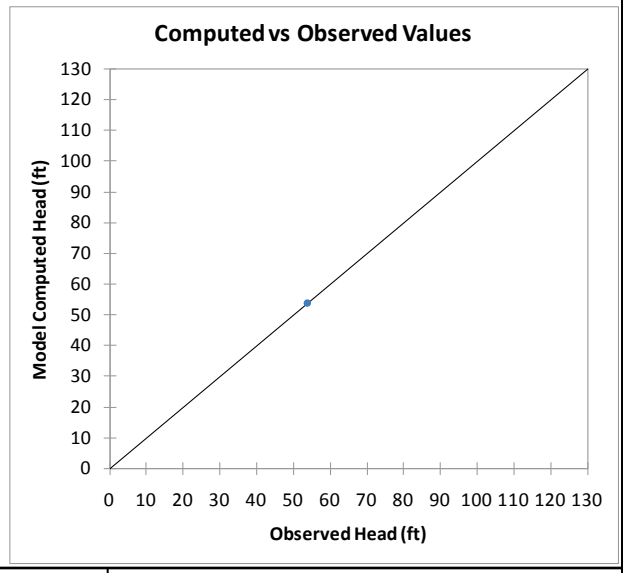

Error Summary

Head

Mean Error:	0.063
Mean Abs. Error:	0.063
Root Mean Sq. Error:	0.063

Regional SEAWAT Calibration
Boulder Zone - February 2004
Final Groundwater Model Calibration Report

Figure 4.5

October 2010

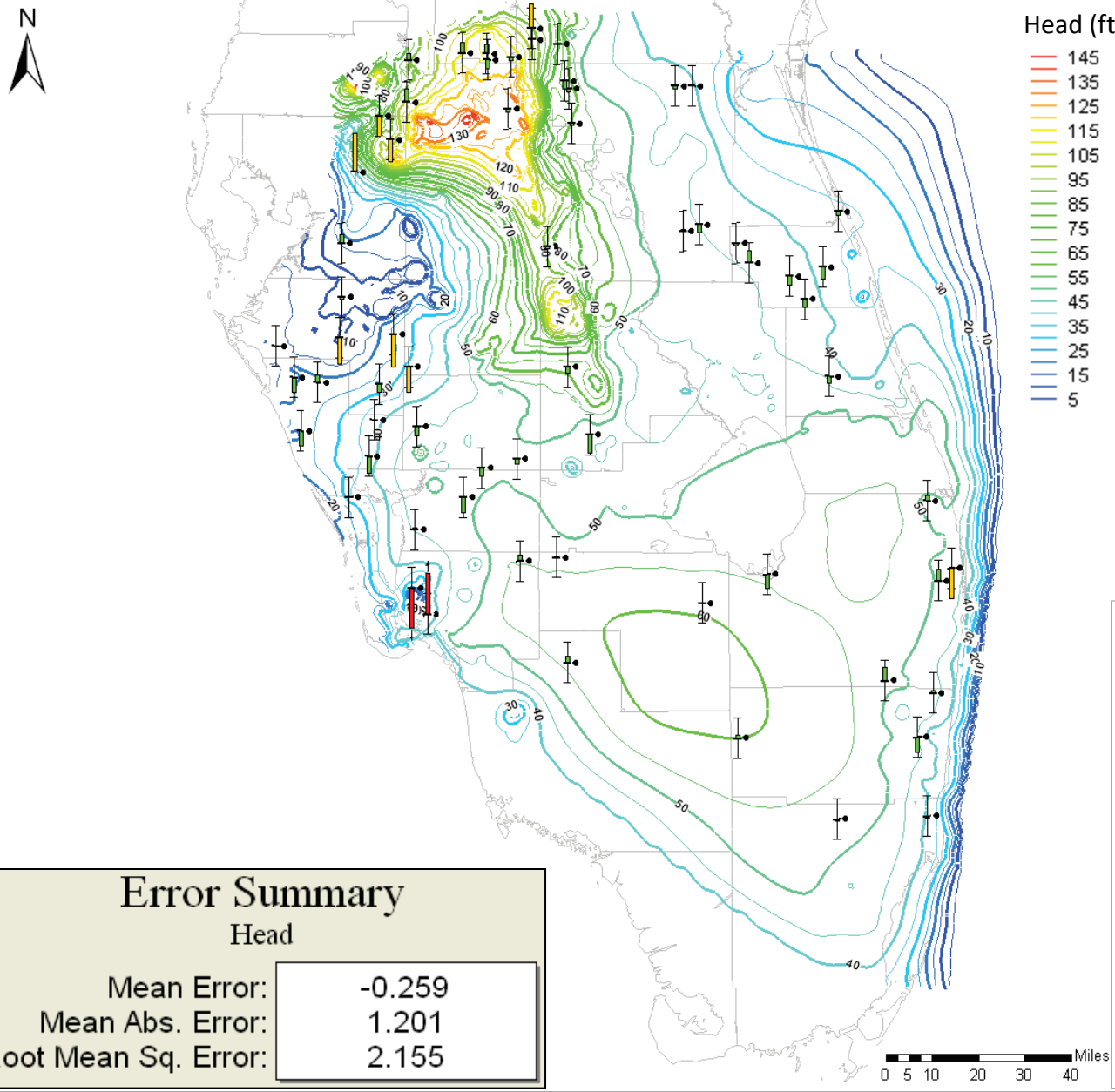

Notes:

Statistics (mean error, mean absolute error and root mean square error) are calculated based on equations presented in Section 4.1.

Calibration targets are green when the calculated value is within 2 feet of the measured head, yellow when within 4 feet and red when the model calculates a head more than 4 feet different from the measured value.

The direction of the colored bar on the calibration target indicates the sign on the residual: bars above the middle line indicate the model calculated higher heads than measured; bars below the middle line indicate negative residuals.

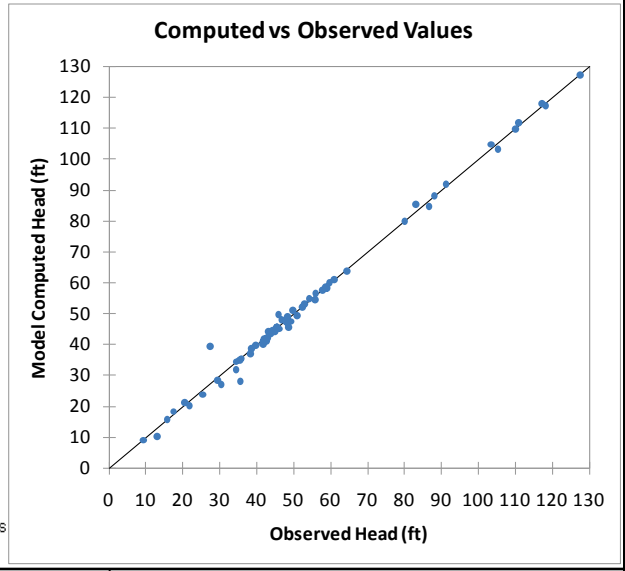

Error Summary

Head

Mean Error:	-0.259
Mean Abs. Error:	1.201
Root Mean Sq. Error:	2.155

Regional SEAWAT Calibration
Upper Floridan Aquifer - October 2003
Final Groundwater Model Calibration Report

Figure 4.6

October 2010

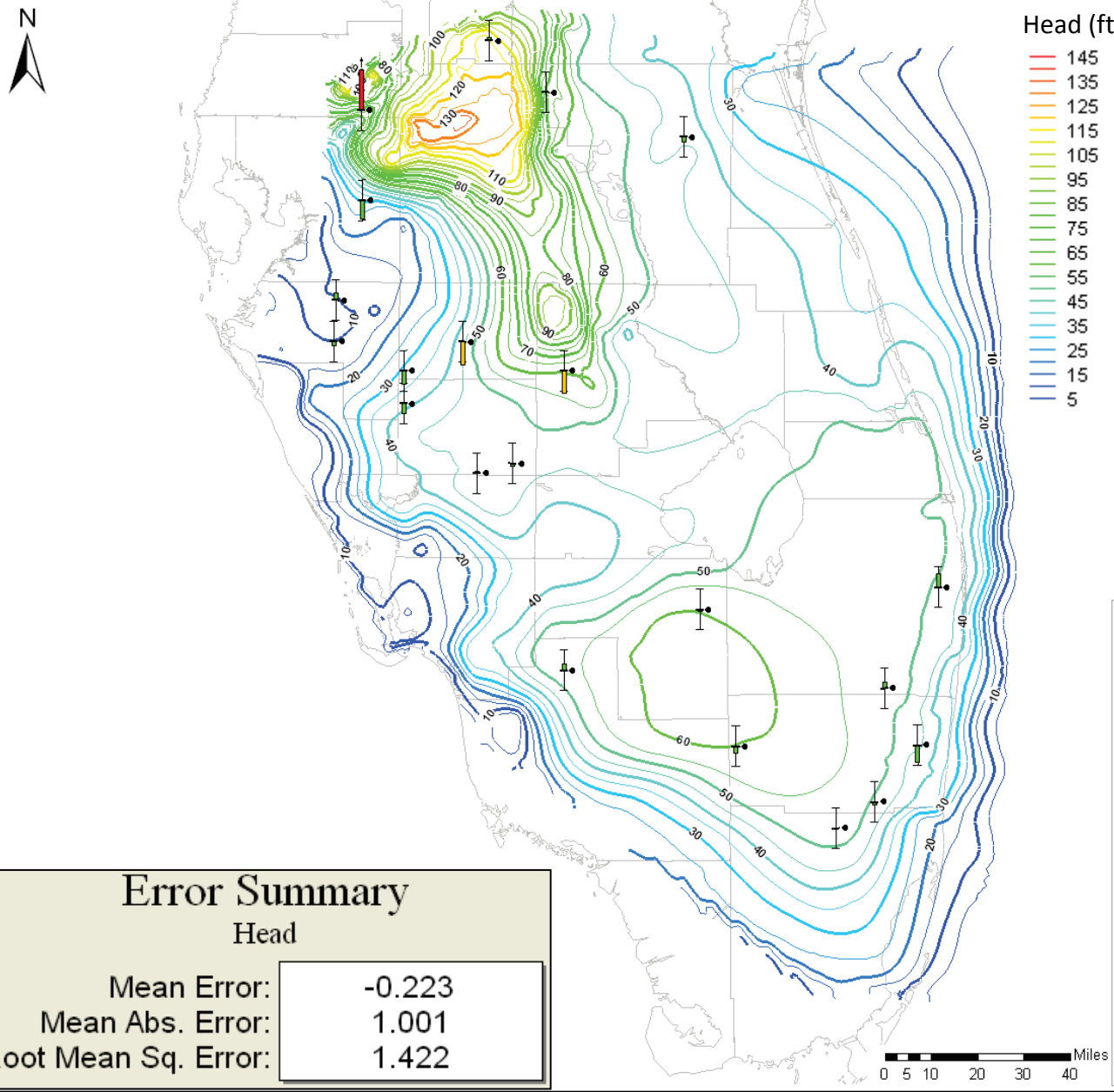

Notes:

Statistics (mean error, mean absolute error and root mean square error) are calculated based on equations presented in Section 4.1.

Calibration targets are green when the calculated value is within 2 feet of the measured head, yellow when within 4 feet and red when the model calculates a head more than 4 feet different from the measured value.

The direction of the colored bar on the calibration target indicates the sign on the residual: bars above the middle line indicate the model calculated higher heads than measured; bars below the middle line indicate negative residuals.

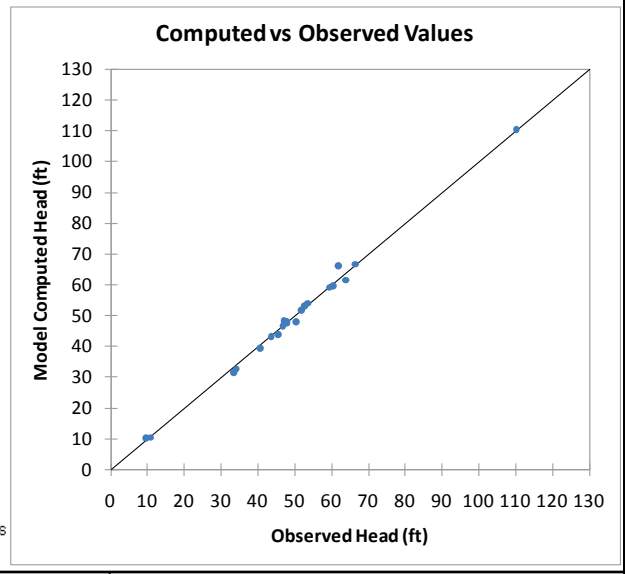

Error Summary

Head

Mean Error:	-0.223
Mean Abs. Error:	1.001
Root Mean Sq. Error:	1.422

Regional SEAWAT Calibration
APPZ Aquifer - October 2003
Final Groundwater Model Calibration Report

Figure 4.7

October 2010

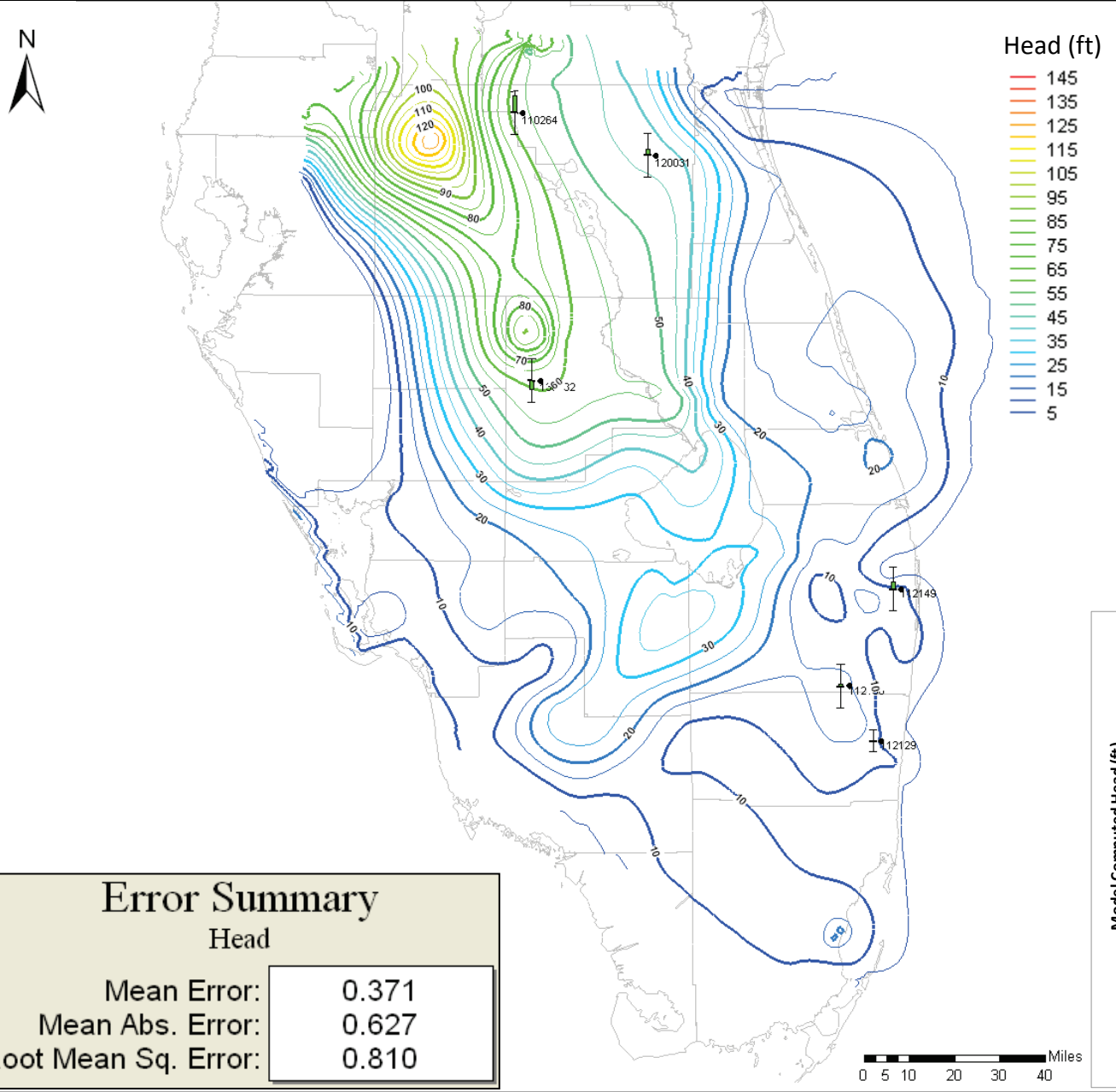

Notes:

Statistics (mean error, mean absolute error and root mean square error) are calculated based on equations presented in Section 4.1.

Calibration targets are green when the calculated value is within 2 feet of the measured head, yellow when within 4 feet and red when the model calculates a head more than 4 feet different from the measured value.

The direction of the colored bar on the calibration target indicates the sign on the residual: bars above the middle line indicate the model calculated higher heads than measured; bars below the middle line indicate negative residuals.

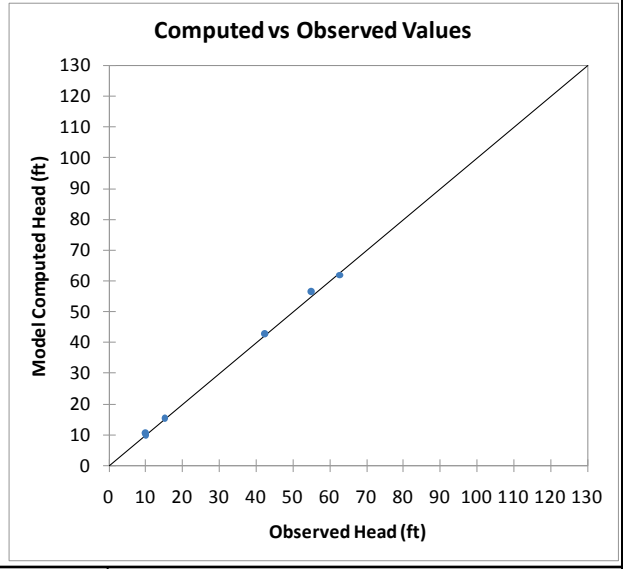

Error Summary

Head

Mean Error:	0.371
Mean Abs. Error:	0.627
Root Mean Sq. Error:	0.810

Regional SEAWAT Calibration

Lower Floridan Aquifer (LF1) - October 2003

Final Groundwater Model Calibration Report

Figure 4.8

October 2010

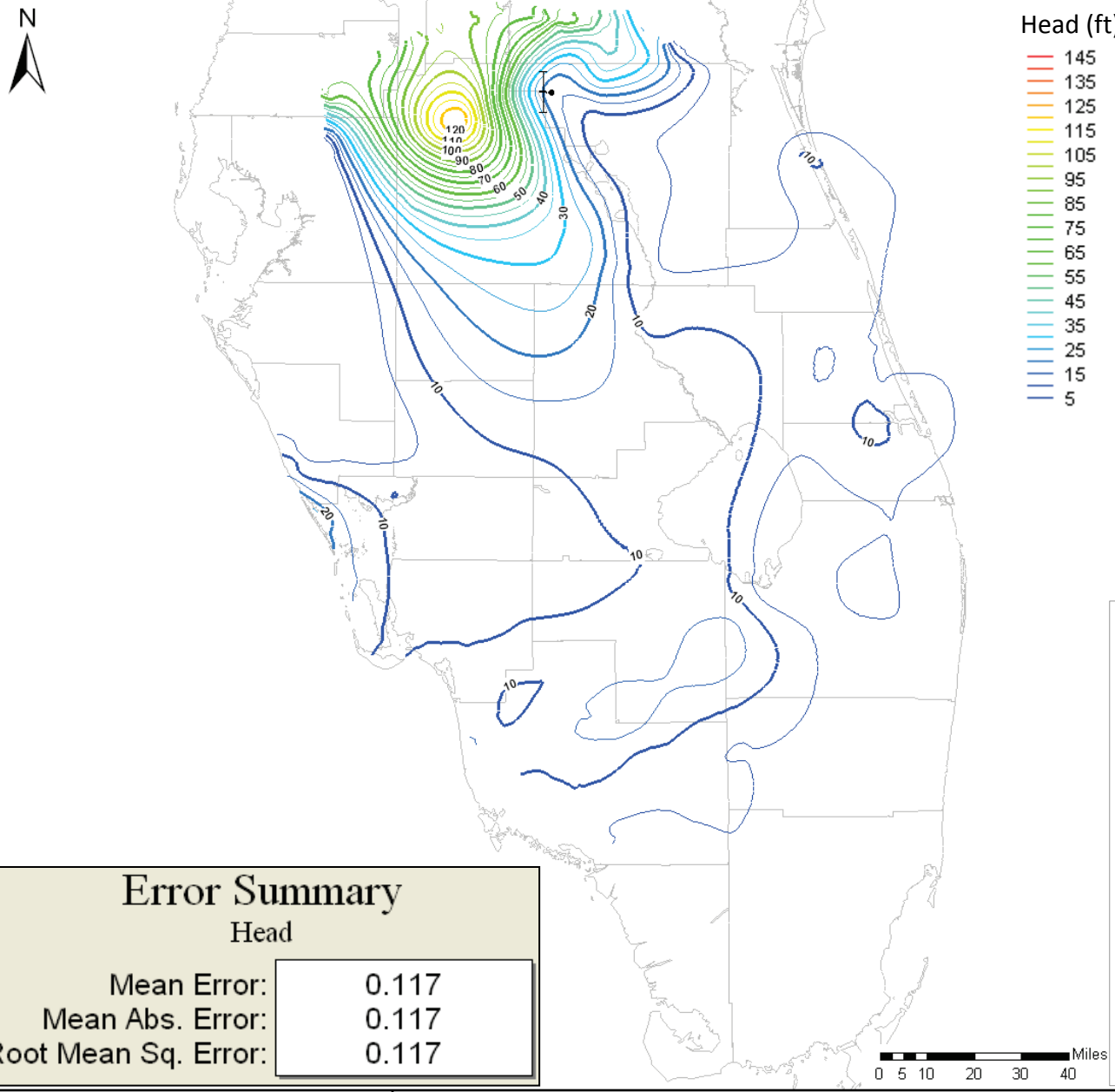

Notes:

Statistics (mean error, mean absolute error and root mean square error) are calculated based on equations presented in Section 4.1.

Calibration targets are green when the calculated value is within 2 feet of the measured head, yellow when within 4 feet and red when the model calculates a head more than 4 feet different from the measured value.

The direction of the colored bar on the calibration target indicates the sign on the residual: bars above the middle line indicate the model calculated higher heads than measured; bars below the middle line indicate negative residuals.

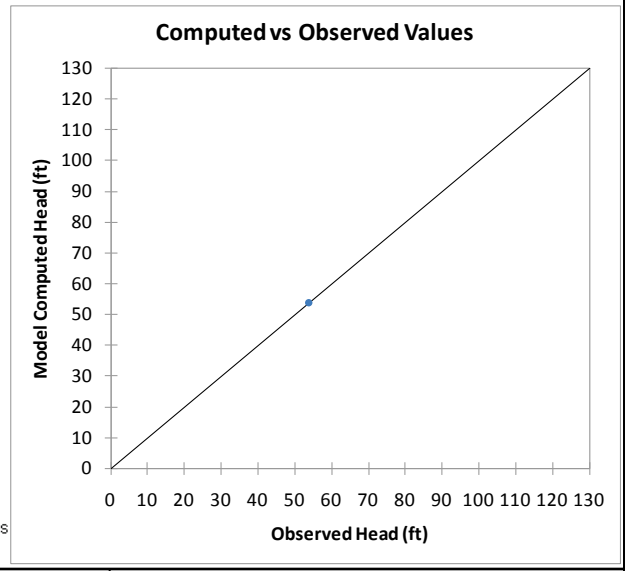

Error Summary

Head

Mean Error:	0.117
Mean Abs. Error:	0.117
Root Mean Sq. Error:	0.117

Regional SEAWAT Calibration
Boulder Zone - October 2003
Final Groundwater Model Calibration Report

Figure 4.9

October 2010

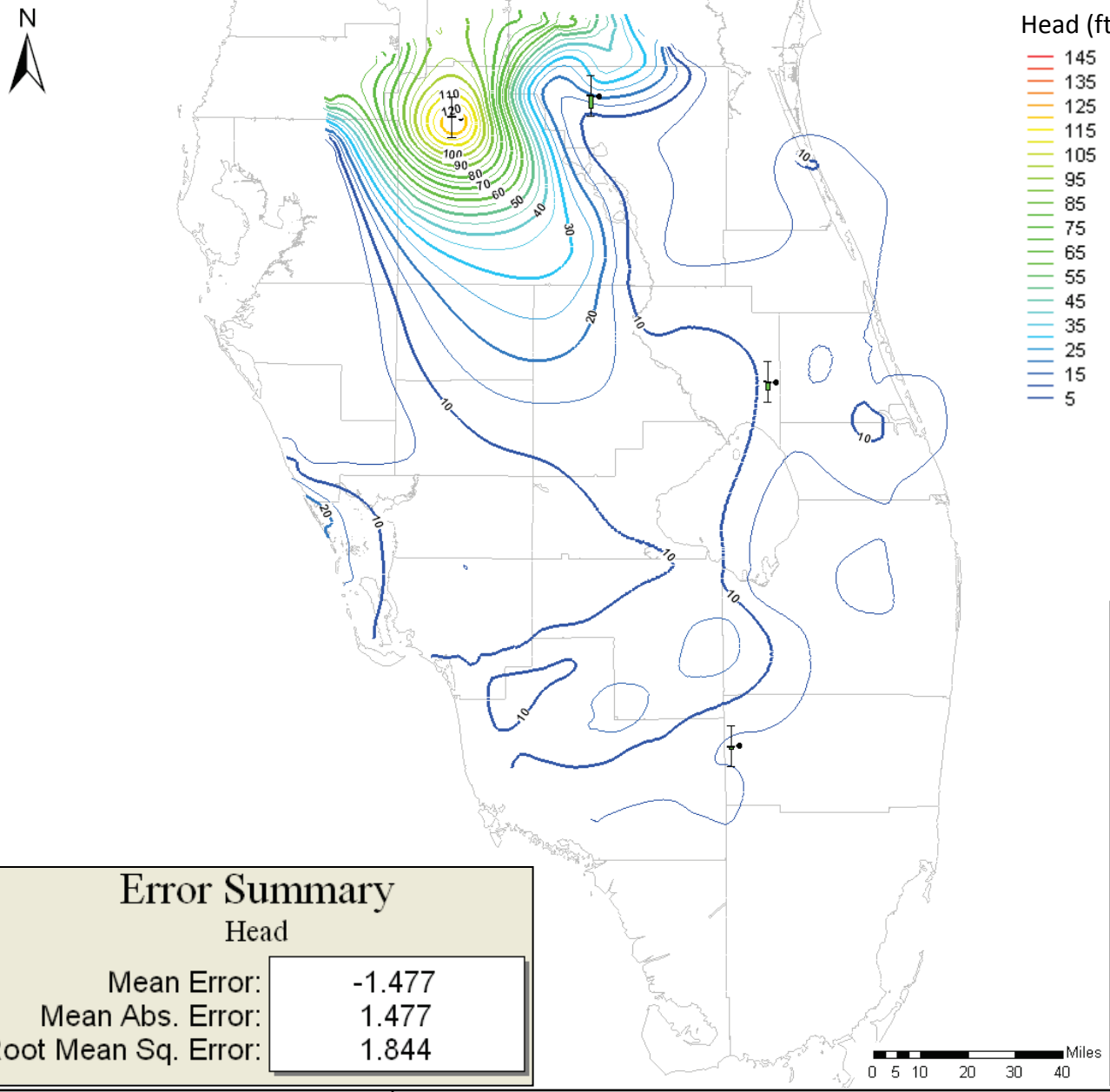

Notes:

Statistics (mean error, mean absolute error and root mean square error) are calculated based on equations presented in Section 4.1.

Calibration targets are green when the calculated value is within 5 feet of the measured head, yellow when within 10 feet and red when the model calculates a head more than 10 feet different from the measured value.

The direction of the colored bar on the calibration target indicates the sign on the residual: bars above the middle line indicate the model calculated higher heads than measured; bars below the middle line indicate negative residuals.

The contours shown are for the BZ.

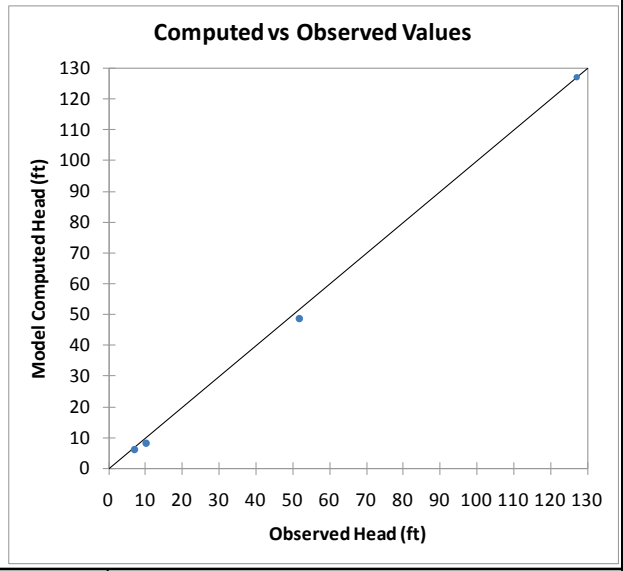

Error Summary

Head

Mean Error:	-1.477
Mean Abs. Error:	1.477
Root Mean Sq. Error:	1.844

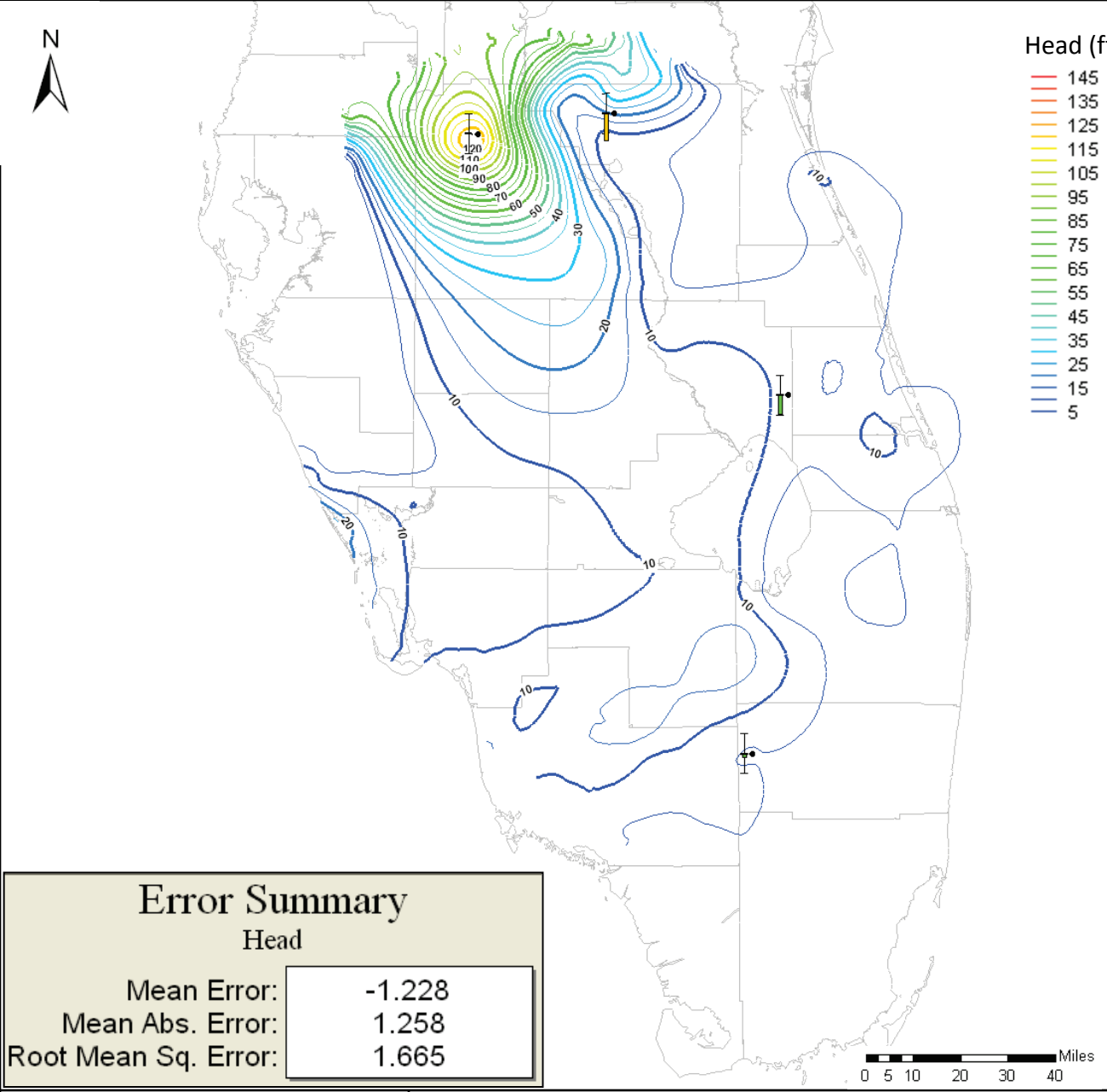

Notes:

Statistics (mean error, mean absolute error and root mean square error) are calculated based on equations presented in Section 4.1.

Calibration targets are green when the calculated value is within 5 feet of the measured head, yellow when within 10 feet and red when the model calculates a head more than 10 feet different from the measured value.

The direction of the colored bar on the calibration target indicates the sign on the residual: bars above the middle line indicate the model calculated higher heads than measured; bars below the middle line indicate negative residuals.

The contours shown are for the BZ.

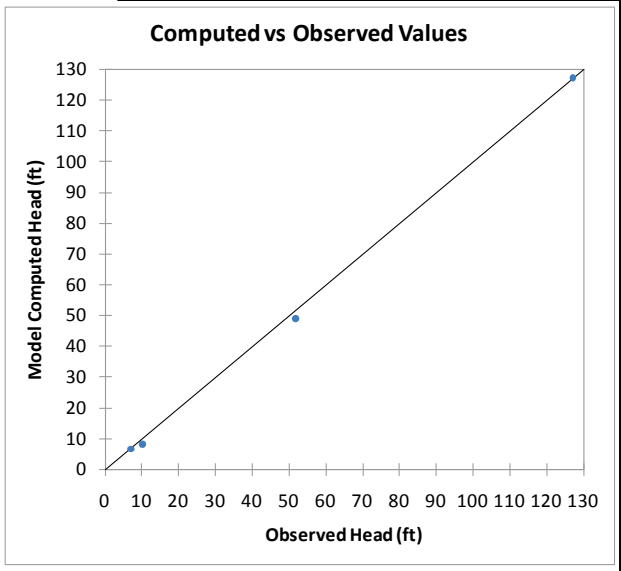

Error Summary

Head

Mean Error:	-1.228
Mean Abs. Error:	1.258
Root Mean Sq. Error:	1.665

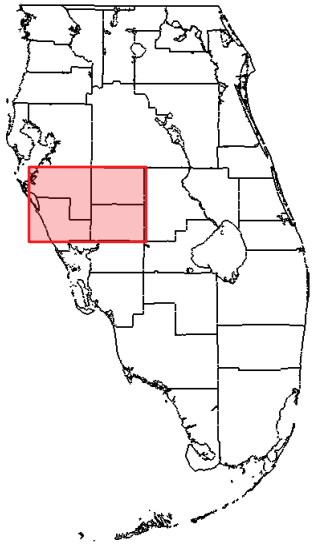

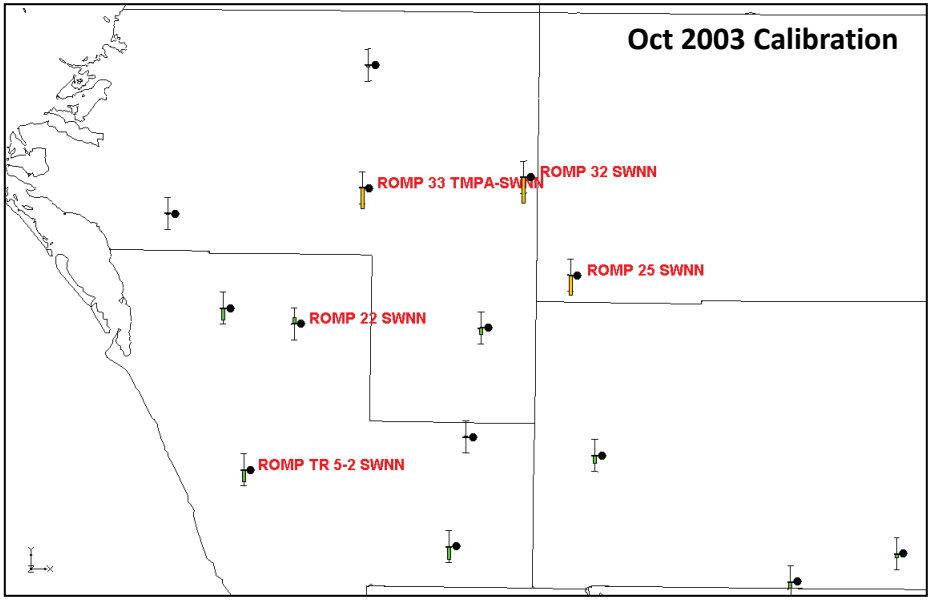

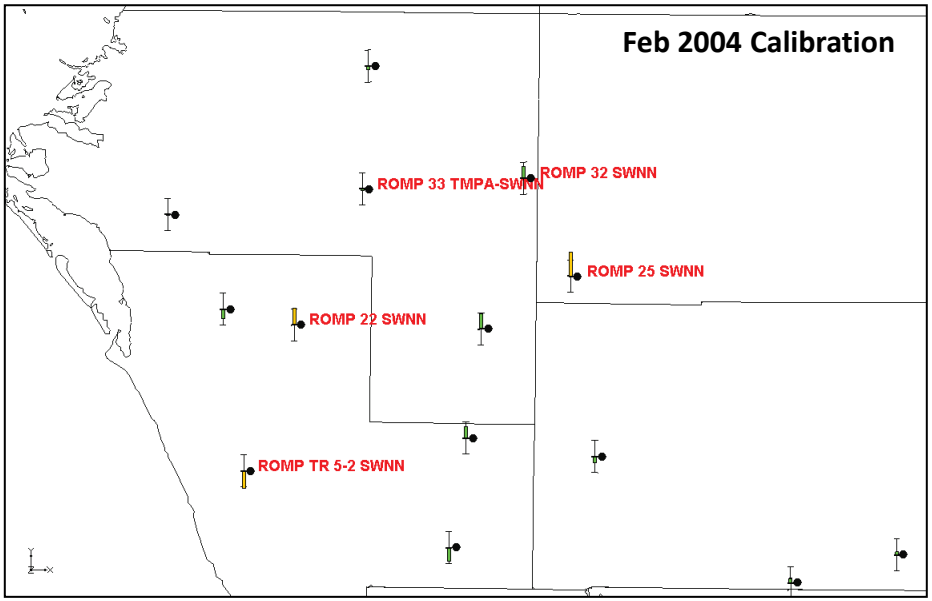

Notes:

This figure is a zoomed view of the October 2003 and February 2004 calibration for the UF. Labeled points are discussed in detail in Section 4.1.1.3. The same information is also shown on Figure 4.2 and 4.6.

Calibration targets are green when the calculated value is within 5 feet of the measured head, yellow when within 10 feet and red when the model calculates a head more than 10 feet different from the measured value.

The direction of the colored bar on the calibration target indicates the sign on the residual: bars above the middle line indicate the model calculated higher heads than measured; bars below the middle line indicate negative residuals.

Regional SEAWAT Calibration
UF Layer, Zoomed
Final Groundwater Model Calibration Report

Figure 4.12

October 2010

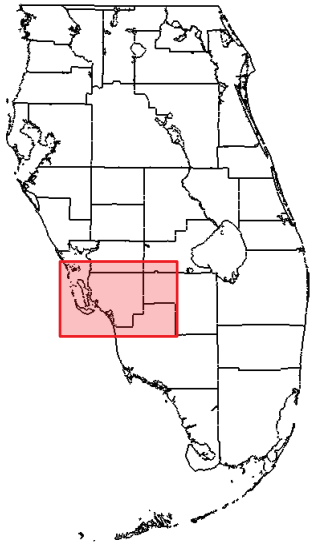

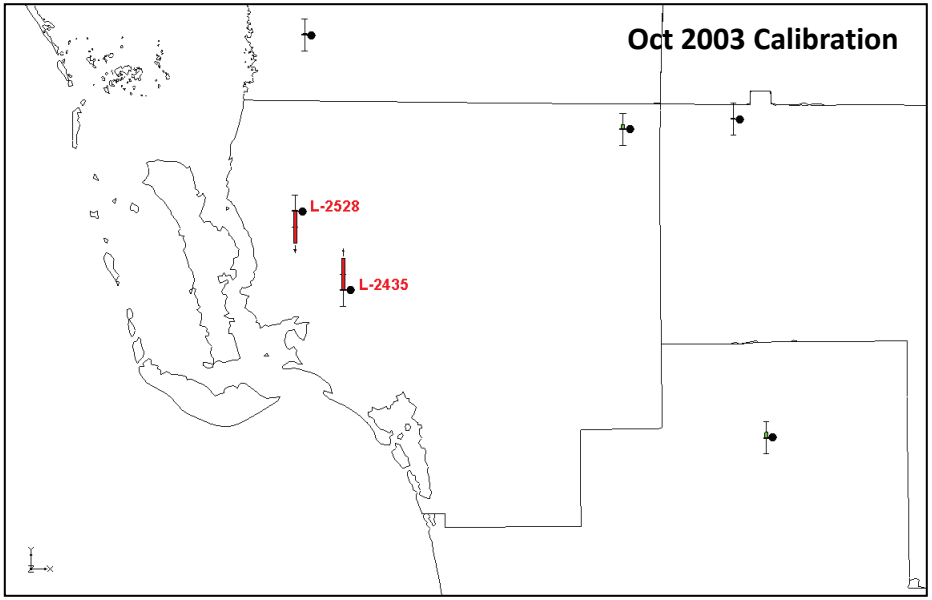

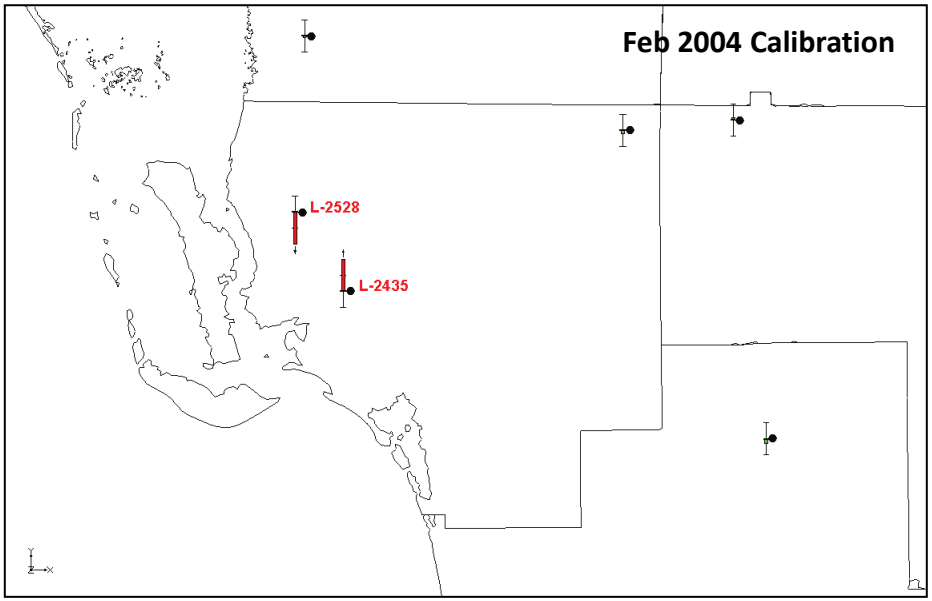

Notes:

This figure is a zoomed view of the October 2003 and February 2004 calibration for the UF. Labeled points are discussed in detail in Section 4.1.1.3. The same information is also shown on Figure 4.2 and 4.6.

Calibration targets are green when the calculated value is within 5 feet of the measured head, yellow when within 10 feet and red when the model calculates a head more than 10 feet different from the measured value.

The direction of the colored bar on the calibration target indicates the sign on the residual: bars above the middle line indicate the model calculated higher heads than measured; bars below the middle line indicate negative residuals.

Regional SEAWAT Calibration
UF Layer, Zoomed
Final Groundwater Model Calibration Report

Figure 4.13

October 2010

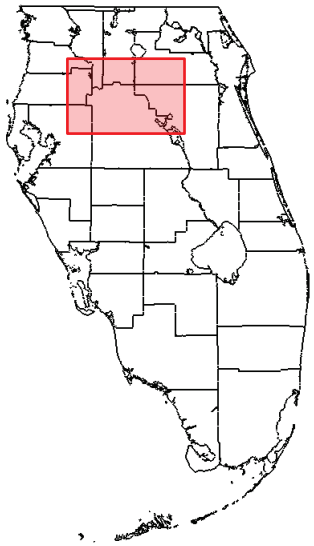

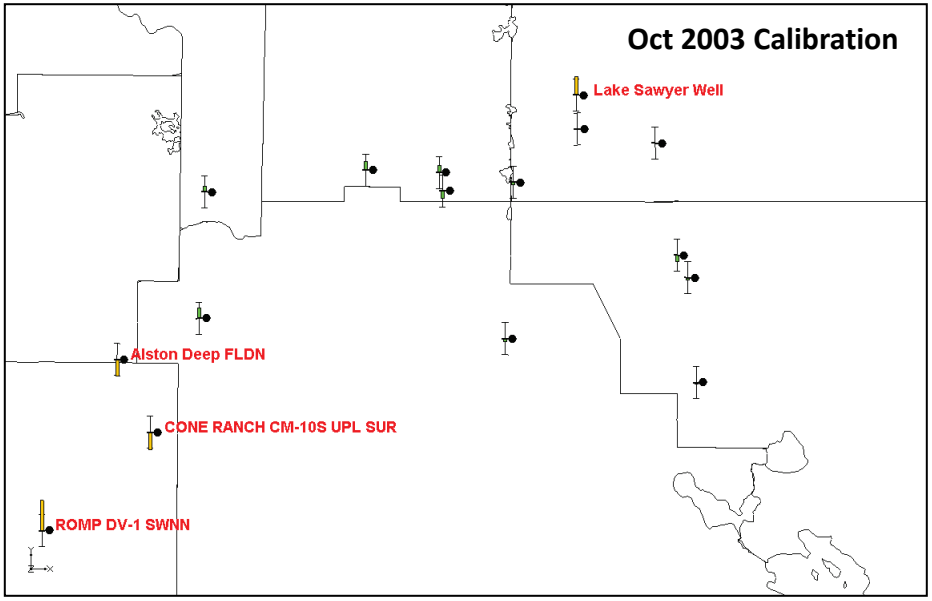

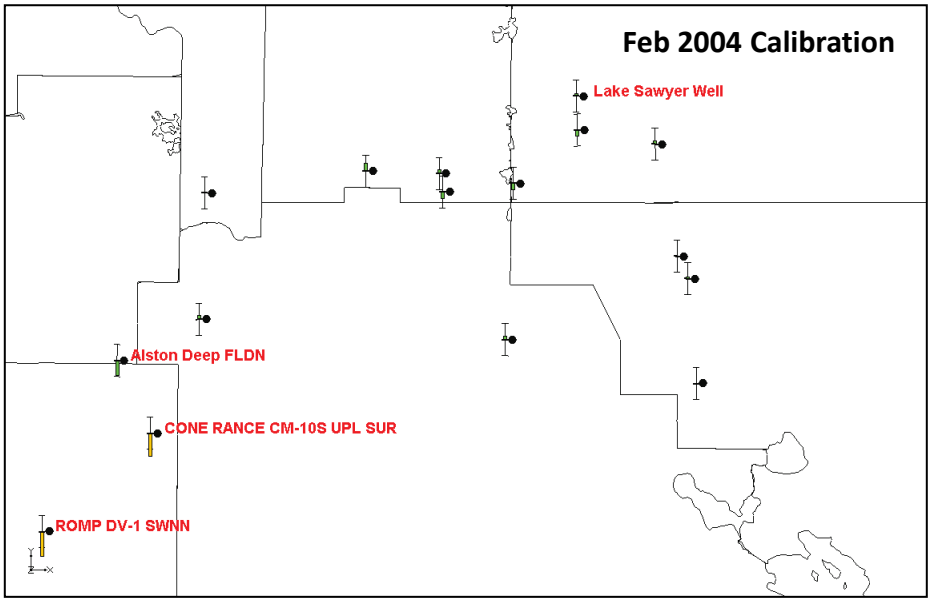

Notes:

This figure is a zoomed view of the October 2003 and February 2004 calibration for the UF. Labeled points are discussed in detail in Section 4.1.1.3. The same information is also shown on Figure 4.2 and 4.6.

Calibration targets are green when the calculated value is within 5 feet of the measured head, yellow when within 10 feet and red when the model calculates a head more than 10 feet different from the measured value.

The direction of the colored bar on the calibration target indicates the sign on the residual: bars above the middle line indicate the model calculated higher heads than measured; bars below the middle line indicate negative residuals.

Regional SEAWAT Calibration
UF Layer, Zoomed
Final Groundwater Model Calibration Report

Figure 4.14

October 2010

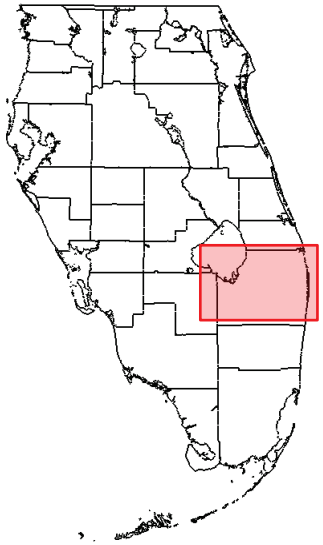

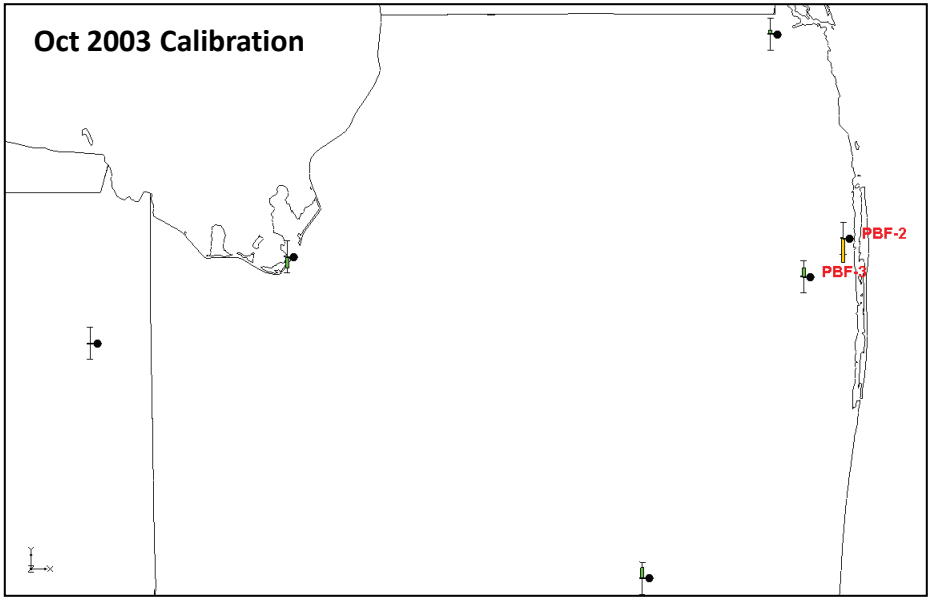

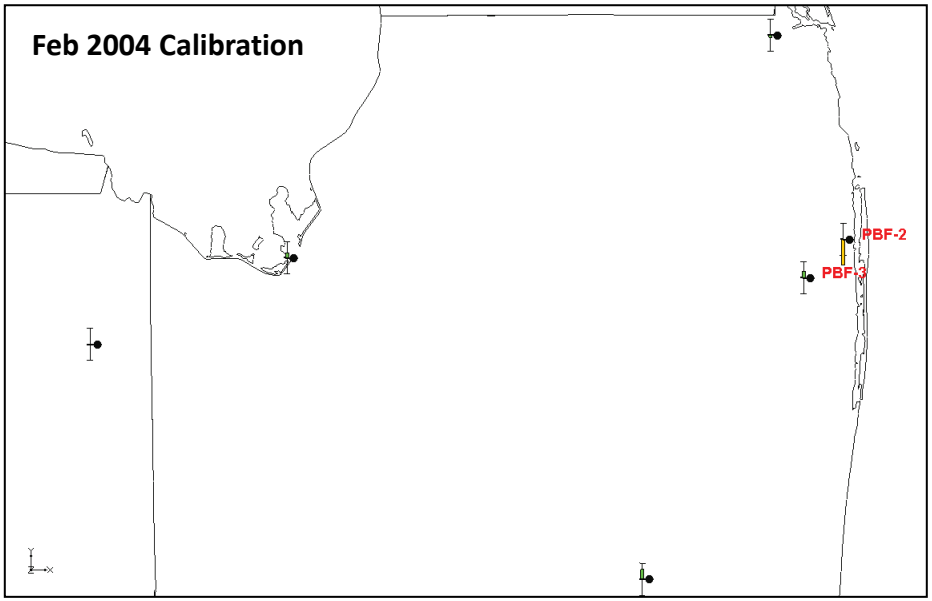

Notes:

This figure is a zoomed view of the October 2003 and February 2004 calibration for the UF. Labeled points are discussed in detail in Section 4.1.1.3. The same information is also shown on Figure 4.2 and 4.6.

Calibration targets are green when the calculated value is within 5 feet of the measured head, yellow when within 10 feet and red when the model calculates a head more than 10 feet different from the measured value.

The direction of the colored bar on the calibration target indicates the sign on the residual: bars above the middle line indicate the model calculated higher heads than measured; bars below the middle line indicate negative residuals.

Regional SEAWAT Calibration
UF Layer, Zoomed
Final Groundwater Model Calibration Report

Figure 4.15

October 2010

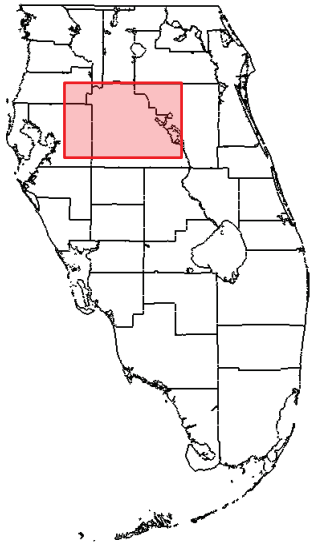

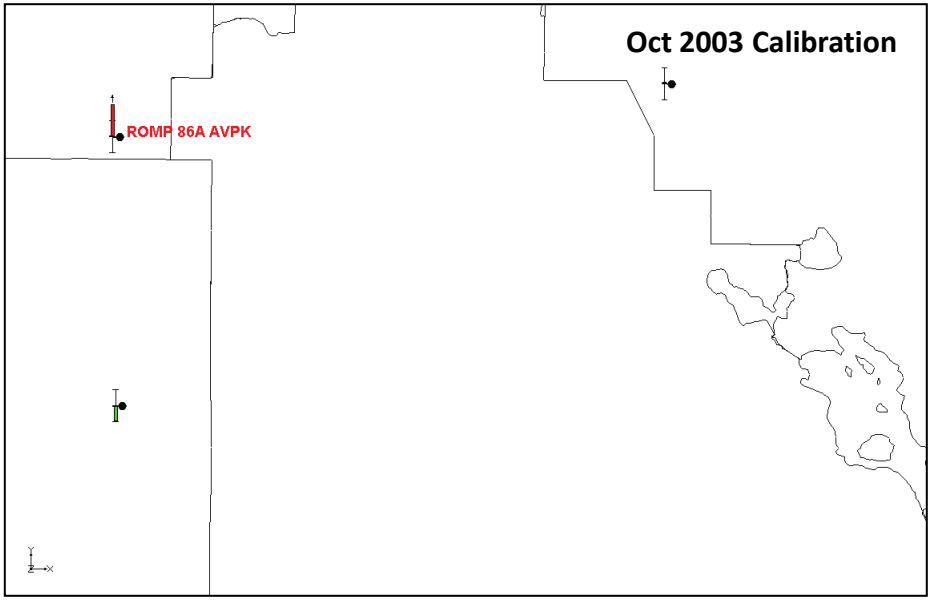

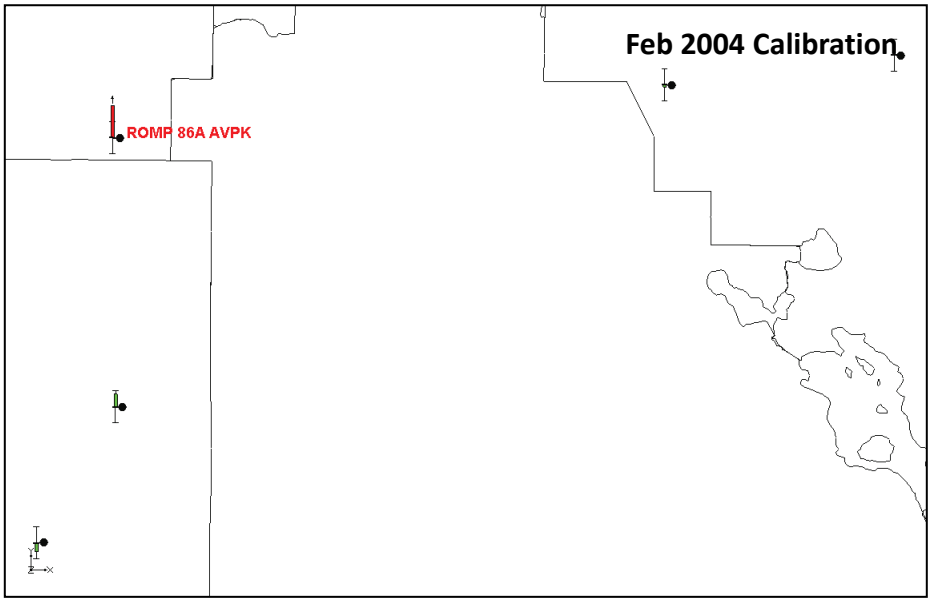

Notes:

This figure is a zoomed view of the October 2003 and February 2004 calibration for the APPZ. Labeled points are discussed in detail in Section 4.1.1.3. The same information is also shown on Figure 4.3 and 4.7.

Calibration targets are green when the calculated value is within 5 feet of the measured head, yellow when within 10 feet and red when the model calculates a head more than 10 feet different from the measured value.

The direction of the colored bar on the calibration target indicates the sign on the residual: bars above the middle line indicate the model calculated higher heads than measured; bars below the middle line indicate negative residuals.

Regional SEAWAT Calibration
APPZ Layer, Zoomed
Final Groundwater Model Calibration Report

Figure 4.16

October 2010

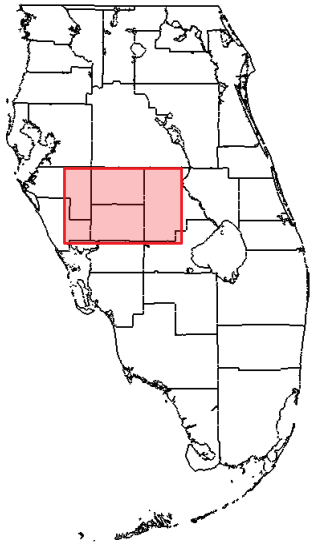

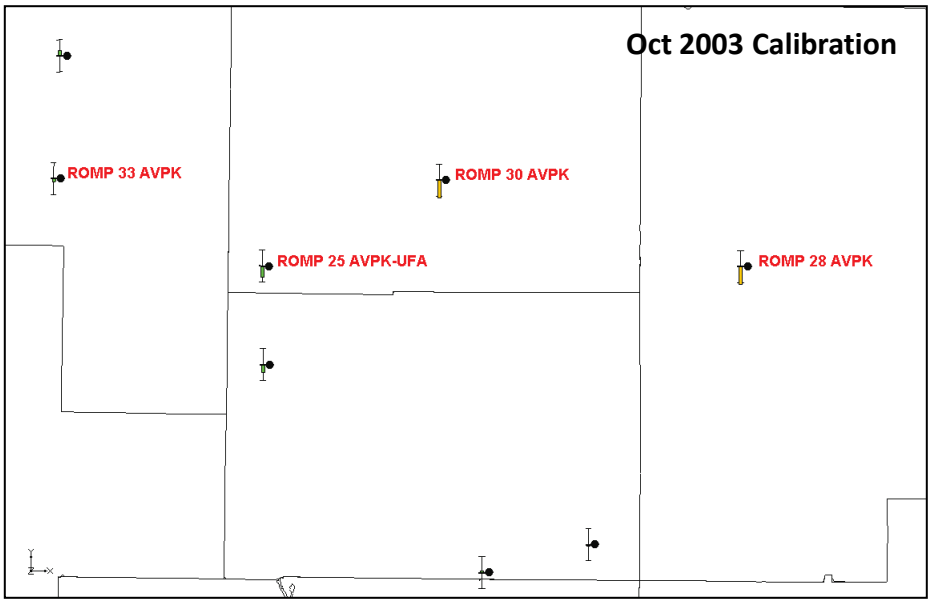

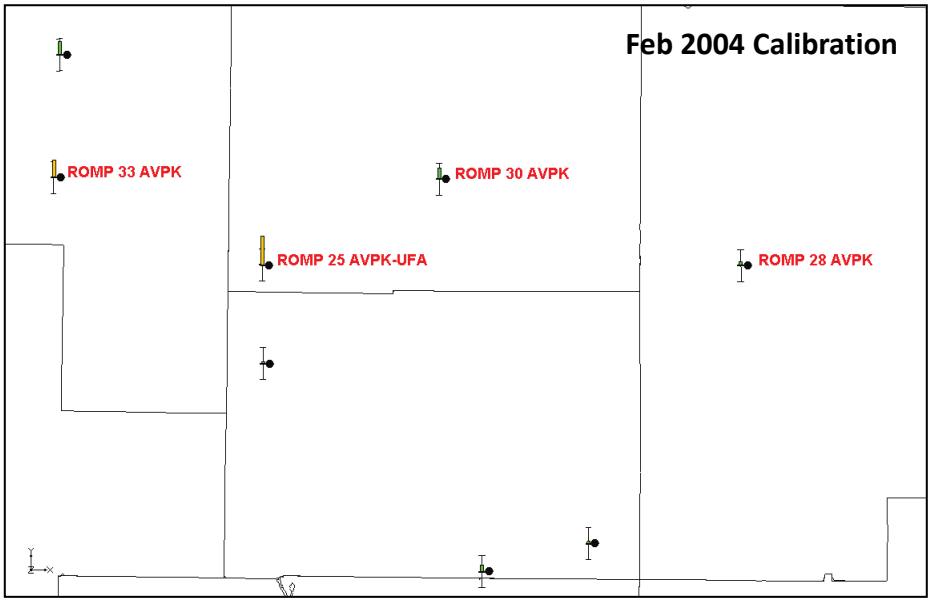

Notes:

This figure is a zoomed view of the October 2003 and February 2004 calibration for the APPZ. Labeled points are discussed in detail in Section 4.1.1.3. The same information is also shown on Figure 4.3 and 4.7.

Calibration targets are green when the calculated value is within 5 feet of the measured head, yellow when within 10 feet and red when the model calculates a head more than 10 feet different from the measured value.

The direction of the colored bar on the calibration target indicates the sign on the residual: bars above the middle line indicate the model calculated higher heads than measured; bars below the middle line indicate negative residuals.

Regional SEAWAT Calibration
APPZ Layer, Zoomed
Final Groundwater Model Calibration Report

Figure 4.17

October 2010

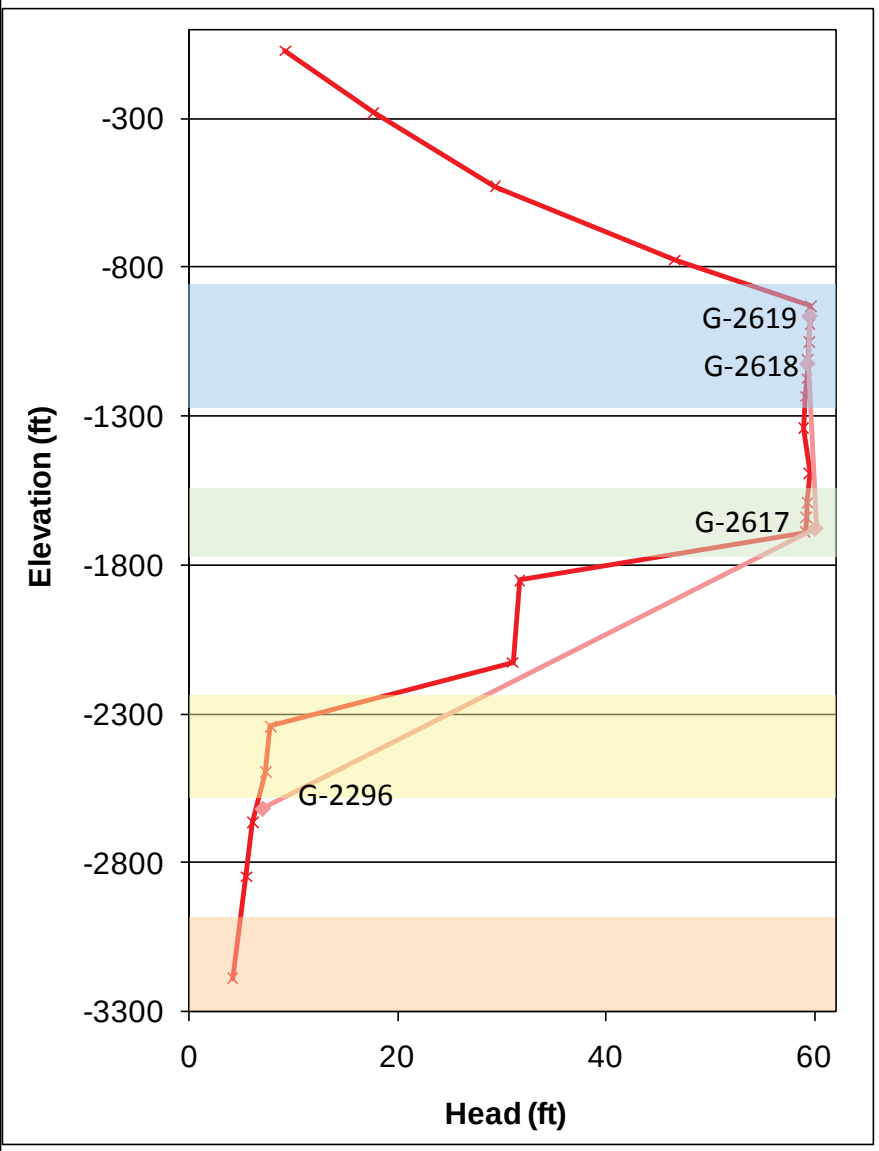

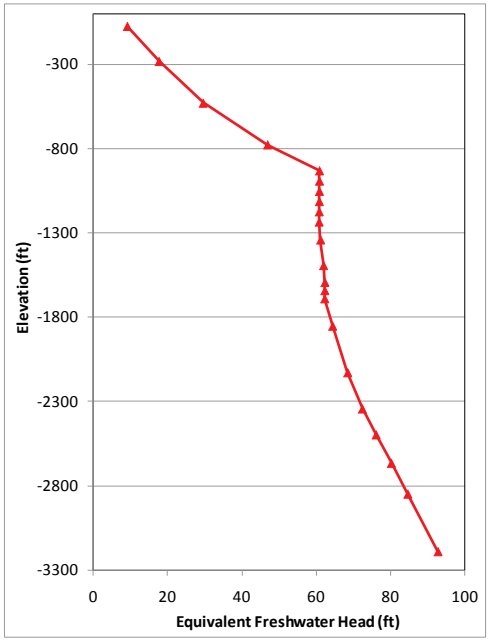

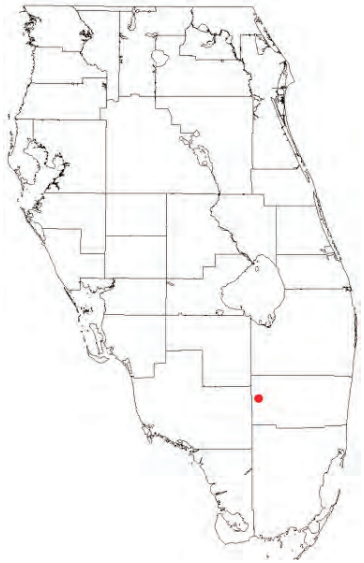

Legend:

- Model Calculated Head- Feb 2004
- Observed Head-Feb 2004
- Cluster Location

Model-Simplified Geology

- Upper Floridan
- APPZ
- Lower Floridan (LF1)
- Boulder Zone

Notes:

The plot at left shows the head changes in a vertical column of the model compared to measurements made at a well cluster. Colored stripes indicate the model-simplified stratigraphic units.

Model calculated heads are from the February 2004 calibrated model. Measured values are averaged for the month of February 2004.

The location of the cluster is marked on the inset map at bottom right.

The plot at left may seem unusual as it seems to indicate downward flow from the APPZ towards the LF1. However, when the heads are converted to equivalent freshwater heads in the plot at top right, the gradient is shown to be upward as expected. Figures on the following pages will not show equivalent freshwater heads.

Regional SEAWAT Calibration
Vertical Gradient Comparison
Final Groundwater Model Calibration Report

Figure 4.18

October 2010

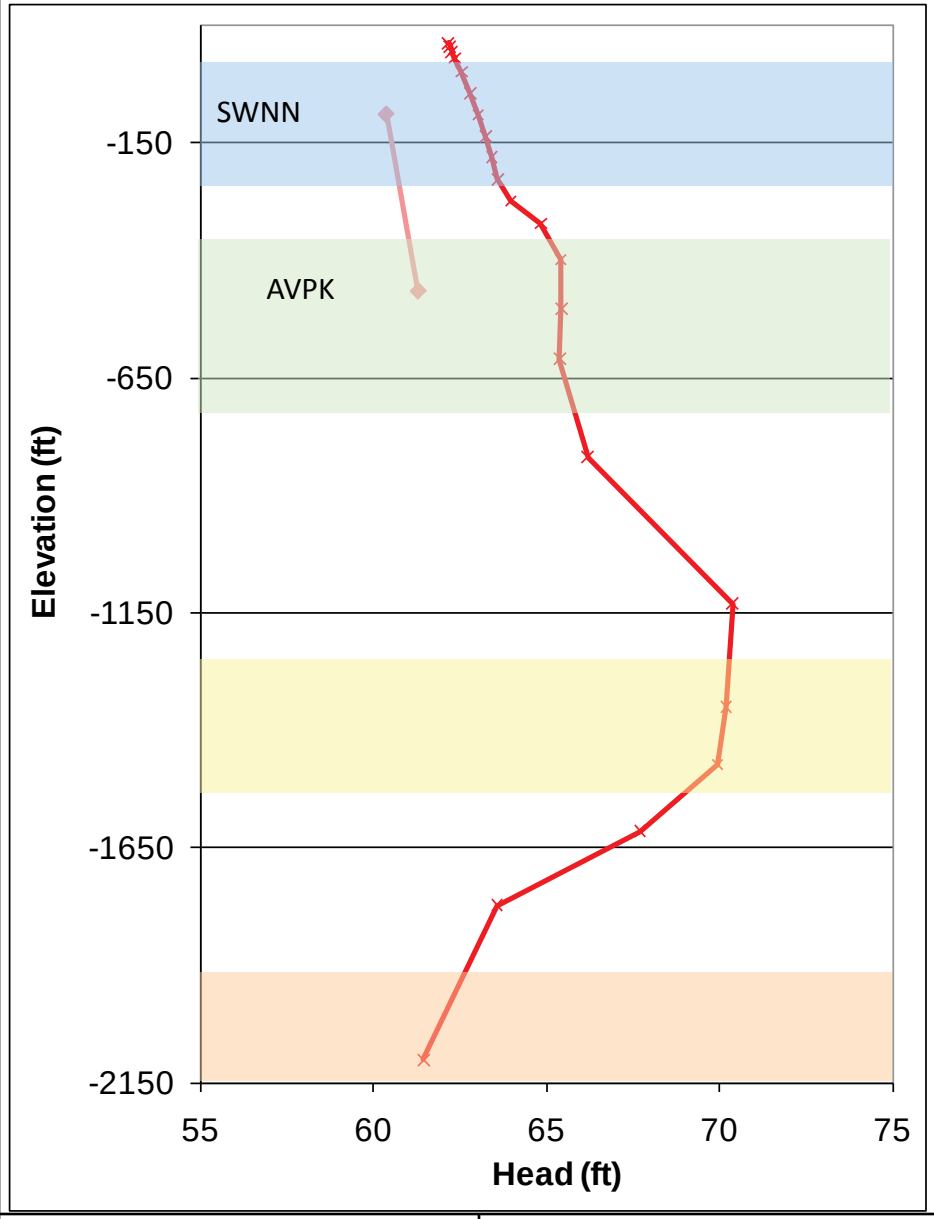

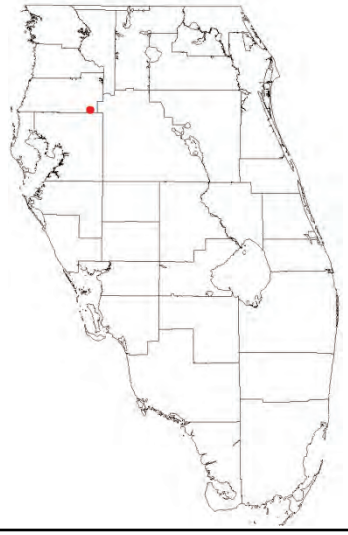

Legend:

Model Calculated Head- Feb 2004

Observed Head-Feb 2004

Cluster Location

Model-Simplified Geology

- Upper Floridan
- APPZ
- Lower Floridan (LF1)
- Boulder Zone

Notes:

These plots show the head changes in a vertical column of the model compared to measurements made at two well clusters. Colored stripes indicate the model-simplified stratigraphic units.

Model calculated heads are from the February 2004 calibrated model. Measured values are averaged for the month of February 2004.

The location of the cluster is marked on the inset map.

Regional SEAWAT Calibration
Vertical Gradient Comparison
Final Groundwater Model Calibration Report

Figure 4.19

October 2010

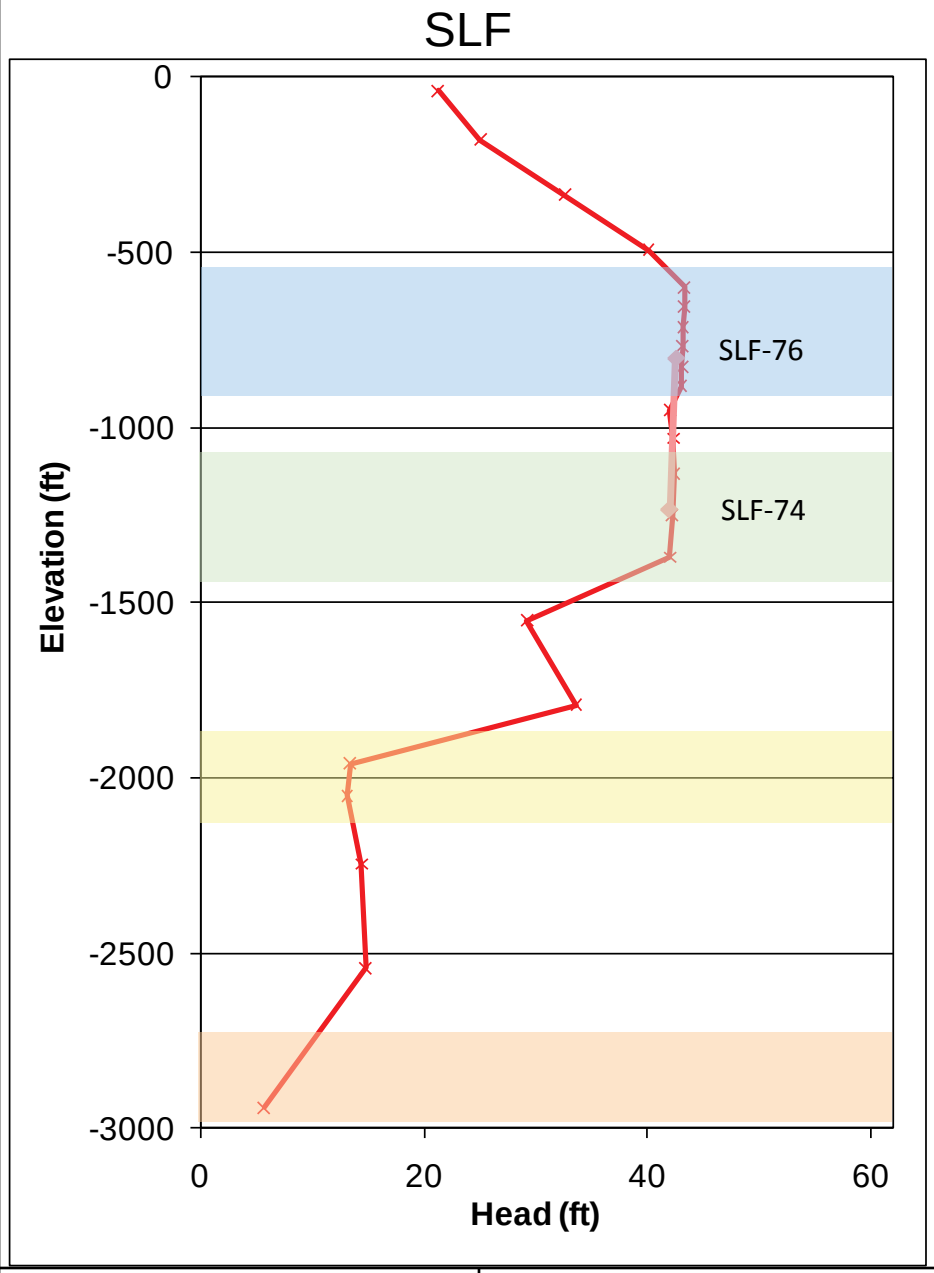

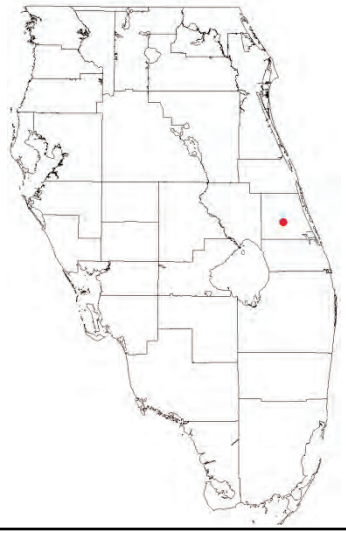

Legend:

- Model Calculated Head- Feb 2004
- Observed Head-Feb 2004
- Cluster Location

Model-Simplified Geology

- Upper Floridan
- APPZ
- Lower Floridan (LF1)
- Boulder Zone

Notes:

These plots show the head changes in a vertical column of the model compared to measurements made at two well clusters. Colored stripes indicate the model-simplified stratigraphic units.

Model calculated heads are from the February 2004 calibrated model. Measured values are averaged for the month of February 2004.

The location of the cluster is marked on the inset map.

Regional SEAWAT Calibration
Vertical Gradient Comparison
Final Groundwater Model Calibration Report

Figure 4.20

October 2010

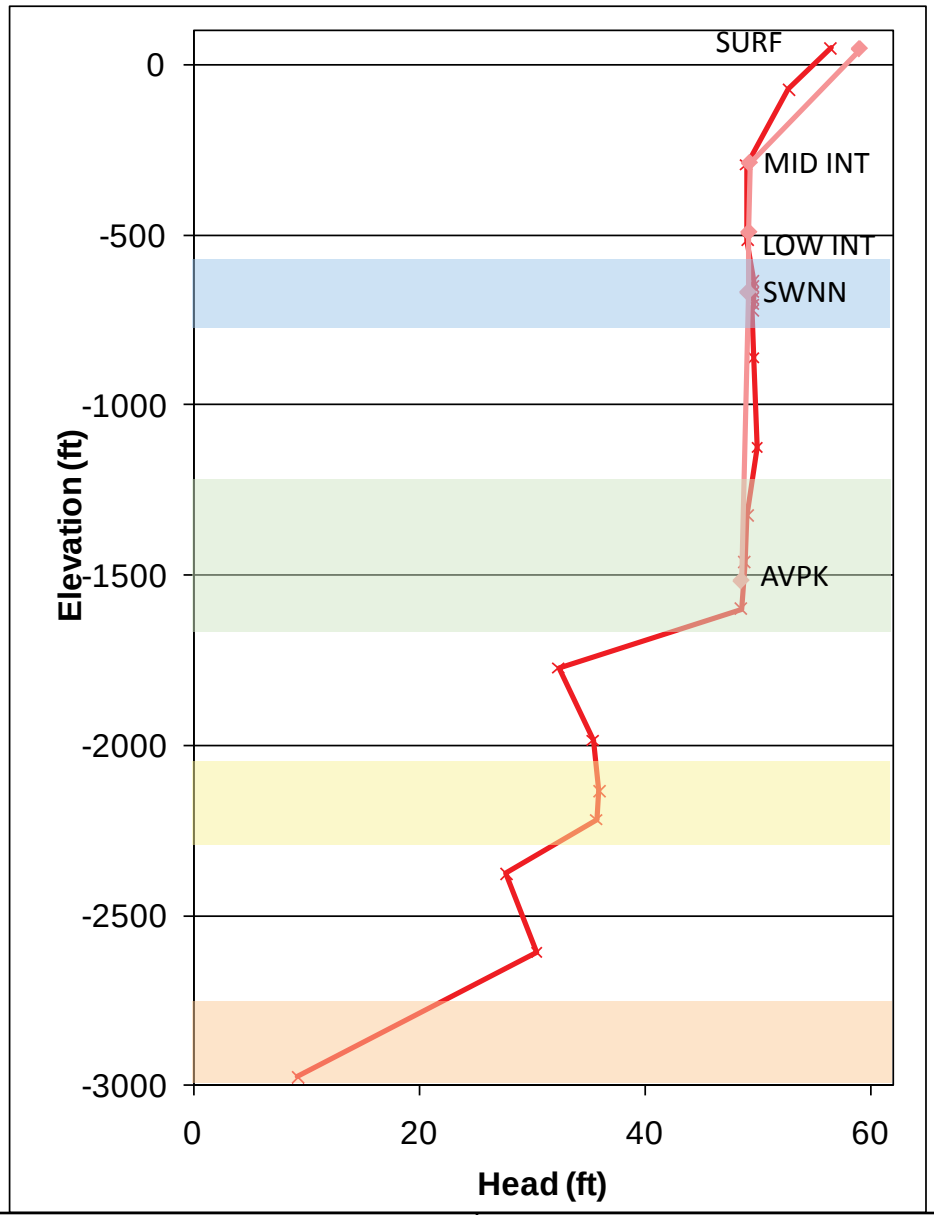

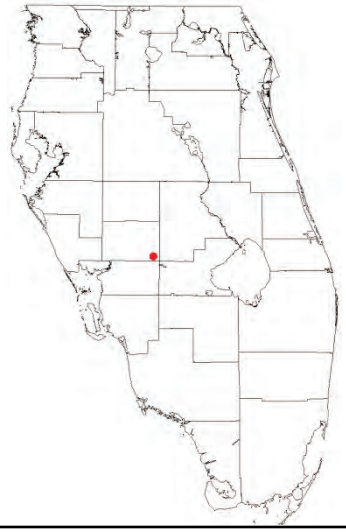

Legend:

- Model Calculated Head- Feb 2004
- Observed Head-Feb 2004
- Cluster Location

Model-Simplified Geology

- Upper Floridan
- APPZ
- Lower Floridan (LF1)
- Boulder Zone

Notes:

These plots show the head changes in a vertical column of the model compared to measurements made at two well clusters. Colored stripes indicate the model-simplified stratigraphic units.

Model calculated heads are from the February 2004 calibrated model. Measured values are averaged for the month of February 2004.

The location of the cluster is marked on the inset map.

Regional SEAWAT Calibration
Vertical Gradient Comparison
Final Groundwater Model Calibration Report

Figure 4.21

October 2010

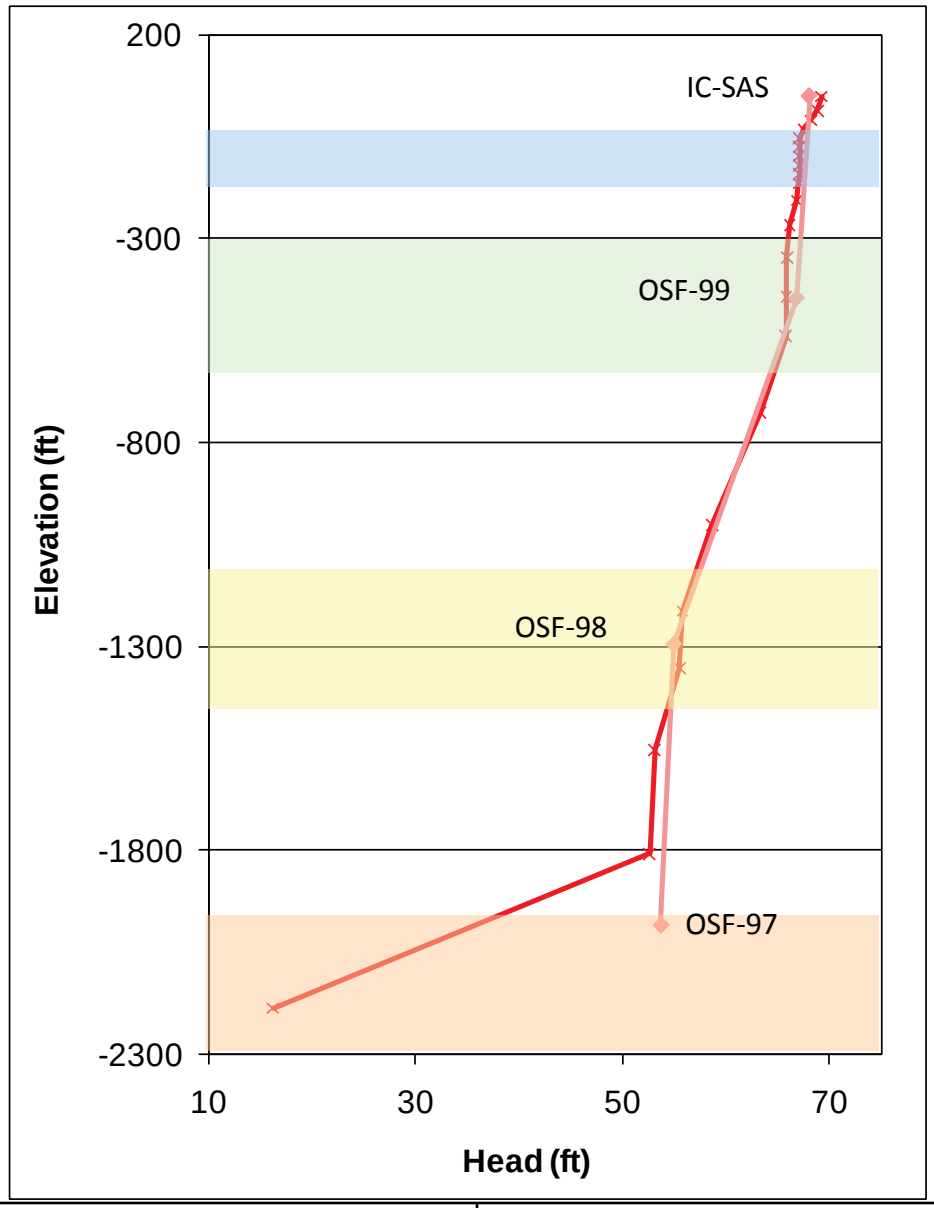

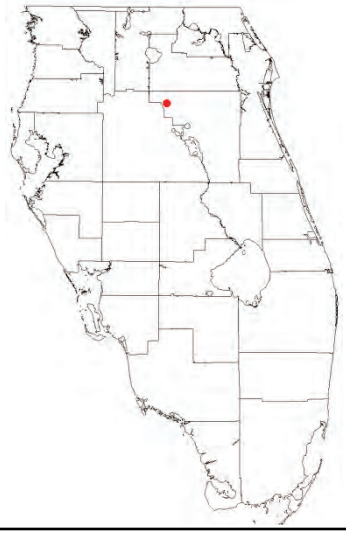

Legend:

Model Calculated Head- Feb 2004

Observed Head-Feb 2004

Cluster Location

Model-Simplified Geology

- Upper Floridan
- APPZ
- Lower Floridan (LF1)
- Boulder Zone

Notes:

These plots show the head changes in a vertical column of the model compared to measurements made at two well clusters. Colored stripes indicate the model-simplified stratigraphic units.

Model calculated heads are from the February 2004 calibrated model. Measured values are averaged for the month of February 2004.

The location of the cluster is marked on the inset map.

Regional SEAWAT Calibration
Vertical Gradient Comparison
Final Groundwater Model Calibration Report

Figure 4.22

October 2010

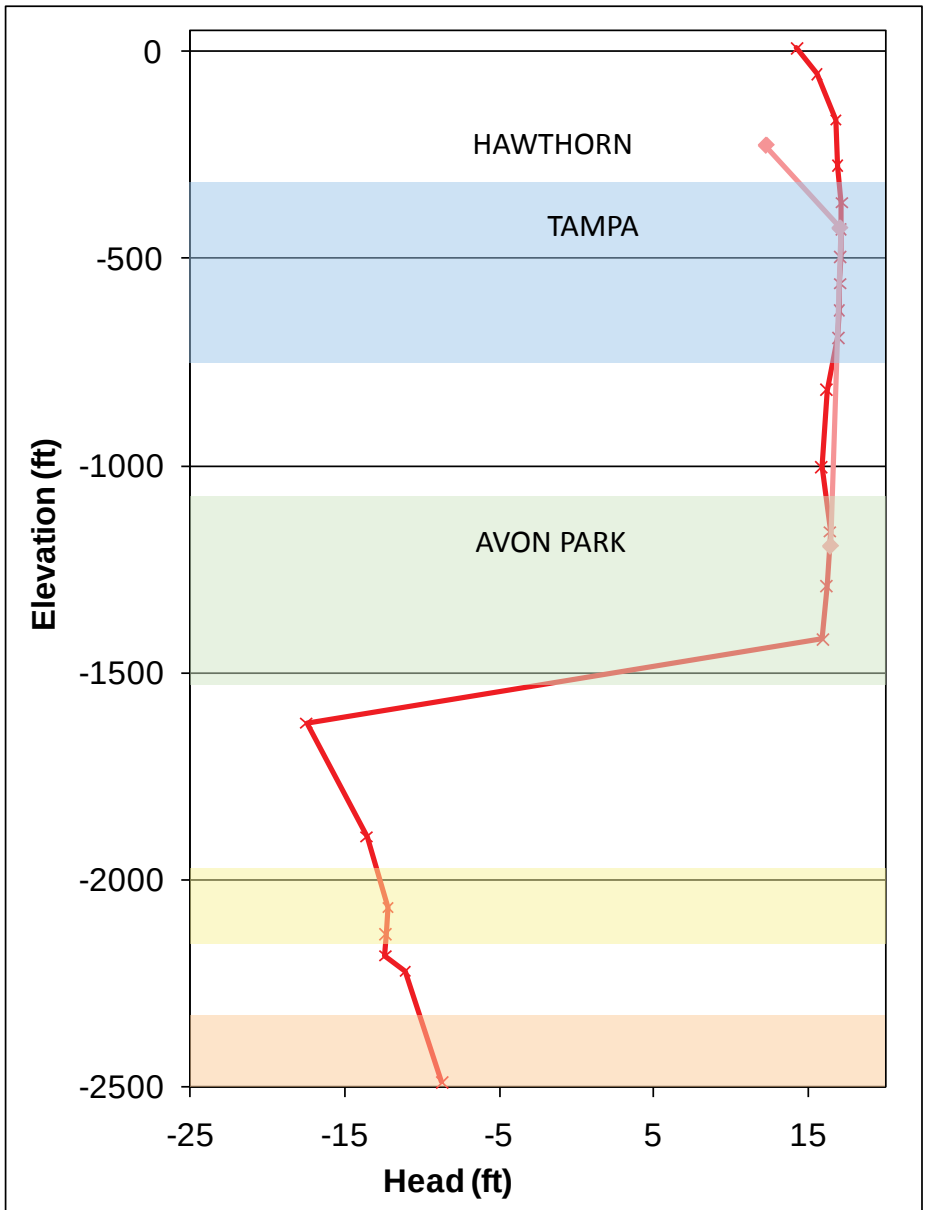

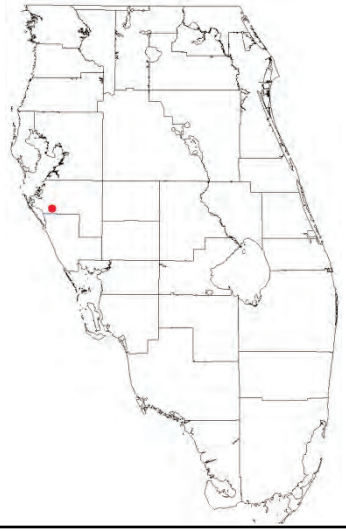

Legend:

Model Calculated Head- Feb 2004

Observed Head-Feb 2004

Cluster Location

Model-Simplified Geology

- Upper Floridan
- APPZ
- Lower Floridan (LF1)
- Boulder Zone

Notes:

These plots show the head changes in a vertical column of the model compared to measurements made at two well clusters. Colored stripes indicate the model-simplified stratigraphic units.

Model calculated heads are from the February 2004 calibrated model. Measured values are averaged for the month of February 2004.

The location of the cluster is marked on the inset map.

Regional SEAWAT Calibration
Vertical Gradient Comparison
Final Groundwater Model Calibration Report

Figure 4.23

October 2010

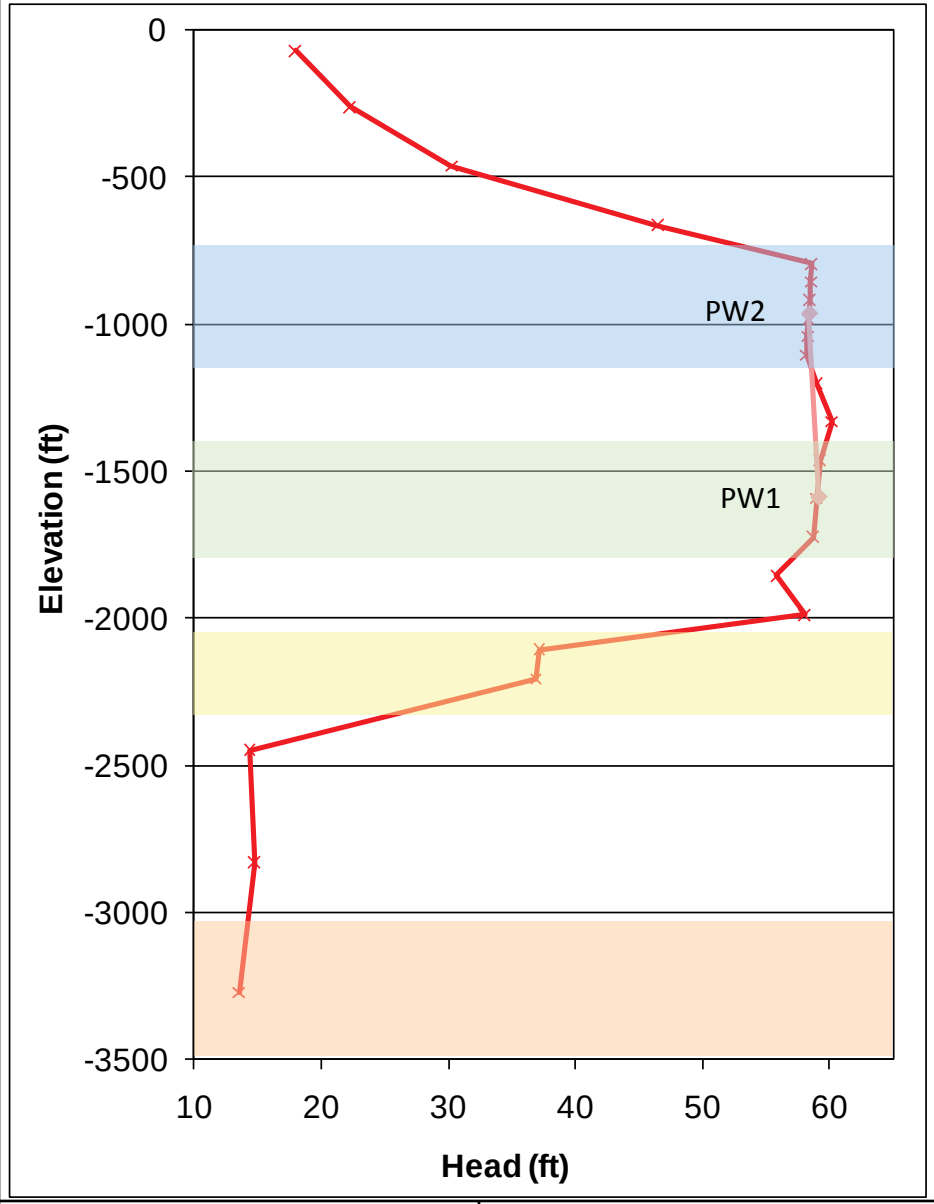

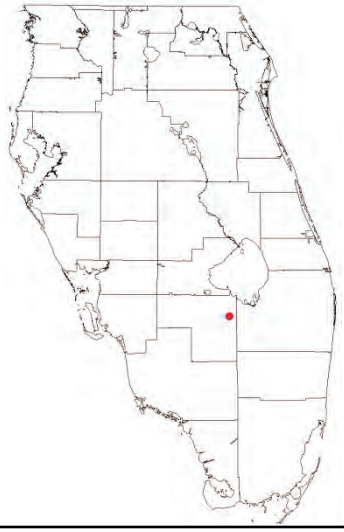

Legend:

- Model Calculated Head- Feb 2004
- Observed Head-Feb 2004
- Cluster Location

Model-Simplified Geology

- Upper Floridan
- APPZ
- Lower Floridan (LF1)
- Boulder Zone

Notes:

These plots show the head changes in a vertical column of the model compared to measurements made at two well clusters. Colored stripes indicate the model-simplified stratigraphic units.

Model calculated heads are from the February 2004 calibrated model. Measured values are averaged for the month of February 2004.

The location of the cluster is marked on the inset map.

Regional SEAWAT Calibration
Vertical Gradient Comparison
Final Groundwater Model Calibration Report

Figure 4.24

October 2010

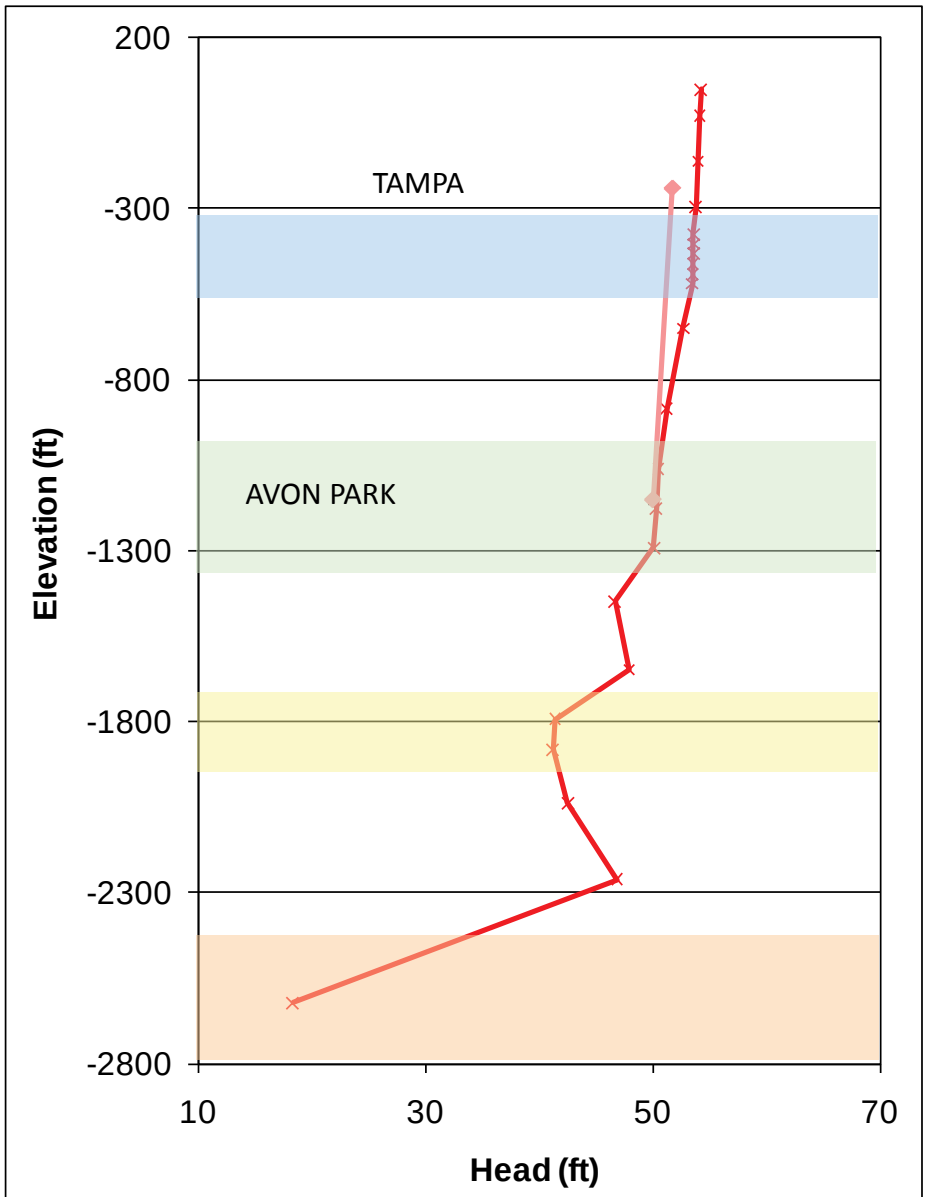

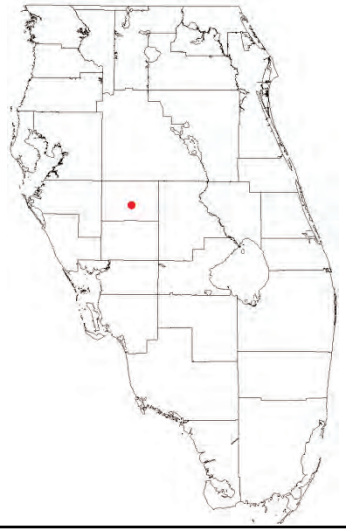

Legend:

Model Calculated Head- Feb 2004

Observed Head-Feb 2004

Cluster Location

Model-Simplified Geology

- Upper Floridan
- APPZ
- Lower Floridan (LF1)
- Boulder Zone

Notes:

These plots show the head changes in a vertical column of the model compared to measurements made at two well clusters. Colored stripes indicate the model-simplified stratigraphic units.

Model calculated heads are from the February 2004 calibrated model. Measured values are averaged for the month of February 2004.

The location of the cluster is marked on the inset map.

Regional SEAWAT Calibration
Vertical Gradient Comparison
Final Groundwater Model Calibration Report

Figure 4.25

October 2010

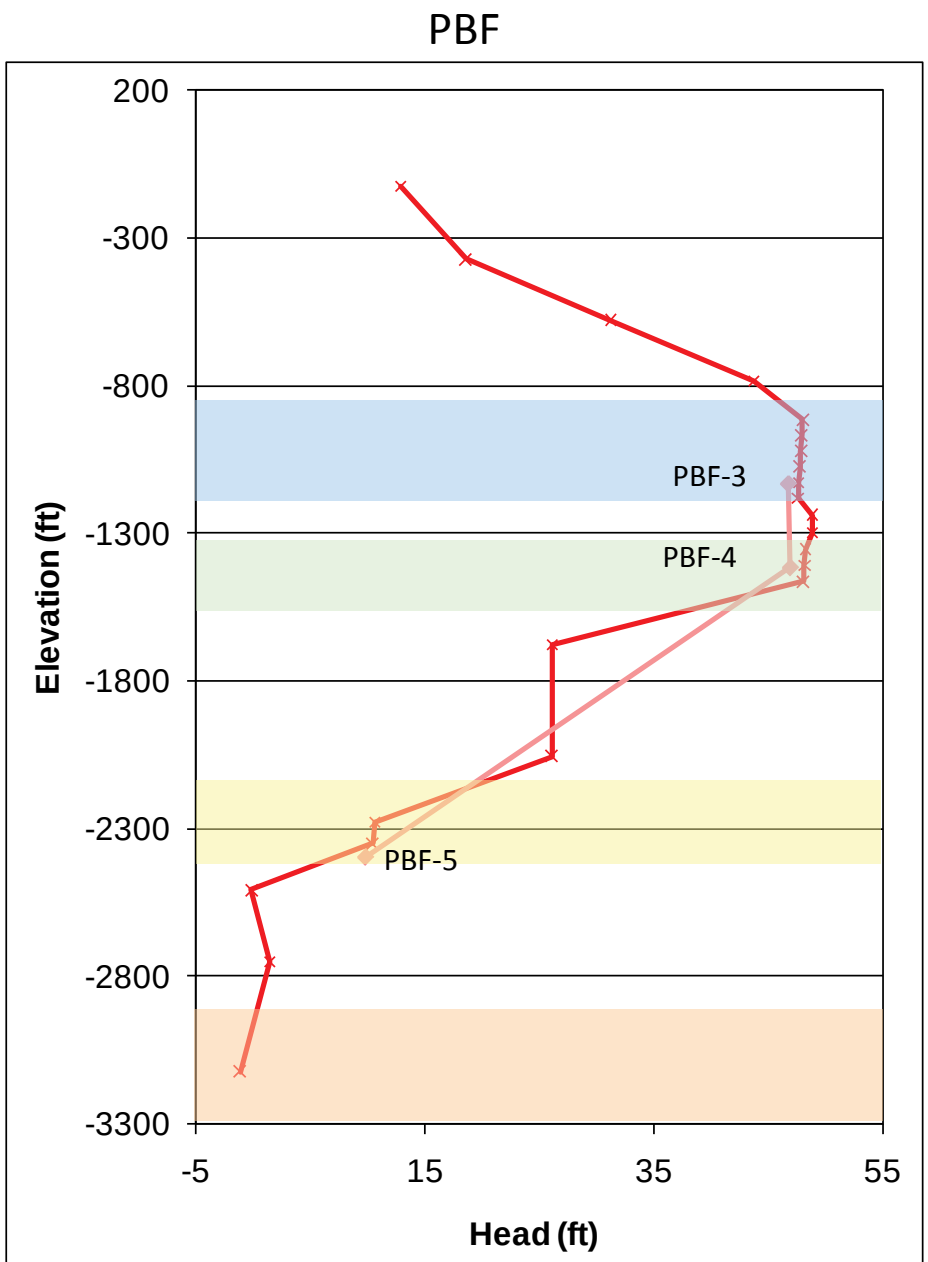

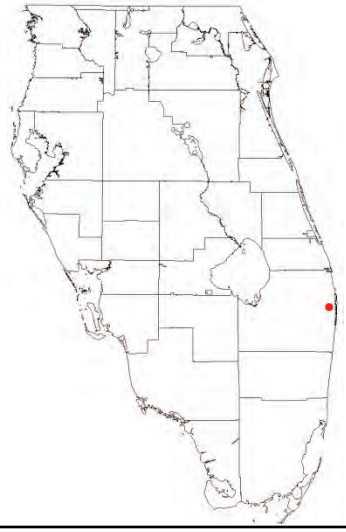

Legend:

Model Calculated Head- Feb 2004

Observed Head-Feb 2004

Cluster Location

Model-Simplified Geology

- Upper Floridan
- APPZ
- Lower Floridan (LF1)
- Boulder Zone

Notes:

These plots show the head changes in a vertical column of the model compared to measurements made at two well clusters. Colored stripes indicate the model-simplified stratigraphic units.

Model calculated heads are from the February 2004 calibrated model. Measured values are averaged for the month of February 2004.

The location of the cluster is marked on the inset map.

Regional SEAWAT Calibration
Vertical Gradient Comparison
Final Groundwater Model Calibration Report

Figure 4.26

October 2010

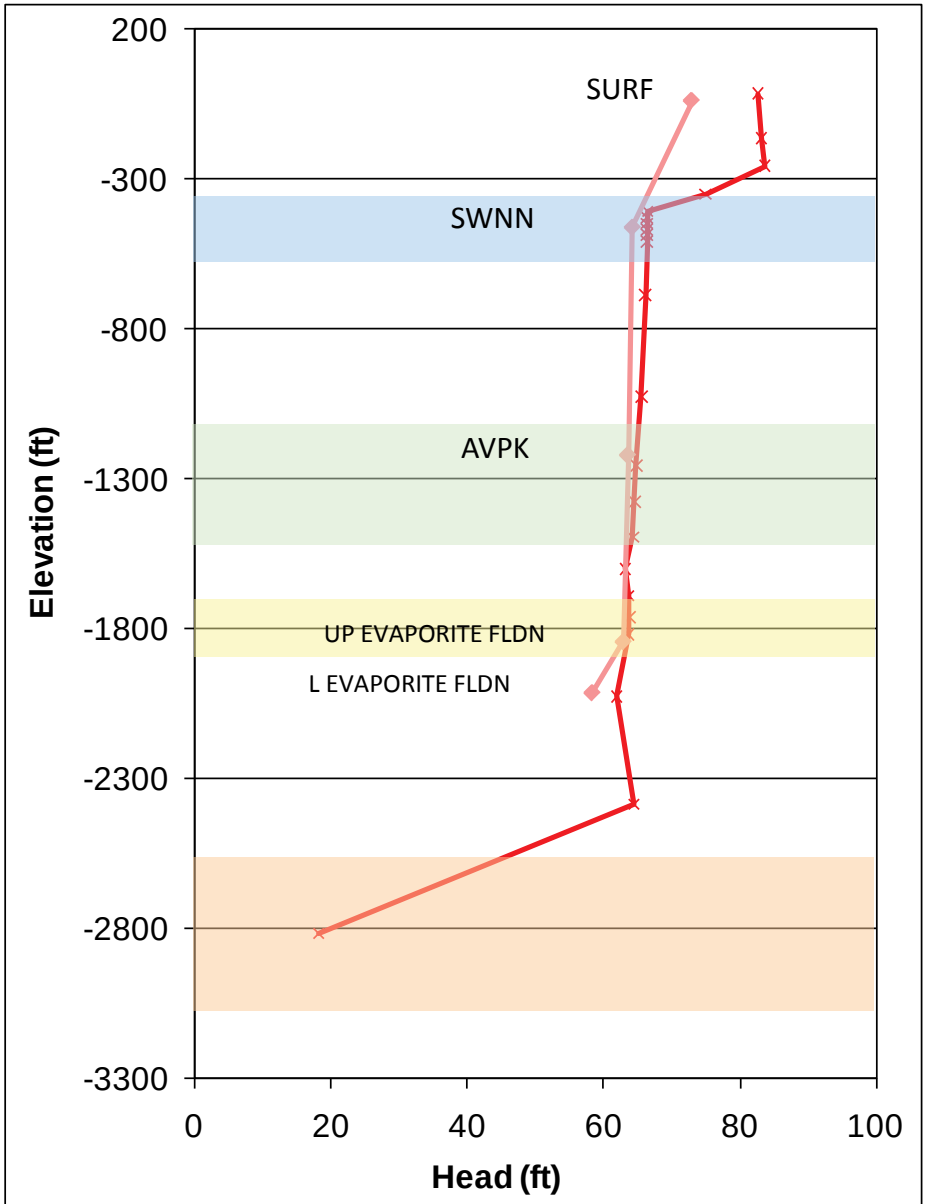

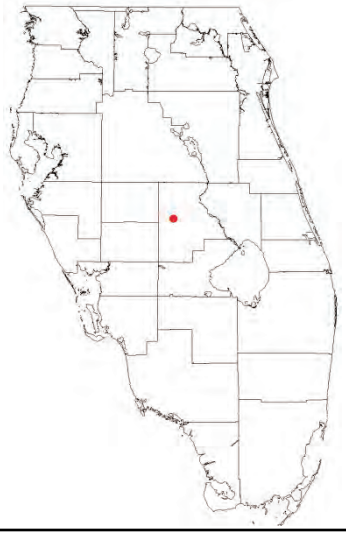

Legend:

Model Calculated Head- Feb 2004

Observed Head-Feb 2004

Cluster Location

Model-Simplified Geology

Upper Floridan

APPZ

Lower Floridan (LF1)

Boulder Zone

Notes:

These plots show the head changes in a vertical column of the model compared to measurements made at two well clusters. Colored stripes indicate the model-simplified stratigraphic units.

Model calculated heads are from the February 2004 calibrated model. Measured values are averaged for the month of February 2004.

The location of the cluster is marked on the inset map.

Regional SEAWAT Calibration
Vertical Gradient Comparison
Final Groundwater Model Calibration Report

Figure 4.27

October 2010

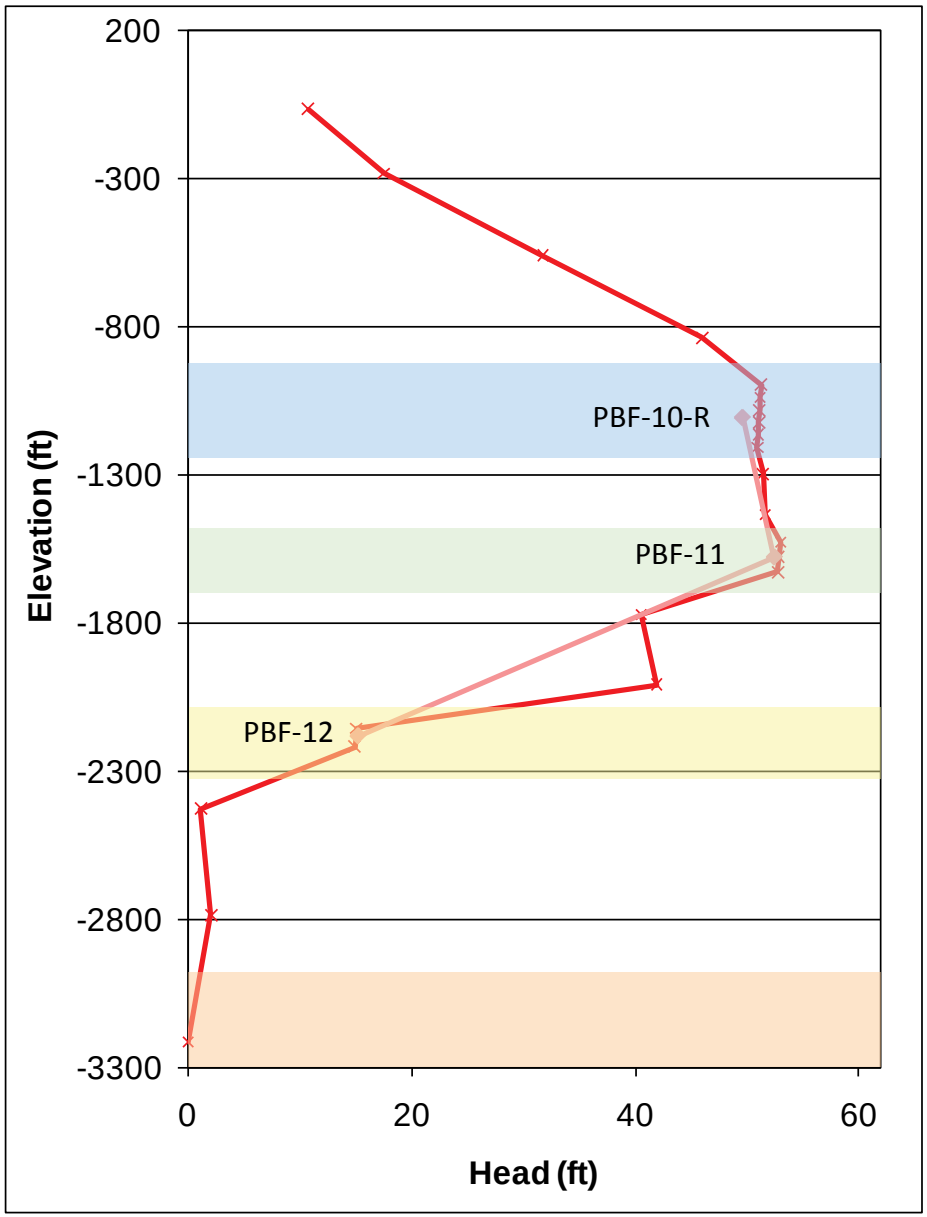

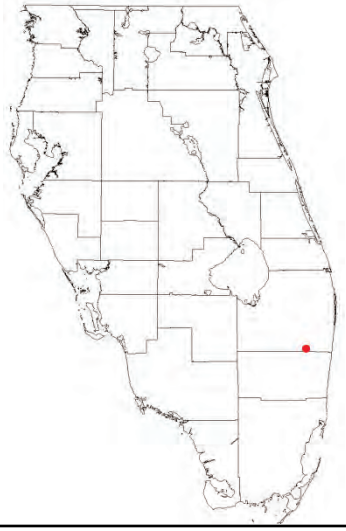

Legend:

- Model Calculated Head- Feb 2004
- Observed Head-Feb 2004
- Cluster Location

Model-Simplified Geology

- Upper Floridan
- APPZ
- Lower Floridan (LF1)
- Boulder Zone

Notes:

These plots show the head changes in a vertical column of the model compared to measurements made at two well clusters. Colored stripes indicate the model-simplified stratigraphic units.

Model calculated heads are from the February 2004 calibrated model. Measured values are averaged for the month of February 2004.

The location of the cluster is marked on the inset map.

Regional SEAWAT Calibration
Vertical Gradient Comparison
Final Groundwater Model Calibration Report

Figure 4.28

October 2010

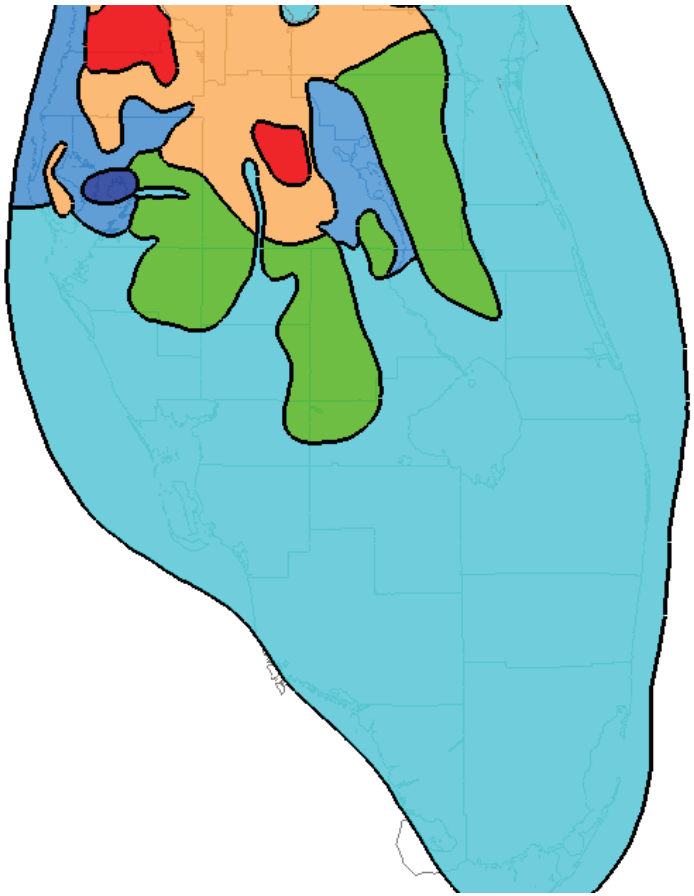

Generalized Recharge (USGS 88-4057)

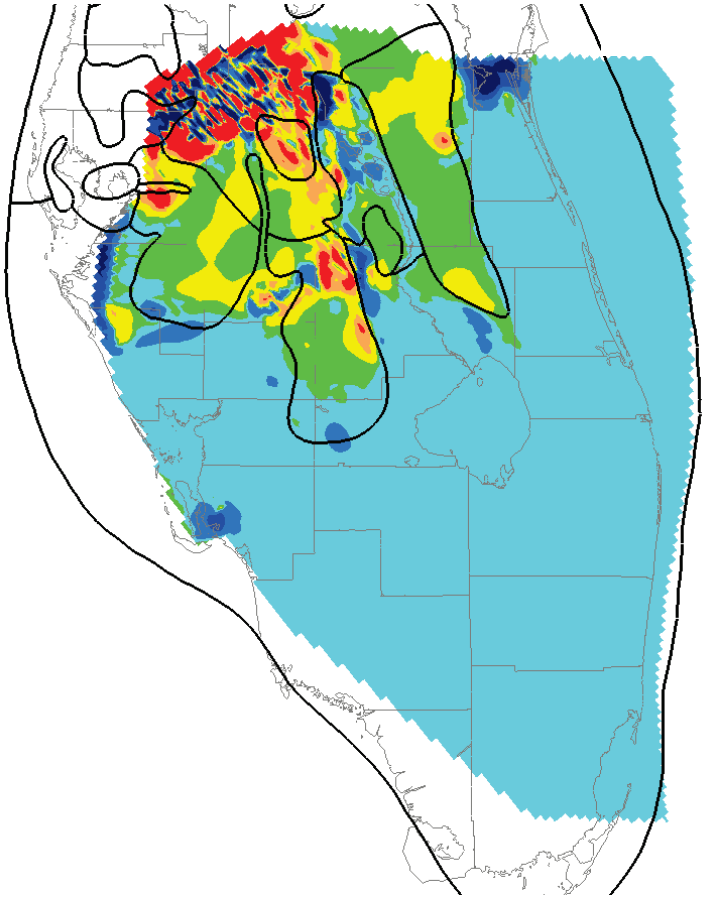

Model Recharge/Discharge

N

Discharge (in/yr):

- Greater than 10
- 5 - 10
- 1 - 5
- Less than 1

Recharge (in/yr):

- Less than 1
- 1 - 5
- 5 - 10
- Greater than 10

Notes:

The model recharge/discharge figure is created from the cell-to-cell flow output from the SEAWAT model. Fluxes in and out of the top of the UF are shown.

Source for generalized recharge is Aucott, 1988.

Regional SEAWAT Calibration
Recharge to the Upper Floridan Comparison
Final Groundwater Model Calibration Report

Figure 4.29

October 2010

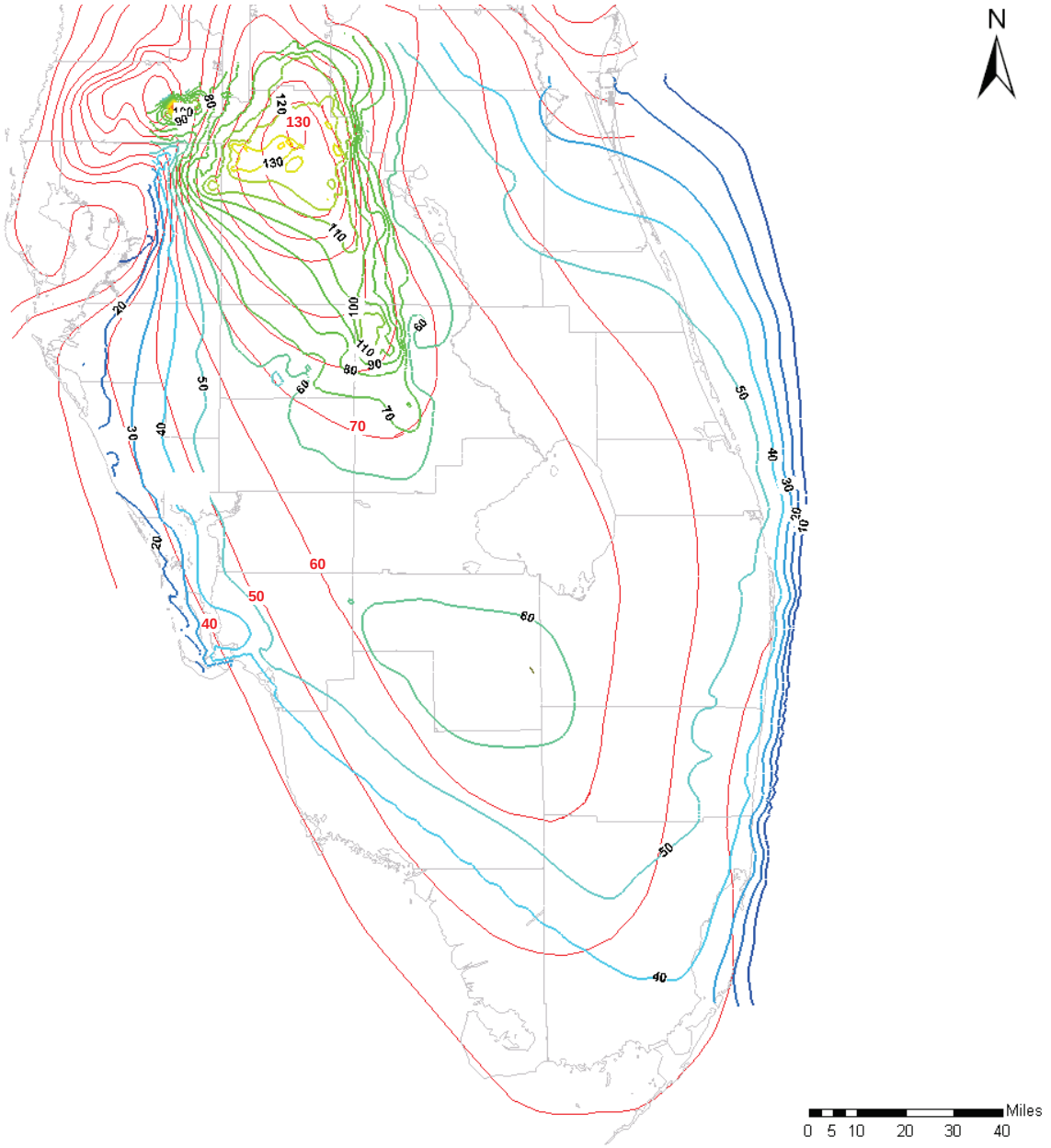

Modeled Head (ft)

180
165
150
135
120
105
90
75
60
45
30
15
0

Predevelopment Heads
(Bush and Johnston, 1988)

Notes:

Pre-Development heads based on U. S. Geological Survey Professional Paper 1403-C (Bush and Johnston, 1988)

Modeled head contours based on the February 2004 calibration simulation with all pumping removed.

Both USGS and model computed head contours are for the UF.

Regional SEAWAT Model
Pre-Development Head Comparison

Final Groundwater Model Calibration Report

Figure 4.30

October 2010

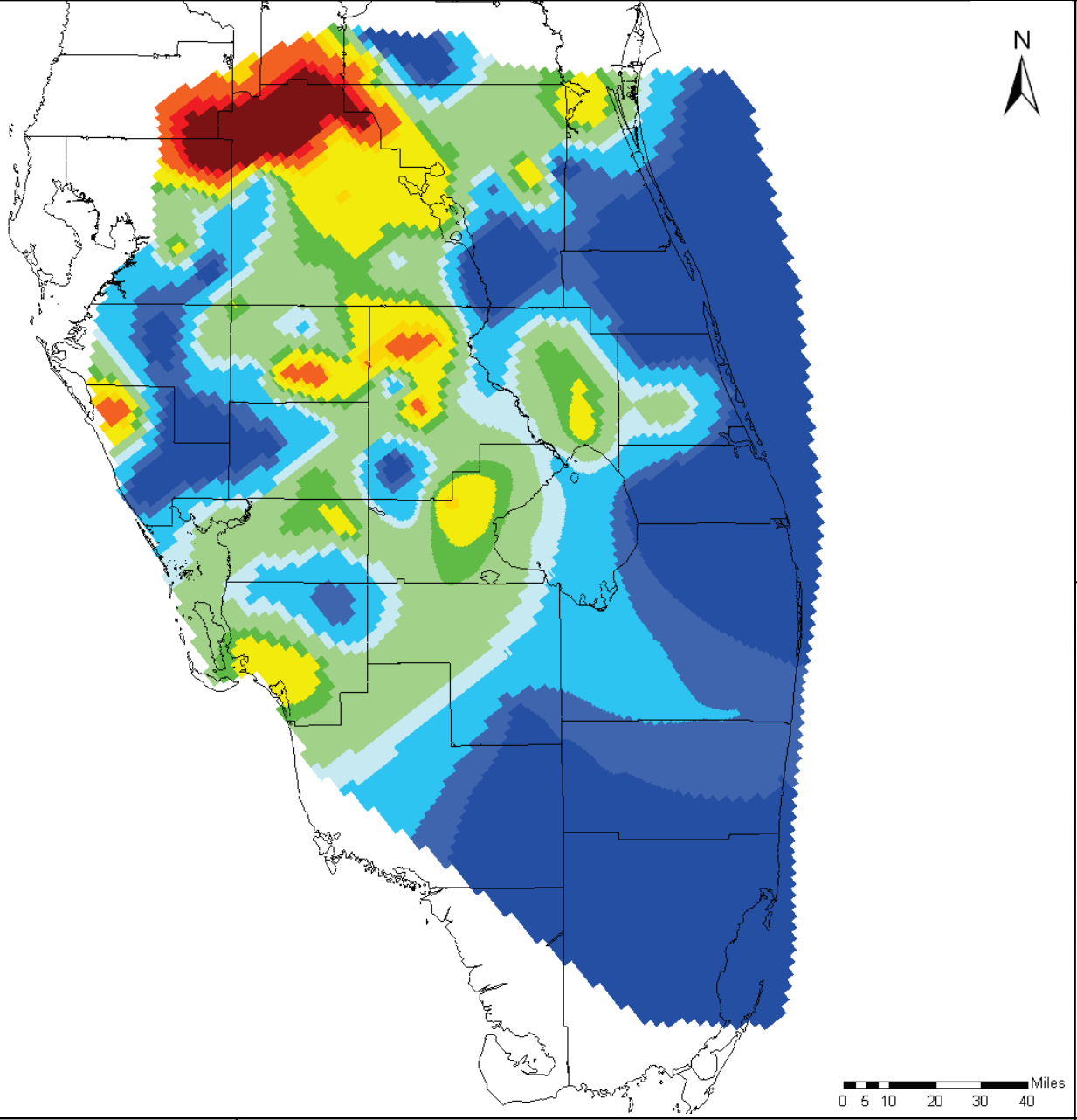

Notes:

This layer (2) overlies the Intermediate Aquifer in the regional model. Where the IA does not exist, (see Figure 4.32) the conductivities match those in layer 3 and 4.

Horizontal hydraulic conductivity was set to twice the vertical value (shown).

Conductivity values were interpolated to the grid from values assigned to a set of pilot points scattered across the model domain.

A combination of automated calibration (PEST) and manual calibration (trial and error) resulted in this conductivity field.

Regional Phase II ASR Vertical Hydraulic Conductivity
Intermediate Aquifer System Layer 2 (SEAWAT)
Final Groundwater Model Calibration Report

Figure 4.31

October 2010

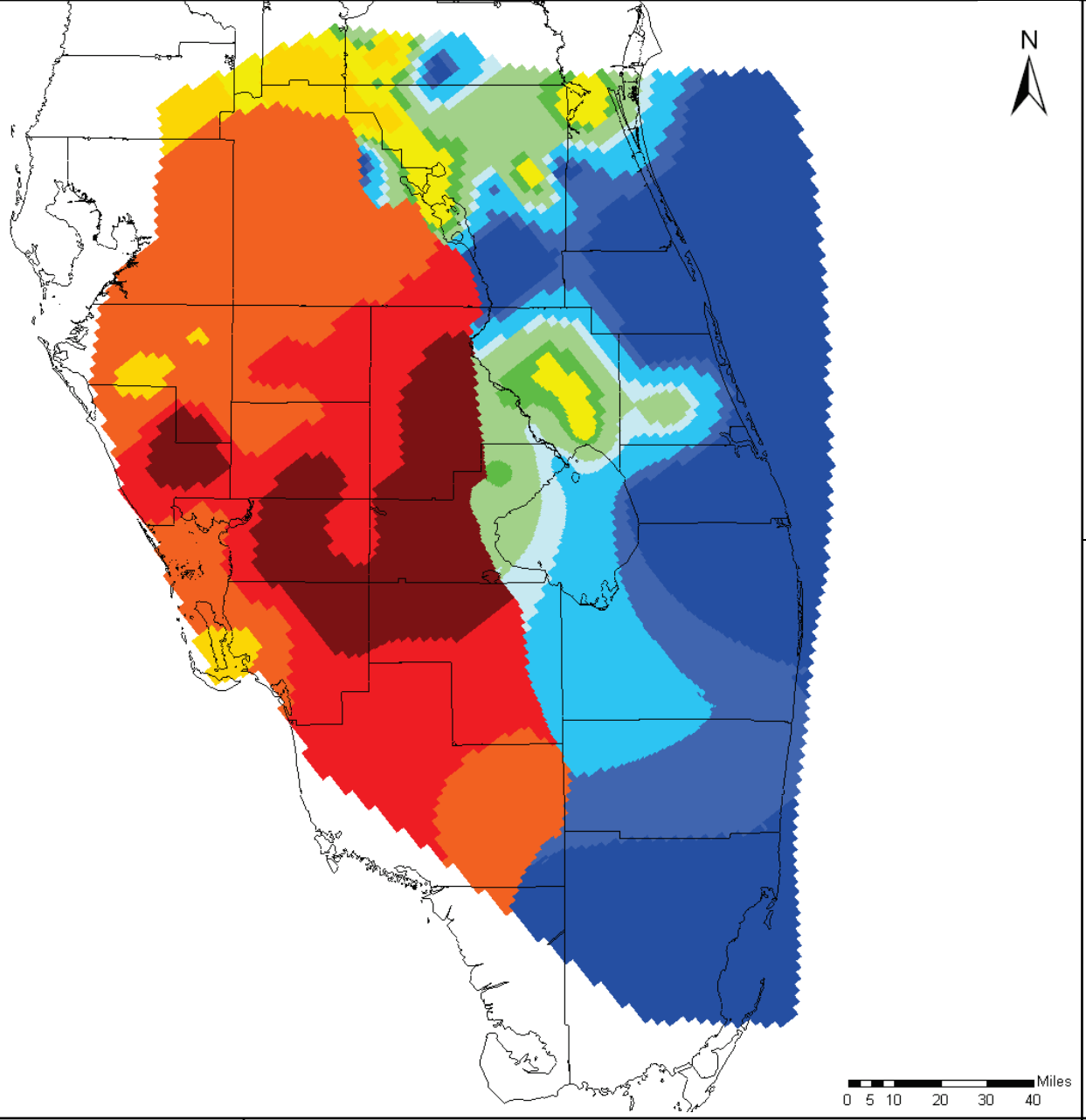

Horizontal Hydraulic Conductivity (ft/d)

- 0.0001 - 0.0005
- 0.0005 - 0.001
- 0.001 - 0.005
- 0.05 - 0.01
- 0.01 - 0.05
- 0.05 - 0.1
- 0.1 - 1
- 1 - 10
- 10 - 50
- 50 - 100
- 100 - 500

Notes:

The western portion of this layer (3) simulates the Intermediate Aquifer (IA). The eastern portion combines with layers 2 and 4 to simulate the Intermediate Confining Unit. Where the IA does not exist, the conductivity match those in layer 2 and 4.

Vertical hydraulic conductivity was set to one tenth of the horizontal value (shown).

Conductivity values were interpolated to the grid from values assigned to a set of pilot points scattered across the model domain.

A combination of automated calibration (PEST) and manual calibration (trial and error) resulted in this conductivity field.

Regional Phase II ASR Horizontal Hydraulic Conductivity Intermediate Aquifer System Layer 3 (SEAWAT)

Final Groundwater Model Calibration Report

Figure 4.32

October 2010

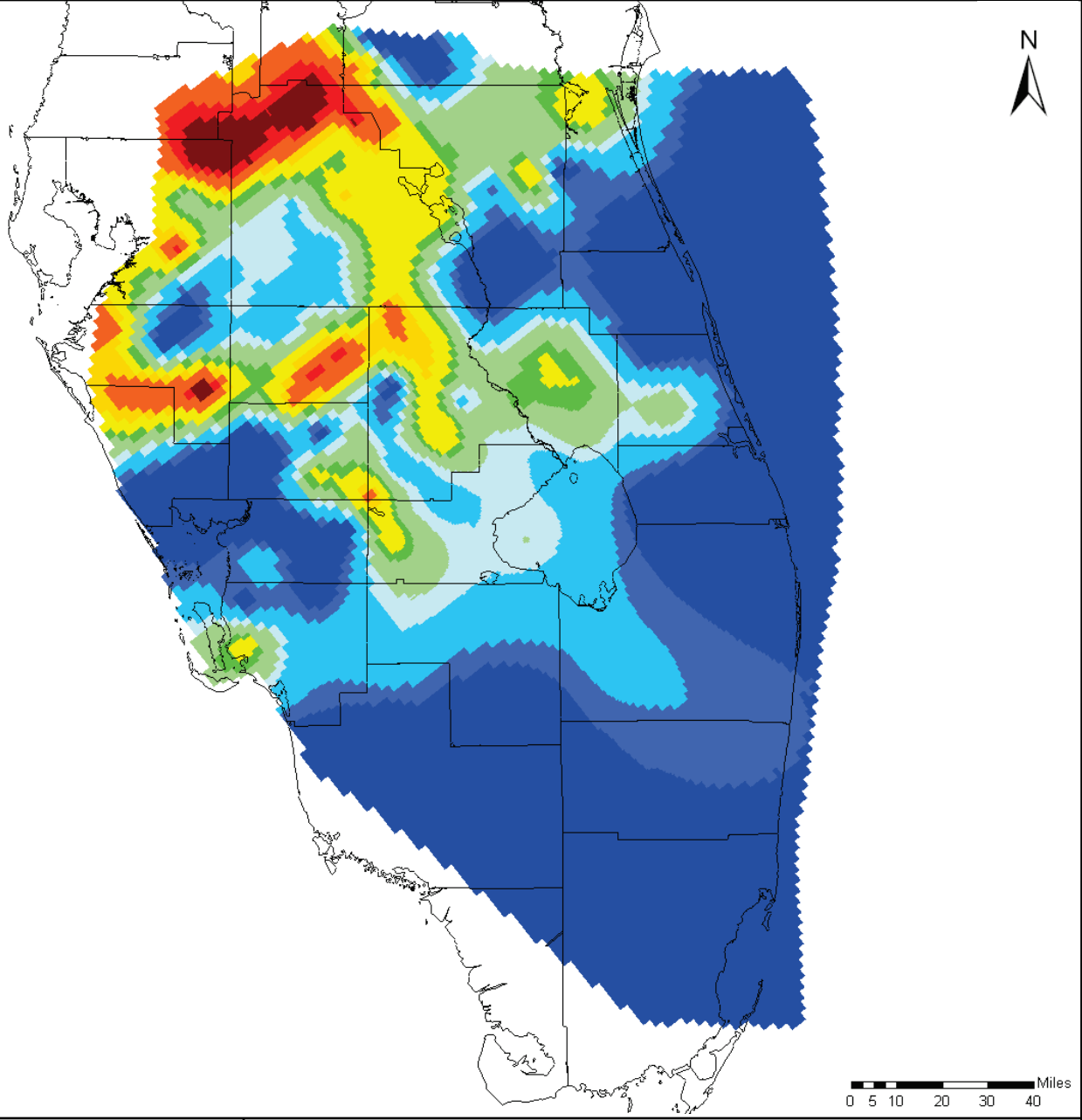

Vertical Hydraulic Conductivity (ft/d)

- 0.00001 - 0.00005
- 0.00005 - 0.0001
- 0.0001 - 0.0005
- 0.0005 - 0.001
- 0.001 - 0.005
- 0.005 - 0.01
- 0.01 - 0.05
- 0.05 - 0.1
- 0.1 - 0.5
- 0.5 - 1
- 1 - 10

Notes:

This layer (4) underlies the Intermediate Aquifer (IA) in the regional model. Where the IA does not exist, (see Figure 4.32) the conductivities match those in layer 2 and 3.

Horizontal hydraulic conductivity was set to twice the vertical value (shown).

Conductivity values were interpolated to the grid from values assigned to a set of pilot points scattered across the model domain.

A combination of automated calibration (PEST) and manual calibration (trial and error) resulted in this conductivity field.

Regional Phase II ASR Vertical Hydraulic Conductivity
Intermediate Aquifer System Layer 4 (SEAWAT)
Final Groundwater Model Calibration Report

Figure 4.33

October 2010

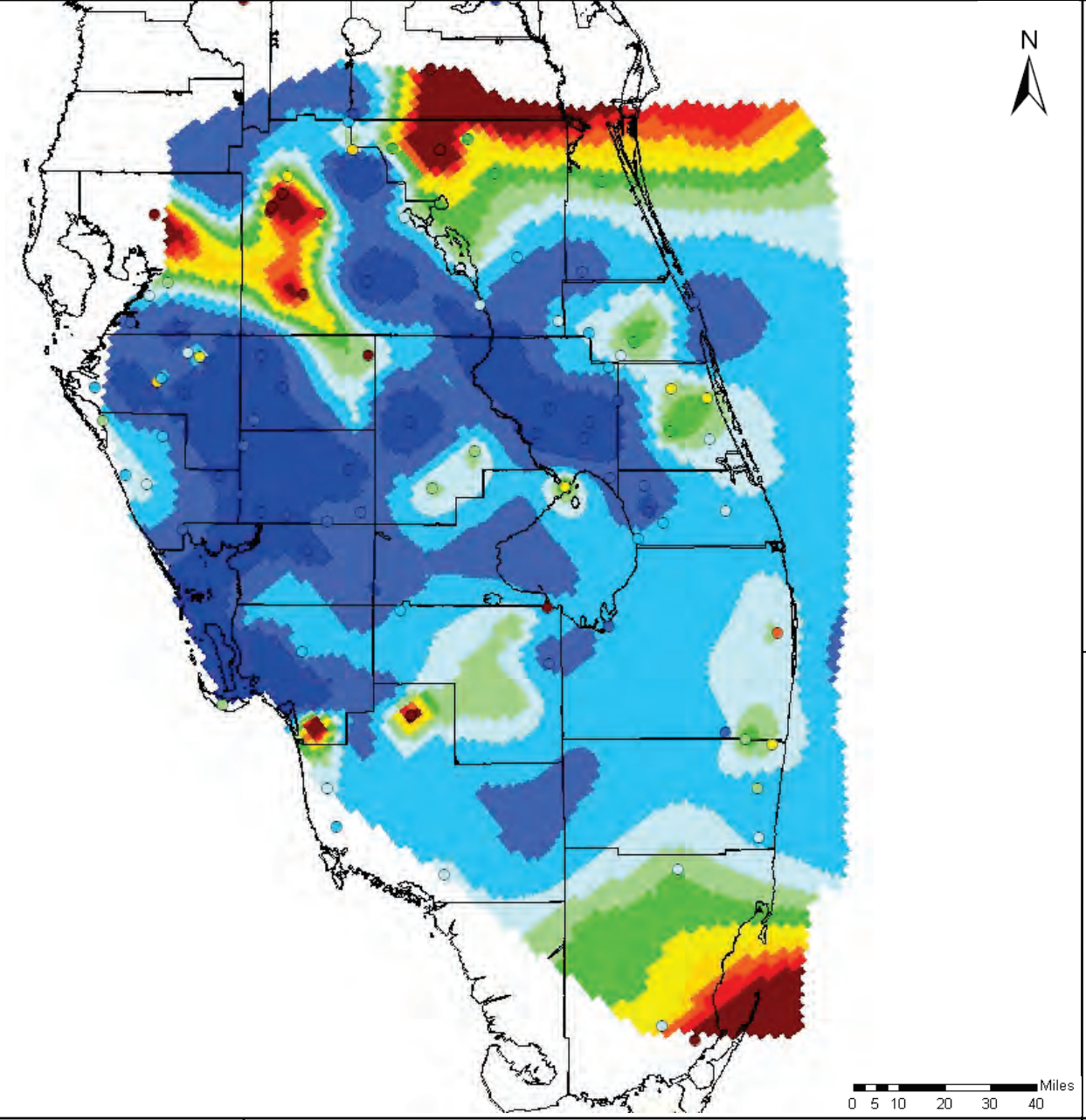

Horizontal Hydraulic Conductivity (ft/d)

- 1 - 20
- 20 - 40
- 40 - 60
- 60 - 80
- 80 - 100
- 100 - 120
- 120 - 140
- 140 - 160
- 160 - 180
- 180 - 200
- 200 - 500
- Locations of APT Data (see Figure 3.2)

Notes:

Vertical hydraulic conductivity was set to one tenth of the horizontal value (shown).

Conductivity values were interpolated to the grid from values assigned to a set of pilot points scattered across the model domain.

A combination of automated calibration (PEST) and manual calibration (trial and error) resulted in this conductivity field.

Colored circles represent field data and are colored on the same color scale for comparison with calibrated values.

Regional Phase II ASR Horizontal Hydraulic Conductivity
Upper Floridan Aquifer (SEAWAT)
Final Groundwater Model Calibration Report

Figure 4.34

October 2010

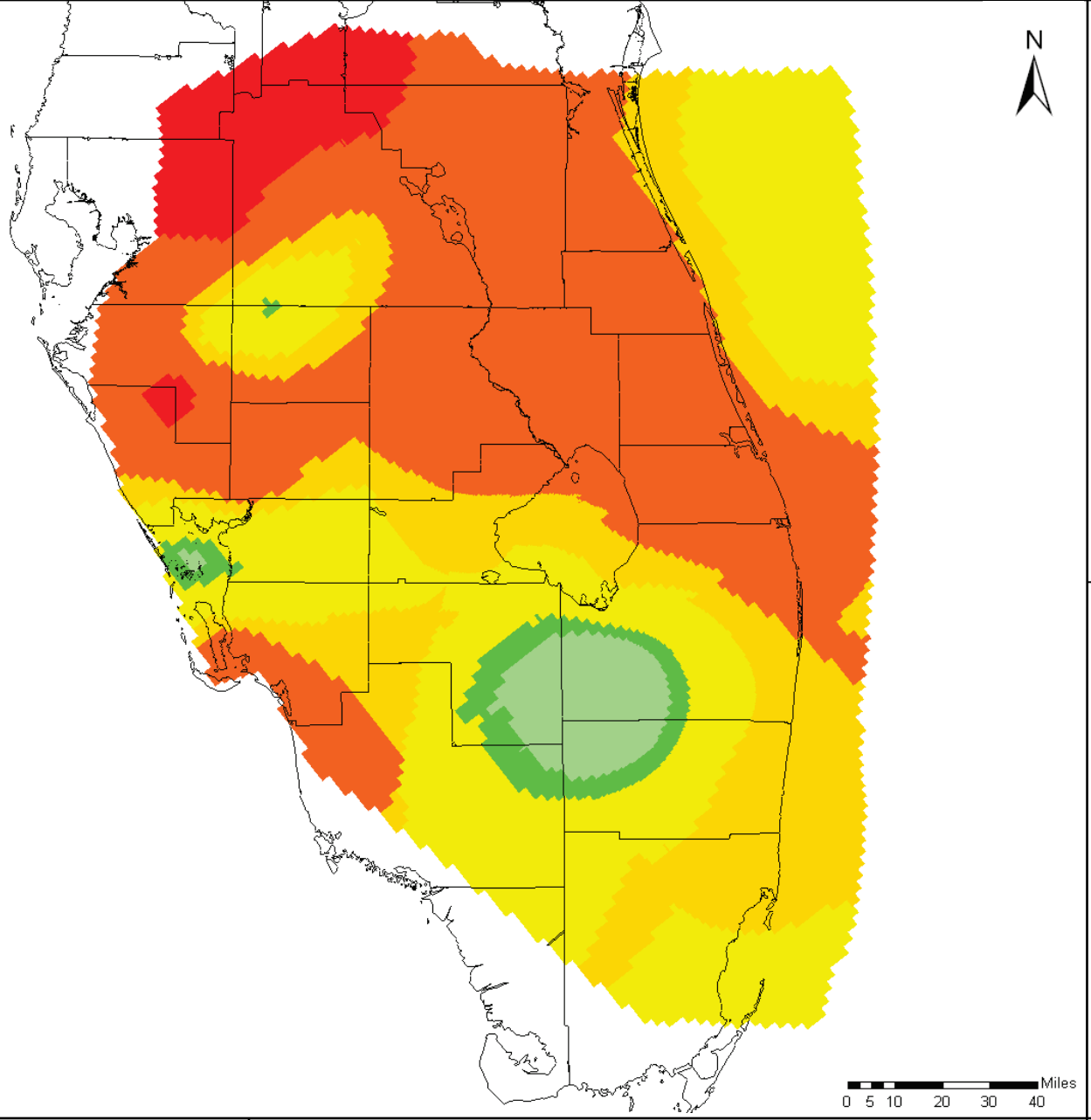

Vertical Hydraulic Conductivity (ft/d)

- $5x10^{-6}$ - $2.5x10^{-5}$
- $2.5x10^{-5}$ - $5x10^{-5}$
- $5x10^{-5}$ - $2.5x10^{-4}$
- $2.5x10^{-4}$ - $5x10^{-4}$
- $5x10^{-4}$ - 0.0025
- 0.0025 - 0.005
- 0.005 - 0.025
- 0.025 - 0.05
- 0.05 - 0.25
- 0.25 - 0.5
- 0.5 - 5

Notes:

Horizontal hydraulic conductivity was set to twice the vertical value (shown).

Conductivity values were interpolated to the grid from values assigned to a set of pilot points scattered across the model domain.

A combination of automated calibration (PEST) and manual calibration (trial and error) resulted in this conductivity field.

Regional Phase II ASR Vertical Hydraulic Conductivity Middle Confining Unit 1 (SEAWAT)

Final Groundwater Model Calibration Report

Figure 4.35

October 2010

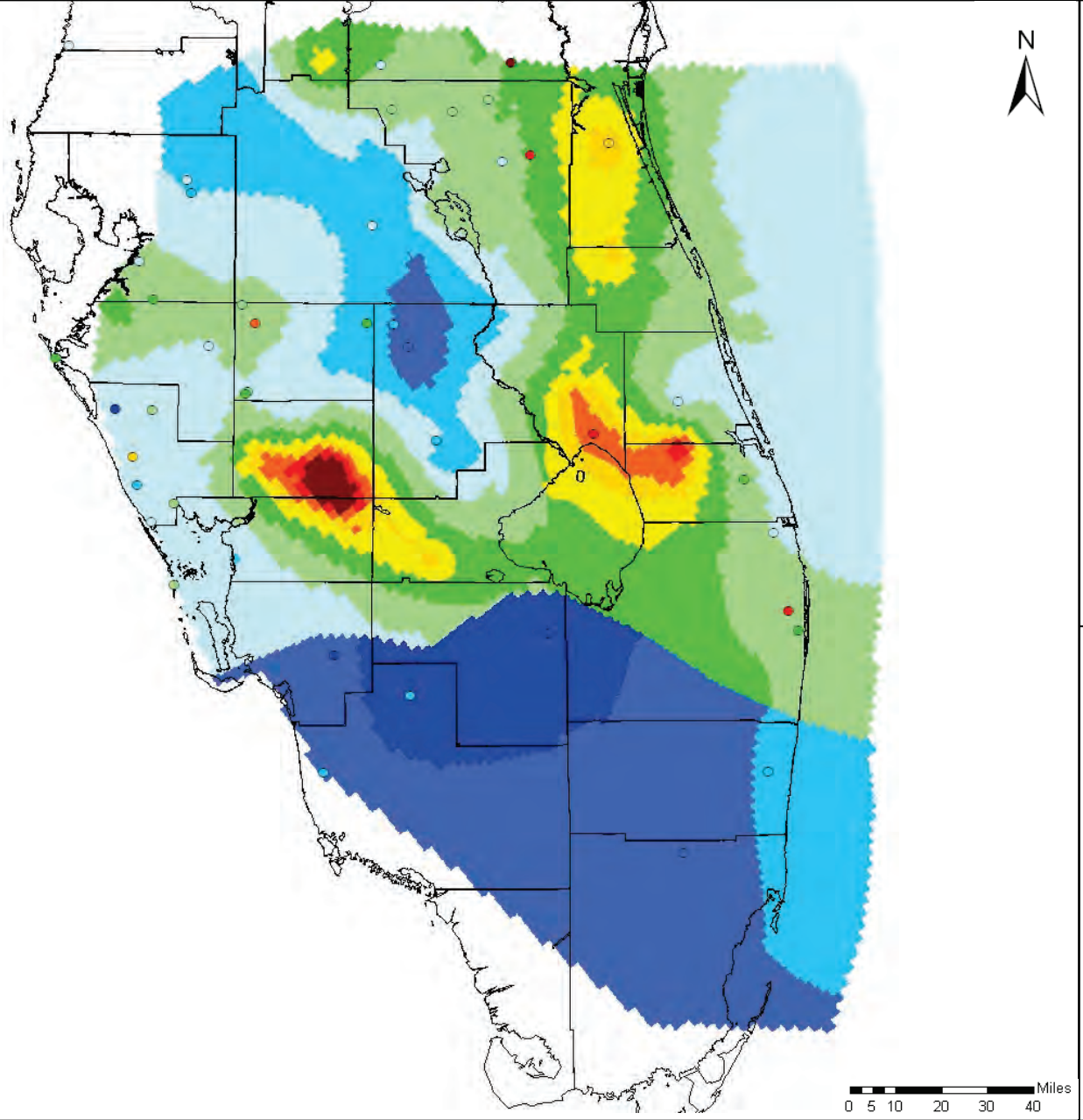

Notes:

Vertical hydraulic conductivity was set to one tenth of the horizontal value (shown).

Conductivity values were interpolated to the grid from values assigned to a set of pilot points scattered across the model domain.

A combination of automated calibration (PEST) and manual calibration (trial and error) resulted in this conductivity field.

Colored circles represent field data and are colored on the same color scale for comparison with calibrated values.

Regional Phase II ASR Horizontal Hydraulic Conductivity
APPZ Aquifer (SEAWAT)
Final Groundwater Model Calibration Report

Figure 4.36

October 2010

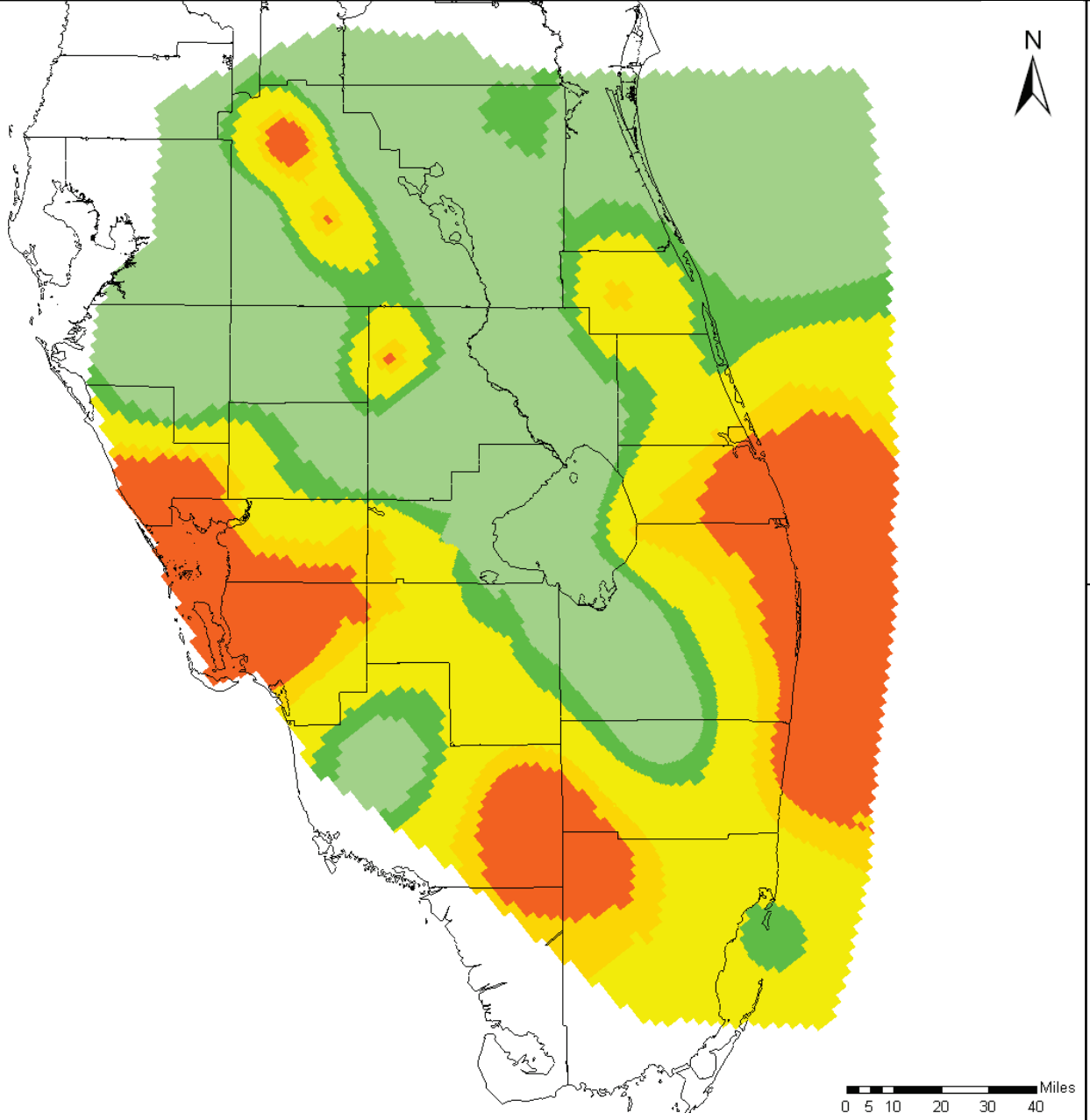

Vertical Hydraulic Conductivity (ft/d)

- $5x10^{-6}$ - $2.5x10^{-5}$
- $2.5x10^{-5}$ - $5x10^{-5}$
- $5x10^{-5}$ - $2.5x10^{-4}$
- $2.5x10^{-4}$ - $5x10^{-4}$
- $5x10^{-4}$ - 0.0025
- 0.0025 - 0.005
- 0.005 - 0.025
- 0.025 - 0.05
- 0.05 - 0.25
- 0.25 - 0.5
- 0.5 - 5

Notes:

Horizontal hydraulic conductivity was set to twice the vertical value (shown).

Conductivity values were interpolated to the grid from values assigned to a set of pilot points scattered across the model domain.

A combination of automated calibration (PEST) and manual calibration (trial and error) resulted in this conductivity field.

Regional Phase II ASR Vertical Hydraulic Conductivity
Middle Confining Unit 2 (SEAWAT)
Final Groundwater Model Calibration Report

Figure 4.37

October 2010

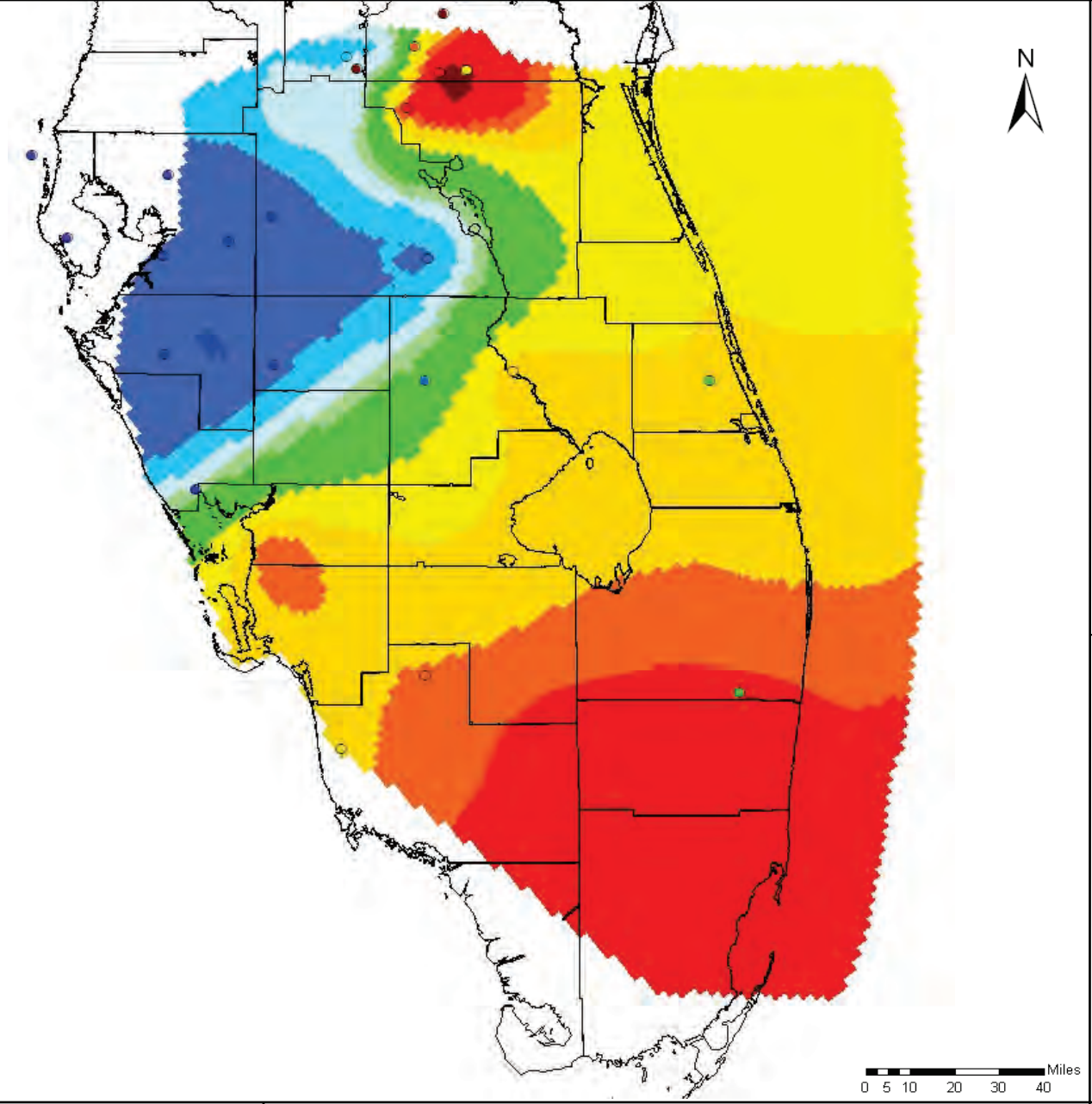

Horizontal Hydraulic Conductivity (ft/d)

- 1 - 20
- 20 - 40
- 40 - 60
- 60 - 80
- 80 - 100
- 100 - 200
- 200 - 300
- 300 - 400
- 400 - 500
- 500 - 1000
- 1000 - 1600
- Locations of APT Data (see Figure 3.3)

Notes:

Vertical hydraulic conductivity was set to one tenth of the horizontal value (shown).

Conductivity values were interpolated to the grid from values assigned to a set of pilot points scattered across the model domain.

A combination of automated calibration (PEST) and manual calibration (trial and error) resulted in this conductivity field.

Colored circles represent field data and are colored on the same color scale for comparison with calibrated values.

Regional Phase II ASR Horizontal Hydraulic Conductivity
Lower Floridan (LF1) Aquifer (SEAWAT)
Final Groundwater Model Calibration Report

Figure 4.38

October 2010

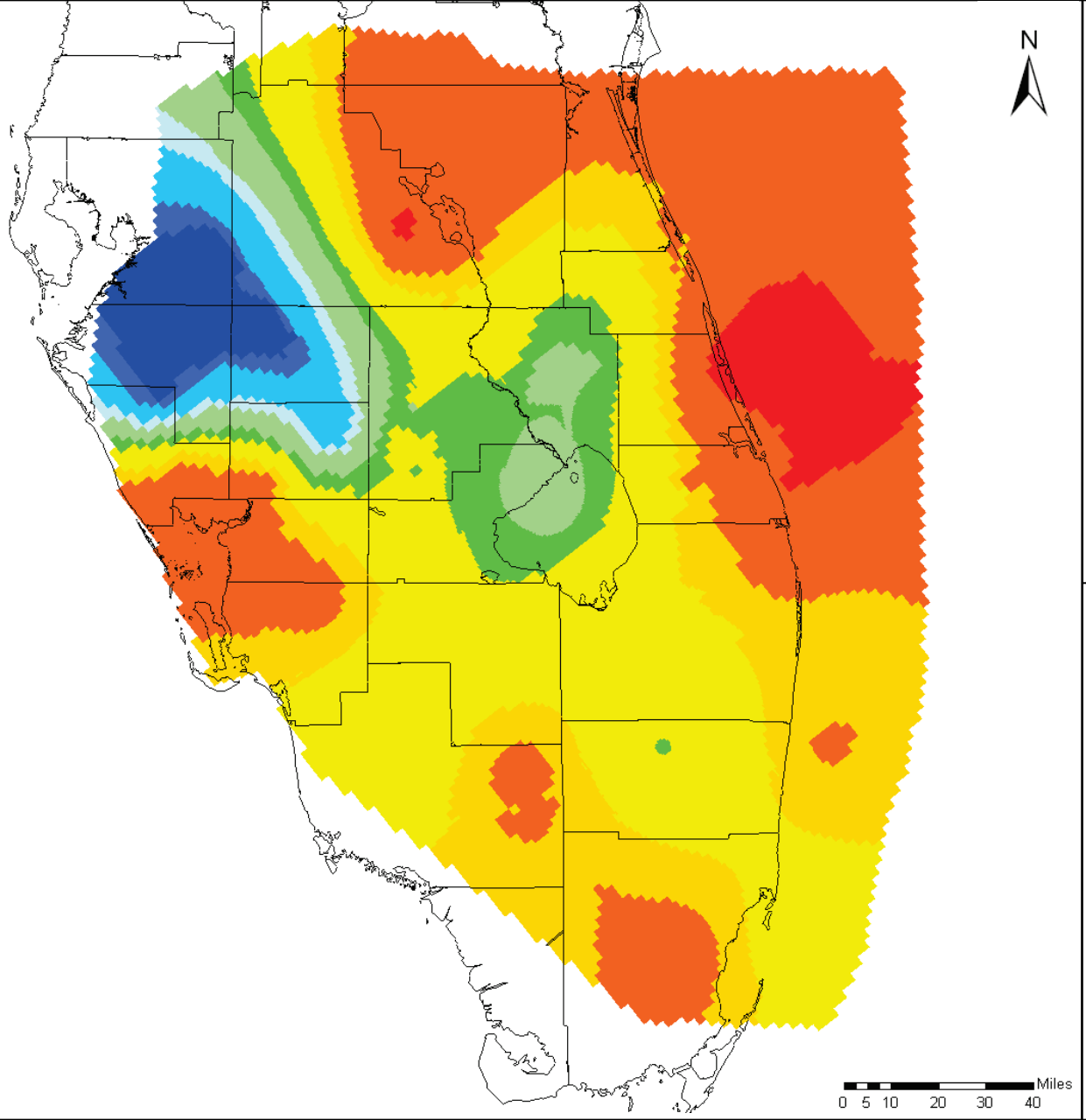

Vertical Hydraulic Conductivity (ft/d)

- $5x10^{-6}$ - $2.5x10^{-5}$
- $2.5x10^{-5}$ - $5x10^{-5}$
- $5x10^{-5}$ - $2.5x10^{-4}$
- $2.5x10^{-4}$ - $5x10^{-4}$
- $5x10^{-4}$ - 0.0025
- 0.0025 - 0.005
- 0.005 - 0.025
- 0.025 - 0.05
- 0.05 - 0.25
- 0.25 - 0.5
- 0.5 - 5

Notes:

Horizontal hydraulic conductivity was set to twice the vertical value (shown).

Conductivity values were interpolated to the grid from values assigned to a set of pilot points scattered across the model domain.

A combination of automated calibration (PEST) and manual calibration (trial and error) resulted in this conductivity field.

Regional Phase II ASR Vertical Hydraulic Conductivity Lower Confining Unit (SEAWAT)

Final Groundwater Model Calibration Report

Figure 4.39

October 2010

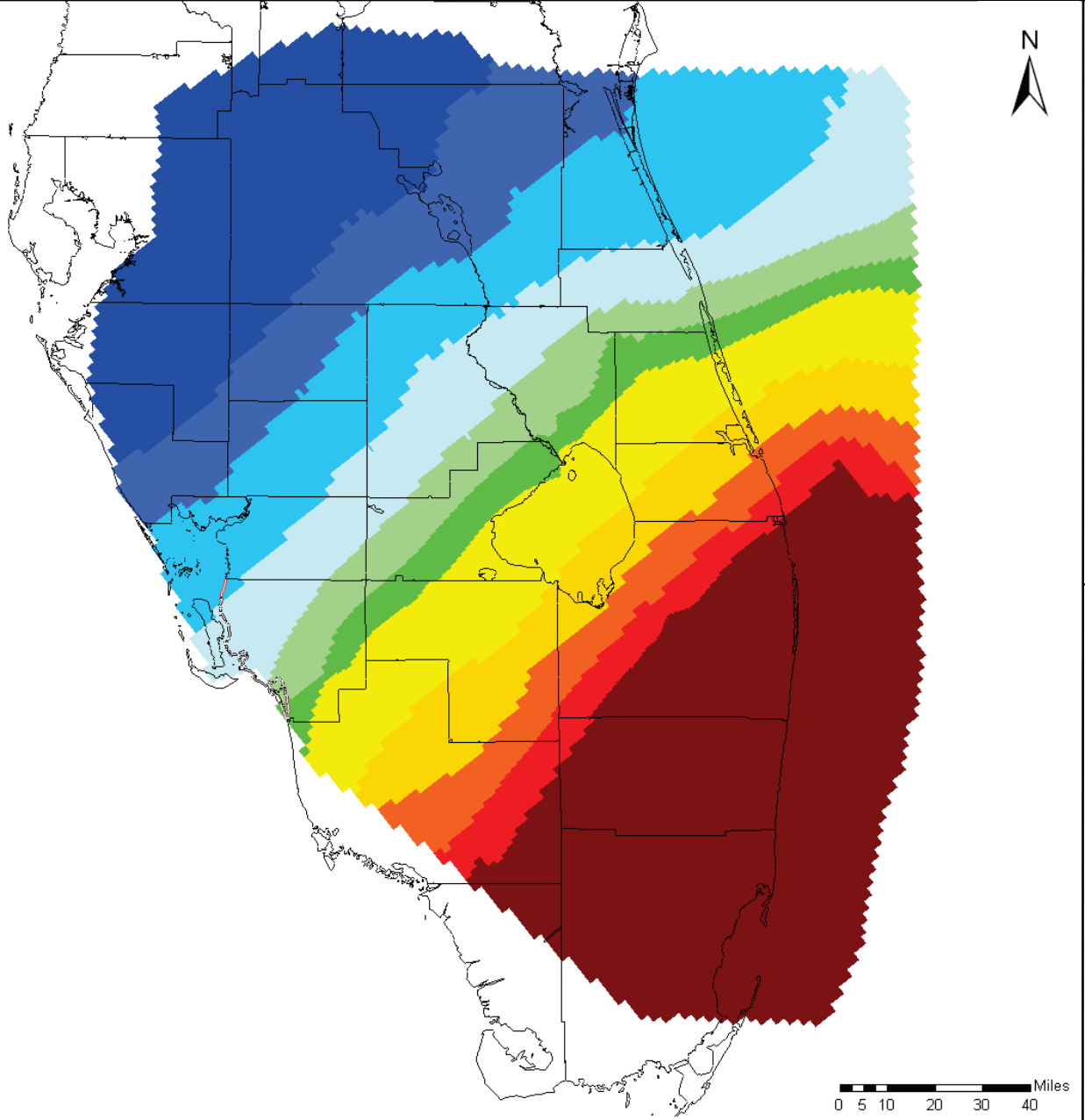

Horizontal Hydraulic Conductivity (ft/d)

- 1 - 50
- 50 - 100
- 100 - 250
- 250 - 500
- 500 - 750
- 750 - 1000
- 1000 - 2000
- 2000 - 3000
- 3000 - 4000
- 4000 - 5000
- 5000 - 10100

Notes:

Vertical hydraulic conductivity was set to one tenth of the horizontal value (shown).

Conductivity values were interpolated to the grid from values assigned to a set of pilot points scattered across the model domain.

A combination of automated calibration (PEST) and manual calibration (trial and error) resulted in this conductivity field.

Regional Phase II ASR Horizontal Hydraulic Conductivity Boulder Zone (SEAWAT)

Final Groundwater Model Calibration Report

Figure 4.40

October 2010

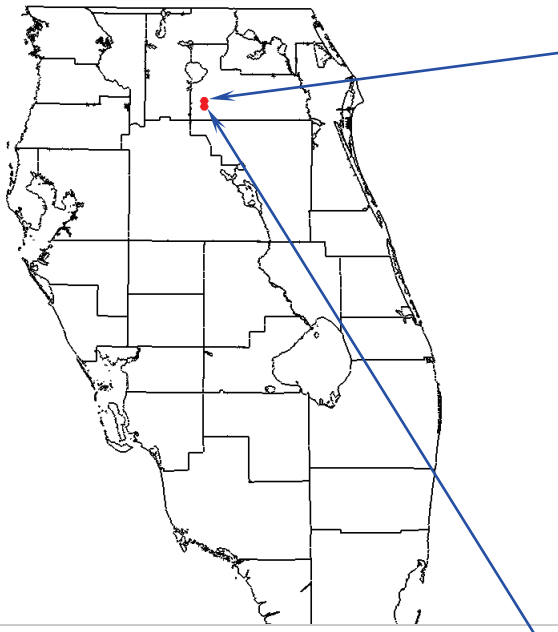

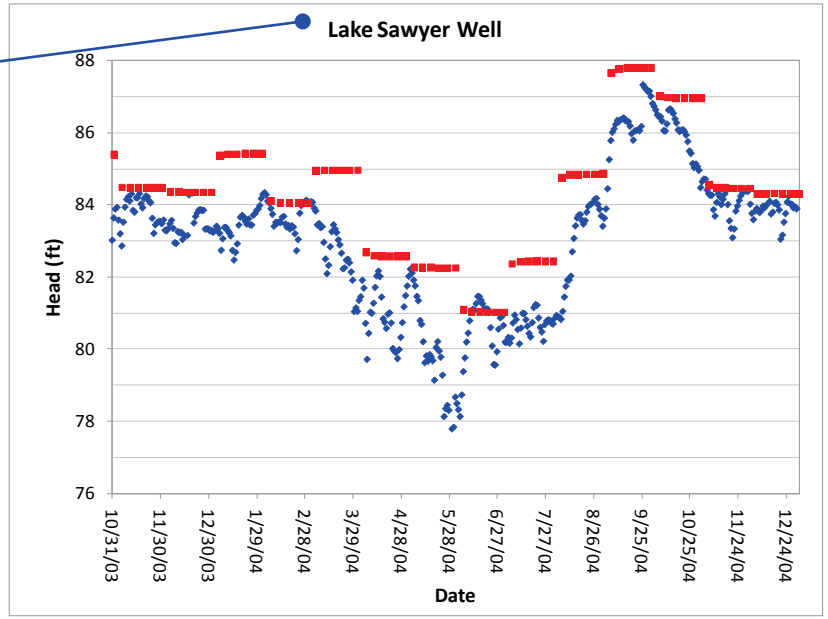

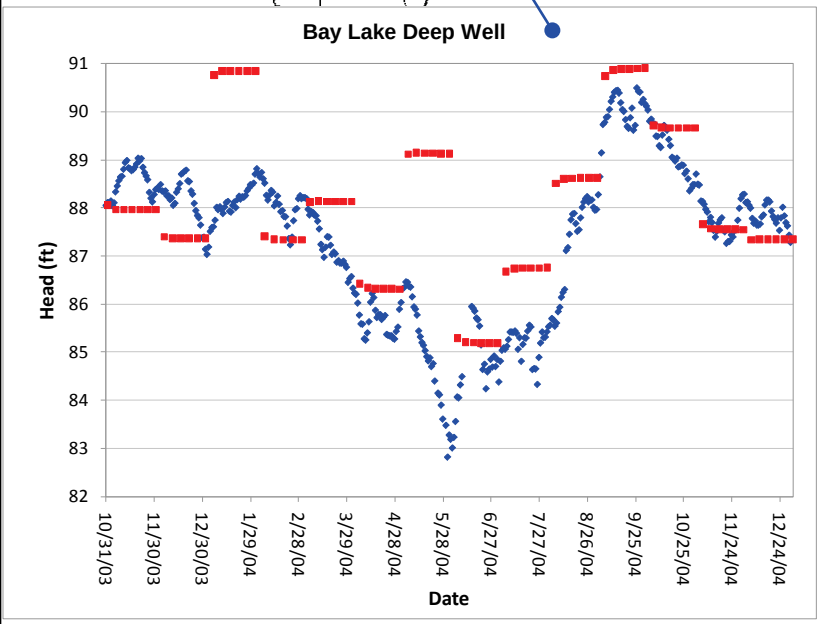

	Bay Lake Well	Lake Sawyer Well
Mean Error	0.760	1.283
Mean Absolute Error	1.036	1.283
Root Mean Square (RMS)	1.350	1.399
Observed Range	7.67	9.56
RMS as Percentage of Range	18%	15%
Coefficient of Determination (r^2)	0.504	0.913
Nash-Sutcliffe Model Efficiency Coefficient	0.244	0.426

Legend

- Measured Head
- Model Calculated Head

Notes:

Figures 4.41 through 4.94 show the comparison between measured head values and model-calculated head values at a number of observation wells for the calibration period. Although the scales vary on each plot, all plots have a horizontal grid line at each foot. This is to make it easy to determine the range of heads at a glance.

The model used month-long stress periods, so pumping and boundary conditions were input as step functions with constant values throughout each month and sudden changes at the end of each month. For this reason, the model cannot be expected to accurately predict day-to-day head variations in any of these wells. Calibration efforts were aimed at matching general trends and monthly averages.

Starting head conditions for this model were based on the October 2003 steady state calibrated model. Transient calibration efforts were focused on matching the head changes, not the actual heads, so it is not uncommon for residuals in the starting condition to be carried through the entire calibration period. This indicates that the model is correctly predicting responses to hydrogeologic forces even if the calculated head values vary somewhat from the measured values.

Transient SEAWAT Calibration Comparison
Upper Floridan Aquifer (2003-2004)
Final Groundwater Model Calibration Report

Figure 4.41

October 2010

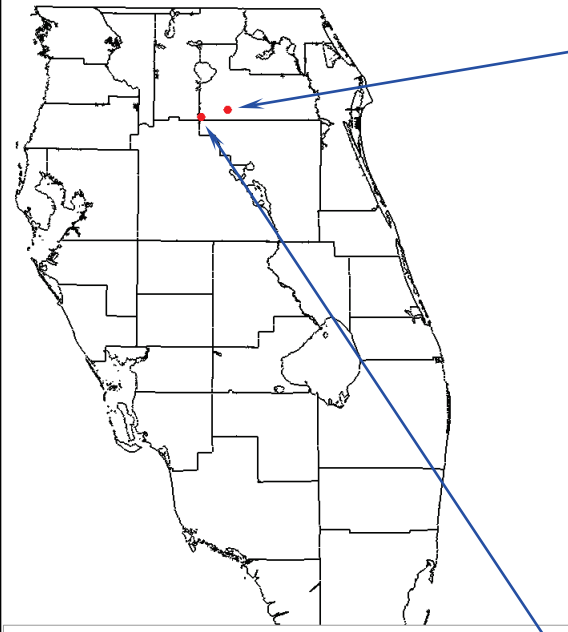

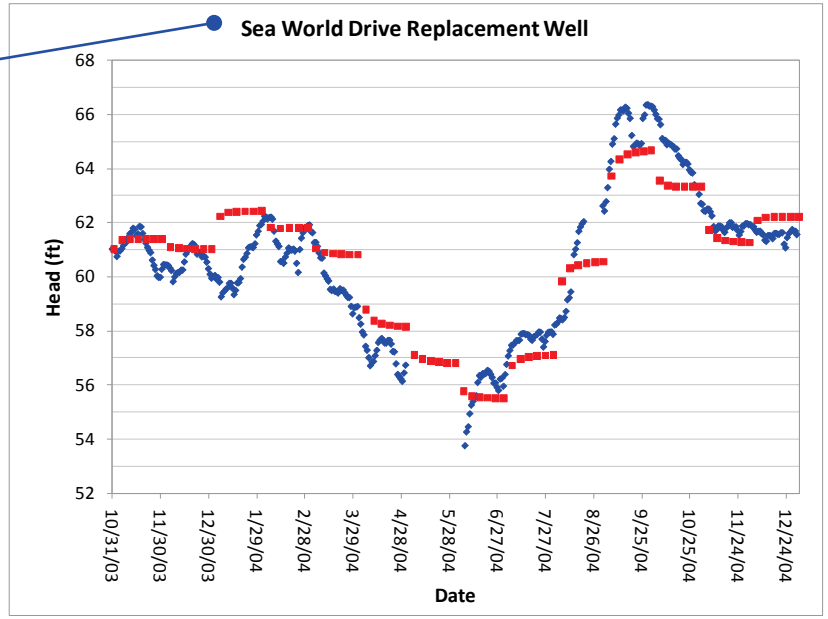

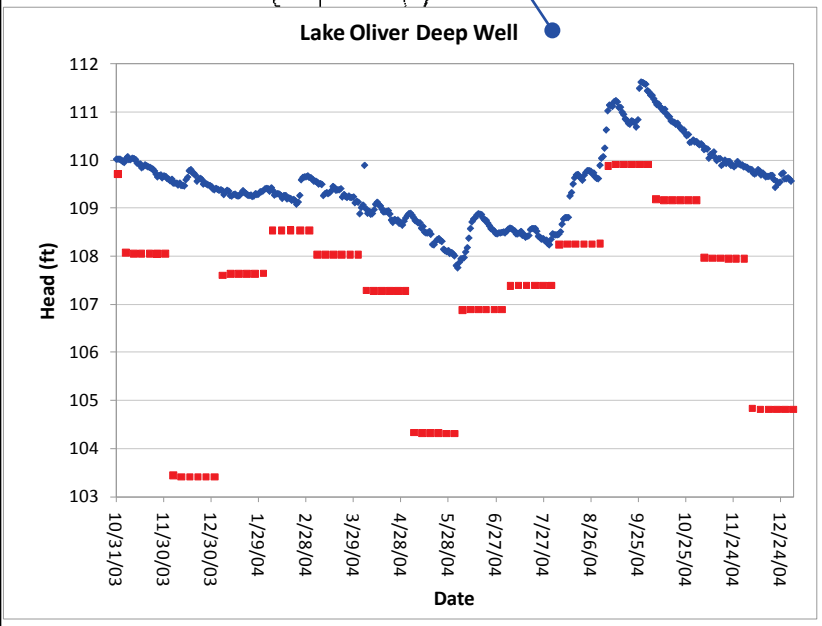

	Lake Oliver Deep Well	Sea World Drive Repl. Well
Mean Error	-2.155	0.222
Mean Absolute Error	2.155	0.743
Root Mean Square (RMS)	2.522	0.927
Observed Range	3.88	12.62
RMS as Percentage of Range	65%	7%
Coefficient of Determination (r^2)	0.309	0.887
Nash-Sutcliffe Model Efficiency Coefficient	-9.806	0.879

Legend

- Measured Head
- Model Calculated Head

Notes:

Figures 4.41 through 4.94 show the comparison between measured head values and model-calculated head values at a number of observation wells for the calibration period. Although the scales vary on each plot, all plots have a horizontal grid line at each foot. This is to make it easy to determine the range of heads at a glance.

The model used month-long stress periods, so pumping and boundary conditions were input as step functions with constant values throughout each month and sudden changes at the end of each month. For this reason, the model cannot be expected to accurately predict day-to-day head variations in any of these wells. Calibration efforts were aimed at matching general trends and monthly averages.

Starting head conditions for this model were based on the October 2003 steady state calibrated model. Transient calibration efforts were focused on matching the head changes, not the actual heads, so it is not uncommon for residuals in the starting condition to be carried through the entire calibration period. This indicates that the model is correctly predicting responses to hydrogeologic forces even if the calculated head values vary somewhat from the measured values.

Transient SEAWAT Calibration Comparison
Upper Floridan Aquifer (2003-2004)
Final Groundwater Model Calibration Report

Figure 4.42

October 2010

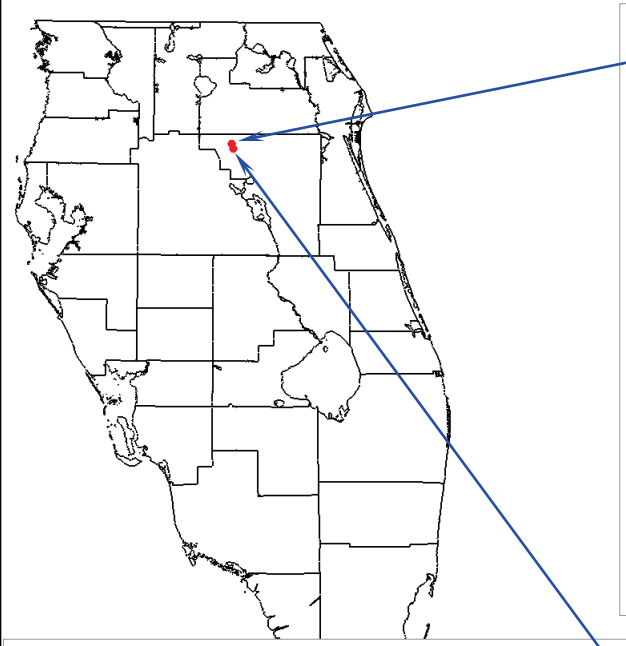

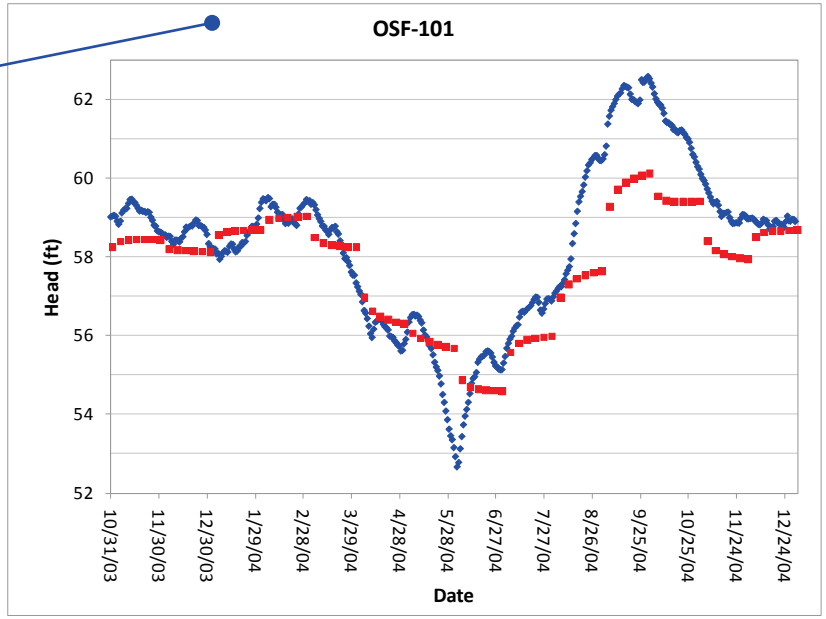

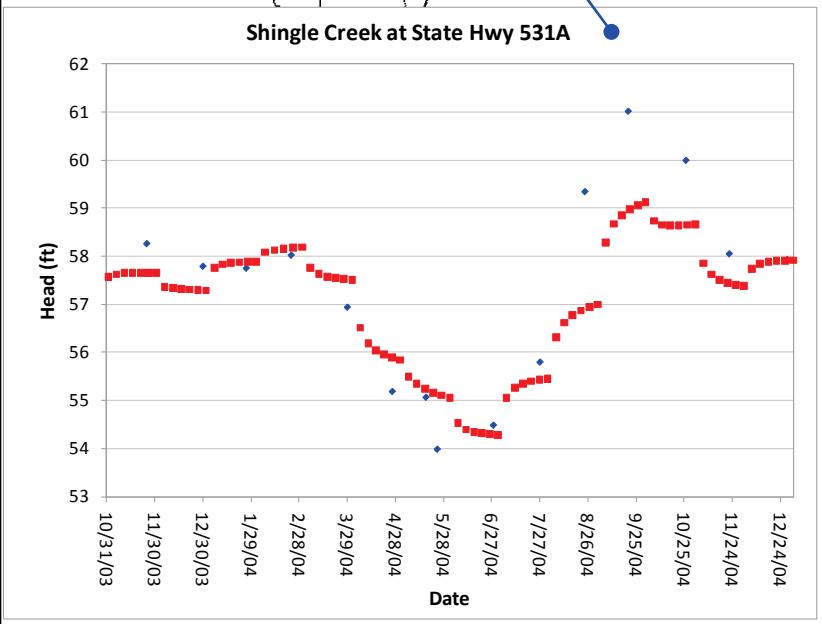

	Shingle Creek	OSF-101
Mean Error	-0.425	-0.591
Mean Absolute Error	0.828	0.793
Root Mean Square (RMS)	1.191	1.050
Observed Range	7.02	9.93
RMS as Percentage of Range	17%	11%
Coefficient of Determination (r^2)	0.676	0.851
Nash-Sutcliffe Model Efficiency Coefficient	0.601	0.717

Legend

- Measured Head
- Model Calculated Head

Notes:

Figures 4.41 through 4.94 show the comparison between measured head values and model-calculated head values at a number of observation wells for the calibration period. Although the scales vary on each plot, all plots have a horizontal grid line at each foot. This is to make it easy to determine the range of heads at a glance.

The model used month-long stress periods, so pumping and boundary conditions were input as step functions with constant values throughout each month and sudden changes at the end of each month. For this reason, the model cannot be expected to accurately predict day-to-day head variations in any of these wells. Calibration efforts were aimed at matching general trends and monthly averages.

Starting head conditions for this model were based on the October 2003 steady state calibrated model. Transient calibration efforts were focused on matching the head changes, not the actual heads, so it is not uncommon for residuals in the starting condition to be carried through the entire calibration period. This indicates that the model is correctly predicting responses to hydrogeologic forces even if the calculated head values vary somewhat from the measured values.

Transient SEAWAT Calibration Comparison
Upper Floridan Aquifer (2003-2004)
Final Groundwater Model Calibration Report

Figure 4.43

October 2010

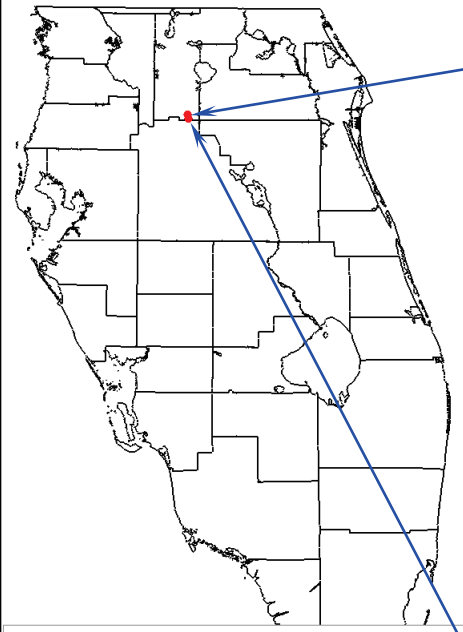

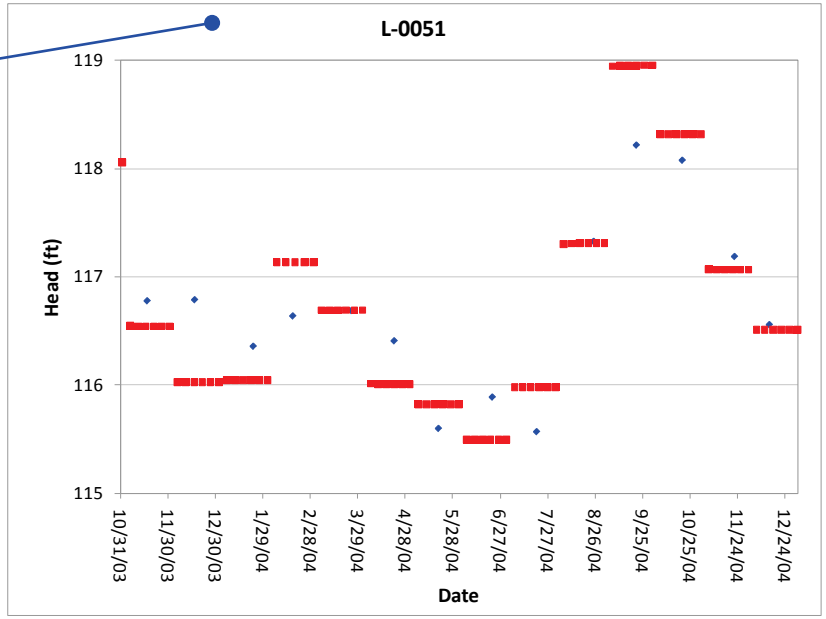

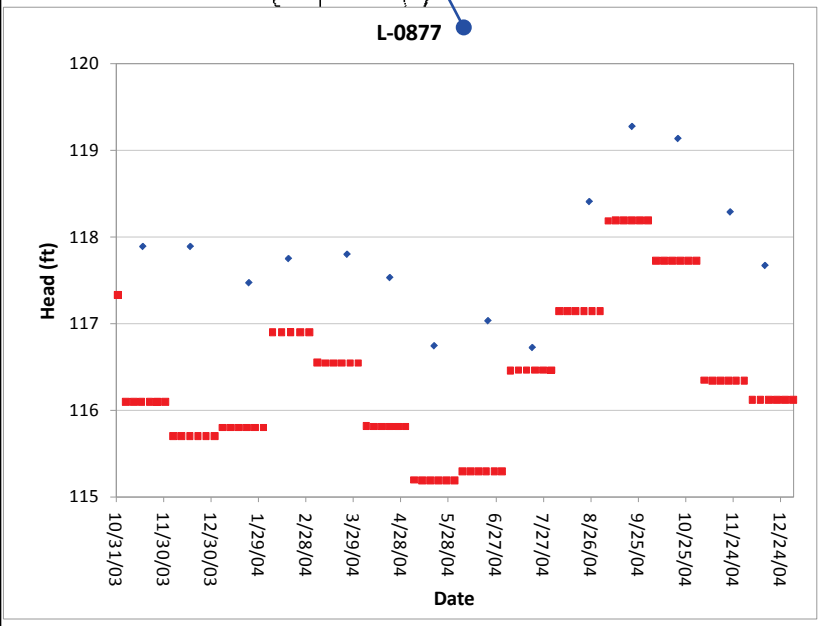

	L-0877	L-0051
Mean Error	-1.439	-0.001
Mean Absolute Error	1.439	0.267
Root Mean Square (RMS)	1.488	0.317
Observed Range	2.56	2.65
RMS as Percentage of Range	58%	12%
Coefficient of Determination (r^2)	0.776	0.881
Nash-Sutcliffe Model Efficiency Coefficient	-3.031	0.828

Legend

- Measured Head
- Model Calculated Head

Notes:

Figures 4.41 through 4.94 show the comparison between measured head values and model-calculated head values at a number of observation wells for the calibration period. Although the scales vary on each plot, all plots have a horizontal grid line at each foot. This is to make it easy to determine the range of heads at a glance.

The model used month-long stress periods, so pumping and boundary conditions were input as step functions with constant values throughout each month and sudden changes at the end of each month. For this reason, the model cannot be expected to accurately predict day-to-day head variations in any of these wells. Calibration efforts were aimed at matching general trends and monthly averages.

Starting head conditions for this model were based on the October 2003 steady state calibrated model. Transient calibration efforts were focused on matching the head changes, not the actual heads, so it is not uncommon for residuals in the starting condition to be carried through the entire calibration period. This indicates that the model is correctly predicting responses to hydrogeologic forces even if the calculated head values vary somewhat from the measured values.

Transient SEAWAT Calibration Comparison
Upper Floridan Aquifer (2003-2004)
Final Groundwater Model Calibration Report

Figure 4.44

October 2010

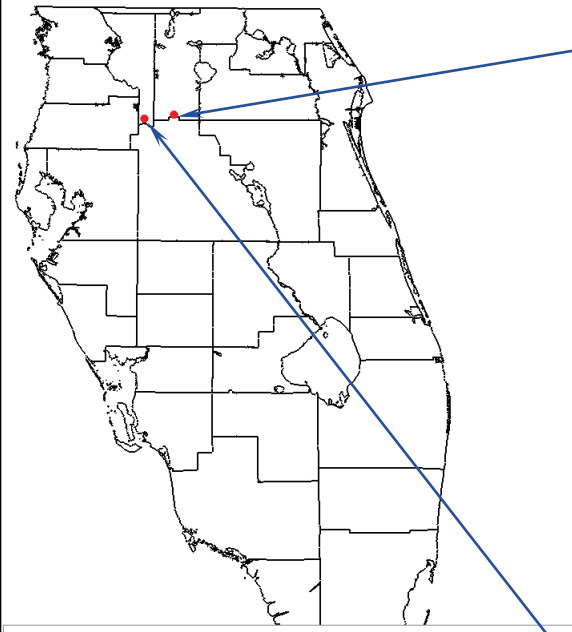

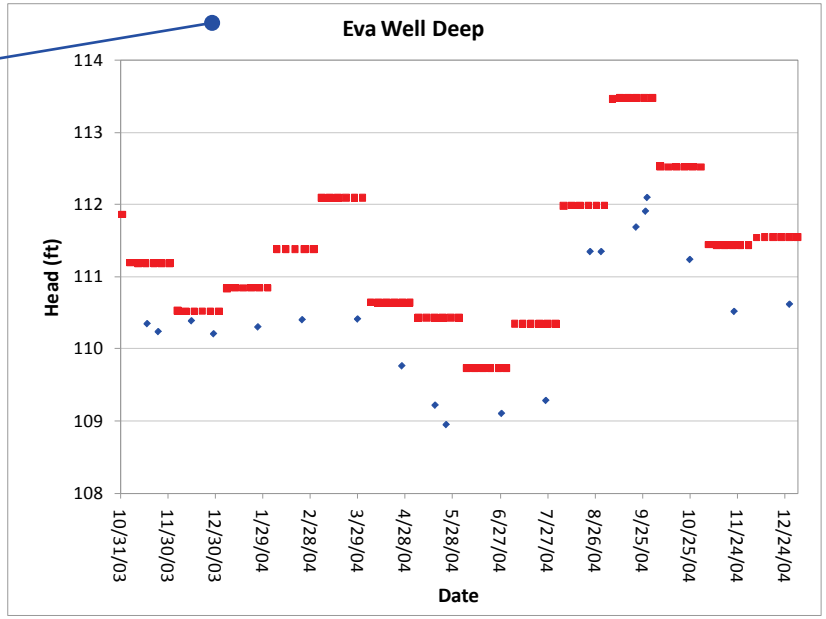

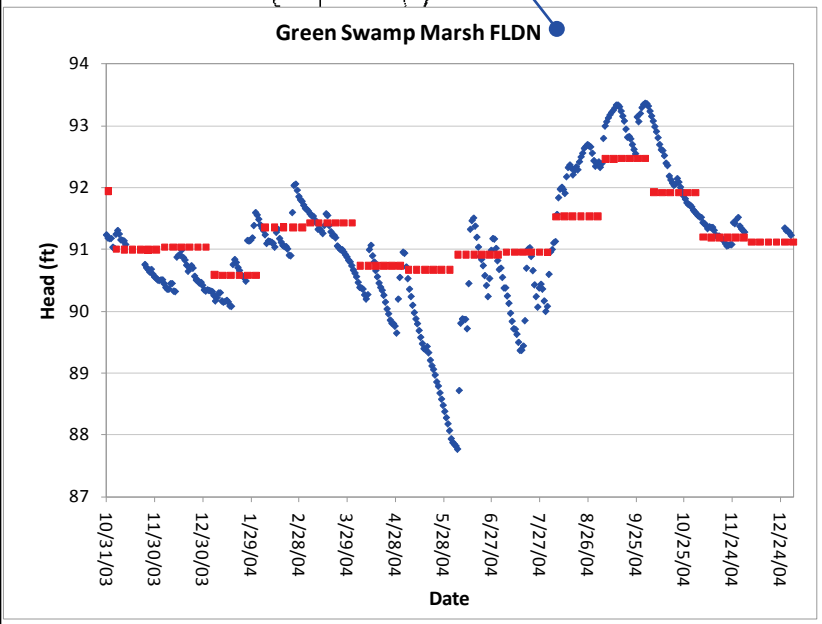

	Green Swamp Marsh	Eva Well Deep
Mean Error	0.159	0.972
Mean Absolute Error	0.430	0.972
Root Mean Square (RMS)	0.536	1.042
Observed Range	5.60	3.15
RMS as Percentage of Range	10%	33%
Coefficient of Determination (r^2)	0.881	0.824
Nash-Sutcliffe Model Efficiency Coefficient	0.656	-0.703

Legend

- Measured Head
- Model Calculated Head

Notes:

Figures 4.41 through 4.94 show the comparison between measured head values and model-calculated head values at a number of observation wells for the calibration period. Although the scales vary on each plot, all plots have a horizontal grid line at each foot. This is to make it easy to determine the range of heads at a glance.

The model used month-long stress periods, so pumping and boundary conditions were input as step functions with constant values throughout each month and sudden changes at the end of each month. For this reason, the model cannot be expected to accurately predict day-to-day head variations in any of these wells. Calibration efforts were aimed at matching general trends and monthly averages.

Starting head conditions for this model were based on the October 2003 steady state calibrated model. Transient calibration efforts were focused on matching the head changes, not the actual heads, so it is not uncommon for residuals in the starting condition to be carried through the entire calibration period. This indicates that the model is correctly predicting responses to hydrogeologic forces even if the calculated head values vary somewhat from the measured values.

Transient SEAWAT Calibration Comparison
Upper Floridan Aquifer (2003-2004)
Final Groundwater Model Calibration Report

Figure 4.45

October 2010

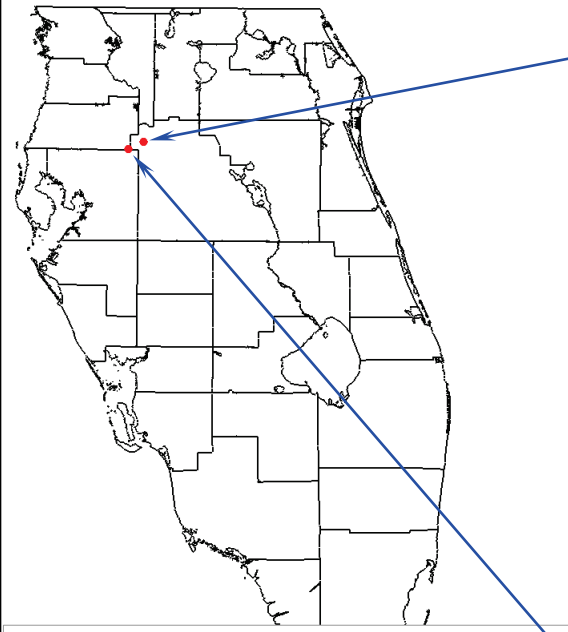

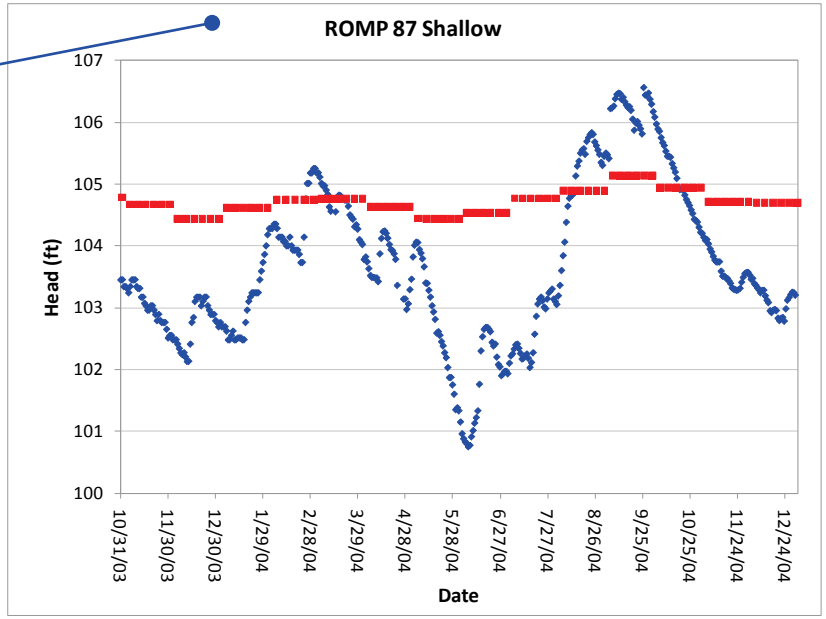

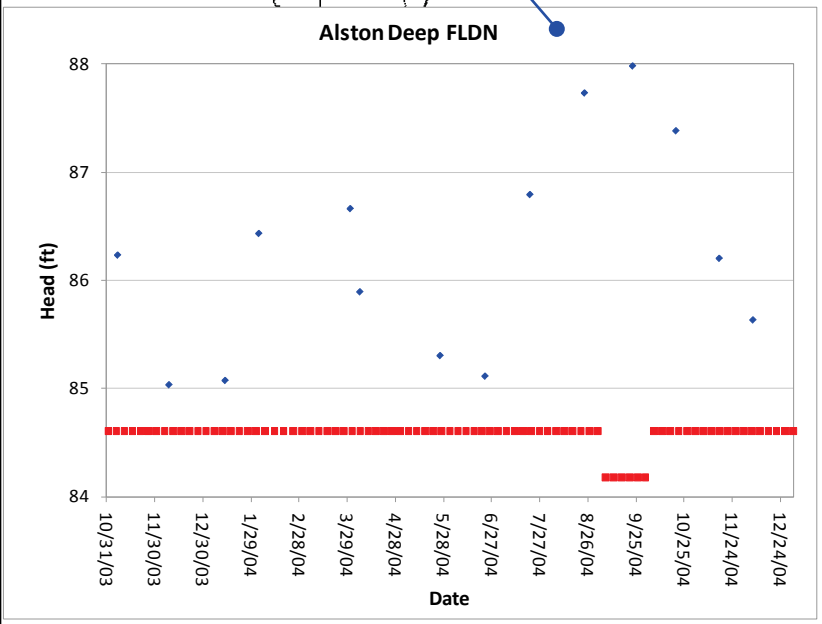

	Alston Deep FLDN	ROMP 87 Shallow
Mean Error	-1.670	1.027
Mean Absolute Error	1.670	1.216
Root Mean Square (RMS)	1.948	1.447
Observed Range	2.95	5.81
RMS as Percentage of Range	66%	25%
Coefficient of Determination (r^2)	0.326	0.779
Nash-Sutcliffe Model Efficiency Coefficient	-3.231	-0.536

Legend

- Measured Head
- Model Calculated Head

Notes:

Figures 4.41 through 4.94 show the comparison between measured head values and model-calculated head values at a number of observation wells for the calibration period. Although the scales vary on each plot, all plots have a horizontal grid line at each foot. This is to make it easy to determine the range of heads at a glance.

The model used month-long stress periods, so pumping and boundary conditions were input as step functions with constant values throughout each month and sudden changes at the end of each month. For this reason, the model cannot be expected to accurately predict day-to-day head variations in any of these wells. Calibration efforts were aimed at matching general trends and monthly averages.

Starting head conditions for this model were based on the October 2003 steady state calibrated model. Transient calibration efforts were focused on matching the head changes, not the actual heads, so it is not uncommon for residuals in the starting condition to be carried through the entire calibration period. This indicates that the model is correctly predicting responses to hydrogeologic forces even if the calculated head values vary somewhat from the measured values.

Transient SEAWAT Calibration Comparison
Upper Floridan Aquifer (2003-2004)
Final Groundwater Model Calibration Report

Figure 4.46

October 2010

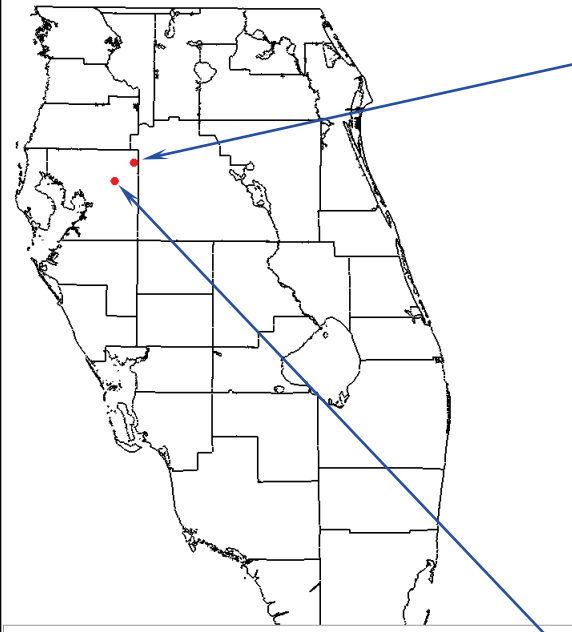

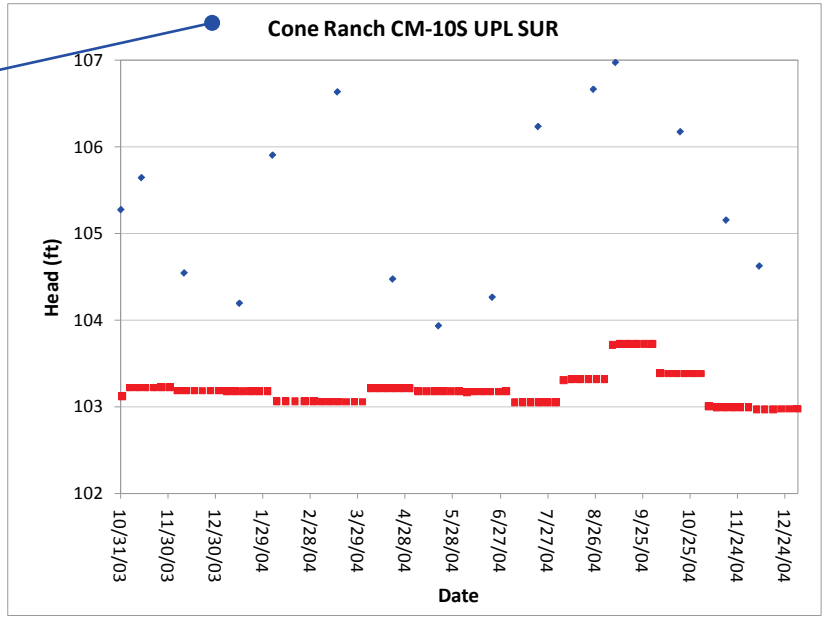

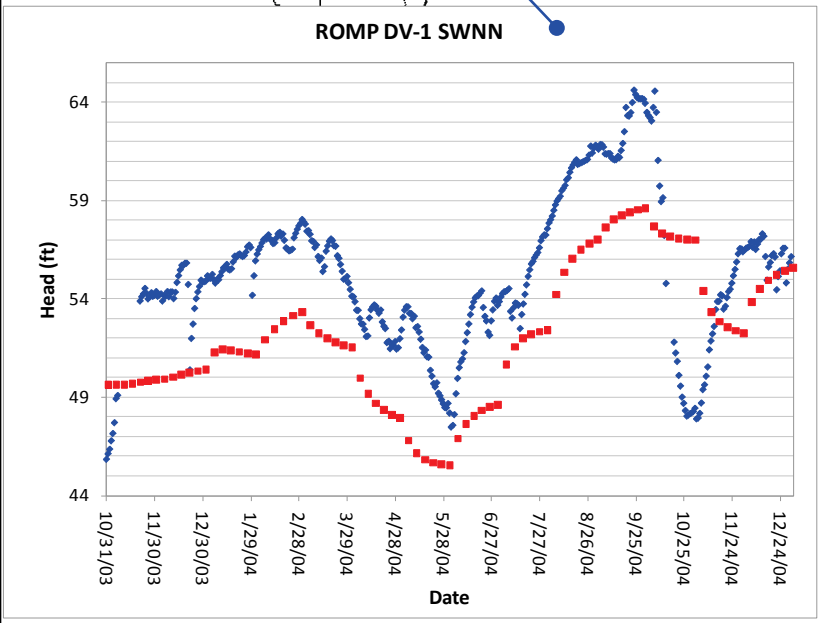

	ROMP DV-1 SWNN	Cone Ranch CM-10S
Mean Error	-3.103	-2.190
Mean Absolute Error	3.541	2.190
Root Mean Square (RMS)	3.770	2.390
Observed Range	18.75	3.04
RMS as Percentage of Range	20%	79%
Coefficient of Determination (r^2)	0.612	0.165
Nash-Sutcliffe Model Efficiency Coefficient	-0.454	-4.572

Legend

- Measured Head
- Model Calculated Head

Notes:

Figures 4.41 through 4.94 show the comparison between measured head values and model-calculated head values at a number of observation wells for the calibration period. Although the scales vary on each plot, all plots have a horizontal grid line at each foot. This is to make it easy to determine the range of heads at a glance.

The model used month-long stress periods, so pumping and boundary conditions were input as step functions with constant values throughout each month and sudden changes at the end of each month. For this reason, the model cannot be expected to accurately predict day-to-day head variations in any of these wells. Calibration efforts were aimed at matching general trends and monthly averages.

Starting head conditions for this model were based on the October 2003 steady state calibrated model. Transient calibration efforts were focused on matching the head changes, not the actual heads, so it is not uncommon for residuals in the starting condition to be carried through the entire calibration period. This indicates that the model is correctly predicting responses to hydrogeologic forces even if the calculated head values vary somewhat from the measured values.

Transient SEAWAT Calibration Comparison
Upper Floridan Aquifer (2003-2004)
Final Groundwater Model Calibration Report

Figure 4.47

October 2010

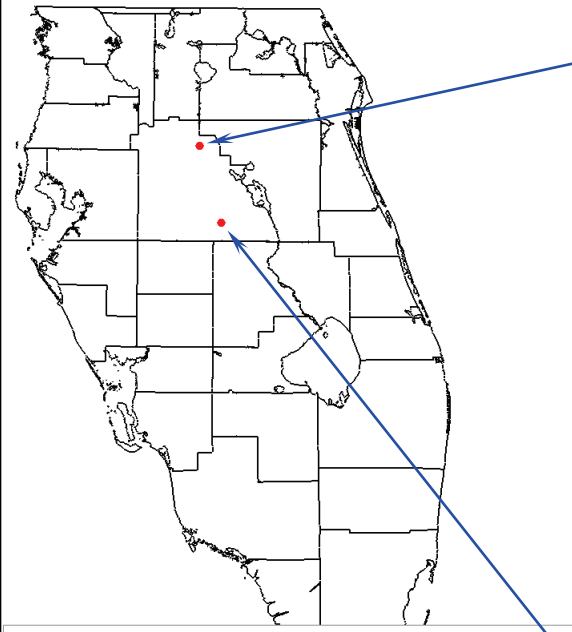

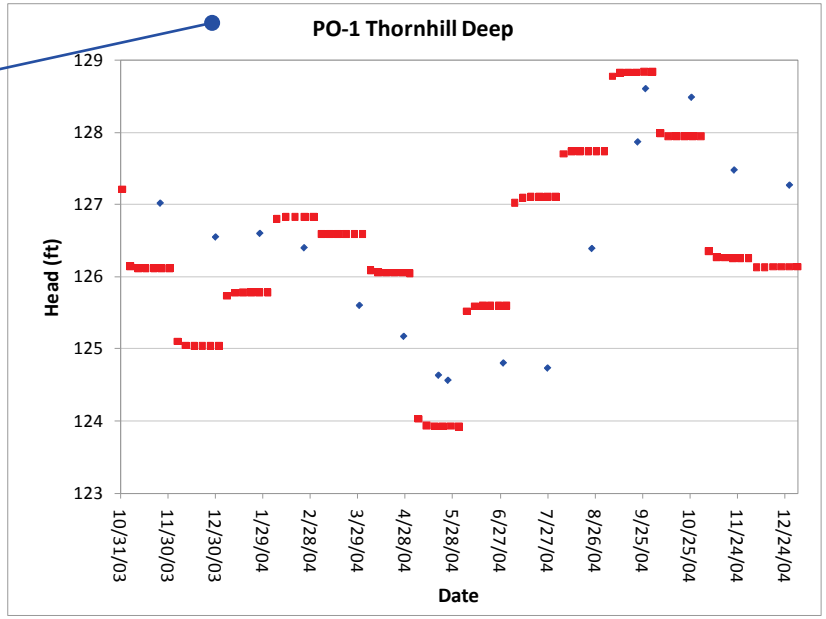

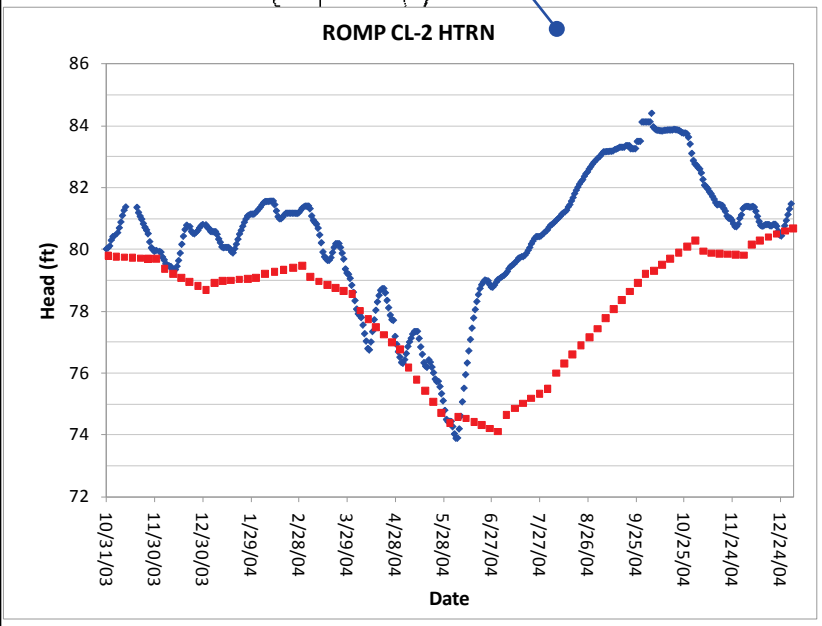

	ROMP CL-2 HTRN	PO-1 Thornhill Deep
Mean Error	-2.265	0.056
Mean Absolute Error	2.265	0.871
Root Mean Square (RMS)	2.872	0.999
Observed Range	10.54	4.05
RMS as Percentage of Range	27%	25%
Coefficient of Determination (r^2)	0.373	0.408
Nash-Sutcliffe Model Efficiency Coefficient	-0.897	0.331

Legend

- Measured Head
- Model Calculated Head

Notes:

Figures 4.41 through 4.94 show the comparison between measured head values and model-calculated head values at a number of observation wells for the calibration period. Although the scales vary on each plot, all plots have a horizontal grid line at each foot. This is to make it easy to determine the range of heads at a glance.

The model used month-long stress periods, so pumping and boundary conditions were input as step functions with constant values throughout each month and sudden changes at the end of each month. For this reason, the model cannot be expected to accurately predict day-to-day head variations in any of these wells. Calibration efforts were aimed at matching general trends and monthly averages.

Starting head conditions for this model were based on the October 2003 steady state calibrated model. Transient calibration efforts were focused on matching the head changes, not the actual heads, so it is not uncommon for residuals in the starting condition to be carried through the entire calibration period. This indicates that the model is correctly predicting responses to hydrogeologic forces even if the calculated head values vary somewhat from the measured values.

Transient SEAWAT Calibration Comparison
Upper Floridan Aquifer (2003-2004)
Final Groundwater Model Calibration Report

Figure 4.48

October 2010

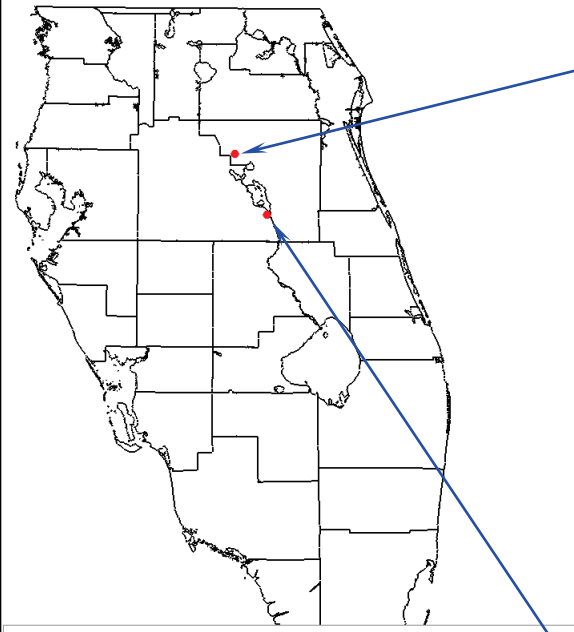

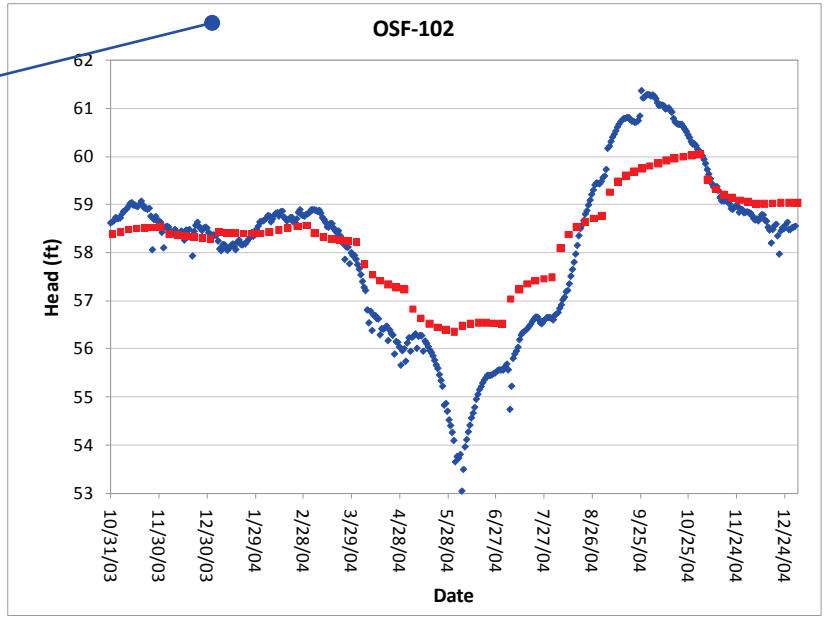

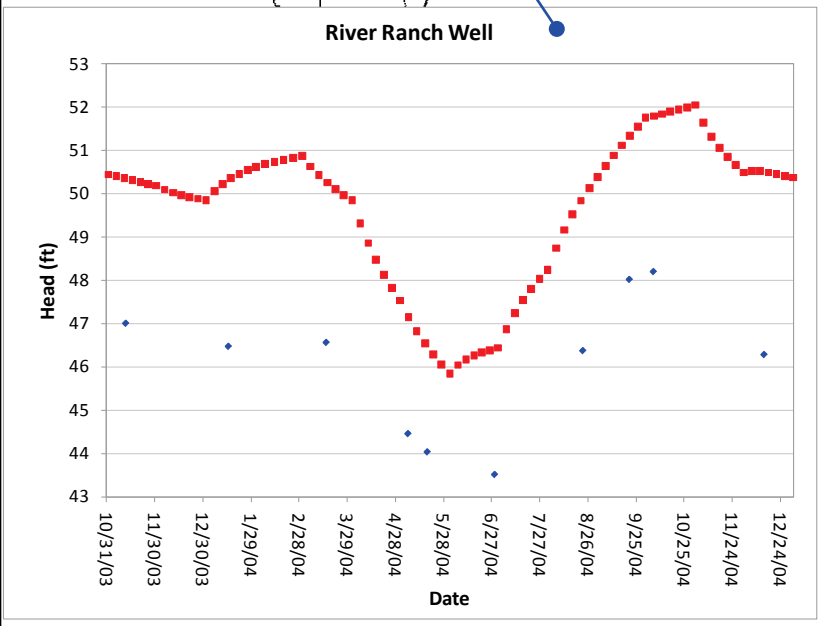

	River Ranch Well	OSF-102
Mean Error	3.312	0.214
Mean Absolute Error	3.312	0.614
Root Mean Square (RMS)	3.358	0.788
Observed Range	4.67	8.33
RMS as Percentage of Range	72%	9%
Coefficient of Determination (r^2)	0.932	0.946
Nash-Sutcliffe Model Efficiency Coefficient	-4.337	0.778

Legend

- Measured Head
- Model Calculated Head

Notes:

Figures 4.41 through 4.94 show the comparison between measured head values and model-calculated head values at a number of observation wells for the calibration period. Although the scales vary on each plot, all plots have a horizontal grid line at each foot. This is to make it easy to determine the range of heads at a glance.

The model used month-long stress periods, so pumping and boundary conditions were input as step functions with constant values throughout each month and sudden changes at the end of each month. For this reason, the model cannot be expected to accurately predict day-to-day head variations in any of these wells. Calibration efforts were aimed at matching general trends and monthly averages.

Starting head conditions for this model were based on the October 2003 steady state calibrated model. Transient calibration efforts were focused on matching the head changes, not the actual heads, so it is not uncommon for residuals in the starting condition to be carried through the entire calibration period. This indicates that the model is correctly predicting responses to hydrogeologic forces even if the calculated head values vary somewhat from the measured values.

Transient SEAWAT Calibration Comparison
Upper Floridan Aquifer (2003-2004)
Final Groundwater Model Calibration Report

Figure 4.49

October 2010

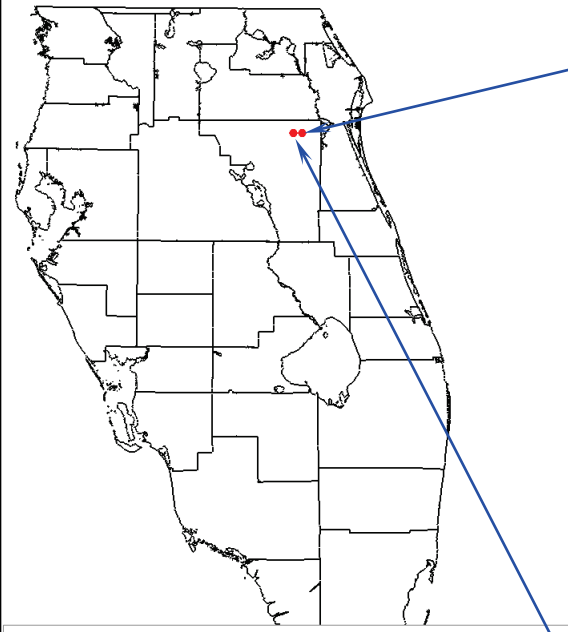

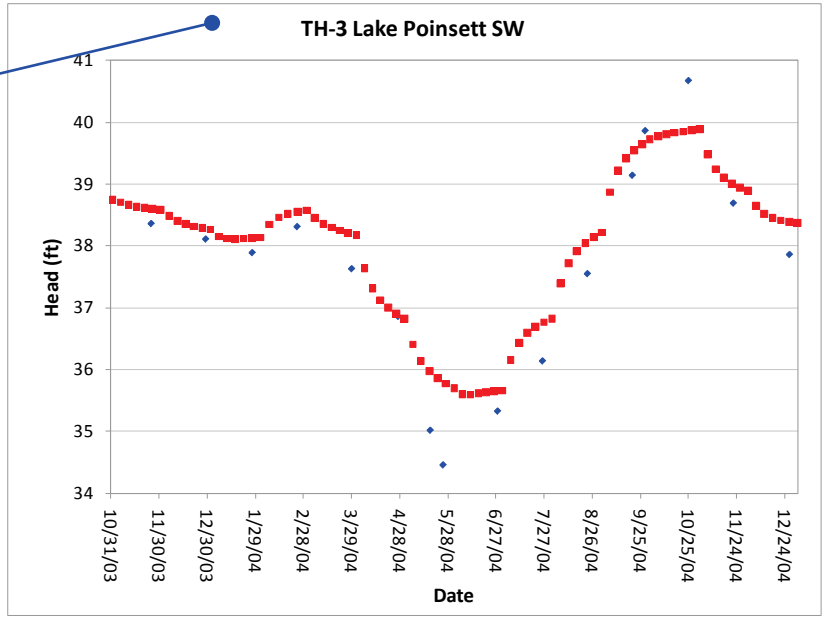

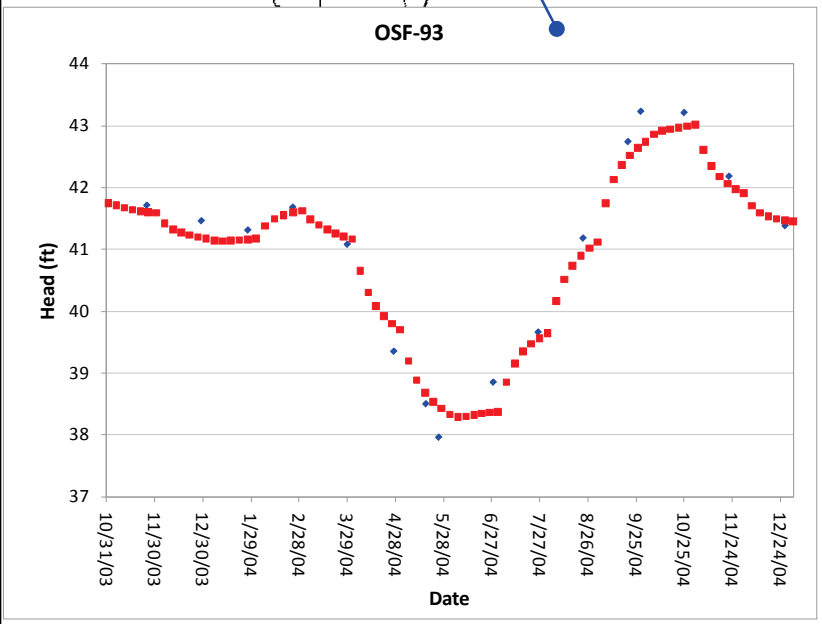

	OSF-93	TH-3 Lake Poinsett
Mean Error	-0.084	0.306
Mean Absolute Error	0.419	0.479
Root Mean Square (RMS)	0.507	0.589
Observed Range	5.27	6.21
RMS as Percentage of Range	10%	9%
Coefficient of Determination (r^2)	0.878	0.917
Nash-Sutcliffe Model Efficiency Coefficient	0.874	0.847

Legend

- Measured Head
- Model Calculated Head

Notes:

Figures 4.41 through 4.94 show the comparison between measured head values and model-calculated head values at a number of observation wells for the calibration period. Although the scales vary on each plot, all plots have a horizontal grid line at each foot. This is to make it easy to determine the range of heads at a glance.

The model used month-long stress periods, so pumping and boundary conditions were input as step functions with constant values throughout each month and sudden changes at the end of each month. For this reason, the model cannot be expected to accurately predict day-to-day head variations in any of these wells. Calibration efforts were aimed at matching general trends and monthly averages.

Starting head conditions for this model were based on the October 2003 steady state calibrated model. Transient calibration efforts were focused on matching the head changes, not the actual heads, so it is not uncommon for residuals in the starting condition to be carried through the entire calibration period. This indicates that the model is correctly predicting responses to hydrogeologic forces even if the calculated head values vary somewhat from the measured values.

Transient SEAWAT Calibration Comparison
Upper Floridan Aquifer (2003-2004)
Final Groundwater Model Calibration Report

Figure 4.50

October 2010

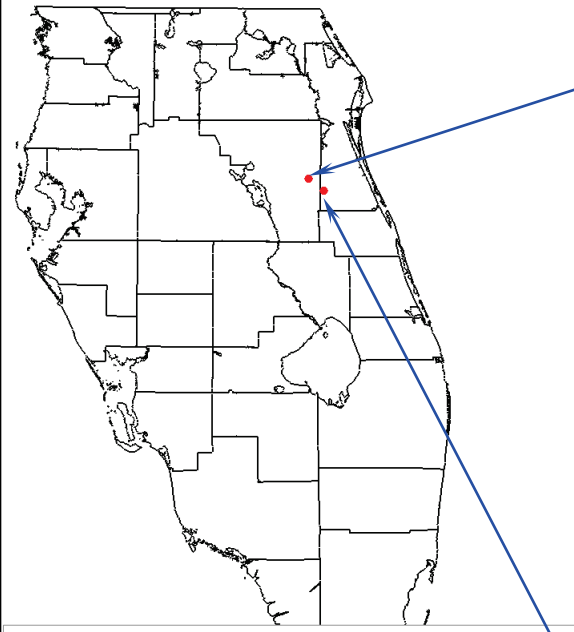

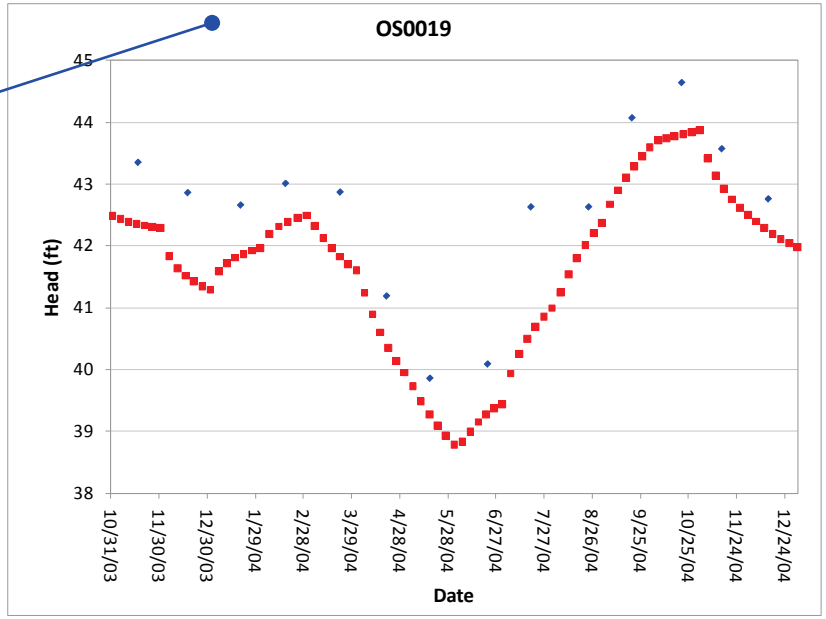

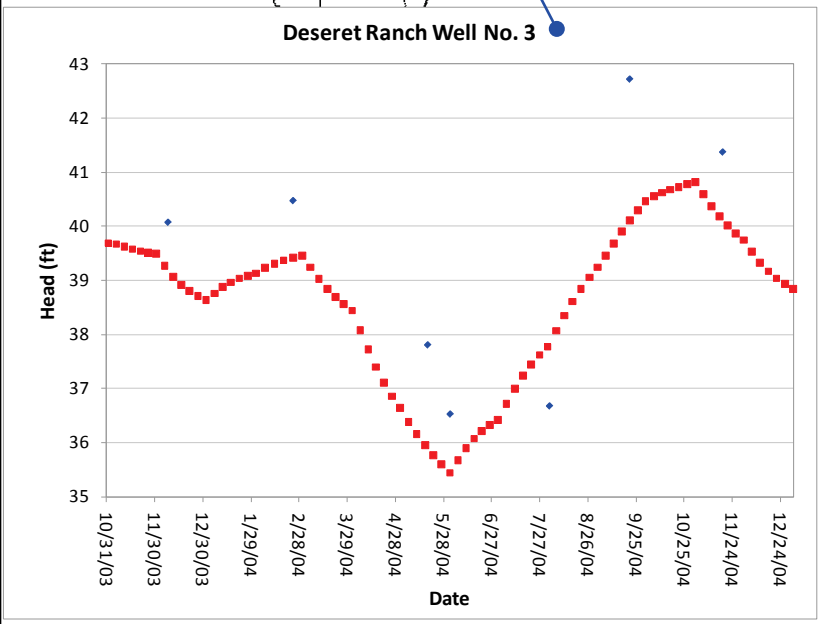

	Deseret Ranch	OS0019
Mean Error	-0.963	-0.919
Mean Absolute Error	1.471	0.919
Root Mean Square (RMS)	1.634	1.033
Observed Range	6.20	4.78
RMS as Percentage of Range	26%	22%
Coefficient of Determination (r^2)	0.657	0.875
Nash-Sutcliffe Model Efficiency Coefficient	0.463	0.377

Legend

- Measured Head
- Model Calculated Head

Notes:

Figures 4.41 through 4.94 show the comparison between measured head values and model-calculated head values at a number of observation wells for the calibration period. Although the scales vary on each plot, all plots have a horizontal grid line at each foot. This is to make it easy to determine the range of heads at a glance.

The model used month-long stress periods, so pumping and boundary conditions were input as step functions with constant values throughout each month and sudden changes at the end of each month. For this reason, the model cannot be expected to accurately predict day-to-day head variations in any of these wells. Calibration efforts were aimed at matching general trends and monthly averages.

Starting head conditions for this model were based on the October 2003 steady state calibrated model. Transient calibration efforts were focused on matching the head changes, not the actual heads, so it is not uncommon for residuals in the starting condition to be carried through the entire calibration period. This indicates that the model is correctly predicting responses to hydrogeologic forces even if the calculated head values vary somewhat from the measured values.

Transient SEAWAT Calibration Comparison
Upper Floridan Aquifer (2003-2004)
Final Groundwater Model Calibration Report

Figure 4.51

October 2010

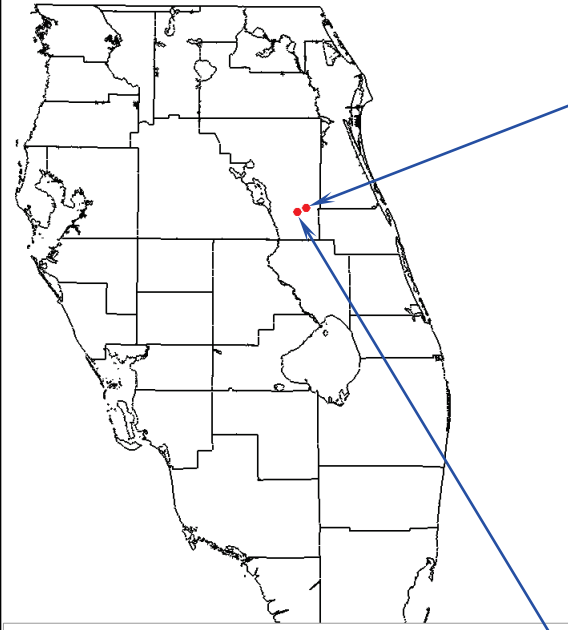

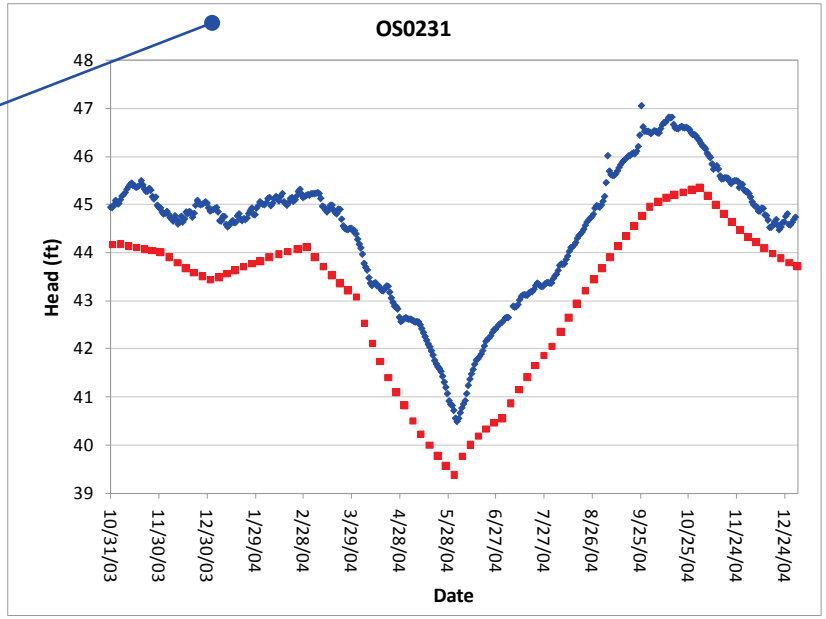

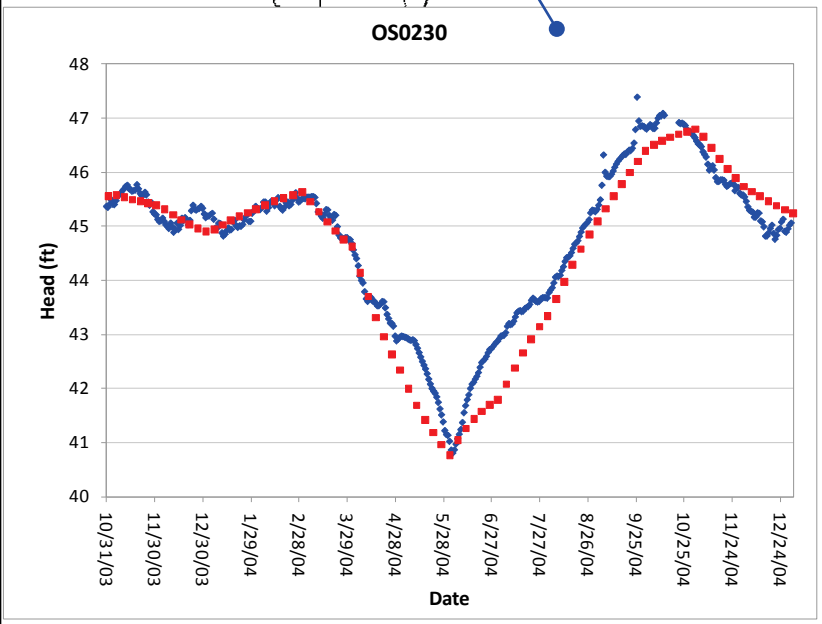

	OS0230	OS0231
Mean Error	-0.199	-1.319
Mean Absolute Error	0.319	1.319
Root Mean Square (RMS)	0.426	1.359
Observed Range	6.59	6.57
RMS as Percentage of Range	6%	21%
Coefficient of Determination (r^2)	0.962	0.968
Nash-Sutcliffe Model Efficiency Coefficient	0.906	0.048

Legend

- Measured Head
- Model Calculated Head

Notes:

Figures 4.41 through 4.94 show the comparison between measured head values and model-calculated head values at a number of observation wells for the calibration period. Although the scales vary on each plot, all plots have a horizontal grid line at each foot. This is to make it easy to determine the range of heads at a glance.

The model used month-long stress periods, so pumping and boundary conditions were input as step functions with constant values throughout each month and sudden changes at the end of each month. For this reason, the model cannot be expected to accurately predict day-to-day head variations in any of these wells. Calibration efforts were aimed at matching general trends and monthly averages.

Starting head conditions for this model were based on the October 2003 steady state calibrated model. Transient calibration efforts were focused on matching the head changes, not the actual heads, so it is not uncommon for residuals in the starting condition to be carried through the entire calibration period. This indicates that the model is correctly predicting responses to hydrogeologic forces even if the calculated head values vary somewhat from the measured values.

Transient SEAWAT Calibration Comparison
Upper Floridan Aquifer (2003-2004)
Final Groundwater Model Calibration Report

Figure 4.52

October 2010

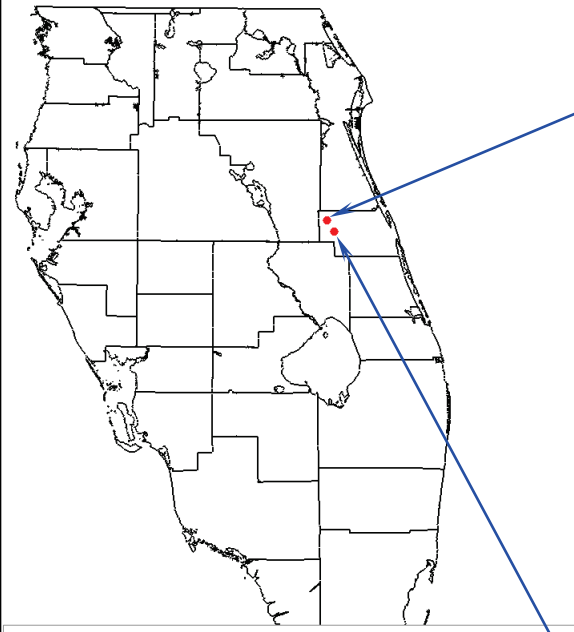

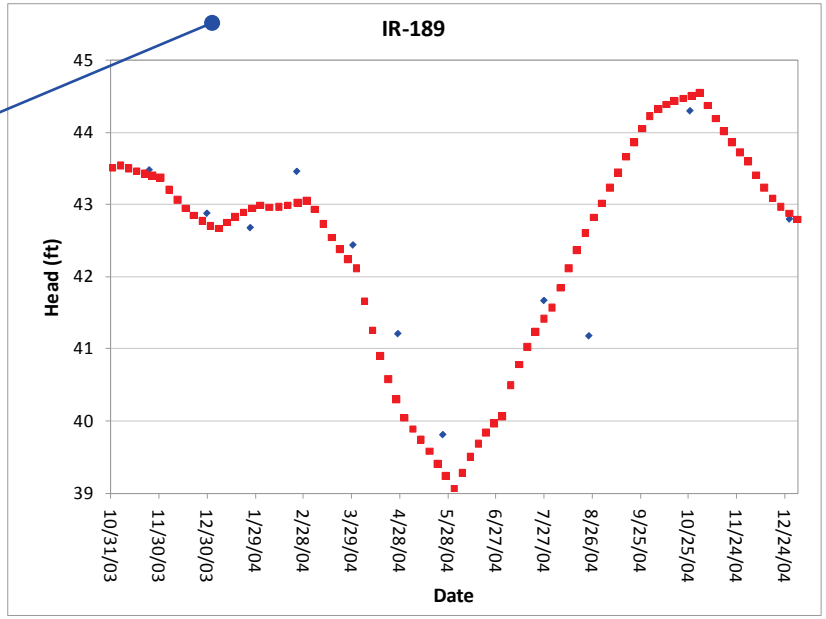

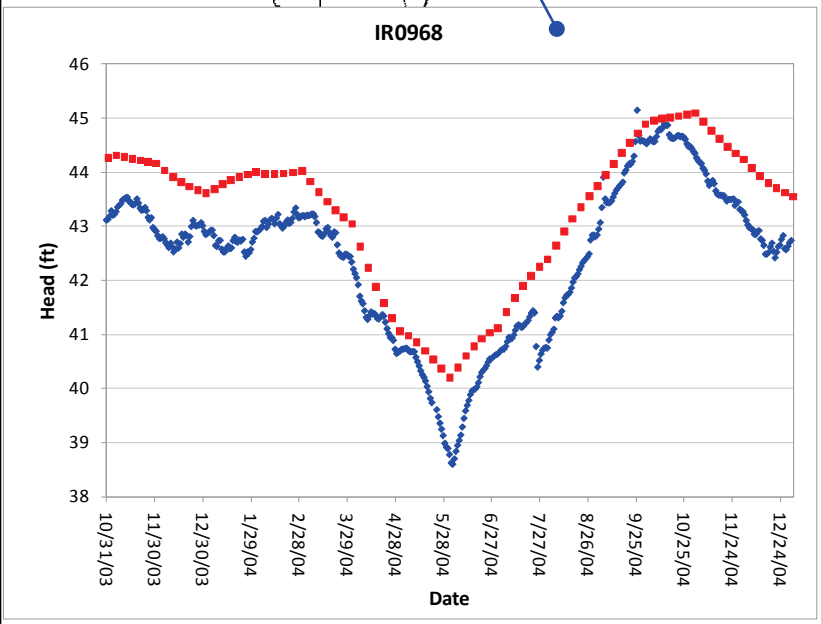

	IR0968	IR-189
Mean Error	0.840	0.038
Mean Absolute Error	0.840	0.319
Root Mean Square (RMS)	0.875	0.452
Observed Range	6.55	4.49
RMS as Percentage of Range	13%	10%
Coefficient of Determination (r^2)	0.968	0.878
Nash-Sutcliffe Model Efficiency Coefficient	0.596	0.864

Legend

- Measured Head
- Model Calculated Head

Notes:

Figures 4.41 through 4.94 show the comparison between measured head values and model-calculated head values at a number of observation wells for the calibration period. Although the scales vary on each plot, all plots have a horizontal grid line at each foot. This is to make it easy to determine the range of heads at a glance.

The model used month-long stress periods, so pumping and boundary conditions were input as step functions with constant values throughout each month and sudden changes at the end of each month. For this reason, the model cannot be expected to accurately predict day-to-day head variations in any of these wells. Calibration efforts were aimed at matching general trends and monthly averages.

Starting head conditions for this model were based on the October 2003 steady state calibrated model. Transient calibration efforts were focused on matching the head changes, not the actual heads, so it is not uncommon for residuals in the starting condition to be carried through the entire calibration period. This indicates that the model is correctly predicting responses to hydrogeologic forces even if the calculated head values vary somewhat from the measured values.

Transient SEAWAT Calibration Comparison
Upper Floridan Aquifer (2003-2004)
Final Groundwater Model Calibration Report

Figure 4.53

October 2010

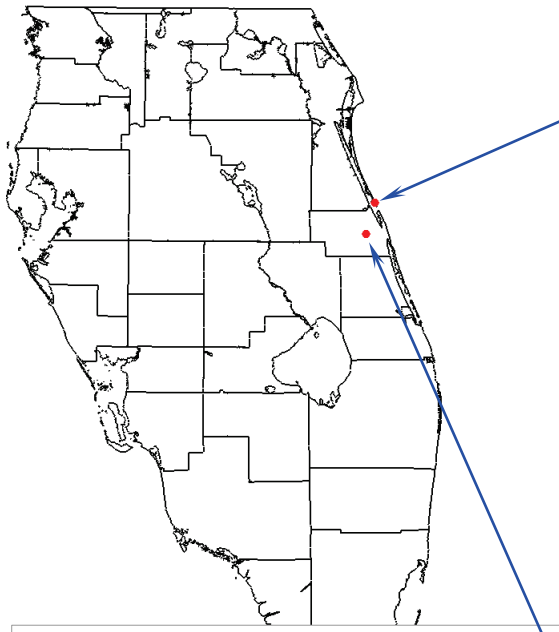

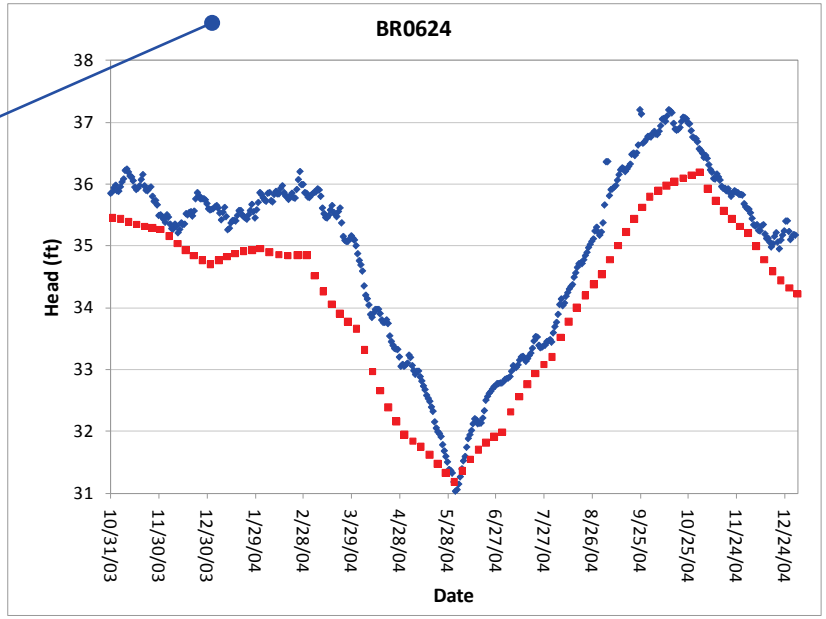

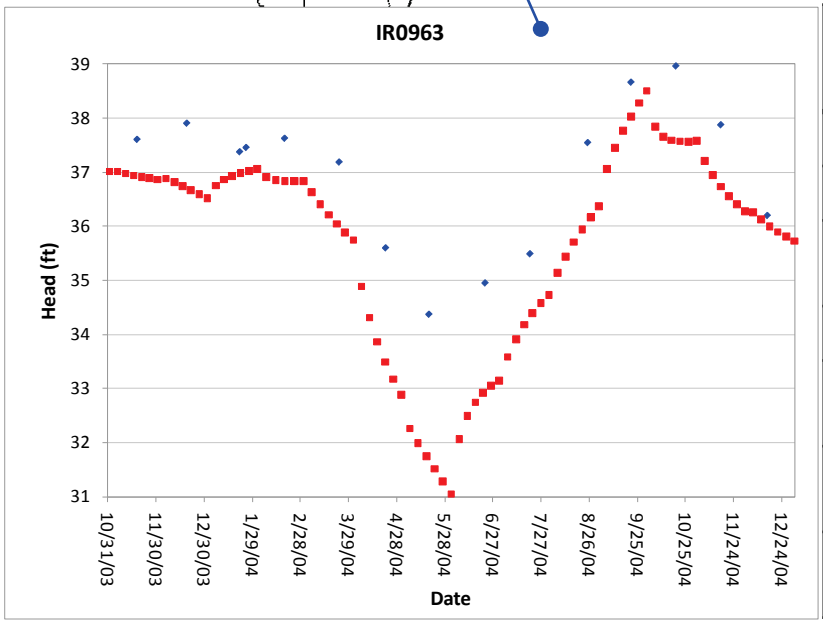

	IR0963	BR0624
Mean Error	-1.244	-0.757
Mean Absolute Error	1.244	0.757
Root Mean Square (RMS)	1.412	0.804
Observed Range	4.6	6.17
RMS as Percentage of Range	31%	13%
Coefficient of Determination (r^2)	0.900	0.965
Nash-Sutcliffe Model Efficiency Coefficient	-0.093	0.688

Legend

- Measured Head
- Model Calculated Head

Notes:

Figures 4.41 through 4.94 show the comparison between measured head values and model-calculated head values at a number of observation wells for the calibration period. Although the scales vary on each plot, all plots have a horizontal grid line at each foot. This is to make it easy to determine the range of heads at a glance.

The model used month-long stress periods, so pumping and boundary conditions were input as step functions with constant values throughout each month and sudden changes at the end of each month. For this reason, the model cannot be expected to accurately predict day-to-day head variations in any of these wells. Calibration efforts were aimed at matching general trends and monthly averages.

Starting head conditions for this model were based on the October 2003 steady state calibrated model. Transient calibration efforts were focused on matching the head changes, not the actual heads, so it is not uncommon for residuals in the starting condition to be carried through the entire calibration period. This indicates that the model is correctly predicting responses to hydrogeologic forces even if the calculated head values vary somewhat from the measured values.

Transient SEAWAT Calibration Comparison
Upper Floridan Aquifer (2003-2004)
Final Groundwater Model Calibration Report

Figure 4.54

October 2010

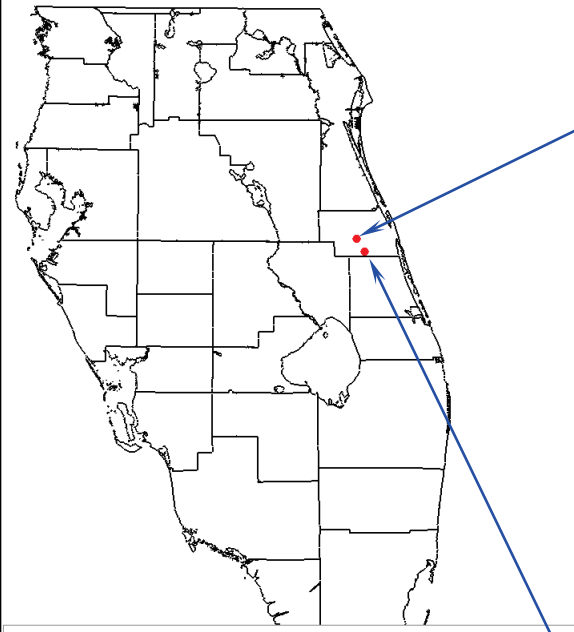

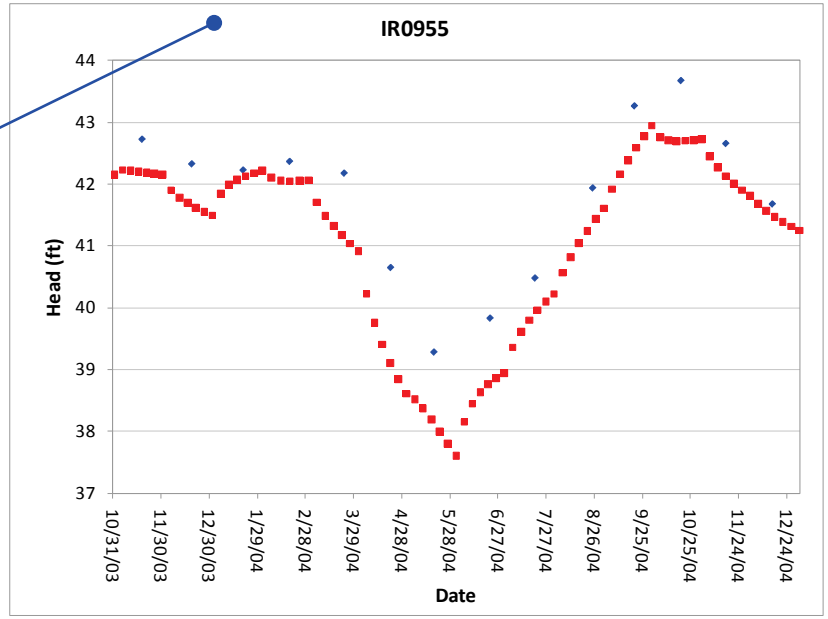

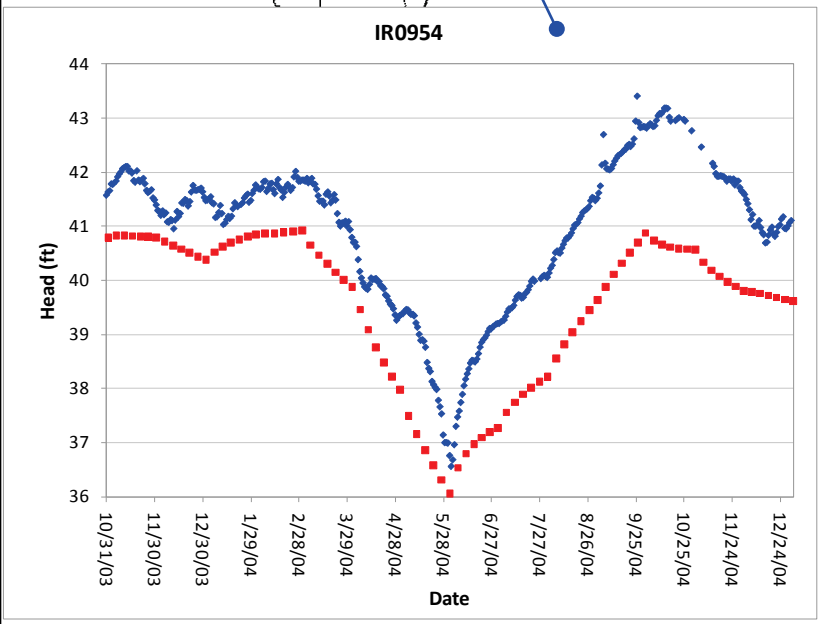

	IR0954	IR0955
Mean Error	-1.417	-0.730
Mean Absolute Error	1.417	0.730
Root Mean Square (RMS)	1.508	0.811
Observed Range	6.84	4.4
RMS as Percentage of Range	22%	18%
Coefficient of Determination (r^2)	0.860	0.950
Nash-Sutcliffe Model Efficiency Coefficient	-0.289	0.573

Legend

- Measured Head
- Model Calculated Head

Notes:

Figures 4.41 through 4.94 show the comparison between measured head values and model-calculated head values at a number of observation wells for the calibration period. Although the scales vary on each plot, all plots have a horizontal grid line at each foot. This is to make it easy to determine the range of heads at a glance.

The model used month-long stress periods, so pumping and boundary conditions were input as step functions with constant values throughout each month and sudden changes at the end of each month. For this reason, the model cannot be expected to accurately predict day-to-day head variations in any of these wells. Calibration efforts were aimed at matching general trends and monthly averages.

Starting head conditions for this model were based on the October 2003 steady state calibrated model. Transient calibration efforts were focused on matching the head changes, not the actual heads, so it is not uncommon for residuals in the starting condition to be carried through the entire calibration period. This indicates that the model is correctly predicting responses to hydrogeologic forces even if the calculated head values vary somewhat from the measured values.

Transient SEAWAT Calibration Comparison
Upper Floridan Aquifer (2003-2004)
Final Groundwater Model Calibration Report

Figure 4.55

October 2010

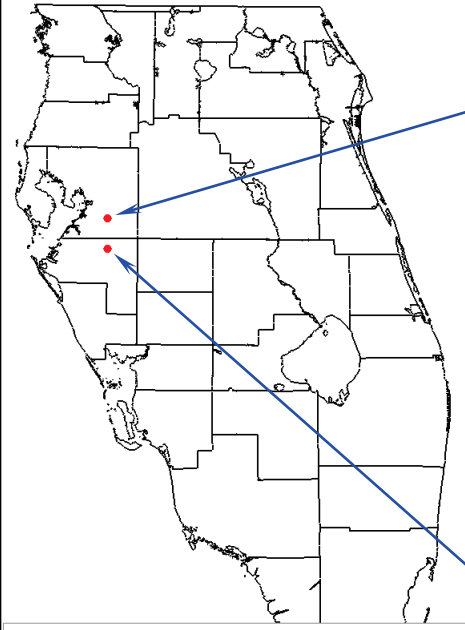

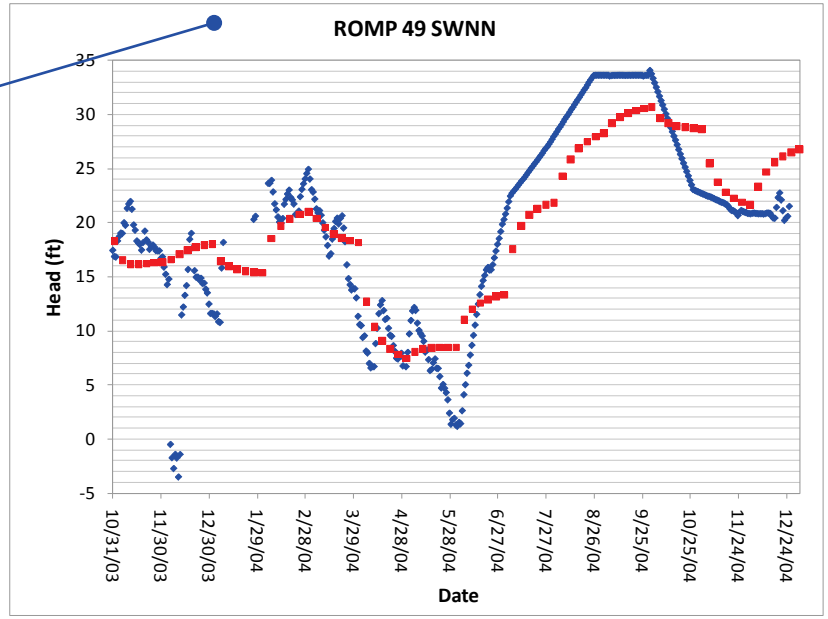

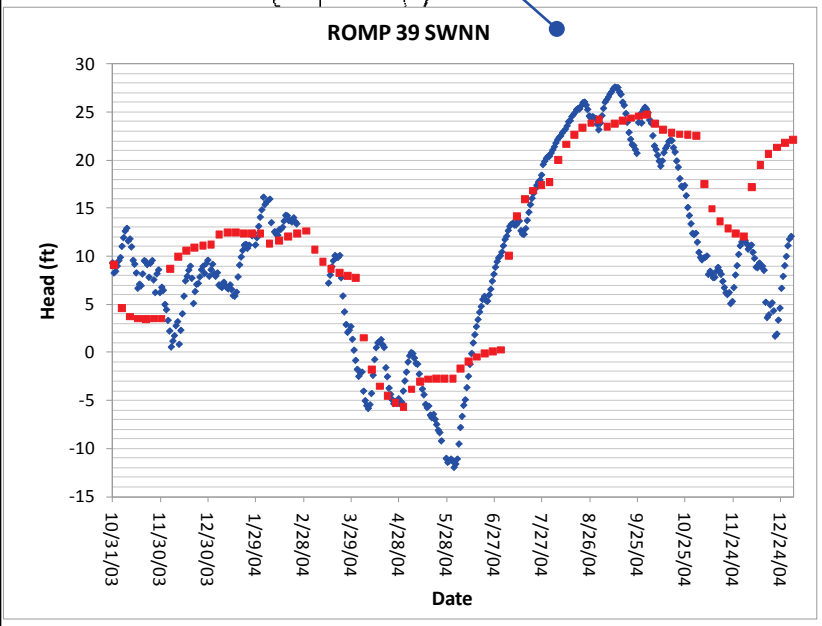

	ROMP 39 SWNN	ROMP 49 SWNN
Mean Error	1.627	0.005
Mean Absolute Error	3.500	2.886
Root Mean Square (RMS)	4.381	3.405
Observed Range	39.52	37.58
RMS as Percentage of Range	11%	9%
Coefficient of Determination (r^2)	0.795	0.824
Nash-Sutcliffe Model Efficiency Coefficient	0.749	0.814

Legend

- Measured Head
- Model Calculated Head

Notes:

Figures 4.41 through 4.94 show the comparison between measured head values and model-calculated head values at a number of observation wells for the calibration period. Although the scales vary on each plot, all plots have a horizontal grid line at each foot. This is to make it easy to determine the range of heads at a glance.

The model used month-long stress periods, so pumping and boundary conditions were input as step functions with constant values throughout each month and sudden changes at the end of each month. For this reason, the model cannot be expected to accurately predict day-to-day head variations in any of these wells. Calibration efforts were aimed at matching general trends and monthly averages.

Starting head conditions for this model were based on the October 2003 steady state calibrated model. Transient calibration efforts were focused on matching the head changes, not the actual heads, so it is not uncommon for residuals in the starting condition to be carried through the entire calibration period. This indicates that the model is correctly predicting responses to hydrogeologic forces even if the calculated head values vary somewhat from the measured values.

Transient SEAWAT Calibration Comparison
Upper Floridan Aquifer (2003-2004)
Final Groundwater Model Calibration Report

Figure 4.56

October 2010

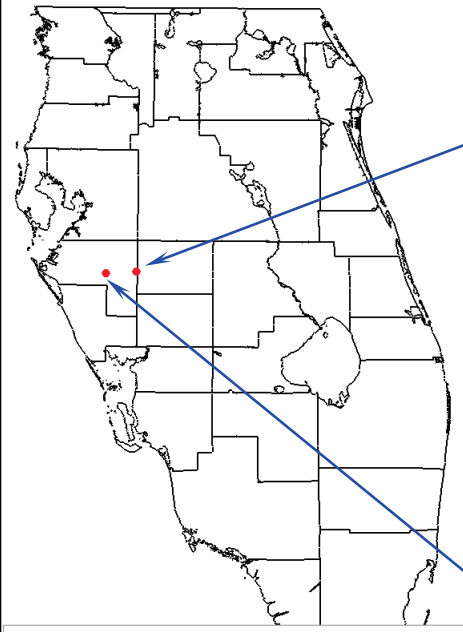

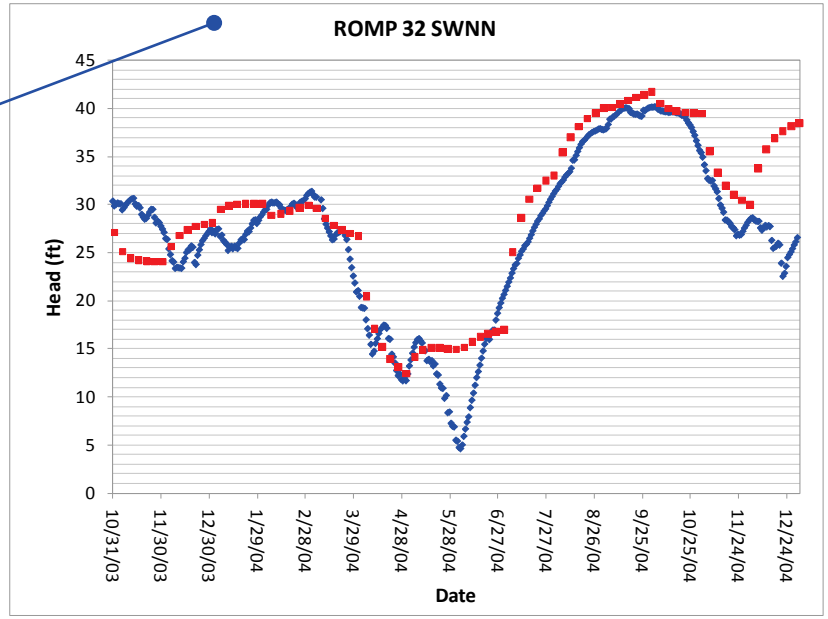

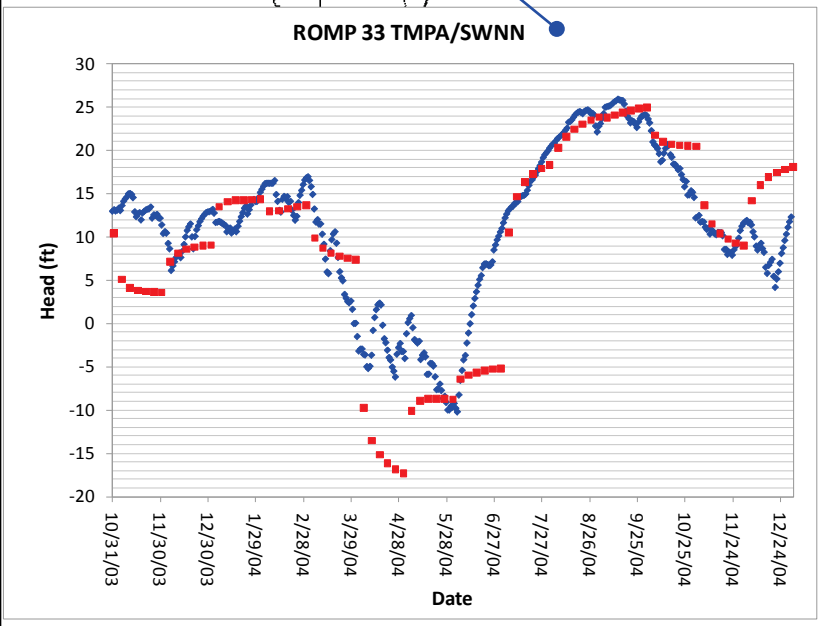

	ROMP 33 TMPA/ SWNN	ROMP 32 SWNN
Mean Error	-1.769	1.894
Mean Absolute Error	3.691	2.623
Root Mean Square (RMS)	4.647	3.427
Observed Range	36.21	35.66
RMS as Percentage of Range	13%	10%
Coefficient of Determination (r^2)	0.875	0.882
Nash-Sutcliffe Model Efficiency Coefficient	0.686	0.826

Legend

- Measured Head
- Model Calculated Head

Notes:

Figures 4.41 through 4.94 show the comparison between measured head values and model-calculated head values at a number of observation wells for the calibration period. Although the scales vary on each plot, all plots have a horizontal grid line at each foot. This is to make it easy to determine the range of heads at a glance.

The model used month-long stress periods, so pumping and boundary conditions were input as step functions with constant values throughout each month and sudden changes at the end of each month. For this reason, the model cannot be expected to accurately predict day-to-day head variations in any of these wells. Calibration efforts were aimed at matching general trends and monthly averages.

Starting head conditions for this model were based on the October 2003 steady state calibrated model. Transient calibration efforts were focused on matching the head changes, not the actual heads, so it is not uncommon for residuals in the starting condition to be carried through the entire calibration period. This indicates that the model is correctly predicting responses to hydrogeologic forces even if the calculated head values vary somewhat from the measured values.

Transient SEAWAT Calibration Comparison
Upper Floridan Aquifer (2003-2004)
Final Groundwater Model Calibration Report

Figure 4.57

October 2010

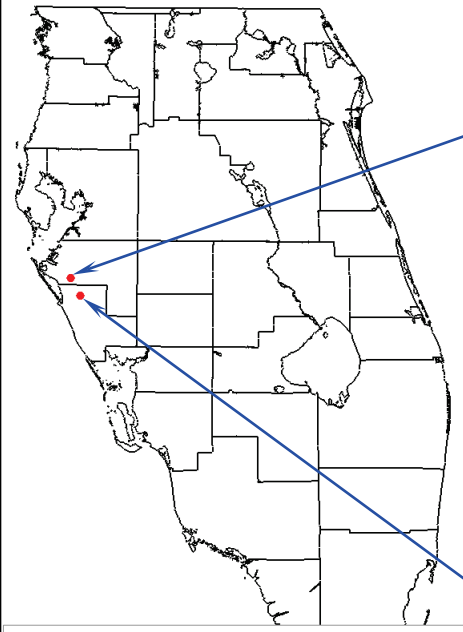

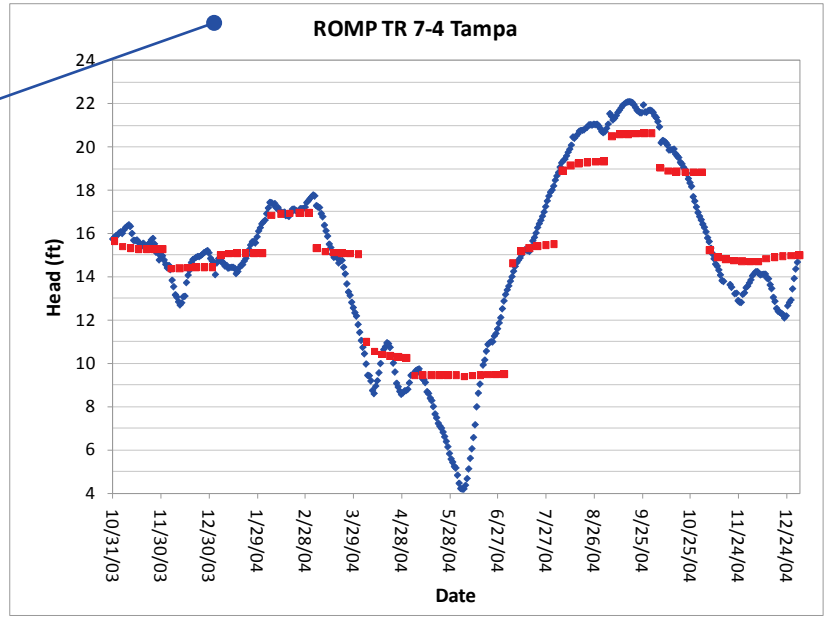

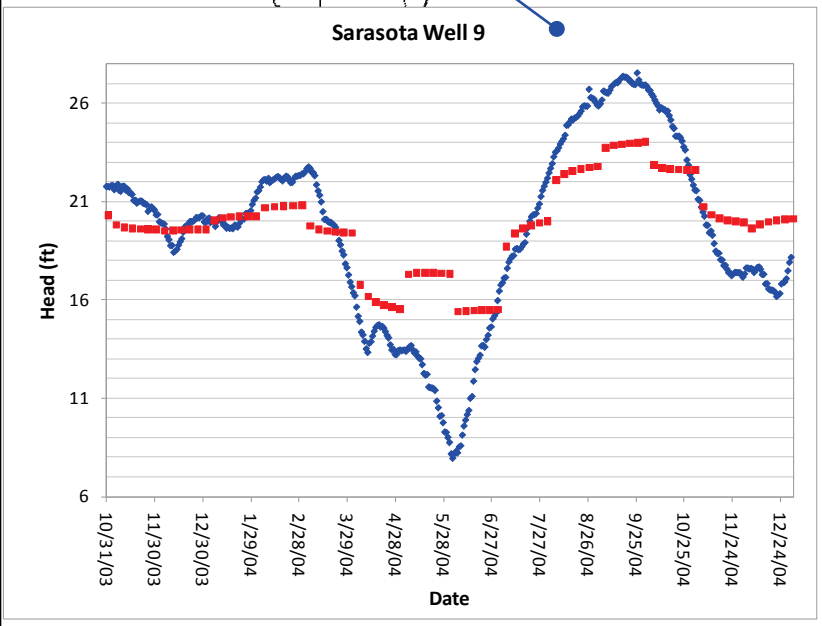

	Sarasota Well 9	ROMP TR 7-4 Tampa
Mean Error	0.346	0.151
Mean Absolute Error	1.991	0.899
Root Mean Square (RMS)	2.479	1.060
Observed Range	19.6	17.9
RMS as Percentage of Range	13%	6%
Coefficient of Determination (r^2)	0.902	0.968
Nash-Sutcliffe Model Efficiency Coefficient	0.687	0.929

Legend

- Measured Head
- Model Calculated Head

Notes:

Figures 4.41 through 4.94 show the comparison between measured head values and model-calculated head values at a number of observation wells for the calibration period. Although the scales vary on each plot, all plots have a horizontal grid line at each foot. This is to make it easy to determine the range of heads at a glance.

The model used month-long stress periods, so pumping and boundary conditions were input as step functions with constant values throughout each month and sudden changes at the end of each month. For this reason, the model cannot be expected to accurately predict day-to-day head variations in any of these wells. Calibration efforts were aimed at matching general trends and monthly averages.

Starting head conditions for this model were based on the October 2003 steady state calibrated model. Transient calibration efforts were focused on matching the head changes, not the actual heads, so it is not uncommon for residuals in the starting condition to be carried through the entire calibration period. This indicates that the model is correctly predicting responses to hydrogeologic forces even if the calculated head values vary somewhat from the measured values.

Transient SEAWAT Calibration Comparison
Upper Floridan Aquifer (2003-2004)
Final Groundwater Model Calibration Report

Figure 4.58

October 2010

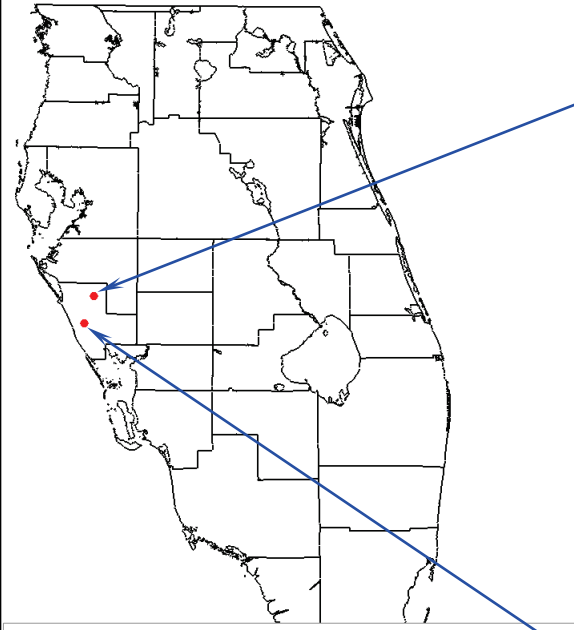

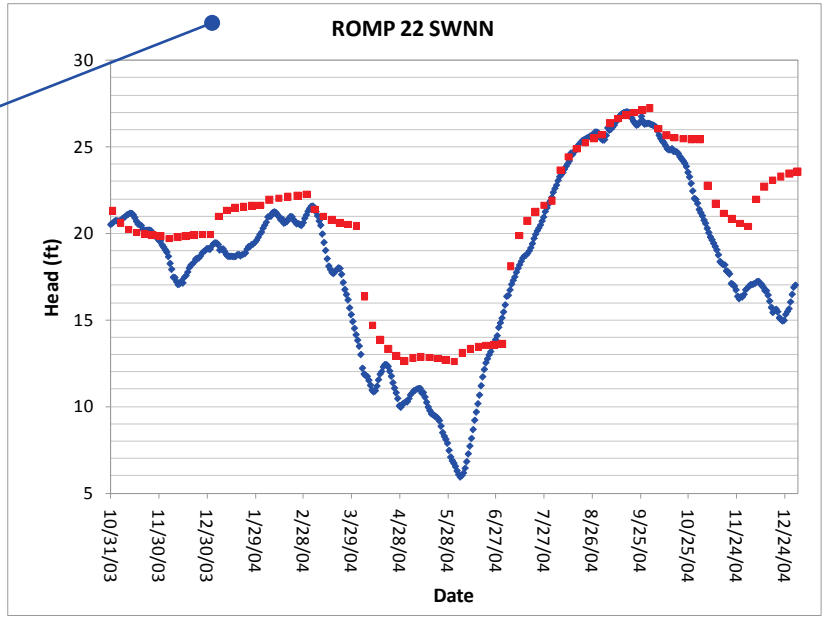

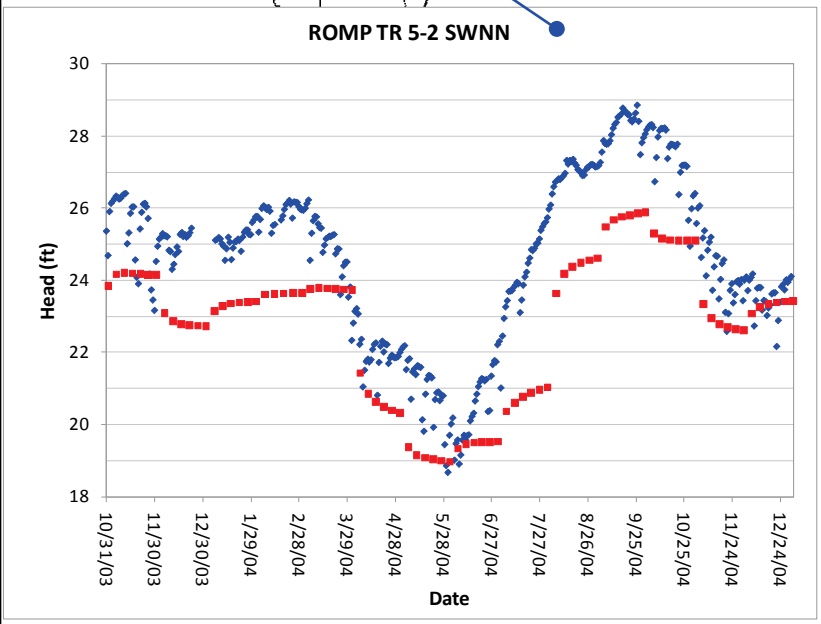

	ROMP TR 5-2 SWNN	ROMP 22 SWNN
Mean Error	-1.818	2.072
Mean Absolute Error	1.818	2.132
Root Mean Square (RMS)	2.013	2.722
Observed Range	10.18	21.06
RMS as Percentage of Range	20%	13%
Coefficient of Determination (r^2)	0.851	0.889
Nash-Sutcliffe Model Efficiency Coefficient	0.166	0.700

Legend

- Measured Head
- Model Calculated Head

Notes:

Figures 4.41 through 4.94 show the comparison between measured head values and model-calculated head values at a number of observation wells for the calibration period. Although the scales vary on each plot, all plots have a horizontal grid line at each foot. This is to make it easy to determine the range of heads at a glance.

The model used month-long stress periods, so pumping and boundary conditions were input as step functions with constant values throughout each month and sudden changes at the end of each month. For this reason, the model cannot be expected to accurately predict day-to-day head variations in any of these wells. Calibration efforts were aimed at matching general trends and monthly averages.

Starting head conditions for this model were based on the October 2003 steady state calibrated model. Transient calibration efforts were focused on matching the head changes, not the actual heads, so it is not uncommon for residuals in the starting condition to be carried through the entire calibration period. This indicates that the model is correctly predicting responses to hydrogeologic forces even if the calculated head values vary somewhat from the measured values.

Transient SEAWAT Calibration Comparison
Upper Floridan Aquifer (2003-2004)
Final Groundwater Model Calibration Report

Figure 4.59

October 2010

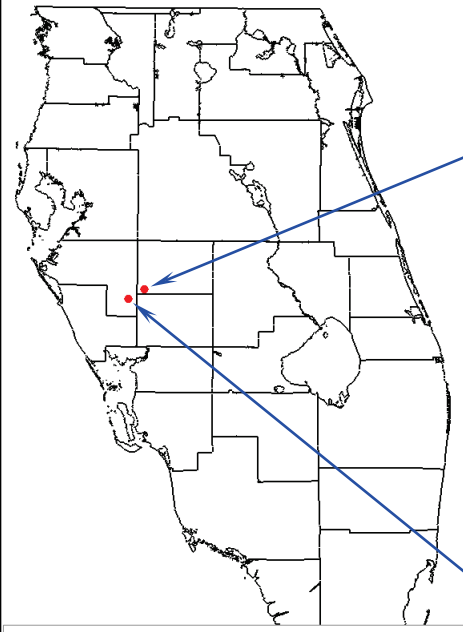

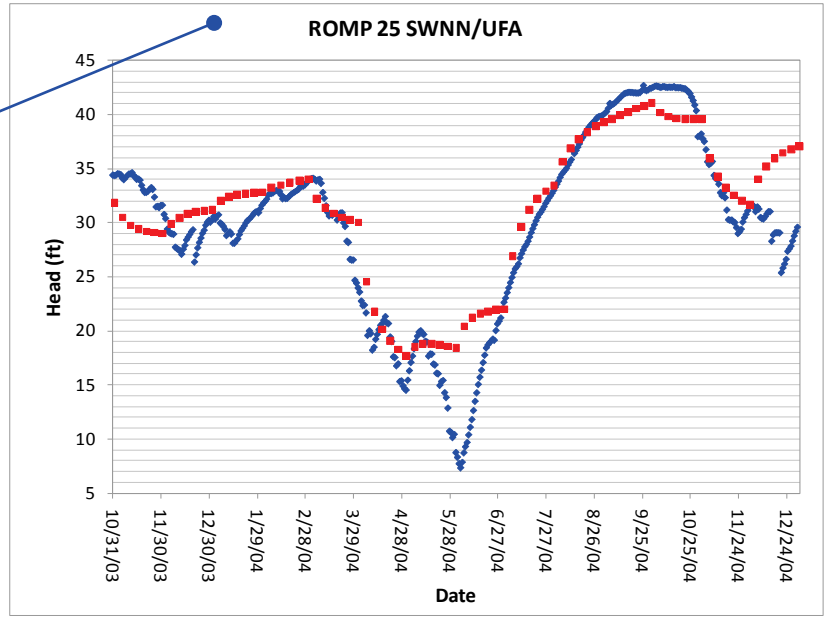

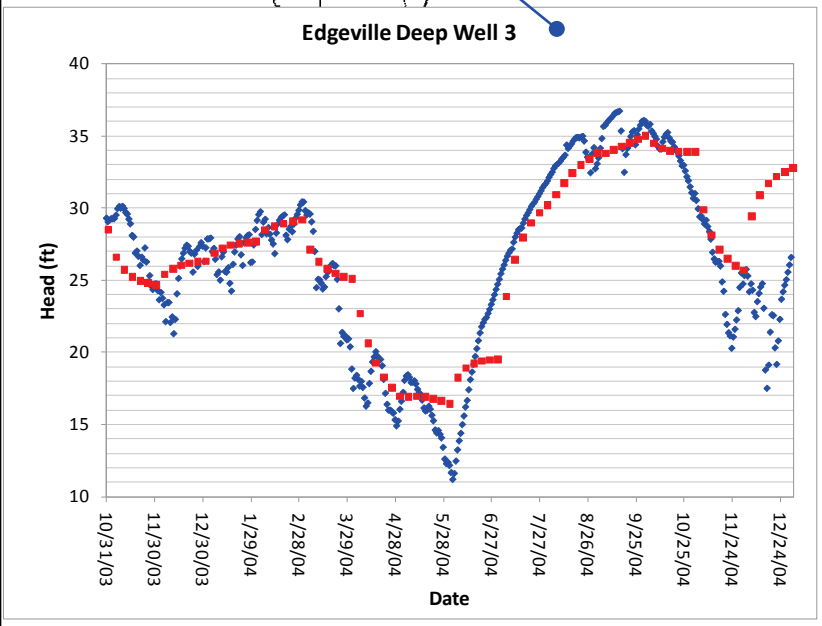

	Edgeville Deep Well 3	ROMP 25 SWNN/ UFA
Mean Error	0.683	1.365
Mean Absolute Error	1.738	2.365
Root Mean Square (RMS)	2.541	2.952
Observed Range	25.57	35.35
RMS as Percentage of Range	10%	8%
Coefficient of Determination (r^2)	0.821	0.916
Nash-Sutcliffe Model Efficiency Coefficient	0.806	0.863

Legend

- Measured Head
- Model Calculated Head

Notes:

Figures 4.41 through 4.94 show the comparison between measured head values and model-calculated head values at a number of observation wells for the calibration period. Although the scales vary on each plot, all plots have a horizontal grid line at each foot. This is to make it easy to determine the range of heads at a glance.

The model used month-long stress periods, so pumping and boundary conditions were input as step functions with constant values throughout each month and sudden changes at the end of each month. For this reason, the model cannot be expected to accurately predict day-to-day head variations in any of these wells. Calibration efforts were aimed at matching general trends and monthly averages.

Starting head conditions for this model were based on the October 2003 steady state calibrated model. Transient calibration efforts were focused on matching the head changes, not the actual heads, so it is not uncommon for residuals in the starting condition to be carried through the entire calibration period. This indicates that the model is correctly predicting responses to hydrogeologic forces even if the calculated head values vary somewhat from the measured values.

Transient SEAWAT Calibration Comparison
Upper Floridan Aquifer (2003-2004)
Final Groundwater Model Calibration Report

Figure 4.60

October 2010

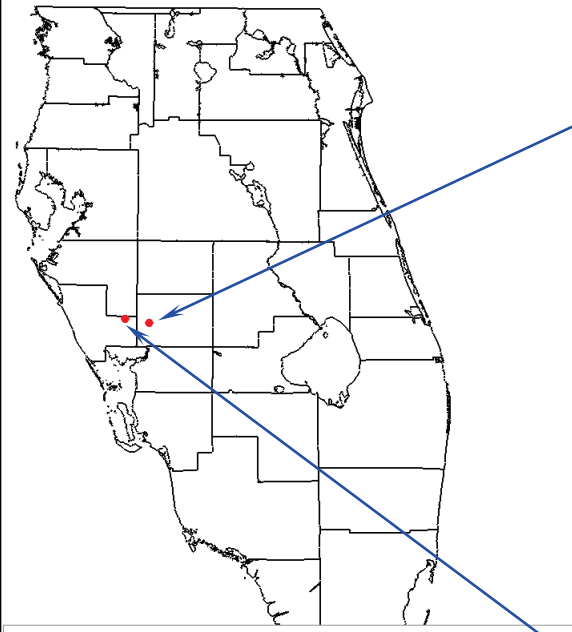

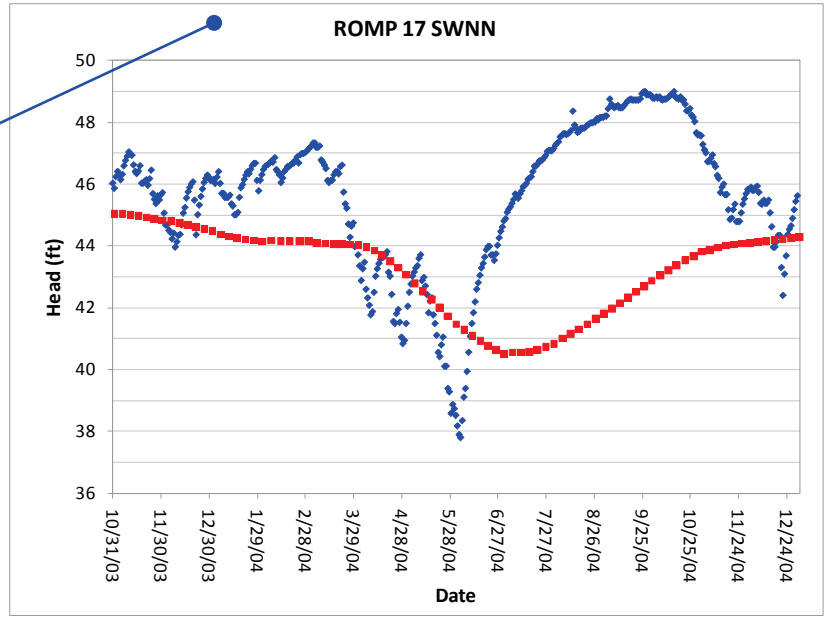

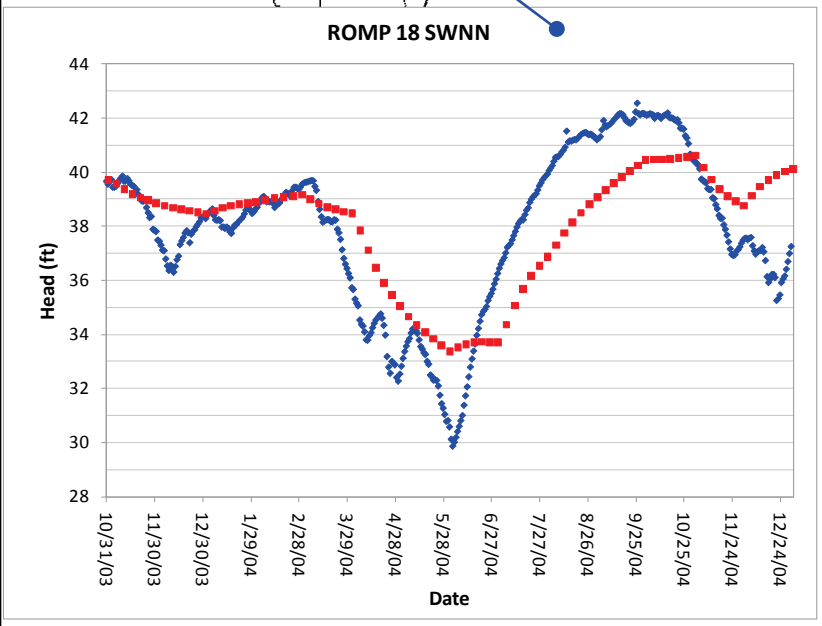

	ROMP 18 SWNN	ROMP 17 SWNN
Mean Error	0.119	-2.371
Mean Absolute Error	1.479	2.653
Root Mean Square (RMS)	1.827	3.419
Observed Range	12.66	11.19
RMS as Percentage of Range	12%	24%
Coefficient of Determination (r^2)	0.578	0.006
Nash-Sutcliffe Model Efficiency Coefficient	0.576	-1.548

Legend

- Measured Head
- Model Calculated Head

Notes:

Figures 4.41 through 4.94 show the comparison between measured head values and model-calculated head values at a number of observation wells for the calibration period. Although the scales vary on each plot, all plots have a horizontal grid line at each foot. This is to make it easy to determine the range of heads at a glance.

The model used month-long stress periods, so pumping and boundary conditions were input as step functions with constant values throughout each month and sudden changes at the end of each month. For this reason, the model cannot be expected to accurately predict day-to-day head variations in any of these wells. Calibration efforts were aimed at matching general trends and monthly averages.

Starting head conditions for this model were based on the October 2003 steady state calibrated model. Transient calibration efforts were focused on matching the head changes, not the actual heads, so it is not uncommon for residuals in the starting condition to be carried through the entire calibration period. This indicates that the model is correctly predicting responses to hydrogeologic forces even if the calculated head values vary somewhat from the measured values.

Transient SEAWAT Calibration Comparison
Upper Floridan Aquifer (2003-2004)
Final Groundwater Model Calibration Report

Figure 4.61

October 2010

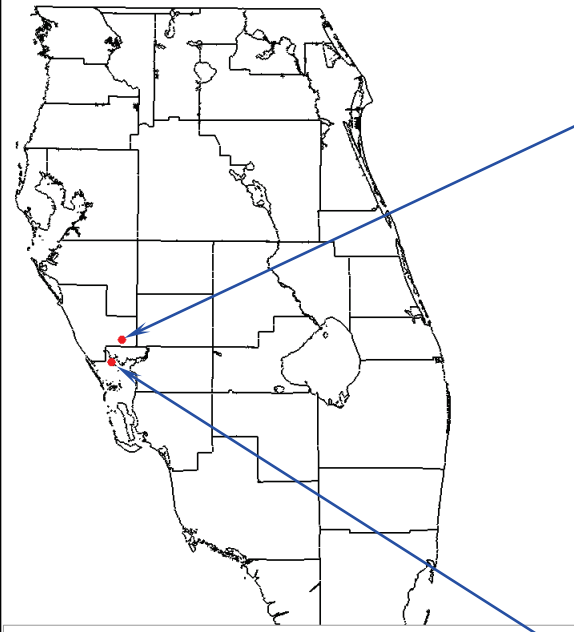

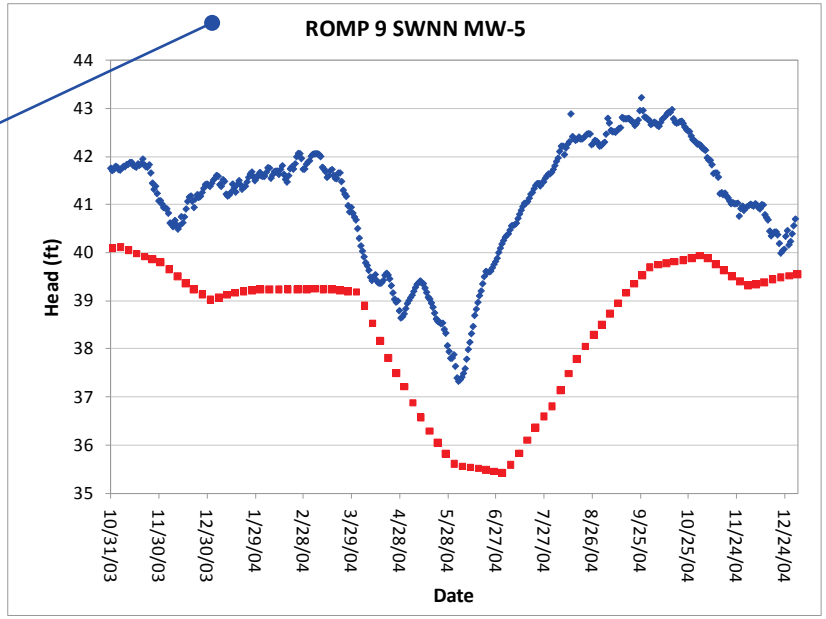

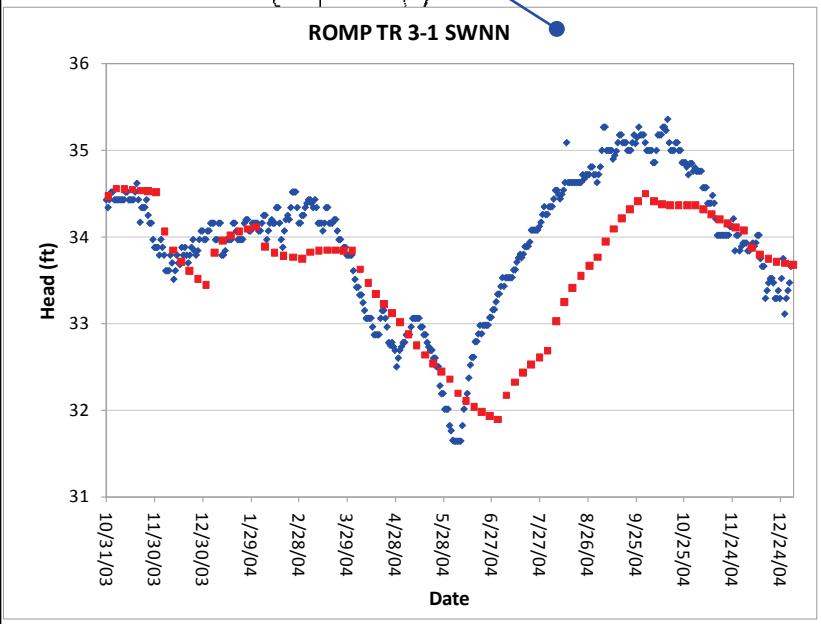

	ROMP TR 3-1	ROMP 9 SWNN MW-5
Mean Error	-0.338	-2.586
Mean Absolute Error	0.453	2.586
Root Mean Square (RMS)	0.643	2.832
Observed Range	3.72	5.91
RMS as Percentage of Range	17%	44%
Coefficient of Determination (r^2)	0.528	0.405
Nash-Sutcliffe Model Efficiency Coefficient	0.271	-4.294

Legend

- Measured Head
- Model Calculated Head

Notes:

Figures 4.41 through 4.94 show the comparison between measured head values and model-calculated head values at a number of observation wells for the calibration period. Although the scales vary on each plot, all plots have a horizontal grid line at each foot. This is to make it easy to determine the range of heads at a glance.

The model used month-long stress periods, so pumping and boundary conditions were input as step functions with constant values throughout each month and sudden changes at the end of each month. For this reason, the model cannot be expected to accurately predict day-to-day head variations in any of these wells. Calibration efforts were aimed at matching general trends and monthly averages.

Starting head conditions for this model were based on the October 2003 steady state calibrated model. Transient calibration efforts were focused on matching the head changes, not the actual heads, so it is not uncommon for residuals in the starting condition to be carried through the entire calibration period. This indicates that the model is correctly predicting responses to hydrogeologic forces even if the calculated head values vary somewhat from the measured values.

Transient SEAWAT Calibration Comparison
Upper Floridan Aquifer (2003-2004)
Final Groundwater Model Calibration Report

Figure 4.62

October 2010

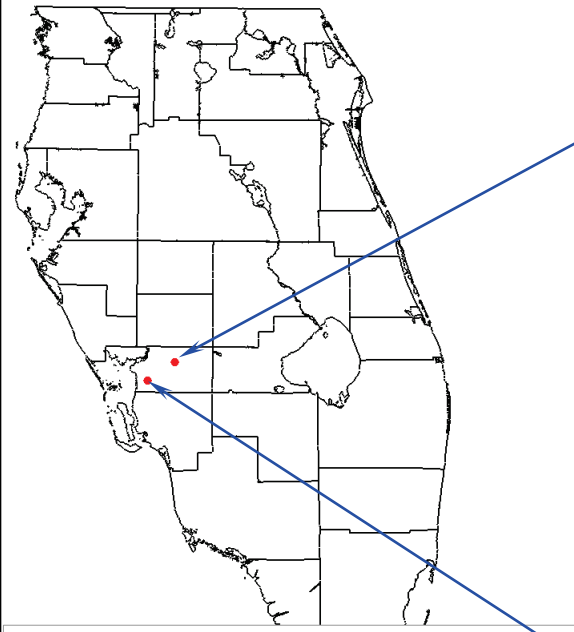

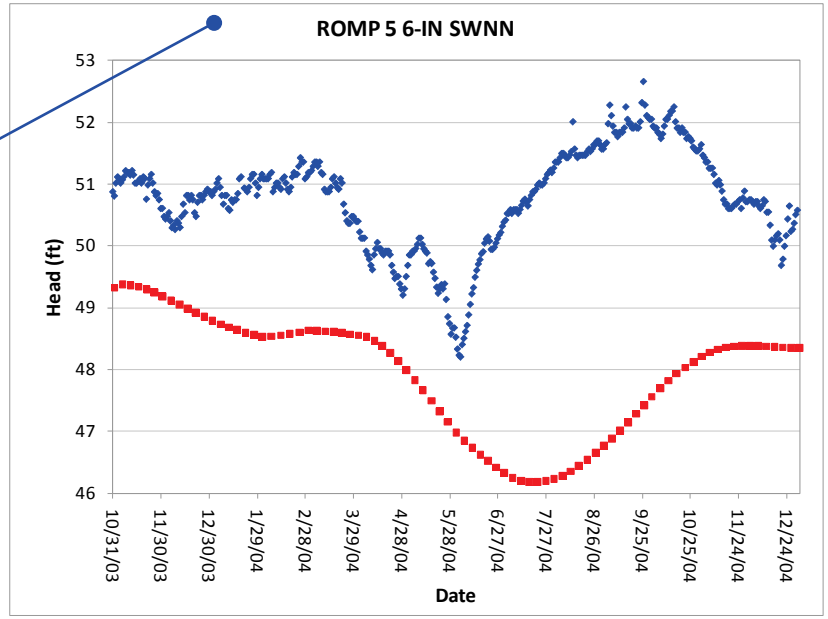

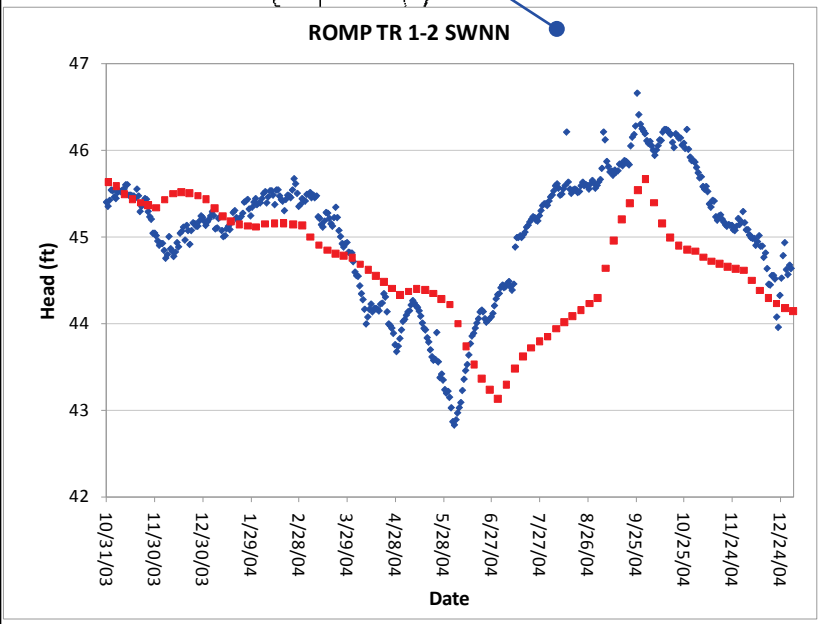

	ROMP TR 1-2 SWNN	ROMP 5 6-IN SWNN
Mean Error	-0.353	-2.718
Mean Absolute Error	0.567	2.718
Root Mean Square (RMS)	0.727	3.036
Observed Range	3.84	4.45
RMS as Percentage of Range	15%	68%
Coefficient of Determination (r^2)	0.290	0.005
Nash-Sutcliffe Model Efficiency Coefficient	-0.069	-10.447

Legend

- Measured Head
- Model Calculated Head

Notes:

Figures 4.41 through 4.94 show the comparison between measured head values and model-calculated head values at a number of observation wells for the calibration period. Although the scales vary on each plot, all plots have a horizontal grid line at each foot. This is to make it easy to determine the range of heads at a glance.

The model used month-long stress periods, so pumping and boundary conditions were input as step functions with constant values throughout each month and sudden changes at the end of each month. For this reason, the model cannot be expected to accurately predict day-to-day head variations in any of these wells. Calibration efforts were aimed at matching general trends and monthly averages.

Starting head conditions for this model were based on the October 2003 steady state calibrated model. Transient calibration efforts were focused on matching the head changes, not the actual heads, so it is not uncommon for residuals in the starting condition to be carried through the entire calibration period. This indicates that the model is correctly predicting responses to hydrogeologic forces even if the calculated head values vary somewhat from the measured values.

Transient SEAWAT Calibration Comparison
Upper Floridan Aquifer (2003-2004)
Final Groundwater Model Calibration Report

Figure 4.63

October 2010

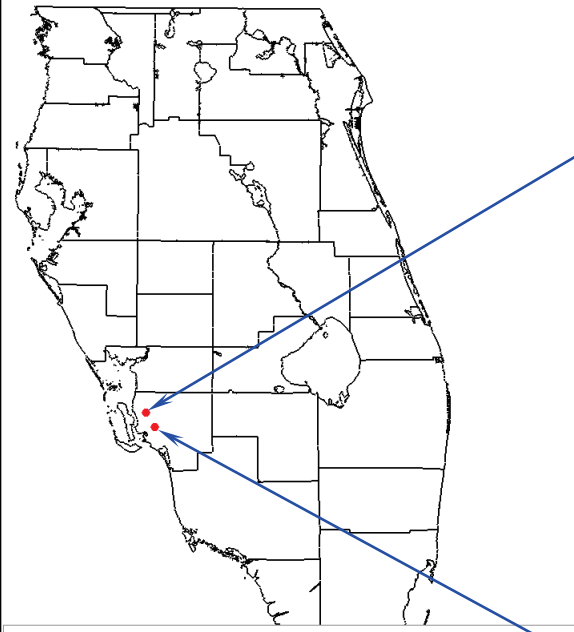

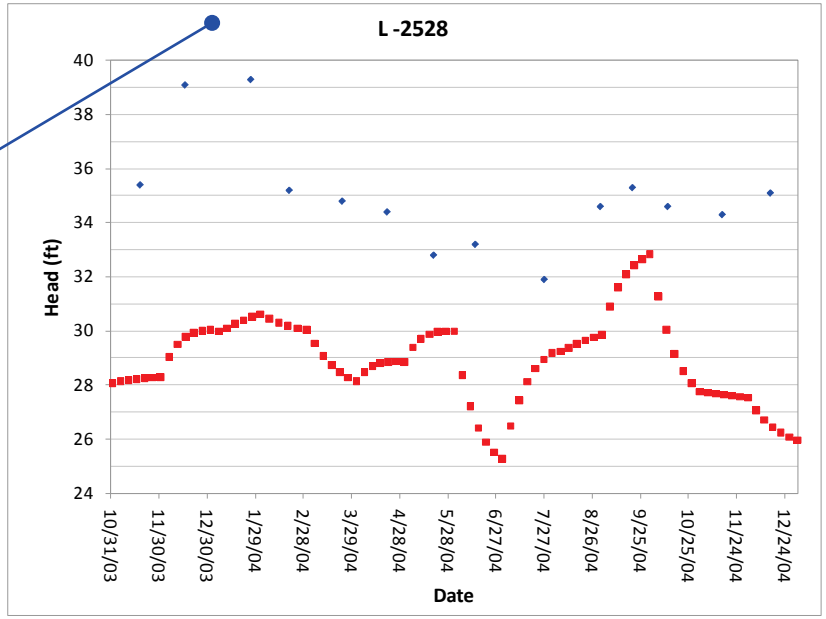

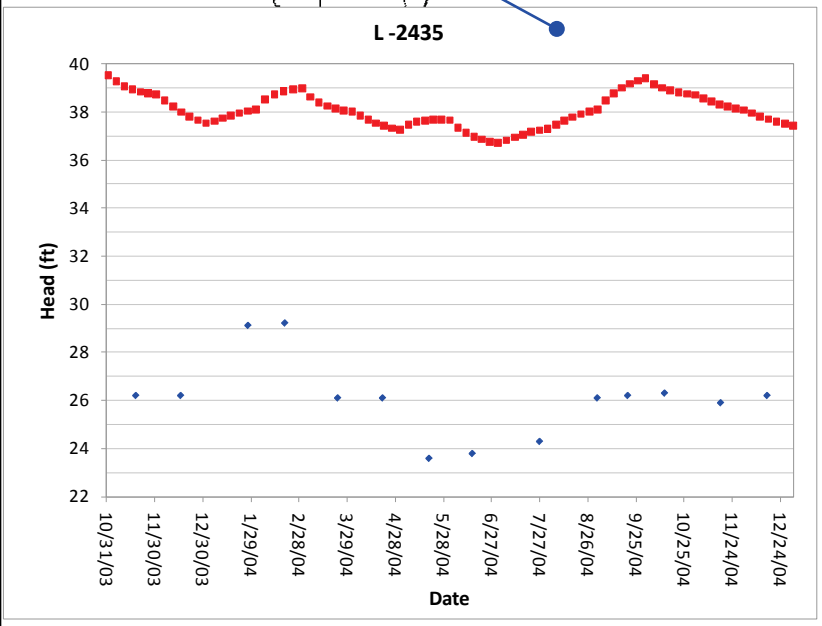

	L-2435	L-2528
Mean Error	12.011	-6.046
Mean Absolute Error	12.011	6.046
Root Mean Square (RMS)	12.094	6.340
Observed Range	5.60	7.40
RMS as Percentage of Range	216%	86%
Coefficient of Determination (r^2)	0.228	0.152
Nash-Sutcliffe Model Efficiency Coefficient	-55.761	-9.327

Legend

- Measured Head
- Model Calculated Head

Notes:

Figures 4.41 through 4.94 show the comparison between measured head values and model-calculated head values at a number of observation wells for the calibration period. Although the scales vary on each plot, all plots have a horizontal grid line at each foot. This is to make it easy to determine the range of heads at a glance.

The model used month-long stress periods, so pumping and boundary conditions were input as step functions with constant values throughout each month and sudden changes at the end of each month. For this reason, the model cannot be expected to accurately predict day-to-day head variations in any of these wells. Calibration efforts were aimed at matching general trends and monthly averages.

Starting head conditions for this model were based on the October 2003 steady state calibrated model. Transient calibration efforts were focused on matching the head changes, not the actual heads, so it is not uncommon for residuals in the starting condition to be carried through the entire calibration period. This indicates that the model is correctly predicting responses to hydrogeologic forces even if the calculated head values vary somewhat from the measured values.

Transient SEAWAT Calibration Comparison
Upper Floridan Aquifer (2003-2004)
Final Groundwater Model Calibration Report

Figure 4.64

October 2010

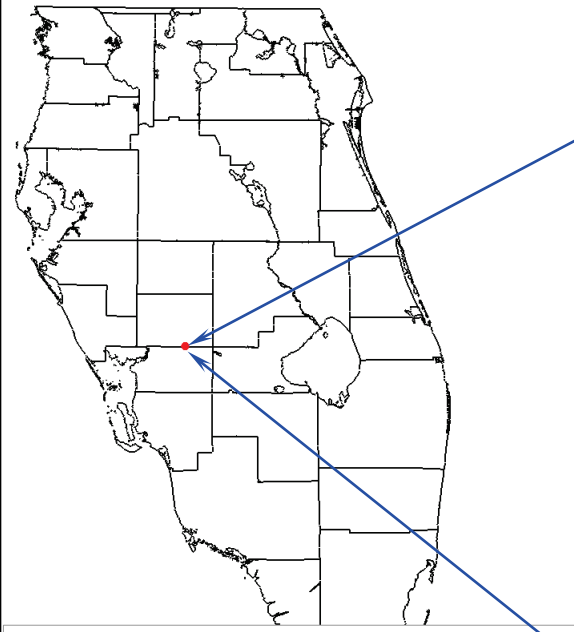

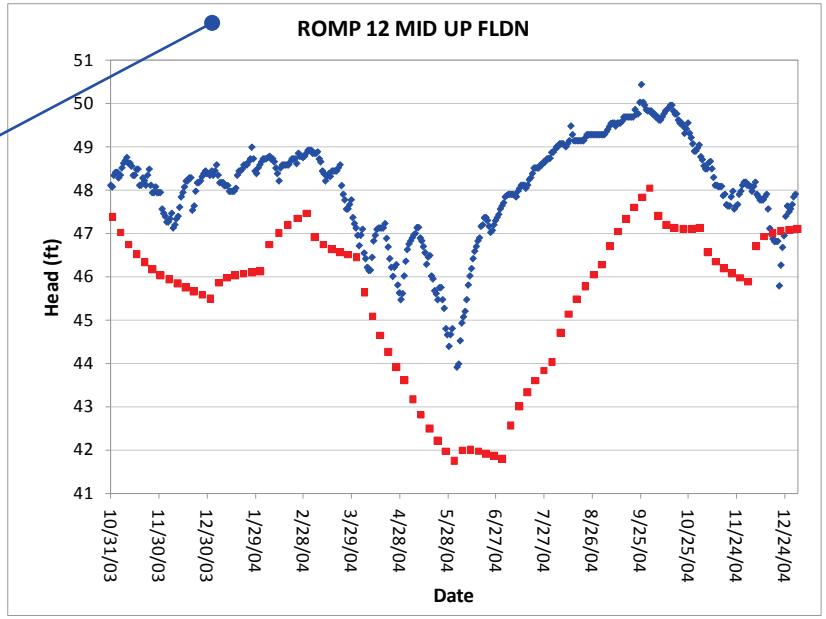

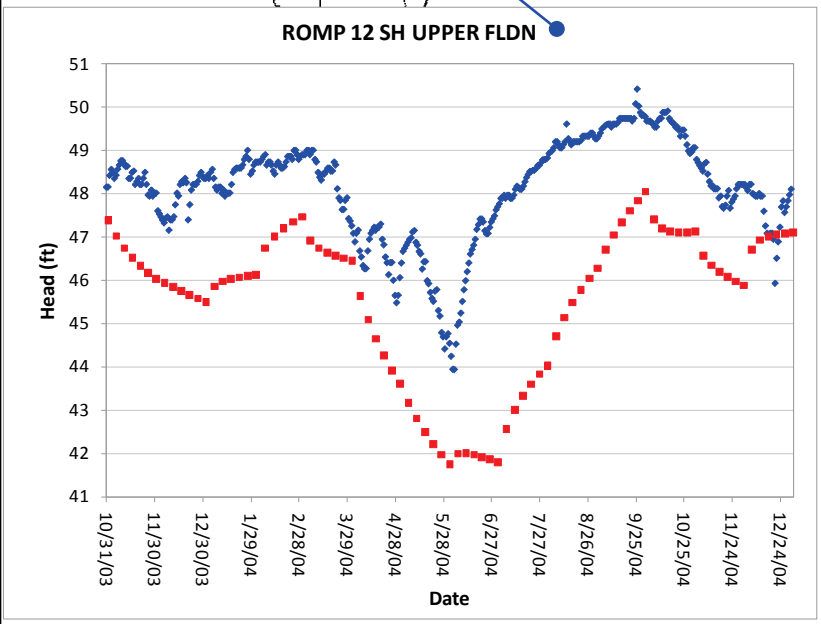

	ROMP 12 SH	ROMP 12 MID
Mean Error	-2.549	-2.514
Mean Absolute Error	2.549	2.514
Root Mean Square (RMS)	2.816	2.802
Observed Range	6.50	6.54
RMS as Percentage of Range	43%	43%
Coefficient of Determination (r^2)	0.518	0.481
Nash-Sutcliffe Model Efficiency Coefficient	-5.754	-5.814

Legend

- Measured Head
- Model Calculated Head

Notes:

Figures 4.41 through 4.94 show the comparison between measured head values and model-calculated head values at a number of observation wells for the calibration period. Although the scales vary on each plot, all plots have a horizontal grid line at each foot. This is to make it easy to determine the range of heads at a glance.

The model used month-long stress periods, so pumping and boundary conditions were input as step functions with constant values throughout each month and sudden changes at the end of each month. For this reason, the model cannot be expected to accurately predict day-to-day head variations in any of these wells. Calibration efforts were aimed at matching general trends and monthly averages.

Starting head conditions for this model were based on the October 2003 steady state calibrated model. Transient calibration efforts were focused on matching the head changes, not the actual heads, so it is not uncommon for residuals in the starting condition to be carried through the entire calibration period. This indicates that the model is correctly predicting responses to hydrogeologic forces even if the calculated head values vary somewhat from the measured values.

Transient SEAWAT Calibration Comparison
Upper Floridan Aquifer (2003-2004)
Final Groundwater Model Calibration Report

Figure 4.65

October 2010

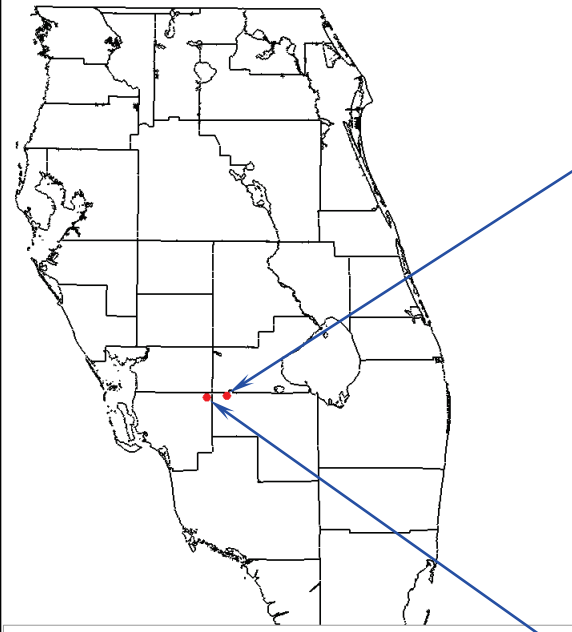

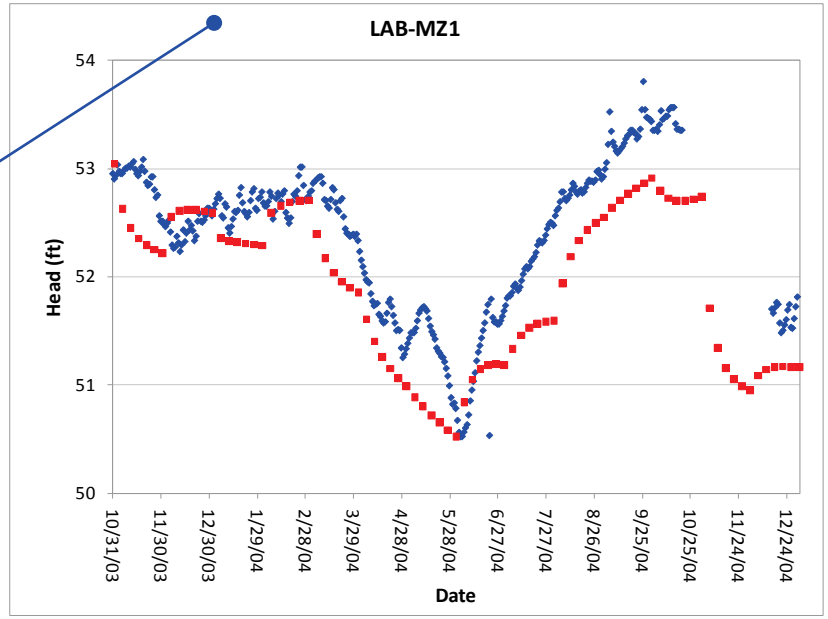

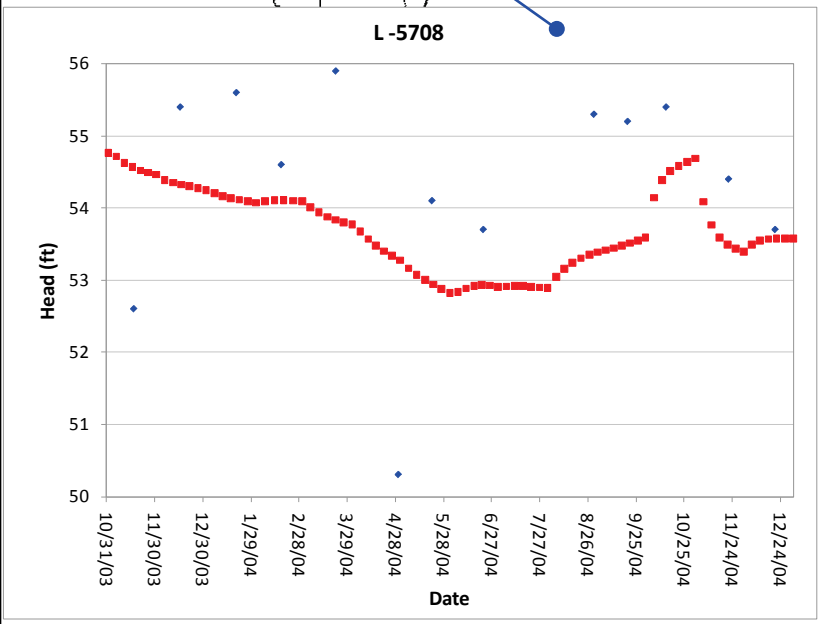

	L-5708	LAB-MZ1
Mean Error	-0.556	-0.413
Mean Absolute Error	1.365	0.428
Root Mean Square (RMS)	1.586	0.472
Observed Range	5.60	3.28
RMS as Percentage of Range	28%	14%
Coefficient of Determination (r^2)	0.024	0.894
Nash-Sutcliffe Model Efficiency Coefficient	-0.158	0.534

Legend

- Measured Head
- Model Calculated Head

Notes:

Figures 4.41 through 4.94 show the comparison between measured head values and model-calculated head values at a number of observation wells for the calibration period. Although the scales vary on each plot, all plots have a horizontal grid line at each foot. This is to make it easy to determine the range of heads at a glance.

The model used month-long stress periods, so pumping and boundary conditions were input as step functions with constant values throughout each month and sudden changes at the end of each month. For this reason, the model cannot be expected to accurately predict day-to-day head variations in any of these wells. Calibration efforts were aimed at matching general trends and monthly averages.

Starting head conditions for this model were based on the October 2003 steady state calibrated model. Transient calibration efforts were focused on matching the head changes, not the actual heads, so it is not uncommon for residuals in the starting condition to be carried through the entire calibration period. This indicates that the model is correctly predicting responses to hydrogeologic forces even if the calculated head values vary somewhat from the measured values.

Transient SEAWAT Calibration Comparison
Upper Floridan Aquifer (2003-2004)
Final Groundwater Model Calibration Report

Figure 4.66

October 2010

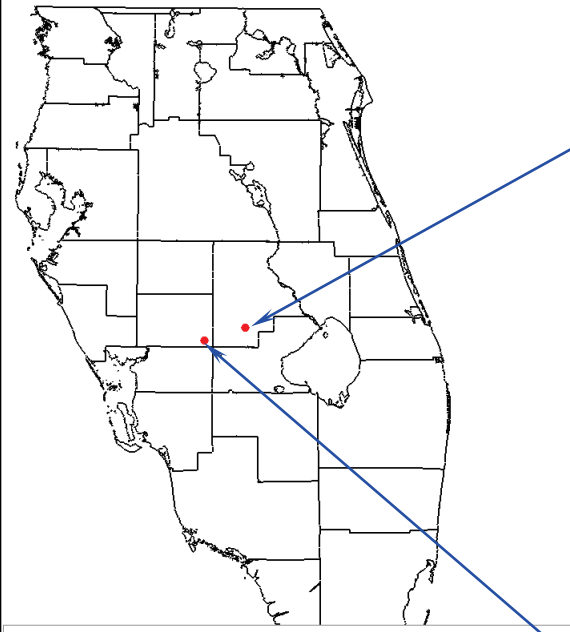

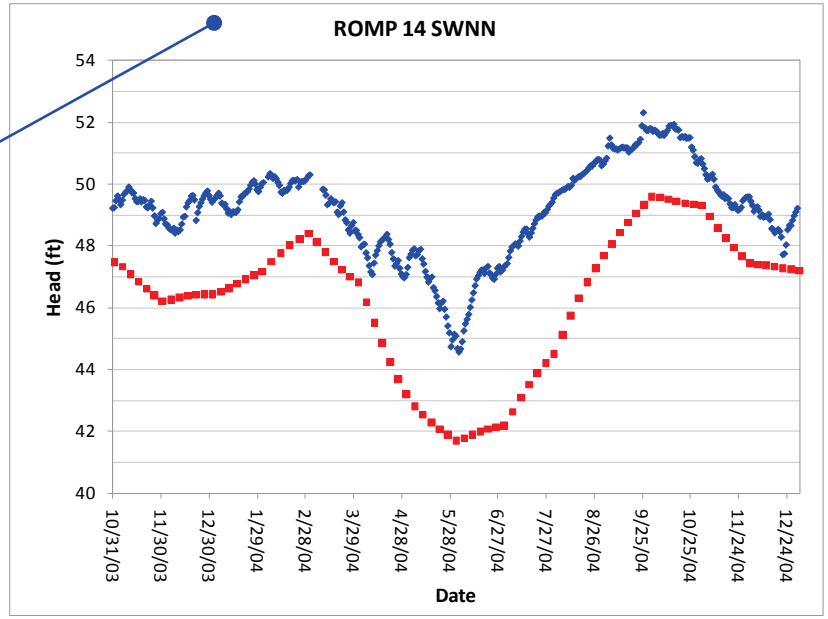

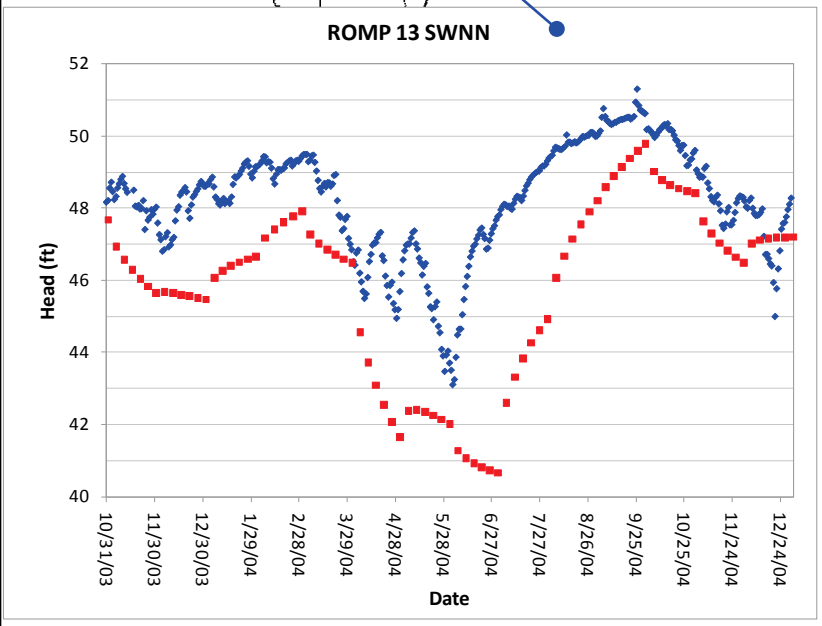

	ROMP 13 SWNN	ROMP 14 SWNN
Mean Error	-2.371	-2.864
Mean Absolute Error	2.371	2.864
Root Mean Square (RMS)	2.746	3.095
Observed Range	8.19	7.73
RMS as Percentage of Range	34%	40%
Coefficient of Determination (r^2)	0.691	0.782
Nash-Sutcliffe Model Efficiency Coefficient	-2.902	-3.680

Legend

- Measured Head
- Model Calculated Head

Notes:

Figures 4.41 through 4.94 show the comparison between measured head values and model-calculated head values at a number of observation wells for the calibration period. Although the scales vary on each plot, all plots have a horizontal grid line at each foot. This is to make it easy to determine the range of heads at a glance.

The model used month-long stress periods, so pumping and boundary conditions were input as step functions with constant values throughout each month and sudden changes at the end of each month. For this reason, the model cannot be expected to accurately predict day-to-day head variations in any of these wells. Calibration efforts were aimed at matching general trends and monthly averages.

Starting head conditions for this model were based on the October 2003 steady state calibrated model. Transient calibration efforts were focused on matching the head changes, not the actual heads, so it is not uncommon for residuals in the starting condition to be carried through the entire calibration period. This indicates that the model is correctly predicting responses to hydrogeologic forces even if the calculated head values vary somewhat from the measured values.

Transient SEAWAT Calibration Comparison
Upper Floridan Aquifer (2003-2004)
Final Groundwater Model Calibration Report

Figure 4.67

October 2010

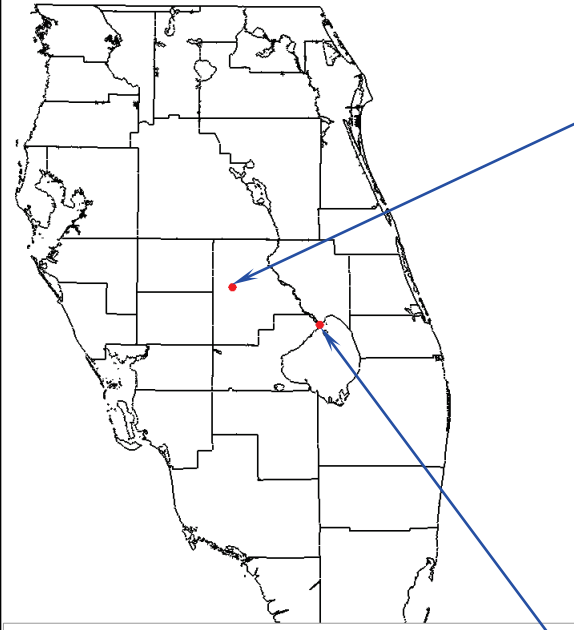

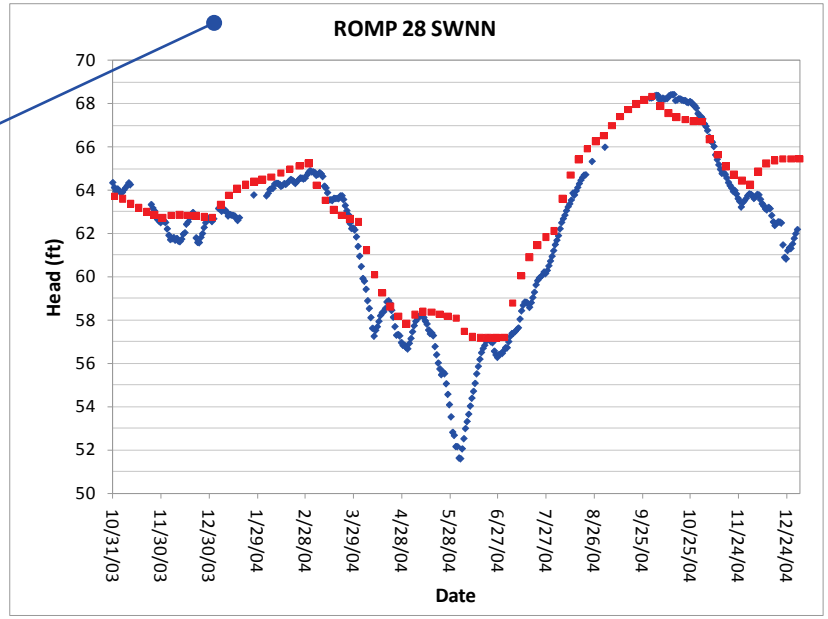

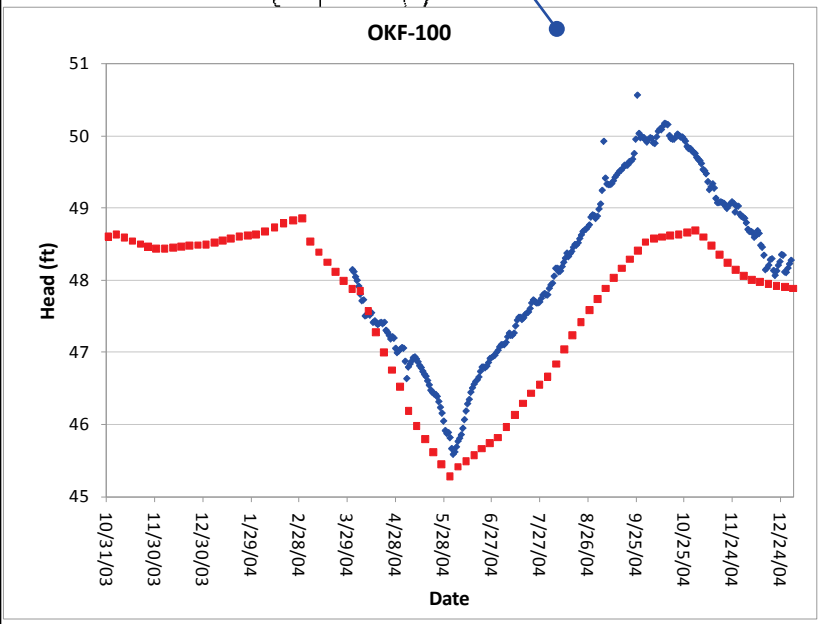

	OKF-100	ROMP 28SWNN
Mean Error	-0.915	0.906
Mean Absolute Error	0.915	1.051
Root Mean Square (RMS)	1.015	1.284
Observed Range	4.98	16.84
RMS as Percentage of Range	20%	8%
Coefficient of Determination (r^2)	0.870	0.959
Nash-Sutcliffe Model Efficiency Coefficient	0.294	0.878

Legend

- Measured Head
- Model Calculated Head

Notes:

Figures 4.41 through 4.94 show the comparison between measured head values and model-calculated head values at a number of observation wells for the calibration period. Although the scales vary on each plot, all plots have a horizontal grid line at each foot. This is to make it easy to determine the range of heads at a glance.

The model used month-long stress periods, so pumping and boundary conditions were input as step functions with constant values throughout each month and sudden changes at the end of each month. For this reason, the model cannot be expected to accurately predict day-to-day head variations in any of these wells. Calibration efforts were aimed at matching general trends and monthly averages.

Starting head conditions for this model were based on the October 2003 steady state calibrated model. Transient calibration efforts were focused on matching the head changes, not the actual heads, so it is not uncommon for residuals in the starting condition to be carried through the entire calibration period. This indicates that the model is correctly predicting responses to hydrogeologic forces even if the calculated head values vary somewhat from the measured values.

Transient SEAWAT Calibration Comparison
Upper Floridan Aquifer (2003-2004)
Final Groundwater Model Calibration Report

Figure 4.68

October 2010

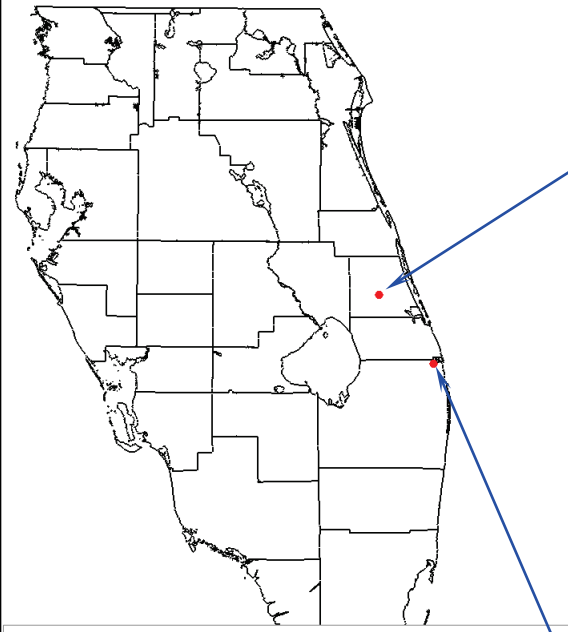

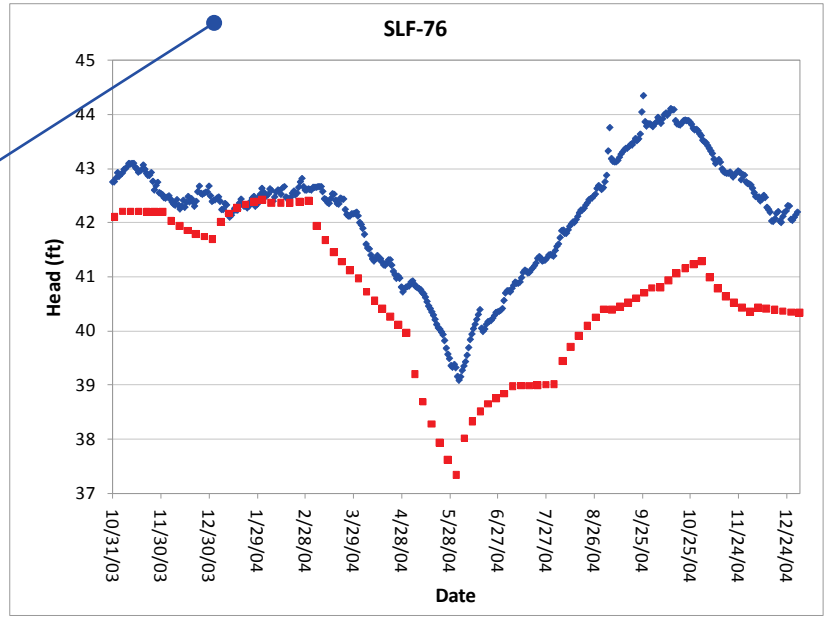

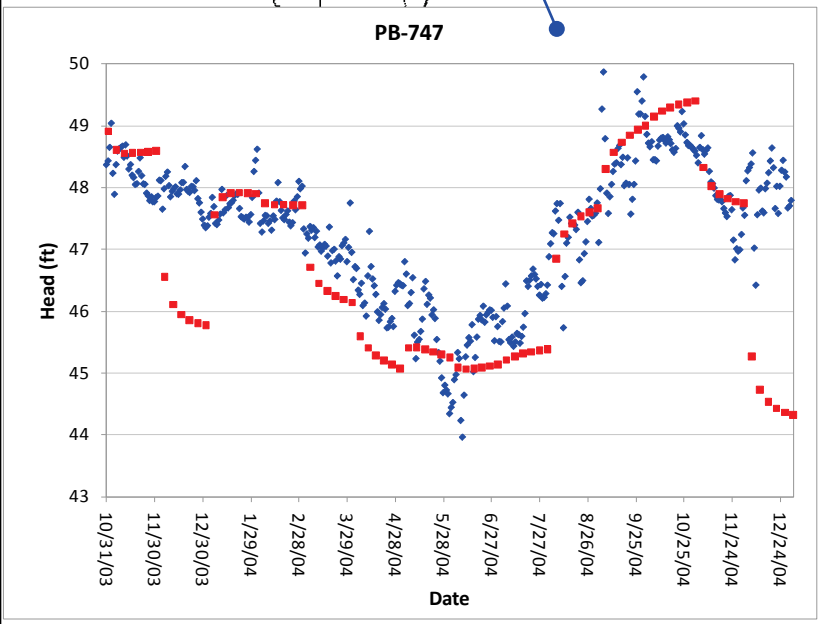

	PB-747	SLF-76
Mean Error	-0.442	-1.501
Mean Absolute Error	0.628	1.501
Root Mean Square (RMS)	0.955	1.762
Observed Range	5.91	5.25
RMS as Percentage of Range	16%	34%
Coefficient of Determination (r^2)	0.647	0.516
Nash-Sutcliffe Model Efficiency Coefficient	0.122	-1.631

Legend

- Measured Head
- Model Calculated Head

Notes:

Figures 4.41 through 4.94 show the comparison between measured head values and model-calculated head values at a number of observation wells for the calibration period. Although the scales vary on each plot, all plots have a horizontal grid line at each foot. This is to make it easy to determine the range of heads at a glance.

The model used month-long stress periods, so pumping and boundary conditions were input as step functions with constant values throughout each month and sudden changes at the end of each month. For this reason, the model cannot be expected to accurately predict day-to-day head variations in any of these wells. Calibration efforts were aimed at matching general trends and monthly averages.

Starting head conditions for this model were based on the October 2003 steady state calibrated model. Transient calibration efforts were focused on matching the head changes, not the actual heads, so it is not uncommon for residuals in the starting condition to be carried through the entire calibration period. This indicates that the model is correctly predicting responses to hydrogeologic forces even if the calculated head values vary somewhat from the measured values.

Transient SEAWAT Calibration Comparison
Upper Floridan Aquifer (2003-2004)
Final Groundwater Model Calibration Report

Figure 4.69

October 2010

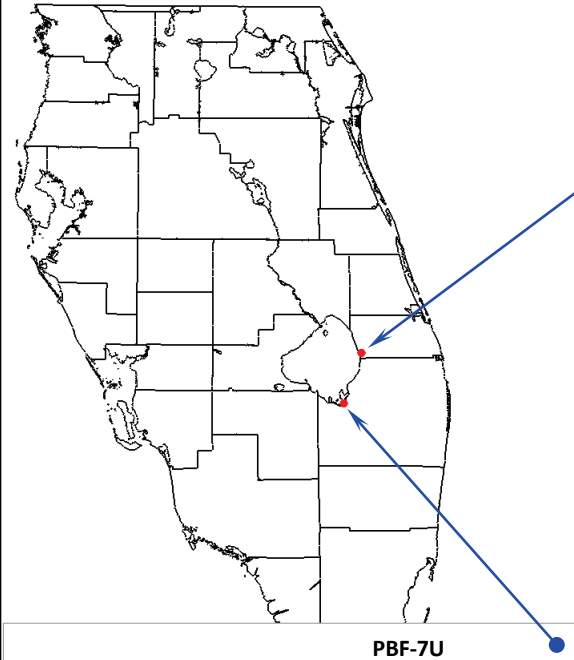

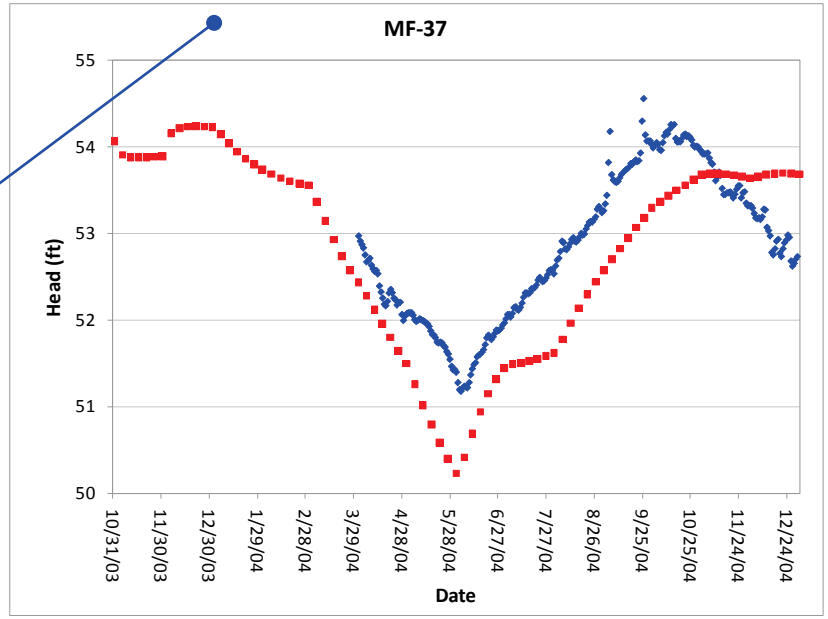

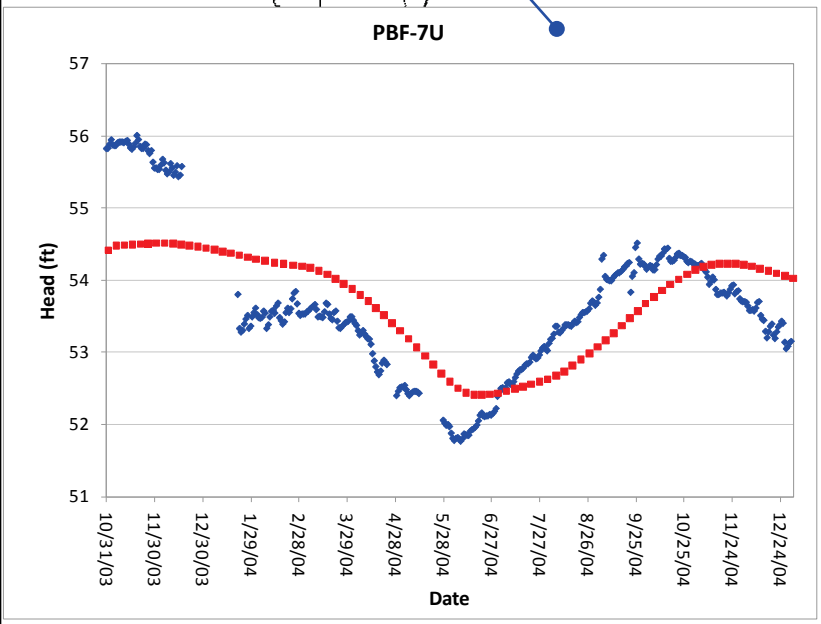

	PBF-7U	MF-37
Mean Error	0.035	-0.506
Mean Absolute Error	0.671	0.678
Root Mean Square (RMS)	0.732	0.729
Observed Range	4.23	3.39
RMS as Percentage of Range	17%	22%
Coefficient of Determination (r^2)	0.499	0.773
Nash-Sutcliffe Model Efficiency Coefficient	0.498	0.230

Legend

- Measured Head
- Model Calculated Head

Notes:

Figures 4.41 through 4.94 show the comparison between measured head values and model-calculated head values at a number of observation wells for the calibration period. Although the scales vary on each plot, all plots have a horizontal grid line at each foot. This is to make it easy to determine the range of heads at a glance.

The model used month-long stress periods, so pumping and boundary conditions were input as step functions with constant values throughout each month and sudden changes at the end of each month. For this reason, the model cannot be expected to accurately predict day-to-day head variations in any of these wells. Calibration efforts were aimed at matching general trends and monthly averages.

Starting head conditions for this model were based on the October 2003 steady state calibrated model. Transient calibration efforts were focused on matching the head changes, not the actual heads, so it is not uncommon for residuals in the starting condition to be carried through the entire calibration period. This indicates that the model is correctly predicting responses to hydrogeologic forces even if the calculated head values vary somewhat from the measured values.

Transient SEAWAT Calibration Comparison
Upper Floridan Aquifer (2003-2004)
Final Groundwater Model Calibration Report

Figure 4.70

October 2010

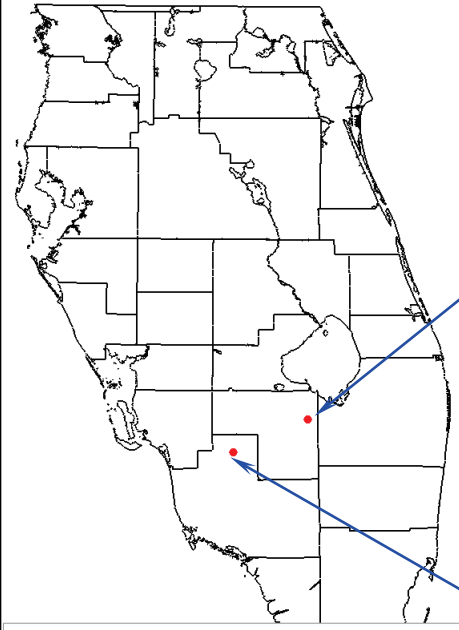

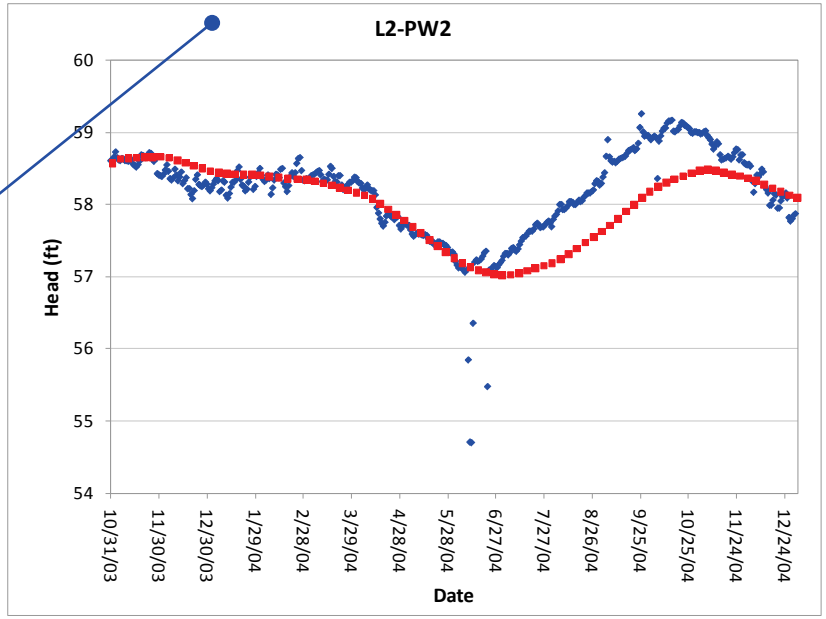

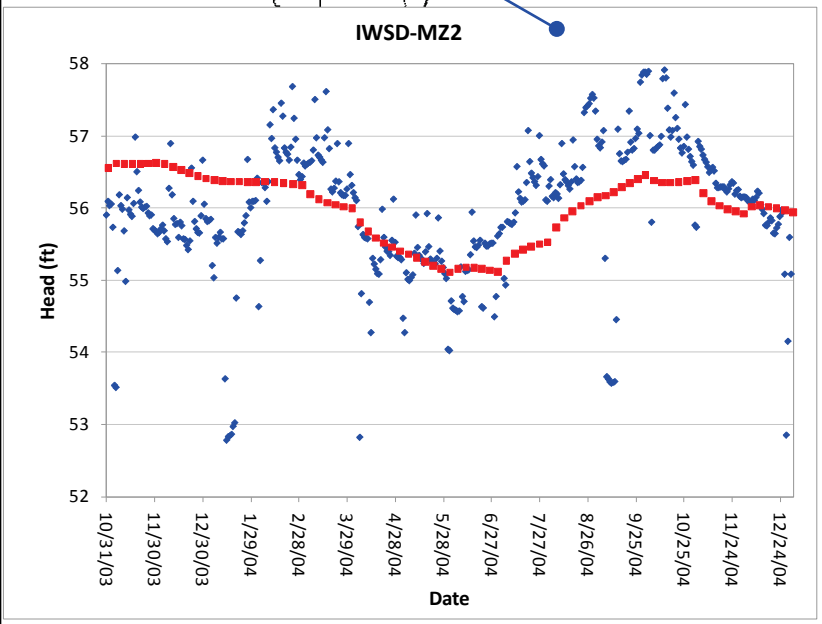

	IWSD-MZ2	L2-PW2
Mean Error	0.022	-0.166
Mean Absolute Error	0.492	0.281
Root Mean Square (RMS)	0.602	0.396
Observed Range	5.13	4.57
RMS as Percentage of Range	12%	9%
Coefficient of Determination (r^2)	0.172	0.600
Nash-Sutcliffe Model Efficiency Coefficient	0.068	0.481

Legend

- Measured Head
- Model Calculated Head

Notes:

Figures 4.41 through 4.94 show the comparison between measured head values and model-calculated head values at a number of observation wells for the calibration period. Although the scales vary on each plot, all plots have a horizontal grid line at each foot. This is to make it easy to determine the range of heads at a glance.

The model used month-long stress periods, so pumping and boundary conditions were input as step functions with constant values throughout each month and sudden changes at the end of each month. For this reason, the model cannot be expected to accurately predict day-to-day head variations in any of these wells. Calibration efforts were aimed at matching general trends and monthly averages.

Starting head conditions for this model were based on the October 2003 steady state calibrated model. Transient calibration efforts were focused on matching the head changes, not the actual heads, so it is not uncommon for residuals in the starting condition to be carried through the entire calibration period. This indicates that the model is correctly predicting responses to hydrogeologic forces even if the calculated head values vary somewhat from the measured values.

Transient SEAWAT Calibration Comparison
Upper Floridan Aquifer (2003-2004)
Final Groundwater Model Calibration Report

Figure 4.71

October 2010

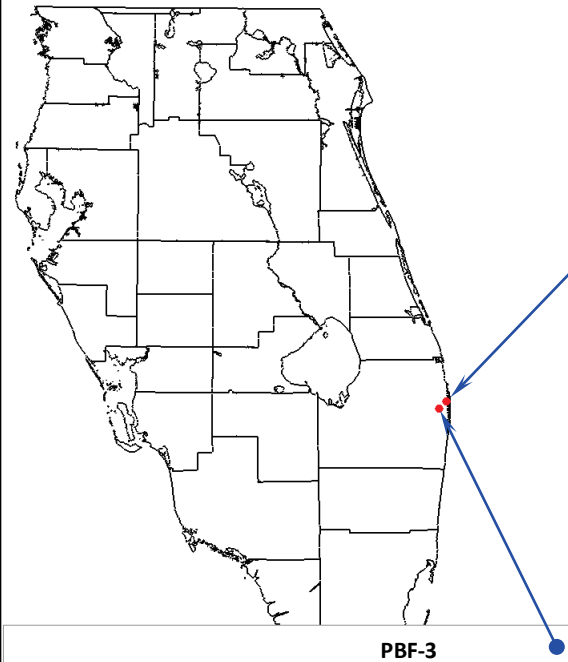

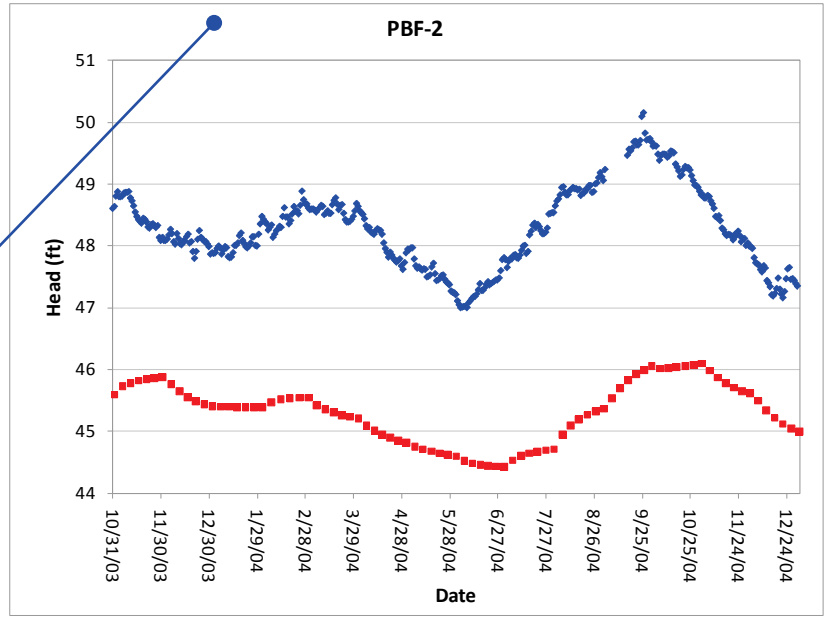

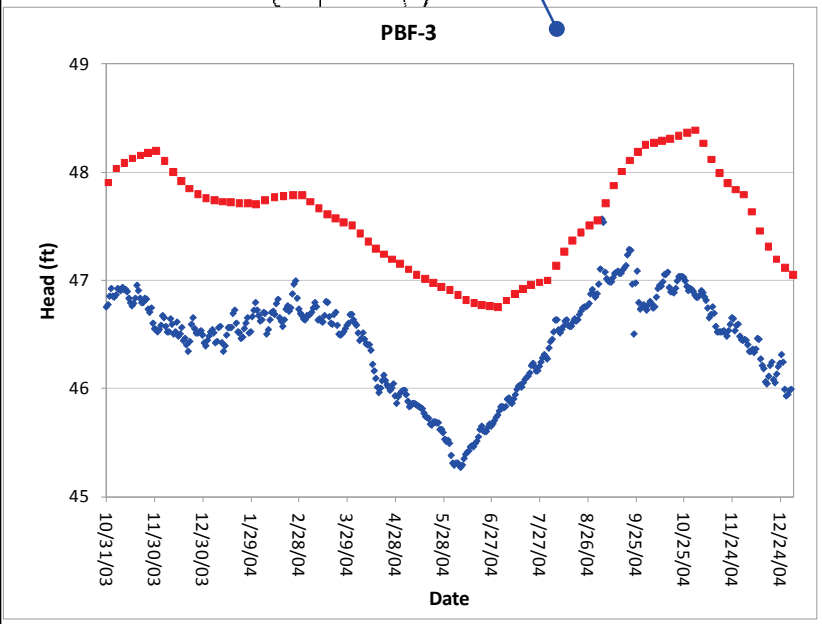

	PBF-3	PBF-2
Mean Error	1.144	-2.997
Mean Absolute Error	1.144	2.997
Root Mean Square (RMS)	1.167	3.036
Observed Range	2.29	3.16
RMS as Percentage of Range	51%	96%
Coefficient of Determination (r^2)	0.750	0.448
Nash-Sutcliffe Model Efficiency Coefficient	-6.436	-21.076

Legend

- Measured Head
- Model Calculated Head

Notes:

Figures 4.41 through 4.94 show the comparison between measured head values and model-calculated head values at a number of observation wells for the calibration period. Although the scales vary on each plot, all plots have a horizontal grid line at each foot. This is to make it easy to determine the range of heads at a glance.

The model used month-long stress periods, so pumping and boundary conditions were input as step functions with constant values throughout each month and sudden changes at the end of each month. For this reason, the model cannot be expected to accurately predict day-to-day head variations in any of these wells. Calibration efforts were aimed at matching general trends and monthly averages.

Starting head conditions for this model were based on the October 2003 steady state calibrated model. Transient calibration efforts were focused on matching the head changes, not the actual heads, so it is not uncommon for residuals in the starting condition to be carried through the entire calibration period. This indicates that the model is correctly predicting responses to hydrogeologic forces even if the calculated head values vary somewhat from the measured values.

Transient SEAWAT Calibration Comparison
Upper Floridan Aquifer (2003-2004)
Final Groundwater Model Calibration Report

Figure 4.72

October 2010

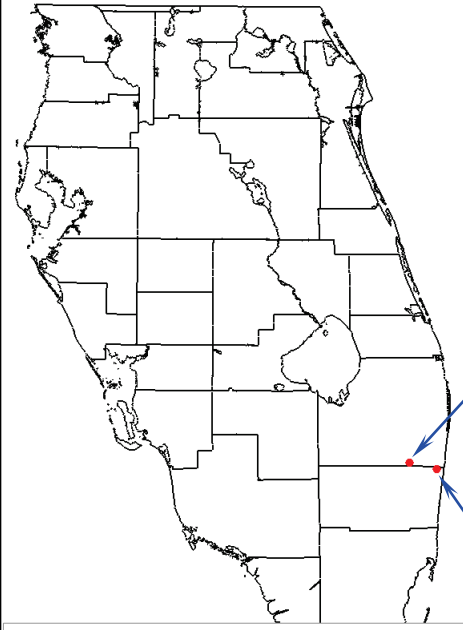

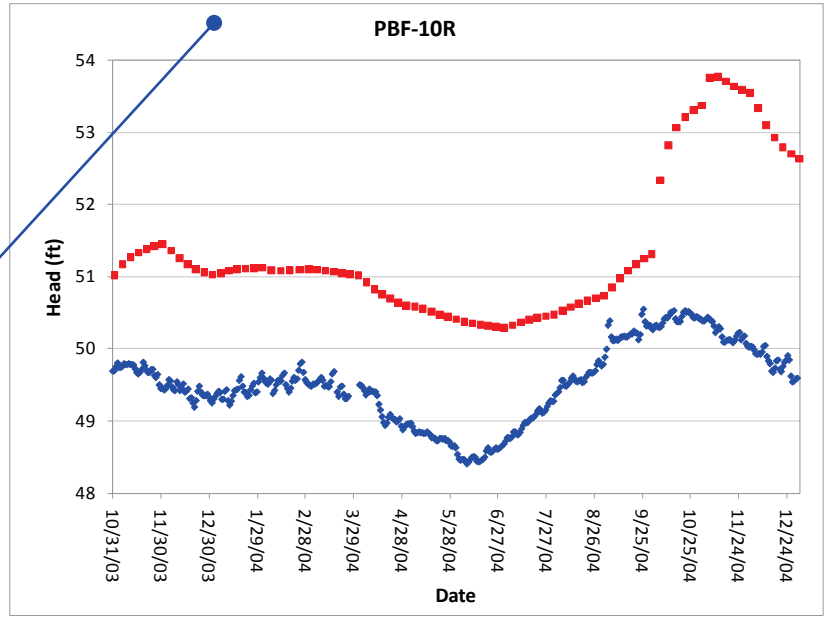

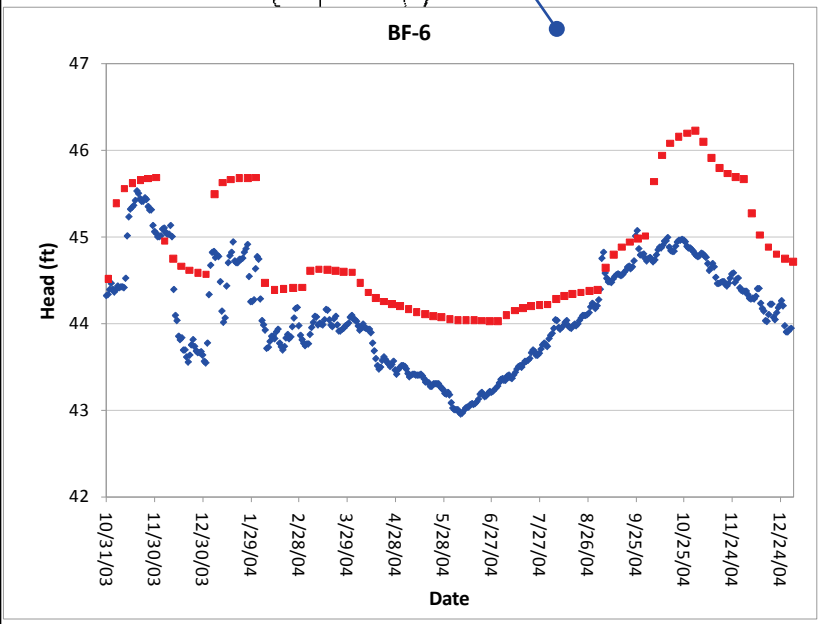

	BF-6	PBF-10R
Mean Error	0.706	1.819
Mean Absolute Error	0.706	1.819
Root Mean Square (RMS)	0.761	1.947
Observed Range	2.58	2.13
RMS as Percentage of Range	27%	91%
Coefficient of Determination (r^2)	0.778	0.550
Nash-Sutcliffe Model Efficiency Coefficient	-0.958	-12.970

Legend

- Measured Head
- Model Calculated Head

Notes:

Figures 4.41 through 4.94 show the comparison between measured head values and model-calculated head values at a number of observation wells for the calibration period. Although the scales vary on each plot, all plots have a horizontal grid line at each foot. This is to make it easy to determine the range of heads at a glance.

The model used month-long stress periods, so pumping and boundary conditions were input as step functions with constant values throughout each month and sudden changes at the end of each month. For this reason, the model cannot be expected to accurately predict day-to-day head variations in any of these wells. Calibration efforts were aimed at matching general trends and monthly averages.

Starting head conditions for this model were based on the October 2003 steady state calibrated model. Transient calibration efforts were focused on matching the head changes, not the actual heads, so it is not uncommon for residuals in the starting condition to be carried through the entire calibration period. This indicates that the model is correctly predicting responses to hydrogeologic forces even if the calculated head values vary somewhat from the measured values.

Transient SEAWAT Calibration Comparison
Upper Floridan Aquifer (2003-2004)
Final Groundwater Model Calibration Report

Figure 4.73

October 2010

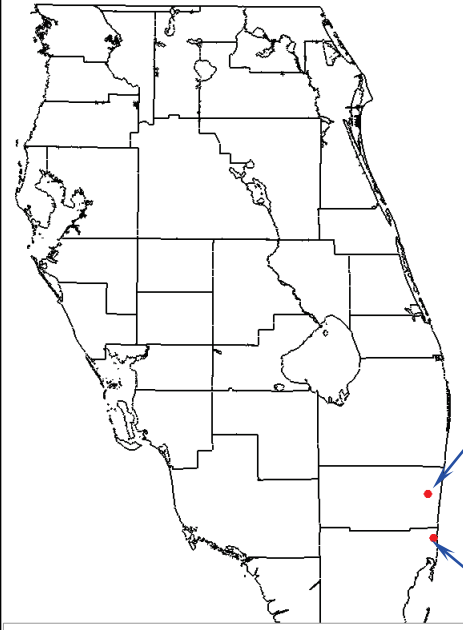

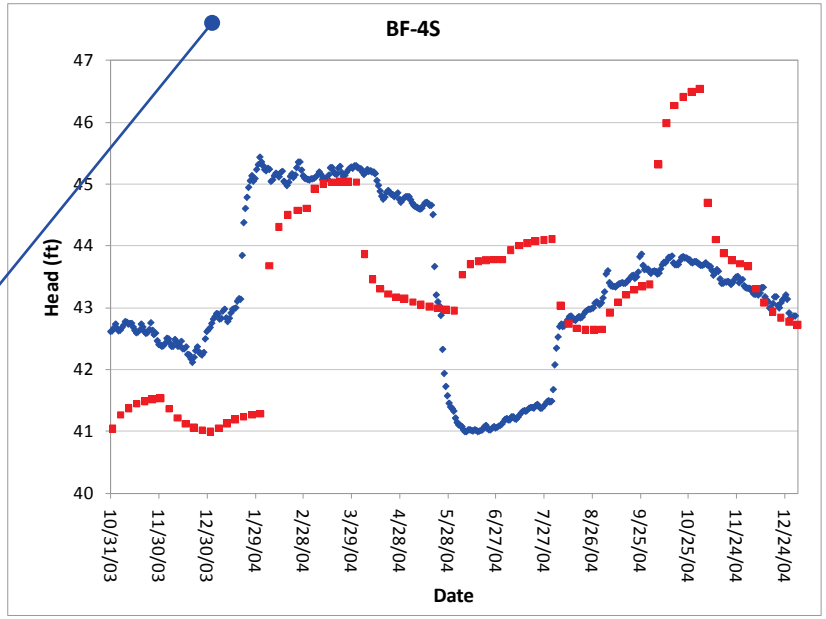

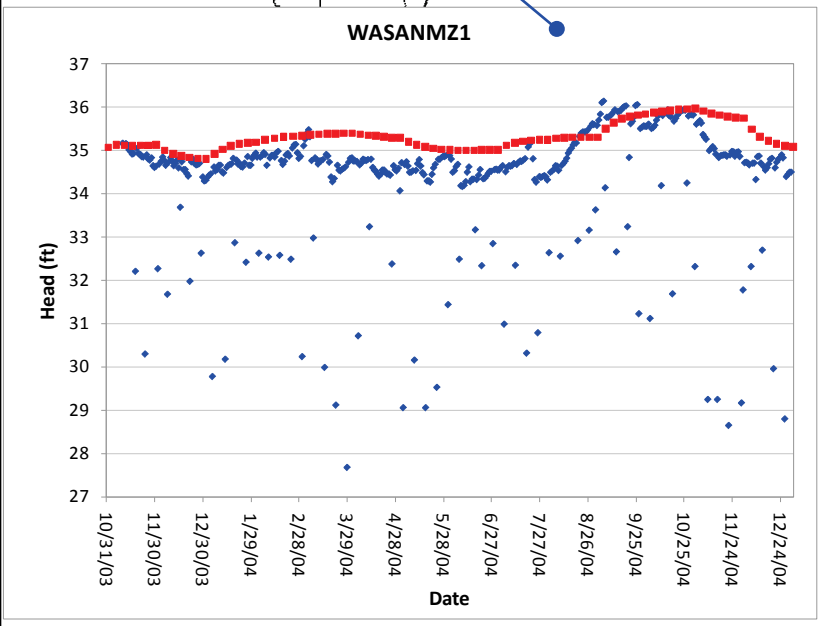

	WASANMZ1	BF-4S
Mean Error	0.876	-0.067
Mean Absolute Error	0.876	1.245
Root Mean Square (RMS)	0.953	1.510
Observed Range	8.46	4.44
RMS as Percentage of Range	11%	34%
Coefficient of Determination (r^2)	0.309	0.080
Nash-Sutcliffe Model Efficiency Coefficient	-3.499	-0.519

Legend

- Measured Head
- Model Calculated Head

Notes:

Figures 4.41 through 4.94 show the comparison between measured head values and model-calculated head values at a number of observation wells for the calibration period. Although the scales vary on each plot, all plots have a horizontal grid line at each foot. This is to make it easy to determine the range of heads at a glance.

The model used month-long stress periods, so pumping and boundary conditions were input as step functions with constant values throughout each month and sudden changes at the end of each month. For this reason, the model cannot be expected to accurately predict day-to-day head variations in any of these wells. Calibration efforts were aimed at matching general trends and monthly averages.

Starting head conditions for this model were based on the October 2003 steady state calibrated model. Transient calibration efforts were focused on matching the head changes, not the actual heads, so it is not uncommon for residuals in the starting condition to be carried through the entire calibration period. This indicates that the model is correctly predicting responses to hydrogeologic forces even if the calculated head values vary somewhat from the measured values.

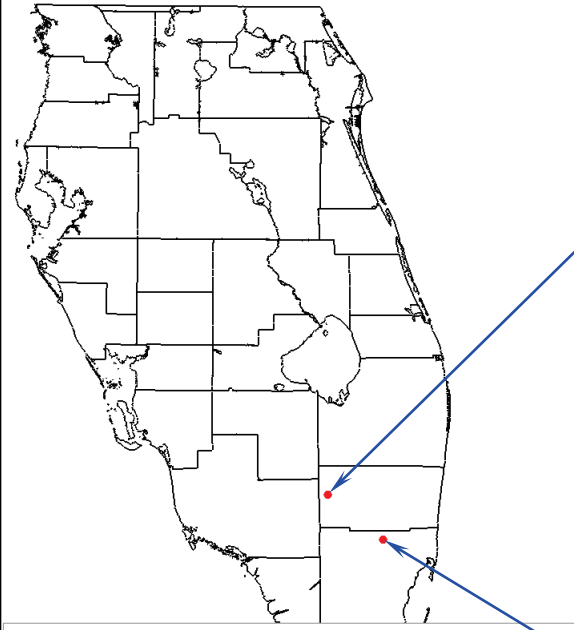

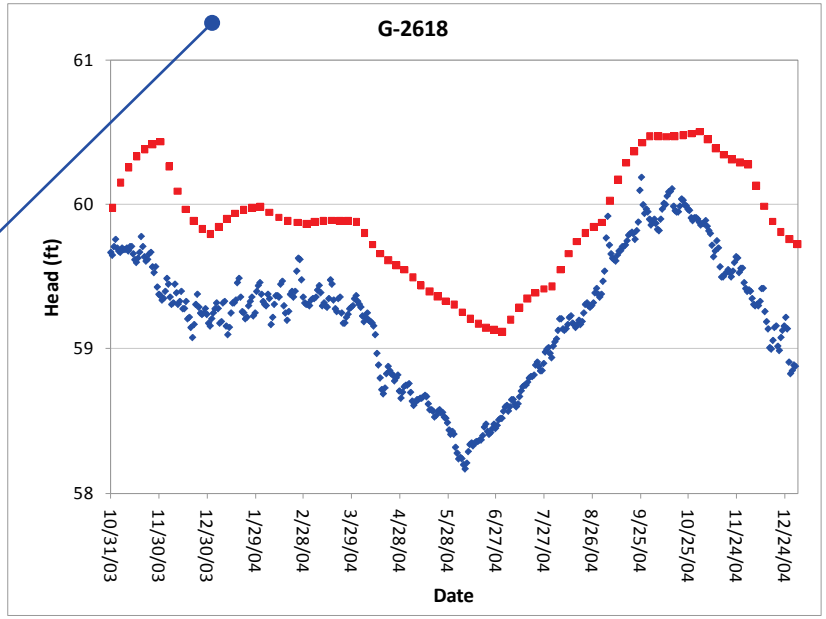

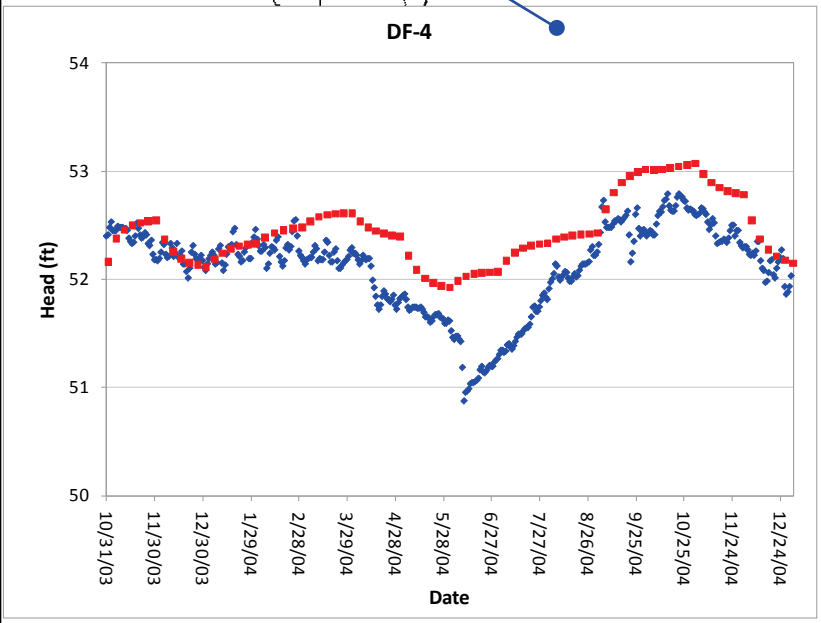

	DF-4	G-2618
Mean Error	0.332	0.640
Mean Absolute Error	0.332	0.640
Root Mean Square (RMS)	0.405	0.654
Observed Range	1.92	2.02
RMS as Percentage of Range	21%	32%
Coefficient of Determination (r^2)	0.629	0.915
Nash-Sutcliffe Model Efficiency Coefficient	-0.130	-1.276

Legend

- Measured Head
- Model Calculated Head

Notes:

Figures 4.41 through 4.94 show the comparison between measured head values and model-calculated head values at a number of observation wells for the calibration period. Although the scales vary on each plot, all plots have a horizontal grid line at each foot. This is to make it easy to determine the range of heads at a glance.

The model used month-long stress periods, so pumping and boundary conditions were input as step functions with constant values throughout each month and sudden changes at the end of each month. For this reason, the model cannot be expected to accurately predict day-to-day head variations in any of these wells. Calibration efforts were aimed at matching general trends and monthly averages.

Starting head conditions for this model were based on the October 2003 steady state calibrated model. Transient calibration efforts were focused on matching the head changes, not the actual heads, so it is not uncommon for residuals in the starting condition to be carried through the entire calibration period. This indicates that the model is correctly predicting responses to hydrogeologic forces even if the calculated head values vary somewhat from the measured values.

Transient SEAWAT Calibration Comparison
Upper Floridan Aquifer (2003-2004)
Final Groundwater Model Calibration Report

Figure 4.75

October 2010

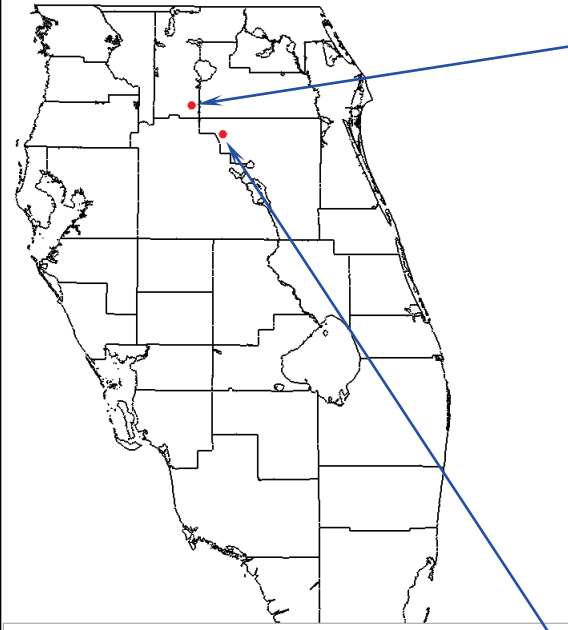

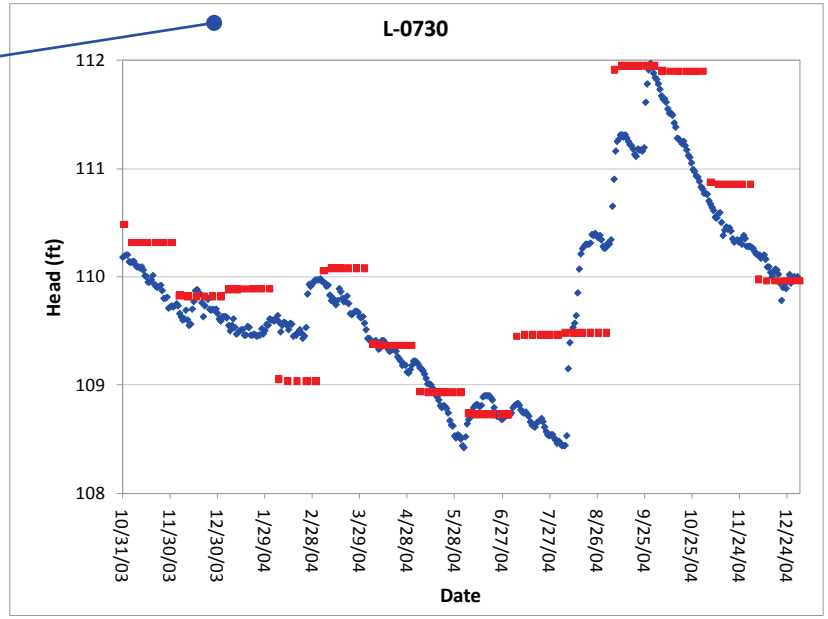

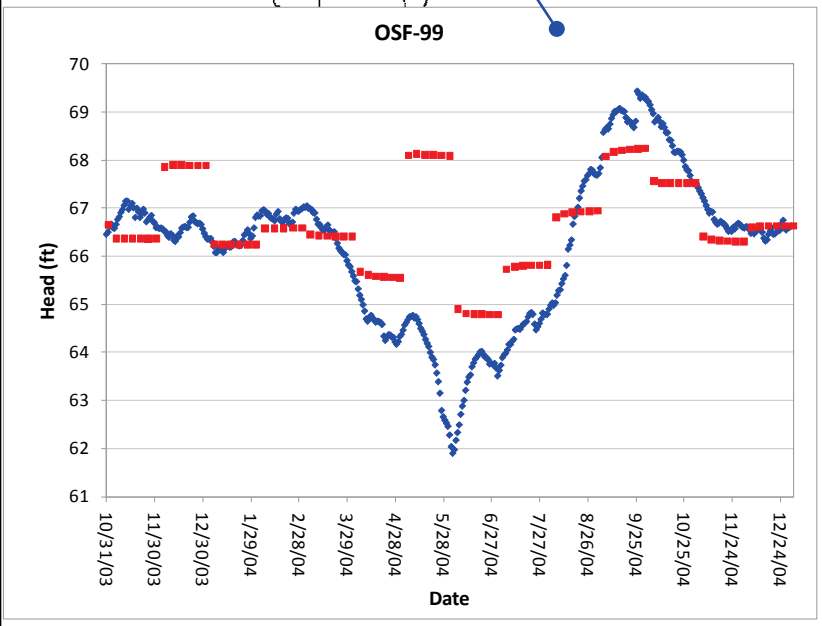

	OSF-99	L-0730
Mean Error	0.487	0.201
Mean Absolute Error	0.886	0.290
Root Mean Square (RMS)	1.287	0.351
Observed Range	7.54	3.55
RMS as Percentage of Range	17%	8%
Coefficient of Determination (r^2)	0.393	0.906
Nash-Sutcliffe Model Efficiency Coefficient	0.277	0.795

Legend

- Measured Head
- Model Calculated Head

Notes:

Figures 4.41 through 4.94 show the comparison between measured head values and model-calculated head values at a number of observation wells for the calibration period. Although the scales vary on each plot, all plots have a horizontal grid line at each foot. This is to make it easy to determine the range of heads at a glance.

The model used month-long stress periods, so pumping and boundary conditions were input as step functions with constant values throughout each month and sudden changes at the end of each month. For this reason, the model cannot be expected to accurately predict day-to-day head variations in any of these wells. Calibration efforts were aimed at matching general trends and monthly averages.

Starting head conditions for this model were based on the October 2003 steady state calibrated model. Transient calibration efforts were focused on matching the head changes, not the actual heads, so it is not uncommon for residuals in the starting condition to be carried through the entire calibration period. This indicates that the model is correctly predicting responses to hydrogeologic forces even if the calculated head values vary somewhat from the measured values.

Transient SEAWAT Calibration Comparison
Avon Park Permeable Zone (2003-2004)
Final Groundwater Model Calibration Report

Figure 4.76

October 2010

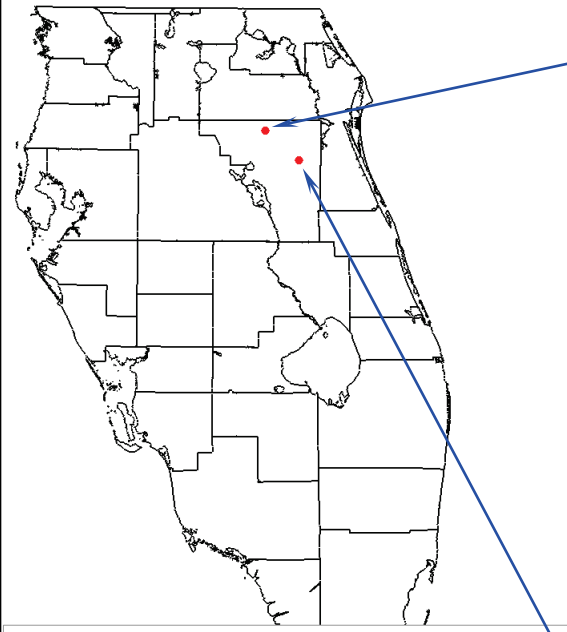

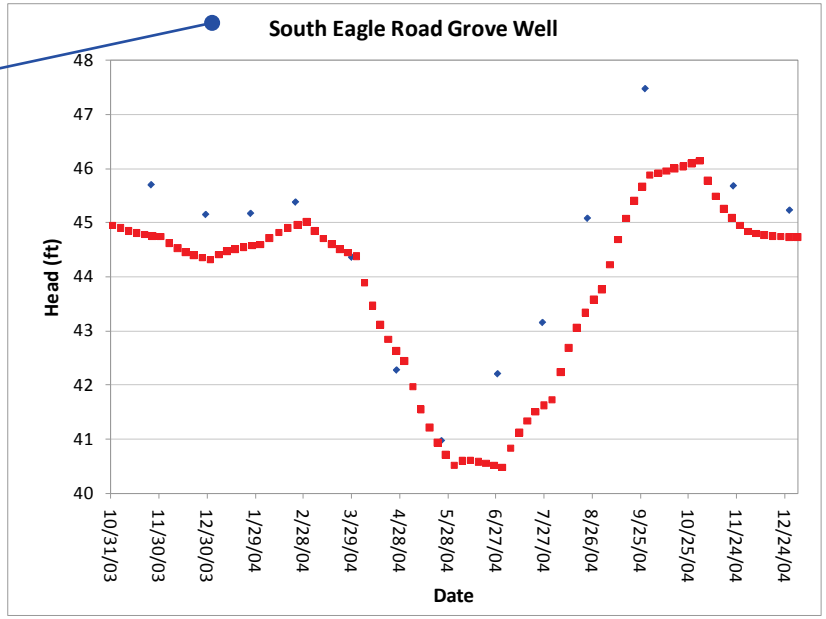

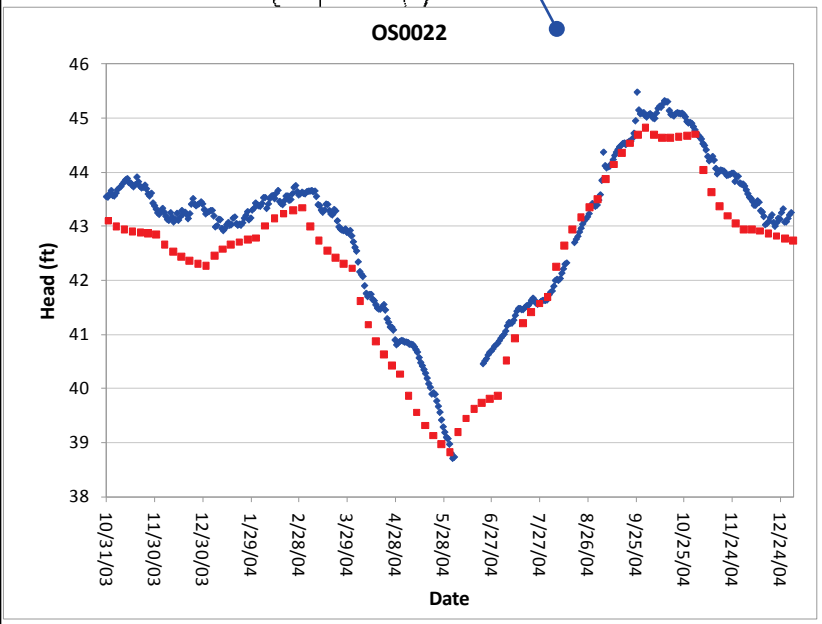

	OS0022	South Eagle Road
Mean Error	-0.482	-0.781
Mean Absolute Error	0.499	1.081
Root Mean Square (RMS)	0.528	1.332
Observed Range	6.77	6.52
RMS as Percentage of Range	8%	20%
Coefficient of Determination (r^2)	0.981	0.626
Nash-Sutcliffe Model Efficiency Coefficient	0.867	0.406

Legend

- Measured Head
- Model Calculated Head

Notes:

Figures 4.41 through 4.94 show the comparison between measured head values and model-calculated head values at a number of observation wells for the calibration period. Although the scales vary on each plot, all plots have a horizontal grid line at each foot. This is to make it easy to determine the range of heads at a glance.

The model used month-long stress periods, so pumping and boundary conditions were input as step functions with constant values throughout each month and sudden changes at the end of each month. For this reason, the model cannot be expected to accurately predict day-to-day head variations in any of these wells. Calibration efforts were aimed at matching general trends and monthly averages.

Starting head conditions for this model were based on the October 2003 steady state calibrated model. Transient calibration efforts were focused on matching the head changes, not the actual heads, so it is not uncommon for residuals in the starting condition to be carried through the entire calibration period. This indicates that the model is correctly predicting responses to hydrogeologic forces even if the calculated head values vary somewhat from the measured values.

Transient SEAWAT Calibration Comparison
Avon Park Permeable Zone (2003-2004)
Final Groundwater Model Calibration Report

Figure 4.77

October 2010

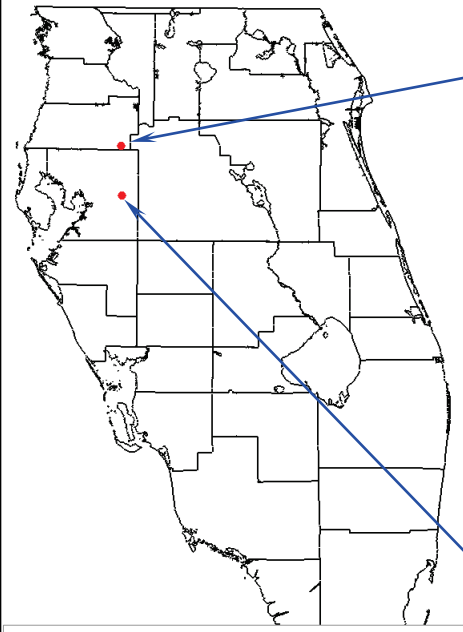

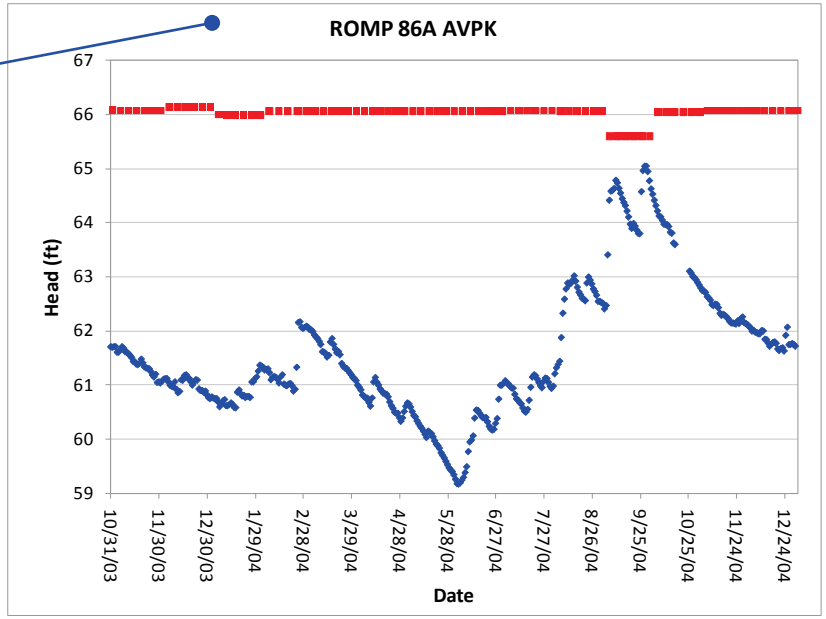

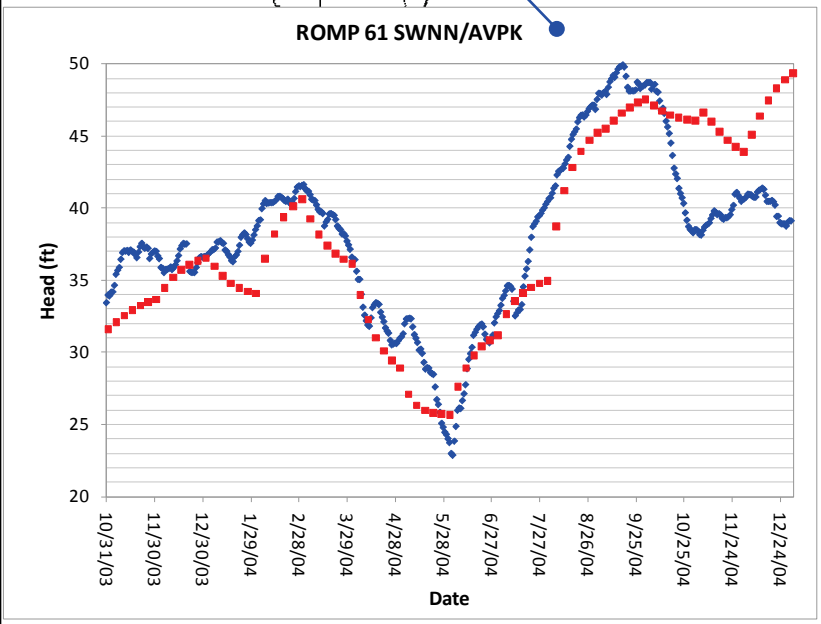

	ROMP 61 SWNN/ AVPK	ROMP 86A AVPK
Mean Error	-0.377	4.419
Mean Absolute Error	2.752	4.419
Root Mean Square (RMS)	3.424	4.596
Observed Range	27.07	5.88
RMS as Percentage of Range	10%	78%
Coefficient of Determination (r^2)	0.732	0.449
Nash-Sutcliffe Model Efficiency Coefficient	0.592	-13.935

Legend

- Measured Head
- Model Calculated Head

Notes:

Figures 4.41 through 4.94 show the comparison between measured head values and model-calculated head values at a number of observation wells for the calibration period. Although the scales vary on each plot, all plots have a horizontal grid line at each foot. This is to make it easy to determine the range of heads at a glance.

The model used month-long stress periods, so pumping and boundary conditions were input as step functions with constant values throughout each month and sudden changes at the end of each month. For this reason, the model cannot be expected to accurately predict day-to-day head variations in any of these wells. Calibration efforts were aimed at matching general trends and monthly averages.

Starting head conditions for this model were based on the October 2003 steady state calibrated model. Transient calibration efforts were focused on matching the head changes, not the actual heads, so it is not uncommon for residuals in the starting condition to be carried through the entire calibration period. This indicates that the model is correctly predicting responses to hydrogeologic forces even if the calculated head values vary somewhat from the measured values.

Transient SEAWAT Calibration Comparison
Avon Park Permeable Zone (2003-2004)
Final Groundwater Model Calibration Report

Figure 4.78

October 2010

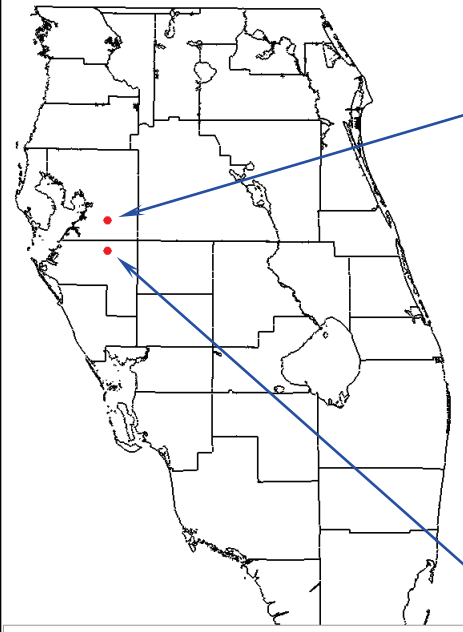

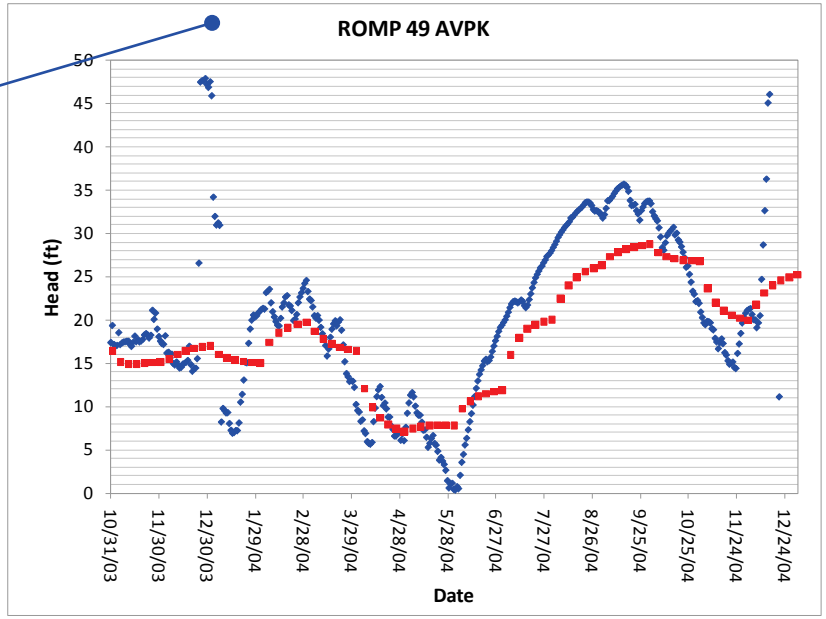

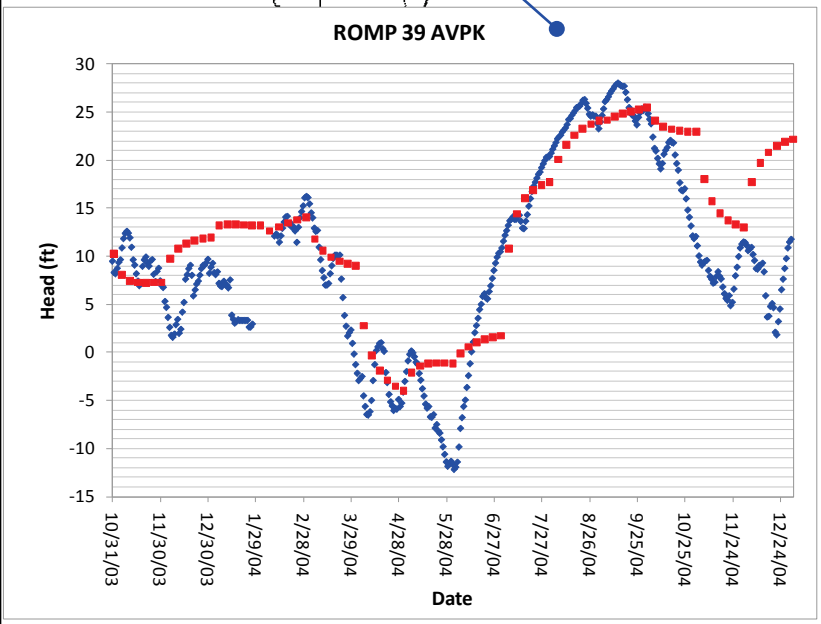

	ROMP 39 AVPK	ROMP 49 AVPK
Mean Error	2.730	-2.172
Mean Absolute Error	3.839	3.285
Root Mean Square (RMS)	4.974	4.004
Observed Range	40.19	47.46
RMS as Percentage of Range	10%	8%
Coefficient of Determination (r^2)	0.787	0.841
Nash-Sutcliffe Model Efficiency Coefficient	0.694	0.741

Legend

- Measured Head
- Model Calculated Head

Notes:

Figures 4.41 through 4.94 show the comparison between measured head values and model-calculated head values at a number of observation wells for the calibration period. Although the scales vary on each plot, all plots have a horizontal grid line at each foot. This is to make it easy to determine the range of heads at a glance.

The model used month-long stress periods, so pumping and boundary conditions were input as step functions with constant values throughout each month and sudden changes at the end of each month. For this reason, the model cannot be expected to accurately predict day-to-day head variations in any of these wells. Calibration efforts were aimed at matching general trends and monthly averages.

Starting head conditions for this model were based on the October 2003 steady state calibrated model. Transient calibration efforts were focused on matching the head changes, not the actual heads, so it is not uncommon for residuals in the starting condition to be carried through the entire calibration period. This indicates that the model is correctly predicting responses to hydrogeologic forces even if the calculated head values vary somewhat from the measured values.

Transient SEAWAT Calibration Comparison
Avon Park Permeable Zone (2003-2004)
Final Groundwater Model Calibration Report

Figure 4.79

October 2010

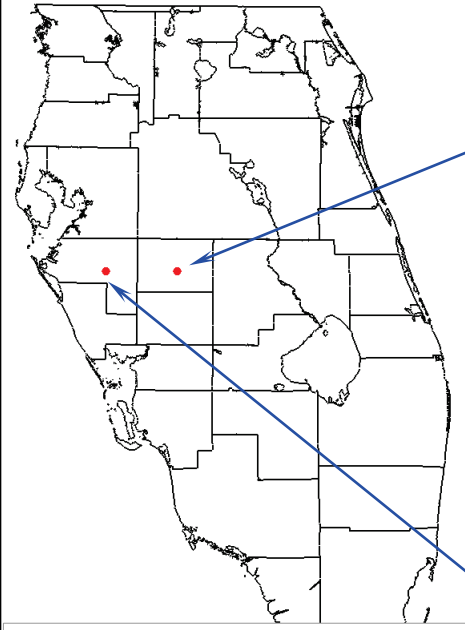

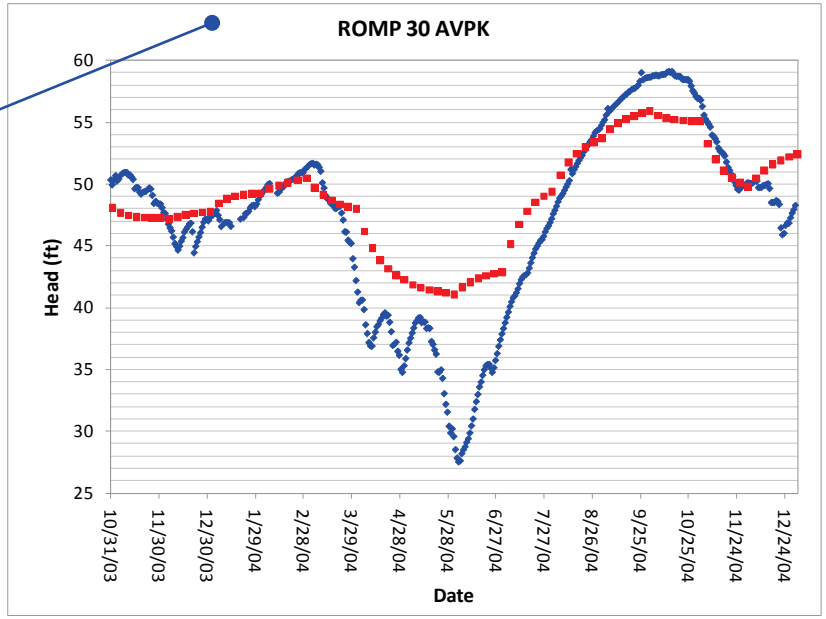

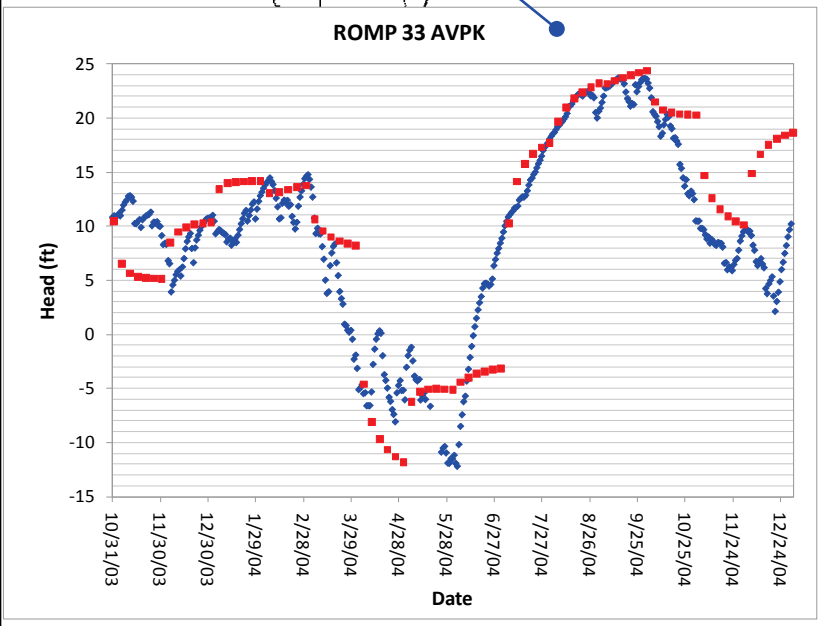

	ROMP 33 AVPK	ROMP 30 AVPK
Mean Error	1.187	1.670
Mean Absolute Error	2.780	2.866
Root Mean Square (RMS)	3.700	3.917
Observed Range	35.91	31.62
RMS as Percentage of Range	10%	12%
Coefficient of Determination (r^2)	0.864	0.925
Nash-Sutcliffe Model Efficiency Coefficient	0.801	0.708

Legend

- Measured Head
- Model Calculated Head

Notes:

Figures 4.41 through 4.94 show the comparison between measured head values and model-calculated head values at a number of observation wells for the calibration period. Although the scales vary on each plot, all plots have a horizontal grid line at each foot. This is to make it easy to determine the range of heads at a glance.

The model used month-long stress periods, so pumping and boundary conditions were input as step functions with constant values throughout each month and sudden changes at the end of each month. For this reason, the model cannot be expected to accurately predict day-to-day head variations in any of these wells. Calibration efforts were aimed at matching general trends and monthly averages.

Starting head conditions for this model were based on the October 2003 steady state calibrated model. Transient calibration efforts were focused on matching the head changes, not the actual heads, so it is not uncommon for residuals in the starting condition to be carried through the entire calibration period. This indicates that the model is correctly predicting responses to hydrogeologic forces even if the calculated head values vary somewhat from the measured values.

Transient SEAWAT Calibration Comparison
Avon Park Permeable Zone (2003-2004)
Final Groundwater Model Calibration Report

Figure 4.80

October 2010

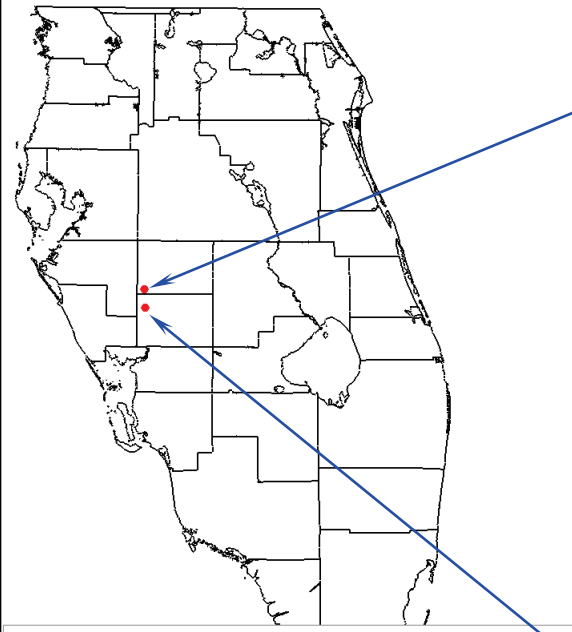

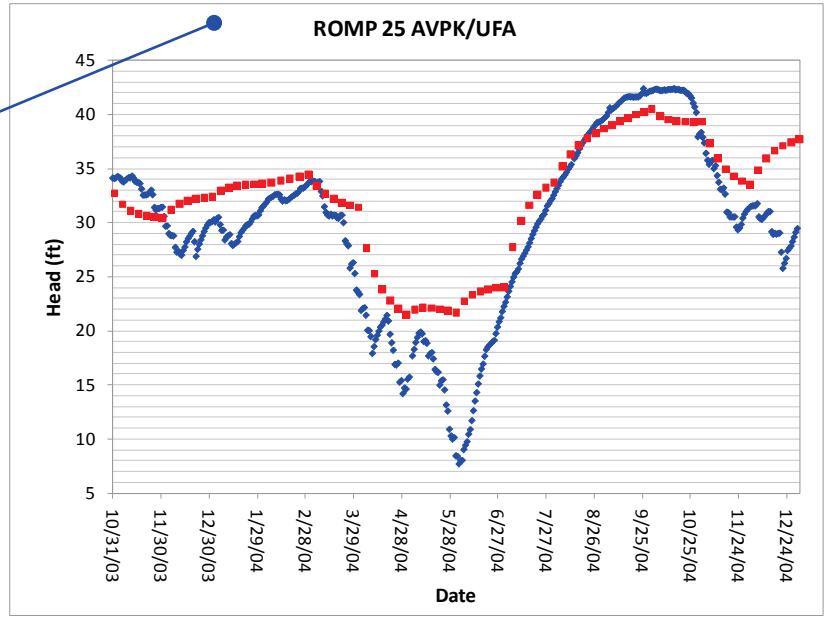

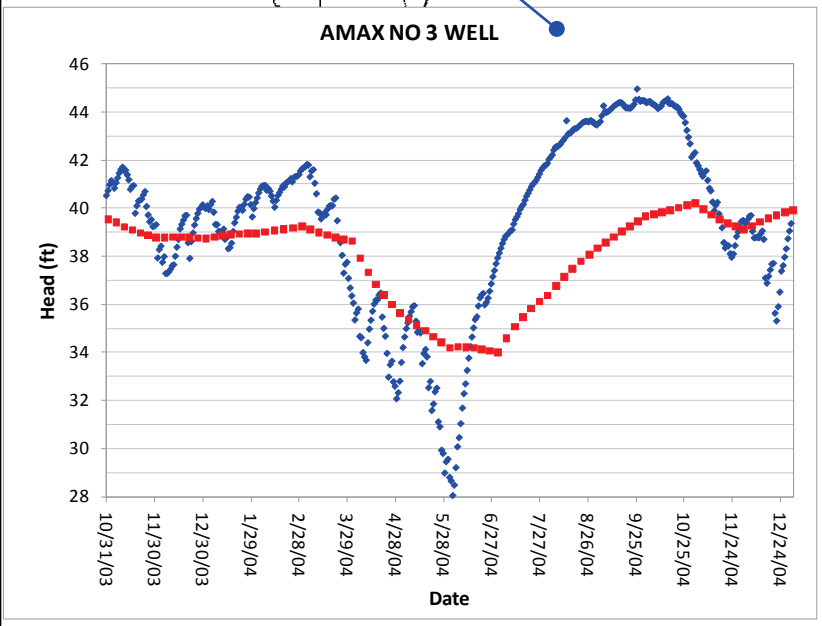

	AMAX NO 3	ROMP 25 AVPK/UFA
Mean Error	-1.355	2.717
Mean Absolute Error	2.249	3.547
Root Mean Square (RMS)	2.937	4.298
Observed Range	16.92	34.73
RMS as Percentage of Range	17%	12%
Coefficient of Determination (r^2)	0.405	0.899
Nash-Sutcliffe Model Efficiency Coefficient	0.234	0.706

Legend

- Measured Head
- Model Calculated Head

Notes:

Figures 4.41 through 4.94 show the comparison between measured head values and model-calculated head values at a number of observation wells for the calibration period. Although the scales vary on each plot, all plots have a horizontal grid line at each foot. This is to make it easy to determine the range of heads at a glance.

The model used month-long stress periods, so pumping and boundary conditions were input as step functions with constant values throughout each month and sudden changes at the end of each month. For this reason, the model cannot be expected to accurately predict day-to-day head variations in any of these wells. Calibration efforts were aimed at matching general trends and monthly averages.

Starting head conditions for this model were based on the October 2003 steady state calibrated model. Transient calibration efforts were focused on matching the head changes, not the actual heads, so it is not uncommon for residuals in the starting condition to be carried through the entire calibration period. This indicates that the model is correctly predicting responses to hydrogeologic forces even if the calculated head values vary somewhat from the measured values.

Transient SEAWAT Calibration Comparison
Avon Park Permeable Zone (2003-2004)
Final Groundwater Model Calibration Report

Figure 4.81

October 2010

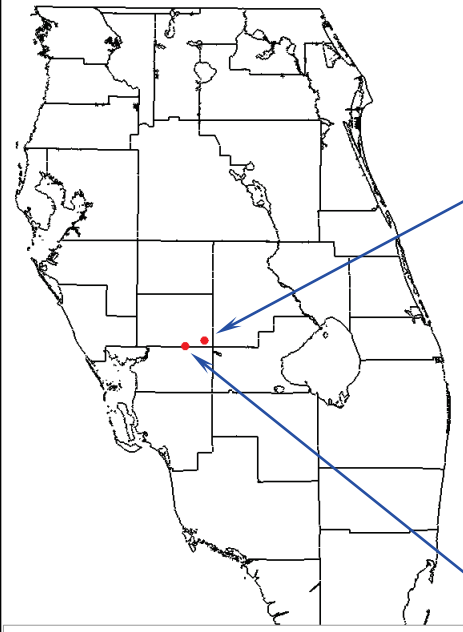

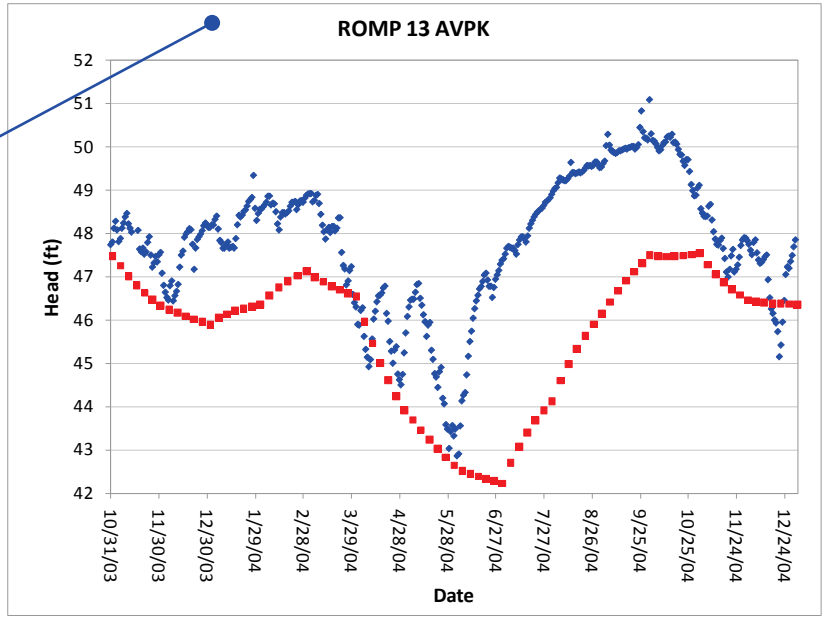

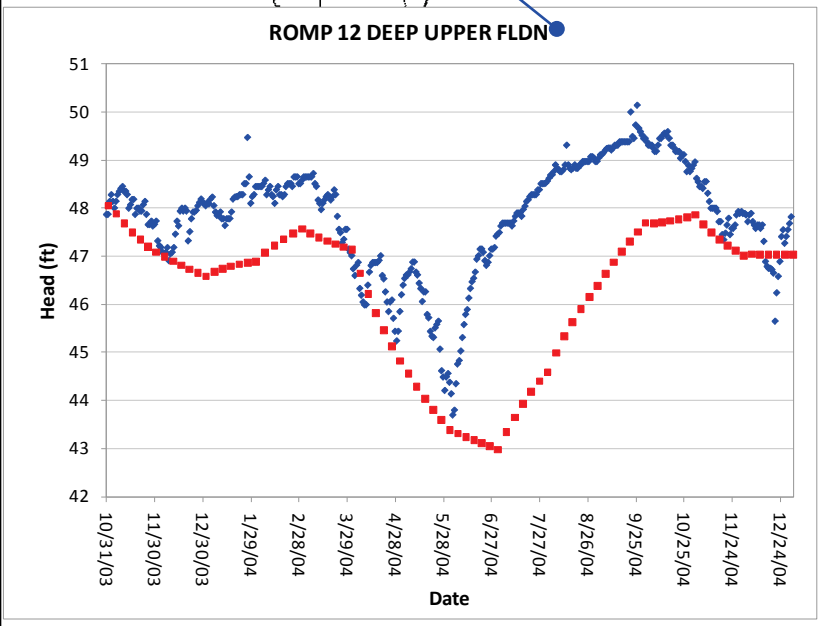

	ROMP 12 DEEP	ROMP 13 AVPK
Mean Error	-1.557	-2.080
Mean Absolute Error	1.557	2.080
Root Mean Square (RMS)	1.966	2.475
Observed Range	6.44	8.23
RMS as Percentage of Range	31%	30%
Coefficient of Determination (r^2)	0.344	0.357
Nash-Sutcliffe Model Efficiency Coefficient	-2.478	-2.043

Legend

- Measured Head
- Model Calculated Head

Notes:

Figures 4.41 through 4.94 show the comparison between measured head values and model-calculated head values at a number of observation wells for the calibration period. Although the scales vary on each plot, all plots have a horizontal grid line at each foot. This is to make it easy to determine the range of heads at a glance.

The model used month-long stress periods, so pumping and boundary conditions were input as step functions with constant values throughout each month and sudden changes at the end of each month. For this reason, the model cannot be expected to accurately predict day-to-day head variations in any of these wells. Calibration efforts were aimed at matching general trends and monthly averages.

Starting head conditions for this model were based on the October 2003 steady state calibrated model. Transient calibration efforts were focused on matching the head changes, not the actual heads, so it is not uncommon for residuals in the starting condition to be carried through the entire calibration period. This indicates that the model is correctly predicting responses to hydrogeologic forces even if the calculated head values vary somewhat from the measured values.

Transient SEAWAT Calibration Comparison
Avon Park Permeable Zone (2003-2004)
Final Groundwater Model Calibration Report

Figure 4.82

October 2010

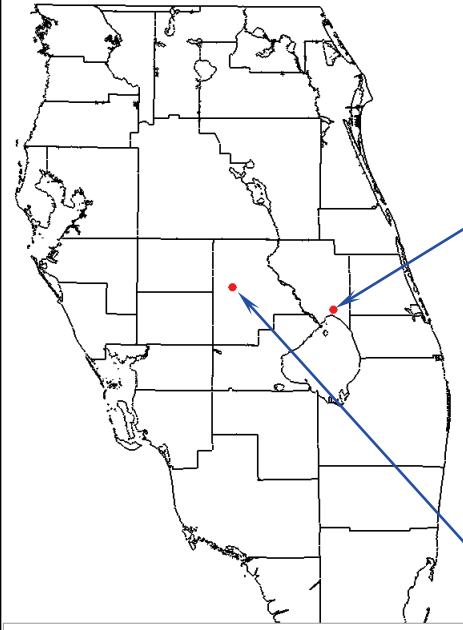

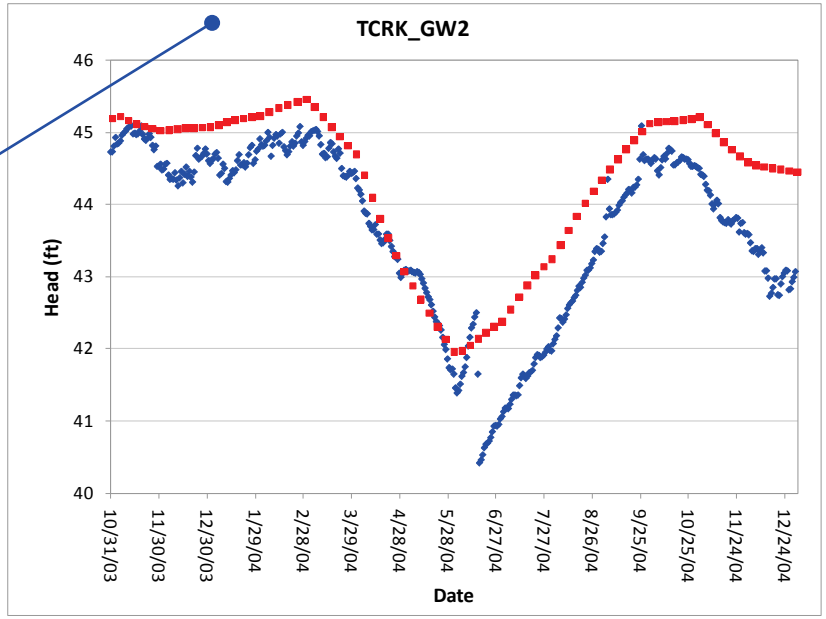

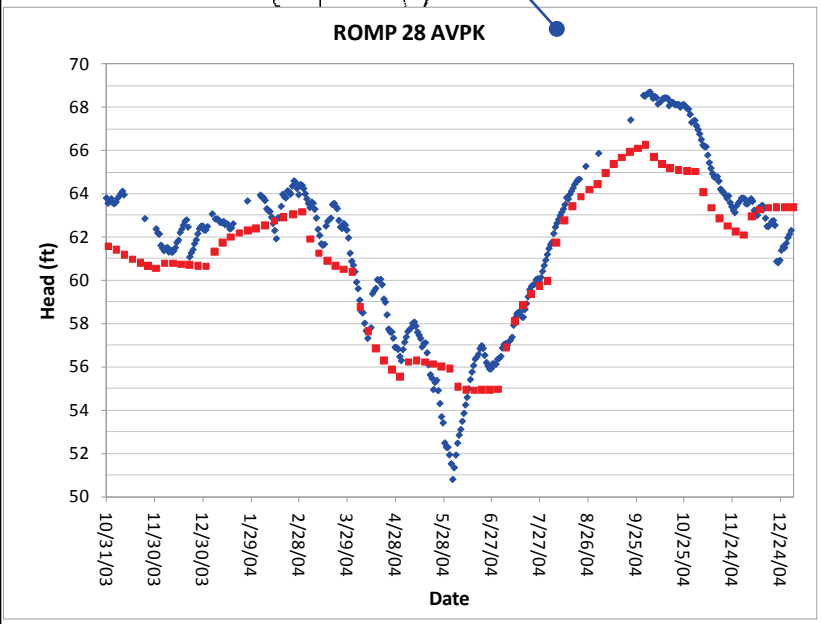

	ROMP 28 AVPK	TCRK_ GW2
Mean Error	-1.053	0.643
Mean Absolute Error	1.173	0.644
Root Mean Square (RMS)	1.408	0.742
Observed Range	17.93	4.67
RMS as Percentage of Range	8%	14%
Coefficient of Determination (r^2)	0.958	0.899
Nash-Sutcliffe Model Efficiency Coefficient	0.857	0.589

Legend

- Measured Head
- Model Calculated Head

Notes:

Figures 4.41 through 4.94 show the comparison between measured head values and model-calculated head values at a number of observation wells for the calibration period. Although the scales vary on each plot, all plots have a horizontal grid line at each foot. This is to make it easy to determine the range of heads at a glance.

The model used month-long stress periods, so pumping and boundary conditions were input as step functions with constant values throughout each month and sudden changes at the end of each month. For this reason, the model cannot be expected to accurately predict day-to-day head variations in any of these wells. Calibration efforts were aimed at matching general trends and monthly averages.

Starting head conditions for this model were based on the October 2003 steady state calibrated model. Transient calibration efforts were focused on matching the head changes, not the actual heads, so it is not uncommon for residuals in the starting condition to be carried through the entire calibration period. This indicates that the model is correctly predicting responses to hydrogeologic forces even if the calculated head values vary somewhat from the measured values.

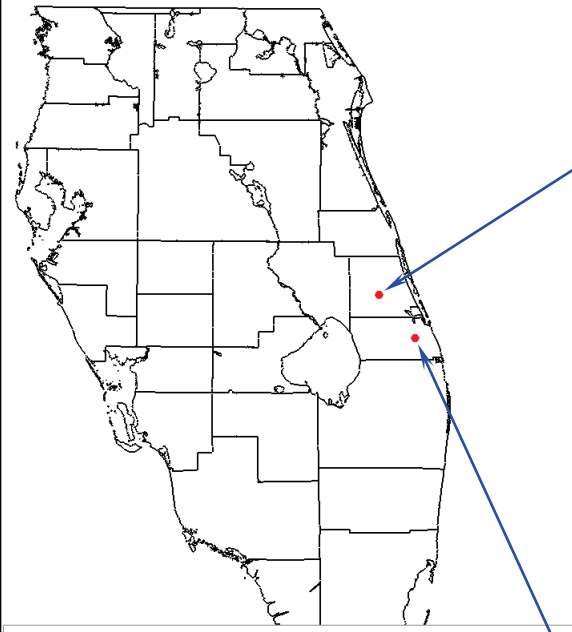

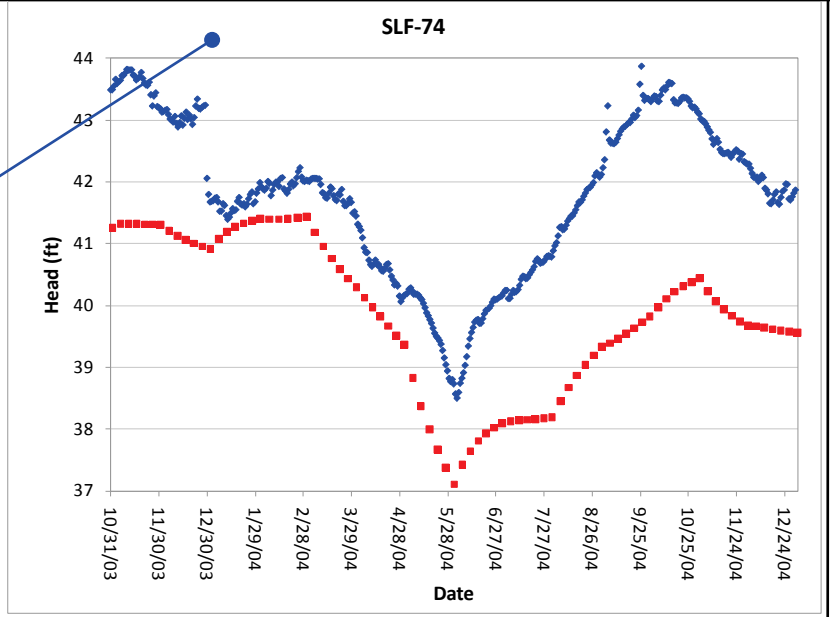

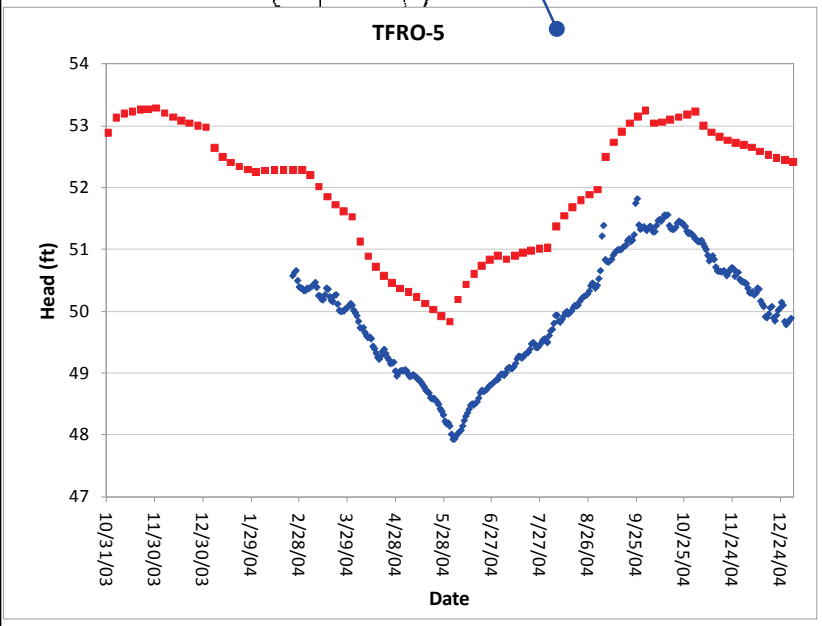

	TFRO-5	SLF-74
Mean Error	1.773	-1.914
Mean Absolute Error	1.773	1.914
Root Mean Square (RMS)	1.797	2.128
Observed Range	3.88	5.36
RMS as Percentage of Range	46%	40%
Coefficient of Determination (r^2)	0.916	0.512
Nash-Sutcliffe Model Efficiency Coefficient	-2.986	-1.924

Legend

- Measured Head
- Model Calculated Head

Notes:

Figures 4.41 through 4.94 show the comparison between measured head values and model-calculated head values at a number of observation wells for the calibration period. Although the scales vary on each plot, all plots have a horizontal grid line at each foot. This is to make it easy to determine the range of heads at a glance.

The model used month-long stress periods, so pumping and boundary conditions were input as step functions with constant values throughout each month and sudden changes at the end of each month. For this reason, the model cannot be expected to accurately predict day-to-day head variations in any of these wells. Calibration efforts were aimed at matching general trends and monthly averages.

Starting head conditions for this model were based on the October 2003 steady state calibrated model. Transient calibration efforts were focused on matching the head changes, not the actual heads, so it is not uncommon for residuals in the starting condition to be carried through the entire calibration period. This indicates that the model is correctly predicting responses to hydrogeologic forces even if the calculated head values vary somewhat from the measured values.

Transient SEAWAT Calibration Comparison
Avon Park Permeable Zone (2003-2004)
Final Groundwater Model Calibration Report

Figure 4.84

October 2010

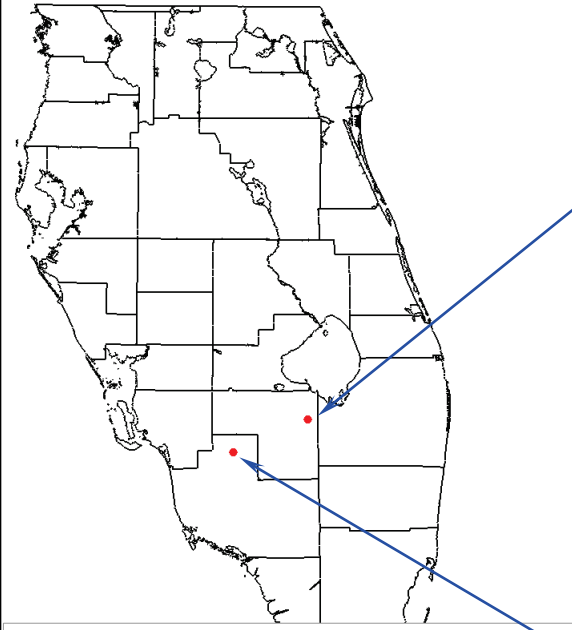

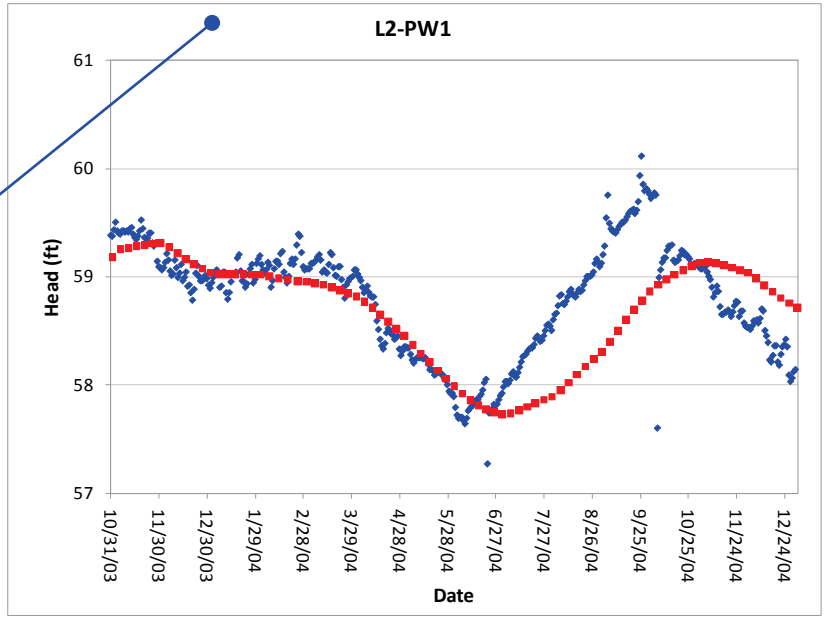

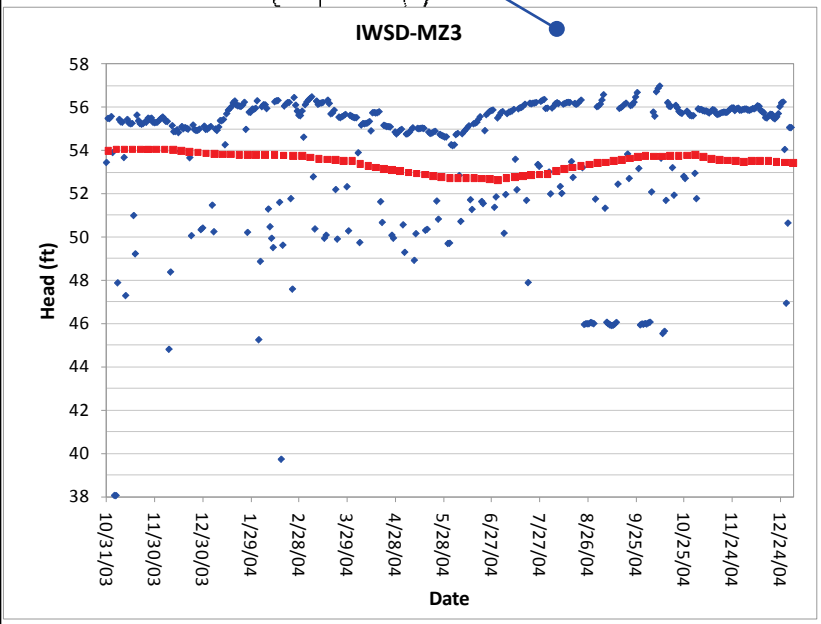

	IWSD-MZ3	L2-PW1
Mean Error	-0.545	-0.124
Mean Absolute Error	1.037	0.293
Root Mean Square (RMS)	1.203	0.414
Observed Range	18.92	2.84
RMS as Percentage of Range	6%	15%
Coefficient of Determination (r^2)	0.003	0.442
Nash-Sutcliffe Model Efficiency Coefficient	-0.558	0.265

Legend

- Measured Head
- Model Calculated Head

Notes:

Figures 4.41 through 4.94 show the comparison between measured head values and model-calculated head values at a number of observation wells for the calibration period. Although the scales vary on each plot, all plots have a horizontal grid line at each foot. This is to make it easy to determine the range of heads at a glance.

The model used month-long stress periods, so pumping and boundary conditions were input as step functions with constant values throughout each month and sudden changes at the end of each month. For this reason, the model cannot be expected to accurately predict day-to-day head variations in any of these wells. Calibration efforts were aimed at matching general trends and monthly averages.

Starting head conditions for this model were based on the October 2003 steady state calibrated model. Transient calibration efforts were focused on matching the head changes, not the actual heads, so it is not uncommon for residuals in the starting condition to be carried through the entire calibration period. This indicates that the model is correctly predicting responses to hydrogeologic forces even if the calculated head values vary somewhat from the measured values.

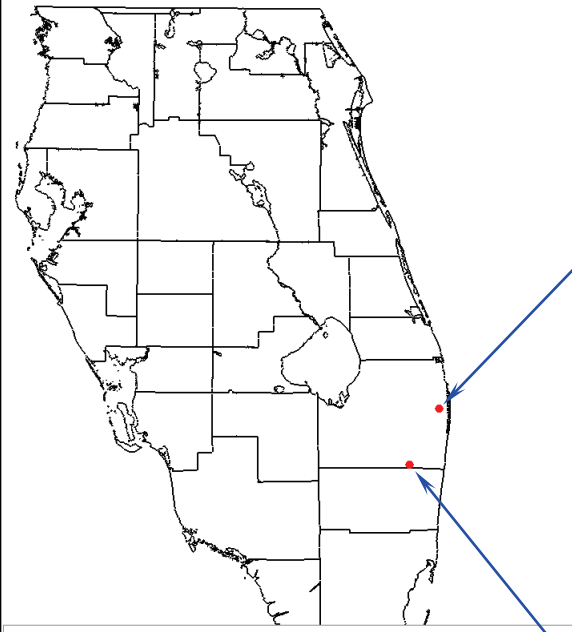

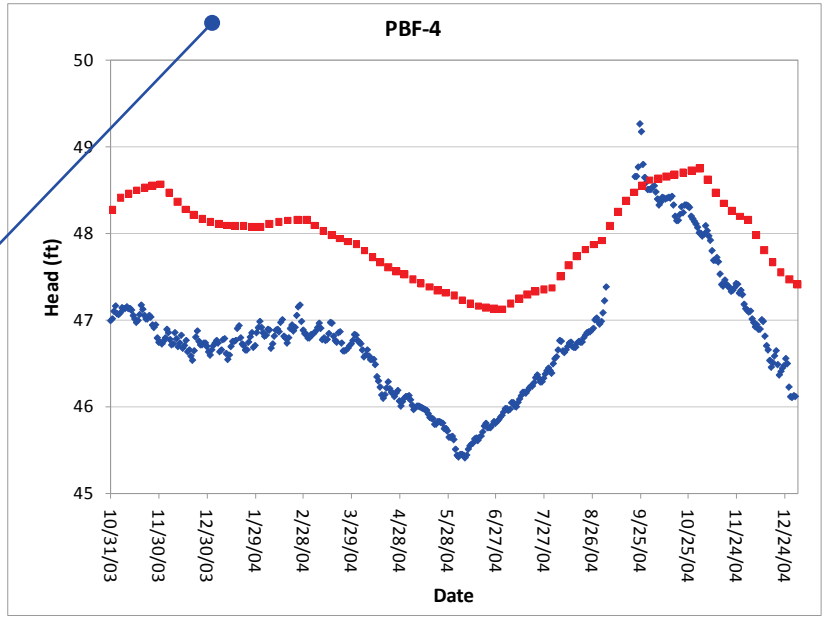

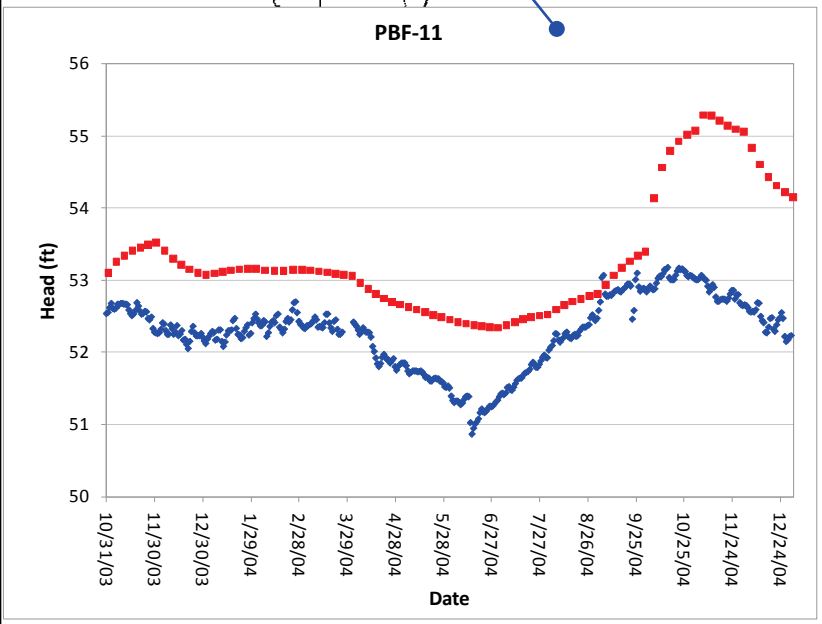

	PBF-11	PBF-4
Mean Error	1.017	1.110
Mean Absolute Error	1.017	1.112
Root Mean Square (RMS)	1.160	1.198
Observed Range	2.32	3.87
RMS as Percentage of Range	50%	31%
Coefficient of Determination (r^2)	0.551	0.708
Nash-Sutcliffe Model Efficiency Coefficient	-4.779	-1.499

Legend

- Measured Head
- Model Calculated Head

Notes:

Figures 4.41 through 4.94 show the comparison between measured head values and model-calculated head values at a number of observation wells for the calibration period. Although the scales vary on each plot, all plots have a horizontal grid line at each foot. This is to make it easy to determine the range of heads at a glance.

The model used month-long stress periods, so pumping and boundary conditions were input as step functions with constant values throughout each month and sudden changes at the end of each month. For this reason, the model cannot be expected to accurately predict day-to-day head variations in any of these wells. Calibration efforts were aimed at matching general trends and monthly averages.

Starting head conditions for this model were based on the October 2003 steady state calibrated model. Transient calibration efforts were focused on matching the head changes, not the actual heads, so it is not uncommon for residuals in the starting condition to be carried through the entire calibration period. This indicates that the model is correctly predicting responses to hydrogeologic forces even if the calculated head values vary somewhat from the measured values.

Transient SEAWAT Calibration Comparison
Avon Park Permeable Zone (2003-2004)
Final Groundwater Model Calibration Report

Figure 4.86

October 2010

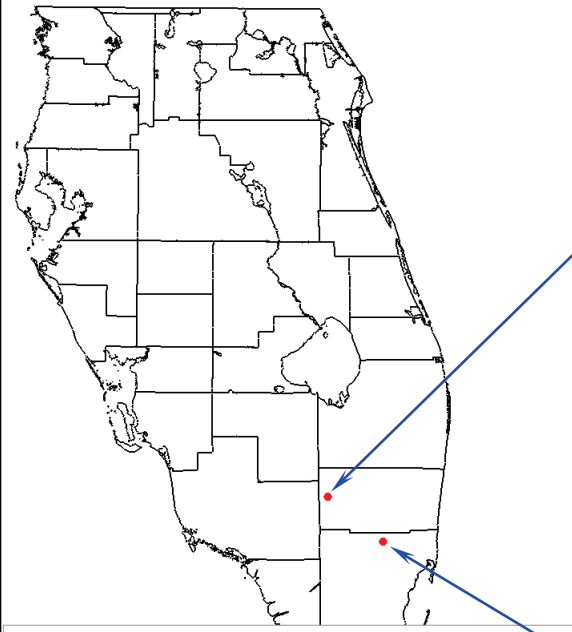

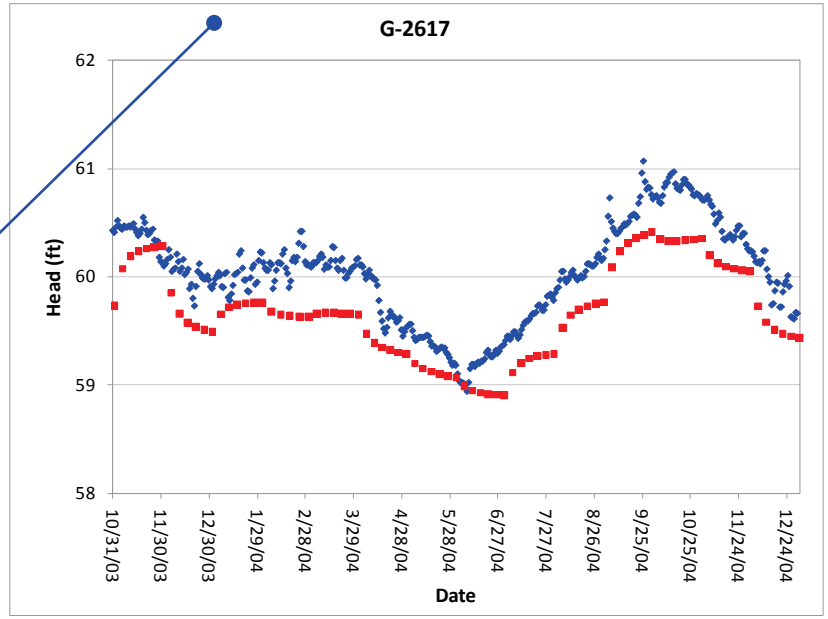

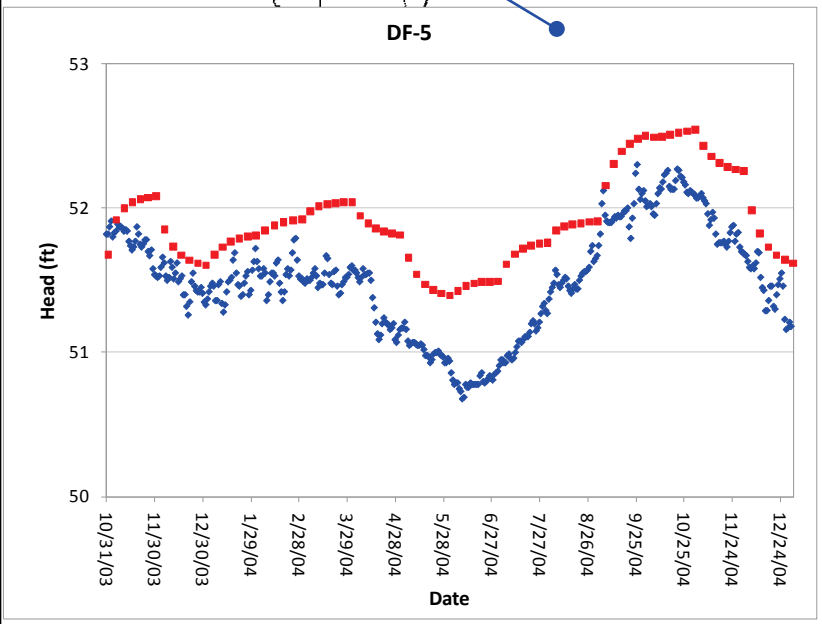

	DF-5	G-2617
Mean Error	0.410	-0.360
Mean Absolute Error	0.410	0.360
Root Mean Square (RMS)	0.432	0.369
Observed Range	1.62	2.13
RMS as Percentage of Range	27%	17%
Coefficient of Determination (r^2)	0.868	0.972
Nash-Sutcliffe Model Efficiency Coefficient	-0.486	0.287

Legend

- Measured Head
- Model Calculated Head

Notes:

Figures 4.41 through 4.94 show the comparison between measured head values and model-calculated head values at a number of observation wells for the calibration period. Although the scales vary on each plot, all plots have a horizontal grid line at each foot. This is to make it easy to determine the range of heads at a glance.

The model used month-long stress periods, so pumping and boundary conditions were input as step functions with constant values throughout each month and sudden changes at the end of each month. For this reason, the model cannot be expected to accurately predict day-to-day head variations in any of these wells. Calibration efforts were aimed at matching general trends and monthly averages.

Starting head conditions for this model were based on the October 2003 steady state calibrated model. Transient calibration efforts were focused on matching the head changes, not the actual heads, so it is not uncommon for residuals in the starting condition to be carried through the entire calibration period. This indicates that the model is correctly predicting responses to hydrogeologic forces even if the calculated head values vary somewhat from the measured values.

Transient SEAWAT Calibration Comparison
Avon Park Permeable Zone (2003-2004)
Final Groundwater Model Calibration Report

Figure 4.87

October 2010

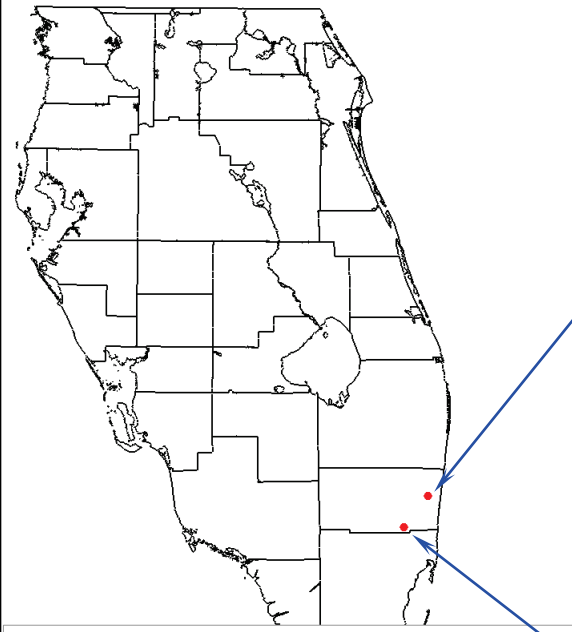

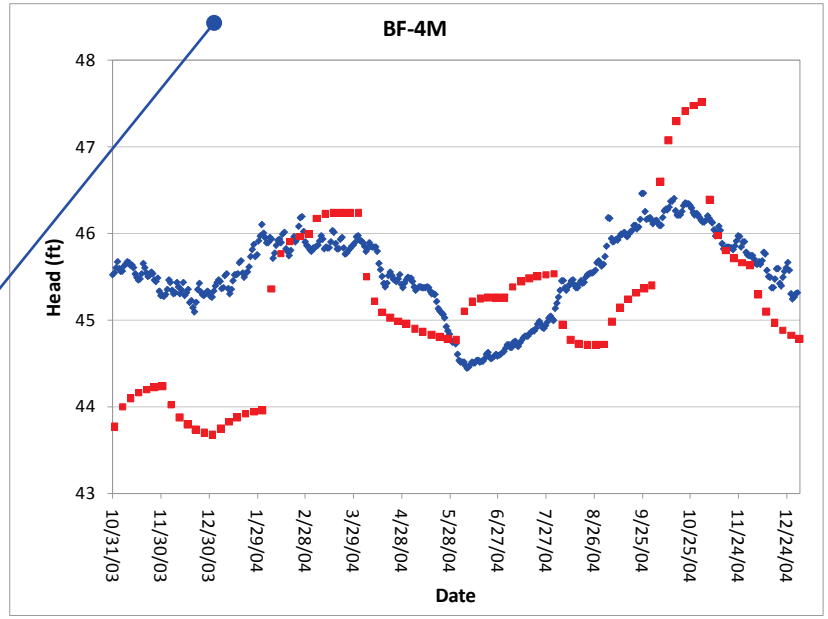

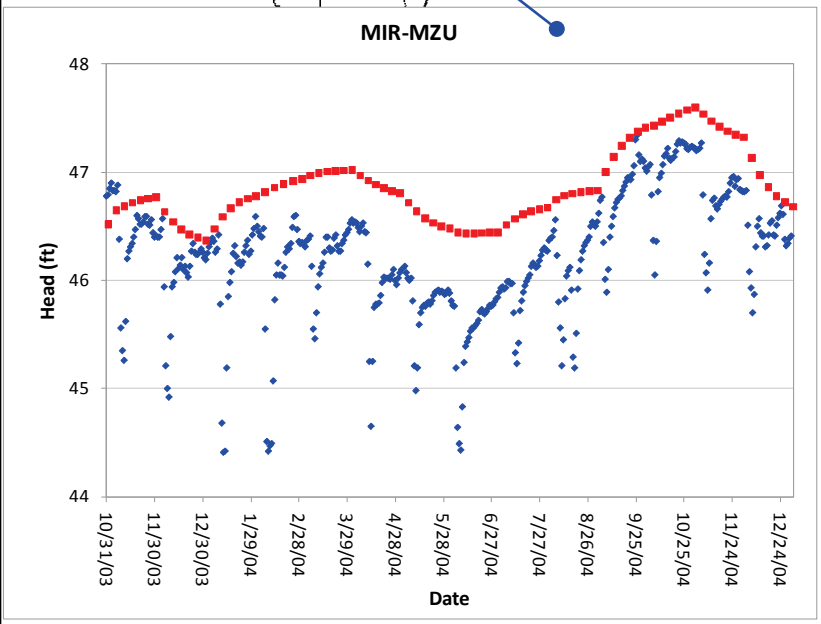

	MIR-MZU	BF-4M
Mean Error	0.631	-0.382
Mean Absolute Error	0.631	0.721
Root Mean Square (RMS)	0.661	0.856
Observed Range	2.93	2.02
RMS as Percentage of Range	22%	42%
Coefficient of Determination (r^2)	0.774	0.185
Nash-Sutcliffe Model Efficiency Coefficient	-1.685	-2.596

Legend

- Measured Head
- Model Calculated Head

Notes:

Figures 4.41 through 4.94 show the comparison between measured head values and model-calculated head values at a number of observation wells for the calibration period. Although the scales vary on each plot, all plots have a horizontal grid line at each foot. This is to make it easy to determine the range of heads at a glance.

The model used month-long stress periods, so pumping and boundary conditions were input as step functions with constant values throughout each month and sudden changes at the end of each month. For this reason, the model cannot be expected to accurately predict day-to-day head variations in any of these wells. Calibration efforts were aimed at matching general trends and monthly averages.

Starting head conditions for this model were based on the October 2003 steady state calibrated model. Transient calibration efforts were focused on matching the head changes, not the actual heads, so it is not uncommon for residuals in the starting condition to be carried through the entire calibration period. This indicates that the model is correctly predicting responses to hydrogeologic forces even if the calculated head values vary somewhat from the measured values.

Transient SEAWAT Calibration Comparison
Avon Park Permeable Zone (2003-2004)
Final Groundwater Model Calibration Report

Figure 4.88

October 2010

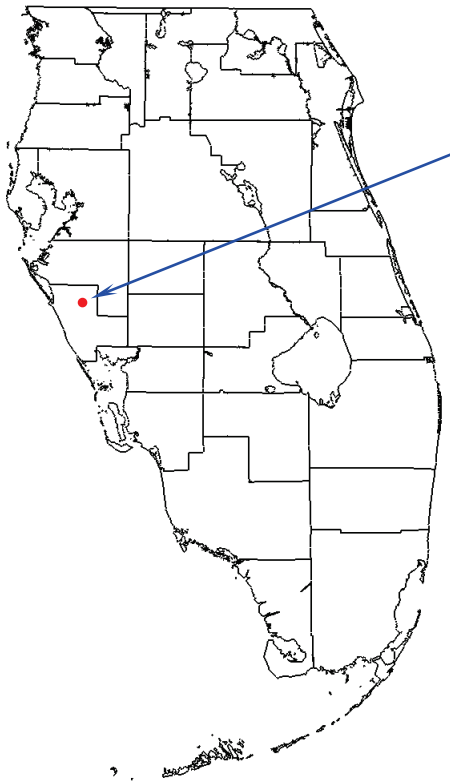

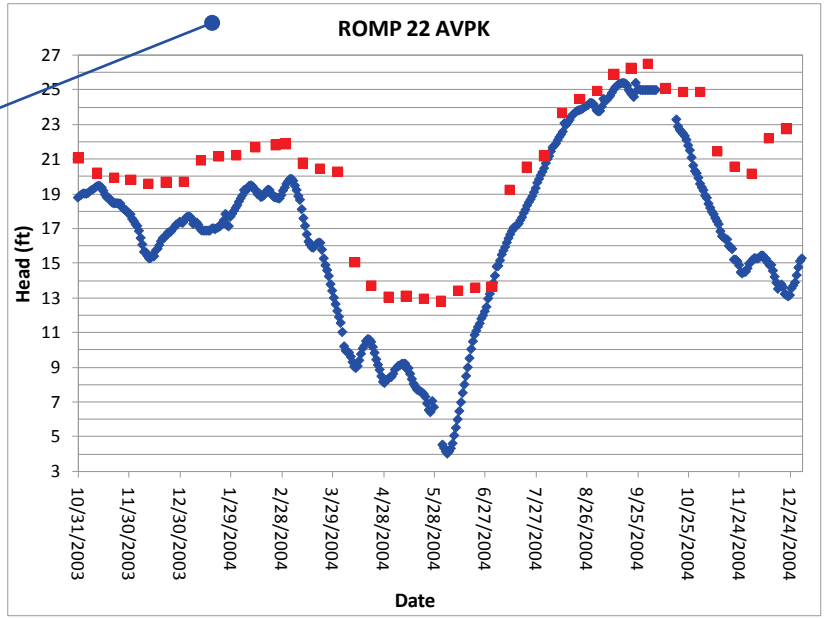

	ROMP 22 AVPK
Mean Error	3.443
Mean Absolute Error	3.443
Root Mean Square (RMS)	4.063
Observed Range	21.39
RMS as Percentage of Range	19%
Coefficient of Determination (r^2)	0.839
Nash-Sutcliffe Model Efficiency Coefficient	0.333

Legend

- Measured Head
- Model Calculated Head

Notes:

Figures 4.41 through 4.94 show the comparison between measured head values and model-calculated head values at a number of observation wells for the calibration period. Although the scales vary on each plot, all plots have a horizontal grid line at each foot. This is to make it easy to determine the range of heads at a glance.

The model used month-long stress periods, so pumping and boundary conditions were input as step functions with constant values throughout each month and sudden changes at the end of each month. For this reason, the model cannot be expected to accurately predict day-to-day head variations in any of these wells. Calibration efforts were aimed at matching general trends and monthly averages.

Starting head conditions for this model were based on the October 2003 steady state calibrated model. Transient calibration efforts were focused on matching the head changes, not the actual heads, so it is not uncommon for residuals in the starting condition to be carried through the entire calibration period. This indicates that the model is correctly predicting responses to hydrogeologic forces even if the calculated head values vary somewhat from the measured values.

Transient SEAWAT Calibration Comparison
Avon Park Permeable Zone (2003-2004)
Final Groundwater Model Calibration Report

Figure 4.89

October 2010

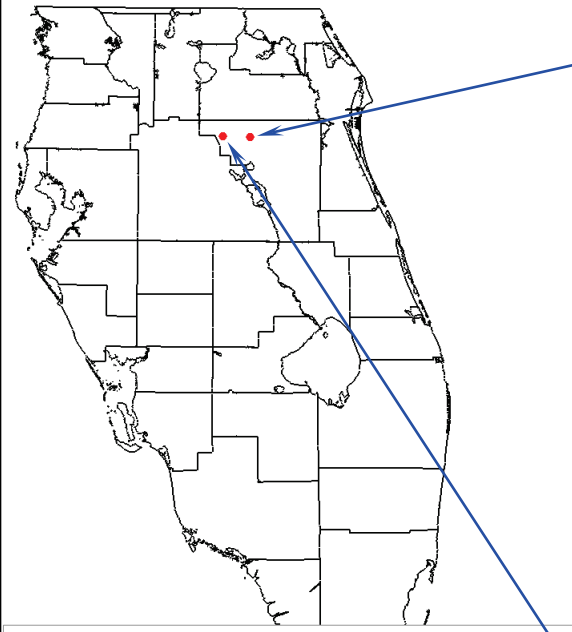

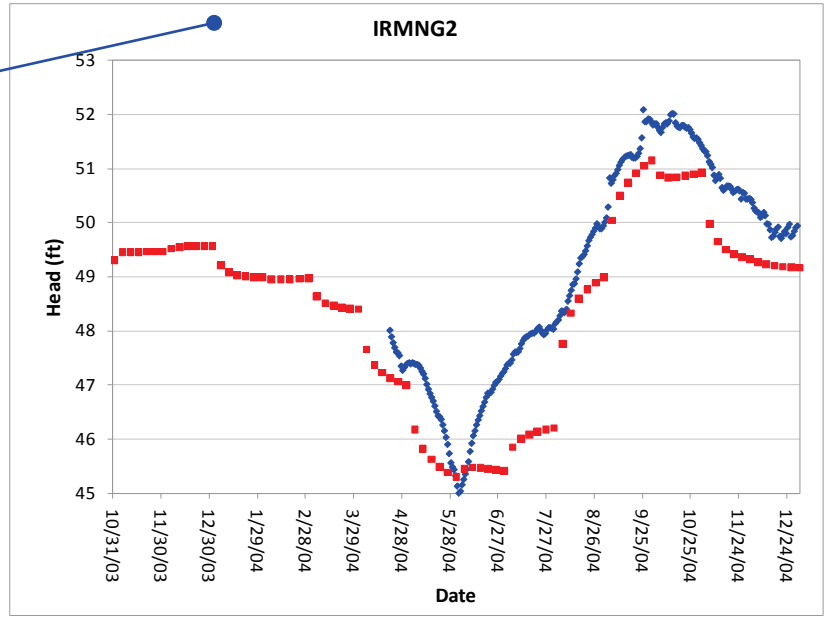

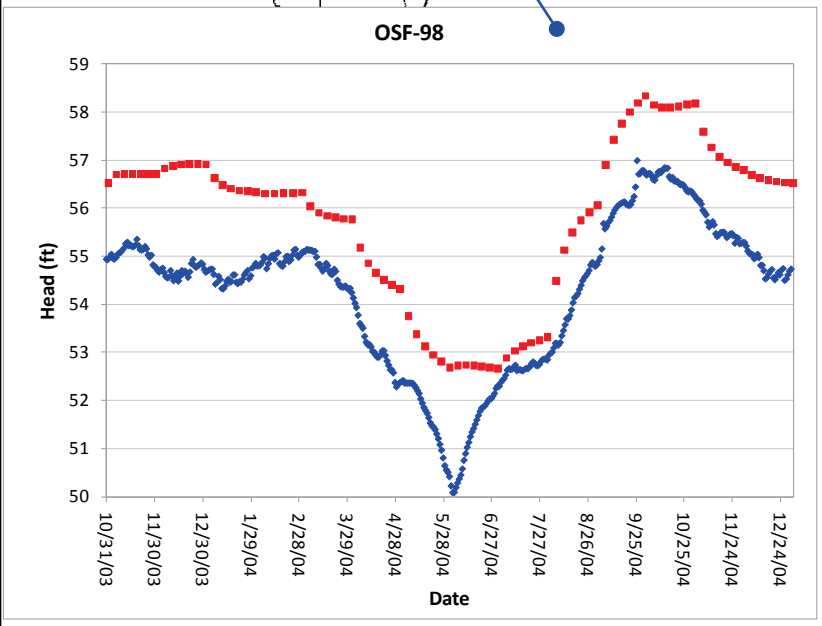

	OSF-98	IRMNG2
Mean Error	1.521	-0.881
Mean Absolute Error	1.521	0.881
Root Mean Square (RMS)	1.576	0.974
Observed Range	6.91	7.09
RMS as Percentage of Range	23%	14%
Coefficient of Determination (r^2)	0.940	0.955
Nash-Sutcliffe Model Efficiency Coefficient	-0.094	0.739

Legend

- Measured Head
- Model Calculated Head

Notes:

Figures 4.41 through 4.94 show the comparison between measured head values and model-calculated head values at a number of observation wells for the calibration period. Although the scales vary on each plot, all plots have a horizontal grid line at each foot. This is to make it easy to determine the range of heads at a glance.

The model used month-long stress periods, so pumping and boundary conditions were input as step functions with constant values throughout each month and sudden changes at the end of each month. For this reason, the model cannot be expected to accurately predict day-to-day head variations in any of these wells. Calibration efforts were aimed at matching general trends and monthly averages.

Starting head conditions for this model were based on the October 2003 steady state calibrated model. Transient calibration efforts were focused on matching the head changes, not the actual heads, so it is not uncommon for residuals in the starting condition to be carried through the entire calibration period. This indicates that the model is correctly predicting responses to hydrogeologic forces even if the calculated head values vary somewhat from the measured values.

Transient SEAWAT Calibration Comparison
Lower Floridan (LF1) Aquifer (2003-2004)
Final Groundwater Model Calibration Report

Figure 4.90

October 2010

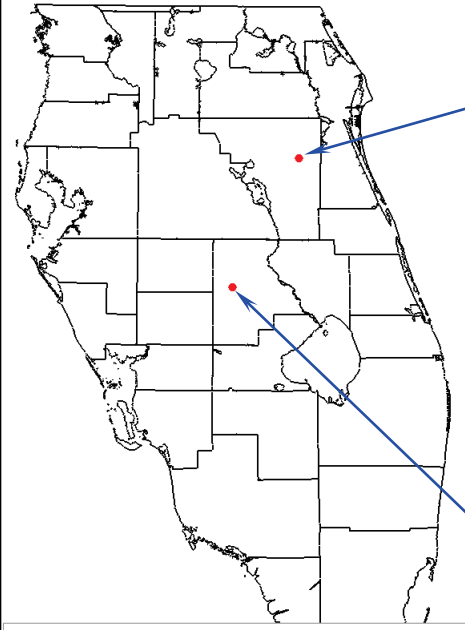

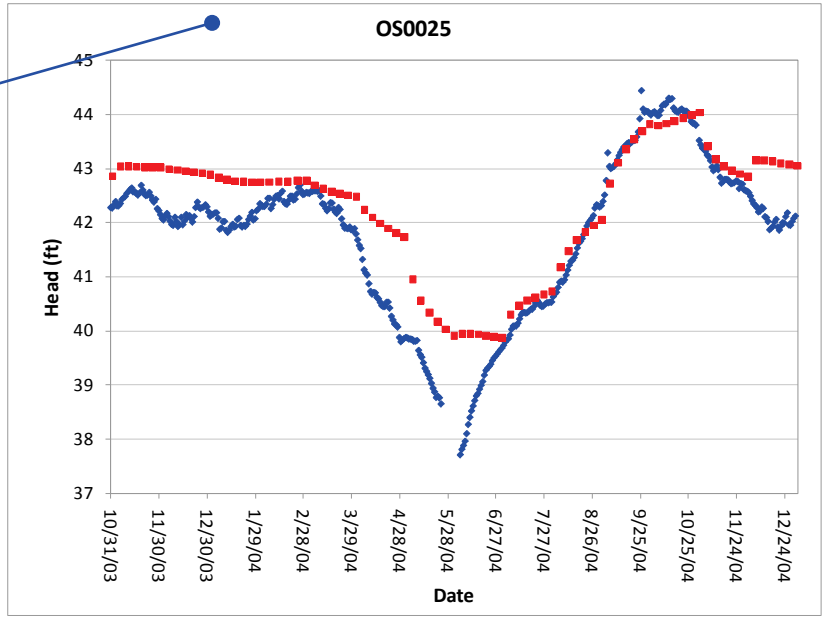

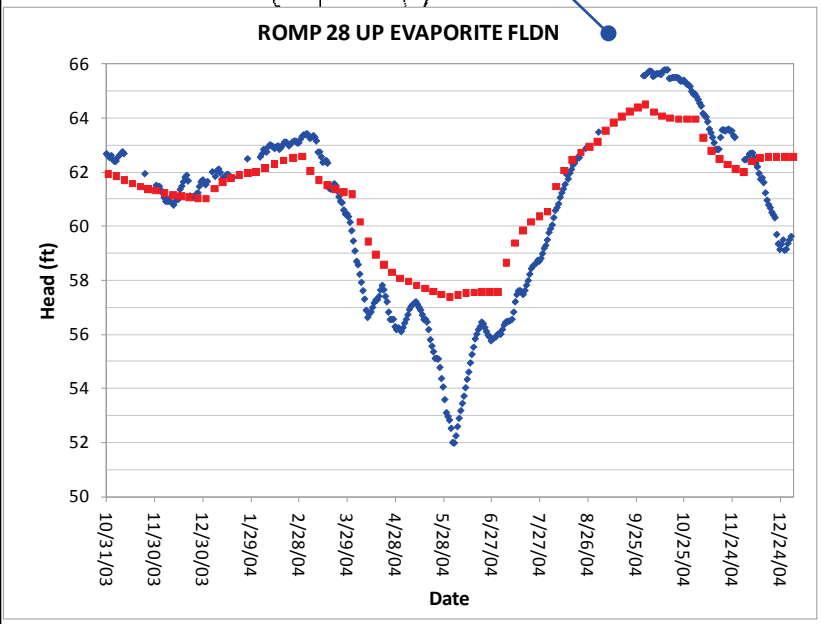

	ROMP 28 UP	OS0025
Mean Error	0.381	0.535
Mean Absolute Error	1.137	0.603
Root Mean Square (RMS)	1.360	0.738
Observed Range	13.81	6.73
RMS as Percentage of Range	10%	11%
Coefficient of Determination (r^2)	0.950	0.889
Nash-Sutcliffe Model Efficiency Coefficient	0.814	0.732

Legend

- Measured Head
- Model Calculated Head

Notes:

Figures 4.41 through 4.94 show the comparison between measured head values and model-calculated head values at a number of observation wells for the calibration period. Although the scales vary on each plot, all plots have a horizontal grid line at each foot. This is to make it easy to determine the range of heads at a glance.

The model used month-long stress periods, so pumping and boundary conditions were input as step functions with constant values throughout each month and sudden changes at the end of each month. For this reason, the model cannot be expected to accurately predict day-to-day head variations in any of these wells. Calibration efforts were aimed at matching general trends and monthly averages.

Starting head conditions for this model were based on the October 2003 steady state calibrated model. Transient calibration efforts were focused on matching the head changes, not the actual heads, so it is not uncommon for residuals in the starting condition to be carried through the entire calibration period. This indicates that the model is correctly predicting responses to hydrogeologic forces even if the calculated head values vary somewhat from the measured values.

Transient SEAWAT Calibration Comparison
Lower Floridan (LF1) Aquifer (2003-2004)
Final Groundwater Model Calibration Report

Figure 4.91

October 2010

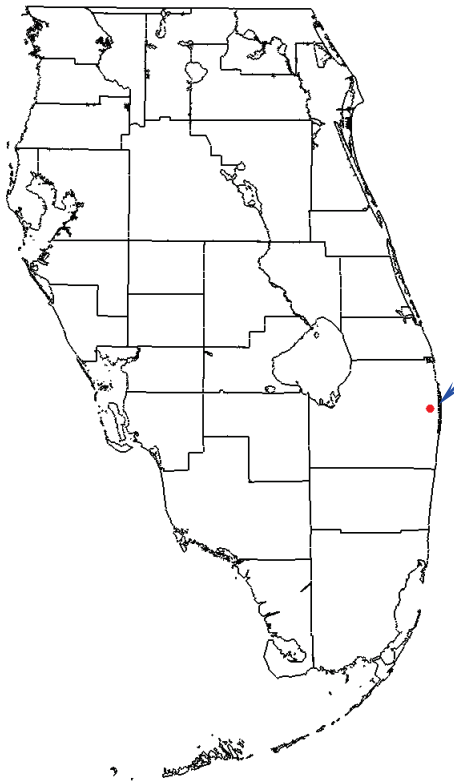

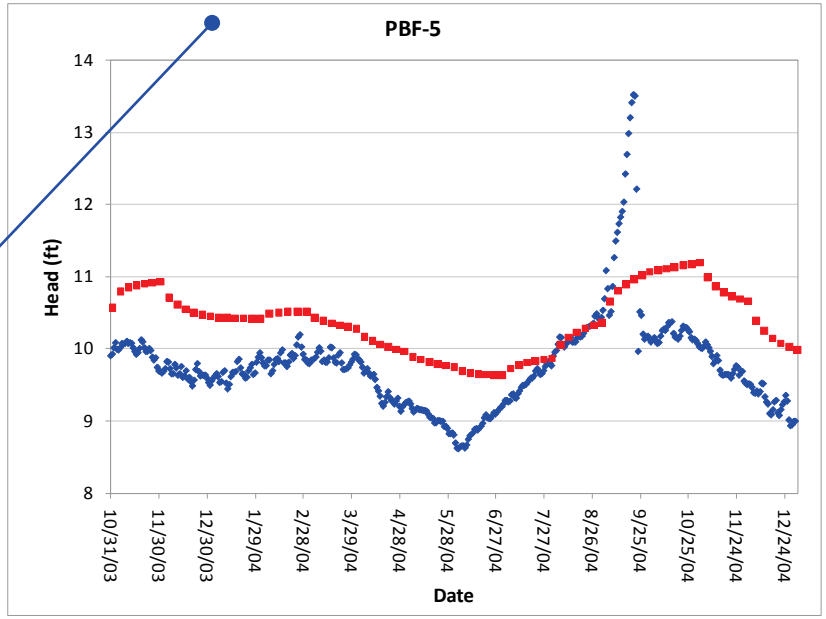

	PBF-5
Mean Error	0.610
Mean Absolute Error	0.704
Root Mean Square (RMS)	0.757
Observed Range	4.91
RMS as Percentage of Range	15%
Coefficient of Determination (r^2)	0.428
Nash-Sutcliffe Model Efficiency Coefficient	-0.645

Legend

- Measured Head
- Model Calculated Head

Notes:

Figures 4.41 through 4.94 show the comparison between measured head values and model-calculated head values at a number of observation wells for the calibration period. Although the scales vary on each plot, all plots have a horizontal grid line at each foot. This is to make it easy to determine the range of heads at a glance.

The model used month-long stress periods, so pumping and boundary conditions were input as step functions with constant values throughout each month and sudden changes at the end of each month. For this reason, the model cannot be expected to accurately predict day-to-day head variations in any of these wells. Calibration efforts were aimed at matching general trends and monthly averages.

Starting head conditions for this model were based on the October 2003 steady state calibrated model. Transient calibration efforts were focused on matching the head changes, not the actual heads, so it is not uncommon for residuals in the starting condition to be carried through the entire calibration period. This indicates that the model is correctly predicting responses to hydrogeologic forces even if the calculated head values vary somewhat from the measured values.

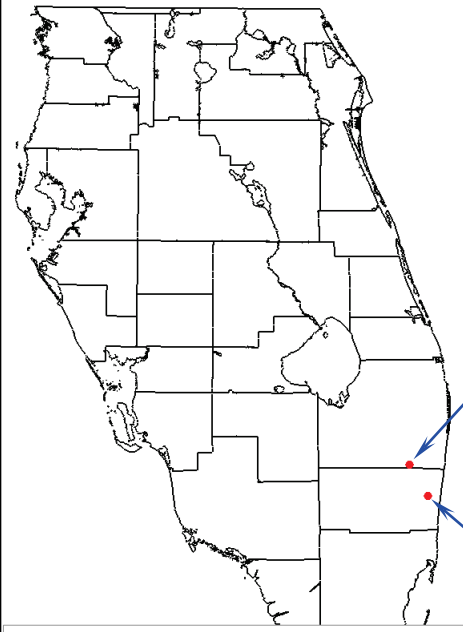

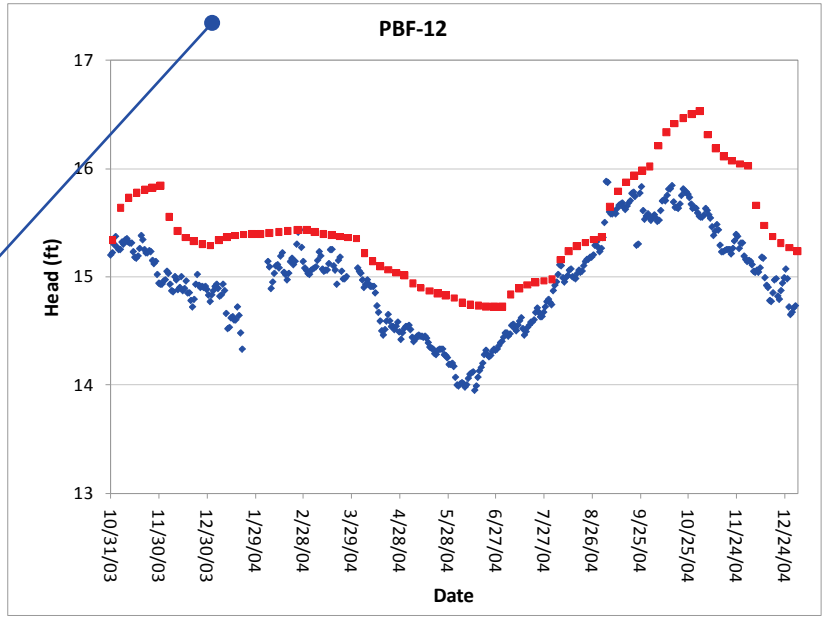

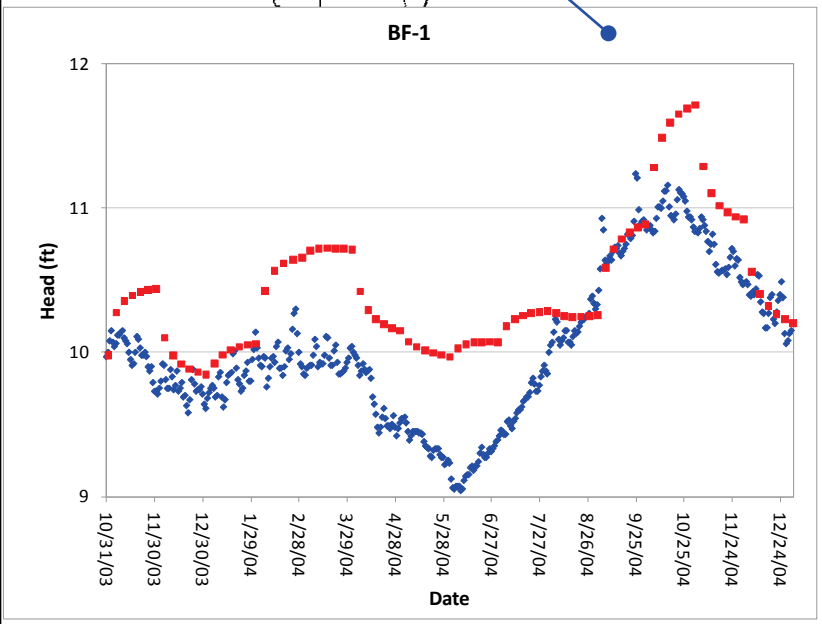

	BF-1	PBF-12
Mean Error	0.410	0.458
Mean Absolute Error	0.424	0.458
Root Mean Square (RMS)	0.491	0.497
Observed Range	2.2	1.93
RMS as Percentage of Range	22%	26%
Coefficient of Determination (r^2)	0.711	0.814
Nash-Sutcliffe Model Efficiency Coefficient	0.040	-0.386

Legend

- Measured Head
- Model Calculated Head

Notes:

Figures 4.41 through 4.94 show the comparison between measured head values and model-calculated head values at a number of observation wells for the calibration period. Although the scales vary on each plot, all plots have a horizontal grid line at each foot. This is to make it easy to determine the range of heads at a glance.

The model used month-long stress periods, so pumping and boundary conditions were input as step functions with constant values throughout each month and sudden changes at the end of each month. For this reason, the model cannot be expected to accurately predict day-to-day head variations in any of these wells. Calibration efforts were aimed at matching general trends and monthly averages.

Starting head conditions for this model were based on the October 2003 steady state calibrated model. Transient calibration efforts were focused on matching the head changes, not the actual heads, so it is not uncommon for residuals in the starting condition to be carried through the entire calibration period. This indicates that the model is correctly predicting responses to hydrogeologic forces even if the calculated head values vary somewhat from the measured values.

Transient SEAWAT Calibration Comparison
Lower Floridan (LF1) Aquifer (2003-2004)
Final Groundwater Model Calibration Report

Figure 4.93

October 2010

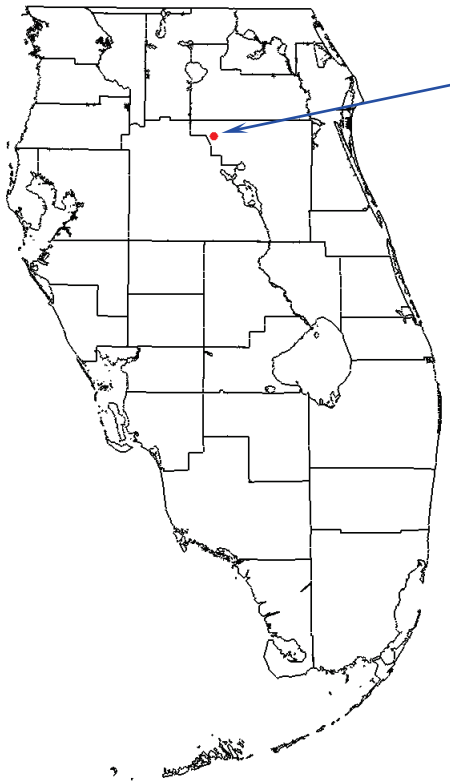

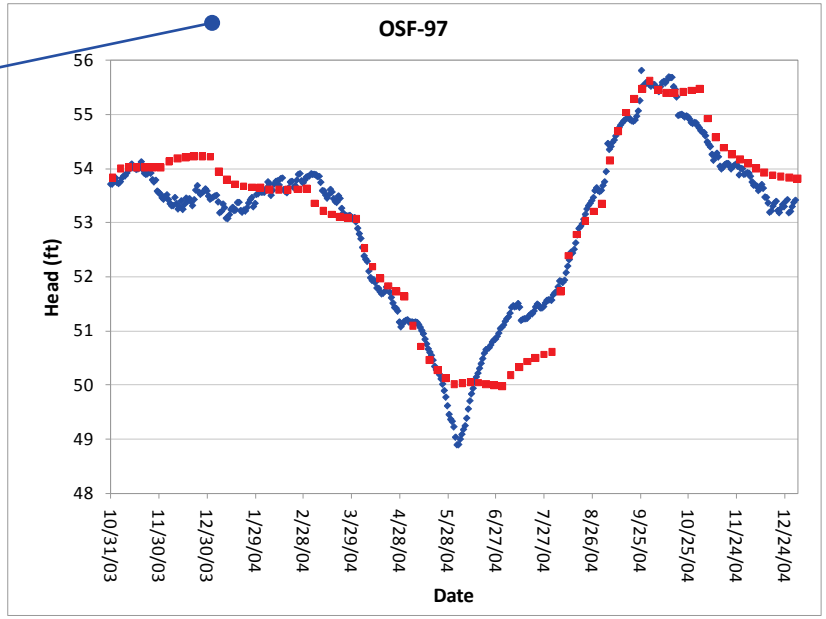

	OSF-97
Mean Error	0.067
Mean Absolute Error	0.335
Root Mean Square (RMS)	0.429
Observed Range	6.92
RMS as Percentage of Range	6%
Coefficient of Determination (r^2)	0.939
Nash-Sutcliffe Model Efficiency Coefficient	0.916

Legend

- Measured Head
- Model Calculated Head

Notes:

Figures 4.41 through 4.94 show the comparison between measured head values and model-calculated head values at a number of observation wells for the calibration period. Although the scales vary on each plot, all plots have a horizontal grid line at each foot. This is to make it easy to determine the range of heads at a glance.

The model used month-long stress periods, so pumping and boundary conditions were input as step functions with constant values throughout each month and sudden changes at the end of each month. For this reason, the model cannot be expected to accurately predict day-to-day head variations in any of these wells. Calibration efforts were aimed at matching general trends and monthly averages.

Starting head conditions for this model were based on the October 2003 steady state calibrated model. Transient calibration efforts were focused on matching the head changes, not the actual heads, so it is not uncommon for residuals in the starting condition to be carried through the entire calibration period. This indicates that the model is correctly predicting responses to hydrogeologic forces even if the calculated head values vary somewhat from the measured values.

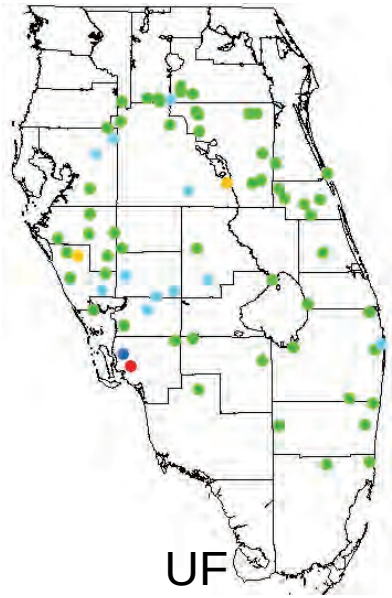

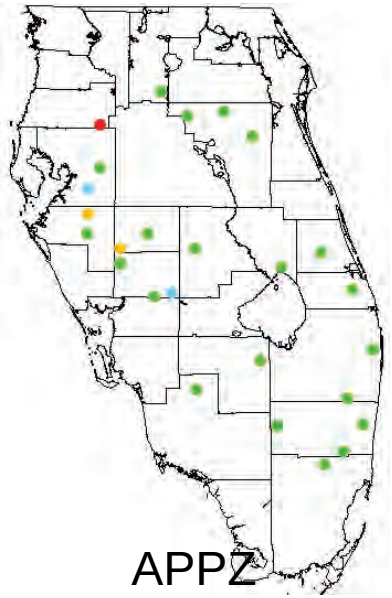

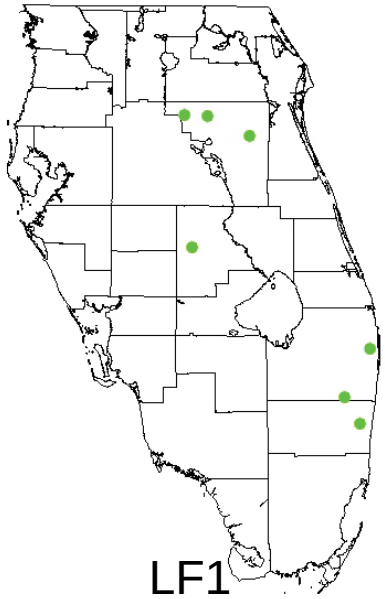

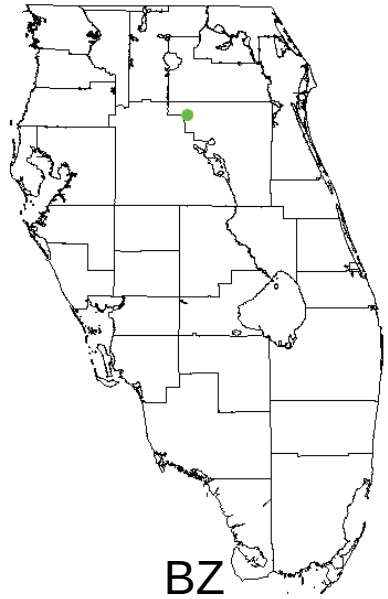

Mean Residual Error

- > 4.0 (model predicts high)
- 2.0 to 4.0
- -2.0 to 2.0 (well calibrated)
- -4.0 to -2.0
- < -4.0 (model predicts low)

Notes:

The mean error (ME) is calculated as described in Section 4.1. The ME statistic is calculated using monthly average heads for both the observed and model calculated data.

A perfectly calibrated point would have an ME value close to zero. In these maps, blue points have negative ME statistics (model prediction is low) and red points have positive ME statistics (model prediction is high). Green points are for well calibrated observation wells.

Transient SEAWAT Calibration Comparison
Mean Residual Error (2003-2004)
Final Groundwater Model Calibration Report

Figure 4.95

October 2010

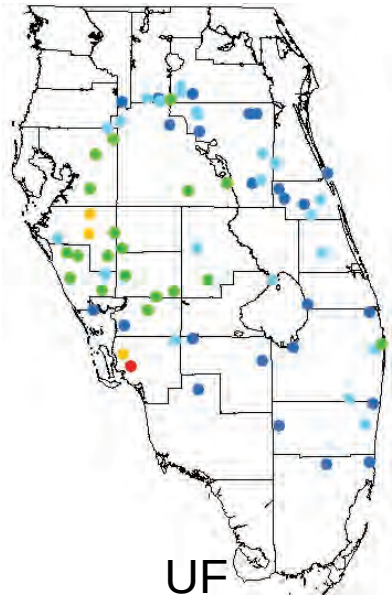

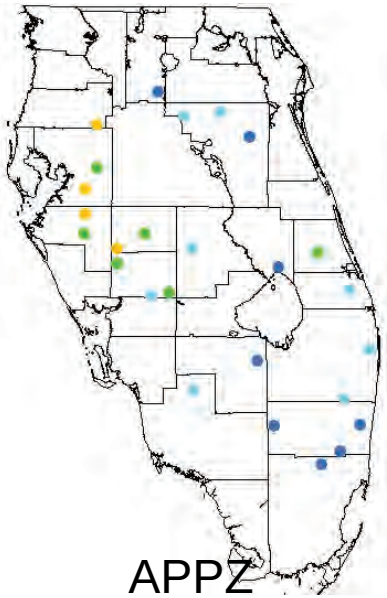

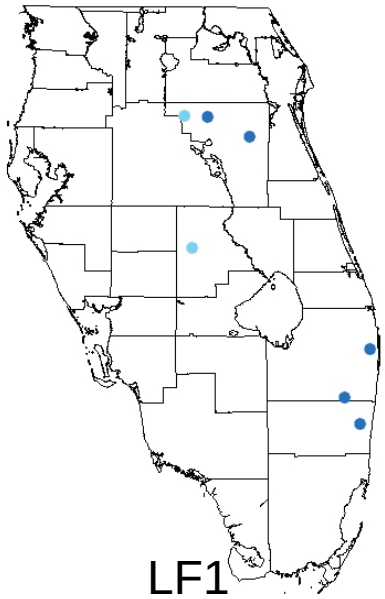

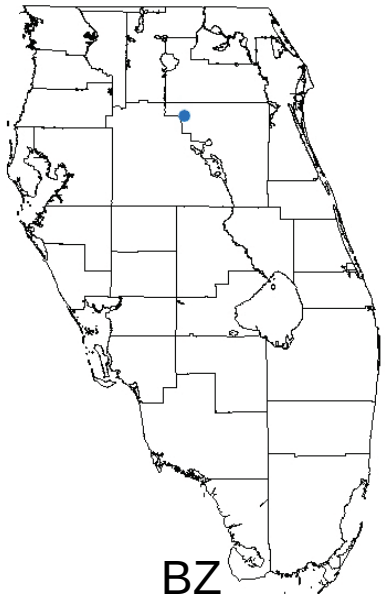

Root Mean Square Error

- < 1.0 (well calibrated)
- 1.0 - 2.0
- 2.0 - 4.0
- 4.0 - 8.0
- > 8.0 (poorly calibrated)

Notes:

The RMS (Root Mean Square) statistic is calculated as described in Section 4.1. The RMS statistic is calculated using monthly average heads for both the observed and model calculated data.

A perfectly calibrated point would have an RMS value close to zero. In these maps, blue points have low RMS statistics (well calibrated) and red points have large RMS (poorly calibrated).

Transient SEAWAT Calibration Comparison
Root Mean Square Error (2003-2004)
Final Groundwater Model Calibration Report

Figure 4.96

October 2010

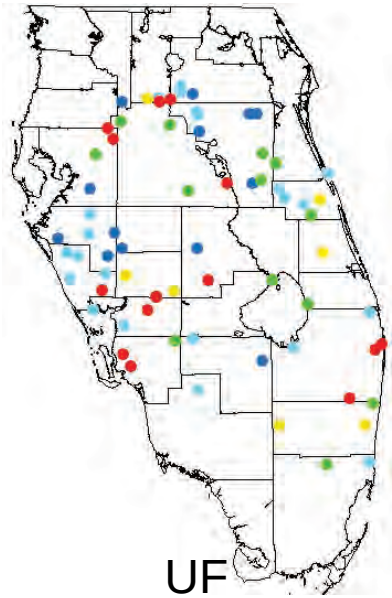

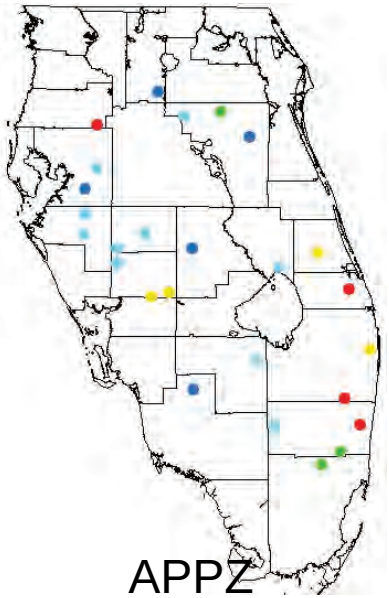

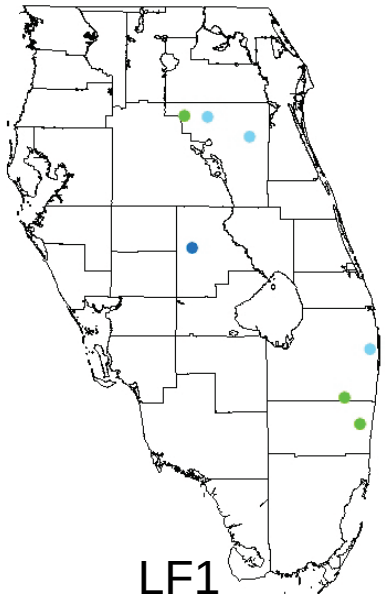

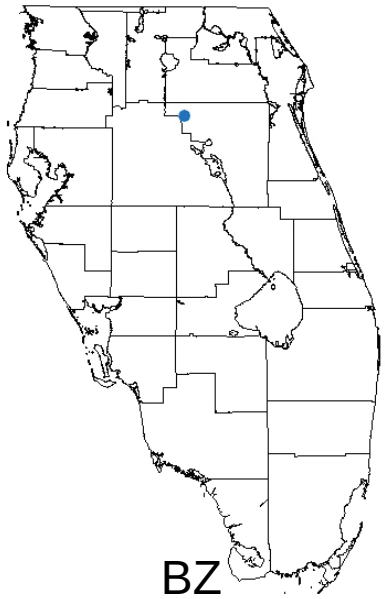

RMS as Percent of Observed Range

- < 10% (well calibrated)
- 10%-20%
- 20%-30%
- 30%-40%
- > 40% (poorly calibrated)

Notes:

The RMS (Root Mean Square) statistic is calculated as described in Section 4.1. This figure shows the RMS for each transient calibration point as a percentage of the range of observed values over the 15 month calibration period. The RMS statistic is calculated using monthly average heads for both the observed and model calculated data.

A perfectly calibrated point would have an RMS value close to zero. When compared to the observed head range, wells with small variability in heads are held to a higher standard. A common rule of thumb is to require that the RMS be less than 10% of the observed range. In these maps, blue points have low RMS statistics compared to the observed head range (well calibrated) and red points have large RMS statistics relative to the observed head range (poorly calibrated).

Transient SEAWAT Calibration Comparison
RMS as Percentage of Range (2003-2004)
Final Groundwater Model Calibration Report

Figure 4.97

October 2010

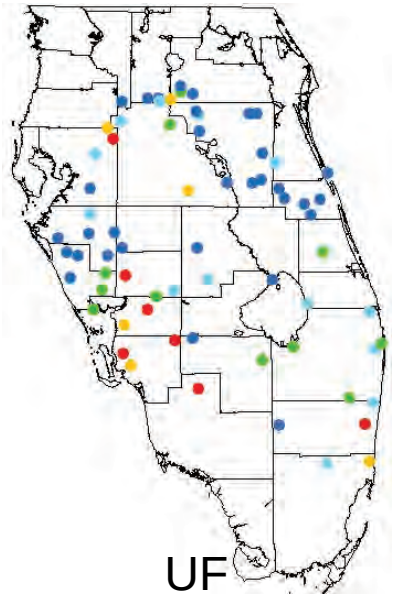

UF

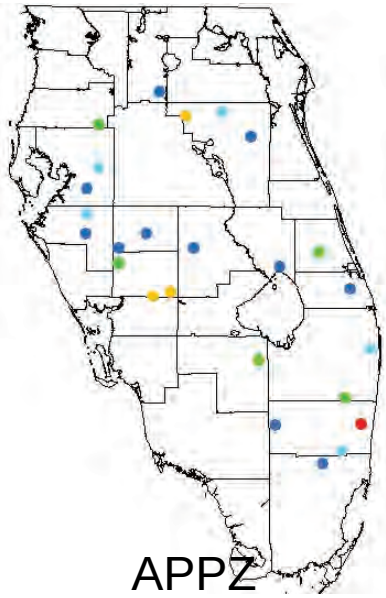

APPZ

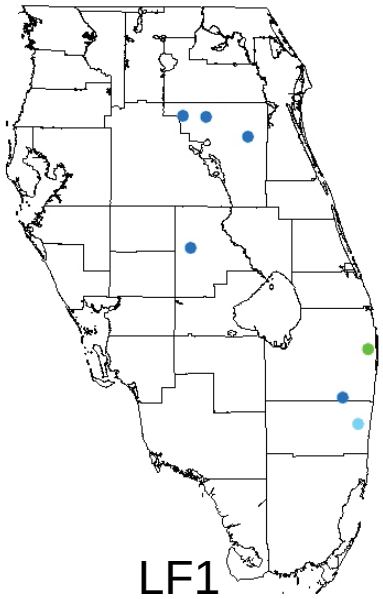

LF1

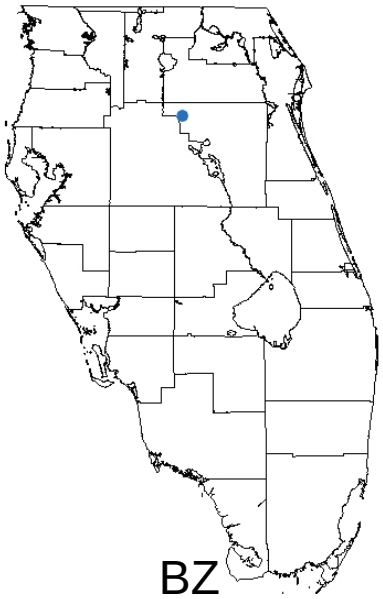

BZ

Coefficient of Determination (r^2)

- > 0.8 (well calibrated)
- 0.6 – 0.8
- 0.4 – 0.6
- 0.2 – 0.4
- < 0.2 (poorly calibrated)

Notes:

The Coefficient of Determination (r^2) is calculated as described in Section 4.2. The r^2 statistic is calculated using monthly average heads for both the observed and model calculated data.

A perfectly calibrated point would have an r^2 value close to 1.0. In these maps, blue points have high r^2 (well calibrated) and red points have small r^2 statistics (poorly calibrated).

Transient SEAWAT Calibration Comparison
Coefficient of Determination (2003-2004)
Final Groundwater Model Calibration Report

Figure 4.98

October 2010

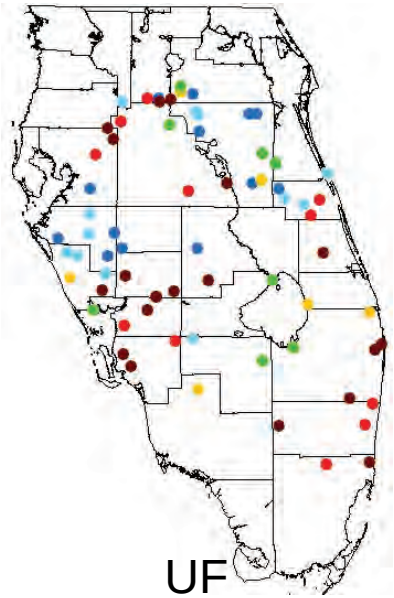

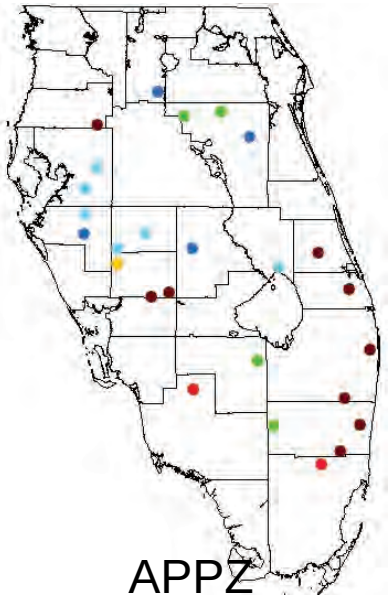

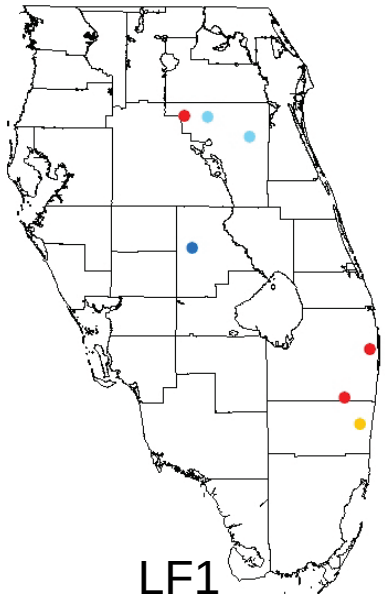

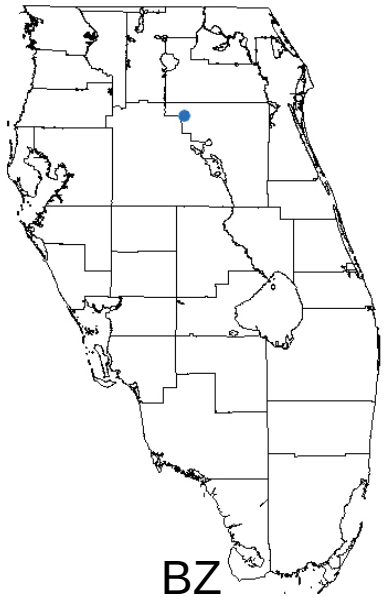

Nash-Sutcliffe Model Efficiency Coefficient

- > 0.75 (well calibrated)
- 0.5 – 0.75
- 0.25 – 0.5
- 0.0 – 0.25
- -1.0 – 0.0
- < -1.0 (poorly calibrated)

Notes:

The Nash-Sutcliffe Model Efficiency Coefficient is calculated as described in Section 4.2. This statistic is calculated using monthly average heads for both the observed and model calculated data.

A perfectly calibrated point would have an efficiency value close to 1.0. A negative efficiency value indicates that the calibration error exceeds the variance in the observed data. In these maps, blue points have high efficiency coefficients (well calibrated) and red points have negative efficiency coefficients (poorly calibrated).

Transient SEAWAT Calibration Comparison
Nash-Sutcliffe Model Efficiency (2003-2004)
Final Groundwater Model Calibration Report

Figure 4.99

October 2010

Alligator Alley

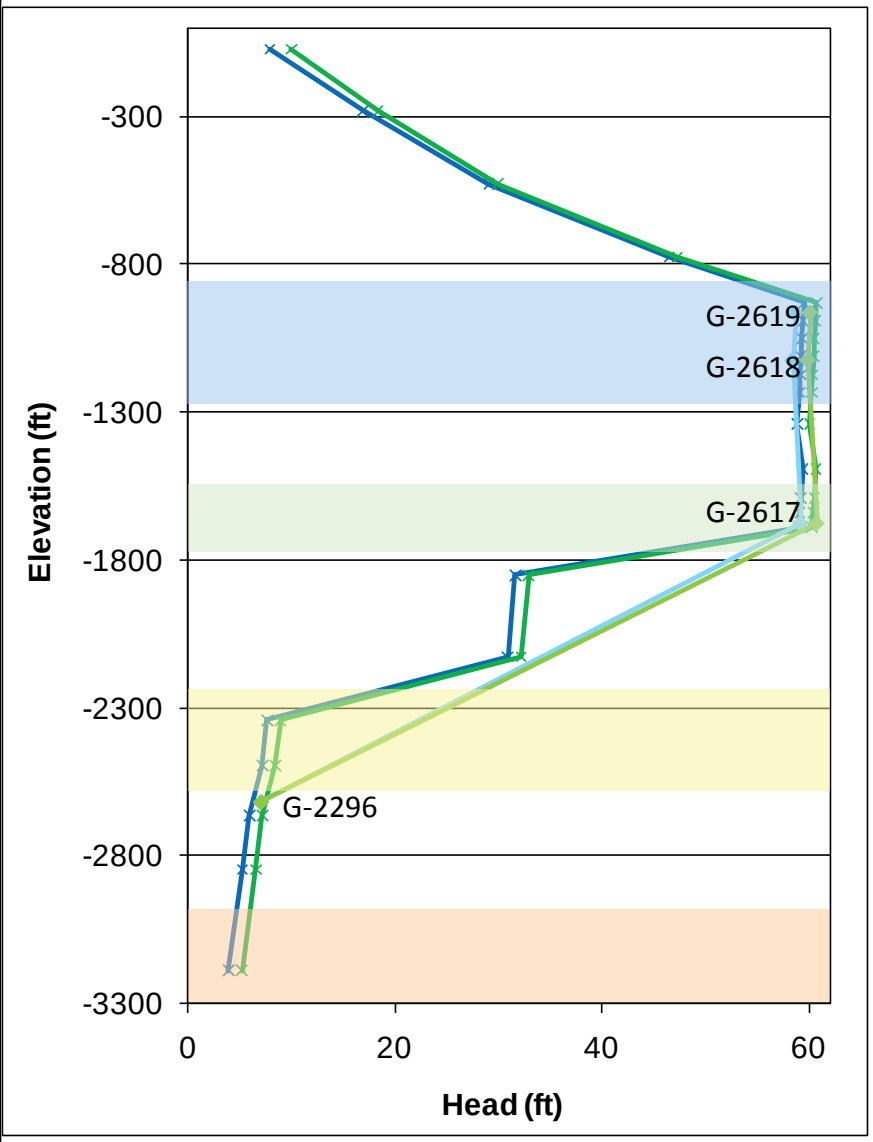

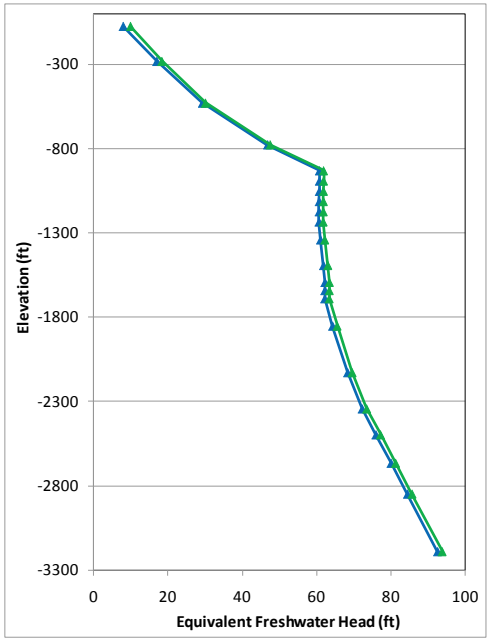

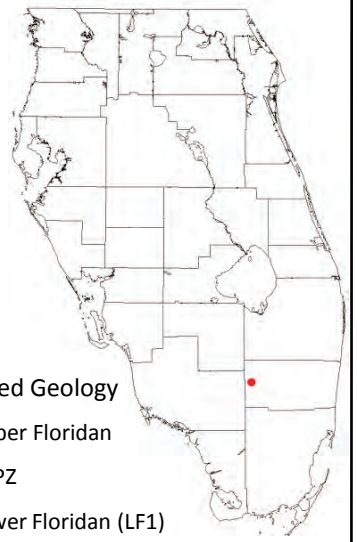

Model-Simplified Geology

- Upper Floridan
- APPZ
- Lower Floridan (LF1)
- Boulder Zone

Legend:

- Model Calculated Head-May 31, 2004
- Observed Head-May 31, 2004
- Model Calculated Head-Oct. 31, 2004
- Observed Head-Oct. 31, 2004
- Cluster Location

Notes:

The plot at left shows the head changes in a vertical column of the model compared to measurements made at a well cluster. Colored stripes indicate the model-simplified stratigraphic units.

Two sets of model calculated heads are shown on the plot:

1) May 31, 2004 from the transient model, representing the dry season
2) October 31, 2004 from the transient model, representing the wet season

Observed head for May 31, 2004 and October 31, 2004 is the measured value for each respective day.

The location of the cluster is marked on the inset map at bottom right.

The plot at left may seem unusual as it seems to indicate downward flow from the APPZ towards the LF1. However, when the heads are converted to equivalent freshwater heads in the plot at top right, the gradient is shown to be upward as expected. Figures on the following pages will not show equivalent freshwater heads.

Regional SEAWAT Calibration
Vertical Gradient Comparison
Final Groundwater Model Calibration Report

Figure 4.100

October 2010

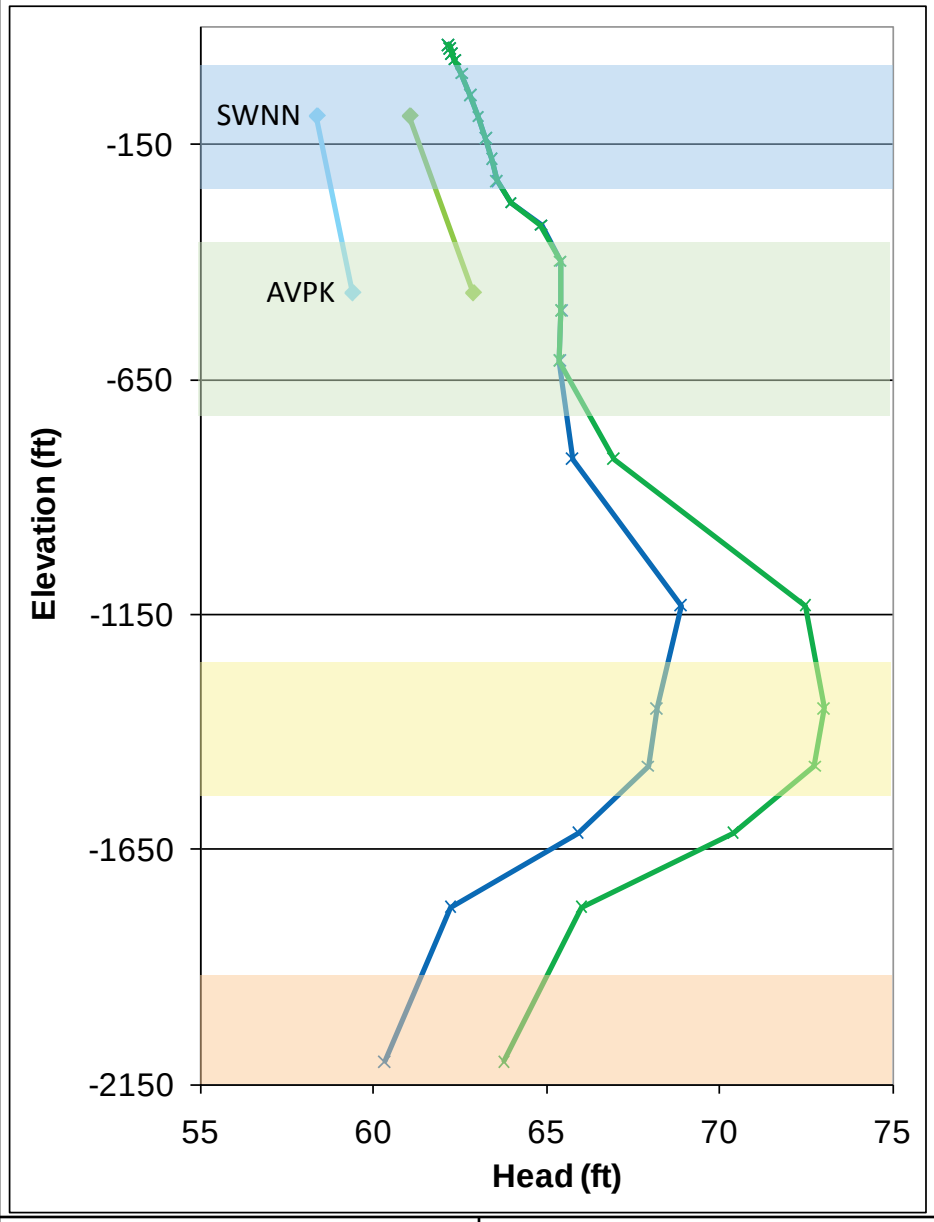

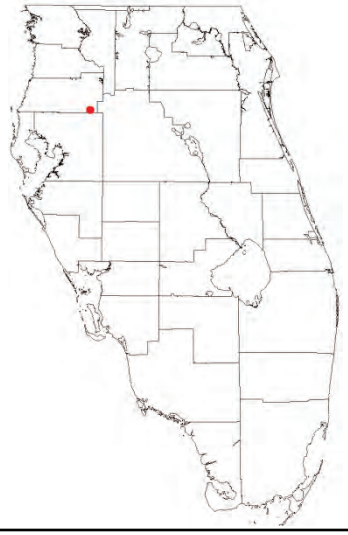

Legend:

- Model Calculated Head-May 31, 2004
- Observed Head-May 31, 2004
- Model Calculated Head-Oct. 31, 2004
- Observed Head-Oct. 31, 2004
- Cluster Location

Model-Simplified Geology

- Upper Floridan
- APPZ
- Lower Floridan (LF1)
- Boulder Zone

Notes:

This plot shows the head changes in a vertical column of the model compared to measurements made at a well cluster.

Two sets of model calculated heads are shown on the plot:

1) May 31, 2004 from the transient model, representing the dry season
2) October 31, 2004 from the transient model, representing the wet season

Observed head for May 31, 2004 and October 31, 2004 is the measured value for each respective day.

Colored stripes indicate the model-simplified stratigraphic units.

The location of the cluster is marked on the inset map.

Regional SEAWAT Calibration
Vertical Gradient Comparison
Final Groundwater Model Calibration Report

Figure 4.101

October 2010

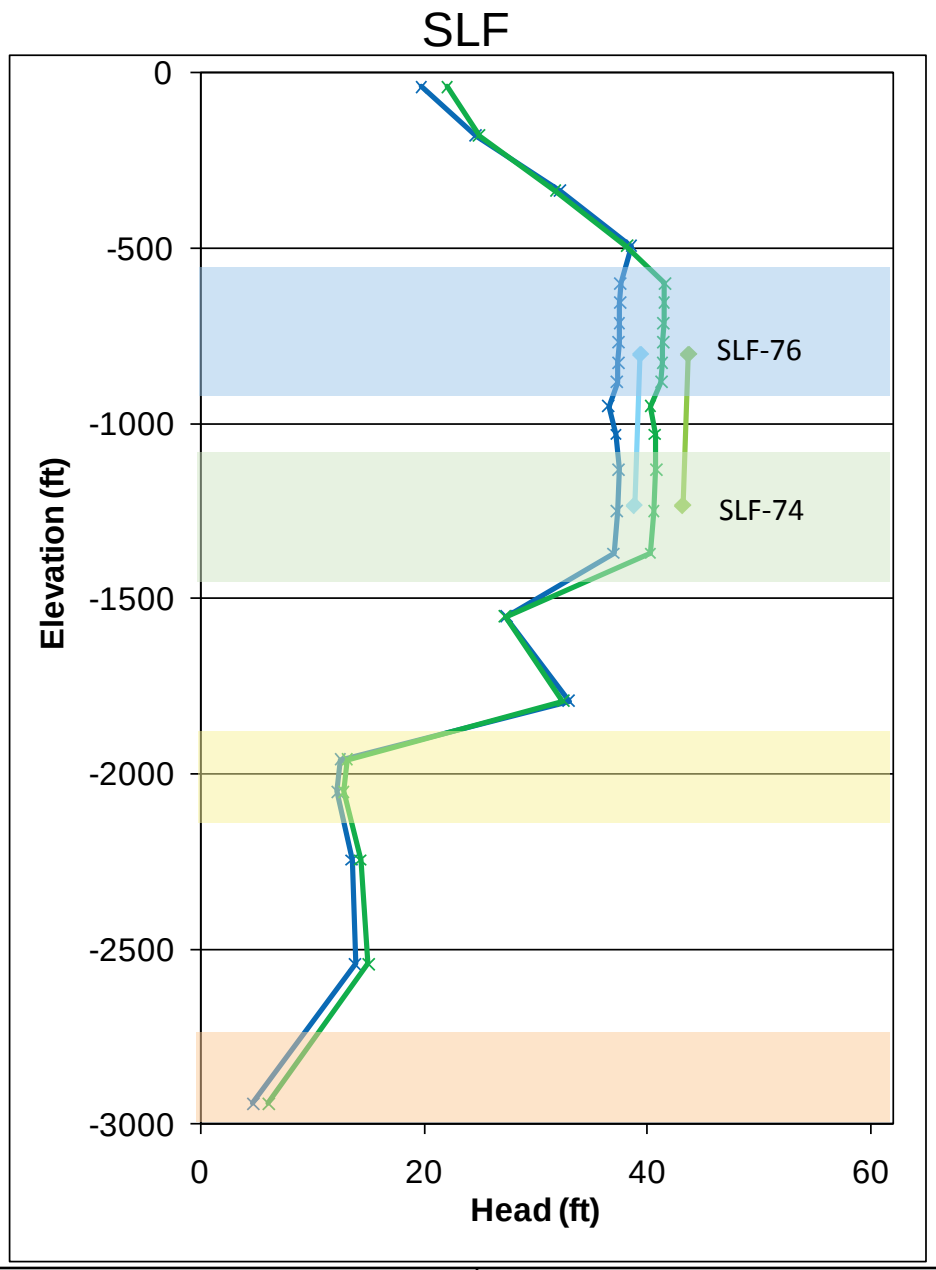

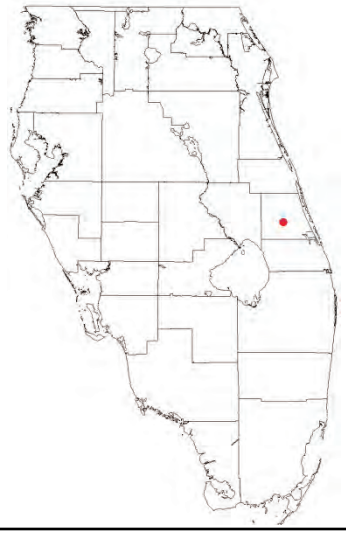

Legend:

- Model Calculated Head-May 31, 2004
- Observed Head-May 31, 2004
- Model Calculated Head-Oct. 31, 2004
- Observed Head-Oct. 31, 2004
- Cluster Location

Model-Simplified Geology

- Upper Floridan
- APPZ
- Lower Floridan (LF1)
- Boulder Zone

Notes:

This plot shows the head changes in a vertical column of the model compared to measurements made at a well cluster.

Two sets of model calculated heads are shown on the plot:

1) May 31, 2004 from the transient model, representing the dry season
2) October 31, 2004 from the transient model, representing the wet season

Observed head for May 31, 2004 and October 31, 2004 is the measured value for each respective day.

Colored stripes indicate the model-simplified stratigraphic units.

The location of the cluster is marked on the inset map.

Regional SEAWAT Calibration
Vertical Gradient Comparison
Final Groundwater Model Calibration Report

Figure 4.102

October 2010

ROMP 13

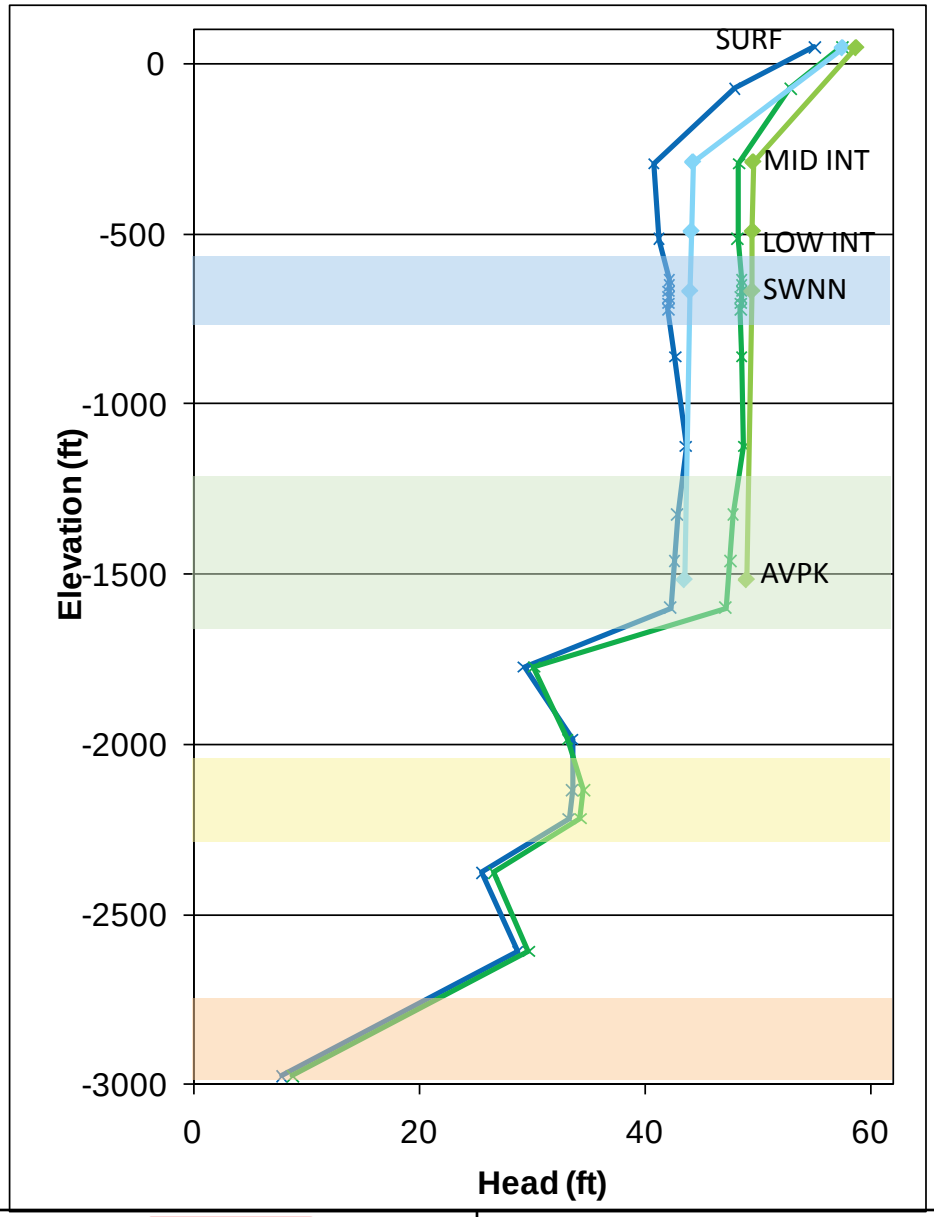

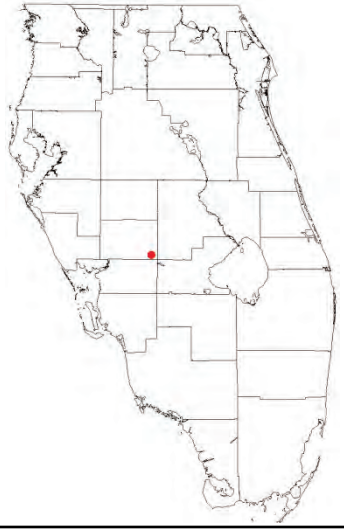

Legend:

- Model Calculated Head-May 31, 2004
- Observed Head-May 31, 2004
- Model Calculated Head-Oct. 31, 2004
- Observed Head-Oct. 31, 2004
- Cluster Location

Model-Simplified Geology

- Upper Floridan
- APPZ
- Lower Floridan (LF1)
- Boulder Zone

Notes:

This plot shows the head changes in a vertical column of the model compared to measurements made at a well cluster.

Two sets of model calculated heads are shown on the plot:

1) May 31, 2004 from the transient model, representing the dry season
2) October 31, 2004 from the transient model, representing the wet season

Observed head for May 31, 2004 and October 31, 2004 is the measured value for each respective day.

Colored stripes indicate the model-simplified stratigraphic units.

The location of the cluster is marked on the inset map.

Regional SEAWAT Calibration
Vertical Gradient Comparison
Final Groundwater Model Calibration Report

Figure 4.103

October 2010

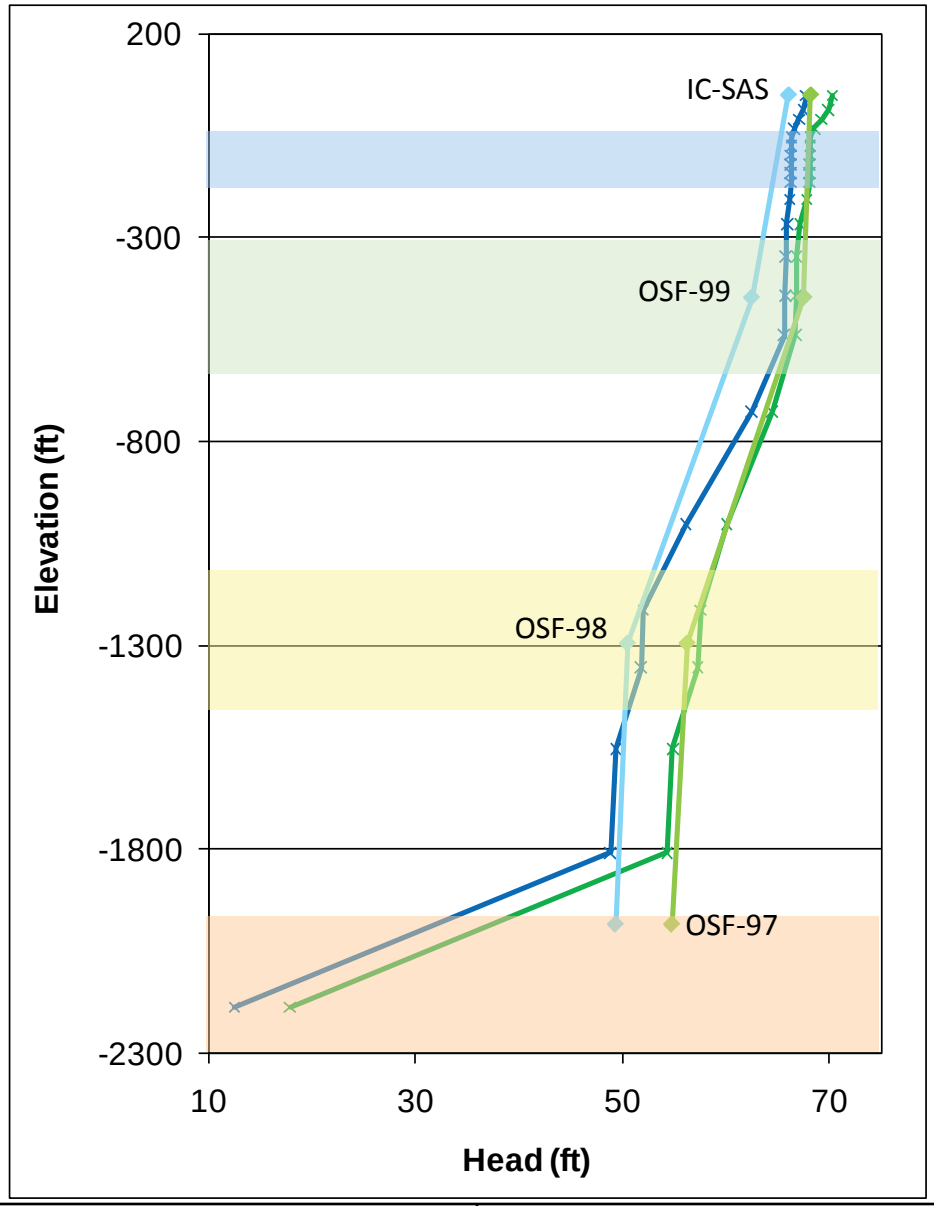

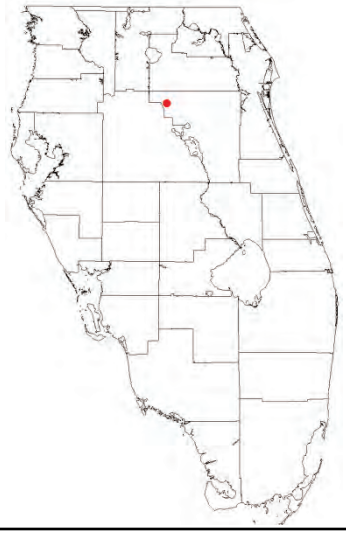

Legend:

- Model Calculated Head-May 31, 2004
- Observed Head-May 31, 2004
- Model Calculated Head-Oct. 31, 2004
- Observed Head-Oct. 31, 2004
- Cluster Location

Model-Simplified Geology

- Upper Floridan
- APPZ
- Lower Floridan (LF1)
- Boulder Zone

Notes:

This plot shows the head changes in a vertical column of the model compared to measurements made at a well cluster.

Two sets of model calculated heads are shown on the plot:

1) May 31, 2004 from the transient model, representing the dry season
2) October 31, 2004 from the transient model, representing the wet season

Observed head for May 31, 2004 and October 31, 2004 is the measured value for each respective day.

Colored stripes indicate the model-simplified stratigraphic units.

The location of the cluster is marked on the inset map.

Regional SEAWAT Calibration
Vertical Gradient Comparison
Final Groundwater Model Calibration Report

Figure 4.104

October 2010

ROMP TR 7-4

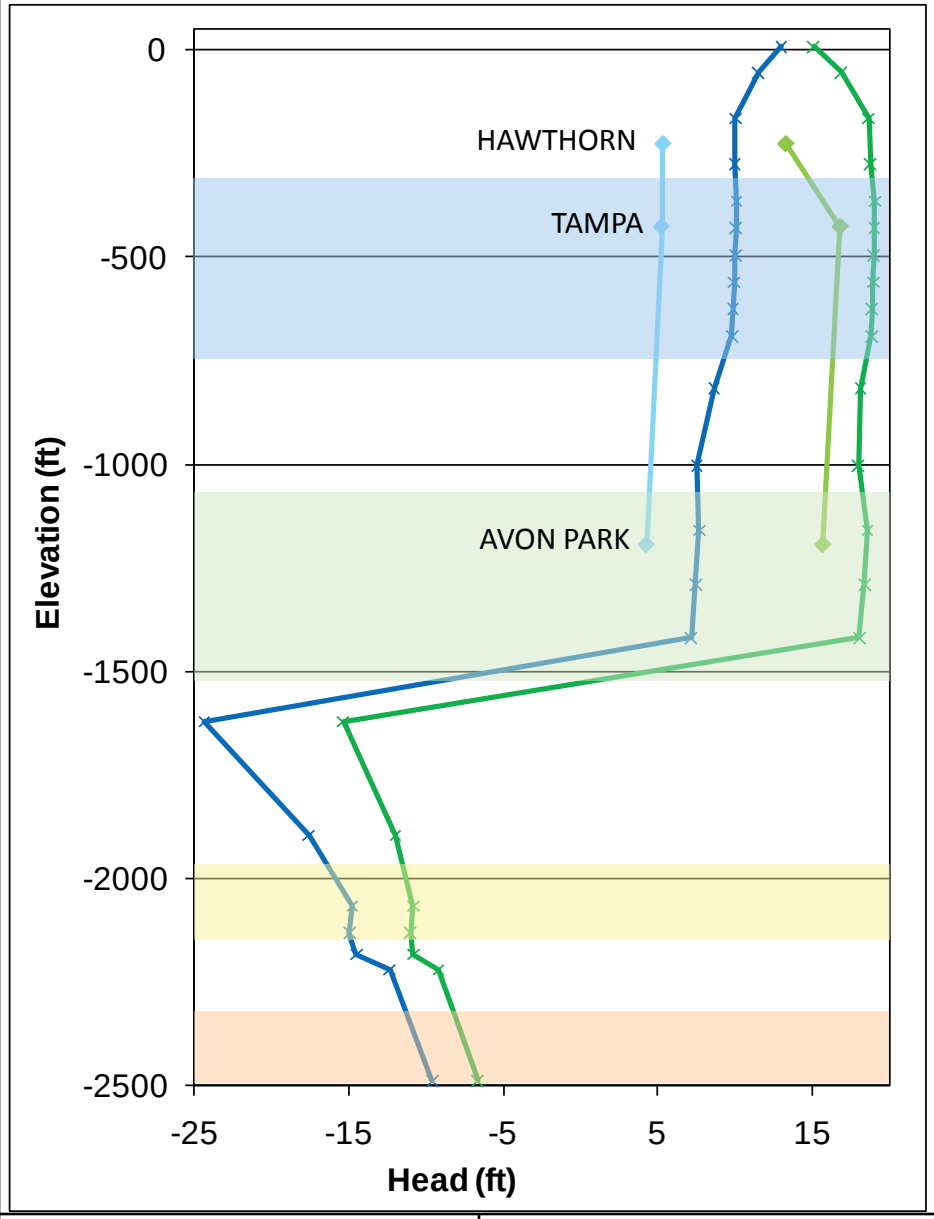

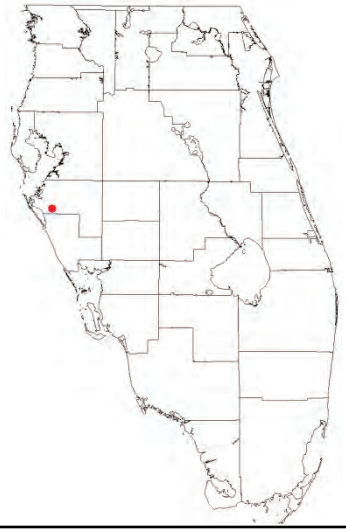

Legend:

- Model Calculated Head-May 31, 2004
- Observed Head-May 31, 2004
- Model Calculated Head-Oct. 31, 2004
- Observed Head-Oct. 31, 2004
- Cluster Location

Model-Simplified Geology

- Upper Floridan
- APPZ
- Lower Floridan (LF1)
- Boulder Zone

Notes:

This plot shows the head changes in a vertical column of the model compared to measurements made at a well cluster.

Two sets of model calculated heads are shown on the plot:

1) May 31, 2004 from the transient model, representing the dry season
2) October 31, 2004 from the transient model, representing the wet season

Observed head for May 31, 2004 and October 31, 2004 is the measured value for each respective day.

Colored stripes indicate the model-simplified stratigraphic units.

The location of the cluster is marked on the inset map.

Regional SEAWAT Calibration
Vertical Gradient Comparison
Final Groundwater Model Calibration Report

Figure 4.105

October 2010

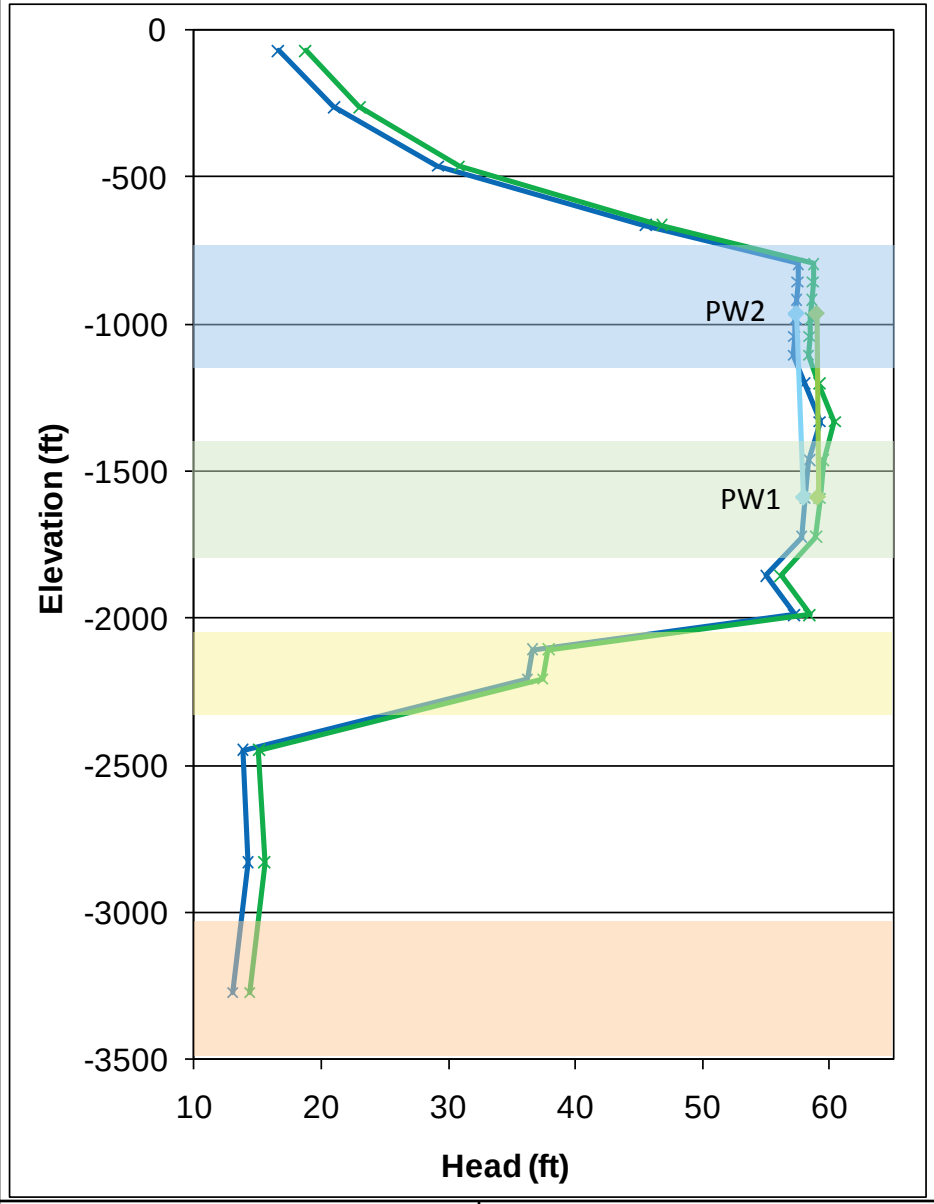

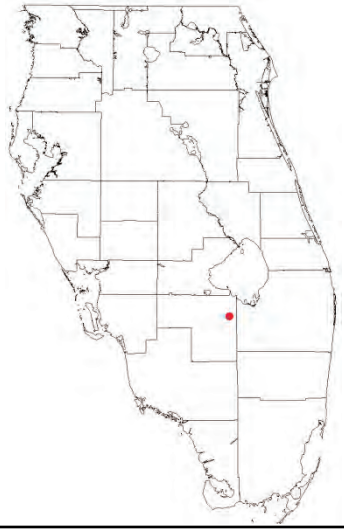

Legend:

- Model Calculated Head-May 31, 2004
- Observed Head-May 31, 2004
- Model Calculated Head-Oct. 31, 2004
- Observed Head-Oct. 31, 2004
- Cluster Location

Model-Simplified Geology

- Upper Floridan
- APPZ
- Lower Floridan (LF1)
- Boulder Zone

Notes:

This plot shows the head changes in a vertical column of the model compared to measurements made at a well cluster.

Two sets of model calculated heads are shown on the plot:

1) May 31, 2004 from the transient model, representing the dry season
2) October 31, 2004 from the transient model, representing the wet season

Observed head for May 31, 2004 and October 31, 2004 is the measured value for each respective day.

Colored stripes indicate the model-simplified stratigraphic units.

The location of the cluster is marked on the inset map.

Regional SEAWAT Calibration
Vertical Gradient Comparison
Final Groundwater Model Calibration Report

Figure 4.106

October 2010

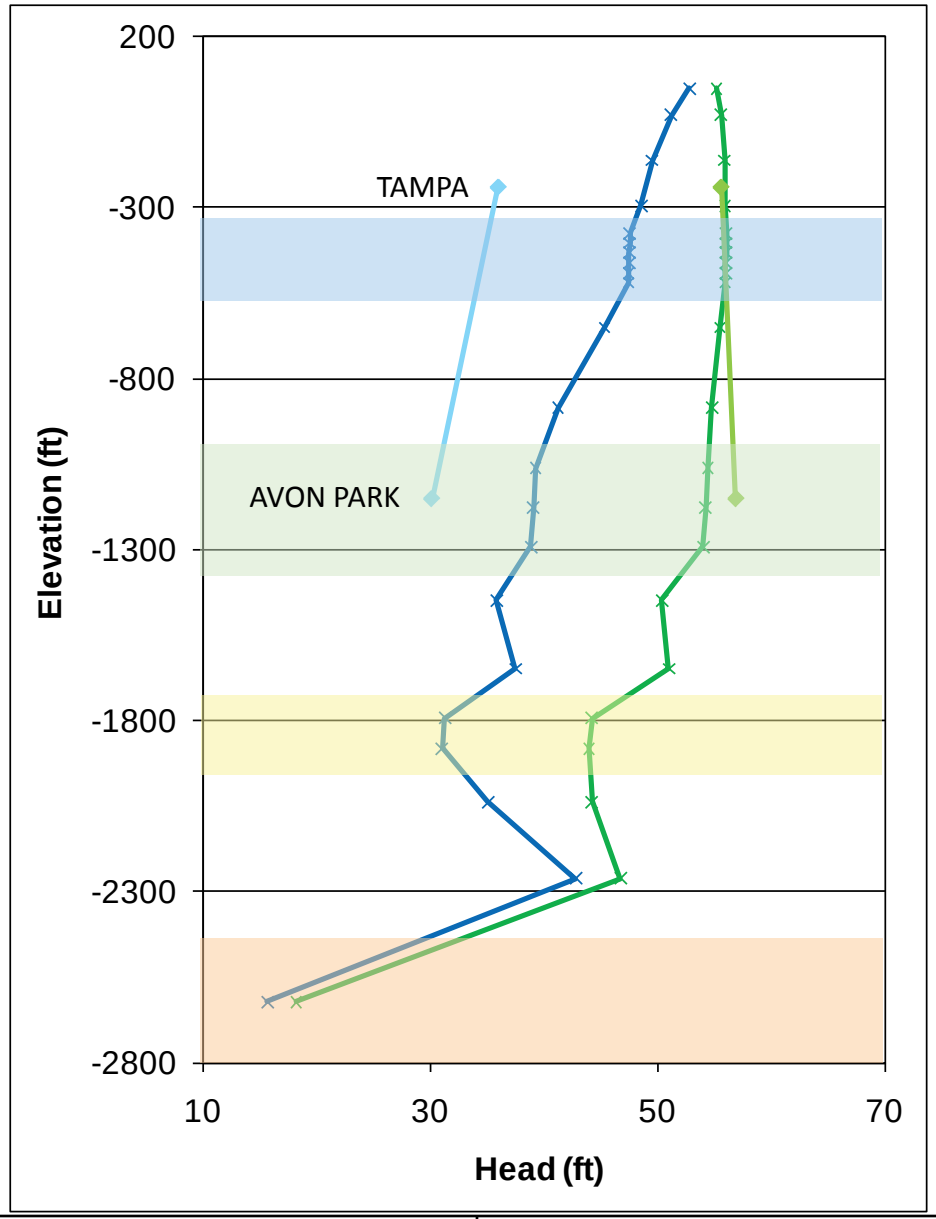

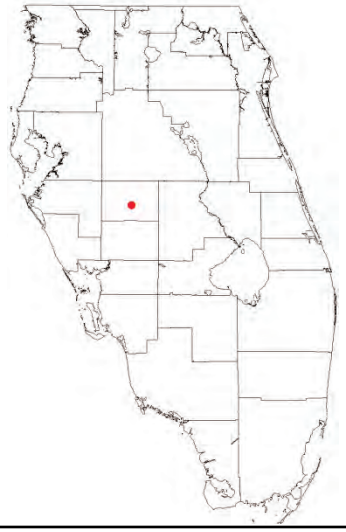

Legend:

- Model Calculated Head-May 31, 2004
- Observed Head-May 31, 2004
- Model Calculated Head-Oct. 31, 2004
- Observed Head-Oct. 31, 2004
- Cluster Location

Model-Simplified Geology

- Upper Floridan
- APPZ
- Lower Floridan (LF1)
- Boulder Zone

Notes:

This plot shows the head changes in a vertical column of the model compared to measurements made at a well cluster.

Two sets of model calculated heads are shown on the plot:

1) May 31, 2004 from the transient model, representing the dry season
2) October 31, 2004 from the transient model, representing the wet season

Observed head for May 31, 2004 and October 31, 2004 is the measured value for each respective day.

Colored stripes indicate the model-simplified stratigraphic units.

The location of the cluster is marked on the inset map.

Regional SEAWAT Calibration
Vertical Gradient Comparison
Final Groundwater Model Calibration Report

Figure 4.107

October 2010

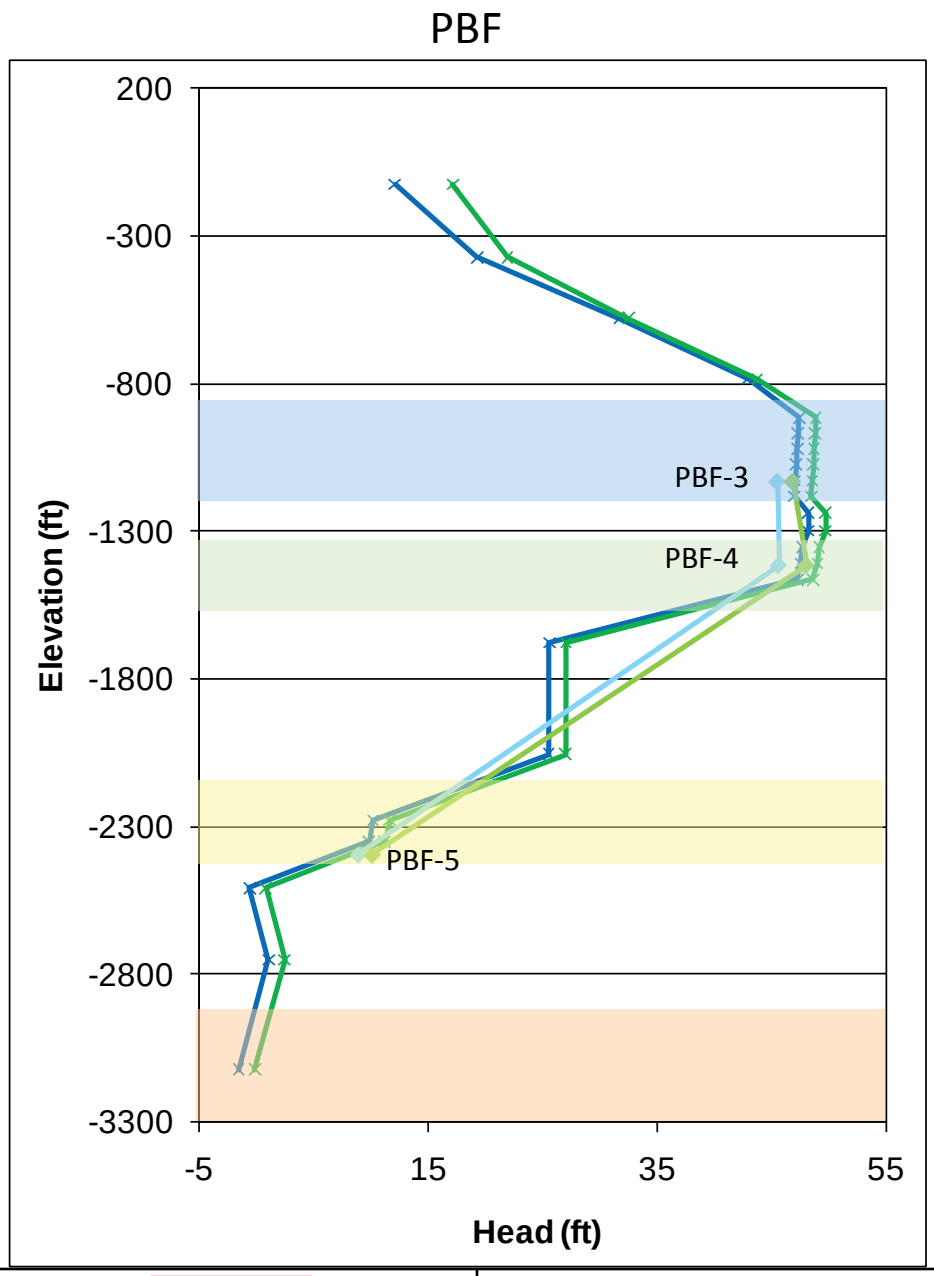

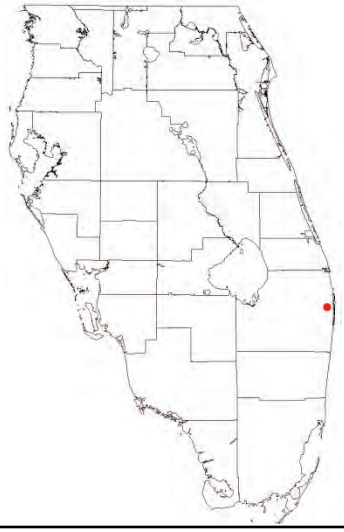

Legend:

- Model Calculated Head-May 31, 2004
- Observed Head-May 31, 2004
- Model Calculated Head-Oct. 31, 2004
- Observed Head-Oct. 31, 2004
- Cluster Location

Model-Simplified Geology

- Upper Floridan
- APPZ
- Lower Floridan (LF1)
- Boulder Zone

Notes:

This plot shows the head changes in a vertical column of the model compared to measurements made at a well cluster.

Two sets of model calculated heads are shown on the plot:

1) May 31, 2004 from the transient model, representing the dry season
2) October 31, 2004 from the transient model, representing the wet season

Observed head for May 31, 2004 and October 31, 2004 is the measured value for each respective day.

Colored stripes indicate the model-simplified stratigraphic units.

The location of the cluster is marked on the inset map.

Regional SEAWAT Calibration
Vertical Gradient Comparison
Final Groundwater Model Calibration Report

Figure 4.108

October 2010

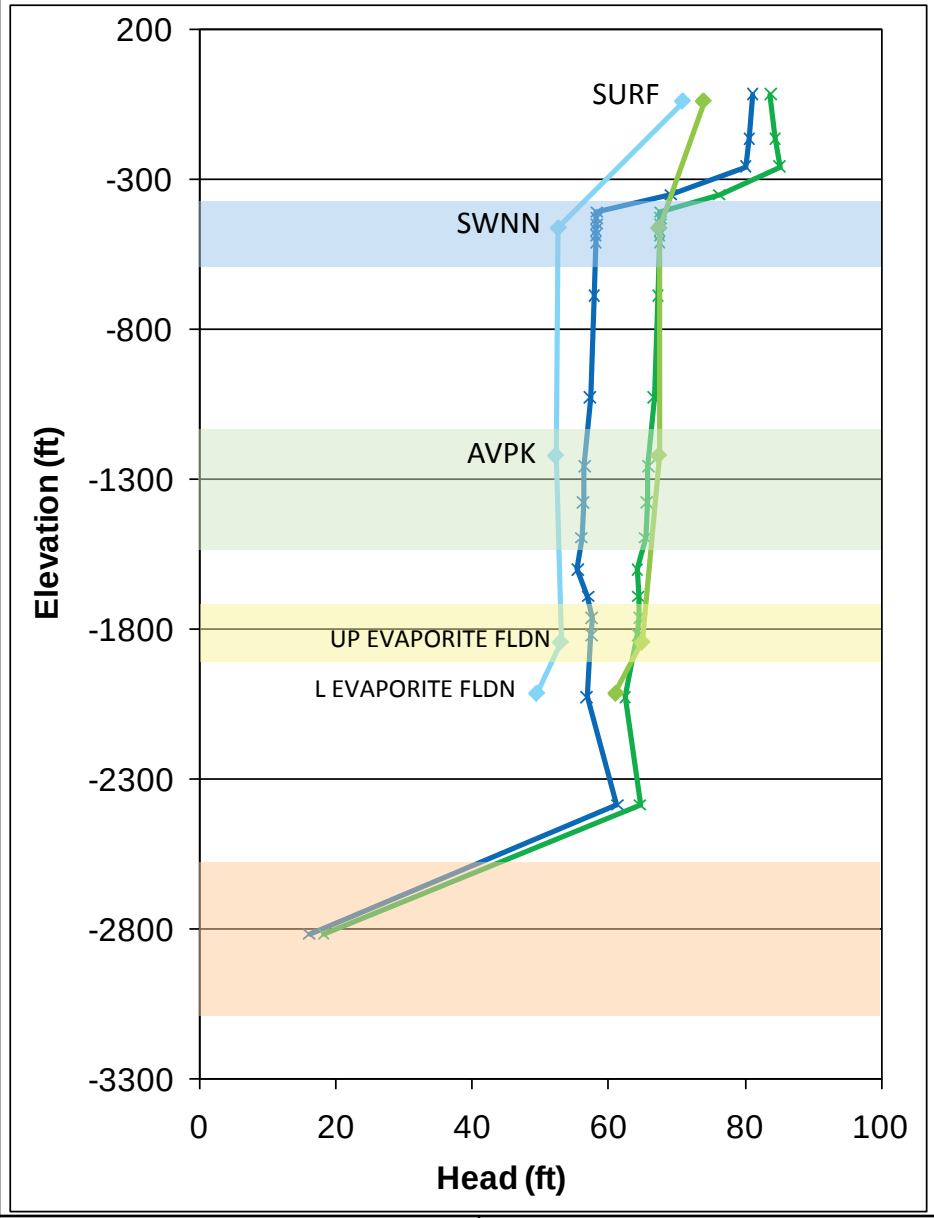

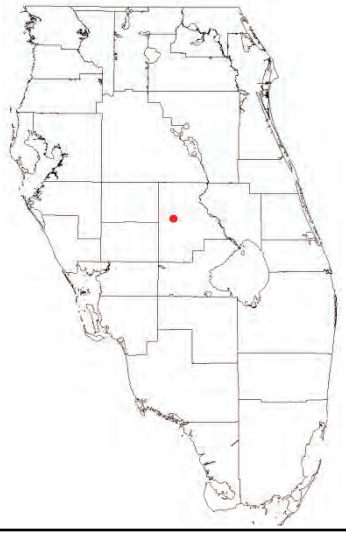

Legend:

- Model Calculated Head-May 31, 2004
- Observed Head-May 31, 2004
- Model Calculated Head-Oct. 31, 2004
- Observed Head-Oct. 31, 2004
- Cluster Location

Model-Simplified Geology

- Upper Floridan
- APPZ
- Lower Floridan (LF1)
- Boulder Zone

Notes:

This plot shows the head changes in a vertical column of the model compared to measurements made at a well cluster.

Two sets of model calculated heads are shown on the plot:

1) May 31, 2004 from the transient model, representing the dry season
2) October 31, 2004 from the transient model, representing the wet season

Observed head for May 31, 2004 and October 31, 2004 is the measured value for each respective day.

Colored stripes indicate the model-simplified stratigraphic units.

The location of the cluster is marked on the inset map.

Regional SEAWAT Calibration
Vertical Gradient Comparison
Final Groundwater Model Calibration Report

Figure 4.109

October 2010

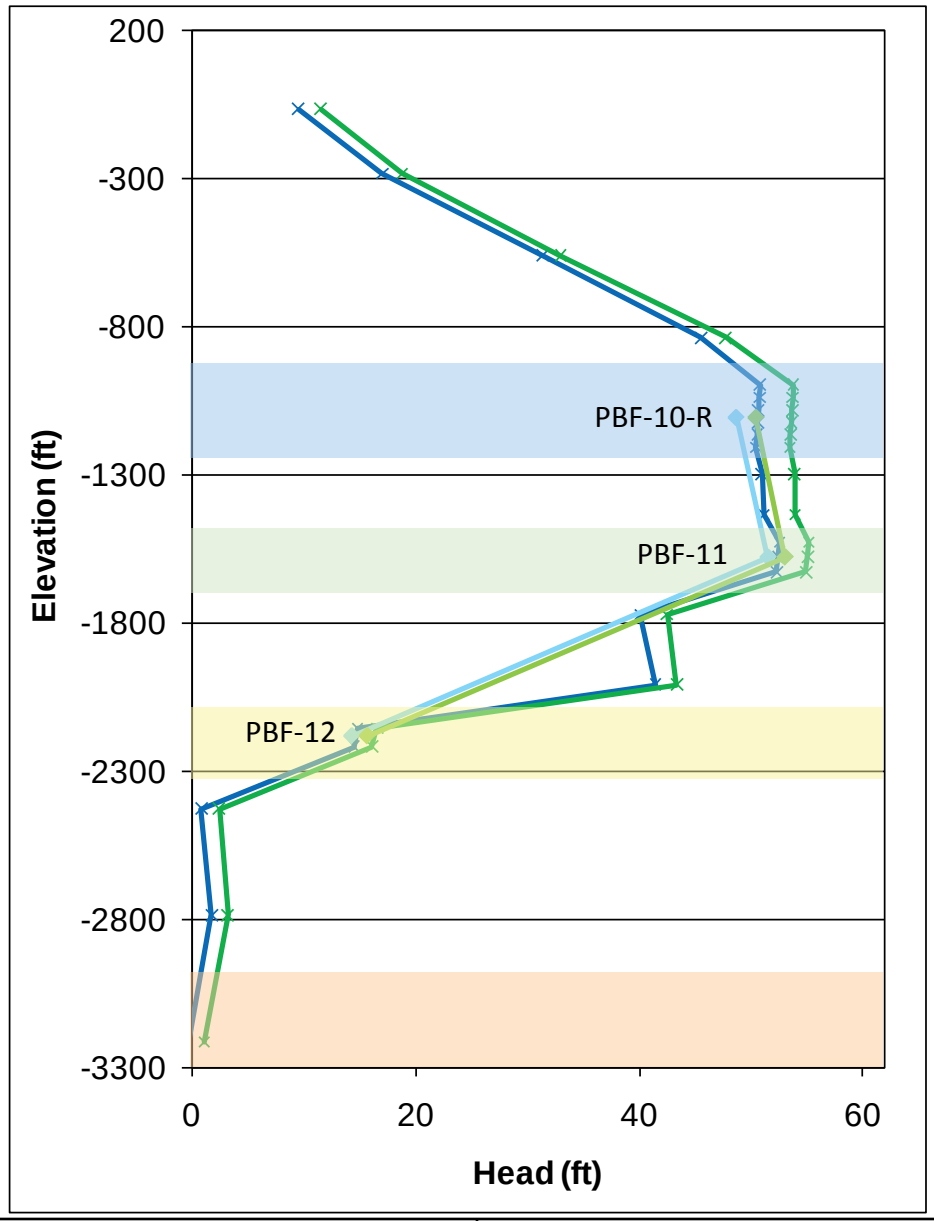

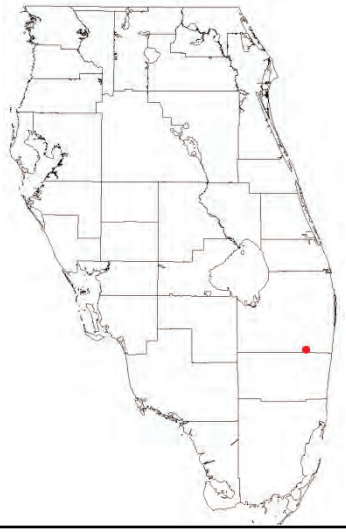

Legend:

- Model Calculated Head-May 31, 2004
- Observed Head-May 31, 2004
- Model Calculated Head-Oct. 31, 2004
- Observed Head-Oct. 31, 2004
- Cluster Location

Model-Simplified Geology

- Upper Floridan
- APPZ
- Lower Floridan (LF1)
- Boulder Zone

Notes:

This plot shows the head changes in a vertical column of the model compared to measurements made at a well cluster.

Two sets of model calculated heads are shown on the plot:

1) May 31, 2004 from the transient model, representing the dry season
2) October 31, 2004 from the transient model, representing the wet season

Observed head for May 31, 2004 and October 31, 2004 is the measured value for each respective day.

Colored stripes indicate the model-simplified stratigraphic units.

The location of the cluster is marked on the inset map.

Regional SEAWAT Calibration
Vertical Gradient Comparison
Final Groundwater Model Calibration Report

Figure 4.110

October 2010

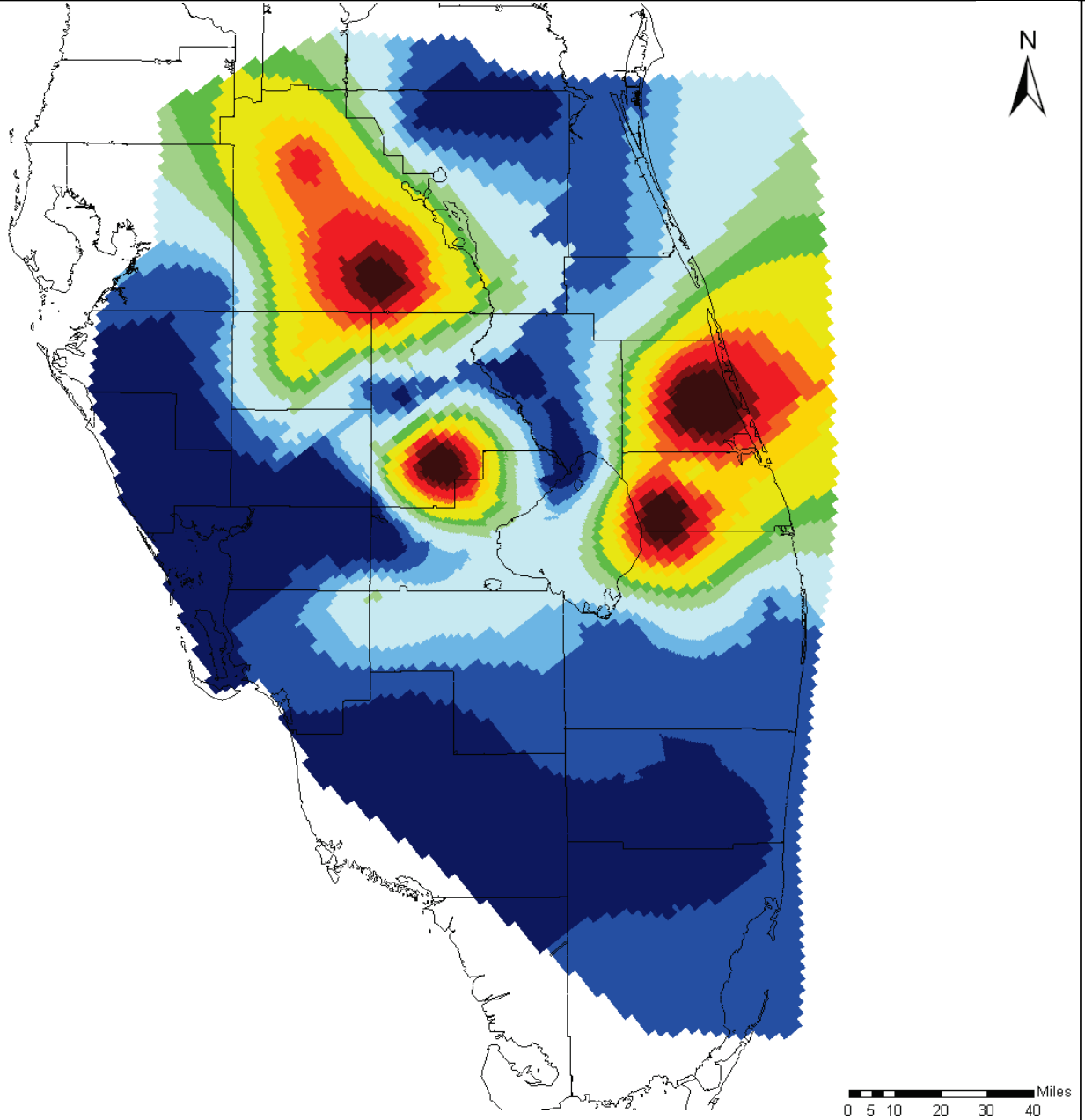

Notes:

Distribution shown was applied to SEAWAT model layers 2 through 4.

Specific Storage values were interpolated to the grid from values assigned to a set of pilot points scattered across the model domain.

A combination of automated calibration (PEST) and manual calibration (trial and error) resulted in this Specific Storage field.

Calibrated SEAWAT Specific Storage Intermediate Aquifer System

Final Groundwater Model Calibration Report

Figure 4.111

October 2010

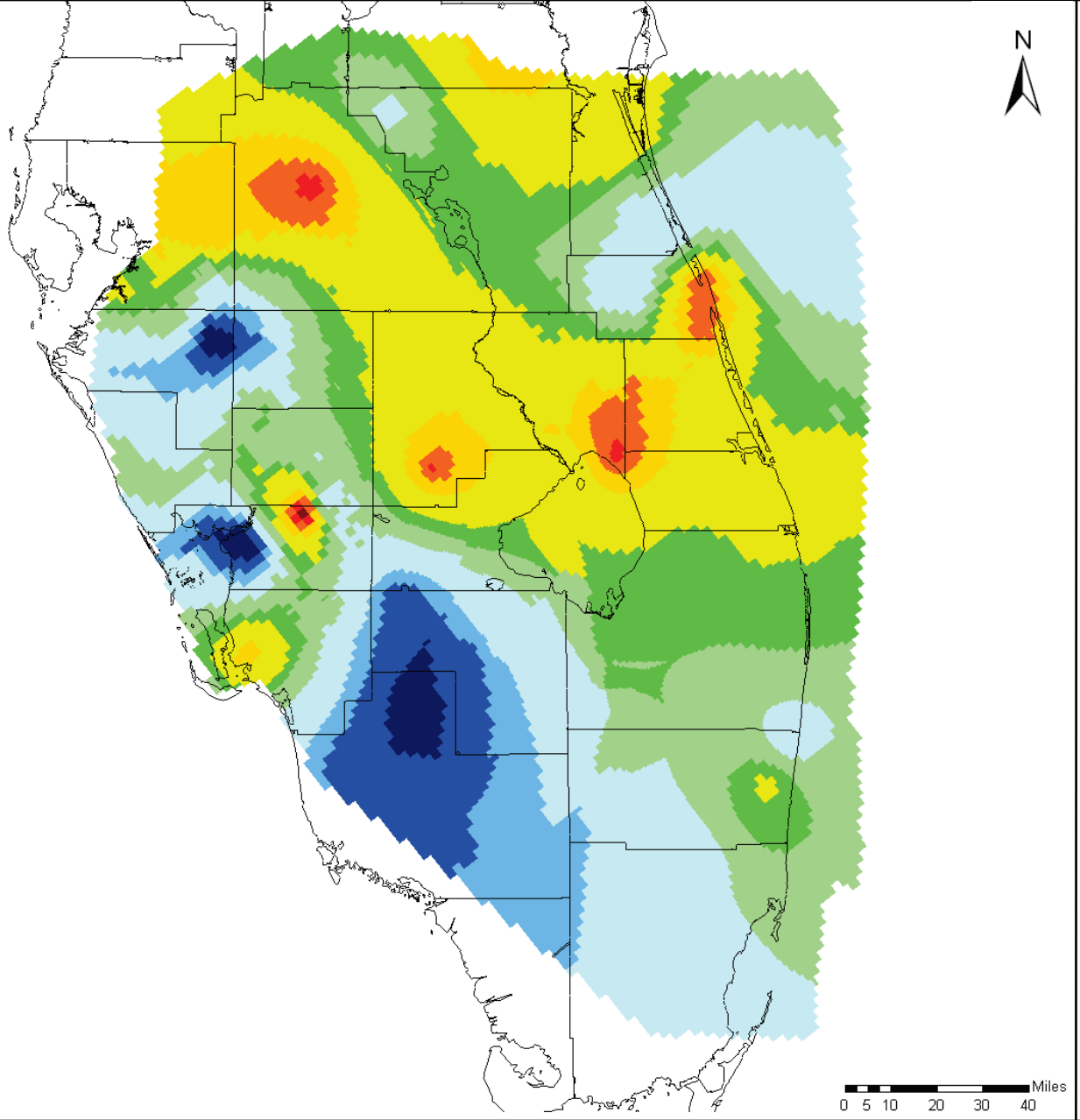

Notes:

Distribution shown was applied to SEAWAT model layers 5 through 10.

Specific Storage values were interpolated to the grid from values assigned to a set of pilot points scattered across the model domain.

A combination of automated calibration (PEST) and manual calibration (trial and error) resulted in this Specific Storage field.

Calibrated SEAWAT Specific Storage
Upper Floridan Aquifer
Final Groundwater Model Calibration Report

Figure 4.112

October 2010

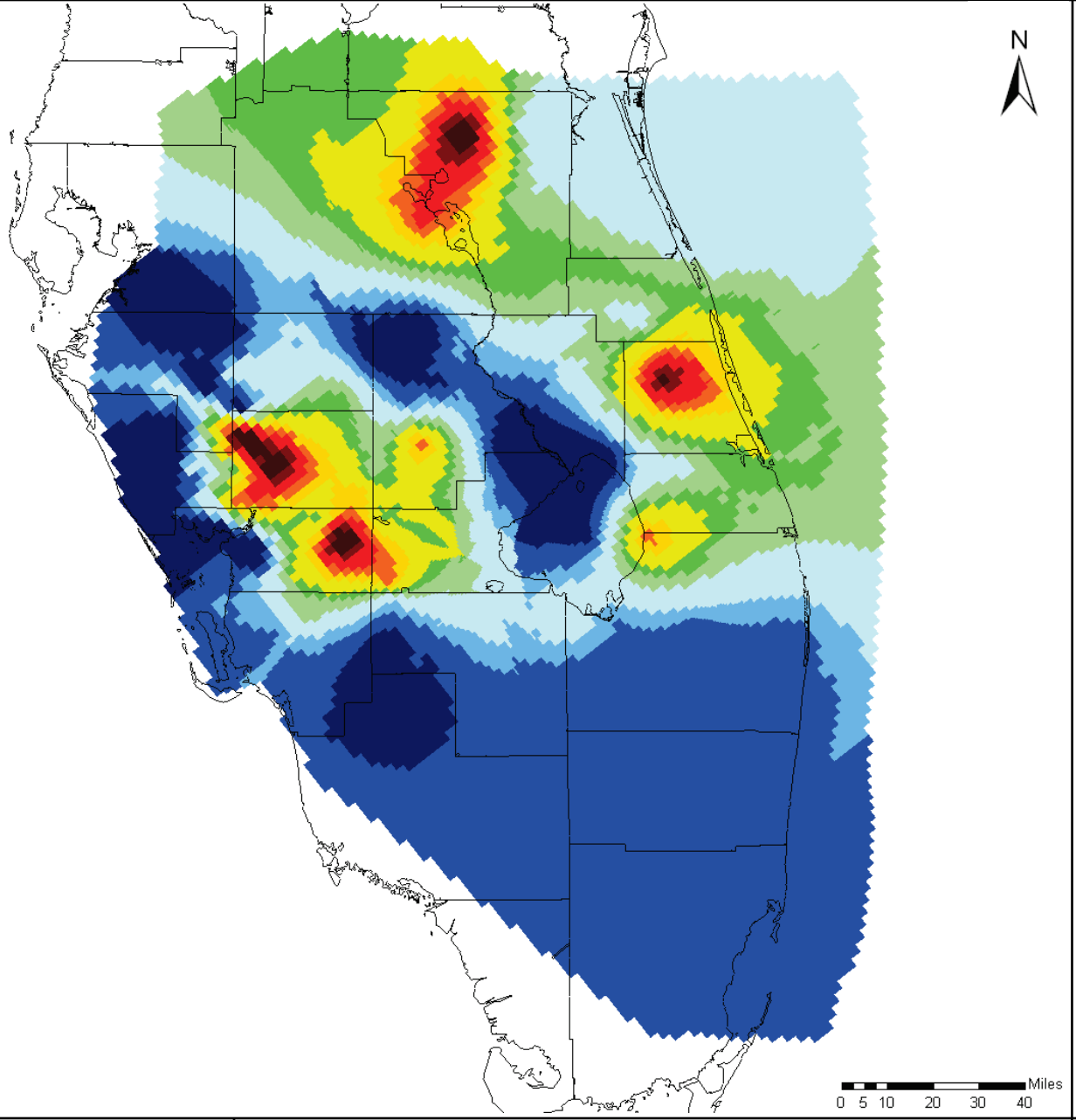

Notes:

Distribution shown was applied to SEAWAT model layers 11 through 12.

Specific Storage values were interpolated to the grid from values assigned to a set of pilot points scattered across the model domain.

A combination of automated calibration (PEST) and manual calibration (trial and error) resulted in this Specific Storage field.

Calibrated SEAWAT Specific Storage
Middle Confining Unit 1

Final Groundwater Model Calibration Report

Figure 4.113

October 2010

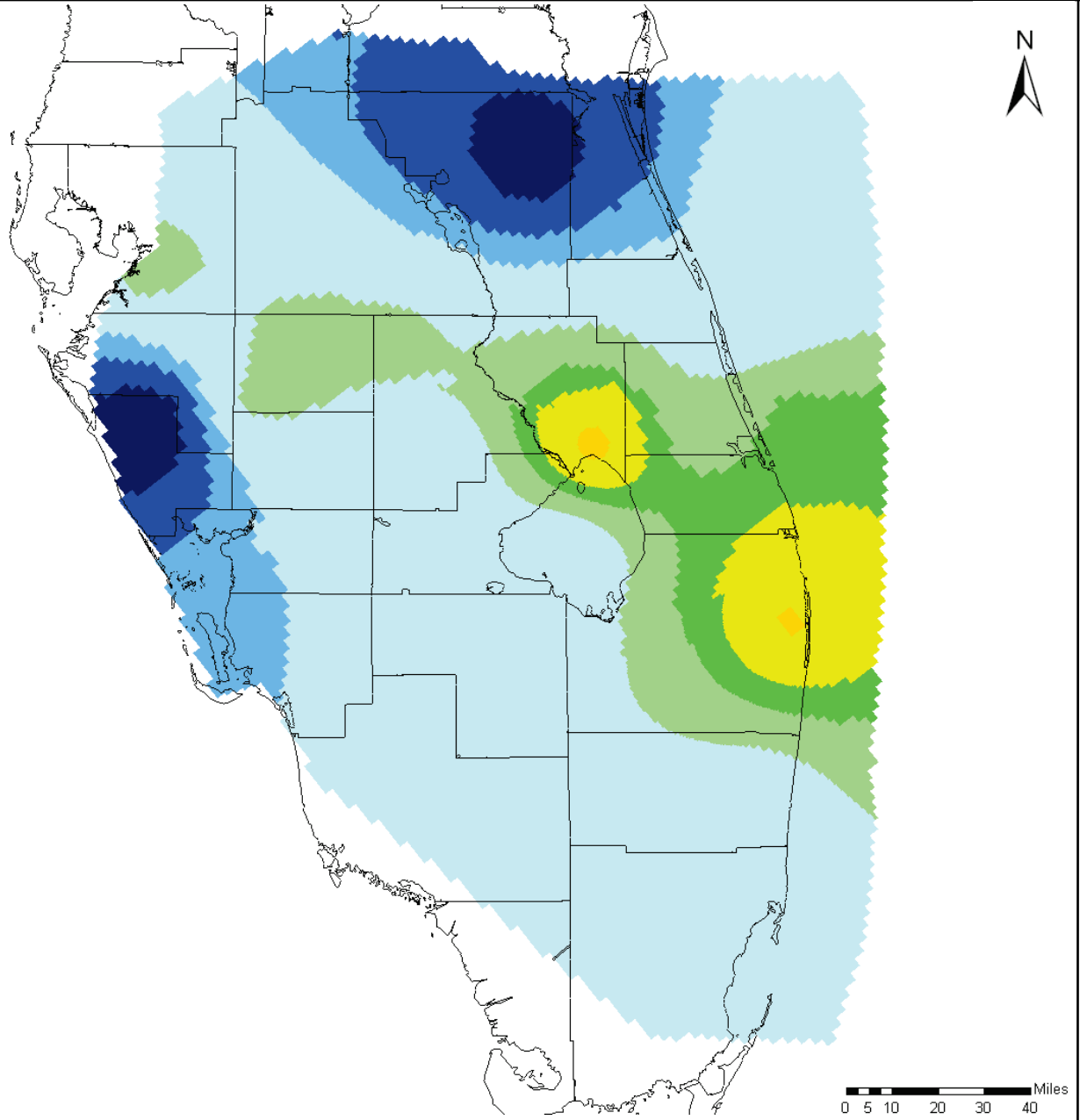

Notes:

Distribution shown was applied to SEAWAT model layers 13 through 15.

Specific Storage values were interpolated to the grid from values assigned to a set of pilot points scattered across the model domain.

A combination of automated calibration (PEST) and manual calibration (trial and error) resulted in this Specific Storage field.

Calibrated SEAWAT Specific Storage
Avon Park Permeable Zone
Final Groundwater Model Calibration Report

Figure 4.114

October 2010

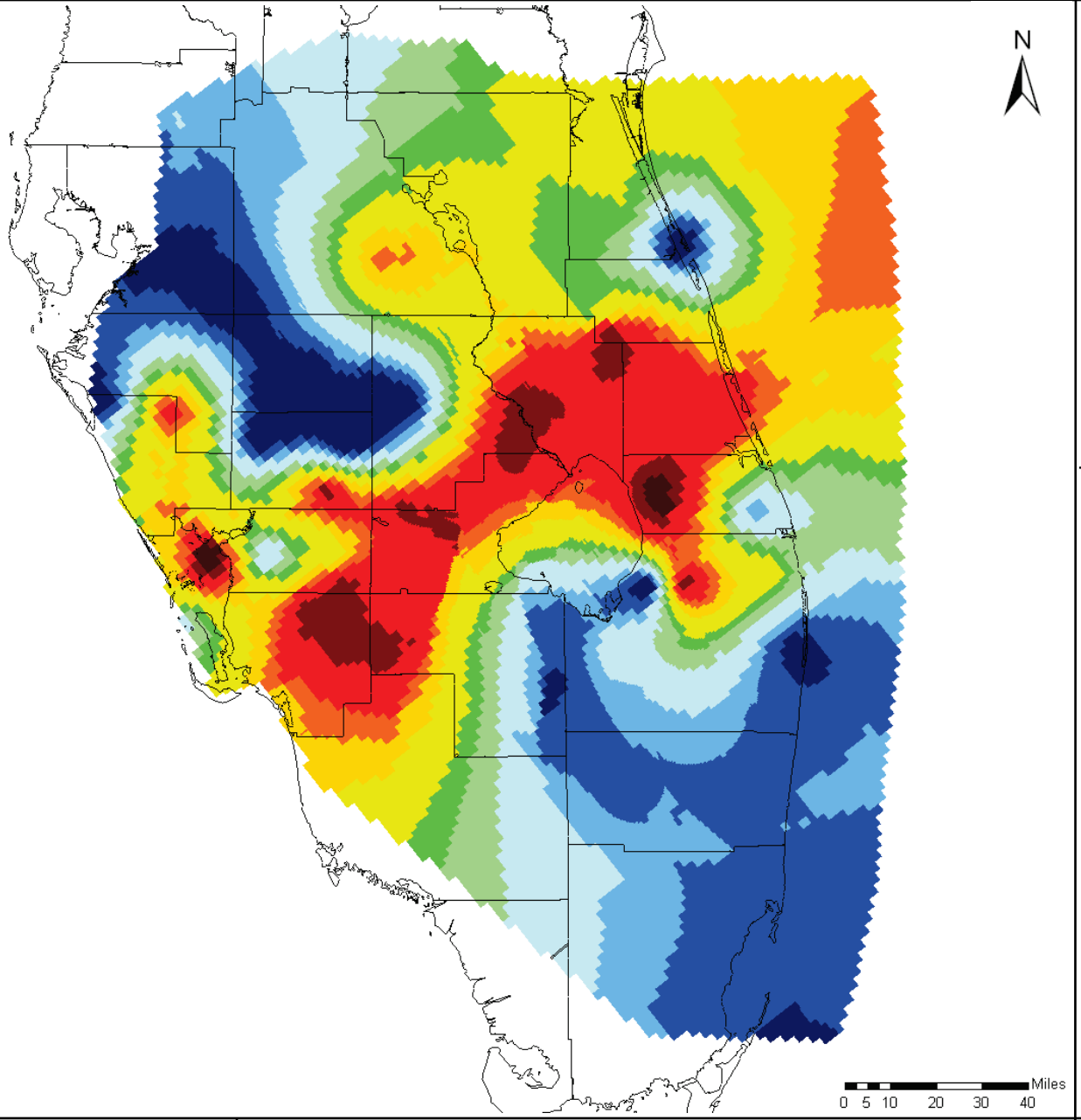

Notes:

Distribution shown was applied to SEAWAT model layers 16 through 17.

Specific Storage values were interpolated to the grid from values assigned to a set of pilot points scattered across the model domain.

A combination of automated calibration (PEST) and manual calibration (trial and error) resulted in this Specific Storage field.

Calibrated SEAWAT Specific Storage
Middle Confining Unit 2
Final Groundwater Model Calibration Report

Figure 4.115

October 2010

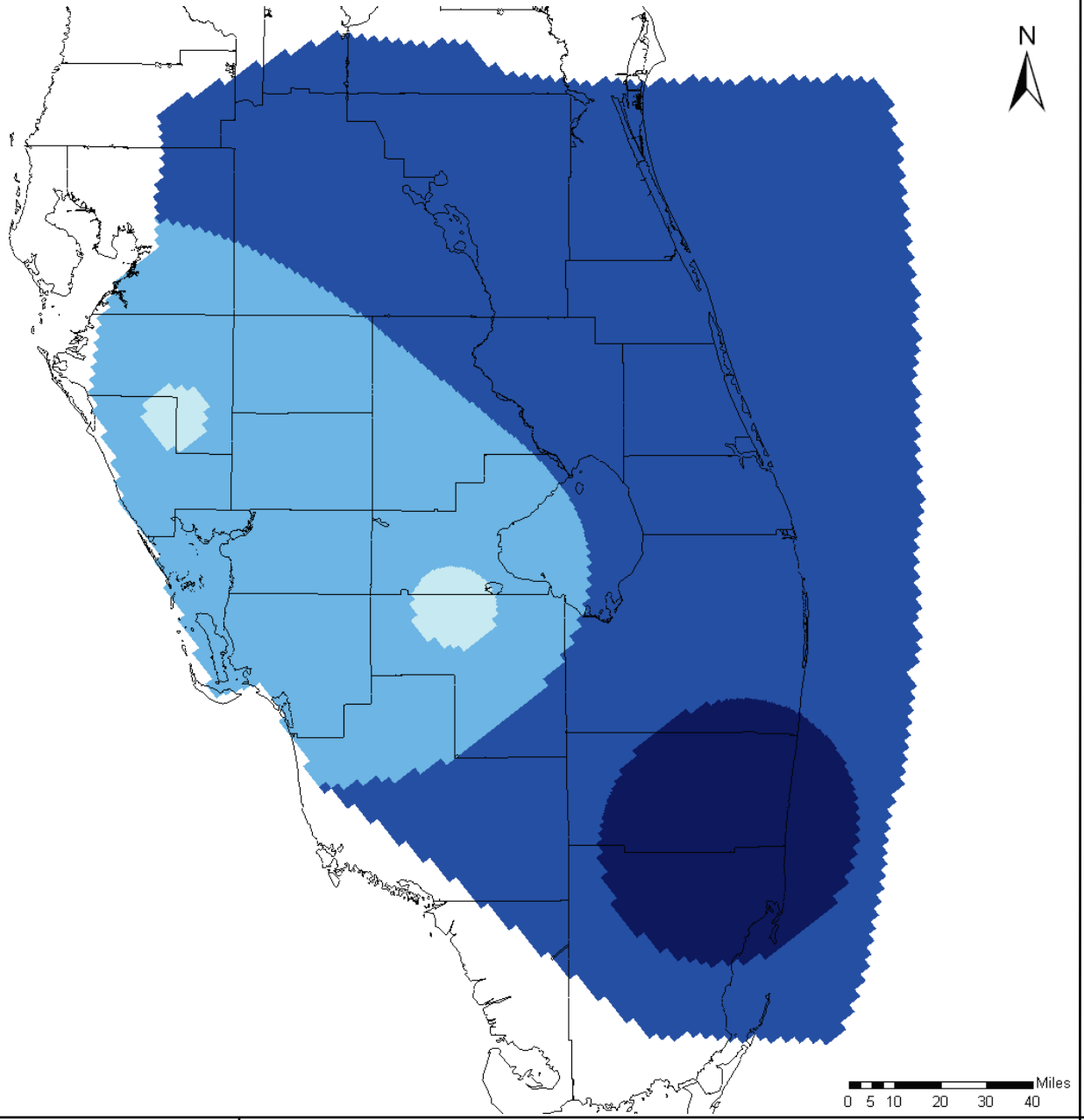

Specific Storage (ft^{-1})

- 1e-003
- 6e-005
- 3e-005
- 1e-005
- 6e-006
- 3e-006
- 1e-006
- 6e-007
- 3e-007
- 1e-007
- 6e-008
- 3e-008
- 1e-008

Notes:

Distribution shown was applied to SEAWAT model layers 18 through 19.

Specific Storage values were interpolated to the grid from values assigned to a set of pilot points scattered across the model domain.

A combination of automated calibration (PEST) and manual calibration (trial and error) resulted in this Specific Storage field.

Calibrated SEAWAT Specific Storage
Lower Floridan (LF1) Aquifer
Final Groundwater Model Calibration Report

Figure 4.116

October 2010

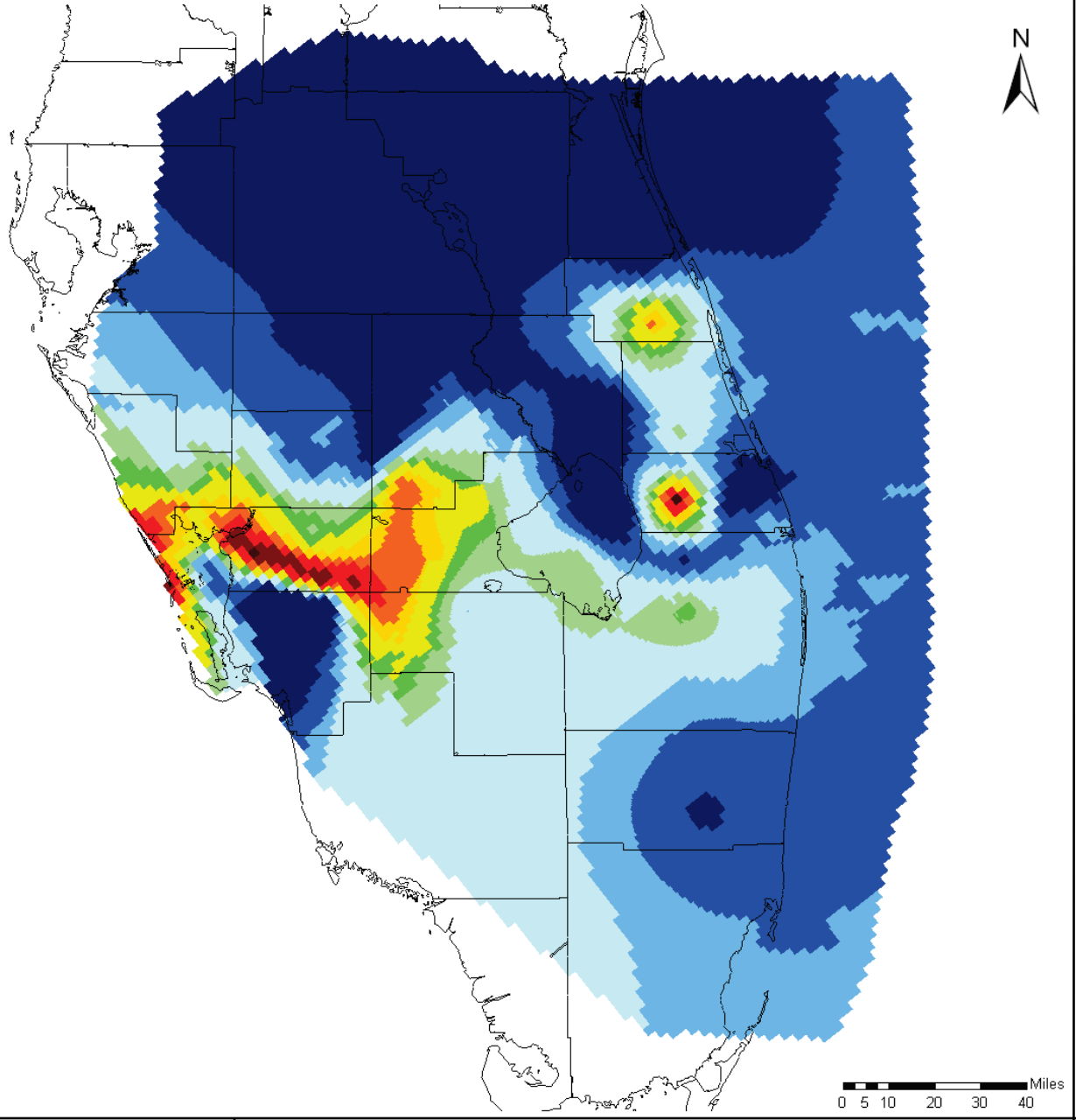

Notes:

Distribution shown was applied to SEAWAT model layers 20 through 21.

Specific Storage values were interpolated to the grid from values assigned to a set of pilot points scattered across the model domain.

A combination of automated calibration (PEST) and manual calibration (trial and error) resulted in this Specific Storage field.

Calibrated SEAWAT Specific Storage
Lower Confining Unit
Final Groundwater Model Calibration Report

Figure 4.117

October 2010

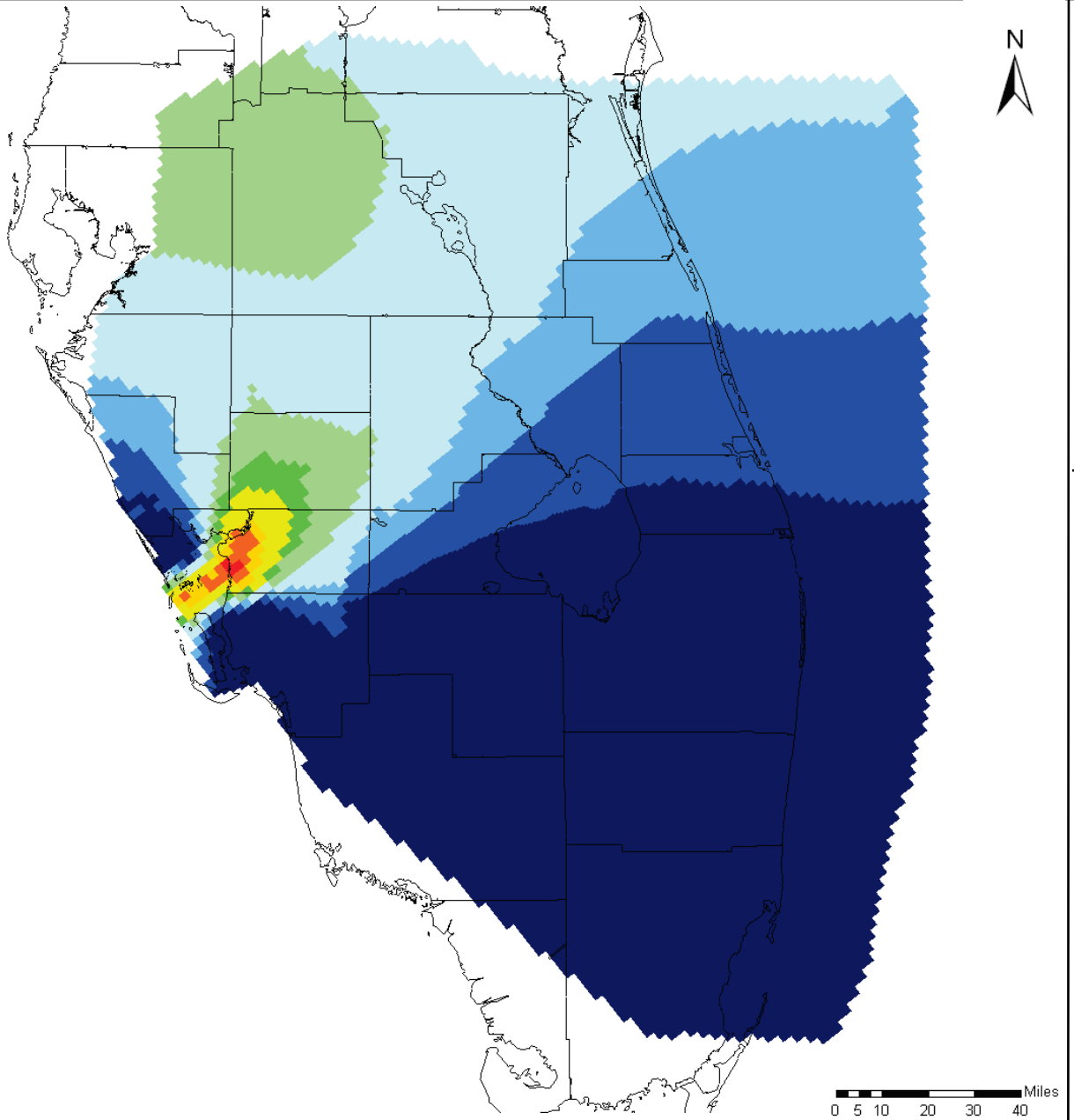

Specific Storage (ft^{-1})

- 1e-003
- 6e-005
- 3e-005
- 1e-005
- 6e-006
- 3e-006
- 1e-006
- 6e-007
- 3e-007
- 1e-007
- 6e-008
- 3e-008
- 1e-008

Notes:

Distribution shown was applied to SEAWAT model layer 22.

Specific Storage values were interpolated to the grid from values assigned to a set of pilot points scattered across the model domain.

A combination of automated calibration (PEST) and manual calibration (trial and error) resulted in this Specific Storage field.

Calibrated SEAWAT Specific Storage
Boulder Zone

Final Groundwater Model Calibration Report

Figure 4.118

October 2010

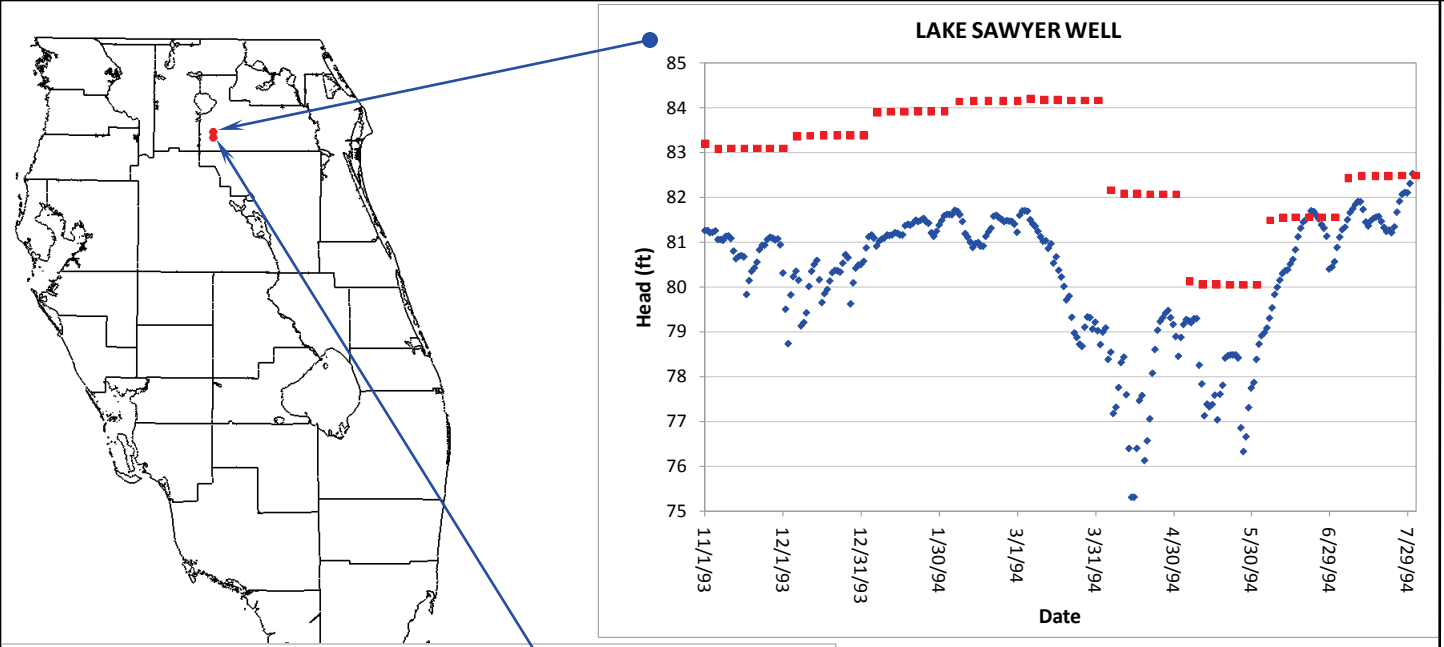

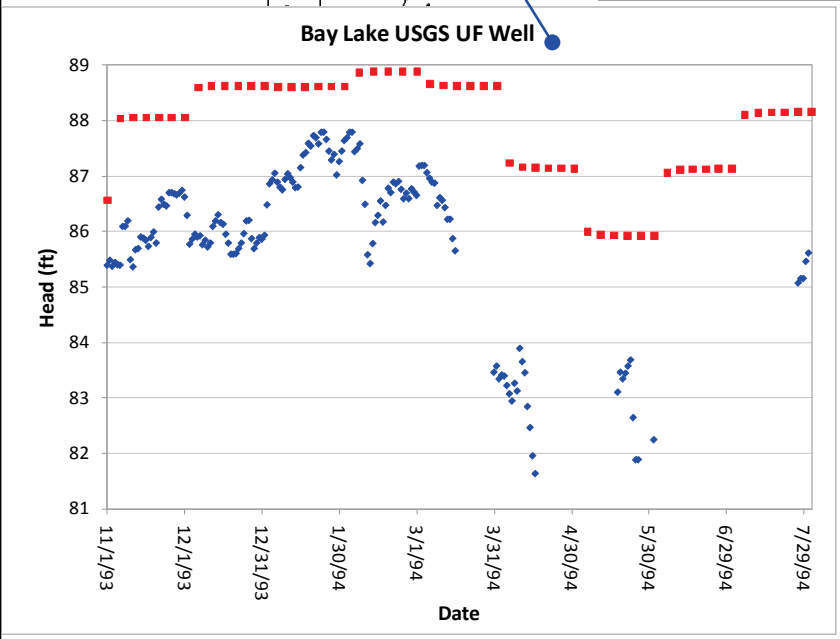

	Bay Lake Well	Lake Sawyer Well
Mean Error	2.772	2.568
Mean Absolute Error	2.772	2.568
Root Mean Square (RMS)	2.961	2.822
Observed Range	6.16	7.23
RMS as Percentage of Range	48%	39%
Coefficient of Determination (r^2)	0.798	0.311
Nash-Sutcliffe Model Efficiency Coefficient	-1.911	-3.993

Legend

- Measured Head
- Model Calculated Head

Notes:

Figures 4.119 through 4.150 show the comparison between measured head values and model-calculated head values at a number of observation wells for the validation period. Although the scales vary on each plot, all plots have a horizontal grid line at each foot. This is to make it easy to determine the range of heads at a glance.

The model used month-long stress periods, so pumping and boundary conditions were input as step functions with constant values throughout each month and sudden changes at the end of each month. For this reason, the model cannot be expected to accurately predict day-to-day head variations in any of these wells. Calibration efforts were aimed at matching general trends and monthly averages.

Starting head conditions for this model were based on the October 1993 steady state solution. Transient calibration efforts were focused on matching the head changes, not the actual heads, so it is not uncommon for residuals in the starting condition to be carried through the entire calibration period. This indicates that the model is correctly predicting responses to hydrogeologic forces even if the calculated head values vary somewhat from the measured values.

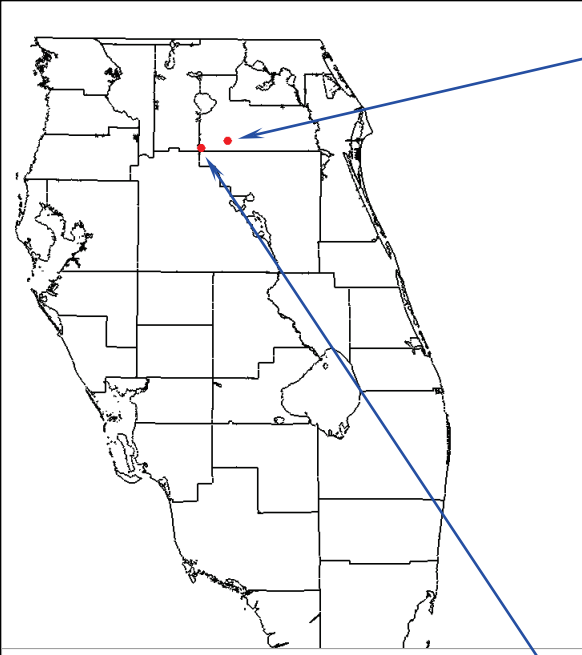

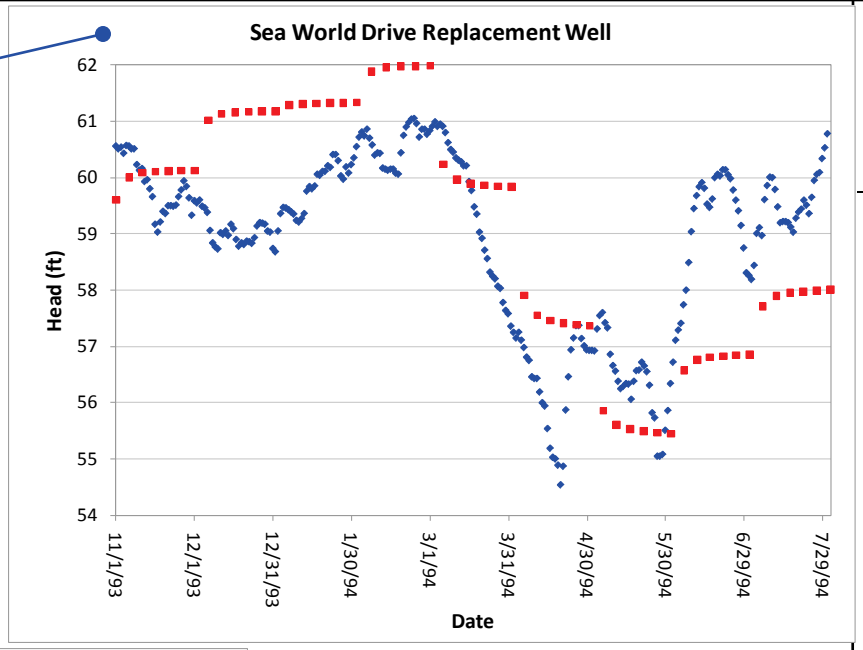

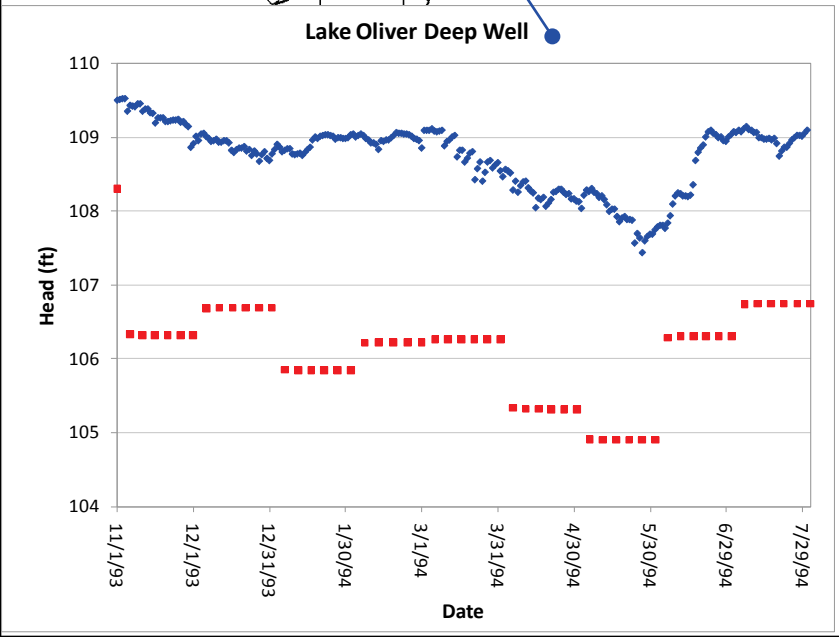

	Lake Oliver Deep Well	Sea World Drive Repl. Well
Mean Error	-2.647	0.248
Mean Absolute Error	2.647	1.312
Root Mean Square (RMS)	2.659	1.485
Observed Range	2.14	6.51
RMS as Percentage of Range	124%	23%
Coefficient of Determination (r^2)	0.0804	0.493
Nash-Sutcliffe Model Efficiency Coefficient	-44.321	-0.113

Legend

- Measured Head
- Model Calculated Head

Notes:

Figures 4.119 through 4.150 show the comparison between measured head values and model-calculated head values at a number of observation wells for the validation period. Although the scales vary on each plot, all plots have a horizontal grid line at each foot. This is to make it easy to determine the range of heads at a glance.

The model used month-long stress periods, so pumping and boundary conditions were input as step functions with constant values throughout each month and sudden changes at the end of each month. For this reason, the model cannot be expected to accurately predict day-to-day head variations in any of these wells. Calibration efforts were aimed at matching general trends and monthly averages.

Starting head conditions for this model were based on the October 1993 steady state solution. Transient calibration efforts were focused on matching the head changes, not the actual heads, so it is not uncommon for residuals in the starting condition to be carried through the entire calibration period. This indicates that the model is correctly predicting responses to hydrogeologic forces even if the calculated head values vary somewhat from the measured values.

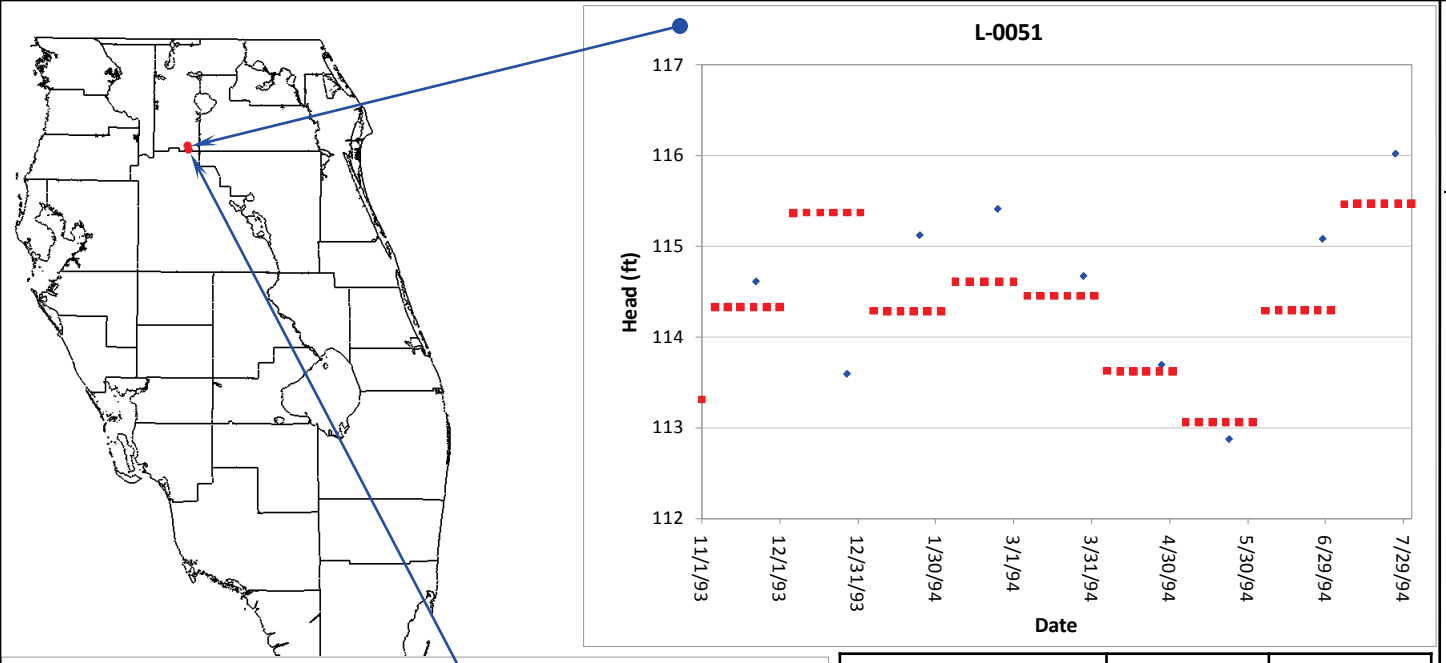

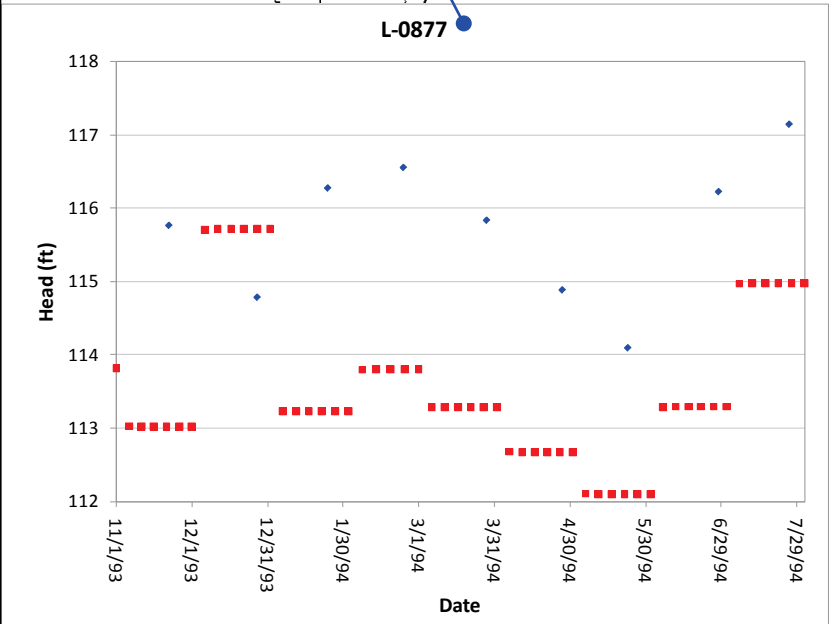

	L-0877	L-0051
Mean Error	-2.192	-0.215
Mean Absolute Error	2.297	0.652
Root Mean Square (RMS)	2.411	0.791
Observed Range	3.05	3.15
RMS as Percentage of Range	79%	25%
Coefficient of Determination (r^2)	0.144	0.354
Nash-Sutcliffe Model Efficiency Coefficient	-5.958	0.297

Legend

- Measured Head
- Model Calculated Head

Notes:

Figures 4.119 through 4.150 show the comparison between measured head values and model-calculated head values at a number of observation wells for the validation period. Although the scales vary on each plot, all plots have a horizontal grid line at each foot. This is to make it easy to determine the range of heads at a glance.

The model used month-long stress periods, so pumping and boundary conditions were input as step functions with constant values throughout each month and sudden changes at the end of each month. For this reason, the model cannot be expected to accurately predict day-to-day head variations in any of these wells. Calibration efforts were aimed at matching general trends and monthly averages.

Starting head conditions for this model were based on the October 1993 steady state solution. Transient calibration efforts were focused on matching the head changes, not the actual heads, so it is not uncommon for residuals in the starting condition to be carried through the entire calibration period. This indicates that the model is correctly predicting responses to hydrogeologic forces even if the calculated head values vary somewhat from the measured values.

Transient SEAWAT Validation Comparison
Upper Floridan Aquifer (1993-1994)
Final Groundwater Model Calibration Report

Figure 4.121

October 2010

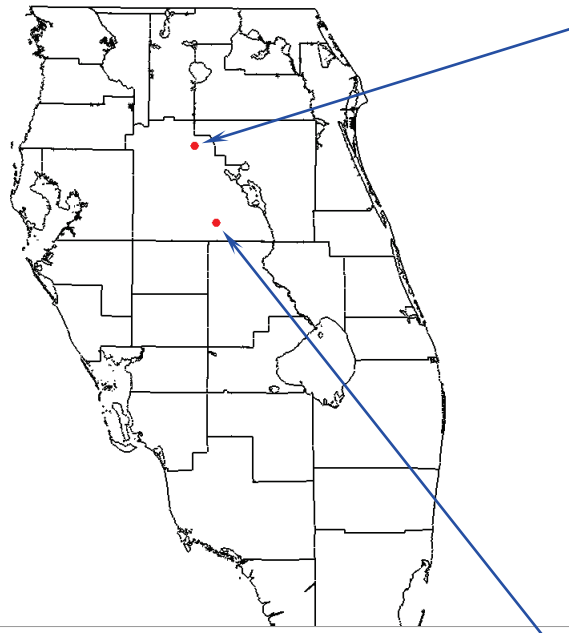

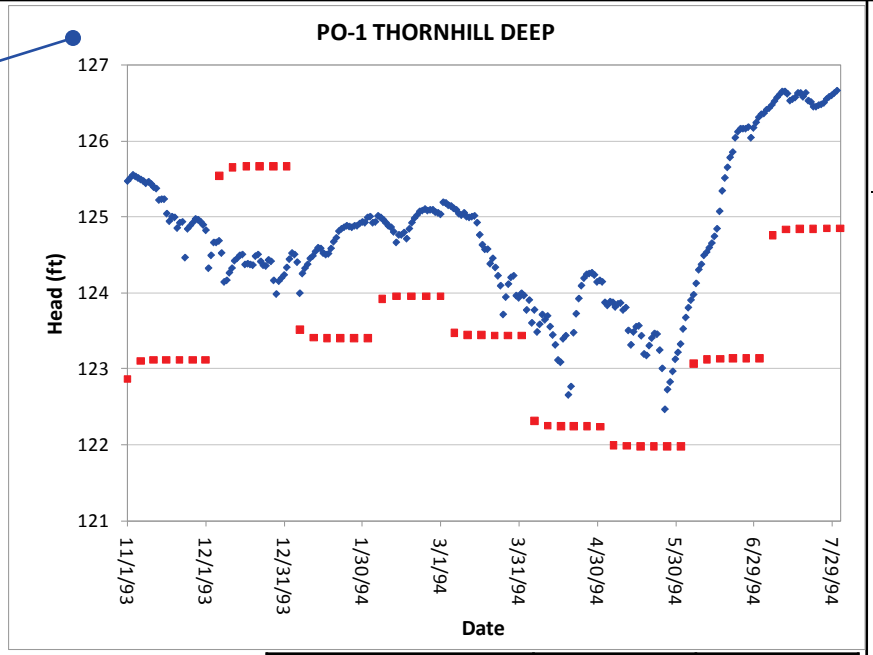

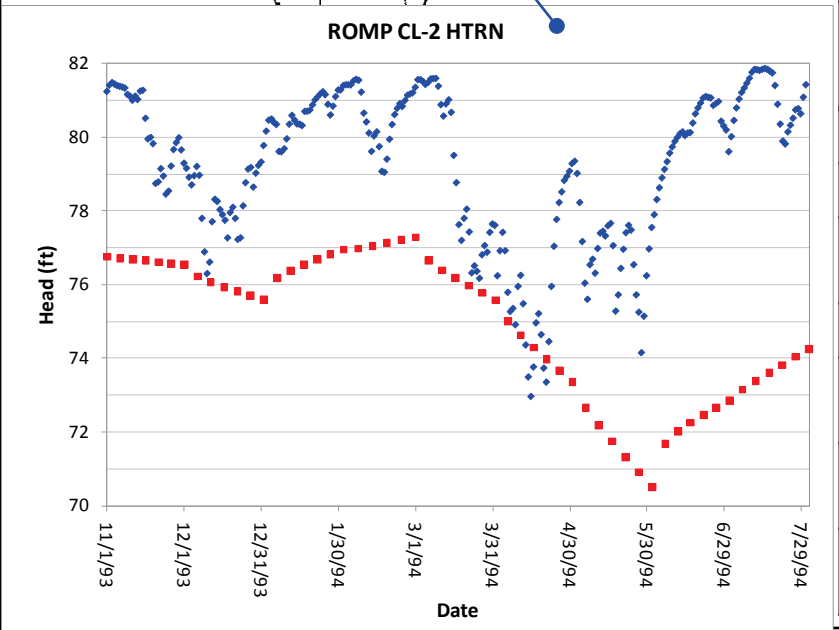

	ROMP CL-2 HTRN	PO-1 Thornhill Deep
Mean Error	-4.278	-1.226
Mean Absolute Error	4.278	1.411
Root Mean Square (RMS)	4.776	1.495
Observed Range	8.91	4.20
RMS as Percentage of Range	54%	36%
Coefficient of Determination (r^2)	0.096	0.300
Nash-Sutcliffe Model Efficiency Coefficient	-6.882	-2.124

Legend

- Measured Head
- Model Calculated Head

Notes:

Figures 4.119 through 4.150 show the comparison between measured head values and model-calculated head values at a number of observation wells for the validation period. Although the scales vary on each plot, all plots have a horizontal grid line at each foot. This is to make it easy to determine the range of heads at a glance.

The model used month-long stress periods, so pumping and boundary conditions were input as step functions with constant values throughout each month and sudden changes at the end of each month. For this reason, the model cannot be expected to accurately predict day-to-day head variations in any of these wells. Calibration efforts were aimed at matching general trends and monthly averages.

Starting head conditions for this model were based on the October 1993 steady state solution. Transient calibration efforts were focused on matching the head changes, not the actual heads, so it is not uncommon for residuals in the starting condition to be carried through the entire calibration period. This indicates that the model is correctly predicting responses to hydrogeologic forces even if the calculated head values vary somewhat from the measured values.

Transient SEAWAT Validation Comparison
Upper Floridan Aquifer (1993-1994)
Final Groundwater Model Calibration Report

Figure 4.122

October 2010

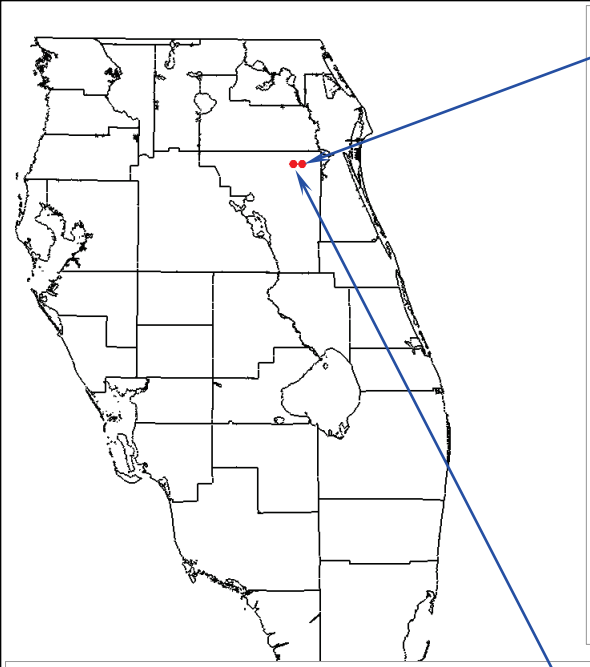

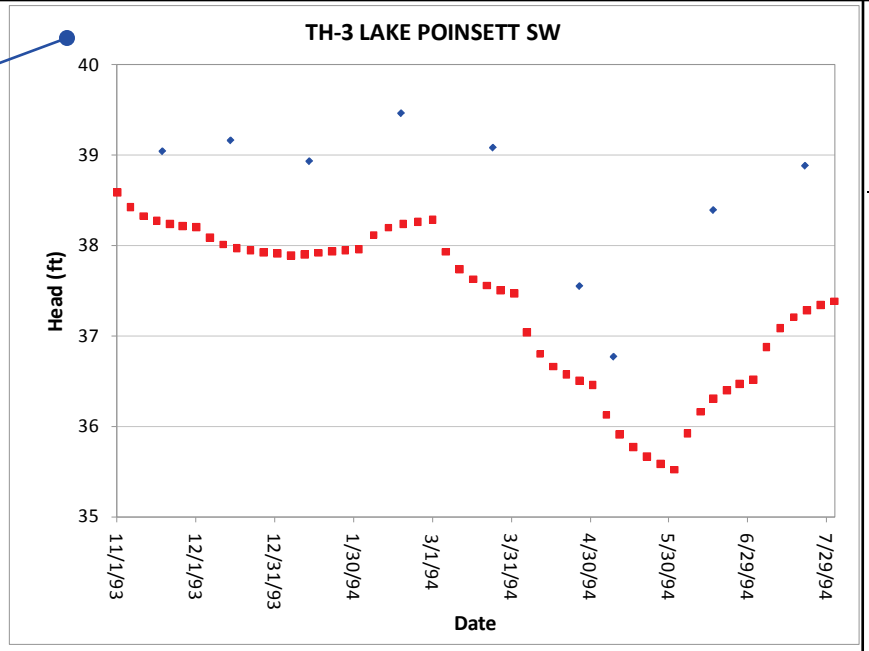

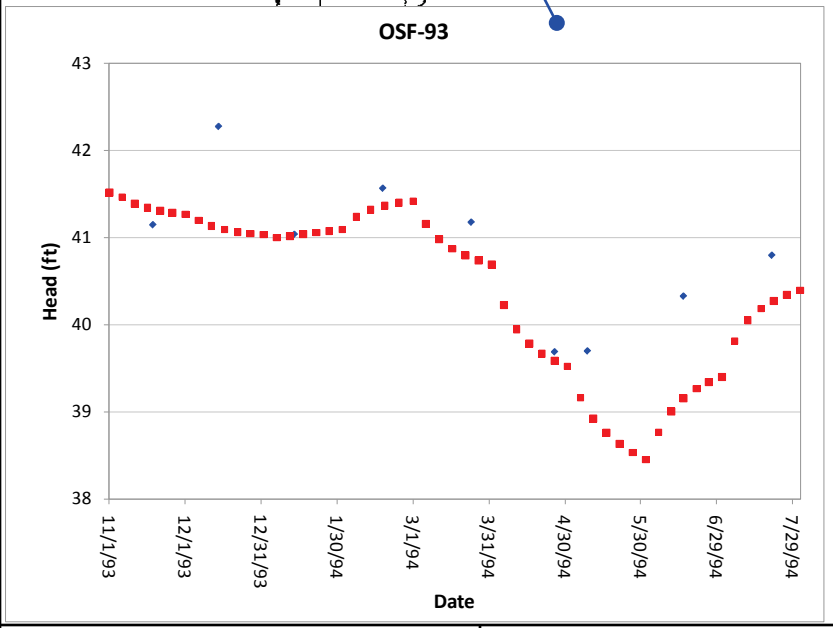

	OSF-93	TH-3 Lake Poinsett
Mean Error	-0.445	-1.234
Mean Absolute Error	0.562	1.234
Root Mean Square (RMS)	0.714	1.329
Observed Range	2.59	2.69
RMS as Percentage of Range	28%	49%
Coefficient of Determination (r^2)	0.633	0.684
Nash-Sutcliffe Model Efficiency Coefficient	0.200	-1.583

Legend

- Measured Head
- Model Calculated Head

Notes:

Figures 4.119 through 4.150 show the comparison between measured head values and model-calculated head values at a number of observation wells for the validation period. Although the scales vary on each plot, all plots have a horizontal grid line at each foot. This is to make it easy to determine the range of heads at a glance.

The model used month-long stress periods, so pumping and boundary conditions were input as step functions with constant values throughout each month and sudden changes at the end of each month. For this reason, the model cannot be expected to accurately predict day-to-day head variations in any of these wells. Calibration efforts were aimed at matching general trends and monthly averages.

Starting head conditions for this model were based on the October 1993 steady state solution. Transient calibration efforts were focused on matching the head changes, not the actual heads, so it is not uncommon for residuals in the starting condition to be carried through the entire calibration period. This indicates that the model is correctly predicting responses to hydrogeologic forces even if the calculated head values vary somewhat from the measured values.

Transient SEAWAT Validation Comparison
Upper Floridan Aquifer (1993-1994)
Final Groundwater Model Calibration Report

Figure 4.123

October 2010

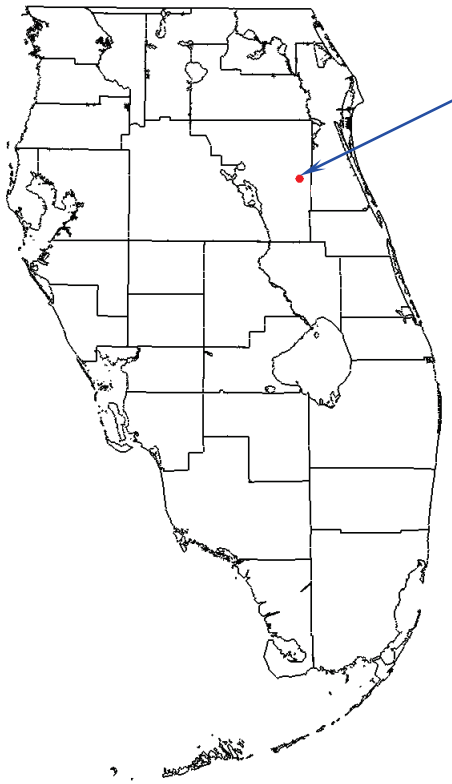

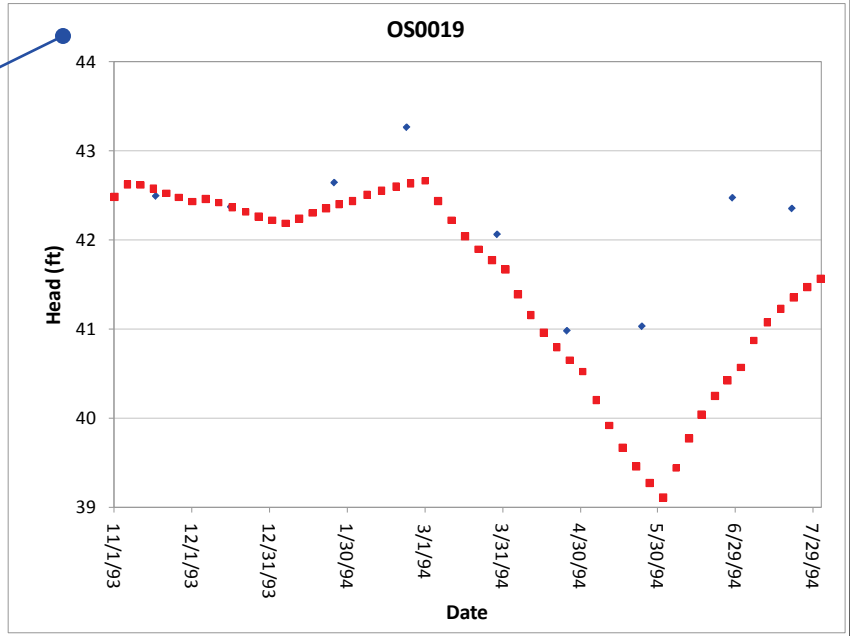

	OS0019
Mean Error	-0.651
Mean Absolute Error	0.717
Root Mean Square (RMS)	1.086
Observed Range	2.28
RMS as Percentage of Range	48%
Coefficient of Determination (r^2)	0.322
Nash-Sutcliffe Model Efficiency Coefficient	-1.413

Legend

- Measured Head
- Model Calculated Head

Notes:

Figures 4.119 through 4.150 show the comparison between measured head values and model-calculated head values at a number of observation wells for the validation period. Although the scales vary on each plot, all plots have a horizontal grid line at each foot. This is to make it easy to determine the range of heads at a glance.

The model used month-long stress periods, so pumping and boundary conditions were input as step functions with constant values throughout each month and sudden changes at the end of each month. For this reason, the model cannot be expected to accurately predict day-to-day head variations in any of these wells. Calibration efforts were aimed at matching general trends and monthly averages.

Starting head conditions for this model were based on the October 1993 steady state solution. Transient calibration efforts were focused on matching the head changes, not the actual heads, so it is not uncommon for residuals in the starting condition to be carried through the entire calibration period. This indicates that the model is correctly predicting responses to hydrogeologic forces even if the calculated head values vary somewhat from the measured values.

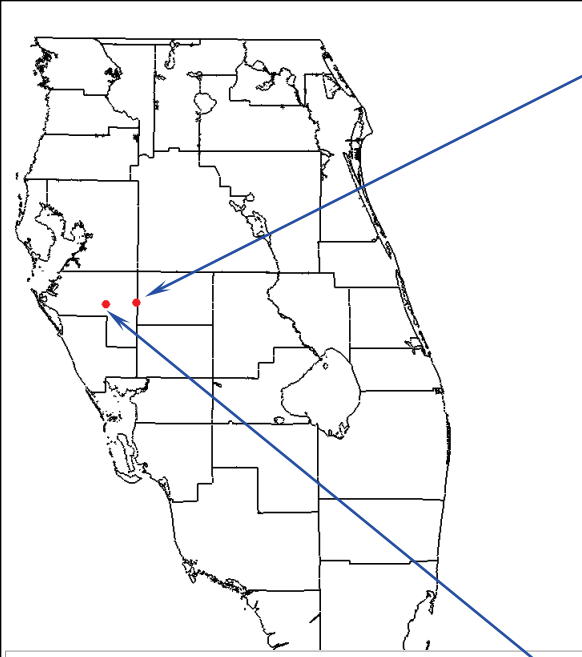

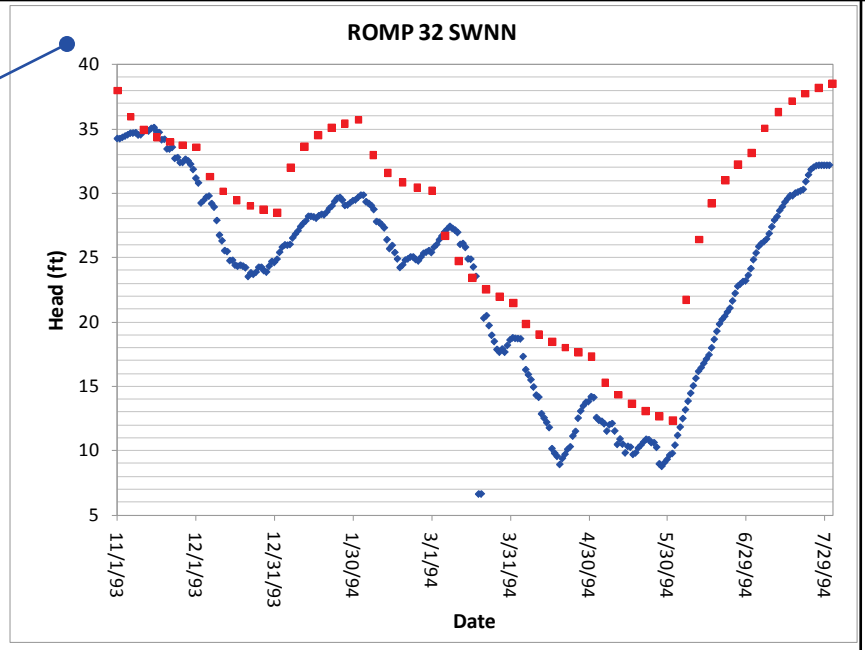

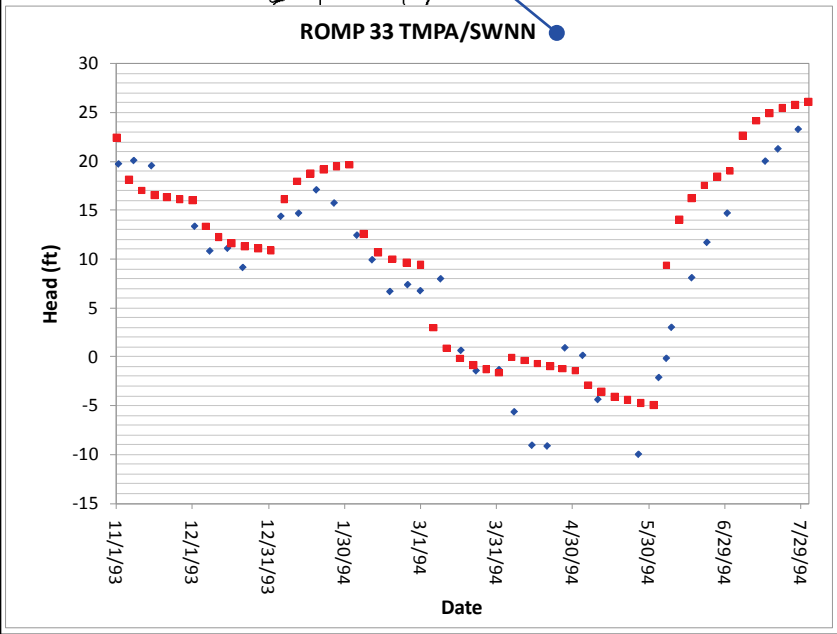

	ROMP 33 TMPA/ SWNN	ROMP 32 SWNN
Mean Error	1.808	4.825
Mean Absolute Error	2.619	4.825
Root Mean Square (RMS)	2.999	5.216
Observed Range	33.28	28.54
RMS as Percentage of Range	9%	18%
Coefficient of Determination (r^2)	0.930	0.926
Nash-Sutcliffe Model Efficiency Coefficient	0.890	0.485

Legend

- Measured Head
- Model Calculated Head

Notes:

Figures 4.119 through 4.150 show the comparison between measured head values and model-calculated head values at a number of observation wells for the validation period. Although the scales vary on each plot, all plots have a horizontal grid line at each foot. This is to make it easy to determine the range of heads at a glance.

The model used month-long stress periods, so pumping and boundary conditions were input as step functions with constant values throughout each month and sudden changes at the end of each month. For this reason, the model cannot be expected to accurately predict day-to-day head variations in any of these wells. Calibration efforts were aimed at matching general trends and monthly averages.

Starting head conditions for this model were based on the October 1993 steady state solution. Transient calibration efforts were focused on matching the head changes, not the actual heads, so it is not uncommon for residuals in the starting condition to be carried through the entire calibration period. This indicates that the model is correctly predicting responses to hydrogeologic forces even if the calculated head values vary somewhat from the measured values.

Transient SEAWAT Validation Comparison
Upper Floridan Aquifer (1993-1994)
Final Groundwater Model Calibration Report

Figure 4.125

October 2010

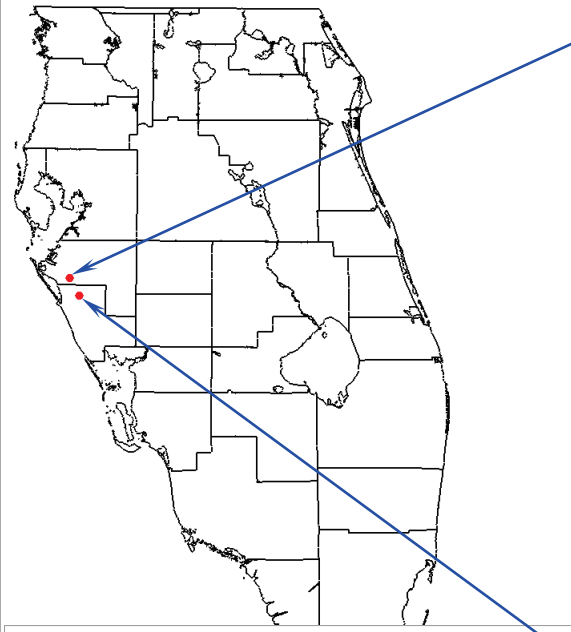

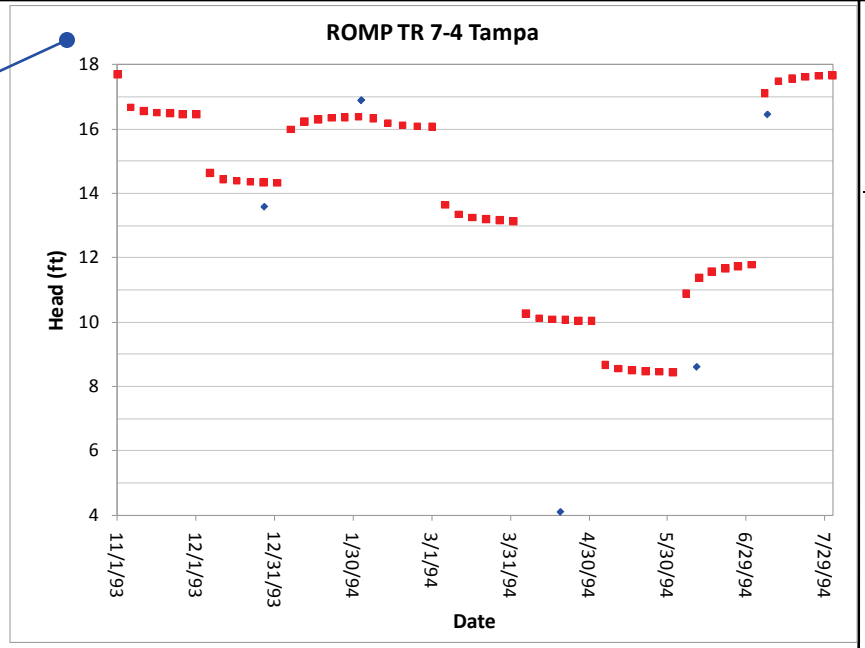

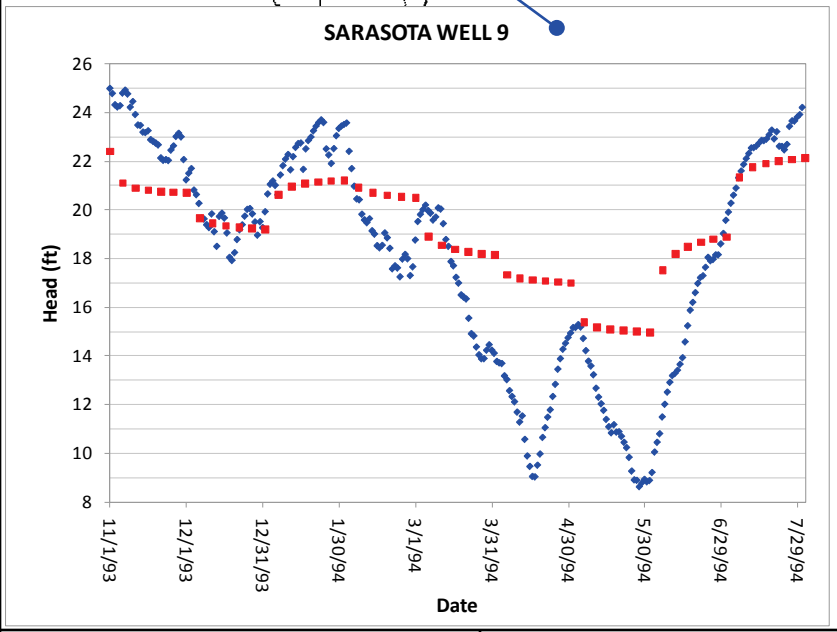

	Sarasota Well 9	ROMP TR 7-4 Tampa
Mean Error	1.113	1.895
Mean Absolute Error	2.211	2.163
Root Mean Square (RMS)	2.663	3.160
Observed Range	16.34	12.8
RMS as Percentage of Range	16%	25%
Coefficient of Determination (r^2)	0.908	0.932
Nash-Sutcliffe Model Efficiency Coefficient	0.593	0.585

Legend

- Measured Head
- Model Calculated Head

Notes:

Figures 4.119 through 4.150 show the comparison between measured head values and model-calculated head values at a number of observation wells for the validation period. Although the scales vary on each plot, all plots have a horizontal grid line at each foot. This is to make it easy to determine the range of heads at a glance.

The model used month-long stress periods, so pumping and boundary conditions were input as step functions with constant values throughout each month and sudden changes at the end of each month. For this reason, the model cannot be expected to accurately predict day-to-day head variations in any of these wells. Calibration efforts were aimed at matching general trends and monthly averages.

Starting head conditions for this model were based on the October 1993 steady state solution. Transient calibration efforts were focused on matching the head changes, not the actual heads, so it is not uncommon for residuals in the starting condition to be carried through the entire calibration period. This indicates that the model is correctly predicting responses to hydrogeologic forces even if the calculated head values vary somewhat from the measured values.

Transient SEAWAT Validation Comparison
Upper Floridan Aquifer (1993-1994)
Final Groundwater Model Calibration Report

Figure 4.126

October 2010

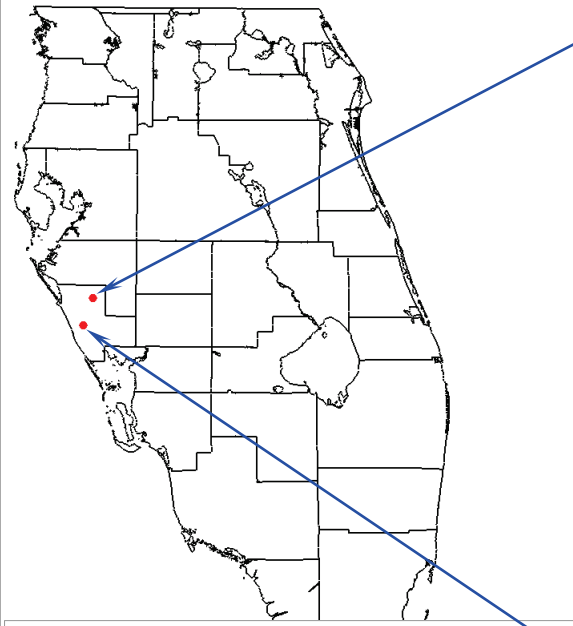

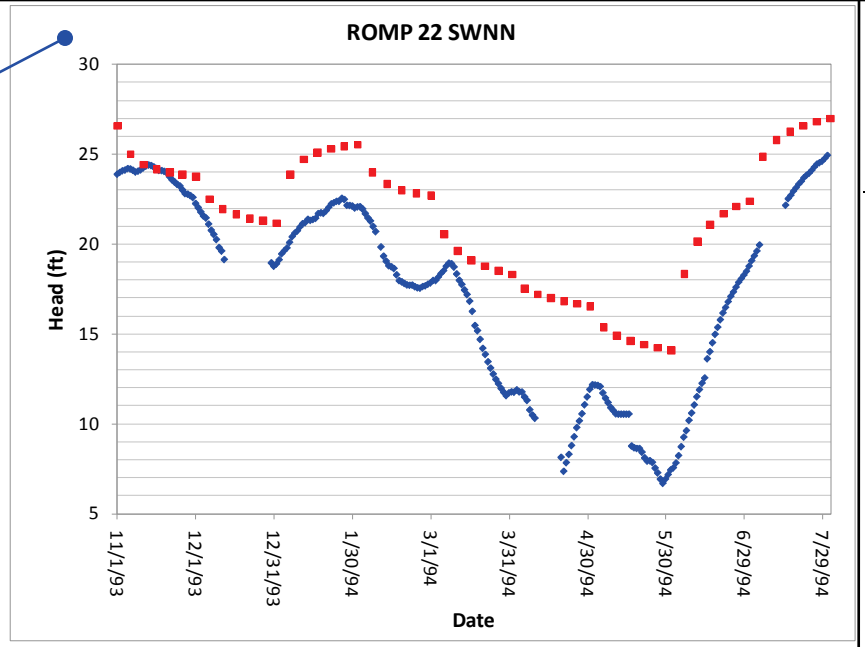

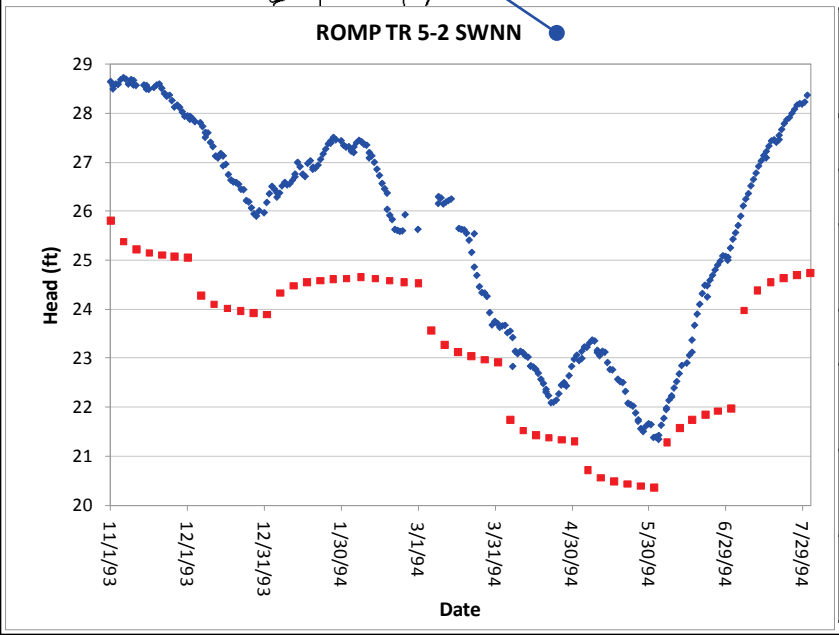

	ROMP TR 5-2 SWNN	ROMP 22 SWNN
Mean Error	-2.258	3.931
Mean Absolute Error	2.258	3.931
Root Mean Square (RMS)	2.345	4.391
Observed Range	7.55	18.24
RMS as Percentage of Range	31%	24%
Coefficient of Determination (r^2)	0.953	0.931
Nash-Sutcliffe Model Efficiency Coefficient	-0.321	0.238

Legend

- Measured Head
- Model Calculated Head

Notes:

Figures 4.119 through 4.150 show the comparison between measured head values and model-calculated head values at a number of observation wells for the validation period. Although the scales vary on each plot, all plots have a horizontal grid line at each foot. This is to make it easy to determine the range of heads at a glance.

The model used month-long stress periods, so pumping and boundary conditions were input as step functions with constant values throughout each month and sudden changes at the end of each month. For this reason, the model cannot be expected to accurately predict day-to-day head variations in any of these wells. Calibration efforts were aimed at matching general trends and monthly averages.

Starting head conditions for this model were based on the October 1993 steady state solution. Transient calibration efforts were focused on matching the head changes, not the actual heads, so it is not uncommon for residuals in the starting condition to be carried through the entire calibration period. This indicates that the model is correctly predicting responses to hydrogeologic forces even if the calculated head values vary somewhat from the measured values.

Transient SEAWAT Validation Comparison
Upper Floridan Aquifer (1993-1994)
Final Groundwater Model Calibration Report

Figure 4.127

October 2010

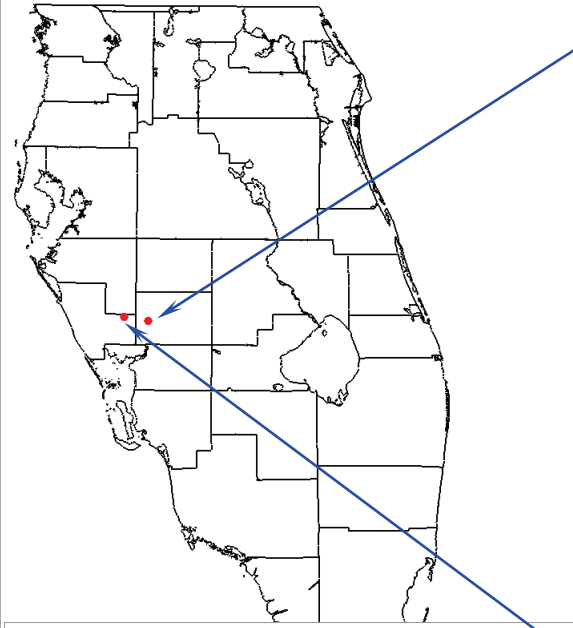

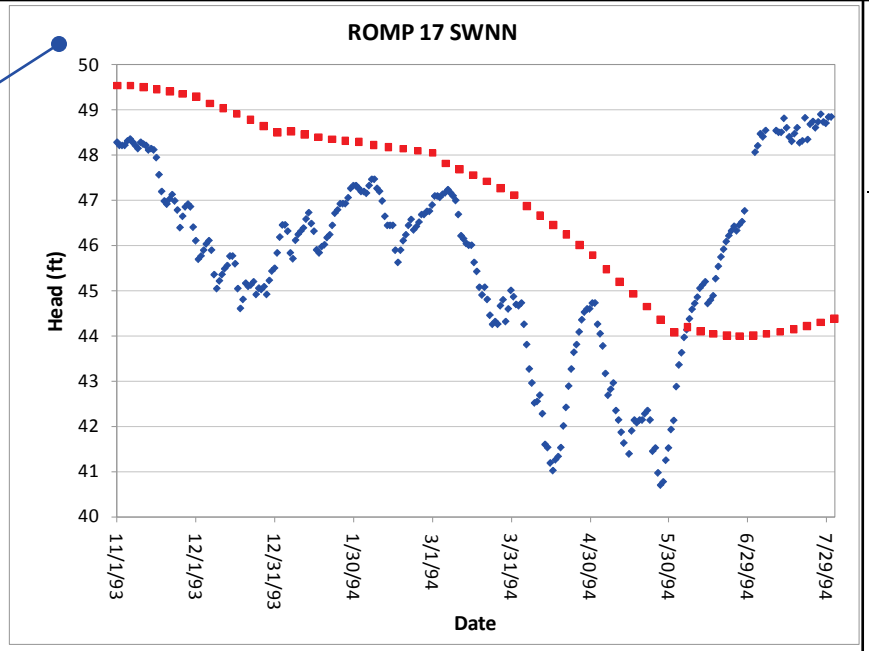

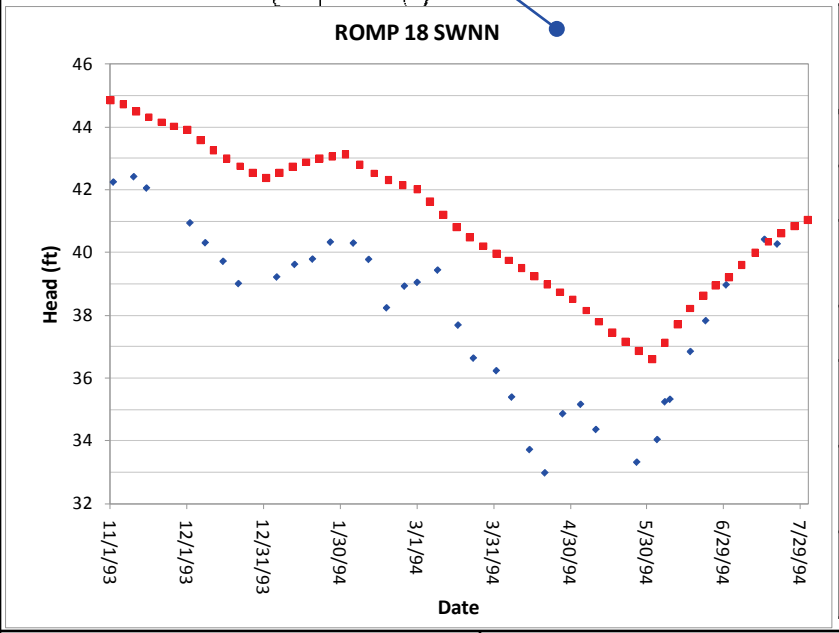

	ROMP 18 SWNN	ROMP 17 SWNN
Mean Error	2.655	1.279
Mean Absolute Error	2.708	2.486
Root Mean Square (RMS)	2.963	2.705
Observed Range	9.42	8.21
RMS as Percentage of Range	31%	33%
Coefficient of Determination (r^2)	0.736	0.053
Nash-Sutcliffe Model Efficiency Coefficient	-0.345	-1.059

Legend

- Measured Head
- Model Calculated Head

Notes:

Figures 4.119 through 4.150 show the comparison between measured head values and model-calculated head values at a number of observation wells for the validation period. Although the scales vary on each plot, all plots have a horizontal grid line at each foot. This is to make it easy to determine the range of heads at a glance.

The model used month-long stress periods, so pumping and boundary conditions were input as step functions with constant values throughout each month and sudden changes at the end of each month. For this reason, the model cannot be expected to accurately predict day-to-day head variations in any of these wells. Calibration efforts were aimed at matching general trends and monthly averages.

Starting head conditions for this model were based on the October 1993 steady state solution. Transient calibration efforts were focused on matching the head changes, not the actual heads, so it is not uncommon for residuals in the starting condition to be carried through the entire calibration period. This indicates that the model is correctly predicting responses to hydrogeologic forces even if the calculated head values vary somewhat from the measured values.

Transient SEAWAT Validation Comparison
Upper Floridan Aquifer (1993-1994)
Final Groundwater Model Calibration Report

Figure 4.128

October 2010

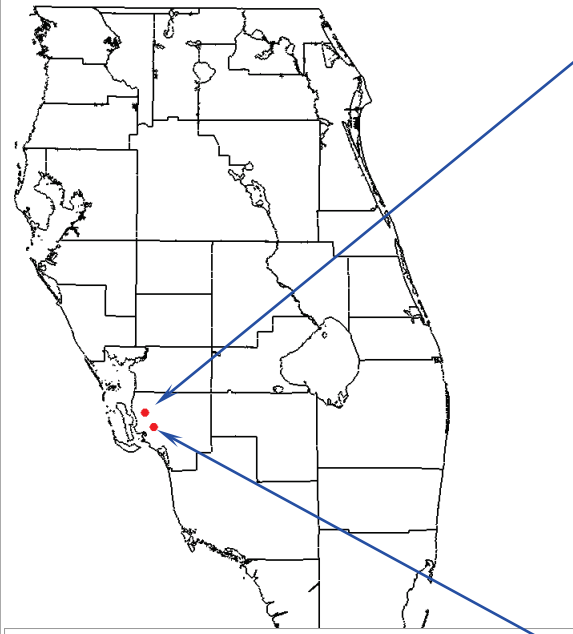

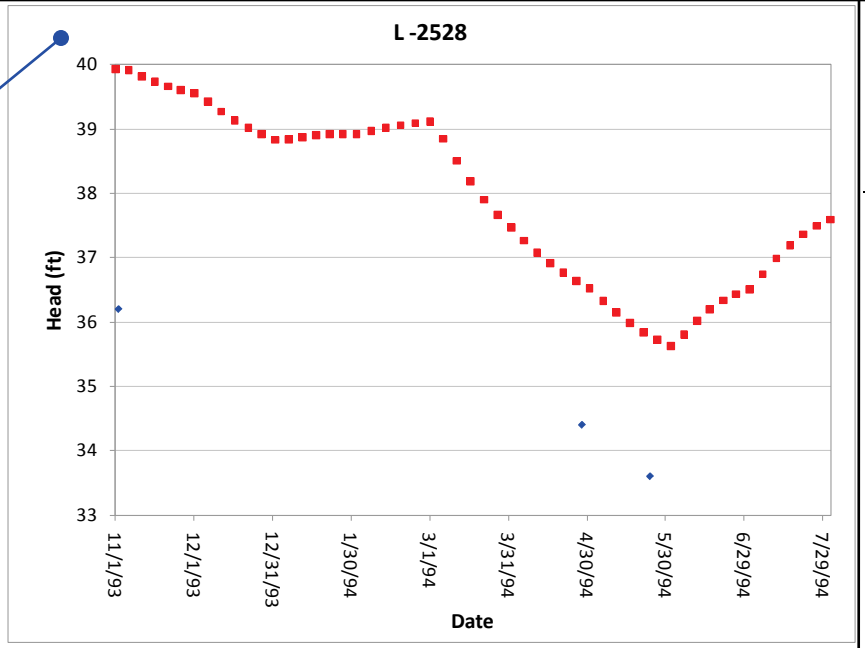

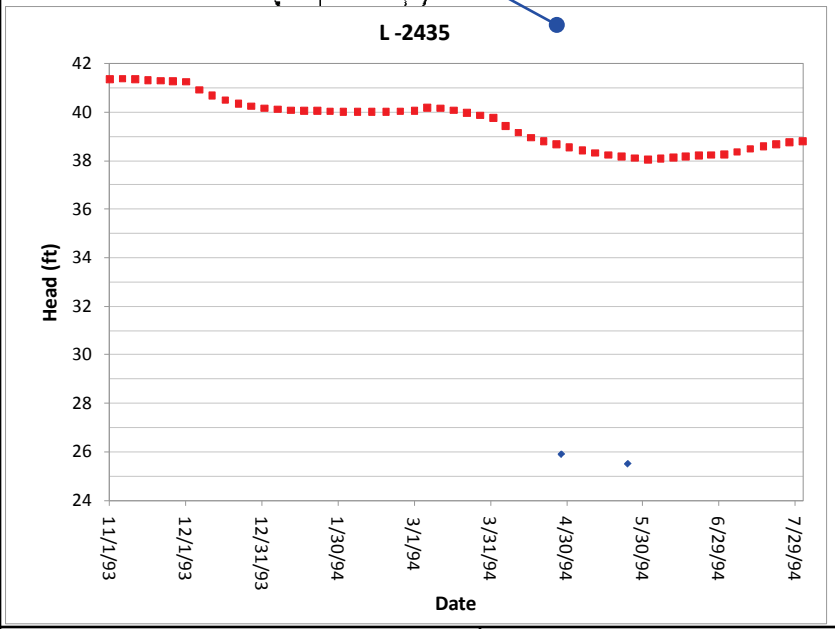

	L-2435	L-2528
Mean Error	13.014	2.897
Mean Absolute Error	13.014	2.897
Root Mean Square (RMS)	13.015	2.937
Observed Range	0.40	2.6
RMS as Percentage of Range	3254%	113%
Coefficient of Determination (r^2)	1.000	0.996
Nash-Sutcliffe Model Efficiency Coefficient	-4233.976	-6.295

Legend

- Measured Head
- Model Calculated Head

Notes:

Figures 4.119 through 4.150 show the comparison between measured head values and model-calculated head values at a number of observation wells for the validation period. Although the scales vary on each plot, all plots have a horizontal grid line at each foot. This is to make it easy to determine the range of heads at a glance.

The model used month-long stress periods, so pumping and boundary conditions were input as step functions with constant values throughout each month and sudden changes at the end of each month. For this reason, the model cannot be expected to accurately predict day-to-day head variations in any of these wells. Calibration efforts were aimed at matching general trends and monthly averages.

Starting head conditions for this model were based on the October 1993 steady state solution. Transient calibration efforts were focused on matching the head changes, not the actual heads, so it is not uncommon for residuals in the starting condition to be carried through the entire calibration period. This indicates that the model is correctly predicting responses to hydrogeologic forces even if the calculated head values vary somewhat from the measured values.

Transient SEAWAT Validation Comparison
Upper Floridan Aquifer (1993-1994)
Final Groundwater Model Calibration Report

Figure 4.129

October 2010

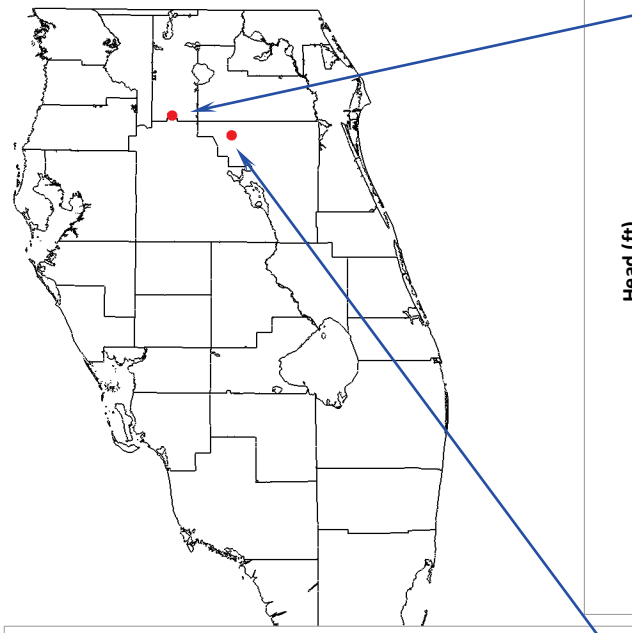

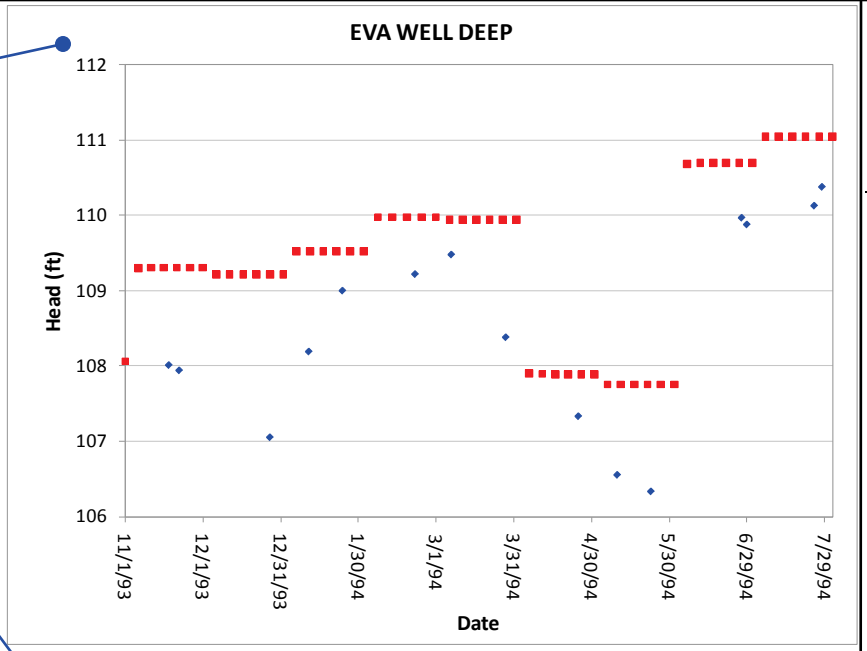

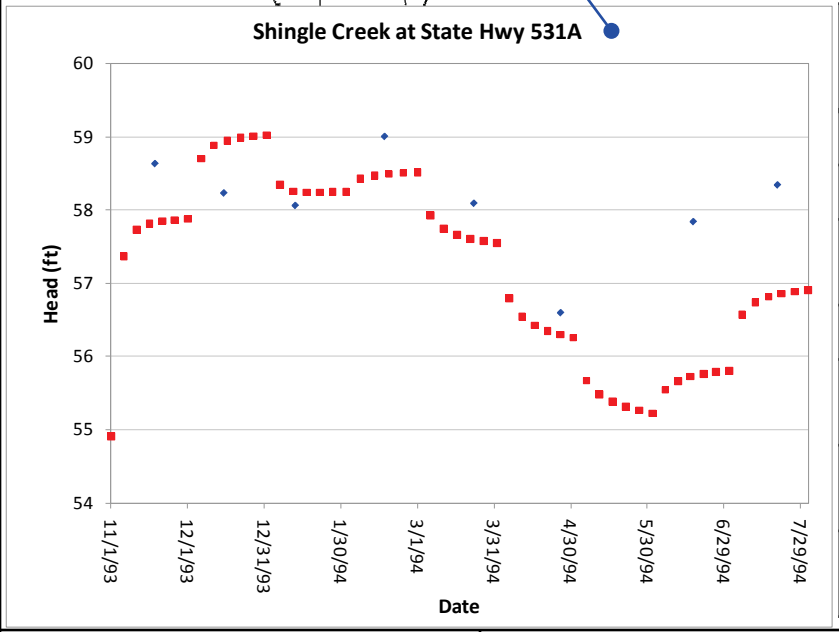

	Shingle Creek	EVA WELL DEEP
Mean Error	-0.655	1.013
Mean Absolute Error	0.880	1.013
Root Mean Square (RMS)	1.148	1.129
Observed Range	2.40	4.05
RMS as Percentage of Range	48%	28%
Coefficient of Determination (r^2)	0.192	0.869
Nash-Sutcliffe Model Efficiency Coefficient	-2.028	0.165

Legend

- Measured Head
- Model Calculated Head

Notes:

Figures 4.119 through 4.150 show the comparison between measured head values and model-calculated head values at a number of observation wells for the validation period. Although the scales vary on each plot, all plots have a horizontal grid line at each foot. This is to make it easy to determine the range of heads at a glance.

The model used month-long stress periods, so pumping and boundary conditions were input as step functions with constant values throughout each month and sudden changes at the end of each month. For this reason, the model cannot be expected to accurately predict day-to-day head variations in any of these wells. Calibration efforts were aimed at matching general trends and monthly averages.

Starting head conditions for this model were based on the October 1993 steady state solution. Transient calibration efforts were focused on matching the head changes, not the actual heads, so it is not uncommon for residuals in the starting condition to be carried through the entire calibration period. This indicates that the model is correctly predicting responses to hydrogeologic forces even if the calculated head values vary somewhat from the measured values.

Transient SEAWAT Validation Comparison
Upper Floridan Aquifer (1993-1994)
Final Groundwater Model Calibration Report

Figure 4.130

October 2010

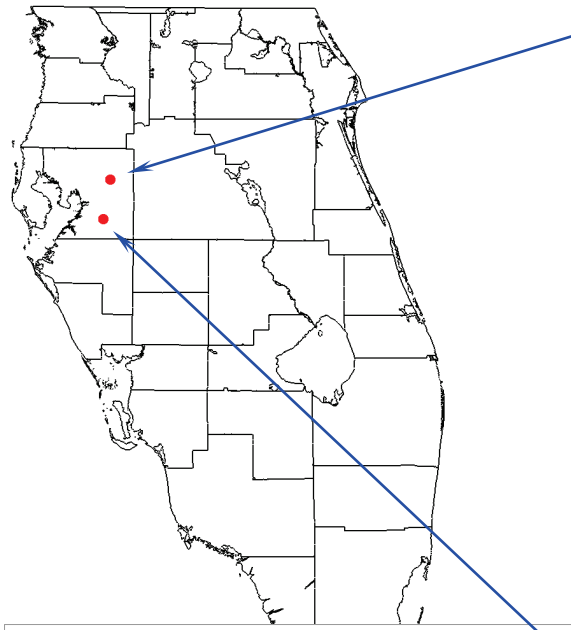

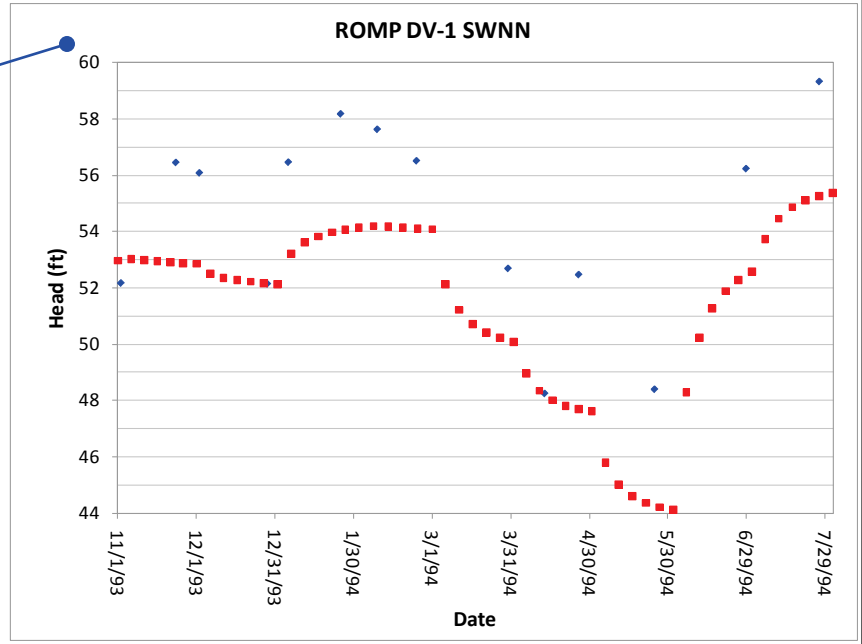

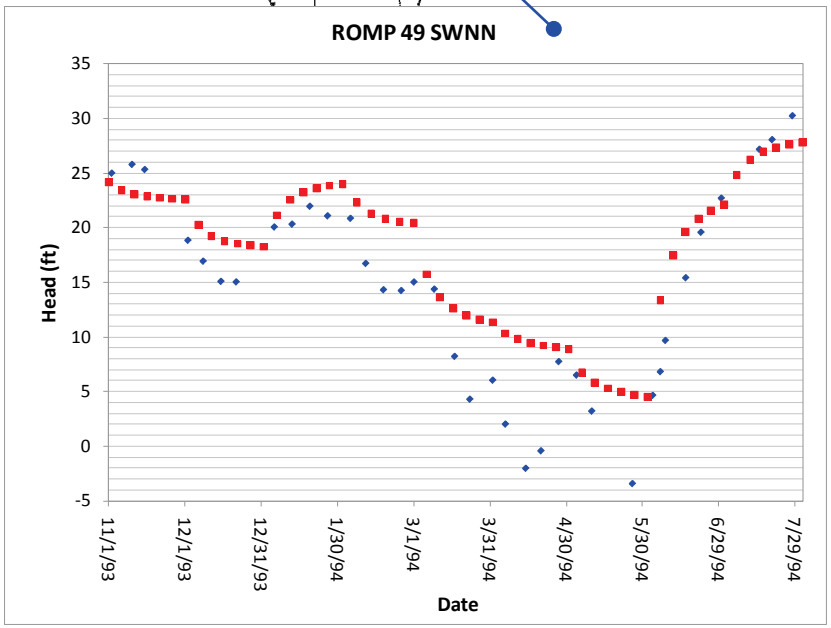

	ROMP 49 SWNN	ROMP DV-1 SWNN
Mean Error	2.522	-3.066
Mean Absolute Error	3.616	3.066
Root Mean Square (RMS)	3.975	3.509
Observed Range	33.69	11.1
RMS as Percentage of Range	12%	87%
Coefficient of Determination (r^2)	0.936	0.735
Nash-Sutcliffe Model Efficiency Coefficient	0.788	-0.119

Legend

- Measured Head
- Model Calculated Head

Notes:

Figures 4.119 through 4.150 show the comparison between measured head values and model-calculated head values at a number of observation wells for the validation period. Although the scales vary on each plot, all plots have a horizontal grid line at each foot. This is to make it easy to determine the range of heads at a glance.

The model used month-long stress periods, so pumping and boundary conditions were input as step functions with constant values throughout each month and sudden changes at the end of each month. For this reason, the model cannot be expected to accurately predict day-to-day head variations in any of these wells. Calibration efforts were aimed at matching general trends and monthly averages.

Starting head conditions for this model were based on the October 1993 steady state solution. Transient calibration efforts were focused on matching the head changes, not the actual heads, so it is not uncommon for residuals in the starting condition to be carried through the entire calibration period. This indicates that the model is correctly predicting responses to hydrogeologic forces even if the calculated head values vary somewhat from the measured values.

Transient SEAWAT Validation Comparison
Upper Floridan Aquifer (1993-1994)
Final Groundwater Model Calibration Report

Figure 4.131

October 2010

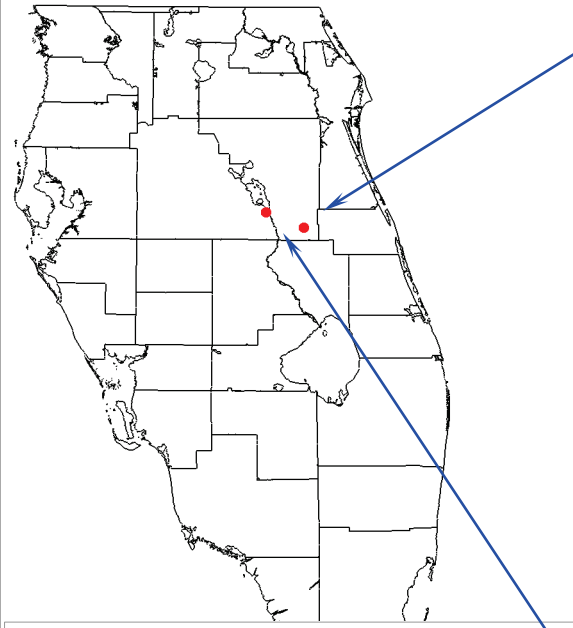

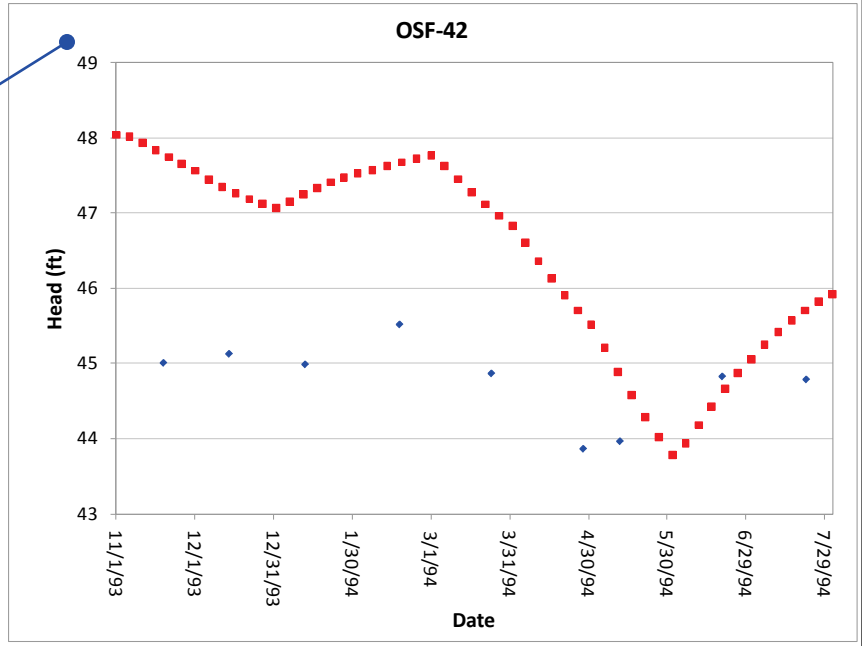

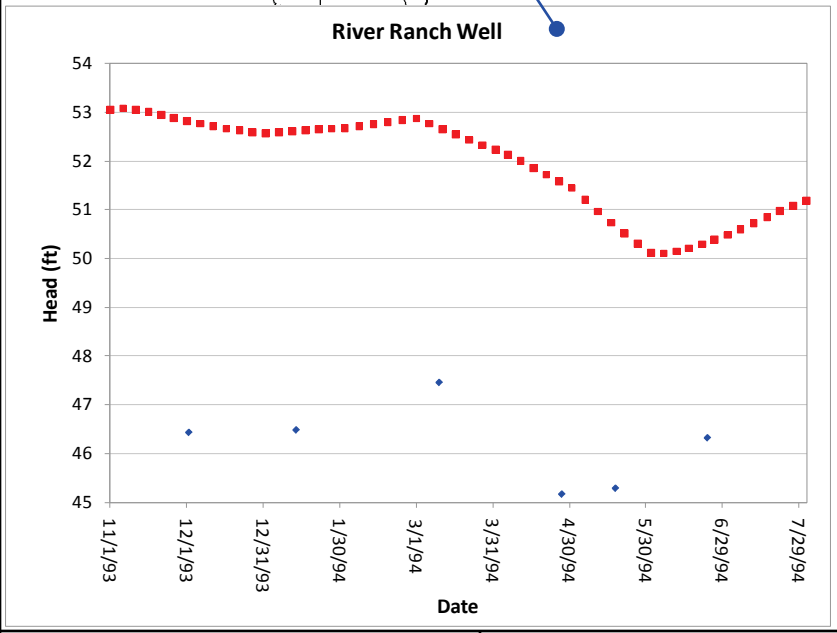

	River Ranch Well	OSF-42
Mean Error	5.628	1.697
Mean Absolute Error	5.628	1.812
Root Mean Square (RMS)	5.704	1.998
Observed Range	2.28	1.65
RMS as Percentage of Range	250%	121%
Coefficient of Determination (r^2)	0.196	0.319
Nash-Sutcliffe Model Efficiency Coefficient	-53.284	-14.883

Legend

- Measured Head
- Model Calculated Head

Notes:

Figures 4.119 through 4.150 show the comparison between measured head values and model-calculated head values at a number of observation wells for the validation period. Although the scales vary on each plot, all plots have a horizontal grid line at each foot. This is to make it easy to determine the range of heads at a glance.

The model used month-long stress periods, so pumping and boundary conditions were input as step functions with constant values throughout each month and sudden changes at the end of each month. For this reason, the model cannot be expected to accurately predict day-to-day head variations in any of these wells. Calibration efforts were aimed at matching general trends and monthly averages.

Starting head conditions for this model were based on the October 1993 steady state solution. Transient calibration efforts were focused on matching the head changes, not the actual heads, so it is not uncommon for residuals in the starting condition to be carried through the entire calibration period. This indicates that the model is correctly predicting responses to hydrogeologic forces even if the calculated head values vary somewhat from the measured values.

Transient SEAWAT Validation Comparison
Upper Floridan Aquifer (1993-1994)
Final Groundwater Model Calibration Report

Figure 4.132

October 2010

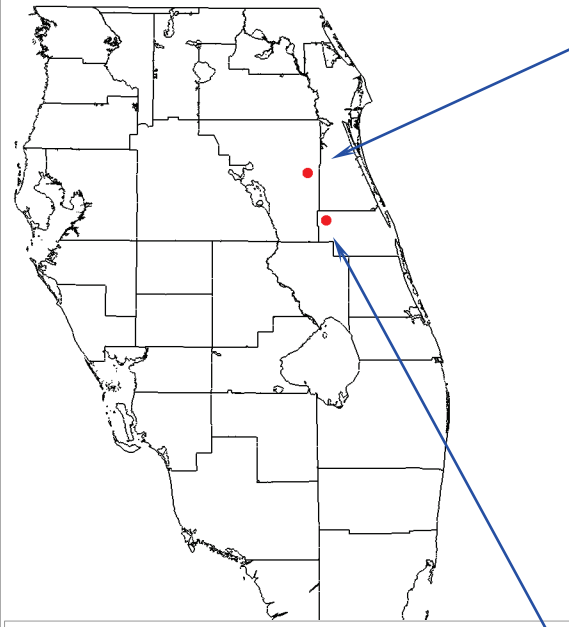

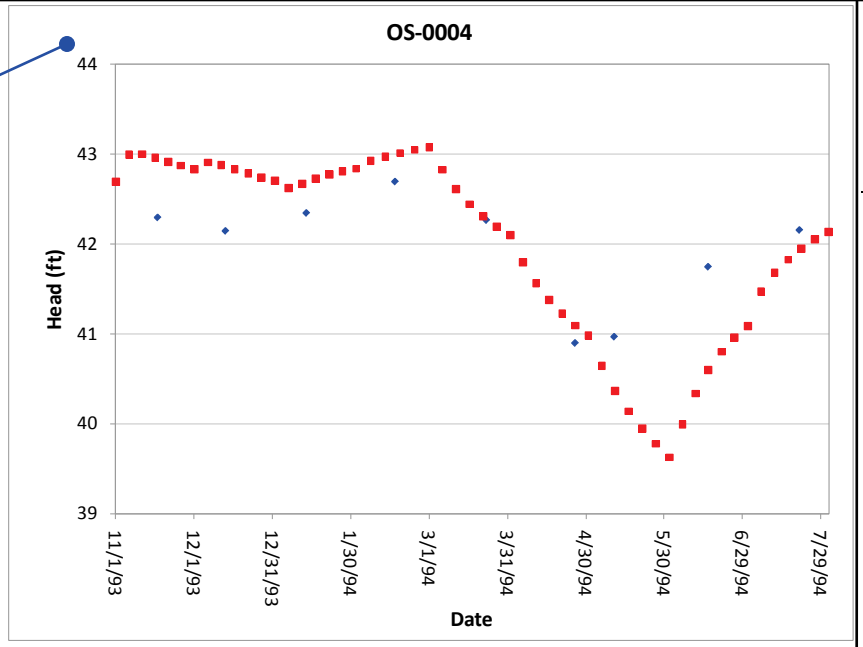

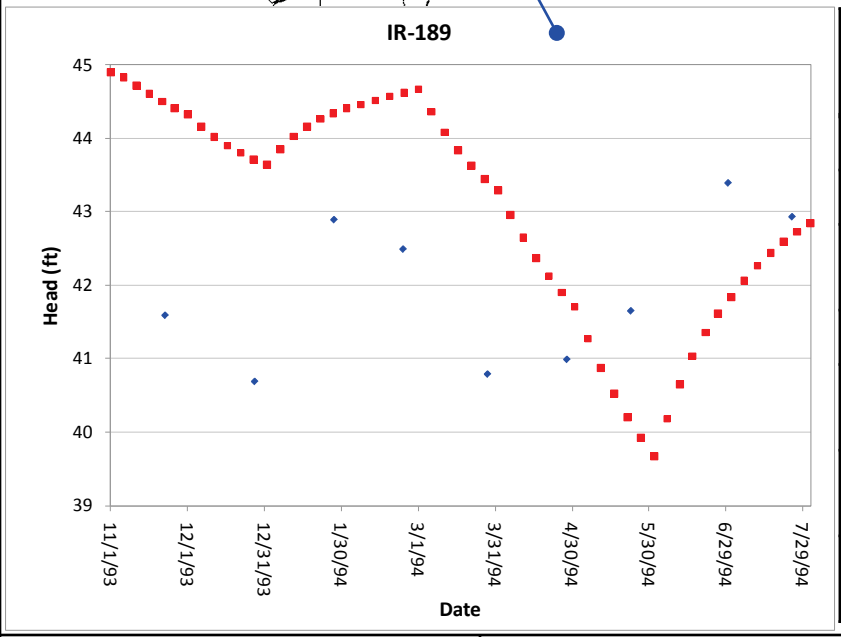

	IR-189	OS-0004
Mean Error	1.129	0.037
Mean Absolute Error	2.052	0.595
Root Mean Square (RMS)	2.276	0.671
Observed Range	2.70	1.80
RMS as Percentage of Range	84%	37%
Coefficient of Determination (r^2)	0.102	0.587
Nash-Sutcliffe Model Efficiency Coefficient	-4.628	-0.293

Legend

- Measured Head
- Model Calculated Head

Notes:

Figures 4.119 through 4.150 show the comparison between measured head values and model-calculated head values at a number of observation wells for the validation period. Although the scales vary on each plot, all plots have a horizontal grid line at each foot. This is to make it easy to determine the range of heads at a glance.

The model used month-long stress periods, so pumping and boundary conditions were input as step functions with constant values throughout each month and sudden changes at the end of each month. For this reason, the model cannot be expected to accurately predict day-to-day head variations in any of these wells. Calibration efforts were aimed at matching general trends and monthly averages.

Starting head conditions for this model were based on the October 1993 steady state solution. Transient calibration efforts were focused on matching the head changes, not the actual heads, so it is not uncommon for residuals in the starting condition to be carried through the entire calibration period. This indicates that the model is correctly predicting responses to hydrogeologic forces even if the calculated head values vary somewhat from the measured values.

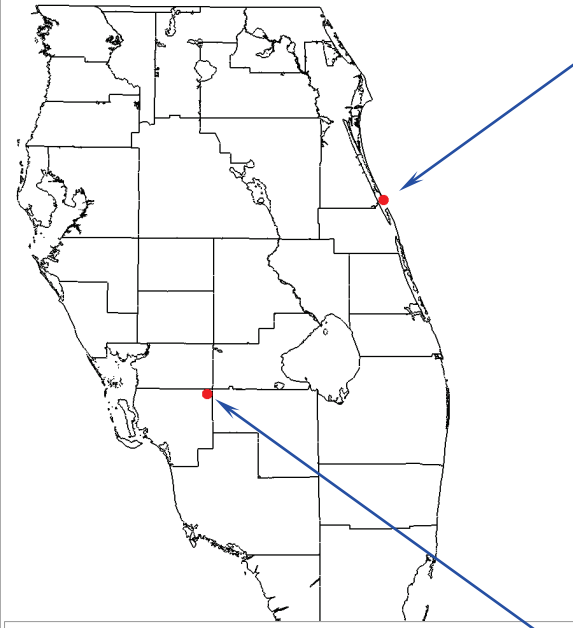

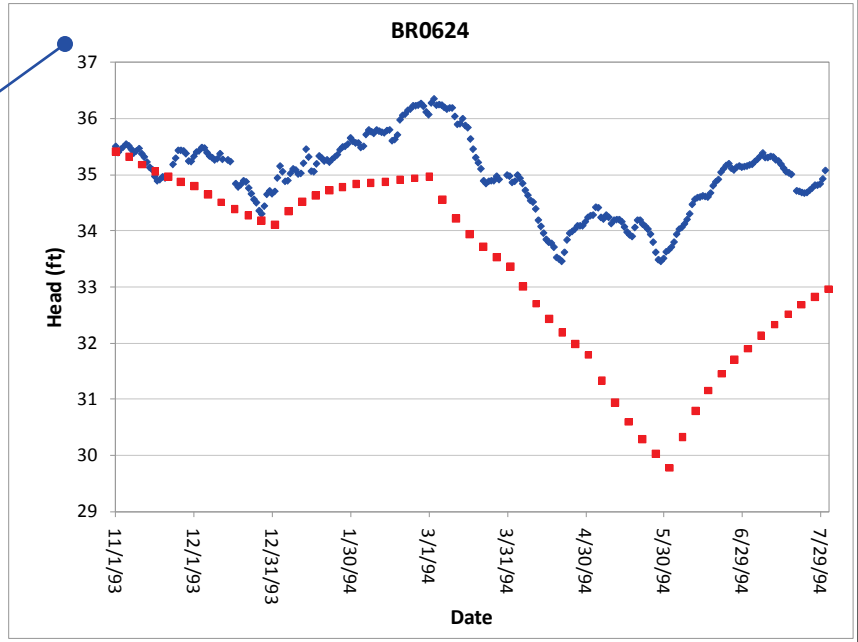

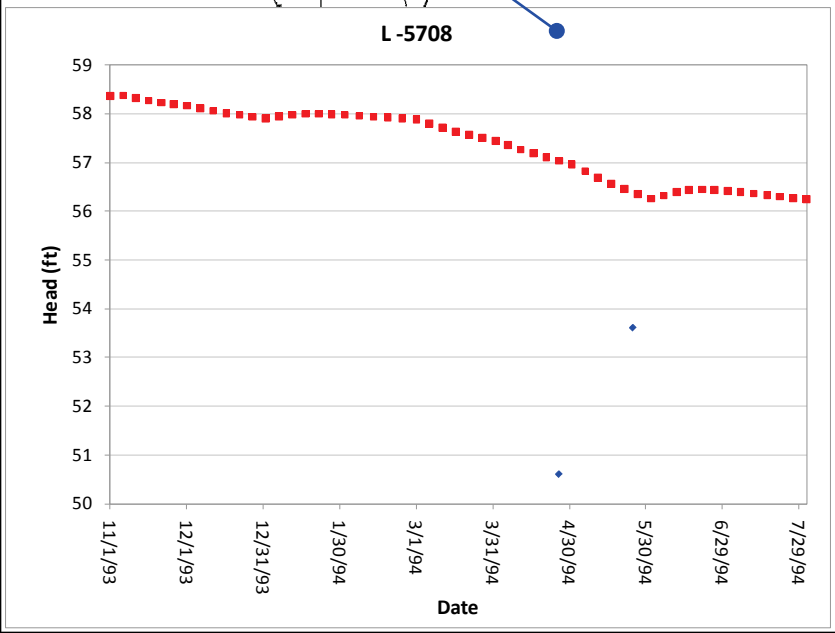

	L-5708	BR0624
Mean Error	4.835	-1.672
Mean Absolute Error	4.835	1.672
Root Mean Square (RMS)	5.158	2.052
Observed Range	3.00	2.88
RMS as Percentage of Range	172%	71%
Coefficient of Determination (r^2)	1.000	0.621
Nash-Sutcliffe Model Efficiency Coefficient	-10.823	-11.699

Legend

- Measured Head
- Model Calculated Head

Notes:

Figures 4.119 through 4.150 show the comparison between measured head values and model-calculated head values at a number of observation wells for the validation period. Although the scales vary on each plot, all plots have a horizontal grid line at each foot. This is to make it easy to determine the range of heads at a glance.

The model used month-long stress periods, so pumping and boundary conditions were input as step functions with constant values throughout each month and sudden changes at the end of each month. For this reason, the model cannot be expected to accurately predict day-to-day head variations in any of these wells. Calibration efforts were aimed at matching general trends and monthly averages.

Starting head conditions for this model were based on the October 1993 steady state solution. Transient calibration efforts were focused on matching the head changes, not the actual heads, so it is not uncommon for residuals in the starting condition to be carried through the entire calibration period. This indicates that the model is correctly predicting responses to hydrogeologic forces even if the calculated head values vary somewhat from the measured values.

Transient SEAWAT Validation Comparison
Upper Floridan Aquifer (1993-1994)
Final Groundwater Model Calibration Report

Figure 4.134

October 2010

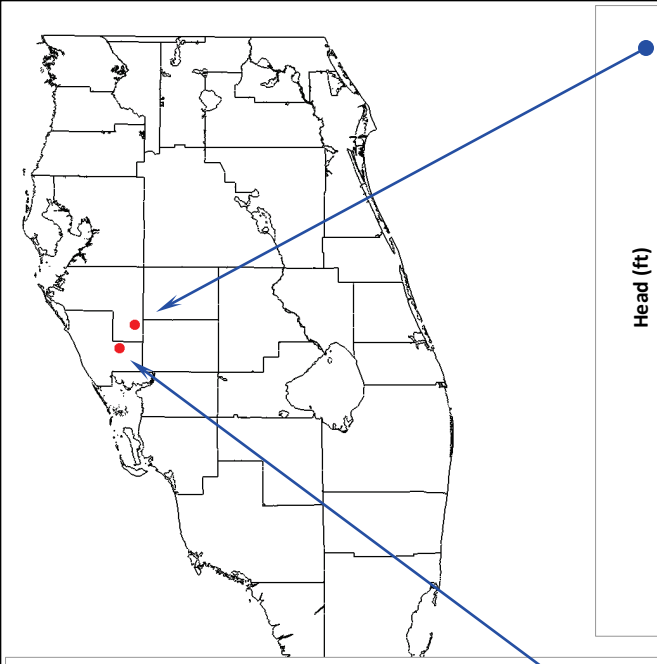

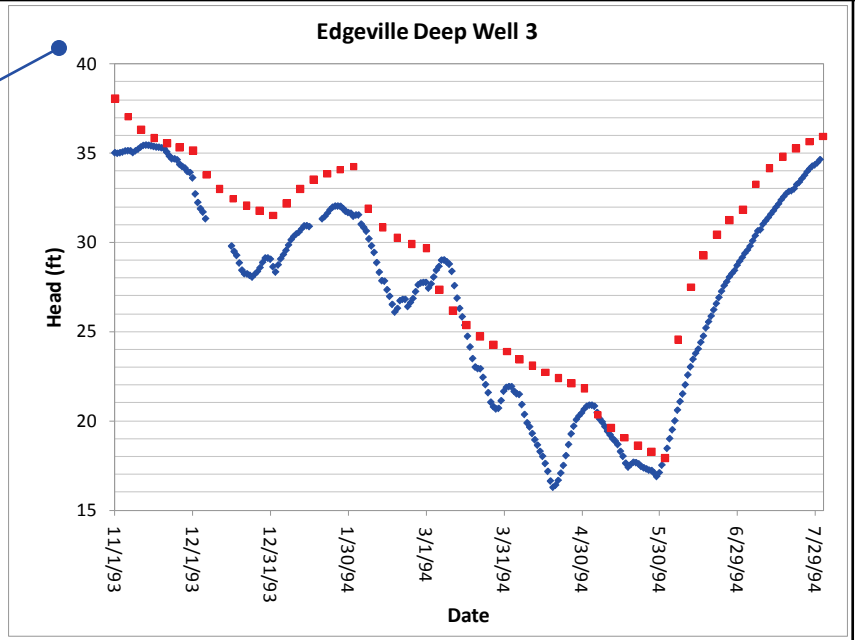

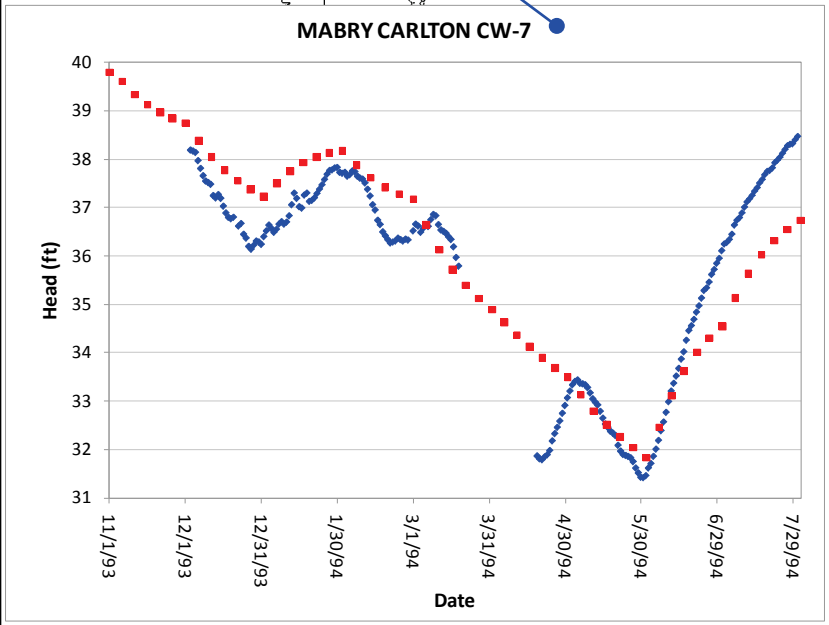

	MABRY CARLTON CW-7	Edgeville Deep Well 3
Mean Error	0.212	2.298
Mean Absolute Error	0.914	2.298
Root Mean Square (RMS)	1.097	2.476
Observed Range	7.05	19.18
RMS as Percentage of Range	16%	13%
Coefficient of Determination (r^2)	0.737	0.970
Nash-Sutcliffe Model Efficiency Coefficient	0.719	0.785

Legend

- Measured Head
- Model Calculated Head

Notes:

Figures 4.119 through 4.150 show the comparison between measured head values and model-calculated head values at a number of observation wells for the validation period. Although the scales vary on each plot, all plots have a horizontal grid line at each foot. This is to make it easy to determine the range of heads at a glance.

The model used month-long stress periods, so pumping and boundary conditions were input as step functions with constant values throughout each month and sudden changes at the end of each month. For this reason, the model cannot be expected to accurately predict day-to-day head variations in any of these wells. Calibration efforts were aimed at matching general trends and monthly averages.

Starting head conditions for this model were based on the October 1993 steady state solution. Transient calibration efforts were focused on matching the head changes, not the actual heads, so it is not uncommon for residuals in the starting condition to be carried through the entire calibration period. This indicates that the model is correctly predicting responses to hydrogeologic forces even if the calculated head values vary somewhat from the measured values.

Transient SEAWAT Validation Comparison
Upper Floridan Aquifer (1993-1994)
Final Groundwater Model Calibration Report

Figure 4.135

October 2010

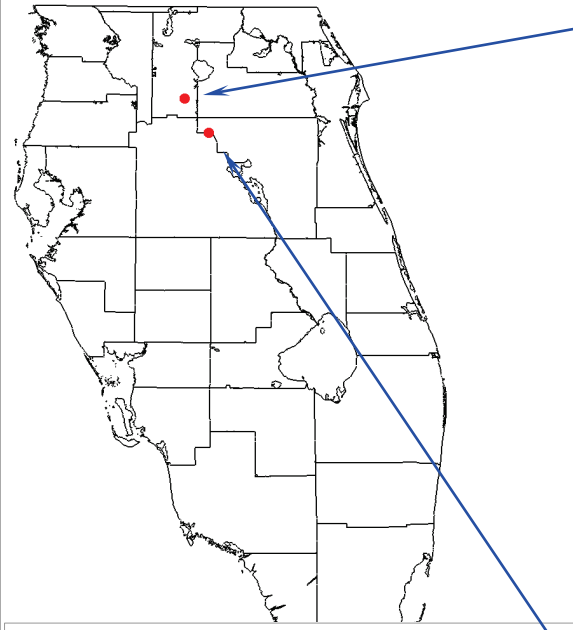

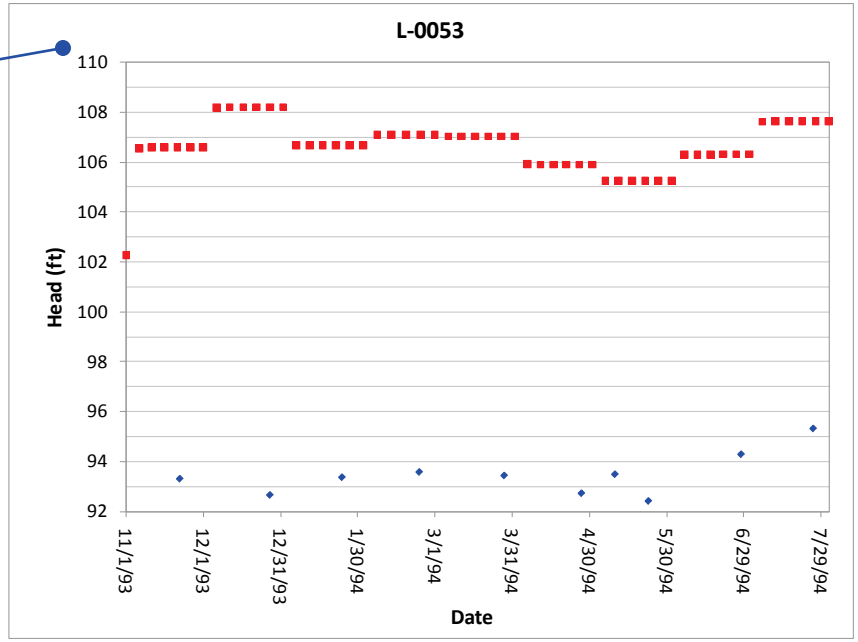

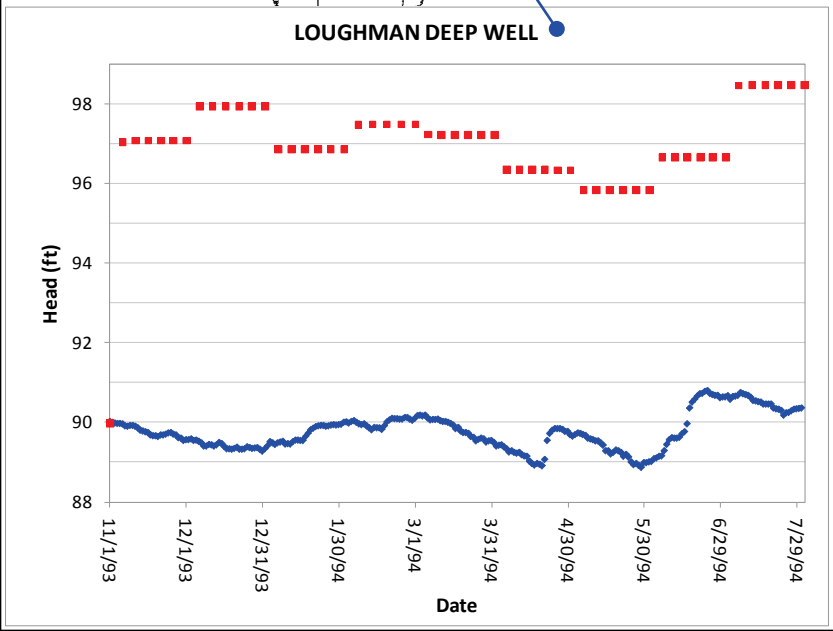

	LOUGHMAN DEEP WELL	L-0053
Mean Error	7.177	13.137
Mean Absolute Error	7.177	13.137
Root Mean Square (RMS)	7.206	13.174
Observed Range	1.94	2.90
RMS as Percentage of Range	371%	454%
Coefficient of Determination (r^2)	0.253	0.043
Nash-Sutcliffe Model Efficiency Coefficient	-419.281	-278.290

Legend

- Measured Head
- Model Calculated Head

Notes:

Figures 4.119 through 4.150 show the comparison between measured head values and model-calculated head values at a number of observation wells for the validation period. Although the scales vary on each plot, all plots have a horizontal grid line at each foot. This is to make it easy to determine the range of heads at a glance.

The model used month-long stress periods, so pumping and boundary conditions were input as step functions with constant values throughout each month and sudden changes at the end of each month. For this reason, the model cannot be expected to accurately predict day-to-day head variations in any of these wells. Calibration efforts were aimed at matching general trends and monthly averages.

Starting head conditions for this model were based on the October 1993 steady state solution. Transient calibration efforts were focused on matching the head changes, not the actual heads, so it is not uncommon for residuals in the starting condition to be carried through the entire calibration period. This indicates that the model is correctly predicting responses to hydrogeologic forces even if the calculated head values vary somewhat from the measured values.

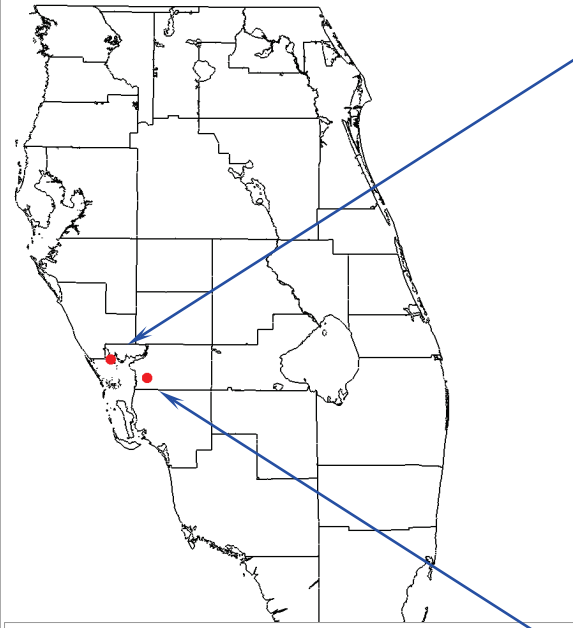

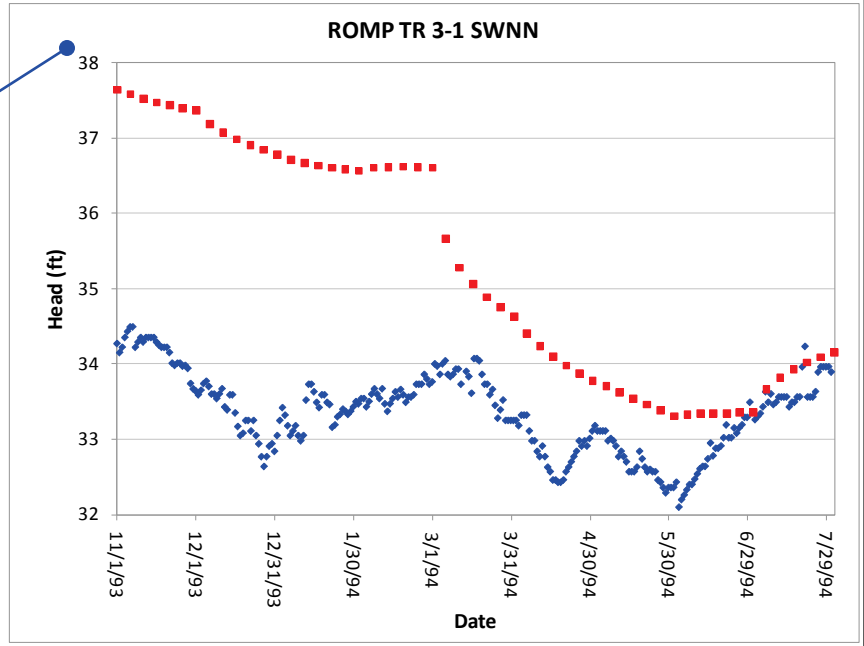

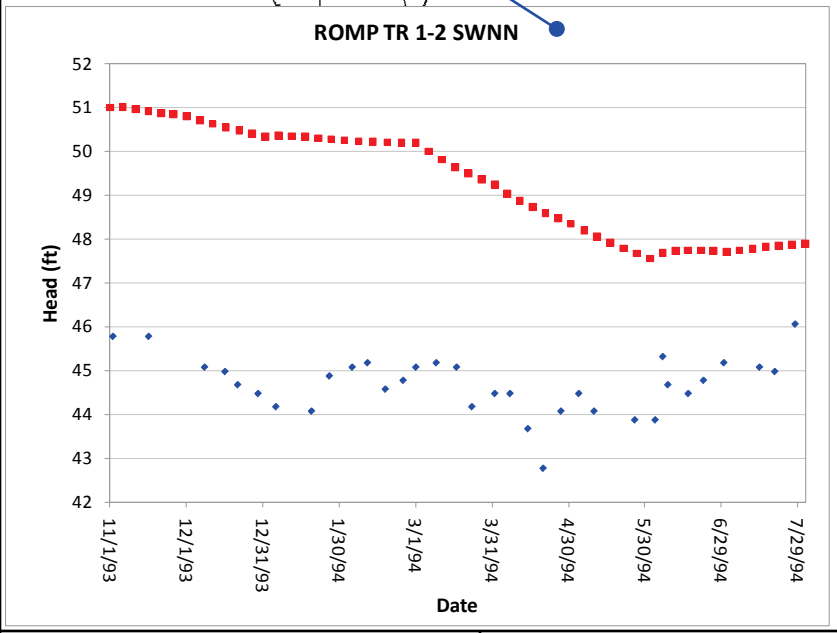

	ROMP TR 1-2 SWNN	ROMP TR 3-1 SWNN
Mean Error	4.596	1.997
Mean Absolute Error	4.596	1.997
Root Mean Square (RMS)	4.742	2.374
Observed Range	3.28	2.60
RMS as Percentage of Range	145%	91%
Coefficient of Determination (r^2)	0.098	0.465
Nash-Sutcliffe Model Efficiency Coefficient	-73.514	-25.251

Legend

- Measured Head
- Model Calculated Head

Notes:

Figures 4.119 through 4.150 show the comparison between measured head values and model-calculated head values at a number of observation wells for the validation period. Although the scales vary on each plot, all plots have a horizontal grid line at each foot. This is to make it easy to determine the range of heads at a glance.

The model used month-long stress periods, so pumping and boundary conditions were input as step functions with constant values throughout each month and sudden changes at the end of each month. For this reason, the model cannot be expected to accurately predict day-to-day head variations in any of these wells. Calibration efforts were aimed at matching general trends and monthly averages.

Starting head conditions for this model were based on the October 1993 steady state solution. Transient calibration efforts were focused on matching the head changes, not the actual heads, so it is not uncommon for residuals in the starting condition to be carried through the entire calibration period. This indicates that the model is correctly predicting responses to hydrogeologic forces even if the calculated head values vary somewhat from the measured values.

Transient SEAWAT Validation Comparison
Upper Floridan Aquifer (1993-1994)
Final Groundwater Model Calibration Report

Figure 4.137

October 2010

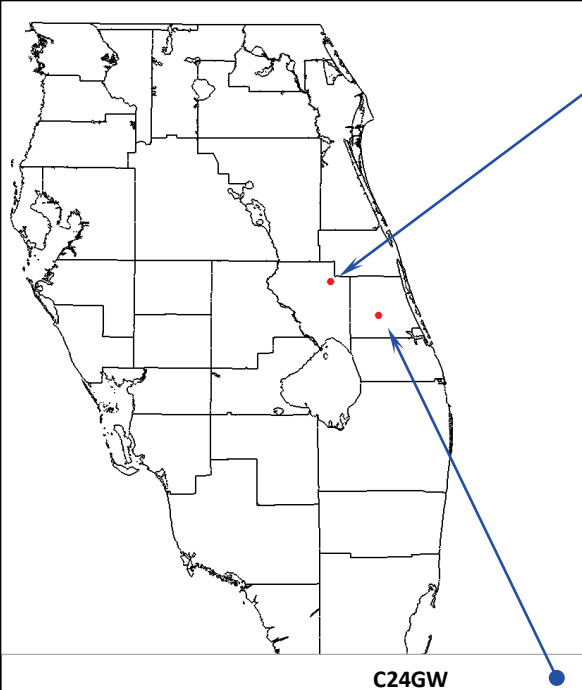

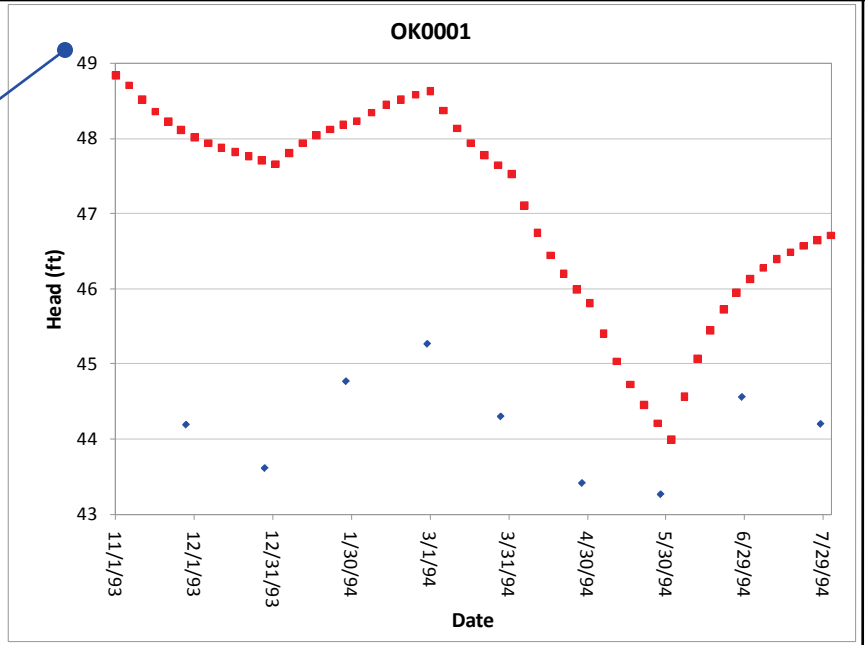

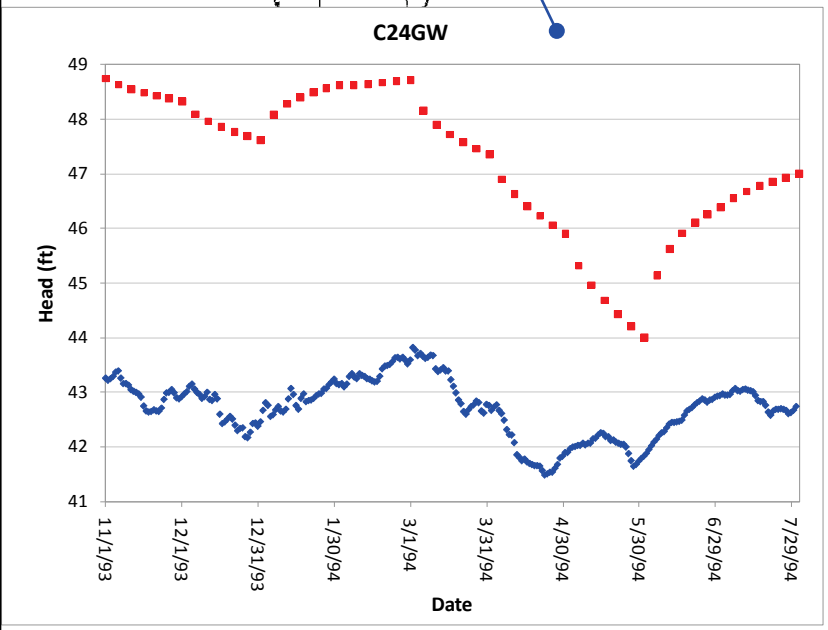

	C24GW	OK0001
Mean Error	4.518	2.931
Mean Absolute Error	4.518	2.931
Root Mean Square (RMS)	4.620	3.153
Observed Range	2.33	2.01
RMS as Percentage of Range	198%	157%
Coefficient of Determination (r^2)	0.621	0.197
Nash-Sutcliffe Model Efficiency Coefficient	-102.953	-24.857

Legend

- Measured Head
- Model Calculated Head

Notes:

Figures 4.119 through 4.150 show the comparison between measured head values and model-calculated head values at a number of observation wells for the validation period. Although the scales vary on each plot, all plots have a horizontal grid line at each foot. This is to make it easy to determine the range of heads at a glance.

The model used month-long stress periods, so pumping and boundary conditions were input as step functions with constant values throughout each month and sudden changes at the end of each month. For this reason, the model cannot be expected to accurately predict day-to-day head variations in any of these wells. Calibration efforts were aimed at matching general trends and monthly averages.

Starting head conditions for this model were based on the October 1993 steady state solution. Transient calibration efforts were focused on matching the head changes, not the actual heads, so it is not uncommon for residuals in the starting condition to be carried through the entire calibration period. This indicates that the model is correctly predicting responses to hydrogeologic forces even if the calculated head values vary somewhat from the measured values.

Transient SEAWAT Validation Comparison
Upper Floridan Aquifer (1993-1994)
Final Groundwater Model Calibration Report

Figure 4.138

October 2010

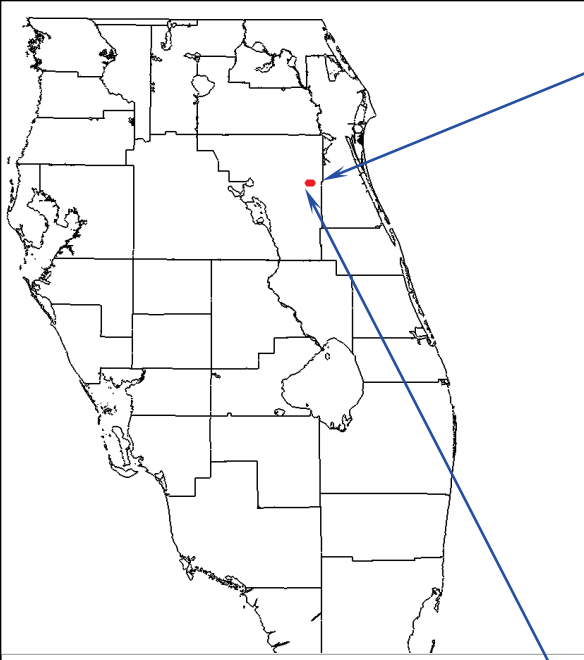

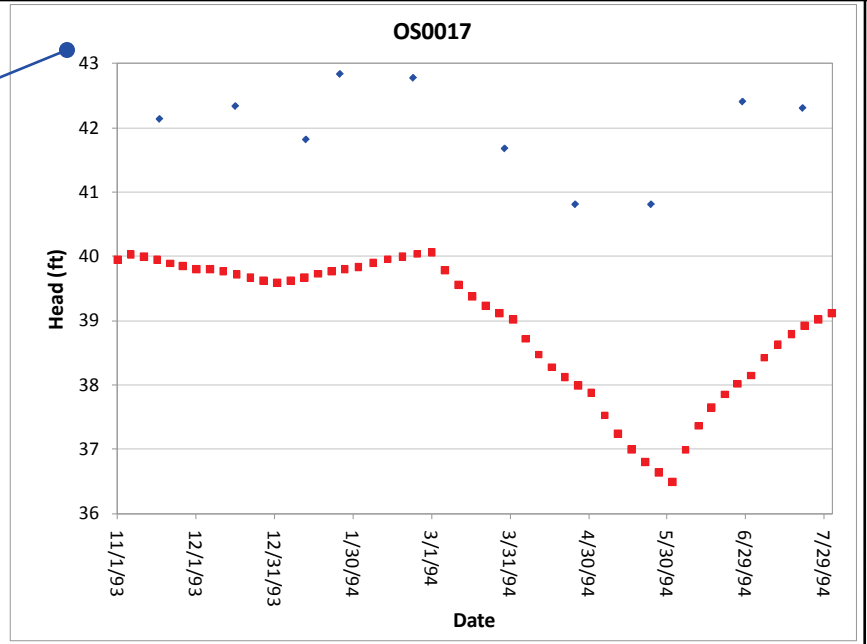

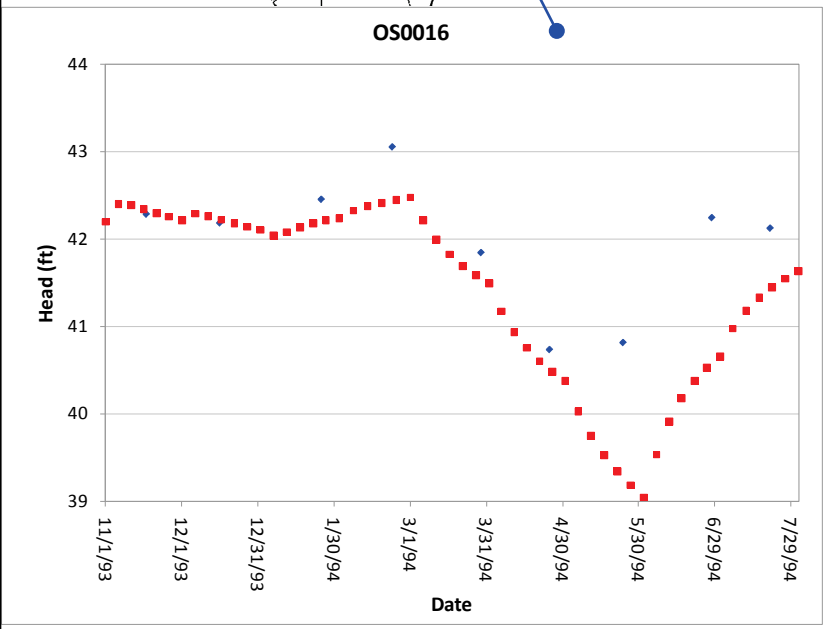

	OS0016	OS0017
Mean Error	-0.556	-3.004
Mean Absolute Error	0.638	3.004
Root Mean Square (RMS)	0.948	3.129
Observed Range	2.32	2.03
RMS as Percentage of Range	41%	154%
Coefficient of Determination (r^2)	0.394	0.276
Nash-Sutcliffe Model Efficiency Coefficient	-0.783	-20.847

Legend

- Measured Head
- Model Calculated Head

Notes:

Figures 4.119 through 4.150 show the comparison between measured head values and model-calculated head values at a number of observation wells for the validation period. Although the scales vary on each plot, all plots have a horizontal grid line at each foot. This is to make it easy to determine the range of heads at a glance.

The model used month-long stress periods, so pumping and boundary conditions were input as step functions with constant values throughout each month and sudden changes at the end of each month. For this reason, the model cannot be expected to accurately predict day-to-day head variations in any of these wells. Calibration efforts were aimed at matching general trends and monthly averages.

Starting head conditions for this model were based on the October 1993 steady state solution. Transient calibration efforts were focused on matching the head changes, not the actual heads, so it is not uncommon for residuals in the starting condition to be carried through the entire calibration period. This indicates that the model is correctly predicting responses to hydrogeologic forces even if the calculated head values vary somewhat from the measured values.

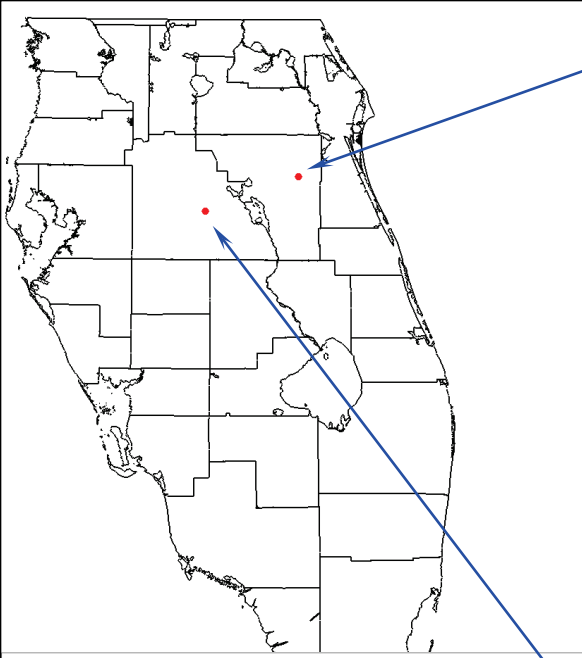

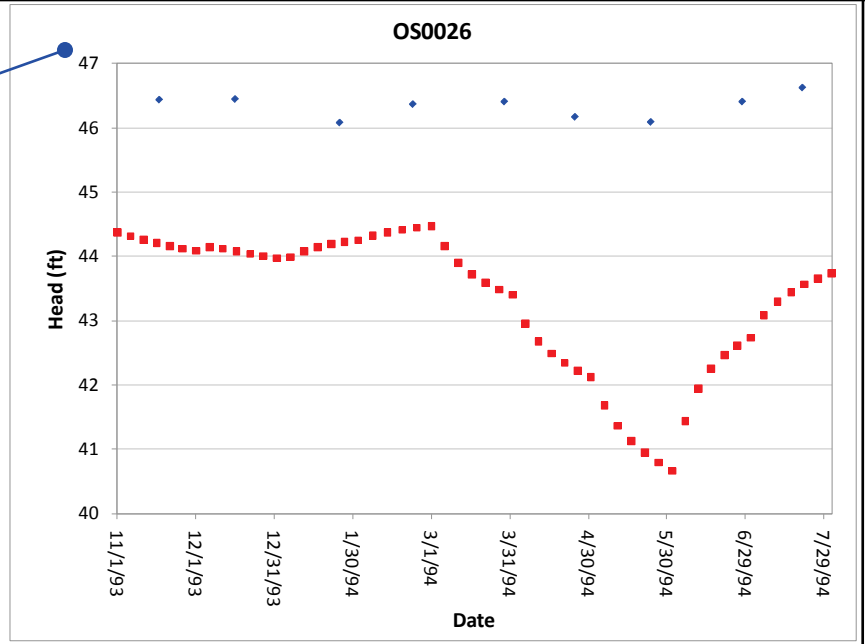

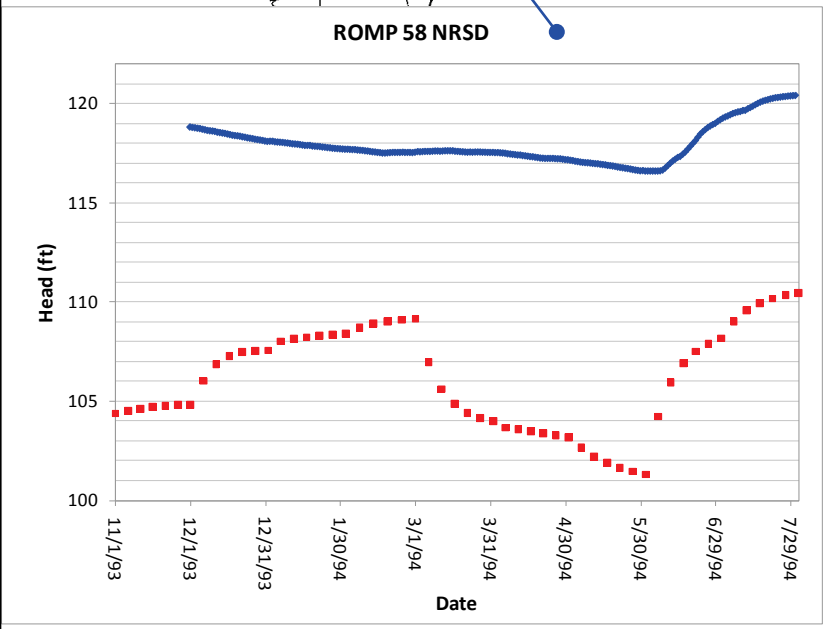

	ROMP 58 NRSD	OS0026
Mean Error	-11.624	-3.021
Mean Absolute Error	11.624	3.021
Root Mean Square (RMS)	11.772	3.182
Observed Range	3.77	0.55
RMS as Percentage of Range	312%	579%
Coefficient of Determination (r^2)	0.524	0.108
Nash-Sutcliffe Model Efficiency Coefficient	-185.748	-329.297

Legend

- Measured Head
- Model Calculated Head

Notes:

Figures 4.119 through 4.150 show the comparison between measured head values and model-calculated head values at a number of observation wells for the validation period. Although the scales vary on each plot, all plots have a horizontal grid line at each foot. This is to make it easy to determine the range of heads at a glance.

The model used month-long stress periods, so pumping and boundary conditions were input as step functions with constant values throughout each month and sudden changes at the end of each month. For this reason, the model cannot be expected to accurately predict day-to-day head variations in any of these wells. Calibration efforts were aimed at matching general trends and monthly averages.

Starting head conditions for this model were based on the October 1993 steady state solution. Transient calibration efforts were focused on matching the head changes, not the actual heads, so it is not uncommon for residuals in the starting condition to be carried through the entire calibration period. This indicates that the model is correctly predicting responses to hydrogeologic forces even if the calculated head values vary somewhat from the measured values.

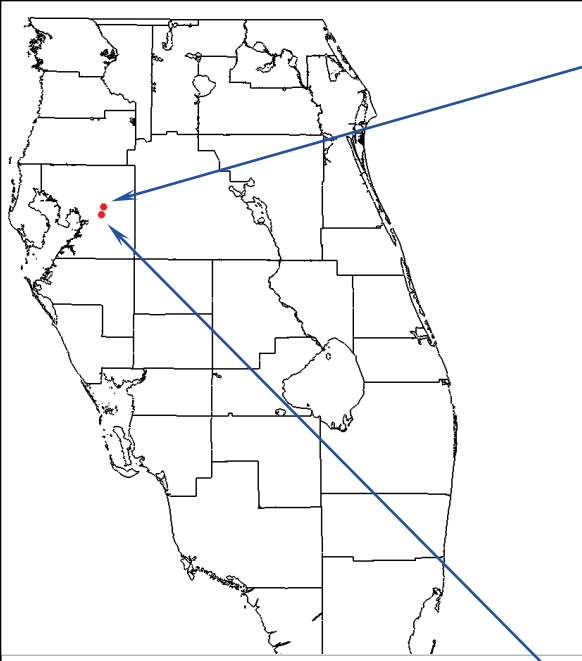

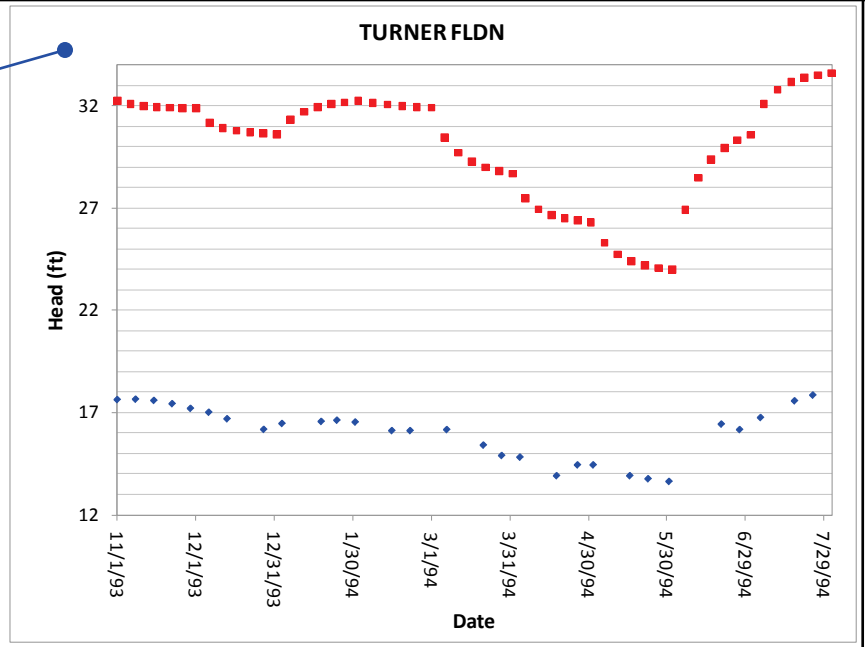

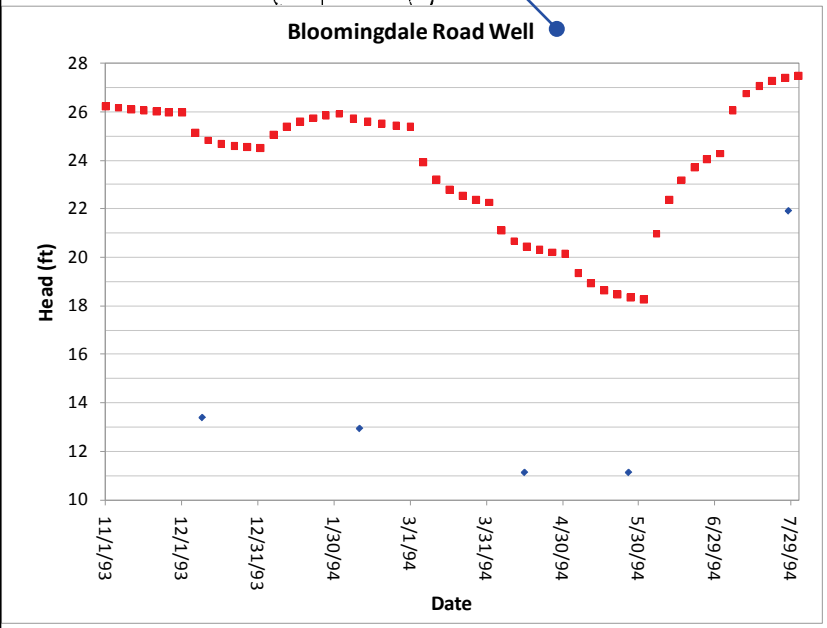

	Blooming-dale Road	TURNER FLDN
Mean Error	9.279	13.904
Mean Absolute Error	9.279	13.904
Root Mean Square (RMS)	9.714	13.994
Observed Range	10.77	4.23
RMS as Percentage of Range	90%	331%
Coefficient of Determination (r^2)	0.487	0.783
Nash-Sutcliffe Model Efficiency Coefficient	-4.873	-144.005

Legend

- Measured Head
- Model Calculated Head

Notes:

Figures 4.119 through 4.150 show the comparison between measured head values and model-calculated head values at a number of observation wells for the validation period. Although the scales vary on each plot, all plots have a horizontal grid line at each foot. This is to make it easy to determine the range of heads at a glance.

The model used month-long stress periods, so pumping and boundary conditions were input as step functions with constant values throughout each month and sudden changes at the end of each month. For this reason, the model cannot be expected to accurately predict day-to-day head variations in any of these wells. Calibration efforts were aimed at matching general trends and monthly averages.

Starting head conditions for this model were based on the October 1993 steady state solution. Transient calibration efforts were focused on matching the head changes, not the actual heads, so it is not uncommon for residuals in the starting condition to be carried through the entire calibration period. This indicates that the model is correctly predicting responses to hydrogeologic forces even if the calculated head values vary somewhat from the measured values.

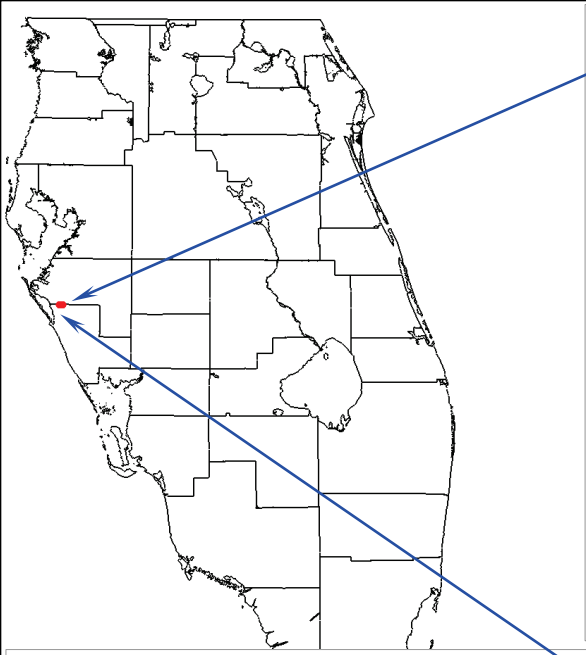

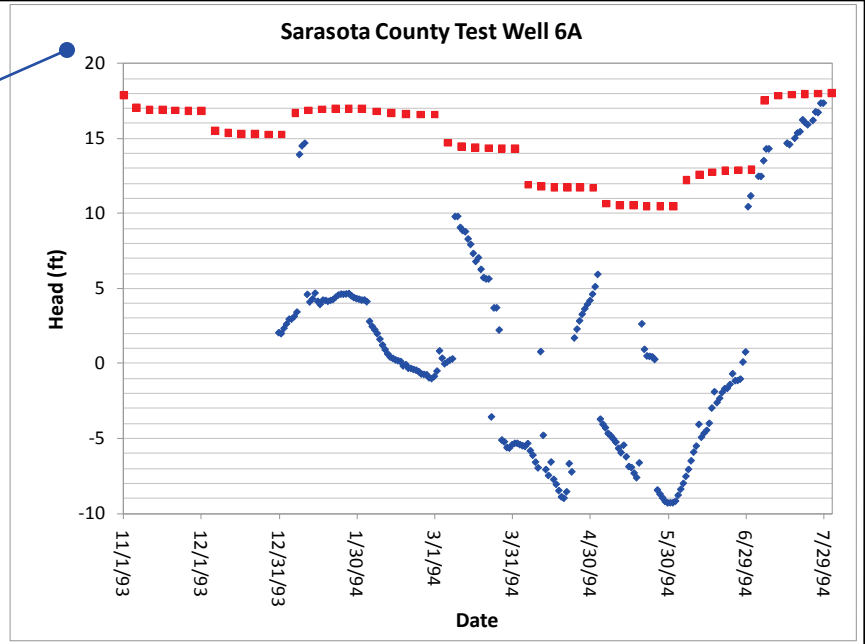

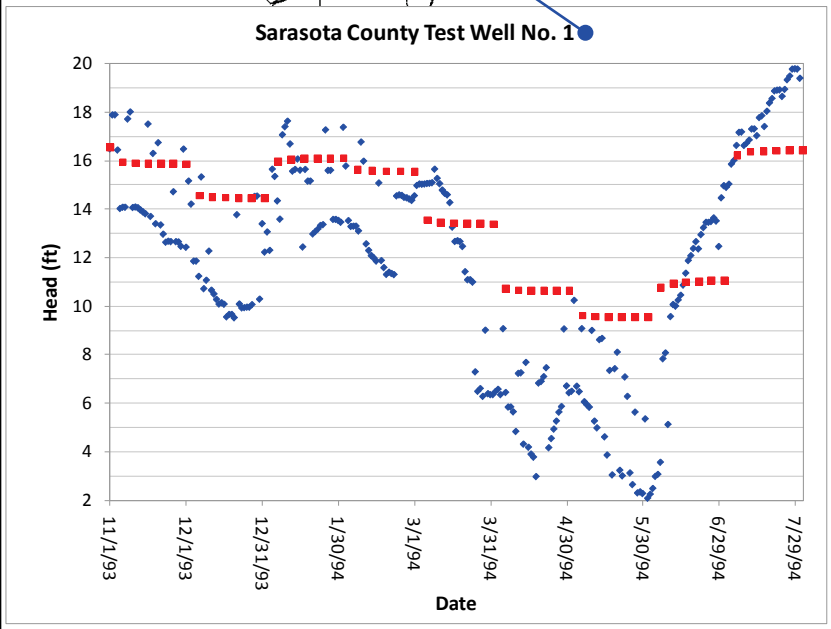

	Sarasota Test Well No. 1	Sarasota Test Well 6A
Mean Error	1.913	12.764
Mean Absolute Error	2.417	12.764
Root Mean Square (RMS)	2.776	13.506
Observed Range	17.71	26.68
RMS as Percentage of Range	16%	51%
Coefficient of Determination (r^2)	0.800	0.623
Nash-Sutcliffe Model Efficiency Coefficient	0.468	-4.090

Legend

- Measured Head
- Model Calculated Head

Notes:

Figures 4.119 through 4.150 show the comparison between measured head values and model-calculated head values at a number of observation wells for the validation period. Although the scales vary on each plot, all plots have a horizontal grid line at each foot. This is to make it easy to determine the range of heads at a glance.

The model used month-long stress periods, so pumping and boundary conditions were input as step functions with constant values throughout each month and sudden changes at the end of each month. For this reason, the model cannot be expected to accurately predict day-to-day head variations in any of these wells. Calibration efforts were aimed at matching general trends and monthly averages.

Starting head conditions for this model were based on the October 1993 steady state solution. Transient calibration efforts were focused on matching the head changes, not the actual heads, so it is not uncommon for residuals in the starting condition to be carried through the entire calibration period. This indicates that the model is correctly predicting responses to hydrogeologic forces even if the calculated head values vary somewhat from the measured values.

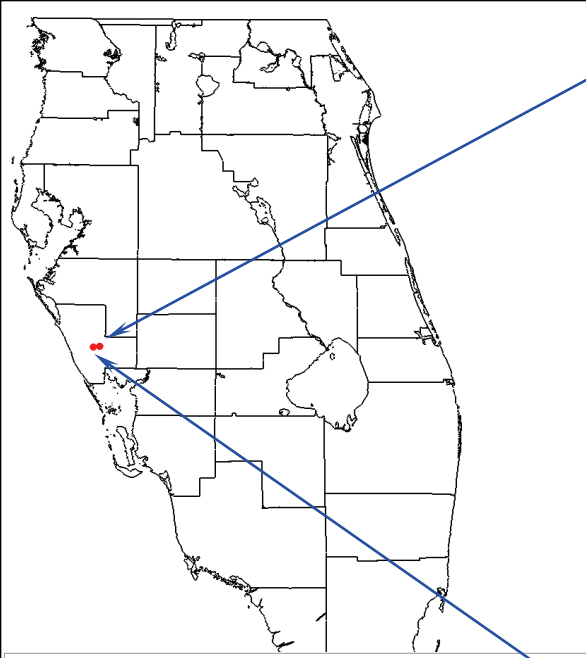

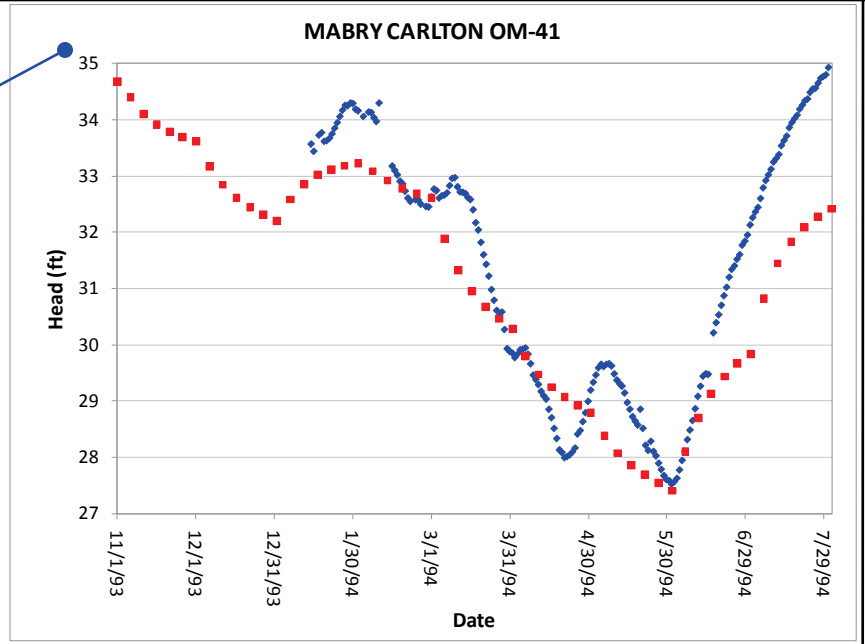

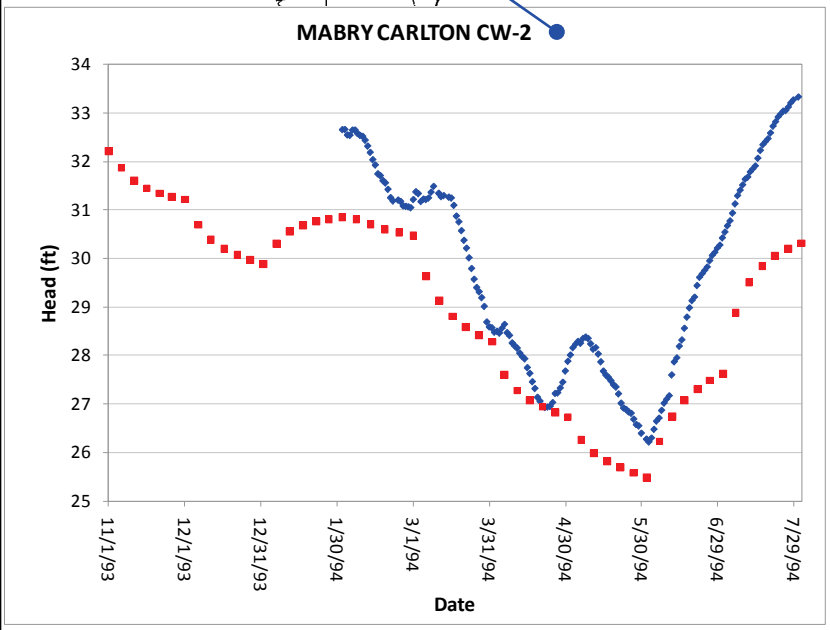

	MABRY CARLTON CW-2	MABRY CARLTON OM-41
Mean Error	-1.481	-0.798
Mean Absolute Error	1.481	0.947
Root Mean Square (RMS)	1.629	1.134
Observed Range	7.10	7.41
RMS as Percentage of Range	23%	15%
Coefficient of Determination (r^2)	0.874	0.856
Nash-Sutcliffe Model Efficiency Coefficient	0.249	0.706

Legend

- Measured Head
- Model Calculated Head

Notes:

Figures 4.119 through 4.150 show the comparison between measured head values and model-calculated head values at a number of observation wells for the validation period. Although the scales vary on each plot, all plots have a horizontal grid line at each foot. This is to make it easy to determine the range of heads at a glance.

The model used month-long stress periods, so pumping and boundary conditions were input as step functions with constant values throughout each month and sudden changes at the end of each month. For this reason, the model cannot be expected to accurately predict day-to-day head variations in any of these wells. Calibration efforts were aimed at matching general trends and monthly averages.

Starting head conditions for this model were based on the October 1993 steady state solution. Transient calibration efforts were focused on matching the head changes, not the actual heads, so it is not uncommon for residuals in the starting condition to be carried through the entire calibration period. This indicates that the model is correctly predicting responses to hydrogeologic forces even if the calculated head values vary somewhat from the measured values.

Transient SEAWAT Validation Comparison
Upper Floridan Aquifer (1993-1994)
Final Groundwater Model Calibration Report

Figure 4.143

October 2010

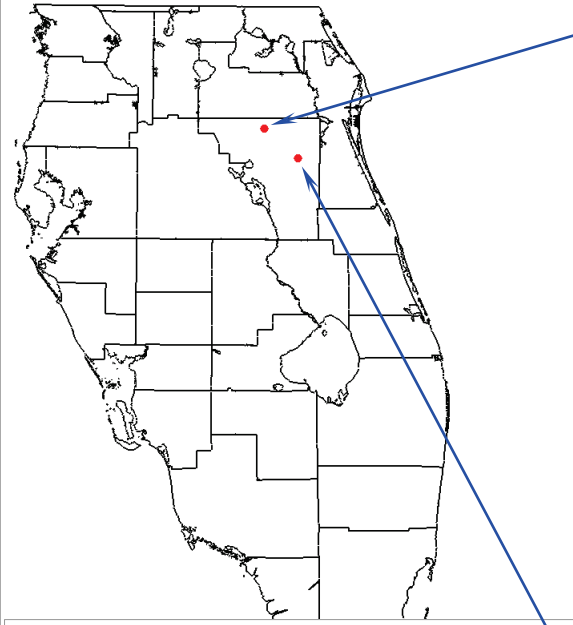

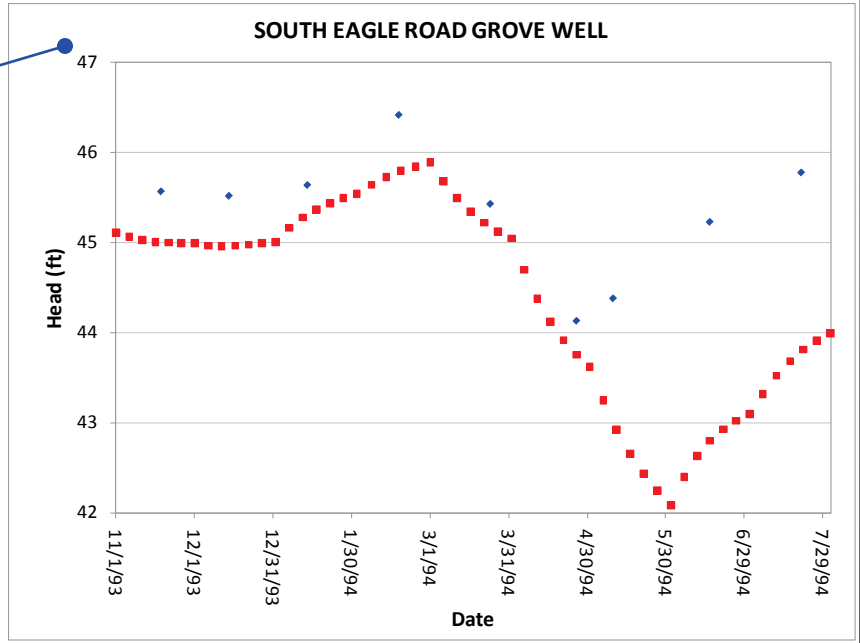

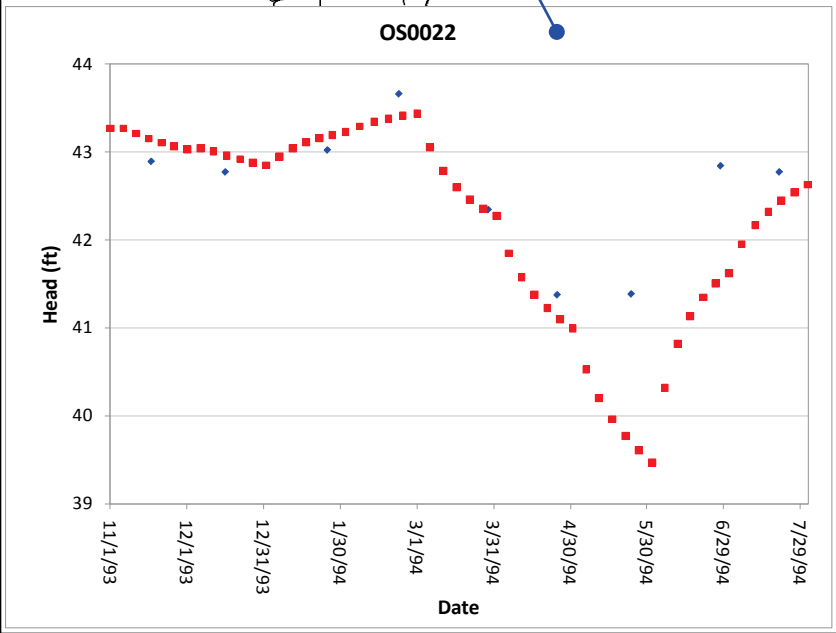

	OS0022	South Eagle Road
Mean Error	-0.338	-0.918
Mean Absolute Error	0.596	0.966
Root Mean Square (RMS)	0.855	1.301
Observed Range	2.29	2.29
RMS as Percentage of Range	37%	57%
Coefficient of Determination (r^2)	0.469	0.283
Nash-Sutcliffe Model Efficiency Coefficient	-0.445	-2.863

Legend

- Measured Head
- Model Calculated Head

Notes:

Figures 4.119 through 4.150 show the comparison between measured head values and model-calculated head values at a number of observation wells for the validation period. Although the scales vary on each plot, all plots have a horizontal grid line at each foot. This is to make it easy to determine the range of heads at a glance.

The model used month-long stress periods, so pumping and boundary conditions were input as step functions with constant values throughout each month and sudden changes at the end of each month. For this reason, the model cannot be expected to accurately predict day-to-day head variations in any of these wells. Calibration efforts were aimed at matching general trends and monthly averages.

Starting head conditions for this model were based on the October 1993 steady state solution. Transient calibration efforts were focused on matching the head changes, not the actual heads, so it is not uncommon for residuals in the starting condition to be carried through the entire calibration period. This indicates that the model is correctly predicting responses to hydrogeologic forces even if the calculated head values vary somewhat from the measured values.

Transient SEAWAT Validation Comparison
Avon Park Permeable Zone (1993-1994)
Final Groundwater Model Calibration Report

Figure 4.144

October 2010

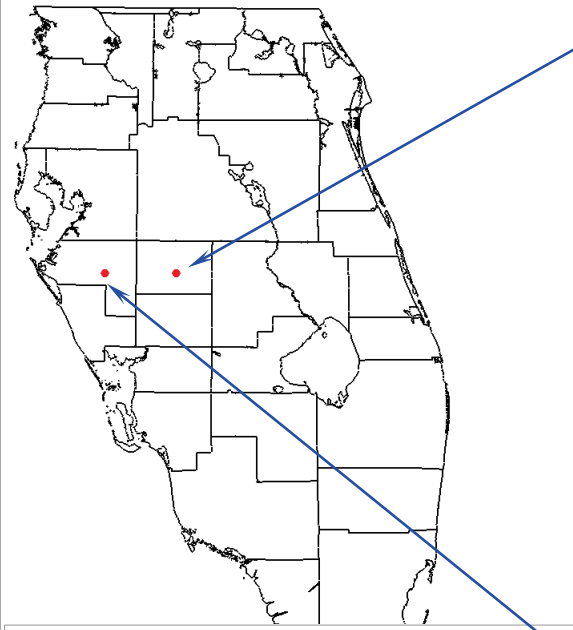

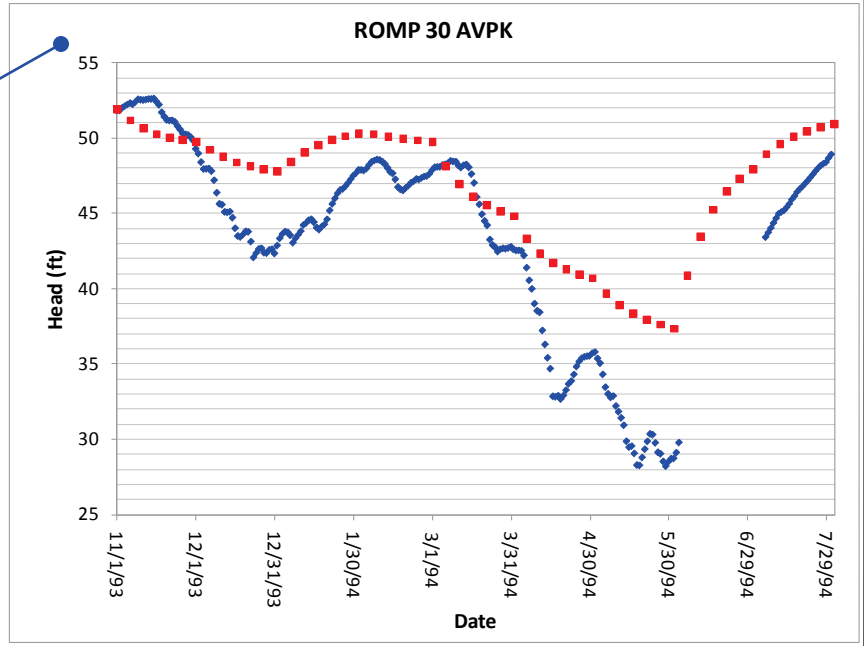

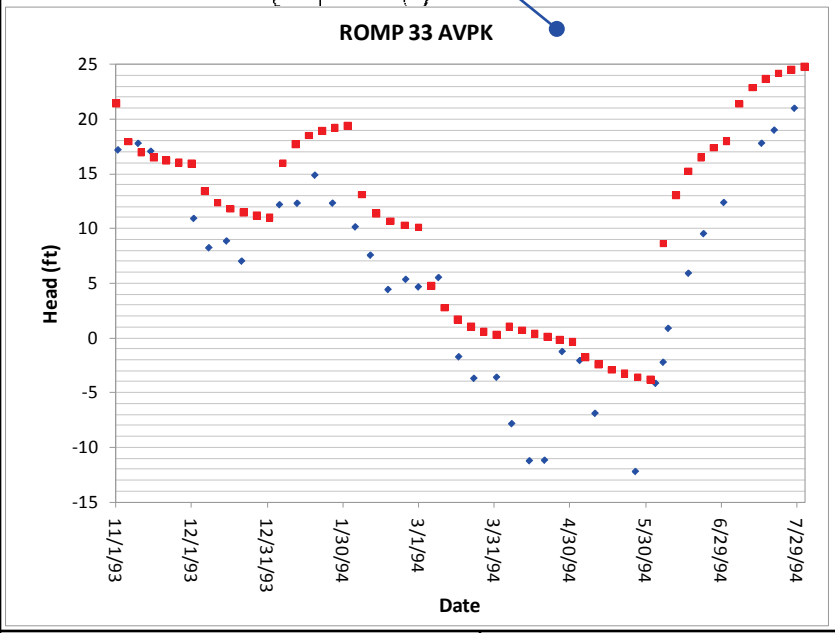

	ROMP 33 AVPK	ROMP 30 AVPK
Mean Error	4.370	4.636
Mean Absolute Error	4.370	4.853
Root Mean Square (RMS)	4.914	6.243
Observed Range	33.22	24.43
RMS as Percentage of Range	15%	26%
Coefficient of Determination (r^2)	0.947	0.823
Nash-Sutcliffe Model Efficiency Coefficient	0.702	0.283

Legend

- Measured Head
- Model Calculated Head

Notes:

Figures 4.119 through 4.150 show the comparison between measured head values and model-calculated head values at a number of observation wells for the validation period. Although the scales vary on each plot, all plots have a horizontal grid line at each foot. This is to make it easy to determine the range of heads at a glance.

The model used month-long stress periods, so pumping and boundary conditions were input as step functions with constant values throughout each month and sudden changes at the end of each month. For this reason, the model cannot be expected to accurately predict day-to-day head variations in any of these wells. Calibration efforts were aimed at matching general trends and monthly averages.

Starting head conditions for this model were based on the October 1993 steady state solution. Transient calibration efforts were focused on matching the head changes, not the actual heads, so it is not uncommon for residuals in the starting condition to be carried through the entire calibration period. This indicates that the model is correctly predicting responses to hydrogeologic forces even if the calculated head values vary somewhat from the measured values.

Transient SEAWAT Validation Comparison
Avon Park Permeable Zone (1993-1994)
Final Groundwater Model Calibration Report

Figure 4.145

October 2010

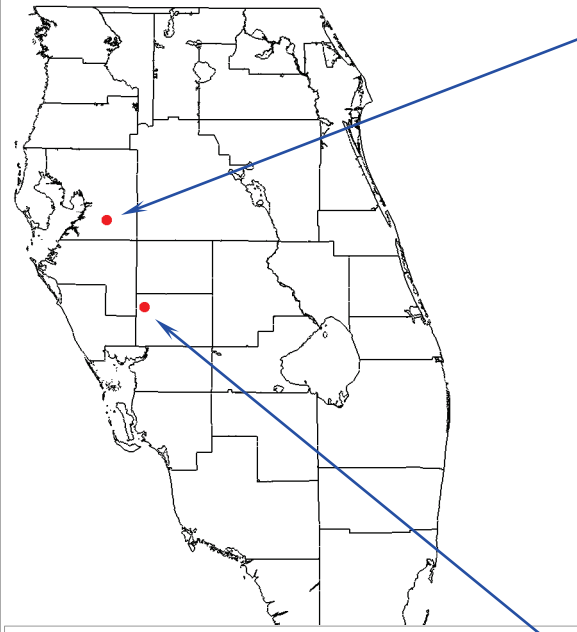

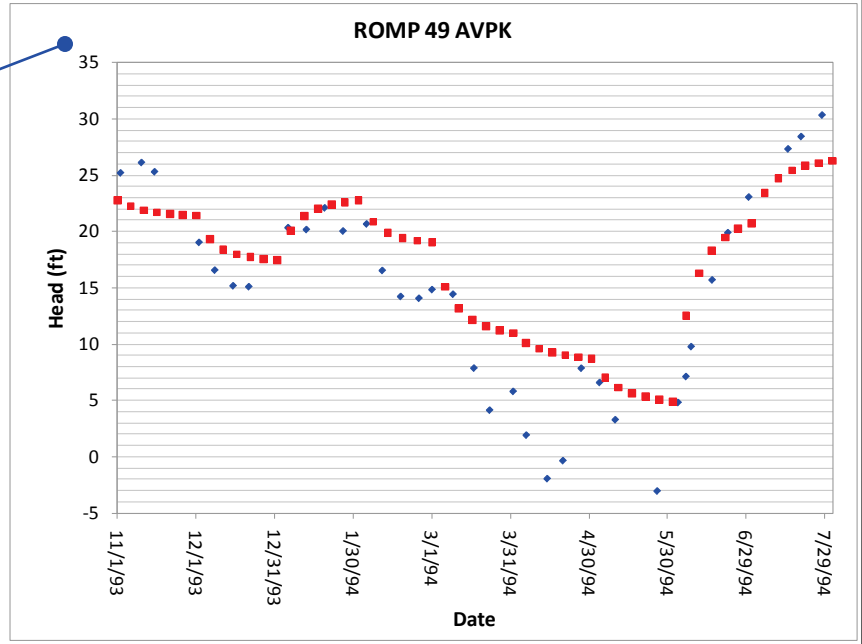

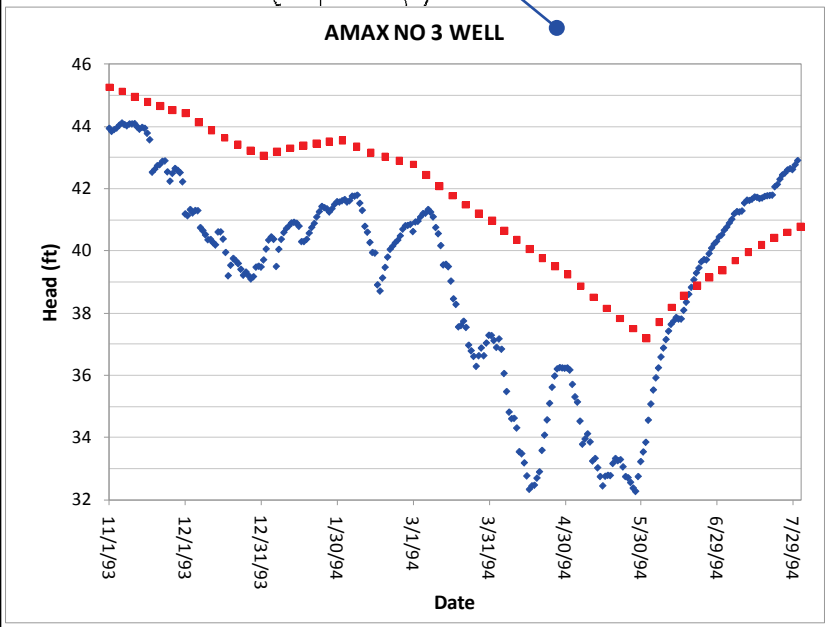

	AMAX NO 3	ROMP 49 AVPK
Mean Error	2.455	1.683
Mean Absolute Error	2.835	3.447
Root Mean Square (RMS)	3.214	3.867
Observed Range	11.86	33.43
RMS as Percentage of Range	27%	12%
Coefficient of Determination (r^2)	0.525	0.935
Nash-Sutcliffe Model Efficiency Coefficient	-0.142	0.801

Legend

- Measured Head
- Model Calculated Head

Notes:

Figures 4.119 through 4.150 show the comparison between measured head values and model-calculated head values at a number of observation wells for the validation period. Although the scales vary on each plot, all plots have a horizontal grid line at each foot. This is to make it easy to determine the range of heads at a glance.

The model used month-long stress periods, so pumping and boundary conditions were input as step functions with constant values throughout each month and sudden changes at the end of each month. For this reason, the model cannot be expected to accurately predict day-to-day head variations in any of these wells. Calibration efforts were aimed at matching general trends and monthly averages.

Starting head conditions for this model were based on the October 1993 steady state solution. Transient calibration efforts were focused on matching the head changes, not the actual heads, so it is not uncommon for residuals in the starting condition to be carried through the entire calibration period. This indicates that the model is correctly predicting responses to hydrogeologic forces even if the calculated head values vary somewhat from the measured values.

Transient SEAWAT Validation Comparison
Avon Park Permeable Zone (1993-1994)
Final Groundwater Model Calibration Report

Figure 4.146

October 2010

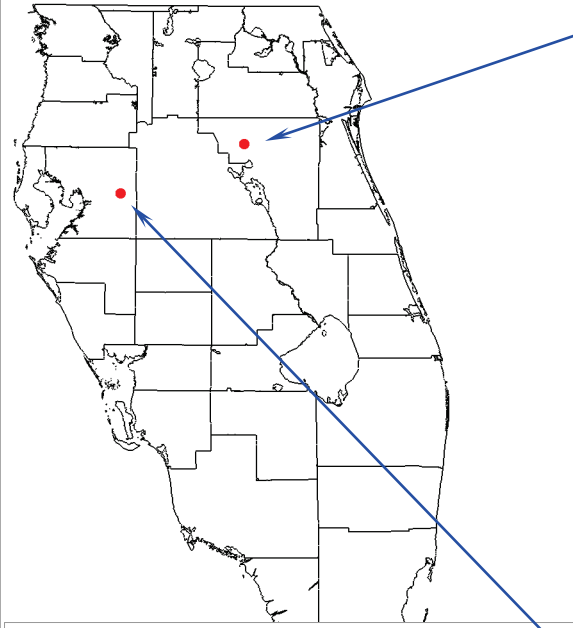

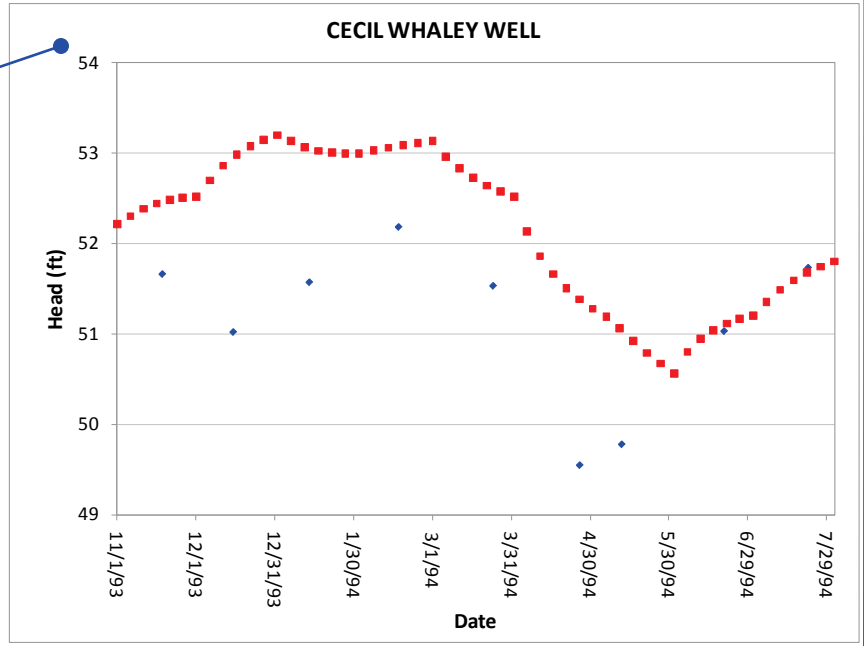

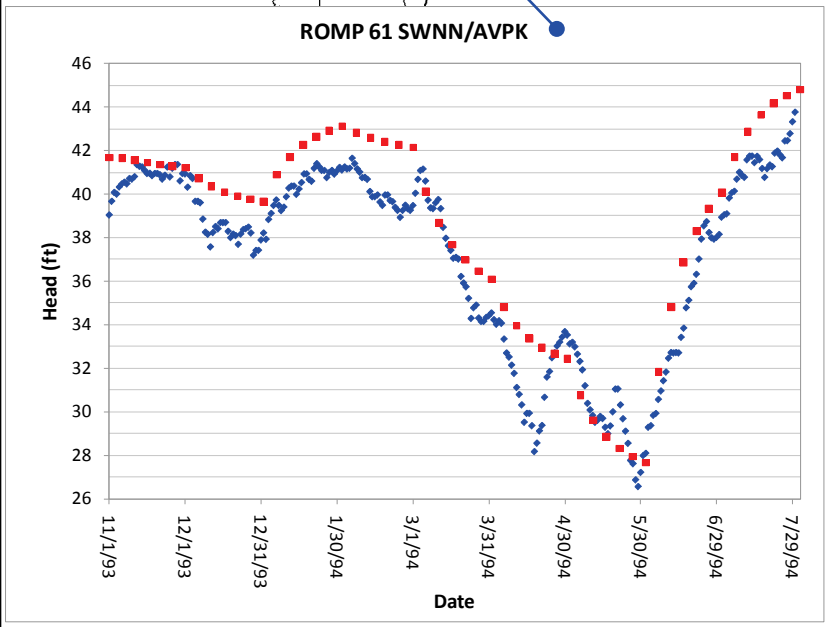

	ROMP 61 SWNN/ AVPK	CECIL WHALEY WELL
Mean Error	1.308	1.048
Mean Absolute Error	1.389	1.117
Root Mean Square (RMS)	1.538	1.309
Observed Range	17.23	2.63
RMS as Percentage of Range	9%	50%
Coefficient of Determination (r^2)	0.972	0.310
Nash-Sutcliffe Model Efficiency Coefficient	0.849	-1.394

Legend

- Measured Head
- Model Calculated Head

Notes:

Figures 4.119 through 4.150 show the comparison between measured head values and model-calculated head values at a number of observation wells for the validation period. Although the scales vary on each plot, all plots have a horizontal grid line at each foot. This is to make it easy to determine the range of heads at a glance.

The model used month-long stress periods, so pumping and boundary conditions were input as step functions with constant values throughout each month and sudden changes at the end of each month. For this reason, the model cannot be expected to accurately predict day-to-day head variations in any of these wells. Calibration efforts were aimed at matching general trends and monthly averages.

Starting head conditions for this model were based on the October 1993 steady state solution. Transient calibration efforts were focused on matching the head changes, not the actual heads, so it is not uncommon for residuals in the starting condition to be carried through the entire calibration period. This indicates that the model is correctly predicting responses to hydrogeologic forces even if the calculated head values vary somewhat from the measured values.

Transient SEAWAT Validation Comparison
Avon Park Permeable Zone (1993-1994)
Final Groundwater Model Calibration Report

Figure 4.147

October 2010

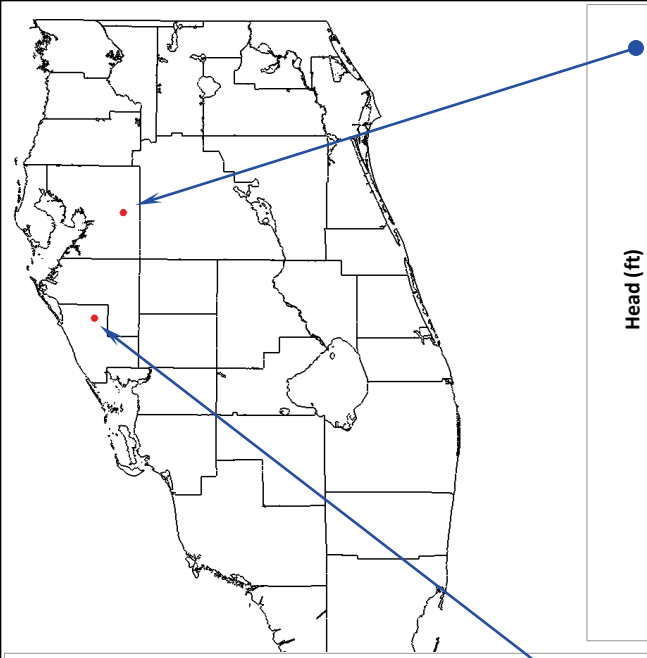

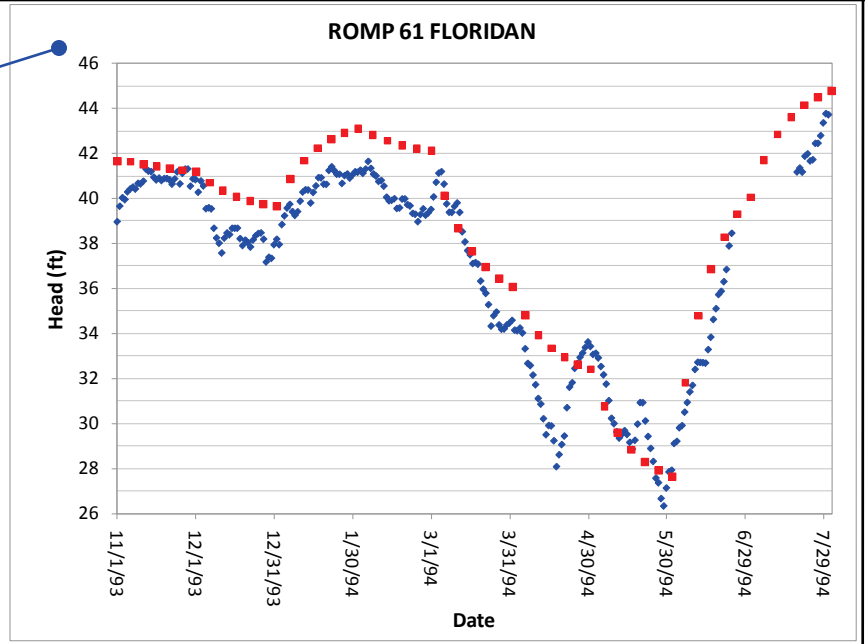

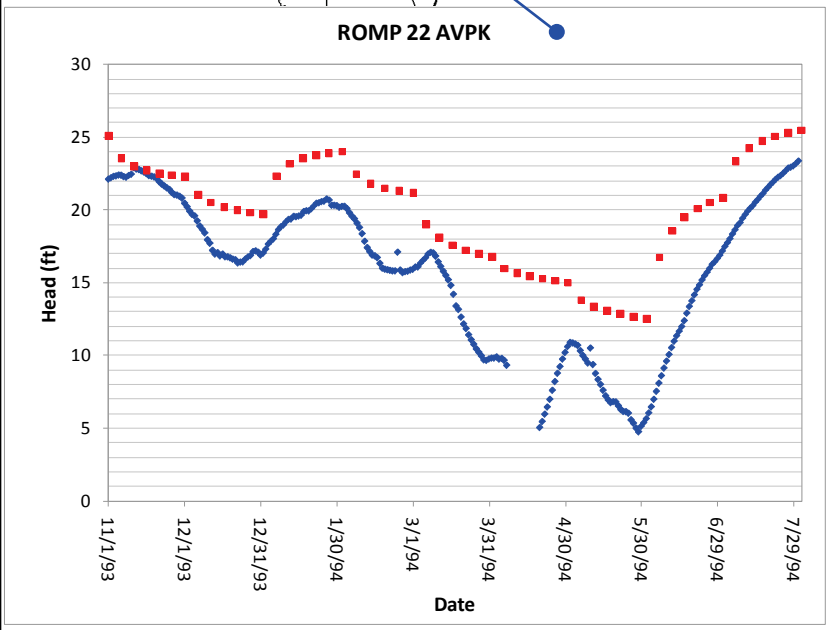

	ROMP 22 AVPK	ROMP 61 FLDN
Mean Error	4.338	1.296
Mean Absolute Error	4.338	1.356
Root Mean Square (RMS)	4.684	1.526
Observed Range	18.64	17.44
RMS as Percentage of Range	25%	9%
Coefficient of Determination (r^2)	0.949	0.966
Nash-Sutcliffe Model Efficiency Coefficient	0.097	0.869

Legend

- Measured Head
- Model Calculated Head

Notes:

Figures 4.119 through 4.150 show the comparison between measured head values and model-calculated head values at a number of observation wells for the validation period. Although the scales vary on each plot, all plots have a horizontal grid line at each foot. This is to make it easy to determine the range of heads at a glance.

The model used month-long stress periods, so pumping and boundary conditions were input as step functions with constant values throughout each month and sudden changes at the end of each month. For this reason, the model cannot be expected to accurately predict day-to-day head variations in any of these wells. Calibration efforts were aimed at matching general trends and monthly averages.

Starting head conditions for this model were based on the October 1993 steady state solution. Transient calibration efforts were focused on matching the head changes, not the actual heads, so it is not uncommon for residuals in the starting condition to be carried through the entire calibration period. This indicates that the model is correctly predicting responses to hydrogeologic forces even if the calculated head values vary somewhat from the measured values.

Transient SEAWAT Validation Comparison
Avon Park Permeable Zone (1993-1994)
Final Groundwater Model Calibration Report

Figure 4.148

October 2010

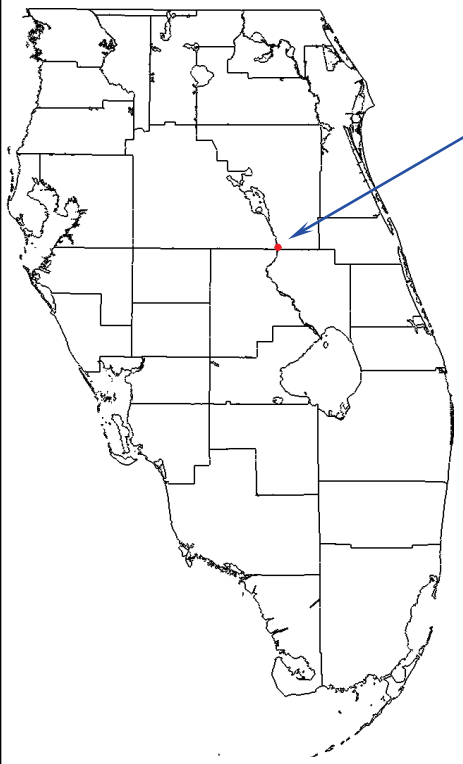

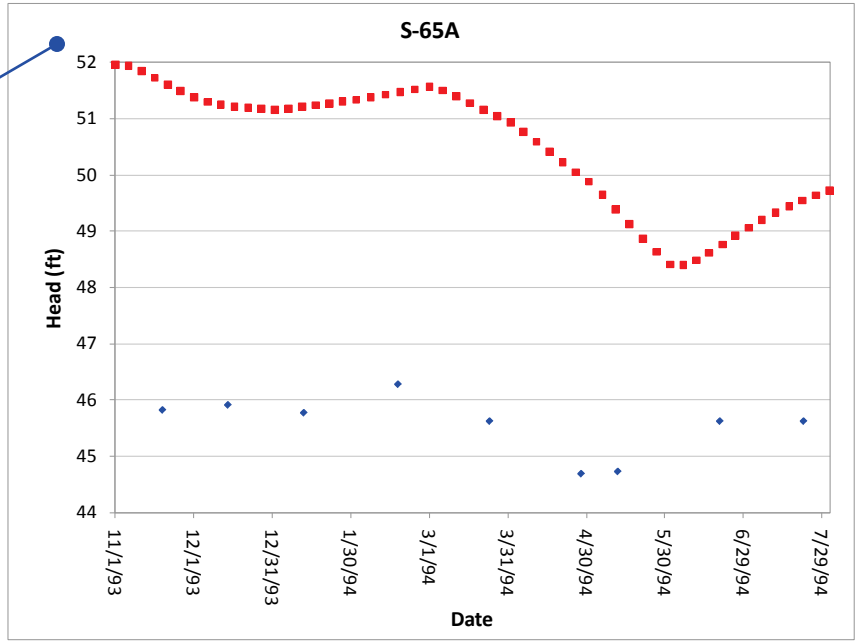

	S-65A
Mean Error	4.962
Mean Absolute Error	4.962
Root Mean Square (RMS)	5.053
Observed Range	1.60
RMS as Percentage of Range	316%
Coefficient of Determination (r^2)	0.226
Nash-Sutcliffe Model Efficiency Coefficient	-101.450

Legend

- Measured Head
- Model Calculated Head

Notes:

Figures 4.119 through 4.150 show the comparison between measured head values and model-calculated head values at a number of observation wells for the validation period. Although the scales vary on each plot, all plots have a horizontal grid line at each foot. This is to make it easy to determine the range of heads at a glance.

The model used month-long stress periods, so pumping and boundary conditions were input as step functions with constant values throughout each month and sudden changes at the end of each month. For this reason, the model cannot be expected to accurately predict day-to-day head variations in any of these wells. Calibration efforts were aimed at matching general trends and monthly averages.

Starting head conditions for this model were based on the October 1993 steady state solution. Transient calibration efforts were focused on matching the head changes, not the actual heads, so it is not uncommon for residuals in the starting condition to be carried through the entire calibration period. This indicates that the model is correctly predicting responses to hydrogeologic forces even if the calculated head values vary somewhat from the measured values.

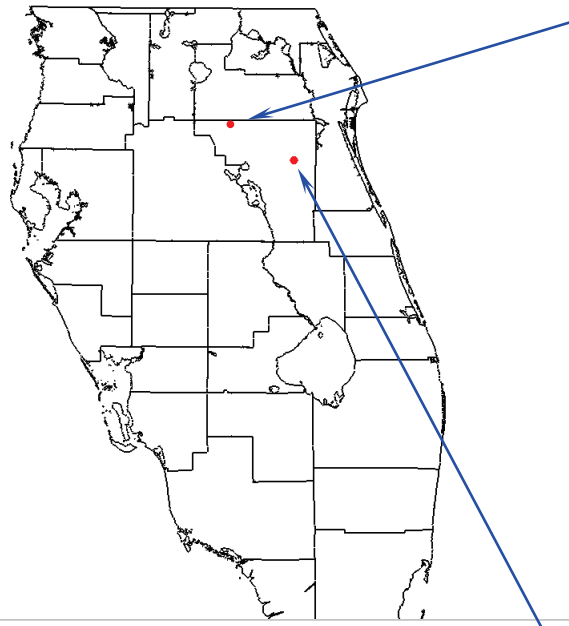

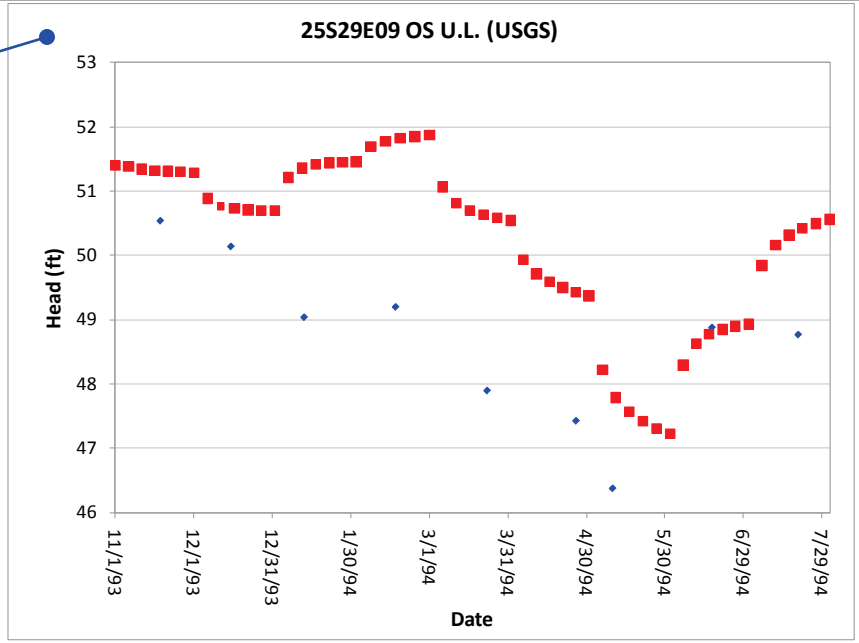

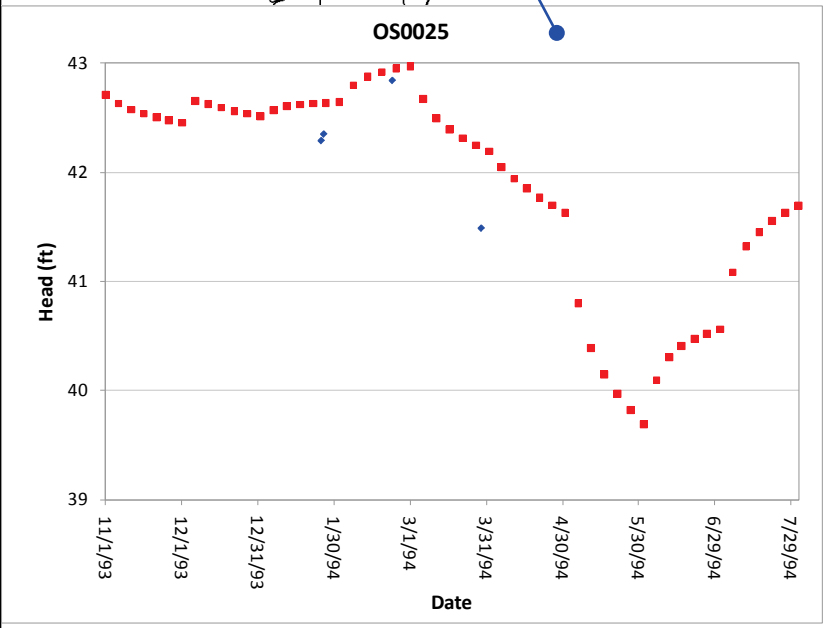

	OS0025	25S29E09 OS U.L. (USGS)
Mean Error	0.432	1.557
Mean Absolute Error	0.435	1.654
Root Mean Square (RMS)	0.613	1.867
Observed Range	1.35	4.16
RMS as Percentage of Range	45%	45%
Coefficient of Determination (r^2)	0.839	0.426
Nash-Sutcliffe Model Efficiency Coefficient	-0.214	-1.325

Legend

- Measured Head
- Model Calculated Head

Notes:

Figures 4.119 through 4.150 show the comparison between measured head values and model-calculated head values at a number of observation wells for the validation period. Although the scales vary on each plot, all plots have a horizontal grid line at each foot. This is to make it easy to determine the range of heads at a glance.

The model used month-long stress periods, so pumping and boundary conditions were input as step functions with constant values throughout each month and sudden changes at the end of each month. For this reason, the model cannot be expected to accurately predict day-to-day head variations in any of these wells. Calibration efforts were aimed at matching general trends and monthly averages.

Starting head conditions for this model were based on the October 1993 steady state solution. Transient calibration efforts were focused on matching the head changes, not the actual heads, so it is not uncommon for residuals in the starting condition to be carried through the entire calibration period. This indicates that the model is correctly predicting responses to hydrogeologic forces even if the calculated head values vary somewhat from the measured values.

Transient SEAWAT Validation Comparison
Lower Floridan Aquifer (1993-1994)
Final Groundwater Model Calibration Report

Figure 4.150

October 2010

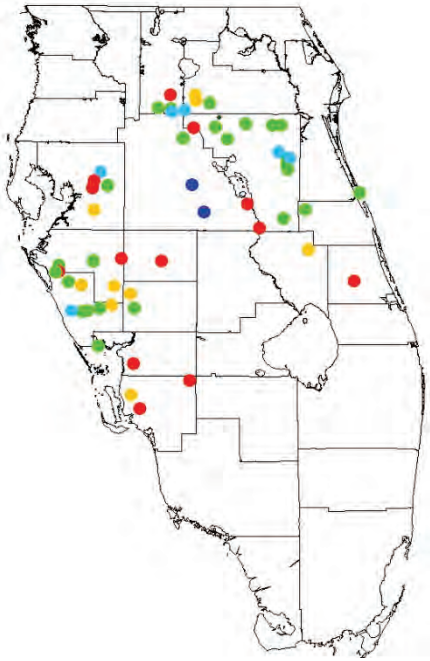

UF

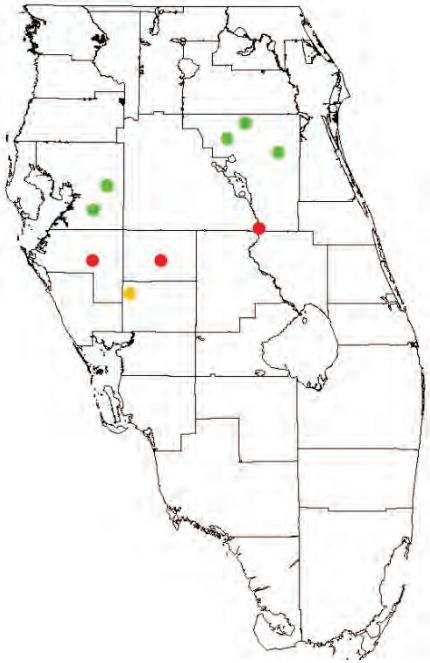

APPZ

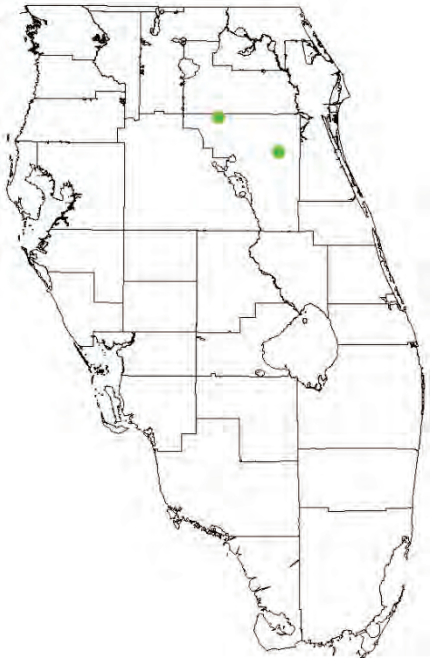

LF1

Mean Residual Error

- > 4.0 (model predicts high)
- 2.0 to 4.0
- -2.0 to 2.0 (well calibrated)
- -4.0 to -2.0
- < -4.0 (model predicts low)

Notes:

The mean error (ME) is calculated as described in Section 4.1. The ME statistic is calculated using monthly average heads for both the observed and model calculated data.

A perfectly calibrated point would have an ME value close to zero. In these maps, blue points have negative ME statistics (model prediction is low) and red points have positive ME statistics (model prediction is high). Green points are for well calibrated observation wells.

Transient SEAWAT Validation Comparison
Mean Residual Error (1993-1994)
Final Groundwater Model Calibration Report

Figure 4.151

October 2010

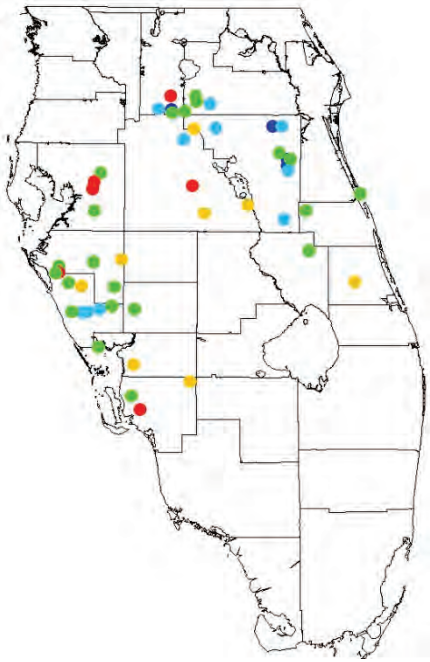

UF

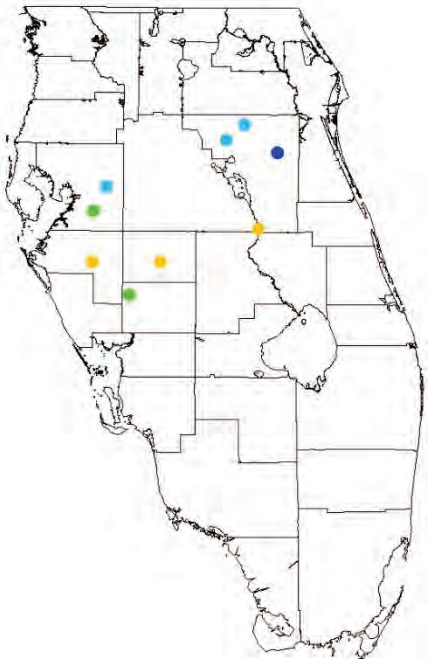

APPZ

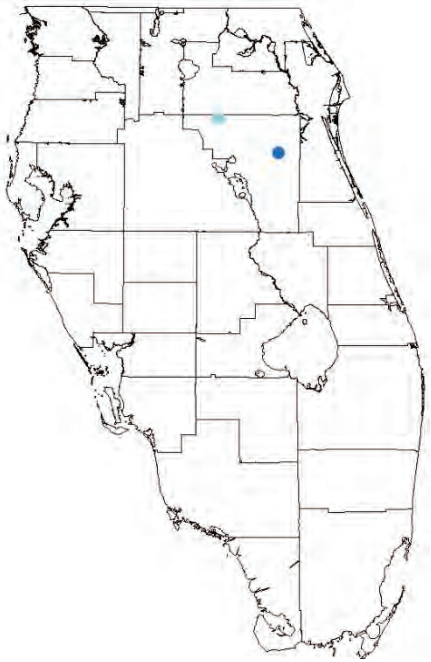

LF1

Root Mean Square Error

- < 1.0 (well calibrated)
- 1.0 - 2.0
- 2.0 - 4.0
- 4.0 - 8.0
- > 8.0 (poorly calibrated)

Notes:

The RMS (Root Mean Square) statistic is calculated as described in Section 4.1. The RMS statistic is calculated using monthly average heads for both the observed and model calculated data.

A perfectly calibrated point would have an RMS value close to zero. In these maps, blue points have low RMS statistics (well calibrated) and red points have large RMS (poorly calibrated).

Transient SEAWAT Validation Comparison
Root Mean Square Error (1993-1994)
Final Groundwater Model Calibration Report

Figure 4.152

October 2010

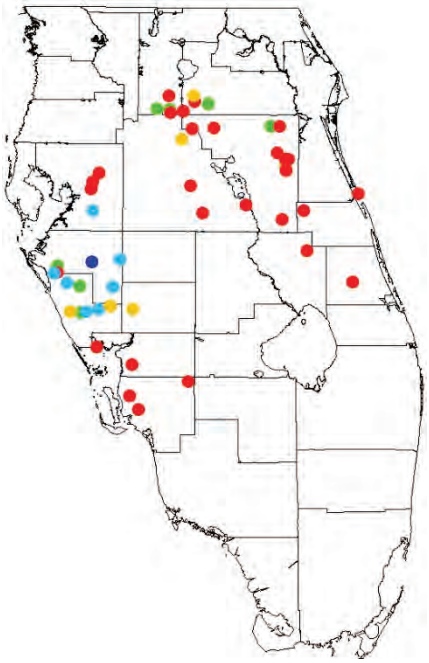

UF

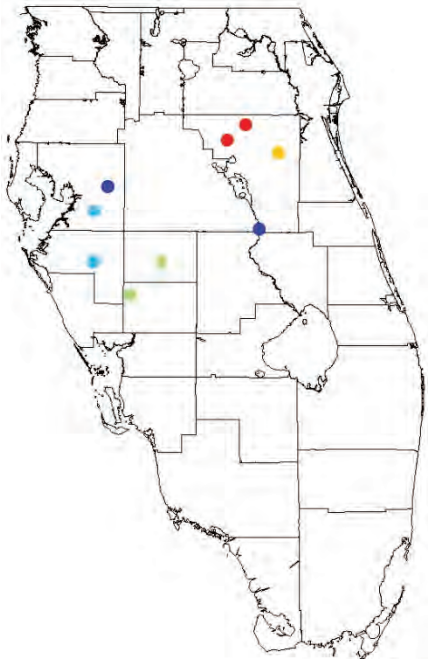

APPZ

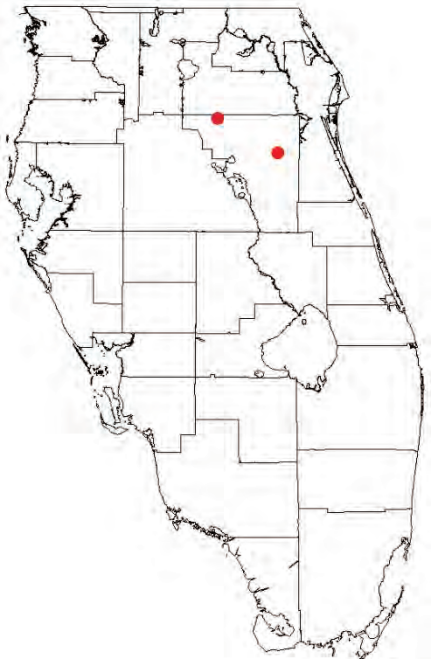

LF1

RMS as Percent of Observed Range

- < 10% (well calibrated)
- 10%-20%
- 20%-30%
- 30%-40%
- > 40% (poorly calibrated)

Notes:

The RMS (Root Mean Square) statistic is calculated as described in Section 4.1. This figure shows the RMS for each transient calibration point as a percentage of the range of observed values over the 15 month calibration period. The RMS statistic is calculated using monthly average heads for both the observed and model calculated data.

A perfectly calibrated point would have an RMS value close to zero. When compared to the observed head range, wells with small variability in heads are held to a higher standard. A common rule of thumb is to require that the RMS be less than 10% of the observed range. In these maps, blue points have low RMS statistics compared to the observed head range (well calibrated) and red points have large RMS statistics relative to the observed head range (poorly calibrated).

Transient SEAWAT Validation Comparison
RMS as Percentage of Range (1993-1994)
Final Groundwater Model Calibration Report

Figure 4.153

October 2010

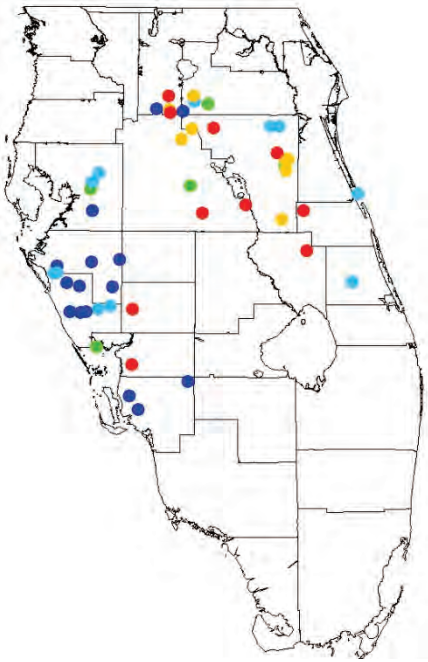

UF

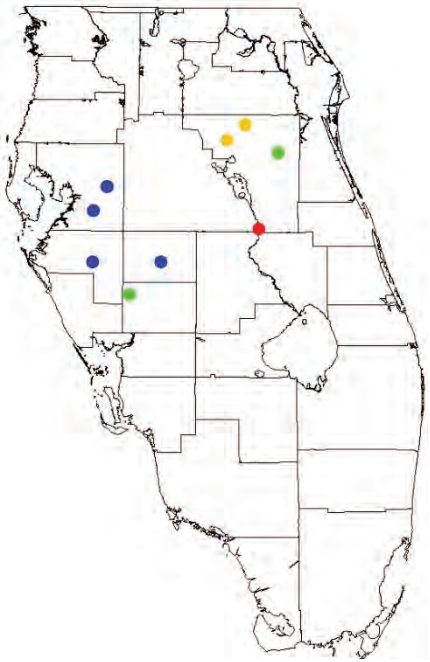

APPZ

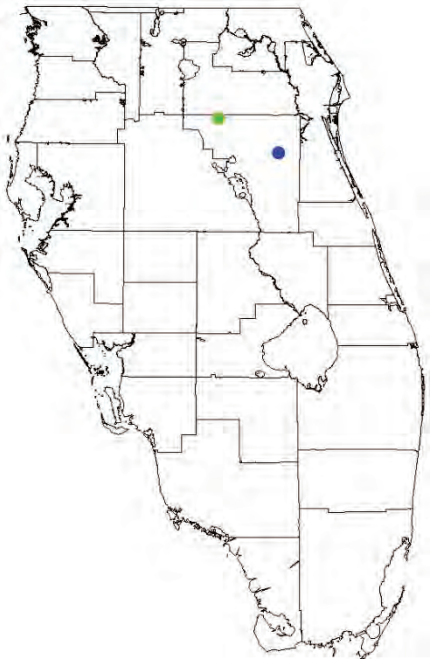

LF1

Coefficient of Determination (r^2)

- > 0.8 (well calibrated)
- 0.6 – 0.8
- 0.4 – 0.6
- 0.2 – 0.4
- < 0.2 (poorly calibrated)

Notes:

The Coefficient of Determination (r^2) is calculated as described in Section 4.2. The r^2 statistic is calculated using monthly average heads for both the observed and model calculated data.

A perfectly calibrated point would have an r^2 value close to 1.0. In these maps, blue points have high r^2 (well calibrated) and red points have small r^2 statistics (poorly calibrated).

Transient SEAWAT Validation Comparison
Coefficient of Determination (1993-1994)
Final Groundwater Model Calibration Report

Figure 4.154

October 2010

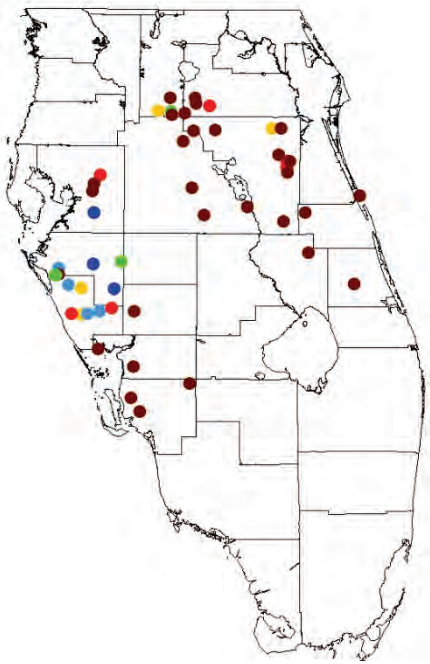

UF

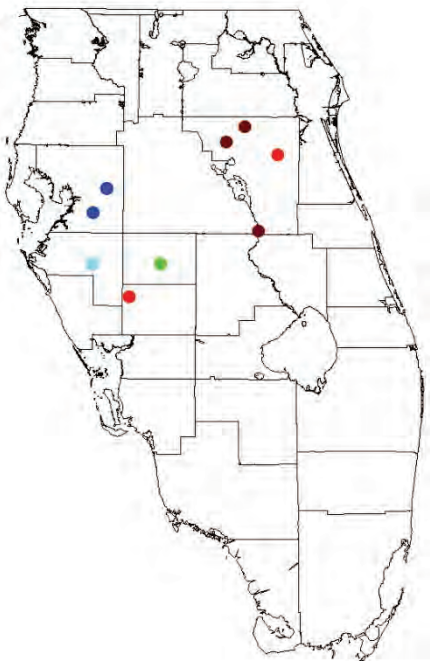

APPZ

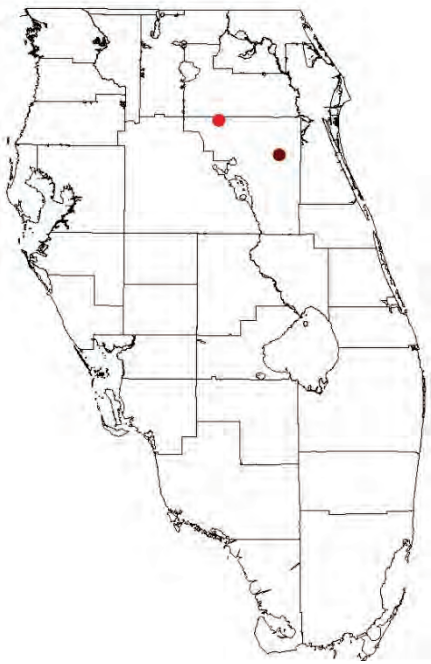

LF1

Nash-Sutcliffe Model Efficiency Coefficient

- > 0.75 (well calibrated)
- 0.5 – 0.75
- 0.25 – 0.5
- 0.0 – 0.25
- -1.0 – 0.0
- < -1.0 (poorly calibrated)

Notes:

The Nash-Sutcliffe Model Efficiency Coefficient is calculated as described in Section 4.2. This statistic is calculated using monthly average heads for both the observed and model calculated data.

A perfectly calibrated point would have an efficiency value close to 1.0. A negative efficiency value indicates that the calibration error exceeds the variance in the observed data. In these maps, blue points have high efficiency coefficients (well calibrated) and red points have negative efficiency coefficients (poorly calibrated).

Transient SEAWAT Validation Comparison
Nash-Sutcliffe Model Efficiency (1993-1994)
Final Groundwater Model Calibration Report

Figure 4.155

October 2010

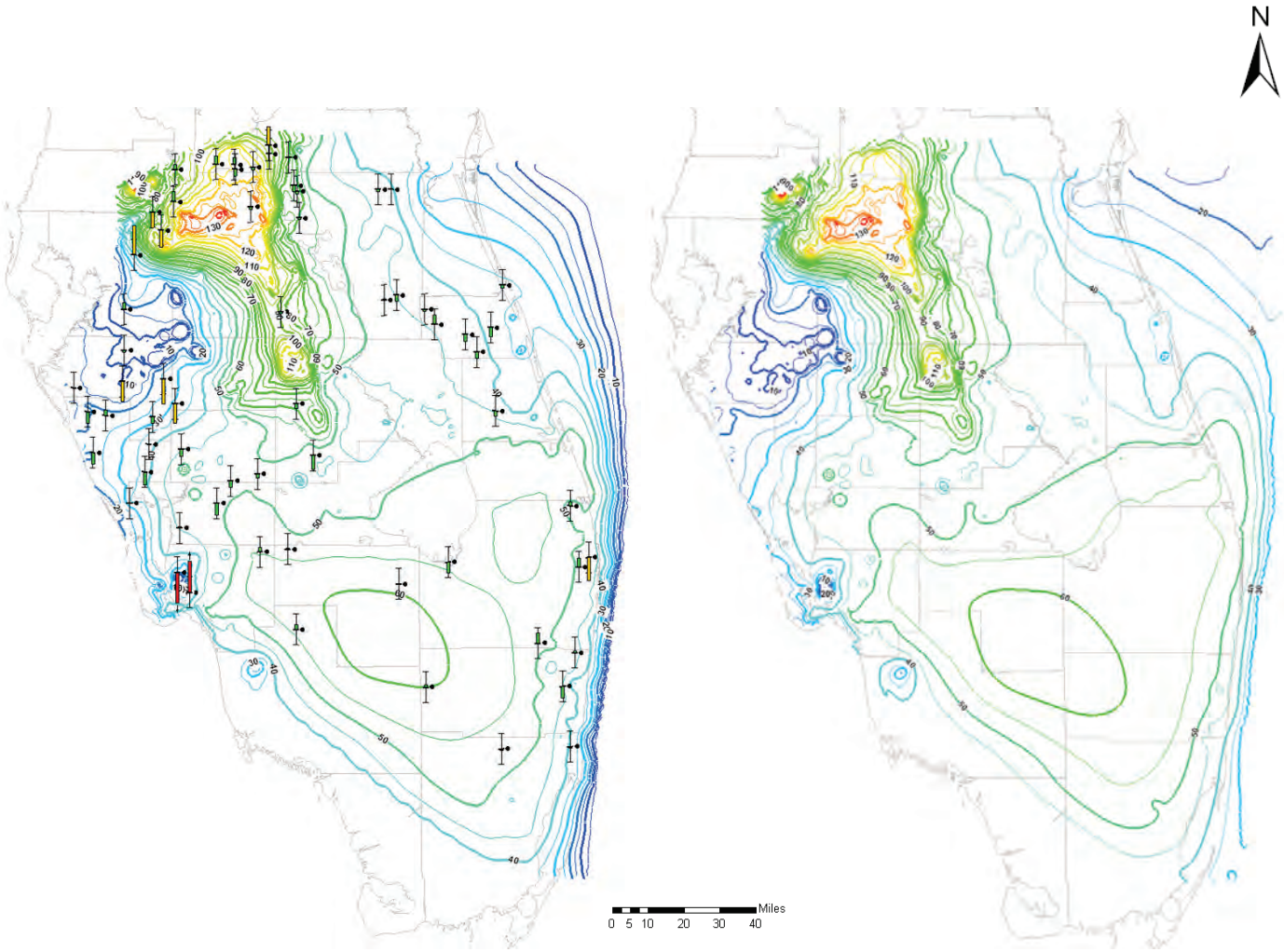

Model Calculated Head

Equivalent Freshwater Head

Notes:

Left figure is the October 2003 model calculated heads (observed heads) as output from the calibrated model. Calibration targets are provided to remind the reader of locations with good or poor calibration.

Right figure is a calculation of the equivalent freshwater head, created by applying Equation 2.2 to the model result in each cell of the model.

Model Calculated and Equivalent Freshwater Head
Upper Floridan Aquifer - October 2003
Final Groundwater Model Calibration Report

Figure 4.156

October 2010

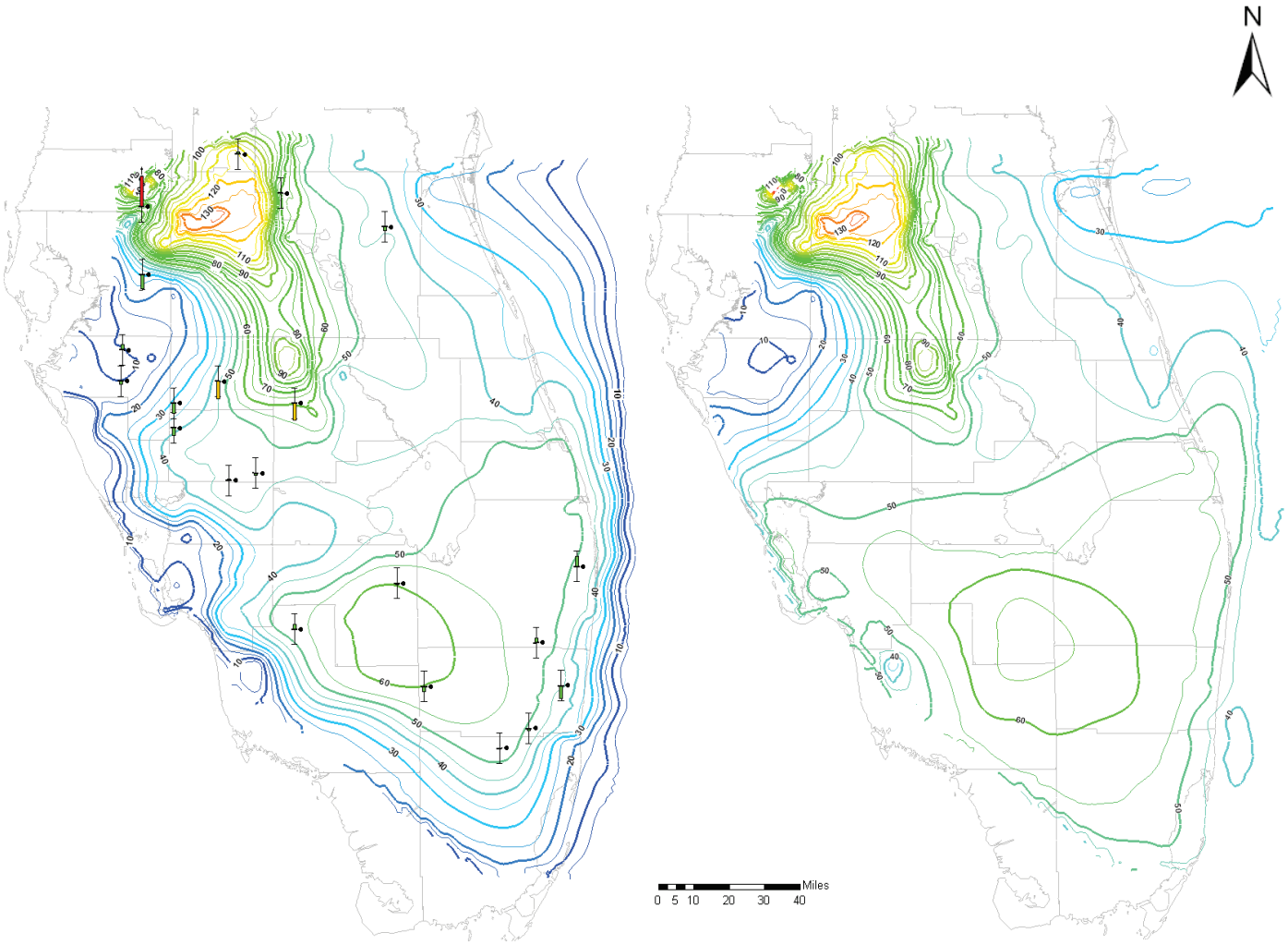

Model Calculated Head

Equivalent Freshwater Head

Head (ft)
145
135
125
115
105
95
85
75
65
55
45
35
25
15
5

Notes:

Left figure is the October 2003 model calculated heads (observed heads) as output from the calibrated model. Calibration targets are provided to remind the reader of locations with good or poor calibration.

Right figure is a calculation of the equivalent freshwater head, created by applying Equation 2.2 to the model result in each cell of the model.

Model Calculated and Equivalent Freshwater Head
APPZ Aquifer - October 2003

Final Groundwater Model Calibration Report

Figure 4.157

October 2010

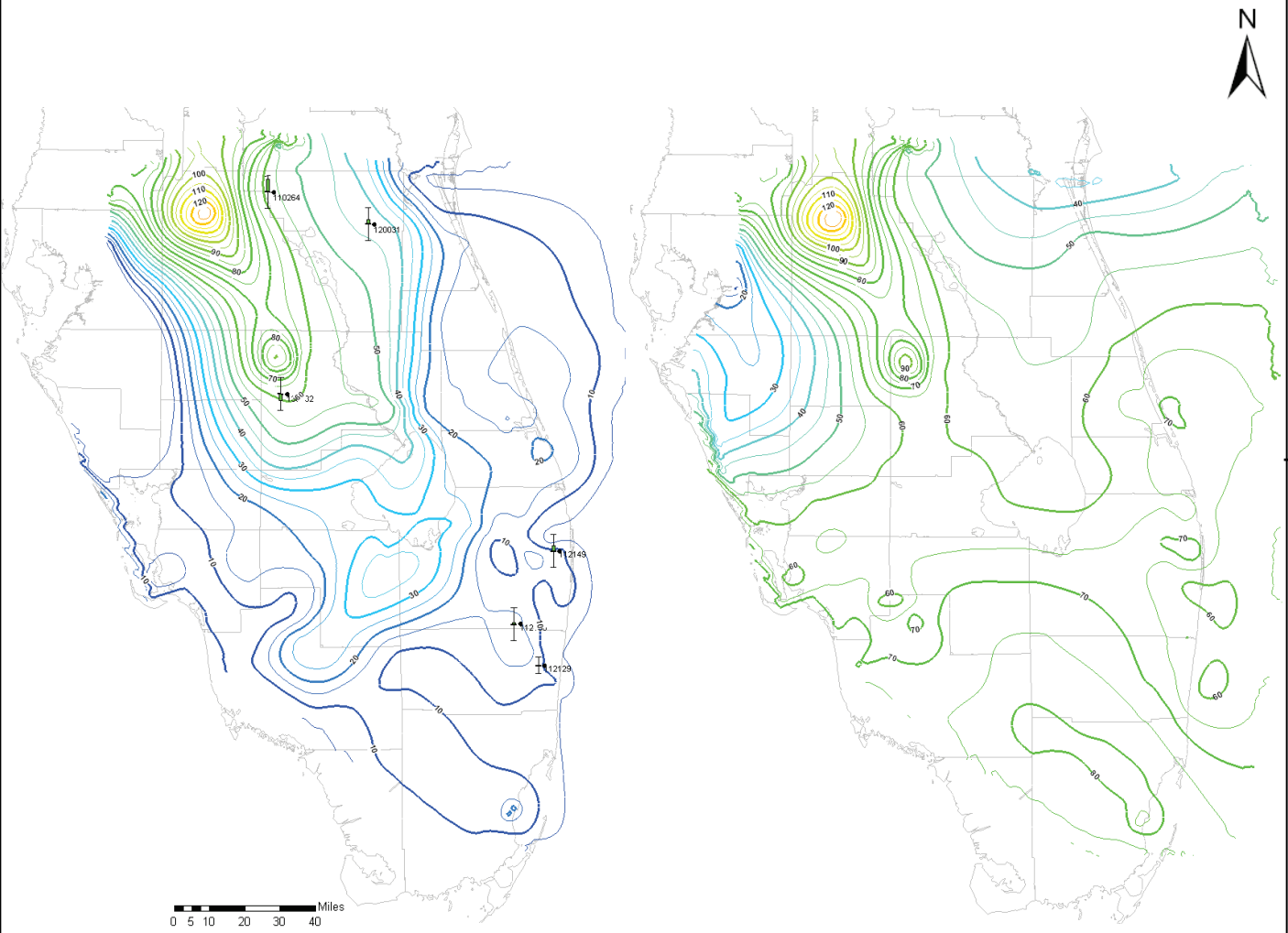

Model Calculated Head

Equivalent Freshwater Head

Legend:

Head (ft)

145
135
125
115
105
95
85
75
65
55
45
35
25
15
5

Notes:

Left figure is the October 2003 model calculated heads (observed heads) as output from the calibrated model. Calibration targets are provided to remind the reader of locations with good or poor calibration.

Right figure is a calculation of the equivalent freshwater head, created by applying Equation 2.2 to the model result in each cell of the model.

Equivalent Freshwater Head
Lower Floridan Aquifer - October 2003

Final Groundwater Model Calibration Report

Figure 4.158

October 2010

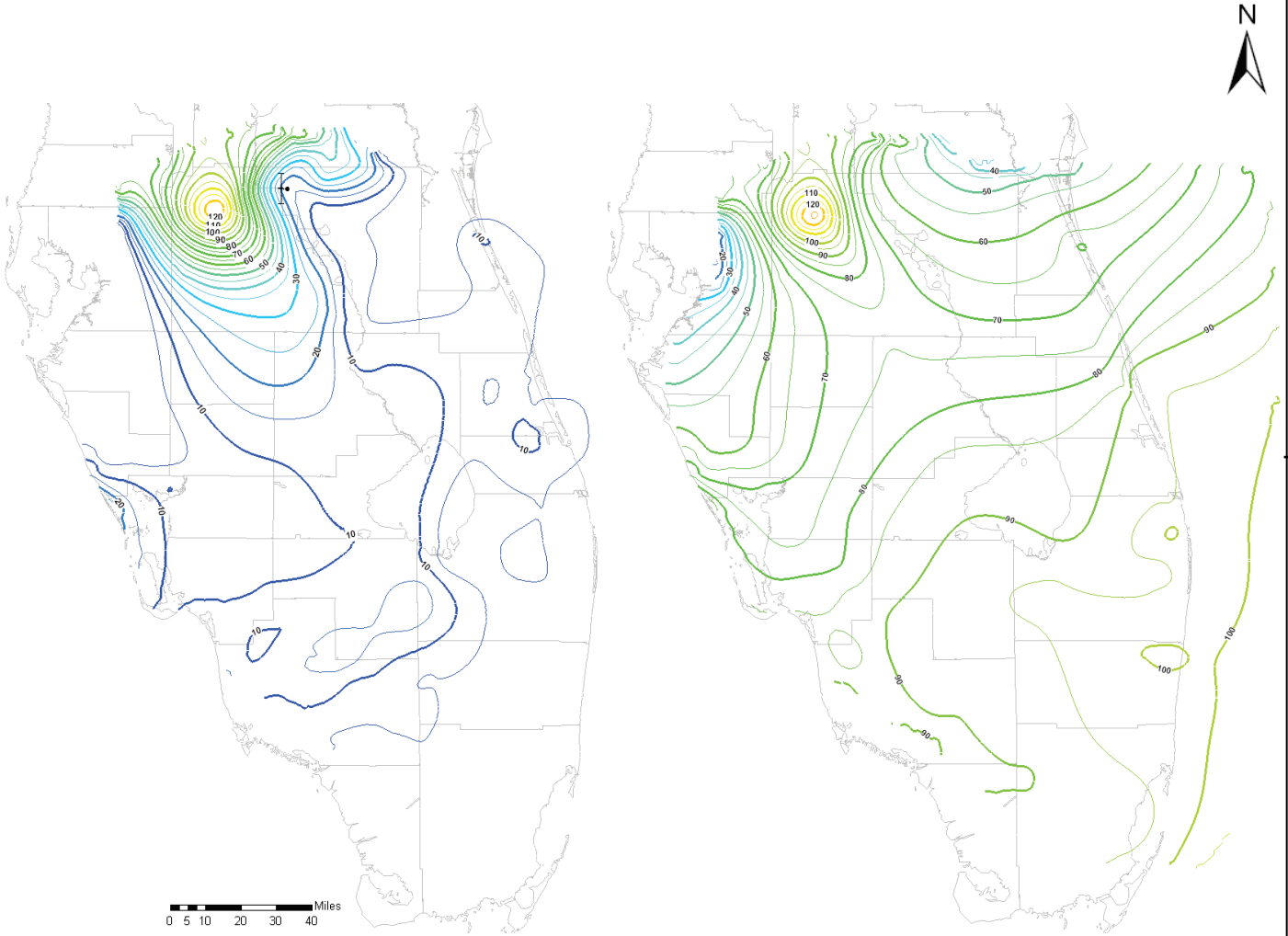

Model Calculated Head

Equivalent Freshwater Head

Legend:

Head (ft)

145
135
125
115
105
95
85
75
65
55
45
35
25
15
5

Notes:

Left figure is the October 2003 model calculated heads (observed heads) as output from the calibrated model. Calibration targets are provided to remind the reader of locations with good or poor calibration.

Right figure is a calculation of the equivalent freshwater head, created by applying Equation 2.2 to the model result in each cell of the model.

Equivalent Freshwater Head
Boulder Zone - October 2003

Final Groundwater Model Calibration Report

Figure 4.159

October 2010

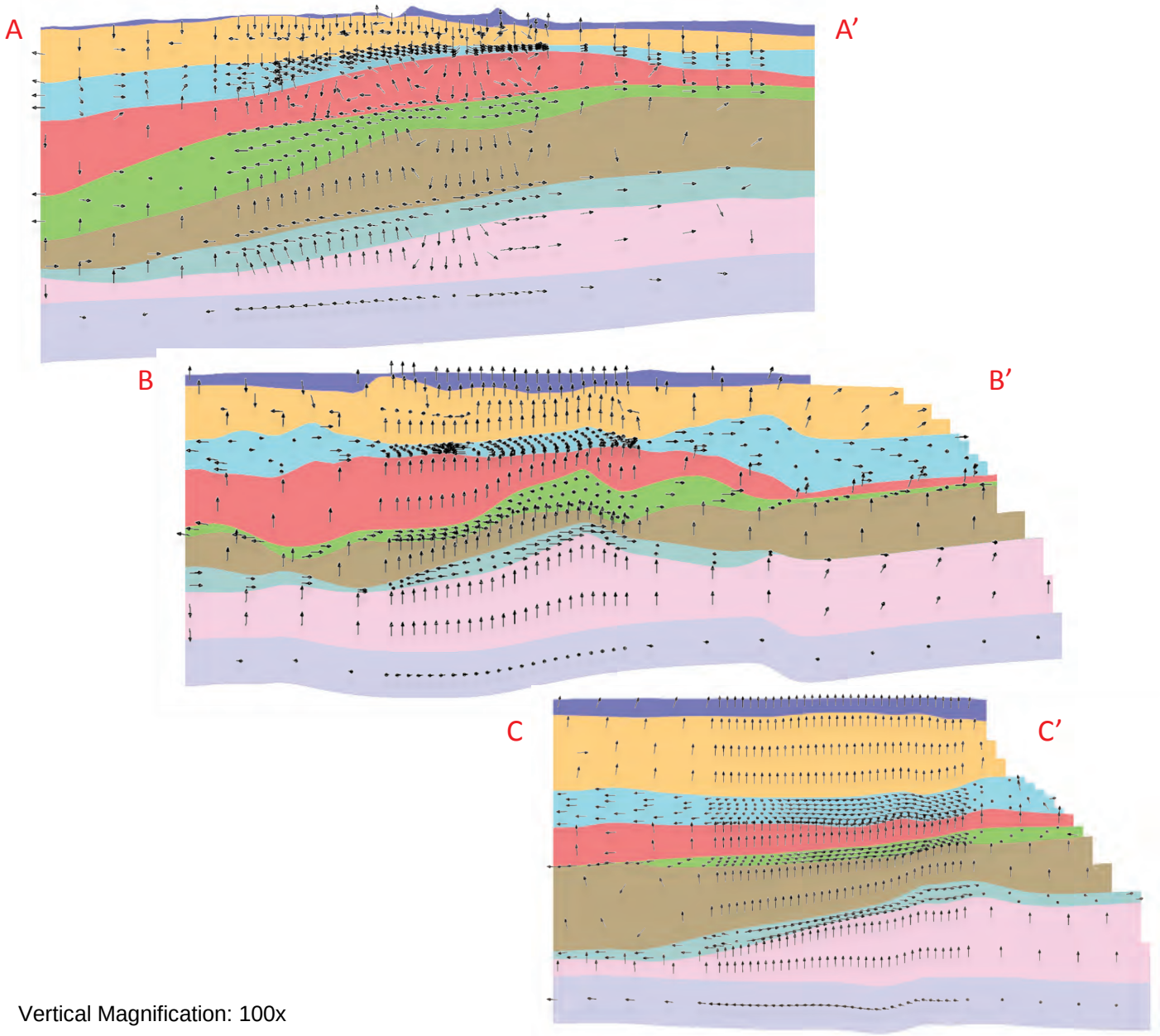

Vertical Magnification: 100x

Hydrogeologic Layers:

- SAS
- IAS
- UF
- MC1
- APPZ
- MC2
- LF1
- LC
- BZ

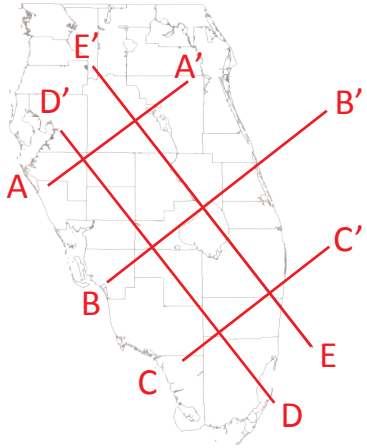

Notes:

These velocity vectors were calculated by dividing the flux vector components (from the MODFLOW cell-by-cell flow file, October 2003 steady state solution) by the area of the corresponding face of the grid cell.

Note that all vectors are the same length; those that seem shorter are pointed slightly into or out of the paper.

Vectors are printed for every sixth cell. Tight clustering of vectors indicates small cell sizes.

Model Results:
Discharge Velocity Vectors on Cross-Sections
Final Groundwater Model Calibration Report

Figure 4.160

October 2010

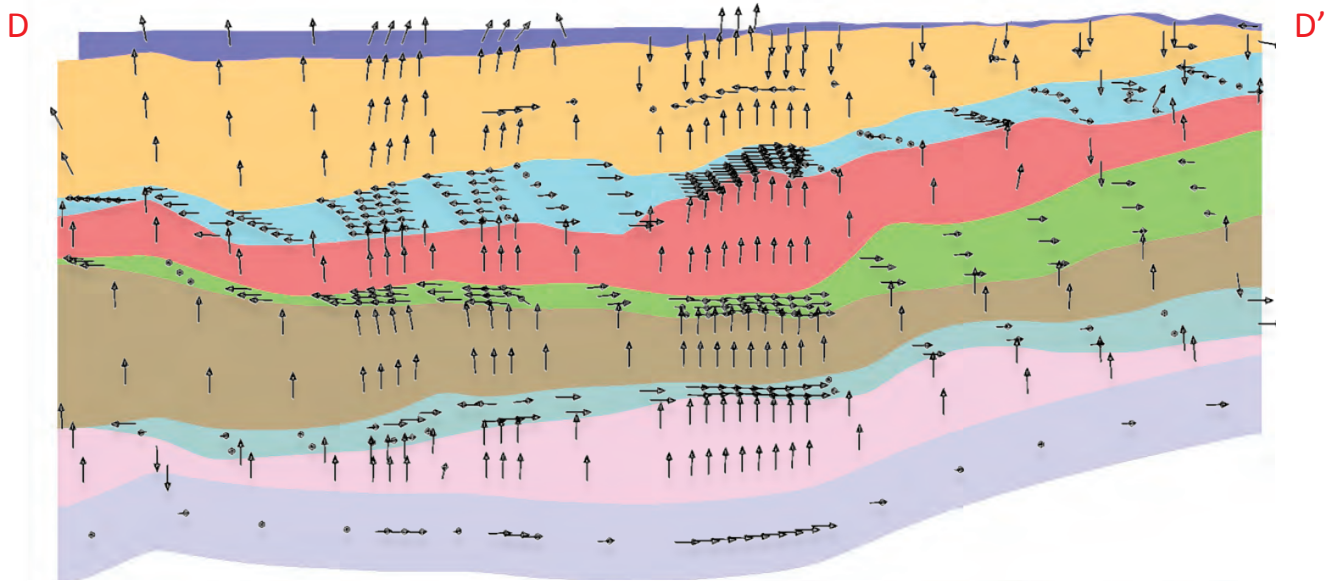

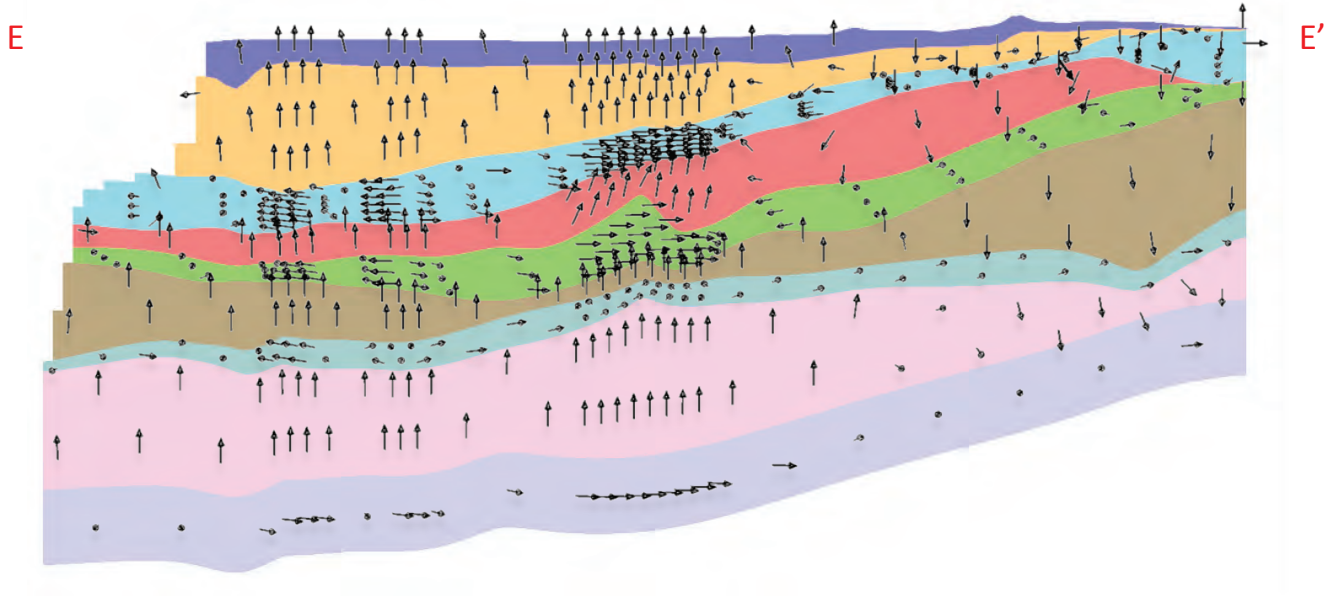

Vertical Magnification: 150x

Hydrogeologic Layers:

- SAS
- IAS
- UF
- MC1
- APPZ
- MC2
- LF1
- LC
- BZ

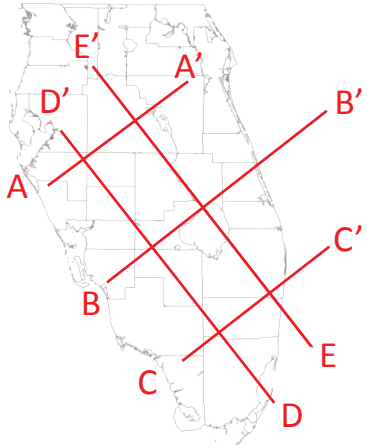

Notes:

These velocity vectors were calculated by dividing the flux vector components (from the MODFLOW cell-by-cell flow file, October 2003 steady state solution) by the area of the corresponding face of the grid cell.

Note that all vectors are the same length; those that seem shorter are pointed slightly into or out of the paper.

Vectors are printed for every sixth cell. Tight clustering of vectors indicates small cell sizes.

Model Results:
Discharge Velocity Vectors on Cross-Sections

Final Groundwater Model Calibration Report

Figure 4.161

October 2010

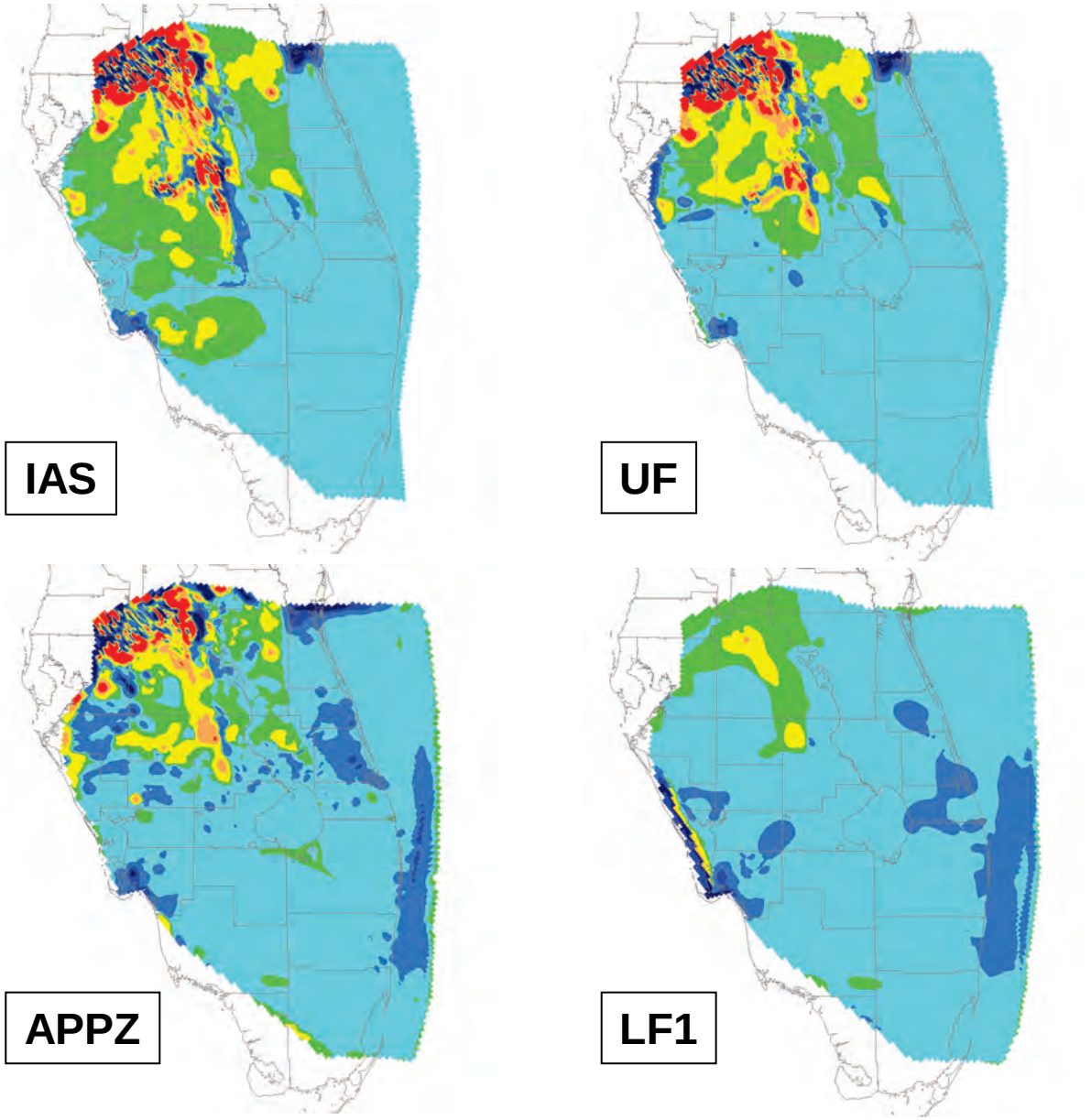

Discharge (in/yr):

- Greater than 10
- 5 - 10
- 1 - 5
- Less than 1

Recharge (in/yr):

- Less than 1
- 1 - 5
- 5 - 10
- Greater than 10

Notes:

These figures were created using the "Bottom" dataset in the MODFLOW cell-to-cell flow solution file corresponding to the bottom of the layer above the primary aquifer. The top of the primary aquifer is coincident with the bottom of the layer above it.

Discharge indicates upward flow; Recharge indicates downward flow.

The recharge and discharge results are from the October 2003 steady state solution.

Model Results: Recharge to and Discharge from the Top of the Primary Aquifers

Final Groundwater Model Calibration Report

Figure 4.162

October 2010

Northern Boundary		
Layer	Flow In (MGD)	Flow Out (MGD)
IAS	7.95	-43.78
UF	350.81	-1437.36
APPZ	343.80	-340.84
LF	100.30	-27.09
BZ	14.80	-109.51

Western Boundary		
Layer	Flow In (MGD)	Flow Out (MGD)
IAS	50.29	-7.49
UF	22.71	-64.87
APPZ	19.05	-832.03
LF	824.82	-60.23
BZ	179.90	-460.28

Atlantic Boundary		
Layer	Flow In (MGD)	Flow Out (MGD)
IAS	N/A	N/A
UF	3.54	-184.12
APPZ	3.70	-4.92
LF	10.60	-21.91
BZ	589.24	0.00

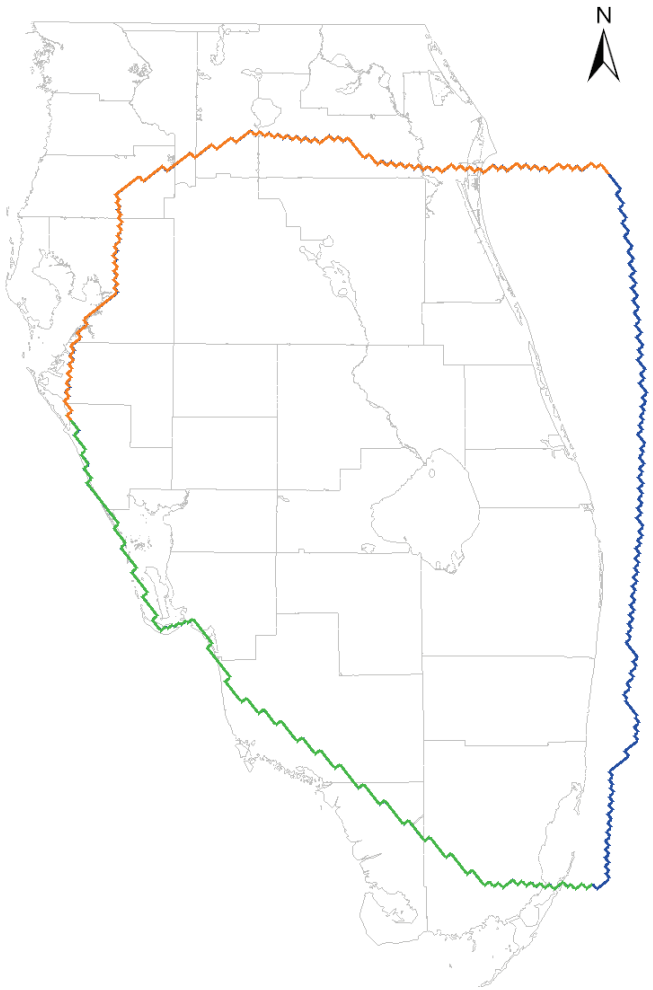

Legend:

- Northern Boundary
- Western Boundary
- Atlantic Boundary

Notes:

The tables list the flow into and out of the specified head boundary cells of the aquifers. The boundary was broken up into three zones, as shown in the legend.

The aquifer portion of the IAS only extends along part of the Northern and Western boundaries in layers 2 and 3. The remainder of the IAS is considered a confining unit and therefore was not included in the flows reported for the Northern and Western boundaries.

Flow rates are for the February 2004 Steady State model results.

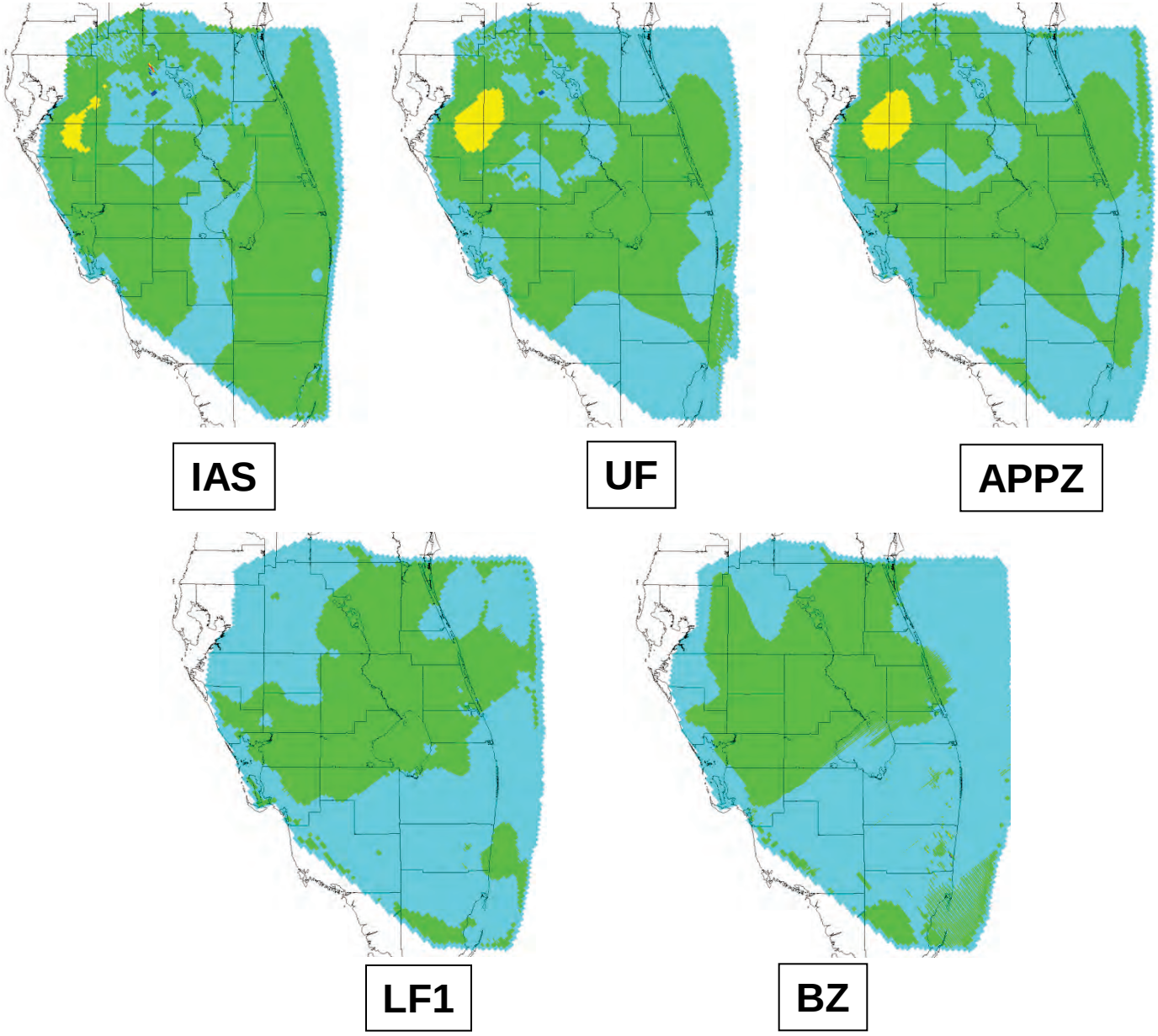

Notes:

Images were made by subtracting the heads calculated using the standard finite difference advection method with upstream weighting from the heads calculated by using the third-order TVD scheme.

Subtraction was made at every cell in the model for the timestep when the maximum differences were observed. This timestep corresponds to December 10, 2004.

Courant number was set to 1.0 for the TVD scheme.

Effect of TVD Advection Solution Technique
On the SEAWAT Model
Final Groundwater Model Calibration Report

Figure 5.1

October 2010

UF-Layer 10

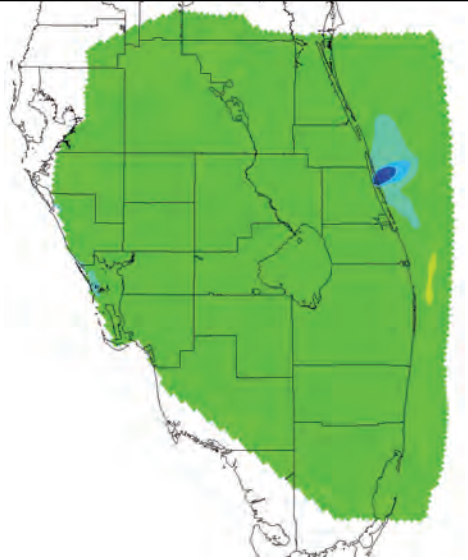

MC1-Layer 12

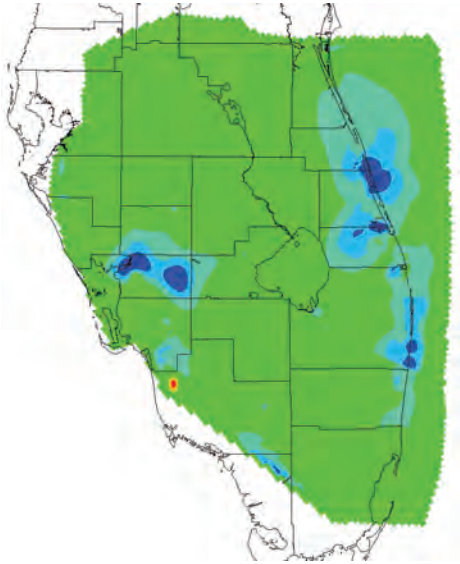

APPZ-Layer 15

Legend: Head difference in ft

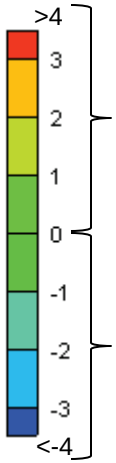

Dispersivity change caused an increase in the model solution.

Dispersivity change caused a decrease in the model solution.

Notes: The figures show the difference between the sensitivity solution and the calibrated model solution during the last timestep. The layers that were chosen to be shown have the maximum head change for each aquifer/confining unit they represent. The maximum head difference for each layer is listed in the table below.

Layer	Maximum Head Difference
UF-Layer 10	-3.1
MC1-Layer 12	-8.9
APPZ-Layer 15	-8.6

Dispersivity Sensitivity Analysis Run 1
Longitudinal Dispersivity = 25.0
Final Groundwater Model Calibration Report

Figure 5.2

October 2010

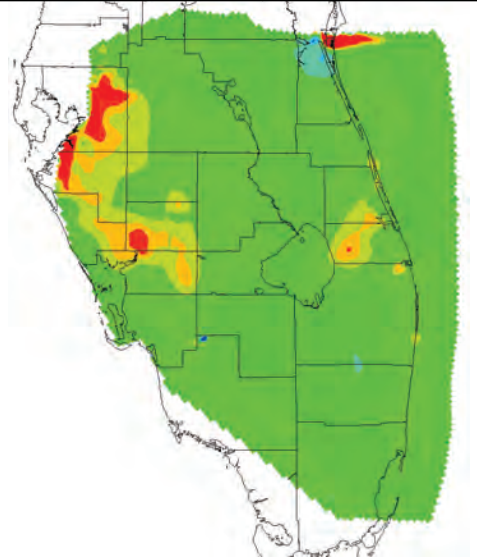

MC2-Layer 16

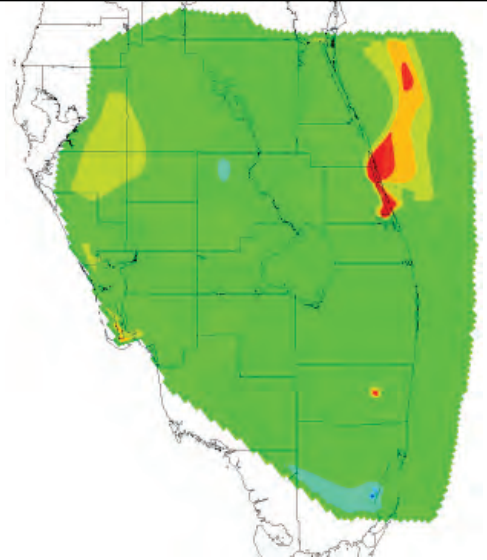

LF-Layer 19

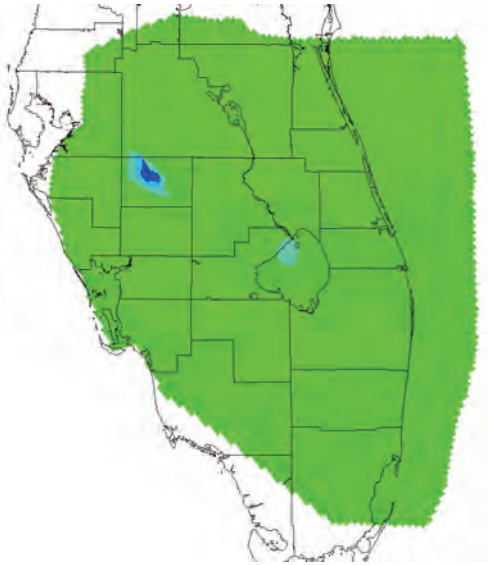

LC-Layer 21

BZ-Layer 22

Legend: Head difference in ft

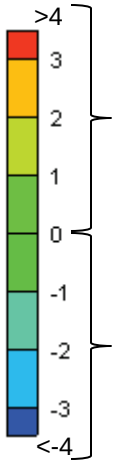

Dispersivity change caused an increase in the model solution.

Dispersivity change caused a decrease in the model solution.

Notes: The figures show the difference between the sensitivity solution and the calibrated model solution during the last timestep. The layers that were chosen to be shown have the maximum head change for each aquifer/confining unit they represent. The maximum head difference for each layer is listed in the table below.

Layer	Maximum Head Difference
MC2-Layer 16	10.3
LF-Layer 19	6.5
LC-Layer 21	-4.6
BZ-Layer 22	0.37

Dispersivity Sensitivity Analysis Run 1
Longitudinal Dispersivity = 25.0
Final Groundwater Model Calibration Report

Figure 5.3

October 2010

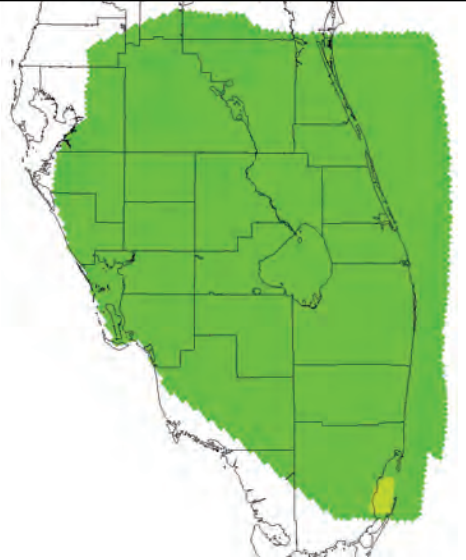

UF-Layer 10

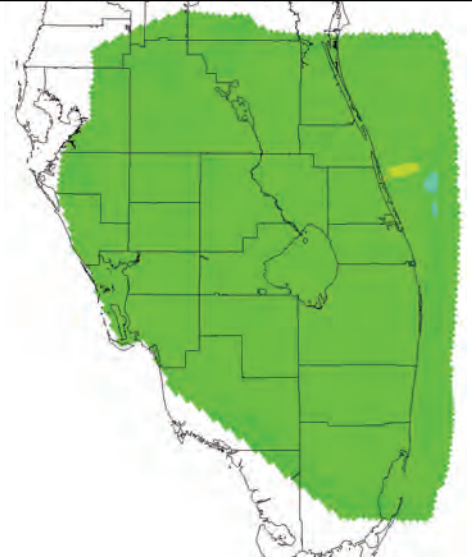

MC1-Layer 12

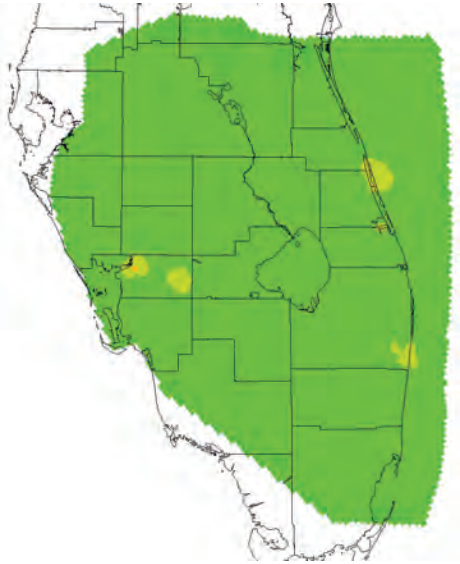

APPZ-Layer 15

Legend: Head difference in ft

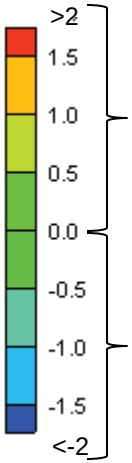

Dispersivity change caused an increase in the model solution.

Dispersivity change caused a decrease in the model solution.

Notes: The figures show the difference between the sensitivity solution and the calibrated model solution during the last timestep. The layers that were chosen to be shown have the maximum head change for each aquifer/confining unit they represent. The maximum head difference for each layer is listed in the table below.

Layer	Maximum Head Difference
UF-Layer 10	0.81
MC1-Layer 12	1.1
APPZ-Layer 15	1.1

Dispersivity Sensitivity Analysis Run 2
Longitudinal Dispersivity = 0.25
Final Groundwater Model Calibration Report

Figure 5.4

October 2010

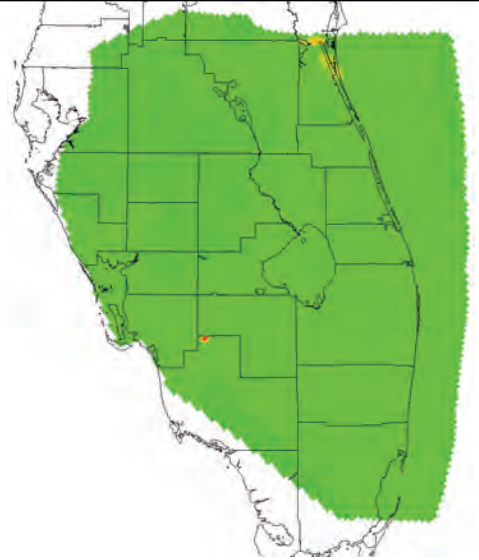

MC2-Layer 17

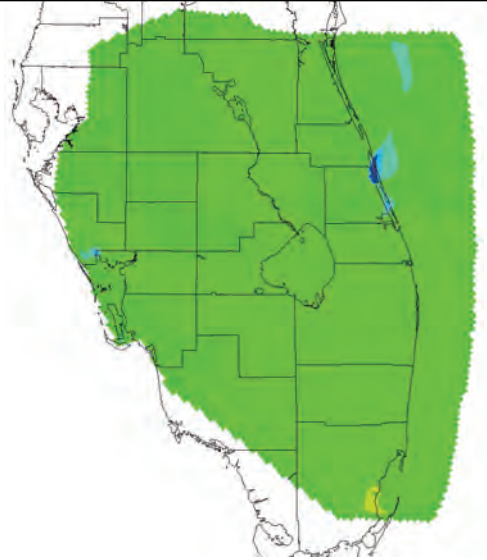

LF-Layer 19

LC-Layer 21

BZ-Layer 22

Legend: Head difference in ft

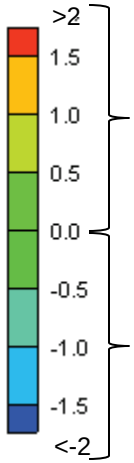

Notes: The figures show the difference between the sensitivity solution and the calibrated model solution during the last timestep. The layers that were chosen to be shown have the maximum head change for each aquifer/confining unit they represent. The maximum head difference for each layer is listed in the table below.

Layer	Maximum Head Difference
MC2-Layer 17	3.7
LF-Layer 19	-2.8
LC-Layer 21	0.5
BZ-Layer 22	0.04

Dispersivity Sensitivity Analysis Run 2
Longitudinal Dispersivity = 0.25
Final Groundwater Model Calibration Report

Figure 5.5

October 2010

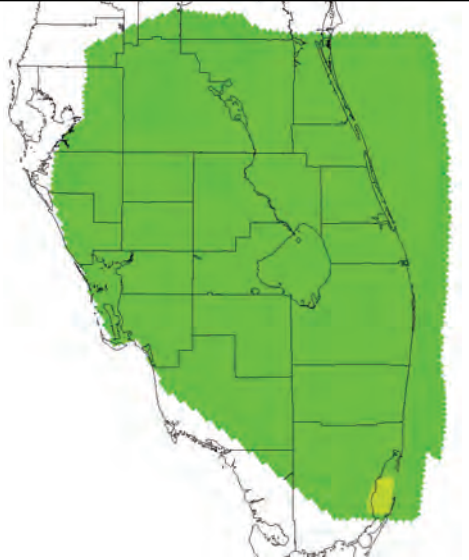

UF-Layer 10

MC1-Layer 12

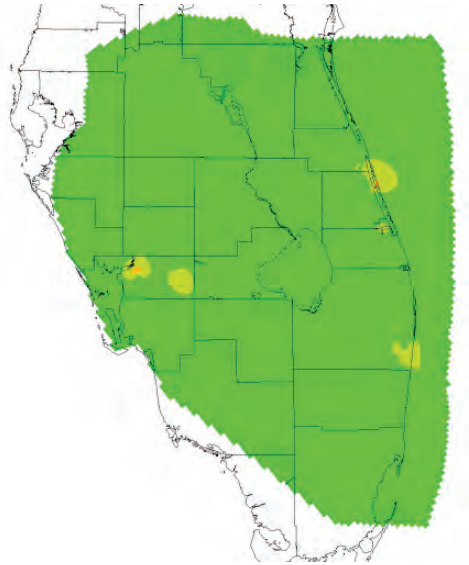

APPZ-Layer 15

Legend: Head difference in ft

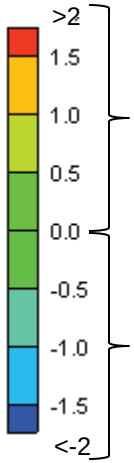

Dispersivity change caused an increase in the model solution.

Dispersivity change caused a decrease in the model solution.

Notes:

The figures show the difference between the sensitivity solution and the calibrated model solution during the last timestep. The layers that were chosen to be shown have the maximum head change for each aquifer/confining unit they represent. The maximum head difference for each layer is listed in the table below.

Ratio of Horizontal Transverse Dispersivity to Longitudinal Dispersivity = 0.5
Ratio of Vertical Transverse Dispersivity to Longitudinal Dispersivity = 0.05

Layer	Maximum Head Difference
UF-Layer 10	0.9
MC1-Layer 12	1.0
APPZ-Layer 15	1.1

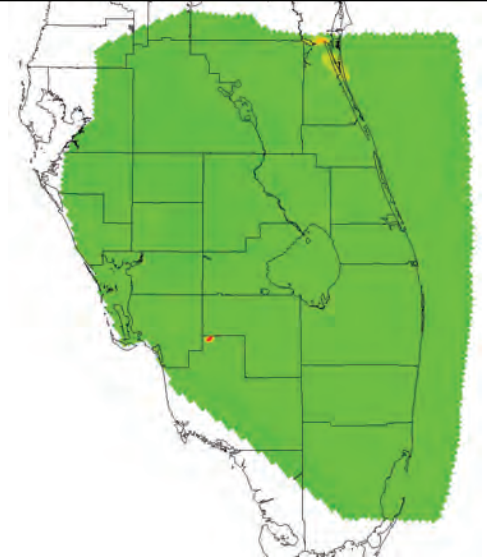

MC2-Layer 17

LF-Layer 19

LC-Layer 21

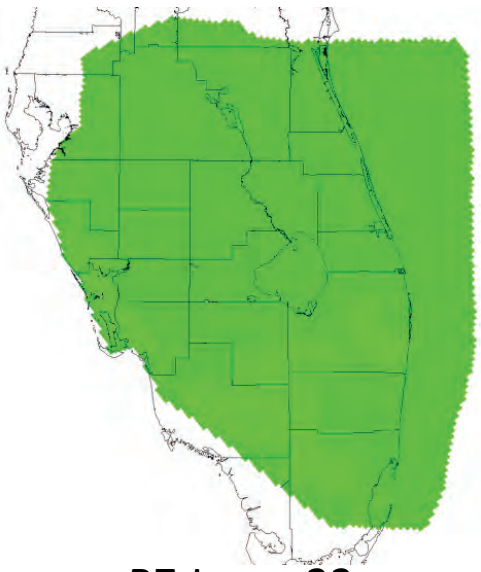

BZ-Layer 22

Legend: Head difference in ft

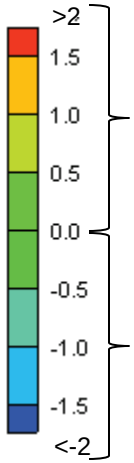

Dispersivity change caused an increase in the model solution.

Dispersivity change caused a decrease in the model solution.

Notes:
The figures show the difference between the sensitivity solution and the calibrated model solution during the last timestep. The layers that were chosen to be shown have the maximum head change for each aquifer/confining unit they represent. The maximum head difference for each layer is listed in the table below.

Ratio of Horizontal Transverse Dispersivity to Longitudinal Dispersivity = 0.5
Ratio of Vertical Transverse Dispersivity to Longitudinal Dispersivity = 0.05

Layer	Maximum Head Difference
MC2-Layer 17	4.0
LF-Layer 19	-3.0
LC-Layer 21	0.5
BZ-Layer 22	-0.05

Dispersivity Sensitivity Analysis Run 3

Final Groundwater Model Calibration Report

Figure 5.7

October 2010

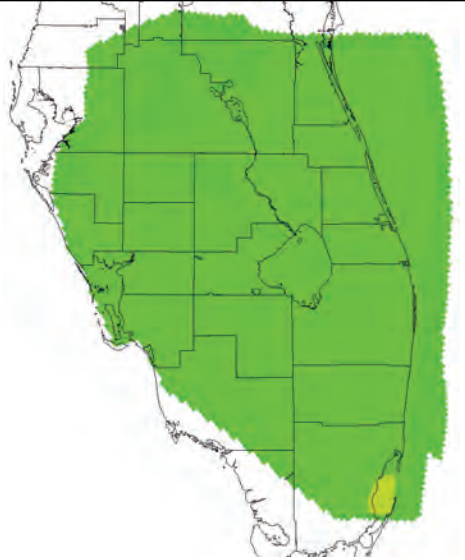

UF-Layer 10

MC1-Layer 12

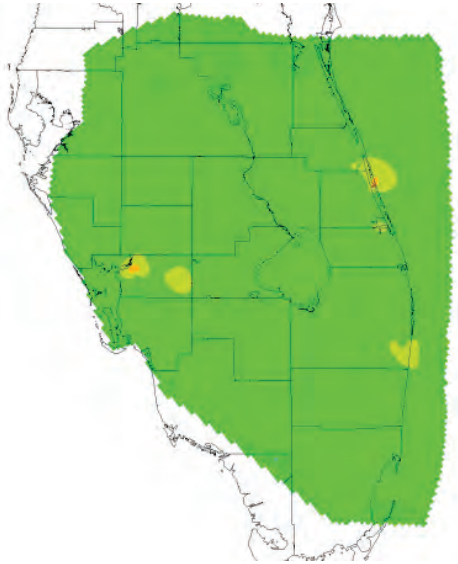

APPZ-Layer 15

Legend: Head difference in ft

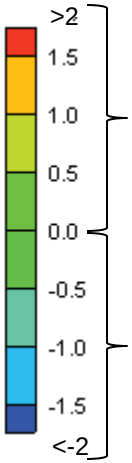

Dispersivity change caused an increase in the model solution.

Dispersivity change caused a decrease in the model solution.

Notes:
The figures show the difference between the sensitivity solution and the calibrated model solution during the last timestep. The layers that were chosen to be shown have the maximum head change for each aquifer/confining unit they represent. The maximum head difference for each layer is listed in the table below.

Ratio of Horizontal Transverse Dispersivity to Longitudinal Dispersivity = 0.1
Ratio of Vertical Transverse Dispersivity to Longitudinal Dispersivity = 0.01

Layer	Maximum Head Difference
UF-Layer 10	0.9
MC1-Layer 12	1.0
APPZ-Layer 15	1.2

Dispersivity Sensitivity Analysis Run 4

Final Groundwater Model Calibration Report

Figure 5.8

October 2010

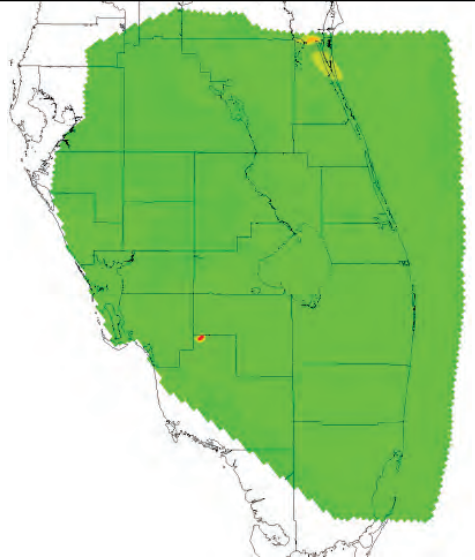

MC2-Layer 17

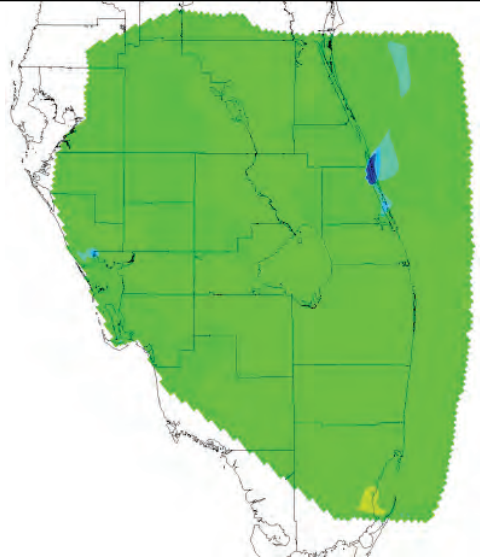

LF-Layer 19

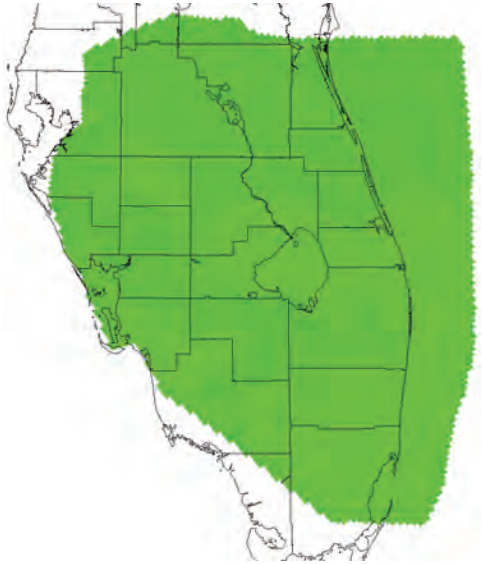

LC-Layer 21

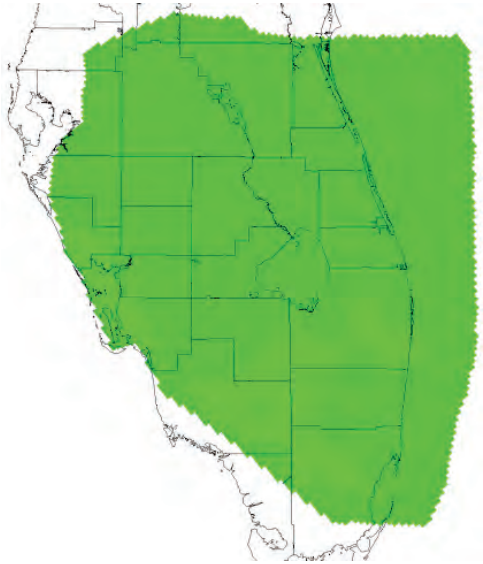

BZ-Layer 22

Legend: Head difference in ft

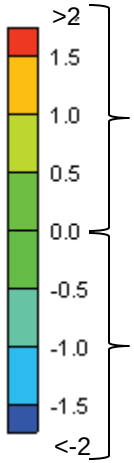

Dispersivity change caused an increase in the model solution.

Dispersivity change caused a decrease in the model solution.

Notes:
The figures show the difference between the sensitivity solution and the calibrated model solution during the last timestep. The layers that were chosen to be shown have the maximum head change for each aquifer/confining unit they represent. The maximum head difference for each layer is listed in the table below.

Ratio of Horizontal Transverse Dispersivity to Longitudinal Dispersivity = 0.1
Ratio of Vertical Transverse Dispersivity to Longitudinal Dispersivity = 0.01

Layer	Maximum Head Difference
MC2-Layer 17	4.2
LF-Layer 19	-3.2
LC-Layer 21	0.5
BZ-Layer 22	-0.05

Dispersivity Sensitivity Analysis Run 4

Final Groundwater Model Calibration Report

Figure 5.9

October 2010

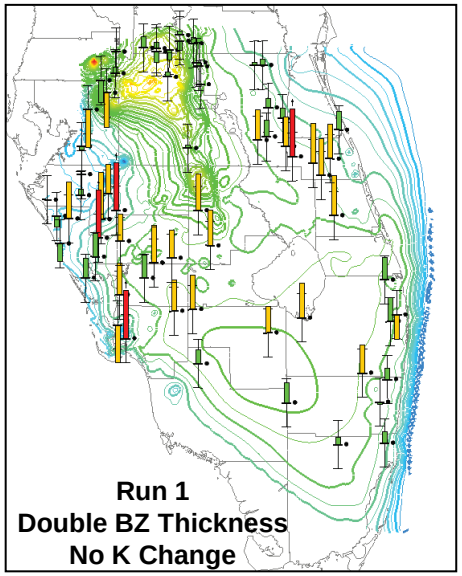

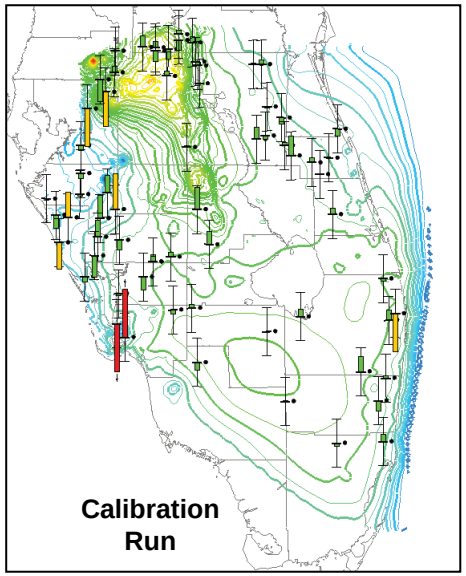

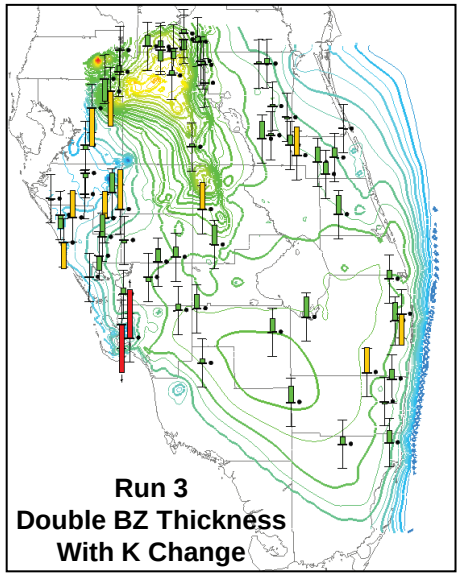

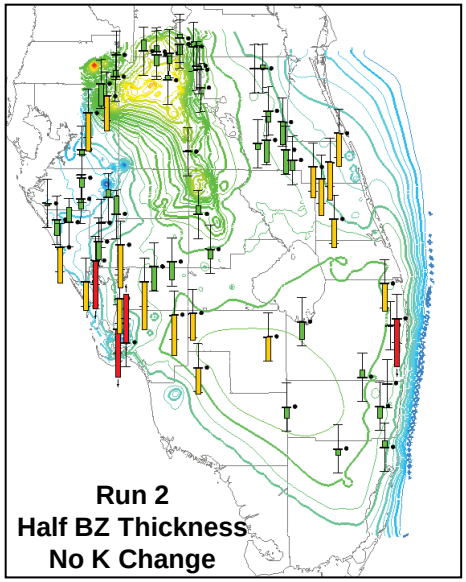

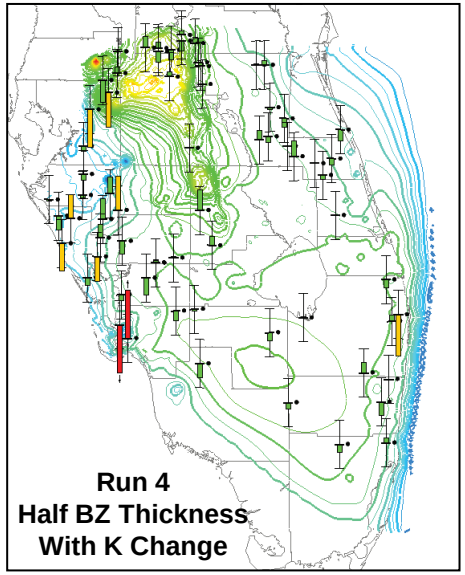

Head (ft)

170
155
140
125
110
95
80
65
50
35
20
5
-10
-25

Notes:

This figure shows the UF steady state February 2004 solution and calibration for the calibration run and four sensitivity runs which analyzed the effect of Boulder Zone thickness and conductivity on the results. Descriptions of these sensitivity runs are available in Section 5.4.

Calibration targets are green when the calculated value is within 2 feet of the measured head, yellow when within 4 feet and red when the model calculates a head more than 4 feet different from the measured value.

The direction of the colored bar on the calibration target indicates the sign on the residual: bars above the middle line indicate the model calculated higher heads than measured; bars below the middle line indicate negative residuals.

Effect of Boulder Zone Thickness
on Upper Floridan Calibration (SEAWAT)
Final Groundwater Model Calibration Report

Figure 5.10

October 2010

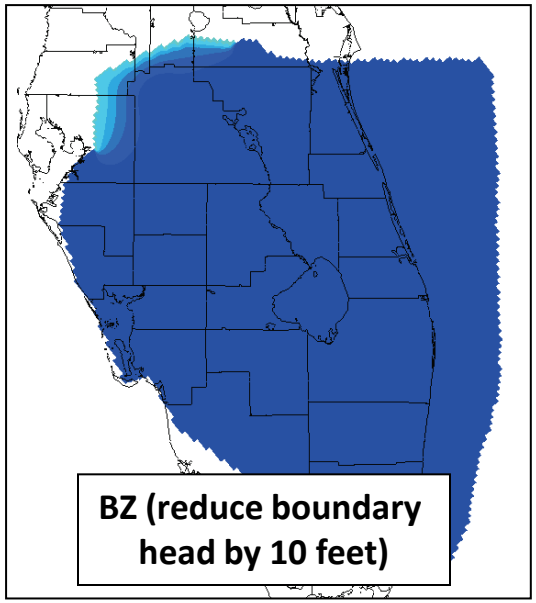

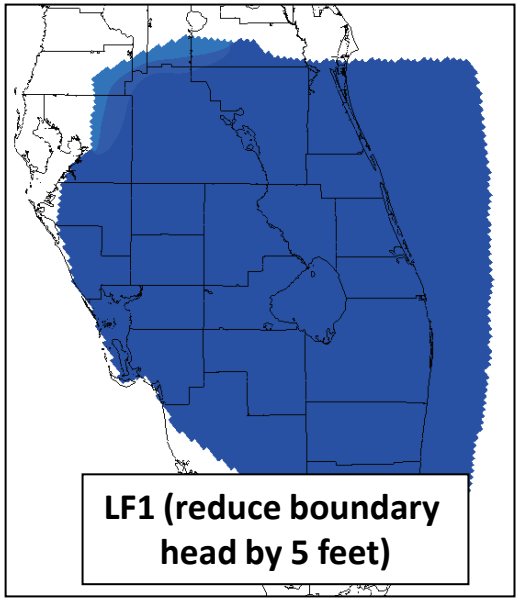

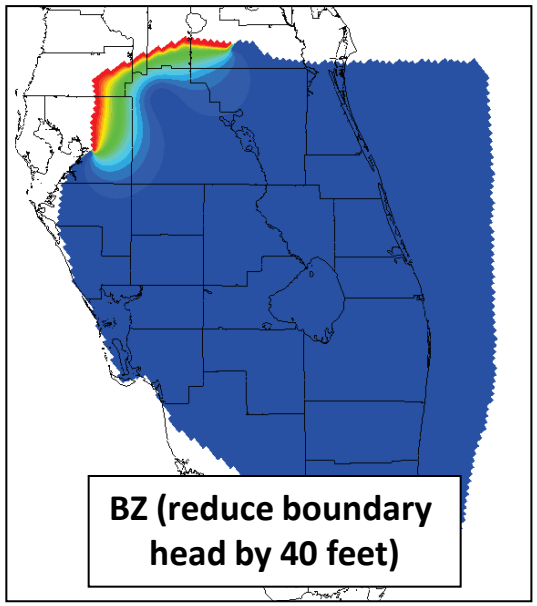

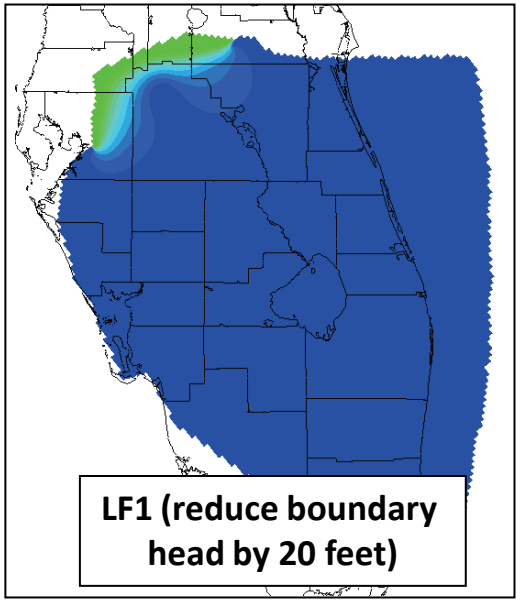

Head Difference (ft)

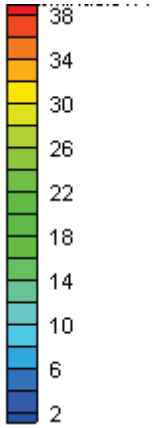

Notes:

The setup of this sensitivity run is described in detail in Section 5.6.1 of this report. Specified heads along the northwest boundary were reduced in the LF1 and BZ layers by the amounts indicated.

The effects on the resulting head solution are shown as the difference between the calibrated head solution and the sensitivity run solution.

No discernible effects were noted in other aquifers.

Head Difference as a Result of North Boundary Specified Head Change

Final Groundwater Model Calibration Report

Figure 5.11

October 2010

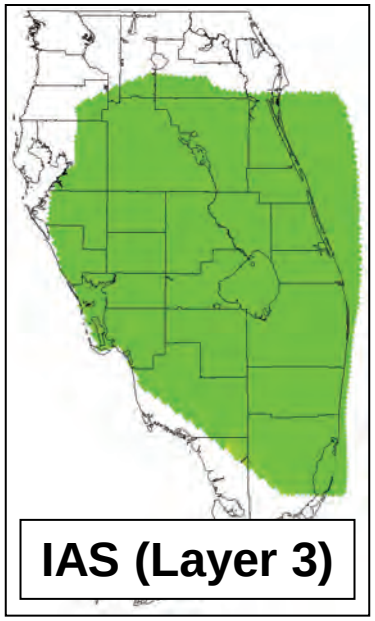

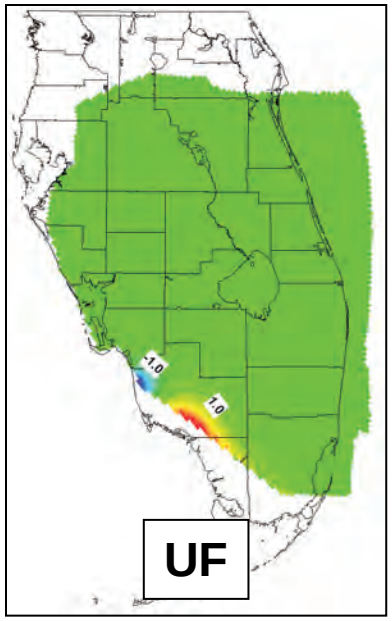

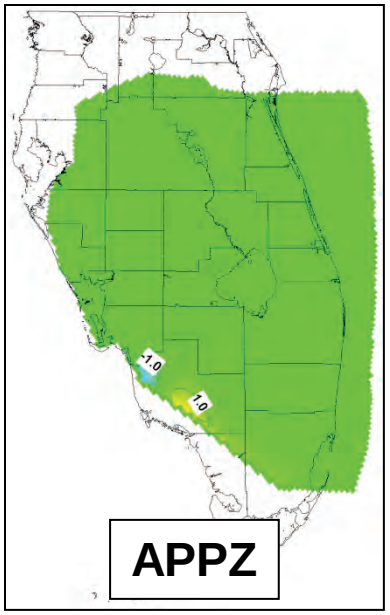

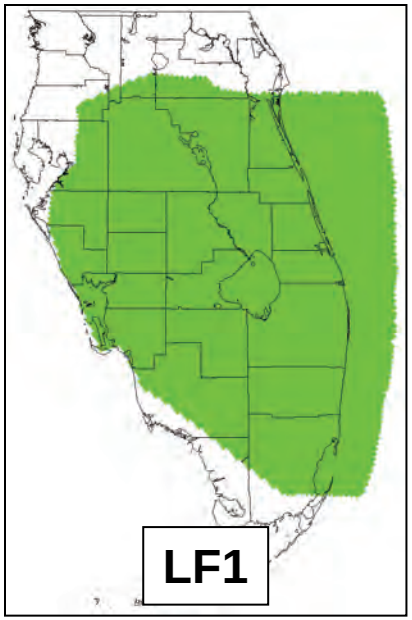

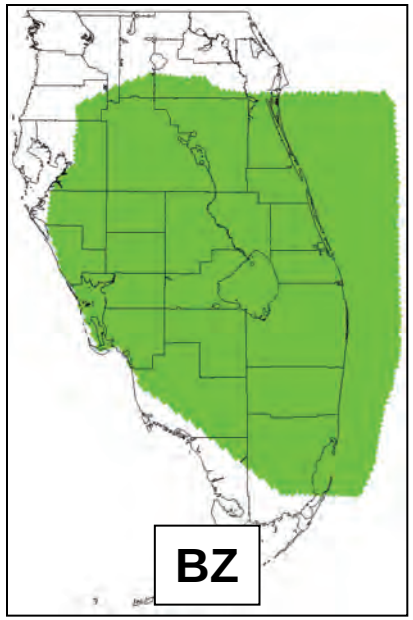

Head Difference (ft)

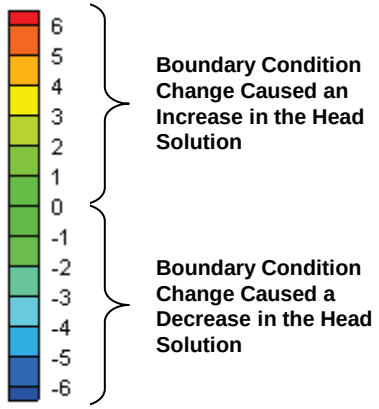

Notes:

The setup of this sensitivity run is described in detail in Section 5.6.2 of this report. Specified heads along the boundary through Everglades National Park in the Upper Floridan aquifer were removed, resulting in a no-flow condition at the boundary.

The effects on the resulting head solution are shown as the difference between the calibrated head solution and the sensitivity run solution.

SEAWAT Head Difference as a Result of Southwest Boundary (Upper Floridan) Specified Head Change

Final Groundwater Model Calibration Report

Figure 5.12

October 2010

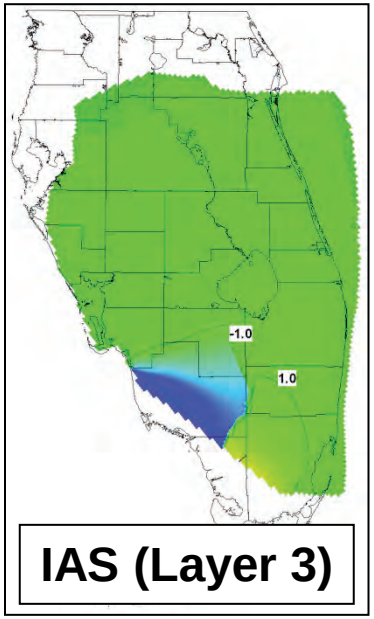

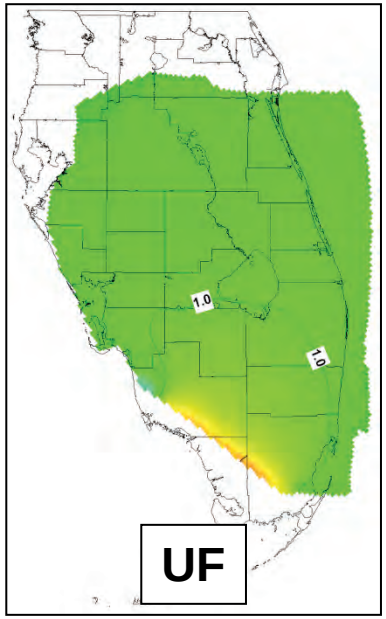

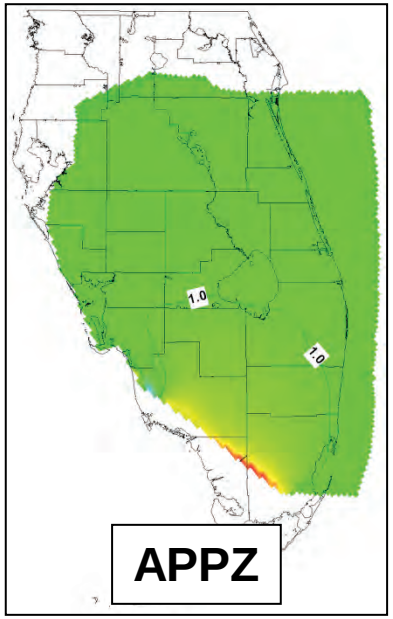

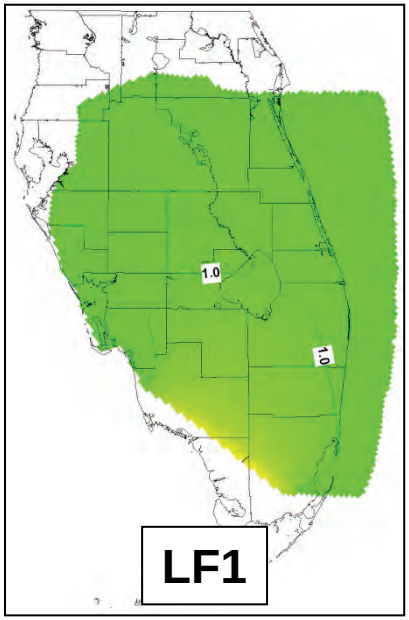

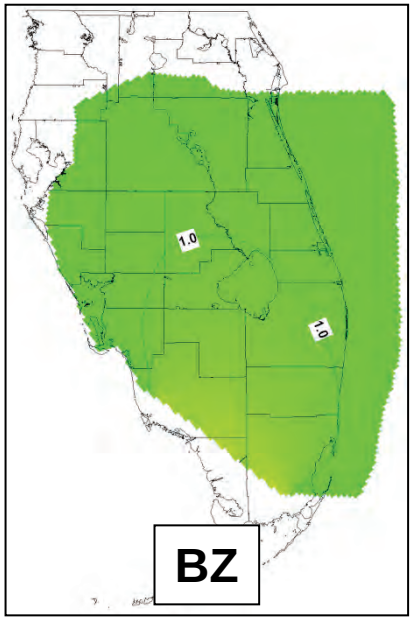

Head Difference (ft)

20
18
14
10
6
2
-2
-6
-10
-14
-18
<-20

Boundary Condition Change Caused an Increase in the Head Solution

Boundary Condition Change Caused a Decrease in the Head Solution

Notes:

The setup of this sensitivity run is described in detail in Section 5.6.2 of this report. Specified heads along the boundary through Everglades National Park in all aquifers were removed, resulting in a no-flow condition at the boundary.

The effects on the resulting head solution are shown as the difference between the calibrated head solution and the sensitivity run solution.

SEAWAT Head Difference as a Result of Southwest Boundary (All Aquifers) Specified Head Change

Final Groundwater Model Calibration Report

Figure 5.13

October 2010

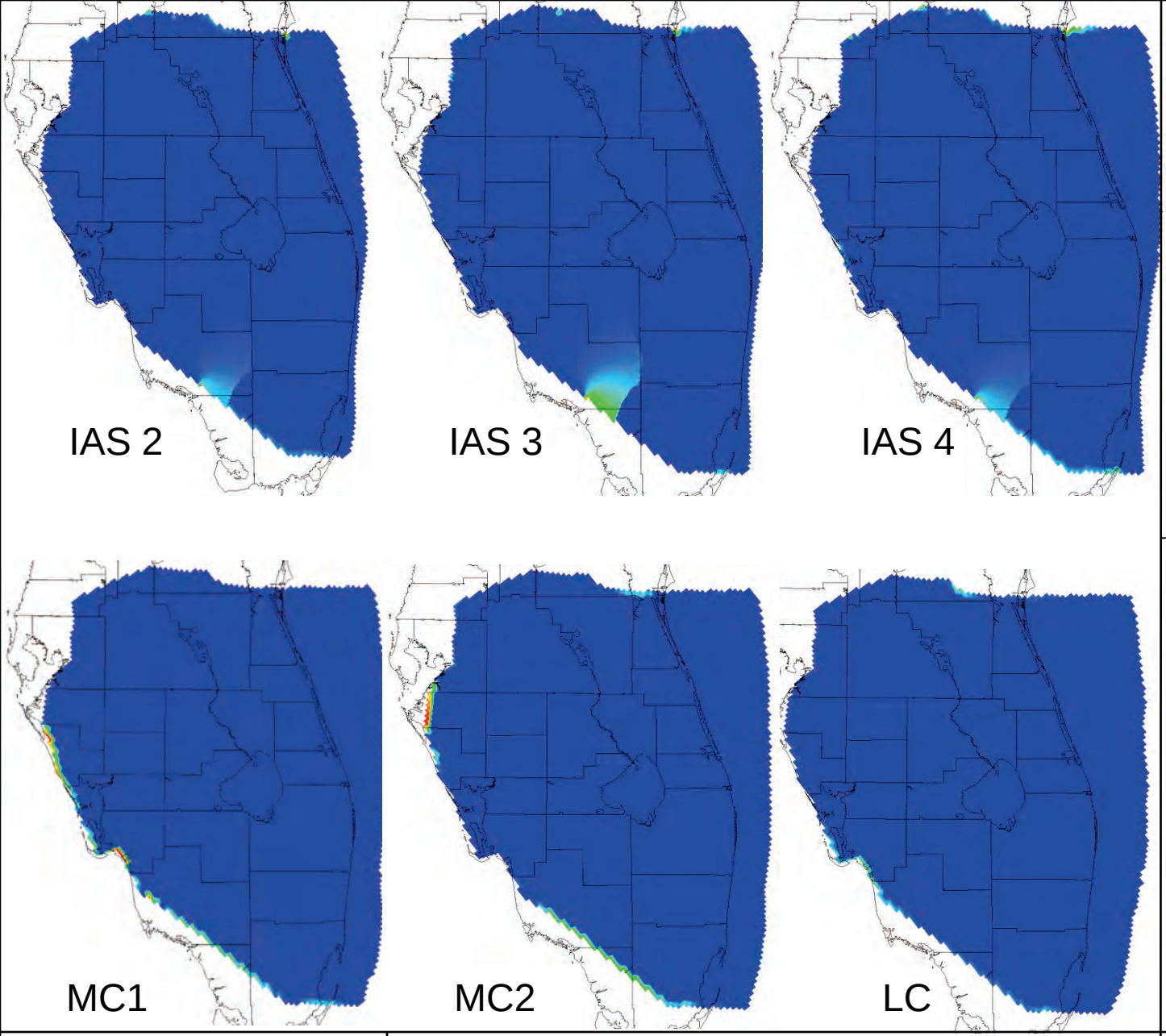

Difference in head (ft)

23
21
19
17
15
13
11
9
7
5
3
1

Notes:

The figures show the difference in head when the calibrated model (with a no-flow boundary condition in the confining units) is compared to the sensitivity which assigned a specified head to the boundary in all layers.

Confining Unit Boundary Sensitivity Analysis

Final Groundwater Model Calibration Report

Figure 5.14

October 2010

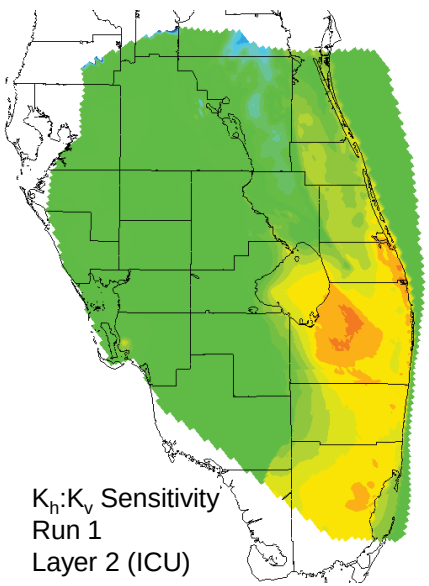

K_h:K_v Sensitivity
Run 1
Layer 2 (ICU)

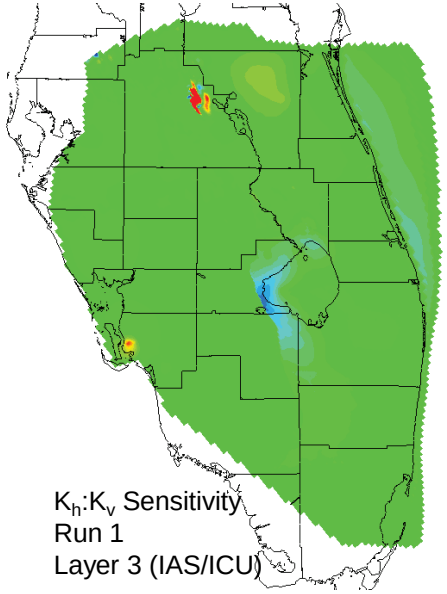

K_h:K_v Sensitivity
Run 1
Layer 3 (IAS/ICU)

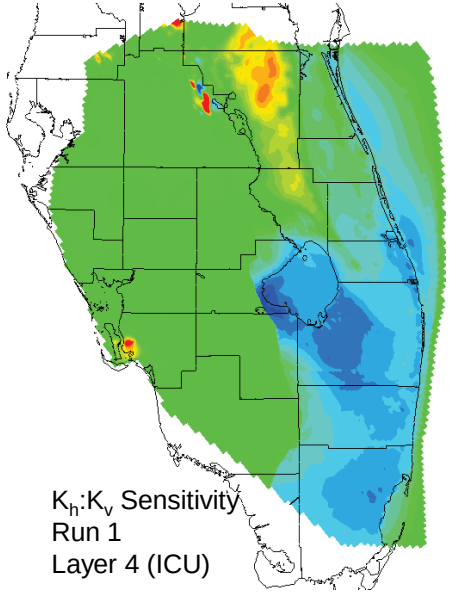

K_h:K_v Sensitivity
Run 1
Layer 4 (ICU)

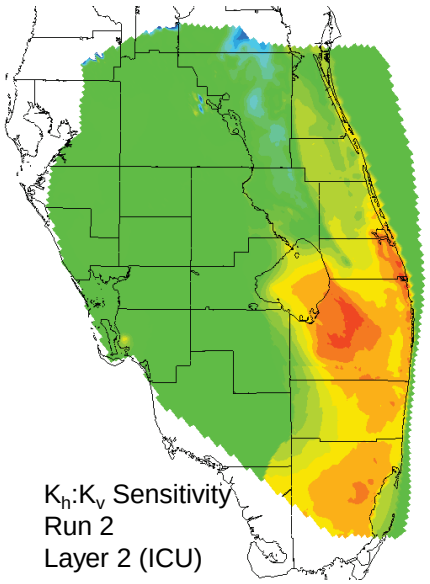

K_h:K_v Sensitivity
Run 2
Layer 2 (ICU)

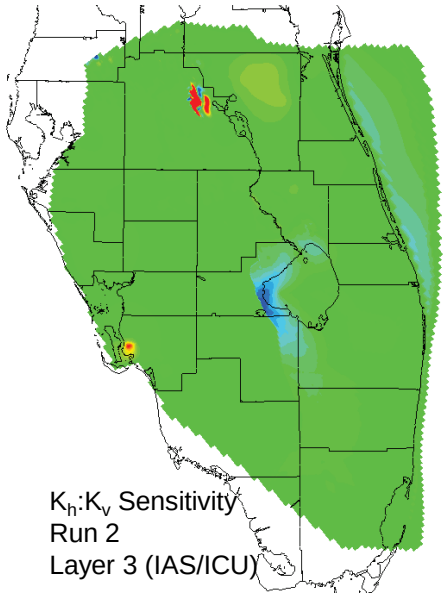

K_h:K_v Sensitivity
Run 2
Layer 3 (IAS/ICU)

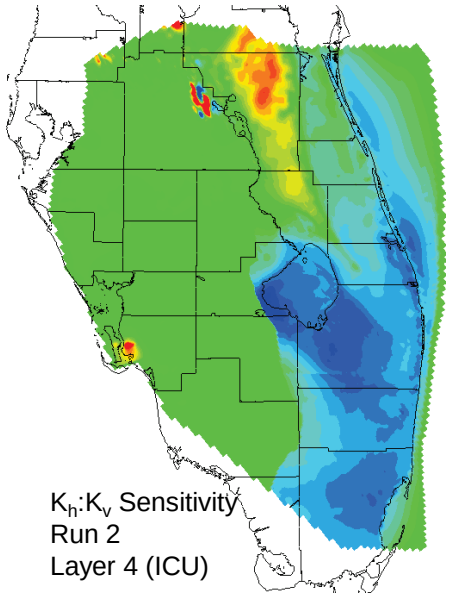

K_h:K_v Sensitivity
Run 2
Layer 4 (ICU)

Head Change Due to K_h:K_v Ratio Changes (ft)

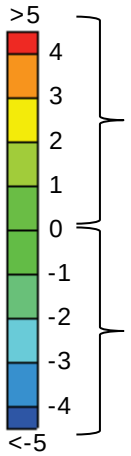

Change in ratio resulted an increase in model calculated head

Change in ratio resulted a decrease in model calculated head

Notes:

The figures show the difference in head when the calibrated model is compared to the sensitivity run which altered the ratio of horizontal to vertical hydraulic conductivity. Head differences were calculated using the February 2004 model.

Horizontal to Vertical Conductivity Ratio Sensitivities Layer 2-4 (IAS/ICU)

Final Groundwater Model Calibration Report

Figure 5.15

October 2010

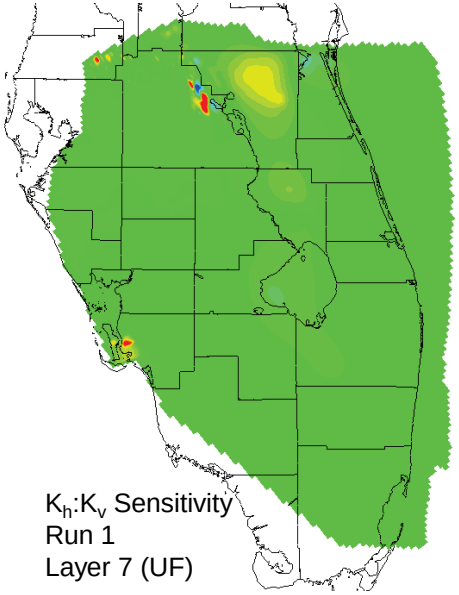

K_h:K_v Sensitivity
Run 1
Layer 7 (UF)

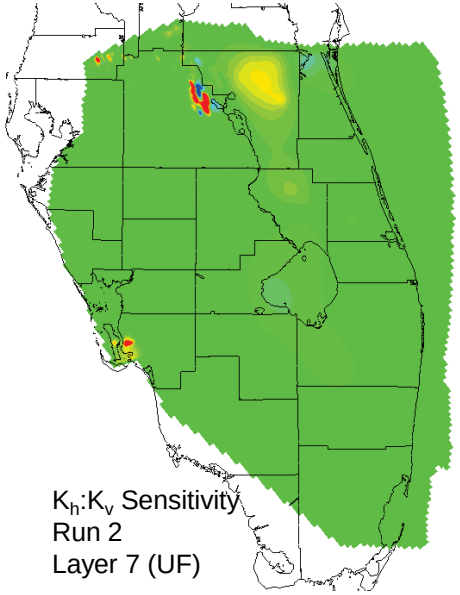

K_h:K_v Sensitivity
Run 2
Layer 7 (UF)

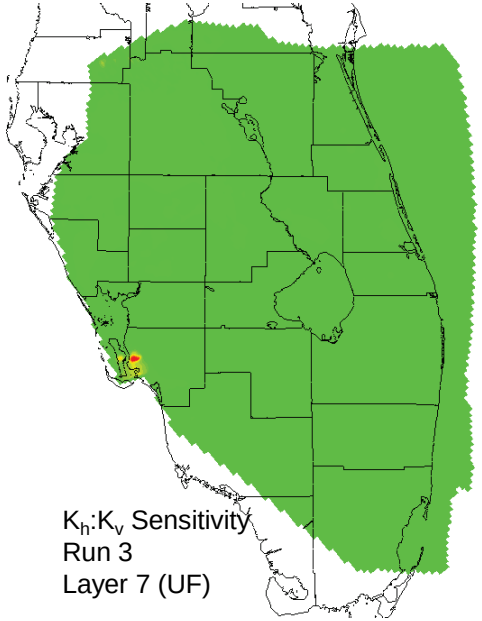

K_h:K_v Sensitivity
Run 3
Layer 7 (UF)

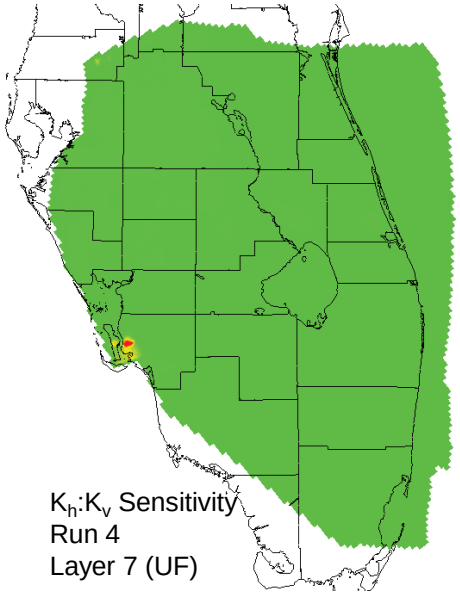

K_h:K_v Sensitivity
Run 4
Layer 7 (UF)

Head Change Due to K_h:K_v Ratio Changes (ft)

>5
4
3
2
1
0
-1
-2
-3
-4
<-5

Change in ratio resulted an increase in model calculated head

Change in ratio resulted a decrease in model calculated head

Notes:

The figures show the difference in head when the calibrated model is compared to the sensitivity run which altered the ratio of horizontal to vertical hydraulic conductivity. Head differences were calculated using the February 2004 model.

Horizontal to Vertical Conductivity Ratio Sensitivities (UF)

Final Groundwater Model Calibration Report

Figure 5.16

October 2010

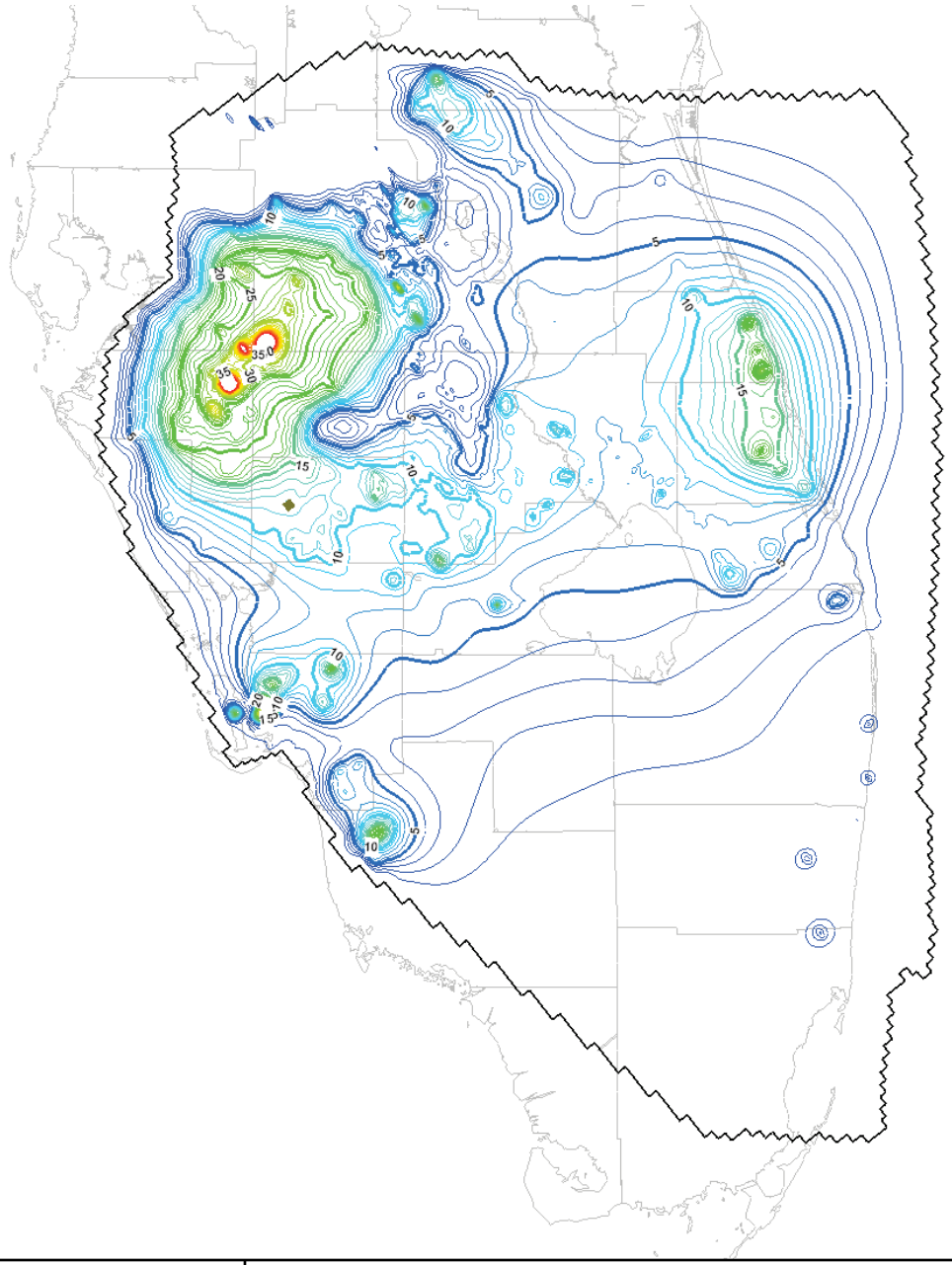

Notes:
Plots show the difference (drawdown) between the SEAWAT February 2004 calibration results and the corresponding simulation with no pumping

Contours are for the Upper Floridan Aquifer

Contour interval is 1 ft

UF Pumping Drawdown
(SEAWAT-February 2004)

Final Groundwater Model Calibration Report

Figure 6.1

October 2010

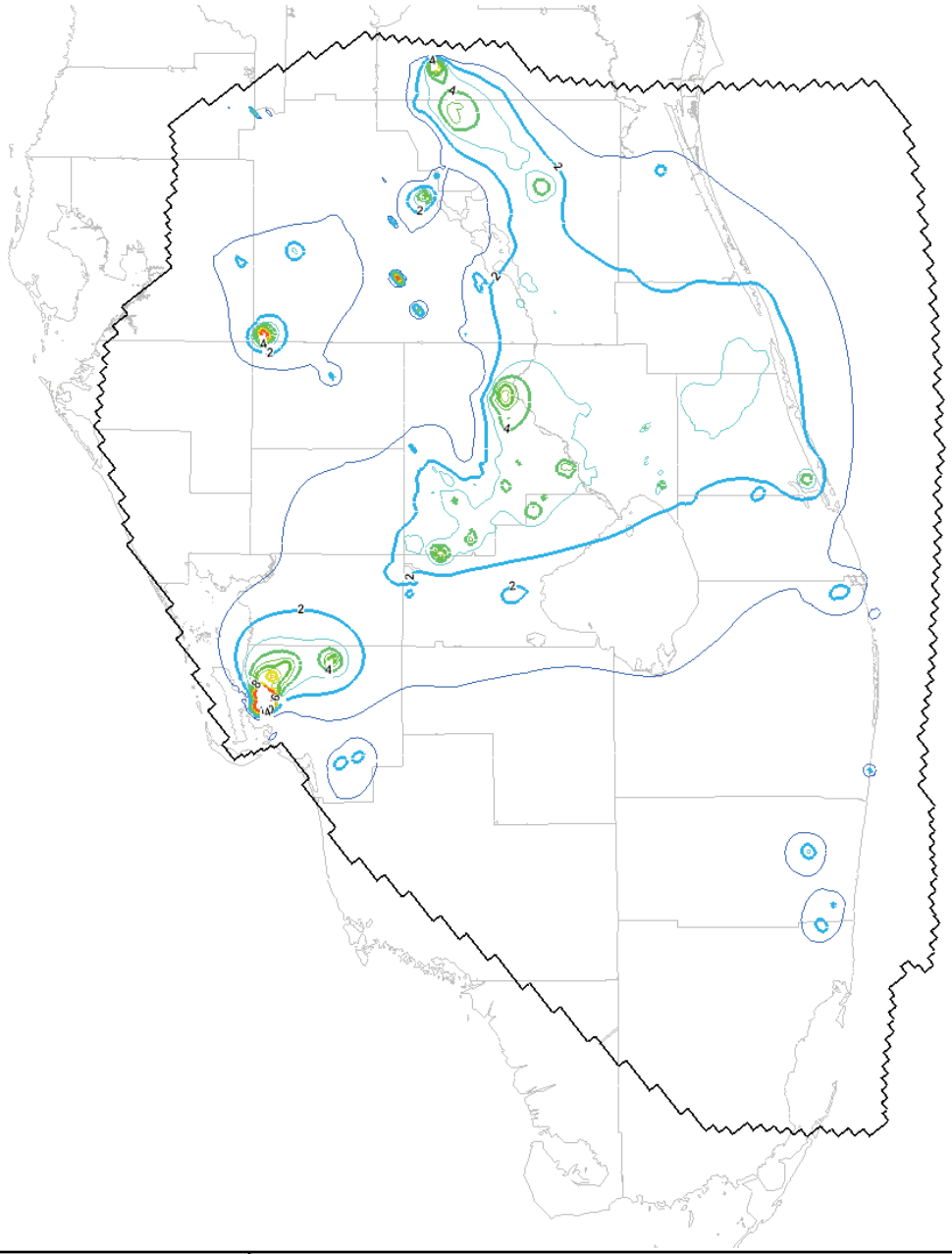

Feet of Drawdown

10
9
8
7
6
5
4
3
2
1
0

Notes:
Plots show the difference (drawdown) between the SEAWAT October 2003 calibration results and the corresponding simulation with all estimated pumping values reduced by 50 percent

Contours are for the Upper Floridan Aquifer

Contour interval is 1 ft

Comparison of Calibration with Reduced (Estimated) Pumping Sensitivity (October 2003, SEAWAT)

Final Groundwater Model Calibration Report

Figure 6.2

October 2010

Table 2.1 Model Assumptions List

Category	Parameter	SEAWAT Package	Assumption	Report Section
Pumping	Pumping Rate	WEL	Missing transient pumping data estimated based on available data and permit	Section 3.5, Appendix D
		WEL	Pumping rates in wells open to different zones were pro-rated based on hydraulic	Section 3.5, Appendix D
	Well Construction	WEL	Open hole/screen interval estimated based on available data if well construction	Appendix A
		WEL	Data collection effort assumed to have captured all significant pumping locations	Appendix A
	Model Input	WEL	Pumping assumed to be from the center of the grid cell	Section 3.5
	Water Quality	SSM	TDS and Temperature at injection wells were estimated based on well type if	Appendix E
Boundary Conditions	Head	CHD	Head boundary assigned to deeper units was correlated with overlying units in the absence of observed data	Appendix C
		CHD	Ocean head based on average monthly tidal data	Appendix C, Section 3.3.2
		CHD	Surface heads assumed to not be significantly impacted by CERP ASR	Appendix C, Section 3.3.1
		CHD	Regional pumping influence at or near model boundary is assumed to be captured by assigned specified heads	Appendix C, Section 3.3.3
	No-Flow	CHD	Lateral flow out of the model boundary in confining units is negligible	Appendix C, Section 5.6.3
	Model Input	CHD	Model boundary is sufficiently far away from CERP ASR influence	Section 3.3, Appendix C
	Water Quality	CHD	TDS /temperature observed at model boundary is indicative of incoming flow water quality	Appendix E
Initial Concentration	Model Input	BTN	Regional TDS/temperature does not vary significantly during the modeled period (except at injection locations)	Appendix E
	TDS	BTN	Natural neighbor interpolation was used to assign the initial TDS between data points	Appendix E
		BTN	TDS concentration generally increases with depth	Appendix E
		BTN	Coastal TDS is equal to seawater concentration at ocean outcrops	Appendix E
		BTN	Seawater TDS concentration is 35,000 mg/l	Appendix E
		BTN	Assumed TDS for SAS is 100 mg/l	Appendix E
	Temperature	BTN	Coastal temperature is based on isotherm evaluation at elevation of ocean outcrops	Appendix E
		BTN	Natural neighbor interpolation was used to assign the initial temperature between data points	Appendix E
		BTN	Assumed temperature for SAS is 24 degrees C	Appendix E

Table 2.1 Model Assumptions List

Category	Parameter	SEAWAT Package	Assumption	Report Section
Hydrogeologic	General	LPF	Geologic/stratagraphic simplifications assumed to be reasonable to address regional CERP ASR questions	Section 3.2
	Model Input	LPF	The hydrogeologic interpretation used to develop the model was based on USGS SIR 2007-5207	Section 3.2
		LPF	Hydraulic conductivity and specific storage in each model cell is indicative of the average hydrogeologic condition for that cell and is determined based on available observed data and ability of the model to reproduce observed head variations	Section 3.2.2, Section 4.0
	Hydraulic Conductivity	LPF	Transmissivity was converted to hydraulic conductivity based on the thickness of the well's open section where available and the aquifer thickness derived from the Hydrogeologic Framework where testing zone information was not available	Section 3.2.2
		LPF	Kriging was used to interpolate hydraulic conductivity between pilot points	Section 4.0
		LPF	The portion of the BZ containing voids was modeled with a very high hydraulic conductivity of approximately 10,000 ft/day	Section 3.2.2
		LPF	Due to data limitations the BZ was modeled at a constant thickness of 500 ft.	Section 3.2
		LPF	No regional anisotropy was incorporated into the model	Section 3.2.3
		LPF	Vertical hydraulic conductivity in aquifers is one tenth of the horizontal hydraulic conductivity	Section 5.7
		LPF	Vertical hydraulic conductivity in confining units is one half of the horizontal hydraulic conductivity	Section 5.7
	Specific Storage	LPF	Kriging was used to interpolate specific storage between pilot points	Section 4.0

Table 2.1 Model Assumptions List

Category	Parameter	SEAWAT Package	Assumption	Report Section
Calibration Data	Water Level	HOB	Due to the limited data in the deeper units of the FAS, some data from dates other than the calibration period were used to refine calibration	Section 4.0
		HOB	Monthly average data was adequate for calibration	Section 6.4
	Well Construction	HOB	Observed values used for calibration are indicative of the zone being evaluated and not a blend of over/under lying units	Section 4.0
		HOB	Open hole/screened intervals were used to determine the representative geologic unit for observation wells	Section 4.0
		HOB	Generally, at least 50% of the screened (open) interval must be in the calibrated unit to be used in calibration	Section 4.0
	Model Input	HOB	Calibration data coverage is adequate to address CERP ASR questions	Section 4.0
		HOB	Modeled results were linearly interpolated from computational points to observation data locations	Section 4.0
Model Parameters	General	N/A	Each cell is representative of average conditions across its area	Section 2.3, Section 3.2.1
		N/A	Steady State solution is reasonable as intial condition for transient simulations	Section 2.4
		DSP	Dispersivity and Diffusion values are reasonable and constant	Section 5.3
		LPF	Porosity values are reasonable and constant	Section 5.2
		N/A	Numerical codes are able to accuratly resolve flow and transport equations	Section 2.2
	Time	N/A	All data is monthly averaged	Section 2.4
		N/A	Calibration/Validation period is sufficient to define system to address CERP ASR questions	Section 2.4
	Density Variation	VDF	Linear relationship between variations in TDS/temperature and density	Section 2.1

Table 2.2: Physical constants used for density dependent flow equations

ρ_{fw}	62.25 lb/ft^3
m_{tds}	1.92 lb/ft^3
TDS_{ref}	0.0
m_{tmp}	-0.0172 lb/ft^3/°C
TMP_{ref}	25 °C
m_p	8.49x10^{-5} lb/ft^4
P_{ref}	0 lb/ft^2

Table 3.1
Comparison of Estimated and Actual Pumping Rates (in GPM)

	Oct 2003		Nov 2003		Dec 2003		Jan 2004		Feb 2004		Mar 2004		April 2004		May 2004	
Well Type	Estimated	Actual	Estimated	Actual	Estimated	Actual	Estimated	Actual	Estimated	Actual	Estimated	Actual	Estimated	Actual	Estimated	Actual
Unspecified	-190	-10,765	-196	-13,471	-566	-13,076	-702	-7,912	-639	-6,759	-1,050	-10,087	-526	-15,920	-600	-16,064
A	0	-210,545	-962	-265,458	0	-276,143	0	-199,155	-83	-159,623	0	-270,720	-73	-445,348	0	-450,933
AC	-59	0	-59	0	-5	-63	0	-45	-3	-48	-7	-109	-4	-160	-8	-154
AG	-2,981	-3,370	-3,463	-3,478	-3,771	-5,926	-2,658	-3,678	-2,304	-5,012	-4,136	-8,530	-6,359	-12,778	-7,067	-8,573
AGR	-7,632	0	-6,869	0	-6,105	0	-5,724	0	-6,105	0	-6,869	0	-7,632	0	-8,395	0
AGR CITRUS	-1,323	0	-1,191	0	-1,058	0	-992	0	-1,058	0	-1,191	0	-1,323	0	-1,455	0
AQC	-19	0	-20	0	-19	0	-16	-1	-71	-1	-102	-2	-8	0	-12	0
ARR	-8	0	-7	0	-7	0	-6	0	-6	0	-6	0	-7	0	-7	0
ASR Injecting	0	5,696	0	5,953	0	1,862	0	3,235	0	2,522	0	5,911	0	2,052	0	0
ASR Pumping	0	-2,439	0	-2,908	0	-1,526	0	-6,795	0	-6,689	0	-8,400	0	-15,366	0	-19,718
C/I	-31,777	0	-28,600	0	-25,422	0	-23,833	0	-25,422	0	-28,600	0	-31,777	0	-34,955	0
CATTLE	0	-1	0	-1	0	-1	0	-1	0	-1	0	-1	0	-1	0	-1
COMM	-21	-427	-6	-210	-9	-245	-6	-222	-5	-220	-2	-200	0	-105	-17	-381
COMM/IRR	0	0	0	0	0	0	0	0	0	-1	0	0	0	-16	0	-2
COMMERCIAL	-271	0	-308	0	-381	0	-345	0	-295	0	-258	0	-292	0	-508	0
DAI	0	-141	0	-130	0	-122	0	-118	0	-116	0	-114	0	-128	0	-135
DOM	-2	0	-2	0	-2	0	-3	0	-1	0	-3	0	-4	0	-6	0
FIR	-54	0	-50	0	-47	0	-45	0	-44	0	-44	0	-49	0	-51	0
FIRE	0	0	0	0	0	0	0	0	0	-1	0	0	0	0	0	-5
FRZ	-1,015	-379	-697	-365	-277	-337	-496	-388	-41	-283	-114	-578	-1,799	-565	-2,059	-668
IC	-4	-30,410	-6	-23,245	-3	-27,827	-3	-24,167	-6	-17,668	-5	-20,762	-3	-30,946	-16	-23,503
IND	-669	-2,563	-660	-2,717	-880	-2,846	-695	-2,350	-743	-2,764	-1,093	-2,511	-1,521	-2,328	-1,782	-2,278
INJ	3,898	246,334	4,468	253,693	3,472	241,907	12,769	226,641	2,395	258,009	1,344	237,810	139	230,680	0	221,968
IRR	-82,183	-46,394	-105,621	-49,393	-104,591	-39,863	-70,039	-46,965	-57,506	-42,658	-107,134	-91,574	-186,259	-118,455	-179,264	-133,298
IRR/CATTLE	-363	-2,209	-422	-2,511	-459	-2,443	-323	-1,743	-280	-2,195	-503	-2,230	-774	-3,438	-860	-4,510
L DRAIN	50	0	67	0	43	0	76	0	105	0	17	0	56	0	44	0
LARGE PWS	-19,733	0	-22,424	0	-27,805	0	-25,114	0	-21,527	0	-18,836	0	-20,630	0	-35,878	0
MD	0	-52,012	0	-30,748	0	-7,505	0	-40,506	0	-15,707	0	-32,040	0	-32,988	0	-19,578
MND	0	0	0	0	-4	0	0	0	-2	0	-5	0	-3	0	-6	0
OTR	-48	0	-48	0	-42	0	-45	0	-48	0	-53	0	-43	0	-61	0
P	0	-97,871	0	-97,110	0	-101,205	0	-95,112	0	-102,301	0	-106,227	0	-119,530	0	-141,908
PH	-33	0	-30	0	-34	0	-27	0	-30	0	-33	0	-33	0	-39	0
PHR	-1	0	0	0	-6	0	0	0	-3	0	-7	0	-4	0	-9	0
PRIVATE	-2,289	0	-2,289	0	-2,289	0	-2,287	0	-2,289	0	-2,289	0	-2,289	0	-2,289	0
PWS	-88,258	-124,893	-72,285	-133,169	-73,292	-126,513	-53,253	-147,326	-79,740	-128,100	-59,586	-161,137	-62,482	-173,783	-68,915	-179,924
R	0	-13,134	0	-14,391	0	-18,562	0	-15,055	0	-13,529	0	-16,911	0	-25,213	0	-25,324
R DRAIN	1	0	1	0	1	0	2	0	2	0	0	0	1	0	1	0
RCG	-12	0	-27	0	-29	0	-14	0	-13	0	-35	0	-33	0	-50	0
REC	0	-18	0	-159	0	-3	0	-48	0	-60	0	-147	0	-21	0	-3
REC GOLF COURSE	-599	0	-540	0	-480	0	-450	0	-480	0	-540	0	-599	0	-659	0
RECLAIMED	0	0	0	0	0	-1	0	0	0	0	0	0	0	0	0	-111
S DRAIN	11	0	15	0	10	0	17	0	24	0	4	0	13	0	10	0
SMALL PWS	-1,455	0	-1,658	0	-2,056	0	-1,864	0	-1,598	0	-1,398	0	-1,535	0	-2,670	0
W DRAIN	1	0	1	0	1	0	2	0	2	0	0	0	1	0	1	0
Total Injection (GPM)	**3,961**	**252,030**	**4,552**	**259,646**	**3,527**	**243,770**	**12,865**	**229,876**	**2,528**	**260,531**	**1,365**	**243,721**	**210**	**232,732**	**56**	**221,968**
Total Extraction (GPM)	**-240,998**	**-597,572**	**-248,436**	**-639,465**	**-249,639**	**-624,206**	**-188,939**	**-591,589**	**-200,346**	**-503,737**	**-233,900**	**-732,279**	**-326,064**	**-997,089**	**-347,640**	**-1,027,071**
Net Pumping (GPM)	**-237,037**	**-345,541**	**-243,884**	**-379,819**	**-246,112**	**-380,437**	**-176,074**	**-361,713**	**-197,818**	**-243,206**	**-232,535**	**-488,558**	**-325,854**	**-764,357**	**-347,583**	**-805,102**
Total Injection (MGD)	**5.7**	**362.9**	**6.6**	**373.9**	**5.1**	**351.0**	**18.5**	**331.0**	**3.6**	**375.2**	**2.0**	**351.0**	**0.3**	**335.1**	**0.1**	**319.6**
Total Extraction (MGD)	**-347.0**	**-860.5**	**-357.7**	**-920.8**	**-359.5**	**-898.9**	**-272.1**	**-851.9**	**-288.5**	**-725.4**	**-336.8**	**-1054.5**	**-469.5**	**-1435.8**	**-500.6**	**-1479.0**
Net Pumping (MGD)	**-341.3**	**-497.6**	**-351.2**	**-546.9**	**-354.4**	**-547.8**	**-253.5**	**-520.9**	**-284.9**	**-350.2**	**-334.9**	**-703.5**	**-469.2**	**-1100.7**	**-500.5**	**-1159.3**
% of Total Pumping	**22%**	**78%**	**22%**	**78%**	**23%**	**77%**	**20%**	**80%**	**21%**	**79%**	**19%**	**81%**	**21%**	**79%**	**22%**	**78%**

Table 3.1 continued
Comparison of Estimated and Actual Pumping Rates (in GPM)

	June 2004		July 2004		Aug 2004		Sept 2004		Oct 2004		Nov 2004		Dec 2004	
Well Type	Estimated	Actual	Estimated	Actual	Estimated	Actual	Estimated	Actual	Estimated	Actual	Estimated	Actual	Estimated	Actual
Unspecified	-258	-12,923	-204	-5,865	-197	-2,135	-236	-2,026	-164	-3,924	-263	-10,315	-178	-8,889
A	-1,233	-372,217	0	-134,059	0	-46,888	0	-4,915	0	-94,371	0	-249,390	0	-165,029
AC	-5	-160	0	0	0	-156	0	-68	0	-95	0	-132	-5	-49
AG	-4,741	-3,115	-2,426	-1,118	-643	-958	-535	-867	-1,821	-483	-4,330	-1,717	-3,344	-5,617
AGR	-9,158	0	-9,540	0	-9,158	0	-8,395	0	-7,632	0	-6,869	0	-6,105	0
AGR CITRUS	-1,588	0	-1,654	0	-1,588	0	-1,455	0	-1,323	0	-1,191	0	-1,058	0
AQC	-13	0	-11	0	-10	0	-10	0	-19	0	-19	0	-19	0
ARR	-8	0	-8	0	-8	0	-8	0	-7	0	-7	0	-7	0
ASR Injecting	0	2,313	0	6,521	0	3,866	0	4,515	958	7,400	0	7,324	0	6,780
ASR Pumping	0	-9,855	0	-1,358	0	-2,099	0	-2,703	0	-1,736	0	-7,934	0	-11,114
C/I	-38,133	0	-39,722	0	-38,133	0	-34,955	0	-31,777	0	-28,600	0	-25,422	0
CATTLE	0	-1	0	-2	0	-2	0	-2	0	-2	0	-2	0	-2
COMM	-22	-449	0	-126	-11	-309	-5	-208	-25	-520	-79	-1,278	-5	-220
COMM/IRR	0	-5	0	-3	0	0	0	0	0	0	0	0	0	0
COMMERCIAL	-521	0	-483	0	-445	0	-381	0	-305	0	-267	0	-294	0
DAI	0	-146	0	-138	0	-142	0	-148	0	-137	0	-131	0	-125
DOM	-2	0	-2	0	-1	0	-1	0	-1	0	-3	0	-2	0
FIR	-56	0	-53	0	-54	0	-57	0	-52	0	-50	0	-48	0
FIRE	0	-10	0	-4	0	-9	0	0	0	0	0	0	0	0
FRZ	-203	-422	-139	-548	-212	-93	-46	-196	-1,104	-153	-1,372	-201	-1,214	-375
IC	-5	-20,375	0	-33,050	-2	-21,912	-2	-13,346	-2	-22,149	-2	-23,928	0	-4,785
IND	-1,288	-2,541	-1,027	-2,406	-2,030	-2,289	-2,068	-2,006	-2,047	-2,154	-1,058	-2,438	-2,475	-2,257
INJ	0	214,439	0	213,662	0	267,910	3,704	287,418	0	286,537	19,606	231,062	6,272	234,946
IRR	-122,940	-54,948	-64,907	-48,794	-20,670	-15,819	-17,027	-21,678	-60,303	-43,377	-117,098	-65,684	-93,258	-55,701
IRR/CATTLE	-577	-1,513	-295	-1,718	-78	-1,562	-65	-253	-222	-2,227	-527	-2,379	-407	-2,187
L DRAIN	204	0	106	0	346	0	303	0	29	0	51	0	41	0
LARGE PWS	-36,775	0	-34,084	0	-31,393	0	-26,908	0	-21,527	0	-18,836	0	-17,939	0
MD	0	-8,981	0	-31,024	0	-17,359	0	-14,037	0	-7,337	0	-25,406	0	-9,378
MND	-4	0	0	0	0	0	0	0	0	0	0	0	-4	0
OTR	-62	0	-62	0	-84	0	-90	0	-90	0	-49	0	-90	0
P	0	-120,738	0	-106,738	0	-91,285	0	-99,153	0	-93,054	0	-83,413	0	-24,298
PH	-38	0	-32	0	-32	0	-34	0	-32	0	-30	0	-37	0
PHR	-5	0	0	0	0	0	0	0	-1	0	0	0	-6	0
PRIVATE	-2,289	0	-2,290	0	-2,291	0	-2,292	0	-2,292	0	-2,293	0	-2,294	0
PWS	-73,528	-164,580	-68,774	-166,963	-68,390	-146,862	-62,667	-142,845	-59,949	-147,821	-56,924	-165,852	-54,791	-158,465
R	0	-22,925	0	-16,620	0	-9,368	0	-6,236	0	-10,358	0	-16,788	0	-13,512
R DRAIN	4	0	2	0	7	0	6	0	1	0	1	0	1	0
RCG	-28	0	-38	0	-35	0	-24	0	-12	0	-27	0	-29	0
REC	0	-143	0	-56	0	-113	0	-23	0	-18	0	-84	0	-81
REC GOLF COURSE	-719	0	-749	0	-719	0	-659	0	-599	0	-540	0	-480	0
RECLAIMED	0	-326	0	0	0	-8	0	0	0	-12	0	0	0	-1
S DRAIN	46	0	24	0	79	0	69	0	7	0	12	0	9	0
SMALL PWS	-2,736	0	-2,536	0	-2,339	0	-2,007	0	-1,607	0	-1,407	0	-1,340	0
W DRAIN	4	0	2	0	7	0	6	0	1	0	1	0	1	0
Total Injection (GPM)	**259**	**216,752**	**135**	**220,183**	**439**	**271,776**	**4,088**	**291,933**	**995**	**293,937**	**19,671**	**238,386**	**6,324**	**241,726**
Total Extraction (GPM)	**-296,934**	**-796,375**	**-229,036**	**-550,589**	**-178,523**	**-359,366**	**-159,927**	**-310,709**	**-192,912**	**-429,928**	**-241,838**	**-657,072**	**-210,850**	**-462,086**
Net Pumping (GPM)	**-296,675**	**-579,623**	**-228,902**	**-330,406**	**-178,083**	**-87,590**	**-155,839**	**-18,776**	**-191,917**	**-135,991**	**-222,167**	**-418,687**	**-204,526**	**-220,359**
Total Injection (MGD)	**0.4**	**312.1**	**0.2**	**317.1**	**0.6**	**391.4**	**5.9**	**420.4**	**1.4**	**423.3**	**28.3**	**343.3**	**9.1**	**348.1**
Total Extraction (MGD)	**-427.6**	**-1146.8**	**-329.8**	**-792.8**	**-257.1**	**-517.5**	**-230.3**	**-447.4**	**-277.8**	**-619.1**	**-348.2**	**-946.2**	**-303.6**	**-665.4**
Net Pumping (MGD)	**-427.2**	**-834.7**	**-329.6**	**-475.8**	**-256.4**	**-126.1**	**-224.4**	**-27.0**	**-276.4**	**-195.8**	**-319.9**	**-602.9**	**-294.5**	**-317.3**
% of Total Pumping	**23%**	**77%**	**23%**	**77%**	**22%**	**78%**	**21%**	**79%**	**21%**	**79%**	**23%**	**77%**	**24%**	**76%**

Table 3.1 Notes:

1.) Well types in this table were based on data from SAJ which used the following abbreviations:

A - Agriculture
AC - Air Conditioning/Withdrawal
AG - Agriculture
AQC - Aquaculture
ARR - Aquifer Remediation and Recovery
ASR Injecting - Aquifer Storage and Recovery Injection
ASR Pumping - Aquifer Storage and Recovery Pumping
CATTLE - Irrigation for Cattle Pasture
COMM - Commercial
COMM/IRR - Commercial and Irrigation
DAI - Dairy
DOM - Single Family
FIR - Fire
FIRE - Fire Protection
FRZ - Freeze Protection
IC - Industrial/Commercial
IND - Industrial
INJ - Injection
IRR - Irrigation
IRR/CATTLE - Irrigation for Cattle Pasture
L DRAIN - Drains Stormwater to Floridan Aquifer
LARGE PWS - Large Public Water Supply
MD - Mining/Dewatering
MND - Mining/Dewatering
OTR - Other
P - Public Supply
PH - Swimming Pool Heating/Withdrawal
PHR - Swimming Pool Heating/Injection
PWS - Public Water Supply
R - Recreation
R DRAIN - Drains Stormwater to Floridan Aquifer
RCG - Recharge (Unspecified)
REC - Water Supply for Recreational Facility (Camp or Marina)
REC GOLF COURSE - Water Supply for Golf Course
S DRAIN - Drains Stormwater to Floridan Aquifer
SMALL PWS - Small Public Water Supply
W DRAIN - Drains Stormwater to Floridan Aquifer

2.) A negative pumping rate indicates extraction; a positive pumping rate indicates injection.

3.) The net pumping rate was calculated as the total injection pumping rate added to the the total extraction pumping rate.

4.) % of Total Pumping was based on the total volume of water passing through the pump within a given month. For example, the percent of total pumping that came from estimated data was calculated as follows:

$$\frac{\left|\text{total estimated injection}\right| + \left|\text{total estimated extraction}\right|}{\left|\text{total estimated injection}\right| + \left|\text{total estimated extraction}\right| + \left|\text{total actual injection}\right| + \left|\text{total actual extraction}\right|}$$

Table 4.1: Usage of SAJ Observation Database in Regional Model Calibration

Model ID[a]	Well Name	Data Source	Easting[b]	Northing[b]	County	Cased Depth (ft)	Drilled Depth (ft)	Dominant Layer[c]	% Open Section in Layer[c]	93/94 Months with Data[d]	03/04 Months with Data[e]	Use for Data in Model Setup/Calibration						Reasoning/Comments
													Observations for Calibration					
												Boundary Conditions[f]	Steady State (Oct 03)	Steady State (Feb 04)	Transient (03/04)	Transient (03/04	Not Used	
100001	754028002 (USGS)	USGS	825635.81	1299236.26	Brevard	400	420	UF	100%	1	2						Not Used	sparse data
120034	BR0202	SJRWMD	724478.88	1470720.30	Brevard	114	129	IAS/ICU	100%	10	0						Not Used	outside IAS (per Miller, 1997)
120037	BR0608	SJRWMD	759211.87	1510816.10	Brevard	84	321	UF	80%	10	15						Not Used	Outside Boundary
120001	BR0624	SJRWMD	832393.04	1285879.97	Brevard	550	650	UF	100%	10	15		UF	UF	UF	UF		
120002	BR0625	SJRWMD	832393.04	1285879.97	Brevard	299	454	UF	74%	10	15						Not Used	Open section of nearby well (120001) completely in UF.
120308	BR0645	SJRWMD	743563.16	1332296.01	Brevard	125	447	UF	62%	10	15						Not Used	Sparse data and only 62% in UF
120006	BR1549	SJRWMD	731152.64	1471898.03	Brevard	60	70	SAS	100%	0	15	SAS						
120007	BR1550	SJRWMD	731152.64	1471898.03	Brevard	20	30	SAS	100%	0	15	SAS						
120311	BR1557	SJRWMD	731104.43	1471740.54	Brevard	150	190	UF	100%	0	15	UF						
120084	BR1558	SJRWMD	740313.67	1451912.56	Brevard	140	180	UF	80%	0	15						Not Used	Near boundary
100002	DESERET RANCH WELL NO. 3 NEAR KENANSVILLE, FL	USGS	705582.88	1311426.42	Brevard	252	272	UF	100%	1	8			UF	UF			This area has a pretty steep drop in Oct 03 (see 120072) so since the only point for this well is 10/20, it is removed from the Oct 03 dataset; sparse 93/94 data
100008	DUDA RANCH L-2	USGS	723267.55	1406484.36	Brevard	430	450	UF	100%	1	2						Not Used	sparse data
100003	FELLSMERE NW TP	USGS	765974.62	1331645.19	Brevard	412	432	UF	100%	1	2						Not Used	sparse data
100009	MERRITT ISLAND INJECTION WELL	USGS	750539.39	1486730.38	Brevard	110	130	IAS/ICU	68%	1	2						Not Used	Outside Boundary
100004	PLATT WELL NEAR MELBOURNE, FL	USGS	743473.52	1332295.81	Brevard	125	447	UF	62%	10	12						Not Used	Duplicate with 120308
111078	2AS7E_GN	SFWMD	848036.92	723841.22	Broward	34.41	36.41	SAS	100%	0	15	SAS						
111077	2AS7E_GN	SFWMD	848036.92	723841.32	Broward	19.69	21.69	SAS	100%	0	15	SAS						
111159	2AS7E_GS	SFWMD	848036.92	723841.32	Broward	64.56	66.56	SAS	100%	0	15	SAS						
111160	2AS7E_GS	SFWMD	848036.92	723841.32	Broward	124.42	126.42	SAS	100%	0	15	SAS						
111042	3AN1W1_G	SFWMD	741323.00	674060.00	Broward	12.5	14.5	SAS	100%	0	15	SAS						
111190	3AN1W1_G	SFWMD	741323.00	674060.00	Broward	33	38	SAS	100%	0	15	SAS						
111189	3AN1W2_GW1	SFWMD	742161.45	673964.66	Broward	28	30	SAS	100%	0	15	SAS						
111188	3AN1W2_GW2	SFWMD	742161.45	673964.66	Broward	14	15	SAS	100%	0	15	SAS						
111187	3AN1W3_GW1	SFWMD	741743.00	672546.00	Broward	34.6	36.6	SAS	100%	0	15	SAS						
111186	3AN1W3_GW2	SFWMD	741743.00	672546.00	Broward	17.7	18.7	SAS	100%	0	15	SAS						
111185	3AN1W4_GW2	SFWMD	741592.00	673548.00	Broward	5.09	7.09	SAS	100%	0	15	SAS						
112129	BF-1	SFWMD	925617.30	669564.23	Broward	2080	2280	LC	52%	0	15		LF	LF	LF	LF		
112138	BF-4M	SFWMD	925172.70	669560.61	Broward	1500	1600	APPZ	100%	0	15		APPZ	APPZ	APPZ			no 93/94 data
112137	BF-4S	SFWMD	925172.70	669560.61	Broward	1000	1200	UF	100%	0	15		UF	UF	UF			no 93/94 data
112139	BF-6	SFWMD	943147.33	720952.19	Broward	960	1128	UF	100%	0	15		UF	UF	UF			no 93/94 data
100173	C-953	USGS	919934.91	678018.91	Broward	35	40	SAS	100%	10	14	SAS						
100092	C-968	USGS	920804.33	627368.70	Broward	94.5	114.5	SAS	100%	10	0	SAS						
100070	F-291	USGS	936336.93	607748.45	Broward	87	107	SAS	100%	10	15	SAS						
111842	F-291	SFWMD	936337.35	607748.12	Broward	107	109	SAS	100%	10	15	SAS						
100115	G-1089	USGS	911381.13	648654.66	Broward	14	16	SAS	100%	2	0						Not Used	sparse data
100103	G-1092	USGS	913418.68	643315.43	Broward	14	16	SAS	100%	2	0						Not Used	sparse data
100086	G-1185	USGS	918710.11	612955.46	Broward	16.3	18.3	SAS	100%	2	0						Not Used	sparse data
100037	G-1212	USGS	934557.13	673133.96	Broward	177.4	197.4	SAS	100%	0	12	SAS						
100129	G-1212A	USGS	934557.13	673133.96	Broward	79	84	SAS	100%	9	0	SAS						
100205	G-1213	USGS	922630.01	713072.20	Broward	13	15	SAS	100%	10	13	SAS						
111324	G-1213_G	SFWMD	922630.64	713071.82	Broward	12	15	SAS	100%	10	14	SAS						
110653	G-1215_G	SFWMD	946875.18	708283.45	Broward	14	20	SAS	100%	10	0	SAS						
100118	G-1220	USGS	936305.24	654395.61	Broward	18	20	SAS	100%	10	15	SAS						
111414	G-1220_G	SFWMD	936305.75	654395.23	Broward	12.08	20	SAS	100%	10	15	SAS						
100093	G-1221	USGS	908975.13	636656.83	Broward	18	20	SAS	100%	10	15	SAS						
111853	G-1221_G	SFWMD	908975.63	636656.57	Broward	11.5	20	SAS	100%	10	15	SAS						
111409	G-1223_G	SFWMD	906972.47	620591.22	Broward	12	20	SAS	100%	10	15	SAS						
110842	G-1224_G	SFWMD	935956.93	624102.39	Broward	12	20	SAS	100%	10	0	SAS						
100073	G-1225	USGS	908312.48	609796.01	Broward	18	20	SAS	100%	9	15	SAS						
110722	G-1225_G	SFWMD	908312.94	609795.78	Broward	18	20	SAS	100%	9	0	SAS						
100084	G-1226	USGS	924721.94	612015.81	Broward	18	20	SAS	100%	10	15	SAS						
111407	G-1226_G	SFWMD	924722.38	612015.52	Broward	14	20	SAS	100%	10	15	SAS						
100231	G-1228	USGS	950243.04	723424.40	Broward	175	195	SAS	100%	9	0	SAS						
100038	G-1232	USGS	935909.04	675364.24	Broward	185	205	SAS	100%	0	12	SAS						
100091	G-1237	USGS	930213.44	625951.72	Broward	180	200	SAS	100%	2	0						Not Used	sparse data
100085	G-1240	USGS	926835.78	611996.26	Broward	180	200	SAS	100%	8	0	SAS						
100064	G-1241	USGS	934633.62	605382.08	Broward	196	216	SAS	100%	9	0	SAS						
100226	G-1260	USGS	945960.04	722211.84	Broward	85	90	SAS	100%	10	15	SAS						
111827	G-1260_G	SFWMD	945960.66	722211.39	Broward	60	90	SAS	100%	10	15	SAS						
110617	G-1262_G	SFWMD	919295.00	678519.00	Broward	13	15	SAS	100%	1	0						Not Used	Sparse data
100216	G-1272	USGS	949271.47	719176.64	Broward	176	196	SAS	100%	7	0	SAS						
100203	G-1315	USGS	934024.37	710520.11	Broward	12	14	SAS	100%	10	15	SAS						
111438	G-1315_G	SFWMD	934025.00	710520.00	Broward	12	14	SAS	100%	10	15	SAS						
100187	G-1316	USGS	922739.69	695605.06	Broward	13	15	SAS	100%	10	15	SAS						
111279	G-1316_G	SFWMD	922740.00	695605.00	Broward	14	16	SAS	100%	10	15	SAS						
100040	G-1340	USGS	937716.26	677597.59	Broward	197	217	SAS	100%	0	10	SAS						
100119	G-1343	USGS	920556.18	653759.06	Broward	190	210	SAS	100%	10	0	SAS						

Table 4.1: Usage of SAJ Observation Database in Regional Model Calibration

Model ID[a]	Well Name	Data Source	Easting[b]	Northing[b]	County	Cased Depth (ft)	Drilled Depth (ft)	Dominant Layer[c]	% Open Section in Layer[c]	93/94 Months with Data[d]	03/04 Months with Data[e]	Use for Data in Model Setup/Calibration						Reasoning/Comments
													Observations for Calibration					
												Boundary Conditions[f]	Steady State (Oct 03)	Steady State (Feb 04)	Transient (03/04)	Transient (03/04	Not Used	
100096	G-1344	USGS	915265.20	639489.69	Broward	162	182	SAS	100%	0	0						Not Used	sparse data
100056	G-1433	USGS	936753.36	602164.81	Broward	130	150	SAS	100%	0	0						Not Used	sparse data
100057	G-1434	USGS	936023.35	602160.05	Broward	172	192	SAS	100%	0	0						Not Used	sparse data
100058	G-1435	USGS	935019.58	602153.52	Broward	184	204	SAS	100%	9	14	SAS						
110616	G-1472_G	SFWMD	936008.00	602294.00	Broward	17.9	20.05	SAS	100%	1	0						Not Used	sparse data
100059	G-1473	USGS	933816.06	602481.79	Broward	112	132	SAS	100%	10	15	SAS						
110910	G-1473	SFWMD	933816.48	602481.46	Broward	126	132	SAS	100%	10	15	SAS						
100083	G-1548	USGS	927931.19	611902.22	Broward	167	187	SAS	100%	9	0	SAS						
100090	G-1569	USGS	931370.10	616265.89	Broward	31	36	SAS	100%	2	0						Not Used	sparse data
100089	G-1570	USGS	927815.01	615839.34	Broward	42	47	SAS	100%	2	0						Not Used	sparse data
100068	G-1585	USGS	917194.86	607089.97	Broward	37	42	SAS	100%	2	0						Not Used	sparse data
100080	G-1588	USGS	930856.39	611012.11	Broward	37	42	SAS	100%	2	0						Not Used	sparse data
100074	G-1597	USGS	928307.64	610087.13	Broward	143	163	SAS	100%	9	0	SAS						
100054	G-1636	USGS	860392.09	594901.79	Broward	22	24	SAS	100%	10	15	SAS						
100081	G-2000	USGS	927935.66	611195.45	Broward	172	192	SAS	100%	9	0	SAS						
100189	G-2001	USGS	949784.37	697672.26	Broward	49	54	SAS	100%	9	0	SAS						
100197	G-2031	USGS	891296.56	700770.66	Broward	20	22	SAS	100%	10	15	SAS						
111327	G-2031_G	SFWMD	891297.19	700770.37	Broward	21	22	SAS	100%	10	15	SAS						
100120	G-2032	USGS	881239.95	656997.81	Broward	20	22	SAS	100%	10	15	SAS						
111337	G-2032_G	SFWMD	881241.00	656998.00	Broward	21	22	SAS	100%	10	15	SAS						
100140	G-2033	USGS	893612.89	677258.16	Broward	21	23	SAS	100%	9	15	SAS						
111323	G-2033_G	SFWMD	893613.00	677258.00	Broward	21	23	SAS	100%	9	15	SAS						
111338	G-2034_G	SFWMD	858090.66	618616.83	Broward	21	22	SAS	100%	10	15	SAS						
100077	G-2035	USGS	925916.22	610710.73	Broward	47	52	SAS	100%	10	15	SAS						
111408	G-2035_G	SFWMD	925917.00	610710.00	Broward	50	52	SAS	100%	10	15	SAS						
100071	G-2037	USGS	924298.37	609254.13	Broward	18	20	SAS	100%	2	0						Not Used	sparse data
100072	G-2038	USGS	924298.37	609254.13	Broward	123	143	SAS	100%	2	0						Not Used	sparse data
100082	G-2040	USGS	926841.52	611087.56	Broward	157	177	SAS	100%	9	0	SAS						
100174	G-2054	USGS	948922.60	690598.02	Broward	122	142	SAS	100%	0	0						Not Used	sparse data
100177	G-2055	USGS	949099.16	691407.04	Broward	160	180	SAS	100%	7	0	SAS						
100192	G-2063	USGS	951697.10	697584.56	Broward	77	82	SAS	100%	6	0	SAS						
100194	G-2064	USGS	950512.76	697677.31	Broward	181	201	SAS	100%	9	0	SAS						
111111	G-2064_G	SFWMD	950588.69	697807.94	Broward	200	201	SAS	100%	0	7	SAS						
100179	G-2065	USGS	944445.40	692788.86	Broward	60	65	SAS	100%	2	0						Not Used	sparse data
100199	G-2072	USGS	948934.99	702008.35	Broward	38	43	SAS	100%	2	0						Not Used	sparse data
100076	G-2073	USGS	927486.53	610081.93	Broward	170	190	SAS	100%	10	0	SAS						
100075	G-2073A	USGS	927486.53	610081.93	Broward	137	157	SAS	100%	10	0	SAS						
100122	G-2091	USGS	929932.43	669771.86	Broward	104	124	SAS	100%	9	0	SAS						
100135	G-2104	USGS	926530.04	674697.81	Broward	50	55	SAS	100%	2	0						Not Used	sparse data
100132	G-2108	USGS	934633.04	675456.85	Broward	50	55	SAS	100%	2	0						Not Used	sparse data
100125	G-2114	USGS	928647.88	671177.25	Broward	58	63	SAS	100%	2	0						Not Used	sparse data
100127	G-2118	USGS	919715.30	671827.85	Broward	62	67	SAS	100%	2	0						Not Used	sparse data
100098	G-2122	USGS	915352.69	640096.05	Broward	115	135	SAS	100%	10	0	SAS						
100095	G-2125	USGS	916454.11	638891.09	Broward	53	58	SAS	100%	9	0	SAS						
100032	G-2129	USGS	922190.45	640138.05	Broward	160	180	SAS	100%	0	8	SAS						
100097	G-2130	USGS	922192.34	639835.15	Broward	55	60	SAS	100%	10	10	SAS						
100110	G-2131	USGS	929806.74	646749.30	Broward	64	69	SAS	100%	2	0						Not Used	sparse data
100106	G-2136	USGS	920795.39	644572.13	Broward	63	68	SAS	100%	2	0						Not Used	sparse data
100111	G-2137	USGS	919773.31	647695.92	Broward	66.5	71.5	SAS	100%	2	0						Not Used	sparse data
100113	G-2140	USGS	917855.98	648188.99	Broward	61.5	66.5	SAS	100%	2	0						Not Used	sparse data
100107	G-2141	USGS	918603.19	645265.40	Broward	56.5	61.5	SAS	100%	2	0						Not Used	sparse data
100109	G-2145	USGS	912123.65	646437.75	Broward	52	57	SAS	100%	2	0						Not Used	sparse data
100193	G-2147	USGS	950588.57	697808.40	Broward	41	46	SAS	100%	10	15	SAS						
111826	G-2147_G	SFWMD	950589.14	697807.94	Broward	154	180	SAS	100%	10	15	SAS						
100191	G-2148	USGS	945416.10	697339.35	Broward	13	15	SAS	100%	2	0						Not Used	sparse data
100178	G-2149	USGS	944908.24	691681.28	Broward	117	137	SAS	100%	9	5	SAS						
100219	G-2156	USGS	912322.91	719239.93	Broward	94.5	99.5	SAS	100%	2	0						Not Used	sparse data
100088	G-2176	USGS	928010.90	613720.19	Broward	151	171	SAS	100%	10	0	SAS						
100087	G-2176A	USGS	928010.90	613720.19	Broward	59	64	SAS	100%	9	0	SAS						
100232	G-2256	USGS	950243.04	723424.40	Broward	90	110	SAS	100%	9	0	SAS						
100227	G-2257	USGS	949977.77	722311.81	Broward	89.5	94.5	SAS	100%	9	0	SAS						
100028	G-2264	USGS	918886.65	628798.79	Broward	183	203	SAS	100%	0	5						Not Used	sparse data
100190	G-2274A	USGS	940231.70	696496.55	Broward	53.1	58.1	SAS	100%	2	0						Not Used	sparse data
100152	G-2275	USGS	930697.70	678258.55	Broward	137	157	SAS	100%	2	0						Not Used	sparse data
100200	G-2277	USGS	948752.91	702007.10	Broward	111	131	SAS	100%	9	0	SAS						
100201	G-2278	USGS	948752.91	702007.10	Broward	183	203	SAS	100%	8	0	SAS						
100055	G-2294	USGS	935479.12	601651.65	Broward	119	139	SAS	100%	10	14	SAS						
100121	G-2296	USGS	713926.40	667921.72	Broward	2711	2811	LC	100%	1	0						Not Used	Model geology puts this well in LC
100181	G-2344A	USGS	944347.49	693797.95	Broward	90.7	95.7	SAS	100%	9	0	SAS						

Table 4.1: Usage of SAJ Observation Database in Regional Model Calibration

Model ID[a]	Well Name	Data Source	Easting[b]	Northing[b]	County	Cased Depth (ft)	Drilled Depth (ft)	Dominant Layer[c]	% Open Section in Layer[c]	93/94 Months with Data[d]	03/04 Months with Data[e]	Use for Data in Model Setup/Calibration						Reasoning/Comments
													Observations for Calibration					
												Boundary Conditions[f]	Steady State (Oct 03)	Steady State (Feb 04)	Transient (03/04)	Transient (03/04	Not Used	
100182	G-2344B	USGS	944347.49	693797.95	Broward	33.2	38.2	SAS	100%	2	0						Not Used	sparse data
100034	G-2352	USGS	924370.30	641464.30	Broward	151	171	SAS	100%	0	12	SAS						
100167	G-2359	USGS	906260.99	682348.73	Broward	80.4	100.4	SAS	100%	2	0						Not Used	sparse data
100168	G-2359A	USGS	906260.99	682348.73	Broward	50.8	55.8	SAS	100%	2	0						Not Used	sparse data
140010	G-2360A	BROWARD CO. via DEP	942596.67	710346.06	Broward	48	51	SAS	100%	1	0						Not Used	sparse data
140011	G-2364	BROWARD CO. via DEP	903757.80	657310.41	Broward	75	80	SAS	100%	1	0						Not Used	sparse data
140012	G-2369A	BROWARD CO. via DEP	879948.05	610918.31	Broward	20	22	SAS	100%	1	0						Not Used	sparse data
100130	G-2370	USGS	918245.24	673838.22	Broward	81.2	101.2	SAS	100%	2	0						Not Used	sparse data
100131	G-2370A	USGS	918245.24	673838.22	Broward	43.6	48.6	SAS	100%	2	0						Not Used	sparse data
140013	G-2372A	BROWARD CO. via DEP	888007.49	672451.19	Broward	27	32	SAS	100%	1	0						Not Used	sparse data
110688	G-2376_G	SFWMD	844253.00	653992.00	Broward	13	15	SAS	100%	10	0	SAS						
100151	G-2389	USGS	917309.48	677871.36	Broward	68	73	SAS	100%	2	0						Not Used	sparse data
100172	G-2394	USGS	911886.04	686017.18	Broward	35	40	SAS	100%	2	0						Not Used	sparse data
100149	G-2395	USGS	919934.91	678018.91	Broward	68	73	SAS	100%	10	15	SAS						
111325	G-2395_G	SFWMD	919935.48	678018.57	Broward	71	73	SAS	100%	10	15	SAS						
100150	G-2396	USGS	919859.98	677887.09	Broward	25	30	SAS	100%	2	0						Not Used	sparse data
100164	G-2405	USGS	922755.87	680934.32	Broward	18	20	SAS	100%	2	0						Not Used	sparse data
100143	G-2406	USGS	913484.34	677747.09	Broward	17.5	19.5	SAS	100%	2	0						Not Used	sparse data
100136	G-2407	USGS	912041.48	675315.06	Broward	17	19	SAS	100%	2	0						Not Used	sparse data
100060	G-2409	USGS	934287.60	602451.68	Broward	79	84	SAS	100%	9	14	SAS						
100061	G-2410	USGS	934196.35	602451.09	Broward	186	206	SAS	100%	10	14	SAS						
100142	G-2411	USGS	921409.13	677795.75	Broward	20	22	SAS	100%	2	0						Not Used	sparse data
100147	G-2412	USGS	921408.50	677896.72	Broward	20	22	SAS	100%	2	0						Not Used	sparse data
100146	G-2415	USGS	921681.77	677898.42	Broward	93	113	SAS	100%	2	0						Not Used	sparse data
100145	G-2416	USGS	921955.04	677900.13	Broward	94	99	SAS	100%	2	0						Not Used	sparse data
100141	G-2417	USGS	921867.10	677394.71	Broward	77	82	SAS	100%	2	0						Not Used	sparse data
100148	G-2418	USGS	921135.24	677895.01	Broward	18	20	SAS	100%	2	0						Not Used	sparse data
100078	G-2425	USGS	932409.95	610618.20	Broward	183	203	SAS	100%	9	13	SAS						
100079	G-2426	USGS	932409.95	610618.20	Broward	86	91	SAS	100%	10	13	SAS						
100166	G-2427	USGS	931677.45	681697.98	Broward	160	180	SAS	100%	2	0						Not Used	sparse data
100162	G-2431	USGS	929040.61	680974.17	Broward	55	60	SAS	100%	2	0						Not Used	sparse data
100163	G-2432	USGS	929040.61	680974.17	Broward	134	154	SAS	100%	2	0						Not Used	sparse data
100157	G-2433	USGS	926041.27	679945.30	Broward	54	59	SAS	100%	2	0						Not Used	sparse data
100158	G-2434	USGS	926041.27	679945.30	Broward	94	114	SAS	100%	2	0						Not Used	sparse data
100159	G-2435	USGS	926041.27	679945.30	Broward	138	158	SAS	100%	2	0						Not Used	sparse data
100155	G-2436	USGS	922492.10	679418.08	Broward	58	63	SAS	100%	1	0						Not Used	sparse data
100156	G-2437	USGS	922492.10	679418.08	Broward	101.5	121.5	SAS	100%	2	0						Not Used	sparse data
100025	G-2441	USGS	932110.91	614554.15	Broward	161	181	SAS	100%	0	14	SAS						
110641	G-2443_G	SFWMD	926332.49	689165.30	Broward	66	145	SAS	100%	10	0	SAS						
110640	G-2444_G	SFWMD	924457.62	683196.24	Broward	83	150	SAS	100%	10	0	SAS						
100046	G-2445	USGS	948611.17	696149.53	Broward	112	132	SAS	100%	0	5						Not Used	sparse data
100144	G-2449	USGS	913484.34	677747.09	Broward	66	71	SAS	100%	2	0						Not Used	sparse data
100137	G-2450	USGS	912041.48	675315.06	Broward	60	65	SAS	100%	2	0						Not Used	sparse data
100165	G-2451	USGS	922755.87	680934.32	Broward	61	66	SAS	100%	2	0						Not Used	sparse data
100160	G-2452	USGS	918754.45	679899.71	Broward	28	33	SAS	100%	2	0						Not Used	sparse data
100161	G-2453	USGS	918754.45	679899.71	Broward	71	76	SAS	100%	2	0						Not Used	sparse data
100169	G-2454	USGS	916551.72	682612.43	Broward	23	28	SAS	100%	2	0						Not Used	sparse data
100170	G-2455	USGS	916551.72	682612.43	Broward	72	77	SAS	100%	2	0						Not Used	sparse data
100153	G-2456	USGS	920035.27	678998.88	Broward	29	34	SAS	100%	2	0						Not Used	sparse data
100154	G-2457	USGS	920035.27	678998.88	Broward	61	66	SAS	100%	1	0						Not Used	sparse data
100133	G-2458	USGS	921429.27	674564.75	Broward	19	21	SAS	100%	2	0						Not Used	sparse data
100134	G-2459	USGS	921429.27	674564.75	Broward	60	65	SAS	100%	2	0						Not Used	sparse data
100138	G-2460	USGS	920779.67	676479.18	Broward	22	24	SAS	100%	2	0						Not Used	sparse data
100139	G-2461	USGS	920779.67	676479.18	Broward	60	65	SAS	100%	2	0						Not Used	sparse data
100065	G-2470	USGS	925317.79	606736.25	Broward	18.6	20.6	SAS	100%	2	0						Not Used	sparse data
100066	G-2471	USGS	925317.79	606736.25	Broward	42.8	47.8	SAS	100%	2	0						Not Used	sparse data
100067	G-2472	USGS	926046.46	606942.77	Broward	20.2	22.2	SAS	100%	2	0						Not Used	sparse data
100069	G-2474	USGS	926317.64	607348.35	Broward	93.4	98.4	SAS	100%	2	0						Not Used	sparse data
100198	G-2475	USGS	921352.11	701524.09	Broward	16.6	18.6	SAS	100%	2	0						Not Used	sparse data
100062	G-2477	USGS	933637.75	604163.98	Broward	75	80	SAS	100%	10	13	SAS						
100063	G-2478	USGS	933637.75	604163.98	Broward	180	200	SAS	100%	10	13	SAS						
100183	G-2479	USGS	947531.71	694223.57	Broward	20	25	SAS	100%	2	0						Not Used	sparse data
100184	G-2480	USGS	947622.77	694224.20	Broward	82	102	SAS	100%	8	0	SAS						
100171	G-2482	USGS	921272.73	685064.94	Broward	18	20	SAS	100%	2	0						Not Used	sparse data
100204	G-2483	USGS	912737.66	710861.64	Broward	17.5	19.5	SAS	100%	2	0						Not Used	sparse data

Table 4.1: Usage of SAJ Observation Database in Regional Model Calibration

Model ID[a]	Well Name	Data Source	Easting[b]	Northing[b]	County	Cased Depth (ft)	Drilled Depth (ft)	Dominant Layer[c]	% Open Section in Layer[c]	93/94 Months with Data[d]	03/04 Months with Data[e]	Use for Data in Model Setup/Calibration						Reasoning/Comments
													Observations for Calibration					
												Boundary Conditions[f]	Steady State (Oct 03)	Steady State (Feb 04)	Transient (03/04)	Transient (03/04	Not Used	
100202	G-2484	USGS	900480.47	705538.65	Broward	17	19	SAS	100%	2	0						Not Used	sparse data
100196	G-2485	USGS	891864.68	699734.52	Broward	17	19	SAS	100%	2	0						Not Used	sparse data
100195	G-2486	USGS	902803.73	697373.34	Broward	19	21	SAS	100%	2	0						Not Used	sparse data
100026	G-2612	USGS	933365.22	618096.23	Broward	253	273	SAS	56%	0	14	SAS						
112123	G-2617	SFWMD	714531.25	668029.48	Broward	1648	1726	APPZ	96%	0	15		APPZ	APPZ	APPZ			no 93/94 data
112124	G-2618	SFWMD	714531.25	668029.48	Broward	1104	1164	UF	100%	0	15		UF	UF	UF			no 93/94 data
112125	G-2619	SFWMD	714531.25	668029.48	Broward	895	1052	UF	89%	0	15						Not Used	Open section of nearby well (112124) completely in UF
100212	G-2704	USGS	942275.88	717412.20	Broward	33	38	SAS	100%	0	0						Not Used	sparse data
100218	G-2708	USGS	939350.18	719412.06	Broward	35	40	SAS	100%	4	0						Not Used	sparse data
100209	G-2711	USGS	945647.93	716728.28	Broward	32	37	SAS	100%	9	0	SAS						
100222	G-2712	USGS	945711.32	720767.77	Broward	33	38	SAS	100%	9	0	SAS						
100206	G-2713	USGS	941203.51	714476.68	Broward	35	40	SAS	100%	4	0						Not Used	sparse data
100223	G-2714	USGS	941252.38	720737.51	Broward	35	40	SAS	100%	4	0						Not Used	sparse data
100207	G-2716	USGS	948567.15	715738.57	Broward	35	40	SAS	100%	9	0	SAS						
100237	G-2718	USGS	944589.75	725102.09	Broward	130	150	SAS	100%	9	0	SAS						
100228	G-2719	USGS	944335.34	722374.00	Broward	155	175	SAS	100%	9	0	SAS						
100210	G-2721	USGS	938183.97	716879.88	Broward	155	175	SAS	100%	4	0						Not Used	sparse data
100214	G-2722	USGS	934257.42	718873.43	Broward	155	175	SAS	100%	4	0						Not Used	sparse data
100213	G-2723	USGS	942364.84	717715.73	Broward	154	174	SAS	100%	4	0	SAS						
100211	G-2724	USGS	952467.16	717684.23	Broward	154	174	SAS	100%	9	0	SAS						
100229	G-2725	USGS	949974.96	722715.70	Broward	150	170	SAS	100%	9	0	SAS						
100221	G-2726	USGS	937340.11	720610.37	Broward	110	130	SAS	100%	4	0						Not Used	sparse data
100208	G-2727	USGS	948477.53	715536.00	Broward	160	180	SAS	100%	5	0						Not Used	sparse data
100233	G-2728	USGS	946328.93	723599.34	Broward	156	176	SAS	100%	9	0	SAS						
100236	G-2729	USGS	947593.80	724920.72	Broward	136	156	SAS	100%	9	0	SAS						
100235	G-2730	USGS	951059.16	723833.98	Broward	142	162	SAS	100%	9	0	SAS						
100234	G-2731	USGS	950607.01	723426.93	Broward	150	170	SAS	100%	9	0	SAS						
100230	G-2733	USGS	951519.06	723130.35	Broward	130	150	SAS	100%	6	0	SAS						
100220	G-2735	USGS	951082.38	720501.91	Broward	130	150	SAS	100%	9	0	SAS						
100217	G-2736	USGS	952545.44	719502.36	Broward	155	175	SAS	100%	9	0	SAS						
100225	G-2737	USGS	948976.81	722304.88	Broward	130	150	SAS	100%	9	0	SAS						
100224	G-2738	USGS	942886.25	721354.40	Broward	91	96	SAS	100%	4	0						Not Used	sparse data
100215	G-2739	USGS	900752.85	718695.56	Broward	19	21	SAS	100%	10	13	SAS						
100019	G-2807	USGS	929873.44	607774.76	Broward	180	200	SAS	100%	0	11	SAS						
101030	G-2852	USGS	928208.44	725498.48	Broward	120	140	SAS	100%	10	0	SAS						
111873	G-2852	SFWMD	931365.16	715623.03	Broward	130	140	SAS	100%	0	15	SAS						
100238	G-2853	USGS	928390.42	725499.65	Broward	17	19	SAS	100%	9	0	SAS						
100049	G-2866	USGS	946786.32	707879.41	Broward	18	20	SAS	100%	0	15	SAS						
100027	G-2900	USGS	920814.33	627378.70	Broward	94.5	114.5	SAS	100%	0	15	SAS						
100116	G-457	USGS	913929.71	649275.79	Broward	19.7	21.7	SAS	100%	2	0						Not Used	sparse data
100112	G-482	USGS	916126.54	647774.54	Broward	17.9	19.9	SAS	100%	2	0						Not Used	sparse data
100108	G-484	USGS	916047.05	645855.61	Broward	18	20	SAS	100%	2	0						Not Used	sparse data
100100	G-561	USGS	938850.95	641589.30	Broward	18.3	20.3	SAS	100%	10	15	SAS						
111415	G-561_G	SFWMD	938851.44	641588.93	Broward	19.7	20.3	SAS	100%	10	15	SAS						
100102	G-582	USGS	916249.04	642625.76	Broward	21	23	SAS	100%	2	0						Not Used	sparse data
100105	G-587	USGS	916605.08	644041.53	Broward	20.8	22.8	SAS	100%	2	0						Not Used	sparse data
100101	G-603	USGS	916071.00	641917.88	Broward	108	128	SAS	100%	2	0						Not Used	sparse data
110644	G-616_G	SFWMD	908355.44	710561.27	Broward	19	23.7	SAS	100%	10	0	SAS						
100094	G-617	USGS	873133.19	638176.45	Broward	24	29	SAS	100%	10	15	SAS						
111336	G-617_G	SFWMD	873133.73	638176.25	Broward	28	29	SAS	100%	10	15	SAS						
110648	G-820A	SFWMD	930777.40	677784.18	Broward	99	100	SAS	100%	10	0	SAS						
100185	G-853	USGS	944051.35	695037.35	Broward	22	27	SAS	100%	10	15	SAS						
111326	G-853_G	SFWMD	944051.93	695036.91	Broward	27	0	Error	0%	10	15	SAS						
100099	G-854	USGS	925835.99	640362.83	Broward	186	206	SAS	97%	10	0	SAS						
100128	G-870	USGS	930007.30	672296.67	Broward	10.5	12.5	SAS	100%	2	0						Not Used	sparse data
100117	G-986	USGS	915284.71	651303.42	Broward	10.5	12.5	SAS	100%	2	0						Not Used	sparse data
100114	G-988	USGS	920678.60	648711.23	Broward	10.5	12.5	SAS	100%	2	0						Not Used	sparse data
100104	G-990	USGS	914329.09	643522.86	Broward	10.5	12.5	SAS	100%	2	0						Not Used	sparse data
100180	GP-1351	USGS	946535.62	693408.95	Broward	14	16	SAS	100%	1	0						Not Used	sparse data
100188	GP-1355	USGS	944414.56	697332.54	Broward	134	154	SAS	100%	2	0						Not Used	sparse data
100186	GP-1357	USGS	944247.53	695109.95	Broward	183	203	SAS	100%	1	0						Not Used	sparse data
112150	MIR-MZU	SFWMD	875503.19	603616.90	Broward	1600	1700	APPZ	71%	0	15		APPZ	APPZ	APPZ			no 93/94 data
111412	S-329_G	SFWMD	916653.00	648718.00	Broward	63	68	SAS	100%	10	15	SAS						
111140	WCA2E4_G3	SFWMD	866899.56	718715.29	Broward	21.7	23.7	SAS	100%	0	15	SAS						
111181	WCA2E4_G4	SFWMD	866909.56	718725.29	Broward	11	13.7	SAS	100%	0	15	SAS						
111999	WCA2E4_G5	SFWMD	866949.56	718765.29	Broward	105.1	125.1	SAS	100%	0	15	SAS						
111180	WCA2E4_G6	SFWMD	866919.56	718735.29	Broward	59.33	64.33	SAS	100%	0	15	SAS						
111179	WCA2E4_G7	SFWMD	866929.56	718745.29	Broward	31.54	36.54	SAS	100%	0	15	SAS						
111178	WCA2E4_G8	SFWMD	866899.56	718715.29	Broward	19.38	21.38	SAS	100%	0	15	SAS						

Table 4.1: Usage of SAJ Observation Database in Regional Model Calibration

Model ID[a]	Well Name	Data Source	Easting[b]	Northing[b]	County	Cased Depth (ft)	Drilled Depth (ft)	Dominant Layer[c]	% Open Section in Layer[c]	93/94 Months with Data[d]	03/04 Months with Data[e]	Use for Data in Model Setup/Calibration						Reasoning/Comments
													Observations for Calibration					
												Boundary Conditions[f]	Steady State (Oct 03)	Steady State (Feb 04)	Transient (03/04)	Transient (03/04	Not Used	
111138	WCA2F4_G3	SFWMD	857574.80	721376.63	Broward	24.3	29.3	SAS	100%	0	15	SAS						
111163	WCA2F4_G4	SFWMD	857574.80	721376.63	Broward	11.05	13.05	SAS	100%	0	15	SAS						
111142	WCA2U1_GW3	SFWMD	867369.01	693780.54	Broward	26.9	28.9	SAS	100%	0	15	SAS						
111141	WCA2U1_GW4	SFWMD	867369.01	693780.54	Broward	19.38	21.38	SAS	100%	0	15	SAS						
111137	WCA2U3_G	SFWMD	849099.15	710755.19	Broward	29.2	34.2	SAS	100%	0	15	SAS						
111182	WCA2U3_G4	SFWMD	849099.15	710755.19	Broward	122.6	124.6	SAS	100%	0	15	SAS						
111177	WCA2U3_G5	SFWMD	849139.15	710795.19	Broward	104.6	124.6	SAS	100%	0	15	SAS						
111176	WCA2U3_G6	SFWMD	849109.15	710765.19	Broward	60.44	65.44	SAS	100%	0	15	SAS						
111175	WCA2U3_G7	SFWMD	849119.15	710775.19	Broward	31.45	36.45	SAS	100%	0	15	SAS						
111162	WCA2U3_G8	SFWMD	849129.15	710785.19	Broward	18.1	20.1	SAS	100%	0	15	SAS						
100271	41S23E10 USGS C3 343 FL	USGS	329732.00	940787.00	Charlotte	185	205	IAS/ICU	100%	1	2						Not Used	No calibration in IAS/ICU
100265	42S20E12 65021501241 FL	USGS	245126.02	912335.64	Charlotte	393	413	IAS/ICU	100%	1	2						Not Used	sparse data
100270	BABCOCK 5 NEAR PUNTA GORDA FL	USGS	413351.95	927244.23	Charlotte	264	284	IAS/ICU	100%	1	2						Not Used	No calibration in IAS/ICU
100274	BROWNS DEEP WELL AT PUNTA GORDA FL	USGS	320426.28	949749.15	Charlotte	800	900	UF	100%	1	2						Not Used	sparse data
112110	BSU-MZL	SFWMD	318215.63	887838.61	Charlotte	1832	1868	MC2	100%	0	7						Not Used	Model geology puts this well in MC2
112111	BSU-MZU	SFWMD	318215.63	887838.61	Charlotte	1207	1287	MC1	100%	0	7						Not Used	Model geology puts this well in MC1
100264	CH-311	USGS	339303.42	910406.55	Charlotte	200	220	IAS/ICU	100%	10	15						Not Used	No calibration in IAS/ICU
100243	CH-323	USGS	405416.78	896849.47	Charlotte	28	33	SAS	100%	0	15	SAS						
100244	CH-324	USGS	405416.78	896849.47	Charlotte	172	192	IAS/ICU	100%	0	15						Not Used	No calibration in IAS/ICU
100267	OLD FAITHFUL DEEP WELL NEAR PUNTA GORDA FL	USGS	322517.27	918415.54	Charlotte	1354	1454	MC1	100%	0	0						Not Used	Model geology puts this well in MC1
100280	PORT CHARLOTTE DEEP WELL A NEAR PORT CHARLOTTE FL	USGS	310172.78	980020.28	Charlotte	330	350	IAS/ICU	100%	7	0						Not Used	No calibration in IAS/ICU
100281	PORT CHARLOTTE SHALLOW NEAR PORT CHARLOTTE FL	USGS	310172.78	980020.28	Charlotte	84	89	IAS/ICU	100%	6	0						Not Used	No calibration in IAS/ICU
130011	PORT CHARLOTTE UTIL DEEP		303788.81	966693.12	Charlotte	128	156	IAS/ICU	100%	0	0						Not Used	No calibration in IAS/ICU
100279	PORT CHARLOTTE UTILITIES DEEP FL	USGS	303726.86	966643.15	Charlotte	128	156	IAS/ICU	100%	7	0						Not Used	No calibration in IAS/ICU
130014	PUNTA GORDA HEIGHTS INT	SWFWMD	328078.59	919987.85	Charlotte	84	125	IAS/ICU	100%	10	0						Not Used	No calibration in IAS/ICU
100269	PUNTA GORDA HEIGHTS WELL NEAR PUNTA GORDA FL	USGS	328145.02	920110.56	Charlotte	84	125	IAS/ICU	100%	7	15						Not Used	No calibration in IAS/ICU
130006	ROMP 10 SURF	SWFWMD	330563.17	981824.78	Charlotte	20	30	IAS/ICU	54%	0	15	SAS						
100258	ROMP 11 HAWTHORN WELL NEAR PUNTA GORDA FL	USGS	351344.37	962010.95	Charlotte	220	335	IAS/ICU	100%	0	2						Not Used	No calibration in IAS/ICU
130010	ROMP 11 HTRN	SWFWMD	351344.20	961987.72	Charlotte	220	335	IAS/ICU	100%	10	15						Not Used	No calibration in IAS/ICU
130029	ROMP 5 12-IN SURF	SWFWMD	393029.00	950317.07	Charlotte	5	85	SAS	79%	0	12	SAS						
130033	ROMP 5 6-IN AVPK	SWFWMD	392952.02	950309.48	Charlotte	1350	1400	MC1	61%	0	15						Not Used	Model geology puts this well in MC1
130032	ROMP 5 6-IN SWNN	SWFWMD	392998.23	950318.27	Charlotte	720	970	UF	100%	0	15		UF	UF	UF			no 93/94 data
130031	ROMP 5 LOWER INT	SWFWMD	393019.05	950318.14	Charlotte	450	600	IAS/ICU	100%	0	15						Not Used	No calibration in IAS/ICU
130028	ROMP 5 SURF	SWFWMD	393031.70	950315.03	Charlotte	5	85	SAS	79%	0	15	SAS						
130030	ROMP 5 UPPER INT	SWFWMD	392998.23	950317.26	Charlotte	130	230	IAS/ICU	100%	0	15						Not Used	No calibration in IAS/ICU
130018	ROMP TR 1-2 L HTRN/TMPA	SWFWMD	336128.10	912400.22	Charlotte	520	600	IAS/ICU	100%	10	15						Not Used	No calibration in IAS/ICU
130025	ROMP TR 1-2 SURF	SWFWMD	336117.22	912399.30	Charlotte	26	46	SAS	100%	10	15	SAS						
130027	ROMP TR 1-2 SWNN	SWFWMD	336126.21	912391.15	Charlotte	980	1184	UF	74%	10	15		UF	UF	UF	UF		
130026	ROMP TR 1-2 UP HTRN	SWFWMD	336114.39	912385.18	Charlotte	218	255	IAS/ICU	100%	10	15						Not Used	No calibration in IAS/ICU
130017	ROMP TR 3-1 HTRN 160	SWFWMD	259340.83	950829.62	Charlotte	140	160	IAS/ICU	100%	10	15						Not Used	No calibration in IAS/ICU
130000	ROMP TR 3-1 HTRN 270	SWFWMD	259335.31	950819.57	Charlotte	250	270	IAS/ICU	100%	0	15						Not Used	No calibration in IAS/ICU
130001	ROMP TR 3-1 HTRN 400	SWFWMD	259335.31	950819.57	Charlotte	380	400	IAS/ICU	100%	10	15						Not Used	No calibration in IAS/ICU
100276	ROMP TR 3-1 PEACE RIVER 400FT WELL NR EL JOBEAN FL	USGS	259340.01	950837.71	Charlotte	380	400	IAS/ICU	100%	1	2						Not Used	No calibration in IAS/ICU
130009	ROMP TR 3-1 SURF	SWFWMD	259343.48	950822.53	Charlotte	14	18	SAS	100%	10	15	SAS						
130002	ROMP TR 3-1 SWNN	SWFWMD	259335.31	950819.57	Charlotte	600	620	UF	100%	10	15		UF	UF	UF	UF		
130016	ROMP TR 3-1 TAMIAMI 75	SWFWMD	259340.83	950829.62	Charlotte	55	75	IAS/ICU	100%	10	15						Not Used	No calibration in IAS/ICU
130022	ROMP TR 3-3 AVPK	SWFWMD	222846.45	944410.16	Charlotte	1602	1652	APPZ	100%	10	15	APPZ						
130019	ROMP TR 3-3 LOW HTRN	SWFWMD	222845.55	944410.17	Charlotte	370	410	IAS/ICU	100%	5	15	IAS-layer 2						
130021	ROMP TR 3-3 OCAL	SWFWMD	222846.45	944410.16	Charlotte	1080	1120	UF	100%	10	15	UF						averaged with 130023
130024	ROMP TR 3-3 SURF	SWFWMD	222844.64	944410.18	Charlotte	10	30	SAS	100%	10	15	SAS						
130023	ROMP TR 3-3 SWNN	SWFWMD	222843.74	944410.19	Charlotte	680	900	UF	100%	5	15	UF						averaged with 130021
130020	ROMP TR 3-3 UP HTRN	SWFWMD	222845.55	944410.17	Charlotte	155	175	IAS/ICU	100%	10	15	IAS-layer 3						
100275	ROMP TR3-1 PEACE RIV 160FT W NR PORT CHARLOTTE FL	USGS	259340.10	950847.81	Charlotte	140	160	IAS/ICU	100%	1	2						Not Used	No calibration in IAS/ICU
100277	ROMP TR3-1 SUWANNEE WELL NR EL JOBEAN FL	USGS	259340.01	950837.71	Charlotte	520	620	UF	92%	1	2						Not Used	sparse data
100253	ROMP TR3-1 TAMIAMI WELL NEAR PORT CHARLOTTE FL	USGS	259312.76	950827.87	Charlotte	55	75	IAS/ICU	100%	0	2						Not Used	No calibration in IAS/ICU
100251	ROMP TR3-3 ARCADIA 175-FT WELL NR ENGLEWOOD FL	USGS	222845.55	944410.17	Charlotte	155	175	IAS/ICU	100%	0	2						Not Used	No calibration in IAS/ICU
100273	ROMP TR3-3 ARCADIA 410-FT WELL NR ENGLEWOOD FL	USGS	222783.60	944287.60	Charlotte	370	410	IAS/ICU	100%	1	0						Not Used	sparse data

Table 4.1: Usage of SAJ Observation Database in Regional Model Calibration

Model ID[a]	Well Name	Data Source	Easting[b]	Northing[b]	County	Cased Depth (ft)	Drilled Depth (ft)	Dominant Layer[c]	% Open Section in Layer[c]	93/94 Months with Data[d]	03/04 Months with Data[e]	Use for Data in Model Setup/Calibration						Reasoning/Comments
													Observations for Calibration					
												Boundary Conditions[f]	Steady State (Oct 03)	Steady State (Feb 04)	Transient (03/04)	Transient (03/04	Not Used	
100272	ROMP TR3-3 SUWANNEE WELL NEAR ENGLEWOOD FL	USGS	222843.74	944410.19	Charlotte	680	900	UF	100%	1	2						Not Used	same as 130023, with sparse data
130012	SR 74 DEEP	SWFWMD	353306.48	950887.90	Charlotte	194	280	IAS/ICU	100%	0	15						Not Used	No calibration in IAS/ICU
130015	SR 74 SHALLOW	SWFWMD	353309.18	950885.86	Charlotte	21	25	SAS	100%	6	15	SAS						
130013	SR 74 SHALLOW	SWFWMD	353334.61	950897.79	Charlotte	75	77	IAS/ICU	100%	9	15						Not Used	No calibration in IAS/ICU
100257	ST HWY 74 DEEP NEAR PUNTA GORDA FL	USGS	353307.39	950887.90	Charlotte	194	280	IAS/ICU	100%	0	2						Not Used	No calibration in IAS/ICU
100278	ST HWY 74 SHALLOW NEAR PUNTA GORDA FL		353460.00	950695.00	Charlotte	21	25	SAS	100%	0	0						Not Used	missing data
100266	TUCKERS CORNER DEEP WELL NEAR PUNTA GORDA FL	USGS	408287.89	917812.38	Charlotte	215	235	IAS/ICU	100%	1	0						Not Used	No calibration in IAS/ICU
100268	USGS C1 121 FL	USGS	365903.30	918391.15	Charlotte	244	264	IAS/ICU	100%	1	0						Not Used	No calibration in IAS/ICU
112128	175-MZ2	SFWMD	416556.67	668295.47	Collier	905	1050	UF	100%	0	15	UF						
112142	BICY-MZ1	SFWMD	554522.19	567147.92	Collier	460	534	IAS/ICU	100%	0	15	IAS-layer 3						
112143	BICY-MZ2	SFWMD	554522.19	567147.92	Collier	838	890	UF	92%	0	15	UF						
112141	BICY-MZ3	SFWMD	554522.19	567147.92	Collier	1550	1785	MC1	99%	0	15	APPZ						
112144	BICY-MZ4	SFWMD	554522.19	567147.92	Collier	2260	2505	MC2	100%	0	15	LF						
100322	C-1003	USGS	393673.68	695247.00	Collier	56	61	SAS	100%	9	0	SAS						
100333	C-1004	USGS	401011.15	705582.29	Collier	55	60	SAS	100%	0	0						Not Used	sparse data
110805	C-1004_G	SFWMD	400992.69	705533.08	Collier	52	60	SAS	100%	10	15	SAS						
100334	C-1004R		400992.72	705734.90	Collier	55	60	SAS	100%	0	0						Not Used	Missing data
100299	C-1053	USGS	403855.91	677212.25	Collier	105	125	SAS	100%	10	0	SAS						
100303	C-1054	USGS	403855.91	677212.25	Collier	20	25	SAS	100%	10	12	SAS						
100306	C-1055	USGS	431194.49	662014.49	Collier	20	25	SAS	100%	8	11	SAS						
100329	C-1057	USGS	403879.29	701092.04	Collier	8.5	10.5	SAS	100%	10	12	SAS						
100330	C-1058	USGS	403879.41	701112.24	Collier	75	80	SAS	100%	10	12	SAS						
100331	C-1059	USGS	393180.55	703832.79	Collier	20	25	SAS	100%	10	15	SAS						
100325	C-1060	USGS	393714.04	697357.10	Collier	20	25	SAS	100%	10	0	SAS						
100311	C-1061	USGS	393800.92	686360.59	Collier	20	25	SAS	100%	10	15	SAS						
100286	C-1067	USGS	478244.97	625747.39	Collier	60	65	SAS	100%	10	0	SAS						
100287	C-1068	USGS	478244.97	625747.39	Collier	180	200	IAS/ICU	100%	10	0						Not Used	sparse data
100292	C-1069	USGS	537441.05	661889.17	Collier	45	50	SAS	100%	10	0	SAS						
100293	C-1070	USGS	537441.05	661889.17	Collier	185	205	IAS/ICU	100%	10	12						Not Used	No calibration in IAS/ICU
100349	C-1071	USGS	555768.20	716089.98	Collier	30	35	SAS	100%	10	15	SAS						
110730	C-1071_G	SFWMD	560046.65	716382.63	Collier	20	35	SAS	100%	10	0	SAS						
100350	C-1072	USGS	555768.20	716089.98	Collier	240	260	IAS/ICU	100%	10	15						Not Used	No calibration in IAS/ICU
110726	C-1072_G	SFWMD	560046.65	716382.63	Collier	140	260	IAS/ICU	100%	10	0						Not Used	No calibration in IAS/ICU
100343	C-1073	USGS	526662.95	713110.02	Collier	140	160	SAS	100%	10	12	SAS						
100365	C-1074		567167.97	759248.04	Collier	110	130	IAS/ICU	90%	0	0						Not Used	No calibration in IAS/ICU
110669	C-1074_G	SFWMD	567054.15	759276.62	Collier	100	130	IAS/ICU	59%	10	15	SAS						
100371	C-1075	USGS	536562.28	778737.46	Collier	18	20	SAS	100%	10	13	SAS						
100372	C-1076	USGS	536404.90	778609.18	Collier	80	85	SAS	100%	10	12	SAS						
100373	C-1077	USGS	536404.90	778609.18	Collier	190	210	IAS/ICU	100%	10	15						Not Used	No calibration in IAS/ICU
100369	C-1078	USGS	508272.96	763351.38	Collier	33	38	SAS	100%	10	15	SAS						
100359	C-1079	USGS	500159.17	739379.42	Collier	370	390	IAS/ICU	100%	10	15						Not Used	No calibration in IAS/ICU
110912	C-1079_G	SFWMD	500159.68	739378.82	Collier	298	390	IAS/ICU	100%	10	15						Not Used	No calibration in IAS/ICU
100361	C-1080	USGS	457995.29	742253.01	Collier	289	309	IAS/ICU	100%	9	14						Not Used	No calibration in IAS/ICU
100347	C-1082	USGS	396842.26	717552.76	Collier	18	20	SAS	100%	10	0	SAS						
110848	C-1083	SFWMD	397326.07	711885.40	Collier	58	74	SAS	100%	10	10	SAS						
100348	C-1083	USGS	397838.12	721171.63	Collier	69	74	SAS	100%	0	0						Not Used	sparse data
100309	C-1085	USGS	404623.44	683770.88	Collier	55	60	SAS	100%	10	0	SAS						
100308	C-1086	USGS	404714.52	683770.34	Collier	86	91	SAS	100%	10	0	SAS						
100317	C-1093	USGS	403845.71	690843.54	Collier	15	17	SAS	100%	10	0	SAS						
100321	C-1094	USGS	397041.99	695125.34	Collier	19	21	SAS	100%	10	12	SAS						
100346	C-1097	USGS	460782.06	715482.94	Collier	16	18	SAS	100%	10	15	SAS						
100362	C-1244	USGS	483352.36	744291.30	Collier	75	80	SAS	100%	0	15	SAS						
100366	C-131		567167.97	759248.04	Collier	49	54	SAS	100%	0	0						Not Used	Missing data
100363	C-258	USGS	519980.87	757657.66	Collier	683	783	IAS/ICU	69%	3	15						Not Used	No calibration in IAS/ICU
111437	C-296	SFWMD	542933.93	646358.80	Collier	8	45	SAS	100%	0	15	SAS						
100289	C-296	USGS	542959.07	646729.63	Collier	40	45	SAS	100%	10	15	SAS						
100364	C-298	USGS	525801.16	758245.06	Collier	283	303	IAS/ICU	100%	10	15						Not Used	No calibration in IAS/ICU
100335	C-303	USGS	430150.20	705538.17	Collier	280	300	IAS/ICU	100%	10	12						Not Used	No calibration in IAS/ICU
100336	C-304	USGS	458211.46	706791.30	Collier	110	130	SAS	100%	10	6	SAS						
100320	C-321	USGS	397131.20	694821.88	Collier	18.3	20.3	SAS	100%	10	0	SAS						
100368	C-363	USGS	522997.59	762898.37	Collier	99	119	SAS	100%	10	12	SAS						
110723	C-391_G	SFWMD	396440.21	675672.46	Collier	70	75	SAS	100%	10	0	SAS						
110740	C-392	SFWMD	399264.32	675656.80	Collier	24.5	30	SAS	100%	10	0	SAS						
100302	C-392	USGS	508197.76	671099.47	Collier	8	10	SAS	100%	10	0	SAS						
110664	C-409A	SFWMD	393761.18	669632.30	Collier	63	73	SAS	100%	10	0	SAS						
100327	C-424	USGS	393610.73	699791.19	Collier	112	132	SAS	100%	1	0						Not Used	Outside Boundary

Table 4.1: Usage of SAJ Observation Database in Regional Model Calibration

Model ID[a]	Well Name	Data Source	Easting[b]	Northing[b]	County	Cased Depth (ft)	Drilled Depth (ft)	Dominant Layer[c]	% Open Section in Layer[c]	93/94 Months with Data[d]	03/04 Months with Data[e]	Use for Data in Model Setup/Calibration						Reasoning/Comments
													Observations for Calibration					
												Boundary Conditions[f]	Steady State (Oct 03)	Steady State (Feb 04)	Transient (03/04)	Transient (03/04	Not Used	
100304	C-430	USGS	403855.91	677212.25	Collier	60	65	SAS	100%	10	0	SAS						
110636	C-430_G	SFWMD	404189.94	676736.53	Collier	63	65	SAS	100%	5	0	SAS						
100318	C-458	USGS	397657.24	691486.57	Collier	58	63	SAS	100%	10	0	SAS						
100319	C-460	USGS	398825.74	691964.15	Collier	61	66	SAS	100%	0	0						Not Used	Outside Boundary
110731	C-460_G	SFWMD	398908.89	692216.33	Collier	64	66	SAS	100%	10	0	SAS						
100370	C-462	USGS	513368.37	772247.18	Collier	90	110	SAS	100%	10	15	SAS						
110672	C-462_G	SFWMD	513368.68	772246.66	Collier	50	110	SAS	100%	10	0	SAS						
100310	C-489	USGS	396450.63	687757.94	Collier	78	83	SAS	100%	10	15	SAS						
100307	C-490	USGS	393802.79	686663.50	Collier	66	71	SAS	100%	10	15	SAS						
100360	C-492	USGS	458060.12	742383.28	Collier	35	40	SAS	100%	10	15	SAS						
111845	C-492	SFWMD	458061.34	742383.41	Collier	60	64	SAS	100%	10	15	SAS						
100283	C-495	USGS	553768.81	592990.60	Collier	65	70	SAS	100%	10	12	SAS						
100284	C-496	USGS	521300.61	608359.88	Collier	52	57	SAS	100%	10	15	SAS						
110729	C-496	SFWMD	521317.03	613206.20	Collier	9	57	SAS	100%	10	0	SAS						
110728	C-503		525728.78	713143.22	Collier	8	20.4	SAS	100%	0	0						Not Used	Missing data
100344	C-503	USGS	526729.03	713241.00	Collier	18.4	20.4	SAS	100%	10	15	SAS						
110670	C-506A_G	SFWMD	393750.45	682657.28	Collier	50	71	SAS	100%	10	0	SAS						
100314	C-515	USGS	393731.67	689895.07	Collier	66	71	SAS	100%	10	0	SAS						
110676	C-531	SFWMD	506314.24	781661.65	Collier	210	237	IAS/ICU	77%	10	0	SAS						
100374	C-532	USGS	505805.00	784967.62	Collier	11	13	SAS	100%	10	8	SAS						
100301	C-54	USGS	694499.48	668536.84	Collier	6.5	8.5	SAS	100%	10	15	SAS						
111382	C-54_G	SFWMD	694318.21	668233.76	Collier	7.2	8.5	SAS	100%	10	15	SAS						
100323	C-575	USGS	393531.45	686968.09	Collier	552	652	IAS/ICU	100%	2	15	IAS-layer 3						
110654	C-598_G	SFWMD	487421.00	692580.00	Collier	31	36	SAS	100%	10	0	SAS						
100341	C-684	USGS	526662.95	713110.02	Collier	470	490	IAS/ICU	100%	2	15						Not Used	No calibration in IAS/ICU
100367	C-687	USGS	499973.97	763005.97	Collier	290	310	IAS/ICU	100%	10	15						Not Used	No calibration in IAS/ICU
100345	C-688	USGS	460782.06	715482.94	Collier	222	242	IAS/ICU	100%	10	15						Not Used	No calibration in IAS/ICU
100342	C-689	USGS	526662.95	713110.02	Collier	245	265	IAS/ICU	100%	10	15						Not Used	No calibration in IAS/ICU
100288	C-690	USGS	478028.72	645974.55	Collier	43	48	SAS	100%	6	15	SAS						
110747	C-690_G	SFWMD	478027.84	645470.06	Collier	43	48	SAS	100%	6	0	SAS						
100316	C-948	USGS	463550.98	689855.65	Collier	400	420	IAS/ICU	100%	6	15						Not Used	No calibration in IAS/ICU
100315	C-951	USGS	463824.17	689854.41	Collier	150	170	SAS	100%	10	15	SAS						
110741	C-951_G	SFWMD	463915.97	689753.20	Collier	120	170	SAS	100%	10	0	SAS						
110732	C-953_G	SFWMD	463915.97	689753.20	Collier	12	40	SAS	100%	10	0	SAS						
100313	C-956	USGS	444544.65	689611.65	Collier	240	260	IAS/ICU	57%	10	0	SAS						
100352	C-963	USGS	459783.74	735681.57	Collier	320	340	IAS/ICU	100%	10	6						Not Used	No calibration in IAS/ICU
100355	C-965	USGS	543290.03	736890.52	Collier	440	460	IAS/ICU	100%	9	15						Not Used	No calibration in IAS/ICU
100354	C-966	USGS	543290.03	736890.52	Collier	35	40	SAS	100%	10	15	SAS						
110661	C-969_G	SFWMD	436158.00	622442.00	Collier	67	72	SAS	100%	10	0	SAS						
100337	C-971	USGS	463948.47	711328.71	Collier	130	150	SAS	100%	10	0	SAS						
100295	C-972	USGS	477744.89	658866.26	Collier	35	40	SAS	100%	10	12	SAS						
100294	C-973	USGS	477836.44	658966.84	Collier	130	150	SAS	100%	10	12	SAS						
100300	C-974	USGS	477677.86	664621.64	Collier	440	460	IAS/ICU	100%	9	15						Not Used	No calibration in IAS/ICU
100297	C-976	USGS	444135.71	662352.05	Collier	35	40	SAS	100%	10	15	SAS						
100298	C-977	USGS	444135.71	662352.05	Collier	120	140	SAS	100%	10	15	SAS						
100351	C-978	USGS	459783.74	735681.57	Collier	35	40	SAS	100%	10	0	SAS						
100353	C-979	USGS	459783.74	735681.57	Collier	93	113	SAS	100%	10	7	SAS						
100312	C-980	USGS	444544.65	689611.65	Collier	25	30	SAS	100%	10	12	SAS						
100356	C-981	USGS	500159.17	739379.42	Collier	55	60	SAS	100%	10	15	SAS						
100358	C-982	USGS	500159.17	739379.42	Collier	140	160	SAS	100%	10	15	SAS						
100357	C-983	USGS	500159.17	739379.42	Collier	420	520	IAS/ICU	100%	6	15						Not Used	No calibration in IAS/ICU
100338	C-984	USGS	498357.73	712802.11	Collier	35	40	SAS	100%	10	15	SAS						
100340	C-985	USGS	498357.73	712802.11	Collier	140	160	SAS	100%	10	15	SAS						
100305	C-986	USGS	542497.80	678837.38	Collier	35	40	SAS	100%	10	15	SAS						
100285	C-987	USGS	506214.67	625270.27	Collier	350	370	IAS/ICU	100%	7	13	IAS-layer 3						
100324	C-988	USGS	498748.72	695535.26	Collier	140	160	SAS	100%	0	0						Not Used	sparse data
110733	C-988_G	SFWMD	498814.20	695364.30	Collier	95	160	SAS	100%	10	0	SAS						
100339	C-989		498357.73	712802.11	Collier	250	270	IAS/ICU	100%	0	0						Not Used	No calibration in IAS/ICU
110665	C-989	SFWMD	498331.52	712428.89	Collier	235	270	IAS/ICU	100%	10	15						Not Used	No calibration in IAS/ICU
100282	C-995	USGS	538058.03	588184.75	Collier	32	37	SAS	100%	10	15	SAS						
100296	C-996	USGS	431102.84	661914.01	Collier	21.5	23.5	SAS	100%	10	0	SAS						
100328	C-997	USGS	430641.40	700417.36	Collier	20	22	SAS	100%	10	15	SAS						
110735	C-997_G	SFWMD	430642.25	700416.28	Collier	12	22	SAS	100%	10	0	SAS						
100332	C-998	USGS	410305.96	705648.56	Collier	57	62	SAS	100%	0	11	SAS						
100290	G-2034	USGS	543025.31	646863.13	Collier	20	22	SAS	100%	10	15	SAS						
111041	HF1_G		483720.29	750093.98	Collier	18	20	SAS	100%	0	0						Not Used	Missing data
111174	HF2_G		484059.75	750152.48	Collier	18	20	SAS	100%	0	0						Not Used	Missing data
111161	HF3_G	SFWMD	482805.40	744432.94	Collier	18	20	SAS	100%	0	14	SAS						
111173	HF4_G		483746.34	747957.87	Collier	18	20	SAS	100%	0	0						Not Used	Missing data

Table 4.1: Usage of SAJ Observation Database in Regional Model Calibration

Model ID[a]	Well Name	Data Source	Easting[b]	Northing[b]	County	Cased Depth (ft)	Drilled Depth (ft)	Dominant Layer[c]	% Open Section in Layer[c]	93/94 Months with Data[d]	03/04 Months with Data[e]	Use for Data in Model Setup/Calibration						Reasoning/Comments
													Observations for Calibration					
												Boundary Conditions[f]	Steady State (Oct 03)	Steady State (Feb 04)	Transient (03/04)	Transient (03/04	Not Used	
111128	HF7_G	SFWMD	483773.56	750525.42	Collier	18	20	SAS	100%	0	15	SAS						
112126	I75-MZ1	SFWMD	416556.67	668295.47	Collier	690	760	UF	95%	0	15						Not Used	close to boundary
112127	I75-MZ3	SFWMD	416556.67	668295.47	Collier	2300	2350	LF	100%	0	15	LF						
112152	IWSD-MZ2	SFWMD	514985.20	756311.02	Collier	1060	1140	UF	100%	0	15		UF	UF	UF			no 93/94 data
112153	IWSD-MZ3	SFWMD	514985.20	756311.02	Collier	1752	1880	APPZ	62%	0	15		APPZ	APPZ	APPZ			no 93/94 data
100326	J.C.BARNETTE NEAR FORT MEADE FL	USGS	389231.16	698303.90	Collier	21	23	SAS	100%	10	12	SAS						
111089	LUCKE_GW	SFWMD	494576.81	659051.59	Collier	18	20	SAS	100%	0	15	SAS						
111110	LUCKW_GW	SFWMD	493246.46	659076.84	Collier	18	20	SAS	100%	0	15	SAS						
100291	S-329	USGS	543025.31	646863.13	Collier	63	68	SAS	100%	10	15	SAS						
111857	SGT1W1	SFWMD	466110.12	659154.39	Collier	10	20	SAS	100%	0	15	SAS						
111861	SGT1W2	SFWMD	469920.55	659637.27	Collier	10	20	SAS	100%	0	15	SAS						
111860	SGT1W4	SFWMD	487616.99	659760.25	Collier	10	20	SAS	100%	0	15	SAS						
111858	SGT1W5	SFWMD	502068.45	658032.38	Collier	10	20	SAS	100%	0	15	SAS						
111702	SGT2W1	SFWMD	463592.49	646700.70	Collier	10	20	SAS	100%	0	15	SAS						
111727	SGT2W2	SFWMD	463619.06	646528.94	Collier	10	20	SAS	100%	0	15	SAS						
111350	SGT2W3	SFWMD	479534.75	645787.53	Collier	10	20	SAS	100%	0	15	SAS						
111703	SGT2W4	SFWMD	493355.14	645805.53	Collier	10	20	SAS	100%	0	15	SAS						
111731	SGT2W5	SFWMD	499888.02	645956.30	Collier	10	20	SAS	100%	0	14	SAS						
111728	SGT2W6	SFWMD	504905.05	639801.92	Collier	10	20	SAS	100%	0	14	SAS						
111441	SGT3W1	SFWMD	468282.35	625667.06	Collier	10	20	SAS	100%	0	13	SAS						
111445	SGT3W2	SFWMD	471277.83	625847.57	Collier	10	20	SAS	100%	0	10	SAS						
111443	SGT3W3	SFWMD	478274.10	624111.02	Collier	10	20	SAS	100%	0	13	SAS						
111447	SGT3W4	SFWMD	492387.60	626132.28	Collier	10	20	SAS	100%	0	15	SAS						
111446	SGT3W5	SFWMD	492308.06	626173.81	Collier	10	20	SAS	100%	0	15	SAS						
111444	SGT3W6	SFWMD	504109.50	620851.95	Collier	10	20	SAS	100%	0	15	SAS						
111442	SGT3W7	SFWMD	511312.93	623351.19	Collier	10	20	SAS	100%	0	15	SAS						
111462	SGT4W5	SFWMD	488328.16	615445.76	Collier	10	20	SAS	100%	0	13	SAS						
111454	SGT4W6	SFWMD	499092.05	615915.45	Collier	10	20	SAS	100%	0	15	SAS						
130047	AMAX 3 NR PINE LEVEL		329280.57	1065319.80	De Soto	340	1547	MC1	43%	0	0						Not Used	Open section straddles multiple layers
100397	AMAX NO 3 WELL NEAR PINE LEVEL FL	USGS	329659.53	1065529.08	De Soto	1447	1547	APPZ	100%	10	15		APPZ	APPZ	APPZ	APPZ		
100414	AMOCO 2 OIL TEST WELL NEAR ARCADIA FL	USGS	442709.79	1092016.38	De Soto	292	312	IAS/ICU	100%	1	2						Not Used	No calibration in IAS/ICU
130042	ARCADIA 1 INT		371976.01	1050059.41	De Soto	84	250	IAS/ICU	100%	0	0						Not Used	No calibration in IAS/ICU
130036	ARCADIA 2 INT		372098.88	1049942.42	De Soto	263	372	IAS/ICU	100%	0	0						Not Used	No calibration in IAS/ICU
100393	ARCADIA WELL 2 AT ARCADIA FL	USGS	372077.56	1049862.78	De Soto	352	372	IAS/ICU	100%	6	10						Not Used	No calibration in IAS/ICU
100396	BERTCHER WELL 704NR ARCADIA FL	USGS	361779.66	1062832.39	De Soto	300	320	IAS/ICU	100%	1	0						Not Used	No calibration in IAS/ICU
100394	BEVIS DEEP IRRIGATION WELL NEAR ARCADIA FL	USGS	409568.48	1055243.34	De Soto	1318	1418	APPZ	100%	1	2						Not Used	sparse data
130050	BONAGUA (HRS) INT		366665.15	1055341.22	De Soto	68	225	IAS/ICU	100%	0	0						Not Used	No calibration in IAS/ICU
130051	BUZZARD ROOST SURFICIAL		331197.34	1056822.02	De Soto	0	0	Error	0%	0	0						Not Used	Data error
100399	CAMP CHANYATAH WELL 49 NEAR ARCADIA FL	USGS	374643.17	1069638.84	De Soto	172	192	IAS/ICU	100%	0	1						Not Used	No calibration in IAS/ICU
100410	CARLTON SURFICIAL WELL NEAR KINSEY FL	USGS	388449.51	1079115.69	De Soto	410	430	IAS/ICU	100%	10	0						Not Used	No calibration in IAS/ICU
100388	CLAVEL RANCH WELL NEAR ARCADIA FL	USGS	315500.67	1044106.02	De Soto	370	390	IAS/ICU	100%	1	0						Not Used	No calibration in IAS/ICU
130034	CUNNINGHAM	SWFWMD	348115.10	1068477.09	De Soto	350	1040	MC1	44%	10	2						Not Used	Open section straddles multiple layers
100398	CUNNINGHAM WELL NEAR ARCADIA FL	USGS	348103.45	1068488.29	De Soto	350	1040	MC1	44%	1	0						Not Used	Open section straddles multiple layers
100375	EMERALD IS FARMS WELL D FL	USGS	446956.71	988082.50	De Soto	1500	1600	APPZ	100%	1	0						Not Used	sparse data
100404	FLA POWER & LIGHT WELL NEAR ARCADIA FL	USGS	409524.09	1077662.67	De Soto	1201	1301	MC1	51%	0	2						Not Used	Model geology puts this well in MC1
100380	GDU WELL M-2 NEAR FORT OGDEN FL	USGS	329744.98	1005016.68	De Soto	797	897	UF	67%	1	2						Not Used	Sparse data
100381	GDU WELL T-2 NEAR FORT OGDEN FL	USGS	329744.98	1005016.68	De Soto	476	496	IAS/ICU	100%	1	2						Not Used	No calibration in IAS/ICU
130041	HOLLINGSWORTH DEEP		335990.78	1069306.08	De Soto	71	1260	MC1	41%	0	0						Not Used	Open section straddles multiple layers
100413	HOLLINGSWORTH WELL 751 NEAR ARCADIA FL	USGS	331784.96	1093055.84	De Soto	410	430	UF	100%	0	0						Not Used	Sparse data
130049	LETTUCE LAKE		337389.07	996080.41	De Soto	105	1190	IAS/ICU	47%	0	0						Not Used	Open section straddles multiple layers
100378	LETTUCE LAKE WELL NEAR FORT OGDEN FL	USGS	337385.60	996099.62	De Soto	105	1190	IAS/ICU	47%	6	9						Not Used	Open section straddles multiple layers
100412	MARSHALL DEEP WELL NEAR GARDNER FL	USGS	394346.54	1092568.76	De Soto	458	478	IAS/ICU	55%	10	15						Not Used	No calibration in IAS/ICU
100402	MCINTYRE WELL NEAR ARCADIA FL	USGS	400132.67	1076307.01	De Soto	1224	1324	APPZ	70%	0	0						Not Used	sparse data
100385	MINUTE MAID WELL 43 FBG D-68 NEAR ARCADIA FL	USGS	361869.40	1037786.26	De Soto	305	325	IAS/ICU	100%	0	0						Not Used	No calibration in IAS/ICU
130048	MORGAN DEEP		347660.18	995731.12	De Soto	208	1010	IAS/ICU	56%	0	0						Not Used	No calibration in IAS/ICU
100377	MORGAN DEEP WELL NEAR FORT OGDEN FL	USGS	347644.04	995748.41	De Soto	208	1010	IAS/ICU	56%	6	8						Not Used	No calibration in IAS/ICU
100376	NAT WOLF CORP IRRIGATION WELL NEAR ARCADIA FL	USGS	390831.30	990336.09	De Soto	1500	1600	APPZ	100%	0	2						Not Used	Sparse data
100382	NUNEZ RED HAWK RANCH WELL NEAR NOCATEE FL	USGS	339976.93	1024892.04	De Soto	408	428	IAS/ICU	100%	1	2						Not Used	No calibration in IAS/ICU
130037	PINDER WELL		421323.58	1047314.09	De Soto	0	1365	MC1	41%	0	0						Not Used	Open section straddles multiple layers
100392	PINDER WELL FL	USGS	421256.99	1047196.32	De Soto	1265	1365	APPZ	66%	0	0						Not Used	sparse data
100379	ROB LANE DESOTO 36 WELL (RUSSELL) NEAR ARCADIA FL	USGS	342287.74	997556.41	De Soto	391	411	IAS/ICU	100%	1	2						Not Used	No calibration in IAS/ICU

Table 4.1: Usage of SAJ Observation Database in Regional Model Calibration

Model ID[a]	Well Name	Data Source	Easting[b]	Northing[b]	County	Cased Depth (ft)	Drilled Depth (ft)	Dominant Layer[c]	% Open Section in Layer[c]	93/94 Months with Data[d]	03/04 Months with Data[e]	Use for Data in Model Setup/Calibration						Reasoning/Comments
													Observations for Calibration					
												Boundary Conditions[f]	Steady State (Oct 03)	Steady State (Feb 04)	Transient (03/04)	Transient (03/04	Not Used	
100260	ROMP 10 ARCADIA WELL NEAR PORT CHARLOTTE FL	USGS	330567.97	981860.09	De Soto	210	276	IAS/ICU	100%	0	2						Not Used	No calibration in IAS/ICU
130004	ROMP 10 HAWTHORN/TAMPA		328154.58	981912.64	De Soto	303	575	IAS/ICU	100%	0	0						Not Used	No calibration in IAS/ICU
130005	ROMP 10 HAWTHORN/TAMPA		328159.10	981912.60	De Soto	110	270	IAS/ICU	100%	0	0						Not Used	No calibration in IAS/ICU
130007	ROMP 10 LOW HTRN/TMPA	SWFWMD	330560.18	981904.59	De Soto	320	473	IAS/ICU	100%	0	15						Not Used	No calibration in IAS/ICU
130003	ROMP 10 OCALA		328158.20	981912.61	De Soto	595	917	UF	91%	0	0						Not Used	missing data
100259	ROMP 10 TAMPA WELL NEAR PORT CHARLOTTE FL	USGS	330555.81	981923.81	De Soto	320	473	IAS/ICU	100%	0	2						Not Used	No calibration in IAS/ICU
130008	ROMP 10 UP HTRN	SWFWMD	330567.97	981860.09	De Soto	130	202	IAS/ICU	100%	0	15						Not Used	No calibration in IAS/ICU
130069	ROMP 12 DEEP UPPER FLDN	SWFWMD	414559.60	984847.37	De Soto	1100	1373	APPZ	55%	0	15		APPZ	APPZ	APPZ			no 93/94 data
130074	ROMP 12 LOW INT	SWFWMD	414558.70	984847.37	De Soto	280	409	IAS/ICU	100%	0	15						Not Used	No calibration in IAS/ICU
130073	ROMP 12 LOW SURF	SWFWMD	414557.79	984847.38	De Soto	12	27	SAS	100%	0	15	SAS						
130070	ROMP 12 MID UP FLDN	SWFWMD	414556.89	984847.38	De Soto	720	905	UF	100%	0	15		UF	UF	UF			no 93/94 data
130071	ROMP 12 SH UPPER FLDN	SWFWMD	414555.98	984847.39	De Soto	505	710	UF	92%	0	15		UF	UF	UF			no 93/94 data
130075	ROMP 12 UP INT	SWFWMD	414555.08	984847.39	De Soto	54	110	IAS/ICU	100%	0	15						Not Used	No calibration in IAS/ICU
130072	ROMP 12 UP SURF	SWFWMD	414554.18	984847.40	De Soto	2	5	SAS	100%	0	15	SAS						
130068	ROMP 13 AVPK	SWFWMD	455624.58	995801.59	De Soto	1550	1600	APPZ	100%	0	15		APPZ	APPZ	APPZ			no 93/94 data
130065	ROMP 13 LOW INT	SWFWMD	455636.45	995825.76	De Soto	514	592	IAS/ICU	100%	0	15						Not Used	No calibration in IAS/ICU
130066	ROMP 13 MID INT	SWFWMD	455650.93	995828.72	De Soto	282	417	IAS/ICU	100%	0	15						Not Used	No calibration in IAS/ICU
130064	ROMP 13 SURF	SWFWMD	455606.50	995801.67	De Soto	7.5	22.5	SAS	100%	0	15	SAS						
130067	ROMP 13 SWNN	SWFWMD	455661.82	995837.76	De Soto	671	786	UF	91%	0	15		UF	UF	UF			no 93/94 data
100390	ROMP 15 AVON PARK WELL NEAR ARCADIA FL	USGS	443001.28	1045872.57	De Soto	1260	1360	MC1	73%	10	2						Not Used	Model geology puts this well in MC1
130080	ROMP 15 INT	SWFWMD	442917.47	1045663.35	De Soto	260	330	IAS/ICU	100%	0	15						Not Used	No calibration in IAS/ICU
100391	ROMP 15 NRSD WELL NEAR ARCADIA FL		442917.47	1045663.35	De Soto	45	55	SAS	100%	0	0						Not Used	Missing data
130057	ROMP 15 SURF	SWFWMD	442935.07	1045747.08	De Soto	45	55	SAS	100%	6	15	SAS						
130055	ROMP 15 SWNN/AVPK		442943.19	1045747.03	De Soto	577	1360	MC1	78%	0	0						Not Used	Model geology puts this well in MC1
130056	ROMP 15 SWNN/AVPK	SWFWMD	442943.19	1045747.03	De Soto	654	1360	MC1	87%	0	15						Not Used	Model geology puts this well in MC1
130081	ROMP 16 INT	SWFWMD	404679.63	1038307.57	De Soto	105	236	IAS/ICU	100%	0	15						Not Used	No calibration in IAS/ICU
100387	ROMP 16 JOSHUA CREEK TAMPA WELL NEAR ARCADIA FL	USGS	404588.70	1038207.14	De Soto	320	340	IAS/ICU	100%	1	2						Not Used	No calibration in IAS/ICU
130058	ROMP 16 OCAL	SWFWMD	404702.18	1038302.38	De Soto	757	942	MC1	88%	10	15						Not Used	Model geology puts this well in MC1
100386	ROMP 16 OCALA WELL NEAR ARCADIA FL	USGS	404588.70	1038207.14	De Soto	757	942	MC1	88%	1	2						Not Used	Model geology puts this well in MC1
130044	ROMP 16 SURF	SWFWMD	404699.45	1038299.36	De Soto	17	27	SAS	100%	10	15	SAS						
130043	ROMP 16 TMPA	SWFWMD	404698.61	1038309.47	De Soto	300	340	IAS/ICU	100%	10	15						Not Used	No calibration in IAS/ICU
131527	ROMP 16.5 AVPK	SWFWMD/TT	368471.98	992452.12	De Soto	715	1539	MC1	58%	0	4						Not Used	Model geology puts this well in MC1
130085	ROMP 16.5 AVPK BACKPLUG	SWFWMD	368468.11	992415.79	De Soto	1440	1537	APPZ	100%	0	4						Not Used	only 3 months of data
130084	ROMP 16.5 AVPK EXPLORATORY		368468.11	992415.79	De Soto	715	1814	MC1	43%	0	0						Not Used	Open section straddles multiple layers
130086	ROMP 16.5 LOWER INT	SWFWMD	368467.21	992415.80	De Soto	347	460	IAS/ICU	100%	0	4						Not Used	No calibration in IAS/ICU
130089	ROMP 16.5 SURF	SWFWMD	368461.78	992415.83	De Soto	4	34	SAS	100%	0	4						Not Used	sparse data
130087	ROMP 16.5 SWNN	SWFWMD	368466.30	992415.80	De Soto	600	826	UF	58%	0	4						Not Used	only 4 months of data, only 59% of open section is in UF
130088	ROMP 16.5 UPPER INT	SWFWMD	368464.49	992415.82	De Soto	56	90	IAS/ICU	92%	0	4						Not Used	No calibration in IAS/ICU
100383	ROMP 17 AVON PARK WELL NEAR NOCATEE FL		338673.44	1033851.99	De Soto	1115	1430	MC1	86%	0	0						Not Used	Model geology puts this well in MC1
130063	ROMP 17 AVPK	SWFWMD	338673.44	1033851.99	De Soto	1115	1430	MC1	86%	10	15						Not Used	Model geology puts this well in MC1
130077	ROMP 17 IAS PZ-2 INT	SWFWMD	338626.46	1033618.05	De Soto	100	160	IAS/ICU	100%	0	15						Not Used	No calibration in IAS/ICU
130061	ROMP 17 LOW HTRN	SWFWMD	338677.19	1033869.13	De Soto	200	240	IAS/ICU	100%	10	15						Not Used	No calibration in IAS/ICU
130060	ROMP 17 LOW HTRN/TMPA	SWFWMD	338690.61	1033852.86	De Soto	395	470	IAS/ICU	100%	10	15						Not Used	No calibration in IAS/ICU
130062	ROMP 17 SURF	SWFWMD	338687.83	1033843.80	De Soto	8	18	IAS/ICU	78%	10	15	SAS						
130059	ROMP 17 SWNN	SWFWMD	338681.48	1033839.81	De Soto	620	670	UF	100%	10	15		UF	UF	UF	UF		
100384	ROMP 17 TAMPA WELL NEAR NOCATEE FL	USGS	338677.19	1033869.13	De Soto	200	240	IAS/ICU	100%	1	2						Not Used	No calibration in IAS/ICU
100407	ROMP 26 AVON PARK WELL NEAR GARDNER FL	USGS	388449.51	1079115.69	De Soto	580	1320	MC1	74%	10	13						Not Used	Model geology puts this well in MC1
100408	ROMP 26 HAWTHORN WELL NEAR GARDNER FL	USGS	388449.51	1079115.69	De Soto	140	180	IAS/ICU	100%	10	15						Not Used	No calibration in IAS/ICU
130040	ROMP 26 HTRN	SWFWMD	388376.10	1078978.30	De Soto	140	180	IAS/ICU	100%	10	0						Not Used	No calibration in IAS/ICU
130082	ROMP 26 INT		388239.64	1078807.52	De Soto	255	429	IAS/ICU	100%	0	0						Not Used	No calibration in IAS/ICU
100406	ROMP 26 NRSD WELL NEAR GARDNER FL	USGS	388449.51	1079115.69	De Soto	10	15	SAS	100%	10	15	SAS						
130038	ROMP 26 SURF	SWFWMD	388382.39	1078975.23	De Soto	10	15	SAS	100%	10	0	SAS						
130039	ROMP 26 SWNN/AVPK	SWFWMD	388352.61	1078973.41	De Soto	580	1320	MC1	74%	10	0						Not Used	Model geology puts this well in MC1
100409	ROMP 26 TAMPA WELL NEAR GARDNER FL	USGS	388449.51	1079115.69	De Soto	255	430	IAS/ICU	100%	0	15						Not Used	No calibration in IAS/ICU
130053	ROMP 35 LOW IAS PERM INT		318063.76	1074323.35	De Soto	230	360	IAS/ICU	100%	0	0						Not Used	No calibration in IAS/ICU
130079	ROMP 35 MW-1 SURF	SWFWMD	318063.78	1074325.37	De Soto	5	20	SAS	100%	0	1						Not Used	sparse data
130054	ROMP 35 SWNN PERM FLDN	SWFWMD	318063.77	1074324.36	De Soto	537.5	741	UF	100%	0	1						Not Used	Sparse data
130052	ROMP 35 UP IAS PERM INT		318063.75	1074322.34	De Soto	120	190	IAS/ICU	100%	0	0						Not Used	No calibration in IAS/ICU
130076	ROMP 9.5 MW-3 SURF	SWFWMD	315650.34	1016693.15	De Soto	12	37	SAS	79%	0	15	SAS						
130078	ROMP 9.5 MW-5 UUPPER FLDN		315559.02	1016686.85	De Soto	500	800	UF	70%	0	0						Not Used	missing data
130083	ROMP 9.5 MW-6 LCU INT	SWFWMD	315557.14	1016677.77	De Soto	475	480	IAS/ICU	100%	0	15						Not Used	No calibration in IAS/ICU
130046	SCARBOROUGH DEEP		456107.14	1088630.65	De Soto	0	1350	MC1	44%	0	0						Not Used	Open section straddles multiple layers

Table 4.1: Usage of SAJ Observation Database in Regional Model Calibration

Model ID[a]	Well Name	Data Source	Easting[b]	Northing[b]	County	Cased Depth (ft)	Drilled Depth (ft)	Dominant Layer[c]	% Open Section in Layer[c]	93/94 Months with Data[d]	03/04 Months with Data[e]	Use for Data in Model Setup/Calibration						Reasoning/Comments
													Observations for Calibration					
												Boundary Conditions[f]	Steady State (Oct 03)	Steady State (Feb 04)	Transient (03/04)	Transient (03/04	Not Used	
100411	SCARBOROUGH DEEP WELL NEAR CREWSVILLE FL	USGS	456039.83	1088514.85	De Soto	1300	1350	APPZ	100%	0	0						Not Used	sparse data
130035	SOUTH TOMATO GROWERS		435842.80	1077527.37	De Soto	225	1248	MC1	55%	0	0						Not Used	Model geology puts this well in MC1
100403	SOUTH TOMATO GROWERS WELL NEAR ARCADIA FL	USGS	435858.16	1077531.33	De Soto	225	1248	MC1	55%	1	2						Not Used	Model geology puts this well in MC1
100389	TOWNSEN RIVER HAWTHORN WELL NEAR ARCADIA FL	USGS	393889.96	1045646.62	De Soto	345	365	IAS/ICU	100%	1	2						Not Used	No calibration in IAS/ICU
100395	TRG WELL J32 NEAR ARCADIA FL	USGS	467704.73	1056144.26	De Soto	710	810	MC1	100%	0	0						Not Used	Model geology puts this well in MC1
100400	TRG WELL J35 NEAR ARCADIA FL	USGS	467598.26	1072100.06	De Soto	1229	1329	MC1	73%	0	0						Not Used	Model geology puts this well in MC1
100405	TRG WELL J36 NEAR ARCADIA FL	USGS	467569.09	1077472.52	De Soto	1261	1361	APPZ	70%	0	2						Not Used	sparse data
130045	TROPICAL RIVER GROVE		451804.25	1077209.55	De Soto	137	698	IAS/ICU	64%	0	0						Not Used	No calibration in IAS/ICU
100401	W FORK BUZZARD ROOST SURFICIAL W NEAR EDGEVILLE FL	USGS	335989.12	1069306.17	De Soto	1160	1260	MC1	100%	9	0						Not Used	Model geology puts this well in MC1
100421	41S30E12 CLEMONS PALMDALE	USGS	564380.95	938173.77	Glades	1000	1100	MC1	100%	1	2						Not Used	Model geology puts this well in MC1
111071	CRS01FM	SFWMD	557891.62	892205.68	Glades	53.72	58.72	SAS	100%	0	15	SAS						
111013	CRS01FS	SFWMD	557891.62	892205.68	Glades	14	19	SAS	100%	0	15	SAS						
111121	CRS01NM	SFWMD	557831.59	892534.39	Glades	52.7	57.7	SAS	100%	0	15	SAS						
111012	CRS01NS	SFWMD	557831.59	892534.39	Glades	14	19	SAS	100%	0	15	SAS						
111152	CRS02FM	SFWMD	579823.69	892487.07	Glades	38.45	43.45	SAS	100%	0	15	SAS						
110926	CRS02FS	SFWMD	579823.69	892487.07	Glades	17.43	22.43	SAS	100%	0	15	SAS						
111076	CRS02NM	SFWMD	579982.84	892796.86	Glades	54.01	59.01	SAS	100%	0	15	SAS						
110925	CRS02NS	SFWMD	579982.84	892796.86	Glades	17.4	22.4	SAS	100%	0	15	SAS						
111072	CRS03FM	SFWMD	600286.92	890027.71	Glades	53.19	58.19	SAS	100%	0	15	SAS						
111117	CRS03FS	SFWMD	600286.92	890027.71	Glades	7.78	12.78	SAS	100%	0	15	SAS						
111120	CRS03NM	SFWMD	600172.00	890109.03	Glades	51.24	56.24	SAS	100%	0	15	SAS						
110927	CRS03NS	SFWMD	600172.00	890109.03	Glades	8.48	13.48	SAS	100%	0	15	SAS						
100424	GL-155 WELL NEAR BRIGHTON FL	USGS	625106.36	1040875.86	Glades	500	600	IAS/ICU	81%	5	9						Not Used	No calibration in IAS/ICU
100422	GL-267 WELL NEAR PALMDALE FL	USGS	553709.00	941934.95	Glades	500	600	IAS/ICU	100%	5	10						Not Used	No calibration in IAS/ICU
100416	GL-319	USGS	503877.32	903819.17	Glades	440	460	IAS/ICU	100%	10	0						Not Used	No calibration in IAS/ICU
100417	GL-320	USGS	503877.32	903819.17	Glades	75	80	SAS	100%	10	0	SAS						
100418	GL-321	USGS	503877.32	903819.17	Glades	440	460	IAS/ICU	100%	1	0						Not Used	No calibration in IAS/ICU
100419	GL-322	USGS	503877.32	903819.17	Glades	75	80	SAS	100%	1	0						Not Used	sparse data
100420	GL-328	USGS	481306.88	907061.57	Glades	105	125	IAS/ICU	100%	0	15						Not Used	No calibration in IAS/ICU
112164	GLF-6	SFWMD	628323.00	910488.00	Glades	840	1560	MC1	66%	0	9						Not Used	Model geology puts this well in MC1
140017	GLWQ-09	USGS ALTAMONTE SPRINGS via DEP	544568.74	979137.86	Glades	18	33	SAS	100%	10	0	SAS						
130115	H-15A NR PALMDALE		544741.79	981257.89	Glades	19	23	SAS	100%	0	0						Not Used	Missing data
110824	H-15A_G	SFWMD	544923.00	981257.00	Glades	21	23	SAS	100%	9	0	SAS						
110828	HE-517	SFWMD	533969.89	885870.77	Glades	128	138	IAS/ICU	100%	10	0						Not Used	No calibration in IAS/ICU
100415	HE-517	USGS	534059.93	886072.50	Glades	118	138	IAS/ICU	100%	10	15						Not Used	No calibration in IAS/ICU
112147	MHGW_GW1	SFWMD	621500.37	904361.66	Glades	1000	1100	UF	60%	0	15						Not Used	DBHYDRO lists open hole depth from 655 to 732. In our geology, this is in the IAS.
111391	MUSEWELLS	SFWMD	495508.19	907627.17	Glades	18	20	SAS	100%	10	15	SAS						
111392	MUSEWELLS	SFWMD	495508.19	907627.17	Glades	80	100	IAS/ICU	100%	10	15						Not Used	No calibration in IAS/ICU
100458	AGRI CHEMICALS W. WELL HA-1 NEAR BOWLING GREEN FL	USGS	375754.74	1203213.50	Hardee	240	260	IAS/ICU	100%	1	0						Not Used	No calibration in IAS/ICU
100443	ANDERSON WELL (HARDEE 601) NO 442 ZOLFO SPRINGS FL	USGS	409499.97	1147546.93	Hardee	120	140	IAS/ICU	100%	1	2						Not Used	No calibration in IAS/ICU
130097	BRUSHY CREEK SURFICIAL		338231.27	1124732.09	Hardee	0	0	Error	0%	0	0						Not Used	Data error
100457	BRYAN HAWTHORN WELL AT BOWLING GREEN FL	USGS	390674.21	1201596.74	Hardee	143	163	IAS/ICU	100%	1	0						Not Used	No calibration in IAS/ICU
100461	C.F.INDUSTRIES WELL UF-5 NEAR FORT GREEN FL	USGS	358319.64	1205056.52	Hardee	340	360	IAS/ICU	100%	1	0						Not Used	No calibration in IAS/ICU
130096	CARGILL FA-1 FLDN	SWFWMD	385209.29	1202274.70	Hardee	408	918	MC1	74%	0	15						Not Used	Model geology puts this well in MC1
100426	CARLTON JR WELL NO 224 NEAR LIMESTONE FL	USGS	351105.31	1095632.51	Hardee	1215	1315	APPZ	100%	1	0						Not Used	sparse data
100432	CARLTON WELL HA-59 NEAR ZOLFO SPRINGS FL	USGS	440924.31	1129289.81	Hardee	211	231	IAS/ICU	100%	1	0						Not Used	No calibration in IAS/ICU
130095	CARLTONS WELL		362793.50	1156154.96	Hardee	110	617	IAS/ICU	69%	0	0						Not Used	No calibration in IAS/ICU
100450	CF INDUSTRIES DEEP WELL LF1 NEAR FORT GREEN FL	USGS	340773.56	1178941.86	Hardee	1100	1200	APPZ	100%	0	2						Not Used	sparse data
100451	CF INDUSTRIES DEEP WELL LF6 NEAR FORT GREEN FL	USGS	377897.44	1178919.52	Hardee	927	1027	MC1	75%	0	2						Not Used	Model geology puts this well in MC1
100449	CF INDUSTRIES UF-3 WELL NEAR WAUCHULA FL	USGS	340412.87	1178853.80	Hardee	355	375	IAS/ICU	100%	0	2						Not Used	No calibration in IAS/ICU
100452	CF INDUSTRIES WELL UF-6 NEAR WAUCHULA FL	USGS	377897.86	1178980.11	Hardee	365	385	IAS/ICU	100%	1	2						Not Used	No calibration in IAS/ICU
100444	CITY ZOLFO SPGS DEEP WELL NO 242 ZOLFO SPRINGS FL	USGS	398529.41	1150241.43	Hardee	902	1002	MC1	100%	1	2						Not Used	Model geology puts this well in MC1

Table 4.1: Usage of SAJ Observation Database in Regional Model Calibration

Model ID[a]	Well Name	Data Source	Easting[b]	Northing[b]	County	Cased Depth (ft)	Drilled Depth (ft)	Dominant Layer[c]	% Open Section in Layer[c]	93/94 Months with Data[d]	03/04 Months with Data[e]	Use for Data in Model Setup/Calibration						Reasoning/Comments
													Observations for Calibration					
												Boundary Conditions[f]	Steady State (Oct 03)	Steady State (Feb 04)	Transient (03/04)	Transient (03/04	Not Used	
140002	CREWSVILLE SH-AGW	SWFWMD via DEP	464898.10	1125599.14	Hardee	6	26	SAS	100%	8	12	SAS						
140003	CREWSVILLE UP INT-AG	SWFWMD via DEP	464891.79	1125598.16	Hardee	96	116	SAS	68%	8	4	SAS						
130090	DURRANCE DEEP		316506.42	1177425.13	Hardee	82	1062	IAS/ICU	34%	0	0						Not Used	Open section straddles multiple layers
100428	FLINT DEEP WELL NEAR CREWSVILLE FL	USGS	444284.12	1099884.99	Hardee	1310	1410	APPZ	100%	1	0						Not Used	sparse data
100429	GRIFFIN WELL NO 723147123221 NEAR ZOLFO SPRINGS FL	USGS	398120.57	1114493.51	Hardee	1096	1196	APPZ	67%	1	0						Not Used	sparse data
100427	HOLLINGSWORTH WELL 620 NEAR LIMESTONE FL	USGS	340665.71	1098439.34	Hardee	315	335	IAS/ICU	100%	1	0						Not Used	No calibration in IAS/ICU
100455	JOHN WHITE WELL 627 NEAR WAUCHULA FL	USGS	437636.28	1187375.91	Hardee	250	270	IAS/ICU	100%	0	2						Not Used	No calibration in IAS/ICU
130098	LETTIS CREEK SURFUCIAL		351586.11	1162702.00	Hardee	0	0	Error	0%	0	0						Not Used	Data error
100425	LIMESTONE LAND 622 WELL NEAR LIMESTONE FL	USGS	368959.34	1095299.94	Hardee	215	235	IAS/ICU	100%	1	2						Not Used	No calibration in IAS/ICU
100431	MARRLS DEEP WELL NO 411 NEAR GARDNER FL	USGS	434860.48	1124374.25	Hardee	1000	1100	MC1	100%	1	2						Not Used	Model geology puts this well in MC1
100448	MITCHELL HAMMOCK SURFICIAL W NR FORT GREEN SPGS FL	USGS	411642.07	1163503.81	Hardee	247	267	IAS/ICU	100%	10	0						Not Used	No calibration in IAS/ICU
130099	MITCHELL HAMMOCK SURFL		332868.25	1175068.95	Hardee	0	0	Error	0%	0	0						Not Used	Data error
100442	PEACE RIVER RANCH NO 231 NR CREWSVILLE FL	USGS	439477.90	1145152.61	Hardee	1063	1163	APPZ	59%	1	2						Not Used	sparse data
100441	ROBERTSON DEEP WELL NO 342 NEAR ZOLFO SPRINGS FL	USGS	433396.12	1136601.82	Hardee	1027	1127	MC1	81%	1	0						Not Used	Model geology puts this well in MC1
130107	ROMP 25 ARC/IAS	SWFWMD	329310.29	1103691.29	Hardee	105	145	IAS/ICU	100%	0	15						Not Used	No calibration in IAS/ICU
130105	ROMP 25 AVPK	SWFWMD	329317.62	1103705.37	Hardee	960	1785	APPZ	67%	0	15		APPZ	APPZ	APPZ			no 93/94 data
130104	ROMP 25 EVAPORITE UP FLDN	SWFWMD	329307.12	1103745.85	Hardee	1866	1911	MC2	100%	0	15						Not Used	Model geology puts this well in MC2
130103	ROMP 25 SURF	SWFWMD	329306.56	1103676.17	Hardee	5	30	SAS	100%	0	15	SAS						
130106	ROMP 25 SWNN	SWFWMD	329307.87	1103726.66	Hardee	300	676	UF	60%	0	15		UF	UF	UF			no 93/94 data
100440	ROMP 30 ARCADIA WELL NEAR ZOLFO SPRINGS FL	USGS	397964.53	1136524.79	Hardee	160	180	IAS/ICU	100%	0	15						Not Used	No calibration in IAS/ICU
100437	ROMP 30 AVON PARK WELL NEAR ZOLFO SGS FL	USGS	397887.01	1137080.71	Hardee	1166	1266	APPZ	100%	10	15		APPZ	APPZ	APPZ	APPZ		
100439	ROMP 30 NRSD WELL NEAR ZOLFO SGS FL	USGS	397887.01	1137080.71	Hardee	13	15	SAS	100%	10	15	SAS						
131528	ROMP 30 AVPK	SWFWMD/TT	397802.94	1136954.70	Hardee	380	1265	MC1	54%	10	4						Not Used	Model geology puts this well in MC1
100438	ROMP 30 TAMPA WELL NEAR ZOLFO SGS FL	USGS	397887.01	1137080.71	Hardee	296	316	IAS/ICU	100%	7	15						Not Used	No calibration in IAS/ICU
100433	ROMP 31 AVON PARK WELL NEAR ONA FL	USGS	359081.81	1135469.82	Hardee	460	1152	MC1	59%	10	15						Not Used	Model geology puts this well in MC1
100434	ROMP 31 HAWTHORN WELL NEAR ONA FL	SWFWMD	359036.83	1135480.25	Hardee	130	350	IAS/ICU	100%	10	15						Not Used	No calibration in IAS/ICU
130092	ROMP 31 HTRN/TMPA		359012.00	1135364.84	Hardee	130	350	IAS/ICU	100%	0	0						Not Used	No calibration in IAS/ICU
100435	ROMP 31 NRSD WELL NEAR ONA FL		359081.81	1135469.82	Hardee	5	15	SAS	100%	0	0						Not Used	Missing data
130093	ROMP 31 SURF	SWFWMD	359063.73	1135415.97	Hardee	5	15	SAS	100%	10	15	SAS						
130102	ROMP 31 SWNN/AVPK	SWFWMD	359081.74	1135414.83	Hardee	460	1152	MC1	59%	10	0						Not Used	Model geology puts this well in MC1
130091	ROWELL DEEP		411595.01	1163411.82	Hardee	39	267	IAS/ICU	97%	0	0						Not Used	No calibration in IAS/ICU
100447	ROWELL DEEP WELL NEAR WAUCHULA FL	USGS	411642.07	1163503.81	Hardee	39	267	IAS/ICU	96%	8	13	SAS						
100454	SHEARER DEEP WELL NO 141 NEAR LEMON GROVE FL	USGS	470268.36	1181454.87	Hardee	993	1093	MC1	81%	1	0						Not Used	Model geology puts this well in MC1
130094	SMITH DEEP	SWFWMD	458436.24	1157855.12	Hardee	66	849	MC1	44%	10	15						Not Used	Open section straddles multiple layers
100445	SMITH DEEP WELL NO. 731136344333 NR LEMON GROVE FL	USGS	458363.84	1157779.73	Hardee	66	849	MC1	44%	1	0						Not Used	Open section straddles multiple layers
100456	ST OF FLORIDA PAYNES CREEK HISTORIC SITE FL	USGS	394320.76	1195311.11	Hardee	110	130	IAS/ICU	100%	1	1						Not Used	No calibration in IAS/ICU
100430	STEPHENS DEEP WELL NO 724201132344 NEAR ONA FL	USGS	321818.55	1120304.76	Hardee	860	960	MC1	100%	0	2						Not Used	Model geology puts this well in MC1
100459	USS AGRI-CHEM LF-5 NEAR BOWLING GREEN FL	USGS	376564.88	1203308.82	Hardee	950	1050	APPZ	100%	1	0						Not Used	sparse data
100453	W.B. GEIGER WELL NEAR WAUCHULA FL	USGS	415015.71	1179678.90	Hardee	273	293	IAS/ICU	100%	1	2						Not Used	No calibration in IAS/ICU
100446	W.D. BOND WELL HA-89 NO. 323 NEAR WAUCHULA FL	USGS	406416.86	1158674.90	Hardee	209	229	IAS/ICU	100%	1	2						Not Used	No calibration in IAS/ICU
130100	WATKINS ROAD SURFICIAL		316861.08	1187422.07	Hardee	0	0	Error	0%	0	0						Not Used	Data error
130101	WEST FORK HORSE CRK SURFL		321509.28	1151428.55	Hardee	0	0	Error	0%	0	0						Not Used	Data error
100460	WHITEHURST DP 73814613422 WELL NR BOWLING GREEN FL	USGS	403728.86	1203633.04	Hardee	750	850	MC1	100%	1	0						Not Used	Model geology puts this well in MC1
100436	WILBUR ROBERTSON WELL NO 124 NR ZOLFO SPRINGS FL	USGS	438521.61	1134857.02	Hardee	323	343	IAS/ICU	100%	1	2						Not Used	No calibration in IAS/ICU
112140	BRY-MW	SFWMD	493917.00	863570.00	Hendry	556	750	IAS/ICU	52%	0	8						Not Used	No calibration in IAS/ICU
110675	C-131	SFWMD	567236.40	759478.16	Hendry	22	54	SAS	100%	10	15	SAS						
111070	CRS04FM	SFWMD	600720.53	879038.22	Hendry	46.15	51.15	SAS	100%	0	15	SAS						
111116	CRS04FS	SFWMD	600720.53	879038.22	Hendry	2.28	7.28	SAS	100%	0	15	SAS						
111119	CRS04NM	SFWMD	599581.34	879071.58	Hendry	47.65	52.65	SAS	100%	0	15	SAS						
111157	CRS04NS	SFWMD	599581.34	879071.58	Hendry	3.02	8.02	SAS	100%	0	15	SAS						
111158	CRS05FM	SFWMD	572553.70	841610.58	Hendry	61	66	SAS	100%	0	15	SAS						
111074	CRS05FS	SFWMD	572553.70	841610.58	Hendry	3.66	8.66	SAS	100%	0	15	SAS						

Table 4.1: Usage of SAJ Observation Database in Regional Model Calibration

Model ID[a]	Well Name	Data Source	Easting[b]	Northing[b]	County	Cased Depth (ft)	Drilled Depth (ft)	Dominant Layer[c]	% Open Section in Layer[c]	93/94 Months with Data[d]	03/04 Months with Data[e]	Use for Data in Model Setup/Calibration						Reasoning/Comments
													Observations for Calibration					
												Boundary Conditions[f]	Steady State (Oct 03)	Steady State (Feb 04)	Transient (03/04)	Transient (03/04	Not Used	
111118	CRS05NM	SFWMD	571719.77	841597.62	Hendry	48.7	53.7	SAS	100%	0	15	SAS						
111156	CRS05NS	SFWMD	571719.77	841597.62	Hendry	4.97	9.97	SAS	100%	0	15	SAS						
111155	CRS06FM	SFWMD	569996.18	872725.16	Hendry	49.29	54.29	SAS	100%	0	15	SAS						
111073	CRS06FS	SFWMD	569996.18	872725.16	Hendry	4.07	9.07	SAS	100%	0	15	SAS						
111154	CRS06NM	SFWMD	569796.59	872701.84	Hendry	48.71	53.71	SAS	100%	0	15	SAS						
111153	CRS06NS	SFWMD	569796.59	872701.84	Hendry	3.78	8.78	SAS	100%	0	15	SAS						
100482	HE-1027	USGS	563390.86	818928.40	Hendry	5	7	SAS	100%	10	0	SAS						
100483	HE-1028	USGS	563390.86	818928.40	Hendry	55	60	SAS	100%	10	0	SAS						
100484	HE-1029	USGS	563390.86	818928.40	Hendry	162	182	IAS/ICU	88%	10	0	SAS						
100479	HE-1036	USGS	633643.94	800859.32	Hendry	8	10	SAS	100%	10	0	SAS						
100480	HE-1037	USGS	633643.94	800859.32	Hendry	100	120	SAS	92%	10	0	SAS						
100471	HE-1042	USGS	593230.86	740623.31	Hendry	75	80	SAS	100%	10	11	SAS						
100472	HE-1043	USGS	593230.86	740623.31	Hendry	8	10	SAS	100%	10	0	SAS						
100473	HE-1044	USGS	593412.45	740421.10	Hendry	380	400	IAS/ICU	100%	1	0						Not Used	No calibration in IAS/ICU
100467	HE-1062	USGS	621834.44	713460.69	Hendry	8	10	SAS	100%	10	14	SAS						
100468	HE-1063	USGS	621834.44	713460.69	Hendry	103	123	SAS	71%	10	15	SAS						
100496	HE-1068	USGS	642811.11	852575.87	Hendry	140	160	IAS/ICU	100%	10	15						Not Used	No calibration in IAS/ICU
100497	HE-1069	USGS	642811.11	852575.87	Hendry	11	13	SAS	100%	10	12	SAS						
100478	HE-1075	USGS	680596.67	800658.45	Hendry	135	155	SAS	100%	10	0	SAS						
100489	HE-1076	USGS	543815.89	840407.47	Hendry	320	340	IAS/ICU	100%	10	13						Not Used	No calibration in IAS/ICU
100488	HE-1077	USGS	543815.89	840407.47	Hendry	8	10	SAS	100%	10	15	SAS						
100487	HE-339	USGS	682483.71	832666.49	Hendry	11	13	SAS	100%	10	0	SAS						
100503	HE-516	USGS	533807.78	884535.01	Hendry	253.3	273.3	IAS/ICU	100%	10	0						Not Used	No calibration in IAS/ICU
110663	HE-529	SFWMD	519208.77	806960.02	Hendry	135	155	SAS	100%	10	0	SAS						
100481	HE-554	USGS	519141.59	806933.45	Hendry	13	15	SAS	100%	10	0	SAS						
100490	HE-555	USGS	513875.02	841003.77	Hendry	250	270	IAS/ICU	100%	10	15						Not Used	No calibration in IAS/ICU
110832	HE-555		514057.03	840801.22	Hendry	250	270	IAS/ICU	100%	0	0						Not Used	No calibration in IAS/ICU
100491	HE-556	USGS	513875.02	841003.77	Hendry	155	175	IAS/ICU	100%	10	15						Not Used	No calibration in IAS/ICU
110831	HE-556	SFWMD	513875.03	841003.38	Hendry	165	175	IAS/ICU	100%	10	0						Not Used	No calibration in IAS/ICU
110666	HE-558	SFWMD	487021.65	864125.17	Hendry	3	14	SAS	100%	10	0	SAS						
100500	HE-558	USGS	487202.17	864225.40	Hendry	12	14	SAS	100%	10	15	SAS						
100493	HE-559	USGS	491596.73	845402.07	Hendry	145	165	SAS	100%	10	0	SAS						
100494	HE-560	USGS	491596.73	845402.07	Hendry	82	87	SAS	100%	10	0	SAS						
100495	HE-569	USGS	491596.73	845402.07	Hendry	15	17	SAS	100%	10	0	SAS						
100501	HE-620	USGS	503034.10	871712.48	Hendry	330	350	IAS/ICU	100%	10	0						Not Used	No calibration in IAS/ICU
100498	HE-629	USGS	633674.45	857502.69	Hendry	124	144	IAS/ICU	93%	10	0	SAS						
100492	HE-851	USGS	514055.80	840801.22	Hendry	8	10	SAS	100%	10	15	SAS						
110833	HE-851		514057.03	840801.22	Hendry	5	13	SAS	100%	0	0						Not Used	Missing data
100485	HE-852	USGS	546969.04	822501.98	Hendry	15	17	SAS	100%	10	0	SAS						
100486	HE-853	USGS	577928.54	825865.56	Hendry	56	61	SAS	100%	10	0	SAS						
100476	HE-855	USGS	614909.77	797871.30	Hendry	85	90	SAS	100%	10	15	SAS						
100477	HE-856	USGS	614909.77	797871.30	Hendry	9	11	SAS	100%	10	15	SAS						
100502	HE-857	USGS	586645.85	882595.41	Hendry	18	20	SAS	100%	10	0	SAS						
100499	HE-858	USGS	613816.06	861153.07	Hendry	15	17	SAS	100%	10	0	SAS						
100475	HE-859	USGS	630243.94	772921.06	Hendry	54	59	SAS	100%	10	15	SAS						
100474	HE-860	USGS	631152.86	773122.44	Hendry	14	16	SAS	100%	10	15	SAS						
100465	HE-861	USGS	691271.89	715783.18	Hendry	65	70	SAS	100%	10	15	SAS						
111852	HE-861_G	SFWMD	690820.40	712350.06	Hendry	37	70	SAS	100%	0	15	SAS						
100466	HE-862	USGS	691271.89	715783.18	Hendry	9	11	SAS	100%	10	15	SAS						
110830	HE-862_G	SFWMD	691272.19	715783.32	Hendry	7	11	SAS	100%	10	0	SAS						
100470	HE-868	USGS	650709.89	741182.56	Hendry	92	97	SAS	100%	10	0	SAS						
100469	HE-884	USGS	632688.01	715038.88	Hendry	62	67	SAS	100%	10	0	SAS						
111124	HE-907	SFWMD	672721.38	826946.58	Hendry	10	20	SAS	100%	0	7	SAS						
111123	HE-908	SFWMD	672721.38	826946.58	Hendry	65	75	SAS	100%	0	7	SAS						
111122	HE-909	SFWMD	672721.38	826946.58	Hendry	130	148	SAS	100%	0	7	SAS						
100770	L-1992	USGS	471667.89	811255.48	Hendry	24	29	SAS	100%	10	0	SAS						
112145	L2-PW1	SFWMD	672708.95	826685.16	Hendry	1400	1810	APPZ	94%	0	15		APPZ	APPZ	APPZ			no 93/94 data
112155	L2-PW2	SFWMD	672708.95	826685.16	Hendry	810	1160	UF	96%	0	15		UF	UF	UF			no 93/94 data
112116	LAB-MZ1	SFWMD	502273.56	879736.84	Hendry	670	837	UF	100%	0	14		UF	UF	UF	UF		
112117	LAB-MZ2	SFWMD	502273.56	879736.84	Hendry	1142	1458	MC1	100%	0	14						Not Used	Model geology puts this well in MC1
112118	LAB-MZ3	SFWMD	502273.56	879736.84	Hendry	1645	1759	APPZ	63%	0	14						Not Used	
110807	USSSUGAR	SFWMD	663144.84	763826.84	Hendry	80	100	SAS	100%	10	15	SAS						
110089	AVON P_G	SFWMD	570433.56	1198899.80	Highlands	6.5	8.5	SAS	100%	10	15	SAS						
130108	AVON PARK WINTER STREET		491780.44	1188441.04	Highlands	0	1300	MC1	49%	0	0						Not Used	Open section straddles multiple layers
100523	BONNET LAKE DEEP NEAR SEBRING FL	USGS	511974.54	1168760.96	Highlands	929	1029	MC1	100%	1	2						Not Used	Model geology puts this well in MC1
130116	BUCHANAN AVENUE SURF	SWFWMD	531079.67	1062746.43	Highlands	9.3	13.3	SAS	100%	0	14	SAS						
111091	BUCK01_G	SFWMD	585755.00	1019050.00	Highlands	16	18	SAS	100%	0	15	SAS						
111093	BUCK02_G	SFWMD	585398.00	1017090.00	Highlands	16.4	18.4	SAS	100%	0	15	SAS						
111094	BUCK03_G	SFWMD	586145.00	1016930.00	Highlands	16.54	18.54	SAS	100%	0	15	SAS						

Table 4.1: Usage of SAJ Observation Database in Regional Model Calibration

Model ID[a]	Well Name	Data Source	Easting[b]	Northing[b]	County	Cased Depth (ft)	Drilled Depth (ft)	Dominant Layer[c]	% Open Section in Layer[c]	93/94 Months with Data[d]	03/04 Months with Data[e]	Use for Data in Model Setup/Calibration						Reasoning/Comments
													Observations for Calibration					
												Boundary Conditions[f]	Steady State (Oct 03)	Steady State (Feb 04)	Transient (03/04)	Transient (03/04	Not Used	
111092	BUCK04_G	SFWMD	586979.00	1016730.00	Highlands	16.27	18.27	SAS	100%	0	15	SAS						
111096	BUCK05_G	SFWMD	588578.00	1017240.00	Highlands	16.41	18.41	SAS	100%	0	15	SAS						
111098	BUCK06_G	SFWMD	589490.00	1017580.00	Highlands	16.46	18.46	SAS	100%	0	15	SAS						
111097	BUCK07_G	SFWMD	590331.00	1018606.00	Highlands	17.09	19.09	SAS	100%	0	15	SAS						
111095	BUCK08_G	SFWMD	590630.00	1017410.00	Highlands	16.36	18.36	SAS	100%	0	15	SAS						
111099	BUCK09_G	SFWMD	592165.00	1016840.00	Highlands	15.28	17.28	SAS	100%	0	15	SAS						
111183	BUCK10_G	SFWMD	592996.00	1016850.00	Highlands	9.79	11.79	SAS	100%	0	15	SAS						
111101	BUCK11_G	SFWMD	593129.00	1018640.00	Highlands	10.12	12.12	SAS	100%	0	15	SAS						
111088	BUCK12_G	SFWMD	596494.00	1021830.00	Highlands	15.76	17.76	SAS	100%	0	15	SAS						
111106	BUCK13_G	SFWMD	597094.00	1021840.00	Highlands	15.22	17.22	SAS	100%	0	15	SAS						
111090	BUCK14_G	SFWMD	597664.00	1021840.00	Highlands	16.6	18.6	SAS	100%	0	15	SAS						
111107	BUCK15_G	SFWMD	598268.00	1021850.00	Highlands	15.02	17.02	SAS	100%	0	15	SAS						
111103	BUCK16_G	SFWMD	598999.00	1021860.00	Highlands	16.37	18.37	SAS	100%	0	15	SAS						
111104	BUCK17_G	SFWMD	599674.00	1021870.00	Highlands	16.13	18.13	SAS	100%	0	15	SAS						
111102	BUCK18_G	SFWMD	600303.00	1021870.00	Highlands	16.37	18.37	SAS	100%	0	15	SAS						
111100	BUCK19_G	SFWMD	600842.00	1021860.00	Highlands	16.81	18.81	SAS	100%	0	15	SAS						
111109	BUCK20_G	SFWMD	596684.00	1020010.00	Highlands	16.29	18.29	SAS	100%	0	15	SAS						
111108	BUCK21_G	SFWMD	599256.00	1020510.00	Highlands	15.43	17.43	SAS	100%	0	15	SAS						
111105	BUCK22_G	SFWMD	600766.00	1020490.00	Highlands	15.78	17.78	SAS	100%	0	15	SAS						
100521	CITY SEBRING DEEP 24 AT SEBRING FL	USGS	512184.15	1151895.77	Highlands	1300	1400	APPZ	100%	1	0						Not Used	sparse data
100528	CLENNY DEEP NW/O AVON PK FL	USGS	481615.59	1204227.00	Highlands	950	1050	MC1	100%	1	2						Not Used	Model geology puts this well in MC1
101170	CLENNY DEEP NW/O AVON PK FL		481615.59	1204227.00	Highlands	950	1050	MC1	100%	0	0						Not Used	Model geology puts this well in MC1
100513	CLYDE PATTERSON WELL 19 NEAR LAKE PLACID FL	USGS	552732.11	1092090.90	Highlands	160	180	SAS	100%	1	0						Not Used	sparse data
100525	DRESSLERS DIARY NR AVON PK FL	USGS	509973.95	1187854.45	Highlands	330	350	IAS/ICU	100%	1	0						Not Used	No calibration in IAS/ICU
100524	FLOYD DEVANE WELL 18 NEAR AVON PARK FL	USGS	495975.15	1174375.84	Highlands	320	340	IAS/ICU	100%	0	2						Not Used	No calibration in IAS/ICU
130114	H-11A NR LAKE PLACID SURF		591264.52	1121208.21	Highlands	13	16	SAS	100%	0	0						Not Used	Missing data
100515	H-11A WELL NEAR LAKE PLACID FL	USGS	591263.00	1121208.13	Highlands	13	16	SAS	100%	10	15	SAS						
112200	HIF-0003	SFWMD	571432.76	1161030.35	Highlands	1180	1280	APPZ	100%	0	0						Not Used	sparse data
112201	HIF-0004	SFWMD	578785.34	1145666.81	Highlands	1200	1300	APPZ	100%	1	0						Not Used	sparse data
112202	HIF-0008	SFWMD	500238.79	1048955.16	Highlands	1350	1450	APPZ	93%	1	0						Not Used	sparse data
112203	HIF-0013	SFWMD	588742.48	1122020.17	Highlands	1006	1106	MC1	63%	1	0						Not Used	Model geology puts this well in MC1
112204	HIF-0014	SFWMD	566109.31	1075009.27	Highlands	1400	1500	APPZ	100%	1	0						Not Used	sparse data
112205	HIF-0032	SFWMD	553390.51	1146632.51	Highlands	250	1360	MC1	53%	1	0						Not Used	Model geology puts this well in MC1
112206	HIF-0037	SFWMD	593589.12	1051127.52	Highlands	619	1450	MC1	72%	0	0						Not Used	Model geology puts this well in MC1
100512	HIF-14 P G PHYPERS	USGS	566040.42	1074892.55	Highlands	1400	1500	APPZ	100%	1	0						Not Used	sparse data
112207	HIF-16_G	SFWMD	481210.84	1095684.68	Highlands	1125	1225	MC1	100%	1	0						Not Used	Model geology puts this well in MC1
100505	HIF-23 GRAHAM CO DAIRY	USGS	485287.46	1008605.63	Highlands	1460	1560	APPZ	100%	1	0						Not Used	sparse data
112208	HIF-23_G	SFWMD	485354.73	1008725.24	Highlands	1460	1560	APPZ	100%	1	0						Not Used	sparse data
112209	HIF-25_G	SFWMD	501809.81	1034711.48	Highlands	680	780	MC1	94%	0	0						Not Used	Model geology puts this well in MC1
112210	HIF-26_G	SFWMD	543542.37	1005393.19	Highlands	1510	1610	MC1	56%	1	0						Not Used	Model geology puts this well in MC1
100520	HIF-32 GUILFORD TOMLINSON	USGS	553321.75	1146518.44	Highlands	1260	1360	APPZ	100%	1	0						Not Used	sparse data
100519	HIF-4 34S31E28 YUCAN RANCH NR LORIDA FL	USGS	578716.13	1145552.72	Highlands	1200	1300	APPZ	100%	1	0						Not Used	sparse data
100506	HIF-5 CHALRES STIDHAM	USGS	527676.09	1039450.94	Highlands	1410	1510	APPZ	78%	1	0						Not Used	sparse data
112211	HIF-5_G	SFWMD	527744.18	1039569.20	Highlands	602	1510	MC1	78%	1	0						Not Used	Model geology puts this well in MC1
100509	HIF-6 LYKES BROW 4IN FLOW	USGS	614019.94	1059667.64	Highlands	420	520	IAS/ICU	100%	1	0						Not Used	No calibration in IAS/ICU
112212	HIF-6_G	SFWMD	614089.64	1059784.85	Highlands	425.5	525.5	IAS/ICU	100%	1	0						Not Used	No calibration in IAS/ICU
100508	HIF-8 BOX RANCH	USGS	500171.18	1048837.15	Highlands	1350	1450	APPZ	93%	1	0						Not Used	sparse data
100522	JOHN MCCULLOCH WELL 11 NEAR SEBRING FL	USGS	528138.73	1156992.00	Highlands	350	370	IAS/ICU	100%	1	2						Not Used	No calibration in IAS/ICU
110245	KRBFFM	SFWMD	600222.66	1136597.09	Highlands	41.77	45.77	SAS	100%	0	15	SAS						
110244	KRBFFS	SFWMD	600228.69	1136590.62	Highlands	21.99	25.99	SAS	100%	0	15	SAS						
110232	KRDFFM	SFWMD	592155.77	1145326.39	Highlands	46.22	51.22	SAS	100%	0	15	SAS						
110231	KRDFFS	SFWMD	592163.78	1145325.77	Highlands	20.54	25.04	SAS	100%	0	15	SAS						
110192	KRDNND1	SFWMD	592209.45	1145839.68	Highlands	77.95	83.35	SAS	100%	0	15	SAS						
110191	KRDNNM1	SFWMD	592195.84	1145833.54	Highlands	45.98	51.48	SAS	100%	0	15	SAS						
110225	KRDNNS1	SFWMD	592189.72	1145835.87	Highlands	19.55	25.05	SAS	100%	0	15	SAS						
130113	LAKE GROVES ROAD SURF	SWFWMD	523798.21	1066489.61	Highlands	13	23	SAS	100%	10	15	SAS						
100511	LAKE GROVES ROAD WELL NEAR LAKE PLACID FL	USGS	523970.60	1066222.46	Highlands	13	23	SAS	100%	1	0						Not Used	sparse data
100507	LAKE PLACID GROVES DEEP SOUTH OF LAKE PLACID FL	USGS	545477.89	1044346.66	Highlands	1100	1200	MC1	100%	1	0						Not Used	Model geology puts this well in MC1
130112	LAKE SIRENA		537325.93	1073668.87	Highlands	0	1680	MC1	40%	0	0						Not Used	Open section straddles multiple layers
110123	LOTELA_G	SFWMD	515067.70	1184414.60	Highlands	8	10	SAS	100%	10	15	SAS						
100518	MARANATHA VILLAGE NEAR SEBRING FL	USGS	519588.19	1157828.01	Highlands	741	841	MC1	100%	1	2						Not Used	Model geology puts this well in MC1
110134	MCARTH_G	SFWMD	589204.13	1128683.90	Highlands	4.4	6.4	SAS	100%	10	15	SAS						
100516	PRAIRIE OAKS GOLF CLUB WELL NEAR SEBRING FL	USGS	487248.68	1132300.68	Highlands	219	239	IAS/ICU	100%	0	0						Not Used	No calibration in IAS/ICU

Table 4.1: Usage of SAJ Observation Database in Regional Model Calibration

Model ID[a]	Well Name	Data Source	Easting[b]	Northing[b]	County	Cased Depth (ft)	Drilled Depth (ft)	Dominant Layer[c]	% Open Section in Layer[c]	93/94 Months with Data[d]	03/04 Months with Data[e]	Use for Data in Model Setup/Calibration						Reasoning/Comments
													Observations for Calibration					
												Boundary Conditions[f]	Steady State (Oct 03)	Steady State (Feb 04)	Transient (03/04)	Transient (03/04	Not Used	
130117	RIDGE WRAP H-1 SURF	SWFWMD	486657.70	1201387.75	Highlands	40	60	SAS	100%	10	15	SAS						
130110	RIDGE WRAP H-10 SURF	SWFWMD	518131.74	1199215.69	Highlands	30	50	SAS	100%	10	15	SAS						
130119	RIDGE WRAP H-2 SURF	SWFWMD	484930.67	1188721.20	Highlands	65	85	SAS	100%	10	15	SAS						
130109	RIDGE WRAP H-4 SURF	SWFWMD	499431.07	1130474.16	Highlands	30	50	SAS	100%	10	14	SAS						
130121	RIDGE WRAP H-5 SURFICIAL	SWFWMD	522812.50	1159243.08	Highlands	35	55	SAS	100%	10	0	SAS						
130123	RIDGE WRAP H-7 SURF	SWFWMD	504968.91	1093523.52	Highlands	20	40	SAS	100%	10	15	SAS						
130124	RIDGE WRAP H-8 SURF	SWFWMD	552784.21	1077155.80	Highlands	45	65	SAS	100%	10	15	SAS						
100527	ROBERT RICHARDS WELL 25 NEAR AVON PARK FL	USGS	521600.23	1193973.82	Highlands	240	260	IAS/ICU	100%	1	2						Not Used	No calibration in IAS/ICU
130137	ROMP 14 AVPK	SWFWMD	541063.55	1023775.44	Highlands	1003	1670	MC1	70%	0	15						Not Used	Model geology puts this well in MC1
130134	ROMP 14 LOW HTRN	SWFWMD	541274.16	1023824.32	Highlands	460	521	IAS/ICU	100%	0	15						Not Used	No calibration in IAS/ICU
130136	ROMP 14 SURF	SWFWMD	541275.91	1023805.13	Highlands	30	300	SAS	100%	0	15	SAS						
130135	ROMP 14 SWNN	SWFWMD	541276.02	1023843.50	Highlands	650	730	UF	100%	0	15		UF	UF	UF			no 93/94 data
130131	ROMP 28 AVPK	SWFWMD	514909.81	1103506.05	Highlands	960	1642	APPZ	52%	0	15		APPZ	APPZ	APPZ			no 93/94 data
130128	ROMP 28 HTRN	SWFWMD	514862.26	1103572.87	Highlands	370	420	IAS/ICU	100%	0	15						Not Used	No calibration in IAS/ICU
130133	ROMP 28 L EVAPORITE FLDN	SWFWMD	514916.06	1103487.85	Highlands	2083	2103	LC	100%	0	15						Not Used	Model geology puts this well in LC
130130	ROMP 28 SURF	SWFWMD	514910.62	1103479.79	Highlands	40	200	SAS	100%	0	15	SAS						
130129	ROMP 28 SWNN	SWFWMD	514856.01	1103589.04	Highlands	485	600	UF	100%	0	15		UF	UF	UF			no 93/94 data
130132	ROMP 28 UP EVAPORITE FLDN	SWFWMD	514916.06	1103487.85	Highlands	1913	1933	LF	94%	0	15		LF	LF	LF	LF		
100510	ROMP 28X FLORIDAN WELL NR LAKE PLACID FL	USGS	545808.20	1066258.25	Highlands	585	1385	MC1	84%	1	2						Not Used	Model geology puts this well in MC1
130126	ROMP 28X SURF	SWFWMD	545854.26	1066272.27	Highlands	50	60	SAS	100%	10	15	SAS						
130125	ROMP 28X SWNN/AVPK	SWFWMD	545851.50	1066253.09	Highlands	585	1385	MC1	84%	10	15						Not Used	Model geology puts this well in MC1
130120	ROMP 43X SURFICIAL	SWFWMD	500327.90	1188608.84	Highlands	180	200	SAS	100%	10	0	SAS						
130118	ROMP 43XX AVPK	SWFWMD	500679.30	1189211.37	Highlands	409	1363	MC1	66%	10	15						Not Used	Model geology puts this well in MC1
100526	ROMP 43XX FLORIDAN WELL NEAR AVON PARK FL	USGS	500685.65	1189222.45	Highlands	409	1363	MC1	66%	0	2						Not Used	Model geology puts this well in MC1
130127	ROMP 43XX SURF	SWFWMD	500685.59	1189208.32	Highlands	32	83	SAS	100%	0	15	SAS						
130111	SEBRING 412 SH DESTROYED		529497.02	1137712.98	Highlands	41	45	SAS	100%	0	0						Not Used	Missing data
130122	SEBRING 412-A NRSD REPL		529475.76	1137827.16	Highlands	40	63	SAS	100%	0	0						Not Used	Missing data
100517	SEBRING 412-A NRSD WELL NEAR SEBRING FL	USGS	529549.94	1137965.73	Highlands	40	63	SAS	100%	10	15	SAS						
100514	SEBRING NRSD WELL NEAR CREWSVILLE FL	USGS	484920.87	1120308.02	Highlands	19.7	21.7	SAS	100%	0	7	SAS						
110125	SEBRING_G	SFWMD	544080.11	1134337.98	Highlands	8	10	SAS	100%	10	15	SAS						
110328	SEBRNG_G	SFWMD	541273.00	1135941.00	Highlands	61.35	66.35	SAS	100%	0	2						Not Used	sparse data
100875	4B38-32-13 PEEK FL	USGS	158381.51	1206844.39	Hillsborough	500	600	UF	75%	1	0						Not Used	Outside Boundary
100596	A.MESSINA,305 SO MACDILL AVE AT TAMPA FL	USGS	173814.81	1314544.42	Hillsborough	130	150	UF	100%	1	2						Not Used	Outside Boundary
130455	ALEXANDER ELEM SCHL FLDN	SWFWMD	167263.93	1334734.77	Hillsborough	49	60	IAS/ICU	100%	0	15						Not Used	Outside Boundary
130456	ALEXANDER ELEM SCHL SURF	SWFWMD	167265.50	1334789.30	Hillsborough	3	24	SAS	100%	10	15	SAS						
130330	ANDREW MESSINA FLDN		173876.23	1314651.77	Hillsborough	84	175	UF	98%	0	0						Not Used	Outside Boundary
130347	ARMISTEAD/PRETTY UPL SURF	SWFWMD	152751.76	1373574.55	Hillsborough	3	23.7	SAS	100%	0	15	SAS						
130346	ARMISTEAD/PRETTY WTL SURF	SWFWMD	152455.66	1373537.94	Hillsborough	2	22.8	SAS	100%	0	15	SAS						
140005	BALM/WIMAUMA SH-AGW	SWFWMD via DEP	245682.42	1233220.83	Hillsborough	7	28	SAS	100%	8	0	SAS						
140006	BALM/WIMAUMA UP INT-	SWFWMD via DEP	245687.91	1233229.86	Hillsborough	80	100	IAS/ICU	54%	8	0	SAS						
100535	BARBER WELL 422 NEAR FORT LONESOME FL	USGS	310535.19	1227035.24	Hillsborough	171	191	IAS/ICU	100%	1	2						Not Used	No calibration in IAS/ICU
130436	BELLAMY ELEM SCHL FLDN	SWFWMD	149938.58	1348535.72	Hillsborough	43	51	IAS/ICU	54%	10	14						Not Used	Outside Boundary
130437	BELLAMY ELEM SCHL SURF	SWFWMD	150278.64	1349396.13	Hillsborough	3	26	SAS	100%	10	15	SAS						
130159	BERGER DEEP	SWFWMD	174261.45	1378032.20	Hillsborough	44	134	UF	88%	10	15						Not Used	Outside Boundary
100646	BERGER DEEP WELL NEAR LUTZ FL	USGS	174244.16	1378082.93	Hillsborough	44	134	UF	88%	1	2						Not Used	Outside Boundary
130158	BERGER SHALLOW	SWFWMD	174260.56	1378032.21	Hillsborough	19	22	SAS	100%	10	15	SAS						
100647	BERGER SHALLOW WELL 2 NEAR CITRUS PARK FL	USGS	174144.41	1377983.13	Hillsborough	19	22	SAS	100%	1	2						Not Used	Outside Boundary
130382	BLACKWATER CRK ELAPP SURF	SWFWMD	275486.98	1380968.62	Hillsborough	2	9	IAS/ICU	53%	0	15	SAS						
130361	BLACKWATER CYP UPL SURF	SWFWMD	284679.63	1387717.79	Hillsborough	2.5	14	IAS/ICU	100%	0	15						Not Used	No calibration in IAS/ICU
130374	BLACKWATER CYP WTL SURF	SWFWMD	284728.24	1387556.72	Hillsborough	2	10	IAS/ICU	100%	0	15						Not Used	No calibration in IAS/ICU
130363	BLACKWATER MSH 1 UPL SURF	SWFWMD	279022.10	1385495.10	Hillsborough	3.5	11.5	IAS/ICU	100%	0	15						Not Used	No calibration in IAS/ICU
130371	BLACKWATER MSH 1 WTL SURF	SWFWMD	279292.51	1385588.45	Hillsborough	0.5	6	IAS/ICU	100%	0	14						Not Used	No calibration in IAS/ICU
130362	BLACKWATER MSH 2 UPL SURF	SWFWMD	281940.01	1383043.83	Hillsborough	2	7.5	IAS/ICU	100%	0	15						Not Used	No calibration in IAS/ICU
130372	BLACKWATER MSH 2 WTL SURF	SWFWMD	282059.40	1382794.20	Hillsborough	1	5	IAS/ICU	96%	0	15	SAS						
130364	BLACKWTR WET PRA UPL SURF	SWFWMD	283245.54	1388023.35	Hillsborough	1	11.5	IAS/ICU	100%	0	15						Not Used	No calibration in IAS/ICU
130373	BLACKWTR WET PRA WTL SURF	SWFWMD	284711.67	1387698.30	Hillsborough	2.5	9	IAS/ICU	100%	0	15						Not Used	No calibration in IAS/ICU
130494	BLKWTR CREEK ELAPP FLDN	SWFWMD	275479.77	1380963.64	Hillsborough	94	154	UF	100%	0	15						Not Used	Hillsborough Basin has a dense coverage of points and is not important for the purposes of the model; remove
130211	BLOOMINGDALE ROAD		247608.86	1296244.64	Hillsborough	168	183	UF	100%	0	0						Not Used	missing data
100579	BLOOMINGDALE ROAD WELL NEAR BLOOMINGDALE FL	USGS	247544.92	1296136.21	Hillsborough	168	183	UF	100%	6	0					UF		no 03/04 data
100601	BRANDON 17 NEAR BRANDON FL	USGS	232919.29	1321543.52	Hillsborough	245	265	UF	100%	1	0						Not Used	sparse data

Table 4.1: Usage of SAJ Observation Database in Regional Model Calibration

Model ID[a]	Well Name	Data Source	Easting[b]	Northing[b]	County	Cased Depth (ft)	Drilled Depth (ft)	Dominant Layer[c]	% Open Section in Layer[c]	93/94 Months with Data[d]	03/04 Months with Data[e]	Use for Data in Model Setup/Calibration						Reasoning/Comments
													Observations for Calibration					
												Boundary Conditions[f]	Steady State (Oct 03)	Steady State (Feb 04)	Transient (03/04)	Transient (03/04	Not Used	
100587	BRANDON RIDGELAND WELL NEAR BRANDON FL	USGS	254928.39	1307373.86	Hillsborough	106	126	IAS/ICU	100%	1	0						Not Used	No calibration in IAS/ICU
100655	BRANT LAKE DEEP WELL 472 NEAR LUTZ FL	USGS	180708.62	1381570.10	Hillsborough	89	94	UF	100%	1	2						Not Used	Outside Boundary
130341	BROOKER CRK HDWTR UPL SUR	SWFWMD	154707.40	1385682.91	Hillsborough	3	20	SAS	100%	0	15	SAS						
130342	BROOKER CRK HDWTR WTL SUR	SWFWMD	156198.97	1387472.23	Hillsborough	1	5	SAS	100%	0	15	SAS						
130425	BUCHANAN SCHOOL FLDN	SWFWMD	182247.87	1368135.52	Hillsborough	76	87	UF	100%	7	15						Not Used	Outside Boundary
130426	BUCHANAN SCHOOL SURF	SWFWMD	182246.98	1368135.53	Hillsborough	4	30	SAS	100%	10	15	SAS						
130384	BWCT1SAS (CM-4) SURF SH	SWFWMD	299083.52	1384968.58	Hillsborough	1	6	IAS/ICU	100%	0	10						Not Used	No calibration in IAS/ICU
130385	BWCT1UFAD (CM-4) UP FL DP	SWFWMD	299083.33	1384948.38	Hillsborough	100	175	UF	100%	0	11						Not Used	Hillsborough Basin has a dense coverage of points and is not important for the purposes of the model; remove
130386	BWCT2SAS SURF SHALLOW	SWFWMD	299050.84	1385312.31	Hillsborough	2.2	6.7	IAS/ICU	100%	0	15						Not Used	No calibration in IAS/ICU
130387	BWCT2UFAD UPPER FLDN DP	SWFWMD	299050.74	1385302.21	Hillsborough	23	26	IAS/ICU	100%	0	15						Not Used	No calibration in IAS/ICU
130390	BWCT3CR SURFICIAL		299122.81	1385742.97	Hillsborough	1	2.1	IAS/ICU	100%	0	0						Not Used	No calibration in IAS/ICU
130388	BWCT3SAS SURF SHALLOW	SWFWMD	298962.97	1385494.93	Hillsborough	4.5	5.6	IAS/ICU	100%	0	15						Not Used	No calibration in IAS/ICU
130389	BWCT3UFAS UP FLDN SHALLOW	SWFWMD	298998.96	1385514.81	Hillsborough	8.6	10.3	IAS/ICU	100%	0	15						Not Used	No calibration in IAS/ICU
130391	BWCT4UFAS UP FLDN SHALLOW	SWFWMD	298914.59	1386081.23	Hillsborough	4.9	8.9	IAS/ICU	100%	0	15						Not Used	No calibration in IAS/ICU
130392	BWCT5UFAS UP FLDN SHALLOW	SWFWMD	298918.01	1386454.93	Hillsborough	11.7	15.7	IAS/ICU	100%	0	15						Not Used	No calibration in IAS/ICU
130393	BWCT6UFAD UPPER FLDN DEEP		298945.23	1386495.09	Hillsborough	43	91	IAS/ICU	54%	0	0						Not Used	No calibration in IAS/ICU
100556	CAMP DOROTHY THOMAS NEAR BOYETTE FL	USGS	252819.77	1273001.15	Hillsborough	120	140	IAS/ICU	100%	1	2						Not Used	No calibration in IAS/ICU
130413	CAMP KEYSTONE FLDN	SWFWMD	141806.79	1394882.37	Hillsborough	41	51	IAS/ICU	66%	10	15						Not Used	Outside Boundary
130421	CAMP KEYSTONE SURF	SWFWMD	141797.44	1394852.18	Hillsborough	3	27	SAS	100%	10	15	SAS						
130283	CARROLL WELL		224492.30	1258611.02	Hillsborough	58	520	UF	60%	0	0						Not Used	Missing data
130170	CARROLLWOOD ELEM DEEP		172830.14	1354467.69	Hillsborough	44	54	SAS	71%	0	0						Not Used	Outside Boundary
130171	CARROLLWOOD ELEM SHALLOW		172827.40	1354463.68	Hillsborough	7	17	SAS	100%	0	0						Not Used	Outside Boundary
130280	CARROLLWOOD MEAD SH SURFL		156043.92	1362256.79	Hillsborough	6	17	SAS	100%	0	0						Not Used	Outside Boundary
130279	CARROLLWOOD MEADOWS PK DP		156050.39	1362272.87	Hillsborough	55	75	UF	100%	0	0						Not Used	Outside Boundary
130445	CHANNEL A BM DEEP TAMPA		137539.42	1341883.93	Hillsborough	100	121	UF	100%	0	0						Not Used	Outside Boundary
100609	CHANNEL G BM DEEP WELL NEAR TAMPA FL	USGS	147865.62	1340035.76	Hillsborough	100	120	UF	100%	7	10						Not Used	Outside Boundary
130447	CHANNEL G BM FLDN		147794.29	1340066.99	Hillsborough	115	120	UF	100%	0	0						Not Used	Outside Boundary
130429	CITRUS PK ELEM SCHL FLDN	SWFWMD	148686.85	1364049.49	Hillsborough	55	66	IAS/ICU	54%	10	15						Not Used	Outside Boundary
130430	CITRUS PK ELEM SCHL SURF	SWFWMD	148674.11	1363964.79	Hillsborough	4	30	SAS	100%	10	15	SAS						
100633	CITY OF ST PETE DEEP WELL E-100 NR CITRUS PARK FL	USGS	140624.54	1371393.93	Hillsborough	656	1200	APPZ	70%	10	15						Not Used	Outside Boundary
130264	CLAPROD		167605.08	1221989.48	Hillsborough	30	143	IAS/ICU	100%	0	0						Not Used	Outside Boundary
130355	CLAY GULLY WTL SURF	SWFWMD	223922.14	1378493.40	Hillsborough	3.5	13.5	IAS/ICU	59%	0	15	SAS						
130258	CLAYWELL ELEM DEEP		165143.23	1370959.43	Hillsborough	40	60	SAS	45%	0	0						Not Used	Outside Boundary
130259	CLAYWELL ELEM SCHOOL SH	SWFWMD	165148.47	1370948.25	Hillsborough	10	17	SAS	100%	8	0	SAS						
100597	CLEVELAND AND HUBERT DEEP WELL AT TAMPA FL	USGS	166696.13	1314925.02	Hillsborough	104	124	UF	100%	1	2						Not Used	Outside Boundary
130490	CONE RANCH 1 UPPER FLDN	SWFWMD	298900.56	1386505.60	Hillsborough	43	93	IAS/ICU	52%	0	15						Not Used	No calibration in IAS/ICU
130404	CONE RANCH 1 WTL SURF	SWFWMD	294727.51	1382543.91	Hillsborough	1	3	SAS	100%	0	15	SAS						
130402	CONE RANCH 2 UPL SURF	SWFWMD	294846.18	1378906.47	Hillsborough	1.5	5	SAS	51%	0	15	SAS						
130401	CONE RANCH 2 WTL SURF	SWFWMD	294872.77	1378875.92	Hillsborough	1	3	SAS	100%	0	15	SAS						
130399	CONE RANCH 3 UPL SURF	SWFWMD	294600.72	1374625.92	Hillsborough	1.5	5	SAS	59%	0	15	SAS						
130400	CONE RANCH 3 WTL SURF	SWFWMD	294672.92	1374685.86	Hillsborough	1.5	5	SAS	64%	0	15	SAS						
130405	CONE RANCH 4 WTL SURF	SWFWMD	302062.36	1375749.70	Hillsborough	2	11	IAS/ICU	68%	0	15	SAS						
130403	CONE RANCH 5 WTL SURF	SWFWMD	307456.28	1369994.38	Hillsborough	2	7	IAS/ICU	79%	0	15	SAS						
130397	CONE RANCH 6 UPL SURF	SWFWMD	301937.78	1379801.29	Hillsborough	1	5	SAS	91%	0	15	SAS						
130398	CONE RANCH 6 WTL SURF	SWFWMD	301885.70	1379983.58	Hillsborough	1	3.5	SAS	100%	0	15	SAS						
130396	CONE RANCH CM-10S UPL SUR	SWFWMD	307652.78	1369932.02	Hillsborough	120	195	UF	100%	0	15		UF	UF	UF			no 93/94 data
130394	CONE RANCH CM-5S SURF	SWFWMD	294530.16	1382505.33	Hillsborough	3	5	IAS/ICU	64%	0	14	SAS						
130395	CONE RANCH CM-6S UPL SURF	SWFWMD	301435.50	1375755.37	Hillsborough	2	7	SAS	55%	0	15	SAS						
130479	CONE RANCH TBW TP-2 FLDN		308616.70	1365499.33	Hillsborough	150	700	APPZ	35%	0	0						Not Used	Open section straddles multiple layers
130300	COSME 3 FLDN	SWFWMD	142991.19	1373206.05	Hillsborough	79	354	UF	100%	10	15						Not Used	Outside Boundary
130326	COSME 7		146150.98	1376725.08	Hillsborough	107	350	UF	100%	0	0						Not Used	Outside Boundary
130340	COUNCIL DEEP NEAR RUSKIN		196024.98	1244082.13	Hillsborough	34	500	UF	67%	0	0						Not Used	Missing data
130441	CRESTWOOD ELEM SCHL FLDN	SWFWMD	165810.46	1342586.26	Hillsborough	45	55	IAS/ICU	84%	10	14	SAS						
130442	CRESTWOOD ELEM SCHL SURF	SWFWMD	165811.36	1342586.25	Hillsborough	3	24	SAS	100%	10	14	SAS						
130369	CYP CRK ELAPP CYP UPL SURF	SWFWMD	208629.33	1384453.56	Hillsborough	1.5	11.5	SAS	72%	0	15	SAS						
130370	CYP CRK ELAPP CYP WTL SUR	SWFWMD	208633.34	1384726.27	Hillsborough	2.5	13.5	SAS	55%	0	15	SAS						
130365	CYP CRK ELAPP MSH UPL SURF	SWFWMD	207021.19	1384704.32	Hillsborough	2	9.5	IAS/ICU	52%	0	15	SAS						
130366	CYP CRK ELAPP MSH WTL SURF	SWFWMD	207158.05	1384925.00	Hillsborough	1	3.5	SAS	100%	0	15	SAS						
130495	CYP CRK ELAPP N FLDN	SWFWMD	207647.02	1391647.37	Hillsborough	80	124	UF	100%	0	15						Not Used	Outside Boundary
130377	CYP CRK ELAPP N SURF	SWFWMD	207646.91	1391637.27	Hillsborough	2	16	IAS/ICU	72%	0	15	SAS						
130367	CYP CRK ELAPP RIV UPL SURF	SWFWMD	206806.80	1387090.87	Hillsborough	2	8	SAS	56%	0	15	SAS						
130368	CYP CRK ELAPP RIV WTL SURF	SWFWMD	206808.66	1387252.48	Hillsborough	4	15.5	IAS/ICU	88%	0	15	SAS						
130375	CYP CRK ELAPP S FLDN	SWFWMD	204398.31	1380127.95	Hillsborough	104	164	UF	100%	0	15						Not Used	Outside Boundary
130378	CYP CRK ELAPP S SURF	SWFWMD	204389.36	1380128.06	Hillsborough	3.5	17.5	IAS/ICU	54%	0	15	SAS						
130172	DEBUEL ROAD DEEP	SWFWMD	188612.02	1381919.46	Hillsborough	118	300	UF	100%	10	15						Not Used	Outside Boundary

Table 4.1: Usage of SAJ Observation Database in Regional Model Calibration

Model ID[a]	Well Name	Data Source	Easting[b]	Northing[b]	County	Cased Depth (ft)	Drilled Depth (ft)	Dominant Layer[c]	% Open Section in Layer[c]	93/94 Months with Data[d]	03/04 Months with Data[e]	Use for Data in Model Setup/Calibration						Reasoning/Comments
													Observations for Calibration					
												Boundary Conditions[f]	Steady State (Oct 03)	Steady State (Feb 04)	Transient (03/04)	Transient (03/04	Not Used	
100656	DEBUEL ROAD DEEP NEAR LUTZ FL	USGS	188672.00	1382015.00	Hillsborough	118	300	UF	100%	10	15						Not Used	Outside Boundary
130173	DEBUEL ROAD SHALLOW	SWFWMD	188594.11	1381919.67	Hillsborough	22	25	SAS	100%	10	15	SAS						
100657	DEBUEL ROAD SHALLOW NEAR LUTZ FL		188672.46	1382014.83	Hillsborough	22	25	SAS	100%	0	0						Not Used	Outside Boundary
130175	DICKMAN WELL		196214.02	1244887.07	Hillsborough	37	536	UF	63%	0	0						Not Used	Missing data
130418	DIOCESE FLDN	SWFWMD	137752.24	1369890.48	Hillsborough	142	180	UF	100%	10	15						Not Used	Outside Boundary
130424	DIOCESE SURF	SWFWMD	137729.52	1369866.53	Hillsborough	19	39.8	SAS	100%	10	15	SAS						
130198	DUNDEE 8 M		167105.56	1390500.60	Hillsborough	65	693	UF	48%	0	0						Not Used	Outside Boundary
130417	EAGLES GOLF CLUB FLDN	SWFWMD	126834.01	1373532.00	Hillsborough	50	60	UF	100%	10	15						Not Used	Outside Boundary
130423	EAGLES GOLF CLUB SURF	SWFWMD	126827.12	1373552.30	Hillsborough	3	28.3	SAS	100%	10	15	SAS						
100566	EDISON JCT FLORIDAN WELL NEAR KEYSVILLE FL	USGS	311525.43	1284990.23	Hillsborough	60	211	IAS/ICU	100%	1	2						Not Used	No calibration in IAS/ICU
130183	EDISON JUNCTION INT	SWFWMD	311514.58	1284982.25	Hillsborough	60	212	IAS/ICU	100%	10	15						Not Used	No calibration in IAS/ICU
130302	ELDRIDGE-WILDE 022 SHALLOW		125353.41	1388822.04	Hillsborough	19	22	SAS	100%	0	0						Not Used	Outside Boundary
130284	ELDRIDGE-WILDE 024 SHALLOW		127372.37	1392431.87	Hillsborough	13	16	SAS	100%	0	0						Not Used	Outside Boundary
130307	EUREKA SPGS LANDFILL DEEP		223982.01	1340870.88	Hillsborough	35	37	IAS/ICU	100%	0	0						Not Used	Outside Boundary
130308	EUREKA SPGS LANDFILL SH		223955.83	1340853.99	Hillsborough	4	10	IAS/ICU	100%	0	0						Not Used	Outside Boundary
100613	EUREKA SPRINGS DEEP WELL NEAR TEMPLE TERRACE FL	USGS	224044.01	1340981.49	Hillsborough	35	37	IAS/ICU	100%	0	15	IAS-layer 2/3						d 3)
100614	EUREKA SPRINGS SHALLOW WELL NEAR TEMPLE TERRACE FL	USGS	224044.01	1340981.49	Hillsborough	4	10	IAS/ICU	100%	10	15						Not Used	part of group represented by 100613 for IAS-bc
130180	FAIRFIELD VILLAGE DEEP		162754.00	1352213.78	Hillsborough	34	45	SAS	100%	0	0						Not Used	Outside Boundary
130181	FAIRFIELD VILLAGE SHALLOW		162750.58	1352226.96	Hillsborough	12	22	SAS	100%	0	0						Not Used	Outside Boundary
130273	FAIRGROUND DEEP	SWFWMD	217145.61	1329868.00	Hillsborough	0	0	Error	0%	10	15	SAS						
130190	FLETCHER LETT FLDN		307697.94	1322438.11	Hillsborough	100	530	UF	43%	0	0						Not Used	Open section straddles multiple layers
100602	FLETCHER LETT WELL NEAR PLANT CITY FL	USGS	307634.19	1322327.56	Hillsborough	100	530	UF	43%	7	8						Not Used	Open section straddles multiple layers
100534	FT LONESOME WELL 88 AT FORT LONESOME FL	USGS	285102.75	1226940.60	Hillsborough	180	200	IAS/ICU	100%	1	2						Not Used	No calibration in IAS/ICU
130317	GATES TRAILER PARK		220655.92	1358654.27	Hillsborough	46	120	UF	61%	0	0						Not Used	Outside Boundary
100610	GRIFFIN 2 DEEP WELL NEAR DOVER FL	USGS	256146.34	1338978.20	Hillsborough	490	590	APPZ	92%	1	2						Not Used	Hillsborough Basin has a dense coverage of points and is not important for the purposes of the model; remove
130228	HARNEY CANAL S-161		213653.32	1341560.46	Hillsborough	0	0	Error	0%	0	0						Not Used	Outside Boundary
130329	HILLS STATE PARK PKNG SH	SWFWMD	259350.65	1388629.07	Hillsborough	15	18	IAS/ICU	100%	0	15						Not Used	No calibration in IAS/ICU
130298	HILLS STATE PK PKNG DEEP	SWFWMD	259352.48	1388633.09	Hillsborough	37	50	UF	59%	10	15						Not Used	Hillsborough Basin has a dense coverage of points and is not important for the purposes of the model; remove
100648	HILLSBOROUGH DEEP WELL 13 NEAR CITRUS PARK FL	USGS	170225.33	1378314.41	Hillsborough	46	347	UF	97%	1	2						Not Used	Outside Boundary
100591	HILLSBOROUGH MEM CEM DEEP NEAR BRANDON FL	USGS	229798.67	1311637.28	Hillsborough	427	527	MC1	100%	1	2						Not Used	Model geology puts this well in MC1
100660	HILLSBOROUGH RD STATE PARK DP NEAR ZEPHYRHILLS FL	USGS	259338.07	1388624.14	Hillsborough	37	50	UF	59%	0	2						Not Used	Hillsborough Basin has a dense coverage of points and is not important for the purposes of the model; remove
100649	HILLSBOROUGH SHALLOW WELL 13 NEAR CITRUS PARK FL	USGS	170118.11	1378335.94	Hillsborough	21	23	SAS	100%	0	2						Not Used	Outside Boundary
130409	HORSE LAKE FLDN	SWFWMD	146401.50	1375737.80	Hillsborough	54.4	94	UF	86%	0	5						Not Used	Outside Boundary
130301	HRSP BOYS CAMP DEEP	SWFWMD	260145.18	1387868.46	Hillsborough	62	74	UF	100%	0	15						Not Used	Hillsborough Basin has a dense coverage of points and is not important for the purposes of the model; remove
130303	HRSP BOYS CAMP SHALLOW	SWFWMD	260127.17	1387858.54	Hillsborough	15	18	IAS/ICU	100%	10	15						Not Used	No calibration in IAS/ICU
130360	HRSP CYPRESS WTL SURF	SWFWMD	259276.98	1387897.46	Hillsborough	1	6	IAS/ICU	73%	0	15	SAS						
130411	HRSP MARSH UPL SURF		260514.49	1388087.97	Hillsborough	9	15	IAS/ICU	100%	0	0						Not Used	No calibration in IAS/ICU
130410	HRSP MARSH WTL SURF		260434.22	1388119.09	Hillsborough	0	11.4	IAS/ICU	75%	0	0						Not Used	No calibration in IAS/ICU
130219	HUTCHINSON FLDN	SWFWMD	156683.81	1371412.79	Hillsborough	49	60	IAS/ICU	55%	9	15						Not Used	Outside Boundary
130222	HUTCHINSON SURF	SWFWMD	156673.95	1371412.91	Hillsborough	3	19.9	SAS	100%	9	15	SAS						
100622	J. W. MORRIS WELL NEAR TEMPLE TERRACE FL	USGS	232278.81	1353673.26	Hillsborough	142	162	UF	100%	1	2						Not Used	sparse data
100650	JAMES DEEP WELL 11 NEAR CITRUS PARK FL	USGS	149610.86	1378696.73	Hillsborough	280	300	UF	100%	1	0						Not Used	Outside Boundary
130321	KEYSTONE PARK FLDN	SWFWMD	148096.78	1384955.87	Hillsborough	59	70	UF	95%	10	15						Not Used	Outside Boundary
130322	KEYSTONE PARK SURF	SWFWMD	148098.55	1384954.84	Hillsborough	3	25	SAS	100%	10	15	SAS						
130246	KUSHMER INT	SWFWMD	206426.63	1266479.51	Hillsborough	41	145	IAS/ICU	97%	9	15	IAS-layer 2						averaged with 130465
130383	LAKE ALICE FLDN	SWFWMD	137916.32	1383042.43	Hillsborough	94	137	UF	100%	0	15						Not Used	Outside Boundary
130380	LAKE ALICE SURF	SWFWMD	137889.86	1383073.09	Hillsborough	2.5	20.1	SAS	100%	0	15	SAS						
130492	LHFDA 22 FLDN	SWFWMD	239762.00	1362987.66	Hillsborough	68	152	UF	94%	0	15	UF						
130379	LHFDA 22 SURF	SWFWMD	239745.37	1363109.06	Hillsborough	2	22	IAS/ICU	100%	0	15						Not Used	No calibration in IAS/ICU
130415	LUTZ PARK FLDN	SWFWMD	180685.97	1391501.06	Hillsborough	60	70	UF	90%	10	15						Not Used	Outside Boundary
130299	LUTZ PARK SURF	SWFWMD	180685.84	1391490.95	Hillsborough	3	25	SAS	100%	10	15	SAS						
130248	LUTZ-LAKE FERN DEEP	SWFWMD	160426.79	1392500.13	Hillsborough	65	375	UF	100%	10	15						Not Used	Outside Boundary
100662	LUTZ-LAKE FERN DEEP NEAR LUTZ FL	USGS	160426.79	1392500.13	Hillsborough	65	375	UF	100%	1	2						Not Used	Outside Boundary
130250	LUTZ-LAKE FERN SHALLOW	SWFWMD	160417.58	1392480.04	Hillsborough	15	22	SAS	100%	10	15	SAS						
100585	M.MURPHY,4317 SAN LUIS AT TAMPA FL	USGS	166045.44	1305143.96	Hillsborough	185	205	UF	100%	1	2						Not Used	Outside Boundary
100627	MA QUAGLIANI WELL NEAR PLANT CITY FL	USGS	300011.44	1359960.42	Hillsborough	196	216	UF	100%	1	2						Not Used	Hillsborough Basin has a dense coverage of points and is not important for the purposes of the model; remove

Table 4.1: Usage of SAJ Observation Database in Regional Model Calibration

Model ID[a]	Well Name	Data Source	Easting[b]	Northing[b]	County	Cased Depth (ft)	Drilled Depth (ft)	Dominant Layer[c]	% Open Section in Layer[c]	93/94 Months with Data[d]	03/04 Months with Data[e]	Use for Data in Model Setup/Calibration						Reasoning/Comments
													Observations for Calibration					
												Boundary Conditions[f]	Steady State (Oct 03)	Steady State (Feb 04)	Transient (03/04)	Transient (03/04	Not Used	
100561	MABRY CARLTON WELL 6 NEAR MYAKKA CITY FL	USGS	284744.13	1281840.53	Hillsborough	700	800	APPZ	94%	0	2						Not Used	sparse data
100629	MARTIN M GRIFFIN ROAD WELL NEAR KNIGHTS FL	USGS	291353.43	1362514.64	Hillsborough	449	469	MC1	100%	1	2						Not Used	Model geology puts this well in MC1
130265	MBWF 1 FLDN	SWFWMD	222414.46	1376681.64	Hillsborough	62	479	UF	65%	10	15						Not Used	Outside Boundary
130266	MBWF 1 SURF	SWFWMD	222415.35	1376681.63	Hillsborough	9	10	IAS/ICU	100%	10	15						Not Used	Outside Boundary
130244	MBWF 10 FLDN		223743.95	1370540.21	Hillsborough	90	500	UF	58%	0	0						Not Used	Outside Boundary
130416	MBWF 11 FLDN		220126.66	1375530.16	Hillsborough	127	500	UF	56%	0	0						Not Used	Outside Boundary
130290	MBWF 12 FLDN		233531.60	1371974.01	Hillsborough	238	520	MC1	40%	0	0						Not Used	Open section straddles multiple layers
130207	MBWF 13 FLDN		237877.16	1376951.95	Hillsborough	50	593	UF	49%	0	0						Not Used	Open section straddles multiple layers
130208	MBWF 13 SURF		237877.17	1376952.96	Hillsborough	0	9	SAS	62%	0	0						Not Used	Missing data
130252	MBWF 17 FLDN	SWFWMD	214034.18	1378470.39	Hillsborough	71	145	UF	100%	10	15						Not Used	Outside Boundary
130271	MBWF 3A FLDN	SWFWMD	228031.98	1377579.53	Hillsborough	100	600	UF	45%	10	0						Not Used	Outside Boundary
130272	MBWF 3A SURF	SWFWMD	228013.29	1377509.02	Hillsborough	12	16	IAS/ICU	100%	10	15						Not Used	outside IAS (per Miller, 1997)
130233	MBWF 6 FLDN	SWFWMD	226062.39	1374388.73	Hillsborough	100	661	UF	40%	10	15						Not Used	Outside Boundary
130234	MBWF 6 SURF	SWFWMD	226151.84	1374377.65	Hillsborough	12	14	IAS/ICU	100%	10	15						Not Used	outside IAS (per Miller, 1997)
130354	MBWF CLAY GULLY CYP WTL SU	SWFWMD	222369.76	1379844.00	Hillsborough	5	25	IAS/ICU	82%	0	15	SAS						
130333	MBWF E BR CLAY GUL WTL SUR	SWFWMD	226627.19	1376069.54	Hillsborough	5	20	IAS/ICU	100%	0	15						Not Used	Outside Boundary
130338	MBWF E CYP MARSH UPL SURF	SWFWMD	233811.03	1381941.35	Hillsborough	5	15	IAS/ICU	100%	0	15						Not Used	Outside Boundary
130357	MBWF E CYP MARSH WTL SURF	SWFWMD	233747.91	1381901.62	Hillsborough	6	12.5	IAS/ICU	100%	0	15						Not Used	Outside Boundary
130217	MBWF P-153 SURF	SWFWMD	224212.64	1378035.62	Hillsborough	0	0	Error	0%	10	15	SAS						
130204	MBWF P-157A SURF	SWFWMD	230883.29	1381175.00	Hillsborough	0	0	Error	0%	10	15	SAS						
130319	MBWF P-159 SURF	SWFWMD	221592.12	1377559.50	Hillsborough	0	0	Error	0%	10	15	SAS						
130163	MBWF RIV FOR SURF	SWFWMD	227709.80	1371047.22	Hillsborough	0	0	Error	0%	0	15						Not Used	Outside Boundary
130485	MBWF S CYP MARSH UPL SURF	SWFWMD	226395.87	1374577.01	Hillsborough	8.3	18.3	IAS/ICU	100%	0	15						Not Used	Outside Boundary
130349	MBWF S CYP MARSH WTL SURF	SWFWMD	226210.01	1374781.08	Hillsborough	4	19	IAS/ICU	100%	0	15						Not Used	Outside Boundary
130408	MBWF SAWGRASS MSH UPL SURF	SWFWMD	222535.56	1372164.79	Hillsborough	0	0	Error	0%	0	8	SAS						
130334	MBWF SAWGRASS MSH WTL SURF	SWFWMD	222285.45	1372228.17	Hillsborough	5	15	IAS/ICU	100%	0	15						Not Used	Outside Boundary
130489	MBWF TROUT CREEK UPL SURF	SWFWMD	217674.97	1375673.68	Hillsborough	8.8	18.8	IAS/ICU	100%	0	15						Not Used	Outside Boundary
130352	MBWF TROUT CREEK WTL SURF	SWFWMD	217862.48	1375621.08	Hillsborough	5	11.5	IAS/ICU	79%	0	15	SAS						
130488	MBWF WELL MARSH UPL SURF	SWFWMD	230859.02	1380589.36	Hillsborough	2.5	15.7	IAS/ICU	78%	0	15	SAS						
130339	MBWF WELL MARSH WTL SURF	SWFWMD	230975.76	1380618.40	Hillsborough	4	13.1	IAS/ICU	86%	0	15	SAS						
130484	MBWF WEST CYP UPL SURF	SWFWMD	221430.37	1377510.79	Hillsborough	8.8	18.8	IAS/ICU	100%	0	15						Not Used	Outside Boundary
130350	MBWF WEST CYP WTL SURF	SWFWMD	221241.75	1377462.37	Hillsborough	2	12	IAS/ICU	57%	0	15	SAS						
130491	MBWF WILD HOG WTL SURF	SWFWMD	231673.59	1377246.96	Hillsborough	5	25	IAS/ICU	100%	0	15						Not Used	Outside Boundary
130335	MBWF X-1 UPL SURF	SWFWMD	219989.39	1378405.66	Hillsborough	5	20	IAS/ICU	89%	0	15	SAS						
130353	MBWF X-1 WTL SURF	SWFWMD	219945.96	1378527.37	Hillsborough	4	29	IAS/ICU	89%	0	15	SAS						
130486	MBWF X-2 UPL SURF	SWFWMD	227027.43	1376630.85	Hillsborough	8.5	18.5	IAS/ICU	100%	0	15						Not Used	Outside Boundary
130348	MBWF X-2 WTL SURF	SWFWMD	226966.85	1376823.45	Hillsborough	2	17	IAS/ICU	95%	0	15	SAS						
130487	MBWF X-3 UPL SURF	SWFWMD	235798.18	1376848.94	Hillsborough	2.7	10.7	IAS/ICU	73%	0	15	SAS						
130336	MBWF X-3 WTL SURF	SWFWMD	235737.45	1377031.42	Hillsborough	5	20	IAS/ICU	100%	0	15						Not Used	No calibration in IAS/ICU
130337	MBWF X-4 UPL SURF	SWFWMD	225326.39	1379952.80	Hillsborough	5	25	IAS/ICU	81%	0	15	SAS						
130356	MBWF X-4 WTL SURF	SWFWMD	225257.42	1380196.00	Hillsborough	4	14	IAS/ICU	53%	0	15	SAS						
130483	MBWF X-6 UPL SURF	SWFWMD	222520.00	1378044.21	Hillsborough	9	19	IAS/ICU	100%	0	15						Not Used	Outside Boundary
130351	MBWF X-6 WTL SURF	SWFWMD	222760.90	1377960.73	Hillsborough	3	28	IAS/ICU	81%	0	15	SAS						
130414	MCDONALD ROGERS FLDN	SWFWMD	149963.52	1392805.88	Hillsborough	48	59	UF	65%	10	15						Not Used	Outside Boundary
130422	MCDONALD ROGERS SURF	SWFWMD	149981.55	1392815.75	Hillsborough	3	25	SAS	100%	10	15	SAS						
130381	MCINTOSH SURF	SWFWMD	289953.81	1359416.58	Hillsborough	1	9	SAS	100%	0	15	SAS						
130493	MCINTOSH SURF	SWFWMD	289955.65	1359421.62	Hillsborough	99	155	IAS/ICU	50%	0	15						Not Used	No calibration in IAS/ICU
100569	MCMULLEN CAMPGROUND SO E RIVERVIEW FL	USGS	240714.21	1287490.00	Hillsborough	705	805	APPZ	100%	1	2						Not Used	sparse data
130293	MORRIS BRDIGE LOWE 1.25		243189.48	1388108.36	Hillsborough	0	0	Error	0%	0	0						Not Used	Data error
100636	MORRIS BRIDGE 11 DEEP NEAR BRANCHTON FL	USGS	220125.09	1375530.54	Hillsborough	127	500	UF	56%	10	0						Not Used	Outside Boundary
130291	MORRIS BRIDGE 12 SHALLOW		233542.38	1371976.92	Hillsborough	20	25	IAS/ICU	100%	0	0						Not Used	No calibration in IAS/ICU
130245	MORRIS BRIDGE 14 DP		234803.83	1382742.83	Hillsborough	82	1783	MC2	33%	0	0						Not Used	Open section straddles multiple layers
130288	MORRIS BRIDGE 2 SHALLOW		224170.12	1376696.59	Hillsborough	8.5	10	IAS/ICU	100%	0	0						Not Used	Outside Boundary
130189	MORRIS BRIDGE 3B DEEP		226578.13	1375760.96	Hillsborough	84	260	UF	100%	0	0						Not Used	Outside Boundary
130138	MORRIS BRIDGE 3C DEEP		227122.11	1376361.11	Hillsborough	1000	1037	MC2	100%	0	0						Not Used	Outside Boundary
100639	MORRIS BRIDGE 3C NEAR THONOTOSASSA FL	USGS	227214.75	1376765.46	Hillsborough	1000	1037	MC2	100%	10	0						Not Used	Outside Boundary
130242	MORRIS BRIDGE 4 SHALLOW		230526.31	1376425.00	Hillsborough	15	17	IAS/ICU	100%	0	0						Not Used	Outside Boundary
130166	MORRIS BRIDGE 5 SHALLOW		223431.37	1374684.38	Hillsborough	8	12.3	IAS/ICU	100%	0	0						Not Used	No calibration in IAS/ICU
130154	MORRIS BRIDGE 537 DEEP		224847.04	1381234.94	Hillsborough	69	71	UF	100%	0	0						Not Used	Outside Boundary
130157	MORRIS BRIDGE 537 SHALLOW		224757.50	1381235.93	Hillsborough	12	22	IAS/ICU	100%	0	0						Not Used	Outside Boundary
130247	MORRIS BRIDGE 7 SHALLOW		228357.14	1374630.31	Hillsborough	10	12	IAS/ICU	100%	0	0						Not Used	No calibration in IAS/ICU
130199	MORRIS BRIDGE 8 SHALLOW		225649.28	1372740.62	Hillsborough	8	10	IAS/ICU	100%	0	0						Not Used	Outside Boundary
100634	MORRIS BRIDGE DEEP 10 NEAR BRANCHTON FL	USGS	223861.19	1370774.29	Hillsborough	90	500	UF	58%	5	2						Not Used	Outside Boundary

Table 4.1: Usage of SAJ Observation Database in Regional Model Calibration

Model ID[a]	Well Name	Data Source	Easting[b]	Northing[b]	County	Cased Depth (ft)	Drilled Depth (ft)	Dominant Layer[c]	% Open Section in Layer[c]	93/94 Months with Data[d]	03/04 Months with Data[e]	Use for Data in Model Setup/Calibration						Reasoning/Comments
													Observations for Calibration					
												Boundary Conditions[f]	Steady State (Oct 03)	Steady State (Feb 04)	Transient (03/04)	Transient (03/04	Not Used	
100643	MORRIS BRIDGE DEEP 13 NEAR BRANCHTON FL	USGS	237981.36	1377148.83	Hillsborough	50	593	UF	49%	10	2						Not Used	Open section straddles multiple layers
100635	MORRIS BRIDGE DEEP WELL 12 NEAR BRANCHTON FL	USGS	233531.62	1371976.03	Hillsborough	238	520	MC1	40%	7	0						Not Used	Open section straddles multiple layers
100658	MORRIS BRIDGE DEEP WELL 14 NEAR BRANCHTON FL	USGS	234740.92	1382638.45	Hillsborough	82	1783	MC2	33%	1	0						Not Used	Open section straddles multiple layers
100651	MORRIS BRIDGE DEEP WELL 17 NEAR BRANCHTON FL	USGS	214184.74	1378319.19	Hillsborough	71	145	UF	100%	2	0						Not Used	Outside Boundary
100638	MORRIS BRIDGE DEEP WELL 2A NEAR BRANCHTON FL	USGS	224107.16	1376592.22	Hillsborough	321	341	UF	66%	2	0						Not Used	Outside Boundary
100640	MORRIS BRIDGE DEEP WELL 3A NEAR BRANCHTON FL	SWFWMD	228030.95	1377567.42	Hillsborough	100	600	UF	45%	10	15						Not Used	Open section straddles multiple layers
100663	MORRIS BRIDGE DEEP WELL 532 NEAR BRANCHTON FL	USGS	246310.86	1392051.53	Hillsborough	41	46	IAS/ICU	100%	1	2						Not Used	No calibration in IAS/ICU
100653	MORRIS BRIDGE DEEP WELL 537 NEAR BRANCHTON FL	USGS	224756.15	1381237.01	Hillsborough	130	150	UF	100%	1	0						Not Used	sparse data
130205	MORRIS BRIDGE LOWE 3-INCH		243368.53	1388106.47	Hillsborough	0	0	Error	0%	0	0						Not Used	Data error
130318	MORRIS BRIDGE P.159 DEEP		221850.64	1377530.37	Hillsborough	0	0	Error	0%	0	0						Not Used	Outside Boundary
130216	MORRIS BRIDGE P-153 DEEP		224364.81	1378108.70	Hillsborough	0	0	Error	0%	0	0						Not Used	Outside Boundary
130203	MORRIS BRIDGE P-157A DEEP		231025.60	1381167.39	Hillsborough	0	0	Error	0%	0	0						Not Used	Outside Boundary
130148	MORRIS BRIDGE P-166 DEEP		231872.91	1376713.45	Hillsborough	0	0	Error	0%	0	0						Not Used	Outside Boundary
130149	MORRIS BRIDGE P-166 SH	SWFWMD	231872.92	1376714.46	Hillsborough	0	0	Error	0%	0	0						Not Used	outside IAS (per Miller, 1997)
100642	MORRIS BRIDGE SH 3A REPLACEMENT NEAR BRANCHTON FL	USGS	228092.59	1377673.05	Hillsborough	500	600	APPZ	100%	1	0						Not Used	too shallow to be representative for BC
130327	MORRIS BRIDGE SHALLOW 11		220126.65	1375529.15	Hillsborough	14.6	24.5	IAS/ICU	100%	0	0						Not Used	Outside Boundary
100641	MORRIS BRIDGE SHALLOW 3A NEAR BRANCHTON FL	USGS	227877.31	1377358.98	Hillsborough	14	16	IAS/ICU	100%	6	0						Not Used	outside IAS (per Miller, 1997)
100644	MORRIS BRIDGE SHALLOW WELL 13 NEAR BRANCHTON FL	USGS	237813.35	1376847.57	Hillsborough	6.67	8.67	IAS/ICU	100%	6	0						Not Used	outside IAS (per Miller, 1997)
100595	NCNB NAT'L BANK,249 SO HYDE PARK AT TAMPA,FL	USGS	183350.74	1314489.66	Hillsborough	125	145	UF	100%	1	2						Not Used	Outside Boundary
130332	NEW RIVER CYP UPL SURF	SWFWMD	249376.87	1390041.64	Hillsborough	5	15	IAS/ICU	100%	0	15						Not Used	No calibration in IAS/ICU
130359	NEW RIVER CYP WTL SURF	SWFWMD	249458.05	1389927.66	Hillsborough	1.5	8	IAS/ICU	100%	0	15						Not Used	No calibration in IAS/ICU
130331	NEW RIVER MARSH UPL SURF	SWFWMD	233891.85	1388603.57	Hillsborough	5	20	IAS/ICU	85%	0	15	SAS						
130358	NEW RIVER MARSH WTL SURF	SWFWMD	250007.47	1388517.84	Hillsborough	1	4	IAS/ICU	100%	0	15						Not Used	No calibration in IAS/ICU
130285	NEWBERGER ROAD FLDN	SWFWMD	189070.72	1394087.27	Hillsborough	50	61	IAS/ICU	100%	9	15						Not Used	Outside Boundary
130419	NEWBERGER ROAD SURF	SWFWMD	189069.82	1394087.28	Hillsborough	3	25	SAS	100%	9	15	SAS						
130311	NORTONS DAIRY		285762.67	1383237.79	Hillsborough	0	45	IAS/ICU	97%	0	0						Not Used	No calibration in IAS/ICU
130449	NWHWRAP 2 DEEP FLDN	SWFWMD	178553.43	1339036.16	Hillsborough	717	771	APPZ	100%	3	0						Not Used	Outside Boundary
130450	NWHWRAP 2 SHALLOW FLDN	SWFWMD	178642.17	1339034.07	Hillsborough	40	55	IAS/ICU	100%	0	15						Not Used	Outside Boundary
130407	NWHWRAP 2 SWNN FLDN	SWFWMD	178588.38	1339034.73	Hillsborough	290	390	UF	98%	0	8						Not Used	Outside Boundary
130431	NWHWRAP 4 DEEP FLDN	SWFWMD	136368.81	1361563.72	Hillsborough	998	1106	APPZ	52%	0	12						Not Used	Outside Boundary
100603	OAK FOREST DEEP AT BRANDON FL	USGS	245858.36	1323831.09	Hillsborough	335	355	UF	100%	1	0						Not Used	sparse data
130451	OAK GROVE JR HI SCHL FLDN	SWFWMD	177691.04	1336833.23	Hillsborough	29	40	SAS	100%	10	15	SAS						
130452	OAK GROVE JR HI SCHL SURF	SWFWMD	177691.93	1336833.22	Hillsborough	3	14	SAS	100%	10	15	SAS						
100584	OAKMONT DEEP NEAR BRANDON FL	USGS	244893.18	1302458.77	Hillsborough	314	334	UF	100%	1	2						Not Used	Hillsborough Basin has a dense coverage of points and is not important for the purposes of the model; remove
130200	PASCO 204 DEEP		166935.53	1398381.79	Hillsborough	45	47	IAS/ICU	100%	0	0						Not Used	Outside Boundary
130201	PASCO 204 SHALLOW		166935.54	1398382.80	Hillsborough	8	10	SAS	100%	0	0						Not Used	Outside Boundary
130191	PASCO 205 DEEP	SWFWMD	165424.78	1392138.07	Hillsborough	80	765	UF	42%	5	0						Not Used	Outside Boundary
130274	PASCO 206 SHALLOW		167034.97	1392016.88	Hillsborough	9	10	SAS	100%	0	0						Not Used	Outside Boundary
130275	PASCO 210 DEEP	SWFWMD	174981.58	1390200.90	Hillsborough	48	52	IAS/ICU	100%	10	0						Not Used	Outside Boundary
130276	PASCO 210 SHALLOW	SWFWMD	174981.59	1390201.91	Hillsborough	11	12	SAS	100%	8	0	SAS						
130220	PASCO SOUTH BM FLDN	SWFWMD	167568.74	1395107.68	Hillsborough	93	700	UF	46%	10	15						Not Used	Outside Boundary
100616	PISTOL CLUB FLORIDAN RMP-14 DEEP NR CITRUS PARK FL	USGS	139306.21	1344380.33	Hillsborough	410	430	MC1	100%	1	0						Not Used	Outside Boundary
100586	PLANT HIGH SCHOOL STADIUM DEEP WELL AT TAMPA FL	USGS	170713.02	1308167.52	Hillsborough	105	125	UF	100%	0	2						Not Used	Outside Boundary
130294	RIVERCREST FLDN		226738.50	1283531.89	Hillsborough	47	175	IAS/ICU	80%	0	0						Not Used	No calibration in IAS/ICU
100562	RIVERCREST WELL NEAR BLOOMINGDALE FL	USGS	226784.13	1283517.25	Hillsborough	47	178	IAS/ICU	78%	1	2						Not Used	No calibration in IAS/ICU
100550	RIVERVIEW NO 3 NEAR ADAMSVILLE FL	USGS	225790.67	1268083.06	Hillsborough	500	600	MC1	100%	1	0						Not Used	Model geology puts this well in MC1
100551	RIVERVIEW WELL 419 NEAR RIVERVIEW FL	USGS	225700.87	1268084.04	Hillsborough	141	161	IAS/ICU	100%	1	0						Not Used	No calibration in IAS/ICU
100661	RMP-01 DEEP WELL NEAR CITRUS PARK FL	USGS	167380.01	1390393.11	Hillsborough	593	693	APPZ	100%	1	2						Not Used	Outside Boundary
100571	ROBINSON HIGH SCHOOL STADIUM DEEP WELL AT TAMPA FL	USGS	166225.78	1289998.45	Hillsborough	79	84	IAS/ICU	100%	1	2						Not Used	Outside Boundary
100530	ROMP 123 FLORIDAN WELL NEAR WIMAUMA FL	USGS	251152.44	1216786.35	Hillsborough	117	620	UF	59%	1	2						Not Used	sparse data
130156	ROMP 123 HTRN/OCAL	SWFWMD	251164.05	1216778.15	Hillsborough	117	620	UF	59%	10	15						Not Used	Open interval is only 59% in UF; 100533 is nearby and completely contained within UF

Table 4.1: Usage of SAJ Observation Database in Regional Model Calibration

Model ID[a]	Well Name	Data Source	Easting[b]	Northing[b]	County	Cased Depth (ft)	Drilled Depth (ft)	Dominant Layer[c]	% Open Section in Layer[c]	93/94 Months with Data[d]	03/04 Months with Data[e]	Use for Data in Model Setup/Calibration						Reasoning/Comments
													Observations for Calibration					
												Boundary Conditions[f]	Steady State (Oct 03)	Steady State (Feb 04)	Transient (03/04)	Transient (03/04	Not Used	
130262	ROMP 48 AVPK	SWFWMD	286583.21	1240198.86	Hillsborough	780	815	MC1	99%	10	15						Not Used	Model geology puts this well in MC1
100541	ROMP 48 FLORIDAN WELL NEAR FORT LONESOME FL	USGS	286601.37	1240218.89	Hillsborough	215	541	UF	70%	0	2						Not Used	sparse data
100542	ROMP 48 HAWTHORN WELL NEAR FORT LONESOME FL	USGS	286583.49	1240229.16	Hillsborough	56	61	IAS/ICU	100%	1	2						Not Used	No calibration in IAS/ICU
130471	ROMP 48 HTRN	SWFWMD	286582.31	1240198.87	Hillsborough	45.5	61	IAS/ICU	100%	10	15						Not Used	No calibration in IAS/ICU
130470	ROMP 48 TMPA/SWNN	SWFWMD	286581.41	1240198.87	Hillsborough	215	541	UF	70%	1	15						Not Used	Nearby wells (130467) with more of the open interval in the UF.
100545	ROMP 49 AVON PARK WELL AT BALM FL	USGS	250496.08	1248580.46	Hillsborough	1140	1575	APPZ	55%	0	2						Not Used	sparse data
130143	ROMP 49 AVPK	SWFWMD	250487.09	1248580.55	Hillsborough	925	1140	APPZ	100%	10	15			APPZ	APPZ	APPZ		A couple of strong pumping events - plus a 40-foot drop in Oct - even with average pumping, we might not get this - remove from Oct, leave in transient, knowing we can't match the pumping events
130144	ROMP 49 HTRN/TMPA	SWFWMD	250505.48	1248620.77	Hillsborough	230	290	IAS/ICU	100%	0	15						Not Used	No calibration in IAS/ICU
130145	ROMP 49 SURF	SWFWMD	250504.86	1248560.17	Hillsborough	37	57	SAS	100%	10	15	SAS						
130467	ROMP 49 SWNN	SWFWMD	250531.91	1248569.99	Hillsborough	410	526	UF	100%	10	15		UF	UF	UF	UF		
100546	ROMP 49 TAMPA WELL AT BALM FL	USGS	250514.15	1248590.38	Hillsborough	290	620	UF	79%	0	2						Not Used	Sparse data
130142	ROMP 49 TAMPA/OCA		250712.31	1248637.85	Hillsborough	195	620	UF	61%	0	0						Not Used	Missing Data
100538	ROMP 50 AVON PARK WELL NEAR WIMAUMA FL	USGS	217117.54	1230349.53	Hillsborough	1330	1430	MC2	100%	10	15						Not Used	Geology places this in MC2
130238	ROMP 50 AVPK	SWFWMD	217060.76	1230229.93	Hillsborough	1393	1430	MC2	100%	10	8						Not Used	Geology places this in MC2
100536	ROMP 50 FLORIDAN WELL NEAR WIMAUMA FL	USGS	217126.19	1230319.13	Hillsborough	200	562	UF	85%	10	15						Not Used	100547/130464 is nearby with a screen more unique to the UF.
100537	ROMP 50 NRSD WELL NEAR WIMAUMA FL	USGS	217118.09	1230400.03	Hillsborough	32.5	37.5	SAS	100%	10	15	SAS						
130236	ROMP 50 SURF	SWFWMD	217065.78	1230278.36	Hillsborough	33	38	SAS	100%	10	3	SAS						
130473	ROMP 50 TMPA/OCAL	SWFWMD	217059.07	1230240.05	Hillsborough	200	562	UF	85%	9	3						Not Used	duplicate with 100536, with sparser data
100582	ROMP 61 FLORIDAN WELL NEAR PLEASANT GROVE FL	USGS	281112.81	1301258.11	Hillsborough	300	1000	APPZ	54%	10	2					APPZ		no 03/04 data
130460	ROMP 61 SWNN/AVPK	SWFWMD	281139.92	1301278.05	Hillsborough	300	1000	APPZ	55%	10	15		APPZ	APPZ	APPZ	APPZ		
130476	ROMP 62 AVPK	SWFWMD	231398.13	1283467.51	Hillsborough	625	692	APPZ	50%	0	15	APPZ						averaged with 100570
130480	ROMP 65 FMW-3 UP FLDN	SWFWMD	176559.82	1374811.63	Hillsborough	92	127	UF	100%	0	15						Not Used	Outside Boundary
130481	ROMP 65 FMW-5 UP FLDN	SWFWMD	177252.53	1376520.58	Hillsborough	90	113	UF	100%	0	13						Not Used	Outside Boundary
100620	ROMP 66 DEEP WELL AT SULPHUR SPRINGS FL	USGS	182783.46	1348871.63	Hillsborough	42	250	UF	86%	10	12						Not Used	Outside Boundary
130438	ROMP 66 TMPA	SWFWMD	182785.20	1348788.23	Hillsborough	42	250	UF	86%	10	15						Not Used	Outside Boundary
130482	ROMP 66 TMPA	SWFWMD	182794.59	1348823.47	Hillsborough	15	21	SAS	100%	0	1						Not Used	Outside Boundary
100623	ROMP 67 AVON PARK WELL NEAR TEMPLE TERRACE FL	USGS	222861.75	1355701.77	Hillsborough	440	490	MC1	68%	10	15						Not Used	Model geology puts this well in MC1
130432	ROMP 67 AVPK	SWFWMD	222781.37	1355564.88	Hillsborough	440	490	MC1	68%	10	15	APPZ						
100624	ROMP 67 TAMPA WELL NEAR TEMPLE TERRACE FL	USGS	222707.57	1355292.94	Hillsborough	70	141	UF	89%	0	2						Not Used	Outside Boundary
130433	ROMP 67 TMPA/SWNN	SWFWMD	222782.26	1355564.87	Hillsborough	70	141	UF	92%	0	15						Not Used	Outside Boundary
100630	ROMP 68 AVON PARK WELL NEAR ANTIOCH FL	USGS	255399.71	1365255.21	Hillsborough	440	490	APPZ	75%	10	15						Not Used	close to boundary
130428	ROMP 68 AVPK	SWFWMD	255379.18	1365186.79	Hillsborough	440	490	APPZ	75%	0	14						Not Used	Duplicate with 100630
100631	ROMP 68 SUWANNEE WELL NEAR ANTIOCH FL	USGS	255356.74	1365269.85	Hillsborough	201	221	UF	100%	0	2						Not Used	Duplicate with 130427
130427	ROMP 68 TMPA/SWNN	SWFWMD	255378.45	1365202.95	Hillsborough	120	221	UF	100%	7	15						Not Used	Hillsborough Basin has a dense coverage of points and is not important for the purposes of the model; remove
130457	ROMP DV-1 AVPK	SWFWMD	265802.77	1331891.27	Hillsborough	530	850	APPZ	92%	10	15						Not Used	pretty strong pumping response
130237	ROMP DV-1 L HTRN/TMPA	SWFWMD	265811.53	1331870.98	Hillsborough	90	140	IAS/ICU	100%	10	15						Not Used	No calibration in IAS/ICU
130239	ROMP DV-1 SURF	SWFWMD	265811.43	1331860.88	Hillsborough	5	15	SAS	100%	10	15	SAS						
130235	ROMP DV-1 SWNN	SWFWMD	265802.47	1331860.97	Hillsborough	160	345	UF	91%	10	15		UF	UF	UF	UF		
130474	ROMP DV-2 L HTRN/TMPA	SWFWMD	285589.40	1322185.14	Hillsborough	108	130	IAS/ICU	100%	5	15						Not Used	No calibration in IAS/ICU
130475	ROMP DV-2 SURF	SWFWMD	285554.83	1322323.85	Hillsborough	15	35	SAS	77%	5	15	SAS						
100581	ROMP TR 10-2 SHALLOW WELL NEAR TAMPA FL	SWFWMD	212665.03	1299007.03	Hillsborough	4	13	SAS	100%	10	15	SAS						
130150	ROMP TR 10-2 SURF		212655.83	1298986.93	Hillsborough	4	13	SAS	100%	0	0						Not Used	Outside Boundary
130461	ROMP TR 10-2 TMPA		212664.58	1298966.63	Hillsborough	115	125	UF	100%	0	0						Not Used	Outside Boundary
100599	ROMP TR 11-2 SUWANNEE WELL NEAR TAMPA FL	SWFWMD	213869.79	1317631.07	Hillsborough	300	315	UF	100%	10	15						Not Used	Outside Boundary
130459	ROMP TR 11-2 SWNN		213863.52	1317632.15	Hillsborough	300	315	UF	100%	0	0						Not Used	Outside Boundary
130478	ROMP TR 12-1 NEW SURF	SWFWMD	156667.91	1325708.79	Hillsborough	12	21	SAS	100%	0	15	SAS						
130477	ROMP TR 12-1 NEW TMPA	SWFWMD	156667.78	1325698.68	Hillsborough	118	132	UF	100%	0	15						Not Used	Outside Boundary
130286	ROMP TR 12-1 SURFICIAL		156734.15	1325697.84	Hillsborough	7	9	SAS	100%	0	0						Not Used	Outside Boundary
130458	ROMP TR 12-1 TAMPA		156718.72	1325683.90	Hillsborough	123	128	UF	100%	0	0						Not Used	Outside Boundary
130328	ROMP TR 12-3		158128.97	1339395.38	Hillsborough	310	345	UF	100%	0	0						Not Used	Outside Boundary
130448	ROMP TR 12-3 SWNN		157396.25	1336478.96	Hillsborough	294	342	UF	100%	0	0						Not Used	Outside Boundary
130260	ROMP TR 13-3 AVPK	SWFWMD	128108.77	1360411.06	Hillsborough	724	807	APPZ	100%	10	15						Not Used	Outside Boundary

Table 4.1: Usage of SAJ Observation Database in Regional Model Calibration

Model ID[a]	Well Name	Data Source	Easting[b]	Northing[b]	County	Cased Depth (ft)	Drilled Depth (ft)	Dominant Layer[c]	% Open Section in Layer[c]	93/94 Months with Data[d]	03/04 Months with Data[e]	Use for Data in Model Setup/Calibration						Reasoning/Comments
													Observations for Calibration					
												Boundary Conditions[f]	Steady State (Oct 03)	Steady State (Feb 04)	Transient (03/04)	Transient (03/04	Not Used	
100626	ROMP TR 13-3 FLRD WELL NEAR CITRUS PARK FL	USGS	128073.00	1360401.00	Hillsborough	724	807	APPZ	100%	1	2						Not Used	Outside Boundary
130261	ROMP TR 13-3 SURF	SWFWMD	128126.15	1360370.42	Hillsborough	8.6	10.6	SAS	100%	10	15	SAS						
130472	ROMP TR 9-1 HTRN/TMPA	SWFWMD	182636.80	1240835.90	Hillsborough	124	288	UF	74%	10	15	UF						
100540	ROMP TR 9-1 TAMPA WELL NEAR RUSKIN FL	USGS	182624.57	1240865.34	Hillsborough	124	288	UF	74%	5	1						Not Used	same as 130472, which has more data
130462	ROMP TR 9-2 AVPK	SWFWMD	205633.64	1249932.08	Hillsborough	714	765	APPZ	100%	10	15						Not Used	close to boundary
130465	ROMP TR 9-2 HTRN/TMPA	SWFWMD	205636.34	1249932.05	Hillsborough	118	148	IAS/ICU	100%	10	15	IAS-layer 2						averaged with 130246
130463	ROMP TR 9-2 OCAL	SWFWMD	205634.54	1249932.07	Hillsborough	622	675	MC1	100%	10	15						Not Used	Model geology puts this well in MC1
130466	ROMP TR 9-2 SURF	SWFWMD	205637.23	1249932.04	Hillsborough	10	20	SAS	100%	10	15	SAS						
130464	ROMP TR 9-2 SWNN	SWFWMD	205635.44	1249932.06	Hillsborough	247	464	UF	100%	10	15						Not Used	close to boundary
100543	ROMP TR 9-3 NRSD WELL NEAR RUSKIN FL	USGS	286645.79	1240340.59	Hillsborough	56	61	IAS/ICU	100%	10	0						Not Used	No calibration in IAS/ICU
130469	ROMP TR 9-3 OCAL/AVPK	SWFWMD	195912.73	1241214.58	Hillsborough	764	779	APPZ	100%	10	15	APPZ						
130257	ROMP TR 9-3 SURF	SWFWMD	195921.72	1241214.47	Hillsborough	20	25	SAS	100%	0	15	SAS						
100544	ROMP TR 9-3 SUWANNEE WELL NEAR RUSKIN FL	USGS	195912.73	1241214.58	Hillsborough	414	514	UF	82%	6	2						Not Used	sparse data
130468	ROMP TR 9-3 SWNN/OCAL	SWFWMD	195912.73	1241214.58	Hillsborough	289	525	UF	87%	10	15						Not Used	close to boundary
100580	ROMP TR10-2 DEEP WELL NEAR TAMPA FL	SWFWMD	212665.03	1299007.03	Hillsborough	115	125	UF	100%	10	15						Not Used	Outside Boundary
130212	ROY HAYNES BALL PARK DEEP		180091.89	1358202.75	Hillsborough	50	70	IAS/ICU	100%	0	0						Not Used	Outside Boundary
130213	ROY HAYNES SHALLOW		180092.01	1358212.85	Hillsborough	7	17	SAS	100%	0	0						Not Used	Outside Boundary
130289	S-161 4 SHALLOW		213740.69	1341357.45	Hillsborough	28.5	30.5	IAS/ICU	100%	0	0						Not Used	Outside Boundary
130305	S-2 DALE MABRY SURFICIAL		171857.26	1376500.00	Hillsborough	0	0	Error	0%	0	0						Not Used	Outside Boundary
130160	S-5 DALE MABRY		171841.03	1375186.87	Hillsborough	0	0	Error	0%	0	0						Not Used	Outside Boundary
100652	SEC 21 GOODWIN WELL NEAR LUTZ FL	USGS	164770.02	1381847.65	Hillsborough	57.5	62.5	UF	100%	1	2						Not Used	Outside Boundary
130168	SHELDON ROAD DEEP		145248.64	1341504.24	Hillsborough	315	325	UF	100%	0	0						Not Used	Outside Boundary
100611	SHELDON ROAD DEEP WELL NEAR CITRUS PARK FL	USGS	145300.00	1341661.94	Hillsborough	315	330	UF	100%	10	15						Not Used	Outside Boundary
130167	SHELDON ROAD SHALLOW		145225.31	1341502.52	Hillsborough	36	88	UF	91%	0	0						Not Used	Outside Boundary
100548	SIMMONS FISH FARM NEAR LITHIA FL	USGS	262745.03	1260588.49	Hillsborough	572	672	MC1	100%	1	2						Not Used	Model geology puts this well in MC1
130202	SIROTOWITZ WELL		170277.91	1364700.63	Hillsborough	65	556	UF	65%	0	0						Not Used	Outside Boundary
100532	SPIVEY GROVE FL	USGS	302143.63	1219452.87	Hillsborough	1100	1200	APPZ	100%	1	0						Not Used	sparse data
100531	SRD WELL ON US 301 NEAR WIMAUMA FL	USGS	220036.84	1218346.51	Hillsborough	135	155	IAS/ICU	100%	1	0						Not Used	No calibration in IAS/ICU
130292	ST PETE 21-7 FLDN	SWFWMD	171675.67	1381155.46	Hillsborough	718	1250	MC2	51%	10	15						Not Used	Outside Boundary
100659	ST PETE 33A NEAR ODESSA FL	USGS	148027.25	1387809.83	Hillsborough	81	359	UF	100%	1	0						Not Used	Outside Boundary
130224	ST PETE CALM 33A FLDN	SWFWMD	148019.61	1387910.96	Hillsborough	81	359	UF	100%	10	15						Not Used	Outside Boundary
130227	ST PETE CALM 34 SHALLOW	SWFWMD	147830.50	1388519.59	Hillsborough	11.2	13.2	SAS	100%	10	15	SAS						
100632	ST PETE DEEP WELL E 102 NEAR CITRUS PARK FL	USGS	135332.86	1367235.13	Hillsborough	697	1200	APPZ	69%	1	2						Not Used	Outside Boundary
130278	ST PETE E-100 FLDN	SWFWMD	140538.32	1371298.47	Hillsborough	656	1200	APPZ	70%	10	3						Not Used	Outside Boundary
130312	ST PETE E-102 FLDN	SWFWMD	135287.00	1367154.91	Hillsborough	697	1200	APPZ	69%	10	15						Not Used	Outside Boundary
130270	ST PETE E-103 DEEP	SWFWMD	124644.41	1372601.82	Hillsborough	605	1111	APPZ	86%	5	15						Not Used	Outside Boundary
101162	ST PETE E-103 DEEP NEAR OLDSMAR FL	USGS	124644.13	1372581.62	Hillsborough	605	1111	APPZ	86%	1	2						Not Used	Outside Boundary
130241	ST PETE E-104 DEEP		145702.13	1355920.06	Hillsborough	715	1120	APPZ	83%	0	0						Not Used	Outside Boundary
130177	ST PETE HILLSBORO 13 DP	SWFWMD	170252.07	1378303.97	Hillsborough	46	347	UF	97%	10	15						Not Used	Outside Boundary
130178	ST PETE HILLSBORO 13 SH	SWFWMD	170251.17	1378303.98	Hillsborough	21	23	SAS	100%	10	15	SAS						
130324	ST PETE IC-6 SHALLOW	SWFWMD	141140.99	1371482.51	Hillsborough	21	23	SAS	100%	10	15	SAS						
130268	ST PETE JACKSON 26A DEEP	SWFWMD	167487.75	1381520.67	Hillsborough	142	300	UF	100%	10	15						Not Used	Outside Boundary
130269	ST PETE JACKSON 26A SH	SWFWMD	167488.65	1381520.66	Hillsborough	0	13	SAS	100%	10	15	SAS						
130151	ST PETE SOUTH SHALLOW	SWFWMD	167675.55	1397207.69	Hillsborough	0	0	Error	0%	10	15	SAS						
100533	STANALAND FL	USGS	268829.55	1224004.57	Hillsborough	330	350	UF	100%	1	0						Not Used	sparse data
100600	STRUCT. 160 WELL NEAR BRANDON FL	SWFWMD	214121.00	1319535.00	Hillsborough	85	240	UF	99%	10	15						Not Used	Outside Boundary
130309	SUNNY BROOK DAILY 604		216454.62	1343549.41	Hillsborough	0	58	IAS/ICU	70%	0	0						Not Used	Outside Boundary
100549	SW HILLS CO 182 NEAR ADAMSVILLE FL	USGS	211103.07	1263800.41	Hillsborough	330	350	UF	100%	1	0						Not Used	sparse data
100539	SW HILLS CO 68 (SUN CITY CENTER W.7) NR WIMAUMA FL	USGS	223328.56	1231644.23	Hillsborough	564	664	MC1	100%	1	0						Not Used	Model geology puts this well in MC1
100554	SW HILLSBOROUGH COUNTY 220 AT ADAMSVILLE FL	USGS	209633.87	1271332.44	Hillsborough	215	235	UF	100%	1	2						Not Used	sparse data
130215	SWFWMD AT S-160 FLDN		213928.53	1319670.95	Hillsborough	85	240	UF	98%	0	0						Not Used	Outside Boundary
100608	SWFWMD WELL NR VANDENBURG AIRPORT NEAR TEMP TER FL	USGS	220580.88	1337504.44	Hillsborough	32	37	IAS/ICU	100%	10	15						Not Used	part of group represented by 100613 for IAS-bc
130304	SWFWMD WMDD		214426.18	1330540.87	Hillsborough	0	88	IAS/ICU	77%	0	0						Not Used	Outside Boundary
130320	TAMPA 15 DEEP		261563.68	1345499.40	Hillsborough	67	413	UF	69%	0	0						Not Used	Missing data
130434	TAMPA BAY DOWNS FLDN	SWFWMD	125335.20	1353256.05	Hillsborough	49	60	UF	100%	10	15						Not Used	Outside Boundary
130435	TAMPA BAY DOWNS SURF	SWFWMD	126125.23	1353149.41	Hillsborough	3	17.4	SAS	100%	10	15	SAS						
100617	TAMPA DEEP WELL 15 NEAR DOVER FL	USGS	261634.63	1345617.03	Hillsborough	67	413	UF	69%	10	13						Not Used	Hillsborough Basin has a dense coverage of points and is not important for the purposes of the model; remove
100575	TAMPA YACHT AND RIDING STABLES AT BALLAST POINT FL	USGS	177314.48	1295358.28	Hillsborough	80	85	IAS/ICU	100%	1	2						Not Used	Outside Boundary
130223	TBC 03 PASTURE		224029.13	1347607.16	Hillsborough	37	100	IAS/ICU	70%	0	0						Not Used	Outside Boundary
130225	TBC 04 CONSTRUCTION SITE		222668.10	1346106.89	Hillsborough	33	110	UF	57%	0	0						Not Used	Outside Boundary

Table 4.1: Usage of SAJ Observation Database in Regional Model Calibration

Model ID[a]	Well Name	Data Source	Easting[b]	Northing[b]	County	Cased Depth (ft)	Drilled Depth (ft)	Dominant Layer[c]	% Open Section in Layer[c]	93/94 Months with Data[d]	03/04 Months with Data[e]	Use for Data in Model Setup/Calibration						Reasoning/Comments
													Observations for Calibration					
												Boundary Conditions[f]	Steady State (Oct 03)	Steady State (Feb 04)	Transient (03/04)	Transient (03/04	Not Used	
130162	TBC 05 VANDENBERG AP FLDN	SWFWMD	221360.83	1336417.64	Hillsborough	55	100	UF	57%	10	15						Not Used	Outside Boundary
130161	TBC 06 EUREKA SPRINGS		219839.32	1341592.40	Hillsborough	57	100	UF	73%	0	0						Not Used	Outside Boundary
130446	TBC 07 DUMP FLDN	SWFWMD	218141.48	1339584.86	Hillsborough	47	100	UF	52%	10	15						Not Used	Outside Boundary
130281	TBC 08 USCE		212760.38	1341873.57	Hillsborough	43	100	IAS/ICU	61%	0	0						Not Used	Outside Boundary
130174	TBC 09 RR GRADE FLDN	SWFWMD	212820.51	1340765.74	Hillsborough	68	110	UF	71%	10	15						Not Used	Outside Boundary
130140	TBC 10 HARVEY ROAD DIARY	SWFWMD	218720.11	1345746.53	Hillsborough	28	56	IAS/ICU	91%	10	0						Not Used	part of group represented by 100613 for IAS-bc
130287	TBC 14 USCE		215843.83	1329009.74	Hillsborough	35	100	IAS/ICU	94%	0	0						Not Used	Outside Boundary
130229	TBC 15 USCE		208616.16	1316464.96	Hillsborough	60	72	IAS/ICU	100%	0	0						Not Used	Outside Boundary
130210	TBC 17 USCE		214034.89	1319636.42	Hillsborough	470	480	MC1	100%	0	0						Not Used	Outside Boundary
130243	TBC 1E-SMC FLDN	SWFWMD	220910.31	1329725.22	Hillsborough	28	79	IAS/ICU	100%	9	15						Not Used	part of group represented by 100613 for IAS-bc
130221	TBC 2E-ES 631 FLDN	SWFWMD	223663.86	1342837.12	Hillsborough	41	91	IAS/ICU	54%	10	15						Not Used	No calibration in IAS/ICU
130155	TBC 2E-SMC FLDN	SWFWMD	221627.94	1329747.60	Hillsborough	37	90	IAS/ICU	100%	10	15						Not Used	part of group represented by 100613 for IAS-bc
130282	TBC 2S-SMC FLDN	SWFWMD	220155.50	1328773.91	Hillsborough	36	86	IAS/ICU	100%	10	15						Not Used	part of group represented by 100613 for IAS-bc
130169	TBC 2W-ES WQ-O2 FDLN		221288.00	1342889.58	Hillsborough	37	87	IAS/ICU	65%	0	0						Not Used	Outside Boundary
130231	TBC 2W-SMC EW-1 SHALLOW		219618.69	1329776.89	Hillsborough	0	0	Error	0%	0	0						Not Used	Outside Boundary
130230	TBC 2W-SMC FLDN	SWFWMD	219618.68	1329775.88	Hillsborough	40	96	IAS/ICU	81%	10	15	UF						
130206	TBC 33-SMC GREENHOUSE		220134.30	1327749.84	Hillsborough	30	80	IAS/ICU	100%	0	0						Not Used	Outside Boundary
130323	TBC 3E-ES USCE		224694.02	1342852.08	Hillsborough	31	84	IAS/ICU	72%	0	0						Not Used	Outside Boundary
130316	TBC 3E-SMC USCE		222398.21	1329745.18	Hillsborough	43	90	IAS/ICU	100%	0	0						Not Used	Outside Boundary
130226	TBC 3S-ES USCE		222609.11	1340753.65	Hillsborough	38	89	IAS/ICU	62%	0	0						Not Used	Outside Boundary
130310	TBC 3W-ES USCE		220570.94	1342897.51	Hillsborough	36	87	IAS/ICU	64%	0	0						Not Used	Outside Boundary
130263	TBC 3W-SMC FLDN		218722.06	1329785.82	Hillsborough	71	121	UF	68%	0	0						Not Used	Outside Boundary
130176	TBC 520		226951.94	1360807.32	Hillsborough	0	0	Error	0%	0	0						Not Used	Outside Boundary
130139	TBC 603 FLDN	SWFWMD	219840.03	1345616.91	Hillsborough	0	0	Error	0%	9	12	SAS						
130232	TBC 609		225542.82	1338499.08	Hillsborough	0	310	UF	76%	0	0						Not Used	Outside Boundary
130297	TBC 611 DEEP		235853.76	1338589.65	Hillsborough	0	200	UF	47%	0	0						Not Used	Open section straddles multiple layers
130325	TBC 621 DEEP		216870.28	1324554.56	Hillsborough	0	63	IAS/ICU	76%	0	0						Not Used	Outside Boundary
130214	TBC 624 DEEP		212513.63	1319956.55	Hillsborough	0	136	IAS/ICU	58%	0	0						Not Used	Outside Boundary
130209	TBC HERVEY 600 FLDN	SWFWMD	226056.80	1350164.89	Hillsborough	0	0	Error	0%	10	15	SAS						
130194	TBC P-SMC USCE		220604.96	1329764.96	Hillsborough	45	306	UF	81%	0	0						Not Used	Outside Boundary
130197	TBC PZ-3 SURF	SWFWMD	221987.41	1351755.19	Hillsborough	0	0	Error	0%	10	15	SAS						
130165	TBC W D FUSSELL 61 FLDN	SWFWMD	213164.13	1327478.05	Hillsborough	0	69	IAS/ICU	66%	10	15	SAS						
130164	TBC WL-01 FLDN	SWFWMD	222747.77	1351625.58	Hillsborough	46	110	IAS/ICU	71%	10	0						Not Used	Outside Boundary
130240	TBC WL-02 FLDN	SWFWMD	221064.66	1350169.32	Hillsborough	40	100	IAS/ICU	93%	10	15						Not Used	part of group represented by 100613 for IAS-bc
130313	TBS FORBES		226156.84	1345462.49	Hillsborough	0	0	Error	0%	0	0						Not Used	Outside Boundary
130315	TEMPLE TERRACE 4		208746.57	1351615.80	Hillsborough	87	510	UF	66%	0	0						Not Used	Outside Boundary
100605	THE WOODLANDS APTS,4714 NO HABANA AT TAMPA FL	USGS	174939.52	1330249.77	Hillsborough	180	200	UF	100%	1	2						Not Used	Outside Boundary
100606	TIA AIRCRAFT MAINTENANCE AT TAMPA FL	USGS	164170.75	1332544.69	Hillsborough	210	230	UF	100%	1	0						Not Used	Outside Boundary
130267	TOURIST CLUB FLDN		188104.19	1342916.82	Hillsborough	80	318	UF	100%	0	0						Not Used	Outside Boundary
130453	TOWN N COUNTRY ELEM FLDN	SWFWMD	152234.47	1336090.07	Hillsborough	20	31	SAS	100%	10	15	SAS						
130454	TOWN N COUNTRY ELEM SURF	SWFWMD	152235.37	1336090.06	Hillsborough	2	6	SAS	100%	10	15	SAS						
130193	TROUT CREEK SUBDIV FLDN	SWFWMD	221411.18	1368510.28	Hillsborough	0	158	UF	65%	10	15						Not Used	Outside Boundary
130192	TROUT CREEK SUBDIV SURF	SWFWMD	220737.36	1368335.92	Hillsborough	0	0	Error	0%	10	15	SAS						
130218	TURNER FLDN	SWFWMD	251794.79	1313274.60	Hillsborough	60	342	UF	76%	10	0					UF		no 03/04 data
100594	TURNER WELL NEAR BRANDON FL	USGS	251838.00	1313343.00	Hillsborough	60	342	UF	76%	10	15						Not Used	Hillsborough Basin has a dense coverage of points and is not important for the purposes of the model; remove
130439	TWIN LAKE ELEM FLDN	SWFWMD	176086.14	1346318.62	Hillsborough	51	62	IAS/ICU	100%	10	15						Not Used	Outside Boundary
130440	TWIN LAKE ELEM SURF	SWFWMD	176056.89	1346346.25	Hillsborough	3	22	SAS	100%	10	15	SAS						
100570	U.S. PHOSPHORIC WELL AT RIVERVIEW FL	USGS	223694.57	1288338.94	Hillsborough	653	658	APPZ	100%	6	10	APPZ						averaged with 130476
100547	UNKNOWN NAME	USGS	205555.12	1249821.85	Hillsborough	444	464	UF	100%	1	0						Not Used	sparse data
130443	UPPER TAMPA BAY PARK FLDN	SWFWMD	128275.18	1342102.10	Hillsborough	55	65	UF	100%	10	15						Not Used	Outside Boundary
130444	UPPER TAMPA BAY PARK SURF	SWFWMD	128397.19	1342107.53	Hillsborough	3	20.3	SAS	100%	10	15	SAS						
130314	US PHOSPHORIC RIVERVIEW		223703.33	1288318.64	Hillsborough	653	658	APPZ	100%	0	0						Not Used	Outside Boundary
100612	USCE TBC-09 NEAR TEMPLE TERRACE FL	USGS	212802.36	1340745.74	Hillsborough	68	110	UF	70%	1	0						Not Used	Outside Boundary
100621	USCE TEST TBC-01 802-220-411 NEAR THONOTOSASSA FL	SWFWMD	222755.95	1351554.77	Hillsborough	46	110	IAS/ICU	71%	10	15						Not Used	Outside Boundary
100619	USCE WELL TBC-03 NEAR TEMPLE TERRACE FL	USGS	224027.27	1347608.01	Hillsborough	37	100	IAS/ICU	70%	10	0						Not Used	Outside Boundary
100618	USCE WELL TBC-04 NEAR TEMPLE TERRACE FL	USGS	222605.08	1346000.50	Hillsborough	33	110	UF	57%	1	0						Not Used	Outside Boundary
100607	USCE WELL TBC-05 NEAR TEMPLE TERRACE FL	USGS	221342.00	1336337.03	Hillsborough	55	100	UF	56%	0	2						Not Used	Outside Boundary
100615	USCE WELL TBC-08 NEAR TEMPLE TERRACE FL	USGS	212758.22	1341874.65	Hillsborough	43	100	IAS/ICU	62%	10	0						Not Used	Outside Boundary
100598	USCE WELL TBC-15 NEAR TAMPA FL	USGS	208553.94	1316357.58	Hillsborough	67	72	IAS/ICU	100%	0	0						Not Used	Outside Boundary
130406	USF GOLF COURSE UPL SURF	SWFWMD	203002.15	1362384.67	Hillsborough	1.5	12.5	SAS	100%	0	15	SAS						
130376	USF GOLF COURSE WTL SURF	SWFWMD	203088.68	1360565.31	Hillsborough	1	9.5	SAS	100%	0	15	SAS						
130182	USGS 511 WELL SHALLOW		207830.85	1373445.43	Hillsborough	4	6	SAS	100%	0	0						Not Used	Outside Boundary
100628	USGS DEEP WELL 402 NEAR LUTZ FL	USGS	178202.17	1361830.22	Hillsborough	65	70	IAS/ICU	100%	1	2						Not Used	Outside Boundary
130153	VALLE DR & PERIO ST DEEP		179893.86	1348961.55	Hillsborough	20	40	SAS	100%	0	0						Not Used	Outside Boundary
130152	VAN DYKE SHALLOW NR LUTZ	SWFWMD	174517.24	1382080.15	Hillsborough	18	22	SAS	100%	10	15	SAS						
130179	VANDENBERG AIRPORT FLDN		220151.98	1337447.24	Hillsborough	0	37	IAS/ICU	97%	0	0						Not Used	Outside Boundary

Table 4.1: Usage of SAJ Observation Database in Regional Model Calibration

Model ID[a]	Well Name	Data Source	Easting[b]	Northing[b]	County	Cased Depth (ft)	Drilled Depth (ft)	Dominant Layer[c]	% Open Section in Layer[c]	93/94 Months with Data[d]	03/04 Months with Data[e]	Use for Data in Model Setup/Calibration						Reasoning/Comments
													Observations for Calibration					
												Boundary Conditions[f]	Steady State (Oct 03)	Steady State (Feb 04)	Transient (03/04)	Transient (03/04	Not Used	
130277	VANDENBERG EAST FLDN	SWFWMD	221309.79	1337478.88	Hillsborough	0	42	IAS/ICU	96%	10	15						Not Used	part of group represented by 100613 for IAS-bc
100604	W.D.FUSSELL 618 WELL NEAR TAMPA FL	USGS	213164.02	1327467.95	Hillsborough	64	69	IAS/ICU	100%	1	2						Not Used	Outside Boundary
100568	WCRWSA GRASSY GULCH FLORIDAN WELL NEAR LITHIA FL	USGS	285278.83	1285829.34	Hillsborough	800	900	APPZ	100%	1	2						Not Used	sparse data
100567	WCRWSA SC-1 FLORIDAN WELL NEAR LITHIA FL	USGS	267367.90	1285372.86	Hillsborough	841	941	APPZ	100%	1	2						Not Used	sparse data
100572	WCRWSA SC-15 UPPER INTERMEDIATE WELL NR LITHIA FL	USGS	303627.36	1289052.48	Hillsborough	80	100	IAS/ICU	100%	1	2						Not Used	No calibration in IAS/ICU
100564	WCRWSA SC-4 LOWER INTERMEDIATE WELL NEAR LITHIA FL	USGS	286475.98	1284642.42	Hillsborough	121	141	IAS/ICU	100%	1	0						Not Used	No calibration in IAS/ICU
100563	WCRWSA SC-4 UPPER FLORIDAN WELL NEAR LITHIA FL	USGS	286121.86	1284307.36	Hillsborough	815	915	APPZ	100%	1	2						Not Used	sparse data
100565	WCRWSA SC-4 UPPER INTERMEDIATE WELL NEAR LITHIA FL	USGS	313865.53	1289244.43	Hillsborough	90	110	IAS/ICU	100%	1	2						Not Used	No calibration in IAS/ICU
100573	WCRWSA SCGM-4 FLORIDAN WELL NEAR LITHIA FL	USGS	313871.80	1289242.35	Hillsborough	800	900	APPZ	100%	1	2						Not Used	sparse data
100557	WCRWSA SCHM-1 UPPER FLORIDAN WELL NEAR LITHIA FL	USGS	259411.00	1277589.18	Hillsborough	840	940	APPZ	100%	1	2						Not Used	sparse data
100576	WCRWSA SCHM-11 FLORIDAN WELL NEAR LITHIA FL	USGS	289855.79	1294351.08	Hillsborough	818	918	APPZ	100%	1	2						Not Used	sparse data
100592	WCRWSA SCHM-2 FLORIDAN WELL NEAR LITHIA FL	USGS	280995.71	1311602.46	Hillsborough	810	910	APPZ	100%	1	2						Not Used	Hillsborough Basin has a dense coverage of points and is not important for the purposes of the model; remove
100593	WCRWSA SCHM-2 INTERMEDIATE WELL NEAR LITHIA FL	USGS	280997.65	1311618.61	Hillsborough	65	70	IAS/ICU	100%	1	2						Not Used	No calibration in IAS/ICU
100589	WCRWSA SCHM-3 FLORIDAN WELL NEAR LITHIA FL	USGS	307435.47	1308666.26	Hillsborough	780	880	APPZ	100%	1	2						Not Used	sparse data
100590	WCRWSA SCHM-3 INTERMEDIATE WELL NEAR LITHIA FL	USGS	307420.05	1308647.21	Hillsborough	85	90	IAS/ICU	100%	1	2						Not Used	No calibration in IAS/ICU
100574	WCRWSA SCHM-4 INTERMEDIATE WELL NEAR LITHIA FL	USGS	286706.32	1284603.91	Hillsborough	82	102	IAS/ICU	100%	1	2						Not Used	No calibration in IAS/ICU
100559	WCRWSA SCHM-5 INTERMEDIATE WELL NEAR LITHIA FL	USGS	309743.76	1279873.75	Hillsborough	90	110	IAS/ICU	100%	1	2						Not Used	No calibration in IAS/ICU
100560	WCRWSA SCHM-5 NRSD WELL NEAR LITHIA FL	USGS	309681.97	1279685.42	Hillsborough	8	10	SAS	100%	1	0						Not Used	sparse data
100558	WCRWSA SCHM-5 UPPER FLORIDAN WELL NEAR LITHIA FL	USGS	309737.41	1279865.73	Hillsborough	805	905	APPZ	100%	1	2						Not Used	sparse data
100553	WCRWSA SCHM-6 INTERMEDIATE WELL NEAR LITHIA FL	USGS	285882.12	1270652.50	Hillsborough	95	115	IAS/ICU	100%	1	2						Not Used	No calibration in IAS/ICU
100552	WCRWSA SCHM-6 UPPER FLORIDAN WELL NEAR LITHIA FL	USGS	285882.90	1270640.38	Hillsborough	810	910	APPZ	100%	1	2						Not Used	sparse data
100555	WCRWSA SCHM-7 FLORIDAN WELL NEAR LITHIA FL	USGS	268640.60	1272221.20	Hillsborough	840	940	APPZ	100%	1	2						Not Used	sparse data
100577	WCRWSA SCHM-8 FLORIDAN WELL NEAR LITHIA FL	USGS	263885.89	1295977.85	Hillsborough	785	885	APPZ	100%	1	2						Not Used	sparse data
100578	WCRWSA SCHM-8 INTERMEDIATE WELL NEAR LITHIA FL	USGS	263896.66	1295977.74	Hillsborough	95	115	IAS/ICU	100%	1	2						Not Used	No calibration in IAS/ICU
100583	WCRWSA SCHM-9 INTERMEDIATE WELL NEAR LITHIA FL	USGS	281109.83	1301227.83	Hillsborough	80	100	IAS/ICU	100%	0	2						Not Used	No calibration in IAS/ICU
100625	WELL 803 233 5455 FL	USGS	151408.98	1359720.72	Hillsborough	80	100	UF	100%	1	2						Not Used	Outside Boundary
130195	WEST VILLAGE DEEP		162250.54	1362996.51	Hillsborough	32	52	SAS	74%	0	0						Not Used	Outside Boundary
130196	WEST VILLAGE SHALLOW		162248.00	1363007.66	Hillsborough	10	20	SAS	100%	0	0						Not Used	Outside Boundary
130188	WHITE SANDS SHALLOW		175790.02	1355461.83	Hillsborough	10	20	SAS	100%	0	0						Not Used	Outside Boundary
130187	WILDER WILLIAMS ROAD		230649.12	1338140.50	Hillsborough	0	0	Error	0%	0	0						Not Used	Data error
120478	IR0040		850386.09	1185444.81	Indian River	850	901	UF	100%	0	0						Not Used	Missing data
120003	IR0114	SJRWMD	848028.94	1210276.16	Indian River	0	105	SAS	100%	6	15	SAS						
120480	IR0189		712816.46	1248733.99	Indian River	0	630	UF	46%	0	0						Not Used	Open section straddles multiple layers
120065	IR0275	SJRWMD	837893.78	1244059.03	Indian River	40	50	SAS	100%	4	0						Not Used	sparse data
120315	IR0312	SJRWMD	840635.49	1179226.54	Indian River	120	568	IAS/ICU	65%	10	15						Not Used	No calibration in IAS/ICU
120005	IR0313	SJRWMD	840842.93	1204718.42	Indian River	390	442	IAS/ICU	100%	10	0						Not Used	No calibration in IAS/ICU
120017	IR0333	SJRWMD	830800.19	1202017.41	Indian River	390	442	IAS/ICU	94%	1	0						Not Used	No calibration in IAS/ICU
120482	IR0365		701444.49	1216406.76	Indian River	0	305	SAS	53%	0	0						Not Used	Missing data
100668	IR-0365 USGS AT YEEHAW,FL	USGS	701386.25	1216292.51	Indian River	285	305	IAS/ICU	100%	1	0						Not Used	No calibration in IAS/ICU
120088	IR0366	SJRWMD	698704.47	1267801.62	Indian River	120	260	IAS/ICU	100%	1	0						Not Used	No calibration in IAS/ICU
120319	IR0372	SJRWMD	845750.45	1201265.80	Indian River	126	671	IAS/ICU	61%	1	0						Not Used	No calibration in IAS/ICU
120484	IR0383		781579.94	1235058.10	Indian River	0	708	UF	48%	0	0						Not Used	Open section straddles multiple layers
120485	IR0655		796926.35	1248930.91	Indian River	130	137	IAS/ICU	100%	0	0						Not Used	No calibration in IAS/ICU
120320	IR0763		720288.43	1257722.37	Indian River	170	671	UF	70%	0	0						Not Used	Missing data
120321	IR0765	SJRWMD	719202.09	1263173.88	Indian River	152	670	UF	69%	1	0						Not Used	sparse data
120322	IR0766	SJRWMD	720010.57	1262973.20	Indian River	115	570	UF	57%	1	0						Not Used	sparse data

Table 4.1: Usage of SAJ Observation Database in Regional Model Calibration

Model ID[a]	Well Name	Data Source	Easting[b]	Northing[b]	County	Cased Depth (ft)	Drilled Depth (ft)	Dominant Layer[c]	% Open Section in Layer[c]	93/94 Months with Data[d]	03/04 Months with Data[e]	Use for Data in Model Setup/Calibration						Reasoning/Comments
													Observations for Calibration					
												Boundary Conditions[f]	Steady State (Oct 03)	Steady State (Feb 04)	Transient (03/04)	Transient (03/04	Not Used	
120066	IR0900	SJRWMD	813677.29	1220619.29	Indian River	40	50	SAS	100%	0	15	SAS						
120012	IR0902	SJRWMD	792731.18	1183086.73	Indian River	15	25	SAS	100%	0	15	SAS						
120488	IR0914		796985.43	1249042.50	Indian River	20	25	SAS	100%	0	0						Not Used	Missing data
120489	IR0915		796985.43	1249042.50	Indian River	253	263	IAS/ICU	100%	0	0						Not Used	No calibration in IAS/ICU
120080	IR0921	SJRWMD	782344.75	1252326.77	Indian River	165	514	IAS/ICU	50%	0	15						Not Used	No calibration in IAS/ICU
120069	IR0944	SJRWMD	728048.51	1226845.14	Indian River	10	15	SAS	100%	0	15	SAS						
120067	IR0946	SJRWMD	813677.29	1220619.29	Indian River	76	86	SAS	100%	0	15	SAS						
120014	IR0947	SJRWMD	792731.18	1183086.73	Indian River	60	70	SAS	100%	0	15	SAS						
120013	IR0954	SJRWMD	792731.18	1183086.73	Indian River	432	482	UF	100%	0	15		UF	UF	UF			no 93/94 data
120071	IR0955	SJRWMD	775195.66	1209891.97	Indian River	380	430	UF	100%	0	15		UF	UF	UF			no 93/94 data
120070	IR0956	SJRWMD	775195.66	1209891.97	Indian River	265	285	IAS/ICU	100%	0	15						Not Used	No calibration in IAS/ICU
120068	IR0963	SJRWMD	813677.29	1220619.29	Indian River	390	442	UF	94%	0	15		UF	UF	UF			no 93/94 data
120011	IR0968	SJRWMD	727961.00	1225532.23	Indian River	303	440	UF	65%	0	15		UF	UF	UF			no 93/94 data
120499	IR0988		851094.99	1242810.07	Indian River	440	490	UF	100%	0	0						Not Used	Missing data
120048	IR0992	SJRWMD	840911.15	1204744.99	Indian River	153	158	IAS/ICU	100%	0	15						Not Used	No calibration in IAS/ICU
120049	IR0993	SJRWMD	840911.15	1204744.99	Indian River	30	40	SAS	100%	0	15	SAS						
120047	IR0999	SJRWMD	848936.14	1245827.72	Indian River	380	400	IAS/ICU	81%	0	15						Not Used	No calibration in IAS/ICU
120085	IR1000	SJRWMD	849564.53	1245931.75	Indian River	547	869	UF	69%	0	15						Not Used	Open sections of nearby wells (120001, 120499) completely in UF
120050	IR1006	SJRWMD	840911.15	1204744.99	Indian River	405	460	IAS/ICU	97%	0	15						Not Used	No calibration in IAS/ICU
120018	IR1008	SJRWMD	857881.07	1200226.08	Indian River	595	685	UF	100%	0	15						Not Used	impacted by some local pumping (which does not impact nearby wells 120068, 120013, 120071)
120504	IR1058		851032.63	1242698.48	Indian River	550	860	UF	71%	0	0						Not Used	Missing data
100670	IR-189 WELL NEAR YEEHAW JUNCTION, FL	USGS	712757.62	1248622.20	Indian River	530	630	UF	100%	10	12		UF	UF	UF	UF		
100667	IR-25 WELL NEAR YEEHAW JUNCTION, FL	USGS	724684.89	1207843.01	Indian River	17	19	SAS	100%	10	14	SAS						
100669	REVERSE OSMOSIS MONITOR W OF OSLO	USGS	827603.34	1217442.94	Indian River	550	650	UF	100%	1	2						Not Used	sparse data
100666	ROMP TR4-2 TAMPA WELL NEAR VENICE FL	USGS	850324.69	1185331.57	Indian River	801	901	UF	100%	1	2						Not Used	sparse data
100665	USDA SOUTH WELL 43RD AVE SW OF OSLO	USGS	840545.97	1179125.14	Indian River	120	568	IAS/ICU	65%	1	2						Not Used	No calibration in IAS/ICU
100671	USGS TH MACE RANCH FELLSMERE GRADE	USGS	698634.37	1267690.93	Indian River	120	260	IAS/ICU	100%	1	2						Not Used	No calibration in IAS/ICU
130504	COLLEGE STREET WELL		370677.24	1628977.43	Lake	90	245	Error	0%	0	0						Not Used	Outside Boundary
100675	EVA DEEP WELL AT EVA, FL	USGS	391237.40	1471462.55	Lake	100	192	UF	100%	0	1						Not Used	Duplicate with 120517 and 130500
130500	EVA WELL DEEP	SWFWMD	391321.18	1471566.01	Lake	100	192	UF	100%	10	15		UF	UF	UF	UF		
130501	EVA WELL SHALLOW	SWFWMD	391318.44	1471557.95	Lake	18	23	SAS	100%	10	15	SAS						
130512	GREEN SWAMP 1 UPL SURF	SWFWMD	351633.04	1465299.09	Lake	1.8	9.8	SAS	100%	0	15	SAS						
130506	GREEN SWAMP 1 WTL SURF	SWFWMD	351741.44	1465449.75	Lake	5	10	SAS	100%	0	15	SAS						
130513	GREEN SWAMP 2 UPL SURF	SWFWMD	351235.30	1476069.66	Lake	1.3	9.3	SAS	100%	0	15	SAS						
130507	GREEN SWAMP 2 WTL SURF	SWFWMD	351102.20	1476181.82	Lake	2	8	SAS	100%	0	15	SAS						
130514	GREEN SWAMP 3 UPL SURF	SWFWMD	357409.95	1470597.45	Lake	8.9	18.9	SAS	100%	0	15	SAS						
130508	GREEN SWAMP 3 WTL SURF	SWFWMD	357285.67	1470699.41	Lake	1	4.5	SAS	100%	0	15	SAS						
130515	GREEN SWAMP 4 UPL SURF	SWFWMD	356784.15	1476319.31	Lake	1.5	9.5	SAS	100%	0	15	SAS						
130509	GREEN SWAMP 4 WTL SURF	SWFWMD	356990.59	1476449.02	Lake	1	4	SAS	100%	0	15	SAS						
130505	GREEN SWAMP BAY UPL SURF	SWFWMD	349395.53	1487376.95	Lake	2	10	SAS	100%	0	15	SAS						
130510	GREEN SWAMP BAY WTL SURF	SWFWMD	349617.96	1487274.18	Lake	1	6	SAS	100%	0	15	SAS						
130498	GREEN SWAMP LK753W		363281.09	1475098.97	Lake	0	0	Error	0%	0	0						Not Used	Data error
100678	JOHNS LAKE WELL NR CLERMONT	USGS	437895.45	1523995.95	Lake	135	155	UF	100%	1	2						Not Used	sparse data
140009	L-0050	SJRWMD via DEP	416871.18	1470891.81	Lake	25	35	SAS	100%	0	0						Not Used	sparse data
120033	L-0050	SJRWMD	419691.14	1470636.77	Lake	25	35	SAS	100%	10	15	SAS						
140008	L-0051	SJRWMD via DEP	416871.18	1470891.81	Lake	85	115	UF	100%	0	0						Not Used	sparse data
120032	L-0051	SJRWMD	419691.14	1470636.77	Lake	85	115	UF	100%	10	15		UF	UF	UF	UF		
120329	L-0052	SJRWMD	437896.59	1524197.95	Lake	73	115	IAS/ICU	100%	7	15						Not Used	outside IAS (per Miller, 1997)
120035	L-0053	SJRWMD	417626.78	1500329.05	Lake	70	85	UF	55%	10	3					UF		sparse 03/04 data
120517	L-0057	SJRWMD	391326.18	1471568.77	Lake	100	192	UF	100%	6	12						Not Used	Duplicate with 100675 and 130500
120523	L-0146		443870.25	1530529.05	Lake	0	0	Error	0%	0	0						Not Used	Outside Boundary
120406	L-0555		363262.20	1475103.43	Lake	64	190	UF	100%	0	0						Not Used	Missing data
120000	L-0677	SJRWMD	425889.32	1489322.58	Lake	160	485	APPZ	44%	0	15						Not Used	Open section straddles multiple layers
120009	L-0709	SJRWMD	426993.88	1487829.32	Lake	81	101	IAS/ICU	100%	0	15						Not Used	No calibration in IAS/ICU
120010	L-0710	SJRWMD	426993.88	1487829.32	Lake	32	42	SAS	100%	0	15	SAS						
120436	L-0719		410246.64	1517296.22	Lake	0	0	Error	0%	0	0						Not Used	Outside Boundary
120437	L-0729	SJRWMD	428494.30	1486472.12	Lake	1300	1410	LC	66%	0	15						Not Used	Model geology puts this well in LC
120015	L-0730	SJRWMD	428559.79	1486575.78	Lake	365	465	APPZ	100%	0	15		APPZ	APPZ	APPZ			no 93/94 data
120444	L-0872		388119.71	1504214.35	Lake	22	32	SAS	100%	0	0						Not Used	Missing data
120446	L-0877	SJRWMD	421044.26	1463498.44	Lake	110	200	UF	100%	10	15		UF	UF	UF	UF		
120449	L-0897		421024.57	1463491.88	Lake	1160	1310	MC2	89%	0	0						Not Used	Model geology puts this well in MC2
120452	L-0906		421060.67	1463498.44	Lake	323	460	APPZ	84%	0	0						Not Used	Missing data
120453	L-0907		421050.83	1463498.44	Lake	10	20	SAS	100%	0	0						Not Used	Missing data
120454	L-0908		421090.21	1463501.73	Lake	75	87	UF	100%	0	0						Not Used	Missing data
100677	LK LOUISA STATE PARK NR CLERMONT		417586.53	1499976.33	Lake	70	85	IAS/ICU	66%	0	0						Not Used	No calibration in IAS/ICU
130497	MASCOTTE DEEP	SWFWMD	362835.90	1528182.17	Lake	63	160	UF	86%	10	15						Not Used	Outside Boundary
130503	MASCOTTE SHALLOW		362834.09	1528178.14	Lake	16	30	SAS	100%	0	0						Not Used	Outside Boundary

Table 4.1: Usage of SAJ Observation Database in Regional Model Calibration

Model ID[a]	Well Name	Data Source	Easting[b]	Northing[b]	County	Cased Depth (ft)	Drilled Depth (ft)	Dominant Layer[c]	% Open Section in Layer[c]	93/94 Months with Data[d]	03/04 Months with Data[e]	Use for Data in Model Setup/Calibration						Reasoning/Comments
													Observations for Calibration					
												Boundary Conditions[f]	Steady State (Oct 03)	Steady State (Feb 04)	Transient (03/04)	Transient (03/04	Not Used	
130511	ROMP 101 6-IN SURF	SWFWMD	358809.11	1499212.33	Lake	5	22	SAS	100%	0	8	SAS						
130502	ROMP 101 AVPK	SWFWMD	358774.33	1499216.64	Lake	118	410	UF	87%	0	8	UF						
130499	S24 E21 211		363164.81	1507016.28	Lake	183	300	UF	100%	0	0						Not Used	Outside Boundary
130496	S24 E29 422		359799.21	1498760.28	Lake	0	260	UF	85%	0	0						Not Used	Missing data
100676	USGS OBSER W EVA SHALLOW AT EVA, FL.		391323.78	1471553.88	Lake	18	23	SAS	100%	0	0						Not Used	Missing data
112115	FMB-MZL	SFWMD	350747.43	785108.32	Lee	1563	1650	APPZ	53%	0	8	APPZ						
112114	FMB-MZU	SFWMD	350747.43	785108.32	Lee	1170	1271	MC1	100%	0	8	UF						
111261	FP10_G	SFWMD	419424.00	763818.00	Lee	14	16	SAS	100%	0	15	SAS						
111053	FP2_GW1	SFWMD	425473.27	770315.65	Lee	11.78	13.78	SAS	100%	0	15	SAS						
111056	FP3_GW1	SFWMD	422268.47	766092.61	Lee	16.9	18.9	SAS	100%	0	15	SAS						
110913	FP4_GW1	SFWMD	421530.56	764178.29	Lee	18	20	SAS	100%	0	15	SAS						
111204	FP5_GW1	SFWMD	420164.16	763681.08	Lee	16	18	SAS	100%	0	15	SAS						
111129	FP6_GW1	SFWMD	420971.02	761657.15	Lee	15.62	17.62	SAS	100%	0	15	SAS						
111055	FP7_GW1	SFWMD	421054.03	760243.10	Lee	13.95	15.95	SAS	100%	0	15	SAS						
111054	FP8_GW1	SFWMD	422521.54	762557.24	Lee	10.68	12.68	SAS	100%	0	15	SAS						
111052	FP9_G	SFWMD	419905.50	760223.32	Lee	18	20	SAS	100%	0	15	SAS						
112112	FPL-MW	SFWMD	400851.96	859414.49	Lee	540	800	UF	84%	0	4						Not Used	sparse data
100819	HE-557	USGS	438263.85	870511.51	Lee	80	100	SAS	78%	10	15	SAS						
112166	IWA-MZL	SFWMD	293008.00	767990.45	Lee	1610	1700	MC1	100%	0	14	APPZ						
112113	IWA-MZU	SFWMD	292806.41	767990.45	Lee	840	869	UF	100%	0	15	UF						
100795	L-1058	USGS	317973.84	838672.72	Lee	126	146	IAS/ICU	100%	9	0						Not Used	No calibration in IAS/ICU
100833	L-1059	USGS	317049.81	881195.47	Lee	169	189	IAS/ICU	100%	10	15						Not Used	No calibration in IAS/ICU
100742	L-1089	USGS	371504.68	796871.65	Lee	205	225	IAS/ICU	100%	10	0						Not Used	No calibration in IAS/ICU
100809	L-1099	USGS	348492.38	854492.90	Lee	205	225	IAS/ICU	100%	1	0						Not Used	No calibration in IAS/ICU
100811	L-1106	USGS	332892.42	854913.98	Lee	209	229	IAS/ICU	100%	10	0						Not Used	No calibration in IAS/ICU
100816	L-1107	USGS	332842.47	860165.57	Lee	171	191	IAS/ICU	100%	10	0						Not Used	No calibration in IAS/ICU
100815	L-1108	USGS	338103.80	860226.03	Lee	205	225	IAS/ICU	100%	10	0						Not Used	No calibration in IAS/ICU
100812	L-1109	USGS	337972.99	854975.85	Lee	210	230	IAS/ICU	100%	10	0						Not Used	No calibration in IAS/ICU
100820	L-1110	USGS	338325.30	865475.53	Lee	218	238	IAS/ICU	100%	10	15						Not Used	No calibration in IAS/ICU
100817	L-1111	USGS	349350.44	860141.63	Lee	145	165	IAS/ICU	100%	10	15						Not Used	No calibration in IAS/ICU
100814	L-1113	USGS	316951.08	857969.33	Lee	210	230	IAS/ICU	100%	10	15						Not Used	No calibration in IAS/ICU
100788	L-1114	USGS	343679.05	833180.87	Lee	152	172	IAS/ICU	100%	10	0						Not Used	No calibration in IAS/ICU
100783	L-1116	USGS	328005.56	831039.03	Lee	185	205	IAS/ICU	100%	10	0						Not Used	No calibration in IAS/ICU
100773	L-1117	USGS	347639.39	816378.31	Lee	228	248	IAS/ICU	100%	10	0						Not Used	No calibration in IAS/ICU
100761	L-1121	USGS	376584.09	809358.85	Lee	200	220	IAS/ICU	100%	10	12						Not Used	No calibration in IAS/ICU
100748	L-1124	USGS	366139.62	805259.40	Lee	210	230	IAS/ICU	100%	10	0						Not Used	No calibration in IAS/ICU
100778	L-1136	USGS	332820.50	822195.72	Lee	18	20	SAS	100%	10	14	SAS						
110662	L-1137	SFWMD	460826.13	847579.86	Lee	15	20	SAS	100%	10	0	SAS						
100802	L-1137	USGS	460849.83	847352.28	Lee	18	20	SAS	100%	0	14	SAS						
100721	L-1138	USGS	470850.10	769961.56	Lee	18	20	SAS	100%	10	14	SAS						
100759	L-1156	USGS	368947.97	808198.76	Lee	200	220	IAS/ICU	100%	10	0						Not Used	No calibration in IAS/ICU
100709	L-1403	USGS	307614.88	764260.64	Lee	10	12	SAS	100%	10	13	SAS						
110739	L-1403	SFWMD	307792.94	763653.38	Lee	2.9	12	SAS	100%	10	0	SAS						
100782	L-1418	USGS	450046.10	827411.24	Lee	57	62	SAS	100%	0	14	SAS						
110660	L-1418_G	SFWMD	449930.39	827438.27	Lee	55	62	SAS	100%	10	0	SAS						
100714	L-1456	USGS	316211.61	766786.32	Lee	28	33	SAS	100%	1	0						Not Used	Outside Boundary
100715	L-1457	USGS	316211.61	766786.32	Lee	9	11	SAS	100%	1	0						Not Used	Outside Boundary
100746	L-1598	USGS	356293.53	803844.29	Lee	156	176	IAS/ICU	100%	10	13						Not Used	No calibration in IAS/ICU
100763	L-1625	USGS	439876.80	809186.18	Lee	198	218	IAS/ICU	100%	10	13						Not Used	No calibration in IAS/ICU
100701	L-1634	USGS	362680.26	755935.03	Lee	850	950	UF	100%	3	12	UF						
100700	L-1635	USGS	362743.13	756065.27	Lee	520	620	IAS/ICU	100%	3	15	IAS-layer 3						
100691	L-1691	USGS	408456.93	731912.31	Lee	64	69	SAS	100%	0	14	SAS						
110658	L-1691_G	SFWMD	406064.97	731956.92	Lee	58	69	SAS	100%	10	0	SAS						
100723	L-1853	USGS	416500.97	770639.87	Lee	190	210	IAS/ICU	100%	10	15						Not Used	No calibration in IAS/ICU
100822	L-1907	USGS	433560.09	867684.40	Lee	52	57	SAS	100%	10	0	SAS						
100765	L-1963	USGS	458498.28	810507.79	Lee	69	74	SAS	100%	10	14	SAS						
100766	L-1964	USGS	458498.28	810507.79	Lee	22	24	SAS	100%	10	11	SAS						
100769	L-1965	USGS	471123.10	811257.89	Lee	205	225	IAS/ICU	72%	10	14	SAS						
100792	L-1968	USGS	421686.63	836446.65	Lee	145	165	IAS/ICU	100%	10	15						Not Used	No calibration in IAS/ICU
100785	L-1973	USGS	390262.62	832595.80	Lee	205	225	IAS/ICU	100%	10	15						Not Used	No calibration in IAS/ICU
100786	L-1974	USGS	390262.62	832595.80	Lee	115	135	IAS/ICU	100%	10	14						Not Used	No calibration in IAS/ICU
100827	L-1975	USGS	423613.80	872787.71	Lee	148	168	IAS/ICU	100%	10	15						Not Used	No calibration in IAS/ICU
100828	L-1976	USGS	423613.80	872787.71	Lee	13	15	SAS	100%	10	15	SAS						
100823	L-1977	USGS	455236.77	868583.80	Lee	165	185	IAS/ICU	100%	10	15						Not Used	No calibration in IAS/ICU
100824	L-1978	USGS	455236.77	868583.80	Lee	15	17	SAS	100%	10	0	SAS						
100734	L-1983	USGS	418895.78	792335.88	Lee	325	345	IAS/ICU	100%	10	14						Not Used	No calibration in IAS/ICU
100727	L-1984	USGS	428410.64	771179.57	Lee	268	288	IAS/ICU	100%	2	0						Not Used	No calibration in IAS/ICU
100728	L-1985	USGS	428773.65	771076.63	Lee	45	50	SAS	100%	10	15	SAS						
100751	L-1993	USGS	407682.59	805656.31	Lee	222	242	IAS/ICU	100%	10	15						Not Used	No calibration in IAS/ICU

Table 4.1: Usage of SAJ Observation Database in Regional Model Calibration

Model ID[a]	Well Name	Data Source	Easting[b]	Northing[b]	County	Cased Depth (ft)	Drilled Depth (ft)	Dominant Layer[c]	% Open Section in Layer[c]	93/94 Months with Data[d]	03/04 Months with Data[e]	Use for Data in Model Setup/Calibration						Reasoning/Comments
													Observations for Calibration					
												Boundary Conditions[f]	Steady State (Oct 03)	Steady State (Feb 04)	Transient (03/04)	Transient (03/04	Not Used	
111828	L-1993_G	SFWMD	408500.54	805550.63	Lee	190	242	IAS/ICU	100%	10	15						Not Used	No calibration in IAS/ICU
100752	L-1994	USGS	407682.59	805656.31	Lee	135	155	IAS/ICU	100%	10	15						Not Used	No calibration in IAS/ICU
111837	L-1994_G	SFWMD	408500.54	805550.63	Lee	125	155	IAS/ICU	100%	10	15						Not Used	No calibration in IAS/ICU
100753	L-1995	USGS	407682.59	805656.31	Lee	22	24	SAS	100%	10	15	SAS						
111836	L-1995_G	SFWMD	408500.54	805550.63	Lee	14	24	SAS	100%	10	15	SAS						
110673	L-1996_G	SFWMD	432785.00	726959.00	Lee	275	295	IAS/ICU	100%	10	0						Not Used	No calibration in IAS/ICU
100686	L-1997	USGS	432721.43	727031.44	Lee	18	20	SAS	100%	0	0						Not Used	sparse data
110657	L-1997_G	SFWMD	432785.00	726959.00	Lee	18	20	SAS	100%	10	0	SAS						
100735	L-1998	USGS	418960.22	792464.63	Lee	140	160	SAS	91%	10	15	SAS						
111840	L-1998	SFWMD	419051.70	792363.31	Lee	105	160	SAS	97%	10	15	SAS						
100736	L-1999	USGS	418960.22	792464.63	Lee	21	26	SAS	100%	10	15	SAS						
100767	L-2186	USGS	458563.46	810635.47	Lee	140	160	SAS	100%	10	15	SAS						
110659	L-2186_G	SFWMD	458564.71	810635.56	Lee	133	160	SAS	100%	10	0	SAS						
100801	L-2187	USGS	460849.83	847352.28	Lee	134	154	SAS	100%	10	14	SAS						
100719	L-2192	USGS	446491.06	769873.92	Lee	164	184	SAS	100%	10	15	SAS						
100726	L-2193	USGS	428793.07	771277.01	Lee	272	292	IAS/ICU	100%	10	15						Not Used	No calibration in IAS/ICU
110720	L-2193	SFWMD	430402.30	769856.49	Lee	220	292	IAS/ICU	100%	10	0						Not Used	No calibration in IAS/ICU
100687	L-2194	USGS	419502.56	727335.72	Lee	117	137	SAS	100%	10	15	SAS						
111851	L-2194_G	SFWMD	419608.26	729858.16	Lee	80	135	SAS	100%	10	15	SAS						
100688	L-2195	USGS	419502.56	727335.72	Lee	13	15	SAS	100%	10	15	SAS						
110724	L-2195_G	SFWMD	419595.83	727636.91	Lee	14	15	SAS	100%	10	0	SAS						
100825	L-2200	USGS	470656.34	869622.89	Lee	143	163	IAS/ICU	52%	10	15	SAS						
100826	L-2202	USGS	470656.34	869622.89	Lee	15.4	17.4	SAS	100%	10	15	SAS						
100762	L-2204	USGS	439876.80	809186.18	Lee	21.4	26.4	SAS	100%	10	14	SAS						
100729	L-2212	USGS	339854.83	779830.54	Lee	216	236	IAS/ICU	100%	10	13						Not Used	sparse data
100744	L-2215	USGS	463883.32	796750.41	Lee	129	149	SAS	100%	10	15	SAS						
100261	L-2216	USGS	407734.94	886006.90	Lee	130	150	IAS/ICU	100%	10	15						Not Used	No calibration in IAS/ICU
100262	L-2217	USGS	407734.94	886006.90	Lee	16	18	SAS	100%	10	15	SAS						
100747	L-2244	USGS	343950.21	805045.21	Lee	187	207	IAS/ICU	100%	10	14						Not Used	No calibration in IAS/ICU
100787	L-2292	USGS	390262.62	832595.80	Lee	516	616	UF	63%	4	15						Not Used	Sparse data, USGS calls this an IAS well
100711	L-2295	USGS	389459.52	763330.32	Lee	510	610	IAS/ICU	100%	3	14						Not Used	No calibration in IAS/ICU
100712	L-2308	USGS	389459.52	763330.32	Lee	11.5	13.5	SAS	100%	10	11	SAS						
100690	L-2310	USGS	401439.86	729934.53	Lee	450	550	IAS/ICU	100%	3	0						Not Used	No calibration in IAS/ICU
100768	L-2311	USGS	458498.28	810507.79	Lee	525	625	IAS/ICU	100%	2	14						Not Used	No calibration in IAS/ICU
100722	L-2313	USGS	470850.10	769961.56	Lee	570	670	UF	57%	3	14						Not Used	USGS calls this an IAS well
100263	L-2328	USGS	407734.94	886006.90	Lee	500	600	IAS/ICU	100%	3	14						Not Used	No calibration in IAS/ICU
100832	L-2341	USGS	376611.00	881054.79	Lee	485	585	IAS/ICU	84%	3	14						Not Used	No calibration in IAS/ICU
100776	L-2434	USGS	323799.77	821788.78	Lee	600	700	UF	100%	10	15						Not Used	Impacted by local pumping
110738	L-2434_G	SFWMD	323801.07	821788.84	Lee	353	700	UF	52%	10	0						Not Used	Impacted by local pumping
100758	L-2435	USGS	351186.61	813474.34	Lee	604	704	UF	100%	3	14		UF	UF	UF	UF		
100791	L-246	USGS	386206.67	836963.93	Lee	23	28	IAS/ICU	100%	7	0						Not Used	No calibration in IAS/ICU
100739	L-2525	USGS	301071.54	796831.17	Lee	545	645	IAS/ICU	100%	3	15	IAS-layer 3						
100834	L-2526	USGS	317320.95	881092.27	Lee	505	605	IAS/ICU	65%	3	15						Not Used	No calibration in IAS/ICU
100803	L-2527	USGS	283215.92	848966.73	Lee	505	605	UF	82%	3	14						Not Used	close to boundary
100800	L-2528	USGS	332536.41	844111.41	Lee	525	625	UF	100%	4	15		UF	UF	UF	UF		
100733	L-2529	USGS	348700.55	784006.08	Lee	445	545	IAS/ICU	100%	3	13	IAS-layer 3						averaged with 100724
100821	L-2530	USGS	434103.62	867580.52	Lee	514	614	UF	83%	3	15						Not Used	USGS calls this an IAS well
100830	L-2531	USGS	458265.56	876243.44	Lee	505	605	IAS/ICU	99%	3	15						Not Used	No calibration in IAS/ICU
100805	L-2549	USGS	283215.92	848966.73	Lee	75	80	IAS/ICU	100%	10	14	IAS-layer 2						
100725	L-2550	USGS	429228.08	771074.18	Lee	114	134	SAS	100%	0	0						Not Used	sparse data
110718	L-2550	SFWMD	430402.30	769856.49	Lee	67	134	SAS	100%	10	0	SAS						
100793	L-2640	USGS	354331.06	837915.56	Lee	160	180	IAS/ICU	100%	10	13						Not Used	No calibration in IAS/ICU
100779	L-2641	USGS	342636.29	822423.94	Lee	150	170	IAS/ICU	100%	10	0						Not Used	No calibration in IAS/ICU
100756	L-2642	USGS	335061.58	806627.10	Lee	140	160	IAS/ICU	100%	10	14						Not Used	No calibration in IAS/ICU
100754	L-2643	USGS	319257.97	806549.22	Lee	180	200	IAS/ICU	100%	10	14						Not Used	No calibration in IAS/ICU
111846	L-2644	SFWMD	316682.06	817200.93	Lee	128	180	IAS/ICU	100%	10	15						Not Used	No calibration in IAS/ICU
100774	L-2644	USGS	317137.20	817500.12	Lee	160	180	IAS/ICU	100%	10	15						Not Used	No calibration in IAS/ICU
100789	L-2645	USGS	306512.59	835535.59	Lee	190	210	IAS/ICU	100%	10	14						Not Used	No calibration in IAS/ICU
100835	L-2646	USGS	355140.47	883123.55	Lee	200	220	IAS/ICU	100%	4	15						Not Used	No calibration in IAS/ICU
100807	L-2700	USGS	321509.73	849550.64	Lee	185	205	IAS/ICU	100%	10	15						Not Used	No calibration in IAS/ICU
100796	L-2701	USGS	335190.73	839068.21	Lee	186	206	IAS/ICU	100%	10	15						Not Used	No calibration in IAS/ICU
110725	L-2701_G	SFWMD	335192.82	839169.23	Lee	175	206	IAS/ICU	100%	10	0						Not Used	No calibration in IAS/ICU
110690	L-2702_G	SFWMD	347900.00	827158.00	Lee	135	155	IAS/ICU	100%	10	0						Not Used	No calibration in IAS/ICU
100771	L-2703	USGS	340557.46	812815.95	Lee	139	159	IAS/ICU	100%	0	0						Not Used	No calibration in IAS/ICU
110671	L-2703_G	SFWMD	340619.00	812671.00	Lee	139	159	IAS/ICU	100%	10	0						Not Used	No calibration in IAS/ICU
100804	L-2820	USGS	283215.92	848966.73	Lee	221	241	IAS/ICU	100%	10	14						Not Used	No calibration in IAS/ICU
100740	L-2821	USGS	301071.54	796831.17	Lee	320	340	IAS/ICU	100%	10	15						Not Used	No calibration in IAS/ICU
100794	L-3203	USGS	354227.00	838394.75	Lee	18	20	IAS/ICU	100%	1	0						Not Used	No calibration in IAS/ICU
100780	L-3204	USGS	342636.29	822423.94	Lee	16	18	SAS	100%	1	0						Not Used	sparse data

Table 4.1: Usage of SAJ Observation Database in Regional Model Calibration

Model ID[a]	Well Name	Data Source	Easting[b]	Northing[b]	County	Cased Depth (ft)	Drilled Depth (ft)	Dominant Layer[c]	% Open Section in Layer[c]	93/94 Months with Data[d]	03/04 Months with Data[e]	Use for Data in Model Setup/Calibration						Reasoning/Comments
													Observations for Calibration					
												Boundary Conditions[f]	Steady State (Oct 03)	Steady State (Feb 04)	Transient (03/04)	Transient (03/04	Not Used	
100757	L-3205	USGS	335007.79	806718.40	Lee	16	18	SAS	100%	1	0						Not Used	sparse data
100755	L-3206	USGS	319077.14	806651.66	Lee	16	18	SAS	100%	10	0	SAS						
100775	L-3207	USGS	317075.04	817372.16	Lee	16	18	SAS	100%	10	14	SAS						
100790	L-3208	USGS	306577.47	835696.62	Lee	16	18	SAS	100%	1	0						Not Used	sparse data
100836	L-3209	USGS	355049.82	883124.21	Lee	16	18	SAS	100%	1	0						Not Used	sparse data
100808	L-3210	USGS	321600.46	849549.91	Lee	16	18	SAS	100%	1	0						Not Used	sparse data
100797	L-3211	USGS	335128.87	839042.18	Lee	16	18	SAS	100%	1	0						Not Used	sparse data
100781	L-3212	USGS	347835.97	827030.46	Lee	16	18	SAS	100%	1	0						Not Used	sparse data
100772	L-3213	USGS	340557.46	812815.95	Lee	16	18	SAS	100%	1	0						Not Used	sparse data
100806	L-3214	USGS	283217.72	849168.70	Lee	16	18	SAS	100%	1	0						Not Used	sparse data
100741	L-3215	USGS	301128.77	796802.32	Lee	16	18	SAS	100%	1	0						Not Used	sparse data
100743	L-331	USGS	376401.13	809158.12	Lee	800	900	UF	100%	1	0						Not Used	sparse data
100810	L-4820	USGS	343750.64	855058.92	Lee	170	190	IAS/ICU	100%	10	15						Not Used	No calibration in IAS/ICU
100737	L-5641	USGS	391481.80	795731.07	Lee	1310	1410	MC1	100%	4	11						Not Used	Model geology puts this well in MC1
100749	L-5648	USGS	394812.31	805404.01	Lee	103	123	IAS/ICU	100%	10	14						Not Used	No calibration in IAS/ICU
110668	L-5649	SFWMD	383850.89	785811.83	Lee	118	128	IAS/ICU	100%	10	0						Not Used	No calibration in IAS/ICU
100731	L-5649	USGS	398742.17	785808.62	Lee	108	128	SAS	100%	10	15	SAS						
100707	L-5664	USGS	439983.51	759304.71	Lee	280	300	IAS/ICU	100%	10	15						Not Used	No calibration in IAS/ICU
100706	L-5665	USGS	439983.51	759304.71	Lee	32	37	SAS	100%	10	0	SAS						
100704	L-5666	USGS	419256.04	759517.12	Lee	200	220	IAS/ICU	100%	7	0						Not Used	No calibration in IAS/ICU
100703	L-5667	USGS	419320.26	759647.06	Lee	27	32	SAS	100%	7	15	SAS						
100705	L-5668	USGS	398152.90	759277.54	Lee	135	155	SAS	100%	10	0	SAS						
100702	L-5669	USGS	398253.28	759337.51	Lee	25	30	SAS	100%	10	0	SAS						
100696	L-5672	USGS	407200.70	750296.96	Lee	33	38	SAS	100%	8	11	SAS						
100697	L-5673	USGS	407200.70	750296.96	Lee	115	135	SAS	100%	8	14	SAS						
100831	L-5708	USGS	459532.85	875833.52	Lee	820	920	UF	100%	3	14		UF	UF	UF	UF		
100750	L-5720	USGS	394812.31	805404.01	Lee	25	30	SAS	100%	10	14	SAS						
100732	L-5721	USGS	398687.35	785689.55	Lee	22	27	SAS	100%	10	0	SAS						
100692	L-5722	USGS	401010.57	734178.03	Lee	19	21	SAS	100%	10	11	SAS						
100693	L-5723	USGS	401010.57	734178.03	Lee	120	140	SAS	100%	8	11	SAS						
100684	L-5724	USGS	388253.28	726522.28	Lee	30	35	SAS	100%	10	0	SAS						
100685	L-5725	USGS	388135.07	726533.13	Lee	108	128	SAS	100%	7	11	SAS						
100680	L-5726	USGS	392480.00	721457.10	Lee	27	32	SAS	100%	8	12	SAS						
100681	L-5727	USGS	396930.01	721480.10	Lee	80	100	SAS	100%	1	0						Not Used	sparse data
100698	L-5730	USGS	389473.14	751112.14	Lee	35	40	SAS	100%	10	14	SAS						
100699	L-5731	USGS	389373.05	751102.67	Lee	100	120	SAS	100%	9	0	SAS						
100682	L-5744	USGS	406227.65	724150.47	Lee	13	15	SAS	100%	10	0	SAS						
100683	L-5745	USGS	406228.07	724221.15	Lee	85	105	SAS	100%	0	0						Not Used	sparse data
100694	L-5746	USGS	398134.14	745807.57	Lee	13	15	SAS	100%	10	11	SAS						
100695	L-5747	USGS	398324.49	745836.34	Lee	85	105	SAS	100%	10	15	SAS						
111876	L-5747	SFWMD	407326.48	740905.92	Lee	59	105	SAS	100%	0	15	SAS						
100738	L-5801	USGS	391481.80	795731.07	Lee	535	635	IAS/ICU	100%	3	11						Not Used	No calibration in IAS/ICU
100717	L-5808	USGS	383174.59	765823.30	Lee	188	208	IAS/ICU	100%	0	15						Not Used	No calibration in IAS/ICU
100777	L-581	USGS	332973.79	822322.73	Lee	157	177	IAS/ICU	100%	9	15						Not Used	No calibration in IAS/ICU
111834	L-581_G	SFWMD	332884.31	822323.49	Lee	110	177	IAS/ICU	100%	9	15						Not Used	No calibration in IAS/ICU
100716	L-5844	USGS	383175.24	765924.27	Lee	30	35	SAS	100%	0	15	SAS						
100724	L-585	USGS	323977.41	771672.46	Lee	455	475	IAS/ICU	100%	2	10	IAS-layer 3						averaged with 100733
100713	L-5874	USGS	421801.95	764479.73	Lee	55	60	SAS	100%	0	15	SAS						
100708	L-588	USGS	419320.26	759647.06	Lee	457	557	IAS/ICU	100%	2	15						Not Used	No calibration in IAS/ICU
112132	L-6433	SFWMD	311448.17	843295.51	Lee	488	645	UF	85%	0	4						Not Used	influenced by IAS, DBHYDRO places it in IAS
112131	L-6436	SFWMD	311364.11	844104.07	Lee	898	1080	UF	57%	0	4						Not Used	only 4 months of data, only 57% of open section in aquifer
100813	L-652	USGS	414325.21	854892.05	Lee	498	598	IAS/ICU	74%	3	15						Not Used	No calibration in IAS/ICU
100818	L-721	USGS	316792.71	860798.24	Lee	16	18	SAS	100%	10	15	SAS						
100829	L-726	USGS	407854.04	875605.30	Lee	17	19	SAS	100%	10	0	SAS						
100799	L-727	USGS	460915.12	847478.43	Lee	66	71	SAS	100%	10	15	SAS						
110744	L-727_G	SFWMD	455353.63	841547.66	Lee	67	71	SAS	100%	10	0	SAS						
100784	L-728	USGS	404844.10	832027.16	Lee	17	19	SAS	100%	10	15	SAS						
100764	L-729	USGS	439854.50	810021.29	Lee	83	103	SAS	100%	10	15	SAS						
110721	L-729_G	SFWMD	439854.69	809819.46	Lee	81	103	SAS	100%	10	0	SAS						
100745	L-730	USGS	463948.58	796878.62	Lee	17	19	SAS	100%	10	15	SAS						
110743	L-730_2_	SFWMD	466510.00	795123.00	Lee	18.7	19	SAS	100%	10	0	SAS						
100720	L-731	USGS	470914.90	769989.76	Lee	223	243	IAS/ICU	100%	10	15						Not Used	No calibration in IAS/ICU
111838	L-731_G	SFWMD	470643.91	770092.04	Lee	165	243	SAS	55%	10	15	SAS						
100730	L-735	USGS	380815.51	780378.87	Lee	250	270	IAS/ICU	100%	10	15						Not Used	No calibration in IAS/ICU
100689	L-738	USGS	401412.47	730066.14	Lee	70	75	SAS	100%	10	15	SAS						
100718	L-739	USGS	413223.72	769749.89	Lee	18	20	SAS	100%	10	12	SAS						
100760	L-742	USGS	370743.60	809324.88	Lee	205	225	IAS/ICU	100%	10	15						Not Used	No calibration in IAS/ICU
111835	L-742_G	SFWMD	370742.79	809022.07	Lee	138	225	IAS/ICU	100%	10	15						Not Used	No calibration in IAS/ICU
100798	L-781	USGS	324888.25	840838.94	Lee	270	290	IAS/ICU	100%	0	0						Not Used	No calibration in IAS/ICU

Table 4.1: Usage of SAJ Observation Database in Regional Model Calibration

Model ID[a]	Well Name	Data Source	Easting[b]	Northing[b]	County	Cased Depth (ft)	Drilled Depth (ft)	Dominant Layer[c]	% Open Section in Layer[c]	93/94 Months with Data[d]	03/04 Months with Data[e]	Use for Data in Model Setup/Calibration						Reasoning/Comments
													Observations for Calibration					
												Boundary Conditions[f]	Steady State (Oct 03)	Steady State (Feb 04)	Transient (03/04)	Transient (03/04	Not Used	
110655	L-781_G	SFWMD	324768.90	840765.44	Lee	82	290	IAS/ICU	100%	10	15						Not Used	No calibration in IAS/ICU
110667	L-954	SFWMD	356459.00	843454.00	Lee	12	14	SAS	100%	8	0	SAS						
140018	LV-01D	SFWMD via DEP	389562.33	730664.08	Lee	18	23	SAS	100%	1	0						Not Used	sparse data
140019	LV-01S	SFWMD via DEP	389620.41	730783.87	Lee	7	17	SAS	100%	1	0						Not Used	sparse data
140020	LV-03	SFWMD via DEP	395400.82	734696.94	Lee	5	15	SAS	100%	1	0						Not Used	sparse data
111136	ST1_G	SFWMD	449330.68	773460.75	Lee	18	20	SAS	100%	0	15	SAS						
111135	ST2_G	SFWMD	449294.19	775022.57	Lee	18	20	SAS	100%	0	15	SAS						
111134	ST3_G	SFWMD	447285.21	774989.29	Lee	18	20	SAS	100%	0	15	SAS						
100710	USGS 262552081485701 L-741	USGS	389459.52	763330.32	Lee	99	119	SAS	100%	10	0	SAS						
110915	WF1_G		466283.81	794547.69	Lee	18	20	SAS	100%	0	0						Not Used	Missing data
111172	WF2_G	SFWMD	463191.13	788549.90	Lee	18	20	SAS	100%	0	15	SAS						
111171	WF3_G	SFWMD	455730.20	785149.36	Lee	18	20	SAS	100%	0	15	SAS						
111170	WF4_G	SFWMD	456105.59	779798.65	Lee	18	20	SAS	100%	0	15	SAS						
111169	WF5_G	SFWMD	460626.73	782660.33	Lee	18	20	SAS	100%	0	15	SAS						
111168	WF6_G	SFWMD	458252.98	780063.53	Lee	18	20	SAS	100%	0	15	SAS						
111039	WF7_G	SFWMD	460482.05	780468.29	Lee	18	20	SAS	100%	0	15	SAS						
100840	2202 FL	USGS	249808.41	1058242.55	Manatee	300	320	IAS/ICU	100%	1	0						Not Used	No calibration in IAS/ICU
101328	AMAX WELL 813 NEAR MYAKKA CITY FL	USGS	291319.16	1046335.35	Manatee	86	106	IAS/ICU	100%	1	0						Not Used	No calibration in IAS/ICU
100869	ARCADIA REPLACE WELL AT RUBONIA FL		155373.77	1184434.12	Manatee	100	160	IAS/ICU	100%	0	0						Not Used	No calibration in IAS/ICU
100864	BEKER W-2 NEAR MYAKKA HEAD FL	USGS	286151.82	1152633.12	Manatee	1125	1225	APPZ	100%	1	0						Not Used	sparse data
130539	BRADENTON STONE WELL		162890.65	1144272.55	Manatee	0	600	IAS/ICU	49%	0	0						Not Used	Open section straddles multiple layers
100861	BRADENTON STONE WELL NEAR BRADENTON FL	USGS	162828.88	1144158.14	Manatee	560	592	UF	100%	0	0						Not Used	sparse data
100872	BUSBY DEEP WELL ON DUETTE ROAD AT DUETTE FL	USGS	293509.48	1189431.59	Manatee	896	996	MC1	55%	1	2						Not Used	Model geology puts this well in MC1
130570	COKER CREEK UPL SURF	SWFWMD	275233.29	1118990.33	Manatee	5	10	SAS	100%	0	10	SAS						
130550	COKER CREEK WTL SURF	SWFWMD	275439.17	1118836.88	Manatee	5	10	SAS	100%	0	10	SAS						
130519	EDGEVILLE 3 DEEP	SWFWMD	294631.08	1083231.28	Manatee	487	600	UF	100%	10	2						Not Used	93/94 data
130520	EDGEVILLE 4 SHALLOW	SWFWMD	294630.34	1083249.47	Manatee	65	70	SAS	100%	10	15	SAS						
100841	EDGEVILLE DEEP WELL 3 AT EDGEVILLE FL	USGS	294699.13	1083347.49	Manatee	487	600	UF	100%	10	15		UF	UF	UF	UF		
100842	EDGEVILLE WELL 4 AT EDGEVILLE FL	USGS	294626.03	1083068.72	Manatee	65	70	SAS	100%	5	0	SAS						
100870	ELLEN MATHESON WELL AT PARRISH FL	USGS	193926.61	1184497.40	Manatee	160	180	IAS/ICU	100%	1	0						Not Used	No calibration in IAS/ICU
100866	ESTECH HAWTHORN 44 NEAR DUETTE FL	USGS	291803.75	1170054.72	Manatee	230	250	IAS/ICU	100%	1	2						Not Used	No calibration in IAS/ICU
130575	FALKNER FARMS 1 SURF	SWFWMD	264180.02	1116005.44	Manatee	9	11	SAS	100%	0	15	SAS						
130576	FALKNER FARMS 2 SURF	SWFWMD	263098.33	1116015.95	Manatee	9	11	SAS	100%	0	15	SAS						
130578	FALKNER FARMS 3 SURF	SWFWMD	264202.46	1116459.73	Manatee	9	11	SAS	100%	0	15	SAS						
130577	FALKNER FARMS 4 SURF	SWFWMD	263111.77	1116470.33	Manatee	9	11	SAS	100%	0	15	SAS						
130571	FARM 5 UPL SURF	SWFWMD	280235.31	1110186.71	Manatee	4	9	SAS	100%	0	14	SAS						
130549	FARM 5 WTL SURF	SWFWMD	280442.66	1110184.78	Manatee	3.5	8.5	SAS	100%	0	14	SAS						
130572	FLATFORD UPL SURF	SWFWMD	286542.95	1113744.32	Manatee	5	10	SAS	100%	0	15	SAS						
130548	FLATFORD WTL SURF	SWFWMD	286281.35	1113726.52	Manatee	5	10	SAS	100%	0	15	SAS						
130542	FLORIDA PWR @ PINEY PT FL	SWFWMD	160092.06	1198246.58	Manatee	104	950	UF	44%	10	4						Not Used	Open section straddles multiple layers
140004	GILLETTE SH-AGW	SWFWMD via DEP	161461.20	1190282.47	Manatee	6	26	SAS	100%	7	0	SAS						
100871	GRIFFIN DEEP WELL AT PARRISH FL	USGS	191621.92	1187554.48	Manatee	476	576	UF	100%	1	0						Not Used	sparse data
130543	JACOBSEN DEEP		304129.08	1068862.79	Manatee	116	1180	IAS/ICU	38%	0	0						Not Used	Open section straddles multiple layers
130540	KIBLER DEEP	SWFWMD	254198.50	1144738.19	Manatee	208	1123	MC1	41%	10	0						Not Used	Open section straddles multiple layers
100862	KIBLER DEEP WELL 26B NEAR BETHANY FL	USGS	254449.76	1144871.50	Manatee	208	1123	MC1	41%	9	15						Not Used	Open section straddles multiple layers
100849	LOCKWOOD RIVER (BARTH) DEEP WELL NEAR BRADENTON FL	USGS	166214.50	1118761.89	Manatee	620	720	UF	100%	1	0						Not Used	sparse data
130535	MA 32 EARL ARNOLD		187624.37	1148219.68	Manatee	31	671	UF	53%	0	0						Not Used	missing data
130533	MA 41 MANATEE FAIRGR FLDN		144293.01	1163821.69	Manatee	216	273	IAS/ICU	78%	0	0						Not Used	Outside Boundary
130522	MA 42 SNEADS ISLAND INT		129502.67	1166453.58	Manatee	200	525	UF	87%	0	0						Not Used	Outside Boundary
130544	MA 45 SWIFT AVON		292049.66	1170368.62	Manatee	980	1220	APPZ	91%	0	0						Not Used	missing data
130516	MA 46 KOEHLER		212115.56	1171577.43	Manatee	0	0	Error	0%	0	0						Not Used	Data error
130518	MA 56 BEN HILL GRIFFIN		191684.42	1187666.89	Manatee	0	576	UF	51%	0	0						Not Used	Missing data
130538	MANATEE SCHROEDER		212985.28	1144296.05	Manatee	168	1103	MC1	41%	0	0						Not Used	Open section straddles multiple layers
100874	MOODY WELL 801 NEAR DUETTE FL	USGS	282521.89	1198016.89	Manatee	260	280	IAS/ICU	100%	1	0						Not Used	No calibration in IAS/ICU
100845	MYAKKA CITY COMM CNTR WELL NEAR MYAKKA CITY FL	USGS	278841.82	1097079.77	Manatee	230	250	IAS/ICU	100%	1	2						Not Used	No calibration in IAS/ICU
100850	PARKS DEEP WELL NEAR MYAKKA HEAD FL	USGS	302964.36	1118445.34	Manatee	1220	1320	APPZ	100%	1	0						Not Used	sparse data
130534	PORT MANATEE 7		154619.80	1203366.82	Manatee	0	0	Error	0%	0	0						Not Used	Data error on cased and drilled depths
130545	ROMP 23 HTRN/TMPA	SWFWMD	273797.60	1085429.25	Manatee	303	363	IAS/ICU	100%	10	15						Not Used	No calibration in IAS/ICU
100843	ROMP 23 MYAKKA CITY OCALA WELL NEAR MYAKKA CITY FL	USGS	273780.38	1085421.34	Manatee	900	1000	MC1	100%	1	2						Not Used	Model geology puts this well in MC1
100844	ROMP 23 MYAKKA CITY TAMPA WELL NEAR MYAKKA CITY	USGS	273798.62	1085441.36	Manatee	354	374	IAS/ICU	100%	1	2						Not Used	No calibration in IAS/ICU
130541	ROMP 23 OCAL	SWFWMD	273783.04	1085416.26	Manatee	904	1000	MC1	100%	10	15						Not Used	Model geology puts this well in MC1
130567	ROMP 23 PZ2 ARC INTER	SWFWMD	273788.49	1085420.25	Manatee	175	250	IAS/ICU	100%	0	15						Not Used	No calibration in IAS/ICU
130568	ROMP 23 SURF	SWFWMD	273787.63	1085424.30	Manatee	10	20	SAS	100%	0	15	SAS						

Table 4.1: Usage of SAJ Observation Database in Regional Model Calibration

Model ID[a]	Well Name	Data Source	Easting[b]	Northing[b]	County	Cased Depth (ft)	Drilled Depth (ft)	Dominant Layer[c]	% Open Section in Layer[c]	93/94 Months with Data[d]	03/04 Months with Data[e]	Use for Data in Model Setup/Calibration						Reasoning/Comments
													Observations for Calibration					
												Boundary Conditions[f]	Steady State (Oct 03)	Steady State (Feb 04)	Transient (03/04)	Transient (03/04	Not Used	
130536	ROMP 32 LOW OCAL/AVPK	SWFWMD	311166.76	1141806.94	Manatee	909	1215	MC1	51%	10	15						Not Used	Model geology puts this well in MC1
130526	ROMP 32 SHALLOW	SWFWMD	311166.69	1141798.86	Manatee	27	47	SAS	100%	0	15	SAS						
100860	ROMP 32 SUWANNEE WELL NEAR MYAKKA HEAD FL	USGS	311150.54	1141806.07	Manatee	560	592	UF	100%	1	2						Not Used	sparse data
130537	ROMP 32 SWNN	SWFWMD	311152.33	1141805.04	Manatee	560	592	UF	100%	10	15		UF	UF	UF	UF		
130529	ROMP 33 ARC	SWFWMD	248483.02	1137666.72	Manatee	215	290	IAS/ICU	100%	10	15						Not Used	No calibration in IAS/ICU
130527	ROMP 33 AVPK	SWFWMD	248473.27	1137682.98	Manatee	1460	1600	APPZ	100%	10	15		APPZ	APPZ	APPZ	APPZ		
100857	ROMP 33 HAWTHORN WELL NEAR BETHANY FL	USGS	248478.80	1137695.04	Manatee	215	290	IAS/ICU	100%	0	2						Not Used	No calibration in IAS/ICU
130569	ROMP 33 INT	SWFWMD	248081.88	1137648.56	Manatee	96	166	IAS/ICU	100%	0	15						Not Used	No calibration in IAS/ICU
100858	ROMP 33 NSRD NEAR BETHANY FL	USGS	248460.48	1137664.92	Manatee	18	30	IAS/ICU	50%	1	2						Not Used	No calibration in IAS/ICU
130530	ROMP 33 SURF	SWFWMD	248461.30	1137656.84	Manatee	18	30	SAS	50%	10	15	SAS						
100856	ROMP 33 SUWANNEE WELL NEAR BETHANY FL	USGS	248487.20	1137634.35	Manatee	404	750	UF	88%	0	2						Not Used	sparse data
130528	ROMP 33 TMPA/SWNN	SWFWMD	248494.57	1137650.44	Manatee	404	750	UF	88%	10	15		UF	UF	UF	UF		
130564	ROMP 39 ARC	SWFWMD	250783.26	1185230.34	Manatee	130	205	IAS/ICU	100%	0	15						Not Used	No calibration in IAS/ICU
130563	ROMP 39 AVPK	SWFWMD	250817.52	1185237.07	Manatee	960	1120	APPZ	89%	0	15		APPZ	APPZ	APPZ			no 93/94 data
130566	ROMP 39 SURF	SWFWMD	250767.92	1185226.46	Manatee	35	75	SAS	75%	0	15	SAS						
130565	ROMP 39 SWNN	SWFWMD	250815.65	1185230.02	Manatee	524	704	UF	100%	0	15		UF	UF	UF			no 93/94 data
130525	ROMP TR 7-1 TMPA	SWFWMD	142777.67	1124984.86	Manatee	320	340	UF	90%	10	15	UF						averaged with 130559
130558	ROMP TR 7-2 AVPK	SWFWMD	153304.59	1131327.52	Manatee	957	1022	MC1	100%	1	15						Not Used	Model geology puts this well in MC1
130560	ROMP TR 7-2 LOW ARC	SWFWMD	153305.41	1131248.71	Manatee	200	290	IAS/ICU	100%	1	15	IAS-layer 3						averaged with 130561
130562	ROMP TR 7-2 SURF	SWFWMD	153311.25	1131282.99	Manatee	12	22	SAS	100%	1	15	SAS						
130559	ROMP TR 7-2 TMPA/SWNN	SWFWMD	153306.29	1131246.68	Manatee	357	465	UF	100%	1	15	UF						averaged with 130525
130561	ROMP TR 7-2 UP ARC	SWFWMD	153306.31	1131248.70	Manatee	60	105	IAS/ICU	100%	1	15	IAS-layer 3						averaged with 130560
100851	ROMP TR 7-4 AVON PARK WELL NEAR BRADENTON FL	USGS	173169.16	1127693.89	Manatee	1162	1250	APPZ	100%	6	15						Not Used	close to boundary
130556	ROMP TR 7-4 AVPK		173085.87	1127548.16	Manatee	1162	1250	APPZ	100%	0	0	APPZ						
100854	ROMP TR 7-4 HAWTHORN WELL NEAR BRADENTON FL	USGS	173169.16	1127693.89	Manatee	213	268	IAS/ICU	100%	10	15						Not Used	No calibration in IAS/ICU
130554	ROMP TR 7-4 HTRN		173127.27	1127618.38	Manatee	213	268	IAS/ICU	100%	0	0						Not Used	No calibration in IAS/ICU
130546	ROMP TR 7-4 NRSD		173109.74	1127584.24	Manatee	15	20	IAS/ICU	100%	0	0						Not Used	No calibration in IAS/ICU
100855	ROMP TR 7-4 NRSD WELL NEAR BRADENTON FL	USGS	173169.16	1127693.89	Manatee	15	20	IAS/ICU	100%	9	15						Not Used	No calibration in IAS/ICU
100852	ROMP TR 7-4 SUWANNEE WELL NEAR BRADENTON FL	USGS	173169.16	1127693.89	Manatee	560	800	UF	73%	10	15						Not Used	Colocated with 100853, which is more clearly in the UF. Datasets almost identical
130555	ROMP TR 7-4 SWNN/OCAL		173098.21	1127600.54	Manatee	560	800	UF	74%	0	0						Not Used	Missing data
100853	ROMP TR 7-4 TAMPA WELL NEAR BRADENTON FL	USGS	173169.16	1127693.89	Manatee	380	500	UF	100%	6	15		UF	UF	UF	UF		
130532	ROMP TR 7-4 TMPA		173107.84	1127576.18	Manatee	380	500	UF	100%	0	0						Not Used	Missing data
130553	ROMP TR 8-1 AVPK	SWFWMD	155334.48	1184331.80	Manatee	1130	1170	APPZ	100%	10	15						Not Used	excessively high TDS due to local pumping
130547	ROMP TR 8-1 HAW/TPA	SWFWMD	155318.94	1184312.80	Manatee	263	321	UF	100%	10	0						Not Used	similar to 130524 with less data
130557	ROMP TR 8-1 SURF	SWFWMD	155321.51	1184302.66	Manatee	17	37	IAS/ICU	97%	1	15	IAS-layer 2						
130524	ROMP TR 8-1 SWNN	SWFWMD	155303.35	1184289.76	Manatee	390	515	UF	100%	10	15	UF						
130552	ROMP TR 8-1 UP AVPK	SWFWMD	155334.48	1184331.80	Manatee	900	940	APPZ	100%	10	15	APPZ						averaged with 100873
130523	ROMP TR 8-1 UP HTRN	SWFWMD	155313.64	1184320.94	Manatee	100	160	IAS/ICU	100%	10	15	IAS-layer 3						
130551	ROMP TR 8-1 UP OCAL	SWFWMD	155328.36	1184274.29	Manatee	627	670	MC1	79%	0	15						Not Used	Outside Boundary, Confining Unit
100868	ROMP TR 8-1 UPPER AVON PARK WELL AT RUBONIA FL	USGS	155219.00	1184154.00	Manatee	900	940	APPZ	100%	6	0						Not Used	Same as 130552, with sparser data
100865	RUTLAND-OAK KNOLL WELL FL	USGS	235400.20	1157071.34	Manatee	800	900	MC1	100%	1	0						Not Used	Model geology puts this well in MC1
101366	SARASOTA COUNTY TEST WELL 6A NEAR SARASOTA FL	USGS	174411.64	1113224.51	Manatee	392	527	UF	95%	8	0					UF		no 03/04 data
100863	SR 64 DEEP WELL NEAR BRADENTON FL	USGS	187561.78	1148105.25	Manatee	32	671	UF	53%	1	0						Not Used	sparse data
100867	SWIFT-AVON PARK ON DUETTE ROAD NEAR DUETTE FL	USGS	291985.61	1170255.07	Manatee	980	1222	APPZ	91%	1	2						Not Used	sparse data
130573	TAYLOR ROAD UPL SURF	SWFWMD	281301.24	1124003.77	Manatee	1	6	SAS	100%	0	15	SAS						
130574	TAYLOR ROAD WTL SURF	SWFWMD	286545.08	1123824.10	Manatee	2	7	SAS	100%	0	15	SAS						
100859	USGS DEEP WELL NEAR MYAKKA HEAD FL	USGS	285387.21	1138065.70	Manatee	460	560	UF	100%	1	2						Not Used	sparse data
131419	VERNA 08 DEEP	SWFWMD	243626.65	1111675.01	Manatee	126	445	IAS/ICU	100%	10	0						Not Used	No calibration in IAS/ICU
130531	VERNA 1A FLDN	SWFWMD	233467.83	1116214.15	Manatee	412	480	IAS/ICU	50%	10	3						Not Used	No calibration in IAS/ICU
100847	VERNA DEEP WELL 1A NEAR VERNA FL	USGS	233548.00	1116350.00	Manatee	412	480	IAS/ICU	51%	10	15						Not Used	No calibration in IAS/ICU
130517	VERNA T 0-1	SWFWMD	243710.20	1117209.22	Manatee	140	480	IAS/ICU	93%	10	4						Not Used	No calibration in IAS/ICU
130521	VERNA T 0-2	SWFWMD	252446.05	1098474.72	Manatee	140	530	IAS/ICU	82%	10	0						Not Used	No calibration in IAS/ICU
100848	VERNA TEST WELL 0-1 NEAR VERNA FL	USGS	243799.09	1117335.11	Manatee	140	480	IAS/ICU	93%	9	15						Not Used	No calibration in IAS/ICU
100846	VERNA TEST WELL 0-2 NEAR VERNA FL	USGS	252492.00	1098603.00	Manatee	140	530	IAS/ICU	82%	6	15						Not Used	No calibration in IAS/ICU
100873	WELL 1 AT PINEY POINT FL	USGS	160125.14	1198349.42	Manatee	104	950	UF	44%	10	15	APPZ						averaged with 130552
111385	JD26_GW1	SFWMD	934359.91	973465.03	Martin	17.14	19.14	SAS	100%	0	15	SAS						
110952	JD6_GW1	SFWMD	933925.41	970836.57	Martin	19.35	21.35	SAS	100%	0	15	SAS						
110951	JDSPMW1_G	SFWMD	947698.52	967700.82	Martin	59	64	SAS	100%	10	15	SAS						

Table 4.1: Usage of SAJ Observation Database in Regional Model Calibration

Model ID[a]	Well Name	Data Source	Easting[b]	Northing[b]	County	Cased Depth (ft)	Drilled Depth (ft)	Dominant Layer[c]	% Open Section in Layer[c]	93/94 Months with Data[d]	03/04 Months with Data[e]	Use for Data in Model Setup/Calibration						Reasoning/Comments
													Observations for Calibration					
												Boundary Conditions[f]	Steady State (Oct 03)	Steady State (Feb 04)	Transient (03/04)	Transient (03/04	Not Used	
110950	JDSPMW3_G	SFWMD	948264.98	964372.40	Martin	59	64	SAS	100%	10	15	SAS						
100928	M-1004	USGS	922012.83	1022158.10	Martin	15	17	SAS	100%	10	15	SAS						
111830	M-1004_G	SFWMD	922014.00	1022157.00	Martin	15	17	SAS	100%	10	15	SAS						
100885	M-1024	USGS	952363.72	960463.89	Martin	78	83	SAS	100%	10	15	SAS						
111329	M-1024_G	SFWMD	952272.20	960463.29	Martin	80	83	SAS	100%	10	15	SAS						
100934	M-1037	USGS	845479.68	1028378.13	Martin	22	24	SAS	100%	4	0						Not Used	sparse data
100936	M-1042	USGS	797515.40	1029092.62	Martin	41	46	SAS	100%	2	0						Not Used	sparse data
100941	M-1043	USGS	908392.64	1050228.51	Martin	132	152	SAS	100%	2	0						Not Used	sparse data
100907	M-1044	USGS	940678.97	990353.62	Martin	143	163	SAS	100%	10	0	SAS						
100883	M-1045	USGS	860027.22	954631.13	Martin	21	23	SAS	100%	4	0						Not Used	sparse data
100900	M-1048	USGS	829688.11	978140.47	Martin	75	80	SAS	100%	10	15	SAS						
111831	M-1048_G	SFWMD	829688.94	978140.06	Martin	25	80	SAS	100%	10	15	SAS						
100909	M-1049	USGS	881996.49	991099.15	Martin	75	80	SAS	100%	1	0						Not Used	sparse data
100927	M-1052	USGS	920050.61	1020511.32	Martin	142	162	SAS	100%	9	0	SAS						
100915	M-1066	USGS	800425.73	997799.38	Martin	25	30	SAS	100%	4	0						Not Used	sparse data
100897	M-1070	USGS	949132.34	971427.61	Martin	100	120	SAS	100%	5	0	SAS						
100894	M-1071	USGS	946335.41	970397.90	Martin	98	118	SAS	100%	9	0	SAS						
111067	M-1071_G	SFWMD	946412.06	970519.23	Martin	114	118	SAS	100%	0	15	SAS						
100895	M-1072	USGS	946335.41	970397.90	Martin	29	34	SAS	100%	10	0	SAS						
111066	M-1072_G	SFWMD	946459.16	970486.63	Martin	30	34	SAS	100%	0	15	SAS						
100899	M-1073	USGS	943478.29	977951.79	Martin	49	54	SAS	100%	3	0						Not Used	sparse data
100903	M-1081	USGS	860515.47	983816.80	Martin	22	24	SAS	100%	4	0						Not Used	sparse data
100891	M-1083	USGS	891453.64	965805.76	Martin	22	24	SAS	100%	10	0	SAS						
100890	M-1085	USGS	824423.41	964971.90	Martin	78	83	SAS	100%	4	0						Not Used	sparse data
100893	M-1088	USGS	795467.79	967186.07	Martin	85	105	SAS	100%	10	0	SAS						
100892	M-1096	USGS	891453.64	965805.76	Martin	85	105	SAS	100%	10	0	SAS						
110634	M-1141_G	SFWMD	906245.00	1029834.00	Martin	89	109	SAS	100%	10	0	SAS						
100937	M-1175	USGS	902989.09	1033128.79	Martin	18	20	SAS	100%	0	0						Not Used	sparse data
110635	M-1179	SFWMD	903618.00	1031332.00	Martin	18.2	20.2	SAS	100%	10	0	SAS						
110633	M-1183_G	SFWMD	906247.00	1029833.00	Martin	19	21	SAS	100%	10	0	SAS						
100929	M-1197	USGS	901605.38	1022920.94	Martin	20	22	SAS	100%	3	0						Not Used	sparse data
100933	M-1198	USGS	908619.24	1028214.95	Martin	20	22	SAS	100%	3	0						Not Used	sparse data
100931	M-1199	USGS	908010.63	1024373.74	Martin	20	22	SAS	100%	3	0						Not Used	sparse data
100886	M-1229	USGS	932909.86	962529.44	Martin	130	150	SAS	100%	10	0	SAS						
100888	M-1230	USGS	942394.73	964715.05	Martin	115	135	SAS	100%	3	0						Not Used	sparse data
100882	M-1231	USGS	904097.40	954368.05	Martin	162	182	IAS/ICU	79%	5	0						Not Used	No calibration in IAS/ICU
100887	M-1232	USGS	932909.86	962529.44	Martin	15.5	17.5	SAS	100%	10	0	SAS						
100889	M-1233	USGS	942394.73	964715.05	Martin	14.5	16.5	SAS	100%	3	0						Not Used	sparse data
100881	M-1234	USGS	904353.69	954390.10	Martin	16	18	SAS	100%	10	15	SAS						
111332	M-1234	SFWMD	904355.00	954289.00	Martin	16	18	SAS	100%	10	15	SAS						
100905	M-1235	USGS	906439.12	985888.96	Martin	140	160	SAS	57%	9	0	SAS						
100913	M-1236	USGS	877715.70	996932.76	Martin	120	140	SAS	50%	10	0	SAS						
100912	M-1237	USGS	840474.61	996546.30	Martin	140	160	SAS	67%	4	0						Not Used	sparse data
100921	M-1238	USGS	840409.60	1010986.19	Martin	102	122	SAS	100%	9	0	SAS						
100910	M-1239	USGS	881996.49	991099.15	Martin	110	130	SAS	100%	1	0						Not Used	sparse data
100940	M-1240	USGS	824731.08	1043939.17	Martin	110	130	SAS	100%	10	0	SAS						
100898	M-1243	USGS	835789.43	972391.43	Martin	53	58	SAS	100%	3	0						Not Used	sparse data
100902	M-1244	USGS	851930.21	982765.13	Martin	25	30	SAS	100%	10	0	SAS						
100938	M-1247	USGS	872133.53	1043960.95	Martin	87	107	SAS	100%	10	0	SAS						
100939	M-1248	USGS	854074.71	1044071.17	Martin	55	60	SAS	100%	4	0						Not Used	sparse data
100926	M-1249	USGS	811572.99	1013895.82	Martin	21	23	SAS	100%	4	0						Not Used	sparse data
100901	M-1252	USGS	802475.54	980640.40	Martin	82.8	87.8	SAS	100%	9	0	SAS						
100923	M-1253	USGS	905361.56	1014359.97	Martin	91	111	SAS	100%	6	0	SAS						
100932	M-1255	USGS	824777.60	1028507.04	Martin	30	35	SAS	100%	10	15	SAS						
110759	M-1255	SFWMD	825242.82	1025479.24	Martin	21.6	26.6	SAS	100%	10	0	SAS						
100924	M-1257	USGS	905361.56	1014359.97	Martin	18	20	SAS	100%	10	0	SAS						
100908	M-1258	USGS	940678.97	990353.62	Martin	16.2	18.2	SAS	100%	10	0	SAS						
100904	M-1259	USGS	928411.85	985927.94	Martin	32.7	37.7	SAS	100%	4	0						Not Used	sparse data
100917	M-1261	USGS	891742.80	1007228.98	Martin	18	20	SAS	100%	10	15	SAS						
111878	M-1261	SFWMD	891743.79	1007228.41	Martin	16.8	19.8	SAS	100%	10	15	SAS						
100911	M-1263	USGS	841390.41	993924.95	Martin	5.3	7.3	SAS	100%	4	0						Not Used	sparse data
100922	M-1264	USGS	839866.98	1011084.73	Martin	14	16	SAS	100%	1	0						Not Used	sparse data
100935	M-1267	USGS	897141.28	1029256.40	Martin	90	110	SAS	100%	10	0	SAS						
100918	M-1269	USGS	924558.34	1008220.36	Martin	21	23	SAS	100%	4	0						Not Used	sparse data
100906	M-1270	USGS	906439.12	985888.96	Martin	19	21	SAS	100%	10	0	SAS						
100916	M-1271	USGS	914215.33	1000276.97	Martin	21	26	SAS	100%	4	0						Not Used	sparse data
100896	M-1272	USGS	915669.80	970394.76	Martin	21	23	SAS	100%	4	0						Not Used	sparse data
100914	M-1273	USGS	877715.70	996932.76	Martin	17.5	19.5	SAS	100%	10	0	SAS						
100925	M-1274	USGS	877893.30	1014201.74	Martin	20.5	22.5	SAS	100%	4	0						Not Used	sparse data

Table 4.1: Usage of SAJ Observation Database in Regional Model Calibration

Model ID[a]	Well Name	Data Source	Easting[b]	Northing[b]	County	Cased Depth (ft)	Drilled Depth (ft)	Dominant Layer[c]	% Open Section in Layer[c]	93/94 Months with Data[d]	03/04 Months with Data[e]	Use for Data in Model Setup/Calibration						Reasoning/Comments
													Observations for Calibration					
												Boundary Conditions[f]	Steady State (Oct 03)	Steady State (Feb 04)	Transient (03/04)	Transient (03/04	Not Used	
100919	M-1276	USGS	865814.65	1008483.02	Martin	122	142	SAS	100%	3	0						Not Used	sparse data
100920	M-1277	USGS	865814.65	1008483.02	Martin	22	27	SAS	100%	3	0						Not Used	sparse data
110632	M-147_G	SFWMD	904384.00	1039011.00	Martin	69	74	SAS	100%	10	0	SAS						
110646	M-933 2_	SFWMD	867321.00	1028503.00	Martin	13	15	SAS	100%	10	0	SAS						
100930	MABRY CARLTON 8-B NRSD WELL NEAR SARASOTA FL	USGS	922012.83	1022158.10	Martin	15	17	SAS	100%	3	0						Not Used	Duplicate with 111830
112213	MF-2	SFWMD	818367.25	1028076.75	Martin	300	800	IAS/ICU	64%	1	0						Not Used	No calibration in IAS/ICU
112214	MF-23	SFWMD	798251.70	996539.65	Martin	456	1119	IAS/ICU	46%	1	0						Not Used	Open section straddles multiple layers
112215	MF-3	SFWMD	922774.20	1047512.71	Martin	543	980	IAS/ICU	55%	1	0						Not Used	No calibration in IAS/ICU
112216	MF-31	SFWMD	924777.60	1024359.42	Martin	844	1092	UF	100%	0	0						Not Used	sparse data
112217	MF-33	SFWMD	789502.05	1016158.11	Martin	1100	1200	MC1	100%	1	0						Not Used	Model geology puts this well in MC1
112218	MF-35	SFWMD	824554.81	970435.35	Martin	390	1340	MC1	37%	1	0						Not Used	Open section straddles multiple layers
112165	MF-35B	SFWMD	824574.85	966362.29	Martin	390	1340	MC1	36%	0	15						Not Used	Open section straddles multiple layers
112103	MF-37	SFWMD	784921.90	965985.04	Martin	765	1039	UF	100%	0	9				UF			This point has full dataset starting in April 2004
112219	MF-3A_G	SFWMD	923032.76	1047999.04	Martin	880	980	UF	100%	1	0						Not Used	sparse data
112163	MF-52	SFWMD	856075.21	1000605.99	Martin	400	1320	MC1	39%	0	15						Not Used	Open section straddles multiple layers
112220	MF-9	SFWMD	828909.34	1031657.18	Martin	360	810	UF	52%	1	0						Not Used	sparse data
100880	PB-1544	USGS	926388.55	963596.90	Martin	210	230	IAS/ICU	100%	4	0						Not Used	No calibration in IAS/ICU
111166	SAV4_G	SFWMD	899455.44	1062712.12	Martin	20.5	22.5	SAS	100%	0	15	SAS						
111165	SAV5_G	SFWMD	898906.70	1063920.64	Martin	21.82	23.82	SAS	100%	0	15	SAS						
111164	SAV6_G	SFWMD	898465.69	1062201.30	Martin	21.35	23.35	SAS	100%	0	15	SAS						
110866	SLAM_G1	SFWMD	911472.00	1043694.00	Martin	55.21	60.21	SAS	100%	0	14	SAS						
110867	SLAM_G2	SFWMD	911472.00	1043696.00	Martin	25	30	SAS	100%	0	14	SAS						
110868	SLPD_G1	SFWMD	893392.00	1038042.00	Martin	80.63	100.63	SAS	100%	0	14	SAS						
110870	SLPD_G2	SFWMD	893394.00	1038038.00	Martin	54.48	59.48	SAS	100%	0	14	SAS						
110869	SLPD_G3	SFWMD	893395.00	1038033.00	Martin	24.63	29.63	SAS	100%	0	14	SAS						
112102	TFRO-5	SFWMD	898492.92	1001979.22	Martin	1106	1350	APPZ	64%	0	11			APPZ	APPZ			no Oct 03 data; no 93/94 data
140056	27-3	DADE CO. via DEP	836135.18	420823.62	Miami-Dade	17	19	SAS	100%	10	0	SAS						
111147	3AS3W1_G	SFWMD	731346.66	553896.56	Miami-Dade	7.7	8.7	SAS	100%	0	15	SAS						
111081	3AS3W1_G	SFWMD	731346.66	553896.56	Miami-Dade	24.4	26.4	SAS	100%	0	15	SAS						
111068	3AS3W2_G	SFWMD	732508.37	553814.90	Miami-Dade	7.5	8.5	SAS	100%	0	15	SAS						
111069	3AS3W2_G	SFWMD	732508.37	553814.90	Miami-Dade	23	25	SAS	100%	0	15	SAS						
111146	3AS3W3_G	SFWMD	732097.39	552418.02	Miami-Dade	7.5	8.5	SAS	100%	0	15	SAS						
111080	3AS3W3_G	SFWMD	732097.39	552418.02	Miami-Dade	26.6	28.6	SAS	100%	0	15	SAS						
111145	3AS3W4_G	SFWMD	731945.46	553625.92	Miami-Dade	9.7	10.7	SAS	100%	0	15	SAS						
111082	3AS3W4_G	SFWMD	731945.46	553625.92	Miami-Dade	28	30	SAS	100%	0	15	SAS						
111079	3BS1W1_G	SFWMD	816927.98	526166.98	Miami-Dade	14	15	SAS	100%	0	15	SAS						
111086	3BS1W1_G	SFWMD	816927.98	526166.98	Miami-Dade	32	34	SAS	100%	0	15	SAS						
111150	3BS1W2_G	SFWMD	818360.43	526241.98	Miami-Dade	12.5	13.5	SAS	100%	0	15	SAS						
111085	3BS1W2_G	SFWMD	818360.43	526241.98	Miami-Dade	28	30	SAS	100%	0	15	SAS						
111149	3BS1W3_G	SFWMD	817560.13	523914.98	Miami-Dade	14	15	SAS	100%	0	15	SAS						
111083	3BS1W3_G	SFWMD	817560.13	523914.98	Miami-Dade	26.5	28.5	SAS	100%	0	15	SAS						
111148	3BS1W4_G	SFWMD	817461.52	525677.48	Miami-Dade	13	14	SAS	100%	0	15	SAS						
111084	3BS1W4_G	SFWMD	817461.52	525677.48	Miami-Dade	32	34	SAS	100%	0	15	SAS						
101560	BW	USGS	890454.78	541004.57	Miami-Dade	40.3	45.3	SAS	100%	2	0						Not Used	sparse data
111126	C2GSW1_GW1	SFWMD	866693.27	496879.81	Miami-Dade	22.5	25	SAS	100%	0	15	SAS						
111125	C2GSW1_GW2	SFWMD	866693.27	496879.81	Miami-Dade	57.5	60	SAS	100%	0	15	SAS						
111115	C2GW1_GW1	SFWMD	866475.26	496774.24	Miami-Dade	22.5	25	SAS	100%	0	15	SAS						
111114	C2GW1_GW2	SFWMD	866475.26	496774.24	Miami-Dade	57.5	60	SAS	100%	0	15	SAS						
112156	DF-4	SFWMD	830843.44	573317.79	Miami-Dade	1140	1230	UF	100%	0	15		UF	UF	UF			no 93/94 data
112154	DF-5	SFWMD	830843.44	573317.79	Miami-Dade	1700	1800	APPZ	51%	0	15		APPZ	APPZ	APPZ			no 93/94 data
112158	ENP-100	SFWMD	787244.43	381470.63	Miami-Dade	620	1333	IAS/ICU	76%	0	14	UF						
101549	F-10	USGS	893670.22	537892.17	Miami-Dade	75.7	80.7	SAS	100%	2	0						Not Used	sparse data
101558	F-12	USGS	890273.66	540700.70	Miami-Dade	51.9	56.9	SAS	100%	2	0						Not Used	sparse data
101559	F-13	USGS	888539.07	540388.45	Miami-Dade	68.3	73.3	SAS	100%	2	0						Not Used	sparse data
101526	F-179	USGS	904208.52	514058.85	Miami-Dade	72	77	SAS	100%	10	15	SAS						
111647	F-179	SFWMD	904208.73	514058.64	Miami-Dade	75	77	SAS	100%	10	15	SAS						
101571	F-239	USGS	895798.16	546723.19	Miami-Dade	47.8	52.8	SAS	100%	10	15	SAS						
111367	F-239_G	SFWMD	895798.00	546723.00	Miami-Dade	48	53	SAS	100%	10	15	SAS						
101581	F-279	USGS	923291.71	565629.09	Miami-Dade	97	117	SAS	100%	2	0						Not Used	sparse data
101507	F-319	USGS	890572.66	499141.96	Miami-Dade	15	17	SAS	100%	10	15	SAS						
111649	F-319	SFWMD	890572.82	499141.80	Miami-Dade	13	17	SAS	100%	10	15	SAS						
101433	F-358	USGS	827512.04	415257.68	Miami-Dade	49	54	SAS	100%	10	15	SAS						
111361	F-358_G	SFWMD	827512.00	415258.00	Miami-Dade	49	54	SAS	100%	10	15	SAS						
101551	F-398	USGS	885079.45	537946.86	Miami-Dade	43.3	48.3	SAS	100%	2	0						Not Used	sparse data
101550	F-410	USGS	885622.40	538959.38	Miami-Dade	56	61	SAS	100%	2	0						Not Used	sparse data
101557	F-411	USGS	886442.70	539367.60	Miami-Dade	51.3	56.3	SAS	100%	1	0						Not Used	sparse data
101565	F-45	USGS	918016.46	544327.87	Miami-Dade	79.9	84.9	SAS	100%	10	15	SAS						
111436	F-45	SFWMD	918016.75	544327.61	Miami-Dade	25	84.9	SAS	100%	10	15	SAS						

Table 4.1: Usage of SAJ Observation Database in Regional Model Calibration

Model ID[a]	Well Name	Data Source	Easting[b]	Northing[b]	County	Cased Depth (ft)	Drilled Depth (ft)	Dominant Layer[c]	% Open Section in Layer[c]	93/94 Months with Data[d]	03/04 Months with Data[e]	Use for Data in Model Setup/Calibration						Reasoning/Comments
													Observations for Calibration					
												Boundary Conditions[f]	Steady State (Oct 03)	Steady State (Feb 04)	Transient (03/04)	Transient (03/04	Not Used	
101522	F-469A	USGS	868314.46	508985.99	Miami-Dade	43	48	SAS	100%	2	0						Not Used	sparse data
101516	F-473	USGS	885724.88	502309.95	Miami-Dade	43	48	SAS	100%	2	0						Not Used	sparse data
101529	F-474	USGS	884561.53	514823.31	Miami-Dade	43	48	SAS	100%	2	0						Not Used	sparse data
111062	FRGPD2_G	SFWMD	799962.58	404458.33	Miami-Dade	9.08	11.08	SAS	100%	0	15	SAS						
101463	G-1000A	USGS	893853.90	487612.94	Miami-Dade	27	32	SAS	100%	2	0						Not Used	sparse data
101471	G-1002B	USGS	891908.53	492044.75	Miami-Dade	8.4	10.4	SAS	100%	2	0						Not Used	sparse data
101468	G-1009A	USGS	887975.87	491821.71	Miami-Dade	27	32	SAS	100%	1	0						Not Used	sparse data
101469	G-1009B	USGS	887975.87	491821.71	Miami-Dade	80	100	SAS	100%	0	2						Not Used	sparse data
101475	G-1010	USGS	887512.02	493030.80	Miami-Dade	12	14	SAS	100%	1	0						Not Used	sparse data
101467	G-1011A	USGS	882945.92	491492.32	Miami-Dade	27	32	SAS	100%	1	0						Not Used	sparse data
101477	G-1013	USGS	889429.31	493747.77	Miami-Dade	12	14	SAS	100%	2	0						Not Used	sparse data
101481	G-1014A	USGS	889058.54	494654.46	Miami-Dade	27	32	SAS	100%	2	0						Not Used	sparse data
101588	G-1047	USGS	933322.06	582352.35	Miami-Dade	12.4	14.4	SAS	100%	2	0						Not Used	sparse data
101591	G-1055	USGS	932020.01	586079.87	Miami-Dade	15.3	17.3	SAS	100%	2	0						Not Used	sparse data
101594	G-1060	USGS	927206.33	596651.11	Miami-Dade	10.7	12.7	SAS	100%	2	0						Not Used	sparse data
101506	G-1074B	USGS	874383.62	498855.89	Miami-Dade	40	45	SAS	100%	10	15	SAS						
111697	G-1074B_G	SFWMD	874383.78	498855.76	Miami-Dade	17	45	SAS	100%	10	15	SAS						
101505	G-1075A	USGS	874950.37	498720.70	Miami-Dade	27	32	SAS	100%	2	0						Not Used	sparse data
101504	G-1078A	USGS	876230.91	498727.16	Miami-Dade	27	32	SAS	100%	2	0						Not Used	sparse data
101511	G-1080A	USGS	878418.39	500252.73	Miami-Dade	27	32	SAS	100%	2	0						Not Used	sparse data
101582	G-1166	USGS	875861.17	568223.06	Miami-Dade	16	18	SAS	100%	10	0	SAS						
110822	G-1166_G	SFWMD	875861.55	568222.91	Miami-Dade	10.5	18	SAS	100%	10	0	SAS						
101438	G-1179	USGS	856455.37	422810.62	Miami-Dade	75	80	SAS	100%	9	3	SAS						
101440	G-1180	USGS	854713.12	423105.59	Miami-Dade	62	67	SAS	100%	10	5	SAS						
111844	G-1183	SFWMD	855807.00	420324.00	Miami-Dade	42	47	SAS	100%	10	15	SAS						
101435	G-1183	USGS	855807.15	420323.68	Miami-Dade	42	47	SAS	100%	10	15	SAS						
101428	G-1264	USGS	850245.47	397341.38	Miami-Dade	54.4	59.4	SAS	100%	9	0	SAS						
101439	G-1270	USGS	854804.74	423106.00	Miami-Dade	22	27	SAS	100%	10	0	SAS						
101563	G-1282	USGS	890074.52	543728.58	Miami-Dade	79	84	SAS	100%	10	11	SAS						
101537	G-1351	USGS	896062.47	534977.37	Miami-Dade	83	103	SAS	100%	9	9	SAS						
101543	G-1354	USGS	897604.88	537005.25	Miami-Dade	84	104	SAS	100%	2	11	SAS						
111343	G-1362_G	SFWMD	838671.29	464568.76	Miami-Dade	11	33	SAS	100%	10	15	SAS						
111340	G-1363	SFWMD	820180.27	439862.42	Miami-Dade	12	33	SAS	100%	10	15	SAS						
101445	G-1363	USGS	820180.30	439862.33	Miami-Dade	28	33	SAS	100%	10	15	SAS						
101567	G-1368A	USGS	890874.06	544878.88	Miami-Dade	34	39	SAS	100%	10	15	SAS						
111365	G-1368A_G	SFWMD	890874.36	544878.71	Miami-Dade	38.4	39	SAS	100%	10	15	SAS						
101561	G-1372	USGS	887073.22	541087.36	Miami-Dade	36.5	41.5	SAS	100%	2	0						Not Used	sparse data
101442	G-1486	USGS	841856.83	425512.20	Miami-Dade	27	32	SAS	100%	10	15	SAS						
111360	G-1486_G	SFWMD	841856.00	425714.00	Miami-Dade	27	32	SAS	100%	10	15	SAS						
101466	G-1487	USGS	821812.25	492566.81	Miami-Dade	7	9	SAS	100%	10	15	SAS						
111823	G-1487_G	SFWMD	821813.00	492567.00	Miami-Dade	18	20	SAS	100%	10	15	SAS						
101541	G-1488	USGS	826473.79	540236.38	Miami-Dade	18	20	SAS	100%	10	15	SAS						
111356	G-1488_G	SFWMD	826474.00	540237.00	Miami-Dade	18	20	SAS	100%	10	15	SAS						
101431	G-1502	USGS	793261.07	466320.54	Miami-Dade	26	31	SAS	100%	10	15	SAS						
111342	G-1502_B	SFWMD	793261.20	466320.65	Miami-Dade	11	31	SAS	100%	10	15	SAS						
101517	G-1555	USGS	868620.39	502525.89	Miami-Dade	30	35	SAS	100%	2	0						Not Used	sparse data
101465	G-1563	USGS	869685.88	490415.65	Miami-Dade	30	35	SAS	100%	2	0						Not Used	sparse data
101483	G-1599A	USGS	871767.03	495070.16	Miami-Dade	55	60	SAS	100%	2	0						Not Used	sparse data
101478	G-1599B	USGS	869760.53	493848.72	Miami-Dade	27	32	SAS	100%	2	0						Not Used	sparse data
101460	G-1604	USGS	881047.72	487040.12	Miami-Dade	57	62	SAS	100%	7	0	SAS						
101461	G-1604A	USGS	883883.45	487155.82	Miami-Dade	86.5	91.5	SAS	100%	2	0						Not Used	sparse data
140014	G-1633	DADE CO. via DEP	920287.53	578938.44	Miami-Dade	44	45	SAS	100%	10	0	SAS						
111278	G-1636_G	SFWMD	860347.35	588709.03	Miami-Dade	22	24	SAS	100%	10	15	SAS						
101592	G-1637	USGS	843351.77	588766.61	Miami-Dade	21	26	SAS	100%	10	15	SAS						
111335	G-1637_G	SFWMD	843352.23	588766.50	Miami-Dade	24	26	SAS	100%	10	15	SAS						
101476	G-176A	USGS	894187.30	493571.61	Miami-Dade	27	32	SAS	100%	1	0						Not Used	sparse data
101568	G-3	USGS	885757.17	544851.44	Miami-Dade	18	20	SAS	100%	10	14	SAS						
111602	G-3_G	SFWMD	885757.47	544851.27	Miami-Dade	11.7	20	SAS	100%	10	14	SAS						
112133	G-3061	SFWMD	890440.09	543986.40	Miami-Dade	955	1105	IAS/ICU	50%	0	15						Not Used	No calibration in IAS/ICU
101495	G-3073	USGS	866617.51	497000.40	Miami-Dade	18	20	SAS	100%	10	0	SAS						
110651	G-3073_G	SFWMD	866618.00	497000.00	Miami-Dade	18	20	SAS	100%	10	0	SAS						
101496	G-3074	USGS	866617.51	497000.40	Miami-Dade	35	40	SAS	100%	10	15	SAS						
111674	G-3074_G	SFWMD	866617.67	497000.30	Miami-Dade	38	40	SAS	100%	10	15	SAS						
101444	G-3162	USGS	857230.03	433717.72	Miami-Dade	87	92	SAS	100%	10	3	SAS						
140015	G-3189	DADE CO. via DEP	811448.94	479467.38	Miami-Dade	20	21	SAS	100%	10	0	SAS						
101530	G-3229	USGS	897269.20	515194.92	Miami-Dade	80	85	SAS	100%	2	11	SAS						
101566	G-3250	USGS	889523.02	544331.39	Miami-Dade	116	260	IAS/ICU	54%	0	11	SAS						
101575	G-3253	USGS	848744.88	548589.15	Miami-Dade	29.5	34.5	SAS	100%	10	15	SAS						
111603	G-3253_G	SFWMD	848552.34	548405.46	Miami-Dade	18	20	SAS	100%	10	15	SAS						

Table 4.1: Usage of SAJ Observation Database in Regional Model Calibration

Model ID[a]	Well Name	Data Source	Easting[b]	Northing[b]	County	Cased Depth (ft)	Drilled Depth (ft)	Dominant Layer[c]	% Open Section in Layer[c]	93/94 Months with Data[d]	03/04 Months with Data[e]	Use for Data in Model Setup/Calibration						Reasoning/Comments
													Observations for Calibration					
												Boundary Conditions[f]	Steady State (Oct 03)	Steady State (Feb 04)	Transient (03/04)	Transient (03/04	Not Used	
101573	G-3259A	USGS	853303.38	548325.98	Miami-Dade	55	60	SAS	100%	10	15	SAS						
111604	G-3259A_G	SFWMD	853303.72	548325.89	Miami-Dade	20	60	SAS	100%	10	15	SAS						
101574	G-3264A	USGS	863078.89	548472.59	Miami-Dade	45	50	SAS	100%	10	4	SAS						
110847	G-3264A_G	SFWMD	863079.22	548472.47	Miami-Dade	20	50	SAS	100%	10	4	SAS						
101457	G-3272	USGS	808027.90	484137.32	Miami-Dade	8	10	SAS	100%	0	15	SAS						
111843	G-3272	SFWMD	808577.64	484139.50	Miami-Dade	7.5	10	SAS	100%	0	15	SAS						
110615	G-3273	SFWMD	795898.93	471578.58	Miami-Dade	7.5	15	SAS	100%	1	0						Not Used	sparse data
101488	G-3284A	USGS	866361.72	496760.07	Miami-Dade	19	21	SAS	100%	2	0						Not Used	sparse data
101489	G-3284B	USGS	866361.72	496760.07	Miami-Dade	20	22	SAS	100%	2	0						Not Used	sparse data
101494	G-3286	USGS	866635.65	496862.36	Miami-Dade	19	21	SAS	100%	2	0						Not Used	sparse data
101492	G-3287	USGS	867001.53	496864.13	Miami-Dade	21	23	SAS	100%	2	0						Not Used	sparse data
101493	G-3287A	USGS	867001.53	496864.13	Miami-Dade	55	60	SAS	100%	2	0						Not Used	sparse data
101490	G-3288	USGS	867916.24	496868.57	Miami-Dade	20	22	SAS	100%	2	0						Not Used	sparse data
101491	G-3288A	USGS	867916.24	496868.57	Miami-Dade	19	21	SAS	100%	2	0						Not Used	sparse data
101486	G-3289	USGS	866270.74	496658.67	Miami-Dade	55	60	SAS	100%	2	0						Not Used	sparse data
101487	G-3290	USGS	866270.74	496658.67	Miami-Dade	11	13	SAS	100%	2	0						Not Used	sparse data
101538	G-3327	USGS	894120.39	536112.93	Miami-Dade	49	54	SAS	100%	10	15	SAS						
111312	G-3327_G	SFWMD	894120.66	536112.75	Miami-Dade	53	54	SAS	100%	10	15	SAS						
101535	G-3328	USGS	895606.09	531880.73	Miami-Dade	49	54	SAS	100%	10	0	SAS						
110826	G-3328_G	SFWMD	895606.35	531880.54	Miami-Dade	53	54	SAS	100%	10	0	SAS						
101536	G-3329	USGS	885180.54	532934.97	Miami-Dade	49	54	SAS	100%	10	15	SAS						
111311	G-3329_G	SFWMD	885180.81	532934.81	Miami-Dade	53	54.6	SAS	100%	10	15	SAS						
101420	G-3342	USGS	832717.63	378691.73	Miami-Dade	73	78	SAS	100%	8	0	SAS						
101424	G-3344	USGS	832140.76	385352.50	Miami-Dade	53	58	SAS	100%	7	0	SAS						
101432	G-3345	USGS	853039.18	408156.25	Miami-Dade	74	79	SAS	100%	6	0	SAS						
101427	G-3348	USGS	844757.74	394288.83	Miami-Dade	85	90	SAS	100%	8	0	SAS						
111417	G-3354_B	SFWMD	829224.78	357174.43	Miami-Dade	6	8	SAS	100%	7	15	SAS						
101423	G-3355	USGS	820842.46	385249.41	Miami-Dade	11	13	SAS	100%	10	15	SAS						
111850	G-3355_G	SFWMD	820842.00	385250.00	Miami-Dade	11	13	SAS	100%	10	15	SAS						
101426	G-3356	USGS	845010.66	395138.56	Miami-Dade	11	13	SAS	100%	10	15	SAS						
111839	G-3356_G	SFWMD	845013.00	394836.00	Miami-Dade	11	13	SAS	100%	10	15	SAS						
101514	G-3423	USGS	875033.71	500336.52	Miami-Dade	12	14	SAS	100%	2	0						Not Used	sparse data
101512	G-3430	USGS	874576.89	500233.26	Miami-Dade	13	15	SAS	100%	2	0						Not Used	sparse data
101447	G-3437	USGS	798719.50	448570.22	Miami-Dade	10.5	12.5	SAS	100%	10	15	SAS						
111829	G-3437_G	SFWMD	798719.56	448570.35	Miami-Dade	10.5	12.5	SAS	100%	10	15	SAS						
101523	G-3439	USGS	842589.40	511428.76	Miami-Dade	10	12	SAS	100%	8	15	SAS						
111696	G-3439_G	SFWMD	842589.63	511428.72	Miami-Dade	10	12	SAS	100%	8	15	SAS						
101539	G-3465	USGS	887266.01	536075.83	Miami-Dade	23.8	28.8	SAS	100%	10	15	SAS						
111848	G-3465_G	SFWMD	887266.28	536075.66	Miami-Dade	26.8	28.8	SAS	100%	10	15	SAS						
101545	G-3466	USGS	890550.10	537204.05	Miami-Dade	17.5	19.5	SAS	100%	10	15	SAS						
110746	G-3466_G	SFWMD	890550.00	537204.00	Miami-Dade	17.5	19.5	SAS	100%	10	0	SAS						
101547	G-3467	USGS	895390.96	537735.32	Miami-Dade	22.5	27.5	SAS	100%	10	15	SAS						
110745	G-3467_G	SFWMD	895391.00	537735.00	Miami-Dade	23	28	SAS	100%	10	0	SAS						
101515	G-3473	USGS	839337.04	502025.92	Miami-Dade	18.4	20.4	SAS	100%	10	15	SAS						
110764	G-3473	SFWMD	839338.00	502026.00	Miami-Dade	18.4	20.4	SAS	100%	10	0	SAS						
101540	G-354	USGS	896054.08	536491.80	Miami-Dade	85.2	90.2	SAS	100%	9	5	SAS						
110766	G-3549	SFWMD	870643.91	421907.59	Miami-Dade	6	11	SAS	100%	5	0						Not Used	sparse data
101437	G-3549	USGS	870644.31	421907.86	Miami-Dade	9	11	SAS	100%	5	15	SAS						
110765	G-3550	SFWMD	867816.59	419168.11	Miami-Dade	8	13	SAS	100%	5	0						Not Used	sparse data
101434	G-3550	USGS	867816.90	419168.37	Miami-Dade	11	13	SAS	100%	5	15	SAS						
101497	G-3551	USGS	822253.09	496909.58	Miami-Dade	16.3	18.3	SAS	100%	3	15	SAS						
111866	G-3551	SFWMD	822253.77	496909.90	Miami-Dade	13.3	18.3	SAS	100%	3	15	SAS						
101482	G-3552	USGS	827840.81	494912.13	Miami-Dade	17.4	19.4	SAS	100%	4	15	SAS						
110914	G-3552	SFWMD	827841.48	494912.46	Miami-Dade	14.4	19.4	SAS	100%	4	15	SAS						
101485	G-3553	USGS	829939.11	496333.83	Miami-Dade	17.9	19.9	SAS	100%	6	15	SAS						
111865	G-3553	SFWMD	829939.77	496334.18	Miami-Dade	14.9	19.9	SAS	100%	6	15	SAS						
101484	G-3554	USGS	833232.14	496347.09	Miami-Dade	18	20	SAS	100%	6	15	SAS						
111354	G-3554	SFWMD	833232.78	496347.46	Miami-Dade	15	20	SAS	100%	6	15	SAS						
101473	G-3555	USGS	835078.60	492215.42	Miami-Dade	17	19	SAS	100%	5	15	SAS						
111353	G-3555	SFWMD	835079.26	492215.80	Miami-Dade	14	19	SAS	100%	5	15	SAS						
101503	G-3556	USGS	830479.46	498456.07	Miami-Dade	17.1	19.1	SAS	100%	0	15	SAS						
101474	G-3557	USGS	822178.55	492467.24	Miami-Dade	17.5	19.5	SAS	100%	4	15	SAS						
111864	G-3557	SFWMD	822179.24	492467.55	Miami-Dade	14.5	19.5	SAS	100%	4	15	SAS						
101519	G-3558	USGS	827518.28	507126.57	Miami-Dade	17	19	SAS	100%	4	15	SAS						
111891	G-3558	SFWMD	827518.90	507126.91	Miami-Dade	14	19	SAS	100%	4	15	SAS						
101527	G-3559	USGS	821731.54	513767.28	Miami-Dade	17.5	19.5	SAS	100%	4	15	SAS						
111890	G-3559	SFWMD	821732.17	513767.60	Miami-Dade	14.5	19.5	SAS	100%	4	15	SAS						
101472	G-3560	USGS	830688.69	491894.75	Miami-Dade	17.5	19.5	SAS	100%	4	15	SAS						
111351	G-3560	SFWMD	830689.36	491895.11	Miami-Dade	14.5	19.5	SAS	100%	4	15	SAS						

Table 4.1: Usage of SAJ Observation Database in Regional Model Calibration

Model ID[a]	Well Name	Data Source	Easting[b]	Northing[b]	County	Cased Depth (ft)	Drilled Depth (ft)	Dominant Layer[c]	% Open Section in Layer[c]	93/94 Months with Data[d]	03/04 Months with Data[e]	Use for Data in Model Setup/Calibration						Reasoning/Comments
													Observations for Calibration					
												Boundary Conditions[f]	Steady State (Oct 03)	Steady State (Feb 04)	Transient (03/04)	Transient (03/04	Not Used	
101462	G-3561	USGS	839535.55	487458.70	Miami-Dade	17	19	SAS	100%	6	15	SAS						
111726	G-3561	SFWMD	839582.69	487287.67	Miami-Dade	14	19	SAS	100%	6	15	SAS						
101578	G-3562	USGS	901152.37	553214.78	Miami-Dade	16.6	18.6	SAS	100%	0	15	SAS						
101521	G-3563	USGS	872420.11	507427.61	Miami-Dade	16.1	18.1	SAS	100%	0	14	SAS						
101562	G-3564	USGS	905421.66	541628.46	Miami-Dade	16.8	18.8	SAS	100%	0	15	SAS						
101508	G-3565	USGS	852155.28	499053.02	Miami-Dade	17	19	SAS	100%	0	15	SAS						
101569	G-3566	USGS	876527.99	544904.42	Miami-Dade	16	18	SAS	100%	0	15	SAS						
101584	G-3567	USGS	841699.59	569678.02	Miami-Dade	16.7	18.7	SAS	100%	0	15	SAS						
101533	G-3568	USGS	866105.28	527285.61	Miami-Dade	14.8	16.8	SAS	100%	0	15	SAS						
101532	G-3570	USGS	889732.98	519228.57	Miami-Dade	16.7	18.7	SAS	100%	0	15	SAS						
101590	G-3571	USGS	886006.48	583824.15	Miami-Dade	16.5	18.5	SAS	100%	0	15	SAS						
101524	G-3572	USGS	853374.49	512586.90	Miami-Dade	17.4	19.4	SAS	100%	0	15	SAS						
101528	G-3574	USGS	821273.98	513866.50	Miami-Dade	4.8	6.8	SAS	100%	0	15	SAS						
101500	G-3575	USGS	822067.07	497716.52	Miami-Dade	6.95	8.95	SAS	100%	0	15	SAS						
101525	G-3576	USGS	816154.32	513645.43	Miami-Dade	7.64	9.64	SAS	100%	0	15	SAS						
101501	G-3577	USGS	820694.64	497812.27	Miami-Dade	6	8	SAS	100%	0	15	SAS						
101502	G-3578	USGS	816485.93	498099.44	Miami-Dade	3.99	5.99	SAS	100%	0	15	SAS						
111887	G-3619	SFWMD	799739.73	380360.62	Miami-Dade	10.75	12	SAS	100%	0	15	SAS						
101421	G-3619	USGS	799766.47	380229.26	Miami-Dade	10	12	SAS	100%	0	15	SAS						
101422	G-3620	USGS	810211.75	383192.02	Miami-Dade	10	12	SAS	100%	0	15	SAS						
111886	G-3620	SFWMD	817956.50	377020.18	Miami-Dade	10.75	12	SAS	100%	0	15	SAS						
111885	G-3622	SFWMD	798499.49	423563.71	Miami-Dade	10.75	12	SAS	100%	0	15	SAS						
101441	G-3622	USGS	798525.02	423836.23	Miami-Dade	10	12	SAS	100%	0	15	SAS						
101453	G-3626	USGS	817239.52	467411.87	Miami-Dade	10	12	SAS	100%	0	15	SAS						
111616	G-3627	SFWMD	819862.25	463778.87	Miami-Dade	10.75	12	SAS	100%	0	15	SAS						
101451	G-3627	USGS	819998.39	463989.67	Miami-Dade	10	12	SAS	100%	0	15	SAS						
101449	G-3628	USGS	809581.56	458601.32	Miami-Dade	10	12	SAS	100%	0	15	SAS						
111874	G-3628	SFWMD	809582.38	458601.56	Miami-Dade	10.75	12	SAS	100%	0	15	SAS						
101534	G-3676	USGS	845436.74	529512.54	Miami-Dade	28	33	SAS	100%	0	15	SAS						
101576	G-3760	USGS	842429.75	548580.68	Miami-Dade	67.69	72.69	SAS	100%	0	15	SAS						
101577	G-3761	USGS	842429.75	548580.68	Miami-Dade	14.3	16.3	SAS	100%	0	15	SAS						
111199	G-3778	SFWMD	821444.82	513814.69	Miami-Dade	101.59	103.59	SAS	100%	0	12	SAS						
111200	G-3779	SFWMD	821445.53	513795.81	Miami-Dade	52.39	54.39	SAS	100%	0	12	SAS						
111201	G-3780	SFWMD	821445.24	513777.14	Miami-Dade	31.61	33.61	SAS	100%	0	12	SAS						
111198	G-3781	SFWMD	821447.34	513753.82	Miami-Dade	16.79	18.79	SAS	100%	0	12	SAS						
111191	G-3784	SFWMD	822062.23	497704.85	Miami-Dade	98.44	100.44	SAS	100%	0	12	SAS						
111202	G-3785	SFWMD	822061.18	497715.04	Miami-Dade	42.64	44.64	SAS	100%	0	12	SAS						
111203	G-3786	SFWMD	822063.32	497683.85	Miami-Dade	26.61	28.61	SAS	100%	0	11	SAS						
111196	G-3787	SFWMD	822063.73	497672.34	Miami-Dade	17.16	19.16	SAS	100%	0	11	SAS						
101520	G-432	USGS	891645.19	506884.99	Miami-Dade	94.5	99.5	SAS	100%	9	11	SAS						
101564	G-440A	USGS	884774.89	543700.24	Miami-Dade	8.4	10.4	SAS	100%	2	0						Not Used	sparse data
101555	G-548	USGS	894028.55	539206.69	Miami-Dade	92.3	97.3	SAS	100%	9	11	SAS						
101480	G-551	USGS	855195.87	494220.85	Miami-Dade	75	80	SAS	100%	10	15	SAS						
111673	G-551_G	SFWMD	855196.03	494220.78	Miami-Dade	71	80	SAS	100%	10	15	SAS						
101479	G-551B	USGS	853751.12	493975.02	Miami-Dade	59.4	64.4	SAS	100%	2	0						Not Used	sparse data
101455	G-553	USGS	874115.13	479369.53	Miami-Dade	86	91	SAS	100%	10	15	SAS						
111646	G-553_G	SFWMD	874115.76	479370.12	Miami-Dade	79	91	SAS	100%	10	15	SAS						
101544	G-570	USGS	894862.69	537091.01	Miami-Dade	82	87	SAS	100%	3	0						Not Used	sparse data
101548	G-571	USGS	893396.62	537789.71	Miami-Dade	89.5	94.5	SAS	100%	9	11	SAS						
101553	G-576	USGS	898509.71	538625.76	Miami-Dade	92.3	97.3	SAS	100%	9	0	SAS						
101546	G-577	USGS	892668.29	537280.90	Miami-Dade	93.7	98.7	SAS	100%	3	0						Not Used	sparse data
101458	G-580A	USGS	885889.14	485285.54	Miami-Dade	20	22	SAS	100%	10	15	SAS						
111884	G-580A	SFWMD	885889.25	485285.39	Miami-Dade	4	22	SAS	100%	10	15	SAS						
110647	G-594_G	SFWMD	836340.84	562790.01	Miami-Dade	13.9	20	SAS	100%	4	0	SAS						
101456	G-596	USGS	816938.91	474477.58	Miami-Dade	14	16	SAS	100%	10	15	SAS						
111824	G-596_B	SFWMD	816939.66	474477.87	Miami-Dade	11	16	SAS	100%	10	15	SAS						
101425	G-613	USGS	813302.91	390774.27	Miami-Dade	18	20	SAS	100%	10	15	SAS						
111363	G-613_B	SFWMD	810205.84	390419.11	Miami-Dade	18.4	21	SAS	100%	10	15	SAS						
101446	G-614	USGS	839129.08	442461.10	Miami-Dade	18	20	SAS	100%	10	15	SAS						
111339	G-614_G	SFWMD	839129.05	442461.12	Miami-Dade	18.1	20	SAS	100%	10	15	SAS						
101531	G-618	USGS	787883.56	519204.01	Miami-Dade	18	20	SAS	100%	10	15	SAS						
111358	G-618_B	SFWMD	787884.28	519204.25	Miami-Dade	10.5	19.7	SAS	100%	10	15	SAS						
101459	G-620	USGS	733090.39	484748.44	Miami-Dade	14.6	16.6	SAS	100%	9	15	SAS						
111841	G-620_B	SFWMD	733090.69	484748.64	Miami-Dade	6	16	SAS	100%	9	15	SAS						
111341	G-757A	SFWMD	827984.00	458468.00	Miami-Dade	28	33	SAS	100%	10	15	SAS						
101448	G-757A	USGS	827984.21	458467.79	Miami-Dade	28	33	SAS	100%	10	15	SAS						
101436	G-789	USGS	802473.92	421123.48	Miami-Dade	18	20	SAS	100%	10	15	SAS						
111822	G-789_G	SFWMD	802473.87	421123.64	Miami-Dade	10	20	SAS	100%	10	15	SAS						
101510	G-847A	USGS	854913.56	499836.07	Miami-Dade	27	32	SAS	100%	2	0						Not Used	sparse data

Table 4.1: Usage of SAJ Observation Database in Regional Model Calibration

Model ID[a]	Well Name	Data Source	Easting[b]	Northing[b]	County	Cased Depth (ft)	Drilled Depth (ft)	Dominant Layer[c]	% Open Section in Layer[c]	93/94 Months with Data[d]	03/04 Months with Data[e]	Use for Data in Model Setup/Calibration						Reasoning/Comments
													Observations for Calibration					
												Boundary Conditions[f]	Steady State (Oct 03)	Steady State (Feb 04)	Transient (03/04)	Transient (03/04	Not Used	
101585	G-852	USGS	927241.91	574068.36	Miami-Dade	18	20	SAS	100%	10	15	SAS						
111825	G-852_G	SFWMD	927242.00	574068.00	Miami-Dade	18	20	SAS	100%	10	15	SAS						
101464	G-855	USGS	831707.20	488870.16	Miami-Dade	18	20	SAS	100%	10	15	SAS						
111344	G-855_G	SFWMD	831707.35	488870.16	Miami-Dade	10	20	SAS	100%	10	15	SAS						
101454	G-860	USGS	879293.33	468896.02	Miami-Dade	18	20	SAS	100%	10	15	SAS						
111650	G-860_G	SFWMD	879293.38	468895.90	Miami-Dade	10.5	20	SAS	100%	10	15	SAS						
101429	G-864	USGS	820598.85	401400.82	Miami-Dade	18	20	SAS	100%	10	15	SAS						
111362	G-864_G	SFWMD	820599.00	401401.00	Miami-Dade	7	20	SAS	100%	10	15	SAS						
110701	G-864A	SFWMD	818309.57	400988.80	Miami-Dade	7	20	SAS	100%	10	0	SAS						
101430	G-864A	USGS	819404.14	402203.99	Miami-Dade	18	20	SAS	100%	10	15	SAS						
101513	G-877A	USGS	869912.23	500210.09	Miami-Dade	27	32	SAS	100%	2	0						Not Used	sparse data
101498	G-881	USGS	874043.28	497201.71	Miami-Dade	18	20	SAS	100%	2	0						Not Used	sparse data
101509	G-884A	USGS	873941.70	499220.45	Miami-Dade	27	32	SAS	100%	1	0						Not Used	sparse data
101583	G-894	USGS	924822.29	569172.50	Miami-Dade	71	76	SAS	100%	5	2	SAS						
101470	G-896	USGS	892915.38	491949.25	Miami-Dade	69	74	SAS	100%	9	11	SAS						
101499	G-901	USGS	892519.84	497399.13	Miami-Dade	91	96	SAS	100%	8	11	SAS						
101452	G-939	USGS	883443.90	466153.37	Miami-Dade	55.2	60.2	SAS	100%	2	2						Not Used	sparse data
101518	G-958A	USGS	854621.20	503772.23	Miami-Dade	27	32	SAS	100%	2	0						Not Used	sparse data
101589	G-968	USGS	837899.36	582988.52	Miami-Dade	45	50	SAS	100%	10	15	SAS						
111357	G-968_G	SFWMD	837900.00	582989.00	Miami-Dade	45	50	SAS	100%	10	15	SAS						
101593	G-970	USGS	860967.55	589048.75	Miami-Dade	13	15	SAS	100%	10	15	SAS						
111854	G-970_G	SFWMD	860968.00	589048.62	Miami-Dade	10	15	SAS	100%	10	15	SAS						
101586	G-972	USGS	838842.21	575925.32	Miami-Dade	13	15	SAS	100%	10	0	SAS						
110682	G-972_G	SFWMD	838842.55	575925.76	Miami-Dade	10	15	SAS	100%	10	0	SAS						
101580	G-973	USGS	867414.06	558791.52	Miami-Dade	13	15	SAS	100%	10	15	SAS						
111605	G-973_G	SFWMD	867414.42	558791.39	Miami-Dade	10	15	SAS	100%	10	15	SAS						
101579	G-975	USGS	833435.19	558537.79	Miami-Dade	13	15	SAS	100%	10	15	SAS						
111855	G-975_G	SFWMD	833435.58	558537.72	Miami-Dade	10	15	SAS	100%	10	15	SAS						
101572	G-976	USGS	845110.58	541424.22	Miami-Dade	13	15	SAS	100%	10	14	SAS						
110849	G-976_G	SFWMD	845111.00	541425.00	Miami-Dade	10	15	SAS	100%	10	14	SAS						
110624	HUMBLE_G	SFWMD	810074.49	448608.74	Miami-Dade	13.13	15.13	SAS	100%	10	15	SAS						
140016	NWW5B	DADE CO. via DEP	854625.68	542743.71	Miami-Dade	20	25	SAS	100%	10	0	SAS						
110623	RUTZKE_G	SFWMD	796393.51	431400.94	Miami-Dade	10.09	12.09	SAS	100%	10	0	SAS						
101587	S-18	USGS	905480.67	578884.28	Miami-Dade	47	52	SAS	100%	10	13	SAS						
111406	S-18_G	SFWMD	905481.00	578884.00	Miami-Dade	47	52	SAS	100%	10	13	SAS						
111648	S-182_G	SFWMD	866705.00	459848.00	Miami-Dade	46	51	SAS	100%	10	15	SAS						
101450	S-182A	USGS	866705.15	459848.38	Miami-Dade	46	51	SAS	100%	10	15	SAS						
101542	S-19	USGS	887443.94	536985.43	Miami-Dade	90	95	SAS	100%	10	15	SAS						
111364	S-19_G	SFWMD	887444.22	536985.26	Miami-Dade	91	95	SAS	100%	10	15	SAS						
101443	S-196A	USGS	821509.74	427349.09	Miami-Dade	18	20	SAS	100%	10	15	SAS						
111847	S-196A	SFWMD	821510.00	427349.00	Miami-Dade	18	20	SAS	100%	10	15	SAS						
101554	S-1B	USGS	889734.65	538981.38	Miami-Dade	35	40	SAS	100%	2	0						Not Used	sparse data
101556	S-68	USGS	890994.46	539528.57	Miami-Dade	56	61	SAS	100%	10	15	SAS						
111366	S-68	SFWMD	890994.74	539528.39	Miami-Dade	51	61	SAS	100%	10	15	SAS						
101552	S-8B	USGS	888549.37	538470.17	Miami-Dade	42	47	SAS	100%	2	0						Not Used	sparse data
101570	S-9A	USGS	884767.95	545012.75	Miami-Dade	40.3	45.3	SAS	100%	2	0						Not Used	sparse data
111037	SYLVA_G	SFWMD	888699.00	517836.00	Miami-Dade	44.2	49.2	SAS	100%	10	15	SAS						
112105	WASANMZ1	SFWMD	936511.00	576823.00	Miami-Dade	1050	1150	UF	100%	0	15		UF	UF	UF			no 93/94 data
112106	WASANMZ2	SFWMD	936510.96	576823.27	Miami-Dade	1410	1510	APPZ	54%	0	8						Not Used	apparent data error
112104	WASASMZ2	SFWMD	871467.29	443172.18	Miami-Dade	1790	1890	MC2	100%	0	15						Not Used	Model geology puts this well in MC2
110083	KRFNNC	SFWMD	593828.10	1255811.77	Oceola	60.9	65.9	IAS/ICU	100%	10	3						Not Used	No calibration in IAS/ICU
111184	ARS B0_G	SFWMD	707647.88	1085645.31	Okeechobee	3.85	5.85	SAS	100%	10	15	SAS						
110187	BASING_G	SFWMD	652451.86	1115905.51	Okeechobee	6.46	8.46	SAS	100%	10	15	SAS						
100949	BASS WELL N OF BASINGER	USGS	652653.50	1135380.28	Okeechobee	915	1015	MC1	100%	1	2						Not Used	Model geology puts this well in MC1
110167	BASSETT_G	SFWMD	681741.26	1118740.87	Okeechobee	8.12	10.12	SAS	100%	10	15	SAS						
100947	DIXIE RANCH	USGS	682499.06	1091361.52	Okeechobee	886	986	MC1	100%	10	0						Not Used	Model geology puts this well in MC1
110093	GRIFFITH_G	SFWMD	679020.56	1149032.49	Okeechobee	5.88	7.88	SAS	100%	10	10	SAS						
100948	JONES WELL S DARK HAMMOCK RD	USGS	725676.36	1102318.41	Okeechobee	412	962	IAS/ICU	41%	9	0						Not Used	Open section straddles multiple layers
110207	KRAFFM	SFWMD	602830.55	1138130.94	Okeechobee	36.37	40.37	SAS	100%	0	15	SAS						
110206	KRAFFS	SFWMD	602825.25	1138139.93	Okeechobee	21.45	23.45	SAS	100%	0	15	SAS						
110228	KRANND	SFWMD	601928.81	1137476.80	Okeechobee	91.86	95.86	SAS	100%	0	15	SAS						
110227	KRANNM	SFWMD	601935.55	1137467.90	Okeechobee	44.52	48.52	SAS	100%	0	15	SAS						
110226	KRANNS	SFWMD	601937.52	1137458.51	Okeechobee	19.4	24.2	SAS	100%	0	15	SAS						
110166	KRBNND	SFWMD	600686.35	1136892.31	Okeechobee	94.01	98.01	SAS	100%	0	15	SAS						
110249	KRBNNM	SFWMD	600679.43	1136901.41	Okeechobee	44.63	48.63	SAS	100%	0	15	SAS						
110248	KRBNNS	SFWMD	600670.88	1136910.31	Okeechobee	25.95	29.95	SAS	100%	0	15	SAS						
110230	KRCFFM	SFWMD	595940.71	1147561.77	Okeechobee	37.77	41.77	SAS	100%	0	15	SAS						
110229	KRCFFS	SFWMD	595935.32	1147572.68	Okeechobee	20.81	24.81	SAS	100%	0	15	SAS						
110210	KRCNND	SFWMD	595270.56	1147179.96	Okeechobee	81.51	85.51	SAS	100%	0	15	SAS						

Table 4.1: Usage of SAJ Observation Database in Regional Model Calibration

Model ID[a]	Well Name	Data Source	Easting[b]	Northing[b]	County	Cased Depth (ft)	Drilled Depth (ft)	Dominant Layer[c]	% Open Section in Layer[c]	93/94 Months with Data[d]	03/04 Months with Data[e]	Use for Data in Model Setup/Calibration						Reasoning/Comments
													Observations for Calibration					
												Boundary Conditions[f]	Steady State (Oct 03)	Steady State (Feb 04)	Transient (03/04)	Transient (03/04	Not Used	
110209	KRCNNM	SFWMD	595268.23	1147189.66	Okeechobee	38.62	42.62	SAS	100%	0	15	SAS						
110208	KRCNNS	SFWMD	595260.23	1147196.64	Okeechobee	16	20	SAS	100%	0	15	SAS						
110132	MAXCEY S_G	SFWMD	623652.00	1166003.21	Okeechobee	6	8	SAS	100%	10	15	SAS						
120337	OK0001	SJRWMD	719451.88	1162089.00	Okeechobee	125	960	UF	51%	10	0						UF	no 03/04 data
120462	OK0018		652710.77	1135496.77	Okeechobee	0	255	SAS	81%	0	0						Not Used	Missing data
120463	OK0019		626041.62	1133284.73	Okeechobee	0	0	Error	0%	0	0						Not Used	Data error
120464	OK0037		592651.03	1151804.79	Okeechobee	0	0	Error	0%	0	0						Not Used	Data error
120465	OK0043		725734.23	1102434.37	Okeechobee	412	962	IAS/ICU	41%	0	0						Not Used	Open section straddles multiple layers
120466	OK0046		724851.38	1196140.70	Okeechobee	0	0	Error	0%	0	0						Not Used	Data error
100951	OK-1 WELL AT FORT DRUM, FL	USGS	719725.62	1159766.84	Okeechobee	860	960	MC1	100%	10	15						Not Used	Model geology puts this well in MC1
111209	OK-2	SFWMD	650017.55	1110150.14	Okeechobee	18	21	SAS	100%	10	15	SAS						
110268	OK-3_G	SFWMD	719095.32	1148267.59	Okeechobee	19	22	SAS	100%	10	15	SAS						
112221	OKF-0018	SFWMD	652723.99	1135495.01	Okeechobee	255	1015	UF	43%	1	0						Not Used	Open section straddles multiple layers
112109	OKF-100	SFWMD	698055.00	1025471.00	Okeechobee	565	1350	APPZ	40%	0	9				UF			OKF-100 has been split into UF and MF sections, with very similar heads. Use for UF
112167	OKF-101	SFWMD	708302.82	1041117.13	Okeechobee	372	800	IAS/ICU	54%	0	6						Not Used	No calibration in IAS/ICU
112222	OKF-17	SFWMD	682570.05	1091477.77	Okeechobee	538	986	UF	53%	1	0						Not Used	sparse data
100946	OKF-23 NR LIVESTOCK MARKET	USGS	703455.53	1061490.89	Okeechobee	825	925	MC1	100%	10	2						Not Used	Model geology puts this well in MC1
100945	OKF-31	USGS	706716.19	1052002.90	Okeechobee	979	1079	MC1	100%	10	2						Not Used	Model geology puts this well in MC1
112223	OKF-31		706716.19	1052002.90	Okeechobee	475	1079	MC1	49%	0	0						Not Used	Open section straddles multiple layers
112224	OKF-34	SFWMD	648495.80	1164880.11	Okeechobee	276	1143	UF	48%	1	0						Not Used	Open section straddles multiple layers
112134	OKF-42	SFWMD	618563.38	1115013.95	Okeechobee	370	1152	MC1	59%	1	7						Not Used	Model geology puts this well in MC1
100950	OKF-42 EXP WELL S65C	USGS	592594.95	1151688.30	Okeechobee	1052	1152	APPZ	100%	1	2						Not Used	sparse data
112226	OKF-54	SFWMD	682141.15	1197504.02	Okeechobee	260	973	UF	58%	1	0						Not Used	sparse data
112227	OKF-7	SFWMD	725748.21	1102434.52	Okeechobee	412	963	IAS/ICU	41%	1	0						Not Used	Open section straddles multiple layers
111027	OPAL_G	SFWMD	729113.09	1086284.15	Okeechobee	8	10	SAS	100%	8	15	SAS						
110091	PEAVINE_G	SFWMD	648586.59	1168919.22	Okeechobee	7	9	SAS	100%	10	10	SAS						
110081	ROCK K_G	SFWMD	712098.46	1172013.84	Okeechobee	52.37	57.37	SAS	100%	10	15	SAS						
112135	TCRK_GW1	SFWMD	725886.34	1056130.64	Okeechobee	990	1075	MC1	100%	0	15						Not Used	Model geology puts this well in MC1
112136	TCRK_GW2	SFWMD	725886.34	1056130.64	Okeechobee	1275	1700	APPZ	75%	0	15				APPZ			Seems to be a data error in the middle of the 0304 dataset. Keep it in transient set for shape comparison only
120168	6037	SJRWMD	457951.00	1514072.00	Orange	19.64	21.64	SAS	100%	10	0	SAS						
120169	6038	SJRWMD	457338.00	1513806.00	Orange	17.68	32.68	SAS	100%	10	0	SAS						
120170	6039	SJRWMD	457877.00	1513227.00	Orange	20.71	22.71	SAS	100%	10	0	SAS						
120257	7-01	SJRWMD	453027.00	1498840.00	Orange	45.39	50.39	SAS	100%	10	0	SAS						
120262	7-06	SJRWMD	454278.00	1498094.00	Orange	48.87	53.87	SAS	100%	10	0	SAS						
120266	7-10	SJRWMD	453035.00	1498085.00	Orange	20	30	SAS	100%	10	0	SAS						
120267	7-11	SJRWMD	453319.00	1497855.00	Orange	20	30	SAS	100%	10	0	SAS						
100992	82912802	USGS	503765.00	1511054.14	Orange	317	337	MC1	100%	1	2						Not Used	Model geology puts this well in MC1
100956	24S29E34 TELY	USGS	526004.59	1464311.92	Orange	317	434	APPZ	53%	1	0						Not Used	sparse data
100961	24S31E23 29-FT SHALLOW AT MOSS PARK FL	USGS	594713.55	1470201.89	Orange	24	29	SAS	100%	1	2						Not Used	sparse data
100960	24S31E23 480-FT WELL AT MOSS PARK FL	USGS	594713.55	1470201.89	Orange	460	480	APPZ	100%	1	2						Not Used	sparse data
110464	AIR19_G	SFWMD	542389.02	1479520.91	Orange	25.56	30.56	SAS	100%	0	15	SAS						
100974	BAY LAKE DEEP WELL NEAR WINDERMERE, FL	USGS	473291.48	1487554.73	Orange	203	223	UF	100%	10	15		UF	UF	UF	UF		
110130	BEELINE_G	SFWMD	598931.96	1497364.00	Orange	7.9	9.9	SAS	100%	10	15	SAS						
100955	BOGGY CREEK ROAD WELL AT COUNTY LINE NEAR TAFT FL	USGS	556701.33	1459275.57	Orange	199	400	UF	58%	10	15						Not Used	Only 58% of open inteval is in UF. Located in unimportant area (between recharge and boundary)
100966	COCOA 11 NR BITHLO FL	USGS	625623.79	1476527.86	Orange	480	580	APPZ	77%	1	0						Not Used	sparse data
100973	COCOA 1-T NEAR BITHLO FL	USGS	625362.78	1485213.61	Orange	180	200	IAS/ICU	100%	8	5						Not Used	outside IAS (per Miller, 1997)
100983	COCOA 2 NR BITHLO FL	USGS	625635.58	1491475.09	Orange	517	617	MC2	68%	1	0						Not Used	Outside Boundary
100975	COCOA 7 NR BITHLO FL	USGS	625632.23	1487233.30	Orange	470	490	APPZ	100%	1	0						Not Used	sparse data
100985	COCOA 9 NR BITHLO FL	USGS	625638.61	1495312.90	Orange	425	525	APPZ	100%	1	0						Not Used	Outside Boundary
100965	COCOA A WELL NEAR BITHLO, FL	USGS	634712.70	1476321.99	Orange	301	516	MC1	42%	10	15	APPZ						averaged with 120051
100978	COCOA B WELL NEAR BITHLO FL	USGS	613668.66	1487446.58	Orange	415	515	APPZ	100%	8	4						Not Used	Sparse data
100979	COCOA C (ZONE 1) WELL NEAR BITHLO FL	USGS	611347.46	1487550.20	Orange	1257	1357	LF	97%	8	5	BZ						Model geology puts this in LF; moved to BZ based on communication with SFWMD
100980	COCOA C (ZONE 3) WELL NEAR BITHLO FL	USGS	611347.46	1487550.20	Orange	1124	1224	LF	100%	8	5	LF						averaged with 120052, 120078, 100969
100981	COCOA C (ZONE 4) WELL NEAR BITHLO FL	USGS	611347.46	1487550.20	Orange	950	1050	MC2	90%	8	5						Not Used	Model geology puts this well in MC2
100982	COCOA C (ZONE 5) WELL NEAR BITHLO FL	USGS	611347.46	1487550.20	Orange	904	1004	MC2	100%	8	5						Not Used	Model geology puts this well in MC2
100977	COCOA D WELL NEAR NARCOOSSEE FL	USGS	602933.80	1487461.83	Orange	226	300	UF	76%	10	15	UF						
100987	COCOA F WELL NEAR BITHLO FL	USGS	625374.77	1500261.89	Orange	200	375	UF	68%	9	0						Not Used	Outside Boundary
100989	COCOA H NEAR BITHLO, FL	USGS	647510.78	1507118.28	Orange	252	495	MC1	51%	9	15						Not Used	Outside Boundary
100990	COCOA K NEAR BITHLO, FL	USGS	647510.78	1507118.28	Orange	6	8	SAS	100%	9	5	SAS						
100972	COCOA M WELL NEAR BITHLO FL	USGS	625362.78	1485213.61	Orange	8	10	SAS	100%	8	5	SAS						
100984	COCOA P WELL NEAR TAFT FL	USGS	572499.29	1492767.45	Orange	419	439	MC1	100%	10	14						Not Used	Model geology puts this well in MC1
100969	COCOA R WELL NEAR BITHLO FL	USGS	604728.96	1478771.86	Orange	1105	1205	LF	100%	7	4	LF						averaged with 120052, 100980, 120078
100976	COCOA-O WELL NEAR BITHLO FL	USGS	625543.03	1487334.36	Orange	85	90	SAS	100%	8	5	SAS						

Table 4.1: Usage of SAJ Observation Database in Regional Model Calibration

Model ID[a]	Well Name	Data Source	Easting[b]	Northing[b]	County	Cased Depth (ft)	Drilled Depth (ft)	Dominant Layer[c]	% Open Section in Layer[c]	93/94 Months with Data[d]	03/04 Months with Data[e]	Use for Data in Model Setup/Calibration						Reasoning/Comments
													Observations for Calibration					
												Boundary Conditions[f]	Steady State (Oct 03)	Steady State (Feb 04)	Transient (03/04)	Transient (03/04	Not Used	
100959	DISNEY SHALLOW WELL AT TREE FARM NEAR VINELAND, FL	USGS	466318.44	1467591.08	Orange	16	18	SAS	100%	10	15	SAS						
100964	E USGS W HARTZOG LK Buena Vista, FL	USGS	456914.14	1475614.30	Orange	97	117	IAS/ICU	55%	1	2						Not Used	No calibration in IAS/ICU
100957	LAKE OLIVER DEEP WELL NEAR VINELAND, FL	USGS	448447.60	1466874.64	Orange	103	318	UF	78%	10	15		UF	UF	UF	UF		
100958	LAKE OLIVER SHALLOW WELL NEAR VINELAND, FL	USGS	448447.60	1466874.64	Orange	33	38	SAS	100%	10	15	SAS						
100986	LAKE SAWYER WELL NEAR WINDERMERE, FL	USGS	472907.32	1500686.07	Orange	158	178	UF	100%	10	15		UF	UF	UF	UF		
110181	MOSSPK_D	SFWMD	594782.95	1470304.77	Orange	240	480	UF	45%	0	15						Not Used	Open section straddles multiple layers
110311	MOSSPK_S	SFWMD	594782.95	1470304.77	Orange	26	29	SAS	100%	0	15	SAS						
100971	OBSER W COCOA 1 NR BITHLO FL	USGS	625362.78	1485213.61	Orange	610	710	MC2	100%	8	0						Not Used	Outside Boundary
120467	OR0003	SJRWMD	647420.26	1507118.88	Orange	252	495	MC1	51%	9	14						Not Used	Outside Boundary
120673	OR0025	SJRWMD	625362.78	1485213.61	Orange	610	710	MC2	100%	8	0						Not Used	Outside Boundary
120470	OR0029	SJRWMD	673459.28	1477029.94	Orange	244	390	UF	100%	10	15						Not Used	Duplicate with 100967
120471	OR0030		556776.00	1459478.05	Orange	199	400	UF	57%	0	0						Not Used	Missing data
120474	OR-0064		448432.16	1466875.57	Orange	103	318	UF	78%	0	0						Not Used	Missing data
120087	OR0082	SJRWMD	602933.80	1487461.83	Orange	226	300	UF	76%	10	0						Not Used	Duplicate with 100977
120476	OR0104		518679.09	1525343.57	Orange	137	400	MC1	52%	0	0						Not Used	Outside Boundary
120560	OR0121		526056.92	1464417.39	Orange	317	434	APPZ	53%	0	0						Not Used	Missing data
120561	OR0248		647567.95	1507220.62	Orange	6	8	SAS	100%	0	0						Not Used	Outside Boundary
120036	OR0265	SJRWMD	625579.46	1500494.32	Orange	200	375	UF	68%	9	12						Not Used	Outside Boundary
120060	OR-0465	SJRWMD	536035.57	1536998.24	Orange	2060	2090	BZ	100%	8	15	BZ						location and depth data not provided by SAJ - source: DBHYDRO
120059	OR-0467	SJRWMD	536306.25	1537602.68	Orange	954	1159	MC2	62%	8	15	LF						location and depth data not provided by SAJ - source: DBHYDRO, assuming station 83312216 is OR-0467
120566	OR0508		684598.23	1508139.57	Orange	152	335	UF	100%	0	0						Not Used	Outside Boundary
120053	OR0613	SJRWMD	618639.70	1487388.78	Orange	1430	1500	LC	100%	0	15	BZ						
120052	OR0614	SJRWMD	618639.70	1487388.78	Orange	1170	1250	LF	100%	0	15	LF						averaged with 100980, 120078 and 100969
120051	OR0615	SJRWMD	618650.42	1487391.80	Orange	900	1050	MC2	100%	0	15	APPZ						averaged with 100965
120346	OR0662	SJRWMD	515568.19	1615040.23	Orange	150	180	SAS	100%	0	15	SAS						
120079	OR-0668	SJRWMD	593337.00	1515350.00	Orange	1490	1537	LC	100%	0	15	BZ						location and depth data not provided by SAJ - source: DBHYDRO
120081	OR0669	SJRWMD	650975.03	1476090.08	Orange	295	315	UF	100%	0	15	UF						
120082	OR0673	SJRWMD	650975.03	1476090.08	Orange	450	540	APPZ	53%	0	15	APPZ						
120083	OR0675	SJRWMD	650975.03	1476090.08	Orange	620	840	MC2	100%	0	15						Not Used	Model geology puts this well in MC2
120078	OR-0676	SJRWMD	593335.24	1515450.47	Orange	1269	1300	LF	100%	0	15	LF						location and depth data not provided by SAJ - source: DBHYDRO
120591	OR0740		634643.62	1476219.29	Orange	301	516	MC1	42%	0	0						Not Used	Open section straddles multiple layers
120595	OR0826		539204.42	1498408.58	Orange	0	0	Error	0%	0	0						Not Used	Data error
120100	OR0827	SJRWMD	537416.32	1521247.79	Orange	365	460	MC1	100%	0	8	UF						
120101	OR0829	SJRWMD	537416.32	1521247.79	Orange	1029	1208	LF	81%	0	5						Not Used	Outside Boundary
120638	OR0883		656757.42	1513686.07	Orange	3	8	SAS	100%	0	0						Not Used	Outside Boundary
120639	OR0884		656757.42	1513686.07	Orange	85	90	SAS	100%	0	0						Not Used	Outside Boundary
120640	OR0886		656701.63	1513581.05	Orange	240	345	UF	99%	0	0						Not Used	Outside Boundary
110190	ORF-29	SFWMD	457250.04	1475816.30	Orange	68	166	UF	59%	0	15						Not Used	Many nearby wells with greater proportion of open interval in UF.
110165	ORF-61	SFWMD	484377.19	1504604.68	Orange	142	650	APPZ	35%	0	10	APPZ						
110193	ORH-1	SFWMD	484377.19	1504604.68	Orange	52	92	SAS	63%	0	10	SAS						
110257	ORS-0029	SFWMD	457250.04	1475816.30	Orange	25	30	SAS	100%	0	15	SAS						
110161	ORS-1	SFWMD	532361.35	1494509.20	Orange	20	30	SAS	100%	0	15	SAS						
110194	ORS-3	SFWMD	484300.54	1504606.53	Orange	22	51	SAS	100%	0	10	SAS						
140023	OV-02S	SFWMD via DEP	525949.00	1487632.29	Orange	18	28	SAS	100%	0	0						Not Used	sparse data
140024	OV-03S	SFWMD via DEP	525965.31	1481865.29	Orange	14	15	SAS	100%	0	0						Not Used	sparse data
140025	OV-04	SFWMD via DEP	536308.73	1477014.35	Orange	5	15	SAS	100%	0	0						Not Used	sparse data
140026	OV-06	SFWMD via DEP	547548.70	1475637.95	Orange	6	16	SAS	100%	0	0						Not Used	sparse data
100988	PALM LAKE DRIVE WELL NEAR WINDERMERE, FL	USGS	493283.52	1506755.63	Orange	215	235	UF	100%	10	15	UF						
100967	PALMETTO WELL NEAR BITHLO, FL	USGS	673402.67	1476923.63	Orange	244	390	UF	100%	10	15	UF						
100968	RCID OBSER. WELL NO. 1	USGS	487380.22	1477893.55	Orange	261	281	UF	100%	1	2						Not Used	sparse
100962	RIBS 2 SHALLOW WELL 16 NR VINELAND	USGS	458233.19	1471567.53	Orange	30.2	35.2	SAS	100%	2	0						Not Used	sparse data
100963	RIBS II SHAL WELL 15	USGS	456914.14	1475614.30	Orange	19.3	21.3	SAS	100%	2	0						Not Used	sparse data
100993	ROSS WELL ON LK BUTLER	USGS	473968.51	1512496.35	Orange	260	280	MC1	96%	1	2						Not Used	Model geology puts this well in MC1
100970	SEA WORLD DRIVE REPLACEMENT WELL NEAR VINELAND, FL	USGS	503448.51	1481970.32	Orange	219	239	UF	100%	10	15		UF	UF	UF	UF		
110160	SKYLAKE_G	SFWMD	532363.72	1494509.34	Orange	100	400	MC1	42%	0	15	APPZ						
110095	TAFT_G	SFWMD	536787.57	1491446.69	Orange	5	7	SAS	100%	10	15	SAS						
110280	TB1_G	SFWMD	482511.00	1494294.00	Orange	25	30	SAS	100%	0	15	SAS						
110281	TB2_G	SFWMD	483596.00	1495309.00	Orange	25	30	SAS	100%	0	15	SAS						
110306	TB3_G	SFWMD	484053.00	1496076.00	Orange	25	30	SAS	100%	0	15	SAS						

Table 4.1: Usage of SAJ Observation Database in Regional Model Calibration

Model ID[a]	Well Name	Data Source	Easting[b]	Northing[b]	County	Cased Depth (ft)	Drilled Depth (ft)	Dominant Layer[c]	% Open Section in Layer[c]	93/94 Months with Data[d]	03/04 Months with Data[e]	Use for Data in Model Setup/Calibration						Reasoning/Comments
													Observations for Calibration					
												Boundary Conditions[f]	Steady State (Oct 03)	Steady State (Feb 04)	Transient (03/04)	Transient (03/04	Not Used	
100991	TOSOHATCHEE GAME PRESERVE NR CHRISTMAS,FL	USGS	684275.94	1507228.54	Orange	152	335	UF	100%	1	2						Not Used	Outside Boundary
110396	TURLAK_G	SFWMD	503070.68	1515087.92	Orange	123.69	143.69	IAS/ICU	62%	0	15						Not Used	No calibration in IAS/ICU
101027	25S 29E09 OS U.L. (USGS)	USGS	522209.24	1451801.30	Osceola	1100	1200	LF	54%	10	2					LF		sparse 03/04 data
110196	ALL1W1	SFWMD	577715.09	1405008.91	Osceola	8	10	SAS	100%	0	15	SAS						
110195	ALL1W2	SFWMD	577715.09	1405008.91	Osceola	18	20	SAS	100%	0	15	SAS						
110199	ALL2W1	SFWMD	578893.98	1404997.87	Osceola	8	10	SAS	100%	0	15	SAS						
110198	ALL2W2	SFWMD	578893.98	1404997.87	Osceola	18	20	SAS	100%	0	15	SAS						
101014	ASHTON FORESTRY TOWER WELL AT ASHTON FL	USGS	580596.25	1421951.72	Osceola	380	400	MC1	100%	10	15						Not Used	Model geology puts this well in MC1
110238	BLACKW1	SFWMD	577641.53	1406516.12	Osceola	5	10	SAS	100%	0	15	SAS						
110237	BLACKW2	SFWMD	577641.53	1406516.12	Osceola	15	20	SAS	100%	0	15	SAS						
101009	CANOE CREEK CAMPGROUND (OSF-18) NR ST CLOUD FL	USGS	567923.02	1394003.36	Osceola	400	500	MC1	100%	10	0						Not Used	Model geology puts this well in MC1
110211	CASTW1	SFWMD	612581.85	1395621.31	Osceola	5	10	SAS	100%	0	15	SAS						
110219	CASTW2	SFWMD	612581.85	1395621.31	Osceola	15	20	SAS	100%	0	15	SAS						
101011	CECIL WHALEY WELL	USGS	541908.88	1404170.03	Osceola	482	582	APPZ	90%	10	2					APPZ		sparse 03/04 data
110078	CHAPMAN_G	SFWMD	593670.91	1333366.11	Osceola	6	8	SAS	100%	10	1	SAS						
110136	ELMAX_G	SFWMD	631171.52	1242843.40	Osceola	5	7	SAS	100%	10	15	SAS						
110189	EXOTGW	SFWMD	619088.89	1389349.30	Osceola	15	20	SAS	100%	0	15	SAS						
101019	FLORIDA POWER WELL	USGS	480186.58	1427628.55	Osceola	241	261	MC1	100%	10	0						Not Used	Model geology puts this well in MC1
101006	HOLOPAW TEST WELL NO 1 NEAR HOLOPAW, FL	USGS	638441.80	1383808.72	Osceola	997	1097	MC2	100%	10	15						Not Used	Model geology puts this well in MC2
110263	IC-HCU		493875.41	1426099.48	Osceola	50	55	IAS/ICU	100%	0	0						Not Used	No calibration in IAS/ICU
110260	IC-SAS	SFWMD	493982.29	1426090.49	Osceola	18	20	SAS	100%	0	15	SAS						
100999	JOE OVERSTREET WELL (OSF-4) NEAR ST CLOUD FL	USGS	584415.26	1309440.92	Osceola	287	400	UF	84%	10	13						Not Used	Open section completely in UF at nearby well (101199)
110197	KENANS1_G	SFWMD	650315.20	1292317.58	Osceola	8	10	SAS	100%	10	10	SAS						
101024	LAKE JOEL WELL NEAR ASHTON FL	USGS	605278.49	1437266.52	Osceola	389	740	MC2	43%	10	15						Not Used	Open section straddles multiple layers
101023	LAKE POINSETT NR ROCKLEDGE,FL	USGS	699976.14	1432911.28	Osceola	233	253	UF	100%	1	2						Not Used	Sparse data
131236	LOUGHMAN DEEP	SWFWMD	469260.91	1427483.51	Osceola	85	250	UF	73%	2	0						Not Used	sparse data
101017	LOUGHMAN DEEP WELL NEAR LOUGHMAN FL	SWFWMD	469333.31	1427592.68	Osceola	85	250	UF	73%	10	4					UF		Sparse 03/04 data
131237	LOUGHMAN SHALLOW	SWFWMD	469267.18	1427486.51	Osceola	29	32	SAS	100%	10	4	SAS						
101018	LOUGHMAN SHALLOW WELL NEAR LOUGHMAN FL		469267.19	1427487.52	Osceola	29	32	SAS	100%	0	0						Not Used	Missing data
110218	MAKO	SFWMD	582810.19	1432573.48	Osceola	15	20	SAS	100%	0	15	SAS						
110128	MAXCEY N_G	SFWMD	648506.07	1217692.19	Osceola	7	9	SAS	100%	10	15	SAS						
101013	MERCANTILE LANE (OS254) NEAR KISSIMMEE FL	USGS	500100.60	1420776.96	Osceola	308	328	MC1	100%	10	15						Not Used	Model geology puts this well in MC1
120643	OS0001		605263.57	1437269.07	Osceola	389	740	MC2	43%	0	0						Not Used	Open section straddles multiple layers
120022	OS0004	SJRWMD	672492.95	1341076.42	Osceola	202	343	UF	61%	0	15						Not Used	nearby well (120025) falls completely in UF
120023	OS0016	SJRWMD	671463.69	1360788.39	Osceola	230	600	UF	69%	10	0					UF		no 03/04 data
120024	OS0017	SJRWMD	678539.60	1361599.64	Osceola	210	380	UF	92%	10	0					UF		no 03/04 data
120021	OS0018	SJRWMD	672992.15	1347357.91	Osceola	235	400	UF	90%	10	0						Not Used	Duplicate with 101002
120020	OS0019	SJRWMD	673501.33	1336592.10	Osceola	240	400	UF	91%	10	15			UF	UF	UF		This area has a pretty steep drop in Oct 03 (see 120072) so since the only point for this well is 10/21, it is removed from the Oct 03 dataset
120295	OS0022	SJRWMD	653838.63	1374816.63	Osceola	700	900	APPZ	54%	10	15		APPZ	APPZ	APPZ	APPZ		
120296	OS0023	SJRWMD	653838.63	1374816.63	Osceola	396	520	UF	66%	9	15						Not Used	Nearby wells (120651, 120025) fall completely in UF
120030	OS0024	SJRWMD	653885.62	1374997.35	Osceola	36	50	SAS	100%	10	15	SAS						
120031	OS0025	SJRWMD	653885.62	1374997.35	Osceola	1470	1480	LC	100%	4	15		LF	LF	LF	LF		Model geology puts this in the LC, but DBHYDRO puts this in the LF.
120025	OS0026	SJRWMD	654128.28	1374979.16	Osceola	280	300	UF	100%	10	0					UF		no 03/04 data
120026	OS0027	SJRWMD	654128.28	1374979.16	Osceola	700	915	APPZ	50%	0	2						Not Used	sparse data
120650	OS0028	SJRWMD	654062.94	1374856.17	Osceola	1050	1054	MC2	100%	0	2						Not Used	Model geology puts this well in MC2
120027	OS0030	SJRWMD	654128.28	1374979.16	Osceola	221	241	IAS/ICU	100%	10	0						Not Used	No calibration in IAS/ICU
120651	OS0031	SJRWMD	653724.89	1375827.63	Osceola	360	460	UF	100%	0	2						Not Used	Sparse data
120652	OS0033		700033.25	1433018.94	Osceola	0	253	IAS/ICU	43%	0	0						Not Used	Open section straddles multiple layers
120653	OS0038		664850.72	1230519.16	Osceola	218	767	UF	59%	0	0						Not Used	Missing data
120654	OS0047		639635.47	1325948.51	Osceola	242	405	UF	69%	0	0						Not Used	Missing data
120655	OS0050		500152.46	1420882.28	Osceola	110	328	UF	56%	0	0						Not Used	Missing data
120656	OS0051		660692.48	1432792.49	Osceola	246	377	UF	100%	0	0						Not Used	Missing data
120657	OS0052		641558.69	1432792.49	Osceola	288	405	UF	100%	0	0						Not Used	Missing data
120089	OS0069	SJRWMD	668880.93	1384198.16	Osceola	220	422	UF	79%	1	15						Not Used	nearby well (120025) falls completely in UF
120659	OS0075		689662.28	1222655.60	Osceola	325	590	UF	82%	0	0						Not Used	Missing data
120660	OS0082		543155.89	1383773.24	Osceola	0	0	Error	0%	0	0						Not Used	Data error
120661	OS0084		687184.41	1399982.80	Osceola	0	0	Error	0%	0	0						Not Used	Data error
120662	OS0090		643124.19	1295147.38	Osceola	0	0	Error	0%	0	0						Not Used	Data error
120664	OS0179		686134.18	1371098.34	Osceola	13	18	SAS	100%	0	0						Not Used	Missing data

Table 4.1: Usage of SAJ Observation Database in Regional Model Calibration

Model ID[a]	Well Name	Data Source	Easting[b]	Northing[b]	County	Cased Depth (ft)	Drilled Depth (ft)	Dominant Layer[c]	% Open Section in Layer[c]	93/94 Months with Data[d]	03/04 Months with Data[e]	Use for Data in Model Setup/Calibration						Reasoning/Comments
													Observations for Calibration					
												Boundary Conditions[f]	Steady State (Oct 03)	Steady State (Feb 04)	Transient (03/04)	Transient (03/04	Not Used	
120063	OS0227	SJRWMD	650031.00	1262861.53	Osceola	15	25	SAS	100%	0	15	SAS						
120073	OS0228	SJRWMD	669437.05	1270635.90	Osceola	20	30	SAS	100%	0	15	SAS						
120064	OS0229	SJRWMD	650031.00	1262861.53	Osceola	215	235	IAS/ICU	100%	0	15						Not Used	No calibration in IAS/ICU
120062	OS0230	SJRWMD	650031.00	1262861.53	Osceola	352	392	UF	100%	0	15		UF	UF	UF			no 93/94 data
120072	OS0231	SJRWMD	669437.05	1270635.90	Osceola	360	420	UF	100%	0	15		UF	UF	UF			no 93/94 data
120074	OS0232	SJRWMD	669437.05	1270635.90	Osceola	62	72	SAS	100%	0	7	SAS						
120086	OS0238	SJRWMD	674839.96	1418958.44	Osceola	173	373	UF	63%	1	15						Not Used	nearby well (120025) falls completely in UF
101026	OS-171 WELL NEAR DEER PARK, FL	SJRWMD	685737.41	1438051.97	Osceola	13	19	SAS	100%	5	15	SAS						
110290	OS-183_G	SFWMD	650039.12	1262931.93	Osceola	22	27	SAS	100%	10	15	SAS						
110188	OSF-101	SFWMD	511852.20	1438600.58	Osceola	160	210	UF	100%	0	15		UF	UF	UF			no 93/94 data
110158	OSF-102	SFWMD	519438.81	1389291.15	Osceola	156	202	UF	100%	0	15		UF	UF	UF			no 93/94 data
120672	OSF-4		584469.12	1309551.87	Osceola	287	400	UF	84%	0	0						Not Used	Missing data
100996	OSF-42	USGS	664793.98	1230405.61	Osceola	218	767	UF	59%	10	2					UF		sparse 03/04 data
110234	OSF-52	SFWMD	592067.96	1261155.76	Osceola	172	880	MC1	61%	0	15						Not Used	Model geology puts this well in MC1
110202	OSF-53	SFWMD	543170.90	1383770.80	Osceola	160	963	MC2	47%	0	15						Not Used	Open section straddles multiple layers
101005	OSF-53 S-61 963-FT WELL NEAR ALCOMA FL	USGS	543102.26	1383664.99	Osceola	863	963	MC2	100%	10	0						Not Used	Model geology puts this well in MC2
110214	OSF53_GW1	SFWMD	542992.66	1383740.16	Osceola	14.35	24.35	SAS	100%	0	15	SAS						
110203	OSF53_GW2	SFWMD	542992.66	1383740.16	Osceola	47.76	57.76	IAS/ICU	100%	0	15						Not Used	No calibration in IAS/ICU
100995	OSF-60A TEST WELL AT YEEHAW JUNCTION, FL	USGS	689604.12	1222541.92	Osceola	305	325	IAS/ICU	100%	10	15						Not Used	No calibration in IAS/ICU
110221	OSF-62	SFWMD	641676.23	1296604.37	Osceola	260	630	UF	58%	0	15						Not Used	Open interval of nearby wells (100997, 120062, 120072) fall completely within UF
100998	OSF-62 TEST WELL nr Kenansville, FL	USGS	643067.30	1295037.71	Osceola	55	60	SAS	100%	10	0	SAS						
110259	OSF62_GW1	SFWMD	641676.23	1296604.37	Osceola	18.04	28.04	SAS	100%	0	15	SAS						
110258	OSF62_GW2	SFWMD	641676.23	1296604.37	Osceola	52.89	62.89	SAS	100%	0	15	SAS						
110222	OSF-64	SFWMD	565998.00	1359130.00	Osceola	310	610	MC1	88%	0	15						Not Used	Model geology puts this well in MC1
101003	OSF-64 TEST WELL (OSS-64D 100 FT) NR SOUTH PORT FL	USGS	569814.54	1358854.12	Osceola	80	100	IAS/ICU	100%	10	0						Not Used	No calibration in IAS/ICU
110233	OSF64_GW1	SFWMD	565998.03	1359130.00	Osceola	19.43	29.43	SAS	100%	0	15	SAS						
110223	OSF64_GW2	SFWMD	565998.00	1359130.00	Osceola	92.15	102.15	IAS/ICU	100%	0	15						Not Used	No calibration in IAS/ICU
110220	OSF-66	SFWMD	594949.39	1342655.05	Osceola	570	670	MC1	100%	0	15						Not Used	Model geology puts this well in MC1
101001	OSF-66 TEST WELL (670 FT) NEAR HOLOPAW FL	USGS	594602.57	1342952.02	Osceola	570	670	MC1	100%	10	0						Not Used	Model geology puts this well in MC1
110213	OSF66_GW1	SFWMD	594949.39	1342655.05	Osceola	21.21	31.21	SAS	100%	0	15	SAS						
110212	OSF66_GW2	SFWMD	594949.39	1342655.05	Osceola	69.24	79.24	SAS	100%	0	15	SAS						
101010	OSF-68 TEST WELL	USGS	613747.21	1395643.65	Osceola	400	500	MC1	54%	10	2						Not Used	Model geology puts this well in MC1
110201	OSF-70	SFWMD	550508.11	1424597.87	Osceola	130	470	MC1	40%	0	15						Not Used	Open section straddles multiple layers
101016	OSF-70 TEST WELL (OSS-70D,55-FT) NR ST CLOUD FL	USGS	550105.95	1424345.61	Osceola	73	78	IAS/ICU	100%	10	0						Not Used	No calibration in IAS/ICU
110200	OSF70_GW1	SFWMD	550508.11	1424597.87	Osceola	16.52	26.52	SAS	100%	0	15	SAS						
110224	OSF70_GW2	SFWMD	550508.11	1424597.87	Osceola	45.13	55.13	IAS/ICU	100%	0	15						Not Used	No calibration in IAS/ICU
110505	OSF-82L	SFWMD	550374.73	1424546.73	Osceola	1230	1503	LF	96%	0	9				LF	LF		Dataset begins 4/27/2004
110491	OSF-82U	SFWMD	550374.73	1424546.73	Osceola	350	583	APPZ	59%	0	3						Not Used	only 3 months of data
110262	OSF-97	SFWMD	493982.24	1426090.34	Osceola	2000	2096	BZ	100%	0	15		BZ	BZ	BZ			Although this is screened in BZ, it's TDS matches the upper BZ or LC layers, so it is placed in the LC for the model (no 93/94 data)
110264	OSF-98	SFWMD	493982.24	1426090.34	Osceola	1220	1501	LF	90%	0	15		LF	LF	LF	LF		
110261	OSF-99	SFWMD	493982.24	1426090.34	Osceola	354	675	APPZ	93%	0	15		APPZ	APPZ	APPZ			no 93/94 data
110236	OSS-72	SFWMD	592067.90	1261155.33	Osceola	105	120	IAS/ICU	100%	0	15						Not Used	No calibration in IAS/ICU
110235	OSS-73	SFWMD	592067.96	1261155.76	Osceola	12	15	SAS	100%	0	15	SAS						
110102	PINE ISL_G	SFWMD	615406.25	1374944.09	Osceola	5.5	10.5	SAS	100%	10	15	SAS						
110110	POINCI_G	SFWMD	499738.96	1447444.36	Osceola	9.39	11.39	SAS	100%	10	15	SAS						
101008	REEDY CREEK OVERLOOK WELL (OSF-11) NR DEER PARK FL	USGS	511069.31	1388012.35	Osceola	378	398	MC1	100%	10	15						Not Used	Model geology puts this well in MC1
101197	S-65 WELL NEAR KENANSVILLE FL	USGS	591960.00	1260752.09	Osceola	750	850	MC1	94%	10	15						Not Used	Model geology puts this well in MC1
101020	SHINGLE CREEK AT STATE HWY 531A NEAR KISSIMMEE, FL	USGS	516053.10	1429805.93	Osceola	180	200	UF	100%	10	15		UF	UF	UF	UF		
101025	SOUTH EAGLE ROAD GROVE WELL AT NARCOOSSEE FL	USGS	582861.73	1437702.34	Osceola	454	474	APPZ	100%	10	13			APPZ	APPZ	APPZ		no Oct03 data
101015	ST CLOUD POWER PLANT WELL (OSF-44) NR ST CLOUD FL	USGS	563428.27	1423301.70	Osceola	514	614	MC2	54%	10	2						Not Used	Model geology puts this well in MC2
110084	SUNGW	SFWMD	562532.31	1396260.58	Osceola	18	20	SAS	100%	0	8	SAS						
101002	TEST HOLE 8NR DEER PARK,FL	USGS	672743.00	1347754.82	Osceola	235	400	UF	90%	10	2					UF		sparse 03/04 data
101000	TH-10 WILLIAMS ROAD WELL NEAR HOLOPAW, FL	USGS	639581.10	1325840.26	Osceola	242	405	UF	69%	9	15						Not Used	Open interval of nearby well (100997) falls completely within UF
101021	TH-3 LAKE POINSETT SW NEAR NEW EDEN, FL	USGS	660637.04	1432684.90	Osceola	340	360	UF	100%	10	15		UF	UF	UF	UF		
101012	TH-4 DEER PARK NW	USGS	674680.64	1418752.10	Osceola	173	373	UF	63%	1	2						Not Used	sparse data
101007	TH-6 DEER PARK NW	USGS	668699.30	1384109.69	Osceola	220	422	UF	78%	1	2						Not Used	sparse data

Table 4.1: Usage of SAJ Observation Database in Regional Model Calibration

Model ID[a]	Well Name	Data Source	Easting[b]	Northing[b]	County	Cased Depth (ft)	Drilled Depth (ft)	Dominant Layer[c]	% Open Section in Layer[c]	93/94 Months with Data[d]	03/04 Months with Data[e]	Use for Data in Model Setup/Calibration						Reasoning/Comments
													Observations for Calibration					
												Boundary Conditions[f]	Steady State (Oct 03)	Steady State (Feb 04)	Transient (03/04)	Transient (03/04	Not Used	
101022	TH-9 NOVA ROAD 532 WEST (OSF-93) NEAR NEW EDEN, FL	USGS	641503.84	1432687.41	Osceola	288	405	UF	100%	10	15		UF	UF	UF	UF		
110184	TOHO1_GW	SFWMD	555547.65	1396041.74	Osceola	32	42	SAS	100%	0	15	SAS						
110204	TOHO1_GW2	SFWMD	555547.65	1396041.74	Osceola	108	118	IAS/ICU	100%	0	15						Not Used	No calibration in IAS/ICU
110169	TOHO10_GW	SFWMD	543295.40	1406485.47	Osceola	16	26	SAS	100%	0	15	SAS						
110150	TOHO12_GW	SFWMD	561669.44	1453805.97	Osceola	20	30	SAS	100%	0	15	SAS						
110149	TOHO13_GW	SFWMD	575792.78	1434265.95	Osceola	20	30	SAS	100%	0	15	SAS						
110256	TOHO14_GW	SFWMD	569848.86	1385256.09	Osceola	20	30	SAS	100%	0	15	SAS						
110168	TOHO15_GW	SFWMD	572732.82	1401045.65	Osceola	66	76	IAS/ICU	71%	0	15	SAS						
110217	TOHO16_W1	SFWMD	568717.72	1393533.63	Osceola	15	25	SAS	100%	0	15	SAS						
110216	TOHO16_W2	SFWMD	568717.72	1393533.63	Osceola	60	75	IAS/ICU	81%	0	15	SAS						
110215	TOHO2_GW	SFWMD	557190.47	1395300.20	Osceola	18	28	SAS	100%	0	15	SAS						
110156	TOHO3_GW		539245.27	1376074.83	Osceola	36	46	SAS	71%	0	0						Not Used	Missing data
110155	TOHO4_GW	SFWMD	530178.16	1386181.12	Osceola	20	30	SAS	100%	0	15	SAS						
110153	TOHO5_GW	SFWMD	514587.76	1405459.13	Osceola	74	84	IAS/ICU	100%	0	15						Not Used	No calibration in IAS/ICU
110152	TOHO6_GW	SFWMD	519440.85	1403599.79	Osceola	20	30	SAS	100%	0	15	SAS						
110151	TOHO7_GW	SFWMD	519679.68	1440603.50	Osceola	20	30	SAS	100%	0	15	SAS						
110242	TOHO8_GW	SFWMD	523957.00	1440281.00	Osceola	53	63	IAS/ICU	100%	0	15						Not Used	No calibration in IAS/ICU
120663	USGS OBSER W OS179 AT DEER PARK, FL.	SJRWMD	685842.09	1437987.82	Osceola	13	19	SAS	100%	0	8	SAS						
101004	USGS OBSER W OS179 AT DEER PARK, FL.	USGS	686075.98	1370990.34	Osceola	13	18	SAS	100%	6	5	SAS						
100997	WELL AT LK MARIAN, NEAR KENANSVILLE, FL	USGS	639385.07	1286455.21	Osceola	300	320	UF	100%	10	9						Not Used	USGS places this in IAS
110241	WR6_GW1	SFWMD	523176.59	1374340.31	Osceola	17.6	19.6	SAS	100%	0	15	SAS						
110240	WR8_GW1	SFWMD	521644.28	1371416.84	Osceola	21.04	23.04	SAS	100%	0	15	SAS						
110239	WR9_GW1	SFWMD	521021.26	1372529.87	Osceola	19.9	21.9	SAS	100%	0	15	SAS						
110704	CA2A-159	SFWMD	837942.06	744226.47	Palm Beach	6.71	8.71	SAS	100%	10	0	SAS						
110924	ENR001W1	SFWMD	859960.36	854585.42	Palm Beach	85	90	SAS	100%	0	15	SAS						
111049	ENR001W2	SFWMD	859960.36	854585.42	Palm Beach	59.97	64.97	SAS	100%	0	15	SAS						
110880	ENR102GW	SFWMD	847551.00	841331.00	Palm Beach	38.28	40.28	SAS	100%	0	12	SAS						
111218	ENR103GW	SFWMD	844744.00	837612.00	Palm Beach	35.51	37.51	SAS	100%	0	15	SAS						
111032	ENR202R3	SFWMD	837792.50	841760.59	Palm Beach	57	62	SAS	100%	0	15	SAS						
111048	ENR202W1	SFWMD	837792.50	841760.59	Palm Beach	170.9	190.9	IAS/ICU	84%	0	15	SAS						
111015	ENR202W2	SFWMD	837792.50	841760.59	Palm Beach	85	90	SAS	100%	0	15	SAS						
111047	ENR202W4	SFWMD	837792.50	841760.59	Palm Beach	21.85	26.85	SAS	100%	0	15	SAS						
111024	ENR203GW	SFWMD	841199.00	839963.00	Palm Beach	35.87	37.87	SAS	100%	0	15	SAS						
111046	ENR204GW	SFWMD	844573.00	842799.00	Palm Beach	35.44	37.44	SAS	100%	0	15	SAS						
111045	ENR303GW	SFWMD	839365.00	828172.00	Palm Beach	34.37	36.37	SAS	100%	0	15	SAS						
111020	ENR401GW	SFWMD	839173.00	835033.00	Palm Beach	35.61	37.61	SAS	100%	0	15	SAS						
110891	MOP2GW1	SFWMD	837258.39	821586.72	Palm Beach	99.65	101.65	SAS	100%	0	15	SAS						
110883	MOP2GW2	SFWMD	837258.39	821586.72	Palm Beach	57.26	59.26	SAS	100%	0	15	SAS						
110892	MOP2GW3	SFWMD	837258.39	821586.72	Palm Beach	29.5	31.5	SAS	100%	0	15	SAS						
110886	MP1-A	SFWMD	847386.10	836209.77	Palm Beach	99.48	101.48	SAS	100%	0	15	SAS						
110888	MP1-B	SFWMD	847386.10	836209.77	Palm Beach	58.03	60.03	SAS	100%	0	15	SAS						
110889	MP1-C	SFWMD	847386.10	836209.77	Palm Beach	18.61	20.61	SAS	100%	0	15	SAS						
110899	MP2-A	SFWMD	843297.16	838391.36	Palm Beach	98.9	100.9	SAS	100%	0	15	SAS						
110897	MP2-B	SFWMD	843297.16	838391.36	Palm Beach	60.8	62.8	SAS	100%	0	15	SAS						
110895	MP2-C	SFWMD	843297.16	838391.36	Palm Beach	23.8	25.8	SAS	100%	0	15	SAS						
101031	PB-1063	USGS	941575.51	726798.25	Palm Beach	114	134	SAS	100%	10	0	SAS						
101108	PB-1089	USGS	934842.25	863579.08	Palm Beach	220	240	SAS	100%	4	0						Not Used	sparse data
101073	PB-1097	USGS	908661.34	798685.23	Palm Beach	140	160	SAS	100%	4	0						Not Used	sparse data
101066	PB-1107	USGS	910882.65	776887.79	Palm Beach	85	105	SAS	100%	10	0	SAS						
101051	PB-1108	USGS	905940.27	752119.28	Palm Beach	180	200	IAS/ICU	100%	10	0						Not Used	No calibration in IAS/ICU
111131	PB-1108	SFWMD	906014.96	752248.36	Palm Beach	80	90	SAS	100%	0	11	SAS						
101099	PB-1152	USGS	892039.84	846855.14	Palm Beach	95	115	SAS	100%	4	0						Not Used	sparse data
101101	PB-1153	USGS	907435.47	851489.09	Palm Beach	40	45	SAS	100%	4	0						Not Used	sparse data
101096	PB-1155	USGS	926040.48	836256.51	Palm Beach	75	80	SAS	100%	10	0	SAS						
101107	PB-1157	USGS	907913.22	862498.66	Palm Beach	80	100	SAS	100%	3	0						Not Used	sparse data
101036	PB-1455	USGS	946794.39	735315.84	Palm Beach	137	157	SAS	100%	1	0						Not Used	sparse data
101046	PB-1456	USGS	955274.58	745371.82	Palm Beach	161	181	SAS	100%	1	0						Not Used	sparse data
101047	PB-1457	USGS	957715.71	747408.75	Palm Beach	173	193	SAS	100%	1	12	SAS						
101048	PB-1491	USGS	941237.16	747826.88	Palm Beach	118	138	SAS	100%	10	15	SAS						
111849	PB-1491_G	SFWMD	941237.82	747826.44	Palm Beach	88	138	SAS	100%	10	15	SAS						
101050	PB-1493	USGS	946234.10	750660.53	Palm Beach	13	15	SAS	100%	0	0						Not Used	sparse data
110637	PB-1495_G	SFWMD	959006.23	755826.19	Palm Beach	18	23	SAS	100%	10	0	SAS						
140028	PB-1521	PALM BEACH CO. via DEP	935139.37	927199.98	Palm Beach	20	22	SAS	100%	1	0						Not Used	sparse data
140029	PB-1524	PALM BEACH CO. via DEP	909627.95	937941.59	Palm Beach	10	20	SAS	100%	1	0						Not Used	sparse data
101129	PB-1525	USGS	914040.65	927163.84	Palm Beach	20	22	SAS	100%	4	0						Not Used	sparse data
101111	PB-1534	USGS	893912.32	884328.65	Palm Beach	20	22	SAS	100%	4	0						Not Used	sparse data

Table 4.1: Usage of SAJ Observation Database in Regional Model Calibration

Model ID[a]	Well Name	Data Source	Easting[b]	Northing[b]	County	Cased Depth (ft)	Drilled Depth (ft)	Dominant Layer[c]	% Open Section in Layer[c]	93/94 Months with Data[d]	03/04 Months with Data[e]	Use for Data in Model Setup/Calibration						Reasoning/Comments
													Observations for Calibration					
												Boundary Conditions[f]	Steady State (Oct 03)	Steady State (Feb 04)	Transient (03/04)	Transient (03/04	Not Used	
101112	PB-1536	USGS	909773.44	884624.48	Palm Beach	20	22	SAS	100%	4	0						Not Used	sparse data
101135	PB-1547	USGS	906408.69	946303.44	Palm Beach	95	115	SAS	100%	10	0	SAS						
101136	PB-1548	USGS	906408.69	946303.44	Palm Beach	55	60	SAS	100%	10	0	SAS						
111167	PB-1548_G	SFWMD	906391.56	946307.68	Palm Beach	20	60	SAS	100%	0	15	SAS						
140030	PB-1552	PALM BEACH CO. via DEP	898764.95	937876.27	Palm Beach	90	100	SAS	100%	1	0						Not Used	sparse data
101057	PB-1573	USGS	916601.31	763291.06	Palm Beach	55	60	SAS	100%	4	0						Not Used	sparse data
101058	PB-1574	USGS	916601.31	763291.06	Palm Beach	203	223	IAS/ICU	100%	4	0						Not Used	No calibration in IAS/ICU
101077	PB-1576	USGS	908981.42	805856.51	Palm Beach	140	160	SAS	100%	4	15	SAS						
101078	PB-1577	USGS	908981.42	805856.51	Palm Beach	126	146	SAS	100%	4	0						Not Used	spares data
101095	PB-1578	USGS	953938.51	831094.14	Palm Beach	206	226	SAS	100%	4	0						Not Used	sparse data
101102	PB-1590A	USGS	900160.62	854475.21	Palm Beach	18	20	SAS	100%	1	0						Not Used	sparse data
140031	PB-1602	PALM BEACH CO. via DEP	948552.75	805070.81	Palm Beach	30	50	SAS	100%	1	0						Not Used	sparse data
101075	PB-1602	USGS	948876.29	802177.97	Palm Beach	45	50	SAS	100%	4	0						Not Used	sparse data
140032	PB-1603	PALM BEACH CO. via DEP	948563.59	805077.95	Palm Beach	60	180	SAS	100%	1	0						Not Used	sparse data
101076	PB-1603	USGS	948876.29	802177.97	Palm Beach	160	180	SAS	100%	4	0						Not Used	sparse data
101061	PB-1605	USGS	948752.00	767844.20	Palm Beach	230	250	IAS/ICU	100%	4	0						Not Used	No calibration in IAS/ICU
101128	PB-1608	USGS	924368.52	926421.75	Palm Beach	130	150	SAS	100%	4	0						Not Used	sparse data
101130	PB-1613	USGS	850342.25	936004.25	Palm Beach	142	162	SAS	100%	10	0	SAS						
111133	PB-1613	SFWMD	850416.17	936025.48	Palm Beach	110	120	SAS	100%	0	15	SAS						
111132	PB-1615_G	SFWMD	850583.40	936163.02	Palm Beach	0	20	SAS	100%	0	15	SAS						
101032	PB-1618	USGS	942030.44	726801.32	Palm Beach	18	20	SAS	100%	4	0						Not Used	sparse data
101045	PB-1619	USGS	945294.68	741768.08	Palm Beach	17.6	19.6	SAS	100%	2	0						Not Used	sparse data
101041	PB-1620	USGS	926931.17	740232.69	Palm Beach	18	20	SAS	100%	4	0						Not Used	sparse data
101060	PB-1621	USGS	935145.48	763510.79	Palm Beach	18	20	SAS	100%	4	0						Not Used	sparse data
101062	PB-1622	USGS	948752.00	767844.20	Palm Beach	19	21	SAS	100%	4	0						Not Used	sparse data
101059	PB-1623	USGS	916601.31	763291.06	Palm Beach	20.5	22.5	SAS	100%	4	0						Not Used	sparse data
101064	PB-1624	USGS	959888.72	773981.85	Palm Beach	19	21	SAS	100%	3	0						Not Used	sparse data
101069	PB-1625	USGS	963406.00	790164.23	Palm Beach	20.5	22.5	SAS	100%	4	0						Not Used	sparse data
101070	PB-1626	USGS	963406.00	790164.23	Palm Beach	88	108	SAS	100%	4	0						Not Used	sparse data
101071	PB-1627	USGS	944959.98	790538.20	Palm Beach	18	20	SAS	100%	4	0						Not Used	sparse data
101072	PB-1628	USGS	945035.76	790665.90	Palm Beach	89	109	SAS	100%	4	15	SAS						
101052	PB-1630	USGS	905940.27	752119.28	Palm Beach	24.8	29.8	SAS	100%	9	0	SAS						
111033	PB-1630	SFWMD	905946.52	752430.24	Palm Beach	25.8	29.8	SAS	100%	0	11	SAS						
101067	PB-1631	USGS	910882.65	776887.79	Palm Beach	24	29	SAS	100%	9	0	SAS						
101074	PB-1632	USGS	908661.34	798685.23	Palm Beach	25	30	SAS	100%	4	0						Not Used	sparse data
101079	PB-1633	USGS	935297.90	808951.93	Palm Beach	100	120	SAS	100%	4	0						Not Used	sparse data
101080	PB-1634	USGS	935297.90	808951.93	Palm Beach	20	25	SAS	100%	3	0						Not Used	sparse data
101087	PB-1635	USGS	945743.62	821746.33	Palm Beach	22	24	SAS	100%	4	0						Not Used	sparse data
101088	PB-1636	USGS	945743.62	821746.33	Palm Beach	74	79	SAS	100%	4	0						Not Used	sparse data
101120	PB-1637	USGS	927721.87	912205.09	Palm Beach	19.7	21.7	SAS	100%	4	0						Not Used	sparse data
101093	PB-1638	USGS	963382.14	830556.62	Palm Beach	20	25	SAS	100%	9	0	SAS						
111413	PB-1639	SFWMD	963457.48	830683.64	Palm Beach	20	25	SAS	100%	10	15	SAS						
101094	PB-1639	USGS	963458.38	830682.94	Palm Beach	20	25	SAS	100%	10	15	SAS						
101085	PB-1641	USGS	913701.96	820930.90	Palm Beach	105	125	SAS	100%	9	0	SAS						
101127	PB-1642	USGS	951439.71	925214.31	Palm Beach	19	21	SAS	100%	10	15	SAS						
111331	PB-1642		956087.54	923004.71	Palm Beach	20	21	SAS	100%	0	0						Not Used	Missing data
101065	PB-1647	USGS	959888.72	773981.85	Palm Beach	93	113	SAS	100%	4	0						Not Used	sparse data
101137	PB-1648	USGS	924598.63	946720.87	Palm Beach	18	20	SAS	100%	4	0						Not Used	sparse data
101138	PB-1649	USGS	924598.63	946720.87	Palm Beach	145	165	SAS	100%	4	0						Not Used	sparse data
101054	PB-1660	USGS	941212.91	753554.64	Palm Beach	20	25	SAS	100%	1	0						Not Used	sparse data
110620	PB-1660	SFWMD	941287.91	753684.43	Palm Beach	15	25	SAS	100%	2	0						Not Used	sparse data
111789	PB-1661	SFWMD	933744.06	753129.23	Palm Beach	15	25	SAS	100%	10	15	SAS						
101053	PB-1661	USGS	934559.02	753739.71	Palm Beach	20	25	SAS	100%	10	15	SAS						
101118	PB-1662	USGS	918082.99	901360.29	Palm Beach	20	25	SAS	100%	10	15	SAS						
111333	PB-1662		920411.15	893678.44	Palm Beach	18	23	SAS	100%	0	0						Not Used	Missing data
101049	PB-1663	USGS	955421.38	750320.79	Palm Beach	18	20	SAS	100%	2	0						Not Used	sparse data
101042	PB-1667	USGS	957489.00	740944.52	Palm Beach	20	22	SAS	100%	2	0						Not Used	sparse data
101043	PB-1669	USGS	957489.00	740944.52	Palm Beach	111	131	SAS	100%	10	12	SAS						
101039	PB-1680	USGS	952569.41	740028.95	Palm Beach	35	40	SAS	100%	9	15	SAS						
110820	PB-1680		957421.26	737611.97	Palm Beach	35	40	SAS	100%	0	0						Not Used	Missing data
101038	PB-1684	USGS	939399.78	737010.40	Palm Beach	35	40	SAS	100%	10	13	SAS						
110821	PB-1684		944346.99	733885.50	Palm Beach	35	40	SAS	100%	0	0						Not Used	Missing data
101034	PB-1686	USGS	947186.07	731279.45	Palm Beach	111	131	SAS	100%	6	11	SAS						
101081	PB-445	USGS	935098.31	809481.05	Palm Beach	9.4	11.4	SAS	100%	10	15	SAS						
111410	PB-445_G	SFWMD	934826.62	809478.80	Palm Beach	10	12	SAS	100%	10	15	SAS						
101035	PB-491	USGS	957345.96	735490.69	Palm Beach	187	207	SAS	100%	1	10	SAS						

Table 4.1: Usage of SAJ Observation Database in Regional Model Calibration

Model ID[a]	Well Name	Data Source	Easting[b]	Northing[b]	County	Cased Depth (ft)	Drilled Depth (ft)	Dominant Layer[c]	% Open Section in Layer[c]	93/94 Months with Data[d]	03/04 Months with Data[e]	Use for Data in Model Setup/Calibration						Reasoning/Comments
													Observations for Calibration					
												Boundary Conditions[f]	Steady State (Oct 03)	Steady State (Feb 04)	Transient (03/04)	Transient (03/04	Not Used	
101040	PB-494	USGS	955676.32	740022.83	Palm Beach	21	23	SAS	100%	2	0						Not Used	sparse data
101109	PB-561	USGS	916957.72	864092.68	Palm Beach	9.3	11.3	SAS	100%	10	14	SAS						
111232	PB-561_G	SFWMD	916958.52	864092.27	Palm Beach	9.3	11.3	SAS	100%	10	15	SAS						
100884	PB-565	USGS	951285.19	959446.30	Palm Beach	19.9	21.9	SAS	100%	10	0	SAS						
111832	PB-565_G	SFWMD	951286.04	959445.82	Palm Beach	19.9	21.9	SAS	100%	10	15	SAS						
101037	PB-567	USGS	952492.79	740000.38	Palm Beach	88	93	SAS	100%	1	0						Not Used	sparse data
101141	PB-595	USGS	952575.94	958021.09	Palm Beach	94	114	SAS	100%	9	0	SAS						
101125	PB-596	USGS	964790.97	921856.66	Palm Beach	57	62	SAS	100%	4	0						Not Used	sparse data
101115	PB-618	USGS	961483.04	891435.59	Palm Beach	31	36	SAS	100%	4	0						Not Used	sparse data
101117	PB-620	USGS	961096.76	894664.25	Palm Beach	31	36	SAS	100%	10	0	SAS						
101113	PB-632	USGS	964846.13	890147.68	Palm Beach	252	272	SAS	64%	4	0						Not Used	sparse data
101114	PB-633	USGS	964846.13	890147.68	Palm Beach	17	19	SAS	100%	4	0						Not Used	sparse data
101084	PB-683	USGS	913776.93	821057.50	Palm Beach	15	17	SAS	100%	10	15	SAS						
111277	PB-683_G	SFWMD	913776.31	821058.15	Palm Beach	15	17	SAS	100%	10	15	SAS						
101106	PB-685	USGS	877338.53	861641.70	Palm Beach	15	17	SAS	100%	7	15	SAS						
111411	PB-685_G	SFWMD	877339.27	861641.28	Palm Beach	15	17	SAS	100%	7	15	SAS						
101140	PB-689	USGS	870718.54	948950.16	Palm Beach	15	17	SAS	100%	7	15	SAS						
111833	PB-689_G	SFWMD	870719.34	948949.72	Palm Beach	15	17	SAS	100%	7	15	SAS						
101063	PB-690	USGS	960906.01	771565.69	Palm Beach	255	275	IAS/ICU	100%	4	0						Not Used	No calibration in IAS/ICU
101068	PB-692	USGS	961922.54	781772.04	Palm Beach	259	279	IAS/ICU	100%	4	0						Not Used	No calibration in IAS/ICU
101086	PB-693	USGS	966080.88	821589.13	Palm Beach	255	275	SAS	100%	4	0						Not Used	sparse data
101126	PB-710	USGS	964689.10	923370.69	Palm Beach	21	23	SAS	100%	10	0	SAS						
101123	PB-715	USGS	887024.17	916704.05	Palm Beach	76	81	SAS	100%	10	0	SAS						
101124	PB-716	USGS	887024.17	916704.05	Palm Beach	13	15	SAS	100%	9	0	SAS						
101133	PB-717	USGS	888062.61	941450.02	Palm Beach	20	25	SAS	100%	4	0						Not Used	sparse data
101119	PB-719	USGS	940500.30	911382.08	Palm Beach	21	26	SAS	100%	4	0						Not Used	sparse data
101044	PB-732	USGS	945643.27	741899.43	Palm Beach	80	100	SAS	100%	10	15	SAS						
111788	PB-732_G	SFWMD	945371.05	741897.11	Palm Beach	19	100	SAS	100%	10	15	SAS						
101142	PB-746	USGS	952482.54	958424.36	Palm Beach	77	82	SAS	100%	9	0	SAS						
112119	PB-747	SFWMD	936328.26	946544.16	Palm Beach	995	1264	UF	71%	0	15		UF	UF	UF			no 93/94 data
101097	PB-750	USGS	894720.46	838186.34	Palm Beach	78	83	SAS	100%	4	0						Not Used	sparse data
101098	PB-751	USGS	894720.46	838186.34	Palm Beach	20	25	SAS	100%	4	0						Not Used	sparse data
101033	PB-752	USGS	947470.12	729665.78	Palm Beach	21	23	SAS	100%	2	0						Not Used	sparse data
101110	PB-767	USGS	941290.18	875538.62	Palm Beach	35	40	SAS	100%	4	0						Not Used	sparse data
101134	PB-789	USGS	942351.35	944921.62	Palm Beach	191	211	SAS	100%	10	0	SAS						
101116	PB-795	USGS	961483.04	891435.59	Palm Beach	180	200	SAS	100%	4	0						Not Used	sparse data
101105	PB-809	USGS	951830.89	857560.23	Palm Beach	130	150	SAS	100%	10	15	SAS						
111334	PB-809	SFWMD	952102.13	857562.80	Palm Beach	145	150	SAS	100%	10	15	SAS						
101121	PB-830	USGS	850528.25	915708.59	Palm Beach	200	220	IAS/ICU	100%	9	0						Not Used	No calibration in IAS/ICU
101122	PB-831	USGS	848056.79	915779.14	Palm Beach	20	25	SAS	100%	10	15	SAS						
111328	PB-831_G	SFWMD	850602.43	915830.99	Palm Beach	21	25	SAS	100%	10	15	SAS						
101139	PB-832	USGS	937449.25	947008.55	Palm Beach	121	141	SAS	100%	10	0	SAS						
101083	PB-834B	USGS	965923.24	818356.54	Palm Beach	181	201	SAS	100%	4	0						Not Used	sparse data
101104	PB-835B	USGS	966464.04	855522.19	Palm Beach	100	120	SAS	100%	4	0						Not Used	sparse data
101082	PB-846	USGS	965923.24	818356.54	Palm Beach	140	160	SAS	100%	4	0						Not Used	sparse data
101103	PB-847	USGS	966464.04	855522.19	Palm Beach	80	100	SAS	100%	4	0						Not Used	sparse data
101132	PB-875	USGS	925110.44	937635.69	Palm Beach	22	24	SAS	100%	10	0	SAS						
101131	PB-880	USGS	925110.44	937635.69	Palm Beach	98	118	SAS	100%	10	0	SAS						
101091	PB-888	USGS	966217.52	827649.07	Palm Beach	21	26	SAS	100%	4	0						Not Used	sparse data
101090	PB-889	USGS	966217.52	827649.07	Palm Beach	180	200	SAS	100%	4	0						Not Used	sparse data
101056	PB-900	USGS	935158.86	761491.33	Palm Beach	58	63	SAS	100%	10	0	SAS						
110684	PB900_G	SFWMD	935235.00	761620.00	Palm Beach	58	63	SAS	100%	10	0	SAS						
101089	PB-935	USGS	919574.73	825410.51	Palm Beach	43	48	SAS	100%	4	0						Not Used	spares data
101055	PB-948	USGS	959109.14	756001.92	Palm Beach	155	175	SAS	100%	10	13	SAS						
101092	PB-949	USGS	965853.69	827747.36	Palm Beach	277	297	SAS	100%	4	0						Not Used	sparse data
101100	PB-99	USGS	963311.23	850675.72	Palm Beach	18	20	SAS	100%	10	15	SAS						
110993	PB-99_G	SFWMD	963310.29	850676.37	Palm Beach	16	18	SAS	100%	10	15	SAS						
112151	PBF-10R	SFWMD	886678.71	735581.37	Palm Beach	1015	1225	UF	100%	0	15		UF	UF	UF			no 93/94 data
112146	PBF-11	SFWMD	886678.71	735581.37	Palm Beach	1515	1670	APPZ	98%	0	15		APPZ	APPZ	APPZ			no 93/94 data
112130	PBF-12	SFWMD	886678.71	735581.37	Palm Beach	2135	2260	LF	96%	0	15		LF	LF	LF	LF		
112120	PBF-2	SFWMD	964547.70	867347.17	Palm Beach	946	1090	UF	100%	0	15		UF	UF	UF			no 93/94 data
112107	PBF-3	SFWMD	949209.57	852482.26	Palm Beach	1050	1252	UF	90%	0	15		UF	UF	UF			no 93/94 data
112148	PBF-4	SFWMD	949209.57	852482.26	Palm Beach	1360	1510	APPZ	98%	0	15		APPZ	APPZ	APPZ			no 93/94 data
112149	PBF-5	SFWMD	949209.57	852482.26	Palm Beach	2340	2490	LF	57%	0	15		LF	LF	LF	LF		
112159	PBF-7L	SFWMD	748904.73	860161.10	Palm Beach	1968	2040	LF	100%	0	15						Not Used	Removed per SFWMD
112157	PBF-7U	SFWMD	748904.73	860161.10	Palm Beach	992	1447	UF	83%	0	15		UF	UF	UF			no 93/94 data
140033	PBMKP-D2	PALM BEACH CO. via DEP	939792.59	761926.18	Palm Beach	100	120	SAS	100%	1	0						Not Used	sparse data

Table 4.1: Usage of SAJ Observation Database in Regional Model Calibration

Model ID[a]	Well Name	Data Source	Easting[b]	Northing[b]	County	Cased Depth (ft)	Drilled Depth (ft)	Dominant Layer[c]	% Open Section in Layer[c]	93/94 Months with Data[d]	03/04 Months with Data[e]	Use for Data in Model Setup/Calibration						Reasoning/Comments
													Observations for Calibration					
												Boundary Conditions[f]	Steady State (Oct 03)	Steady State (Feb 04)	Transient (03/04)	Transient (03/04	Not Used	
140034	PBMKP-S2	PALM BEACH CO. via DEP	939792.59	761926.18	Palm Beach	34	44	SAS	100%	1	0						Not Used	sparse data
111051	PGAW04	SFWMD	925623.90	912244.64	Palm Beach	10	15	SAS	100%	0	11	SAS						
140035	PV13E31N	SFWMD via DEP	925518.25	789883.88	Palm Beach	10	15	SAS	100%	1	0						Not Used	sparse data
140036	PV18W21S	SFWMD via DEP	924656.24	789002.88	Palm Beach	20	30	SAS	100%	1	0						Not Used	sparse data
140037	PV18W29S	SFWMD via DEP	924654.42	788860.49	Palm Beach	10	15	SAS	100%	1	0						Not Used	sparse data
140038	PV20E10N	SFWMD via DEP	925696.74	789535.64	Palm Beach	10	15	SAS	100%	1	0						Not Used	sparse data
140039	PV21E20N	SFWMD via DEP	925722.06	789695.35	Palm Beach	20	30	SAS	100%	1	0						Not Used	sparse data
140040	PV21W8N	SFWMD via DEP	924798.19	789394.57	Palm Beach	10	15	SAS	100%	1	0						Not Used	Sparse data
140041	PV22E31S	SFWMD via DEP	925754.80	788840.28	Palm Beach	10	15	SAS	100%	1	0						Not Used	sparse data
140042	PV24E16S	SFWMD via DEP	925801.33	789093.02	Palm Beach	20	30	SAS	100%	1	0						Not Used	sparse data
140043	PV27W23N	SFWMD via DEP	924875.07	789733.34	Palm Beach	20	30	SAS	100%	1	0						Not Used	Sparse data
140044	PV31W11S	SFWMD via DEP	924987.78	789156.47	Palm Beach	10	15	SAS	100%	1	0						Not Used	Sparse data
140045	PV32W26N	SFWMD via DEP	925005.56	789784.66	Palm Beach	10	15	SAS	100%	1	0						Not Used	Sparse data
140046	PV34E29N	SFWMD via DEP	926052.68	789848.94	Palm Beach	10	15	SAS	100%	1	0						Not Used	sparse data
140047	PV39E7S	SFWMD via DEP	926181.91	789250.97	Palm Beach	10	15	SAS	100%	1	0						Not Used	sparse data
140048	PV4W30N	SFWMD via DEP	924308.26	789856.95	Palm Beach	10	15	SAS	100%	1	0						Not Used	sparse data
140049	PV7E8S	SFWMD via DEP	925382.58	789221.61	Palm Beach	10	15	SAS	100%	1	0						Not Used	sparse data
140050	PV8W9S	SFWMD via DEP	924403.34	789195.14	Palm Beach	10	15	SAS	100%	1	0						Not Used	sparse data
111065	S10C_GW1		868241.97	741338.83	Palm Beach	62.59	64.59	SAS	100%	0	0						Not Used	Missing data
111064	S10C_GW2	SFWMD	868241.97	741338.83	Palm Beach	99.39	101.39	SAS	100%	0	15	SAS						
111063	S10C_GW3	SFWMD	868241.97	741338.83	Palm Beach	29.47	31.47	SAS	100%	0	15	SAS						
111060	WCA2E1_G3	SFWMD	868015.80	734077.81	Palm Beach	22.2	27.2	SAS	100%	0	15	SAS						
111059	WCA2E1_G4	SFWMD	868005.80	734067.81	Palm Beach	13.68	15.68	SAS	100%	0	15	SAS						
111058	WCA2F1_GW3	SFWMD	862669.25	737365.87	Palm Beach	31.95	33.95	SAS	100%	0	15	SAS						
111057	WCA2F1_GW4	SFWMD	862669.25	737365.87	Palm Beach	12.55	14.55	SAS	100%	0	15	SAS						
140051	WCAS-7D	SFWMD via DEP	807457.87	727947.71	Palm Beach	85.8	95.8	SAS	100%	1	0						Not Used	sparse data
140052	WCAS-7S	SFWMD via DEP	807466.96	727948.75	Palm Beach	5.9	15.9	SAS	100%	1	0						Not Used	sparse data
131078	ALSTON DEEP FLDN	SWFWMD	294773.69	1398107.15	Pasco	59	98	UF	99%	0	15		UF	UF	UF			no 93/94 data
131074	AUSTIN SMITH FLDN	SWFWMD	263944.65	1428895.60	Pasco	68	102	IAS/ICU	56%	0	15						Not Used	No calibration in IAS/ICU
101145	B WEICHT DEEP WELL NO 2 NEAR CRYSTAL SPRINGS FL	USGS	291388.67	1398029.50	Pasco	60	100	UF	99%	6	7						Not Used	Hillsborough Basin has a dense coverage of points and is not important for the purposes of the model; remove
130643	CARVER LOIS		280522.46	1397024.30	Pasco	60	105	UF	100%	0	0						Not Used	missing data
130679	CCWF SR-4 SURF	SWFWMD	199333.27	1437082.61	Pasco	0	6.3	SAS	63%	10	15	SAS						
130702	CCWF T2-D SURF	SWFWMD	206483.06	1442868.78	Pasco	0	9.5	IAS/ICU	100%	10	15						Not Used	Outside Boundary
130666	CCWF T3-A SURF	SWFWMD	202017.12	1429494.66	Pasco	0	10.8	IAS/ICU	55%	9	15	SAS						
130581	CCWF T3-B SURF	SWFWMD	201892.74	1429566.83	Pasco	0	6.2	SAS	78%	9	15	SAS						
130963	CCWF TMR-3 DEEP	SWFWMD	207224.03	1442920.83	Pasco	160	625	UF	46%	10	15						Not Used	Outside Boundary
130695	CCWF TMR-3 SHALLOW	SWFWMD	207207.24	1442860.41	Pasco	7	11	IAS/ICU	100%	10	15						Not Used	Outside Boundary
130964	CCWF TMR-4 DEEP	SWFWMD	201567.98	1437451.45	Pasco	99	592	UF	55%	10	15						Not Used	Outside Boundary
130644	CCWF TMR-4 SHALLOW	SWFWMD	201564.40	1437450.48	Pasco	20	24	IAS/ICU	100%	10	15						Not Used	Outside Boundary
131071	CHANCEY RD FLDN	SWFWMD	287157.60	1415455.35	Pasco	50	87	UF	100%	0	15						Not Used	Hillsborough Basin has a dense coverage of points and is not important for the purposes of the model; remove
130906	CYP CRK W-29 B2CTRDP SURF		209801.81	1443770.05	Pasco	7	8.7	IAS/ICU	100%	0	0						Not Used	Outside Boundary
130908	CYP CRK W-29 B2MS SURF		209934.06	1443606.90	Pasco	6	13.3	IAS/ICU	100%	0	0						Not Used	Outside Boundary
130909	CYP CRK W-29 B2MSE SURF		209997.80	1443707.19	Pasco	13	19	IAS/ICU	100%	0	0						Not Used	Outside Boundary
130910	CYP CRK W-29 B2MSW SURF		209728.20	1443589.06	Pasco	14	20.9	IAS/ICU	100%	0	0						Not Used	Outside Boundary
130638	CYPRESS CREEK T4-C		202027.11	1421293.50	Pasco	0	0	Error	0%	0	0						Not Used	Outside Boundary
130603	DOYLES RANCH FLDN		159920.60	1402915.43	Pasco	38	438	UF	83%	0	0						Not Used	Outside Boundary
131070	EILAND BLVD FLDN	SWFWMD	255831.58	1424820.31	Pasco	49	99	IAS/ICU	100%	0	15						Not Used	No calibration in IAS/ICU
131076	EILAND BLVD SURF	SWFWMD	255822.64	1424821.42	Pasco	4	9	IAS/ICU	54%	0	15	SAS						
130823	FOX RIDGE FLDN	SWFWMD	239711.85	1413809.60	Pasco	104	155	UF	100%	0	15	UF						averaged with 130614 and 130859
130828	FOX RIDGE SURF	SWFWMD	239668.41	1413931.29	Pasco	1.3	8	SAS	100%	0	15	SAS						
130748	GREEN SWAMP W CYP UPL SURF	SWFWMD	307013.51	1458543.63	Pasco	1	5	SAS	100%	0	15	SAS						
130798	GREEN SWAMP W CYP WTL SURF	SWFWMD	306815.29	1458363.59	Pasco	2	5	SAS	100%	0	15	SAS						
130649	HARRY MATTS DEEP	SWFWMD	176066.03	1402458.11	Pasco	59	60	UF	100%	0	15						Not Used	Outside Boundary
130650	HARRY MATTS SHALLOW	SWFWMD	176074.98	1402458.00	Pasco	8	10	SAS	100%	0	15	SAS						
131088	HILLS RIV @ HWY 39 FLDN	SWFWMD	281146.35	1404298.26	Pasco	44	112	UF	100%	0	15						Not Used	Hillsborough Basin has a dense coverage of points and is not important for the purposes of the model; remove
130843	HRSR391UFAS UP FLDN SH	SWFWMD	281145.67	1404227.56	Pasco	16.7	20.7	IAS/ICU	100%	0	15						Not Used	No calibration in IAS/ICU
130844	HRSR392UAS SHALLOW	SWFWMD	280907.26	1404563.19	Pasco	8.4	12.4	IAS/ICU	100%	0	15						Not Used	No calibration in IAS/ICU
130846	HRSR393NO (UFAS) U FLD SH	SWFWMD	280766.31	1404796.87	Pasco	14.9	18.9	IAS/ICU	100%	0	15						Not Used	No calibration in IAS/ICU
130847	HRSR393NO SURF	SWFWMD	280775.26	1404796.79	Pasco	2.5	4.5	IAS/ICU	100%	0	15						Not Used	No calibration in IAS/ICU
130845	HRSR393SO (UFAS) U FLD SH	SWFWMD	280854.93	1404705.11	Pasco	8.8	9.8	IAS/ICU	100%	0	15						Not Used	No calibration in IAS/ICU
130848	HRSR394UFAS UPPER FLDN SH	SWFWMD	280421.50	1405234.54	Pasco	13.9	17.9	IAS/ICU	100%	0	15						Not Used	No calibration in IAS/ICU
130849	HRSR395UFAS UPPER FLDN SH	SWFWMD	280245.54	1405549.37	Pasco	16.5	20.5	IAS/ICU	100%	0	15						Not Used	No calibration in IAS/ICU
130593	J ALSTON FLDN	SWFWMD	294812.06	1398674.47	Pasco	47	55	IAS/ICU	100%	10	15						Not Used	No calibration in IAS/ICU
101147	J O ALSTON WELL NEAR CRYSTAL SPRINGS FL	USGS	294813.85	1398674.45	Pasco	47	55	IAS/ICU	100%	1	2						Not Used	No calibration in IAS/ICU
101150	KING DEEP NEAR LUTZ FL	USGS	205743.71	1407509.38	Pasco	450	550	APPZ	100%	0	0						Not Used	Outside Boundary

Table 4.1: Usage of SAJ Observation Database in Regional Model Calibration

Model ID[a]	Well Name	Data Source	Easting[b]	Northing[b]	County	Cased Depth (ft)	Drilled Depth (ft)	Dominant Layer[c]	% Open Section in Layer[c]	93/94 Months with Data[d]	03/04 Months with Data[e]	Use for Data in Model Setup/Calibration						Reasoning/Comments
													Observations for Calibration					
												Boundary Conditions[f]	Steady State (Oct 03)	Steady State (Feb 04)	Transient (03/04)	Transient (03/04	Not Used	
130860	NEW RIVER LIBRARY FLDN	SWFWMD	252703.71	1414642.86	Pasco	80	135	UF	87%	0	15						Not Used	Hillsborough Basin has a dense coverage of points and is not important for the purposes of the model; remove
130861	NEW RIVER LIBRARY SURF	SWFWMD	252703.82	1414652.96	Pasco	2	9	SAS	100%	0	15	SAS						
130595	NORTH SHALLOW	SWFWMD	167944.32	1405104.62	Pasco	0	0	Error	0%	10	15	SAS						
130608	PASCO 207 DEEP		177032.52	1404116.20	Pasco	72	173	UF	100%	0	0						Not Used	Outside Boundary
130636	PASCO 220 SHALLOW	SWFWMD	170637.57	1403585.97	Pasco	14	15	SAS	100%	10	15	SAS						
130667	PASCO 305 DEEP		152259.59	1398871.30	Pasco	37	39	SAS	100%	0	0						Not Used	Outside Boundary
130668	PASCO 305 SHALLOW		152259.60	1398872.31	Pasco	9	10	SAS	100%	0	0						Not Used	Outside Boundary
131090	PLAZA MATERIALS FLDN	SWFWMD	290027.76	1413262.62	Pasco	71	137	UF	100%	0	15						Not Used	Hillsborough Basin has a dense coverage of points and is not important for the purposes of the model; remove
131091	PLAZA MATERIALS SURF	SWFWMD	290038.57	1413269.58	Pasco	25	28	IAS/ICU	100%	0	15						Not Used	No calibration in IAS/ICU
130796	RIVER RD RIVERINE UPL SURF	SWFWMD	293411.00	1461345.21	Pasco	1.5	5	SAS	100%	0	15	SAS						
130797	RIVER RD RIVERINE WTL SURF	SWFWMD	293544.94	1461333.86	Pasco	4	29	IAS/ICU	59%	0	15	SAS						
130585	ROMP 80 SURFICIAL		200305.85	1404140.76	Pasco	9	19	SAS	100%	0	0						Not Used	Outside Boundary
101151	ROMP 85 AVON PARK WELL NEAR ZEPHYRHILLS FL	USGS	230043.11	1422493.34	Pasco	450	505	APPZ	100%	0	13						Not Used	Outside Boundary
130613	ROMP 85 AVPK	SWFWMD	229950.53	1422405.65	Pasco	450	505	APPZ	100%	0	15	APPZ						
101152	ROMP 85 FLORIDAN WELL NEAR ZEPHYRHILLS FL		229954.17	1422410.66	Pasco	160	300	UF	100%	0	0						Not Used	Outside Boundary
130884	ROMP 85 SURFICIAL		229953.73	1422370.26	Pasco	0	0	Error	0%	0	0						Not Used	Outside Boundary
130614	ROMP 85 TMPA/SWNN	SWFWMD	229945.83	1422384.48	Pasco	160	300	UF	100%	1	15	UF						averaged with 130859 and 130823
101153	ROMP 86 AVON PARK DEEP WELL NEAR ZEPHYRHILLS FL		276217.98	1425720.30	Pasco	425	434	APPZ	100%	0	0						Not Used	missing data
130612	ROMP 86 AVPK	SWFWMD	276226.93	1425720.22	Pasco	425	434	APPZ	100%	1	15						Not Used	sparse data and very close to 131043
131043	ROMP 86A AVPK	SWFWMD	279977.38	1405582.26	Pasco	500	560	APPZ	100%	0	15		APPZ	APPZ	APPZ			no 93/94 data
131044	ROMP 86A SWNN	SWFWMD	279977.28	1405572.16	Pasco	135	175	UF	100%	0	15						Not Used	Hillsborough Basin has a dense coverage of points and is not important for the purposes of the model; remove
130962	ROMP 90 AVPK	SWFWMD	288873.65	1465363.80	Pasco	424	665	MC2	58%	10	15	APPZ						location and depth data not provided by SAJ - source: SWFWMD WMIS
130986	ROMP 90 OCAL	SWFWMD	288873.65	1465363.80	Pasco	62	160	UF	100%	10	15	UF						location and depth data not provided by SAJ - source: SWFWMD WMIS
131046	ROMP BR-3 UP FLDN	SWFWMD	258193.96	1453665.59	Pasco	133	246	UF	100%	0	15	UF						location and depth data not provided by SAJ - source: SWFWMD WMIS
130973	ROMP TR 16-2 OCAL	SWFWMD	105232.85	1429344.03	Pasco	350	370	Error	0%	9	14						Not Used	Outside Boundary
130974	ROMP TR 16-2 SWNN	SWFWMD	105232.85	1429344.03	Pasco	210	230	Error	0%	0	15						Not Used	Outside Boundary
130810	RT 54 APRILE CYP WTL SURF	SWFWMD	165243.98	1406754.90	Pasco	3.5	23.5	SAS	100%	0	15	SAS						
130771	RT 54 NELSON WTL SURF	SWFWMD	178781.04	1406344.62	Pasco	3	18	SAS	100%	0	15	SAS						
130590	SOUTH PASCO WEST DEEP	SWFWMD	162600.58	1403686.67	Pasco	0	0	Error	0%	10	15	SAS						
130634	SOUTH PASCO WEST SHALLOW	SWFWMD	162600.46	1403676.57	Pasco	0	0	Error	0%	10	15	SAS						
131057	SPWF 1 WTL SURF	SWFWMD	168361.90	1401270.49	Pasco	2.7	3.7	SAS	100%	0	15	SAS						
130827	SPWF 2 TRANS SURF	SWFWMD	170420.42	1402679.43	Pasco	3	17	SAS	100%	0	15	SAS						
131052	SPWF 2 WTL SURF	SWFWMD	170392.82	1402619.15	Pasco	3.4	6.4	SAS	100%	0	14	SAS						
130826	SPWF 6 TRANS SURF	SWFWMD	170410.13	1404300.02	Pasco	3.5	22	SAS	100%	0	15	SAS						
130812	SPWF 6 WTL SURF	SWFWMD	170376.53	1404189.31	Pasco	2	22	SAS	100%	0	15	SAS						
130596	SR 54 DEEP	SWFWMD	168619.20	1406823.75	Pasco	178	345	UF	100%	10	15						Not Used	Outside Boundary
131072	SR 54 EAST FLDN	SWFWMD	297612.07	1428497.41	Pasco	45	98	UF	100%	0	15						Not Used	Hillsborough Basin has a dense coverage of points and is not important for the purposes of the model; remove
131075	SR 54 EAST SURF	SWFWMD	297594.37	1428517.77	Pasco	5	15	IAS/ICU	100%	0	15						Not Used	No calibration in IAS/ICU
130769	SR 54 GRAND OAKS UPL SURF	SWFWMD	211489.86	1416969.82	Pasco	1	4	SAS	100%	0	15	SAS						
130770	SR 54 GRAND OAKS WTL SURF	SWFWMD	211338.35	1417022.05	Pasco	1	4	SAS	100%	0	15	SAS						
130599	SR 54 SHALLOW	SWFWMD	168601.30	1406823.98	Pasco	3	5	SAS	100%	10	15	SAS						
130594	SR 577 DEEP	SWFWMD	244608.88	1439456.50	Pasco	57	150	IAS/ICU	72%	10	13						Not Used	No calibration in IAS/ICU
130597	SR 577 SHALLOW	SWFWMD	244599.94	1439456.59	Pasco	18	20.7	SAS	100%	10	14	SAS						
130655	ST PETE 41 SHALLOW	SWFWMD	167740.50	1398823.31	Pasco	17	19	SAS	100%	10	15	SAS						
130662	ST PETE 42 DP	SWFWMD	167731.07	1400217.59	Pasco	70	398	UF	94%	10	15						Not Used	Outside Boundary
130663	ST PETE 42 SHALLOW	SWFWMD	167749.22	1400237.57	Pasco	20	22	SAS	100%	10	15	SAS						
130682	ST PETE 43 SHALLOW	SWFWMD	169042.52	1400575.02	Pasco	20	22	SAS	100%	10	15	SAS						
130584	ST PETE 44 SHALLOW	SWFWMD	170435.25	1400992.10	Pasco	21	22	SAS	100%	10	15	SAS						
130669	ST PETE 45 DEEP	SWFWMD	170842.12	1402037.72	Pasco	59	707	UF	49%	10	15						Not Used	Outside Boundary
130670	ST PETE 45 SHALLOW	SWFWMD	170797.24	1402028.18	Pasco	18	20	SAS	100%	10	15	SAS						
130697	ST PETE 46 SHALLOW	SWFWMD	167524.35	1401584.04	Pasco	20	22	SAS	100%	10	15	SAS						
130609	ST PETE 47 SHALLOW	SWFWMD	167113.32	1403074.27	Pasco	19	21	SAS	100%	10	15	SAS						
130621	ST PETE 48 SHALLOW	SWFWMD	165833.85	1403120.62	Pasco	14	16	SAS	100%	10	15	SAS						
130642	ST PETE 49 SHALLOW	SWFWMD	167701.28	1404279.24	Pasco	20	22	SAS	100%	10	15	SAS						
130582	ST PETE 50 SHALLOW	SWFWMD	169581.83	1405063.99	Pasco	17	19	SAS	100%	10	15	SAS						
130882	ST PETE E-105 2-IN SHALLOW	SWFWMD	167170.64	1401931.95	Pasco	0	18	SAS	100%	10	15	SAS						
130714	ST PETE E-105 6-IN SHALLOW		167125.13	1401871.91	Pasco	18	20	SAS	100%	0	0						Not Used	Outside Boundary
130713	ST PETE E-105 DEEP	SWFWMD	167170.51	1401921.85	Pasco	1012	1360	MC2	100%	9	15						Not Used	Outside Boundary
130628	ST PETE EAST SHALLOW	SWFWMD	165595.25	1403366.08	Pasco	0	0	Error	0%	10	15	SAS						

Table 4.1: Usage of SAJ Observation Database in Regional Model Calibration

Model ID[a]	Well Name	Data Source	Easting[b]	Northing[b]	County	Cased Depth (ft)	Drilled Depth (ft)	Dominant Layer[c]	% Open Section in Layer[c]	93/94 Months with Data[d]	03/04 Months with Data[e]	Use for Data in Model Setup/Calibration						Reasoning/Comments
													Observations for Calibration					
												Boundary Conditions[f]	Steady State (Oct 03)	Steady State (Feb 04)	Transient (03/04)	Transient (03/04	Not Used	
130660	ST PETE NEW SHALLOW	SWFWMD	169928.19	1401968.26	Pasco	0	0	Error	0%	10	15	SAS						
101148	ST PETE SHALLOW 105 NEAR LAND O LAKES FL	USGS	167185.18	1401986.72	Pasco	18	20	SAS	100%	10	15	SAS						
101146	ST PETE WELL 42 NEAR LAND O LAKES FL	USGS	167731.07	1400217.59	Pasco	70	398	UF	94%	1	2						Not Used	Outside Boundary
101154	U.S. HIGHWAY 98 WELL NEAR DADE CITY, FL	USGS	296847.69	1436767.21	Pasco	41	200	UF	100%	6	10						Not Used	Hillsborough Basin has a dense coverage of points and is not important for the purposes of the model; remove
130762	UHFDA CYPRESS 1 UPL SURF	SWFWMD	287771.15	1415054.59	Pasco	5	25	IAS/ICU	100%	0	15						Not Used	No calibration in IAS/ICU
130808	UHFDA CYPRESS 1 WTL SURF	SWFWMD	287681.62	1414953.42	Pasco	5	20	IAS/ICU	100%	0	15						Not Used	No calibration in IAS/ICU
130758	UHFDA CYPRESS 2 UPL SURF	SWFWMD	290489.76	1413295.66	Pasco	2	7	IAS/ICU	86%	0	15	SAS						
130807	UHFDA CYPRESS 2 WTL SURF	SWFWMD	290824.88	1413348.07	Pasco	1	5	IAS/ICU	82%	0	15	SAS						
130760	UHFDA CYPRESS 3 UPL SURF	SWFWMD	293627.59	1416473.49	Pasco	2.5	7.5	IAS/ICU	100%	0	15						Not Used	No calibration in IAS/ICU
130806	UHFDA CYPRESS 3 WTL SURF	SWFWMD	293493.03	1416434.34	Pasco	1.5	8.5	IAS/ICU	92%	0	15	SAS						
130805	UHFDA CYPRESS 4 UPL SURF	SWFWMD	295382.17	1434748.41	Pasco	2.5	7.5	IAS/ICU	100%	0	15						Not Used	No calibration in IAS/ICU
130804	UHFDA CYPRESS 4 WTL SURF	SWFWMD	295326.19	1434690.34	Pasco	2	7	IAS/ICU	100%	0	15						Not Used	No calibration in IAS/ICU
130763	UHFDA NORTH MARSH UPL SURF	SWFWMD	291137.77	1422113.98	Pasco	2.5	12.5	IAS/ICU	100%	0	15						Not Used	No calibration in IAS/ICU
130803	UHFDA NORTH MARSH WTL SURF	SWFWMD	291029.38	1421810.95	Pasco	3.5	8.5	IAS/ICU	100%	0	15						Not Used	No calibration in IAS/ICU
130757	UHFDA RIVERINE 1 UPL SURF	SWFWMD	295950.73	1424091.46	Pasco	2	10	IAS/ICU	100%	0	15						Not Used	No calibration in IAS/ICU
130801	UHFDA RIVERINE 1 WTL SURF	SWFWMD	295887.27	1423806.18	Pasco	2	7	IAS/ICU	100%	0	15						Not Used	No calibration in IAS/ICU
130761	UHFDA RIVERINE 2 UPL SURF	SWFWMD	294730.05	1421036.05	Pasco	3	8	IAS/ICU	100%	0	15						Not Used	No calibration in IAS/ICU
130800	UHFDA RIVERINE 2 WTL SURF	SWFWMD	294679.57	1420898.13	Pasco	1	4	IAS/ICU	100%	0	15						Not Used	No calibration in IAS/ICU
130799	UHFDA RIVERINE 3 WTL SURF	SWFWMD	302232.21	1433000.65	Pasco	2	7	IAS/ICU	100%	0	15						Not Used	No calibration in IAS/ICU
131053	UHFDA SOUTH MARSH UPL SURF	SWFWMD	289658.35	1418702.54	Pasco	2.3	7.3	IAS/ICU	100%	0	15						Not Used	No calibration in IAS/ICU
130802	UHFDA SOUTH MARSH WTL SURF	SWFWMD	289361.63	1418543.71	Pasco	1	5.3	IAS/ICU	100%	0	15						Not Used	No calibration in IAS/ICU
130759	UHFDA WET PRA UPL SURF	SWFWMD	287917.91	1416289.60	Pasco	2	10	IAS/ICU	100%	0	15						Not Used	No calibration in IAS/ICU
130809	UHFDA WET PRAIRIE WTL SURF	SWFWMD	287908.73	1416264.43	Pasco	2	7	IAS/ICU	100%	0	15						Not Used	No calibration in IAS/ICU
130850	UHR1T1UFAD UPPER FLDN DEEP		292842.86	1411945.38	Pasco	41	93	UF	100%	0	0						Not Used	missing data
130851	UHRT1SAS SURF SHALLOW	SWFWMD	292807.17	1411955.81	Pasco	3.1	5.1	IAS/ICU	100%	0	14						Not Used	No calibration in IAS/ICU
130852	UHRT2UFAS UPPER FLDN SH	SWFWMD	292476.61	1412009.40	Pasco	15	19	IAS/ICU	100%	0	15						Not Used	No calibration in IAS/ICU
130855	UHRT3CR (UFAS) UP FLDN SH	SWFWMD	292139.55	1412325.67	Pasco	6.8	10.8	IAS/ICU	100%	0	15						Not Used	No calibration in IAS/ICU
130854	UHRT3SAS SURF SHALLOW	SWFWMD	292156.87	1412264.90	Pasco	4.3	6.3	IAS/ICU	100%	0	15						Not Used	No calibration in IAS/ICU
130853	UHRT3UFAS UPPER FLDN SH	SWFWMD	292148.12	1412285.19	Pasco	20	24	IAS/ICU	100%	0	14						Not Used	No calibration in IAS/ICU
130856	UHRT4UFAS UPPER FLDN SH	SWFWMD	291954.02	1412579.93	Pasco	6	10.6	IAS/ICU	100%	0	14						Not Used	No calibration in IAS/ICU
130858	UHRT5SAS SURF SHALLOW	SWFWMD	291687.88	1412824.85	Pasco	3.2	5.2	IAS/ICU	100%	0	15						Not Used	No calibration in IAS/ICU
130857	UHRT5UFAD UPPER FLDN DEEP		291696.83	1412824.76	Pasco	54	93	UF	100%	0	0						Not Used	missing data
131087	UP HILLS 1 WTL UP FLDN	SWFWMD	292824.78	1411925.34	Pasco	41	93	UF	100%	0	15						Not Used	Hillsborough Basin has a dense coverage of points and is not important for the purposes of the model; remove
131086	UP HILLS 5 WTL UP FLDN	SWFWMD	291679.41	1412875.43	Pasco	54	93	UF	100%	0	15						Not Used	Hillsborough Basin has a dense coverage of points and is not important for the purposes of the model; remove
130615	US 98 NR DADE CITY FLDN		296908.95	1436914.13	Pasco	41	200	UF	100%	0	0						Not Used	missing data
130586	WEICHT DEEP		291406.76	1398049.53	Pasco	60	100	UF	99%	0	0						Not Used	sparse data
130859	WESLEY CHAPEL WWTP FLDN	SWFWMD	228306.34	1432025.57	Pasco	94	116	UF	71%	0	15	UF						averaged with 130614 and 130823
130832	WESLEY CHAPEL WWTP SURF	SWFWMD	228306.01	1431995.27	Pasco	1.5	14.5	SAS	100%	0	15	SAS						
131080	WILSON ROAD FLDN REPL	SWFWMD	180359.16	1406577.93	Pasco	95	135	UF	100%	0	15						Not Used	Outside Boundary
131081	WILSON ROAD SURF REPL	SWFWMD	180350.45	1406598.24	Pasco	5	25	SAS	100%	0	15	SAS						
130981	WILSON WELL 25	SWFWMD	179738.36	1405800.53	Pasco	60	71	UF	86%	10	0						Not Used	Outside Boundary
130988	WILSON WELL 26	SWFWMD	179738.38	1405801.54	Pasco	3	30	SAS	100%	10	0	SAS						
101149	WINTER QUARTERS ROAD WELL NEAR CITRUS PARK FL	USGS	185705.71	1404613.90	Pasco	415	435	MC1	100%	1	2						Not Used	Outside Boundary
131069	WIRE ROAD FLDN	SWFWMD	276423.23	1431084.16	Pasco	92	139	UF	100%	0	15						Not Used	Hillsborough Basin has a dense coverage of points and is not important for the purposes of the model; remove
131073	ZEPHYRHILLS PARK FLDN	SWFWMD	274772.06	1418724.07	Pasco	55	100	UF	90%	0	15						Not Used	Hillsborough Basin has a dense coverage of points and is not important for the purposes of the model; remove
130720	ZEPHYRHILLS PARK SURF	SWFWMD	274780.90	1418713.88	Pasco	15	35	IAS/ICU	100%	0	15						Not Used	No calibration in IAS/ICU
131077	ZEPHYRHILLS PRISON FLDN	SWFWMD	269459.46	1405151.63	Pasco	42	99	UF	84%	0	15						Not Used	Hillsborough Basin has a dense coverage of points and is not important for the purposes of the model; remove
101167	1S E LAKE WELL NEAR TARPON SPRINGS FL	USGS	111951.21	1375968.63	Pinellas	10	12	SAS	100%	0	0						Not Used	Outside Boundary
131168	BISHOP FLDN	SWFWMD	109549.39	1393865.03	Pinellas	65	76	UF	100%	10	15						Not Used	Outside Boundary
131175	BISHOP SURF	SWFWMD	109653.18	1393282.62	Pinellas	3	29	SAS	100%	10	15	SAS						
131153	BROOKER CREEK DEEP		107669.34	1366638.15	Pinellas	300	310	UF	100%	0	0						Not Used	Outside Boundary
131152	BROOKER CREEK SHALLOW		107669.32	1366637.14	Pinellas	80	90	UF	100%	0	0						Not Used	Outside Boundary
131117	CITY OF OLDSMAR TEST		117932.57	1350531.88	Pinellas	108	174	UF	100%	0	0						Not Used	Outside Boundary
131171	DUNN WRAP-55F FLDN	SWFWMD	111089.13	1380971.71	Pinellas	57	77	UF	100%	10	15						Not Used	Outside Boundary
131176	DUNN WRAP-56S SURF	SWFWMD	111094.01	1380936.28	Pinellas	3	27.4	SAS	100%	10	15	SAS						
101163	E LAKE WELL 3S NEAR OLDSMAR FL	USGS	112628.54	1373130.28	Pinellas	4	9.4	SAS	100%	0	0						Not Used	Outside Boundary
101159	E LAKE WELL 7S NEAR OLDSMAR FL	USGS	113660.11	1369983.94	Pinellas	7	12.3	SAS	100%	0	0						Not Used	Outside Boundary
101158	E LAKE WELL 8S NEAR OLDSMAR FL	USGS	113720.36	1367861.41	Pinellas	7	12.4	SAS	100%	0	0						Not Used	Outside Boundary
131113	EAST LAKE 1 SHALLOW		112011.79	1376072.86	Pinellas	10	12	SAS	100%	0	0						Not Used	Outside Boundary
131115	EAST LAKE 17 DEEP		123511.49	1365307.53	Pinellas	57	305	UF	100%	0	0						Not Used	Outside Boundary
131148	EAST LAKE 17 DEEP		123593.78	1371368.33	Pinellas	57	305	UF	100%	0	0						Not Used	Outside Boundary

Table 4.1: Usage of SAJ Observation Database in Regional Model Calibration

Model ID[a]	Well Name	Data Source	Easting[b]	Northing[b]	County	Cased Depth (ft)	Drilled Depth (ft)	Dominant Layer[c]	% Open Section in Layer[c]	93/94 Months with Data[d]	03/04 Months with Data[e]	Use for Data in Model Setup/Calibration						Reasoning/Comments
													Observations for Calibration					
												Boundary Conditions[f]	Steady State (Oct 03)	Steady State (Feb 04)	Transient (03/04)	Transient (03/04	Not Used	
131102	EAST LAKE 2 SHALLOW		111987.95	1374355.61	Pinellas	12	14	SAS	100%	0	0						Not Used	Outside Boundary
131103	EAST LAKE 2A SHALLOW		111987.96	1374356.62	Pinellas	7	10	SAS	100%	0	0						Not Used	Outside Boundary
131101	EAST LAKE 3 SHALLOW		112689.11	1373234.51	Pinellas	4.4	9.4	SAS	100%	0	0						Not Used	Outside Boundary
131107	EAST LAKE 4 SHALLOW		113754.23	1372513.54	Pinellas	6	11	SAS	100%	0	0						Not Used	Outside Boundary
131108	EAST LAKE 4A SHALLOW		113754.25	1372514.55	Pinellas	8	12	SAS	100%	0	0						Not Used	Outside Boundary
131147	EAST LAKE 5 SHALLOW		113783.57	1374633.83	Pinellas	9	12	SAS	100%	0	0						Not Used	Outside Boundary
131118	EAST LAKE 6 SHALLOW		113992.05	1376752.65	Pinellas	10	12	SAS	100%	0	0						Not Used	Outside Boundary
131100	EAST LAKE 7 SHALLOW		113720.70	1370089.19	Pinellas	7	12	SAS	100%	0	0						Not Used	Outside Boundary
131146	EAST LAKE 8 SHALLOW		113780.95	1367966.65	Pinellas	7	12	SAS	100%	0	0						Not Used	Outside Boundary
131172	EAST LAKE 9 SHALLOW		116535.24	1372778.26	Pinellas	8	10	SAS	100%	0	0						Not Used	Outside Boundary
101160	EAST LAKE DEEP WELL 14 NEAR OLDSMAR FL	USGS	123498.21	1371324.17	Pinellas	57	305	UF	100%	1	2						Not Used	Outside Boundary
101157	EAST LAKE DEEP WELL 17 NEAR TARPOPN SPRINGS FL	USGS	123655.47	1365088.36	Pinellas	57	305	UF	100%	0	2						Not Used	Outside Boundary
131150	EAST LAKE M2 DEEP		112077.52	1374354.37	Pinellas	507	538	MC1	100%	0	0						Not Used	Outside Boundary
101164	EAST LAKE MON M2 DEEP W NEAR TARPON SPRINGS FL	USGS	112016.94	1374250.13	Pinellas	507	538	MC1	100%	1	0						Not Used	Outside Boundary
101165	EAST LAKE SHALLOW WELL 2A NEAR OLDSMAR FL	USGS	111927.37	1374251.38	Pinellas	7	9.7	SAS	100%	0	0						Not Used	Outside Boundary
101161	EAST LAKE SHALLOW WELL 4A NEAR OLDSMAR FL	USGS	113693.65	1372408.29	Pinellas	8	11.8	SAS	100%	0	0						Not Used	Outside Boundary
131181	EAST LAKE WOODLAND FLDN	SWFWMD	110949.12	1365747.80	Pinellas	97	107	UF	100%	10	15						Not Used	Outside Boundary
131182	EAST LAKE WOODLAND SURF	SWFWMD	110972.92	1365783.84	Pinellas	3	20.5	IAS/ICU	44%	10	15						Not Used	Outside Boundary
101166	EL-5S NEAR OLDSMAR FL	USGS	113723.00	1374529.59	Pinellas	9	12	SAS	100%	0	0						Not Used	Outside Boundary
131139	ELDRIDGE-WILDE 114 SHALLOW		123094.27	1393904.40	Pinellas	16	19	SAS	100%	0	0						Not Used	Outside Boundary
131129	ELDRIDGE-WILDE 13 SHALLOW		124105.39	1389243.12	Pinellas	26	28	SAS	100%	0	0						Not Used	Outside Boundary
101169	ELDRIDGE-WILDE 2S NEAR TARPON SPRINGS FL	USGS	117869.08	1390688.32	Pinellas	61	290	UF	100%	1	2						Not Used	Outside Boundary
131104	ELDRIDGE-WILDE MONITOR 5		120379.44	1391819.79	Pinellas	58	229	UF	100%	0	0						Not Used	Outside Boundary
131163	EWWF 1 UPL SURF	SWFWMD	117862.15	1391486.58	Pinellas	4	35	SAS	100%	0	15	SAS						
131204	EWWF 1 WTL SURF	SWFWMD	117752.78	1391347.65	Pinellas	4.9	8	SAS	100%	0	15	SAS						
131140	EWWF 11 FLDN	SWFWMD	124030.59	1391381.99	Pinellas	110	400	UF	100%	9	15						Not Used	Outside Boundary
131141	EWWF 11 SURF	SWFWMD	124030.73	1391392.09	Pinellas	21.9	26	SAS	100%	9	15	SAS						
131167	EWWF 1A W FLDN	SWFWMD	119517.83	1393178.38	Pinellas	68	70	UF	100%	10	15						Not Used	Outside Boundary
131132	EWWF 1B W SURF	SWFWMD	119515.60	1393211.75	Pinellas	0	23.5	SAS	100%	10	15	SAS						
131133	EWWF 1C W SURF	SWFWMD	119506.37	1393191.67	Pinellas	0	11.8	SAS	100%	10	15	SAS						
131134	EWWF 1D W SURF	SWFWMD	119506.09	1393171.46	Pinellas	0	5.6	SAS	100%	10	15	SAS						
131135	EWWF 2A WEST SURF	SWFWMD	119369.72	1393021.78	Pinellas	0	23.3	SAS	100%	9	15	SAS						
131136	EWWF 2B W SURF	SWFWMD	119324.82	1393012.30	Pinellas	0	14.5	SAS	100%	9	15	SAS						
131137	EWWF 2C W SURF	SWFWMD	119323.93	1393012.31	Pinellas	0	9.5	SAS	100%	9	15	SAS						
131145	EWWF 2S DEEP	SWFWMD	117869.08	1390688.32	Pinellas	61	290	UF	100%	10	15						Not Used	Outside Boundary
131160	EWWF 3 UPL SURF	SWFWMD	122532.53	1390533.51	Pinellas	5	38.9	SAS	100%	0	15	SAS						
131203	EWWF 3 WTL SURF	SWFWMD	122478.39	1390503.94	Pinellas	5.7	8.7	SAS	100%	0	15	SAS						
131174	EWWF 3A W SURF	SWFWMD	119245.96	1392876.98	Pinellas	15.5	17.5	SAS	100%	10	15	SAS						
131138	EWWF 3B W SURF	SWFWMD	119251.26	1392871.86	Pinellas	0	31.6	SAS	100%	10	15	SAS						
131111	EWWF 3C W SURF	SWFWMD	119260.35	1392881.84	Pinellas	0	11.9	SAS	100%	10	15	SAS						
131112	EWWF 3D WEST SURF	SWFWMD	119233.49	1392882.21	Pinellas	0	6.9	SAS	100%	10	15	SAS						
131161	EWWF 5 UPL SURF	SWFWMD	120280.69	1392847.64	Pinellas	4	18.6	SAS	100%	0	15	SAS						
131162	EWWF 5 WTL SURF	SWFWMD	120230.44	1393100.91	Pinellas	5	20.1	SAS	100%	0	15	SAS						
131116	HORST ROAD SHALLOW		117726.07	1387713.83	Pinellas	7	8	SAS	100%	0	0						Not Used	Outside Boundary
131166	JOHNSON SALT BAYOU FLDN	SWFWMD	99635.48	1393842.16	Pinellas	64	74	UF	100%	10	15						Not Used	Outside Boundary
131173	JOHNSON SALT BAYOU SURF	SWFWMD	99632.69	1393835.13	Pinellas	3	25.9	SAS	88%	10	15	SAS						
101155	KOGER DEEP AT ST PETERSBURG FL	USGS	125963.81	1285455.74	Pinellas	120	140	UF	100%	1	0						Not Used	Outside Boundary
131165	LANSBROOK EAST UPL SURF	SWFWMD	110228.04	1374456.87	Pinellas	3	13.7	SAS	100%	0	15	SAS						
131164	LANSBROOK EAST WTL SURF	SWFWMD	110332.85	1374263.44	Pinellas	2	9.4	SAS	100%	0	14	SAS						
131158	LANSBROOK WEST WTL SURF	SWFWMD	108844.99	1373637.57	Pinellas	4	29	UF	41%	0	15						Not Used	Outside Boundary
131149	NORTH LAKE TARPON FLDN	SWFWMD	109449.23	1390542.37	Pinellas	758	780	APPZ	100%	10	15						Not Used	Outside Boundary
101168	NORTH LAKE TARPON NEAR TARPON SPRINGS FL	USGS	109448.95	1390522.16	Pinellas	758	780	APPZ	100%	1	2						Not Used	Outside Boundary
131170	NWHWRAP 1 DEEP	SWFWMD	111274.24	1381335.89	Pinellas	571	627	APPZ	100%	0	14						Not Used	Outside Boundary
131184	OLDSMAR ELEM SCHL FLDN	SWFWMD	117509.05	1349389.96	Pinellas	51	62	UF	100%	10	15						Not Used	Outside Boundary
131183	OLDSMAR ELEM SCHL SURF	SWFWMD	117558.85	1349425.65	Pinellas	4	19.1	SAS	83%	10	15	SAS						
131157	PINE RIDGE CYP UPL SURF	SWFWMD	111233.16	1381666.84	Pinellas	3	10.4	SAS	100%	0	15	SAS						
131159	PINE RIDGE CYP WTL SURF	SWFWMD	111303.82	1381595.13	Pinellas	8	23.5	SAS	100%	0	15	SAS						
131131	PRESIDENTIAL ESTATES		106869.48	1386349.15	Pinellas	105	115	UF	100%	0	0						Not Used	Outside Boundary
131194	ROMP TR 14-1 SURF	SWFWMD	110736.24	1336835.02	Pinellas	8.8	9	SAS	100%	8	15	SAS						
101156	ROMP TR 14-1 TAMPA WELL NEAR SAFETY HARBOR FL	USGS	110673.48	1336835.89	Pinellas	170	343	UF	100%	0	2						Not Used	Outside Boundary
131192	ROMP TR 14-1 TMPA	SWFWMD	110721.45	1336802.90	Pinellas	70	170	UF	100%	0	15						Not Used	Outside Boundary
131193	ROMP TR-14-1 SWNN	SWFWMD	110721.45	1336802.90	Pinellas	264	284	UF	100%	0	15						Not Used	Outside Boundary

Table 4.1: Usage of SAJ Observation Database in Regional Model Calibration

Model ID[a]	Well Name	Data Source	Easting[b]	Northing[b]	County	Cased Depth (ft)	Drilled Depth (ft)	Dominant Layer[c]	% Open Section in Layer[c]	93/94 Months with Data[d]	03/04 Months with Data[e]	Use for Data in Model Setup/Calibration						Reasoning/Comments
													Observations for Calibration					
												Boundary Conditions[f]	Steady State (Oct 03)	Steady State (Feb 04)	Transient (03/04)	Transient (03/04	Not Used	
131155	SAULS DIARY		116095.91	1392889.03	Pinellas	0	0	Error	0%	0	0						Not Used	Outside Boundary
131154	TARPON ROAD DEEP	SWFWMD	104228.53	1391828.09	Pinellas	205	305	UF	100%	10	8						Not Used	Outside Boundary
131156	TARPON ROAD SHALLOW	SWFWMD	104227.64	1391828.11	Pinellas	10	12.4	SAS	100%	10	15	SAS						
101194	119 FL	USGS	338231.40	1257427.90	Polk	90	110	IAS/ICU	100%	0	0						Not Used	No calibration in IAS/ICU
131256	1-4 DEEP WELL NR POLK CITY		366812.74	1385283.09	Polk	55	93	IAS/ICU	67%	0	0						Not Used	No calibration in IAS/ICU
101206	164 FL	USGS	352159.22	1279225.69	Polk	147	167	IAS/ICU	100%	0	2						Not Used	No calibration in IAS/ICU
101222	210 FL	USGS	408111.17	1300459.19	Polk	81	101	IAS/ICU	100%	1	2						Not Used	No calibration in IAS/ICU
101226	222 FL	USGS	458980.14	1311090.09	Polk	130	150	IAS/ICU	100%	1	2						Not Used	No calibration in IAS/ICU
101263	25S25E32	USGS	390581.35	1427732.41	Polk	211	231	UF	100%	1	2						Not Used	Sparse data
101228	29S29E28 L ROSALIE NW	USGS	519573.97	1310924.85	Polk	475	575	MC1	100%	1	1						Not Used	Model geology puts this well in MC1
101229	29S30E19 KISS STPK NR LK KISSIMMEE	USGS	541550.88	1312066.81	Polk	460	560	MC1	100%	1	6						Not Used	Model geology puts this well in MC1
101208	30S29E21 E LK WALES UTILITY	USGS	519295.02	1282143.71	Polk	737	837	APPZ	76%	1	6						Not Used	sparse data
101174	33S30E06 USAF AVON PARK #1	USGS	542145.75	1206735.12	Polk	935	1035	APPZ	51%	1	2						Not Used	sparse data
131270	ALSTON BAY UPL SURF	SWFWMD	304930.60	1399857.99	Polk	2.5	7.5	IAS/ICU	100%	0	15						Not Used	No calibration in IAS/ICU
131276	ALSTON BAY WTL SURF	SWFWMD	304804.66	1399886.39	Polk	2	5	IAS/ICU	93%	0	15	SAS						
131271	ALSTON CYPRESS 1 UPL SURF	SWFWMD	302159.69	1401054.70	Polk	2.5	7.5	IAS/ICU	63%	0	15	SAS						
131275	ALSTON CYPRESS 1 WTL SURF	SWFWMD	302128.94	1400920.64	Polk	1	16	IAS/ICU	77%	0	15	SAS						
131272	ALSTON CYPRESS 2 UPL SURF	SWFWMD	300707.65	1409963.86	Polk	3	15	IAS/ICU	100%	0	15						Not Used	No calibration in IAS/ICU
131274	ALSTON CYPRESS 2 WTL SURF	SWFWMD	300726.59	1409980.85	Polk	2	5	IAS/ICU	75%	0	15	SAS						
131384	ALSTON TRACT FLDN	SWFWMD	304859.71	1400236.40	Polk	50	112	UF	90%	0	15						Not Used	Hillsborough Basin has a dense coverage of points and is not important for the purposes of the model; remove
131329	ALSTON TRACT SURF	SWFWMD	304861.62	1400249.51	Polk	1	9	IAS/ICU	81%	0	15	SAS						
131273	ALSTON WET PRA UPL SURF	SWFWMD	305189.32	1400761.72	Polk	2.5	7.5	IAS/ICU	89%	0	15	SAS						
131277	ALSTON WET PRA WTL SURF	SWFWMD	305259.93	1400750.98	Polk	2	10	IAS/ICU	86%	0	15	SAS						
131210	ALTMAN DEEP		458593.08	1208990.77	Polk	80	700	IAS/ICU	41%	0	0						Not Used	Open section straddles multiple layers
101177	ALTMAN DEEP WELL NEAR WEST FROSTPROOF FL	USGS	458525.98	1208879.00	Polk	80	700	IAS/ICU	41%	6	0						Not Used	Open section straddles multiple layers
101256	ANNULAR MONITOR AT POLK CITY	USGS	388603.13	1400071.27	Polk	840	908	MC2	100%	1	2						Not Used	Model geology puts this well in MC2
101210	BARTOW SENIOR HIGH SCHOOL NEAR BARTOW FL	USGS	384895.15	1290511.90	Polk	125	145	IAS/ICU	100%	1	0						Not Used	No calibration in IAS/ICU
131248	BETHLEHEM ROAD DEEP	SWFWMD	322863.81	1238171.66	Polk	100	1000	MC1	35%	10	0						Not Used	Open section straddles multiple layers
101186	BETHLEHEM ROAD DEEP WELL NEAR BRADLEY JUNCTION FL	USGS	322861.92	1238172.80	Polk	100	1000	MC1	35%	10	0						Not Used	Open section straddles multiple layers
131320	BEVIS FLDN		467123.22	1319328.67	Polk	0	190	SAS	53%	0	0						Not Used	Missing data
131221	BREWSTER WELL		339992.92	1244899.95	Polk	394	834	MC1	74%	0	0						Not Used	Model geology puts this well in MC1
101190	CL-3 HAWTHORN WELL NEAR FROSTPROOF FL	USGS	470797.04	1246822.48	Polk	140	197	IAS/ICU	100%	0	2						Not Used	No calibration in IAS/ICU
131265	CLAUDE HARDIN WELL		342130.76	1332954.15	Polk	325	643	MC1	73%	0	0						Not Used	Model geology puts this well in MC1
101209	CLEAR SPRINGS DEV. 8-IN IAS WELL NEAR BARTOW FL	USGS	397680.52	1287204.09	Polk	123	143	IAS/ICU	100%	0	15						Not Used	No calibration in IAS/ICU
101232	CNTL HAWTHORN AT HIGHLAND CITY FL	USGS	373719.96	1321596.84	Polk	80	100	IAS/ICU	100%	1	2						Not Used	No calibration in IAS/ICU
101223	CNTRL FL TRUSS HTRNN AT BARTOW FL	USGS	389096.14	1301290.07	Polk	55	60	IAS/ICU	100%	0	2						Not Used	No calibration in IAS/ICU
131254	COLEY DEEP	SWFWMD	484908.45	1240141.40	Polk	208	319	IAS/ICU	78%	10	15						Not Used	No calibration in IAS/ICU
101251	COMBEE RD SHAL AT SR33 NR LAKELAND,FL		363281.07	1376820.03	Polk	8	9	SAS	100%	0	0						Not Used	Missing data
131211	COMBEE ROAD DEEP		363408.17	1376812.01	Polk	31	55	IAS/ICU	100%	0	0						Not Used	No calibration in IAS/ICU
101250	COMBEE ROAD DEEP WELL NEAR LAKELAND, FL	USGS	363371.37	1376920.36	Polk	31	55	IAS/ICU	100%	6	9						Not Used	No calibration in IAS/ICU
101246	CRESENT DR DEEP AT LAKELND FL	USGS	345180.34	1366323.74	Polk	727	827	APPZ	100%	1	2						Not Used	Hillsborough Basin has a dense coverage of points and is not important for the purposes of the model; remove
131216	CROSBY		379537.52	1348831.65	Polk	45	265	UF	56%	0	0						Not Used	Missing data
131325	DRAUDT FLDN		464321.83	1314898.48	Polk	0	480	IAS/ICU	36%	0	0						Not Used	Open section straddles multiple layers
101255	DRILL PIPE INNER MONITOR AT POLK CITY	USGS	388603.13	1400071.27	Polk	808	908	MC2	100%	1	2						Not Used	Model geology puts this well in MC2
101207	EAST LAKE WALES UTILITY SHALLOW W NR NALCREST FL	USGS	519181.73	1282153.15	Polk	20	22	SAS	100%	0	9	SAS						
131321	ESTEVE FLDN		463878.35	1315910.58	Polk	0	460	IAS/ICU	37%	0	0						Not Used	Open section straddles multiple layers
131249	FISH LAKE DEEP NR LAKELAND		358149.72	1364542.39	Polk	265	311	UF	96%	0	0						Not Used	Missing data
101245	FISH LAKE DEEP WELL NEAR LAKELAND, FL	USGS	358082.62	1364435.83	Polk	265	311	UF	97%	6	9						Not Used	Hillsborough Basin has a dense coverage of points and is not important for the purposes of the model; remove
101231	FOODTWN DEEP NEAR EAGLE LAKE FL	USGS	403555.79	1317657.53	Polk	280	300	UF	100%	1	0						Not Used	sparse data
131244	FORT GREEN SPRINGS INT		346113.25	1224306.62	Polk	280	300	IAS/ICU	100%	0	0						Not Used	No calibration in IAS/ICU
101182	FT GREEN SPRINGS NEAR FORT GREEN FL	USGS	346129.52	1224318.61	Polk	208	302	IAS/ICU	100%	7	10						Not Used	No calibration in IAS/ICU
101261	FUSSELL RD DP	USGS	392009.23	1414087.36	Polk	197	217	UF	100%	1	2						Not Used	sparse data
131214	GARDINIER NR BOWLING GREEN		378302.23	1223809.82	Polk	410	908	MC1	75%	0	0						Not Used	Model geology puts this well in MC1
101181	GARDINIER WELL NEAR BOWLING GREEN FL	USGS	378461.19	1223787.50	Polk	410	908	MC1	75%	0	2						Not Used	Model geology puts this well in MC1
131279	GREEN SWAMP 7 UPL SURF	SWFWMD	363006.30	1447464.65	Polk	0.5	3.5	SAS	100%	0	15	SAS						
131278	GREEN SWP DOME 7 WTL SURF	SWFWMD	362908.58	1447546.19	Polk	0.5	3.5	SAS	100%	0	15	SAS						
131322	HART FLDN		466209.50	1315798.29	Polk	0	0	Error	0%	0	0						Not Used	Data error
131323	HART NRSD SURF		466029.65	1315698.16	Polk	0	80	SAS	100%	0	0						Not Used	Missing data
101202	HOMELAND NO 4 WELL NEAR HOMELAND FL	USGS	397285.84	1268018.01	Polk	182	202	IAS/ICU	100%	0	12						Not Used	No calibration in IAS/ICU

Table 4.1: Usage of SAJ Observation Database in Regional Model Calibration

Model ID[a]	Well Name	Data Source	Easting[b]	Northing[b]	County	Cased Depth (ft)	Drilled Depth (ft)	Dominant Layer[c]	% Open Section in Layer[c]	93/94 Months with Data[d]	03/04 Months with Data[e]	Use for Data in Model Setup/Calibration						Reasoning/Comments
													Observations for Calibration					
												Boundary Conditions[f]	Steady State (Oct 03)	Steady State (Feb 04)	Transient (03/04)	Transient (03/04	Not Used	
101200	HOMELAND NO 9 WELL NEAR HOMELAND FL	USGS	396773.55	1265203.66	Polk	646	746	MC1	100%	1	15						Not Used	Model geology puts this well in MC1
131385	HOWARD STREET FLDN	SWFWMD	302468.11	1423523.68	Polk	134	172	UF	100%	0	15						Not Used	Hillsborough Basin has a dense coverage of points and is not important for the purposes of the model; remove
131328	HOWARD STREET SURF	SWFWMD	302531.72	1423634.21	Polk	4	24	IAS/ICU	100%	0	15						Not Used	No calibration in IAS/ICU
131319	HUTCHINSON FLDN		466941.94	1318925.56	Polk	0	347	IAS/ICU	52%	0	0						Not Used	No calibration in IAS/ICU
101205	IMC TEST WELL ON HWY 98 NEAR BARTOW FL	USGS	389560.94	1277047.59	Polk	207	227	IAS/ICU	100%	1	4						Not Used	No calibration in IAS/ICU
110253	INDIAN L_G	SFWMD	550527.22	1255699.44	Polk	6.64	8.64	SAS	100%	10	15	SAS						
101187	J.C.BARNETTE NEAR FORT MEADE FL	USGS	388971.99	1240187.99	Polk	209	229	IAS/ICU	100%	1	2						Not Used	No calibration in IAS/ICU
101244	JOHNSON HTHN NEAR LAKELAND FL	USGS	322158.41	1364119.13	Polk	110	130	IAS/ICU	67%	1	0						Not Used	No calibration in IAS/ICU
131231	KAISER ANNULUS A DEEP		333512.23	1298581.71	Polk	2791	2920	Error	0%	0	0						Not Used	missing data
131232	KAISER ANNULUS B DEEP		333512.24	1298582.72	Polk	1270	1348	MC2	100%	0	0						Not Used	missing data
131262	KELLEY WELL NR ARTURAS		451834.82	1258811.16	Polk	306	959	MC1	68%	0	0						Not Used	Model geology puts this well in MC1
101249	KIMBELL WELL NR LK MARION	USGS	485296.91	1369230.38	Polk	379	399	MC1	100%	1	2						Not Used	Model geology puts this well in MC1
100588	KNOX DEEP WELL NEAR MULBERRY FL	USGS	315399.77	1307714.98	Polk	280	300	UF	100%	1	0						Not Used	sparse data
110247	KREFFM	SFWMD	597673.63	1241463.48	Polk	25.86	40.86	SAS	100%	0	15	SAS						
110451	KREFFS	SFWMD	597659.02	1241489.15	Polk	15.51	20.51	SAS	100%	0	15	SAS						
110172	KRENND	SFWMD	598893.62	1242073.87	Polk	106.39	116.39	IAS/ICU	100%	0	15						Not Used	No calibration in IAS/ICU
110171	KRENNM1	SFWMD	598884.66	1242090.64	Polk	21.97	36.97	SAS	100%	0	15	SAS						
110170	KRENNS	SFWMD	598881.26	1242099.84	Polk	16.35	21.35	SAS	100%	0	15	SAS						
110183	KRFFFM	SFWMD	593375.50	1255492.63	Polk	21.01	36.01	SAS	100%	0	15	SAS						
110182	KRFFFS	SFWMD	593369.22	1255500.52	Polk	16.4	21.4	SAS	100%	0	15	SAS						
110265	KRFNND	SFWMD	593855.11	1255783.01	Polk	112.35	116.35	IAS/ICU	100%	0	15						Not Used	No calibration in IAS/ICU
110267	KRFNNM	SFWMD	593849.92	1255797.16	Polk	19.4	34.4	SAS	100%	0	15	SAS						
110266	KRFNNS	SFWMD	593846.08	1255807.67	Polk	16.26	21.26	SAS	100%	0	15	SAS						
131226	KUDER CITRUS DEEP		377912.49	1296426.36	Polk	180	662	MC1	66%	0	0						Not Used	Model geology puts this well in MC1
101247	LAKE ALFRED DEEP WELL AT LAKE ALFRED, FL	USGS	423665.75	1366820.39	Polk	282	555	MC1	99%	10	15						Not Used	Model geology puts this well in MC1
101252	LAKE ALFRED DEEP WELL NEAR LAKE ALFRED, FL	USGS	418347.93	1394935.61	Polk	102	425	MC1	60%	10	15						Not Used	Model geology puts this well in MC1
101253	LAKE ALFRED SHALLOW W. NEAR LAKE ALFRED, FL	USGS	418282.77	1394829.36	Polk	6	9	SAS	100%	10	5	SAS						
131208	LAKE HATCHINEHA ROAD		479754.22	1348102.70	Polk	137	463	MC1	68%	0	0						Not Used	Model geology puts this well in MC1
101239	LAKE HATCHINEHA ROAD WELL NEAR LAKE HAMILTON FL	USGS	479756.88	1348096.62	Polk	137	463	MC1	68%	7	10						Not Used	Model geology puts this well in MC1
101230	LAKE KISSIMMEE ST PARK SHALLOW W NR LAKE WALES FL	USGS	541889.28	1312982.70	Polk	23	28	SAS	100%	0	9	SAS						
131334	LAKE LOWERY ST 900	SWFWMD	431529.81	1381524.28	Polk	0	6.1	SAS	100%	0	1	SAS						
131233	LAKE MCLEOD SHALLOW		415761.17	1322941.16	Polk	24	26	SAS	100%	0	0						Not Used	Missing data
101233	LAKE MCLEOD SHALLOW WELL NEAR EAGLE LAKE FL	USGS	415694.16	1322833.50	Polk	24	26	SAS	100%	6	9	SAS						
131280	LAKE STARR STLE NRSD SURF		468374.75	1318514.74	Polk	0	20	SAS	100%	0	0						Not Used	Missing data
131281	LAKE STARR STLN NRSD SURF		465863.94	1318526.77	Polk	0	15	SAS	100%	0	0						Not Used	Missing data
131282	LAKE STARR STLNE NRSD SUR		467570.12	1319023.55	Polk	0	25	SAS	100%	0	0						Not Used	Missing data
131286	LAKE STARR STLNW NRSD SUR		464606.07	1318027.90	Polk	0	13	SAS	100%	0	0						Not Used	Missing data
131283	LAKE STARR STLS NRSD SURF		466120.30	1315899.71	Polk	0	22	SAS	100%	0	0						Not Used	Missing data
131284	LAKE STARR STLSE NRSD SUR		467651.10	1317205.28	Polk	0	12	SAS	100%	0	0						Not Used	Missing data
131285	LAKE STARR STLW NRSD SURF		464871.09	1317016.68	Polk	0	19	SAS	100%	0	0						Not Used	Missing data
131287	LAKE STARR STUE NRSD SURF		468734.88	1318816.01	Polk	0	74	SAS	100%	0	0						Not Used	Missing data
131288	LAKE STARR STUN NRSD SURF		465864.91	1318728.76	Polk	0	35	SAS	100%	0	0						Not Used	Missing data
131289	LAKE STARR STUNW NRSD SUR		464338.04	1318231.19	Polk	0	35	SAS	100%	0	0						Not Used	Missing data
131290	LAKE STARR STUS NRSD SURF		466208.04	1315495.32	Polk	0	50	SAS	100%	0	0						Not Used	Missing data
131291	LAKE STARR STUSE NRSD SUR		468097.55	1316799.18	Polk	0	80	SAS	100%	0	0						Not Used	Missing data
131303	LAKE STARR WTS-1 NRSD SUR		463707.86	1317729.29	Polk	0	50	SAS	100%	0	0						Not Used	Missing data
131308	LAKE STARR WTS-11 NRSD SUR		468191.56	1317707.67	Polk	0	20	SAS	100%	0	0						Not Used	Missing data
131309	LAKE STARR WTS-14 NRSD SU		467020.47	1316602.34	Polk	0	10	SAS	100%	0	0						Not Used	Missing data
131310	LAKE STARR WTS-15 NRSD SU		467016.12	1315693.42	Polk	0	75	SAS	100%	0	0						Not Used	Missing data
131311	LAKE STARR WTS-17 NRSD SU		466301.12	1316201.82	Polk	0	8	SAS	100%	0	0						Not Used	Missing data
131312	LAKE STARR WTS-19 NRSD SU		466387.39	1315494.46	Polk	0	15	SAS	100%	0	0						Not Used	Missing data
131313	LAKE STARR WTS-21 NRSD SU		465403.86	1316105.16	Polk	0	20	SAS	100%	0	0						Not Used	Missing data
131314	LAKE STARR WTS-22 NRSD SU		464770.72	1314997.30	Polk	0	65	SAS	100%	0	0						Not Used	Missing data
131315	LAKE STARR WTS-23 NRSD SU		463790.64	1316314.98	Polk	0	85	SAS	100%	0	0						Not Used	Missing data
131316	LAKE STARR WTS-25 NRSD SU		464688.44	1316522.70	Polk	0	13	SAS	100%	0	0						Not Used	Missing data
131317	LAKE STARR WTS-26 NRSD SU		466833.37	1314987.35	Polk	0	24	SAS	100%	0	0						Not Used	Missing data
131304	LAKE STARR WTS-4 NRSD SUR		464346.88	1320049.02	Polk	0	80	SAS	100%	0	0						Not Used	Missing data
131305	LAKE STARR WTS-7 NRSD SUR		467756.21	1320436.56	Polk	0	90	SAS	100%	0	0						Not Used	Missing data
131306	LAKE STARR WTS-8 NRSD SUR		469535.23	1317398.31	Polk	0	102	SAS	100%	0	0						Not Used	Missing data
131307	LAKE STARR WTS-9 NRSD SUR		464606.08	1318028.91	Polk	0	130	SAS	65%	0	0						Not Used	Missing data
101201	LAKE WEOHYAKAPKA WELL NEAR FROSTPROOF FL	USGS	514296.84	1264892.16	Polk	179	199	IAS/ICU	100%	6	10						Not Used	No calibration in IAS/ICU

Table 4.1: Usage of SAJ Observation Database in Regional Model Calibration

Model ID[a]	Well Name	Data Source	Easting[b]	Northing[b]	County	Cased Depth (ft)	Drilled Depth (ft)	Dominant Layer[c]	% Open Section in Layer[c]	93/94 Months with Data[d]	03/04 Months with Data[e]	Use for Data in Model Setup/Calibration						Reasoning/Comments
												Boundary Conditions[f]	Observations for Calibration: Steady State (Oct 03)	Observations for Calibration: Steady State (Feb 04)	Observations for Calibration: Transient (03/04)	Observations for Calibration: Transient (03/04	Not Used	
101242	LAKELAND STADIUM WELL AT LAKELAND FL	USGS	349215.73	1360029.73	Polk	820	920	APPZ	93%	0	2						Not Used	Hillsborough Basin has a dense coverage of points and is not important for the purposes of the model; remove
110205	LAKWEO_G	SFWMD	514343.43	1265366.63	Polk	18	20	SAS	100%	0	14	SAS						
101180	LASTINGER ROAD NEAR FORT MEADE FL	USGS	441801.85	1220892.21	Polk	115	135	IAS/ICU	100%	1	2						Not Used	No calibration in IAS/ICU
131245	LK ALFRED DP AT LK ALFRED	SWFWMD	423067.80	1366879.49	Polk	282	555	MC1	96%	3	3						Not Used	Model geology puts this well in MC1
131219	LK ALFRED DP NR LK ALFRED	SWFWMD	418516.65	1394727.94	Polk	102	425	MC1	60%	10	15						Not Used	Model geology puts this well in MC1
131220	LK ALFRED SH NR LK ALFRED	SWFWMD	418478.63	1394656.47	Polk	6	9	SAS	100%	9	0	SAS						
101238	LK HATCHI NR HAINES CITY	USGS	507323.39	1344397.36	Polk	391	411	MC1	100%	1	2						Not Used	Model geology puts this well in MC1
131295	LK STARR 1PNS-100 ICU INT		465773.30	1318328.26	Polk	0	100	SAS	73%	0	0						Not Used	Missing data
131296	LK STARR 1PNS-125 FLDN		465773.31	1318329.26	Polk	0	125	SAS	59%	0	0						Not Used	Missing data
131292	LK STARR 1PNS-25 NRSD SUR		465773.29	1318325.23	Polk	0	25	SAS	100%	0	0						Not Used	Missing data
131293	LK STARR 1PNS-50 NRSD SUR		465773.29	1318326.24	Polk	0	50	SAS	100%	0	0						Not Used	Missing data
131294	LK STARR 1PNS-75 NRSD SUR		465773.30	1318327.25	Polk	0	75	SAS	98%	0	0						Not Used	Missing data
131297	LK STARR 2PNS-10 NRSD SUR		466120.79	1316000.70	Polk	0	10	SAS	100%	0	0						Not Used	Missing data
131300	LK STARR 2PNS-101 NRSD SU		466120.80	1316003.73	Polk	0	101	SAS	76%	0	0						Not Used	Missing data
131301	LK STARR 2PNS-156 NRSD SU		466120.81	1316004.74	Polk	0	156	IAS/ICU	50%	0	0						Not Used	No calibration in IAS/ICU
131298	LK STARR 2PNS-27 NRSD SUR		466120.79	1316001.71	Polk	0	27	SAS	100%	0	0						Not Used	Missing data
131299	LK STARR 2PNS-51 NRSD SUR		466120.80	1316002.72	Polk	0	51	SAS	100%	0	0						Not Used	Missing data
131302	LK STARR 3PNS-40 NRSD SUR		468374.76	1318515.75	Polk	0	40	SAS	100%	0	0						Not Used	Missing data
131223	LKLAND HILLS DEEP NR LAKEL		352114.35	1371758.94	Polk	63	103	IAS/ICU	100%	0	0						Not Used	No calibration in IAS/ICU
131247	MADDOX DEEP WELL	SWFWMD	380061.96	1205416.51	Polk	50	737	IAS/ICU	47%	10	0						Not Used	Open section straddles multiple layers
101171	MADDOX WELL NEAR BOWLING GREEN FL	USGS	380060.17	1205417.66	Polk	50	737	IAS/ICU	47%	10	0						Not Used	Open section straddles multiple layers
101185	MOBIL WELL UF 1 NORTH WELL NEAR FORT MEADE FL	USGS	429983.59	1229380.17	Polk	223	243	IAS/ICU	100%	0	2						Not Used	No calibration in IAS/ICU
101178	MOBIL WELL UF5 HAWTHORN WELL NEAR BOWLING GREEN FL	USGS	411493.71	1212966.95	Polk	197	217	IAS/ICU	100%	1	2						Not Used	No calibration in IAS/ICU
101184	MOBILE WELL UF 7 NORTH WELL NEAR FORT MEADE FL	USGS	407742.51	1227139.24	Polk	195	215	IAS/ICU	100%	1	0						Not Used	No calibration in IAS/ICU
101179	MOBILE WELL UF9 NORTH WELL NEAR FORT MEADE FL	USGS	398523.04	1219219.24	Polk	215	235	IAS/ICU	100%	1	0						Not Used	No calibration in IAS/ICU
101241	N FLORIDA AVE D AT LAKELAND FL	USGS	347486.40	1355437.52	Polk	765	865	APPZ	100%	0	2						Not Used	Hillsborough Basin has a dense coverage of points and is not important for the purposes of the model; remove
131324	NELSON FLDN		467369.03	1314479.82	Polk	0	300	SAS	50%	0	0						Not Used	Missing data
101175	NEUMAN WEGUAR WELL 29 NEAR BEREAH FL	USGS	476449.33	1207299.73	Polk	220	240	IAS/ICU	100%	1	2						Not Used	No calibration in IAS/ICU
131340	OAK HILL OLD AG WELL UP FL		371330.26	1325957.04	Polk	60	80	IAS/ICU	100%	0	0						Not Used	No calibration in IAS/ICU
131339	OAK HILL OLD TREE FARM SUR		372234.86	1327061.51	Polk	3	10	IAS/ICU	100%	0	0						Not Used	No calibration in IAS/ICU
131338	OAK HILL PUMP HOUSE SURF		371250.09	1327270.62	Polk	15	25	IAS/ICU	100%	0	0						Not Used	No calibration in IAS/ICU
131326	ORANGE-CO INC FLDN		469344.41	1314975.38	Polk	0	495	IAS/ICU	37%	0	0						Not Used	Open section straddles multiple layers
101237	ORLEANS ST DEEP AT LAKELAND FL	USGS	347735.80	1339254.85	Polk	673	773	APPZ	100%	0	2						Not Used	Hillsborough Basin has a dense coverage of points and is not important for the purposes of the model; remove
110114	OSS-74	SFWMD	612721.77	1208412.98	Polk	75	90	SAS	100%	0	12	SAS						
110115	OSS-75	SFWMD	612721.77	1208412.98	Polk	17	32	SAS	100%	0	12	SAS						
131209	P E WILLIAMS P-44		459188.50	1399756.78	Polk	81	180	SAS	48%	0	0						Not Used	Open section straddles multiple layers
101198	P-49 WELL NEAR FROSTPROOF FL	USGS	553594.17	1261448.12	Polk	15	17	SAS	100%	10	15	SAS						
131217	PEBBLEDALE ROAD DEEP INT		363969.46	1274335.37	Polk	288	303	IAS/ICU	53%	0	0						Not Used	No calibration in IAS/ICU
131218	PEBBLEDALE ROAD SHALLOW	SWFWMD	363968.61	1274342.44	Polk	53	58	IAS/ICU	100%	10	0						Not Used	No calibration in IAS/ICU
131318	PERRY FLDN		469362.58	1318813.03	Polk	0	450	IAS/ICU	41%	0	0						Not Used	Open section straddles multiple layers
101234	PIPER WATER TOWER NEAR LAKELAND FL	USGS	330257.32	1325265.22	Polk	450	550	MC1	100%	0	0						Not Used	Model geology puts this well in MC1
101243	PLANT CITY QUAD FL	USGS	321682.88	1364032.28	Polk	124	144	UF	100%	1	2						Not Used	Hillsborough Basin has a dense coverage of points and is not important for the purposes of the model; remove
120058	PO-0014	SJRWMD	423730.80	1366927.75	Polk	0	0	Error	0%	10	0	SAS						
120091	PO-0023	SJRWMD	431595.09	1381631.05	Polk	68	73	IAS/ICU	100%	0	15						Not Used	No calibration in IAS/ICU
120092	PO-0024	SJRWMD	432752.70	1381933.46	Polk	75	80	IAS/ICU	100%	0	15						Not Used	No calibration in IAS/ICU
101258	PO-1 THORNHILL DEEP NEAR DAVENPORT, FL	USGS	445284.30	1406188.17	Polk	131	151	UF	100%	10	15		UF	UF	UF	UF		
101259	PO-2 THORNHILL SH NR DAVENPORT	USGS	445284.30	1406188.17	Polk	13	15	SAS	100%	6	2	SAS						
110113	POF-20	SFWMD	612721.77	1208412.98	Polk	260	1000	MC1	49%	0	12						Not Used	Open section straddles multiple layers
110179	POF-22	SFWMD	527306.87	1350493.07	Polk	200	460	MC1	77%	0	15						Not Used	Model geology puts this well in MC1
101254	POLK CITY ROMP 76A WELL NR POLK CITY FL	USGS	388602.43	1399970.27	Polk	264	315	MC1	58%	0	12						Not Used	Model geology puts this well in MC1
101236	POLK COUNTY LANDFILL NEAR LAKELAND FL	USGS	383328.78	1337820.40	Polk	100	120	IAS/ICU	100%	1	2						Not Used	No calibration in IAS/ICU
110178	POS-11	SFWMD	527306.87	1350493.07	Polk	5	10	SAS	100%	0	15	SAS						
110243	POS-12	SFWMD	527306.87	1350493.07	Polk	26	36	SAS	100%	0	15	SAS						
110180	POS-13	SFWMD	527306.87	1350493.07	Polk	108	122	IAS/ICU	100%	0	15						Not Used	No calibration in IAS/ICU
101240	PRECISION TRUSS NEAR LAKELAND FL	USGS	323812.29	1349954.17	Polk	120	140	IAS/ICU	100%	1	2						Not Used	No calibration in IAS/ICU
131240	R PERDUE		434292.35	1285667.50	Polk	266	783	MC1	75%	0	0						Not Used	Model geology puts this well in MC1
131235	RIDGE WRAP CLP-1 SURF	SWFWMD	471605.78	1275853.54	Polk	60	70	SAS	100%	10	15	SAS						
131383	RIDGE WRAP CLP-3 SURF	SWFWMD	483752.43	1276021.03	Polk	30	60	SAS	100%	10	15	SAS						
131386	RIDGE WRAP CLP-5 SURF	SWFWMD	486167.34	1271859.90	Polk	48	58	SAS	100%	10	15	SAS						
131368	RIDGE WRAP CLP-7 SURF	SWFWMD	482016.10	1262889.77	Polk	180	200	SAS	100%	10	14	SAS						
131378	RIDGE WRAP CLP-9 SURF	SWFWMD	472286.44	1244472.60	Polk	25	35	SAS	100%	10	15	SAS						

Table 4.1: Usage of SAJ Observation Database in Regional Model Calibration

Model ID[a]	Well Name	Data Source	Easting[b]	Northing[b]	County	Cased Depth (ft)	Drilled Depth (ft)	Dominant Layer[c]	% Open Section in Layer[c]	93/94 Months with Data[d]	03/04 Months with Data[e]	Use for Data in Model Setup/Calibration						Reasoning/Comments
													Observations for Calibration					
												Boundary Conditions[f]	Steady State (Oct 03)	Steady State (Feb 04)	Transient (03/04)	Transient (03/04	Not Used	
131344	RIDGE WRAP P-1 SURF	SWFWMD	395182.43	1388229.85	Polk	55	75	SAS	91%	9	15	SAS						
131379	RIDGE WRAP P-10 SURF	SWFWMD	464374.19	1236476.18	Polk	20	42	SAS	100%	10	14	SAS						
131346	RIDGE WRAP P-2 SURF	SWFWMD	427050.05	1351700.36	Polk	66	86	SAS	88%	10	15	SAS						
131350	RIDGE WRAP P-3 SURF	SWFWMD	424324.19	1329155.68	Polk	41	61	SAS	100%	10	15	SAS						
131342	RIDGE WRAP P-4 SURF	SWFWMD	446034.72	1420919.79	Polk	90	110	SAS	100%	9	15	SAS						
131215	RIDGE WRAP P-5 SURF	SWFWMD	453344.90	1385269.35	Polk	95	115	SAS	100%	10	15	SAS						
131345	RIDGE WRAP P-6 SURF	SWFWMD	460538.40	1366508.09	Polk	85	105	SAS	100%	10	15	SAS						
131348	RIDGE WRAP P-7 SURF	SWFWMD	458131.45	1350633.59	Polk	125	145	SAS	100%	10	15	SAS						
131351	RIDGE WRAP P-8 SURF	SWFWMD	465863.81	1326861.77	Polk	90	110	SAS	100%	10	15	SAS						
131361	RIDGE WRAP VC-1 SURF	SWFWMD	484564.91	1281218.53	Polk	45	65	SAS	100%	10	15	SAS						
131366	RIDGE WRAP VC-10A FLDN	SWFWMD	492507.06	1265438.55	Polk	245	263	IAS/ICU	100%	10	15						Not Used	No calibration in IAS/ICU
131367	RIDGE WRAP VC-10B SURF	SWFWMD	492513.34	1265436.51	Polk	10	21	SAS	100%	10	15	SAS						
131253	RIDGE WRAP VC-11A FLDN	SWFWMD	477273.21	1308848.80	Polk	162	260	IAS/ICU	100%	10	15						Not Used	No calibration in IAS/ICU
131353	RIDGE WRAP VC-11B SURF	SWFWMD	477216.69	1308845.02	Polk	40	60	SAS	100%	10	15	SAS						
131352	RIDGE WRAP VC-12 SURF	SWFWMD	474741.46	1319266.63	Polk	50	70	SAS	100%	10	14	SAS						
131349	RIDGE WRAP VC-13A FLDN	SWFWMD	466755.55	1341327.88	Polk	178	200	IAS/ICU	100%	10	14						Not Used	No calibration in IAS/ICU
131222	RIDGE WRAP VC-13B SURF	SWFWMD	466763.62	1341327.84	Polk	77	97	SAS	100%	10	15	SAS						
131257	RIDGE WRAP VC-2 SURF	SWFWMD	479361.73	1262910.59	Polk	130	150	SAS	100%	10	15	SAS						
131246	RIDGE WRAP VC-3 SURF	SWFWMD	474543.16	1277438.67	Polk	70	90	SAS	100%	10	15	SAS						
131261	RIDGE WRAP VC-4 SURF	SWFWMD	479325.91	1257690.56	Polk	85	105	SAS	100%	10	15	SAS						
131372	RIDGE WRAP VC-5 SURF	SWFWMD	493787.58	1249196.22	Polk	19	37	SAS	100%	10	15	SAS						
131369	RIDGE WRAP VC-6 SURF	SWFWMD	487990.65	1261242.11	Polk	35	55	SAS	100%	10	15	SAS						
131212	RIDGE WRAP VC-7 SURF	SWFWMD	477308.99	1304270.66	Polk	67	87	SAS	100%	10	15	SAS						
131259	RIDGE WRAP VC-8 SURF	SWFWMD	469413.00	1327185.14	Polk	59	79	SAS	100%	10	14	SAS						
131347	RIDGE WRAP VC-9 SURF	SWFWMD	465561.41	1350678.66	Polk	69	89	SAS	100%	10	15	SAS						
101199	RIVER RANCH WELL NEAR INDIAN LAKE ESTATES, FL	USGS	585855.04	1261570.32	Polk	280	300	UF	100%	6	9					UF	UF		Missing data for OCt03 and Feb04
131260	RODGER WELL		445454.26	1325296.16	Polk	91	612	MC1	57%	0	0						Not Used	Model geology puts this well in MC1
101172	ROMP 40 AVON PARK WELL NEAR DUETTE FL	USGS	314914.35	1206150.91	Polk	408	1140	MC1	38%	1	0						Not Used	Open section straddles multiple layers
101173	ROMP 40 HAWTHORN WELL NEAR DUETTE FL	USGS	314914.00	1206151.00	Polk	76	180	IAS/ICU	100%	10	0						Not Used	No calibration in IAS/ICU
131229	ROMP 40 HTRN	SWFWMD	314911.64	1206149.93	Polk	76	180	IAS/ICU	100%	10	15						Not Used	No calibration in IAS/ICU
131230	ROMP 40 SURF	SWFWMD	314922.31	1206135.69	Polk	38	43	IAS/ICU	100%	10	15						Not Used	No calibration in IAS/ICU
131228	ROMP 40 SWNN/AVPK	SWFWMD	314905.24	1206137.86	Polk	408	1140	MC1	38%	10	15						Not Used	Open section straddles multiple layers
101203	ROMP 44 FLORIDAN WELL NEAR BABSON PARK FL	USGS	462875.25	1269340.79	Polk	232	402	UF	50%	0	2						Not Used	sparse data
101204	ROMP 44 NRSD WELL NEAR BABSON PARK FL		462940.62	1269451.30	Polk	382	402	MC1	87%	0	0						Not Used	Model geology puts this well in MC1
131365	ROMP 44 SURF	SWFWMD	462883.35	1269344.79	Polk	25	75	SAS	100%	9	15	SAS						
131364	ROMP 44 SWNN/OCAL	SWFWMD	462872.50	1269328.69	Polk	232	402	UF	50%	10	15						Not Used	Open section straddles multiple layers
101192	ROMP 45 HAWTHORN WELL AT FORT MEADE FL	USGS	402029.13	1247374.09	Polk	172	192	IAS/ICU	100%	1	2						Not Used	No calibration in IAS/ICU
131381	ROMP 45 SHALLOW	SWFWMD	401924.20	1247825.20	Polk	38	58	IAS/ICU	100%	0	15						Not Used	No calibration in IAS/ICU
101193	ROMP 45 SUWANNEE WELL AT FORT MEADE FL	USGS	402029.13	1247374.09	Polk	420	440	UF	57%	1	2						Not Used	Sparse data
101195	ROMP 55 FLORIDAN WELL NEAR BABSON PARK FL	USGS	475013.54	1257376.72	Polk	212	1200	MC1	47%	0	2						Not Used	Open section straddles multiple layers
101196	ROMP 55 NRSD WELL NEAR BABSON PARK FL	USGS	475079.16	1257487.55	Polk	1100	1200	MC2	97%	10	0						Not Used	Model geology puts this well in MC2
131371	ROMP 55 SURF	SWFWMD	475021.63	1257378.71	Polk	23	73	SAS	100%	0	15	SAS						
131370	ROMP 55 SWNN/AVPK	SWFWMD	475013.58	1257386.82	Polk	212	1200	MC1	47%	10	15						Not Used	Open section straddles multiple layers
101219	ROMP 57 FLORIDAN WELL NEAR LAKE WALES FL	USGS	455176.83	1298292.05	Polk	160	634	MC1	63%	10	15						Not Used	Model geology puts this well in MC1
101220	ROMP 57 HAWTHORN WELL NEAR LAKE WALES FL	USGS	455176.83	1298292.05	Polk	95	140	IAS/ICU	100%	10	15						Not Used	No calibration in IAS/ICU
131357	ROMP 57 HTRN		455102.55	1298176.43	Polk	95	140	IAS/ICU	100%	0	0						Not Used	No calibration in IAS/ICU
101221	ROMP 57 NRSD WELL NEAR LAKE WALES FL	USGS	455176.83	1298292.05	Polk	20	40	SAS	100%	6	15	SAS						
131330	ROMP 57 SURF REPL		455106.98	1298166.31	Polk	20	40	SAS	100%	0	0						Not Used	Missing data
131225	ROMP 57 SURFICIAL		455107.88	1298166.31	Polk	20	40	SAS	100%	0	0						Not Used	Missing data
131356	ROMP 57 SWNN/AVPK	SWFWMD	455099.78	1298162.31	Polk	160	634	MC1	63%	10	15						Not Used	Model geology puts this well in MC1
101217	ROMP 57A NRSD WELL NEAR LAKE WALES FL	USGS	473333.27	1295628.57	Polk	115	135	SAS	100%	10	13	SAS						
101216	ROMP 57A OCALA WELL NEAR LAKE WALES FL	USGS	473333.27	1295628.57	Polk	274	315	IAS/ICU	100%	10	15						Not Used	No calibration in IAS/ICU
131360	ROMP 57X HTRN		473649.64	1295665.69	Polk	192	210	IAS/ICU	88%	0	0						Not Used	No calibration in IAS/ICU
131359	ROMP 57X OCAL		473649.64	1295665.69	Polk	274	315	IAS/ICU	100%	0	0						Not Used	No calibration in IAS/ICU
131358	ROMP 57X SURF		473470.19	1295666.52	Polk	114	135	SAS	100%	0	0						Not Used	Missing data
101225	ROMP 58 NRSD WELL NEAR LAKE WALES FL	USGS	464428.68	1304133.71	Polk	310	330	UF	100%	9	0					UF		no 03/04 data
131354	ROMP 58 OCAL	SWFWMD	464367.63	1304014.24	Polk	155	330	IAS/ICU	71%	0	15						Not Used	No calibration in IAS/ICU
101224	ROMP 58 OCALA WELL NEAR LAKE WALES FL	USGS	464363.19	1304024.36	Polk	155	330	IAS/ICU	71%	10	2						Not Used	No calibration in IAS/ICU
131355	ROMP 58 SURF	SWFWMD	464365.84	1304016.27	Polk	45	60	SAS	100%	0	15	SAS						
101212	ROMP 59 AVON PARK WELL AT BARTOW FL	USGS	377078.00	1291606.00	Polk	200	1048	MC1	39%	10	15						Not Used	Open section straddles multiple layers

Table 4.1: Usage of SAJ Observation Database in Regional Model Calibration

Model ID[a]	Well Name	Data Source	Easting[b]	Northing[b]	County	Cased Depth (ft)	Drilled Depth (ft)	Dominant Layer[c]	% Open Section in Layer[c]	93/94 Months with Data[d]	03/04 Months with Data[e]	Use for Data in Model Setup/Calibration						Reasoning/Comments
													Observations for Calibration					
												Boundary Conditions[f]	Steady State (Oct 03)	Steady State (Feb 04)	Transient (03/04)	Transient (03/04	Not Used	
101183	ROMP 59 AVON PARK WELL AT BARTOW FL	USGS	378524.86	1223899.73	Polk	808	908	MC1	83%	10	0						Not Used	Model geology puts this well in MC1
101213	ROMP 59 HAWTHORN WELL AT BARTOW FL	USGS	377077.52	1291605.98	Polk	122	142	IAS/ICU	100%	10	15						Not Used	No calibration in IAS/ICU
131242	ROMP 59 HTRN		376993.01	1291505.13	Polk	50	60	IAS/ICU	100%	0	0						Not Used	No calibration in IAS/ICU
131239	ROMP 59 SWNN/AVPK	SWFWMD	377013.59	1291495.89	Polk	200	1050	MC1	38%	10	15						Not Used	Open section straddles multiple layers
131241	ROMP 59 TMPA	SWFWMD	376995.71	1291506.12	Polk	122	142	IAS/ICU	100%	0	2						Not Used	No calibration in IAS/ICU
101214	ROMP 59 UPPER HAWTHORN WELL AT BARTOW FL	USGS	377077.52	1291605.98	Polk	50	60	IAS/ICU	100%	6	15						Not Used	No calibration in IAS/ICU
101215	ROMP 60 FLORIDAN WELL AT MULBERRY FL	USGS	338705.54	1294188.51	Polk	237	710	MC1	62%	10	2						Not Used	Model geology puts this well in MC1
131207	ROMP 60 OCAL/AVPK	SWFWMD	338833.88	1294301.61	Polk	237	710	MC1	62%	10	15						Not Used	Model geology puts this well in MC1
131255	ROMP 60X SWNN/AVPK	SWFWMD	349430.81	1318637.13	Polk	212	806	MC1	43%	4	13						Not Used	Open section straddles multiple layers
131264	ROMP 70 FLDN		348049.22	1359907.56	Polk	185	645	MC1	46%	0	0						Not Used	Open section straddles multiple layers
131382	ROMP 70 SURF		348050.11	1359907.55	Polk	22	35	SAS	100%	0	0						Not Used	missing data
131251	ROMP 73 TMPA/OCAL	SWFWMD	420250.43	1340985.39	Polk	161	389	UF	40%	0	15						Not Used	Open section straddles multiple layers
131337	ROMP 74X PERM LOWER FLDN		474028.89	1390055.84	Polk	1250	1400	LF	81%	0	0						Not Used	Missing data
131336	ROMP 74X PERM SURF		474038.02	1390096.20	Polk	25	225	SAS	85%	0	0						Not Used	Missing data
131331	ROMP 74X PERM UPPER FLDN		474038.17	1390126.49	Polk	450	740	APPZ	98%	0	0						Not Used	Missing data
131335	ROMP 76X 4-INCH SURF	SWFWMD	388602.85	1400030.87	Polk	25	35	IAS/ICU	100%	0	10						Not Used	No calibration in IAS/ICU
131206	ROMP 76X OCAL/AVPK	SWFWMD	388585.77	1400019.88	Polk	264	315	MC1	58%	10	15						Not Used	Model geology puts this well in MC1
131343	ROMP 87 AVPK	SWFWMD	326586.03	1414130.63	Polk	300	380	MC1	100%	10	15						Not Used	Model geology puts this well in MC1
101260	ROMP 87 NR LAKELAND , FL	USGS	327326.35	1414073.88	Polk	300	380	MC1	100%	0	12						Not Used	Model geology puts this well in MC1
131380	ROMP 87 SHALLOW	SWFWMD	326593.29	1414142.69	Polk	28	38	UF	100%	0	15		UF	UF	UF			no 93/94 data
131341	ROMP 88 AVPK	SWFWMD	362926.77	1446758.20	Polk	195	385	UF	83%	10	15						Not Used	Hillsborough Basin has a dense coverage of points and is not important for the purposes of the model; remove
131363	ROMP CL-1 6-IN SURF	SWFWMD	482814.69	1275075.81	Polk	29	49	SAS	100%	0	15	SAS						
131362	ROMP CL-1 SWNN/OCAL	SWFWMD	482797.56	1275059.73	Polk	220	315	IAS/ICU	86%	9	15						Not Used	No calibration in IAS/ICU
131375	ROMP CL-2 DEEP SURF	SWFWMD	490976.33	1244539.07	Polk	200	220	IAS/ICU	100%	10	15						Not Used	No calibration in IAS/ICU
131376	ROMP CL-2 FLDN	SWFWMD	490980.79	1244529.96	Polk	412	442	MC1	100%	1	15						Not Used	Model geology puts this well in MC1
131377	ROMP CL-2 HTRN	SWFWMD	490980.79	1244529.96	Polk	330	346	UF	100%	10	15		UF	UF	UF	UF		
131374	ROMP CL-2 SURF	SWFWMD	490976.34	1244540.08	Polk	17	22	SAS	100%	10	15	SAS						
101188	ROMP CL-2 WELL NEAR FROSTPROOF FL	USGS	490973.61	1244532.01	Polk	412	442	MC1	100%	0	2						Not Used	Model geology puts this well in MC1
101189	ROMP CL-3 FLORIDAN WELL NEAR FROSTPROOF FL	USGS	470797.04	1246822.48	Polk	228	440	UF	45%	0	2						Not Used	Open section straddles multiple layers
131252	ROMP CL-3 HTRN	SWFWMD	470800.59	1246814.39	Polk	140	197	IAS/ICU	100%	1	15						Not Used	No calibration in IAS/ICU
101191	ROMP CL-3 NRSD WELL NEAR FROSTPROOF FL	USGS	470862.54	1246933.69	Polk	420	440	MC1	100%	10	0						Not Used	Model geology puts this well in MC1
131205	ROMP CL-3 SURF	SWFWMD	470815.05	1246832.50	Polk	20	49	SAS	100%	0	15	SAS						
131373	ROMP CL-3 SWNN/OCAL	SWFWMD	470784.42	1246814.46	Polk	228	440	UF	45%	10	15						Not Used	Open section straddles multiple layers
101176	S-65A (POF-20R 397-FT) WELL NR YEEHAW JUNCTION FL	USGS	612466.77	1208414.07	Polk	900	1000	APPZ	90%	9	0					APPZ		no 03/04 data
101235	SANLON RANCH DEEP WELL NEAR EATON PARK FL	USGS	358372.27	1334019.98	Polk	293	1220	APPZ	36%	10	13						Not Used	Open section straddles multiple layers
131238	SANLON RANCH FLDN	SWFWMD	358317.23	1333911.15	Polk	293	1220	APPZ	36%	10	15						Not Used	Open section straddles multiple layers
131327	SAXONS FLDN		465953.61	1318526.34	Polk	0	150	SAS	51%	0	0						Not Used	Missing data
131227	SMITH WELL NR HAINES CITY		453539.83	1363225.90	Polk	110	549	MC1	60%	0	0						Not Used	Model geology puts this well in MC1
110098	SNIVELY_G	SFWMD	521386.03	1322640.39	Polk	10.67	12.67	SAS	100%	9	10	SAS						
101262	SPREAD EAGLE RNCH DP	USGS	423905.76	1422267.45	Polk	80	285	UF	85%	1	2						Not Used	Sparse data
131213	SR 33/COMBEE ROAD SHALLOW	SWFWMD	363388.15	1376768.73	Polk	8	9	SAS	100%	10	15	SAS						
101218	SR 60 DEEP WELL NEAR LAKE WALES FL	USGS	444995.06	1297265.64	Polk	1400	1500	MC2	100%	1	2						Not Used	Model geology puts this well in MC2
101248	TENNOROCK ROAD WELL NEAR LAKELAND, FL	USGS	369049.67	1369707.17	Polk	45	72	IAS/ICU	100%	6	9						Not Used	No calibration in IAS/ICU
131266	TENOROC FLRD NR LAKELAND		376372.33	1370064.31	Polk	400	430	MC1	100%	0	0						Not Used	Model geology puts this well in MC1
131224	TENOROC RD NR LAKELAND IN		369116.72	1369812.73	Polk	45	72	IAS/ICU	100%	0	0						Not Used	No calibration in IAS/ICU
131267	TENOROC REPLACEMENT NRSD		371356.29	1369999.42	Polk	18	20	IAS/ICU	100%	0	0						Not Used	No calibration in IAS/ICU
131332	THORNHILL RANCH DEEP	SWFWMD	445373.35	1406440.19	Polk	108	151	UF	68%	0	12						Not Used	Located near 101258, which is open only in the UF and has more data
131333	THORNHILL RANCH SHALLOW	SWFWMD	445375.14	1406440.18	Polk	10	15	SAS	100%	0	12	SAS						
110174	TICK ISL_G	SFWMD	595826.79	1218544.64	Polk	6.7	8.7	SAS	100%	10	15	SAS						
101257	USGS CORE HOLE 2 AT POLK CITY	USGS	388603.13	1400071.27	Polk	1896	1996	LC	99%	1	2						Not Used	Model geology puts this well in LC
131263	USGS GREEN SWAMP DEEP	SWFWMD	423987.90	1422393.21	Polk	80	285	UF	85%	1	0						Not Used	sparse data
131234	USGS P-47 SHALLOW		460706.24	1399042.18	Polk	60	67	SAS	100%	0	0						Not Used	Missing data
131243	USGS P-48 SHALLOW	SWFWMD	484431.00	1226719.00	Polk	59	62	SAS	100%	10	15	SAS						
131250	VARN CITRUS		420619.79	1250298.54	Polk	497	890	MC1	95%	0	0						Not Used	Model geology puts this well in MC1
101227	WARREN HAWTHORN NEAR MULBERRY FL	USGS	321326.43	1311563.05	Polk	107	127	IAS/ICU	100%	1	2						Not Used	No calibration in IAS/ICU
131258	WEST WELL		429527.61	1221263.02	Polk	0	928	MC1	49%	0	0						Not Used	Open section straddles multiple layers
101211	WILDWOOD BAPTIST CHURCH AT BARTOW FL	USGS	381225.65	1291951.19	Polk	130	150	IAS/ICU	100%	1	0						Not Used	No calibration in IAS/ICU
131269	WILLIAMS CLAY MONITOR		365794.87	1380947.49	Polk	28	31	IAS/ICU	100%	0	0						Not Used	No calibration in IAS/ICU
131268	WILLIAMS MONITOR CW-3		369002.56	1378802.79	Polk	22	26	SAS	100%	0	0						Not Used	Missing data
110177	WR11_GW1	SFWMD	525736.74	1363324.06	Polk	19.39	21.39	SAS	100%	0	15	SAS						
110176	WR15_GW1	SFWMD	530392.73	1362803.72	Polk	19.27	21.27	SAS	100%	0	15	SAS						

Table 4.1: Usage of SAJ Observation Database in Regional Model Calibration

Model ID[a]	Well Name	Data Source	Easting[b]	Northing[b]	County	Cased Depth (ft)	Drilled Depth (ft)	Dominant Layer[c]	% Open Section in Layer[c]	93/94 Months with Data[d]	03/04 Months with Data[e]	Use for Data in Model Setup/Calibration						Reasoning/Comments
													Observations for Calibration					
												Boundary Conditions[f]	Steady State (Oct 03)	Steady State (Feb 04)	Transient (03/04)	Transient (03/04	Not Used	
110175	WR16_GW1	SFWMD	529670.95	1361190.21	Polk	21.05	23.05	SAS	100%	0	15	SAS						
110698	C24GW	SFWMD	819193.11	1092402.93	Saint Lucie	600	775	UF	100%	10	0					UF		no 03/04 data
110851	IRLMG1	SFWMD	904532.29	1066442.42	Saint Lucie	93.42	98.42	SAS	100%	0	14	SAS						
110853	IRLMG2	SFWMD	904538.13	1066435.49	Saint Lucie	51.7	56.7	SAS	100%	0	12	SAS						
110854	IRLMG3	SFWMD	904544.06	1066426.43	Saint Lucie	24.47	29.47	SAS	100%	0	12	SAS						
110104	IRMNG1	SFWMD	878950.14	1122632.13	Saint Lucie	53.35	58.35	SAS	100%	0	14	SAS						
110105	IRMNG2	SFWMD	878953.27	1122623.83	Saint Lucie	24.31	29.31	SAS	100%	0	14	SAS						
101402	PG-1	USGS	876911.74	1128107.71	Saint Lucie	31	36	SAS	100%	8	0	SAS						
101393	PG-10	USGS	837415.05	1114984.82	Saint Lucie	21	26	SAS	100%	2	0						Not Used	sparse data
101410	PG-12	USGS	834558.62	1169706.28	Saint Lucie	20	22	SAS	100%	3	0						Not Used	sparse data
101401	PG-15E	USGS	827447.18	1127564.37	Saint Lucie	53	58	SAS	100%	3	0						Not Used	sparse data
101405	PG-16	USGS	814163.07	1137507.58	Saint Lucie	20	25	SAS	100%	4	0						Not Used	sparse data
101383	PG-25	USGS	874563.59	1079015.57	Saint Lucie	7	27	SAS	100%	4	0						Not Used	sparse data
101386	PG-26	USGS	809732.90	1094370.58	Saint Lucie	21	23	SAS	100%	4	0						Not Used	sparse data
101407	PG-5	USGS	864834.50	1146120.10	Saint Lucie	20	25	SAS	100%	10	0	SAS						
101394	PG-7	USGS	861918.71	1117424.88	Saint Lucie	22	24	SAS	100%	4	0						Not Used	sparse data
111061	SAV1_G	SFWMD	892044.82	1079936.52	Saint Lucie	20.75	22.75	SAS	100%	0	15	SAS						
110860	SLCM_G1	SFWMD	880460.00	1058053.00	Saint Lucie	80.17	100.17	SAS	100%	0	14	SAS						
110862	SLCM_G2	SFWMD	880455.00	1058045.00	Saint Lucie	52.28	57.28	SAS	100%	0	14	SAS						
110861	SLCM_G3	SFWMD	880457.00	1058049.00	Saint Lucie	26.67	31.67	SAS	100%	0	14	SAS						
140055	SLF-0051	USGS ALTAMONTE SPRINGS via DEP	867726.02	1092713.32	Saint Lucie	600	775	UF	100%	0	0						Not Used	sparse data
112228	SLF-11	SFWMD	791281.52	1164690.00	Saint Lucie	224	946	UF	69%	1	0						Not Used	sparse data
112229	SLF-14	SFWMD	795303.17	1092197.81	Saint Lucie	318	1286	UF	28%	1	0						Not Used	Open section straddles multiple layers
112230	SLF-17	SFWMD	795581.10	1087367.68	Saint Lucie	320	1286	UF	27%	1	0						Not Used	Open section straddles multiple layers
112231	SLF-21	SFWMD	850164.05	1125344.56	Saint Lucie	156	707	IAS/ICU	56%	1	0						Not Used	No calibration in IAS/ICU
112232	SLF-23	SFWMD	828573.74	1049525.83	Saint Lucie	350	894	UF	50%	1	0						Not Used	sparse data
120632	SLF-27		814054.87	1111164.37	Saint Lucie	300	900	UF	63%	0	0						Not Used	Missing data
112233	SLF-27	SFWMD	814069.64	1111164.76	Saint Lucie	300	900	UF	63%	1	0						Not Used	sparse data
112234	SLF-3	SFWMD	838909.34	1151174.63	Saint Lucie	310	1106	UF	74%	1	0						Not Used	sparse data
112235	SLF-4	SFWMD	823514.09	1141685.71	Saint Lucie	492	993	UF	100%	1	0						Not Used	sparse data
120633	SLF-4		823575.81	1141601.20	Saint Lucie	482	993	UF	100%	0	0						Not Used	Missing data
112236	SLF-40	SFWMD	820708.50	1122891.04	Saint Lucie	376	786	UF	72%	1	0						Not Used	sparse data
112237	SLF-46	SFWMD	880298.42	1155847.66	Saint Lucie	666	1100	UF	100%	1	0						Not Used	sparse data
120634	SLF-46		880895.13	1152379.13	Saint Lucie	666	1100	UF	100%	0	0						Not Used	Missing data
112238	SLF-47	SFWMD	905882.88	1089007.18	Saint Lucie	850	1230	UF	88%	0	0						Not Used	sparse data
112239	SLF-50	SFWMD	819191.80	1092403.42	Saint Lucie	600	775	UF	100%	1	0						Not Used	sparse data
112108	SLF-62B	SFWMD	836003.27	1082784.18	Saint Lucie	355	733	IAS/ICU	51%	0	15						Not Used	No calibration in IAS/ICU
112101	SLF-69	SFWMD	836548.22	1101782.47	Saint Lucie	420	866	UF	78%	0	9						Not Used	Open section of nearby well (112161) completely in UF.
112162	SLF-74	SFWMD	821840.68	1092293.33	Saint Lucie	1068	1450	APPZ	90%	0	15				APPZ			Seems to be a data error in the middle of the 0304 dataset. Keep it in transient set for shape comparison only
112160	SLF-75	SFWMD	821825.10	1092287.51	Saint Lucie	480	700	UF	50%	0	15						Not Used	Open section of nearby well (112161) completely in UF.
112161	SLF-76	SFWMD	821840.68	1092293.33	Saint Lucie	790	860	UF	100%	0	15		UF	UF	UF			no 93/94 data
120635	SLF-9		788839.62	1132080.25	Saint Lucie	263	1060	UF	49%	0	0						Not Used	Open section straddles multiple layers
112240	SLF-9	SFWMD	789049.08	1131963.83	Saint Lucie	263	1058	UF	49%	1	0						Not Used	Open section straddles multiple layers
110876	SLHR_G1	SFWMD	881382.00	1055006.00	Saint Lucie	54.04	59.04	SAS	100%	0	14	SAS						
110877	SLHR_G2	SFWMD	881382.00	1049996.00	Saint Lucie	24.79	29.79	SAS	100%	0	14	SAS						
101385	STL-123	USGS	804360.80	1083848.44	Saint Lucie	11	13	SAS	100%	3	0						Not Used	sparse data
101397	STL-125	USGS	848353.12	1123633.58	Saint Lucie	9.77	11.77	SAS	100%	0	15	SAS						
110456	STL-125_G	SFWMD	848354.51	1123632.99	Saint Lucie	0	11.77	SAS	100%	0	15	SAS						
101391	STL-130	USGS	843408.08	1105418.60	Saint Lucie	13	15	SAS	100%	4	0						Not Used	sparse data
101384	STL-134	USGS	819344.73	1081179.45	Saint Lucie	13	15	SAS	100%	3	0						Not Used	sparse data
101395	STL-136	USGS	858673.18	1117610.44	Saint Lucie	12	14	SAS	100%	2	0						Not Used	sparse data
101392	STL-172	USGS	880325.77	1110771.65	Saint Lucie	25	30	SAS	100%	10	15	SAS						
110742	STL-172_G	SFWMD	880325.59	1110771.91	Saint Lucie	26	30	SAS	100%	10	0	SAS						
101382	STL-173	USGS	881784.48	1078348.19	Saint Lucie	42	47	SAS	100%	8	0	SAS						
101378	STL-174	USGS	888370.66	1078284.37	Saint Lucie	21	26	SAS	100%	10	0	SAS						
101380	STL-175	USGS	897104.43	1078553.39	Saint Lucie	180	200	SAS	51%	10	15	SAS						
111448	STL-175_G	SFWMD	897105.66	1078552.68	Saint Lucie	13	200	SAS	94%	10	15	SAS						
101381	STL-176	USGS	897104.43	1078553.39	Saint Lucie	25	30	SAS	100%	10	15	SAS						
110737	STL-176_G	SFWMD	897105.66	1078552.68	Saint Lucie	26	30	SAS	100%	10	0	SAS						
101379	STL-177	USGS	897752.34	1078440.13	Saint Lucie	182	202	IAS/ICU	56%	5	0	SAS						
101370	STL-185	USGS	819147.72	1058474.44	Saint Lucie	95	115	SAS	100%	10	15	SAS						
101404	STL-191	USGS	873457.91	1133643.26	Saint Lucie	113	133	IAS/ICU	100%	10	0						Not Used	No calibration in IAS/ICU
101406	STL-192	USGS	870721.33	1139990.81	Saint Lucie	98	118	SAS	66%	4	0	SAS						
101396	STL-213	USGS	850723.82	1117888.97	Saint Lucie	95	115	SAS	100%	10	15	SAS						
110758	STL-213		850879.05	1107776.24	Saint Lucie	110	115	SAS	100%	0	0						Not Used	Missing data
101375	STL-214	USGS	845908.02	1068486.53	Saint Lucie	65	70	SAS	100%	10	15	SAS						
110719	STL-214		847822.08	1067772.44	Saint Lucie	40	70	SAS	100%	0	0						Not Used	Missing data

Table 4.1: Usage of SAJ Observation Database in Regional Model Calibration

Model ID[a]	Well Name	Data Source	Easting[b]	Northing[b]	County	Cased Depth (ft)	Drilled Depth (ft)	Dominant Layer[c]	% Open Section in Layer[c]	93/94 Months with Data[d]	03/04 Months with Data[e]	Use for Data in Model Setup/Calibration						Reasoning/Comments
													Observations for Calibration					
												Boundary Conditions[f]	Steady State (Oct 03)	Steady State (Feb 04)	Transient (03/04)	Transient (03/04	Not Used	
101408	STL-264	USGS	834231.43	1158407.56	Saint Lucie	85	90	SAS	100%	10	15	SAS						
101411	STL-266	USGS	857324.06	1171126.76	Saint Lucie	36.5	41.5	SAS	100%	9	0	SAS						
101409	STL-267	USGS	819390.46	1159038.23	Saint Lucie	18	20	SAS	100%	4	0						Not Used	sparse data
101390	STL-269	USGS	854858.86	1105170.29	Saint Lucie	20	22	SAS	100%	4	0						Not Used	sparse data
101371	STL-270	USGS	878003.45	1060351.98	Saint Lucie	21	23	SAS	100%	4	0						Not Used	sparse data
101372	STL-271	USGS	865903.79	1061398.58	Saint Lucie	21	23	SAS	100%	4	0						Not Used	sparse data
101374	STL-272	USGS	845745.47	1068267.41	Saint Lucie	21	23	SAS	100%	1	0						Not Used	sparse data
101376	STL-276	USGS	889220.85	1071624.16	Saint Lucie	20.5	22.5	SAS	100%	4	0						Not Used	sparse data
101377	STL-277	USGS	894270.71	1072158.39	Saint Lucie	19.5	21.5	SAS	100%	3	0						Not Used	sparse data
101387	STL-278	USGS	884649.90	1098157.56	Saint Lucie	21.5	26.5	SAS	100%	3	0						Not Used	sparse data
101389	STL-279	USGS	813758.53	1102666.64	Saint Lucie	79	84	SAS	100%	4	0						Not Used	sparse data
111127	STL-279_G	SFWMD	813856.73	1102754.47	Saint Lucie	79	84	SAS	100%	0	14	SAS						
101399	STL-286	USGS	803120.54	1127266.44	Saint Lucie	75	80	SAS	100%	3	0						Not Used	sparse data
110186	STL-286_G	SFWMD	803175.50	1127391.75	Saint Lucie	75	80	SAS	100%	0	11	SAS						
101400	STL-287	USGS	803120.54	1127266.44	Saint Lucie	30	35	SAS	100%	3	0						Not Used	sparse data
110185	STL-287_G	SFWMD	803175.50	1127391.75	Saint Lucie	30	35	SAS	100%	0	11	SAS						
101398	STL-294	USGS	876288.74	1126690.48	Saint Lucie	133	153	IAS/ICU	79%	5	0	SAS						
101388	STL-313	USGS	776962.36	1100535.82	Saint Lucie	102	122	SAS	100%	10	15	SAS						
110754	STL-313		779505.28	1100225.33	Saint Lucie	40	122	SAS	100%	0	0						Not Used	Missing data
101373	STL-41	USGS	780157.64	1064076.01	Saint Lucie	15	17	SAS	100%	9	0	SAS						
101403	STL-42	USGS	762902.57	1132506.55	Saint Lucie	16	18	SAS	100%	10	15	SAS						
101332	BEE RIDGE WELL 15 NEAR SARASOTA FL	USGS	200608.74	1080349.38	Sarasota	100	120	IAS/ICU	100%	1	2						Not Used	No calibration in IAS/ICU
131408	BIG SLOUGH DEEP	SWFWMD	280501.24	1041161.63	Sarasota	78	100	IAS/ICU	100%	10	15						Not Used	No calibration in IAS/ICU
101323	BIG SLOUGH DEEP WELL NR ARCADIA FL	USGS	280533.81	1041280.87	Sarasota	80	100	IAS/ICU	100%	10	15						Not Used	No calibration in IAS/ICU
131409	BIG SLOUGH SHALLOW	SWFWMD	280500.35	1041162.65	Sarasota	19	25	IAS/ICU	100%	10	4						Not Used	No calibration in IAS/ICU
101324	BIG SLOUGH SHALLOW WELL NEAR ARCADIA FL	USGS	280533.81	1041280.87	Sarasota	20	25	IAS/ICU	100%	10	10						Not Used	No calibration in IAS/ICU
101339	CELERY FARM NRSD WELL 1 NEAR SARASOTA FL	USGS	189644.70	1094443.74	Sarasota	17.7	19.7	SAS	100%	3	0						Not Used	sparse data
101336	CELERY FARM NRSD WELL 11 NEAR SARASOTA FL	USGS	187169.68	1091037.95	Sarasota	10.5	12.5	SAS	100%	4	0						Not Used	sparse data
101338	CELERY FARM NRSD WELL 3 NEAR SARASOTA FL	USGS	191611.62	1092905.97	Sarasota	16.5	18.5	SAS	100%	3	0						Not Used	sparse data
101337	CELERY FARM NRSD WELL 4 NEAR SARASOTA FL	USGS	191235.75	1091597.15	Sarasota	17.2	19.2	SAS	100%	3	0						Not Used	sparse data
101334	CELERY FARM NRSD WELL 9 NEAR SARASOTA FL	USGS	190854.07	1089783.34	Sarasota	18.7	20.7	SAS	100%	3	0						Not Used	sparse data
131416	CITY OF SARASOTA 23RD/COCONUT		155072.29	1102348.09	Sarasota	450	570	UF	100%	0	0						Not Used	Missing data
131399	CITY OF SARASOTA INJECTION		158276.55	1098874.01	Sarasota	1108	1500	APPZ	56%	0	0						Not Used	Missing data
101342	CITY SARASOTA 11TH ST AND OREGON WELL SARASOTA FL	SWFWMD	154481.77	1098517.10	Sarasota	43	479	IAS/ICU	81%	10	15						Not Used	No calibration in IAS/ICU
101346	CITY SARASOTA 23RD AND COCONUT W NEAR SARASOTA FL	USGS	154944.20	1102349.83	Sarasota	450	570	UF	100%	10	15						Not Used	appears to be impated by local pumping
101348	CITY SARASOTA 27TH ST WELL NEAR SARASOTA FL	USGS	154298.99	1103048.63	Sarasota	45	343	IAS/ICU	100%	10	2	IAS-layer 2						averaged with 101344
101347	CITY SARASOTA HICKORY AVE WELL AT SARASOTA FL	USGS	152867.01	1102860.45	Sarasota	38	591	IAS/ICU	62%	10	15						Not Used	Outside Boundary
131414	ENGLEWOOD 14 DEEP	SWFWMD	219736.37	962919.09	Sarasota	44	55	IAS/ICU	100%	10	15	IAS-layer 2						
131415	ENGLEWOOD 14A SHALLOW	SWFWMD	219731.82	962916.11	Sarasota	10	20	SAS	100%	10	15	SAS						
131392	ENGLEWOOD 3 DEEP		212981.83	978349.77	Sarasota	109	135	IAS/ICU	100%	0	0						Not Used	No calibration in IAS/ICU
131424	ENGLEWOOD 5 PROD ZONE INT		208311.16	979163.03	Sarasota	37	66	IAS/ICU	97%	0	0						Not Used	No calibration in IAS/ICU
131425	ENGLEWOOD 5 WT		208330.19	979165.86	Sarasota	10	15	SAS	100%	0	0						Not Used	Missing data
131397	ENGLEWOOD 8 PRODUCTION ZON		213711.96	978947.91	Sarasota	58	70	IAS/ICU	100%	0	0						Not Used	No calibration in IAS/ICU
131391	ENGLEWOOD C-10		213582.33	975313.21	Sarasota	42	70	IAS/ICU	96%	0	0						Not Used	No calibration in IAS/ICU
101274	ENGLEWOOD DEEP ZONE 3 NEAR ENGLEWOOD FL	USGS	212584.23	978221.75	Sarasota	109	135	IAS/ICU	100%	1	2						Not Used	No calibration in IAS/ICU
101271	ENGLEWOOD TEST C10 NR ENGLEWOOD FL	USGS	213519.50	975191.68	Sarasota	42	70	IAS/ICU	96%	1	0						Not Used	No calibration in IAS/ICU
131418	ENGLEWOOD TW6 INT		223738.21	960357.86	Sarasota	45	65	IAS/ICU	100%	0	0						Not Used	No calibration in IAS/ICU
101268	ENGLEWOOD WATER DT R-2 NEAR ENGLEWOOD FL	USGS	216763.37	954501.96	Sarasota	90	110	IAS/ICU	100%	1	2						Not Used	sparse data
101266	ENGLEWOOD WD PO 1 NEAR ENGLEWOOD FL	USGS	226943.46	952526.07	Sarasota	300	320	IAS/ICU	100%	1	0						Not Used	sparse data
101267	ENGLEWOOD WD RIVER 2 NEAR ENGLEWOOD FL	USGS	217187.12	954345.94	Sarasota	290	310	IAS/ICU	100%	1	0						Not Used	sparse data
101270	ENGLEWOOD WELL 14 NE ENGLEWOOD FL	USGS	219720.66	962803.11	Sarasota	44	55	IAS/ICU	100%	1	0						Not Used	duplicate with 131414, sparse data
101265	ENGLEWOOD WELL 150 NEAR ENGLEWOOD FL	USGS	227539.85	952428.96	Sarasota	81	101	IAS/ICU	100%	1	2						Not Used	sparse data
101269	ENGLEWOOD WELL TW 6 NR ENGLEWOOD FL	USGS	223548.07	960177.05	Sarasota	45	65	IAS/ICU	100%	1	2						Not Used	No calibration in IAS/ICU

Table 4.1: Usage of SAJ Observation Database in Regional Model Calibration

Model ID[a]	Well Name	Data Source	Easting[b]	Northing[b]	County	Cased Depth (ft)	Drilled Depth (ft)	Dominant Layer[c]	% Open Section in Layer[c]	93/94 Months with Data[d]	03/04 Months with Data[e]	Use for Data in Model Setup/Calibration						Reasoning/Comments
													Observations for Calibration					
												Boundary Conditions[f]	Steady State (Oct 03)	Steady State (Feb 04)	Transient (03/04)	Transient (03/04	Not Used	
131398	ENGLEWOOD WT 8A		213711.97	978948.92	Sarasota	14	16	SAS	100%	0	0						Not Used	Missing data
101331	FLA CITIES TEST 1 NR SARASOTA FL	USGS	201107.00	1070392.00	Sarasota	426	446	IAS/ICU	100%	9	15						Not Used	No calibration in IAS/ICU
131421	FLORIDA CITIES TEST 1	SWFWMD	201062.23	1070252.53	Sarasota	104	446	IAS/ICU	100%	10	7						Not Used	No calibration in IAS/ICU
101289	HENRY RANCH WELL 1 NEAR MURDOCK FL	USGS	205263.57	1022349.70	Sarasota	266	286	IAS/ICU	100%	1	0						Not Used	No calibration in IAS/ICU
101291	HENRY RANCH WELL 3 NEAR VENICE FL	USGS	207090.63	1024147.67	Sarasota	73	78	IAS/ICU	100%	1	0						Not Used	No calibration in IAS/ICU
101345	KENSINGTON PARK WELL 1 NEAR SARASOTA FL	USGS	169991.84	1102250.93	Sarasota	190	210	IAS/ICU	100%	1	2						Not Used	No calibration in IAS/ICU
101361	KME 02 WELL NEAR SARASOTA FL	USGS	227614.57	1110892.17	Sarasota	760	860	MC1	100%	4	0						Not Used	Model geology puts this well in MC1
131420	KME 09		249273.27	1106643.33	Sarasota	123	575	IAS/ICU	71%	0	0						Not Used	No calibration in IAS/ICU
131406	KME 09 WT		232714.01	1110436.42	Sarasota	21	42	SAS	100%	0	0						Not Used	Missing data
101355	KME RECHARGE WELL NEAR VERNA FL	USGS	237767.00	1110297.00	Sarasota	1100	1200	MC1	100%	10	0						Not Used	Model geology puts this well in MC1
101358	KME WATER TABLE 09 WELL NEAR SARASOTA FL	USGS	232811.75	1110651.36	Sarasota	21	42	SAS	100%	9	0	SAS						
101359	KME WELL 04 NEAR SARASOTA FL	USGS	224157.00	1110743.00	Sarasota	420	440	IAS/ICU	90%	10	0						Not Used	No calibration in IAS/ICU
101360	KME WELL 04-A NEAR VERNA NEAR SARASOTA FL	USGS	224095.28	1110626.62	Sarasota	18	20	SAS	100%	5	0	SAS						
101364	KME WELL 08 NEAR SARASOTA FL	SWFWMD	243551.00	1111550.00	Sarasota	126	445	IAS/ICU	100%	10	15						Not Used	No calibration in IAS/ICU
101352	KME WELL 14A NR VERNA FL	USGS	235055.15	1109617.91	Sarasota	87	107	IAS/ICU	100%	10	0						Not Used	No calibration in IAS/ICU
131400	KME WT 11 NR VERNA		234164.90	1110535.39	Sarasota	18	21	SAS	100%	0	0						Not Used	Missing data
101290	MABRY CARLTON (STM-24A) TAMPA WELL NR SARASOTA FL	USGS	223924.00	1023581.00	Sarasota	380	400	IAS/ICU	100%	9	0						Not Used	No calibration in IAS/ICU
131394	MABRY CARLTON 13 NR MYAK C		276969.66	1030829.96	Sarasota	65	287	IAS/ICU	100%	0	0						Not Used	No calibration in IAS/ICU
101304	MABRY CARLTON 26 NRSD WELL NEAR SARASOTA FL	USGS	245165.34	1028533.12	Sarasota	91	96	IAS/ICU	100%	5	0						Not Used	No calibration in IAS/ICU
101305	MABRY CARLTON 27 NRSD WELL NEAR SARASOTA FL	USGS	245175.34	1028543.12	Sarasota	91	96	IAS/ICU	100%	5	0						Not Used	No calibration in IAS/ICU
101311	MABRY CARLTON 4-B NRSD WELL NEAR SARASOTA FL	USGS	219976.31	1032107.41	Sarasota	185	205	IAS/ICU	100%	7	0						Not Used	No calibration in IAS/ICU
131396	MABRY CARLTON 6 INT		283425.04	1046432.08	Sarasota	311	369	IAS/ICU	100%	0	0						Not Used	No calibration in IAS/ICU
101287	MABRY CARLTON CW-1 (3E) HTRN WELL NEAR SARASOTA FL	USGS	225647.84	1021644.24	Sarasota	210	230	IAS/ICU	100%	9	0						Not Used	No calibration in IAS/ICU
101286	MABRY CARLTON CW-1 (3F) SWNN WELL NEAR SARASOTA FL	USGS	225675.00	1021614.00	Sarasota	454	554	IAS/ICU	60%	9	2						Not Used	No calibration in IAS/ICU
101294	MABRY CARLTON CW-2 (HM-21)HTRN WELL NR SARASOTA FL	USGS	225244.05	1026193.46	Sarasota	220	240	IAS/ICU	100%	6	0						Not Used	No calibration in IAS/ICU
101292	MABRY CARLTON CW-2 (OM-21) OCALA W NR SARASOTA FL	USGS	225244.00	1026193.00	Sarasota	900	1000	MC1	100%	6	0						Not Used	Model geology puts this well in MC1
101293	MABRY CARLTON CW-2 (SM 21A)SWNN W NR SARASOTA FL	USGS	224929.00	1026318.00	Sarasota	590	690	UF	100%	6	0					UF		no 03/04 data
101319	MABRY CARLTON CW-3 (6E) HTRN WELL NEAR SARASOTA FL	USGS	236500.47	1038025.63	Sarasota	220	240	IAS/ICU	100%	6	2						Not Used	No calibration in IAS/ICU
101318	MABRY CARLTON CW-3 (6F) SWNN WELL NEAR SARASOTA FL	USGS	236518.53	1038025.44	Sarasota	451	551	IAS/ICU	63%	6	2						Not Used	No calibration in IAS/ICU
101320	MABRY CARLTON CW-3 (6G) NRSD WELL NEAR SARASOTA FL	USGS	236562.03	1038144.80	Sarasota	220	240	IAS/ICU	100%	3	0						Not Used	No calibration in IAS/ICU
101301	MABRY CARLTON CW-5 (14-EN) HAWTHORN NR SARASOTA FL	USGS	245145.34	1028513.12	Sarasota	91	96	IAS/ICU	100%	4	0						Not Used	No calibration in IAS/ICU
101300	MABRY CARLTON CW-5 (14-FN) SUWANNEE NR SARASOTA FL	USGS	245156.33	1028433.23	Sarasota	450	550	IAS/ICU	73%	8	2						Not Used	No calibration in IAS/ICU
101302	MABRY CARLTON CW-5 (14-GN) NRSD NR SARASOTA FL	USGS	245155.34	1028523.12	Sarasota	91	96	IAS/ICU	100%	3	0						Not Used	No calibration in IAS/ICU
101282	MABRY CARLTON CW-6 (14-ES) HTRN W NR SARASOTA FL	USGS	247351.49	1020562.74	Sarasota	190	210	IAS/ICU	100%	8	0						Not Used	No calibration in IAS/ICU
101280	MABRY CARLTON CW-6 (14-FS) SWNN W. NR SARASOTA FL	USGS	247280.85	1020453.05	Sarasota	450	550	IAS/ICU	75%	9	2						Not Used	No calibration in IAS/ICU
101283	MABRY CARLTON CW-6 (14S) NRSD WELL NR SARASOTA FL	USGS	247351.49	1020562.74	Sarasota	190	210	IAS/ICU	100%	9	0						Not Used	No calibration in IAS/ICU
101315	MABRY CARLTON CW-7 (20) NRSD WELL NEAR SARASOTA FL	USGS	263272.52	1033495.37	Sarasota	230	250	IAS/ICU	100%	8	0						Not Used	No calibration in IAS/ICU
101314	MABRY CARLTON CW-7 (20E) HTRN WELL NR SARASOTA FL	USGS	263262.52	1033485.37	Sarasota	230	250	IAS/ICU	100%	8	0						Not Used	No calibration in IAS/ICU
101313	MABRY CARLTON CW-7 (20F) SWNN WELL NR SARASOTA FL	USGS	263291.10	1033395.48	Sarasota	529	629	UF	100%	8	2					UF		no 03/04 data
101303	MABRY CARLTON OM-41 SWNN WELL NEAR SARASOTA FL	USGS	236602.00	1028873.00	Sarasota	650	750	UF	100%	7	0					UF		no 03/04 data
101307	MABRY CARLTON WELL 13 NEAR MYAKKA CITY FL	USGS	276968.00	1030831.00	Sarasota	65	287	IAS/ICU	100%	10	0						Not Used	No calibration in IAS/ICU
101321	MABRY CARLTON WELL 16 NEAR MYAKKA CITY FL	USGS	285566.38	1039317.51	Sarasota	281	301	IAS/ICU	100%	1	0						Not Used	No calibration in IAS/ICU

Table 4.1: Usage of SAJ Observation Database in Regional Model Calibration

Model ID[a]	Well Name	Data Source	Easting[b]	Northing[b]	County	Cased Depth (ft)	Drilled Depth (ft)	Dominant Layer[c]	% Open Section in Layer[c]	93/94 Months with Data[d]	03/04 Months with Data[e]	Use for Data in Model Setup/Calibration						Reasoning/Comments
													Observations for Calibration					
												Boundary Conditions[f]	Steady State (Oct 03)	Steady State (Feb 04)	Transient (03/04)	Transient (03/04	Not Used	
101327	MABRY CARLTON WELL 6 NEAR MYAKKA CITY FL	USGS	283462.71	1046305.49	Sarasota	349	369	IAS/ICU	100%	10	1						Not Used	No calibration in IAS/ICU
101281	MACARTHUR TRACT WELL 14GS NEAR MURDOCK FL	USGS	247171.82	1020393.54	Sarasota	280	300	IAS/ICU	100%	1	0						Not Used	No calibration in IAS/ICU
131410	MANASOTA 14 DEEP	SWFWMD	201049.83	981682.15	Sarasota	263	305	IAS/ICU	100%	10	15						Not Used	duplicate with 101275
101275	MANASOTA DEEP 14 NR ENGLEWOOD FL	USGS	201113.03	981792.50	Sarasota	263	305	IAS/ICU	100%	10	15	IAS-layer 3						averaged with 131441
101306	MYAKKA RIVER NURSERY WELL NEAR MURDOCK FL	USGS	192967.57	1029759.84	Sarasota	80	100	IAS/ICU	100%	1	0						Not Used	No calibration in IAS/ICU
101272	N PORT ON SITE MON WELL NEAR NORTH PORT FL	USGS	246984.37	977187.81	Sarasota	650	750	UF	100%	0	2						Not Used	Sparse data
101273	N PORT ONSITE SH MONITOR WELL NEAR NORTH PORT FL	USGS	246984.37	977187.81	Sarasota	500	600	UF	82%	1	2						Not Used	Sparse data
101354	NE SCHROEDER-MANATEE FLORIDAN WELL NR SARASOTA FL	USGS	202813.82	1110455.67	Sarasota	1180	1280	MC1	87%	1	0						Not Used	Model geology puts this well in MC1
101341	NEW HOG FLORIDAN WELL NEAR SARASOTA FL	USGS	153478.00	1097620.00	Sarasota	84	531	IAS/ICU	69%	10	0						Not Used	Outside Boundary
131393	NEW HOG WELL		153480.26	1097620.08	Sarasota	84	531	IAS/ICU	69%	0	0						Not Used	Outside Boundary
101284	OMP TR5-1 SUWANNEE WELL AT LAUREL FL	USGS	184128.69	1021407.71	Sarasota	492	510	UF	95%	0	2						Not Used	sparse data
131402	ORANGE AVENUE		156849.74	1100204.79	Sarasota	22	534	IAS/ICU	71%	0	0						Not Used	No calibration in IAS/ICU
101322	OSPREY WELL 9 NEAR OSPREY FL	USGS	174632.39	1040597.03	Sarasota	235	255	IAS/ICU	100%	10	0	IAS-layer 3						averaged with 131440
101329	PALMER WELL NEAR SARASOTA FL	USGS	239399.16	1064408.07	Sarasota	340	360	IAS/ICU	100%	1	0						Not Used	No calibration in IAS/ICU
101277	PLANTATION TMIM WELL NEAR VENICE FL	USGS	211307.22	996426.30	Sarasota	60	65	IAS/ICU	100%	1	0						Not Used	No calibration in IAS/ICU
101312	RMR WELL 20C NEAR SARASOTA FL	USGS	263379.19	1033162.33	Sarasota	233.5	253.5	IAS/ICU	100%	1	0						Not Used	No calibration in IAS/ICU
131450	ROMP 18 SURF	SWFWMD	288792.59	1041032.51	Sarasota	2	17	SAS	100%	0	15	SAS						
101325	ROMP 18 SUWANNEE WELL NEAR SARASOTA FL	USGS	288742.95	1041035.99	Sarasota	745	845	UF	67%	1	2						Not Used	Sparse data
131412	ROMP 18 SWNN	SWFWMD	288799.88	1041039.51	Sarasota	505	845	UF	78%	10	15		UF	UF	UF	UF		
131433	ROMP 19 EAST HTRN	SWFWMD	248302.87	1034017.30	Sarasota	80	121	IAS/ICU	100%	10	15						Not Used	No calibration in IAS/ICU
131435	ROMP 19 EAST LOW HTRN	SWFWMD	248302.87	1034017.30	Sarasota	211	221	IAS/ICU	100%	10	15						Not Used	No calibration in IAS/ICU
131434	ROMP 19 EAST LOW HTRN	SWFWMD	248302.87	1034017.30	Sarasota	410	425	IAS/ICU	100%	10	15						Not Used	No calibration in IAS/ICU
131432	ROMP 19 EAST SURF	SWFWMD	248297.48	1034020.39	Sarasota	14.5	34.5	IAS/ICU	77%	10	15	SAS						
131436	ROMP 19 WEST HTRN		219963.21	1032260.17	Sarasota	87	205	IAS/ICU	100%	0	0						Not Used	No calibration in IAS/ICU
131438	ROMP 19 WEST SURF		219966.64	1032242.96	Sarasota	32	62	IAS/ICU	99%	0	0						Not Used	No calibration in IAS/ICU
131437	ROMP 19 WEST SWNN	SWFWMD	219963.21	1032260.17	Sarasota	410	420	IAS/ICU	100%	1	0						Not Used	No calibration in IAS/ICU
101308	ROMP 19 WLAM WELL NEAR SARASOTA FL	USGS	219976.00	1032107.00	Sarasota	410	425	IAS/ICU	100%	5	15						Not Used	No calibration in IAS/ICU
101310	ROMP 19 WS WELL NEAR SARASOTA FL	USGS	219976.31	1032107.41	Sarasota	32	67	IAS/ICU	99%	10	15	SAS						
101309	ROMP 19 WUAM WELL NEAR SARASOTA FL	USGS	219976.00	1032107.00	Sarasota	87	205	IAS/ICU	100%	10	15						Not Used	No calibration in IAS/ICU
101316	ROMP 19X ELAM SUWANNEE WELL NEAR SARASOTA FL	USGS	248300.96	1033916.32	Sarasota	410	419	IAS/ICU	100%	3	0						Not Used	No calibration in IAS/ICU
101317	ROMP 19X EUAM TAMIAMI WELL NEAR SARASOTA FL		248301.00	1033916.00	Sarasota	80	101	IAS/ICU	100%	0	0						Not Used	No calibration in IAS/ICU
131447	ROMP 20 OCAL	SWFWMD	175321.94	1042551.86	Sarasota	1105	1150	MC1	100%	2	15	UF						
131448	ROMP 20 SURF	SWFWMD	175322.98	1042563.97	Sarasota	12	32	IAS/ICU	86%	2	15	SAS						
131443	ROMP 22 ARC	SWFWMD	222126.10	1084973.85	Sarasota	95	125	IAS/ICU	100%	10	15						Not Used	No calibration in IAS/ICU
131444	ROMP 22 ARC/TMPA	SWFWMD	222160.30	1084966.41	Sarasota	230	290	IAS/ICU	100%	10	15						Not Used	No calibration in IAS/ICU
101333	ROMP 22 AVON PARK WELL NEAR UTOPIA FL	USGS	222133.98	1084951.54	Sarasota	1200	1660	APPZ	69%	0	2						Not Used	Duplicate with 131446, but sparse data
131446	ROMP 22 AVPK	SWFWMD	222123.05	1084941.56	Sarasota	1200	1660	APPZ	69%	10	15				APPZ	APPZ		
131442	ROMP 22 SURF	SWFWMD	222133.98	1084951.54	Sarasota	7	17	SAS	99%	10	15	SAS						
131445	ROMP 22 SWNN	SWFWMD	222153.63	1084933.15	Sarasota	400	635	UF	76%	10	15		UF	UF	UF	UF		
131462	ROMP 24 INT	SWFWMD	244184.79	1091306.90	Sarasota	74	171	IAS/ICU	100%	0	15						Not Used	No calibration in IAS/ICU
131466	ROMP 9 AVPK MW-6	SWFWMD	282265.18	998622.90	Sarasota	1180	1230	MC1	100%	0	15						Not Used	Model geology puts this well in MC1
131456	ROMP 9 LOW HTRN MW-4	SWFWMD	282284.22	998628.79	Sarasota	190	320	IAS/ICU	100%	0	15						Not Used	No calibration in IAS/ICU
131455	ROMP 9 MID INT MW-3	SWFWMD	282298.75	998635.72	Sarasota	122	163	IAS/ICU	100%	0	15						Not Used	No calibration in IAS/ICU
131457	ROMP 9 SURF MW-1	SWFWMD	282317.67	998628.48	Sarasota	5	27.5	SAS	100%	0	15	SAS						
131458	ROMP 9 SWNN MW-5	SWFWMD	282263.44	998629.99	Sarasota	545	860	UF	90%	0	15		UF	UF	UF			no 93/94 data
131461	ROMP 9 UP HTRN MW-2	SWFWMD	282270.66	998628.91	Sarasota	40	65	IAS/ICU	100%	0	15						Not Used	No calibration in IAS/ICU
131459	ROMP TR 4-1 LOW INT	SWFWMD	187097.14	992923.73	Sarasota	272	645	IAS/ICU	61%	0	15						Not Used	No calibration in IAS/ICU
131464	ROMP TR 4-1 MID INT	SWFWMD	187088.24	992935.95	Sarasota	121	224	IAS/ICU	100%	0	15						Not Used	No calibration in IAS/ICU
131463	ROMP TR 4-1 SURF	SWFWMD	187075.77	992953.27	Sarasota	12	25	SAS	100%	0	15	SAS						
131468	ROMP TR 4-1 SWNN	SWFWMD	187110.38	992895.30	Sarasota	765	821	UF	100%	0	15	UF						
131465	ROMP TR 4-1 UP INT	SWFWMD	187066.86	992964.48	Sarasota	30	112	IAS/ICU	100%	0	15						Not Used	TDS is unusually high - removed as anomaly
131460	ROMP TR 4-2 SURF	SWFWMD	200647.30	987953.97	Sarasota	2	19	SAS	100%	0	15	SAS						
131441	ROMP TR 4-2 TMPA	SWFWMD	200635.54	987954.10	Sarasota	460	475	IAS/ICU	100%	10	15	IAS-layer 3						averaged with 101275
131439	ROMP TR 5-1 SWNN	SWFWMD	184128.69	1021407.71	Sarasota	492	510	UF	95%	10	15	UF						
131449	ROMP TR 5-1 TAMIAMI	SWFWMD	184124.06	1021397.66	Sarasota	40	60	IAS/ICU	100%	0	15	IAS-layer 2						averaged with 101279 and 131411
131440	ROMP TR 5-1 TMPA	SWFWMD	184118.67	1021400.75	Sarasota	275	289	IAS/ICU	100%	10	15	IAS-layer 3						averaged with 101322
131389	ROMP TR 5-2 LOW HTRN	SWFWMD	202559.30	1028318.81	Sarasota	245	265	IAS/ICU	100%	10	15						Not Used	No calibration in IAS/ICU
131387	ROMP TR 5-2 OCAL	SWFWMD	202560.28	1028325.87	Sarasota	850	890	MC1	100%	10	15						Not Used	Model geology puts this well in MC1
131403	ROMP TR 5-2 SURF	SWFWMD	202569.30	1028323.75	Sarasota	8	13	SAS	100%	10	15	SAS						

Table 4.1: Usage of SAJ Observation Database in Regional Model Calibration

Model ID[a]	Well Name	Data Source	Easting[b]	Northing[b]	County	Cased Depth (ft)	Drilled Depth (ft)	Dominant Layer[c]	% Open Section in Layer[c]	93/94 Months with Data[d]	03/04 Months with Data[e]	Use for Data in Model Setup/Calibration						Reasoning/Comments
													Observations for Calibration					
												Boundary Conditions[f]	Steady State (Oct 03)	Steady State (Feb 04)	Transient (03/04)	Transient (03/04	Not Used	
131404	ROMP TR 5-2 SWNN	SWFWMD	202561.02	1028310.71	Sarasota	510	630	UF	100%	10	15		UF	UF	UF	UF		
131388	ROMP TR 5-2 TMPA	SWFWMD	202560.28	1028325.87	Sarasota	360	400	IAS/ICU	100%	10	15						Not Used	No calibration in IAS/ICU
131390	ROMP TR 5-2 UP HTRN	SWFWMD	202559.30	1028318.81	Sarasota	100	120	IAS/ICU	100%	10	12						Not Used	No calibration in IAS/ICU
131429	ROMP TR 5-3 FLDN	SWFWMD	199913.24	1029804.82	Sarasota	1080	1125	MC1	100%	0	15						Not Used	Model geology puts this well in MC1
131428	ROMP TR 5-3 UPPER INT	SWFWMD	199776.51	1029696.25	Sarasota	63	140	IAS/ICU	100%	0	15						Not Used	No calibration in IAS/ICU
131422	ROMP TR 6-1 HTRN	SWFWMD	152418.63	1069370.12	Sarasota	300	315	IAS/ICU	100%	10	15						Not Used	Outside Boundary
131453	ROMP TR SA-1 AVPK	SWFWMD	154321.04	1098425.86	Sarasota	995	1015	MC1	100%	0	15						Not Used	Outside Boundary
131454	ROMP TR SA-1 SURF	SWFWMD	154329.07	1098418.69	Sarasota	4	28	SAS	100%	0	15	SAS						
131452	ROMP TR SA-1 SWNN	SWFWMD	154331.80	1098420.68	Sarasota	708	738	UF	100%	0	15	UF						
131451	ROMP TR SA-1 UP INT	SWFWMD	154324.72	1098431.88	Sarasota	328	388	IAS/ICU	100%	0	15	IAS-layer 3						
131467	ROMP TR SA-3 UP FLDN	SWFWMD	165884.36	1098967.02	Sarasota	1096	1218	MC1	100%	0	15						Not Used	Model geology puts this well in MC1
101326	ROMP TR-20 UPPER HAWTHORN WELL AT OSPREY FL	USGS	175302.03	1042549.06	Sarasota	105	125	IAS/ICU	100%	1	2						Not Used	sparse data
101276	ROMP TR4-2 TAMPA WELL NEAR VENICE FL	USGS	200661.13	987978.05	Sarasota	460	475	IAS/ICU	100%	0	2						Not Used	duplicate with 131441
101285	ROMP TR5-1 HAWTHORN WELL AT LAUREL FL	USGS	184118.67	1021400.75	Sarasota	275	289	IAS/ICU	100%	1	2						Not Used	sparse data
101298	ROMP TR5-2 LOWER HAWTHORN MONITOR NEAR LAUREL FL	USGS	202559.30	1028318.81	Sarasota	245	265	IAS/ICU	100%	0	2						Not Used	No calibration in IAS/ICU
101296	ROMP TR5-2 SURFICIAL MONITOR NEAR LAUREL FL	USGS	202526.57	1028137.36	Sarasota	8	13	SAS	100%	5	0	SAS						
101299	ROMP TR5-2 SUWANNEE MONITOR NEAR LAUREL FL	USGS	202561.02	1028310.71	Sarasota	510	630	UF	100%	0	2						Not Used	Same as 131404, but sparse data
101297	ROMP TR5-2 UPPER HAWTHORN MONITOR NEAR LAUREL FL	USGS	202559.30	1028318.81	Sarasota	100	120	IAS/ICU	100%	6	2						Not Used	No calibration in IAS/ICU
131426	SARASOTA 11TH ST DEEP	SWFWMD	154385.67	1098400.82	Sarasota	43	479	IAS/ICU	81%	10	0						Not Used	No calibration in IAS/ICU
131401	SARASOTA 21ST ST INT		155644.75	1101888.46	Sarasota	123	561	IAS/ICU	60%	0	0						Not Used	No calibration in IAS/ICU
131405	SARASOTA 27TH ST INT		154245.63	1102964.44	Sarasota	45	343	IAS/ICU	100%	0	0						Not Used	No calibration in IAS/ICU
131407	SARASOTA CO TEST 1 FLADN		167088.27	1113189.42	Sarasota	350	606	UF	81%	0	0						Not Used	Missing data
131417	SARASOTA CO TEST 6A FLADN		174413.03	1113223.66	Sarasota	392	527	UF	95%	0	0						Not Used	Missing data
101365	SARASOTA COUNTY TEST WELL 1 NEAR SARASOTA FL	USGS	167107.72	1113211.22	Sarasota	350	606	UF	81%	10	0					UF		no 03/04 data
131395	SARASOTA HICKORY AVE INT		152910.45	1102575.95	Sarasota	38	591	IAS/ICU	63%	0	0						Not Used	Outside Boundary
101335	SARASOTA WELL 9 NEAR SARASOTA FL	USGS	194598.85	1090969.45	Sarasota	630	730	UF	100%	10	15		UF	UF	UF	UF		
131423	SCHROEDER-MANATEE		202321.88	1109365.24	Sarasota	430	1367	MC1	55%	0	0						Not Used	Model geology puts this well in MC1
101343	STA INJ DEEP MTR 2 NEAR SARASOTA FL	USGS	158214.68	1098757.60	Sarasota	1108	1500	APPZ	56%	10	2						Not Used	close to boundary
101330	SUNRISE UTILITIES WELL 3 NEAR SARASOTA FL		182545.29	1065838.97	Sarasota	433	453	IAS/ICU	100%	0	0						Not Used	No calibration in IAS/ICU
131431	UTOPIA 1	SWFWMD	218596.15	1092373.16	Sarasota	0	0	Error	0%	7	0	SAS						
131411	VENICE 35 INT	SWFWMD	188539.04	1006263.41	Sarasota	86	163	IAS/ICU	100%	10	15	IAS-layer 2						averaged with 131449 and 101279
131430	VENICE 36 INT	SWFWMD	188560.65	1006255.09	Sarasota	58	68	IAS/ICU	100%	0	15						Not Used	No calibration in IAS/ICU
101278	VENICE GARDENS SUWANNEE WELL NEAR VENICE FL	USGS	205536.50	997903.43	Sarasota	700	800	UF	100%	0	2						Not Used	Sparse data
101279	VENICE WELL 35 NEAR VENICE FL	USGS	188533.64	1006265.49	Sarasota	143	163	IAS/ICU	100%	2	2	IAS-layer 2						averageed with 131449 and 131411
101357	VERNA LINGER LODGE WELL 11 NEAR SARASOTA FL	USGS	234101.48	1110419.89	Sarasota	18	21	SAS	100%	5	0	SAS						
101353	VERNA LINGER LODGEL 1 NEAR SARASOTA FL	USGS	223999.73	1110122.61	Sarasota	18	20	SAS	100%	1	0						Not Used	sparse data
101362	VERNA PRODUCTION WELL 1 NEAR SARASOTA FL	USGS	228610.54	1111285.65	Sarasota	500	600	UF	100%	0	0						Not Used	sparse data
101351	VERNA PRODUCTION WELL 20 NEAR SARASOTA FL	USGS	237968.75	1109470.65	Sarasota	474	494	UF	100%	1	0						Not Used	sparse data
101350	VERNA PRODUCTION WELL 23 NEAR SARASOTA FL	USGS	239500.38	1109353.83	Sarasota	341	361	IAS/ICU	100%	1	0						Not Used	No calibration in IAS/ICU
101356	VERNA PRODUCTION WELL 24 NEAR SARASOTA FL	USGS	240232.03	1110356.34	Sarasota	400	500	IAS/ICU	54%	1	0						Not Used	No calibration in IAS/ICU
101349	VERNA PRODUCTION WELL 37 NEAR SARASOTA FL	USGS	248938.38	1106429.55	Sarasota	614	714	UF	100%	0	0						Not Used	sparse data
101363	VERNA PRODUCTION WELL 4 NEAR SARASOTA FL	USGS	230144.22	1111370.46	Sarasota	438	458	UF	64%	1	0						Not Used	sparse data
131413	VERNA T 0-4		224338.26	1094697.31	Sarasota	140	500	IAS/ICU	84%	0	0						Not Used	No calibration in IAS/ICU
101340	VERNA TEST WELL 0-4 NEAR VERNA FL	USGS	224402.00	1094822.00	Sarasota	140	500	IAS/ICU	84%	10	15						Not Used	No calibration in IAS/ICU
101344	WHITAKER BAY WELL NEAR SARASOTA FL	USGS	153899.43	1101376.72	Sarasota	54	337	IAS/ICU	100%	10	2	IAS-layer 2						averaged with 101348
131427	WHITAKER BAYOU INT		153902.27	1101387.80	Sarasota	54	337	IAS/ICU	100%	0	0						Not Used	No calibration in IAS/ICU
131512	GREEN SWAMP 5 UPL SURF	SWFWMD	347091.91	1484051.89	Sumter	0	13.9	SAS	100%	0	15	SAS						
131487	GREEN SWAMP 5 WTL SURF	SWFWMD	347244.28	1484121.38	Sumter	3	15	SAS	100%	0	15	SAS						
131513	GREEN SWAMP 6 UPL SURF	SWFWMD	343841.56	1477451.78	Sumter	0.9	8.9	SAS	100%	0	15	SAS						
131488	GREEN SWAMP 6 WTL SURF	SWFWMD	343984.05	1477400.13	Sumter	1	4	SAS	100%	0	15	SAS						
131481	GREEN SWAMP L-11K DEEP	SWFWMD	327859.20	1466573.84	Sumter	0	36	UF	47%	7	15						Not Used	Open section straddles multiple layers
131482	GREEN SWAMP L-11K SHALLOW	SWFWMD	327877.07	1466573.68	Sumter	0	17	SAS	74%	7	15	SAS						

Table 4.1: Usage of SAJ Observation Database in Regional Model Calibration

Model ID[a]	Well Name	Data Source	Easting[b]	Northing[b]	County	Cased Depth (ft)	Drilled Depth (ft)	Dominant Layer[c]	% Open Section in Layer[c]	93/94 Months with Data[d]	03/04 Months with Data[e]	Use for Data in Model Setup/Calibration						Reasoning/Comments
													Observations for Calibration					
												Boundary Conditions[f]	Steady State (Oct 03)	Steady State (Feb 04)	Transient (03/04)	Transient (03/04	Not Used	
131473	GREEN SWAMP L-11M DEEP	SWFWMD	327470.17	1454395.35	Sumter	0	49	UF	69%	7	15						Not Used	Hillsborough Basin has a dense coverage of points and is not important for the purposes of the model; remove
131474	GREEN SWAMP L-11M MED DEEP	SWFWMD	327425.74	1454426.03	Sumter	0	18	IAS/ICU	49%	7	15						Not Used	Open section straddles multiple layers
131475	GREEN SWAMP L-11M SHALLOW	SWFWMD	327461.23	1454395.42	Sumter	0	9	SAS	65%	7	15	SAS						
101415	GREEN SWAMP L11MD NR DADE CITY, FL		327309.13	1454376.51	Sumter	44	49	UF	100%	0	0						Not Used	missing data
101416	GREEN SWAMP L11MM NR DADE CITY, FL		327309.13	1454376.51	Sumter	16	18	UF	100%	0	0						Not Used	missing data
101417	GREEN SWAMP L11MS NR DADE CITY, FL		327309.13	1454376.51	Sumter	7	9	IAS/ICU	100%	0	0						Not Used	No calibration in IAS/ICU
131514	GREEN SWAMP MARSH FLDN	SWFWMD	328795.44	1463171.99	Sumter	44	122	UF	100%	0	15		UF	UF	UF			no 93/94 data
131511	GREEN SWAMP MARSH UPL SUR	SWFWMD	328866.24	1463090.59	Sumter	1.2	9.2	SAS	100%	0	15	SAS						
131486	GREEN SWAMP MARSH WTL SURF	SWFWMD	328945.21	1462918.20	Sumter	1	6	SAS	100%	0	15	SAS						
131485	GREEN SWAMP RIV UPL SURF	SWFWMD	339925.43	1474786.61	Sumter	1	5	SAS	100%	0	15	SAS						
131484	GREEN SWAMP WET PRA UPL S	SWFWMD	342531.30	1453482.94	Sumter	3	8	IAS/ICU	98%	0	15	SAS						
131476	ROMP 89 OCAL	SWFWMD	321689.24	1464128.57	Sumter	20	143	UF	98%	10	15						Not Used	Hillsborough Basin has a dense coverage of points and is not important for the purposes of the model; remove

Notes:

(a) The Model ID is a 6-digit identification number assigned in the SAJ monitoring well database.

(b) Easting and Northing are in feet and are based on the State Plane NAD83 Florida East coordinate system

(c) Dominant Layer and "% Open Section in Layer" describe a comparison between the model-simplified geology and the reported open section of each well (between the cased and drilled depths). For example, ROMP 18 SUWANEE (101325) is listed with a dominant layer of UF and a % Open Section in Layer of 67%. This indicates that 67% of the open section of the well overlaps the UF, as defined by the model grid. The other third of the open section coincides with other layers of the model.

(d) The column labeled "93/94 Months with Data" indicates the number of months between October 1993 and July 1994 (validation period) with at least one head measurement for each well.

(e) The column labeled "03/04 Months with Data" indicates the number of months between October 2003 and December 2004 (calibration period) with at least one head measurement for each well.

(f) Boundary condition assignments are described in Appendix C

Table 4.2: Steady State Calibration Results

Station	Layer	X Coordinate (ft) State Plane NAD83 FL East	Y coordinate (ft) State Plane NAD83 FL East	Observed Water Level (October 2003)	Computed Water Level (October 2003)	Observed Water Level (February 2004)	Computed Water Level (February 2004)
ALSTON DEEP FLDN	UF	294773.69	1398107.15	86.62	84.61	86.43	84.61
BAY LAKE DEEP WELL NEAR WINDERMERE, FL	UF	473291.48	1487554.73	88.05	88.06	88.13	87.34
BF-4S	UF	925172.70	669560.61	42.62	41.04	45.18	44.36
BF-6	UF	943147.33	720952.19	44.32	44.52	43.98	44.19
BR0624	UF	832393.04	1285879.97	35.85	35.46	35.86	35.30
CONE RANCH CM-10S UPL SUR	UF	307652.78	1369932.02	105.27	103.12	105.90	103.06
DESERET RANCH WELL NO. 3 NEAR KENANSVILLE, FL	UF	705582.88	1311426.42	--	--	40.47	39.97
DF-4	UF	830843.44	573317.79	52.40	52.16	52.30	52.06
EDGEVILLE DEEP WELL 3 AT EDGEVILLE FL	UF	294699.13	1083347.49	29.30	28.49	28.77	30.68
EVA WELL DEEP	UF	391321.18	1471566.01	110.81	111.87	110.41	111.38
G-2618	UF	714531.25	668029.48	59.67	59.98	59.37	59.45
GREEN SWAMP MARSH FLDN	UF	328795.44	1463171.99	91.23	91.94	91.33	91.36
IR0954	UF	792731.18	1183086.73	41.57	40.79	41.75	41.84
IR0955	UF	775195.66	1209891.97	43.04	42.15	42.37	42.81
IR0963	UF	813677.29	1220619.29	38.24	37.01	37.63	37.58
IR0968	UF	727961.00	1225532.23	43.11	44.27	43.07	44.74
IR-189 WELL NEAR YEEHAW JUNCTION, FL	UF	712757.62	1248622.20	43.80	43.51	43.46	43.74
IWSD-MZ2	UF	514985.20	756311.02	55.90	56.56	56.63	55.98
L-0051	UF	419691.14	1470636.77	117.12	118.06	116.64	117.14
L-0877	UF	421044.26	1463498.44	118.22	117.33	117.75	116.90
L-2435	UF	351186.61	813474.34	27.40	39.53	29.20	38.86
L-2528	UF	332536.41	844111.41	35.50	28.07	35.20	29.87
L2-PW2	UF	672708.95	826685.16	58.61	58.57	58.39	58.31
L-5708	UF	459532.85	875833.52	54.20	54.77	54.60	54.22
LAB-MZ1	UF	502273.56	879736.84	52.95	53.04	52.72	53.02
LAKE OLIVER DEEP WELL NEAR VINELAND, FL	UF	448447.60	1466874.64	110.02	109.71	109.33	108.54
LAKE SAWYER WELL NEAR WINDERMERE, FL	UF	472907.32	1500686.07	83.02	85.39	83.69	84.05
OS0019	UF	673501.33	1336592.10	--	--	43.01	42.93
OS0230	UF	650031.00	1262861.53	45.36	45.55	45.41	46.44
OS0231	UF	669437.05	1270635.90	44.94	44.16	45.10	44.85
OSF-101	UF	511852.20	1438600.58	59.03	58.26	59.17	59.13
OSF-102	UF	519438.81	1389291.15	58.61	58.39	58.73	58.70
PB-747	UF	936328.26	946544.16	48.37	48.91	47.67	47.44

Table 4.2: Steady State Calibration Results

Station	Layer	X Coordinate (ft) State Plane NAD83 FL East	Y coordinate (ft) State Plane NAD83 FL East	Observed Water Level (October 2003)	Computed Water Level (October 2003)	Observed Water Level (February 2004)	Computed Water Level (February 2004)
PBF-10R	UF	886678.71	735581.37	49.69	51.02	49.57	50.82
PBF-2	UF	964547.70	867347.17	48.60	45.59	48.45	45.30
PBF-3	UF	949209.57	852482.26	46.75	47.90	46.71	47.54
PBF-7U	UF	748904.73	860161.10	55.82	54.42	53.55	54.20
PO-1 THORNHILL DEEP NEAR DAVENPORT, FL	UF	445284.30	1406188.17	127.53	127.22	126.40	126.84
ROMP 12 MID UP FLDN	UF	414556.89	984847.38	48.12	47.38	48.66	49.22
ROMP 12 SH UPPER FLDN	UF	414555.98	984847.39	48.15	47.38	48.75	49.22
ROMP 13 SWNN	UF	455661.82	995837.76	48.17	47.67	49.19	49.56
ROMP 14 SWNN	UF	541276.02	1023843.50	49.22	47.46	50.04	51.11
ROMP 17 SWNN	UF	338681.48	1033839.81	46.02	45.02	46.62	45.83
ROMP 18 SWNN	UF	288799.88	1041039.51	39.65	39.71	39.04	40.42
ROMP 22 SWNN	UF	222153.63	1084933.15	20.51	21.31	20.73	22.83
ROMP 25 SWNN/UFA	UF	329307.87	1103726.66	34.36	31.86	32.65	35.65
ROMP 28 SWNN	UF	514856.01	1103589.04	64.35	63.72	64.31	66.17
ROMP 32 SWNN	UF	311152.33	1141805.04	30.37	27.11	29.91	31.37
ROMP 33 TMPA/SWNN	UF	248494.57	1137650.44	12.97	10.38	14.75	14.59
ROMP 39 SWNN	UF	250815.65	1185230.02	9.30	9.08	13.94	13.53
ROMP 49 SWNN	UF	250531.91	1248569.99	17.43	18.30	22.14	21.77
ROMP 5 6-IN SWNN	UF	392998.23	950318.27	50.87	49.32	51.09	50.03
ROMP 87 SHALLOW	UF	326593.29	1414142.69	103.45	104.78	104.24	104.75
ROMP 9 SWNN MW-5	UF	282263.44	998629.99	41.76	40.09	41.72	39.94
ROMP CL-2 HTRN	UF	490980.79	1244529.96	80.01	79.80	81.28	81.40
ROMP DV-1 SWNN	UF	265802.47	1331860.97	45.84	49.63	56.94	53.81
ROMP TR 1-2 SWNN	UF	336126.21	912391.15	45.40	45.63	45.46	45.29
ROMP TR 3-1 SWNN	UF	259335.31	950819.57	34.43	34.47	34.20	33.75
ROMP TR 5-2 SWNN	UF	202561.02	1028310.71	25.37	23.84	25.90	23.67
ROMP TR 7-4 TAMPA WELL NEAR BRADENTON FL	UF	173169.16	1127693.89	15.75	15.66	17.05	16.94
SARASOTA WELL 9 NEAR SARASOTA FL	UF	194598.85	1090969.45	21.75	20.29	22.04	20.92
SEA WORLD DRIVE REPLACEMENT WELL NEAR VINELAND, FL	UF	503448.51	1481970.32	61.02	61.03	61.34	61.83
SHINGLE CREEK AT STATE HWY 531A NEAR KISSIMMEE, FL	UF	516053.10	1429805.93	57.87	57.57	58.02	58.31
SLF-76	UF	821840.68	1092293.33	42.75	42.10	42.56	43.07
TH-3 LAKE POINSETT SW NEAR NEW EDEN, FL	UF	660637.04	1432684.90	38.64	38.75	38.31	38.71

Table 4.2: Steady State Calibration Results

Station	Layer	X Coordinate (ft) State Plane NAD83 FL East	Y coordinate (ft) State Plane NAD83 FL East	Observed Water Level (October 2003)	Computed Water Level (October 2003)	Observed Water Level (February 2004)	Computed Water Level (February 2004)
TH-9 NOVA ROAD 532 WEST (OSF-93) NEAR NEW EDEN, FL	UF	641503.84	1432687.41	41.96	41.74	41.68	41.82
WASANMZ1	UF	936511.00	576823.00	35.32	35.07	34.57	35.17
AMAX NO 3 WELL NEAR PINE LEVEL FL	APPZ	329659.53	1065529.08	40.53	39.53	40.85	41.04
BF-4M	APPZ	925172.70	669560.61	45.52	43.77	45.93	45.75
DF-5	APPZ	830843.44	573317.79	51.82	51.68	51.56	51.51
G-2617	APPZ	714531.25	668029.48	60.43	59.73	60.13	59.19
IWSD-MZ3	APPZ	514985.20	756311.02	53.42	53.98	53.26	53.39
L-0730	APPZ	428559.79	1486575.78	110.18	110.48	109.60	109.03
L2-PW1	APPZ	672708.95	826685.16	59.38	59.18	59.12	58.90
MIR-MZU	APPZ	875503.19	603616.90	46.78	46.52	45.99	46.63
OS0022	APPZ	653838.63	1374816.63	43.54	43.10	43.51	43.71
OSF-99	APPZ	493982.24	1426090.34	66.46	66.65	66.84	66.60
PBF-11	APPZ	886678.71	735581.37	52.54	53.10	52.43	52.88
PBF-4	APPZ	949209.57	852482.26	46.99	48.27	46.89	47.91
ROMP 12 DEEP UPPER FLDN	APPZ	414559.60	984847.37	47.87	48.05	48.43	49.25
ROMP 13 AVPK	APPZ	455624.58	995801.59	47.73	47.48	48.59	48.83
ROMP 25 AVPK/UFA	APPZ	329317.62	1103705.37	34.12	32.74	32.41	36.08
ROMP 28 AVPK	APPZ	514909.81	1103506.05	63.81	61.57	63.61	64.12
ROMP 30 AVON PARK WELL NEAR ZOLFO SGS FL	APPZ	397887.01	1137080.71	50.32	48.06	50.06	51.48
ROMP 33 AVPK	APPZ	248473.27	1137682.98	10.84	10.45	12.55	14.71
ROMP 39 AVPK	APPZ	250817.52	1185237.07	9.51	10.24	13.25	14.91
ROMP 49 AVPK	APPZ	250487.09	1248580.55	--	--	21.60	20.50
ROMP 61 SWNN/AVPK	APPZ	281139.92	1301278.05	33.42	31.59	40.37	42.01
ROMP 86A AVPK	APPZ	279977.38	1405582.26	61.71	66.08	61.31	66.06
SOUTH EAGLE ROAD GROVE WELL AT NARCOOSSEE FL	APPZ	582861.73	1437702.34	--	--	45.38	45.50
TFRO-5	APPZ	898492.92	1001979.22	--	--	50.52	52.18
BF-1	LF1	925617.30	669564.23	9.97	9.98	9.99	10.38
OS0025	LF1	653885.62	1374997.35	42.28	42.86	42.44	42.93
OSF-98	LF1	493982.24	1426090.34	54.93	56.52	54.93	56.45
PBF-12	LF1	886678.71	735581.37	15.20	15.34	15.13	15.07
PBF-5	LF1	949209.57	852482.26	9.90	10.57	9.87	10.23
PBF-7L	LF1	748904.73	860161.10	41.72	31.59	39.24	31.27
ROMP 28 UP EVAPORITE FLDN	LF1	514916.06	1103487.85	62.69	61.92	62.97	63.42
OSF-97	BZ	493982.24	1426090.34	53.72	53.84	53.70	53.76

Table 4.2: Steady State Calibration Results

Station	Layer	X Coordinate (ft) State Plane NAD83 FL East	Y coordinate (ft) State Plane NAD83 FL East	Observed Water Level (October 2003)	Computed Water Level (October 2003)	Observed Water Level (February 2004)	Computed Water Level (February 2004)
Alligator Alley Test Well (G-2296)	LF/BZ (Expanded Calibration)*	713926.40	667921.72	7.00	6.63	--	6.10
OLI-IW1	LF/BZ (Expanded Calibration)*	756443.00	1091566.68	10.10	8.21	--	8.13
OSF-82L	LF/BZ (Expanded Calibration)*	550374.73	1424546.73	51.77	49.06	--	48.78
USGS CORE HOLE 2 AT POLK CITY	LF/BZ (Expanded Calibration)*	388669.96	1400176.12	127.10	127.16	--	127.04

* The expanded calibration for the LF1/BZ layers included wells which had available data for time periods other than the calibration or validation periods. They were included as loose constraints because of the small amount of data available for the calibration and validation periods in these layers. Reported observed data for these points in this table is not for October 2003.

Table 4.3: Mass Balance for Flow Solution (Calibrated Model)

	Flow in (ft^3/d)				Flow out (ft^3/d)				
Time	Storage	Constant Head	Wells	Total	Storage	Constant Head	Wells	Total	Percent Discrepancy
1.0	0.00E+00	6.83E+08	4.90E+07	7.32E+08	0.00E+00	5.81E+08	1.52E+08	7.33E+08	0.0539 %
11.0	1.23E+07	6.94E+08	5.05E+07	7.57E+08	8.27E+06	5.87E+08	1.62E+08	7.57E+08	0.0265 %
21.0	8.89E+06	6.93E+08	5.05E+07	7.53E+08	4.48E+06	5.87E+08	1.62E+08	7.53E+08	0.0258 %
31.0	7.64E+06	6.93E+08	5.05E+07	7.51E+08	2.93E+06	5.86E+08	1.62E+08	7.51E+08	0.0258 %
41.3	2.44E+07	6.27E+08	4.73E+07	6.98E+08	4.90E+06	5.35E+08	1.59E+08	6.99E+08	0.0268 %
51.7	1.64E+07	6.30E+08	4.73E+07	6.93E+08	2.29E+06	5.33E+08	1.59E+08	6.94E+08	0.0272 %
62.0	1.35E+07	6.31E+08	4.73E+07	6.91E+08	1.29E+06	5.32E+08	1.59E+08	6.92E+08	0.0272 %
72.3	9.19E+06	6.97E+08	4.64E+07	7.53E+08	1.66E+07	5.95E+08	1.42E+08	7.53E+08	0.0244 %
82.7	5.69E+06	6.94E+08	4.64E+07	7.46E+08	8.83E+06	5.95E+08	1.42E+08	7.46E+08	0.0249 %
93.0	4.16E+06	6.92E+08	4.64E+07	7.43E+08	5.98E+06	5.95E+08	1.42E+08	7.43E+08	0.0252 %
104.6	5.44E+06	6.81E+08	5.04E+07	7.36E+08	1.51E+07	5.94E+08	1.27E+08	7.37E+08	0.0243 %
116.2	2.74E+06	6.79E+08	5.04E+07	7.32E+08	1.03E+07	5.95E+08	1.27E+08	7.33E+08	0.0251 %
122.0	2.22E+06	6.79E+08	5.04E+07	7.31E+08	9.05E+06	5.95E+08	1.27E+08	7.31E+08	0.0253 %
132.3	2.43E+07	7.07E+08	4.70E+07	7.78E+08	3.15E+06	5.99E+08	1.76E+08	7.79E+08	0.0268 %
142.7	1.92E+07	7.09E+08	4.70E+07	7.75E+08	1.05E+06	5.97E+08	1.76E+08	7.75E+08	0.0257 %
153.0	1.67E+07	7.10E+08	4.70E+07	7.73E+08	4.81E+05	5.96E+08	1.76E+08	7.73E+08	0.0255 %
163.0	6.57E+07	7.27E+08	4.47E+07	8.37E+08	3.65E+05	5.95E+08	2.42E+08	8.37E+08	0.0280 %
173.0	5.38E+07	7.34E+08	4.47E+07	8.33E+08	1.69E+05	5.91E+08	2.42E+08	8.33E+08	0.0262 %
183.0	4.79E+07	7.38E+08	4.47E+07	8.31E+08	1.15E+05	5.89E+08	2.42E+08	8.31E+08	0.0257 %
193.3	6.09E+07	7.21E+08	4.26E+07	8.25E+08	1.93E+06	5.73E+08	2.50E+08	8.25E+08	0.0248 %
203.7	5.16E+07	7.27E+08	4.26E+07	8.21E+08	4.05E+05	5.71E+08	2.50E+08	8.21E+08	0.0249 %
214.0	4.73E+07	7.30E+08	4.26E+07	8.20E+08	2.23E+05	5.70E+08	2.50E+08	8.20E+08	0.0248 %
224.0	2.73E+07	7.53E+08	4.16E+07	8.22E+08	2.17E+07	6.03E+08	1.98E+08	8.22E+08	0.0198 %
234.0	2.10E+07	7.50E+08	4.16E+07	8.12E+08	1.16E+07	6.03E+08	1.98E+08	8.13E+08	0.0216 %
244.0	1.80E+07	7.49E+08	4.16E+07	8.08E+08	7.32E+06	6.03E+08	1.98E+08	8.08E+08	0.0222 %
254.3	9.43E+06	7.38E+08	4.23E+07	7.90E+08	4.23E+07	6.07E+08	1.41E+08	7.90E+08	0.0204 %
264.7	6.16E+06	7.31E+08	4.23E+07	7.79E+08	2.79E+07	6.10E+08	1.41E+08	7.79E+08	0.0226 %
275.0	4.54E+06	7.27E+08	4.23E+07	7.74E+08	2.16E+07	6.12E+08	1.41E+08	7.74E+08	0.0233 %
285.3	2.20E+06	7.03E+08	5.21E+07	7.58E+08	5.62E+07	6.06E+08	9.57E+07	7.58E+08	0.0224 %
295.7	1.29E+06	6.96E+08	5.21E+07	7.49E+08	4.40E+07	6.10E+08	9.57E+07	7.50E+08	0.0241 %
306.0	8.27E+05	6.92E+08	5.21E+07	7.45E+08	3.77E+07	6.12E+08	9.57E+07	7.45E+08	0.0247 %
316.0	6.39E+05	6.85E+08	5.68E+07	7.43E+08	5.53E+07	5.99E+08	8.84E+07	7.43E+08	0.0252 %
326.0	2.56E+05	6.79E+08	5.68E+07	7.36E+08	4.53E+07	6.03E+08	8.84E+07	7.36E+08	0.0257 %
336.0	1.49E+05	6.76E+08	5.68E+07	7.33E+08	4.02E+07	6.04E+08	8.84E+07	7.33E+08	0.0262 %
346.3	8.14E+06	6.57E+08	5.65E+07	7.21E+08	2.43E+07	5.85E+08	1.12E+08	7.22E+08	0.0274 %
356.7	2.99E+06	6.58E+08	5.65E+07	7.17E+08	2.04E+07	5.85E+08	1.12E+08	7.17E+08	0.0274 %
367.0	1.29E+06	6.57E+08	5.65E+07	7.15E+08	1.85E+07	5.85E+08	1.12E+08	7.15E+08	0.0275 %
377.0	3.51E+07	6.68E+08	4.94E+07	7.52E+08	7.12E+06	5.82E+08	1.63E+08	7.52E+08	0.0311 %
387.0	2.21E+07	6.73E+08	4.94E+07	7.45E+08	4.07E+06	5.78E+08	1.63E+08	7.45E+08	0.0291 %
397.0	1.63E+07	6.76E+08	4.94E+07	7.42E+08	2.54E+06	5.76E+08	1.63E+08	7.42E+08	0.0287 %
407.3	1.34E+07	6.58E+08	4.69E+07	7.18E+08	1.38E+07	5.82E+08	1.22E+08	7.18E+08	0.0279 %
417.7	8.08E+06	6.57E+08	4.69E+07	7.12E+08	8.63E+06	5.82E+08	1.22E+08	7.13E+08	0.0287 %
428.0	6.05E+06	6.57E+08	4.69E+07	7.10E+08	6.23E+06	5.82E+08	1.22E+08	7.10E+08	0.0288 %

Table 4.4: Mass Balance Discrepancy (Transport Equations)

Time (d)	TDS Discrepancy (%) (Total In-Out)	Temperature Discrepancy (%) (Total In-Out)
1.0	-1.12E-06 %	2.56E-06 %
6.0	-8.93E-08 %	-7.30E-07 %
11.0	9.66E-08 %	-5.50E-07 %
16.0	2.66E-07 %	-1.68E-06 %
21.0	3.11E-07 %	-1.61E-06 %
26.0	2.52E-07 %	-1.11E-06 %
31.0	2.02E-07 %	-5.02E-07 %
36.2	1.73E-07 %	-3.62E-07 %
41.3	1.82E-07 %	-1.00E-07 %
46.5	1.59E-07 %	-1.24E-06 %
51.7	1.39E-07 %	-2.14E-06 %
56.8	1.15E-07 %	-2.83E-06 %
62.0	9.29E-08 %	-3.35E-06 %
67.2	9.64E-08 %	-3.08E-06 %
72.3	8.36E-08 %	-2.78E-06 %
77.5	8.14E-08 %	-2.49E-06 %
82.7	7.08E-08 %	-2.22E-06 %
87.8	6.43E-08 %	-2.43E-06 %
93.0	5.03E-08 %	-2.18E-06 %
98.8	-1.60E-08 %	-1.81E-06 %
104.6	-4.81E-08 %	-1.59E-06 %
110.4	-8.96E-08 %	-1.41E-06 %
116.2	-1.04E-07 %	-1.25E-06 %
122.0	-1.47E-07 %	-1.11E-06 %
127.2	-1.63E-07 %	-1.36E-06 %
132.3	-1.71E-07 %	-1.38E-06 %
137.5	-1.75E-07 %	-1.38E-06 %
142.7	-1.64E-07 %	-1.31E-06 %
147.8	-1.75E-07 %	-1.27E-06 %
153.0	-1.70E-07 %	-1.07E-06 %
158.0	-1.70E-07 %	-1.02E-06 %
163.0	-2.00E-07 %	-9.99E-07 %
168.0	-1.99E-07 %	-9.29E-07 %
173.0	-2.25E-07 %	-8.89E-07 %
178.0	-2.25E-07 %	-7.37E-07 %
183.0	-2.50E-07 %	-6.60E-07 %
188.2	-2.68E-07 %	-7.76E-07 %
193.3	-3.03E-07 %	-8.44E-07 %
198.5	-3.21E-07 %	-8.79E-07 %
203.7	-3.48E-07 %	-9.07E-07 %
208.8	-3.60E-07 %	-8.56E-07 %
214.0	-3.60E-07 %	-8.69E-07 %
219.0	-4.20E-07 %	-9.16E-07 %

Table 4.4: Mass Balance Discrepancy (Transport Equations)

Time (d)	TDS Discrepancy (%) (Total In-Out)	Temperature Discrepancy (%) (Total In-Out)
224.0	-4.20E-07 %	-9.50E-07 %
229.0	-4.63E-07 %	-9.35E-07 %
234.0	-4.61E-07 %	-9.58E-07 %
239.0	-5.02E-07 %	-1.07E-06 %
244.0	-5.19E-07 %	-1.06E-06 %
249.2	-5.65E-07 %	-1.14E-06 %
254.3	-5.64E-07 %	-1.19E-06 %
259.5	-6.04E-07 %	-1.05E-06 %
264.7	-6.15E-07 %	-1.04E-06 %
269.8	-6.51E-07 %	-9.25E-07 %
275.0	-6.60E-07 %	-8.43E-07 %
280.2	-6.64E-07 %	-7.80E-07 %
285.3	-6.50E-07 %	-7.24E-07 %
290.5	-6.47E-07 %	-7.26E-07 %
295.7	-6.38E-07 %	-6.03E-07 %
300.8	-6.33E-07 %	-6.07E-07 %
306.0	-6.22E-07 %	-5.48E-07 %
311.0	-6.27E-07 %	-6.09E-07 %
316.0	-6.08E-07 %	-6.35E-07 %
321.0	-6.12E-07 %	-5.52E-07 %
326.0	-5.90E-07 %	-4.68E-07 %
331.0	-5.93E-07 %	-1.66E-06 %
336.0	-5.73E-07 %	-1.47E-06 %
341.2	-5.66E-07 %	-1.42E-06 %
346.3	-5.49E-07 %	-1.37E-06 %
351.5	-5.45E-07 %	-1.22E-06 %
356.7	-5.31E-07 %	-1.07E-06 %
361.8	-5.29E-07 %	-7.76E-07 %
367.0	-5.18E-07 %	-8.60E-07 %
372.0	-5.18E-07 %	-9.74E-07 %
377.0	-5.16E-07 %	-9.10E-07 %
382.0	-5.15E-07 %	-9.24E-07 %
387.0	-5.13E-07 %	-1.03E-06 %
392.0	-5.12E-07 %	-1.16E-06 %
397.0	-5.10E-07 %	-1.33E-06 %
402.2	-5.10E-07 %	-1.49E-06 %
407.3	-5.13E-07 %	-1.63E-06 %
412.5	-5.14E-07 %	-1.75E-06 %
417.7	-5.13E-07 %	-1.95E-06 %
422.8	-5.13E-07 %	-2.19E-06 %
428.0	-5.11E-07 %	-2.37E-06 %

Table 4.5: Transport Parameters used in Calibrated Transient Model

Porosity	SAS	0.25
	IAS	0.25
	ICU	0.4
	UF	0.25
	MC1	0.3
	APPZ	0.25
	MC2	0.3
	LF1	0.25
	LC	0.3
	BZ	0.25
Longitudinal Dispersivity		2.5 ft
Horizontal Transverse Dispersivity		2.5 ft
Vertical Transverse Dispersivity		2.5 ft
Effective Molecular Diffusion Coefficient		0.0 ft^2/d

Table 5.1: Porosity values for sensitivity runs

	Calibration Run	Porosity Sensitivity Run 1	Porosity Sensitivity Run 2	Porosity Sensitivity Run 3
Aquifer porosity (SAS, UF, APPZ, LF1, BZ)	0.25	0.4	0.25	0.3
ICU porosity	0.4	0.4	0.25	0.25
Confining Unit Porosity (MC1, MC2, LC)	0.3	0.4	0.25	0.25

Table 5.2: Dispersivity values for sensitivity runs

	Calibration Run	Dispersion Sensitivity Run 1	Dispersion Sensitivity Run 2	Dispersion Sensitivity Run 3	Dispersion Sensitivity Run 4
Longitudinal Dispersivity (ft)	2.5	25.0	0.25	2.5	2.5
Ratio of Horizontal Transverse Dispersivity to Longitudinal Dispersivity	1.0	1.0	1.0	0.5	0.1
Ratio of Vertical Transverse Dispersivity to Longitudinal Dispersivity	1.0	1.0	1.0	0.05	0.01

Table 5.3: Boulder Zone thickness and hydraulic conductivity values for sensitivity runs

	Calibration Run	BZ Thickness Run 1	BZ Thickness Run 2	BZ Thickness Run 3	BZ Thickness Run 4
BZ Thickness (ft)	500	1000	250	1000	250
BZ Horizontal Hydraulic Conductivity (ft/d)	Varies (1 to 10,000)	Same as Calibration (1-10,000)	Same as Calibration (1-10,000)	Half Calibration (0.5-5,000)	Twice Calibration (2-20,000)
BZ Vertical Hydraulic Conductivity (ft/d)	Varies (0.1 to 1,000)	Same as Calibration (0.1-1,000)	Same as Calibration (0.1-1,000)	Twice Calibration (0.2-2,000)	Half Calibration (0.05-500)

Table 5.4: Root Mean Square Statistics for Each Boulder Zone Thickness Sensitivity Run (Steady State February 2004)

Aquifer	Calibration	Run 1 (Double BZ Thickness; No K Change)	Run 2 (Half BZ Thickness; No K Change)	Run 3 (Double BZ Thickness; With K Change)	Run 4 (Half BZ Thickness; With K Change)
UF	1.748	2.512	2.281	1.867	1.752
MF	1.530	2.448	1.621	1.782	1.498
LF1	0.711	1.702	0.865	1.027	0.707
BZ	0.063	0.504	0.508	0.184	0.186

Note: RMS is calculated using Equation 4.3

Table 5.5: RMS Statistics for each Aquifer for the Calibration and Everglades Head Sensitivity Runs (Steady State February 2004)

Layer	Calibration Run	No-Flow on UF through Everglades	No-Flow on all aquifers through Everglades
UF	1.748	1.748	1.898
APPZ	1.530	1.530	1.917
LF	0.711	0.712	1.143
BZ	0.063	0.063	0.120

Note: RMS is calculated according to Equation 4.3.

APPENDIX E

Supporting documents for Regional ASR Study groundwater model

Phase II Appendices to USACE (2011)

A. Phase II Model Data Collection

B. Phase II Model Grid Resolution Study

C. Selection of Boundary Conditions

D. Pumping Data Report

E. Total Dissolved Solids and Temperature Data Evaluation

F. WASH123 and SEAWAT Comparison

G. Interagency Modeling Center Review Comments on Draft Report with Responses

H. Interagency Modeling Center Comments on Final Report with Responses

Appendix A: Phase II Groundwater Model Data Collection

1.0 Phase II Groundwater Model Data Collection

1.1 Model Boundaries, Spatial and Temporal

1.1.1 Horizontal Boundaries

The Phase II Groundwater Model will be developed, as part of the Aquifer Storage and Recovery (ASR) Regional Study. The model originally included all of peninsular Florida, from Orlando southward to the Keys. This includes all of the South Florida Water Management District (SFWMD), and parts of the Southwest Florida Water Management District (SWFWMD) and the St. Johns River Water Management District (SJRWMD), hereafter regarded collectively as the Water Management Districts or WMD's. As the data collection progressed, the Phase II model has been refined. See Figure 1.1

Figure 1.1: Refined Phase II Model Boundary

1.1.2 Vertical Boundaries

The aquifers included for study are the Floridan Aquifer System (FAS), which includes the Lower-Hawthorne, Suwannee, and Avon Park Aquifers, and the Boulder Zone; and the Intermediate Aquifer, which includes the Mid-Hawthorne and Sandstone Aquifers. Pumping records within these aquifers were collected. Water use in the Surficial Aquifer System (SAS) is not part of the model, so pumping from the SAS was not collected. However, since the SAS is the top boundary layer, water level data in the Surficial Aquifer was collected.

1.1.3 Temporal Boundaries

The period of record (POR) was determined based on the period with the best data representation. A similar groundwater model, "Simulation of Ground-Water Flow in the Intermediate and Floridan Aquifer Systems in Peninsular Florida," (known as the "Mega Model) was produced by Nicasio Sepulveda of USGS for the August 1993 through July 1994 POR (a "USGS water year"). As data collection progressed, it was determined that pumping and groundwater data from the WMD's for calendar year 2004 were the most comprehensive. Thus,

the ASR Regional Groundwater Model was set to be calibrated for the POR spanning October 2003 through December 2004. The last three months of 2003 were added to include a continuous water year. The calibrated model would be verified using the groundwater data from the Mega Model for the 1993-1994 POR. Data collection then focused on these two PORs.

1.2 Data Required

The data required for this model can be separated into three categories: pumping data, transient water level data, and water quality data. Each well with data also needed to have accurate location and depth data. Each type of data came from different well types. The pumping data came from production, injection, and ASR wells, while the water level and water quality data came from monitoring well records, ASR wells, and some production wells (public supply). Each type of well had many different agencies as data sources. The following paragraphs describe the three main types of data, in the order in which they were collected:

1.2.1 Pumping Data

Water is pumped by three types of wells: production, injection, and ASR wells. Production wells, or consumptive use permit (CUP) wells, are wells that only recover water from the aquifer or pump out (a few are free-flowing). Underground injection control (UIC) wells are wells that only inject water into the aquifer or recharge. UIC wells in Florida are either Class I or Class V, based on a state UIC category system. ASR wells both recharge and recover, and are considered Class V UICs (though not all Class V wells are ASRs). There are also a few drainage wells that drain storm water runoff and control lake levels. Monthly pumped volumes were converted to average cubic feet per day (cfd) for each month during the PORs. All water pumped out, or recovered, is reported as negative values. All water pumped in, or recharged, is reported as positive values.

1.2.2 Water Level Data

Water level (WL) data are retrieved from monitoring wells, which are different from pumping wells in that they are designed to monitor groundwater conditions, not recharge or recover large volumes of water. Most of the monitoring wells recorded water levels on a daily basis, providing comprehensive information for the model. Many of the monitoring wells had screened intervals at up to three different depths, and would thus provide water levels for three different aquifers in one location. Water levels are reported as either elevation in feet NGVD or feet below the ground surface (to be converted to feet NGVD in the model).

1.2.3 Water Quality Data

The water quality (WQ) parameters necessary for the model were chlorides, total dissolved solids (TDS), and conductivity. Most of the water quality monitoring was performed on monitoring well water, though the frequency was seasonally or annually instead of daily. Water quality data were also provided for ASR wells

during cycle testing and for public supply CUP wells. These data were collected even less frequently.

2.0 Data Sources

Data was collected from the following sources: SFWMD, SWFWMD, SJRWMD, U.S. Geological Survey (USGS), the Florida Department of Environmental Protection (FDEP), the Florida Department of Health (FDOH), USACE, the Groundwater Protection Council (GWPC), private contractors, and individual facility owners and operators. Agency data sources included permit databases, permitting engineers, general data databases (CERP and DRAM), GIS databases, hydro-geologic reports, and modelers who compiled similar data for similar models. Each source had many types of data, but each had a different strength. The WMDs and FDOH provided the most comprehensive CUP data, both wellhead and pumping records. FDEP and USGS provided the most comprehensive ASR well data. FDEP provided the most comprehensive UIC data. FDOH provided the most comprehensive private well records. The WMDs and USGS provided the most comprehensive water level and water quality data. Comprehensive data sets of each type of well were compiled using data from these respective sources, and the rest of the data were used to fill in data gaps, such as missing depths, capacities, and individual wells.

Data Source Table

Well Type	Subtype	Well Head Data Source	Daily Data Source (Pumping, WL, WQ)
Production/CUP	Surface Water	omitted	n/a
	Ground Water	WMDs, USGS, FDOH, FDEP	WMDs, FDEP
Injection/UIC	Class I	FDEP, GWPC	FDEP, Facility owners
	Class V ASR	FDEP, USGS	Cycle tests, MORs, facility operators, PEs of record, FDEP, USGS
	Class V nonASR	FDEP	None fell within model boundary
Monitoring Well	General	WMD & USGS databases, SFWMD	
	ASR	SFWMD	
	Class I	SFWMD	Tetra Tech

Table 1.1: Data Source Table

3.0 Ensuring Completeness of Wellhead Data

3.1 Production/CUP Data

To ensure the most comprehensive database, geographically overlapping data with incomparable nomenclature were compared using GIS ArcInfo. Once this was complete, data gaps were addressed. Essential CUP wellhead data included the location, drilled and cased depths, and capacities. Locating accurate data, if not provided, was imperative, as any wellhead missing even one piece of the data could not be used. Various methods were used to track down missing data depending on available resources, and logical assumptions were made when necessary. The resources available varied by the original data source. Each WMD had a web-based permit database, which was consulted first for missing information. For the most part, these databases had the same information that we had obtained previously from other sources. When missing data could not be found or was not available, the following assumptions were made:

3.1.1 Assumed Well Depths.

The following methods were used to assume missing depth information:

a. For wells in which only one of the two interval depths was provided, the cased OR drilled depth, the missing depth was assumed based on a 20 foot open interval.
b. Many permits encompassed several wells (henceforth referred to as “co-located” wells). Wells within the same permit (and thus the same use type) were assumed to have similar depths.
c. Many wells had no depth information, and no co-located wells. For these, USGS data was cross-referenced to obtain the aquifer designation. Then, depths were assumed based on other wells in the area with the same aquifer designation and same use type (irrigation, PWS, etc.).
d. FDOH provided a very comprehensive well database, including domestic wells, with precise locations (latitude and longitude instead of row and column in a model). However, most of these wells had no depth information. The following steps were taken to determine how many, if any, of the wells could be reasonably assumed to pull from the IAS or FAS.
    a. Using data from several USGS tables, % withdrawals by aquifer and total households with wells, by county, was assessed. The number of domestic wells provided by the FDOH was also compared to the total number reported by USGS. It was assumed by the data provided that more domestic wells exist than data is available for. See table 3.1.

b. Of the FDOH domestic well depths provided, % withdrawal by aquifer, by county was assessed. The numbers corresponded with those provided by USGS.

WATER USE REPORTED BY USGS

County	% Total Water usage from FAS	% Total Water Usage from IAS	% Total Water Usage from Biscayne/SAS	# of Domestic Wells per USGS	# of Domestic Wells from FDOH
Brevard	86.1%	0.00%	13.9%	22,458	227
Broward	0.0%	0.00%	100.0%	7,778	122
Charlotte	20.4%	75.41%	4.2%	6,670	93
Collier	2.2%	57.22%	40.6%	11,382	55
DeSoto	88.8%	11.19%	0.0%	7,235	248
Glades	36.4%	3.38%	60.2%	1,252	34
Hardee	90.3%	9.72%	0.0%	5,394	293
Hendry	0.1%	64.01%	35.9%	3,717	132
Highlands	85.0%	14.90%	0.1%	14,284	2626
Hillsborough	98.7%	1.19%	0.1%	70,947	1815
Indian River	84.7%	0.00%	15.3%	18,773	311
Lake	99.5%	0.00%	0.5%	29,839	4869
Lee	16.1%	27.08%	56.9%	29,384	196
Manatee	96.7%	3.31%	0.0%	7,388	142
Martin	13.3%	0.00%	86.7%	19,247	770
Miami-Dade	0.7%	0.00%	99.3%	19,193	607
Monroe	86.7%	0.00%	13.3%	1,255	3
Okeechobee	79.9%	0.00%	20.1%	6,915	177
Orange	99.7%	0.00%	0.3%	26,115	3840
Osceola	97.6%	0.00%	2.4%	13,375	808
Palm Beach	2.4%	0.00%	97.6%	43,021	444
Pasco	99.7%	0.00%	0.3%	43,376	615
Pinellas	99.9%	0.00%	0.1%	4,385	240
Polk	96.1%	3.50%	0.4%	45,174	6921
St. Lucie	58.1%	0.00%	41.9%	29,577	414
Sarasota	67.5%	32.45%	0.1%	28,710	881
Sumter	98.3%	0.00%	1.7%	11,287	164

Table 3.1

c. For the counties that USGS reported pulled more than 95% of their water from aquifers deeper than the SAS, aquifer designations and depths were assumed for all FDOH wells for which no depths were originally provided. IAS and FAS designations were applied according to % given in table 3.1. The counties with 95% or higher are highlighted in red.

If no depth could be logically determined using these methods, the well was omitted.

3.1.2 Assumed Locations.

Two methods were used to assume missing location information:

a. When there were co-located wells in the same permit with only one XY coordinate and missing individual location data, ten feet were added to the known X and Y coordinate values of wells on the same property (then 20 feet, then 30 feet, depending on the number of co-located wells with unknown locations).
b. If no co-located wells with data existed, addresses were looked up and XY values obtained by using Google Earth and GIS, when feasible.

If no location could be determined using any of these methods for a well, it was omitted.

3.1.3 Assumed Capacities.

Seven methods were used to obtain missing capacity information:

a. For wells with no capacity data that did have pumping records, the highest pumping value (i.e., converted to a pumping rate) was used.
b. Data provided by FDEP and FDOH was used to find permitted capacities.
c. Well capacities were were assumed based on known capacities of other wells with the same diameter and same use type.
d. For wells that had only annual averages and no information on diameter or use type, the annual average was used as the capacity. However, if the annual average was 0 for that year, the annual average of a well in the same area with the same use type was used.
e. As a last resort, if no capacity or pumping information was provided, a similar co-location process was used to assume well capacities for wells with the same use type.
f. The private well data provided had no capacity data. Average household flows were calculated per county using average people per household and average daily use per capita, as reported by USGS. Q = (avg. gal/day per person)(avg persons per household)/(7.47 gal/cf).
g. Only annual average flows were provided for the free-flowing wells. Because the free-flowing wells have no pump with a capacity, the annual average was used as the capacity.

If not enough data was present to make a logical capacity assumption, the well was omitted.

3.2 Injection/UIC Data

As with CUP pumping data, the same wellhead data is essential for UIC wells. FDEP provided the most comprehensive wellhead data for all UIC wells, and nearly complete pumping data for the Class I UIC wells. Additional data sources cited to verify comprehensive and accurate ASR wellhead data included several contacts at the SFWMD, the SFWMD on-line permit database, and several technical reports from USGS.

In addition to the WMDs, FDEP, USGS, and USACE, the individual facilities and engineers of record were also contacted to verify wellhead and pumping information during the QA/QC phase, as detailed in a later section.

Additional data sources sited to verify comprehensive and accurate Class I and Class V well head data included FDEP's UIC Program, FDEP's Oil and Gas section (part of Florida Geologic Society (FGS), and GWPC. These data sources verified location, depth, and capacity information. The facilities and engineers of record were contacted for this information during the QA/QC phase, as detailed in a later section.

3.3 Monitoring Well Data

USGS and the WMDs all maintain web-based databases for their monitoring well data. Water level and water quality data was downloaded from these sites. Coordination with hydrologists and GIS personnel at each agency was necessary to expedite the process and ensure accurate data. Monitoring well data were also collected from FDEP, which does not maintain their database online. Other databases maintained by FGS and USACE were consulted to ensure a comprehensive data set. FAS water level and water quality data collected by Tetra-Tech were also used. One set collected by Tetra-Tech included internal water pressures for injection wells. However, no depth or aquifer information was available for these pressures, and it was verified by the FDEP injection well specialist that no reference elevations exist for this data. Therefore, these wells were not included in this data set.

It must be noted that many monitoring wells have more than one interval within a single hole, and many well fields exist with several different holes clustered in close proximity with similar depths and therefore similar transient data. Both scenarios could look like a duplicate at first glance, and each case was carefully scrutinized by database comparison and even verification from a source groundwater expert. Each separate interval, even within the same hole, is listed as a separate well with a unique model ID number. This ensures the appropriate water level data is paired with the correct interval.

3.3.1 USGS Monitoring Well Data

Transient water level data maintained by USGS was downloaded from their National Water Information System, or NWIS. Because NWIS monitoring wells are throughout the model domain, this database was compared to the wellhead databases obtained from the water management districts to eliminate duplication. Duplicate wells were matched by name, USGS ID number, XY coordinates, and depth. Transient data between the duplications was spot-checked to ensure the readings were the same. When a duplicate was found, missing data in one of the databases was filled in using the other database (usually the cased depth), so both databases matched. The larger set of transient data was used in each case. There were a few discrepancies in total depths between NWIS and DBHydro (SFWMD's database). It was confirmed by the SFWMD groundwater data department that NWIS data is more reliable, so depths provided by NWIS were used in these cases.

Assumptions were made for cased depths that were not provided. These assumptions were based on the provided total depths and a probable open hole interval at that depth based on cased depths provided for other wells. The open hole interval assumptions used were as follows:

Total Depth, feet below surface	Open Hole Interval, feet
< 25	2
25 – 99.9	5
100 – 499	20
> 500	100

The assumptions listed in this table were used for estimating cased depths in every monitoring well data set collected, from every data source.

Once the duplicates were removed from the dataset, casing depths assumed, and location accuracy verified by GIS, the corresponding transient data was linked to the wellhead data set.

3.3.2 SFWMD Monitoring Well Data

The SFWMD's DBHydro browser was the main source for monitoring well data from that district. DBHydro is the SFWMD's corporate environmental database, which includes hydrologic (including groundwater), hydro-geologic (including well construction), and water quality data. From the transient groundwater level database, both transient water levels and wellhead information were downloaded. The wellhead database downloaded from the transient groundwater section was compared to the well construction data from the hydro-geologic database. It was confirmed by the SFWMD groundwater data department that the well construction data from the hydro-geologic database was more accurate, so the XY coordinates and depths from this database were used where discrepancies existed.

A different set of wells maintained in a separate database are also included in this data set. They are known to the District as the "POT run", a twice a year snapshot of water-level (and in some cases water-quality) from the Upper Floridan Aquifer. It was determined during the compilation that DBHydro included a few wells that fall within the SJRWMD. Only DBHydro provided transient data for these four wells, and they were also included in the data set.

It is worth noting that a little over 10% of the wellheads listed in DBHydro had transient data recorded during ASR's POR. Only those wells with applicable transient data were included in the data set for this model.

Once the duplicates were removed from the dataset, casing depths assumed, and location accuracy verified by GIS, the corresponding transient data was linked to the wellhead data set.

3.3.3 SJRWMD Monitoring Well Data

Monitoring well data from five different sources was compared for duplication and accuracy and then compiled. These five data sources were: the web-based groundwater monitoring network GIS data (known as the ORACLE DB), the web-based archived groundwater level database (known as the WEB HYDRON), monitoring station records for piezometers in the Floridan and shallower aquifers surrounding the Conserv II facility in western Orange County, monitoring well data collected by Tetra-Tech, and the groundwater data set used in the East Central Florida model. With the exception of the Conserv II data, all the data sets included data on the same wells, each using a different mix of three separate and distinct naming systems. A senior hydrologist at the District provided a groundwater monitoring network list showing all three names for each well, which was used to determine duplicate wells.

Once the duplicates were removed from the dataset, casing depths assumed, and location accuracy verified by GIS, the corresponding transient data was linked to the wellhead data set.

3.3.4 SWFWMD Monitoring Well Data

A complete list of monitoring wellheads and the corresponding transient data was available on the district's web-based database, and was also provided directly to the Corps by a senior hydrologist. Data from the same monitoring wells was also collected by Tetra-Tech.

Once the duplicates were removed from the dataset, casing depths assumed, and location accuracy verified by GIS, the corresponding transient data was linked to the wellhead data set.

3.3.5 FDEP Monitoring Well Data

Some water level data was also provided by FDEP. It was verified that their data sources were the same as listed above; the water management districts and USGS. However, after checking for duplications, a few wells had no matches and were incorporated into the data set.

3.3.6 Correcting Water Levels.

Water levels in DBHydro were converted from pressure in psi to equivalent freshwater head in feet above the well's pressure transducer. This methodology assumes a water density with a standard temperature and salinity within the well. It does not account for actual variations in these parameters. Based on information from SFWMD, the converted heads in DBHydro were very close to what they would be if they had been corrected for density and temperature, for TDS values under 10,000 mg/l. These did not need further correction, and were used as reported.

However, for TDS values over 10,000 mg/l, DBHydro heads did not equal what the water levels would be if corrected for the effects of both temperature and

water quality (salinity). SFWMD provided a spreadsheet containing the appropriate formulas for this density correction. Generally, the water quality (salinity) for the wells are reasonably well known; however, accurate temperature readings were not readily available for most wells. In wells where accurate temperatures were not well known, a temperature of 24 degrees Celsius was assumed based on discussions with SFWMD.

Figure 3.1, below, illustrates the relationships between DBHydro water levels, and the affects of density correction.

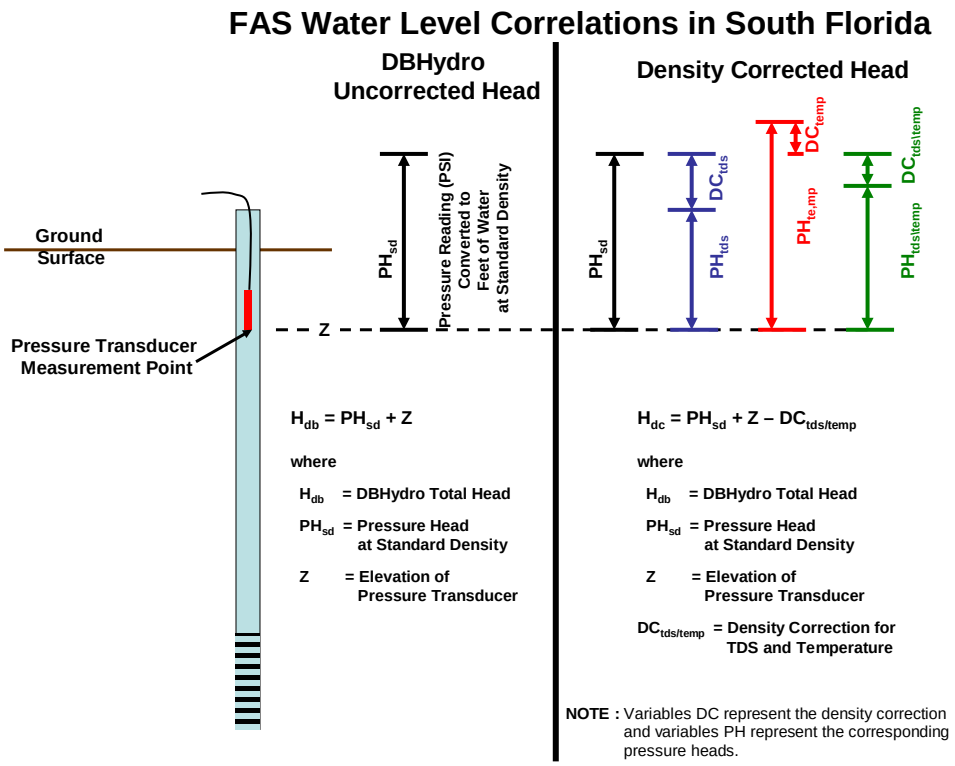

Figure 3.1

The left side shows the ground elevation and transducer elevation in the well. The transducer's reading in psi is divided by 0.4335 to convert to equivalent feet of freshwater (assuming an equivalent freshwater density of 1000.38 kg/m^3), then added to the elevation of the transducer. This is what is reported in DBHydro. Though they are not density corrected, the values are very close to what they would be if density corrected, for TDS levels below 10,000 mg/l. The heads on the right show the relationship between the total heads in DBHydro with and without density correction. The black line shows the unchanged DBHydro values. The blue line shows what the level would be if density corrected only for TDS. The red line shows the water levels for temperature density corrections. The green line shows the water levels after density correction for both TDS and temperature. The black and green lines are equal heads for TDS values below 10,000 mg/l. They are not equal for TDS values above 10,000 mg/l.

Water level data from USGS had not been density corrected and had the same above calculation applied to each reading to give equivalent freshwater heads. However, discussions with USGS verified that their monitoring wells were not deep enough in South Florida to reach water with 10,000 mg/l salinity. This was verified, and the same principles applied.

4.0 Quality Assurance/Quality Control of Pumping Wellhead Data

A large amount of data was collected, all from different sources, all with varying degrees of QA/QC provided prior to dissemination. In short, the data as received included many errors, the nature of which varied by agency. Thus, QA/QC was

required continually throughout the compilation process. Once the pumping wellhead location data was collected, it had to undergo a rigorous QA/QC process before adding the pumping records to it. The following paragraphs describe the compilation QA/QC process.

4.1 Ensure Compatibility

In order for the data to be useful for the model, all wellheads needed to have a location, depth, and either water level, pumping, or water quality data, all with uniform units. Due to the fact that each data source used different nomenclature systems, different reporting requirements of the facilities, and different data management, separate SFWMD, SWFWMD, SJRWMD, DEP, and USGS files were maintained initially. Not only did each agency have a different nomenclature system, but the USGS, FDEP, FDOH, and contractor data overlapped the WMD data, as well as each other. Thus, each file had to be organized identically to easily combine the files later and check for duplicates.

All data had to be in the same vertical and horizontal datum. They are as follows:

Horizontal Datum: NAC 83 State Plane 0901 Florida East, US Survey Foot

Vertical Datum: NGVD 29, US Survey Foot

CorpsCon was used for the horizontal datum conversion, after which the well locations were plotted in GIS to ensure proper conversion and to detect and correct any outliers.

4.2 Eliminate Wells out of the Model Boundary

Wells that fell outside the model boundary were confirmed as having correct location data and omitted. Upon closer inspection, it was found that some wells, though they plotted inside the model boundary, were still in the wrong place. This prompted a more thorough location assessment via GIS.

4.3 Verify Correct Location Data

The remaining wells inside the model boundary were analyzed to determine if the XY locations were correct. Since the ASR and injection well data sets were relatively small (400 wells total), each well could be addressed. However, that could not be done to the 21,000 CUP wells, so a representative number were addressed. The SFWMD CUP well permit numbers were different for each county, so they were plotted by county to determine if their location data was correct. SJRWMD and SWFWMD CUP nomenclature was not by county, so a representative sample of the wells was analyzed individually.

4.4 Eliminate Duplicates

Duplicates were found and eliminated by analyzing multiple wells with the same permit number, owner, well name, depth, capacity, and XY location. All of these parameters were analyzed to make sure it was a duplicate well. Fortunately,

relatively few duplicates were found in these data sets. Most wells with the same permit number and owner had different well names (well 1, well 2, etc.), different depths, well diameters, capacities, or a combination of differences. Some permits with multiple wells provided one XY location for the entire permit; thus the same location for all wells. Each co-located well XY was changed enough to be on the same property, but to avoid being in the exact location of another well (see Section 2.1.2).

The only outstanding issue found was that over 200 wells in the SWFWMD data set were confirmed as all being different wells with different permit numbers, well names, depths, and capacities, yet all having the exact same XY location. The data source was notified of this, and the correct locations were provided.

4.5 Fill in Pumping Gaps

Once the QA/QC procedure for the wellhead data was complete, the product was a comprehensive and corrected pumping wellhead data set. Historic pumping records provided by the WMDs were then added to the respective well heads. It was then determined not only how many wells did not have pumping data, but also how much pumping data did not have a matching wellhead. Phone calls were made to the data sources to discuss the findings and determine appropriate data representation. Again, it was different for each district. The pumping data gaps were handled as follows:

4.5.1 Data sources at one district ensured that their historical pumping data set was complete, and that any "missing" pumping data indicated no pumping at all. A representative sample of the wells was checked on this district's web-based permit data base to confirm the zero pumping for the unreported months. After that, each well was checked individually to confirm that each month of its operation was represented, and that zero pumping was reported appropriately.

4.5.2 Another district provided CUP pumping records for wells for which they previously did not provide wellhead data. There were few of these and it was feasible to look up each permit on the web-based permit database. This procedure provided the permit start date (showing if active during model POR), water source (aquifer name or surface water), how many wells, and the relative location. It was easy to fill in the wellhead information for the pumping records, and determine if it belonged in the model.

4.5.3 Some of the pumping records provided were given in totals per permit, all wells combined. This required a detailed 4-step procedure for properly distributing the provided pumping data, and filling in the gaps. As an example, Bob's Citrus Grove has 6 wells, but only one total pumping value for each month from August 1993 through July 1994.

a. The drill and abandoned dates were noted. Only the wells operating during the pumping dates were used in this process. For example,

wells A, B, and C were drilled in 1978, while wells D, E, and F were drilled in 2000. As a result, only wells A, B, and C can be considered at this point.

b. The capacities of the wells in operation were summed. Well A was 250,000 cfd, Well B was 200,000 cfd, and Well C was 100,000 cfd. A combined capacity of 550,000 cfd was used.
c. For each month, the percentage of the total permit capacity that was pumped was calculated. The total pumped in August 1993 was 20% of 550,000 cfd, 18% in September, and so forth.
d. It was assumed that each individual well pumped at the same capacity percentage, and the monthly percentages were applied to each well. Therefore, well A was reported as having pumped 20% of its 250,000 cfd capacity in August 1993, 18% of its 250,000 cfd capacity in September, and so forth. This was calculated and reported as monthly cfd.

Note from the example that there are no pumping data for any well for the October 2003 through December 2004 POR. The data filling for this period was handled differently.

a. First, the county and the type of well were noted. Bob's Citrus Grove is in Lee County and has all irrigation wells.
b. Another irrigation well in Lee County for which historical pumping records were provided was located. Sunny Groves, also in Lee County, had historical pumping data for both PORs.
c. The monthly percentages were determined for Sunny Groves, as in c. above, FOR BOTH PORs.
d. If the 1993-1994 monthly percentage numbers for Sunny Groves were similar to those of Bob's, it was assumed the 2003-2004 usage percentages were also similar.
e. Sunny Grove's 2003-2004 monthly percentages were applied to Bob's wells for the same POR.
f. If the 1993-1994 monthly percentage numbers for Sunny Groves were NOT similar to those of Bob's, it was assumed the 1993-1994 usage percentages for Bob's may be a more accurate representation of his usage ten years later.

4.5.4 Wellheads with no historical pumping records represented a majority of the pumping data gaps. In this case, only the above steps a, b, c, and e, were followed.

4.5.5 Monthly flow records are not kept for drainage wells. Annual averages were available for two years; 1995 and the 1993-1994 water year. Using the acreages and monthly rainfall totals in the area, calculations were run in an effort to determine a runoff coefficient for each well. A coefficient was determined when the calculated annual average matched the furnished annual average. This process did not provide useful runoff coefficients, as each well had a different runoff coefficient for each year an

average was provided. Thus, the 1993-1994 annual averages (in cubic feet per day) were used for monthly drainage flows for that POR. Monthly flows for the 2003-2004 POR were calculated using the same annual average and the total annual rainfall ratio between the PORs. The 1993-1994 annual average dataset was used for the 2003-2004 calculations instead of the 1995 averages for two reasons. The first reason was to maintain calculation consistency. The second reason was that the runoff coefficients calculated for this POR more closely resembled expected runoff coefficients for the land use types and soil type of the surrounding area. Monthly and annual rainfall totals were retrieved from NOAA and the water management district web sites.

4.5.6 For CUP wells in which the annual average was reported as the capacity, monthly flows were calculated by multiplying the annual average by a flow/annual average ratio computed for a nearby well of the same use type with furnished capacity and flow data.

4.5.7 The capacities calculated for the domestic wells were also used as monthly averages.

4.5.8 Since there were only about 400 UIC and ASR wells, it was feasible to call each owner, lead operator, or engineer of record, and obtain any missing data. During this process, the locations, depths, capacities, and drilled and abandoned dates were double-checked, and any wells that were drilled after 2004 were noted for later modeling.

5.0 Quality Assurance/Quality Control of all Monthly Pumping Data

Once every wellhead had pumping data paired with it for each month it was in operation, the second QA/QC process was initiated. For this, a highly objective approach was necessary. A procedure was established, listing what to look for, but not denoting methodology. Some of the QA/QC steps required were already performed, but it was assumed that an objective party completing the same tasks using a different method may find more mistakes. This proved to be the case. Below are the steps the objective QA/QC team followed:

<u>Pumping locations</u>.

1. Check for duplicates.
2. Check for units. All pumping capacities should be in cfd.
3. Check for possible order of magnitude problems (i.e., if most are in the order of 10,000, but one is on the order of 10).
4. There should be no zeros. If depth or location data are not provided, space should be left blank.
5. Make sure all columns contain data consistent with the heading, and that headings are consistent with guidelines.

<u>Pumping data.</u>

1. Ensure each well had a reported pump rate (including zeros) for every POR month in existence.
2. Check to see that actual pumping rates reported are consistent with the pump capacities. Some reported pumping rates were a magnitude of 10 or more too high. These values were changed to be similar to appropriate pumping rates in other months for the same well.
3. Make sure all pumping data are reported in cfd.
4. Make sure all columns contain data consistent with the heading, and that headings are consistent with model needs.
5. There can be zeros reported in the pumping, which indicate it was recorded that no pumping occurred that month. Spaces indicate no data available.

Once this was completed, the wellhead and pumping data were ready to be included in the model. At this point, the water level and water quality data could be addressed.

6.0 Quality Assurance/Quality Control of Water Level Data

The water level data underwent a similar QA/QC process as the transient pumping data. A majority of the time was spent ensuring the accuracy of the location and depths of the well heads, and verifying accurate intervals, well fields, and corresponding transient data. Careful attention was given to check wells with multiple names, multiple wells with similar depths in close geographic proximity, and wells with multiple intervals. As with the pumping wellheads, all locations were converted to NAD83 State Plane XY coordinates, and every depth was converted to feet below ground surface. Every water level was given in feet, NGVD. Wellheads were mapped in GIS to determine gross outliers and eliminate those out of the model boundary. GIS was also used to help determine duplicate wells.

The transient water level data was handled differently than the monthly pumping data. One major difference is that the daily recorded water levels were used instead of monthly averages. Though daily records for each and every monitoring well was preferred, if data was not recorded for every well, it could not be assumed. The QA/QC process for the transient water level data involved ensuring all water level data available was collected, and paired up with the right wellhead, at the right interval. Many wells had several sets of the same water level data from different projects; only the largest set was included in the data set.

7.0 Quality Assurance/Quality Control of Water Quality Data

The water quality data underwent a QA/QC process similar to that of the transient water level data. It was not necessary to ensure the accuracy of the monitoring well head locations and depths, as water level readings had been

collected from the same monitoring wells, and this step had already been completed..

The transient water quality data was compiled in a similar manner to the water level data. Daily recorded samples, which were infrequent, were used. Though data for each monitoring well is preferred, data cannot be assumed for a well with no records. The QA/QC process for the transient water quality data involved ensuring all water quality data available was collected, and paired up with the right wellhead, at the right interval.

After compilation of TDS, Chlorides, and Specific Conductance data was all complete, the TDS data was analyzed for comprehensiveness. Only the TDS data was needed for the model. However, since it was known that there are large water quality data gaps, both spatially and temporally, the other two species were collected to be converted to TDS to fill any data gaps. However, if the TDS data was comprehensive enough, the conversion of Chloride and Specific Conductance data would not be necessary. This turned out to be the case, and only the original TDS data was used in the model.

References

Groundwater Protection Council, 2007, “Class I Inventory of the United States.” An inventory of Class I Injection wells provided on their web site.

Florida Stormwater, Erosion, and Sedimentation Control Inspector’s Manual, The.

Marella, Richard L., 1999. “Water Withdrawals, Use, Discharge, and Trends in Florida, 1995,” U.S. Geological Survey Water-Resources Investigations Report 99-4002: prepared in cooperation with the Florida Department of Environmental Protection.

Marella, Richard L., 2004. “Water Withdrawals, Use, Discharge, and Trends in Florida, 2000,” U.S. Geological Survey Scientific Investigations Report 2004-5151: prepared in cooperation with the Florida Department of Environmental Protection.

Reese, Ronald S., 2002. “Inventory and Review of Aquifer Storage and Recovery in Southern Florida,” Water-Resources Investigations Report 02-4036; prepared as part of the U.S. Geological Survey Place-Based Studies Program.

Reese and Alvarez-Zarikian, 2007 “Hydrology and Aquifer Storage and Recovery Performance in the Upper Floridan Aquifer, Southern Florida,” U.S. Geological Survey, Reston, Virginia: prepared as part of the U.S. Geological Survey Greater Everglades Priority Ecosystems Science Initiative.

Sepulveda, Nicasio, 2002, “Simulation of Ground-Water Flow in the Intermediate and Floridan Aquifer Systems in Peninsular Florida,” U.S. Geological Survey, Water-Resources Investigations Report 02-4009.

Reese, R.S., 2000, “Hydrogeology and the Distribution of Salinity in the Floridan Aquifer System, Southwestern Florida,” U.S. Geological Survey, Water-Resources Investigations Report 98-4253.

Torres, A.E., Sacks, L.A., Yobbi, D.K., Knochenmus, L.A., and B.G. Katz, 2001. “Hydrogeologic Framework and Geochemistry of the Intermediate Aquifer System in Parts of Charlotte, De Soto, and Sarasota Counties, Florida,” U.S. Geological Survey, Water-Resources Investigations Report 01-4015.

Reese, Ronald S., 2002. “Inventory and Review of Aquifer Storage and Recovery in Southern Florida,” U.S.Geological Survey, Water-Resources Investigations Report 02-4036.

O’Reilly, Andrew M., Spechler, Rick M., and McGurk, Brian E., 2002. “Hydrogeology and Water-Quality Characteristics of the Lower Floridan Aquifer in

East-Central Florida," U.S. Geological Survey, Water Resources Investigations Report 02-4193.

Reese, R.S., 2004. "Hydrogeology, Water Quality, and Distribution and Sources of Salinity in the Floridan Aquifer System, Martin and St. Lucie Counties, Florida," U.S. Geological Survey Water-Resources Investigations Report 03-4242.

Merritt, M.L., 1997. "Computation of the Time-Varying Flow Rate from an Artesian Well in Central Dade County, Florida, by Analytical and Numerical Simulation Methods," U.S. Geological Survey, Water-Supply Paper 2491.

SFWMD/DBHydro; Monitoring Well database for locations, depths, water levels, and water quality data.

SFWMD - Emily Richardson
- Injection well and monitoring well data
- Representative BZ TDS data (October 2007)
- Packer Test data (November 2008)
  - Application Permit 13-01556-W
  - ARCADIS, July 2004, V.1
  - CDM (April, 2006 and July, 2007 V.1)
  - CH2MHILL (May 1991, June 1992, Nov 2002, March 2003, Oct 2004, and Aug 2007)
  - Fiveash ASR Report, Sept. 1998
  - FKAA Exploratory Well Report, Nov. 2003
  - Geraghty & Miller, (Feb. 1990 and July, 1991)
  - Hazen & Sawyer, Nov. 2001
  - Highland Beach ASR Report, Oct. 2001
  - JLA Geosciences, January 2008
  - MHC, June 2007
  - Missimer Assoc., Jan. 1993
  - Missimer International, Feb. 1997
  - MWH, (Aug. 2006 and April, 2007)
  - N. Miami Beach Exp. Floridan Rpt., Jan. 2004
  - PBS&J, June, (2008 V.1 and Sept. 2008)
  - Sunrise ASR Report, Mar. 1998
  - USGS WRIR 02-4036
  - USGS WRIR 94-4010
  - WASA Monthly Reports
  - Witt & Assoc., (Feb. 2002 and 2007)
  - WRS, (January 2004 V.1 and January 2005)
  - LEC Model Report (April 2006), Table 4-4 TDS data

SWFWMD; Pumping well data provided by Mike Kelley, Water level data provided by Margit Crowell, and water quality data provided by Robert Peterson and Catherine Wolden.

SJRWMD; data provided by web data base with guidance and supplements from Bill Osburn

USGS web database: http://fl.water.usgs.gov/infodata/groundwater.html

FDOH; data provided by Lawrence Gordon, P.G.

FDEP data base; with guidance and supplements from Cathleen McCarty, Joe Haberfeld, and Kenna Study; with special thanks to John Davis

Cocoa/Dyal plant Monthly Operating Reports (MORs) for ASR wells, for the modeling periods of record (PORs).

Palm Beach County System 9 plant records MORs for ASR wells, for the PORs.

Sunrise/Springtree Water Treatment Plant MORs for ASR wells, for the modeling PORs.

Miami-Dade Water And Sewer Authority, West Wellfield MORs for ASR wells, for the modeling PORs.

Boynton Beach cycle history records and MORs for the ASR wells, for the modeling PORs.

Palm Bay ASR well cycle test data for the modeling PORs, collected by Chris Brown.

Fiveash ASR well cycle test data for the modeling PORs.

Lee County - North Reservoir ASR well cycle test data for the modeling PORs.

Birdie and Blandford, Hydrogeologic, 1994

Compilation of UF data provided by Chris Brown (May 2006)

INTERAGENCY MODELING CENTER (IMC)

Modeling Service Request (MSR) Form

Jul. 14, 2008

Project Name		Project Manager	Requesting Agency	Request Date
ASR Regional Study Model Development Effort	☑ PDT ☐ RECOVER	SFWMD: Robert Verastro USACE: Orlando Ramos-Gines	USACE	**14 JUL 2008**

Contact Information	Name: Orlando Ramos-Gines Phone: 904-232-1662 Email: Orlando.Ramos-Gines@usace.army.mil
Service Duration	Start Date (M/D/Y): 07/14/2008 Due Date (M/D/Y): Varies (see attached)

Brief Description of Service (See attached SOW for details):	☐ **New Work**	☐ **Change Order**

1. Review Data Compilation Report for the ASR Regional Study (Task 1B) – Available for review 01 Dec 08 – Deadline for IMC Review 01 Jan 09.
2. Reports and papers documenting the hydrogeologic framework for the ASR Regional Study (Task 3) - Available for review 11 Aug 08 – Deadline for IMC Review 29 Aug 08.
3. Phase I model Report for the ASR Regional Study (Task 4A) - Available for review 11 Aug 08 – Deadline for IMC Review 29 Aug 08.
4. Interim Phase II Model Report for the ASR Regional Study (Task 4B) - Available for review 27 Feb 09 – Deadline for IMC Review 20 Mar 09.
5. Final Phase II Model Report for the ASR Regional Study (Task 4B) - Available for review 30 Sep 09 – Deadline for IMC Review 22 Oct 09.
6. Regional Optimization Report for the ASR Regional Study (Task 4C) - Available for review 30 Jul 10 – Deadline for IMC Review 20 Aug 10.
7. Final Inset Model Report for the ASR Regional Study (Task 5) - Available for review 30 Mar 11 – Deadline for IMC Review 15 Apr 11.

Service Type

☐ Review

☐ Model Application

Project Estimated Service Amount	In-Kind Service: Hours: __~ 24 ____ Contractual Amount: $ _____	**Activity Code & Job #**	COE: SFWMD:

Fund #		**Budget Line Item #**		**Funding Amount**	$

APPROVALS

	To	Title	Agency/Organization	Action Code(s) *	Initials	Date
1	Orlando Ramos-Gines	Proj Manager	USACE	A		
	Robert Verastro	Proj Manager	SFWMD	A		
2	Larry Stout	IMC Director	USACE	A		
3	Akin Owosina	IMC Director	SFWMD	A		

Project Name		Project Manager	Requesting Agency	Request Date
ASR Regional Study Model Development Effort	☑ PDT ☐ RECOVER	SFWMD: Robert Verastro USACE: Orlando Ramos-Gines	USACE	**14 JUL 2008**

Contact Information	Name: Orlando Ramos-Gines Phone: 904-232-1662 Email: Orlando.Ramos-Gines@usace.army.mil
Service Duration	Start Date (M/D/Y): 07/14/2008 Due Date (M/D/Y): Varies (see attached)

Brief Description of Service (See attached SOW for details): ☐ **New Work** ☐ **Change Order**

1. Review Data Compilation Report for the ASR Regional Study (Task 1B) – Available for review 01 Dec 08 – Deadline for IMC Review 01 Jan 09.
2. Reports and papers documenting the hydrogeologic framework for the ASR Regional Study (Task 3) - Available for review 11 Aug 08 – Deadline for IMC Review 29 Aug 08.
3. Phase I model Report for the ASR Regional Study (Task 4A) - Available for review 11 Aug 08 – Deadline for IMC Review 29 Aug 08.
4. Interim Phase II Model Report for the ASR Regional Study (Task 4B) - Available for review 27 Feb 09 – Deadline for IMC Review 20 Mar 09.
5. Final Phase II Model Report for the ASR Regional Study (Task 4B) - Available for review 30 Sep 09 – Deadline for IMC Review 22 Oct 09.
6. Regional Optimization Report for the ASR Regional Study (Task 4C) - Available for review 30 Jul 10 – Deadline for IMC Review 20 Aug 10.
7. Final Inset Model Report for the ASR Regional Study (Task 5) - Available for review 30 Mar 11 – Deadline for IMC Review 15 Apr 11.

Service Type

☐ Review

☐ Model Application

FOR IMC USE ONLY

Request NO.		**Work Assigned to**		**Date Assigned**		**Priority**	
IMC Estimated Service Amount	In-Kind Service: _____ Hours			Contractual Amount: $ _____			
Completion Date		**Final Cost**	**Hour: and/or $**		**Product Delivery Date**		
IMC Manager Sign Off	**Akin Owosina**		**Signature**			**Date**	
	Larry Stout		**Signature**			**Date**	

*** Action Codes:** A = Approve C = Comment R = Reject

The intent of this updated MSR is to augment the original strategy document (submitted via MSR in December 2004), outline the current status and plan for the ASR modeling, identify documents for future review, and anticipated review dates for upcoming work products. See following summary of ASR modeling Tasks.

Task 1 - Literature Search and Data Compilation:

The ASR Regional Study encompasses a large study area extending from Orlando in the north to the Florida Keys in the south. Over the years a considerable volume of geotechnical, geological and hydrogeological information has been collected by governmental agencies and private companies. The existing data types are many and varied. The purpose of this task is two fold. The first component is to assemble, review and evaluate computer model related data. Both published and un-published hydrogeologic and modeling reports concerning the Floridan Aquifer are of interest. The second component is to collect and compile existing data for the calibration of the ASR Regional and Inset Models. Existing databases such as the Florida Geological Survey well database and the SFWMD DBHYDRO database will be of particular interest.

Task 1A: Literature Search

This task included the compilation and organization of existing groundwater modeling efforts to support development of a large regional model as well as several high-resolution inset models that will simulate the Floridan Aquifer System in response to the proposed CERP ASR program.

Status: This task was completed by CH2MHill in December 2005 and a report generated. (Sub-Task No. 3 – Groundwater Numerical Model Development Support and Data Collection Report).

IMC Review: Not Performed

Task 1B: Data Compilation

This task will provide the data sets necessary for numerical model development and calibration tasks. Data will be compiled into a spreadsheet or a database, evaluated and "scrubbed" in order to expedite development of model data sets and graphical output. The main scope of the task will be to synthesize the data into coherent data sets and graphical displays. Three primary data sets will be compiled: groundwater pumping, hydraulic head, and concentration in TDS. Data compiled from this task will assist with the development of the overall Floridan Aquifer System hydrogeologic framework.

Status: This task is currently underway. Data compilation is anticipated to be complete by the end of September 2008. A summary report documenting the data compilation efforts is anticipated by December 2008.

IMC Review: To be performed upon completion of the Data Compilation Report. Anticipated review date 01DEC08.

Task 2 - Bench-scale Modeling Study:

In order to balance the needs of the project with the current technical capabilities of software and hardware, the model development team recommended the development of a bench-scale model to evaluate various model codes and approaches in order to aid the model code selection task. The primary objectives of the bench-scale modeling effort were:

- Provide an improved estimate of model run times
- Provide a preliminary understanding of model development issues relating to resolution requirements, boundary types, and starting conditions
- Uncover model limitations and short comings
- Aid in determining what class of model (constant density standard flow and transport, uncoupled density-dependent flow and transport, fully density dependent flow and transport) is required to address CERP ASR issues
- Provide comparison performance metrics for various bench marked codes including relative accuracy, and model stability and run-times
- Aid in the evaluation of hardware needs & pre/post processing requirements

The four codes were selected in a collaborative fashion among members of the modeling sub-team of the PDT. These codes included:

- MODFLOW and MT3DMS using equivalent freshwater heads to represent saltwater boundaries (e.g., standard flow and transport model)
- MODFLOW using SWI package (Salt-water intrusion package)
- SEAWAT (fully density-dependent)
- WASH123 (fully density-dependent)

Each model included a model boundary consisting of a 40-mile by 40-mile square box with vertical layers representing the Surficial Aquifer System (SAS), Hawthorn Group confining unit, and the Floridan Aquifer System (FAS). Weighing all of the factors and considering improvements that could be made to the model grid or mesh for future models, it appears that both the SEAWAT and WASH123 codes are appropriate to utilize for the ASR Regional Study model development effort.

Status: This task was completed and a final report (ASR Regional Study – Benchscale Modeling) published in July 2006.

IMC Review: The work product from this task was reviewed by IMC and comments were incorporated into the final report.

Task 3 - Hydrogeologic Framework Studies:

Numerous reports and papers documenting the hydrogeologic framework used in the models and testing of various hydrogeologic theories have been performed to date. These include:

- "Preliminary Hydrogeologic Framework Report", Reese and Richardson 2004.
- "Synthesis of the Hydrogeologic Framework of the Floridan Aquifer System and Delineation of a Major Avon Park Permeable Zone in Central and Southern Florida", USGS Scientific Investigation Report 2007-5207.
- "Lineament Analysis South Florida Region", Fies 2004.
- "Using Density-Dependent Numerical Models To Evaluate Regional Ground Water Flow Patterns In South Florida", Bittner et all. 2007.

These reports and papers document the data and approach to be used in the Phase II ASR Regional Model calibration.

Status: These tasks have been completed; however, updates are planned in some cases as the modeling proceeds.

IMC Review: IMC has not reviewed these documents to date. However, subsequent to the17APR08 meeting with IMC, it was determined that a limited review of these documents would be appropriate. This review should focus on the applicability of the data presented and revisions or suggestions to facilitate the development of the Phase II model.

Task 4 - Regional Screening Model:

This task will focus on the development, calibration, verification, and documentation of a regional screening-level numerical computer model of the FAS. The regional screening-level numerical model is intended to be a peninsular size model with low grid/mesh resolution in areas outside the focus of the model which would be north of Lake Okeechobee, adjacent to the C-43 reservoir, and along the Florida lower east coast. In the model focus areas, grid/mesh resolution would be increased to provide greater accuracy in simulating groundwater heads and salinity. The intended use of the screening model is to aid the PDT in evaluating the feasibility of the proposed CERP ASR program. The model will simulate the changes in flow and head within the FAS resulting from various plan scenarios. Performance measures will be developed related to maximum aquifer pressures, hydrofracturing, and others. Model output will be compared to these various measures to determine feasible plans. The intent of this regional screening model is to evaluate the regional impacts of CERP ASR clusters, not to evaluate local scale impacts of individual wells.

Due to the complexity of the FAS and the large scale of the modeling to be undertaken, this regional modeling effort will be divided into the phases described below.

Task 4A (Phase I):

The Phase I model was a coarse test bed for the more refined Phase II model.
Specific goals of the Phase I model were to:

- Identify model boundaries and test model boundary parameters
- Identify regional flow and salt migration pathways
- Identify the timing of salt water intrusion
- Evaluate model run times and model sensitivity to time step sizes
- Test hydraulic and transport parameter sensitivity
- Compare WASH123D and SEAWAT results

The Phase I effort included regional conceptualization, estimates of hydraulic and transport parameters, density dependent 3-D groundwater model construction, gross comparisons to head and concentration data, evaluation of flow and transport patterns, and sensitivity analyses to several model parameters. Each of these tasks and analyses provided a greater understanding of the flow and transport system that makes up the majority of the Florida subsurface. This increased understanding provided a platform on which to build in the additional complexities of the Phase II model.

Status: Task was completed and a draft report (Draft ASR Regional Study Phase I - Groundwater Modeling) published in December 2006.

IMC Review: The work product was not reviewed be IMC, since it was considered to be an interim work product. However, subsequent to the 17APR08 meeting with IMC, it was determined that a limited review of this document would be appropriate. Since this model was not calibrated and several key hydrogeologic features (such as groundwater pumping) were not incorporated into

the model, this review should focus on the revisions or suggestions to facilitate the development of the Phase II model.

Task 4B (Phase II):

The Phase II model will consist of several parts. First, a comprehensive data review will be completed to ensure that all available head, concentration, and groundwater withdrawal data is incorporated (See Task 1B, above). Phase II model construction will accompany the data review since the model construction will depend heavily on data availability and data requirements. Once the Phase II model is constructed, a flow only calibration will be performed. For the flow-only transient calibration, concentration values and transport parameters will be held constant. Flow parameters will be adjusted until the computed heads reasonably match observed data. Once a satisfactory flow-only calibration is obtained, full transient calibrations, with variable flow and concentration data, will be completed. Regional model calibration data will encompass flow and water quality data in approximately 200 monitoring wells in multiple geologic units. Regional model calibration will be performed where computed and observed data are correlated over a duration of approximately 1 year (2003-2004). Flow and water quality data for a different 1-year time period (1993-1994), representing a different hydraulic condition, will be used for model validation. The goal of this effort is a fully-calibrated Phase II Regional Model. The calibrated Phase II model will ultimately be used in the evaluation of proposed ASR project alternatives.

Status: Task has been on hold pending the completion of the data collection effort. Although the data collection work defined in Task 1B is not yet complete, the Phase II model construction has begun. It is anticipated that the first level (flow-only) calibration will be completed in January 2009 and the Phase II model calibration will be completed in September 2009.

IMC Review: The Phase II Regional Model Calibration Report will be reviewed by IMC. The anticipated review date for this report is 30SEP09. However, due to the large and complex nature of this regional model calibration, an interim review of the first level (flow-only) calibration is warranted. This interim review is anticipated to be in the form of a presentation to the PDT in February 2009.

Task 4C (Regional Optimization Simulations):

Upon the successful calibration of the Phase II Regional Model, numerous optimization simulations will be performed to evaluate the impacts of the proposed CERP ASR system. Initially, the ASR configuration and flows from D13R (or the appropriate update thereof) will be simulated. The model output will be compared to a set of performance criteria that are currently under development. If the simulated model output exceeds the performance measures at a particular ASR cluster, the number of ASR wells at that location will be reduced systematically until the simulated ASR configuration successfully meets the performance goals. This effort will be coordinated with other

modeling efforts (surface water, ecological, etc.) to evaluate the regional impacts of the proposed CERP ASR system.

Status: This task will be performed after the calibration of the regional model and is anticipated to be complete in July 2010. However, some D13R simulations will be performed during calibration to ensure reasonable runtimes and model stability when the stress of the ASR systems is incorporated into the model.

IMC Review: The ASR Regional Optimization Report will be reviewed by IMC. The anticipated review date for this report is 30JUL10.

Task 5 - High Resolution Inset Models:

In conjunction with the regional model, smaller scale transient stress-test "inset" models will be developed in the vicinity of operational ASR wells. Data collected during the on-going operations or cycle testing will be used to facilitate the calibration of transport parameters for the regional model. Boundary conditions and hydrogeologic parameters will be assigned based on information obtained during the regional model calibration. The calibration of these "inset" models will be done in two steps. The first step will use data from the first cycle testing of the Pilot Projects. The second step will be performed later, after cycle two of the Pilot Projects has been completed. Once the "inset" models have been calibrated to both sets of cycle test data (as wells as regional well data), optimization simulations will be made to evaluate the performance of the ASR configuration determined in the regional modeling. Since these "inset" models will have substantially greater resolution than the regional model, local scale effects of individual wells within each ASR well cluster can be evaluated.

Status: This task will proceed incrementally. The calibration to cycle test one is planned to be complete in September 2009 and the calibration and optimization to cycle test two to be complete in March 2011.

IMC Review: The calibration and optimization report generated for this task will be reviewed by IMC. The anticipated review date for this report is 30MAR11. However, a review of the interim work product during the September 2009 PDT meeting should also be coordinated with the IMC.

MSR 324, Task 1B

IMC Review Comments

On

Aquifer Storage and Recovery

Phase II Groundwater Model Data Collection

In accordance with Modeling Service Request (MSR) 324, the Interagency Modeling Center (IMC) was tasked to review the well data collection and analysis effort of the project Phase II Groundwater Model Data Collection report. The IMC concentrated its efforts on missing information in the report, methodology accuracy of correlating varying data types into a single database with correct translation techniques, evaluation methods of correlation among the data groups, assumptions used in data correlation, criteria used for removing bad data or data scrubbing, data sets assumptions about inflows and outflow parameters within the aquifer system, sufficiency of the data to prescribe inland boundary conditions for the model, and sufficiency of the data to support model calibration with acceptable accuracy for the project.

The project team conducted a comprehensive data collection of thousands of wells and an analysis of the Floridian Aquifer in South Florida for the Phase II groundwater model as part of the Aquifer Storage and Recovery (ASR) Regional Study. The study area is very large and encompasses an area of about 20,000 square miles from Orlando southward to the Keys. The project team acquired data from the United State Geology Survey (USGS), South Florida Water Management District (SFWMD), Southwest Florida Water Management District (SWFWMD), St. Johns River Water Management District (SJRWMD) and independent contractors. They analyzed the data for accuracy and quality, removed redundancy from the various sources and added required missing well data with respect to location, depth, and well screen under some assumptions. Overall the project team did a monumental job in taking various types of data from thousands of wells, with various types of formats from various agencies, and compiling and combining the data into a single data set.

1. Additional Information

1.1. Section 1.2 of the report defined the water well data requirements for the project. It considers accurate location of wells, the depth from which the data was acquired in each well, and the type of water well (pumping, flowing, injection, and monitoring). The project may also consider acquiring seismology and bore-log data from bedrock investigations that were conducted along major roadway, gasoline pipelines, and pre-construction investigations of highways bridges, high-rise structures, and power stations.

1.2. The collected data will help to increase the geologic detail and accuracy of the Phase II modeling effort. Providing fence-diagrams of the aquifer, showing their

structures, well penetration, and well screen, will assist the reviewers, other modelers that may conduct future modeling tasks for the project, and the engineers that will develop the initial and final design of the project.

1.3. The report discusses very well how the modeling team obtained and analyzed the data. The report could be more useful if it included the data or provided a link for it.

1.4. The report could further help to understand the geologic structure of the model domain and the conceptual flow model if it provided a map for each aquifer layer (geologic unit) showing the location of the wells, with unique symbol and color code for each well category, the location where pumping tests took place, model boundaries, and potential ASR locations.

1.5. The reader could benefit by the inclusion of contour maps in the report showing the elevations of the top and bottom of each aquifer layer, and maps showing the thickness of each aquifer layer, model boundaries, and potential ASR locations. This would increase the understanding of the model domain and decrease error in data utilization.

2. Methodology accuracy of correlating varying data types into a single database with correct translation techniques

The project team conducted rigorous work in acquiring data from different sources and merging them into a single database. The work included downloading the data, verifying database attributes, translating elevations to a common datum, and converting pumping rates to common units. The work was automated by employing database analysis routines and Geographic Information Systems (GIS) tools. The manuscript briefly describes this work. The IMC recommends expanding the document to include the following points:

2.1. Explain in Section 1.1.3 whether the "ASR Regional Groundwater model" and the "Mega Model for 1993-1994" boundaries match/relate for employing the mega model for verification.

2.2. Disclose in Sections 1.2.1 and 3.1.3g the source and the location of the annual average flow data and how data was measured for the "free flowing wells".

2.3. Explain the use of a 20-foot open interval assumption in section 3.1.1a., and expand the discussion on using only one of the two interval depths that were provided.

2.4. Expand the discussion in Section 3.1.1c on how drill depths were converted from/to? NGVD elevation for wells which were cross-referenced in local vicinity and aquifer designation. State all the assumptions employed for this conversion, e.g. was GIS or another tool used to average surface elevation for a given location referenced?

2.5. From Section 3.1.1d.c (Table 3.1) would counties such as DeSoto, Hardee, Highlands, and Sarasota be highlighted in red (95% use deeper than SAS) and require aquifer designations and depths assumed for the well figures listed under the FDOH column? Please revise.

2.6. Provide detailed information in Section 3.2, last paragraph, on how "These data sources verified location, depth, and capacity information."

2.7. Specify in Section 3.3 how "Other databases maintained by FGS and USACE were consulted to ensure a comprehensive data set."

2.8. Specify in Section 3.3 the number SFWMD CUP wells that were used as a sample to verify the correct location of the wells, and how verification of all SFWMD wells was done by using only one sample of wells.
2.9. Discuss the error that could occur in operation such as the one described in Section 3.3.1, namely, "… NWIS monitoring wells … database was compared to the wellhead databases obtained from the water management districts to eliminate duplication." Please include a justification for not using a systemic approach such as using Oracle or a VBA to find the data duplication, which would process all incidences.
2.10. Include a justification in Section 3.3.1 for the statement "It was confirmed by the SFWMD groundwater data department that NWIS data is more reliable, so depths provided by NWIS were used in these cases." It is possible that the SFWMD data for some of the SFWMD wells not used are correct. Thus, though preferring the NWIS database indeed assures proper data analysis for most of the wells, data analysis should be done for each of the wells to reduce uncertainty in model input.
2.11. Detail in Section 3.3.1 how the project derived the probability distribution of the "probable open hole interval at that depth based on cased depths provided for other wells. "
2.12. Explain in Section 3.3.2 how the project assumed the casing depth for the SFWMD wells and provide justification for each assumption.
2.13. Explain in Section 3.3.3 how the project assumed the casing depth for the SJRWMD wells and provide justification for each assumption.
2.14. Explain in Section 3.3.4 how the project assumed the casing depth for the SWFWMD wells and provide justification for each assumption.
2.15. Define in Section 3.3.6 the terms 'standard temperature' and 'standard salinity'.
2.16. Quantify in Section 3.3.6 the term "reasonably well known."
2.17. Provide a synopsis of the discussion with the SFWMD in Section 3.3.6 on well-water temperature and explain the reason for assuming well-water temperature of 24^{o}C when the temperature was not provided in the database.
2.18. Explain in Section 4.3 the reason for elimination of all well data outside the model domain, considering that data from outside and adjacent to the model boundary provided information for proper prescription of boundary conditions.
2.19. List in Section 4.5.1 both the number of wells and their percentage of the total wells used as a sample to confirm that no pumping data represent no pumping. Additionally, the section should discuss how the project conducted the examination.
2.20. Describe in Section 6.0 how monthly pumping data correlate with daily water level data.

3. Evaluation methods of correlation

The IMC commends the project team for their work in correlating data from the various data sets and considers this work to be adequate considering the uncertainty in these records. The correlation included cross-referencing data among the agencies data bases; correlating well-screen depth when necessary from drilling depth, other wells in the same permit and same water use in the same proximity; resolving discrepancies among the agencies' databases; verifying the data in each agency

database; assigning well coordinates, when necessary, based on co-located wells; assigning well pumping capacities, when necessary, based on maximum pumping rates, permits, well capacities of other wells of the same type, diameter, use type, water use and required amounts; resolving interval data issues for monitoring wells; and converting monitoring wells water pressures to water heads.

4. Assumptions used in data correlation

Some assumptions were required in order to perform the data correlation due to incomplete database records and/or insufficient data to verify the entries in some databases. Most of the assumptions employed in this process were reasonable and acceptable. The IMC recommends expanding the document to include justifications and explanations for the following assumptions:

4.1. The project should justify the assumption under Item 3.1.1.a, namely, that when only the drilling depth or the casing depth is provided, the other depth was assumed based on a 20-foot open interval.

4.2. The project should justify the assumption under Item 3.1.1.b, namely, that wells within the same permit were assumed to have similar depths. The report should also quantify the term ‘similar’.

4.3. The project should justify the assumption under Item 3.1.1.c, namely, that in the case where records of a few wells do not have the information in their depth, the project assumed that their depth are the same as other wells in the area. In addition, the project should quantify a unit distance that bounds the other wells to be considered in the ‘area’. Additionally, the document should state the actions that were taken when wells in the ‘area’ do not have the same depth.

4.4. The project should justify the assumption under Item 3.1.1.d to assign a depth for a well.

4.5. The project should justify the assumptions under Item 3.1.2.a, namely, that co-located wells are 10 feet apart and that the coordinates of these wells are always increasing (it could be decreasing) from the location specified in the permit.

4.6. The project should justify the assumptions under Item 3.1.3.a, namely, if a well capacity is not given in the records, it is equal to the highest pumping rate in record.. A well capacity could be determined from the well’s equation for maximum drawdown condition, subject to the maximum capacity of the pump.

4.7. The project should justify the assumptions under Item 3.1.3.c, namely, if a well capacity is not given, it is equal to the capacity of other wells in the area with the same diameter. This assumption could be true only if the wells penetration in to the aquifer is the same, the screen length is the same, and the hydraulic conductivity of the aquifer around each well is the same.

4.8. The project should justify the assumptions under Item 3.1.3.d, namely, if a well’s capacity, use type, and diameter are not given, its capacity equals to its average annual pumping rate. This is especially difficult to justify for wet years, where the average annual pumping rate is less than for dry years. Good engineering design would require that the well capacity be higher than the anticipated pumping rate for a dry year.

4.9. The project team should justify the assumptions under Item 3.1.3.e, namely, if no information about the well is given except its location, its capacity equals to another well for the same use type in the co-location. This argument may be

questionable. For example, in a small sub-division where different contractors were hired to construct irrigation wells, each contractor constructed wells according to their individual contract. Some wells depth were only 60 feet deep with 10 feet casing and pumping from the surficial oleic layer, while other wells were 120 to 160 feet deep with 10 to 20 feet casing, pumping from a limestone layer beneath.

4.10. The document should justify the assumptions used to estimate the total depth of a well in the table of Section 3.3.1.

4.11. The document should justify the assumptions used in Section 3.3.6 when "Correcting Water Levels", using water temperature of 24 degrees Celsius.

4.12. When assuming 24 degrees Celsius, the project could use density of 997.2 kg/m3 instead of 1000.38 kg/m3 according to CRC Handbook of chemistry.

4.13. The same section of the document should explain the value of the conversion factor (0.4335) when converting from psi to equivalent feet (head) of freshwater.

4.14. The document should explain in Section 4.1 the conversion of the vertical datum to "Ensure Compatibility."

4.15. The document should explain in Section 4.5.3 the clause "Fill in Pumping Gaps", bullet 'f'. The project may elect to increase the wells' pumping rates by a percentage based on population growth, instead of assuming no increase in water usage from 1993 to 2004.

4.16. The document should explain in Section 4.5.5 using monthly flow records, were wet vs. dry seasons considered in flows, or were all months of the year averaged together. In addition, the project could explain propagation of uncertainty errors in model predictions under this assumption.

4.17. The document should explain in Section 4.5.6, how "nearby" CUP wells were used to extrapolate missing flow data and how the project considered the distance between the wells in the correlation.

5. Criteria used for removing bad data or data scrubbing

Based on the descriptions in the document regarding the data removal, the IMC considers the methodology used by the project team to remove data from the dataset as appropriate, especially when the data was incomplete or unaccountable. The IMC recommends that the document discuss the procedure for which the well data was validated against construction data in order to determine if a given datum is 'bad.' Furthermore, the document should mention whether the CUP, UIC, and ASR wells have been validated against construction dates.

6. Data sets assumption about inflows and outflow parameters within the aquifer system

The document discusses how the project acquired, merged, and correlated water-well data from the model domain. The IMC recommends including a discussion of the data pertaining to flow along the model boundaries, within each aquifer layer, and among the layers, areas as described below:

6.1. The document should discuss data to support any assumption with respect to leakage between the aquifer units.

6.2. The addition of data in three categories: pumping data, water-level data, and water-quality data as mentioned in Section 1.2 above, should be adequately discussed. The document should also discuss information with respect to aquifer flow and transport parameters. The project team should verify if information gathered during the first phase of the modeling effort and in the current task were sufficient with respect to aquifer conductivity, storativity, and dispersion parameters.

6.3. The primary datasets discussed in the document pertaining to inflows and outflows of the aquifer are ground water pumping and hydraulic head. The document should also discuss whether the hydraulic head accounts for precipitation, recharge, and seepage from rivers, canals, lakes, and reservoirs. If not, the project should discuss how these parameters are addressed.

7. Sufficiency of the data to prescribe inland boundary conditions of the model

The IMC was unable to evaluate whether the data gathered is sufficient to prescribe the inland boundary conditions of the model due to the lack of information described above.

8. Sufficiency of the data to support model calibration with acceptable accuracy for the project

The project has already collected a large amount of information about the geology, hydrology, and operation of the model domain. This information may be sufficient for model calibration. The IMC recommends that the following issues be considered and addressed as the project team continues development of the regional ASR model:

8.1. Determination of the maximum uncertainty for model predictions, considering the project purposes.

8.2. Recognition that a potential for model assumption errors could be the result of assumed well depths. Many regions with numerous local wells do not have "standard" depths per well type. Depths may be varied based upon the drilling company and not the well type.

9. Miscellaneous

The document is written quite well, but could be improved by addressing the following issues:

9.1. Stating the purpose of the data collection effort for the Phase II Groundwater Model.

9.2. Having a caption for each table and figure.

9.3. Defining each of the acronyms at their first appearance.

9.4. Defining each term at its first appearance.

9.5. Careful editing to improve readability, way of expression, correcting all typo and grammatical mistakes, and capitalizing the first letter of a name.

9.6. Grammatical – changing sub-titles of Figure 3.1 from "DBHydro Uncorrected Head" to "DBHydro Density Uncorrected Head" and changing "Density Corrected Head" to "DBHydro Density Corrected Head". Another alternative is to take "DBHydro" out of the two sub-titles and add it to the primary title.

Overall the IMC believes that the project team has successfully conducted a monumental data acquisition task. The project obtained the data from various agencies, removed redundancy, converted the data to a uniform datum and units, assigned values to missing data attributes under careful consideration, conducted a quality assurance program, and employed a quality control protocol. The project team could improve the report by giving a link to the database, providing figures to show the geology of the model domain, conceptual model, and depiction of the location and penetration of the water wells. Further improvement of the report could be achieved by expanding the discussion on how the work was done, listing and justifying all the assumptions used in this work, and addressing the miscellaneous items described above.

Appendix B: Grid Resolution Study

Table of Contents

1.0 Spatial Discretization

The numerical solutions presented as output from SEAWAT or WASH123D merely represent approximations of the "true" solution. The nearness of the model output to the "true" solution (accuracy) is dependent on a multitude of factors, including the validity of the conceptual model, and the density and accuracy of model parameters and boundary conditions. In addition to these factors, the construction of the computational grid (or mesh) and the temporal discretization of the model can have a large effect on the accuracy of the model solution. Temporal discretization will be discussed in the following section.

The selection of the grid cell size (or mesh node spacing) is based on a number of factors:

- The discretization of the grid or mesh must be fine enough to sufficiently define the problem. Since solutions are only calculated at the grid cell centers or mesh node points, these calculation points must be sufficiently dense to describe slopes, changes, topographic features, etc. A too-coarse mesh or grid may result in blocky results that do not accurately describe the conditions of the site.

- The discretization of the grid or mesh must be fine enough to provide stability and convergence for the solver.

- The discretization of the grid or mesh must be coarse enough that the solver can produce a solution on available computers in a reasonable amount of time.

- For transport simulations, the discretization of the grid or mesh must be fine enough to minimize numerical dispersion and unnatural oscillations. The impact of numerical dispersion and solution oscillation is also dependent on the solver used.

Thus, the selection of a computational grid or mesh requires the balancing of several differing needs. The following sub-sections describe the process used to create the SEAWAT grid and the WASH123D mesh as well as testing which indicated that the grid/mesh was sufficient for the use intended.

1.1 SEAWAT Grid Selection and Testing

The SEAWAT grid was designed mainly for sufficient discretization to describe the problem while aiming to keep the computational time manageable. This grid has 232 cells per row, 214 cells per column and a total of 22 layers. Horizontal grid cell dimensions vary from 10000 feet to 2000 feet. The smaller cells are placed near possible ASR sites where greater detail of the results will be required. Because of the structured nature of the mesh, horizontal cell sizes must be carried to the edge of the grid, resulting in bands of smaller cells. The structured nature of the grid also results in a number of inactive cells (those located outside the model area, but within the square grid zone. Nearly 25% of the cells in this grid are inactive. The grid is shown in Figure B1-1. To account for anisotropy and the predominant flow directions, the grid was rotated 38 degrees from north. The layer thicknesses are dependent on the thickness of the hydrogeologic layers. In each case, the number of computational layers was selected

and the hydrogeologic layer was equally divided into the grid layers. See the inset to Figure B1-1 for clarification.

Although this grid is sufficiently fine to describe the features, slopes and changes of the regional model, it was not immediately clear whether this grid was sufficiently fine to result in a stable, convergent, accurate solution. Further, because several of the layers become very thin in the northwest area of the model, aspect ratios become very large, raising fears of inaccuracies and instabilities. Tests were run on a number of grids to determine the possible impacts to solution accuracy that might be caused by numerical dispersion, oscillation or other inaccuracies.

1.1.1 Accuracy Testing Grids

Six additional grids were built for the model area. Identical parameters, starting conditions, and boundary conditions were applied to each grid and the results were compared to determine what grid size was necessary for sufficient accuracy in the result. The six grids are compared in Table B1 and shown in Figures B1-2 through B1-7.

Table B1: Test Grid Statistics

Grid Name	**20k11**	**20k20**	**10k11**	**10k20**	**5k11**	**5k20**
Approximate Horizontal Cell Size (ft)	20,000	20,000	10,000	10,000	5,000	5,000
Number of Rows	69	69	138	138	275	275
Number of Columns	55	55	109	109	217	217
Number of Layers	11	20	11	20	11	20
Number of Cells	41,745	75,900	165,462	300,840	656,425	1,193,500
Number of Active Cells	21,161	39,556	84,027	157,054	333,552	623,477

1.1.2 Steady State Testing

Steady state SEAWAT models were set up on each of the six testing grids. Although the models were similar to the calibration model discussed in Section 4.1 of this report, the tests were run before the final versions of all data were available and before the calibration process had been completed. Starting

conditions for both salinity and temperature changed substantially after this testing process. During the calibration period, some boundary conditions were altered slightly, and parameter values were changed. These changes are not reflected in these testing models and the results are not intended to reflect either reality or the calibrated conditions of the model. The general idea was simply to run six identical models on each of the grids and compare the results.

In these models, the starting conditions for salinity and temperature were developed and included in the model. The model did not compute the transport equation, but simply used the starting concentration and temperature conditions to develop equivalent heads (accounting for density variation due to salinity and temperature) for the calculation of the flow portion of the model. Output heads are point-water heads (the level to which water would rise in a standpipe).

In reality, it was impossible to make each of the models exactly identical. Because of the varying sizes of the grids, interpolations of heads on the surface and around the side boundaries varied slightly. Also, starting conditions for both salinity and temperature varied slightly due to the interpolation to slightly different points. These differences account for some of the variability in the results explained below.

The results were compared in two ways. First, a set of points were selected in the model domain and the heads at the cells covering these points were extracted and compared. Some of these points were set at known points of interest, such as potential ASR sites. Other points were selected simply to obtain good coverage of the model domain. The locations of these comparison points are shown in Figure B1-8. The comparison of solution heads for each of the aquifer systems shown in Figures B1-9 through B1-13 is the absolute value of the difference between the indicated grid solution and the solution on the 5000 ft grid with 20 layers. This grid was selected for the comparison since it has the highest resolution and should therefore have the most accurate result.

In extracting the heads at these points, no attempt was made to interpolate between the cell centers to the exact point. The head reported at the cell covering the point of interest was extracted and tabulated unchanged. This means that the point's proximity to the cell center could affect the reliability of the comparison. Figure B1-14 shows an example of this issue. Point M is shown overlain with each of the three test grids. Images a, b, and c each have a single cell from one of the test grids highlighted for clarity. Notice that the point is near the center of the grid cell for the 20000 foot grid, so the extracted value for that cell would be similar to the expected value at the comparison point. For the 10000 ft grid and the 5000 foot grid, the point is near the edge or corner of the cell, so even a set of highly accurate solutions would be expected to yield slightly different results for the point in question. Some of the differences shown in Figures B1-9 through B1-13 are attributable to this issue.

The second comparison of the results was done by overlaying the contour maps for each of the solutions and observing the spread of the contour locations. These results are shown in Figures B1-15 through B1-24. These contours were computed by interpolating from the cell centers using GMS. On these maps, the results from the 10000-ft grid are shown bolded. This is the size of the largest cells in the ASR production grid (see Figure B1-1).

The results of the steady state test runs indicate that there is very little difference between an 11-layer grid and a 20-layer grid in terms of the head solution when the horizontal discretization is the same. The head differences at the comparison points seldom vary by more than a few tenths of a foot, which is well within the expected accuracy of this large-scale regional model. Further, the contours plotted in Figures B1-15 through B1-24 show almost identical results for solutions from grids with the same horizontal grid spacing. Normally, the contour lines are indistinguishable. One significant exception is the 50-foot contour in the Upper Floridian Aquifer as it crosses Lake Okeechobee and continues northwest-ward nearly parallel to the Kissimmee River (See Figure B1-18). Here the 50-foot contour lines for the solutions to the 10,000-ft/11 layer model and the 10,000-ft/20 layer model can be 3 to 4 miles apart. However, the water table here is flat enough that this makes little difference to the actual head values at the comparison points (see Figure B1-10).

Differences between the 10,000-ft grid solutions and the 5,000-ft grid solutions are also minor in most locations. The differences are generally around 1-2 feet at the comparison points. Contour line locations vary by less than a mile in most cases. The main exceptions to these generalizations occur in the northwest section of the model (near comparison point M) and along some of the boundaries. The differences near the boundaries are most likely caused by differences in interpolation of boundary conditions to grids of different sizes and cells with centroids in varying locations. These differences are caused by the difficulty in assigning exactly identical boundary conditions and are not attributable to solver issues.

The northwest section of the grid generally has the greatest head differences and the largest contour movement. In this area, many of the upper layers are extremely thin and, in reality, pinch out. This means that the use of larger cell sizes can cause aspect ratios approaching 5000.

Differences between the 10,000-ft grid and the 20,000-ft grid are more important. The contours may be located 3 or 4 miles away from the location on the smaller grid, but the head differences seldom exceed 2 feet. As with the smaller grids, the worst variation is found in the northwestern portion of the model where aspect ratios are the highest. In the Lower Floridian (LF1) Aquifer and the Boulder Zone, head differences in the northwest corner of the model, exceed 12 feet.

The test results indicate that for the purposes of a steady state regional model, the 10,000-ft grid is likely sufficient from a solver accuracy standpoint. Differences between the 10,000-ft grid and the 5,000 ft grid are minor in most cases and the additional time and computational effort required for a 5,000-ft grid are not warranted with the minor improvement achieved. The results also show that downgrading the grid to 20,000-foot spacing would sacrifice some accuracy, especially in the northwest section of the model. This sacrifice is caused primarily by the interpolation of data to a coarser grid, which cannot sufficiently describe the data. Errors do not seem to propagate into the interior of the model during a steady state run.

1.1.3 Transient Testing

Once the steady state testing had shown that a 10,000-ft grid was sufficient for an accurate result, the same model was expanded to a transient, 12-month run and the results were compared in similar ways

to determine the effect of grid size on the transient head and concentration results. In this case, the transport equation was calculated for salinity and temperature, coupled with the head calculation from MODFLOW. The model was run on the same six computational grids. Specific storage was set to 1.0 x 10^{-5} to allow for sufficient propagation of boundary condition changes. Computational timesteps were 1 day long and solutions were output at the end of each month.

Only a few of the comparison points were used because of the much larger amount of output data. Point C was used because of its proximity to so many of the proposed ASR sites. Point K was used since it is on the far southeast edge of the model and because it is near some of the proposed ASR sites not directly north of Lake Okeechobee. Finally, Point M was used because it had the worst error in the steady state testing. Comparison of output at this point will indicate whether errors are compounded in subsequent timesteps.

Computed heads at point C are shown in Figures B1-25 through B1-29 as an example. Head changes in the solutions on separate grids track each other very closely although the initial head value is often slightly different. Initial heads were slightly different because of interpolation differences for starting conditions and boundary conditions and some differences in the solution of the steady state model. These figures show that head increases and decreases continued for each model, irrespective of the initial head value. Similar plots could be made for any point of interest in the model, but they are not shown in this report.

The differences among the grid solutions can be shown more clearly and concisely in Figures B1-30 through B1-34. Here, the absolute value of the difference in head between the 5000-ft grid with 20 layers and each of the other grids is plotted. In each case, a different color represents a different comparison point and a different symbol represents a different aquifer system. Figure B1-30 clearly shows that, like the steady state solutions, there is no significant difference in the solutions for the 11-layer grids and the 20-layer grids. A similar conclusion can be drawn by noting the similarity between the plots on Figure B1-31 and Figure B1-32 and the similarity between Figure B1-33 and B1-34. Figures B1-31 through B1-34 indicate that at points C (near Lake Okeechobee) and K (southeast part of the model), the horizontal resolution of the grid makes little difference. However, the difference in heads for the various solutions at Point M (northwest part of the model) is often significant. Comparisons of Figures B1-31 and B1-32 with Figures B1-33 and B1-34 also show that the 20000-ft grid has a greater head difference than the 10000-ft grid.

Another important conclusion from these tests is that the head differences do not compound as the model proceeds. This shows that the errors are probably due to differences in interpolation of starting conditions and boundary conditions and not a result of solver errors or numerical dispersion.

Although not shown, the salinity and temperature for these comparison points were also extracted. They showed almost no difference among the solutions (maximum 700 mg/L TDS and 3°C) and no change in concentration with time (maximum of 150 mg/L TDS and 0.07°C change over 1 year). The differences in among the grid solutions are easily explained by differences in interpolation for starting conditions to grids of differing resolutions.

2.0 Temporal Discretization

Temporal discretization can be as important as spatial discretization. Computational timesteps (times at which the solution is computed) must be placed often enough to allow changes in boundary conditions and to describe output head or concentration slopes, but too many computational timesteps can also substantially increase computational time. Output timesteps (times at which the output is reported) must be sufficient to describe the model output, but, too many output timesteps increases computational time, the size of the output files and the RAM required to view results.

2.1 Temporal Discretization in SEAWAT Model

The SEAWAT model requires the definition of both stress periods and timesteps. The stress periods define periods of constant boundary conditions. For this regional scale model, the stress periods were 1 month long. This means that all pumping rates and boundary heads can only change at the end of each month. Pumping is assumed to be constant for the entire month. If more than one measurement was made at a boundary well during a month, the average head was assigned for the entire month. The flow model timesteps were then set to be 1 day long.

2.1.1 SEAWAT Timestep Testing

In SEAWAT, the flow solution is computed and output according to user-defined options. For the transport solution using the standard finite-difference method with upstream weighting, the user has the option to define the transport timestep sizes or allow the model to select them based on a maximum Courant Number. Three tests were run using the 10,000-ft, 11 layer grid as follows:

- Allow the model to select timesteps that will keep the Courant Number below 0.5. (This resulted in timesteps of approximately 0.23 days.)
- Force the model to use 1-day timesteps
- Force the model to use 5-day timesteps

The three solutions were read onto the grid and compared as with the previous tests. One main difference was that since all three models were run on the same grid, problems with interpolation of starting conditions and boundary conditions and the location in the cell of the comparison points were eliminated. Figure B2-1 shows the absolute value of the difference in head at three comparison points for the 1-day timestep run and the model-selected timestep run. (The scale is large to match Figure B2-2.) The maximum difference in head is 0.03 ft, which is well within the expected error of the model and the accuracy of the input data. It is likely that the Courant number is high in a few small areas of the model, forcing the model-calculated timestep to be small. It is also possible that the 0.5 limit for the Courant number was too restrictive. Clearly, the tiny change in the results of the model do not warrant the computational time increase caused by reducing the timestep size below 6 hours.

The comparison between a 1 day timestep and a 5-day timestep is shown in Figure B2-2. This figure clearly shows a nearly 20-foot difference in computed heads in the Lower Floridan (LF1) and Boulder

Zone layers at comparison point M, which is located in the northwest portion of the model. Some error is to be expected at this location where the layers are so thin and the aspect ratio is high. However, even point C (just north of Lake Okeechobee) shows a difference of nearly 6 feet between the two runs.

The differences are also shown in Figures B2-3 through B2-12. These figures are plan view contour maps of each of the aquifer systems, each comparing two solutions. For all aquifers, the comparison between the 1-day and 0.23-day timesteps is so close, the lines are indistinguishable on the map at that scale. The maps showing the 5-day timestep indicate some serious convergence problems. There are numerous unexplained depressions and mounds in the water table and the shapes of the contours are often significantly changed.

Because the 5-day timestep simulation runs significantly faster than the 1-day timestep, calibration was performed using the larger timestep. A sensitivity analysis in Section 5 of the main report shows that when the TVD solution scheme (with timesteps smaller than 1 day) was used, differences in computed head were minor. Although this seems to contradict the conclusion of this appendix, significant changes to the model set up during calibration improved the convergences issues and prevented the need for the smaller timesteps.

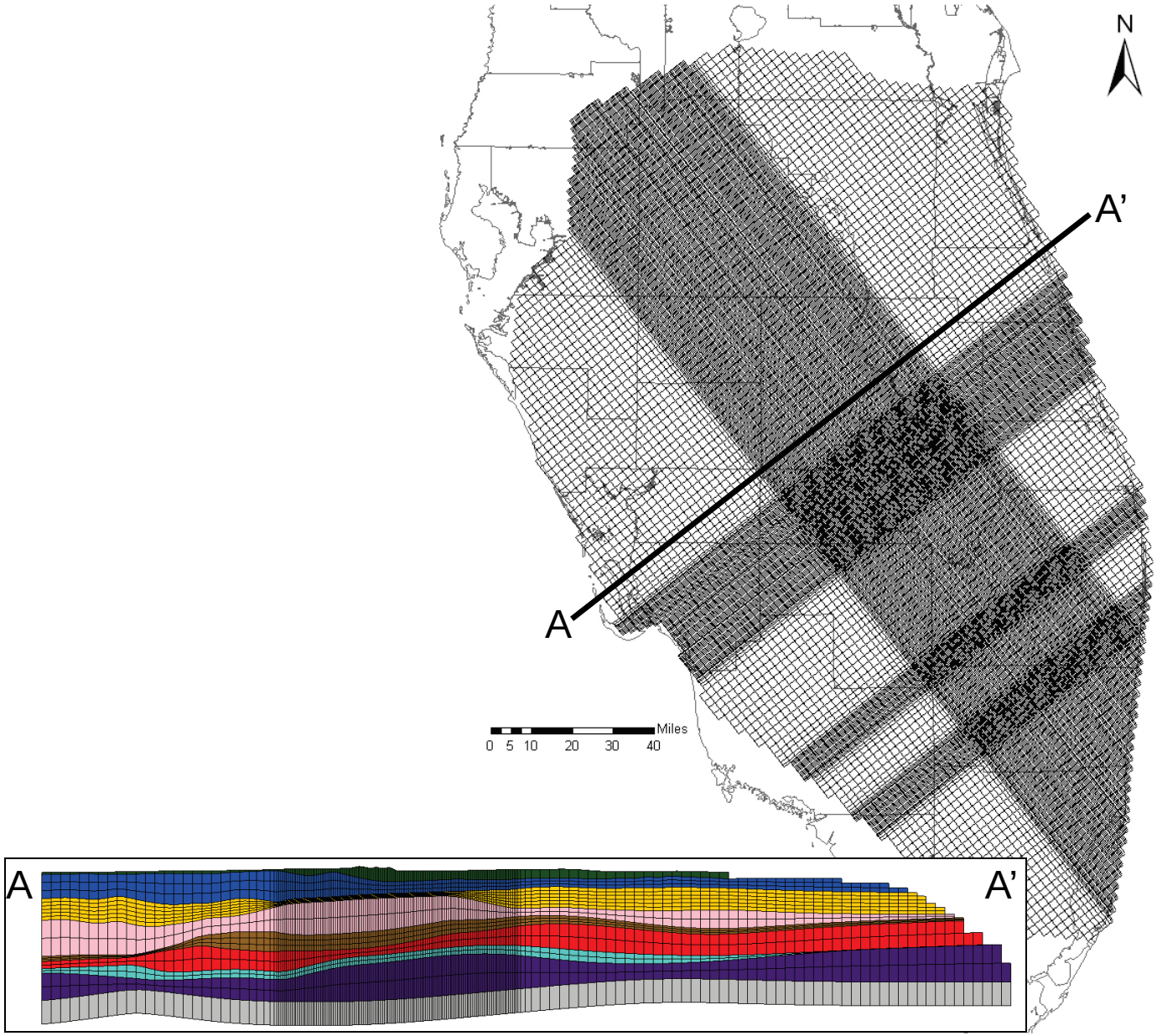

Notes:

Number of cells: 1,092,256

Number of active cells: 823,038

Horizontal grid cell size: Variable 2000 ft to 10000 ft

Number of layers: 22

Map image shows the extent of the upper layer of the grid. Lower layers extend further to the east, underneath the ocean (see inset).

Inset shows a typical cross-section (vertical magnified 50 times)

Legend:

- Surficial Aquifer System
- Intermediate Aquifer Syst./ Intermediate Confining Unit
- Upper Floridan Aquifer
- Middle Confining Unit 1
- Avon Park Permeable Zone
- Middle Confining Unit 2
- Lower Floridan (LF1) Aquifer
- Lower Confining Unit
- Boulder Zone

Regional Phase II ASR SEAWAT Production Grid

Final Groundwater Model Calibration Report

Figure B1-1

October 2010

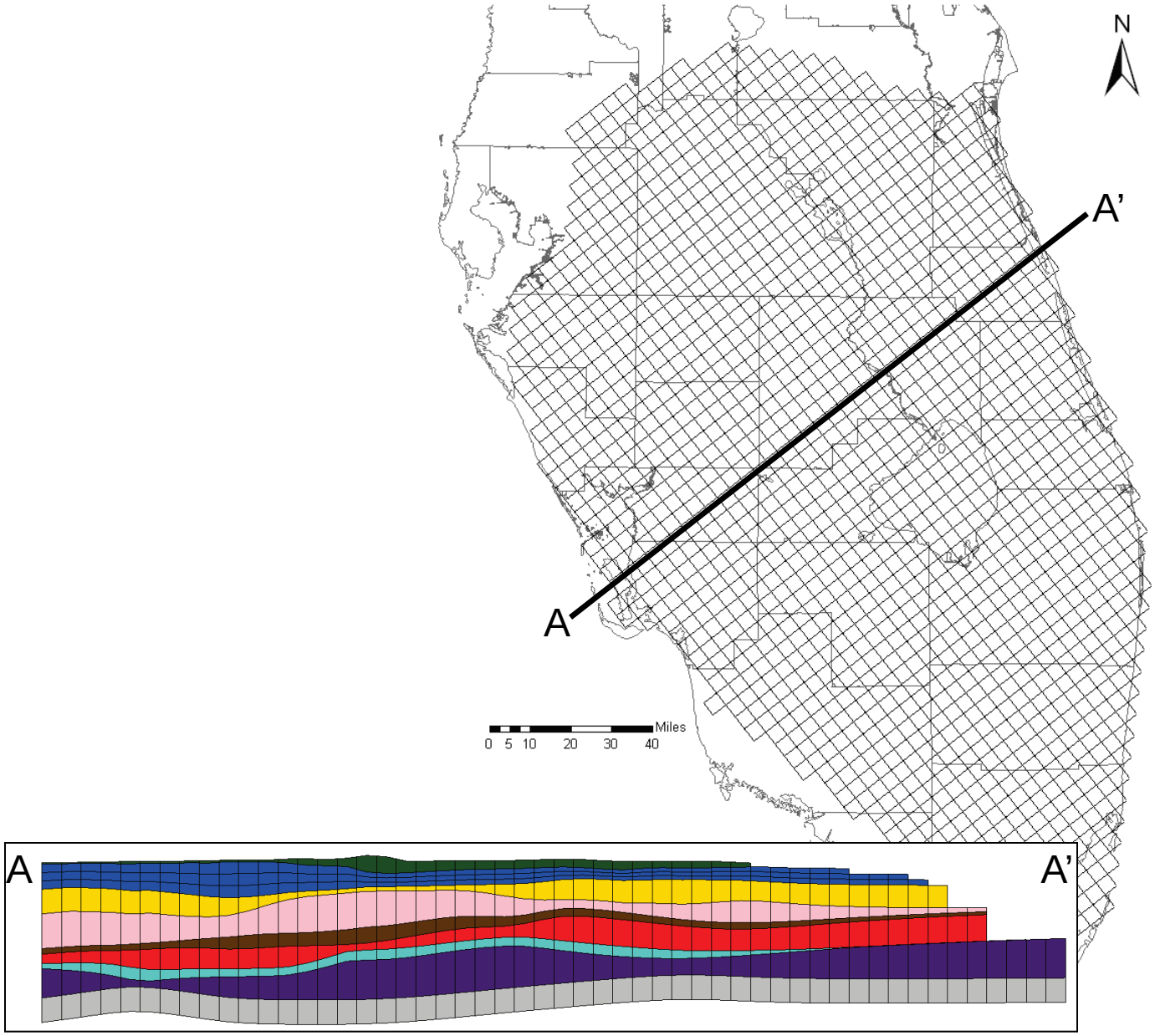

Notes:

Number of cells: 41,745

Number of active cells: 21,161

Horizontal grid cell size: 20000 ft

Number of layers: 11

Map image shows the extent of the upper layer of the grid. Lower layers extend further to the east, underneath the ocean (see inset).

Inset shows a typical cross-section (vertical magnified 50 times)

Legend:

- Surficial Aquifer System
- Intermediate Aquifer Syst./ Intermediate Confining Unit
- Upper Floridan Aquifer
- Middle Confining Unit 1
- Avon Park Permeable Zone
- Middle Confining Unit 2
- Lower Floridan (LF1) Aquifer
- Lower Confining Unit
- Boulder Zone

20000 ft Test Grid (11 Layers)

Final Groundwater Model Calibration Report

Figure B1-2

October 2010

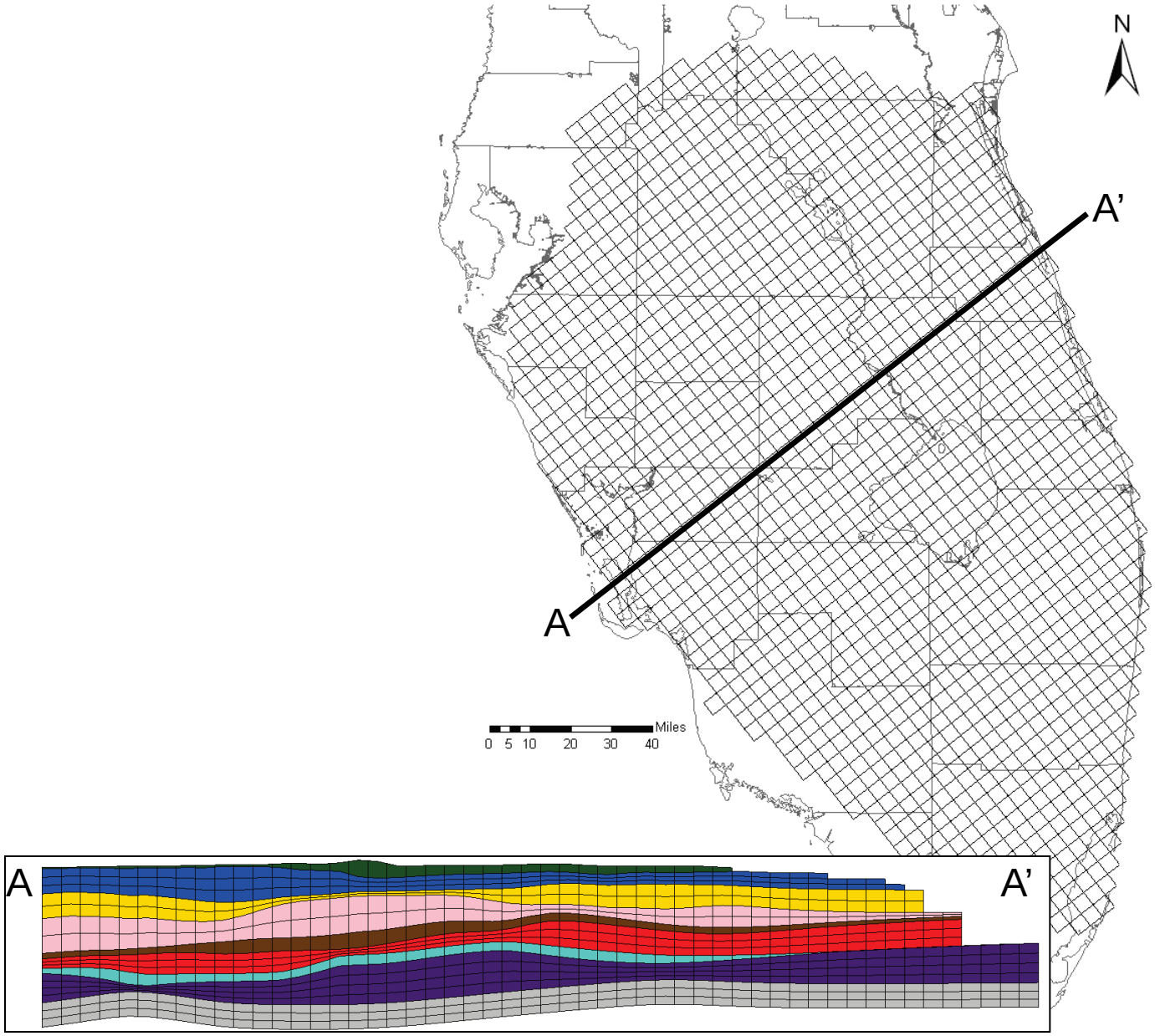

Notes:

Number of cells: 75,900

Number of active cells: 39,556

Horizontal grid cell size: 20000 ft

Number of layers: 20

Map image shows the extent of the upper layer of the grid. Lower layers extend further to the east, underneath the ocean (see inset).

Inset shows a typical cross-section (vertical magnified 50 times)

Legend:

- Surficial Aquifer System
- Intermediate Aquifer Syst./ Intermediate Confining Unit
- Upper Floridan Aquifer
- Middle Confining Unit 1
- Avon Park Permeable Zone
- Middle Confining Unit 2
- Lower Floridan (LF1) Aquifer
- Lower Confining Unit
- Boulder Zone

20000 ft Test Grid (20 Layers)

Final Groundwater Model Calibration Report

Figure B1-3

October 2010

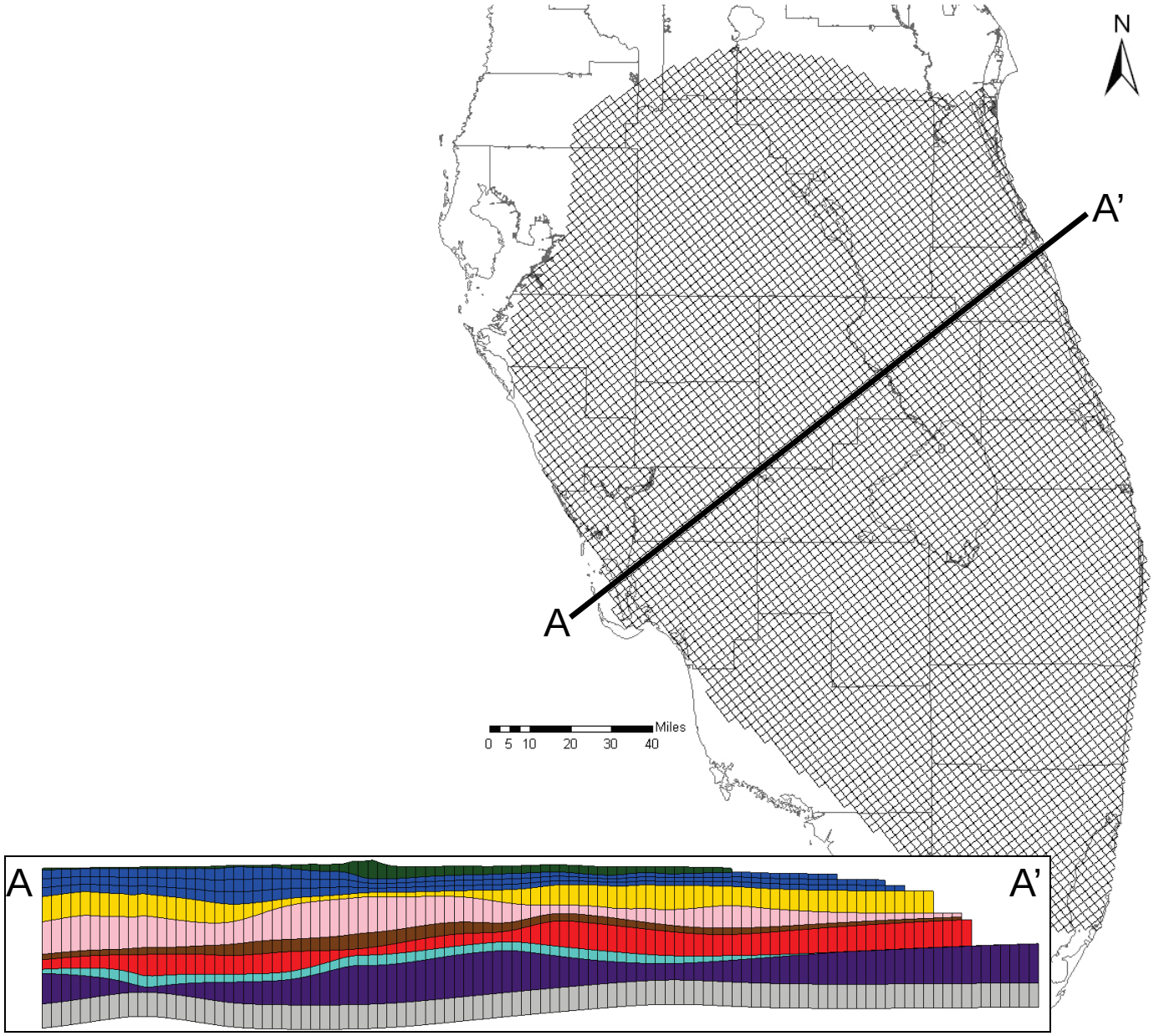

Notes:

Number of cells: 165,462

Number of active cells: 84,027

Horizontal grid cell size: 10000 ft

Number of layers: 11

Map image shows the extent of the upper layer of the grid. Lower layers extend further to the east, underneath the ocean (see inset).

Inset shows a typical cross-section (vertical magnified 50 times)

Legend:

- Surficial Aquifer System
- Intermediate Aquifer Syst./ Intermediate Confining Unit
- Upper Floridan Aquifer
- Middle Confining Unit 1
- Avon Park Permeable Zone
- Middle Confining Unit 2
- Lower Floridan (LF1) Aquifer
- Lower Confining Unit
- Boulder Zone

10000 ft Test Grid (11 Layers)

Final Groundwater Model Calibration Report

Figure B1-4

October 2010

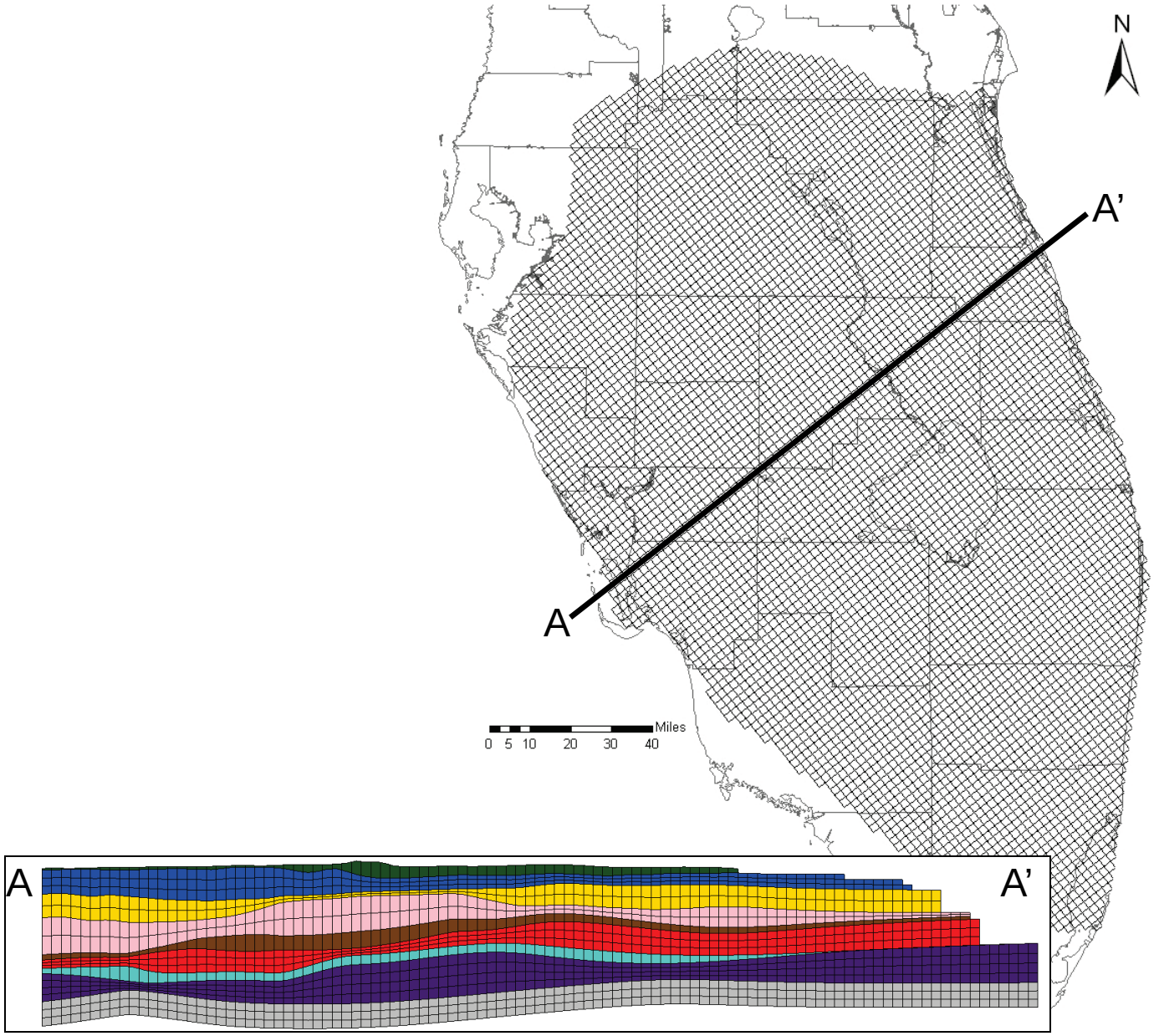

Notes:

Number of cells: 300,840

Number of active cells: 157,054

Horizontal grid cell size: 10000 ft

Number of layers: 20

Map image shows the extent of the upper layer of the grid. Lower layers extend further to the east, underneath the ocean (see inset).

Inset shows a typical cross-section (vertical magnified 50 times)

Legend:

- Surficial Aquifer System
- Intermediate Aquifer Syst./ Intermediate Confining Unit
- Upper Floridan Aquifer
- Middle Confining Unit 1
- Avon Park Permeable Zone
- Middle Confining Unit 2
- Lower Floridan (LF1) Aquifer
- Lower Confining Unit
- Boulder Zone

10000 ft Test Grid (20 Layers)

Final Groundwater Model Calibration Report

Figure B1-5

October 2010

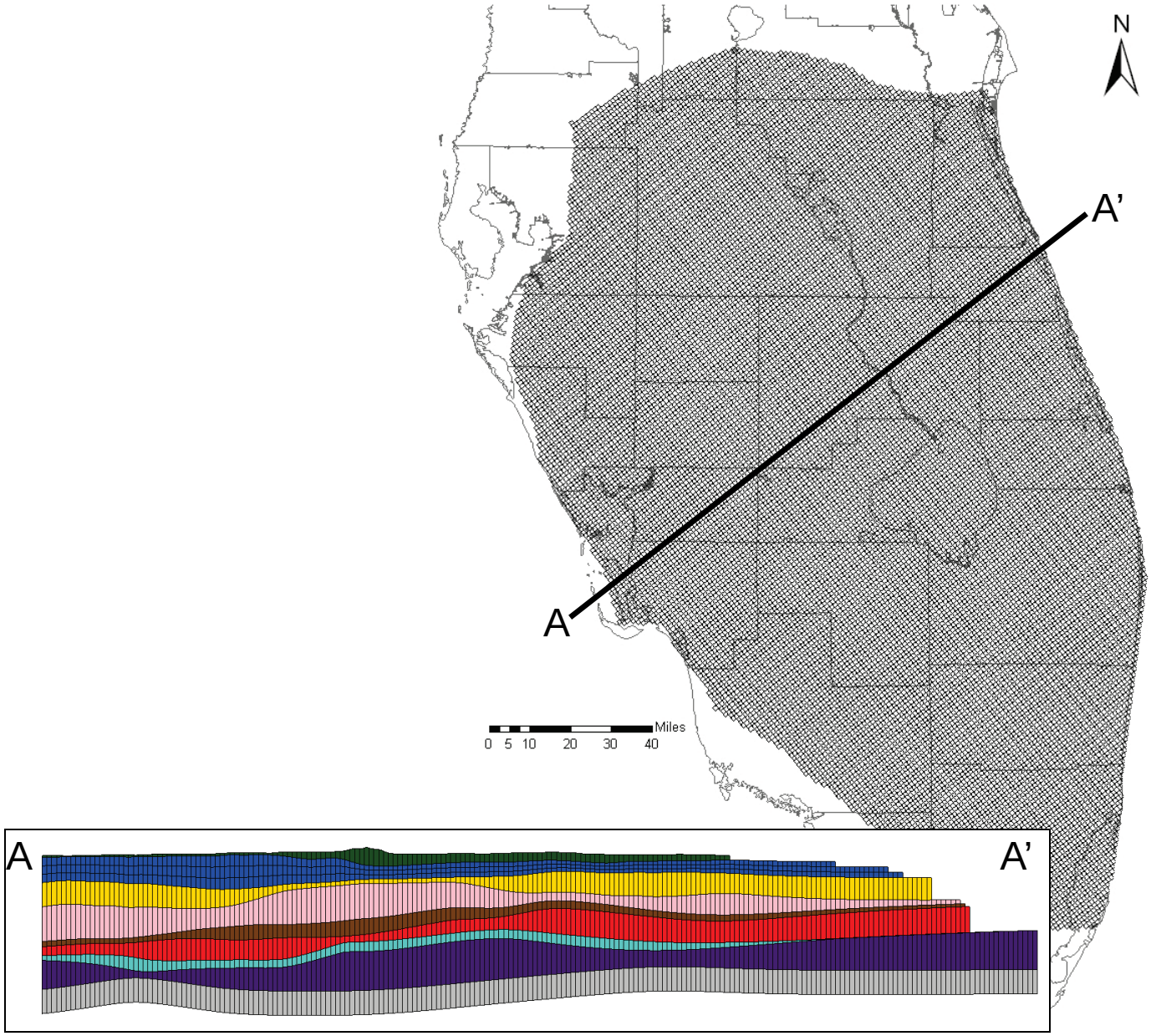

Notes:

Number of cells: 656,425

Number of active cells: 333,552

Horizontal grid cell size: 5000 ft

Number of layers: 11

Map image shows the extent of the upper layer of the grid. Lower layers extend further to the east, underneath the ocean (see inset).

Inset shows a typical cross-section (vertical magnified 50 times)

Legend:

- Surficial Aquifer System
- Intermediate Aquifer Syst./ Intermediate Confining Unit
- Upper Floridan Aquifer
- Middle Confining Unit 1
- Avon Park Permeable Zone
- Middle Confining Unit 2
- Lower Floridan (LF1) Aquifer
- Lower Confining Unit
- Boulder Zone

5000 ft Test Grid (11 Layers)

Final Groundwater Model Calibration Report

Figure B1-6

October 2010

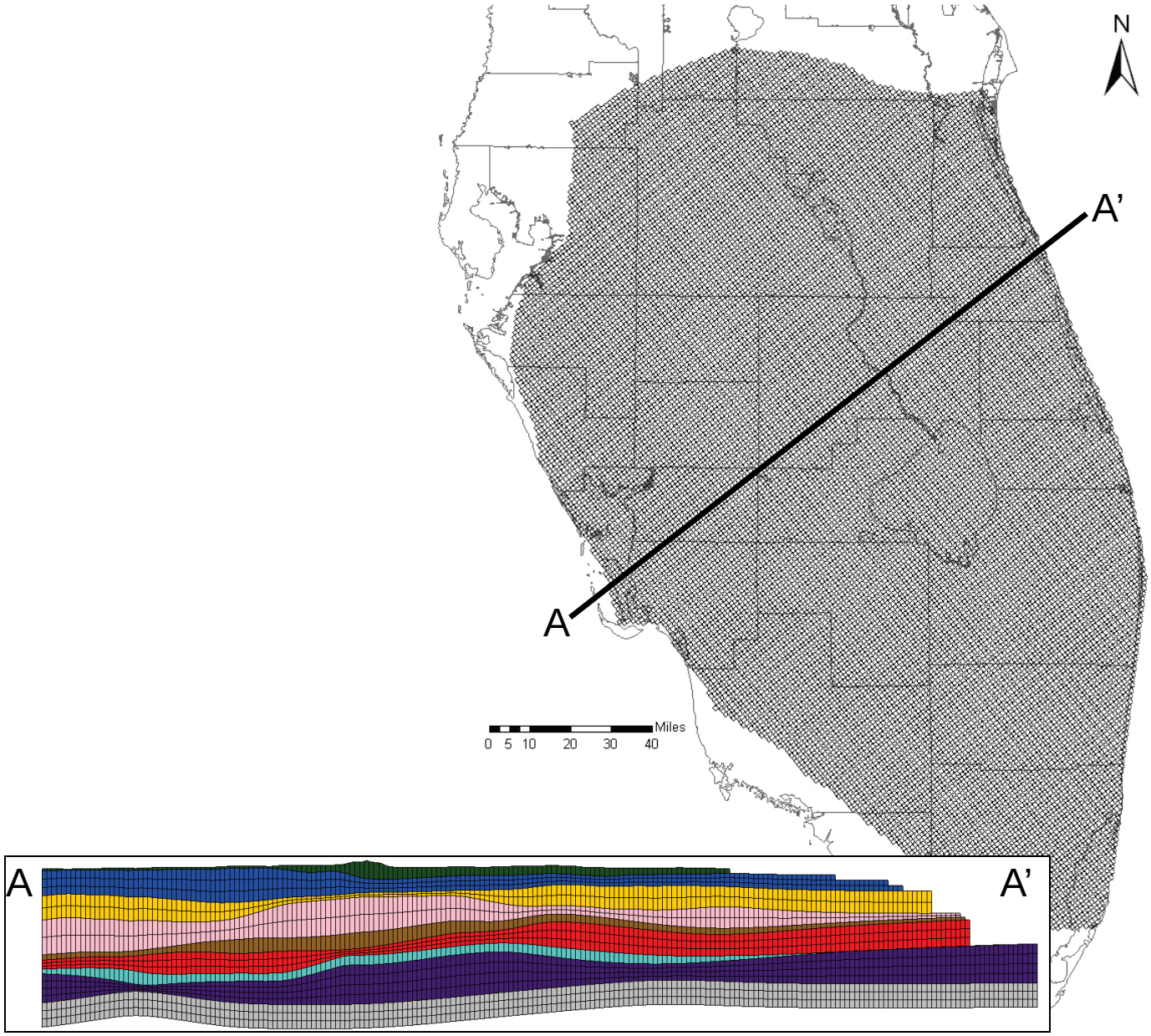

Notes:

Number of cells: 1,193,500

Number of active cells: 623,477

Horizontal grid cell size: 5000 ft

Number of layers: 20

Map image shows the extent of the upper layer of the grid. Lower layers extend further to the east, underneath the ocean (see inset).

Inset shows a typical cross-section (vertical magnified 50 times)

Legend:

- Surficial Aquifer System
- Intermediate Aquifer Syst./ Intermediate Confining Unit
- Upper Floridan Aquifer
- Middle Confining Unit 1
- Avon Park Permeable Zone
- Middle Confining Unit 2
- Lower Floridan (LF1) Aquifer
- Lower Confining Unit
- Boulder Zone

5000 ft Test Grid (20 Layers)

Figure B1-7

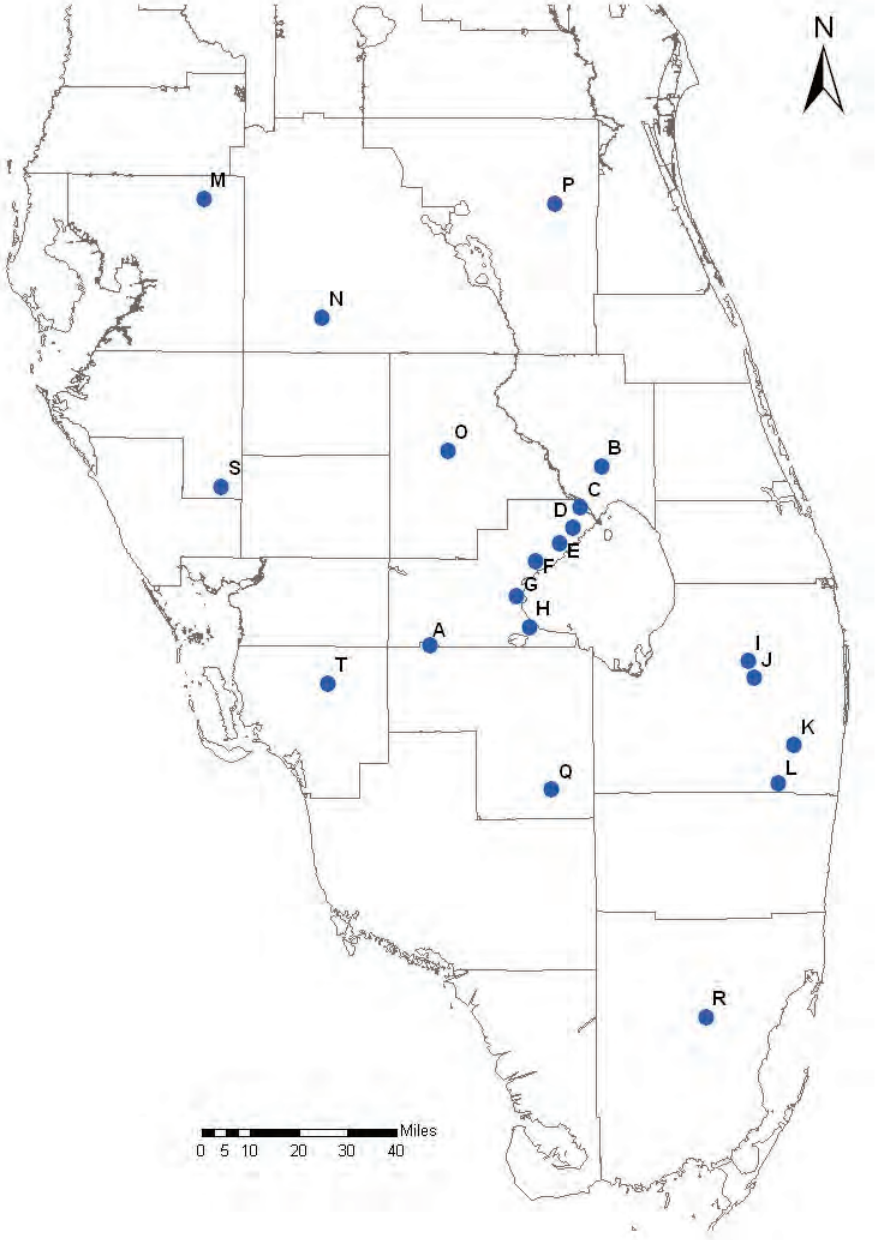

Notes:
This map shows the locations for comparison of head solutions from each of the six test grids. Points A through L were selected to coincide with potential ASR locations. Points M through T were selected solely to provide coverage of the entire model area.

Comparison Locations for SEAWAT Grid Testing

Final Groundwater Model Calibration Report

Figure B1-8

October 2010

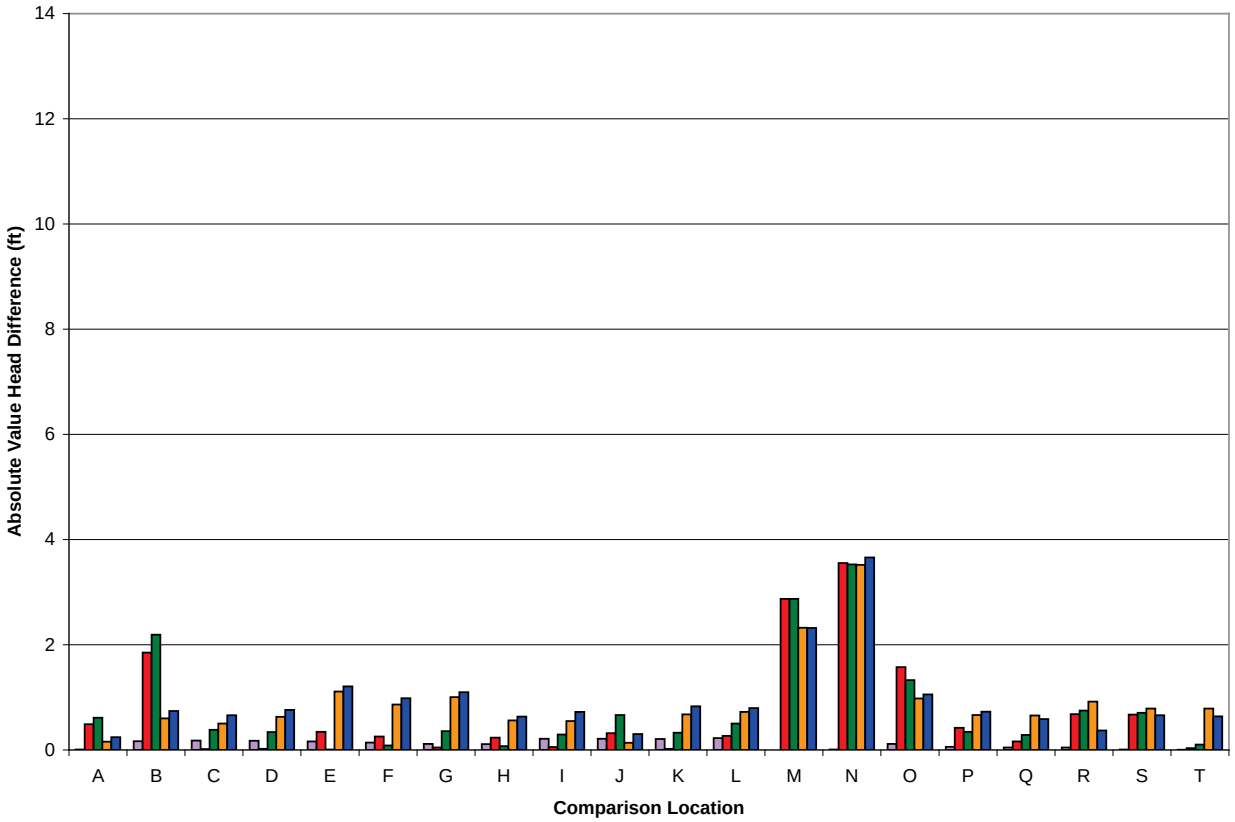

Legend (Comparison Grid):

- 5000-ft Grid/11 Layers
- 10000-ft Grid/20 Layers
- 10000-ft Grid/11 Layers
- 20000-ft Grid/20 Layers
- 20000-ft Grid/11 Layers

Notes:

This plot shows the absolute value of the difference between the model-calculated head at each location on the 5000-ft/20 layer grid and the grid indicated by the bar color.

Heads were extracted from the center of Layer 3, the middle of the three layers representing the Intermediate Aquifer System and Intermediate Confining Unit.

See Figure B1-8 for the horizontal locations of each of the 20 comparison points.

Head Differences in IAS Layer
(Compared to 5000-ft Grid with 20 Layers)
Final Groundwater Model Calibration Report

Figure B1-9

October 2010

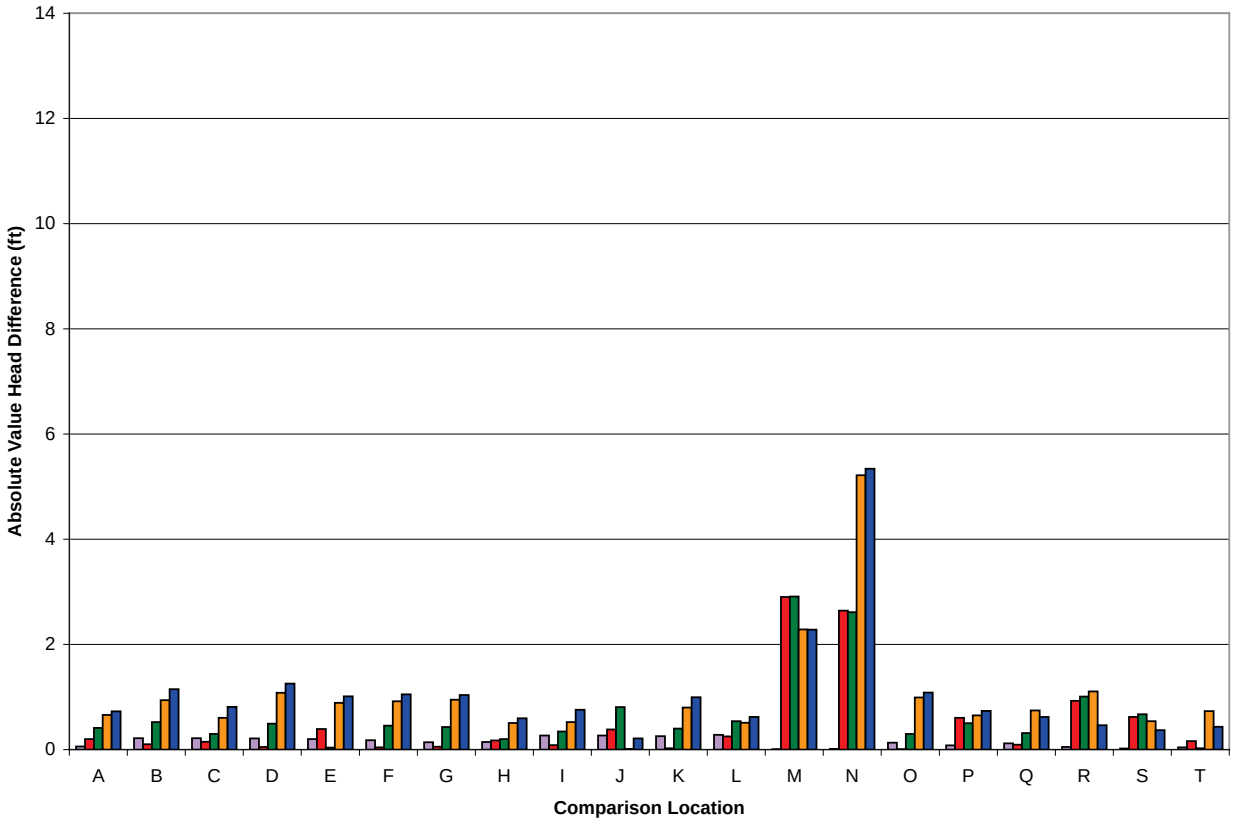

Legend (Comparison Grid):

- 5000-ft Grid/11 Layers
- 10000-ft Grid/20 Layers
- 10000-ft Grid/11 Layers
- 20000-ft Grid/20 Layers
- 20000-ft Grid/11 Layers

Notes:

This plot shows the absolute value of the difference between the model-calculated head at each location on the 5000-ft/20 layer grid and the grid indicated by the bar color.

Heads were extracted from the center of the Upper Floridan Aquifer. For the 11-layer grids, this was layer 5; for the 20-layer grids, the results from layer 5 and 6 were averaged.

See Figure B1-8 for the horizontal locations of each of the 20 comparison points.

Head Differences in Upper Floridan Layer
(Compared to 5000-ft Grid with 20 Layers)
Final Groundwater Model Calibration Report

Figure B1-10

October 2010

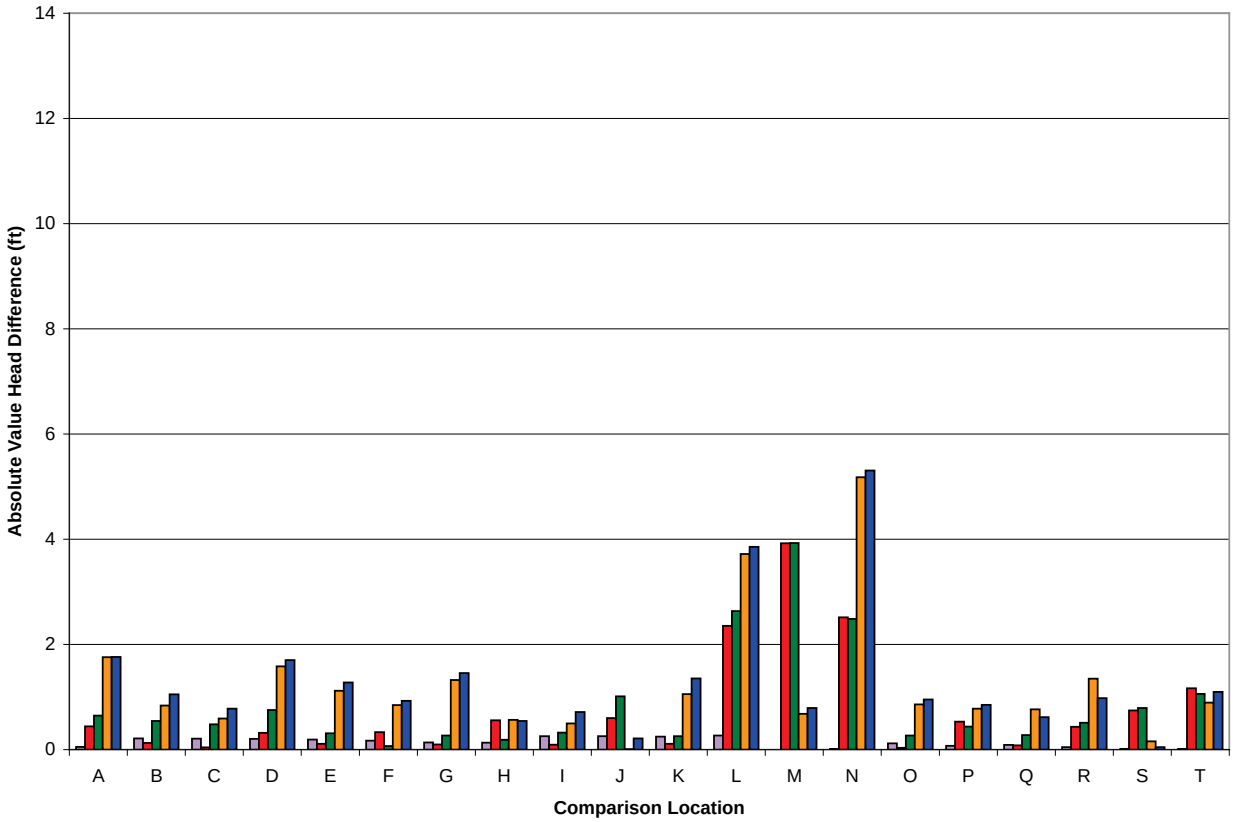

Legend (Comparison Grid):

- 5000-ft Grid/11 Layers
- 10000-ft Grid/20 Layers
- 10000-ft Grid/11 Layers
- 20000-ft Grid/20 Layers
- 20000-ft Grid/11 Layers

Notes:

This plot shows the absolute value of the difference between the model-calculated head at each location on the 5000-ft/20 layer grid and the grid indicated by the bar color.

Heads were extracted from the center of the Avon Park Permeable Zone. For the 11-layer grids, this was layer 7; for the 20-layer grids, this was layer 9.

See Figure B1-8 for the horizontal locations of each of the 20 comparison points.

Head Differences in APPZ Layer
(Compared to 5000 ft Grid with 20 Layers)
Final Groundwater Model Calibration Report

Figure B1-11

October 2010

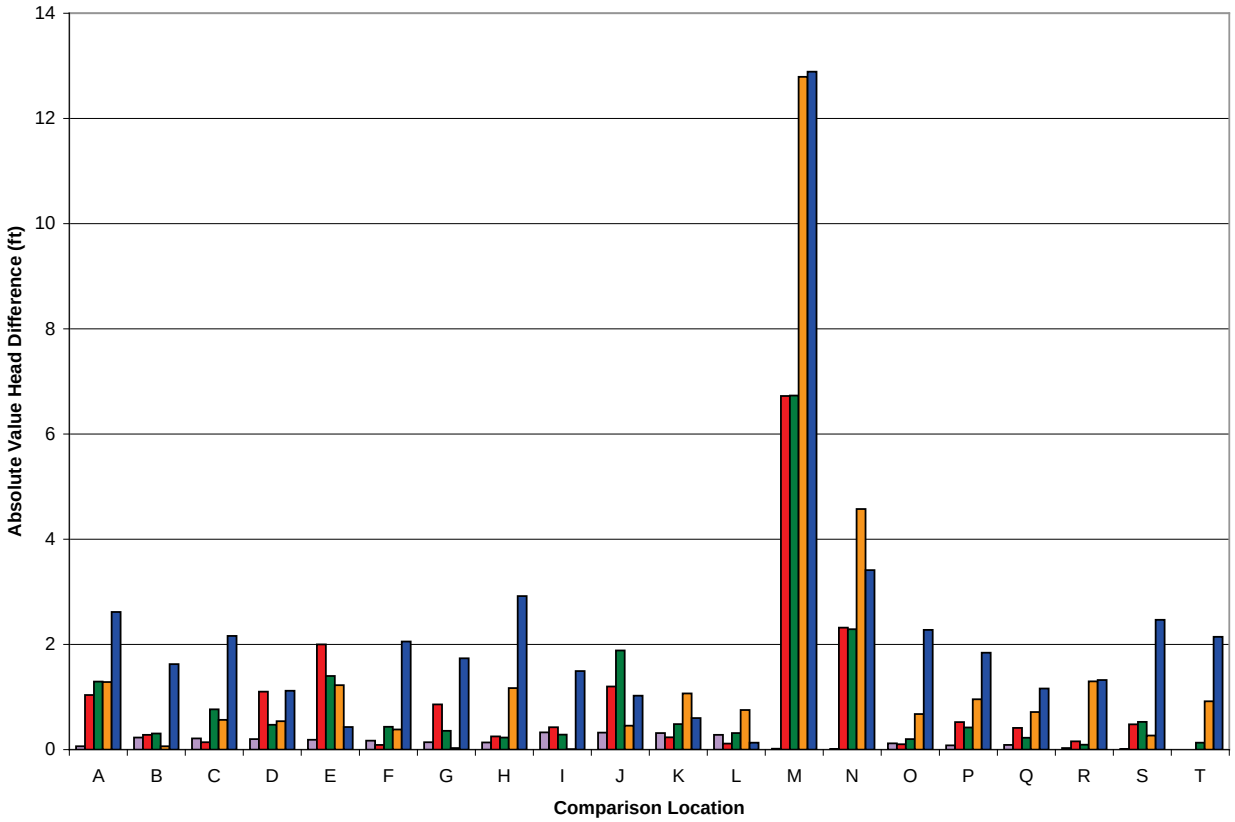

Legend (Comparison Grid):

- 5000-ft Grid/11 Layers
- 10000-ft Grid/20 Layers
- 10000-ft Grid/11 Layers
- 20000-ft Grid/20 Layers
- 20000-ft Grid/11 Layers

Notes:

This plot shows the absolute value of the difference between the model-calculated head at each location on the 5000-ft/20 layer grid and the grid indicated by the bar color.

Heads were extracted from the center of the Lower Floridan (LF1) Aquifer. For the 11-layer grids, this was layer 9; for the 20-layer grids, this was layer 13.

See Figure B1-8 for the horizontal locations of each of the 20 comparison points.

Head Differences in Lower Floridan (LF1) Layer
(Compared to 5000 ft Grid with 20 Layers)
Final Groundwater Model Calibration Report

Figure B1-12

October 2010

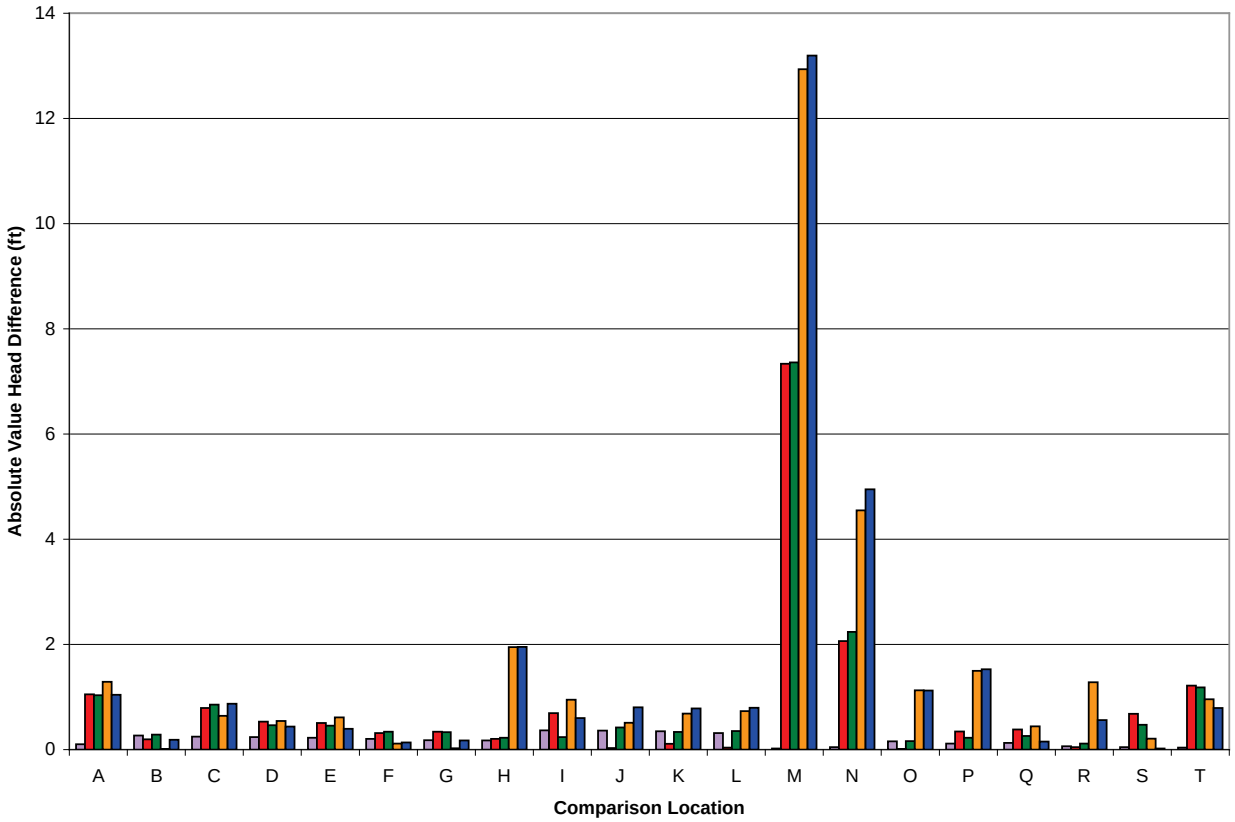

Legend (Comparison Grid):

- 5000-ft Grid/11 Layers
- 10000-ft Grid/20 Layers
- 10000-ft Grid/11 Layers
- 20000-ft Grid/20 Layers
- 20000-ft Grid/11 Layers

Notes:

This plot shows the absolute value of the difference between the model-calculated head at each location on the 5000-ft/20 layer grid and the grid indicated by the bar color.

Heads were extracted from the center of the Boulder Zone. For the 11-layer grids, this was layer 11; for the 20-layer grids, this was layer 19.

See Figure B1-8 for the horizontal locations of each of the 20 comparison points.

Head Differences in Boulder Zone Layer
(Compared to 5000 ft Grid with 20 Layers)
Final Groundwater Model Calibration Report

Figure B1-13

October 2010

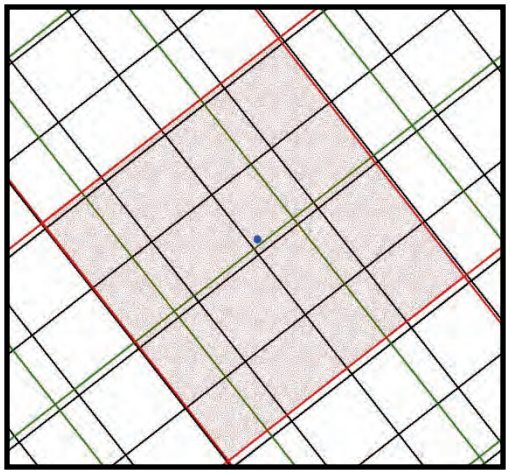

(a)

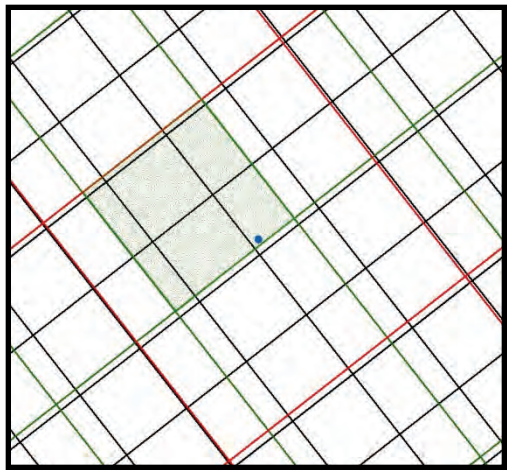

(b)

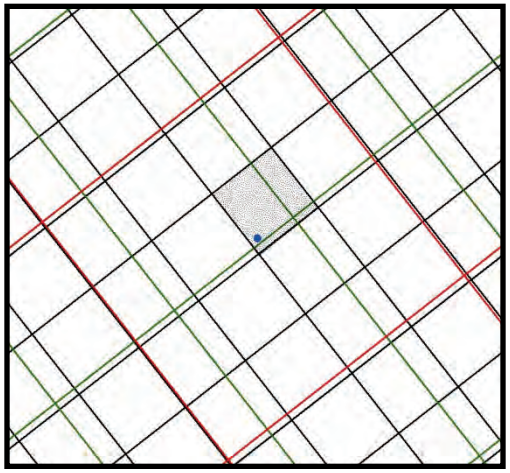

(c)

Legend:

- 20,000-ft grid
- 10,000-ft grid
- 5,000-ft grid

Notes:

These images show the location of comparison point M and the three test grids (each in a different color).

In Image (a), the 20,000 foot grid cell containing Point M is shaded. Notice that the point is near the centroid of the cell.

In Image (b), the 10,000 foot grid cell containing Point M is shaded. Notice that the point is near the edge of the cell, thus nearly 5,000 feet from the computational point at the center of the cell.

In Image (c), the 5,000 foot grid cell containing Point M is shaded. Notice that the point is near the corner of the cell, over 3,000 feet from the computational point at the center of the cell.

Location of Comparison Point M in Each Test Grid

Figure B1-14

Final Groundwater Model Calibration Report

October 2010

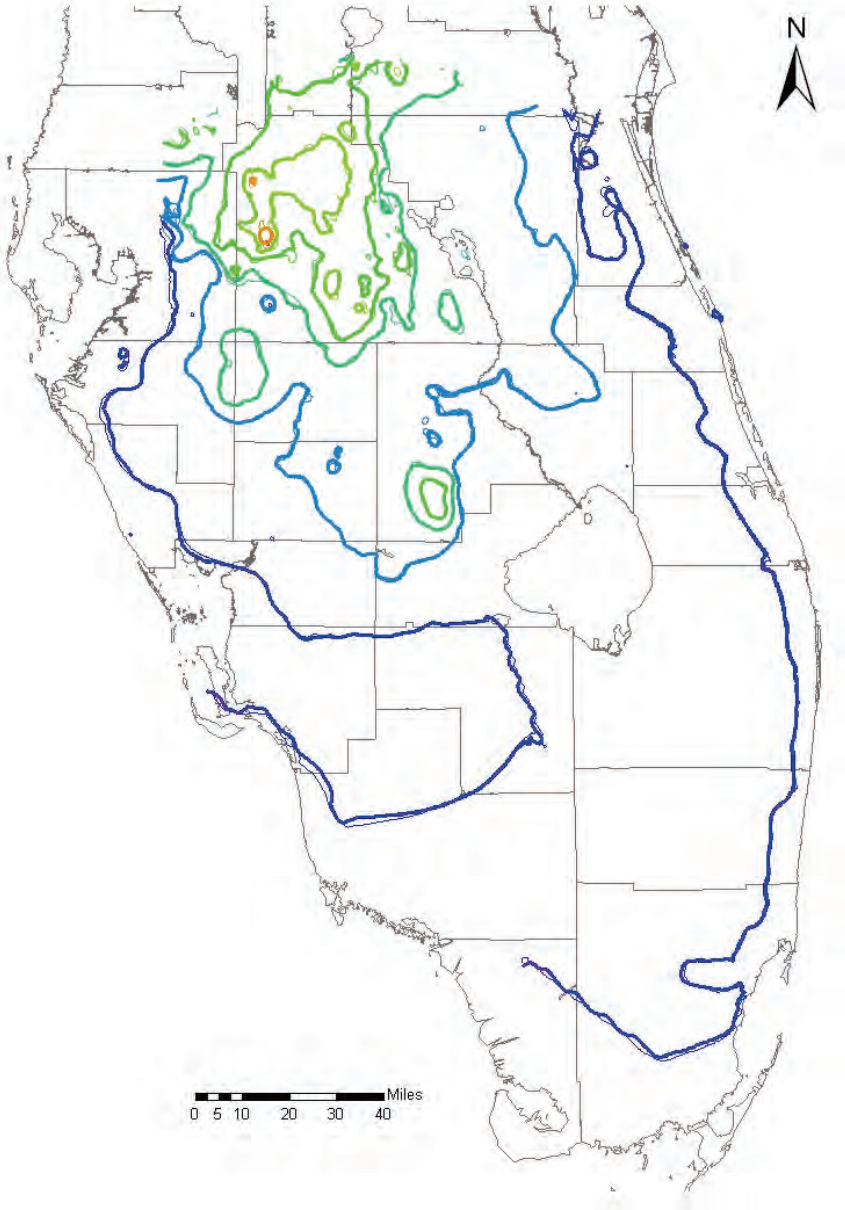

Legend (Test Grid):

- 5,000-ft grid / 20 Layers
- 5,000-ft grid / 11 Layers
- 10,000-ft grid / 20 Layers
- 10,000-ft grid / 11 Layers

Legend (Head):

- 25 ft
- 50 ft
- 75 ft
- 100 ft
- 125 ft
- 150 ft
- 175 ft

Notes:

Solutions from grids with identical horizontal resolution, but differing numbers of layers are nearly indistinguishable at this scale. Here, both are shown, but with the same line type.

These heads are point-water heads (the level to which water would rise in a standpipe). The model was computed using equivalent freshwater head, which accounts for density variations due to salinity and temperature.

These solutions are from layer 3 of each grid.

Steady State Head Solutions for IAS on Test Grids
(5,000 ft grid and 10,000 ft grid)
Final Groundwater Model Calibration Report

Figure B1-15

October 2010

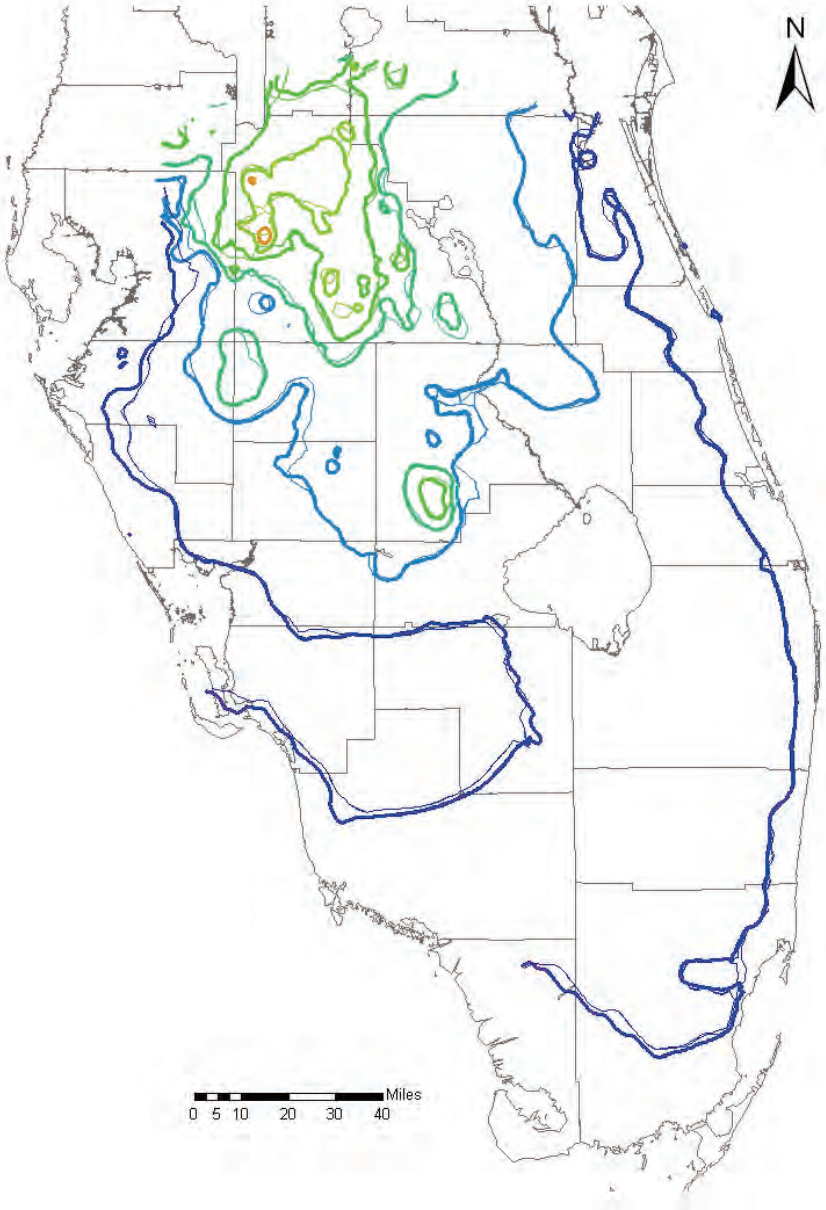

Legend (Test Grid):

- 20,000-ft grid / 20 Layers
- 20,000-ft grid / 11 Layers
- 10,000-ft grid / 20 Layers
- 10,000-ft grid / 11 Layers

Legend (Head):

- 25 ft
- 50 ft
- 75 ft
- 100 ft
- 125 ft
- 150 ft
- 175 ft

Notes:

Solutions from grids with identical horizontal resolution, but differing numbers of layers are nearly indistinguishable at this scale. Here, both are shown, but with the same line type.

These heads are point-water heads (the level to which water would rise in a standpipe). The model was computed using equivalent freshwater head, which accounts for density variations due to salinity and temperature.

These solutions are from layer 3 of each grid.

Steady State Head Solutions for IAS on Test Grids
(20,000 ft grid and 10,000 ft grid)
Final Groundwater Model Calibration Report

Figure B1-16

October 2010

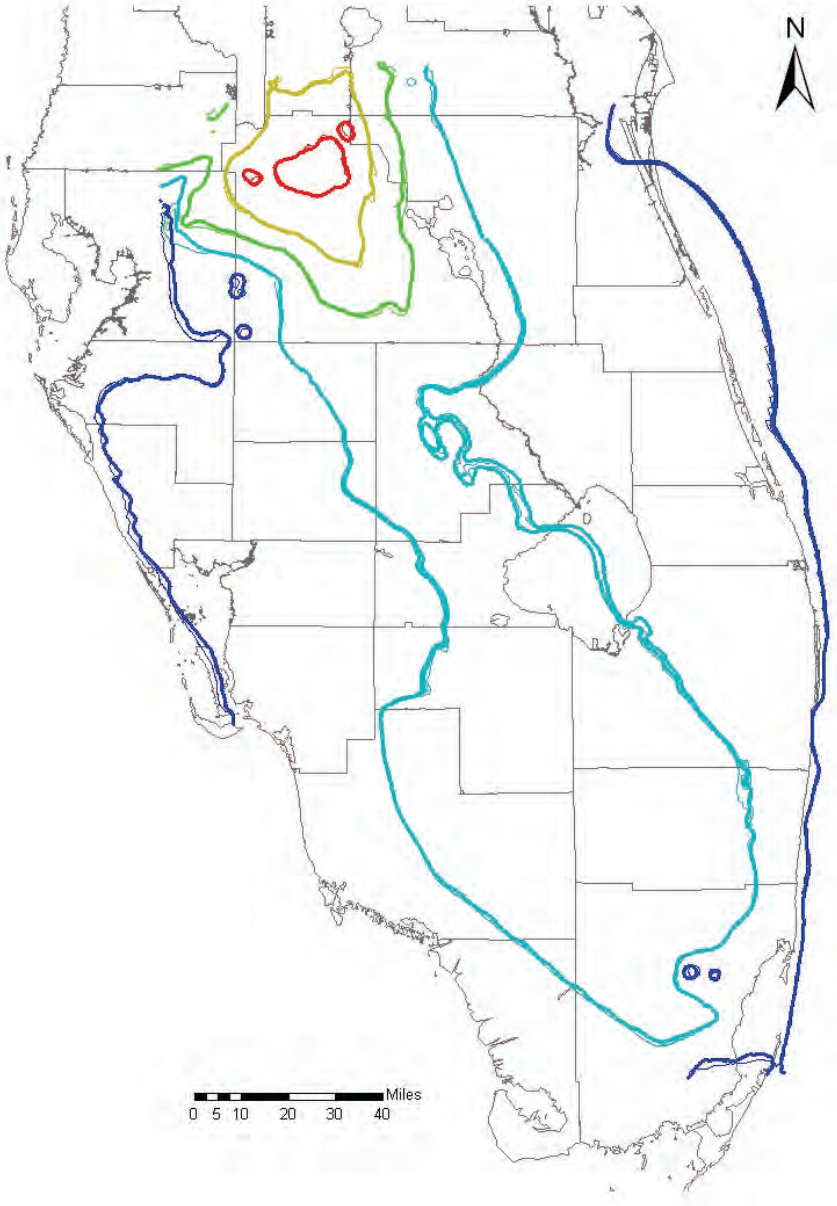

Legend (Test Grid):

- 5,000-ft grid / 20 Layers
- 5,000-ft grid / 11 Layers
- 10,000-ft grid / 20 Layers
- 10,000-ft grid / 11 Layers

Legend (Head):

- 25 ft
- 50 ft
- 75 ft
- 100 ft
- 125 ft

Notes:

Solutions from grids with identical horizontal resolution, but differing numbers of layers are nearly indistinguishable at this scale. Here, both are shown, but with the same line type.

These heads are point-water heads (the level to which water would rise in a standpipe). The model was computed using equivalent freshwater head, which accounts for density variations due to salinity and temperature.

These solutions are from layer 5 of each grid.

Steady State Head Solutions for UF on Test Grids
(5,000 ft grid and 10,000 ft grid)
Final Groundwater Model Calibration Report

Figure B1-17

October 2010

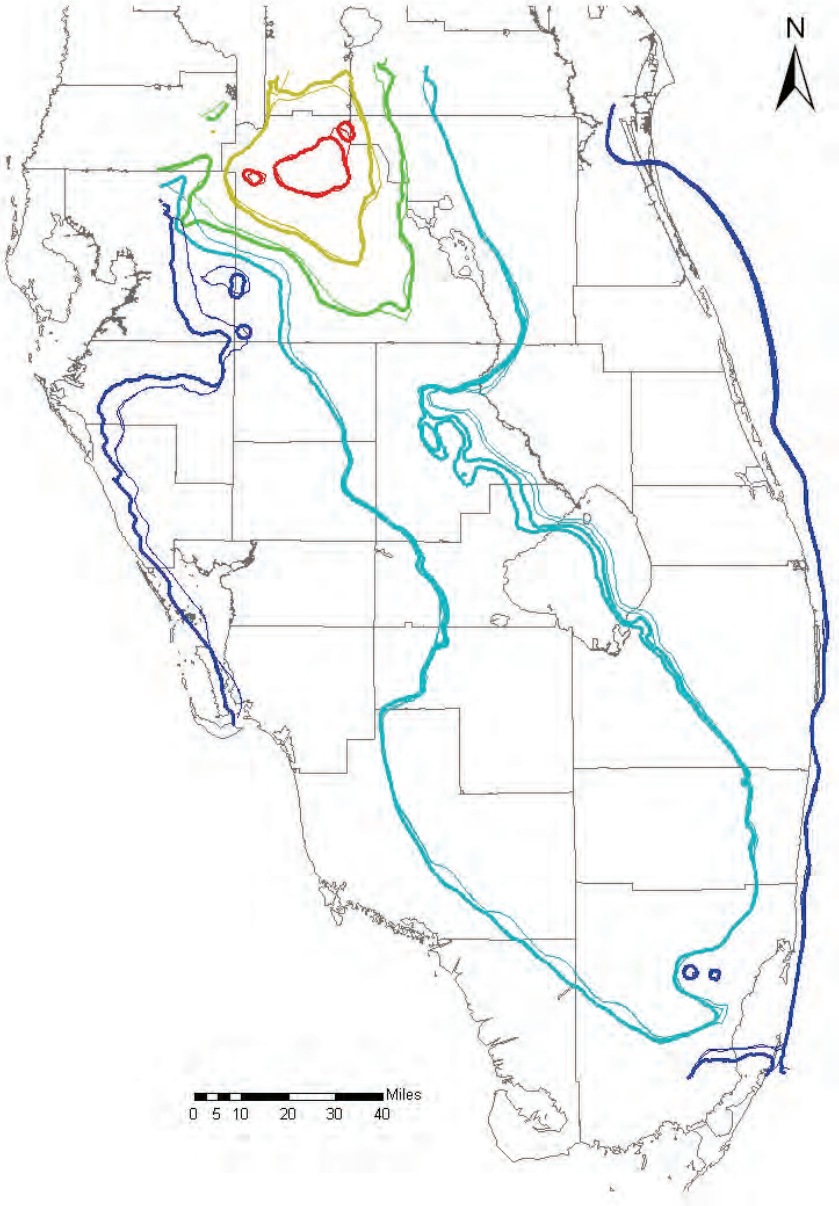

Legend (Test Grid):

- 20,000-ft grid / 20 Layers
- 20,000-ft grid / 11 Layers
- 10,000-ft grid / 20 Layers
- 10,000-ft grid / 11 Layers

Legend (Head):

- 25 ft
- 50 ft
- 75 ft
- 100 ft
- 125 ft

Notes:

Solutions from grids with identical horizontal resolution, but differing numbers of layers are nearly indistinguishable at this scale. Here, both are shown, but with the same line type.

These heads are point-water heads (the level to which water would rise in a standpipe). The model was computed using equivalent freshwater head, which accounts for density variations due to salinity and temperature.

These solutions are from layer 5 of each grid.

Steady State Head Solutions for UF on Test Grids
(20,000 ft grid and 10,000 ft grid)
Final Groundwater Model Calibration Report

Figure B1-18

October 2010

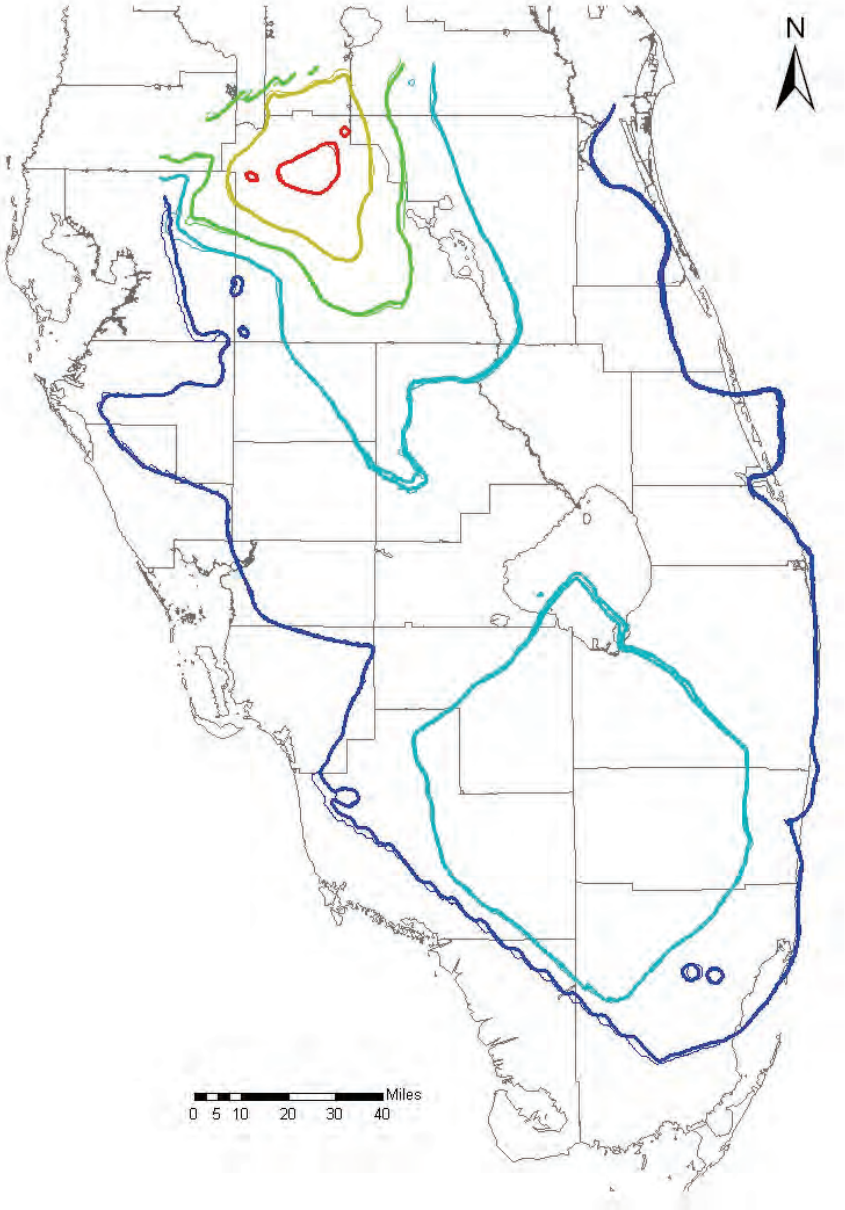

Legend (Test Grid):

- 5,000-ft grid / 20 Layers
- 5,000-ft grid / 11 Layers
- 10,000-ft grid / 20 Layers
- 10,000-ft grid / 11 Layers

Legend (Head):

- 25 ft
- 50 ft
- 75 ft
- 100 ft
- 125 ft

Notes:

Solutions from grids with identical horizontal resolution, but differing numbers of layers are nearly indistinguishable at this scale. Here, both are shown, but with the same line type.

These heads are point-water heads (the level to which water would rise in a standpipe). The model was computed using equivalent freshwater head, which accounts for density variations due to salinity and temperature.

These solutions are from layer 7 of the 11-layer grids and layer 9 of the 20-layer grids.

Steady State Head Solutions for APPZ on Test Grids
(5,000 ft grid and 10,000 ft grid)
Final Groundwater Model Calibration Report

Figure B1-19

October 2010

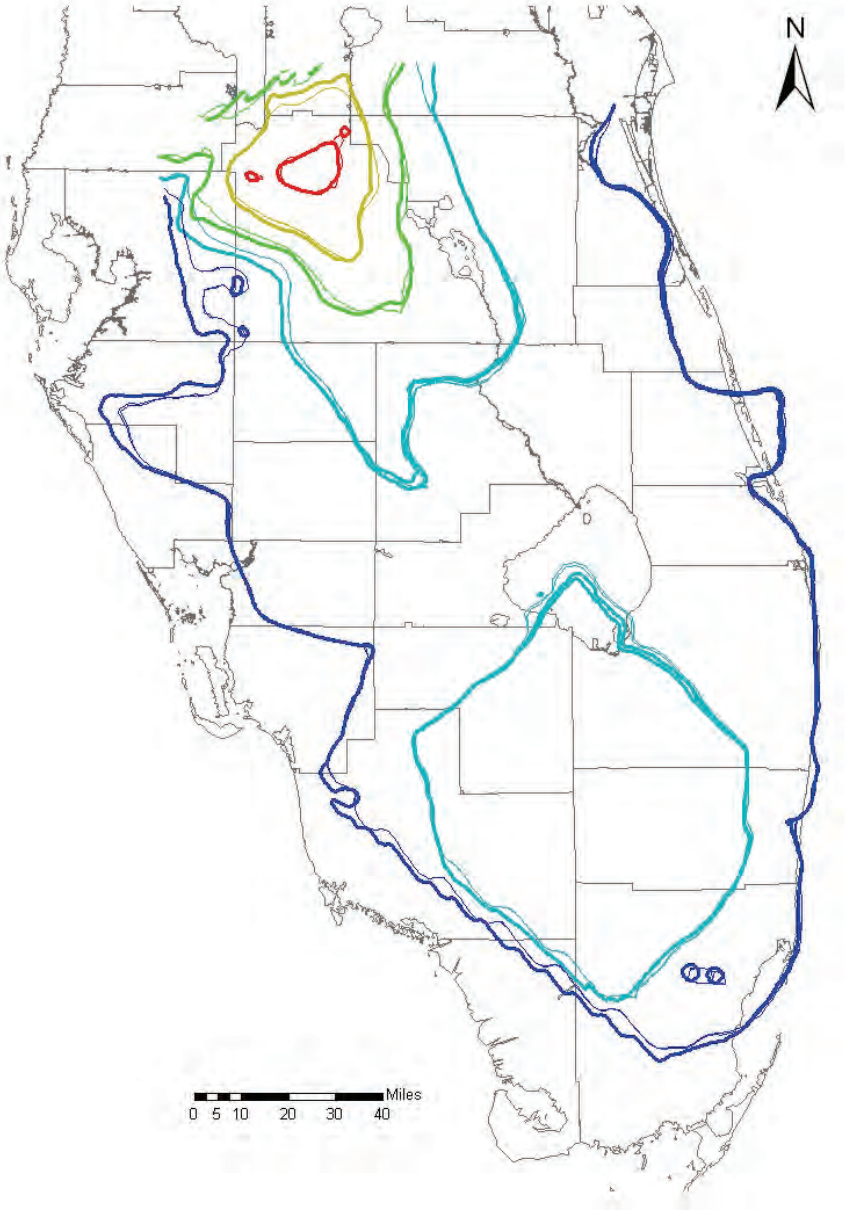

Legend (Test Grid):

- 20,000-ft grid / 20 Layers
- 20,000-ft grid / 11 Layers
- 10,000-ft grid / 20 Layers
- 10,000-ft grid / 11 Layers

Legend (Head):

- 25 ft
- 50 ft
- 75 ft
- 100 ft
- 125 ft

Notes:

Solutions from grids with identical horizontal resolution, but differing numbers of layers are nearly indistinguishable at this scale. Here, both are shown, but with the same line type.

These heads are point-water heads (the level to which water would rise in a standpipe). The model was computed using equivalent freshwater head, which accounts for density variations due to salinity and temperature.

These solutions are from layer 7 of the ll-layer grids and layer 9 of the 20-layer grids.

Steady State Head Solutions for APPZ on Test Grids
(20,000 ft grid and 10,000 ft grid)
Final Groundwater Model Calibration Report

Figure B1-20

October 2010

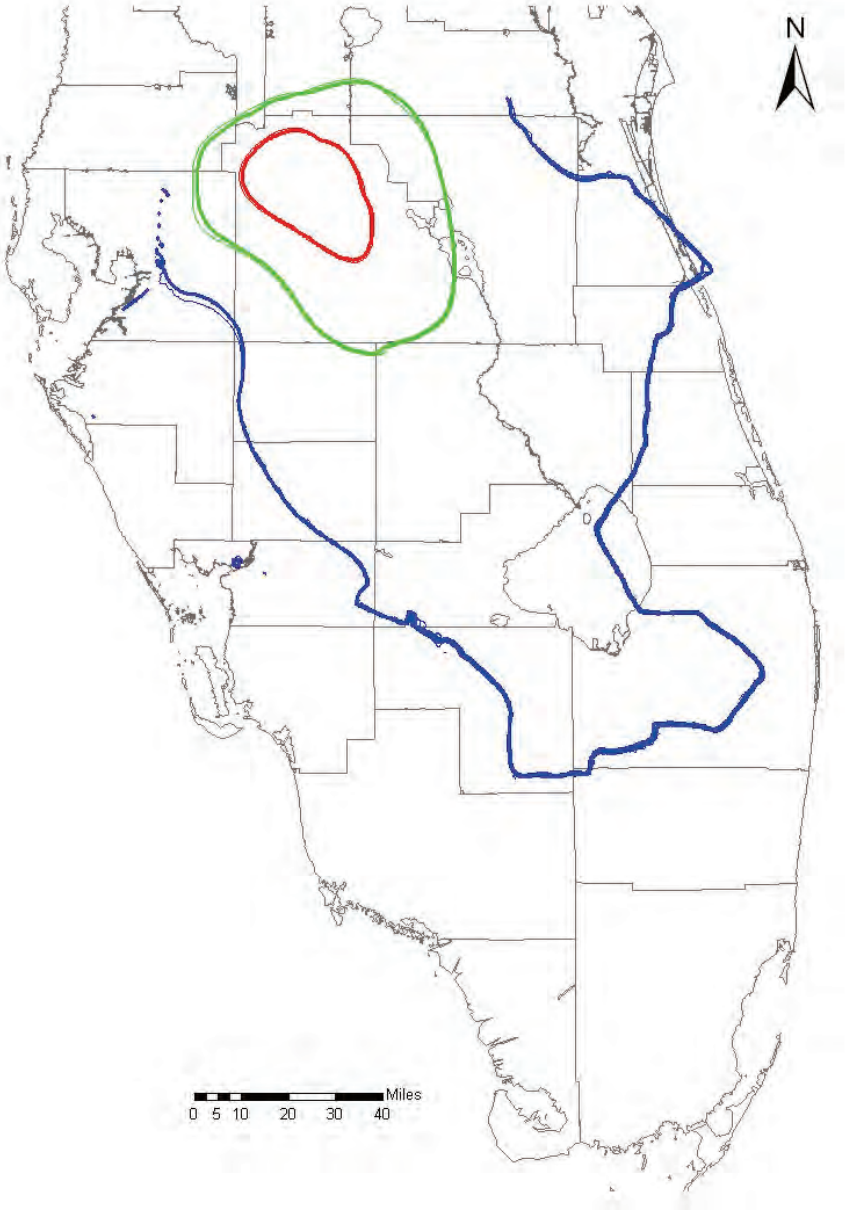

Legend (Test Grid):

- 5,000-ft grid / 20 Layers
- 5,000-ft grid / 11 Layers
- 10,000-ft grid / 20 Layers
- 10,000-ft grid / 11 Layers

Legend (Head):

- 25 ft
- 50 ft
- 75 ft

Notes:

Solutions from grids with identical horizontal resolution, but differing numbers of layers are nearly indistinguishable at this scale. Here, both are shown, but with the same line type.

These heads are point-water heads (the level to which water would rise in a standpipe). The model was computed using equivalent freshwater head, which accounts for density variations due to salinity and temperature.

These solutions are from layer 9 of the 11-layer grids and layer 13 of the 20-layer grids.

Steady State Head Solutions for LF1 on Test Grids
(5,000 ft grid and 10,000 ft grid)
Final Groundwater Model Calibration Report

Figure B1-21

October 2010

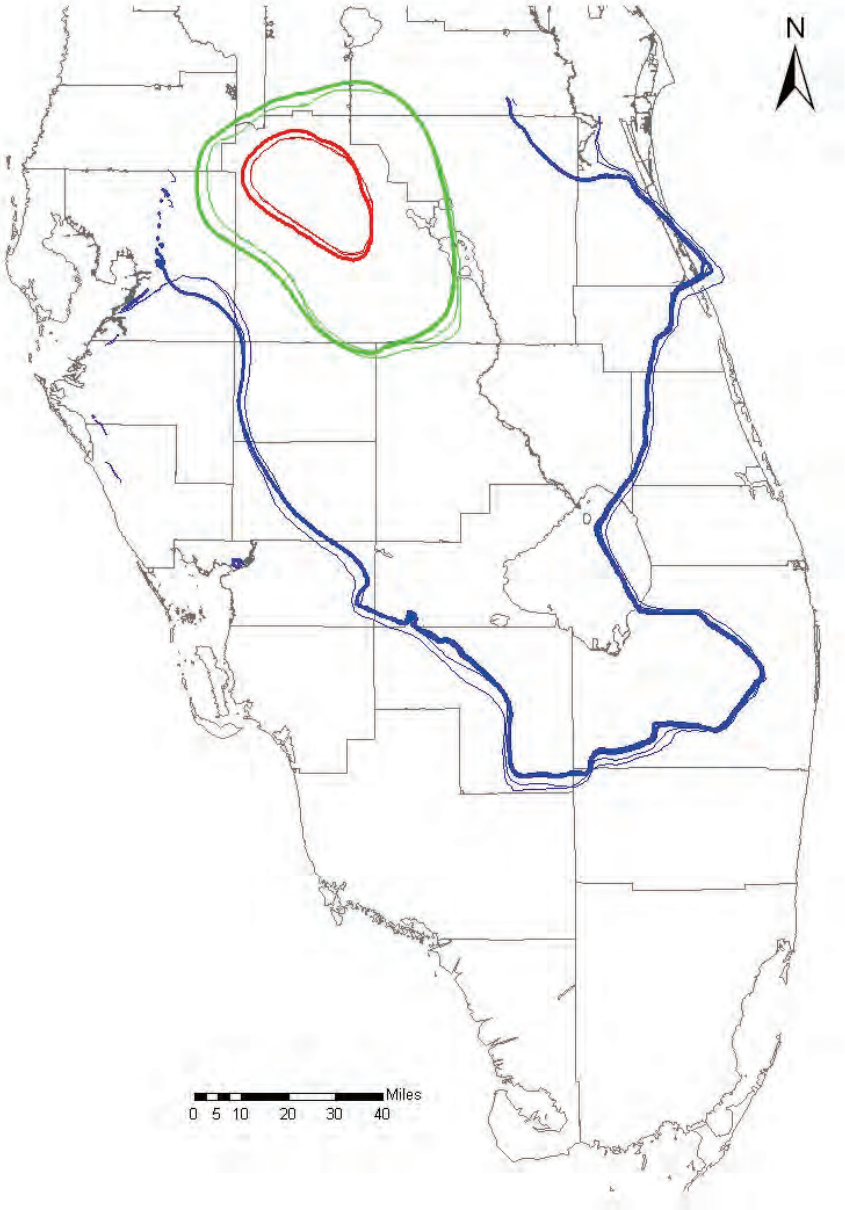

Legend (Test Grid):

- 20,000-ft grid / 20 Layers
- 20,000-ft grid / 11 Layers
- 10,000-ft grid / 20 Layers
- 10,000-ft grid / 11 Layers

Legend (Head):

- 25 ft
- 50 ft
- 75 ft

Notes:

Solutions from grids with identical horizontal resolution, but differing numbers of layers are nearly indistinguishable at this scale. Here, both are shown, but with the same line type.

These heads are point-water heads (the level to which water would rise in a standpipe). The model was computed using equivalent freshwater head, which accounts for density variations due to salinity and temperature.

These solutions are from layer 9 of the 11-layer grids and layer 13 of the 20-layer grids.

Steady State Head Solutions for LF1 on Test Grids
(20,000 ft grid and 10,000 ft grid)
Final Groundwater Model Calibration Report

Figure B1-22

October 2010

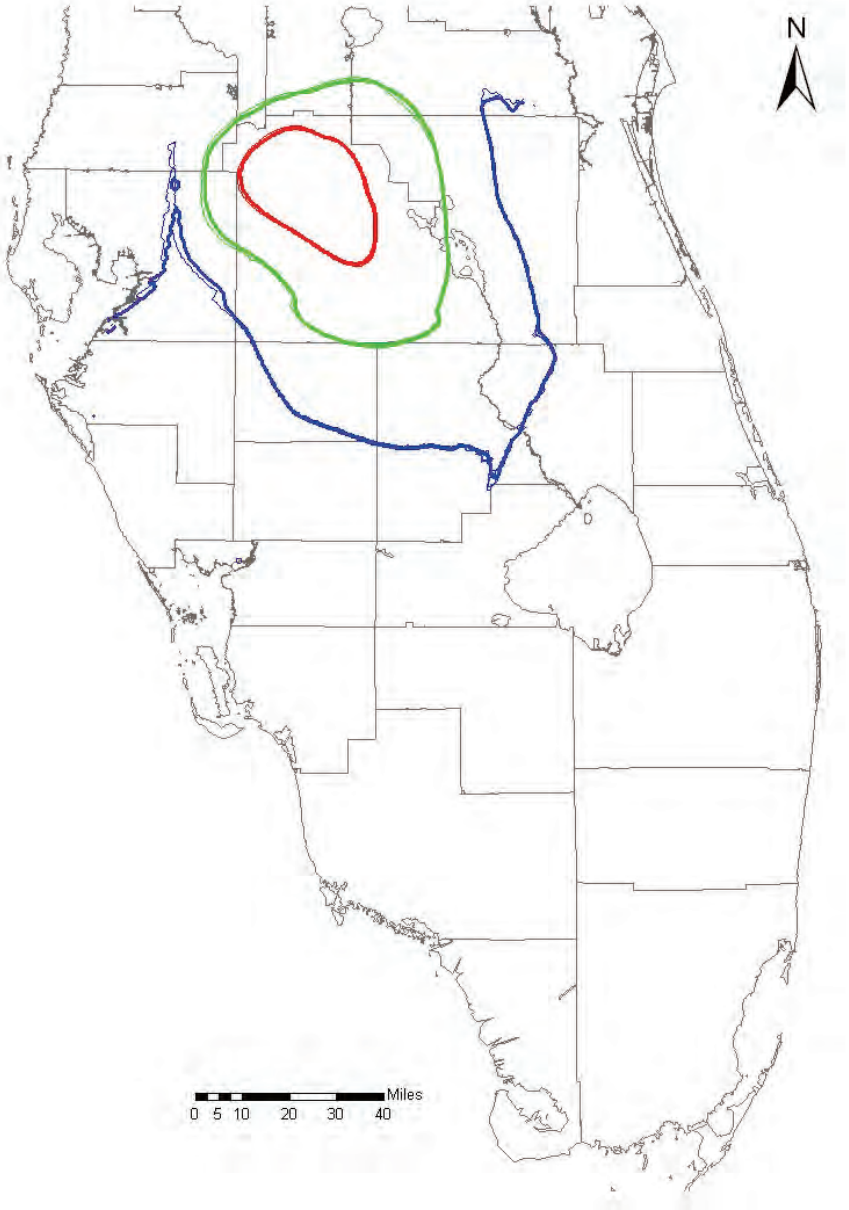

Legend (Test Grid):

- 5,000-ft grid / 20 Layers
- 5,000-ft grid / 11 Layers
- 10,000-ft grid / 20 Layers
- 10,000-ft grid / 11 Layers

Legend (Head):

- 25 ft
- 50 ft
- 75 ft

Notes:

Solutions from grids with identical horizontal resolution, but differing numbers of layers are nearly indistinguishable at this scale. Here, both are shown, but with the same line type.

These heads are point-water heads (the level to which water would rise in a standpipe). The model was computed using equivalent freshwater head, which accounts for density variations due to salinity and temperature.

These solutions are from layer 11 of the 11-layer grids and layer 19 of the 20-layer grids.

Steady State Head Solutions for BZ on Test Grids
(5,000 ft grid and 10,000 ft grid)
Final Groundwater Model Calibration Report

Figure B1-23

October 2010

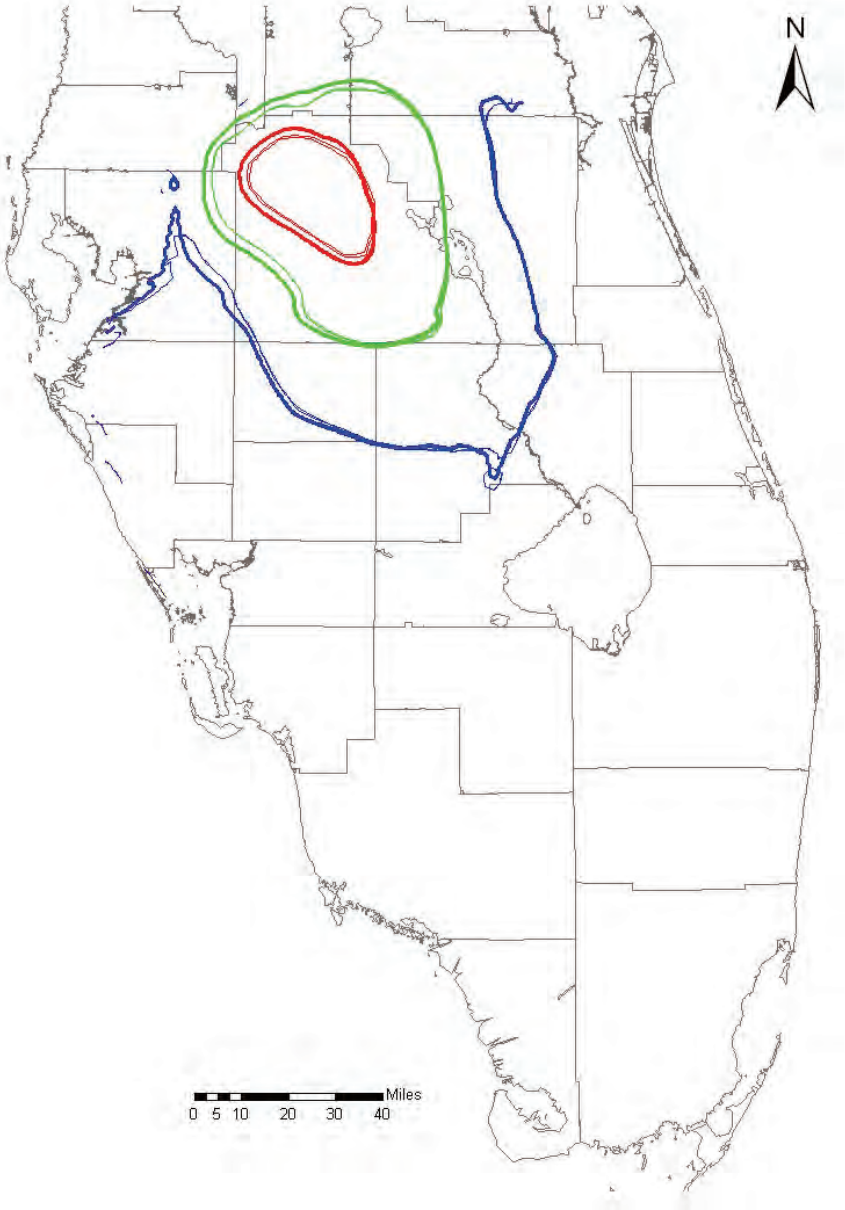

Legend (Test Grid):

- 20,000-ft grid / 20 Layers
- 20,000-ft grid / 11 Layers
- 10,000-ft grid / 20 Layers
- 10,000-ft grid / 11 Layers

Legend (Head):

- 25 ft
- 50 ft
- 75 ft

Notes:

Solutions from grids with identical horizontal resolution, but differing numbers of layers are nearly indistinguishable at this scale. Here, both are shown, but with the same line type.

These heads are point-water heads (the level to which water would rise in a standpipe). The model was computed using equivalent freshwater head, which accounts for density variations due to salinity and temperature.

These solutions are from layer 11 of the 11-layer grids and layer 19 of the 20-layer grids.

Steady State Head Solutions for BZ on Test Grids
(20,000 ft grid and 10,000 ft grid)
Final Groundwater Model Calibration Report

Figure B1-24

October 2010

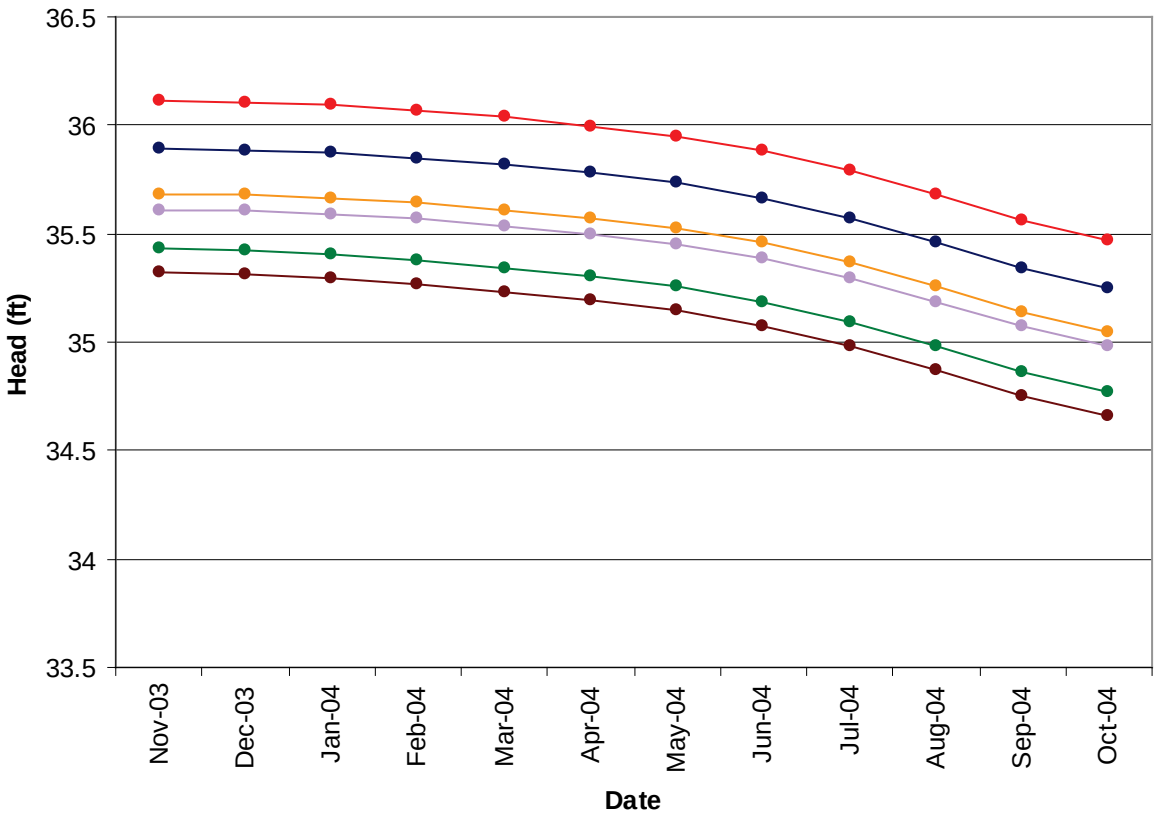

Legend:

- 5,000-ft grid / 20 layers
- 5,000-ft grid / 11 layers
- 10,000-ft grid / 20 layers
- 10,000-ft grid / 11 layers
- 20,000-ft grid / 20 layers
- 20,000-ft grid / 11 layers

Notes:

Heads were extracted from the center of Layer 3, the middle of the three layers representing the Intermediate Aquifer System and Intermediate Confining Unit.

These heads are point-water heads (the level to which water would rise in a standpipe). The model was computed using equivalent freshwater head, which accounts for density variations due to salinity and temperature.

See Figure B1-8 for the horizontal locations of comparison point C.

Comparison of Transient Heads at Point C (IAS)

Figure B1-25

Final Groundwater Model Calibration Report

October 2010

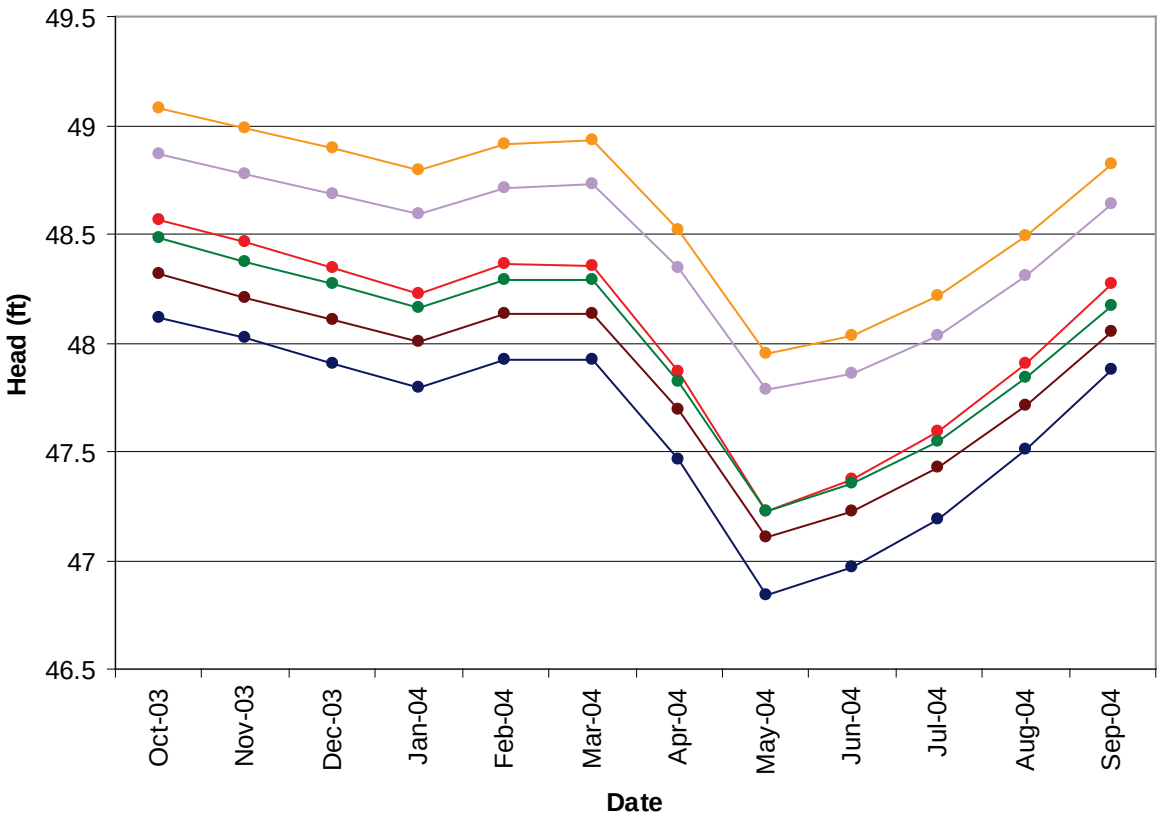

Legend:

- 5,000-ft grid / 20 layers
- 5,000-ft grid / 11 layers
- 10,000-ft grid / 20 layers
- 10,000-ft grid / 11 layers
- 20,000-ft grid / 20 layers
- 20,000-ft grid / 11 layers

Notes:

Heads were extracted from the center of the Upper Floridan Aquifer. For the 11-layer grids, this was layer 5; for the 20-layer grids, the results from layer 5 and 6 were averaged.

These heads are point-water heads (the level to which water would rise in a standpipe). The model was computed using equivalent freshwater head, which accounts for density variations due to salinity and temperature.

See Figure B1-8 for the horizontal locations of comparison point C.

Comparison of Transient Heads at Point C (UF)

Final Groundwater Model Calibration Report

Figure B1-26

October 2010

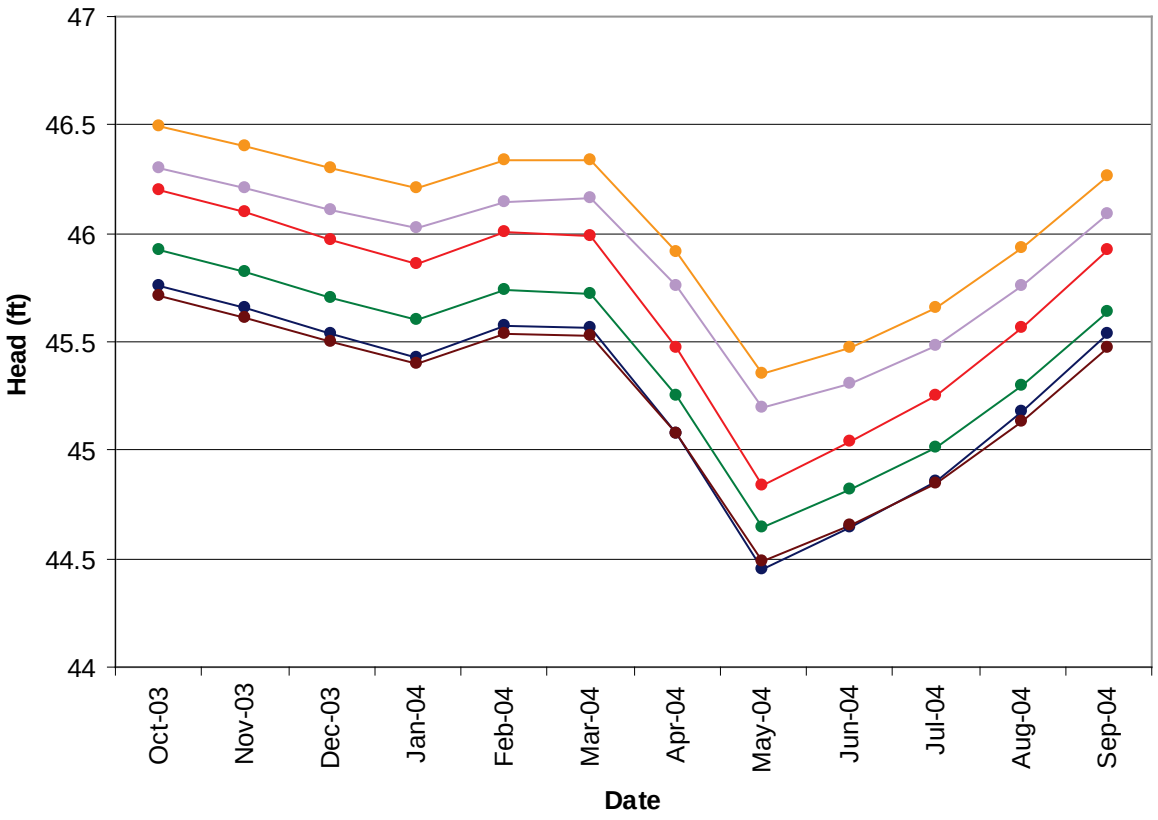

Legend:

- 5,000-ft grid / 20 layers
- 5,000-ft grid / 11 layers
- 10,000-ft grid / 20 layers
- 10,000-ft grid / 11 layers
- 20,000-ft grid / 20 layers
- 20,000-ft grid / 11 layers

Notes:

Heads were extracted from the center of the Avon Park Permeable Zone. For the 11-layer grids, this was layer 7; for the 20-layer grids, this was layer 9.

These heads are point-water heads (the level to which water would rise in a standpipe). The model was computed using equivalent freshwater head, which accounts for density variations due to salinity and temperature.

See Figure B1-8 for the horizontal locations of comparison point C.

Comparison of Transient Heads at Point C (APPZ)

Figure B1-27

Final Groundwater Model Calibration Report

September 2009

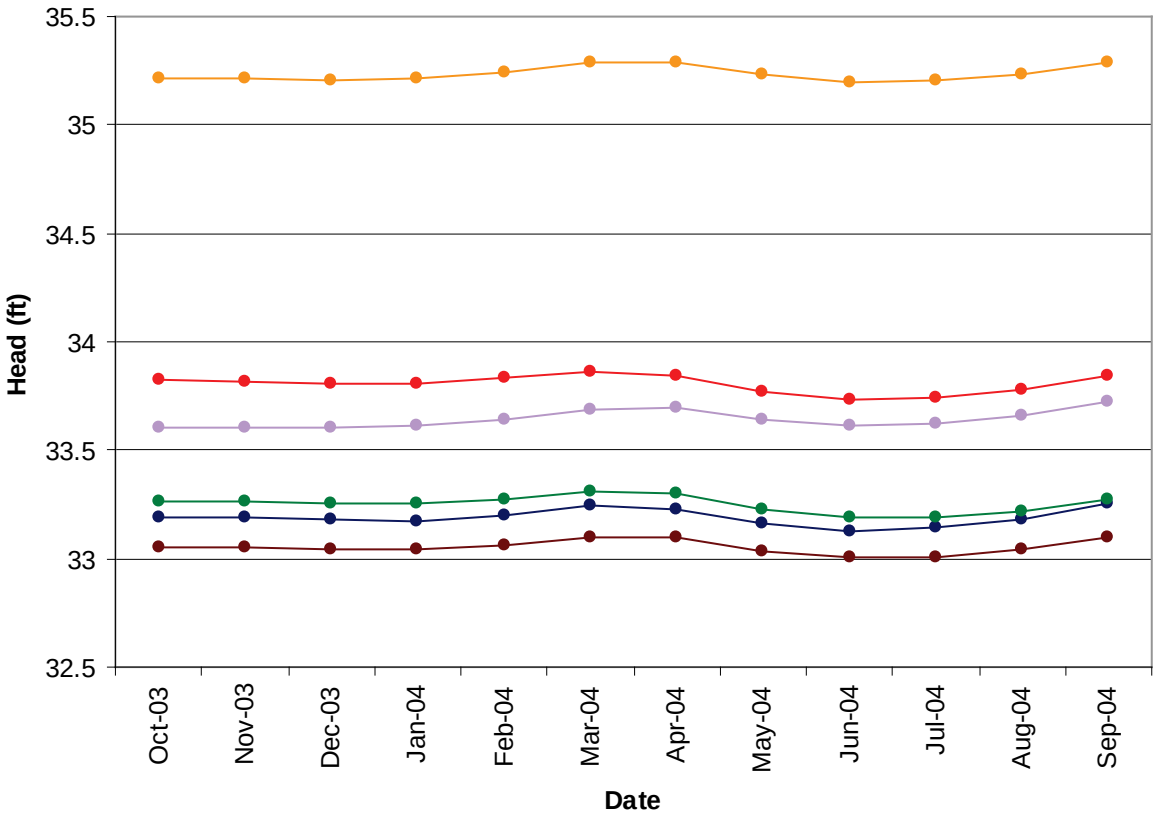

Legend:

- 5,000-ft grid / 20 layers
- 5,000-ft grid / 11 layers
- 10,000-ft grid / 20 layers
- 10,000-ft grid / 11 layers
- 20,000-ft grid / 20 layers
- 20,000-ft grid / 11 layers

Notes:

Heads were extracted from the center of the Lower Floridan (LF1) Aquifer. For the 11-layer grids, this was layer 9; for the 20-layer grids, this was layer 13.

These heads are point-water heads (the level to which water would rise in a standpipe). The model was computed using equivalent freshwater head, which accounts for density variations due to salinity and temperature.

See Figure B1-8 for the horizontal locations of comparison point C.

Comparison of Transient Heads at Point C (LF1)

Final Groundwater Model Calibration Report

Figure B1-28

October 2010

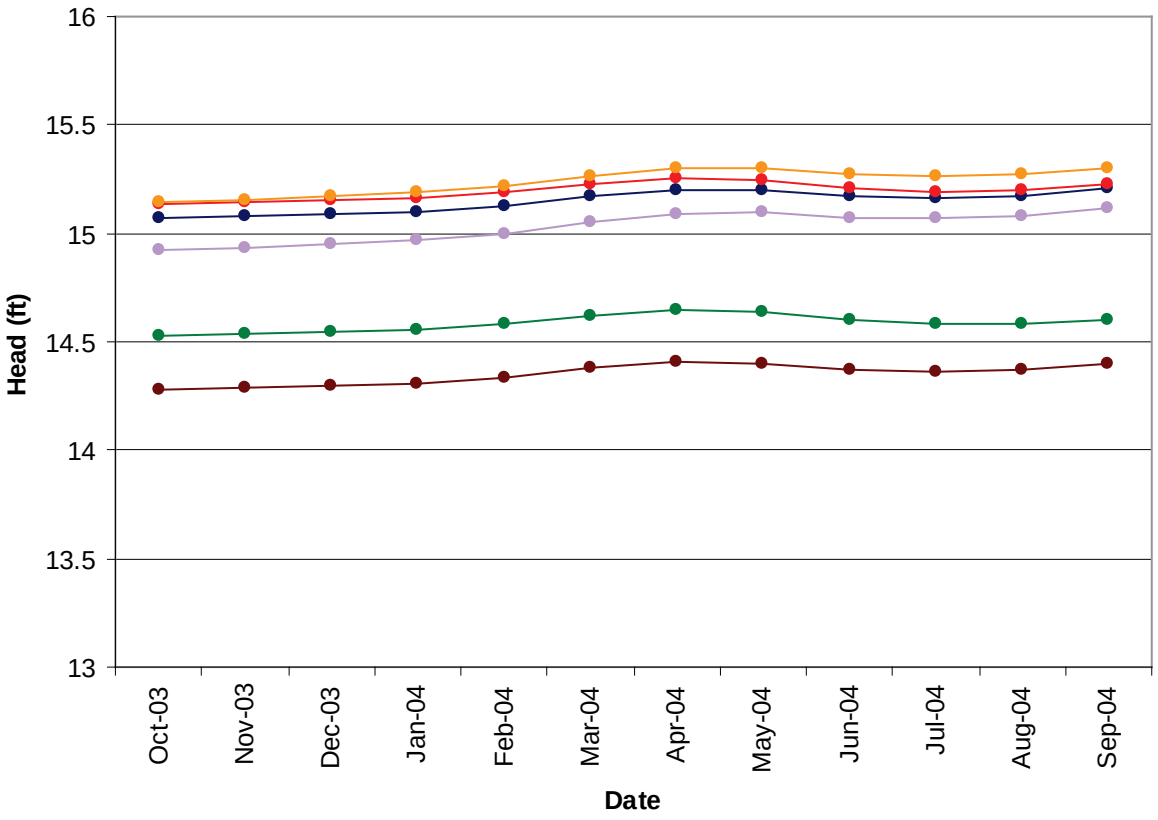

Legend:

- 5,000-ft grid / 20 layers
- 5,000-ft grid / 11 layers
- 10,000-ft grid / 20 layers
- 10,000-ft grid / 11 layers
- 20,000-ft grid / 20 layers
- 20,000-ft grid / 11 layers

Notes:

Heads were extracted from the center of the Boulder Zone. For the 11-layer grids, this was layer 11; for the 20-layer grids, this was layer 19.

These heads are point-water heads (the level to which water would rise in a standpipe). The model was computed using equivalent freshwater head, which accounts for density variations due to salinity and temperature.

See Figure B1-8 for the horizontal locations of comparison point C.

Comparison of Transient Heads at Point C (BZ)

Final Groundwater Model Calibration Report

Figure B1-29

October 2010

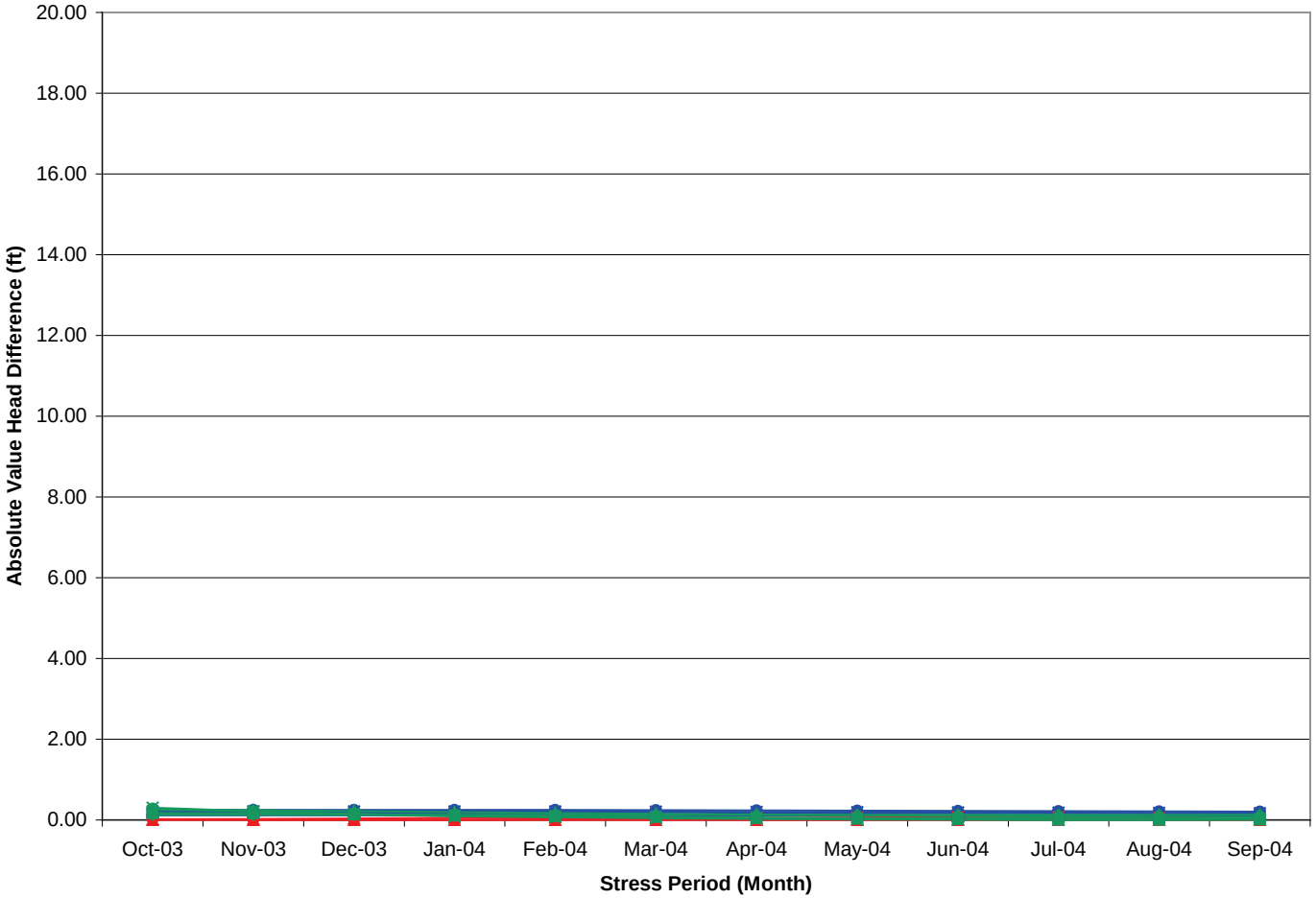

Legend:

- Point C
- Point M
- Point K
- Intermediate Aquifer System
- Upper Floridan
- Avon Park Permeable Zone
- Lower Floridan (LF1)
- Boulder Zone

Notes:

Solutions on the two grids are compared by computing the absolute value of the head difference at each point.

The scale is set to match that on the following 4 figures.

Vertical locations of the comparison points are in the center of the indicated aquifer.

See Figure B1-8 for the horizontal locations of the comparison points.

Comparison of Transient Heads for 5000-ft / 11 Layer Grid vs. 5000-ft / 20 Layer Grid

Final Groundwater Model Calibration Report

Figure B1-30

October 2010

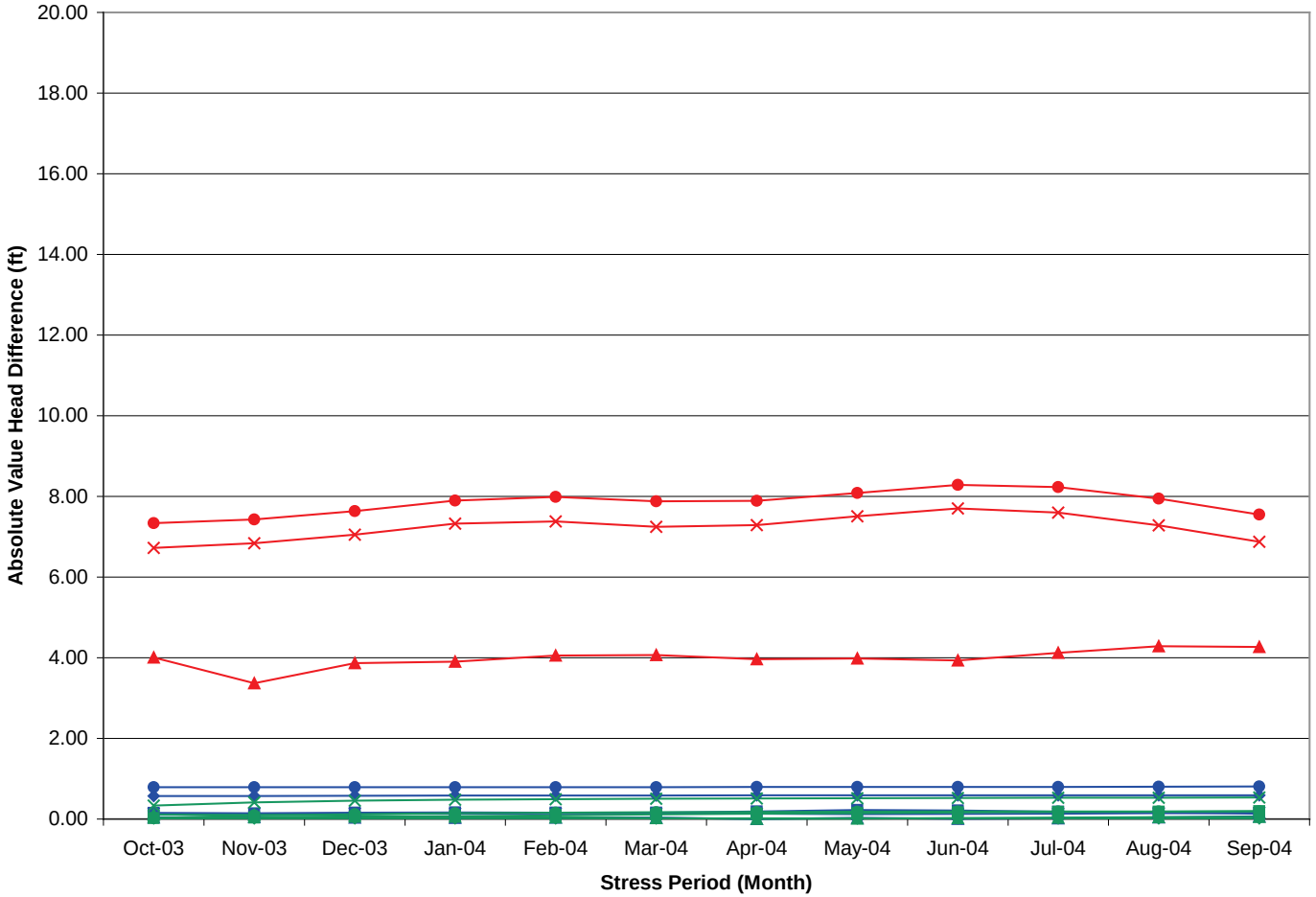

Legend:

- Point C
- Point M
- Point K
- Intermediate Aquifer System
- Upper Floridan
- Avon Park Permeable Zone
- Lower Floridan (LF1)
- Boulder Zone

Notes:

Solutions on the two grids are compared by computing the absolute value of the head difference at each point.

Vertical locations of the comparison points are in the center of the indicated aquifer.

See Figure B1-8 for the horizontal locations of the comparison points.

Comparison of Transient Heads for 10000-ft / 20 Layer Grid vs. 5000-ft / 20 Layer Grid

Final Groundwater Model Calibration Report

Figure B1-31

October 2010

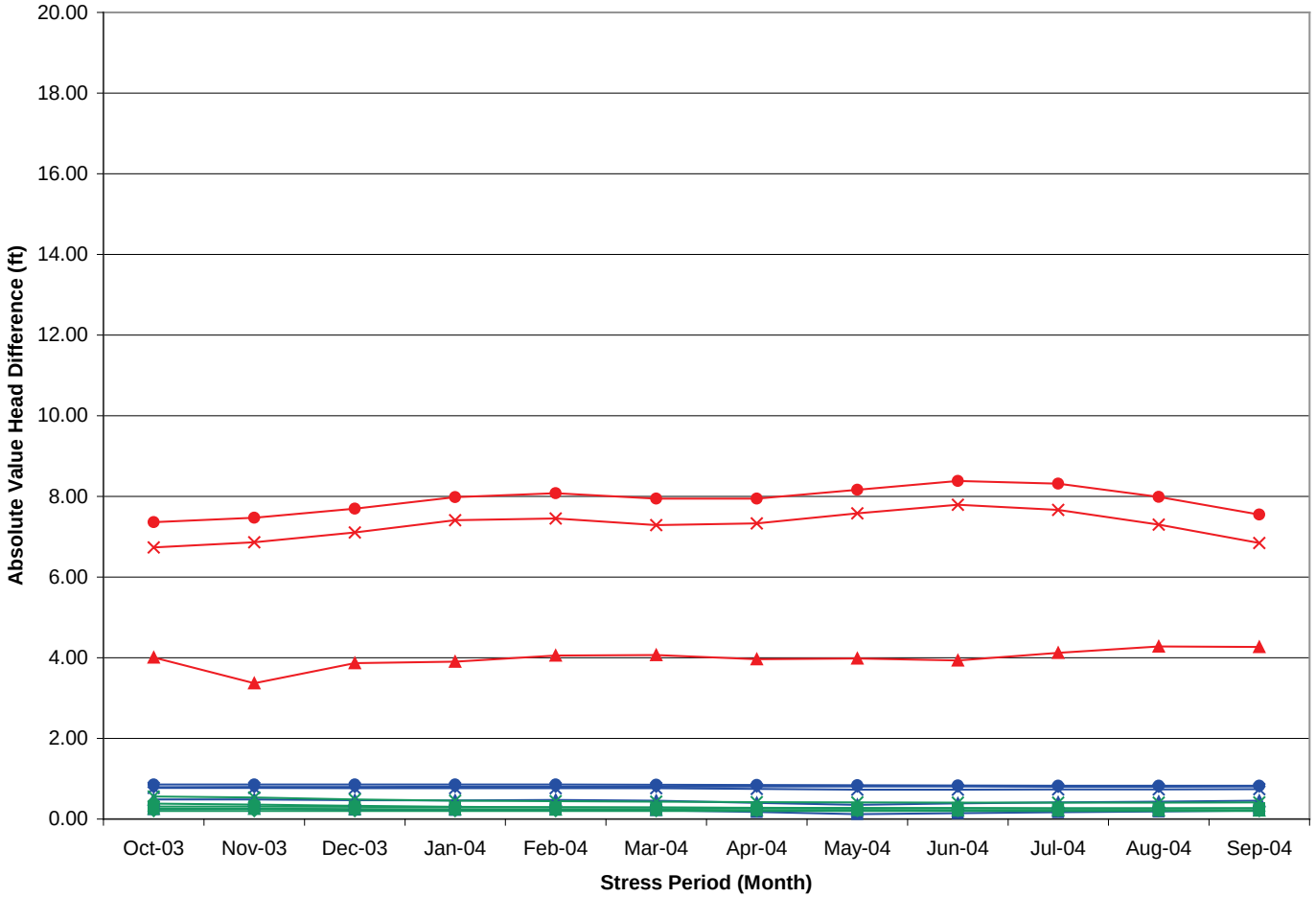

Legend:

- Point C
- Point M
- Point K
- Intermediate Aquifer System
- Upper Floridan
- Avon Park Permeable Zone
- Lower Floridan (LF1)
- Boulder Zone

Notes:

Solutions on the two grids are compared by computing the absolute value of the head difference at each point.

Vertical locations of the comparison points are in the center of the indicated aquifer.

See Figure B1-8 for the horizontal locations of the comparison points.

Comparison of Transient Heads for 10000-ft / 11 Layer Grid vs. 5000-ft / 20 Layer Grid

Final Groundwater Model Calibration Report

Figure B1-32

October 2010

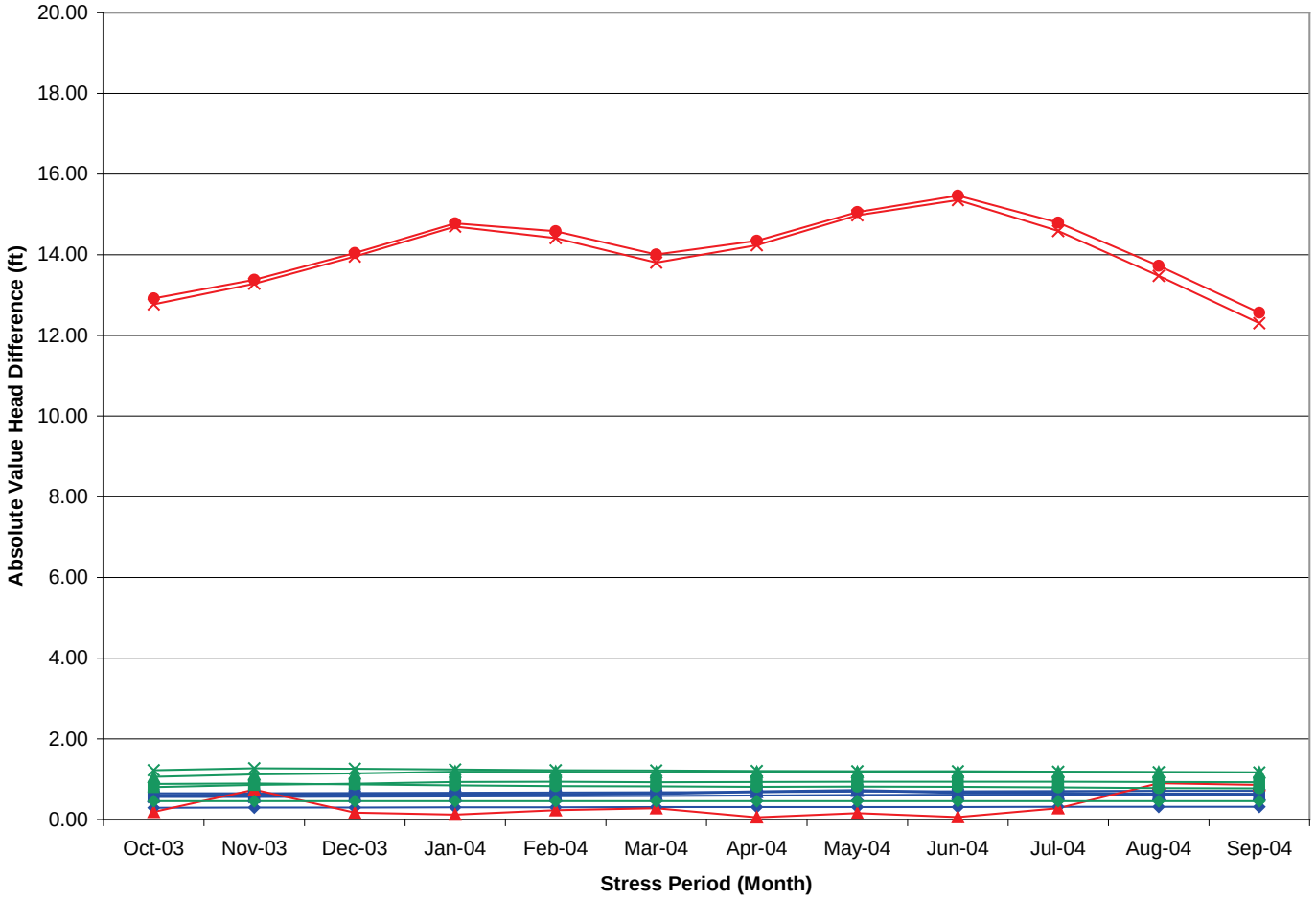

Legend:

- Point C
- Point M
- Point K
- Intermediate Aquifer System
- Upper Floridan
- Avon Park Permeable Zone
- Lower Floridan (LF1)
- Boulder Zone

Notes:

Solutions on the two grids are compared by computing the absolute value of the head difference at each point.

Vertical locations of the comparison points are in the center of the indicated aquifer.

See Figure B1-8 for the horizontal locations of the comparison points.

Comparison of Transient Heads for 20000-ft / 20 Layer Grid vs. 5000-ft / 20 Layer Grid

Final Groundwater Model Calibration Report

Figure B1-33

October 2010

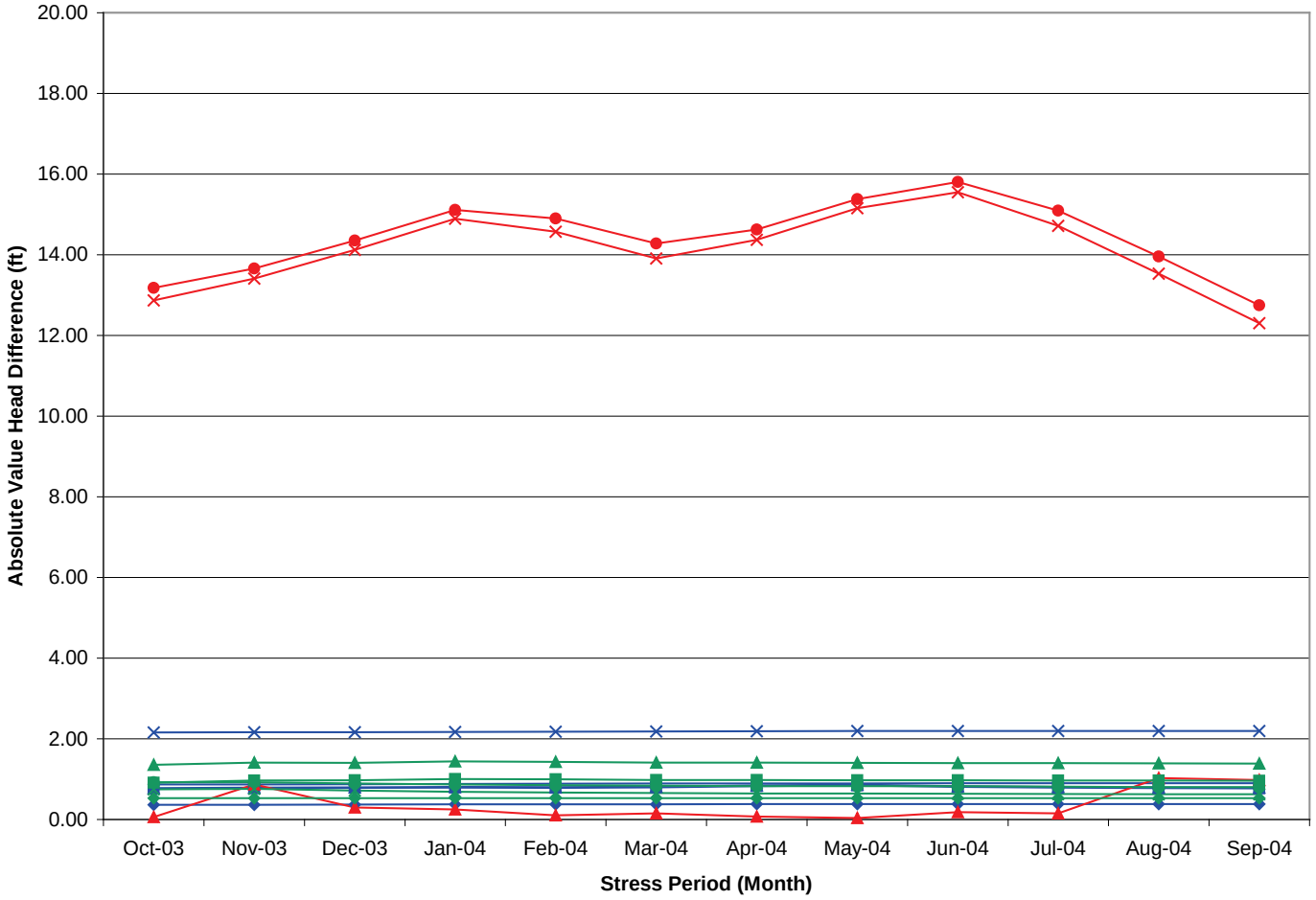

Legend:

- Point C
- Point M
- Point K
- Intermediate Aquifer/Confining Unit
- Upper Floridan
- Avon Park Permeable Zone
- Lower Floridan (LF1)
- Boulder Zone

Notes:

Solutions on the two grids are compared by computing the absolute value of the head difference at each point.

Vertical locations of the comparison points are in the center of the indicated aquifer.

See Figure B1-8 for the horizontal locations of the comparison points.

Comparison of Transient Heads for 20000-ft / 11 Layer Grid vs. 5000-ft / 20 Layer Grid

Final Groundwater Model Calibration Report

Figure B1-34

October 2010

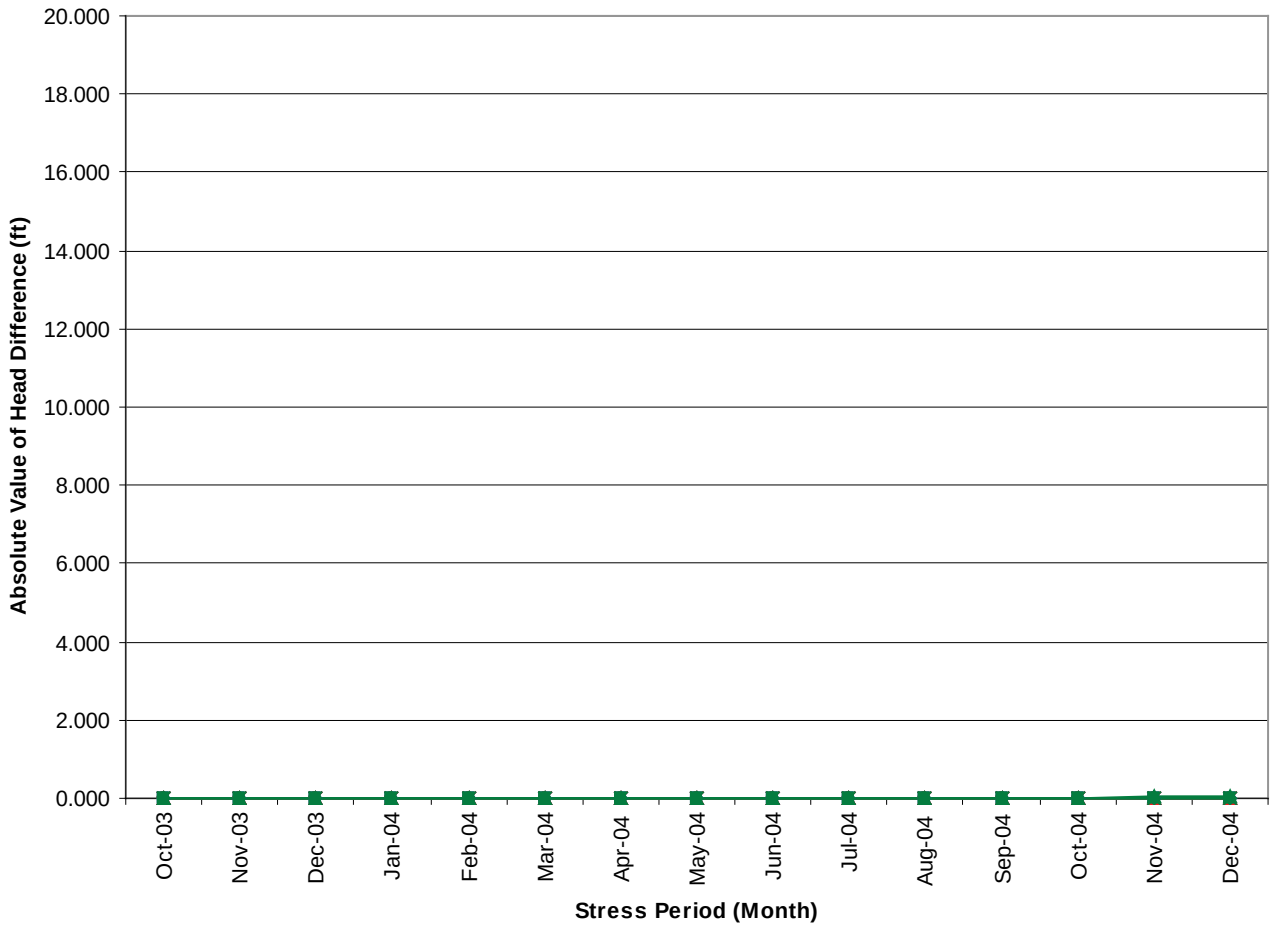

Legend:

- Point C
- Point M
- Point K
- Intermediate Aquifer System
- Upper Floridan
- Avon Park Permeable Zone
- Lower Floridan (LF1)
- Boulder Zone

Notes:

The two solutions are compared by computing the absolute value of the head difference at each point.

The scale is set to match that on Figure B2-2.

Vertical locations of the comparison points are in the center of the indicated aquifer.

See Figure B1-8 for the horizontal locations of the comparison points.

Comparison of Transient Heads for 1-Day Timestep vs. Model-Computed Timestep (0.23 d)

Final Groundwater Model Calibration Report

Figure B2-1

October 2010

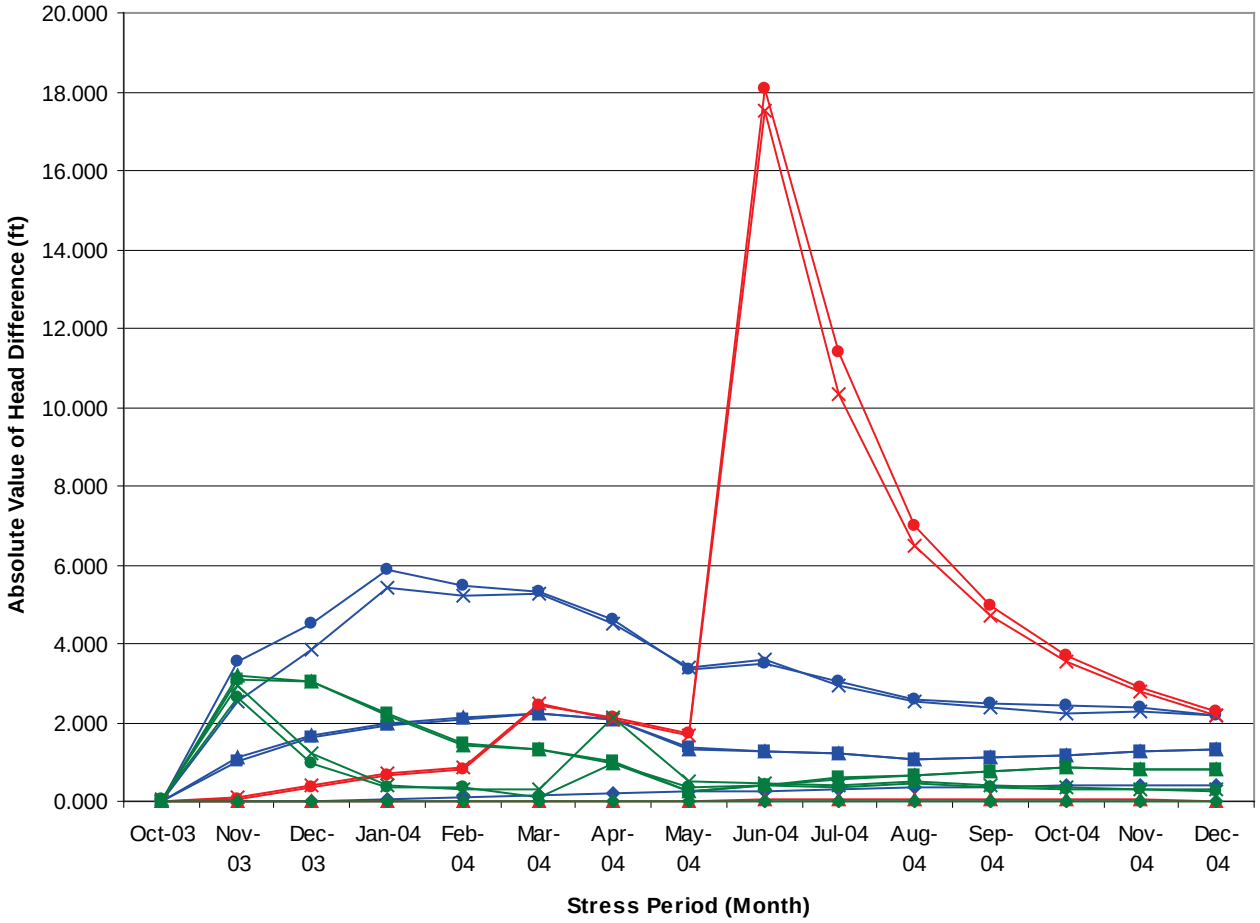

Legend:

- Point C
- Point M
- Point K
- Intermediate Aquifer System
- Upper Floridan
- Avon Park Permeable Zone
- Lower Floridan (LF1)
- Boulder Zone

Notes:

The two solutions are compared by computing the absolute value of the head difference at each point.

The scale is set to match that on Figure B2-1.

Vertical locations of the comparison points are in the center of the indicated aquifer.

See Figure B1-8 for the horizontal locations of the comparison points.

Comparison of Transient Heads for 1-Day Timestep vs. 5-Day Timestep

Final Groundwater Model Calibration Report

Figure B2-2

October 2010

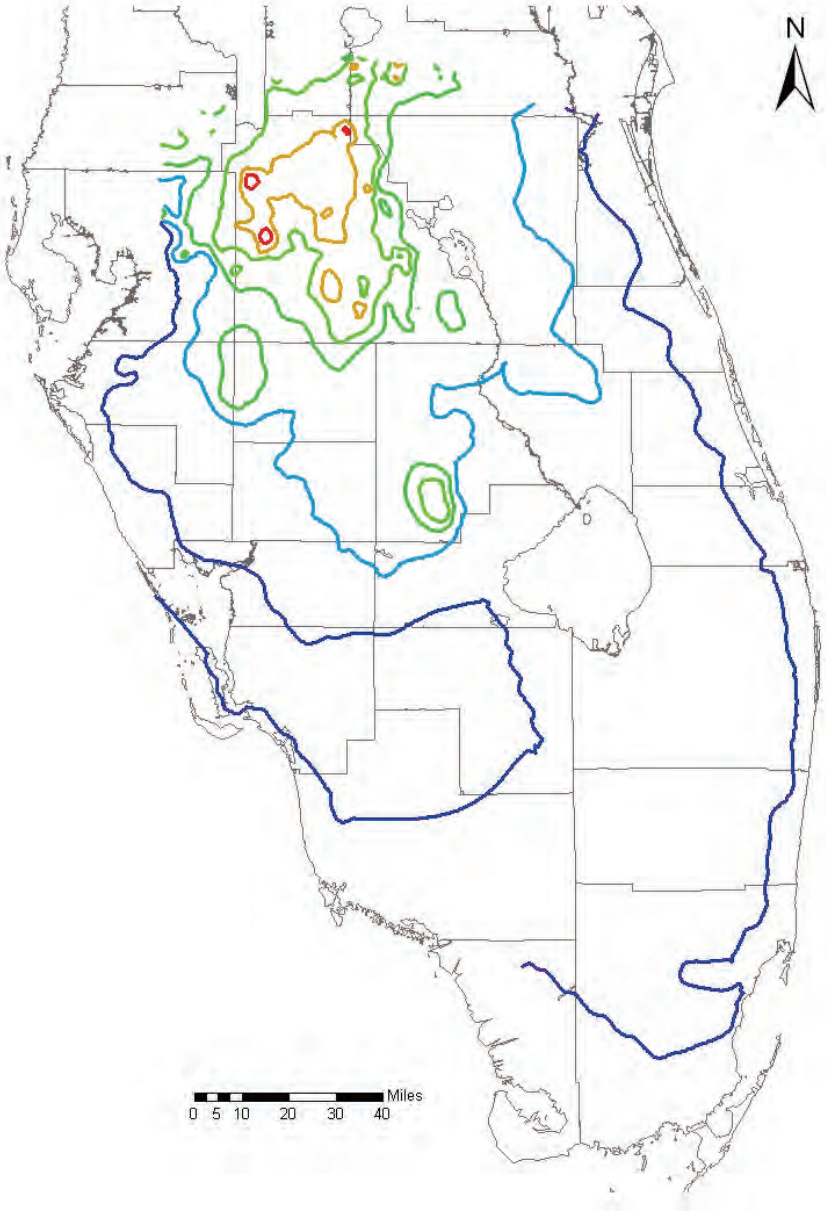

Legend:

- 1-day Timesteps
- Model-Computed Timesteps (0.23 day)

Legend (Head):

- 25 ft
- 50 ft
- 75 ft
- 100 ft
- 125 ft
- 150 ft

Notes:

The two solutions shown here are virtually indistinguishable

These heads are point-water heads (the level to which water would rise in a standpipe). The model was computed using equivalent freshwater head, which accounts for density variations due to salinity and temperature.

These solutions are from layer 3 of the 10,000-ft grid with 11 layers.

Transient Head Solutions (T=366 days) for IAS with 1-Day Timesteps and Model-Computed Timesteps)

Final Groundwater Model Calibration Report

Figure B2-3

October 2010

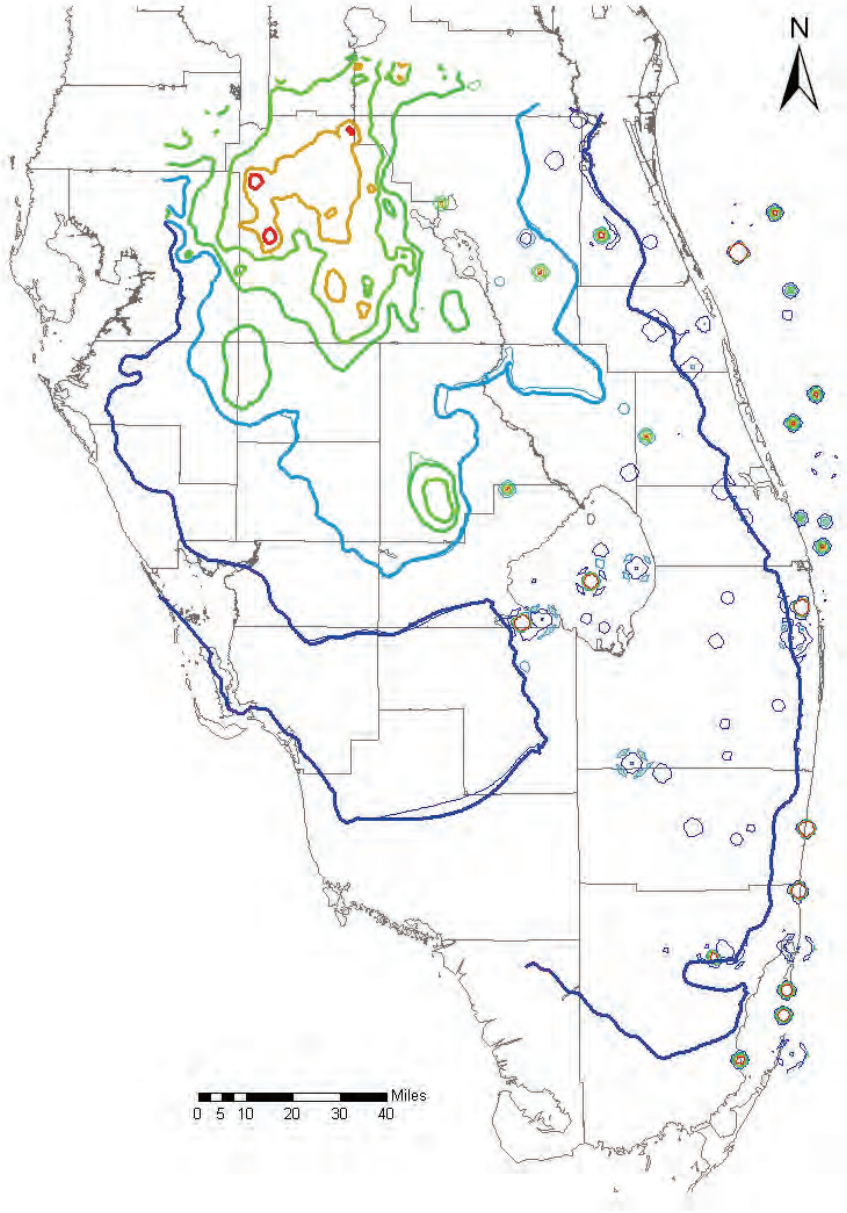

Legend:

- 1-Day Timesteps
- 5-Day Timesteps

Legend (Head):

- -600 ft
- 25 ft
- 50 ft
- 75 ft
- 100 ft
- 125 ft
- 150 ft
- 2400 ft

Notes:

These heads are point-water heads (the level to which water would rise in a standpipe). The model was computed using equivalent freshwater head, which accounts for density variations due to salinity and temperature.

These solutions are from layer 3 of the 10,000-ft grid with 11 layers.

Transient Head Solutions (T=366 days) for IAS with 1-Day Timesteps and 5-Day Timesteps)

Final Groundwater Model Calibration Report

Figure B2-4

October 2010

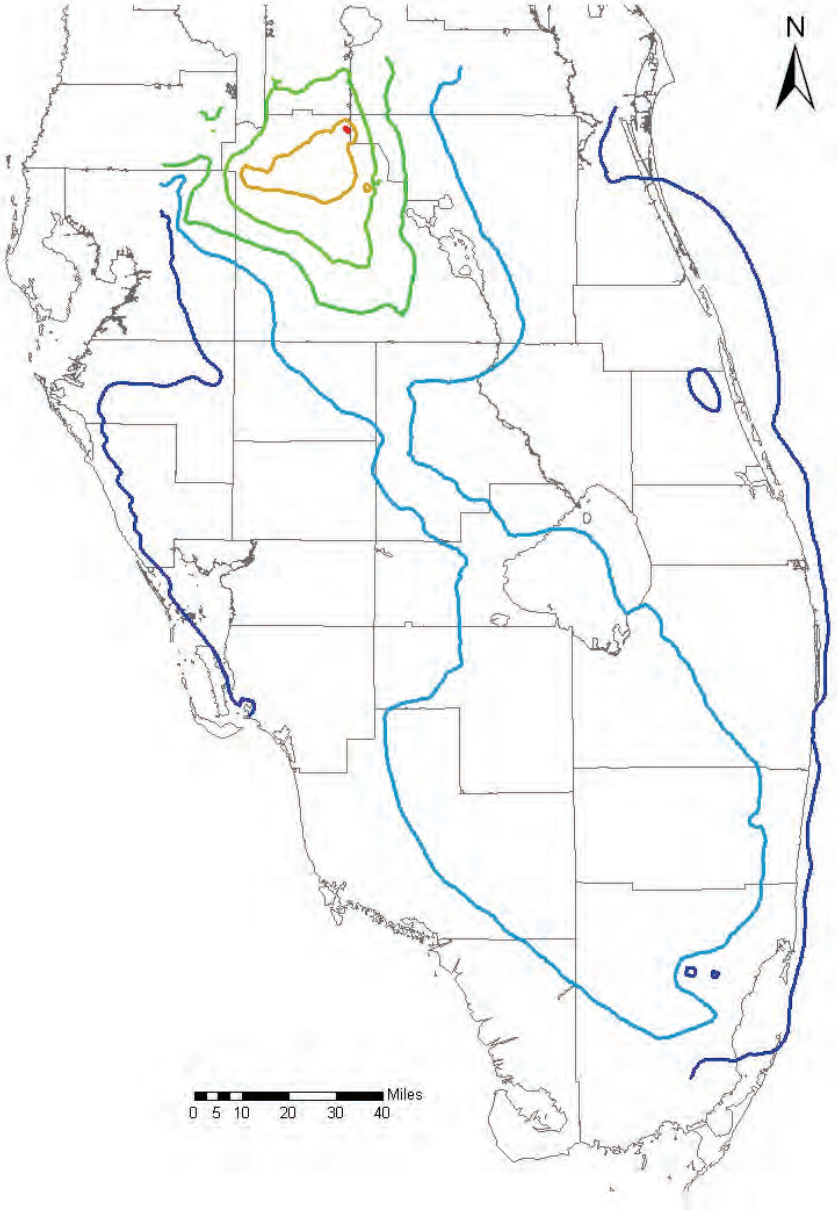

Legend:

- 1-day Timesteps
- Model-Computed Timesteps (0.23 day)

Legend (Head):

- 25 ft
- 50 ft
- 75 ft
- 100 ft
- 125 ft
- 150 ft

Notes:

The two solutions shown here are virtually indistinguishable

These heads are point-water heads (the level to which water would rise in a standpipe). The model was computed using equivalent freshwater head, which accounts for density variations due to salinity and temperature.

These solutions are from layer 5 of the 10,000-ft grid with 11 layers.

Transient Head Solutions (T=366 days) for UF with 1-Day Timesteps and Model-Computed Timesteps)

Final Groundwater Model Calibration Report

Figure B2-5

October 2010

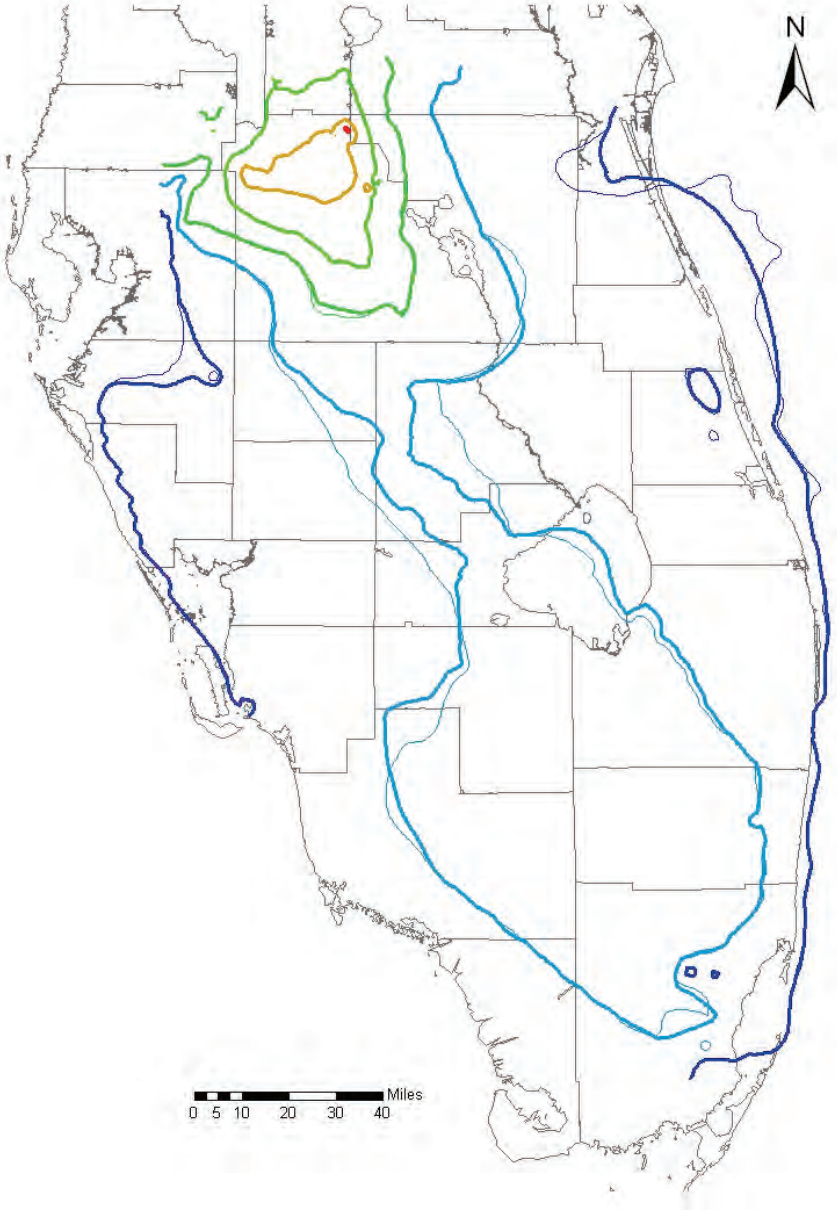

Legend:

- 1-Day Timesteps
- 5-Day Timesteps

Legend (Head):

- 25 ft
- 50 ft
- 75 ft
- 100 ft
- 125 ft
- 150 ft

Notes:

These heads are point-water heads (the level to which water would rise in a standpipe). The model was computed using equivalent freshwater head, which accounts for density variations due to salinity and temperature.

These solutions are from layer 5 of the 10,000-ft grid with 11 layers.

Transient Head Solutions (T=366 days) for UF with 1-Day Timesteps and 5-Day Timesteps)

Final Groundwater Model Calibration Report

Figure B2-6

October 2010

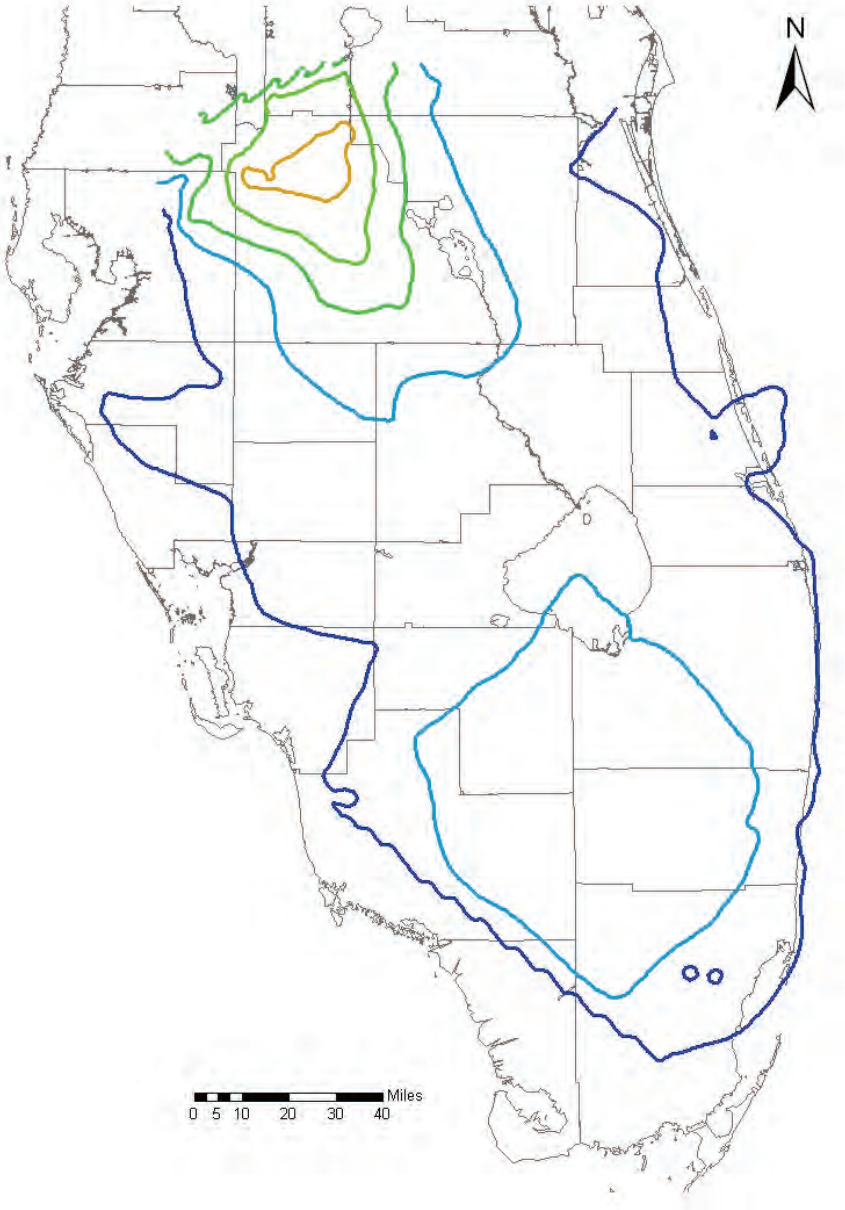

Legend:

- 1-day Timesteps
- Model-Computed Timesteps (0.23 day)

Legend (Head):

- 25 ft
- 50 ft
- 75 ft
- 100 ft
- 125 ft
- 150 ft

Notes:

The two solutions shown here are virtually indistinguishable

These heads are point-water heads (the level to which water would rise in a standpipe). The model was computed using equivalent freshwater head, which accounts for density variations due to salinity and temperature.

These solutions are from layer 7 of the 10,000-ft grid with 11 layers.

Transient Head Solutions (T=366 days) for APPZ with 1-Day Timesteps and Model-Computed Timesteps)

Final Groundwater Model Calibration Report

Figure B2-7

October 2010

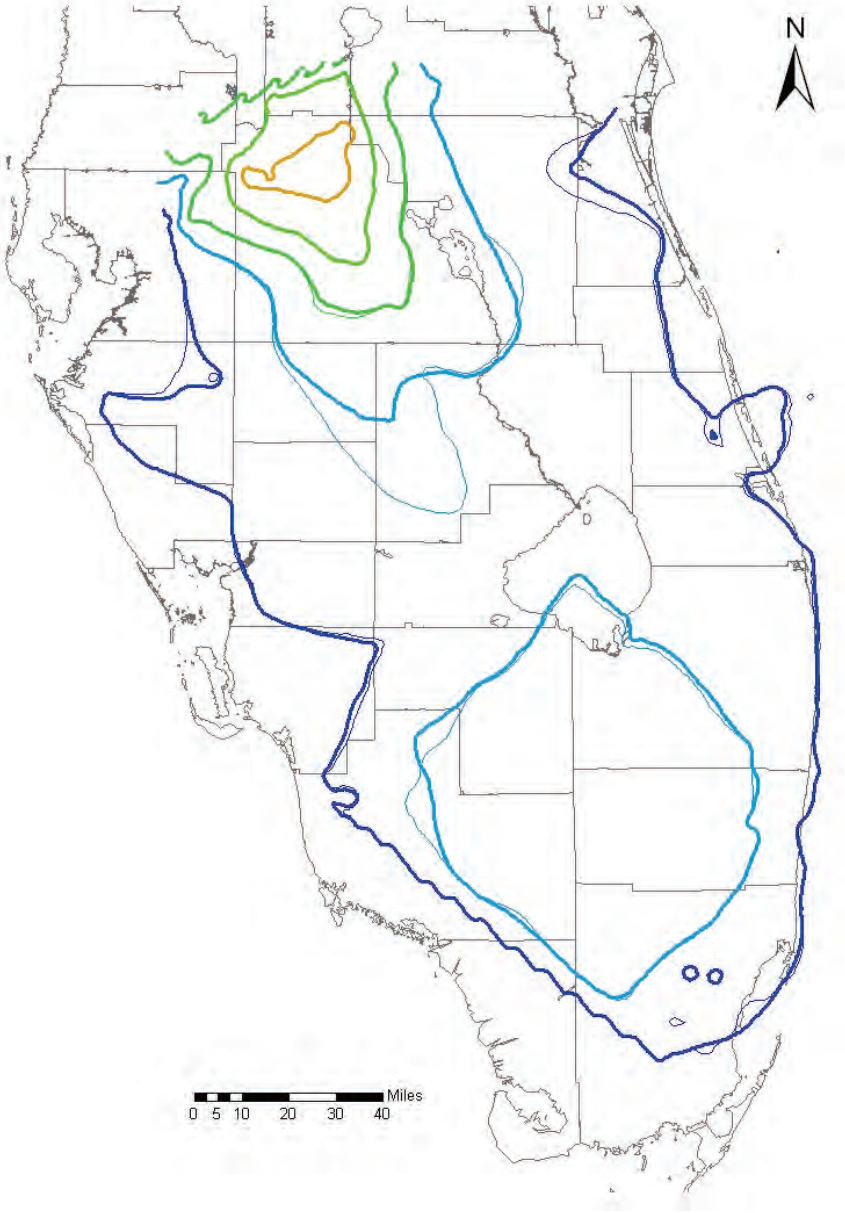

Legend:

- 1-Day Timesteps
- 5-Day Timesteps

Legend (Head):

- 25 ft
- 50 ft
- 75 ft
- 100 ft
- 125 ft
- 150 ft

Notes:

These heads are point-water heads (the level to which water would rise in a standpipe). The model was computed using equivalent freshwater head, which accounts for density variations due to salinity and temperature.

These solutions are from layer 7 of the 10,000-ft grid with 11 layers.

Transient Head Solutions (T=366 days) for APPZ with 1-Day Timesteps and 5-Day Timesteps)

Final Groundwater Model Calibration Report

Figure B2-8

October 2010

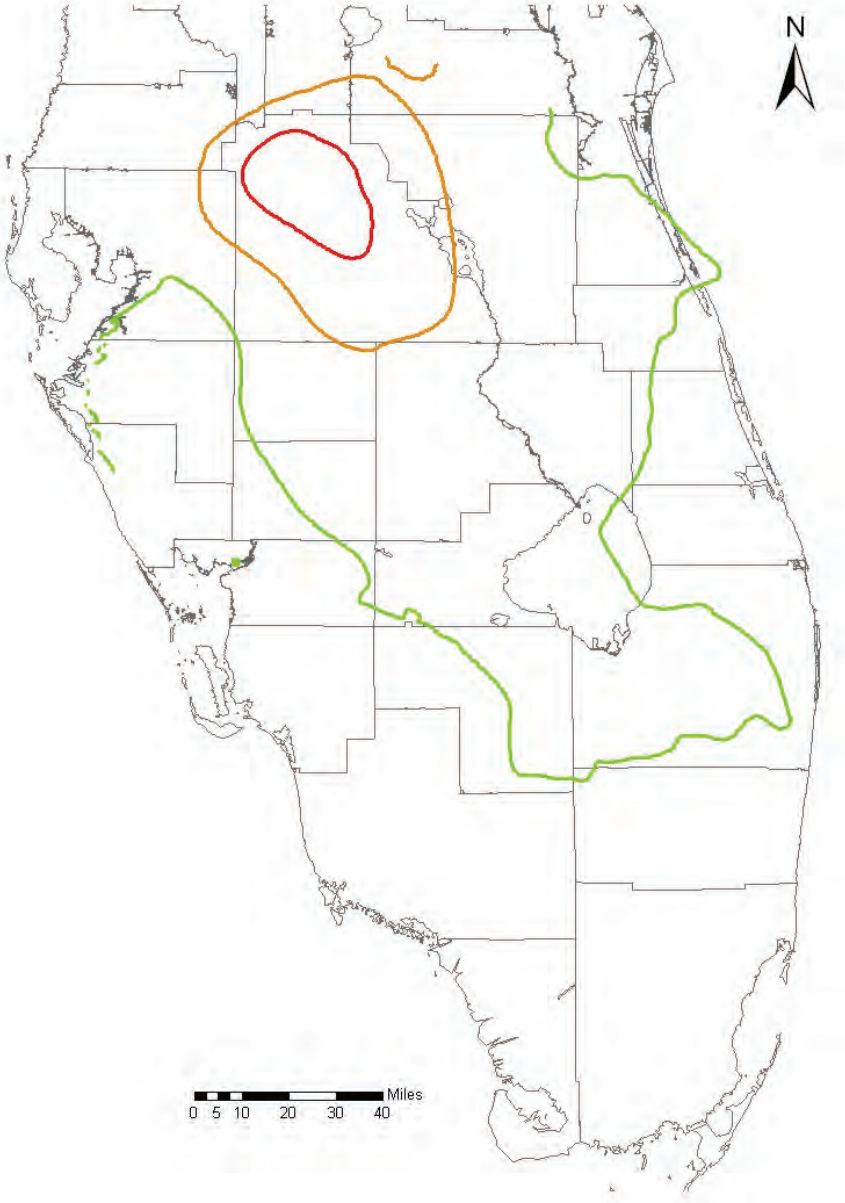

Legend:

1-day Timesteps

Model-Computed Timesteps (0.23 day)

Legend (Head):

25 ft

50 ft

75 ft

Notes:

The two solutions shown here are virtually indistinguishable

These heads are point-water heads (the level to which water would rise in a standpipe). The model was computed using equivalent freshwater head, which accounts for density variations due to salinity and temperature.

These solutions are from layer 9 of the 10,000-ft grid with 11 layers.

Transient Head Solutions (T=366 days) for LF1 with 1-Day Timesteps and Model-Computed Timesteps)

Final Groundwater Model Calibration Report

Figure B2-9

October 2010

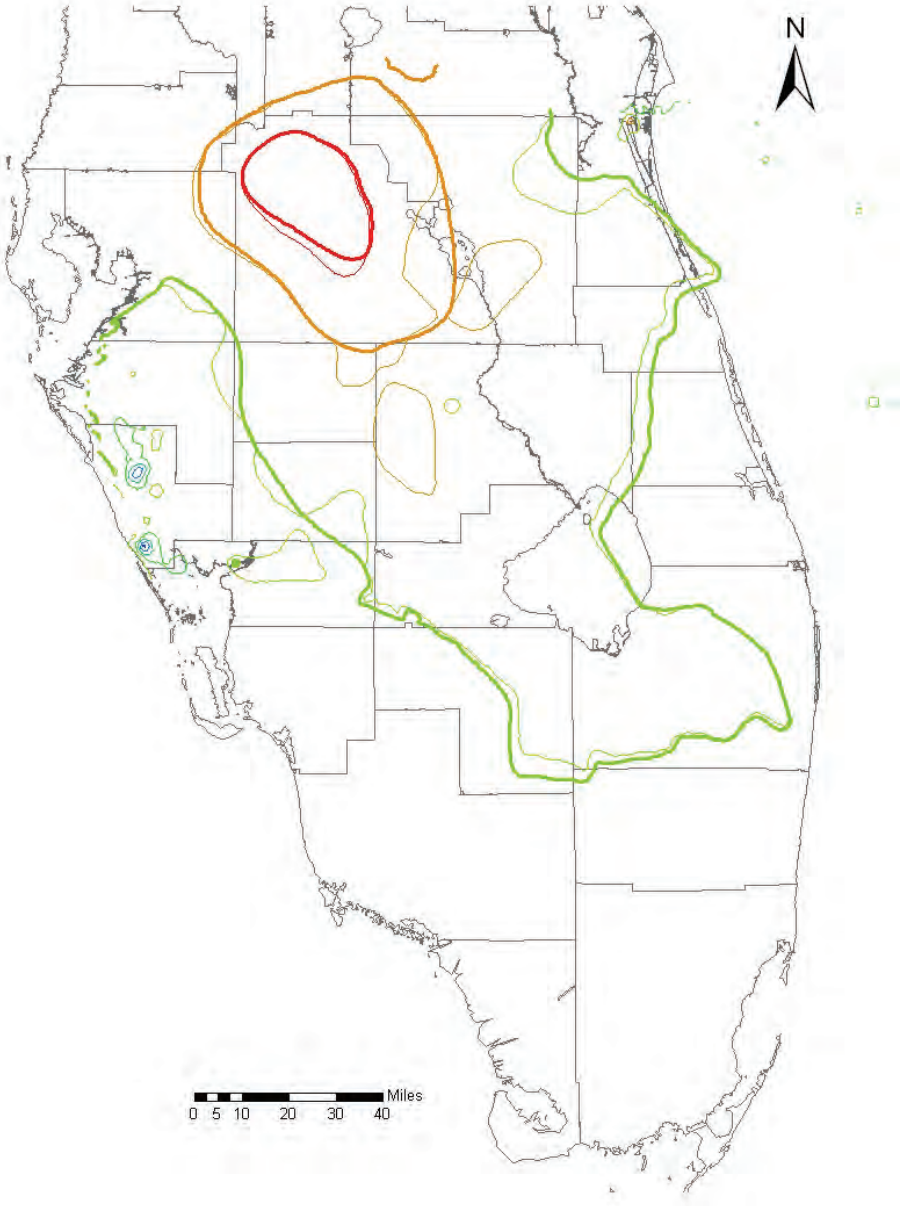

Legend:

- 1-Day Timesteps
- 5-Day Timesteps

Legend (Head):

- -75 ft
- -50 ft
- -25 ft
- 0 ft
- 25 ft
- 50 ft
- 75 ft

Notes:

These heads are point-water heads (the level to which water would rise in a standpipe). The model was computed using equivalent freshwater head, which accounts for density variations due to salinity and temperature.

These solutions are from layer 9 of the 10,000-ft grid with 11 layers.

Transient Head Solutions (T=366 days) for LF1 with 1-Day Timesteps and 5-Day Timesteps)

Final Groundwater Model Calibration Report

Figure B2-10

October 2010

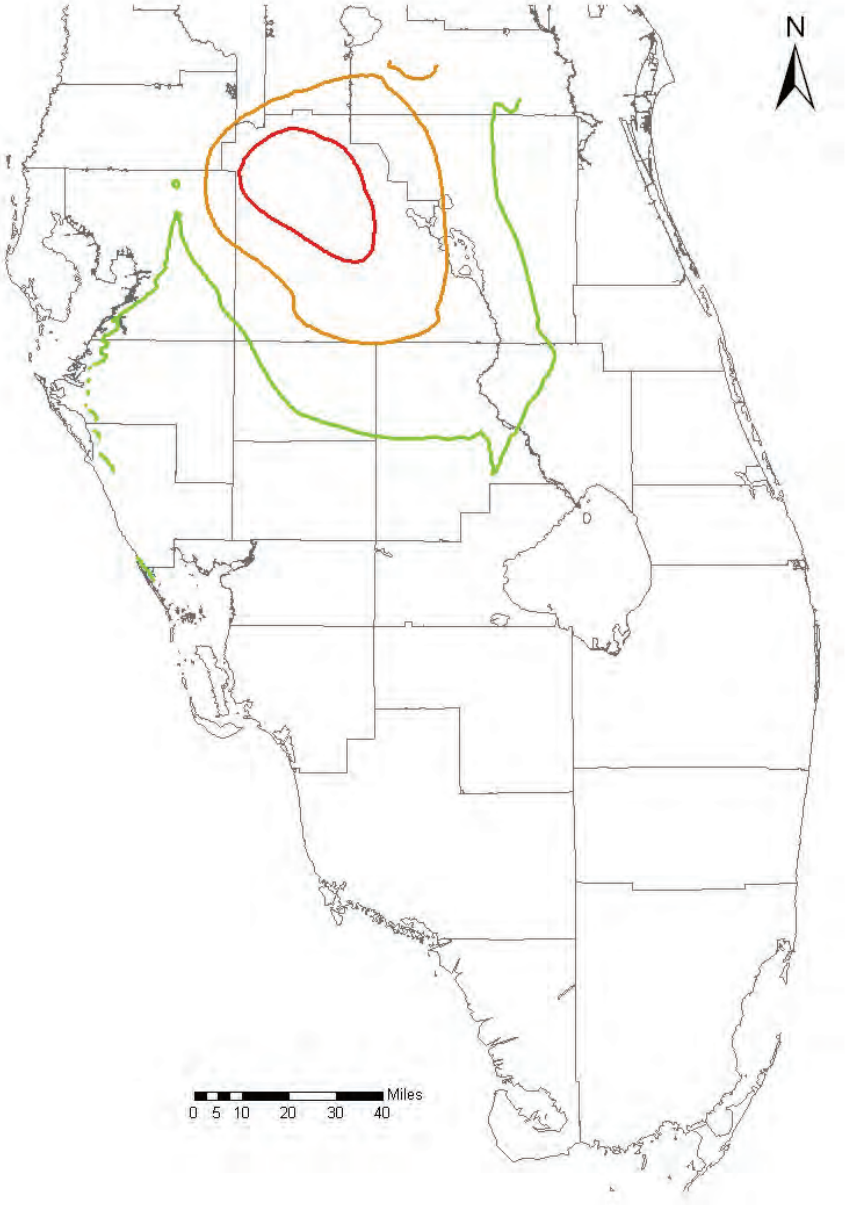

Legend:

1-day Timesteps

Model-Computed Timesteps (0.23 day)

Legend (Head):

25 ft

50 ft

75 ft

Notes:

The two solutions shown here are virtually indistinguishable

These heads are point-water heads (the level to which water would rise in a standpipe). The model was computed using equivalent freshwater head, which accounts for density variations due to salinity and temperature.

These solutions are from layer 11 of the 10,000-ft grid with 11 layers.

Transient Head Solutions (T=366 days) for BZ with 1-Day Timesteps and Model-Computed Timesteps)

Final Groundwater Model Calibration Report

Figure B2-11

October 2010

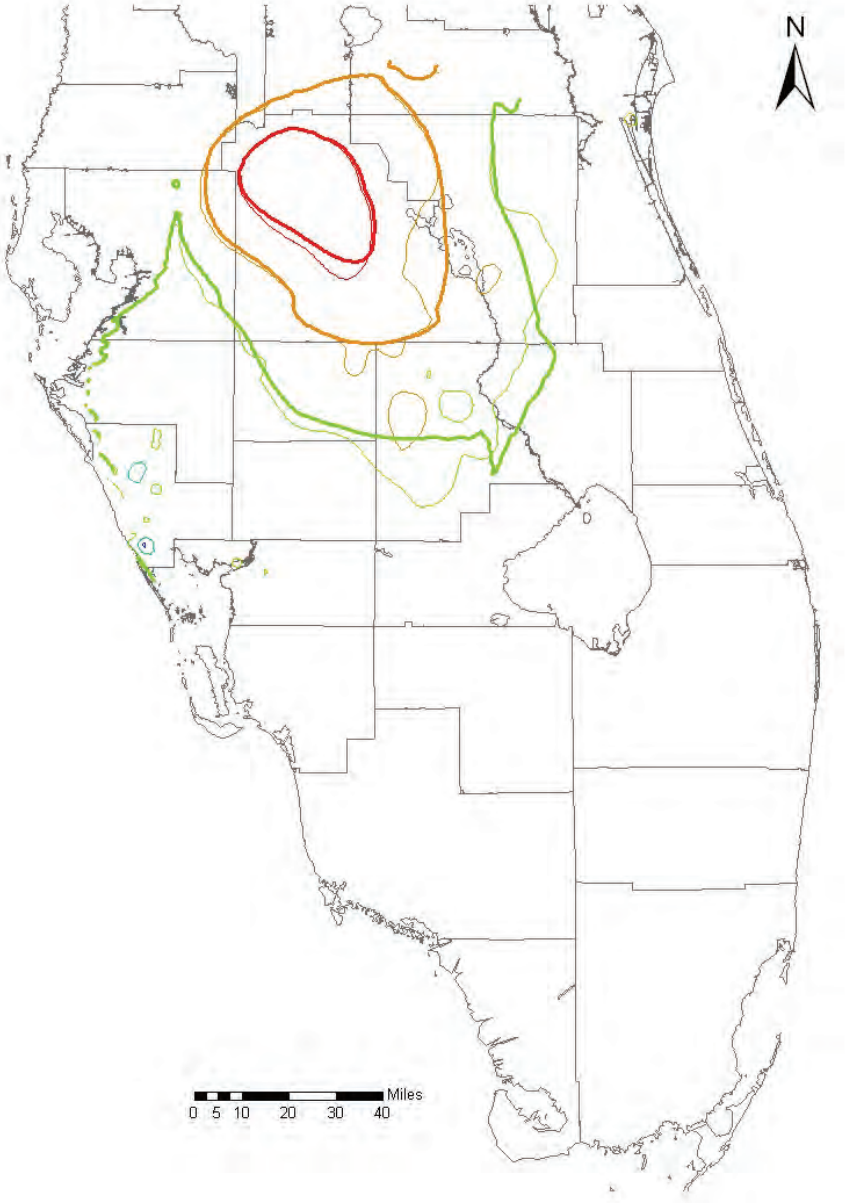

Legend:

- 1-Day Timesteps
- 5-Day Timesteps

Legend (Head):

- -75 ft
- -25 ft
- 25 ft
- 50 ft
- 75 ft

Notes:

These heads are point-water heads (the level to which water would rise in a standpipe). The model was computed using equivalent freshwater head, which accounts for density variations due to salinity and temperature.

These solutions are from layer 11 of the 10,000-ft grid with 11 layers.

Transient Head Solutions (T=366 days) for BZ with 1-Day Timesteps and 5-Day Timesteps)

Final Groundwater Model Calibration Report

Figure B2-12

October 2010

Appendix C: Selection of Boundary Conditions

Table of Contents

1.0 Introduction

The selection of appropriate boundary conditions is crucial to the creation of a groundwater model which is both credible and functional. The solutions from SEAWAT and WASH123D models are derived from partial differential governing equations which can only yield unique solutions if the model is provided with a set of boundary conditions.

Suitable boundary conditions must account for any interior stresses in the model. For example, if an extraction well is located near the boundary, its drawdown must be considered in the boundary condition. For a calibration model which is reproducing historic conditions, this is not difficult, provided the data is available. However, in a predictive model, accurately forecasting the drawdown can be difficult and is often the purpose of the model. Ideally, model boundaries coincide with static features that are not affected by internal stresses. Examples include no-flow boundaries occurring at groundwater divides or impermeable boundaries; and specified head boundaries occurring at large surface water features which are directly connected with the groundwater and provide a large source (or sink) of water. Often, these ideal boundaries are either non-existent, or they are too far from the point of interest to be of use. In their absence, modelers must settle for static, estimated boundary conditions at locations far enough from the point of interest to be unaffected by changes in the interior of the model.

Specified head boundary conditions force the model to honor the assigned head values at the boundary cells or nodes. To meet this requirement, the model will remove or add as much water as necessary. This type of boundary is best set at a large surface water body, which can take significant withdrawals or inputs without a substantial change in water level. If it is set at a more arbitrary location with the head based on estimated or measured head values at wells, the user must be aware that the model may be making unacceptable flux changes at that boundary.

Specified flux boundary conditions force the model to honor the assigned flux value – either in or out with no requirement for head. If the flux is too large in the negative direction (out of the model), the stability of the model might be compromised as the model attempts to withdraw water that is not readily available. If the flux is too large in the positive direction (into the model), unreasonably high heads may build up at the boundary.

A no-flow boundary is a specified flux boundary whose flux is set to zero. No water is allowed in or out at this boundary. These types of boundary conditions are often used to simulate groundwater divides, which often occur in unconfined aquifers at ridges where recharge provides an input of water from the surface. Since water must flow horizontally to one side of the ridge or the other, no horizontal flow is expected to cross the divide. No-flow boundaries may also be assigned at impermeable boundaries, which are often assumed to exist on the bottom of a model. When other options are not available, no-flow boundaries are sometimes aligned perpendicular to known groundwater head contours with the assumption that flow will be along the boundary and not across it. This is a dangerous practice since the contours may not be based on sufficient data; interior stresses or seasonal changes may change the shape of the contours; or different hydrogeologic layers may not all have contours with the same shape.

Similar boundary conditions for constituent concentration must be assigned at all boundaries when the model is to solve the groundwater transport equations. For specified head and specified flux boundaries, a concentration is assigned, which the model applies whenever the flux is inward. Fluxes out of the model take the concentration calculated by the model.

1.1 Overview of Head Boundary Conditions for the ASR Regional Model

The ASR regional model has been built to investigate the regional effects of the operation of numerous ASR wells located in the interior of southern Florida. Most of the proposed sites are located along the north and west shores of Lake Okeechobee in Okeechobee and Glades Counties. Additional sites are located in Palm Beach County. Early testing indicated that the proposed flow rates at the ASR sites may have far-reaching effects on the groundwater system throughout southern Florida. The model boundary was designed based on these tests. See Figure C1-1 for the boundary locations.

1.1.1 East Boundary

On the east, the boundary extends to the layer outcrops in the Atlantic Ocean for each hydrogeologic layer. Each layer is cut when it intersects the bathymetry data for the Atlantic Ocean floor and assigned as a specified head boundary. The head value for the boundary condition was based on the monthly mean sea level measured at two tide gauges – one at Virginia Key, near Miami, and the other at Naples, on the west coast of the Florida peninsula. There is some monthly variation in the ocean level, with slightly higher levels in the fall and lower levels in the spring and summer. However, the annual variation of monthly mean sea levels is about 0.5 feet, much smaller than the variation in nearly every other parameter of the model. Since all layers of the model outcrop in the Atlantic Ocean, the ocean is expected to be closely connected, hydraulically, to the groundwater conditions in the model. The ocean is such a large source of water that changes in the interior of the model can be assumed to have no effect on the ocean level. In other words, no amount of pumping in Florida is going to change the level of the Atlantic Ocean!

1.1.2 West, South and North Boundaries

Ideally, the west and south boundaries would also extend out to the locations of the outcrops for each layer in the Gulf of Mexico. However, these outcrops occur nearly 150 miles from the Florida coastline. Extension of the model boundary to these outcrops would add significantly to the model size, RAM requirements and computational time. This would also add a large area to the model which has not been extensively studied and for which there is no significant data regarding heads, water quality or aquifer characteristics. Instead, the west boundary follows the coastline from Tampa Bay down to the north boundary of Collier County. At this point, the model boundary cuts inland and follows a southeasterly line that passes through the Everglades about 10 to 30 miles from the coastline. This section of the Everglades was eliminated from the model because of a lack of data and because of significant surface water, which suggests that ASR pumping is not likely to affect groundwater heads in this area.

The north boundary passes through Brevard, Orange, Lake, Sumter, and Pasco Counties, then cuts down to follow the east coast of Tampa bay down to the Gulf of Mexico. This north boundary was selected to be beyond the area of groundwater recharge in Polk County and the area affected by the ASR wells.

The north, west and south boundaries are located to coincide with available data points. Heads assigned at these locations are based on measured values at wells located on or near the boundary. Although the heads at many of these locations have been measured frequently over long periods of time, the wells are seldom fully penetrating, so they may not represent the conditions in the entire aquifer. Also, heads for cells between well locations must be estimated. Generally, linear interpolations of the measured heads along the boundaries are used for simplicity. Initial testing of the expected effects of the ASR wells indicated that the north, west and south boundaries are well away from the area of impact for the wells. This was later verified with some sensitivity runs on the calibrated model as explained in Section 5.6 of the Groundwater Model Calibration Report.

1.1.3 Top and Bottom Boundaries

The top boundary of the model coincides with the ground surface where recharge of precipitation (less runoff and evapotranspiration) is a primary source of water to the model. In practice, a flux boundary condition is often applied to the surface of a groundwater model to simulate recharge. In these cases, the magnitude of the flux is calculated using a flow budget, subtracting such sinks as evapotranspiration and runoff from precipitation to determine the volume of water seeping through surface soils into the model. This type of calculation is often complicated by land use and soil type variations as well as the typical unavailability of sufficient data. Recharge often becomes a calibration parameter and is varied, along with hydrogeologic material properties such as conductivity and storage, until the model result matches measured aquifer conditions.

For this regional ASR model, the decision was made to assign a specified head to the surface of the model. Although this is an unusual practice, it saves the trouble and inaccuracies inherent in calculation of a recharge value. The use of a specified head at the surface is warranted since the ASR pumping is not expected to affect the heads in the Surficial Aquifer System (SAS), and because there is a wealth of SAS head data in many areas of the model. In the SEAWAT model, the SAS was included as the top layer of cells. In the WASH123D model, the SAS was not included as a model layer but the SAS heads were assigned to the top layer of model nodes. Each surface cell and node was assigned a specified head based on an interpolation of the available head data in the SAS for each month of the calibration and validation periods. See Section 4.0 of this appendix for details on the interpolation process. Since the head was specified in every cell, SEAWAT and WASH123D made no calculations in the top layer of cells or nodes. As explained above, this method allowed the models to calculate the necessary flux in order to honor the user-defined specified head boundary condition. The calculated flux was compared to available estimates on recharge in the model domain and found to be generally similar (See Section 4.1.4 in the main report).

The bottom of the model was set to coincide with the bottom of the Boulder Zone. The exact depth of the bottom of the Boulder Zone is generally unknown and was estimated. The bottom boundary was assumed to be a no-flow boundary. Since the conductivity of the Boulder Zone is so much higher than

the conductivity of the Sub-Floridan confining unit, the majority of the flow in this layer would be horizontal or upward and little, if any, water would flow downward. Thus, it is probably valid to assume no flow through the bottom of the model.

1.2 Equivalent freshwater heads

Because of the close hydraulic relationship between the aquifers in South Florida and the Atlantic Ocean and Gulf of Mexico, there are significant variations in the salinity of the groundwater. Deep aquifers are almost entirely saline, with the exception of some areas in the north of the model. Surface aquifers are fed more by rainfall, resulting in generally low salinity. These salinity variations can have a marked effect on density and flow. This section describes how these variations were incorporated into the model.

TDS was used as a proxy for salinity in the ASR regional model and the two terms are used interchangeably in this report. TDS data was normalized by dividing each measured value by 35,000 mg/L, a commonly accepted TDS value for seawater. This results in a unitless value of approximately 1.0 for seawater and 0.0 for freshwater.

Comments from reviewers early in the modeling process indicated that temperature variations might also play a significant role in the density and flow conditions in the model. Deeper aquifers are generally warmer, likely due to geothermal effects. Temperature does not have as great an effect on water density as salinity, but it is included in the model and treated as another constituent concentration.

Both SEAWAT and WASH123D can solve the flow equations with density dependence, calculating flow and transport simultaneously. Both models require the user to enter head boundary conditions and initial conditions as observed head based on local density, or the water level measured in a well. The models then use the temperature and salinity to calculate the *equivalent freshwater head*, which takes into account both TDS and temperature to determine the potential energy at a given location. The flow equations are solved based on equivalent freshwater heads and then the solutions are converted back to observed heads for viewing and analysis.

Because model results are reported as observed heads, the solutions sometimes appear to show unusual flow patterns. When there are significant changes in salinity, flow may appear to be moving "uphill." Since the equivalent freshwater head is actually the potential energy of the water at a given point, fluid flow would be expected to occur from locations of high equivalent freshwater head to locations of lower equivalent freshwater head. If the salinity is markedly different between two points, high observed heads may not correspond to high equivalent freshwater heads.

Equivalent freshwater head is calculated by first calculating the observed density, using Equation C1:

$$\rho_{obs} = \rho_{fw} + m_{tds}\left(TDS - TDS_{ref}\right) + m_{tmp}\left(TMP - TMP_{ref}\right) \qquad \text{Equation C1}$$

where:

ρ_{obs} = Observed density
ρ_{fw} = Density of water at the reference TDS and temperature
m_{tds} = Slope of the assumed linear relationship between density and TDS

TDS = Total dissolved solids in the water (proxy for salinity) normalized by dividing by 35,000 mg/L
TDS_{ref} = Reference TDS
m_{tmp} = Slope of the assumed linear relationship between density and temperature
TMP = Temperature in the water (°C)
TMP_{ref} = Reference temperature

Once the observed density has been calculated, the equivalent freshwater head can be directly calculated by using Equation C2:

$$EFH = \left(\frac{\rho_{obs}}{\rho_{fw}}\right)h_{obs} - \left(\frac{\rho_{obs} - \rho_{fw}}{\rho_{fw}}\right)Z \qquad \text{Equation C2}$$

where:
EFH = Equivalent freshwater head
ρ_{obs} = Observed density (calculated using Equation C1)
ρ_{fw} = Density of water at the reference TDS and temperature
h_{obs} = Observed head
Z = Elevation of point (using NGVD29 as a datum)

The following physical constants were used in the models:

Table C1: Physical constants used for density dependent flow equations

ρ_{fw}	62.25 lb/ft^3
m_{tds}	1.92 lb/ft^3
TDS_{ref}	0.0
m_{tmp}	-0.0166 lb/ft^3/°C
TMP_{ref}	25 °C

Some analysis of Equations C1 and C2 can be instructive in understanding the great effect salinity can have on the pressure and, therefore, the potential energy of the groundwater. The subsurface water temperatures within the model domain generally vary from about 20°C to 40°C, with some small areas having temperatures outside that range. With the reference temperature at 25°C and the temperature/density slope so low, temperature variations can only contribute to a drop in density of about 0.25 lb/ft^3 from freshwater density or an increase in density of less than 0.1 lb/ft^3. Normalized TDS levels in the groundwater vary across the spectrum from 0 (freshwater) to slightly above 1 (seawater). With a TDS/density slope of 1.92, it is clear that salinity variations can contribute to a change in density of nearly 2 lb/ft^3 from the density of freshwater. These variations in both temperature and TDS result in a range of possible observed density from 62.0 lb/ft^3, just below freshwater density (62.25 lb/ft^3), to about 64.25 lb/ft^3.

At maximum, the first term in Equation C2 can result in a value about 103% of the observed head. The greater difference between equivalent freshwater head and observed head is obtained from the second term in Equation C2. Where the elevation is not much below zero, the second term has little effect, but

at significant depths where *Z* is greatly negative, the effect on the equivalent freshwater head can be startling. The Boulder Zone can reach elevations of -3,500 ft, making the equivalent freshwater head approximately 115 feet higher than the observed head if the TDS is high and the temperature is low!

Most of the analysis of the available data described in the following sections was based on the equivalent freshwater heads calculated from the available data. If measured TDS data was available for the well in question, that value was used to calculate equivalent freshwater head. If no data point was available at that location, the interpolated starting condition for the cell containing the point in question was used to estimate the TDS. For temperature, the interpolated starting condition was always used. Section 3.4 describes the development of initial conditions. Depths used in the calculations were the middle of the open interval for the well.

2.0 Aquifer Boundary Heads

Specified head boundary conditions were assigned to all the cells or nodes around the edge of the model domain in each aquifer layer. Sea level heads were applied to the eastern boundary at the layer outcrop location. Layers 2 and 3 were assigned aquifer heads on the western side of the model within the area designated as IA (Intermediate Aquifer) by Randazzo and Jones (1997). No boundary condition (no-flow) was defined outside the IA area. Other aquifers were assigned heads on all sides of the model. Confining units were assigned sea level heads on the east, but were left as no-flow boundaries for the north, west and south sides of the model.

Early iterations of this regional ASR model followed conventional modeling practice in the application of boundary conditions. For the side boundaries, this process involved gathering available head data at the boundary and linearly interpolating the heads for all cells between the data points. The team found that some of these methods were not applicable to the ASR regional model either because of lack of data, special conditions or the density dependent calculations planned. Here, we present a short explanation of some of the shortcomings of linear interpolation of aquifer boundary heads along the edges of the model.

- Interpolation of observed head data near the edges of the model domain in an aquifer occasionally resulted in sudden, large head variations, which are troublesome for the model's solver routine. This is generally a result of the simplification of the geology in the model. For example, the model includes a hydrogeologic unit referred to as the Upper Floridan aquifer. Many researchers divide this aquifer into the Suwannee and Ocala aquifers in some areas of the domain. Sometimes a Suwanee well and an Ocala well are placed near each other and have significantly different observed heads or TDS measurements, but in the model, both are considered part of the Upper Floridan aquifer. Simple linear interpolation of the heads at these wells can lead to steep head slopes like those shown in Figure C2-1a. Since the model aims to reproduce field conditions on a regional scale, some averaging of nearby well heads often helps smooth out these boundary conditions.
- Sparse data, especially in the lower aquifers, led to different flow conditions in deeper aquifers than in shallow aquifers. For example, both the Upper Floridan aquifer and the Avon Park

Permeable Zone of the Upper Floridan aquifer show high heads in Polk County compared to surrounding areas, due to extensive infiltration of precipitation. This high head is also shown in the wells along the model boundary, which makes it possible for the model to reproduce field conditions. There are very few monitoring wells in the Lower Floridan aquifer and none along the model boundary in this recharge area. A simple linear interpolation of existing data for use as a boundary condition would not include a high water table at this point (Figure C2-1b). However, TDS data (Section 3.4.1) shows very low salinity in the deep aquifers of Polk County, indicating that the source of the groundwater is recharge and the mound in the water table probably extends to the deeper aquifers. This problem can be remedied by adding synthetic points to the boundary that help shape the boundary conditions according to knowledge of the site.

- Combinations of head distributions, TDS distributions and temperature distributions may result in equivalent freshwater head distributions that contain sudden changes or unexpected flow conditions, which pose a challenge to the model solver (Figure C2-2). This problem can be remedied by performing the interpolation on the equivalent freshwater heads and then using site conditions to back out the observed head for assignment as boundary conditions.

The following subsections describe the process, which was developed to address the concerns listed above, and was used to assign boundary conditions to the edges of the layers.

2.1 Using an Azimuth Angle to Plot Data

A common issue with 3-dimensional modeling is the difficulty in viewing, displaying and analyzing 3-D data and results using a 2-D sheet of paper or computer screen. Generally, model images are displayed by viewing contours of a single layer or cross-section cut through the 3-D model. For boundary conditions, the cells or nodes can be colored by the assigned head value and viewed one layer at a time, but this prevents the user from observing subtle changes and slopes. It also makes it difficult to compare heads in different layers.

In reality, the selection of boundary conditions for the side (vertical) boundaries of this model was a 1-dimensional interpolation process of assigning head values to points along a line, which is arranged in a closed loop around the model. To make the analysis of the boundary conditions easier, the line around the model was stretched out along the x-axis of a data plot, which is termed an azimuth plot in this report. The points were arranged by calculating the east-based azimuth between the cell or node in question and a center point. Each cell or node, then, is assigned an angle between 0° and 360°, where 0° (and 360°) correspond to points directly east of the center point; 90° corresponds to a point directly north of the center point, with the angle increasing in a counter-clockwise manner around the model. Head, TDS, temperature, elevation and equivalent freshwater head for boundary cells can then be plotted on the y-axis. Figure C2-3 shows the location of the center point and indicates the angle measurements at various locations around the model. The center point was selected to provide a unique angle value for each cell by preventing any boundary cells from being collinear or nearly collinear with another boundary cell and the center point.

For clarity, Figure C2-4 shows an empty azimuth plot. These plots were used extensively in creating the boundary conditions for the regional ASR model. It is important that the reader fully understand these plots before continuing to read other sections of this appendix. Figure C2-4 includes a small inset map of the Florida Peninsula with a few key cities labeled. These same cities are labeled on the azimuth figure with vertical lines. Beginning from the left of the plot, points represent locations along the eastern (Atlantic) coast of Florida beginning just south of Vero Beach and continuing north toward Cocoa Beach. From 90° to about 120°, the points on the plot represent locations between Cocoa and Orlando drawn from east to west. Points on the plot continue counter-clockwise around the model, passing down the western coast, through the Everglades and then up through Miami, West Palm Beach and Port St. Lucie and back to where it started. The points shown at 360° should have the same values as the points shown at 0° for any given data set as they represent the same location on the map.

All of the azimuth plots in this appendix will be laid out in this manner with the inset map and the vertical city labels on the plot.

This type of display allows us to clearly see trends along the boundary of the model and we can compare heads in different layers simultaneously. It also allows us to more easily compare estimated values with measured values and recognize statistical outliers.

2.2 Selection of Data Points

Most of the data points used to construct the specified head boundary conditions for each aquifer were selected from the database of well data provided by SAJ. The database included a table containing information on the horizontal location of the well and the open interval of each well. This table was used with the interpolated geologic data to determine which of the hydrogeologic layers were expected to provide water to the well. A second table in the database presented water level measurements for each well during the periods of interest: October 2003 through December 2004 (calibration period) and August 1993 through July 1994 (validation period). Data for a few additional wells (not provided in the SAJ database) was obtained by NAP using databases such as DBHYDRO (SFWMD), WMIS (SWFWMD), the SJRWMD Hydrologic Data and the USGS NWISWeb Water Data, all of which are available online.

The wells listed in the database were separated into groups based on the hydrogeologic unit represented, using a database query. To be categorized with a given hydrogeologic unit, the query required that at least 90% of the open length be within that unit. Wells were generally assumed to be on the boundary of the model if they were within 10,000 feet of the boundary (using a GIS selection by location). Since the largest model cells (elements) in the SEAWAT (WASH123D) models are 10,000 feet wide, this corresponds to about 1 cell width from the boundary. On occasion, when data was sparse, additional wells were added to the group even if less than 90% of their screen was in the specified unit or if they were located more than 10,000 feet from the boundary.

Once all of the boundary wells had been compiled, average monthly heads were calculated and the available data was examined to determine which wells had sufficient data for the two time periods of interest. It was important that the head distributions in the boundary conditions for different months be similar. The deleterious effect of missing data is illustrated in Figure C2-5. Here, the available data

for April and May 2004 at three monitoring wells is shown. Since April and May generally have similar heads, the 30-foot difference at ROMP 101 AVPK is unexpected and caused only by the lack of data in April at this well. This problem was prevented in the boundary conditions by ensuring that data was provided for each well in every month of the modeling periods. If a certain well was missing only a few months of data, statistical comparisons could be used to estimate the heads in months with no available data (see Section 2.3 below). If the well was missing data for numerous months, estimating the missing data became a risky process. To prevent the introduction of this level of uncertainty, wells with insufficient data were removed from the group and not used for developing boundary conditions for the model. This determination was generally made if there were less than about 5 unique months of data available in the calibration time periods. Additional wells were removed if they were clearly impacted by local pumping or if other local conditions (such as TDS) made them unsuitable for use in a regional model. Table C2 lists all of the wells extracted from the database and provides explanations for those that were removed.

Modeling the IAS (Intermediate Aquifer System) presented unique challenges for this regional scale model. In reality, the IAS, as its name suggests, is actually a system of poorly defined aquifers interspersed with less conductive materials. Because of the lack of good conceptual data for this system, this ASR regional model lumps the entire system into a single layer of the model. If the data is also lumped into a single layer, the sudden, erratic changes in head cause difficulties for the model solver. Figure C2-6 is an azimuth plot showing the average monthly head for the months of concern (calibration and validation periods only) for the IAS layer. It clearly shows that there are wells located very near each other, which have starkly different heads. The head differences are most likely a result of adjacent wells being open in different flow zones and do not represent the system on a regional scale. The sudden head changes caused by strict linear interpolation of the available data can be difficult for the model to resolve. However, a comparison of the monitoring data and the screened elevations for each well (Figure C2-7) indicates the presence of several different conductive units with unique hydraulic signatures. Consider, for example, the data for wells with Model ID 131440 and 131449. (Model IDs were assigned to each well in the SAJ database.) These wells are located only 1,000 feet apart, but the head at 131440 is consistently 5 to 6 feet higher than at 131449, indicating that they might be tapping different units. This theory can be solidified by an analysis of their open hole intervals, which shows that at 131440, the open hole is more than 200 feet deeper than the open hole at 131449. The well names do not always help with this type of analysis, but in this case, knowing that well 131440 is called ROMP TR 5-1 TMPA and well 131449 is called ROMP TR 5-1 TAMIAMI makes us confident that these two wells belong in separate flow units.

The same process was followed for the rest of the IAS well data to determine if other wells could be separated in this manner. The final division of the wells is indicated by a set of red lines on Figure C2-8. Generally, wells open at higher elevations have lower average monthly heads. The lines on the figure separate the two groups. Clearly, the separation is not perfect. Wells 101348 (City of Sarasota 27th Street Well) and 101344 (Whitaker Bay Well near Sarasota, FL) have rather large screens that span both sub-sections of the aquifer. They are included with the upper group because their head data is more consistent with that group. Conversely, Well 100700 (L-1635) has a head distribution that matches

more closely the upper group of wells, but its screen is so deep, that it remains with the lower group. This causes an area of rather steep slope on the boundary of the model, but since no information was available to eliminate the data from that well and since the open hole is so deep, it was left with the deep well group. Figure C2-9 shows the two separate groups of wells on an azimuth plot. When compared to Figure C2-6, it shows an improvement in the smoothness of the data. The upper section was assigned to Layer 2 of the SEAWAT model the second layer of nodes in the WASH123D model. The lower section was assigned to Layer 3 of the SEAWAT model and the third and fourth layers of nodes in the WASH123D model. It is likely that the models will more easily come to a solution and that the results will be more accurate because of the removal of a simplification that was not warranted by the data.

This comparison of head data and open hole elevations was also critical in determining where nearby wells could be merged for simplification of the boundary condition. Wells were merged for one of two reasons. First, there were often two wells near each other with very similar vertical locations and head data. In some cases they were determined to be duplicates in the SAJ database, but other times, they were simply similar wells in close proximity. Combining the two wells by averaging their data was an easy way to fill in missing data in one well and resulted in simplification of the boundary conditions. The second reason for combining two nearby wells was to average out starkly different head conditions in the same model layer. The actual geology of every layer in the model is more complicated than the model and can often contain sub-aquifers or small areas with different hydrogeologic conditions. Averaging the heads is a good way to ensure that the model accurately represents regional conditions, but does not require the modeler to make a decision as to which of the different heads is more "accurate." (Figure C2-1a.) Table C2 indicates which wells were combined and presents criteria for each decision.

In addition to the monitoring well points around the boundary of the model, two additional points were added to the data set to enforce the ocean boundary on the east boundary of the model. These points were added to the outcrop location for each layer, one point at the northeast corner of the model where the outcrop line intersects the north model boundary, and one point at the southeast corner of the model where the outcrop line intersects the south model boundary. Because the heads are interpolated linearly along a line circumscribing the model, this will ensure that each cell at the ocean boundary is given the head obtained from tide gauge data.

2.3 Filling in Missing Data

Table C2 also indicates the availability of data for each well in the database, which was selected for use as a boundary well. While the water levels at many wells are regularly measured, others have extremely sparse data. As described above, wells with data available for less than about 5 unique months of the periods of interest (calibration and validation periods), were removed early in the process. For the remaining wells, missing data was estimated using one of two methods described in this section, to ensure that the boundary conditions for all periods of interest had similar head characteristics and incorporated seasonal changes. All estimates of missing data were made after the observed head had been converted to equivalent freshwater head as described above and presented in Equations C1 and

C2. Use of the equivalent freshwater head ensures that the TDS and temperature data are taken into account (Figure C2-2).

2.3.1 Using Seasonal Trends to Estimate Heads

The first method was used for filling in missing data for a given month, when the database provided data for same month in a different year. We will use a UF well, ROMP 90 OCAL, as an example to illustrate the method for filling in the missing data. This well is located in Dade City, in the county of Pasco. The SAJ database contained monthly head data from September 1993 through July 1994 and daily head data from October 2003 through December 2004. This is consistent with the SWFWMD website, which indicates a monthly monitoring program beginning in 1994 and continued until daily monitoring became available beginning December 1, 1997. The daily head data for each month in the calibration period (October 2003 – December 2004) was averaged to obtain a single average head value for each month of concern. All months of the calibration and validation periods are accounted for, except August 1993, when no water level value is available for this well.

To ensure consistency between the months of concern, the August 1993 data point was estimated by calculating a linear correlation between all other boundary wells with August 1993 data and August 2004 data. There are a total of 39 such wells. Using the Excel SLOPE and INTERCEPT functions, the following correlations were obtained:

$$WL_{93} = 0.977WL_{04} - 1.073$$ Equation C3

$$WL_{04} = 1.015WL_{93} + 1.377$$ Equation C4

where:

WL_{93} = Water level measured in August 1993

WL_{04} = Water level measured in August 2004

Correlation coefficients (r^2) values for both equations were 0.992, well above the minimum level for statistical significance. The two correlations are not exactly identical because Excel uses a vertical offset least squares linear regression instead of a perpendicular offset to determine the best-fit trendline. This causes slight differences when x and y are reversed. To account for this difference, which is more unsettling than inaccurate, the two equations were solved for WL_{93} and the slopes and intercepts were averaged to obtain a single equation that can be used to estimate the August 1993 head value for any well which has August 2004 data available. This equation is listed below as Equation 5:

$$WL_{93} = 0.981WL_{04} - 1.215$$ Equation C5

where:

WL_{93} = Water level measured in August 1993

WL_{04} = Water level measured in August 2004

Since the August 2004 average monthly head at ROMP 90 OCAL was 70.9 ft, the August 1993 average monthly head at this well can be estimated to be 68.4 ft.

The months of October, November and December appear three times in the periods of interest. When data was available for two of the years, the above process was followed once for each available year, resulting in two estimates for the missing month. These two estimates were then averaged to obtain a single value for use in the model. When data was available for only one of the years, it was used as the basis for estimating heads for both missing years following the procedure outlined here.

This process was followed for every missing data point with available data in the same month of a different year. The correlation was always very good, with r^2 values normally above 0.990. The only exception to this rule was for the comparison between October 1993 and October 2004 data sets when the r^2 value was a substantial 0.988.

The r^2 value is not always the best way to quantify the quality of a regression analysis. Additional investigation of the quality of the regression was done by using the regression equation (Equation C5) to calculate the heads for wells which had measurements for that month. For example, in the August 1993/August 2004 data sets, there were 40 wells with data for both months. (These were the 40 wells used to compute a regression equation.) For each of these wells, the 1993 head was calculated from the 2004 head using Equation C5. This calculated head was compared to the observed head for that month to obtain a residual between calculated and observed heads. Because of the nature of the least squares analysis with a vertical offset, the average of these residuals was 0.0. But when the absolute value of the residuals was averaged, the result was 2.2 feet. This means that, on average, this method of estimating the missing data results in a head that is erroneous by just more than 2 feet. The root mean square (RMS) is calculated by squaring the residuals, averaging the results and then taking the square root. This method gives greater weight to large residuals. For the August 1993/ August 2004 regression results, the RMS was 2.5 feet. Both of these statistics are well within the calibration error expected in a regional model of this scale. All of the other pairs of months show similar regression quality. The worst correlations are between October 1993 and October 2004 and September 1993 and September 2004, where the mean absolute error was 2.2 and the RMS was 2.8.

2.3.2 Estimating Heads Using Similar Wells

The process for estimating head values for wells with a few missing months of data is described in section 2.3.1 and was used successfully to fill in nearly all the missing data for the boundary wells. Seven of the wells, however, were missing a given month in every year of the data set and a second method was developed to handle them. As before, we will illustrate the process by using an example, FMB-MZL. This is an APPZ well located in Lee County. The SAJ database provides daily water level measurements at this well from 19 May 2004 through 8 December 2004. From this data, we can average the measurements in each month and obtain average monthly heads for May through December 2004. Using the process described in section 2.3.1, the heads for the missing months of October through December of 2004 and August through December of 1993 can be easily estimated. The remaining months with no available data, then, are January through April of 1994 and the same period in 2004.

A linear regression was used as before, but this time, the regression correlated the monthly average data from other wells, which have a full data set. It would have been appropriate to select a few nearby

wells in the same aquifer for the correlation, but often there are no wells particularly close and the open interval is seldom the same. So, a comparison was made between the well in question and all other boundary wells in the data set. The five wells with the closest correlation (measured using the r^2 value) were used to estimate the missing data points, even if these wells were located far away or in different aquifers. In the case of FMB-MZL, the correlation coefficients for all the boundary wells varied from 0.001 (the average of ROMP TR 3-3 SWNN and ROMP TR 3-3 OCAL) to 0.888 (IWA-MZL). As would be expected, the best correlation is obtained from a nearby well in the same unit: IWA-MZL and FMB MZL are located about 11 miles apart and their screens are only about 50 feet different in elevation. The five wells with the best correlations were compiled for use in filling in the missing data. For FMB-MZL, the five best correlated wells are:

- IWA-MZL,
- USGS Cocoa D Well near Narcoossee, FL
- USGS Palm Lake Drive Well near Windermere, FL,
- ROMP 85 AVPK, and
- BICY-MZ1

These wells are not all located near FMB-MZL, nor are they all in the APPZ layer, but statistically, they have the best correlated data sets. Figure C2-10 shows these five data sets along with the available data for FMB-MZL. The hydrogeologic layer for each well is indicated in the legend and an inset map shows their locations. The five best-correlated data sets were averaged and then, the correlation between the average and FMB-MZL was used to construct a linear relationship to fill in the missing data. The linear equation is shown in Equation C6 below:

$$WL_{FMB-MZL} = 1.366 WL_{avg} + 37.366 \qquad \text{Equation C6}$$

where:

$WL_{FMB\text{-}MZL}$ = Water level measured at FMB-MZL for a given month

WL_{avg} = Average of the water levels measured at the five most statistically correlated boundary wells for the same month

Equation C6 fit the available data with an r^2 correlation value of 0.889. The estimates for the missing data are added to Figure C2-11. The correlation coefficients (r^2) for the other wells whose data sets were completed using this method varied from 0.46 to 0.93.

As with the regression presented in Section 2.3.1, the residual between measured and calculated heads was calculated for each month and then the mean absolute error and RMS were calculated. For the regression on the data at FMB-MZL, the mean absolute error was 0.3 feet and the RMS was 0.4 feet. The worst RMS for the wells correlated in this way was 1.7, found for the combination of two Boulder Zone wells: OR0613 and the USGS Cocoa C (Zone 1) Well near Bithlo, FL.

Although the r^2 values seem to indicate that these estimates are less trustworthy than those determined by comparing months across years, the residual statistics show that these errors are clearly within the expected calibration error.

2.4 Interpolation

Once the data sets had been cleaned by removing sparse data, removing data with local effects, combining wells located near each other and filling in missing data, the azimuth plots were used to analyze the available data. The interpolation process described here was repeated for each month of the calibration and validation periods.

Figure C2-12 shows the equivalent freshwater heads for October 2003. All data points are connected with straight lines. Where the head is marked with an open circle symbol, there is at least one head measurement available at that location for the month of October 2003. Wherever there is a change of slope in the connecting line without a circle symbol, the head value at that location has been estimated using one of the two methods described in the previous section. Open circles that appear offset from the line indicate that heads at two or more wells in the same area were averaged. Several observations of the data can be drawn from Figure C2-12.

- The highest heads in the Upper Floridan and Avon Park Permeable Zone aquifers are found in the area between Orlando and Tampa. This is known to be the main recharge area for the region and high heads in this area are not surprising. (Low salinities in this area in the Lower Floridan and Boulder Zone indicate that the recharge is likely affecting the deeper aquifers. There are no head data points in this area in the deep aquifers.)

- Between Tampa and Venice, where the boundary follows the coast line of the Gulf of Mexico, the equivalent freshwater heads are low, often lower than the ocean level, indicating flow from the ocean into the model domain in this area.

- Equivalent freshwater heads increase somewhat in the area between Venice and Everglades National Park. This increase is probably caused by movement of the boundary inland, where salinity may be lower and observed heads may be higher.

- From about 100° (just east of Orlando) until about 160° (just south of Tampa), the IAS, UF, APPZ, and LF have very similar equivalent freshwater heads, indicating very little vertical movement and close hydraulic connections between the different layers.

- Along all coastlines, there is a great difference between the equivalent freshwater heads in the different layers. Generally, the highest equivalent freshwater heads are found in the deepest layers, indicating upward movement.

- The points at 50° (east of Cocoa) and 285°(east of Miami) are the locations where tide gauge data was used to set the boundary conditions. On the model, all areas between Cocoa and Miami will be assigned this same observed head value, although variations in salinity, temperature and depth can alter the equivalent freshwater head. The slope of the equivalent

freshwater head on Figure C2-12 towards these points can indicate the direction of water exchange between the ocean and the inland groundwater. For the Boulder Zone and the Lower Floridan Aquifer, these lines slope inland, indicating movement of ocean water into the main section of the model. For the Upper Floridan and Avon Park Permeable Zone layers, these slopes are directed seaward, indicating movement from the peninsular groundwater outward to the ocean. This observation combined with the previous one supports the idea that ocean water enters through the deeper layers, flows upward and then back out towards the ocean.

An examination of these plots also shows that a linear interpolation between the available data points is not sufficient. This is most apparent in the area between Orlando and Tampa. Both the Upper Floridan and Avon Park Permeable Zone aquifers show a distinct increase in head of over 200% around Orlando followed by a precipitous drop in head towards Tampa. The head in the Lower Floridan appears to be following the same trend, but then cuts across the other lines to meet its next data point, near Naples, skipping the high heads in Polk County. The Boulder Zone data follows a similar trend, but with no data points available between Orlando and Miami. It is believed that these anomalies are the result of using a linear interpolation scheme on excessively sparse data. If wells were drilled in the deeper layers between Orlando and Naples, their heads would be expected to more closely follow the trends exhibited in the upper layers. The low salinity found in the Lower Floridan and Boulder Zone indicate that precipitation which recharges the upper aquifers also reaches the deeper layers of the system.

A number of synthetic points were added to the data sets to form the head signatures to the expected shape. Figure C2-13 shows the October 2003 azimuth plot with these synthetic points indicated with small x's. The majority of the synthetic points are added to the Boulder Zone and Lower Floridan lines, and result in a peak in equivalent freshwater heads between Orlando and Tampa and a low point between Tampa and Venice. The upward gradient has been enforced in most places outside the Polk County recharge zone. A few minor changes have been made by adding points to the Avon Park Permeable Zone or Upper Floridan layers.

Since SEAWAT and WASH123D require that boundary conditions be entered as observed head values, not equivalent freshwater heads, the points on Figure C2-13 had to be converted to observed head using forms of Equations C1 and C2. The first step in a SEAWAT model, though, is to convert user-supplied observed heads to equivalent freshwater heads. In this conversion, the user-supplied TDS and temperature initial conditions are used. In order to ensure that the model calculated equivalent freshwater head matches what was developed in Figure C2-13, the conversion back to observed head needed to be done using the TDS and temperature extracted from the initial conditions, not the actual measured values, when available. In most cases, these two values were similar, but on a few occasions, the TDS measured at a well was determined to represent a local phenomena and the measurement was not used in the development of the initial conditions data set. (Section 3.4.1 and 3.4.2)

The resulting observed heads were used to interpolate the specified head boundary condition to the grid. The azimuth angle was used as the basis for the interpolation by calculating the angle from the center point to the center of each cell on the boundary. Heads at cells between each pair of neighboring

boundary data points (and synthetic data points) were linearly interpolated using the following equation:

$$h_{cell} = h_{obs1} - \frac{(\theta_{obs1} - \theta_{cell})(h_{obs1} - h_{obs2})}{(\theta_{obs1} - \theta_{obs2})}$$ Equation C7

where:

h_{cell}	=	The observed head to be assigned to the cell in question
θ_{cell}	=	The azimuth angle of the center of the cell in question
h_{obs1}, h_{obs2}	=	Observed head at two data points (or synthetic data points), which bound the group of cells to be interpolated
θ_{obs1}, θ_{obs2}	=	Azimuth angles of two data points (or synthetic data points), which bound the group of cells to be interpolated

2.5 Additional Data Tweaking

Although SEAWAT and WASH123D require the modeler to provide boundary conditions as observed heads, the model immediately converts the observed heads to equivalent freshwater heads using the user-provided TDS and temperature initial conditions. The model calculations are then made using the equivalent freshwater heads.

As a final check of the boundary conditions, the cells along the boundary were extracted from the grid and the observed head, TDS, temperature and elevation of each of these boundary cells was tabulated. Microsoft Access was used to calculate the equivalent freshwater head at each computational cell or node just as SEAWAT and WASH123D would do at the start of the model run (see Equations C1 and C2). Figures C2-14 through C2-19 show the observed head assigned as a boundary condition and the equivalent freshwater head calculated at each boundary cell. As with other figures in this report, the cells are plotted using their azimuth angle calculated from the same center point. These equivalent freshwater heads are the boundary conditions seen by the model.

Some locations on these plots seem to have “wavy” equivalent freshwater head changes. An example of this phenomenon is the Upper Floridan Aquifer heads (Figure C2-16) between the angles of 240 and 270 degrees. Here, the applied head boundary condition is linear (with a slope change at the data point), but the calculated equivalent freshwater head is “wavy.” This unusual shape to the plot is caused by the different methods of interpolating each of the data sets that affect the final equivalent freshwater head and should not cause a problem for the model since the variations are very small. The TDS, temperature and elevation data sets are interpolated in 2 dimensions using a linear or natural neighbor scheme. Contours may be perpendicular to the boundary, but more often, they touch the boundary at some angle or may even be approximately parallel to the boundary. Conversely, the head assigned to the boundary is interpolated in 1 dimension along a line circumscribing the model. This means that when all the data sets are combined, the contours may be peculiar.

An example of this issue is shown in Figures C2-20 and C2-21. These two figures show the pertinent data sets for calculating the equivalent freshwater heads for a set of 13 boundary cells located near the

southwest coast of Florida, just north of Everglades National Park. Figure C2-20a shows the temperature distribution as a plan view contour plot and as subset of an azimuth plot. Here, the contours on the right half of the section intersect the boundary at nearly a right angle. This results in a relatively smooth azimuth plot. In Figure C2-20b, the TDS distribution is displayed in the same manner. These contours are nearly parallel to the boundary and so sharp declines in the TDS for each cell occur when the boundary moves to the next column of the grid. The layer elevation is presented in Figure C2-20c. These contours are much closer to parallel with the boundary and so the jump in elevation that occurs as the boundary moves to the next column is much more pronounced than with the TDS plot. Figure C2-21a shows the assigned observed heads for these boundary cells. Notice that the lines in the azimuth plot are perfectly straight due to the linear interpolation of the cells by the azimuth angle. The slope change at 237° is caused by a synthetic well point which was added in an effort to smooth out the boundary condition. (This process is explained in Section 2.5.) Figure C2-21b presents the calculated equivalent freshwater head in each cell (See Equations C1 and C2). Because of the sudden changes in TDS and especially elevation which occur when the boundary moves to the next column, the azimuth plot appears to be oscillating. A few rough contours have been added to the plan view image for Figure C2-21b to show that the apparent oscillation is a product only of the azimuth plotting method. Therefore, these unusual line shapes with small oscillations in head can be disregarded in the examination of these equivalent freshwater head azimuth plots.

For each of the Floridan aquifers (Figures C2-16 through C2-18), there are multiple lines indicating the calculated equivalent freshwater heads. Boundary heads, initial TDS and initial temperature are all constant across the layers of any given aquifer. So, for the Upper Floridan Aquifer, each cell along the boundary in layer 5 has exactly the same specified head, initial TDS and initial temperature as the same cell in layer 6, 7, 8, 9 and 10. The only difference between the cells is the elevation of the centroid, which is used in the calculation of the equivalent freshwater head (See Equation C1 and C2). Thus, where the lines are further spread apart on the equivalent freshwater heads plots, the cells are thicker, leading to more divergent elevations and, therefore, equivalent freshwater heads. Note also, that if the observed density is close to freshwater density (low salinity and temperature close to 25°), the elevation differences become less important. This is why the lines always plot on top of each other in the areas between Orlando and Tampa. Salinity is low and so the observed head is nearly equal to the equivalent freshwater head.

Figure C2-22 shows the equivalent freshwater heads calculated for all aquifer layers of the model on one plot. They are overlain with x's showing the calculated equivalent freshwater head at each monitoring well used in the interpolation. Occasionally, the x symbol does not fall close to the line. This occurs either because the TDS of the data point differs from the initial condition TDS or because the elevation of the center of the open section of the well differs from the center of the cell.

Figure C2-22 also highlights an additional problem with this method of assigning the boundary heads. In some cases, there are unusual or unexpected shapes to the lines, beyond what can be explained by the interpolation issues ("wavy" sections) discussed above. These variations are generally the result of assuming that all the pertinent data sets (TDS, temperature and elevation) are linear within the zones of

linear assigned heads. Some of these problems, such as the dropping of the Avon Park Permeable Zone EFH below the Upper Floridan EFH at around 60° can be resolved.

Additional break points were added where nonlinearities in the TDS or elevation data sets caused unusual results in the equivalent freshwater heads. (Non-linearities in temperature rarely caused these types of anomalies.) At each breakpoint, a value for equivalent freshwater head was selected to smooth the plot. Then, the assigned head was back-calculated using the TDS, temperature and elevation at that location. Figures C2-23 through C2-26 show the effect of these breakpoints on the boundary condition expressed as observed head and equivalent freshwater head. No breakpoints were added to the IAS layers. The locations of the breakpoints are obvious from the plots because the new observed head line (solid red) varies from the previous observed head line (dashed red). In each case, the breakpoints smoothed the equivalent freshwater head and removed unexplained anomalies.

It is important to stress that despite the apparently arbitrary nature of some of these edits to the data sets, the applied head boundary condition still matches the measured head at each monitoring well – except where nearby wells were averaged as shown in Table C2. The measured head values for all aquifers are shown as red dots on Figures C2-23 through C2-26.

2.6 Final Results

The resulting equivalent freshwater heads for all aquifer layers of the model are shown together on an azimuth plot in Figure C2-27 for October 2003. The flow directions are preserved much better now that break points have been added. Except for the area between Orlando and Tampa, the flow is generally upward. There is a close communication between upper and lower aquifer layers between Orlando and Tampa. The x's on the figure indicate that there is a close correlation between the measured heads (converted to equivalent freshwater heads) and the applied boundary conditions. The actual head values applied to the model for October 2003 are shown in Figure C2-28. These are observed heads, not equivalent freshwater heads. Notice again that the applied heads match the available data at all locations. Figure C2-29 shows plan view images of each aquifer with the October 2003 specified heads indicated in each cell with a colored circle. The same process was followed to create side boundary conditions for the aquifers for each month of the calibration and validation periods.

3.0 Surficial Aquifer System Surface Heads

As described in Section 1.1 of this appendix, the surface of the model was given a specified head boundary condition. This type of boundary condition sets the required head for each cell and the model adds or removes any amount of water necessary to achieve that head. This imitates the water flux caused by rainfall and evapotranspiration cycles, but does not require exhaustive data analysis and large assumptive leaps to come up with the flux values. This type of boundary on the surface of the model is only valid because there is significant shallow head data available in the Surficial Aquifer System (SAS) and because we are not actually concerned with the flow through this upper layer. None of the forces applied to the final model (ASR well pumping) are expected to have effects on the SAS. The heads applied to the SAS cells directly impact the addition (and removal) of water through the surface to the Intermediate Aquifer System (IAS) layers.

Early iterations of this regional ASR model followed conventional modeling practice in the application of boundary conditions. For the SAS surface head boundaries, 2-dimensional interpolation was used to convert discrete head measurements to an array of head values, one for each surface cell. The team found that some of these methods were not applicable to the current situation either because of lack of data, special conditions or the density dependent calculations planned. Here, we present a short explanation of some of the shortcomings of previous methods of assigning boundary conditions. Two-dimensional linear interpolation of observed head data in the SAS sometimes resulted in unacceptable interactions with the topography, such as:

- The interpolated head was above the ground surface where no surface water was expected, or the interpolated head was below the elevation of the bottom of the SAS. This was often caused by interpolation across an area of sparse data where topographic changes were not linear. (See Figure C3-1a)
- The interpolated water table did not rise underneath hills and ridges in known recharge areas. This was due to monitoring wells being found in river valleys, not at higher ground levels. (See Figure C3-1b)

The following sections describe the process that was designed to avoid those problems and create a smooth, accurate distribution of head in the SAS layer.

3.1 Selection of Data Points

The heads assigned to the upper layer of the model were based on available data for wells open in the Surficial Aquifer System (SAS). The data for these wells was provided by SAJ in a database. Wells were assumed to represent the heads in the SAS layer if the top of their open interval was in the top layer of the model and if the bottom of their open interval was in the first or second layer of the model. These were extracted using a query in Microsoft Access. The measured data for each well was averaged for each month in the calibration period (October 2003 to December 2004) and the validation period (August 1993 to July 1994). The query also extracted the x and y locations, ground elevation and open interval elevations.

Wells with obvious errors or local phenomena were removed from the data set. These errors include:

- Wells with water level more than 10 feet above the ground surface elevation (flooded areas)
- Wells with water level lower than the level of the ocean (affected by pumping)
- Wells with data errors such as the cased elevation below the drilled elevation or the ground surface elevation exactly 0.0 ft.

Additional analyses were used to remove duplicate wells and to remove upper wells in a nested set. This was done by gathering all wells located within 25 feet of each other. In each set of wells only the well with the deepest open interval was used. This deeper well would be expected to better represent

the head conditions which directly affect the IAS layers. This method also removed duplicates in the database.

3.2 Filling in Missing Data

As with the aquifer boundary wells (Section 2.3), it was important to have the same set of points for each month to ensure uniformity among the months. Because many of the wells were not measured in every month of the calibration and validation periods, a procedure was developed to estimate the heads for the months with missing data. The procedure was nearly identical to that described in Section 2.3 for the aquifer boundary heads.

In the first step, a regression of head measurements for the same month in different years was used to estimate many of the missing head values. All r^2 values were above 0.992 indicating a close linear correlation. The quality of the head estimates was also calculated by comparing the available data values to those that would be calculated using the regression equation. The residual between the computed and estimated value for each month was tabulated and the mean absolute error and root mean square error were calculated. The largest mean absolute error was 1.76 for the comparison between June 1994 and June 2004. The largest root mean square error was 3.34, calculated for the November 1993 and November 2004 data. These errors are within the error expected on the calibrated model.

At this point, wells with sparse data were removed from the data set. Sparse data wells were defined as those that had less than five months of data before this regression step or less than ten months of data after this regression step. The removal of sparse data was important for the reliability of the final step in the process of estimating missing data.

The second step to filling in missing data was to correlate the monthly average heads for each month still missing data with five wells whose data was statistically most similar. The similar wells were determined by calculating the r^2 value and the regression line slope for each pair of wells. The r^2 values were ranked and the five highest values which corresponded to positive slopes were assumed to be the most similar wells. The data at these five wells was averaged and the result was compared to the well with missing data using the Excel SLOPE and INTERCEPT functions to determine a linear relationship which could be used to estimate missing data. The r^2 values for the comparison between the average of the five best wells and the well of concern varied from very good (0.99) to rather poor (0.5). The worst r^2 value of 0.5 was found for the well G-2063 located in Broward County. As before, additional comparisons were made for each month with available data for both the well in question and the average of the five best wells. The regression equation was used to estimate the head and this estimate was compared to the actual data with the calculation of a residual error. The mean absolute error and root mean square (RMS) error for these comparisons was less than the expected calibration quality. The worst mean absolute error was 1.57 ft and the worst RMS was 2.1; both occurred at the SWFWMD well MBWF X-1 UPL SURF located in Hillsborough County.

3.3 Regression/Interpolation

The boundary condition for the top of the model was designed to imitate recharge by allowing the model to calculate the flux required to duplicate the measured heads in the SAS layer. This was implemented by assigning a head value to every cell on the surface of the model. This interpolation process was repeated for each month of the calibration and validation period. Initially, the cell heads were determined using an interpolation scheme to convert the occasionally sparse well data to individual cell values. For simplicity's sake, a linear interpolation scheme was selected; however, the density of the data points can have a great effect on the resulting head values. Figure C3-1 shows two examples of how linear interpolation can cause unexpected results when the data points are too sparse to correctly define the water table surface. To account for these and other problems, the following process was designed:

First the model area was divided into five zones based on topography, presence of water and data availability as follows:

1. Ocean areas, placed visually using a map;
2. Lake Okeechobee, placed visually using an areal photo and map;
3. Ridge peaks where linear regression was not consistent with the majority of observed data, based on the zones labeled as Lake Wales Ridge, Winter Haven Ridge, Lakeland Ridge, Bombing Range Ridge, Orlando Ridge, Mount Dora Ridge, Brooksville Ridge, Marion Upland and Deland Ridge in Figure 2 of Sepúlveda, 2002;
4. Dry land areas with a reasonable linear relationship between measured head and ground surface elevation;
5. Remaining dry land where observed data did not fit the linear regression equation developed for Zone 4.

Figure C3-2 shows the zones designated for the model domain. Specified heads were assigned differently in each zone. The cells in the ocean areas and Lake Okeechobee were assigned a specified head according to the mean monthly ocean level and lake level, respectively. The remaining inland areas were assigned a specified head by using either a linear regression or linear interpolation. Figure C3-3 shows the wells used for creating the linear regression (696 data points) and the wells used for linear interpolation (616 data points). For the the inland area (the area shown in green in Figure C3-2), data could be fit to a linear regression which correlated the observed head in the SAS wells to the ground surface elevation at that well. The upper plot on Figure C3-4 shows all of the water level data used to develop the SAS boundary condition for October 2003 plotted against the ground surface elevation at each well, overlain with a linear trend line. From this plot it is apparent that the water level data in the upper elevations does not correlate well with the ground surface elevation. These locations correspond to the ridges. Here, the water surface is much deeper because of the steepness of the ridge slopes. The inclusion of these wells in the regression tended to skew the slope of the regression line downward, so they were removed and categorized in Zone 3. Similarly, wells near the southeast and

southwest coastlines did not appear to follow the general regression of the data. These wells were also removed from the regression and categorized separately (Zone 5) for the development of SAS boundary condition. The lower plot on Figure C3-4 contains the wells used for the regression analysis (Zone 3 and 5 wells removed) for October 2003. The wells in this data set (Zone 4) show a reasonable correlation between the observed water level and the ground surface elevation. Since the water levels varied throughout the year, a separate regression equation was created for each month, using the same set of wells. Plots of head versus elevation for all monthly data sets are similar. R^2 values for all months vary between 0.975 and 0.984, and the root mean square error (RMS) ranges from 3.72 in September 2004 to 4.54 in May 2004, indicating that the data is well correlated in all months. Once a regression equation for each month was developed, this equation was used to calculate a head value for each cell in the SAS layer of the model based on the ground surface elevation assigned to that cell in the model.

Once heads had been assigned in each zone according to the process outlined below, the heads were checked against the ground surface elevation and the elevation of the bottom of the SAS. Heads were required to be at least one foot above the bottom of the SAS (to prevent dry cells) and no more than 10 feet above the ground surface (to remove some anomalous data points).

3.4 Final Results

The final set of specified heads applied to the surface of the regional model is shown in Figure C3-5. As expected the heads trend with the ground surface elevation. Higher heads are seen in Polk County and surrounding areas where ground surface elevations are high and significant recharge occurs. The water table gently slopes down towards the flat areas of the peninsula, south of Lake Okeechobee. The heads assigned in coastal areas are at or close to sea level.

4.0 Differences in Assigning Boundary Conditions for SEAWAT vs. WASH123D

The processes described in Sections 2 and 3 generally refer to the assignment of boundary conditions to the SEAWAT grid. This model was built first and so, was used exclusively while the process was being developed. The same process was also applied to the WASH123D model, except that interpolations were made to mesh node locations, which were not the same as the grid cell centers used in the SEAWAT model.

5.0 References

Google Earth Pro v5.1

Miller, James A. 1997. *Hydrogeology of Florida.* in *The Geology of Florida*. eds. Anthony F. Randazzo and Douglas S. Jones.

Sepúlveda, Nicasio. 2002. *Simulation of Ground-Water Flow in the Intermediate and Floridan Aquifer System in Peninsular Florida*. U.S. Geological Survey Water-Resources Investigations Report 02-4009.

South Florida Water Management Districts Environmental Database (DBHYDRO), http://my.sfwmd.gov/dbhydroplsql/show_dbkey_info.main_menu

Southwest Florida Water Management Districts Water Management Information System (WMIS), http://www8.swfwmd.state.fl.us/WMIS/ResourceData/ExtDefault.aspx

St. Johns River Water Management Districts Hydrologic Dataport, http://webapub.sjrwmd.com/agws93/hdsnew/map.html

U.S. Geological Survey (USGS). NWISWeb Water Data, http://waterdata.usgs.gov/nwis/gw

Table C2: Description of data availability and decisions for inclusion in the definition of side boundary conditions for aquifer layers (not including Surficial Aquifer System).

Layer	SAJ Model ID	Well Name(s)	X	Y	Water Level Data Availability	TDS Data Availability	Boundary Head Decisions
IAS	120034	BR0202	724478.88	1470720.30	Significant head data for 93/94 calibration period provided by SAJ	None	Removed - Outside the IAS area (Miller, 1997)
IAS	100973	USGS 282510081054503 COCOA 1-T	625362.78	1485213.61	One head data point for most months in 93/94 and 03/04 calibration periods provided by SAJ	None	Removed – Outside the IAS area (Miller, 1997)
IAS	120329	L-0052	437896.59	1524197.95	One head data point for most months in 93/94 and 03/04 calibration periods provided by SAJ	None	Removed – Outside the IAS area (Miller, 1997)
IAS	100644	USGS 280659082175202 MORRIS BRIDGE SH 13	237813.35	1376847.57	Bimonthly head data points for 93/94 calibration period provided by SAJ	None	Removed – Outside the IAS area (Miller, 1997)
IAS	130149	MORRIS BRIDGE P-166 SH	231872.92	1376714.46	One head data point (9/1993) provided by SAJ	None	Removed – Outside the IAS area (Miller, 1997)
IAS	130272	MBWF 3A SURF	228013.29	1377509.02	One to three head data points for all months in 93/94 and 03/04 calibration periods provided by SAJ	None	Removed – Outside the IAS area (Miller, 1997)

Table C2: Description of data availability and decisions for inclusion in the definition of side boundary conditions for aquifer layers (not including Surficial Aquifer System).

Layer	SAJ Model ID	Well Name(s)	X	Y	Water Level Data Availability	TDS Data Availability	Boundary Head Decisions
IAS	100641	USGS 280655082193002 MORRIS BRIDGE SH 3A	227877.31	1377358.98	Bimonthly head data points for 93/94 calibration periods provided by SAJ	None	Removed – Outside the IAS area (Miller, 1997)
IAS	130234	MBWF 6 SURF	226151.84	1374377.65	One to two head data points for most months in 93/94 and 03/04 calibration periods provided by SAJ	None	Removed – Outside the IAS area (Miller, 1997)
IAS	130240	TBC WL-02 FLDN	221064.66	1350169.32	Monthly head data points for 93/94 and 03/04 calibration periods provided by SAJ	None	Removed – this group of wells represented by 100613
IAS	130140	TBC 10 HARNEY RD DAIRY	218720.11	1345746.53	Monthly head data points for 93/94 calibration period provided by SAJ	None	Removed – this group of wells represented by 100613

Table C2: Description of data availability and decisions for inclusion in the definition of side boundary conditions for aquifer layers (not including Surficial Aquifer System).

Layer	SAJ Model ID	Well Name(s)	X	Y	Water Level Data Availability	TDS Data Availability	Boundary Head Decisions
IAS	100613	USGS 280058082202201 EUREKA SPRINGS DEEP	224044.01	1340981.49	Daily head data points for 03/04 calibration period provided by SAJ. Additional daily head data points for 93/94 calibration period obtained from USGS by NAP. No data available 8/11/93 to 10/5/93. 8/93 value is the average of first 10 days of the month; 10/93 value is the average of the last 26 days of the month; 9/93 value was estimated based on the least squares analysis of 9/93 and 9/04 data points at all wells.	Available	This well assumed to be representative of a group of wells in this area. Used in definition of boundary conditions (layer 2 and 3)
IAS	100614	USGS 280058082202202 EUREKA SPRINGS SHALL	224044.01	1340981.49	Daily head data points for 93/94 and 03/04 calibration periods provided by SAJ	None	Removed – this group of wells represented by 100613
IAS	130277	VANDENBERG EAST FLDN	221309.79	1337478.88	Monthly head data points for 93/94 and 03/04 calibration periods provided by SAJ	None	Removed – this group of wells represented by 100613

Table C2: Description of data availability and decisions for inclusion in the definition of side boundary conditions for aquifer layers (not including Surficial Aquifer System).

Layer	SAJ Model ID	Well Name(s)	X	Y	Water Level Data Availability	TDS Data Availability	Boundary Head Decisions
IAS	100608	USGS 280022082210501 SWFWMD NR VANDENBERG	220580.88	1337504.44	Daily head data points for 93/94 and 03/04 calibration periods provided by SAJ	None	Removed – this group of wells represented by 100613
IAS	130155	TBC 2E-SMC FLDN	221627.94	1329747.60	Monthly head data points for 93/94 calibration period and daily head data points for most of 03/04 calibration period provided by SAJ	None	Removed – this group of wells represented by 100613
IAS	130243	TBC 1E-SMC FLDN	226151.84	1374377.65	Monthly head data points for 93/94 and 03/04 calibration periods provided by SAJ	None	Removed – this group of wells represented by 100613
IAS	130282	TBC 2S-SMC FLDN	220155.50	1328773.91	Monthly head data points for 93/94 and 03/04 calibration periods provided by SAJ	None	Removed – this group of wells represented by 100613
IAS	130246	KUSHMER INT	206426.63	1266479.51	Monthly head data points for 93/94 and 03/04 calibration periods provided by SAJ. 10/93 data is missing so the 130465 head value was used (not averaged) for this month.	None	Used in definition of boundary conditions (layer 2). Averaged with 130465.

Table C2: Description of data availability and decisions for inclusion in the definition of side boundary conditions for aquifer layers (not including Surficial Aquifer System).

Layer	SAJ Model ID	Well Name(s)	X	Y	Water Level Data Availability	TDS Data Availability	Boundary Head Decisions
IAS	130465	ROMP TR 9-2 HTRN/TMPA	205636.34	1249932.05	Weekly head data points for 93/94 calibration period and daily head data points for 03/04 calibration period provided by SAJ	None	Used in definition of boundary conditions (layer 2). Averaged with 130246.
IAS	130523	ROMP TR 8-1 UP HTRN	155313.64	1184320.94	Daily head data points for 93/94 and 03/04 calibration periods provided by SAJ. Data before 10/16/93 missing. Weekly head data points obtained from USGS by NAP for the months of 8/93 and 9/93.	Available for well called ROMP TR 8-1 INT (determined to be the same well based on location and open interval)	Used in definition of boundary conditions (layer 3).
IAS	130557	ROMP TR 8-1 SURF	155321.51	1184302.66	Daily head data points for 03/04 calibration period plus one data point in June 1994 provided by SAJ. Missing months estimated using least squares estimates comparing the same month in different years.	None	Used in definition of boundary conditions (layer 2).

Table C2: Description of data availability and decisions for inclusion in the definition of side boundary conditions for aquifer layers (not including Surficial Aquifer System).

Layer	SAJ Model ID	Well Name(s)	X	Y	Water Level Data Availability	TDS Data Availability	Boundary Head Decisions
IAS	130560	ROMP TR 7-2 LOW ARC	153305.41	1131248.71	Daily head data points for 03/04 calibration period plus one data point in June 1994 provided by SAJ. Missing months estimated using least squares estimates comparing the same month in different years.	Available for well called ROMP TR 7-2 LOWER INT (determined to be the same well based on location and open interval)	Used in definition of boundary conditions (layer 3). Averaged with 130561.
IAS	130561	ROMP TR 7-2 UP ARC	153306.31	1131248.70	Daily head data points for 03/04 calibration period plus one data point in June 1994 provided by SAJ. Missing months estimated using least squares estimates comparing the same month in different years.	Available for well called ROMP TR 7-2 UP HAWTHORN (determined to be the same well based on location and open interval)	Used in definition of boundary conditions (layer 3). Averaged with 130560.
IAS	101348	USGS 272133082324701 CITY SARASOTA 27TH ST	154298.99	1103048.63	Daily head data points for 93/94 calibration period plus one data point in May 2004 and one in Sept 2004 provided by SAJ. Missing months estimated using least squares estimates comparing the same month in different years.	Available	Used in definition of boundary conditions (layer 2). Averaged with 101344.

Table C2: Description of data availability and decisions for inclusion in the definition of side boundary conditions for aquifer layers (not including Surficial Aquifer System).

Layer	SAJ Model ID	Well Name(s)	X	Y	Water Level Data Availability	TDS Data Availability	Boundary Head Decisions
IAS	101344	USGS 272119082325101 WHITAKER BAY WELL	153899.43	1101376.72	Daily head data points for 93/94 calibration period plus one data point in May 2004 and one in Sept 2004 provided by SAJ. Missing months estimated using least squares analysis comparing the same month in different years.	None	Used in definition of boundary conditions (layer 2). Averaged with 101348.
IAS	131451	ROMP TR SA-1 UP INT	154324.72	1098431.88	Daily head data points for 03/04 calibration period. 93/94 calibration period heads estimated using least squares analysis comparing the same month in different years	None	Used in definition of boundary conditions (layer 3)
IAS	101326	USGS 271137082284503 ROMP TR-20 UP HTRN	175302.03	1042549.06	One head data point for the 93/94 calibration period (May 1994) and two head data points for the 03/04 calibration period (May and Sept 2004) were provided by SAJ. No additional data was found by NAP	None	Removed – sparse data

Table C2: Description of data availability and decisions for inclusion in the definition of side boundary conditions for aquifer layers (not including Surficial Aquifer System).

Layer	SAJ Model ID	Well Name(s)	X	Y	Water Level Data Availability	TDS Data Availability	Boundary Head Decisions
IAS	101322	USGS 271118082285301 OSPREY WELL 9	174632.39	1040597.03	Daily head data points for the 93/94 calibration period were provided by SAJ. Head values for the 03/04 calibration period were estimated using least squares analysis comparing the measured heads in the same month for different years.	None	Used in definition of boundary conditions (layer 3). Averaged with 131440.
IAS	131440	ROMP TR 5-1 TMPA	184118.67	1021400.75	Daily head data points for the 93/94 and 03/04 calibration periods were provided by SAJ	Available	Used in definition of boundary conditions (layer3). Averaged with 101322.
IAS	101285	USGS 270808082270503 ROMP TR-20 UP HTRN	184118.67	1021400.75	Two head data points for the 93/94 calibration period and two head data points for the 03/04 calibration period were provided by SAJ (May/Sept).	None	Removed – sparse data

Table C2: Description of data availability and decisions for inclusion in the definition of side boundary conditions for aquifer layers (not including Surficial Aquifer System).

Layer	SAJ Model ID	Well Name(s)	X	Y	Water Level Data Availability	TDS Data Availability	Boundary Head Decisions
IAS	131449	ROMP TR 5-1 TAMIAMI	184124.06	1021397.66	Daily head data points for the 03/04 calibration period were provided by SAJ. Head values for the 93/94 calibration period were estimated using least squares analysis comparing measured heads in the same month for different years	Available for well called ROMP TR 5-1 INTERMED. (determined to be the same well based on location and open interval)	Used in definition of boundary conditions (layer 2). Averaged with 101279 and 131411.
IAS	101279	USGS 270542082261801 VENICE 35	200661.13	987978.05	Daily head data points from 8/1/93 through 10/7/93 and single points for 5/94, 5/04 and 9/04 were provided by SAJ. A few additional months' values were estimated using least squares analysis comparing measured heads in the same month for different years.	Available	Used in definition of boundary conditions (layer 2). Averaged with 131449 and 131411. This well is probably the same as 131411. The data from SAJ match the USGS data, but not that for 131411.

Table C2: Description of data availability and decisions for inclusion in the definition of side boundary conditions for aquifer layers (not including Surficial Aquifer System).

Layer	SAJ Model ID	Well Name(s)	X	Y	Water Level Data Availability	TDS Data Availability	Boundary Head Decisions
IAS	131411	VENICE 35 INT	188539.04	1006263.41	One to four head data points for each month in the 93/94 and 03/04 calibration periods were provided by SAJ.	Available	Used in definition of boundary conditions (layer 2). Averaged with 131449 and 131411. This well is probably the same as 101279. The data from SAJ match the DBHYDRO data, but not that for 101279.
IAS	131465	ROMP TR 4-1 UP INT	187066.86	992964.48	Daily head data points for the 03/04 calibration period provided by SAJ.	Available	Removed – the TDS value at this well is unusually high and may indicate a data error or an anomaly not accounted for in the model.

Table C2: Description of data availability and decisions for inclusion in the definition of side boundary conditions for aquifer layers (not including Surficial Aquifer System).

Layer	SAJ Model ID	Well Name(s)	X	Y	Water Level Data Availability	TDS Data Availability	Boundary Head Decisions
IAS	101276	USGS 270240082235701 ROMP TR 4-2 TAMPA	200661.13	987978.05	Two head data points (May and Sept) for the 03/04 calibration period provided by SAJ. NAP obtained additional daily head data points for the 93/94 calibration period from USGS. Heads for additional months in the 03/04 period were estimated using a least squares analysis comparing the same month in different years.	Available	Removed – this is the same well as 131441
IAS	131441	ROMP TR 4-2 TMPA	200635.54	987954.10	Daily head data points for the 93/94 and 03/04 calibration periods provided by SAJ	Available (well called ROMP TR 4-2 SWWN)	Used for definition of boundary conditions (layer 3). Averaged with 101275.
IAS	101275	USGS 270137082235301 MANASOTA DEEP 14	201113.03	981792.50	Daily head data points for the 93/94 and 03/04 calibration periods provided by SAJ	Available	Used for definition of boundary conditions (layer 3). Averaged with 131441.

Table C2: Description of data availability and decisions for inclusion in the definition of side boundary conditions for aquifer layers (not including Surficial Aquifer System).

Layer	SAJ Model ID	Well Name(s)	X	Y	Water Level Data Availability	TDS Data Availability	Boundary Head Decisions
IAS	131410	MANASOTA 14 DEEP	201049.83	981682.15	One to four head data points for each month in the 93/94 and 03/04 calibration periods were provided by SAJ.	Available	Removed – this is the same well as 101275
IAS	131414	ENGLEWOOD 14 DEEP	219736.37	962919.09	One to four head data points for each month in the 93/94 and 03/04 calibration periods were provided by SAJ. (Daily data after 11/8/04)	Available	Used for definition of boundary conditions (layer 2).
IAS	101270	USGS 265834082202401 ENGLEWOOD 14	219720.66	962803.11	Two head data points (9/93 and 5/94) provided by SAJ	Available	Removed – this is the same well as 131414 and data is too sparse.
IAS	101268	USGS 265712082205701 ENGLEWOOD WATER DT R-2	216763.37	954501.96	Four head data points provided by SAJ. (Two points for each calibration period.)	None	Removed – sparse data
IAS	101267	USGS 265710082205101 ENGLEWOOD WD RIVER 2	217187.12	954345.94	Two head data points for the 93/94 calibration period provided by SAJ	None	Removed – sparse data
IAS	101266	USGS 265653082190301 ENGLEWOOD WD PO 1	226943.46	952526.07	Two head data points for the 93/94 calibration period provided by SAJ	None	Removed sparse data

Table C2: Description of data availability and decisions for inclusion in the definition of side boundary conditions for aquifer layers (not including Surficial Aquifer System).

Layer	SAJ Model ID	Well Name(s)	X	Y	Water Level Data Availability	TDS Data Availability	Boundary Head Decisions
IAS	101265	USGS 265652082185801 ENGLEWOOD WELL 150	227539.85	952428.96	Four head data points provided by SAJ. (Two points for each calibration period.)	None	Removed sparse data
IAS	130019	ROMP TR 3-3 LOW HTRN	222845.55	944410.17	One to six head data points for the 93/94 calibration period for each month beginning with March 1994 and daily head data points for the 03/04 calibration period were provided by SAJ. First seven months of 93/94 period were estimated using a least squares analysis comparing the same month in different years.	Available (well called ROMP TR 3-3 L INT)	Used to define boundary conditions (layer 2).
IAS	130020	ROMP TR 3-3 UP HTRN	222845.55	944410.17	One to six head data points for the 93/94 calibration period for each month beginning with October 1993 and daily head data points for the 03/04 calibration period were provided by SAJ. First seven months of 93/94 period were estimated using a least squares analysis comparing the same month in different years.	Available (well called ROMP TR 3-3 U HAWTH)	Used to define boundary conditions (layer 3)

Table C2: Description of data availability and decisions for inclusion in the definition of side boundary conditions for aquifer layers (not including Surficial Aquifer System).

Layer	SAJ Model ID	Well Name(s)	X	Y	Water Level Data Availability	TDS Data Availability	Boundary Head Decisions
IAS	100273	USGS 265531082194804 ROMP TR 3-3 ARCADIA	222783.60	944287.60	Two head data points for the 93/94 calibration period provided by SAJ	None	Removed – sparse data
IAS	100265	USGS 265017082153701 42S20E12	245126.02	912335.64	Four head data points provided by SAJ. (Two points for each calibration period.)	None	Removed – sparse data
IAS	100805	USGS 263955082083103 L-2549	283215.92	848966.73	Monthly head data points for most months in the 93/94 and 03/04 calibration periods provided by SAJ. Missing months (Sept 93 and Aug 04) estimated using a least squares analysis comparing the same month in different years.	Available	Used to define boundary conditions (layer 2).
IAS	100739	USGS 263117082051001 L-2525	301071.54	796831.17	Six head data points for the 93/94 calibration period, plus daily head data points for the 03/04 calibration period provided by SAJ. Head during the remaining months was estimated using a least squares analysis comparing the same month in different years.	Available	Used for definition of boundary conditions (layer 3).

Table C2: Description of data availability and decisions for inclusion in the definition of side boundary conditions for aquifer layers (not including Surficial Aquifer System).

Layer	SAJ Model ID	Well Name(s)	X	Y	Water Level Data Availability	TDS Data Availability	Boundary Head Decisions
IAS	100724	USGS 262710082005301 L-585	323977.41	771672.46	Monthly head data points for most months in the 93/94 and 03/04 calibration periods provided by SAJ. Head during the remaining months was estimated using a least squares analysis comparing the same month in different years. After averaging the head with 100733, heads for Feb 94 and Feb 04 were estimated using a least squares analysis comparing all monthly average heads at these two points against those at 130556, 131452, 131441, 101275, 100700, 130559 and 130525, which were shown to have the most similar head changes.	None	Used for definition of boundary conditions (layer 3). Averaged with 100733.
IAS	100729	USGS 262831081575901 L-2212	339854.83	779830.54	Monthly head data points for about half of the months in the 93/94 and 03/04 calibration periods provided by SAJ.	None	Removed – sparse data

Table C2: Description of data availability and decisions for inclusion in the definition of side boundary conditions for aquifer layers (not including Surficial Aquifer System).

Layer	SAJ Model ID	Well Name(s)	X	Y	Water Level Data Availability	TDS Data Availability	Boundary Head Decisions
IAS	100733	USGS 262944081560801 L-2529	348700.55	784006.08	Monthly head data points for most of the months in the 93/94 and 03/04 calibration periods provided by SAJ. Head during the remaining months was estimated using a least squares analysis comparing the same month in different years. After averaging the head with 100724, heads for Feb 94 and Feb 04 were estimated using a least squares analysis comparing all monthly average heads at these two points against those at 130556, 131452, 131441, 101275, 100700, 130559 and 130525, which were shown to have the most similar head changes.	None	Used for definition of boundary conditions (layer 3). Averaged with 100724.
IAS	100700	USGS 262435081535001 L-1635	362743.13	756065.27	Six head data points for the 93/94 calibration period, plus daily head data points for the 03/04 calibration period provided by SAJ. Head during the remaining months was estimated using a least squares analysis comparing the same month in different years.	None	Used for definition of boundary conditions (layer 3).

Table C2: Description of data availability and decisions for inclusion in the definition of side boundary conditions for aquifer layers (not including Surficial Aquifer System).

Layer	SAJ Model ID	Well Name(s)	X	Y	Water Level Data Availability	TDS Data Availability	Boundary Head Decisions
IAS	100323	USGS 261438081481001 C-575	393531.45	686968.09	Monthly head data points for most of the months in the 93/94 and 03/04 calibration periods provided by SAJ. Head during the remaining months was estimated using a least squares analysis comparing the same month in different years.	None	Used for definition of boundary conditions (layer 3).
IAS	100287	USGS 260314081323102 C-1068	478244.97	625747.39	Monthly head data points for most of the months in the 93/94 calibration period provided by SAJ.	None	Removed – sparse data
IAS	100285	USGS 260309081272601 C-987	506214.67	625270.27	Nine head data points for the 93/94 calibration period, plus daily head data points for the 03/04 calibration period beginning 12/7/03 provided by SAJ. Head during the remaining months was estimated using a least squares analysis comparing the same month in different years.	None	Used for definition of boundary conditions (layer 3).

Table C2: Description of data availability and decisions for inclusion in the definition of side boundary conditions for aquifer layers (not including Surficial Aquifer System).

Layer	SAJ Model ID	Well Name(s)	X	Y	Water Level Data Availability	TDS Data Availability	Boundary Head Decisions
IAS	112142	BICY-MZ1	554522.19	567147.92	Daily head data points for the 03/04 calibration period provided by SAJ. Heads for the 93/94 calibration period were estimated using a least squares analysis comparing the same month in different years.	Available	Used for definition of boundary conditions (layer 3).
UF	120311	BR1557	731104.4	1471740.54	Daily head data points for the 03/04 calibration period provided by SAJ. Heads for the 93/94 calibration period were estimated using a least squares analysis comparing the same month in different years.	None	Used for definition of boundary conditions
UF	120470	OR0029	673459.3	1477029.94	One to two head data points for each month in the 93/94 and 03/04 calibration periods were provided by SAJ.	None	Removed – this is identical to 100967.
UF	100967	USGS 282348080564701 PALMETTO WELL	673402.7	1476923.63	One to two head data points for each month in the 93/94 and 03/04 calibration periods were provided by SAJ.	None	Used for definition of boundary conditions.

Table C2: Description of data availability and decisions for inclusion in the definition of side boundary conditions for aquifer layers (not including Surficial Aquifer System).

Layer	SAJ Model ID	Well Name(s)	X	Y	Water Level Data Availability	TDS Data Availability	Boundary Head Decisions
UF	120081	OR0669	650975	1476090.08	Daily head data points for 03/04 calibration period provided by SAJ. Heads for the 93/94 calibration period were estimated using a least squares analysis comparing the same month in different years.	Available	Used for definition of boundary conditions.
UF	999993	OR0678	589521.2	1515254.41	No data provided by SAJ. NAP obtained daily head data from SJRWMD website for the 03/04 calibration period. Heads for the 93/94 calibration period were estimated using a least squares analysis comparing the same month in different years.	Available	Used for definition of boundary conditions. (Note: the Model ID listed here is not consistent with the water level database obtained from SAJ, which did not include OR0678.)
UF	100977	USGS 282531081095701 COCOA D WELL	602933.8	1487461.83	Daily head data points for the 93/94 and 03/04 calibration periods provided by SAJ.	Available	Used for definition of boundary conditions.

Table C2: Description of data availability and decisions for inclusion in the definition of side boundary conditions for aquifer layers (not including Surficial Aquifer System).

Layer	SAJ Model ID	Well Name(s)	X	Y	Water Level Data Availability	TDS Data Availability	Boundary Head Decisions
UF	120100	OR0827	537416.3	1521247.79	Daily head data points for the 03/04 calibration period from 3/23/04 to 11/21/04 provided by SAJ. Least squares analysis comparing the same month in different years was used to fill in some of the missing data points. The rest (Jan, Feb, Jun, Dec) were filled in using a least squares analysis comparing heads at this point to heads at 110160, 130492, OR0678, 100570, 130476, 101348 and 101344.	None	Used for definition of boundary conditions.
UF	100988	USGS 282835081305201 PALM LAKE DRIVE WELL	493283.5	1506755.63	Daily head data points for the 93/94 and 03/04 calibration periods provided by SAJ.	Available	Used for definition of boundary conditions
UF	100678	USGS 283128081404701 JOHNS LAKE WELL	437895.5	1523995.95	Four head data points for the calibration periods provided by SAJ (Two points for the 93/94 period; two points for the 03/04 period)	Available	Removed – sparse data

Table C2: Description of data availability and decisions for inclusion in the definition of side boundary conditions for aquifer layers (not including Surficial Aquifer System).

Layer	SAJ Model ID	Well Name(s)	X	Y	Water Level Data Availability	TDS Data Availability	Boundary Head Decisions
UF	130502	ROMP 101 AVPK	358774.3	1499216.64	Daily head data points for the 03/04 calibration period (5/28/04 through 12/31/04) provided by SAJ. Heads in additional months were estimated using a least squares analysis comparing the same month in different years. Heads for Jan, Feb, Mar and Apr for both calibration periods were estimated by a least squares analysis comparing heads at this well to those at 130613, 130986, 100988, 112144, and 112127, which were shown to have the most similar head changes during the periods in question.	None	Used for definition of boundary conditions. (This is also listed as an MF well.)
UF	130986	ROMP 90 OCAL	288426.96	1465372.08	Monthly head data points for most months of the 93/94 calibration period and daily head data points for the 03/04 calibration period provided by SAJ. August 1993 head data was estimated using a least squares analysis comparing August 1993 heads with August 3004 heads.	None	Used for definition of boundary conditions

Table C2: Description of data availability and decisions for inclusion in the definition of side boundary conditions for aquifer layers (not including Surficial Aquifer System).

Layer	SAJ Model ID	Well Name(s)	X	Y	Water Level Data Availability	TDS Data Availability	Boundary Head Decisions
UF	131046	ROMP BR-3 UP FLDN	258185.17	1453679.83	Daily head data points for the 03/04 calibration period provided by SAJ. Heads for the 93/94 calibration period were estimated using a least squares analysis comparing the same month in different years.	None	Used in definition of boundary conditions
UF	130859	Wesley Chapel WWTP FLDN	228306.3	1432025.57	Daily head data points for the 03/04 calibration period provided by SAJ. Heads for the 93/94 calibration period were estimated using a least squares analysis comparing the same month in different years.	None	Used in definition of boundary conditions. (Averaged with 130614 and 130823)
UF	130614	ROMP 85 TMPA/SWNN	229945.8	1422384.48	One to two head data points for each month in the 03/04 calibration period plus one point (5/94) in the 93/94 calibration period were provided by SAJ Heads for missing months were estimated using a least squares analysis comparing the same month in different years.	Available	Used in definition of boundary conditions. (Averaged with 130859 and 130823)

Table C2: Description of data availability and decisions for inclusion in the definition of side boundary conditions for aquifer layers (not including Surficial Aquifer System).

Layer	SAJ Model ID	Well Name(s)	X	Y	Water Level Data Availability	TDS Data Availability	Boundary Head Decisions
UF	130823	Fox Ridge FLDN	239711.9	1413809.6	Daily head data points for most of the 03/04 calibration period, with monthly data for the first two months of the period were provided by SAJ. Heads for missing months were estimated using a least squares analysis comparing the same month in different years.	None	Used in definition of boundary conditions. (Averaged with 130614 and 130859)
UF	100653	USGS 280736082201901 MORRIS BRIDGE DEEP WELL 537	224756.2	1381237.01	Daily head data points 7/8/94 to 7/31/94 provided by SAJ	None	Removed – sparse data
UF	130492	LHFDA 22 FLDN	239762	1362987.66	Daily head data points for the 03/04 calibration period provided by SAJ. Heads for the 93/94 calibration period were estimated using a least squares analysis comparing the same month in different years.	None	Used for definition of boundary condition
UF	100622	USGS 280305082185101 J.W. MORRIS WELL	232278.8	1353673.26	Four head data points for the calibration periods provided by SAJ (Two points for the 93/94 period; two points for the 03/04 period)	None	Removed – sparse data

Table C2: Description of data availability and decisions for inclusion in the definition of side boundary conditions for aquifer layers (not including Surficial Aquifer System).

Layer	SAJ Model ID	Well Name(s)	X	Y	Water Level Data Availability	TDS Data Availability	Boundary Head Decisions
UF	130230	TBC 2W-SMC FLDN	219618.7	1329775.88	Monthly head data points for all months of the 93/94 calibration period and daily head data points for the 03/04 calibration period provided by SAJ.	None	Used for definition of boundary condition
UF	100601	USGS 275747082184001 BRANDON 17	232919.3	1321543.52	Two head data points for the 93/94 calibration period provided by SAJ	None	Removed – sparse data
UF	100554	USGS 274928082225501 SW HILLSBOROUGH CO 220	209633.9	1271332.44	Four head data points for the calibration periods provided by SAJ (Two points for the 93/94 period; two points for the 03/04 period)	None	Removed – sparse data
UF	100549	USGS 274813082223601 SW HILLS CO 182	211103.1	1263800.41	Two head data points for the 93/94 calibration period provided by SAJ	None	Removed – sparse data
UF	130472	ROMP TR 9-1 HTRN/TMPA	182636.8	1240835.9	Daily head data points for the 93/94 and 03/04 calibration periods provided by SAJ.	Available	Used in definition of boundary conditions

Table C2: Description of data availability and decisions for inclusion in the definition of side boundary conditions for aquifer layers (not including Surficial Aquifer System).

Layer	SAJ Model ID	Well Name(s)	X	Y	Water Level Data Availability	TDS Data Availability	Boundary Head Decisions
UF	130547	ROMP TR 8-1 HAW/TPA	155318.9	1184312.8	Three to five head data points for each month in the 93/94 calibration period provided by SAJ.	None	Removed – it has similar heads to 130524, but less head data and no TDS data
UF	130524	ROMP TR 8-1 SWNN	155303.4	1184289.76	Three to five head data points for each month in the 93/94 calibration period and daily head data points for the 03/04 calibration period provided by SAJ.	Available	Used in definition of boundary conditions
UF	130559	ROMP TR 7-2 TMPA/SWNN	153306.29	1131246.68	Daily head data points for 03/04 calibration period plus one head data point in the 93/94 calibration period (6/94) provided by SAJ. Heads for missing months were estimated using a least squares analysis comparing the same month in different years.	Available	Used in definition of boundary conditions. (Averaged with 130525)
UF	130525	ROMP TR 7-1 TMPA	142777.67	1124984.86	Daily head data points for the 93/94 and 03/04 calibration periods provided by SAJ.	Available	Used in definition of boundary conditions. (Averaged with 130559)

Table C2: Description of data availability and decisions for inclusion in the definition of side boundary conditions for aquifer layers (not including Surficial Aquifer System).

Layer	SAJ Model ID	Well Name(s)	X	Y	Water Level Data Availability	TDS Data Availability	Boundary Head Decisions
UF	101346	USGS 272127082323801 CITY SARASOTA 23RD AND COCONUT	154944.20	1102349.83	Daily head data points for the 93/94 and 03/04 calibration periods (except missing 8/93) provided by SAJ.	None	Removed – this well appears to be located in a small local area affected by pumping.
UF	131452	ROMP TR SA-1 SWNN	154331.80	1098420.68	Daily head data points for the 03/04 calibration period provided by SAJ. Heads for the 93/94 calibration period were estimated using a least squares analysis comparing the same month in different years.	None	Used in definition of boundary conditions
UF	131467	ROMP TR SA-3 UP FLDN	165884.36	1098967.02	Daily head data points for the 03/04 calibration period provided by SAJ. Heads for the 93/94 calibration period were estimated using a least squares analysis comparing the same month in different years.	None	Removed – open section of this well is very deep, possibly in the MC1 layer. If it is in the UF, it represents a deeper section of that unit, which is not accounted for in the model.

Table C2: Description of data availability and decisions for inclusion in the definition of side boundary conditions for aquifer layers (not including Surficial Aquifer System).

Layer	SAJ Model ID	Well Name(s)	X	Y	Water Level Data Availability	TDS Data Availability	Boundary Head Decisions
UF	131447	ROMP 20 OCAL	175321.94	1042551.86	Daily head data points for the 03/04 calibration period plus 5 head data points for the final two months of the 93/94 calibration period were provided by SAJ. Heads for the remaining months of the 93/94 calibration period were estimated using a least squares analysis comparing the same month in different years.	Available	Used in definition of boundary conditions
UF	131439	ROMP TR 5-1 SWNN	184128.69	1021407.71	Daily head data points for the 93/94 and 03/04 calibration periods provided by SAJ.	Available	Used in definition of boundary conditions
UF	131468	ROMP TR 4-1 SWNN	187110.38	992895.30	Daily head data points for the 03/04 calibration period provided by SAJ. Heads for the 93/94 calibration period were estimated using a least squares analysis comparing the same month in different years.	Available	Used in definition of boundary conditions

Table C2: Description of data availability and decisions for inclusion in the definition of side boundary conditions for aquifer layers (not including Surficial Aquifer System).

Layer	SAJ Model ID	Well Name(s)	X	Y	Water Level Data Availability	TDS Data Availability	Boundary Head Decisions
UF	130023	ROMP TR 3-3 SWNN	222843.74	944410.19	Daily head data points for the 03/04 calibration period plus 17 head data points for the final 7 months of the 93/94 calibration period were provided by SAJ. Heads for the remaining months of the 93/94 calibration period were estimated using a least squares analysis comparing the same month in different years.	Available	Used in definition of boundary conditions. (Averaged with 130021)
UF	100272	USGS 265531082194803 ROMP TR 3-3 SUWANNEE	222843.74	944410.19	Four head data points for the calibration periods provided by SAJ (Two points for the 93/94 period; two points for the 03/04 period)	Available	Removed – this is the same well as 130023 and has sparse data
UF	130021	ROMP TR 3-3 OCAL	222846.45	944410.16	One to six head data points for each month in 93/94 calibration period (missing Aug through Sept) and daily head data points for the 03/04 calibration period. Heads for the remaining months of the 93/94 calibration period were estimated using a least squares analysis comparing the same month in different years.	Available	Used in definition of boundary conditions. (Averaged with 130023)

Table C2: Description of data availability and decisions for inclusion in the definition of side boundary conditions for aquifer layers (not including Surficial Aquifer System).

Layer	SAJ Model ID	Well Name(s)	X	Y	Water Level Data Availability	TDS Data Availability	Boundary Head Decisions
UF	112113	IWA-MZU	292806.41	767990.45	Daily head data points for the 03/04 calibration period provided by SAJ. Heads for the 93/94 calibration period were estimated using a least squares analysis comparing the same month in different years.	Available	Used in definition of boundary conditions
UF	112114	FMB-MZU	350747.43	785108.32	Daily head data points from 5/19/04 to 12/31/04 provided by SAJ. Many missing months were estimated using a least squares analysis comparing heads from the same month in different years. The months from Jan to Apr in both years were estimated using a least squares analysis comparing the heads at this well to those at 120311, 130245, 100868, 130556, and 130022	Available (Note: This well screen is very low. The TDS for this well was not used in the interpolation of the starting conditions, but is used here to estimate the effective freshwater head for definition of the boundary conditions.)	Used in definition of boundary conditions

Table C2: Description of data availability and decisions for inclusion in the definition of side boundary conditions for aquifer layers (not including Surficial Aquifer System).

Layer	SAJ Model ID	Well Name(s)	X	Y	Water Level Data Availability	TDS Data Availability	Boundary Head Decisions
UF	100701	USGS 262435081535101 L-1634	362680.26	755935.03	One to two head data points available for most months in both the 93/94 and the 03/04 calibration periods. Heads for the missing months were estimated using a least squares analysis comparing heads from the same month in different years. Feb 94 and Feb04 heads were estimated using a least squares analysis comparing the heats at this well to those at 130557, 130556, 130472, 130524, 100570, and 130552.	None	Used in definition of boundary conditions
UF	112128	I75-MZ2	416556.67	668295.47	Daily head data points for the 03/04 calibration period provided by SAJ. Heads for the 93/94 calibration period were estimated using a least squares analysis comparing the same month in different years.	Available	Used in definition of boundary conditions
UF	112143	BICY-MZ2	554522.19	567147.92	Daily head data points for the 03/04 calibration period provided by SAJ. Heads for the 93/94 calibration period were estimated using a least squares analysis comparing the same month in different years.	Available	Used in definition of boundary conditions

Table C2: Description of data availability and decisions for inclusion in the definition of side boundary conditions for aquifer layers (not including Surficial Aquifer System).

Layer	SAJ Model ID	Well Name(s)	X	Y	Water Level Data Availability	TDS Data Availability	Boundary Head Decisions
UF	112158	ENP-100	787244.43	381470.63	Daily head data points for the 03/04 calibration period provided by SAJ. (Missing first 9 days of Oct 2003.) Heads for the 93/94 calibration period were estimated using a least squares analysis comparing the same month in different years.	Available	Used in definition of boundary conditions
MF	120082	OR0673	650975.03	1476090.08	Daily head data points for the 03/04 calibration period provided by SAJ. Heads for the 93/94 calibration period were estimated using a least squares analysis comparing the same month in different years.	Available	Used in definition of boundary conditions
MF	100965	USGS 282341081040101 COCOA A WELL	634712.70	1476321.99	Daily head data points for the 93/94 and 03/04 calibration periods provided by SAJ	Available	Used in definition of boundary conditions (Averaged with 120051)
MF	100975	USGS 282530081054201 COCOA 7	625632.23	1487233.30	One head data point (4/20/94) provided by SAJ.	Available	Removed – sparse data

Table C2: Description of data availability and decisions for inclusion in the definition of side boundary conditions for aquifer layers (not including Surficial Aquifer System).

Layer	SAJ Model ID	Well Name(s)	X	Y	Water Level Data Availability	TDS Data Availability	Boundary Head Decisions
MF	120051	OR0615	618650.42	1487391.80	Daily head data points for the 03/04 calibration period provided by SAJ. Heads for the 93/94 calibration period were estimated using a least squares analysis comparing the same month in different years.	None	Used in definition of boundary conditions (Averaged with 100965)
MF	100978	USGS 282532081075601	613668.66	1487446.58	Monthly head data points for most months of the 93/94 calibration period and a few months of the 03/04 calibration period provided by SAJ	None	Removed – sparse data. There are other nearby wells with better data to use.
MF	110160	UP211 / SKYLAKE_G	532363.72	1494509.34	Daily head data points for the 03/04 calibration period provided by SAJ. (Missing first 10 days of Oct 2003.) Heads for the 93/94 calibration period were estimated using a least squares analysis comparing the same month in different years.	None	Used for definition of boundary conditions

Table C2: Description of data availability and decisions for inclusion in the definition of side boundary conditions for aquifer layers (not including Surficial Aquifer System).

Layer	SAJ Model ID	Well Name(s)	X	Y	Water Level Data Availability	TDS Data Availability	Boundary Head Decisions
MF	110165	UD209 / ORF-61	484377.19	1504604.68	Daily head data points from 3/11/04 to 12/31/04 provided by SAJ. Some missing months were filled using a least squares analysis comparing the same month in different years. The heads for the months of Jan and Feb for both years were estimated using a least squares analysis comparing the heads at this well to the heads at 120082, 999993, 120081, 130523, and 131046.	Available	Used for definition of boundary conditions

Table C2: Description of data availability and decisions for inclusion in the definition of side boundary conditions for aquifer layers (not including Surficial Aquifer System).

Layer	SAJ Model ID	Well Name(s)	X	Y	Water Level Data Availability	TDS Data Availability	Boundary Head Decisions
MF	130502	ROMP 101 AVPK	358774.33	1499216.64	Daily head data points for the 03/04 calibration period (5/28/04 through 12/31/04) provided by SAJ. Heads in additional months were estimated using a least squares analysis comparing the same month in different years. Heads for Jan, Feb, Mar and Apr for both calibration periods were estimated by a least squares analysis comparing heads at this well to those at 130613, 130986, 100988, 112144, and 112127, which were shown to have the most similar head changes during the periods in question.	None	Removed. (This is also listed as a UF well. 88% UF, 11% MF)
MF	130962	ROMP 90 AVPK	288873.50	1465347.64	Daily head data points for the 93/94 and 03/04 calibration periods provided by SAJ. (Missing Aug 93, Sep93 and part of Oct 93). Heads for the missing months were estimated using a least squares analysis comparing the same month in different years.	None	Used for definition of boundary conditions.

Table C2: Description of data availability and decisions for inclusion in the definition of side boundary conditions for aquifer layers (not including Surficial Aquifer System).

Layer	SAJ Model ID	Well Name(s)	X	Y	Water Level Data Availability	TDS Data Availability	Boundary Head Decisions
MF	130613	ROMP 85 AVPK	229950.53	1422405.65	Monthly head data points for the 03/04 calibration period provided by SAJ. Heads for the 93/94 calibration period were estimated using a least squares analysis comparing heads in the same months, but different years.	None	Used for definition of boundary conditions
MF	100642	USGS 280655082193003 MORRIS BRIDGE SH 3A	228092.59	1377673.05	Daily head data points for the period from 7/6/94 to 7/31/94 provided by SAJ.	None	Removed – too shallow
MF	100640	USGS 280655082193001 MORRIS BRIDGE DEEP WELL 3A	228030.95	1377567.42	Daily head data points for the 93/94 calibration period plus 2 points from the 03/04 calibration period provided by SAJ.	None	Removed - It is 45% UF and 32% MF)
MF	130432	ROMP 67 AVPK	222781.37	1355564.88	One to two head data points for each month of the two calibration periods provided by SAJ.	Available	Used for definition of boundary conditions
MF	100570	USGS 275215082201901 US PHOSPHORIC WELL	223694.57	1288338.94	Monthly head data points for most months in the two calibration periods provided by SAJ.	Available	Used for definition of boundary conditions (Averaged with 130476)

Table C2: Description of data availability and decisions for inclusion in the definition of side boundary conditions for aquifer layers (not including Surficial Aquifer System).

Layer	SAJ Model ID	Well Name(s)	X	Y	Water Level Data Availability	TDS Data Availability	Boundary Head Decisions
MF	130476	ROMP 62 AVPK	231398.13	1283467.51	Daily head data points for the 03/04 calibration period provided by SAJ. Head values for the 93/94 calibration period estimated based on least squares analysis comparing monthly average heads from the same months, but different years.	Available	Used for definition of boundary conditions (Averaged with 100570)
MF	130469	ROMP TR 9-3 OCAL/AVPK	195912.73	1241214.58	Two to four head data points for each month in the 93/94 calibration period and daily head data points for the 03/04 calibration period provided by SAJ.	Available	Used in definition of boundary conditions
MF	100873	USGS 273718082315501 FP&L WELL 1	160125.14	1198349.42	Daily head data points for the 93/94 and 03/04 calibration periods provided by SAJ	None	Used in definition of boundary conditions (averaged with 130552)
MF	100868	USGS 273458082324703 ROMP TR 8-1 UP AVPK	155219.00	1184154.00	Eight head data points for the 93/94 calibration period provided by SAJ	Available	Remove – same as 130552 with sparser data

Table C2: Description of data availability and decisions for inclusion in the definition of side boundary conditions for aquifer layers (not including Surficial Aquifer System).

Layer	SAJ Model ID	Well Name(s)	X	Y	Water Level Data Availability	TDS Data Availability	Boundary Head Decisions
MF	130552	ROMP TR 8-1 UP AVPK	155334.48	1184331.80	Three to five head data points for each month in the 93/94 calibration period and daily head data points for the 03/04 calibration period provided by SAJ	Available	Used in definition of boundary conditions (averaged with 100873)

Table C2: Description of data availability and decisions for inclusion in the definition of side boundary conditions for aquifer layers (not including Surficial Aquifer System).

Layer	SAJ Model ID	Well Name(s)	X	Y	Water Level Data Availability	TDS Data Availability	Boundary Head Decisions
MF	130553	ROMP TR 8-1 AVPK	155334.48	1184331.80	Three to five head data points for each month in the 93/94 calibration period and daily head data points for the 03/04 calibration period provided by SAJ	Available	The TDS here is exceptionally high. According to Emily, excessive pumping here has caused upconing of saline water. This well has a TDS about 1 order of magnitude higher than 130552 at about the same location, but higher in the aquifer. Since the upconing will not be simulated in the model, this well is removed.

Table C2: Description of data availability and decisions for inclusion in the definition of side boundary conditions for aquifer layers (not including Surficial Aquifer System).

Layer	SAJ Model ID	Well Name(s)	X	Y	Water Level Data Availability	TDS Data Availability	Boundary Head Decisions
MF	130556	ROMP TR 7-4 AVPK	173085.87	1127548.16	No data provided by SAJ. NAP obtained daily head data points for the 03/04 calibration period. Head values for the 93/94 calibration period estimated based on least squares analysis comparing monthly average heads from the same months, but different years.	Available	Used in definition of boundary conditions
MF	130022	ROMP TR 3-3 AVPK	222846.45	944410.16	Two to five head data points for each month from 10/93 to 7/93 plus daily head data points for the 03/04 calibration period provided by SAJ. Missing months (August and September 1993) estimated based on least squares analysis comparing monthly average heads from the same months, but different years.	Available	Used in definition of boundary conditions

Table C2: Description of data availability and decisions for inclusion in the definition of side boundary conditions for aquifer layers (not including Surficial Aquifer System).

Layer	SAJ Model ID	Well Name(s)	X	Y	Water Level Data Availability	TDS Data Availability	Boundary Head Decisions
MF	112166	IWA-MZL	293008.00	767990.45	Daily head data points beginning 11/21/03 and continuing through the 03/04 calibration period provided by SAJ. Heads for the 93/94 calibration period and the month of 10/93 estimated based on least squares analysis comparing monthly average heads from the same months, but different years.	Available (because well is high, this TDS is not used in the initial conditions interpolation.)	Used in definition of boundary conditions
MF	112115	FMB-MZL	350747.43	785108.32	Daily head data points from 5/19/04 to 12/31/04 provided by SAJ. Heads for some missing months estimated based on least squares analysis comparing monthly average heads from the same months, but different years. Heads for Jan through Apr of both years estimated using a least squares analysis comparing heads at this well to heads at 112166, 100988, 100977, 130613, and 112142	Available	Used in definition of boundary conditions

Table C2: Description of data availability and decisions for inclusion in the definition of side boundary conditions for aquifer layers (not including Surficial Aquifer System).

Layer	SAJ Model ID	Well Name(s)	X	Y	Water Level Data Availability	TDS Data Availability	Boundary Head Decisions
MF	112141	BICY-MZ3	554522.19	567147.92	Daily head data points for the 03/04 calibration period provided by SAJ. Head values for the 93/94 calibration period estimated based on least squares analysis comparing monthly average heads from the same months, but different years.	Available	Used in definition of boundary conditions
LF1	120052	OR0614	618639.70	1487388.78	Daily head data points for the 03/04 calibration period provided by SAJ. Head values for the 93/94 calibration period estimated based on least squares analysis comparing monthly average heads from the same months, but different years.	Available	Used in definition of boundary condition (Averaged with 100980, 120078 and 100969)
LF1	100979	USGS 282533081082202 COCOA C (ZONE 1)	611347.46	1487550.20	17 head data points covering most of the 93/94 calibration period and some of the 03/04 calibration period provided by SAJ Head values for missing months estimated based on least squares analysis comparing monthly average heads from the same months, but different years.	Available, but removed based on conversation with Emily 22 Apr 09	Moved to boulder zone

Table C2: Description of data availability and decisions for inclusion in the definition of side boundary conditions for aquifer layers (not including Surficial Aquifer System).

Layer	SAJ Model ID	Well Name(s)	X	Y	Water Level Data Availability	TDS Data Availability	Boundary Head Decisions
LF1	100980	USGS 282533081082204 COCOA C (ZONE 3)	611347.46	1487550.20	16 head data points covering most of the 93/94 calibration period and some of the 03/04 calibration period provided by SAJ Head values for missing months estimated based on least squares analysis comparing monthly average heads from the same months, but different years.	Available	Used in definition of boundary condition (Averaged with 120052, 120078 and 100969)
LF1	120078	OR0676	593335.24	1515450.47	Daily head data points for the 03/04 calibration period provided by SAJ. Head values for the 93/94 calibration period estimated based on least squares analysis comparing monthly average heads from the same months, but different years.	None	Used in definition of boundary condition (Averaged with 120052, 100980 and 100969)

Table C2: Description of data availability and decisions for inclusion in the definition of side boundary conditions for aquifer layers (not including Surficial Aquifer System).

Layer	SAJ Model ID	Well Name(s)	X	Y	Water Level Data Availability	TDS Data Availability	Boundary Head Decisions
LF1	100969	USGS 282406081093602	604728.96	1478771.86	13 head data points covering most of the 93/94 calibration period and some of the 03/04 calibration period provided by SAJ Head values for missing months estimated based on least squares analysis comparing monthly average heads from the same months, but different years.	None	Used in definition of boundary condition (Averaged with 120052, 100980 and 120078)
LF1	120059	OR0467	536076.97	1537120.31	25 head data points covering most of the 93/94 calibration period and all months of the 03/04 calibration period provided by SAJ Head values for missing months estimated based on least squares analysis comparing monthly average heads from the same months, but different years.	None	Used in definition of boundary condition

Table C2: Description of data availability and decisions for inclusion in the definition of side boundary conditions for aquifer layers (not including Surficial Aquifer System).

Layer	SAJ Model ID	Well Name(s)	X	Y	Water Level Data Availability	TDS Data Availability	Boundary Head Decisions
LF1	112127	I75-MZ3	416556.67	668295.47	Daily head data points for the 03/04 calibration period provided by SAJ. Head values for the 93/94 calibration period estimated based on least squares analysis comparing monthly average heads from the same months, but different years.	Available	Used in definition of boundary condition
LF1	112144	BICY-MZ4	554522.19	567147.92	Daily head data points for the 03/04 calibration period provided by SAJ. Head values for the 93/94 calibration period estimated based on least squares analysis comparing monthly average heads from the same months, but different years.	Available	Used in definition of boundary condition

Table C2: Description of data availability and decisions for inclusion in the definition of side boundary conditions for aquifer layers (not including Surficial Aquifer System).

Layer	SAJ Model ID	Well Name(s)	X	Y	Water Level Data Availability	TDS Data Availability	Boundary Head Decisions
BZ	120053	OR0613	618639.70	1487388.78	Daily head data points for the 03/04 calibration period provided by SAJ. Head values for the 93/94 calibration period estimated based on least squares analysis comparing monthly average heads from the same months, but different years.	None. The interpolated value in the BZ is about 34000. Since this well is actually in the LC, the EFH will be calculate using the interpolated LC TDS, which is 14800.	Used in definition of boundary condition (averaged with 100979 and 120079)

Table C2: Description of data availability and decisions for inclusion in the definition of side boundary conditions for aquifer layers (not including Surficial Aquifer System).

Layer	SAJ Model ID	Well Name(s)	X	Y	Water Level Data Availability	TDS Data Availability	Boundary Head Decisions
BZ	100979	USGS 282533081082202 COCOA C (ZONE 1)	611347.46	1487550.20	17 head data points covering most of the 93/94 calibration period and some of the 03/04 calibration period provided by SAJ Head values for missing months estimated based on least squares analysis comparing monthly average heads from the same months, but different years.	Available. This value is not used for the TDS starting condition interpolation. The interpolated TDS at this location is about 34000. The EFH will be calculated using the measured value of 7620.	Used in definition of boundary condition (averaged with 120053 and 120079)

Table C2: Description of data availability and decisions for inclusion in the definition of side boundary conditions for aquifer layers (not including Surficial Aquifer System).

Layer	SAJ Model ID	Well Name(s)	X	Y	Water Level Data Availability	TDS Data Availability	Boundary Head Decisions
BZ	120079	OR0668	593335.24	1515450.47	Daily head data points for the 03/04 calibration period provided by SAJ. Head values for the 93/94 calibration period estimated based on least squares analysis comparing monthly average heads from the same months, but different years.	None. The interpolated value in the BZ is about 34000. Since this well is actually in the LC, the EFH will be calculate using the interpolated LC TDS, which is 9926.	Used in definition of boundary conditions (averaged with 120053 and 100979)
BZ	120060	OR0465	536035.57	1536998.24	25 head data points covering most of the 93/94 calibration period and all months of the 03/04 calibration period provided by SAJ Head values for missing months estimated based on least squares analysis comparing monthly average heads from the same months, but different years.	None	Used in definition of boundary conditions

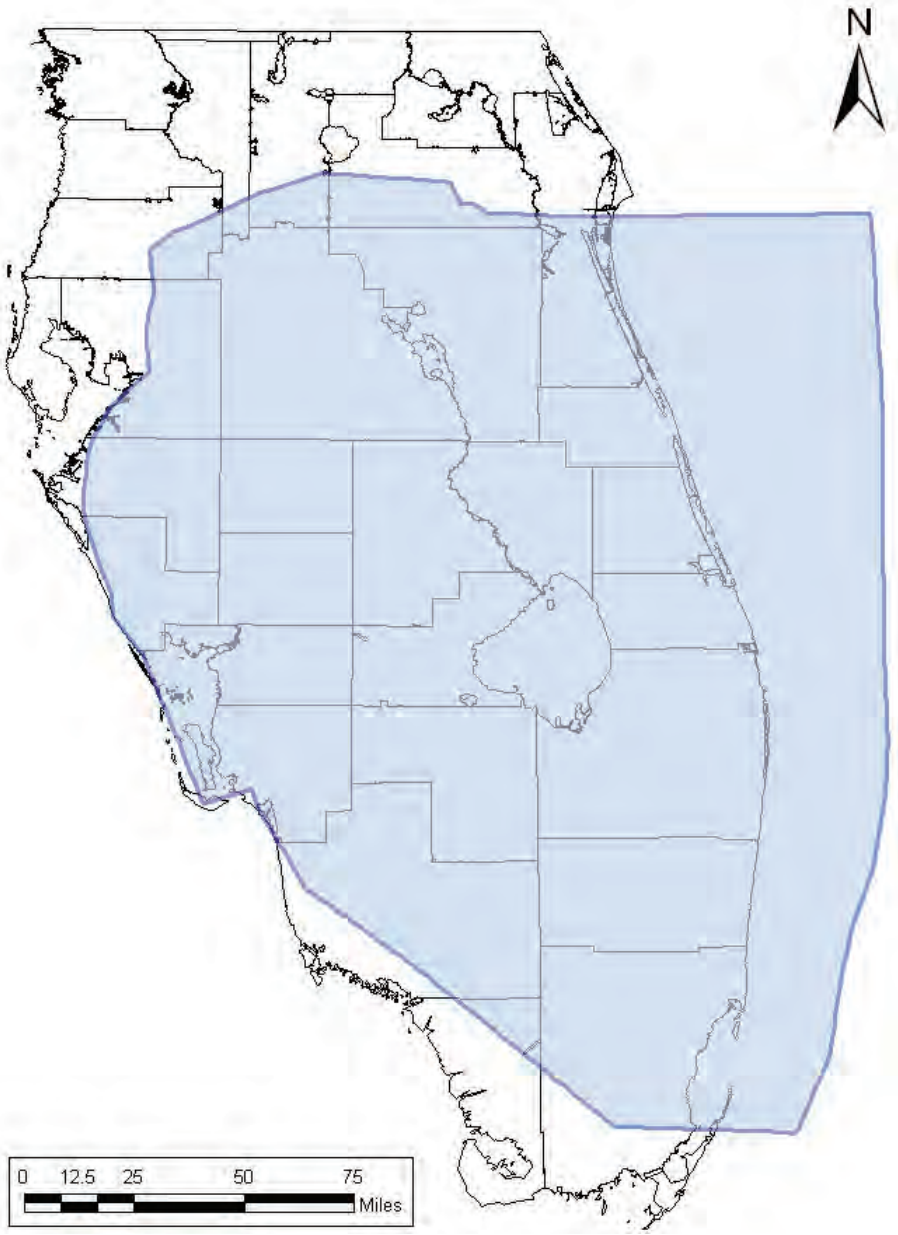

Notes:

This model boundary was developed based on bench-scale and Phase 1 modeling.

North, west and south boundaries are placed to pass through convenient monitoring wells.

The east boundary roughly corresponds with the layer outcrops in the Atlantic Ocean floor. Layers above the Boulder Zone do not extend all the way to the pictured boundary, but cut off at the approximate location of the ocean outcrop. The SAS (surface layer) extends only to the coast line on the east coast.

Model Boundary

Final Groundwater Model Calibration Report

Figure C1-1

April 2010

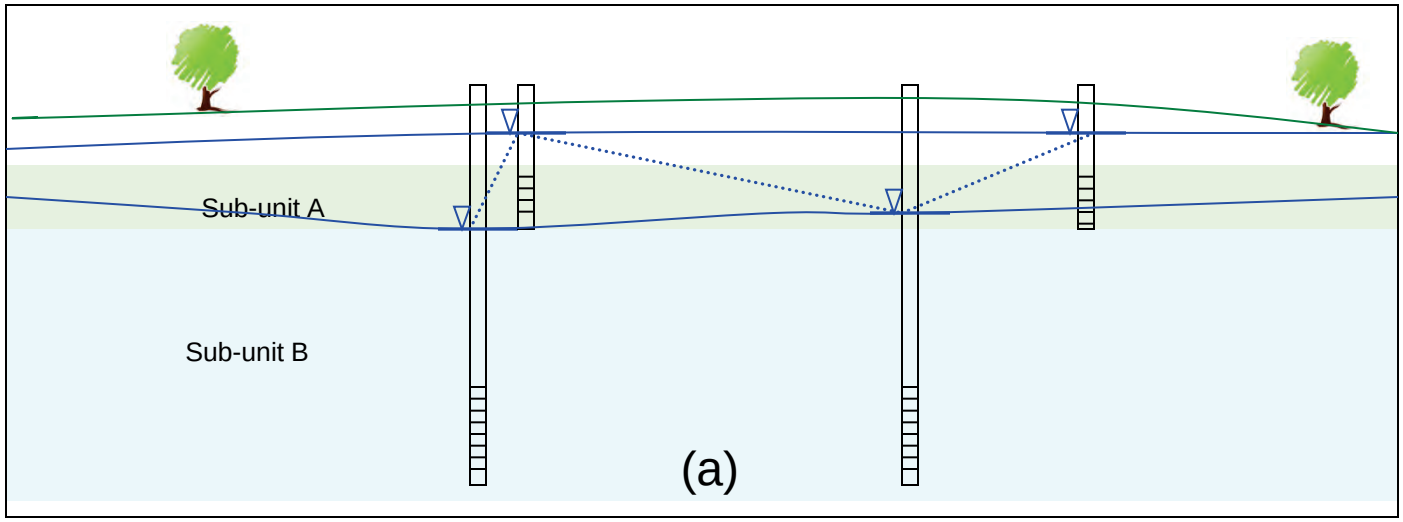

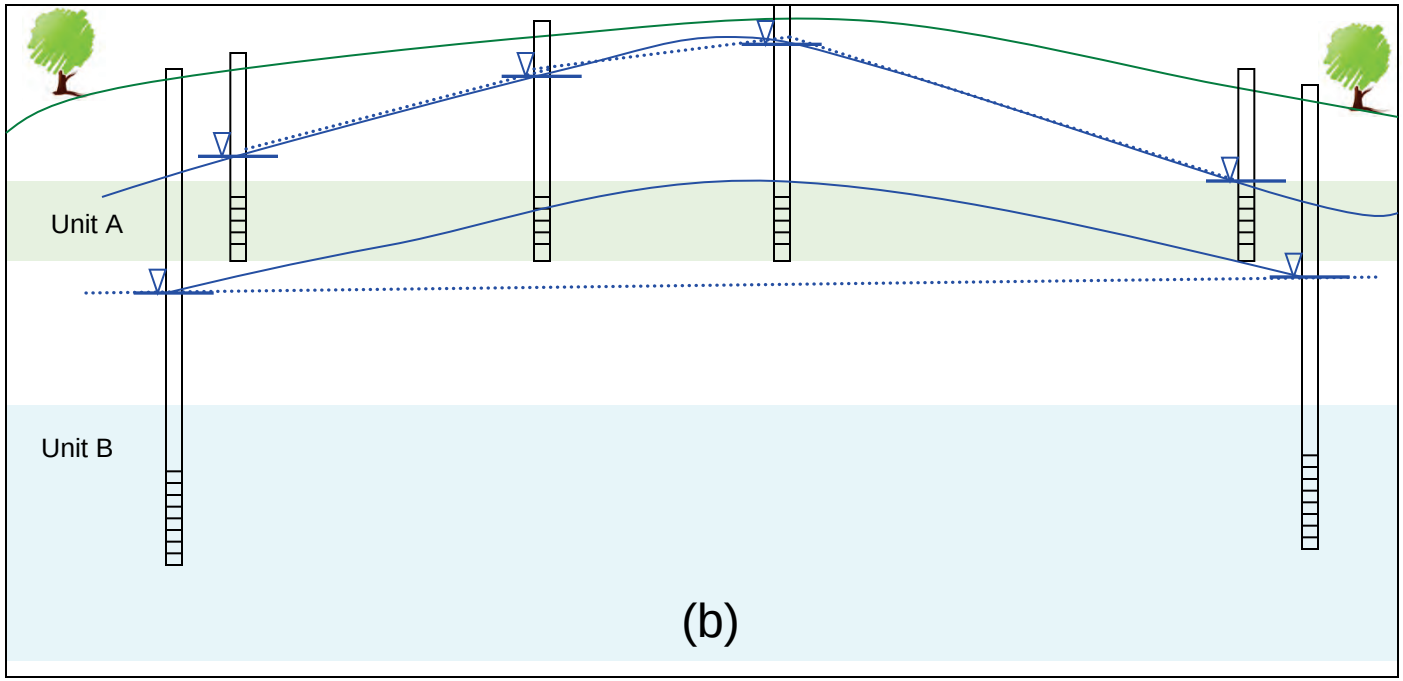

Legend

- Ground Surface
- Water Table
- Interpolated Water Table
- Measured Water Level
- Monitoring Well

Notes:

(a) Because the hydrogeologic framework had to be simplified for the regional ASR model, sometimes there are areas where more than one distinct sub-unit is included in a single unit of the model. When wells are screened in separate units and are placed close together, the disparate heads can cause steep slopes in the linearly interpolated heads when all wells are used.

(b) Deeper layers often have sparser data sets. In this example, the center of the image is a recharge area and it affects both shallow and deep aquifers. Because of the sparse data in Unit B, the recharge area is not delineated by the available data. In some cases this can lead to significant differences in the interpolated water tables between deep and shallow zones.

Interpolation Problems for FAS Boundary Conditions

Final Groundwater Model Calibration Report

Figure C2-1

April 2010

Linearly Interpolate Observed Head

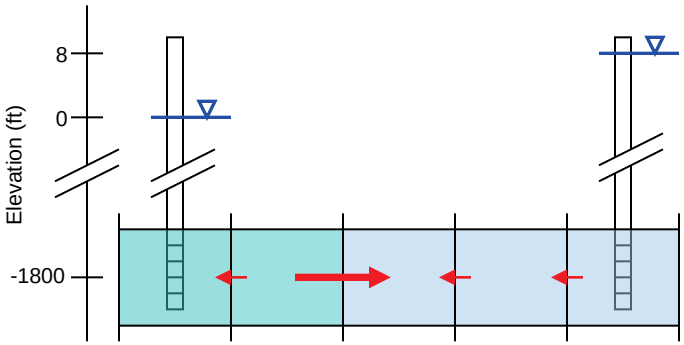

TDS (mg/L)	35000	35000	1000	500	100
Head (ft)	0.0	2.0	4.0	6.0	8.0
EFH (ft)	55.5	57.6	5.6	6.8	8.2

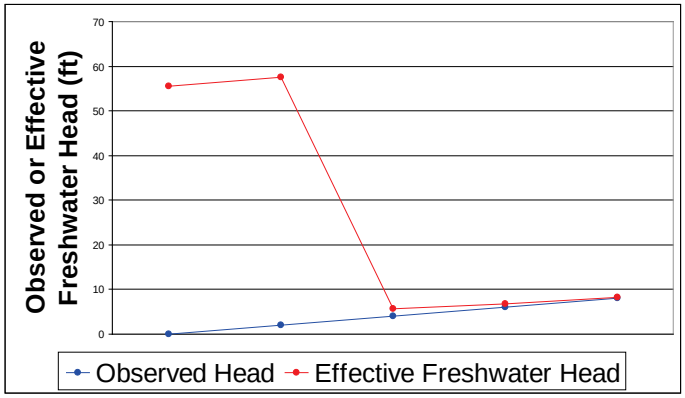

(a)

Linearly Interpolate Equivalent Freshwater Head

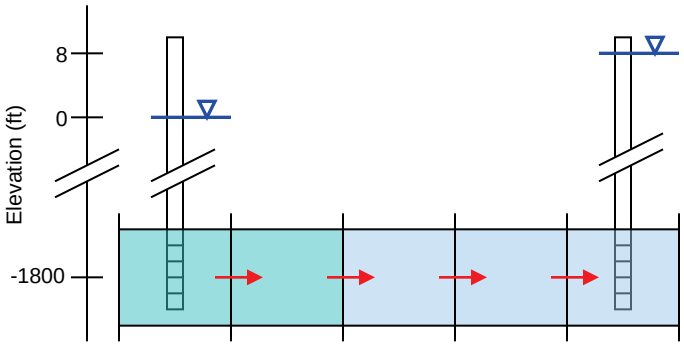

TDS (mg/L)	35000	35000	1000	500	100
EFH (ft)	55.5	43.7	31.8	20.0	8.2
Head (ft)	0.0	-11.5	30.2	19.2	8.0

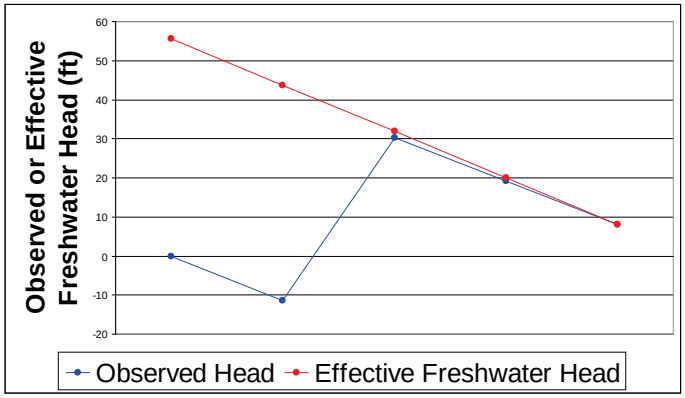

(b)

Legend

- Grid Cell (high TDS)
- Grid Cell (low TDS)
- GW Flow Direction
- Measured Water Level
- Monitoring Well

Notes:

(a) In this cartoon, two heads have been measured and a linear interpolation of the measured heads is used to assign boundary conditions to the three cells between the monitoring wells. Because a sudden change in TDS occurs between these wells, the Equivalent freshwater head results in unusual flow conditions between the measured heads. Since the model solves the flow equations using the Equivalent freshwater heads, these steep slopes and slope changes may prove difficult for the solver.

(b) In the second cartoon, the same measured heads have been converted to Equivalent freshwater heads and the linear interpolation was performed using these Equivalent freshwater heads. This makes the flow conditions smooth and regular and will be simpler for the model to resolve. Either condition fits the measured data, but the second will result in a more stable model.

Interpolation Problems for FAS Boundary Conditions

Final Groundwater Model Calibration Report

Figure C2-2

April 2010

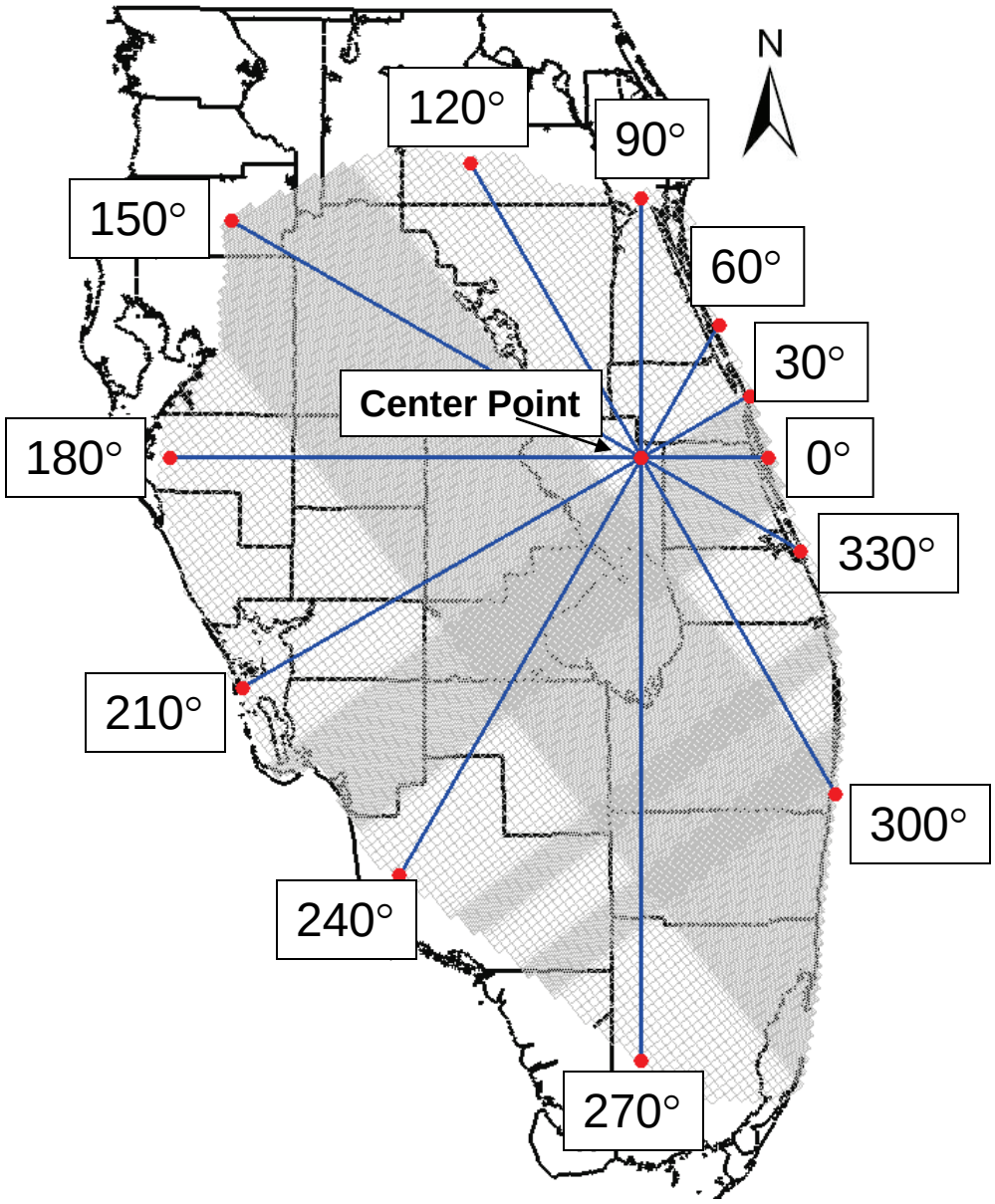

Legend

- County Boundaries
- SEAWAT Cell Edges
- Azimuth Angle Lines

Azimuth Angle Locations

Figure C2-3

Final Groundwater Model Calibration Report

April 2010

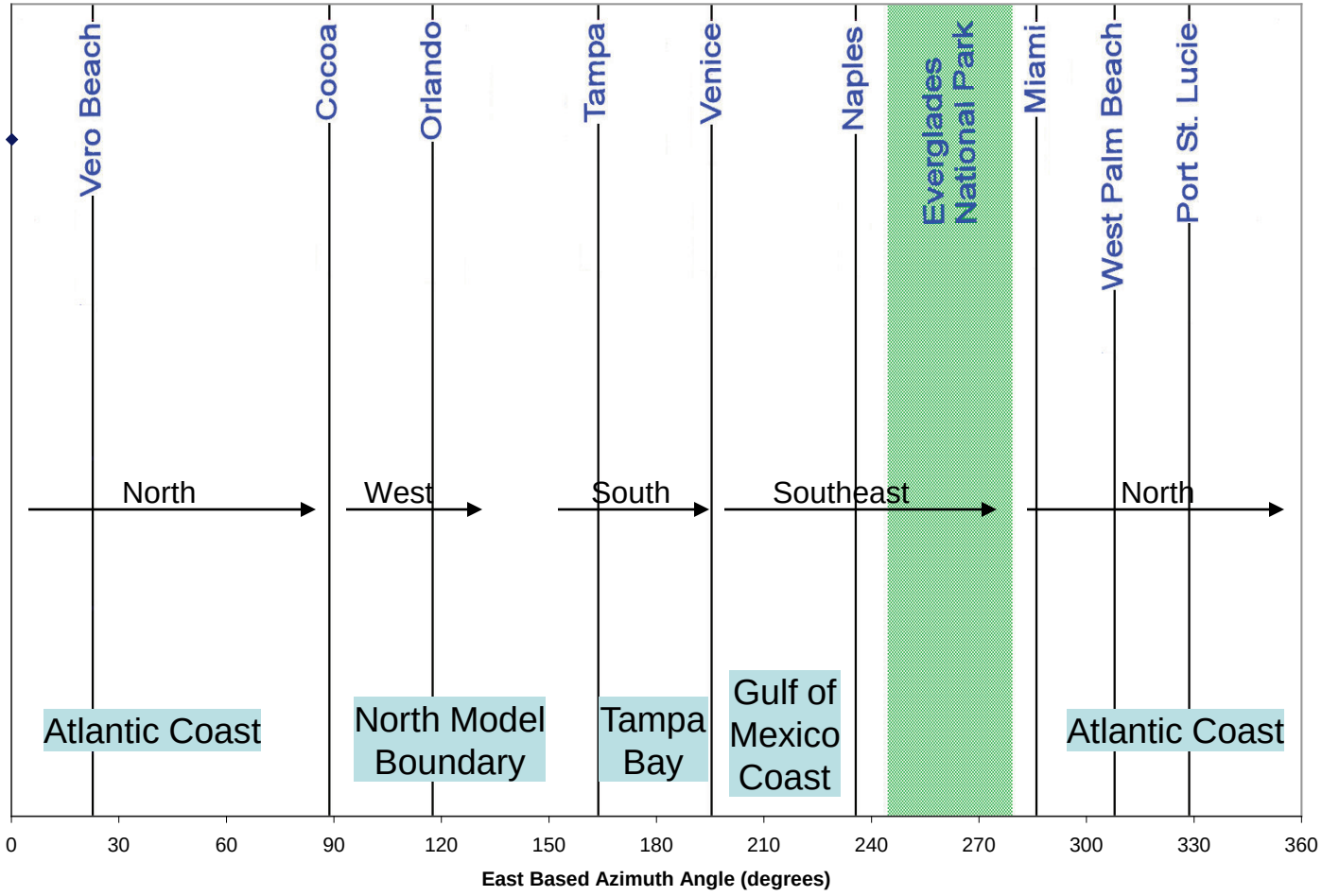

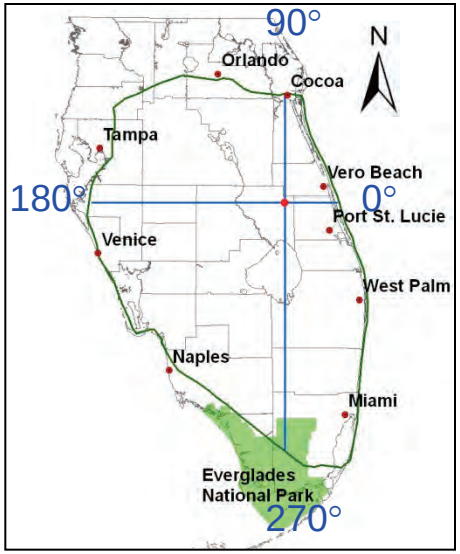

Layout of Azimuth Figures

Figure C2-4

Final Groundwater Model Calibration Report

April 2010

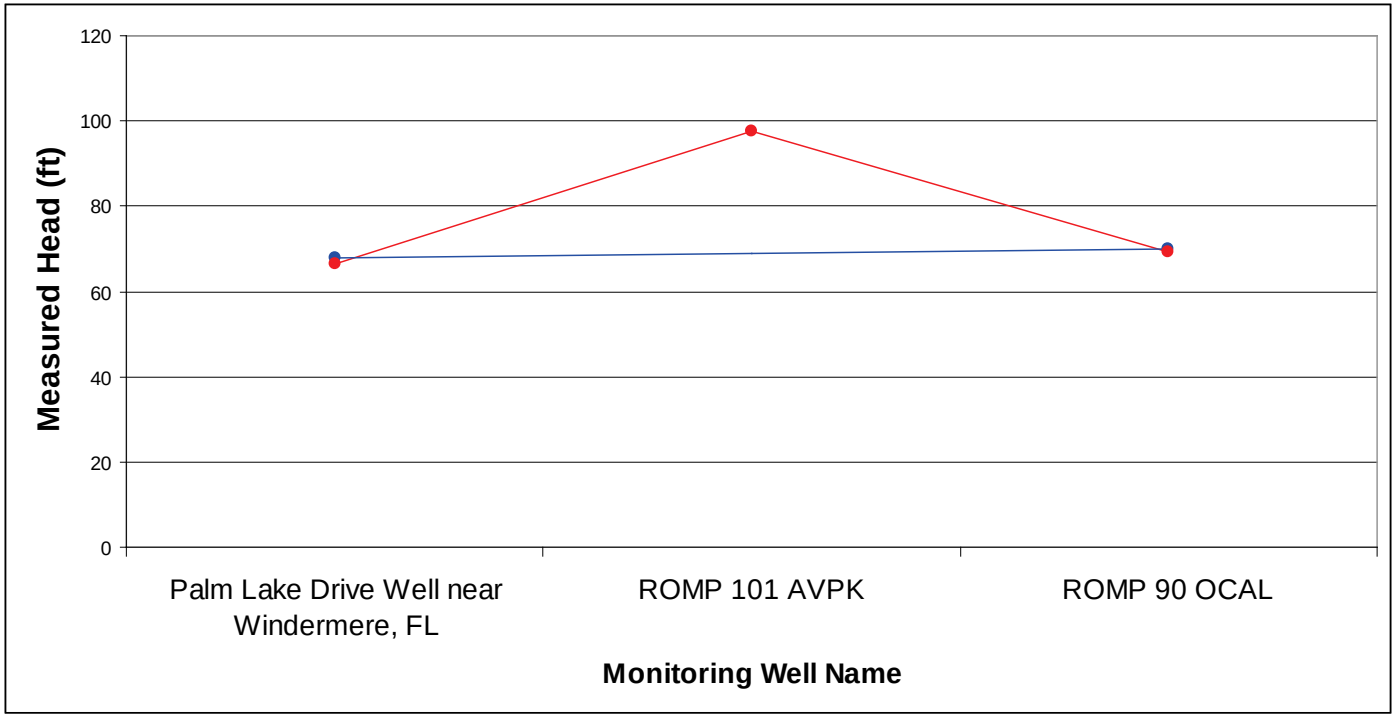

Legend

- Apr 2004 Measured Heads
- May 2004 Measured Heads
- Apr 2004 Interpolation
- May 2004 Interpolation

Notes:

This plot shows the heads measured at three wells designated as boundary wells in the Upper Floridan Aquifer. They are located in the north of the model. In May 2004, the water levels in all three wells were measured, showing a higher head around ROMP 101 (Polk County recharge area). Because this well was not measured in April, a strict linear interpolation of the available data does not show this high water level.

Making changes like this to the boundary conditions from month to month can cause difficulties in calibration of the model and may contribute to its instability. In this case, the model would be forced to add nearly 15 feet of water in a single stress period. This is not likely to happen naturally.

For this reason, it is important that data be available for all months of the calibration and validation period for all wells used to develop boundary conditions.

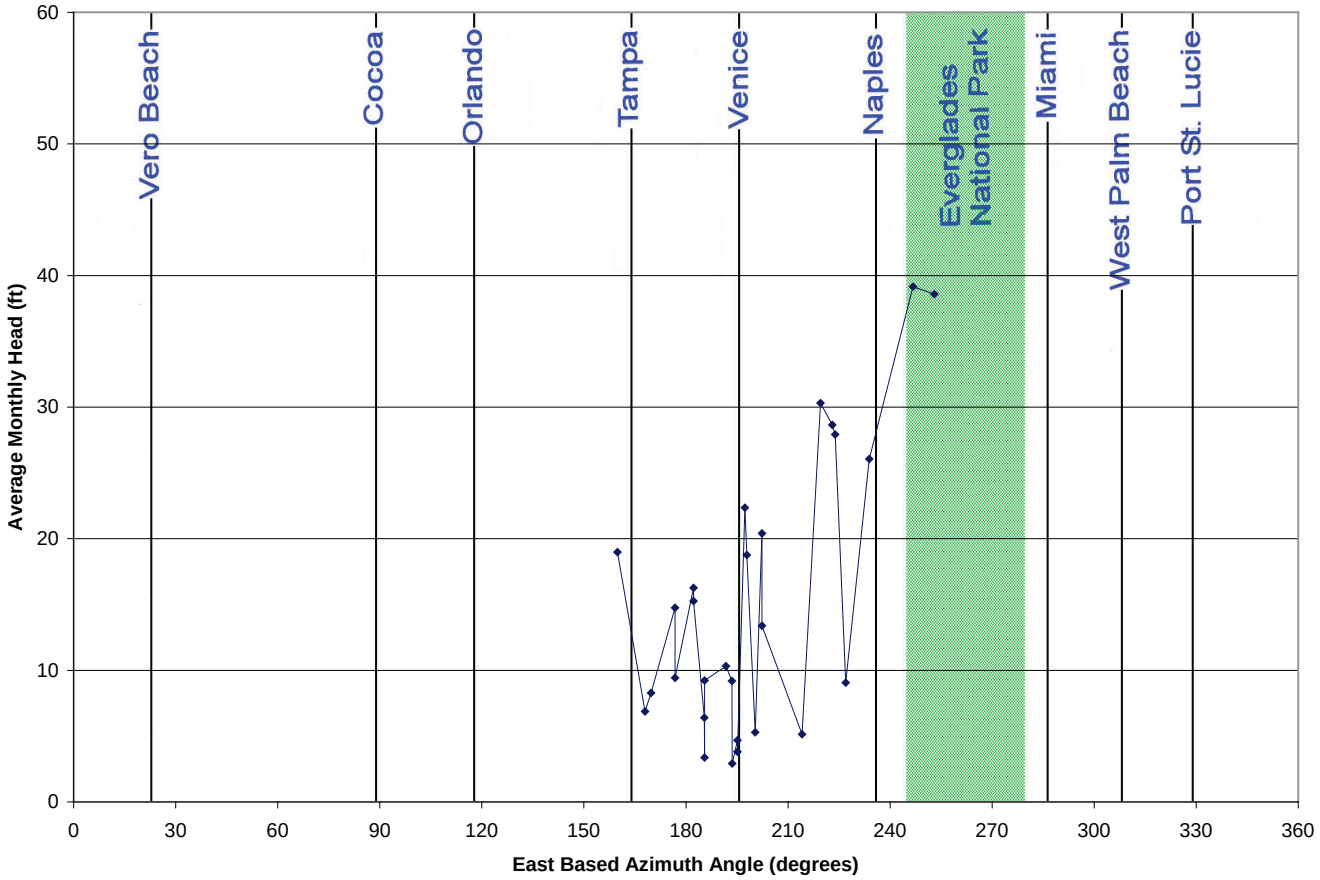

Legend

Measured IAS head data

Notes:

1. Well locations are along the western coast of Florida, extending from just north of Tampa to the northern borders of Everglades National Park.
2. See the inset map below for locations of the monitoring wells as defined by their east-based azimuth angle.
3. Figures C2-3 and C2-4 show the method used to create these plots.

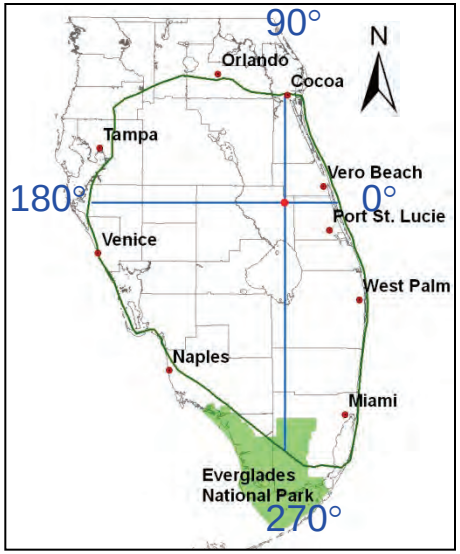

Observed Head Distributions and Screen Elevations for IAS Monitoring Wells

Final Groundwater Model Calibration Report

Figure C2-6

April 2010

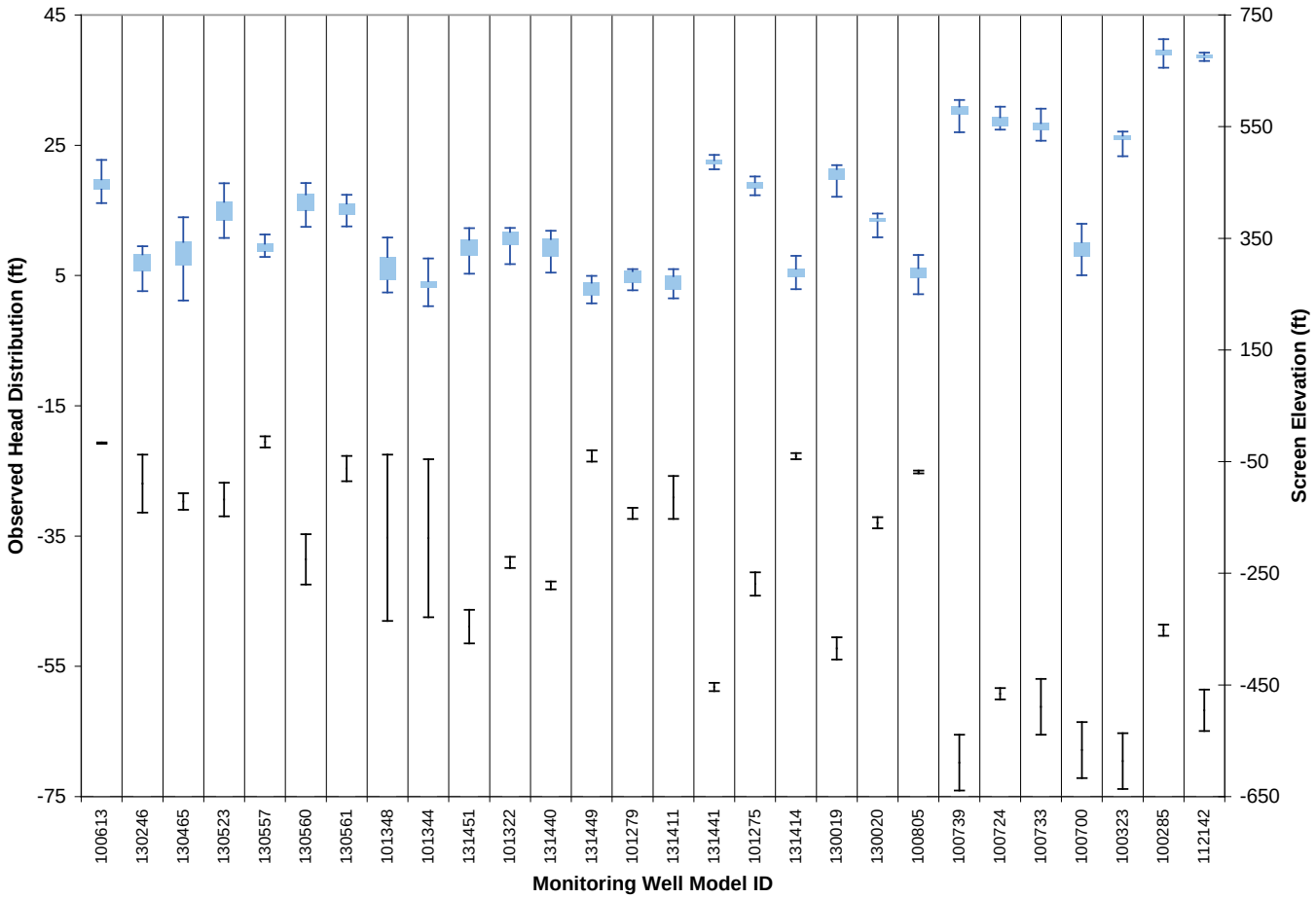

Legend

Observed Head Distribution (left axis)

- Maximum Head
- Upper Quartile
- Lower Quartile
- Minimum Head

Screen Elevation (right axis)

- Top of Screen
- Bottom of Screen

Notes:

1. Well locations are shown in the map below as blue squares.
2. Wells are shown in the plot in order from north to south, with northernmost wells at left.
3. Head statistics (maximum, minimum and quartiles) were performed on monthly average head values for the calibration and validation periods only.

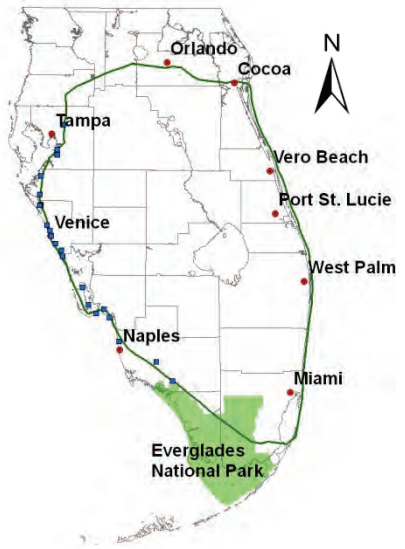

Observed Head Distributions and Screen Elevations for IAS Monitoring Wells

Final Groundwater Model Calibration Report

Figure C2-7

April 2010

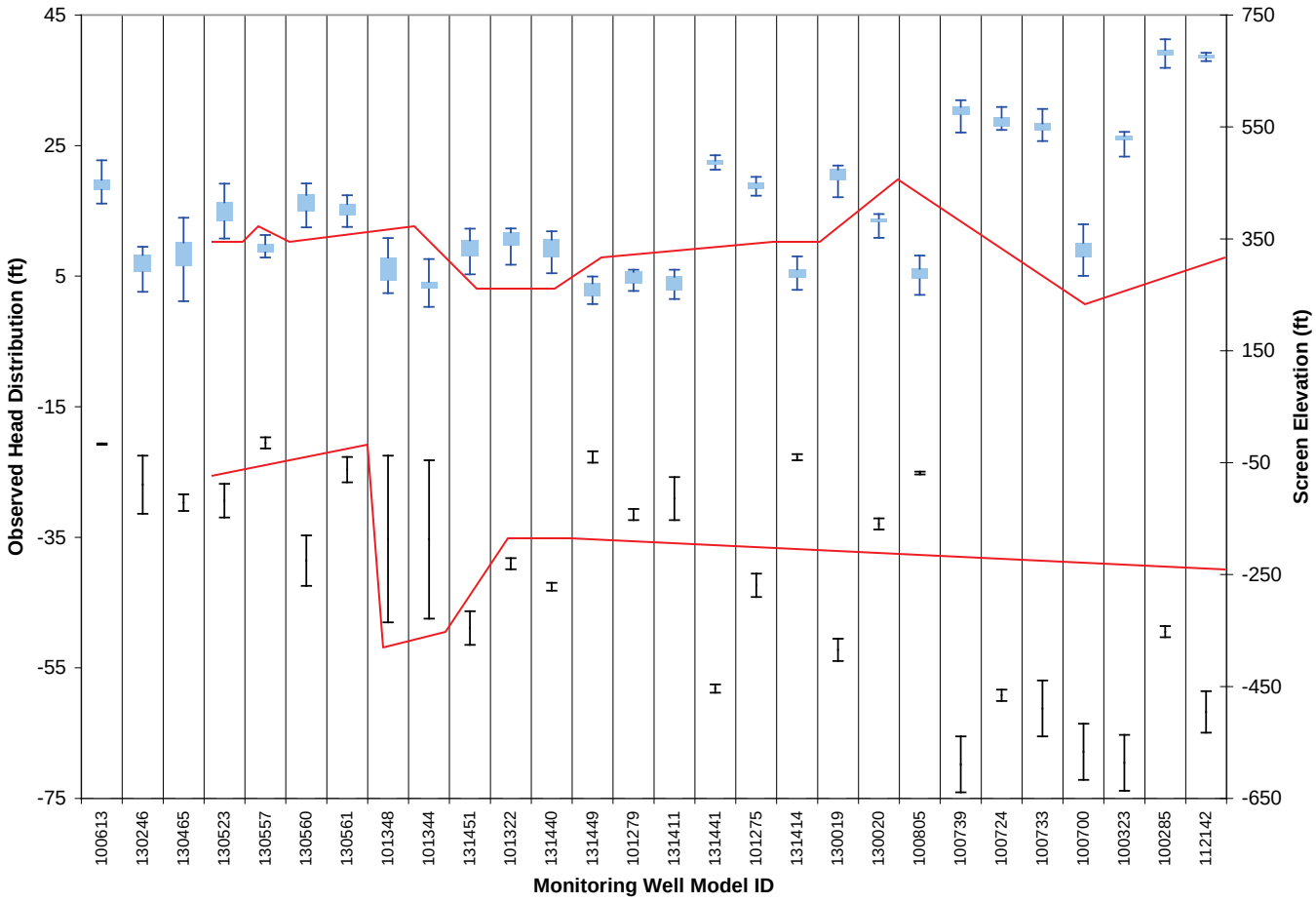

Legend

Observed Head Distribution (left axis)

- Maximum Head
- Upper Quartile
- Lower Quartile
- Minimum Head

Screen Elevation (right axis)

- Top of Screen
- Bottom of Screen

Estimated division for upper and lower sections of the aquifer

Notes:

1. Well locations are shown in the map below as blue squares.
2. Wells are shown in the plot in order from north to south, with northernmost wells at left.
3. The red lines indicate the estimated division of wells belonging to the higher section of the aquifer and those belonging to the lower section of the aquifer. See the text for more details.

Observed Head Distributions and Screen Elevations for IAS Monitoring Wells

Final Groundwater Model Calibration Report

Figure C2-8

April 2010

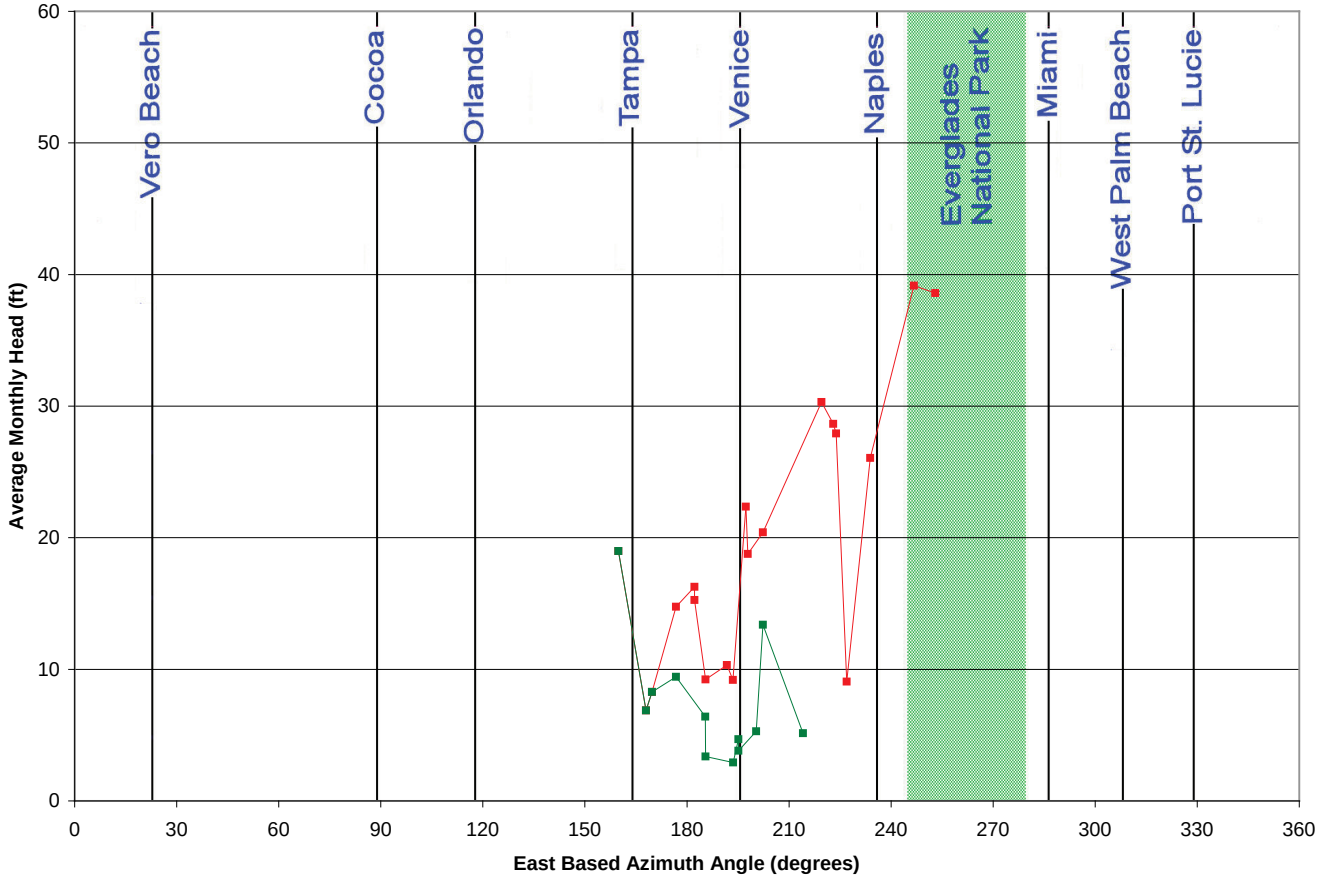

Legend

- Measured IAS head data – upper section
- Measured IAS head data – lower section

Notes:

1. Well locations are along the western coast of Florida, extending from just north of Tampa to the northern borders of Everglades National Park.
2. See the inset map below for locations of the monitoring wells as defined by their east-based azimuth angle.
3. Figures C2-3 and C2-4 in this appendix show the method used to create these plots.

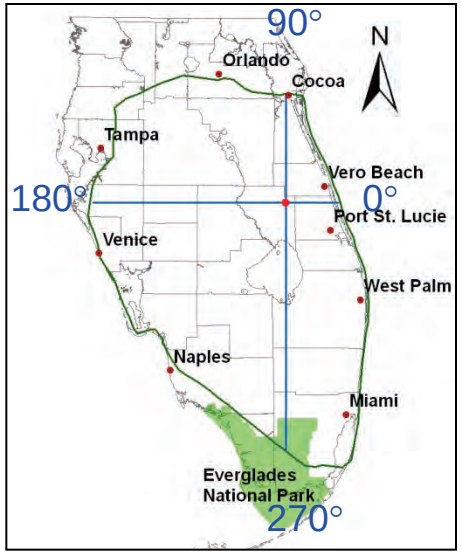

Observed Head Distributions and Screen Elevations for IAS Monitoring Wells

Final Groundwater Model Calibration Report

Figure C2-9

April 2010

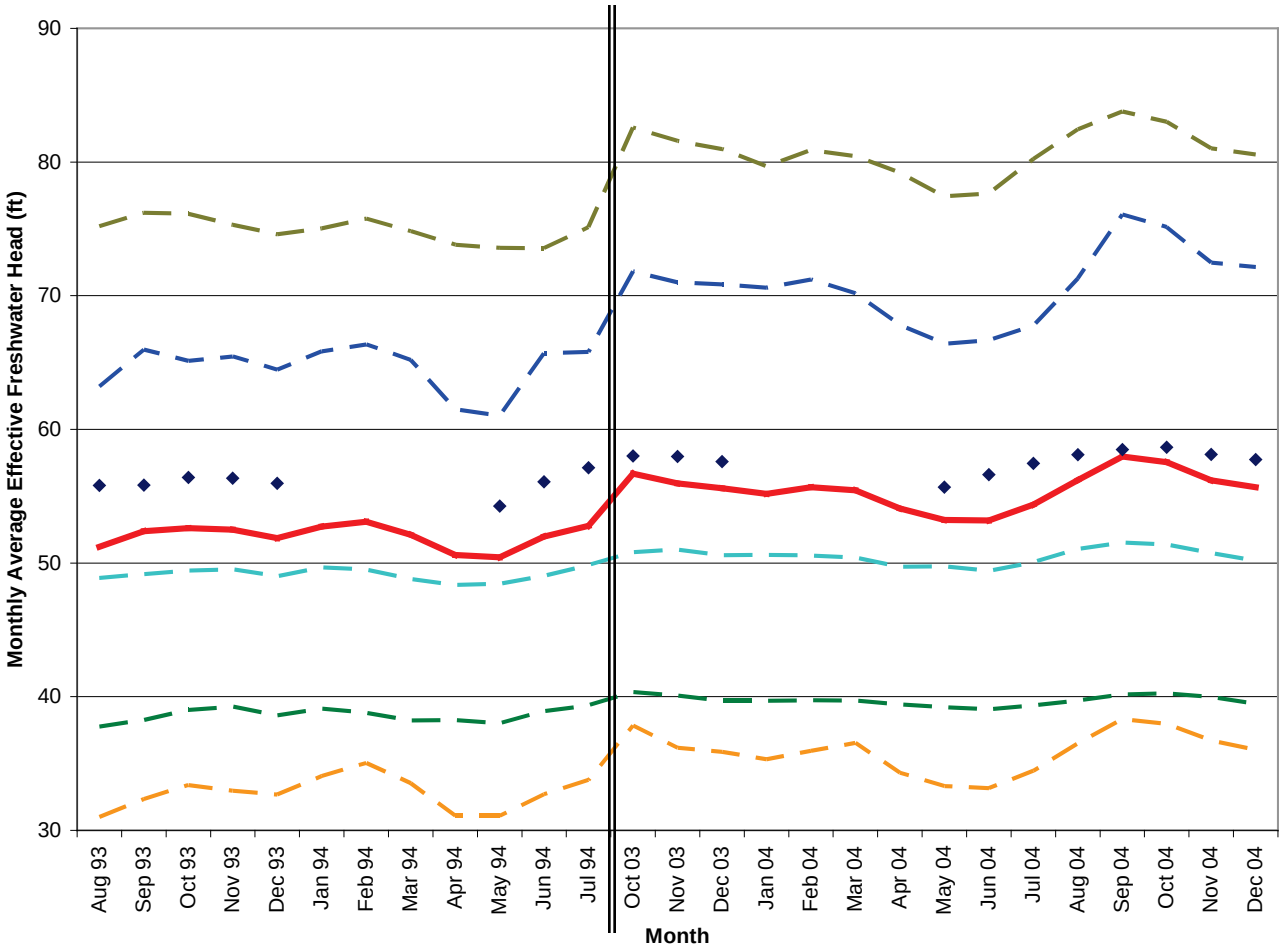

Legend

- FMB-MZL (APPZ)
- IWA-MZL (APPZ)
- Cocoa D (UF)
- Palm Lake Drive (UF)
- ROMP 85 AVPK (APPZ)
- BICY-MZ1 (IAS)
- Average of Five Complete data sets

Notes:

1. Note that since this plot only shows data for the calibration and validation periods, the x-axis is not linear – it skips directly from July 1994 to October 2003.

2. Locations of the wells are shown in the map below.

3. The five complete data sets (dotted lines) are statistically best correlated with the existing data at FMB-MZL. The average of these five data sets is shown with a thick red line.

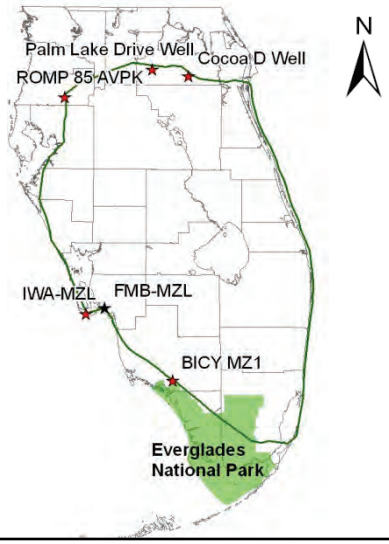

Equivalent Freshwater Heads for FMB-MZL and the five best correlated wells

Final Groundwater Model Calibration Report

Figure C2-10

April 2010

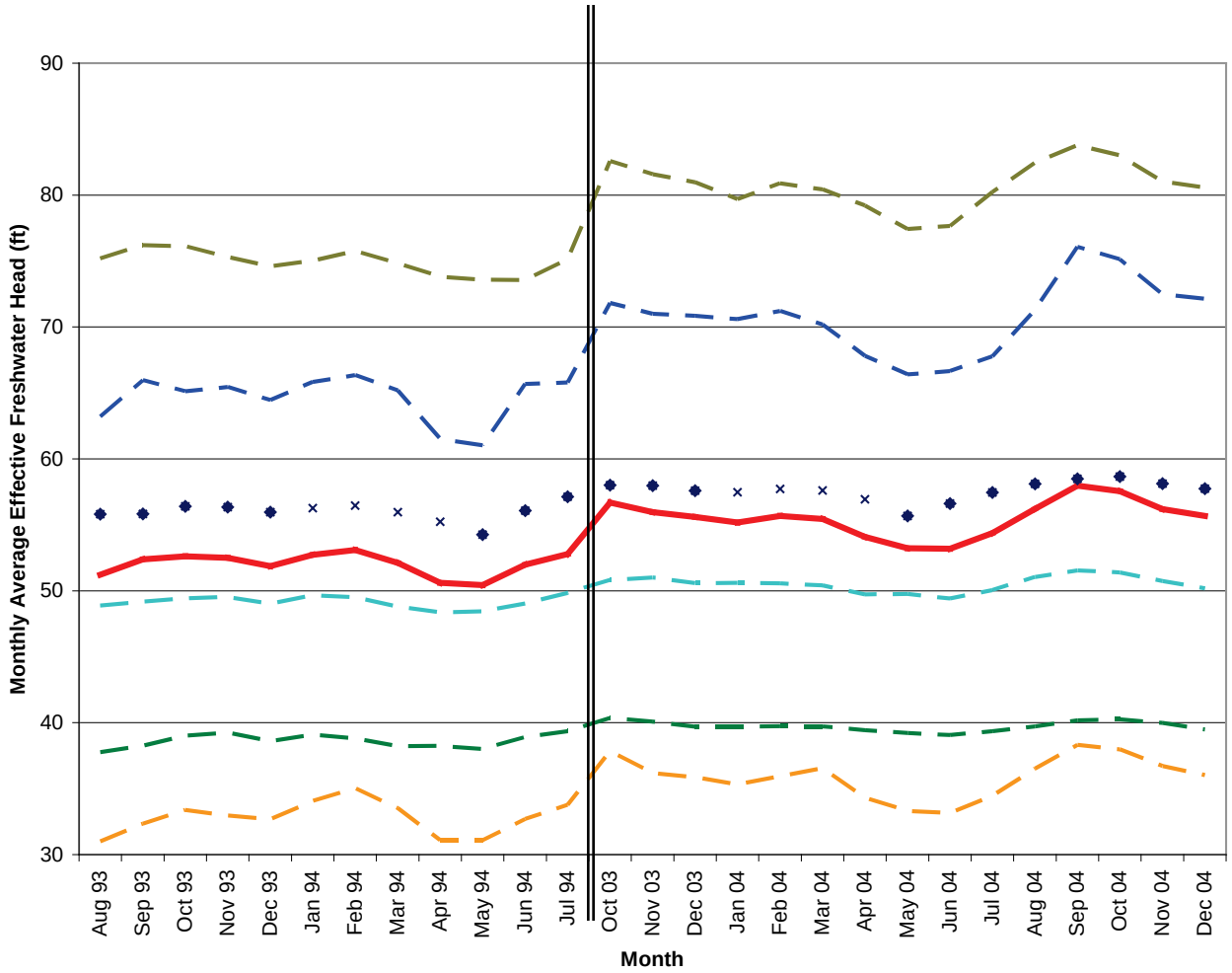

Legend

- FMB-MZL (APPZ)
  - Actual Data
  - Estimated Data
- IWA-MZL (APPZ)
- Cocoa D (UF)
- Palm Lake Drive (UF)
- ROMP 85 AVPK (APPZ)
- BICY-MZ1 (IAS)
- Average of Five Complete data sets

Notes:

1. Note that since this plot only shows data for the calibration and validation periods, the x-axis is not linear – it skips directly from July 1994 to October 2003.

2. Locations of the wells are shown in the map below.

3. The five complete data sets (dotted lines) are statistically best correlated with the existing data at FMB-MZL. The average of these five data sets (thick red line) was used to fill in the missing data (small blue x's).

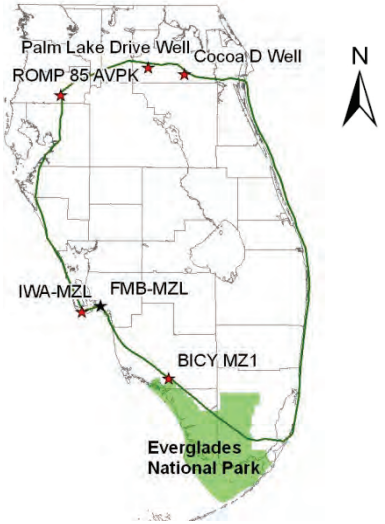

Equivalent Freshwater Heads for FMB-MZL and the five best correlated wells

Final Groundwater Model Calibration Report

Figure C2-11

April 2010

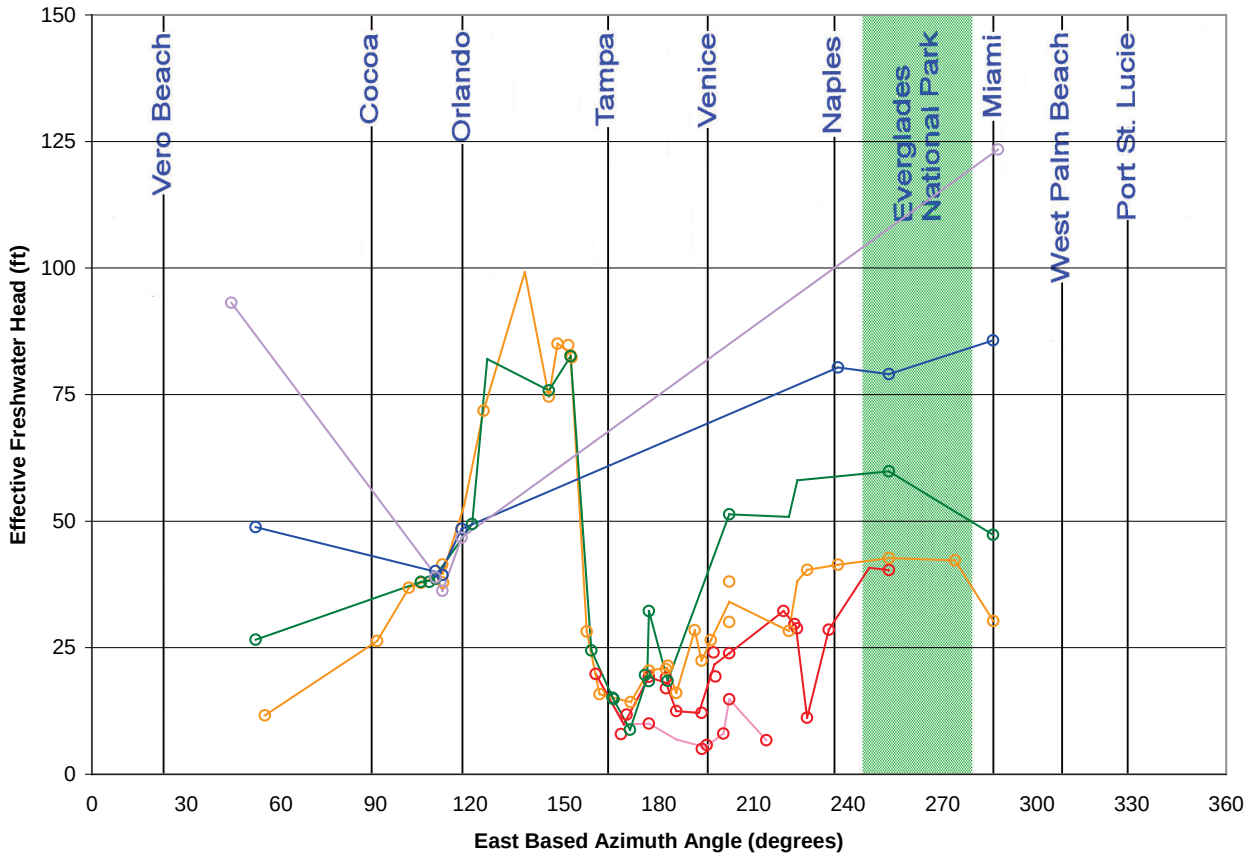

Legend

- Applied Boundary Condition (each cell)
- Measured Head Value

Layers:

- Intermediate Aquifer System (layer 2)
- Intermediate Aquifer System (layer 3)
- Upper Floridan Aquifer
- Avon Park Permeable Zone
- Lower Floridan Aquifer
- Boulder Zone

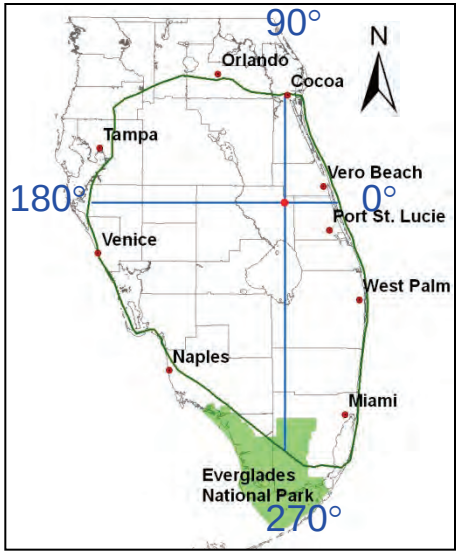

Equivalent Freshwater Head – October 2003 (Measured Points and Interpolated Values)

Final Groundwater Model Calibration Report

Figure C2-12

April 2010

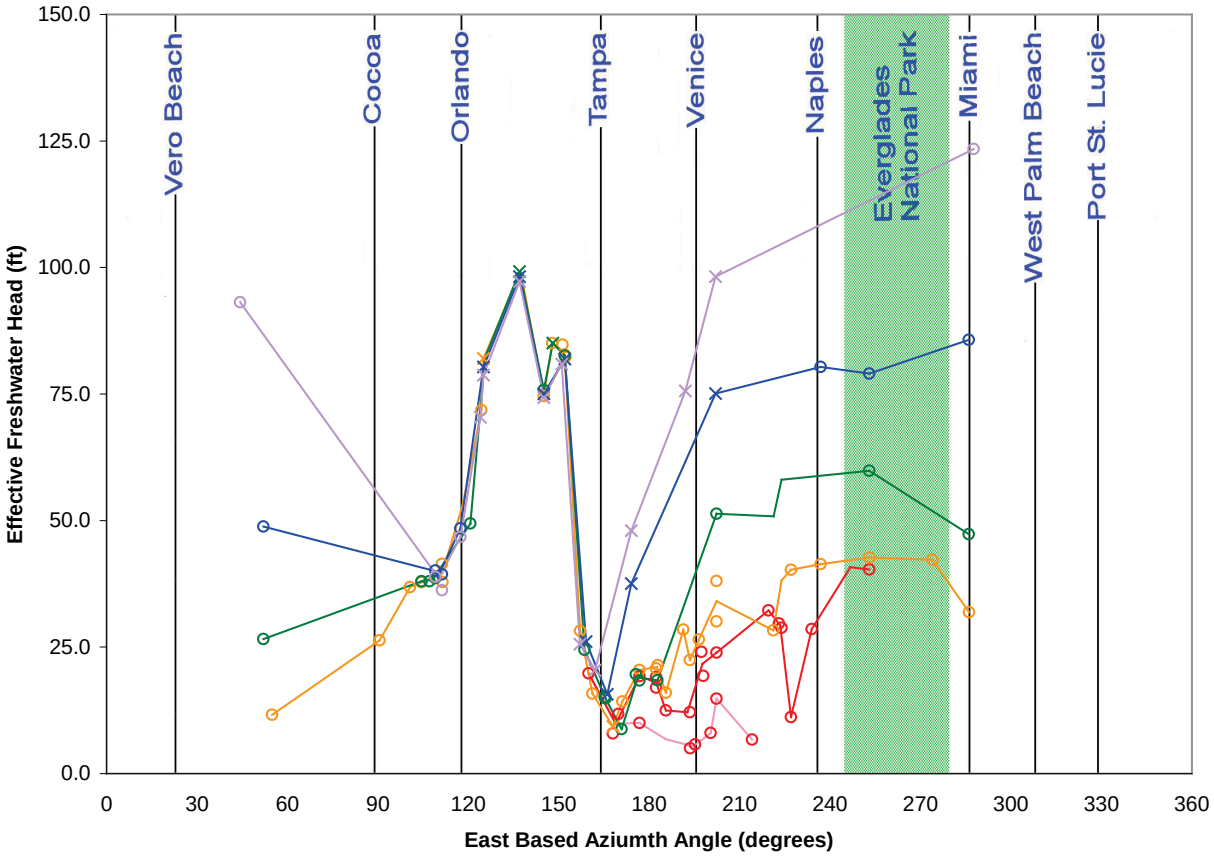

Legend

- Applied Boundary Condition (each cell)
- Measured Head Value
- Synthetic Head Value

Layers:

- Intermediate Aquifer System (layer 2)
- Intermediate Aquifer System (layer 3)
- Upper Floridan Aquifer
- Avon Park Permeable Zone
- Lower Floridan Aquifer
- Boulder Zone

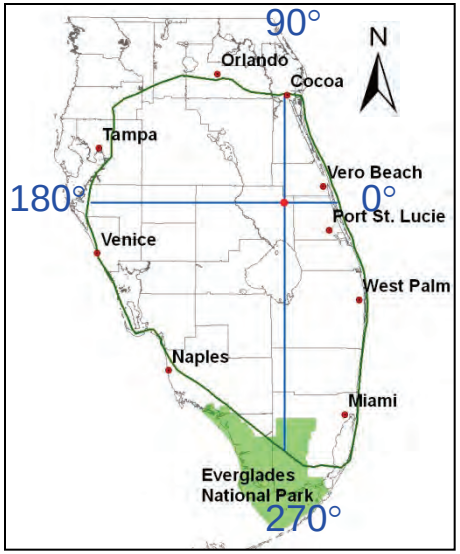

Equivalent Freshwater Head – October 2003

(Measured Points, Synthetic Points and Interpolated Values)

Final Groundwater Model Calibration Report

Figure C2-13

April 2010

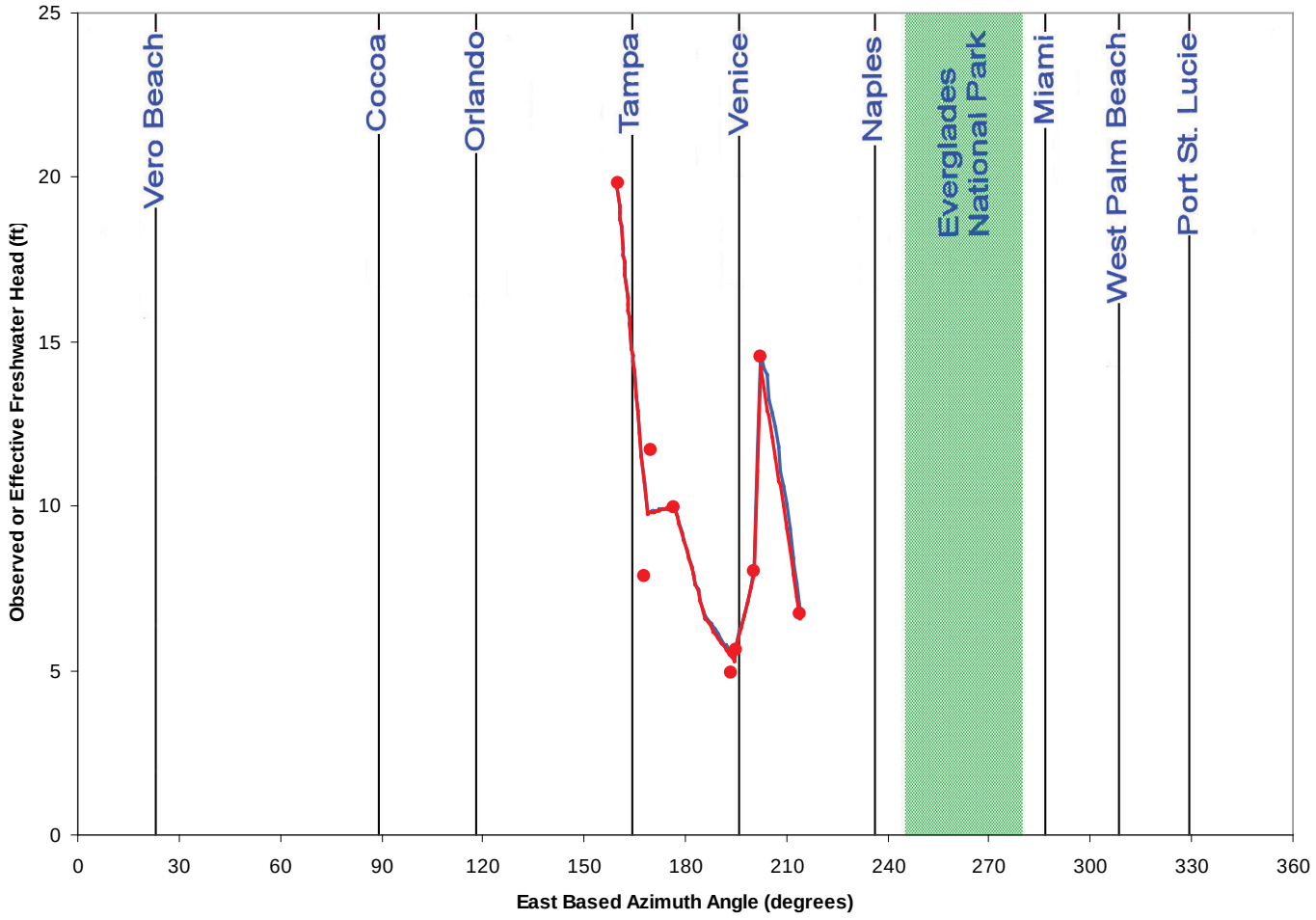

Legend

- Applied Observed Head Boundary Condition
- Calculated Equivalent Freshwater Head
- Measured Heads from Monitoring Wells

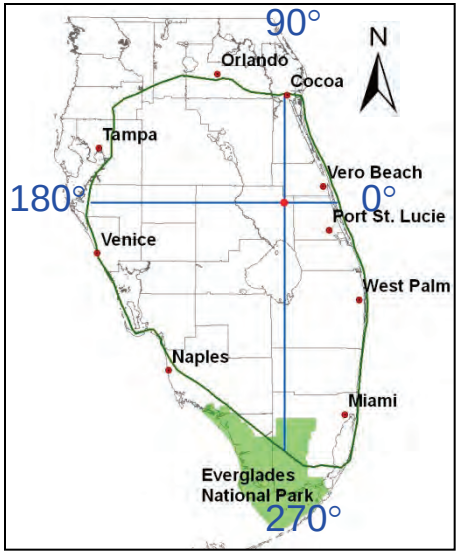

Applied Head Boundary Condition vs. Calculated Equivalent Freshwater Head – IAS Layer 2

Final Groundwater Model Calibration Report

Figure C2-14

April 2010

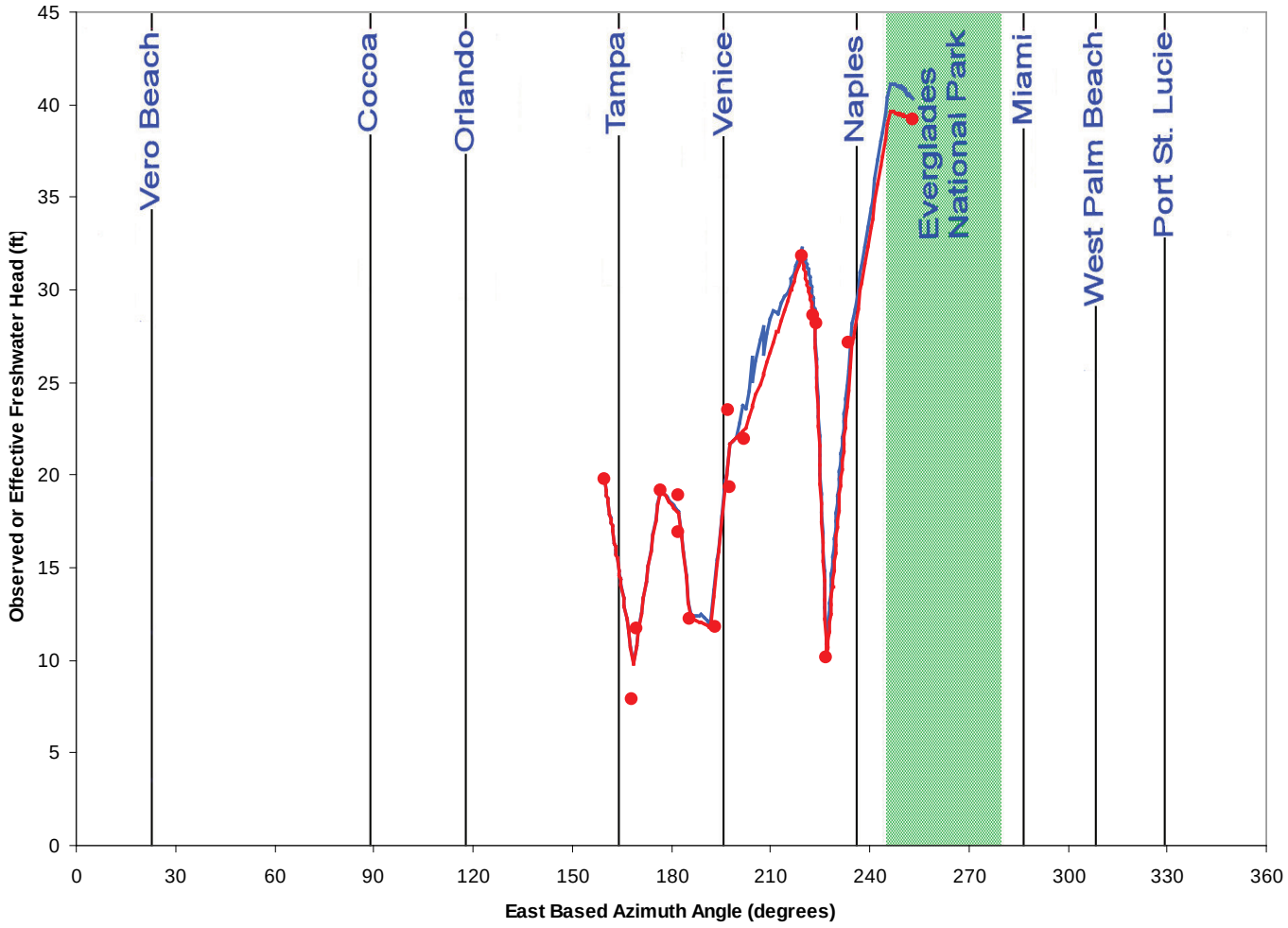

Legend

- Applied Observed Head Boundary Condition
- Calculated Equivalent Freshwater Head
- Measured Heads from Monitoring Wells

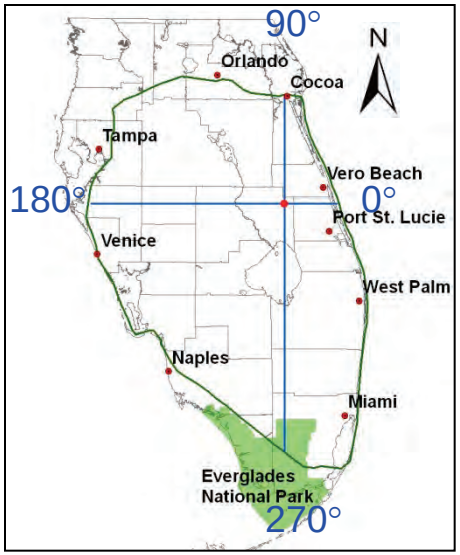

Applied Head Boundary Condition vs. Calculated Equivalent Freshwater Head – IAS Layer 3

Final Groundwater Model Calibration Report

Figure C2-15

April 2010

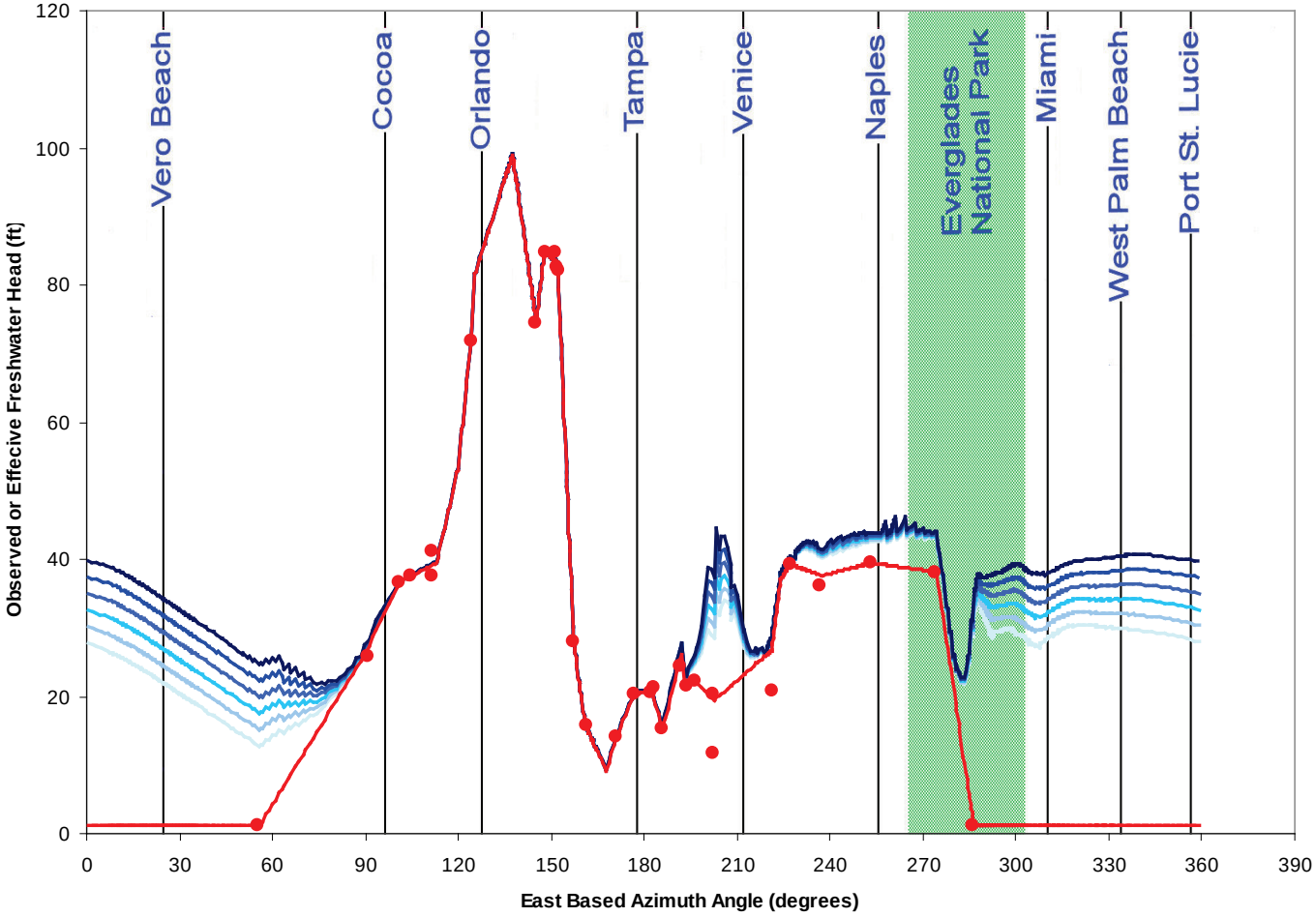

Legend

- Applied Observed Head Boundary Condition
- Calculated Equivalent Freshwater Head
  - Layer 5
  - Layer 6
  - Layer 7
  - Layer 8
  - Layer 9
  - Layer 10
- Measured Heads from Monitoring Wells

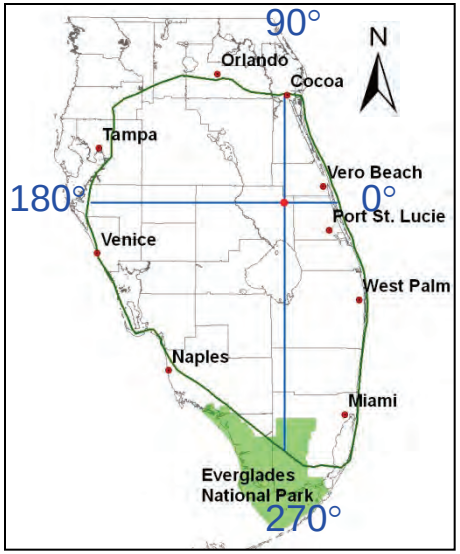

Applied Head Boundary Condition vs. Calculated Equivalent Freshwater Head – Upper Floridan Aquifer

Final Groundwater Model Calibration Report

Figure C2-16

April 2010

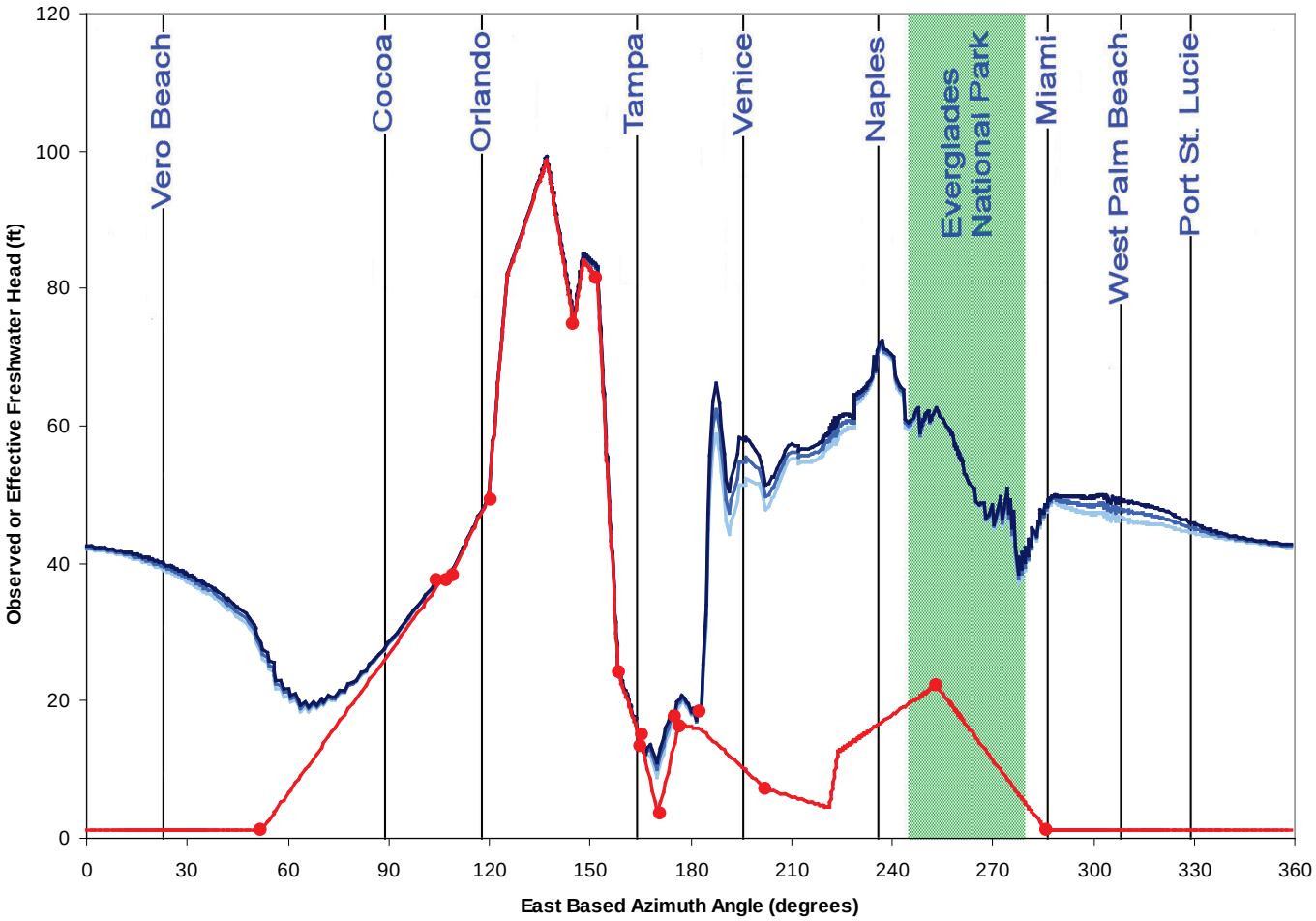

Legend

- Applied Observed Head Boundary Condition
- Calculated Equivalent Freshwater Head
  - Layer 13
  - Layer 14
  - Layer 15
- Measured Heads from Monitoring Wells

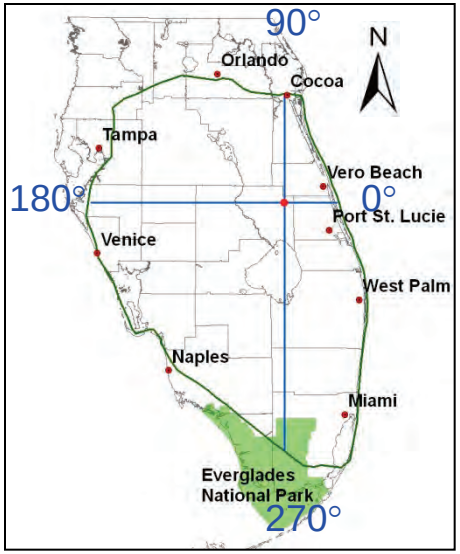

Applied Head Boundary Condition vs. Calculated Equivalent Freshwater Head – Avon Park Permeable Zone

Final Groundwater Model Calibration Report

Figure C2-17

April 2010

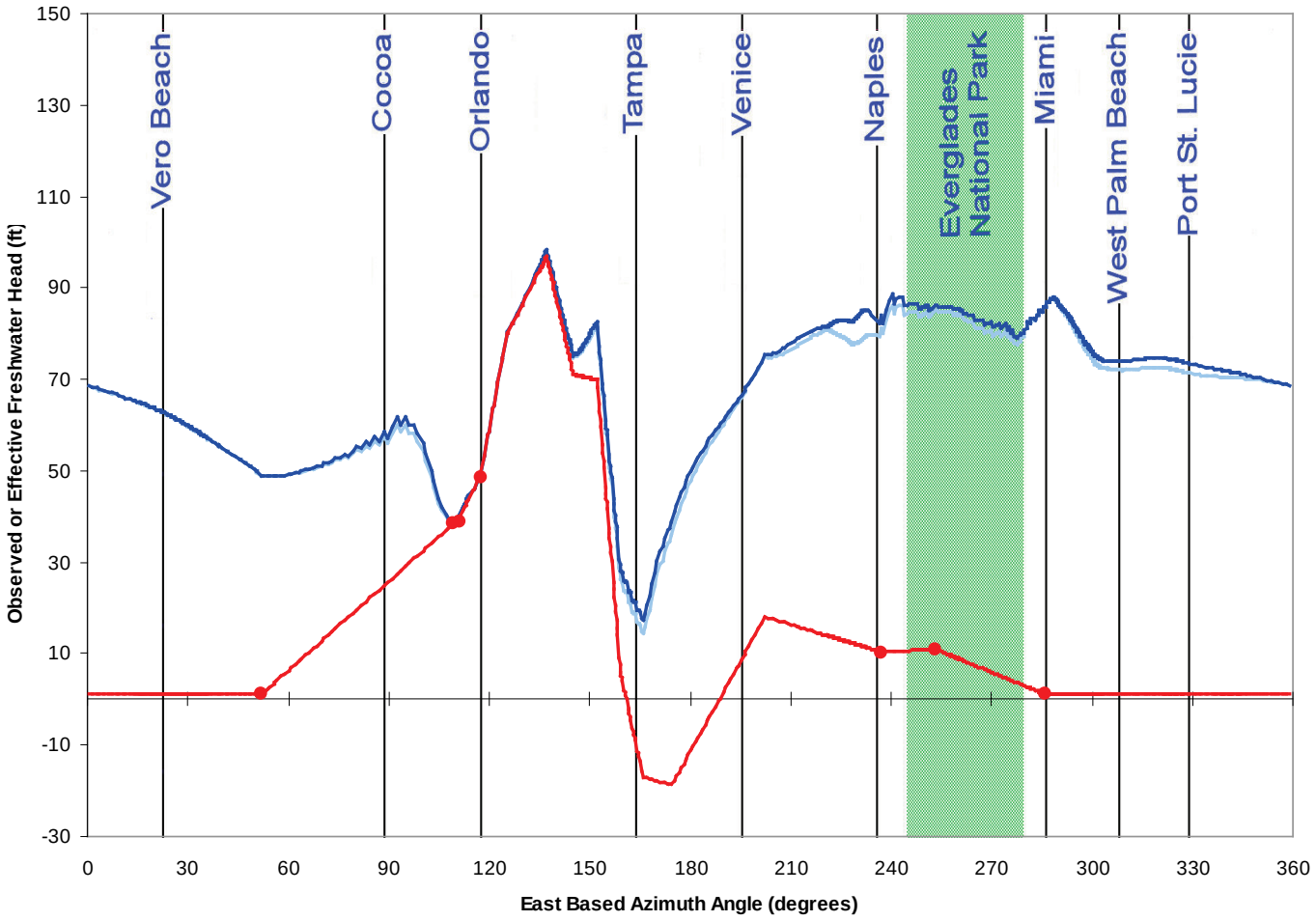

Legend

- Applied Observed Head Boundary Condition
- Calculated Equivalent Freshwater Head
  - Layer 18
  - Layer 19
- Measured Heads from Monitoring Wells

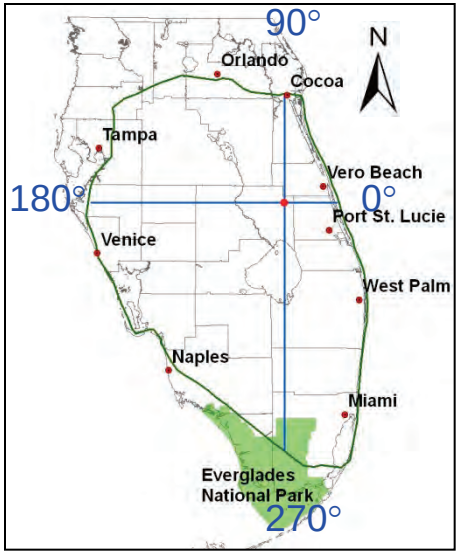

Applied Head Boundary Condition vs. Calculated Equivalent Freshwater Head – Lower Floridan Aquifer

Final Groundwater Model Calibration Report

Figure C2-18

April 2010

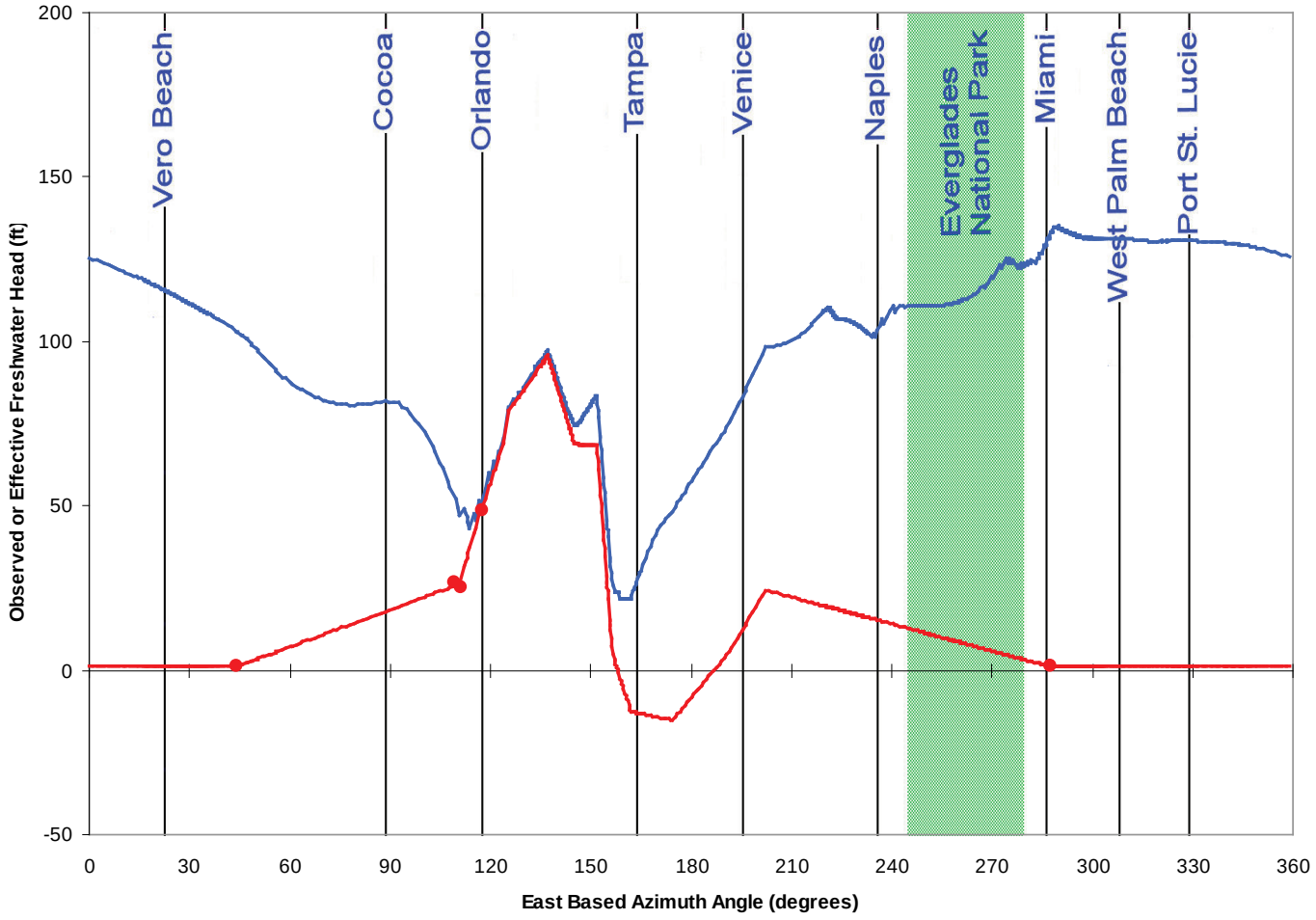

Legend

- Applied Observed Head Boundary Condition
- Calculated Equivalent Freshwater Head
- Measured Heads from Monitoring Wells

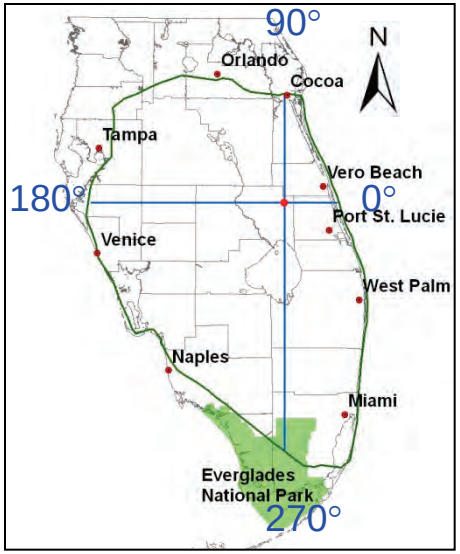

Applied Head Boundary Condition vs. Calculated Equivalent Freshwater Head – Boulder Zone

Final Groundwater Model Calibration Report

Figure C2-19

April 2010

Temperature

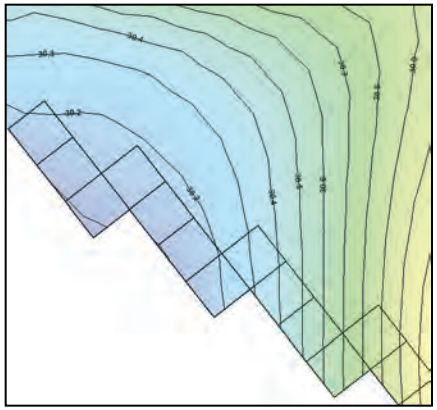

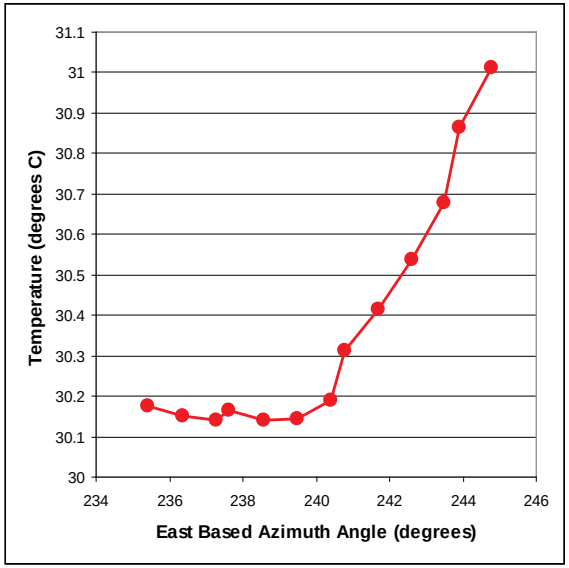

(a)

TDS

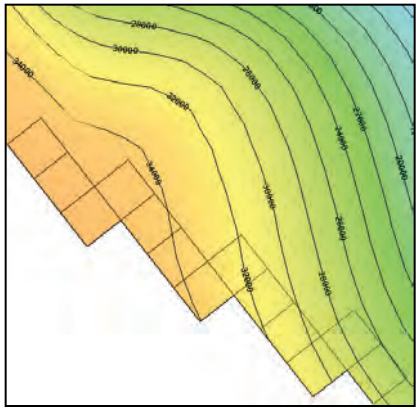

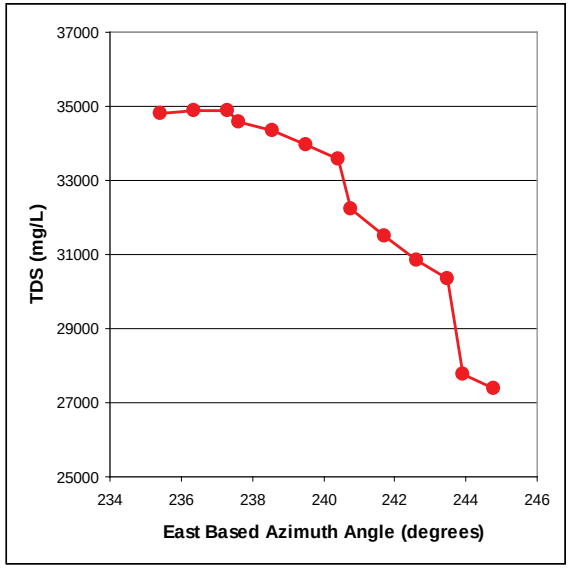

(b)

Elevation

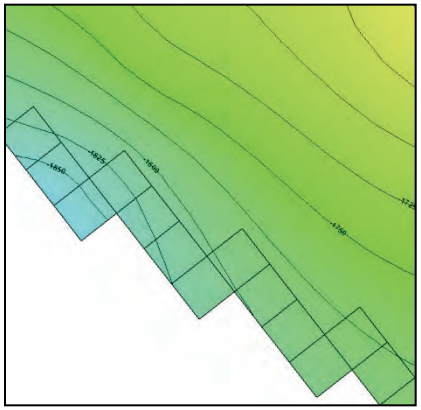

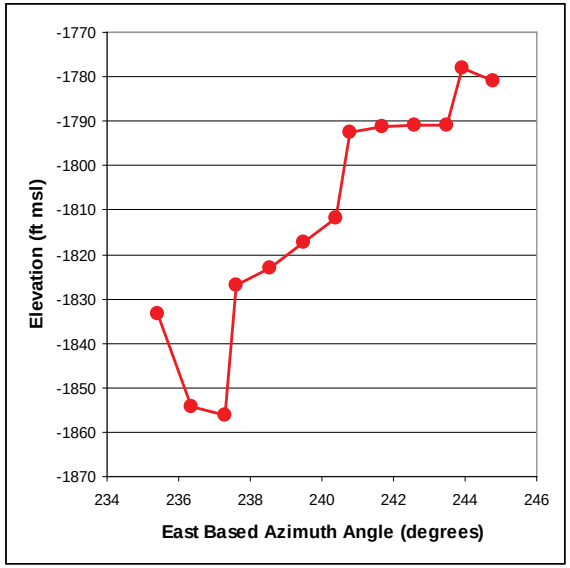

(c)

TDS, Temperature and Elevation Variations on an Example Set of Boundary Cells

Final Groundwater Model Calibration Report

Figure C2-20

April 2010

Observed Head

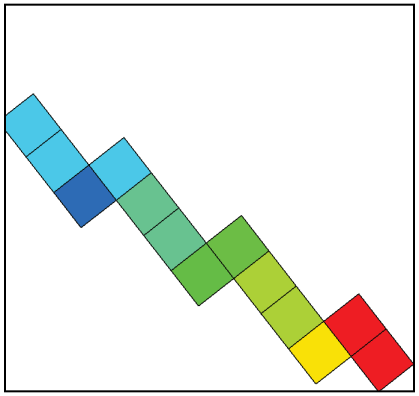

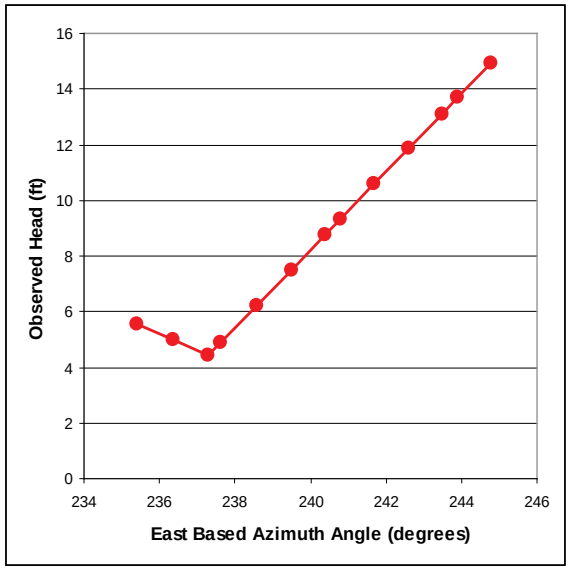

(a)

Equivalent Freshwater Head

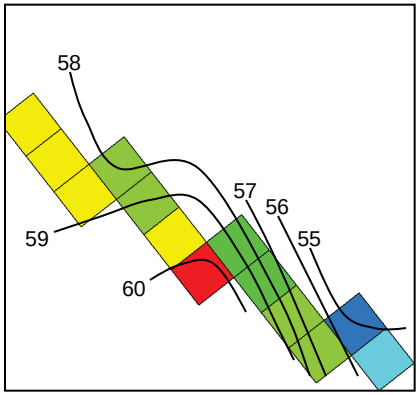

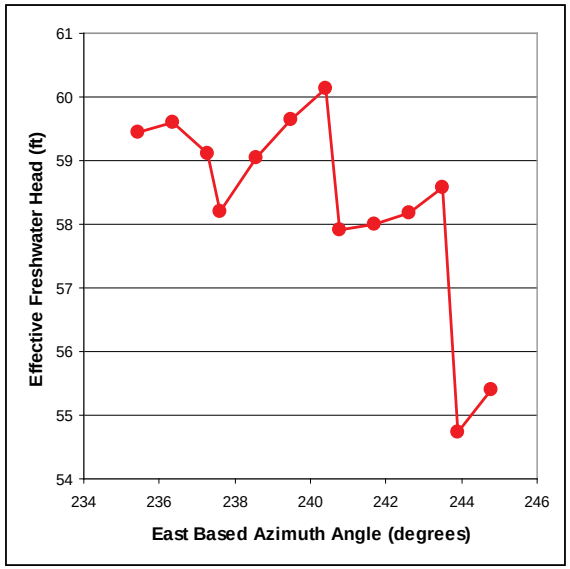

(b)

Notes:

1. This figures should be examined in combination with Figure 20.

2. The TDS, Temperature and Elevation data sets on this small set of boundary cells (Figure C2-20(a), C2-20(b) and C2-20(c)) are based in 2-dimensional interpolations of available data to the computational grid.

3. The Observed Head (Figure C2-21(a)) was assigned based on a 1-dimensional linear interpolation of available boundary data around the edge of the model. The slope change which occurs at the third cell from the left is a result of a break point added as described in Section 2.5

4. The Equivalent Freshwater Head (Figure C2-21(b)) was calculated using Equations 1 and 2 presented in Section 1.2.

5. The unusual oscillations of the Equivalent freshwater head are due to variations mainly in the elevations and TDS of the cells. Because the elevation and TDS contours are nearly parallel to the edge of the model in some areas, the blocky nature of the boundary results in these oscillations.

Observed Head and Equivalent Freshwater Head Variations on an Example Set of Boundary Cells

Final Groundwater Model Calibration Report

Figure C2-21

April 2010

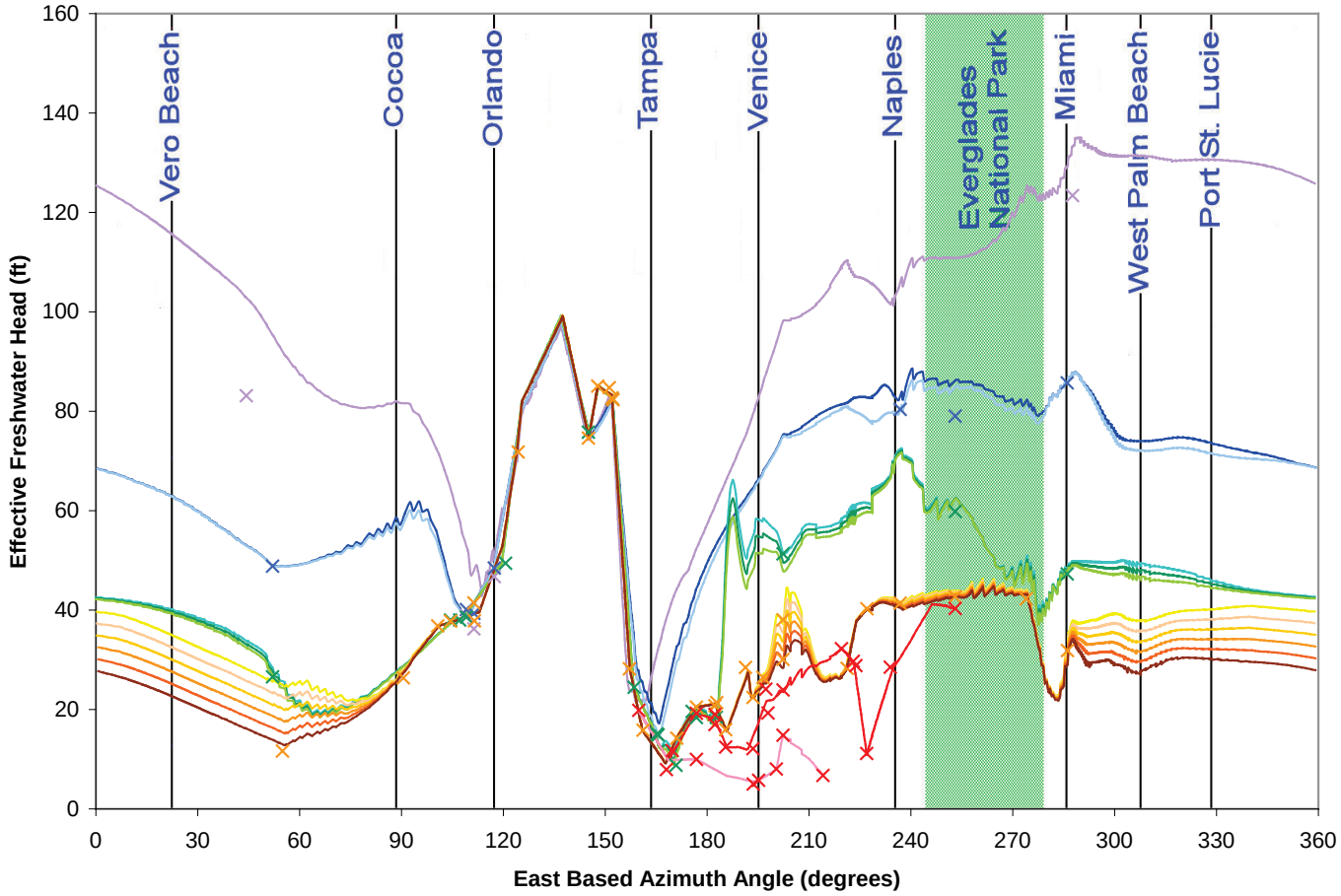

Legend

- Applied Boundary Condition (each cell converted to EFH)
- Measured Head Value (converted to EFH)
- Boulder Zone
  - Layer 22
- Lower Floridan
  - Layer 19
  - Layer 18
- Avon Park Permeable Zone
  - Layer 15
  - Layer 14
  - Layer 13
- Upper Floridan
  - Layer 10
  - Layer 9
  - Layer 8
  - Layer 7
  - Layer 6
  - Layer 5
- Intermediate Aquifer System
  - Layer 3
  - Layer 2

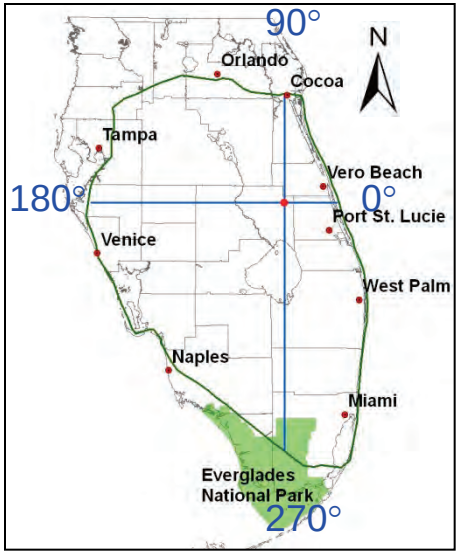

October 2003 Equivalent Freshwater Head as Calculated by Model With Measured Points (No Breakpoints Added)

Final Groundwater Model Calibration Report

Figure C2-22

April 2010

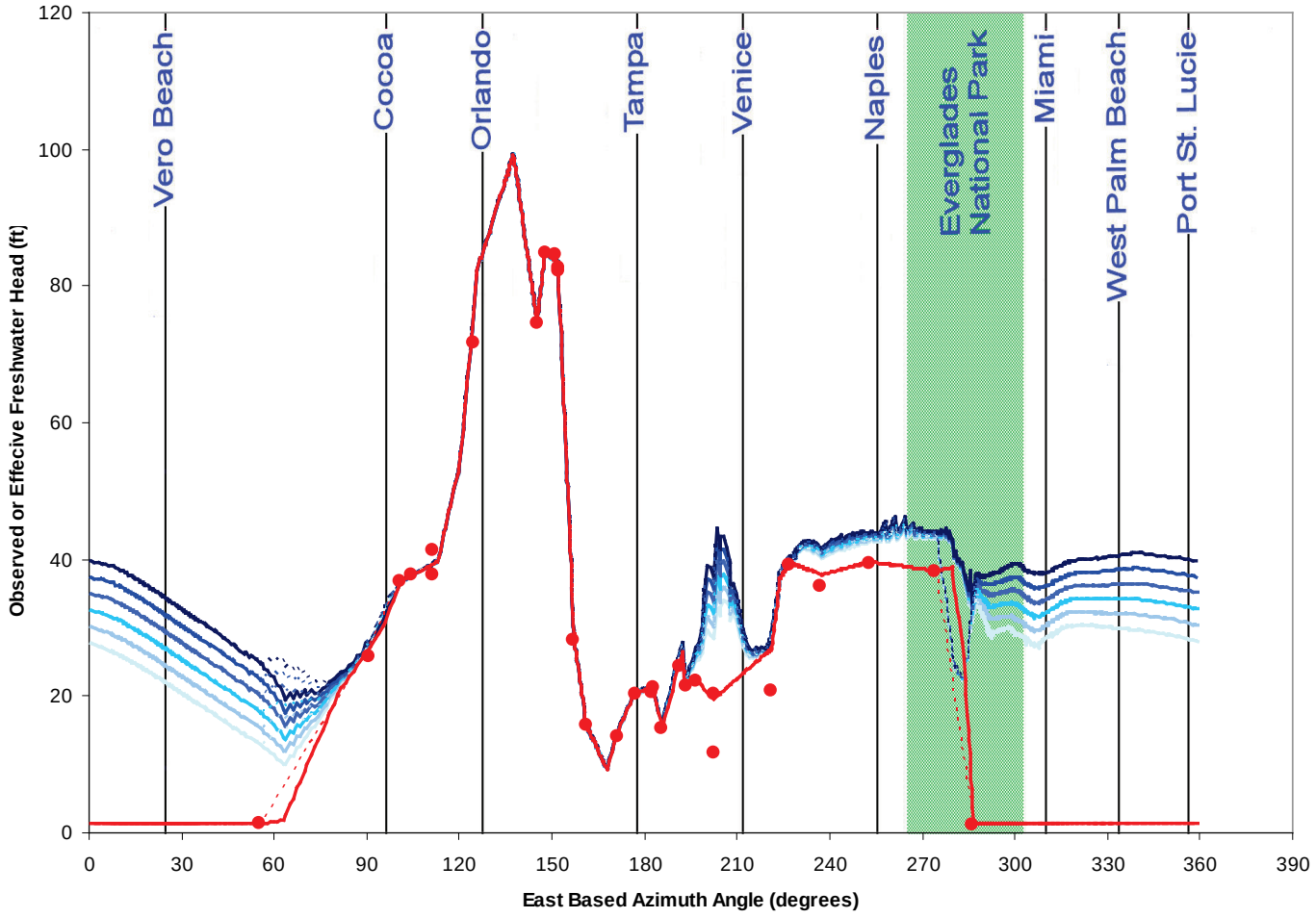

Legend

- Heads without Breakpoints
- Heads with Breakpoints
- Observed Head (all layers)
- EFH (Layer 5)
- EFH (Layer 6)
- EFH (Layer 7)
- EFH (Layer 8)
- EFH (Layer 9)
- EFH (Layer 10)
- Measured Heads from Monitoring Wells

Note: EFH = Equivalent Freshwater Head

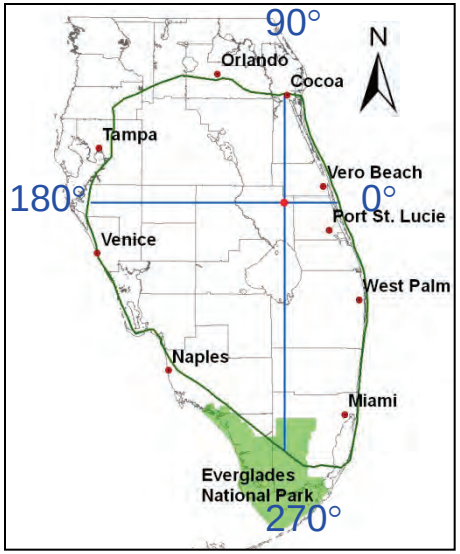

October 2003 Boundary Heads (Upper Floridan Aquifer) – Effect of Breakpoints

Final Groundwater Model Calibration Report

Figure C2-23

April 2010

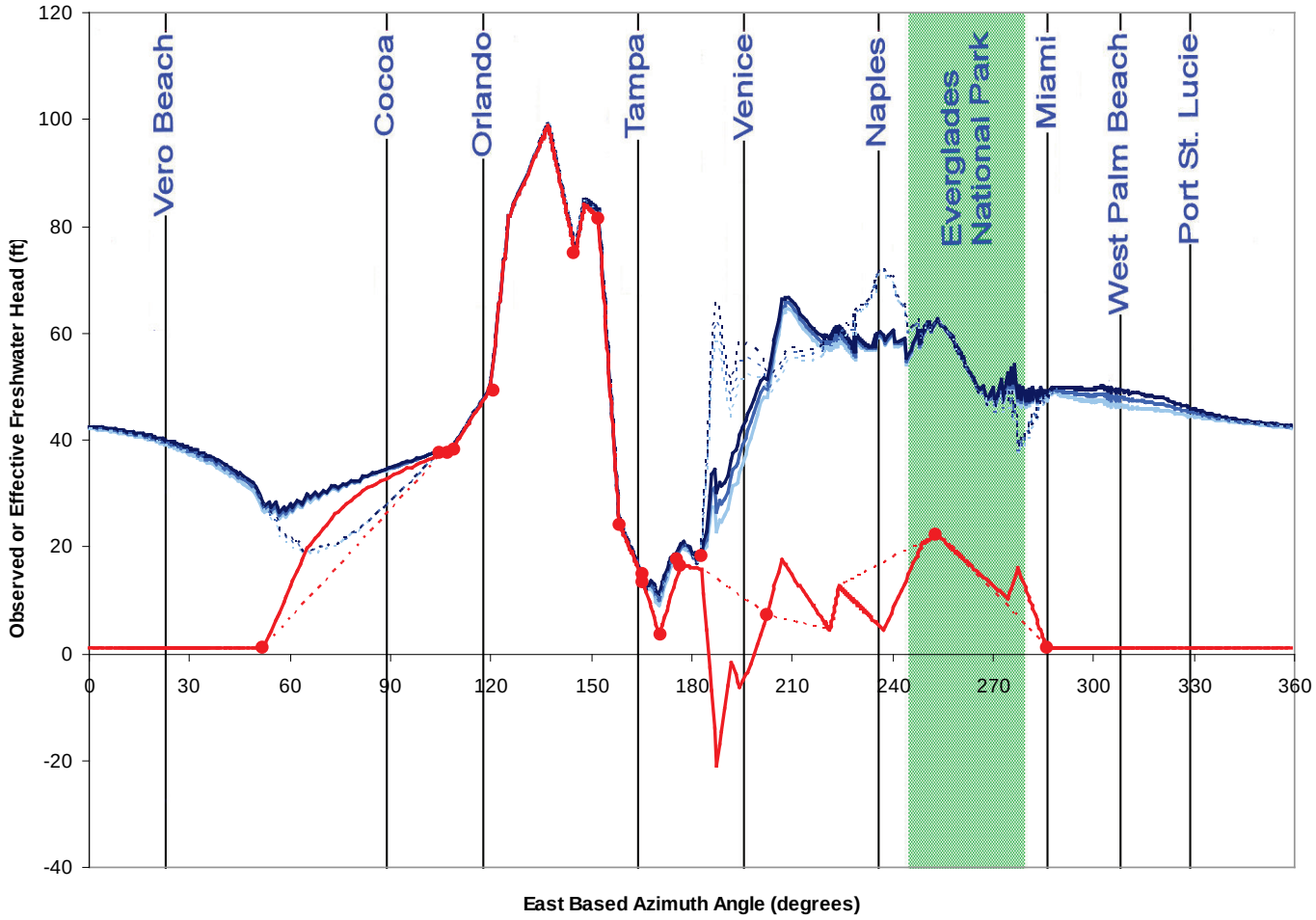

Legend

- Heads without Breakpoints
- Heads with Breakpoints
- Observed Head (all layers)
- EFH (Layer 13)
- EFH (Layer 14)
- EFH (Layer 15)
- Measured Heads from Monitoring Wells

Note: EFH = Equivalent Freshwater Head

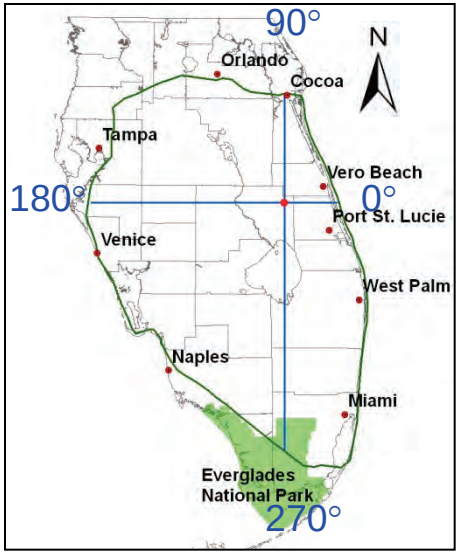

October 2003 Boundary Heads (Avon Park Permeable Zone) – Effect of Breakpoints

Final Groundwater Model Calibration Report

Figure C2-24

April 2010

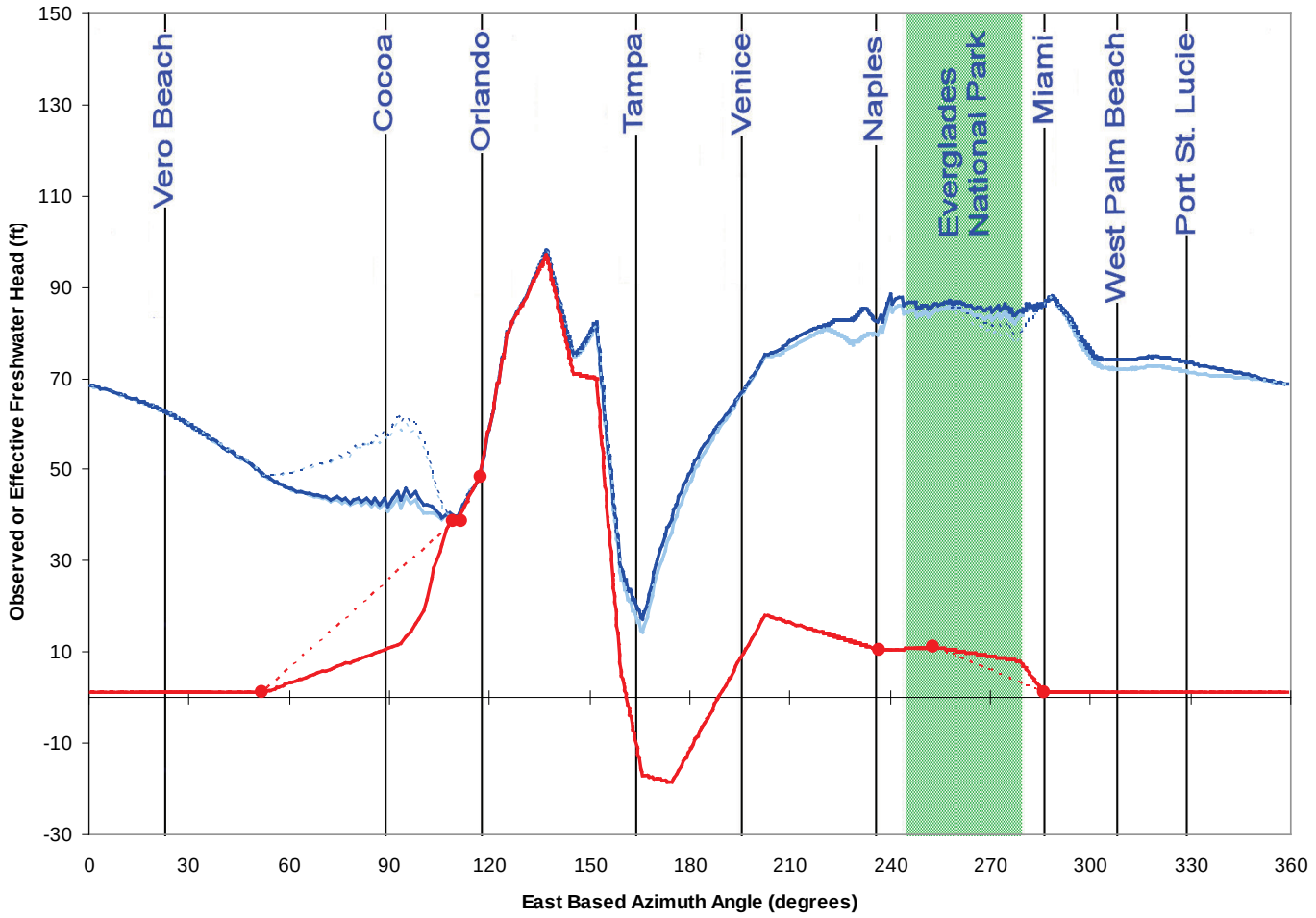

Legend

- Heads without Breakpoints
- Heads with Breakpoints
- Observed Head (all layers)
- EFH (Layer 18)
- EFH (Layer 19)
- Measured Heads from Monitoring Wells

Note: EFH = Equivalent Freshwater Head

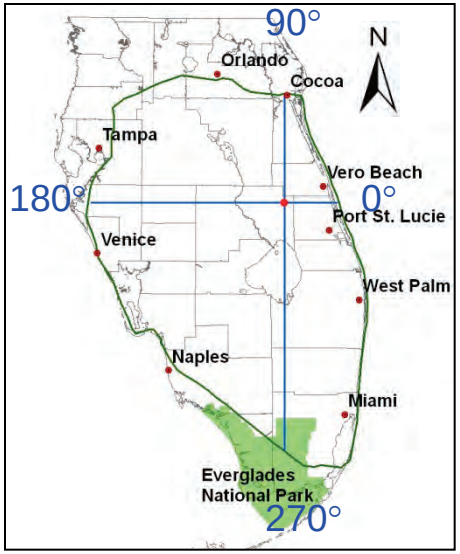

October 2003 Boundary Heads (Lower Floridan Aquifer) – Effect of Breakpoints

Final Groundwater Model Calibration Report

Figure C2-25

April 2010

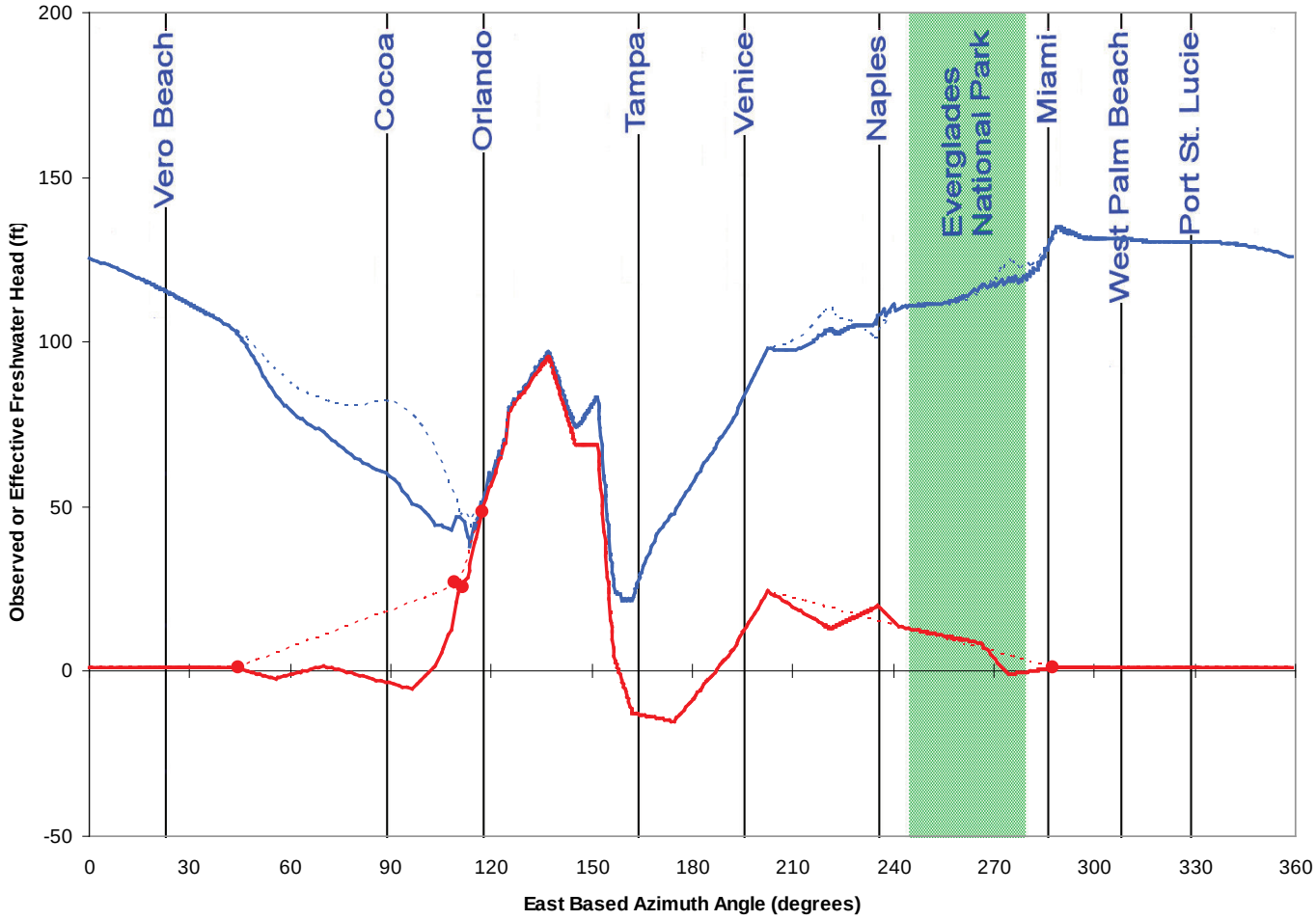

Legend

- Heads without Breakpoints
- Heads with Breakpoints
- Observed Head
- Equivalent Freshwater Head
- Measured Heads from Monitoring Wells

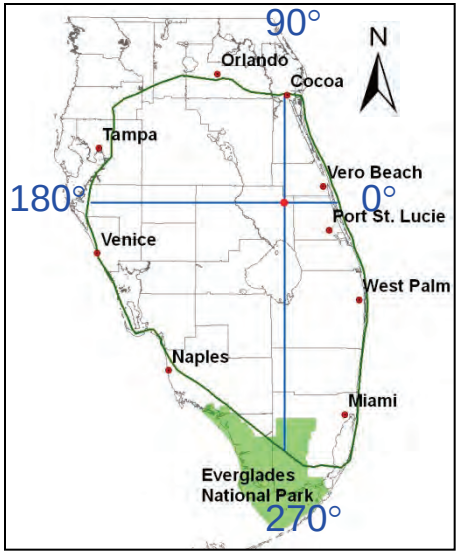

October 2003 Boundary Heads (Boulder Zone) – Effect of Breakpoints

Final Groundwater Model Calibration Report

Figure C2-26

April 2010

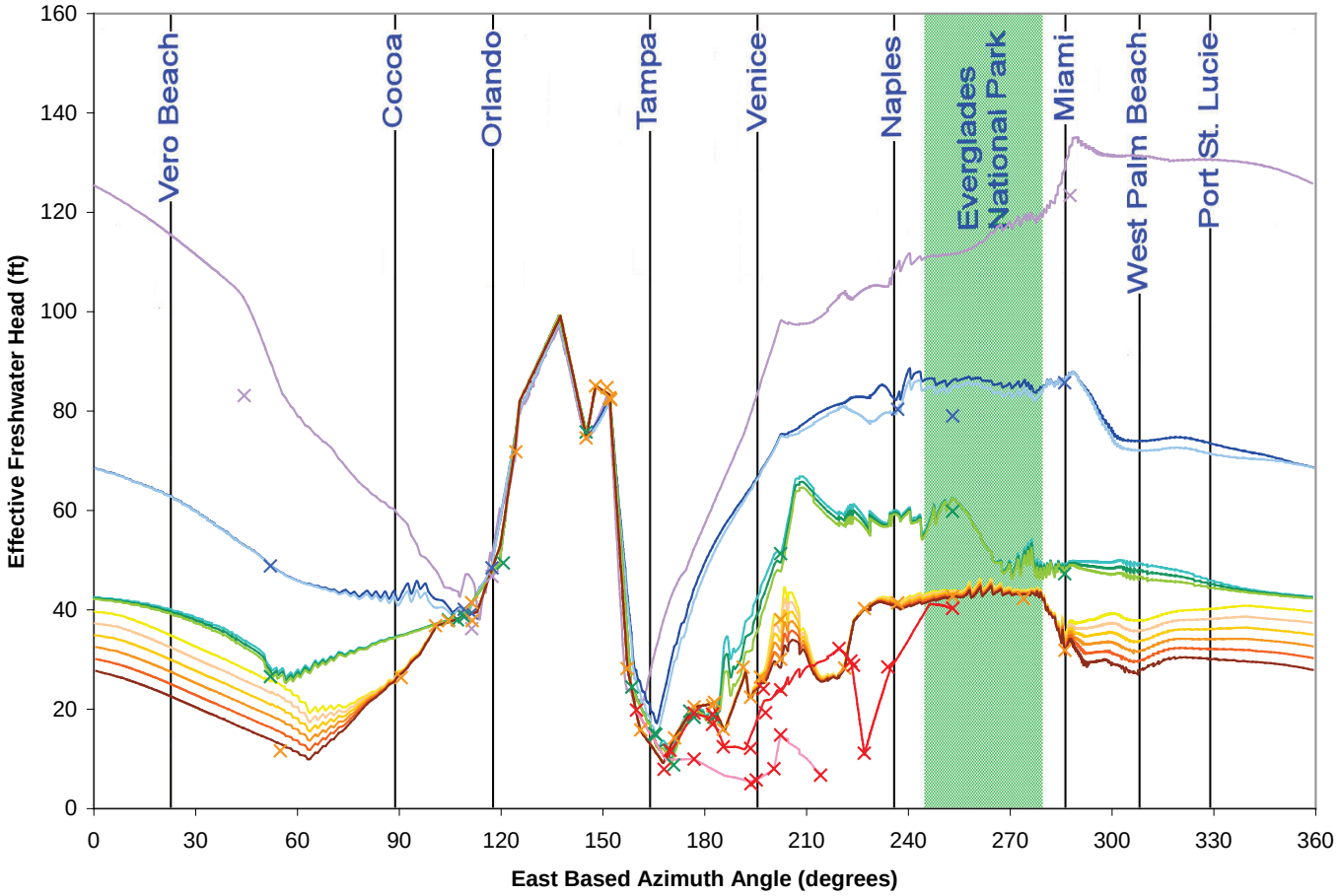

Legend

- Applied Boundary Condition (each cell converted to EFH)
- Measured Head Value (converted to EFH)
- Boulder Zone
  - Layer 22
- Lower Floridan
  - Layer 19
  - Layer 18
- Avon Park Permeable Zone
  - Layer 15
  - Layer 14
  - Layer 13
- Upper Floridan
  - Layer 10
  - Layer 9
  - Layer 8
  - Layer 7
  - Layer 6
  - Layer 5
- Intermediate Aquifer System
  - Layer 3
  - Layer 2

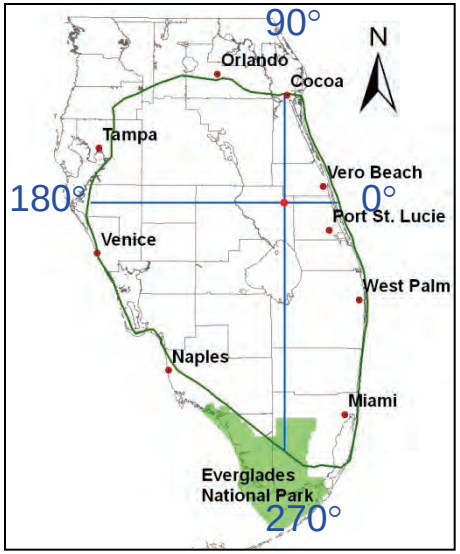

October 2003 Equivalent Freshwater Head as Calculated by Model With Measured Points (With Breakpoints Added)

Final Groundwater Model Calibration Report

Figure C2-27

April 2010

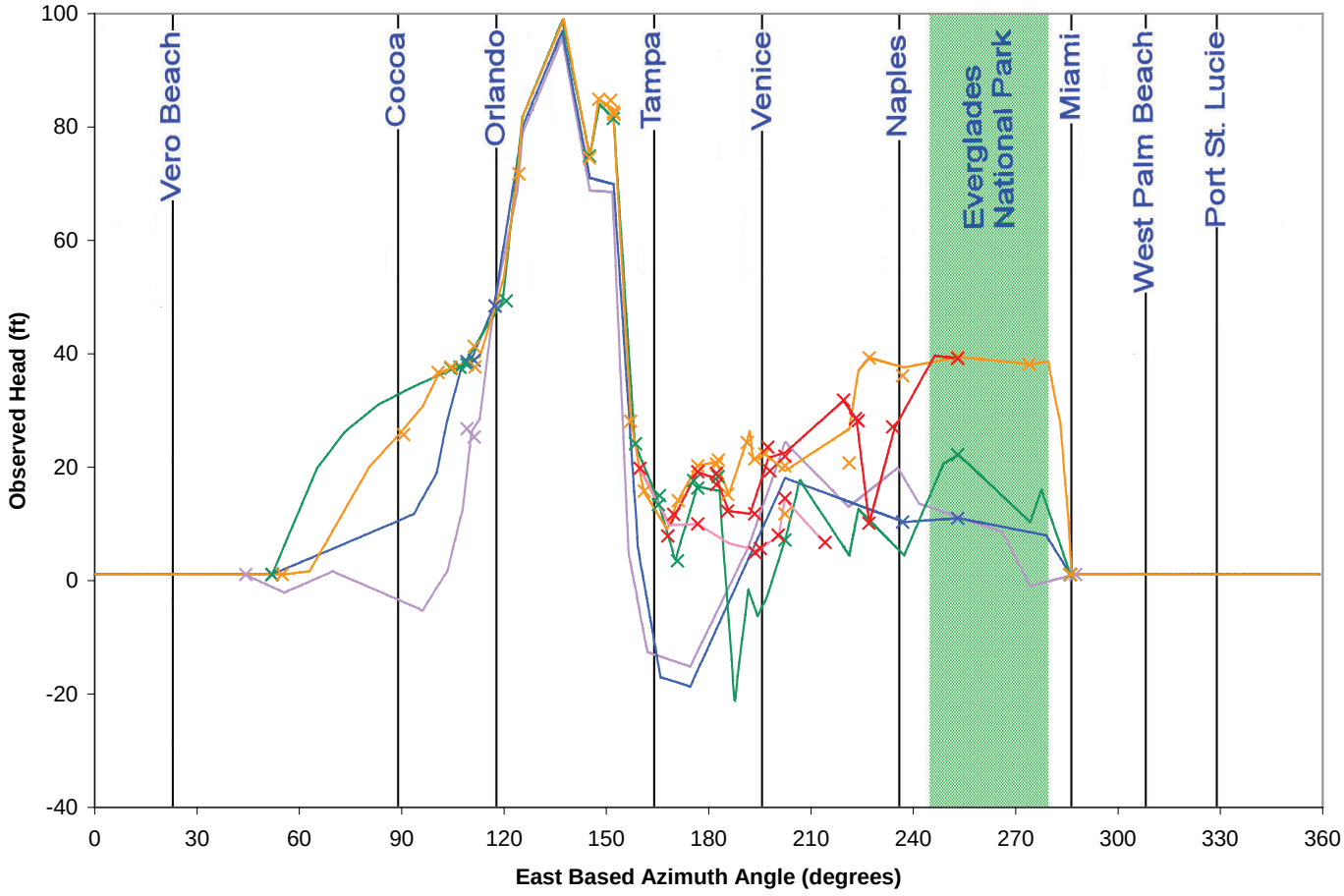

Legend

- Applied Boundary Condition (each cell)
- × Measured Head Value

Layers:

- Intermediate Aquifer System (layer 2)
- Intermediate Aquifer System (layer 3)
- Upper Floridan Aquifer
- Avon Park Permeable Zone
- Lower Floridan Aquifer
- Boulder Zone

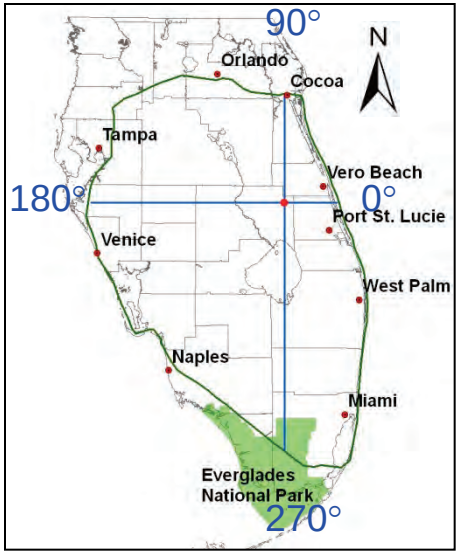

Observed Head – October 2003
(Measured Points and Applied Boundary Condition)

Final Groundwater Model Calibration Report

Figure C2-28

April 2010

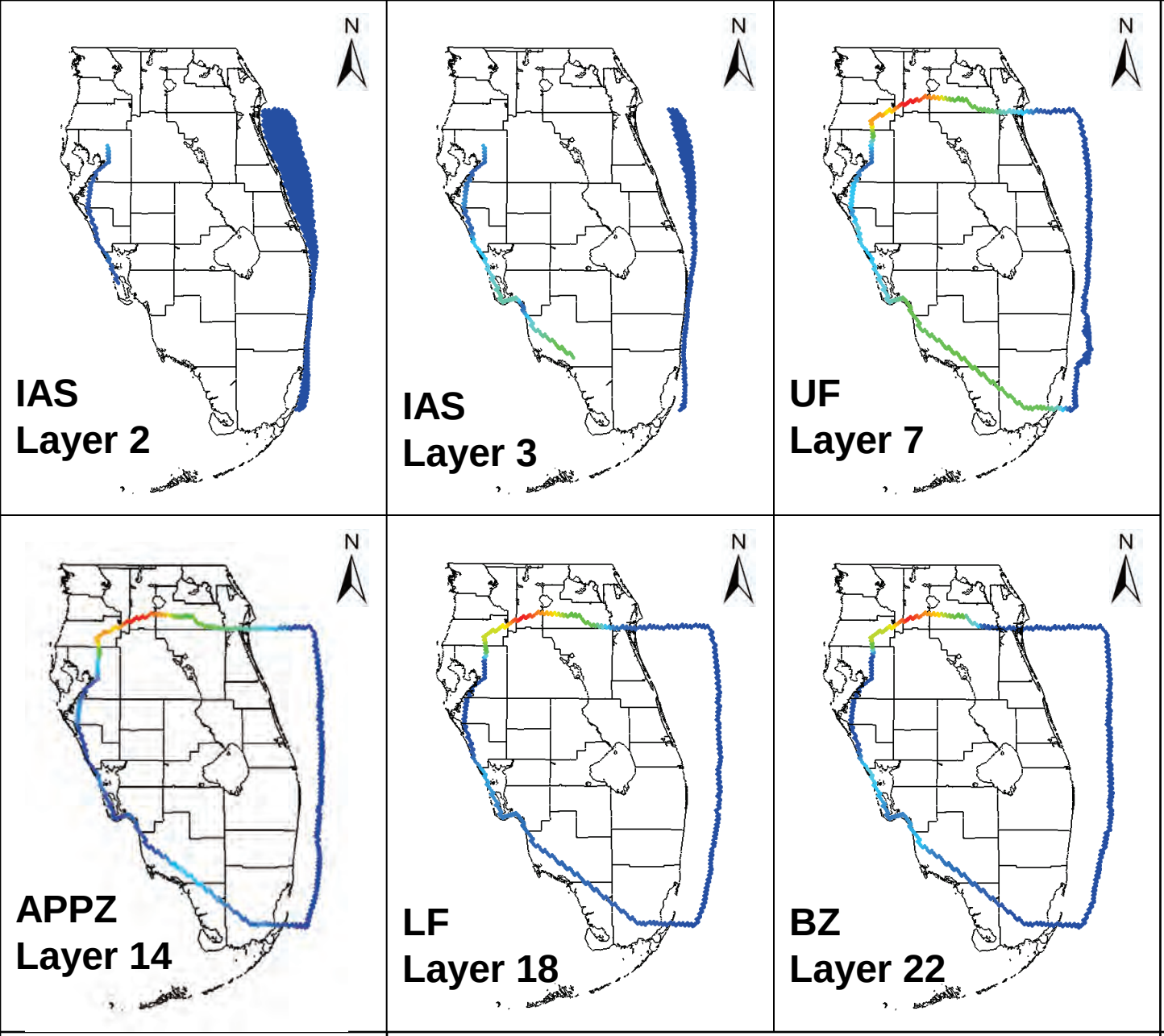

Notes:
The specified heads for each aquifer are the same regardless of the layer. Thus, the heads shown for Layer 7 are the same as those applied to Layers 5, 6, 8, 9 and 10.

IAS = Intermediate Aquifer System
UF = Upper Floridan Aquifer
APPZ = Avon Park Permeable Zone
LF = Lower Floridan Aquifer
BZ = Boulder Zone

Applied Specified Head Boundary Conditions – October 2003

Final Groundwater Model Calibration Report

Figure C2-29

April 2010

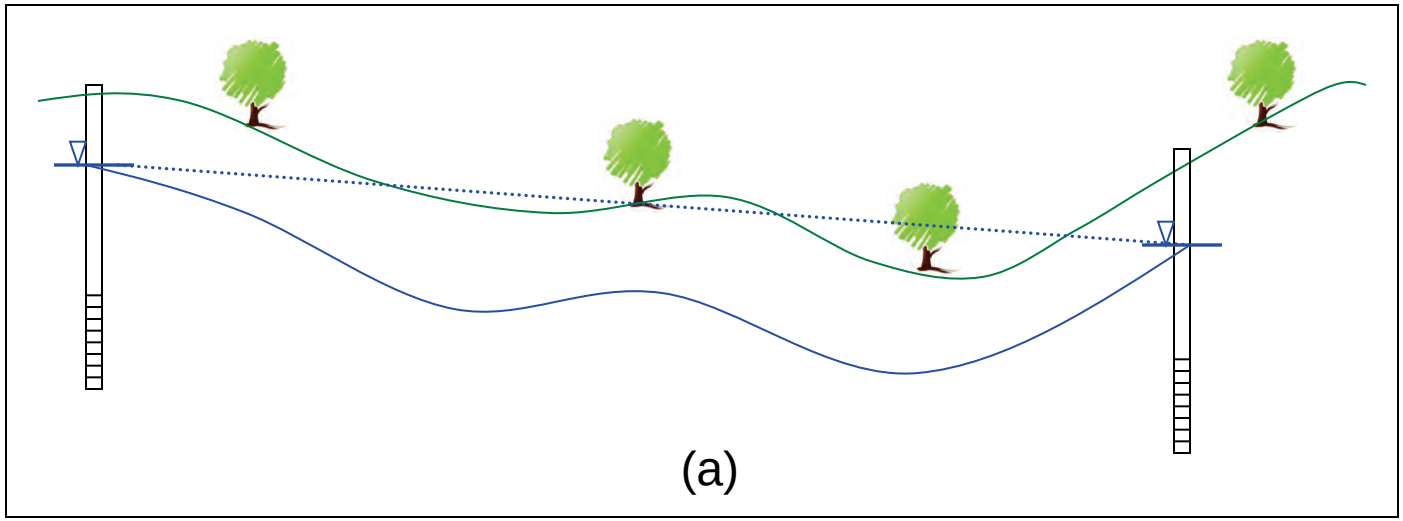

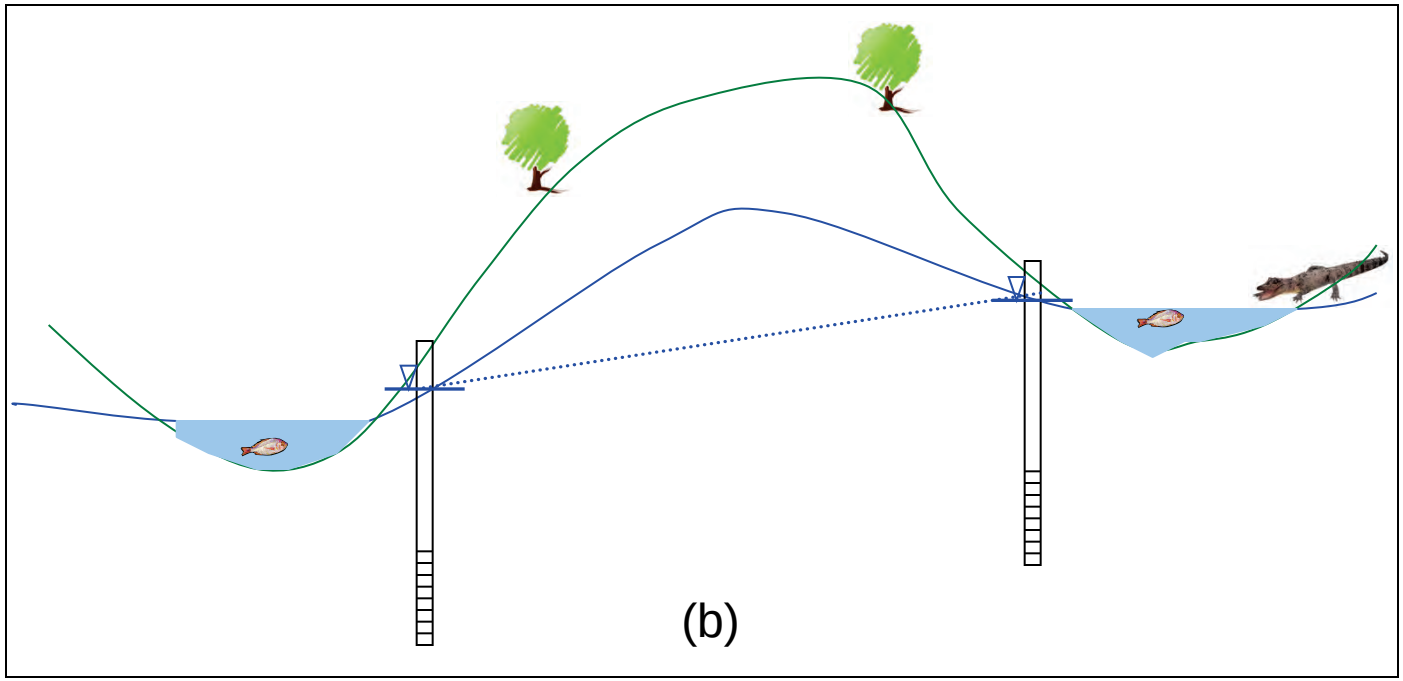

Legend

- Ground Surface
- Water Table
- Interpolated Water Table
- Measured Water Level
- Monitoring Well
- Surface Water

Notes:

(a) In some cases, the ground surface has some variability which is not reflected in the available water level data. If a simple linear interpolation of the available data is used, some areas may appear to have standing water where none is known to exist. The interpolation technique used for assigning heads to the SAS layer did not allow the assigned head to be above the ground surface except in areas where surface water was known to be found.

(b) Sometimes, wells are found near river valleys which are separated by higher ground. In these cases, we would expect the groundwater table to be lower between the rivers where recharge occurs. If no monitoring wells are placed on the higher ground, a linear interpolation will not be sufficient to accurately portray site conditions. The interpolation technique used for assigning heads to the SAS layer used a correlation relationship between head and ground surface elevation to assign heads to high ground areas with sparse data.

Interpolation Problems for SAS Surface Boundary Conditions

Final Groundwater Model Calibration Report

Figure C3-1

April 2010

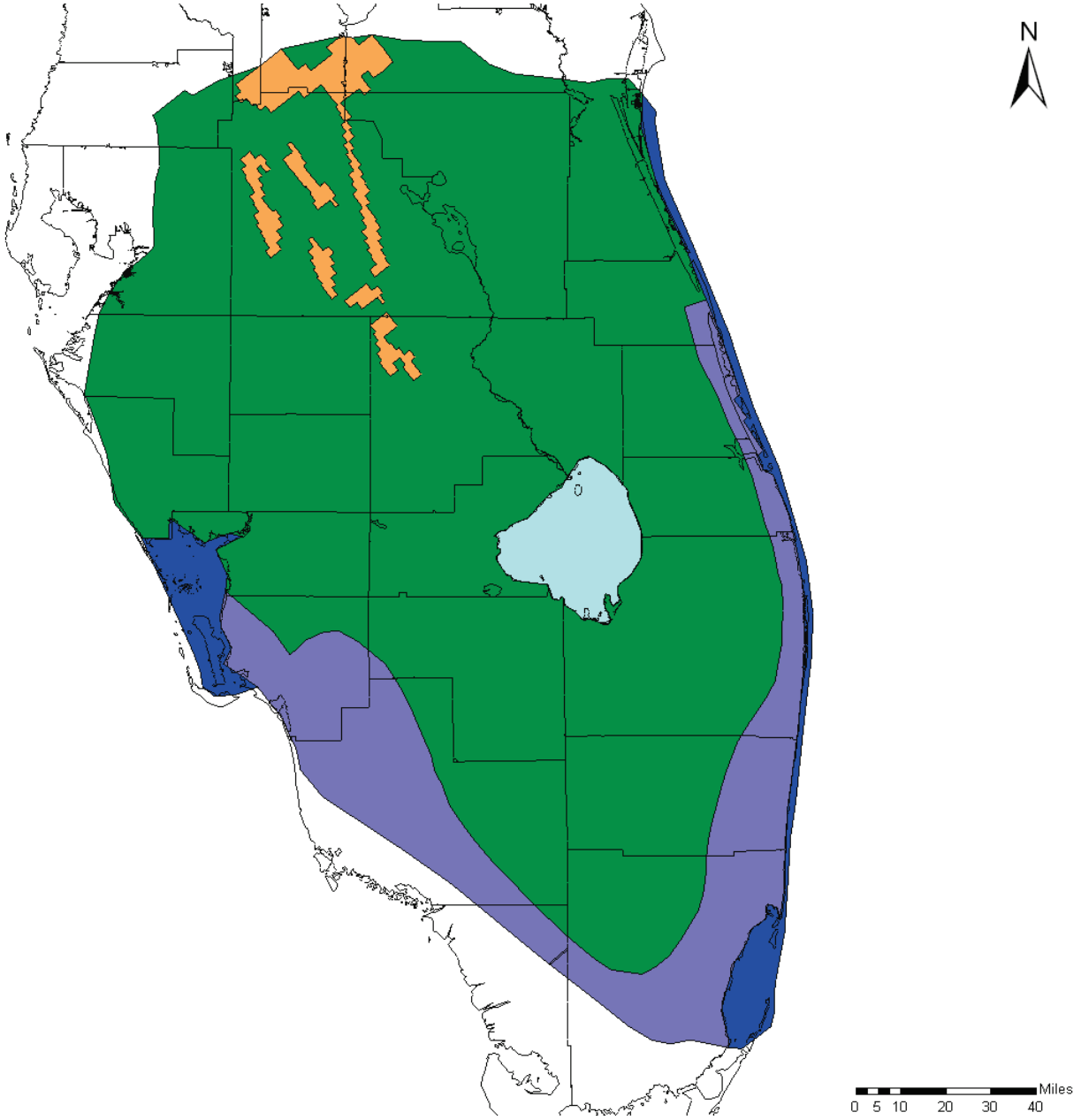

Legend:

- Zone 1 - Ocean
- Zone 2 - Lake Okeechobee
- Zone 3 - Ridges
- Zone 4 - Dry land with data fit to a linear regression
- Zone 5 - Dry land with data that did not fit linear regression

Zones for Assigning Specified Head Boundary Conditions to the SAS

Final Groundwater Model Calibration Report

Figure C3-2

October 2010

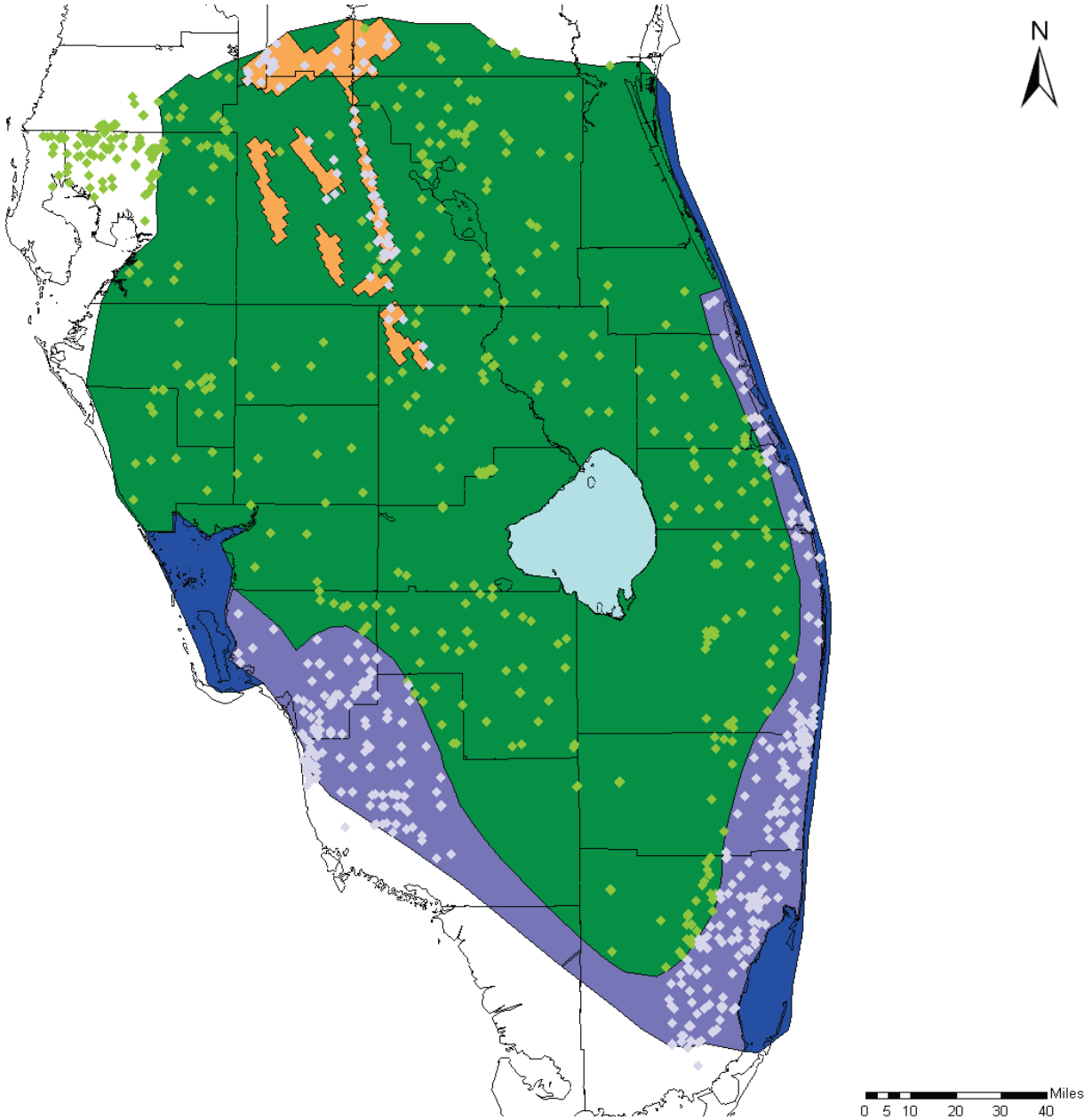

Legend:

- Zone 1 - Ocean
- Zone 2 - Lake Okeechobee
- Zone 3 - Ridges
- Zone 4 - Dry land with data fit to a linear regression
- Zone 5 - Dry land with data that did not fit linear regression
- Wells with data that was fit to a linear regression
- Wells with data that was linearly interpolated

Zones for SAS Regression/Interpolation

Figure C3-3

Final Groundwater Model Calibration Report

October 2010

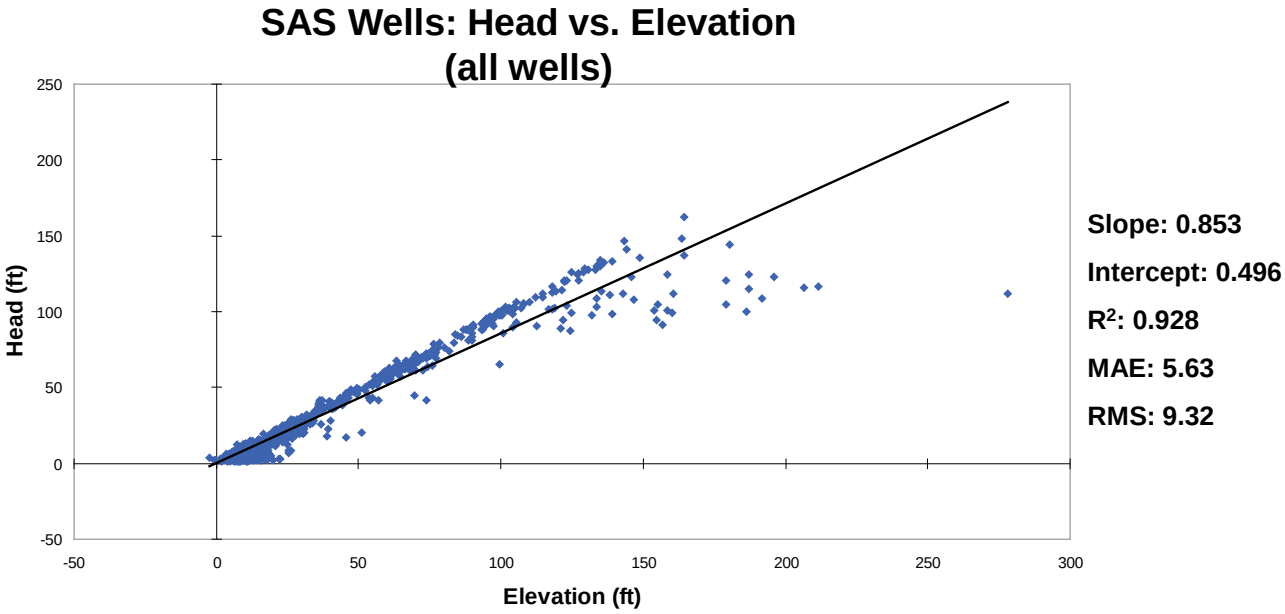

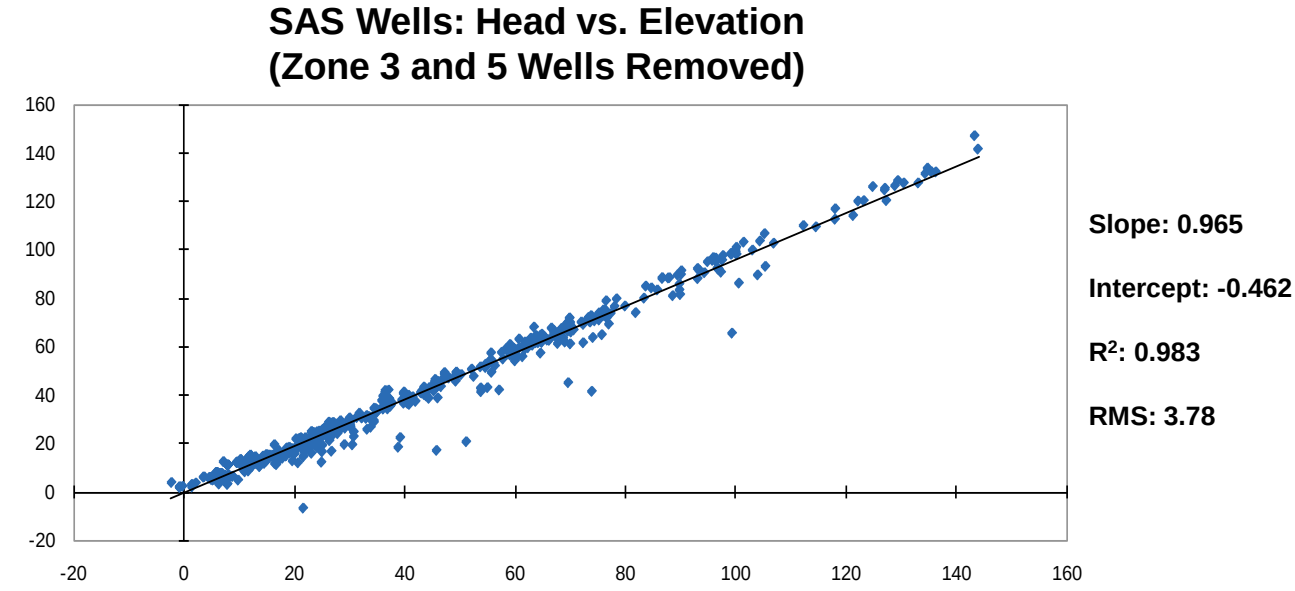

Notes:

The upper plot shows the correlation between head and ground surface elevation for the month of October 2003 at each well open in the SAS layer of the model. The lower plot is the same, but the points in zones 3 (ridges) and 5 (coastal areas) were removed.

Slope, intercept and r^2 values were calculated by Excel, using the SLOPE, INTERCEPT and RSQ functions to fit the data to a straight line.

MAE (Mean absolute error) and RMS (Root mean square error) were calculated by using the regression equation to estimate the head at each point and comparing this estimated head to the measured head. The MAE is the average of the absolute value of the residual at each well. To calculate the RMS, each residual was squared, they were averaged and then the square root was taken. This gives additional weight to points that have the greatest residual.

The best-fit line on the lower plot has a slope that matches well with the general trend of the majority of the points. This is the line that was used to estimate the head in zone 4. The RMS and MAE values are similar in magnitude to the expected calibration error.

Regressions for other months of the calibration and validation periods had similar statistics.

See Figure C3-3 for zone locations.

Regression for Heads and Elevations for SAS wells, October 2003

Final Groundwater Model Calibration Report

Figure C3-4

April 2010

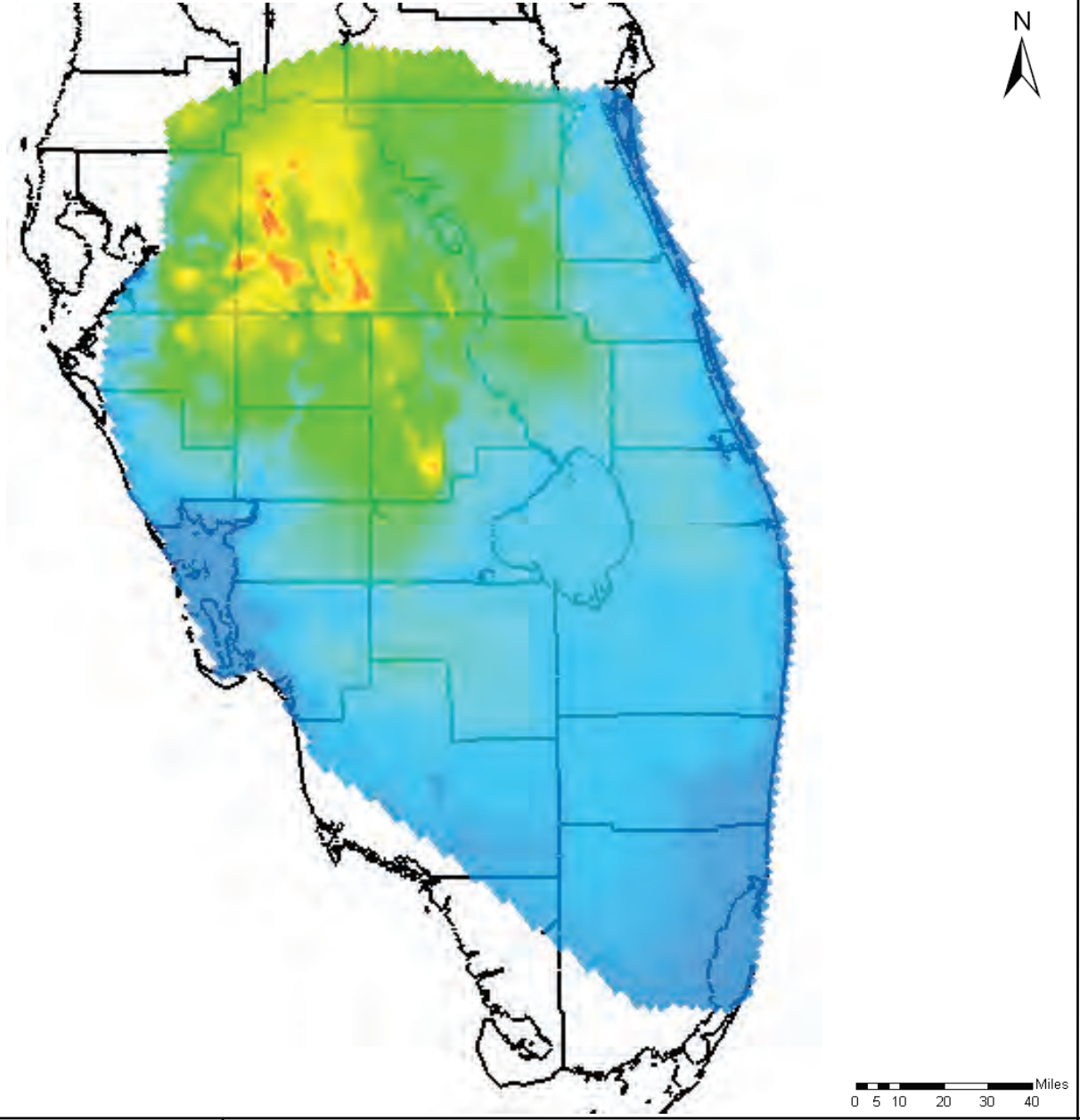

Legend

Head (ft)

- 175
- 150
- 125
- 100
- 75
- 50
- 25
- 0

Notes:
Figure shows specified heads applied to the SAS layer for October 2003.

Separate interpolations were made for each month of the calibration and validation period.

The model used month-long stress periods, which required constant heads during each month.

Specified Head Applied to SAS (surface) Layer
October 2003
Final Groundwater Model Calibration Report

Figure C3-5

April 2010

Appendix D: Pumping Data Report

Table of Contents

1.0 Introduction

The purpose of the ASR Regional model is to evaluate the large scale impacts of the proposed Comprehensive Everglades Restoration Program (CERP) ASR system on the surrounding groundwater. Prior to using this model as a predictive tool, the model must be calibrated to ensure that it reasonably simulates system responses to historic stresses. For the ASR regional model, these stresses are primarily water removal in water supply and agricultural wells scattered throughout the model domain. As with all inputs to the model, the quality of the data entered has a direct impact on the quality of the final solution. Unfortunately, pumping data is not always uniformly tabulated and collected. There were many pumping wells which provided no pumping data and many that had holes in their data sets.

The Jacksonville District (SAJ) of the Corps of Engineers was tasked with collecting, organizing and providing the pumping data to the groundwater modeling team. An exhaustive search of available data was performed as described in their Data Collection Report provided in Appendix A of the Groundwater Model Calibration Report. In order to correctly represent the pumping in the model, it was important that all wells with missing or incomplete pumping records be assigned an estimate of the pumping for each month of the calibration and validation periods. SAJ also provided the modelers with these estimated pump rates when the data was not available. The methods used to estimate these rates are also described in their Data Collection Report.

The pumping data provided by SAJ was incorporated into the regional SEAWAT and WASH123D models. It should be understood that because SEAWAT and WASH123D calculate the flow equation at their computational points (i.e. cell centers and nodes, respectively), all wells falling on the same computational point are effectively combined. For a regional scale model, this is sufficient, but near-field effects of individual wells are not well-portrayed on a regional scale with coarse resolution like that used in the regional grid and mesh, whose cell and element sizes are as large as 10,000 ft on a side. The methodology explaining how well pumping is assigned to SEAWAT cells and WASH123D nodes is described in Section 2.0 of this Appendix.

The process of model-setup and calibration of the regional model began with a steady-state model representing October 2003. None of the model results for this month caused concern. With October 2003 nearly calibrated, several other months were run to validate the original calibration. With May 2004 and September 2004, a pattern of unusual results began to emerge, indicating a problem with the pumping data. Section 3.0 of this appendix presents an evaluation of the problems and the process used to select and implement a solution.

2.0 Pumping Rate Assignment in the Regional Model

The results of the SAJ data collection effort were several tables of regional pumping data for consumptive use wells, deep injection wells and existing ASR wells. The tables contained well location information including well name, well identification number (Model ID), horizontal coordinates in Florida State Plane 1983 East, aquifer designation, depth from the ground surface to the top of open hole (cased depth), and depth from the ground surface to the bottom of the open hole (drilled depth). The tables also contained transient pumping rate data including well type, pump capacity, date

pumping, pumping rate, and a flag to indicate whether the pumping rate was reported or estimated. This data needed to be reworked into a format that could be incorporated into the SEAWAT and WASH123D models.

The first step was to determine the vertical elevations for the pumping wells. The ground surface elevation was estimated at each pump using the topographic data described in Section 3.1 of the calibration report, and then the given cased and drilled depths were subtracted from the estimated ground surface elevations to determine the open hole cased and drilled elevations. These elevations were compared against the hydrostratigraphic surface elevations for each layer to determine the aquifer(s) where the casing is open. If a pump's open hole interval overlapped more than one aquifer, the pumping rate for that pump was divided among the multiple aquifers based on the percentage of the open hole in each aquifer. The confining units were not considered in this computation. For example, if 15% of a pump's open hole overlapped the Upper Floridan (UF), 50% overlapped the Upper Middle Confining Unit (MC1), and 35% overlapped the Avon Park Permeable Zone (APPZ), then the pumping rate was distributed so that 30% of the rate was assigned to the UF and 70% was assigned to the APPZ. If the pump's open hole interval completely overlapped a confining unit, then judgment was used to determine the vertical location of the pump based on the proximity to aquifers, the pump's aquifer designation, the pump name, well drilling reports, or other available data.

Special consideration had to be given to pumping assignments in the Surficial Aquifer System (SAS) and the Intermediate Aquifer System (IAS) as a result of their geologic conceptualizations, described in Section 3.0 of the main report. Because the SAS has an assigned head, no head computation will occur in the SAS layer so pumping stresses will have no impact on the SAS heads. Therefore any wells found to pump from the SAS were removed from the data set. The Intermediate Aquifer (IA) portion of the IAS only occurs in the western portion of the model in the middle third of the IAS layer. For pumps found to be located horizontally and vertically within the IA, pumping rates were distributed by the percentage of the open hole overlapping the conceptualized aquifer. For example, for an open hole whose open interval was 10% in the SAS, 15% in the upper third of the IAS (ICU), 20% in the middle third of the IAS (IA), 20% in the lower third of the IAS (ICU), and 35% in the UF, the distribution of the pumping rate would be assigned with 54% of the rate coming from the UF and 31% of the rate from the IA. The 15% of the pumping rate in the SAS is removed from the data set. Pumps located horizontally outside the boundary of the IA but located vertically within the IAS were determined to be within the SAS or the UF based on proximity to the SAS or UF, the pump's aquifer designation, the pump name, well drilling reports, or other available data.

Once aquifers were identified for each pump, their pumping rates were assigned to the grid and mesh. The pumping rates were incorporated into the SEAWAT grid using the *Map to MODFLOW* tool in GMS and into the WASH123D mesh using the *Map to FEMWATER* tool. These tools determine the location of the model computational point(s) for each pumping well given the well horizontal and vertical location. For SEAWAT, the location is the center point of the model grid cell containing the well and for WASH123D, the location is the node nearest to the well location. Due to the differences in computational points for the two codes, the pumping rates were applied somewhat differently in the two models.

For the SEAWAT grid, if a pump was horizontally and vertically located within a cell, its pumping rate was applied to the center of that cell. Therefore in the case of a 10,000-foot by 10,000-foot cell, the rates of all wells existing within that cell are totaled and applied to the same computational point. If the pump's open hole overlaps several vertical cells, the pumping rate for that pump is split up among the vertical column of cells in proportion to the coverage of each of the cells by the well open interval. The GMS tool *Map to MODFLOW* totals and applies the pumping rates for each cell automatically.

For the WASH123D mesh, pumping wells must have horizontal coordinates that coincide with its computational points, the mesh nodes, to be assigned correctly with the *Map to FEMWATER* tool in GMS. Thus, the actual horizontal locations of the pumping wells must be manually adjusted to match mesh nodes. This adjustment was made by generating a two-dimensional mesh with horizontal node locations coincidingwith pumps (or pumping centers made up of several pumps) having rates higher than 100,000 cubic feet per day. The remainder of the 2D mesh to the model boundary was filled in with nodes at 10,000-foot spacing. The locations of pumps with lesser rates were moved to coincide with the nearest 2D mesh node. Once each pump was adjusted to coincide with a mesh node, the open hole intervals were evaluated to ensure that each pump's open hole interval overlapped the appropriate aquifer nodes in the 3D mesh. If the pump's open hole interval overlapped several vertical nodes, the pumping rate for that pump was split up among the vertical column of nodes in proportion to the hydraulic conductivity of the elements surrounding the nodes. The GMS tool *Map to FEMWATER* was used to total and apply the pumping rates to the mesh nodes.

3.0 Pumping Rate Problem Identification

During the calibration process, a reasonable preliminary steady state calibration to October 2003 data was achieved (see Figure D3-1). Further, initial testing of a transient model for the period data between October 2003 and December 2004 showed a coarse agreement between calculated and observed heads. However, with the development of steady state models for other months of the period, distinct patterns were computed by the numerical models that were not supported by the existing water level data. Figures D3-2 and D3-3 show examples of these patterns. Figure D3-2 shows the model results of the Upper Floridan aquifer for May 2004, using parameter values developed during the steady state calibration of October 2003. In this figure, distinct cones of depression can be seen northwest of Lake Okeechobee, primarily in Highlands County (within the red box). These cones of depression are relatively widespread and can reach up to 100 ft in depth. Available water level data does not indicate a water table depression of this magnitude in this area. The inset verifies (as expected) that these depressed areas are caused by the presence of wells which pump at high rates. It also indicates that most of the wells at the centers of these cones are irrigation wells. A second example of an anomalously large cone of depression can be seen in Figure D3-3. This figure shows the computed results for the Upper Floridan aquifer for the September 2004 period. During this period the large cones of depression seen in Highlands County are no longer present; instead, a distinct cone of depression in northern St. Lucie County (within the red box) is predicted by the model. Again these water levels were not supported by the available water level data.

The poor calibration achieved for May 2004 and September 2004 when the same parameter values yielded a good calibration for October 2003 indicated a problem with either the data or the conceptualization of the system. The fact that the areas of greatest concern for both May 2004 and September 2004 corresponded with the locations of pumping wells with large pump rates, pointed to a problem with the pumping data. For this reason, a closer look was taken at the pumping data and the methodology used to provide estimated pump rates for wells without a complete pump record. The following sections describe the evaluation performed, the search for a solution and the selection of a path forward.

3.1 Problem Evaluation

Since the pumping was suspected to be the cause of the calibration problems, the modeling team re-evaluated the pumping data provided by SAJ, beginning with the September 2004 period. As shown in Figure D3-3, a significant cone of depression was computed in the vicinity of St. Lucie County. The pumping data provided for September 2004 calibration was compared to the results of an analysis provided in February 2007 by the SFWMD (Center for Hydrology & Water Resources, 2007). The water management district provided this information in response to concerns raised during the initial data evaluation subsequent to the Phase I modeling effort regarding the significant pumping data gaps identified. Although it had been expected that this data would be integrated into the pumping data, some discrepancy still existed between the original data provided by SFWMD and the final pumping data set. The inset figure (right side of Figure D3-3) shows a blow up of the September 2004 St. Lucie cone of depression, as well as the pumping well locations. Data from SFWMD is indicated with an "X" and the SAJ database data is marked with a "DOT." Each pumping location is colored based on the magnitude of the pumping with blue being lower magnitude pumping and red being higher magnitude pumping (up to 250,000 cfd). Remember that the dots indicate the pumping magnitude that was used in the calculation of the head contours shown. The map shows numerous locations where the pumping in September 2004 is significantly higher in the SAJ data set than the SFWMD data set (blue X's over red dots). These locations correspond to the deepest portions of the cones of depression shown. The figure also shows that the overall pumping in the area is much higher in the SAJ data than in the SFWMD data – few of the x's are any closer to the red end of the spectrum than a light blue or green color.

Further analysis compared the September 2004 pump rates from the data base with the October 2003 pump rates. Remember that the October 2003 pump rates yielded a reasonable calibration. In Figure D3-4, the magnitude of the October 2003 pumping is indicated by the color of the "X" marking the well location. Similarly, the September 2004 pump rates are indicated by the color of the "DOT" at the same location. Each pumping location is again color coded by magnitude with blue being lower magnitude pumping and red being higher magnitude pumping (up to 250,000 cfd). The contours shown on this figure are from the September 2004 model run using parameter values which resulted in a well-calibrated October 2003 steady state run. At several locations the pumping reported for September 2004 in the SAJ database is significantly higher than that provided for October 2003 (red dots over blue X's). This higher pumping causes the significant computed cone of depression in September 2004, which does not appear in the October 2003 calibration runs.

Based on this initial evaluation, it appeared that the high magnitude pumping at a few wells in the September 2004 SAJ data set was the cause of the unexpected cone of depression in the St. Lucie County area. Discussions with SFWMD indicated that their pumping data was from an in-depth study of irrigation pumping in the St. Lucie County area. Since the SAJ estimates were based simply on the comparison of known pump rates to the pump capacity or allocation, the SFWMD pumping estimate would be more representative of the actual pumping. Unfortunately, since the SFWMD data is only available in a small area of the model domain, it could not solve the data problem for the entire model domain.

The next step in the evaluation was to determine if the high magnitude pumping observed in the SAJ database was based on reported or estimated data. Reported data consists of pumping rates provided by one of the data sources for each month of the calibration period. For wells where no reported data was provided but there was reasonable certainty that the well was pumping, the rates were estimated. In all cases examined, large pumping rates which caused significant and unexpected cones of depression were the result of estimated pumping data, not reported data. This evaluation also indicated that the types of wells causing this problem were primarily irrigation/farming wells. Notice that Figure D3-2 shows that almost all of the wells located near the centers of the anomalous cones of depression in Highland County for May 2004 are irrigation wells.

The SAJ pumping data (including both reported and estimated pumping rates) indicated that nearly 2000 irrigation wells in the model domain were pumping at 85% or more of their pump capacity in September 2004 (Figure D3-5). However during September 2004, Florida was affected by three major hurricanes (Frances, Ivan and Jeanne). Both Frances and Jeanne caused significant precipitation across a large swath of the model domain, resulting in one of the wettest months in the last 15 years. With so much rain in such a short period of time, it would be unlikely that irrigation needs from the wells would be so high. Figure D3-6 shows the location of irrigation wells listed in the SAJ database with pump rates more than 85% of their capacities. This figure shows that these high pumping rate irrigation wells are in all three of the Water Management Districts covered by the model and many are in the vicinity of the two problem areas already identified in Highlands and St. Lucie Counties (Figures D3-2 and D3-3).

Additional analyses compared the long term trends of the reported and estimated pumping data at wells divided into geographic zones shown in Figure D3-7. These zones were roughly based on similar physiographic and hydrogeologic properties, not necessarily on Water Management District Boundaries. Due to the availability of the SFWMD study of irrigation wells in Zone 1 and lack of major Floridan irrigation pumping in Zone 2, the following evaluation is only presented for Zones 3, 4, and 5. For the October 2003 to December 2004 period, there were 5,669 irrigation wells with reported pump data for all months, 4,206 irrigation wells with reported data in some of the months, and 6,628 wells with no reported data. For each zone the reported and estimated pumping data was normalized by dividing the reported rate by the pump capacity/allocation. The distribution of the average normalized pumping rate for wells with reported data is shown by month (October 2003 to December 2004) on Figure D3-8. Although there are minor variations between the zones, the general trend shows higher pumping in the dry season (spring and early summer) and lower pumping in the wet season (late summer and fall) as expected. When compared to the monthly rainfall data in Polk County, shown in Figure D3-9, a distinct

inverse correlation can be seen, where pumping increases in low rainfall months and decreases in high rainfall months. The data in Figure D3-8 also shows that the reported pumping rate is on average less than 20 percent of the capacity/allocation even in the driest months. This average percentage of pumping capacity is also consistent with the data provided by SFWMD for Zone 1.

Figure D3-10 shows the comparison between the reported and estimated pump rates as a percentage of the capacity/allocation averaged across all irrigation wells in Zone 5. There are two main concerns illustrated in Figure D3-10. First, the estimated data is five to thirty times higher than the reported data when considered as a percentage of capacity or allocation. Secondly, the seasonal variations applied to the estimated data do not match either the reported data or the expected variations. Generally, pumping would be expected to be highest during dry periods when rainfall is not sufficient for the fields and orchards. When rain is abundant, pump rates would be expected to fall. The highest pump rates in the estimated data occur in July 2004. Although Figure D3-9 shows that although July's precipitation is about half of September's, it is quite a bit larger than nearly all other months of data. (This same precipitation trend is repeated in numerous weather stations throughout Florida.) Further, the lowest estimated pumping rates occur in January 2004, which has one of the lowest rainfall measurements of the period. The estimated pumping rates clearly do not correlate with the known meteorological conditions at the time.

The concerns with the methodology for estimating missing pump data are further illustrated by looking at selected individual wells. An example of this can be seen on Figure D3-11 at the irrigation wells in Northern St. Lucie County in the center of the anomalous water table depression computed by the model in September 2004. This figure shows that the maximum pumping rate (94 % of capacity) was estimated in September 2004, which has already been shown to be one of the wettest on record. The pump rates for the entire period seem completely uncorrelated to the precipitation data. It is also suspicious that exact pump rates are repeated for seemingly unrelated months. For example, March 2004 and September 2004 have identical estimated pump rates. Similarly, February 2004, August 2004 and December 2004 have identical rates.

This analysis clearly indicates that the original methodology used to fill gaps in the available pumping data was flawed. When it is totaled up across all the irrigation wells in the model domain, the difference between the estimated and reported pump volumes is on the order of tens to hundreds of millions of gallons of water per day (depending on the month). Clearly, this discrepancy severely impacts model calibration. A new process for estimating missing pump rates was necessary in order to adequately calibrate the model for all time periods of concern.

3.2 Solution

In order to calibrate the regional ASR model, it was necessary to revisit the available pump data and develop a new methodology for estimating pump rates where data was not available. The majority of the problems found in the data set from SAJ were with the agricultural or irrigation wells, so they have been handled separately from the remainder of the wells. This section describes the process used to analyze the data and estimate missing values.

3.2.1 Agricultural/Irrigation Wells

In the SAJ Data Collection Report (provided in Appendix A), the method employed to estimate pump rates for irrigation/agricultural wells with missing data is described. The methodology involved dividing the wells up by county, calculating the average pumping across each county as a percentage of capacity/allocation and then applying this percentage to the wells and months with missing data. Our analysis showed that some errors must have been introduced during the process because those percentages do not hold true for all wells and are significantly larger than the percentages calculated on the wells with sufficient data. The main concerns with this method are twofold. First, it separates the data into groups based on county boundaries, which have no known physical relationship to either water availability or water needs. Secondly, it assumes that pump capacity or allocation is directly related to the water needs of each user. The available data shows that this is not always true. For example, based on the reported pump rates, the average usage for October 2003 was 5.8% of the capacity. But the standard deviation is over 10% and the median rate as a percentage is only 2.4%, meaning that there is a wide spread in the values and 50% of the values are below 2.4%. These statistics indicate that there are a lot of agricultural wells whose reported (not estimated) usage in October 2003 was nowhere near the average usage of 5.8%. These may be permit owners who did not correctly calculate their usage requirements or who have changed their usage since receiving a permit.

The issue is clarified in Figure D3-12, which shows the pumping data for four randomly selected wells from the data set. These four wells all have complete data sets in the SAJ database and are scattered across the model domain. The only one of the four that appears to follow the general seasonal usage which is inversely proportional to rainfall is the Palm Beach Country Club. Aerial photos indicate that this water is most likely used to irrigate a golf course. Water usage at this well is low in August and September when rainfall is high. Conversely, water usage is highest earlier in the summer when rainfall is low. However, although the shape is similar to the average usage seen in the rest of the data set, the percentages of capacity are significantly higher than average. In October 2003, the average usage was 5.8% of the capacity, while this well used nearly 30% of its capacity.

The other three wells all have unusual usage rates. Aerial photos show all of these wells are near farmland which appears to be growing various tree crops such as citrus fruit. The Oak Island Citrus well has low usage rate throughout most of the first year, with a sudden, stark increase in usage during August, September and October. These are the months when evapotranspiration would be expected to be highest, but these are also the months when rainfall was highest. There is also no known explanation for the high usage in December 2004. The Evans Properties and Lykes Block wells have similar unexplainable variations in usage during the period in question. Figure D3-13 presents the same data as a normalized pump rate for all four wells together.

These problems were addressed by first attempting to find a geographic method of separating the wells into groups based on their data or other available characteristics – not on something as arbitrary as the county boundaries. A geographic separation of groups would allow us to assign the wells with no data or very little data to the appropriate group. Making the division based on the available data would assure that the known data in each group could be used to accurately estimate the pump data for the

wells with sparse or non-existent data in the same group. Unfortunately, all efforts to divide the wells into groups based on their data failed, despite analysis of the data as reported pump rates, percentages of capacity, percentages of another month's data, etc. Only about 50% of the wells have data closely correlated with precipitation data. These wells are scattered all across the domain and are interspersed with wells that seem to have no correlation to any seasonal changes. The zones described in Section 2 were chosen somewhat arbitrarily, with some attention to physiographic regions. Although these zones spread across two-thirds of the model domain and include the majority of the wells, there is very little variation in the pump rates when expressed as percentages of the capacity or allocation.

Some effort was expended in looking for a way to divide the wells based on the type of crop being irrigated. Although SFWMD was very helpful in providing extensive information on the methods used to calculate water needs based on crop type, no data was easily available to determine what crop was being served by each well. SAJ was unable to provide this type of data. Land-use GIS coverages indicated only that the land was used for agriculture – not the specific type of agricultural activity. Internet searches yielded little information and well permit applications obtained online did not request information on the use of the water being allocated. It might be possible to use aerial photographs to make assumptions on water use based on the types of fields nearby. However, this would be a time-consuming and likely inaccurate process. Aerial photos might be out of date and the wells might not be located exactly at the field they are irrigating.

Additional work was performed to find a statistically significant correlation between rainfall at the nearest weather station and the pump rate at each well. However, the correlation was weak and not within acceptable confidence intervals.

In an effort to remove the dependence of this methodology on the capacity or allocation of each well, comparisons of pump rates were made between months. However, this analysis ignored nearly 42% of the wells since they had no reported data in the database. Further, an additional 2% of the wells were removed from the analysis because they had only three or fewer months with available data. Using this month-to-month comparison of available data, it was found that nearly 50% of the wells statistically fit into a group in which the May 2004 pumping was approximately three times the January 2004 pumping rate and April 2004 pumping was approximately 22 times the September 2004 pumping rate, for example. Similar ratios were calculated between all other months of the period. Although only 50% of all agricultural wells fit into this group, it was actually 86% of the agricultural wells with sufficient data. And these wells were spread across the entire model domain. Additional groupings of wells were found, but were all very small and none were geographically grouped. Without a geographical grouping, it was impossible to determine the grouping of wells with no data or very little data. For this reason, only the first grouping (including about 86% of the wells) was used to estimate missing pumping data.

Using this month-to-month comparison of pumping rates, missing data was filled in for all wells with a partial data set. If a well had no available data, the average pump rate as a percentage of capacity was used to estimate one month and then the month-to-month ratios were used to calculate the remaining months. The pumping obtained in this way was compared to the pumping obtained using only the average ratio of pumping to capacity for each month (described below). The differences were negligible

– especially on a regional scale. For this reason, the simpler of the two methods was used and is described in detail in the following section.

3.2.1.1 Final Method for Estimating Missing Pumping for Agricultural Wells

The method selected for estimating the missing pumping data for agricultural wells involved comparing the pump rate for each well and each month to the capacity or allocation for that well. Where all the data was missing, the average percentage of capacity being pumped across all the wells was used to fill in estimated pump rates. Where some data was missing, the available data was used to offset the average percentages for filling in the missing months. The method is described in detail here.

1. Reported data was separated from estimated data in the SAJ database. If the flag was zero, the data value was assumed to be a reported value. The exception was for those wells with model IDs between 20000 and 39999 (Southwest Florida Water Management District data). In these cases, if the data value was a zero, it was assumed to be a reported data value regardless of the flag. (See the SAJ Data Collection Report provided in Appendix A.) Values estimated by SAJ were removed from the data and replaced with empty cells.

2. For all reported data values, the fraction of the capacity/allocation was computed by dividing the pump rate by the capacity or allocation. No calculation was made for empty cells (missing data).

3. For each month all of the calculated fractions were averaged by summing them and dividing by the number of wells with reported data in that month. Figure D3-14 shows these averages. As observed above, these averages show an inverse correlation to precipitation (see Figure D3-9 for Polk County precipitation as an example).

4. The ratio between each known pump rate as a fraction of capacity and the average pump rate as a fraction of capacity was computed by dividing the result of step 2 by the result of step 3 for each known data point. For example, if a certain well was pumping 11.6% of its capacity/allocation for the month of October 2003, the ratio to the average would be 2, since the average pumping for October 2003 among known data points was 5.8%. This would tell us that this well was pumping at twice the average when reported as a percent of capacity or allocation.

5. For wells with at least one month of data, the ratios computed in step 4 were averaged for each well. For the example presented in step 4, imagine that in November, the pump rate was 6.9% of the capacity/allocation. Since this is the average rate among all wells, the ratio for November calculated in step 4 would be 1.0. If these were the only two data points, the average for this well would be 1.5 (the average of 1 for November and 2 for October), indicating that on average, this well was pumping 150% of the average when reported as a fraction of the capacity/allocation.

6. Fractions of the capacity/allocation are listed for every well and every month.

a. If reported data is available for every month, the fractions calculated in step 2 is listed.

b. If reported data is available for some, but not all of the months in the period, the fractions calculated in step 2 are listed for the months with available data. For the months with no available data, the fraction is estimated by multiplying the average for the well calculated in step 5 by the average for all the wells for the month in question calculated in step 3. For the hypothetical well mentioned above, the averages for months missing data (December 2003 through December 2004) were multiplied by 1.5 to obtain an estimated fraction. For December 2003, the average pumping for all wells with data was 7.3% of the capacity/allocation. Thus, for this hypothetical well, the fraction for December would be 10.95% (1.5 times 7.3%) of the capacity/allocation.

c. If reported data was not available for any month of the period, the averages calculated in step 3 were assigned to each month.

7. Pump rates were calculated by multiplying the capacity/allocation reported for each well by the fraction calculated in step 6 for each month. Pump rates were not allowed to exceed the capacity/allocation. If the fraction was over 1.0, the capacity/allocation was assumed to be the pump rate for that month.

There were two exceptions to the above process. First, for wells which had a drill date or abandonment date within the calibration period, the zero pumping months before drilling or after abandonment were not included in the average calculated in step 5.

Secondly, initial runs with this pumping data indicated too much pumping in the area just north of Lake Okeechobee (see Figure D3-15). Agricultural wells in this area were separated and their pump rates as ratios to their capacities were averaged separately. The averages were slightly different than the average calculated for the data set as a whole and are presented in Figure D3-15. These averages were used in place of those shown in Figure D3-14 for missing pumping data in this area.

3.2.2 Other Wells

As a result of so many questionable pumping rates estimated for the irrigation wells, the pumping rates for other well types were analyzed to see if their estimated rates appeared to be reasonable. These pumping well types included recreational wells, mining/dewatering wells, commercial/industrial wells, air conditioning wells, domestic/private wells, aquaculture wells, freeze protection wells, Orlando drain wells, injection wells, and public water supply wells. These well types are not generally related to rainfall or meteorological conditions so a comparison to the reported data is the only means of assessing whether the estimated pumping appears reasonable. For each well type, the reported pumping rates for wells of each type were normalized by the well capacity and compared to the estimated values normalized by the well capacity. The results for each well type are summarized below. It should be noted that existing ASR wells are not included on this list. As described in the Data Collection Report, each ASR facility was contacted to obtain daily pumping data during the time periods of interest so none of the existing ASR pumping rates were estimated.

1. Recreational wells (671 wells), Mining/Dewatering wells (90 wells), Commercial/Industrial wells (471 wells) and Air Conditioning wells (5 wells): A comparison of the estimated pumping rates to the reported pumping rates demonstrated that the estimated values are reasonable for these well types. For the recreational wells, all pumping rates within the 2003/2004 time period were reported data and some estimates were required for the 1993/1994 time period using the ratio of reported pumping rate to pump capacity for each well per month. For the mining/dewatering wells, only 2 wells required calculating estimated values. The ratio of reported value to pump capacity used to compute the mining/dewatering estimates is reasonable. For the commercial/industrial wells, only 104 wells required pumping rate estimates to be calculated. The reported pumping rate to pump capacity ratio used to make the estimates is slightly low but the estimated values are not unreasonable. For the air conditioning wells, only one well was completely estimated and 4 wells were partially estimated. The reported pumping rate to pump capacity ratio used to make the estimates is slightly low but reasonable for these minor pumping wells.

2. Domestic/Private wells (10,165 wells): There are no reported values for these well types. These well pumping rates are estimated based on the logical methodology described in the Data Collection Report. These pumping rates are all very low values, as expected for domestic and private wells. The range of values is from a low withdrawal of 0.2 cubic feet per day (cfd) to a high of approximately 2,300 cfd but the majority of the withdrawal rates are in the 40 to 50 cfd range. Because the rates are so low, it is not likely that these rates have a significant impact on the regional model calibration. No adjustment was made to these estimates.

3. Aquaculture wells (20 wells): There are 18 wells that are completely estimated and 2 wells that are partially estimated. The reported values have a maximum pumping rate of approximately 300 cfd. The estimated values were as large as 141,000 cfd and 81,000 cfd at 11 of the estimated wells. These estimates were too high compared to the reported data. It was confirmed by SAJ that these well types were lumped with agricultural well types because the term “farms” was included in the well name. However, these farms are seafood farms and there rates vary differently than agricultural wells. The rates for these wells were revised by normalizing the reported data by the pump capacity and using that ratio to determine the pumping rate estimates. The resulting maximum estimated pumping withdrawal was 1,400 cfd.

4. Freeze Protection Wells (124 wells): There are two general areas where wells labeled “freeze protection” are located: northeast of Lake Okeechobee and southwest of Lake Okeechobee. The maximum reported values provided for these two areas, respectively, was 10,000 cfd and 35,000 cfd. Estimated values provided for these two areas were as high as 76,000 cfd (northeast of Lake Okeechobee) and 200,000 cfd (southwest of Lake Okeechobee). Also the maximum ratio of reported data to pump capacity is 30% while the maximum for the same ratio in the provided estimated data was 80%. These pumping rate estimates were too high. In looking at the data provided, six facilities were identified that have reported pumping rates:

a. Six L's Farms has many pumps that pump all year long. It's possible that these wells are actually used for irrigation rather than freeze protection, since it is expected that freeze protection would only be required during certain parts of the year.

b. Highlands Citrus Grove has reported data and estimated data. The reported pumping rates are approximately 30% of the pump capacity.

c. Southern Grove and LaBelle Grove have rates of 0.0 cfd for each month.

d. A Green's Citrus Grove has reported values of approximately 3% of the pump capacity and is located within Hendry County

e. River Country Land and Cattle – reported pumping in 1993 and 1994 only at rates approximately 6% of the pump capacity and is located within Okeechobee County

Based on the reported rates at these facilities, it was decided that Six L's Farms wells would not be used to estimate pumping rates since it seems likely that these are actually irrigation wells. Also the Highland Citrus Grove reported well rate to pump capacity ratio appeared high for these well types and was used to estimate the unknown pumping rates at Highland Citrus Grove only. The known pumping rate to pump capacity ratio at A Green's Citrus Grove was used to estimate the unknown pumping rates southwest of Lake Okeechobee. The known pumping rate to pump capacity ratio at River Country Land and Cattle was used to estimate the unknown pumping northeast of Lake Okeechobee. With these changes, the resulting pumping rate estimates were considerably lower than the estimates provided. For example, at LaBelle Drainage District, the maximum estimated pumping rate was revised from 200,000 cfd to 16,000 cfd.

5. Orlando Drain Wells (25 wells): All of the pumping for the Orlando drain wells is estimated. Drain wells are used to inject street runoff in the City of Orlando area to the UF aquifer in order to minimize flooding and control lake levels. The estimates provided did not appear to be related to rainfall patterns although it seems likely that months with high rainfall values, like September 2004 as mentioned in Section 3.1 of this appendix, should have the highest injection values. Adjustments were made to the computation of the drain wells estimates described in the Data Collection Report as follows. As part of the study by Sepulveda (2002), these drain wells estimates were made in cubic feet per second per year for the 1993/1994 time period. These estimates were converted to cfd units and the value was adjusted in each month based on the percentage rainfall in that month to the total for the 1993/1994 time period. The rainfall data was collected from the NOAA rainfall gage at Orlando, Florida. To find the 2003/2004 values, the 1993/1994 cfd/year was adjusted by the ratio of the 2003/2004 rainfall over the 1993/1994 rainfall. That new 2003/2004 yearly cfd was adjusted for the percent of rainfall for each month in the 2003/2004 time period. As a result of the changes the maximum estimated injection for the drain well decreased from approximately 75,000 cfd to 16,000 cfd.

6. Injection wells (120 wells): As stated in the Data Collection Report, the pumping rate data for these wells was verified by calling each facility. A few updates were made to these data sets including correcting pumping rates that were not placed in the correct month, changing an assumption that led to very small injection rates instead of a more appropriate rate (for example 0.13 cfd was revised to be 19,295 cfd) and re-contacting a facility to obtain data not previously received. Of the 120 wells, only 4 wells required updated pumping rates.

7. Public Water Supply wells (2,046 wells): Of the well total, there are 385 wells with reported pumping rates, 475 wells with partially reported data and partially estimated pumping rates, and 1,186 wells with all estimated pumping rates. The Data Collection Report states that the public water supply wells were estimated based on the ratios of reported pumping to pump capacity on a per county basis. These ratios were pro-rated by pump use within the county if possible. For example, municipality pump rates tend to be higher than business pump rates which tend to be higher than church pump rates. Questions arose in a backcheck of these assumptions. For a few public water supply wells, reported pumping to pump capacity ratios for irrigation wells were inadvertently used to estimate public water supply pumping rates. The use of nearby similar-use public water supply wells revised the maximum pumping rates from approximately 17,000 cfd to 3,000 cfd. The largest inconsistency was found at the two locations with the highest pumping rates in the model. One is a public water supply well in Kissimmee with a maximum rate of 1.4 million cfd and the other consists of two wells at Reedy Creek Improvement District (RCID) with a maximum pumping rate of 1.1 million cfd each. While the Kissimmee public water supply well and the RCID wells are large pumpers, these estimates are incredibly high. Further investigation revealed that the Kissimmee well rates were doubled compared to an appropriate estimate. The RCID wells were duplicates of other RCID wells already present in the data set for which some reported data was provided. The reported values ranged from 0 to 600,000 cfd.

4 References

Sepúlveda, Nicasio. 2002. Simulation of Ground-Water Flow in the Intermediate and Floridan Aquifer System in Peninsular Florida, U.S. Geological Survey Water-Resources Investigations Report 02-4009.

South Florida Water Management District's environmental database (DBHYDRO), http://my.sfwmd.gov/dbhydroplsql/show_dbkey_info.main_menu

Center for Hydrology & Water Resources. 2007. *Methodology for Estimating the Magnitude, Spatial and Temporal Variation of Irrigation Demand from the Floridan Aquifer System Within the Upper East Coast Planning Area, Florida.*

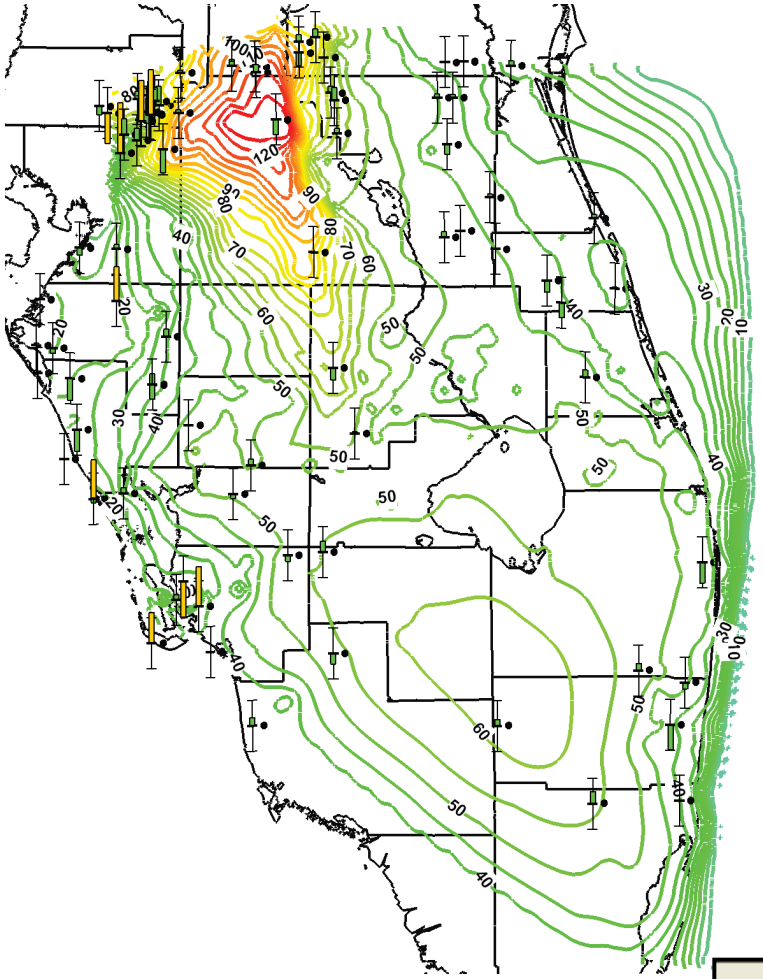

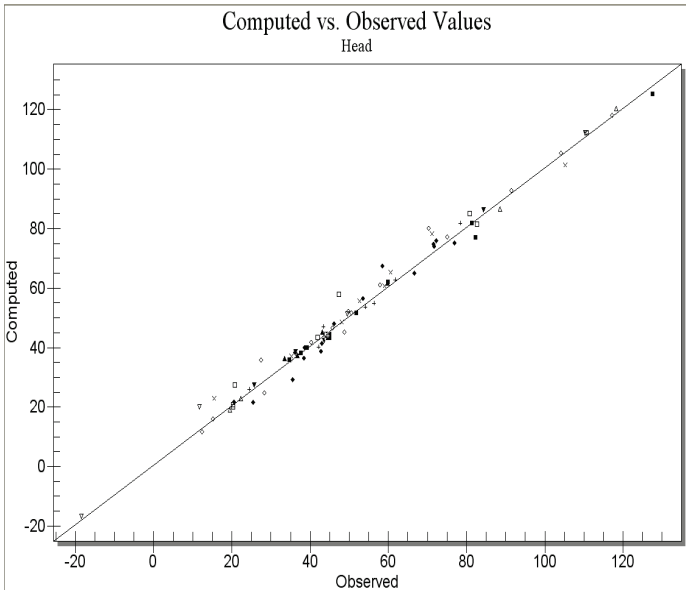

Error Summary

Head

Mean Error:	0.636
Mean Abs. Error:	2.219
Root Mean Sq. Error:	3.180

Notes:
This calibration (figure, plot and statistics) represents the results at an interim point in the calibration process. This does not represent the final selected calibration.

It was at this point that the problems with the pumping data were discovered.

Comparison to Figure 4.3 in the Calibration Report shows that significant improvement occurred in the following months.

October 2003 Steady State Preliminary Calibrated Heads

Final Groundwater Model Calibration Report

Figure D3-1

October 2010

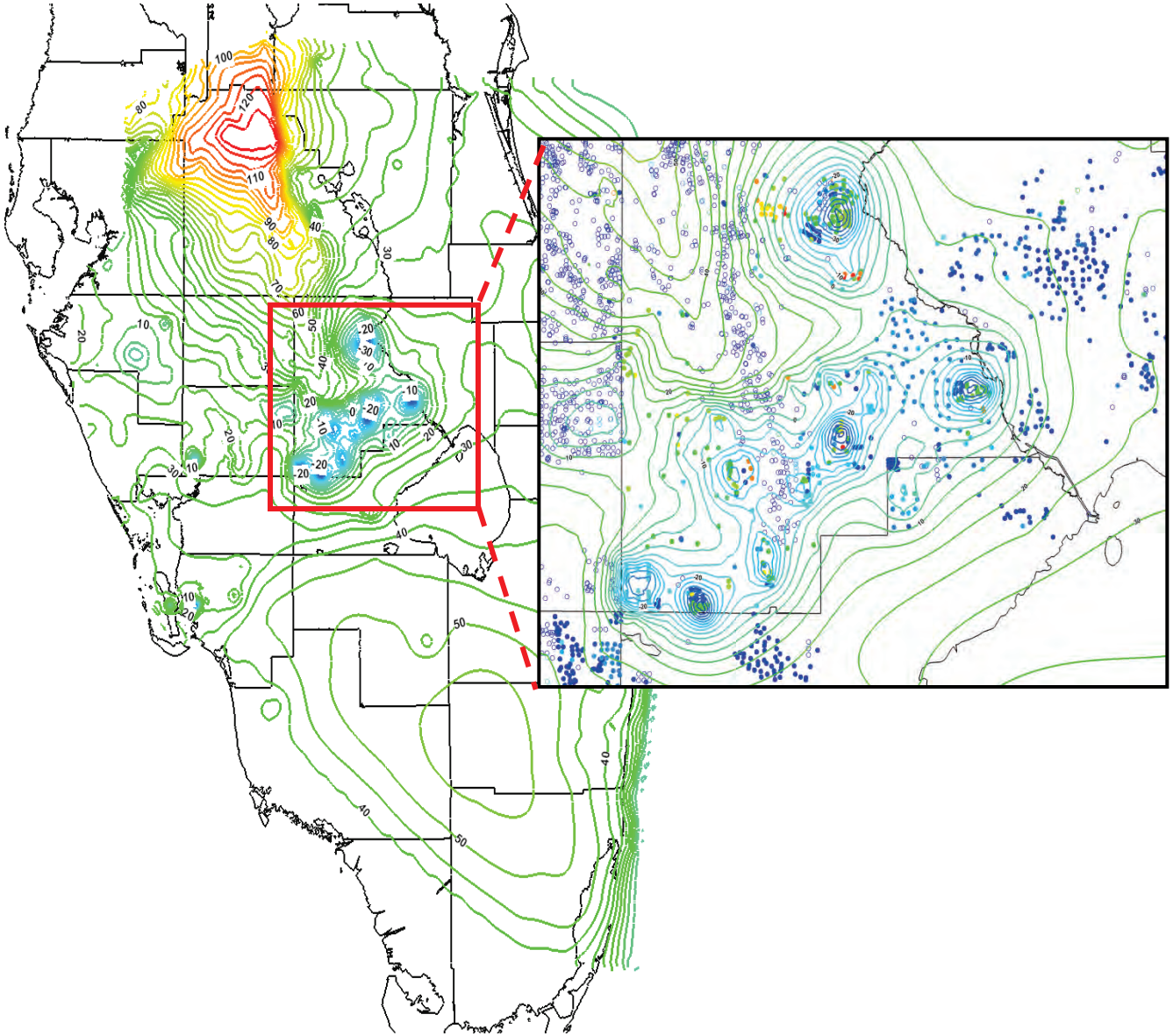

Legend

- Irrigation Wells
- Other Wells

Pumping rate color coded

- Red – large magnitude pumping
- Blue – small magnitude pumping

Notes:

These heads were calculated by applying the preliminary calibration conductivity values (used to make Figure D3-1) to the pumping rates provided by SAJ for the month of May 2004.

This figure is based on a preliminary calibration and uses pump rates that were determined to be faulty. This is not the final solution for May 2004.

UF May 2004 Steady State Model Results (Preliminary)

Final Groundwater Model Calibration Report

Figure D3-2

October 2010

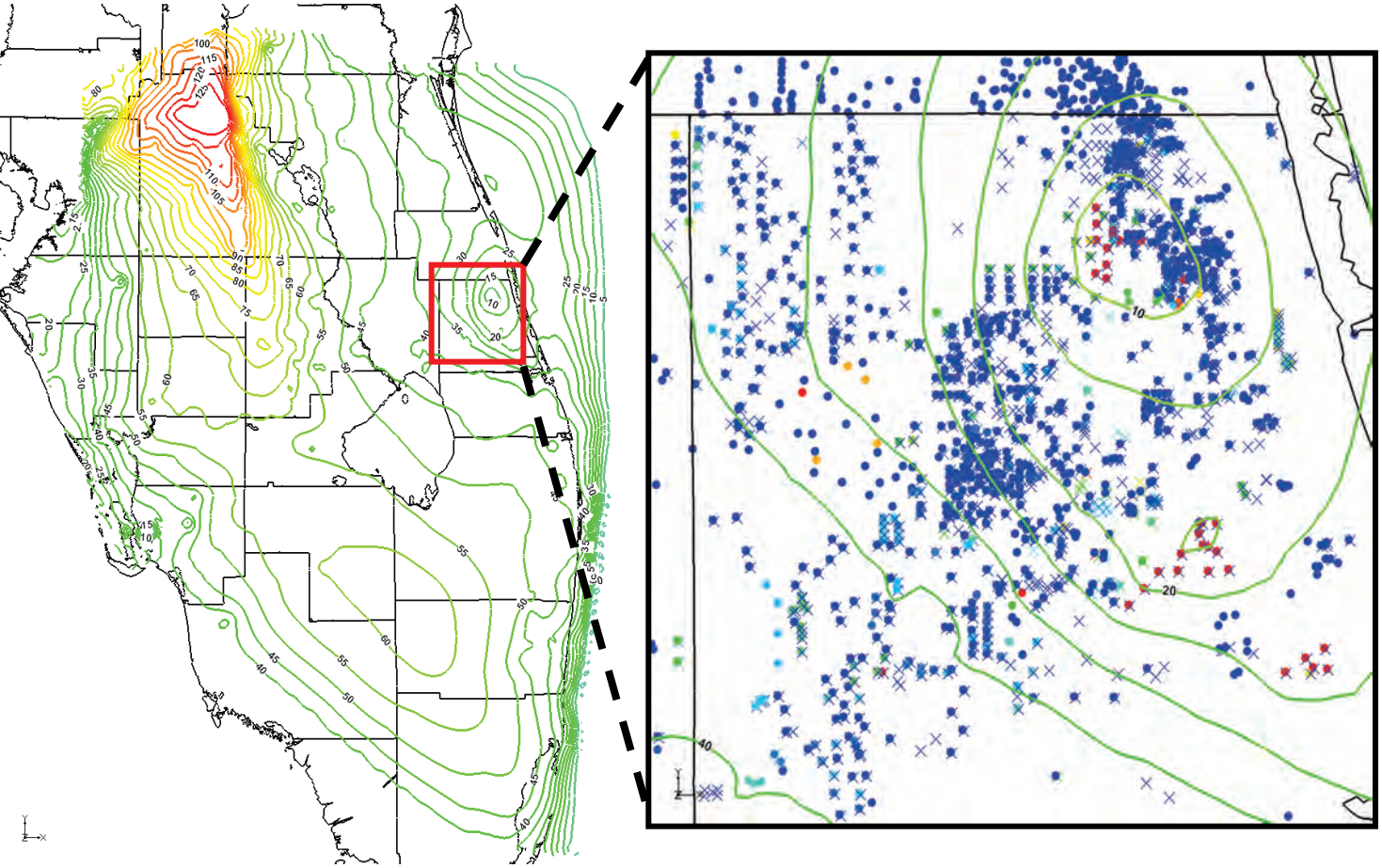

Legend

- SAJ Estimated Pump Rate (September 04)
- SFWMD Estimated Pump Rate (September 04)

Pumping rate color coded
Red – large magnitude pumping
Blue – small magnitude pumping

Notes

These model results were calculated by applying the conductivity values from the preliminary October 2003 calibration to the estimated pumping rates provided by SAJ for September 2004.

This figure is based on a preliminary calibration and uses pumping rates that were found to be erroneous. This is not the final solution for September 2004.

The SFWMD estimates are from the report by Center for Hydrology & Water Resources (2007).

UF - Sept 2004 Steady State Model (Preliminary)

Pumping Distribution in relation to Cone of Depression

Final Groundwater Model Calibration Report

Figure D3-3

October 2010

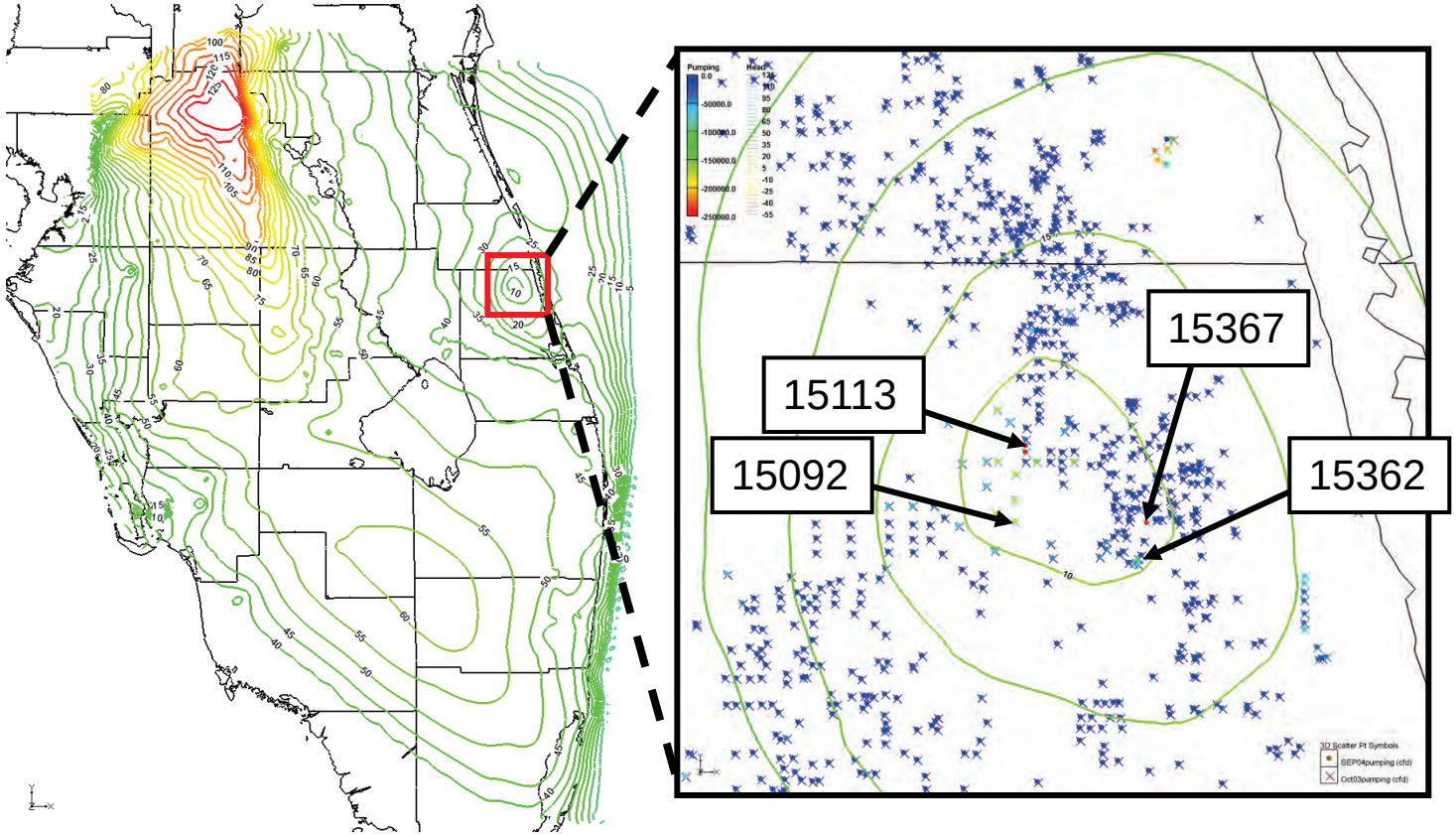

ModelID	seq-permitID-Name
15092	56-00091-W-23273-13-ALCO GROVES/BROWN RANCH
15367	56-00099-W-14919-3-D B PALMER
15362	56-01881-W-168911-Well 2-EDSALL GROVES E 12 - E 13
15113	56-00092-W-14899-7-EGAN GROVES BLOCKS 1-10 12 AND 13

Legend

- September 2004 Pump Rates
- October 2003 Pump Rates

Pumping rate color coded
Red – large magnitude pumping
Blue – small magnitude pumping

Notes

Contours are the model results for September 2004 (preliminary calibration).

All pump rates (designated with the color of the markers) are from the SAJ database, which includes reported pump rates and estimated rates.

The four wells called out on the figure were selected because they are located near the lowest head in this cone and because their September 2004 pump rates are much higher than the October 2003 rates as reported by SAJ.

Comparison of September 2004 and October 2003 Pump Rates

Final Groundwater Model Calibration Report

Figure D3-4

October 2010

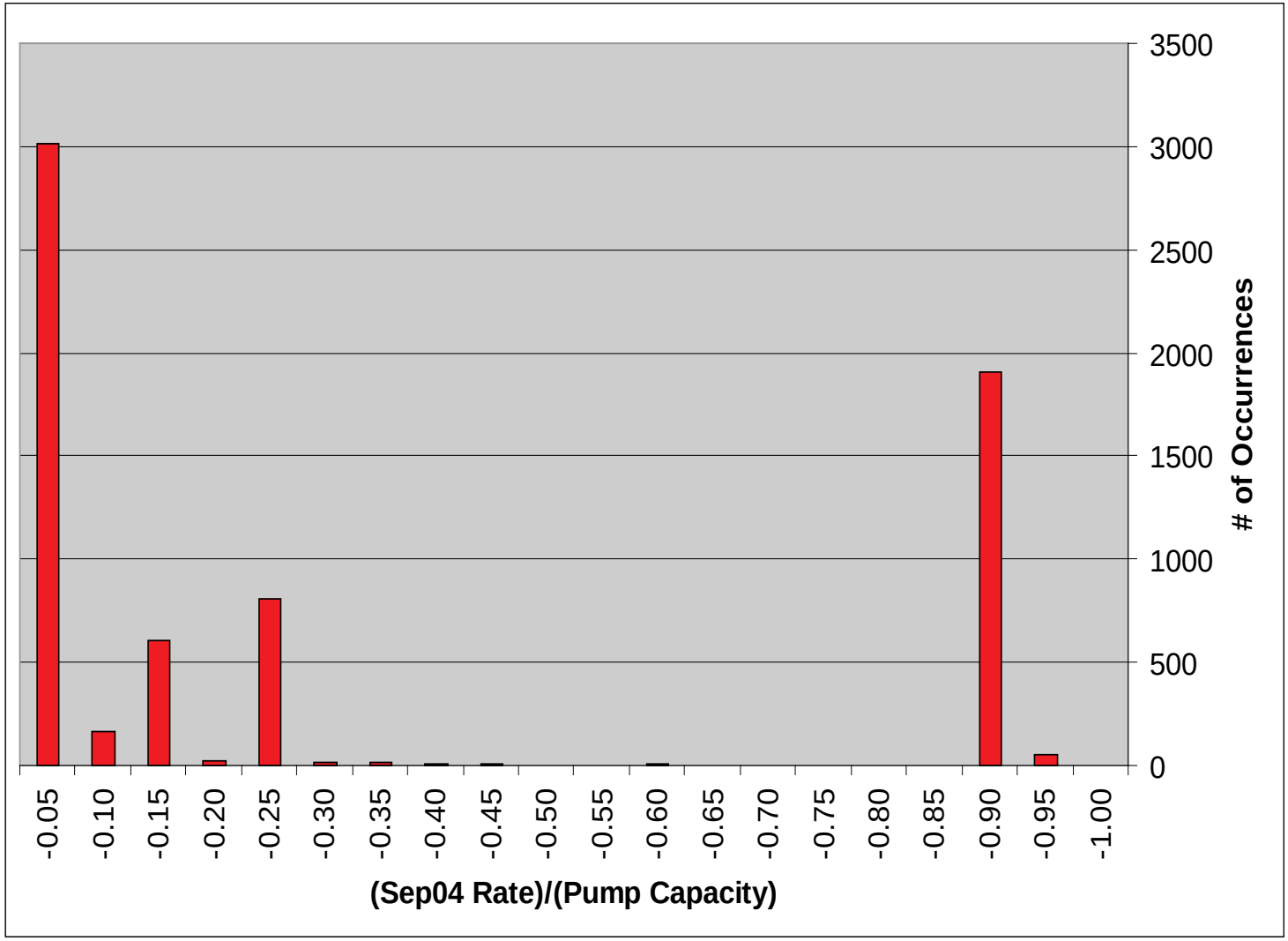

Notes

This histogram shows the distribution of irrigation well pump rates for September 2004 (reported in the SAJ database) as a ratio of the reported pump capacity.

This includes both reported pump rates and estimated pump rates.

The ratios are negative since the pump rates are reported as negative values (for extraction) but the capacities are reported as positive numbers.

Normalized Pumping Distribution (September 04) for Irrigation Wells

Final Groundwater Model Calibration Report

Figure D3-5

October 2010

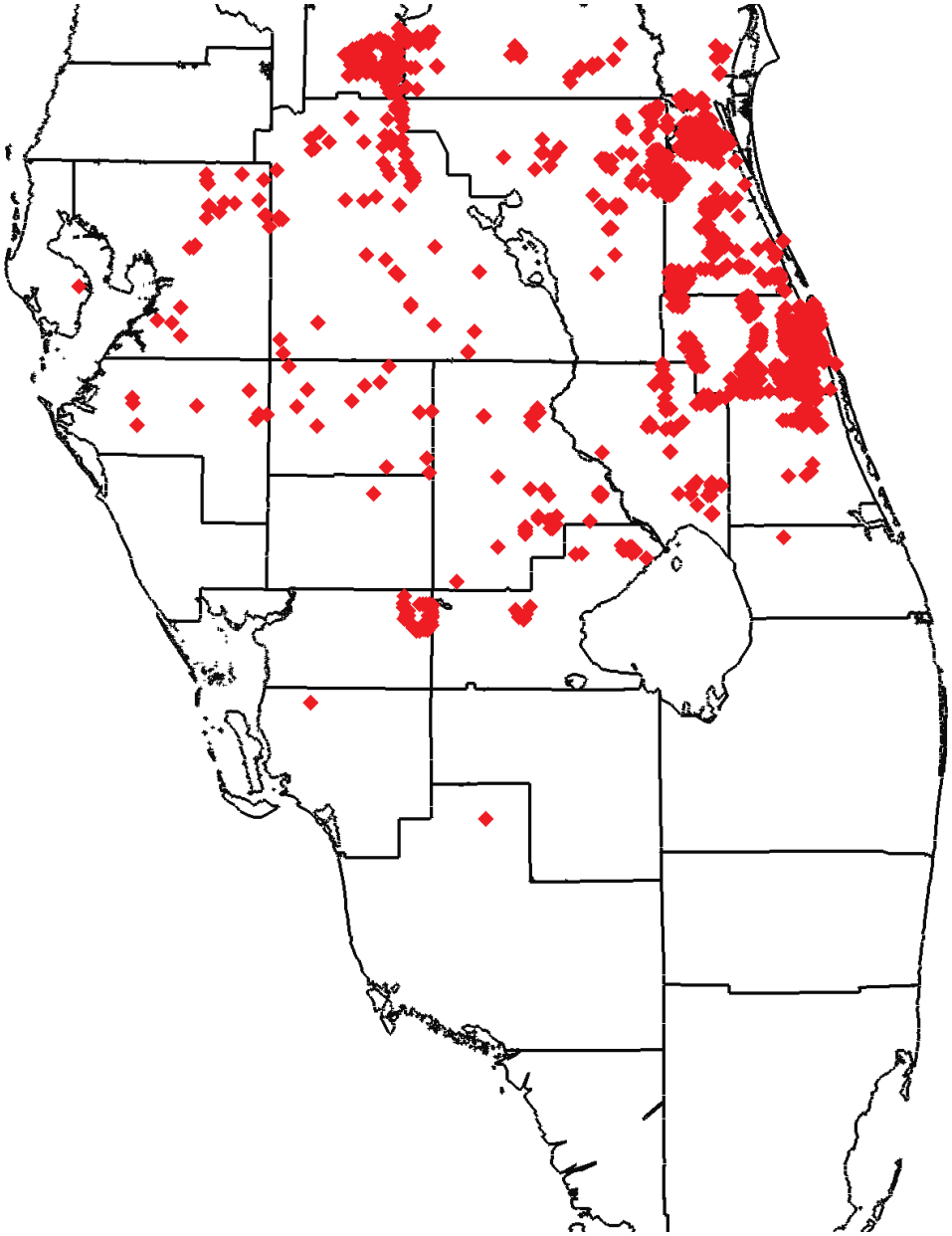

Notes
Each red symbol on this map indicates a well listed in the SAJ database with a pump rate greater than 85% of the capacity.

Location of Irrigation Wells with Pump Rates Greater than 85% of Capacity (September 2004)

Final Groundwater Model Calibration Report

Figure D3-6

October 2010

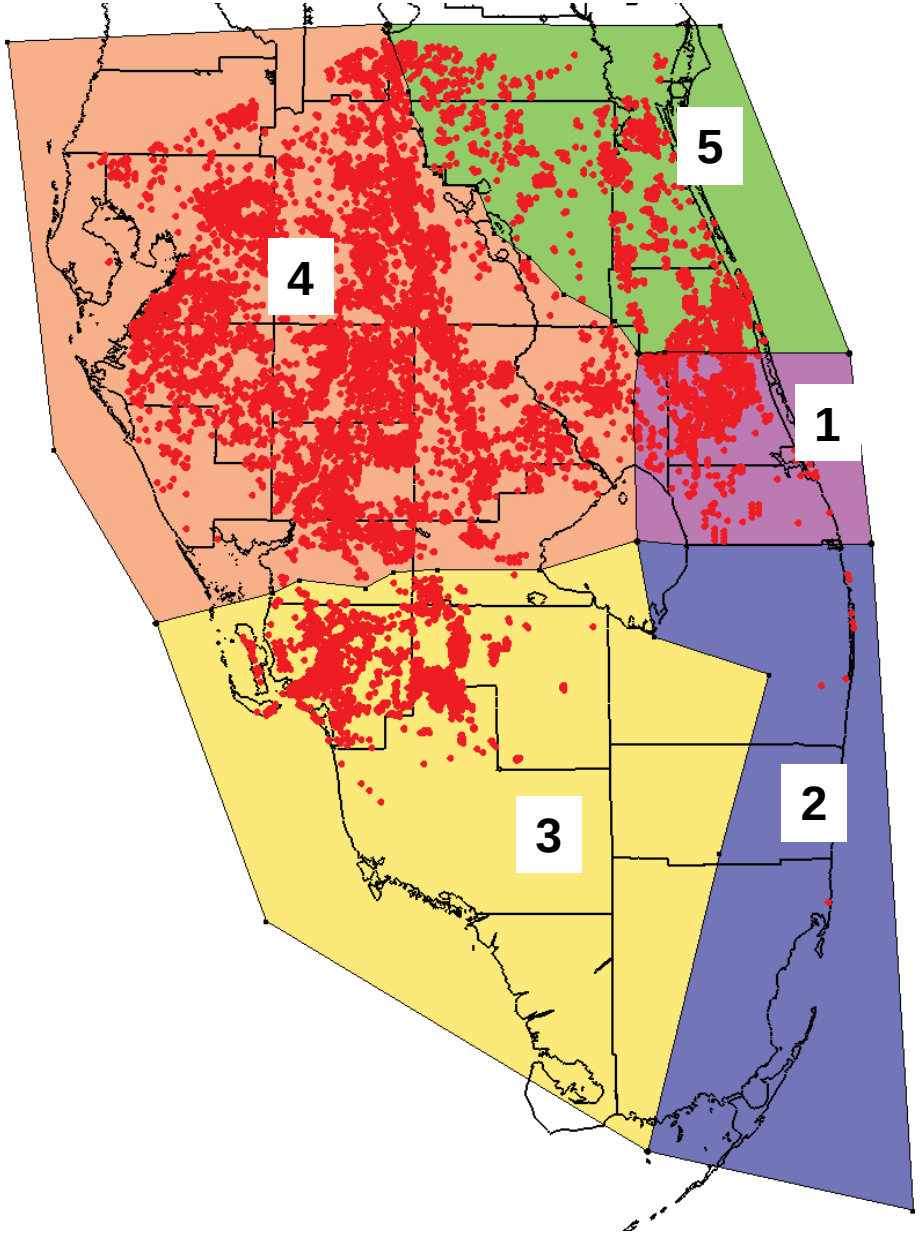

Legend

- Irrigation Wells

Notes:

Zones were selected for the irrigation well analysis and were roughly based on physiographic and hydrogeologic zones. Zone 2 was eliminated from the analysis because of very little pumping. Zone 1 was eliminated because of the additional work already accomplished by SFWMD.

Zones Used for Irrigation Well Analysis

Final Groundwater Model Calibration Report

Figure D3-7

October 2010

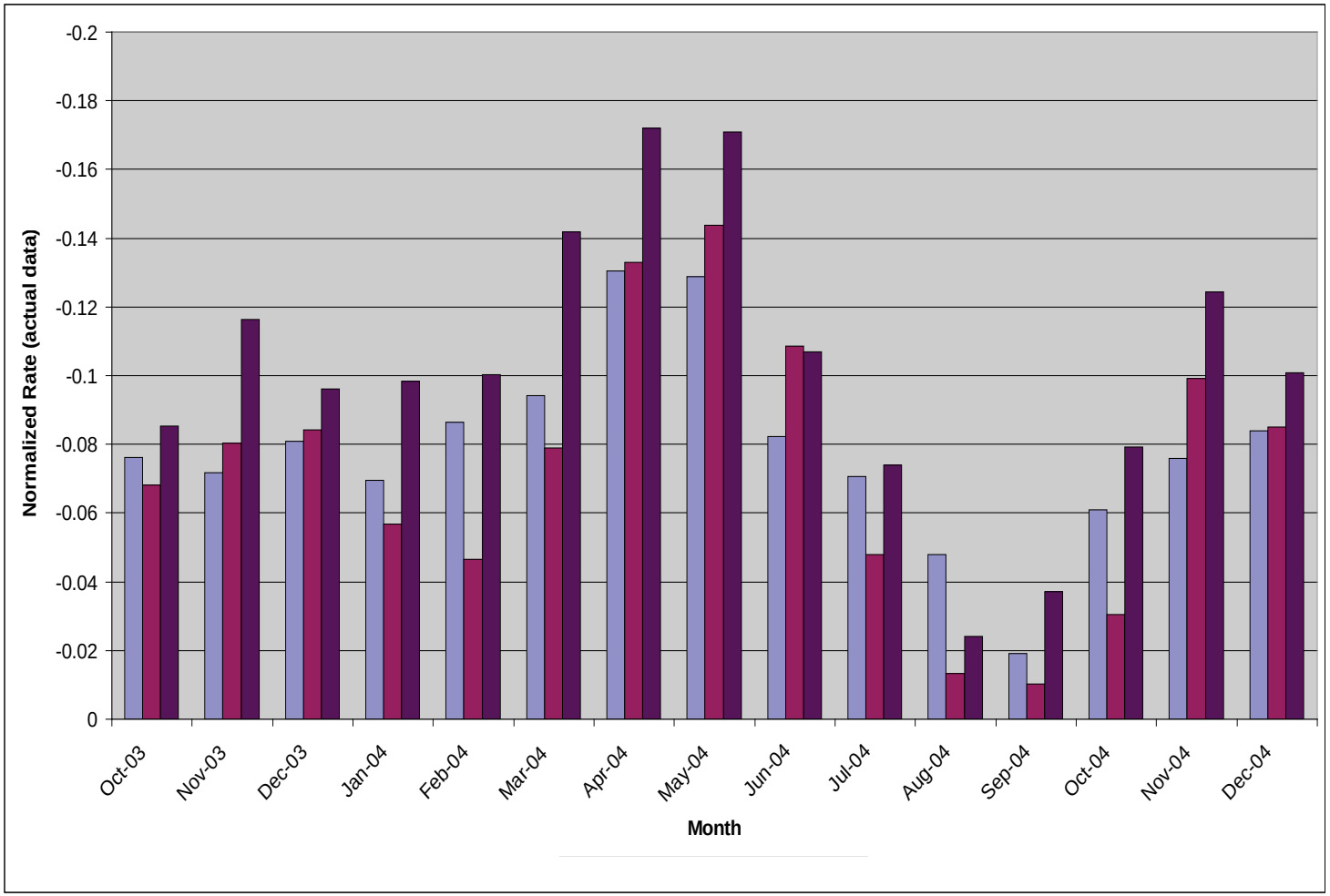

Legend

- Zone 5
- Zone 4
- Zone 3

Notes

Normalized pump rates were averaged for all agricultural wells with actual reported data to create this plot. Normalization was to pump capacity/allocation.

Zones are depicted on Figure D3-7.

Normalized Pumping Distribution Of Actual Data for Irrigation Wells

Final Groundwater Model Calibration Report

Figure D3-8

October 2010

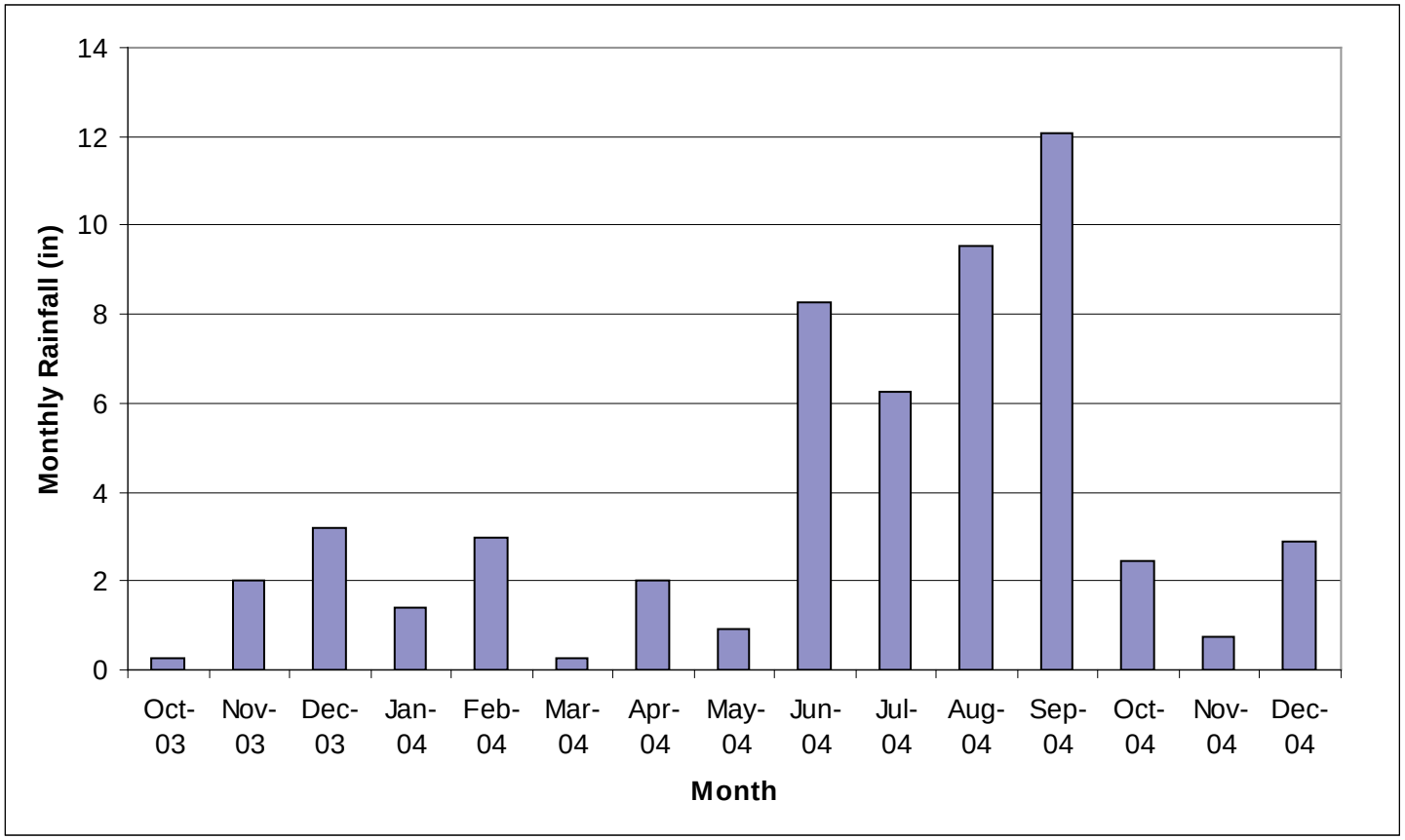

Notes

Rainfall is from station 265A_R.
Data provided by SAJ.

Polk County Monthly Precipitation Data

Final Groundwater Model Calibration Report

Figure D3-9

October 2010

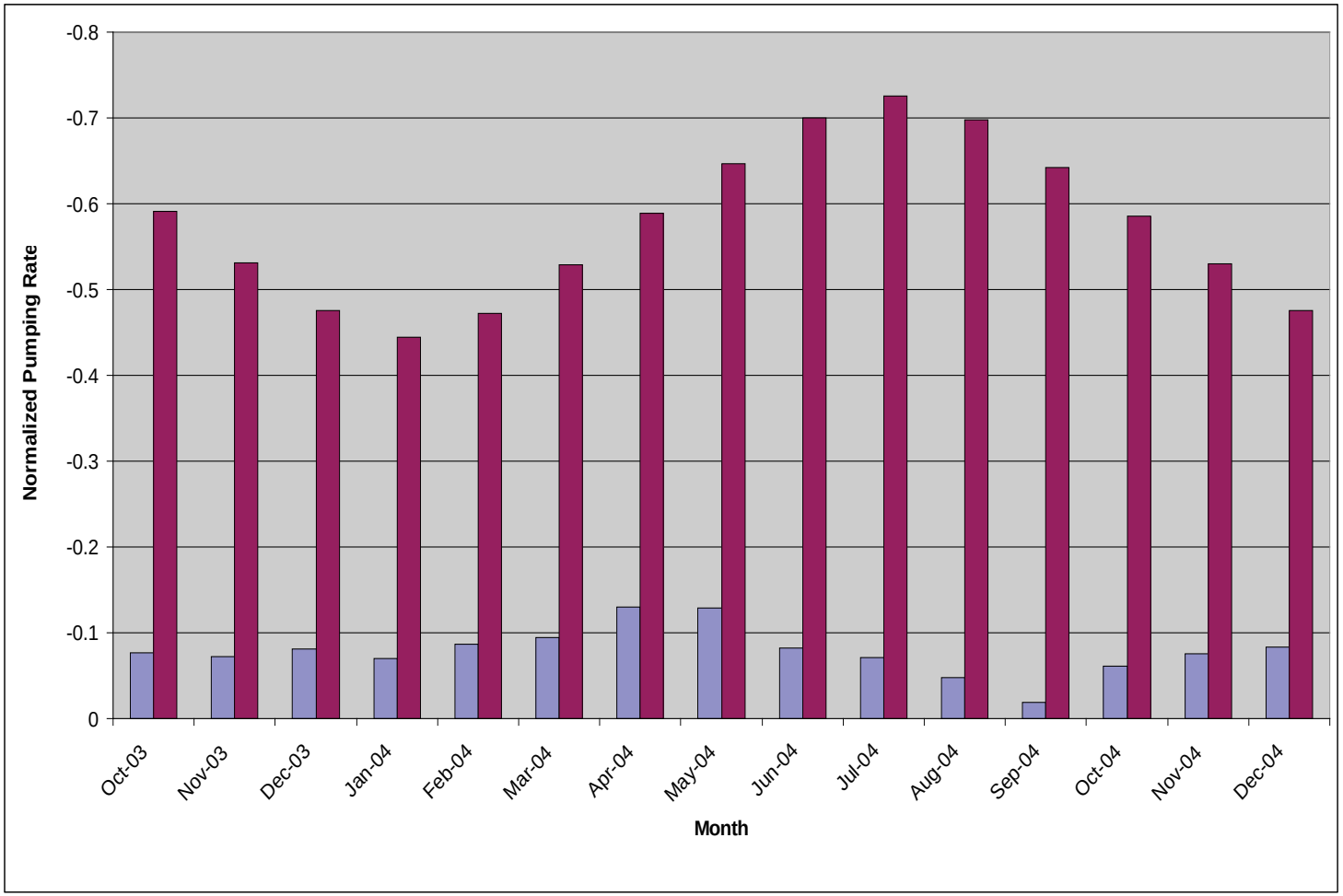

Legend

- Actual (Reported) Normalized Pump Rate
- Estimated Normalized Pump Rate

Notes

This figure presents average normalized pump rates for agricultural wells in Zone 5 (see figure D3-7).

Rates are normalized to capacity/allocation data for each well.

Reported and Estimated pump rates are based on SAJ database.

Normalized Pumping Distribution of Actual and Estimated Data for Irrigation Wells

Final Groundwater Model Calibration Report

Figure D3-10

October 2010

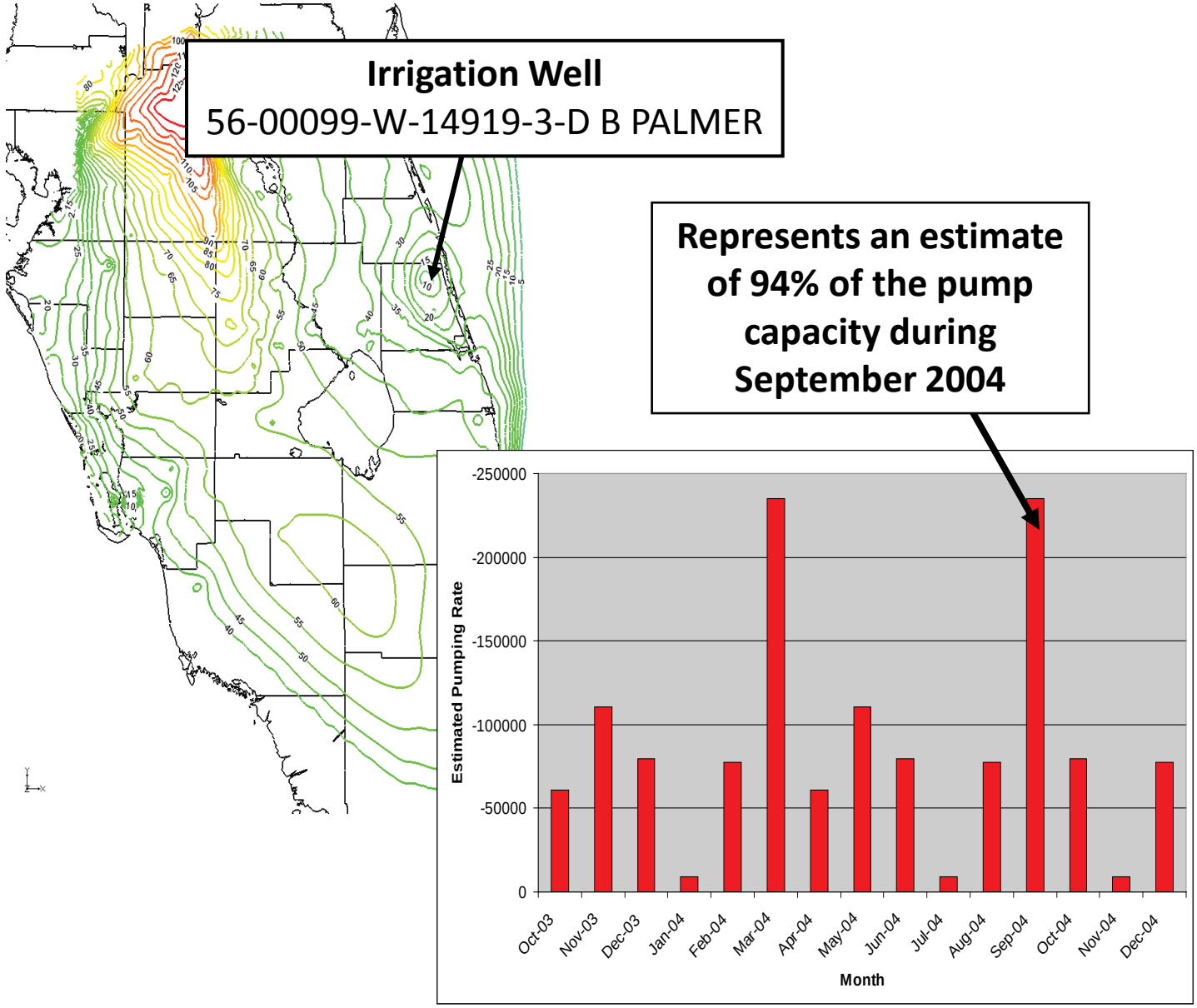

Notes

This is an example of a well with estimated pump rates that are suspicious.

According to the estimates provided by SAJ, September 2004 and May 2004 had identical pump rates at 94% of the capacity of the well. Several other groups of months show exactly equal pump rates, as well.

There is no correlation between the pump rates and the known meteorological conditions. For example, three hurricanes caused significant rainfall during September 2004, so agricultural pumping would be expected to be minimal.

Estimated Pumping Rates for an Irrigation Well in Northern St. Lucie County

Final Groundwater Model Calibration Report

Figure D3-11

October 2010

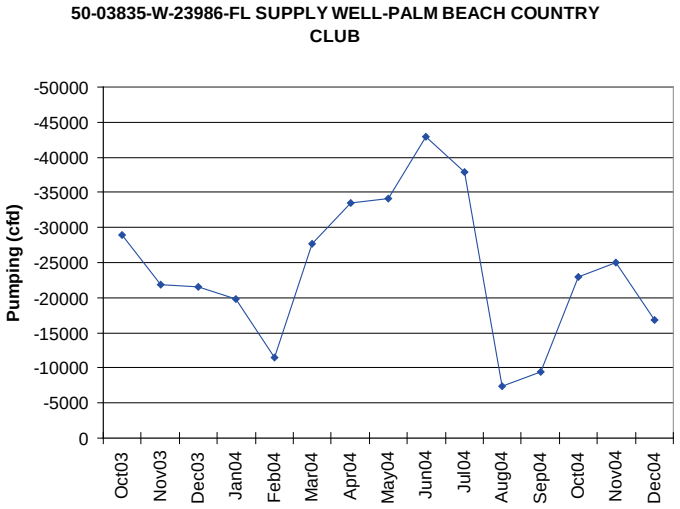

(a)

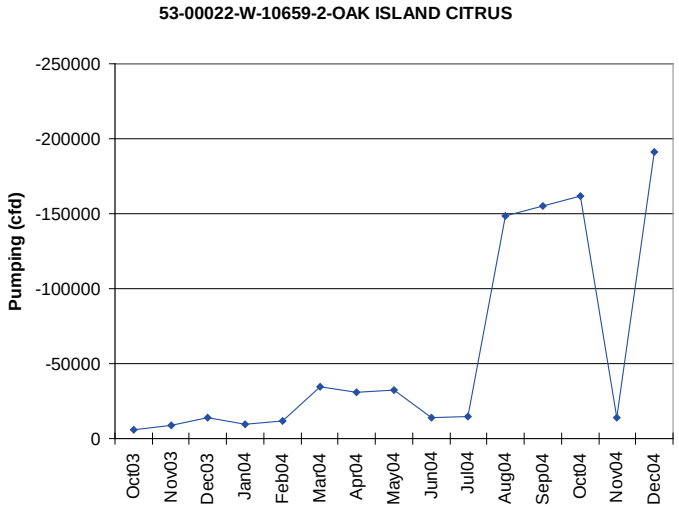

(b)

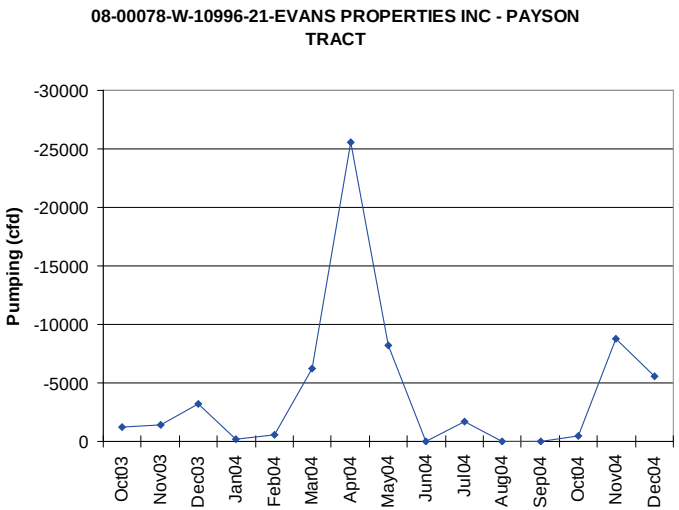

(c)

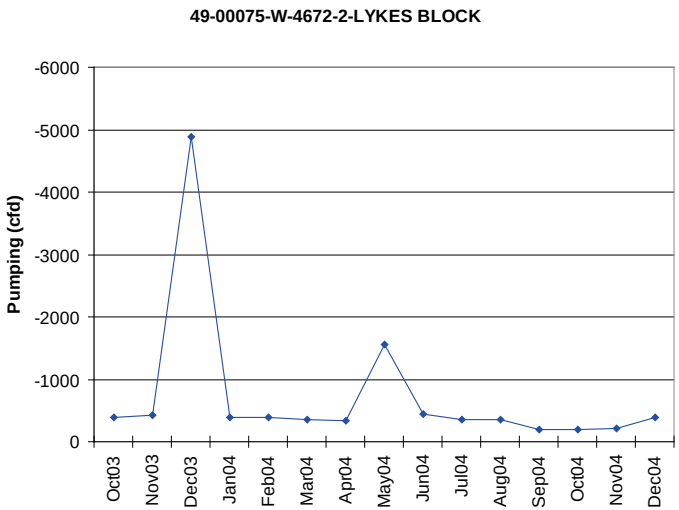

(d)

Notes:

Pump rates reported for four wells is provided to aid in the discussion in the text. All four wells had actual, reported values for each month in the period. Only the Palm Beach Country Club well seems well-correlated with precipitation (high pumping during dry periods and low pumping during wet periods).

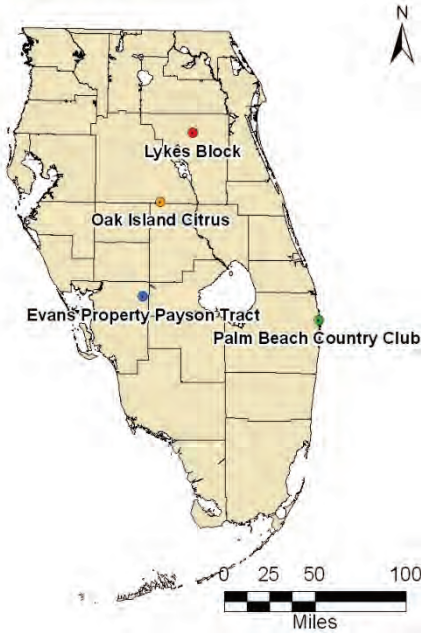

Four Examples of Pumping Well Data

Final Groundwater Model Calibration Report

Figure D3-12

October 2010

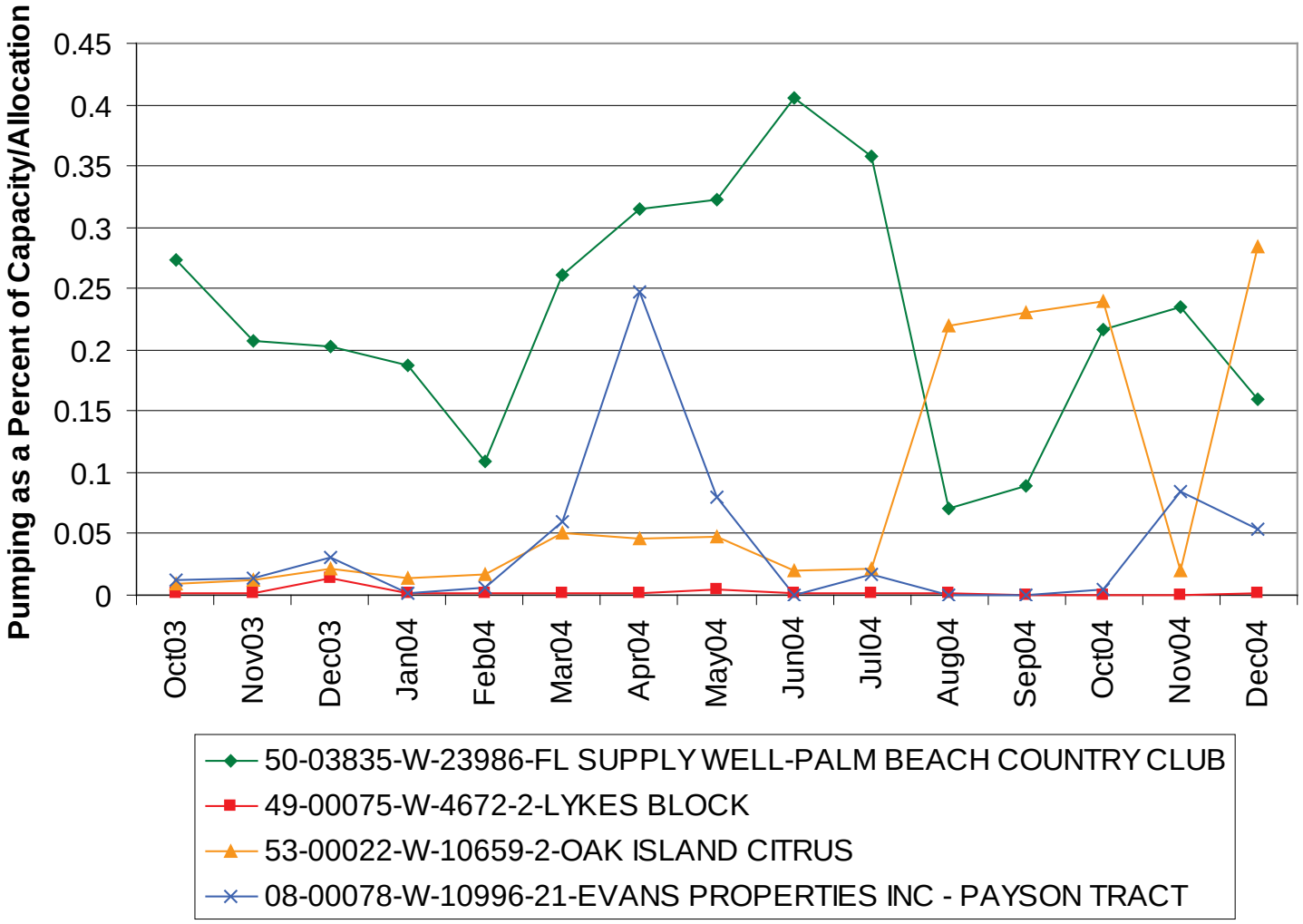

Notes

The normalized pump rates for the four wells presented on Figure D3-12 are presented on a single plot for comparison.

Pump rates are normalized to reported pump allocation/capacity information.

Four Examples of Pumping Well Data

Final Groundwater Model Calibration Report

Figure D3-13

October 2010

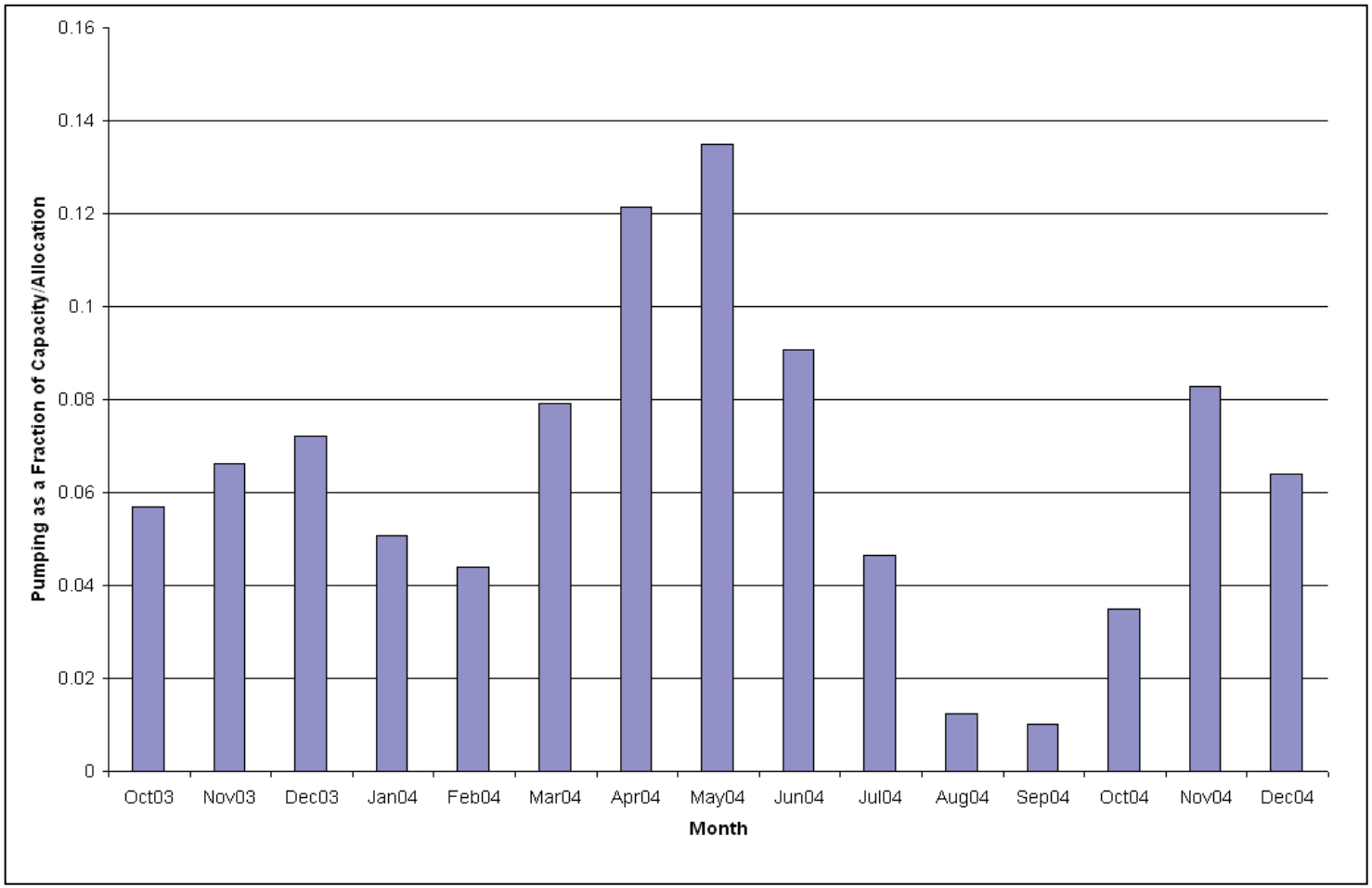

Notes

This plot presents the average pumping as a fraction of capacity/allocation for all wells with reported data in a month of the period. These averages were used to fill in missing data at other wells as described in the text.

Average Pumping as a Fraction of Capacity/Allocation

Final Groundwater Model Calibration Report

Figure D3-14

October 2010

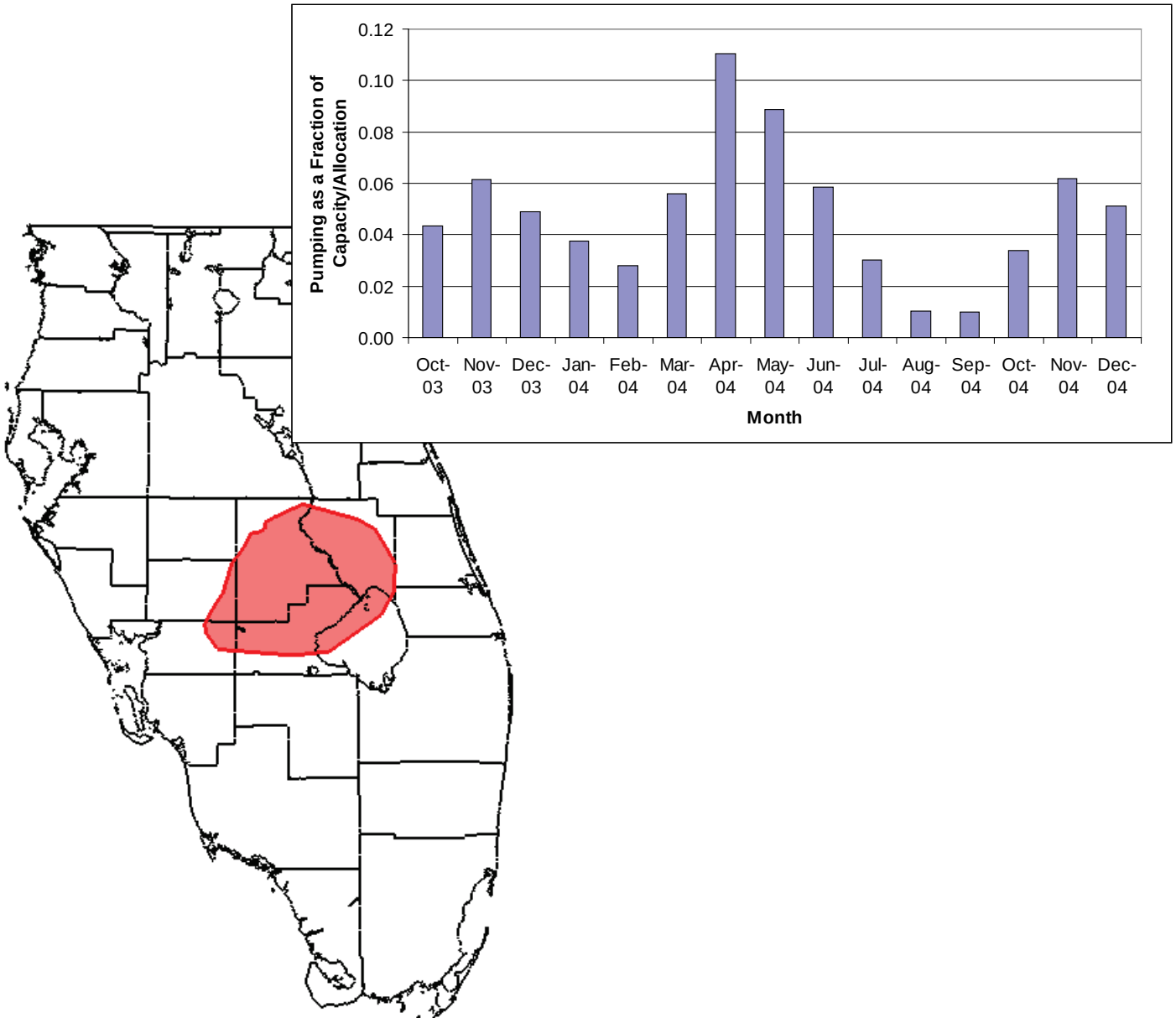

Notes

This plot presents the average pumping as a fraction of capacity/allocation for all wells in the area indicated on the map with reported data in a month of the period. These averages were used to fill in missing data at other wells in this area.

The pump rates are similar, but not exactly the same as those presented on Figure D3-14 and used for all other agricultural wells in the model.

Average Pumping as a Fraction of Capacity/Allocation North of Lake Okeechobee

Final Groundwater Model Calibration Report

Figure D3-15

October 2010

Appendix E: Total Dissolved Solids (TDS) and Temperature Data Evaluation

Table of Contents

1.0 Introduction

Groundwater density variations can affect groundwater heads and regional groundwater flow patterns. The impact of this density effect is magnified as depth is increased. That density affects regional groundwater flow patterns in the Floridan Aquifer System is supported by several studies [Hughes, Vacher, and Sanford (2007), Meyer (1989), Sanford et al (1998), Kohout (1965), Kohout et al (1977)]. The SEAWAT and WASH123D codes were chosen for use in the ASR Regional Groundwater Model study because both codes have the ability to model density-dependent flow based on variations in both salinity and temperature.

To compute the density variations in the model, salinity and temperature values representing two conditions are required: initial conditions and boundary conditions. For the initial conditions, salinity and temperature assignments are required at every computational point in the model domain. These datasets form the salinity and temperature initial condition for the steady state and transient simulations. Because data was sparse in deeper model layers and because data during the calibration time period was often unavailable, available data from the last few decades was evaluated. It should be noted that although current values of salinity and temperature were used to begin the steady state simulation, salinity and temperature are not considered to be in equilibrium. The steady state simulation was used to generate heads that agreed with the current salinity and temperature datasets. The steady state heads were then used as the initial condition heads for the transient simulation.

Boundary conditions for salinity and temperature are required when flow is entering the model at a boundary. When flow is leaving the model at the boundary, the salinity and temperature values are computed by the model. The initial conditions values coincident with the model boundary were assumed to be the boundary conditions. The boundary changes to salinity and temperature in this model are expected to be small given the time scale being modeled. Boundary conditions for salinity and temperature are also required at each well where injection occurs within the model domain, since the injected water quality often differs from that of the native aquifer water quality.

This appendix contains a discussion of the data collection, evaluation, and interpolation used to define the initial and boundary conditions for salinity and temperature.

2.0 Salinity (TDS) and Temperature Data Collection

For this study, reported measurements of total dissolved solids (TDS) are used as proxy for salinity. An extensive TDS and temperature data collection effort was undertaken to identify representative water quality data from the SAS to the BZ. Water quality data for injected water was also gathered. A variety of data sources were used to collect the available data. The primary data source for TDS was the SAJ data collection effort, which is summarized in Appendix A. For temperature, the primary data source was SFWMD. In order to augment this data, additional TDS information was collected from a variety of sources, including USGS Water-Resources Investigations and Scientific Investigations Reports, the SFWMD DBhydro database, databases maintained by SWFWMD and SJRWMD, individual well

completion reports, packer test data, personal communications, and, to a limited extent, data from previous modeling efforts.

3.0 Regional TDS and Temperature Data Evaluation

Once all of the data sources were compiled, the available TDS and temperature data was evaluated to ensure representative data was used in setting the initial TDS concentrations and temperatures in each model layer. Since data was compiled from a variety of sources, the master data file contained duplicate data with different well names for the same well. This often occurred due to the different naming conventions of the agencies collecting the well data. Care was taken to remove duplicate wells from the representative data sets developed for each model layer. Once the duplicate well data was removed, the data was reviewed to determine which water quality values were representative of existing conditions in the FAS. Where possible, water quality data from the beginning of the calibration period (October 2003) was used; however, in areas where data was sparse, reported measurements from other time periods were used to fill data gaps. Since the regional water quality does not change drastically over a period of a few years, this method of filling data gaps was considered to be sufficient.

In some cases, the TDS and temperature data collected was accompanied by an identification of the particular aquifer or confining unit where the data was sampled. Because many of the sources of TDS and temperature data provided only depths of the tested intervals, vertical locations for the data had to be estimated. The ground surface elevation at each monitoring well was approximated from the topographic data described in Section 3.1 of the calibration report. Then the given tested interval depths were subtracted from the estimated ground surface elevations to determine the vertical interval where the water quality was measured. These vertical elevations were compared against the hydrostratigraphic surface elevations for each layer to determine the layer(s) where each measurement was taken. Although each data measurement was taken only in an interval of the hydrogeologic layer, the measurement was assumed to represent the entire vertical column of the aquifer or confining unit. In some cases, the measurement interval straddled two hydrogeologic units. In that case, the TDS and temperature values were considered applicable in both layers.

As the data was reviewed, the time series data indicated that the TDS and temperature at several wells was being influenced by on-going injection or ASR operations. Data of this type was considered to be suspect since the lateral extent of the impacted groundwater quality should be limited to the area very near the injection well. As a result of the sparse data measurements and coarse resolution of the model, the injected water quality applied to the model could impact a much larger area. Consequently, data at or near injection wells was not used if the samples appeared to reflect the quality of the injected water instead of the native water quality. In some cases, TDS or temperature values found in the well completion reports could be used to represent the water quality prior to injection. Examples of locations where well completion TDS and temperature values were adopted are Big Cypress Preserve (BICY), Immokalee Water and Sewer District (IWSD), and I-75 Canal (I75).

Another data quality issue was discovered as the TDS data was processed. Typically, salinity increases with depth throughout the model domain. However, some recorded TDS data from multi-zone wells

were determined to be inverted. This resulted in data in select locations to appear saltier in shallower units in comparison to the deeper monitoring zones. Data at these locations were reviewed in detail and coordinated with the SFWMD. Numerous corrections were made to the TDS database developed for this study to rectify problems with the raw data that had been collected. In these instances, the source of this raw data was contacted and consulted. However, at several locations, the verified data confirmed that more saline water was observed in the UF than the underlying APPZ. This TDS inversion primarily occurred in coastal southeastern Florida. Prominent examples of inversion are located at the SFWMD test wells near City of Oakland Park and the Hillsboro ASR Pilot Project.

The City of Oakland Park wells are located in Broward County near the Atlantic coast. The wells in this location where TDS data are available for the UF are designated BF-1, BF-3, and BF-4S. The recorded TDS for these UF wells varies between 7,500 mg/l and 8,731 mg/l. In addition to these UF wells, there are two wells, BF-2 and BF-4M, that have TDS data for the APPZ. The recorded TDS levels for these wells range from 4,810 mg/l to 5,520 mg/l, which is noticeably fresher than that observed in the UF.

The Hillsboro ASR Pilot Project wells are located in southern Palm Beach County. The wells in this location where TDS data are available for the UF are PBF-10R and PBF-13. The recorded TDS for these UF wells varies between 2,932 mg/l and 6,500 mg/l. The corresponding APPZ well at this location, PBF-11, again has a lower TDS range of between 1,262 mg/l and 3,200 mg/l.

Additional locations along the southeastern coast of Florida have also been identified as having higher TDS levels in the UF than the APPZ. These include the deep injection facility for the Coral Springs Improvement District (CS-M2), the Sawgrass Water Treatment Plant at the City of Sunrise (SUN-BTW), and the reverse osmosis facility at the Town of Jupiter (JUP_RO). A variety of published reports document these areas of known TDS inversion. As shown in Figure 3.18 in the main report, the use of observed data to set the UF TDS distribution resulted in isolated areas of elevated TDS in the UF along the southeast coast.

During the TDS and temperature data evaluation process, close coordination was maintained with the SFWMD to ensure the data used to set the initial distributions in the model were representative of each modeled geologic layer. The lower hydrogeologic units generally contained fewer TDS and temperature data points than shallower units. Table 3.1 summarizes the TDS data and Table 3.2 summarizes the temperature data used for this modeling effort.

The following sub-sections describe how the available TDS and temperature data was used to generate a representative distribution in each geologic layer and also documents any assumptions/simplifications made for this study.

4.0 Regional TDS and Temperature Distributions

The evaluated TDS and temperature data were used to generate representative TDS and temperature distributions in each hydrogeologic layer. For TDS, the interpolation methodology and assumptions to create the final distribution for each model layer can be grouped as follows: the SAS, the aquifers, the

confining units, and the IAS. Interpolation methodology and assumptions for the final temperature distribution in each layer are split into two groups: the SAS and the other model layers. Below is a discussion of each group used to create the final distribution.

4.1 TDS Distributions

4.1.1 SAS Layer TDS Distribution

In the SEAWAT Phase II Regional Model, the top layer (representing the SAS) is set as a constant head boundary condition. Since this layer is shallow and fresh, the density impact on the computed heads in the model is negligible. Consequently, several simplifying assumptions were made in setting the TDS distribution in this layer. These include setting the TDS concentration to 100 mg/l in the land areas and 35,000 mg/l at the ocean. Although some variability does exist in the observed SAS TDS data, this assumption is reasonable for the scope and purpose of this modeling effort. Since the WASH123D model did not include model elements for the SAS, the TDS assumptions for the SAS are only applied to the top layer of nodes in the WASH123D model.

4.1.2 Aquifer Layers TDS Distribution

Once the TDS data were collected and evaluated by the modeling team, GMS was used to interpolate the data to each modeled aquifer in the FAS (UF, APPZ, LF1, and BZ). A variety of interpolation schemes were tested to ensure a reasonable fit with the observed data. Based on the density of available data, the natural neighbor interpolation routine (Sibson, 1981) with a constant nodal function was adopted. For this interpolation the TDS at the ocean outcrops for each geologic layer was set to 35,000 mg/l. As the TDS distribution for each layer was interpolated, it was critically evaluated to ensure that it was reasonable. Numerous error checking routines were used to ensure deeper aquifers were progressively more saline than shallower layers. The primary exception to this guideline was between the UF and APPZ along the southeastern coast of Florida. As previously discussed, the observed data indicates that a TDS inversion may exist in this area. As such, the APPZ was allowed to be fresher in this area so that the model was able to properly account for this phenomenon. Figures 3.18, 3.20, 3.22 and 3.24 in the main report show the TDS distribution adopted for each modeled aquifer in the FAS.

4.1.3 Confining Layers TDS Distribution

For the modeled confining units within the FAS (MC1, MC2, and LC), GMS was again used to interpolate the data to each modeled layer. However, during the evaluation of the confining unit data a high degree of variability in salinity was identified at numerous locations within the confining units. Often a large TDS gradient (generally becoming significantly saltier with depth) was observed within the confining unit. This was particularly apparent at locations where packer test or continuous measurement data was available. It must be noted that the observed TDS in an individual well open within a confining unit may be very dependent on open interval of well, with shallower open intervals generally fresher and deeper open intervals generally saltier. This high degree of variability in observed salinity with depth necessitated a thorough review of the data used to develop a representative initial TDS distribution for the confining units. Wells where significant TDS gradients existed were evaluated individually to prevent skewing of the interpolation. The natural neighbor interpolation routine (Sibson, 1981) with a

constant nodal function was again used to develop the TDS distribution for each FAS confining unit. For this interpolation the TDS at the ocean outcrops for each geologic layer was set to 35,000 mg/l, consistent with the methodology used in the aquifer layers. As the TDS distribution for each layer was interpolated, it was critically evaluated to ensure that it was reasonable. In areas of significant TDS variability, the TDS data, the depth interval of the sample, and data available from underlying/overlying aquifers were used to determine if sampled data was representative of confining unit conditions in a particular area.

Once a representative data set was derived, numerous error checking routines were used to ensure that the interpolated TDS value in the confining units was no fresher than that in the overlying aquifer and no saltier than that in the underlying aquifer. The primary exception to this guideline was again in the area along the southeastern coast of Florida where the UF observations are saltier than those in the APPZ in some locations. In the areas where this TDS inversion was observed, the average of the UF and APPZ was used for the MC1, in the absence of observed data. Figures 3.19, 3.21, and 3.23 in the main report show the TDS distribution adopted for each modeled confining unit in the FAS.

4.1.4 IAS Layers TDS Distribution

Due to the highly variable nature of the hydrogeology in the IAS (inter-bedded aquifers in the west and primarily confining in the east), a separate approach was adopted to determine the TDS distribution in these layers. In the western "aquifer" portion of the IAS substantial data was available, while in the east "confining" portion of the IAS only limited data was available. Accordingly, the TDS distribution for the IAS was developed in two phases.

First, the available data in the "aquifer" portion of the IAS was interpolated consistent with the methodology adopted for the FAS aquifers. In this portion of the IAS, 196 observed TDS data points were available for this interpolation. No attempt was made to vertically differentiate the TDS interpolation in this area, since the observed TDS was generally relatively fresh (less than a few thousand mg/l TDS) and modeled geology is grossly simplified for the purposes of this study. The second step in the process was to develop a TDS distribution in the "confining" portion of the IAS. Since only limited data was available in this portion of the model domain, an average of the assumed SAS and the interpolated UF TDS distributions was used in this portion of the model. As with the SAS, the depths of the IAS layers are relatively shallow. Consequently, the density impact on the computed heads in the model is negligible.

4.2 Temperature Distributions

4.2.1 SAS Layer Temperature

Because shallow density variations have little impact on model results, temperature data in the SAS layer was not evaluated. An average temperature value of 24^{o}C was assumed for the entire layer. For the SEAWAT model, this constant temperature value was applied to the top layer of cells whereas the top layer of nodes was assigned the constant value in the WASH123D model.

4.2.2 IAS and FAS Temperature Distribution

The temperature datasets for each of the other layers (IAS, UF, MC1, APPZ, MC2, LF1, LC, and BZ) were imported to GMS. The 2-D natural neighbor interpolation scheme (Sibson, 1981) with a constant nodal function was used to interpolate the data to each computational point for the grid/mesh for these layers. The temperature on the ocean boundary for the aquifers was approximated by a general temperature-depth of ocean water profile (Middle Latitude Thermocline) compiled by the University Corporation for Atmospheric Research (Figure 3.27 of the main report). Use of this general thermocline to estimate ocean temperatures in the model is supported by measured data from studies of the Floridan Current at latitude 27°N, between Jupiter Island and Grand Bahama Island (Morrissey and Clark, 2009 and Chester, 1989). For the confining units, the ocean boundary temperature was interpolated from the estimates of the aquifer temperature above and below each confining unit.

Temperature data points used in the interpolation of a particular hydrogeologic layer were from monitoring wells with open intervals completely or partly within that hydrogeologic layer. In the shallower model layers, sufficient temperature data was available for interpolation. In the deeper layers, some temperature data points were added from adjacent layers to fill data gaps and smooth sharp variations. For example, the LF1 well, W-17073, in Pinellas County was used in the interpolations for the BZ, LC and LF1. Because the BZ does not exist in this area, the LF1 temperature data value at W-17073 should be representative for all of these layers.

The temperature interpolation in the LF1 layer also included the addition of data points for consistency. The initial interpolation of the LF1 temperature data showed that the layer was cooler than the layers above and below (MC2 and LC) in areas west of Lake Okeechobee and in Brevard County. Several temperature values measured at monitoring wells estimated to be within the MC2 and LC were added to the LF1 interpolation to make the LF1 warmer in both areas.

Although layer interpolations were checked for consistency with layers above and below, it should be noted that no method was employed to ensure that temperature increased or decreased with depth as was done for the TDS analysis. Generally, on the east coast, temperature decreases with depth while on the west coast, temperature increases with depth as shown in Figures 3.28 through 3.36 of the main report.

5.0 Injection Well TDS and Temperature Evaluation

The model requires the assignment of TDS and temperature values for injected water. There are three types of injection wells within the model domain: 1) Drain wells that inject excess stormwater, 2) Class I deep injection wells, and 3) ASR wells. For all three types of wells, the injected temperature was assumed to have a value consistent with the regional water temperature assumed for the SAS, 24°C. For salinity, TDS data was gathered for Class I deep injection wells and ASR wells as discussed in Appendix A. Salinity injected at drain wells was assumed to be 250 mg/l. The drain wells are near the northern model boundary and have negligible impact on the model results.

The injected TDS values provided as a result of the data collection effort were average monthly values. The date range of the injected TDS values did not always overlap the calibration and validation time periods but generally, the average monthly injected TDS data values for a particular well do not vary significantly over time. If the date range of the injected TDS dataset was after the model time period, the first monthly value was used for the entire model time period. Conversely, if the date range of the dataset was before the model time period, the last monthly value was used for the entire model time period. For example, for Cooper City Water Treatment Plant, monthly injected TDS data values were available from March 2005 to December 2005 so the March 2005 value was used for the entire calibration period from October 2003 to December 2004.

Injected TDS data were not available at all injection wells. Consequently, injected TDS values were based on assumptions at some wells. In cases where the injection well is associated with an oil and gas facility, the injected water is brine, so a value of 35,000 mg/l was assumed. In cases where there were several wells pumping for one facility and at least one of the wells had known TDS injection values, the other facility wells were assumed to inject the same TDS. In some cases, injected TDS data from a nearby similar facility could be used to generate a TDS injection dataset where none was available. Table 5.1 lists the wells, their locations, the average injected TDS, the date range of available data, and the applied assumptions.

The injected TDS and temperature have very little impact on the calibration or flow patterns of the regional model. As a result of the coarse model resolution and limited model time period, the impact is only to the model cells where the injection wells are located.

6.0 References

Bennett, M.W., 2004. Hydrogeologic Investigation of the Floridan Aquifer System, Big Cypress Preserve, Collier County, Florida, Technical Publication WS-18, South Florida Water Management District.

Bennett, M.W., 2002. Hydrogeologic Investigation of the Floridan Aquifer System, Immokalee Water & Sewer District Wastewater Treatment Plant, Collier County, Florida, Technical Publication WS-14, South Florida Water Management District.

Bennett, M.W. and E. E. Rectenwald, 2003. Hydrogeologic Investigation of the Floridan Aquifer System, Intercession City, Osceola County, Florida, Technical Publication WS-23, South Florida Water Management District.

CDM, 1987. Deep Injection Well No. 1, Final Well Completion Report, City of Plantation, Florida.

Chester, David Brian, 1989. Acoustic Tomography in the Straits of Florida, Master of Science Thesis at Massachusetts Institute of Technology and the Woods Hole Oceanographic Institution.

Geraghty and Miller, 1984.Construction and Testing of an Exploratory Well for Injection Feasibility, Merritt Island, Brevard County, Florida, U.S..

Hazen and Sawyer, 2001. Injection Well No. 1 Construction Completion Report, Water/Wastewater Treatment Plant, City of Cooper City, Florida.

Merritt, M.L., 1997, Computation of the Time-Varying Flow Rate from an Artesian Well in Central Dade County, Florida, by Analytical and Numerical Simulation Methods, U.S. Geological Survey Water-Supply Paper 2491.

Meyer, Fredrick W., 1989. Hydrogeology, Ground-Water Movement, and Subsurface Storage in the Floridan Aquifer System in Southern Florida, U.S. Geological Survey Professional Paper 1403-G.

Miami-Dade Water and Sewer Department, 2006. Engineering Report for North District Wastewater Treatment Plant Injection Wells IW-1N & IW-4N, Volume 1, Miami-Dade County, Florida.

Missimer & Associates, Inc, undated. SSU-Southern State Utilities, Marco Island Injection Well No. 1, Well Completion Report, Volume 1.

Morrissey, S.K. and J. F. Clark, 2009 Isotopic Measurements from the Floridan Aquifer: Years 1 to 5 Results, unpublished.

MWH, 2004. Class 1 Injection Well and Dual Zone Monitoring Well Drilling and Testing Report, North Lee County Water Treatment Plant.

Reese, Ronald S., 2002. Inventory and Review of Aquifer Storage and Recovery in Southern Florida, U.S. Geological Survey Water Resources Investigations Report 02-4036.

Reese, Ronald S., 1994. Hydrogeology and the Distribution and Origin of Salinity in the Floridan Aquifer System, Southeastern Florida, U.S. Geological Survey Water Resources Investigations Report 94-4010.

Reese, Ronald S., 2004. Hydrogeology, Water Quality, and Distribution and Sources of Salinity in the Floridan Aquifer System, Martin and St. Lucie Counties, Florida, U.S. Geological Survey Water Resources Investigations Report 03-4242.

Reese, Ronald S. and Carlos A. Alvarez-Zarikian, 2007. Hydrogeology and Aquifer Storage and Recovery Performance in the Upper Floridan Aquifer, Southern Florida, U.S. Geological Survey Scientific Investigations Report 2006-5239.

Sibson, R., 1981. A brief description of natural neighbor interpolations, In Interpreting Multivariate Data, Ed. V. Barnett, Chichester, 21-36, John Wiley.

Torres, A.E., L.A. Sacks, D.K. Yobbi, L.A. Knochenmus, and B.G. Katz, 2001. Hydrogeologic Framework and Geochemistry of the Intermediate Aquifer System in Parts of Charlotte, De Soto, and Sarasota Counties, Florida, U.S. Geological Survey Water Resources Investigations Report 01-4015.

Station	X coordinate (ft FL State Plane 1983)	Y coordinate (ft FL State Plane 1983)	TDS (mg/l)	Date	Source
113TH AVE REC CTR ICGU WELL AT TEMPLE TERRACE FL	212928.361	1353513.016	395	9-Dec-03	USGS
36-00003-W - Corkscrew (Lee County) - MH ASR#1 Corkscrew wf	425770.205	775260.399	179	1-May-04	Facility
AAC3914	335222.969	1301072.646	170	3-Mar-05	FDOH
AAD1201	398884.635	1386270.158	170	10-Jun-96	FDOH
AAD1251	382319.867	1364239.005	270	30-Apr-07	FDOH
AAE9522	333769.039	1298603.855	280	8-Mar-05	FDOH
AAG7229	469793.096	1353101.423	160	13-May-96	FDOH
AAI2585	473747.876	1350410.555	170	29-Apr-96	FDOH
AAJ0229	202328.518	1256367.989	630	20-Jul-04	FDOH
AAJ2397	202518.705	1256343.593	620	20-Jul-04	FDOH
AMERICAN CITRUS PRODUCTS CORP P-1 (DID# 5)	426845.844	969846.653	1840	3-Aug-04	SWFWMD
AMERICAN CITRUS PRODUCTS CORP P-2 (DID# 6)	427789.777	968303.447	1742	3-Aug-04	SWFWMD
AMERICAN CITRUS PRODUCTS CORP P-3 (DID# 7)	425595.641	968379.315	1972	3-Aug-04	SWFWMD
AMERICAN CITRUS PRODUCTS CORP P-4 (DID# 8)	426866.232	967177.595	1742	3-Aug-04	SWFWMD
ARCADIA FISH INC #1 (DID# 1)	390127.193	1024420.344	399	12-Jan-04	SWFWMD
BABCOCK 2126	414724.039	929143.712	486	23-Dec-93	SWFWMD
BICY-MZ1	554522.187	567147.922	3340	1-Feb-05	SFWMD
BLACKBURN PT SH TEST NEAR OSPREY FL	169994.812	1038025.912	441	4-Nov-93	USGS
BR0202	724478.877	1470720.295	3059	3-May-94	SJRWMD
BRADBURN WELL	226348.569	1288995.276	345	28-Dec-93	SWFWMD
BRUSHY CREEK SURFICIAL WELL NEAR ONA FL	338229.638	1124732.024	237	27-Jan-94	USGS
CARLTON SURFICIAL WELL NEAR KINSEY FL	350867.574	1079694.298	121	15-Jun-94	USGS
CITY OF SARA 27TH ST	154245.622	1102964.265	1479	30-Jan-04	SWFWMD
CLAPROD WL NR RUSKIN	167604.639	1221989.429	807	9-Feb-04	SWFWMD
COCOA 2T NR BITHLO, FL	630606.537	1479455.21	423	19-Apr-94	USGS
COCOA 3T NR BITHLO, FL	627926.949	1478750.153	387	19-Apr-94	USGS
CYPRESS CK CYPRESS W19 H NRSD WELL NEAR DREXEL FL	206316.295	1436397.63	381	20-Oct-03	USGS
CYPRESS CK CYPRESS W19 I NRSD WELL NEAR DREXEL FL	206588.064	1436697.54	106	17-Oct-03	USGS
CYPRESS CK CYPRESS W19 J NRSD WELL NEAR DREXEL FL	206315.128	1436296.625	130	20-Oct-03	USGS
CYPRESS CK CYPRESS W19 L NRSD WELL NEAR DREXEL FL	206049.191	1436501.739	460	16-Oct-03	USGS
CYPRESS CK CYPRESS W19 M NRSD WELL NEAR DREXEL FL	206768.075	1436796.477	220	17-Oct-03	USGS
CYPRESS CK CYPRESS W19 N NRSD WELL NEAR DREXEL FL	205963.27	1436805.788	251	16-Oct-03	USGS
CYPRESS CK CYPRESS W19 O NRSD WELL NEAR DREXEL FL	206590.396	1436899.549	136	17-Oct-03	USGS
CYPRESS CRK CYPRESS W19 K2 HTRN WELL NR DREXEL FL	206139.782	1436601.708	327	16-Oct-03	USGS
CYPRESS CRK CYPRESS W19 P NRSD WELL NR DREXEL FL	206497.474	1436597.57	189	20-Oct-03	USGS
CYPRESS CRK CYPRESS W19 Q HTRN WELL NR DERXEL FL	206411.551	1436901.618	434	17-Oct-03	USGS
CYPRESS CRK W5 NO. 1 NRSD WELL NR DREXEL FL	211628.483	1446162.508	467	23-Apr-04	USGS
CYPRESS CRK W5 NO. 2 NRSD WELL NR DREXEL FL	211839.538	1446166.154	201	21-Apr-04	USGS
CYPRESS CRK W5 NO. 3 NRSD WELL NR DREXEL FL	211733.856	1446542.139	292	23-Apr-04	USGS
CYPRESS CRK W5 NO. 4 NRSD WELL NR DREXEL FL	211153.168	1446662.938	205	19-Nov-03	USGS
CYPRESS CRK W5 NO. 5 NRSD WELL NR DREXEL FL	211417.72	1446497.269	459	22-Apr-04	USGS
CYPRESS CRK W5 NO. 6 NRSD WELL NR DREXEL FL	211339.377	1446057.729	170	22-Apr-04	USGS
DT BROWN #4	413804.591	982226.286	849	31-Mar-94	SWFWMD
DT BROWN #6	406600.156	982264.495	440	31-Mar-94	SWFWMD
EAST CHARLOTTE DRAINAGE DIST #1 (DID# 1)	429339.68	951294.691	1696	17-Mar-04	SWFWMD
EDWARD O VARNER #2 (DID# 2)	427510.293	965057.435	958	30-Mar-04	SWFWMD
EDWARD O VARNER #3 (DID# 3)	424636.329	965410.797	510	16-Mar-04	SWFWMD
EDWARD O VARNER #55 (DID# 4)	426394.12	961853.456	878	16-Mar-04	SWFWMD
ENGLEWOOD	217511.745	954911.113	6700	1-Oct-03	DEP
ENGLEWOOD # 14	219736.737	962919.39	520	11-Mar-94	SWFWMD
ENGLEWOOD #5 HAWTHORNE	208316.518	979164.792	1661	26-Nov-03	SWFWMD
ENGLEWOOD #5 HAWTHORNE	208311.371	979163.162	683	26-Nov-03	SWFWMD
EUREKA SPRINGS DEEP WELL NEAR TEMPLE TERRACE FL	223982.938	1340873.897	274	9-Dec-04	USGS
FLORIDA CITIES TEST	201062.496	1070252.325	1075	31-Dec-03	SWFWMD
FORT FOSTER FLRD WELL NEAR ZEPHYRHILLS FL	263271.154	1388084.125	156	29-Nov-04	USGS
Gasparilla Island RO DZMW-1	247354.383	922372.781	20700	1-Oct-03	Facility
GDU WELL T-2	329741.437	1005025.289	663	12-Apr-04	SWFWMD
HARVESTER UNITED METHODIST FLRD WELL NEAR LUTZ FL	194782.893	1405732.09	181	8-Sep-03	USGS
HE-517	533969.886	885870.773	371.1	13-Dec-88	SFWMD
HE-556	513875.027	841003.382	690	15-Dec-88	SFWMD
HILLSBOROUGH WELL 71	180607.12	1234068.076	698	22-Dec-93	SWFWMD
JAMES BYRD NR RIVERVIEW	211231.326	1303257.127	691	18-Feb-04	SWFWMD
KNIGHTS TRAIL UP INT	199776.56	1029696.352	708	31-Mar-04	SWFWMD
KREFFD	597669	1241470	314	25-Jul-00	SFWMD
KRENND	598893.622	1242073.866	350	29-Jan-01	SFWMD
KRFNND	593855.11	1255783.011	530	29-Jan-01	SFWMD
L-1186	310130.216	767946.682	3280	29-Mar-75	WRI 98-4253
L-2190	372993.32	859595.7	777	25-Oct-88	SFWMD
L-2295	389250.93	763361.128	1411	7-Nov-90	SFWMD

Station	X coordinate (ft FL State Plane 1983)	Y coordinate (ft FL State Plane 1983)	TDS (mg/l)	Date	Source
L-2311	458564.707	810635.557	2960.1	7-Nov-90	SFWMD
L-2525	301072.837	796831.245	1176.9	25-Oct-88	SFWMD
L-2549	283280.7	849295.479	554	4-Apr-90	SFWMD
L-2646	355114.412	883249.321	350	4-Apr-90	SFWMD
L-2820	283280.7	849295.479	2083	25-Oct-88	SFWMD
L-2821	301072.837	796831.245	1356	4-Apr-90	SFWMD
L-5649	383850.888	785811.828	815.1	24-Oct-88	SFWMD
L-5812	402912.289	747899.097	2900		SIR2006-5239
L-5814	402911.077	747697.155	3000		SIR2006-5239
L-5815	402912.289	747899.097	920		SIR2006-5239
L-5856	426224.607	775257.912	348	4-Apr-97	WRI 02-4036
L-5873	368222.769	825698.94	2410	1-Nov-99	WRI 02-4036
L-588	301965.174	762591.221	3465	24-Oct-88	SFWMD
L-591	278867.774	779222.828	2090	29-Mar-75	WRI 98-4253
LADY MOON FARMS G-1 - BP (DID #1)	437313.576	952695.564	636	4-Nov-03	SWFWMD
LIGHTFOOT RET POND HTRN WELL AT TEMPLE TERRACE FL	207306.259	1352475.728	278	10-Aug-04	USGS
M-1041	761194	1027082	352	6-Apr-93	SFWMD
MABRY CARLTON # 6	283425.309	1046432.182	642	30-Mar-94	SWFWMD
MACARTHUR TRACT 10H	237446.862	1048329.766	756	30-Mar-04	SWFWMD
MANASOTA DEEP # 14	201049.645	981681.75	371	11-May-94	SWFWMD
MANATEE FAIRGROUNDS	144293.119	1163821.99	1626	26-Dec-03	SWFWMD
NAFCO GROVES INT	472800.179	1003887.663	812	7-Jan-94	SWFWMD
NORTH PORT/MYAKKA	253268.969	988013.266	2600	21-Mar-05	DEP
NWHWRAP-2	178637.842	1339032.408	334	27-Jan-04	SWFWMD
ODESSA COMMUNITY CENTER FLRD WELL NEAR ODESSA FL	147575.371	1402984.654	295	2-Dec-04	USGS
OKF-0003	755117.318	1037466.918	2284.1	17-Apr-90	SFWMD
OKF-24	739284.46	1052173.835	3532	5-Sep-79	SFWMD
OKS-86	669299	1137517	204	7-Apr-93	SFWMD
OKS-93P1	683291	1092690	219	14-Apr-93	SFWMD
OKS95DP1	733351	1134155	269	6-Apr-93	SFWMD
OR-0004	449729	1472422	123.9	24-Jan-89	SFWMD
OSF-64 TEST WELL (OSS-64D 100ft) nr South Port FL	569882.071	1358961.453	307	26-Oct-93	USGS
OSF-70 TEST WELL (OSS-70D, 55-ft) nr St Cloud, FL	550173.202	1424451.036	419	27-Oct-93	USGS
PALMA SOLA-W DAVIS	117158.211	1160034.619	2078	20-Dec-93	SWFWMD
PEACE RIVER	329942.479	1003712.319	224	3-Mar-03	DEP
PEACE RIVER	328469.147	1002926.26	596	1-Oct-03	DEP
PEACE RIVER	328451.925	1002920.338	292	1-Oct-03	DEP
PEACE RIVER	323639.02	1001758.365	268	6-Oct-03	DEP
PEACE RIVER	323687.904	1001767.057	292	1-Oct-03	DEP
PEACE RIVER	329938.189	1008842.695	548	2-Oct-03	DEP
PEACE RIVER	318141.605	1001266.109	460	2-Oct-03	DEP
PEACE RIVER	324133.44	1001530.151	352	3-Jun-05	DEP
Peace River-1/T-1	329714.356	1003691.924	364	7-Apr-04	Facility
PLANTATION HAWTHORNE	211853.631	996409.058	364	24-Feb-94	SWFWMD
POF-8	514365.002	1265001.786	90.9	14-Nov-90	SFWMD
POH-1	613132.741	1208901.403	310	4-Jun-07	SFWMD
PORT CHAR UTIL DEEP	303788.822	966693.096	309	29-Mar-94	SWFWMD
PORT CHARLOTTE DEEP	307712.596	981353.38	1698	29-Mar-94	SWFWMD
PORT CHARLOTTE SHALL	307713.345	981356.403	594	29-Mar-94	SWFWMD
PRAIRIE CR UP INT-AG	402189.654	986602.463	635	13-Apr-04	SWFWMD
PUNTA GORDA HEIGHTS	328078.859	919987.644	994	25-Feb-04	SWFWMD
ROB LANE (G.V. RUSSELL)	342312.8	997585.334	1015	14-Apr-04	SWFWMD
ROLEN PROPERTIES ENTERPRISES #11 (DID# 11)	389330.015	977065.307	729	14-Jul-04	SWFWMD
ROLEN PROPERTIES ENTERPRISES #4 (DID# 4)	379116.741	966554.745	919	14-Jul-04	SWFWMD
ROLEN PROPERTIES ENTERPRISES #5 (DID# 5)	380433.998	963863.729	956	14-Jul-04	SWFWMD
ROLEN PROPERTIES ENTERPRISES #7 (DID# 7)	383416.243	971671.171	306	14-Jul-04	SWFWMD
ROLEN PROPERTIES ENTERPRISES #9 (DID# 9)	380549.911	975209.635	660	14-Jul-04	SWFWMD
ROMP 10 HAWTHORN	330568.152	981860.495	879	20-Nov-03	SWFWMD
ROMP 10 LIMESTONE	330559.728	981904.391	1176	16-May-94	SWFWMD
ROMP 11 DEEP	351344.288	961987.417	1535	29-Mar-94	SWFWMD
ROMP 12 UP INTERMEDIATE	414562.136	984832.707	478	27-Jan-04	SWFWMD
ROMP 13 LOW INT	455636.905	995825.861	312	28-Jan-04	SWFWMD
ROMP 13 MW2	455674.364	995814.469	360	26-Sep-96	WRI 01-4015
ROMP 13 MW3	455674.364	995814.469	320	26-Sep-96	WRI 01-4015
ROMP 16.5 LOWER INTERMEDIATE	368468.715	992386.096	608	27-Jan-04	SWFWMD
ROMP 17 IAS LPZ	338718.349	1033819.321	542	2-Oct-96	WRI 01-4015
ROMP 17 PZ2	338626.458	1033618.054	378	9-Apr-04	SWFWMD
ROMP 17 SAS	338718.349	1033819.321	492	28-Aug-96	WRI 01-4015

Table 3.1a: TDS data (IAS)

Station	X coordinate (ft FL State Plane 1983)	Y coordinate (ft FL State Plane 1983)	TDS (mg/l)	Date	Source
ROMP 17 UFA	338718.349	1033819.321	628	28-Aug-96	WRI 01-4015
ROMP 19 ELAM	248308.981	1034022.798	1017	3-Mar-94	SWFWMD
ROMP 19 ES WELL NEAR SARASOTA FL	248362.745	1034035.652	593	15-Feb-94	USGS
ROMP 19 WLAM	219981.864	1032239.361	1363	28-Apr-04	SWFWMD
ROMP 20 LOWER INT	175288.269	1042538.416	2580	17-May-94	SWFWMD
ROMP 20 UPPER INT	175301.848	1042548.66	1304	15-Jan-04	SWFWMD
ROMP 22 L INTERMEDIATE	222160.573	1084966.407	632	18-Feb-94	SWFWMD
ROMP 22 UPPER INT	222126.545	1084973.538	496	26-Jan-04	SWFWMD
ROMP 23 HAW-TAMPA	273797.24	1085429.459	206	11-Jan-94	SWFWMD
ROMP 5 MW2	393007.309	950322.253	702	24-Sep-96	WRI 01-4015
ROMP 5 MW3	393007.309	950322.253	1850	24-Sep-96	WRI 01-4015
ROMP 5 UPPER INT	392998.406	950316.958	641	13-Jan-04	SWFWMD
ROMP 9 INTERMEDIATE	282298.786	998635.854	1017	15-Jan-04	SWFWMD
ROMP 9 OW13	282304.265	998645.772	1270	27-Aug-96	WRI 01-4015
ROMP 9 OW14	282304.265	998645.772	1400	27-Aug-96	WRI 01-4015
ROMP 9.5 LOW INT	315550.255	1016676.011	434	10-Oct-03	SWFWMD
ROMP 9.5 MW18	315723.041	1016633.972	468	20-Aug-97	WRI 01-4015
ROMP 9.5 MW2	315632.684	1016634.725	414	19-Aug-97	WRI 01-4015
ROMP 9.5 UPPER INT	315715.129	1016595.459	469	10-Oct-03	SWFWMD
ROMP TR 1-2 L HAW	336134.02	912404.923	2052	9-May-94	SWFWMD
ROMP TR 1-2 UP INT	336114.479	912384.977	977	9-Dec-03	SWFWMD
ROMP TR 3-1 L HAWTHO	259334.744	950817.66	1817	17-May-94	SWFWMD
ROMP TR 3-1 U HAWTHO	259340.467	950829.22	2172	23-Feb-04	SWFWMD
ROMP TR 3-3 U HAWTH/L INT (average	222975.07	944398.504	3545		SWFWMD
ROMP TR 4-2 SUWANNEE	200635.719	987953.69	1794	14-Mar-94	SWFWMD
ROMP TR 5-1 INTERMED	184118.583	1021401.157	1664	11-Mar-94	SWFWMD
ROMP TR 5-2 L HAW	202559.044	1028318.317	1789	16-Feb-94	SWFWMD
ROMP TR 6-1 HAWTHORN	152418.509	1069368.004	2582	24-May-94	SWFWMD
ROMP TR 7-2 LOWER INT	153306.038	1131248.301	547	29-Jan-04	SWFWMD
ROMP TR 7-2 UP HAWTHORN	153306.038	1131248.301	382	29-Jan-04	SWFWMD
ROMP TR 8-1 INT	155313.458	1184321.047	514	8-Jan-94	SWFWMD
ROTUNDA WATER PLANT 18	235682.113	923361.196	8600	21-Mar-94	SWFWMD
RTA-007	503672.944	903943.886	497.1	8-Nov-90	SFWMD
SARASOTA - VENICE GARDENS	205188.84	998354.71	5380	1-Oct-03	DEP
SARASOTA HISTORICAL SOC	169381.847	1047123.974	1911	27-Apr-04	SWFWMD
SHELDON & ELSIE KODNER #1 (DID# 1)	425519.13	954570.532	1090	30-Mar-04	SWFWMD
SHELL CREEK RV PARK INT	364534.647	960246.013	1117	24-Feb-04	SWFWMD
SOUTHBAY UTILITIES DEEP	174077.046	1036377.138	3035	3-Feb-94	SWFWMD
SR 74 DEEP WELL	353306.209	950887.398	555	26-Feb-04	SWFWMD
STARKEY S63 UNW NRSD WELL NEAR ODESSA FL	146086.593	1426735.204	74	11-Nov-03	USGS
STEVE E VARNER 34-B (DID# 1)	427012.808	954513.72	1716	17-Mar-04	SWFWMD
TAMPA YACHT & STABLES	177168.11	1295011.632	506	11-Feb-04	SWFWMD
TEST 18 BLACKBURN WELL	245020.235	1015638.821	1224	27-Apr-04	SWFWMD
USGS 530371401	474746.409	1352238.977	71	6-May-96	FDOH
USGS C-1	367376.945	918584.922	2440	25-Feb-94	SWFWMD
USGS C-3	329739.483	940778.922	356	30-Mar-94	SWFWMD
USGS TUCKERS CORNER	408400.07	918138.887	354	23-Dec-93	SWFWMD
VENICE # 35	188538.777	1006263.718	948	31-Dec-03	SWFWMD
VENICE SH WF 33	192238.284	1007970.691	1485	25-Feb-94	SWFWMD
VENICE SH WF 59	196210.126	1007947.545	472	2-Apr-04	SWFWMD
VENICE SH WF 68	199809.177	1007893.384	798	31-Dec-03	SWFWMD
VENICE TEST WELL 38 NEAR VENICE FL	188242.831	1006501.121	331	26-Aug-93	USGS
VO #3	282154.051	1024824.345	1267	22-Mar-94	SWFWMD
WCRWSA WT-9-100	215177.711	1396461.721	216	18-Nov-03	SWFWMD
WHITAKER BAYOU WELL	153902	1101388	659	29-Dec-03	SWFWMD
WILLIAMS FARMS PARTNERSHIP #4 (DID# 4)	416380.431	966205.386	566	18-Mar-04	SWFWMD
WILLIAMS FARMS PARTNERSHIP #5 (DID# 5)	418052.949	969452.341	378	18-Mar-04	SWFWMD
WILLIAMS FARMS PARTNERSHIP #6 (DID# 6)	417991.181	967066.489	602	18-Mar-04	SWFWMD
Winkler Avenue MHMW-1	368159.414	825572.738	2410	1-Nov-99	SIR2006-5239

Station	X coordinate (ft FL State Plane 1983)	Y coordinate (ft FL State Plane 1983)	TDS (mg/l)	Date	Source
36-00003-W - LEE COUNTY UTILITIES - LH ASR#1 - North Reservoir	382564.0864	865453.9572	1617	10-Mar-99	SFWMD
36-00003-W - LEE COUNTY UTILITIES (only one pumping) - LH ASR#1 Olga	432240	868000	2284	4-Feb-99	SFWMD
3OAK-DZMW1	396637.988	777523.078	1500		SFWMD
4B 38-32-13 PEEK	158442.823	1206956.177	787	1-Feb-94	SFWMD
AAD4875	110802.696	1341631.138	310	28-Mar-01	FDOH
AAD5622	105330.07	1393232.123	130	28-Mar-01	FDOH
AAD7528	472434	1353024.348	70	6-May-96	FDOH
AAE9695	194476.224	1226063.671	600	25-Jan-01	FDOH
AAE9699	223282.21	1330137.499	230	31-Jan-01	FDOH
AAH1593	469496.754	1353147.267	120	29-Apr-96	FDOH
ADRIAN CHAPMAN (DID# 4)	396214.693	984937.301	1473	14-Jan-04	SFWMD
ADRIAN CHAPMAN (DID# 6)	405250.756	979736.924	1168	14-Jan-04	SFWMD
ADRIAN CHAPMAN (DID# 7)	399395.215	978907.705	1033	14-Jan-04	SFWMD
AFMW-1 (Bradenton HSPS ASR MW)	146286.871	1154162.979	1000	15-Nov-04	Facility
BARDMOOR DEEP WELL	90440.742	1286320.726	1255	16-Dec-03	SWFWMD
BCOES	948766.599	713215.538	3952	6-Oct-03	DEP
BELLE GLADE, CITY OF	757542.016	858452.196	2900	1-Oct-03	SFWMD
BF-1	925617.3	669564.23	7730		ECFAS Table 4-4
BF-3	925364.134	669470.163	8360	12-Jun-97	SFWMD
BF-4S	925172.703	669560.613	7500	8-Jun-07	SFWMD
BGTP-1	759840	877795	2500	15-Mar-05	SFWMD
BICY-MZ2	554522.187	567147.922	5570	1-Feb-05	SFWMD
BLUE GOOSE GROVES #15 (DID# 15)	398723.283	994900.767	731	10-Nov-03	SWFWMD
BOYRO_EPXU	953221.774	786238.388	4400	5-Mar-07	SFWMD
BR0202	724478.877	1470720.295	3059	3-May-94	SJRWMD
BR0585	704359.147	1560270.518	340	25-Oct-03	SJRWMD
BR0608	758316.067	1510787.462	3000	24-Jan-04	SJRWMD
BR0624	832407.57	1285842.671	549	26-Oct-03	SJRWMD
BR0645	743634.232	1332404.269	1150	28-Apr-04	SJRWMD
BR0660	667663.773	1555092.422	3400	25-Jan-94	SJRWMD
BR1526	667734.073	1555192.53	3530	28-Apr-04	SJRWMD
BR1557	731175.964	1471843.54	3680	25-Jan-04	SJRWMD
BR1572	704359.147	1560270.518	6900	25-Oct-03	SJRWMD
BR1835	694239.309	1610656.053	1655	25-Oct-03	SJRWMD
BROWARD CO. NORTH DIST.	933012.638	700321.94	4324	1-Oct-03	SFWMD
BUTLER S C B S15 #1	93366.845	1277073.912	1006	15-Mar-94	SWFWMD
C-1108	433465.791	695524.542	4900	10-Jan-94	WRI 98-4253
C-1133	634291.75	650423.49	1870		WRI 98-4253
C-1206	428564.292	630122.3	5500	24-Jun-97	SIR2006-5239
C-1207	428836.253	629817.95	5620	1-Jul-97	SIR2006-5239
C-21	513815.52	789687.03	1850		WRI 98-4253
C-22	514272.1	763128.92	2500		WRI 98-4254
C-236	530034.464	714513.379	2070	16-Mar-59	WRI 98-4253
C-258	519890.286	757758.918	2660	7-Oct-81	WRI 98-4253
CASEY RANCH WELL	111714.208	1374057.281	440	24-Jan-94	SWFWMD
CCRO-10A	323631.051	817186.174	1252	28-Feb-02	SFWMD
CH-315	351547.305	961312.632	1900	7-Aug-99	SIR2006-5239
CH-316	351547.305	961312.632	2020	19-Mar-02	SIR2006-5239
CH-317	351547.305	961312.632	1860	19-Mar-02	SIR2006-5239
CH-318	242983.961	936404.355	21100	26-Feb-00	SIR2006-5239
CH-319	242983.961	936404.355	22100	20-Apr-00	SIR2006-5239
CH-325	351547.305	961312.632	1640	19-Mar-02	SIR2006-5239
CH-326	351547.305	961312.632	760	21-Mar-02	SIR2006-5239
CH-327	351547.305	961312.632	1860	19-Mar-02	SIR2006-5239
City Ice & Fuel	921046.473	529569.745	3016	29-Apr-59	SFWMD
City of FT. Lauderdale	941140.043	641402.613	7352	1-Oct-03	SFWMD
City of FT. Lauderdale	941340.043	641402.613	7296	1-Nov-03	SFWMD
CITY OF NORTH PORT LOWER	247037.887	977111.531	13580	1-Oct-03	SFWMD
CITY OF NORTH PORT UPPER	247037.887	977111.531	8140	1-Oct-03	SFWMD
CLAYWELL ELEM AGWQMP ID-057VF092 FL	165250.958	1371229.439	219	2-Dec-04	USGS
CLEARWATER 15 (DUNEDIN 6)	88180.356	1344019.847	553	23-Dec-03	SWFWMD
CLEARWATER 18 PRODUCTION	83415.149	1322657.307	302	29-Dec-93	SWFWMD
CLEARWATER WELL 67	103212.912	1338833.441	378	23-Dec-03	SWFWMD
CLEARWATER-DUN WELL 17	95664.97	1354379.973	1110	27-Dec-93	SWFWMD
CLEWRO-PW1	676273.795	875746.668	2700	17-Aug-05	SFWMD
CM-I1	950934.951	702426.034	5120	2-Jun-59	SFWMD
CNB #3	219951.866	1340650.075	347	23-Mar-04	SWFWMD
Cocoa - Claude H. Dyal - 1	741538.367	1462517.858	475	25-Jul-94	Facility
COCOA D WELL NEAR NARCOOSSEE, FL	602933.8	1487461.832	381	12-May-03	USGS

Station	X coordinate (ft FL State Plane 1983)	Y coordinate (ft FL State Plane 1983)	TDS (mg/l)	Date	Source
COCOA DYAL	674095.793	1474755.598	369	20-Jun-04	DEP
COH_F3	925987	613161	4750		ECFAS Table 4-4
COHWTP_TW	926387	611661	4500	12-Jun-07	SFWMD
CORAL SPRINGS IMP DIST / DIW	897697.466	695859.819	10962	1-Oct-03	SFWMD
D MICHAEL-HRS	242923.436	1388414.351	258	19-Nov-03	SWFWMD
DF-4	830843.436	573317.791	3590	25-Jan-05	SFWMD
DINER CITRUS & CATTLE CO #11 (DID# 11)	388319.349	964235.747	2017	13-Jul-04	SWFWMD
DINER CITRUS & CATTLE CO #12 (DID# 12)	393745.426	967712.982	1224	13-Jul-04	SWFWMD
DINER CITRUS & CATTLE CO #7 (DID# 7)	404801.46	971047.018	477	13-Jul-04	SWFWMD
DINER CITRUS & CATTLE CO #8 (DID# 8)	407887.038	964929.898	518	13-Jul-04	SWFWMD
DIOCESE OF ST PETE	98940.5	1257267.34	3435	29-Dec-93	SWFWMD
DOBENECH WELL	215354.449	1425735.061	294	17-Nov-03	SWFWMD
DT BROWN G-36	427381.31	984369.81	652	12-Aug-93	SWFWMD
DUNEDIN #4	79277.444	1338309.139	457	23-Dec-03	SWFWMD
EAST LAKE WOODLANDS FL	110948.838	1365733.96	1125	28-Jan-04	SWFWMD
ENGLEWOOD	217507.049	954810.162	19350	31-Jul-00	SIR2006-5239
ENP-100	787244.43	381470.63	5510	25-Jan-05	SFWMD
EVERCLUB	970850.4	860146.62	5000	9-Oct-01	SFWMD
EXBRY-1	475404.088	855772.73	2200	21-Jun-04	SFWMD
EXKR-1	696704.82	1025434.635	825	12-Mar-04	SFWMD
EXPM-1	784620	965030	1680	7-Oct-03	SFWMD
FKAA - J. Robert Dean WTP - Deep Injection Well IW-1	818797.282	402379.894	4732	4-Sep-08	SFWMD
FKAAFCEW1	818318	403673	4550	10-Oct-03	ECFAS Table 4-4
FPL-MW	400851.962	859414.492	2000	21-Mar-06	SFWMD
FPU-MZU	878265.367	1135536.726	1960	11-Dec-02	SFWMD
FTL-MZU2	941689.959	641434.042	6795	7-Sep-99	SFWMD
G2-1	809186.06	1119715.22	2317	5-Mar-96	WRI 03-4242
G-2618	713926.399	667921.717	1650	14-Jan-92	WRI 98-4253
G-2887	943158.561	721457.218	3800	3-Sep-92	SIR2006-5239
G-2914	898496.586	670288.232	4520	31-Jul-97	SIR2006-5239
G-2917	933649.07	670332.132	7880	16-Mar-98	SFWMD
G-3061	890348.097	543831.021	2920	4-Dec-74	SIR2006-5239
G-3062	890255.085	544133.413	2830	20-Nov-74	SIR2006-5239
G-3709	829113	497139	4300		ECFAS Table 4-4
G7-1	820522.52	1124304.06	3640	29-Feb-96	WRI 03-4242
Gasparilla Island RO DZMW-1	247354.383	922372.781	19900	1-Nov-03	Facility
GB-1	863403.824	402995.169	2720	18-Dec-75	SFWMD
GDU WELL M-2	329751.283	1005001.882	807	14-Mar-94	SWFWMD
GL-331	628313.697	910475.205	4096	20-Nov-01	SIR2006-5239
GL-5B	553452.381	957446.536	285	2-Sep-99	SFWMD
GLF-0002	650450.743	983226.511	1322	24-Apr-86	SFWMD
GLF-1	681167.674	1022612.581	1058	10-Jul-97	SFWMD
HANCOCK & LAWRENCE	399652.38	986532.418	809	25-Mar-94	SWFWMD
HB-TPW1	961554.365	755841.765	6700	1-Jul-01	SFWMD
HC-0001	522027.684	1112997.903	184.9	6-Jan-86	SFWMD
HE-1141	474134.238	856278.868	2040	26-Mar-04	SIR2006-5239
HE-116	482148.372	864019.621	2950	7-Mar-75	WRI 98-4253
HE-278	472878.359	838815.856	2300	10-Dec-53	WRI 98-4253
HE-46	613982.665	868850.67	2131	7-May-53	SFWMD
HE-9	640460.757	873880.568	3053	1-May-43	SFWMD
HENNINGSEN WELL	210684.695	1435134.791	509	17-Nov-03	SWFWMD
HIF-0001	627351	1051594	581	23-Jan-89	SFWMD
HIF-0002	617742.781	1106330.952	368	10-May-82	SFWMD
HIF-0003	571434.113	1161030.424	257	12-Oct-78	SFWMD
HIF-0006	614631.388	1059582.346	415		SAJ
HIF-0008	500239.881	1048955.277	343	12-May-81	SFWMD
HIF-0013	588743.239	1122020.312	430	23-Jan-89	SFWMD
HIF-0014	566108.881	1075009.248	180	23-Jan-89	SFWMD
HIF-0027	542022.841	1011152.896	298		SAJ
HIF-0032	553390.84	1146632.417	174		SAJ
HIF-42U	671099	1048400	708	30-May-08	SFWMD
HILLS CO ASR SMW-1	197182.145	1341540.848	551	25-Feb-04	SWFWMD
HOLLYWOOD WASTEWATER TRTMT. PLANT	940986.481	616553.093	4132	1-Oct-03	SFWMD
I75-MZ1_2	416556.672	668295.467	5100	31-Jan-05	SFWMD
ICW-2	814300	983904	1900		ECFAS Table 4-4
INTERSIL	782721.548	1345725	1600	1-Oct-03	DEP
IR0312	840707.965	1179340.383	765	24-Jan-04	SJRWMD
IR0313	840788.518	1204575.203	578	28-Jul-94	SJRWMD

Station	X coordinate (ft FL State Plane 1983)	Y coordinate (ft FL State Plane 1983)	TDS (mg/l)	Date	Source
IR0921	782344.751	1252326.768	1590	25-Jan-04	SJRWMD
IR1000	849564.527	1245931.752	1660	25-Jan-04	SJRWMD
IR-373	776390	1201917	625	14-Apr-93	SFWMD
IWSD-MZ2	514985.196	756311.019	2820	4-Feb-05	SFWMD
IZ MANN GOLF COURSE WL	171399.42	1061935.384	2596	10-Mar-94	SWFWMD
JENSEN WELL	235801.349	1417177.853	198	17-Nov-03	SWFWMD
JUDY WILLIAMS WELL	187376.807	1401700.967	510	17-Nov-03	SWFWMD
JUP_RO_DZM	931130.107	942241.032	6780	24-Sep-93	SFWMD
KING WELL	103712.335	1327391.917	301	15-Mar-94	SWFWMD
L-0040	473512.189	1737834.95	183	21-Nov-03	SJRWMD
L-0045	485680.778	1755865.384	1473		SAJ
L-0051	419637.798	1470470.817	128		SAJ
L-0052	437896.589	1524197.949	148		SAJ
L-0053	417653.254	1500280.404	108	29-Jan-04	SJRWMD
L-00588	302146.525	762690.799	3465		SAJ
L-0059	531493.038	1701337.877	509	16-Mar-04	SJRWMD
L-0066	471326.333	1726229.828	758	21-Nov-03	SJRWMD
L-0095	369008.143	1584445.43	194	29-Jan-04	SJRWMD
L-0199	435370.202	1538959.02	165	29-Jan-04	SJRWMD
L-02527	283740.318	850099.185	3457		SAJ
L-02528	332968.604	844942.385	2018		SAJ
L-0455	480080.258	1757601.061	233	19-Jan-04	SJRWMD
L-0620	403271.966	1660665.851	214	30-Nov-03	SJRWMD
L-1186	310130.22	767946.8	3280	29-Mar-75	WRI 98-4253
L-1634	362405.378	755634.012	3160	28-Aug-80	WRI 98-4253
L-1646	274352.98	782394.73	2350		SAJ
L-2003	380722.83	817409.86	2820	24-Dec-74	WRI 98-4253
L-2115	355041.639	806579.738	1690	30-Jun-75	WRI 98-4253
L-2201	317795.619	839078.109	2390	20-Aug-80	WRI 98-4253
L-2292	390261.62	832496.16	2320	7-Jun-78	WRI 98-4253
L-2313	470578.15	769961.66	2790	7-Jun-78	WRI 98-4253
L-2319	428590.96	771178.31	1250	8-Jun-78	WRI 98-4253
L-2401	323061.43	770972.54	2900	10-Nov-77	WRI 98-4253
L-2426	349057.811	820356.653	1090	26-Jan-77	WRI 98-4253
L-2433	414594.885	849816.112	1980	10-Feb-77	WRI 98-4253
L-2434	323738.2	821662.76	1200	16-Jun-78	WRI 98-4253
L-2525	301010.19	796702.86	1230	30-Nov-77	WRI 98-4253
L-2527	283219.18	849169.61	3660	19-Dec-77	WRI 98-4253
L-2528	332534.848	843909.448	2220	9-Jun-78	WRI 98-4253
L2-PW2	672708.954	826685.164	1560	2-Feb-05	SFWMD
L-468	267535.79	792051.54	1970		SAJ
L-591	278868.87	779223.75	2090	29-Mar-75	WRI 98-4253
L-6433	311448.17	843295.51	2760	27-May-05	SFWMD
LAB-MZ1	502273.564	879736.844	1800	10-Dec-97	SFWMD
Lake Manatee - B-1	216224.213	1149498.875	355	4-Nov-03	Facility
Lake Manatee - B-2	216934.848	1148582.027	218	4-Feb-03	Facility
LIBRARY DP WL ON PAULA	150715.84	1335636.426	1027	4-Dec-03	SWFWMD
LM-7974	293119	823885	3912		SFWMD
M-1034	900051.28	1041088.96	4784	10-Jul-00	WRI 03-4242
M-106	915988.05	1034219.39	1950	28-May-57	WRI 03-4242
M-1121	922765.31	1047492.46	2560	18-Jul-01	WRI 03-4242
M-1326	924813.6	1024379.86	2377	10-Jul-00	WRI 03-4242
M-1349	926014.18	1034082.53	2156	31-May-90	WRI 03-4242
M-1357	897286.987	1059562.996	2728	22-Jun-05	SFWMD
M-143	867931.9	1035860.22	2110	24-Oct-61	WRI 03-4242
M-186	823199.91	1043024.04	2480	30-Dec-77	WRI 03-4242
M-255	818473.64	1028160.8	2430	24-Jul-01	WRI 03-4242
M-30	817278.2	987663.47	1126	25-Mar-58	WRI 03-4242
M-740	888113.44	996687.89	2570	24-May-78	WRI 03-4242
M-744	790924.29	1027959.27	1000	10-May-79	WRI 03-4242
M-745	828936.52	1031637.1	2850	24-Jul-01	WRI 03-4242
M-841	901286.45	1030896.85	6080	4-Sep-57	WRI 03-4242
M-901	813633.77	995021.55	778	29-May-57	WRI 03-4242
M-927	815926.03	1032896.82	2130	23-Oct-61	WRI 03-4242
M-940	929068.64	1036526.55	1250	31-Aug-59	WRI 03-4242
MACARTHUR TRACT 14FS	247299.3	1020454.277	1107	24-Feb-94	SWFWMD
MANATEE FRUIT #3	114493.264	1143417.651	2010	10-Jan-94	SWFWMD
MANATEE FRUIT-MIDWAY	122323.446	1140293.276	857	20-Dec-93	SWFWMD

Station	X coordinate (ft FL State Plane 1983)	Y coordinate (ft FL State Plane 1983)	TDS (mg/l)	Date	Source
MAN-F14	965578	815102	4100	14-Aug-03	SFWMD
MARGATE, CITY OF DIW	912732.054	694130.554	6562	1-Oct-03	SFWMD
MARSH CITRUS GROVES (OLD EMERALD GROVE) -BP DID #1	400237.376	1007020.566	587	7-Nov-03	SWFWMD
MARTIN MURPHEY	166065.612	1305204.354	406	11-Feb-04	SWFWMD
MDWSA_BZ1	876311	442379	2750	3-Jun-05	SFWMD
MF-23	798425.377	996296.651	953	15-Sep-87	SFWMD
MF-31	923812.783	1023381.027	2500	23-Oct-03	SFWMD
MF-33	789229.622	1016157.62	1052	19-Sep-83	SFWMD
MF-35	824627.12	970556.95	2975		ECFAS Table 4-4
MF-37U	784921.897	965985.038	1611	5-Sep-07	SFWMD
MF-40U	826580.032	1044391.078	2400	6-Jun-07	SFWMD
MF-52	856075.205	1000605.991	2500	23-Oct-03	SFWMD
MF-9	829647.569	1030546.579	2800	23-Oct-03	SFWMD
MIAMI-DADE SOUTH DISTRICT WWTP DUAL-ZONE MONITOR WELL FA-3	871526	442422	1928	1-Oct-03	Facility
MIAMI-DADE SOUTH DISTRICT WWTP MONITORING WELL FA2	873227	441122	1840	1-Oct-03	Facility
MIDWAY GROVES	154048.856	1121654.079	987	9-Mar-94	SWFWMD
MILLER WELL- KENNETH CITY	103344.672	1270241.221	425	2-Jan-04	SWFWMD
MIR-F2	877300.478	595660.559	2520	20-Aug-08	SFWMD
MIU-MZ1	418501.641	591506.133	31100	2-Feb-05	SFWMD
MO-130	884358.756	339295.521	5730	18-Dec-75	SFWMD
MYAKKA HEAD #5 USGS	285400.859	1138060.422	339	23-Dec-03	SWFWMD
NCCWTMZ2	433829.989	695522.633	4690	27-Feb-96	SFWMD
NCWRF-MW1	398257.361	701832.649	5920	###########	SFWMD
NMB-2F	913635	588117	3353	17-Jun-03	SFWMD
NORTH PORT/MYAKKA	253358.403	987911.389	3700	8-Mar-05	DEP
NORTHEAST INJECTION B-11	133467.495	1273194.614	22960	9-Mar-04	SWFWMD
NPSL-MZU	866749	1092495	2440	17-Nov-99	SFWMD
NRCS1-1	828575	1099139	2400	3-Dec-03	SFWMD
NRCS11-1	849058.89	1145082.44	1236		ECFAS Table 4-4
NRCS12-1	852004	1147554	1000	5-Dec-03	SFWMD
NRCS121-1	820466.46	1138324.51	2133		ECFAS Table 4-4
NRCS14-1	852413	1145484	1200	14-Sep-04	SFWMD
NRCS201-1	845039	1153829	1400	5-Dec-03	SFWMD
NRCS202-1	806894	1102027	1500	3-Dec-03	SFWMD
NRCS202-2	808150.53	1102042.11	1500		ECFAS Table 4-4
NRCS203-1	763751.16	1136675.34	1672.7		ECFAS Table 4-4
NRCS204-3	783480.55	1064593.21	1239		ECFAS Table 4-4
NRCS2-2	810793.26	1119669.24	2081		ECFAS Table 4-4
NRCS29-8	831644	1167169	1500	5-Dec-03	SFWMD
NRCS3-2	810077	1089551	1500	7-Mar-05	SFWMD
NRCS35-1	814193.07	1081499.97	3490		ECFAS Table 4-4
NRCS5-1	825919.34	1101665.61	1954.5		ECFAS Table 4-4
NRCS6-1	801011	1127976	2200	4-Dec-03	SFWMD
NRCS7-2	820523	1126953	1600	4-Sep-03	SFWMD
NRCS8-4	857779	1129801	1200	1-Mar-02	SFWMD
NWHWRAP 18-F	117509.322	1349389.855	1350	9-Mar-04	SWFWMD
NWHWRAP-3	105055.002	1407538.902	337	12-Jan-04	SWFWMD
NWHWRAP-3D	105004.468	1407535.473	2199	12-Jan-04	SWFWMD
OK-23	703455.53	1061490.89	982	31-May-00	WRI 03-4242
OK-31	706715.81	1052305.83	1146	19-Sep-84	WRI 03-4242
OK-72	742249.27	1151932.14	2930	19-Jul-01	WRI 03-4242
OKF-0001	748649.92	1140549.123	585		SAJ
OKF-0003	755117.33	1037467.017	2290		SAJ
OKF-0019	667498.118	1132972.159	471		SAJ
OKF-0022	676184.524	1058051.272	815		SAJ
OKF-0025	670768.269	1057947.908	925		SAJ
OKF-0027	712614	1081411	600	27-Sep-78	SFWMD
OKF-0036	647234.487	1159326.522	419		SAJ
OKF-0037	656416.317	1144178.945	551		SAJ
OKF-0040	635058.968	1117728.594	485		SAJ
OKF-0042	618562.178	1115014.125	437		SAJ
OKF-0075	671124.387	1070267.008	684		SAJ
OKF-0076	674105.08	1065421.394	1033		SAJ
OKF-0077	647226.196	1121964.986	536		SAJ
OKF-106	725843.941	1055704.198	1500	27-Aug-08	SFWMD
OKF-17	682589.18	1091462.55	548	31-May-00	WRI 03-4242
OKF-6A	676157.86	1110457.61	842		ECFAS Table 4-4
OKF-7	725677.45	1102318.13	332	15-Jul-87	SFWMD

Station	X coordinate (ft FL State Plane 1983)	Y coordinate (ft FL State Plane 1983)	TDS (mg/l)	Date	Source
OKF-71	739965	1159211	1430	23-Nov-93	SFWMD
OKF-74	725338	1078805	3950	2-Dec-93	SFWMD
OKF-94	733921	1118606	320	12-Apr-93	SFWMD
OKF-96D1	671812	1159531	661	6-Apr-93	SFWMD
OM-41 SARASOTA COUNTY	236547.038	1028750.65	1305	24-May-94	SWFWMD
OR0068	512767.738	1609897.479	670	13-Jul-94	SJRWMD
OR0106	470041.776	1590790.602	135	29-Aug-04	SJRWMD
OR0265	625553.35	1500362.74	810		SAJ
OR0547	507000.144	1591638.751	187	19-Feb-04	SJRWMD
OR0548	506933.443	1591539.371	170		SAJ
OR0617	620131.362	1524303.479	267		SAJ
OR0662	515635.201	1615138.752	658	30-Nov-03	SJRWMD
OR0669	650699.054	1476013.364	492	25-Oct-03	SJRWMD
OR0678	589589.347	1515356.409	196	30-Oct-03	SJRWMD
OR0796	493128.945	1575434.517	206	30-Nov-03	SJRWMD
ORC-PW5	894415	360131	7700	13-Jun-07	SFWMD
ORF-0029	457250.285	1475816.306	135		SAJ
ORF-0030	459137.042	1495602.108	132	26-Mar-79	SFWMD
ORF-0031	472907.318	1500686.066	160	29-May-79	SFWMD
ORF-32	493284.92	1506754.934	157	29-May-79	SFWMD
OS0004	672546.755	1340995.653	433	26-Oct-03	SJRWMD
OS0017	678629.23	1361498.705	681	28-Jul-94	SJRWMD
OS0019	674271.486	1336343.735	528		SAJ
OS0031	653818.524	1375933.495	635	26-Oct-03	SJRWMD
OSF-0008	516120.362	1429910.073	119		SAJ
OSF-0010	522099.862	1451905.505	125		SAJ
OSF-0014	500169.35	1420881.432	222		SAJ
OSF-0017	574939.755	1421765.026	227		SAJ
OSF-0025	457228	1454001	118	23-Jan-79	SFWMD
OSF-0052	592028.257	1260760.907	566		SAJ
OSF-100	493879.859	1426094.407	172	7-Feb-05	SFWMD
OSF-104U	613202.432	1208993.173	190	4-Jun-07	SFWMD
OSF-11	511137.595	1388117.915	109	10-Aug-93	SFWMD
OSF-12	580665	1422057	242	28-Jul-93	SFWMD
OSF-19	616853.016	1299405.369	438	12-Sep-79	SFWMD
OSF-21	657674	1265758.65	436		ECFAS Table 4-4
OSF-24	614087.023	1397162.754	394	6-Dec-79	SFWMD
OSF-27	583686.414	1459215.15	593	10-Aug-93	SFWMD
OSF-3	639311.788	1286553.304	296	24-Jan-89	SFWMD
OSF-32	469652	1454445	113	11-Sep-79	SFWMD
OSF-35	466287.011	1442543.455	167	11-Sep-79	SFWMD
OSF-37	641830.752	1401081.199	343	26-Mar-79	SFWMD
OSF-4	584484.602	1309549.116	154	12-Sep-79	SFWMD
OSF-5	480254.627	1427732.738	145	29-Jul-93	SFWMD
OSF-6	539947.203	1383477.259	153	25-Jan-89	SFWMD
OSF-60	689768	1222465	419	2-Aug-93	SFWMD
OSF-62	641676.227	1296604.37	321	2-Aug-93	SFWMD
OSF-66	594949.386	1342655.05	122	2-Aug-93	SFWMD
OSF-68	613817	1395749	212	26-Jul-93	SFWMD
OSF-7	627406	1376145	385	3-Oct-78	SFWMD
OSF-8	516122	1429910	119	4-Sep-79	SFWMD
OSF-84	639651.485	1325948.319	193	4-Aug-93	SFWMD
OSF-85	672811.605	1347862.301	397	2-Dec-92	SFWMD
OSF-86	685793.16	1365744.215	848	3-Aug-93	SFWMD
OSF-92	660707.881	1432789.033	286	5-Aug-93	SFWMD
PAHOKEE, CITY OF STP	764969.483	896737.978	3780	1-Oct-03	SFWMD
PALM BAY	785880.641	1342135.073	1780	1-Oct-03	DEP
PALM BCH CO. SOUTHERN REGION	928806.304	785408.436	5000	1-Oct-03	SFWMD
PALM BEACH COUNTY SYSTEM 9 NORTH, DUAL ZONE MW-1	917035.986	749286.617	5260	1-Oct-04	Facility
PAUL R WHARTON HS WELL	219912.828	1392525.987	290	16-Feb-04	SWFWMD
PB-1137	718008	728333.104	2086	28-May-05	SFWMD
PB-1167	882763.74	933847.04	2990	7-Dec-94	WRI 03-4242
PB-1179	936684.66	886110.9	4500		SAJ
PB-1183	939190.65	917432.11	6280	29-Sep-88	WRI 03-4242
PB-1194	962654.126	793592.078	3910	21-May-92	SIR2006-5239
PB-1690	939741	874642	7390	15-Oct-86	USGS WRIR 99-4061
PB-1692	961842.59	867202.079	5056	17-Jul-97	SIR2006-5239
PB-1702	950601.494	776339.311	4234	6-Sep-96	SIR2006-5239

Station	X coordinate (ft FL State Plane 1983)	Y coordinate (ft FL State Plane 1983)	TDS (mg/l)	Date	Source
PB-1776	910905.637	727915.122	4500	30-Apr-02	Facility
PB-203	776091.15	848379.22	3670		SAJ
PB-734	769973.28	863105.52	3630		SAJ
PB-747	936320.999	946546.435	4060	19-Jun-74	SIR2006-5239
PBF-1	953618.172	959048.572	2600.1	31-May-90	SFWMD
PBF-10R	886678.707	735581.372	5830	3-Sep-03	SFWMD
PBF-13	886997.951	735463.946	4064	16-Nov-00	SFWMD
PBF-15U	863897.133	874380.647	3400	7-Jun-07	SFWMD
PBF-3	949209.57	852482.255	4850	23-Oct-00	SFWMD
PBF-7U	748904.73	860161.101	2848	19-Jan-00	SFWMD
PEACE RIVER	323512.974	992692.397	944	1-Oct-03	DEP
PEACE VALLEY GROVES W3 - BP (DID #3)	414004.292	991413.544	555	4-Nov-03	SWFWMD
PEELED-MW1	918682.652	643742.172	4930	15-Jun-07	SFWMD
PEMBROKE PINES WWTP/DIW	875724.648	604016.271	3250	1-Oct-03	SFWMD
PERICO ISLAND WELL	112383.823	1153609.596	1942	24-Dec-03	SWFWMD
PLANTATION SUWANNEE	211776.254	996561.201	3468	24-Feb-94	SWFWMD
POF-0002	444203.999	1425387.265	179	5-Sep-79	SFWMD
POF-0003	459187.071	1399757.272	154		SAJ
POF-0008	514364.754	1265001.79	90		SAJ
POF-0010	537910.69	1211706.391	94	12-Sep-79	SFWMD
POF-0012	539700	1208167	88	12-Sep-79	SFWMD
POF-0015	519640.709	1311032.803	101		SAJ
POF-0019	519363.605	1282252.625	78		SAJ
POF-1	469343.022	1427379.5	170	14-Sep-79	SFWMD
POF-14	485364.816	1369336.474	96	11-Sep-79	SFWMD
POF-4	479538.11	1348255.194	118	5-Dec-79	SFWMD
POF-5	585924.446	1261680.07	484	22-May-79	SFWMD
POF-6	507391.509	1344504.24	148	5-Sep-79	SFWMD
PROGRESS VIL NR RIVERVIEW	217409.644	1300507.625	543	21-Jan-94	SWFWMD
PROPERTY RESERVE INC #1 (DID# 1)	204400.676	1238996.034	644	29-Jun-04	SWFWMD
PROPERTY RESERVE INC #4 (DID# 4)	207980.721	1240521.3	552	12-Jul-04	SWFWMD
PROPERTY RESERVE INC #5 - BP (DID# 5)	204766.428	1241923.336	922	20-Sep-04	SWFWMD
PROPERTY RESERVE INC #5 (DID# 5)	204766.428	1241923.336	1770	29-Jun-04	SWFWMD
Punta Gorda / Shell Creek - ASR-3 (9120)	351447.1045	960000.5407	1860	31-Jan-02	SFWMD
QUAIL HOLLOW FLORIDAN	210365.966	1435785.407	289	17-Nov-03	SWFWMD
ROBERT NORRIS #8 (DID# 8)	361786.896	1014692.711	763	29-Jan-04	SWFWMD
ROLEN PROPERTIES ENTERPRISES #2 (DID# 2)	389885.489	981270.744	1374	14-Jul-04	SWFWMD
ROLEN PROPERTIES ENTERPRISES #3 (DID# 3)	379167.8	971848.043	843	14-Jul-04	SWFWMD
ROMP 12 SH UP FLORIDAN	414516.068	984825.607	762	27-Jan-04	SWFWMD
ROMP 13 MW4	455674.364	995814.469	416	27-Sep-96	WRI 01-4015
ROMP 16.5 SUWANNEE	368470.14	992421.633	625	27-Jan-04	SWFWMD
ROMP 17 SWNN	338718.349	1033819.321	791	27-May-92	WRI 01-4015
ROMP 18 SUWANNEE	288795.939	1041033.084	615	23-May-94	SWFWMD
ROMP 20 SWNN	175273.794	1042521.112	3047	1-Oct-03	SWFWMD
ROMP 22 SWNN	222153.447	1084932.848	767	10-May-94	SWFWMD
ROMP 33 SWNN	248494.573	1137650.741	339	23-May-94	SWFWMD
ROMP 39 SWNN	250815.293	1185230.222	419	19-May-94	SWFWMD
ROMP 48 FLORIDAN	286579.982	1240209.795	235	9-Feb-94	SWFWMD
ROMP 49 SWN	250521.978	1248556.155	285	14-Jul-94	SWFWMD
ROMP 5 MW4	393007.309	950322.253	1100	25-Sep-96	WRI 01-4015
ROMP 50 FLORIDAN	217059.247	1230239.943	429	6-May-94	SWFWMD
ROMP 85 FLORIDAN	229946.1	1422384.683	145	18-Nov-03	SWFWMD
ROMP 9 OW15	282304.265	998645.772	1560	26-Aug-96	WRI 01-4015
ROMP 9.5 MW1	315632.684	1016634.725	806	19-Aug-97	WRI 01-4015
ROMP TR 10-2 DEEP	212664.273	1298987.337	600	21-Jan-94	SWFWMD
ROMP TR 11-2	213863.602	1317631.64	726	3-Dec-03	SWFWMD
ROMP TR 1-2 SWNN	336126.665	912391.043	2221	9-May-94	SWFWMD
ROMP TR 12-1 DP (NEW)	156718.877	1325682.075	1228	18-Feb-04	SWFWMD
ROMP TR 12-3 (NEW)	157401.341	1336484.449	347	18-Feb-04	SWFWMD
ROMP TR 13-1 SUWANNEE	82073.291	1306464.807	1249	2-Jan-04	SWFWMD
ROMP TR 13-1 TAMPA	82079.245	1306460.78	565	29-Dec-93	SWFWMD
ROMP TR 13-2X SUWANNEE	100493.65	1303502.465	7560	27-Jan-04	SWFWMD
ROMP TR 14-2 TAMPA	89117.762	1346205.234	1930	23-Dec-03	SWFWMD
ROMP TR 14-3 SWNN	98301.457	1344665.269	715	6-Dec-03	SWFWMD
ROMP TR 15-1 TAMPA	82285.339	1385680.917	1430	23-Dec-03	SWFWMD
ROMP TR 15-2 TAMPA	89620.504	1383708.113	796	31-Dec-03	SWFWMD
ROMP TR 15-3 SWNN	95631.161	1382456.759	454	6-Dec-03	SWFWMD
ROMP TR 3-1 SUWANNEE	259349.31	950816.914	1512	17-May-94	SWFWMD

Station	X coordinate (ft FL State Plane 1983)	Y coordinate (ft FL State Plane 1983)	TDS (mg/l)	Date	Source
ROMP TR 3-3 SUWANNEE	222958.177	944410.6	15010	16-May-94	SWFWMD
ROMP TR 4-1 SUWANNEE	187110.785	992895.211	6720	1-Oct-03	SWFWMD
ROMP TR 5-1 SUWANNEE	184128.421	1021407.911	2514	24-May-94	SWFWMD
ROMP TR 5-2 SUWANNEE	202560.658	1028310.714	2704	16-Feb-94	SWFWMD
ROMP TR 7-1	142781.145	1124988.852	840	25-May-94	SWFWMD
ROMP TR 7-2 SH FL	153306.642	1131246.172	849	3-Feb-04	SWFWMD
ROMP TR 7-4 SWNN	173097.758	1127600.243	754	10-Jan-04	SWFWMD
ROMP TR 7-4 TAMPA	173108.201	1127576.581	546	26-Jan-94	SWFWMD
ROMP TR 8-1 OCALA	155318.85	1184313.201	1030	8-Jan-04	SWFWMD
ROMP TR 8-1 SWNN	155303.439	1184290.059	1051	9-May-94	SWFWMD
ROMP TR 9-1	182636.985	1240836.299	733	4-Feb-04	SWFWMD
ROMP TR 9-2 SWNN	205615.938	1249932.074	1022	4-May-94	SWFWMD
ROMP TR 9-3 SWNN	195911.376	1241198.428	2098	5-May-94	SWFWMD
ROPER GROVES WELL	386722.511	998507.612	895	25-Mar-94	SWFWMD
ROY HAYNE AGWQMP FLRD WELL NR SULPHUR SPRINGS FL	174589.743	1358385.11	136	11-Aug-04	USGS
ROYAL PALM BCH VILLAGE UTIL DIW	906289.579	873438.945	4095	1-Oct-03	SFWMD
S-0001	618147.147	1592176.004	206		SAJ
S-0025	642809.739	1588927.461	9600		SAJ
S-0028	609870.944	1595821.114	251		SAJ
S-0034	627148.499	1603278.054	214		SAJ
S-0037	524356.421	1634502.429	3030		SAJ
S-0038	605686.251	1595624.414	2640		SAJ
S-0086	628139.145	1618932.316	804		SAJ
S-0097	526230.059	1636213.042	3856		SAJ
S-0829	557607.913	1595112.17	152		SAJ
S-1014	542251.849	1580913.734	294		SAJ
S-1056	568151.474	1572765.445	176		SAJ
S-1193	589263.96	1572419.763	227		SAJ
S-1201	619382.134	1580155.906	3730		SAJ
S-1328	618778.523	1600457.341	118		SAJ
S-1397	554860.345	1633297.947	229		SAJ
S-1408	539193.256	1600113.168	190		SFWMD
S-1533_G	851722.97	370030.571	6100	30-Dec-74	SFWMD
S-156	943090	547430	5188	14-Oct-40	SFWMD
S-158	939775.926	531000.872	4770	3-Mar-40	SFWMD
S-524	793171.97	465815.69	2900		ECFAS Table 4-4
SALT BAYOU FL-JOHNSON	99635.339	1393842.931	2104	16-Dec-03	SWFWMD
SARASOTA - CENTER RD	201199.204	1001330.007	3732	1-Oct-03	DEP
SARASOTA - VENICE GARDENS	205188.84	998354.71	7860	1-Oct-03	DEP
SARASOTA CO TEST WELL #1	167087.899	1113189.295	1079	31-Dec-03	SWFWMD
SCC-MZU	418846.924	641207.277	5900	14-Apr-05	SFWMD
SEABOARD UTIL #8	218634.999	1312047.81	470	1-Feb-94	SWFWMD
SHELDON RD DEEP	145260.18	1341495.097	5470	26-Jan-04	SWFWMD
SLF-11	791552.296	1164690.831	1800		SAJ
SLF-21	850060.323	1124953.851	901		SAJ
SLF-27	814069.64	1111164.76	2354		ECFAS Table 4-4
SLF-3	838497.52	1151155.28	1748	16-Sep-83	ECFAS Table 4-4
SLF-36	807907.866	1143252.88	1851		SAJ
SLF-40	818715.86	1121382.12	1707	16-Sep-87	ECFAS Table 4-4
SLF-48	843339	1077966	1284	21-Sep-83	SFWMD
SLF-51	819191.255	1092504.729	2104	19-Jan-83	SFWMD
SLF-60	786161.606	1071987.075	2100	23-Oct-03	SFWMD
SLF-62	828482	1075057	3100	23-Oct-03	SFWMD
SLF-62B	836003.27	1082784.18	3100	6-Jul-04	ECFAS Table 4-4
SLF-63	783767.26	1144482.06	2080		ECFAS Table 4-4
SLF-64	777699.12	1155672.11	2091.3		ECFAS Table 4-4
SLF-67	767932.93	1105760.25	942.5		ECFAS Table 4-4
SLF-9	788851.74	1132077.92	2896.8		ECFAS Table 4-4
SNEAD'S ISLAND	129502.403	1166453.54	1424	24-Dec-03	SWFWMD
SOUTH BEACHES	802480.018	1347810.495	1190	1-Oct-03	DEP
SOUTH CROSS BAYOU W S9	94918.191	1271343.174	468	15-Mar-94	SWFWMD
ST PETE	129741.927	1250160.14	1580	1-Oct-03	DEP
ST PETE	130344.596	1250066.295	1690	1-Oct-03	DEP
STL-216	823514.09	1141685.72	1900	1-Jun-00	WRI 03-4242
STL-223	760681.93	1127233.64	2200		SAJ
STL-225	828500.08	1049407.94	2437	30-May-90	WRI 03-4242
STL-228	879797.19	1111460.7	2260	9-May-79	WRI 03-4242
STL-229	813996.65	1111047.67	2224		SAJ

Station	X coordinate (ft FL State Plane 1983)	Y coordinate (ft FL State Plane 1983)	TDS (mg/l)	Date	Source
STL-230	851973.12	1067994	2190	29-Sep-77	WRI 03-4242
STL-244	807643.23	1146370.48	1050		SAJ
STL-248	851159.36	1049510.17	2510	29-Sep-77	WRI 03-4242
STL-255	883868.24	1060687.36	3046	12-Jul-00	WRI 03-4242
STL-352	880271.13	1155898	2540	16-Jul-01	WRI 03-4242
STL-353	905807.58	1088890.63	701	6-Jun-00	WRI 03-4242
STL-355	818938.08	1092588.85	2008	31-Aug-87	WRI 03-4242
STL-371	772377.83	1164528.37	2480		SFWMD
STL-375	836572.78	1101752.11	1562	7-Jun-00	WRI 03-4242
STL-376	849441.51	1163211.01	951	25-Jul-01	WRI 03-4242
STL-377	875281.02	1096489.97	2774	31-May-90	WRI 03-4242
STL-381	821825.06	1092297.6	2220	18-Jul-01	WRI 03-4242
STL-382	821825.06	1092297.6	2634	7-Jun-00	WRI 03-4242
STL-385	865817.08	1130371.21	924	25-Jul-01	WRI 03-4242
STL-392	840437.67	1064708.58	3026	11-Jul-00	WRI 03-4242
SUA_F1	949620.149	919515.319	5000	16-Feb-07	SFWMD
SUN-BTW	881184.653	648814.988	8700	6-Nov-07	SFWMD
SUNRISE SAWGRASS WWTP	873510.516	653626.482	5790	1-Oct-03	SFWMD
SWF-10776	141866.229	1394987.374	199		SAJ
SWF-10777	99694.08	1393947.225	2102		SAJ
SWF-10796	103786.549	1413396.648	271		SAJ
SWF-10859	110736.24	1336835.02	150		SAJ
SWF-10872	464367.626	1304014.241	200		SAJ
SWF-10903	250593.65	1248680.941	280		SAJ
SWF-10904	470784.421	1246814.462	235		SAJ
SWF-10937	248302.873	1034017.304	1003		SAJ
SWF-11390	153306.26	1131244.66	849		SAJ
SWF-11876	514856.007	1103589.044	200		SAJ
SWF-13344	151377.963	1578110.887	2349		SAJ
SWF-17312	329307.869	1103726.659	900		SAJ
SWF-18055	180359.16	1406577.93	211		SAJ
SWF-259	155363.48	1184402.937	1035		SAJ
SWFWMD WELL AT S-160	213930.616	1319656.782	485	30-Jan-04	SWFWMD
SYKES CREEK	750648.17	1486790.229	5080	1-Oct-03	DEP
SYMONS GROVES #2 - BP (DID #2)	401541.673	992800.856	649	6-Nov-03	SWFWMD
SYMONS GROVES #6 - BP (DID #6)	406723.803	990267.614	460	6-Nov-03	SWFWMD
TAMPA BAY DOWNS WRAP-57F	125335.019	1353255.952	1189	27-Jan-04	SWFWMD
TARPON ROAD DEEP WELL	104213.6	1391819.412	315	15-Jan-04	SWFWMD
TBC - 09	212811.124	1340768.064	314	30-Jan-04	SWFWMD
TR3-3U	222842.353	944208.652	28080	12-Apr-00	SFWMD
USGS 280310082290000	180091.89	1358202.746	234		SFWMD
USGS 280341082325702	156420	1357797	220		SFWMD
USGS 280550082310000	165143.234	1370959.43	204		SFWMD
USGS 280727082025301	318347.62	1379302.8	204		SFWMD
USGS 280852082140000	259352.481	1388633.089	320		SFWMD
VC HOLLINGSWORTH JR #8 (DID# 8)	470555.261	982575.565	437	1-Oct-04	SWFWMD
VENICE 2E	195250.049	1017845.69	2896	2-Apr-04	SWFWMD
W-14920	502146.892	584193.351	5735	19-Dec-80	SFWMD
W-15371	585797.587	769236.207	1684	2-Apr-83	SFWMD
W-466	697360.57	535378.311	2806	3-Jun-41	SFWMD
W-7362	851901.808	287756.505	5470	16-Jul-76	SFWMD
WCRWSA CYX-3 SWNN	219893.696	1393907.426	255	19-Nov-03	SWFWMD
West Port DZMW-1	260104	947308	5304	1-Oct-03	Facility
West Port DZMW-1	260104	947308	12486	1-Oct-03	Facility
WEST VILLAGE AGWQMP ID-057VS104 FL	162280.307	1362982.932	343	30-Nov-04	USGS
Winkler Avenue ASR-1	368159.414	825572.738	1770	1-Nov-99	SIR2006-5239
Winkler Avenue SZMW-1	368159.414	825572.738	2998	16-Sep-99	SIR2006-5239
WOODLANDS APTS	174873.312	1330196.744	251	11-Jan-94	SWFWMD

Station	X coordinate (ft FL State Plane 1983)	Y coordinate (ft FL State Plane 1983)	TDS (mg/l)	Date	Source
AAB3915	473608.326	1349495.186	100	13-May-96	FDOH
BICY-TW	554522.19	567147.92	26336.5		ECFAS Table 4-4
BONITA WTP	408816.685	731203.392	6200	6-Apr-04	DEP
BROWARD CO. NORTH DIST.	932271.456	702401.458	5545	1-Oct-03	SFWMD
BROWARD CO. NORTH DIST.	932546.542	702100.325	5013	1-Oct-03	SFWMD
BS_WRF-MW1	392865.487	742437.245	10800		SFWMD
Burnt Store Utilities Dual Zone Injection Monitor Injection Well	318215.632	887838.612	1600	1-Oct-03	Facility
C-1108	433465.791	695524.542	16600	22-Jul-92	WRI 98-4253
C-1111	416466.849	668152.969	27300		WRI 98-4253
C-284	506801.882	784257.273	2660	8-Oct-59	WRI 98-4253
CH-313	341447.731	894535.428	7880	3-Mar-92	WRI 98-4253
CITY OF NORTH PORT	247497.408	981290.32	18340	1-Oct-03	DEP
COCOA 39 NR BITHLO,FL	625957.434	1472591.231	782	25-May-04	USGS
EASTPORT	318533.848	961241.123	3434	1-Oct-03	DEP
EPU-MZU	318357.546	961258.729	3043	5-Oct-99	SFWMD
FORT MYERS BEACH WWTP DUAL ZONE MONITOR WELL	350747.433	785108.319	4450	1-Oct-03	Facility
Fort Myers RO WTP DZMW-1	385929.456	834794.663	3200	1-Oct-03	Facility
FTL-MW2	941690	641434	6795		ECFAS Table 4-4
G3-1	810107.03	1090837.62	3210	26-Jul-01	WRI 03-4242
G-3709	829040.164	496999.604	7220	6-Feb-97	SIR2006-5239
G6-1	801045.66	1127965.81	2044	5-Mar-96	WRI 03-4242
GEN DEV CORP AVON PARK	327631.631	1006356.222	974	10-May-94	SWFWMD
GL-5C	553433.737	957444.26	1263	2-Sep-99	SFWMD
GREATER PINE ISLAND DUAL-ZONE INJECTION MONITOR WELL	293119	823885	32000	17-May-05	Facility
HE-1087	672690.195	826805.29	1370	1-Jan-94	USGS
HE-1105	493958.05	822674.002	2090	20-Oct-82	WRI 98-4253
HIF-0002	617744	1106331	368	10-May-82	SFWMD
HILLS CO ASR SZMW-1	197219.936	1341775.582	2347	2-Feb-94	SWFWMD
IWA-MZL	293008	767990.447	31420	22-May-00	SFWMD
KNIGHTS TRAIL FLORIDAN	199913.225	1029804.86	2824	3-Feb-94	SWFWMD
L-5803	368478.02	871718.971	1580	12-Dec-90	WRI 98-4253
L-6436	311364.107	844104.065	24900	15-Jul-05	SFWMD
LAB-MZ2	502273.564	879736.844	1340	3-Feb-05	SFWMD
LAGORCECC	943094.41	547438.11	12000	7-May-02	SFWMD
LHA-LZMWB	443062.822	830683.434	3460	20-Aug-07	SFWMD
LM-7973	293068.888	823834.691	32000		SFWMD
MF-33	789502	1016158	1297	16-Aug-88	SFWMD
NCWRF-IW1	398375.711	701831.93	31500		SFWMD
NFM-MZU	368708.027	871747.836	1590	27-Feb-96	SFWMD
NMB-1F	914032	588133	11880	6-Feb-03	SFWMD
OKF-0016	682120	1090771	538	5-Dec-78	SFWMD
OKF-0075	671125	1070267	684	18-Sep-84	SFWMD
OKF-19	667497	1132973	471	29-Nov-79	SFWMD
OKF-36	647234	1159327	419	29-Jun-88	SFWMD
OKF-73	719014	1084450	4889.1	31-Oct-89	SFWMD
OKF-76	674104	1065422	1033	15-Sep-80	SFWMD
OKF-77	647226	1121965	536	12-Sep-80	SFWMD
OKF-81	613376	1152179	410	23-Nov-93	SFWMD
OR0827	535539.962	1521143.537	204	23-Oct-03	SJRWMD
OSF-13	499798	1417550	178	8-Dec-78	SFWMD
OSF-14	500168.878	1420881.49	222	10-Sep-79	SFWMD
OSF-15	629284	1372407	577	22-Mar-79	SFWMD
OSF-18	567992	1394109	219	28-Jul-93	SFWMD
OSF-66	594949	1342655	150	18-Feb-05	SFWMD
PB-1775	910616.289	730639.677	4200	18-Sep-01	SIR2006-5239
PB-747	936328.256	946544.161	4060	19-Jun-74	SFWMD
PELICAN GROVES-C (DID# 3)	410060.486	994105.025	672	12-Nov-03	SWFWMD
POF-0010	537912	1211707	94	12-Sep-79	SFWMD
POF-11	538001	1211201	110	12-Sep-79	SFWMD
POF-15	519642	1311033	101	13-Nov-90	SFWMD
POF-17	546494	1258841	130	22-May-79	SFWMD
POF-18	591918	1247330	370	6-Sep-79	SFWMD
ROMP 20 OCALA	175321.482	1042551.458	4961	20-Oct-93	SWFWMD
ROMP 22 AVON PARK	222123.22	1084941.05	2481	10-May-94	SWFWMD
ROMP 23-1 DEEP	273782.683	1085416.467	813	10-Jan-94	SWFWMD
ROMP TR 5-2 OCALA	202560.464	1028325.766	2304	15-Jan-04	SWFWMD
ROMP TR 7-2 DEEP FL	153305.044	1131327.612	1575	3-Feb-04	SWFWMD
ROMP TR 9-2 OCALA	205647.891	1249897.165	2228	29-Jan-04	SWFWMD

Table 3.1c: TDS data (MC1)

Station	X coordinate (ft FL State Plane 1983)	Y coordinate (ft FL State Plane 1983)	TDS (mg/l)	Date	Source
ROMP TR SA-3 UP FLORIDAN	165861.476	1099006.789	1907	30-Jan-04	SWFWMD
SANIBEL	292808.852	767978.51	32900	1-Oct-03	DEP
SARASOTA - CENTER RD	201199.204	1001330.007	18164	1-Oct-03	DEP
SCRWWTPIW1	418931.625	641111.679	26978	29-Apr-96	SFWMD
SLF-63	783767	1144482	2544	30-May-90	SFWMD
SLF-64	777699	1155672	2340	14-Apr-93	SFWMD
SLF-65	772451	1164644	2480	14-Apr-93	SFWMD
SO COLLIER CO WTP	432218.045	666047.877	9100	11-Oct-04	DEP
STL-229	813996.28	1111049.16	2224	23-May-90	WRI 03-4242
SUN-BTW	881184.653	648814.988	15520		SFWMD
SYKES CREEK	750956.259	1486766.743	16500	1-Oct-03	DEP
TCRK_GW1	725886.339	1056130.635	497	9-Feb-05	SFWMD
TREE O #3 (THREE L GROVES) DID #3	356379.683	1008670.663	654	9-Mar-04	SWFWMD
USGS 530374501	472776.56	1351746.18	92	13-May-96	FDOH
USSC_ASR	830689	890903.505	3700	11-Dec-92	SFWMD

Station	X coordinate (ft FL State Plane 1983)	Y coordinate (ft FL State Plane 1983)	TDS (mg/l)	Date	Source
271813082201301 ROMP 22 AVON PARK WELL	219697.00	1082391.00	2500	11-Aug-93	SFWMD
82410503 COCOA 5	625430.14	1483397.64	448	12-May-03	USGS
82510503 COCOA 7 NR BITHLO, FL	625701.14	1487336.07	731	13-May-03	USGS
82510504 COCOA 3 NR BITHLO, FL	625702.58	1489153.91	568	12-May-03	USGS
82610504 COCOA 9 NR BITHLO, FL	625707.54	1495415.36	766	12-May-03	USGS
82710501 COCOA 10 NR BITHLO, FL	625441.84	1498041.35	441	12-May-03	USGS
ACME IMPROVEMENT DISTRICT / DIW	909414.06	836783.47	5510	1-Oct-03	SFWMD
ATLANTIC UTILITIES OF SARASOTA INJECTION WELL	179085.70	1086384.66	36100	29-Nov-88	SFWMD
BF-2	925545.72	669572.28	5380	21-Oct-93	SFWMD
BF-4	925172.70	669560.61	4810		ECFAS Table 4-4
BICY-MZ3	554522.19	567147.92	27400	31-Jan-05	SFWMD
BITHLO 1 WELL AT BITHLO, FL	626548.02	1531792.13	355	13-May-03	USGS
BOYRO_EPXL	953221.77	786238.39	4900	5-Mar-07	SFWMD
BREX-1	617719.00	997587.00	1876	4-Jul-04	SFWMD
BROWARD CO. NORTH DIST.	932412.64	700321.94	6612	1-Oct-03	SFWMD
BROWARD CO. NORTH DIST.	932271.46	702401.46	9614	1-Oct-03	SFWMD
Burnt Store Utilities Dual Zone Injection Monitor Injection Well	318215.63	887838.61	34000		Facility
C-1111	416466.85	668152.97	34900		WRI 98-4253
C-1124	561565.94	693228.60	5170	10-Dec-82	WRI 98-4253
CCUD-IW1	885050.40	627681.26	5170		SFWMD
CCUEP-IW-2	318258.02	961258.21	10000	1-Jan-97	SFWMD
CH-314	341357.11	894536.12	34900	23-Jun-92	WRI 98-4253
City of FT. Lauderdale	941140.04	641402.61	9252	1-Oct-03	SFWMD
City of FT. Lauderdale	934417.44	636310.57	6145	1-Nov-03	SFWMD
COCOA 25 NR BITHLO,FL	605860.31	1472208.27	364		USGS
COCOA 40 NR BITHLO,FL	626045.65	1471177.30	636	13-May-03	USGS
COCOA A WELL NEAR BITHLO, FL	634712.70	1476321.99	802	12-May-03	USGS
COCOA DYAL	674185.15	1474654.65	1935	20-Jun-04	DEP
COCOA H NEAR BITHLO, FL	647580.26	1507220.16	469	13-May-03	USGS
CORAL SPRINGS IMP DIST / DIW	897697.47	695859.82	5776	1-Oct-03	SFWMD
DF-1	828433.00	575983.00	3400	16-Oct-93	SFWMD
ENCON	936488.57	942378.59	3292	1-Oct-03	SFWMD
FKAA - J. Robert Dean WTP - Deep Injection Well IW-1	818797.28	402379.89	20100		SFWMD
FORT MYERS BEACH WWTP DUAL ZONE MONITOR WELL	350747.43	785108.32	33800	1-Oct-03	SFWMD
Fort Myers RO WTP DZMW-1	385929.46	834794.66	29000	1-Sep-03	SFWMD
FPU_RO-IW1	866322.66	1130448.90	1700		SFWMD
FPU_RO-MW1	866257.66	1130468.89	1739.8		ECFAS Table 4-4
G-2617	714531.25	668029.48	2410	26-Jan-05	SFWMD
GL-331	628313.70	910475.21	9109	9-Nov-01	SIR2006-5239
HAL-DZMW1	933151.51	602290.81	5720	20-Sep-06	SFWMD
HB-TPW1	961554.37	755841.77	11900	1-Jul-01	SFWMD
HIF-0003	571433.00	1161030.00	257	12-Oct-78	SFWMD
HIF-0004	578785.00	1145667.00	715	7-Jan-81	SFWMD
HIF-0008	500239.00	1048955.00	343	12-May-81	SFWMD
HIF-0013	588742.00	1122020.00	430.9	23-Jan-89	SFWMD
HIF-0014	566109.00	1075009.00	180.1	23-Jan-89	SFWMD
HIF-42L	671099.00	1048400.00	4034	30-May-08	SFWMD
HILLS CO ASR DMW-1	197159.81	1341401.40	4224	25-Feb-04	SWFWMD
L2-TW	672740.65	826627.02	2160	8-Feb-94	SFWMD
LAB-MZ3	502273.56	879736.84	16800	3-Feb-05	SFWMD
LHA-DIW	443004.58	830652.43	19000	3-Feb-08	SFWMD
M-1353	900502.16	1041192.65	2148	10-Jul-00	WRI 03-4242
M-1356	895336.92	1059642.37	2610	30-Aug-01	WRI 03-4242
MANATEE INJECTION WELL	127992.68	1136454.08	8850	3-Oct-03	SWFWMD
MARGATE, CITY OF DIW	912732.05	694130.55	6331	1-Jan-88	SFWMD
MF-37L	784921.90	965985.04	3600	6-Jun-07	SFWMD
MF-40L	826580.03	1044391.08	2600	6-Jun-07	SFWMD
MIR_RO-MW1	880764.90	594372.97	6712.9		ECFAS Table 4-4
MIU-MZ2	418501.64	591506.13	36800	2-Feb-05	SFWMD
MO-130	884359.00	339296.00	34200		ECFAS Table 4-4
NFM-MZL	368708.03	871747.84	30400		SFWMD
NMC-MW	895887.98	1057447.65	2144		ECFAS Table 4-4
NRCS205-6	777179.00	1155399.00	2900	2-Dec-03	SFWMD
NWHWRAP-1D	111274.52	1381336.28	3185	16-Dec-03	SWFWMD
NWHWRAP-2D	178553.43	1339036.06	2126	27-Jan-04	SWFWMD
OKF-35	709756.00	1059798.00	4953	4-Sep-79	SFWMD
OKF-40	635056.00	1117729.00	485	5-Sep-79	SFWMD

Station	X coordinate (ft FL State Plane 1983)	Y coordinate (ft FL State Plane 1983)	TDS (mg/l)	Date	Source
OKF-73	719014.00	1084450.00	4889.1		SFWMD
OR0673	650699.05	1476013.36	1660	25-Jan-04	SJRWMD
OS0027	654176.63	1374923.61	999	9-May-04	SJRWMD
OSF-0001	505832.00	1451359.00	191	11-Sep-79	SFWMD
OSF-0030	645661.00	1336146.00	343	24-Jan-89	SFWMD
OSF-104M	613202.43	1208993.17	200	4-Jun-07	SFWMD
OSF-16	537241.00	1435294.00	127	13-Sep-79	SFWMD
OSF-2	467092.00	1442540.00	110	4-Dec-79	SFWMD
OSF-21	657674.00	1265758.65	436	11-Aug-93	SFWMD
OSF-22	605279.77	1437265.82	298		SFWMD
OSF-26	578575.00	1405498.00	369	19-Jun-78	SFWMD
OSF-27	583686.03	1459215.01	593	10-Aug-93	SFWMD
OSF-33	569400.00	1423393.00	253	13-Sep-79	SFWMD
OSF-38	563050.00	1423508.00	210	11-Dec-78	SFWMD
OSF-44	563391.20	1423388.08	186	28-Nov-79	SFWMD
PB-1186	757541.77	858553.16	3033	10-Feb-90	SFWMD
PB-1196	930965.75	942016.59	3890	17-Jul-01	WRI 03-4242
PB-1693	961753.39	866999.46	3650	14-Sep-96	SIR2006-5239
PB-1775	910616.29	730639.68	4600	6-Sep-01	SIR2006-5239
PBC3-MZU	936083.96	781079.00	4660		SFWMD
PBF-11	886678.71	735581.37	2830	3-Sep-03	SFWMD
PBF-15M	863897.13	874380.65	4100	7-Jun-07	SFWMD
PBF-6	949133.50	852463.54	3960	1-Jul-96	SFWMD
PEELED-MW1	918682.65	643742.17	6930	15-Jun-07	SFWMD
PELICAN GROVES-A (DID# 1)	409191.50	999169.55	540	12-Nov-03	SWFWMD
PELICAN GROVES-B (DID# 2)	410088.32	996782.95	507	12-Nov-03	SWFWMD
PINE-IW1	408463.41	767091.70	13200	18-Sep-04	SFWMD
PLT-ROI1	896118.72	652838.90	5490	1-Nov-90	SFWMD
POF-0002	444203.00	1425387.00	179	5-Sep-79	SFWMD
POF-19	519363.00	1282253.00	78	6-Sep-79	SFWMD
POF-21	585924.00	1261680.00	359	12-Aug-93	SFWMD
POF-7	482377.00	1321581.00	120.1	25-Jan-89	SFWMD
POF-9	542212.00	1206039.00	95	12-Sep-79	SFWMD
PORT ST. LUCIE - SOUTH PORT WWTP/DIW	883856.42	1060920.25	3200	1-Oct-03	SFWMD
PSL-EW2	828206.79	1061344.00	3050	2-Mar-06	SFWMD
PSLWPT-IW1	866386.80	1055240.95	4600	17-Jan-03	SFWMD
ROCKLEDGE	745964.86	1451849.85	2380		DEP
ROMP 12 DP UP FLORIDAN	414503.61	984829.32	1127	27-Jan-04	SWFWMD
ROMP 17 AP	338673.72	1033852.39	916	10-May-94	SWFWMD
ROMP 33 AVON PARK	248473.19	1137683.48	2098	19-May-94	SWFWMD
ROMP 39 AVON PARK	250817.97	1185236.56	405	23-May-94	SWFWMD
ROMP 48 AVON PARK	286605.65	1240216.12	252	18-Jan-94	SWFWMD
ROMP 49 AVON PARK	250491.08	1248584.05	277	13-Jan-94	SWFWMD
ROMP 62 - CAMPO	231391.64	1283456.77	368	23-Feb-04	SWFWMD
ROMP 67-1 AVON PARK	222763.64	1355541.94	577	10-Feb-04	SWFWMD
ROMP TR 7-4 AP	173085.59	1127547.76	1599	5-May-94	SWFWMD
ROMP TR 8-1 U AV PK	155334.48	1184331.80	3252	9-May-94	SWFWMD
ROMP TR 8-2 AVON PARK	165325.08	1181491.81	4926	12-Jan-04	SWFWMD
ROMP TR 9-3 AP	195912.45	1241198.42	8430	5-May-94	SWFWMD
ROMP TR AB-1	201614.25	1254692.82	7120	28-Mar-94	SWFWMD
ROMP20	177627.00	1040684.00	26790	2-Mar-92	SFWMD
ROMP43	465545.00	1181679.00	130	2-Jun-06	SWFWMD
SCC-MZL	418846.92	641207.28	31000		SFWMD
SFWMD Tri-Zone Monitor Well Immokalee Water & Sewer District WWTP	514985.20	756311.02	5050	2-Oct-03	Facility
SLF-54	763186.00	1059904.00	3562	21-Mar-84	SFWMD
SLF-74	821840.68	1092293.33	5200	23-Oct-03	SFWMD
STL-387	869858.22	1081717.11	2766	11-Jul-00	WRI 03-4242
STUART, CITY OF DIW	899651.00	1045042.00	2100	1-Oct-03	SFWMD
SUNRISE SAWGRASS (RO) CW-1	875680.63	664308.62	3518	1-Oct-03	SFWMD
SUNRISE SAWGRASS WWTP	874563.07	653556.60	5070	1-Oct-03	SFWMD
SUNRISE SAWGRASS WWTP	873510.52	653626.48	3720	21-Feb-85	SFWMD
SYKES CREEK	750956.26	1486766.74	16500		DEP
TCRK_GW2	725891.34	1056130.64	4260	11-Feb-05	SWFWMD
TFRO-4	898108.00	1003309.00	1310	8-May-03	SFWMD
TR3-3L	222842.35	944208.65	32900	12-Apr-00	SFWMD
US PHOSPHORIC	223672.99	1288319.27	3316	18-Feb-04	SWFWMD
USSC_ASR	830689.00	890903.51	4400	14-Dec-92	SFWMD

Table 3.1d: TDS data (APPZ)

Station	X coordinate (ft FL State Plane 1983)	Y coordinate (ft FL State Plane 1983)	TDS (mg/l)	Date	Source
Venice Gardens Deep Injection Well	205536.50	997903.43	32100	10-Jun-85	SFWMD
W-17001	541152.26	1023575.29	1073	11-Oct-96	SFWMD
W-17073	92615.00	1273195.00	20000	4-Jun-05	SFWMD
W-18116	368567.94	992516.04	3288	18-Dec-00	SFWMD
WASANMZ2	936510.96	576823.27	19900	27-Jan-05	SFWMD
WCRWSA RMP 13PZ	150836.03	1347605.13	1410	22-Jun-04	SWFWMD
ZEMEL ROAD LANDFILL MONITOR WELL NO. - DUAL ZONE	341615.60	894342.18	34362	1-Oct-03	Facility

Station	X coordinate (ft FL State Plane 1983)	Y coordinate (ft FL State Plane 1983)	TDS (mg/l)	Date	Source
3OAK-IW1	396728.86	777522.52	36300.0	7-Apr-05	SFWMD
82310501 COCOA 11 NR BITHLO, FL	625692.67	1476631.06	810.0	13-May-03	USGS
82510502USGS OBSER W. COCOA 1 NR BITHLO, FL.	625431.68	1485316.47	519.0	13-May-03	USGS
82510702 COCOA 7A NR BITHLO, FL	615879.77	1487244.12	930.0	12-May-03	USGS
82510801 COCOA 14 NR BITHLO, FL	611415.78	1487451.04	550.0	24-May-04	USGS
82510802 COCOA 15 NR BITHLO, FL	608558.57	1487353.48	785.0	12-May-03	USGS
82510902 COCOA 16 NR BITHLO, FL	606505.03	1487356.07	511.0	12-May-03	USGS
82610502 COCOA 2 NR BITHLO, FL	625704.50	1491577.69	775.0	12-May-03	USGS
AAD7578	473992.55	1349649.94	80.0	13-May-96	FDOH
BF-1	925617.30	669564.23	31900.0		ECFAS Table 4-4
BICY-MZ4	554522.19	567147.92	37700.0	1-Feb-05	SFWMD
BS_WRF_IW1	392920.25	742467.20	38000.0		SFWMD
Burnt Store Utilities Dual Zone Injection Monitor Injection Well	318215.63	887838.61	34000.0	1-Oct-03	Facility
C-1108	433465.79	695524.54	37300.0	20-Oct-92	WRI 98-4253
C-1111	416466.85	668152.97	34600.0		WRI 98-4253
CCUD-IW1	885050.40	627681.26	27500.0		SFWMD
CCUD-MW1	885121.07	627681.78	31400.0		SFWMD
CITY OF MIRAMAR WWTP	874249.45	603698.28	28000.0	1-Oct-03	SFWMD
CLEW_IW-1	674629.73	868695.76	9056.0		SFWMD
COCOA 18 NR BITHLO, FL	604455.01	1489984.54	613.0	12-May-03	USGS
COCOA 19 NR BITHLO	607672.59	1492808.11	621.0	12-May-03	USGS
COCOA 20 NR BITHLO, FL	604799.76	1480692.89	595.0	12-May-03	USGS
COCOA 21 NR BITHLO, FL	604797.34	1478875.06	698.0	13-May-03	USGS
COCOA 22 16IN WELL NR BITHLO, FL	606314.20	1477863.16	387.0	13-May-03	USGS
COCOA 23 NR BITHLO,FL	604614.02	1475340.62	567.0	13-May-03	USGS
COCOA 24 NR BITHLO,FL	604790.49	1473724.54	483.0	12-May-03	USGS
COCOA 25 NR BITHLO,FL	605860.31	1472208.27	364.0	13-May-03	USGS
COCOA C (ZONE 5) WELL NEAR BITHLO, FL	611416.02	1487653.02	725.0	14-May-03	USGS
CORAL SPRINGS IMP DIST / DIW	897444.59	695121.17	11724.0	1-Oct-03	SFWMD
DF-1	828433.47	575983.36	34200.0	12-Dec-96	SFWMD
FORT PIERCE UTILITY AUTHORITY	878265.37	1135536.73	25000.0	1-Oct-03	SFWMD
FPL-EW2	860450.42	856499.91	8060.0		SFWMD
FPU_RO-IW1	866322.66	1130448.90	18000.0		SFWMD
HE-1087/L2-TW	672685.20	826805.29	5550.0	1-Jan-94	WRI 98-4253
HE-1104	586281.62	773044.45	13200.0	4-Apr-83	WRI 98-4253
HOLLYWOOD WASTEWATER TRTMT. PLANT	940986.48	616553.09	34508.0	1-Oct-03	SFWMD
L-5803	368478.02	871718.97	35200.0	12-Dec-90	WRI 98-4253
MARGATE, CITY OF DIW	912732.05	694130.55	12700.0	1-Oct-03	SFWMD
Melbourne Lake Washington, BR-0910	742259.00	1387439.00	2300.0	16-Jul-98	WRI 02-4193
NCCWTMZ1	433829.99	695522.63	33000.0	18-Jun-96	SFWMD
NCWRF-IW1	398375.71	701831.93	35000.0		SFWMD
NFM-MZL	368708.03	871747.84	30400.0	27-Feb-96	SFWMD
NWHWRAP-4D	136367.21	1361554.24	904.0	26-Jan-04	SWFWMD
OR0675	650699.05	1476013.36	1254.0	25-Oct-03	SJRWMD
OS0028	654176.63	1374923.61	941.0	9-May-04	SJRWMD
OSF-22	605279.77	1437265.82	298.0	6-Dec-79	SFWMD
OSF-28	504800.82	1416015.61	173.0	23-Jun-72	SFWMD
OSF-34	541977.51	1404275.22	168.0	14-Sep-79	SFWMD
OSF-99	493982.24	1426090.34	951.0	9-Jun-08	SFWMD
PALM BEACH COUNTY SYSTEM 9 NORTH, DUAL ZONE MW-1	917035.99	749286.62	15000.0	1-Sep-03	Facility
PBCSWA RRF SITE #7	936624.00	886562.00	25000.0	1-Oct-03	SFWMD
PBP-MZL	875725.00	604016.00	26311.0	3-Aug-99	SFWMD
PEMBROKE PINES WWTP/DIW	875724.65	604016.27	30305.0	1-Oct-03	SFWMD
POMPANO BEACH RO	944610.28	695379.29	34681.0	1-Nov-03	SFWMD
PORT ST. LUCIE - NORTH PORT WWTP/DIW	866749.30	1092494.57	23000.0	1-Mar-04	SFWMD
PORT ST. LUCIE - SOUTH PORT WWTP/DIW	883760.93	1060835.06	23000.0	1-Oct-03	SFWMD
Port St. Lucie LTC WTP	850741.00	1104482.00	22000.0	7-Oct-03	SFWMD
PSLWPT-IW1	866386.80	1055240.95	26000.0	15-Jan-03	SFWMD
PUNTA GORDA WWTP DUAL-ZONE MONITOR (EW-1)	347720.61	944325.90	30200.0	1-Oct-03	Facility
ROCKLEDGE	745964.86	1451849.85	2380.0	1-Oct-03	DEP
ROMP 50 AVON PARK	217060.85	1230230.13	8060.0	4-Feb-04	SWFWMD
ROMP TR 8-1 L AV PK	155337.15	1184329.94	35360.0	28-Mar-94	SWFWMD
ROMP TR AB-3	213774.11	1249673.91	13380.0	14-Jan-04	SWFWMD
ROMP-25	329309.49	1103748.46	4646.0	12-Apr-00	SFWMD
SCC-MZL	418846.92	641207.28	31000.0	14-Apr-05	SFWMD
SCRWWTPIW1	418931.63	641111.68	33270.0	2-May-96	SFWMD
SOUTH BEACHES	802377.81	1347827.28	9780.0	1-Oct-03	DEP

Table 3.1e: TDS data (MC2)

Station	X coordinate (ft FL State Plane 1983)	Y coordinate (ft FL State Plane 1983)	TDS (mg/l)	Date	Source
STL-333	880745.64	1135400.00	25000.0	24-May-93	WRI 03-4242
SUN-MW	875680.63	664308.62	12393.9		ECFAS Table 4-4
SUN-MW2	874563.06	653556.59	23643.9		ECFAS Table 4-4
SUNRISE SAWGRASS WWTP	874563.07	653556.60	21970.0	1-Oct-03	SFWMD
TCRK_GW2	725886.34	1056130.64	4260.0	11-Feb-05	SFWMD
W-16226	750698.47	1487741.81	23630.0	6-Jun-05	SFWMD
W-16882	943433.87	798935.63	14000.0	7-Jun-91	SFWMD
W-17052	764969.48	896737.98	8485.0	13-Jun-89	SFWMD

Station	X coordinate (ft FL State Plane 1983)	Y coordinate (ft FL State Plane 1983)	TDS (mg/l)	Date	Source
3OAK-IW1	396728.86	777522.52	36700	4-Apr-05	SFWMD
ACME ID	906862.90	837170.98	30820	1-Oct-98	DEP
BF-1	925617.30	669564.23	31900	11-Sep-97	SFWMD
BOYNTON BEACH PTBLE.WATER TRMNT PLT	943503.87	798935.63	31270	1-Jan-99	SFWMD
BS_WRF_IW1	392920.25	742467.20	36100		SFWMD
Bull Creek OS-0025	653838.63	1374917.62	2040		WRI 02-4193
C-820	556755.64	699802.30	26000	8-Feb-77	WRI 98-4253
CCUD-IW1	885050.40	627681.26	32300		SFWMD
CLEW_IW-1	674629.73	868695.76	24236		SFWMD
COCOA 13R NR BITHLO, FL	613737.17	1487448.41	601	12-May-03	USGS
COCOA C (ZONE 3) WELL NEAR BITHLO, FL	611416.02	1487653.02	606	13-May-03	USGS
Conway #3	550702.00	1519786.00	184	28-Mar-00	WRI 02-4193
CORAL SPRINGS IMP DIST / DIW	897444.59	695121.17	29800	1-Oct-03	SFWMD
DF-1	828433.00	575983.00	34200	13-Oct-93	SFWMD
EAST CENTRAL REGIONAL WWTP / DIW	940009.00	875149.00	38000	1-Oct-03	SFWMD
FKAA - J. Robert Dean WTP - Deep Injection Well IW-1	818797.28	402379.90	30867	13-Oct-08	SFWMD
FORT PIERCE RO	866257.66	1130468.90	31000	3-Nov-03	SFWMD
FPL-EW2	860450.42	856499.91	37300		SFWMD
FTL-MZL2	941689.96	641434.04	31443	1-Oct-03	Facility
G-2296	713926.40	667921.72	37200	15-Jan-92	WRI 98-4253
GLF-6	628323.00	910488.00	24000		SFWMD
HE-1087	672685.20	826805.29	19100	1-Jan-94	WRI 98-4253
I75-MZ3	416556.67	668295.47	35700	13-Apr-95	SFWMD
Lake Louisa State Park L-0729	422238.40	1486918.46	210	15-Feb-00	WRI 02-4193
LHA-DIW	443004.58	830652.43	30700	5-Feb-08	SFWMD
Long Branch near Bithlo, OR-0618	619951.93	1523192.69	3280	14-Apr-99	WRI 02-4193
MARTIN COUNTY UTILITY NORTH/DIW	895887.98	1057447.65	35100	2-Oct-03	SFWMD
MF-37	784921.90	965985.04	25750		SFWMD
Navy #1	554765.00	1538248.00	160	28-Mar-00	WRI 02-4193
OK-100	698032.64	1025476.47	12800	17-Dec-01	SIR2006-5239
OKF-105	619115.79	1115332.23	2897		SFWMD
OKF-15	660476.00	1087834.00	1415.1	29-Jun-88	SFWMD
OLI-MW1-LMZ	756558.00	1091566.68	30300		SFWMD
OR0614	618639.70	1487388.78	1470	14-May-03	Facility
OSF-98	493982.24	1426090.34	740	9-Jun-08	SFWMD
PAHOKEE, CITY OF STP	764969.48	896737.98	21900	1-Oct-03	SFWMD
PBF-12	886678.71	735581.37	30300	3-Sep-03	SFWMD
PBF-15L	863897.13	874380.65	34416		SFWMD
PBF-5	949209.57	852482.26	32500	28-Jan-05	SFWMD
PSLLTC-IW1	850609.01	1104256.19	34200	22-Jun-02	SFWMD
PSLWPT-IW1	866386.80	1055240.95	31000	14-Jan-03	SFWMD
PSLWPT-MW1	866386.79	1055180.00	32017.9		ECFAS Table 4-4
PUNTA GORDA WWTP DUAL-ZONE MONITOR (EW-1)	347720.61	944325.90	31500	1-Oct-03	Facility
ROCKLEDGE	745915.71	1451847.72	31400	1-Oct-03	DEP
ROMP 28 UP EVAPORITE FLDN	514916.06	1103487.55	2292	17-Mar-04	SWFWMD
ROMP TR 8-1 L AV PK	155337.15	1184329.94	35360		SFWMD
SFWMD Tri-Zone Monitor Well Immokalee Water & Sewer District WWTP	514985.20	756311.02	36600	30-Jul-03	Facility
Sky Lake #2	532428.00	1496612.00	174	12-Apr-99	WRI 02-4193
Southeast #2	565397.00	1471676.00	360	27-Apr-99	WRI 02-4193
Southeast test well near Lake, Nona OR-0636	568198.61	1485909.54	290	29-Nov-95	WRI 02-4193
STL-332	880745.64	1135400.00	31500	29-Sep-92	WRI 03-4242
STUART, CITY OF DIW	899651.00	1045042.00	30000	1-Oct-03	SFWMD
STU-MZL	900443.37	1041253.19	30313.9	16-Dec-02	SFWMD
UNITED TECH PRATT & WHITNEY DIW	882487.53	934220.52	30780	1-Oct-03	SFWMD
USGS CORE HOLE 2 AT POLK CITY	388669.96	1400176.12	1340	4-Nov-80	WRI 02-4193
W-16616	928726.30	785408.44	36477	7-Jun-90	SFWMD

Table 3.1g: TDS data (LC)

Station	X coordinate (ft FL State Plane 1983)	Y coordinate (ft FL State Plane 1983)	TDS (mg/l)	Date	Source
CCUD-IW1	885050.40	627681.26	35600		SFWMD
CLEW_IW-1	674629.73	868695.76	35440		SFWMD
CLEWDZMW-1	674637.98	868696.07	32000		SFWMD
COCOA Average of C and S	611416.02	1487653.02	11070		USGS
FPL-EW2	860450.42	856499.91	37300		SFWMD
FPU_RO-IW1	866322.66	1130448.90	33000		SFWMD
HH-LFADEW	442149.85	1447196.59	428	13-Jul-07	SFWMD
OK-100	698032.64	1025476.47	14300	6-Dec-01	SIR2006-5239
OSF-104	613202.43	1208993.17	23604	16-Jun-06	SFWMD
PSLLTC-IW1	850609.01	1104256.19	34000	20-Jun-02	SFWMD
PSLWPT-IW1	866386.80	1055240.95	34000	13-Jan-03	SFWMD
ROMP 28 EVAPORITE	514916.06	1103487.55	4358	17-Mar-04	SWFWMD
USGS CORE HOLE 2 AT POLK CITY	388613.13	1400081.27	1340	2-Nov-82	WRI 02-4193
W-16226	750698.47	1487741.81	34300	6-Jun-05	SFWMD

Table 3.1h: TDS data (BZ)

Station	X coordinate (ft FL State Plane 1983)	Y coordinate (ft FL State Plane 1983)	TDS (mg/l)	Date	Source
CCUD-IW1	885050.40	627681.26	37200	23-Jun-05	SFWMD
CLEW_IW-1	674629.73	868695.76	36000	29-Jun-05	SFWMD
FKAA - J. Robert Dean WTP - Deep Injection Well IW-1	818797.28	402379.90	39133	12-Oct-08	SFWMD
FPU_RO-IW1	866322.66	1130448.90	36000	13-Apr-02	SFWMD
M-1324	895891.55	1057423.94	34260	30-Jul-87	WRI 03-4242
MO-189	625069.70	137339.45	37200	4-May-90	WRI 02-4036
NLCWTP-IW1	397888.01	872374.10	36900	25-Jun-05	SFWMD
OLI-IW1	756443.00	1091566.70	39000		SFWMD
OR-0465 Lake Ivanhoe	536035.57	1536998.20	180		SFWMD
OSF-104	613202.43	1208993.20	36350		SFWMD
OSF-106	562378.69	1367126.00	32700		SFWMD
OSF-97	493982.24	1426090.34	26447.7	26-Feb-02	SFWMD
PB-1186	757541.77	858553.16	39927	13-Jun-05	SFWMD
PSLLTC-IW1	850609.01	1104256.19	35800	4-Oct-02	SFWMD
PSLWPT-IW1	866386.80	1055240.95	34000	26-Apr-03	SFWMD
ROMP TR 8-1 L AV PK	155337.15	1184329.94	35360		SWFWMD
SCRWTP-IW1	432103.00	666004.00	36100	24-Jun-05	SFWMD
SEPOLK-DEW	517726.16	1248260.30	25000		SFWMD
STL-254	883868.24	1060687.36	35300	2-Nov-82	WRI 03-4242
STL-332	880745.64	1135400.00	36700	1-Feb-93	WRI 03-4242
USGS CORE HOLE 2 AT POLK CITY	388603.13	1400071.27	1340	4-Nov-80	WRI 02-4193
W-16226	750698.47	1487741.81	35300	6-Jun-05	SFWMD
W-16234	939265.37	917555.90	38200	11-Jun-05	SFWMD
W-17052	764969.48	896737.98	40863	13-Jun-05	SFWMD
W-17480 Orlando Utilities Commission Southeast test well	568198.61	1485909.50	6090	19-Aug-96	SFWMD
West Melborne-IW1 (W-15961)	770271.14	1358628.00	36200		SFWMD

Table 3.2a: Temperature data (IAS)

Station	X coordinate (ft FL State Plane 1983)	Y coordinate (ft FL State Plane 1983)	Temperature (°C)	Date	Source
WEL1840001186800	93341.00	1277116.00	25.0	02-Sep-02	SFWMD
WEL0062001076800	103667.00	1413270.00	25.0	18-May-90	SWFWMD
WEL0057001076300	105846.00	1425669.00	26.0	19-Dec-03	SWFWMD
WEL1569000110800	117158.00	1160035.00	26.0	30-Sep-03	SWFWMD
WEL2984000242100	124060.00	1113638.00	26.0	16-Jun-05	SWFWMD
WEL2983000242000	128882.00	1107180.00	25.0	16-Jun-05	SWFWMD
WEL2409000170600	129105.00	1109772.00	27.0	24-Oct-00	SWFWMD
ROY CLAYTON-HRS	134255.00	1485884.00	22.0	28-Feb-06	SWFWMD
WEL0210001092400	136666.00	1129955.00	27.0	17-Feb-98	SWFWMD
WEL1565000110400	139617.00	1177290.00	24.0	17-Feb-04	SWFWMD
WEL0066001077200	140093.00	1406406.00	24.0	16-Sep-99	SWFWMD
WEL0070001077600	141771.50	1394764.00	23.0	16-Sep-99	SWFWMD
WEL0738000047200	144293.00	1163822.00	25.0	26-Dec-03	SWFWMD
WEL0068001077400	144415.00	1404089.00	24.0	10-Sep-97	SWFWMD
WEL0403000013700	147507.00	1405197.00	24.0	16-Sep-99	SWFWMD
WEL0128001083400	150249.00	1349444.00	24.0	16-Sep-99	SWFWMD
WEL2698003490500	150311.00	1166307.00	24.0	13-Mar-01	SWFWMD
WEL0152001086100	152109.00	1336031.00	25.0		SFWMD
ROMP TR 6-1 HAWTHORN	152419.00	1069368.00	27.0	03-Oct-03	SWFWMD
ROMP TR 7-2 UP HAWTHORN	153306.00	1131248.00	25.0	29-Jan-04	SWFWMD
ROMP TR 7-2 LOWER INT	153307.00	1131248.00	25.0	29-Jan-04	SWFWMD
WEL0997000073100	153902.00	1101388.00	25.0	29-Dec-03	SWFWMD
WEL0539000027300	154246.00	1102964.00	27.0	18-Nov-02	SWFWMD
ROMP TR SA-1 INTERMEDIATE	154325.00	1098432.00	26.0	29-Sep-03	SWFWMD
ROMP TR 8-1 INT	155313.00	1184321.00	26.0	17-Sep-03	SWFWMD
ROMP TR 8-1 SURF	155321.00	1184303.00	25.0	19-Mar-03	SWFWMD
WEL0463000019700	155641.00	1101904.50	28.0	29-Dec-03	SWFWMD
WEL2411000170900	156247.00	1072916.00	26.0	23-Oct-00	SWFWMD
WEL0597000033100	156681.00	1371422.00	24.0	12-Jun-01	SWFWMD
WEL0803000053700	157465.00	1456058.00	25.0	08-Sep-97	SWFWMD
WEL0496000023000	162222.00	1362978.00	25.5		SFWMD
WEL0447000018100	162714.00	1352263.00	24.6		SFWMD
WEL1876000132800	162820.50	1373660.50	25.0	29-Jun-99	SWFWMD
WEL0739000047300	165121.00	1370941.50	25.0	28-Mar-02	SWFWMD
WEL0139001084700	165760.50	1342580.00	25.0	09-May-90	SWFWMD
WEL2397000169300	166929.00	1199567.00	25.0	14-Feb-01	SWFWMD
WEL0154001086300	167277.50	1334782.50	25.0	09-May-90	SWFWMD
WEL0061001076700	167399.00	1414035.00	25.0	14-May-90	SWFWMD
WEL0767000050100	167584.00	1221987.00	27.0	16-Sep-03	SWFWMD
WEL2696003490300	169304.00	1141707.00	24.0	12-Mar-01	SWFWMD
WEL1702000124100	169382.00	1047124.00	25.0	27-Apr-04	SWFWMD
WEL0417000015100	172849.50	1354463.50	24.0	13-Sep-99	SWFWMD
ROMP TR 7-4 SURF	173110.00	1127584.00	28.0	15-Jun-98	SWFWMD
ROMP TR 7-4 HAWTH	173111.00	1127581.00	25.0	18-Sep-03	SWFWMD
WEL1704000124300	174077.00	1036377.00	26.0	19-Dec-01	SWFWMD
WEL2407000170400	174171.00	1036005.00	26.0	23-Oct-00	SWFWMD
WEL0281000001500	174616.00	1040796.00	28.0	17-Aug-98	SWFWMD
ROMP 20 LOWER INT	175288.00	1042538.00	26.0	22-Sep-03	SWFWMD
ROMP 20 UPPER INT	175302.00	1042549.00	24.0	22-Sep-03	SWFWMD
ROMP 20 SURFICIAL	175323.00	1042564.00	25.0	22-May-01	SWFWMD
WEL0135001084100	176026.50	1346292.00	25.0	09-May-90	SWFWMD
WEL1556000109500	177167.50	1295009.00	24.0	22-Nov-04	SWFWMD
WEL1578000111700	177265.00	1135758.50	26.0	10-Mar-86	SWFWMD
WEL0149001085700	177497.00	1337028.00	25.0		SFWMD
WEL0147001085600	178617.50	1339033.50	24.0	05-Sep-03	SWFWMD
WEL0346000008000	179883.00	1348919.00	26.5		SFWMD
WEL0577000031100	180088.50	1358207.00	24.0	28-Mar-00	SWFWMD
WEL0075001078100	180487.05	1391341.83	25.0		SFWMD
WEL1445000098400	180607.00	1234068.00	24.0	17-Sep-03	SWFWMD

Table 3.2a: Temperature data (IAS)

Station	X coordinate (ft FL State Plane 1983)	Y coordinate (ft FL State Plane 1983)	Temperature (°C)	Date	Source
WEL2464000176500	180805.51	1102223.45	26.6		SFWMD
ROMP TR 5-1 INTERMED	184119.00	1021401.00	25.0	30-Sep-03	SWFWMD
WEL0224001142500	184124.00	1021397.00	25.0	09-Jul-98	SWFWMD
WEL0892000062700	185070.00	1491201.00	27.0	19-Aug-85	SWFWMD
WEL0892000062600	185136.00	1491145.00	25.0	14-Nov-94	SWFWMD
WEL2559000183700	186225.00	1071756.00	24.0	09-Feb-01	SWFWMD
WEL2527001269000	186355.50	1029035.00	26.0	23-Oct-00	SWFWMD
ROMP TR 4-1 UP INT	187067.00	992965.00	26.0	19-Sep-03	SWFWMD
ROMP TR 4-1 MID INT	187088.00	992936.00	26.0	19-Sep-03	SWFWMD
ROMP TR 4-1 LOW INT	187097.00	992924.00	27.0	19-Sep-03	SWFWMD
WEL1444000098300	188013.00	1227710.00	26.0	16-Jan-98	SWFWMD
WEL0676000041000	188539.00	1006264.00	25.0	31-Dec-03	SWFWMD
WEL1579000111800	188626.00	1117780.00	24.0	14-May-01	SWFWMD
WEL2406000170300	188721.00	1006071.00	25.0	02-Feb-01	SWFWMD
WEL1754000129300	189086.00	1009017.00	24.0	19-Oct-00	SWFWMD
WEL3030002390100	189134.00	1057884.00	27.0	24-Jan-06	SFWMD
WEL1577000111600	189918.00	1128497.00	25.0	25-Aug-99	SWFWMD
WEL0097000060300	189951.50	1394109.00	25.0	22-Sep-99	SWFWMD
WEL1005000073900	190691.00	1432409.00	25.0	09-Sep-97	SWFWMD
WEL0644000037800	190899.00	1452514.00	25.0	15-Feb-06	SWFWMD
WEL1697000123600	192238.00	1007971.00	25.0	28-Dec-94	SWFWMD
WEL1427000096600	192640.00	1244212.00	25.5		SFWMD
WEL1733000127200	192745.00	1099980.00	25.0	24-Aug-99	SWFWMD
WEL0827000056100	194558.50	1090852.00	26.0	10-Nov-03	SWFWMD
WEL1731000127000	195424.00	1086106.00	24.0	13-Oct-03	SWFWMD
WEL1711000125000	195873.00	1100265.00	25.0	14-May-01	SWFWMD
WEL2405000170200	195935.00	1012454.00	27.0	02-Feb-01	SWFWMD
WEL1719000125800	196210.00	1007948.00	26.0	02-Apr-04	SWFWMD
WEL1732000127100	199049.00	1099100.00	25.0	24-Aug-99	SWFWMD
WEL1766000130500	199777.00	1029696.00	26.0	31-Mar-04	SWFWMD
WEL1855001174500	199799.00	1021218.00	25.0	19-Oct-00	SWFWMD
WEL1715000125400	199809.00	1007893.00	25.0	31-Dec-03	SWFWMD
WEL1722000126100	200271.00	1087471.00	25.0	25-Aug-99	SWFWMD
WEL2538001689900	200379.00	1016445.00	26.0	02-Feb-01	SWFWMD
ROMP TR 4-2 SUWANNEE	200635.00	987956.00	27.0	25-Sep-03	SWFWMD
WEL0670000040400	201050.00	981682.00	27.0	25-Sep-03	SWFWMD
WEL0889000062300	201081.00	1070262.50	28.0	30-Dec-03	SWFWMD
WEL1744000128300	201368.00	1011809.00	25.0	13-Feb-01	SWFWMD
WEL2691000189100	201417.00	1080523.00	24.0	22-May-01	SWFWMD
ROMP TR 5-2 U HAW	202555.00	1028322.00	24.0	02-Jun-99	SWFWMD
ROMP TR 5-2 L HAW	202559.00	1028318.00	25.0	12-Sep-03	SWFWMD
WEL2460000176100	204247.00	998016.00	25.0	07-Dec-00	SWFWMD
WEL2403000170000	205337.00	998936.00	27.0	07-Dec-00	SWFWMD
ROMP TR 9-2 TAMPA	205569.00	1249935.00	25.0	15-Sep-03	SWFWMD
WEL0695000042900	206444.00	1266478.00	24.0	23-Dec-02	SWFWMD
WEL1864001173800	207799.00	1099204.00	26.0	18-Jul-01	SWFWMD
WEL1741001159300	208208.00	1095362.00	26.0	13-Jul-01	SWFWMD
WEL0989000072300	208311.00	979163.00	24.0	26-Nov-03	SWFWMD
WEL0989000136000	208317.00	979165.00	25.0	26-Nov-03	SWFWMD
WEL1446000098500	209651.50	1271288.50	24.0	12-Feb-04	SWFWMD
WEL2695003490200	211155.00	1158915.00	25.0	12-Mar-01	SWFWMD
WEL1422000096100	211209.50	1303277.00	24.0	19-Dec-02	SWFWMD
WEL1729000126800	211854.00	996409.00	25.0	30-Dec-02	SWFWMD
WEL1648000118700	212492.00	1408552.00	25.0	12-May-03	SWFWMD
WEL2408000170500	212686.00	977870.00	23.0	19-Oct-00	SWFWMD
WEL2466000176700	213054.00	1276025.00	26.0	16-Feb-01	SWFWMD
WEL1751000129000	213975.00	1011770.00	27.0	13-Oct-00	SWFWMD
WEL1547000108600	215178.00	1396462.00	26.0	18-Nov-03	SWFWMD
WEL1900000136200	217502.00	1095664.00	25.0	18-Aug-99	SWFWMD

Table 3.2a: Temperature data (IAS)

Station	X coordinate (ft FL State Plane 1983)	Y coordinate (ft FL State Plane 1983)	Temperature (°C)	Date	Source
WEL2408002544100	218098.00	954841.00	27.0	15-Oct-01	SWFWMD
SAWYER CB 4E FLDN REPL	218186.00	1473149.00	23.0	15-Feb-06	SWFWMD
WEL0729000046300	219737.00	962919.00	25.0	25-Sep-03	SWFWMD
ROMP 19 WS	219966.00	1032243.00	25.0	24-May-01	SWFWMD
ROMP 19 WLAM	219995.00	1032214.00	26.0	25-Nov-02	SWFWMD
ROMP 19 WUAM	220071.00	1032244.00	25.0	28-Apr-04	SWFWMD
WEL0391000012500	221350.50	1336407.00	24.0	26-Jan-99	SWFWMD
ROMP 22 UPPER INT	222127.00	1084974.00	24.0	29-Sep-03	SWFWMD
ROMP 22 L INTERMEDIATE	222161.00	1084966.00	24.0	29-Sep-03	SWFWMD
WEL1217001171100	222707.00	1259641.00	24.0	16-Feb-01	SWFWMD
ROMP TR 3-3 L INT	222972.00	944407.00	26.0	11-Sep-03	SWFWMD
ROMP TR 3-3 U HAWTH	222975.00	944399.00	24.0	23-Feb-04	SWFWMD
WEL0944000068200	223979.00	1340867.00	23.0	26-Jan-99	SWFWMD
WEL0944000067800	223982.00	1340852.00	24.0	26-Jan-99	SWFWMD
WEL0372000010600	224126.50	1110685.00	25.0	19-May-99	SWFWMD
WEL0722000045600	224337.00	1094695.00	25.0	10-Oct-03	SWFWMD
WEL1437000097600	226349.00	1288995.00	23.0	30-Dec-97	SWFWMD
WEL0909000064300	226752.50	1283530.00	25.0	04-Dec-03	SWFWMD
WEL1718000125700	227094.00	1064453.00	25.0	25-Aug-99	SWFWMD
WEL1708000124700	227581.00	1093435.00	27.0	18-Aug-99	SWFWMD
WEL1469000100800	229901.50	1296680.00	24.0	25-Jun-92	SWFWMD
WEL1450000098900	230553.50	1298895.50	24.0	30-Apr-92	SWFWMD
WEL0633000036700	233460.50	1116203.50	26.0	10-Dec-98	SFWMD
WEL0879000061500	233546.50	1371960.00	22.0	07-Jan-99	SWFWMD
WEL1231001184700	233757.50	1304821.00	25.0	23-Jun-92	SWFWMD
WEL1447000098600	234459.50	1311682.00	28.0	24-Sep-91	SWFWMD
WEL1720000125900	235023.00	1089115.00	24.0	17-Aug-98	SWFWMD
WEL0309000004300	235094.00	1109673.00	25.0	25-Aug-99	SWFWMD
WEL1880000133200	235661.50	1315103.50	25.0	24-Jun-92	SWFWMD
WEL1235000077400	235682.00	923361.00	25.0	19-Nov-02	SWFWMD
WEL1516000105500	236461.00	1277574.00	24.0	20-Sep-91	SWFWMD
WEL1581000112000	236655.00	1185050.00	24.0	29-Oct-96	SWFWMD
WEL1730000126900	237438.00	1048349.50	25.0	30-Mar-04	SWFWMD
WEL1714000125300	237483.00	1048408.00	23.0	09-May-01	SWFWMD
WEL1727000126600	237535.00	1048347.00	25.0	28-Jul-98	SWFWMD
WEL1505000104400	237688.50	1294677.50	25.0	24-Sep-91	SWFWMD
WEL1212001184500	237858.50	1302252.00	26.0	22-Jun-92	SWFWMD
WEL1517000105600	238492.50	1319821.00	24.0	03-Apr-00	SWFWMD
WEL1901000136300	238790.00	1078168.00	24.0	24-Feb-97	SWFWMD
WEL1497000103600	239073.50	1281329.50	24.0	22-Jun-92	SWFWMD
WEL1783001184600	239278.00	1275166.00	26.0	22-Jun-92	SWFWMD
WEL1724000126300	239536.00	1064477.00	24.0	10-Oct-03	SWFWMD
WEL1222001184100	240272.50	1284347.50	23.0	20-Sep-91	SWFWMD
WEL1803001184800	240784.50	1281816.50	24.0	23-Jun-92	SWFWMD
WEL1698000123700	241270.00	1082486.00	24.0	24-Feb-97	SWFWMD
WEL1991001314700	241360.00	1460251.00	24.0	11-May-99	SWFWMD
WEL2033001320700	241561.00	1411864.00	24.0	14-Sep-98	SWFWMD
WEL1574000111300	241727.00	1082986.00	24.0	25-Aug-99	SWFWMD
WEL1750000128900	241741.00	1082237.00	22.0	21-Feb-01	SWFWMD
WEL1710000124900	241868.00	1084250.00	24.0	14-May-01	SWFWMD
WEL1488000102700	242157.50	1275741.50	25.0	23-Jun-92	SWFWMD
WEL1769000130800	243157.00	1090546.00	24.0	18-Aug-99	SWFWMD
WEL1480000101900	243218.00	1274114.50	24.0	23-Jun-92	SWFWMD
WEL1771000131000	243520.50	1111492.00	27.0	24-Aug-99	SWFWMD
WEL1717000125600	243562.00	1085997.00	24.0	10-Oct-96	SWFWMD
WEL0375000010900	243711.00	1117201.00	26.0	23-Sep-03	SWFWMD
WEL1510000104900	243960.50	1328046.50	26.0	12-Sep-91	SWFWMD
WEL1085001294900	244042.00	1091241.00	26.0	10-Oct-03	SWFWMD
WEL1533000107200	244080.00	1296530.00	25.0	19-Sep-91	SWFWMD

Table 3.2a: Temperature data (IAS)

Station	X coordinate (ft FL State Plane 1983)	Y coordinate (ft FL State Plane 1983)	Temperature (°C)	Date	Source
WEL1707000124600	244345.00	1092049.00	25.0	14-May-01	SWFWMD
WEL2697003490400	244526.00	1116880.00	26.0	15-Feb-01	SWFWMD
WEL0361000009800	244608.00	1439450.00	25.0	13-Mar-03	SWFWMD
WEL0361000009500	244610.00	1439462.00	25.0	13-May-99	SWFWMD
WEL1758000129700	244785.00	1109109.00	25.0	14-May-01	SWFWMD
WEL1483000102200	244866.00	1285814.50	24.0	22-Jun-92	SWFWMD
WEL1768000130700	244915.00	1085983.00	23.0	24-Oct-00	SWFWMD
WEL1712000125100	245020.00	1015639.00	25.0	27-Apr-04	SWFWMD
WEL1772000131100	245762.00	1086746.00	25.0	14-May-01	SWFWMD
WEL1700000123900	245909.00	1095063.00	24.0	11-Jun-97	SWFWMD
WEL1703000124200	247243.00	1020537.00	25.0	21-Jul-98	SWFWMD
WEL1716000125500	247276.00	1020504.00	24.0	21-Jul-98	SWFWMD
WEL1723000126200	247281.00	1020474.00	26.0	10-Nov-03	SWFWMD
WEL1761000130000	247621.00	1085956.00	23.0	21-Oct-96	SWFWMD
WEL1767000136400	248036.65	1082417.00	25.0	04-Nov-96	SWFWMD
WEL1767000130600	248037.65	1082417.00	27.0	04-Nov-96	SWFWMD
WEL1899000135900	248077.00	1086456.00	24.0	27-May-99	SWFWMD
ROMP 19 ES	248297.00	1034020.00	24.0	24-May-01	SWFWMD
ROMP 19 EUAM	248303.00	1034018.00	24.0	13-Oct-03	SWFWMD
ROMP 19 ELAM	248305.50	1034020.00	26.0	13-Oct-03	SWFWMD
ROMP 33 SURF	248461.00	1137663.00	26.0	03-May-01	SWFWMD
WEL1981001315700	248463.00	1124630.00	25.0	23-Aug-99	SWFWMD
ROMP 33 INT	248483.00	1137667.00	25.0	03-Oct-03	SWFWMD
WEL1524000106300	248835.50	1313854.00	24.0	17-Sep-91	SWFWMD
WEL2543001797500	248904.00	1104417.50	28.0	24-Oct-00	SWFWMD
WEL1494000103300	249145.00	1274154.50	24.0	22-Jun-92	SWFWMD
WEL2700003490700	249207.00	1120949.00	25.0	21-Feb-01	SWFWMD
WEL0840000057400	249241.50	1106586.00	27.2	25-Aug-99	SFWMD
WEL1575000111400	250013.00	1099567.00	24.0	31-Aug-99	SWFWMD
WEL1495000103400	250335.50	1311415.00	24.0	25-Sep-91	SWFWMD
ROMP 49 INT	250508.00	1248601.00	26.0	16-Sep-03	SWFWMD
ROMP 39 INTERMEDIATE	250784.00	1185230.00	24.0	21-Sep-04	SWFWMD
ROMP 123 DEEP	251149.50	1216792.50	24.0	24-Oct-03	SWFWMD
WEL0489000022300	252446.00	1098475.00	27.0	15-May-01	SWFWMD
WEL1528000106700	252626.50	1298563.00	25.0	17-Sep-91	SWFWMD
WEL1531000107000	253340.00	1315727.00	24.0	18-Sep-91	SWFWMD
WEL1448000098700	253356.00	1307597.00	25.0	29-Apr-92	SWFWMD
WEL2008001317400	254103.00	1447895.00	27.0	15-Sep-98	SWFWMD
WEL1228001170900	255421.00	1270105.00	25.0	16-Mar-00	SWFWMD
WEL2291001767800	255823.00	1424821.00	21.0	21-Dec-99	SWFWMD
WEL2291001760300	255831.00	1424819.00	23.0	17-Jan-00	SWFWMD
WEL1508000104700	256358.50	1294888.50	23.0	20-Sep-91	SWFWMD
WEL1213001183700	256830.00	1296811.50	26.0	17-Sep-91	SWFWMD
WEL1440000097900	257053.50	1306847.50	24.0	24-Sep-91	SWFWMD
WEL1219001183800	257651.00	1132169.00	25.0	17-Sep-91	SWFWMD
WEL2000001313700	258906.00	1462997.00	24.0	17-Sep-98	SWFWMD
WEL1498000103700	259050.50	1285871.50	26.0	13-Nov-91	SWFWMD
ROMP TR 3-1 L HAWTHO	259335.00	950818.00	27.0	22-Sep-03	SWFWMD
ROMP TR 3-1 U HAWTHO	259340.00	950829.00	26.0	20-Nov-02	SWFWMD
WEL1482000102100	259351.00	1388629.00	23.0	03-May-00	SWFWMD
WEL1455000099400	259470.50	1300918.00	24.0	26-Sep-91	SWFWMD
WEL1641000118000	259724.00	1481878.00	22.0	01-Dec-94	SWFWMD
WEL1580000111900	260893.00	1096227.00	25.0	25-Aug-99	SWFWMD
WEL1221001183900	261030.00	1295346.50	25.0	17-Sep-91	SWFWMD
WEL1227001183600	262544.00	1312605.50	23.0	17-Sep-91	SWFWMD
WEL1502000104100	263418.00	1300834.00	24.0	01-Oct-91	SWFWMD
WEL1499000103800	263472.50	1288251.50	23.0	30-Sep-91	SWFWMD
WEL2319001767600	263945.00	1428895.00	23.0	20-Dec-99	SWFWMD
WEL2681000188100	264564.00	948278.00	24.0	08-May-01	SWFWMD

Table 3.2a: Temperature data (IAS)

Station	X coordinate (ft FL State Plane 1983)	Y coordinate (ft FL State Plane 1983)	Temperature (°C)	Date	Source
WEL1464000100300	265546.50	1343584.50	24.0	04-Sep-91	SWFWMD
WEL1790001170200	265661.00	1333940.00	26.0	11-Sep-91	SWFWMD
ROMP DV-1	265872.50	1331257.50	24.0	10-Sep-91	SWFWMD
WEL2028001320200	265880.00	1454441.00	24.0	14-Sep-98	SWFWMD
WEL1478000101700	267214.50	1285386.50	23.0	01-Oct-91	SWFWMD
WEL1234001182800	267781.50	1342955.50	23.0	04-Sep-91	SWFWMD
WEL1784001182700	267864.00	1351339.00	23.0	04-Sep-91	SWFWMD
WEL1988001315000	267984.00	1450279.00	24.0	13-May-99	SWFWMD
WEL1810001184300	268611.00	1272141.00	24.0	01-Oct-91	SWFWMD
WEL2699003490600	270705.00	981231.00	24.0	21-Feb-01	SWFWMD
WEL1576000111500	272131.00	1101876.00	24.0	23-Aug-99	SWFWMD
WEL0574000030800	272973.00	1466694.00	24.0	08-Oct-85	SWFWMD
WEL1477000101600	273395.00	1330275.00	24.0	09-Sep-91	SWFWMD
WEL1795001183000	273640.00	1337040.00	25.0	05-Sep-91	SWFWMD
ROMP 23 PZ2	273788.00	1085421.00	26.0	01-Sep-03	SWFWMD
ROMP 23 HAW-TAMPA	273797.00	1085429.00	27.0	02-Jul-01	SWFWMD
WEL0684000041800	274159.00	1496380.00	23.0	08-Oct-85	SWFWMD
WEL0991000072500	274775.00	1418708.00	26.0	11-Apr-00	SWFWMD
WEL1996001314000	275011.00	1410109.00	24.0	14-Sep-98	SWFWMD
WEL1507000104600	276560.00	1277013.50	23.0	02-Oct-01	SWFWMD
WEL1491000103000	276834.00	1314888.50	25.0	11-Sep-91	SWFWMD
WEL2041001321900	277339.00	1401096.00	24.0	26-May-98	SWFWMD
WEL1553000109200	278090.00	1296190.50	24.0	01-Oct-91	SWFWMD
WEL1537000107600	278576.00	1318912.00	24.0	18-Sep-91	SWFWMD
WEL1459000099800	278700.00	1331840.00	25.0	09-Sep-91	SWFWMD
WEL1518000105700	278904.00	1312398.00	24.0	18-Sep-91	SWFWMD
WEL1476000101500	280259.00	1335461.50	25.0	05-Sep-91	SWFWMD
WEL0614000034800	280508.00	1041161.00	26.0	31-Oct-03	SWFWMD
WEL1538000107700	280650.00	1291721.50	25.0	19-Sep-91	SWFWMD
WEL1706000124500	282154.00	1024824.00	25.0	28-Oct-04	SWFWMD
ROMP 9 LOWER INT	282284.00	998629.00	25.0	19-Sep-03	SWFWMD
ROMP 9 INTERMEDIATE	282299.00	998636.00	25.0	19-Sep-03	SWFWMD
ROMP 9 OW13	282309.00	998646.00	27.0	27-Aug-96	USGS (Torres et al, WRI01-4015)
ROMP 9 OW14	282314.00	998646.00	25.0	27-Aug-96	USGS (Torres et al, WRI01-4015)
L-2549	283281.00	849295.00	25.0	22-Aug-90	DBHYDRO
L-2820	283282.00	849295.00	26.0	25-Oct-88	DBHYDRO
L-2527	283283.00	849295.00	28.0	22-Aug-90	DBHYDRO
WEL0390000012400	283425.00	1046432.00	26.0	31-Oct-03	SWFWMD
WEL1211001182600	283461.00	1351693.00	23.0	03-Sep-91	SWFWMD
ROMP DV-2 FL	285564.50	1322327.50	25.0	21-Mar-00	SWFWMD
WEL1809001184400	286015.00	1270359.00	24.0	01-Oct-91	SWFWMD
ROMP 48 HAWTHORN	286578.00	1240208.00	25.0	19-Nov-03	SWFWMD
ROMP 48 FLORIDAN	286590.50	1240204.50	25.0	15-Jun-04	SWFWMD
WEL1230001183100	286734.00	1328026.50	23.0	06-Sep-91	SWFWMD
WEL1539000107800	287322.00	1314183.00	24.0	19-Sep-91	SWFWMD
WEL1490000102900	288142.50	1353972.00	23.0	16-Mar-00	SWFWMD
WEL1801001182900	289013.50	1332045.50	25.0	05-Sep-91	SWFWMD
WEL1210001184000	289193.50	1293560.50	24.0	19-Sep-91	SWFWMD
WEL1563000110200	291655.00	1116844.00	25.0	26-Sep-03	SWFWMD
WEL1568000110700	291801.00	1169960.00	25.0	06-Oct-03	SWFWMD
WEL1582000112100	292448.00	1134814.00	26.0	12-Mar-01	SWFWMD
WEL1536000107500	292852.50	1310798.50	24.0	19-Sep-91	SWFWMD
WEL1879000133100	292907.00	1326454.00	24.0	06-Sep-91	SWFWMD
WEL1462000100100	294281.50	1349167.50	22.0	04-Sep-91	SWFWMD
WEL0347000008100	294812.00	1398675.00	25.0	14-Sep-98	SWFWMD
WEL1781001182500	296893.50	1360355.50	24.0	03-Sep-91	SWFWMD
WEL2289001767700	297618.00	1428476.00	22.0	21-Dec-99	SWFWMD
L-2525	301072.00	796831.00	27.0	25-Oct-88	DBHYDRO
L-2821	301073.00	796831.00	26.0	22-Aug-90	DBHYDRO

Table 3.2a: Temperature data (IAS)

Station	X coordinate (ft FL State Plane 1983)	Y coordinate (ft FL State Plane 1983)	Temperature (°C)	Date	Source
L-588	301965.00	762591.00	26.0	24-Oct-88	DBHYDRO
WEL0778000051200	303789.00	966693.00	25.0	11-Nov-03	SWFWMD
WEL2039001321300	304255.00	1388320.00	27.0	17-Sep-98	SWFWMD
WEL1529000106800	306080.50	1285024.50	24.0	18-Sep-91	SWFWMD
WEL0932000066600	307713.00	981353.00	26.0	20-Jun-03	SWFWMD
WEL0932000066900	307713.00	981356.00	25.0	12-Jan-98	SWFWMD
WEL1523000106200	309179.00	1395645.00	22.8		SFWMD
WEL0452000018600	311767.00	1285030.00	24.0	14-Jan-99	SWFWMD
WEL1215001172300	313996.00	1231178.00	24.0	16-Mar-00	SWFWMD
WEL2088001338100	314788.00	1291771.00	24.0	03-Apr-00	SWFWMD
ROMP 40 HAWTHORNE	314911.00	1206150.00	25.0	25-Nov-03	SWFWMD
ROMP 40 SHALLOW WELL	314922.00	1206135.00	25.0	01-Dec-98	SWFWMD
ROMP 9.5 LOW INT	315550.00	1016676.00	25.0	10-Oct-03	SWFWMD
ROMP 9.5 UPPER INT	315715.00	1016595.00	25.0	10-Oct-03	SWFWMD
ROMP 35 UPPER INT	318094.00	1074297.00	25.0	15-Mar-05	SWFWMD
ROMP 35 LOWER INT	318096.00	1074280.00	25.0	15-Mar-05	SWFWMD
WEL2450000175100	319642.00	891196.00	27.0	04-Oct-00	SWFWMD
WEL1356000089500	321341.00	1186890.00	26.0	25-Sep-85	SWFWMD
WEL2026001320000	323541.00	1410874.00	23.6		SFWMD
ROMP 87 SHALLOW	326612.00	1414182.00	23.9		SFWMD
WEL0971000070500	328079.00	919988.00	25.0	25-Feb-04	SWFWMD
ROMP 25 LILY ARCADIA	329310.00	1103691.00	26.0	17-Sep-03	SWFWMD
WEL1236000077500	329739.00	940779.00	26.0	20-Nov-03	SWFWMD
WEL1153001167100	329741.00	1005025.00	25.0	21-Nov-02	SWFWMD
ROMP 10 LIMESTONE	330560.00	981904.00	27.0	22-Sep-03	SWFWMD
ROMP 10 WT MONITOR	330563.00	981824.00	24.0	05-Jan-98	SWFWMD
ROMP 10 HAWTHORN	330568.00	981860.00	24.0	20-Nov-03	SWFWMD
WEL1692000123100	332534.00	1299701.00	26.0	02-Oct-85	SWFWMD
L-2528	332599.00	844036.00	27.0	06-Jan-87	DBHYDRO
ROMP TR 1-2 UP INT	336114.00	912385.00	27.0	09-Dec-03	SWFWMD
ROMP TR 1-2 L HAW	336134.00	912405.00	29.0	11-Sep-03	SWFWMD
ROMP 17 PZ2	338626.00	1033618.00	24.0	24-Sep-03	SWFWMD
ROMP 17 INT	338677.00	1033869.00	25.0	24-Sep-03	SWFWMD
ROMP 17 U FL	338691.00	1033853.00	26.0	04-Nov-97	SWFWMD
WEL2829003576300	339099.00	955606.00	25.0	06-Feb-02	SWFWMD
WEL1847001173400	339657.00	1359468.00	26.0	21-Mar-00	SWFWMD
WEL2661000187300	342026.00	1244995.00	23.0	08-May-00	SWFWMD
WEL1338000087700	342313.00	997585.00	28.0	14-Apr-04	SWFWMD
WEL1686000122500	343404.00	1241031.00	26.0	10-Nov-98	SWFWMD
WEL2011001312700	343456.47	1406163.79	23.7		SFWMD
WEL0226001094300	344391.00	998521.00	25.0	05-Nov-97	SWFWMD
WEL0802000053600	346113.00	1224306.00	26.0	17-Oct-03	SWFWMD
ROMP 70 SURFICIAL	348043.00	1359898.00	26.0	11-Nov-98	SWFWMD
ROMP 11 DEEP	351344.00	961987.00	26.0	19-Sep-03	SWFWMD
WEL0532000026600	352114.00	1371760.00	24.0	05-Sep-85	SWFWMD
WEL0832000056600	353306.00	950887.00	25.0	26-Feb-04	SWFWMD
L-2646	355114.00	883249.00	26.0	01-Nov-91	DBHYDRO
WEL1140001162300	357777.00	1037531.00	21.0	06-Feb-02	SWFWMD
ROMP 31 HAWTHORN	359012.00	1135365.00	25.0	20-Oct-03	SWFWMD
WEL1336000087500	361741.00	1037916.00	27.0	20-Nov-95	SWFWMD
WEL0357000009100	363408.00	1376812.00	24.0	10-Nov-98	SWFWMD
WEL0510000024500	363969.00	1274342.00	25.0	09-Nov-98	SWFWMD
WEL2333001774400	364535.00	960246.00	25.0	24-Feb-04	SWFWMD
WEL0914000064800	366812.00	1385283.00	24.0	23-Oct-85	SWFWMD
WEL1339000087800	367089.00	1064225.00	25.0	11-Feb-02	SWFWMD
WEL1867000131900	367377.00	918585.00	29.0	29-Sep-03	SWFWMD
WEL2824003575800	367930.00	1102029.00	22.0	05-Feb-02	SWFWMD
ROMP 16.5 LOWER INTERMEDIATE	368469.00	992386.00	26.0	22-Sep-04	SWFWMD
ROMP 16.5 UPPER INTERMEDIATE	368469.00	992397.00	24.0	29-Sep-03	SWFWMD

Table 3.2a: Temperature data (IAS)

Station	X coordinate (ft FL State Plane 1983)	Y coordinate (ft FL State Plane 1983)	Temperature (°C)	Date	Source
ROMP 16.5 SUWANNEE	368504.00	992395.00	28.0	29-Sep-03	SFWMD
WEL2911002928000	371050.00	967759.50	30.0	15-Apr-02	SWFWMD
WEL0546000028000	371976.00	1050060.00	24.0	26-Oct-00	SWFWMD
WEL1907000136800	372062.00	1049945.00	26.0	17-Nov-97	SWFWMD
WEL0344000007800	372098.00	1049943.00	26.0	24-Sep-03	SWFWMD
L-2191	372992.00	859596.00	28.0	25-Oct-88	DBHYDRO
L-2190	372993.00	859596.00	26.0	25-Oct-88	DBHYDRO
WEL1352000089100	374668.00	1069594.00	24.0	14-Oct-03	SWFWMD
WEL2826003576000	375242.00	1156522.00	24.0	25-Feb-02	SWFWMD
ROMP 59 U HAWTHORN	376993.00	1291505.00	24.0	26-Feb-04	SWFWMD
ROMP 59 HAWTHORN	377887.00	1292791.00	25.0	20-Jun-85	SWFWMD
WEL2337003447600	378364.00	977265.50	27.0	06-Sep-05	SWFWMD
WEL2545001797700	378857.00	953079.00	26.0	30-Oct-00	SWFWMD
WEL2337003448000	380430.50	963849.50	27.0	07-Sep-05	SWFWMD
WEL2337003464500	380572.00	975228.00	26.0	06-Sep-05	SWFWMD
WEL2561001001900	381569.50	951911.50	26.0	17-Jul-01	SWFWMD
WEL2337001841200	382934.00	1039653.00	29.0	06-Sep-05	SWFWMD
WEL2561003116500	382935.00	951879.00	29.0	19-Jun-02	SWFWMD
WEL2561001001900	382972.00	951902.00	26.0		SFWMD
WEL2561003116100	383006.00	957682.00	28.0	19-Jun-02	SWFWMD
WEL2561003115700	383088.00	953561.00	28.0	19-Jun-02	SWFWMD
WEL2917000229200	383174.00	954448.00	25.0	12-Sep-05	SWFWMD
WEL2917000229400	383499.00	959878.00	27.0	12-Sep-05	SWFWMD
WEL1328000086700	383660.00	1058860.00	24.0	11-Oct-00	SWFWMD
WEL2337003448100	383786.50	980091.50	25.0	06-Sep-05	SWFWMD
L-5649	383851.00	785812.00	28.0	24-Oct-88	DBHYDRO
WEL2561000232700	384220.50	951805.00	30.0	19-Jun-02	SWFWMD
WEL2561003116600	384638.00	958942.00	29.0	19-Jun-02	SWFWMD
WEL2561003116000	385173.00	955714.00	26.0	19-Jun-02	SWFWMD
WEL2907002921300	385193.00	986828.00	24.0	20-Feb-03	SFWMD
WEL2560001002400	385468.00	959864.00	27.0	17-Jul-01	SWFWMD
WEL2561003116300	385502.00	959725.00	28.0	19-Jun-02	SWFWMD
WEL2561003115600	385804.00	953161.00	30.0	19-Jun-02	SWFWMD
ROMP 26 HAWTHORN	388354.00	1078994.00	26.0	30-Sep-03	SWFWMD
WEL1982001315600	388882.00	1370529.00	23.0	04-Mar-02	SWFWMD
L-2295	389251.00	763361.00	26.0	27-Nov-90	DBHYDRO
WEL2337001842100	389310.00	977086.00	28.0	06-Sep-05	SWFWMD
WEL2938001232200	390140.00	1024464.00	25.0	12-Jan-04	SFWMD
KWDZMW-1	391524.00	86220.00	25.0		SFWMD
WEL2547002299500	391877.00	985674.00	30.0	14-Jan-04	SFWMD
ROMP 5 UPPER INT	392998.00	950317.00	27.0	19-Sep-03	SWFWMD
ROMP 5 LOWER INT	393019.00	950318.00	29.0	19-Sep-03	SWFWMD
WEL2138000149400	393193.00	1035653.00	26.0	03-Aug-05	SFWMD
C-575	393505.00	687101.00	27.0	20-Aug-90	DBHYDRO
WEL2189000153500	393639.00	1034742.00	25.0	03-Aug-05	SFWMD
WEL0431000016500	394276.00	1092452.00	26.0	24-Nov-97	SWFWMD
WEL1908000136900	394411.00	1195387.00	23.0	14-Oct-03	SWFWMD
WEL1344000088300	394988.00	1019768.00	28.0	03-Oct-03	SWFWMD
WEL2547002299200	395836.00	982518.00	30.0	14-Jan-04	SFWMD
WEL1137001166900	396283.00	985767.00	26.0	17-Jul-01	SWFWMD
WEL2913001062900	396509.00	974536.00	28.0	02-Jan-03	SFWMD
WEL2913001062800	396516.00	975748.00	28.0	02-Jan-03	SFWMD
WEL1689000122800	397191.00	1267881.00	23.0	15-Oct-03	SWFWMD
ROMP 30 TAMPA	397814.50	1136938.00	26.0	27-Oct-03	SWFWMD
WEL2547000237800	400609.00	979358.00	26.0	14-Jan-04	SFWMD
ROMP 45 SHALLOW	401925.00	1247825.00	26.0	16-Nov-98	SWFWMD
ROMP 45 HAWTHORNE	401957.00	1247806.00	25.0	19-Nov-03	SWFWMD
WEL1165001161100	402190.00	986602.00	25.0	13-Apr-04	SWFWMD
ROMP 16 SHALLOW	404699.00	1038300.00	25.0	19-Nov-97	SWFWMD

Table 3.2a: Temperature data (IAS)

Station	X coordinate (ft FL State Plane 1983)	Y coordinate (ft FL State Plane 1983)	Temperature (°C)	Date	Source
ROMP 16 HAWTHORNE	404699.00	1038309.00	26.0	14-Oct-03	SWFWMD
WEL2547001797900	404785.00	981957.00	28.0	14-Jan-04	SFWMD
CHWQ-03	405961.00	896745.00	26.0	20-May-92	DBHYDRO
WEL1872000132400	406600.00	982264.00	27.0	13-Jan-04	SWFWMD
WEL2692002271000	407925.00	992744.00	29.0	22-Oct-02	SFWMD
WEL1147001163700	408142.00	1002860.00	24.0	11-Oct-00	SWFWMD
WEL1866000131800	408400.00	918139.00	25.0	29-Sep-03	SWFWMD
WEL3024003757200	410112.00	968007.00	24.0	17-Nov-05	SWFWMD
WEL2827003576100	410579.00	1234189.50	21.0	05-Feb-02	SWFWMD
WEL3024003757300	411587.00	968080.00	24.0	17-Nov-05	SWFWMD
WEL0302000003600	411595.00	1163412.00	24.0	20-Oct-03	SWFWMD
WEL1325000086400	413805.00	982226.00	27.0	28-Jun-00	SWFWMD
L-00652A	413970.00	855904.00	28.0	08-Jan-87	DBHYDRO
ROMP 12 LO INTERMEDIATE	414528.00	984839.00	27.0	18-Sep-03	SWFWMD
ROMP 12 UP INTERMEDIATE	414562.00	984833.00	26.0	18-Sep-03	SWFWMD
WEL1868000132000	414709.00	929164.50	25.0	19-Jun-01	SWFWMD
WEL2953001636700	415481.50	968584.00	30.0	18-Mar-04	SWFWMD
WEL2953001746900	416369.50	966220.50	28.0	18-Mar-04	SWFWMD
I75-TW	416557.00	668295.00	29.0	19-Sep-94	DBHYDRO
WEL3003001725300	417519.50	963204.50	27.0	16-Feb-06	SWFWMD
WEL2953003781000	417991.50	967050.00	27.0	18-Mar-04	SWFWMD
WEL2953003781100	418074.50	969454.50	28.0	18-Mar-04	SWFWMD
WEL3003001347000	421346.00	964612.00	27.0	16-Feb-06	SWFWMD
L-1968	421848.00	837381.00	25.0	04-Jan-88	DBHYDRO
WEL2401002196300	423886.50	967202.00	30.0	16-Mar-04	SWFWMD
WEL2401002196200	424185.00	961953.50	29.0	16-Mar-04	SWFWMD
WEL2825003575900	424212.00	1356086.00	24.0	07-Feb-02	SWFWMD
WEL2401002196100	424226.50	969704.50	30.0	16-Mar-04	SWFWMD
WEL2401002197300	424342.00	969823.00	28.0	16-Mar-04	SWFWMD
WEL2969001440100	424636.00	965411.00	25.0	16-Mar-04	SWFWMD
WEL2902001609800	425596.00	968379.00	30.0	08-May-06	SWFWMD
WEL2933003032100	425727.00	975170.00	33.0	12-Mar-03	SFWMD
WEL2401002196700	425852.00	964867.00	27.0	17-Mar-04	SWFWMD
WEL2969001064900	426385.00	961844.50	27.0	16-Mar-04	SWFWMD
WEL2931003032200	426705.00	972135.00	30.0	12-Mar-03	SFWMD
WEL2902002271600	426866.00	967178.00	30.0	08-May-06	SWFWMD
WEL2970001403600	426991.00	954538.00	30.0	17-Mar-04	SWFWMD
WEL0123001082900	427050.00	1351701.00	26.0	24-May-99	SWFWMD
WEL2902001609700	427790.00	968303.00	29.0	08-May-06	SWFWMD
WEL2928000232000	428541.00	971719.00	28.0	12-Mar-03	SWFWMD
L-2319	428658.00	771308.00	28.0	08-Jan-86	DBHYDRO
WEL2932003032300	428890.00	974748.00	33.0	12-Mar-03	SFWMD
WEL2401002196500	429052.00	968588.00	28.0	16-Mar-04	SWFWMD
WEL2401000169800	429303.00	951318.00	30.0	11-Oct-00	SWFWMD
WEL2401002195600	429304.00	951318.00	30.0	17-Mar-04	SFWMD
WEL2401002199000	429366.00	962323.00	27.0	02-Mar-05	SWFWMD
WEL2401002195700	429390.00	954044.00	30.0	17-Mar-04	SWFWMD
WEL2401002195900	429425.50	959920.50	28.0	17-Mar-04	SWFWMD
WEL1688000122700	429968.50	1229407.50	26.0	12-Mar-96	SWFWMD
WEL2401002198900	430206.00	967064.00	25.0	16-Mar-04	SWFWMD
C-303	430214.00	705468.00	26.0	24-Nov-87	DBHYDRO
WEL2401002195800	433267.50	968652.50	28.0	16-Mar-04	SWFWMD
WEL1348000088700	433391.00	1041693.00	27.0	26-Sep-85	SWFWMD
WEL2929000232100	433880.00	973533.00	32.0	12-Mar-03	SWFWMD
WEL2544001797600	434702.50	964628.00	28.0	11-Feb-03	SWFWMD
WEL2863003646900	434838.00	952786.00	29.0	06-Sep-02	SWFWMD
WEL2541001797300	435168.00	967150.00	31.0	18-Dec-00	SWFWMD
WEL2906000232500	435881.50	979175.00	27.0	20-Mar-02	SWFWMD
WEL2927000230000	436712.00	973964.00	31.0	14-Jul-03	SFWMD

Table 3.2a: Temperature data (IAS)

Station	X coordinate (ft FL State Plane 1983)	Y coordinate (ft FL State Plane 1983)	Temperature (°C)	Date	Source
WEL2902000231800	437174.00	964684.00	26.0	11-Feb-03	SWFWMD
WEL2863003089801	437314.00	952696.00	25.0	04-Nov-03	SWFWMD
WEL2927000230100	437423.00	976318.00	28.0	14-Jul-03	SWFWMD
WEL2862000232400	438492.00	994589.00	25.0	19-Mar-02	SFWMD
WEL2902000231900	438675.00	973130.00	28.0	22-Oct-02	SWFWMD
WEL2902002001400	439826.00	973174.00	27.0	22-Oct-02	SFWMD
ROMP 57-2 HAWTHORNE	455103.00	1298176.00	25.0	17-Oct-03	SWFWMD
ROMP 13 LOW INT	455637.00	995826.00	26.0	23-Sep-03	SWFWMD
ROMP 13 MID INT	455651.00	995829.00	25.0	23-Sep-03	SWFWMD
CHWQ-01	457778.00	949678.00	26.0	21-May-92	DBHYDRO
L-2531	458056.00	875562.00	28.0	13-Dec-88	DBHYDRO
C-1080	458061.00	742383.00	25.0	24-Nov-87	DBHYDRO
WEL0125001083100	458131.00	1350634.00	30.0	22-Oct-03	SWFWMD
L-2311	458565.00	810636.00	26.0	31-Oct-91	DBHYDRO
ORF-0030	459137.00	1495602.00	24.0	26-Mar-79	DBHYDRO
WEL0322000005600	459154.00	1399704.50	24.0	29-Aug-85	SWFWMD
POF-3	459188.00	1399757.00	24.0	14-Sep-79	DBHYDRO
C-688	460757.00	715514.00	26.0	26-Nov-90	DBHYDRO
ROMP 44 FLORIDAN	462869.50	1269340.00	24.0	17-May-99	SWFWMD
ROMP 58 OCALA	464374.50	1303999.50	25.0	17-Oct-03	SWFWMD
OSF-35	466287.00	1442543.00	24.0	11-Sep-79	DBHYDRO
WEL0138001084600	466734.50	1341333.50	25.0	10-Oct-03	SWFWMD
ROMP CL-3 FLORIDAN	470768.00	1246803.00	25.0	19-May-99	SWFWMD
ROMP CL-3 INTERMEDIATE	470800.00	1246814.00	24.0	15-Oct-03	SWFWMD
WEL1351000089000	472800.00	1003888.00	25.0	03-Oct-03	SWFWMD
ORF-0031	472907.00	1500686.00	24.0	29-May-79	DBHYDRO
WEL0162000060200	477252.00	1308860.50	25.0	10-Oct-03	SWFWMD
ROMP CL-1 FL	482810.50	1275037.50	24.0	16-Feb-00	SWFWMD
WEL2823000209800	483887.00	1143332.00	24.0	27-Feb-02	SWFWMD
WEL0871000060500	484914.00	1240153.00	26.0	15-Oct-03	SWFWMD
WEL1694000123300	485723.50	1284088.00	25.0	14-Sep-99	SWFWMD
ROMP CL-2 DEEP SURF	490976.00	1244539.00	26.0	17-Feb-00	SWFWMD
WEL0179001089100	492493.00	1265459.50	25.0	10-Oct-03	SWFWMD
GLWQ-08	496963.00	949407.00	26.0	20-May-92	DBHYDRO
C-687	500066.00	763006.00	25.0	27-Nov-90	DBHYDRO
LAB-TW-IAS	502271.00	879737.00	27.0	11-Mar-97	DBHYDRO
RTA-007	503673.00	903944.00	26.0	12-May-92	DBHYDRO
C-269	504260.00	587923.00	25.0	09-Jan-90	DBHYDRO
C-531	506314.00	781662.00	25.0	24-Nov-87	DBHYDRO
HE-556	513875.00	841003.00	25.0	15-Dec-88	DBHYDRO
POF-8	514365.00	1265002.00	24.0	06-Dec-90	DBHYDRO
ROMP 28 INTERMEDIATE	514862.00	1103573.00	25.0	16-Oct-03	SWFWMD
ROMP 28 INTERMEDIATE OB-4	514873.00	1103487.00	25.0	21-Jun-04	SWFWMD
C-684	525728.00	713042.00	25.0	23-Nov-87	DBHYDRO
C-689	525729.00	713042.00	26.0	23-Nov-87	DBHYDRO
C-298	526050.00	758172.00	25.0	24-Nov-87	DBHYDRO
HE-517	533970.00	885871.00	25.0	18-May-92	DBHYDRO
C-311	534795.00	572682.00	26.0	19-Oct-87	DBHYDRO
OR0824	535473.00	1520941.00	24.0	09-May-04	SJRWMD
C-00039	536800.00	538351.00	27.0	19-Oct-87	DBHYDRO
ROMP 14 INTERMEDIATE	541274.00	1023824.00	26.0	24-Sep-03	SWFWMD
GLWQ-02	544974.00	933497.00	26.0	18-May-92	DBHYDRO
GL-5A	553437.00	957447.00	26.0	02-Sep-99	DBHYDRO
BICY-MZ1	554522.00	567148.00	28.0	24-Jun-04	DBHYDRO
C-308	568854.00	662350.00	24.0	26-Nov-90	DBHYDRO
POF-5	585924.00	1261680.00	24.0	22-May-79	DBHYDRO
OR0664	589520.00	1515255.00	22.0	29-Oct-00	SJRWMD
KRFNND	593855.00	1255783.00	24.0	24-Oct-00	DBHYDRO
KRENND	598894.00	1242074.00	23.0	24-Oct-00	DBHYDRO

Table 3.2a: Temperature data (IAS)

Station	X coordinate (ft FL State Plane 1983)	Y coordinate (ft FL State Plane 1983)	Temperature (°C)	Date	Source
POH-1	613133.00	1208901.00	24.0	04-Jun-07	DBHYDRO
OSF-19	616853.00	1299405.00	24.0	12-Sep-79	DBHYDRO
OR0017	625452.00	1485214.00	24.0	06-Aug-96	SJRWMD
OSF-3	639312.00	1286553.00	24.0	24-Jan-89	DBHYDRO
OSF-37	641831.00	1401081.00	24.0	26-Mar-79	DBHYDRO
OKF-2	650018.00	1110150.00	23.0	27-Jun-85	DBHYDRO
GLF-0002	650450.00	983226.00	25.0	24-Apr-86	DBHYDRO
OKF-22	676184.00	1058051.00	25.0	15-Sep-80	DBHYDRO
GLF-1	681169.00	1022612.00	27.0	14-May-87	DBHYDRO
OKF-101	708303.00	1041117.00	25.0	08-Aug-05	DBHYDRO
W-1115	711700.00	324712.00	28.9		SFWMD
G-2296	714530.00	668029.00	26.0	18-Dec-96	DBHYDRO
BR0586	722281.00	1513032.00	23.0	26-Oct-03	SJRWMD
BR0202	724408.00	1470617.00	24.0	11-Jul-99	SJRWMD
IR0854	735401.00	1200087.00	25.0	17-May-95	SJRWMD
BR0925	745020.00	1282310.00	24.0	09-Jan-91	SJRWMD
PBF-7	748907.00	860161.00	25.6		SFWMD
OKF-0003	755117.00	1037467.00	24.0	29-Nov-90	DBHYDRO
STL-373	767860.00	1105644.00	27.0	24-May-90	USGS (Reese, WRI03-4242)
SLF-67	767933.00	1105760.00	27.0	17-Nov-93	DBHYDRO
WA-1119	768272.00	1119581.00	27.0	15-Apr-88	USGS (Reese, WRI03-4242)
IR0629	773795.00	1263904.00	25.0	10-Apr-95	SJRWMD
IR0631	775049.00	1264918.00	25.0	05-Apr-95	SJRWMD
IR0956	775395.00	1209780.00	25.0	18-Oct-98	SJRWMD
WA-1148	778505.00	1013380.00	26.0	20-May-88	USGS (Reese, WRI03-4242)
IR0628	779996.00	1262509.00	25.0	11-Apr-95	SJRWMD
IR0921	782273.00	1252215.00	26.0	25-Jan-04	SJRWMD
SLF-60	786163.00	1071987.00	25.0	24-Jan-01	DBHYDRO
IR0287	791268.00	1248508.00	24.0	03-Nov-98	SJRWMD
STL-218	791281.00	1164690.00	28.0	01-Jun-00	USGS (Reese, WRI03-4242)
SLF-11	791282.00	1164690.00	27.0	06-Jul-04	DBHYDRO
WA-547	792007.00	1109556.00	27.0	01-Aug-85	USGS (Reese, WRI03-4242)
S-524	793172.00	465816.00	24.0	03-Nov-83	USGS(Merritt, WSP2491)
STL-47	811844.00	1131540.00	25.0	16-Jul-80	USGS (Reese, WRI03-4242)
SLF-27	814070.00	1111165.00	28.0	16-Sep-87	DBHYDRO
M-255	818474.00	1028161.00	29.0	24-Jul-01	USGS (Reese, WRI03-4242)
WA-875	819378.00	1117634.00	27.0	18-Aug-87	USGS (Reese, WRI03-4242)
WA-1136	820060.00	1105014.00	26.0	05-May-88	USGS (Reese, WRI03-4242)
WA-1140	820061.00	1105014.00	28.0	16-May-88	USGS (Reese, WRI03-4242)
SLF-75	821825.00	1092288.00	28.0	05-Oct-04	DBHYDRO
SLF-76	821843.00	1092293.00	21.0	24-Jan-01	DBHYDRO
M-189	821861.00	994649.00	29.0	02-Mar-53	USGS (Reese, WRI03-4242)
M-192	822622.00	985261.00	29.0	16-Apr-57	USGS (Reese, WRI03-4242)
WA-1188	822805.00	1095533.00	28.0	21-Jul-88	USGS (Reese, WRI03-4242)
M-186	823200.00	1043024.00	31.0	30-Dec-77	USGS (Reese, WRI03-4242)
WA-1113	825032.00	1101702.00	26.0	14-Apr-88	USGS (Reese, WRI03-4242)
SLF-62	828481.00	1075057.00	27.0	24-Jan-01	DBHYDRO
STL-225	828500.00	1049408.00	30.0	30-May-90	USGS (Reese, WRI03-4242)
SLF-23	828574.00	1049526.00	32.0	30-May-90	DBHYDRO
MF-9	828909.00	1031657.00	30.0	06-Jul-04	DBHYDRO
M-745	828937.00	1031637.00	30.0	24-Jul-01	USGS (Reese, WRI03-4242)
WA-829	830583.00	1089810.00	29.0	05-Aug-87	USGS (Reese, WRI03-4242)
KRM-TZMW	830843.00	573318.00	24.0	21-Mar-94	DBHYDRO
SLF-62B	836003.00	1082784.00	29.0	06-Jul-04	DBHYDRO
SLF-69	836548.00	1101782.00	25.0	23-Jan-01	DBHYDRO
STL-367	838262.00	1066920.00	26.0	25-May-90	USGS (Reese, WRI03-4242)
IR0312	840635.00	1179227.00	25.0	26-Jul-03	SJRWMD
IR0992	840788.00	1204575.00	24.0	21-Apr-01	SJRWMD
IR1006	840789.00	1204575.00	25.0	24-Jan-04	SJRWMD

Table 3.2a: Temperature data (IAS)

Station	X coordinate (ft FL State Plane 1983)	Y coordinate (ft FL State Plane 1983)	Temperature (^{o}C)	Date	Source
STL-243	849471.00	1119585.00	25.0		USGS (Reese, WRI03-4242)
STL-224	850163.00	1125345.00	25.0	06-Jun-00	USGS (Reese, WRI03-4242)
SLF-21	850164.00	1125345.00	26.0	06-Jul-04	DBHYDRO
WA-580	854245.00	1083254.00	29.0	27-Jan-86	USGS (Reese, WRI03-4242)
M-602	867808.00	1042423.00	26.0	16-Nov-53	USGS (Reese, WRI03-4242)
M-143	867932.00	1035860.00	26.0	24-Oct-61	USGS (Reese, WRI03-4242)
WA-708	871779.00	1127575.00	24.0	29-Dec-86	USGS (Reese, WRI03-4242)
SUN-MZU	873511.00	653626.00	24.0	21-Sep-99	DBHYDRO
WA-1179	873513.00	1140208.00	26.0	19-Jul-88	USGS (Reese, WRI03-4242)
M-47	875108.00	1028122.00	25.0	07-Jun-46	USGS (Reese, WRI03-4242)
PBP-MZU	875726.00	604016.00	24.0	03-Aug-99	DBHYDRO
M-748	882309.00	1032605.00	27.0	23-Apr-57	USGS (Reese, WRI03-4242)
STL-71	891351.00	1093349.00	24.0	16-Jul-80	USGS (Reese, WRI03-4242)
M-443	891669.00	1038313.00	24.0	23-Apr-57	USGS (Reese, WRI03-4242)
M-244	896585.00	1000978.00	25.0	23-Mar-53	USGS (Reese, WRI03-4242)
M-65	910016.00	1050441.00	24.0	19-Jul-46	USGS (Reese, WRI03-4242)
M-64	916798.00	1062905.00	26.0	18-Jul-46	USGS (Reese, WRI03-4242)
M-1121	922765.00	1047492.00	25.0	18-Jul-01	USGS (Reese, WRI03-4242)
MF-3	922774.00	1047513.00	25.0	31-May-90	DBHYDRO
MF-31	924777.00	1024359.00	24.0	25-Jan-01	DBHYDRO
M-1349	926014.00	1034083.00	22.0	31-May-90	USGS (Reese, WRI03-4242)
LYTAL-TW	949208.00	852482.00	23.0		SFWMD

Table 3.2b: Temperature data (UF)

Station	X coordinate (ft FL State Plane 1983)	Y coordinate (ft FL State Plane 1983)	Temperature (°C)	Date	Source
82510503_G	625702.00	1487335.00	24.0		SFWMD
82510702_G	615881.00	1487243.00	24.7		SFWMD
82510802_G	608560.00	1487353.00	25.0		SFWMD
82510902_G	606506.00	1487355.00	25.0		SFWMD
82510903_G	604453.00	1487358.00	25.0		SFWMD
82610502_G	625706.00	1491577.00	25.0		SFWMD
82610504_G	625709.00	1495415.00	25.0		SFWMD
83210501_G	626629.00	1531670.00	24.0		SFWMD
84612602_G	515726.00	1615340.00	23.8		SFWMD
AMERICAN CITRUS PRODUCTS #18 (DID #4)	440519.00	967004.00	28.0	11-Feb-03	SWFWMD
AMERICAN CITRUS PRODUCTS #22 (DID #6)	440441.00	969738.00	26.0	11-Feb-03	SWFWMD
AMERICAN CITRUS PRODUCTS #22 (DID #6)	440472.00	969696.00	27.0	11-Feb-03	SWFWMD
BF-1	925615.00	669564.00	22.0	01-Mar-93	DBHYDRO
BF-3	925364.00	669470.00	22.0	24-Oct-00	DBHYDRO
BF-4S	925174.00	669561.00	23.0	08-Jun-07	DBHYDRO
BICY-MZ2	554523.00	567148.00	30.0		SFWMD, packer test
BOYRO_EPXU	953222.00	786238.00	25.0	05-Mar-07	DBHYDRO
BR0202	724408.00	1470617.00	24.2		SFWMD
BR0585	704288.00	1560171.00	24.0		SFWMD
BR0586	722281.00	1513032.00	23.1		SFWMD
BR0608	758244.00	1510686.00	24.0	24-Jul-03	SJRWMD
BR0624	832335.00	1285733.00	26.0	26-Jul-03	SJRWMD
BR0625	832336.00	1285733.00	25.0	26-Oct-03	SJRWMD
BR0645	743563.00	1332296.00	25.0	26-Apr-03	SJRWMD
BR1187	808653.00	1306034.00	25.0	09-Feb-95	SJRWMD
BR1473	740933.00	1470145.00	23.0	31-Jan-95	SJRWMD
BR1486	750943.00	1504002.00	24.0	23-May-95	SJRWMD
BR-1526	667842.00	1555294.00	24.2		SFWMD
BR1557	731104.00	1471741.00	25.0	27-Apr-03	SJRWMD
BR1558	740258.00	1451762.00	24.0	26-Apr-03	SJRWMD
BR1559	799357.00	1272168.00	25.0	26-Oct-03	SJRWMD
BR1572	704288.00	1560332.00	24.0		SFWMD
BR1748	760099.00	1517458.00	23.0	24-Jul-03	SJRWMD
BR1835	694168.00	1610558.00	23.3		SFWMD
BRY-MW	493917.00	863570.00	30.0	09-Jan-06	DBHYDRO
CBARWF 2W CREWS LAKE DP	161314.00	1473675.00	23.0	20-Feb-06	SWFWMD
CCRO-225	326927.00	835100.00	29.2		SFWMD
CH-R5	392978.00	949940.00	29.0		SFWMD
City of Sarasota V39	248918.04	1104409.68	27.7		SFWMD
CO-2318	433829.00	695523.00	29.0		SFWMD
COCOA D_G	602935.00	1487461.00	24.0		SFWMD
COCOA F_G	625445.00	1500363.00	24.0		SFWMD
COCOA H_G	647580.00	1507220.00	24.0		SFWMD
COH_F3	925987.00	613161.00	23.1		SFWMD
CR 581 NORTH FLDN	217000.00	1461175.00	22.0	15-Feb-06	SWFWMD
CS-M2	897623.00	695829.00	23.0	13-Sep-00	USGS (Reese, WRI03-4242)
DF-2	830645.00	573066.00	23.8	06-Dec-96	SFWMD
DF-4	830843.00	573318.00	23.0	09-Jun-04	DBHYDRO
ENP-100	787244.00	381471.00	28.0	14-Jun-04	DBHYDRO
EXKR-1	696705.00	1025435.00	25.0	12-Mar-04	DBHYDRO
EXPM-1	784620.00	965030.00	27.0	10-Nov-03	DBHYDRO
FPL-MW	400852.00	859414.00	28.0	21-Mar-06	DBHYDRO
FPU-MZU	878266.00	1135537.00	24.0	11-Dec-02	DBHYDRO
FTL-MZU2	941690.00	641434.00	22.0	07-Sep-99	DBHYDRO
FTPIERCEUT	865826.00	1130401.00	25.0		SFWMD
G-2618	714531.00	668029.00	25.0	22-Sep-04	DBHYDRO
GL-5B	553452.00	957447.00	25.0	02-Sep-99	DBHYDRO
GLF-1	681169.00	1022612.00	27.0	14-May-87	DBHYDRO
GLF-6	628323.00	910488.00	30.0	15-Nov-01	DBHYDRO

Table 3.2b: Temperature data (UF)

Station	X coordinate (ft FL State Plane 1983)	Y coordinate (ft FL State Plane 1983)	Temperature (°C)	Date	Source
HC-0001	522028.00	1112998.00	23.0	06-Jan-86	DBHYDRO
I75-MZ2	416557.00	668295.00	29.0	13-Apr-95	SFWMD
IC-TW	493980.00	1426090.00	22.6		SFWMD
IR0312	840635.00	1179227.00	25.0	26-Jul-03	SJRWMD
IR0342	849565.00	1245558.00	25.0		SFWMD
IR0628	779996.00	1262509.00	25.0	11-Apr-95	SJRWMD
IR0629	773795.00	1263904.00	25.0	10-Apr-95	SJRWMD
IR0631	775049.00	1264918.00	25.0	05-Apr-95	SJRWMD
IR0814	817805.00	1217099.00	25.0	16-May-95	SJRWMD
IR0854	735401.00	1200087.00	25.0	17-May-95	SJRWMD
IR0921	782273.00	1252215.00	26.0	25-Jan-04	SJRWMD
IR0954	792660.00	1182973.00	25.0	27-Jul-03	SJRWMD
IR0955	775394.00	1209780.00	26.0	27-Jul-03	SJRWMD
IR0963	813657.00	1220415.00	26.0	26-Jul-03	SJRWMD
IR0968	727890.00	1225420.00	26.0	27-Jul-03	SJRWMD
IR1000	849492.00	1245820.00	24.0	26-Jul-03	SJRWMD
IR1006	840788.00	1204575.00	24.9		SFWMD
IWA-MZU	292806.00	767990.00	28.0	22-May-00	DBHYDRO
IWSD-MZ2	515034.00	756360.00	31.0	25-Jun-96	DBHYDRO
IWSD-PW2	514933.43	756198.61	28.0		SFWMD
KME TEST WELL 09	249209.89	1106527.82	27.2		SFWMD
KME WELL 04	224095.28	1110626.62	25.3		SFWMD
KWDZMW-1	391525.00	86220.00	23.6		SFWMD
L-2319	428658.00	771308.00	28.0	08-Jan-86	DBHYDRO
L-2435	351159.00	813502.00	27.0	06-Jan-87	DBHYDRO
L-2460	461451.00	845658.00	29.6		SFWMD
L-2528	332599.00	844036.00	28.0	25-Oct-88	DBHYDRO
L2-PW2	672710.00	826685.00	26.0	22-Jun-04	DBHYDRO
L-5602	356507.00	799527.00	30.0		SFWMD
L-5609	336730.00	790989.00	28.3		SFWMD
L-5708	459534.00	875835.00	26.0		SFWMD
L-5812	402976.00	748028.00	32.2		SFWMD
L-6433	311448.00	843296.00	28.0	27-May-05	DBHYDRO
LAB-MZ1	502272.00	879737.00	29.0	22-Jun-04	DBHYDRO
LM-7733	408591.00	766596.00	30.6		SFWMD
M-1034	900051.00	1041089.00	26.0	10-Jul-00	USGS (Reese, WRI03-4242)
M-106	915988.00	1034219.00	24.0	28-May-57	USGS (Reese, WRI03-4242)
M-1121	922765.00	1047492.00	25.0	18-Jul-01	USGS (Reese, WRI03-4242)
M-113	909445.00	1026099.00	24.0	03-May-57	USGS (Reese, WRI03-4242)
M-1326	924814.00	1024380.00	24.0	10-Jul-00	USGS (Reese, WRI03-4242)
M-1349	926014.00	1034083.00	22.0	31-May-90	USGS (Reese, WRI03-4242)
M-1360	784887.00	966243.00	27.0	13-Nov-01	USGS (Reese, WRI03-4242)
M-143	867932.00	1035860.00	26.0	24-Oct-61	USGS (Reese, WRI03-4242)
M-145	815526.00	996543.00	28.3		SFWMD
M-146	795138.00	1011110.00	27.0		SFWMD
M-150	913991.00	1007143.00	24.5		SFWMD
M-168_G	798320.00	1000537.00	27.0		SFWMD
M-169	793915.00	1025546.00	27.5		SFWMD
M-170	795827.00	1021109.00	27.5		SFWMD
M-171	796025.00	1016061.00	27.8		SFWMD
M-173	797330.00	1004352.00	26.5		SFWMD
M-186	823200.00	1043024.00	31.0	30-Dec-77	USGS (Reese, WRI03-4242)
M-189	821861.00	994649.00	29.0	02-Mar-53	USGS (Reese, WRI03-4242)
M-192	822622.00	985261.00	29.0	16-Apr-57	USGS (Reese, WRI03-4242)
M-244	896585.00	1000978.00	25.0	23-Mar-53	USGS (Reese, WRI03-4242)
M-254	824040.00	1014450.00	28.0		USGS (Reese, WRI03-4242)
M-27	886167.00	989103.00	26.7		SFWMD
M-306	912468.00	1005113.00	24.5		SFWMD
M-43	877394.00	1022985.00	25.0		USGS (Reese, WRI03-4242)

Table 3.2b: Temperature data (UF)

Station	X coordinate (ft FL State Plane 1983)	Y coordinate (ft FL State Plane 1983)	Temperature (°C)	Date	Source
M-443	891669.00	1038313.00	24.0	23-Apr-57	USGS (Reese, WRI03-4242)
M-602	867808.00	1042423.00	26.0	16-Nov-53	USGS (Reese, WRI03-4242)
M-741	883583.00	998480.00	24.0		SFWMD
M-745	828937.00	1031637.00	30.0	24-Jul-01	USGS (Reese, WRI03-4242)
M-747	806619.00	1034174.00	27.0	16-Dec-55	USGS (Reese, WRI03-4242)
M-748	882309.00	1032605.00	27.0	23-Apr-57	USGS (Reese, WRI03-4242)
M-841	901286.00	1030897.00	24.0	04-Sep-57	USGS (Reese, WRI03-4242)
M-86	911900.00	1052371.00	25.0	23-Jul-46	USGS (Reese, WRI03-4242)
M-88	917033.00	1040285.00	24.0	23-Jul-46	USGS (Reese, WRI03-4242)
M-901	813633.00	995021.00	27.8		SFWMD
M-919	801317.00	975890.00	26.0		SFWMD
M-922	827718.00	977608.00	27.0	07-Mar-57	USGS (Reese, WRI03-4242)
M-926	886259.00	1036969.00	25.0	23-Apr-57	USGS (Reese, WRI03-4242)
M-927	815926.00	1032897.00	28.0	23-Oct-61	USGS (Reese, WRI03-4242)
M-95	919584.00	1036868.00	24.0	24-Jul-46	USGS (Reese, WRI03-4242)
MDWNA_FA3N	936514.00	576823.00	23.4		SFWMD
MDWSA_FA3	871526.00	442422.00	25.0		SFWMD
MF-10	887371.00	997408.00	26.2		SFWMD
MF-20	781792.00	1025928.00	26.5		SFWMD
MF-23	798252.00	996540.00	27.6		SFWMD
MF-3	922774.00	1047513.00	25.0	31-May-90	DBHYDRO
MF-31	924778.00	1024359.00	25.0	06-Jul-04	DBHYDRO
MF-33	789502.00	1016158.00	24.4		SFWMD
MF-35	824555.00	970435.00	28.9		SFWMD
MF-37-MC1	784923.00	965985.00	28.0	01-Nov-01	DBHYDRO
MF-40U	826581.00	1044391.00	29.0	06-Jun-07	DBHYDRO
MF-52	856075.00	1000606.00	28.7		SFWMD
MF-54	926088.00	1034202.00	22.0		SFWMD
MF-6	791722.00	1027980.00	27.2		SFWMD
MF-9	828909.00	1031657.00	30.0	06-Jul-04	DBHYDRO
MIU-MZ1	418494.25	591527.00	29.0	21-Oct-04	DBHYDRO
NBC-MZU2	933485.00	701513.00	23.0	07-Sep-99	DBHYDRO
NCCWTMZ1	433915.00	695501.00	29.0	18-Jun-96	DBHYDRO
NPSL-MZU	866749.00	1092495.00	26.0	17-Nov-99	DBHYDRO
NRCS205-5	778001.00	1159128.00	27.9		SFWMD
OK-72	742249.00	1151932.00	27.0	19-Jul-01	USGS (Reese, WRI03-4242)
OKF-100U	698055.00	1025471.00	25.0	05-May-04	DBHYDRO
OKF-101	708303.00	1041117.00	25.0	08-Aug-05	DBHYDRO
OKF-13	742962.00	1155367.00	26.0	31-May-00	USGS (Reese, WRI03-4242)
OKF-17	682589.00	1091463.00	26.0	31-May-00	USGS (Reese, WRI03-4242)
OKF-2	650018.00	1110150.00	23.0	27-Jun-85	DBHYDRO
OKF-2	749670.00	1167109.00	25.0	12-Sep-80	DBHYDRO
OKF-22	676184.00	1058051.00	26.8		SFWMD
OKF-23	703527.00	1061608.00	26.2		SFWMD
OKF-42	618563.00	1115014.00	26.3	17-Jun-04	SFWMD
OKF-7	725748.00	1102435.00	24.9		SFWMD
OR0003	647422.00	1507118.00	24.0	17-Feb-03	SJRWMD
OR0025	625363.00	1485214.00	24.0	13-May-03	SJRWMD
OR0033	604383.00	1487256.00	25.0	24-May-04	SJRWMD
OR0037	608490.00	1487251.00	25.0	12-May-03	SJRWMD
OR0038	606437.00	1487253.00	25.0	12-May-03	SJRWMD
OR0055	625632.00	1487233.00	24.0	13-May-03	SJRWMD
OR0057	625636.00	1491475.00	24.0	12-May-03	SJRWMD
OR0059	625639.00	1495313.00	24.0	24-May-04	SJRWMD
OR0062	625373.00	1497939.00	24.0	12-May-03	SJRWMD
OR0068	512768.00	1609897.00	23.0		SFWMD
OR0082	602865.00	1487359.00	24.0	26-May-04	SJRWMD
OR0106	371643.00	1591395.00	23.9		SFWMD
OR0265	625553.00	1500363.00	24.0	28-Apr-02	SJRWMD

Table 3.2b: Temperature data (UF)

Station	X coordinate (ft FL State Plane 1983)	Y coordinate (ft FL State Plane 1983)	Temperature (°C)	Date	Source
OR0548	506933.00	1591539.00	23.8		SFWMD
OR0617	620131.00	1524303.00	25.0	25-Jul-03	SJRWMD
OR0662	515568.00	1615040.00	24.0		SFWMD
OR0669	650630.00	1475910.00	25.0	25-Oct-03	SJRWMD
OR0740	634644.00	1476219.00	24.0	12-May-03	SJRWMD
OR0796	493063.00	1575334.00	24.0		SFWMD
ORF-0030	459137.00	1495602.00	24.0	26-Mar-79	DBHYDRO
ORF-32	493285.00	1506755.00	24.0	29-May-79	DBHYDRO
ORF-60	467178.00	1470886.00	23.2		SFWMD
OS0004	672477.00	1340887.00	23.0	26-Oct-03	SJRWMD
OS0017	678559.00	1361391.00	24.0	05-May-01	SJRWMD
OS0031	653749.00	1375827.00	26.0	26-Oct-03	SJRWMD
OS0230	649971.00	1262720.00	24.0	27-Jul-03	SJRWMD
OS0231	669454.00	1270498.00	24.0	26-Oct-03	SJRWMD
OSF-100	493880.00	1426094.00	24.0	30-Jun-04	DBHYDRO
OSF-104U	613138.00	1209263.00	24.0	04-Jun-07	DBHYDRO
OSF-11	511138.00	1388118.00	22.0	10-Aug-93	DBHYDRO
OSF-19	616853.00	1299405.00	24.0	12-Sep-79	DBHYDRO
OSF-21	657675.00	1265759.00	25.7		SFWMD
OSF-24	614087.00	1397163.00	22.0	22-Mar-79	DBHYDRO
OSF-3	639313.00	1286553.00	24.0	01-Aug-05	DBHYDRO
OSF-35	466287.00	1442543.00	24.0	11-Sep-79	DBHYDRO
OSF-37	641831.00	1401081.00	24.0	26-Mar-79	DBHYDRO
OSF-4	584485.00	1309549.00	24.0	12-Sep-79	DBHYDRO
OSF-5	480255.00	1427733.00	24.0	29-Jul-93	DBHYDRO
OSF-52	592068.00	1261156.00	26.2		SFWMD
OSF-6	539947.00	1383477.00	23.0	25-Jan-89	DBHYDRO
OSF-60	689768.00	1222465.00	25.0	01-Aug-05	DBHYDRO
OSF-62	641676.00	1296604.00	25.0	02-Aug-93	DBHYDRO
OSF-70	550509.00	1424598.00	25.0	02-Dec-92	DBHYDRO
OSF-84	639651.00	1325948.00	24.0	04-Aug-93	DBHYDRO
OSF-85	672812.00	1347862.00	23.0	02-Dec-92	DBHYDRO
OSF-86	685793.00	1365744.00	26.0	03-Aug-93	DBHYDRO
OSF-92	660708.00	1432789.00	25.0	05-Aug-93	DBHYDRO
OSFWQ-01	550086.00	1424652.00	25.0	25-Jan-93	DBHYDRO
PAHO-MZU	764969.00	896738.00	28.0	14-Jul-99	DBHYDRO
PB-1144	953654.00	959039.00	25.0	13-Jul-00	USGS (Reese, WRI03-4242)
PB-1194	962730.00	793720.00	25.0	21-May-92	USGS (Reese, WRI02-4036)
PB-1196	930965.00	942017.00	23.0	17-Jul-01	USGS (Reese, WRI03-4242)
PB-1763	938731.00	782344.00	24.0	28-Jan-99	USGS (Reese, WRI02-4036)
PB-1765	886941.00	735451.00	24.0	10-Apr-00	USGS (Reese and Alvarez-Zarikian, SIR2006-5239
PB-747	936275.00	946597.00	24.0	19-Jun-74	USGS (Reese, WRI03-4242)
PBCSR-MZU	928806.00	785408.00	25.0	21-Sep-99	DBHYDRO
PBF-1	953618.00	959049.00	26.0	31-May-90	DBHYDRO
PBF-10R	886679.00	735581.00	24.0	03-Sep-03	DBHYDRO
PBF-13	886998.00	735464.00	24.0	16-Nov-00	DBHYDRO
PBF-15U	863877.00	874383.00	27.0	07-Jun-07	DBHYDRO
PBF-3	949210.00	852482.00	22.0	23-Sep-04	DBHYDRO
PBF-7U	749013.00	860161.00	26.0	22-Sep-04	DBHYDRO
PBP-MZU	875725.00	604016.00	23.6		SFWMD
PCU #5	271259.62	1409007.72	24.0		SWFWMD
PLESS PARK FLDN	234068.00	1489746.00	22.0	16-Feb-06	SWFWMD
POF-1	469343.00	1427380.00	24.0	14-Sep-79	DBHYDRO
POF-13	541620.00	1312175.00	24.0	25-Jan-89	DBHYDRO
POF-20	612722.00	1208413.00	25.0		SFWMD
POF-20R	613137.00	1208894.00	26.0	24-Mar-06	DBHYDRO
POF-3	459188.00	1399757.00	24.0	14-Sep-79	DBHYDRO

Table 3.2b: Temperature data (UF)

Station	X coordinate (ft FL State Plane 1983)	Y coordinate (ft FL State Plane 1983)	Temperature (°C)	Date	Source
POF-5	585924.00	1261680.00	24.0	22-May-79	DBHYDRO
POF-6	507392.00	1344504.00	24.0	23-May-79	DBHYDRO
PSL-RO1	869489.00	1081564.00	25.0		SFWMD
PWU-MZU	882488.00	934221.00	27.0	17-Jan-01	DBHYDRO
ROMP 10 OLIGOCENE	328127.00	981852.50	27.0	17-Jul-85	SWFWMD
ROMP 101 DEEP	358775.00	1499216.00	23.0	19-Feb-97	SWFWMD
ROMP 12 MID UP FLORIDAN	414558.50	984828.00	29.0	18-Sep-03	SWFWMD
ROMP 12 SH UP FLORIDAN	414497.00	984827.00	28.0	25-Sep-03	SWFWMD
ROMP 123 DEEP	251149.50	1216792.50	24.0	24-Oct-03	SWFWMD
ROMP 13 SWNN	455667.50	995825.50	28.0	23-Sep-03	SWFWMD
ROMP 14 SH FLORIDAN	541271.50	1023851.50	26.0	09-Mar-04	SWFWMD
ROMP 15 DEEP	442918.00	1045764.00	28.2		SFWMD
ROMP 16.5 AVON PARK	368488.50	992452.00	30.0	29-Sep-03	DBHYDRO
ROMP 16.5 SUWANNEE	368470.00	992422.00	27.0	29-Sep-03	DBHYDRO
ROMP 17 SWNN	338699.00	1033829.50	28.0	25-Sep-03	SWFWMD
ROMP 18 SUWANNEE	288814.50	1041019.00	27.0	13-Oct-03	SWFWMD
ROMP 20 SWNN	175296.00	1042505.00	28.0	01-Oct-03	SWFWMD
ROMP 22 SWNN	222174.50	1084911.50	25.0	29-Sep-03	SWFWMD
ROMP 25 LILY SUWANNEE	329332.00	1103695.33	28.0	17-Sep-03	SWFWMD
ROMP 26 AVON PARK	388342.00	1078991.00	31.0	30-Sep-03	SWFWMD
ROMP 28 SUWANNEE	514876.50	1103602.50	25.0	16-Oct-03	SWFWMD
ROMP 28 SUWANNEE OB-5	514895.50	1103500.00	26.0	21-Jun-04	SWFWMD
ROMP 28X DEEP	545830.00	1066255.50	25.0	24-Aug-00	SWFWMD
ROMP 30 AVON PARK	397813.00	1136915.00	26.6		SFWMD
ROMP 31 AVON PARK	359056.00	1135365.50	30.0	11-Mar-02	SWFWMD
ROMP 32 SUWANNEE	311169.00	1141807.50	27.0	17-Nov-03	SWFWMD
ROMP 33 SWNN	248513.50	1137647.50	26.0	03-Oct-03	SWFWMD
ROMP 35 SWNN	318100.00	1074282.00	28.0	15-Mar-05	SWFWMD
ROMP 39 SWNN	250814.50	1185212.50	27.0	10-Sep-03	SWFWMD
ROMP 40 AVON PARK	314896.00	1206124.50	27.0	22-Apr-04	SWFWMD
ROMP 43XX FLORIDAN	500713.00	1189202.00	26.1		SFWMD
ROMP 44 FLORIDAN	462869.50	1269340.00	24.0	17-May-99	SWFWMD
ROMP 45 SUWANNEE	401941.00	1247857.00	27.0	19-Nov-03	SWFWMD
ROMP 48 FLORIDAN	286590.50	1240204.50	24.0	19-Nov-03	SWFWMD
ROMP 49 SWN	250546.00	1248538.00	26.0	16-Sep-03	SWFWMD
ROMP 5 SWNN	393064.67	950320.67	30.0	22-Sep-03	SWFWMD
ROMP 5 SWNN	393098.00	950322.00	30.0	25-May-04	SWFWMD
ROMP 50 FLORIDAN	217039.50	1230219.00	25.0	24-Oct-03	SWFWMD
ROMP 51 - ELAPP	195944.50	1217491.00	28.0	17-Sep-03	SWFWMD
ROMP 57-1 FLORIDAN	455111.00	1298172.00	24.8		SFWMD
ROMP 58 OCALA	464380.93	1303983.88	25.7		SFWMD
ROMP 59 AVON PARK	377821.00	1292682.00	22.5		SFWMD
ROMP 60 DEEP	338815.00	1294295.50	26.5	17-Oct-03	SWFWMD
ROMP 61 AT PLEASANT	281144.00	1301241.00	26.0	04-Apr-00	SWFWMD
ROMP 67-2	222784.50	1355589.50	23.0	24-Jun-96	SWFWMD
ROMP 68-2 SUWANNEE	255359.00	1365226.50	24.0	11-Jan-99	SWFWMD
ROMP 70 FLORIDAN	348016.50	1359883.50	26.0	05-Mar-02	SWFWMD
ROMP 76A POLK CITY	388594.00	1399995.00	24.0	25-May-99	SWFWMD
ROMP 85 FLORIDAN	229946.00	1422385.00	24.0	14-Aug-03	SWFWMD
ROMP 86A SUWANNEE	280069.00	1405716.00	23.0	14-Feb-00	SWFWMD
ROMP 87 SHALLOW	326603.00	1414162.00	24.0	05-May-99	SWFWMD
ROMP 88 ROCK RIDGE	362919.00	1446738.00	24.0	05-May-99	SWFWMD
ROMP 9 OW15	282319.00	998646.00	27.0	26-Aug-96	USGS (Torres et al, WRI01-4015)
ROMP 9 SWNN	282283.50	998638.00	28.0	30-Sep-03	SWFWMD
ROMP 9.5 UP FL	315548.50	1016714.00	26.0	10-Oct-03	SWFWMD
ROMP 90 FLORIDAN	288873.66	1465346.33	25.0	07-Jun-94	SWFWMD
ROMP 93 DEEP	198470.00	1452908.00	25.0	17-Sep-97	SWFWMD
ROMP CL-1 FL	482823.00	1275015.00	24.4		SFWMD
ROMP CL-2 DEEP FL	490955.00	1244482.00	26.5		SFWMD

Table 3.2b: Temperature data (UF)

Station	X coordinate (ft FL State Plane 1983)	Y coordinate (ft FL State Plane 1983)	Temperature (°C)	Date	Source
ROMP CL-3 FLORIDAN	470768.00	1246803.00	25.0	19-May-99	SWFWMD
ROMP DV-1 SUWANNEE	265866.00	1331901.00	26.0	15-Sep-03	SWFWMD
ROMP TR 10-2 DEEP	212664.50	1299012.00	25.0	23-Sep-03	SWFWMD
ROMP TR 11-2	213862.50	1317621.50	25.0	03-Dec-03	SWFWMD
ROMP TR 1-2 SWNN	336141.00	912363.67	31.0	29-Apr-03	SWFWMD
ROMP TR 12-1 DEEP	156724.50	1325676.00	25.0	16-Apr-92	SWFWMD
ROMP TR 12-1 DP (NEW)	156724.50	1325675.00	25.0	22-Nov-04	SWFWMD
ROMP TR 12-3	158098.50	1339342.50	26.0	16-Apr-92	SWFWMD
ROMP TR 12-3 (NEW)	157403.00	1336476.50	25.0	18-Feb-04	SWFWMD
ROMP TR 13-1 SUWANNEE	82092.00	1306477.00	24.0	02-Jan-04	SFWMD
ROMP TR 13-2X SUWANNEE	100537.00	1303485.00	25.0	27-Jan-04	SFWMD
ROMP TR 14-1 SUWANNE	110780.00	1336784.00	24.0	23-Aug-88	SFWMD
ROMP TR 14-1 TAMPA	110691.00	1336785.00	24.0	24-Aug-99	SFWMD
ROMP TR 14-2 OCALA	89033.00	1346083.00	26.0	17-May-91	SFWMD
ROMP TR 14-2 TAMPA	89124.00	1346183.00	26.0	23-Dec-03	SFWMD
ROMP TR 14-3 SWNN	98337.00	1344637.00	25.0	05-Dec-03	SFWMD
ROMP TR 15-1 TAMPA	82261.00	1385688.00	25.0	23-Dec-03	SFWMD
ROMP TR 15-2 TAMPA	89576.00	1383661.00	25.0	31-Dec-03	SFWMD
ROMP TR 15-3 SWNN	95650.00	1382463.00	25.0	05-Dec-03	SFWMD
ROMP TR 16-2	105239.00	1429354.00	26.0	24-Sep-03	SWFWMD
ROMP TR 16-2 SHALLOW TRIPLE ZONE	105233.00	1429345.00	26.0	24-Sep-03	SWFWMD
ROMP TR 17-1 DEEP	108585.00	1453422.00	24.0	27-Nov-03	SWFWMD
ROMP TR 17-3 SUWANNE	116317.00	1453657.00	25.0	08-Sep-97	SWFWMD
ROMP TR 3-1 SUWANNEE	259339.50	950802.00	28.0	22-Sep-03	SWFWMD
ROMP TR 4-1 SUWANNEE	187117.50	992876.50	28.0	01-Oct-03	SWFWMD
ROMP TR 5-1 SUWANNEE	184117.50	1021392.50	26.0	30-Sep-03	SWFWMD
ROMP TR 5-2 SUWANNEE	202545.00	1028325.00	28.0	12-Sep-03	SWFWMD
ROMP TR 7-1	142781.00	1124989.00	26.0	26-Sep-03	SWFWMD
ROMP TR 7-2 SH FL	153302.00	1131245.50	26.0	03-Feb-04	SWFWMD
ROMP TR 7-4 SWNN	173098.00	1127600.00	27.0	18-Sep-03	SWFWMD
ROMP TR 8-1 NR RUBIO	155249.50	1184210.50	26.0	18-Sep-85	SWFWMD
ROMP TR 8-1 OCALA	155315.00	1184334.00	27.0	16-Sep-03	SWFWMD
ROMP TR 9-1	182630.50	1240815.50	25.0	04-Feb-04	SWFWMD
ROMP TR 9-2 SWNN	205631.00	1249927.00	27.0	15-Sep-03	SWFWMD
ROMP TR 9-3 SWNN	195921.00	1241221.50	27.0	05-Sep-03	SWFWMD
ROMP TR SA-1 SUWANNEE	154331.50	1098411.00	28.0	29-Sep-03	SWFWMD
ROMP20	177628.00	1040684.00	27.2		SFWMD
ROMP28_4	514895.00	1103485.00	25.0		SFWMD
ROMP29A	519841.00	1152172.00	23.3		SFWMD
ROY CLAYTON-HRS	134255.00	1485884.00	22.0	28-Feb-06	SWFWMD
RPB-MZU	906290.00	873439.00	24.0	12-Jan-00	DBHYDRO
SAWYER CB 4E FLDN REPL	218186.00	1473149.00	23.0	15-Feb-06	SWFWMD
SCC-MZU	418811.50	641147.50	29.0	14-Apr-05	DBHYDRO
SCRWWTPMW1	418849.00	641207.00	29.0		SFWMD
SCU-MZU	939265.00	917657.00	24.0	12-Oct-99	DBHYDRO
SLF-0049	819012.00	1092706.00	30.0	31-Aug-87	DBHYDRO
SLF-11	791282.00	1164690.00	27.0	06-Jul-04	DBHYDRO
SLF-13	781694.00	1116100.00	27.9		SFWMD
SLF-14	795303.00	1092198.00	29.0	06-Jul-04	SFWMD
SLF-16	795393.00	1089992.00	29.2		SFWMD
SLF-17	795581.00	1087368.00	27.8		SFWMD
SLF-18	800962.00	1071027.00	30.7		SFWMD
SLF-21	850164.00	1125345.00	26.0	06-Jul-04	DBHYDRO
SLF-23	828574.00	1049526.00	32.0	30-May-90	DBHYDRO
SLF-26	879872.00	1111576.00	24.0		SFWMD
SLF-27	814071.00	1111165.00	27.0		SFWMD
SLF-28	891152.00	1093968.00	24.0		SFWMD
SLF-31	852047.00	1068111.00	28.0		SFWMD
SLF-42	878899.00	1157115.00	25.0		SFWMD

Table 3.2b: Temperature data (UF)

Station	X coordinate (ft FL State Plane 1983)	Y coordinate (ft FL State Plane 1983)	Temperature (°C)	Date	Source
SLF-44	911120.00	1073791.00	24.0		SFWMD
SLF-45	877700.00	1162259.00	24.0		SFWMD
SLF-47	905883.00	1089007.00	24.0	31-May-90	DBHYDRO
SLF-48	843339.00	1077966.00	26.0	18-Nov-81	DBHYDRO
SLF-50	819192.00	1092403.00	28.0	15-Sep-87	DBHYDRO
SLF-53	803991.00	1131121.00	28.0		SFWMD
SLF-6	849545.00	1119700.00	25.0		SFWMD
SLF-60	786162.00	1071987.00	28.0	06-Jul-04	DBHYDRO
SLF-61	838334.00	1067038.00	25.6		SFWMD
SLF-62B	836003.00	1082784.00	29.0	04-Oct-04	DBHYDRO
SLF-63	783767.00	1144482.00	26.0		SFWMD
SLF-64	777699.00	1155672.00	26.6		SFWMD
SLF-65	772451.00	1164644.00	27.3		SFWMD
SLF-67	767933.00	1105760.00	27.0	17-Nov-93	DBHYDRO
SLF-69	836548.00	1101782.00	25.0	23-Jan-01	DBHYDRO
SLF-7	807717.00	1146483.00	27.6		SFWMD
SLF-75	821825.00	1092288.00	28.0	05-Oct-04	DBHYDRO
SLF-76	821842.00	1092293.00	29.0	16-Jun-04	DBHYDRO
SLF-9	789049.00	1131964.00	26.6		SFWMD
STL-216	823514.00	1141686.00	28.0	01-Jun-00	USGS (Reese, WRI03-4242)
STL-218	791281.00	1164690.00	28.0	01-Jun-00	USGS (Reese, WRI03-4242)
STL-224	850163.00	1125345.00	25.0	06-Jun-00	USGS (Reese, WRI03-4242)
STL-225	828500.00	1049408.00	30.0	30-May-90	USGS (Reese, WRI03-4242)
STL-228	879797.00	1111461.00	24.0	09-May-79	USGS (Reese, WRI03-4242)
STL-230	851973.00	1067994.00	28.0	29-Sep-77	USGS (Reese, WRI03-4242)
STL-243	849471.00	1119585.00	25.0		USGS (Reese, WRI03-4242)
STL-248	851159.00	1049510.00	30.0	29-Sep-77	USGS (Reese, WRI03-4242)
STL-255	883869.00	1060687.00	25.0	12-Jul-00	USGS (Reese, WRI03-4242)
STL-335	866645.00	1092405.00	27.0	12-Jul-00	USGS (Reese, WRI03-4242)
STL-346	820708.00	1122891.00	27.0	01-Jun-00	USGS (Reese, WRI03-4242)
STL-348	878824.00	1157001.00	25.0		USGS (Reese, WRI03-4242)
STL-350	911044.00	1073674.00	24.0		USGS (Reese, WRI03-4242)
STL-351	877625.00	1162145.00	24.0		USGS (Reese, WRI03-4242)
STL-352	880271.00	1155898.00	24.0	16-Jul-01	USGS (Reese, WRI03-4242)
STL-353	905808.00	1088891.00	24.0	06-Jun-00	USGS (Reese, WRI03-4242)
STL-355	818938.00	1092589.00	30.0	31-Aug-87	USGS (Reese, WRI03-4242)
STL-356	819119.00	1092388.00	28.0	20-Mar-96	USGS (Reese, WRI03-4242)
STL-357	819191.00	1092403.00	28.0	12-Mar-82	USGS (Reese, WRI03-4242)
STL-359	803918.00	1131006.00	28.0		USGS (Reese, WRI03-4242)
STL-375	836573.00	1101752.00	28.0	07-Jun-00	USGS (Reese, WRI03-4242)
STL-376	849442.00	1163211.00	27.0	25-Jul-01	USGS (Reese, WRI03-4242)
STL-382	821827.00	1092298.00	28.0	07-Jun-00	USGS (Reese, WRI03-4242)
STL-385	865817.00	1130371.00	25.0	25-Jul-01	USGS (Reese, WRI03-4242)
STL-388	869498.00	1081614.00	25.0	11-Jul-00	USGS (Reese, WRI03-4242)
STL-389	870587.00	1080408.00	25.0	11-Jul-00	USGS (Reese, WRI03-4242)
STL-391	836026.00	1082765.00	30.0	18-Jul-01	USGS (Reese, WRI03-4242)
STL-392	840438.00	1064709.00	31.0	11-Jul-00	USGS (Reese, WRI03-4242)
STL-47	811844.00	1131540.00	25.0	16-Jul-80	USGS (Reese, WRI03-4242)
STU-MZU	900033.00	1041129.00	24.0	15-Mar-06	DBHYDRO
SUN-MZU	873511.00	653626.00	24.0	21-Sep-99	DBHYDRO
W-14385	401942.00	1247879.00	27.0		SFWMD
W-14920	502147.00	584193.00	29.8		SFWMD
W-15332	254588.00	950250.00	25.1		SFWMD
W-15683	222843.00	944209.00	29.0	11-Sep-03	SFWMD
W-15826	157915.00	1182383.00	26.0		SFWMD
W-17001	541152.00	1023575.00	26.0		SFWMD
W-17056	282273.00	998464.00	28.0		SFWMD
W-17392	455829.00	995732.00	26.0		SFWMD
W-17452	154392.00	1098518.00	27.0		SFWMD

Table 3.2b: Temperature data (UF)

Station	X coordinate (ft FL State Plane 1983)	Y coordinate (ft FL State Plane 1983)	Temperature (°C)	Date	Source
W-17725	728142.00	1224927.00	25.5		SFWMD
W-18116	368569.00	992516.00	25.0		SFWMD
W-2861	866295.00	1034961.00	26.1		SFWMD
WA-1001	827924.00	1100200.00	28.0	03-Nov-87	USGS (Reese, WRI03-4242)
WA-1005	844869.00	1101386.00	28.0		SFWMD
WA-1016	836461.00	1106498.00	28.0		USGS (Reese, WRI03-4242)
WA-1032	884260.00	1151174.00	25.0		SFWMD
WA-1083	828066.00	1109188.00	25.0		USGS (Reese, WRI03-4242)
WA-1085	772299.00	1129690.00	27.0		USGS (Reese, WRI03-4242)
WA-1087	773959.00	1116467.00	26.0		USGS (Reese, WRI03-4242)
WA-1107	826918.00	1103629.00	26.0		SFWMD
WA-1113	825032.00	1101702.00	26.0	14-Apr-88	USGS (Reese, WRI03-4242)
WA-1119	768272.00	1119581.00	27.0	15-Apr-88	USGS (Reese, WRI03-4242)
WA-1121	817331.00	1111163.00	27.0	02-May-88	USGS (Reese, WRI03-4242)
WA-1136	820060.00	1105014.00	26.0		SFWMD
WA-1139	846147.00	1155419.00	27.0	06-May-88	USGS (Reese, WRI03-4242)
WA-1140	820061.00	1105014.00	28.0	16-May-88	USGS (Reese, WRI03-4242)
WA-1143	844301.00	1145817.00	27.0	18-May-88	USGS (Reese, WRI03-4242)
WA-1146	856101.00	1145672.00	26.0	18-May-88	USGS (Reese, WRI03-4242)
WA-1147	833504.00	1040644.00	28.0		SFWMD
WA-1151	835161.00	1115076.00	31.0	07-Jun-88	USGS (Reese, WRI03-4242)
WA-1155	849767.00	1132917.00	27.2		SFWMD
WA-1158	861258.00	1123380.00	28.0		USGS (Reese, WRI03-4242)
WA-117	788426.00	1074503.00	25.0		USGS (Reese, WRI03-4242)
WA-1183	822804.00	1095533.00	25.0	20-Jul-88	USGS (Reese, WRI03-4242)
WA-1186	820737.00	1093707.00	25.0	20-Jul-88	USGS (Reese, WRI03-4242)
WA-546	782854.00	1009455.00	27.8		SFWMD
WA-547	792007.00	1109556.00	27.0	01-Aug-85	USGS (Reese, WRI03-4242)
WA-562	846046.00	1081195.00	27.0	13-Nov-85	USGS (Reese, WRI03-4242)
WA-580	854245.00	1083254.00	29.0	27-Jan-86	USGS (Reese, WRI03-4242)
WA-611	858081.00	1073679.00	26.0		USGS (Reese, WRI03-4242)
WA-612	849801.00	1069296.00	26.0		USGS (Reese, WRI03-4242)
WA-625	871581.00	1046079.00	28.0		USGS (Reese, WRI03-4242)
WA-699	855680.00	1121534.00	26.0	25-Nov-86	USGS (Reese, WRI03-4242)
WA-708	871779.00	1127575.00	24.0	29-Dec-86	USGS (Reese, WRI03-4242)
WA-727	837980.00	1169520.00	29.0		USGS (Reese, WRI03-4242)
WA-815	875082.00	1133147.00	26.0	25-Jun-87	USGS (Reese, WRI03-4242)
WA-820	837880.00	1111856.00	26.0	27-Jul-87	USGS (Reese, WRI03-4242)
WA-829	830583.00	1089810.00	29.0	05-Aug-87	USGS (Reese, WRI03-4242)
WA-875	819378.00	1117634.00	27.0	18-Aug-87	USGS (Reese, WRI03-4242)
WA-877	857161.00	1131741.00	26.0	19-Aug-87	USGS (Reese, WRI03-4242)
WA-878	804694.00	1115861.00	28.0	25-Aug-87	USGS (Reese, WRI03-4242)
WA-879	859341.00	1128217.00	25.0	26-Aug-87	USGS (Reese, WRI03-4242)
WEL0055001095700	151613.00	1425227.00	24.0	11-Sep-97	SWFWMD
WEL0058000075400	423992.00	1422380.50	24.0	03-May-99	SWFWMD
WEL0062001079600	103728.00	1413292.00	26.0	17-Dec-03	SWFWMD
WEL0063001079500	115010.00	1411494.00	25.0	18-May-90	SWFWMD
WEL0064001077000	105004.00	1407535.00	26.0	09-Sep-03	SWFWMD
WEL0064001077100	105055.00	1407539.00	24.0	09-Sep-03	SWFWMD
WEL0067001077300	179659.00	1405766.00	24.0	11-Jun-01	SWFWMD
WEL0067001805500	180357.00	1406540.00	24.0	11-Jun-01	SWFWMD
WEL0070001077600	141771.50	1394764.00	23.0	16-Sep-99	SWFWMD
WEL0071001077700	99663.00	1393823.00	25.0	16-Dec-03	SFWMD
WEL0073001077900	149956.50	1392759.50	24.0	13-Jun-01	SWFWMD
WEL0074001078000	109594.00	1393177.00	25.0	15-May-90	SFWMD
WEL0075001078100	180517.50	1391394.00	25.0	22-Sep-99	SWFWMD
WEL0079001078500	111033.00	1380831.00	24.0	05-Feb-97	SFWMD
WEL0081001078700	126809.00	1373547.50	24.0	11-Jun-01	SWFWMD
WEL0083001078900	137756.00	1369875.00	23.0	11-Jun-01	SWFWMD

Table 3.2b: Temperature data (UF)

Station	X coordinate (ft FL State Plane 1983)	Y coordinate (ft FL State Plane 1983)	Temperature (°C)	Date	Source
WEL0108001081400	96447.00	1369316.00	26.0	20-Sep-93	SFWMD
WEL0110001081600	182205.00	1368037.50	24.0	13-Sep-99	SWFWMD
WEL0114001082100	102326.00	1366808.00	25.0	13-Feb-97	SFWMD
WEL0116001082200	110914.00	1365779.00	24.0	06-Dec-02	SFWMD
WEL0118001082400	148690.50	1364049.00	24.0	11-Jun-01	SWFWMD
WEL0126001083200	125342.50	1353255.50	24.0	27-Jan-04	SWFWMD
WEL0128001083400	150219.00	1349391.00	24.4		SFWMD
WEL0130001083600	182733.50	1348771.00	26.0	30-Jun-99	SWFWMD
WEL0131001083800	117500.00	1349421.00	25.0	09-Mar-04	SFWMD
WEL0133001084000	100634.00	1348545.00	25.0	15-May-90	SFWMD
WEL0138001084600	466713.00	1341340.00	25.4		SFWMD
WEL0141001084900	128277.00	1342054.50	25.0	10-May-90	SWFWMD
WEL0147000240900	178606.00	1338994.00	26.0	27-Jun-05	SWFWMD
WEL0274000000800	104967.00	1357072.00	24.0	13-Feb-97	SFWMD
WEL0293000002700	348103.00	1068488.00	26.1		SFWMD
WEL0295000002900	227615.00	1110892.00	27.5		SFWMD
WEL0311000004500	479739.00	1348147.00	24.9		SFWMD
WEL0322000005600	459154.00	1399704.50	24.0	29-Aug-85	SWFWMD
WEL0326000006000	123326.00	1395514.00	24.0	13-Aug-85	SFWMD
WEL0327000006100	291357.00	1397428.00	23.0	14-Aug-85	SWFWMD
WEL0347001774200	294771.01	1398103.18	23.0	14-Feb-00	SWFWMD
WEL0356000009300	174243.50	1378075.00	26.0	13-Jun-01	SWFWMD
WEL0361000009500	244610.00	1439462.00	25.0	13-May-99	SWFWMD
WEL0391000012500	221350.50	1336407.00	24.0	26-Jan-99	SWFWMD
WEL0408000014200	294629.50	1083251.00	26.0	23-Sep-03	SWFWMD
WEL0411000014500	145205.50	1341489.00	25.0	10-Aug-99	SWFWMD
WEL0411000014600	145267.50	1341484.50	27.0	09-Sep-03	SWFWMD
WEL0419000015300	458454.00	1157880.00	26.7		SFWMD
WEL0420000015400	188606.00	1381935.00	24.0	22-Sep-99	SWFWMD
WEL0435000016900	212793.50	1340762.00	24.0	30-Jan-04	SWFWMD
WEL0437000017100	296909.00	1436914.00	24.0	21-Sep-98	SWFWMD
WEL0439000017300	362836.00	1528182.00	24.0	08-May-96	SWFWMD
WEL0463000019700	155641.00	1101904.50	28.0	29-Dec-03	SWFWMD
WEL0495000022900	129502.00	1166454.00	25.0	30-Sep-03	SWFWMD
WEL0508000024200	115168.00	1472823.00	26.0	28-Nov-03	SWFWMD
WEL0510000024400	363962.50	1274317.50	24.0	28-Aug-85	SWFWMD
WEL0514000024800	418534.00	1394727.50	24.0	04-May-99	SWFWMD
WEL0545003730200	470530.00	982617.00	29.0	01-Oct-04	SFWMD
WEL0563000029700	103186.00	1338809.00	24.0	22-Dec-03	SFWMD
WEL0569000030300	118990.00	1399311.00	24.0	23-Jul-96	SFWMD
WEL0573000030700	101097.00	1336919.00	25.0	15-May-90	SFWMD
WEL0577000031100	180085.00	1358211.00	24.9		SFWMD
WEL0591000032500	213884.00	1313583.50	25.0	16-Sep-03	SWFWMD
WEL0595000032900	251771.00	1313261.50	24.0	19-Nov-03	SWFWMD
WEL0597000033100	156684.00	1371433.00	24.6		SFWMD
WEL0597000162500	158565.50	1371409.00	22.0	09-Feb-00	SWFWMD
WEL0608000034200	167068.50	1113192.50	26.0	31-Dec-03	SWFWMD
WEL0633000036700	233460.50	1116203.50	25.0	17-Feb-99	SWFWMD
WEL0684000041800	274159.00	1496380.00	23.0	08-Oct-85	SWFWMD
WEL0695000042900	206463.00	1266479.00	24.0		SFWMD
WEL0697000043100	121696.00	1411343.00	25.0	03-Sep-97	SWFWMD
WEL0700000043400	160205.00	1392454.50	24.0	22-Sep-99	SWFWMD
WEL0702000043600	391321.00	1471566.00	24.0	11-Aug-94	SWFWMD
WEL0739000047300	165099.00	1370923.00	24.7		SFWMD
WEL0743000047700	469268.50	1427480.50	24.0	12-May-99	SWFWMD
WEL0764000049800	220237.00	1453011.00	24.0	16-Feb-06	SWFWMD
WEL0777000051100	451834.00	1077226.00	26.5		SFWMD
WEL0786000052000	188126.00	1342939.00	26.0	24-Nov-03	SWFWMD
WEL0804000053800	423039.00	1366925.00	25.3		SFWMD

Table 3.2b: Temperature data (UF)

Station	X coordinate (ft FL State Plane 1983)	Y coordinate (ft FL State Plane 1983)	Temperature (°C)	Date	Source
WEL0815000054900	379996.00	1205305.00	26.5		SFWMD
WEL0827000056100	194558.50	1090852.00	26.0	10-Nov-03	SWFWMD
WEL0830000056400	254370.00	1144757.00	26.6		SFWMD
WEL0851000058500	156039.50	1362260.00	25.0	29-Jun-99	SWFWMD
WEL0859000059300	134469.00	1437376.00	24.0	03-Sep-97	SWFWMD
WEL0871000060500	484918.00	1240165.00	25.4		SFWMD
WEL0879000061300	233541.50	1371958.50	24.0	14-Mar-00	SWFWMD
WEL0909000064300	226766.00	1283528.00	24.8		SFWMD
WEL0919000065300	160074.00	1198237.00	27.1		SFWMD
WEL0921000065500	149641.00	1378749.50	24.0	22-Sep-99	SWFWMD
WEL0926000066000	259345.50	1388638.50	24.0	14-Mar-00	SWFWMD
WEL0938000067200	347644.00	995779.00	28.0		SFWMD
WEL0991001766200	274787.00	1418695.00	26.0	20-Dec-99	SWFWMD
WEL0994000072800	107609.00	1366532.00	24.0	10-May-91	SFWMD
WEL0994000072900	107610.00	1366532.00	24.0	10-May-91	SFWMD
WEL0996000073000	337430.00	996059.00	27.9		SFWMD
WEL1003000073700	261581.00	1345494.00	24.0	25-Jan-99	SWFWMD
WEL1006000074000	148088.50	1384968.00	24.0	12-Jun-01	SWFWMD
WEL1014000074800	104202.00	1391839.00	25.0	15-Jan-04	SFWMD
WEL1035000075800	385201.00	1202274.00	28.0	14-Oct-03	SWFWMD
WEL1148001167200	427348.00	984309.50	31.0	19-Sep-03	SWFWMD
WEL1212001184500	237827.00	1302198.00	26.0		SFWMD
WEL1213001183700	256830.00	1296811.50	26.0	17-Sep-91	SWFWMD
WEL1216001170700	306699.50	1324511.00	24.0	06-Sep-91	SWFWMD
WEL1218001184900	240547.50	1276364.50	24.0	25-Jun-92	SWFWMD
WEL1219001183800	259301.00	1313996.00	25.0	17-Sep-91	SWFWMD
WEL1220001184200	268423.00	1298809.00	24.0	01-Oct-91	SWFWMD
WEL1221001183900	260998.00	1295292.00	25.0		SFWMD
WEL1222001184100	240241.00	1284293.00	23.0		SFWMD
WEL1223001169600	242891.50	1388362.00	23.0	19-Nov-03	SWFWMD
WEL1227001183600	262603.00	1312246.00	23.0		SFWMD
WEL1231001184700	233757.50	1304821.00	25.0	23-Jun-92	SWFWMD
WEL1234001182800	267750.00	1342902.00	23.0		SFWMD
WEL1323000086200	329739.00	1005004.50	26.0	10-Oct-03	SWFWMD
WEL1327000086600	386720.00	998520.50	30.0	30-Oct-03	SWFWMD
WEL1329000086800	418815.00	998153.50	28.0	13-Feb-03	SWFWMD
WEL1332000087100	442352.50	991013.00	28.5	19-Sep-03	SFWMD
WEL1333000087200	399655.50	986532.50	30.0	26-Jun-00	SWFWMD
WEL1416000095500	526397.50	1122259.50	23.0	09-Jan-01	SWFWMD
WEL1420000095900	147079.00	1388380.00	24.0	23-Sep-99	SWFWMD
WEL1421000096000	217378.50	1300453.50	24.0	12-Feb-99	SWFWMD
WEL1422000262500	211231.00	1303261.00	24.0	21-Feb-07	SWFWMD
WEL1425000096400	129888.00	1384430.50	25.0	12-Jun-01	SWFWMD
WEL1426000096500	240487.50	1296264.50	25.0	30-Sep-91	SWFWMD
WEL1427000096600	192649.00	1244227.00	25.0	13-Jan-04	SWFWMD
WEL1428000096700	169537.00	1362200.00	24.0	20-Sep-99	SWFWMD
WEL1429000096800	156424.00	1357776.50	25.0	30-Jun-99	SWFWMD
WEL1431000097000	166070.00	1305224.50	24.0	11-Feb-04	SWFWMD
WEL1432000097100	218638.50	1312025.00	24.0	14-Feb-01	SWFWMD
WEL1433000097200	180666.50	1314818.50	22.0	29-Apr-92	SWFWMD
WEL1434000097300	143169.50	1378173.50	24.0	13-Jun-01	SWFWMD
WEL1438000097700	174842.50	1330143.50	22.0	24-Jan-97	SWFWMD
WEL1439000097800	245132.50	1311434.00	25.0	24-Sep-91	SWFWMD
WEL1441000098000	259514.00	1305261.00	25.0	26-Sep-91	SWFWMD
WEL1446000098500	209651.50	1271288.50	24.0	12-Feb-04	SWFWMD
WEL1447000098600	234459.50	1311682.00	28.0	24-Sep-91	SWFWMD
WEL1449000098800	130450.00	1383750.50	24.0	27-Sep-99	SWFWMD
WEL1450000098900	230553.50	1298895.50	24.0	30-Apr-92	SWFWMD
WEL1454000099300	150737.50	1335640.00	25.0	04-Dec-03	SWFWMD

Table 3.2b: Temperature data (UF)

Station	X coordinate (ft FL State Plane 1983)	Y coordinate (ft FL State Plane 1983)	Temperature (°C)	Date	Source
WEL1456000099500	249911.50	1339903.50	23.0	05-Sep-91	SWFWMD
WEL1457000099600	131295.00	1386669.00	22.0	23-Sep-99	SWFWMD
WEL1458000099700	146085.00	1390073.50	26.0	12-Jun-01	SWFWMD
WEL1461000100000	153771.50	1372533.50	24.0	20-Sep-99	SWFWMD
WEL1464000100300	265546.50	1343584.50	24.0	04-Sep-91	SWFWMD
WEL1466000100500	257254.50	1330233.00	24.0	11-Sep-91	SWFWMD
WEL1468000100700	152357.50	1374067.00	23.0	23-Sep-99	SWFWMD
WEL1472000101100	136675.00	1387203.50	24.0	23-Sep-99	SWFWMD
WEL1473000101200	150073.00	1370560.50	24.0	23-Sep-99	SWFWMD
WEL1474000101300	154097.50	1373813.50	24.0	13-Jun-01	SWFWMD
WEL1475000101400	143821.50	1385795.50	26.0	20-Sep-00	SWFWMD
WEL1476000101500	280259.00	1335461.50	25.0	05-Sep-91	SWFWMD
WEL1481000102000	239195.50	1301429.50	26.0	22-Jun-92	SWFWMD
WEL1483000102200	244834.00	1285760.00	24.0		SFWMD
WEL1484000102300	263034.50	1298357.00	24.0	26-Sep-91	SWFWMD
WEL1485000102400	257208.50	1334576.50	24.0	12-Nov-91	SWFWMD
WEL1488000102700	242126.00	1275687.00	25.0		SFWMD
WEL1489000102800	242380.50	1305638.50	26.0	25-Sep-91	SWFWMD
WEL1491000103000	276834.00	1314888.50	25.0	11-Sep-91	SWFWMD
WEL1495000103400	250304.00	1311361.00	24.0		SFWMD
WEL1496000103500	266386.00	1301556.00	25.0	02-Oct-91	SWFWMD
WEL1497000103600	239042.00	1281275.00	24.0		SFWMD
WEL1499000103800	263441.00	1288197.00	23.0		SFWMD
WEL1503000104200	244297.00	1308750.00	24.0	24-Sep-91	SWFWMD
WEL1504000104300	286325.00	1284294.50	24.0	20-Sep-91	SWFWMD
WEL1505000104400	237657.00	1294623.00	25.0		SFWMD
WEL1506000104500	266221.00	1321153.00	25.0	12-Sep-91	SWFWMD
WEL1508000104700	256327.00	1294834.00	23.0		SFWMD
WEL1512000105100	137748.50	1339605.00	25.0	20-Nov-91	SWFWMD
WEL1513000105200	249126.50	1324659.50	24.0	16-Sep-91	SWFWMD
WEL1517000105600	238492.50	1319821.00	24.0	03-Apr-00	SWFWMD
WEL1519000105800	150827.00	1347653.50	25.0	06-May-91	SWFWMD
WEL1520000105900	173845.50	1314598.00	28.0	08-May-91	SWFWMD
WEL1521000106000	233820.50	1319063.00	24.0	16-Sep-91	SWFWMD
WEL1523000106200	309212.00	1395697.50	23.0	14-Sep-98	SWFWMD
WEL1524000106300	248835.50	1313854.00	24.0	17-Sep-91	SWFWMD
WEL1525000106400	179936.50	1387764.50	23.0	21-Nov-96	SWFWMD
WEL1526000106500	254603.50	1289957.00	24.0	17-Sep-91	SWFWMD
WEL1528000106700	252595.00	1298509.00	25.0		SFWMD
WEL1530000106900	251859.50	1302510.00	25.0	18-Sep-91	SWFWMD
WEL1532000107100	250718.50	1322522.00	25.0	16-Sep-91	SWFWMD
WEL1534000107300	248640.50	1303654.00	26.0	19-Sep-91	SWFWMD
WEL1535000107400	244349.50	1287941.50	24.0	19-Sep-91	SWFWMD
WEL1540000107900	248946.50	1299788.50	25.0	18-Sep-91	SWFWMD
WEL1542000108100	238346.50	1289014.50	24.0	23-Sep-91	SWFWMD
WEL1549000108800	219904.50	1392512.50	25.0	13-Aug-03	SWFWMD
WEL1550000108900	219902.50	1393910.00	25.0	13-Aug-03	SWFWMD
WEL1552000109100	197184.00	1341541.00	24.0	25-Feb-04	SWFWMD
WEL1553000109200	278058.00	1296136.00	24.0		SFWMD
WEL1554000109300	249555.50	1305362.00	24.0	02-Oct-91	SWFWMD
WEL1564000110300	154018.50	1121596.50	27.0	16-Feb-95	SWFWMD
WEL1565000110400	139617.00	1177290.00	24.0	17-Feb-04	SWFWMD
WEL1566000110500	114524.00	1143466.00	26.0	26-Sep-03	SWFWMD
WEL1567000110600	112408.00	1153597.00	26.0	26-Sep-03	SWFWMD
WEL1570000110900	285394.00	1138078.00	26.0	22-Dec-03	SWFWMD
WEL1571000111000	122322.00	1140331.00	25.0	10-Dec-01	SWFWMD
WEL1578000111700	177265.00	1135758.50	27.0		SFWMD
WEL1636000117500	163501.00	1473588.00	24.0	13-Oct-94	SWFWMD
WEL1638000117700	110149.00	1456744.00	25.0	27-Nov-03	SWFWMD

Table 3.2b: Temperature data (UF)

Station	X coordinate (ft FL State Plane 1983)	Y coordinate (ft FL State Plane 1983)	Temperature (°C)	Date	Source
WEL1639000117800	166702.00	1458192.00	24.0	13-Oct-94	SWFWMD
WEL1640000117900	106086.00	1438703.00	25.0	17-Dec-03	SWFWMD
WEL1643000118200	168963.00	1488774.00	25.0	29-Aug-95	SWFWMD
WEL1644000118300	215354.00	1425735.00	23.0	17-Nov-03	SWFWMD
WEL1646000118500	118309.00	1472695.00	25.0	08-Dec-03	SWFWMD
WEL1647000118600	204859.00	1422048.00	23.0	16-Oct-01	SWFWMD
WEL1648000187500	212471.00	1408531.00	25.0	12-May-03	SWFWMD
WEL1649000118800	235801.00	1417178.00	24.0	11-Aug-03	SWFWMD
WEL1651000119000	122328.00	1484411.00	23.0	08-Dec-03	SWFWMD
WEL1652000119100	210685.00	1435135.00	22.0	17-Nov-03	SWFWMD
WEL1653000119200	121197.00	1493142.00	24.0	28-Nov-03	SWFWMD
WEL1653000135400	121277.00	1493243.00	24.0	28-Nov-03	SWFWMD
WEL1654000119300	207648.00	1435473.00	22.0	21-Nov-96	SWFWMD
WEL1655000119400	98073.00	1437854.00	25.0	27-Nov-03	SWFWMD
WEL1656000119500	96012.00	1411521.00	26.0	08-Dec-03	SWFWMD
WEL1657000119600	126679.00	1285244.00	26.0	27-Nov-91	SFWMD
WEL1661000120000	84416.00	1398286.00	27.0	25-Nov-91	SFWMD
WEL1662000120100	86290.00	1373302.00	26.0	13-May-91	SFWMD
WEL1664000120300	133432.00	1273031.00	26.0	07-May-91	SFWMD
WEL1664000135600	133435.00	1273233.00	24.0	09-Mar-04	SFWMD
WEL1670000120900	88196.00	1343974.00	25.0	23-Dec-03	SFWMD
WEL1671000121000	95605.00	1354274.00	25.0	03-Apr-97	SFWMD
WEL1672000121100	94876.00	1271335.00	23.0	27-Nov-02	SFWMD
WEL1673000121200	90419.00	1286352.00	24.0	16-Dec-03	SFWMD
WEL1674000121300	103652.00	1327285.00	24.0	19-Feb-96	SFWMD
WEL1675000121400	79237.00	1338345.00	24.6	23-Dec-03	SFWMD
WEL1676000121500	83402.00	1322623.00	25.0	07-Dec-99	SFWMD
WEL1678000121700	103304.00	1270207.00	24.0	02-Jan-04	SFWMD
WEL1679000121800	128034.00	1279063.00	25.0	24-Mar-95	SFWMD
WEL1682000122100	112021.00	1374553.00	23.0	26-Feb-97	SFWMD
WEL1683000122200	98900.00	1257235.00	25.0	16-Jan-98	SFWMD
WEL1684000122300	111654.00	1373952.00	24.0	05-Mar-96	SFWMD
WEL1690000122900	336089.50	1356714.50	27.0	21-Mar-00	SWFWMD
WEL1696000123500	433489.00	1330001.00	25.5		SFWMD
WEL1699000123800	236526.00	1028767.50	29.0	03-Oct-03	SWFWMD
WEL1701000124000	195261.00	1017830.50	28.0	30-Sep-03	SWFWMD
WEL1723000126200	247281.00	1020474.00	26.0	10-Nov-03	SWFWMD
WEL1725000126400	171397.00	1061932.50	27.0	14-Jan-99	SWFWMD
WEL1726000126500	211768.00	996541.50	26.0	29-Jan-03	SWFWMD
WEL1783001184600	239246.45	1275111.25	25.5		SFWMD
WEL1784001182700	267832.00	1351286.00	23.0		SFWMD
WEL1789001183500	240007.50	1318896.00	24.0	16-Sep-91	SFWMD
WEL1792001170400	164771.50	1320771.50	26.0	29-Mar-00	SWFWMD
WEL1796001183300	229054.00	1317902.00	24.0	13-Sep-91	SWFWMD
WEL1798001183200	291181.00	1333742.50	24.0	10-Sep-91	SWFWMD
WEL1801001182900	288981.06	1331991.62	25.0	05-Sep-91	SWFWMD
WEL1802001183400	233605.50	1332499.50	24.0	13-Sep-91	SWFWMD
WEL1805001170100	268733.50	1348603.00	24.0	05-Sep-91	SWFWMD
WEL1811001172800	177372.00	1184204.00	27.0	17-Sep-03	SWFWMD
WEL1876000132800	162820.50	1373660.50	26.0	09-Sep-99	SWFWMD
WEL1880000133200	235630.00	1315050.00	25.0		SFWMD
WEL1895000135200	92893.00	1406266.00	22.0	08-Dec-03	SWFWMD
WEL1898000135700	444313.00	1425080.00	25.5		SFWMD
WEL1910000137200	228369.50	1204272.00	25.0	10-Nov-03	SWFWMD
WEL1912000137400	123480.00	1387126.00	24.0	17-Feb-97	SFWMD
WEL1915000137800	124277.00	1379841.00	23.0	19-Feb-97	SFWMD
WEL1918000138100	117926.00	1373966.00	22.0	19-Feb-97	SFWMD
WEL1938000140500	103446.00	1363660.00	25.0	26-Feb-97	SFWMD
WEL1939000140600	244662.00	1081887.00	26.0	18-Aug-99	SWFWMD

Table 3.2b: Temperature data (UF)

Station	X coordinate (ft FL State Plane 1983)	Y coordinate (ft FL State Plane 1983)	Temperature (°C)	Date	Source
WEL1941000140800	337962.50	1408786.00	24.0	26-May-98	SWFWMD
WEL1955000142200	270718.00	1428433.00	25.0	11-May-99	SWFWMD
WEL1956000142300	290908.00	1445006.00	24.0	12-May-99	SWFWMD
WEL1962001312100	124618.00	1487576.00	23.0	28-Nov-03	SWFWMD
WEL1979001315900	112300.00	1362324.00	24.0	26-Feb-97	SFWMD
WEL1987001315100	318380.50	1379356.00	24.0	27-May-98	SWFWMD
WEL1989001314900	248232.00	1399470.00	23.0	14-Sep-98	SWFWMD
WEL1990001314800	255171.00	1438792.00	24.0	03-Apr-00	SWFWMD
WEL1992001314600	275719.00	1445960.00	24.0	12-May-99	SWFWMD
WEL1993001314500	259172.00	1410165.00	25.0	19-May-98	SWFWMD
WEL1994001314400	293021.00	1422260.00	23.0	10-May-00	SWFWMD
WEL1995001314300	233175.00	1447208.00	24.0	11-May-99	SWFWMD
WEL1996001314000	275011.00	1410109.00	24.0	14-Sep-98	SWFWMD
WEL1997001313900	273959.00	1403250.00	24.0	15-Sep-98	SWFWMD
WEL1998001319400	269973.00	1434501.00	24.0	26-May-98	SWFWMD
WEL1999001313800	271274.00	1439539.00	23.0	12-May-99	SWFWMD
WEL2002001313500	284434.00	1403553.00	22.0	14-Sep-98	SWFWMD
WEL2003001313400	268617.00	1433101.00	24.0	12-May-99	SWFWMD
WEL2005001313200	336092.00	1387994.50	24.0	27-May-98	SWFWMD
WEL2006001313100	296603.50	1387326.50	24.0	20-May-98	SWFWMD
WEL2007001313000	278757.00	1427345.00	26.0	10-May-99	SWFWMD
WEL2010001312800	344205.50	1406210.50	23.0	26-May-98	SWFWMD
WEL2011001312700	343489.50	1406216.00	24.0	26-May-98	SWFWMD
WEL2014001053100	261611.00	1447716.00	25.0	15-Sep-98	SWFWMD
WEL2018001318500	258502.00	1422091.00	24.0	28-May-98	SWFWMD
WEL2019001318600	264297.00	1419834.00	25.0	11-May-99	SWFWMD
WEL2020001318700	254576.00	1410075.00	24.0	16-Sep-98	SWFWMD
WEL2022001318900	290854.00	1408016.00	26.0	28-May-98	SWFWMD
WEL2025001319900	210366.00	1435785.00	23.0	17-Nov-03	SWFWMD
WEL2026001320000	323574.00	1410926.00	24.0	27-May-98	SWFWMD
WEL2027001320100	329116.00	1399566.50	24.0	27-May-98	SWFWMD
WEL2030001320400	262103.00	1408014.00	24.0	19-May-98	SWFWMD
WEL2031001320500	265250.00	1409498.00	25.0	10-May-99	SWFWMD
WEL2032001320600	261225.00	1418528.00	26.0	10-May-99	SWFWMD
WEL2034001320800	276448.00	1438276.00	24.0	12-May-99	SWFWMD
WEL2035001320900	266126.00	1443328.00	23.0	13-May-99	SWFWMD
WEL2036001321000	278884.00	1412697.00	23.0	12-May-99	SWFWMD
WEL2037001321100	288056.00	1455336.00	24.0	12-May-99	SWFWMD
WEL2038001321200	304222.00	1388267.50	24.0	14-Feb-00	SWFWMD
WEL2040001321800	273026.00	1399320.00	24.0	26-May-98	SWFWMD
WEL2040001321801	273027.00	1399320.00	26.0	26-May-98	SWFWMD
WEL2041001321901	277339.00	1401096.00	24.0	26-May-98	SWFWMD
WEL2042001322001	272062.00	1401451.00	24.0	26-May-98	SWFWMD
WEL2044001321700	258097.00	1453813.00	22.0	14-Feb-00	SWFWMD
WEL2045001324000	277948.50	1134132.00	29.0	24-Feb-03	SWFWMD
WEL2076001334300	219949.50	1340663.00	24.0	04-Mar-03	SWFWMD
WEL2118001342500	187377.00	1401701.00	24.0	17-Nov-03	SWFWMD
WEL2120000147700	186851.00	1401775.00	24.0	30-Nov-98	SWFWMD
WEL2136000149200	394280.00	1036151.00	28.0	03-Aug-05	SFWMD
WEL2289001760500	297618.00	1428486.00	22.0	17-Jan-00	SWFWMD
WEL2290001760400	287157.00	1415455.00	22.0	17-Jan-00	SWFWMD
WEL2292001760200	276423.00	1431085.00	24.0	17-Jan-00	SWFWMD
WEL2318001767900	269460.00	1405152.00	23.0	20-Dec-99	SWFWMD
WEL2337003447700	389872.00	981257.50	29.0	06-Sep-05	SWFWMD
WEL2337003447800	379146.00	971835.00	26.0	07-Sep-05	SWFWMD
WEL2391000168700	231830.50	1110148.50	28.0	24-Oct-00	SWFWMD
WEL2392000168800	175057.50	1113107.50	27.0	27-Oct-00	SWFWMD
WEL2400001804700	115204.00	1471463.00	24.0	19-Dec-03	SWFWMD
WEL2401002196500	429036.98	968587.36	28.1		SFWMD

Table 3.2b: Temperature data (UF)

Station	X coordinate (ft FL State Plane 1983)	Y coordinate (ft FL State Plane 1983)	Temperature (°C)	Date	Source
WEL2430002073600	382129.00	1028758.00	31.0	20-Feb-03	SFWMD
WEL2448000174800	240012.00	1181288.00	26.0	14-Feb-01	SWFWMD
WEL2449000175000	140534.00	1094045.00	28.0	23-Oct-00	SWFWMD
WEL2451000175200	347539.00	995586.00	26.0	02-Jan-01	SWFWMD
WEL2453000175400	305245.00	1183469.00	24.9		SFWMD
WEL2454000175500	412845.00	1149647.00	28.3		SFWMD
WEL2456000175700	246510.00	1204329.00	26.8		SFWMD
WEL2457000175800	243624.50	1161235.00	26.0	27-Jul-01	SWFWMD
WEL2459000176000	206031.00	1237498.00	25.0	25-Jul-01	SWFWMD
WEL2464000176500	180810.50	1102214.50	27.0	26-Oct-00	SWFWMD
WEL2466000176700	213054.00	1276025.00	26.0	16-Feb-01	SWFWMD
WEL2467000176800	191129.50	1223829.50	24.0	16-Feb-01	SWFWMD
WEL2473002812200	408723.00	1034950.00	30.0	13-Oct-05	SFWMD
WEL2473003536900	410221.00	1028781.00	30.0	13-Oct-05	SFWMD
WEL2474000177500	465243.00	1184306.00	30.5		SFWMD
WEL2476000177700	206775.50	1166573.00	30.0	12-Feb-01	SWFWMD
WEL2523001063300	393977.00	974653.00	31.0	02-Jan-03	SFWMD
WEL2523001252500	395427.00	974257.00	27.0	04-Dec-01	SWFWMD
WEL2526001253700	238366.50	1128357.50	26.0	10-Jan-01	SWFWMD
WEL2527001269000	186355.50	1029035.00	26.0	23-Oct-00	SWFWMD
WEL2528001383400	207326.00	1249284.00	26.0	01-Mar-01	SWFWMD
WEL2531001583800	206866.00	1238594.00	26.8		SFWMD
WEL2532001592900	287533.00	1293525.00	26.0	24-Sep-01	SWFWMD
WEL2533001602800	405466.00	1034162.00	30.3	13-Oct-00	SFWMD
WEL2533001602801	405467.00	1034162.00	29.0	16-Apr-03	SFWMD
WEL2534001603300	301143.00	1289966.50	26.7	24-Sep-01	SFWMD
WEL2536001628000	352159.50	1004918.50	31.0	15-Oct-03	SWFWMD
WEL2539001795600	398465.00	1069853.00	32.0	16-Nov-00	SWFWMD
WEL2541001797300	435180.42	967140.14	31.2		SFWMD
WEL2542001797400	193809.00	1087830.00	28.6		SFWMD
WEL2547000237800	400608.99	979357.59	25.9		SFWMD
WEL2547001293900	399430.00	978860.00	30.0	14-Jan-04	SFWMD
WEL2547001797900	404785.04	981957.38	27.5		SFWMD
WEL2547002299400	396213.00	984939.00	29.0	14-Jan-04	SFWMD
WEL2547002299500	391877.00	985674.00	30.0	14-Jan-04	SFWMD
WEL2547002299600	405224.00	979733.00	29.0	14-Jan-04	SFWMD
WEL2558001820100	132080.00	1101916.00	25.0	12-Feb-01	SWFWMD
WEL2561000232700	384238.00	951793.00	28.0		SFWMD
WEL2561001634000	385030.50	958951.00	32.0	19-Jun-02	SWFWMD
WEL2561003116400	385788.50	954389.00	32.0	19-Jun-02	SWFWMD
WEL2562000183800	264229.00	1249806.00	26.7		SFWMD
WEL2564001820200	388150.00	1202619.00	25.0	09-Jan-01	SWFWMD
WEL2587001831700	107389.00	1344409.00	24.0	29-Mar-00	SFWMD
WEL2648001843700	228734.00	1422793.00	23.0	29-Mar-00	SWFWMD
WEL2649001843800	137947.00	1384002.00	25.0	29-Mar-00	SWFWMD
WEL2692001305500	402757.00	990251.00	30.0	05-Jun-01	SFWMD
WEL2692001305501	402756.00	990251.00	28.0	11-Feb-02	SFWMD
WEL2692001601600	402674.00	991564.00	28.0	25-Mar-03	SFWMD
WEL2692002270800	401507.00	992783.00	30.0	05-Jun-01	SFWMD
WEL2692002270801	401506.00	992783.00	28.0	05-Nov-03	SFWMD
WEL2692002271000	407925.02	992743.52	28.6		SFWMD
WEL2692002271101	406734.00	990226.00	28.0	05-Nov-03	SFWMD
WEL2692003803000	407472.00	992645.00	29.0	09-Mar-04	SFWMD
WEL2702001064500	389998.00	1016588.00	31.0	26-Jun-01	SFWMD
WEL2702001064501	389999.00	1016588.00	31.0	16-Apr-03	SFWMD
WEL2702001259300	390397.00	1008405.00	33.0	26-Jun-01	SFWMD
WEL2702001492000	389472.00	1005079.00	30.9	26-Jun-01	SFWMD
WEL2702001561200	388693.00	1010436.00	30.0	26-Jun-01	SFWMD
WEL2702002732300	389398.00	1007604.00	31.0	26-Jun-01	SFWMD

Table 3.2b: Temperature data (UF)

Station	X coordinate (ft FL State Plane 1983)	Y coordinate (ft FL State Plane 1983)	Temperature (°C)	Date	Source
WEL2702002732400	393663.00	1010303.00	30.0	26-Jun-01	SFWMD
WEL2702002732501	396194.00	1010388.00	28.0	05-Nov-03	SFWMD
WEL2702002732600	393458.00	1006568.00	32.3	22-Apr-03	SFWMD
WEL2702002732700	394886.00	1003731.00	30.0		SFWMD
WEL2702002732800	397339.00	1005533.00	31.0	26-Jun-01	DBHYDRO
WEL2702002732801	397338.00	1005533.00	29.0	05-Nov-03	DBHYDRO
WEL2702002732901	395096.00	1008375.00	30.0	05-Nov-03	SFWMD
WEL2702002733001	395089.00	1007163.00	30.0	05-Nov-03	SFWMD
WEL2702002733200	389391.00	1006594.00	30.0	26-Jun-01	DBHYDRO
WEL2702002733201	389392.00	1006594.00	28.0	05-Nov-03	DBHYDRO
WEL2705001285300	395238.00	1002315.00	30.0		SFWMD
WEL2706000189201	400239.00	1007030.00	28.0	06-Nov-03	SFWMD
WEL2707000189301	358858.00	1008723.00	29.0		SFWMD
WEL2707000189400	357071.00	1011463.00	30.9	18-Jun-02	SFWMD
WEL2707000189401	357072.00	1011463.00	29.1	22-Apr-03	SFWMD
WEL2719001430900	233731.50	1255982.00	27.0	02-Oct-01	SWFWMD
WEL2723003105700	414773.00	988865.00	31.0	11-Sep-01	SFWMD
WEL2724003105600	409345.00	988393.00	28.7	11-Sep-01	SFWMD
WEL2725003105500	412239.00	988274.00	29.0	11-Sep-01	SFWMD
WEL2725003105501	412238.00	988274.00	29.0	04-Nov-03	SFWMD
WEL2726003105400	412789.00	989584.00	29.0	11-Sep-01	SFWMD
WEL2726003105401	412788.00	989584.00	29.0	04-Nov-03	SFWMD
WEL2727003105300	412254.00	990799.00	28.0	11-Sep-01	SFWMD
WEL2727003105301	412253.00	990799.00	28.0	04-Nov-03	SFWMD
WEL2728003105200	408996.00	990212.00	29.0	11-Sep-01	SFWMD
WEL2728003105201	408995.00	990212.00	29.0	19-Oct-04	SFWMD
WEL2729003105100	413975.00	991395.00	30.0	11-Sep-01	SFWMD
WEL2729003105102	413974.00	991395.00	28.0	04-Nov-03	SFWMD
WEL2730003105000	412172.00	992213.00	28.0	11-Sep-01	SFWMD
WEL2730003105001	412171.00	992213.00	29.0	22-Apr-03	SFWMD
WEL2731003104900	409731.00	992228.00	30.0	11-Sep-01	SFWMD
WEL2731003104902	409730.00	992228.00	30.0	19-Oct-04	SFWMD
WEL2791002647700	143425.00	1183995.00	30.0	30-Aug-01	SWFWMD
WEL2793002392100	181201.50	1204445.00	26.0	01-Mar-01	SWFWMD
WEL2794003144200	154441.50	1101654.00	27.0	12-Feb-01	SWFWMD
WEL2844000215300	359018.00	1018316.00	31.0	09-May-02	DBHYDRO
WEL2862001114400	456568.00	993690.00	28.0	19-Mar-02	SFWMD
WEL2862001114500	457647.00	992372.00	31.0	19-Mar-02	SFWMD
WEL2862001114501	457646.00	992372.00	28.0	28-Feb-03	SFWMD
WEL2862001114600	457189.00	991162.00	28.0	19-Mar-02	SFWMD
WEL2862001115200	459542.00	991555.00	31.0	19-Mar-02	SFWMD
WEL2862001115201	459541.00	991555.00	29.0		SFWMD
WEL2862001115300	456106.00	991672.00	28.0	19-Mar-02	SFWMD
WEL2862001115600	458722.00	990448.00	28.0	19-Mar-02	SFWMD
WEL2862001115700	456823.00	990457.00	30.0	19-Mar-02	SFWMD
WEL2862001232100	456566.00	993286.00	28.0	19-Mar-02	SFWMD
WEL2897001000600	460763.00	1001344.00	27.9	13-Mar-03	SFWMD
WEL2897001003600	457334.00	1002572.00	29.3	13-Mar-03	SFWMD
WEL2897002697500	455097.00	1007127.00	29.6	13-Mar-03	SFWMD
WEL2897002697600	462308.00	1003053.00	30.0	13-Mar-03	SFWMD
WEL2897002697700	460842.00	999021.00	29.5	13-Mar-03	SFWMD
WEL2898000233600	468439.00	999894.00	30.0	13-Mar-03	SFWMD
WEL2898001003000	470389.00	991302.00	28.0	13-Mar-03	SFWMD
WEL2898001003100	468038.00	991313.00	30.0		SFWMD
WEL2898001003200	468231.00	994038.00	30.0	13-Mar-03	SFWMD
WEL2898002698100	468959.00	994944.00	27.9	13-Mar-03	SFWMD
WEL2898002698300	466098.00	1001925.00	29.8	13-Mar-03	SFWMD
WEL2898002698400	468174.00	1001208.00	28.3	13-Mar-03	SFWMD
WEL2900000231300	404827.00	1032853.00	30.0	22-Jan-03	SFWMD

Table 3.2b: Temperature data (UF)

Station	X coordinate (ft FL State Plane 1983)	Y coordinate (ft FL State Plane 1983)	Temperature (°C)	Date	Source
WEL2900000231301	404828.00	1032853.00	28.0	04-Jun-03	SFWMD
WEL2900001004300	407168.00	1031728.00	31.0	22-Jan-03	SFWMD
WEL2900001004301	407169.00	1031728.00	29.0	16-Apr-03	SFWMD
WEL2900001228900	406075.00	1030018.00	31.0	22-Jan-03	SFWMD
WEL2900001228901	406074.00	1030018.00	28.0	19-Oct-04	SFWMD
WEL2900001810100	404262.00	1029120.00	29.0	22-Jan-03	SFWMD
WEL2900001810101	404263.00	1029120.00	28.0	22-Apr-03	SFWMD
WEL2900001810200	407510.00	1028394.00	30.0	22-Jan-03	SFWMD
WEL2900001810201	407509.00	1028394.00	28.0	06-Nov-03	SFWMD
WEL2900002569300	403093.00	1030037.00	30.0	22-Jan-03	SFWMD
WEL2900002569301	403094.00	1030037.00	29.4	04-Jun-03	SFWMD
WEL2900002569500	408354.00	1033741.00	31.0	22-Jan-03	SFWMD
WEL2900002569501	408355.00	1033741.00	31.0	04-Jun-03	SFWMD
WEL2901000231100	472178.00	987154.00	29.0	13-Feb-03	SFWMD
WEL2901003343300	470642.00	987262.00	28.0	13-Feb-03	SFWMD
WEL2901003343400	470274.00	985951.00	30.0	13-Feb-03	SFWMD
WEL2901003343500	471992.00	985943.00	28.0	13-Feb-03	SFWMD
WEL2901003642400	472277.00	988971.00	28.0	13-Feb-03	SFWMD
WEL2902002001400	439825.74	973174.28	26.9		SFWMD
WEL2903001417000	273828.50	1142846.50	30.0	12-Mar-03	SWFWMD
WEL2903001798700	430867.00	972415.00	30.0	12-Mar-03	SFWMD
WEL2904000232300	463039.00	1099993.00	31.5		SFWMD
WEL2904001105000	462419.00	1102319.00	31.4		SFWMD
WEL2905000231400	395685.00	1044019.00	26.6		SFWMD
WEL2906000232600	438126.00	993683.00	30.0	20-Mar-02	SFWMD
WEL2908003040600	381235.00	989884.00	29.2		SFWMD
WEL2908003735400	379969.00	989893.00	30.3		SFWMD
WEL2910001164600	411374.00	1040186.00	31.0	12-Mar-03	SFWMD
WEL2912002961300	395920.00	1024224.00	29.6	18-Feb-03	SFWMD
WEL2913001063200	404656.00	975697.00	29.0	02-Jan-03	SFWMD
WEL2913001065000	393985.00	975865.00	31.0	02-Jan-03	SFWMD
WEL2913001065300	393960.00	971927.00	30.0	02-Jan-03	SFWMD
WEL2913001065800	399308.00	973812.00	31.0	02-Jan-03	SFWMD
WEL2913001066000	399411.00	975730.00	29.0	02-Jan-03	SFWMD
WEL2913001113400	407183.00	975593.50	27.0	02-Jan-03	SWFWMD
WEL2913001222300	399495.00	974719.00	30.0	02-Jan-03	SFWMD
WEL2913001247200	404018.00	974792.00	31.0	02-Jan-03	SFWMD
WEL2913001247300	407188.00	975581.00	29.0	02-Jan-03	SFWMD
WEL2914001634700	415009.00	998255.00	31.0	05-Jun-02	SFWMD
WEL2914002917000	417540.00	998240.00	31.0	05-Jun-02	SFWMD
WEL2914002917100	416275.00	998248.00	30.0	05-Jun-02	SFWMD
WEL2922003704100	352477.00	1013517.00	30.9	22-Apr-03	SFWMD
WEL2922003704101	352478.00	1013517.00	29.4		SFWMD
WEL2923001434100	385708.00	1023584.00	31.0	04-Jun-03	SFWMD
WEL2924001434200	385690.00	1020857.00	28.4	04-Jun-03	SFWMD
WEL2927000230000	436755.00	973998.00	32.0	14-Jul-03	SWFWMD
WEL2927000230100	437423.00	976318.00	28.0	14-Jul-03	SWFWMD
WEL2930000232200	422916.00	972612.00	32.5	12-Mar-03	SFWMD
WEL2931003032200	426704.85	972134.68	29.9		SFWMD
WEL2932003032300	428890.14	974748.05	33.3		SFWMD
WEL2933003032100	425726.91	975169.61	32.8		SFWMD
WEL2934003032400	428973.00	973435.00	33.0	12-Mar-03	SFWMD
WEL2938001117200	390590.00	1024158.00	31.0	12-Jan-04	SFWMD
WEL2941003562800	331677.00	1079624.00	30.4		SFWMD
WEL2945001352800	400301.00	1002485.00	31.0	10-Nov-03	SFWMD
WEL2945001352900	398855.00	1002494.00	30.0	10-Nov-03	SFWMD
WEL2945001353100	398839.00	999868.00	30.0	10-Nov-03	SFWMD
WEL2945001353200	401460.00	999953.00	30.0	10-Nov-03	SFWMD
WEL2945001710700	399437.00	994412.00	30.0	12-Nov-03	SFWMD

Table 3.2b: Temperature data (UF)

Station	X coordinate (ft FL State Plane 1983)	Y coordinate (ft FL State Plane 1983)	Temperature (°C)	Date	Source
WEL2945001710701	399438.00	994412.00	29.0	01-Mar-05	SFWMD
WEL2945001780000	404786.00	996903.00	30.0	12-Nov-03	SFWMD
WEL2945002741400	398717.00	994921.00	30.0	10-Nov-03	SFWMD
WEL2945002741700	401523.00	995408.00	30.0	12-Nov-03	SFWMD
WEL2945002741701	401524.00	995408.00	28.0	09-May-06	SFWMD
WEL2947000236900	378277.00	1006971.00	31.0	13-Nov-03	SFWMD
WEL2947000237000	386416.00	1007724.00	28.0	13-Nov-03	SFWMD
WEL2953001636700	415467.87	968563.61	29.5		SFWMD
WEL2957000238000	378600.00	987882.00	28.8		SFWMD
WEL2967003527100	470491.00	1073400.00	31.0	09-Mar-04	SFWMD
WEL2969001555200	421235.50	967940.50	29.0	17-Mar-04	SWFWMD
WEL2976003831500	410473.00	995556.00	28.3	16-Feb-05	SFWMD
WEL2990001002801	372548.00	986914.00	29.5		SFWMD
WEL2996003926700	442470.00	994669.00	28.0	11-Jan-05	SFWMD
WEL2997000244400	95576.00	1263647.00	24.0	14-Feb-05	SFWMD
WEL3004001574200	372300.00	1005194.00	31.0	11-May-05	SFWMD
WEL3004001574300	374849.00	1007903.00	28.0	11-May-05	SFWMD
WEL3004001574400	372500.00	1008020.00	31.0	11-May-05	SFWMD
WEL3004001574500	374831.00	1005278.00	31.0	11-May-05	SFWMD
WEL3004001587400	373660.00	1005892.00	29.0	11-May-05	SFWMD
WEL3004001602000	372336.00	1010445.00	30.0	11-May-05	SFWMD
WEL3004001604200	375067.00	1013254.00	28.0	11-May-05	SFWMD
WEL3004001604300	372446.00	1013272.00	30.0	11-May-05	SFWMD
WEL3007001559400	414378.00	1150042.00	29.6		SFWMD
WEL3007002477700	414381.00	1150547.00	25.4		SFWMD
WEL3011001164500	393083.00	1032524.00	30.8	21-Jul-05	SFWMD
WEL3030002390100	189134.00	1057884.00	27.0	24-Jan-06	SFWMD
WEL3048002276100	170089.00	1207913.00	26.1		SFWMD

Table 3.2c: Temperature data (MC1)

Station	X coordinate (ft FL State Plane 1983)	Y coordinate (ft FL State Plane 1983)	Temperature (°C)	Date	Source
MIU-MZ2	418494.50	591527.00	32.0	21-Oct-04	DBHYDRO
OK-1	719797.00	1159881.00	26.0	12-Oct-93	DBHYDRO
WA-119	807750.00	1045690.00	28.0		USGS (Reese, WRI03-4242)
MF-32	789490.00	1019793.00	28.0	17-Nov-81	DBHYDRO
MIR-MZU	875549.00	603698.00	23.0	16-Feb-00	DBHYDRO
POF-6	507392.00	1344504.00	26.0	05-Sep-79	DBHYDRO
POF-14	485365.00	1369336.00	24.0	11-Sep-79	DBHYDRO
OSF-11	511138.00	1388118.00	22.0	10-Aug-93	DBHYDRO
OSF-34	541978.00	1404275.00	24.0	14-Sep-79	DBHYDRO
WASANMZ2	936511.00	576823.00	20.0	27-Jan-05	DBHYDRO
POF-13	541620.00	1312175.00	24.0	25-Jan-89	DBHYDRO
WEL2900001810100	404262.00	1029120.00	29.0	22-Jan-03	SFWMD
WEL2900002569501	408355.00	1033741.00	31.0	04-Jun-03	SFWMD
M-1360	784888.00	966243.00	28.0	01-Nov-01	USGS (Reese, WRI03-4242)
M-911	823635.00	980923.00	26.0	16-Jul-80	USGS (Reese, WRI03-4242)
M-32	817818.00	988271.00	28.0	25-Jan-57	USGS (Reese, WRI03-4242)
M-29	773143.00	1024269.00	26.0		USGS (Reese, WRI03-4242)
M-110	915194.00	1031185.00	24.0	13-Aug-46	USGS (Reese, WRI03-4242)
OK-31	706716.00	1052306.00	27.0	19-Jul-01	USGS (Reese, WRI03-4242)
OK-9001	725846.00	1056171.00	28.0	24-Jul-01	USGS (Reese, WRI03-4242)
STL-389	870587.00	1080408.00	25.0	11-Jul-00	USGS (Reese, WRI03-4242)
G3-1	810107.00	1090838.00	29.0	26-Jul-01	USGS (Reese, WRI03-4242)
STL-380	821828.00	1092298.00	31.0	18-Jul-01	WRI 03-4242
STL-229	813996.00	1111049.00	27.0	23-May-90	USGS (Reese, WRI03-4242)
WEL2901000231100	472178.00	987154.00	29.0	13-Feb-03	SFWMD
WEL2901003343300	470642.00	987262.00	28.0	13-Feb-03	SFWMD
WEL2901003343400	470274.00	985951.00	30.0	13-Feb-03	SFWMD
WEL2901003343500	471992.00	985943.00	28.0	13-Feb-03	SFWMD
WEL2901003642400	472277.00	988971.00	28.0	13-Feb-03	SFWMD
WEL1500000103900	158412.50	1206900.00	25.0	10-Jan-95	SWFWMD
MF-40L	826580.00	1044391.00	31.0	06-Jun-07	DBHYDRO
OKF-100L	698056.00	1025471.00	27.0	05-Jun-07	DBHYDRO
BOYRO_EPXL	953223.00	786238.00	25.0	05-Mar-07	DBHYDRO
OSF-6	539947.00	1383477.00	23.0	25-Jan-89	DBHYDRO
OSFWQ-01	550086.00	1424652.00	24.0	18-Feb-93	DBHYDRO
WEL2547002299400	396213.00	984939.00	29.0	14-Jan-04	SFWMD
OR0678	589521.00	1515255.00	24.0	30-Oct-03	SJRWMD
WEL2938001117200	390590.00	1024158.00	31.0	12-Jan-04	SFWMD
WEL2531001583800	206866.00	1238594.00	27.0		SFWMD
STL-357	819191.00	1092403.00	28.0	12-Mar-82	USGS (Reese, WRI03-4242)
WEL2903001417000	273828.50	1142846.50	30.0	12-Mar-03	SWFWMD
WEL2930000232200	422916.00	972612.00	33.0	12-Mar-03	SFWMD
WEL2934003032400	428973.00	973435.00	33.0	12-Mar-03	SFWMD
BICY-MZ3	554524.00	567148.00	28.0	24-Jun-04	DBHYDRO
WEL2945001353100	398839.00	999868.00	30.0	10-Nov-03	SFWMD
WEL2945001353200	401460.00	999953.00	30.0	10-Nov-03	SFWMD
WEL2945002741400	398717.00	994921.00	30.0	10-Nov-03	SFWMD
WEL2945001710701	399438.00	994412.00	29.0	01-Mar-05	SFWMD
WEL2945001142400	398731.00	997143.00	30.0	10-Nov-03	SFWMD
WEL2996003926700	442470.00	994669.00	28.0	11-Jan-05	SFWMD
WEL2473003536900	410221.00	1028781.00	30.0	13-Oct-05	SFWMD
BSU-MZU	317716.50	887559.00	31.0	06-Jul-04	SFWMD
C-781	558001.00	775754.00	37.8		SFWMD
WEL1035000075800	385201.00	1202274.00	28.0	14-Oct-03	SWFWMD
WEL2462000176300	242654.00	1110541.00	30.0	25-Jul-01	SWFWMD
OR0055	625632.00	1487233.00	24.0	13-May-03	SJRWMD
OR0059	625639.00	1495313.00	27.0	12-May-03	SJRWMD
OR0003	647422.00	1507118.00	24.0	26-May-04	SJRWMD
CS-M2	897624.00	695829.00	22.0	13-Sep-00	USGS (Reese, WRI03-4242)

Table 3.2c: Temperature data (MC1)

Station	X coordinate (ft FL State Plane 1983)	Y coordinate (ft FL State Plane 1983)	Temperature (°C)	Date	Source
WEL0293000002700	348103.00	1068488.00	26.0		SFWMD
WEL1696000123500	433489.00	1330001.00	26.0		SFWMD
WEL2136000149200	394280.00	1036151.00	28.0	03-Aug-05	SFWMD
WEL2862001114600	457189.00	991162.00	28.0	19-Mar-02	SFWMD
WEL2862001114501	457646.00	992372.00	28.0	28-Feb-03	SFWMD
WEL2862001114400	456568.00	993690.00	28.0	19-Mar-02	SFWMD
WEL2862001232100	456566.00	993286.00	28.0	19-Mar-02	SFWMD
WEL2862001115201	459541.00	991555.00	29.0	20-Nov-03	SFWMD
WEL2793002392100	181201.50	1204445.00	26.0	01-Mar-01	SWFWMD
WEL2528001383400	207326.00	1249284.00	26.0	01-Mar-01	SWFWMD
EPU-MZU	318594.00	961362.00	31.0	05-Oct-99	DBHYDRO
WEL2536001628000	352159.50	1004918.50	31.0	15-Oct-03	SWFWMD
WEL0919000065300	160074.00	1198237.00	27.0		SFWMD
WEL2792002837900	178595.50	1218998.00	27.0	18-Oct-01	SWFWMD
FMB-MZL	350747.00	785108.00	31.0	28-Jul-99	DBHYDRO
FMB-MZU	350811.00	785238.00	32.0	28-Jul-99	DBHYDRO
FTL-MZU2	941690.00	641434.00	21.5		SFWMD
WEL2562000183800	264229.00	1249806.00	27.0		SFWMD
WEL1331000087000	327599.50	1006296.00	32.0	09-Jul-98	SWFWMD
GL-5B	553452.00	957447.00	25.0	02-Sep-99	DBHYDRO
GL-5C	553434.00	957444.00	28.0	02-Sep-99	DBHYDRO
GLF-6	628327.00	910488.00	29.6		SFWMD
HE-1105	493958.00	822674.00	30.0		SFWMD
WEL2476000177700	206775.50	1166573.00	30.0	12-Feb-01	SWFWMD
WEL1552000133500	197204.00	1341759.50	26.0	17-Dec-02	SWFWMD
WEL2526001253700	238366.50	1128357.50	26.0	10-Jan-01	SWFWMD
I75-TW	416557.00	668295.00	29.0	25-Jan-95	DBHYDRO
IWA-MZL	293008.00	767990.00	31.0	22-May-00	DBHYDRO
IWSD-MZ3	515034.00	756360.00	31.0	22-Feb-96	Bennett, 2002, packer test
WEL2920000230500	356357.00	1012680.00	31.0	04-Jun-03	SFWMD
WEL2921000230600	407577.00	1039502.00	29.0	14-Jul-03	SFWMD
WEL0830000056400	254370.00	1144757.00	27.0		SFWMD
WEL0295000002900	227615.00	1110892.00	27.0		SFWMD
WEL0318000005200	237778.50	1110401.50	29.0	15-May-01	SWFWMD
WEL1766000136100	199919.00	1029793.50	28.0	22-Oct-04	SWFWMD
WEL2542001797400	193809.00	1087830.00	29.0		SFWMD
OSF-86	685793.00	1365744.00	26.0	03-Aug-93	DBHYDRO
OSF-27	583686.00	1459215.00	26.0	10-Aug-93	DBHYDRO
OSF-64	565998.00	1359130.00	24.0	03-Aug-93	DBHYDRO
L2-PW1	672709.00	826685.00	26.0	06-Oct-04	DBHYDRO
OSF-62	641676.00	1296604.00	25.0	02-Aug-93	DBHYDRO
L2-TW-MC1	672743.00	826627.00	27.0	07-Feb-94	DBHYDRO
ZRL-MZ1	341554.00	894221.00	28.0	27-Feb-96	DBHYDRO
L-6462	432888.00	763510.00	34.4		SFWMD
L-6463	420506.00	776501.00	31.7		SFWMD
L-6471	245196.00	882875.00	28.9		SFWMD
LAB-MZ2	502274.00	879737.00	34.0	22-Jun-04	DBHYDRO, Geophysical Log
WEL0311000004500	479739.00	1348147.00	25.0		SFWMD
WEL3048002276100	170089.00	1207913.00	26.0		SFWMD
WEL0996000073000	337430.00	996059.00	28.0		SFWMD
WEL0804000053800	423053.50	1366902.00	26.0	20-May-99	SWFWMD
WEL0514000024800	418534.00	1394727.50	24.0	04-May-99	SWFWMD
M-1356	895337.00	1059642.00	25.0	30-Aug-01	USGS (Reese, WRI03-4242)
WEL0815000054900	379996.00	1205305.00	26.0		SFWMD
WEL2706000189201	400239.00	1007030.00	28.0	06-Nov-03	SFWMD
WEL0938000067200	347644.00	995779.00	28.0		SFWMD
WEL0879000061300	233552.00	1371943.00	23.7		SFWMD
WEL1811001172800	177372.00	1184204.00	27.0	24-Sep-04	SWFWMD
NFM-MZU	368708.00	871748.00	28.0	27-Feb-96	DBHYDRO

Table 3.2c: Temperature data (MC1)

Station	X coordinate (ft FL State Plane 1983)	Y coordinate (ft FL State Plane 1983)	Temperature (°C)	Date	Source
NLCWTP-IW1	397889.00	872374.00	32.1		SFWMD
WEL0147001085500	178597.00	1339035.00	25.8		SFWMD
OKF-17	682589.00	1091463.00	26.0	31-May-00	USGS (Reese, WRI03-4242)
OR0673	650629.00	1475910.00	26.0	25-Jul-03	SJRWMD
OR0827	535473.00	1521042.00	24.0	09-May-04	SJRWMD
ORF-60	467178.00	1470886.00	23.0		SFWMD
OR0047	503492.00	1532164.00	25.0	19-Mar-03	SJRWMD
WEL2563001029400	373772.50	1127691.50	28.0	06-Sep-01	SWFWMD
PB-1196	930967.00	942017.00	23.1		USGS (Reese, WRI03-4242)
PB-747	936275.00	946597.00	24.0	19-Jun-74	USGS (Reese, WRI03-4242)
PBF-7U	749013.00	860161.00	26.0	10-Jun-04	DBHYDRO
WEL2908000232800	380894.00	992916.00	26.0	06-Nov-02	SFWMD
WEL2976003831500	410473.00	995556.00	28.0	16-Feb-05	SFWMD
WEL2730003105001	412171.00	992213.00	29.0	22-Apr-03	SFWMD
WEL2729003105102	413974.00	991395.00	28.0	04-Nov-03	SFWMD
WEL2980002816100	410103.00	994144.00	30.0	12-Nov-03	SFWMD
WEL2453000175400	305245.00	1183469.00	25.0		SFWMD
WEL2702001259300	390397.00	1008405.00	33.0	26-Jun-01	SFWMD
WEL3004001604300	372446.00	1013272.00	30.0	11-May-05	SFWMD
WEL3004001604200	375067.00	1013254.00	28.0	11-May-05	SFWMD
WEL3004001587400	373660.00	1005892.00	29.0	11-May-05	SFWMD
WEL3004001574500	374831.00	1005278.00	31.0	11-May-05	SFWMD
WEL3004001574200	372300.00	1005194.00	31.0	11-May-05	SFWMD
WEL3004001574400	372500.00	1008020.00	31.0	11-May-05	SFWMD
WEL3004001602000	372336.00	1010445.00	30.0	11-May-05	SFWMD
PWU-MZU	882488.00	934221.00	27.0	17-Jan-01	DBHYDRO
ROMP 12 DP UP FLORIDAN	414491.00	984828.50	30.0	18-Sep-03	SWFWMD
ROMP 14 AVON PARK	541075.00	1023767.00	27.0	24-Sep-03	SWFWMD
ROMP 15 DEEP	442930.50	1045755.50	29.0	30-Oct-03	SWFWMD
ROMP 16 OCALA	404691.00	1038305.00	30.0	19-Nov-97	SWFWMD
ROMP 17 AP	338696.00	1033835.50	32.0	24-Sep-03	SWFWMD
ROMP 20	177627.00	1040684.00	28.0		SFWMD
ROMP 20 OCALA	175320.50	1042570.50	30.0	22-Sep-03	SWFWMD
ROMP 22 AVON PARK	222114.50	1084916.00	31.0	24-Sep-04	SWFWMD
ROMP 23-1 DEEP	273795.00	1085398.50	31.0	01-Sep-03	SWFWMD
ROMP 25 LILY SUWANNEE	329326.00	1103703.00	28.0	19-Apr-04	SWFWMD
ROMP 28 UP AVON PARK	514903.00	1103510.50	27.0	27-Jun-03	SWFWMD
ROMP 28_4	514895.00	1103485.00	25.0		SFWMD
ROMP 29A	519838.00	1152172.00	25.0		SFWMD
ROMP 30 AVON Park	397802.76	1136955.11	26.6		add point from MF to improve interpolation
ROMP 32 AVON PARK	311177.00	1141806.50	29.0	17-Nov-03	SWFWMD
ROMP 39 AVON PARK	250816.50	1185216.00	29.0	10-Sep-03	DBHYDRO
ROMP 45 AVON PARK	401944.50	1247858.00	25.0	19-Nov-03	SWFWMD
ROMP 48 AVON PARK	286606.00	1240216.00	27.0	19-Nov-03	SWFWMD
ROMP 49 AVON PARK	250470.00	1248631.00	27.5		SFWMD
ROMP 5 AVON PARK	392934.50	950316.00	32.0	19-Sep-03	SWFWMD
ROMP 57-1 FLORIDAN	455111.00	1298172.00	25.0		SFWMD
ROMP 60 DEEP	338815.00	1294295.50	27.0	17-Oct-03	DBHYDRO
ROMP 62 - CAMPO	231413.00	1283467.00	27.0	23-Feb-04	SWFWMD
ROMP 67-1 AVON PARK	222781.50	1355518.00	24.0	23-Sep-03	SWFWMD
ROMP 68-1 AVON PARK	255358.50	1365168.00	24.0	11-Jan-99	SWFWMD
ROMP 87	326599.50	1414156.00	25.0	15-Mar-00	SWFWMD
ROMP 9 AVON PARK	282286.50	998634.50	31.0	19-Sep-03	SWFWMD
WEL0017001090700	490968.00	1244506.00	26.0	10-Feb-00	SWFWMD
ROMP TR 1-2 SWNN	336137.50	912370.50	30.0	11-Sep-03	SWFWMD
ROMP TR 13-1 OCALA	82093.00	1306477.00	27.0	31-Aug-99	SFWMD
ROMP TR 13-2 L SWNN	100538.00	1303485.00	26.0	06-May-91	SFWMD
ROMP TR 13-3	128135.00	1360390.00	26.1		SFWMD
ROMP TR 7-2 DEEP FL	153302.00	1131337.00	30.0	18-Sep-03	SWFWMD

Table 3.2c: Temperature data (MC1)

Station	X coordinate (ft FL State Plane 1983)	Y coordinate (ft FL State Plane 1983)	Temperature (°C)	Date	Source
ROMP TR 7-4 SWNN	173090.00	1127584.00	27.0	14-Sep-04	SWFWMD
ROMP TR 8-1 NR RUBIO	155249.50	1184210.50	26.0	18-Sep-85	SWFWMD
ROMP TR 8-2 AVON PARK	165358.00	1181504.00	28.1		SFWMD
ROMP TR 9-2 OCALA	205646.50	1249909.50	28.0	15-Sep-03	SWFWMD
ROMP TR 9-3 AP	195932.00	1241245.00	28.0		SFWMD
ROMP TR AB-1	201657.00	1254715.00	27.1		SFWMD
ROMP TR AB-3	213730.00	1249629.00	28.2		SFWMD
ROMP TR SA-1 AVON PARK	154326.50	1098413.50	29.0	29-Sep-03	SWFWMD
ROMP TR SA-3 UP FLORIDAN	165872.50	1098987.00	30.0	12-Sep-03	SWFWMD
WEL1327000086600	386720.00	998520.50	30.0	30-Oct-03	SWFWMD
WEL1802001183400	233605.50	1332499.50	24.0	13-Sep-91	SWFWMD
WEL2911001627500	368499.50	967229.50	31.0	15-Apr-02	SWFWMD
SLF-63	783767.00	1144482.00	26.0	18-Nov-93	DBHYDRO
SLF-64	777699.00	1155672.00	28.0	18-Nov-93	DBHYDRO
SLF-65	772451.00	1164644.00	27.0	18-Nov-93	DBHYDRO
WEL0419000015300	458454.00	1157880.00	27.0		SFWMD
STL-255	883869.00	1060687.00	25.0	12-Jul-00	USGS (Reese, WRI03-4242)
WEL2719001430900	233731.50	1255982.00	27.0	02-Oct-01	SWFWMD
WEL2430002073600	382129.00	1028758.00	31.0	20-Feb-03	SFWMD
WEL2430003489400	378062.00	1028483.00	31.0	20-Feb-03	SFWMD
WEL2451000175200	347539.00	995586.00	26.0	02-Jan-01	SWFWMD
WEL2897002697600	462308.00	1003053.00	30.0	13-Mar-03	SFWMD
WEL2898002698100	468959.00	994944.00	28.0	13-Mar-03	SFWMD
WEL2898001003200	468231.00	994038.00	30.0	13-Mar-03	SFWMD
WEL2898001003100	468038.00	991313.00	30.0	13-Mar-03	SFWMD
WEL2898001003000	470389.00	991302.00	28.0	13-Mar-03	SFWMD
WEL2898000233600	468439.00	999894.00	30.0	13-Mar-03	SFWMD
WEL2923001434100	385708.00	1023584.00	31.0	04-Jun-03	SFWMD
WEL2692002270801	401506.00	992783.00	28.0	05-Nov-03	SFWMD
WEL2692002271101	406734.00	990226.00	28.0	05-Nov-03	SFWMD
WEL2692001305501	402756.00	990251.00	28.0	11-Feb-02	SFWMD
WEL2692001305500	402757.00	990251.00	30.0	05-Jun-01	SFWMD
WEL2692003803000	407472.00	992645.00	29.0	09-Mar-04	SFWMD
WEL2534001603300	301143.00	1289966.50	27.0	24-Sep-01	SFWMD
WEL2532001592900	287533.00	1293525.00	26.0	24-Sep-01	SWFWMD
TCRK_GW1	725886.00	1056131.00	26.0	16-Jun-04	DBHYDRO
WEL2465000176600	206683.50	1143450.00	25.0	09-Jan-01	SWFWMD
WEL2474000177500	465254.00	1184276.00	31.0	05-Sep-01	SWFWMD
WEL2913001247200	404018.00	974792.00	31.0	02-Jan-03	SFWMD
WEL2913001066000	399411.00	975730.00	29.0	02-Jan-03	SFWMD
WEL2913001222300	399495.00	974719.00	30.0	02-Jan-03	SFWMD
WEL2913001065000	393985.00	975865.00	31.0	02-Jan-03	SFWMD
WEL2913001065300	393960.00	971927.00	30.0	02-Jan-03	SFWMD
WEL2896003700800	356418.00	1008640.00	29.0	09-Mar-04	SFWMD
WEL0777000051100	451834.00	1077226.00	27.0		SFWMD
WEL2456000175700	246510.00	1204329.00	27.0		SFWMD
WEL2844000215300	359018.00	1018316.00	31.0	09-May-02	SFWMD
WEL0969000070300	223676.00	1288309.00	25.7		SFWMD
WEL1898000135700	444307.50	1425087.50	25.0	12-May-99	SWFWMD
WEL0545003730200	470530.00	982617.00	29.0	01-Oct-04	SFWMD
W-15826	157916.00	1182383.00	27.5		SFWMD
WA-1111	768272.00	1119581.00	28.0		USGS (Reese, WRI03-4242)
IR1000	849492.00	1245820.00	24.0	26-Jul-03	SJRWMD
WEL1519001172400	150823.00	1347565.00	26.4		SFWMD
WEL2914002917000	417540.00	998240.00	31.0	05-Jun-02	SFWMD
WEL2957000238000	378600.00	987882.00	29.0		SFWMD

Table 3.2d: Temperature data (APPZ)

Station	X coordinate (ft FL State Plane 1983)	Y coordinate (ft FL State Plane 1983)	Temperature (°C)	Date	Source
MIR-MZU	875549.00	603698.00	23.0	16-Feb-00	DBHYDRO
OSF-0010	522099.00	1451905.00	24.0	20-Mar-79	DBHYDRO
OSF-17	574941.00	1421765.00	24.0	27-Mar-79	DBHYDRO
OSF-28	504801.00	1416016.00	26.0	23-Jun-72	DBHYDRO
OSF-34	541978.00	1404275.00	24.0	14-Sep-79	DBHYDRO
SLF-41	779260.00	1056819.00	30.0	22-Jul-80	DBHYDRO
SLF-54	763186.00	1059904.00	28.0	21-Mar-84	DBHYDRO
SUNSHINE FOLIAGE WORLD A (DID #3)	414378.39	1150042.06	29.6		SFWMD
PBF-15M	863877.00	874383.00	27.0	07-Jun-07	DBHYDRO
OSF-104M	613139.00	1209263.00	24.0	04-Jun-07	DBHYDRO
P-375	196619.00	914697.00	37.8		SFWMD
WEL2900001228901	406074.00	1030018.00	31.0	06-Nov-03	DBHYDRO
WEL2900001810101	404263.00	1029120.00	28.0	22-Apr-03	SFWMD
WEL2900001810201	407509.00	1028394.00	28.0	06-Nov-03	DBHYDRO
WEL2900000231300	404827.00	1032853.00	29.3	22-Jan-03	SFWMD
WEL2900001004300	407168.00	1031728.00	31.0	22-Jan-03	DBHYDRO
MF-37	784889.00	966243.00	29.0	30-Oct-01	USGS (Reese, WRI03-4242)
OK-9000	725576.00	1055666.00	35.0	17-Apr-91	USGS (Reese, WRI03-4242)
OK-9002	725846.00	1056171.00	28.0	24-Jul-01	USGS (Reese, WRI03-4242)
STL-387	869858.00	1081717.00	25.0	11-Jul-00	USGS (Reese, WRI03-4242)
STL-380	821828.00	1092298.00	31.0	18-Jul-01	USGS (Reese, WRI03-4242)
WEL2901000231100	472178.00	987154.00	28.7		SFWMD
WEL2533001602800	405466.00	1034162.00	30.3	13-Oct-00	SFWMD
MF-40L	826580.00	1044391.00	31.0	06-Jun-07	DBHYDRO
OKF-100L	698056.00	1025471.00	27.0	05-Jun-07	DBHYDRO
BOYRO_EPXL	953223.00	786238.00	25.0	05-Mar-07	DBHYDRO
82510702_G	615881.00	1487243.00	24.7		SFWMD
83210501_G	626629.00	1531670.00	24.0		SFWMD
OSF-22	605280.00	1437266.00	26.0	31-Jul-85	DBHYDRO
AID-MZU	906926.00	837211.00	26.0	12-Nov-02	DBHYDRO
ALLY-TW	714532.00	668029.00	25.0	09-Jun-04	DBHYDRO
WEL2899000228300	393788.00	1029792.00	30.0	18-Feb-03	SFWMD
WEL2899000228400	396398.00	1028261.00	30.0	18-Feb-03	SFWMD
BCN-M2	933013.00	700322.00	22.9		SFWMD
WEL2904001105000	462419.00	1102319.00	31.4		SFWMD
BF-4M	925173.00	669561.00	22.0	08-Jun-07	DBHYDRO
BICY-MZ3	554524.00	567148.00	32.0	29-Jan-98	Bennett, 2004, temperature log
WEL2945001780000	404786.00	996903.00	30.0	12-Nov-03	SFWMD
WEL2945002741701	401524.00	995408.00	28.0	09-May-06	SFWMD
WEL2945001710700	399437.00	994412.00	30.0	12-Nov-03	SFWMD
WEL2945001352800	400301.00	1002485.00	31.0	10-Nov-03	SFWMD
WEL2945001352900	398855.00	1002494.00	30.0	10-Nov-03	SFWMD
WEL2473002812200	408723.00	1034950.00	30.0	13-Oct-05	SFWMD
WEL2473002812300	410508.00	1031405.00	30.0	13-Oct-05	SFWMD
CH-R5	392979.00	949940.00	32.0		SFWMD
WEL2564001820200	388150.00	1202619.00	25.0	09-Jan-01	SWFWMD
OR0014	625624.00	1476528.00	24.0	13-May-03	DBHYDRO
OR0037	608490.00	1487251.00	25.0	12-May-03	SJRWMD
OR0038	606437.00	1487253.00	25.0	12-May-03	SJRWMD
OR0033	604383.00	1487256.00	25.0	24-May-04	SJRWMD
OR0057	625636.00	1491475.00	24.0	12-May-03	DBHYDRO
OR0740	634644.00	1476219.00	24.0	12-May-03	SJRWMD
COCOA H_G	647580.00	1507220.00	23.9		SFWMD
WEL1329000086800	418815.00	998153.50	28.0	26-Sep-02	SWFWMD
CS-M2	897624.00	695829.00	22.0	13-Sep-00	USGS (Reese, WRI03-4242)
WEL3011001164500	393083.00	1032524.00	30.8	21-Jul-05	SFWMD
WEL2947000236900	378277.00	1006971.00	31.0	13-Nov-03	SFWMD
WEL2947000237000	386416.00	1007724.00	28.0	13-Nov-03	SFWMD

Table 3.2d: Temperature data (APPZ)

Station	X coordinate (ft FL State Plane 1983)	Y coordinate (ft FL State Plane 1983)	Temperature (°C)	Date	Source
WEL2862001115600	458722.00	990448.00	28.0	19-Mar-02	SFWMD
WEL2862001115700	456823.00	990457.00	30.0	19-Mar-02	SFWMD
WEL2862001115300	456106.00	991672.00	28.0	19-Mar-02	SFWMD
WEL2862001115200	459542.00	991555.00	31.0	19-Mar-02	SFWMD
WEL1660000119900	109821.00	1390244.00	24.0	06-Oct-86	SFWMD
WEL2906000232600	438126.00	993683.00	30.0	20-Mar-02	SFWMD
WEL2539001795600	398465.00	1069853.00	32.0	16-Nov-00	SWFWMD
WEL2045001324000	277948.50	1134132.00	29.0	24-Feb-03	SWFWMD
FMB-MZL	350747.00	785108.00	31.0	28-Jul-99	DBHYDRO
WEL1331000087000	327567.00	1006236.00	30.2		SFWMD
GLF-6	628324.00	910488.00	31.0	09-Nov-01	DBHYDRO
PBF-11	886680.00	735581.00	23.0	03-Sep-03	DBHYDRO
HE-1106	477332.00	803987.00	40.0		SFWMD
WEL1552000133600	197159.81	1341401.40	26.0		SFWMD
I75-TW	416557.00	668295.00	30.2	20-Dec-94	DBHYDRO, packer test
IC-TW	493981.00	1426090.00	24.0	17-Dec-02	DBHYDRO
IWSD-MZ3	515034.00	756360.00	31.0	22-Feb-96	Bennett, 2002, packer test
WEL2919000230400	353906.00	1011284.00	31.0	04-Jun-03	SFWMD
OSF-27	583686.00	1459215.00	26.0	10-Aug-93	DBHYDRO
SUN-MZL	873512.00	653626.00	24.0	21-Sep-99	DBHYDRO
OSF-64	565999.00	1359130.00	25.0	16-Aug-05	DBHYDRO
OSF-70	550508.00	1424598.00	26.0	10-Aug-05	DBHYDRO
DF-5	830843.00	573318.00	23.0	09-Jun-04	DBHYDRO
MOSSPK_D	594783.00	1470305.00	24.0	02-Aug-05	DBHYDRO
L2-TW	672741.00	826627.00	26.0		SFWMD
ZRL-MZ2	341555.00	894221.00	32.0	27-Feb-96	DBHYDRO
PBF-6	949133.50	852463.54	22.0	01-Jul-96	DBHYDRO
L-6471	245197.00	882875.00	30.0		SFWMD
LAB-MZ3	502275.00	879737.00	34.0	22-Jun-04	DBHYDRO
WEL1690000122900	336089.50	1356714.50	27.0	21-Mar-00	SWFWMD
WEL2990001002801	372548.00	986914.00	29.5		SFWMD
WEL0804000053800	423053.50	1366902.00	26.0	20-May-99	SWFWMD
M-1353	900502.00	1041193.00	25.0	10-Jul-00	USGS (Reese, WRI03-4242)
WEL1573000111200	127993.00	1136454.00	30.0	03-Oct-03	SWFWMD
WEL0879000061300	233541.50	1371958.50	24.0	14-Mar-00	SWFWMD
WEL0486000022000	112234.67	1430728.78	25.0	04-Jan-96	SWFWMD
WEL0078001078400	111309.00	1381332.00	26.0	12-Sep-03	SFWMD
WEL0147001085500	178575.00	1339035.50	26.0		SFWMD
WEL0120001082600	136367.00	1361554.00	27.0		SFWMD
WEL2922003704101	352478.00	1013517.00	30.9		SFWMD
OKF-13	742962.00	1155367.00	26.0	31-May-00	USGS (Reese, WRI03-4242)
OR0547	506821.00	1591437.00	25.0		SFWMD
OR0617	620131.00	1524303.00	25.0	25-Jul-03	SJRWMD
OR0652	515569.00	1615040.00	25.2		SFWMD
OR0673	650629.00	1475910.00	26.0	25-Jul-03	SJRWMD
OR0827	535472.83	1521041.59	24.3		SFWMD
OR-47_G	503292.00	1532266.00	25.0		SFWMD
OS0027	654107.00	1374817.00	26.0	26-Oct-03	SJRWMD
OSF-21	657674.00	1265759.00	26.0	11-Aug-93	DBHYDRO
WEL2563001029400	373772.50	1127691.50	28.0	06-Sep-01	SWFWMD
SCC-MZL	418847.00	641207.00	30.0	07-Jun-99	DBHYDRO
WASANMZ2	936511.00	576823.00	20.0	27-Jan-05	DBHYDRO
PB-1196	930966.00	942017.00	23.0	17-Jul-01	USGS (Reese, WRI03-4242)
PB-1774	952122.00	958220.00	23.1		SFWMD
PBF-7	748906.00	860161.00	26.3		SFWMD
WEL2019001318600	264297.00	1419834.00	25.0	11-May-99	SWFWMD
WEL2908003735400	379969.00	989893.00	30.3		SFWMD
WEL2908003040600	381235.00	989884.00	29.2		SFWMD
WEL2731003104902	409730.00	992228.00	30.0	04-Nov-03	SFWMD

Table 3.2d: Temperature data (APPZ)

Station	X coordinate (ft FL State Plane 1983)	Y coordinate (ft FL State Plane 1983)	Temperature (°C)	Date	Source
WEL2728003105201	408995.00	990212.00	29.0	04-Nov-03	SFWMD
WEL2727003105301	412253.00	990799.00	28.0	04-Nov-03	SFWMD
WEL2726003105401	412788.00	989584.00	29.0	04-Nov-03	SFWMD
WEL2725003105501	412238.00	988274.00	29.0	04-Nov-03	SFWMD
WEL2724003105600	409345.00	988393.00	28.7	11-Sep-01	SFWMD
WEL2723003105700	414773.00	988865.00	31.0	11-Sep-01	SFWMD
WEL2978002815900	409230.00	999199.00	29.0	12-Nov-03	SFWMD
WEL2979002816000	410119.00	996770.00	29.0	12-Nov-03	SFWMD
PLA-MZU	906523.00	657665.00	21.0	19-Feb-03	DBHYDRO
WEL2702002732700	394886.00	1003731.00	30.0		SFWMD
WEL2702002732801	397338.00	1005533.00	31.0	05-Nov-03	SFWMD
WEL2702002732901	395096.00	1008375.00	30.0	05-Nov-03	SFWMD
WEL2702002733001	395089.00	1007163.00	30.0	05-Nov-03	SFWMD
WEL2702002733201	389392.00	1006594.00	28.0	05-Nov-03	SFWMD
WEL2702001492000	389472.00	1005079.00	30.9	26-Jun-01	SFWMD
WEL2702001561200	388693.00	1010436.00	29.6	26-Jun-01	SFWMD
WEL2702001064500	389998.00	1016588.00	31.0	26-Jun-01	SFWMD
WEL2702002732300	389398.00	1007604.00	31.0	26-Jun-01	SFWMD
WEL2702002732400	393663.00	1010303.00	30.0	26-Jun-01	SFWMD
WEL2702002732501	396194.00	1010388.00	28.0	05-Nov-03	SFWMD
WEL2702002732600	393458.00	1006568.00	32.3		SFWMD
WEL3004001574300	374849.00	1007903.00	28.0	11-May-05	SFWMD
ROMP 12 DP UP FLORIDAN	414491.00	984828.50	30.0	18-Sep-03	SWFWMD
ROMP 13 AVON PARK	455604.50	995808.00	28.0	23-Sep-03	SWFWMD
ROMP 14 AVON PARK	541075.00	1023767.00	27.0	24-Sep-03	SWFWMD
ROMP 15 DEEP	442918.00	1045764.00	28.2		SFWMD
ROMP 16.5 AVON PARK	368488.50	992452.00	30.0	29-Sep-03	DBHYDRO
WEL1027001104600	338696.00	1033835.50	32.0	24-Sep-03	SWFWMD
WEL1029001117700	222106.27	1084891.23	30.8		SFWMD
ROMP 22_S	222258.00	1085008.00	30.2		SFWMD
ROMP 25 LILY AVON PARK	329331.00	1103692.50	32.0	17-Sep-03	SWFWMD
ROMP 26 AVON PARK	388342.00	1078991.00	31.0	30-Sep-03	SWFWMD
ROMP 28 UP AVON PARK	514903.00	1103510.50	24.0	16-Oct-03	DBHYDRO
ROMP 28X DEEP	545830.00	1066255.50	25.0	24-Aug-00	SWFWMD
ROMP 30 AVON PARK	397813.00	1136915.00	27.0		SFWMD
ROMP 31 AVON PARK	359056.00	1135365.50	30.0	11-Mar-02	SWFWMD
ROMP 32 AVON PARK	311177.00	1141806.50	29.0	03-Jul-03	SWFWMD
ROMP 33 AVON PARK	248473.00	1137683.00	30.0		SFWMD
ROMP 39 AVON PARK	250816.50	1185216.00	29.0	10-Sep-03	SWFWMD
ROMP 40 AVON PARK	314896.00	1206124.50	26.0	18-Mar-03	SWFWMD
WEL0203001091600	500713.00	1189202.00	26.1		SFWMD
ROMP 48 AVON PARK	286604.00	1240207.50	28.0	25-Jun-03	SWFWMD
ROMP 49 AVON PARK	250480.50	1248607.50	27.0	16-Sep-03	SWFWMD
WEL1090001172600	195927.00	1217506.00	28.0		SFWMD
WEL0169001088000	281130.00	1301224.00	26.0	28-Dec-05	SWFWMD
WEL1034001141300	231413.00	1283467.00	27.0	23-Feb-04	SWFWMD
WEL0121001082700	222781.50	1355518.00	25.0		SFWMD
ROMP 68-1 AVON PARK	255358.50	1365168.00	25.0		SFWMD
WEL1905000136600	348016.50	1359883.50	26.0	05-Mar-02	SWFWMD
ROMP 85 AVON PARK	229950.00	1422406.00	24.0	22-Sep-98	SWFWMD
ROMP 86A AVON PARK	280067.00	1405716.00	26.0	14-Feb-00	SWFWMD
WEL0384000011800	198470.00	1452908.00	25.0	17-Sep-97	SWFWMD
WEL0751000048500	128113.00	1360391.00	26.0		SFWMD
WEL2666003472800	114568.63	1431615.76	25.0	17-Feb-04	SWFWMD
WEL2831000210000	119725.00	1429953.00	26.0	09-Sep-03	SWFWMD
WEL0211001092700	173084.00	1127558.00	30.0	18-Sep-03	SWFWMD
WEL0005001092000	155322.50	1184343.50	27.0	16-Sep-03	SWFWMD
WEL2190001715500	165341.50	1181498.00	28.0	17-Sep-03	SWFWMD
WEL0186001089800	205555.00	1249937.50	28.0	15-Sep-03	SWFWMD

Table 3.2d: Temperature data (APPZ)

Station	X coordinate (ft FL State Plane 1983)	Y coordinate (ft FL State Plane 1983)	Temperature (°C)	Date	Source
WEL0004001090901	195922.00	1241221.50	28.0		SFWMD
WEL1071001290600	201614.25	1254692.82	27.0	10-Dec-98	SWFWMD
WEL1091001172700	213752.00	1249651.50	28.0	12-Sep-03	SWFWMD
ROMP 29A	519840.00	1152172.00	25.7		SFWMD
WEL2967003527100	470491.00	1073400.00	31.0	09-Mar-04	SFWMD
WEL1770000130900	158216.00	1098859.00	27.7		SFWMD
WEL2705001285300	395238.00	1002315.00	31.0		SFWMD
WA-1082	823097.00	1111894.00	29.0		USGS (Reese, WRI03-4242)
WEL2910001164600	411374.00	1040186.00	31.0	12-Mar-03	SFWMD
WEL2457000175800	243624.50	1161235.00	26.0	27-Jul-01	SWFWMD
STL-255	883868.00	1060687.00	25.0	12-Jul-00	USGS (Reese, WRI03-4242)
WEL2912002961300	395920.00	1024224.00	30.0	18-Feb-03	SFWMD
WEL2430003489400	378062.00	1028483.00	31.0		SFWMD
WEL2897001000600	460763.00	1001344.00	27.9	13-Mar-03	SFWMD
WEL2897002697500	455097.00	1007127.00	29.6	13-Mar-03	SFWMD
WEL2897001003600	457334.00	1002572.00	29.3	13-Mar-03	SFWMD
WEL2898001003100	468038.00	991313.00	30.0		SFWMD
WEL2898001003000	470389.00	991302.00	28.5		SFWMD
WEL2898002698300	466098.00	1001925.00	29.8	13-Mar-03	SFWMD
WEL2898002698400	468174.00	1001208.00	28.3	13-Mar-03	SFWMD
WEL2924001434200	385690.00	1020857.00	28.4	04-Jun-03	SFWMD
WEL3007002477700	414381.00	1150547.00	25.4		SFWMD
WEL2692002270800	401507.00	992783.00	30.0		SFWMD
WEL2692001601600	402674.00	991564.00	28.0	25-Mar-03	SFWMD
WEL2477000177800	169188.50	1207810.00	25.0	15-Feb-01	SWFWMD
TCRK_GW2	725887.00	1056131.00	27.0	16-Jun-04	DBHYDRO
WEL2474000177500	465243.00	1184306.00	30.0	05-Sep-01	SFWMD
WEL2707000189300	358858.00	1008723.00	31.3		SFWMD
WEL2523001063300	393977.00	974653.00	31.0	02-Jan-03	SFWMD
WEL2707000189401	357071.00	1011463.00	30.9		SFWMD
WEL2844000215300	359018.00	1018316.00	31.4		SFWMD
WEL2941003562800	331677.00	1079624.00	30.4		SFWMD
WEL0969000070300	223674.50	1288314.00	26.0	18-Feb-04	SWFWMD
WEL1898000135700	444307.50	1425087.50	25.0	12-May-99	SWFWMD
W-15683	222842.00	944209.00	32.0		SFWMD
WEL1648000187500	212471.00	1408531.00	25.0	12-May-03	SWFWMD
WEL1519001172400	150829.50	1347585.00	27.0	09-Sep-03	SWFWMD
WEL2914002917100	416275.00	998248.00	30.0	05-Jun-02	SFWMD
WEL2914001634700	415009.00	998255.00	31.0	05-Jun-02	SFWMD
WEL2708000222300	402781.00	1008832.00	25.0	17-Jul-01	SFWMD
WEL3008003877800	437153.50	1392396.00	25.0	20-Jul-05	SWFWMD
WEL1953000142000	273621.00	1423556.00	25.0	11-May-99	SWFWMD

Table 3.2e: Temperature data (MC2)

Station	X coordinate (ft FL State Plane 1983)	Y coordinate (ft FL State Plane 1983)	Temperature (°C)	Date	Source
CLW-A1	105102.00	1321910.00	29.1		SFWMD
W-15831	130588.00	1138073.00	31.7		SFWMD
NWHWRAP-4D	136396.00	1361594.00	27.0		SFWMD
ST PETE DEEP # 105	167169.00	1401909.00	25.0	12-Aug-85	SWFWMD
W-16274	177807.00	1083591.00	36.7		SFWMD
ROMP 50 AVON PARK	217020.00	1230198.00	25.0	18-Feb-03	SWFWMD
ZEPHYRHILLS 006	274634.00	1417385.00	25.0	11-May-99	SWFWMD
BSU-MZL	317716.50	887559.00	32.0	6-Jul-04	DBHYDRO
ROMP 25 LILY EVAPORITE	329346.00	1103781.00	27.0	7-Oct-03	SWFWMD
ZRL-MZ2	341555.00	894221.00	32.0	27-Feb-96	DBHYDRO
NFM-MZL	368709.00	871748.00	33.0	27-Feb-96	DBHYDRO
Polk City USGS core hole 2	388670.00	1400176.00	26.0	4-Nov-80	USGS (O'Reilly et al, WRI02-4193)
CH-R5	392980.00	949940.00	32.5		SFWMD
NLCWTP-IW1	397890.00	872374.00	35.8		SFWMD
ROMP 12	414514.00	984827.00	30.8		SFWMD
I75-TW	416557.00	668295.00	30.0	20-Dec-94	DBHYDRO
SCC-MZL	418847.00	641207.00	29.0	14-Apr-05	DBHYDRO
NCCWTMZ2	433984.00	695249.00	31.0	27-Feb-96	DBHYDRO
OR0794	469976.00	1590792.00	25.8		SFWMD
OR0559	484034.00	1528509.00	25.0	8-Mar-00	SJRWMD
HE-1105	493959.00	822674.00	33.3		SFWMD
OSF-28	504801.00	1416016.00	26.0	23-Jun-72	DBHYDRO
ROMP 28 EVAPORITE	514896.00	1103515.00	27.0	18-Mar-02	SWFWMD
IWSD-TW	514984.00	756311.00	31.0	22-Feb-96	Bennett, 2002, packer test
C-1130	519068.00	736284.00	31.7		SFWMD
ROMP 29A	519839.00	1152172.00	26.3		SFWMD
Sky Lake #2	532428.00	1496612.00	26.0	12-Apr-99	USGS (O'Reilly et al, WRI02-4193)
BICY-MZ4	554525.00	567148.00	33.0	29-Jan-98	Bennett, 2004, temperature log
C-1124	561566.00	693229.00	30.6		SFWMD
W-15371	585798.00	769236.00	34.4		SFWMD
ORF-62	604253.00	1476241.00	25.0	15-Aug-05	DBHYDRO
OSF-22	605280.00	1437266.00	26.0	31-Jul-85	DBHYDRO
GLF-6	628326.00	910488.00	31.0	2-Nov-01	DBHYDRO
OR0675	650628.00	1475910.00	27.0	25-Oct-03	SJRWMD
OS0028	654107.00	1374817.00	27.0	26-Oct-03	SJRWMD
L2-TW	672744.00	826627.00	27.0	10-Jan-97	DBHYDRO
C-1127	683726.00	562928.00	27.8		SFWMD
C-962	687903.00	598265.00	32.8		SFWMD
W-12542	710023.00	1129877.00	28.9		SFWMD
BR-0910	742259.00	1387439.00	29.0	16-Jul-98	USGS (O'Reilly et al, WRI02-4193)
DF-1	828433.00	575983.00	22.0	12-Dec-96	DBHYDRO
STL-335	866646.00	1092405.00	27.0	12-Jul-00	USGS (Reese, WRI03-4242)
NPSL-MZL	866750.00	1092495.00	27.0	17-Nov-99	DBHYDRO
MDWSA_FA3	871527.00	442422.00	24.3		SFWMD
MIR-MW1	875503.00	603617.00	23.0	16-Feb-00	DBHYDRO
PBP-MZL	875725.00	604016.00	25.0		SFWMD
FPU-MZL	878265.00	1135537.00	24.0	11-Dec-02	DBHYDRO
PWU-MZL	882488.00	934221.00	27.0	17-Jan-01	DBHYDRO
STL-386	883688.00	1060686.00	25.0	12-Jul-00	USGS (Reese, WRI03-4242)
M-1325	895889.00	1057448.00	24.0	11-Dec-02	DBHYDRO
M-1353	900502.00	1041193.00	25.0	10-Jul-00	USGS (Reese, WRI03-4242)
RPB-MZL	906291.00	873439.00	24.0	12-Jan-00	DBHYDRO
MAR-MZL2	912732.00	694131.00	21.5	7-Sep-99	DBHYDRO
BF-1	925619.00	669564.00	20.0	23-Feb-93	DBHYDRO
PBC3-MZU	936079.00	781079.00	25.6	24-Nov-99	DBHYDRO
WPB-MZL	940194.00	874545.00	22.0	19-Mar-03	DBHYDRO
FTL-MZL2	941689.00	641434.00	20.0	7-Sep-99	DBHYDRO

Table 3.2f: Temperature data (LF1)

Station	X coordinate (ft FL State Plane 1983)	Y coordinate (ft FL State Plane 1983)	Temperature (°C)	Date	Source
W-17073	92615.00	1273195.00	33.6	25-Mar-74	DBHYDRO
L-5609	336731.00	790989.00	28.0		SFWMD
Polk City USGS core hole 2	388670.00	1400176.00	26.0	04-Nov-80	USGS (O'Reilly et al, WRI02-4193)
I75-MZ3	416557.00	668295.00	30.0	19-Dec-94	DBHYDRO, packer test
Lake Louisa State Park L-0729	422238.00	1486918.00	25.0	15-Feb-00	USGS (O'Reilly et al, WRI02-4193)
ORF-60	467177.00	1470886.00	25.0		SFWMD
OR0559	484034.00	1528509.00	25.0	08-Mar-00	SJRWMD
IC-TW	493981.00	1426090.00	25.0		SFWMD
IWSD-TW	514991.00	756311.00	31.0	22-Feb-96	Bennett, May 2002, packer test
ROMP 28 L AVON PARK	514906.00	1103501.50	27.0		SFWMD
Sky Lake #2	532428.00	1496612.00	26.0	12-Apr-99	USGS (O'Reilly et al, WRI02-4193)
BICY-TW	554526.00	567148.00	33.6	29-Jan-98	Bennett, 2004, temperature log
OR0560	557300.00	1509971.00	26.0		SJRWMD
OR0636	568198.61	1485909.54	28.0	23-Aug-96	USGS (Adamski and German, WRI03-4257)
OR0676	593335.24	1515450.47	27.0	30-Oct-03	SJRWMD
OR0021	611347.00	1487550.00	24.0	12-May-03	SJRWMD
OR0022	611348.00	1487550.00	24.0	13-May-03	SJRWMD
COCOA 13R NR BITHLO, FL	613737.17	1487448.41	24.0	30-Jun-99	USGS (Adamski and German, WRI03-4257)
OR0614	619094.00	1487342.00	28.0	27-Jan-01	SJRWMD
OR0618	620131.00	1524303.00	27.0	17-Feb-03	SJRWMD
GLF-6	628322.00	910488.00	31.0	22-Oct-01	DBHYDRO
OS0025	653839.00	1374817.00	26.0		SFWMD
L2-TW	672742.00	826627.00	26.0	01-Feb-94	DBHYDRO
C-962	687902.00	598265.00	34.0		SFWMD
OKF-100	697988.00	1025436.00	29.0	17-Dec-01	DBHYDRO
ALLY-TW	714531.00	668029.00	27.0		SFWMD
PAHO-MZL	764969.00	896738.00	28.0	14-Jul-99	DBHYDRO
MF-37	784922.00	965985.00	30.0	23-Oct-01	DBHYDRO
DF-2	830646.00	573066.00	19.0		SFWMD
PBF-15L	863877.00	874383.00	27.0	07-Jun-07	DBHYDRO
FPU-MW	878265.37	1135536.73	24.4	19-Apr-05	DBHYDRO
PWU-MZL	882488.00	934221.00	27.0	17-Jan-01	DBHYDRO
PBF-12	886681.00	735581.00	23.0	03-Sep-03	DBHYDRO
NMC-MW	895888.00	1057448.00	27.0		SFWMD
CS-I1	897445.00	695121.00	26.0	13-Sep-00	USGS (Reese, WRI03-4242)
STU-MZL	900443.00	1041253.00	27.0		SFWMD
PLA-MZL	906523.00	657665.00	21.0	19-Feb-03	DBHYDRO
AID-MZL	906925.00	837211.00	26.0	12-Nov-02	DBHYDRO
MAR-MZL1	913306.00	693654.00	22.0		SFWMD
BF-1	925618.00	669564.00	20.0	17-Feb-93	DBHYDRO
PBCSR-MZL	928807.00	785408.00	25.0	21-Sep-99	DBHYDRO
PBC3-MZL	936080.00	781079.00	27.0	24-Nov-99	DBHYDRO
SCU-MZL	939266.00	917657.00	24.0	12-Oct-99	DBHYDRO
FTL-MZL2	941689.00	641434.00	20.0	07-Sep-99	DBHYDRO
PBF-5	949211.00	852482.00	22.0	23-Sep-04	DBHYDRO
BR-0910	742259.00	1387439.00	29.0	16-Jul-98	USGS (O'Reilly et al, WRI02-4193)
OR0613	618644.70	1487393.78	28.5	23-Aug-99	USGS (Adamski and German, WRI03-4257)
OR0668	589432.00	1515255.00	28.0	27-Oct-04	SJRWMD
NFM-MZL	368709.00	871748.00	33.0	27-Feb-96	DBHYDRO
BSU-MZL	317716.50	887559.00	32.0	06-Jul-04	DBHYDRO
EPU-MZL	318594.00	961362.00	30.5	05-Oct-99	DBHYDRO

Table 3.2g: Temperature data (LC)

Station	X coordinate (ft FL State Plane 1983)	Y coordinate (ft FL State Plane 1983)	Temperature (°C)	Date	Source
EPU-MZL	318594.00	961362.00	30.5		SFWMD
L-5013	368627.00	805198.00	43.0		SFWMD
Lake Louisa State Park L-0729	422238.00	1486918.00	25.0	15-Feb-00	USGS (O'Reilly et al, WRI02-4193)
ORF-60	467176.00	1470886.00	27.0		SFWMD
IC-TW	493983.00	1426090.00	27.0	28-Dec-02	Bennett and Rectenwald, December 2003
C-415	517887.00	791920.00	36.0		SFWMD
C-820	556756.00	699802.00	41.0	30-Oct-03	DBHYDRO
W-15317	602750.00	662193.00	30.0	18-Dec-07	DBHYDRO
OR0021	611347.00	1487550.00	24.0	26-Oct-03	SJRWMD
OSF-104L	613202.00	1208993.00	27.0	06-Dec-01	DBHYDRO
OS0025	653839.00	1374817.00	27.0	26-Oct-03	SJRWMD
CLEW_IW-1	674630.00	868696.00	29.0		SFMWD
OKF-100	697988.00	1025436.00	31.0		USGS (Reese, WRI03-4242),use avg packer test
ALLY-TW	714533.00	668029.00	26.0		USGS (Meyer, 1989 Site 10)
W-15890	801396.00	1347824.00	32.0	12-May-03	DBHYDRO
MDWSA_I1	874120.00	440883.00	16.0		SFWMD
NMC-MW	895888.00	1057448.00	27.0		SFWMD
MAR-MZL1	913305.00	693654.00	15.0	20-Apr-05	DBHYDRO
BF-1	925617.00	669564.00	21.0	26-Jan-01	DBHYDRO
OR0613	618644.70	1487393.78	28.5	23-Aug-99	USGS (Adamski and German, WRI03-4257)
W-17073	92500.00	1273200.00	33.6	25-Mar-74	DBHYDRO, Added to the BZ layer to improve interpolation
ROMP 28 Evaporite	514906.00	1103501.50	27.0		SFWMD
OR0668	589432.00	1515255.00	28.0		SJRWMD, Added from LF layer

Table 3.2g: Temperature data (BZ)

Station	X coordinate (ft FL State Plane 1983)	Y coordinate (ft FL State Plane 1983)	Temperature (^{o}C)	Date	Source
W-17073	92615.00	1273195.00	33.6	25-Mar-74	DBHYDRO, Added to the BZ layer to improve interpolation
L-5000	226013.00	857117.00	43.0		USGS (Meyer, 1989 Site 15)
NPORT_DIW	250794.00	975534.00	44.0	20-Mar-87	DBHYDRO, AVG near base (NO BZ this well)
W-18091	293009.00	767918.00	39.0		SFWMD, Temperature Log
W-6674	373753.00	899294.00	38.0		USGS (Meyer, 1989 Site 2)
NLCWTP-IW1	397888.00	872374.00	36.0		MWH, April 2004
NCWRF-IW1	398376.00	701832.00	36.0		SFWMD, Temperature Log
C-1104	418384.00	591642.00	33.3		Missimer & Associates, undated
L-6461	427827.00	835731.00	38.0		SFWMD
W-16884	433375.00	695525.00	34.0		SFWMD, Geophysical Log
ORF-60	467175.00	1470886.00	26.0		SFWMD
OSF-97	493981.00	1426090.00	24.0	07-Feb-05	DBHYDRO
C-1246	514885.00	756362.00	36.0		SFWMD
IWSD-TW	514989.00	756311.00	36.0	09-Jan-02	DBHYDRO
W-1916	538479.00	715689.00	40.0		SFWMD
W-6150	544716.00	710707.00	42.0		SFWMD
P-311	549306.00	705484.00	37.0		SFWMD
C-819	556274.00	698824.00	41.0		SFWMD
C-746	558825.00	699828.00	43.0		SFWMD
HE-970	600120.00	808591.00	35.0		SFWMD
StCloud_OSF-0081	603920.00	1424341.00	29.0	06-Jan-00	USGS
OSF-104	613203.00	1208993.00	31.0		SFWMD
C-1125	641104.00	642475.00	29.0		SFWMD
W-15813	669849.00	1104902.00	43.0		SFWMD
CLEW_IW-1	674631.00	868696.00	32.0		SFWMD
C-962	687901.00	598265.00	31.0		SFWMD
PB-1138	697390.00	787876.00	41.0		SFWMD
ALLY-TW	714534.00	668029.00	26.0		USGS (Meyer, 1989 Site 10)
G-3240	730287.00	519875.00	23.0		USGS (Meyer, 1989 Site 11)
W-16226	750698.00	1487742.00	32.0		Geraghty & Miller, 1984
PB-1186	757542.00	858553.00	28.0		SFWMD, AVG over stable length of inversion on temp log
W-17052	764969.00	896738.00	30.0		SFWMD, Minimum BZ value from Temp Logs
W-15890	801397.00	1347824.00	32.0		SFWMD
IR-1001	823796.00	1182081.00	32.0		USGS (Meyer, 1989 Site 4)
PU-I2	848795.00	493789.00	16.0		USGS (Meyer, 1989 Site 12)
PSLLTC-IW1	850609.00	1104256.00	26.0		SFWMD, AVG over inverted temp section of log
FPL-EW2	860128.00	860441.00	31.0		SFWMD, AVG over STABLE length of log temp inversion
FPU_RO-IW1	866323.00	1130449.00	24.0		SFWMD, AVG over STABLE length of log temp inversion
PSLWPT-IW1	866387.00	1055241.00	25.0		SFWMD, Mean BZ value from Temp Log
I-1_g	870014.00	494695.00	16.0		SFWMD
MDWSA_I1	874120.00	440883.00	16.0		SFWMD
W-15748	882294.00	934068.00	27.0		SFWMD, Minimum BZ value from Temp Log
STL-254	883870.00	1060687.00	26.0	02-Nov-82	USGS (Reese, WRI03-4242)
PTSL_SPORT	883942.00	1060806.00	22.0		USGS (Meyer, 1989 Site 5)
CCUD-IW1	885050.00	627681.00	15.0		Hazen & Sawyer, 2001, Downhole probe
TFIW-2	896683.00	1005771.00	24.0		SFWMD, BHT from temp log, inversion dosen't stabilize
M-1034	900053.00	1041089.00	21.0		SFWMD
PLT-I1	906662.00	657847.00	18.0		CDM, 1987, downhole probe
MAR-MZL1	913305.00	693654.00	15.0		SFWMD
W-15886	917036.00	749287.00	18.0		SFWMD, AVG over stable length of inversion on temp log
BCN-I1	932263.00	700322.00	14.0		SFWMD, AVG over stable length of inversion on temp log
MDWNA_I-1N	936512.00	576823.00	10.0		Miami-Dade Water and Sewer Dept, 2006
PB-1180	936548.00	886438.00	16.0		USGS (Meyer, 1989 Site 7)
HOL-IW1	941045.00	616691.00	9.0		SFWMD, BHT temperature inversion not stable at TD
FTL-I1	941769.00	641407.00	10.0		USGS (Meyer, 1989 Site 9)

Table 5.1: Injection well TDS

Facility	X coordinate (ft FL State Plane 1983)	Y coordinate (ft FL State Plane 1983)	Average Injected TDS (mg/l)	Dataset date range		Comment
Acme Improvement District/Wellington-1	906651.34	830985.82	1307	01-Jan-00	01-Dec-05	
Bear Island-2	561780.88	689979.08	35000			Assume TDS injected is 35,000 mg/L (seawater) - brine discharge from oil and gas prod.
Beeline Community (Pratt & Whitney) PBC-1	882294.17	934067.52	31526	08-Jan-92	01-Nov-05	
Belle Glade	757470.63	858427.59	1517	01-Jan-99	01-Dec-05	
Berry Groves - Caloosahatchee ASR exploratory well-EXBRY-1	382340.63	856298.6	250			Assume TDS injected is 250 mg/L
Bonita Springs Utilities (San Carlos Estates WTP)-ASR - 1	402992	747797	154	01-Jul-04	01-Oct-05	Assume that Bonita Springs Utilities injects the same TDS as Corkscrew Lee County
Bonita Springs WTP-1	408963	731293	15820	01-Apr-04	01-Dec-05	
Boynton Beach ASR-ASR 1	962564	793682	201	24-Feb-94	21-Apr-94	
Boynton Beach RO-1	943358.88	798807.49	28075	01-Dec-98	01-Dec-03	
Broward County 2A-1	948842	713346	226	01-Nov-98	01-Feb-04	
Broward County North Regional-1	933459.65	701702.45	730	01-Jun-99	01-Dec-05	Assume same TDS dataset for all facility locations
Broward County North Regional-2	933461.65	701704.45	730	01-Jun-99	01-Dec-05	Assume same TDS dataset for all facility locations
Broward County North Regional-3	933463.65	701706.45	730	01-Jun-99	01-Dec-05	Assume same TDS dataset for all facility locations
Broward County North Regional-4	933465.65	701708.45	730	01-Jun-99	01-Dec-05	Assume same TDS dataset for all facility locations
Broward County North Regional-5	933467.65	701710.45	730	01-Jun-99	01-Dec-05	Assume same TDS dataset for all facility locations
Broward County North Regional-6	933469.65	701712.45	730	01-Jun-99	01-Dec-05	Assume same TDS dataset for all facility locations
Burnt Store-1	317655.5	888764.57	7953	01-Jan-96	01-Dec-05	
Charlotte County East Port-1	318518	960964.54	3511	01-Dec-98	01-Dec-05	
Charlotte County East Port-2	318520	960960	23601	01-Dec-98	01-Dec-05	
Charlotte County West Port-1	236938.15	947373.17	11333	01-Oct-98	01-Dec-05	
City of Orlando 8229 Drain well	516637	1517602	250			Assume TDS injected is 250 mg/L
City of Sunrise-ASR-1	898007	670372	24	23-Jan-04	23-Jan-04	
Cocoa - Claude H. Dyal-1	741538.36	1462517.85	419	31-Aug-93	22-Dec-93	
Cocoa - Claude H. Dyal-2	741540.36	1462519.85	419	31-Aug-93	22-Dec-93	
Cocoa - Claude H. Dyal-3	741542.36	1462521.85	419	31-Aug-93	22-Dec-93	
Cocoa - Claude H. Dyal-4	741544.36	1462523.85	419	31-Aug-93	22-Dec-93	
Cocoa - Claude H. Dyal-5	741546.36	1462525.85	419	31-Aug-93	22-Dec-93	
Cocoa - Claude H. Dyal-6	741548.36	1462527.85	419	31-Aug-93	22-Dec-93	
Cocoa - Claude H. Dyal-7	741550.36	1462529.85	419	31-Aug-93	22-Dec-93	Assume that Cocoa Dyal 7 injects same TDS as Cocoa Dyal 1
Cocoa - Claude H. Dyal-8	741552.36	1462531.85	419	31-Aug-93	22-Dec-93	Assume that Cocoa Dyal 8 injects same TDS as Cocoa Dyal 1
Cocoa - Claude H. Dyal-9	741554.36	1462533.85	419	31-Aug-93	22-Dec-93	Assume that Cocoa Dyal 9 injects same TDS as Cocoa Dyal 1
Cooper City-1	885050.4	627681.26	2880	01-Mar-05	01-Dec-05	
Coral Springs IW-1-CS-I1	897444.59	695121.17	29256	01-Oct-03	01-Dec-04	
Coral Springs IW-2-SC-I2	897697.46	695859.81	12119	01-Oct-03	01-Dec-04	
Corkscrew (Lee County)-MH ASR#1	425597	775414	136	01-Jul-04	01-Oct-05	Assume same TDS dataset for all facility locations
Corkscrew (Lee County)-MH ASR#2	425807	774493	136	01-Jul-04	01-Oct-05	Assume same TDS dataset for all facility locations
Corkscrew (Lee County)-MH ASR#3	424279	777794	136	01-Jul-04	01-Oct-05	Assume same TDS dataset for all facility locations
Corkscrew (Lee County)-MH ASR#4	424765	776404	136	01-Jul-04	01-Oct-05	Assume same TDS dataset for all facility locations
Corkscrew (Lee County)-MH ASR#5	423688	779149	136	01-Jul-04	01-Oct-05	Assume same TDS dataset for all facility locations
East-Central Regional-1	938580.56	874005.38	664	01-Mar-98	01-Nov-05	Assume same TDS dataset for all facility locations
East-Central Regional-2	938582.56	874007.38	664	01-Mar-98	01-Nov-05	Assume same TDS dataset for all facility locations
East-Central Regional-3	938584.56	874009.38	664	01-Mar-98	01-Nov-05	Assume same TDS dataset for all facility locations
East-Central Regional-4	938586.56	874011.38	664	01-Mar-98	01-Nov-05	Assume same TDS dataset for all facility locations
East-Central Regional-5	938588.56	874013.38	664	01-Mar-98	01-Nov-05	Assume same TDS dataset for all facility locations
East-Central Regional-6	938590.56	874015.38	664	01-Mar-98	01-Nov-05	Assume same TDS dataset for all facility locations
Encon/Jupiter-1	936485.26	942356.69	501	01-Apr-98	01-Dec-05	
Englewood IW-1-1	214000	954416.9	20840	01-Dec-92	01-Dec-05	
Englewood-ASR-1	230438.76	936885.38	415	01-Oct-01	01-May-05	
Fiveash Wellfield (FTL)-ASR 1	933649	670331	231	01-Nov-98	01-Feb-04	Assume that Fiveash Wellfield injects same TDS as Broward County 2A-1
Fort Myers Beach-1	359112.55	791504.65	32827	09-Oct-98	07-Dec-05	
Fort Myers WTP-1	385993	834835	8833	01-Apr-00	01-Dec-05	
Fort Pierce Util. Authority RO-1	866322.66	1130448.89	5557	01-Jan-03	01-Dec-05	
Fort Pierce Util. Authority WWTP-1	878222.11	1135587.99	515	01-Jan-99	01-Dec-05	
G.T. Lohmeyer in Ft. Lauderdale-1	941769.4	641407.48	1229	01-Jan-00	01-Dec-05	Assume same TDS dataset for all facility locations
G.T. Lohmeyer-2	941587.06	641406.26	1229	01-Jan-00	01-Dec-05	Assume same TDS dataset for all facility locations

Facility	X coordinate (ft FL State Plane 1983)	Y coordinate (ft FL State Plane 1983)	Average Injected TDS (mg/l)	Dataset date range		Comment
G.T. Lohmeyer-3	941310.04	641402.61	1229	01-Jan-00	01-Dec-05	Assume same TDS dataset for all facility locations
G.T. Lohmeyer-4	943327.12	642496.2	1229	01-Jan-00	01-Dec-05	Assume same TDS dataset for all facility locations
G.T. Lohmeyer-5	941040.04	641400	1229	01-Jan-00	01-Dec-05	Assume same TDS dataset for all facility locations
Gasparilla Island WTP-1	247335.93	922338.62	22183	01-Dec-01	01-Dec-05	
Hollywood-1	941221.38	616431.22	2662	01-Oct-03	01-Dec-05	Assume same TDS dataset for all facility locations
Hollywood-2	941223.38	616433.22	2662	01-Oct-03	01-Dec-05	Assume same TDS dataset for all facility locations
Immokalee-1	514885	756362	34861	14-Aug-02	01-Jun-05	
Intersil-1	784700	1345725	2131	01-Jan-98	01-Oct-05	Assume same TDS dataset for all facility locations
Intersil-2	784710	1345720	2131	01-Jan-98	01-Oct-05	Assume same TDS dataset for all facility locations
Kaiser-1	333168.41	1297465.4	779	01-Mar-96	01-Dec-05	Assume that Kaiser-1 injects the same TDS as Zemel Road
Kissimmee River/CERP exploratory well - OK-100	696704.82	1025434.635	180	01-Mar-09	01-Mar-09	Value from preliminary Kissimmee ASR data
Lake Manatee-B-1	216224.21	1149498.87	295	04-Aug-93	09-Dec-04	Assume that Lake Manatee B-1 injects the same TDS as Peace River-1/T-1
Lake Manatee-B-2	216934.84	1148582.02	295	04-Aug-93	09-Dec-04	Assume that Lake Manatee B-1 injects the same TDS as Peace River-1/T-1
Lee County Utilities (Olga)-LH ASR#1 Olga	432240	868000	309	01-Jun-01	01-Jul-05	
Lee County Utilities-LH ASR#1 North Reservoir	382550	865500	320	07-Oct-03	29-Dec-03	
Lehigh (oil and gas)-1	427279.01	835868.32	35000			Assume TDS injected is 35,000 mg/L (seawater) - brine discharge from oil and gas prod.
Margate-1	914118.7	693300.69	345	01-Mar-00	01-Dec-02	
Margate-2	914120.7	693302.69	491	01-Mar-00	01-Dec-05	
Melbourne-Grant Street-1	782020.2	1359774.64	577	01-Jun-98	01-Dec-05	
Miami-Dade North District-1	936410.96	577893.27	454	01-May-96	01-Dec-05	Assume that Miami-Dade North wellfield injects same TDS as Miami-Dade South wellfield
Miami-Dade North District-2	936510.96	577443.27	454	01-May-96	01-Dec-05	Assume that Miami-Dade North wellfield injects same TDS as Miami-Dade South wellfield
Miami-Dade North District-3	869717.03	427820.14	454	01-May-96	01-Dec-05	Assume that Miami-Dade North wellfield injects same TDS as Miami-Dade South wellfield
Miami-Dade North District-4	935970.96	576943.27	454	01-May-96	01-Dec-05	Assume that Miami-Dade North wellfield injects same
Miami-Dade South District-1	874120	440883	454	01-May-96	01-Dec-05	Assume same TDS dataset for all facility locations
Miami-Dade South District-10	869719.03	427822.14	454	01-May-96	01-Dec-05	Assume same TDS dataset for all facility locations
Miami-Dade South District-11	869710	427810	454	01-May-96	01-Dec-05	Assume same TDS dataset for all facility locations
Miami-Dade South District-12	871369.33	442406.13	454	01-May-96	01-Dec-05	Assume same TDS dataset for all facility locations
Miami-Dade South District-13	869712.03	427828.14	454	01-May-96	01-Dec-05	Assume same TDS dataset for all facility locations
Miami-Dade South District-14	874126	440881	454	01-May-96	01-Dec-05	Assume same TDS dataset for all facility locations
Miami-Dade South District-15	874122	440885	454	01-May-96	01-Dec-05	Assume same TDS dataset for all facility locations
Miami-Dade South District-16	874124	440887	454	01-May-96	01-Dec-05	Assume same TDS dataset for all facility locations
Miami-Dade South District-17	874142	443078	454	01-May-96	01-Dec-05	Assume same TDS dataset for all facility locations
Miami-Dade South District-2	874870	440840	454	01-May-96	01-Dec-05	Assume same TDS dataset for all facility locations
Miami-Dade South District-3	875618	440887	454	01-May-96	01-Dec-05	Assume same TDS dataset for all facility locations
Miami-Dade South District-4	875910	441553	454	01-May-96	01-Dec-05	Assume same TDS dataset for all facility locations
Miami-Dade South District-5	876304	442461	454	01-May-96	01-Dec-05	Assume same TDS dataset for all facility locations
Miami-Dade South District-6	876313	443061	454	01-May-96	01-Dec-05	Assume same TDS dataset for all facility locations
Miami-Dade South District-7	875607	443133	454	01-May-96	01-Dec-05	Assume same TDS dataset for all facility locations
Miami-Dade South District-8	874869	443127	454	01-May-96	01-Dec-05	Assume same TDS dataset for all facility locations
Miami-Dade South District-9	873259	441100	454	01-May-96	01-Dec-05	Assume same TDS dataset for all facility locations
Miami-Dade West Wellfield-1	831784.23	497010.59	287	22-Apr-04	08-Jun-04	
Miami-Dade West Wellfield-2	831834.23	497060.59	291	20-Feb-04	01-Aug-04	
Miami-Dade West Wellfield-3	831884.23	497110.59	287	22-Apr-04	08-Jun-04	
Mid Felda-1	489120.45	793239.59	35000			Assume TDS injected is 35,000 mg/L (seawater) - brine discharge from oil and gas prod.
Miramar RO-1	880764.9	594262.97	2631	01-Nov-95	01-Dec-05	
Miramar RO-2	880673.72	594262.55	2920	01-Jul-96	01-Oct-05	
Miramar WWTP-1	875549.45	603608.27	394	01-Aug-97	01-Dec-05	
Miramar WWTP-2	874249.45	603548.27	2920	01-Jul-96	01-Oct-05	Assume that Miramar WWTP-2 injects same TDS as
North Collier County WTP-1	431275.78	694627.34	8356	01-Feb-95	01-Dec-05	Assume same TDS dataset for all facility locations

Table 5.1: Injection well TDS

Facility	X coordinate (ft FL State Plane 1983)	Y coordinate (ft FL State Plane 1983)	Average Injected TDS (mg/l)	Dataset date range		Comment
North Collier County WTP-2	431277.78	694629.34	8356	01-Feb-95	01-Dec-05	Assume same TDS dataset for all facility locations
North Collier County WWTP-2	398139	701823	8356	01-Feb-95	01-Dec-05	Assume that North Collier County WWTP-2 injects
North Fort Myers Utility-1	375252.55	854404.85	499	01-Jul-96	01-Jan-02	
North Martin County-1	895891.55	1057423.94	4259	01-Jul-98	01-Dec-05	Assume same TDS dataset for all facility locations
North Martin County-2	895893.55	1057425.94	4259	01-Jul-98	01-Dec-05	Assume same TDS dataset for all facility locations
North Port St. Lucie-1	866826.31	1092304.69	19483	01-Oct-03	01-Dec-04	
North Port, City of -1	250475.77	989050.79	13764	11-Apr-94	01-Nov-05	
North Port/Sarasota (Mayakkahatchee Creek)-SWI_51730	250924.06	988658.52	280	01-Sep-05	01-Oct-05	
Ocean Spray Cranberries-1	823795.81	1182081.2	2224	01-Apr-98	01-Dec-05	
Orange Co 8038 Drain well	530948	1501497	250			Assume TDS value of 250 mg/L
Orange Co 8040 Drain well	536840	1501687	250			Assume TDS value of 250 mg/L
Orange Co 8041 Drain well	537689	1487242	250			Assume TDS value of 250 mg/L
Orange Co 8142 Drain well	528939	1514331	250			Assume TDS value of 250 mg/L
Orange Co 8143 Drain well	530257	1508469	250			Assume TDS value of 250 mg/L
Orange Co 8144 Drain well	530342	1507159	250			Assume TDS value of 250 mg/L
Orange Co 8145 Drain well	539069	1500967	250			Assume TDS value of 250 mg/L
Orange Co 8146 Drain well	539858	1496325	250			Assume TDS value of 250 mg/L
Orange Co 8151 Drain well	555167	1513141	250			Assume TDS value of 250 mg/L
Orange Co 8224 Drain well	523942	1514451	250			Assume TDS value of 250 mg/L
Orange Co 8225 Drain well	524837	1515251	250			Assume TDS value of 250 mg/L
Orange Co 8226 Drain well	518137	1512851	250			Assume TDS value of 250 mg/L
Orange Co 8227 Drain well	523233	1515762	250			Assume TDS value of 250 mg/L
Pahokee-1	768956.47	903692.76	1256	01-Jan-99	01-Dec-05	
Palm Bay-1	785481.61	1342510.45	2542	01-Apr-98	01-Dec-05	
Palm Bay-ASR 1	785480.61	1342510.45	419	31-Aug-93	22-Dec-93	Assume that Palm Bay ASR injects the same TDS as Cocoa-Dyal
Palm Beach County So. Region Pumping Station (Sys. 9) North-1	916961.46	749156.72	3271	01-Dec-01	01-Apr-05	
Palm Beach County Southern Region WRF-1	928640.74	785279.25	7932	01-Oct-03	01-Dec-04	
Palm Beach County Southern Region WRF-2	928642	785280	25720	01-Oct-03	01-Dec-04	
Palm Beach County System 3 /Sroc/diw1-1	937150.02	776449.24	2094	01-Dec-96	01-Dec-05	
PBCWU DEPT/Hillsboro Canal East-WTP 9 - ASR 1	910616.28	730639.67	485	14-Oct-04	28-Dec-04	
PBCWU DEPT/System 3-WTP 3 - ASR - 1	935525	781439	485	14-Oct-04	28-Dec-04	Assume that PBCWU System 3 injects the same TDS as PBCWU System 9
Peace River-1/T-1	329986.7	1003590.77	295	04-Aug-93	09-Dec-04	
Peace River-10/S-9R	329253.94	1002384.73	315	01-Oct-03	09-Dec-04	
Peace River-11/S-4	324454.39	1001312.43	296	01-Dec-93	09-Dec-04	
Peace River-12/S-10	324809.41	1000501.63	315	01-Oct-03	09-Dec-04	
Peace River-13/S-11	324811.86	1000804.58	315	01-Oct-03	09-Dec-04	
Peace River-14/S-12	324538.23	1000503.82	315	01-Oct-03	09-Dec-04	
Peace River-15/S-13	324450.29	1000807.51	315	01-Oct-03	09-Dec-04	
Peace River-16/S-14	324176.66	1000506.75	315	01-Oct-03	09-Dec-04	
Peace River-17/S-15	324178.3	1000708.72	315	01-Oct-03	09-Dec-04	
Peace River-18/S-16	324814.31	1001107.54	295	04-Aug-93	09-Dec-04	Assume that Peace River-18/S-16 injects same TDS as Peace River-1/T-1
Peace River-19/S-17	324816.76	1001410.49	288	04-Aug-93	09-Dec-04	
Peace River-2/S-2	329987.51	1003691.76	300	04-Aug-93	09-Dec-04	
Peace River-20/S-18	324543.14	1001109.73	315	01-Oct-03	09-Dec-04	
Peace River-21/S-19	324180.76	1001011.68	315	01-Oct-03	09-Dec-04	
Peace River-22/S-20	324184.03	1001415.62	295	04-Aug-93	09-Dec-04	Assume that Peace River-18/S-16 injects same TDS as Peace River-1/T-1
Peace River-3/S-1	330168.28	1003690.32	303	01-Dec-93	09-Dec-04	
Peace River-4/S-6	328258.87	1002291.7	283	08-Oct-03	09-Dec-04	
Peace River-5/S-7	328345.21	1001786.05	306	01-Nov-03	09-Dec-04	
Peace River-6/S8	327621.29	1001690.86	283	01-Oct-03	09-Dec-04	

Table 5.1: Injection well TDS

Facility	X coordinate (ft FL State Plane 1983)	Y coordinate (ft FL State Plane 1983)	Average Injected TDS (mg/l)	Dataset date range		Comment
Peace River-8/S-3R	330072.26	1002984.15	315	08-Oct-03	09-Dec-04	
Peace River-9/S-5R	329258.78	1002990.64	315	08-Oct-03	09-Dec-04	
Pembroke Pines-1	874696.32	602710.94	3327	01-Oct-03	01-Dec-04	
Pembroke Pines-2	874698.32	602712.94	29710	01-Oct-03	01-Dec-04	
Plantation Central RO-1	896046.17	652402.62	2353	01-Jan-97	01-Dec-05	
Plantation East RO-1	903158.23	651938.33	1925	01-Feb-00	01-Dec-05	
Plantation Regional WWTP-1	906500.35	657107.3	432	01-May-00	01-Dec-05	Assume same TDS dataset for all facility locations
Plantation Regional WWTP-2	906502.35	657105.3	432	01-May-00	01-Dec-05	Assume same TDS dataset for all facility locations
Plantation RO(Sarasota) -SWI_51740	211618.82	996810.77	5121	01-Nov-03	01-Dec-04	
Pompano Beach-1	944610.27	695314.29	2492	01-Sep-02	01-Dec-05	
Port Mayaca/CERP expoloratory well-EXPM-1	784619.67	965030.23	250			Assume TDS injected is 250 mg/L
Port St. Lucie James E. Anderson WTP (formerly LTC, per DEP)-1	850609.01	1104256.18	5273	01-Apr-03	01-Nov-05	
Punta Gorda / Shell Creek-ASR - 4R	351729.75	961513.25	323	01-Jun-03	01-Nov-05	
Punta Gorda / Shell Creek-ASR-3	351447.1	960000.54	312	01-Jun-03	01-Nov-05	
Punta Gorda-1	347624.63	947389.46	28393	01-Aug-01	01-Dec-05	
Raccoon Pt. Field-1	687840.16	598360.42	35000			Assume TDS injected is 35,000 mg/L (seawater) - brine discharge from oil and gas prod.
Rockledge-1	744814.41	1452378.44	586	01-Apr-99	01-Dec-05	
Royal Palm Beach/Northern Region Op'n Ctr/WTP 10-1	906398.99	872991.35	596	01-May-95	01-Dec-05	
Sarasota Co.- Brentwood (Atlantic Utilities)-1	177416.54	1082565.99	2840	19-Dec-98	01-Dec-05	
Sarasota Co.- Center Road -1	201506.27	1001382.14	6122	01-Jun-96	01-Dec-05	
Sarasota Co.- Venice Gardens/ Jacaranda WTP-1	205536.5	997903.43	4875	01-May-96	01-Dec-05	
Seacoast Utilities-1	939171.99	920158.54	7180	01-Mar-04	01-Dec-04	
South Beaches-1	801395.8	1347823.83	7905	01-Jul-98	01-Dec-05	
South Collier County WTP-1	432819	666004	8356	01-Feb-95	01-Dec-05	Assume that South Collier County WTP-1 injects same TDS as North Collier County WTP-1
South Collier County WTP-2	431808	666010	8356	01-Feb-95	01-Dec-05	Assume that South Collier County WTP-2 injects same TDS as North Collier County WTP-1
South Port St. Lucie-1	883777.98	1060686.85	26223	01-Oct-03	01-Nov-04	
Stuart-1	900051.27	1041088.96	30440	01-Oct-03	01-Dec-04	
Stuart-2	900053.27	1041086.96	12000	01-Oct-03	01-Dec-04	
Sunniland-1	537748.46	713980.22	35000			Assume TDS injected is 35,000 mg/L (seawater) - brine discharge from oil and gas prod.
Sunrise Sawgrass RO-1	875750.72	664308.69	3275	01-Aug-01	01-Dec-05	
Sunrise-1	873390.51	653626.48	410	01-Apr-98	01-Dec-05	
Sunrise-2	873511	653101	458	01-Apr-98	01-Oct-05	
Sunrise-3	874513.06	653631.59	361	01-Dec-96	01-Mar-04	
West Felda Field-	466408.7	807639.91	35000			Assume TDS injected is 35,000 mg/L (seawater) - brine discharge from oil and gas prod.
West Melbourne-1	771000.29	1360340.97	484	01-Mar-98	01-Dec-05	
Westport St Lucie -	866386.79	1055240.94	1453	01-Nov-03	01-Nov-05	
Zemel Road Landfill-1	343965.46	894302.3	779	01-Mar-96	01-Dec-05	

Appendix F: WASH123D and SEAWAT Comparison

Table of Contents

1.0 Introduction

During the model construction process, a WASH123D model was developed for the same domain as that of the SEAWAT model. Calibration models were completed and compared in the Draft Calibration report for the two models. After receiving comments from the Project Delivery Team and the Interagency Modeling Center, the model was recalibrated to produce the final calibration results documented in the final ASR Regional Calibration Report. The final calibration was completed using only the SEAWAT model. The WASH123D model was not recalibrated for two main reasons: 1) It is much more difficult to incorporate heterogeneity of the hydrogeologic parameters into the WASH123D model as described later in this appendix, and 2) WASH123D has fewer solver options. A less accurate but faster solver allows for a coarse calibration in SEAWAT followed by a more refined calibration with its more accurate, slower solver. The WASH123D code has only a more accurate but slower solver resulting in a longer time to develop a calibrated solution.

The draft calibration results are retained in this appendix for both the SEAWAT and WASH123D models to demonstrate their similarity. This similarity supports the reliability of the final SEAWAT calibration results. Sensitivity runs from the Draft Calibration Report that were related to the WASH123D model are also found in this appendix.

2.0 Draft Steady State Calibration

Using the same methodology as described in Section 4.1 of the final report, model hydraulic conductivities for the draft SEAWAT and WASH123D models were varied until the computed heads matched observed heads at selected wells for both October 2003 and February 2004. The goodness of fit to the observed data was evaluated using error statistics, calibration target figures, gradient analysis at well clusters, and comparison to other published information. Only the error statistics and calibration target figures for the draft SEAWAT and WASH123D are retained within this appendix. In comparing these statistics and figures, it can be shown that the model results using the two different codes are very similar.

For the draft SEAWAT model, both trial-and-error and automated methods were used to vary the hydraulic conductivities. Also smooth, interpolated conductivity fields were generated through use of “pilot points” rather than zonal conductivity fields. This process was identical to the calibration process for the final SEAWAT model described in detail in Section 4.1 of the main report.

During the Phase I model study, it was determined that the SEAWAT and WASH123D codes should provide similar results given similar hydrogeologic parameters, initial conditions and boundary conditions. To take advantage of these similarities, the initial hydraulic conductivities used for the WASH123D model were based on the draft calibrated hydraulic conductivities from the SEAWAT model. Using this method allowed for a time savings because only one model (the SEAWAT model) had to be calibrated using both “trial and error” methods and automated methods. Once the draft calibrated SEAWAT conductivities were determined and input to the WASH123D model, adjustments were made to the WASH123D model conductivities by the “trial and error” method.

2.1 SEAWAT

2.1.1 Draft Conductivity Fields

Figures F2-1 through F2-4 show the draft calibrated maps of hydraulic conductivity for all aquifer layers of the FAS. Aquifers are shown with horizontal hydraulic conductivities (vertical conductivities were always 1/10 of the horizontal value). Figures F2-5 through F2-7 show the draft calibrated maps of hydraulic conductivity for all confining units of the FAS. Confining units are shown with vertical hydraulic conductivities (horizontal conductivities were always twice the vertical value).

The IAS layers are shown in Figures F2-8 through F2-10. In reality, this geologic layer is a complex combination of interbedded confining units and sub-regional aquifers. Because of the complexity of this system and because the ASR wells are not expected to impact this layer substantially, the IA and ICU were combined into layers 2 through 4 of the SEAWAT model and Layers 1 through 4 of the WASH123D model. For this modeling effort, the aquifer portions of this geologic system were simplified into a single aquifer layer between two confining unit layers. The aquifer layer was modeled located in the northwestern portion of the model domain in layer 3 of the SEAWAT model and layers 2 and 3 of the WASH123D model. The boundary between the aquifer and aquitard in this model layer is based on a figure in "The Hydrogeology of Florida" (Miller, 1997). All ICU layers have identical vertical hydraulic conductivities in the areas outside of this aquifer zone in both models. (Note that Figure F2-9 shows horizontal hydraulic conductivity, not vertical, so the colors are slightly different.) Variability was allowed between the ICU conductivities overlying and underlying the aquifer portion of the IAS. This allowed for some variation in the source of pumped water in the IA. It is important to remember that these layers are not expected to replicate reality. The model was not calibrated in the IAS and no attempt has been made to correctly simulate flow in this section. These layers act simply as a conduit for recharge water traveling to the UF and discharge water traveling to the surface. The objective was merely to correctly define these flows.

Figures F2-1 and F2-2 show the horizontal hydraulic conductivity values for the UF and APPZ. There was a significant amount of data available for both these layers and the calibration process did not allow model conductivities to vary significantly from what has been measured. The UF (Figure F2-1) shows a zone of somewhat low conductivity along the Kissimmee River, with higher conductivities in the southern portion of the model. It is important to note that the lower conductivities found in the west portion of the model coincide with greater thickness, so the transmissivity does not drop as low as it may seem from this figure. This is also the area where the Hawthorn and Suwannee units are found. This model has combined both of these units into the UF, so the conductivities may vary somewhat from known measurements in either of these units. It is also interesting to note that the Kissimmee River ASR Pilot Project (KASR) is at the eastern side of a small area of high conductivity. The drop in conductivity towards the east is documented, but the exact location and nature of this drop is unknown. The area of lower conductivity to the East of KASR may significantly impact the efficiency of the proposed CERP ASR wells in this area.

The conductivities in the APPZ (Figure F2-2) are lowest along the north-south ridges west of Kissimmee River and reach higher levels on the east side of the model, including an area of very high conductivity directly beneath the low conductivity area in the UF near KASR. The line between the northern dolomite rock and the southern limestone is one of the few sudden changes in conductivity in this model. The location of the interface between the two rocks is based on USGS Scientific Investigation Report 2007-5207 (Reese and Richardson, 2008) though its exact location may be unknown. Suggestions were made to try to soften the conversion from dolomite to limestone. Some sensitivity analyses were run to determine the importance of the placement of that line, but the effects were minor and localized. Since the precise location of this line did not affect the regional calibration, the location of this interface was kept consistent that depicted in USGS Scientific Investigation Report 2007-5207 (Reese and Richardson, 2008).

Figures F2-3 and F2-4 present the horizontal hydraulic conductivity fields for the LF1 and BZ layers of the model. Very little data was available for either layer. The draft calibrated results show generally increasing conductivity to the southeastern portion of the model domain. This distribution is consistent with the current understanding of these deeper aquifers (Reese and Richardson, 2008).

Finally, Figures F2-5 through F2-7 show the vertical hydraulic conductivity values selected for the three confining units in the Floridan system. Although some data was available for these layers, it was used only as a loose constraint on the range of conductivities in each layer. The conductivity values in these layers were valuable tools in the calibration process since the model was highly sensitive to these values.

2.1.2 Description of the Steady State Calibration Quality

Figures F2-11 through F2-20 show the calibration target plots and the error statistics separated by layer and month. The UF steady state head solution and corresponding calibration targets in Figures F2-11 and F2-15 (February 2004 and October 2003, respectively) shows a good calibration. The RMS in both months is 1.9 feet or less with the mean error values very close to zero. The majority of the calibration targets are green, indicating a match within 2 feet of the measured head value. The exceptions are due to steep head gradients, near-well pumping effects or the inability to calibrate both months simultaneously (likely due to errors in the pumping estimates or lack of a local steady state condition).

The statistics and calibration targets for the APPZ steady state calibration are shown on Figures F2-12 and F2-16 (February 2004 and October 2003, respectively). These plots show slightly more error than the UF but with the RMS still less than 2.4 in both months. Most of the calibration points in this layer show a close similarity between calculated and measured heads. A few exceptions, skew the statistics, but do not materially affect the usefulness of the model.

Figures F2-13 and F2-17 show the head solution and calibration information for the LF1, while Figures F2-14 and F2-18 show the same data for the BZ. The unusual shapes in the head contours are due to the influence of density as caused by salinity and temperature and a great depth. At this great depth, there is much less data for comparison, but the figure shows that all data has been matched very closely and the RMS values are impressive at less than 1 foot. Due to the small number of calibration points in the

LF1 and BZ, an expanded calibration was performed in these layers. Figures F2-19 and F2-20 show the head solution and calibration information of the calibration of data from the LF1 and BZ to data that has been collected for these units during a time period other than the calibration period. Since the water level data used for this expanded calibration was not from the modeled period, these figures use a confidence interval of 5 ft rather than the 2 ft interval used in the other calibration plots (i.e. green bars indicate agreement within 5 feet). The error statistics for this expanded calibration are consistent with that seen in the other layers of the model. The reasonable fit of the calibration and expanded calibration in these lower layers of the model indicates that the flow to and from these units into the units more directly affected by the CERP ASR program is reasonable on a regional basis.

2.2 WASH123D Comparison to SEAWAT

The following sub-sections compare the hydraulic conductivities in the SEAWAT and WASH123D models and describe the correlation of the WASH123D draft calibration results to those generated in the SEAWAT draft calibration model.

2.2.1 Draft Conductivity Fields

The initial hydraulic conductivity values for the WASH123D model varied somewhat from the draft calibrated SEAWAT model conductivities. For the SEAWAT model, "pilot points" were used as described in Section 4.1, to provide a smooth conductivity field with a different value at every cell across the domain. In WASH123D, hydraulic conductivity is assigned to each finite element using a material zone. The material zone associates the element properties such as porosity, hydraulic conductivity, and storage coefficient, to each element within the model domain. A different hydraulic conductivity value for each element in this model would require 740,637 material zones, which would be difficult to implement and would tax the memory requirements of the code. To reduce the number of material zones, the draft calibrated SEAWAT conductivities were contoured by layer at contour intervals sufficient to replicate the regional flow fields. Then the contours were used to create zones of similar hydraulic conductivity with one material for each zone. A total of 297 material zones were assigned for the steady state WASH123D model.

The WASH123D heads produced using SEAWAT draft calibrated conductivities resulted in an RMS of approximately 5 feet. Trial and error adjustments were made to the WASH123D material zone shapes, the number of zones, and zone conductivity values, primarily in the confining units, to improve the calibration.

Figures F2-21 through F2-30 show the draft calibrated hydraulic conductivities for the WASH123D steady state ASR Regional Model.

The WASH123D calibrated hydraulic conductivities for the IAS (Layers 1 through 4) are shown in Figures F2-21 through F2-23. A comparison to the SEAWAT conductivities for corresponding Layer 2 through 4 (Figures F2-8 through F2-10) reveals that the values are very similar with minor differences resulting from efforts to reduce the number of material zones.

Figures F2-24 through F2-27 show the calibrated WASH123D Floridan Aquifer horizontal hydraulic conductivities. These values are nearly identical to the SEAWAT aquifer horizontal hydraulic conductivity values (Figures F2-1 through F2-4). Differences are the result of condensing similar values to reduce the total number of material zones. Few changes were made to these layers to establish the draft calibration.

The WASH123D vertical conductivities for the confining units are shown in Figures F2-28 through F2-30. Conductivities in these layers were adjusted to improve the calibration. Even with the adjustments, overall the conductivities are very similar to the values from the SEAWAT model (Figures F2-5 through F2-7). The most sensitive area was the MC2 layer where adjustments of a few hundredths of a ft/d in the southern part of the model had a significant impact on several calibration wells across the model. The MC2 conductivity change from SEAWAT to WASH123D is apparent in the figures where the "bright green" area, indicating a vertical conductivity range of 0.005 to 0.01 ft/d in the SEAWAT model, was adjusted to a "yellow" area of 0.01 to 0.05 ft/d in the WASH123D model. This change resulted in increasing the amount of upward flow from the LF1 to the APPZ and UF in these areas. Minor differences in vertical flow between the two models are to be expected based on based on differences in the way vertical conductivities and initial conditions are applied to the computational points as described in this section and Section 3.4 of the main report.

2.2.2 Comparison of Steady State Calibration

The Floridan Aquifer WASH123D calibrated head contours, error statistics and calibration targets for February 2004 are shown in Figures F2-31 through F2-34 and for October 2003 on Figures F2-35 through F2-38. The WASH123D calibrated head contours are also compared to the SEAWAT calibrated head contours in Figures F2-39 through F2-46. In the comparison figures, the WASH123D contours are colored by elevation and overlay the black head contours from the SEAWAT model.

As found for the SEAWAT model, the WASH123D UF calibration is very good with RMS values for both February 2004 and October 2003 (Figure F2-31 and F2-35, respectively) of less than 1.9 feet. The majority of the calibration locations show results within 2 feet of the observed data. Discrepancies described in Section F2.1.2 for the SEAWAT model also occur in the WASH123D model and for the same reasons. For both February 2004 and October 2003 (Figures F2-39 and F2-40, respectively), the WASH123D and SEAWAT head contours nearly align. The largest contour discrepancies are in the southern part of the model where the WASH123D heads are a foot or two higher than the SEAWAT heads.

The error statistics for the APPZ are larger than for the UF with RMS values of 2.8 ft and 2.6 ft for February 2004 and October 2003 (Figure F2-32 and F2-36, respectively), respectively. Also, the WASH123D APPZ RMS values are approximately 0.5 foot greater than those computed using SEAWAT. Despite the slightly larger error, most of the calibration wells are within two feet of the observed data. The WASH123D APPZ calibration locations with the greatest error are the same as those for the SEAWAT model (Section F2.1.2). The APPZ WASH123D and SEAWAT head contours track closely for both calibration months (Figures F2-41 and F2-42). The heads are slightly higher in the southern part of the WASH123D model.

The WASH123D LF1 RMS values are 1.7 ft and 1.1 ft for October 2003 and February 2004 (Figure F2-33 and F2-37), respectively. The February 2004 WASH123D calibration is similar to the SEAWAT draft calibration for the same month but the October 2003 calibrations differ slightly between the two models. The greatest difference occurs at ROMP 28 in Highlands County where the October 2003 computed head is about 3.5 feet lower than the observed head. Despite the difference at this one point, the head contour comparison between WASH123D and SEAWAT (Figures F2-43 and F2-44) show a close contour alignment throughout the area surrounding ROMP 28. Near the coast, some minor head contour differences are found.

As described in Section F2.1.2, an expanded calibration was done for the deeper units of the FAS (LF1 and BZ). Figures F2-34 and F2-38 show the calibration targets when October 2003 or February 2004 model results are compared to calibration locations that are not from the same date. These figures show head contours from the BZ and have calibration targets that use a 5 ft confidence interval instead of the 2 ft confidence interval used for the other calibration plots. Because the calibration points were not from the calibration time periods, less effort was expended to match the points exactly. The RMS values are between 2.5 ft and 3 ft for both months indicating that the computed heads are within a reasonable range. Comparing the SEAWAT and WASH123D head contours for the BZ (Figures F2-45 and F2-46) reveals that the models are computing similar heads. In the BZ layers of the models, the density impacts from the largest changes in salinity, temperature and pressure are greatest. The compatibility of the head contours in this layer verifies that the two codes are computing the density-dependent calculations in a similar way improving the reliability of the results.

3.0 Draft Transient Calibration

Draft transient calibrations were performed for the SEAWAT and WASH123D models for the time period from October 2003 to December 2004. The quality of the calibration was determined through visual analysis of the computed head variation over time at each calibration point compared to the observed head variation. The results of the 2 draft transient calibrations are very similar, except in the western part of the model domain. Differences between the SEAWAT and WASH123D draft calibrations appear to be due to differences in pumping locations and differences in assignment of specific storage.

Although transport parameters such as porosity, dispersivity, and molecular diffusion coefficient vary over time, their effect was insignificant at the time scale (15 months) of the model. Model sensitivity to these parameters can be found in Section 5.0 of the main report. For transient calibration, the most sensitive parameter was specific storage.

3.1 Specific Storage

Specific storage was varied using “trial and error” and automated methods for the draft SEAWAT transient model. Rather than zonal distributions of specific storage, interpolated “pilot points” were used to generate smooth specific storage fields. This process was identical to that used for the hydraulic conductivity fields for the steady state calibration for the final SEAWAT model described in detail in Section 4.1 of the main report.

Specific storage is not specifically used in WASH123D as shown in Equations 2.5 and 2.6 of the main report. The WASH123D code requires an effective aquifer compressibility to determine the storage term used in the governing equation. The relationship between specific storage and the compressibility parameters is shown in Equation 3.1.1.

$$S_s = \rho_\omega g(\alpha + n\beta)$$ Equation F3.1.1

where

S_s = Specifc storage (L^{-1})
ρ_ω = Density of water (M/L^3)
g = Acceleration of gravity (L/T^2)
α = Compressibility of the aquifer skeleton ($1/(M/LT^2)$)
n = Porosity (L^3/L^3)
β = Compressibility of water ($1/(M/LT^2)$)

In WASH123D, the equation is rearranged by multiplying density and gravity into the parenthesis as follows:

$$S_s = \alpha' + n\beta'$$ Equation F3.1.2

where

α' = Modified compressibility of the aquifer skeleton, $\rho_\omega g\alpha$ (L^{-1})
β' = Modified compressibility of water, $\rho_\omega g\beta$ (L^{-1})

The WASH123D code hardwires the value for the modified compressibility of water (β') at a value of 1.22×10^{-6} ft^{-1}. This is based on an assumed water compressibility of 1.96×10^{-8} ft^2/lbf and cannot be changed without reprogramming and recompiling WASH123D. Using the constant value for modified water compressibility as well as the specific storage and porosity values from the calibrated SEAWAT model, the modified aquifer compressibility values were calculated. Zonal distributions of these values were applied to the model.

In some cases, the SEAWAT specific storage values were so small that the corresponding modified aquifer compressibility was negative. Further discussion related to negative aquifer compressibilities and their negligible affects on the calibration are discussed in Section 4.0 of this appendix.

3.2 SEAWAT

Figures F3-1 through F3-21 show the SEAWAT calibration at a number of observation wells which had significant data available. In each case, the observed and calculated heads are plotted during the 15 month calibration period (October 2003 through December 2004). Note that because of differing ranges of heads measured and calculated at each well, each plot has a different head scale on the y-axis. In order to facilitate the analysis of these plots, every graph has a horizontal grid line at every foot of head. In this way, the reader can tell, at a glance, whether the well has a large swing in heads (many grid lines) or has very little head variation (few grid lines).

Because of the time discretization (constant boundary conditions and pumping for each month) it is impossible for the model to correctly calculate the head every single day. The main purpose of the calibration effort was to correctly calculate the average head during the driest period (usually during the month of June 2004) and the average head during the wettest period (usually late fall 2004).

Because the model can only attempt a calculation of the average monthly heads, it is not surprising that the model will seldom match the lowest measured head (usually during the first few days of June 2004). Further, the time discretization often results in the lowest model-calculated head occurring several weeks after the lowest measured head. During June 2004, the head changes on nearly all observation wells indicate that significant pumping occurred during the first few days of the month and then abruptly stopped, causing a steep rise in water levels. Because of the ASR regional model's time discretization, this high pumping is averaged over the entire month, resulting in the lowest heads being calculated at the end of the month. See for example, the results at ROMP 9 SWNN in Sarasota County (Figure F3-9). The continued pumping during the month of June causes the model to calculate a lower head for the whole month of June, but the measured data shows a sudden, steep increase in head beginning in the first week of June.

In some cases, the October 2003 steady state calculated head differed by a few feet from the measured head at the end of October. In these cases, the transient calibration sought to match the head changes each month, instead of the actual heads. This ensures that the aquifer response to hydrogeologic forces is accurate, even if the initial computed head value is slightly different from that observed. See for example, ROMP 13 SWNN in De Soto County (Figure F3-10). The October 31 calculated head (steady state) is nearly 2 feet lower than the measured head value. However, the difference between the October 2003 heads and the June 2004 heads is 5 to 6 feet in the measured data and just over 6 feet in the model results. Similarly, the head rise between June 2004 and October 2004 is 8 feet in the measured data and about 7 feet in the model output. This indicates that the model is doing a good job of reproducing the effect of temporal changes such as seasonal rainfall changes and pumping effects. Although the steady state model did not perfectly reproduce the heads at this point, the head variation is reasonable.

Similarly, MF-37 on the east coast of Lake Okeechobee (Figure F3-11) was installed during the calibration period. Thus, there was no data available for either the October 2003 or February 2004 steady state calibration. It appears that if data had been available, the model would have underpredicted the head at this well by approximately 3 feet. However, during the transient calibration, it becomes clear that the temporal effects on this well are being correctly reproduced in the transient model. It is important, when viewing Figures F3-1 through F3-21 to mentally move the model calculated heads up or down until the initial value matches the measured value at that time before determining the quality of the calibration.

It is significant that the pumping across the region exerts a much greater effect on the transient head data than the specific storage values. Section 3.5 of the main report and Appendix D present the difficulties in collecting and using the pumping data. A huge percentage of the pumping data had to be estimated based on well type and seasonal averages.

These estimates of pumping caused additional problems during calibration. These are made clear by comparing the results at Edgeville Deep Well 3 in Manatee County (Figure F3-9) and BF-6 in Broward County (Figure F3-14). At Edgeville, the model results indicate a significant reduction in pumping during the last month of the model (December 2004). The measured data at this well do not show such a sudden and large increase in head. This indicates that the pumping in the model in this area is incorrect – likely due to the failure of the assumptions made during the pumping estimated (described in Appendix D). Conversely, at BF-6, there is clearly a reduction in pumping during the months of November 2003 and January 2004, with an increase in pumping during the months of October 2003 and December 2003. In this case, the estimates made in the model appear to closely match reality, as shown by the close similarity of the heads at this well. Pumping estimation errors can also be the cause of the failure of the model to reproduce the low heads in the summer of 2004 or the high heads in the Fall of 2004. As will be explained later in Section 6, the pumping data quality represents the single largest source of error to this model. The estimates made to fill in missing data were planned in order to provide a model accurate enough to make gross, regional-scale estimates of the effects of the CERP ASR program. Because of pumping errors, the regional model cannot be used for near-scale problems or to answer questions requiring high accuracy.

In general, the transient calibration is considered to be of a high enough quality to answer the questions required by the regional ASR model. The model was able to roughly reproduce both the scale and timing of the main head changes during the 15-month calibration period.

The storage terms used in the calibrated transient model are presented in Figures F3-22 through F3-29. Conductivity values were the same as those used for the steady state model (See Section F2.1). Table 4.1 in the main report presents the other transport parameters used in the transient model. These parameters were selected to be similar to generally accepted values. Their sensitivity is discussed in Section 5 of the main report.

3.3 WASH123D

A transient WASH123D model was developed for the same domain and calibration time period as the transient SEAWAT model. As stated in Section F2.0, the Phase I study indicated that similar results are expected for the WASH123D and SEAWAT models given similar model inputs. To use this similarity to limit the number of transient WASH123D calibration runs, the draft calibrated transient SEAWAT input parameters were used to estimate the initial transient WASH123D input parameters. The input parameters include specific storage, porosity, dispersivity, and molecular diffusion coefficient; however the primary transient calibration parameter in SEAWAT was specific storage. Hydraulic conductivity values used in the WASH123D transient model were the same as the values used for the draft calibrated WASH123D steady state model.

Like the hydraulic conductivity values, the aquifer compressibility values are assigned in WASH123D using material zones. Because the zones created for the hydraulic conductivity and the zones created for the compressibility do not align, much smaller zones with common conductivities and compressibilities are necessary to adequately define the aquifer heterogeneity. Establishing the

material zones required several steps. First, the calibrated SEAWAT specific storage values were contoured by layer at sufficient contour intervals to define the storage variation. The contours were used to create zones of similar specific storage with one value for each zone. Using the polygons representing storage zones and the polygons representing the WASH123D calibrated hydraulic conductivity zones, an "intersect" analysis was performed in the Environmental Systems Research Institute's ArcMap 9.3 program. The result of this analysis was a set of refined polygon zones that defined a set of conductivity and storage values consistent with the original independent sets of polygons for these parameters. The storage values for each material zone were then converted to modified aquifer compressibility using Equation F3.1.2. A total of 1,974 material zones were assigned for the transient WASH123D model.

Because it is difficult to make incremental changes with so many zones and because automated parameter calibration programs cannot revise zone boundaries, no additional calibration by trial and error or automated methods was performed for the WASH123D transient model.

The WASH123D head results over the calibration period are shown in Figures F3-30 to F3-50. These figures are the same format as Figures F3-1 through F3-21 for the SEAWAT transient calibration with the addition of the WASH123D model results.

For the wells in the north, east and south parts of the model, the WASH123D heads are very similar to the SEAWAT heads in the UF, APPZ and LF1. Note that at many of these wells, apparent differences between the two models are only due to differences in the initial condition. Other than this starting head value, the two codes show the same aquifer response in these areas.

West of Lake Okeechobee, the head results differ between the two codes. Figure F3-38 shows 3 wells where this occurs in the UF. The starting heads for these 3 wells are approximately the same for SEAWAT and WASH123D. However, the WASH123D low point in May 2004 is not as low as the SEAWAT low point and the WASH123D recovery from May 2004 to October 2004 is lower and lagged compared to the SEAWAT solution. This same pattern is found at many other western UF and APPZ wells. Further, the observed data displays a larger recovery from May to October 2004 than the SEAWAT solution so the WASH123D solution does not provide a better match to observed data than the SEAWAT solution in these areas. Lowering the modified compressibility values west of Lake Okeechobee could yield an improvement in the recovery. Because the majority of the pumping in the model domain occurs west of Lake Okeechobee, it is likely that the differences between the two models are due to a combination of the differences in assignment of storage coefficient and pumping locations (see Appendix D).

Head differences are also notable at the BZ well, OSF-97, shown on Figure F3-50. The pattern of the head results in the SEAWAT and WASH123D solutions is similar with a slightly lagged and lower recovery in the WASH123D model. The biggest difference, though, is the magnitude of the heads. The SEAWAT heads and observed heads vary between 49 ft and 56 ft whereas the WASH123D heads vary between 16 ft and 20 ft. This difference results from the differences between the two models in TDS assignment (See Section 3.4.1 of the main report) and the impact of TDS on head. The open hole interval for OSF-97 extends up near the top of the BZ aquifer in both models. In the WASH123D model, the top interface of

the BZ aquifer has a nodal computational point where the TDS is set at the BZ aquifer TDS value of 26,400 mg/l. The TDS value used to calculate the OSF-97 head for comparison with the WASH123D model results is the BZ TDS value of 26,400 mg/l. In the SEAWAT model, there is no computational point at the top BZ aquifer interface. The initial condition is set at the center of the BZ aquifer cell at 26,400 mg/l and at the center of the LC confining unit cell at 3,700 mg/l. Thus, the TDS value used to determine the head in the calibration well in the SEAWAT model near the top of the BZ aquifer is an average of the high BZ TDS and the lower LC TDS. This significant difference in TDS value used to compute the calibration well head causes the difference in computed head between the two models.

4.0 Sensitivity Simulations from the Draft Calibration

4.1 WASH123D Timestep Sensitivity

To ensure that the selected timestep size does not affect the numerical accuracy, the WASH123D transient model was run using several timestep sizes. A smaller timestep size should provide a more accurate solution, however the model run time will be longer. The goal is to limit the error in the solution while limiting the execution time. The timestep sizes tested were 1 day, 5 days and 10 days.

Figure F4-1 shows plots of the computed heads for the 3 timestep sizes at 3 UF wells across the model domain. The differences in timestep size have little effect on the head solution across the majority of the model. Proximity to large pumping centers increases the head differences because as the pumps turn on and off, the finer timestep intervals can capture the changes more accurately. In Figure F4-1, it's clear that ROMP 39 SWNN is near a large pumping center because the head range over 15 months is more than 20 feet. At the beginning of July 2004, recovery of the head at ROMP 39 SWNN begins as pumping decreases or stops. On July 16, 2004, the maximum difference in head, 1 foot, between the 1 day and 5 day timestep solutions occurs because with the finer timestep, 15 computations were performed instead of only 3 computations with the coarser timestep. Because no change in pumping rates occur in the middle of the month, the difference in the solutions decreases toward the end of July 2004 as additional computations are performed in both models.

Near a few very large pumping centers, the head differences between the 1 day timestep and 5 day timestep solutions are as large as 10 to 13 feet at specific times when large changes in pumping occur. These differences occur at the nodes where pumping is assigned. As a result of the estimates in pumping locations and pumping rates (see Appendix D), it is impossible to accurately predict the heads at these locations using this regional model.

The 5 day timestep was chosen to compute the transient draft calibration for consistency with the 5 day timestep used for the SEAWAT transient draft calibration. Although the 1 day timestep provides a slightly more accurate solution, the difference in head across the majority of the model is within the calibration error. In addition, the model run time using the 1 day timestep size was unreasonably long at 1 week. The run time for the 5 day timestep solution was 48 hours which is comparable with the SEAWAT 5 day timestep run using the TVD advection scheme.

4.2 Specific Storage in SEAWAT vs. Compressibility in WASH123D

During draft calibration of the transient SEAWAT model, specific storage terms were varied within acceptable range until the model output matched the measured field values as closely as possible. The available data includes some measurements as low as 2 x 10^{-10} ft^{-1}. The minimum storage term in the draft calibrated model was 1 x 10^{-8} ft^{-1}. Since the WASH123D model draft calibration lagged slightly behind the SEAWAT model in the schedule, the SEAWAT draft calibration parameters were used as a starting point for the WASH123D parameters. Instead of specific storage, WASH123D requires the user to input the modified compressibility of the matrix, which it then uses to calculate the specific storage term required by the governing equation. The calculation is made according to equation F3.1.2.

To transfer the draft calibrated storage terms from SEAWAT to WASH123D, it was necessary to back calculate the modified aquifer compressibility that would result in the desired specific storage term. This resulted in a number of negative values for aquifer compressibility for some areas of the model. There is no physical explanation for a negative compressibility.

Because there are field measured values of specific storage that are lower than the threshold of positive aquifer compressibility, it is clear that this equation is an estimate and that there are other parameters involved in the storage response to driving forces in the aquifer. It is possible that a negative aquifer compressibility could be the best value for this parameter if the goal is to produce a model that accurately reproduces field conditions. However, these negative values would be difficult to defend.

To determine the effect of the negative compressibility values, the SEAWAT model was rerun for two additional sensitivity runs. In the first, the specific storage terms were truncated at 2.65 x 10^{-8} ft^{-1}, the minimum storage term reported in the Preliminary Hydrogeologic Framework. This resulted in only a slight change to a few storage values (13% of the LC values, 3% of the MC1 values, less than 2% for BZ, MC2, APPZ and IAS, and none of the UF values). For the second storage sensitivity run, the specific storage values were truncated at 3.05 x 10^{-7} ft^{-1}. This ensured no negative compressibility terms when the values were converted to the WASH123D model.

The effects of truncating the storage terms had minimal effects on the draft calibration. Those wells which did see changes to the model calculated heads were generally located in the south of the model or in the deeper layers. All noticeable changes occurred in the second of the two sensitivity runs (with storage truncated at 3.05x10^{-7} ft^{-1}). Figure F4-2 shows the effects for the three observation wells which showed the greatest effect. In each case, the truncation of the storage term (increasing it in some areas) resulted in a reduction in the range of heads over the 15 month calibration period. The low heads in June and the high heads in October 2004 occur later when the storage terms are increased significantly. The draft calibration might be said to be less precise when the storage terms are increased, but the difference is minor.

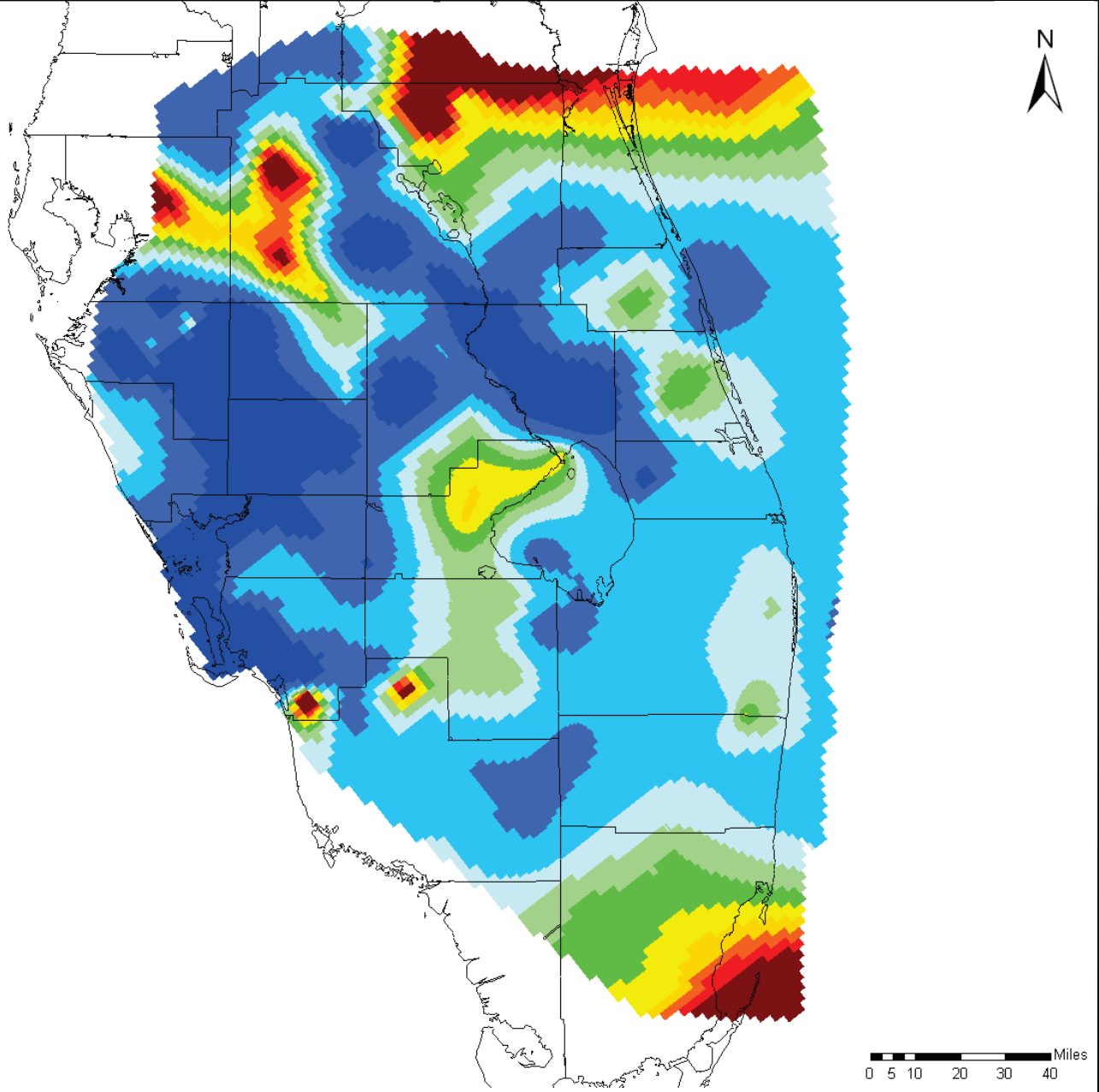

Horizontal Hydraulic Conductivity (ft/d)

- 1 - 20
- 20 - 40
- 40 - 60
- 60 - 80
- 80 - 100
- 100 - 120
- 120 - 140
- 140 - 160
- 160 - 180
- 180 - 200
- 200 - 500

Notes:

Vertical hydraulic conductivity was set to one tenth of the horizontal value (shown).

Conductivity values were interpolated to the grid from values assigned to a set of pilot points scattered across the model domain.

A combination of automated calibration (PEST) and manual calibration (trial and error) resulted in this conductivity field.

Regional Phase II ASR Horizontal Hydraulic Conductivity Upper Floridan Aquifer (SEAWAT)

Final Groundwater Model Calibration Report

Figure F2-1

October 2010

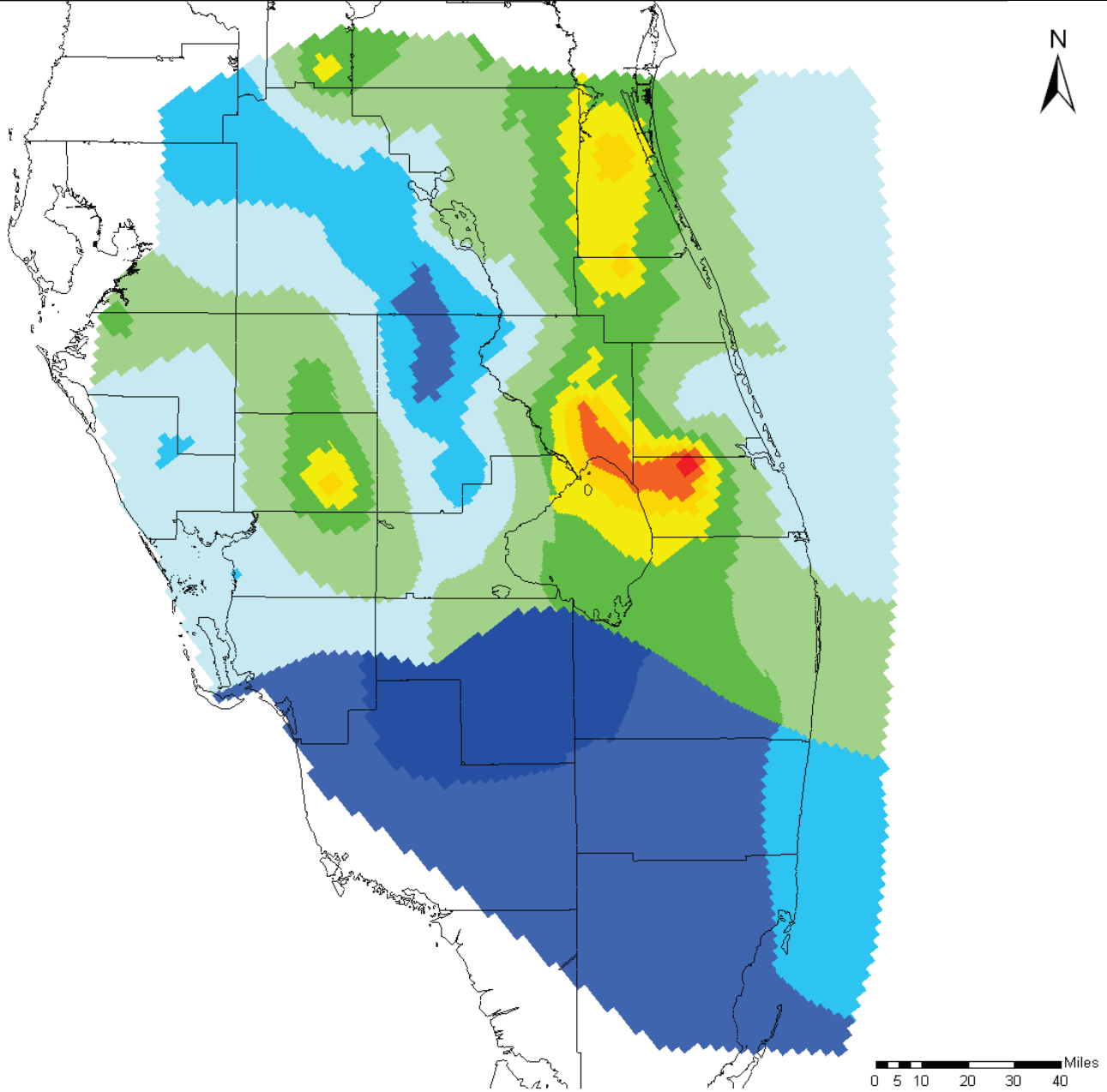

Horizontal Hydraulic Conductivity (ft/d)

- 5 - 20
- 20 - 50
- 50 - 100
- 100 - 200
- 200 - 400
- 400 - 600
- 600 - 800
- 800 - 1000
- 1000 - 1250
- 1250 - 1500
- 1500 - 1700

Notes:

Vertical hydraulic conductivity was set to one tenth of the horizontal value (shown).

Conductivity values were interpolated to the grid from values assigned to a set of pilot points scattered across the model domain.

A combination of automated calibration (PEST) and manual calibration (trial and error) resulted in this conductivity field.

Regional Phase II ASR Horizontal Hydraulic Conductivity
APPZ Aquifer (SEAWAT)
Final Groundwater Model Calibration Report

Figure F2-2

October 2010

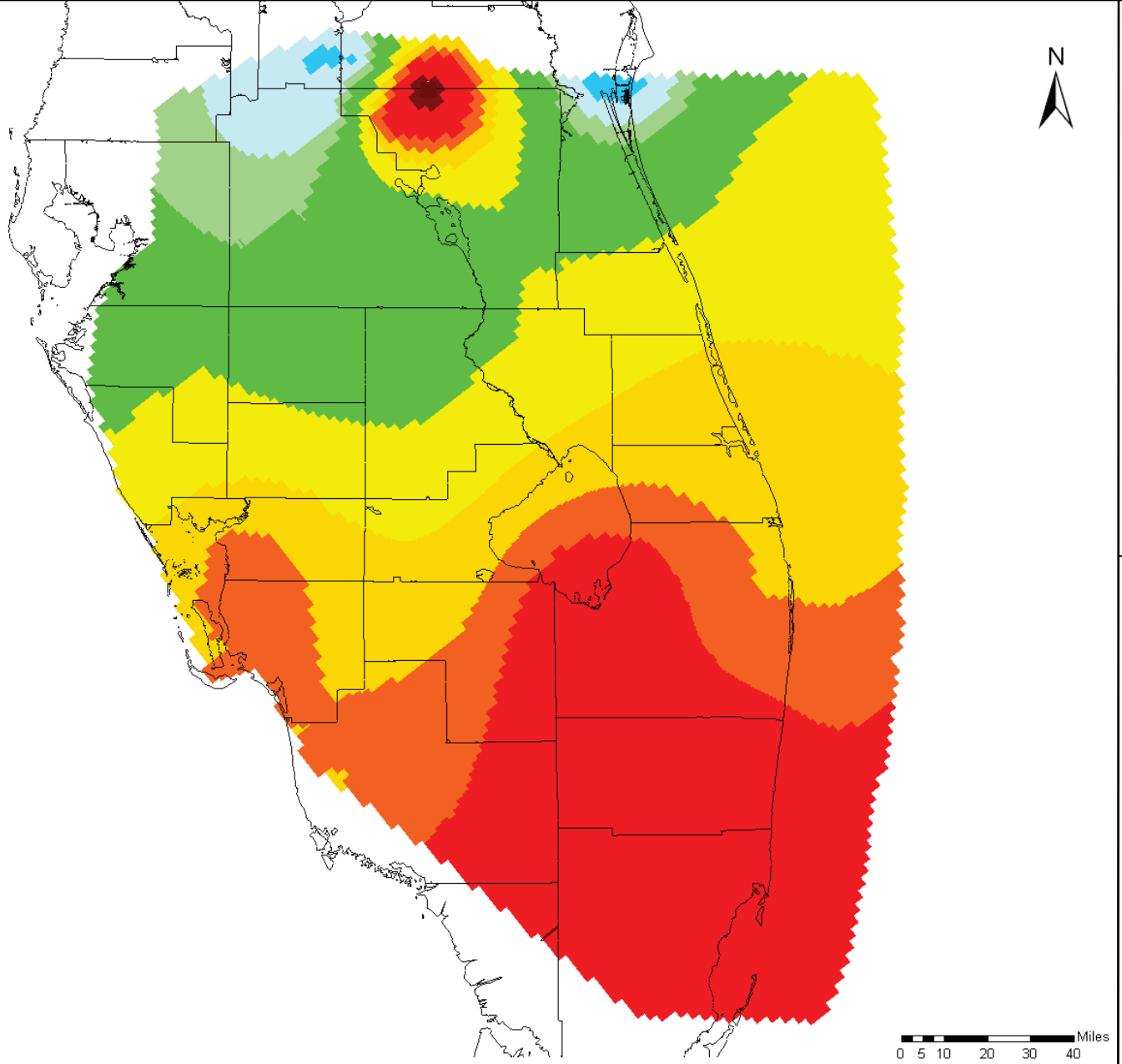

Horizontal Hydraulic Conductivity (ft/d)

- 1 - 20
- 20 - 40
- 40 - 60
- 60 - 80
- 80 - 100
- 100 - 200
- 200 - 300
- 300 - 400
- 400 - 500
- 500 - 1000
- 1000 - 1520

Notes:

Vertical hydraulic conductivity was set to one tenth of the horizontal value (shown).

Conductivity values were interpolated to the grid from values assigned to a set of pilot points scattered across the model domain.

A combination of automated calibration (PEST) and manual calibration (trial and error) resulted in this conductivity field.

Regional Phase II ASR Horizontal Hydraulic Conductivity
Lower Floridan (LF1) Aquifer (SEAWAT)
Final Groundwater Model Calibration Report

Figure F2-3

October 2010

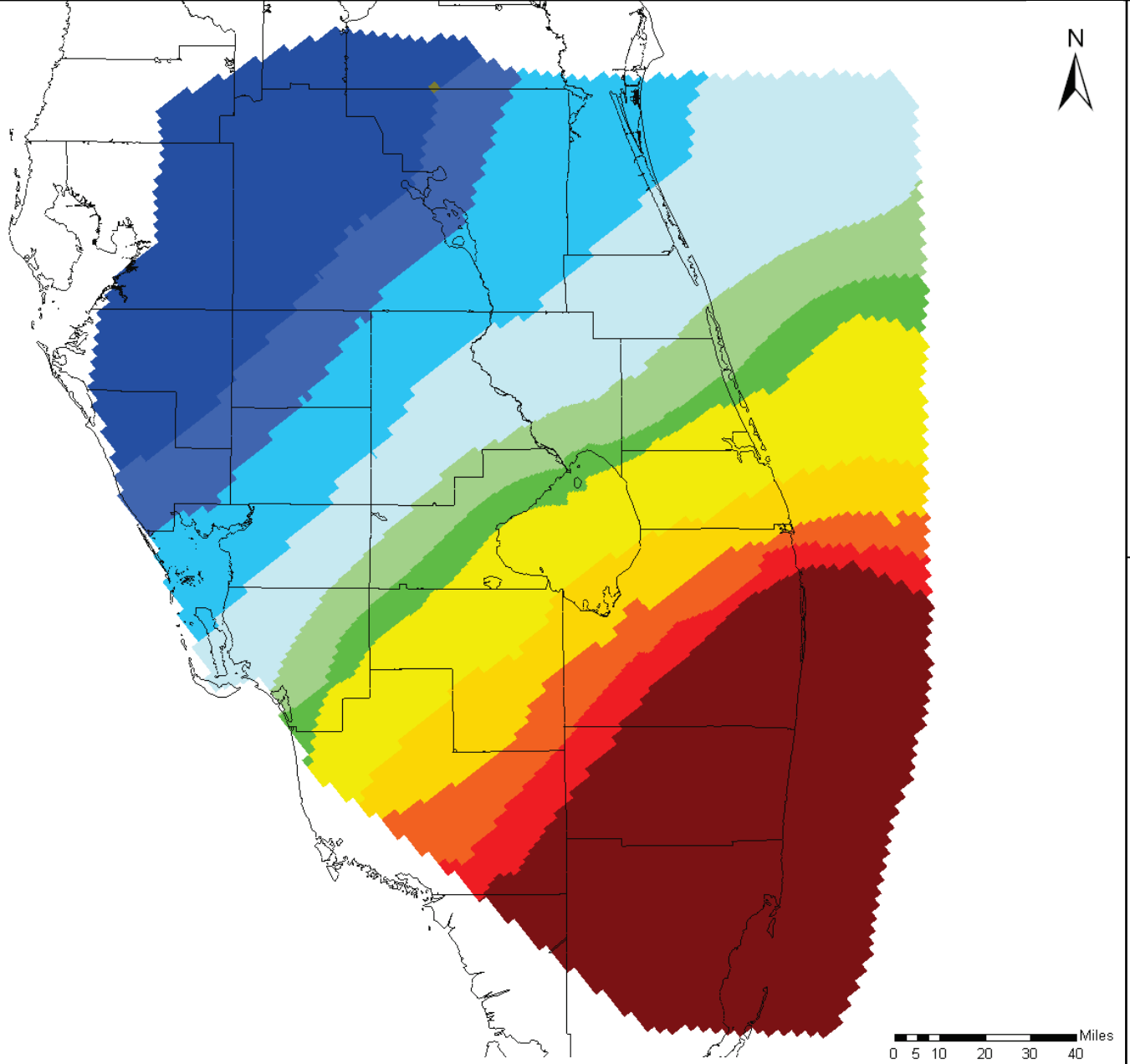

Horizontal Hydraulic Conductivity (ft/d)

- 1 - 50
- 50 - 100
- 100 - 250
- 250 - 500
- 500 - 750
- 750 - 1000
- 1000 - 2000
- 2000 - 3000
- 3000 - 4000
- 4000 - 5000
- 5000 - 10000

Notes:

Vertical hydraulic conductivity was set to one tenth of the horizontal value (shown).

Conductivity values were interpolated to the grid from values assigned to a set of pilot points scattered across the model domain.

A combination of automated calibration (PEST) and manual calibration (trial and error) resulted in this conductivity field.

Regional Phase II ASR Horizontal Hydraulic Conductivity Boulder Zone (SEAWAT)

Final Groundwater Model Calibration Report

Figure F2-4

October 2010

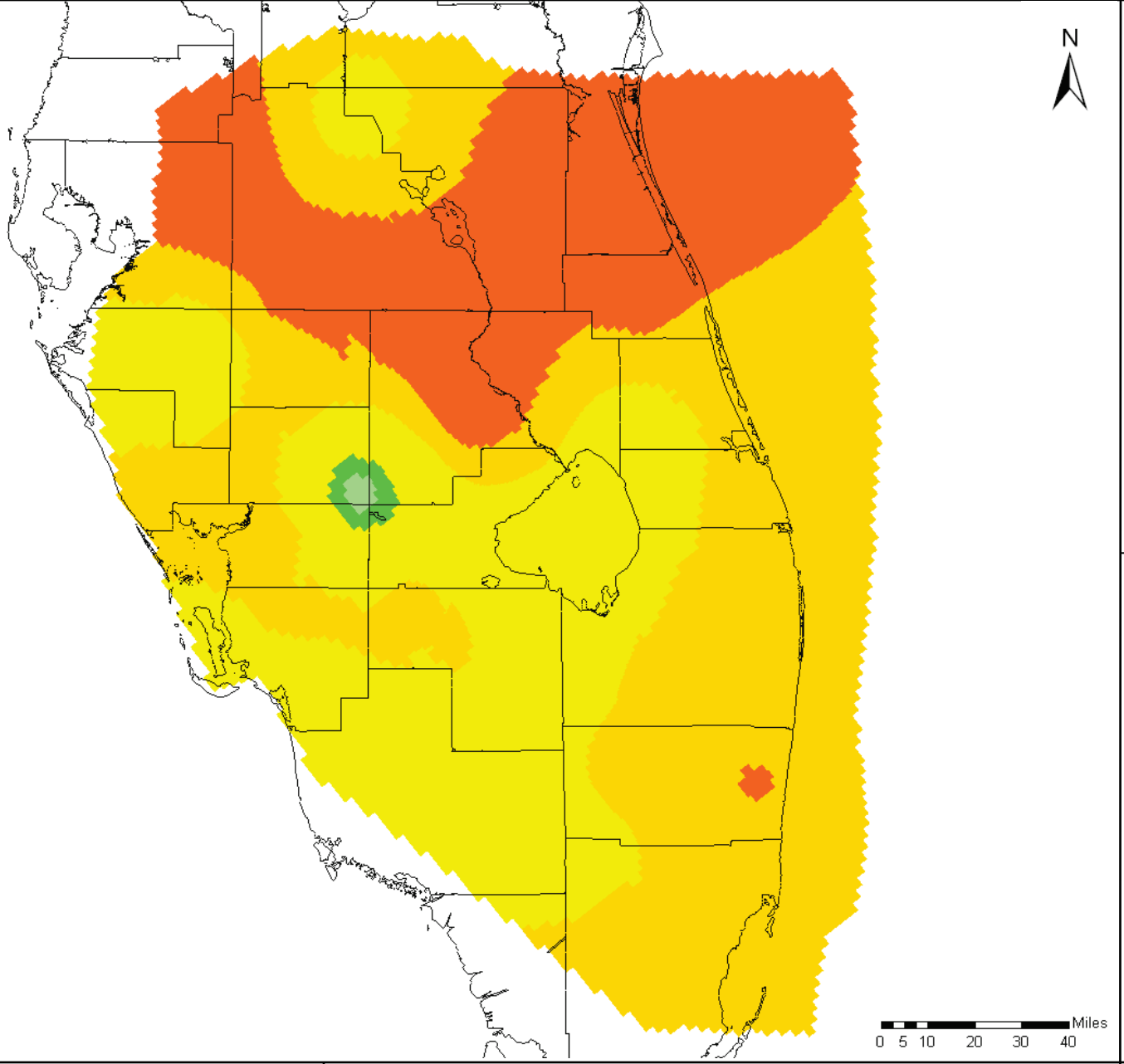

Vertical Hydraulic Conductivity (ft/d)

- 0.00001 - 0.00005
- 0.00005 - 0.0001
- 0.0001 - 0.0005
- 0.0005 - 0.001
- 0.001 - 0.005
- 0.005 - 0.01
- 0.01 - 0.05
- 0.05 - 0.1
- 0.1 - 0.5
- 0.5 - 1
- 1 - 10

Notes:

Horizontal hydraulic conductivity was set to twice the vertical value (shown).

Conductivity values were interpolated to the grid from values assigned to a set of pilot points scattered across the model domain.

A combination of automated calibration (PEST) and manual calibration (trial and error) resulted in this conductivity field.

Regional Phase II ASR Vertical Hydraulic Conductivity
Middle Confining Unit 1 (SEAWAT)
Final Groundwater Model Calibration Report

Figure F2-5

October 2010

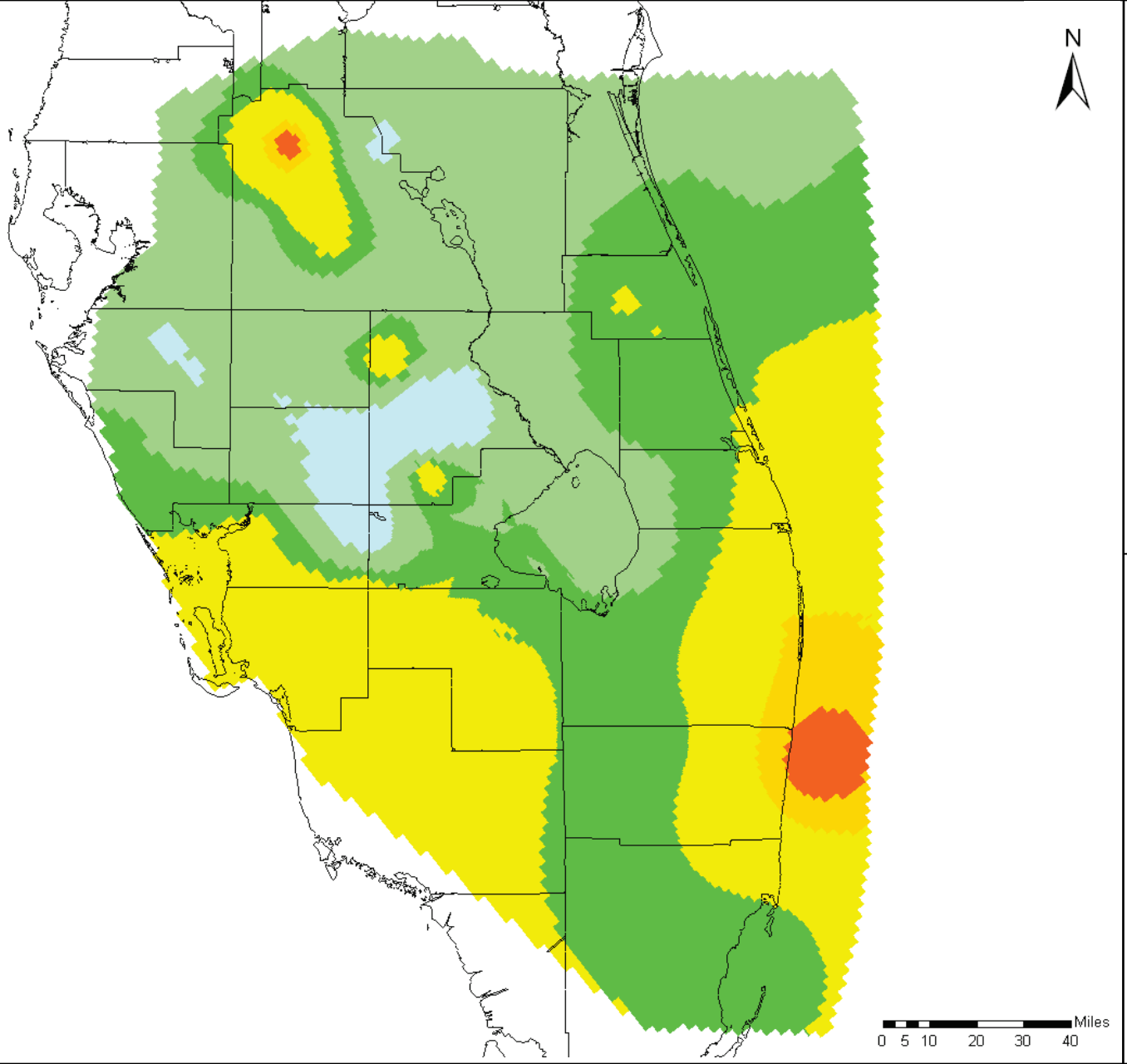

Vertical Hydraulic Conductivity (ft/d)

- 0.00001 - 0.00005
- 0.00005 - 0.0001
- 0.0001 - 0.0005
- 0.0005 - 0.001
- 0.001 - 0.005
- 0.005 - 0.01
- 0.01 - 0.05
- 0.05 - 0.1
- 0.1 - 0.5
- 0.5 - 1
- 1 - 10

Notes:

Horizontal hydraulic conductivity was set to twice the vertical value (shown).

Conductivity values were interpolated to the grid from values assigned to a set of pilot points scattered across the model domain.

A combination of automated calibration (PEST) and manual calibration (trial and error) resulted in this conductivity field.

Regional Phase II ASR Vertical Hydraulic Conductivity
Middle Confining Unit 2 (SEAWAT)
Final Groundwater Model Calibration Report

Figure F2-6

October 2010

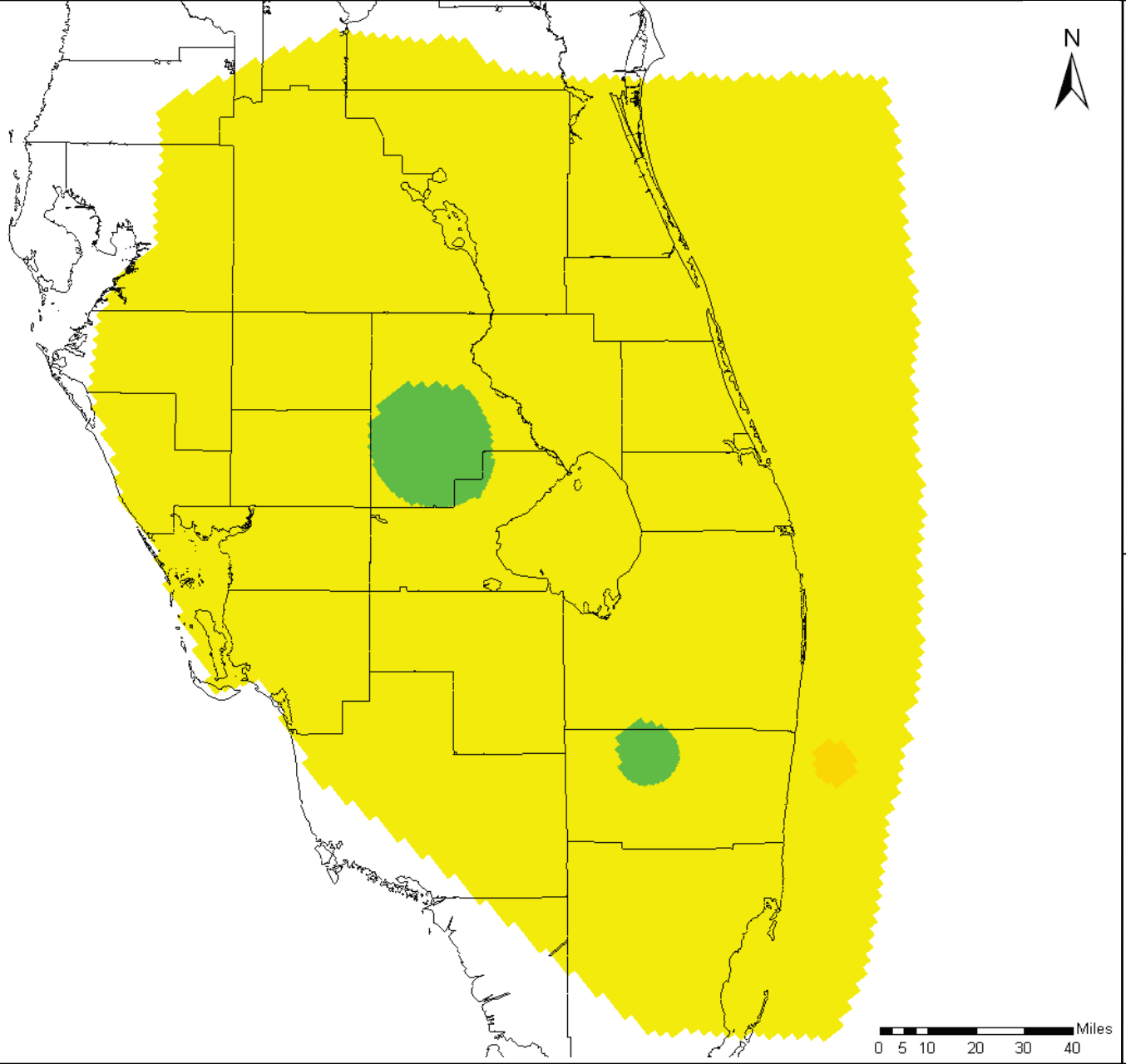

Vertical Hydraulic Conductivity (ft/d)

- 0.00001 - 0.00005
- 0.00005 - 0.0001
- 0.0001 - 0.0005
- 0.0005 - 0.001
- 0.001 - 0.005
- 0.005 - 0.01
- 0.01 - 0.05
- 0.05 - 0.1
- 0.1 - 0.5
- 0.5 - 1
- 1 - 10

Notes:

Horizontal hydraulic conductivity was set to twice the vertical value (shown).

Conductivity values were interpolated to the grid from values assigned to a set of pilot points scattered across the model domain.

A combination of automated calibration (PEST) and manual calibration (trial and error) resulted in this conductivity field.

Regional Phase II ASR Vertical Hydraulic Conductivity Lower Confining Unit (SEAWAT)

Final Groundwater Model Calibration Report

Figure F2-7

October 2010

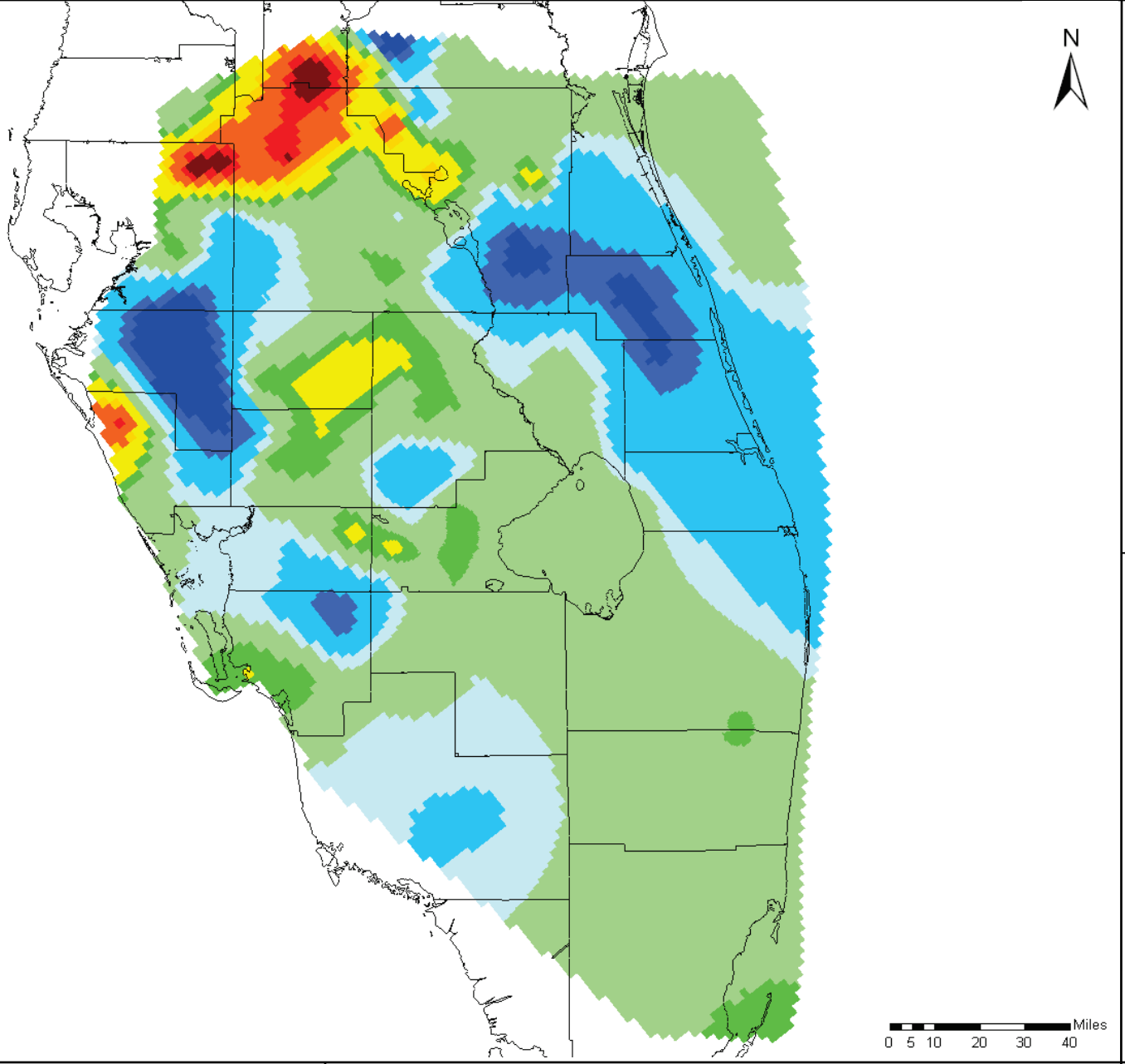

Notes:

This layer (2) overlies the Intermediate Aquifer in the regional model. Where the IA does not exist, (see Figure 4.28) the conductivities match those in layer 3 and 4.

Horizontal hydraulic conductivity was set to twice the vertical value (shown).

Conductivity values were interpolated to the grid from values assigned to a set of pilot points scattered across the model domain.

A combination of automated calibration (PEST) and manual calibration (trial and error) resulted in this conductivity field.

Regional Phase II ASR Vertical Hydraulic Conductivity
Intermediate Aquifer System Layer 2 (SEAWAT)
Final Groundwater Model Calibration Report

Figure F2-8

October 2010

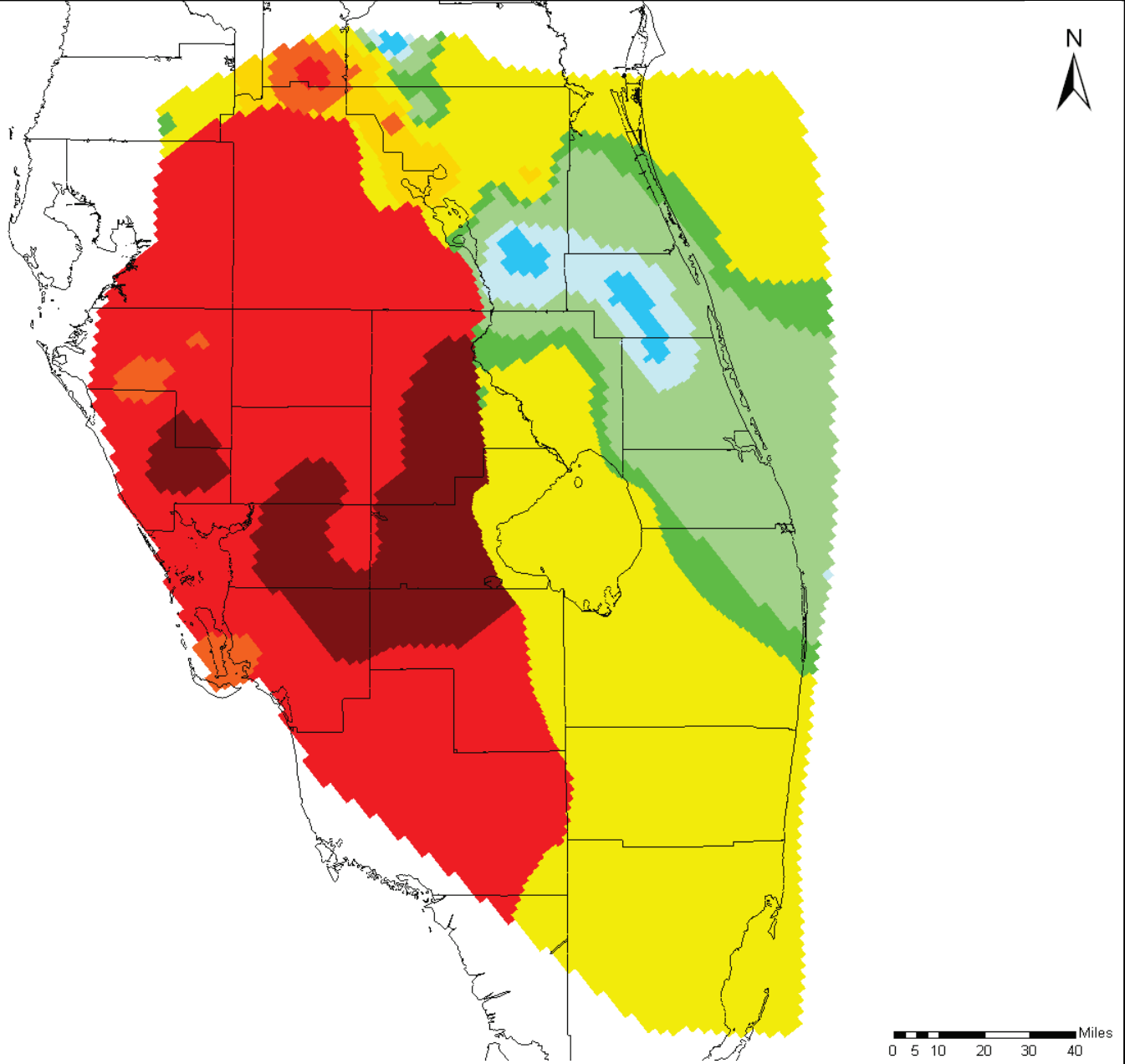

Horizontal Hydraulic Conductivity (ft/d)

- 0.00001 - 0.00005
- 0.00005 - 0.0001
- 0.0001 - 0.0005
- 0.005 - 0.001
- 0.001 - 0.005
- 0.005 - 0.01
- 0.01 - 0.1
- 0.1 - 1
- 1 - 10
- 10 - 100
- 100 - 500

Notes:

The western portion of this layer (3) simulates the Intermediate Aquifer (IA). The eastern portion combines with layers 2 and 4 to simulate the Intermediate Confining Unit. Where the IA does not exist, the conductivity match those in layer 2 and 4.

Vertical hydraulic conductivity was set to one tenth of the horizontal value (shown).

Conductivity values were interpolated to the grid from values assigned to a set of pilot points scattered across the model domain.

A combination of automated calibration (PEST) and manual calibration (trial and error) resulted in this conductivity field.

Regional Phase II ASR Horizontal Hydraulic Conductivity Intermediate Aquifer System Layer 3 (SEAWAT)

Final Groundwater Model Calibration Report

Figure F2-9

October 2010

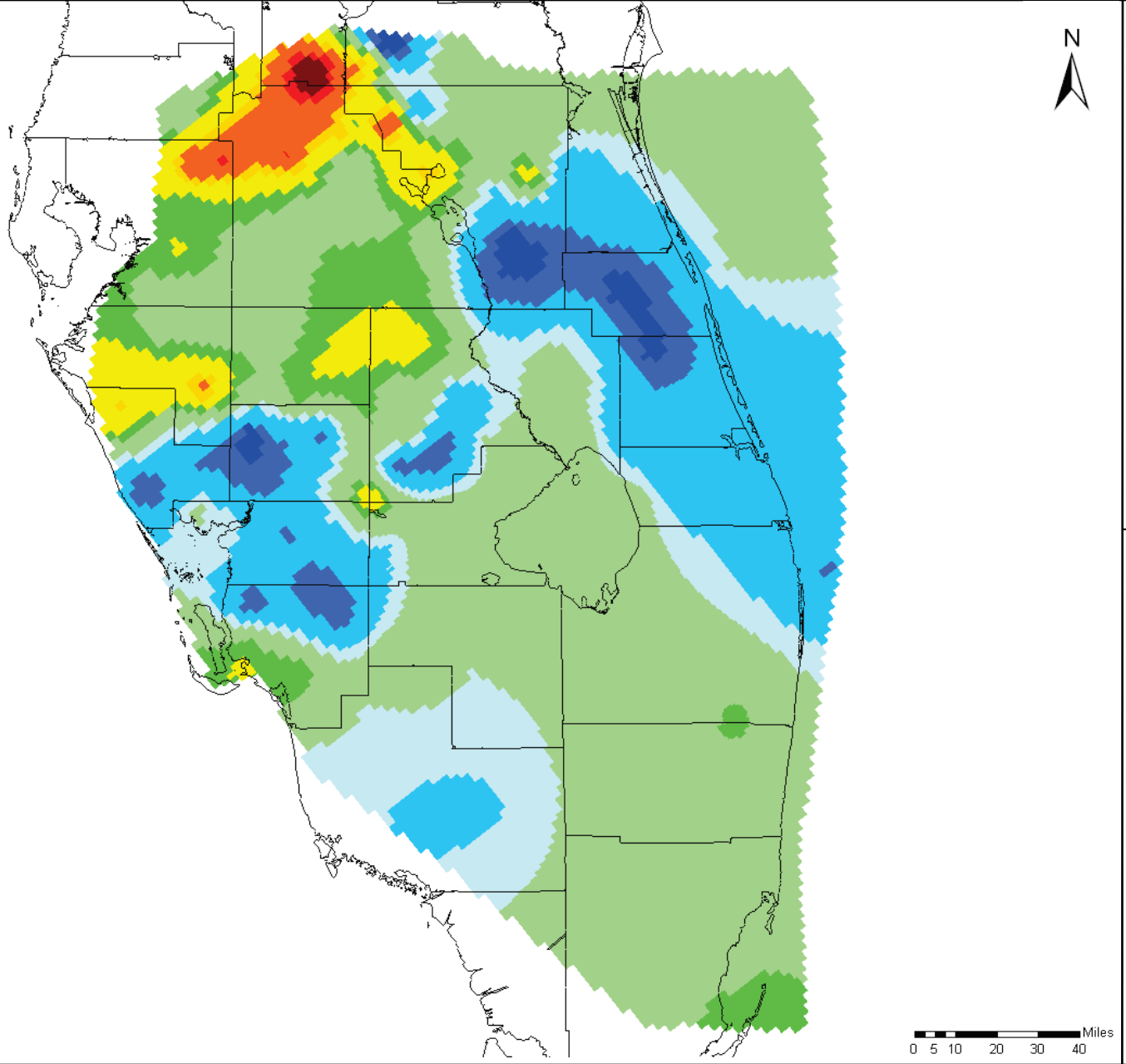

Vertical Hydraulic Conductivity (ft/d)

- 0.00001 - 0.00005
- 0.00005 - 0.0001
- 0.0001 - 0.0005
- 0.0005 - 0.001
- 0.001 - 0.005
- 0.005 - 0.01
- 0.01 - 0.05
- 0.05 - 0.1
- 0.1 - 0.5
- 0.5 - 1
- 1 - 10

Notes:

This layer (4) underlies the Intermediate Aquifer (IA) in the regional model. Where the IA does not exist, (see Figure 4.28) the conductivities match those in layer 2 and 3.

Horizontal hydraulic conductivity was set to twice the vertical value (shown).

Conductivity values were interpolated to the grid from values assigned to a set of pilot points scattered across the model domain.

A combination of automated calibration (PEST) and manual calibration (trial and error) resulted in this conductivity field.

Regional Phase II ASR Vertical Hydraulic Conductivity
Intermediate Aquifer System Layer 4 (SEAWAT)
Final Groundwater Model Calibration Report

Figure F2-10

October 2010

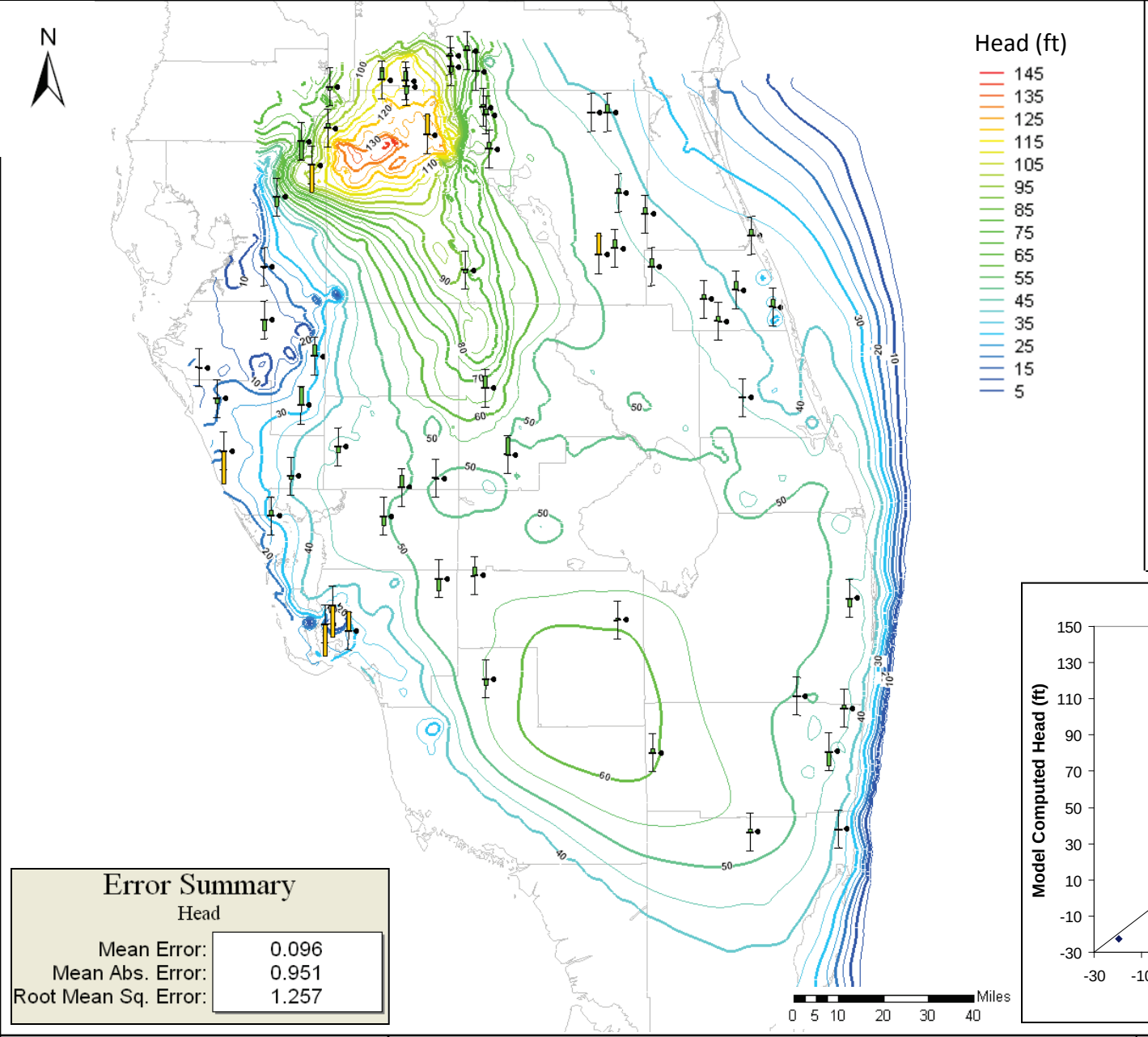

Notes:

Statistics (mean error, mean absolute error and root mean square error) are calculated based on equations presented in Section 4.1.

Calibration targets are green when the calculated value is within 2 feet of the measured head, yellow when within 4 feet and red when the model calculates a head more than 4 feet different from the measured value.

The direction of the colored bar on the calibration target indicates the sign on the residual: bars above the middle line indicate the model calculated higher heads than measured; bars below the middle line indicate negative residuals.

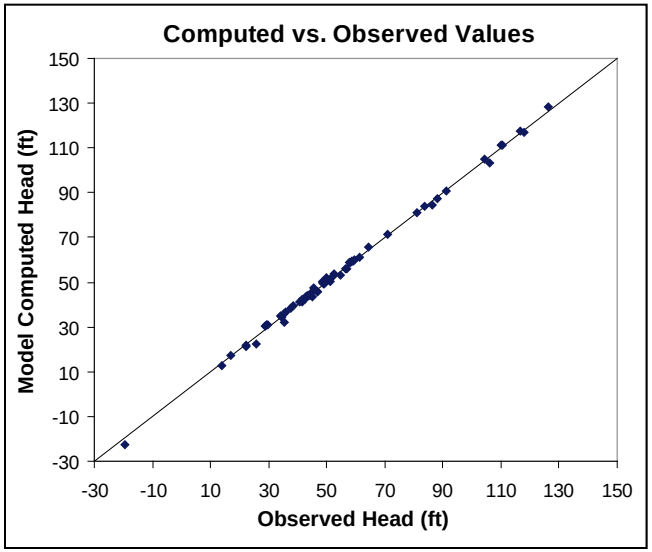

Error Summary

Head

Mean Error:	0.096
Mean Abs. Error:	0.951
Root Mean Sq. Error:	1.257

Regional SEAWAT Calibration
Upper Floridan Aquifer - February 2004
Final Groundwater Model Calibration Report

Figure F2-11

October 2010

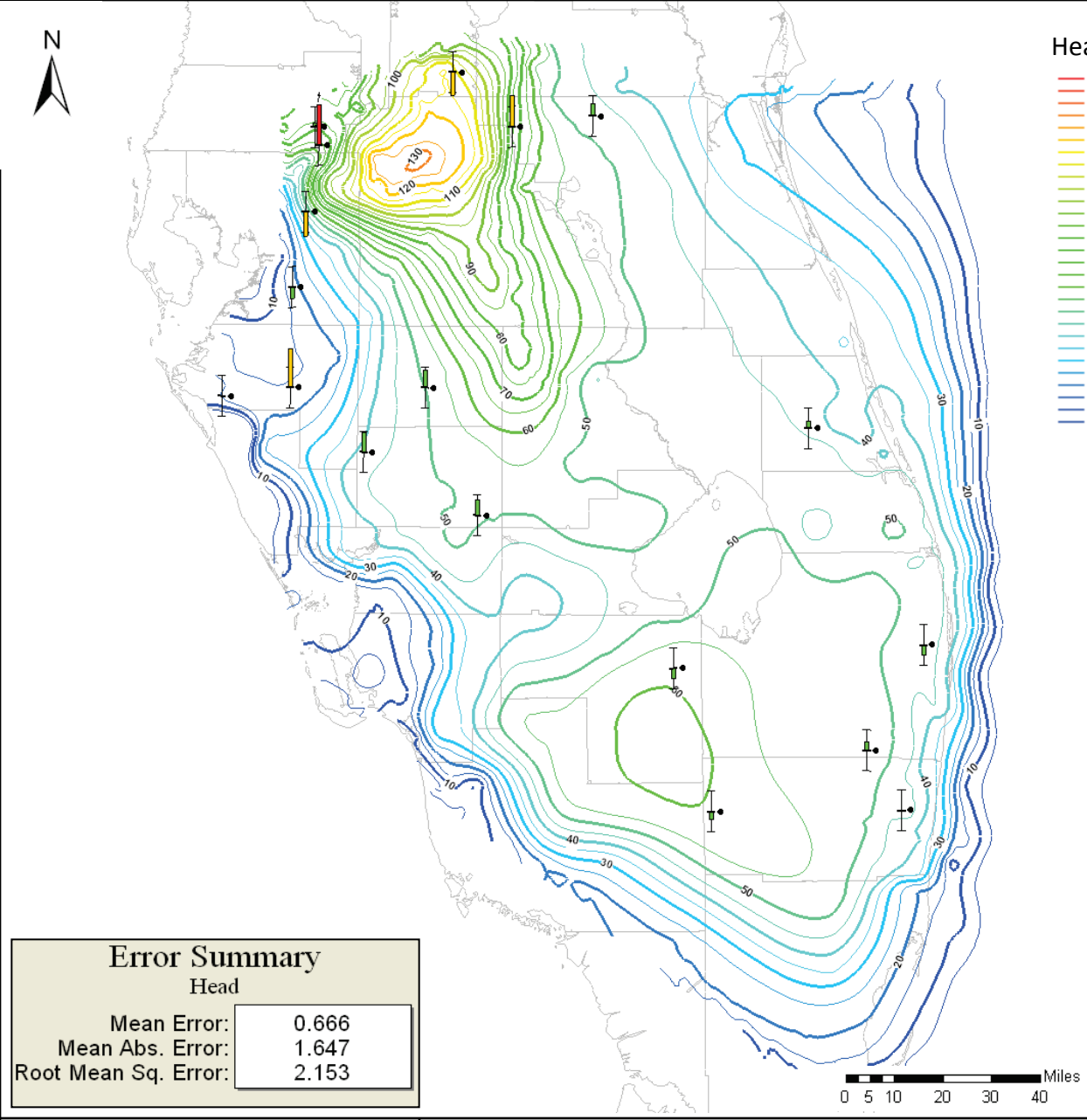

Notes:

Statistics (mean error, mean absolute error and root mean square error) are calculated based on equations presented in Section 4.1.

Calibration targets are green when the calculated value is within 2 feet of the measured head, yellow when within 4 feet and red when the model calculates a head more than 4 feet different from the measured value.

The direction of the colored bar on the calibration target indicates the sign on the residual: bars above the middle line indicate the model calculated higher heads than measured; bars below the middle line indicate negative residuals.

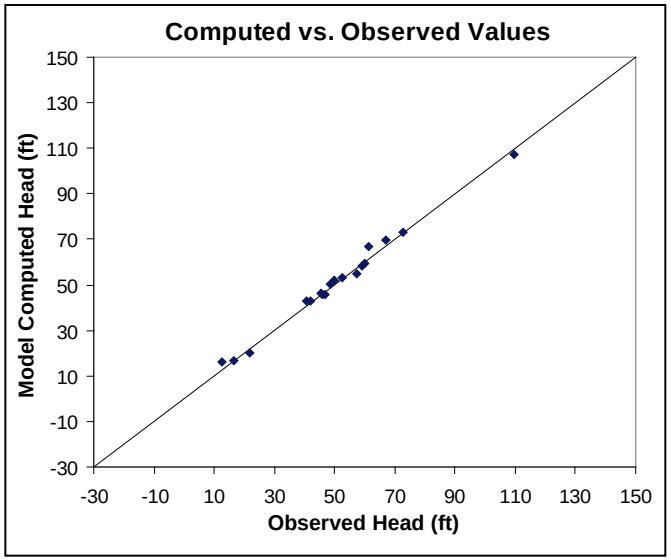

Error Summary

Head

Mean Error:	0.666
Mean Abs. Error:	1.647
Root Mean Sq. Error:	2.153

Regional SEAWAT Calibration
APPZ Aquifer - February 2004
Final Groundwater Model Calibration Report

Figure F2-12

October 2010

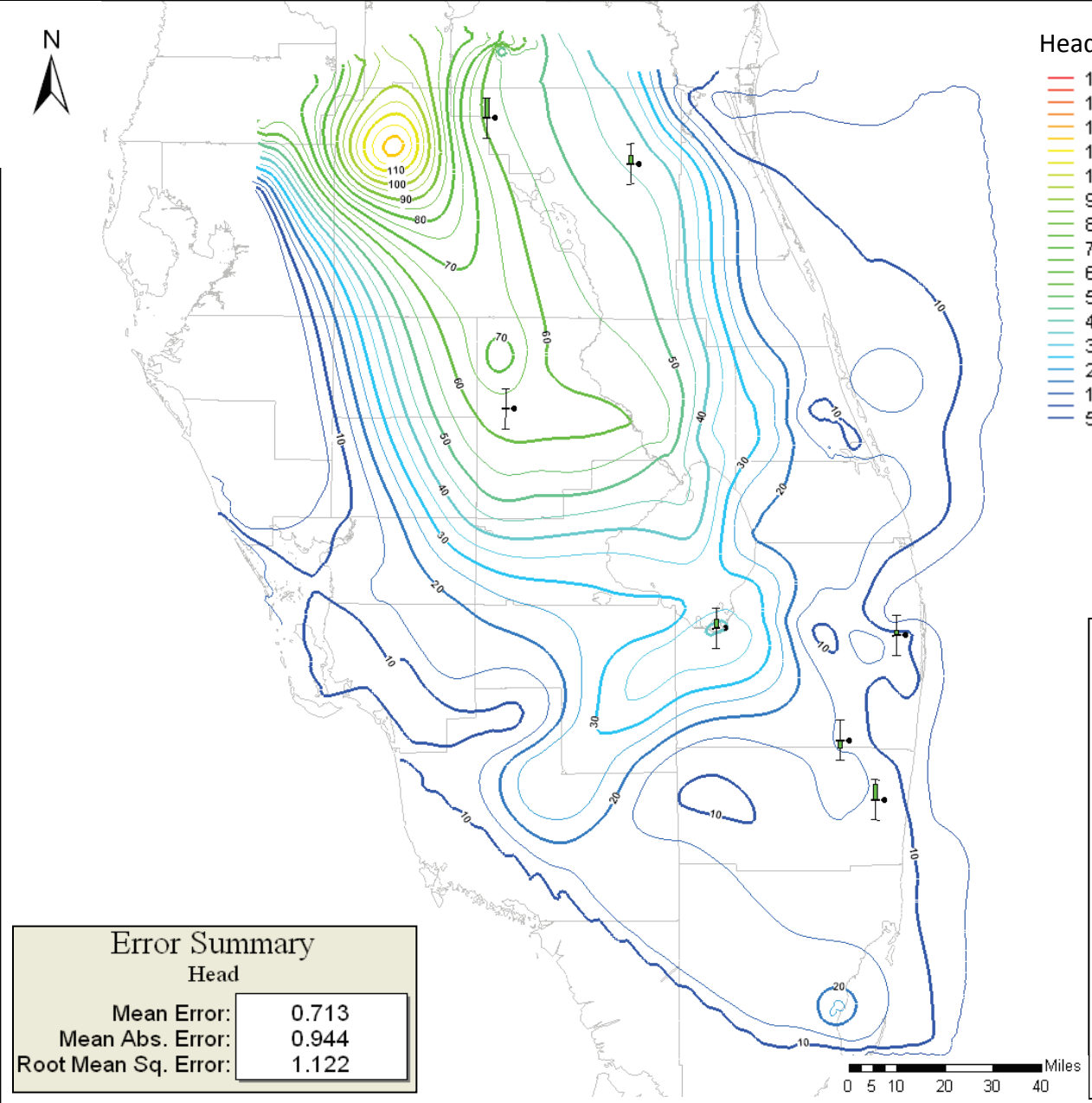

Notes:

Statistics (mean error, mean absolute error and root mean square error) are calculated based on equations presented in Section 4.1.

Calibration targets are green when the calculated value is within 2 feet of the measured head, yellow when within 4 feet and red when the model calculates a head more than 4 feet different from the measured value.

The direction of the colored bar on the calibration target indicates the sign on the residual: bars above the middle line indicate the model calculated higher heads than measured; bars below the middle line indicate negative residuals.

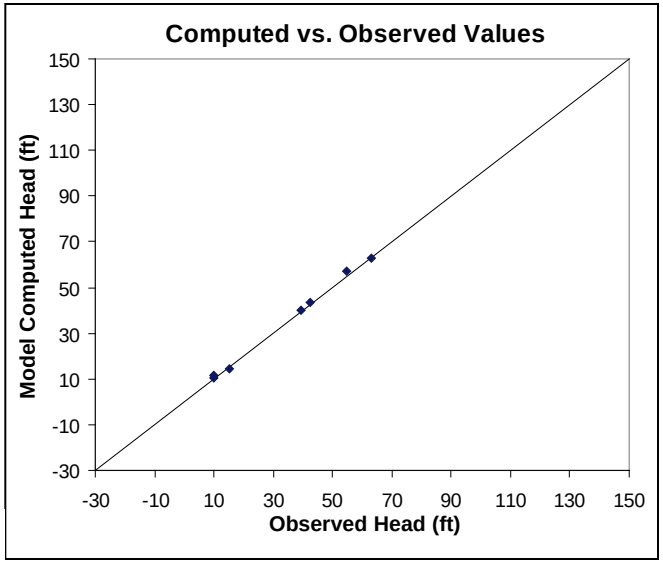

Error Summary

Head

Mean Error:	0.713
Mean Abs. Error:	0.944
Root Mean Sq. Error:	1.122

Regional SEAWAT Calibration
Lower Floridan (LF1) Aquifer - February 2004
Final Groundwater Model Calibration Report

Figure F2-13

October 2010

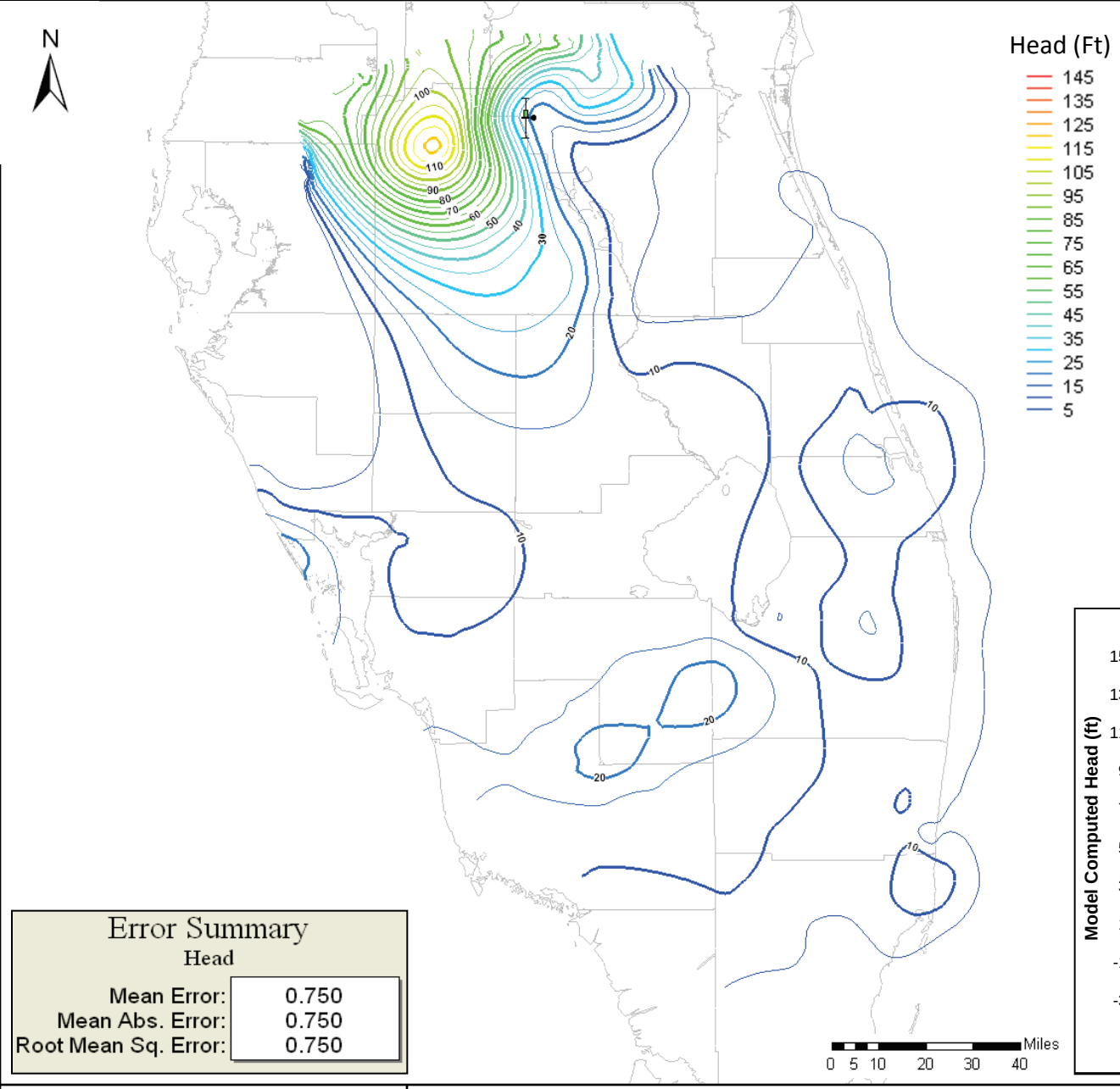

Notes:

Statistics (mean error, mean absolute error and root mean square error) are calculated based on equations presented in Section 4.1.

Calibration targets are green when the calculated value is within 2 feet of the measured head, yellow when within 4 feet and red when the model calculates a head more than 4 feet different from the measured value.

The direction of the colored bar on the calibration target indicates the sign on the residual: bars above the middle line indicate the model calculated higher heads than measured; bars below the middle line indicate negative residuals.

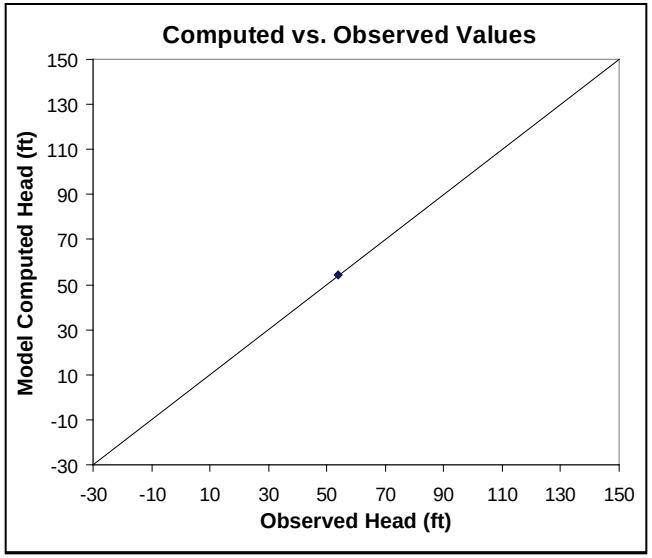

Error Summary

Head

Mean Error:	0.750
Mean Abs. Error:	0.750
Root Mean Sq. Error:	0.750

Regional SEAWAT Calibration
Boulder Zone - February 2004
Final Groundwater Model Calibration Report

Figure F2-14

October 2010

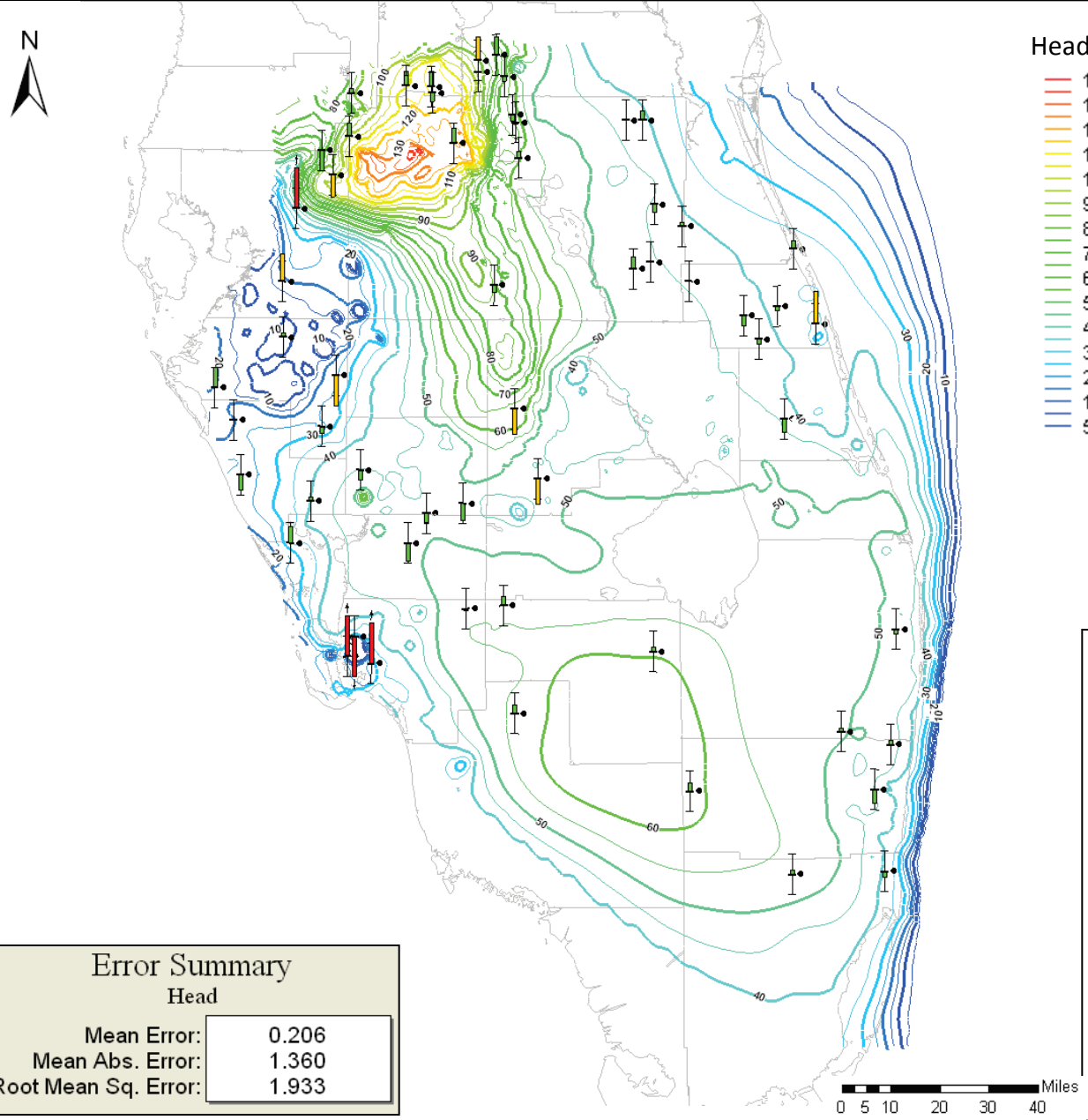

Notes:

Statistics (mean error, mean absolute error and root mean square error) are calculated based on equations presented in Section 4.1.

Calibration targets are green when the calculated value is within 2 feet of the measured head, yellow when within 4 feet and red when the model calculates a head more than 4 feet different from the measured value.

The direction of the colored bar on the calibration target indicates the sign on the residual: bars above the middle line indicate the model calculated higher heads than measured; bars below the middle line indicate negative residuals.

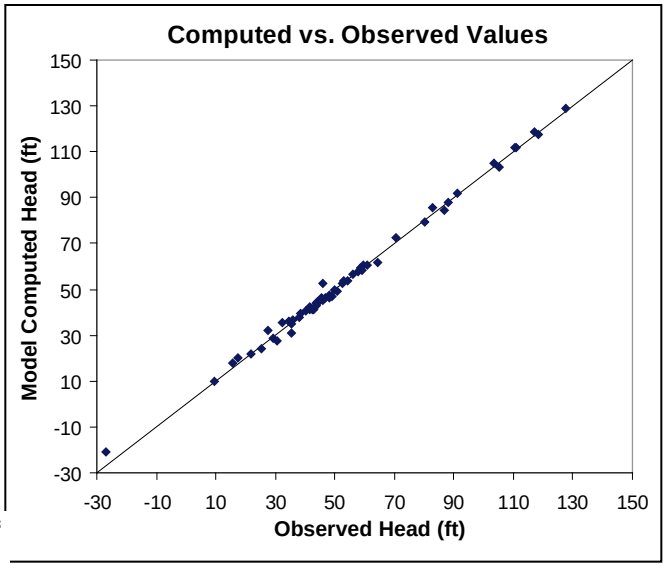

Error Summary

Head

Mean Error:	0.206
Mean Abs. Error:	1.360
Root Mean Sq. Error:	1.933

Regional SEAWAT Calibration
Upper Floridan Aquifer - October 2003
Final Groundwater Model Calibration Report

Figure F2-15

October 2010

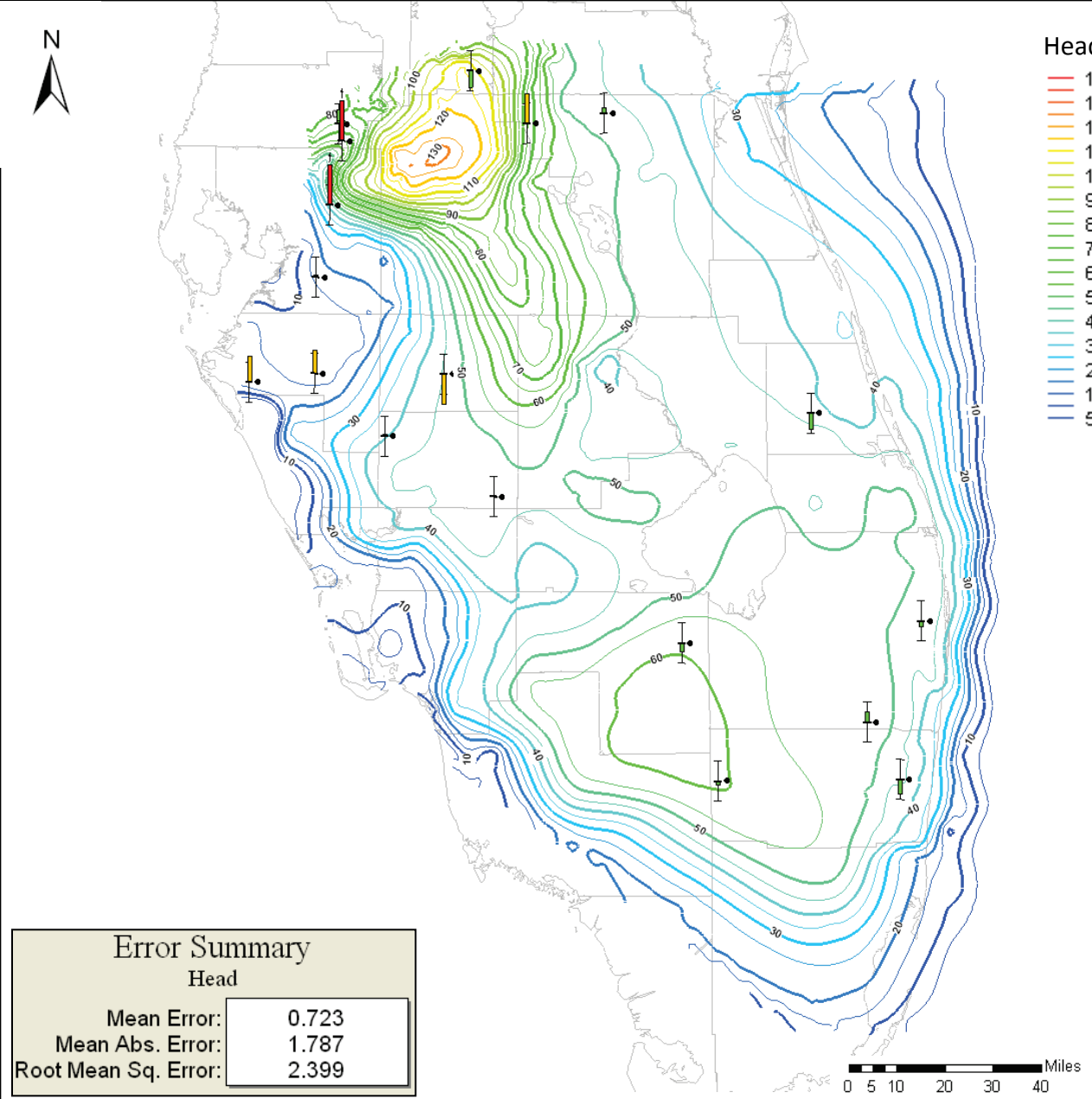

Notes:

Statistics (mean error, mean absolute error and root mean square error) are calculated based on equations presented in Section 4.1.

Calibration targets are green when the calculated value is within 2 feet of the measured head, yellow when within 4 feet and red when the model calculates a head more than 4 feet different from the measured value.

The direction of the colored bar on the calibration target indicates the sign on the residual: bars above the middle line indicate the model calculated higher heads than measured; bars below the middle line indicate negative residuals.

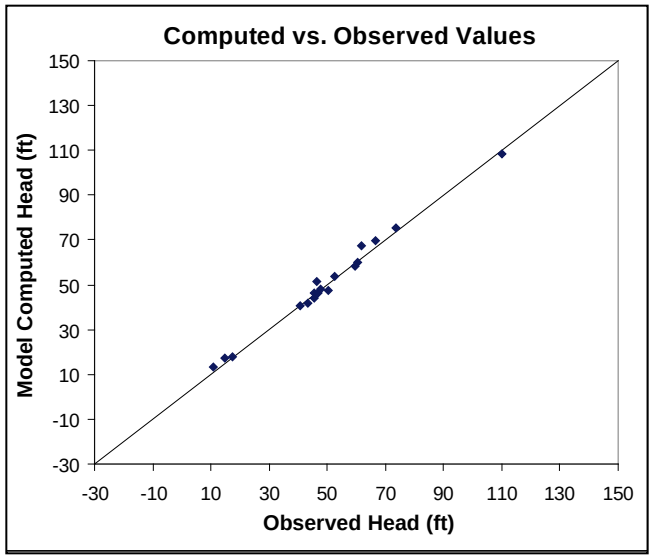

Error Summary

Head

Mean Error:	0.723
Mean Abs. Error:	1.787
Root Mean Sq. Error:	2.399

Regional SEAWAT Calibration
APPZ Aquifer - October 2003
Final Groundwater Model Calibration Report

Figure F2-16

October 2010

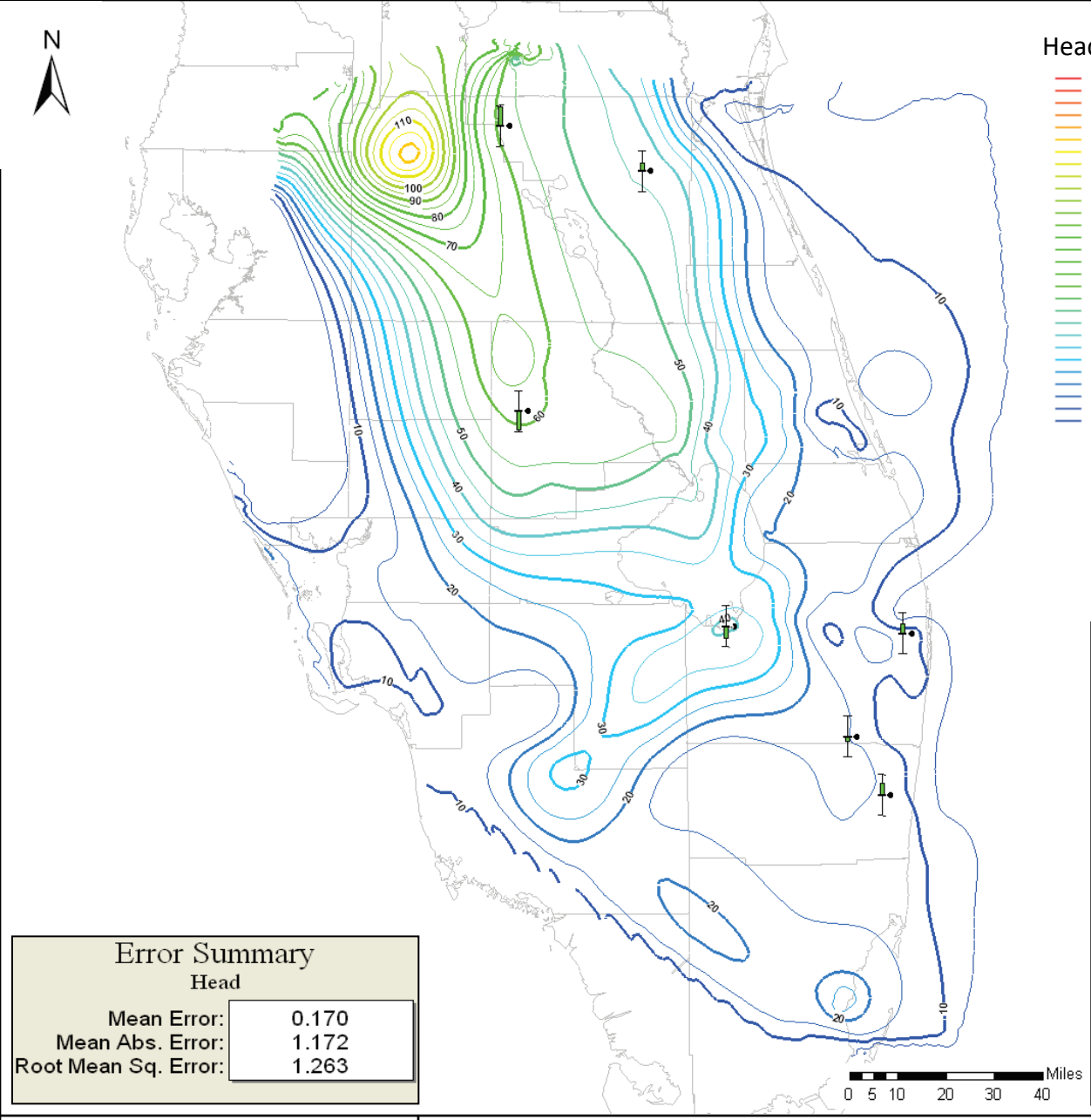

Notes:

Statistics (mean error, mean absolute error and root mean square error) are calculated based on equations presented in Section 4.1.

Calibration targets are green when the calculated value is within 2 feet of the measured head, yellow when within 4 feet and red when the model calculates a head more than 4 feet different from the measured value.

The direction of the colored bar on the calibration target indicates the sign on the residual: bars above the middle line indicate the model calculated higher heads than measured; bars below the middle line indicate negative residuals.

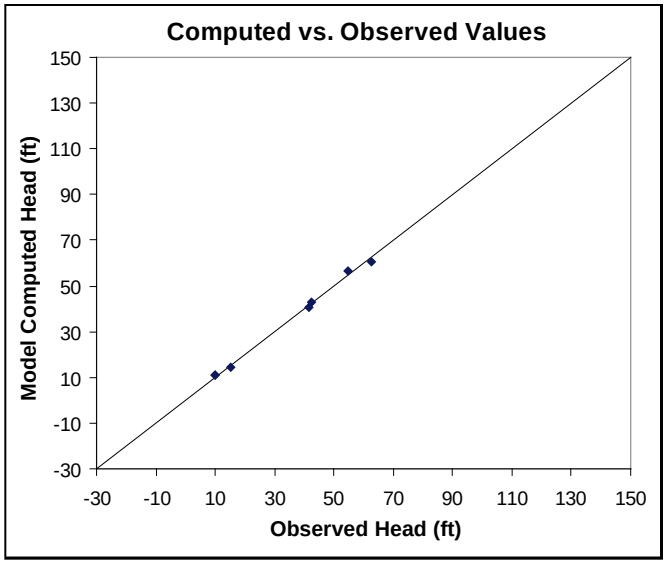

Error Summary
Head

Mean Error:	0.170
Mean Abs. Error:	1.172
Root Mean Sq. Error:	1.263

Regional SEAWAT Calibration
Lower Floridan (LF1) Aquifer - October 2003
Final Groundwater Model Calibration Report

Figure F2-17

October 2010

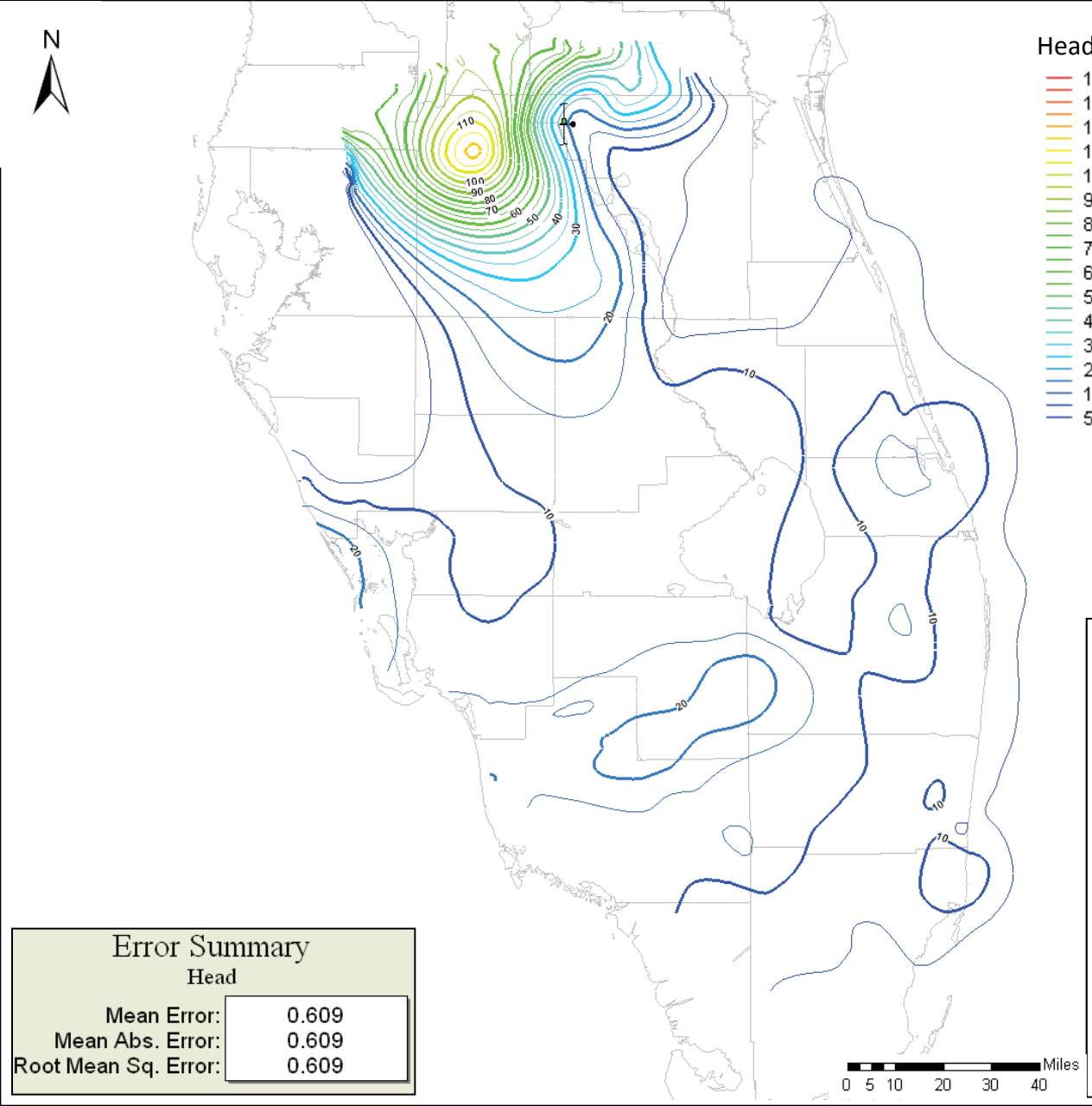

Notes:

Statistics (mean error, mean absolute error and root mean square error) are calculated based on equations presented in Section 4.1.

Calibration targets are green when the calculated value is within 2 feet of the measured head, yellow when within 4 feet and red when the model calculates a head more than 4 feet different from the measured value.

The direction of the colored bar on the calibration target indicates the sign on the residual: bars above the middle line indicate the model calculated higher heads than measured; bars below the middle line indicate negative residuals.

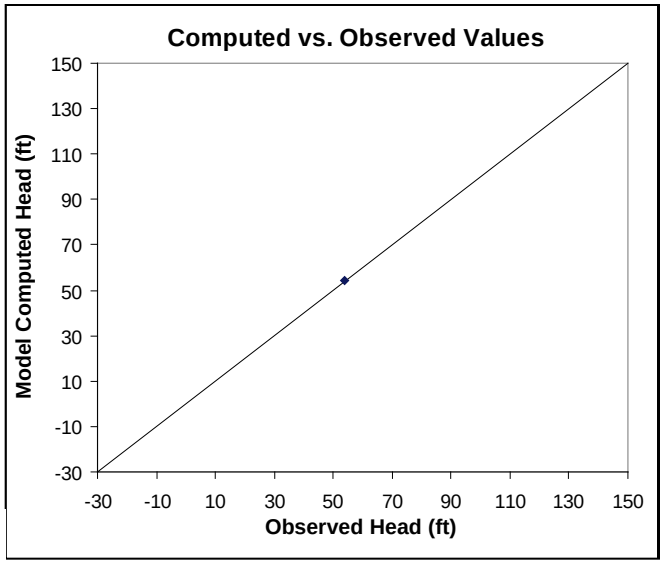

Error Summary	
Head	
Mean Error:	0.609
Mean Abs. Error:	0.609
Root Mean Sq. Error:	0.609

Regional SEAWAT Calibration
Boulder Zone - October 2003
Final Groundwater Model Calibration Report

Figure F2-18

October 2010

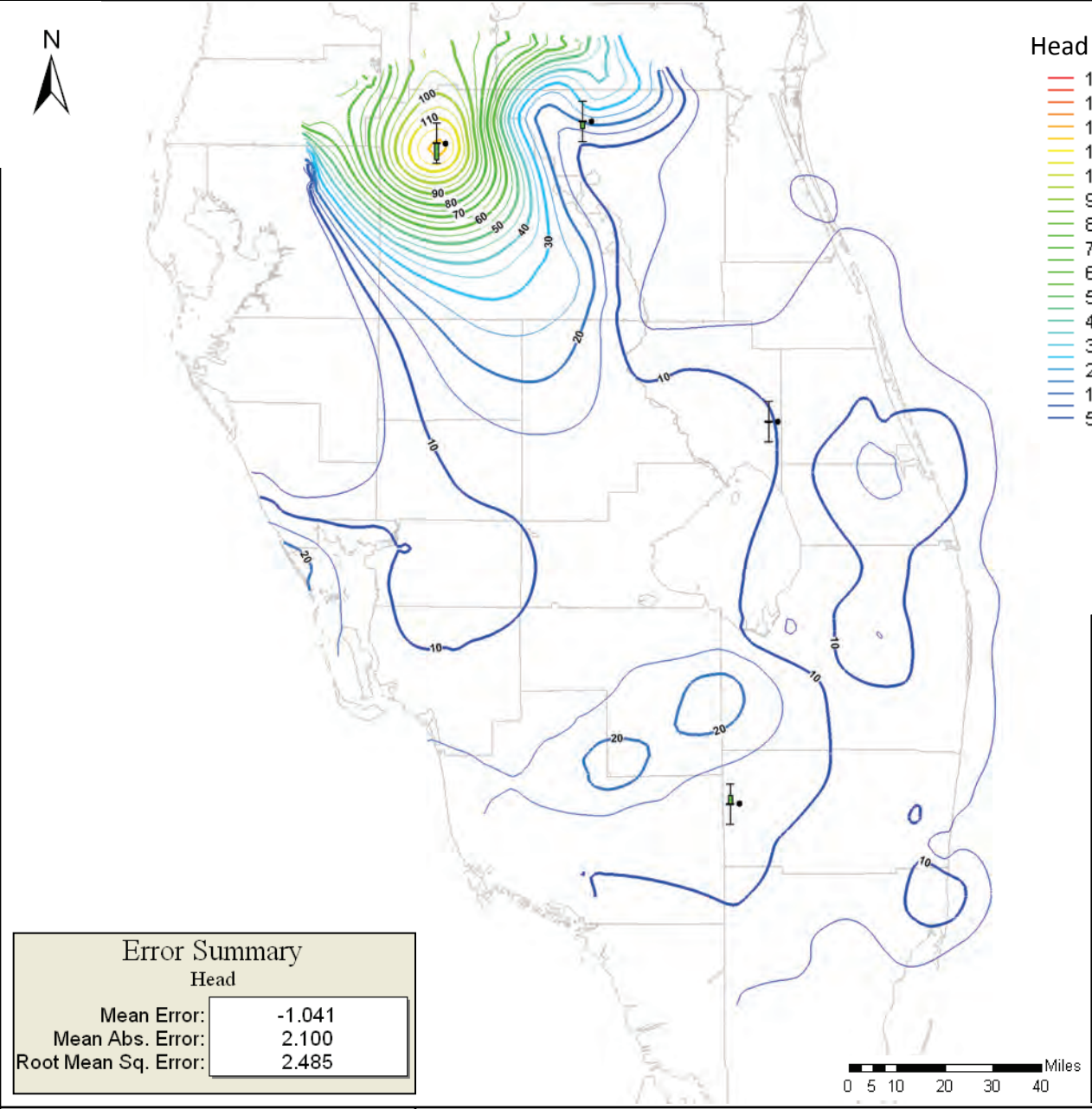

Notes:

Statistics (mean error, mean absolute error and root mean square error) are calculated based on equations presented in Section 4.1.

Calibration targets are green when the calculated value is within 5 feet of the measured head, yellow when within 10 feet and red when the model calculates a head more than 10 feet different from the measured value.

The direction of the colored bar on the calibration target indicates the sign on the residual: bars above the middle line indicate the model calculated higher heads than measured; bars below the middle line indicate negative residuals.

The contours shown are for the BZ.

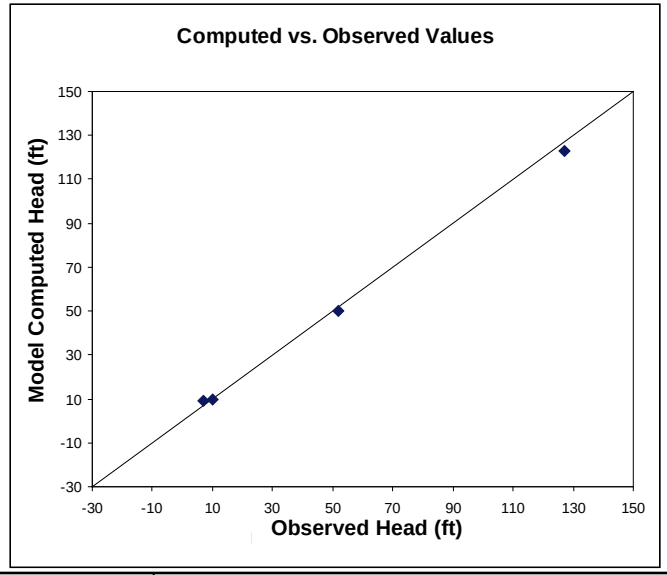

Error Summary Head	
Mean Error:	-1.041
Mean Abs. Error:	2.100
Root Mean Sq. Error:	2.485

Regional SEAWAT Calibration
LF1/BZ Expanded Calibration - February 2004 Model
Final Groundwater Model Calibration Report

Figure F2-19

October 2010

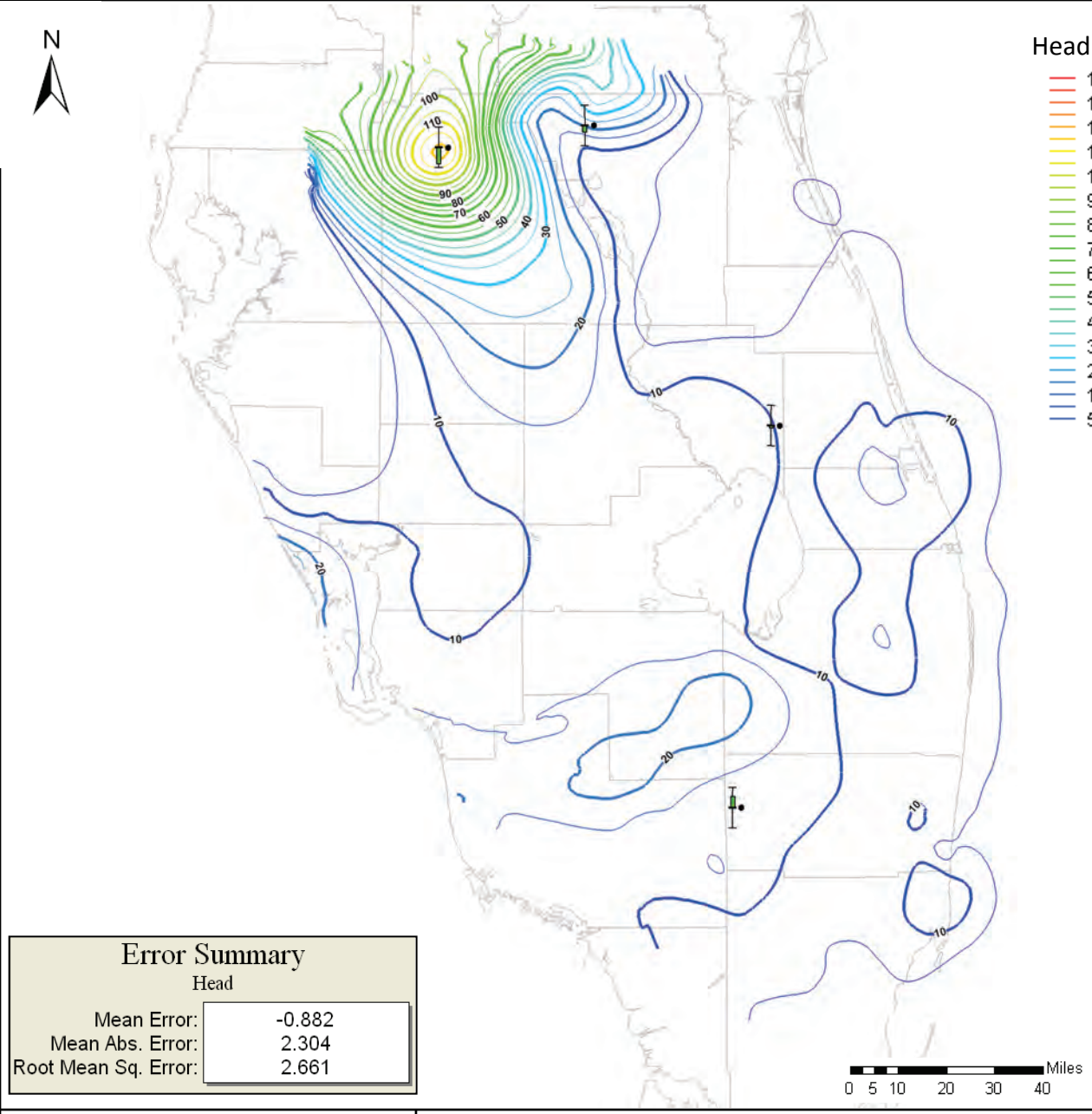

Notes:

Statistics (mean error, mean absolute error and root mean square error) are calculated based on equations presented in Section 4.1.

Calibration targets are green when the calculated value is within 5 feet of the measured head, yellow when within 10 feet and red when the model calculates a head more than 10 feet different from the measured value.

The direction of the colored bar on the calibration target indicates the sign on the residual: bars above the middle line indicate the model calculated higher heads than measured; bars below the middle line indicate negative residuals.

The contours shown are for the BZ.

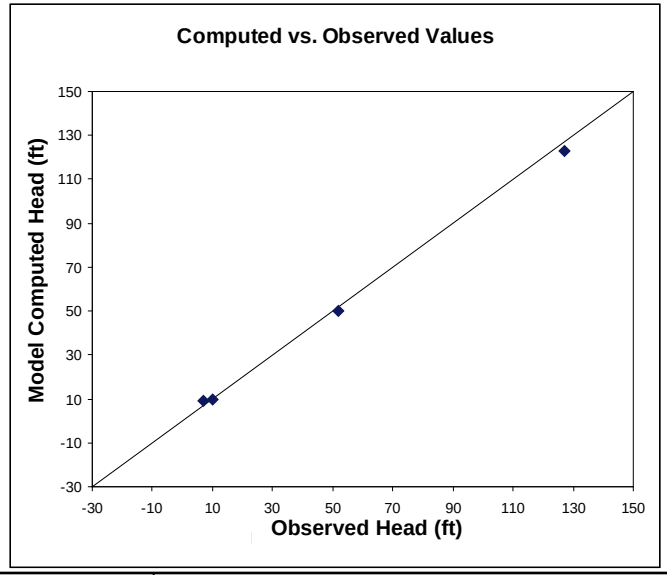

Error Summary	
Head	
Mean Error:	-0.882
Mean Abs. Error:	2.304
Root Mean Sq. Error:	2.661

Regional SEAWAT Calibration

LF1/BZ Expanded Calibration – October 2003 Model

Final Groundwater Model Calibration Report

Figure F2-20

October 2010

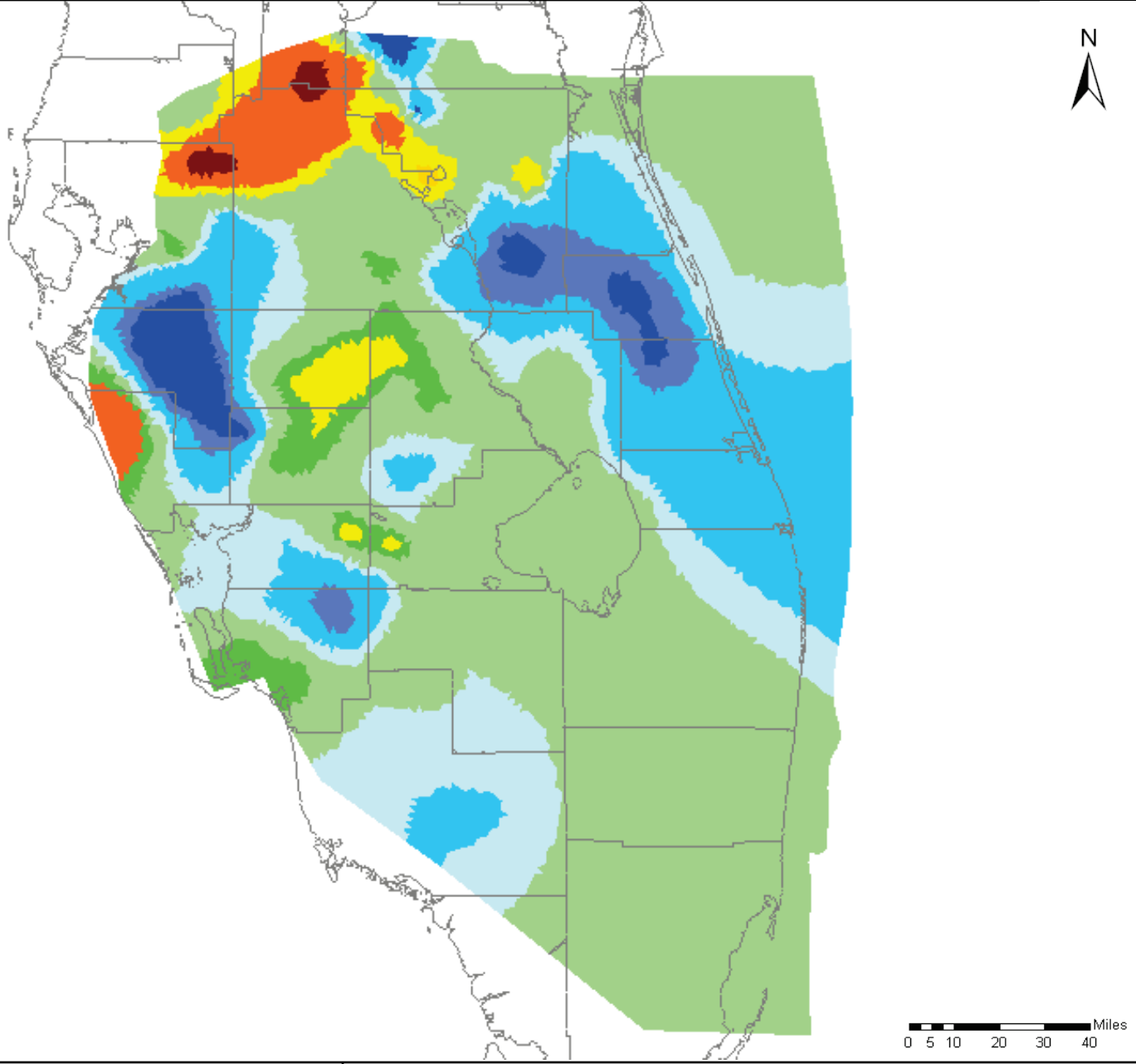

Notes:

This layer (2) overlies the Intermediate Aquifer in the regional model. Where the IA does not exist, (see Figure 4.31) the conductivities match those in layer 3 and 4.

Horizontal hydraulic conductivity was set to twice the vertical value (shown).

These conductivity values were organized in zones with constant values arranged to match the SEAWAT values as closely as possible. Some changes were then made during the WASH123D calibration.

Compare to Figure 4.27.

Regional Phase II ASR Vertical Hydraulic Conductivities
Intermediate Aquifer System Layer 2 (WASH123D)
Final Groundwater Model Calibration Report

Figure F2-21

October 2010

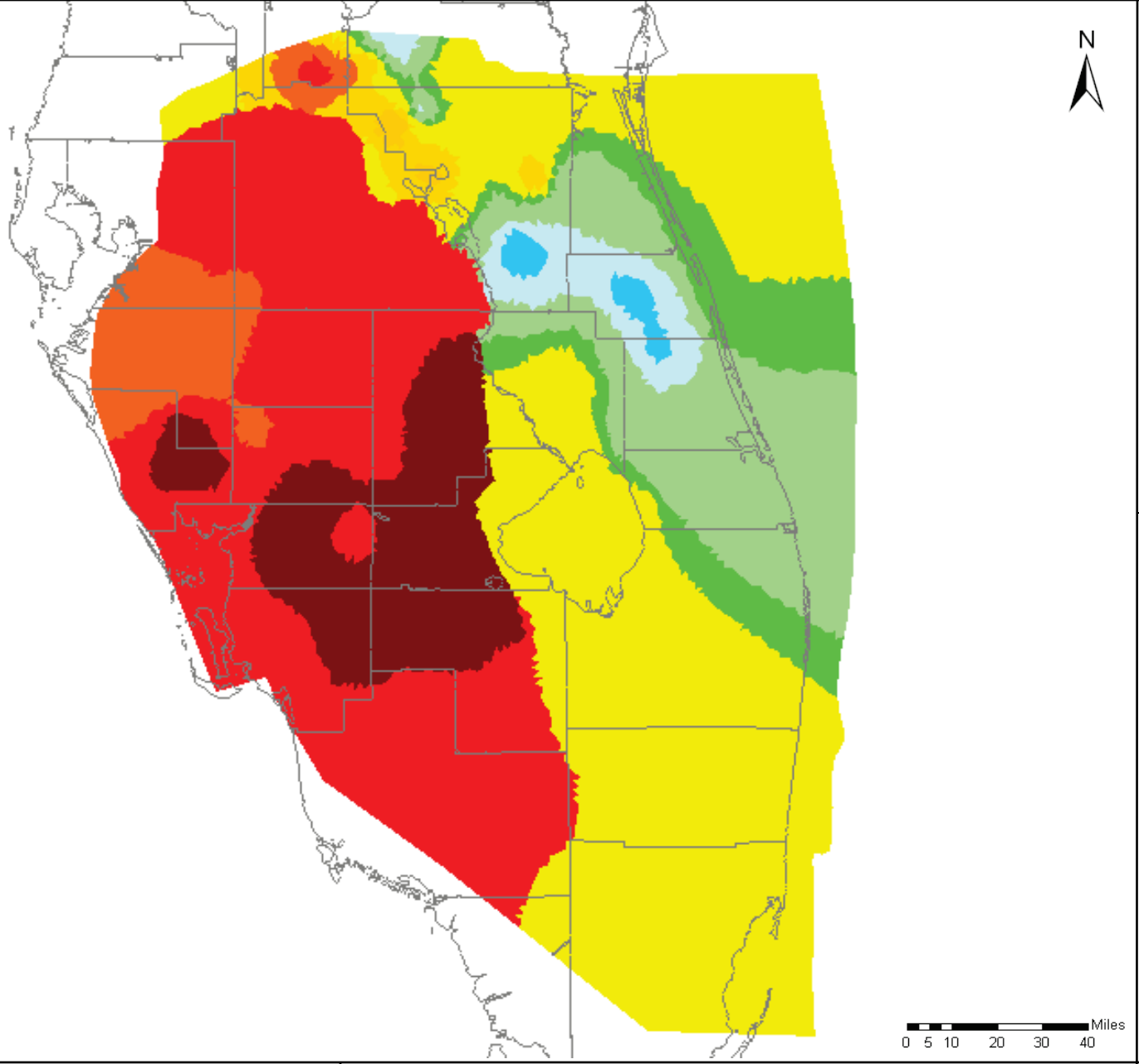

Horizontal Hydraulic Conductivity (ft/d)

- 0.00001 - 0.00005
- 0.00005 - 0.0001
- 0.0001 - 0.0005
- 0.0005 - 0.001
- 0.001 - 0.005
- 0.005 - 0.01
- 0.01 - 0.1
- 0.1 - 1
- 1 - 10
- 10 - 100
- 100 - 500

Notes:

The western portion of this layer (3) simulates the Intermediate Aquifer (IA). The eastern portion combines with layers 2 and 4 to simulate the Intermediate Confining Unit. Where the IA does not exist, the conductivity match those in layer 2 and 4.

Vertical hydraulic conductivity was set to one tenth of the horizontal value (shown).

These conductivity values were organized in zones with constant values arranged to match the SEAWAT values as closely as possible. Some changes were then made during the WASH123D calibration.

Compare to Figure 4.28.

Regional Phase II ASR Horizontal Hydraulic Conductivities
Intermediate Aquifer System Layer 3 (WASH123D)
Final Groundwater Model Calibration Report

Figure F2-22

October 2010

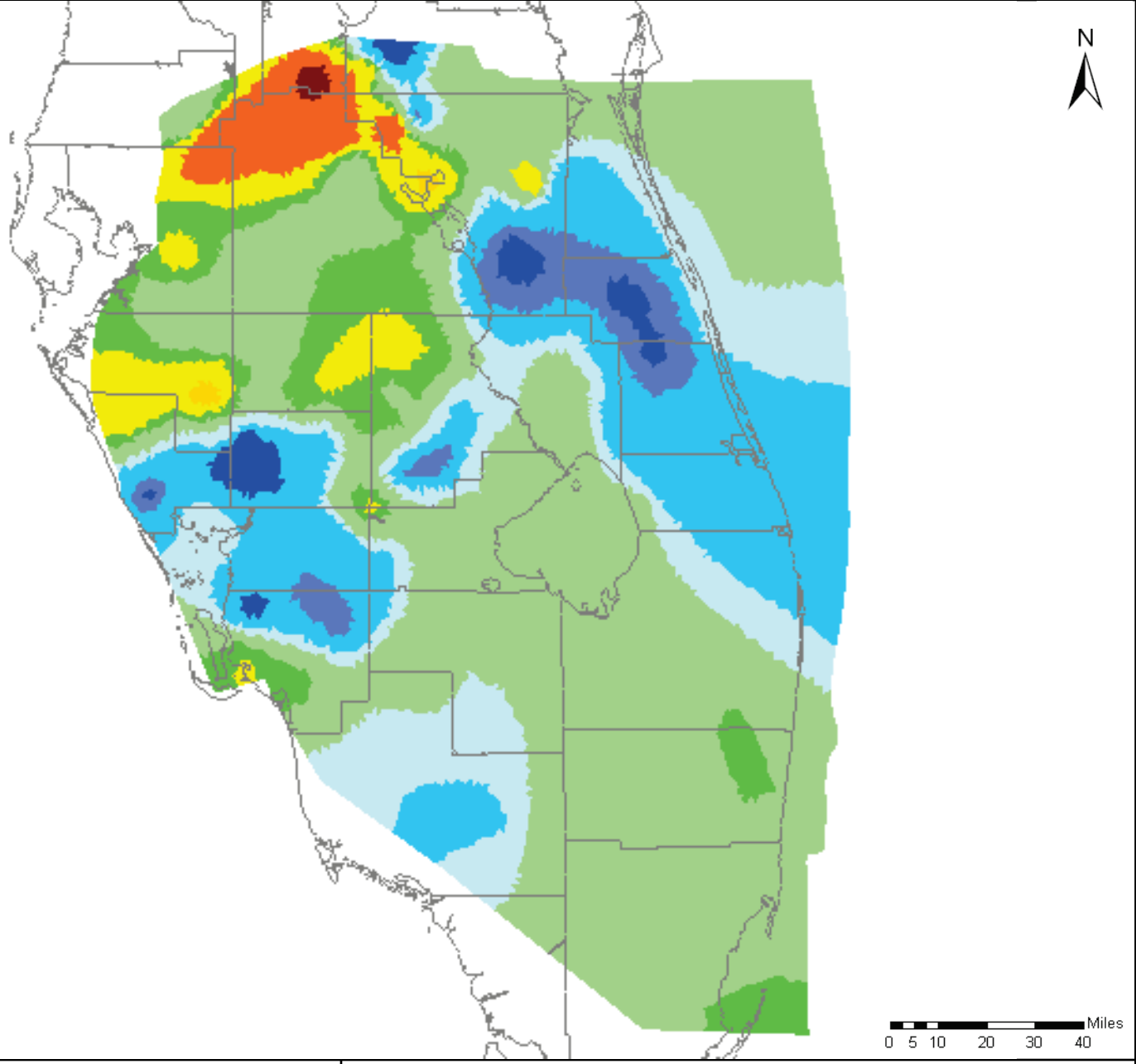

Vertical Hydraulic Conductivity (ft/d)

- 0.00001 - 0.00005
- 0.00005 - 0.0001
- 0.0001 - 0.0005
- 0.0005 - 0.001
- 0.001 - 0.005
- 0.005 - 0.01
- 0.01 - 0.05
- 0.05 - 0.1
- 0.1 - 0.5
- 0.5 - 1
- 1 - 10

Notes:

This layer (4) underlies the Intermediate Aquifer (IA) in the regional model. Where the IA does not exist, (see Figure 4.28) the conductivities match those in layer 2 and 3.

Horizontal hydraulic conductivity was set to twice the vertical value (shown).

These conductivity values were organized in zones with constant values arranged to match the SEAWAT values as closely as possible. Some changes were then made during the WASH123D calibration.

Compare to Figure 4.29.

Regional Phase II ASR Vertical Hydraulic Conductivities Intermediate Aquifer System Layer 4 (WASH123D)

Final Groundwater Model Calibration Report

Figure F2-23

October 2010

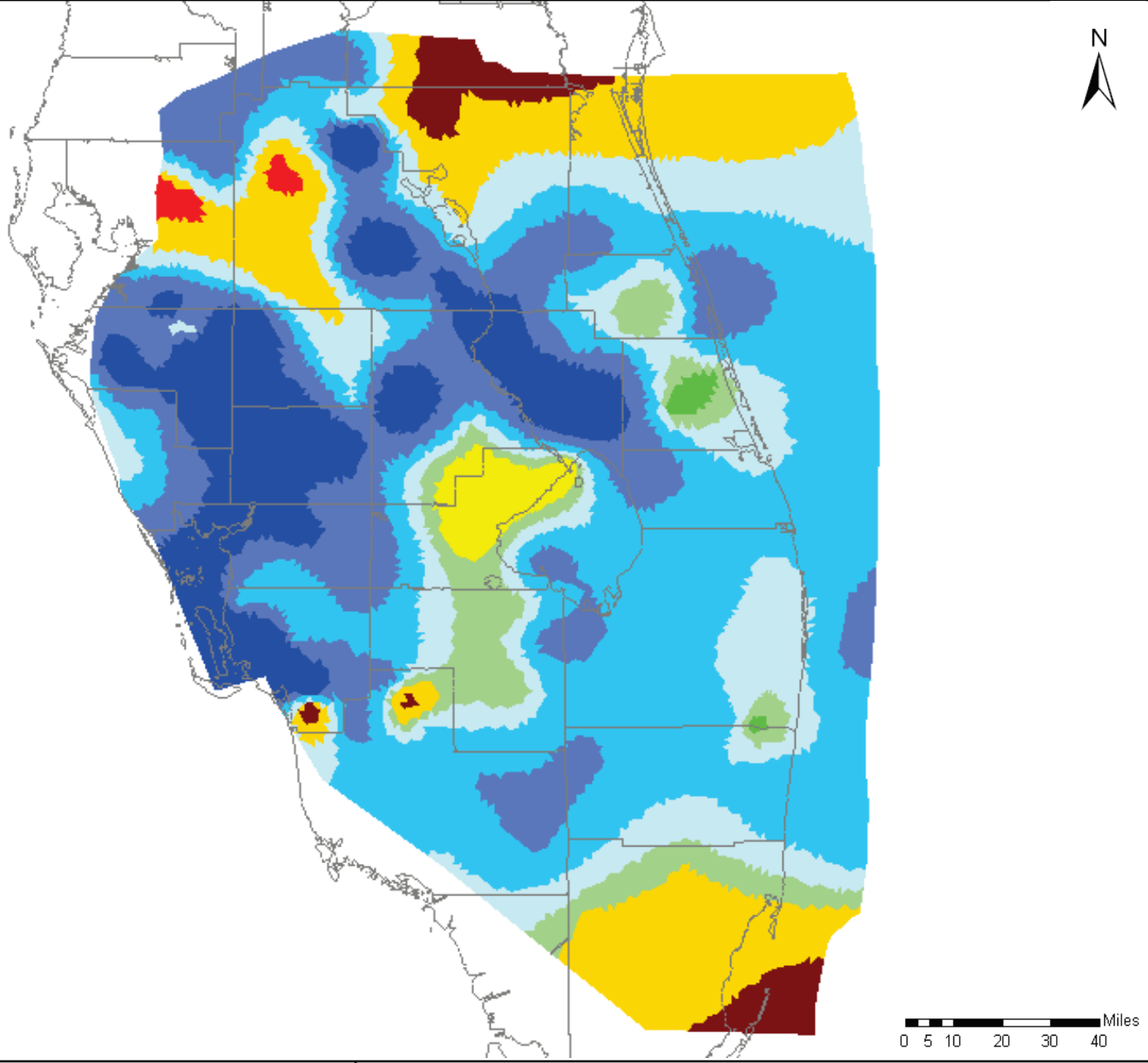

Horizontal Hydraulic Conductivity (ft/d)

- 1 - 20
- 20 - 40
- 40 - 60
- 60 - 80
- 80 - 100
- 100 - 120
- 120 - 140
- 140 - 160
- 160 - 180
- 180 - 200
- 200 - 500

Notes:

Vertical hydraulic conductivity was set to one tenth of the horizontal value (shown).

Conductivity values were interpolated to the grid from values assigned to a set of pilot points scattered across the model domain.

These conductivity values were organized in zones with constant values arranged to match the SEAWAT values as closely as possible. Some changes were then made during the WASH123D calibration.

Compare to Figure 4.20.

Regional Phase II ASR Horizontal Hydraulic Conductivities Upper Floridan Aquifer System (WASH123D)

Final Groundwater Model Calibration Report

Figure F2-24

October 2010

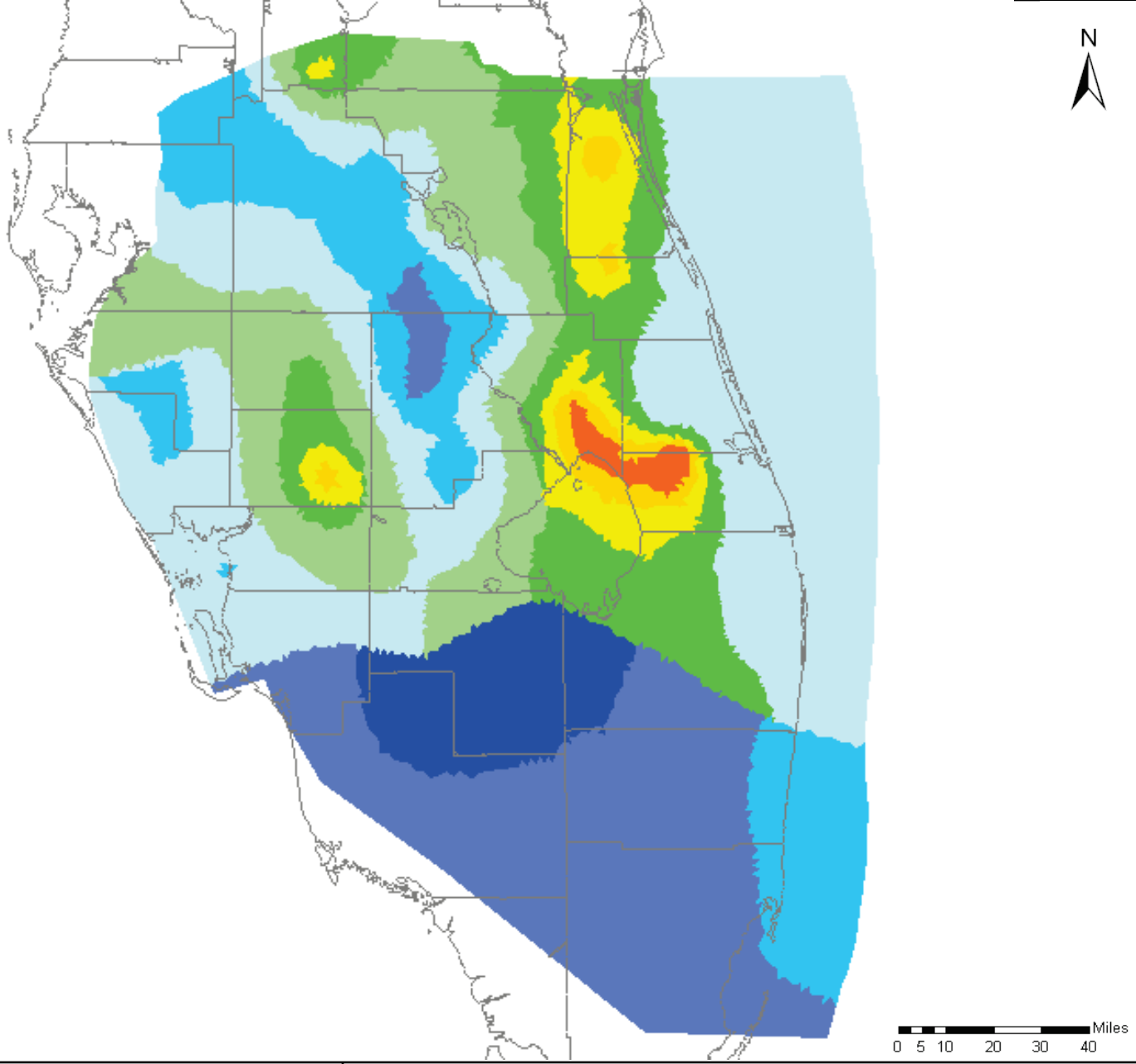

Horizontal Hydraulic Conductivity (ft/d)

- 5 - 20
- 20 - 50
- 50 - 100
- 100 - 200
- 200 - 400
- 400 - 600
- 600 - 800
- 800 - 1000
- 1000 - 1250
- 1250 - 1500
- 1500 - 1700

Notes:

Vertical hydraulic conductivity was set to one tenth of the horizontal value (shown).

Conductivity values were interpolated to the grid from values assigned to a set of pilot points scattered across the model domain.

These conductivity values were organized in zones with constant values arranged to match the SEAWAT values as closely as possible. Some changes were then made during the WASH123D calibration.

Compare to Figure 4.21.

Regional Phase II ASR Horizontal Hydraulic Conductivities
APPZ Aquifer (WASH123D)
Final Groundwater Model Calibration Report

Figure F2-25

October 2010

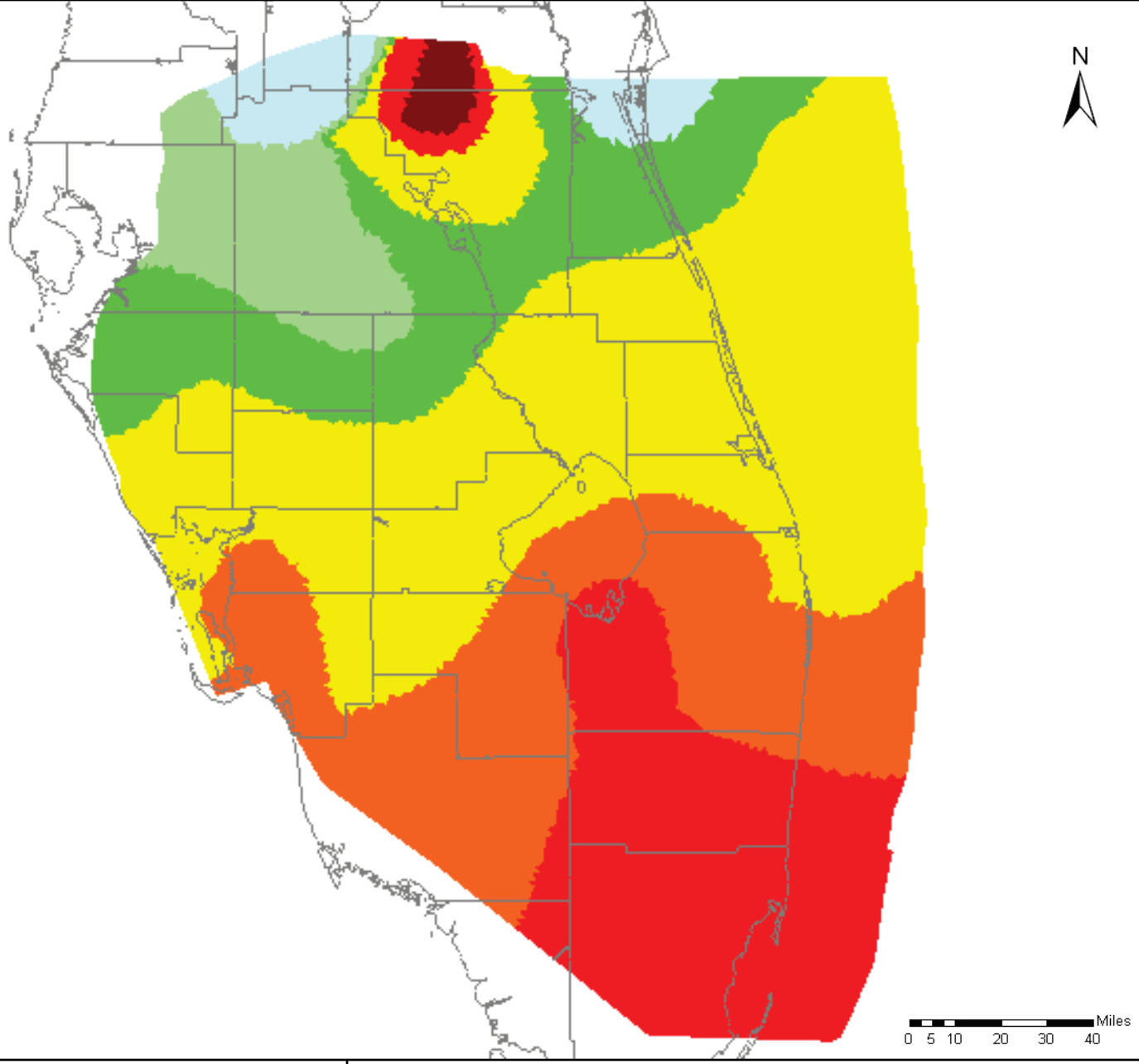

Horizontal Hydraulic Conductivity (ft/d)

- 1 - 20
- 20 - 40
- 40 - 60
- 60 - 80
- 80 - 100
- 100 - 200
- 200 - 300
- 300 - 400
- 400 - 500
- 500 - 1000
- 1000 - 1520

Notes:

Vertical hydraulic conductivity was set to one tenth of the horizontal value (shown).

Conductivity values were interpolated to the grid from values assigned to a set of pilot points scattered across the model domain.

These conductivity values were organized in zones with constant values arranged to match the SEAWAT values as closely as possible. Some changes were then made during the WASH123D calibration.

Compare to Figure 4.22.

Regional Phase II ASR Horizontal Hydraulic Conductivities
Lower Floridan (LF1) Aquifer (WASH123D)
Final Groundwater Model Calibration Report

Figure F2-26

October 2010

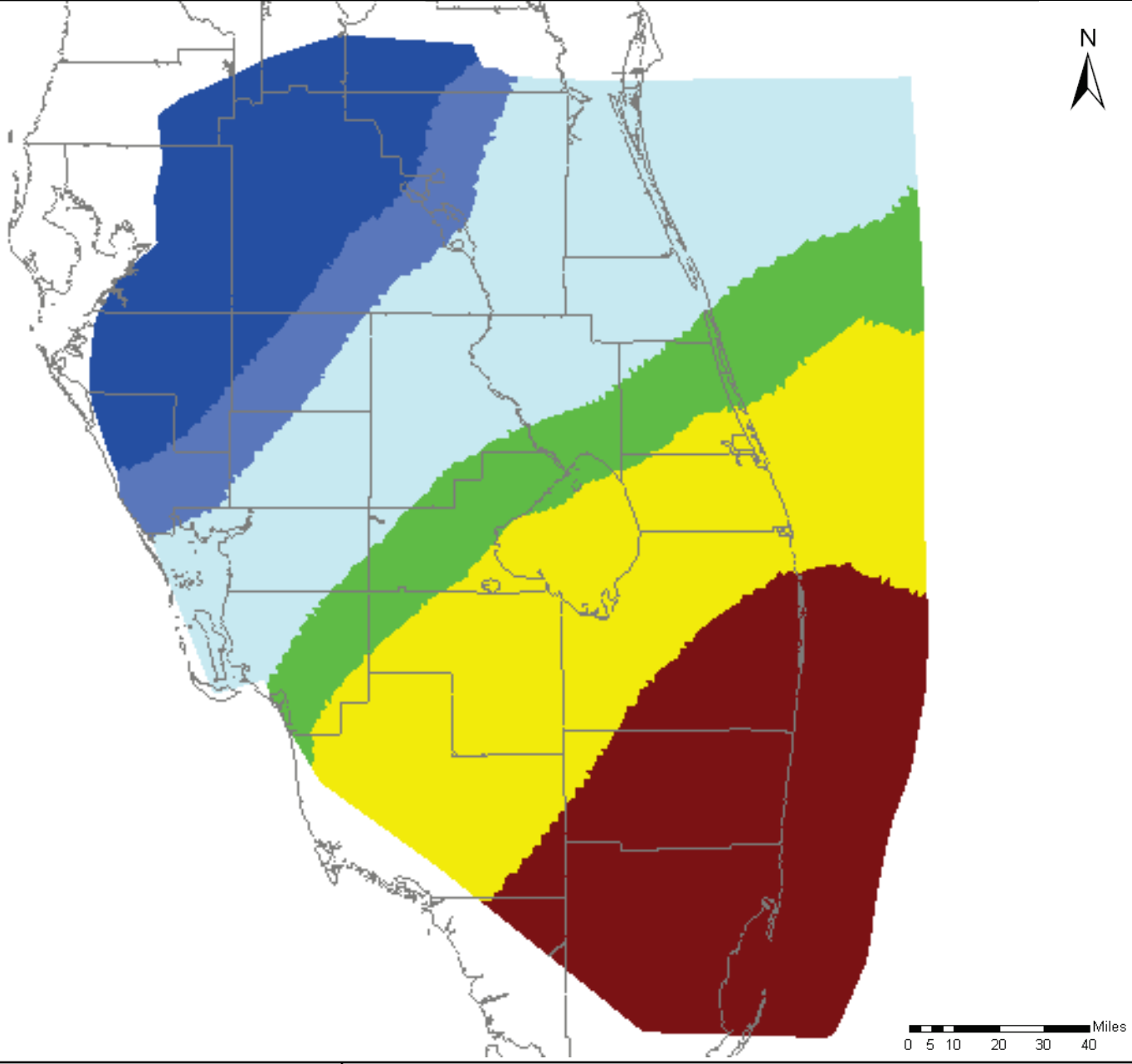

Horizontal Hydraulic Conductivity (ft/d)

- 1 - 50
- 50 - 100
- 100 - 250
- 250 - 500
- 500 - 750
- 750 - 1000
- 1000 - 2000
- 2000 - 3000
- 3000 - 4000
- 4000 - 5000
- 5000 - 10000

Notes:

Vertical hydraulic conductivity was set to one tenth of the horizontal value (shown).

Conductivity values were interpolated to the grid from values assigned to a set of pilot points scattered across the model domain.

These conductivity values were organized in zones with constant values arranged to match the SEAWAT values as closely as possible. Some changes were then made during the WASH123D calibration.

Compare to Figure 4.23.

Regional Phase II ASR Horizontal Hydraulic Conductivities Boulder Zone (WASH123D)

Final Groundwater Model Calibration Report

Figure F2-27

October 2010

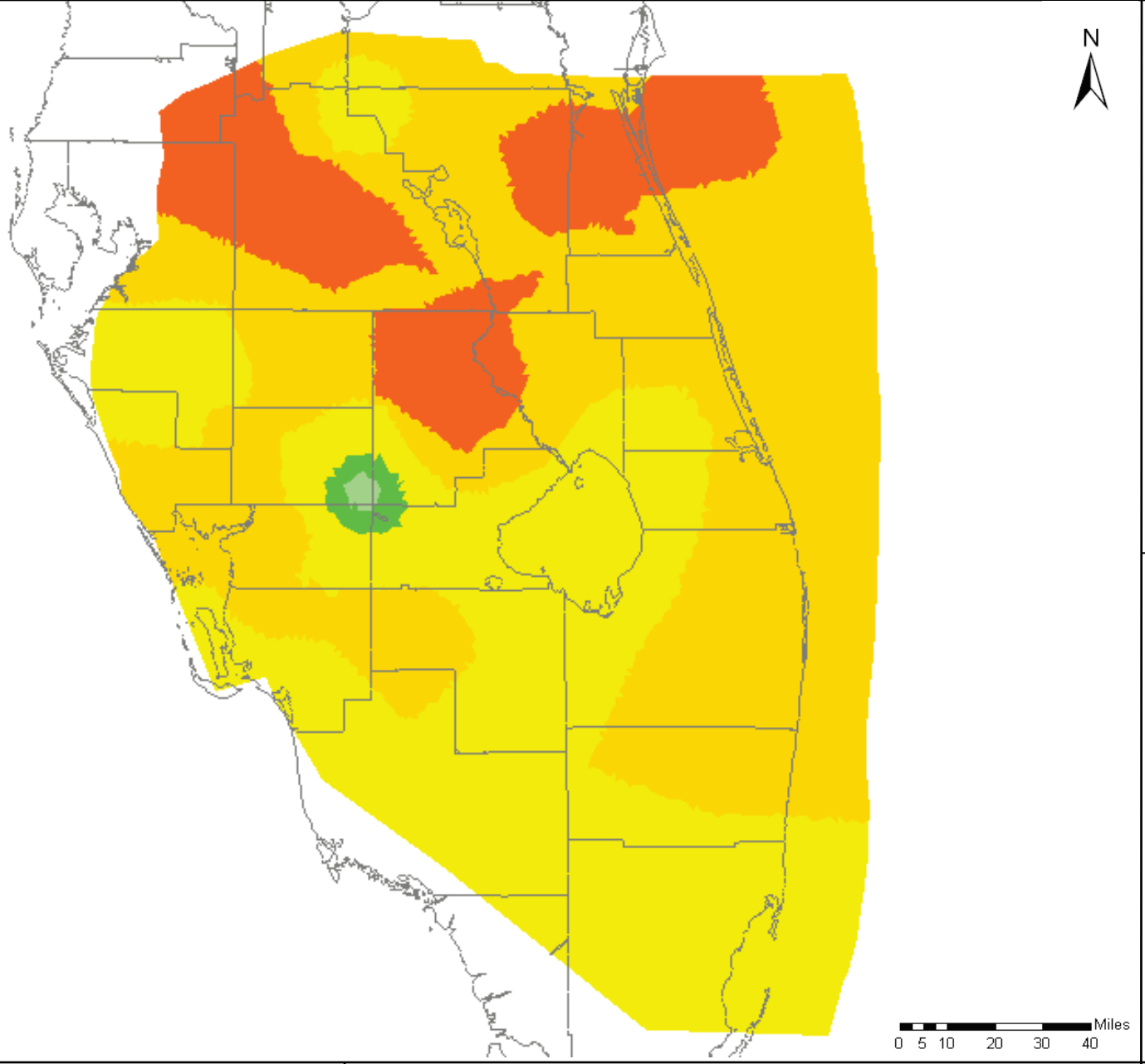

Vertical Hydraulic Conductivity (ft/d)

- 0.00001 - 0.00005
- 0.00005 - 0.0001
- 0.0001 - 0.0005
- 0.0005 - 0.001
- 0.001 - 0.005
- 0.005 - 0.01
- 0.01 - 0.05
- 0.05 - 0.1
- 0.1 - 0.5
- 0.5 - 1
- 1 - 10

Notes:

Horizontal hydraulic conductivity was set to twice the vertical value (shown).

Conductivity values were interpolated to the grid from values assigned to a set of pilot points scattered across the model domain.

These conductivity values were organized in zones with constant values arranged to match the SEAWAT values as closely as possible. Some changes were then made during the WASH123D calibration.

Compare to Figure 4.24.

Regional Phase II ASR Vertical Hydraulic Conductivities Middle Confining Unit 1 (WASH123D)

Final Groundwater Model Calibration Report

Figure F2-28

October 2010

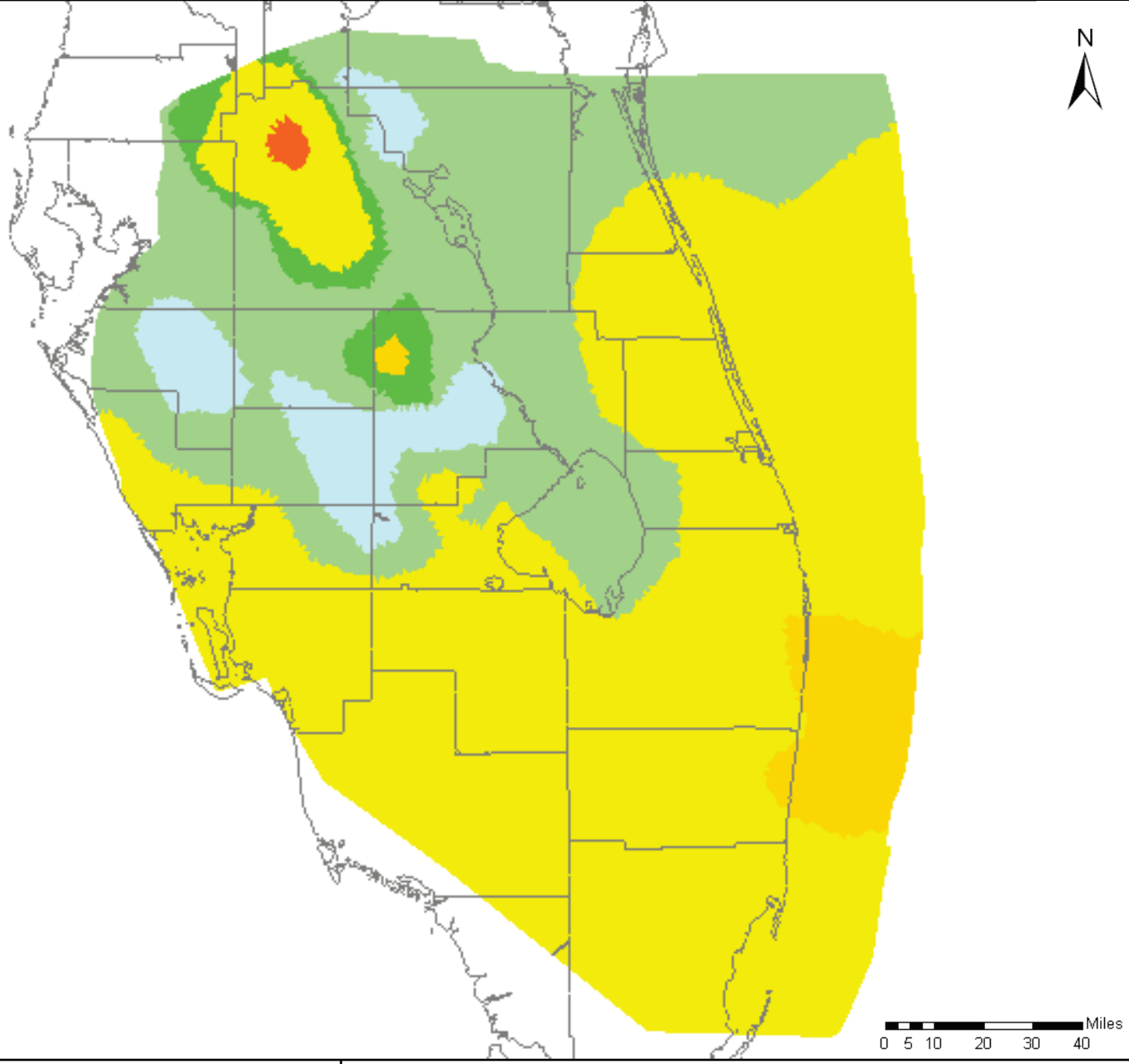

Vertical Hydraulic Conductivity (ft/d)

- 0.00001 - 0.00005
- 0.00005 - 0.0001
- 0.0001 - 0.0005
- 0.0005 - 0.001
- 0.001 - 0.005
- 0.005 - 0.01
- 0.01 - 0.05
- 0.05 - 0.1
- 0.1 - 0.5
- 0.5 - 1
- 1 - 10

Notes:

Horizontal hydraulic conductivity was set to twice the vertical value (shown).

Conductivity values were interpolated to the grid from values assigned to a set of pilot points scattered across the model domain.

These conductivity values were organized in zones with constant values arranged to match the SEAWAT values as closely as possible. Some changes were then made during the WASH123D calibration.

Compare to Figure 4.25.

Regional Phase II ASR Vertical Hydraulic Conductivities
Middle Confining Unit 2 (WASH123D)
Final Groundwater Model Calibration Report

Figure F2-29

October 2010

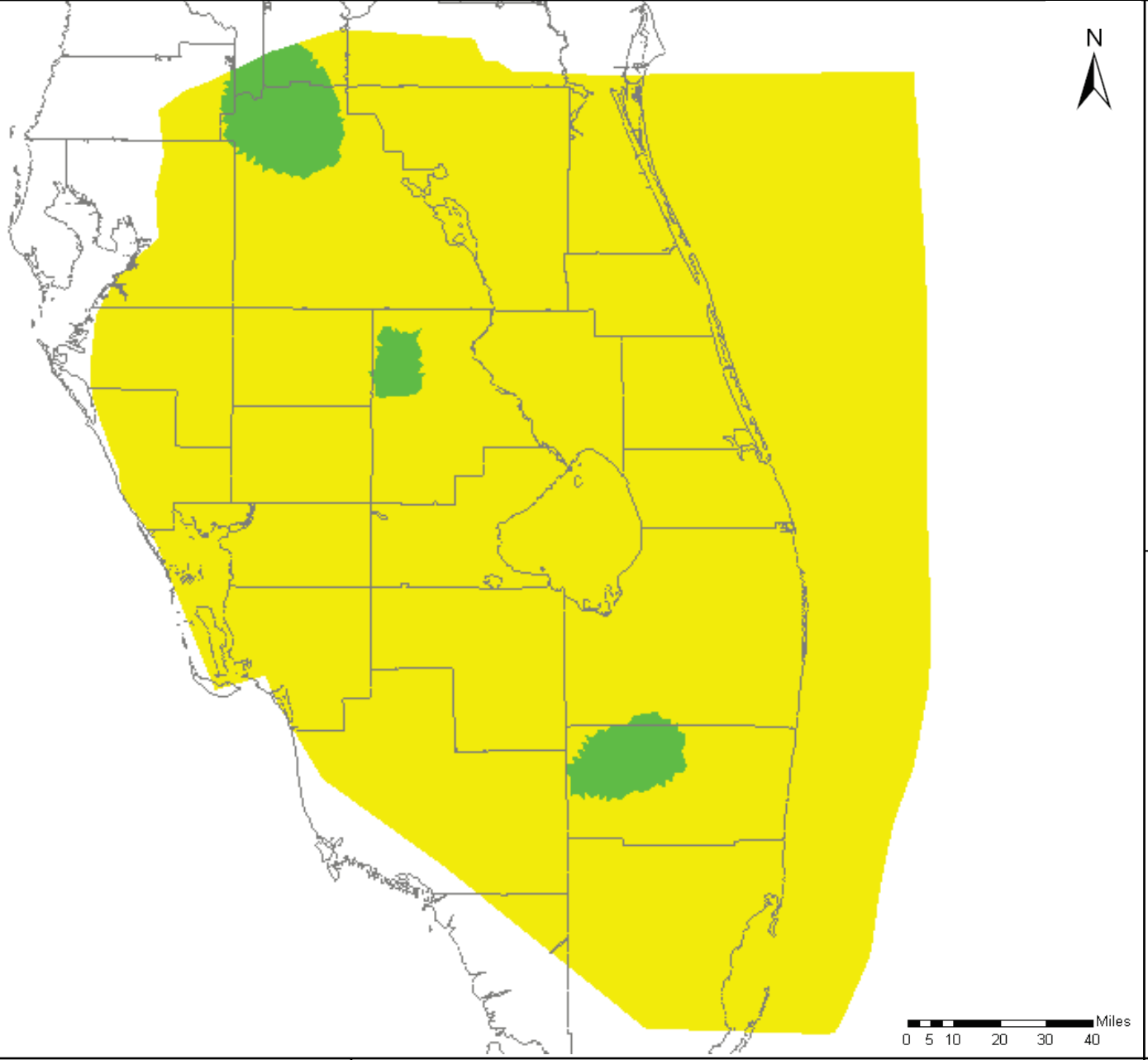

Vertical Hydraulic Conductivity (ft/d)

- 0.00001 - 0.00005
- 0.00005 - 0.0001
- 0.0001 - 0.0005
- 0.0005 - 0.001
- 0.001 - 0.005
- 0.005 - 0.01
- 0.01 - 0.05
- 0.05 - 0.1
- 0.1 - 0.5
- 0.5 - 1
- 1 - 10

Notes:

Horizontal hydraulic conductivity was set to twice the vertical value (shown).

Conductivity values were interpolated to the grid from values assigned to a set of pilot points scattered across the model domain.

These conductivity values were organized in zones with constant values arranged to match the SEAWAT values as closely as possible. Some changes were then made during the WASH123D calibration.

Compare to Figure 4.26.

Regional Phase II ASR Vertical Hydraulic Conductivities Lower Confining Unit (WASH123D)

Final Groundwater Model Calibration Report

Figure F2-30

October 2010

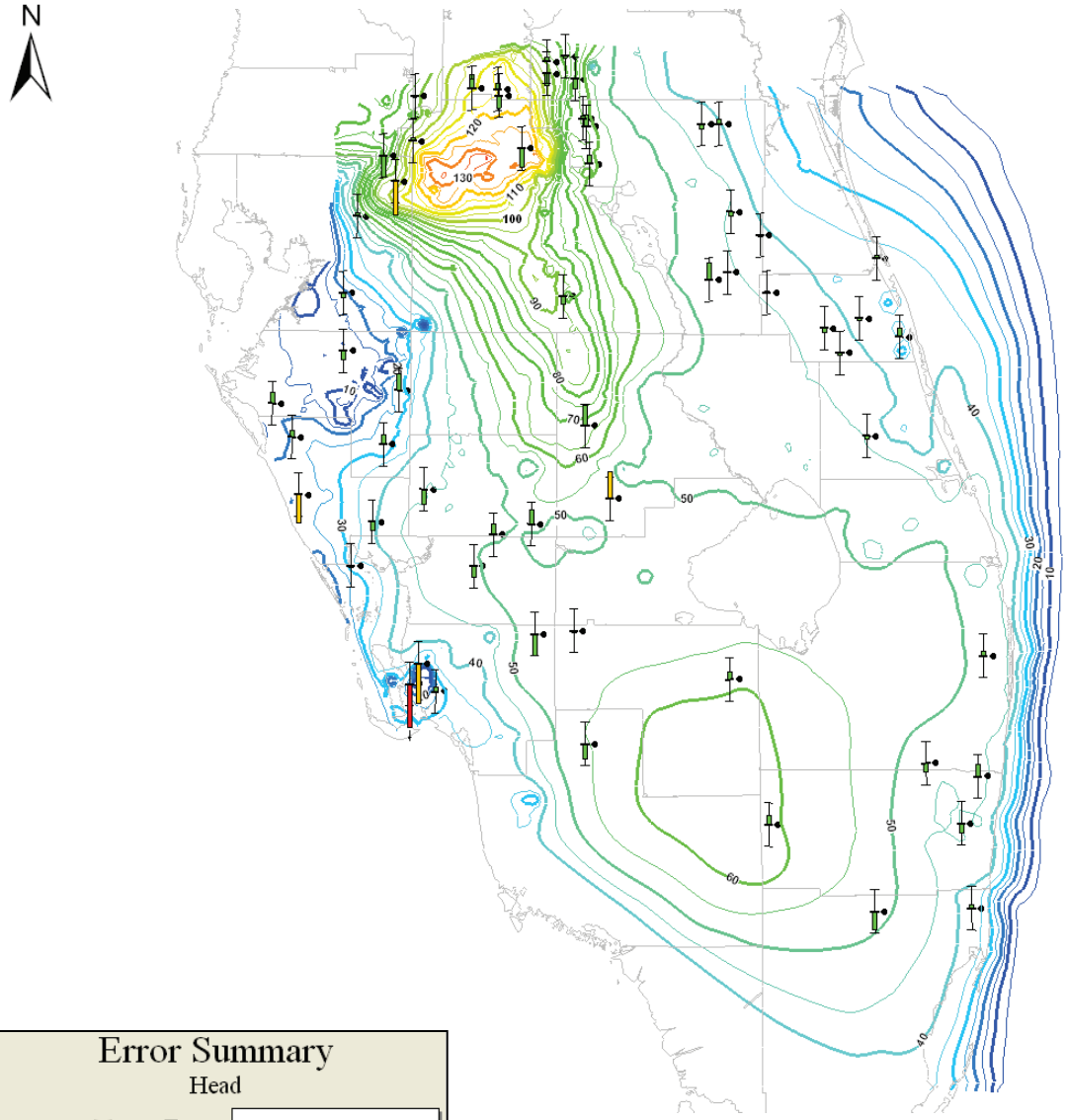

Notes:

Statistics (mean error, mean absolute error and root mean square error) are calculated based on equations presented in Section 4.1.

Calibration targets are green when the calculated value is within 2 feet of the measured head, yellow when within 4 feet and red when the model calculates a head more than 4 feet different from the measured value.

The direction of the colored bar on the calibration target indicates the sign on the residual: bars above the middle line indicate the model calculated higher heads than measured; bars below the middle line indicate negative residuals.

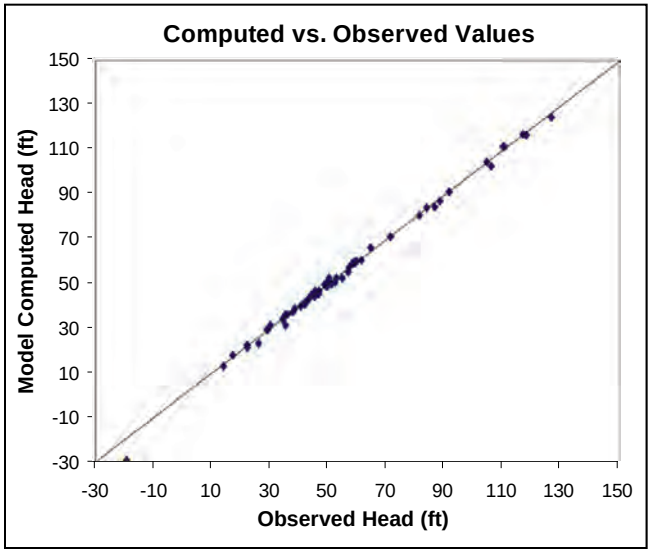

Error Summary

Head

Mean Error:	**-0.262**
Mean Abs. Error:	**1.067**
Root Mean Sq. Error:	**1.714**

Regional WASH123D Calibration
Upper Floridan Aquifer - February 2004
Final Groundwater Model Calibration Report

Figure F2-31

October 2010

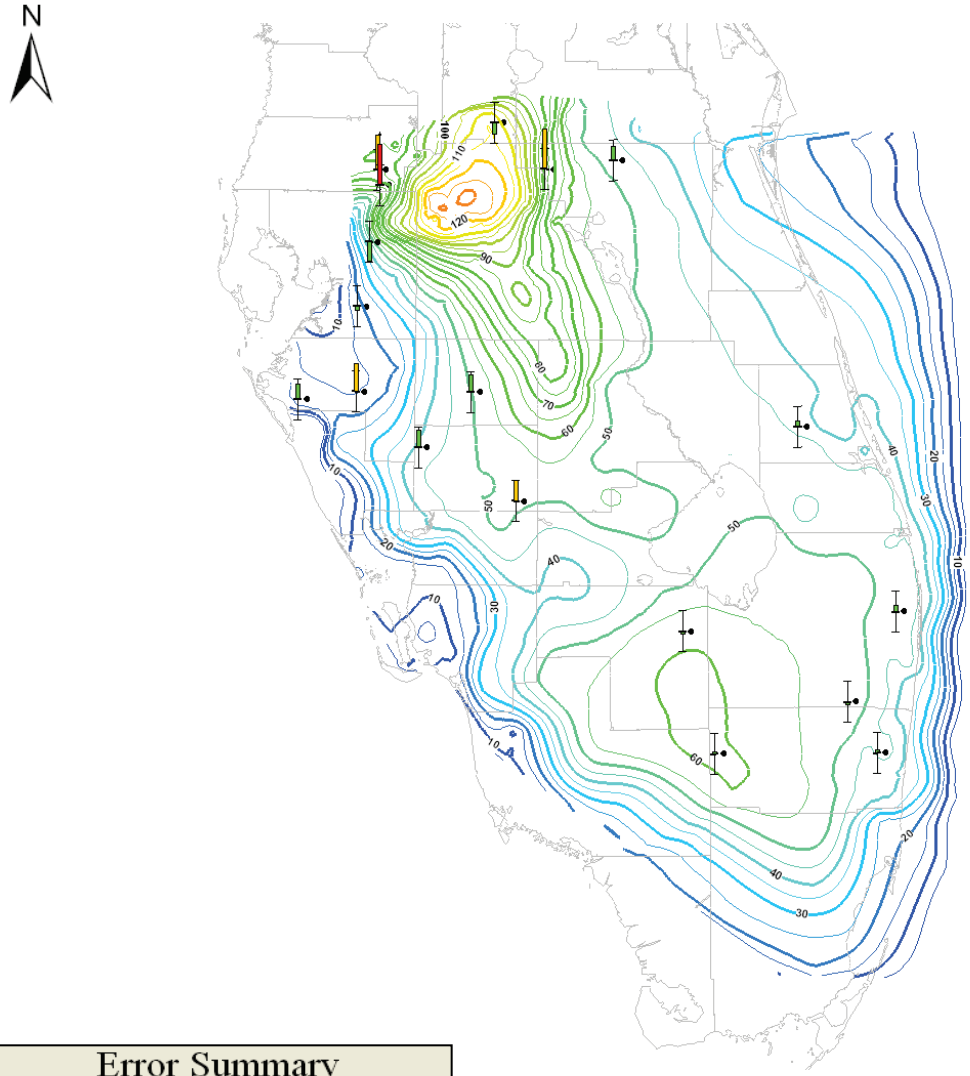

Notes:

Statistics (mean error, mean absolute error and root mean square error) are calculated based on equations presented in Section 4.1.

Calibration targets are green when the calculated value is within 2 feet of the measured head, yellow when within 4 feet and red when the model calculates a head more than 4 feet different from the measured value.

The direction of the colored bar on the calibration target indicates the sign on the residual: bars above the middle line indicate the model calculated higher heads than measured; bars below the middle line indicate negative residuals.

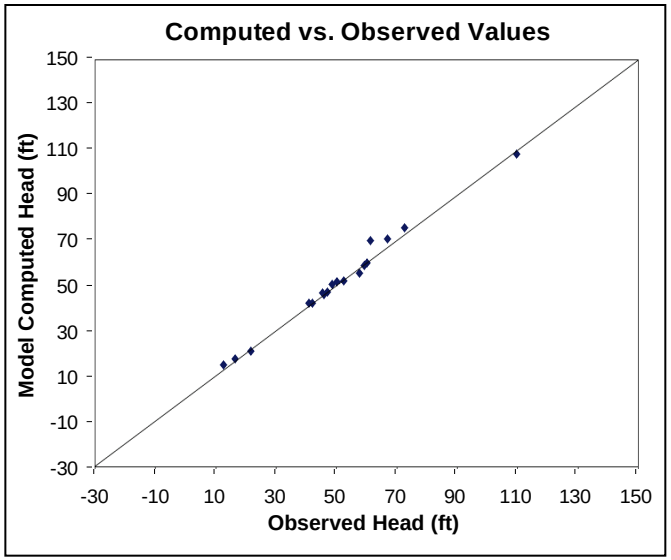

Error Summary

Head

Mean Error:	1.356
Mean Abs. Error:	1.795
Root Mean Sq. Error:	2.651

Regional WASH123D Calibration
APPZ Aquifer - February 2004
Final Groundwater Model Calibration Report

Figure F2-32

October 2010

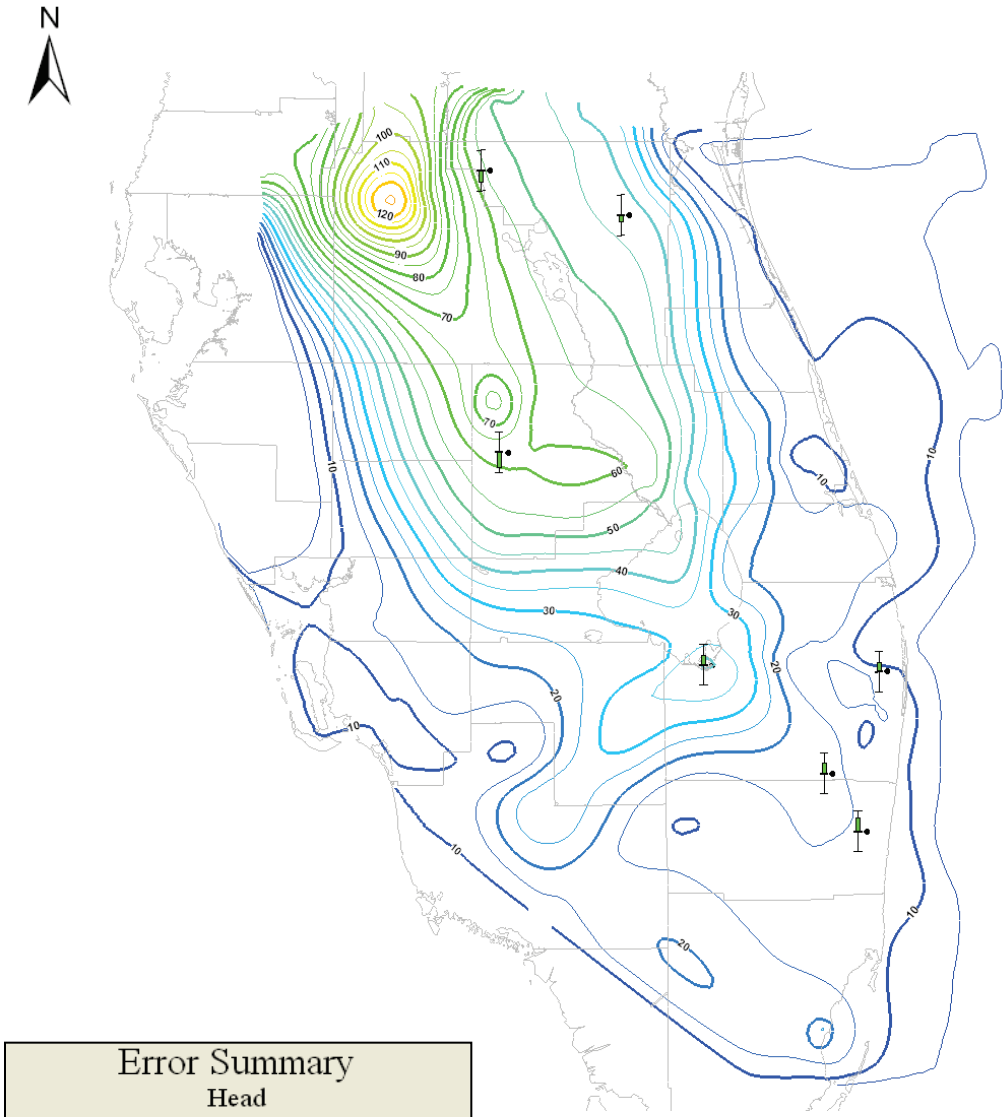

Notes:

Statistics (mean error, mean absolute error and root mean square error) are calculated based on equations presented in Section 4.1.

Calibration targets are green when the calculated value is within 2 feet of the measured head, yellow when within 4 feet and red when the model calculates a head more than 4 feet different from the measured value.

The direction of the colored bar on the calibration target indicates the sign on the residual: bars above the middle line indicate the model calculated higher heads than measured; bars below the middle line indicate negative residuals.

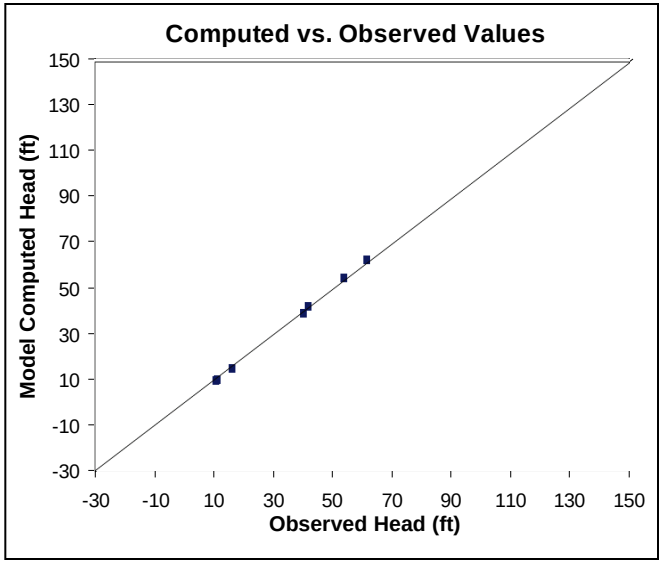

Error Summary

Head

Mean Error:	0.131
Mean Abs. Error:	1.055
Root Mean Sq. Error:	1.088

Regional WASH123D Calibration
Lower Floridan (LF1) Aquifer - February 2004
Final Groundwater Model Calibration Report

Figure F2-33

October 2010

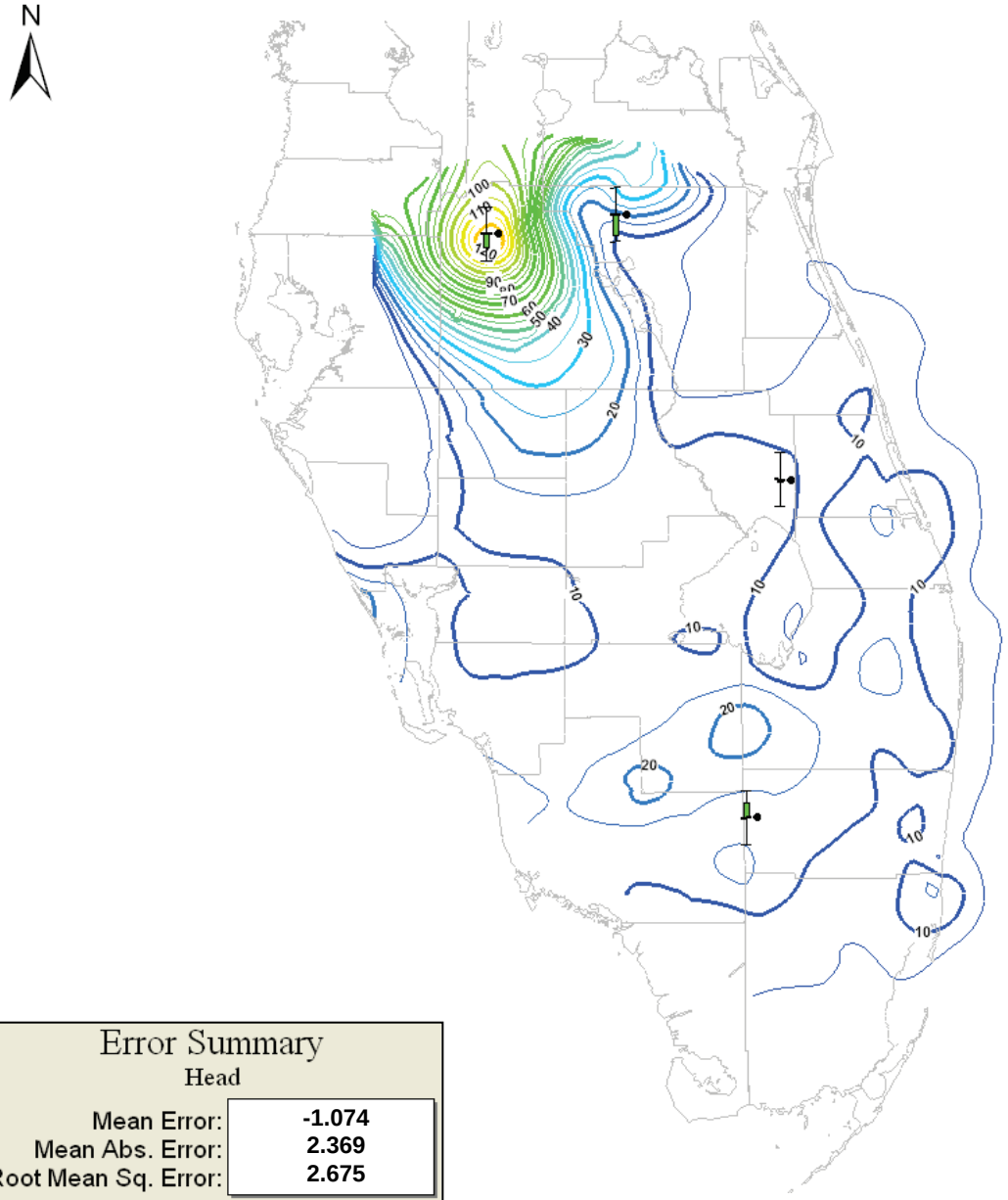

Notes:

Statistics (mean error, mean absolute error and root mean square error) are calculated based on equations presented in Section 4.1.

Calibration targets are green when the calculated value is within 5 feet of the measured head, yellow when within 10 feet and red when the model calculates a head more than 10 feet different from the measured value.

The direction of the colored bar on the calibration target indicates the sign on the residual: bars above the middle line indicate the model calculated higher heads than measured; bars below the middle line indicate negative residuals.

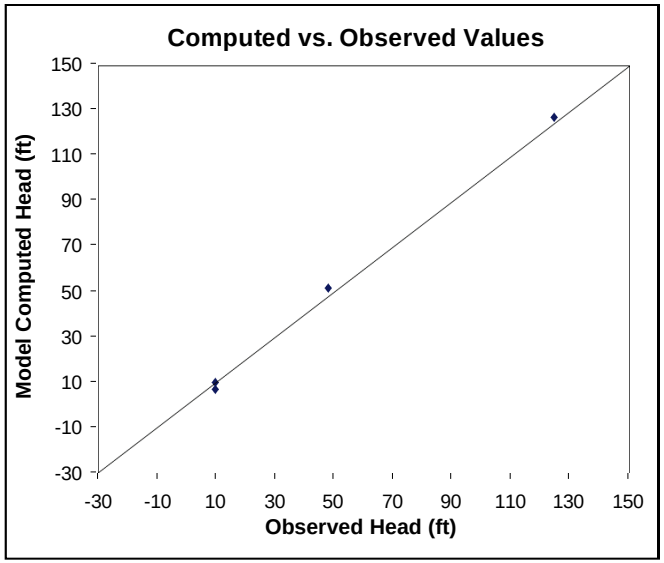

Error Summary

Head

Mean Error:	-1.074
Mean Abs. Error:	2.369
Root Mean Sq. Error:	2.675

Regional WASH123D Calibration
LF1/BZ Expanded Calibration - February 2004

Final Groundwater Model Calibration Report

Figure F2-34

October 2010

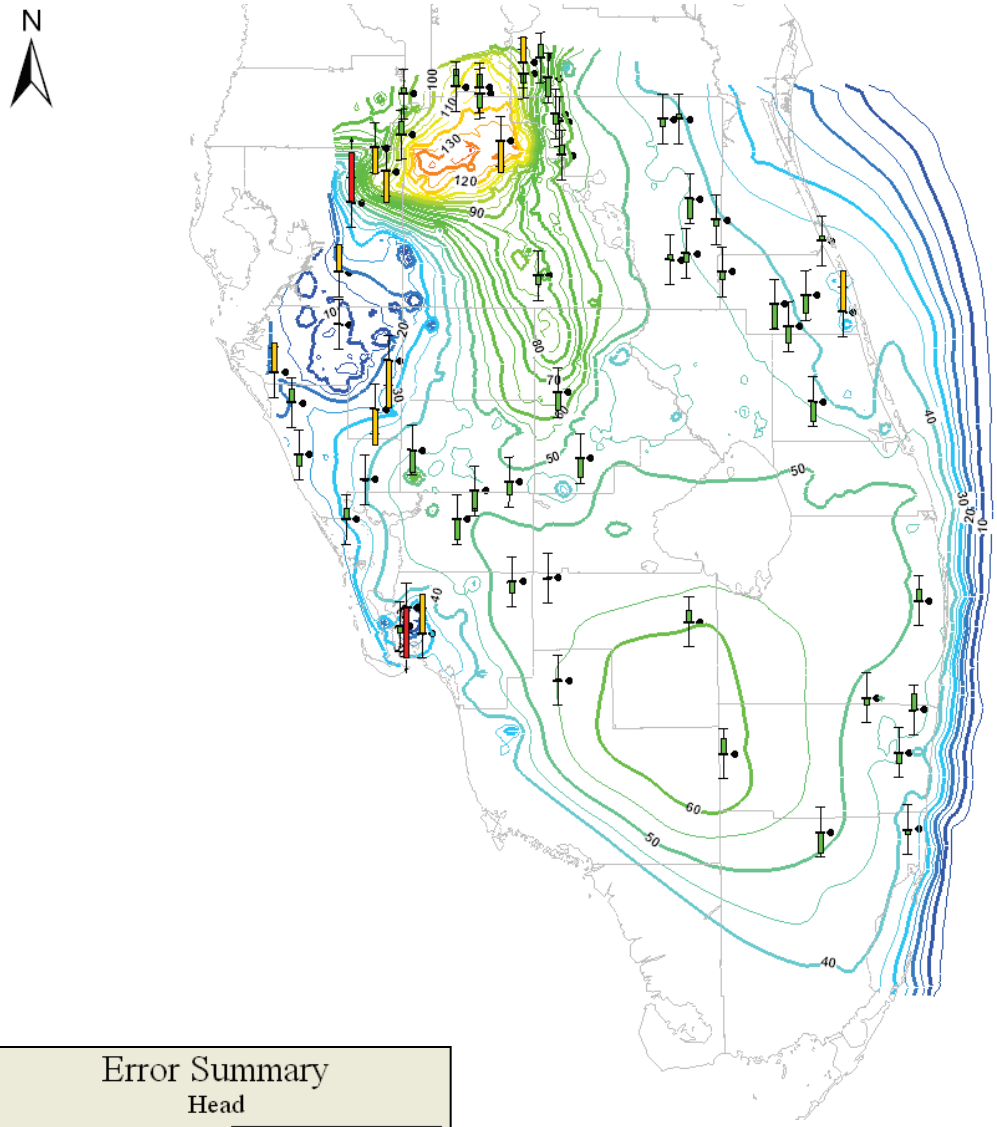

Notes:

Statistics (mean error, mean absolute error and root mean square error) are calculated based on equations presented in Section 4.1.

Calibration targets are green when the calculated value is within 2 feet of the measured head, yellow when within 4 feet and red when the model calculates a head more than 4 feet different from the measured value.

The direction of the colored bar on the calibration target indicates the sign on the residual: bars above the middle line indicate the model calculated higher heads than measured; bars below the middle line indicate negative residuals.

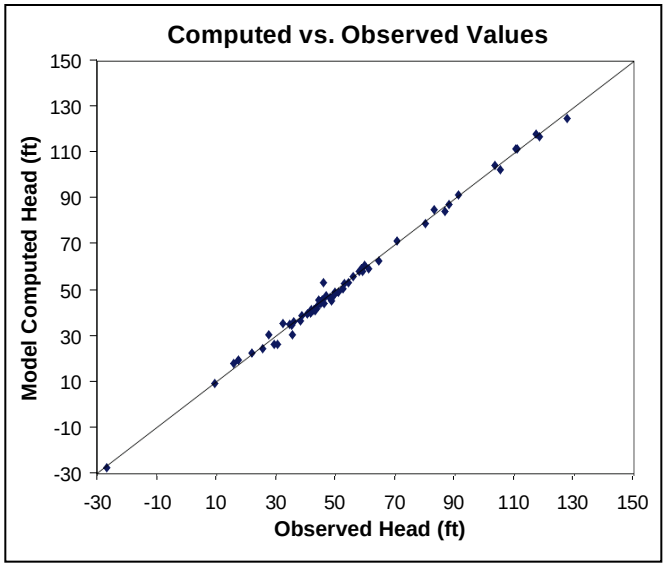

Error Summary

Head

Mean Error:	-0.235
Mean Abs. Error:	1.411
Root Mean Sq. Error:	1.874

Regional WASH123D Calibration
Upper Floridan Aquifer - October 2003
Final Groundwater Model Calibration Report

Figure F2-35

October 2010

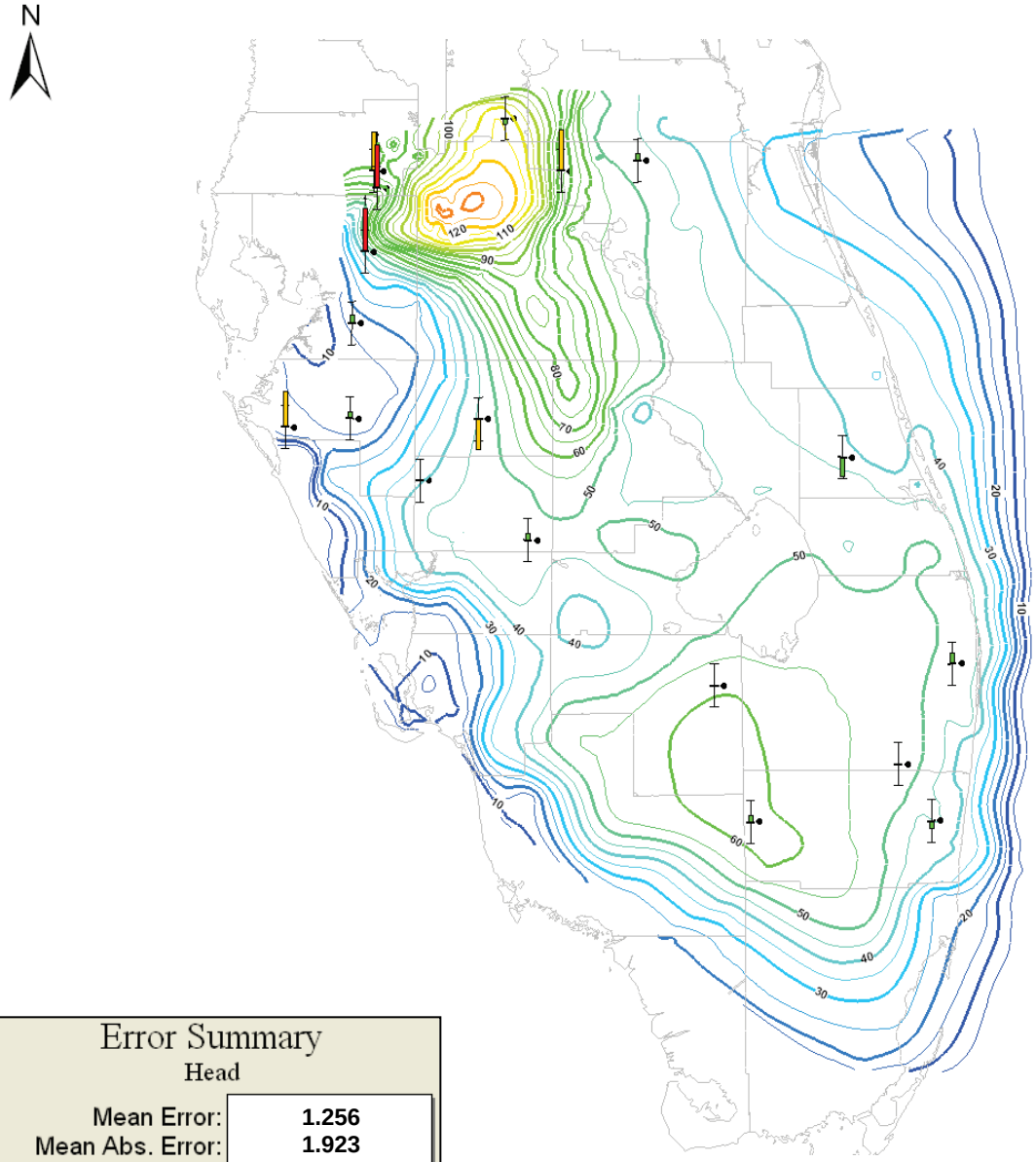

Notes:

Statistics (mean error, mean absolute error and root mean square error) are calculated based on equations presented in Section 4.1.

Calibration targets are green when the calculated value is within 2 feet of the measured head, yellow when within 4 feet and red when the model calculates a head more than 4 feet different from the measured value.

The direction of the colored bar on the calibration target indicates the sign on the residual: bars above the middle line indicate the model calculated higher heads than measured; bars below the middle line indicate negative residuals.

Error Summary

Head

Mean Error:	1.256
Mean Abs. Error:	1.923
Root Mean Sq. Error:	2.874

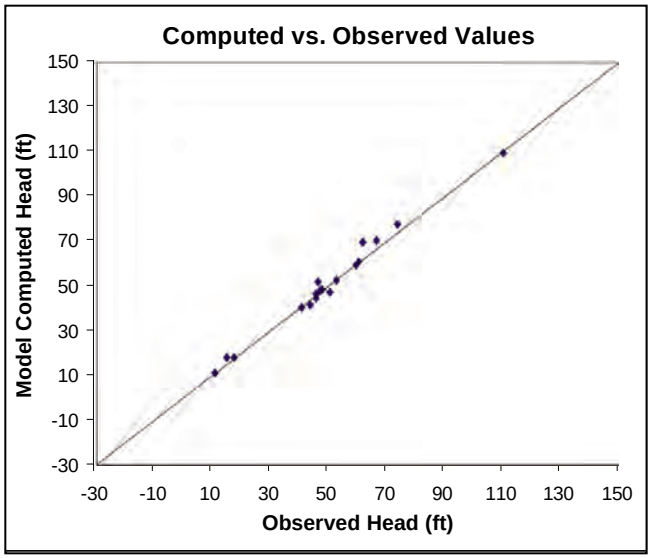

Regional WASH123D Calibration
APPZ Aquifer - October 2003
Final Groundwater Model Calibration Report

Figure F2-36

October 2010

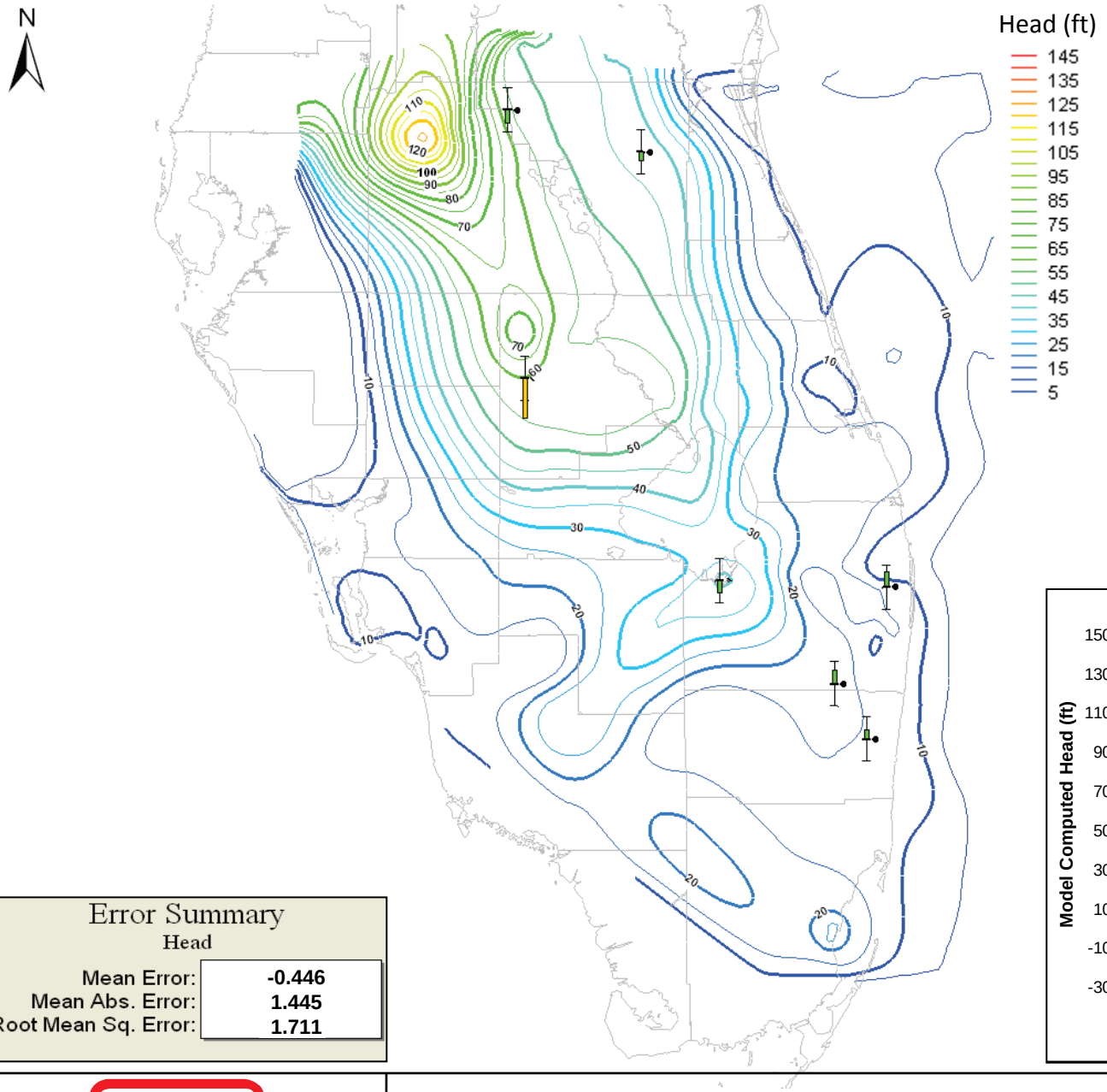

Notes:

Statistics (mean error, mean absolute error and root mean square error) are calculated based on equations presented in Section 4.1.

Calibration targets are green when the calculated value is within 2 feet of the measured head, yellow when within 4 feet and red when the model calculates a head more than 4 feet different from the measured value.

The direction of the colored bar on the calibration target indicates the sign on the residual: bars above the middle line indicate the model calculated higher heads than measured; bars below the middle line indicate negative residuals.

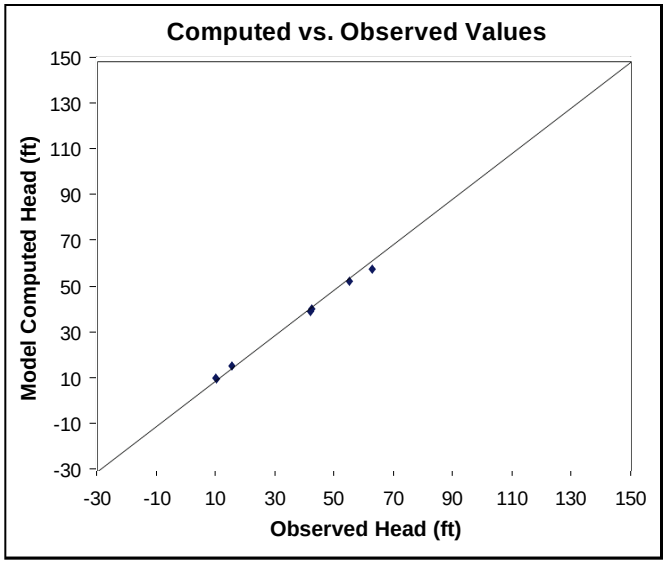

Error Summary

Head

Mean Error:	-0.446
Mean Abs. Error:	1.445
Root Mean Sq. Error:	1.711

Regional WASH123D Calibration
Lower Floridan (LF1) Aquifer - October 2003
Final Groundwater Model Calibration Report

Figure F2-37

October 2010

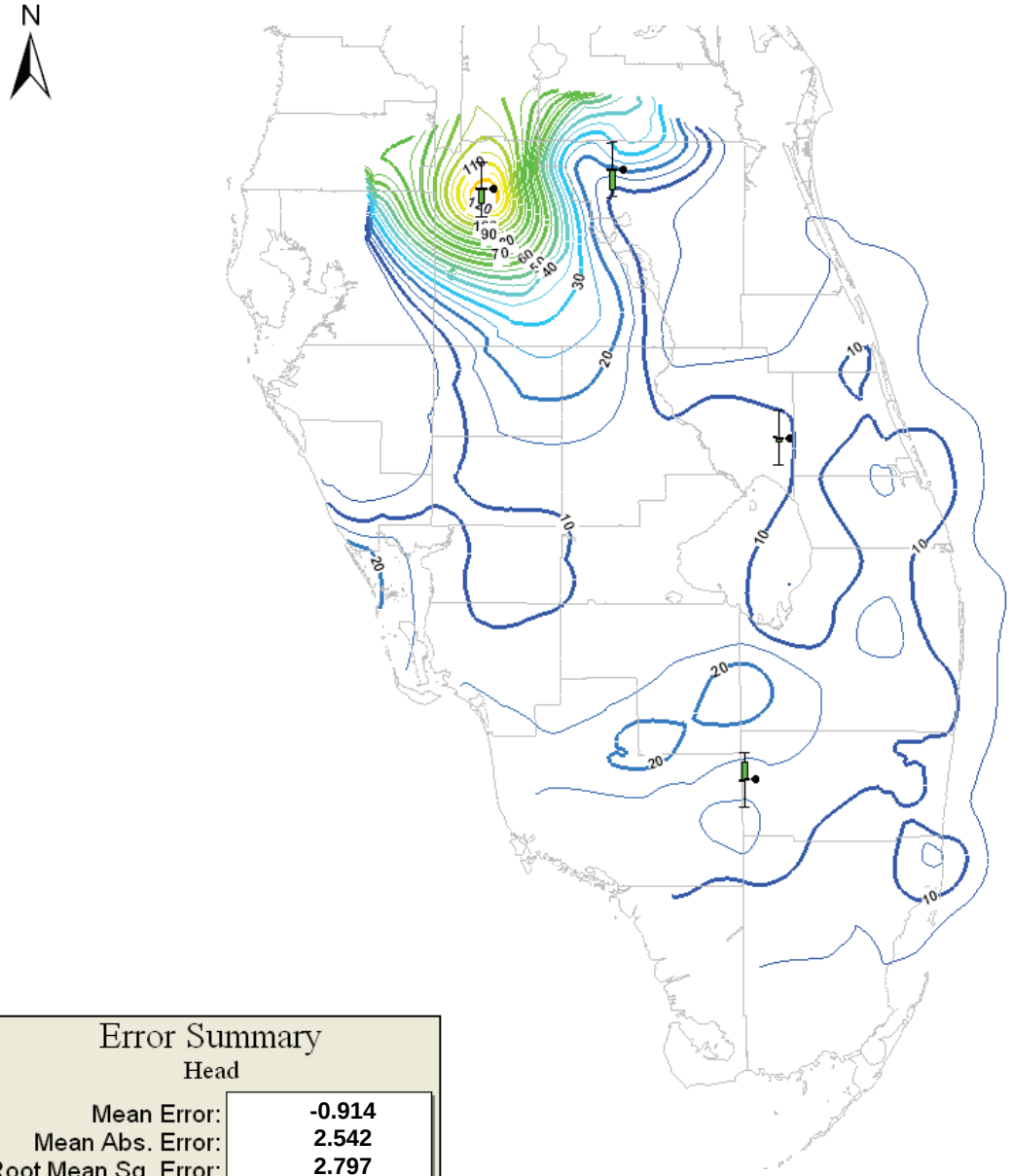

Notes:

Statistics (mean error, mean absolute error and root mean square error) are calculated based on equations presented in Section 4.1.

Calibration targets are green when the calculated value is within 5 feet of the measured head, yellow when within 10 feet and red when the model calculates a head more than 10 feet different from the measured value.

The direction of the colored bar on the calibration target indicates the sign on the residual: bars above the middle line indicate the model calculated higher heads than measured; bars below the middle line indicate negative residuals.

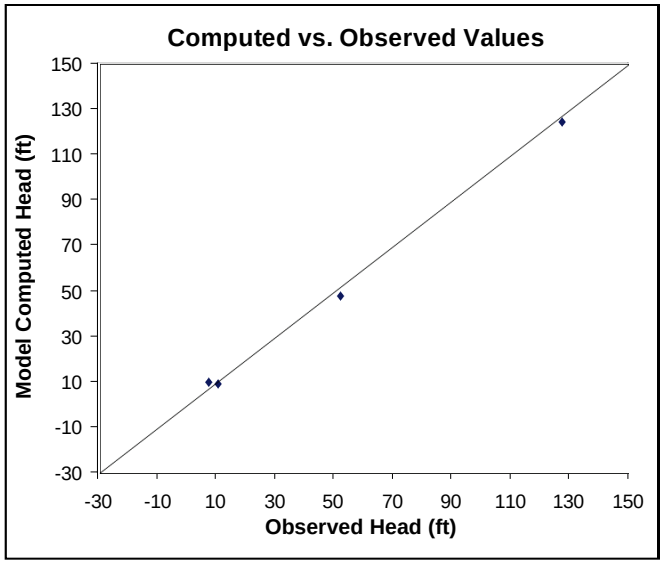

Error Summary Head	
Mean Error:	-0.914
Mean Abs. Error:	2.542
Root Mean Sq. Error:	2.797

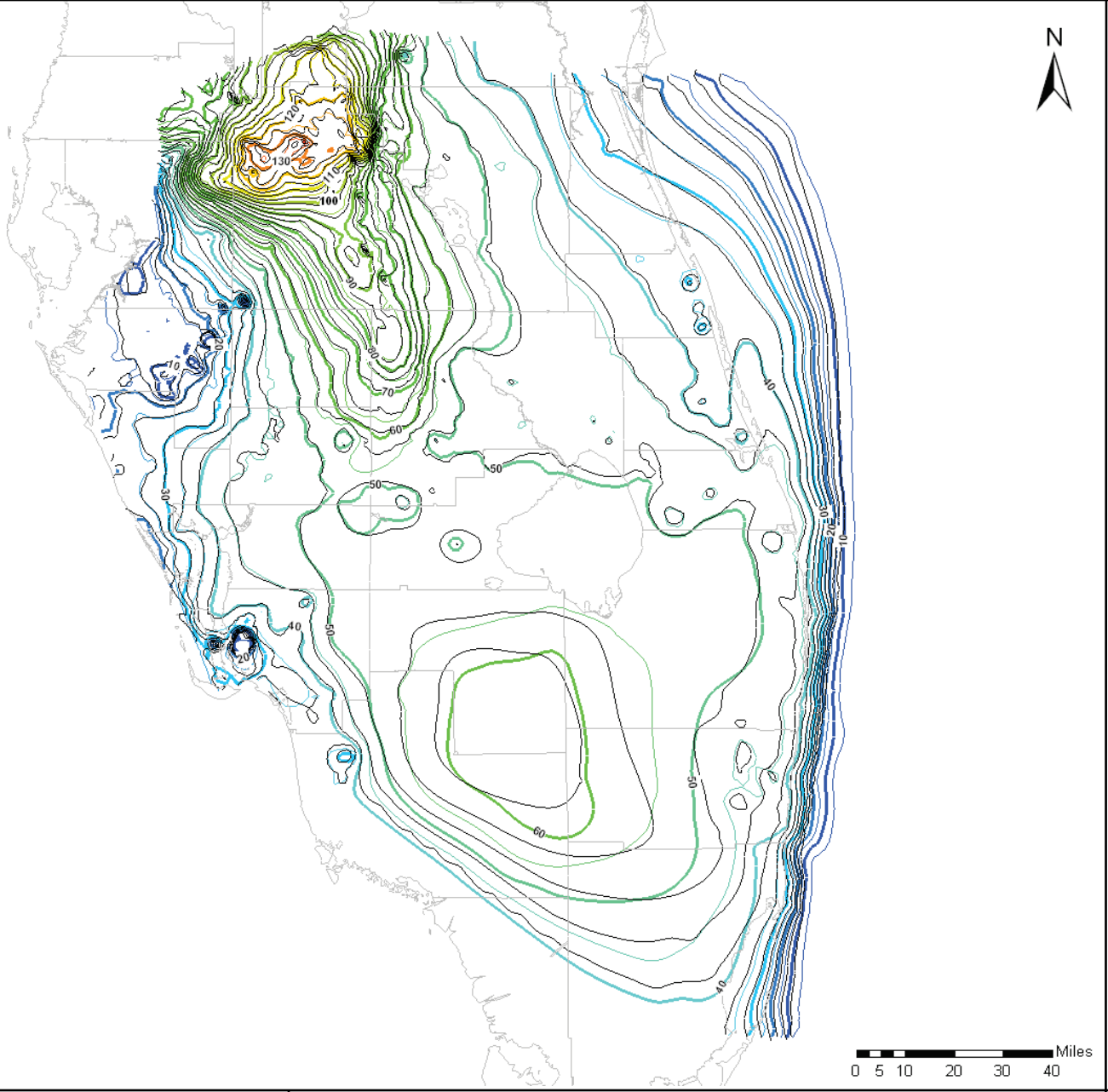

Notes:

Colored contours are heads generated in the WASH123D model

Black contours are heads generated in the SEAWAT model

WASH123D Head (ft)

- 145
- 135
- 125
- 115
- 105
- 95
- 85
- 75
- 65
- 55
- 45
- 35
- 25
- 15
- 5

Regional Phase II ASR SEAWAT to WASH123D Comparison
Upper Floridan Aquifer – February 2004
Final Groundwater Model Calibration Report

Figure F2-39

October 2010

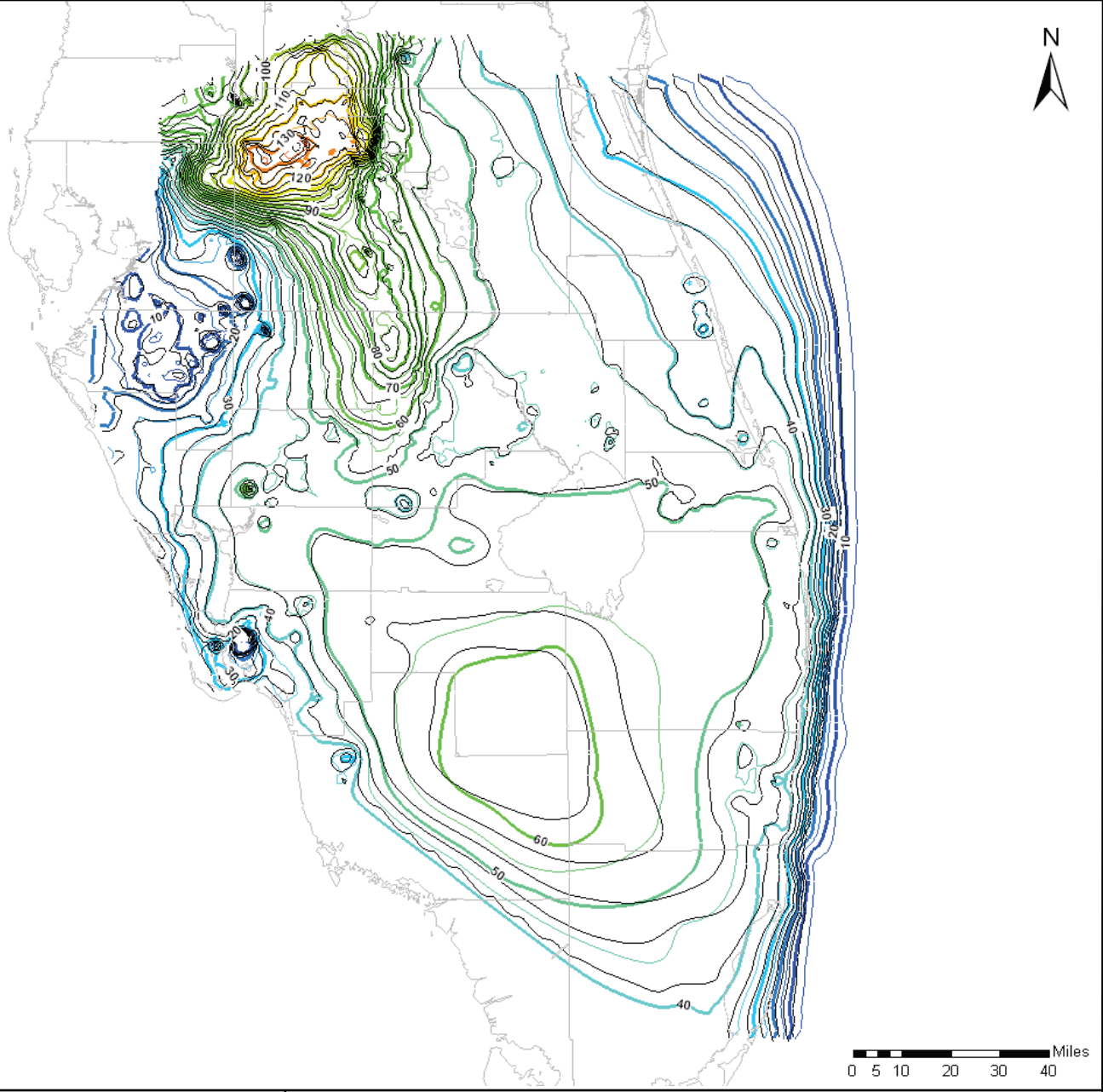

Notes:

Colored contours are heads generated in the WASH123D model

Black contours are heads generated in the SEAWAT model

WASH123D Head (ft)

145
135
125
115
105
95
85
75
65
55
45
35
25
15
5

Regional Phase II ASR SEAWAT to WASH123D Comparison
Upper Floridan Aquifer – October 2003
Final Groundwater Model Calibration Report

Figure F2-40

October 2010

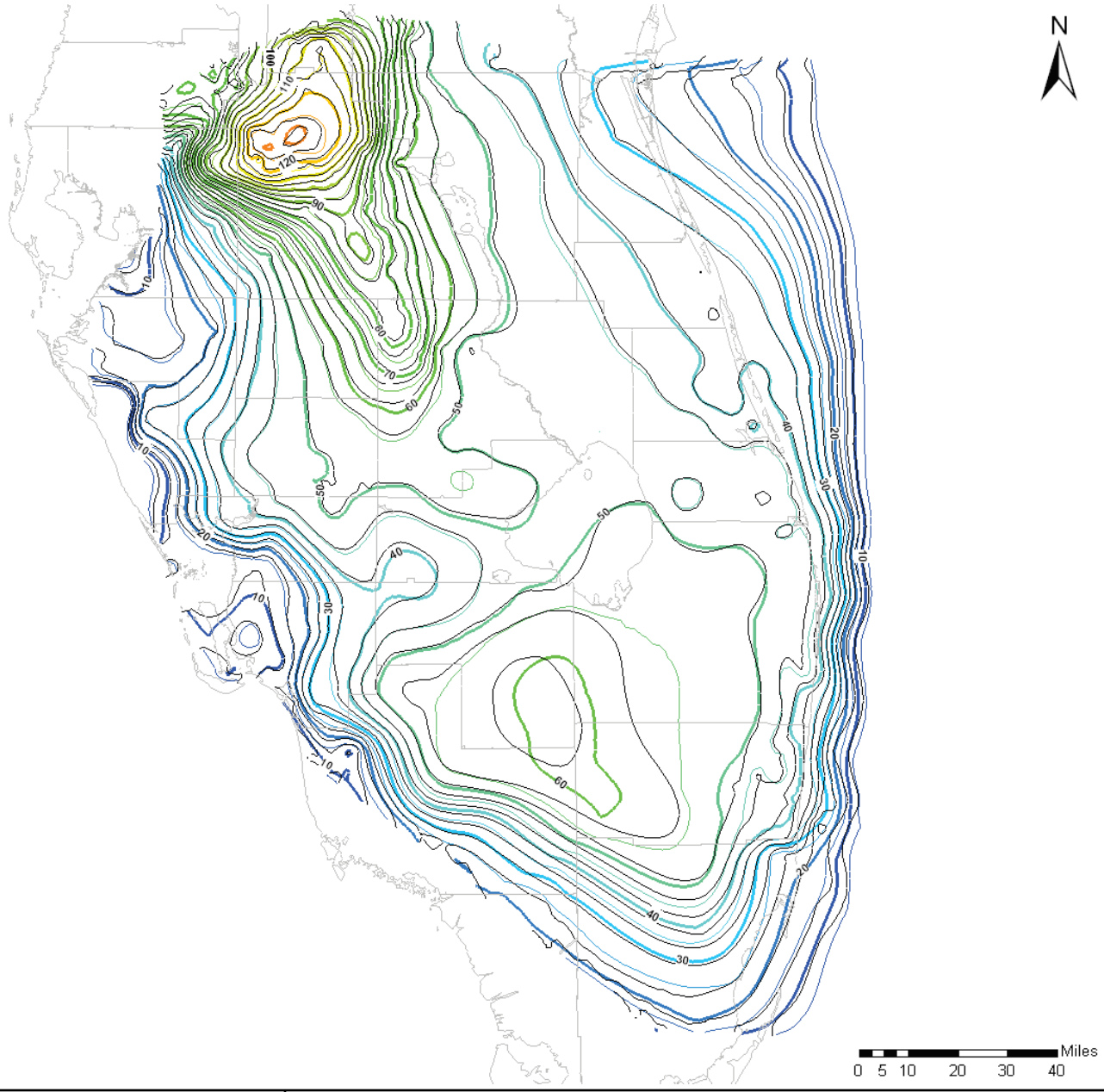

Notes:

Colored contours are heads generated in the WASH123D model

Black contours are heads generated in the SEAWAT model

WASH123D Head (ft)

145
135
125
115
105
95
85
75
65
55
45
35
25
15
5

Regional Phase II ASR SEAWAT to WASH123D Comparison Avon Park Permeable Zone – February 2004

Final Groundwater Model Calibration Report

Figure F2-41

October 2010

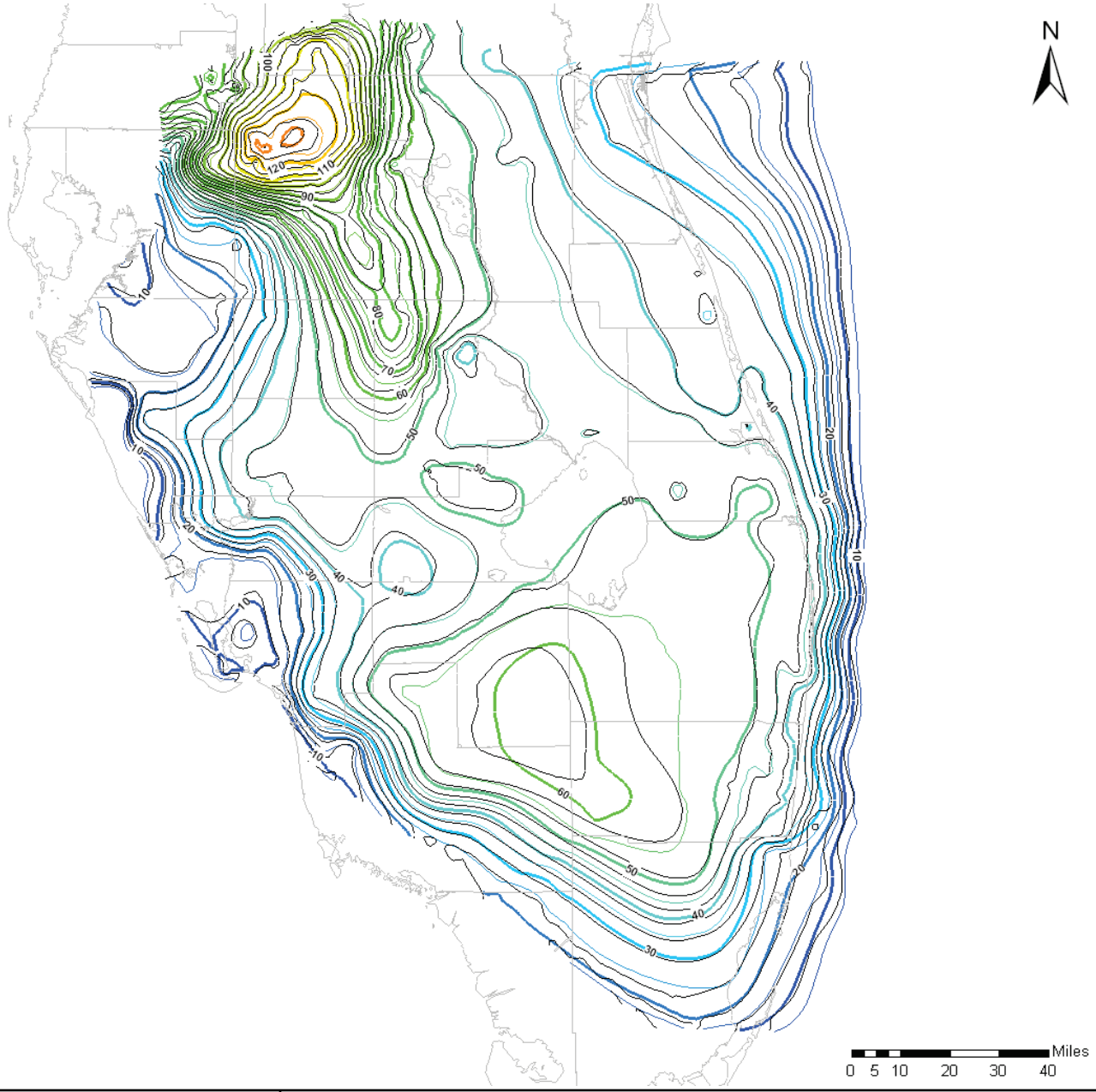

Notes:

Colored contours are heads generated in the WASH123D model

Black contours are heads generated in the SEAWAT model

WASH123D Head (ft)

- 145
- 135
- 125
- 115
- 105
- 95
- 85
- 75
- 65
- 55
- 45
- 35
- 25
- 15
- 5

Regional Phase II ASR SEAWAT to WASH123D Comparison
Avon Park Permeable Zone – October 2003
Final Groundwater Model Calibration Report

Figure F2-42

October 2010

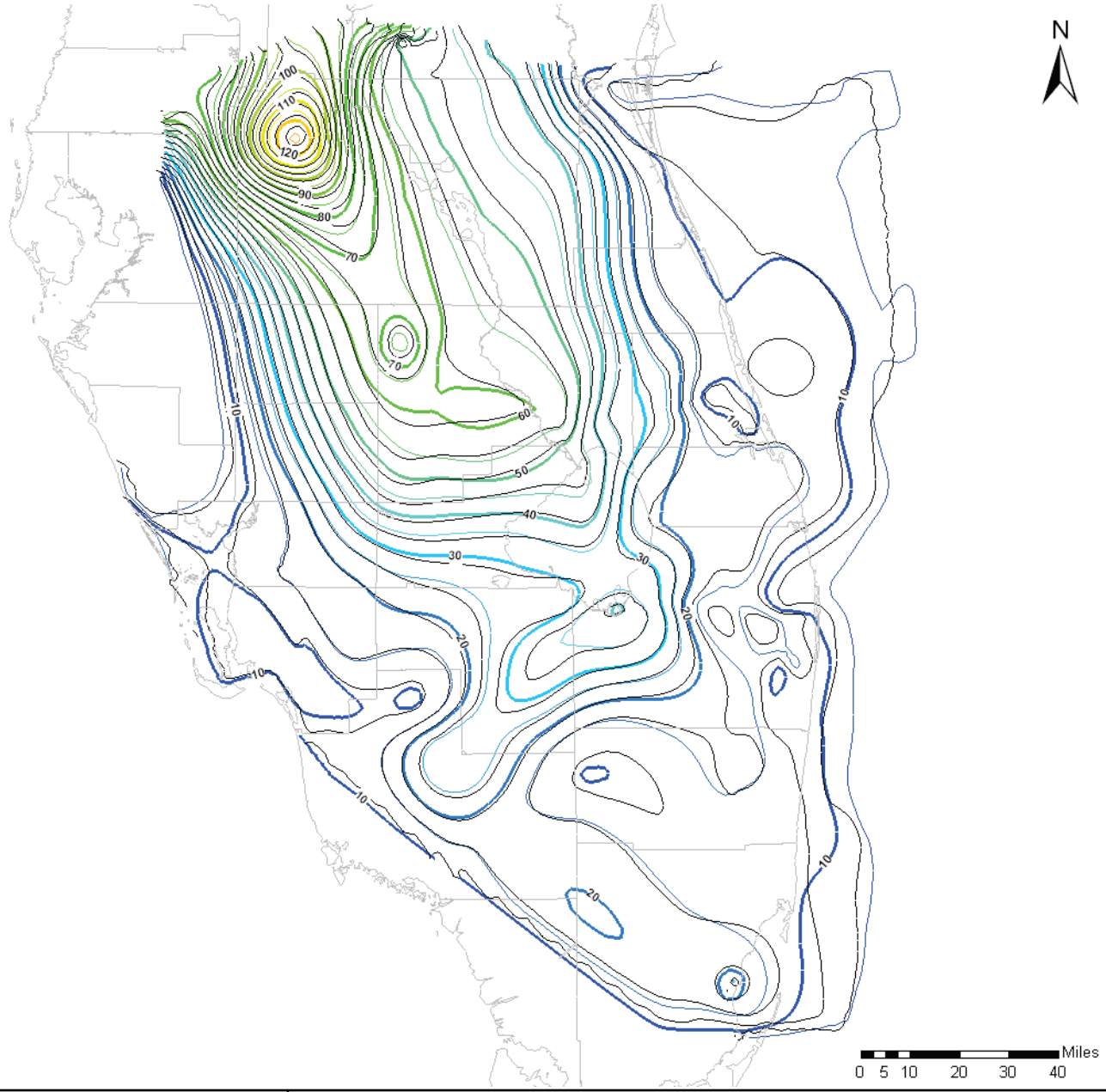

Notes:

Colored contours are heads generated in the WASH123D model

Black contours are heads generated in the SEAWAT model

WASH123D Head (ft)

145
135
125
115
105
95
85
75
65
55
45
35
25
15
5

Regional Phase II ASR SEAWAT to WASH123D Comparison
Lower Floridan (LF1) Aquifer – February 2004
Final Groundwater Model Calibration Report

Figure F2-43

October 2010

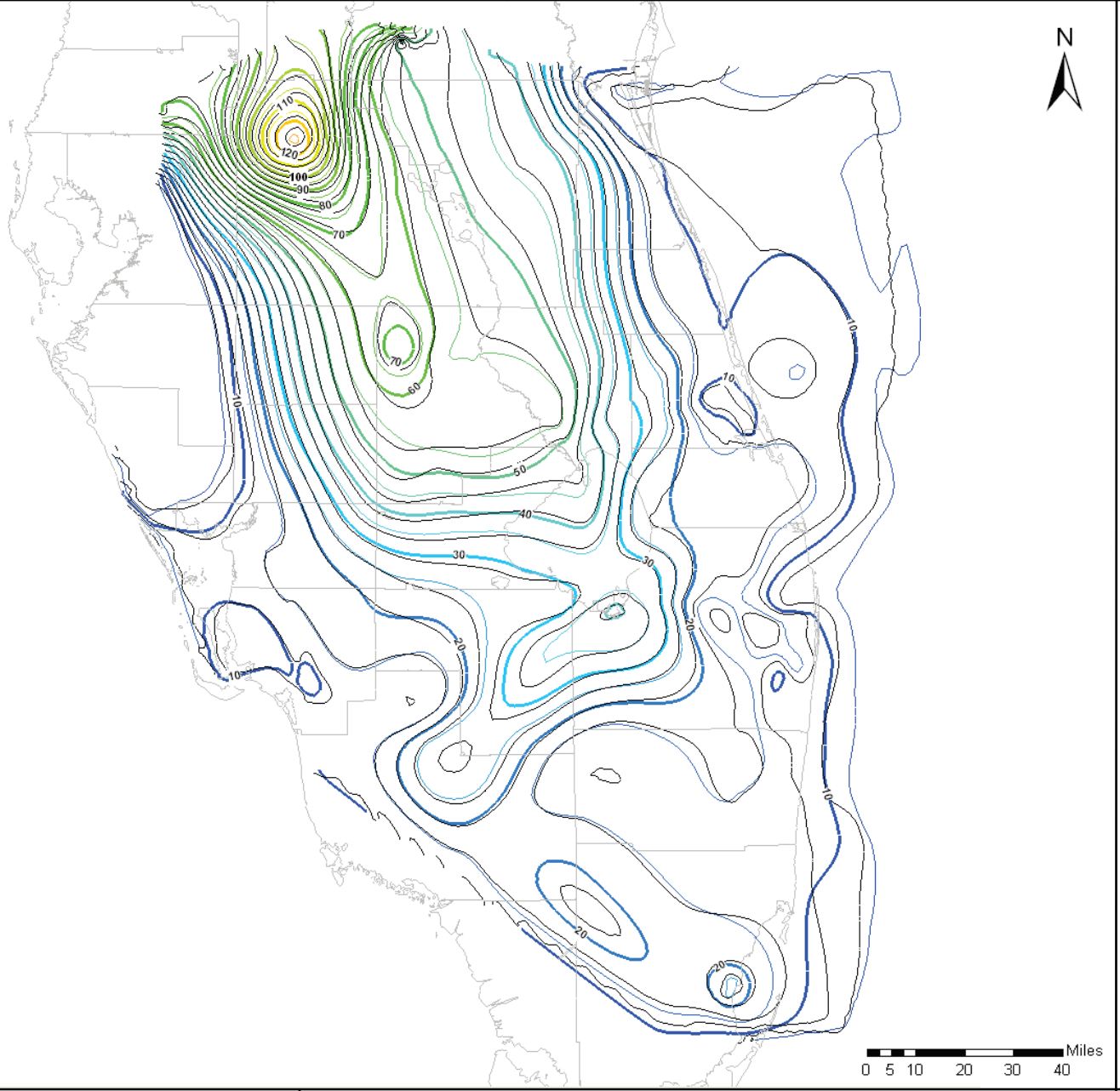

Notes:

Colored contours are heads generated in the WASH123D model

Black contours are heads generated in the SEAWAT model

WASH123D Head (ft)

- 145
- 135
- 125
- 115
- 105
- 95
- 85
- 75
- 65
- 55
- 45
- 35
- 25
- 15
- 5

Regional Phase II ASR SEAWAT to WASH123D Comparison
Lower Floridan (LF1) Aquifer – October 2003
Final Groundwater Model Calibration Report

Figure F2-44

October 2010

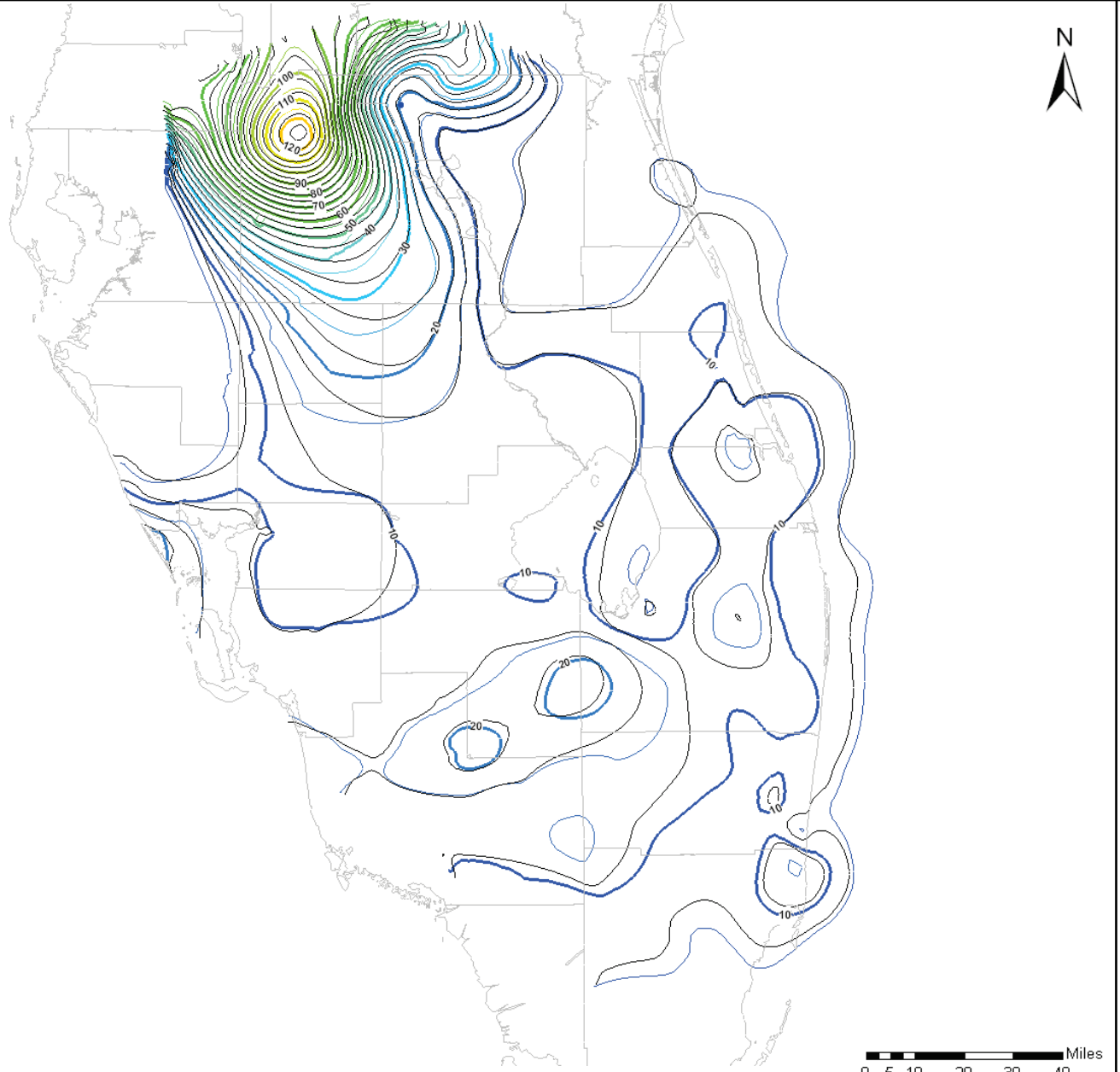

Notes:

Colored contours are heads generated in the WASH123D model

Black contours are heads generated in the SEAWAT model

WASH123D Head (ft)

145
135
125
115
105
95
85
75
65
55
45
35
25
15
5

Regional Phase II ASR SEAWAT to WASH123D Comparison Boulder Zone – February 2004

Final Groundwater Model Calibration Report

Figure F2-45

October 2010

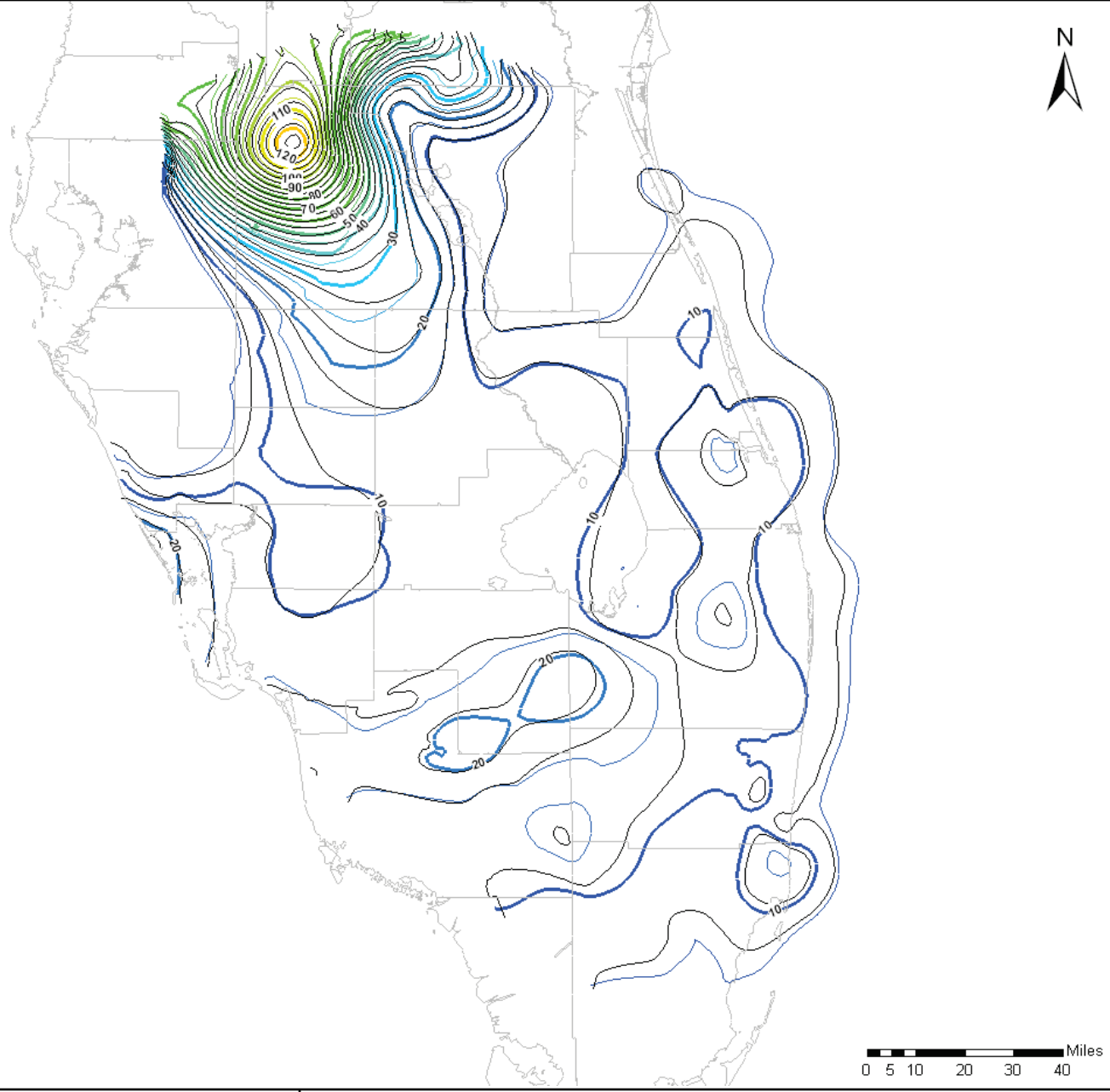

Notes:

Colored contours are heads generated in the WASH123D model

Black contours are heads generated in the SEAWAT model

WASH123D Head (ft)

145
135
125
115
105
95
85
75
65
55
45
35
25
15
5

Regional Phase II ASR SEAWAT to WASH123D Comparison
Boulder Zone – October 2003
Final Groundwater Model Calibration Report

Figure F2-46

October 2010

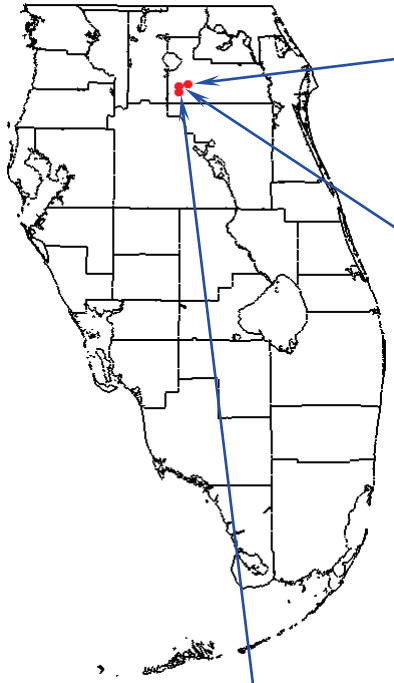

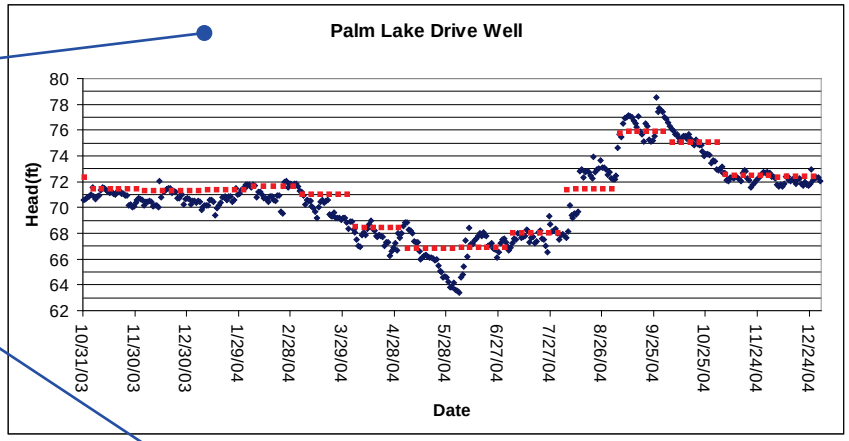

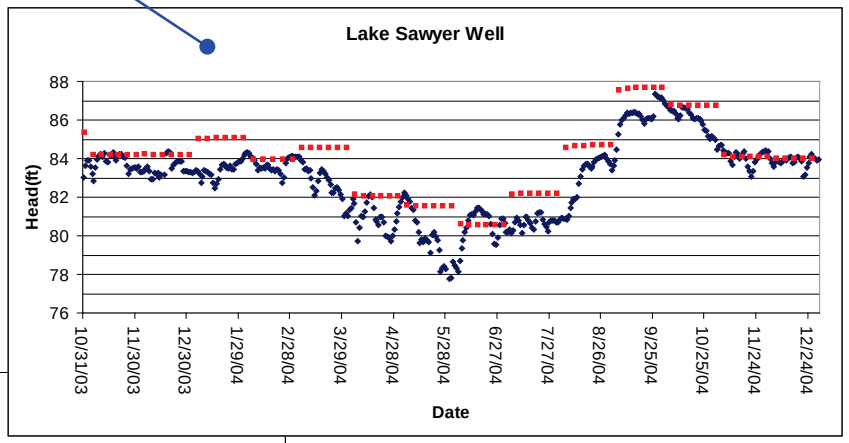

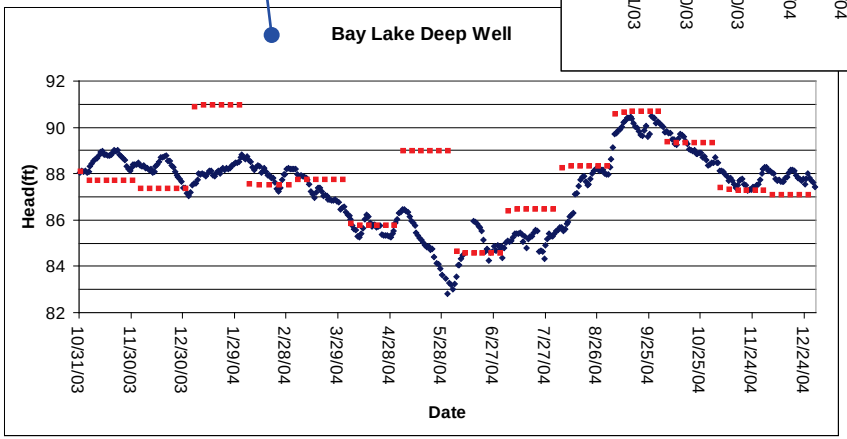

Legend

- Measured Head
- Model Calculated Head

Notes:

Figures 4.57 through 4.77 show the comparison between measured head values and model-calculated head values at a number of observation wells for the calibration period. Although the scales vary on each plot, all plots have a horizontal grid line at each foot. This is to make it easy to determine the range of heads at a glance.

The model used month-long stress periods, so pumping and boundary conditions were input as step functions with constant values throughout each month and sudden changes at the end of each month. For this reason, the model cannot be expected to accurately predict day-to-day head variations in any of these wells. Calibration efforts were aimed at matching general trends and monthly averages.

Starting head conditions for this model were based on the October 2003 steady state calibrated model. Transient calibration efforts were focused on matching the head changes, not the actual heads, so it is not uncommon for residuals in the starting condition to be carried through the entire calibration period. This indicates that the model is correctly predicting responses to hydrogeologic forces even if the calculated head values vary somewhat from the measured values.

Transient SEAWAT Calibration Comparison
Upper Floridan Aquifer (2003-2004)
Final Groundwater Model Calibration Report

Figure F3-1

October 2010

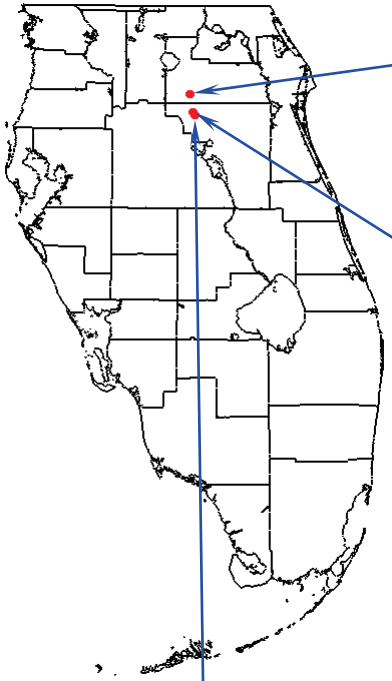

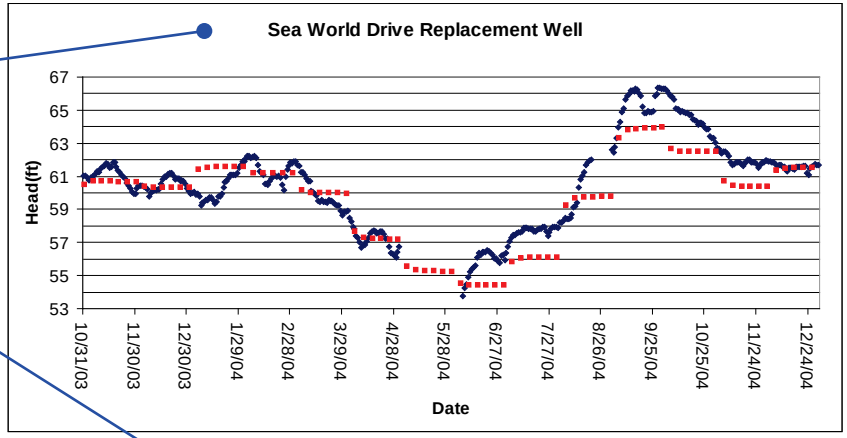

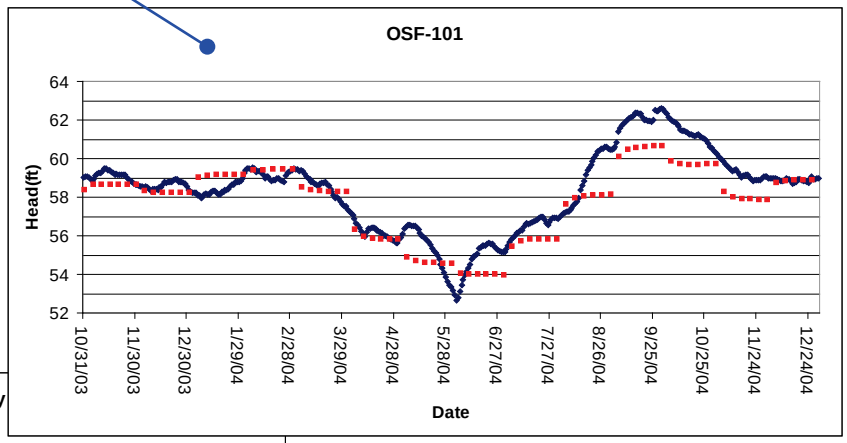

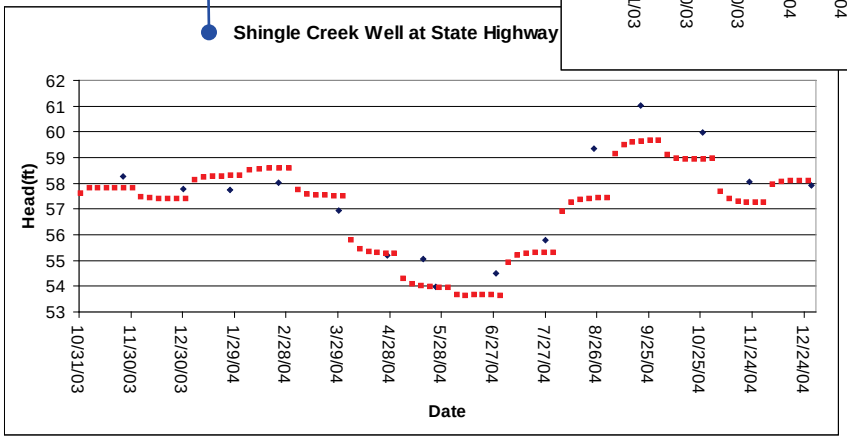

Legend

- Measured Head
- Model Calculated Head

Notes:

Figures 4.57 through 4.77 show the comparison between measured head values and model-calculated head values at a number of observation wells for the calibration period. Although the scales vary on each plot, all plots have a horizontal grid line at each foot. This is to make it easy to determine the range of heads at a glance.

The model used month-long stress periods, so pumping and boundary conditions were input as step functions with constant values throughout each month and sudden changes at the end of each month. For this reason, the model cannot be expected to accurately predict day-to-day head variations in any of these wells. Calibration efforts were aimed at matching general trends and monthly averages.

Starting head conditions for this model were based on the October 2003 steady state calibrated model. Transient calibration efforts were focused on matching the head changes, not the actual heads, so it is not uncommon for residuals in the starting condition to be carried through the entire calibration period. This indicates that the model is correctly predicting responses to hydrogeologic forces even if the calculated head values vary somewhat from the measured values.

Transient SEAWAT Calibration Comparison
Upper Floridan Aquifer (2003-2004)
Final Groundwater Model Calibration Report

Figure F3-2

October 2010

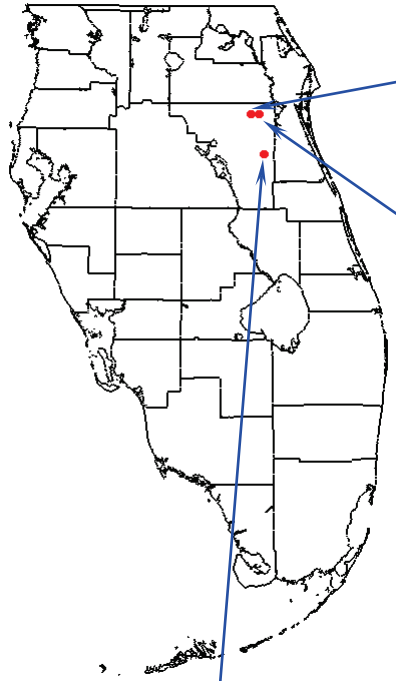

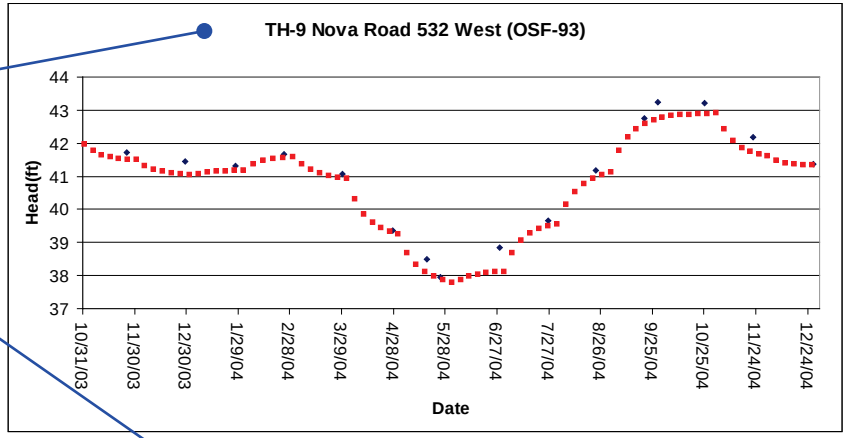

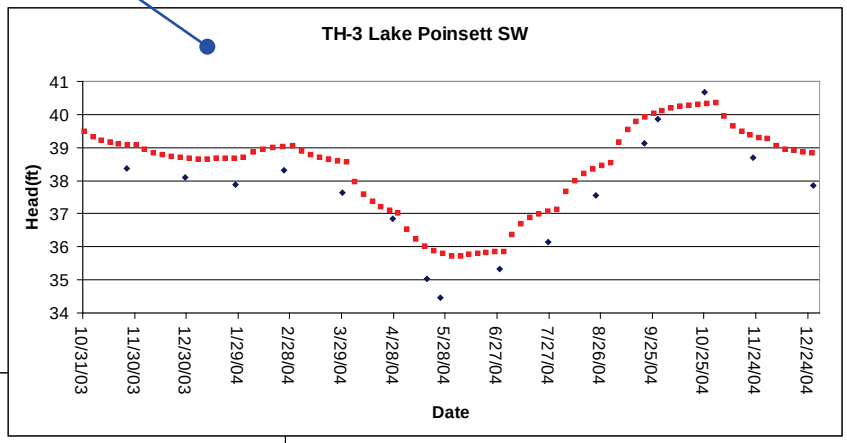

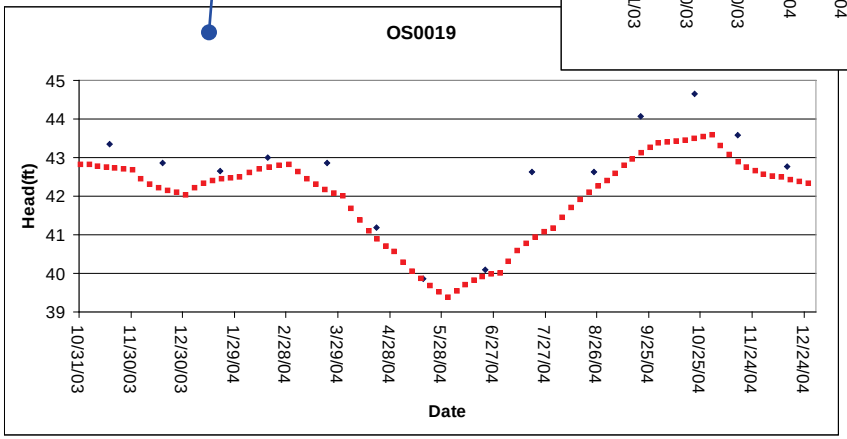

Legend

- Measured Head
- Model Calculated Head

Notes:

Figures 4.57 through 4.77 show the comparison between measured head values and model-calculated head values at a number of observation wells for the calibration period. Although the scales vary on each plot, all plots have a horizontal grid line at each foot. This is to make it easy to determine the range of heads at a glance.

The model used month-long stress periods, so pumping and boundary conditions were input as step functions with constant values throughout each month and sudden changes at the end of each month. For this reason, the model cannot be expected to accurately predict day-to-day head variations in any of these wells. Calibration efforts were aimed at matching general trends and monthly averages.

Starting head conditions for this model were based on the October 2003 steady state calibrated model. Transient calibration efforts were focused on matching the head changes, not the actual heads, so it is not uncommon for residuals in the starting condition to be carried through the entire calibration period. This indicates that the model is correctly predicting responses to hydrogeologic forces even if the calculated head values vary somewhat from the measured values.

Transient SEAWAT Calibration Comparison
Upper Floridan Aquifer (2003-2004)
Final Groundwater Model Calibration Report

Figure F3-3

October 2010

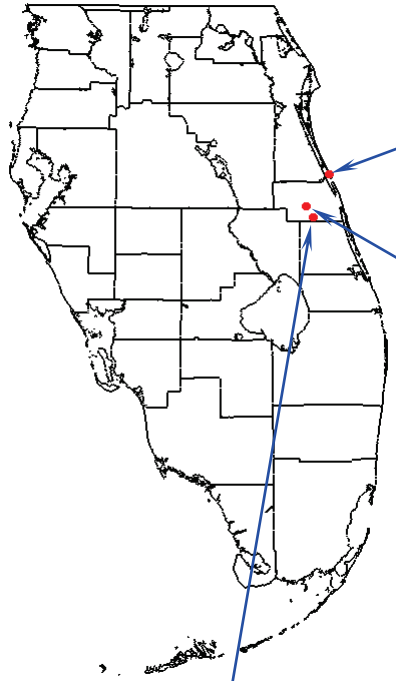

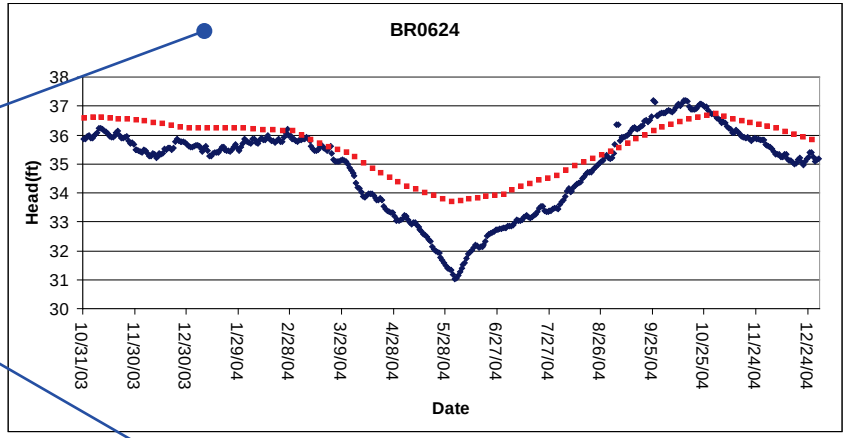

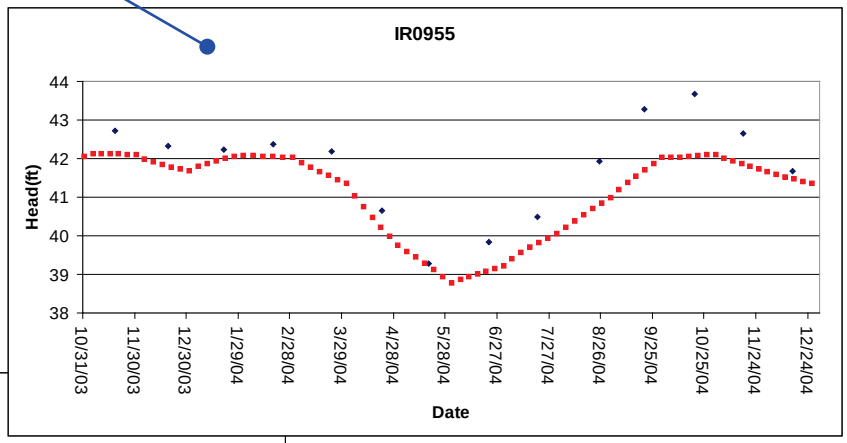

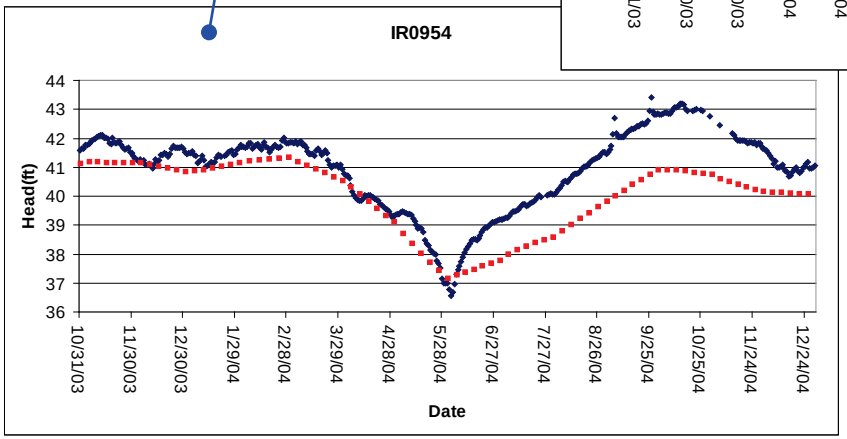

Legend

- Measured Head
- Model Calculated Head

Notes:

Figures 4.57 through 4.77 show the comparison between measured head values and model-calculated head values at a number of observation wells for the calibration period. Although the scales vary on each plot, all plots have a horizontal grid line at each foot. This is to make it easy to determine the range of heads at a glance.

The model used month-long stress periods, so pumping and boundary conditions were input as step functions with constant values throughout each month and sudden changes at the end of each month. For this reason, the model cannot be expected to accurately predict day-to-day head variations in any of these wells. Calibration efforts were aimed at matching general trends and monthly averages.

Starting head conditions for this model were based on the October 2003 steady state calibrated model. Transient calibration efforts were focused on matching the head changes, not the actual heads, so it is not uncommon for residuals in the starting condition to be carried through the entire calibration period. This indicates that the model is correctly predicting responses to hydrogeologic forces even if the calculated head values vary somewhat from the measured values.

Transient SEAWAT Calibration Comparison
Upper Floridan Aquifer (2003 – 2004)
Final Groundwater Model Calibration Report

Figure F3-4

October 2010

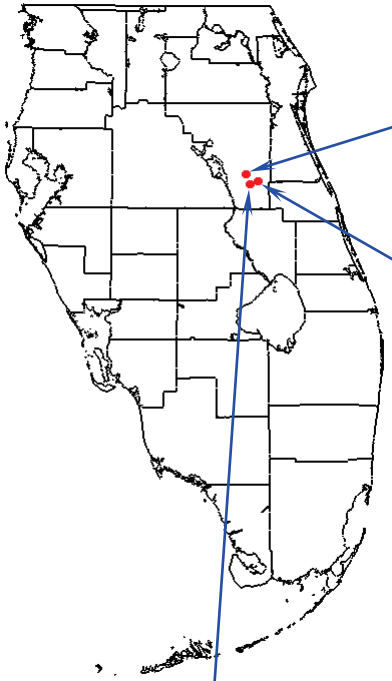

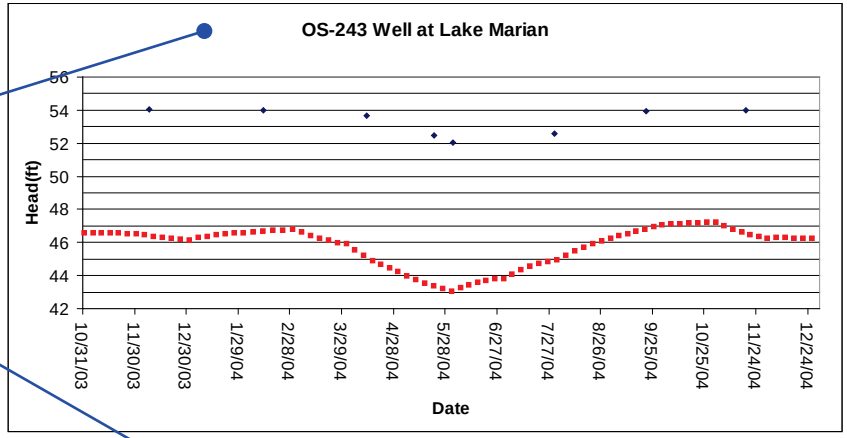

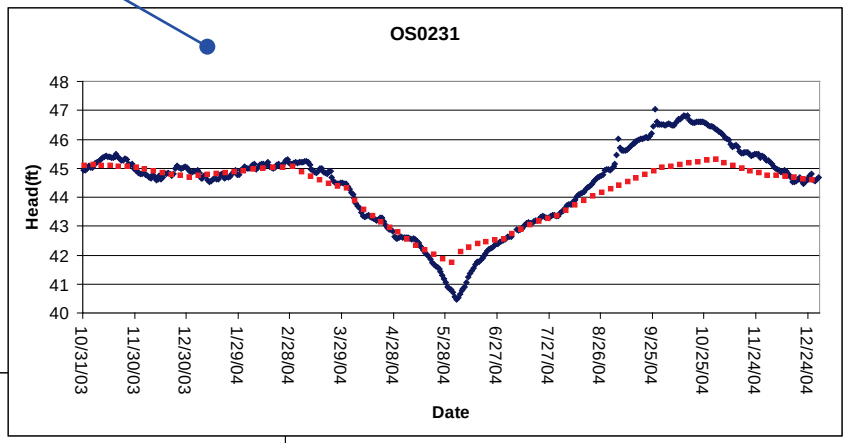

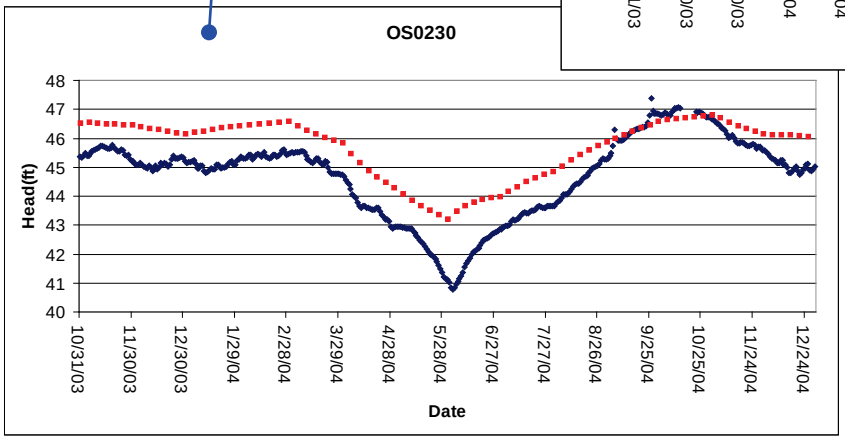

Legend

- Measured Head
- Model Calculated Head

Notes:

Figures 4.57 through 4.77 show the comparison between measured head values and model-calculated head values at a number of observation wells for the calibration period. Although the scales vary on each plot, all plots have a horizontal grid line at each foot. This is to make it easy to determine the range of heads at a glance.

The model used month-long stress periods, so pumping and boundary conditions were input as step functions with constant values throughout each month and sudden changes at the end of each month. For this reason, the model cannot be expected to accurately predict day-to-day head variations in any of these wells. Calibration efforts were aimed at matching general trends and monthly averages.

Starting head conditions for this model were based on the October 2003 steady state calibrated model. Transient calibration efforts were focused on matching the head changes, not the actual heads, so it is not uncommon for residuals in the starting condition to be carried through the entire calibration period. This indicates that the model is correctly predicting responses to hydrogeologic forces even if the calculated head values vary somewhat from the measured values.

Transient SEAWAT Calibration Comparison
Upper Floridan Aquifer (2003-2004)
Final Groundwater Model Calibration Report

Figure F3-5

October 2010

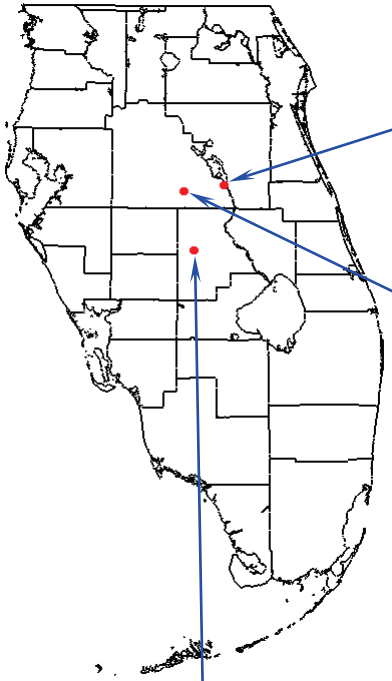

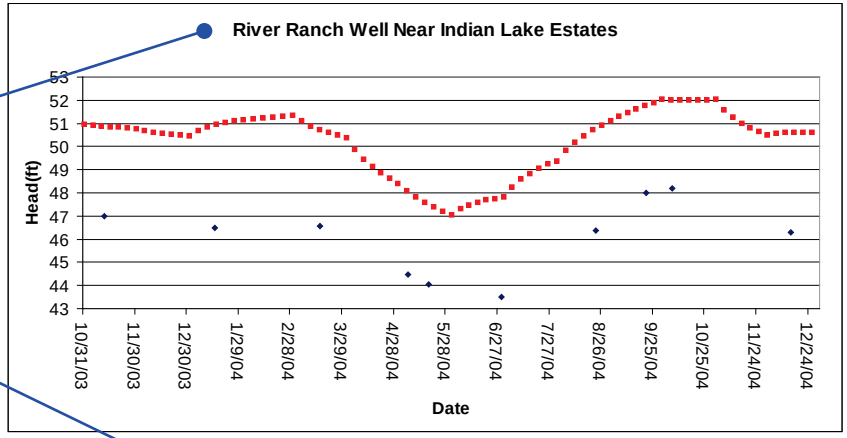

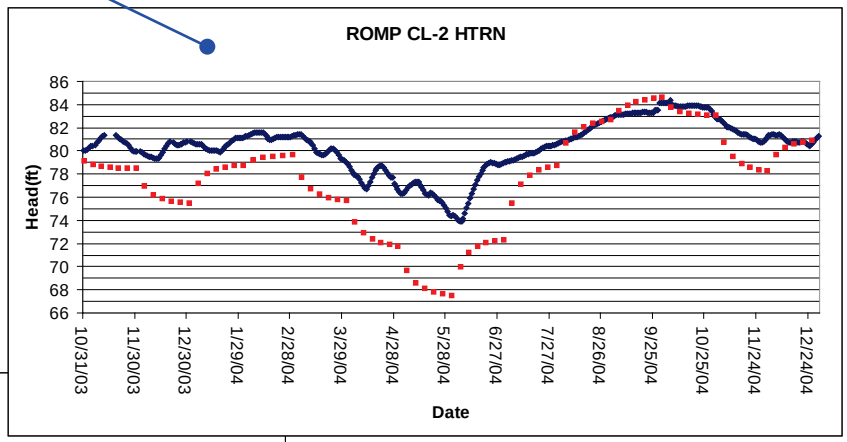

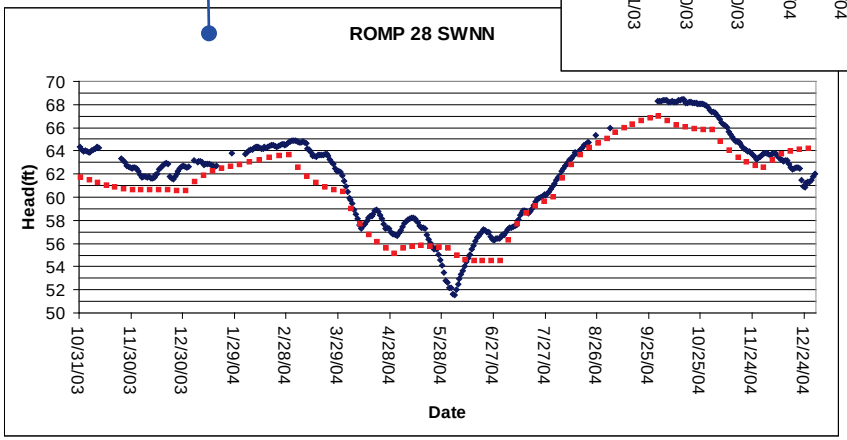

Legend

- Measured Head
- Model Calculated Head

Notes:

Figures 4.57 through 4.77 show the comparison between measured head values and model-calculated head values at a number of observation wells for the calibration period. Although the scales vary on each plot, all plots have a horizontal grid line at each foot. This is to make it easy to determine the range of heads at a glance.

The model used month-long stress periods, so pumping and boundary conditions were input as step functions with constant values throughout each month and sudden changes at the end of each month. For this reason, the model cannot be expected to accurately predict day-to-day head variations in any of these wells. Calibration efforts were aimed at matching general trends and monthly averages.

Starting head conditions for this model were based on the October 2003 steady state calibrated model. Transient calibration efforts were focused on matching the head changes, not the actual heads, so it is not uncommon for residuals in the starting condition to be carried through the entire calibration period. This indicates that the model is correctly predicting responses to hydrogeologic forces even if the calculated head values vary somewhat from the measured values.

Transient SEAWAT Calibration Comparison
Upper Floridan Aquifer (2003-2004)
Final Groundwater Model Calibration Report

Figure F3-6

October 2010

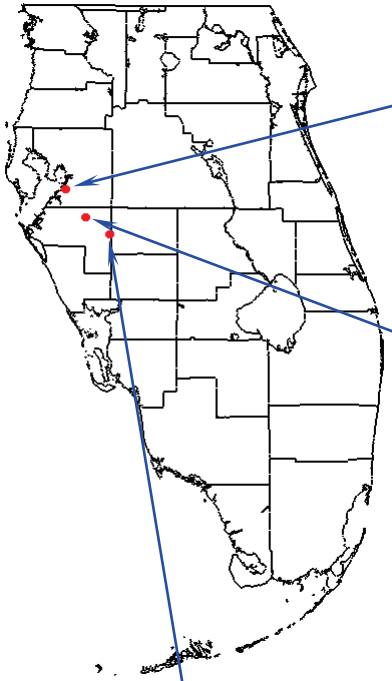

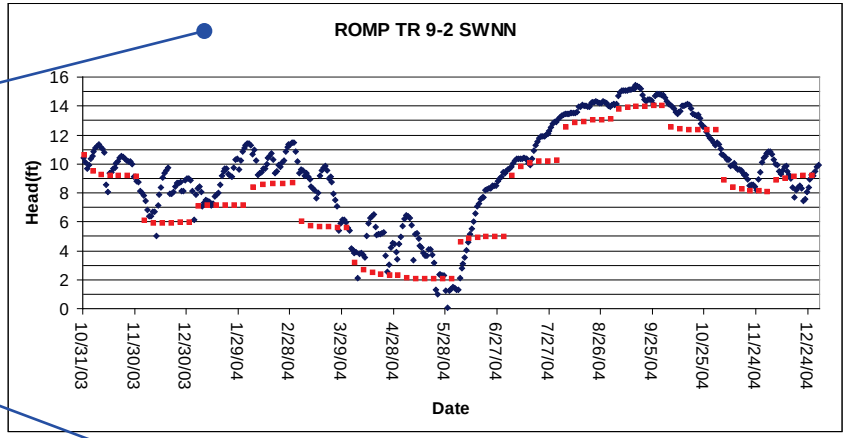

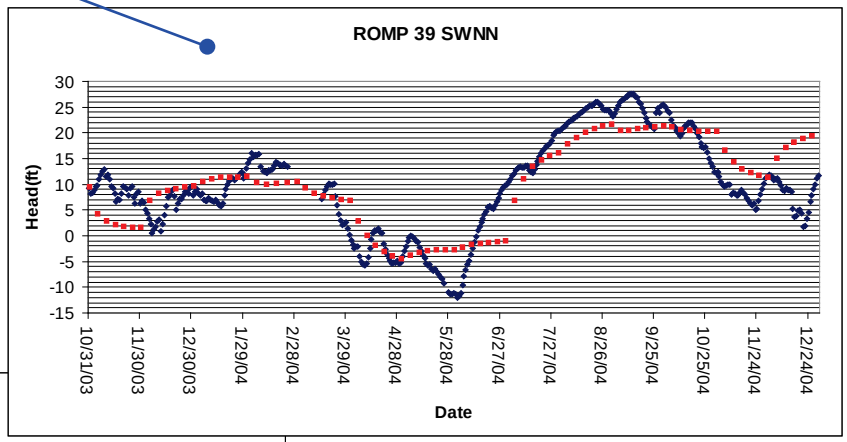

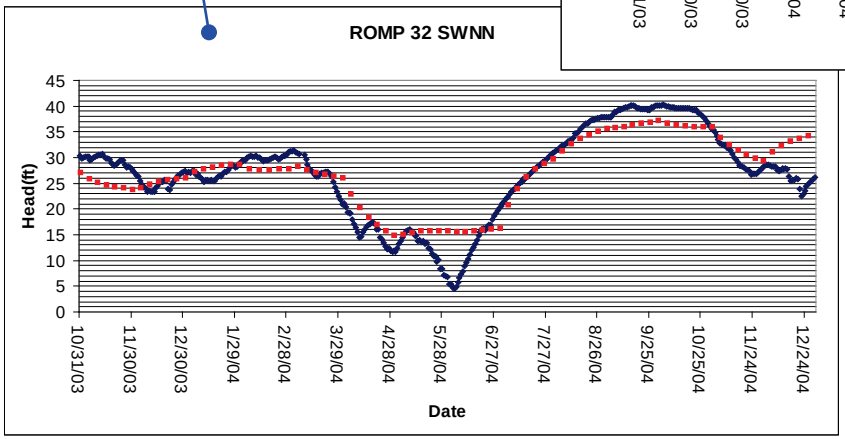

Legend

- Measured Head
- Model Calculated Head

Notes:

Figures 4.57 through 4.77 show the comparison between measured head values and model-calculated head values at a number of observation wells for the calibration period. Although the scales vary on each plot, all plots have a horizontal grid line at each foot. This is to make it easy to determine the range of heads at a glance.

The model used month-long stress periods, so pumping and boundary conditions were input as step functions with constant values throughout each month and sudden changes at the end of each month. For this reason, the model cannot be expected to accurately predict day-to-day head variations in any of these wells. Calibration efforts were aimed at matching general trends and monthly averages.

Starting head conditions for this model were based on the October 2003 steady state calibrated model. Transient calibration efforts were focused on matching the head changes, not the actual heads, so it is not uncommon for residuals in the starting condition to be carried through the entire calibration period. This indicates that the model is correctly predicting responses to hydrogeologic forces even if the calculated head values vary somewhat from the measured values.

Transient SEAWAT Calibration Comparison
Upper Floridan Aquifer (2003-2004)
Final Groundwater Model Calibration Report

Figure F3-7

October 2010

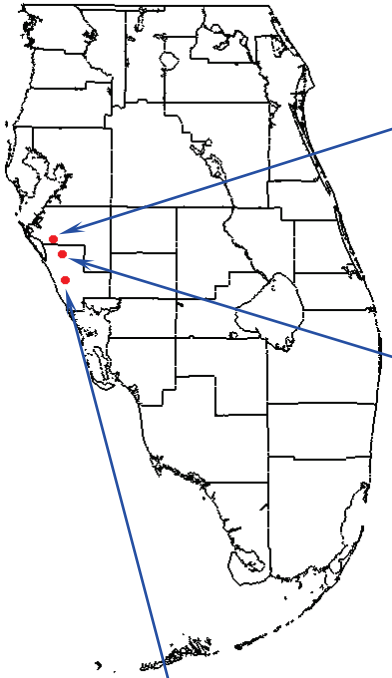

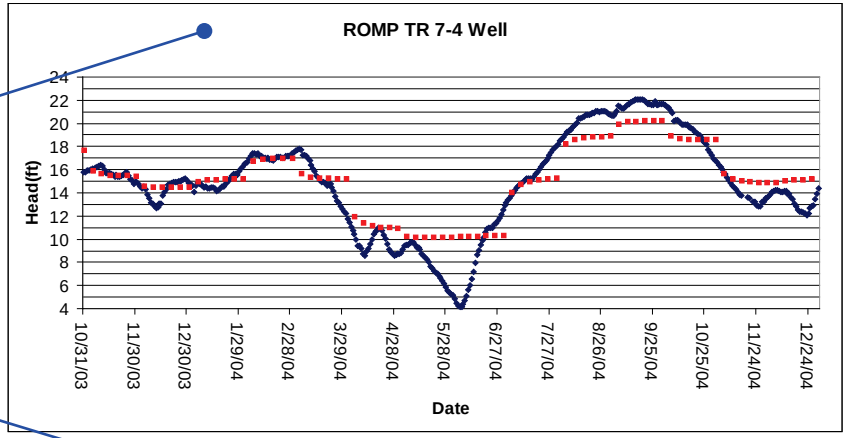

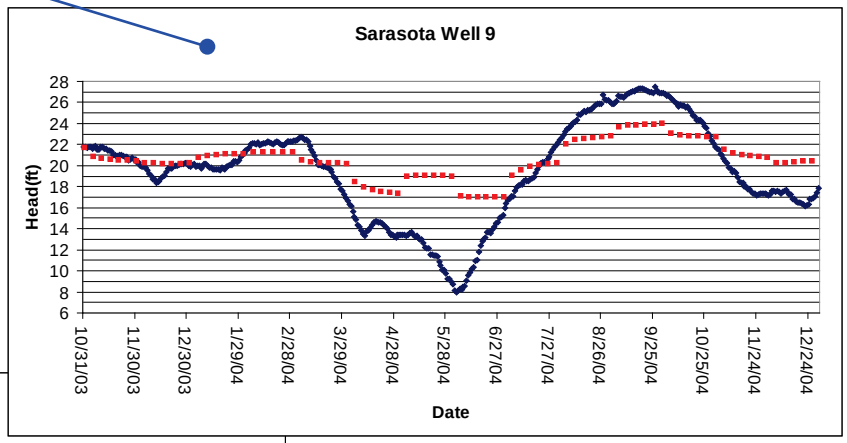

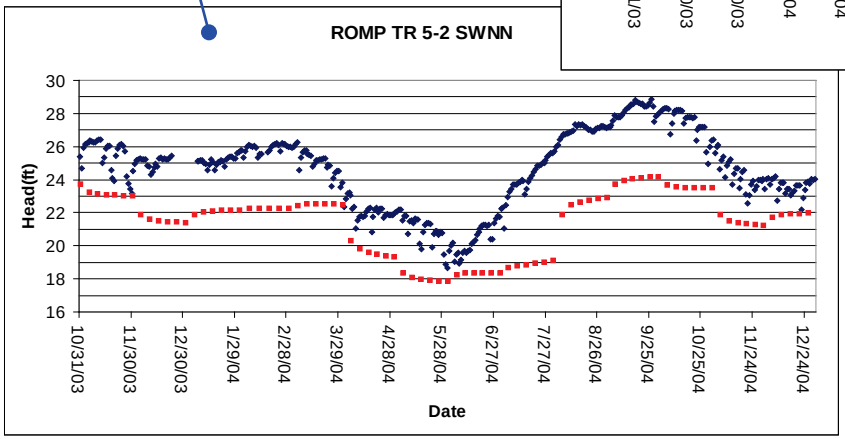

Legend

- Measured Head
- Model Calculated Head

Notes:

Figures 4.57 through 4.77 show the comparison between measured head values and model-calculated head values at a number of observation wells for the calibration period. Although the scales vary on each plot, all plots have a horizontal grid line at each foot. This is to make it easy to determine the range of heads at a glance.

The model used month-long stress periods, so pumping and boundary conditions were input as step functions with constant values throughout each month and sudden changes at the end of each month. For this reason, the model cannot be expected to accurately predict day-to-day head variations in any of these wells. Calibration efforts were aimed at matching general trends and monthly averages.

Starting head conditions for this model were based on the October 2003 steady state calibrated model. Transient calibration efforts were focused on matching the head changes, not the actual heads, so it is not uncommon for residuals in the starting condition to be carried through the entire calibration period. This indicates that the model is correctly predicting responses to hydrogeologic forces even if the calculated head values vary somewhat from the measured values.

Transient SEAWAT Calibration Comparison
Upper Floridan Aquifer (2003-2004)
Final Groundwater Model Calibration Report

Figure F3-8

October 2010

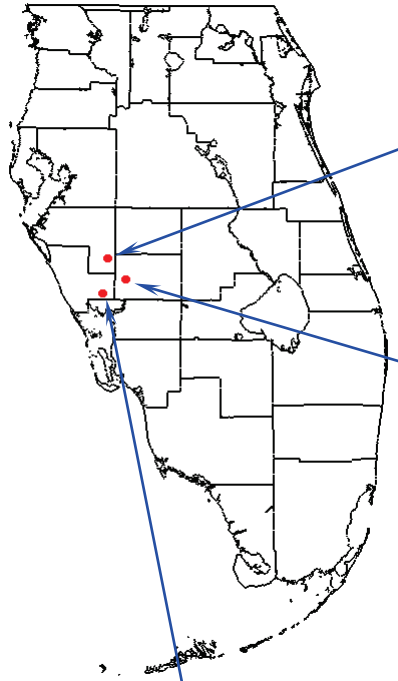

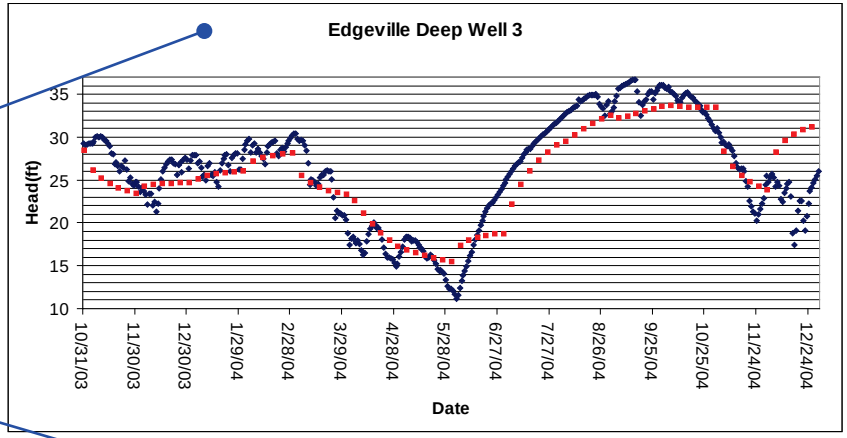

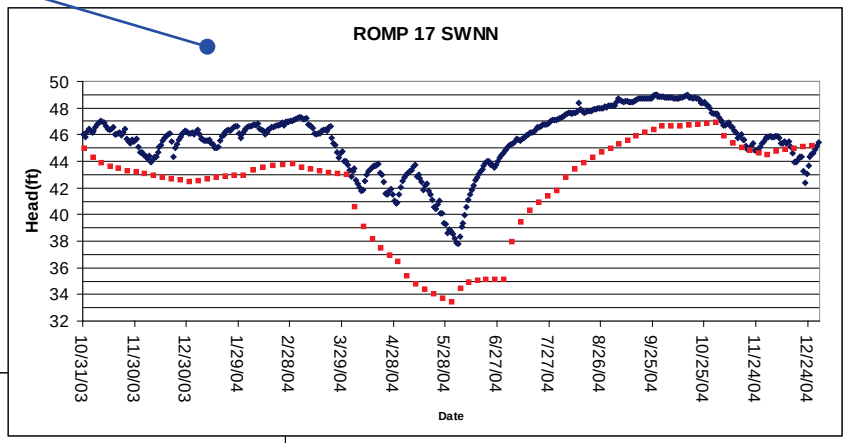

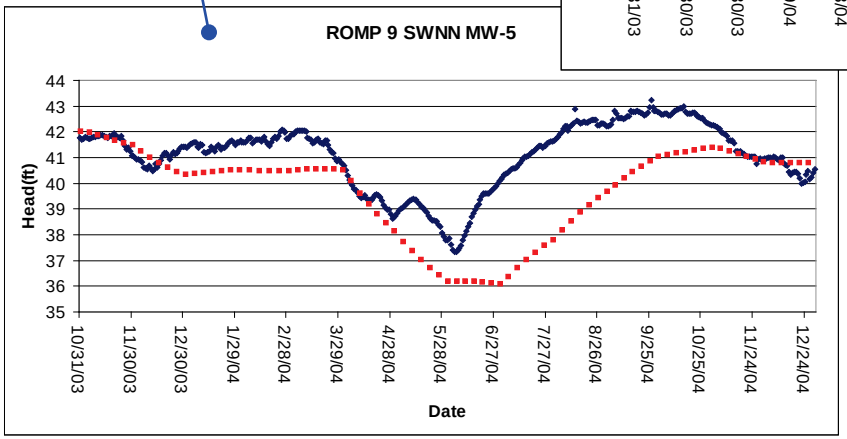

Legend

- Measured Head
- Model Calculated Head

Notes:

Figures 4.57 through 4.77 show the comparison between measured head values and model-calculated head values at a number of observation wells for the calibration period. Although the scales vary on each plot, all plots have a horizontal grid line at each foot. This is to make it easy to determine the range of heads at a glance.

The model used month-long stress periods, so pumping and boundary conditions were input as step functions with constant values throughout each month and sudden changes at the end of each month. For this reason, the model cannot be expected to accurately predict day-to-day head variations in any of these wells. Calibration efforts were aimed at matching general trends and monthly averages.

Starting head conditions for this model were based on the October 2003 steady state calibrated model. Transient calibration efforts were focused on matching the head changes, not the actual heads, so it is not uncommon for residuals in the starting condition to be carried through the entire calibration period. This indicates that the model is correctly predicting responses to hydrogeologic forces even if the calculated head values vary somewhat from the measured values.

Transient SEAWAT Calibration Comparison
Upper Floridan Aquifer (2003-2004)
Final Groundwater Model Calibration Report

Figure F3-9

October 2010

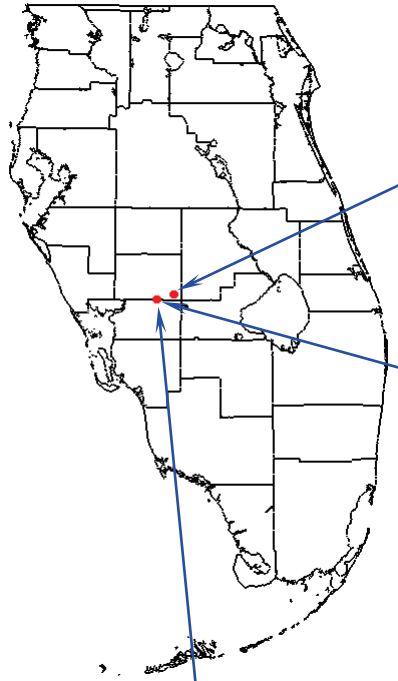

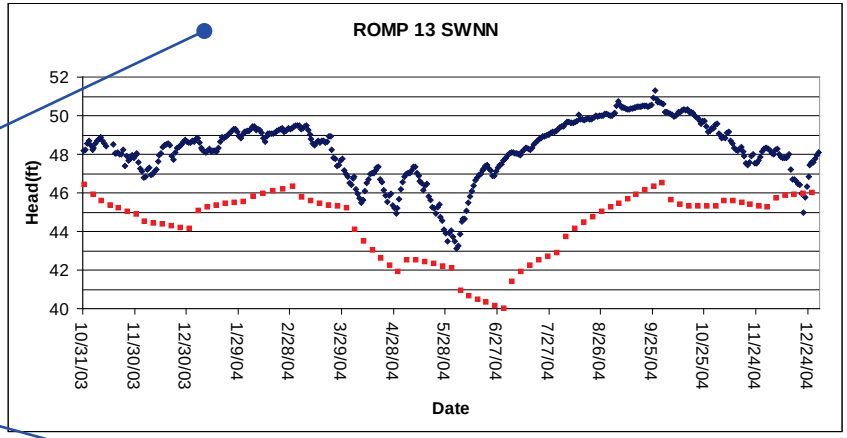

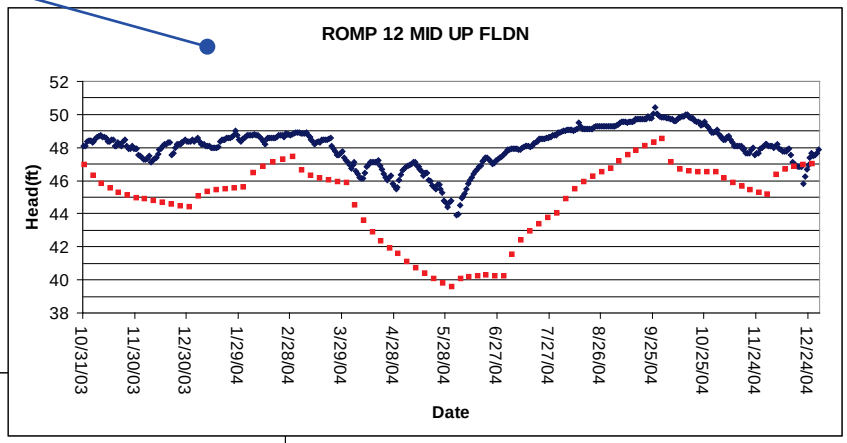

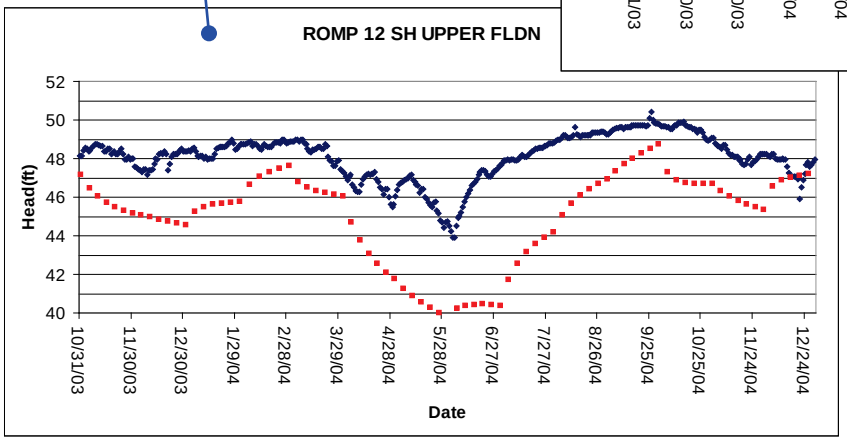

Legend

- Measured Head
- Model Calculated Head

Notes:

Figures 4.57 through 4.77 show the comparison between measured head values and model-calculated head values at a number of observation wells for the calibration period. Although the scales vary on each plot, all plots have a horizontal grid line at each foot. This is to make it easy to determine the range of heads at a glance.

The model used month-long stress periods, so pumping and boundary conditions were input as step functions with constant values throughout each month and sudden changes at the end of each month. For this reason, the model cannot be expected to accurately predict day-to-day head variations in any of these wells. Calibration efforts were aimed at matching general trends and monthly averages.

Starting head conditions for this model were based on the October 2003 steady state calibrated model. Transient calibration efforts were focused on matching the head changes, not the actual heads, so it is not uncommon for residuals in the starting condition to be carried through the entire calibration period. This indicates that the model is correctly predicting responses to hydrogeologic forces even if the calculated head values vary somewhat from the measured values.

Transient SEAWAT Calibration Comparison
Upper Floridan Aquifer (2003-2004)
Final Groundwater Model Calibration Report

Figure F3-10

October 2010

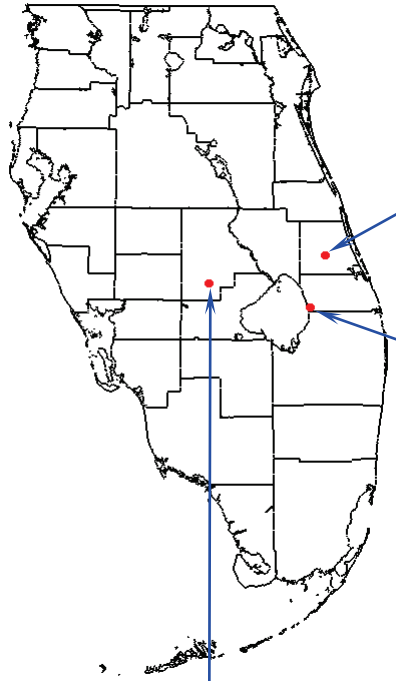

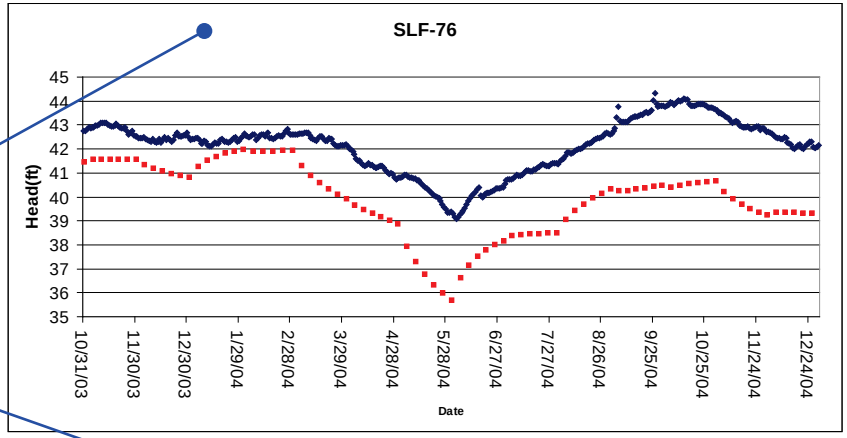

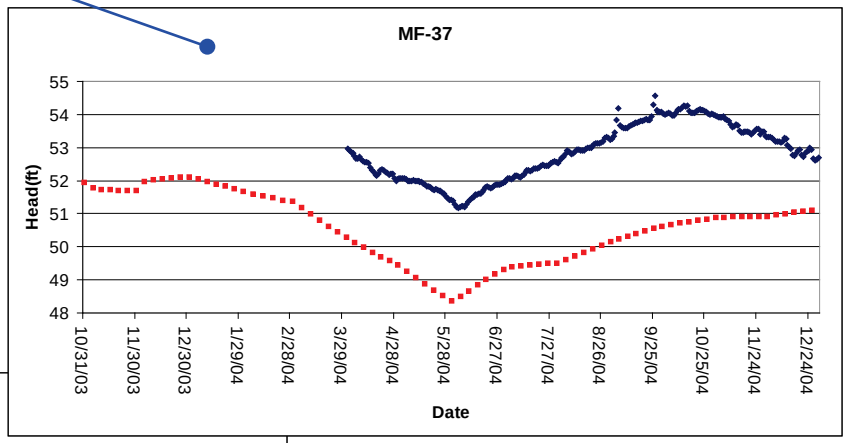

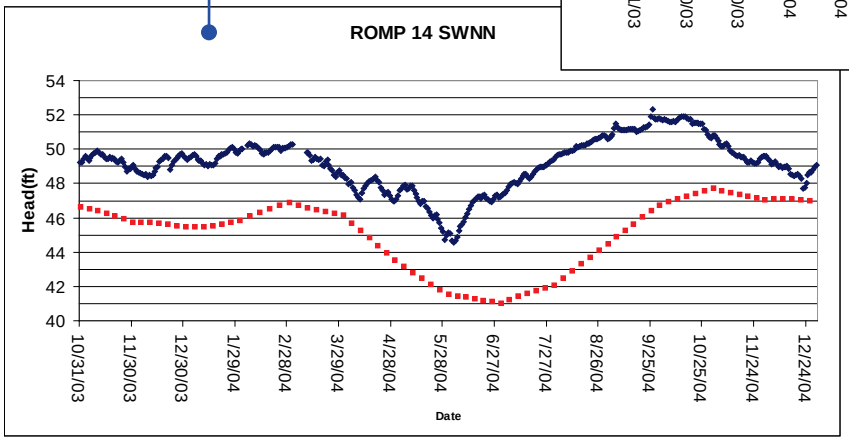

Legend

- Measured Head
- Model Calculated Head

Notes:

Figures 4.57 through 4.77 show the comparison between measured head values and model-calculated head values at a number of observation wells for the calibration period. Although the scales vary on each plot, all plots have a horizontal grid line at each foot. This is to make it easy to determine the range of heads at a glance.

The model used month-long stress periods, so pumping and boundary conditions were input as step functions with constant values throughout each month and sudden changes at the end of each month. For this reason, the model cannot be expected to accurately predict day-to-day head variations in any of these wells. Calibration efforts were aimed at matching general trends and monthly averages.

Starting head conditions for this model were based on the October 2003 steady state calibrated model. Transient calibration efforts were focused on matching the head changes, not the actual heads, so it is not uncommon for residuals in the starting condition to be carried through the entire calibration period. This indicates that the model is correctly predicting responses to hydrogeologic forces even if the calculated head values vary somewhat from the measured values.

Transient SEAWAT Calibration Comparison
Upper Floridan Aquifer (2003-2004)
Final Groundwater Model Calibration Report

Figure F3-11

October 2010

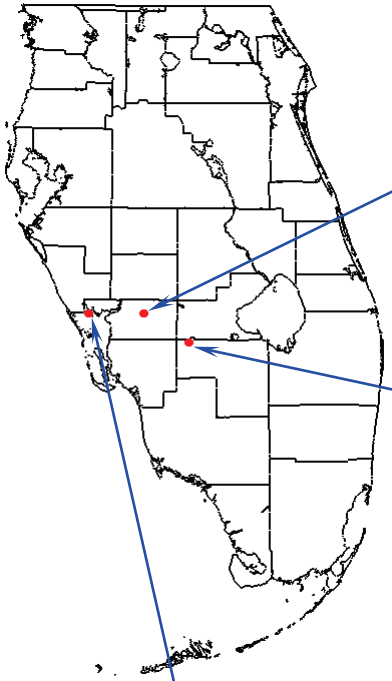

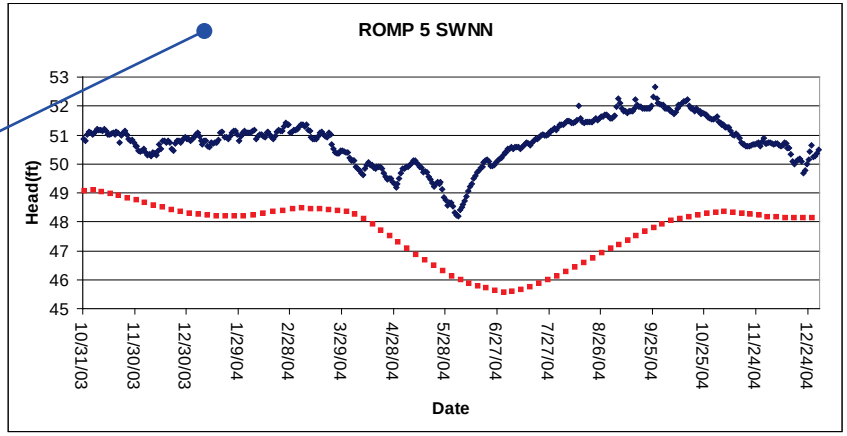

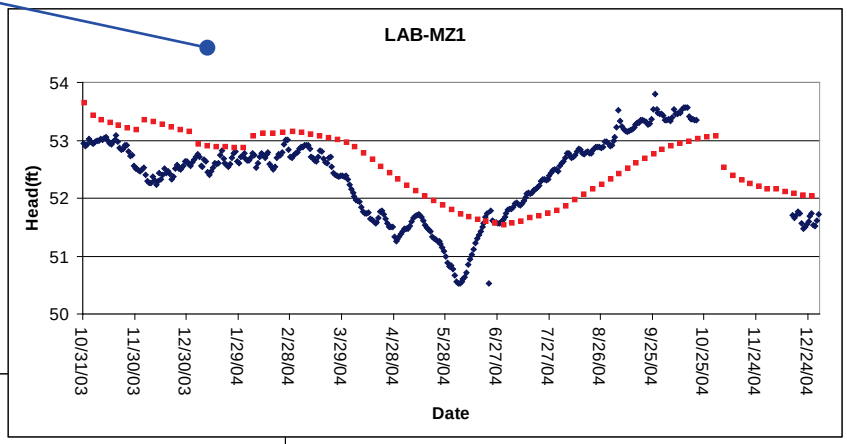

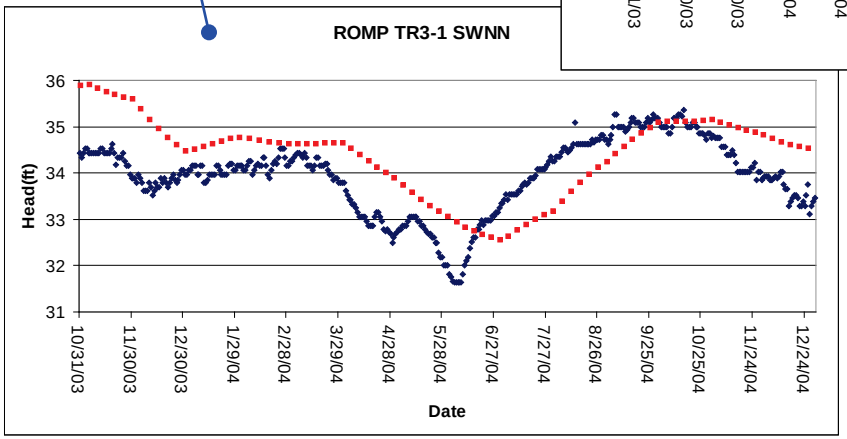

Legend

- Measured Head
- Model Calculated Head

Notes:

Figures 4.57 through 4.77 show the comparison between measured head values and model-calculated head values at a number of observation wells for the calibration period. Although the scales vary on each plot, all plots have a horizontal grid line at each foot. This is to make it easy to determine the range of heads at a glance.

The model used month-long stress periods, so pumping and boundary conditions were input as step functions with constant values throughout each month and sudden changes at the end of each month. For this reason, the model cannot be expected to accurately predict day-to-day head variations in any of these wells. Calibration efforts were aimed at matching general trends and monthly averages.

Starting head conditions for this model were based on the October 2003 steady state calibrated model. Transient calibration efforts were focused on matching the head changes, not the actual heads, so it is not uncommon for residuals in the starting condition to be carried through the entire calibration period. This indicates that the model is correctly predicting responses to hydrogeologic forces even if the calculated head values vary somewhat from the measured values.

Transient SEAWAT Calibration Comparison
Upper Floridan Aquifer (2003-2004)
Final Groundwater Model Calibration Report

Figure F3-12

October 2010

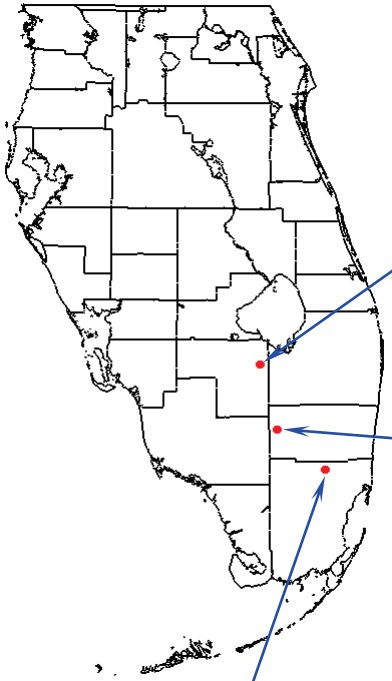

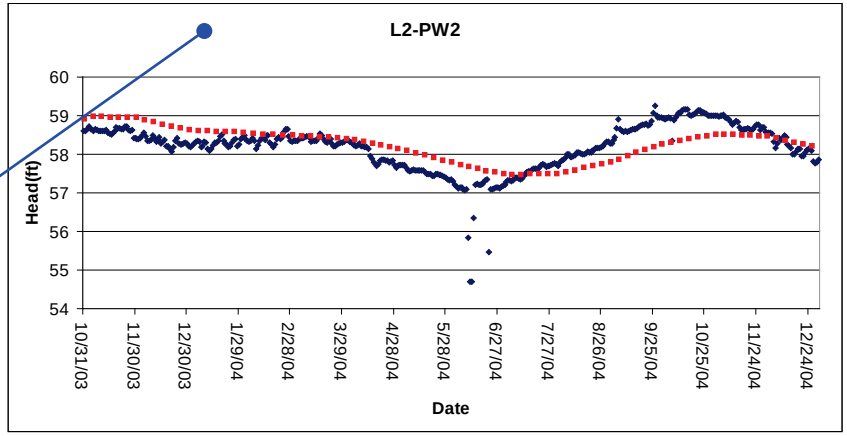

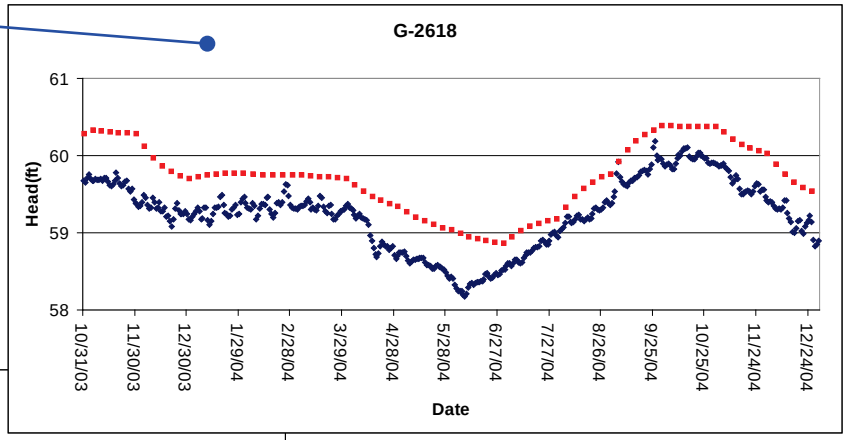

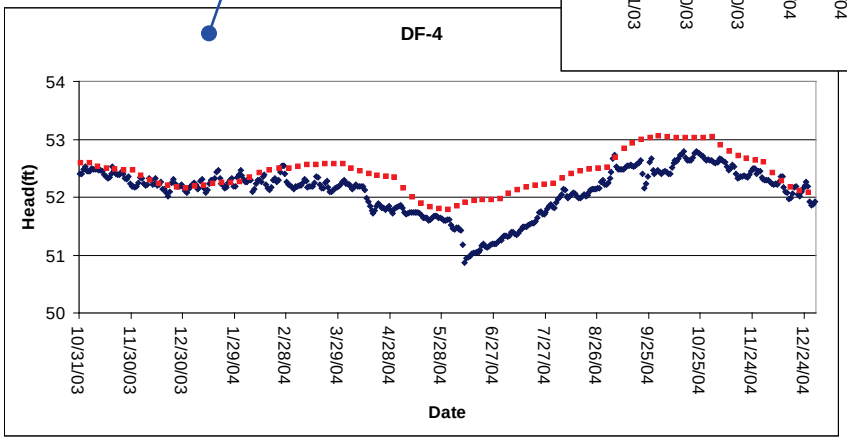

Legend

- Measured Head
- Model Calculated Head

Notes:

Figures 4.57 through 4.77 show the comparison between measured head values and model-calculated head values at a number of observation wells for the calibration period. Although the scales vary on each plot, all plots have a horizontal grid line at each foot. This is to make it easy to determine the range of heads at a glance.

The model used month-long stress periods, so pumping and boundary conditions were input as step functions with constant values throughout each month and sudden changes at the end of each month. For this reason, the model cannot be expected to accurately predict day-to-day head variations in any of these wells. Calibration efforts were aimed at matching general trends and monthly averages.

Starting head conditions for this model were based on the October 2003 steady state calibrated model. Transient calibration efforts were focused on matching the head changes, not the actual heads, so it is not uncommon for residuals in the starting condition to be carried through the entire calibration period. This indicates that the model is correctly predicting responses to hydrogeologic forces even if the calculated head values vary somewhat from the measured values.

Transient SEAWAT Calibration Comparison
Upper Floridan Aquifer (2003-2004)
Final Groundwater Model Calibration Report

Figure F3-13

October 2010

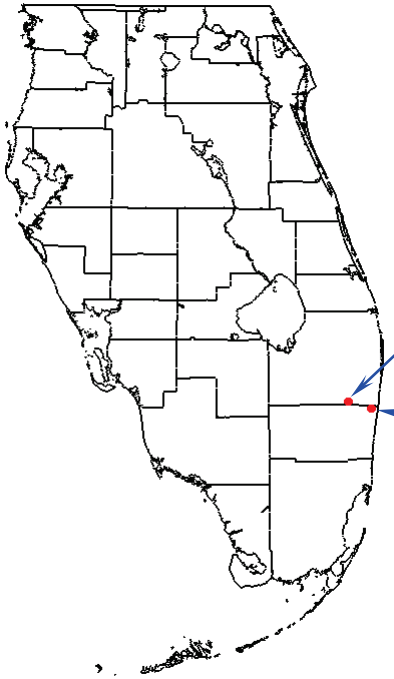

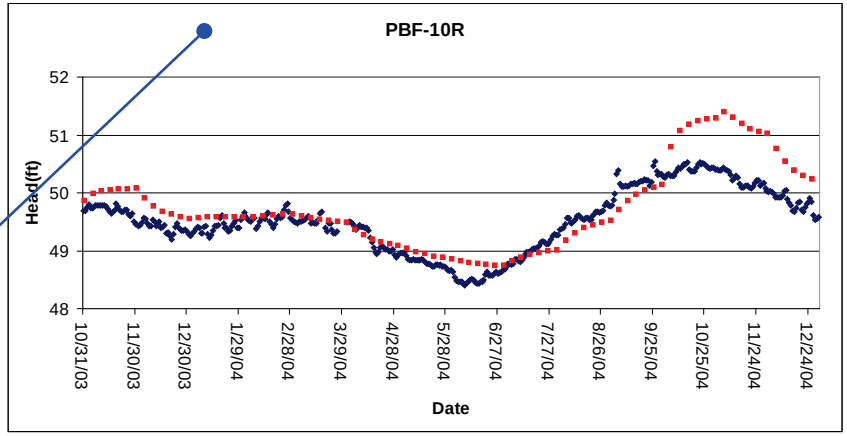

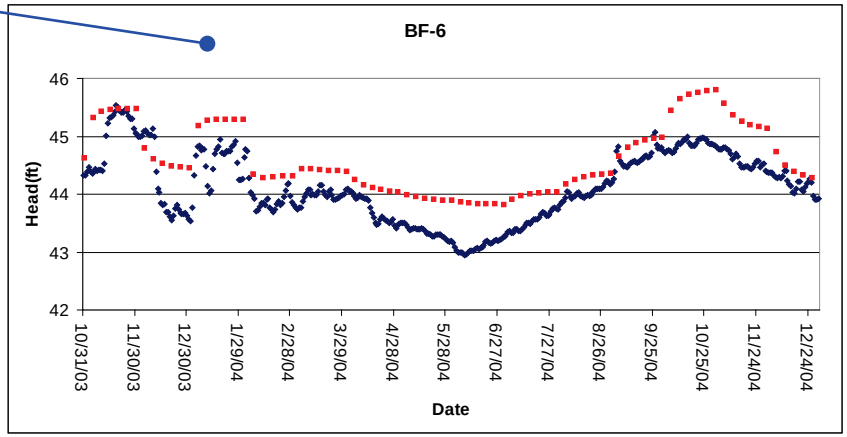

Legend

- Measured Head
- Model Calculated Head

Notes:

Figures 4.57 through 4.77 show the comparison between measured head values and model-calculated head values at a number of observation wells for the calibration period. Although the scales vary on each plot, all plots have a horizontal grid line at each foot. This is to make it easy to determine the range of heads at a glance.

The model used month-long stress periods, so pumping and boundary conditions were input as step functions with constant values throughout each month and sudden changes at the end of each month. For this reason, the model cannot be expected to accurately predict day-to-day head variations in any of these wells. Calibration efforts were aimed at matching general trends and monthly averages.

Starting head conditions for this model were based on the October 2003 steady state calibrated model. Transient calibration efforts were focused on matching the head changes, not the actual heads, so it is not uncommon for residuals in the starting condition to be carried through the entire calibration period. This indicates that the model is correctly predicting responses to hydrogeologic forces even if the calculated head values vary somewhat from the measured values.

Transient SEAWAT Calibration Comparison
Upper Floridan Aquifer (2003-2004)
Final Groundwater Model Calibration Report

Figure F3-14

October 2010

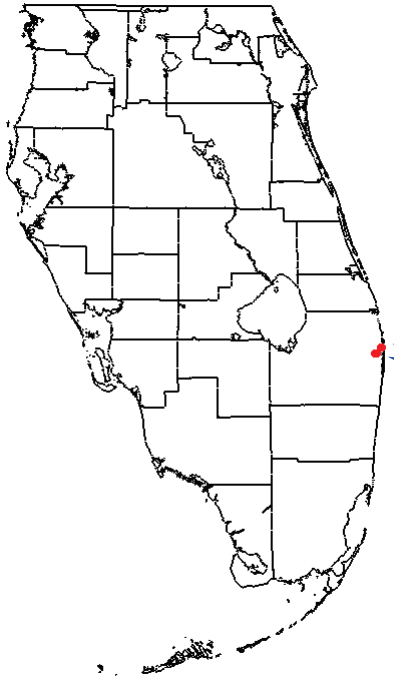

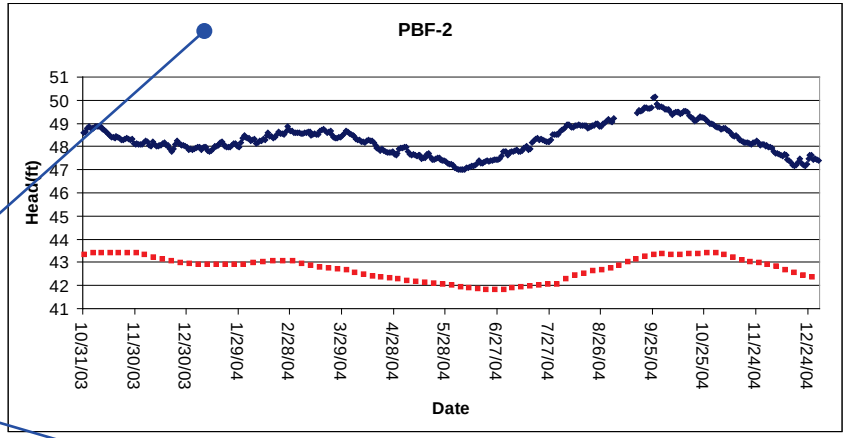

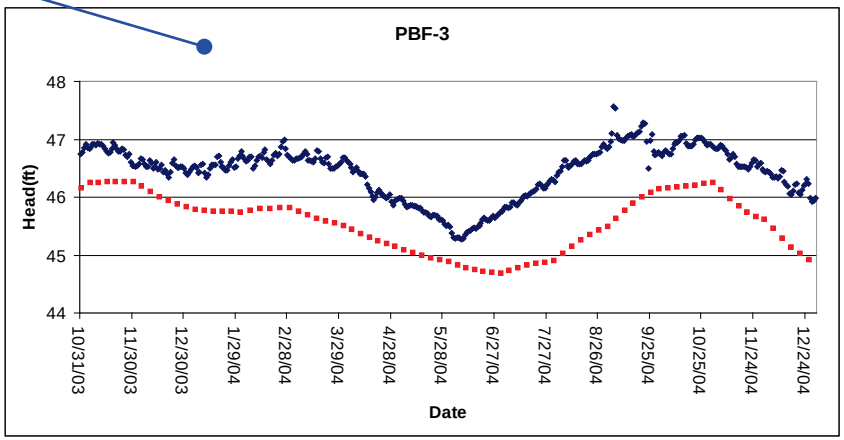

Legend

- Measured Head
- Model Calculated Head

Notes:

Figures 4.57 through 4.77 show the comparison between measured head values and model-calculated head values at a number of observation wells for the calibration period. Although the scales vary on each plot, all plots have a horizontal grid line at each foot. This is to make it easy to determine the range of heads at a glance.

The model used month-long stress periods, so pumping and boundary conditions were input as step functions with constant values throughout each month and sudden changes at the end of each month. For this reason, the model cannot be expected to accurately predict day-to-day head variations in any of these wells. Calibration efforts were aimed at matching general trends and monthly averages.

Starting head conditions for this model were based on the October 2003 steady state calibrated model. Transient calibration efforts were focused on matching the head changes, not the actual heads, so it is not uncommon for residuals in the starting condition to be carried through the entire calibration period. This indicates that the model is correctly predicting responses to hydrogeologic forces even if the calculated head values vary somewhat from the measured values.

Transient SEAWAT Calibration Comparison
Upper Floridan Aquifer (2003-2004)
Final Groundwater Model Calibration Report

Figure F3-15

October 2010

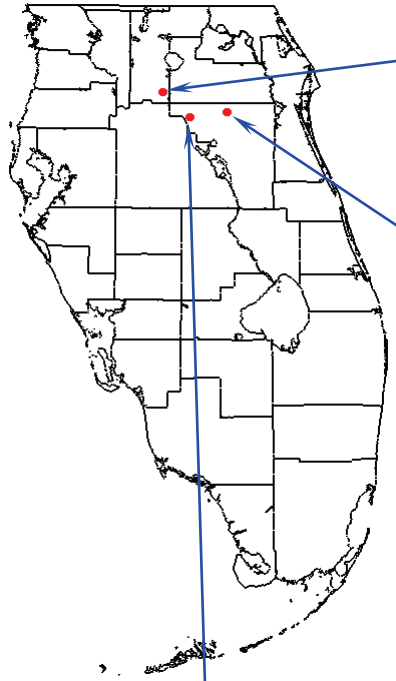

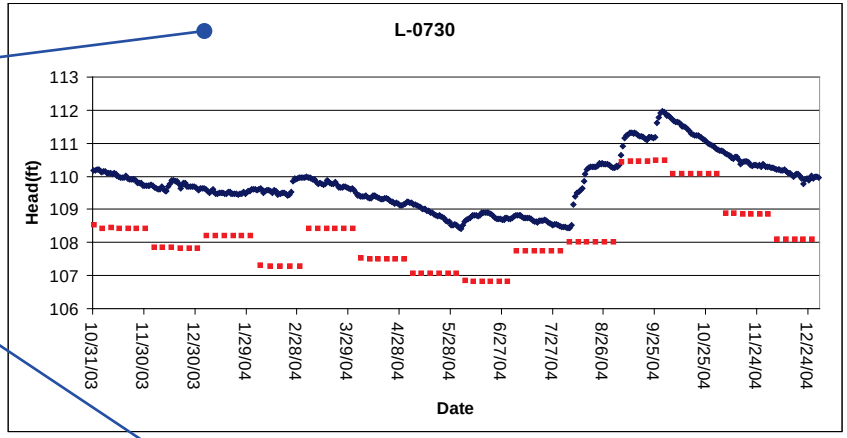

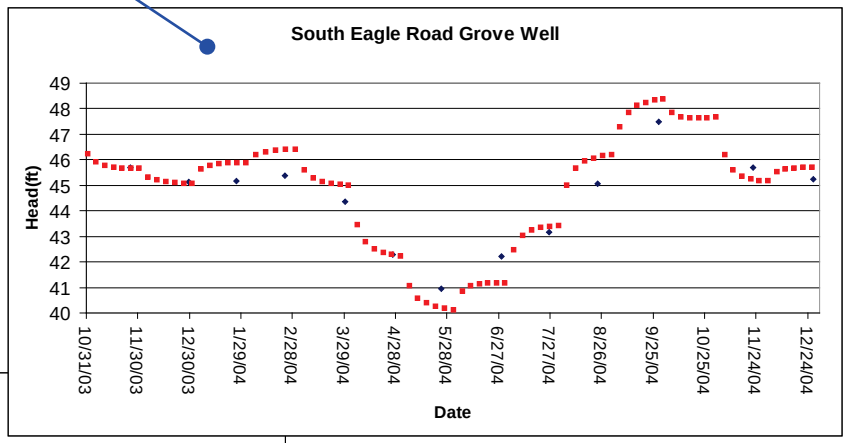

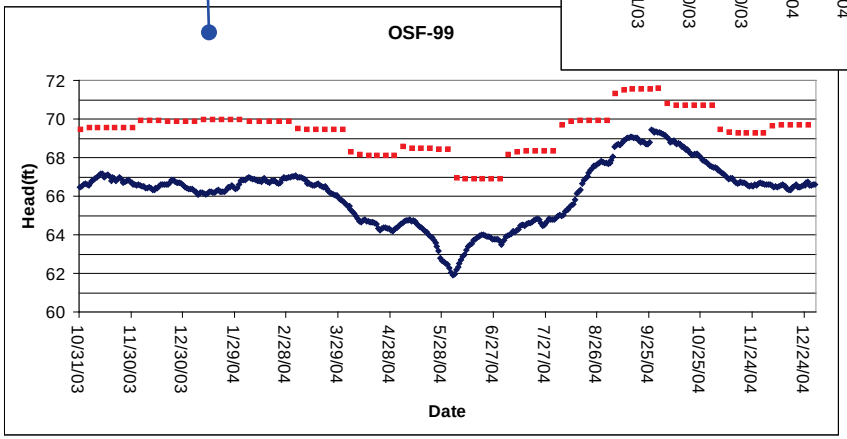

Legend

- Measured Head
- Model Calculated Head

Notes:

Figures 4.57 through 4.77 show the comparison between measured head values and model-calculated head values at a number of observation wells for the calibration period. Although the scales vary on each plot, all plots have a horizontal grid line at each foot. This is to make it easy to determine the range of heads at a glance.

The model used month-long stress periods, so pumping and boundary conditions were input as step functions with constant values throughout each month and sudden changes at the end of each month. For this reason, the model cannot be expected to accurately predict day-to-day head variations in any of these wells. Calibration efforts were aimed at matching general trends and monthly averages.

Starting head conditions for this model were based on the October 2003 steady state calibrated model. Transient calibration efforts were focused on matching the head changes, not the actual heads, so it is not uncommon for residuals in the starting condition to be carried through the entire calibration period. This indicates that the model is correctly predicting responses to hydrogeologic forces even if the calculated head values vary somewhat from the measured values.

Transient SEAWAT Calibration Comparison
Avon Park Permeable Zone (2003-2004)
Final Groundwater Model Calibration Report

Figure F3-16

October 2010

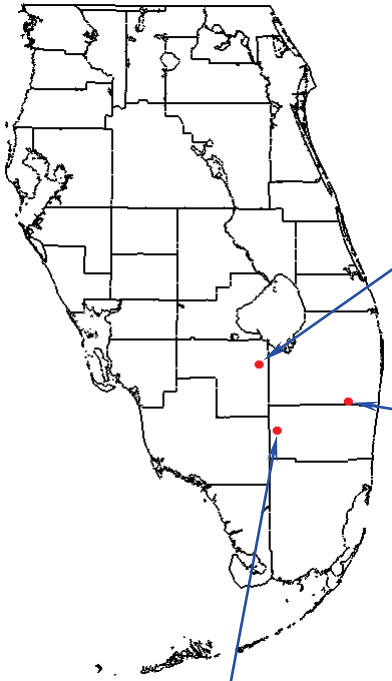

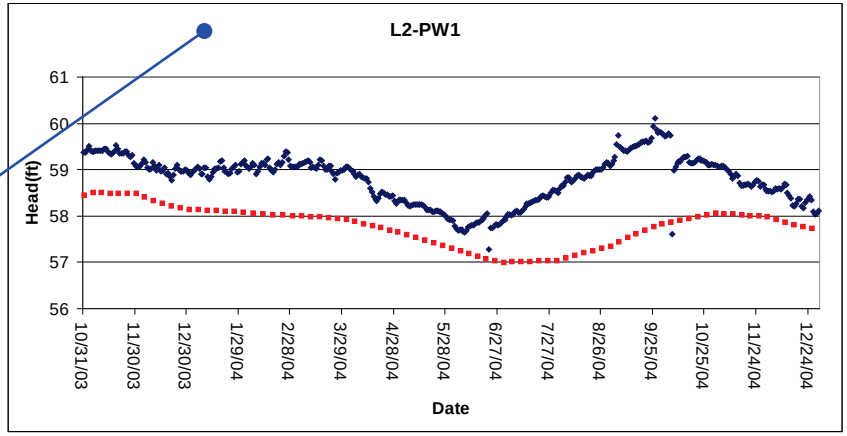

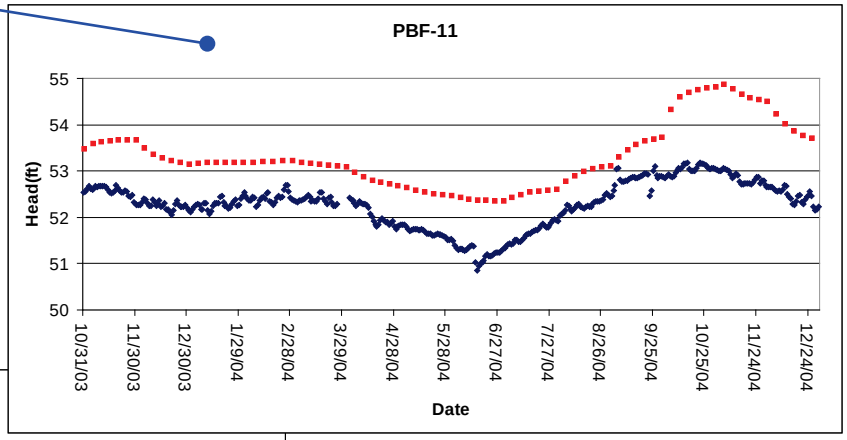

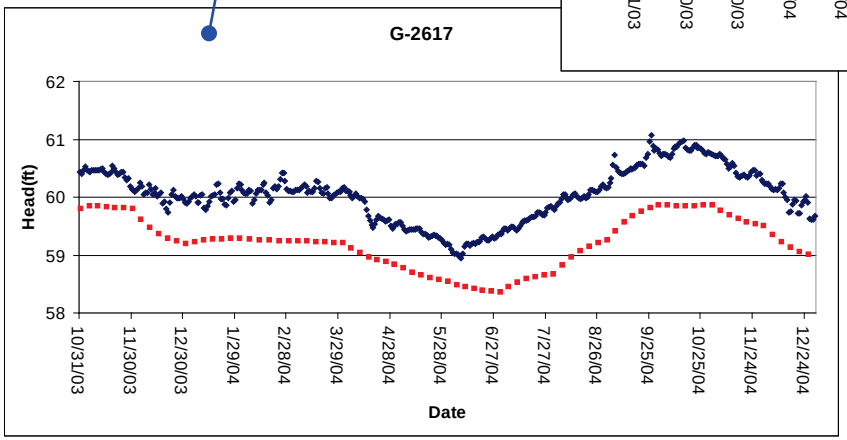

Legend

- Measured Head
- Model Calculated Head

Notes:

Figures 4.57 through 4.77 show the comparison between measured head values and model-calculated head values at a number of observation wells for the calibration period. Although the scales vary on each plot, all plots have a horizontal grid line at each foot. This is to make it easy to determine the range of heads at a glance.

The model used month-long stress periods, so pumping and boundary conditions were input as step functions with constant values throughout each month and sudden changes at the end of each month. For this reason, the model cannot be expected to accurately predict day-to-day head variations in any of these wells. Calibration efforts were aimed at matching general trends and monthly averages.

Starting head conditions for this model were based on the October 2003 steady state calibrated model. Transient calibration efforts were focused on matching the head changes, not the actual heads, so it is not uncommon for residuals in the starting condition to be carried through the entire calibration period. This indicates that the model is correctly predicting responses to hydrogeologic forces even if the calculated head values vary somewhat from the measured values.

Transient SEAWAT Calibration Comparison
Avon Park Permeable Zone (2003-2004)
Final Groundwater Model Calibration Report

Figure F3-17

October 2010

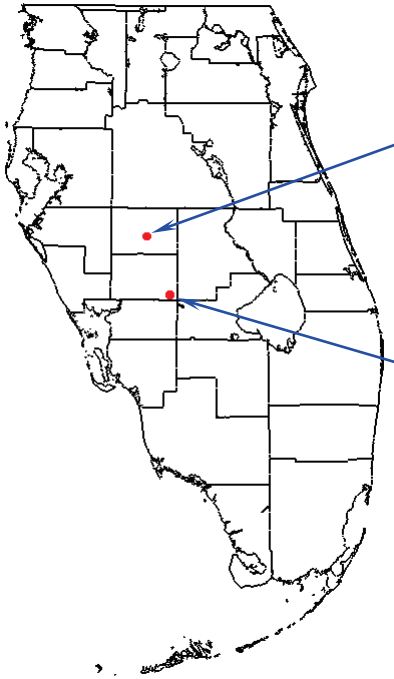

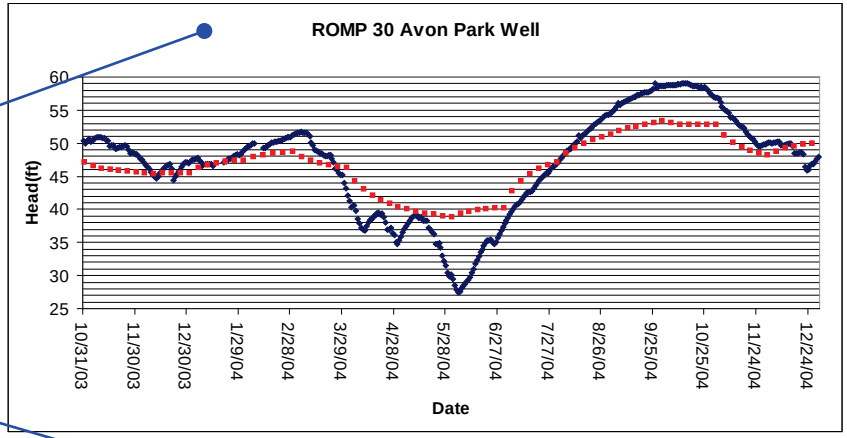

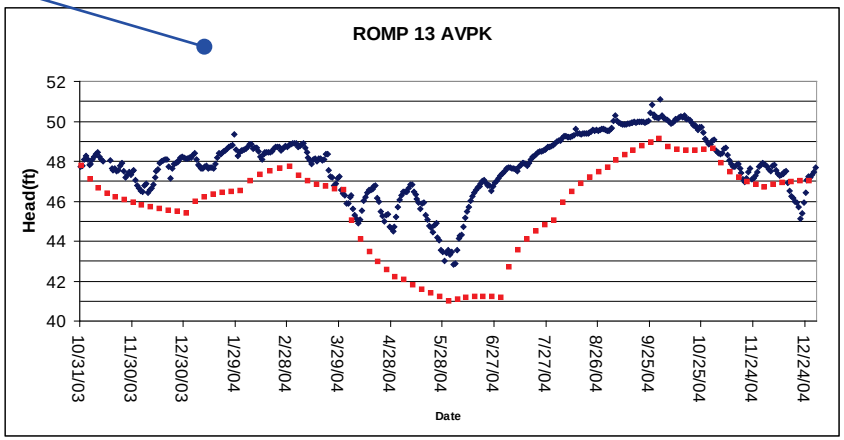

Legend

- Measured Head
- Model Calculated Head

Notes:

Figures 4.57 through 4.77 show the comparison between measured head values and model-calculated head values at a number of observation wells for the calibration period. Although the scales vary on each plot, all plots have a horizontal grid line at each foot. This is to make it easy to determine the range of heads at a glance.

The model used month-long stress periods, so pumping and boundary conditions were input as step functions with constant values throughout each month and sudden changes at the end of each month. For this reason, the model cannot be expected to accurately predict day-to-day head variations in any of these wells. Calibration efforts were aimed at matching general trends and monthly averages.

Starting head conditions for this model were based on the October 2003 steady state calibrated model. Transient calibration efforts were focused on matching the head changes, not the actual heads, so it is not uncommon for residuals in the starting condition to be carried through the entire calibration period. This indicates that the model is correctly predicting responses to hydrogeologic forces even if the calculated head values vary somewhat from the measured values.

Transient SEAWAT Calibration Comparison
Avon Park Permeable Zone (2003-2004)
Final Groundwater Model Calibration Report

Figure F3-18

October 2010

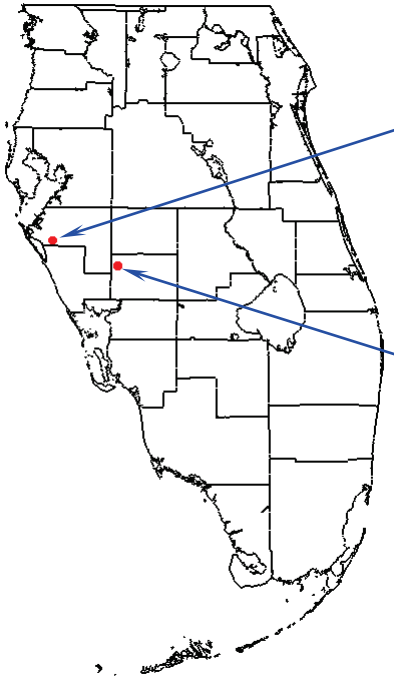

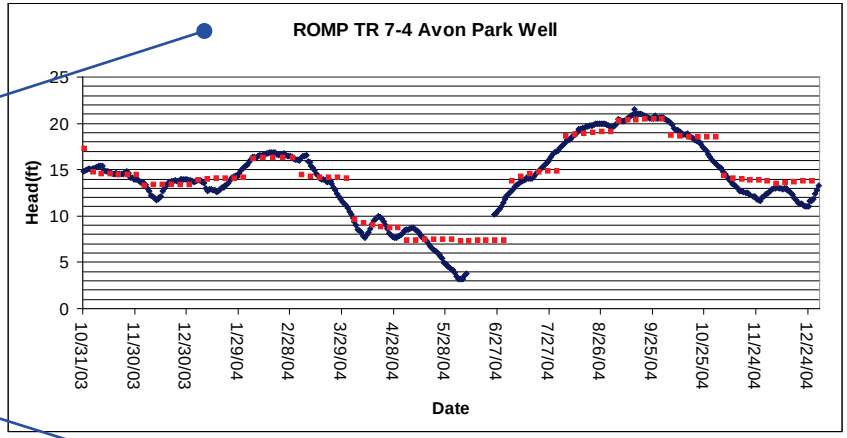

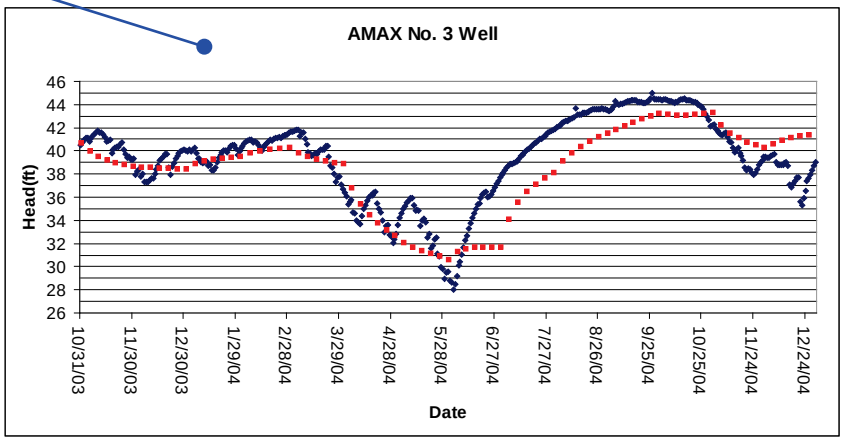

Legend

- Measured Head
- Model Calculated Head

Notes:

Figures 4.57 through 4.77 show the comparison between measured head values and model-calculated head values at a number of observation wells for the calibration period. Although the scales vary on each plot, all plots have a horizontal grid line at each foot. This is to make it easy to determine the range of heads at a glance.

The model used month-long stress periods, so pumping and boundary conditions were input as step functions with constant values throughout each month and sudden changes at the end of each month. For this reason, the model cannot be expected to accurately predict day-to-day head variations in any of these wells. Calibration efforts were aimed at matching general trends and monthly averages.

Starting head conditions for this model were based on the October 2003 steady state calibrated model. Transient calibration efforts were focused on matching the head changes, not the actual heads, so it is not uncommon for residuals in the starting condition to be carried through the entire calibration period. This indicates that the model is correctly predicting responses to hydrogeologic forces even if the calculated head values vary somewhat from the measured values.

Transient SEAWAT Calibration Comparison
Avon Park Permeable Zone (2003-2004)
Final Groundwater Model Calibration Report

Figure F3-19

October 2010

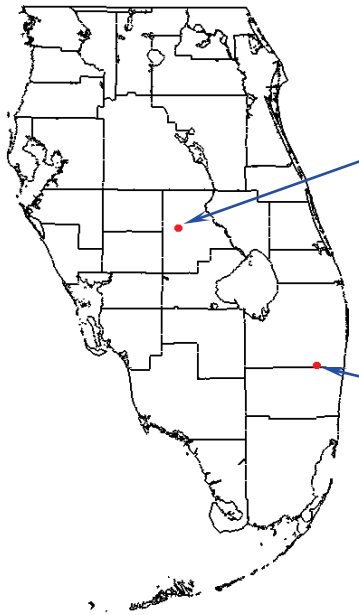

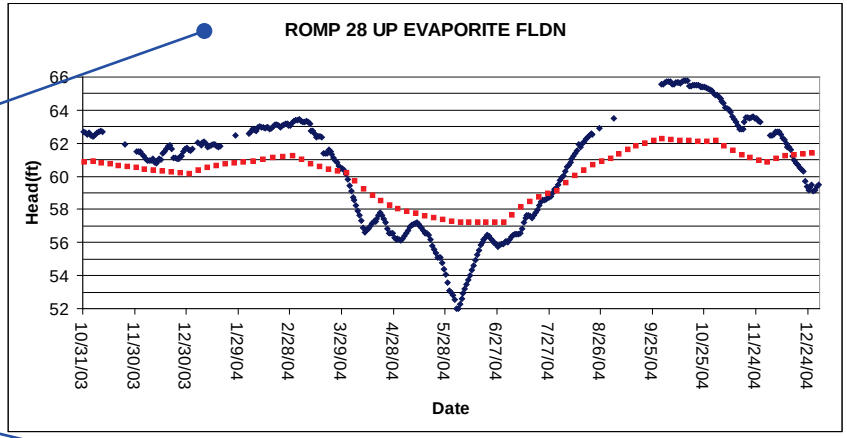

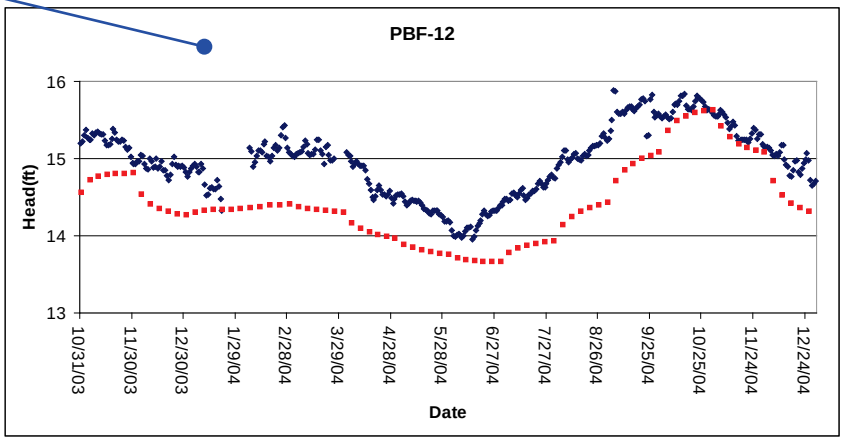

Legend

- Measured Head
- Model Calculated Head

Notes:

Figures 4.57 through 4.77 show the comparison between measured head values and model-calculated head values at a number of observation wells for the calibration period. Although the scales vary on each plot, all plots have a horizontal grid line at each foot. This is to make it easy to determine the range of heads at a glance.

The model used month-long stress periods, so pumping and boundary conditions were input as step functions with constant values throughout each month and sudden changes at the end of each month. For this reason, the model cannot be expected to accurately predict day-to-day head variations in any of these wells. Calibration efforts were aimed at matching general trends and monthly averages.

Starting head conditions for this model were based on the October 2003 steady state calibrated model. Transient calibration efforts were focused on matching the head changes, not the actual heads, so it is not uncommon for residuals in the starting condition to be carried through the entire calibration period. This indicates that the model is correctly predicting responses to hydrogeologic forces even if the calculated head values vary somewhat from the measured values.

Transient SEAWAT Calibration Comparison
Lower Floridan (LF1) Aquifer (2003-2004)
Final Groundwater Model Calibration Report

Figure F3-20

October 2010

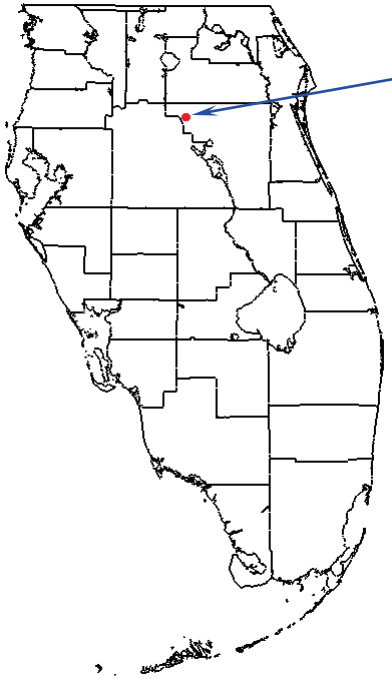

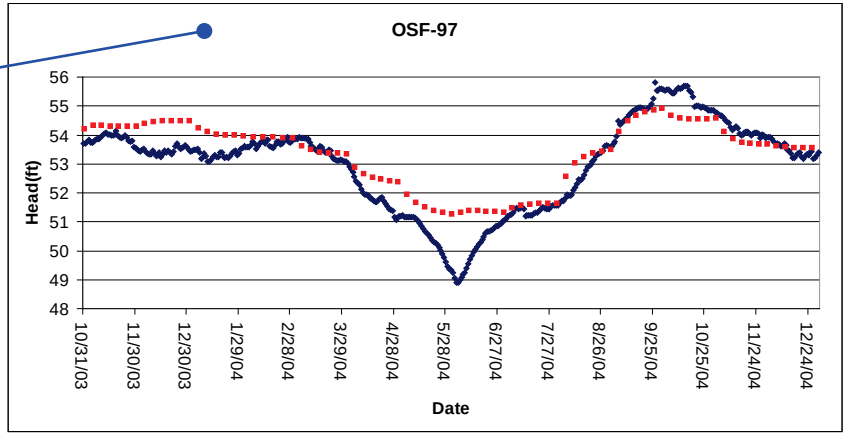

Legend

- Measured Head
- Model Calculated Head

Notes:

Figures 4.57 through 4.77 show the comparison between measured head values and model-calculated head values at a number of observation wells for the calibration period. Although the scales vary on each plot, all plots have a horizontal grid line at each foot. This is to make it easy to determine the range of heads at a glance.

The model used month-long stress periods, so pumping and boundary conditions were input as step functions with constant values throughout each month and sudden changes at the end of each month. For this reason, the model cannot be expected to accurately predict day-to-day head variations in any of these wells. Calibration efforts were aimed at matching general trends and monthly averages.

Starting head conditions for this model were based on the October 2003 steady state calibrated model. Transient calibration efforts were focused on matching the head changes, not the actual heads, so it is not uncommon for residuals in the starting condition to be carried through the entire calibration period. This indicates that the model is correctly predicting responses to hydrogeologic forces even if the calculated head values vary somewhat from the measured values.

Transient SEAWAT Calibration Comparison
Boulder Zone (2003-2004)
Final Groundwater Model Calibration Report

Figure F3-21

October 2010

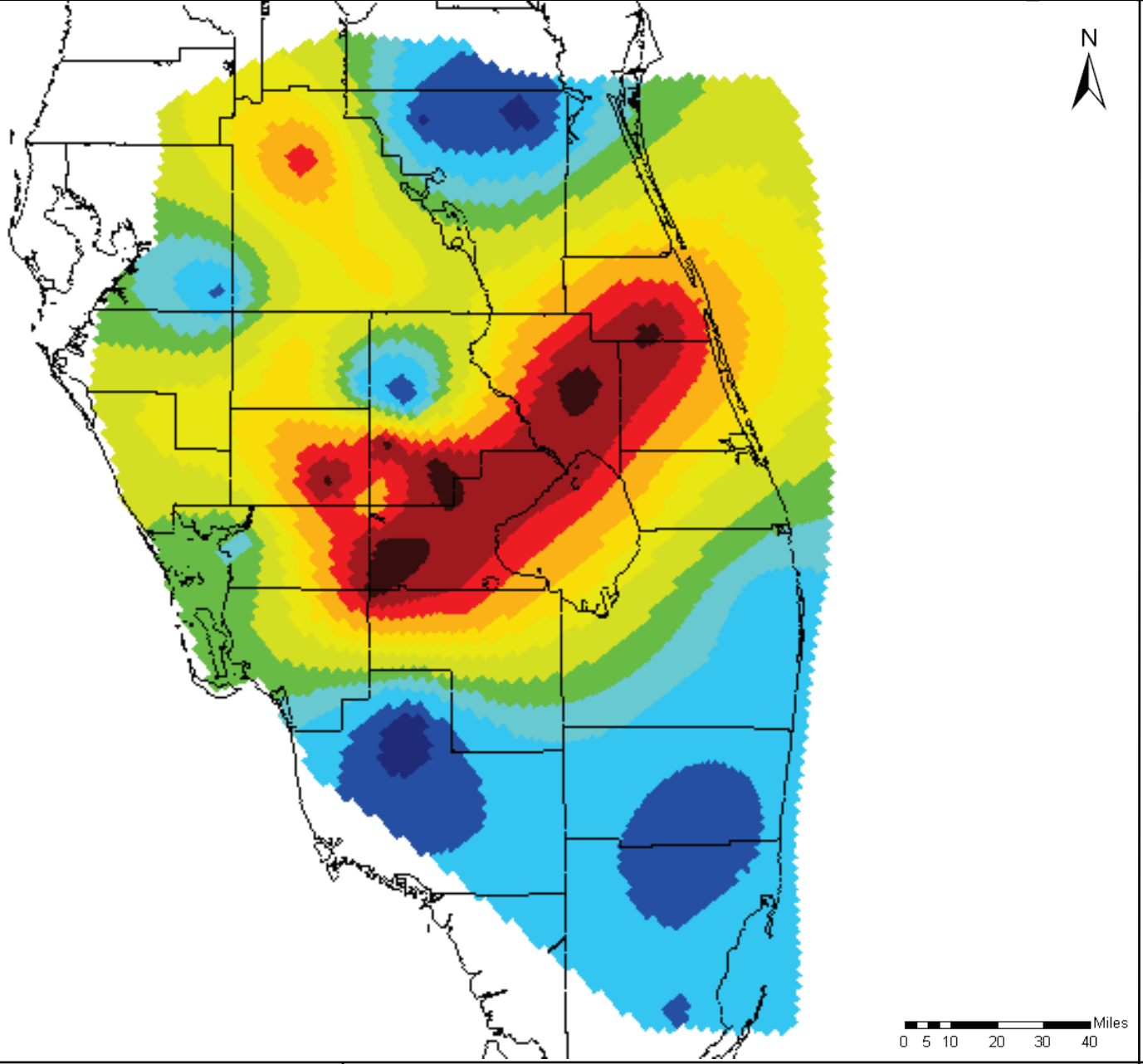

Notes:

Distribution shown was applied to SEAWAT model layers 2 through 4.

Specific Storage values were interpolated to the grid from values assigned to a set of pilot points scattered across the model domain.

A combination of automated calibration (PEST) and manual calibration (trial and error) resulted in this Specific Storage field.

Calibrated SEAWAT Specific Storage
Intermediate Aquifer System
Final Groundwater Model Calibration Report

Figure F3-22

October 2010

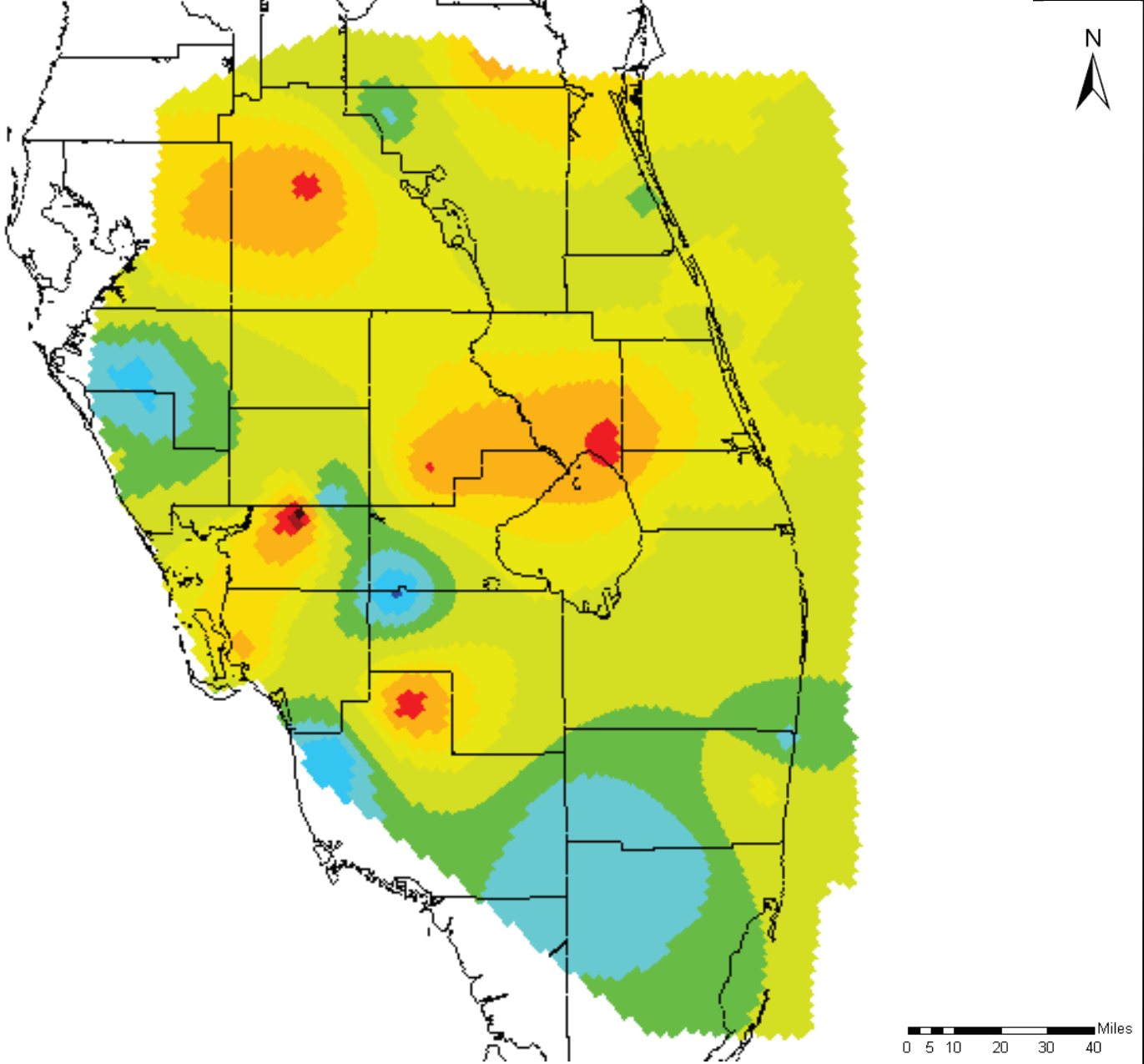

Notes:

Distribution shown was applied to SEAWAT model layers 5 through 10.

Specific Storage values were interpolated to the grid from values assigned to a set of pilot points scattered across the model domain.

A combination of automated calibration (PEST) and manual calibration (trial and error) resulted in this Specific Storage field.

Calibrated SEAWAT Specific Storage
Upper Floridan Aquifer
Final Groundwater Model Calibration Report

Figure F3-23

October 2010

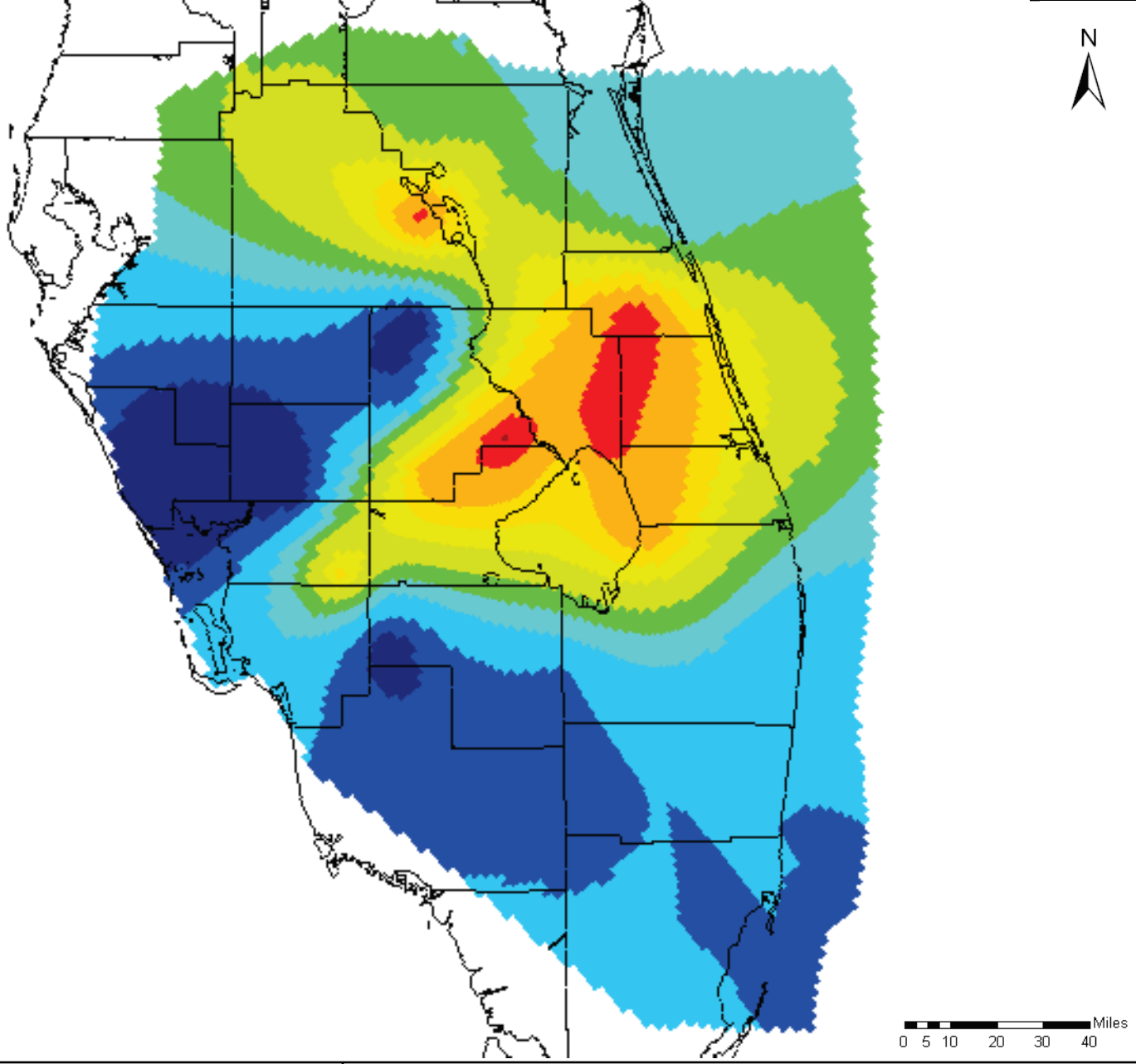

Notes:

Distribution shown was applied to SEAWAT model layers 11 through 12.

Specific Storage values were interpolated to the grid from values assigned to a set of pilot points scattered across the model domain.

A combination of automated calibration (PEST) and manual calibration (trial and error) resulted in this Specific Storage field.

Calibrated SEAWAT Specific Storage
Middle Confining Unit 1
Final Groundwater Model Calibration Report

Figure F3-24

October 2010

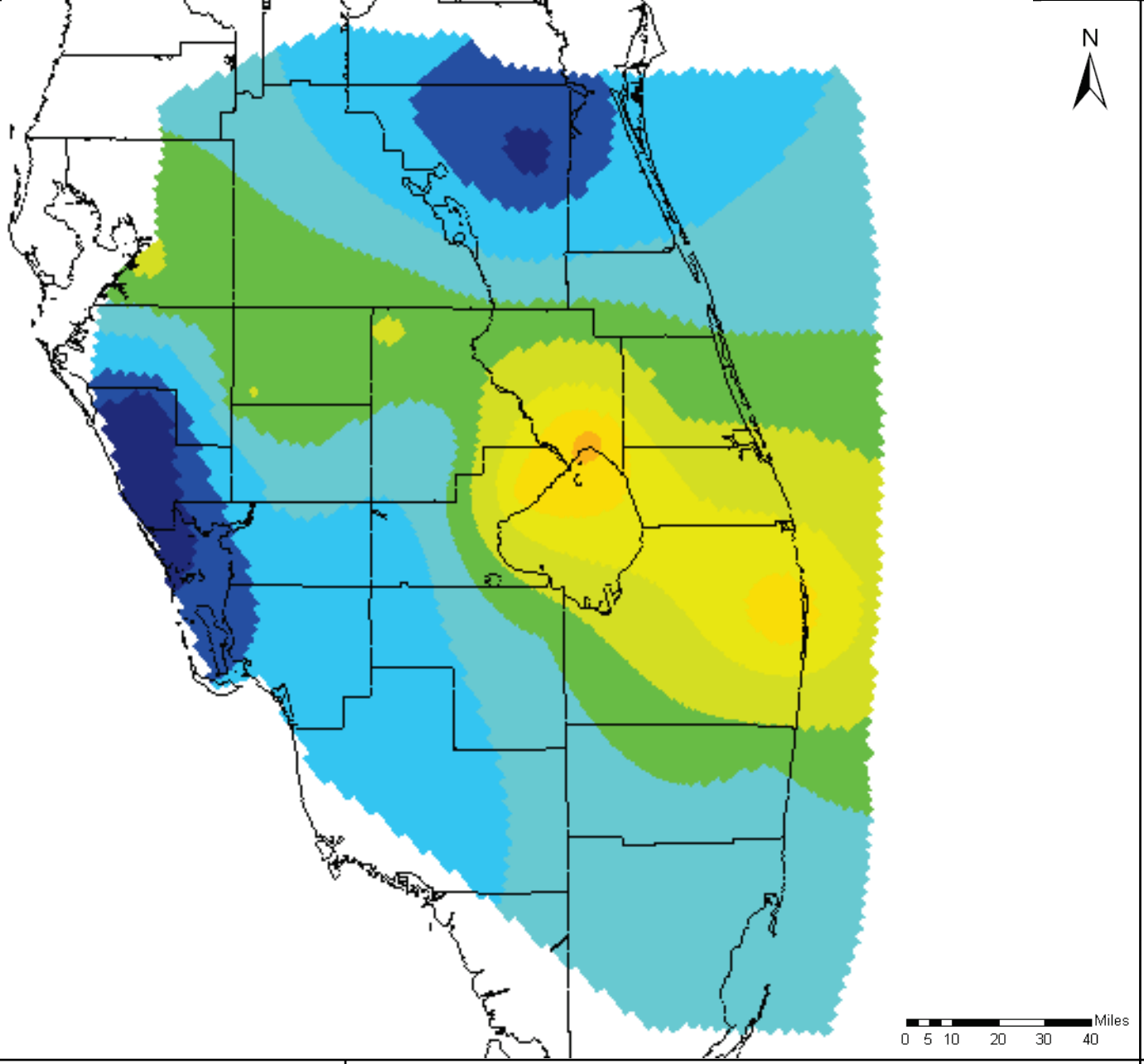

Notes:

Distribution shown was applied to SEAWAT model layers 13 through 15.

Specific Storage values were interpolated to the grid from values assigned to a set of pilot points scattered across the model domain.

A combination of automated calibration (PEST) and manual calibration (trial and error) resulted in this Specific Storage field.

Calibrated SEAWAT Specific Storage
Avon Park Permeable Zone
Final Groundwater Model Calibration Report

Figure F3-25

October 2010

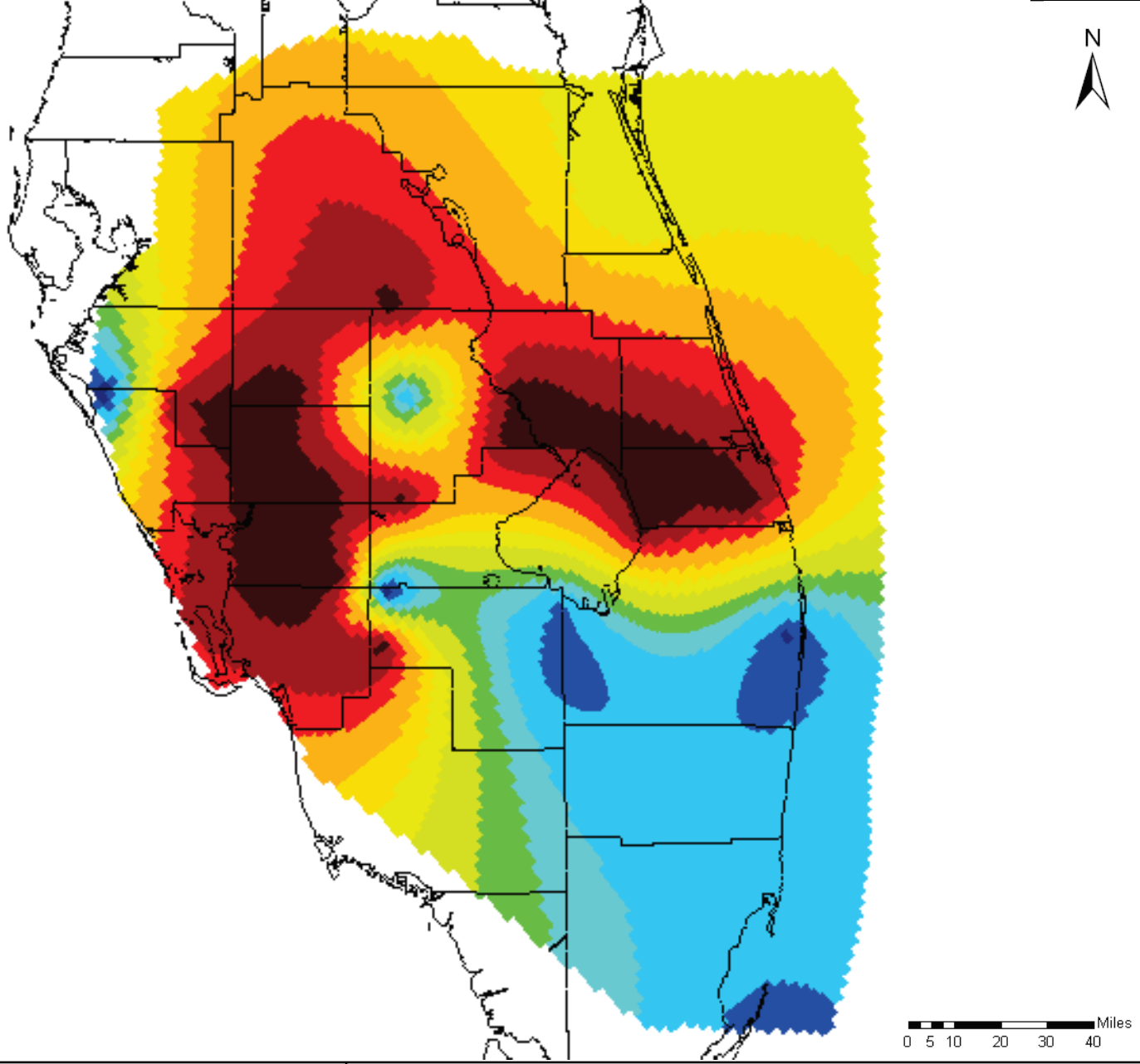

Notes:

Distribution shown was applied to SEAWAT model layers 16 through 17.

Specific Storage values were interpolated to the grid from values assigned to a set of pilot points scattered across the model domain.

A combination of automated calibration (PEST) and manual calibration (trial and error) resulted in this Specific Storage field.

Calibrated SEAWAT Specific Storage
Middle Confining Unit 2
Final Groundwater Model Calibration Report

Figure F3-26

October 2010

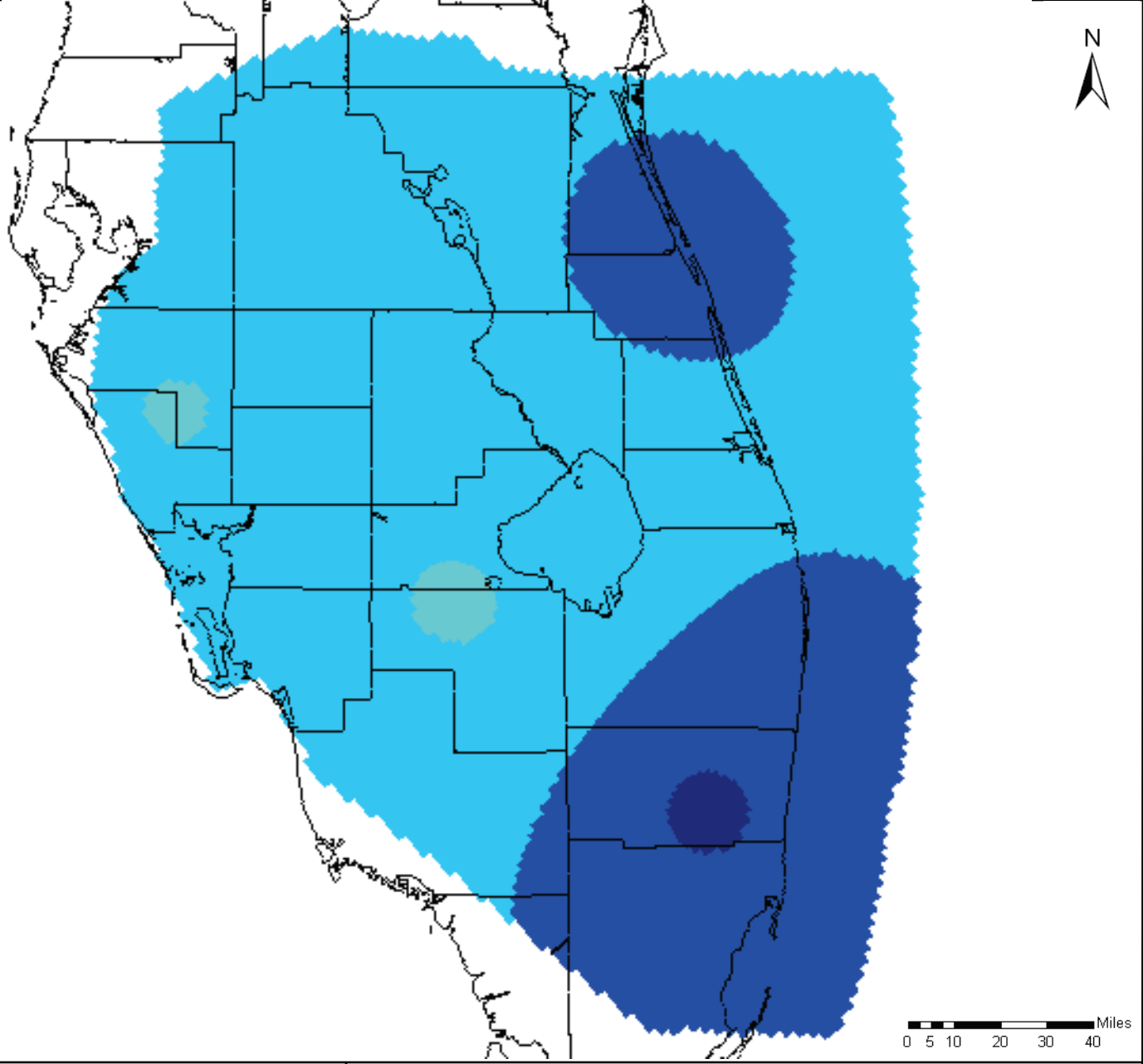

Notes:

Distribution shown was applied to SEAWAT model layers 18 through 19.

Specific Storage values were interpolated to the grid from values assigned to a set of pilot points scattered across the model domain.

A combination of automated calibration (PEST) and manual calibration (trial and error) resulted in this Specific Storage field.

Calibrated SEAWAT Specific Storage
Lower Floridan (LF1) Aquifer
Final Groundwater Model Calibration Report

Figure F3-27

October 2010

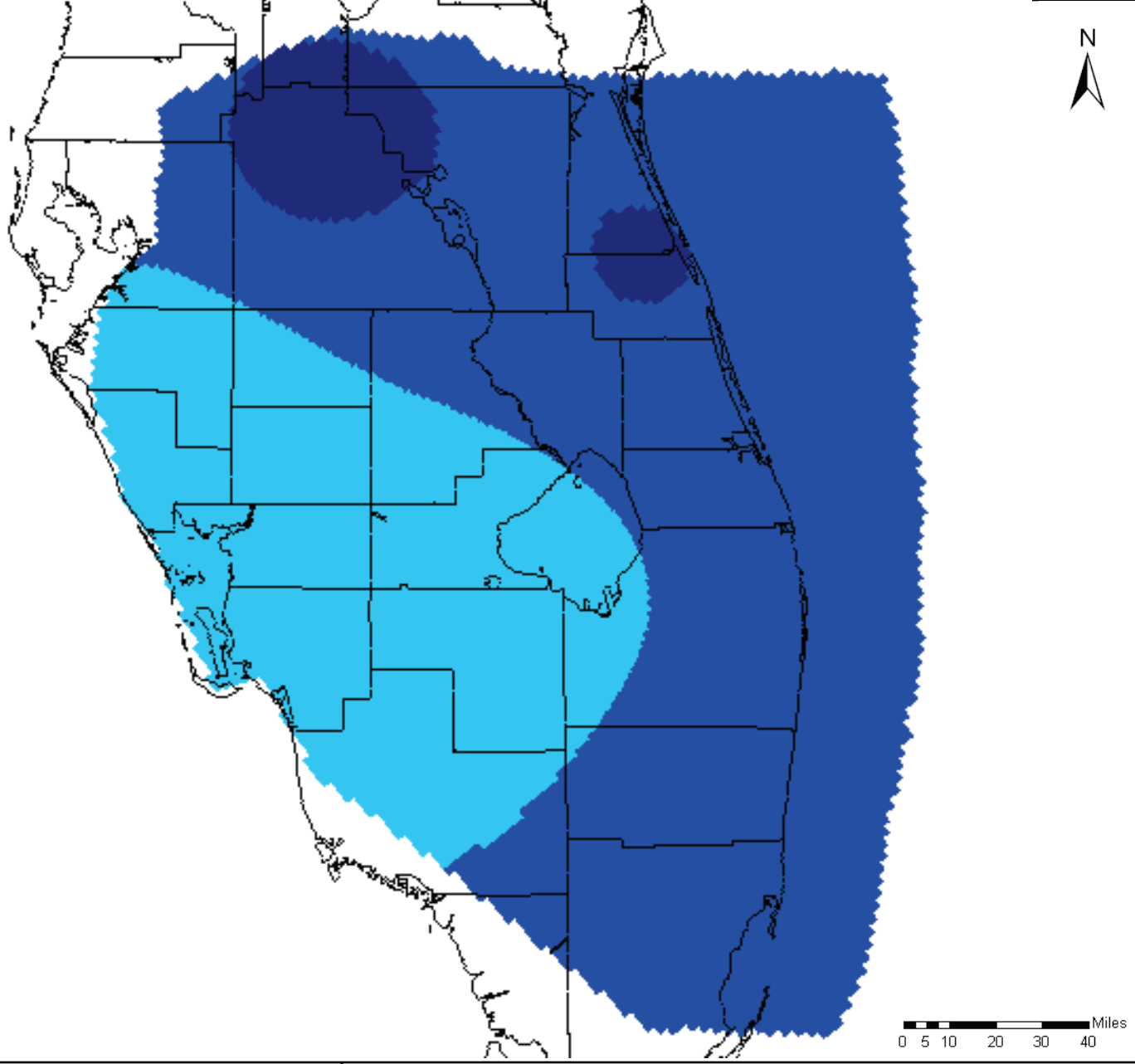

Notes:

Distribution shown was applied to SEAWAT model layers 20 through 21.

Specific Storage values were interpolated to the grid from values assigned to a set of pilot points scattered across the model domain.

A combination of automated calibration (PEST) and manual calibration (trial and error) resulted in this Specific Storage field.

Calibrated SEAWAT Specific Storage
Lower Confining Unit
Final Groundwater Model Calibration Report

Figure F3-28

October 2010

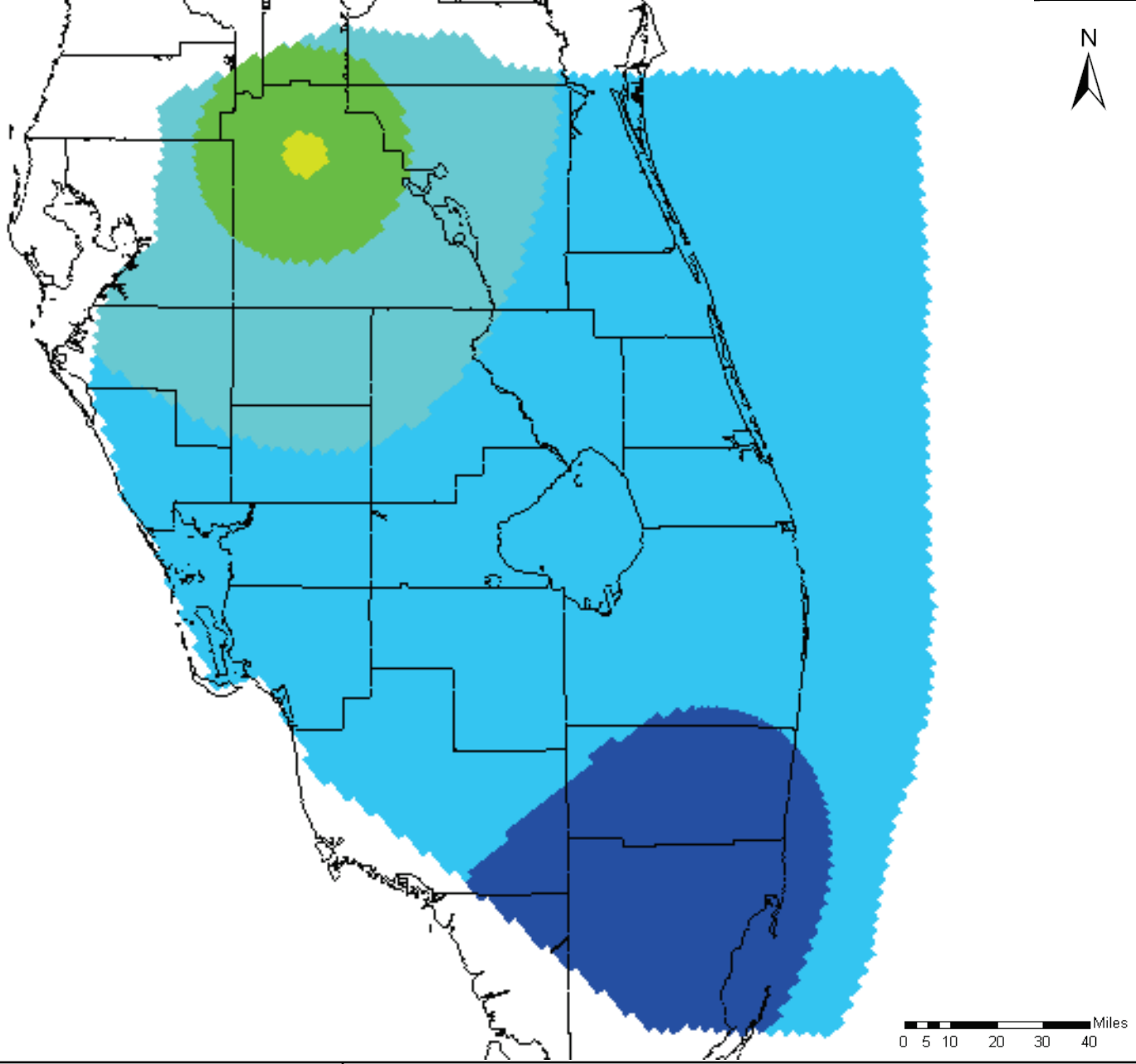

Notes:

Distribution shown was applied to SEAWAT model layer 22.

Specific Storage values were interpolated to the grid from values assigned to a set of pilot points scattered across the model domain.

A combination of automated calibration (PEST) and manual calibration (trial and error) resulted in this Specific Storage field.

Calibrated SEAWAT Specific Storage
Boulder Zone
Final Groundwater Model Calibration Report

Figure F3-29

October 2010

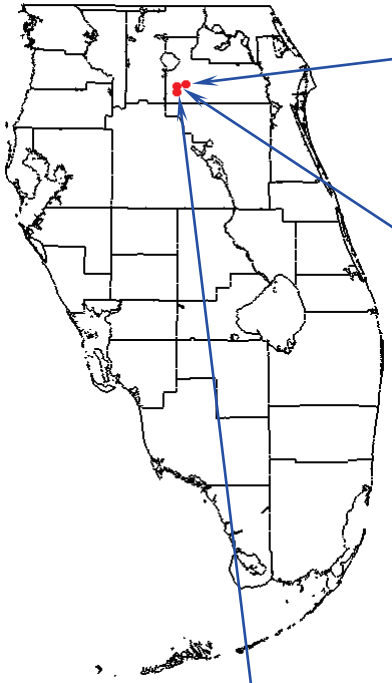

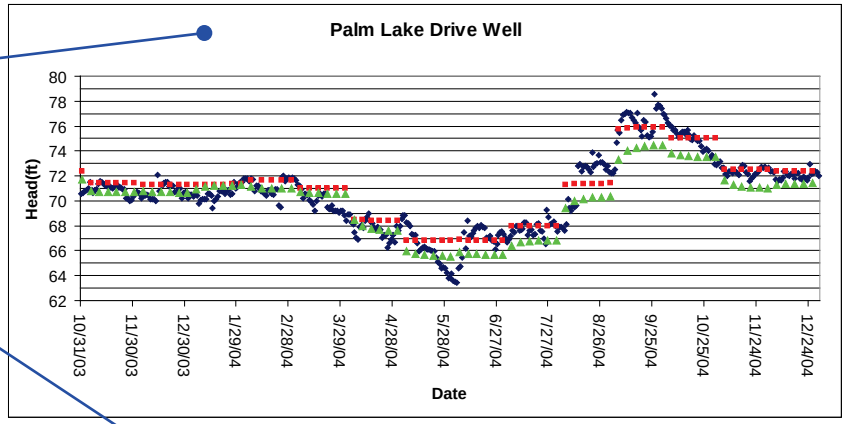

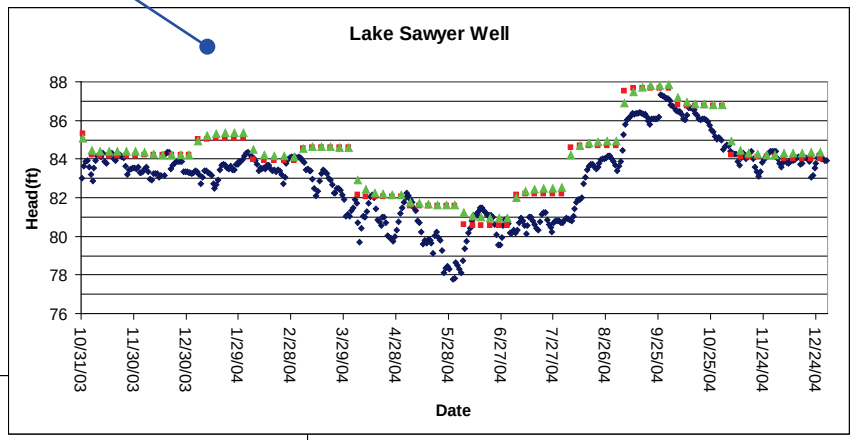

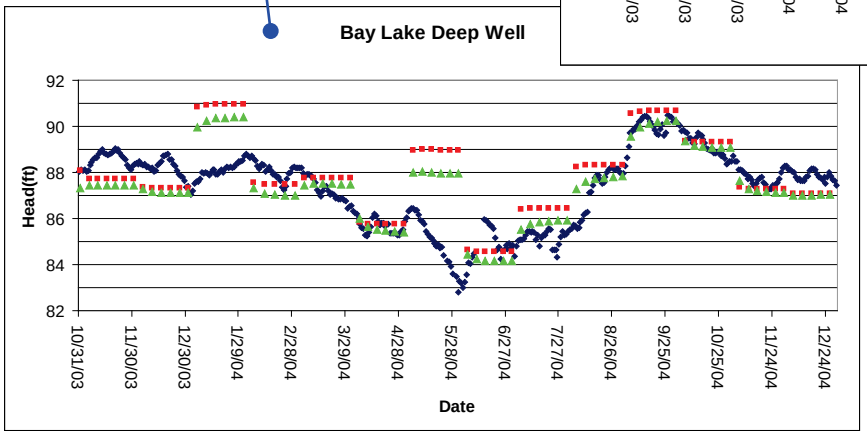

Legend

- Measured Head
- SEAWAT Calculated Head
- WASH123D Calculated Head

Notes:

Figures 4.102 through 4.122 show the comparison between measured head values, model-calculated head values from the SEAWAT model and model-calculated head values from the WASH123D model at a number of observation wells for the calibration period. Although the scales vary on each plot, all plots have a horizontal grid line at each foot. This is to make it easy to determine the range of heads at a glance.

The model used month-long stress periods, so pumping and boundary conditions were input as step functions with constant values throughout each month and sudden changes at the end of each month. For this reason, the model cannot be expected to accurately predict day-to-day head variations in any of these wells. Calibration efforts were aimed at matching general trends and monthly averages.

Starting head conditions for this model were computed in WASH123D based on October 2003 steady state conditions. Transient calibration efforts incorporated values of hydraulic conductivity and storage that were consistent with the SEAWAT model. As with the SEAWAT model, it is not uncommon for residuals in the starting condition to be carried through the entire calibration period. This indicates that the model is correctly predicting responses to hydrogeologic forces even if the calculated head values vary somewhat from the measured values.

Transient WASH123D Calibration Comparison
Upper Floridan Aquifer (2003-2004)

Final Groundwater Model Calibration Report

Figure F3-30

October 2010

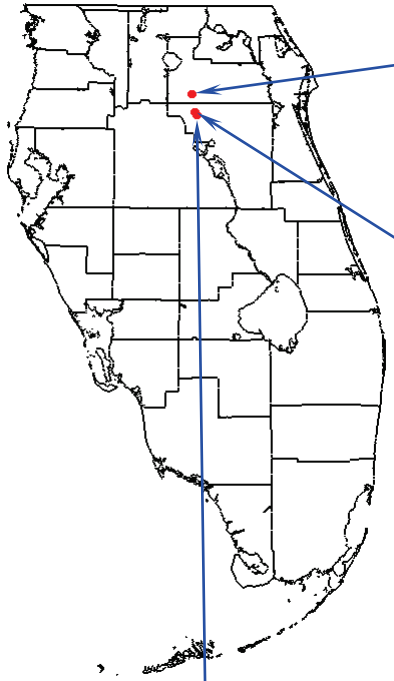

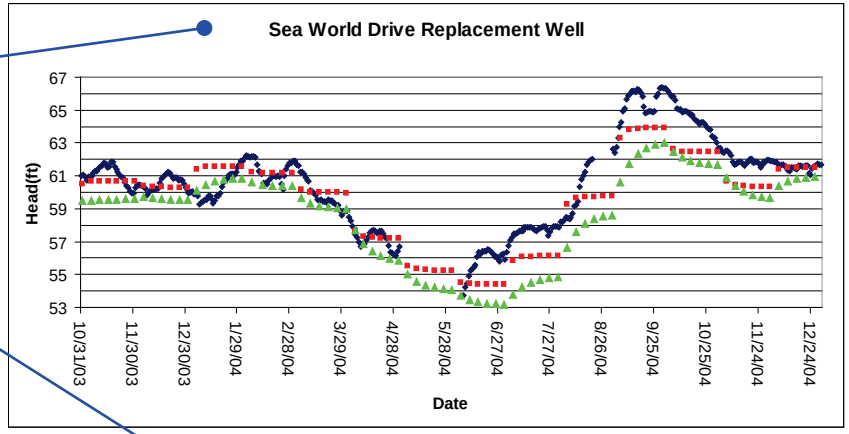

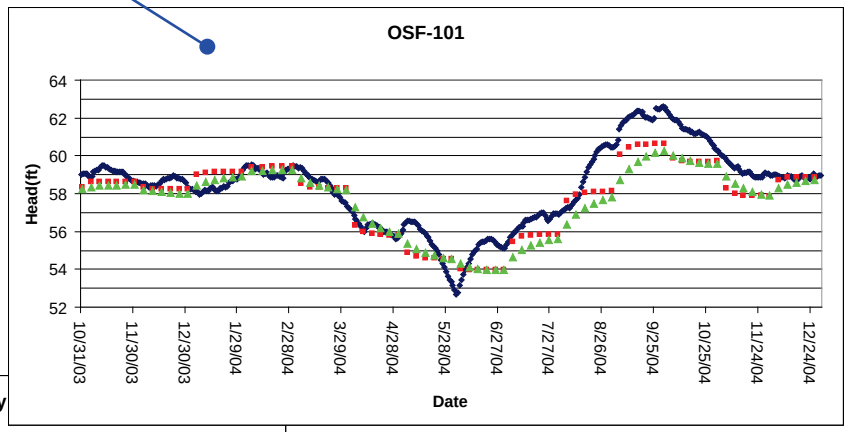

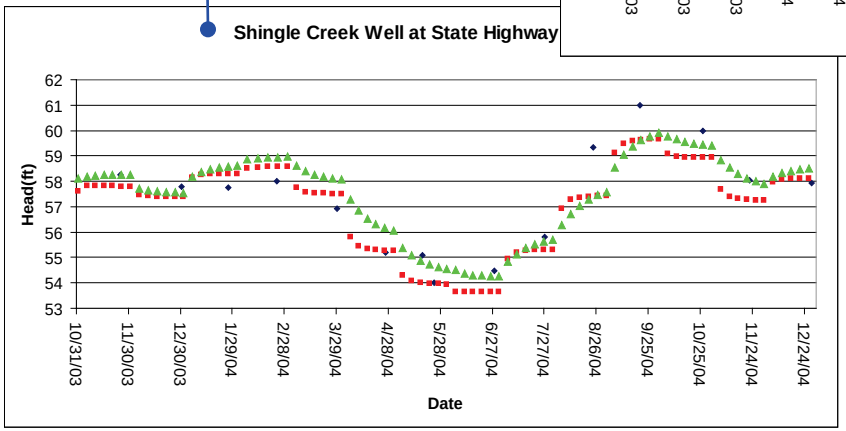

Legend

- Measured Head
- SEAWAT Calculated Head
- WASH123D Calculated Head

Notes:

Figures 4.102 through 4.122 show the comparison between measured head values, model-calculated head values from the SEAWAT model and model-calculated head values from the WASH123D model at a number of observation wells for the calibration period. Although the scales vary on each plot, all plots have a horizontal grid line at each foot. This is to make it easy to determine the range of heads at a glance.

The model used month-long stress periods, so pumping and boundary conditions were input as step functions with constant values throughout each month and sudden changes at the end of each month. For this reason, the model cannot be expected to accurately predict day-to-day head variations in any of these wells. Calibration efforts were aimed at matching general trends and monthly averages.

Starting head conditions for this model were computed in WASH123D based on October 2003 steady state conditions. Transient calibration efforts incorporated values of hydraulic conductivity and storage that were consistent with the SEAWAT model. As with the SEAWAT model, it is not uncommon for residuals in the starting condition to be carried through the entire calibration period. This indicates that the model is correctly predicting responses to hydrogeologic forces even if the calculated head values vary somewhat from the measured values.

Transient WASH123D Calibration Comparison
Upper Floridan Aquifer (2003-2004)

Final Groundwater Model Calibration Report

Figure F3-31

October 2010

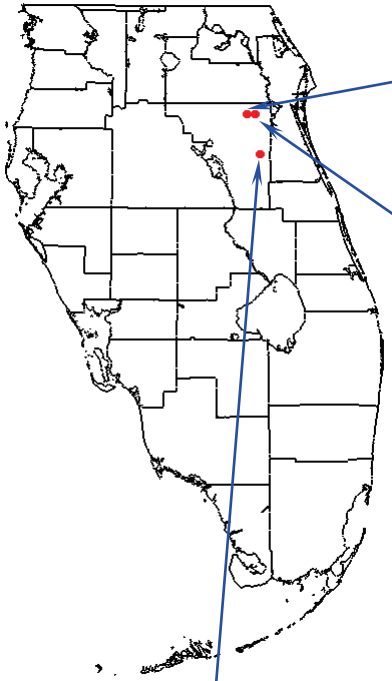

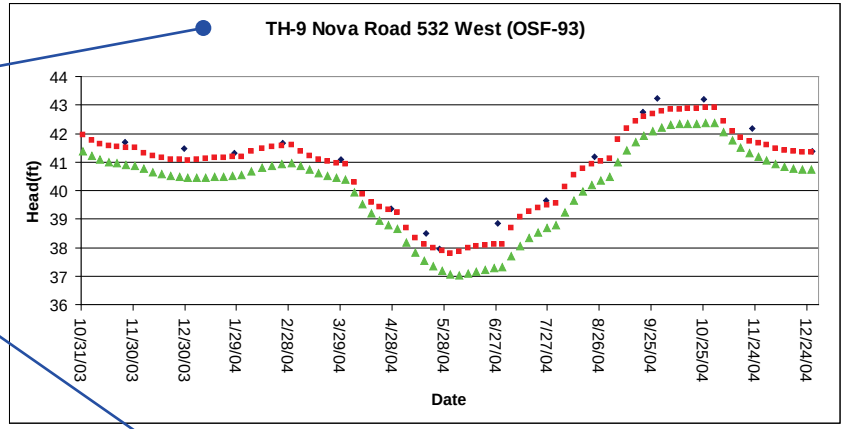

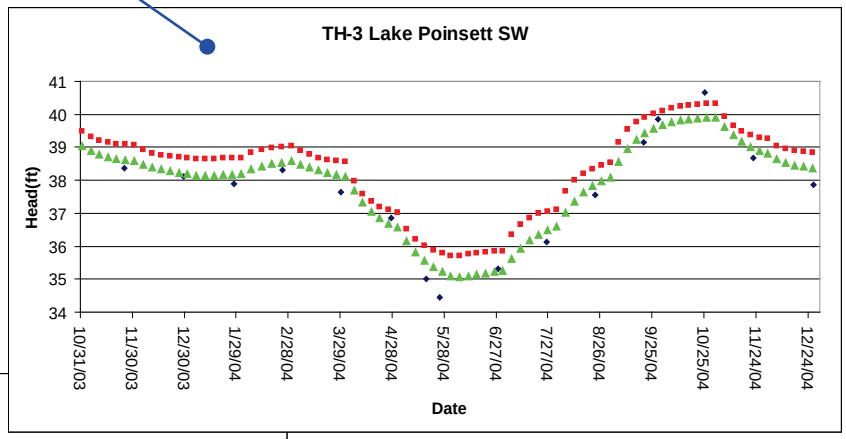

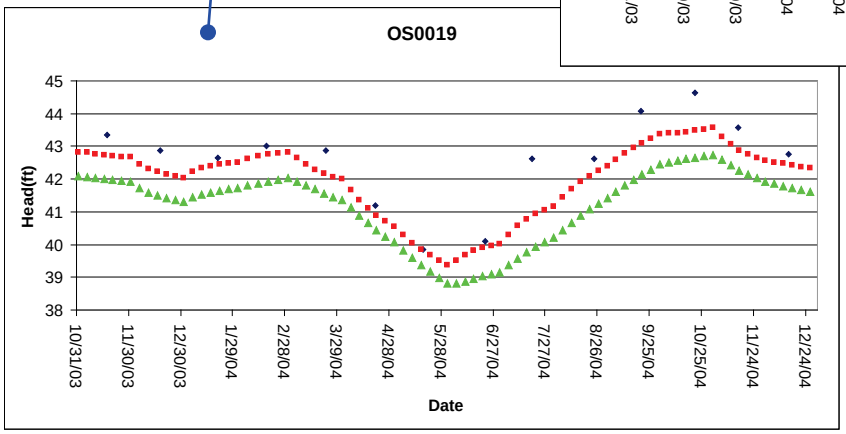

Legend

- Measured Head
- SEAWAT Calculated Head
- WASH123D Calculated Head

Notes:

Figures 4.102 through 4.122 show the comparison between measured head values, model-calculated head values from the SEAWAT model and model-calculated head values from the WASH123D model at a number of observation wells for the calibration period. Although the scales vary on each plot, all plots have a horizontal grid line at each foot. This is to make it easy to determine the range of heads at a glance.

The model used month-long stress periods, so pumping and boundary conditions were input as step functions with constant values throughout each month and sudden changes at the end of each month. For this reason, the model cannot be expected to accurately predict day-to-day head variations in any of these wells. Calibration efforts were aimed at matching general trends and monthly averages.

Starting head conditions for this model were computed in WASH123D based on October 2003 steady state conditions. Transient calibration efforts incorporated values of hydraulic conductivity and storage that were consistent with the SEAWAT model. As with the SEAWAT model, it is not uncommon for residuals in the starting condition to be carried through the entire calibration period. This indicates that the model is correctly predicting responses to hydrogeologic forces even if the calculated head values vary somewhat from the measured values.

Transient WASH123D Calibration Comparison
Upper Floridan Aquifer (2003-2004)

Final Groundwater Model Calibration Report

Figure F3-32

October 2010

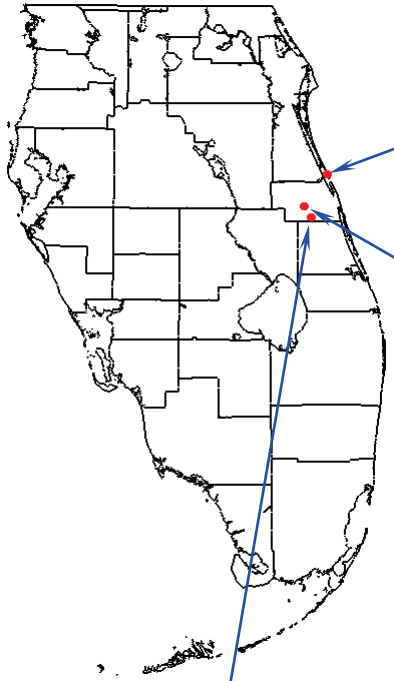

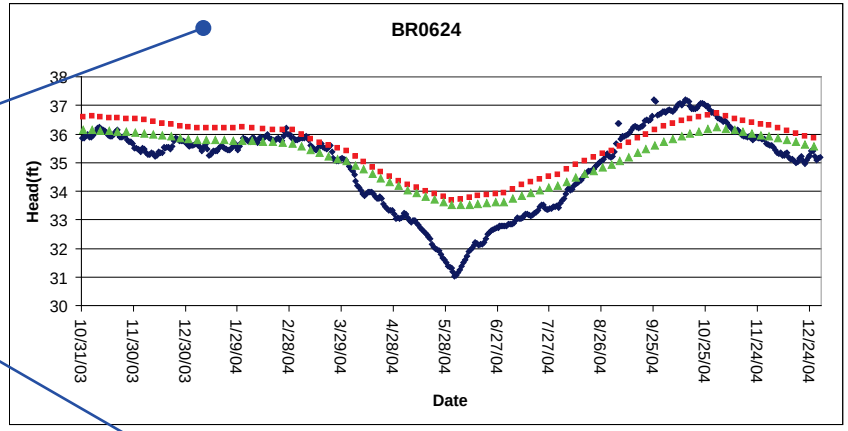

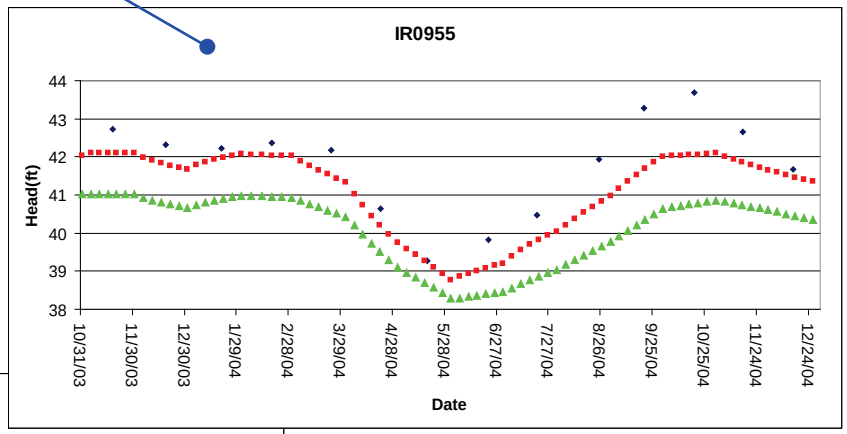

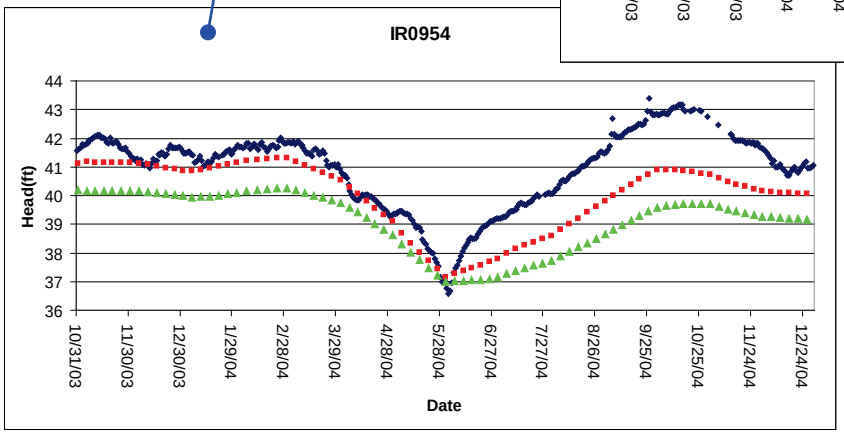

Legend

- Measured Head
- SEAWAT Calculated Head
- WASH123D Calculated Head

Notes:

Figures 4.102 through 4.122 show the comparison between measured head values, model-calculated head values from the SEAWAT model and model-calculated head values from the WASH123D model at a number of observation wells for the calibration period. Although the scales vary on each plot, all plots have a horizontal grid line at each foot. This is to make it easy to determine the range of heads at a glance.

The model used month-long stress periods, so pumping and boundary conditions were input as step functions with constant values throughout each month and sudden changes at the end of each month. For this reason, the model cannot be expected to accurately predict day-to-day head variations in any of these wells. Calibration efforts were aimed at matching general trends and monthly averages.

Starting head conditions for this model were computed in WASH123D based on October 2003 steady state conditions. Transient calibration efforts incorporated values of hydraulic conductivity and storage that were consistent with the SEAWAT model. As with the SEAWAT model, it is not uncommon for residuals in the starting condition to be carried through the entire calibration period. This indicates that the model is correctly predicting responses to hydrogeologic forces even if the calculated head values vary somewhat from the measured values.

Transient WASH123D Calibration Comparison
Upper Floridan Aquifer (2003 – 2004)

Final Groundwater Model Calibration Report

Figure F3-33

October 2010

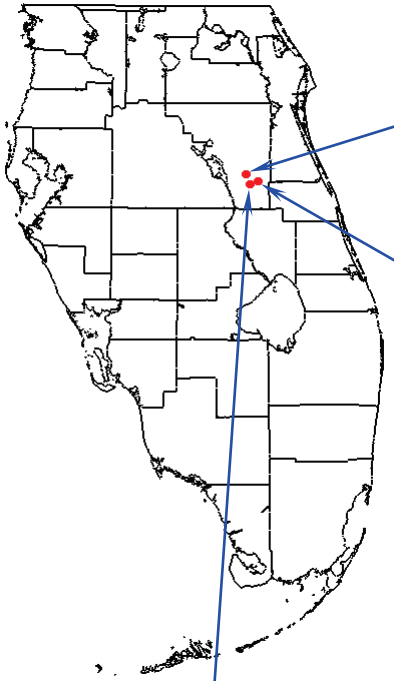

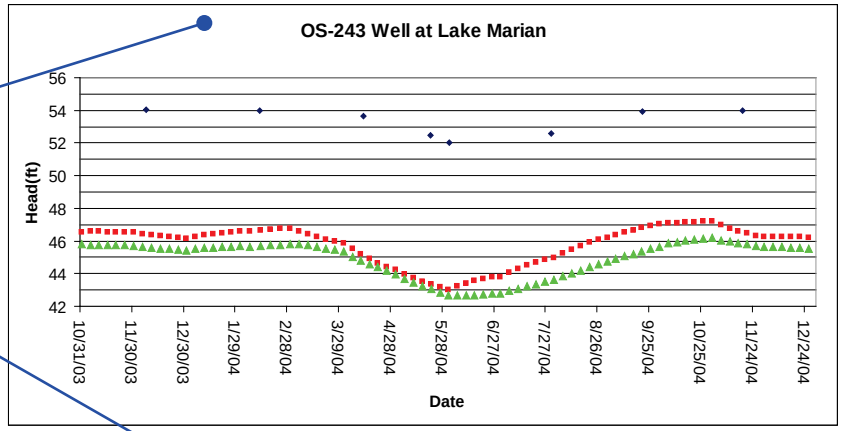

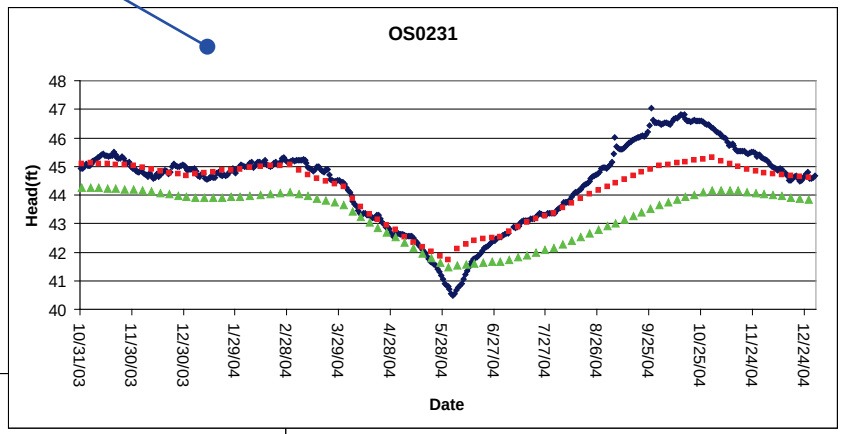

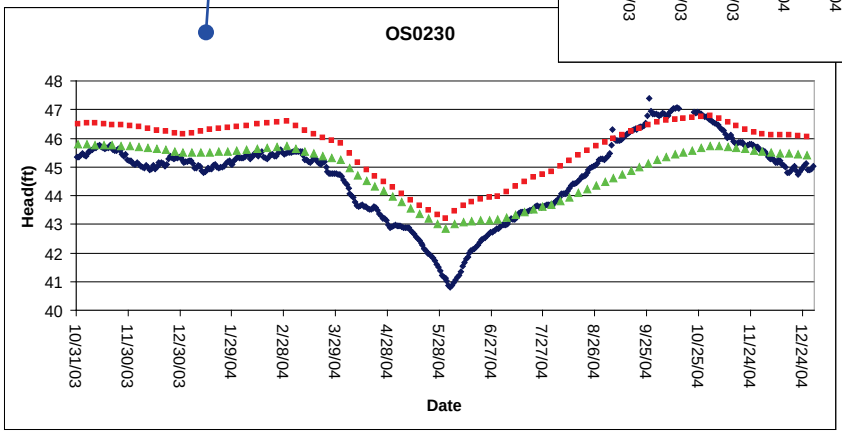

Legend

- Measured Head
- SEAWAT Calculated Head
- WASH123D Calculated Head

Notes:

Figures 4.102 through 4.122 show the comparison between measured head values, model-calculated head values from the SEAWAT model and model-calculated head values from the WASH123D model at a number of observation wells for the calibration period. Although the scales vary on each plot, all plots have a horizontal grid line at each foot. This is to make it easy to determine the range of heads at a glance.

The model used month-long stress periods, so pumping and boundary conditions were input as step functions with constant values throughout each month and sudden changes at the end of each month. For this reason, the model cannot be expected to accurately predict day-to-day head variations in any of these wells. Calibration efforts were aimed at matching general trends and monthly averages.

Starting head conditions for this model were computed in WASH123D based on October 2003 steady state conditions. Transient calibration efforts incorporated values of hydraulic conductivity and storage that were consistent with the SEAWAT model. As with the SEAWAT model, it is not uncommon for residuals in the starting condition to be carried through the entire calibration period. This indicates that the model is correctly predicting responses to hydrogeologic forces even if the calculated head values vary somewhat from the measured values.

Transient WASH123D Calibration Comparison
Upper Floridan Aquifer (2003-2004)
Final Groundwater Model Calibration Report

Figure F3-34

October 2010

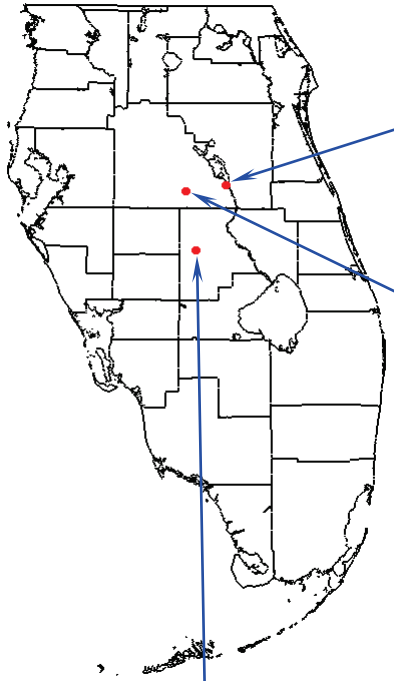

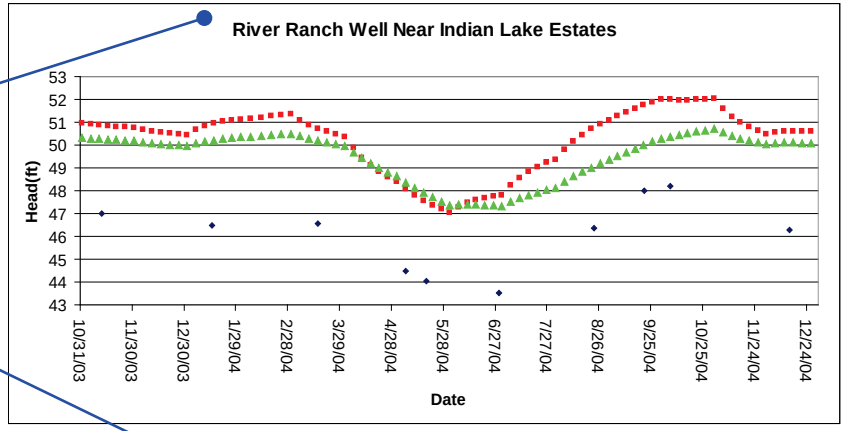

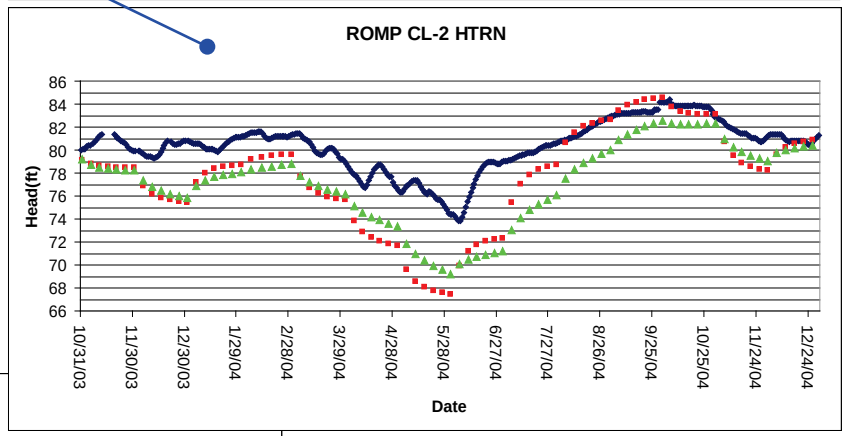

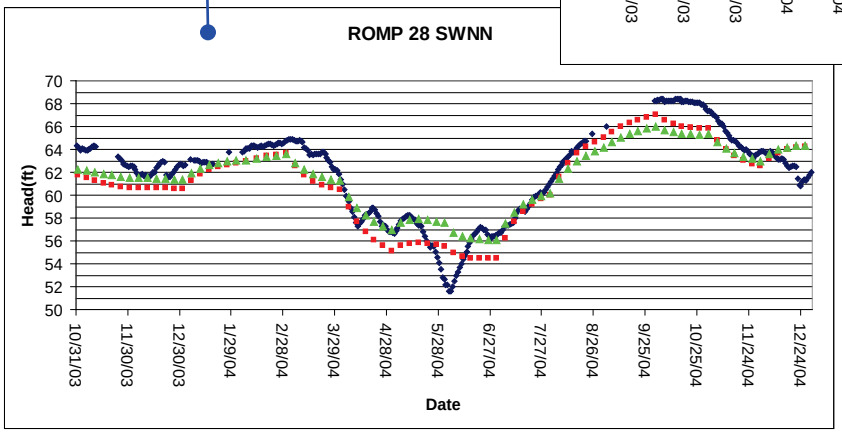

Legend

- Measured Head
- SEAWAT Calculated Head
- WASH123D Calculated Head

Notes:

Figures 4.102 through 4.122 show the comparison between measured head values, model-calculated head values from the SEAWAT model and model-calculated head values from the WASH123D model at a number of observation wells for the calibration period. Although the scales vary on each plot, all plots have a horizontal grid line at each foot. This is to make it easy to determine the range of heads at a glance.

The model used month-long stress periods, so pumping and boundary conditions were input as step functions with constant values throughout each month and sudden changes at the end of each month. For this reason, the model cannot be expected to accurately predict day-to-day head variations in any of these wells. Calibration efforts were aimed at matching general trends and monthly averages.

Starting head conditions for this model were computed in WASH123D based on October 2003 steady state conditions. Transient calibration efforts incorporated values of hydraulic conductivity and storage that were consistent with the SEAWAT model. As with the SEAWAT model, it is not uncommon for residuals in the starting condition to be carried through the entire calibration period. This indicates that the model is correctly predicting responses to hydrogeologic forces even if the calculated head values vary somewhat from the measured values.

Transient WASH123D Calibration Comparison
Upper Floridan Aquifer (2003-2004)

Final Groundwater Model Calibration Report

Figure F3-35

October 2010

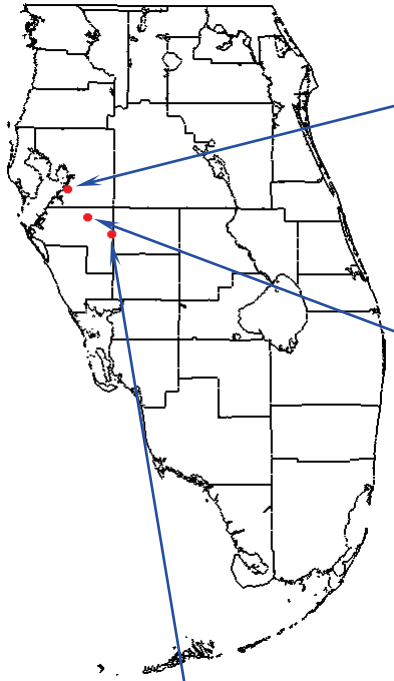

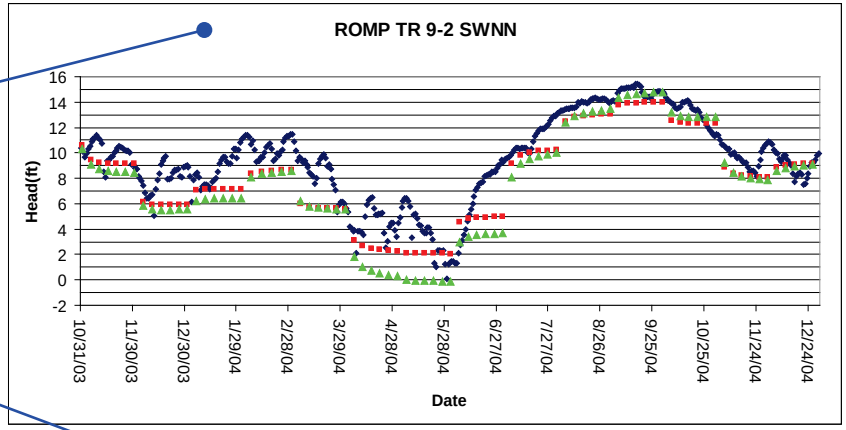

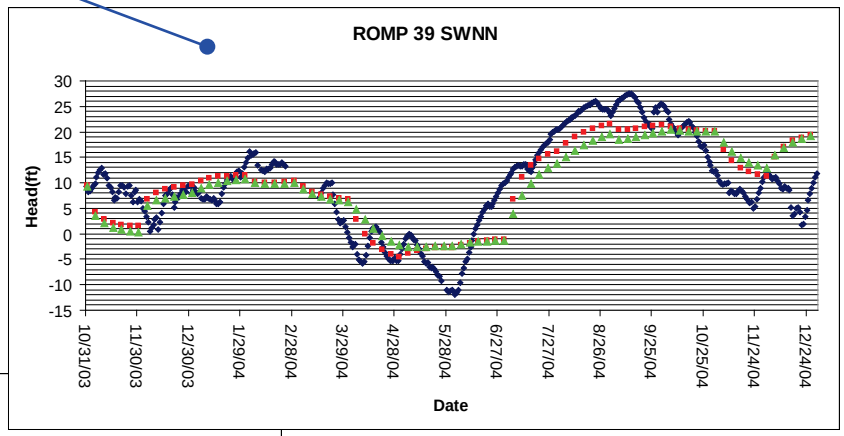

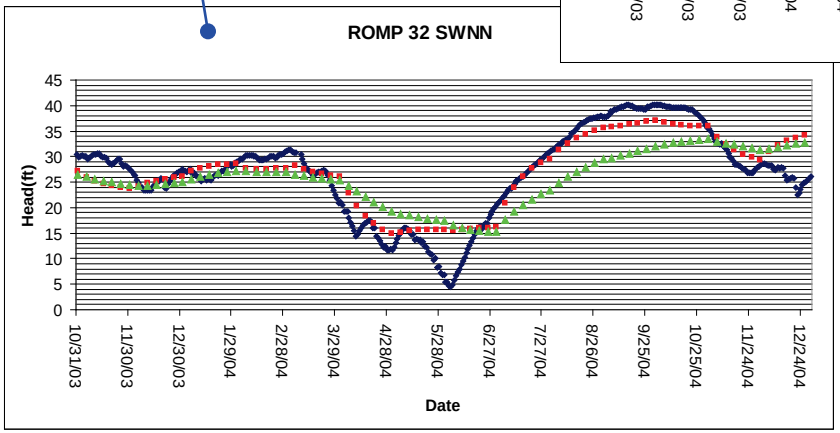

Legend

- Measured Head
- SEAWAT Calculated Head
- WASH123D Calculated Head

Notes:

Figures 4.102 through 4.122 show the comparison between measured head values, model-calculated head values from the SEAWAT model and model-calculated head values from the WASH123D model at a number of observation wells for the calibration period. Although the scales vary on each plot, all plots have a horizontal grid line at each foot. This is to make it easy to determine the range of heads at a glance.

The model used month-long stress periods, so pumping and boundary conditions were input as step functions with constant values throughout each month and sudden changes at the end of each month. For this reason, the model cannot be expected to accurately predict day-to-day head variations in any of these wells. Calibration efforts were aimed at matching general trends and monthly averages.

Starting head conditions for this model were computed in WASH123D based on October 2003 steady state conditions. Transient calibration efforts incorporated values of hydraulic conductivity and storage that were consistent with the SEAWAT model. As with the SEAWAT model, it is not uncommon for residuals in the starting condition to be carried through the entire calibration period. This indicates that the model is correctly predicting responses to hydrogeologic forces even if the calculated head values vary somewhat from the measured values.

Transient WASH123D Calibration Comparison
Upper Floridan Aquifer (2003-2004)
Final Groundwater Model Calibration Report

Figure F3-36

October 2010

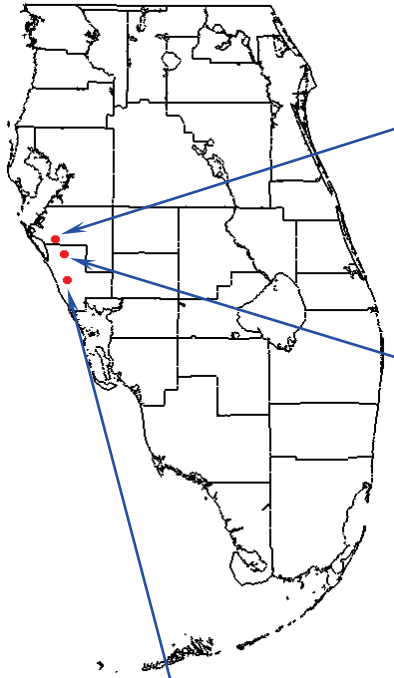

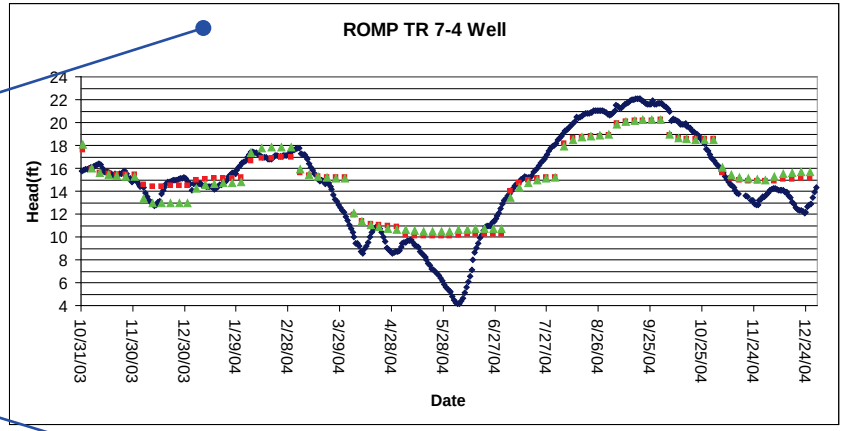

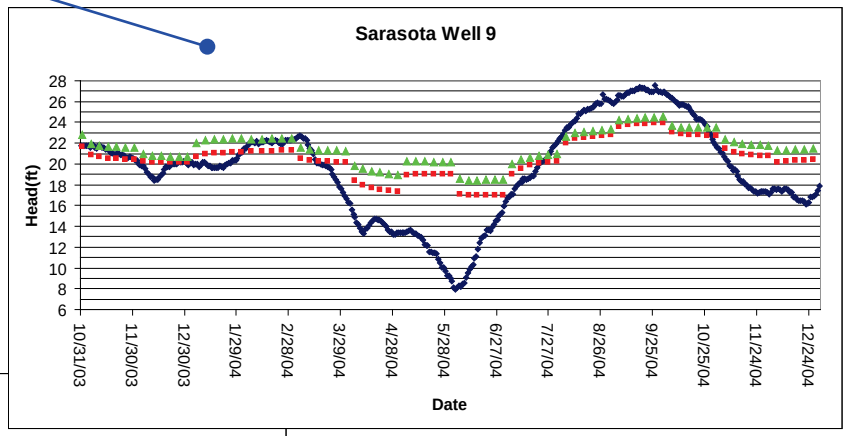

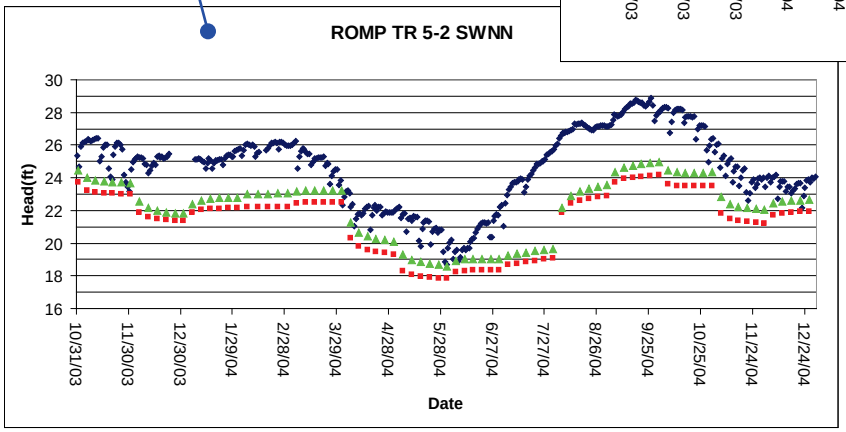

Legend

- Measured Head
- SEAWAT Calculated Head
- WASH123D Calculated Head

Notes:

Figures 4.102 through 4.122 show the comparison between measured head values, model-calculated head values from the SEAWAT model and model-calculated head values from the WASH123D model at a number of observation wells for the calibration period. Although the scales vary on each plot, all plots have a horizontal grid line at each foot. This is to make it easy to determine the range of heads at a glance.

The model used month-long stress periods, so pumping and boundary conditions were input as step functions with constant values throughout each month and sudden changes at the end of each month. For this reason, the model cannot be expected to accurately predict day-to-day head variations in any of these wells. Calibration efforts were aimed at matching general trends and monthly averages.

Starting head conditions for this model were computed in WASH123D based on October 2003 steady state conditions. Transient calibration efforts incorporated values of hydraulic conductivity and storage that were consistent with the SEAWAT model. As with the SEAWAT model, it is not uncommon for residuals in the starting condition to be carried through the entire calibration period. This indicates that the model is correctly predicting responses to hydrogeologic forces even if the calculated head values vary somewhat from the measured values.

Transient WASH123D Calibration Comparison
Upper Floridan Aquifer (2003-2004)
Final Groundwater Model Calibration Report

Figure F3-37

October 2010

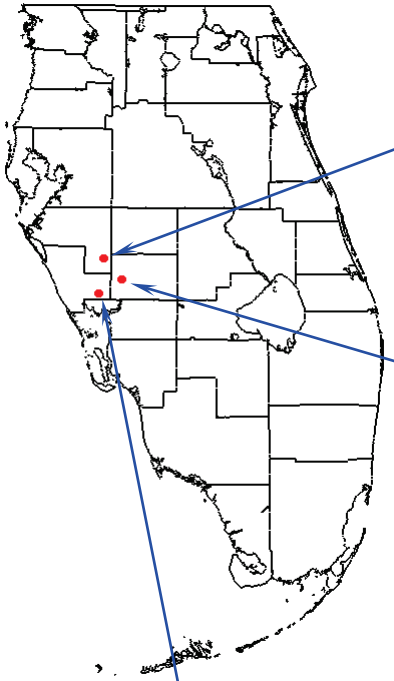

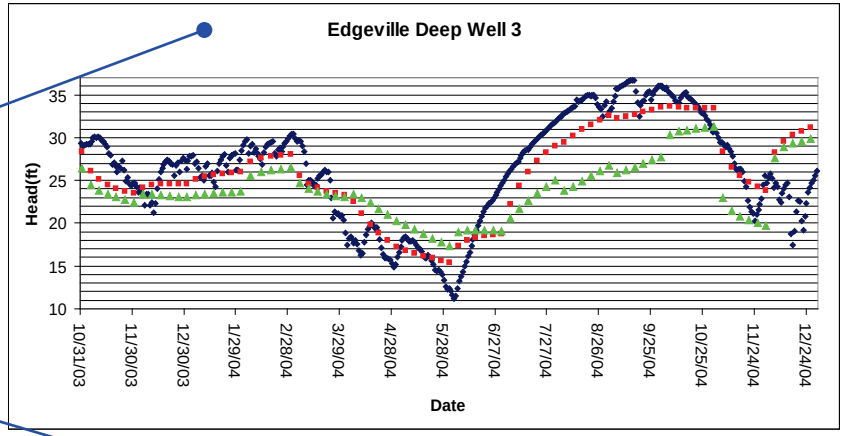

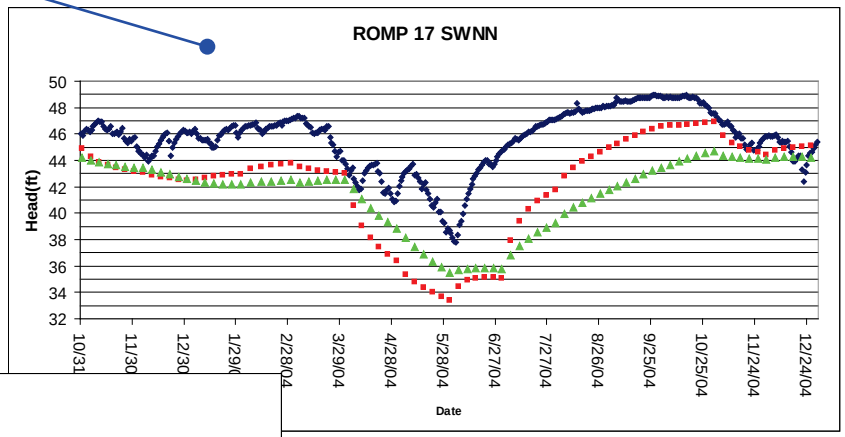

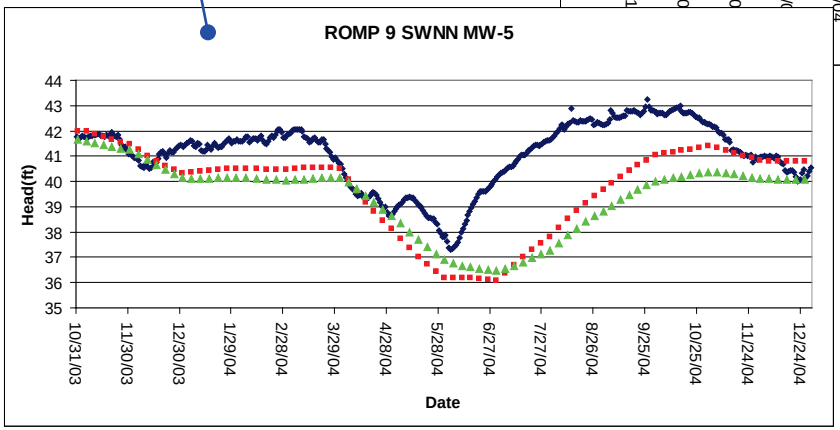

Legend

- Measured Head
- SEAWAT Calculated Head
- WASH123D Calculated Head

Notes:

Figures 4.102 through 4.122 show the comparison between measured head values, model-calculated head values from the SEAWAT model and model-calculated head values from the WASH123D model at a number of observation wells for the calibration period. Although the scales vary on each plot, all plots have a horizontal grid line at each foot. This is to make it easy to determine the range of heads at a glance.

The model used month-long stress periods, so pumping and boundary conditions were input as step functions with constant values throughout each month and sudden changes at the end of each month. For this reason, the model cannot be expected to accurately predict day-to-day head variations in any of these wells. Calibration efforts were aimed at matching general trends and monthly averages.

Starting head conditions for this model were computed in WASH123D based on October 2003 steady state conditions. Transient calibration efforts incorporated values of hydraulic conductivity and storage that were consistent with the SEAWAT model. As with the SEAWAT model, it is not uncommon for residuals in the starting condition to be carried through the entire calibration period. This indicates that the model is correctly predicting responses to hydrogeologic forces even if the calculated head values vary somewhat from the measured values.

Transient WASH123D Calibration Comparison
Upper Floridan Aquifer (2003-2004)
Final Groundwater Model Calibration Report

Figure F3-38

October 2010

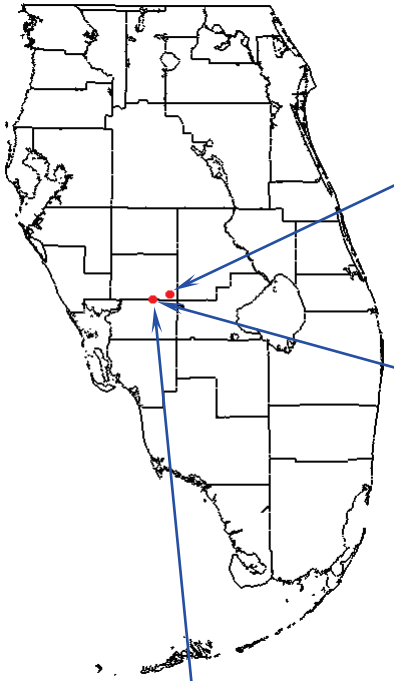

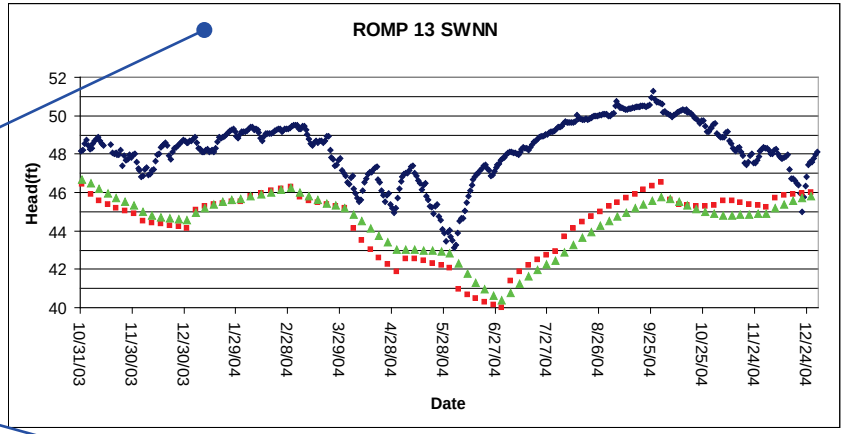

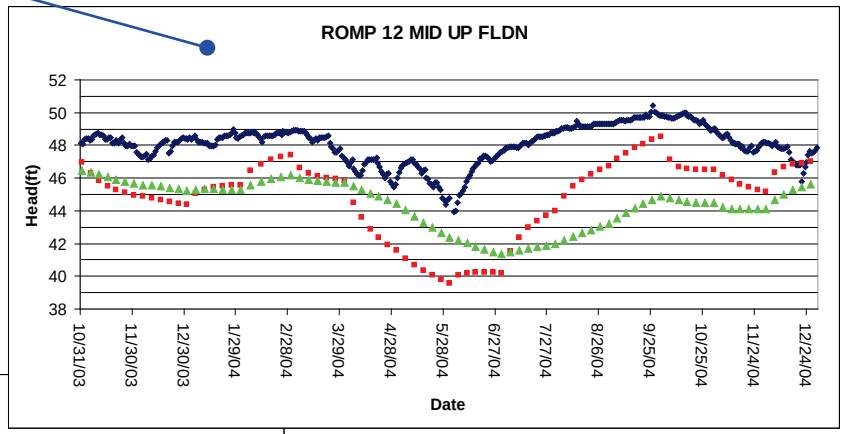

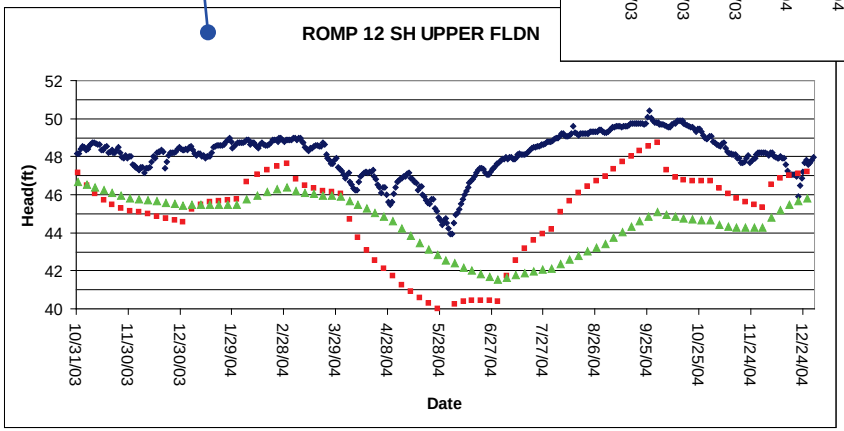

Legend

- Measured Head
- SEAWAT Calculated Head
- WASH123D Calculated Head

Notes:

Figures 4.102 through 4.122 show the comparison between measured head values, model-calculated head values from the SEAWAT model and model-calculated head values from the WASH123D model at a number of observation wells for the calibration period. Although the scales vary on each plot, all plots have a horizontal grid line at each foot. This is to make it easy to determine the range of heads at a glance.

The model used month-long stress periods, so pumping and boundary conditions were input as step functions with constant values throughout each month and sudden changes at the end of each month. For this reason, the model cannot be expected to accurately predict day-to-day head variations in any of these wells. Calibration efforts were aimed at matching general trends and monthly averages.

Starting head conditions for this model were computed in WASH123D based on October 2003 steady state conditions. Transient calibration efforts incorporated values of hydraulic conductivity and storage that were consistent with the SEAWAT model. As with the SEAWAT model, it is not uncommon for residuals in the starting condition to be carried through the entire calibration period. This indicates that the model is correctly predicting responses to hydrogeologic forces even if the calculated head values vary somewhat from the measured values.

Transient WASH123D Calibration Comparison
Upper Floridan Aquifer (2003-2004)
Final Groundwater Model Calibration Report

Figure F3-39

October 2010

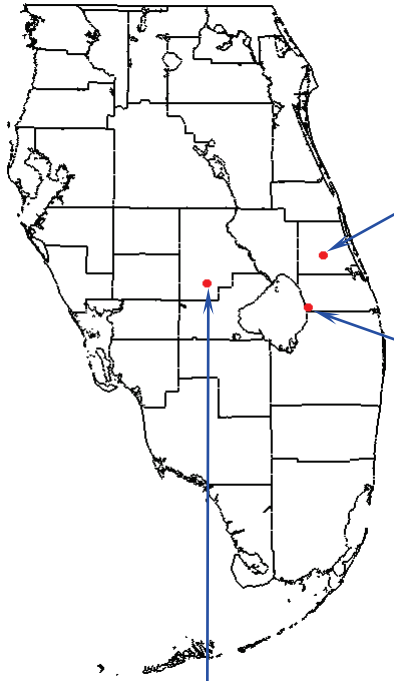

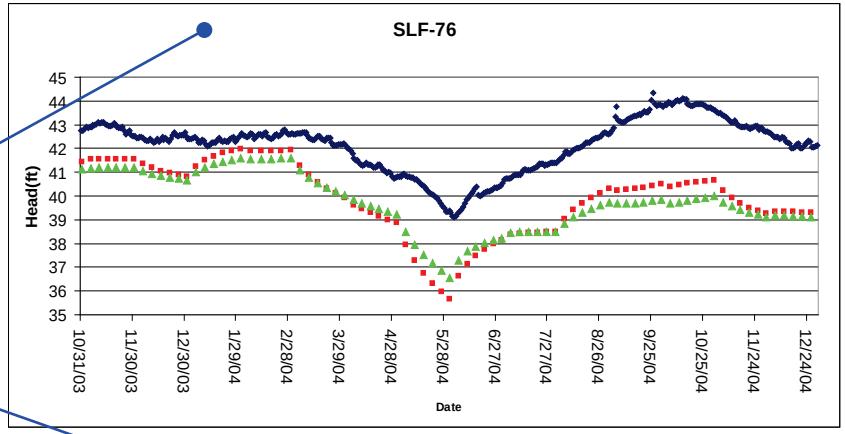

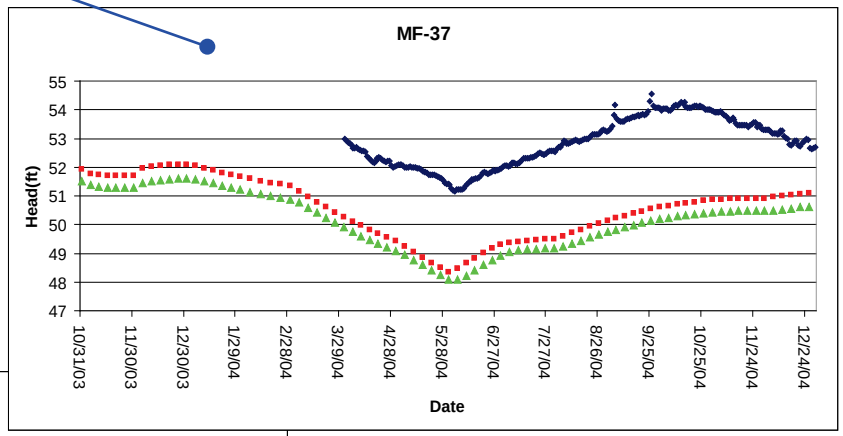

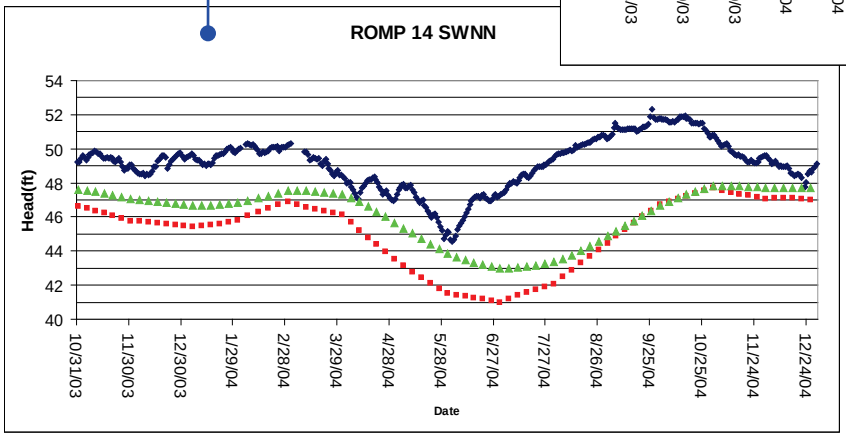

Legend

- Measured Head
- SEAWAT Calculated Head
- WASH123D Calculated Head

Notes:

Figures 4.102 through 4.122 show the comparison between measured head values, model-calculated head values from the SEAWAT model and model-calculated head values from the WASH123D model at a number of observation wells for the calibration period. Although the scales vary on each plot, all plots have a horizontal grid line at each foot. This is to make it easy to determine the range of heads at a glance.

The model used month-long stress periods, so pumping and boundary conditions were input as step functions with constant values throughout each month and sudden changes at the end of each month. For this reason, the model cannot be expected to accurately predict day-to-day head variations in any of these wells. Calibration efforts were aimed at matching general trends and monthly averages.

Starting head conditions for this model were computed in WASH123D based on October 2003 steady state conditions. Transient calibration efforts incorporated values of hydraulic conductivity and storage that were consistent with the SEAWAT model. As with the SEAWAT model, it is not uncommon for residuals in the starting condition to be carried through the entire calibration period. This indicates that the model is correctly predicting responses to hydrogeologic forces even if the calculated head values vary somewhat from the measured values.

Transient WASH123D Calibration Comparison
Upper Floridan Aquifer (2003-2004)

Final Groundwater Model Calibration Report

Figure F3-40

October 2010

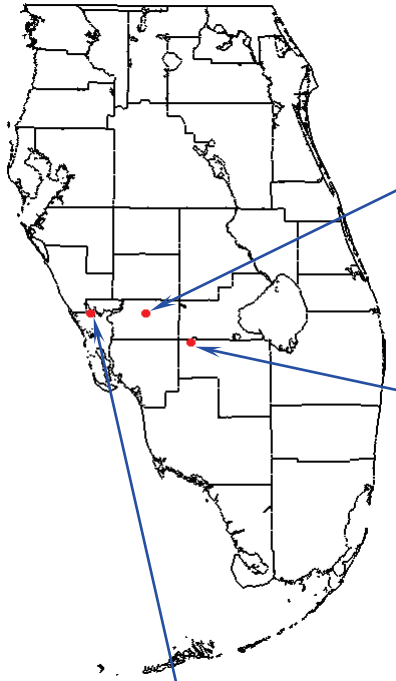

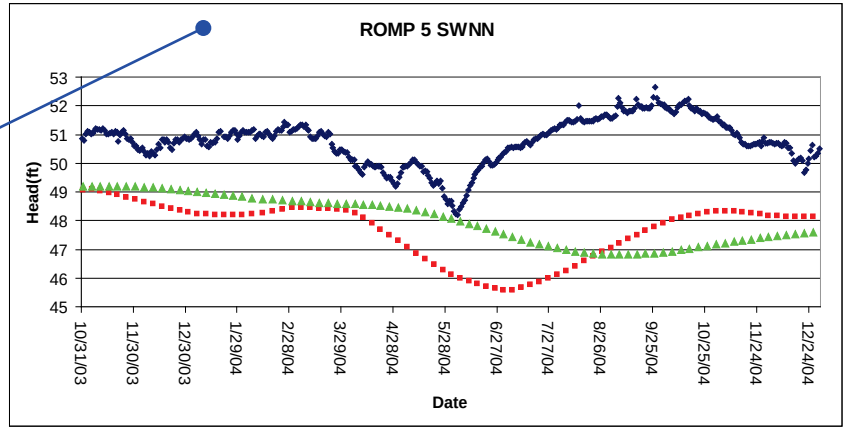

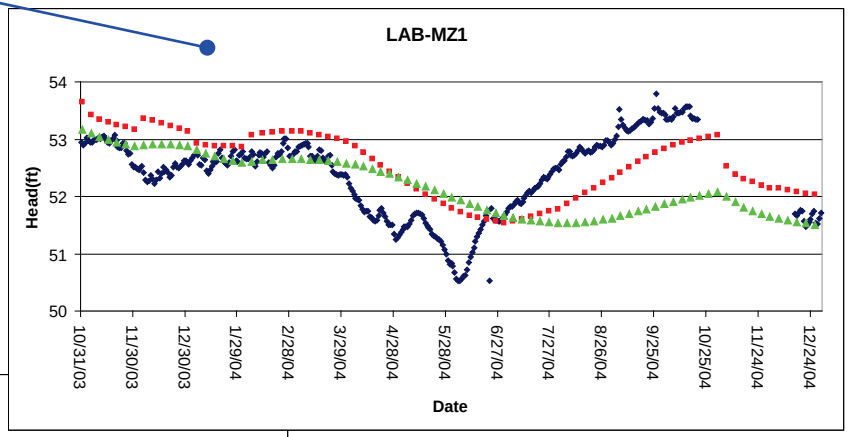

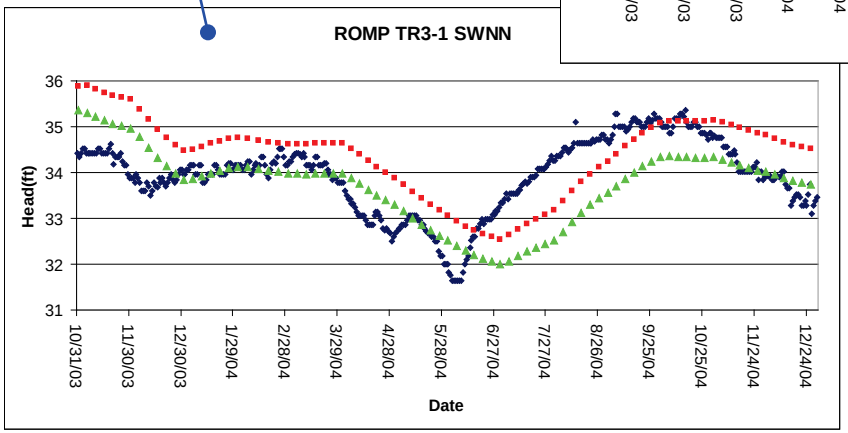

Legend

- Measured Head
- SEAWAT Calculated Head
- WASH123D Calculated Head

Notes:

Figures 4.102 through 4.122 show the comparison between measured head values, model-calculated head values from the SEAWAT model and model-calculated head values from the WASH123D model at a number of observation wells for the calibration period. Although the scales vary on each plot, all plots have a horizontal grid line at each foot. This is to make it easy to determine the range of heads at a glance.

The model used month-long stress periods, so pumping and boundary conditions were input as step functions with constant values throughout each month and sudden changes at the end of each month. For this reason, the model cannot be expected to accurately predict day-to-day head variations in any of these wells. Calibration efforts were aimed at matching general trends and monthly averages.

Starting head conditions for this model were computed in WASH123D based on October 2003 steady state conditions. Transient calibration efforts incorporated values of hydraulic conductivity and storage that were consistent with the SEAWAT model. As with the SEAWAT model, it is not uncommon for residuals in the starting condition to be carried through the entire calibration period. This indicates that the model is correctly predicting responses to hydrogeologic forces even if the calculated head values vary somewhat from the measured values.

Transient WASH123D Calibration Comparison
Upper Floridan Aquifer (2003-2004)

Final Groundwater Model Calibration Report

Figure F3-41

October 2010

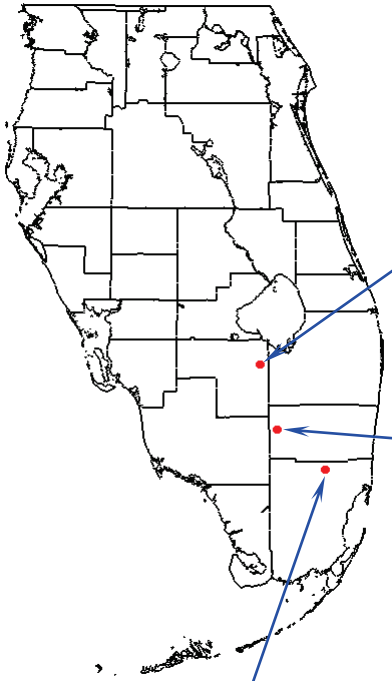

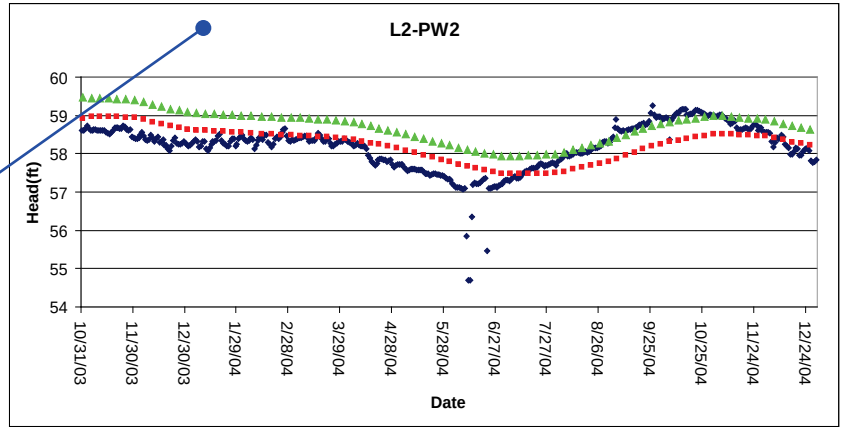

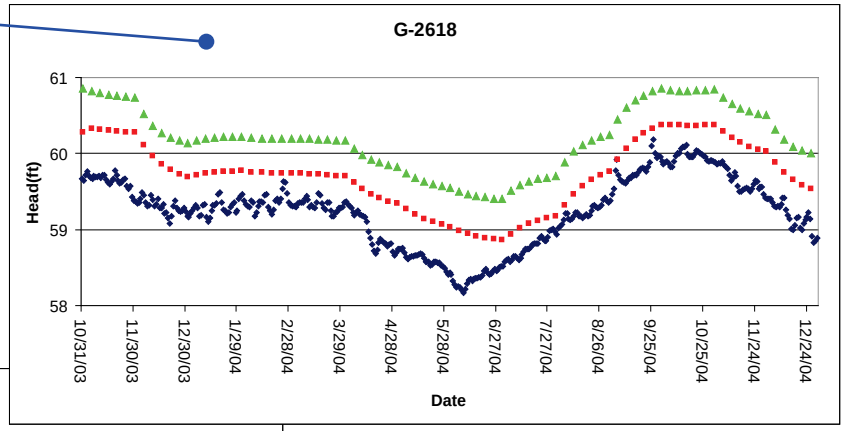

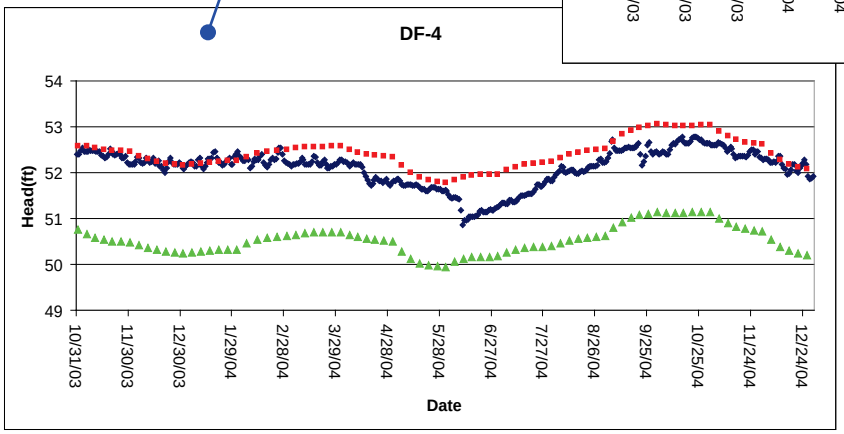

Legend

- Measured Head
- SEAWAT Calculated Head
- WASH123D Calculated Head

Notes:

Figures 4.102 through 4.122 show the comparison between measured head values, model-calculated head values from the SEAWAT model and model-calculated head values from the WASH123D model at a number of observation wells for the calibration period. Although the scales vary on each plot, all plots have a horizontal grid line at each foot. This is to make it easy to determine the range of heads at a glance.

The model used month-long stress periods, so pumping and boundary conditions were input as step functions with constant values throughout each month and sudden changes at the end of each month. For this reason, the model cannot be expected to accurately predict day-to-day head variations in any of these wells. Calibration efforts were aimed at matching general trends and monthly averages.

Starting head conditions for this model were computed in WASH123D based on October 2003 steady state conditions. Transient calibration efforts incorporated values of hydraulic conductivity and storage that were consistent with the SEAWAT model. As with the SEAWAT model, it is not uncommon for residuals in the starting condition to be carried through the entire calibration period. This indicates that the model is correctly predicting responses to hydrogeologic forces even if the calculated head values vary somewhat from the measured values.

Transient WASH123D Calibration Comparison
Upper Floridan Aquifer (2003-2004)
Final Groundwater Model Calibration Report

Figure F3-42

October 2010

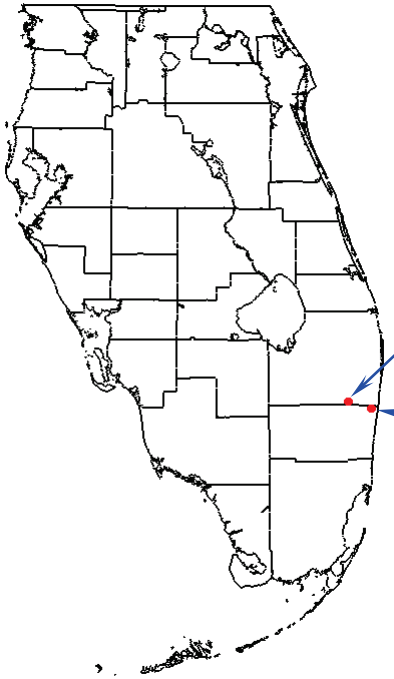

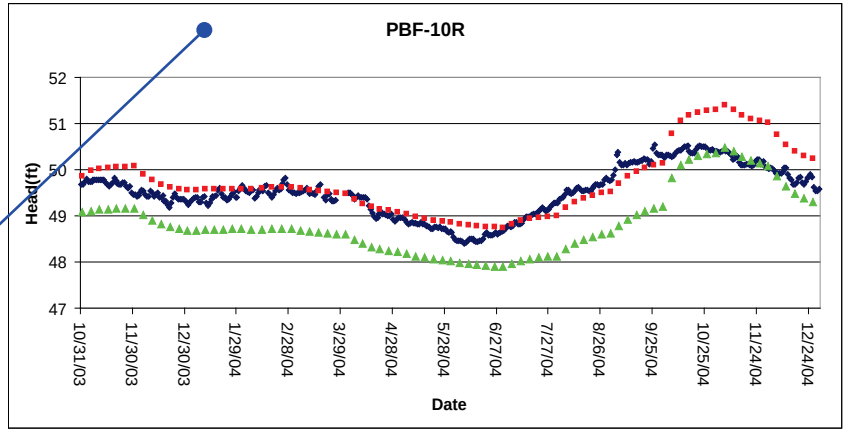

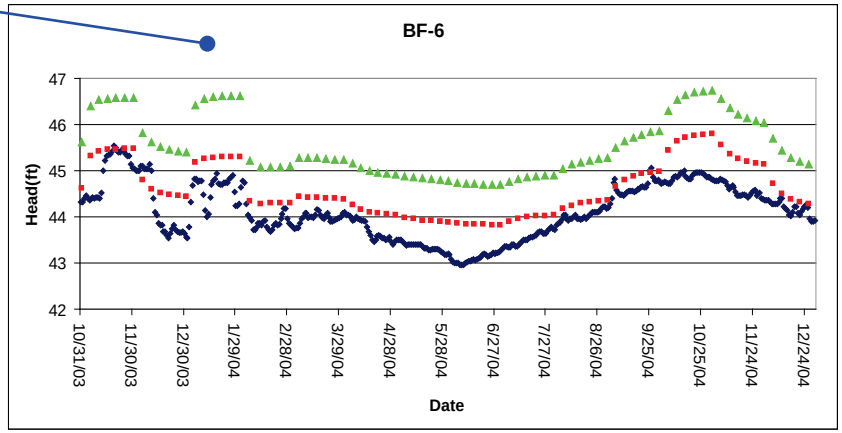

Legend

- Measured Head
- SEAWAT Calculated Head
- WASH123D Calculated Head

Notes:

Figures 4.102 through 4.122 show the comparison between measured head values, model-calculated head values from the SEAWAT model and model-calculated head values from the WASH123D model at a number of observation wells for the calibration period. Although the scales vary on each plot, all plots have a horizontal grid line at each foot. This is to make it easy to determine the range of heads at a glance.

The model used month-long stress periods, so pumping and boundary conditions were input as step functions with constant values throughout each month and sudden changes at the end of each month. For this reason, the model cannot be expected to accurately predict day-to-day head variations in any of these wells. Calibration efforts were aimed at matching general trends and monthly averages.

Starting head conditions for this model were computed in WASH123D based on October 2003 steady state conditions. Transient calibration efforts incorporated values of hydraulic conductivity and storage that were consistent with the SEAWAT model. As with the SEAWAT model, it is not uncommon for residuals in the starting condition to be carried through the entire calibration period. This indicates that the model is correctly predicting responses to hydrogeologic forces even if the calculated head values vary somewhat from the measured values.

Transient WASH123D Calibration Comparison
Upper Floridan Aquifer (2003-2004)
Final Groundwater Model Calibration Report

Figure F3-43

October 2010

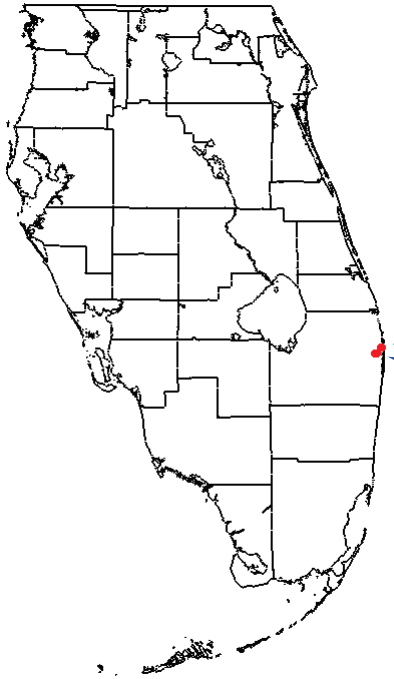

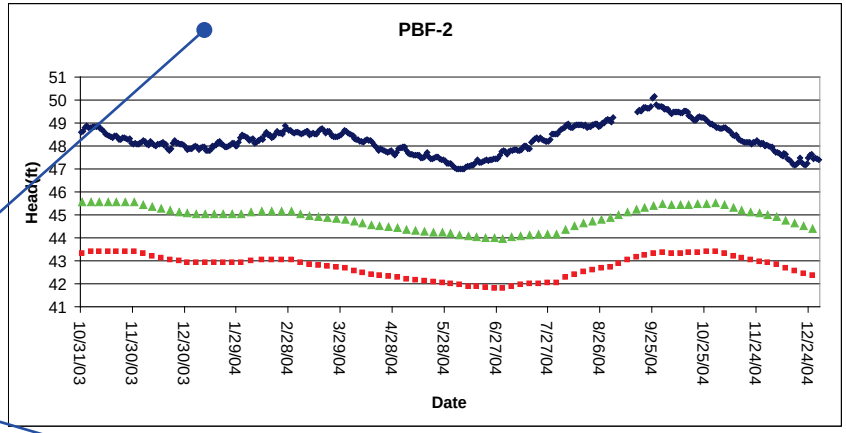

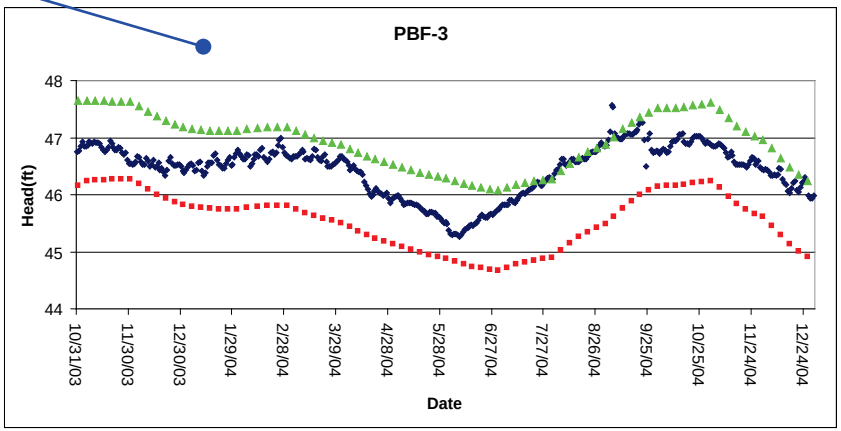

Legend

- Measured Head
- SEAWAT Calculated Head
- WASH123D Calculated Head

Notes:

Figures 4.102 through 4.122 show the comparison between measured head values, model-calculated head values from the SEAWAT model and model-calculated head values from the WASH123D model at a number of observation wells for the calibration period. Although the scales vary on each plot, all plots have a horizontal grid line at each foot. This is to make it easy to determine the range of heads at a glance.

The model used month-long stress periods, so pumping and boundary conditions were input as step functions with constant values throughout each month and sudden changes at the end of each month. For this reason, the model cannot be expected to accurately predict day-to-day head variations in any of these wells. Calibration efforts were aimed at matching general trends and monthly averages.

Starting head conditions for this model were computed in WASH123D based on October 2003 steady state conditions. Transient calibration efforts incorporated values of hydraulic conductivity and storage that were consistent with the SEAWAT model. As with the SEAWAT model, it is not uncommon for residuals in the starting condition to be carried through the entire calibration period. This indicates that the model is correctly predicting responses to hydrogeologic forces even if the calculated head values vary somewhat from the measured values.

Transient WASH123D Calibration Comparison
Upper Floridan Aquifer (2003-2004)
Final Groundwater Model Calibration Report

Figure F3-44

October 2010

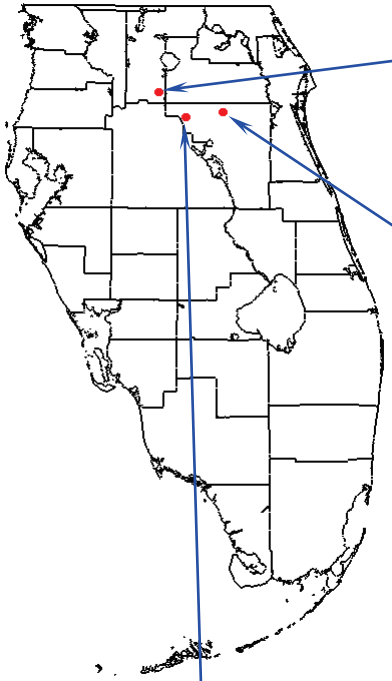

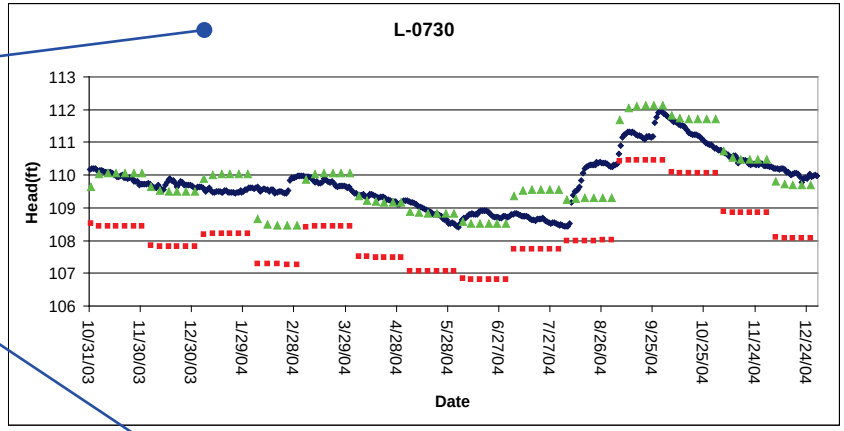

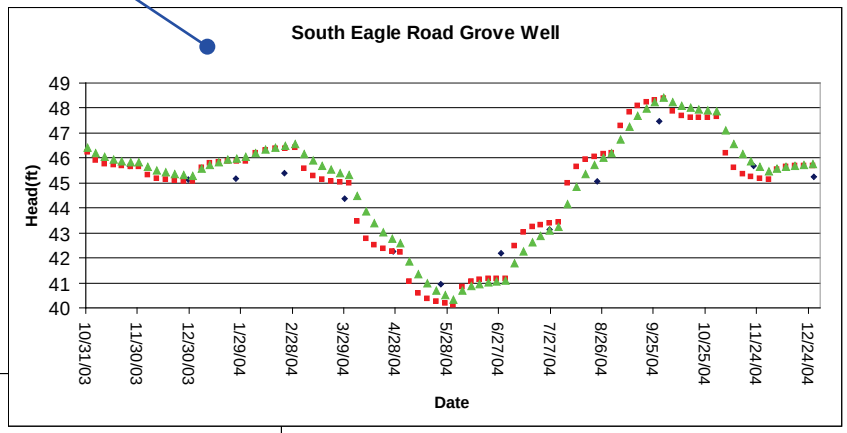

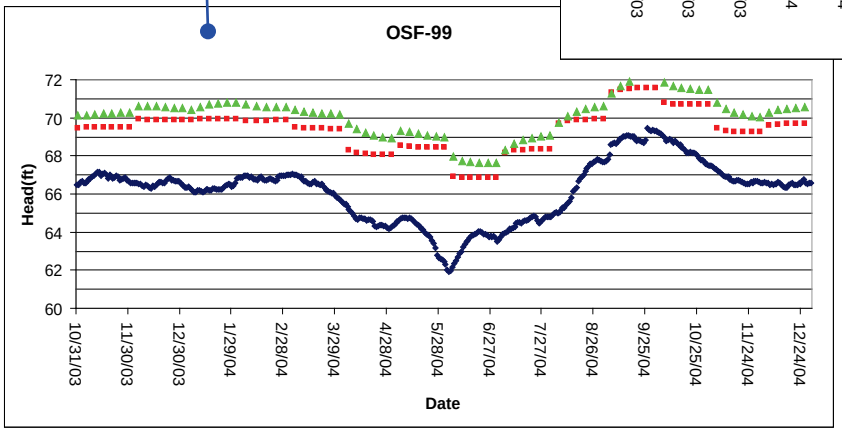

Legend

- Measured Head
- SEAWAT Calculated Head
- WASH123D Calculated Head

Notes:

Figures 4.102 through 4.122 show the comparison between measured head values, model-calculated head values from the SEAWAT model and model-calculated head values from the WASH123D model at a number of observation wells for the calibration period. Although the scales vary on each plot, all plots have a horizontal grid line at each foot. This is to make it easy to determine the range of heads at a glance.

The model used month-long stress periods, so pumping and boundary conditions were input as step functions with constant values throughout each month and sudden changes at the end of each month. For this reason, the model cannot be expected to accurately predict day-to-day head variations in any of these wells. Calibration efforts were aimed at matching general trends and monthly averages.

Starting head conditions for this model were computed in WASH123D based on October 2003 steady state conditions. Transient calibration efforts incorporated values of hydraulic conductivity and storage that were consistent with the SEAWAT model. As with the SEAWAT model, it is not uncommon for residuals in the starting condition to be carried through the entire calibration period. This indicates that the model is correctly predicting responses to hydrogeologic forces even if the calculated head values vary somewhat from the measured values.

Transient WASH123D Calibration Comparison
Avon Park Permeable Zone (2003-2004)
Final Groundwater Model Calibration Report

Figure F3-45

October 2010

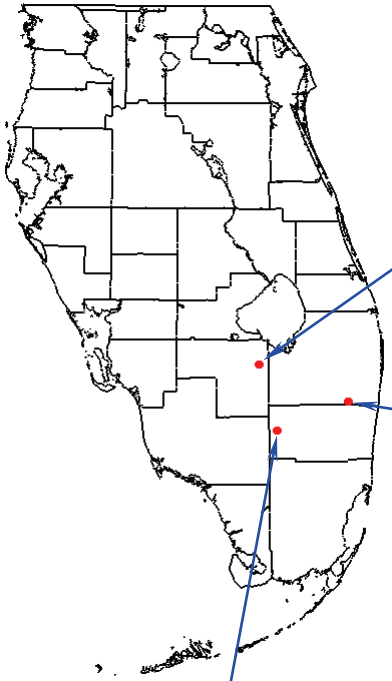

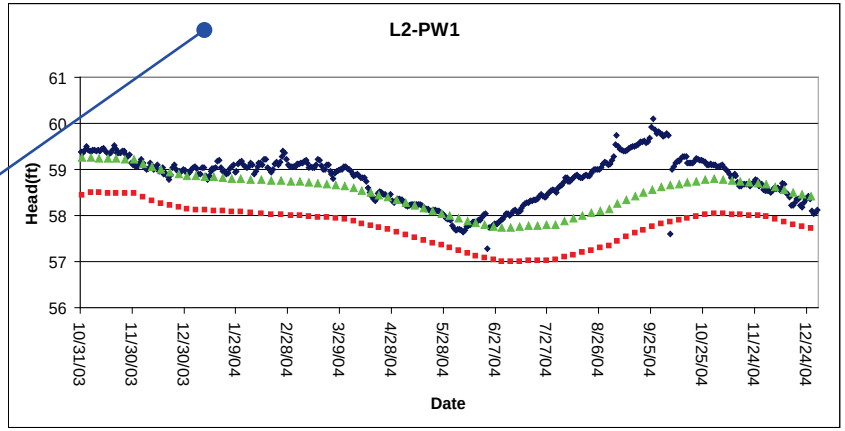

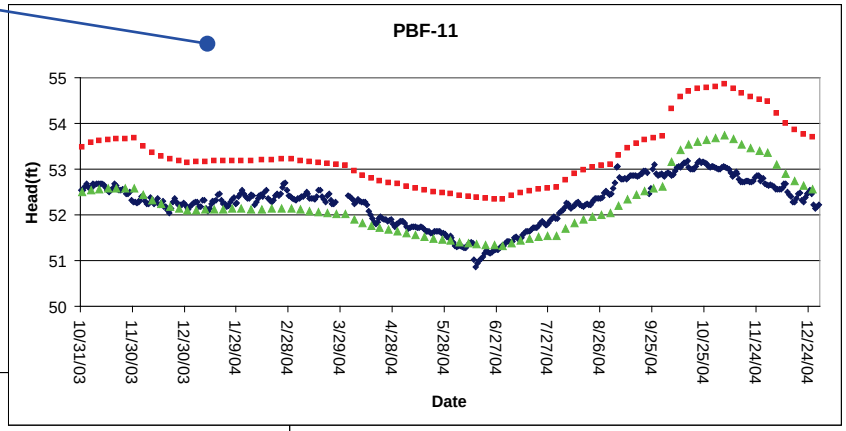

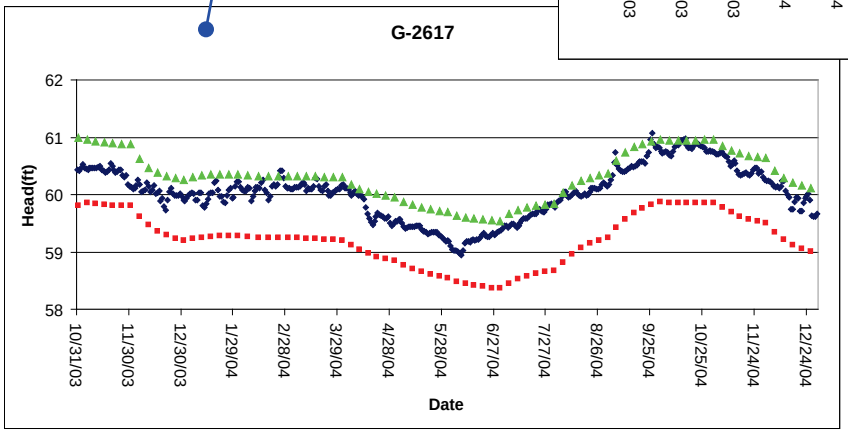

Legend

- Measured Head
- SEAWAT Calculated Head
- WASH123D Calculated Head

Notes:

Figures 4.102 through 4.122 show the comparison between measured head values, model-calculated head values from the SEAWAT model and model-calculated head values from the WASH123D model at a number of observation wells for the calibration period. Although the scales vary on each plot, all plots have a horizontal grid line at each foot. This is to make it easy to determine the range of heads at a glance.

The model used month-long stress periods, so pumping and boundary conditions were input as step functions with constant values throughout each month and sudden changes at the end of each month. For this reason, the model cannot be expected to accurately predict day-to-day head variations in any of these wells. Calibration efforts were aimed at matching general trends and monthly averages.

Starting head conditions for this model were computed in WASH123D based on October 2003 steady state conditions. Transient calibration efforts incorporated values of hydraulic conductivity and storage that were consistent with the SEAWAT model. As with the SEAWAT model, it is not uncommon for residuals in the starting condition to be carried through the entire calibration period. This indicates that the model is correctly predicting responses to hydrogeologic forces even if the calculated head values vary somewhat from the measured values.

Transient WASH123D Calibration Comparison
Avon Park Permeable Zone (2003-2004)
Final Groundwater Model Calibration Report

Figure F3-46

October 2010

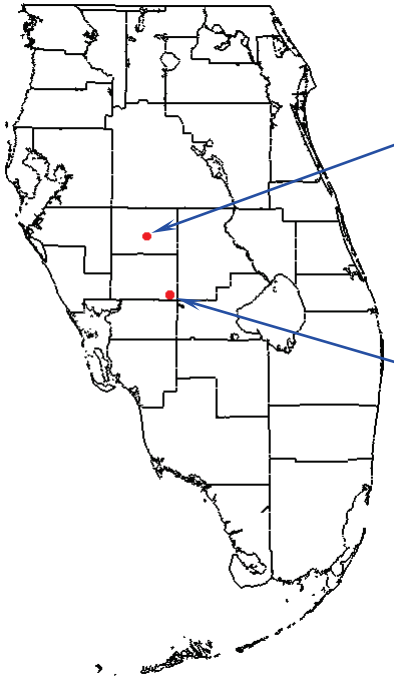

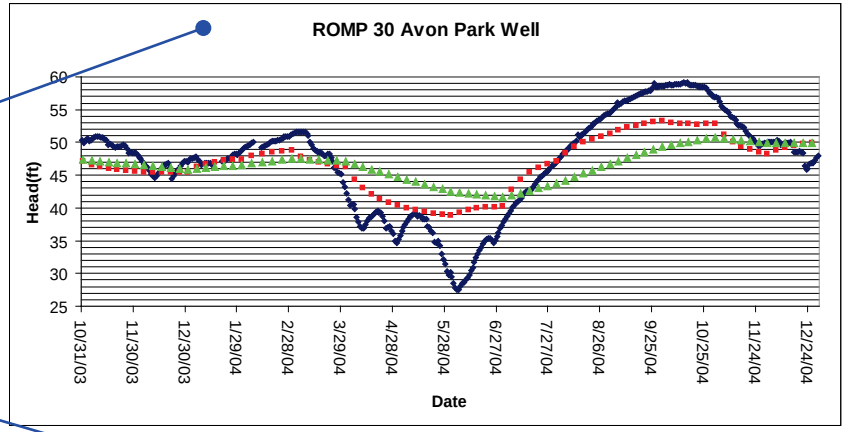

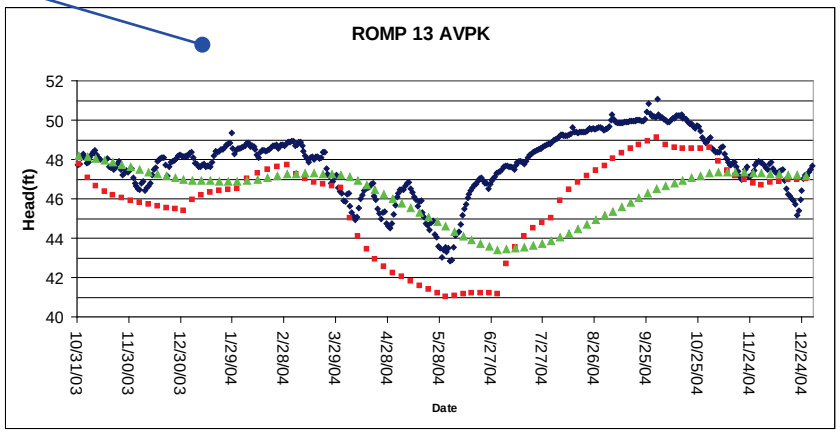

Legend

- Measured Head
- SEAWAT Calculated Head
- WASH123D Calculated Head

Notes:

Figures 4.102 through 4.122 show the comparison between measured head values, model-calculated head values from the SEAWAT model and model-calculated head values from the WASH123D model at a number of observation wells for the calibration period. Although the scales vary on each plot, all plots have a horizontal grid line at each foot. This is to make it easy to determine the range of heads at a glance.

The model used month-long stress periods, so pumping and boundary conditions were input as step functions with constant values throughout each month and sudden changes at the end of each month. For this reason, the model cannot be expected to accurately predict day-to-day head variations in any of these wells. Calibration efforts were aimed at matching general trends and monthly averages.

Starting head conditions for this model were computed in WASH123D based on October 2003 steady state conditions. Transient calibration efforts incorporated values of hydraulic conductivity and storage that were consistent with the SEAWAT model. As with the SEAWAT model, it is not uncommon for residuals in the starting condition to be carried through the entire calibration period. This indicates that the model is correctly predicting responses to hydrogeologic forces even if the calculated head values vary somewhat from the measured values.

Transient WASH123D Calibration Comparison
Avon Park Permeable Zone (2003-2004)
Final Groundwater Model Calibration Report

Figure F3-47

October 2010

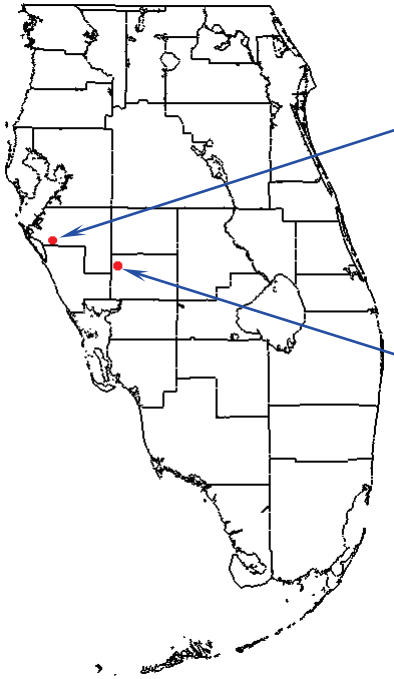

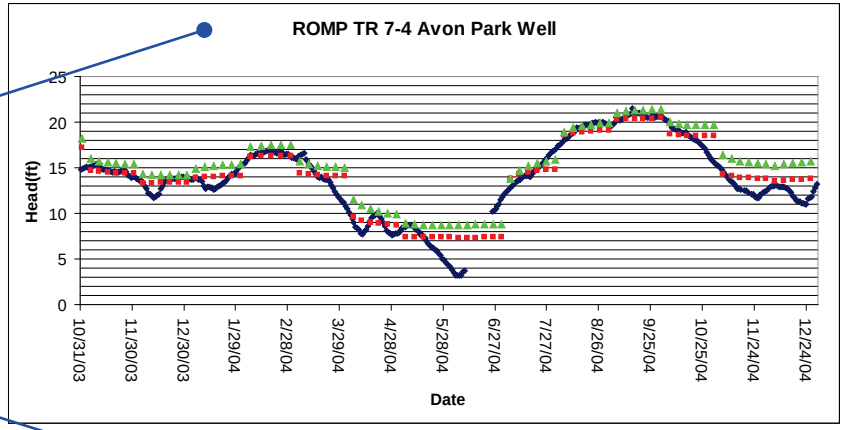

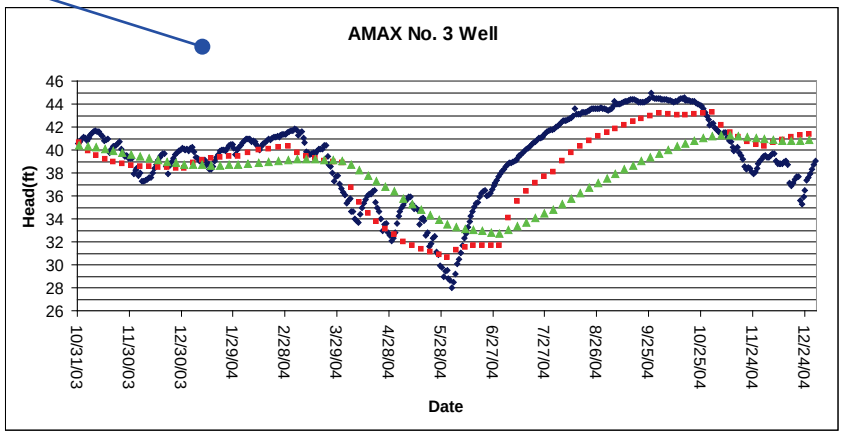

Legend

- Measured Head
- SEAWAT Calculated Head
- WASH123D Calculated Head

Notes:

Figures 4.102 through 4.122 show the comparison between measured head values, model-calculated head values from the SEAWAT model and model-calculated head values from the WASH123D model at a number of observation wells for the calibration period. Although the scales vary on each plot, all plots have a horizontal grid line at each foot. This is to make it easy to determine the range of heads at a glance.

The model used month-long stress periods, so pumping and boundary conditions were input as step functions with constant values throughout each month and sudden changes at the end of each month. For this reason, the model cannot be expected to accurately predict day-to-day head variations in any of these wells. Calibration efforts were aimed at matching general trends and monthly averages.

Starting head conditions for this model were computed in WASH123D based on October 2003 steady state conditions. Transient calibration efforts incorporated values of hydraulic conductivity and storage that were consistent with the SEAWAT model. As with the SEAWAT model, it is not uncommon for residuals in the starting condition to be carried through the entire calibration period. This indicates that the model is correctly predicting responses to hydrogeologic forces even if the calculated head values vary somewhat from the measured values.

Transient WASH123D Calibration Comparison
Avon Park Permeable Zone (2003-2004)
Final Groundwater Model Calibration Report

Figure F3-48

October 2010

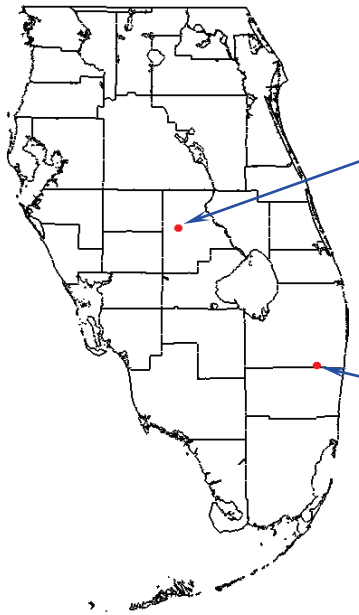

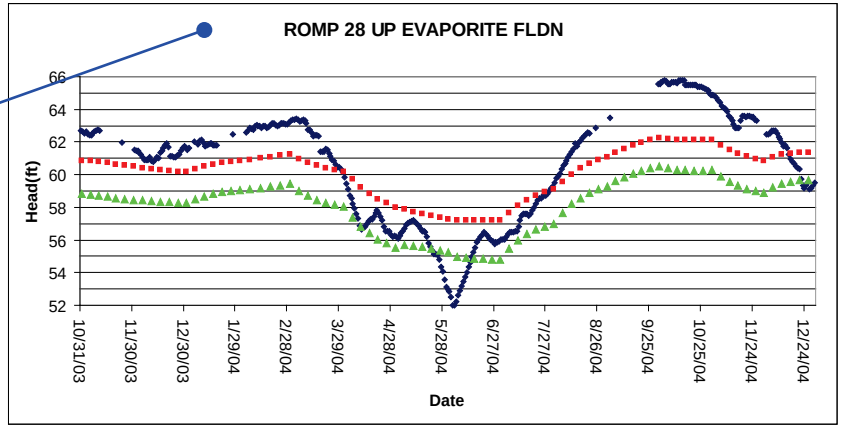

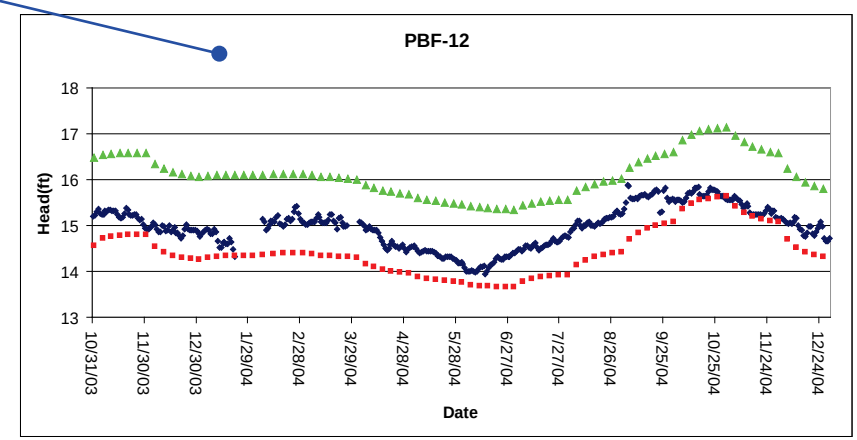

Legend

- Measured Head
- SEAWAT Calculated Head
- WASH123D Calculated Head

Notes:

Figures 4.102 through 4.122 show the comparison between measured head values, model-calculated head values from the SEAWAT model and model-calculated head values from the WASH123D model at a number of observation wells for the calibration period. Although the scales vary on each plot, all plots have a horizontal grid line at each foot. This is to make it easy to determine the range of heads at a glance.

The model used month-long stress periods, so pumping and boundary conditions were input as step functions with constant values throughout each month and sudden changes at the end of each month. For this reason, the model cannot be expected to accurately predict day-to-day head variations in any of these wells. Calibration efforts were aimed at matching general trends and monthly averages.

Starting head conditions for this model were computed in WASH123D based on October 2003 steady state conditions. Transient calibration efforts incorporated values of hydraulic conductivity and storage that were consistent with the SEAWAT model. As with the SEAWAT model, it is not uncommon for residuals in the starting condition to be carried through the entire calibration period. This indicates that the model is correctly predicting responses to hydrogeologic forces even if the calculated head values vary somewhat from the measured values.

Transient WASH123D Calibration Comparison
Lower Floridan (LF1) Aquifer (2003-2004)
Final Groundwater Model Calibration Report

Figure F3-49

October 2010

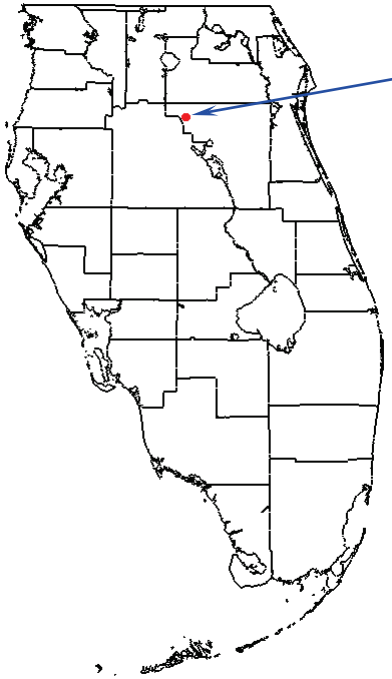

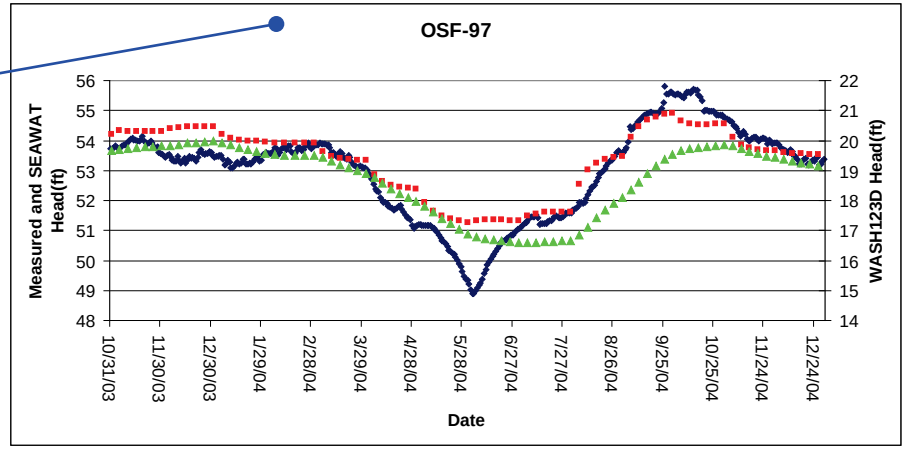

Legend

- Measured Head
- SEAWAT Calculated Head
- WASH123D Calculated Head

Notes:

Figures 4.102 through 4.122 show the comparison between measured head values, model-calculated head values from the SEAWAT model and model-calculated head values from the WASH123D model at a number of observation wells for the calibration period. Although the scales vary on each plot, all plots have a horizontal grid line at each foot. This is to make it easy to determine the range of heads at a glance.

The model used month-long stress periods, so pumping and boundary conditions were input as step functions with constant values throughout each month and sudden changes at the end of each month. For this reason, the model cannot be expected to accurately predict day-to-day head variations in any of these wells. Calibration efforts were aimed at matching general trends and monthly averages.

Starting head conditions for this model were computed in WASH123D based on October 2003 steady state conditions. Transient calibration efforts incorporated values of hydraulic conductivity and storage that were consistent with the SEAWAT model. As with the SEAWAT model, it is not uncommon for residuals in the starting condition to be carried through the entire calibration period. This indicates that the model is correctly predicting responses to hydrogeologic forces even if the calculated head values vary somewhat from the measured values.

Transient WASH123D Calibration Comparison
Boulder Zone (2003-2004)
Final Groundwater Model Calibration Report

Figure F3-50

October 2010

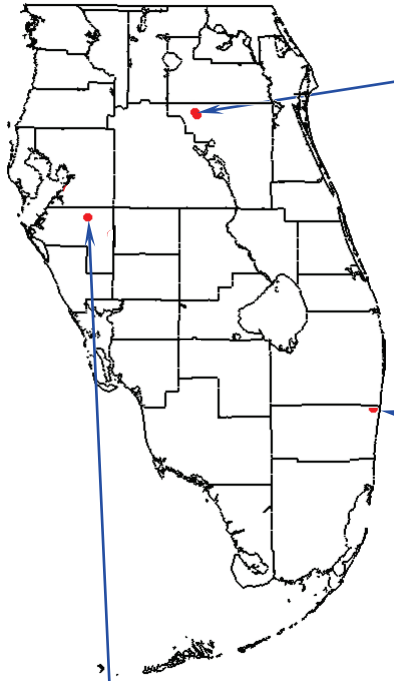

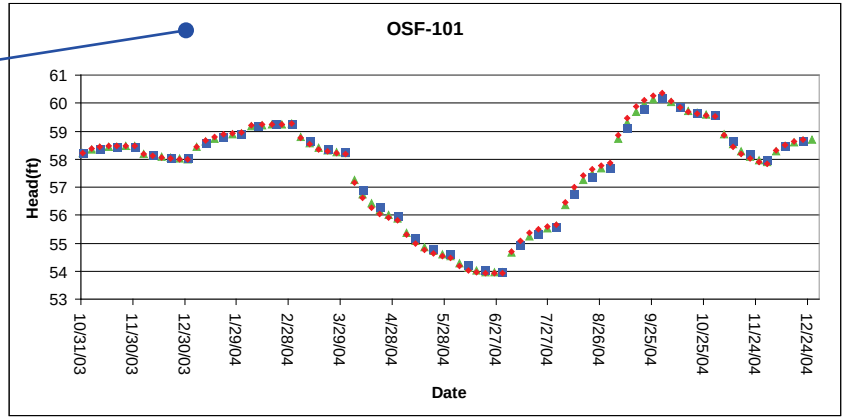

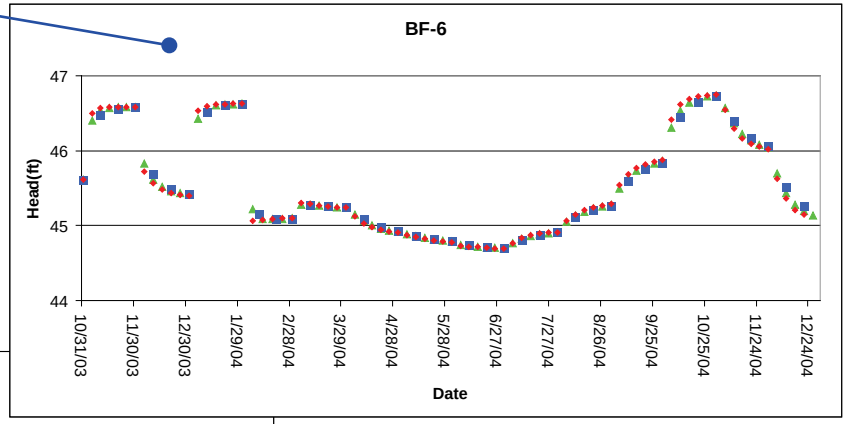

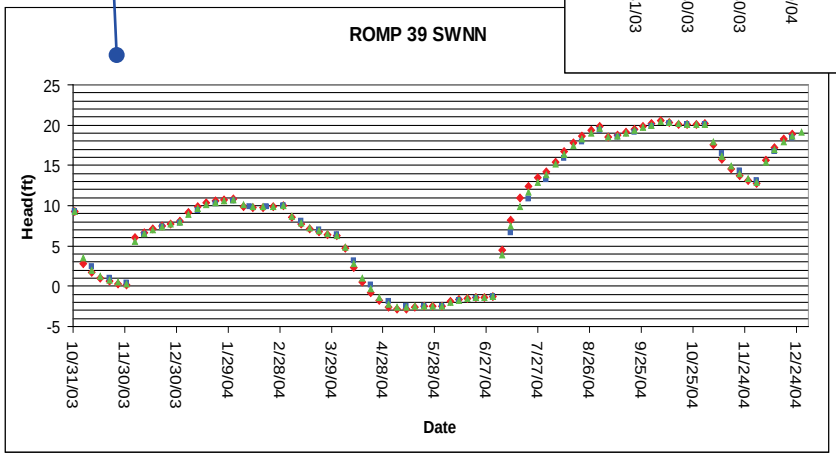

Legend

- 1 Day Timestep
- 5 Day Timestep
- 10 Day Timestep

Notes:

The transient WASH123D draft calibration model run used a 5 day time step size.

Timestep sizes were varied to investigate the effects on the head solution. Head solutions for 3 UF wells across the model domain show that using a 1 day, 5 day or 10 day timestep produces head solutions with minor differences.

The largest difference of the wells shown is at ROMP 39 SWNN. In the middle of July 2004, the difference between the 1 day timestep head and the 5 day and 10 day timestep heads is 1.0 ft and 1.5 ft, respectively. ROMP 39 SWNN is near a large pumping center where the timing as pumps turn on and off is important.

While the 1 day timestep may more accurately compute heads in areas near pumping centers, the differences between the head solutions for the different timesteps is within the model error. A 5 day timestep size is appropriate for this regional application.

Effect of Timestep on WASH123D Solution at Selected Upper Floridan Aquifer Wells

Final Groundwater Model Calibration Report

Figure F4-1

October 2010

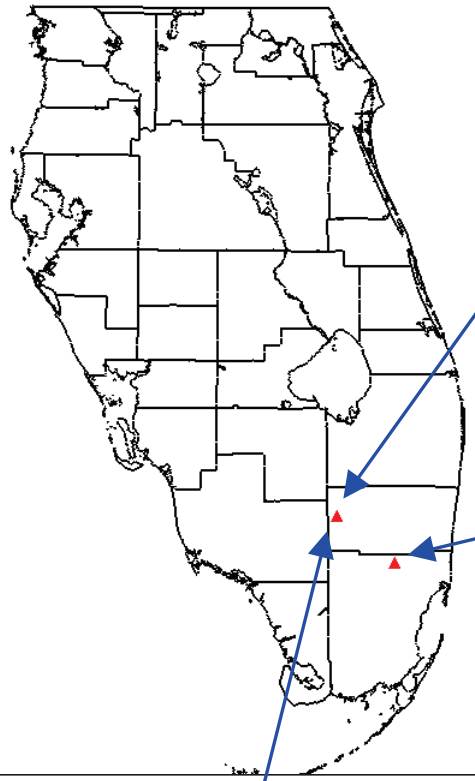

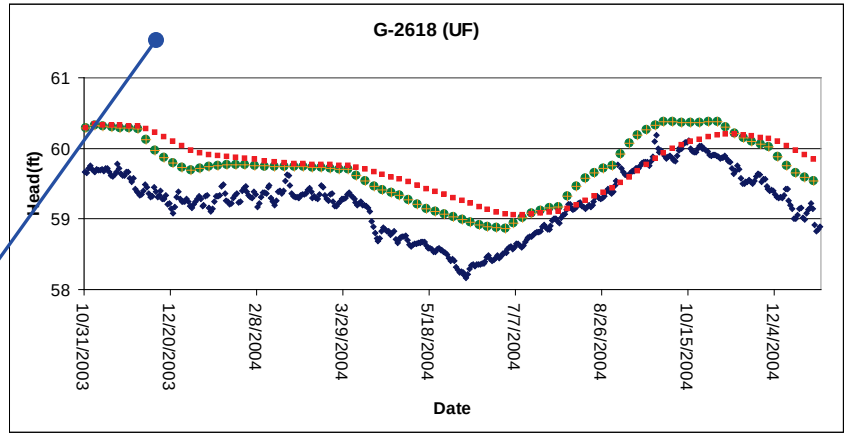

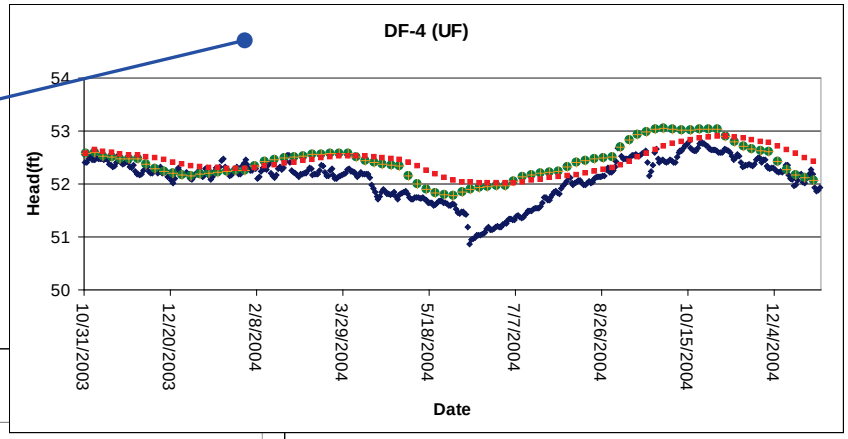

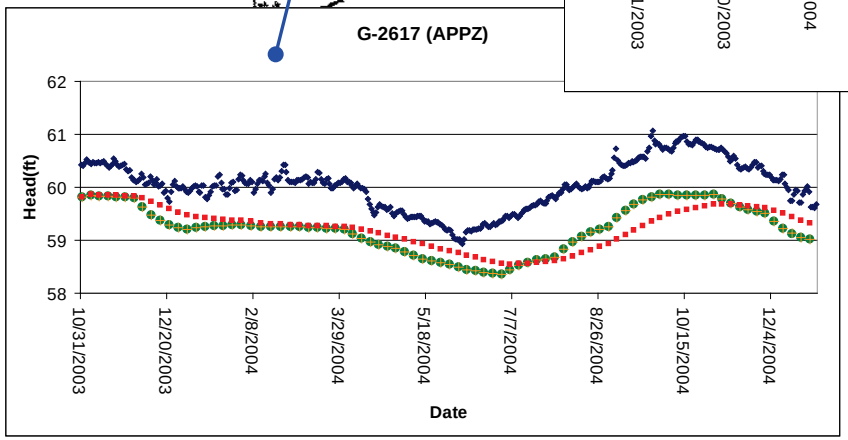

- **Observed Head**
- **Calibrated Model Calculated Head**
- **Sensitivity Calculated Head (Truncate Ss at 2.65×10^{-8} ft^{-1})**
- **Sensitivity Calculated Head (Truncate Ss at 3.05×10^{-7} ft^{-1})**

Notes:

This figure shows the results from three observation wells, which showed the greatest impact from truncation of the Specific Storage value. Setup of these sensitivity runs and the selection of the Cutoff values are described in Section 4.2 of Appendix F.

All other observation wells showed negligible changes to the result calculated by the calibrated model run.

The layer tapped by each observation well is indicated on the plot title.

G-2618 and G-2617 are part of a well cluster.

Result of SEAWAT Specific Storage Truncation at Three Most-Impacted Observation Wells

Final Groundwater Model Calibration Report

Figure F4-2

October 2010

Appendix G: IMC Comments to Draft Report With Responses

USACE Response to IMC Comments on "Draft Groundwater Model Calibration Report, Aquifer Storage and Recovery Regional Modeling Study"

The groundwater team at the Philadelphia District, USACE, is grateful to the IMC for their comments on the recently completed document, "Draft Groundwater Model Calibration Report, Aquifer Storage and Recovery Regional Modeling Study." Many of the comments were incorporated in their entirety to improve the report and model. Others of the comments indicate a lack of clarity in the presentation of the material in the report. In these cases, revisions and/or additions to the text and figures of the report were incorporated to better explain model construction, assumptions and/or conclusions. A few comments indicate a difference of opinion between USACE groundwater modelers/PDT and the IMC reviewers. This document contains individual responses to each comment and a description of the action taken, if any, to change the model and/or the report. The original text of the IMC comments are provided as black text, while the responses to comments are provided as red, italic text.

The SEAWAT model has been recalibrated based on IMC comments, as described in this document, and additional PDT comments. The WASH123D model has not been recalibrated but an appendix has been added to the final report to document the similarity in the results of the draft SEAWAT and WASH123D calibrations.

IMC MSR 324 – Task 4B: Review of "Draft Groundwater Model Calibration Report, Aquifer Storage and Recovery Regional Modeling Study"

Interagency Modeling Center (IMC)

Purpose

The purpose of this document is to provide comments based upon the review of documents submitted in support of the Aquifer Storage and Recovery (ASR) modeling study to develop and calibrate a regional groundwater flow and transport model.

Documents Reviewed

The document shown below was submitted for IMC review:

- "Draft Groundwater Model Calibration Report Aquifer Storage and Recovery Regional Modeling Study ." US Army Corps of Engineers, April, 2010.

Individual reviewers in some cases reviewed additional documents when certain parts of the report above needed further clarification.

This document is divided into the following two sections: (1) technical comments and (2) general comments.

Technical Comments

The review was limited to the document above, and therefore does not extend to the model code, model input or model output files.

The comments are listed following the table of contents of the review document for ease of reference.

0.0 Executive Summary

1. Paragraph 1: The authors should briefly introduce the "four documents" within the Executive Summary.

Fixed.

2. Paragraph 3: The authors should briefly introduce all performance goals/objectives within the Executive Summary.

Language has been added to the Executive Summary to list the major performance goals that will be discussed in detail in the fourth report. Because the specifics to meet each of the goals are still evolving, only broad descriptions are included. These descriptions are detailed enough to define the scale and accuracy of the model necessary to meet the goals Those objectives which are beyond the ability of the regional model to examine, will be examined using the local scale models.

3. Paragraph 3: The authors should detail "various constraints" in the Executive Summary.

This phrase has been removed from the Executive Summary.

4. Paragraph 3: The authors should quantitatively characterize "well calibrated" in the Executive Summary. The authors state in Paragraph 1 that the objective of the present report is to detail the construction, calibration, and sensitivity of the Phase II Regional Model. The authors should explicitly and quantitatively detail construction and sensitivity in the Executive Summary.

The purpose of the Executive Summary is to provide a quick overview for readers who do not have the background or knowledge to understand the details of the technical report or who do not have the time to read the lengthy report. We believe that the inclusion of detailed quantitative statistics on the calibration quality is unnecessary and undesired in an Executive Summary. The qualitative description of the calibration has been expanded and the reader who is interested in more details is directed to the calibration chapter of the main report.

1.0 Introduction

1. Paragraph 1: The authors should consistently identify the objective of the fourth report as either "The final document in the series will summarize the local scale model development and evaluation of various CERP ASR alternatives." (from the present paragraph) OR " The calibrated model described in this report will be used to evaluate CERP ASR against a variety of performance objectives. This evaluation will be documented in the fourth and final ASR groundwater modeling report." (from the Executive Summary).

The two descriptions are both true. Both descriptions have been expanded to mention both the regional aspect and the local-scale aspects of the planned analysis.

2.0 Regional Modeling Approach

1. Paragraphs 1 and 2: The authors state that "The first and most important step in the modeling process is to define clear, achievable goals and objectives for each stage of the process based on the desired end results." The authors do not explicitly identify model goals within Section 2.0. The authors identify a primary objective in Section 2.0, and allude to "different project objectives". The authors introduce four "large-scale issues". The authors should explicitly identify all goals, objectives, and issues upon introducing these concepts in Section 2.0. Alternatively, if goals, objectives, and issues are formally introduced at another location within the document, the authors may wish to defer introduction of goals, objectives, and issues to the location within the document in which these concepts are discussed.

As mentioned in the comment, four large-scale issues were identified that will be addressed using the regional model. A fifth issue, potential for rock fracturing, has been added to this list. Two smaller scale issues were also identified in the original report. Those are well-to-well interaction within an ASR well cluster and ASR well recovery efficiency. The smaller scale issues will be addressed using the local scale models. Details regarding how these issues are evaluated and the criteria for the evaluation will be provided in the fourth report in this series. The modelers believe that this general definition of the objectives is sufficient for moving forward with the calibration. The PDT is aware that their objectives must not exceed the reliability or resolution of the model.

2. The authors should include a section that details previous studies. For example the USGS Regional Aquifer System Analysis (RASA) program generated a considerable volume of information specifically related to the study area. The authors may want to detail the RASA program, and identify elements of the RASA program that are of use to satisfying the ASR Regional Modeling objectives. Specifically, the authors may find the following reports relevant:

Miller, J.A., 1986, Hydrogeologic framework of the Floridan aquifer system in Florida, and in parts of Georgia, Alabama, and South Carolina: U.S. Geological Survey Professional Paper 1403-B, 91 p. 33 pls.

Bush, P.W., R.H. Johnston, 1988, Ground-water hydraulics, regional flow and ground-water development of the Floridan aquifer system in Florida and in parts of Georgia, South Carolina, and Alabama: U.S. Geological Survey Professional Paper 1403-C, 80 p., 17 pls.

Meyer, F.W., 1989, Hydrogeology, ground-water movement, and subsurface storage in the Floridan aquifer system in southern Florida: U. S. Geological Survey Professional Paper 1403-G, 59 p.

Sprinkle, C.L., 1989, Geochemistry of the Floridan aquifer system in Florida and parts of Georgia, South Carolina, and Alabama: U.S. Geological Survey Professional Paper 1403-I, 105 p, 9 pls.

A summary of previous modeling work was provided by CH2MHill. This report had been included as a reference in the draft report. A few sentences have been added to the Introduction to direct the readers to this report. In addition, aspects of the USGS RASA program that were used to generate the hydrogeologic framework are described in Reese and Richardson (2008), referenced as the major basis for the hydrogeologic construction of this model.

3. The authors should summarize other previous studies in a section that is devoted to previous work.

Same response as for #2 above.

2.1 Modeling Codes

1. Paragraph 1: The authors state that "Substantial density variations in the groundwater (due to variations in temperature and salinity) are observed across the model domain". The authors should replace qualitative statements with quantitative statements throughout the document. For example, the authors should state the numerical variation in density across the model domain in place of the qualitative term "Substantial".

Fixed.

2.1.1 SEAWAT

1. Paragraph 1: The authors may wish to eliminate the bullets, and associated sentence, as this information is not particularly relevant.

Agreed.

2. Paragraph 1: The authors should include Guo and Bennett (1998) in the reference as the first occurrence of SEAWAT within the published literature. (Guo, W., Bennett, G. D., 1998. Simulation of saline/fresh water flows using MODFLOW. In: MODFLOW '98 Conference, Golden, Colorado. pp. 267–274.)

Reference added.

3. Equation 2.1 is not "the variable-density form of Darcy's law for groundwater flow." Equation 2.1 is more correctly characterized as "the governing equation for flow in a porous medium, as a function of freshwater head" (Equation 37, Guo and Langevin, 2001). The authors should appropriately cite Guo and Langevin (2001). The authors should explain the freshwater head concept, and include and reference Equation 3 of Guo and Langevin (2001).

The name of the equation (now 2.3) has been changed with citation. The description of equivalent freshwater head with equations was previously found in Appendix C, but has been moved to this chapter as new Section 2.1.

4. The authors may wish to correctly typeset the denominator of the dimensionless density term for the gamma axis in Equation 2.1. The authors may wish to identify alpha, beta, and gamma as "Orthogonal coordinate axes" following "Where".

Fixed.

5. Equation 2.2 is not "the advective-dispersion equation". Equation 2.2 is more correctly characterized as "the governing equation for fate and transport of contaminants of species k in a three dimensional, transient groundwater flow system". If the authors do not employ reactive species, the authors should eliminate the fourth term on the right-hand side of Equation 2.2. The authors should appropriately cite Zheng and Wang (1999) Equation 1. What is the difference between C in Equation 2.1 and C^k in Equation 2.2? The authors should use a lower case k in Equation 2.2 as is done by Zheng and Wang (1999), to differentiate between this species counter and the use of a capital K symbol for hydraulic conductivity. The authors should identify D_{ij} as the "hydrodynamic dispersion coefficient tensor", as is done by Zheng and Wang (1999). The authors may wish to cast Equations 2.1 and 2.2 in a parallel form, such that the implied summation in i and j on Equation 2.2 is expanded, or such that the implied summation in i and j is employed in Equation 2.1.

The errors in format and definition have been fixed. Equation 2.2 (now 2.4) has been written as found in equation 38 of Guo and Langevin, 2002 in place of the previous form copied from Zheng and Wang, 1999. Both equations are written exactly as found in the 2002 SEAWAT USGS published User's Guide.

2.1.2 WASH123D

1. The authors may wish to cast Equation 2.3 in a form that is parallel to the form chosen for Equations 2.1 and 2.2. Specifically, Equation 2.3 uses a tensor dot product form that is not used by Equations 2.1 and 2.2. The authors may wish to note that it is possible to write Equations 2.1 and 2.2 in a tensor dot product form.

Since Equation 2.2 (now Equation 2.4) is now written in the form of Guo and Langevin, 2002, it is in tensor dot product form and matches Equation 2.3 (now Equation 2.5). Since the USGS SEAWAT User's Guide does not present all equations in parallel form, we have not done so in this project report.

2. The authors should use a bold typeface for hydraulic conductivity K, and for the gradient operator del, to distinguish these elements as tensors, and differentiate them from, for example, an element of K, such as K_{xx}, which would not be typeset with a bold font.

The conductivity tensor K in equation 2.5 (old equation 2.3) has been bolded. The gradient operators have also been bolded.

3. What is the difference between "referenced pressure head" in Equation 2.3 and head? What is the difference between "potential head" z in Equation 2.3 and "elevation at the measurement point" Z in Equation 2.1? What is the difference between "density of source/sink water" rho^star in Equation 2.3 and "fluid density source or sink water" rho_s in Equation 2.1? What is the difference between "volumetric flow rate of source or sink" q in Equation 2.3, "source/sink volumetric flow rate per unit volume of aquifer" q_s in Equation 2.2, and "volumetric flow rate of sources and sinks per unit volume of aquifer" q_s in Equation 2.1?

The original equations were written exactly as found in the respective model documentation. The model documentation is referenced in Section 8.0 so that the reader may research the source document to answer additional questions on the governing equation or model descriptions. In response to this comment, the variables used in the equations have been made to match.

4. The authors define time with the symbol t on both Page 4 and Page 5. The volumetric flow rate of sources and sinks is defined after both Equations 2.1 and 2.2. Throughout the entire document, the authors may wish to define variables once, on first use, and refrain from redefinition throughout the remainder of the document.

The second definition of time and source/sink flow rate has been removed.

5. Paragraph 2: The authors refer to Equation 2.2 as both the "advective-dispersion" equation and the "subsurface transport equation". The authors should use a consistent textual description of this equation.

We see no contradiction between the two terms.

6. Paragraph 2: The authors should explicitly state goals of the Phase II modeling effort.

The purpose of this section is to provide a general overview of the equations solved by each model. The model objectives are summarized at the beginning of Section 2.0.

2.2 Model Extent and Spatial Discretization

1. Figure 2.2: Do surfaces represent the tops of hydrogeologic units? Bottoms of hydrogeologic units? The mid-point of hydrogeologic units? Please explain.

A note has been added to Figure 2.2 indicating that these surfaces represent the tops of each hydrogeologic unit.

2. In the Phase I report, the model domain was rotated 18 degrees counterclockwise. In this Phase II model, the domain appears to have been rotated 38 degrees west of north. Has the rotation been changed from Phases I to II and why?

As stated in Bittner et al (2008), "… it would seem more reasonable for the axis to be similar to that of the gravity anomaly axis… Additional simulations are planned using a grid alignment rotated to correspond with the gravity anomalies direction…" During the construction of the Phase II model grid, several gravity anomaly publications and recent field work performed by SFWMD were reviewed to determine a reasonable average angle for preferential flow paths. The resulting grid angle was N38W. A statement has been added to the new text to explain the change in grid angle. It should be noted that since regional anisotropy was not activated for the final calibration, the angle of the grid has no bearing on the results.

3. Some additional clarification regarding the vertical layering is needed. The authors need to explain the vertical layering. It is clear that they use the major hydrogeologic units (Figure 2.4). However, they should explain the discretization of those layers. The APPZ zone in southwestern Florida is missing or non-productive (Reese and Richardson, 2007) based upon observed data. Similarly, the Boulder zone is also missing or generally non-productive in the northern portion of the model. How these units were dealt with in the model should be discussed.

Additional paragraphs have been added to Section 3.2.1 to describe the subdivision of the hydrogeologic layers into model layers. The missing APPZ zone in SW Florida was modeled by making the layer very thin in that area. The missing BZ zone was modeled

by making the conductivity values similar to the LF in this area. Both of these descriptions are included in the new text in Section 3.2.1.

4. The model's horizontal extent is not sufficiently extensive near the northwestern corner, western, and southern boundaries. These boundaries should be extended to where outcrops of Floridan Aquifers occur. On the Gulf side of the model, the boundaries should be extended as far as possible into the Gulf, with consideration of model run time, to include the estimated position of the saltwater/freshwater interface. Using observed data instead of natural boundaries to specify constant heads and/or concentrations along these boundaries will limit the use of the model for evaluating saltwater intrusion in those areas. It may also create challenges in drawing defensible conclusions if ASR wells are analyzed close to these boundaries.

The current model boundaries were based on the recommendations in the conclusion of the Phase 1 model report (previously reviewed by IMC). Although it would be desirable to extend all layers to their outcrop locations, this would greatly increase the computational time for each model run and the RAM necessary to interact with the model or solution. This would also add vast areas to the model where little or no geologic information is available. The layer outcrops occur over 150 miles west of the Floridan peninsula. Including this area would double the area of the model without adding additional relevant data. Half of the model would be void of any calibration points or data on layer thicknesses, hydraulic conductivity or storage.

The risks inherent in a larger, more unwieldy model with a large uncalibrated zone, have been determined to outweigh the risks that the ASR wells will impact the specified head boundary conditions on either the west or north boundary. We have developed a plan to determine the effect of the ASR pumping on the boundary conditions. The plan is to extract the flux rate for each specified head boundary cell on the north, west and south boundaries of the model and reapply that rate as a specified flux boundary condition during the ASR regional production runs. These solutions can be compared against those solutions obtained using the specified head boundary conditions. If the differences are minimal, we will be assured that the simplification to the model was warranted and that the boundary is not impacted by the CERP ASR pumping. If the differences are significant, the two solutions will allow us to bound the possible effects of the pumping and provide a more probabilistic solution to the decision-makers. This process will be described in detail in the next report, which describes the use of the regional model and the local-scale model to predict the effects of the CERP ASR program.

2.3 Model Time Discretization

1. Both the transient calibration and validation simulation periods are much too short to show any TDS concentration changes in the modeled aquifers if only 10 and 15 monthly stress periods are used. The Kissimmee River ASR project alone will exceed 15 months just for the 4 cycles. In addition, this short of a timeframe does

not address variations in climatic conditions which drive the head in the upper aquifers.

It was not the intent of this model to reproduce TDS concentration changes. There are very few wells with long term TDS data, so calibration of this type of model would be difficult. The TDS and temperature were included in the model only because they impact the flow of groundwater. The PDT is interested in possible long-term effects of the CERP ASR program on saltwater intrusion. To answer these questions, we will be running a much longer-term version of the model and a number of sensitivities or Monte Carlo type simulations will be run because of the uncertainty inherent in the use of the model for something it has not been calibrated to do.

Regarding the shortness of the timeframe for addressing climatic conditions, we have tried to balance the time requirements of an enormous data collection effort with the need to calibrate to a wide variety of hydrologic conditions. Clearly the model would be better with longer or more-varied calibration period, but the time and money required to collect the necessary data is prohibitive. SAJ can, perhaps, provide an estimate of the cost of collection of 27 months of head and pumping data. The data collection effort performed to date involved searches of numerous databases, a QA/QC effort and many phone calls to individual well owners.

2. Discussion of the time steps in Section 2.3 is confusing. Flow time steps are defined in the report as 5 or 6 days, but in each flow timestep, transport timesteps are determined during transport modeling, either using a fixed step or being calculated by transport model. In addition, it is unusual to run a steady state SEAWAT model to obtain steady state solutions directly. It is usual to set up as a transient model with a single stress period of significant duration so that a steady solution is obtained when both heads and concentrations do not change much or approach constant values as time increases.

Section 2.3 (now Section 2.4) has been clarified to indicate that both flow and transport timesteps were approximately 5 days long. (31-day months had timestep sizes of 5.2 days; 30-day months had timstep sizes of 5 days; 29-day months had timestep sizes of 5.6 days; 28-day months had timestep sizes of 5.8 days). The flow and transport timesteps were the same. We believe this to be valid because the TDS and temperature are not expected to change significantly at this scale. For the future local scale models, it is expected that both the flow and transport timesteps will need to be smaller in order to effectively model the freshwater bubble.

There is an option in MT3D to allow the transport simulation to select the timestep size based on the user-specified Courant number. When this option was selected, the model required a very small timestep size (less than 1 day) because of a few cells in the northwest portion of the model with large aspect ratios. This area is far from the proposed ASR locations and not important for the goals of this model, so this timestep selection option was not used. A sensitivity analysis of the selection of timestep size is presented in Appendix B. It indicated very little material improvement in the model with a timestep size less than 5 days.

The reviewer indicates that it is unusual to run a steady state SEAWAT model to obtain steady state solutions, but we believe it is the best option in this case. The purpose of this initial steady state run was to develop a starting condition for the transient model in which the equivalent freshwater heads are at equilibrium. This is done by holding the TDS concentration (and temperature) at the initial conditions and solving for the head condition which matches the boundary conditions, model parameters and initial TDS and temperature fields. In this way, the transient model will be starting with our best estimate for conditions during October 2003 (or October 1993 for the validation period). Otherwise, the initial stress periods (or perhaps all of the stress periods) in the transient model will be taken up with bringing the heads to an equilibrium condition rather than trying to reproduce the heads in the calibration wells.

As mentioned by the reviewer, a true steady state transport condition for TDS or temperature can only be obtained by running the transient model for a long period of time, until the concentrations do not change with time. Tests presented in the Phase 1 report (see Section 5.1) indicate that when allowed to run for 35,000 years, the TDS concentrations increase significantly in all areas of the model other than the recharge area. If this type of steady state starting condition was used for the start of the transient model, the initial conditions would have been nothing like the TDS levels which have been measured in the Floridan peninsula over the last few decades. This model would not have accurately reproduced conditions in 2003 or in any other period for the foreseeable future. The TDS condition in the peninsula does not seem to be in a steady state condition currently, in part due to the variety of significant pumping stresses that are being placed on the Floridan Aquifer.

3. Please explain why the period from October 1993 through July 1994 was chosen for the validation period (page 8). There are fewer observation wells active during this time period.

The period from August 1993 through July 1994 was chosen to reduce the data collection effort. The August 1993 through July 1994 time period is the same time period used for the regional model performed by USGS (Sepulveda, 2002). Choosing the same time period allowed SAJ and the modelers to make use of data collected as part of the USGS study.

4. Paragraph 3: The authors initially use a one-day, steady-state stress period "to provide a starting condition for the rest of the model." This steady-state stress period solves for a steady state head; however, the concentration solution will not instantaneously adjust to this steady-state head solution. The concentration solution may take significantly longer than one day, and in some instances or at some locations, perhaps months, years, or decades, to adjust to the instantaneous, steady-state head solution. This longer-term adjustment to the initial concentration condition may affect the estimation of transport parameters with an automated method like PEST. The authors may wish to include an additional transient stress period after the steady-state period and prior to the start of the time

period of interest. The concentration solution will migrate toward a steady state during this additional stress period. The length of the additional transient stress period is a function of the time needed for the concentration solution to migrate to a steady state, in response to the steady-state head solution.

We do not believe that the salinity is currently in a steady state. The Phase 1 report included some tests of that model running for 35,000 years. At the end of those runs, a significant portion of all aquifers had a larger TDS concentration than what exists currently (based on water quality data for the last few decades). The purpose of the one-day steady state run was to obtain a head condition that agreed with the interpolated TDS field. Put simply, the transient starting condition for the temperature and TDS concentrations was based on an interpolation of the available data while the transient starting condition for the head was based on a steady state calibration of hydraulic conductivity values until the starting condition matched available data.

It is true that a longer period run may require the adjustment of transport parameters. However, there is not enough data to do this type of calibration. Substantial uncertainty exists in estimating the ocean level 35,000 years ago and consequently the boundary heads for a simulation starting 35,000 years ago. The changes to the TDS in this model are expected to be small given the time scale being modeled. The transport parameters are expected to become more important for the local scale models. If the data for the local scale calibration is not available, sensitivity runs will be used to determine the range of possible results.

The inclusion of an additional transient stress period prior to the time period of interest would need to be exceedingly long (perhaps 35,000 years) and there is not sufficient data for calibration or boundary conditions for that length of time.

3.0 Conceptual Model

1. Paragraph 1: It is mentioned that additional conceptualizations of temperature and salinity are required. Has salinity been analyzed in previous model efforts? Please clarify.

The purpose of this sentence was to indicate that while much of the conceptualization for the hydrogeology was available in the Framework (Reese and Richardson, 2008), the TDS and temperature data had not been analyzed in that report. The sentence has been clarified in the report and a new Appendix describing the analyses of the salinity and temperature data has been added.

3.1 Topography

Paragraph 3: How did the authors parse well data where the well is open within more than one hydrogeologic unit?

For monitoring wells, the database was queried to find all wells with more than 50% of the open interval within a single hydrogeologic unit. Some wells were omitted if they were deemed to not represent regional conditions. A table presenting the well names and the reasons for inclusion or removal has been added to the report as Table 4.1.

For pumping wells, the pump rate was prorated among the aquifers tapped by the open interval based on the thickness of each aquifer covered by the well and the approximate conductivity found in each aquifer. Wells which partially tapped confining units had all their pump volume moved to the aquifer portions of the wells. (Rounding occasionally resulted in a small amount of water being pulled from confining unit cells.) For additional details, please see Appendix D Section 2.0 Pumping Rate Assignment in the Regional Model.

3.2.1 Regional Geology

Paragraph 2: The authors should describe briefly the UF and APPZ before describing the LF.

The descriptions of all aquifers are provided in the Hydrogeologic Framework (Reese and Richardson, 2008) and readers are invited to look in that document for additional information. The statement about the LF is made because the Hydrogeologic Framework divides the LF into a number of subunits (LF1, LF2, and LF3). The model does not differentiate between these layers, so the statement in Paragraph 2 is made to address this difference. The statement has been clarified in the report.

3.2.2 Hydrogeologic Properties

1. Paragraph 2: The authors should provide the specific subsection of Section 3, in which the final calibrated parameters are presented. The authors should reference figure numbers.

Fixed

3.2.3 Regional Anisotropy

1. Bittner, Richardson, Langevin, England, and Stevens (2008) concluded that regional anisotropy and the effects of pressure and temperature on fluid density and viscosity improve agreement between head observations in southern Florida, and numerical models of variable density flow and transport. The authors state that "SFWMD performed additional hydrogeologic investigations to quantify the extent and magnitude of regional anisotropy in the FAS. Initial findings from an analysis of flowing fractures in selected wells indicate that evidence may exist for [regional anisotropy in the FAS]. However, further unpublished analysis ultimately concluded that, although there are indications of a preferential flow direction in some areas, this is not a widespread, regional feature. Based on these findings, regional anisotropy was not included." Given the conclusions of Bittner

et al. and the SFWMD field study, the authors should fully detail the unpublished analyses.

Unfortunately, these unpublished results are still not available for inclusion in this report. They are planned for completion in time for inclusion in the TDR for the Regional Study. Conversations with Emily Richardson at SFWMD have given us a clearer understanding of the basics of the study and this section has been clarified. Although Bittner et al (2008) concluded that the inclusion of anisotropy might improve the calibration of the model, there is currently no evidence to support the use of a regional anisotropy, so the model was calibrated without this option. Readers who require additional information on this study are invited to wait for the TDR or to contact Ms. Richardson directly.

2. Paragraph 2. Regional anisotropy may be present due to stratigraphy and the development of higher permeability facies along depositional strike. The direction of this strike would probably be roughly parallel to the axis of the peninsula, which is 10 to 30 degrees west of North. This may be more important in the UF than in the APPZ. Perhaps this could be confirmed by aquifer tests, provided enough monitoring wells in different directions were used in the tests.

This is an interesting theory, but its analysis is outside the scope of this study.

3.3 Boundary Conditions

3.3.1 Surficial Head Boundary Conditions

1. Paragraph 2: The authors detail an assumption that ASR pumping does not affect head in the SAS. The authors may wish to include a table or list, in which all model assumptions are clearly listed. For example, the authors would include a number of standard assumptions in the table or list, such as principal axes of anisotropy are aligned with Cartesian axes of the model grid. The authors may wish to detail methods, such as sensitivity analyses, used to justify all assumptions, including the assumption that ASR pumping or injection does not change SAS head. What happens if ASR pumping or injection occurs for a very long period of time, such that the SAS is potentially drawn down or up in some locations? Is the SAS sufficiently disconnected from the FAS at all locations within the model domain? What if ASR pumping occurred at locations where the FAS and SAS are not sufficiently disconnected? Would the head in the SAS be affected?

We have added Table 2.1 detailing assumptions, their basis and sensitivities in Section 2.0.

Regarding the assumption of principal axes of anisotropy being aligned with the Cartesian axes of the grid, since anisotropy was set to 1.0 on all layers, the orientation of the grid has no effect on the result.

Regarding the assumption with the SAS, we cannot be certain of the validity of this assumption until we have run the production runs with the ASR wells. The modelers are planning a sensitivity run which will extract the calculated fluxes at all specified head boundary cells (other than those on the ocean) and then rerun the model using those fluxes as specified flux boundary conditions. The comparison between the results of these two models will tell us what impact this assumption has had on the ASR analysis. If the impact is important, the two models may help bound the results. The PDT has been kept aware of our assumptions and their possible effects on the ASR analysis.

2. Appendix Page C-3: The authors state that "The calculated flux was compared to available estimates on recharge in the model domain and found to be generally similar." The authors should detail the comparison of calculated flux and available estimates of recharge with a table or graph. The authors should provide documentation to support the available estimates of recharge, such as report reference or well identification information.

This analysis was described in Section 4.1.4 and in Figure 4.18 (now Figure 4.29). The statement from the Appendix has been updated.

3. Paragraph : The authors may wish to detail whether the specified head boundary condition at the surface is transient or steady. If specified boundary conditions at the surface are steady state, the authors may wish to justify the steady state assumption. The authors may wish to provide a table of observed aquifer heads, with associated well or location identification information, and ranges in observed head.

The specified head boundary condition at the surface is transient and based on average monthly heads for a large number of wells. The text has been clarified in several locations to make this clear. Table 4.1 lists all the wells used in the SAS interpolation

3.3.2 Simulation of Ocean Boundary

1. Paragraph 1: The authors state that "the annual variation of monthly mean sea levels is about 0.5 feet, which is much smaller than the variation in nearly every other parameter of the model." The authors may wish to detail how an annual variation in mean sea level, measured in feet, is compared with variation in other model parameters, such as hydraulic conductivity, that are not measured in feet and/or not transient. The authors may wish to re-word this sentence.

The sentence has been revised to clarify the original meaning – that the variation in head at the ocean boundary is smaller than the variation in heads seen at nearly all observation wells in the model.

2. Paragraph 1: The authors should provide a figure that details ocean boundary elevation versus time for both the Virginia Key and Naples gages. The authors should tabulate the phase and amplitude of major tidal constituents at Virginia Key, Naples, and at other tidal gages in Florida, to prove that Virginia Key and Naples are representative time series for the east and west coasts of Florida. The Virginia Key tidal gage is inside Biscayne Bay, at the end of a pier that is near a causeway. Are the phase and amplitude of major tidal constituents at this location equivalent to the phase and amplitude of major tidal constituents 40 miles off the coast of Melbourne Beach, or 15 miles off the coast of Fort Lauderdale?

A figure of the ocean boundary elevation has been added to the report (Figure 3.16). We see no need to tabulate the phase and amplitude of major tidal constituents at the gages in Florida because we are using only the Monthly Average water level in the model. The stress periods in the model are a month long and so, cannot hope to reproduce any tidal signatures. In response to the request that Virginia Key and Naples data be revisited to ensure they are representative, the NOAA Tides and Currents Database was searched for any other tidal gages in the modeling domain with data available for the calibration or validation periods. A number of additional tidal gauges were found. The Trident Pier gage is located just north of the model boundary on the east coast. In the 2003/2004 period, its water level is up to 0.6 feet lower than the modeled boundary condition. If it had been averaged with the only other east coast gage, the head at the eastern boundary would have dropped by approximately 0.25 feet during the spring and summer of 2004. However, since this gage has no available data during the 1993/1994 validation period, it was not used in the selection of boundary conditions. The 0.25 foot change is less than the calibration errors and would have been of minimal impact to the model overall.

Three gauges were found in the Florida Keys. These are beyond the boundary of the model, and so were eliminated from the model. However, the monthly average water level is very close to that measured at Virginia Key. Inclusion of these points in an average would have changed the boundary condition head by perhaps 0.1 feet in some months. This is well within the error inherent in the model.
Finally, a single gauge (Port Manatee) was found on the west coast, about 15 miles from the entrance to Tampa Bay. This gauge had available data only for the calibration period, and generally had water levels similar to those at Naples.

The entire range of all the available data for all months of the calibration and validation periods is less than 1.5 feet. The sea levels do not change significantly over this time period when averaged over each month. The use of the Naples and Virginia Key gauges was sufficiently accurate for the model of this scale. The plots of water levels at each gauge and the locations of the gauges are shown below:

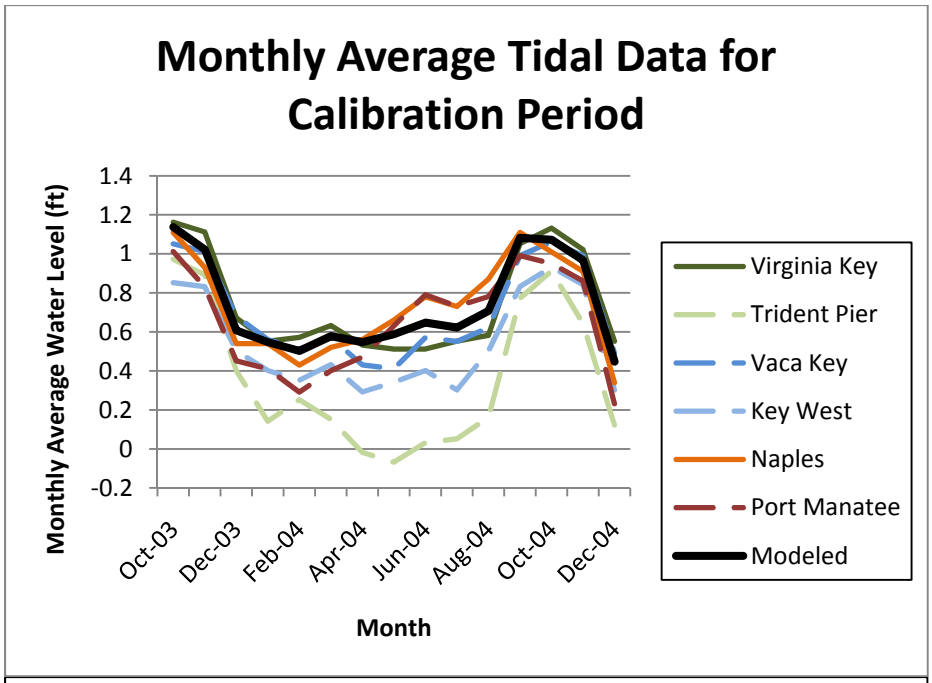
Monthly Average Tidal Data for Calibration Period
Monthly Average Water Level (ft)
1.4
1.2
1
0.8
0.6
0.4
0.2
0
-0.2
Oct-03
Dec-03
Feb-04
Apr-04
Jun-04
Aug-04
Oct-04
Dec-04
Month
Virginia Key
Trident Pier
Vaca Key
Key West
Naples
Port Manatee
Modeled

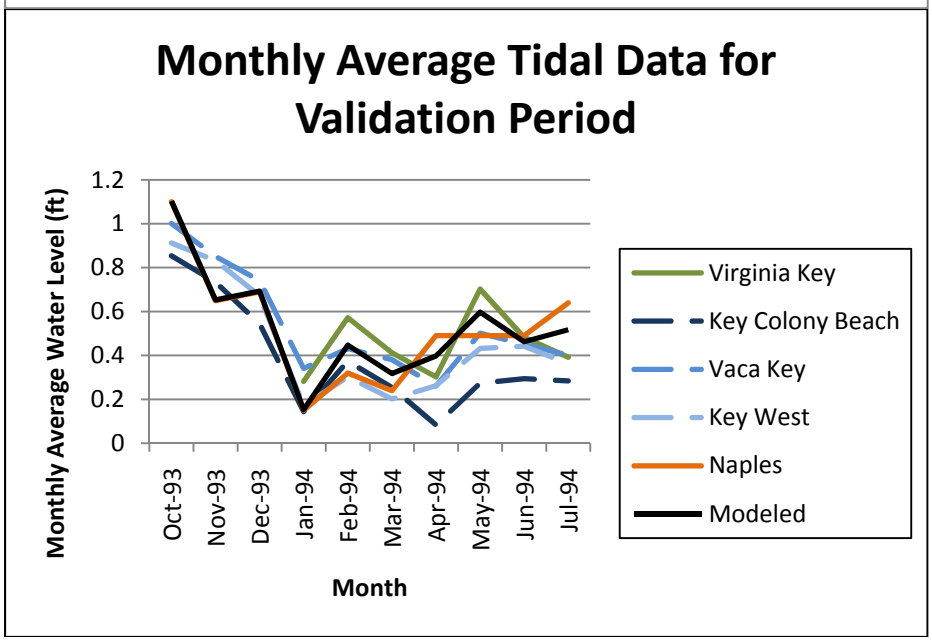
Monthly Average Tidal Data for Validation Period
Monthly Average Water Level (ft)
1.2
1
0.8
0.6
0.4
0.2
0
Oct-93
Nov-93
Dec-93
Jan-94
Feb-94
Mar-94
Apr-94
May-94
Jun-94
Jul-94
Month
Virginia Key
Key Colony Beach
Vaca Key
Key West
Naples
Modeled

3.3.3 Aquifer Head Boundary Conditions

1. Paragraph 1: The authors should explain whether aquifer head boundary conditions are transient or steady state. If aquifer head boundary conditions are steady state, the authors should justify the steady state assumption. The authors should provide a table of observed aquifer heads shown on Figure 3.10, with associated well or location identification information, and ranges in observed head.

The aquifer head boundary conditions are transient. The head values for each stress period were selected by averaging the available data over the month. A few sentences have been added to the text to emphasize this point. Table C2 (in Appendix C) contains information on all of the wells shown in Figure 3.10 (now Figure 3.17). The table has been expanded to include location information. Since the aquifer boundary conditions are transient (averaged over each month), the inclusion of ranges of observed head is less useful. More useful, might be the inclusion of the ranges of observed heads in each stress period, however, as this would make the size of the table and report unwieldy, the readers are invited to extract the desired data from the appropriate online database (e.g. USGS or DBHydro).

3.3.4 Confining Unit Head Boundary Conditions

1. Paragraph 1: The authors should justify the no-flow boundary condition on boundaries of confining units. The authors should compare the vertical flux between confining unit and aquifer, at the boundary, to the vertical flux between confining unit and aquifer a few cells into the domain. If both vertical fluxes are within 10%, the assumption may be acceptable. Alternately, the authors may wish to use a specified head on confining unit boundaries, which is equivalent to the average of the head used in the bounding aquifers.

A comparison of the model results with and without specified heads assigned on the confining unit boundaries has been added in the sensitivity section (Section 5.5.3) of the report. No appreciable difference was observed, indicating that the assumption is acceptable.

3.3.5TDS and Temperature at the Boundaries

3.4 Initial Conditions

3.4.1 Salinity (TDS) Distribution

1. The TDS along the ocean boundary in BZ was set above sea water at 40,000 mg/l. The report suggests that it could be caused by minerals in BZ and injections of wastewater with high salt, but this high value is still used in the model at the boundaries where these conditions may not exist. Was the selection of this value derived from model calibration? This high concentration will largely increase equivalent freshwater water heads in BZ and thus change flow directions and patterns in upper layers.

This issue was brought up at the February 2010 PDT meeting and was addressed as a sensitivity run in Section 5.5 in the original Draft document. The recommended plan forward was to recalibrate the model using the new lower BZ salinities at the ocean boundary. As planned, the model has been recalibrated for the final version of the modeling report. As such, Section 5.5 was removed as being unnecessary and the TDS interpolation plots were updated.

2. Relating to the previous question, the eastern boundary temperature was set at approximately 4 degrees C in the BZ to account for temperature and density changes observed in the deep ocean. Considering that one of the largest warm water currents runs along the eastern boundary, is there a reference from the coast of SE Florida which supports the standard middle latitude thermocline used to calculate the temperature at depth for the aquifers?

The temperature along the eastern boundary of the BZ varies from approximately 7°C at the northern edge of the Phase II ASR Regional model to 5°C at the southern edge.

The temperature variation was read from Figure 3.19 (now Figure 3.27) of the Draft Groundwater Calibration Model Report based on the variation in the BZ layer depth.

At latitude 27°N, between Jupiter Island and Grand Bahama Island, several studies have been performed to estimate the transport of the Florida Current. Data collection for these studies included temperature along the latitude line from the ocean surface to its floor. The figure below, from Figure 2.3 of Chester, 1989 (which was adapted from Leaman et al., 1987), shows the temperature profile throughout the cross section at latitude 27°N. The temperature at the base of the cross section, approximately 750 m (2,460 ft) deep, is 5°C which is consistent with the temperature values used in the Phase II model at this depth. In 2001, NOAA obtained temperature data from the same site which was reported in a study to determine groundwater flow patterns in the Floridan Aquifer based on isotopic measurements. At a depth of 630 m (2,065 ft), the temperature reported was 7.8°C. (Table 2 of Morrissey and Clark, 2009). In the Phase II model, this location is on the boundary of the LC where the assigned temperature is 8°C. Data from these reports supports the use of the middle latitude thermocline along the Florida coast to assign the temperature boundary condition.

References:

1) Acoustic Tomography in the Straits of Florida, David Brian Chester, B.S. Southampton College of Long Island University (1989), Master of Science at the Massachusetts Institute of Technology and the Woods Hole Oceanographic Institution

2) Leaman, K.D., R. Molinari, and P. Vertes, 1987: Structure and Variability of the Florida Current at 27N: April 1982-July 1984, Journal of Physical Oceanography, 17, 565-583.

3) Morrissey, S.K. and J. F. Clark, 2009 Isotopic Measurements from the Floridan Aquifer: Years 1 to 5 Results, unpublished.

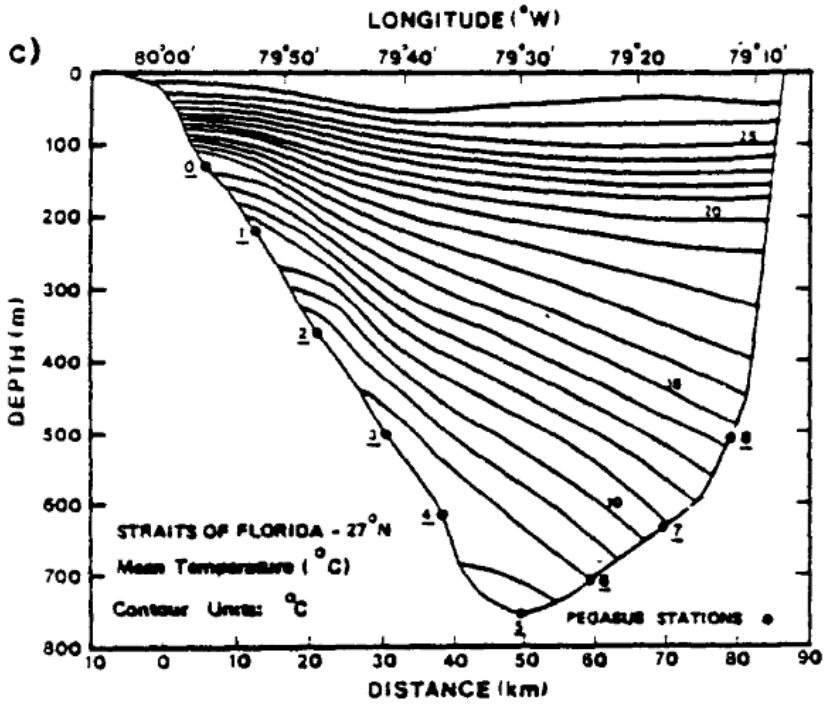

3. Reese (1994) investigated the distribution of TDS in the Floridan aquifer system, in southeastern Florida. The authors do not reference Reese (1994). The following TDS distributions, using the Reese and Richardson (2008) hydrostratigraphic framework, can be generated by interpolating Reese (1994) data to cell centers:

[Figures removed.]

These figures may not be directly quoted or referenced by others, or identified as a personal communication. The information may be useful to the authors in answering specific questions concerning TDS distributions based on Reese (1994).

The 1994 Reese report (WRI 94-4010) referenced in this comment was used in the generation of the salinity distribution for this model. The omission of this reference was corrected in the final modeling report. In addition to the referenced report, a variety of other data sources were used, including more recent USGS publications, data from the Florida Department of Health, the DBhydro on-line data base, data collected for previous modeling efforts, well completion reports, etc.

Based on discussions with the reviewer, the above figures were generated based on Table 7 (WRI 94-4010), which identifies the depth to the brackish and saline water interfaces at 24 locations. These interface depths were primarily based on resistivity curves and not measured water quality data. For the Phase II regional modeling effort, measured water quality data, including data from Tables 2 and 3 of WRI 94-4010, were used to establish the salinity distribution in each model layer. The data used were critically evaluated by both the modelers and SFWMD to ensure that the data were representative and reliable. After the data were interpolated to the model grid/mesh, a variety of error-checking routines were performed to ensure consistency between vertical layers. This was especially important in the confining layers, where the salinity data were more limited than in the aquifers. Appendix E has been added to the final modeling report to more fully describe the procedures used to generate the TDS distribution in the Phase II regional model.

4. The authors TDS distributions are somewhat different at some locations in southeastern Florida than the distributions shown above in Figures 1 – 4 ***[Figures removed]***. The authors show "islands" of high or low TDS concentration at some locations. For example, TDS of less than 5 ppt in the MCU Lower, in northern Miami-Dade County, where the Reese (1994) distribution shows greater than 30 ppt. The authors may wish to explain---at some locations---the transient geologic process that lead to the presence of these "islands" of TDS concentration, or re-contour the TDS distribution such that the islands do not exist, and a classic saltwater wedge shape remains, as is shown in the above Figures 1 – 4 ***[Figures removed]***. The authors may wish to re-order Figures 3.11 through 3.17 in stratigraphic order, such that the reader can progress from top to bottom, or bottom to top, and rationalize TDS distributions that deviate from the classic saltwater wedge shape.

In evaluating this review comment, an error in the DBhydro database was discovered at wells DF-1 and DF-5. These wells were used to generate the TDS distribution for the MC2 and are at the location in northern Miami-Dade County referenced above. The corrected TDS for this location is 34,200 mg/l. This error has been corrected in the DBhydro database and updated in the final calibrated model.

During model construction the "islands" of high TDS concentration were evaluated throughout the model domain. Some are the results of TDS inversions (high TDS overlying lower TDS) which are supported in the data. Prominent examples of this inversion are located at the SFWMD test wells near City of Oakland Park and the Hillsboro ASR Pilot Project.

The City of Oakland Park wells are located in Broward County near the Atlantic coast. The wells in this location where TDS data are available for the UF are designated BF-1, BF-3, and BF-4S. The recorded TDS for these UF wells varies between 7500 mg/l and 8731 mg/l. In addition to these UF wells, there are two wells, BF-2 and BF-4M, that have TDS data for the APPZ. The recorded TDS levels for these wells range from 4810 mg/l to 5520 mg/l, which is noticeably fresher than that observed in the UF.

The Hillsboro ASR Pilot Project wells are located in southern Palm Beach County. The wells in this location where TDS data are available for the UF are PBF-10R and PBF-13. The recorded TDS for these UF wells varies between 2932 mg/l and 6500 mg/l. The corresponding APPZ well at this location, PBF-11, again has a lower TDS range of between 1262 mg/l and 3200 mg/l.

In summary, the TDS data was collected from numerous sources in addition to WRI 94-4010 and critically reviewed during the Phase II model construction and calibration. As discussed during the October 28, 2008, PDT meeting with IMC, observed data was used to the maximum extent possible to set the initial TDS concentrations. The data at the "island" locations referenced in this comment is based on observed data and the lateral extent of elevated TDS is limited within the model. As such, the modelers feel that the TDS representation is reasonable, accurate, and consistent with the approach previously presented to the IMC.

3.4.2 Temperature Distribution

1. Figure 3.24: What causes the 22-28 degree C temperature in the Boulder Zone, within Miami-Dade County, near the county boundary that divides Miami-Dade County and Broward County, within 10 kilometers of the Atlantic Ocean? Is this 22-28 degree C temperature due to injection? If so, are there other locations within the model domain that also would exhibit relatively higher temperature due to injection, such as at the North and South District Wastewater Treatment Plants in Miami-Dade County, where very large volumes of wastewater treatment plant effluent have been injected into the Boulder Zone?

The higher temperature in the Boulder Zone near the Miami-Dade/Broward County boundary is due to injection. This temperature data point should have been removed from the data set. Because injection well temperature data or temperature influences at monitoring wells due to injection wells represent local conditions and do not reflect the regional aquifer temperature, temperature data affected by injection should be omitted. The temperature dataset was reanalyzed for injection impacts and adjustments were made to the temperature distributions in the Boulder Zone and Lower Floridan layers. Appendix E has been added to the report to detail the data used in each layer to construct the temperature distribution and their sources.

3.5 Sources and Sinks

4.0 Calibration/Validation

4.1 Steady State Calibration

1. On page 21, the authors indicate that there is no standard protocol for selecting a calibration range during the calibration process. It should be noted that the calibration statistics are within an acceptable range for previous models developed for the Floridan aquifer (Figures 4.2 through 4.11).

The modelers continue to believe that despite the variety of statistical measures of calibration quality, the decision to accept a calibration is primarily a qualitative one, and is based on numerous considerations, including the intended use of the model and the precision required to answer the questions to be posed. That the calibration statistics for this model are within the ranges deemed acceptable by previous modelers is auspicious, but these previous models were not likely designed for the same purposes, so a comparison of statistical calibration may not be practical.

Figure 4.19: The authors show a saddle feature in the modeled predevelopment head distribution for the 60-foot contour, west of Lake Okeechobee. This region is of particular importance, as it is an area where ASR is being evaluated. The following text may not be directly quoted or referenced by others, or identified as a personal communication. However, the information may be useful to the authors in answering specific questions concerning historic potentiometric surface delineations. The authors may also find it useful to review the cited literature.

[Text removed].

Stringfield, V.T., 1936, Artesian water in the Florida peninsula: U.S. Geological Survey Water-Supply Paper 773-C, p 115-195.

Stringfield, V.T., 1938, Groundwater supplies in Florida: Civil Engineering, Vol. 8, No. 7.

Stringfield, V.T., 1966, Artesian water in Tertiary limestone in the southeastern states: U.S. Geological Survey Professional Paper 517, 226 pp.

Cooper, H.H., 1944, Groundwater investigations in Florida: American Water Works Association Journal, Vol. 36, No. 2.

Parker, G.G., Ferguson, G.E., Love, S.K., and others, 1955, Water resources of southeastern Florida, with special reference to geology and ground water of the Miami area: U.S. Geological Survey Water Supply Paper 1255, 965 pp.

Healy, H.G., 1962, Piezometric surface of the Floridan aquifer in Florida, July 6-17, 1961: Florida Bureau of Geology Map Series No 1, 1 map.

Healy, H.G., 1975, Potentiometric surface and areas of artesian flow of the Floridan aquifer in Florida, May 1974: Florida Bureau of Geology Map Series No 73, 1 map.

Healy, H.G., 1978, Appraisal of uncontrolled flowing artesian wells in Florida: U.S. Geological Survey Water-Resources Investigations 78-95, 26 pp.

Healey, H.G., 1982, Potentiometric surface of the Floridan aquifer in Florida, May 1980: Florida Bureau of Geology Map Series 104, 1 map.

Kohout, F.A., 1965, A hypothesis concerning cyclic flow of salt water related to geothermal heating in the Floridan aquifer: Transactions of The New York Academy of Sciences Series II, Vol. 28, No. 2, p 249-271.

Johnston, R.H., Healy, H.G., and Hayes, L.R., 1981, Potentiometric surface of the Tertiary limestone aquifer system, southeastern United States, May 1980: U.S. Geological Survey Open-File Report 81-486, 1 map.

Johnston, R.H., Krause, R.E., Meyer, F.W., Ryder, P.D., Tibbals, C.H., and Hunn, J.D., 1980, Estimated potentiometric surface for the Tertiary limestone aquifer system, southeastern United States, prior to development: U.S. Geological Survey Open-File Report 80-406, 1 map.

Bush, P.W., Barr, G.L., Clarke, J.S., and Johnston, R.H., 1987, Potentiometric surface of the upper Floridan aquifer in Florida and in parts of Georgia, South Carolina, and Alabama, May 1985: U.S. Geological Survey Water-Resources Investigations Report 86-4316.

Bush, P.W., R.H. Johnston, 1988, Ground-water hydraulics, regional flow and ground-water development of the Floridan aquifer system in Florida and in parts of Georgia, South Carolina, and Alabama: U.S. Geological Survey Professional Paper 1403-C, 80 p., 17 pls.

Barr, G.L., 1985, Potentiometric surface of the Upper Floridan aquifer, west central Florida, May 1985: U.S. Geological Survey Open-File Report 85-482, 1 sheet.

Barr, G.L., 1987, Potentiometric surface of the Upper Floridan aquifer in Florida, May 1985: Florida Geological Survey Map Series 119, 1 sheet.

Barr, G.L., 1993, Potentiometric surface of the Upper Floridan aquifer in Florida, May 1990: Florida Geological Survey Map Series 138, 1 sheet.

Meyer, F.W., 1989, Hydrogeology, ground-water movement, and subsurface storage in the Floridan aquifer system in southern Florida: U. S. Geological Survey Professional Paper 1403-G, 59 p.

Miller, J.A., 1990, Ground water atlas of the United States: Segment 6, Alabama, Florida, Georgia, and South Carolina: U.S. Geological Survey HA 730-G, 28 pp.

> Given the eventual conclusion that "the Floridan aquifer system south of Lake Okeechobee can only be replenished by groundwater flow from central Florida" (Bush and Johnston, 1988), what causes the modeled potentiometric high south of Lake Okeechobee on Figure 4.19 (and also on Figure 4.2, 4.3, 4.6, 4.7)? Is this the result of some assumed initial condition in head, salinity, or temperature? Perhaps some assumed initial condition within the modeled trough, west of Lake Okeechobee? Is the assumed initial condition the result of one of the above-described, historic, superseded hypotheses? Is the existence of this trough in the pre-development model realistic? Given the importance of comparing pre-development conditions in the Lake Okeechobee region to post ASR conditions, the presence of this trough may considerably affect study conclusions, and conclusions about the impact of the ASR program. The authors may wish to specifically, explicitly, and quantitatively explain why the trough exists within the pre-development model, or alter the model to eliminate the trough.

The reviewer has identified a trough feature that occurs between the 50-foot and 60-foot contours in the modeled predevelopment Upper Floridan head contours in the vicinity of Lake Okeechobee as shown on Figure 4.19 of the Draft Groundwater Model Calibration Report (now Figure 4.30). In addition, the reviewer provided a history of the major contributions to the development of the published Upper Floridan potentiometric surface in south Florida. In the earliest cited publications, Stringfield (1936), Parker and others (1955), Healy (1962), the trough is not shown. Two later publications, Healy (1975) and Johnston et al (1981), show a trough based on additional head data in the Lake Okeechobee area. Bush and Johnston (1988) reanalyzed the data and removed the trough from the 1980 potentiometric surface based on three factors (1) some wells used to delineate the trough were open to depths shallower than the Floridan aquifer or not open exclusively to the Floridan aquifer (2) water level fluctuations at Belle Glade (PB-203) suggest replenishment from the recharge area north of the trough and (3) the higher head water south of Lake Okeechobee has not dissipated over time.

The comparison to the predevelopment heads (Bush and Johnston, 1988) in the Draft Groundwater Model Calibration Report was made by running the calibrated 2004 steady state SEAWAT model without any pumping wells. The head boundary conditions on the surface and aquifer side boundaries represent hydraulic conditions for 2004 (i.e. with drawdown from pumping included). It is possible that because the surface heads defining the recharge represent 2004 conditions rather than predevelopment conditions, less recharge is entering the model and it is not sufficient head to push the flow further to the south in the Upper Floridan aquifer. However, in areas other than the trough area, it was surprising how closely the modeled predevelopment contours matched the Bush and Johnston (1988) contours.

The model initial conditions are independent of the data in any of the publications of the Upper Floridan potentiometric surfaces. The initial head condition for each model cell was set arbitrarily at an elevation higher than the bottom of the SEAWAT grid cell. The initial head conditions affect how quickly the model reaches a solution but does not impact the numerical result. The salinity and temperature initial conditions were based on available total dissolved solid and temperature data to determine the native values for the aquifer. In the figures showing the distribution of the salinity and temperature data for the initial conditions (Figures 3.18 to 3.25 and 3.28 to 3.36), the area west of Lake Okeechobee exhibits salinities and temperatures much higher than the surrounding areas in the MC1 and APPZ layers for salinity and in all layers below the UF for temperature. It is possible that these patterns contribute to the formation of the trough, but not enough information is available for salinity and temperature in predevelopment times to know whether the patterns have existed long-term or have developed more recently.

The model can be altered to remove the trough for predevelopment conditions. One way this can be done is to lower the values of the vertical hydraulic conductivity in the ICU and/or IAS in Glades County. The topography and surface heads in the area along Caloosahatchee River up to Lake Okeechobee are lower than those in the UF so to keep the water from discharging to the surface, a tighter ICU/IAS is necessary. Another way to increase the UF heads is to increase the vertical hydraulic conductivities in the confining units below the UF. Although these changes can yield a predevelopment solution without a trough, the computed UF heads for calibration time periods become too high compared to the observed heads or the hydraulic conductivity values necessary to complete the change are beyond reasonable ranges.

A significant problem in deciding whether or not a trough exists is the lack of head data. Even for 2004 calibration conditions, there are only a few well clusters that could be used to determine the direction of flow and none of them are in Glades County, the area where the trough may exist. The well clusters surrounding Glades County (clockwise starting in the north) are ROMP 28 (UF, APPZ, and LF), OKF-100 (UF and APPZ), PBF-7 (UF and LF), L2 (UF and APPZ), and LAB (UF and APPZ). Of these wells, the UF well furthest north and south, ROMP 28, L2 and PBF-7, have heads higher than 55 ft. The UF wells closer to the border of Glades County, OKF-100

and LAB, have values less than 53 ft indicating a shallow trough like that shown in the model results. Of course, with current conditions, the heads are affected by pumping and may not represent the pattern of the heads in predevelopment conditions.

A study that may provide insight regarding the question of whether the Upper Floridan aquifer in south Florida is recharged from areas north of the lake will be published later this year. The study states that analyses of geochemical data indicates that "most of the Upper Floridan aquifer contains groundwater recharged during the last glacial period" rather than from recently recharged groundwater (Morrissey, S. K., et al., 2010). While evidence to show that the higher head water in the south Florida Upper Floridan aquifer is "relic" water doesn't prove that the trough was always present, it doesn't preclude the presence of a trough.

With the predevelopment trough removed from the model or not, the modeled flow directions that occur in the UF are unchanged. At wells PBF-7 and L2 south of Lake Okeechobee, an upward gradient exists that is replicated in the model. At ROMP 28 in Highlands County, a downward gradient exists that is replicated in the model. The location of the gradient direction change varies based on recharge and pumping conditions. This area is the location where many of the proposed ASR wells are planned. Sensitivity and Monte Carlo analyses will be performed for the with-project scenarios to better define the uncertainty and determine the impact of the CERP ASR program for different aquifer pumping conditions.

Reference:
Morrissey, S. K., J. F. Clark, M. Bennett, E. Richardson, and M. Stute (2010) Groundwater reorganization in the Floridan aquifer following Holocene sea-level rise. Nature Geoscience, doi:10.1038/NGEO956.

2. Paragraph 13: The authors use a statement by Anderson (1992) to suggest that "The judgment of when the fit between model and reality is good enough is a subjective one. To date, there is no standard protocol for evaluating the calibration process…" Anderson made this statement almost 20 years ago in 1992. A considerable volume of work has occurred since 1992, in which standard protocols for evaluating calibration are more quantitative than in 1992. For example, the authors may wish to refer to and incorporate concepts available in the vast literature on parameter estimation, and from parameter estimation codes such as UCODE or PEST. The authors may wish to remove the Anderson quote, abandon the position that calibration is entirely subjective, and provide more quantitative calibration methods and metrics.

A considerable volume of work has, indeed, been published since 1992, and there are numerous statistical measures and analyses that have been put forward in an effort to standardize the calibration of models. However, we continue to support Anderson's opinion that the decision to accept a calibration is primarily a subjective one. This decision must take into account the purpose for which the model is designed as well as the data available and the resolution in both time and space. For example, despite its

calibration metrics, this regional model is not calibrated well enough to provide estimates of well-to-well interactions for ASR wells. With the same calibration statistics, this model is calibrated well enough to provide an estimate of the regional impacts of the CERP ASR program as a whole.

4.1.1 SEAWAT

1. Figures 4.20-4.29: The authors may wish to re-order the figures in stratigraphic order, either from top to bottom, or from bottom to top; and to re-order the figures such that WASH123 and SEAWAT figures are adjacent, for identical layers. The reader can then easily confirm that the same distribution is being used for both models. The authors show orders of magnitude changes in regional horizontal hydraulic conductivities across sharp interfaces, at some locations. For example, south of Lake Okeechobee, in the APPZ for the SEAWAT model, horizontal hydraulic conductivity changes from 5-20 feet per day to 400-600 feet per day across a sharp line near the edge of the lake. The authors may wish to offer geologic justification for such a sharp, regional delineation; or, the authors may wish to introduce a more gradual, continuous transition zone, in which regional hydraulic conductivity changes continuously along a continuous gradient. The authors may wish to use pilot points and an interpolation method such as kriging to define hydrogeologic parameters that vary in space, in a reasonable and defensible fashion. Some sharp-change locations under the proposed conductivity distribution are in regions where ASR will be analyzed by the model. The adopted hydraulic conductivity may affect conclusions drawn from the model. The authors may wish to contour all hydrogeologic parameters with a continuous contour method (such as is used on Figure 5.3), as opposed to the method of bins (used on Figures 4.20-4.29).

Figures 4.20 through 4.29 for the SEAWAT model were ordered according to their descriptions in the text, which discussed the aquifers first. They have been reordered according to their stratigraphic order. The WASH123D model has not been recalibrated for the final report. An appendix has been added to show the similarity of the draft calibrations between the SEAWAT model and the WASH123D model. We prefer to keep the SEAWAT and WASH123D figures separate since they are discussed in different sections of the report.

All of the changes in hydraulic conductivity which occur across sharp interfaces are explained in the report. Section 4.1.2 describes both the location of the change from the ICU to IAS based on Miller (1997) and the location of the change from limestone to dolomite in the APPZ, based on the Framework report (Reese and Richardson, 2008). In addition, a sensitivity analysis was run on the location of the APPZ change and the location of this line was found to be unimportant to the calibration. Since this line runs near some of the proposed ASR locations, some additional sensitivities are planned for the regional ASR runs.

The conductivity fields were developed using pilot points and ordinary kriging. (See Section 4.1.1 and the notes on Figures 4.31 through 4.40)

We avoided using a continuous contour method because of the sharp interfaces in hydraulic conductivity seen in layer 3 (IAS/ICU) and the APPZ. A continuous contour method would have placed a number of very close contour lines across that interface and might have given the impression that the conductivity changed gradually (albeit with a sharp slope). The use of bins in the figures makes clear that a sudden change of several orders of magnitude was used in the model and is consistent with the format of numerous existing studies of the Floridan Aquifer.

4.1.1.2 Calibrated Hydraulic Conductivity Fields

1. Please add the APT data to the calibrated horizontal and vertical hydraulic conductivity fields, and provide a discussion about changes between observed data and simulated values.

APT results have been overlain on the calibration conductivity field figures (see Figures 4.34, 4.36 and 4.38).

2. On page 24, the authors state that the boundary between the aquifer and aquitard was based on Miller (1997). Please explain why Reese and Richardson (2007) were not used. On page 27 and Figure 4.12, the authors discuss and illustrate the vertical gradient for the Alligator Alley well. They indicate that if equivalent fresh water heads were used, the water level actually increases with depth (for the simulated wells).

Reese and Richardson (2008) do not include a figure showing the boundary between the aquifer and aquitard in the IAS/ICU layer.

- The authors should show the observed data on the equivalent freshwater head graph. Will the simulated and observed still match?

Equivalent freshwater head is generally not measured in the field. TDS and temperature data are much sparser than head data. In order to show the "observed data" on this figure (4.18) we would need to use the TDS, temperature and head data to calculate the equivalent freshwater head. This would be the same calculation made on the model calculated data, so this exercise does not appear to be relevant. The purpose of the equivalent freshwater head plot in Figure 4.18 was to clear up any confusion that might result from the observed head plot at left. Readers without a clear understanding of equivalent freshwater head or without a clear knowledge of salinity conditions deep below south Florida may be confused by the apparent downward gradient between the APPZ and the Boulder Zone in the observed head plot. The equivalent freshwater head plot is included and discussed in the text as a reminder to the reader that flow conditions are controlled by the equivalent freshwater head, not

by the observed head. Therefore, the head gradient driving the groundwater flow at the Alligator Alley well is upward from the Boulder Zone to the surface.

- The authors should provide the formula for converting to freshwater equivalent heads

The description of the concept of equivalent freshwater heads and the equation have been moved from Appendix C to a new section (2.1) in the main report.

- The authors should demonstrate the vertical flow under transient conditions by doing wet and dry season graphs.

Wet and dry season (May 2004 and October 2004) results have been plotted together on the vertical gradient plots and included in the analysis of the transient calibration. See Figures 4.100 through 4.110.

- A similar graph for ROMP 86A would be helpful. At this well, the observed and simulated data do not provide a good match.

See the response above. Plotting the equivalent freshwater head involves subjecting both the observed and model calculated heads to the same calculations. Further, since the observed heads at ROMP 86A are shallow and because the groundwater in all layers has low salinity in this area, the calculation would have a minimal effect on the results. The purpose of the equivalent freshwater head plot on Figure 4.18 was not to allow comparison of the calculated and observed heads, but to show that the vertical movement of groundwater is governed by the gradient in the equivalent freshwater heads and not that in the measured heads.

3. Figures 3.1 and 4.20, and Section 4.1.1.2, concerning the horizontal hydraulic conductivity field in the UF: The area of high K along the northwest side of Lake Okeechobee in Glades County (> 120 ft/d) is questionable. The only data point that supports this is the Kissimmee River ASR pilot site, and this site is at the far northeastern extent of this area. Is this level of K in the Suwannee and upper Ocala supported by the new test well in Glades County, BREX-1?

The model is quite insensitive to this area of high K except in the immediate vicinity of pumping wells. Since there are no observation points nearby, this K value does not affect the calibration quality. Because this area is so important to the ASR project, a number of sensitivities are planned for the production runs to ensure that the model can bound the possible outcomes of the CERP ASR program.

BREX-1 was not included in the model because it did not meet the standards specified for the project in several ways:

- ***It was a 'natural flow' test with no applied stress***
- ***It was a single well test. (Other single well tests were used, but they were all applied stress tests conducted using conventional methods)***
- ***The test lasted less than an hour***

4. Figures 3.2 and 4.21, and Section 4.1.1.2, concerning the horizontal hydraulic conductivity field in the APPZ: There are some large areas in Figure 3.2 without data that could be important to the model and to the implementation of ASR. These areas are:

- Southern Glades and northern Hendry Counties

- Southern Osceola and northern Okeechobee Counties

K in the APPZ in these areas could be large, for example, in wells GLF-6 and LAB-TW in the first of these areas. However, these areas are not indicated to have high K in Figure 4.21. Has data been collected in test wells drilled in Okeechobee and Osceola Counties since the preliminary framework study concerning the K of the APPZ in the second of these areas? (If not hydraulic tests data, then maybe indications of high K, such as fracturing indicated on geophysical logs and development of thick zones of dolomite.)

There was no APPZ test run during the construction of LAB-TW. However, LAB-PW2 was re-constructed as part of the Regional study and a test of the APPZ was conducted at that time, resulting in a transmissivity of over 560,000 ft2/d in a 100 foot interval. This test result has been included in the latest calibration of the model.

The GLF-6 test was not used because at a discharge rate of 290 gpm, the test would not have stressed that portion of the aquifer, which has large open fractures.

5. Figures 3.3 and 4.22, and Section 4.1.1.2, concerning the horizontal hydraulic conductivity field in the LF: Similar to the APPZ, could an area of high K in the LF extend from northern Osceola County southward down through Okeechobee County? This is a large data gap area. Has data been collected in test wells drilled in Okeechobee and Osceola Counties since the preliminary framework study concerning the K of the LF in this area? (If not hydraulic tests data, then maybe indications of high K, such as fracturing indicated on geophysical logs and the development of thick zones of dolomite.)

According the SFWMD, the Toho Water Authority has done a single-well test in Osceola County in the LF, but the results have not been released yet.

Northeast of OSF-104, there was a test well called LATMAX_B-6, but it was open to both the UF and APPZ. The open hole was long and there was some semi-confinement in the middle and there are no logs to indicate the locations of permeable zones, so there is no way to parse out hydraulic conductivities from the reported transmissivity value.

We are aware of no other data in this area.

6. Figure 4.22: The area of relatively high K (200 to 300 ft/d) in the LF in Sarasota, southern Manatee, and Desoto Counties is not supported by the data shown in

Figure 3.3. Low K in this area is also indicated by the possible presence of pore-filling evaporate at the depth of the LF.

These conductivities have been reduced in the latest calibration of the model.

7. Figures 3.6 and 4.26, concerning vertical K of LC: The moderate K (0.01 to 0.05) of this unit probably does not extend into the northwestern part of the modeled area (west-central Florida). We would expect very low K in this area because of possible or probable presence of pore-filling evaporate at the depth of the LC in this area.

The conductivities have been reduced in the latest calibration of the model.

8. Observed confinement provided by Lower Floridan confining unit (LC) below the Lower Floridan aquifer (LF1) is generally tight. Reese and Richardson (2007) indicate that this unit provides good confinement in areas where there has been infilling of the pore space with gypsum and anhydrite. The Glauconitic bed can also provide tight confinement in some areas. Maliva and Walker (1998) found in southwestern Florida that unfractured dolomite beds provide the primary confinement. Conductivity of dolomite is as low as 3e-5 ft/day. However, calibrated vertical hydraulic conductivity (Kv) of LC presented in the report is globally around 0.01-0.05 ft/day, which is 100 to 1000 times higher than those measured. High Kv values in LC have significant effects on simulated heads in upper layers due to large equivalent freshwater heads in Boulder Zone (BZ) caused by the depth of the aquifer and the high concentrations assigned in the model. Please provide an explanation as to why the observed Kv values were not used in the model to limit upper flow from the boulder zone which has generally not been observed around the deep well injection sites.

In the northwest part of the model (west-central Florida), the LC vertical conductivities have been reduced. In this area the Boulder Zone is not present and the Lower Floridan conductivities have also been reduced to reflect the possible presence of pore-filling evaporate (see the two previous comments). Because the aquifers above and below the LC layer are not present or not very permeable, the model is not very sensitive to changes in the LC conductivity values in this area.

In the remaining portions of the model, the LC vertical conductivities have also been revised as part of the recalibration. The recalibrated LC conductivities in the southwestern portion of the model are in the range from 0.01 to 0.1 ft/d. This is much higher than the conductivity for dolomite shown in Maliva and Walker (1998). However, it is important to remember that for this model, the LF represents the first permeable zone (LF1) of the Lower Floridan Aquifer and the LC represents all of the permeable and confining units between the LF1 and the BZ. As such, the conductivities in the LC are a composite of all of those layers which are made up dolomite as well as many other materials. For these deep zones, not much is known about their combined permeability or continuity. Any discontinuities created by

fractures or facies changes are represented in the model by a higher vertical conductivity.

It is possible that upward migration at injection sites has not been observed because not enough time has passed for the injected fluid to migrate up through the confining layer(s). A MODPATH analysis of the travel time of a particle from the BZ upward through the LC (Kv=0.1 ft/d) to the LF in the model yielded a value on the order of 5,000 years. The monitoring period since injection began is less than 100 years.

For the above reasons, we have maintained the LC vertical conductivities in the 0.01 to 0.1 ft/d range.

9. Figures 3.10 - layer 22, Figure 3.14, and Figure 4.23, concerning extent of BZ: We don't think the BZ extends into the northwestern part of the modeled area. (See Reese and Richardson, 2008, Figure 24). It does appear to be present in east-central Florida, including Oceola and Orange Counties, but it is probably absent in most of west-central Floridan (north of Charlotte County). Can the northwestern boundary of the layer including the BZ be modified to more correctly reflect the extent of the BZ in this area?

See our response to Comment 3 in Section 2.2. The absence of the BZ in the northwest part of the model is accommodated by making the conductivity close to that of the LF.

10. Figure 4.19, the area of high head doesn't extend far enough to the south. Predevelopment heads in the northern Keys was as high as 40 ft, but the modeled head is 30 ft (or less?).

As described in Section 4.1.4, the predevelopment heads were computed by removing all interior pumping in the model. This allows a close comparison to the figure published by Bush and Johnston in 1988 for areas interior of the model boundaries. Unfortunately, because of the nature of the specified head boundary conditions, any pumping which impacts the boundary cannot be removed. The specified heads along the southern boundary are based on measured head values in the 2003/2004 time period, specifically heads at I75-MZ2, BICY-MZ2 and ENP-100, so no comparison near these boundaries should be made for predevelopment conditions.

11. For Figures 3.12, 3.22, 4.19,and 4.21, and maps of the APPZ, there is a correlation between salinity, temperature, head, and possibly K in the APPZ in an area southwest of the Lake along the Caloosahatchee River Basin in southern Glades and northern Hendry Counties. Salinity and temperature are high in this area, head drops down some (see saddle in axis of area of high head extending southeast into southern Florida on Figure 4.19), and K could be high in this area. Can this correlation be explained by the model? One theory might be that there is increased upwelling of saline water in this area. Also, a map that Emily Richardson and Reese created of the altitude of the base of the brackish-water zone (base of the USDW – water with less than 10,000 mg/L dissolved-solids

concentration) indicates a saddle in this same area. This surface approximates the saltwater interface and the depth of this interface is substantially shallower in this area than to the north or south. This would seem to suggest that the low head in the UF in this area was present even before development (pumping) of the Floridan.

Salinity and temperature fields were interpolated from the available data. Conductivity has been tweaked until the heads matched measured field values. There is likely a correlation between these four parameters, but the model cannot explain it. The time scale of the model does not extend far enough back into the past to determine if the upwelling of saline water caused the other parameters to change. This type of explanation is beyond the scope of this model; the model has not been designed to be able to answer this question.

12. P. 23, bottom sentence, Section 4.1.1.2: The 2:1 ratio for horizontal to vertical K of confining units needs to be referenced and better explained. Did this come from Reese and Richardson, 2004, p. 41? What Reese and Richardson (2004, p.41) are saying is that this 2:1 ratio was derived from comparison of horizontal to vertical K values from core analyses, and this ratio was used to estimate the vertical K values from horizontal K values determined from packer or aquifer test in confining units.

The 2:1 ratio was an average based on core data where both vertical and horizontal permeability was measured. Most of the data came from SWFWMD ROMP wells. A sensitivity of this ratio has been run and a new section (Section 5.6) has been added to the report to describe the results.

13. P. 24, middle second paragraph, Figure 4.20, Concerning the greater thickness of UF due to inclusion of Ocala in the northwest portion of the model area, and the lower K values in this area: In most of west-central Florida, Reese and Richardson did not include the Ocala Limestone in the UF because it was considered to be more of a semiconfining unit (MC1) than part of an aquifer. (See Reese and Richardson, 2008, p. 43 and 46, Middle Confining Unit, and Figure 20).

This statement was a mistake. It has been corrected to state that the UF is a combination of the Hawthorn and Suwannee units.

14. P. 24, bottom paragraph and P. 53: The citation for the USGS report is Reese and Richardson, 2008, not 2007. The report came out in 2008.

Agreed

15. P. 25, 3rd paragraph, concerning vertical K values for confining units: Given the importance of the K values for these units in the model, should more work be done to compile, interpret, and review this data. The data was rather hastily

pulled together and perhaps was not as thoroughly reviewed as it should have been.

The compilation of the database of vertical K values was begun as a pre-PMP task. The main body of work occurred over the period of about a year, ending in 2003, but it continued as more data became available.

It is unclear what has convinced the reviewer that the data was "rather hastily pulled together" and "was not as thoroughly reviewed as it should have been." If this is based on the impression that there is not enough data available, this can be explained by the process which was used to evaluate the available data. Most leakance values available are based on partially penetrating or overly penetrating tests, which would not allow for the determination of a representative leakance value and the data had to be omitted. The preliminary framework report provides extensive detail on the criteria used for these analyses and the reviewers are invited to look there for additional detail.

16. After reviewing the steady state calibration maps, it looks like some possible observation wells are missing. An example may be OSF-66. Also, many injection well sites should have monitor wells which monitor the boulder zone and possible 1 or 2 layers above the Boulder Zone. The authors should verify that all observation wells were included. If a well was omitted, the authors should explain why.

An additional look at the monitoring well database has led to the loosening of the criteria for selecting wells for use in calibration. Previously, the well was required to have at least 90% of its screen in a given aquifer layer in order to be selected. Further analysis determined that because the geology is simplified and interpolated, wells with at least 50% of their open intervals in a single aquifer could be included. This necessarily eliminates some useful wells because of simplifications to the model geology. However, it was important to eliminate any wells which did not provide head data representative of a single aquifer layer and an in-depth study of the conditions at each of the thousands of monitoring wells was impossible given the time schedule and budget and out of the scope of the study.

OSF-66, according to the simplified geology of the model, is open entirely in the MC1 confining unit, and so was not used in the calibration.

A table of all wells in the database and the basis for their inclusion or elimination has been added to the report. (Table 4.1)

4.1.1.4 Comparison of Model Result to Some Published Information

1. P. 29, second paragraph, concerning slight drop in head along the Calooshatchee River computed by the model (Figure 4.19): We question that the lower head in this area is the result of the stage in the Calooshatchee River. How about the alternate explanation provided in 4.1.1.2 regarding increased upwelling of saline water in this area?

Although both mechanisms driving flow in this comment, (1) low surface heads, and (2) high equivalent freshwater heads in the APPZ due to high salinities along the Caloosahatchee River in that unit, act to create an upward gradient in the UF, neither provide a full explanation of the reason for the lower head in the UF along the Caloosahatchee River. The reason for the slight drop in head computed by the model for predevelopment conditions along the Caloosahatchee River is dependent on many uncertain factors. A discussion of this "trough" area and its implications for the with-project conditions modeling is found in the response to Comment 4.1 Figure 4.19 above.

4.1.2 WASH123D Comparison to SEAWAT

4.2 Transient Calibration/Validation

1. Please present the simulated TDS concentrations for the transient model in primary aquifers. Little to no discussion on water quality was presented in the report. The report would benefit from a detailed discussion concerning water quality since the model was developed as a variable density tool.

This model was not meant to be used as a water quality tool. The TDS and temperature data was included only because of its impact on groundwater flow. Further, the calibration period was so short that the final TDS was not appreciably different from the initial TDS, except in areas of injection of freshwater. Figures of the final TDS distribution would look quite similar to the figures of initial TDS distribution, and plots of the changing TDS at individual points would be flat lines. Water quality will be addressed in greater detail using the local-scale models. Text has been added to the report to clarify this.

2. The horizontal hydraulic conductivities in layer 3 (IA/ICU) was not presented and should be added to the report.

The horizontal hydraulic conductivities for layer 3 were presented in Figures 4.28 and 4.31. They are now found in Figure 4.32.

3. Please provide vector plots of cross sections through model domain. At least three cross sections from north to south and three from west to east of model domain should be provided. In addition, a 3-D display of saltwater/freshwater interface in the modeled aquifers would also be helpful.

These plots and figures have been added to the report. The cross-sections with vectors are Figure 4.160 and 4.161. The 3-d display of salinity is found in Figure 3.25.

4. The flux exchanges between primary aquifers, and discharges to Atlantic Ocean and the Gulf of Mexico should be summarized and discussed for such a large regional model.

These statistics have been summarized in Figure 4.163.

5. The model report should have a table listing the calibration statistics (ME, MAE, and RMS for each observation well). Also, the authors should provide these metrics for each layer and for the model in its entirety. In addition, the table should include the correlation coefficient (r) and coefficient of determination (r^2), which quantifies the relationship between the observed and simulated water levels (Triola 1993). These comments also apply to the validation and transient WASH123D analyses.

These statistics have been calculated and are presented on maps in new figures added to the report.

6. Page 33: Regarding figures 4.57 through 4.77, what is the output frequency for the model calculated heads? The red squares (symbol for heads) occur more frequently than monthly (stress period length) and seem to vary from well to well.

The output frequency for the model calculated heads is approximately every 5 days. The actual frequency varies from month to month based on the number of days in the month. However, there is no variance in frequency from well to well. It is unclear what wells the reviewer feels have more or less output than others. Additional text has been added to clarify that the output timesteps for observation points are the same as the timestep length.

7. An examination of figures 4.57 through 4.77 indicates that at times there is very little correlation between the observed and simulated data. Some examples are given below:

FIGURE	WELL NAME	PERIOD (M/YR)
4.63	ROMP 39 SWNN	3/2004 – 6/2004
4.64	SARASOTA WELL 9	3/2004 – 7/2004
4.66	ROMP 12 MID UP FLDN	3/2004 – 8/2004
4.74	ROMP 13 AVPK	3/2004 – 9/2004
4.76	PBF-12	3/2004 – 11/2004

Some of the listed wells do represent the poorest locations in the calibration. However, as mentioned in the report, the model stress periods are too coarse to be able to match

the steep drop in head and sudden recovery which occurred in almost all wells during the first week of June 2004. This is the case for both ROMP 39 and ROMP 13.

ROMP 12 and the Sarasota well are examples of locations where the model was unable to exactly match the field measured data, likely because of errors in the pumping estimates or over simplifications of the geology in this area.

We feel that the calibration at PBF-12 is reasonable. With the exception of November 2003, the seasonal changes are reproduced by the model (e.g. the head drop from December 2003 to June 2004 is about 1.5 feet; the head rise from June 2004 to October 2004 is nearly 2 feet). On average the model is over-predicting the heads by only about 0.5 feet.

See Section 4.2.2 for an analysis of the transient calibration in each region of the model.

8. Figures 4.76 and 4.121: Well OSF-98 was included for the steady state calibration but not for the transient calibration. Since data is available for this well, it should be included.

This was an oversight that has been corrected.

9. A review of the water levels from the various simulations for the boulder zone suggests an extremely high water level in Polk County with heads similar to the overlying aquifers. Is there evidence that supports this?

There is no direct evidence to support the high heads on the boundary in Polk County in the BZ. There are, however, a number of minor lines of evidence which were the basis for setting the heads as explained in the report. First, there are a number of wells in Orange County (mostly Cocoa USGS wells and OR wells) which showed a similarity in heads among the BZ, LF and UF. These wells were used in the interpolation of the boundary condition and are marked with red diamonds on Figure 3.17. Next, the TDS data in the BZ in Polk County is generally much fresher than in other areas of the layer. This is only based on 2 or 3 measured TDS data points, but led us to the conclusion that the recharge in Polk County must be impacting the BZ and therefore, be in close connection.

Finally, the assumption seems valid since there is a single observation point from the BZ in Polk County, USGS Core Hole 2 at Polk City. This well does not have very much data and there are no head measurements available for either February 2004 or October 2003, but a measurement in September 2003 indicates a head of 127 ft. The model closely reproduces this head in the October model (see Figure 4.11). Although this cannot be a strong calibration point because of the lack of data at the time of interest, it does indicate that the heads in Polk County in the BZ are being predicted at levels similar to what would be expected in the field.

10. The use of the constant heads for the Surficial Aquifer System (SAS) raises some issues. Although this approach is acceptable for the southern portion of the model where the Hawthorn Group is thick and provides sufficient confinement, this is not the case in the northern portion of the model. The Upper Floridan in the northern portion of the model acts in a semi-confined nature with the SAS and seasonal trends in these two aquifers generally follow each other due to the high connection between them. Water levels in the SAS may change several feet during the year. Without this seasonal representation in the model for the transient simulations, the degree of calibration of the northern wells needs to be tempered.

The specified heads applied to the SAS were transient – they were reinterpolated for each month of the calibration and validation periods. Text has been added to the report in several sections to clarify this.

11. Some of the calibration wells appear to have a series of flat lines for each month. Please provide an explanation as to why this is occurring.

The flat lines indicate that the combination of stress changes, hydraulic conductivity and specific storage allow the model to reach an equilibrium condition at this well very quickly within some or all of the stress periods. The model cannot be expected to match daily head changes at the observation wells when it is designed with monthly stress periods. The PDT was part of the decision to use such coarse time discretization and they are aware of the impact to the model results.

Note that wells located near a boundary often show these flat lines because the boundary effect is felt so quickly.

12. The authors should discuss the volumetric flows from the calibrated model:

- Please provide documentation and graphics for the mass balance and percent discrepancy. Discuss any anomalies that you notice.

- Did all of the stress periods reach closure? If not, please discuss.

This information is presented in Tables 4.3 and 4.4.

13. Figures 4.57-4.77, and 4.86-4.122: The authors may wish to include mean error, mean absolute error, root mean square error, and/or the Nash-Sutcliff model efficiency coefficient for each time series. The authors may wish to provide contour plots of mean error, mean absolute error, root mean square error, and/or the Nash-Sutcliff model efficiency coefficient. These contour plots will allow the reader to judge where the model is more effective in replicating observation, and where the model is less effective. The authors may wish to develop tables of error metrics, for both the steady state and transient models. The authors may wish to

offer conclusions about the quality of the calibration, using quantitative metrics to support each conclusion.

These statistics are now presented on additional maps and tables in the calibration section (Section 4.0) of the report. We disagree with the method of contouring error since there can be no guarantee that the error between observation wells is related to the error at the wells themselves. The maps are provided with colored dots for each observation point (Figures 4.95 through 4.99).

5.0 Sensitivity Simulations

1. Regarding the Sensitivity Analysis, to the extent possible, the authors should follow the ASTM guidelines for conducting a Sensitivity Analysis (ASTM D5611)

The ASTM guidelines indicate that input parameters should be varied to determine the effects of that variation on both the calibration of the model and the question for which the model was designed. The Sensitivity section of this report (Section 5) discusses the first half of that direction (determination of the sensitivity of the calibration to each of the input parameters). The second half of the guidelines (determination of the sensitivity of the impact of the CERP ASR wells on the regional groundwater system) will be included in the next report, discussing the production ASR runs.

2. Regarding the Porosity and Dispersion/Diffusion, it would be beneficial to see the sensitivity results either in tables or as figures. According to the authors, some areas changed as much as 15 ft.

With so many model layers and so many timesteps, it is difficult to show the sensitivity results in figures without greatly multiplying the number of figures in the report. Figures are reserved for those sensitivity analyses that showed an impact on the model. An effort has been made to provide figures, tables, or a detailed analysis of the results so that readers can draw their own conclusions about the sensitivities or each parameter.

3. Figure 5.5 is difficult to analyze. The authors may wish to expand the size of the graphs to make them clearer.

This analysis was deemed unimportant since the north boundary head has been analyzed with a sensitivity analysis. This figure has been removed.

5.5 Boulder Zone Salinity

1. P. 41. We would agree that interior salinity values for the BZ can be higher than ocean values because of long-term buildup of dissolved solids (mineralization of the water). We also think that the salinity at the outcrop points should be about the same as the salinity of seawater (TDS of 35,000 to 36,000 mg/L). In southeastern

Florida (Miami-Dade and Broward Counties) eight samples of water from the BZ had an average TDS of 37,000 mg/L, but the TDS in the Lower Floridan was as high as 40,000 mg/L (Reese, WRIR 94-4010, 1994, p. 40).

The TDS at all ocean outcrops (including the BZ) has been set to 35,000 mg/l. As discussed in the response to comment 3.4.1.1 the model has been recalibrated based on this revision. The TDS distribution within the model domain was based on a variety of data sources, including the referenced report.

6.0 Sources of Uncertainty

1. The report states that the principle error in the model is the pumpage data limitations. The authors may want to rephrase this to the principle stress error in the model is due to the lack of aquifer parameter knowledge throughout the model domain and the uncertainty within each aquifer especially at depth.

We continue to believe that pumping data represents the principal error in the model. It is true that the lack of aquifer knowledge in some areas of the domain, especially at depth, is an important data gap, but this data could be estimated through calibration if other parameters (primarily pumping) were better known. Pumping exerts an enormous effect on the groundwater conditions in south Florida and is quite difficult to obtain.

2. The Floridan aquifer is a karst aquifer, with large solution holes and caverns. However, the SEAWAT and WASH123D models are essentially porous media models. Is it justified to use this type of model when attempting to look at transport phenomena in the Floridan aquifer? Could the conduit flow model developed by the USGS be worth looking into for future ASR modeling? Shoemaker, W.B., Kuniansky, E.L., Birk, S., Bauer, S., and Swain, E.D., 2008, Documentation of a Conduit Flow Process (CFP) for MODFLOW-2005: U.S. Geological Survey Techniques and Methods, Book 6, Chapter A24, 50 p. - http://pubs.usgs.gov/tm/tm6a24/

The selection of the modeling code was outlined in the Benchscale Report (Brown, et al 2006). The IMC had the opportunity to comment on that analysis at that time. Perhaps the use of conduit modeling could be considered in the future, but it is outside the scope of the current modeling project.

7.0 Conclusions/Recommendations

1. Paragraph 2: The authors state that "the calibrated regional models do an excellent job reproducing the FAS flow system." The authors may wish to replace the qualitative "excellent" description with a number of quantitative measures that describe the degree to which model predictions match observations. This is particularly important given that the objective of the report is to describe model calibration. The conclusion should be more scientific than "excellent".

For example, as is detailed above, the authors may wish to provide contour plots of mean error, mean absolute error, root mean square error, and/or the Nash-Sutcliff model efficiency coefficient. These contour plots will allow the reader to judge where the model is more effective in replicating observation, and where the model is less effective.

Quantitative measures of the calibration quality are provided in Section 4.1 and 4.2. The reader is directed to these section and the accompanying tables and figures to draw their own conclusion about the calibration. In the Conclusion section of the report, a quick overview of the results and conclusions drawn during the report is presented. A qualitative analysis is appropriate here.

2. Paragraph 5: The authors state that the "calibrated model not only calibrates to steady state snap shots of the aquifers, but also reasonably replicates the observed flow dynamics in the FAS as the aquifers respond to a variety of stresses." The authors do not discuss, or provide figures or illustrations, that detail flow dynamics. For example, the authors do not provide plots of transient velocity, with vectors. The authors do not detail dynamic flow observations, to which model results could be compared to draw the conclusion. Where do the authors make a comparison of modeled and observed flow dynamics? The authors may wish to substantiate this conclusion with technical model data and observations of flow dynamics, or abandon the claim that flow dynamics are replicated.

This was an unfortunate choice of words. The intent of the sentence was to indicate that the model calibrated well to both steady state and transient conditions. The phrase "flow dynamics" has been removed from the revised sentence.

Editorial Comments

0.0 Executive Summary

1. Paragraph 1: The authors should use quotation marks to identify the following verbatim quote from 114 STAT. 2687 TITLE VI SEC 601 Paragraph (h)(1): "is the restoration, preservation, and protection of the South Florida Ecosystem while providing for other water-related needs of the region, including water supply and flood protection."

Fixed.

2. Paragraph 1: The authors should note that ecosystem is capitalized in TITLE VI.

Fixed.

3. Paragraph 1: The authors may wish to use a verb other than "help".

This sentence was revised in the process of rewriting the Executive Summary

4. Paragraph 1: The authors should replace "of CERP ASR program" with "of the CERP ASR program".

Fixed.

5. Paragraph 2: The authors use an entire paragraph in a three paragraph Executive Summary to describe planned content of another report---a future report. The authors should focus the Executive Summary on the present report.

The Executive Summary has been rewritten and expanded.

6. Paragraph 2: The authors should consistently refer to "the CERP ASR program", in place of "CERP ASR" (at two locations in Paragraph 2 and at other locations within the document).

Fixed

7. Paragraph 2 Line 7: The authors should strike "an".

Fixed.

8. Paragraph 2 Line 8: The authors should consistently identify "analyses" (from Line 7) or "analysis" (from Line 8).

Fixed.

9. Paragraph 3: The authors should consistently identify "performance goals" (this paragraph) or "performance objectives" (previous paragraph); OR clearly differentiate the difference between performance goals and performance objectives.

The phrases "performance goals" and "performance objectives" are used interchangeably in this report. However, during the rewriting of the Executive Summary, the term "performance goals" has been removed.

10. Paragraph 3: The authors defined and used the acronym PDT in the previous paragraph. The authors should use the acronym PDT here, as the acronym is defined and was used in the previous paragraph.

Fixed.

1.0 Introduction

1. Paragraph 1: The authors should eliminate passive voice throughout the document.

We do not feel that passive voice should be entirely eliminated, especially in a technical report. We have made an effort to provide variety of sentence structure while maintaining grammatical accuracy. The inclusion of passive voice is useful for emphasizing results and eliminating first person subjects, as is common in technical writing.

2. Paragraph 1: The authors should consistently identify "the CERP ASR program" (from Executive Summary) or "the CERP ASR system" (this paragraph) throughout the document.

Fixed

3. Paragraph 2: The authors should use a verb other than "help".

Please see our response to Comment #3 in the Executive Summary section above.

4. Paragraph 2: The authors state, “Figure 1.1 shows the study area and Figure 1.2 shows the approximate location of the proposed ASR well clusters envisioned in the CERP”. However, Figures 1.1 and Figure 1.2 do not cover the same area. Moreover, Figure 1.1 is not labeled as the site map and does not include the SFWMD boundary. The authors should clarify.

We do not see any reason that the two figures should cover the same area. Each has a separate purpose. Figure 1.1 shows all of the place names mentioned in the report so that any reader unfamiliar with Florida geography can find the location of a city, county or water body mentioned in the text. Since the text does not discuss the boundary of the SFWMD and does not use this boundary to direct readers to any location, there is no need to include this boundary on Figure 1.1. Figure 1.2 is a map of the propose ASR well locations.

5. Caloosahatchee River is misspelled.

Fixed

2.2 Model Extent and Spatial Discretization

1. Paragraph 2 Line 5: The authors should refer to the Florida peninsula, as is done in Paragraph 2 on Line 8.

Fixed

2. Paragraph 6: The authors may wish to clarify whether "budgets" refers to project funds or water budgets.

Fixed

3.0 Conceptual Model

1. Paragraph 1: The authors may wish to rephrase as "(represented by total dissolved solids [TDS])."

Fixed

2. Paragraph 2: The authors may wish to rephrase as "have greatest effect on groundwater flow and constituent transport."

We see no reason to change this sentence.

3.2.1 Regional Geology

1. Paragraph 2: The authors may wish to refer to the Upper Floridan aquifer and Lower Floridan

The cited paragraph refers to both the Upper Floridan and Lower Floridan as written.

Appendix

1. The appendices are very long (217 pages). A table of contents would be helpful.

A list of appendices has been added to the end of the table of contents. To aid readers, the appendices will be provided in separate pdf files and the pdf files have been set up with bookmarks.

Acronyms

1. The acronym IMC is used for Interagency Modeling Center not Interagency Modeling Commission.

Fixed.

Conclusion

The models may need to be revised if the review comments stated above are taken into consideration. The models are acceptable products that could be improved with the suggestions provided. There is also a need to demonstrate how the rock fracturing potential resulting from increased pressures in the FAS during ASR injection would be addressed. It is not clear from the report how the rock fracturing potential was used to guide model construction and calibration.

Rock fracturing potential will be addressed using an analysis from Nicholas Geibel completed in 2010. His report will be available with the final TDR. The analysis provides a head threshold that should not be exceeded for each ASR well location. The

Appendix H: IMC Comments to Final Report With Responses

Comments on the Final Groundwater Model Calibration Report, Aquifer Storage and Recovery Regional Model Study were provided to the groundwater team at the Philadelphia District, USACE from the IMC reviewers via an email from Mr. Larry Stout, P.E., Chief, Interagency Modeling Section, Water Resources Engineering Branch, Jacksonville District, USACE on December 14, 2010. This appendix contains the text of the email and responses to each comment. The groundwater team would like to thank the IMC for their comprehensive review.

The original text of the IMC email is provided as black text, while the responses to comments are provided as red, italic text.

Thank you for providing the Final Groundwater Model Calibration Report for the ASR Regional Study. The IMC team has reviewed the revised report, and want to commend the authors for their excellent work in addressing the large volume of comments provided by the review team. The text is efficient and the figures are informative. After reviewing the Final report, the IMC review team continues to have the following consensus concerns:

1. With respect to the response to Item Number 4, which begins on Page 10 of Appendix G: the model should reach a quasi-steady equilibrium with respect to TDS, temperature, and head, prior to the beginning of the calibration or verification period. A quasi-steady state is defined as an equilibrium, in which any oscillation of TDS, temperature, and/or head is about some mean value, and the mean value does not change or trend as a function of time. A spin-up period that converges on a quasi-steady state is necessary for conclusions developed with the model to be meaningful and defensible.

We continue to believe that the TDS, temperature and head are not currently in a steady state or quasi-steady state condition and that no benefit would be provided to the model by including a spin-up time. Indications of the likely results of a long spin-up time or short spin-up time are provided by model tests performed during Phase 1 and, more recently, in preparation for the "with project" conditions model.

A long spin-up period would lead to significantly increased TDS concentrations and decreased heads compared to those observed today. These results were found during the Phase I model runs where total run lengths of 10,000 to 35,000 years were tested and the Floridan aquifers became significantly saltier south of Lake Okeechobee. Using these TDS values, which are much higher than those currently observed, as initial conditions would not provide reasonable model results.

Recently, an additional model run has been completed with a total run length of 13-years. This run was used to test the boundary conditions for the future "with-project" regional model but without the proposed ASR wells. No appreciable change in TDS occurred during the 13-year timeframe indicating that a short term spin-up would have no impact on the model results.

2. With respect to the response that begins on Page 27: authors state that the "head boundary conditions on the surface and aquifer side boundaries represent hydraulic conditions for 2004 (i.e. with drawdown from pumping included). It is possible that because the surface heads defining the recharge represent 2004 conditions rather than predevelopment conditions, less recharge is entering the model and it is not sufficient head to push the flow further to the south in the Upper Floridan aquifer." Authors may wish to construct a head boundary condition that initially represents a pre-development condition, and then employ a transient boundary condition that changes to reflect historic development. Authors may, for example, defensibly adopt one of the older head distributions cited in the comment as pre-development---such as Stringfield (1936), Parker and others (1955), or Healy (1962). Some of these head distributions were based on extensive data collection campaigns. A defensible initial boundary condition that changes with historic development is necessary for conclusions developed with the model to be meaningful and defensible.

The construction of a head boundary condition based on previous studies would be difficult, time-consuming, and too inaccurate to provide a defensible boundary condition. The calibration model head boundary condition includes side boundaries for each of the major aquifers identified in Reese and Richardson (2008) – the Upper Floridan, the Avon Park Permeable Zone, the Lower Floridan, and the Boulder Zone. Many of the older publications report head data as a potentiometric surface of the Floridan Aquifer as a whole and additional research would need to be undertaken to determine if the actual data is available and to correlate the data to the Regional ASR model aquifers. Also, the main driver to potentially push additional recharge into the trough area near Lake Okeechobee would be high heads in the Surficial Aquifer. The older publications focused on the Floridan Aquifer and artesian heads rather than the Surficial Aquifer heads. Developing a pre-development boundary condition would involve a large amount of guesswork and would not add much value to the modeling effort.

3. With respect to the response that begins on Page 27: the stated objective of the model is to evaluate a number of ASR related issues near Lake Okeechobee. The model predicts that a trough area will exist near Lake Okeechobee: an area of relatively higher head south of Lake Okeechobee is separated from areas of relatively higher head north of Lake Okeechobee by a depression or trough in head contours near Lake Okeechobee. Authors state that "in areas other than the trough area, it was surprising how closely the modeled predevelopment contours matched the Bush and Johnston (1988) contours." It is also necessary to have a clear understanding of the trough area, and this does not currently exist. A head distribution that is supported by observation data within the area of interest near Lake Okeechobee is necessary for conclusions developed with the model within the area of interest---near Lake Okeechobee---to be meaningful and defensible.

The head distribution provided by the calibration model results is supported by the observation data within the area of interest near Lake Okeechobee for the steady state

calibration time periods of February 2004 and October 2003 and the transient time period from October 2003 to December 2004. Thus, the model conclusions are meaningful and defensible. When comparing the model results representing pre-development conditions to the pre-development heads, the model predicts the pre-development heads closely except that the model shows a depression in the Upper Floridan head contours (i.e. a trough) west of Lake Okeechobee, whereas the estimated pre-development contours do not show a trough. No pre-development observation data exists in the area to determine whether the trough existed during pre-development conditions.

Our purpose in comparing the model results to the pre-development heads was simply to show an additional line of evidence for the accuracy of the model – the fact that the model produces results similar to other published work. The pre-development conditions results will not be used for any of the production runs as the project continues. The calibrated model runs that do match observed data in the area near Lake Okeechobee will be used as the base to construct the "with project" conditions model. Uncertainties in the trough area will be evaluated using sensitivity analyses.

It is the consensus opinion of the IMC Review Team to recommend that the authors take one of the following actions: (a) address the limitations associated with these concerns, with additional analyses, data collection, and appropriate revision to both the model and the report; or (b) prominently acknowledge the limitations associated with these concerns in both the Executive Summary and in Section 7 Conclusions/Recommendations. Acknowledgement of all three concerns may take the following efficient and concise form:

> The model has limitations, which include but are not limited to the following: (1) The model did not achieve a quasi-steady state---with respect to TDS, temperature, and head distributions---prior to the beginning of the calibration period. (2) The boundary condition on the surface and sides of the domain is fixed and represents 2004. Transience that deviates from 2004 may exist on the boundary. (3) The model predicts a trough in the head distribution north and west of Lake Okeechobee. Insufficient data exists in this area to determine whether the trough actually exists. The model may underestimate head in the trough area by as much as 15 feet, with respect to published potentiometric surfaces for the area.

The following sentences have been added to the Executive Summary. "The Interagency Modeling Center (IMC) has reviewed this study and their comments on the draft report are listed in Appendix G with responses from the modeling team. While the modeling team addressed most of their comments with additional analyses or text, there are some differences of opinion between the two groups. The IMC comments on the final report and the modeler responses are provided in Appendix H and illustrate the two sides of each issue."

In addition to the above, the IMC recommends that Appendix G be modified as follows:

4. The following statement is made at the top of Page 21 of Appendix G: "These figures may not be directly quoted or referenced by others, or identified as a personal communication. The information may be useful to the authors in answering specific questions concerning TDS distributions based on Reese (1994)." IMC recommends that the referenced figures be removed from Appendix G. The information was provided to the authors, to assist the authors in addressing specific concerns related to the TDS distribution. The information was not intended for publication by the USACE.

The figures provided in the comments from the IMC have been removed from Appendix G.

5. The following statement is made on Page 23 of Appendix G: "The following text may not be directly quoted or referenced by others, or identified as a personal communication. However, the information may be useful to the authors in answering specific questions concerning historic potentiometric surface delineations." IMC recommends that the referenced text be removed from Appendix G. The information was provided to the authors, to assist the authors in addressing specific concerns related to the saddle feature near Lake Okeechobee. The information was not intended for publication by the USACE.

The referenced text provided in the comments from the IMC has been removed from Appendix G.

In conclusion, it is the opinion of the IMC review team that the authors did a commendable job in developing the referenced model. The hydrogeology of this area is quite complex. The report is clearly written and informative.

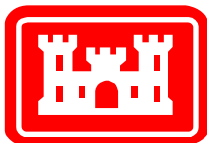

U.S. Army Corps of Engineers
Philadelphia District

REGIONAL MODEL PRODUCTION SCENARIO REPORT

AQUIFER STORAGE AND RECOVERY REGIONAL MODELING STUDY

PREPARED FOR
U.S. ARMY CORPS OF ENGINEERS
JACKSONVILLE DISTRICT

PREPARED BY
U.S. ARMY CORPS OF ENGINEERS
PHILADELPHIA DISTRICT

June 2013

CONTENTS

ABBREVIATIONS

APPA	Artesian Pressure Protection Area
APPZ	Avon Park Permeable Zone
ASR	Aquifer Storage and Recovery
BZ	Boulder Zone
CERP	Comprehensive Everglades Restoration Plan
ERDC	Engineer Research and Development Center (USACE)
FAS	Floridan Aquifer System
FDM	Finite Difference Method
IAS	Intermediate Aquifer System
ICU	Intermediate Confining Unit
IMC	Interagency Modeling Center
LC	Lower Confining Unit
LF	Lower Floridan Aquifer
MC1, MC2	Middle Confining Units 1 and 2
NAP	Philadelphia District (USACE)
NWIS	National Water Information System (USGS)
NWO	Omaha District (USACE)
NWQMC	National Water Quality Montoring Council
PDT	Project Delivery Team
RASRSM	Regional ASR Study Model
SAJ	Jacksonville District (USACE)
SAS	Surficial Aquifer System
SFWMD	South Florida Water Management District
SFWMM	South Florida Water Management Model
STA	Stormwater Treatment Area
TDR	Technical Data Report
TDS	Total Dissolved Solids
TVD	Total-Variation-Diminishing
UF	Upper Floridan Aquifer
USACE	US Army Corps of Engineers
USGS	United States Geological Survey

EXECUTIVE SUMMARY

This report details the use of a calibrated regional model to analyze the effects of the proposed Comprehensive Everglades Restoration Plan (CERP) Aquifer Storage and Recovery (ASR) system, consisting of 333 ASR wells with the potential to inject or extract 5 mgd each. The model indicated that this number of wells was too large for the established performance measures and instead, recommended a smaller system consisting of 94 ASR wells in the Upper Floridan (UF) Aquifer, 37 wells in the Avon Park Permeable Zone (APPZ), and 101 wells in the Boulder Zone (BZ). Wells in the BZ would have 10 mgd capacity. While this design meets the requirements for pump pressure and protection of the artesian pressure in St. Lucie and Martin Counties, the head impacts of the system are significant and widespread. Further, although the system can support the full amount of recharge envisioned by the CERP, there will be a significant reduction in the recovery potential of the system. A second design recommendation was also presented which removed the BZ wells which would be expensive to install and have little possibility of recovering stored water.

A Monte Carlo analysis was used to investigate the uncertainty in the model results. It concluded that a few sites may need to have a slight reduction in the number of ASR wells in order to meet the pump pressure requirements, but there is very little uncertainty in the ability to protect the artesian pressure in St. Lucie and Martin Counties or in the widespread nature of drawdown and "drawup" impacts from the proposed ASR system.

It is recommended that additional study in the form of field pilot studies and local scale modeling at the proposed sites be used to confirm the assumptions from this model and reduce the uncertainty in the results.

1 INTRODUCTION

The U.S. Army Corps of Engineers (USACE), Philadelphia District (NAP), has prepared this report for the USACE, Jacksonville District (SAJ), and the South Florida Water Management District (SFWMD) in support of the CERP. This report documents the evaluation of CERP ASR scenarios using the regional groundwater model. It is the final installment of a series of four documents describing the multi-phased modeling approach undertaken to evaluate the proposed CERP ASR system. The four documents are:

- ASR Regional Study – Benchscale Modeling (Brown, et al, 2006). This report evaluated several model code options and concluded with the selection of WASH123D and SEAWAT as the best-suited to the ASR regional evaluation.
- Draft ASR Regional Study Phase I – Groundwater Modeling (NAP, 2006). This report described the first phase of the model development, including identification of boundaries and regional flow and salt migration pathways; evaluation of model run times and sensitivity to time step sizes; testing of boundary parameters and the sensitivity of hydraulic and transport parameters; and a comparison of results from WASH123D and SEAWAT.
- Final Groundwater Model Calibration Report, Aquifer Storage and Recovery Regional Modeling Study (NAP, 2011). This document presents the model setup, boundary condition development and calibration for the regional model, which is the basis of the model evaluation of the CERP ASR plan.
- Regional Model Production Scenario Report (this report). This document describes the evaluation of the CERP ASR plan against regional performance objectives including rock fracture potential, pump pressures, and impacts to nearby wells. The evaluations were performed on the calibrated regional model with the addition of the ASR wells described in the South Florida Water Management Model (SFWMM), D13R scenario (SFWMD and USACE, 1999). The number of ASR wells was reduced in order to meet the performance objectives and the final design was subjected to a Monte Carlo sensitivity analysis.

In addition to these modeling reports, an evaluation of the effects of various hydrogeologic theories on groundwater flow in South Florida was presented in the conference paper “Using Density-Dependent Numerical Models to Evaluate Regional Groundwater Flow Patterns in South Florida” (Bittner et al, 2008). This study was also preceded and is supported by “Groundwater Numerical Model Development Support and Data Collection Report” (CH2MHill, 2005).

Simultaneously with work on the regional model, significant effort has been expended developing local-scale SEAWAT models of pilot study sites at Kissimmee River and Hillsboro (Site 1) which have been running since January 2009 and January 2010, respectively. These models were built to investigate near field effects of the ASR wells which cannot be suitably studied on a large, regional scale model. The original plans called for inclusion of the local scale modeling work in this report. However, further discussions among members of the Project Delivery Team (PDT) have determined that this modeling

information would be better suited for the Pilot Study Technical Data Report (TDR) developed by SAJ, which is currently in review.

ASR is one of the alternatives proposed by the CERP to provide fresh water storage in South Florida. The CERP recommends the installation of 333 ASR wells open in the Floridan Aquifer System (FAS) and distributed over a large region with well field clusters near Lake Okeechobee, along the Caloosahatchee River, and at several locations along existing canals in the Lower East Coast Region (Palm Beach and Broward Counties). Figure 1.1 shows the approximate location of the proposed ASR well clusters envisioned in the CERP. The proposed plan, with total recharge and recovery pumping rates of approximately 1.65 billion gallons per day, may be larger than any currently operating ASR project (SFWMD and USACE, 2008). To evaluate the numerous design considerations and the variation in aquifer response on regional, sub-regional, and local scales, density-dependent numerical modeling of the FAS was required as discussed in the ASR Regional Study Project Management Plan (SAJ and SFWMD, 2003).

The focus of this report is the application of the previously calibrated model to answer a variety of questions about the impacts of the CERP ASR system on a regional scale. This report begins with a description of the conversion of the calibration model to allow investigation of the regional impacts of the full CERP ASR system. The CERP design was then scaled back in a series of scenarios until the impacts were within the requirements of a set of performance measures. These performance measures included rock fracture potential, pump pressure, impacts to neighboring users (artesian pressure protection, maximum drawdown, and water quality migration), and the ability to provide the storage and recovery volumes designated in D13R. During the process of scaling back the CERP design, wells were removed and some were added to other aquifers, including the APPZ and the BZ. The final scenario was then subjected to a robust Monte Carlo sensitivity analysis.

1.1 Acknowledgements

This report is part of a study prepared for and in cooperation with the SAJ and SFWMD. Thanks are given to the USACE Engineering Research and Development Center (ERDC) and the United States Geological Survey (USGS) for their cooperation, modeling code development assistance, and technical guidance during this study. Special thanks to the IMC (Interagency Modeling Center) for their cooperation in the review of the various phases of this study.

2 MODEL SETUP

The regional impact of the proposed CERP ASR system was evaluated by applying the storage and recovery rates from the November 1998 D13R simulation on the South Florida Water Management Model (USACE and SFWMD, 1999) to the regional ASR study model described in NAP, 2011. The November 1998 D13R simulation on the SFWMM is the "official" simulation recognized by the IMC and constituted the correction of a few errors found in the CERP Yellow Book document (personal communication, Dan Crawford, SAJ).

After first running the model with the CERP ASR design, the plan was scaled back until limits on the performance measures were met. These performance measures were developed by the Project Delivery Team (PDT). During the process, additional changes were made to the plan based on requests from and discussions with the PDT.

For clarity, some discussion of model names is necessary. 'D13R' refers to the run on either model, which incorporates a set of ASR wells into the area surrounding Lake Okeechobee and extending to the Lower East Coast. This report refers to the implementation of the D13R scenario on two models: The South Florida Water Management Model (SFWMM) and the Regional ASR Study Model (RASRSM). Table 2.1 lists some important information about each of the models.

The SFWMM is a regional-scale, physically-based model which combines hydrology and water management practices in southern Florida. Its development began at SFWMD in the 1970s and it has been through several major revisions in the last 4 decades. Although the SFWMM includes a groundwater component, it looks only at surficial, unconfined flows and it addresses them as 2d, vertically averaged flow. ASR wells are incorporated as reservoirs without the evapotranspiration losses. The model simply keeps track of the volumes of injected water (removed from the modeled system), applies a 70% recovery efficiency and tracks the volume of the bubble (net accumulation of excess water injected). Recovered water is limited to the volume of the bubble. The SFWMM is only able to look at the impacts of the ASR system on the water demands in the surface system. ASR wells are included as an additional management option for removal of excess water or supplementation during periods of water deficiency (SFWMD, 2005). The SFWMM is not able to look at regional-scale hydrogeologic impacts of the ASR wells in the FAS. The RASRSM was developed to investigate these hydrogeologic impacts which the SFWMM was not able to examine.

The SFWMM-D13R included CERP and non-CERP projects and determined the volumes of water that would need to be removed or restored by ASR wells in six different basins. The maximum required rate turned out to be 1.65 billion gallons per day. Assuming that all wells are sized to be able to pump 5 mgd, 333 ASR wells would be required to meet that maximum rate.

The PDT for the Regional ASR Study selected a number of property sites near water sources and divided the 333 ASR wells among the sites. The RASRSM-D13R adds the ASR wells to the selected sites and then investigates the regional hydrogeologic impacts of these wells. The 'calibration model' referenced in

this report is the RASRSM before the addition of the ASR wells, when it was calibrated to field data from 2003 and 2004. The setup and calibration of that model are outlined in NAP, 2011.

The RASRSM-D13R model was built using the same computational grid and geologic layering as the calibration (RASRSM) model. Horizontally, the model extended from Orlando to the Everglades and from the west coast of the Floridan peninsula to the bench outcrop of each unit in the Atlantic Ocean. Vertically, the model extended from the ground surface to the base of the Boulder Zone (BZ) and included the following hydrogeologic units:

- Surficial Aquifer System (SAS) – a combination of all units above and including the Hawthorn unit
- Intermediate Aquifer System (IAS) – a combination of the intermediate aquifer and the intermediate confining unit (ICU)
- Upper Floridan Aquifer (UF)
- Middle Confining Unit 1 (MC1)
- Avon Park Permeable Zone (APPZ)
- Middle Confining Unit 2 (MC2)
- Lower Floridan Aquifer (LF)
- Lower Confining Unit (LC)
- Boulder Zone (BZ)

See the Calibration Report (NAP, 2011) for additional information on the extent of the model domain, these hydrogeologic units and their properties.

2.1 BASINS

SAJ provided the daily volumes of recharge and recovery at ASR wells from the SFWMM-D13R scenario for each of 6 basins: Lake Okeechobee, Caloosahatchee River, L-8, C-51, Central Palm Beach, and Hillsboro. The number of wells required in each basin was determined by dividing the maximum flow rate by the expected individual well capacity of 5 mgd. See Figure 1.1 for the general locations of these basins and numbers of required wells. Based on discussions with the ASR Regional Study PDT, a total of 16 sites were selected for the installation of ASR wells. The L-8, C-51, Central Palm Beach and Hillsboro basins each have only one possible site for ASR wells. The Caloosahatchee River Basin has three sites and the Lake Okeechobee Basin has nine.

The wells in each basin were divided among the available sites based roughly on the perimeter length of the sites. As will be described in Section 4, as additional scenarios were developed, the numbers of wells at each site changed from the original design. Well locations were sometimes altered slightly since SEAWAT only allows the placement of wells in the centers of computational cells. At each proposed site, ASR cells were selected to be as far apart as possible given the property size, number of wells and cell

sizes in order to minimize well-to-well interaction as much as possible. It was occasionally necessary to place two wells in the same cell by doubling the pump rate.

2.2 Choice of Time Period

The SFWMM-D13R scenario covered the 30-year period from 1965 to 1995. File size limitations and run times make it difficult to run the RASRSM for such a long period of time. The input and output files for a single 30-year RASRSM-D13R run required nearly 52 GB of storage space and the run-time was between 18 and 30 hours depending on the machine used and the number of processes being run simultaneously. In addition, some of the input files were too large for the allocation of memory for the file buffer. This problem was solved by dividing the RASRASM-D13R run into separate chunks of 38-40 months, each successive chunk being hot-started from the final solution of the previous chunk. In order to address the problems of run-times and space requirements, additional computer resources were acquired and the decision was made to run a shorter section of the D13R period.

Since recharge flows (injection) greatly exceed recovery flows (extraction) at most of the sites for most of the 30-year period, the D13R plan indicates a gradual build-up of freshwater in the aquifers. (Figures 2.1 through 2.6 show the recharge and recovery rates and available aquifer storage at each basin.) The year 1965 was selected as the start time for the regional model run so that the starting condition would not be impacted by previous injection periods. The year 1977 was selected as the end time for the regional model run to include periods covered by SAJ Lake Okeechobee models and to incorporate the entire first cycle of the Lake Okeechobee basin wells (which return to zero stored volume in 1977). As the following paragraphs will show, this shortened period covers a wide variety of hydrologic conditions similar to what would have been seen with the full 30-year time period.

The annual precipitation data for the proposed time period at 13 sites within and near the model domain was compared to the distribution of precipitation data over a 71-year period (1929-1999) in Figure 2.7, which shows a nice range of conditions (Winsberg, 2011). At most of the sites analyzed, several of the years from the model period lie in each of the quartiles of the larger dataset. Note, for example that 1968 and 1969 were very wet years at most of the sites while 1975 was a very dry year. In order to look at the model domain as a whole, Thiessen polygons were developed for the sites and clipped to the model domain. In this way, the recharge values were area-averaged using the polygon areas. This average is shown at the right end of the plot in Figure 2.7 and shows a similar wide distribution of precipitation conditions during the 13-year period.

As a second analysis of the variability of hydrologic conductions during the 13-year evaluation period, Figures 2.8 and 2.9 show the comparison of the annual extracted/injected volumes in each basin for the 13-year period (used in RASRSM-D13R) to the distribution of extracted/injected volumes for the full 30-year period (from the SFWMM-D13R). Similar to the precipitation analysis described above, the values for the 13-year model period are widely spread across the range of values from the 30-year period. Note, for example, that 1971 has generally low injection rates and high extraction rates, indicating a dry period when ASR water was used to supply surface water needs. Similarly, 1969 has generally high injection rates and low extraction rates, indicating a surplus of water in the system.

Since both of these analyses indicate wide variability in the period from 1965 to 1977, we can be assured that the shortened time period of the RASRSM-D13R will still adequately investigate a variety of hydrologic conditions.

2.3 Model Time steps and Stress Periods

The RASRSM was developed using the USGS density-dependent groundwater code, SEAWAT (Langevin, 2003), which is an extension of MODFLOW. SEAWAT (and MODFLOW) require the division of the simulation time into stress periods and time steps. Sources, sinks and boundary conditions generally are allowed to change only at the end of stress periods, resulting in step-functions for many model inputs. Time steps are smaller than or equal to stress periods. Model results are calculated and output may be generated at the end of each time step. In the RASRSM calibration, stress periods were one month long. All boundary conditions and sources and sinks were averaged over each month and applied as a step function to the model. The RASRSM calibration flow and transport time steps were 5 days long, with full output generated at the end of every other time step. The selection of the 5-day time step was based on the results of model testing described in the Calibration Report (NAP, 2011) which indicated that 5 days would be sufficiently accurate without overpowering data storage limits with unduly large output files.

At the start of development of the RASRSM-D13R simulation, the plan was to continue with month-long stress periods and 5-day time steps for the reasons stated above. Month-long stress periods would require the averaging of ASR pumping over each month. However, the pumping rates obtained from the SFWMM-D13R scenario for the ASR wells were found to vary significantly on a daily basis at most of the basins. Figure 2.10 shows one example when this averaging would have resulted in a significant loss of detail, although the total volume of water entering and leaving the ASR well would have been correct. Instead, 10-day stress periods were used to balance the need for simplicity in this large, regional model with the desire to correctly reproduce the pump rates from the SFWMM-D13R design. To coincide with the monthly boundary condition changes, some of the stress periods were shortened or lengthened by a few days. Each month was divided into 3 stress periods: one from the 1st to the 10th of the month, another from the 11th to the 20th of the month and the final period from the 21st to the last day of the month. The last stress period of the month might be as short as 8 days (for February) or as long as 11 days.

Despite the shortened stress period lengths, boundary conditions and regional (non-ASR) pumping remained on monthly step functions in order to simplify the conversion of the calibration model to the D13R model. Time steps remained at the 5-day length used in the calibration model. The comparison between stress periods and time steps for the RASRSM calibration model and the RASRSM-D13R scenario are shown pictorially in Figure 2.11.

2.4 Boundary Conditions

In the calibration model, the boundary cells on the north, west and south edges of all aquifers were given specified head boundary conditions based on the available head data. All cells in the top layer

(SAS) were also given specified head boundary conditions, which allowed the model to calculate and apply recharge or discharge to the surface, as necessary, to meet observed conditions. These applied head values were based on interpolations of measured head values and the process used to develop these boundary condition values is described in the Calibration Report (NAP, 2011).

Although this methodology worked well for the calibration model, it presented some difficulties in applying the model to a separate time period. There is far less head data available for the D13R model period (1965-1977), especially in the deeper hydrogeologic units, making it impossible to repeat the interpolation process which was used to set the 2003-2004 and 1993-1994 boundary conditions on the calibration model. Instead, a separate method was developed which used the available data to form a correlation between the sparse data from the 1960s and 1970s and the more dense data already used in the calibration periods. This correlation was then applied to the boundary conditions from the calibration model, to produce a new set of specified heads for the D13R model.

The first step in developing this correlation was to find as much data as possible for all of the monitoring wells which had data during any part of the D13R model period (1965-1977) and during the calibration or validation periods. The data collection process for the calibration model was lengthy and tedious (see Appendix A of the Calibration Report, NAP, 2011) and it was not desirable to repeat that process, which would have been magnified by the additional length of the model time period. Since the USGS National Water Information System (NWIS) provides significant data and allows a search of wells by county and time period, this website was used to collect the data. Although, there is likely additional data available from other sources, including DBHYDRO, the NWIS site was used alone to save time and effort. The data obtained at this site seemed sufficient for the task since the goal was to develop correlations between time periods, instead of using the data directly in the model.

A total of 186 wells were found with data for the D13R period and the calibration and validation periods and the records were downloaded and tabulated. Initial, optimistic plans had assumed that there would be sufficient data to develop distinct correlations for each county and aquifer, but not all counties and aquifers were well-represented. Most of these 186 wells were open in the SAS with very few tapping the deepest layers of the model. Because of the insufficient data, separate correlations could not be calculated for each aquifer and county, and all wells were combined for analysis.

The tabulated data was condensed by calculating a monthly average head at each well for each month with available data. The Excel functions RSQ, SLOPE and INTERCEPT were used to calculate a linear correlation between months in the D13R period and months in the calibration datasets. The linear equations were then applied to all boundary conditions on the north, west, south and top boundary of the calibration model. The resulting estimated heads were applied to the regional D13R model. It is important to note that the correlations were always quite good, with the lowest correlation coefficient (r^2) being 0.956.

The details of the process can best be explained by using an example such as January 1974. Of the 186 wells downloaded from the USGS NWIS website, 123 wells have data available for both January 1974

and January 1993 and 111 have data in both January 1974 and January 2004. When a linear correlation is fit to these data points (see Figure 2.12), r^2 is 0.976 between 1974 and 1993 and 0.977 between 1974 and 2004. Since the correlation to the 2004 data is slightly better, the equation for that line was used to convert January 2004 boundary conditions to January 1974.

Boundary conditions were converted cell by cell. To develop the boundary conditions for January 1974, the assigned heads for January 2004 at each model cell were altered by applying the equation: $y=0.95x+1.10$ where x is the assigned head for January 2004 in the calibration model (already interpolated from available January 2004 data points) and y is the head to be assigned for January 1974 in the RASRSM-D13R scenario. This equation is then applied to each specified head cell of the model to create a set of specified head boundary conditions for January 1974 from the January 2004 dataset. The same process was followed for each month of the 13-year period. Two examples of the conversion from the 1993/1994 and 2003/2004 specified heads to the 1965-1977 specified heads are shown in Figures 2.13 and 2.14. Note that the general seasonal trends are preserved, while magnitudes are shifted up and down slightly to reflect annual variations in weather patterns.

2.5 Regional Pumping

A significant effort was expended by SAJ to collect and tabulate the groundwater pumping in the model domain for the calibration and validation periods (see Appendices A and D of NAP, 2011). This data is much more difficult to track using public records than most of the other data used in the model. The collection process involved numerous phone calls to well owners and state agencies and the resulting dataset still had significant gaps, which were filled using estimation processes described in Appendix D of the Calibration Report (NAP, 2011). Repetition of this tiresome process for the period of the D13R scenario was not possible within the budget and schedule. This old data may not even be available any more. Like other data in the model, a method was developed to estimate conditions during the period 1965-1977 using the data already collected for the calibration and validation models.

This analysis was made possible by the Historical Water-Use tables published online (USGS Florida Water Science Center). These tables provide estimates of freshwater withdrawals for each year from 1965 to 2000, separated by county and use type. Missing or unavailable data in the downloaded tables was first estimated by using linear interpolation. Then, a ratio was calculated between each year from 1965 to 1977 and 1993 or 1994 for each county and each water use type. That ratio was applied to each well in that county with that water use type. In this way, the locations of the wells and seasonal variations are preserved but the volumes are altered based on water demand. Table 2.2 lists the well type codes from the SAJ pumping database and the corresponding water use from the USGS tables. Where a match was not possible, this table also provides the methodology for estimating pumping rates for the D13R time period.

This process probably does not accurately capture all groundwater withdrawals. The use of linear interpolation assumes a continuous, predictable trend from year to year and this method does not account for wells that might have been abandoned before 1993. But, it is expected that on a regional scale, the volumes of water extracted will be close to reality.

An example will clarify the process. The USGS tables referenced above indicate that agricultural groundwater withdrawals in Hillsborough County totaled about 44.73 mgd in 1965, 64.20 mgd in 1970, 64.74 mgd in 1993 and 62.79 mgd in 1994. If we want to estimate the 1966 flow rate for an agricultural well in Hillsborough County, we begin by linearly interpolating the 1965 and 1970 data to get an estimate for 1966. The result is 48.62 mgd. We then calculate the ratio between agricultural extraction rates in 1993 and 1966 by dividing 48.62 by 64.74, resulting in a ratio of 0.751. This means that all agricultural wells in Hillsborough County can be converted to 1966 flow rates by multiplying the 1993 rate (from the calibration model) by 0.751. One example Hillsborough County agricultural well is owned by Dooley Groves and is reported to have extracted 0.024 mgd during August 1993. By applying the conversion ratio, the August 1966 extraction rate can be estimated at 0.018 mgd. This is the value that was input into the D13R regional model. Figure 2.15 shows all of the pumping in a portion of Hillsborough County in the calibration model and the D13R regional model.

These estimates are not expected to be accurate at individual wells. It is quite possible that the Dooley Groves well did not exist in 1966 and it is also likely that other wells existed in 1966 which have been abandoned in the decades since then. However, it is expected that generally, the extraction from the groundwater on a regional scale will be sufficient to reproduce groundwater conditions during the 1960s and 1970s. As with the specified heads, the objective is to preserve the seasonal variations in regional pumping, while varying the magnitudes according to estimated demand.

2.6 CERP ASR Wells

The recharge and recovery rates assigned to the ASR wells were obtained from the output from the SFWMM-D13R model. Daily flow rates were extracted from *.dss files provided by SAJ using the structure codes in Table 2.3.

The output from the SFWMM-D13R model consists of daily average flow rates to and from ASR wells in each of the six basins. These were incorporated into the RASRSM using positive values for injection rates and negative values for extraction rates, which is the MODFLOW sign convention. See Figure 2.16 for a plot of three months of D13R data at the C-51 basin with the conversion to positive and negative flow rates for the SEAWAT model.

Generally, this process worked well. One exception was at the Central Palm Beach basin, where the wells were occasionally injecting and extracting at the same time and at the same rates (see Figure 2.17). The reason for this apparent inconsistency was that the injection and extraction rates were not connected by the SFWMM. Injection in this basin was a function of the stage levels in the Palm Beach County Agricultural Reserve reservoir, while extraction depended on water supply demands in central and southern Palm Beach County. It is not clear how this type of condition would be handled in reality once the system is built. For the sake of this model, it was assumed that net flow would be 0 mgd during this period.

As described above, the model was run with 10-day stress periods. This means that source/sink terms can only change once every 10 days. For the ASR wells, this meant averaging flow rates over the 10-day

time periods. As shown in Figure 2.10, this eliminates some of the extremes in the pumping schedules, but it provides a better picture of conditions than monthly stress periods.

2.6.1 Incorporation of ASR Well Recovery Efficiency

Recovery efficiency is a measure of the portion of stored water that can be recovered from an ASR well. Efficiency can be reduced by mixing of fresh water with the native, high concentration total dissolved solids (TDS) water, or movement of the freshwater bubble during storage periods. The RASRSM is not able to estimate recovery efficiency because it is affected by primarily small-scale processes (near-well mixing and near-well water quality). The RASRSM was designed to look at regional questions related to the CERP ASR plan. ASR well recovery efficiency can best be investigated through local scale modeling and local pilot studies (SAJ, in review).

The SFWMM-D13R scenario was also not able to calculate the ASR well recovery efficiency. Instead, it assumed 70% recovery efficiency on the ASR wells. This assumption was incorporated in the model by not allowing the model to remove more than 70% of the previously recharged water. Not all RASRSM-D13R scenarios made this same efficiency assumption, for several reasons. First, early data from the Kissimmee River and Hillsboro Pilot studies indicated that recovery efficiency at Kissimmee River was near 100% because of the low background TDS, while at Hillsboro, recovery efficiency was much lower, near 40%, because of higher background TDS (SAJ, in review). Second, later project scenarios (described in Section 4) involved the addition of ASR wells to the APPZ and BZ, aquifers whose high TDS was expected to preclude high recovery efficiencies.

To accommodate the lower recovery efficiencies at Hillsboro, in the APPZ and in the BZ in the RASRSM-D13R scenario, the volume of available water in the aquifers was tracked through each stress period. Injection rates were applied as delineated by SFWMM-D13R, but extraction rates were set at the minimum of the reported SFWMM-D13R rate or the available volume of previously injected water multiplied by efficiency. Thus, if the full design number of wells is used, injection rates will match D13R-SFWMM rates, but extraction could stop sooner than designed if the recovery efficiency is assumed to be less than 70%. Although pilot testing at the Kissimmee River site indicated nearly 100% recovery efficiency, this high value could not be incorporated into the RASRSM-D13R scenario because there is no way to know how high the extraction rates might have gone had efficiency been assumed to be higher in the SFWMM-D13R scenario. More detailed analysis of recovery efficiency is possible with the local scale models (SAJ, in review).

Based on discussions with the PDT, all recovery efficiencies in the UF were assumed to be 70%, except for Hillsboro, which was set to 40%. All recovery efficiencies in the APPZ were assumed to be 30%, except for Hillsboro, which was set to 40%. All recovery efficiencies in the BZ were assumed to be 0%.

2.7 Initial Conditions

Numeric models require the selection of initial conditions as a starting place for the solver. For this model, three sets of starting conditions were required: head, TDS and temperature.

The initial head conditions were of no importance since the first stress period of the model was set to be steady state and was only 1 day in length. No ASR wells were pumping during the first day of the model, but all boundary conditions and regional pumping were set to January 1965 conditions as described in sections 2.4 and 2.5. The model determined a steady state condition that would meet those conditions and then used it as the starting condition for the following stress period.

The TDS and temperature starting conditions from the calibration model (2003) were used as the starting conditions for this D13R model (beginning in 1965) since the scarcity of TDS and temperature data available for the 1960s makes it unreasonable to attempt a new interpolation of field data to determine the initial TDS and temperature for this simulation. It is not expected that significant, regional changes to TDS concentrations and groundwater temperature would occur on the timescale of several decades in most areas of the model. Significant water quality changes might be expected to occur near the coast or near extraction wells, but large scale changes in the majority of the aquifers would occur only over large (geologic) time periods.

To verify this expectation, an analysis was made of long term water quality data for wells in the model domain. TDS, chlorides and specific conductance data was collected from the National Water Quality Monitoring Council (NWQMC) Water Quality Portal for all wells in counties within or touching the model boundaries with at least 40 years of data. (Forty years was selected since it is the approximate difference between the 2003 starting condition for the calibration model and the 1965 starting condition for the RASRSM-D13R model.)

A Mann Kendall analysis was used to determine if a statistically significant trend existed in the data (using a 95% confidence interval). If the Mann Kendall analysis showed a significant trend, a Sen's slope analysis was used to quantify the slope of the trend (USEPA, 2000). The resulting slope value was then multiplied by 40 years to determine the approximate change in water quality that could be expected between 1965 and 2003. Finally, the approximated water quality change was divided by the estimated seawater value for each characteristic to make possible comparisons among the water quality parameters. The estimated seawater values were 35,000 mg/L TDS, 19,400 mg/L chlorides and 50,000 uS/cm specific conductance. In many cases, this percentage change as related to seawater was similar for the three water quality parameters at a given well.

The wells were divided by aquifer and are presented spatially in Figures 2.18 through 2.24. Note that the majority of the wells had no significant trend or a very small median slope. The majority of the points which had a significant water quality change (greater than 10% of seawater levels) were located in the Biscayne Aquifer near Biscayne Bay. One additional point with significant change was located in the SAS aquifer along the lower east coast of the peninsula. The SAS is used as a boundary for this model and no calculations are made in this layer. Additionally, since the depth is small, the equivalent freshwater head will be similar to the measured head and an error in the starting TDS will have little effect on the results of the model.

The only other point which shows a significant change in water quality over a 40-year period was located in the Floridan Aquifer system in Orange County. However, this well is closely surrounded by a number of other wells from the same aquifer which show no significant trend. This leads to the conclusion that the large water quality change at this well is caused by a local anomaly.

Figures 2.25 through 2.31 show the TDS, chlorides and specific conductance data for each of the wells which showed a significant trend and a median slope whose 40-year water quality change could be more than 10% of the seawater level. Finally Figures 2.32 and 2.33 show the TDS, chlorides and specific conductance data for two example wells which do not show a large change in water quality.

The results of this analysis show that the use of the 2003 starting conditions for the RASRSM model beginning in 1965 will have minimal effects on the final results of the model. TDS changes quite slowly in the majority of the model domain. A similar condition is expected with temperature changes.

2.8 Validation of Boundary Conditions and Initial Conditions

In order to ensure that the methodology presented above was reasonable, the RASRSM-D13R was run without any ASR wells and the results were compared to a few observation wells which had head data available for some part of the period from 1965-1977. These comparisons are shown on Figures 2.34 through 2.79 with summary statistics in Figure 2.80. Although the comparison is not as close as for a well-calibrated model, the correlations are good considering the methodology described above. The majority of the wells have mean errors and mean absolute errors within 5 feet and seasonal changes are nearly always well timed. Unfortunately, since most of these wells are located in the northwest portion of the domain and tap the upper aquifers they may not represent all parts of the model domain, but the close comparisons lend some credibility to the model setup process.

3 PERFORMANCE MEASURES

The PDT developed a number of performance measures for analyzing the D13R scenarios from a regional standpoint. The purpose of these performance measures was to provide decision-makers with the data and information necessary to understand the probable hydrogeologic impact of the proposed ASR program on the region. Local scale models are required to assess near-field issues (SAJ, in review).

3.1 ROCK FRACTURE

One of the initial concerns, expressed early in the regional ASR study process, was that large volume, high pressure injection into the aquifers would cause fracturing of the rock, resulting in significant, permanent changes to the subsurface hydrogeologic conditions of South Florida. The PDT turned to Nick Geibel of USACE Omaha District (NWO) to analyze the strength of the rock and the pressures that would cause rock fracturing (Geibel, 2012).

A thorough explanation of the calculation is given in the Giebel report, but a short overview of the equations (Tensile Method) is presented here.

The rock fracture limit is assumed to be reached when the water pressure, P, reaches the critical water pressure stress level, P_f, at the top of the aquifer due to ASR injection. The critical water pressure is described by Equation 3.1.

$$P_f = \sigma_v K_o - P_o\left(K_o - 1\right) \qquad \text{Equation 3.1}$$

where:

σ_v = Overburden stress, defined by:

$$\sigma_v = \sum \gamma t \qquad \text{Equation 3.2}$$

where:

γ = Specific weight of overlying units

t = Thickness of overlying units

K_o = Coefficient of Lateral Earth Pressure, defined by:

$$K_o = 1 - \sin\phi \qquad \text{Equation 3.3}$$

where:

ϕ = Angle of friction

P_o = Ambient pre-fracture water pressure at top of unit (estimated as pressure head from February 2004 calibration)

The water pressure during injection is described by Equation 3.4:

$$P = \gamma_w h_p \qquad \text{Equation 3.4}$$

where

γ_w = Specific weight of water

h_p = Pressure head, defined by:

$$h_p = h_t - h_e \qquad \text{Equation 3.5}$$

where:

h_e = Elevation head

h_t = Total head

Thus, fracturing would be expected to occur when the pressure caused by pumping (Equation 3.5) meets or exceeds the critical water pressure (Equation 3.1). For analysis in the regional model, Equations 3.1 and 3.4 were set equal and rearranged to determine the limiting total head. After simplification, the result is Equation 3.6:

$$h_t = h_e + \frac{(1-\sin\phi)\sum \gamma t}{\gamma_w} + (h_{to} - h_e)(\sin\phi) \qquad \text{Equation 3.6}$$

where:

h_{to} = Ambient pre-fracture total head

For this analysis, the following constants were used:

γ = 130 lb/ft^3 (for all materials)

γ_w = 62.4 lb/ft^3

ϕ = 28.9°

The pre-fracture total head was taken from the February 2004 calibration model. The elevation head and unit thicknesses were based on the geologic units as incorporated into the calibration model.

This calculation was run on each cell in the UF and APPZ aquifers in the regional model. Figure 3.1 shows the resulting maximum allowable total head to prevent rock fracturing. Note that in the UF, maximum total head values in the areas of the proposed ASR sites range from about 300 feet to 600 feet. In the APPZ they range from 600 feet to nearly 1000 feet. Because these limits were so high, other performance measures become limiting factors. D13R scenarios will not be compared to these limits in this report.

3.2 Pump Pressure

As the PDT discussed the ramifications of early model results, it became clear that a limit should be set on the pressure the ASR pumps were required to overcome. The well package in SEAWAT forces the user-defined fluxes into the model without regard to the size of the pump that would be required to achieve this flux rate. The PDT determined that it would be unlikely that an ASR pump would be able to

overcome more than 100 psi of head. This is also the pressure at which most FAS wells are tested and the pressure at which both the Kissimmee River and Hillsboro Pilot Study ASR wells were tested. This performance measure was used in the first few RASRSM-D13R scenarios to eliminate ASR wells from sites where this pressure would be exceeded.

Figure 3.2 shows a simplified schematic of an ASR well injecting into an artesian aquifer. The source of the injected water is assumed to be a surface water body located near the ASR site. Thus, the head to overcome is approximately equal to the difference between the model-calculated aquifer head and the ground surface elevation at the well, if headlosses and pump efficiency are ignored. This head difference can be converted to pressure using the density of water.

One of the problems with using a regional model to estimate the pressure requirements of the ASR pumps, is that the cells are much too large to accurately portray heads near the well. Figure 3.3 shows the results of a simple injection well model run with three different grid resolutions. These plots were developed by running models with identical well pump schedules and boundary conditions on three different grids. The model computed a much higher head at the well when run on the grid with the smallest grid cells. The results of the three models become more similar as the distance from the well increases. These plots were made using a small, generic model. It was not possible to run the RASRSM-D13R model with cell sizes of two feet with the existing computer resources, schedule and budget. Instead, the Theim equation (Equation 3.7) was used to estimate the result on a two-foot grid using the results from the 2000-ft grid.

$$h_w = h_{i,j} + \frac{Q}{2\pi T}\ln\left(\frac{r_e}{r_w}\right) \qquad \text{Equation 3.7}$$

where

h_w = Head at the well
$h_{i,j}$ = Head computed in the cell by the model
Q = Flow rate to the well (positive for injection)
T = Transmissivity of the aquifer
r_e = Effective radius of the grid cell
r_w = Radius of the well (assumed to be 1 foot)

The effective radius can be calculated as 0.208 times the grid cell size for a uniform grid (Anderson and Woesner,1992, p 147-149). This calculation was used for most of the ASR sites, since the grid is regular with a cell size of 200 feet for most proposed sites and their surrounding areas. A few sites, notably Lakeside Ranch and Riverbend had some ASR wells assigned to irregularly sized grid cells. The relationship between the effective radius and the cell size was rederived, but it was found to be only slightly different from multiplying the average of the cell size in each Cartesian direction by 0.208.

Equation 3.7 was applied to the aquifer heads calculated by the model at each ASR well. The head was compared to the ground surface elevation and converted to pressure. The maximum well pump pressure was reported at each ASR site for each scenario on the RASRSM-D13R.

3.3 Artesian Pressure Protection Area (APPA)

Another performance measure requested by the PDT had to do with the impact of ASR on the artesian pressure in the UF and APPZ aquifers in Saint Lucie and Martin Counties. Water users in that area depend on the artesian heads for water withdrawal and the permits for ASR sites will require that the flow from artesian aquifers not be reduced by more than 10% as a result of the project.

Merritt (1997) presents an equation to estimate the flow from an artesian aquifer as shown in Equation 3.8.

$$Q = \left(\log_{10}\left(\frac{2.25Tt}{r_w^2 S} \right) \right)^{-1} \left(\frac{4\pi s_w T}{2.3} \right) \quad \text{Equation 3.8}$$

where

Q = Flow from the artesian well
T = Transmissivity
t = Time
r_w = Well radius
S = Storage coefficient
s_w = Difference between aquifer head and height of spigot

If we wish to use this equation to compare the artesian flows before and after the construction of the D13R ASR system, the only variable which will change with the addition of ASR wells is s_w since the head in the aquifer will change. All other parameters are constant characteristics of either the aquifer or the well. Therefore, we can define a variable, *A*, as follows and simplify the equation.

$$A = \left(\log_{10}\left(\frac{2.25Tt}{r_w^2 S} \right) \right)^{-1} \left(\frac{4\pi T}{2.3} \right) \quad \text{Equation 3.9}$$

$$Q = As_w \quad \text{Equation 3.10}$$

$$Q = A\left(h_{aq} - gse\right) \quad \text{Equation 3.11}$$

where

h_{aq} = Model-calculated aquifer head
gse = Ground surface elevation (estimation of spigot elevation)

The comparison between artesian flow before and after ASR installation can be computed as follows:

$$\%QR = \frac{Q_{noASR} - Q_{ASR}}{Q_{noASR}} \quad \text{Equation 3.12}$$

$$\%QR = \frac{A\left(H_{aq-noASR} - gse\right) - A\left(H_{aq-ASR} - gse\right)}{A\left(H_{aq-noASR} - gse\right)} \quad \text{Equation 3.13}$$

$$\%QR = \frac{H_{aq-noASR} - H_{aq-ASR}}{H_{aq-noASR} - gse} \quad \text{Equation 3.14}$$

where

$\%QR$	=	Percent flow reduction from artesian well
$Q_{no\text{-}ASR}$	=	Flow rate with D13R ASR system
Q_{ASR}	=	Flow rate without D13R ASR system
$H_{aq\text{-}noASR}$	=	Head in the aquifer without D13R ASR system
$H_{aq\text{-}ASR}$	=	Head in the aquifer with D13R ASR system

The results from the D13R scenarios were analyzed for the impact to the artesian conditions in Saint Lucie and Martin Counties by comparing the head results at each output timestep for the RASRSM covering 1965-1977 without ASR wells and the RASRSM covering the same period with ASR wells using Equation 3.14. The result was reported with maps of the UF and APPZ layers with the cells colored by the maximum percent flow reduction across the time period. A second set of maps is provided where the cells are colored based on the number of days out of the 13 year period that the 10% rule is exceeded.

It is important to remember that although the rule apparently applies to the two counties in their entirety, there is one section of Saint Lucie County that (according to the RASRSM) does not have artesian groundwater conditions even before the installation of the ASR wells. This is caused by a ridge coming down from the northwest, which increases the ground surface elevation, but does not significantly increase the head in the aquifers. Figure 3.4 shows the ground surface elevations in Saint Lucie and Martin Counties with the surrounding areas. The ridge comes down through Okeechobee County and extends into the corner of Saint Lucie County. The calibrated models did not predict artesian conditions on the spine of this ridge, and only predicted slightly artesian conditions on the side slopes. Even tiny ASR pumping rates can affect these areas significantly enough to exceed the 10% rule. In the analysis that follows here, areas around the ridge were removed from the analysis.

3.4 Head Impacts

Another matter of importance in analyzing the regional effects of the CERP ASR program is the drawdown which might be experienced by neighboring water users due to the extraction cycles on the ASR wells. Head impacts, which vary spatially (horizontally and vertically) and with time, are difficult to show in a 2-dimensional static figure such as those provided with this report. In an effort to better illustrate these effects on neighboring users, head impacts for each RASRSM-D13R scenario are presented in two different ways.

For permitting purposes, it is important to know the extent of the 1-foot and 5-foot drawdown contours. Since each basin of CERP ASR wells has a different pumping schedule and varying rates, it is not reasonable to select a specific time period during the 13-year model run, at which maximum drawdown would be expected for the entire model. Instead, the drawdown was calculated for each cell of the model at each output time step by subtracting the head in the no project run from that in the ASR simulation. Then, at each cell, the maximum drawdown was extracted and combined with the maximums in other cells into a single dataset representing the maximum drawdown over the model run period (1965-1977). Note that the maximum drawdown may not occur at the same time in each cell of

the model. The 1-foot contour and the 5-foot contour were delineated for each aquifer and these contours are plotted in output figures.

Although neighboring users may, at some periods, experience reductions in water levels due to ASR recovery, they will also, at other periods, experience increases in water levels due to ASR recharge. In this report, we refer to this increase in water level due to ASR pumping as "drawup," which is calculated by subtracting the head in the ASR simulation from the head in the no-project run in each cell. Similar to the drawdown analysis, the maximum "drawup" in each cell was combined into a single dataset and the 1-foot and 5-foot "drawup" contours for each aquifer are presented on maps. Note again that the maximum "drawup" may not occur at the same time in each cell of the model.

The maximum drawdown and "drawup" figures give a good picture of the worst-case scenario for head impacts. However, this worst case may be a rare occurrence over the 13-year simulation. In addition, the "drawup" is generally greater and longer lasting than the drawdown. These details are not evident in the previously described maximum drawdown and "drawup" map figures. To give an idea of the temporal component of head impacts to neighboring users, additional figures are provided for each scenario that show time plots of drawdown and "drawup" at numerous locations near the ASR sites. These locations are located at distances of five, 15 and 25 miles from the proposed ASR well sites and have been chosen in all radial directions.

Although the drawdown/"drawup" analysis is listed here as a performance measure, the PDT has not selected a drawdown/"drawup" limit beyond which the ASR scenario would be rejected. Although these results did not impact scenario selection in the same way that the other performance measures did, they are believed to be important to stakeholders and decision-makers.

In Section 4, the results of the D13R scenarios will be presented and will show that in many of the scenarios, ASR pumping causes significant head changes throughout the model, including adjacent to the north, west and southern boundaries of the model. These boundaries were defined as specified heads based on available head measurements. An assumption inherent in this boundary condition was that the ASR pumping effects would not reach the boundary. Appendix A addresses this assumption and concludes that the boundary effects on the performance measures are minimal.

3.5 Water Quality Migration and Saltwater Intrusion

Because the ASR wells will be injecting high quality water to mostly saline aquifers, and because the injection volumes will exceed extraction volumes, it is reasonable to expect that the CERP ASR plan will have a beneficial impact on seawater intrusion and overall water quality in the Floridan peninsula. The PDT wished to be able to quantify this impact since it is an advantage of ASR system over some other components of CERP. Other members of the PDT expressed some concern that the ASR systems might push low quality water into the zone of influence of a water supply well and requested that this possible impact be investigated.

Unfortunately, this regional model is not well-suited to answering these questions for at least two reasons. First, the cells are too large to accurately portray TDS transport, especially near the wells.

Second, impacts to salinity at locations far from the ASR wells are highly dependent on transport parameters such as dispersion, which could not be calibrated due to lack of TDS time series data and the short time period of the calibration models.

Investigations of water quality migration are better suited to pilot study cycle testing with associated local-scale models (SAJ, in review).

3.6 Ability to Provide Storage/Recovery Designated in SFWMM-D13R

SFWMM-D13R was developed to be able to meet urban, agricultural and ecological water supply requirements. It also provides storage for excess water that may be required later. Many of the scenarios tested in the RASRSM-D13R involved a reduction in the number of ASR wells from the SFWMM-D13R design, or a reduction in the volume pumped. The amount of storage and extracted water that can be provided by each scenario will be important for decision-makers.

Like the drawdown performance measure, the PDT defined no limit beyond which the scenario would be rejected based on storage and recovery rates. Instead, plots are provided showing the total annual injected and extracted volumes for each scenario compared to the volumes defined by SFWMM-D13R. This allows decision makers to quickly analyze the water volumes that would need to be made up using other components of CERP.

4 PROJECT SCENARIOS

After the calibrated RASRSM model had been adjusted to reflect the 1965-1977 period as described in Section 2, the model was first set up to run the entire suite of 333 ASR wells as designated in SFWMM-D13R. The locations of these wells are shown on Figure 1.1. The results were compared to the full suite of performance measures and then the PDT designed a number of follow-up simulations, which were also analyzed against the performance measures. The following section will present the scenario descriptions and their results when compared to important performance measures.

4.1 DESCRIPTIONS OF SELECTED SCENARIOS

The following scenarios were run using the regional model and are discussed below:

1. Full D13R design from SFWMM
2. Scale back Scenario 1 to meet pump pressure requirement by successively removing wells from the model until pump pressures are near or below 100 psi. This is not a unique design – there may be other arrangements of the wells that will meet this requirement, but will have more or fewer wells or a different distribution of the same number of wells.
3. Add all wells that were removed for Scenario 2 to the APPZ. This simulation allows for full injection capacity, but because of lower recovery efficiency in the APPZ, the extraction volumes are often lower than the original SFWMM-D13R design.
4. Scale back Scenario 3 to meet pump pressure requirement by successively removing wells from the model (APPZ layer) until pump pressures are near or below 100 psi. This is not a unique design– there may be other arrangements of the wells that will meet this requirement, but will have more or fewer wells or a different distribution of the same number of wells.
9. Add all wells that were removed for Scenario 4 to the BZ. These wells are to have capacities of 10 mgd and 0% efficiency. Because of the doubled capacity, the number of wells in the BZ is half what had been removed from Scenario 4. Some well counts in upper layers were adjusted slightly to prevent the inclusion of "half wells."
10. Scale back Scenario 9 to meet APPA performance measure and to eliminate drawdown greater than one foot at a distance of one mile from each site.
11. Scale back Scenario 9 to meet APPA performance measure (allow drawdown of any magnitude outside the APPA.)
12. Remove BZ wells from Scenario 11.

Simulation 5 was similar to Simulation 9 and was removed from this analysis because it added no unique information. Simulations 6 through 8 investigated the possibility of using gravity drainage to extract water during recovery periods. The application of the RASRSM to these scenarios was questionable and the PDT ultimately decided to eliminate these runs from the analysis.

Figures 4.1 through 4.12 show the injection and extraction flow rates in the SFWMM-D13R and in each of the RASRSM-D13R scenario runs, providing a visual description of each scenario.

4.2 Scenario 1 – Full Design

Scenario 1 followed the injection and extraction schedules used in the SFWMM-D13R as closely as possible. Some small differences in flow rates were caused by the need to average pump rates over 10-day periods. This averaging did not affect the total volume added or removed from the aquifer. Scenario 1 included all 333 recommended ASR wells, which were distributed among the proposed sites as shown in Figure 4.13. All wells were placed in the UF aquifer and were assumed to be fully penetrating. The SFWMM-D13R scenario assumed 70% recovery efficiency for all wells. However, since data at the Hillsboro pilot site has indicated much lower recovery efficiency, the RASRSM assumed 40% efficiency at that site. Because of this reduction in efficiency, some extraction at this site was removed to ensure sufficient water quality on the extracted water. The results from this simulation are presented in Figures 4.13 through 4.31.

The addition of all these ASR wells to the UF aquifer clearly has some very significant effects on the regional hydrogeology. The head rise is so great, that pumps at all sites would need to be able to overcome pressures much greater than 100 psi (see Figure 4.17). The greatest pressure requirements occur at L-63N and Taylor Creek where hydraulic conductivities are lower and the pressure to overcome is over 800 psi and over 400 psi, respectively.

The effect on the artesian conditions in St. Lucie and Martin Counties is also significant. Figure 4.18 shows that a large portion of the two counties loses all artesian pressure at least once during the 13-year model period. Figure 4.19 indicates that most of this area loses more than 10% of artesian flow for more than 40% of the model time period. All areas of the counties are predicted to lose at least 20% of the artesian flow capacity at some point during the model.

The maximum drawdown experienced due to the ASR wells is greater than one foot in the majority of the model (see Figure 4.20). The 5-foot drawdown area is only slightly smaller. Significant impacts are felt in all layers of the model and across the whole domain from boundary to boundary. The time series plots of drawdown and “drawup” at individual points (Figures 4.21 through 4.28) support the conclusion that this scenario would cause excessive head changes at numerous locations for extended and repeated time periods.

This scenario allows for nearly all of the recommended injection and extraction flows defined in D13R (see Figure 4.29 through 4.31) but the regional effects of the system are widespread and significant and all performance measures are exceeded.

4.3 Scenario 2 – Original Design, Scaled Back for Pump Pressures

Scenario 2, a scaled back version of Scenario 1, was developed by removing wells until the pump pressure requirement of 100 psi was met at each site. The process of removing wells was a trial-and-error process where wells were removed from areas of the highest pump pressure. This would naturally result in the removal of wells from areas of low hydraulic conductivity or high density of ASR wells. Because of the arbitrary nature of the procedure to remove wells, the resulting arrangement of wells

(shown in Figure 4.32) is not the only design that would work. Like Scenario 1, all wells were screened across the UF aquifer. This run reduced the total number of wells from 333 to 97.

Results from Scenario 2 are presented in Figures 4.33 through 4.50. In this scenario, the model estimated that the pumps would need to overcome 80 to 100 psi for most sites (See Figure 4.36). Note that the pressure predicted at the C-41 Canal site is slightly over 100 psi. However, the difference (1 psi) is well within the error tolerance of the model. Interestingly, no ASR wells were placed at the Nicodemus Slough, Taylor Creek and L-63N sites in this scenario. Because of the low hydraulic conductivity at these sites the model predicted that pump pressures would exceed the 100 psi limit even with just a single well.

The preservation of artesian conditions in St. Lucie and Martin Counties is slightly better than Scenario 1 (see Figures 4.37 and 4.38). Only areas right around the ridge and near the well sites lose artesian conditions altogether at any time during the model run. Areas near the coast preserve artesian conditions and the reduction in flow is estimated to be less than 10%. More than 10% artesian pressure loss is predicted to occur in about half the area for more than 11% of the 13-year model run period.

For all aquifers, the area impacted by significant drawdown is slightly smaller for Scenario 2 than it was for Scenario 1 (see Figure 4.39). The "drawup" contours extend slightly further in all aquifers. Time series plots of drawdown and "drawup" (Figures 4.40 through 4.47) show a significant reduction in impact, but sites within 15 miles of the ASR wells still show significant head impacts over long periods of time.

Although this run results in an improvement in all of the performance measures, it also is unable to meet the storage and recovery needs specified in the SFWMM-D13R design (see Figures 4.48 through 4.50). All basins see significant reductions in their ability to store and provide recovered water. This scenario can provide 30% - 56% of designed storage volume and 23% - 78% of designed recovery volume.

4.4 Scenario 3 – Add Remainder of Wells to APPZ

Since the results of Scenarios 1 and 2 indicated that the SFWMM-D13R design cannot be entirely incorporated into the UF, Scenario 3 was developed to try to put the rest of the wells into the APPZ. This well distribution is shown in Figure 4.51. Because of higher TDS concentrations, the recovery efficiency for wells in the APPZ is expected to be much lower than the 70% assumed by the SFWMM-D13R for UF wells. Although neither of the pilot studies looked at APPZ ASR wells, the PDT estimated a recovery efficiency of 30% in the APPZ, except at Hillsboro, where the recovery efficiency was assumed to be 40%. These lower efficiencies were incorporated into the RASRSM by cumulatively tracking the volumes of water injected and extracted and stopping extraction once the volume stored in the aquifer had been recovered. This reduced recovery efficiency means that the addition of ASR wells to the APPZ will provide additional storage capacity, but will not be able to fully provide the recovery volumes designated by the SFWMM-D13R design. Results are shown in Figures 4.52 through 4.69.

The addition to the APPZ of all 236 wells which had been removed from Scenario 2 resulted in a significant increase in the required pump pressures at most of the APPZ sites (see Figure 4.55). This is especially true at Hillsboro, which is located in the limestone portion of the unit. It is also noteworthy that the addition of ASR wells to the APPZ resulted in an increase in the pressures that must be overcome by pumps in the UF layer. Many of these UF sites were already near the 100 psi limit with Scenario 2 and the addition of even one APPZ well pushed the UF pressure over the limit, although the APPZ pressure may remain below the limit.

The effects of the ASR system on the APPA in St. Lucie and Martin Counties are shown in Figures 4.56 and 4.57. Although there is little change in the land area which meets the 10% limit, the area that loses artesian pressure completely is much larger in Scenario 3 than in Scenario 2 for both the UF and APPZ aquifers. Model results indicate that most of the water users in the two counties will experience significant reductions in artesian flow during ASR extraction periods.

The areas affected by significant drawdown and "drawup" for Scenario 3 are shown in Figure 4.58 and the time series plots are in Figures 4.59 through 4.66. Generally, the "drawup" is similar to Scenario 1 since there is a close connection between the UF and APPZ and both scenarios inject the same volume of water. Drawdown is slightly less than Scenario 1 due to the reduced extraction volumes in the APPZ wells.

The comparisons of the injection and extraction flow rates to the design rates (Figures 4.67 through 4.69) show, as expected, that this scenario allows for a full injection capacity. Extraction volumes are lessened, however, due to the lower assumed recovery efficiency in the APPZ. Reductions in flow tend to increase towards the end of the simulation as stored water is gradually used up. This simulation is able to extract between 40% and 98% of the annual volumes designated by SFWMM-D13R.

4.5 Scenario 4 – UF and APPZ Wells, Meeting Pump Pressure Requirements

To develop Scenario 4, the number of wells in the APPZ was reduced until pump pressures again met the 100 psi requirement. The results of Scenario 3 and Scenario 4 indicate communication between the UF and APPZ layers at many of the proposed ASR sites. Since the UF ASR wells had already put the UF pump pressures close to the limit, it was often impossible to add any APPZ wells without causing the UF pump pressure to again exceed the limit. In most cases, only a few APPZ wells could remain. Most of the APPZ wells in this scenario were at sites that had no UF wells, such as Nicodemus Slough, Taylor Creek, and L-63 N. All three of these sites have low conductivities in the UF, but much higher conductivities in the APPZ. In total, this scenario included 41 wells in the APPZ. When combined with the 95 UF wells, this resulted in a total of 136 ASR wells for this scenario. The full details of the design are provided in Figure 4.70 with the results shown in Figures 4.71 through 4.88.

Pump pressure requirements are shown in Figure 4.74. Although the maximum pressures in the UF at Kissimmee River / Paradise Run and Lakeside Ranch are slightly over the 100 psi limit, the exceedance is within the error of the model.

The effects of ASR extraction on the artesian pressure in St. Lucie and Martin Counties are shown in Figures 4.75 and 4.76. These effects are quite similar to those for Scenario 2. Coastal areas meet the requirement that artesian flow be reduced by no more than 10%. Inland areas near the Lakeside Ranch and Port Mayaca ASR well sites and near the ridge in St. Lucie County lose all artesian flow for more than 40% of the 13-year simulation.

Drawdown and "drawup" impacts (Figures 4.77 through 4.85) show a slightly smaller impact than Scenario 3, but not as small as Scenario 2.

Because of the smaller total number of ASR wells, the amount of water recharged or recovered in all basins has been reduced, often by significant percentages. Injection volumes have been reduced to 43-64% of the design because of the diminished number of ASR wells. Extraction volumes have shrunk to 26-83% of SFWMM-D13R volumes because of the reduced number of ASR wells, but also because of the lower assumed recovery efficiency at Hillsboro and at all APPZ sites.

4.6 Scenario 9 – Larger, Less Efficient BZ Wells

Scenario 9 was developed by using the same well distribution from Scenario 4 and adding the remaining wells from the SFWMM-D13R design to the BZ. BZ wells were assumed to have capacities of 10 mgd, so only half as many wells were added to Scenario 9 as had been removed from Scenario 4. The design of this scenario is shown on Figure 4.89. The recovery efficiency of the BZ wells was assumed to be 0%, making these wells more like disposal wells than ASR wells. Although the use of the term ASR for these BZ wells may not be appropriate because there is no recovery cycle, these wells are able to provide removal of excess water during wet seasons, preventing flooding and helping keep the salinity of coastal estuaries at appropriate levels. Figures 4.90 through 4.107 show the results of this scenario.

Pump pressure requirements in the UF and APPZ have remained approximately the same as for Scenario 4, but there has been an increase in pump pressures in the BZ, although the levels remain well below the 100 psi limit (see Figure 4.93).

This scenario represents a slight improvement over Scenario 4 in terms of artesian pressure in the APPA (see Figure 4.94 and 4.95).

The zones of significant "drawup" have expanded slightly but areas of significant drawdown have shrunk due to the additional injected water (Figures 4.96 through 4.104).

Because of the additional injection in the BZ, this scenario is able to meet the D13R volumes for storage (injection). Extraction volumes are smaller for this scenario than for Scenario 4 because of the 0% recovery efficiency in the BZ. This scenario was able to extract between 28% and 60% of the D13R annual volumes (Figures 4.124 through 4.126).

4.7 Scenario 10 – Eliminating Drawdown Beyond 1 Mile and Meeting APPA Requirements

Scenario 10 was developed to meet both performance measures and greatly reduce drawdown impacts of the system. It began with the set up for Scenario 9 (which already met the pump pressure requirements) and then the extraction was gradually reduced until the artesian pressure loss in the APPA was less than 10% and maximum drawdown 1 mile from each site was less than or equal to 1 foot. This scenario was designed to virtually eliminate all impacts to neighboring users (other than increased head).

The reduction in extraction was accomplished by applying a percentage to the extraction volumes used in Scenario 9. The percentages used at each site are listed in the second table on Figure 4.108. Note that this is not the recovery efficiency. Recovery efficiency (shown in the upper table) was still applied to the pump rates, but this extraction percentage was applied additionally to further reduce the drawdown (see Section 4.10).

The results for this scenario are presented in Figures 4.109 through 4.126. This scenario allows for full injection capacity, but the allowable extraction is much smaller than that required by SFWMM-D13R. In some areas, nearly all extraction was eliminated from the model.

As expected, there is little impact to the pump pressures since injection volumes are unchanged. (See Figure 4.112.) Artesian pressure remains within the 10% limit in all areas of Saint Lucie and Martin Counties for both the UF and APPZ. (See Figures 4.113 and 4.114) Large losses in artesian pressure occur only in the immediate vicinity of ASR wells. Most of both counties lose less than 5% of the existing artesian pressure.

There was no major change in areas of "drawup" compared to Scenario 9. As expected, however, the areas of significant drawdown have changed greatly. Drawdown greater than 1 foot is now only found in the immediate vicinity of the ASR wells. Note that the apparent drawdown in the BZ is not due to extraction, but is caused by salinity changes which impact the equivalent freshwater head. There is no extraction from the BZ ASR wells in this scenario. Drawdown and "drawup" data are shown in Figures 4.115 through 4.123.

Although this run was able to meet the SFWMM-D13R scenario requirements for storage, recovery was reduced to between 1% and 4% of the SFWMM-D13R extraction volumes in each year of the simulation. (See Figures 4.124 through 4.126.)

4.8 Scenario 11 – Final Selected Scenario

When the PDT analyzed the results of Scenario 10, it was determined that the requirement to reduce drawdown below 1 foot at locations more than 1 mile from the ASR wells was likely too stringent. Scenario 10 is more like an expensive water disposal system than an ASR system. Some informal research indicated that other ASR sites in Florida are not held to that standard. Therefore, Scenario 11 was designed to meet all performance measures other than the 1 foot drawdown at 1 mile requirement.

It was developed by starting with Scenario 10 and gradually increasing extraction volumes until just before the APPA requirement was exceeded. The resulting design is shown in Figure 4.127. Note that most sites have their full extraction capacity (already decreased by recovery efficiencies) except for those that are near St. Lucie and Martin Counties, where the artesian pressure protection rules are in force.

Because injection volumes are unchanged, the pump pressures that must be overcome during injection are quite similar to results from Scenarios 9 and 10 (Figure 4.131). Artesian pressure reductions in Saint Lucie and Martin counties are greater than they were for Scenario 10, but still meet the 10% requirement in both the UF and APPZ. Areas outside these counties see greater loss of artesian pressure during the extraction periods of the ASR pumping schedule.

"Drawup" areas and magnitudes are similar to those seen in both Scenario 9 and Scenario 10. (See Figures 4.134 through 4.142.) Drawdown areas are somewhat similar in size to those seen in Scenario 9 but the shape of the maximum drawdown contours have shifted slightly to avoid St. Lucie and Martin Counties. Time series plots show drawdown magnitudes similar to Scenario 9 for points away from the APPA, but they are smaller in the APPA.

Annual extraction volumes are still not able to meet SFWMM-D13R levels, but they can provide between 12% and 60% of the recovery water volumes during each year of the 13-year simulation, which is an improvement over Scenario 10. (See Figures 4.143 through 4.145.)

This simulation was selected by the PDT as the final recommendation and it was used in all of the analyses of Sections 5 and 6 including the Monte Carlo simulation.

4.9 Scenario 12 – Selected Scenario Without BZ Wells

After the completion of all the production scenario analyses and the Monte Carlo simulation (presented in Section 6) discussions with the PDT and the IMC model reviewers revealed some concerns about the BZ ASR wells from people not originally involved in the scenario decisions. Concerns included:

- Drilling to BZ depths is quite expensive, perhaps prohibitively so,
- With no recovery cycle, these wells are not truly "ASR wells,"
- Despite the ecological and flood-protection advantages of disposing of excess water through these BZ wells, this water is desperately needed in the Everglades and although there is no current mechanism to transport it there, the idea of disposing of needed water is not palatable to some.

To address these concerns, an additional scenario was added which was identical to Scenario 11, except it did not include any BZ wells. The design is summarized on Figure 4.146. Note that the reduction in extraction which was used to prevent significant loss of artesian pressure in St. Lucie and Martin Counties is still included. The results of this scenario are shown in Figures 4.147 to 4.164.

Pump pressures (shown on Figure 4.150) are similar to the results of Scenario 4 and are slightly lower in the BZ than the results of Scenarios 9, 10 and 11 because of the removal of BZ wells.

The reduction of artesian flow in the APPA for this scenario is shown in Figures 4.151 and 4.152. A few small areas exceed the 10% limit slightly. Extraction impacts are increased because there was less injection previously. This performance measure exceedance could easily be eliminated with a slight additional reduction to recovery rates in the ASR wells near these counties.

Drawdown and "drawup" results are shown on Figures 4.153 through 4.161. The area of significant "drawup" has been reduced slightly due to the removal of the BZ wells. Drawdown areas have changed only trivially.

Unlike Scenario 11, this scenario cannot meet the storage volumes defined by D13R. As shown in Figures 4.162 through 4.164, annual injection volumes for this scenario are between 42% and 62% of the D13R volumes from the SFWMM. Extraction volumes have increased slightly and range from 12% to 82%.

4.10 Recovery Efficiency, Extraction Percentage, and Comparison to Designed Flow Rates

In the above subsections, a number of percentages are reported for each of the scenarios. During conversations with members of the PDT, presentations to various groups and the IMC and internal reviews of the draft report, the authors noted that many had difficulty understanding the differences between these reported percentages. Although the text has been clarified as much as possible to explain their meanings, this section is provided as an additional aid to understanding.

- **Recovery Efficiency**: The recovery efficiency is a comparison between the amount of water injected into the ASR well and the volume which can be recovered. This percentage is generally less than 100% due to water quality, uncertainties regarding heterogeneities in the rock, movement of the freshwater bubble, density stratification, etc. Section 2.6.1 explains how recovery efficiency was incorporated into this model. The SFWMM-D13R assumed 70% recovery efficiency for all ASR wells. Thus, the extracted volumes never exceed 70% of what has already been injected. The recovery efficiency is also an assumption and an input for the RASRSM-D13R. When the assumed recovery efficiency is less than 70% (such as in the APPZ), the extraction rates are set to zero in the MODFLOW well package as soon as the recovered volumes reach 30% of the previously injected volumes. Once additional injection periods had added to the volume of stored water, extraction was again allowed. The inclusion of recovery efficiencies usually impacted the length of time for extraction and not flow rates. Until the stored volume in the aquifer reached zero, extraction rates matched those designated by SFWMM-D13R. Recovery efficiencies for each proposed ASR site are provided on the upper tables of the design figures for each scenario (Figures 4.13, 4.32, 4.51, 4.70, 4.89, 4.108, 4.127, and 4.146).
- Extraction Percentage: In order to meet the performance measure requiring that artesian flows not be reduced by more than 10% in the APPA (St. Lucie and Martin Counties), extraction rates at some proposed ASR sites were reduced beyond the recovery efficiency for Scenarios 10, 11 and 12. In Scenario 10, these extraction percentages were also used to reduce the drawdown at

distances more than 1 mile from the proposed ASR sites. Unlike recovery efficiency, these extraction percentages were added as a reduction in flow rate for all extraction periods during the modeled period regardless of the volumes of stored water in the aquifer. These percentage, which range from 0% to 100% are shown on the lower tables of the design figures for Scenarios 10, 11 and 12 (Figures 4.108, 4.127, and 4.146).

- Comparison to Designed Flow Rates: In order to analyze the success of each scenario at meeting the storage and recovery volumes defined by SFWMM-D13R, tables of percentages are provided for each scenario listing the comparison of annual volumes injected and extracted as a percentage of the SFWMM-D13R volumes. These are not inputs to the model, but are analyses of the scenario for its ability to meet the designated volumes. These percentages are shown on three figures for each scenario and are accompanied by bar charts showing the actual volumes each year. If the percentage reported is 100%, this means the scenario was able to exactly meet the volumes designated in SFWMM-D13R. Lower percentages mean a reduction in the ability of the scenario to storage or recovery needs of the basin. See Figures 4.29-4.31, 4.48-4.50, 4.67-4.69, 4.86-4.88, 4.105-4.107, 4.124-4.126, 4.143-4.145, and 4.162-4.164.

A short example may help clarify these three reported percentages. Assume that the SFWMM-D13R design for a given basin defined 30 days of injection at 20 mgd followed by 30 days of extraction at 14 mgd. This rate could be met by using four ASR wells. The injected volume would be 600 million gallons. Assuming 70% recovery efficiency, 420 million gallons would be available for recovery. This is exactly the volume that is removed during the second 30-day period.

In one scenario, this flow rate might be achieved in the RASRSM-D13R by using 4 UF wells with 70% recovery efficiency. This allows us to exactly match the designated flow rates from the SFWMM-D13R design. Now, let us assume that this site is near St. Lucie or Martin Counties and that its extraction percentage is set to 50% to prevent a loss of artesian pressure. This would mean reducing the extraction rate during the second 30 days from 14 mgd to 7 mgd, with a resulting extracted volume of 210 million gallons. When we compare this to the D13R design, this is 100% of the designed injection volume but only 50% of the designed extraction volume.

Let us assume that in a second scenario, this flow rate is to be divided evenly between two UF wells at 70% recovery efficiency and 2 APPZ wells at 30% recovery efficiency. The two UF wells would be set to inject at a total rate of 10 mgd for the first 30 days of the scenario. During the second 30 days, the extraction rate would be 7 mgd (3.5 mgd per well). If we continue with the assumption that the extraction percentage is 50% for protection of the APPA, the extraction rate would be further reduced to 3.5 mgd (1.75 mgd per well). This is a total injection volume of 300 million gallons and a total extraction volume of 105 million gallons.

In order to add the two APPZ wells, we begin with 30 days of injection at a rate of 10 mgd. This is a total injected volume of 300 million gallons, but since the recovery efficiency is only 30% in the APPZ, only 90 million gallons are available for recovery. During the first 10 days of extraction, the extraction rate is set to 7 mgd to match the requirements from the SFWMM-D13R design. This removes a volume of 70

million gallons and reduces the stored available volume to only 20 million gallons. Thus, during the second 10 days of extraction, the maximum possible rate is 2 mgd (1 mgd per well). This extraction period removes the last of the available stored freshwater so the extraction rate during the final 10 days of the scenario is 0 mgd. Then, if we apply the 50% reduction required to protect artesian pressure, the three extraction rates for the last 30 days of the scenario are reduced to: 3.5 mgd, 1 mgd, and 0 mgd, divided evenly between the two wells. This is a total extracted volume of 45 million gallons.

In order to compare to the SFWMM-D13R design, the volumes from the UF and APPZ are added together and divided by the design volume. For the injection comparison, we add the 300 million gallons injected into the UF to the 300 million gallons injected into the APPZ and divide by the 600 million gallons in the D13R design. The result is 100%, meaning that this scenario is able to fully meet the injection requirements of D13R. For the extraction comparison, we add the 105 million gallons removed from the UF to the 45 million gallons removed from the APPZ. The result (150 million gallons) is divided by the design volume of 420 million gallons and we can show that this scenario provides only 36% of the extracted volumes designated by SFWMM-D13R.

4.11 Validity of Drawdown Plots

The maximum drawdown plots shown on Figures 4.20, 4.39, 4.58, 4.77, 4.96, 4.115, 4.134, and 4.153 show widespread impacts caused by the ASR pumping. Some might question the validity of a model that indicates ASR impacts occurring many tens of miles away in aquifers not tapped by the ASR wells. There are three reasons that the modeling team feels that these results are valid.

1. First, impacts to groundwater conditions are already being felt on a regional scale. Figure 4.165 shows the measured heads during the calibration period at six monitoring wells scattered throughout the regional domain and found in all four aquifers. Each one experienced a steep decline in head, with a minimum occurring between June 2 and June 4, 2004, followed by an abrupt increase in head. Each well has a different magnitude of head and the ranges vary, but the shape of the head plot for each well is startlingly similar. This same signature is seen at nearly every observation well in the model domain. (See Figures 4.41 through 4.94 in the Calibration Report, NAP, 2011.)

   To more closely evaluate the head signature, heads at 74 wells were normalized to their head range where 1.0 is the maximum measured head and 0.0 is the minimum measured head (over the 14-month calibration period of November 2003 to December 2004). These 74 wells were located in all areas of the model domain and in all aquifers. They were selected only when more than 400 daily observations were reported during the calibration period. To prevent the over-selection of wells containing the head signature, no wells were removed from the analysis for unexplained anomalies or possible data errors. Figure 4.166 shows these normalized heads distributed into bins of 10% of the wells with data for that day (between 6 and 8 wells). Note that while the outer bands are quite large, the inner bands are extremely narrow. For example,

if the outer two bands (lightest blue and lightest red bands) are removed, 80% of the observation wells would fall into the remaining envelope, which is very thin. Note also that at the beginning of June 2004, all but the outermost (light blue) band are small, indicating nearly universal head minimums occurring within a few days of each other at all observation wells.

The main cause of this head signature is likely the regional pumping occurring in the FAS. Figure 4.167 compares this normalized head distribution to the monthly averaged extraction pumping in the model domain. When the extraction pumping is compared to the head (upper plot on Figure 4.167), there is a close correlation with a slight lag in the head changes. In the lower plot on Figure 4.167, the extraction pumping has been adjusted by summing 80% of the previous month's pumping rate with 20% of the current month's pumping rate. (The 80% and 20% multipliers were selected by trial and error in a search for a good correlation.) These two plots show a close relationship between FAS withdrawals and groundwater levels.

Some may argue that precipitation would be the main driver for head changes. Figure 4.168 shows the same normalized head distribution plots overlain with daily precipitation data for four sites. This precipitation data has been smoothed by summing the previous 30 days of precipitation. The lower plot on Figure 4.168 shows the average 30-day precipitation calculated using relative areas of Thiessen polygons clipped to the model domain. Both plots show poor correlation between precipitation and groundwater heads during the fall, winter and spring seasons. Precipitation is the likely cause of the sharp dip in heads which reached a low point between June 2, 2004 and June 4, 2004 at the vast majority of the observation points. Although the heads were already dropping due to increased extraction pumping, the descent was sharpened by approximately 2 weeks of dry weather. All four weather stations reported several days of rain beginning between June 2, 2004 and June 5, 2004, which caused the water levels to begin to rise.

Because the majority of the groundwater withdrawals from the FAS in the model domain are for agricultural purposes, there is some relationship between precipitation and groundwater withdrawals during the growing season. During the spring and early summer of 2004, when agricultural demands were high, extraction pumping also increased because precipitation remained low. Precipitation then increased during the summer and early fall and so agricultural water demands were largely met by rainfall and groundwater extraction diminished. Although precipitation rates were quite low during the late fall and winter of both 2003 and 2004, agricultural water demands were also low, so pumping did not need to be increased.

The groundwater extraction is not evenly distributed across the model domain. (See Figures 3.37 to 3.41 of the Calibration Report, NAP, 2011). The greatest rates are generally near Lake Okeechobee and the vast majority of the wells are located in the northern half of the model. Despite this irregular distribution, the effects of the pumping are felt nearly uniformly in all parts of the model domain with very little delay. This seems to support the data from the RASRSM-

D13R model which shows head impacts at great distances within short periods of time from the ASR wells.

2. Secondly, as shown in Figure 4.169, the proposed ASR pumping is enormous. This plot shows the sum of all existing extraction wells within the model domain based on the SAJ-developed pumping database and separated into the months of the calibration period. (Details on the development of this database are available in NAP, 2011, especially Appendix A.) At 5 mgd each, 333 ASR wells could remove a maximum of 1.67 billion gallons each day. This is more than the total volume of water removed from the entire model domain during any month of the calibration period other than April and May 2004. The volumes of water being considered for CERP ASR are large and beyond anything that has previously been seen on this peninsula. It is reasonable that its impact might be larger than what has been seen previously.

3. Finally, critics of the drawdown plots might argue that the impacts of the pilot ASR systems were not felt very far away. The left image on Figure 4.170 shows the results from the RASRSM with the pumping from the Kissimmee pilot test applied and calibrated to available field data. The contours show the location of 0.01 feet of maximum drawdown for each aquifer. The right image is an early RASRSM-D13R simulation which included 97 wells scattered throughout the proposed ASR sites, all screened in the UF. In this figure, the contour line is set at 1 foot of maximum drawdown. Thus, the figure on the right has almost 100 times as many wells as the figure on the left and the drawdown shown is 100 times that shown on the left. The area of impact for the two images is strikingly similar. Differences in the shape of the contours are due to the placement of the ASR wells in the D13R run, not all of which were located near the Kissimmee River pilot site.

   Although the Kissimmee cycle test model is calibrated fairly well to the measured data, all of that data is located very close to the ASR well where the drawdown magnitudes are large enough to be measured. Because a drawdown of 0.01 feet is far too small to be measured or noticed in any outlying well, the location of the 0.01 feet maximum drawdown shown in the model output cannot be validated against field data. But, the model results lend some credence to the idea that the placement of about 100 ASR wells would have the impact shown on the right. Note that this is from an early simulation and does not exactly match the results presented previously in this report.

Bredehoeft (2011) discusses the possible reason for this large-area impact. He states that the distance at which cyclical signals from pumping wells can be detected increases with aquifer transmissivity and artesian conditions. The conditions in the FAS are artesian in nearly all areas and the transmissivity is quite large compared to other aquifer systems.

For these three reasons, it is reasonable to believe that impacts from the CERP ASR system might be felt throughout the Floridan peninsula. It is important to remember that these impacts represent the movement of a pressure wave and not the movement of individual molecules of water or the movement

of the freshwater bubble. Pressure can move rapidly through an aquifer without impacting the locations of many water molecules in the same way that a person pushing on one end of an air mattress or water bed can see an immediate movement at the other end of the bed although it is not expected that the molecules of air or water have traveled across the bed instantaneously.

5 TVD Model Run

As explained in the Calibration Report (NAP, 2011), SEAWAT is equipped with several advection solvers. Most of the model runs described in this and other reports, were run using the standard finite difference method (FDM) using upstream weighting. This method is quite fast, though it is not considered to be as accurate as the third order Total-Variation-Diminishing (TVD) method, which is also supported by SEAWAT. The TVD method is significantly slower and so, was not a reasonable choice for the majority of the model runs for this project.

Section 5.1 of the Calibration Report (NAP, 2011) presents the results of a sensitivity analysis which involved running the model using the TVD method and then comparing the results to determine what, if anything, was lost by using the more efficient FDM solver. The results indicated that differences were minor, but were most pronounced for areas impacted by significant, sudden changes in pumping. Because the ASR design includes this type of a pumping signature, the team decided to make intermediate D13R scenarios using the standard FDM solver, but that the final run would be made using the TVD solver. This was considered to be a good compromise between necessary computational speed and desired accuracy.

Accordingly, when Scenario 11 was selected as the final D13R scenario run, it was repeated using the TVD method. Unfortunately, the problem was beyond the capabilities of the TVD method and the simulation repeatedly crashed before completing even one-quarter of the 13-year simulation. The TVD solver requires the user to enter a desired Courant number and then the model automatically sizes the time steps to meet that requirement. Although a full range of Courant numbers were tried, the model was never able to get beyond 983 days into the simulation before crashing due to a severely non-diagonally dominant matrix.

The reason for this failure is probably due to the fact that grid cells near the ASR wells were too large. Generally, small cells are required in areas where sudden, drastic changes to the head or constituent concentrations are expected. The ASR pumping scenarios include numerous sudden changes in pump rates, often changing from full injection to full extraction (or vice versa) in subsequent time steps. While the TVD solver can reduce the time step size to mitigate these changes, it is powerless to change the cell sizes.

Although the existing grid had its smallest cells at the locations of most ASR wells, they were still 2000 feet on a side and were probably not small enough to handle the pumping schedules for D13R. The cells could not be made any smaller because of computational requirements of the computers used to run the models. The grid, as it was, was already taxing the limits of the computers and time constraints with over 1 million cells and requiring more than 12 hours for a single RASRSM-D13R run using the FDM solver. Further, changes to the grid at this point would have required recalibration and rerunning of all 8 RASRSM-D13R scenarios, which was beyond the scope and budget for the project. Fortunately, the comparison of the first 983 days of the results indicated that the differences were minor and the standard FDM solution was sufficient for the needs of the project.

Comparisons of the results are presented for three example areas in Figures 5.1 through 5.3. In each case, the model calculated heads are presented as a time series for a set of points located at increasing distances from the ASR wells. Plots at right show the calculated heads from each of the two solution methods and the difference (TVD solution minus standard FDM solution).

The greatest differences between the two solutions are in the ICU (layer 4) directly above the Moorehaven ASR site, which includes six UF ASR wells and 4 BZ ASR wells in Scenario 11 (See Figure 5.1). During the first 983 days of the D13R simulation, the TVD solution exceeds the FDM solution by greater than 2 feet at only two times, both when the ASR wells switch suddenly from extraction to injection. In addition, the TVD solution head is less than the FDM solution head by more than 2 feet about a half dozen times during the two and a half year simulation when the ASR Wells switch suddenly from injection to extraction. Although the head impact of the pumping continues through the period of pumping, the difference between the two solution methods is only significant for a few weeks or months after the change in pumping. The TVD solution is more accurate during these sudden changes, but only for a short period. Once the model begins to equilibrate to the new condition, both solution techniques are similar with differences well within the error tolerance of the model. In addition, differences between the two solutions are greatest at the ASR site and quickly drop off as distance from the site increases. In fact, differences are within error tolerances when the distance exceeds a few miles.

Comparable results are shown in Figures 5.2 and 5.3, though the differences are smaller and more minor. Similar conditions are seen throughout the model when sudden changes impact the model.

The purpose of the RASRSM-D13R scenarios was to estimate the ability of the CERP system to meet regional performance measures, as described in previous sections. There are two reasons that the use of the standard FDM solution is sufficient for this purpose despite its differences from the TVD solution:

- The performance measure results are presented as worst-case, or maximum conditions. These conditions generally occur at the ends of long periods of either injection or extraction at the ASR wells. Since the differences between the two solutions occur at the beginning of an injection or extraction period, and quickly drop to acceptable levels, the use of the more accurate TVD solution would not significantly affect the performance measure results.
- Most of the performance measures are meant to measure regional impacts of the ASR pumping. Although the differences between the two solution techniques can be significant, the differences are seen only in the immediate vicinity of the ASR wells (usually within a mile or two). This is a regional model, whose purpose is to show the regional effects of D13R over a long time period. It was never expected that this model would be able to reproduce near-well effects. The local scale models (SAJ, in review) were developed for these purposes. The standard FDM solution is considered sufficiently accurate on a regional scale.

This analysis showed that the FDM solutions are sufficiently accurate for the analysis of the performance measures on the regional scale model. All solutions presented in this report were computed using the standard FDM method.

6 MONTE CARLO SENSITIVITY ANALYSIS

Often, numerical groundwater modeling is treated in a deterministic way – i.e. the modeler inputs his best guess for all parameters and treats the result as the "correct answer." In reality, there is uncertainty in all models. Model uncertainty can stem from uncertainty in the input parameters, simplifications made to force the system to fit a mathematical model, error caused by spatial and temporal discretization, etc. It is often more advisable to approach groundwater modeling from a probabilistic standpoint and use the uncertainty in the input parameters to estimate the uncertainly in the output. In a probabilistic model, there is not just one "correct answer;" instead there are a range of possible answers. The decision makers can then provide for a range of possible results in their planning.

A Monte Carlo sensitivity analysis is one way to quantify the uncertainty in the output. In this type of analysis, the input parameters are given probability distributions instead of discrete values. The range and distribution of the values should be an indication of the uncertainty in the parameter. Parameters that are well known or have been measured at the site might be given a narrower range of values than parameters that are unknown or obtained from the literature. The model is then run multiple times with different sets of randomized parameter values selected from those distributions. Assuming that the input distributions are valid, this methodology results in a number of equally probable model results. Instead of reporting a single answer, modelers can report the range and distribution of the model results and planners can design for contingencies based on those distributions. Also, if the results of the Monte Carlo analysis indicate a wide variability in output, it can signal the need to collect more data to reduce the uncertainty and tighten the variability of the model output. See Figure 6.1 for a schematic of a Monte Carlo analysis.

During the Monte Carlo analysis of the RASRSM, the input parameters for Scenario 11 were randomized and the ASR and no project scenarios were run on each randomized set of parameters. The results were then analyzed in comparison to the performance measures. The entire process was automated so that the computer could run a large number of randomized scenarios and provide statistics on output without user intervention.

6.1 INPUT PARAMETER DISTRIBUTIONS

The designation of probability distributions for the input parameters is often a challenge. If sufficient samples or measurements have been taken, distributions of the results can be applied to the model parameters. However, there is seldom that much data available for groundwater models. Testing for parameters such as hydraulic conductivity and storage parameters or analyzing geology can be expensive. Often, information is known at just a few points and must be interpolated to other areas of the model. In some cases, including the present model, probability distributions are simply estimated based on a range of values that would be considered acceptable by the engineer's judgment.

The parameters that were varied for this Monte Carlo analysis were porosity, dispersivity, molecular diffusion, hydraulic conductivity, specific storage, starting TDS concentrations, starting temperature, the thickness of the BZ and horizontal anisotropy. A total of five different methods were used to vary these

parameters during the randomized Monte Carlo runs. In all, 2894 different sets of parameters were developed using the techniques described here.

6.1.1 Uniform Distribution of Values

The first group of parameters was varied uniformly within a range considered acceptable. This group included porosity, longitudinal dispersivity and molecular diffusion for TDS and temperature. These parameters are transport parameters which could not be calibrated due to the short time period of the calibration model and the lack of sufficient time varying TDS and temperature data. The parameter values used in the calibration model were best guesses with little basis in field data, so the best option was to allow the Monte Carlo scenarios to use any value within plausible limits.

Each layer of the model was given a different random value for porosity and longitudinal dispersivity, but a single diffusion value for each constituent was selected to be applied to the entire model. The random numbers were generated using the RANDOM_NUMBER function in FORTRAN. Each random number was generated independently; there was no assumed correlation between the parameters. The allowable ranges for these parameters are shown in Table 6.1. The range was incorporated using the following formula:

$$Random\ Parameter\ Value = R \times (UB - LB) + LB \qquad \text{Equation 6.1}$$

where

R = Random number generated by FORTRAN (between 0.0 and 1.0)
UB = Upper bound of acceptable values
LB = Lower bound of acceptable values

Randomized distributions of a few of these parameters are shown in Figure 6.2. It is beyond the scope of this report to show all of them. These examples are indicative of all of the parameters in this group. Notice that each plot divides the range into 20 bins. Therefore, if an infinite number of simulations had been run, 5% of the values would have fallen into each bin. Because of the random nature of the parameter selection, there is some variation among the bins, but generally, all are between 4% and 6%.

6.1.2 Log Distribution of Values

The second group of parameters was varied using a log distribution with the range set according to acceptable values. This group included the ratio of longitudinal to transverse dispersivity, the ratio of longitudinal to vertical dispersivity and the ratios of horizontal to vertical conductivity for each geologic unit. These distributions placed the greatest probability on the lower bound of the acceptable range.

The allowable ranges for these parameters are listed in Table 6.2. The random numbers were generated using the RANDOM_NUMBER function in FORTRAN and then adjusted using the following formula. All random parameters were developed independently without any assumed correlation between parameters.

$$Random\ Parameter\ Value = 10\text{^}\left(R \times \left(log(UB) - log(LB)\right) + log(LB)\right)$$ Equation 6.2

where

R = Random number generated by FORTRAN (between 0.0 and 1.0)
UB = Upper bound of acceptable values
LB = Lower bound of acceptable values

Distributions of a few of these parameters are shown in Figure 6.3. It is beyond the scope of this report to show all of them. Notice that the applied distribution made it more likely that a value would be selected from the low end of each range. For example, more than 16% of the 2892 Monte Carlo selections applied a longitudinal to transverse dispersivity ratio between 0.1 and 0.15 while only 2% of the simulations applied a ratio close to 1.0. This is in keeping with general rules of thumb for this ratio.

For the hydraulic conductivity ratios in the aquifers (UF, APPZ, LF, BZ), the calibrated model used a value of 0.1. This was assumed to be the most likely value and the log scale was set up to place most random selections close to this value.

Unfortunately, an error was made in the setup for the hydraulic conductivity ratios for the confining units (MC1, MC2, LC). Here, the model calibration used a value of 0.5, and this should have been the most common value in the Monte Carlo selections. However, the same distribution was used here as with the other log scale parameters and the most likely value was again, 0.1. Similar situations occurred for the IAS and ICU. Although this error is unfortunate, it is believed to have a minimal impact on the results of the analysis. The hydraulic conductivity ratios were not used as calibration parameters so the 0.5 value is the initial guess made as the model was being set up, not a calibrated value. Further, as will be described below, each Monte Carlo simulation was tested against the calibration data before being added to the set. Thus, if the calibration was sensitive to these parameter values, bad values would have automatically been removed from the set before continuing. See Section 6.2.3 for additional information on this issue.

6.1.3 Parameter Distributions Applied to Pilot Points

Two of the most sensitive calibration parameters (hydraulic conductivity and specific storage) were included in the calibration model as pilot points. As described in Section 4.1.1 of the Calibration Report (NAP, 2011), the parameter values were applied to a set of mostly randomly placed points. Then these parameters were interpolated to the computational grid using a kriging technique.

In order to apply the Monte Carlo analysis to these parameters, a distribution was applied to the pilot point values and the interpolation was regenerated to produce a new conductivity or storage field for each run. Since hydraulic conductivity was closely calibrated and based on significant field data, itsr uncertainty was considered to be somewhat low and the values were not allowed to vary as much as more uncertain parameters. Each pilot point hydraulic conductivity value was allowed to vary between half of the calibrated value and twice the calibrated value. Uniform distributions were applied using Equation 6.1. A few examples of the conductivity fields for the UF are shown in Figures 6.4 and 6.5.

This method allowed each randomized hydraulic conductivity distribution to remain true to any measured data and close to calibrated values. General trends and orders of magnitude are preserved, but subtle changes are introduced in each randomization. The Monte Carlo simulation can investigate the sensitivity of some of these values while remaining true to known information.

The distributions for specific storage were set in a similar manner. Again, random values were selected for each pilot point, but a log distribution was used spanning four orders of magnitude, ranging from one hundredth of the calibrated value to 100 times the calibrated value. The larger range was selected because there was less data for selecting storage values and therefore, more uncertainty. Also, selection of the best calibration was more difficult for the transient model because of the additional parameters and the difficulty in defining a "well-calibrated" scenario. The log distribution was selected because of the large range and the fact that these parameters tend to fall along a log scale. Figures similar to Figures 6.4 and 6.5 could be supplied but are omitted for simplicity since they would provide no new information.

6.1.4 Invertible Distributions Applied to Pilot Points

Another type of distribution was developed for parameters whose ranges straddled unity, but were not appropriately distributed with either a uniform or log distribution. Horizontal anisotropy in the UF and APPZ were varied in the Monte Carlo simulation using this type of invertible distribution. MODFLOW and SEAWAT incorporate this parameter by applying a ratio to each cell of the model, representing the ratio of hydraulic conductivity along the columns to hydraulic conductivity along the rows.

Early work on the regional ASR study demonstrated the existence of a preferential flow direction along the spine of the Floridan peninsula based on some lineament studies (Fries, 2004). It was this information that led to the rotation of the grid by 38°. Later study (Bittner, et al, 2008) indicated that this anisotropy did not affect calibration and so it was removed from the RASRSM. The PDT asked that it be re-introduced in the Monte Carlo simulation. At that time, some early information at the Kissimmee River pilot site seemed to indicate localized preferential flow to the east and west, nearly perpendicular to that indicated by the SFWMD work. This issue has continued to progress and is described in greater detail in the cycle test report (SAJ, in review). Here, it is sufficient to mention that at the time the Monte Carlo simulations were being set up, it was unclear if there was any anisotropy and which direction it might go. Further, there were theories that localized effects might not match regional effects. So the Monte Carlo simulations were developed to include preferential flows in both directions with anisotropy values varying spatially (rather than being constant across the model). Horizontal anisotropy was varied in the UF and APPZ layers – all other layers had anisotropy values of 1.0, meaning equal conductivity in both directions.

The range selected for horizontal anisotropy was 0.1 to 10.0. This allows the conductivity in either direction to be as much as 10 times or as little as one tenth of the conductivity in the perpendicular direction. If a uniform distribution had been applied across this range, the likelihood of selection of a value between 1.0 and 10.0 would have been ten times the likelihood of selection of a value between 0.1 and 1.0, placing an undue emphasis on values above 1, where the conductivity along the columns is

greater than that along the rows. If a log distribution had been applied, the opposite would have occurred. Instead, the range was set to 1 to 10 and a uniform distribution was applied as in Equation 6.1. Then, a second random value was selected between 0 and 1. If the second number was greater than 0.5, the original random value was inverted. This puts half of the selected values on each side of unity making anisotropy in each direction equally likely.

Figure 6.6 shows the resulting distribution. Note that in the plot at left, the inverted bins are sized at 0.1, while the bins for the non-inverted values are sized at 0.9. This makes the distribution look uniform for the upper values and logarithmic for the lower values. If we think of these values in terms of ratios instead of decimals, the distribution becomes uniform as in the plot at right. Thus, for this Monte Carlo simulation, it is just as likely that the preferential flow is along the columns as along the rows.

To provide spatially varying horizontal anisotropy, the randomized values were applied to a small set of pilot points and interpolated to the surface. A few example anisotropy distributions are shown in Figure 6.7. There is quite a bit of variability in these values due to the uncertainty, but, as will be described in section 6.2, the algorithm for developing these scenarios was set up to eliminate randomizations that could not match the calibration.

6.1.5 Multiplier distributions applied to Pilot Points

As described in Section 2.7, the starting conditions for TDS and temperature on the RASRSM-D13R model matched the starting conditions from the calibration model. The development of the starting conditions for TDS concentration and temperature for the calibration model is described in the Calibration Report (NAP, 2011). The process entailed interpolation of available data, but also involved some engineering judgment and comparison to underlying layers to ensure consistency. Because this method required user intervention, it could not easily be automated for the Monte Carlo simulations like all of the other parameter selection processes. Thus, a separate process was employed to vary the starting conditions.

A set of pilot points was created and values associated with each point were randomized with a range of 0.8 to 1.2 and a uniform distribution (Equation 6.1). The narrow range was used because there was a significant amount of field data employed, so the uncertainty was considered to be somewhat low. The values assigned to these pilot points were interpolated to the grid using the kriging method to apply a value to each cell. The interpolated values on each grid cell were then multiplied by the starting condition value for TDS and temperature from the calibration model for that cell. The final starting TDS concentrations and temperatures varied between 80% and 120% of the values developed for the calibration model. In this way, the resulting randomized starting values remained close to available data and were consistent with other layers and surrounding areas.

Figures 6.8 and 6.9 show a few example randomizations for TDS starting values. Note that all randomizations remain true to the available data and consistent with surrounding data, but subtle differences have been introduced to each randomization. A similar process was followed for setting the initial temperature condition.

Multiplier distributions were also used to change the thickness of the BZ. In the calibration model, the BZ was 500 ft thick over the entire model domain. For the Monte Carlo runs, the multipliers were set from a range of 0.5 to 2.0, resulting in a BZ thickness varying from 250 ft to 1000 ft. An invertible distribution (see Section 6.1.4) was used to prevent the random numbers from favoring one end or the other of the range.

6.2 Selection of Monte Carlo Simulations

For each Monte Carlo simulation, the above processes were used to obtain random values for the 1485 parameters. Every random value was developed independently with no pre-conceived correlations between parameters. Next, any necessary kriging was performed and model input files were developed. Then, the calibration simulations were run with the new set of randomized data to compare the results against the calibration data. Only those scenarios that met minimum calibration requirements were run through the D13R scenarios and the post-processing routines to compare the results to the performance measures. See the flow chart in Figure 6.10 for a visual summary of the process.

6.2.1 Steady State Calibration Check

To test the steady state calibration, the October 2003 and February 2004 calibration models were run with the randomized parameter sets described in Section 6.1. See the Calibration Report (NAP, 2011) for details on these two calibration periods. In the original calibration, some calibration points were considered to be less important than others due to model simplifications, local effects, etc. For this calibration check, everything had to be automated, so all calibration points were given the same weight. The residual error at each point was calculated and the root mean square for the entire calibration set was calculated using Equation 6.3 for each of the two models.

$$RMS = \sqrt{\frac{\sum_{i=1}^{n} c_i - o_i}{n}} \qquad \text{Equation 6.3}$$

where:

c_i = Model calculated head at observation point, i
o_i = Observed head at observation point, i
n = Number of observation points

When the calibrated parameters were used, the RMS for October 2003 was 2.08 and for February 2004 was 1.78. The percentage change for each RMS value was calculated as follows:

$$\%chng = \frac{\left|RMS_c - RMS_m\right|}{RMS_c} \times 100 \qquad \text{Equation 6.4}$$

where

RMS_c = Calibrated RMS
RMS_m = Monte Carlo scenario RMS

Only those scenarios that had a percent change less than 150% were used in the Monte Carlo analysis (RMS less than 5.20 for October 2003 and less than 4.44 for February 2004). Figure 6.11 shows the February 2004 and October 2003 RMS values for each of the randomized parameter sets compared to the calibrated values and the cutoff points for the Monte Carlo analysis. Approximately 55% of the parameter sets passed the steady state calibration test and continued to the next step of the analysis. Those parameter sets which did not pass this test were eliminated from the analysis.

6.2.2 Transient Calibration Check

The calibration check for the transient model was based on the Nash-Sutcliffe statistic (Nash and Sutcliffe, 1970). The 15-month transient calibration model (October 2003 – December 2004) was run with the Monte Carlo randomizations and then the Nash-Sutcliffe statistic was calculated using Equation 6.5 for each observation point.

$$E = 1 - \frac{\sum (o_i - c_i)^2}{\sum (o_i - \bar{o})^2}$$ Equation 6.5

where

E = Nash-Sutcliffe statistic
o_i = Observed head for given time step
c_i = Model calculated head for given time step
$\bar{o}$ = Average observed head across all time steps

When the Nash-Sutcliffe statistic is greater than zero, variation in the model output is smaller than the variation in observed data. When it is less than zero, the model is inefficient, i.e. the variation between calculated and observed values is greater than the variance in the observed data. The optimum value is 1.0. The negative values can be much greater than the positive numbers, so a simple summation would put far too much emphasis on the few poorly calibrated points. To prevent this, points were awarded to each observation point based on the system shown in Table 6.3.

The points awarded to each observation point were summed and a score was assigned to each randomization. The calibration model score was 180. Higher numbers indicate a better calibration. For the Monte Carlo randomization to be selected, the score needed to be higher than 153, 85% of the calibrated value.

Figure 6.12 shows the results of the transient calibration test when compared to the steady state calibration results. It is interesting to note that there are a number of Monte Carlo randomizations with apparently better transient calibrations than the accepted calibration model described in the Calibration Report (NAP, 2011). This is due to the fact that during calibration, the quality of each transient test run was assessed both quantitatively, using a suite of statistical measures, and qualitatively, using the engineering judgment of the modeling team. In order to automate the Monte Carlo analysis, only the quantitative analyses could be used and in this case, only one of the statistical measures was employed.

About 53% of the randomizations that passed the steady state test also passed the transient test and continued to the next step of the Monte Carlo analysis. All other parameter sets were eliminated from the analysis.

6.2.3 Effects of Removing Poorly Calibrated Scenarios

As explained earlier, it is often difficult to select the probability distributions for input parameters, especially when there is minimal data available. In this analysis, the best effort has been made to select reasonable ranges for the input parameters and to develop reasonable distributions that placed greater emphasis on more likely values. But it was also important to ensure that the model results for each simulation matched available calibration data to a reasonable degree. In many cases, when the calibration data was used to whittle down the simulations, the distribution of the parameters was affected. One example of this phenomenon is shown in Figure 6.13. The plot on the left shows the distribution of a parameter whose distribution was not affected by the Monte Carlo selection process. Note that the distribution of all randomized scenarios is quite similar to the distribution of the selected scenarios. The plot on the right shows the distribution for a parameter that was affected by the selection process. Here, a greater percentage of the randomized scenarios with low ratios were not selected because of poor calibration. Thus the distribution has changed as a result of the selection process. During analysis of the input for this report, a few errors were found in the setup of the randomization algorithm, including that described in Section 6.1.2. This method of selecting the scenarios helps mitigate the effect of these errors in setup.

6.3 Monte Carlo Analysis Results

Once the calibration tests had been used to select the best of the randomized scenarios, the results of the RASRSM-D13R runs were compared to the performance measures. Instead of a single, deterministic answer, like those presented in Section 4, this method resulted in a distribution of results, helping to quantify the uncertainty in the model.

In all, 825 full Monte Carlo iterations were run. These had been whittled down from 2836 randomizations of the input parameters. About 55% (1551 randomizations) passed the steady state calibration test and, of those, 53% of those passed the transient calibration test.

The time required to make these runs was significant. It took about 4 to 7 minutes to make the steady state calibration check and 60 to 90 minutes to make the transient calibration check. If those tests were passed, it took 10 to 15 hours to run the D13R scenario and an additional 9 to 14 hours to run a no project scenario for comparison. Another 10 to 30 minutes were required to run the post processing codes and update the running pass rates. In total, a complete Monte Carlo scenario would take 20-30 hours to run to completion.

Variations in run times are due to differences in computer speeds. A total of 14 different computers were used for varying amounts of time over a period of 3 months to complete the simulation.

6.3.1 Monte Carlo Output and Performance Measure Statistics

Because of storage limitations, it was not possible to save the entire set of output files for each Monte Carlo run. On average, the output files totaled nearly 26 GB for a single run of the D13R scenario. Much of that space (39% for flow files, 30% for concentration results and 23% for text output files) was not used for any of the performance measure analyses. But there was still a large amount of disk space needed to store just the head output files - 2 GB for each run. And the results of the no project scenario were of similar size. For 825 runs, that would require over 3 TB just to store the head output files.

Instead of storing the actual output files, each scenario was compared to the performance measures and either passed or failed each one. The number of passing scenarios was summed up as the scenarios finished and new scenarios overwrote the previous solution files. In the case of APPA and drawdown results, this summation was done for each cell in the model. In the case of the pump pressure requirement, the summation was done for each proposed ASR site. Since there were so few sites (16) compared to grid cells (1.2 million), the actual maximum pump pressures were also tabulated.

The final result of the Monte Carlo simulation included:

- A grid dataset showing the number of Monte Carlo simulations with a loss of more than 10% of the artesian pressure at each cell,
- A grid dataset showing the number of Monte Carlo simulations with less than 1 foot of maximum drawdown at each cell,
- A grid dataset showing the number of Monte Carlo simulations with less than 5 feet of maximum drawdown at each cell, and
- A list of the maximum pump pressures encountered at each proposed ASR site for each Monte Carlo iteration.

This space-saving output setup precludes the ability to present distributions of output data such as the maximum drawdown or the percent artesian pressure loss. Instead, we can present the percentage of Monte Carlo simulations meeting each performance measure. If the percentage is close to 100%, we can be fairly certain that the Scenario 11 ASR system design will meet the given performance measure. Conversely, if the percentage is close to 0%, we can be fairly certain that the performance measure will not be met at that location. If the percentage is in the middle, near 50%, we cannot say one way or the other what will happen. If the area of middle percentages is unreasonably large or covers an important area, additional data collection or modeling work are required to tighten up the uncertainty in the output.

One important decision for this type of analysis was how many iterations to run. In reality, the decision was made based on available computers and time allotted, but it was important to be able to determine the accuracy of the results. It was desirable to stop the Monte Carlo simulation only when it was determined that additional iterations would not appreciably improve the reliability of the results. This was done by computing the 95% confidence interval using the following equations:

First, the equation for the sample mean is:

$$\overline{Y} = \frac{1}{N}\sum_{i=1}^{N} Y_i$$ Equation 6.6

where

$\overline{Y}$ = Mean

N = Number of Monte Carlo simulations

Y_i = Result of simulation i

Because the results for this Monte Carlo simulation are binary (either pass or fail), Equation 6.6 can be reworked with $\overline{Y}$ becoming the percent of the runs passing the performance measure:

$$\overline{Y} = \frac{1}{N}\left(P \times 1 + F \times 0\right)$$

$$\overline{Y} = \frac{P}{N}$$ Equation 6.7

where

N = Total number of Monte Carlo simulations

P = Number of passing simulations

F = Number of failing simulations

Second, the variance is computed using Equation 6.8:

$$S^2 = \frac{1}{N-1}\sum_{i=1}^{N}\left(Y_i - \overline{Y}\right)^2$$ Equation 6.8

where

S^2 = Variance (note that S is the standard deviation)

Then, the half-width of the confidence interval is computed as:

$$HW = z_{1-\alpha/2}\frac{S}{\sqrt{N}}$$ Equation 6.9

where

HW = Half-width of the confidence interval

$Z_{1-\alpha/2}$ = Z statistic where α is 5% (1.96)

Equation 6.8 can be inserted into Equation 6.9 and because of the binary nature of the results, it can be reworked as:

$$HW = \frac{1.96}{N}\sqrt{\frac{P\left(N-P\right)}{\left(N-1\right)}}$$ Equation 6.10

Note that the half-width of the 95% confidence interval is dependent only on the number of Monte Carlo simulations and on the number of passing simulations. Figure 6.14 shows how the confidence interval changes as the number of simulations increases for different pass rates. The half-width of the 95% confidence interval is greatest when the pass rate is 50%. As the number of Monte Carlo simulations increases, the effect of the pass rate on the confidence interval lessens. At 825 simulations, the half width of the 95% confidence interval is 3.41% at most. To reduce the half-width of the 95% confidence interval by one percentage point (from 3.4% to 2.4%) an additional 825 simulations would be required and the same set of computers would require about three more months to reach this point. The advantages from the improvement in the confidence interval are outweighed by the time required to achieve these improvements.

6.3.2 Pump Pressure

The method for calculating the pressure that would need to be overcome by the ASR pumps to inject the required flows is explained in Section 3.2. The same method was applied to each of the 825 selected Monte Carlo simulations. Figures 6.15 through 6.26 show the histograms of the results at each ASR site. Bars for pressure values meeting the 100 psi requirement are blue; bars for values not meeting the requirement are red.

For all of the UF sites, the majority of the Monte Carlo runs met the pressure requirements. The percentages and the spread of the results vary significantly, however. For example, at Hillsboro in the UF (Figure 6.15), 66% of the Monte Carlo runs met the 100 psi requirement. But there was a wide range of maximum pressures, from 46 psi to 195 psi. The maximum value of 195 is nearly twice the requirement. This indicates that the uncertainty in the input parameters has led to significant uncertainty in this output parameter. Conversely, at Flaghole in the UF (Figure 6.18), 86% of the Monte Carlo runs met the 100 psi requirement and the range is a bit narrower, from 58 psi to 140 psi. The uncertainty in the input parameters has a lesser impact on this performance measure. Note that all Monte Carlo simulations met the pump pressure requirement at all sites in the APPZ and BZ.

Figure 6.27 shows the change in percentage of passing simulations for the UF site at Lakeside Ranch as the number of simulations increases. The 95% confidence interval (calculated using Equation 6.10) is also plotted on this figure. Note that there is significant variation in the percentage when the number of Monte Carlo simulations is less than 200. After that point, there is less variation and the width of the 95% confidence interval gradually decreases. By the time the Monte Carlo analysis was stopped (at 825 iterations) the improvement in confidence with each additional iteration was trivial. The “return on investment” of time and computational power had become very small.

Figure 6.28 shows the percentage of Monte Carlo simulations that met the pump pressure requirement at each proposed ASR site in the UF with the 95% confidence interval shown as error bars. Note that, as expected, the largest confidence intervals are on the points where the percentage passing is closest to 50%.

Only four sites passed the criteria for every Monte Carlo run, but these are the four sites that have no ASR wells assigned to the UF in Scenario 11. All other sites failed the criteria at least part of the time, so there is a possibility that the number of ASR wells would need to be reduced at some or all of the sites. The most critical sites are Kissimmee River and Lakeside Ranch, both of which slightly exceeded the 100 psi requirement in Scenario 11. Hillsboro is the third most critical site, although it was below the limit in Scenario 11. (See Figure 4.131.)

6.3.3 Artesian Pressure Protection Area (APPA)

The results of the Monte Carlo analysis on the loss of artesian pressure are shown in Figures 6.29 and 6.30. As explained in Section 3.3, one of the performance criteria was that not more than 10% of artesian well flow be lost in the APPA, which consists of Saint Lucie and Martin Counties. As the Monte Carlo simulations finished, each cell was investigated and the loss of artesian pressure was calculated. The number of simulations where more than 10% of the artesian pressure was lost was summed up for each cell in the model. Figures 6.29 and 6.30 each show the percentage of Monte Carlo runs where more than 10% was lost (see upper left images). Note that in both the UF and APPZ, both St. Lucie and Martin Counties are completely blue, indicating fewer than 5% of the runs exceeded the 10% limit. There are a few cells that exceed 5% slightly, but they are not visible with the existing color ramp and at the existing scale. These cells are mostly in the northwest of Martin County and southwest of St. Lucie County. These results show that the distribution of ASR wells in Scenario 11 is very likely to be able to meet this performance measure.

The other three images on each of Figure 6.29 and Figure 6.30 show that the 95% confidence interval is quite small, with the maximum being about 3.4%. In St. Lucie and Martin Counties, the maximum 95% confidence interval is even smaller, less than 2%. The bottom two images on each figure show the upper and lower bound of this 95% confidence interval. The differences between the two are nearly impossible to discern. This is an indication that the number of Monte Carlo simulations was sufficient for the regional nature of the model. Additional simulations would have made little impact to the result.

It is important to remember that this plot represents the worst time step of the 13-year period. The areas in red will lose more than 10% of their artesian pressure at least once during the period. At other times, the head will actually rise and artesian flow will increase.

6.3.4 Drawdown

Drawdown was not a specific performance measure, since there was no specific limit on how much drawdown would be allowable or the distance at which impacts could be felt. However, the drawdown impacts to the neighboring areas were investigated and incorporated into the Monte Carlo simulation. After each Monte Carlo run, the maximum drawdown was computed for each cell of the grid. It is important to note that this magnitude of drawdown is a worst-case condition and would not be found during most of the run period. In fact the figures in Section 4 show that the water table actually rises during much of the period. As the Monte Carlo analysis progressed, the scenarios with greater than 1 foot drawdown, and greater than 5 feet drawdown, were counted for each cell.

Figures 6.31 through 6.34 include an image (top left) of the percentage of Monte Carlo scenarios that had a maximum drawdown greater than 1 foot. Similarly, Figures 6.35 through 6.38 include an image (top left) of the percentage of Monte Carlo scenarios that had a maximum drawdown greater than 5 feet. Like the APPA figures described in the previous section, each figure also shows the half width of the 95% confidence interval and the upper and lower bounds of that confidence interval. There is very little difference between the upper and lower bounds. The half width of the confidence interval is less than 3.5% everywhere. This indicates that a sufficient number of Monte Carlo simulations were run to provide the accuracy desired for a regional model of this scale.

Impacts to the head surrounding the ASR sites are significant. Red areas, indicating nearly all Monte Carlo simulations exceeded 1-foot or 5-foot drawdown, are large. It is likely that maximum drawdown across Glades County, Palm Beach County, Broward County and Lake Okeechobee will exceed 1 foot, with a large part of the area also exceeding 5 feet of drawdown in the UF. Impacts to the APPZ will be similar. Impacts to the LF are centered around the southeast corner of Palm Beach County – most of the county will likely see more than 1 foot drawdown, while only the southeast quadrant will be likely to see 5 feet.

7 SOURCES OF UNCERTAINTY

As with all models, there are numerous sources of uncertainty. Every effort has been made to minimize uncertainty, and where that was impossible, we have endeavored to quantify the impact of the uncertainties on the goals of the model. The purpose of the RASRSM was to investigate the regional effects of the CERP ASR plan. This model was meant to give a broad-brushed, order-of-magnitude estimate of the number of ASR wells which could be placed in the FAS. It cannot be used to look at near-field well effects or at small-scale TDS transport. Local scale modeling and pilot studies (SAJ, in review) are better tools for those types of investigations.

Here we discuss some of the sources of uncertainty in the RASRSM and the possible impact on the model results.

7.1 MODEL SETUP

As discussed in Section 6 of the Calibration Report (NAP, 2011) the model set up introduced a number of uncertainties including,

- time and spatial discretization,
- simplification of the geology,
- interpolation of starting TDS and temperature conditions,
- interpolation of specified head boundary conditions to the SAS and aquifer sides,
- data gaps in regional pumping data,
- inability to calibrate to transport parameters,
- non-uniqueness of calibration (hydraulic conductivity and specific storage).

All of these uncertainties were discussed in detail in the Calibration Report (NAP, 2011). Despite these uncertainties, the calibration of the RASRSM to field data was good and many of these parameters were included in the Monte Carlo analysis, which showed very little variability in the output.

7.2 CONVERSION OF CALIBRATION MODEL TO D13R MODEL

In order to set up the RASRSM-D13R model, the boundary conditions, source/sink terms (regional pumping) and initial conditions were converted from the 2003/2004 or 1993/1994 time periods of the calibration and validation models to the 1965-1977 time period required for the D13R analysis. Generalized data and statistical trends were used to ensure that the conditions in the aquifers were similar to those that existed in the 1960s and 1970s and which informed the selection of ASR pumping rates in the SFWMM-D13R model. The resulting model (run without ASR) was compared to available head data from the 1965-1977 period and found to match fairly well, though not as well as would be required of a calibrated model. The available data was mostly from upper sections of the aquifer system and from the north and west areas of the model domain. The paucity of data in some areas of the model and the fact that model did not always match the data as well as would be desired adds some additional uncertainty to the model results.

7.3 ASR Pumping Data

The SFWMM-D13R model provided daily pumping data for each of the proposed ASR basins. Implementation of daily pumping changes was beyond the scope of this regional model, so the pumping data was averaged over 10-day periods. The averages were calculated so that the total volumes of water injected into or extracted from the aquifers were correct, but the averaging can cause a loss of some high pumping rates, when they are short-lived. Since the performance measures all look at worst-case conditions which generally occur at the end of a long period of injection or extraction, this averaging is unlikely to significantly impact the performance measure results.

The SFWMM-D13R simulation assumed 70% recovery efficiency on injected water. In the RASRSM-D13R, smaller recovery efficiencies were assumed at Hillsboro and in the APPZ and BZ layers. Recovery efficiency is a local-scale effect caused by such processes as mixing of fresh water with the native high-TDS water in the aquifer, buoyancy stratification, local groundwater gradients, etc. Only a highly detailed local scale model could adequately investigate these processes. Field verification of these assumptions can only be effected by pilot studies at the specific site in question.

Recovery efficiency affects the volumes of water which could be removed at each site. However, the APPA performance measure is already a limiting factor on extraction volumes at many sites, so the use of an assumed recovery efficiency will have little impact on the model results. At sites far from St. Lucie and Martin Counties, errors in the recovery efficiency assumptions will impact the volumes that can be removed during dry periods. It is expected that additional near-field study to investigate recovery efficiency will be necessary at each site before construction of the ASR system. This study should include both field pilot studies and local scale numerical modeling as was done for the Kissimmee and Hillsboro pilot sites (SAJ, in review).

7.4 Performance Measures

The use of the RASRSM to investigate the performance measures involved some additional uncertainties. The estimate of the pressures which a pump would be required to overcome assumes that the elevation of the source water is equal to the ground surface elevation at the well location. Pressure calculations ignore headlosses (from pipe flow, pumps, and the treatment system), and skin effects at the well. The use of the Theim equation to account for large grid cells assumes homogeneous, isotropic conditions with an infinite, uniform-thickness aquifer.

The use of the Merritt equation to estimate the percent loss of artesian flow in the APPA also assumes homogeneous, isotropic conditions with an infinite, uniform-thickness aquifer.

The errors introduced by these analyses are probably minor and within the error of the model. Since the purpose of the model is to obtain an order-of-magnitude level accuracy on the number of ASR wells which can be constructed, these estimates and calculations are sufficient. Readers should remember that the recommended numbers of ASR wells may need to be slightly altered as additional study continues.

8 CONCLUSIONS/RECOMMENDATIONS

The RASRSM calibration model was broadened to include the D13R scenario with ASR pumping rates and schedules drawn from SFWMM-D13R. Changes to the design were made to meet PDT-developed performance measures, including the pressure that well pumps would be required to overcome and the effect of the ASR system on the APPA in St. Lucie and Martin Counties. The results show that pump pressure requirements and protection of the APPA can be met with approximately 94 ASR wells in the UF, 37 ASR wells in the APPZ and 101 ASR wells in the BZ if the extraction at sites near the APPA is significantly reduced (Scenario 11). (UF and APPZ wells will have a 5 mgd capacity; BZ wells will have a 10 mgd capacity.) The suggested arrangement of these wells is indicated in Figure 4.127. Although full recharge potential will be available, a significant reduction in the available water for recovery will limit the effectiveness of the system. The model also indicates that this arrangement of wells will result in significant head impacts over a large area of the Floridan peninsula.

Due to the depth and poor water quality in the BZ, it is unlikely that so many BZ wells could be built. Scenario 12 was developed to simulate a more likely scenario including only the UF and APPZ wells (see Figure 1.146). The comparison of these results to the performance measures is only slightly different from Scenario 11 but it involves a significant reduction in storage capacity for the system.

A Monte Carlo analysis of the results of Scenario 11 showed that some additional reduction in the number of wells or the extraction rates may be necessary at a few sites due to pump pressure limitations. The sites most likely to require a small reduction in ASR wells are Lakeside Ranch, Kissimmee River/Paradise Run and Hillsboro (Site 1). It is unlikely that any further reduction will be necessary in protection of artesian conditions in St. Lucie or Martin Counties, though the design for Scenario 11 already includes significant reductions in extraction volumes for several sites around the northeast shore of Lake Okeechobee.

This regional model run makes assumptions about the conditions of the aquifer, the seasonal variations during the 1960s and 1970s and the recovery efficiencies expected from the aquifers. All of these assumptions will need to be closely analyzed through pilot studies at the proposed ASR sites and local scale models to predict the local effects of the ASR well system.

9 REFERENCES

Anderson, M.P. and Woesner, W.W., 1992. *Applied Groundwater Modeling: Simulation of Flow and Advective Transport*, Academic Press, London.

Bittner, L.D., Richardson, E., Langevin, C.D., England, S.M., and Stevens, G.T., 2008. *Using Density-Dependent Numerical Models to Evaluate Regional Groundwater Flow Patterns in South Florida*.

Bredehoeft, J.D., 2011. *Monitoring Regional Groundwater Extraction: The Problem*: Ground Water, Vol 49, pp 808-814.

Brown, C.J., England, S.M., Stevens, G.T., Cheng, H-P, and Richardson, E., 2006. *ASR Regional Study – Benchscale Modeling, Final Report*. Availabe at http://www.evergladesplan.org/pm/projects/project_docs/pdp_asr_combined/082206_asr_benchscale_study.pdf.

CH2MHill, 2005. *Sub-Task No. 3 – Groundwater Numerical Model Development Support and Data Collection Report*.

Fies, M., 2004. *Comprehensive Everglades Restoration Plan, Lineament Analysis South Florida Regional Aquifer Storage and Recovery Study.* U.S. Army Corps of Engineers, Jacksonville, Fl. Available from http://www.evergladesplan.org/pm/projects/project_docs/pdp_asr_combined/013007_asr_lineament_dtmt.pdf

Geibel, N.M. and Brown, C.J., 2012. *Hydraulic Fracturing of the Floridan Aquifer from Aquifer Storage and Recovery Operations*: Environmental & Engineering Geoscience, Vol. 18, pp 159-174.

Kohout, F.A., 1965. *A Hypothesis Concerning Cyclic Flow of Salt Water Related to Geothermal Heating in the Floridan Aquifer:* New York Academy of Science Transactions, v. 28, no. 2, p. 249-271.

Kohout, F.A., Meisler, Harold, Meyer, F.W., Johnston, R.H., Leve, G.W., Wait, R.L. 1988, *Hydrogeology of the Atlantic Continental Margin*, in Sheridan, R.E., and Grow, J.A., eds, The Geology of North America, Volume 1-2, The Atlantic Continental Margin, US.: Geological Society of America.

Langevin, C.D., Shoemaker, W.B., and Guo, W., 2003. *MODFLOW-2000, the US Geological Survey Modular Ground-Water Model – Documentation of the SEAWAT-2000 Version with the Variable Density Flow Process (VDF) and the Integrated MT3DMS Transport Process (IMT)*, U.S. Geological Survey Open-File Report 03-426, 43 p.

Merritt, M.L., 1997. *Computation of the Time-Varying Flow Rate from and Artesian Well in Central Dade County, Florida, by Analytical and Numerical Simulation Methods.* USGS WSP 2491.

National Climatic Data Center. *Local Climatological Data*. http://climatecenter.fsu.edu/products-services/data. Accessed 9/25/2012.

National Water Information System (NWIS), US Geological Survey. http://waterdata.usgs.gov/nwis/gw.

National Water Quality Monitoring Council. Water Quality Portal. http://waterqualitydata.us

South Florida Water Management District's environmental database (DBHYDRO). http://my.sfwmd.gov/dbhydroplsql.

South Florida Water Management District, 2005. *Documentation of the South Florida Water Management Model, Version 5.5*. Available from http://www.sfwmd.gov/portal/page/portal/xrepository/sfwmd_repository_pdf/sfwmm_final_121605.pdf.

South Florida Water Management District and U.S.Army Corps of Engineers. 2008. *Aquifer Storage & Recovery Program Interim Report.* Available from http://www.evergladesplan.org/pm/projects/project_docs/pdp_asr_combined/052808_asr_report/052808_asr_interim_rpt.pdf

U.S. Army Corps of Engineers and the South Florida Water Management District, 1999. *Central & South Florida Projects, Comprehensive Review Study. Final Integrated Feasibility Report and Programmatic Environmental Impact Statement.* Report signed by Congress, April 1999, 4033 p.

U.S. Army Corps of Engineers, Philadelphia District (NAP), 2006. *Draft ASR Regional Study Phase I – Groundwater Modeling.* Available at http://www.evergladesplan.org/pm/projects/project_docs/pdp_asr_combined/021908_asr_draft_phase1_gw_rpt.pdf.

U.S. Army Corps of Engineers, Philadelphia District (NAP), 2011. *Final Groundwater Model Calibration Report – Aquifer Storage and Recovery Regional Modeling Study.* Available at http://www.evergladesplan.org/pm/projects/pdp_32_33_34_44_asr_combined.aspx.

U.S. Army Corps of Engineers, Jacksonville District (SAJ), in review. *Lake Okeechobee ASR Pilot Project Technical Data Report.*

U.S. Army Corps of Engineers, Jacksonville District (SAJ) and South Florida Water Management District (SFWMD). 2003. *Project Management Plan, Aquifer Storage and Recovery Regional Study.* Available at http://www.evergladesplan.org/pm/pmp/pmp_44_regional.aspx.

U.S. Environmental Protection Agency (EPA). 2000. *Guidance for Data Quality Assessment, Practical Methods for Data Analysis.* EPA QA/G-9, QA00 Update.

U.S. Geological Survey Florida Water Science Center. *Historical Water-Use in Florida – Counties*. http://fl.water.usgs.gov/infodata/wateruse/counties.html.

Winsberg, M.D. *Long-Term Precipitation Data.* Florida Climate Center, Office of the State Climatologist. http://climatecenter.fsu.edu/products-services/data. Accessed 11/15/11.

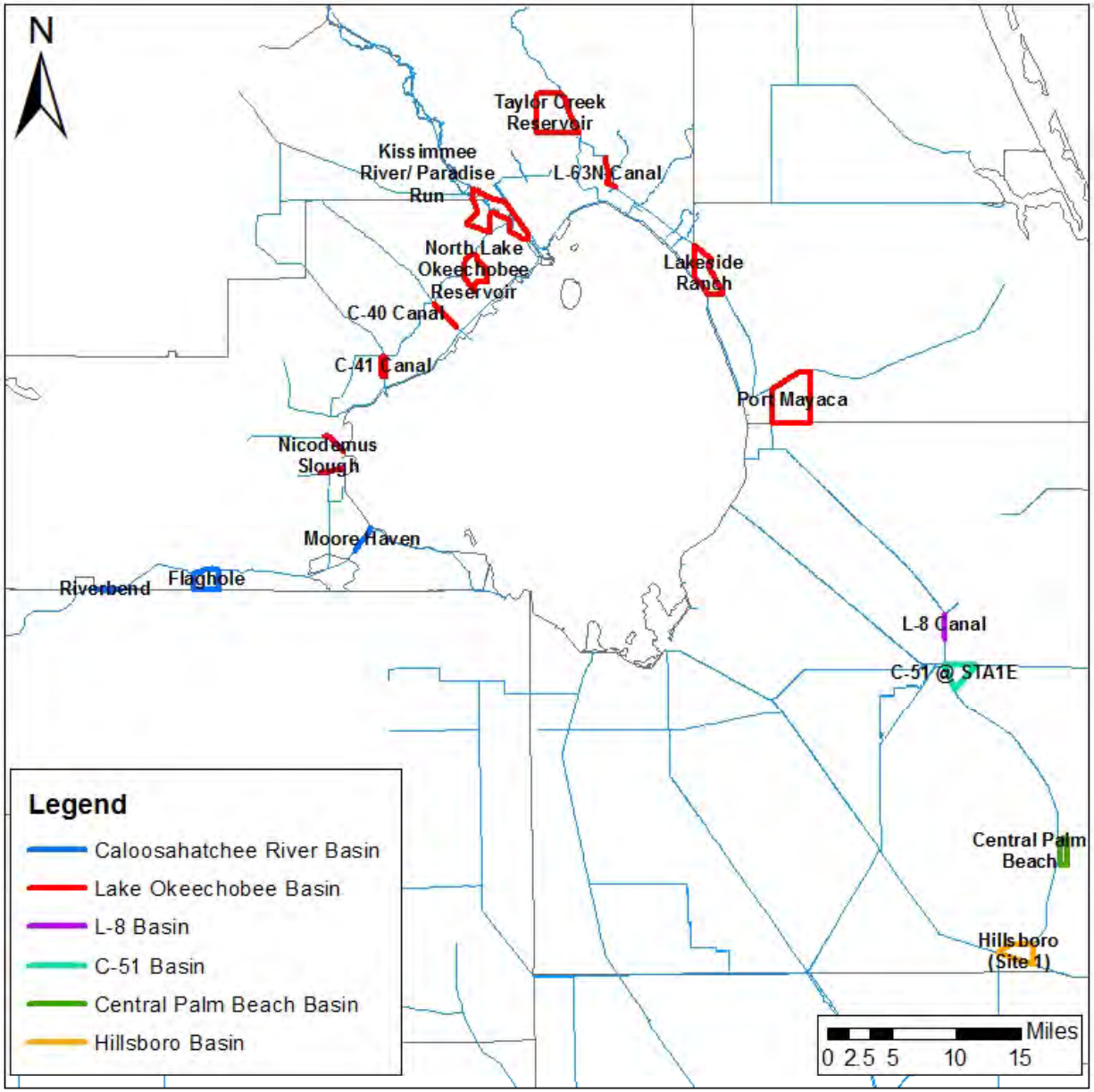

Notes:

The SFWMM-D13R design for the CERP ASR plan divides the system into 6 basins and assigns flows to each basin. The proposed distribution of ASR wells among the basins is shown in the table below.

The CERP ASR Regional Study PDT developed a suite of proposed ASR sites which were selected to be close to water sources and near plots of land owned by SFWMD. The wells for each basin were then parsed out to each of the proposed sites based on the size of property at each site.

Number of CERP D13R ASR Wells Planned for Each Basin	
Caloosahatchee River	44
Lake Okeechobee	200
L-8	10
C-51	34
Central Palm Beach	15
Hillsboro	30
Total	**333**

D13R Basin Locations and Proposed ASR Sites

Regional Model Production Scenario Report

Figure 1.1

June 2013

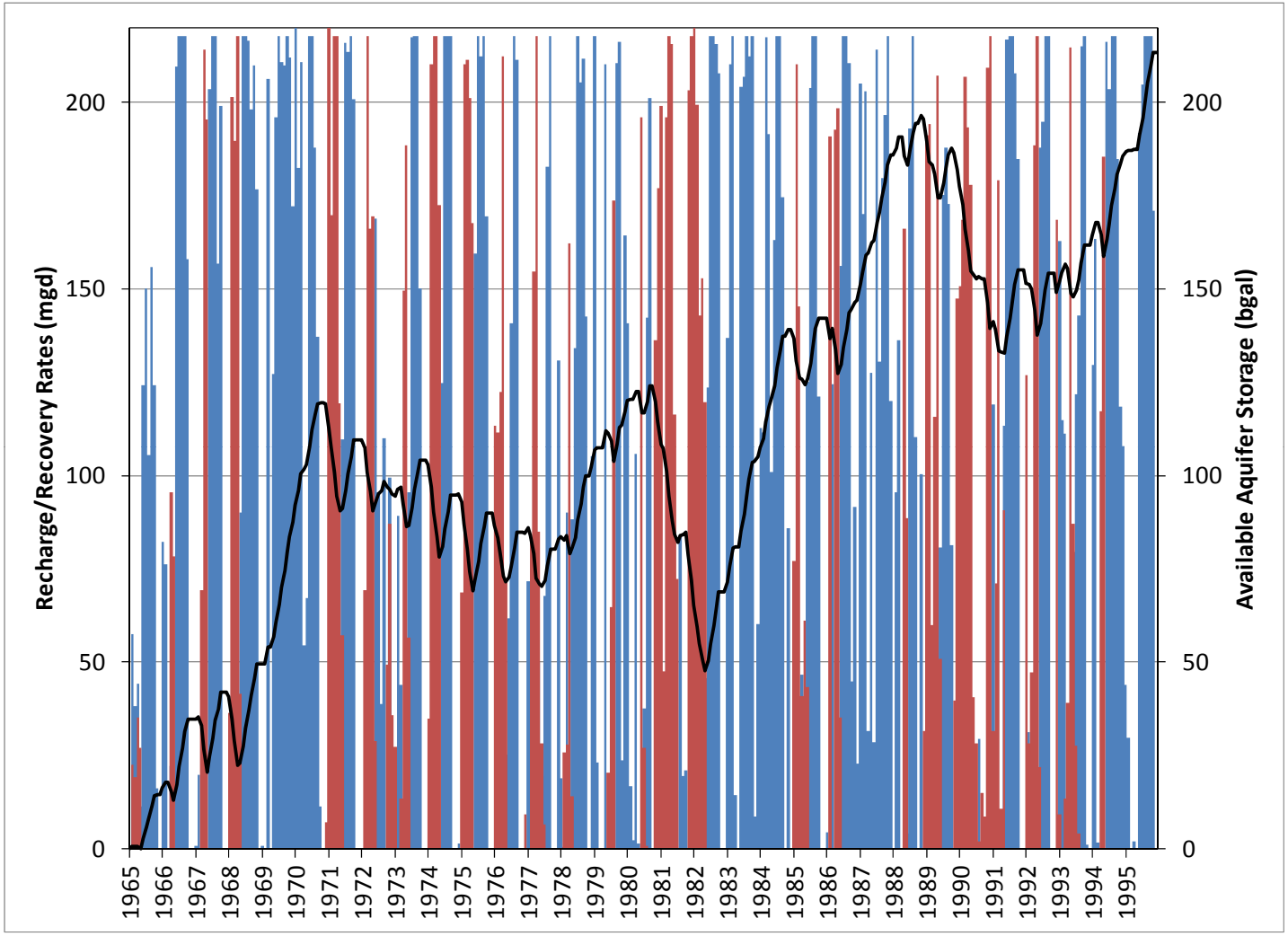

Legend

- Recharge (Injection)
- Recovery (Extraction)
- Aquifer Storage (right axis)

Notes:

This figure shows the ASR flow rates defined by the SFWMM-D13R scenario for the Caloosahatchee River Basin.

Blue and red bars indicate monthly flow rates in mgd (see left axis).

The black line indicates the available storage volume (in billion gallons) in the aquifer assuming 70% recovery efficiency (see right axis). This line is calculated by cumulatively adding 70% of recharge volumes and subtracting recovery volumes. In the SFWMM-D13R scenario, extraction was not allowed if this volume was less than or equal to zero.

Note that the RASRSM-D13R scenarios used 10-day averages of daily flow rates, not the monthly averages shown here.

The maximum flow rate in this basin is 220 mgd. Since each ASR well is to have a 5 mgd capacity, there are 44 ASR wells assigned to this basin.

CALOOSAHATCHEE RIVER BASIN
SFWMM-D13R ASR PUMPING RATES

REGIONAL MODEL PRODUCTION SCENARIO REPORT

FIGURE 2.1

JUNE 2013

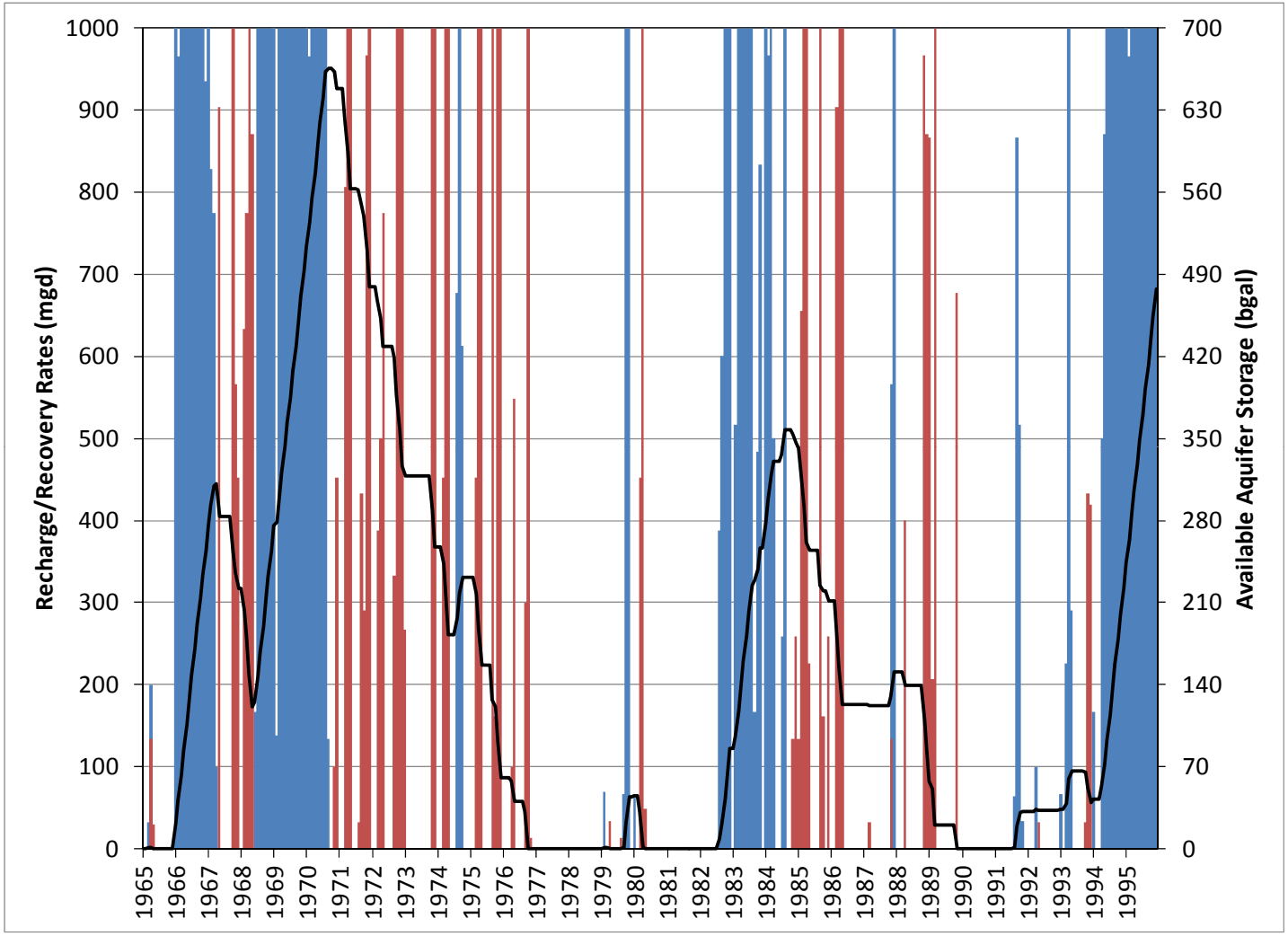

Legend

- Recharge (Injection)
- Recovery (Extraction)
- Aquifer Storage (right axis)

Notes:

This figure shows the ASR flow rates defined by the SFWMM-D13R scenario for the Lake Okeechobee Basin.

Blue and red bars indicate monthly flow rates in mgd (see left axis).

The black line indicates the available storage volume (in billion gallons) in the aquifer assuming 70% recovery efficiency (see right axis). This line is calculated by cumulatively adding 70% of recharge volumes and subtracting recovery volumes. In the SFWMM-D13R scenario, extraction was not allowed if this volume was less than or equal to zero.

Note that the RASRSM-D13R scenarios used 10-day averages of daily flow rates, not the monthly averages shown here.

The maximum flow rate in this basin is 1000 mgd. Since each ASR well is to have a 5 mgd capacity, there are 200 ASR wells assigned to this basin.

Lake Okeechobee Basin
SFWMM-D13R ASR Pumping Rates

Regional Model Production Scenario Report

Figure 2.2

June 2013

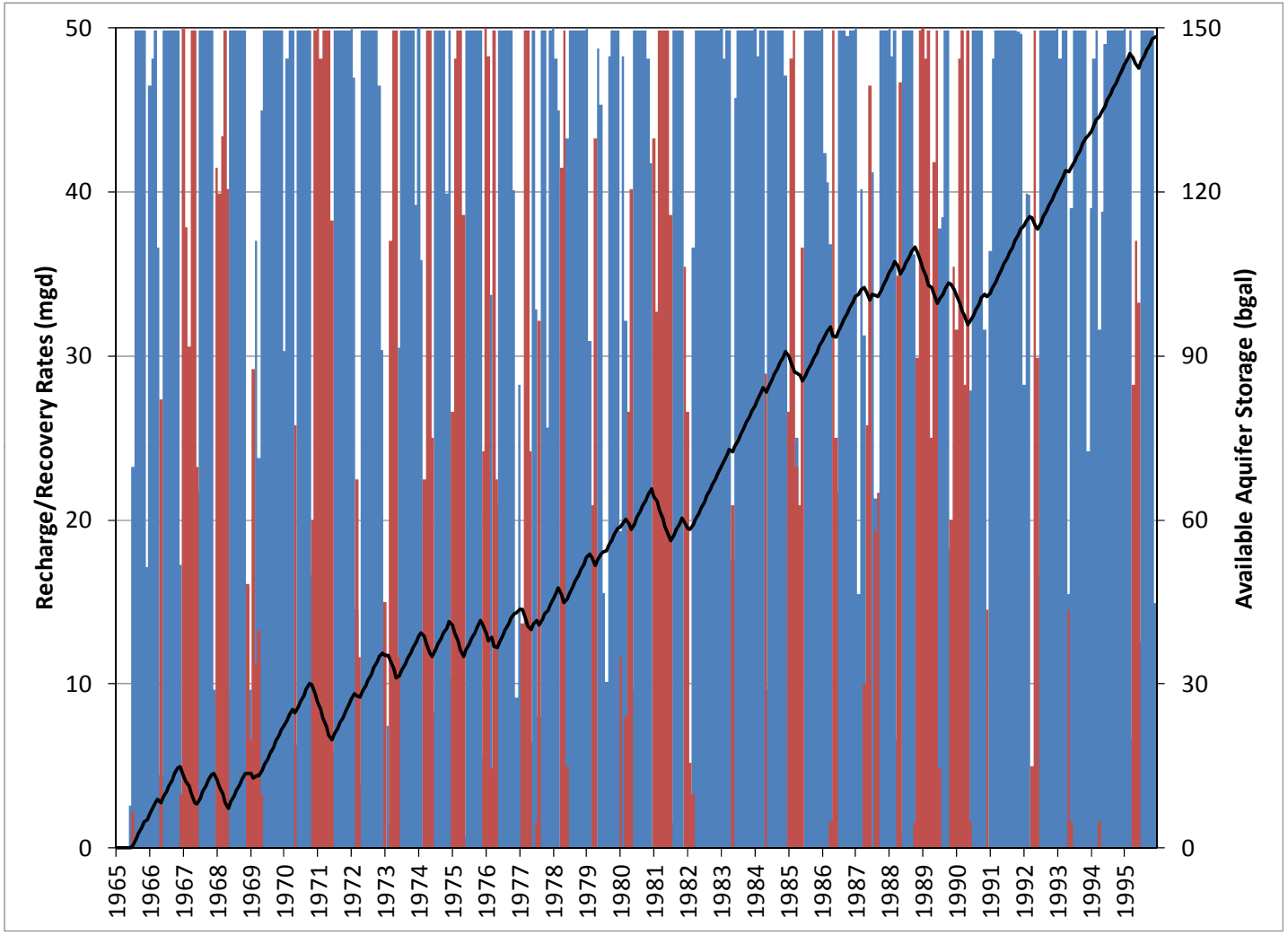

Legend

- Recharge (Injection)
- Recovery (Extraction)
- Aquifer Storage (right axis)

Notes:

This figure shows the ASR flow rates defined by the SFWMM-D13R scenario for the L-8 Basin.

Blue and red bars indicate monthly flow rates in mgd (see left axis).

The black line indicates the available storage volume (in billion gallons) in the aquifer assuming 70% recovery efficiency (see right axis). This line is calculated by cumulatively adding 70% of recharge volumes and subtracting recovery volumes. In the SFWMM-D13R scenario, extraction was not allowed if this volume was less than or equal to zero.

Note that the RASRSM-D13R scenarios used 10-day averages of daily flow rates, not the monthly averages shown here.

The maximum flow rate in this basin is 50 mgd. Since each ASR well is to have a 5 mgd capacity, there are 10 ASR wells assigned to this basin.

L-8 BASIN
SFWMM-D13R ASR PUMPING RATES
REGIONAL MODEL PRODUCTION SCENARIO REPORT

FIGURE 2.3

JUNE 2013

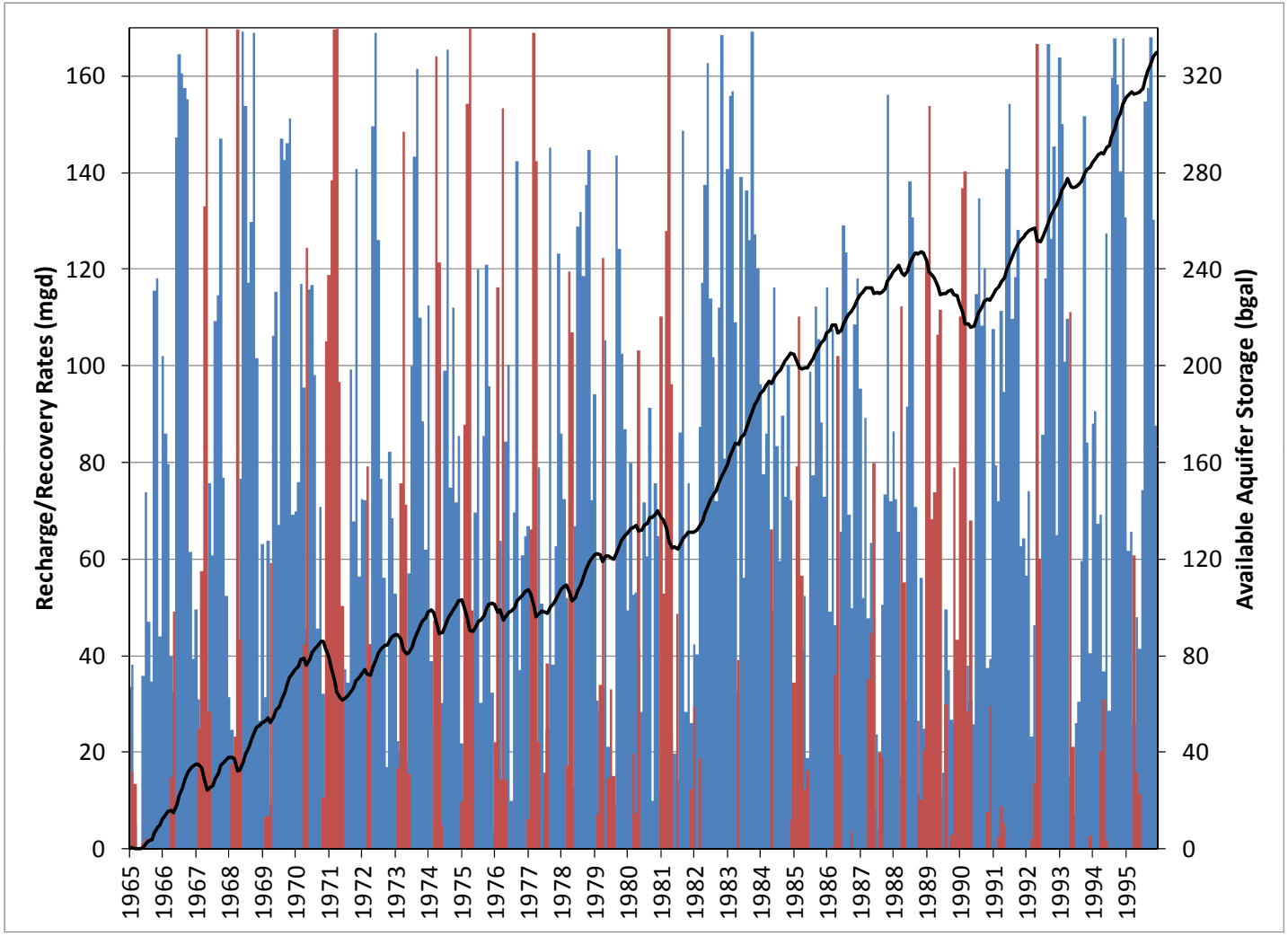

Legend

- Recharge (Injection)
- Recovery (Extraction)
- Aquifer Storage (right axis)

Notes:

This figure shows the ASR flow rates defined by the SFWMM-D13R scenario for the C-51 (STA1E) Basin.

Blue and red bars indicate monthly flow rates in mgd (see left axis).

The black line indicates the available storage volume (in billion gallons) in the aquifer assuming 70% recovery efficiency (see right axis). This line is calculated by cumulatively adding 70% of recharge volumes and subtracting recovery volumes. In the SFWMM-D13R scenario, extraction was not allowed if this volume was less than or equal to zero.

Note that the RASRSM-D13R scenarios used 10-day averages of daily flow rates, not the monthly averages shown here.

The maximum flow rate in this basin is 170 mgd. Since each ASR well is to have a 5 mgd capacity, there are 34 ASR wells assigned to this basin.

C-51 Basin (at STA1E)
SFWMM-D13R ASR Pumping Rates

Regional Model Production Scenario Report

Figure 2.4

June 2013

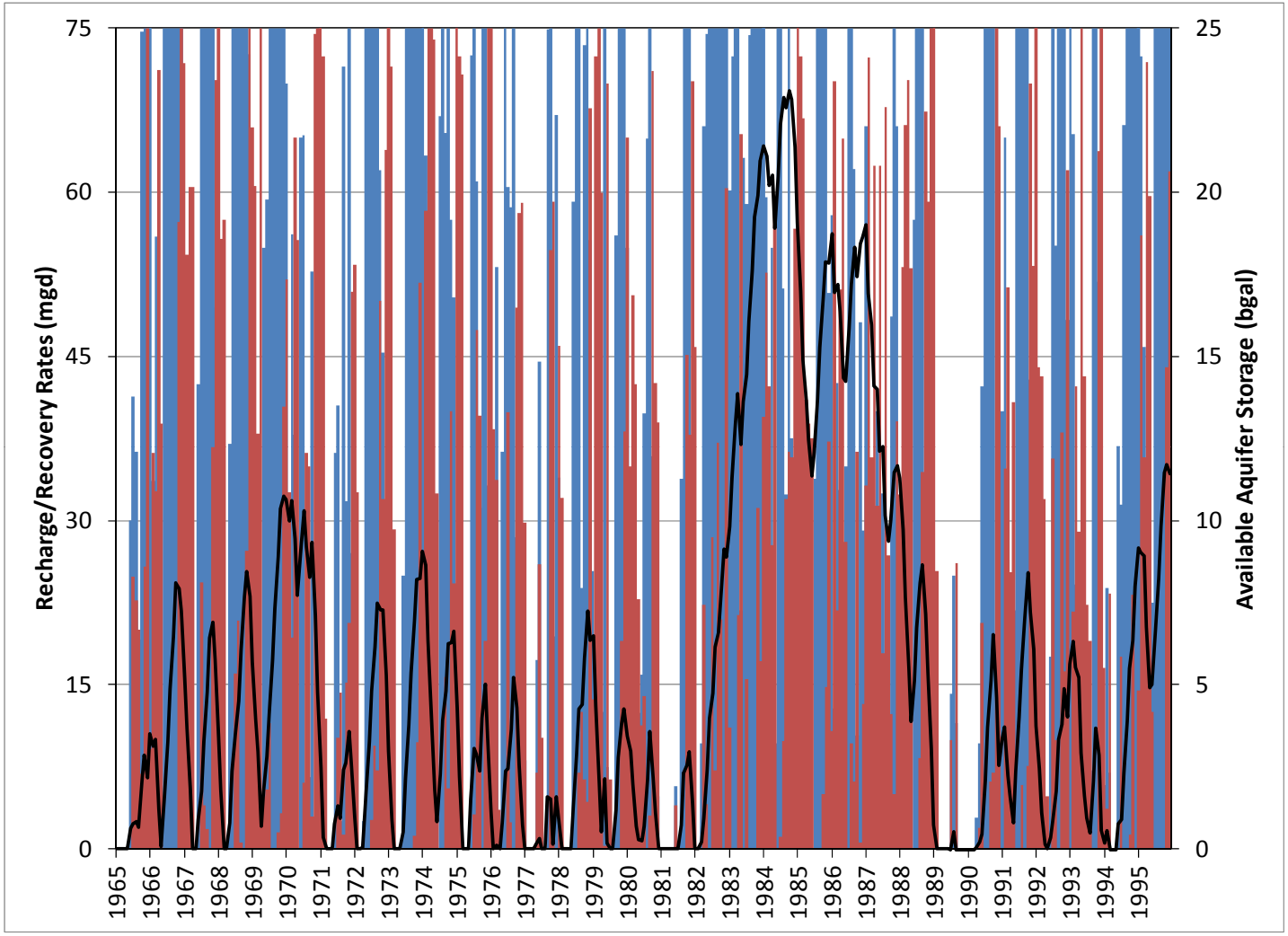

Legend

- Recharge (Injection)
- Recovery (Extraction)
- Aquifer Storage (right axis)

Notes:

This figure shows the ASR flow rates defined by the SFWMM-D13R scenario for the Central Palm Beach Basin.

Blue and red bars indicate monthly flow rates in mgd (see left axis).

The black line indicates the available storage volume (in billion gallons) in the aquifer assuming 70% recovery efficiency (see right axis). This line is calculated by cumulatively adding 70% of recharge volumes and subtracting recovery volumes. In the SFWMM-D13R scenario, extraction was not allowed if this volume was less than or equal to zero.

Note that the RASRSM-D13R scenarios used 10-day averages of daily flow rates, not the monthly averages shown here.

The maximum flow rate in this basin is 75 mgd. Since each ASR well is to have a 5 mgd capacity, there are 15 ASR wells assigned to this basin.

CENTRAL PALM BEACH BASIN
SFWMM-D13R ASR PUMPING RATES

REGIONAL MODEL PRODUCTION SCENARIO REPORT

FIGURE 2.5

JUNE 2013

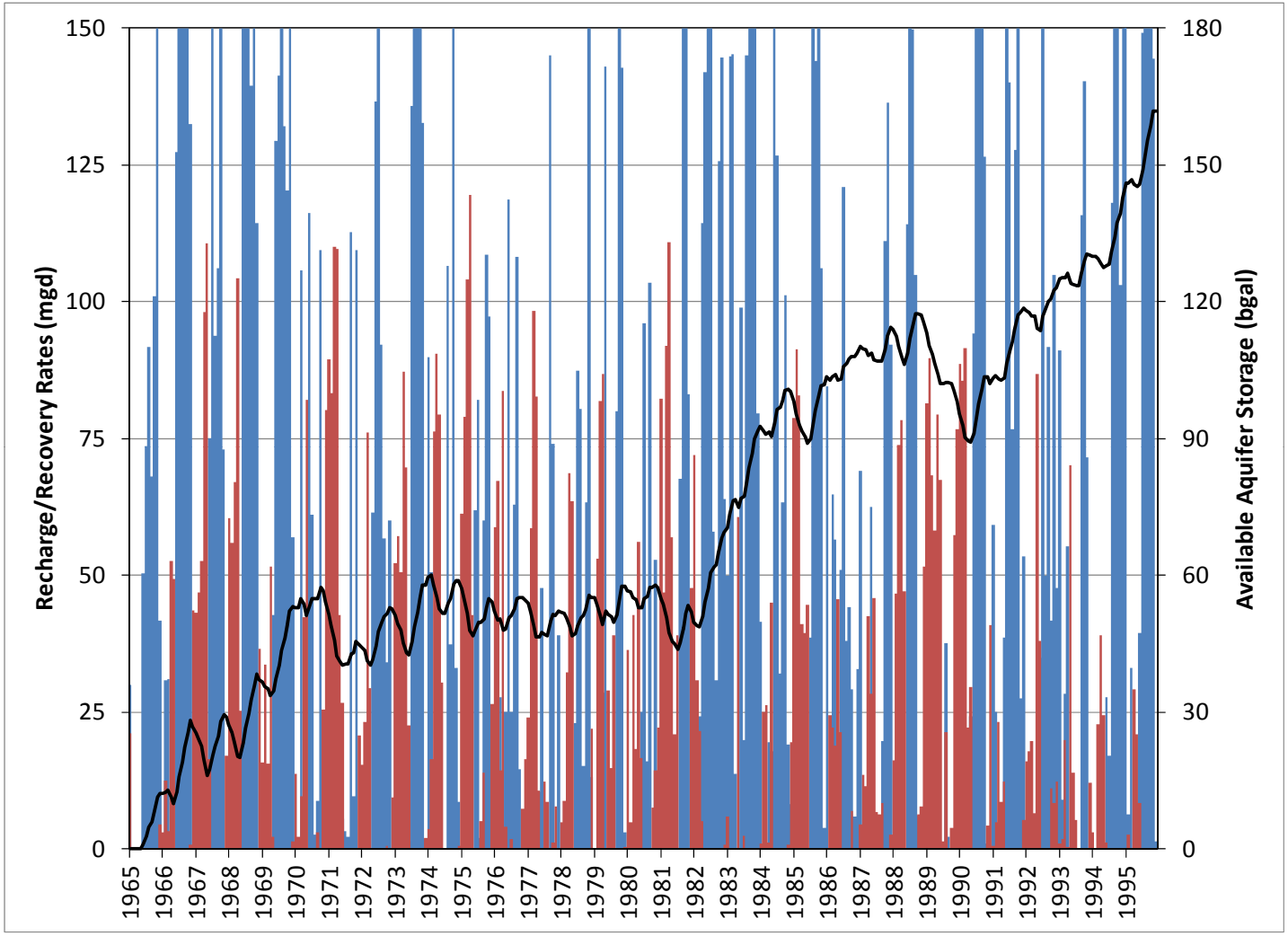

Legend

- Recharge (Injection)
- Recovery (Extraction)
- Aquifer Storage (right axis)

Notes:

This figure shows the ASR flow rates defined by the SFWMM-D13R scenario for the Hillsboro (Site 1) Basin.

Blue and red bars indicate monthly flow rates in mgd (see left axis).

The black line indicates the available storage volume (in billion gallons) in the aquifer assuming 70% recovery efficiency (see right axis). This line is calculated by cumulatively adding 70% of recharge volumes and subtracting recovery volumes. In the SFWMM-D13R scenario, extraction was not allowed if this volume was less than or equal to zero.

Note that the RASRSM-D13R scenarios used 10-day averages of daily flow rates, not the monthly averages shown here.

The maximum flow rate in this basin is 150 mgd. Since each ASR well is to have a 5 mgd capacity, there are 30 ASR wells assigned to this basin.

HILLSBORO (SITE 1) BASIN
SFWMM-D13R ASR PUMPING RATES

REGIONAL MODEL PRODUCTION SCENARIO REPORT

FIGURE 2.6

JUNE 2013

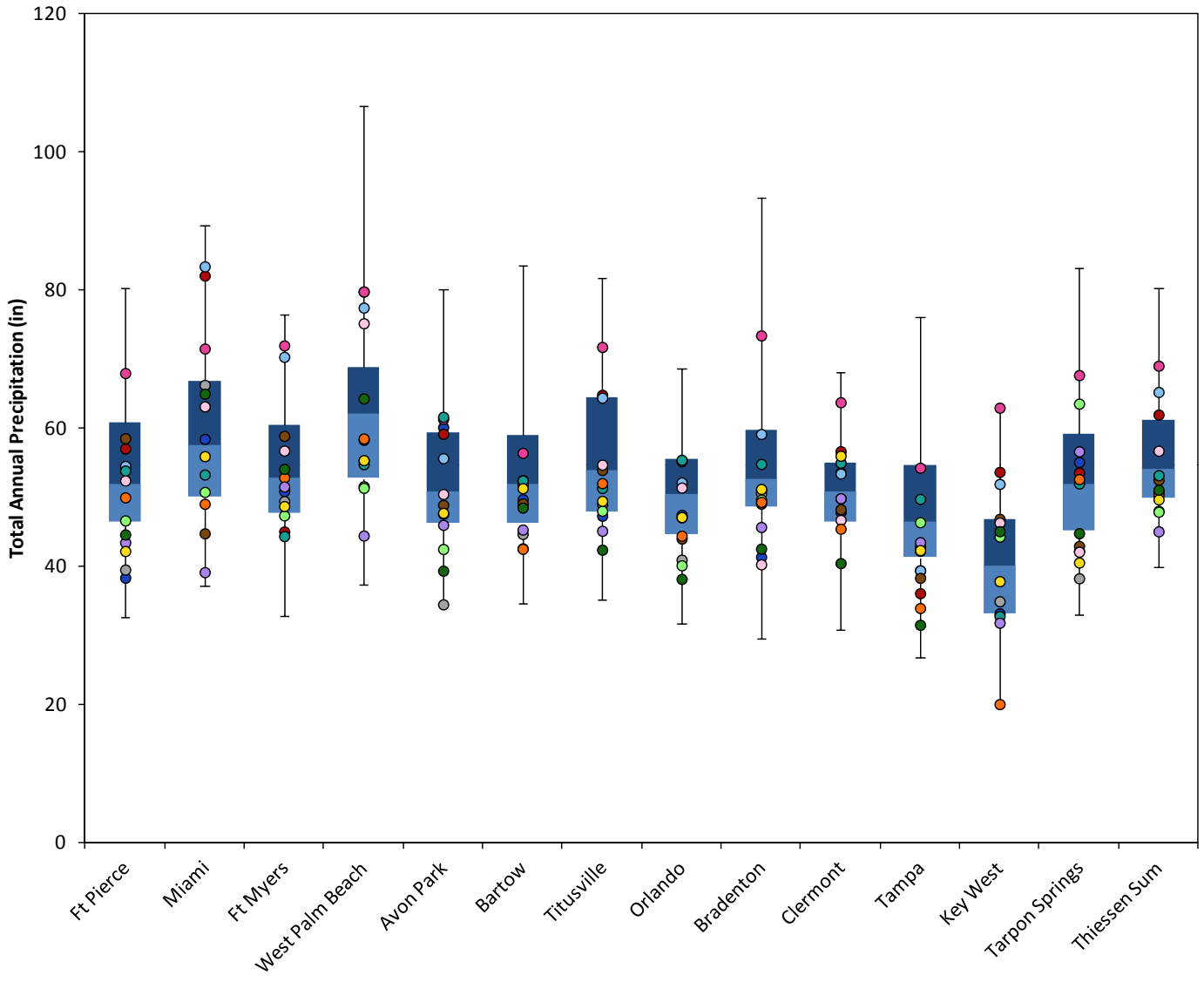

Legend

- Maximum
- Upper Quartile
- Median
- Lower Quartile
- Minimum

(1929-1999)

- 1965
- 1966
- 1967
- 1968
- 1969
- 1970
- 1971
- 1972
- 1973
- 1974
- 1975
- 1976
- 1977

Notes:

This figure compares total annual precipitation for the years of the RASRSM-D13R scenario (1965-1977) to the distribution of data for the period 1929-1999. The data for the D13R scenario are well spread across the range of data for the larger period. There are wet and dry years represented in the D13R scenario period.

The Thiessen Sum was calculated by constructing Thiessen polygons for each site and clipping them to the model boundaries. The percentage area represented by each polygon was computed and applied to the annual precipitation to obtain an area-weighted sum of all precipitation in the model area. Polygons for Tarpon Springs and Key West did not intersect the model area and were given a weight of 0% resulting in no impact to the Thiessen Sum.

Precipitation data source: Winsberg, 2011

COMPARISON OF 1965-1977 PRECIPITATION TO 1929-1999 STATISTICS

REGIONAL MODEL PRODUCTION SCENARIO REPORT

FIGURE 2.7

JUNE 2013

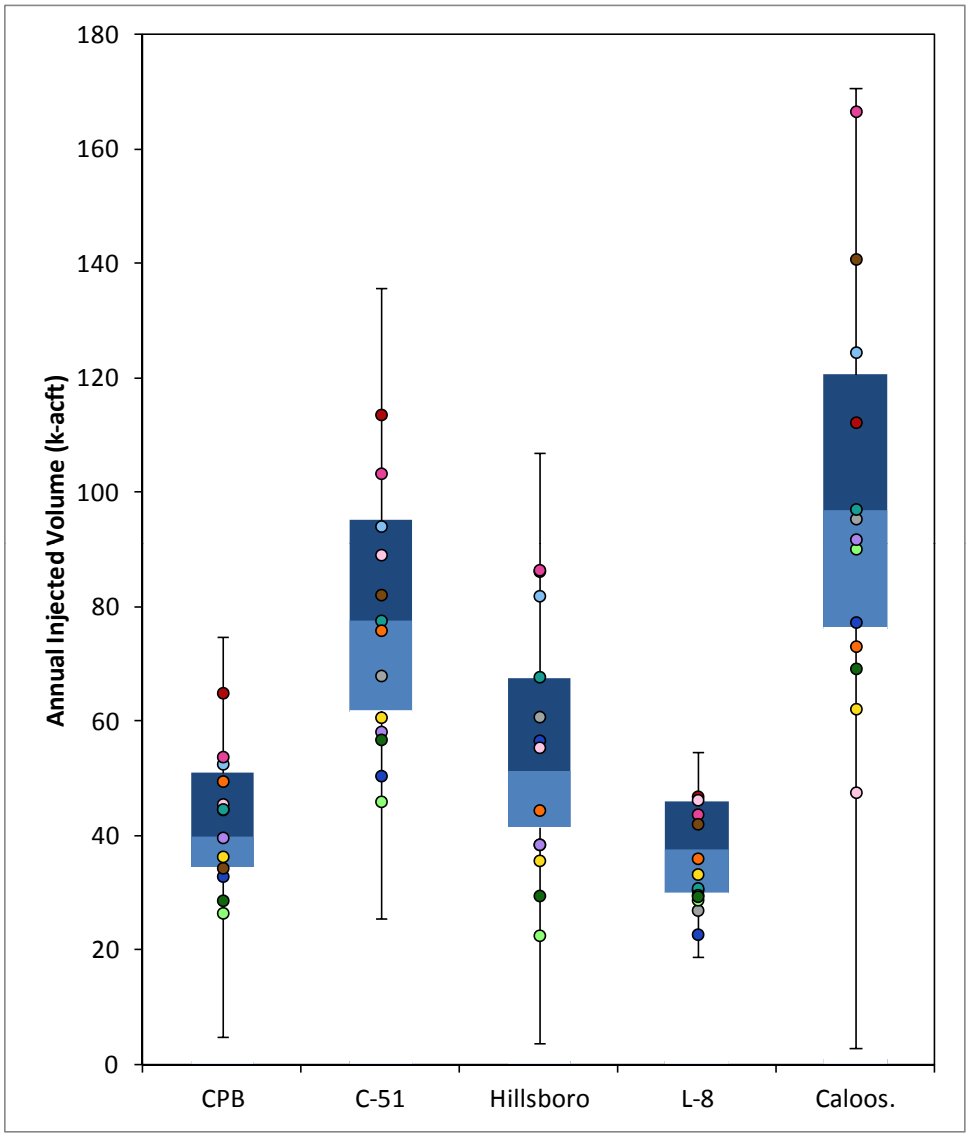

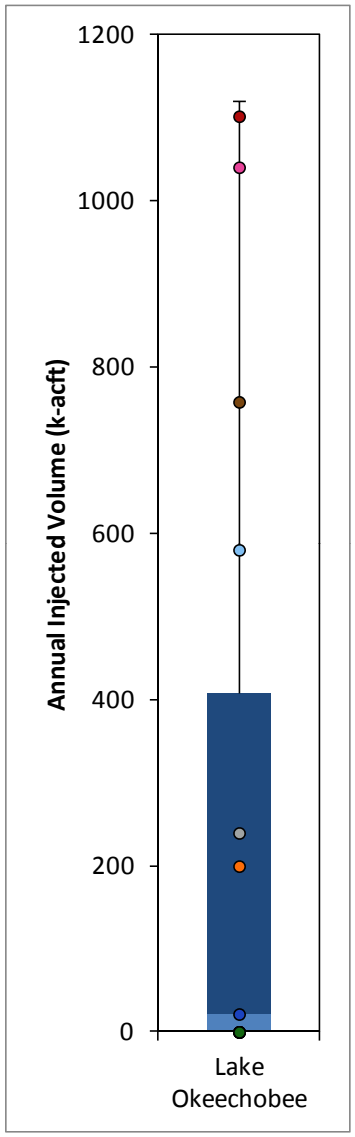

Legend

- Maximum
- Upper Quartile
- Median
- Lower Quartile
- Minimum

1965-1995

1965	1972
1966	1973
1967	1974
1968	1975
1969	1976
1970	1977
1971	

Notes:

This figure compares total annual ASR injection volumes for the years of the RASRSM-D13R scenario (1965-1977) to the distribution of annual ASR injection volumes for the SFWMM-D13R scenario for the period 1965-1995. The data for RASRSM are well spread across the range of data for the larger period. There are years of high and low injection volumes represented in the RASRSM period.

Comparison of 1965-1977 D13R Annual Injection Volumes to 1965-1995 D13R Annual Injection Volume Statistics

Regional Model Production Scenario Report

Figure 2.8

June 2013

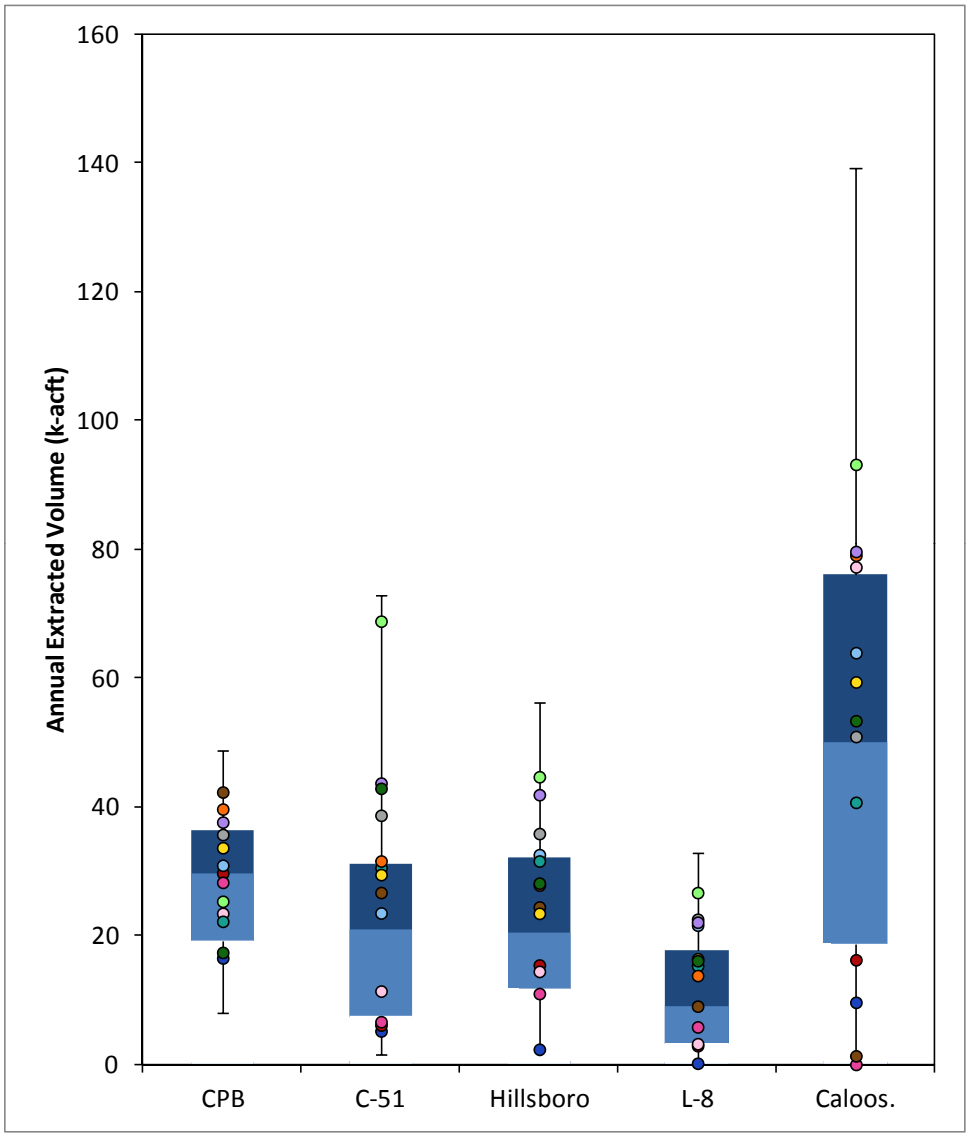

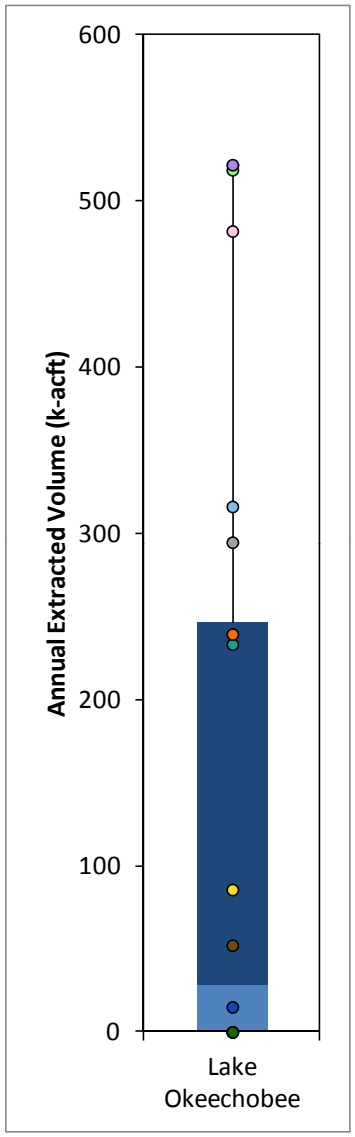

Legend

- Maximum
- Upper Quartile
- Median
- Lower Quartile
- Minimum

1965-1995

- 1965
- 1966
- 1967
- 1968
- 1969
- 1970
- 1971
- 1972
- 1973
- 1974
- 1975
- 1976
- 1977

Notes:

This figure compares total annual ASR extraction volumes for the years of the RASRSM-D13R scenario (1965-1977) to the distribution of annual ASR extraction volumes for the SFWMM-D13R scenario for the period 1965-1995. The data for RASRSM are well spread across the range of data for the larger period. There are years of high and low extraction volumes represented in the RASRSM period.

COMPARISON OF 1965-1977 D13R ANNUAL EXTRACTION VOLUMES TO 1965-1995 D13R ANNUAL EXTRACTION VOLUME STATISTICS

REGIONAL MODEL PRODUCTION SCENARIO REPORT

FIGURE 2.9

JUNE 2013

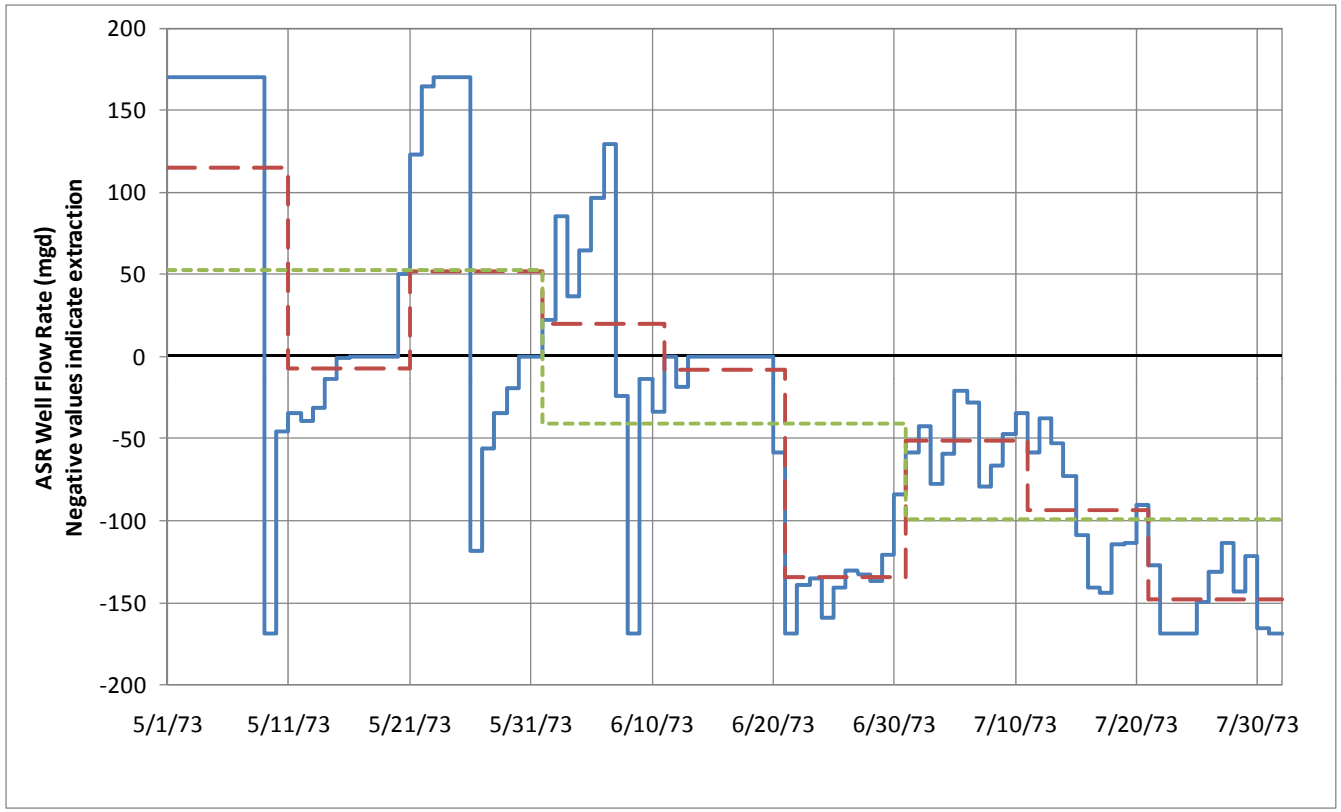

Legend

- Daily Average Flow Rate
- 10-Day Average Flow Rate
- Monthly Average Flow Rate

Notes:

Here, an example of the daily SFWMM-D13R output for ASR pumping (injection and extraction) is shown for a three month period with the 10-day and monthly averaged values superimposed.

The 10-day stress period was selected for this model because it balances the need to incorporate this detailed data with limitations of computer resources and time constraints.

Generally, the 10-day average does a good job of estimating the flow rates when there are not too many switches between injection and extraction.

Calibration Model (RASRSM)

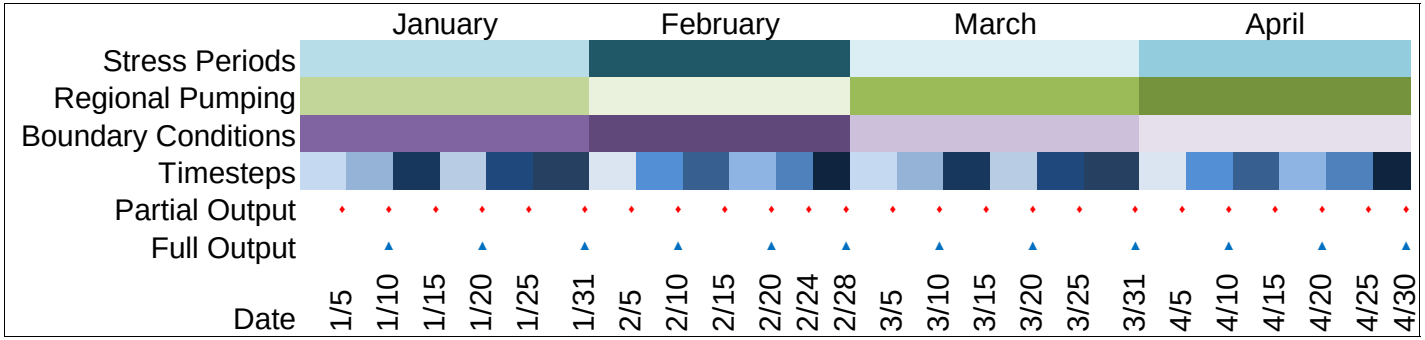

RASRSM-D13R

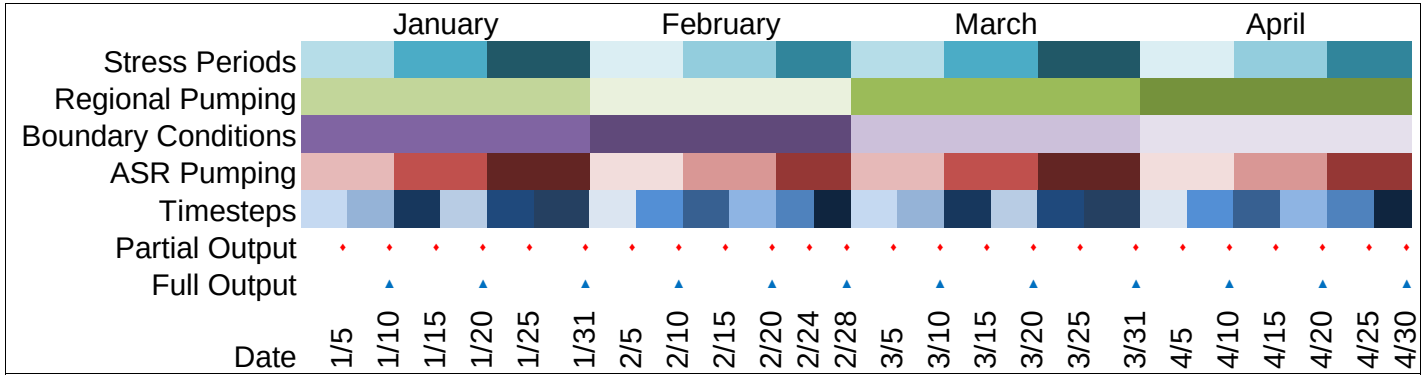

Partial Output: Heads at observation points, TDS at all grid cells
Full Output: Heads, fluxes and TDS at all grid cells

Notes:

These figures indicate, with colored boxes, the lengths of stress periods and time steps for the RASRSM model during calibration and during the D13R runs.

In the calibration model (top figure) stress periods were one month long. Thus, regional pumping and boundary condition heads were averaged over each month and input as step functions. Time steps were 5 days long with full output printed every 10 days.

In the D13R scenarios (lower figure), the daily variation in the ASR pumping was not sufficiently captured by the month-long stress periods. Instead, stress periods of 10 days were implemented and the ASR pumping was averaged over each 10-day period. In order to make use of the boundary condition and regional pumping data used in the calibration model, these parameters continued to be averaged over each month and input as month-long step functions. In this model, the 5-day timesteps were retained along with full output every 10 days.

Note that variations in the lengths of the months necessitate slight variations in the lengths of stress periods and time steps. For example, the last stress period and the last two time steps of February are slightly shorter than others since February is a shorter month.

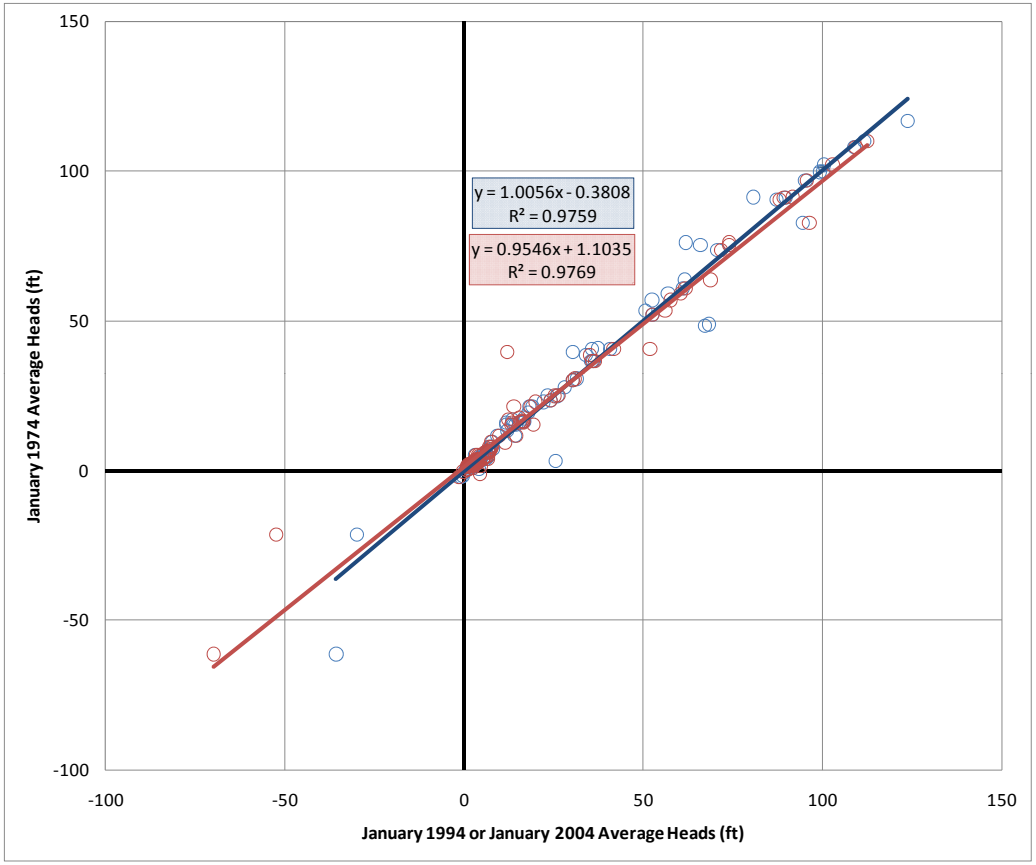

Legend

- 1994/1974 Average Monthly Heads
- 2004/1974 Average Monthly Heads
- 1994/1974 Trendline
- 2004/1974 Trendline

Notes:

A plot like this was used to determine the best way to estimate the specified head boundary condition for the period 1965 to 1977 when very little head data was available.

The available data for the area of the model was compiled and each month was compared to the same month in the calibration and validation periods.

In this example, January 1974 is compared to both January 1994 and January 2004, when boundary conditions have already been developed by interpolation of the available data. In this case, the correlation to 2004 is better, so the equation y=0.95x+1.1 was applied to the January 2004 boundary condition to estimate conditions in January 1974.

This same process was followed for each month of the 13-year period.

Because of sparse data, all available wells with long term data were combined for this analysis, without accounting for aquifer or location.

D13R Boundary Conditions: Correlation Example – January 1974

Regional Model Production Scenario Report

Figure 2.12

June 2013

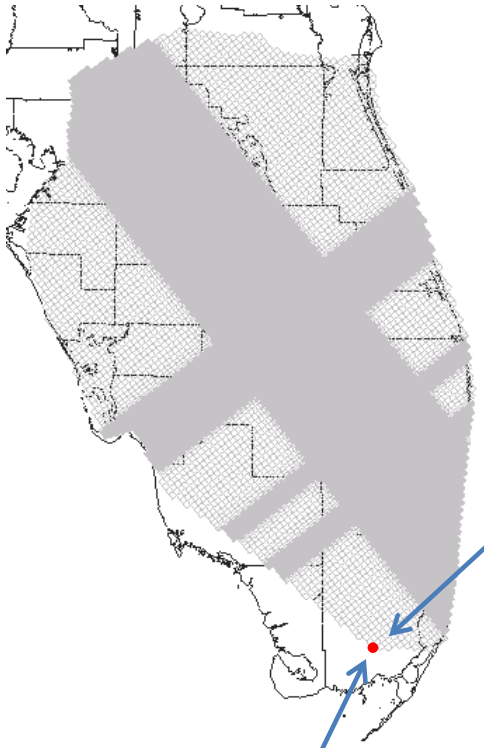

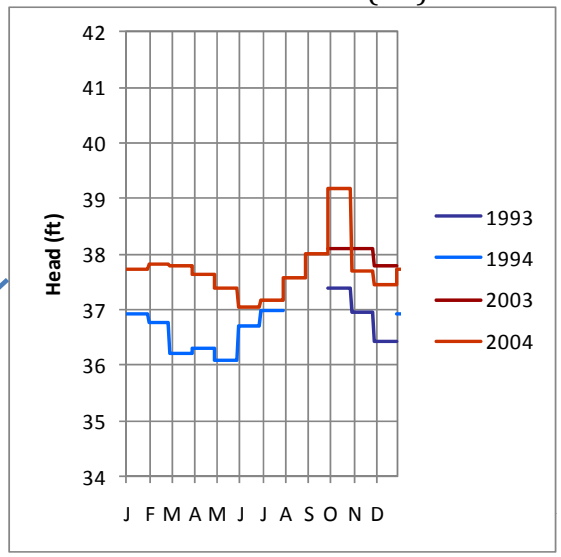

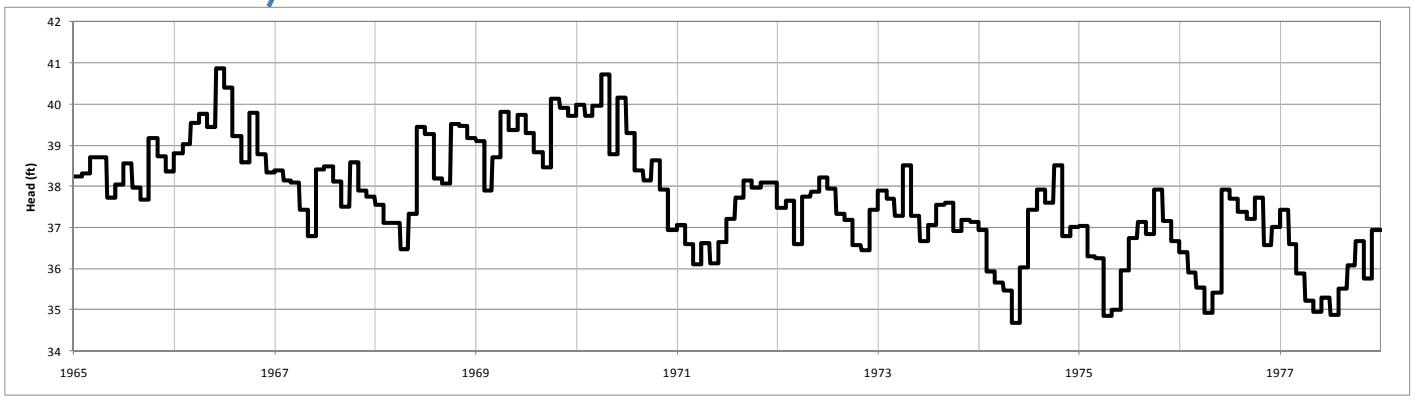

Notes:

The monthly correlations between heads in the RASRSM calibration and validation and the D13R models (see Figure 2.12) were used to estimate the boundary heads between 1965 and 1977 based on the calibration and validation specified heads, which were interpolated from data.

The upper plot shows the boundary conditions applied to the indicated cell for the calibration and validation models. These heads were based on interpolations of available measured head data for the calibration and validation periods (see NAP, 2011).

The lower plot shows the boundary conditions applied to the indicated cell for the RASRSM-D13R. Here, correlations between the heads from periods of calibration and validation and the D13R model period were used to convert the calibration/validation data to estimated head levels during the 1960s and 1970s.

Note that general seasonal trends are retained, but variations are added to reflect wet or dry years

ESTIMATION OF SPECIFIED HEAD BOUNDARY CONDITIONS - EXAMPLE

REGIONAL MODEL PRODUCTION SCENARIO REPORT

FIGURE 2.13

JUNE 2013

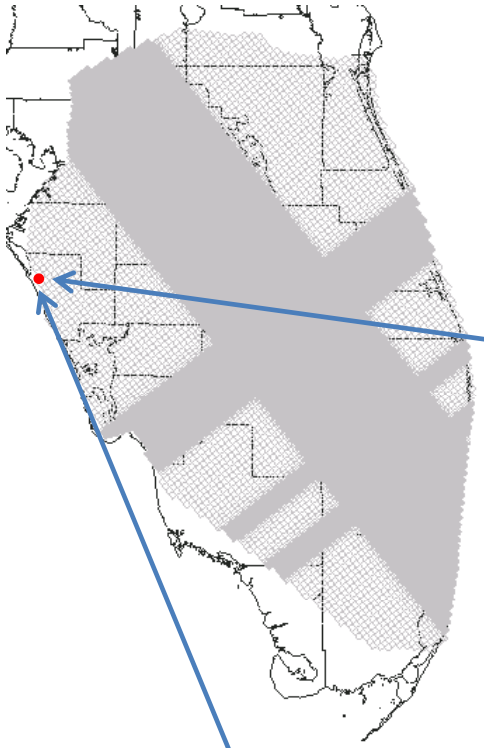

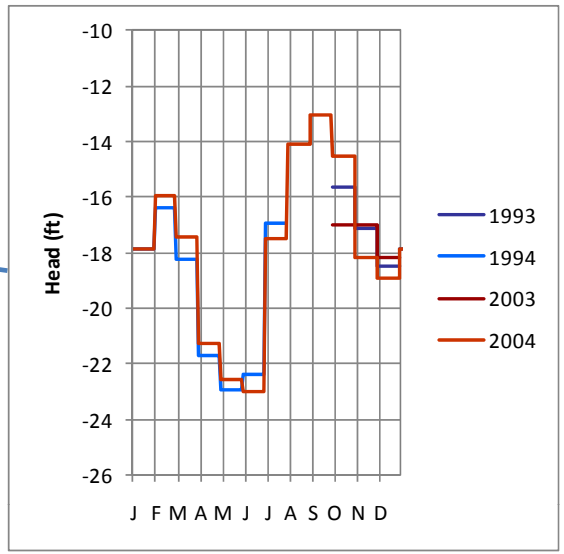

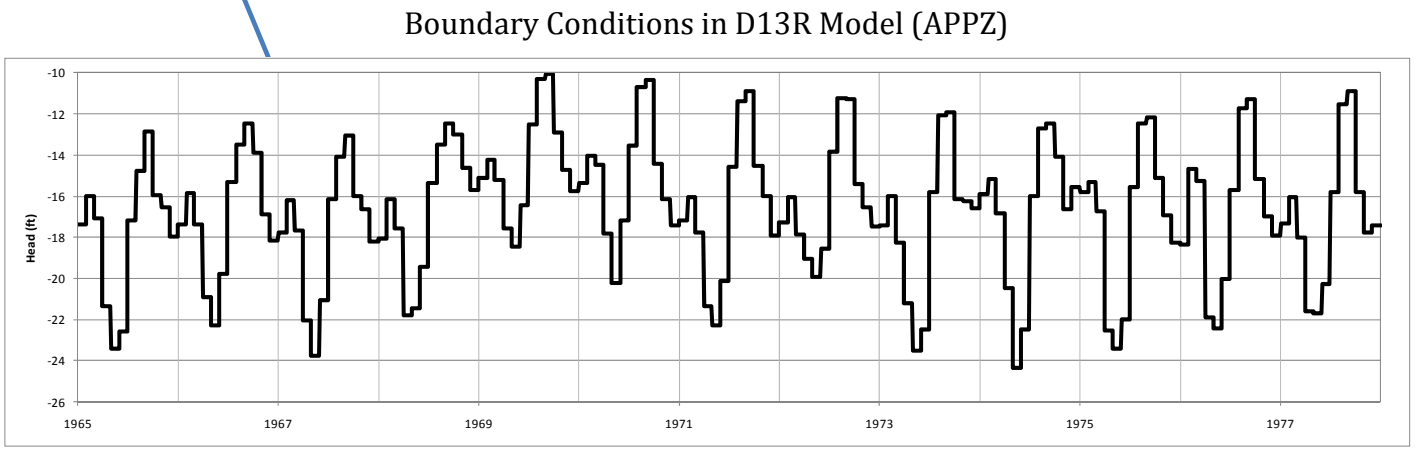

Notes:

The correlations between heads in months of the RASRSM calibration and validation and the D13R models (see Figure 2.12) were used to estimate the boundary heads between 1965 and 1977 based on the calibration and validation specified heads, which were interpolated from data.

The upper plot shows the boundary conditions applied to the indicated cell for the calibration and validation models. These heads were based on interpolations of available measured head data for the calibration and validation periods (see NAP, 2011).

The lower plot shows the boundary conditions applied to the indicated cell for the RASRSM-D13R. Here, correlations between the periods of calibration and validation and the D13R model period were used to convert the interpolated data to estimated head levels during the 1960s and 1970s.

Note that general seasonal trends are retained, but variations are added to reflect wet or dry years

ESTIMATION OF SPECIFIED HEAD BOUNDARY CONDITIONS - EXAMPLE

REGIONAL MODEL PRODUCTION SCENARIO REPORT

FIGURE 2.14

JUNE 2013

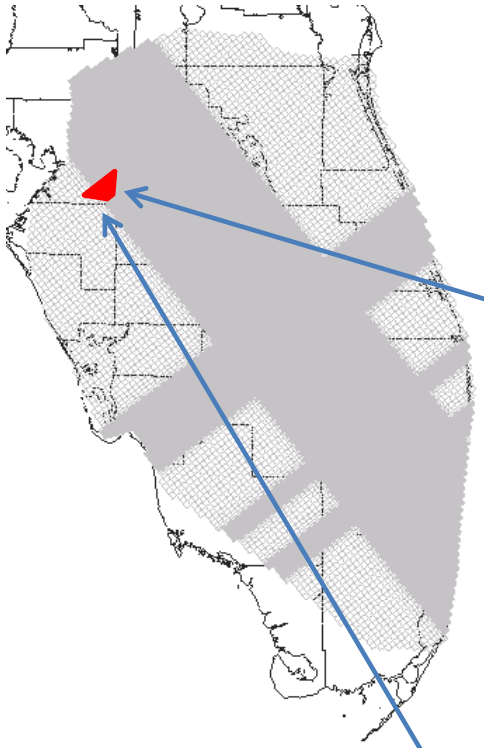

Pumping in Validation Model (UF)

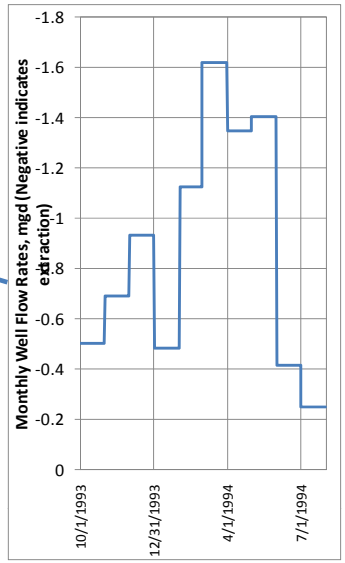

Pumping in D13R Model (UF)

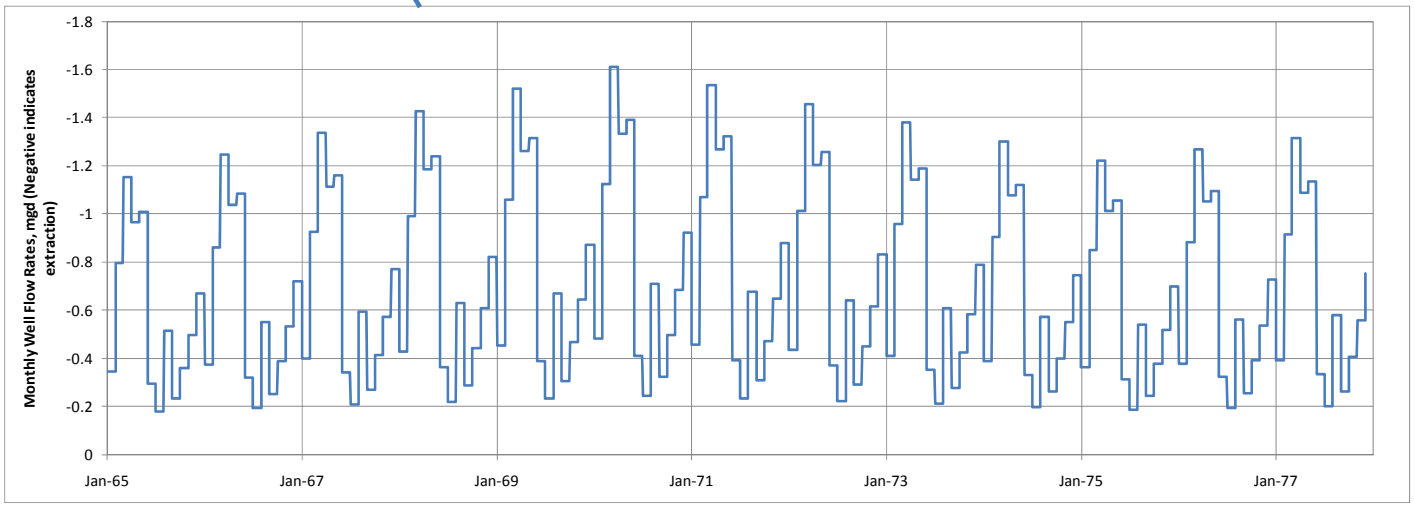

Notes:

The upper plot shows the monthly averaged groundwater extraction for a small section of Hillsborough County used in the RASRSM validation model, which covered the period from October 1993 to September 1994.

The pumping from the validation modeling was used with some long term pumping data provided by the USGS Florida Water Science Center to estimate the groundwater extraction for the RASRSM-D13R model for the period from 1965 to 1977. This result is shown in the lower plot for the same section of Hillsborough County.

Note that general seasonal trends are retained, but variations are added to reflect wet or dry years

ESTIMATION OF REGIONAL PUMPING - EXAMPLE

REGIONAL MODEL PRODUCTION SCENARIO REPORT

FIGURE 2.15

JUNE 2013

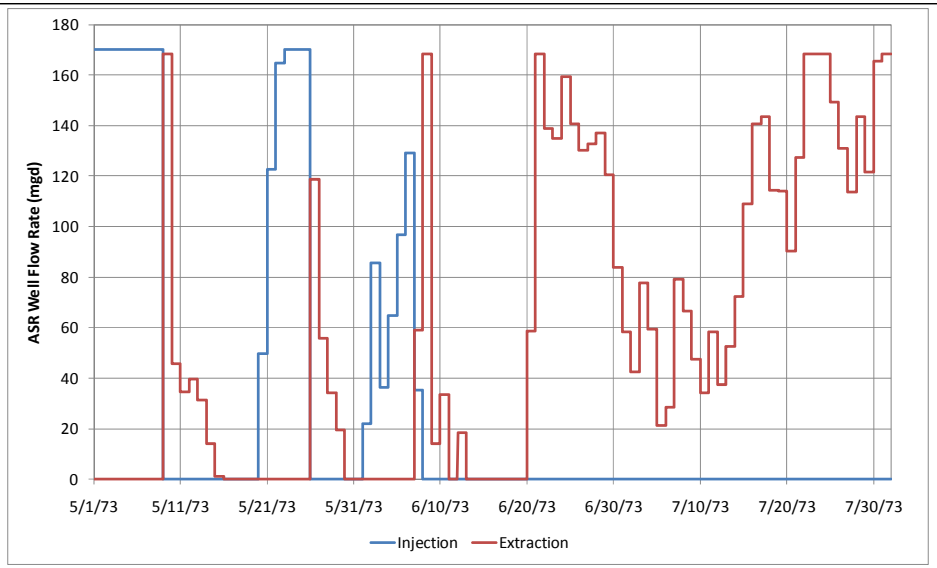

(a)

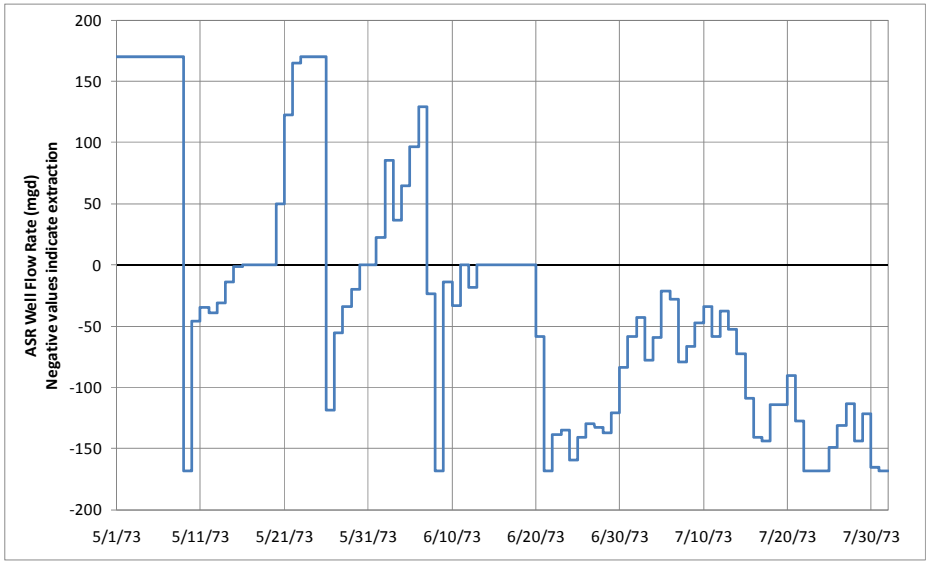

(b)

Notes:

Plot (a) shows the output from SFWMM-D13R for three months at the C-51 ASR basin.

To prepare the data for the regional model, extraction rates were subtracted from injection rates to obtain plot (b), which can be applied to the model.

Notice that on one day (June 7) there is both injection and extraction occurring on the same day.

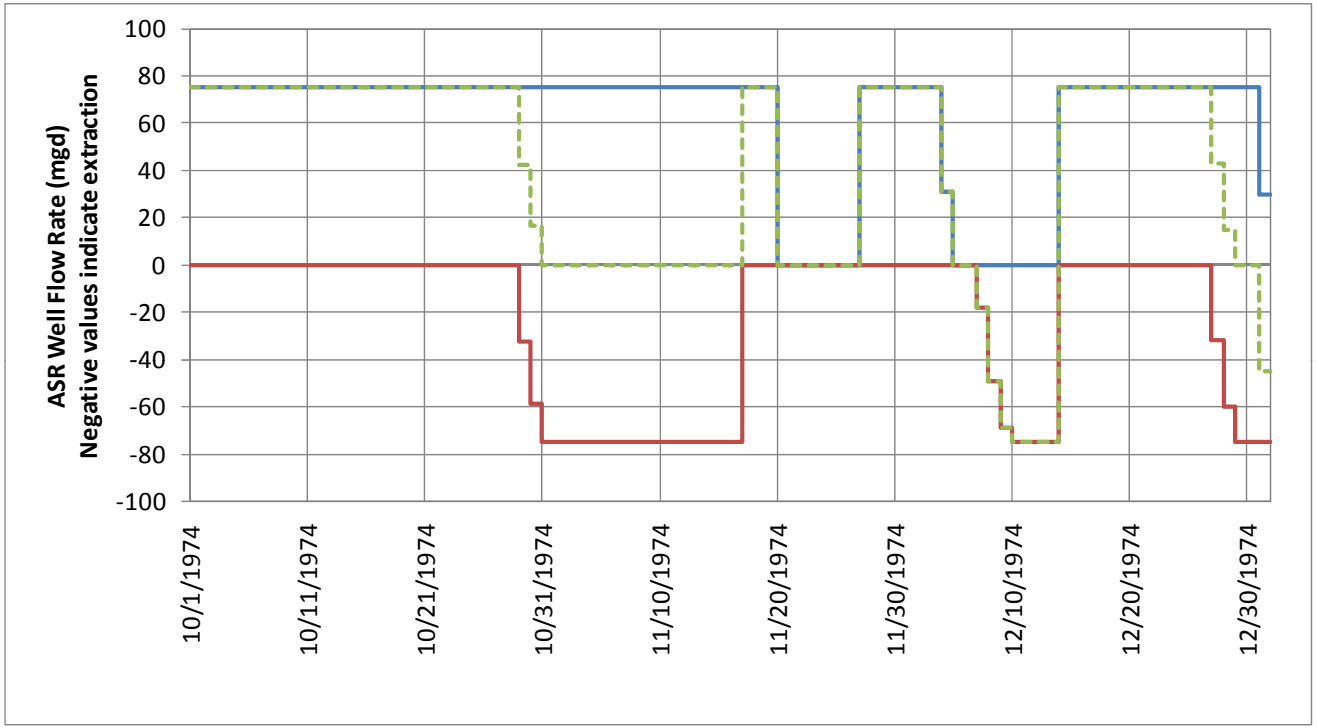

Legend

- Injection Rate (positive)
- Extraction Rate (negative)
- Modeled Rate

Notes:

This plot illustrates the problems caused when an ASR well is injecting and extracting at the same rate in the D13R model output. The plot shows the flow rates for a three-month period in the Central Palm Beach ASR basin.

Between October 31 and November 16, the D13R output shows that all wells in this basin were both injecting and extracting at their full capacity (15 wells at 5mgd each). It is unclear how this would be handled in reality. In the model, this results in a net zero flow rate.

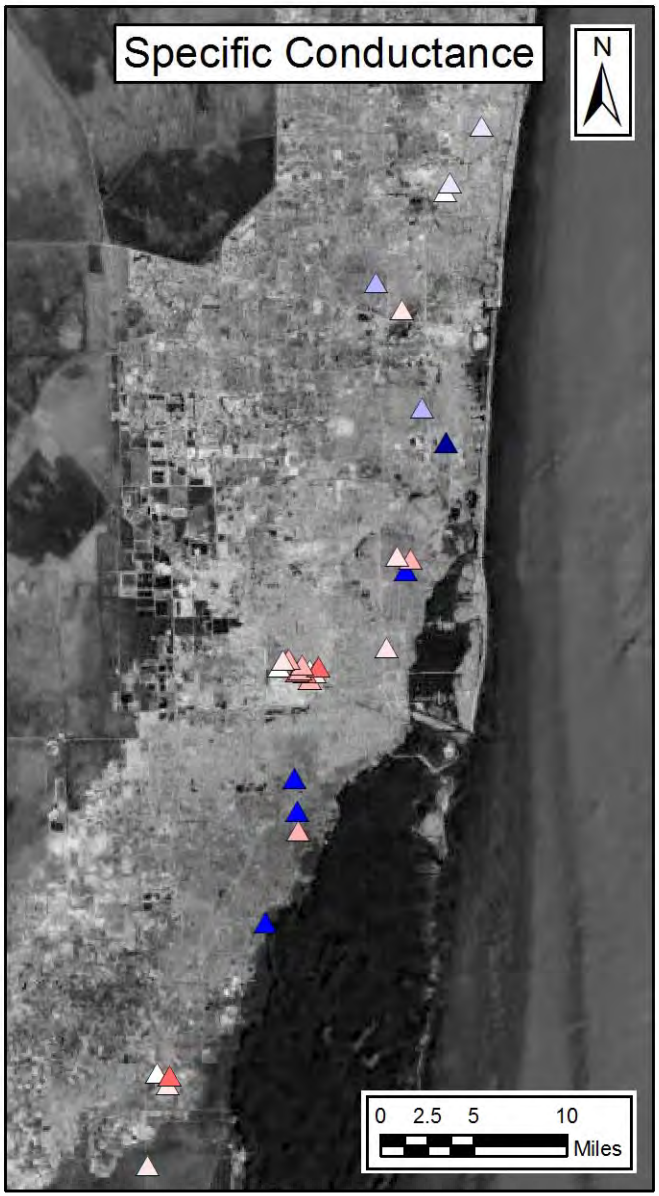

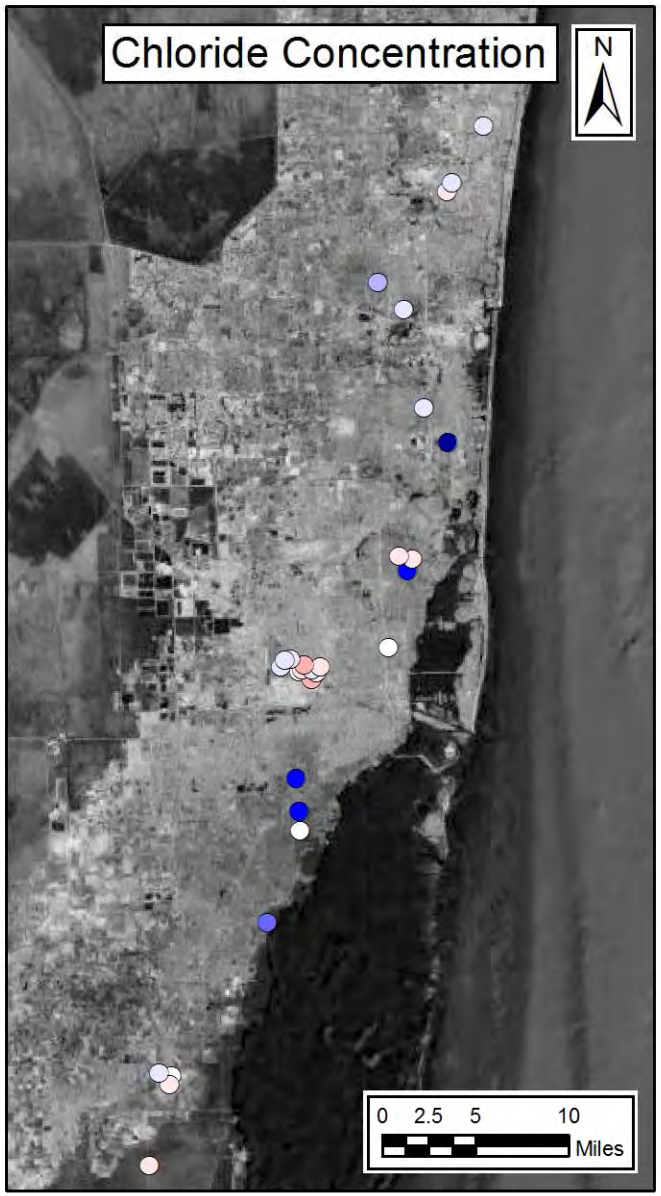

40-year Change as a Percentage of Seawater Characteristics

- No significant slope
- -10% to -5%
- -5% to -1%
- -1% to 0%
- 0% to 1%
- 1% to 5%
- 5% to 10%
- 10% to 50%
- > 50%

Mann Kendall analysis was used to determine if a significant slope (confidence 95%) exists.

Sen's slope analysis was used to calculate the median slope in the data.

The median slope (change per year) was multiplied by 40 and then divided by the seawater value to determine the 40-year change as a percentage of seawater. Negative percentages indicate falling values.

Specific conductance of seawater was assumed to be 50,000 uS/cm. Chloride concentration of seawater was assumed to be 19,400 mg/L.

Data source: www.waterqualitydata.us

Background map source: Google Earth

LONG-TERM SALINITY CHANGES IN BISCAYNE AQUIFER WELLS

REGIONAL MODEL PRODUCTION SCENARIO REPORT

Figure 2.18

June 2013

40-year Change as a Percentage of Seawater Characteristics

- No significant slope
- -10% to -5%
- -5% to -1%
- -1% to 0%
- 0% to 1%
- 1% to 5%
- 5% to 10%
- 10% to 50%
- > 50%

Mann Kendall analysis was used to determine if a significant slope (confidence 95%) exists.

Sen's slope analysis was used to calculate the median slope in the data.

The median slope (change per year) was multiplied by 40 and then divided by the seawater value to determine the 40-year change as a percentage of seawater. Negative percentages indicate falling values.

Specific conductance of seawater was assumed to be 50,000 uS/cm. Chloride concentration of seawater was assumed to be 19,400 mg/L.

Data source: www.waterqualitydata.us

Background map source: Google Earth

LONG-TERM SALINITY CHANGES IN FLORIDAN AQUIFER WELLS

REGIONAL MODEL PRODUCTION SCENARIO REPORT

Figure 2.19

June 2013

40-year Change as a Percentage of Seawater Characteristics

- No significant slope
- -10% to -5%
- -5% to -1%
- -1% to 0%
- 0% to 1%
- 1% to 5%
- 5% to 10%
- 10% to 50%
- > 50%

Mann Kendall analysis was used to determine if a significant slope (confidence 95%) exists.

Sen's slope analysis was used to calculate the median slope in the data.

The median slope (change per year) was multiplied by 40 and then divided by the seawater value to determine the 40-year change as a percentage of seawater. Negative percentages indicate falling values.

Specific conductance of seawater was assumed to be 50,000 uS/cm. Chloride concentration of seawater was assumed to be 19,400 mg/L.

Data source: www.waterqualitydata.us

Background map source: Google Earth

LONG-TERM SALINITY CHANGES IN INTERMEDIATE AQUIFER SYSTEM WELLS

REGIONAL MODEL PRODUCTION SCENARIO REPORT

Figure 2.20

June 2013

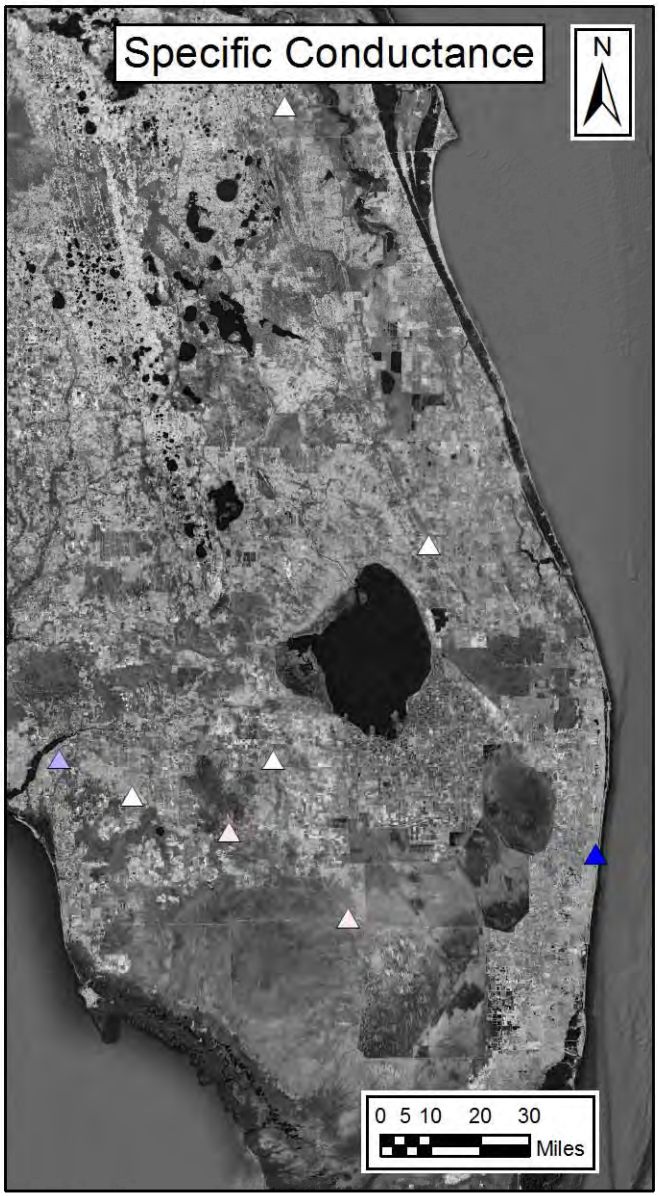

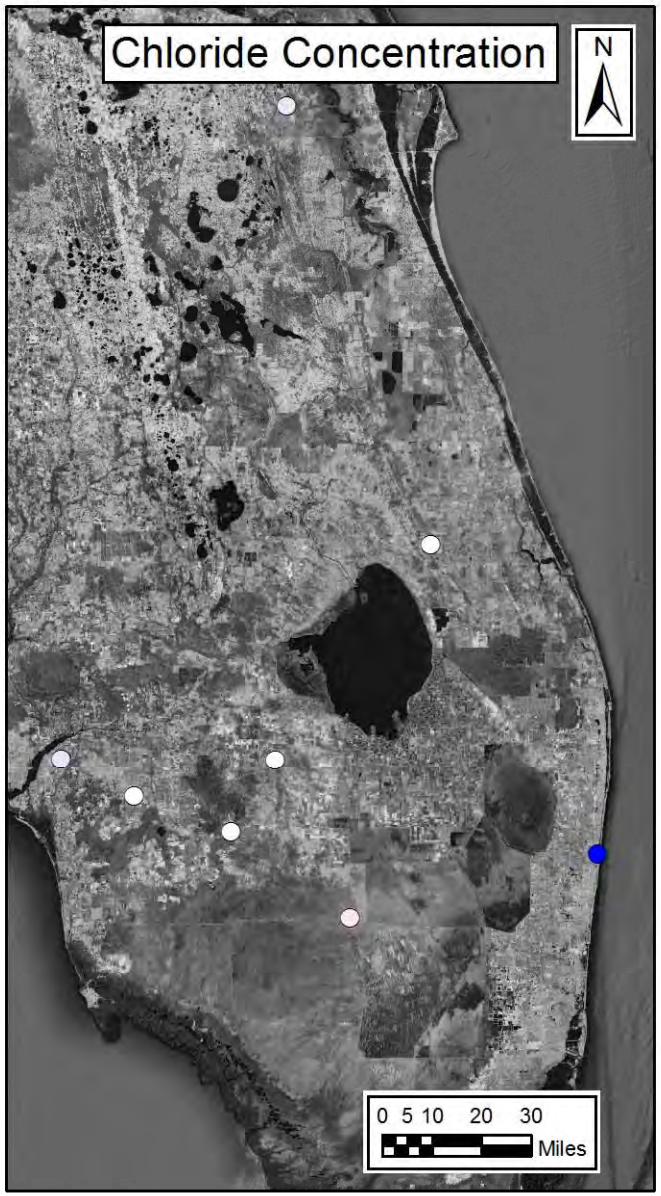

40-year Change as a Percentage of Seawater Characteristics

- No significant slope
- -10% to -5%
- -5% to -1%
- -1% to 0%
- 0% to 1%
- 1% to 5%
- 5% to 10%
- 10% to 50%
- > 50%

Mann Kendall analysis was used to determine if a significant slope (confidence 95%) exists.

Sen's slope analysis was used to calculate the median slope in the data.

The median slope (change per year) was multiplied by 40 and then divided by the seawater value to determine the 40-year change as a percentage of seawater. Negative percentages indicate falling values.

Specific conductance of seawater was assumed to be 50,000 uS/cm. Chloride concentration of seawater was assumed to be 19,400 mg/L.

Data source: www.waterqualitydata.us

Background map source: Google Earth

Long-Term Salinity Changes in Surficial Aquifer System Wells

Regional Model Production Scenario Report

Figure 2.21

June 2013

40-year Change as a Percentage of Seawater Characteristics

- No significant slope
- -10% to -5%
- -5% to -1%
- -1% to 0%
- 0% to 1%
- 1% to 5%
- 5% to 10%
- 10% to 50%
- > 50%

Mann Kendall analysis was used to determine if a significant slope (confidence 95%) exists.

Sen's slope analysis was used to calculate the median slope in the data.

The median slope (change per year) was multiplied by 40 and then divided by the seawater value to determine the 40-year change as a percentage of seawater. Negative percentages indicate falling values.

Specific conductance of seawater was assumed to be 50,000 uS/cm. Chloride concentration of seawater was assumed to be 19,400 mg/L.

Data source: www.waterqualitydata.us

Background map source: Google Earth

LONG-TERM SALINITY CHANGES IN WELLS OF UNKNOWN AQUIFER

REGIONAL MODEL PRODUCTION SCENARIO REPORT

Figure 2.22

June 2013

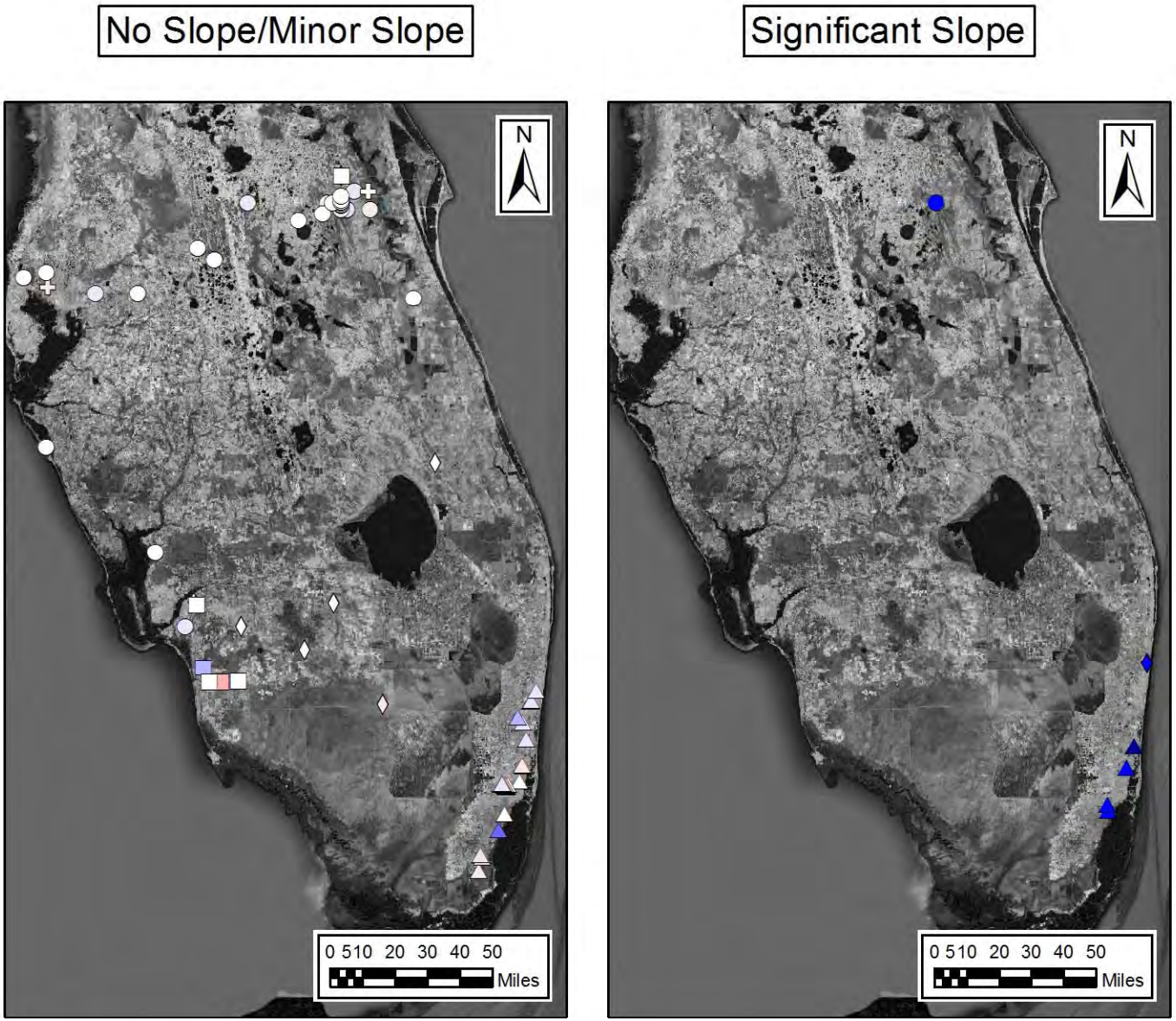

40-year Change as a Percentage of Seawater Characteristics

- No significant slope
- -10% to -5%
- -5% to -1%
- -1% to 0%
- 0% to 1%
- 1% to 5%
- 5% to 10%
- 10% to 50%
- > 50%

- Floridan Aquifer
- Biscayne Aquifer
- Intermediate Aquifer System
- Surficial Aquifer System
- Unknown Aquifer

Mann Kendall analysis was used to determine if a significant slope (confidence 95%) exists.

Sen's slope analysis was used to calculate the median slope in the data.

The median slope (change per year) was multiplied by 40 and then divided by the seawater value to determine the 40-year change as a percentage of seawater. Negative percentages indicate falling values.

Chloride concentration of seawater was assumed to be 19,400 mg/L.

Data source: www.waterqualitydata.us

Background map source: Google Earth

LONG-TERM CHLORIDE CONCENTRATION CHANGES IN WELLS OF ALL AQUIFERS

REGIONAL MODEL PRODUCTION SCENARIO REPORT

Figure 2.23

June 2013

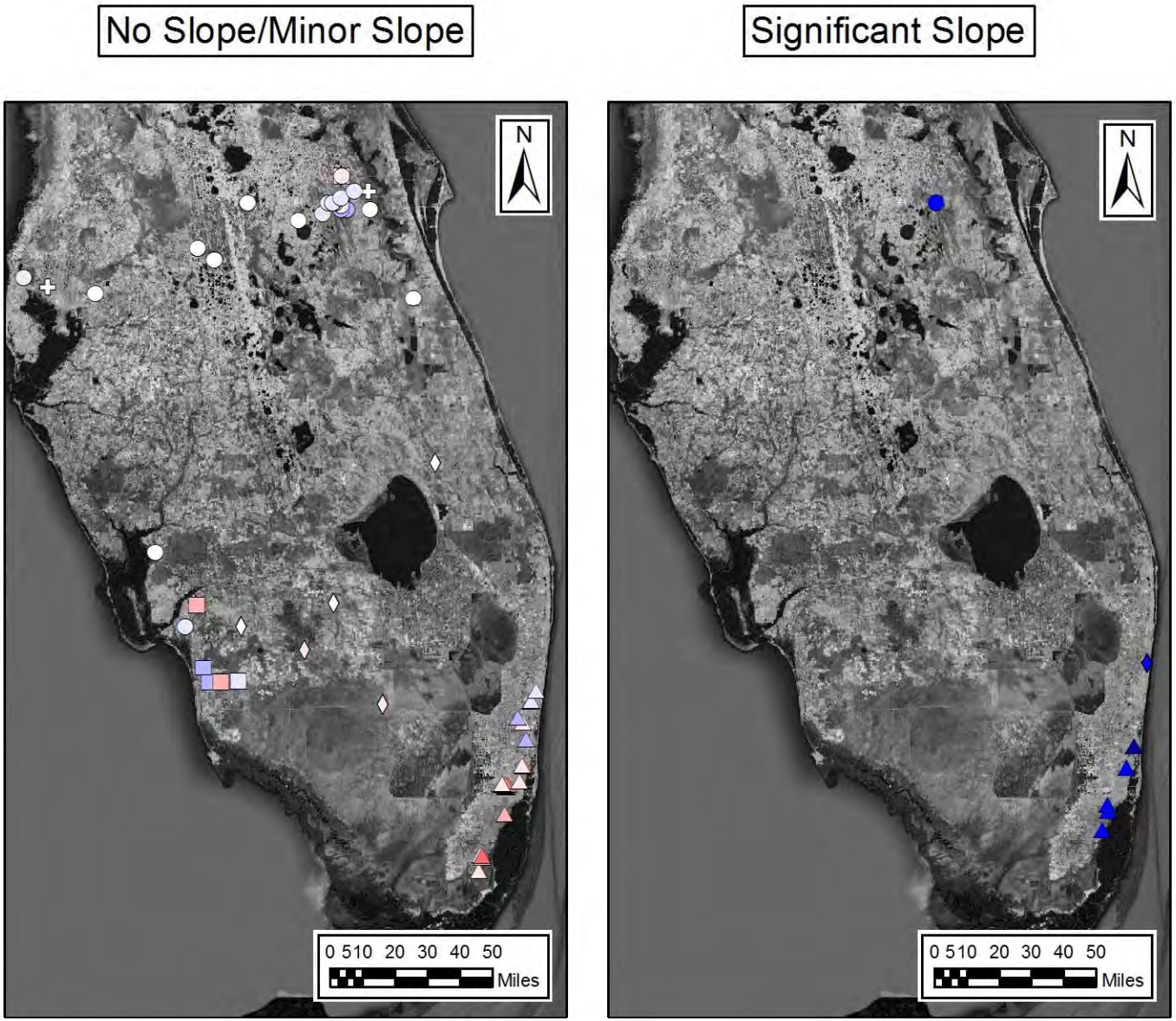

40-year Change as a Percentage of Seawater Characteristics

- No significant slope
- -10% to -5%
- -5% to -1%
- -1% to 0%
- 0% to 1%
- 1% to 5%
- 5% to 10%
- 10% to 50%
- > 50%

- Floridan Aquifer
- Biscayne Aquifer
- Intermediate Aquifer System
- Surficial Aquifer System
- Unknown Aquifer

Mann Kendall analysis was used to determine if a significant slope (confidence 95%) exists.

Sen's slope analysis was used to calculate the median slope in the data.

The median slope (change per year) was multiplied by 40 and then divided by the seawater value to determine the 40-year change as a percentage of seawater. Negative percentages indicate falling values.

Specific conductance of seawater was assumed to be 50,000 uS/cm.

Data source: www.waterqualitydata.us

Background map source: Google Earth

LONG-TERM SPECIFIC CONDUCTANCE CHANGES IN WELLS OF ALL AQUIFERS

REGIONAL MODEL PRODUCTION SCENARIO REPORT

Figure 2.24

June 2013

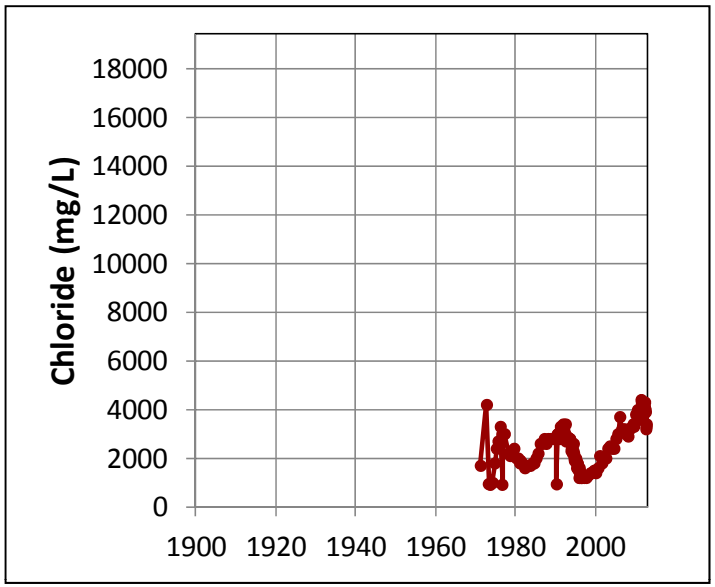

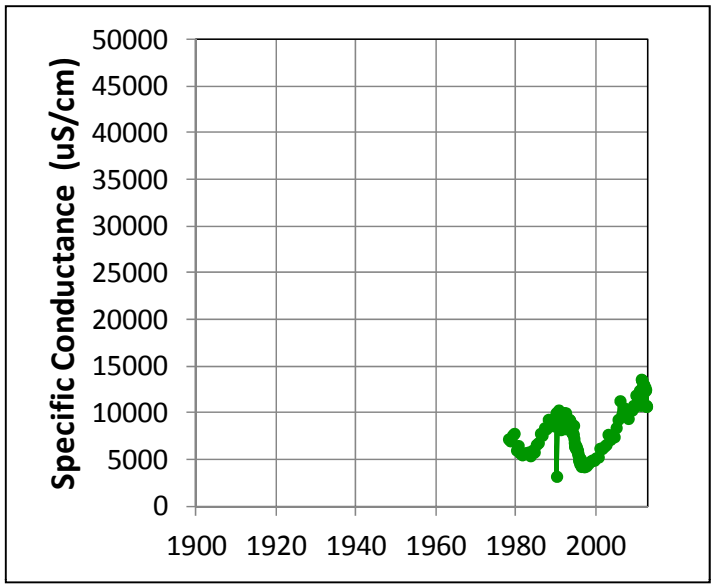

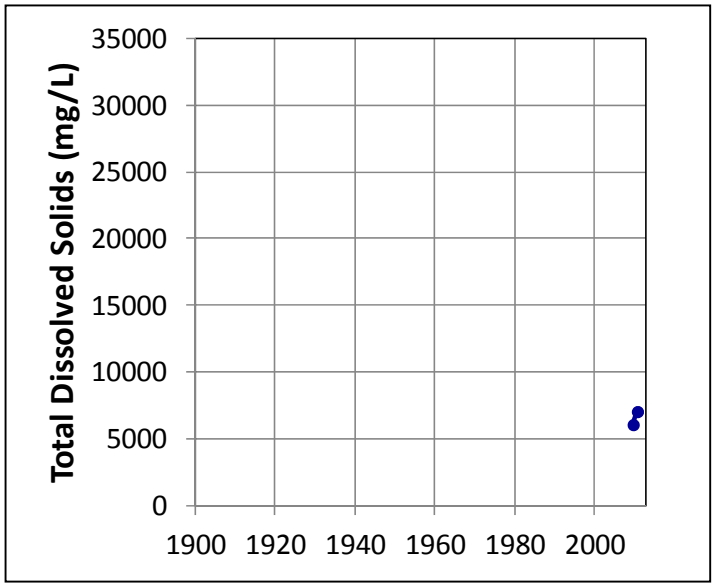

	Chloride (mg/L)	Specific Conductance (uS/cm)	Total Dissolved Solids (mg/L)
Number of Points	164	152	2
Mann Kendall Trend	Statistically significant upward	Statistically significant upward	Insufficient Data
Sen's Slope (per year)	37.42	127.05	-
40-Year Change	1497	5082	-
40-Year Change as % of Seawater	7.7%	10.2%	-

Notes:

This well is open in the Biscayne Aquifer.

Top of y-axis scales are assumed seawater characteristics 19,400 mg/L Chloride; 50,000 uS/cm Specific Conductance; 35,000 mg/L TDS

Data source: www.waterqualitydata.us

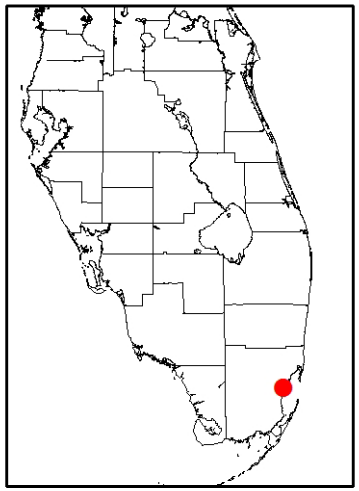

SALINITY VARIATIONS AT USGS-253652080183701

REGIONAL MODEL PRODUCTION SCENARIO REPORT

Figure 2.25

June 2013

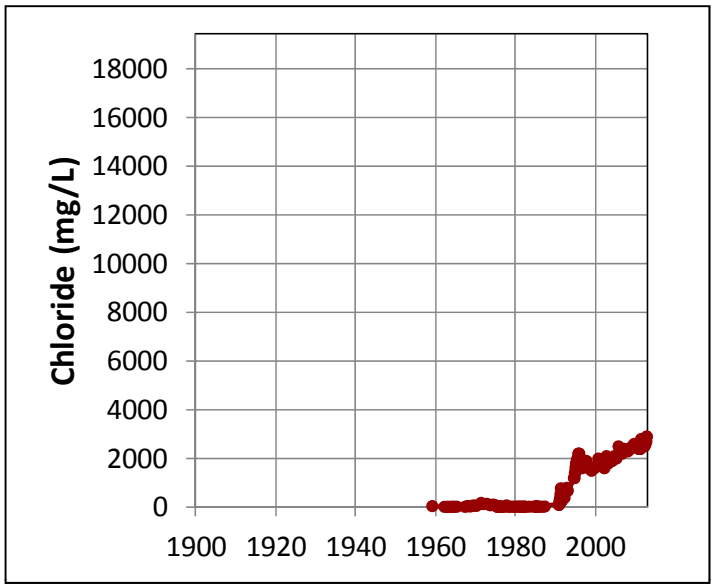

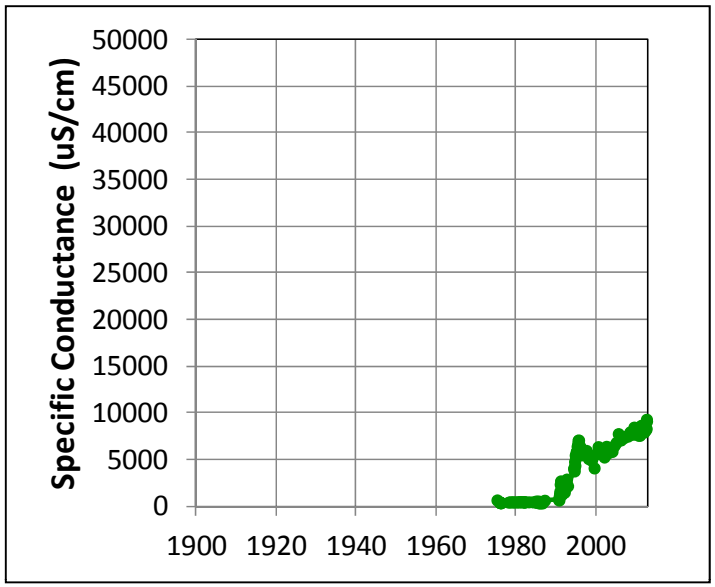

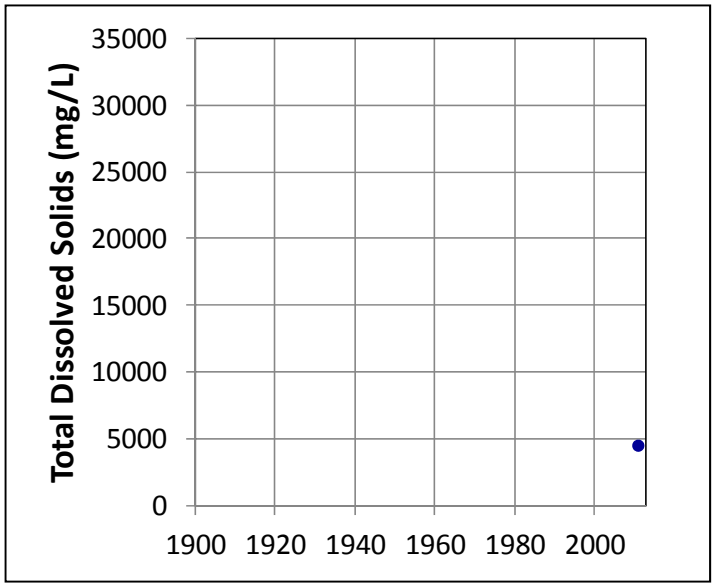

	Chloride (mg/L)	Specific Conductance (uS/cm)	Total Dissolved Solids (mg/L)
Number of Points	164	136	1
Mann Kendall Trend	Statistically significant upward	Statistically significant upward	Insufficient Data
Sen's Slope (per year)	68.57	257.21	-
40-Year Change	2743	10288	-
40-Year Change as % of Seawater	14.1%	20.6%	-

Notes:

This well is open in the Biscayne Aquifer.

Top of y-axis scales are assumed seawater characteristics 19,400 mg/L Chloride; 50,000 uS/cm Specific Conductance; 35,000 mg/L TDS

Data source: www.waterqualitydata.us

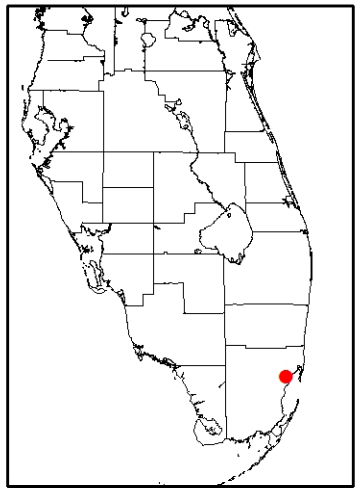

SALINITY VARIATIONS AT USGS-254201080173001

REGIONAL MODEL PRODUCTION SCENARIO REPORT

Figure 2.26

June 2013

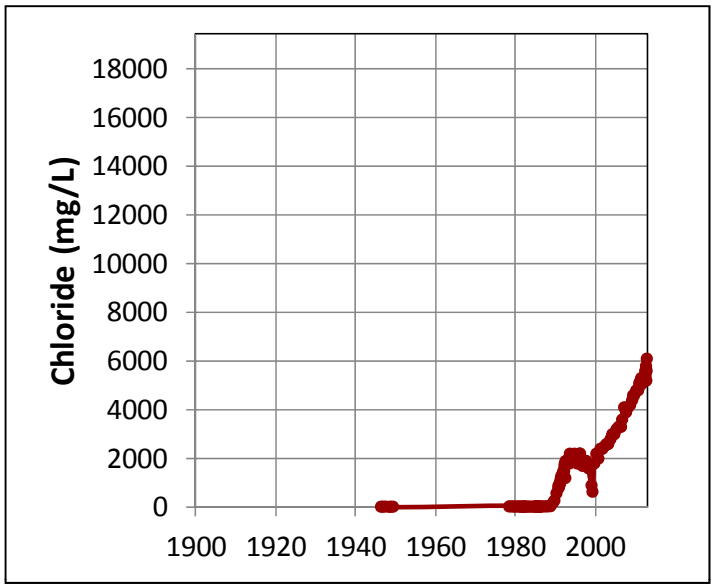

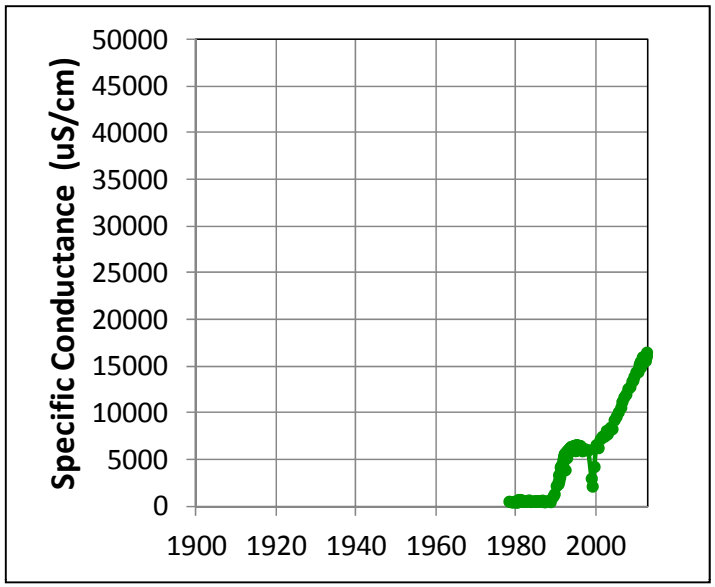

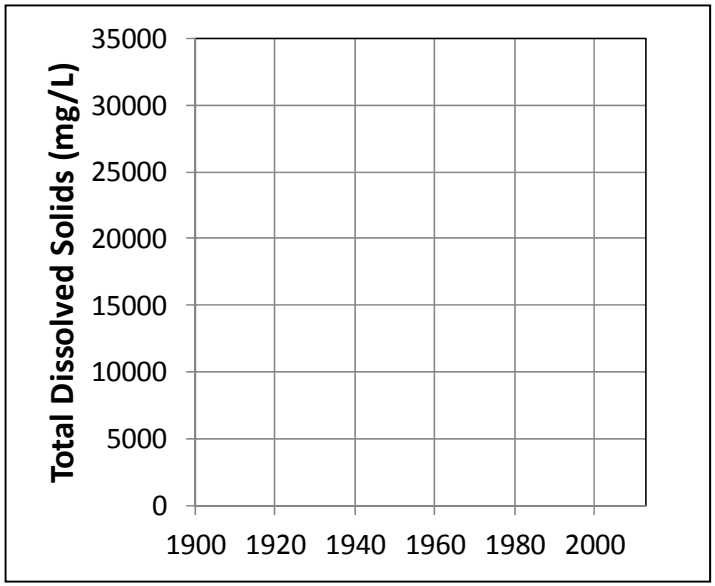

	Chloride (mg/L)	Specific Conductance (uS/cm)	Total Dissolved Solids (mg/L)
Number of Points	175	169	0
Mann Kendall Trend	Statistically significant upward	Statistically significant upward	Insufficient Data
Sen's Slope (per year)	171.58	511.02	-
40-Year Change	6863	20441	-
40-Year Change as % of Seawater	35.4%	40.9%	-

Notes:

This well is open in the Biscayne Aquifer.

Top of y-axis scales are assumed seawater characteristics 19,400 mg/L Chloride; 50,000 uS/cm Specific Conductance; 35,000 mg/L TDS

Data source: www.waterqualitydata.us

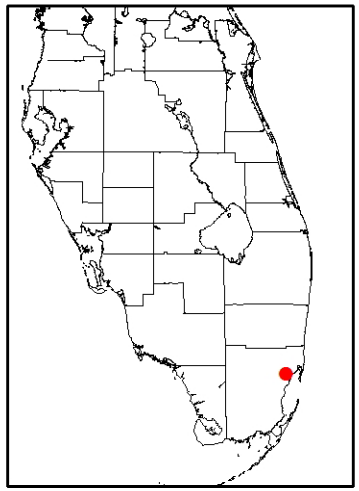

SALINITY VARIATIONS AT USGS-254335080170501

REGIONAL MODEL PRODUCTION SCENARIO REPORT

Figure 2.27

June 2013

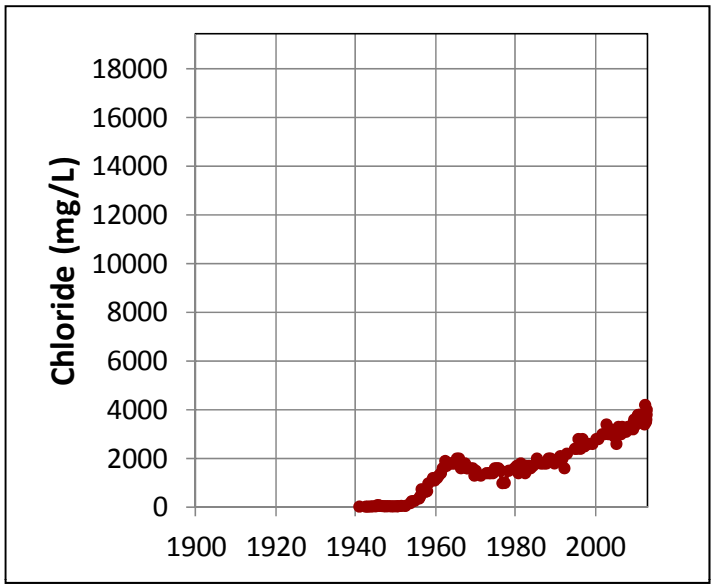

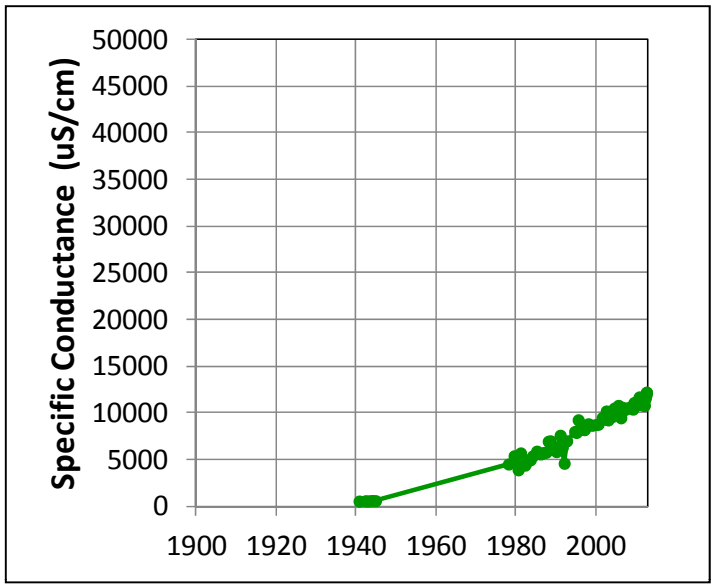

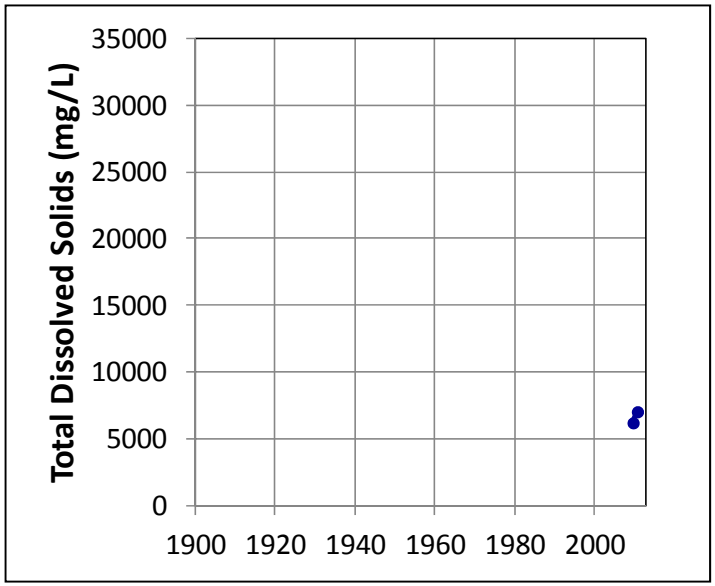

	Chloride (mg/L)	Specific Conductance (uS/cm)	Total Dissolved Solids (mg/L)
Number of Points	149	92	2
Mann Kendall Trend	Statistically significant upward	Statistically significant upward	Insufficient Data
Sen's Slope (per year)	52.66	207.16	-
40-Year Change	2107	8286	-
40-Year Change as % of Seawater	10.9%	16.6%	-

Notes:

This well is open in the Biscayne Aquifer.

Top of y-axis scales are assumed seawater characteristics 19,400 mg/L Chloride; 50,000 uS/cm Specific Conductance; 35,000 mg/L TDS

Data source: www.waterqualitydata.us

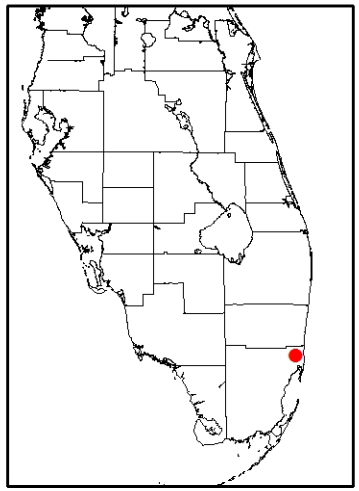

SALINITY VARIATIONS AT USGS-255315080111501

REGIONAL MODEL PRODUCTION SCENARIO REPORT

Figure 2.28

June 2013

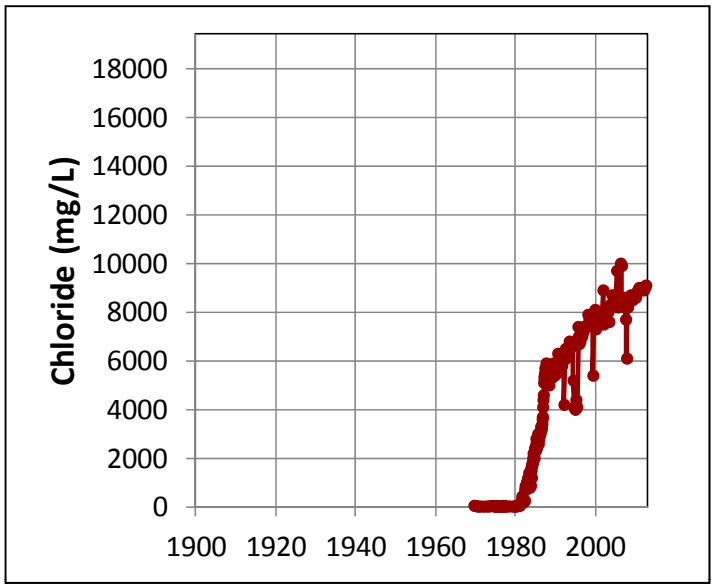

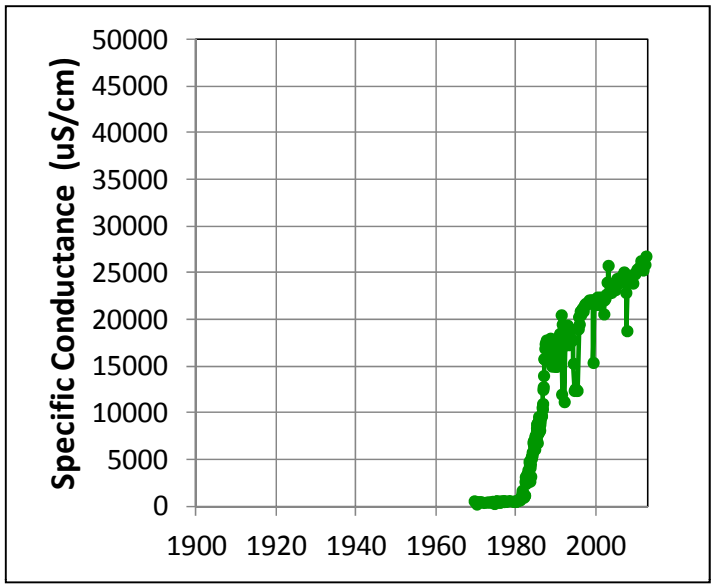

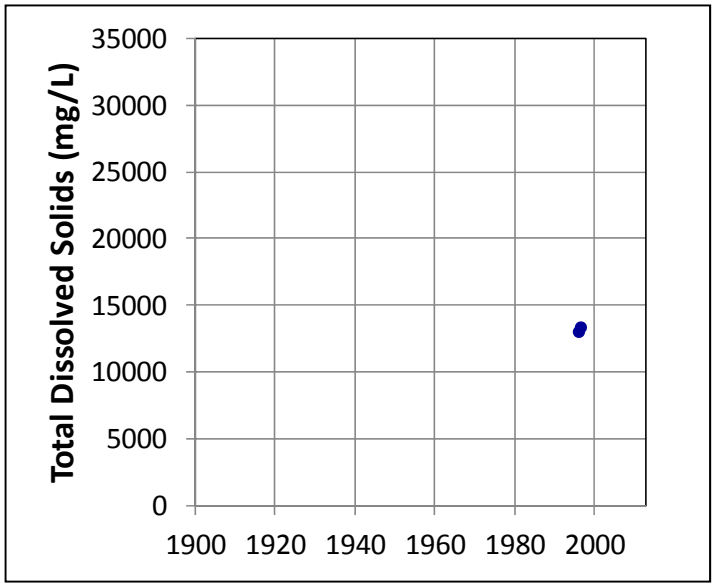

	Chloride (mg/L)	Specific Conductance (uS/cm)	Total Dissolved Solids (mg/L)
Number of Points	308	307	2
Mann Kendall Trend	Statistically significant upward	Statistically significant upward	Insufficient Data
Sen's Slope (per year)	316.86	877.90	-
40-Year Change	12674	35116	-
40-Year Change as % of Seawater	65.3%	70.2%	-

Notes:

This well is open in the Biscayne Aquifer.

Top of y-axis scales are assumed seawater characteristics 19,400 mg/L Chloride; 50,000 uS/cm Specific Conductance; 35,000 mg/L TDS

Data source: www.waterqualitydata.us

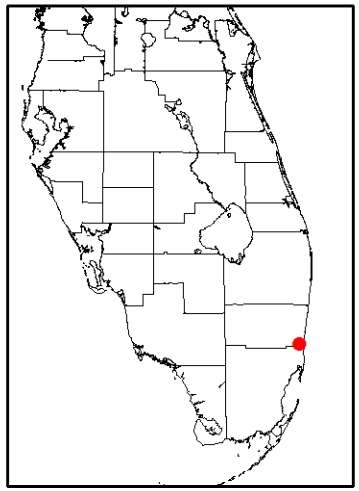

SALINITY VARIATIONS AT USGS-255916080090401

REGIONAL MODEL PRODUCTION SCENARIO REPORT

Figure 2.29

June 2013

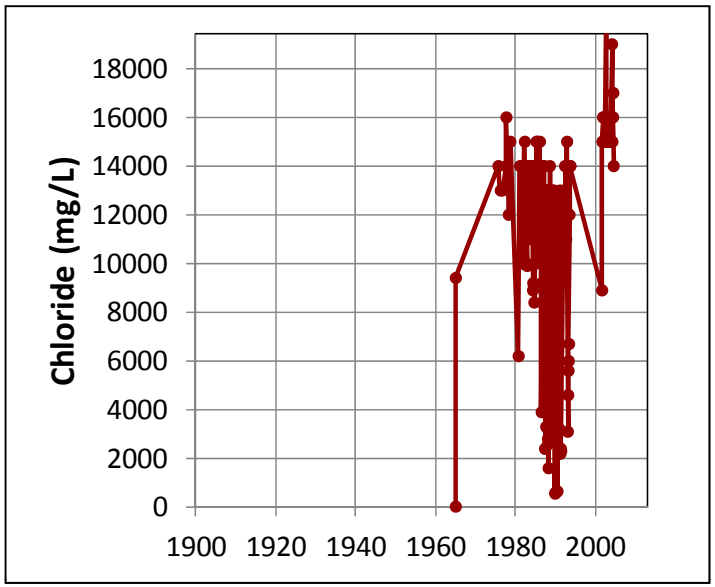

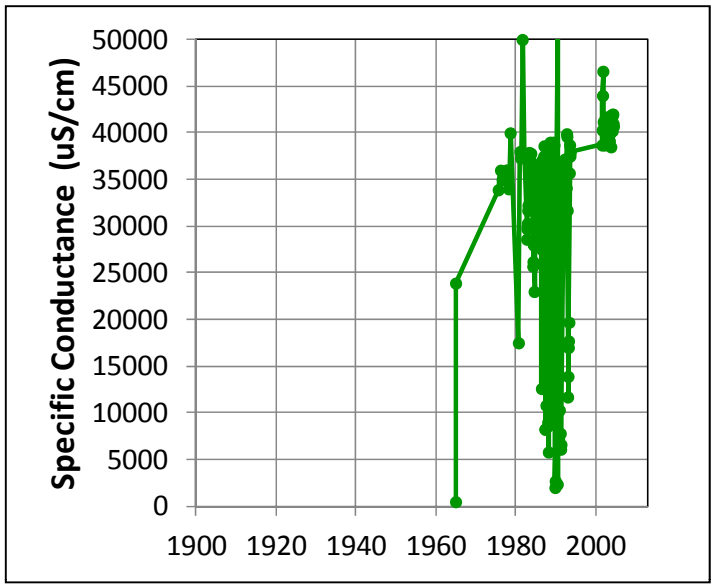

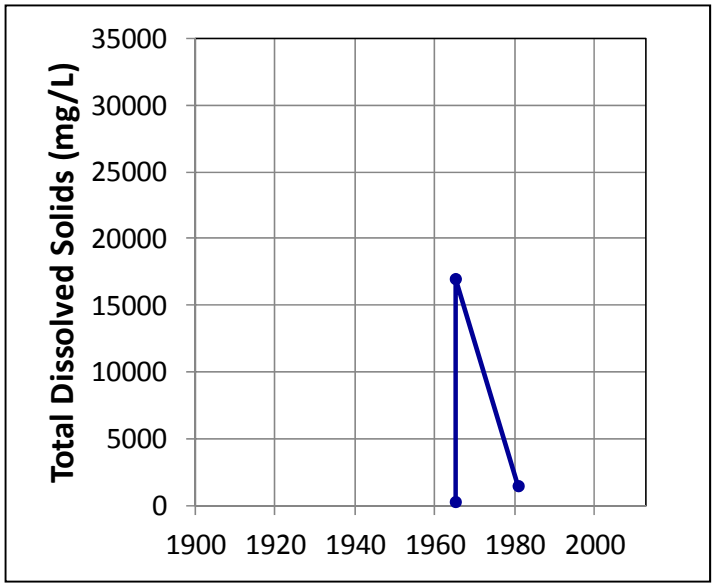

	Chloride (mg/L)	Specific Conductance (uS/cm)	Total Dissolved Solids (mg/L)
Number of Points	164	164	3
Mann Kendall Trend	Statistically significant upward	Statistically significant upward	Insufficient Data
Sen's Slope (per year)	67.98	246.07	-
40-Year Change	2719	9843	-
40-Year Change as % of Seawater	14.0%	19.7%	-

Notes:

This well is open in the Surficial Aquifer System.

Top of y-axis scales are assumed seawater characteristics 19,400 mg/L Chloride; 50,000 uS/cm Specific Conductance; 35,000 mg/L TDS

Data source: www.waterqualitydata.us

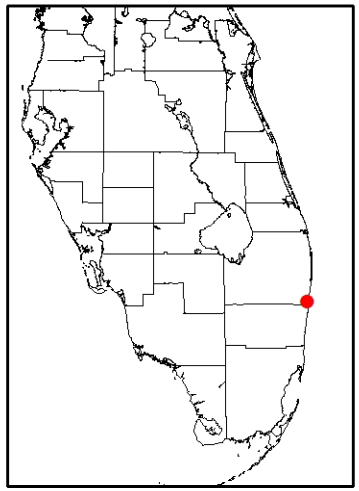

SALINITY VARIATIONS AT USGS-262114080054001

REGIONAL MODEL PRODUCTION SCENARIO REPORT

Figure 2.30

June 2013

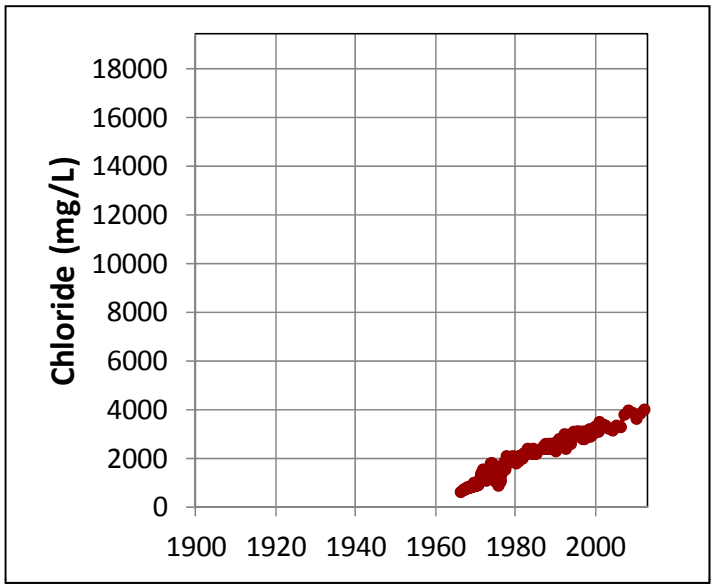

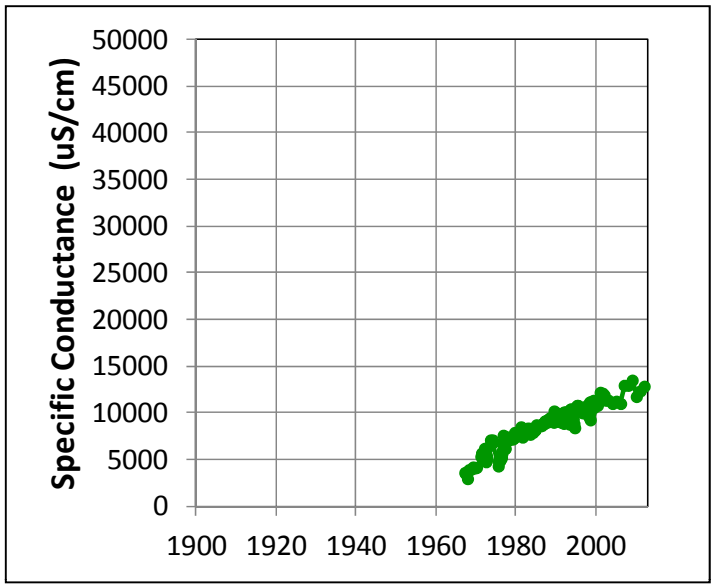

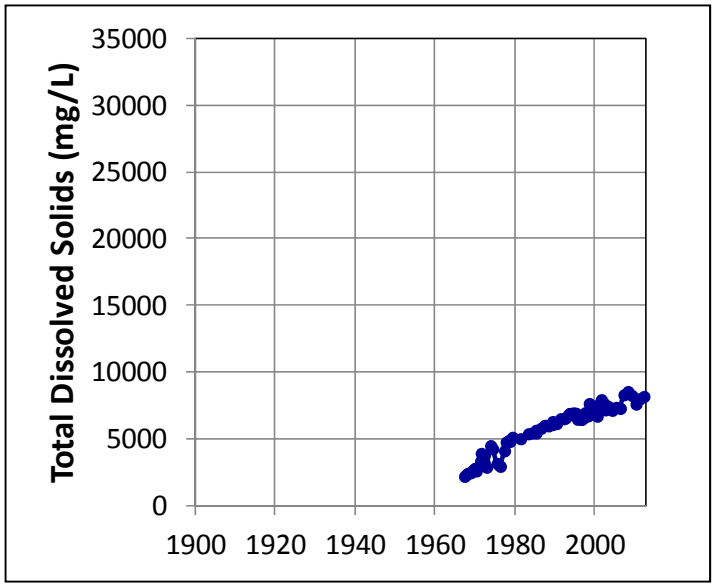

	Chloride (mg/L)	Specific Conductance (uS/cm)	Total Dissolved Solids (mg/L)
Number of Points	362	256	65
Mann Kendall Trend	Statistically significant upward	Statistically significant upward	Statistically significant upward
Sen's Slope (per year)	71.71	194.52	128.90
40-Year Change	2868	7781	5156
40-Year Change as % of Seawater	14.8%	15.6%	14.7%

Notes:

This well is open in the Floridan Aquifer System.

Top of y-axis scales are assumed seawater characteristics 19,400 mg/L Chloride; 50,000 uS/cm Specific Conductance; 35,000 mg/L TDS

Data source: www.waterqualitydata.us

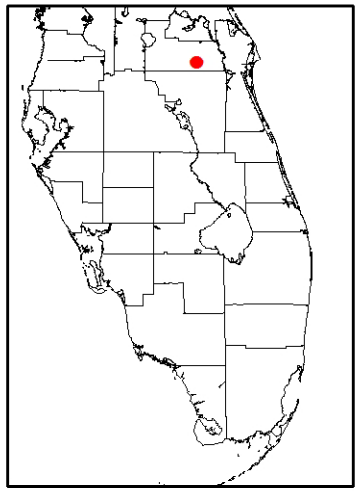

SALINITY VARIATIONS AT USGS-282533081082202

REGIONAL MODEL PRODUCTION SCENARIO REPORT

Figure 2.31

June 2013

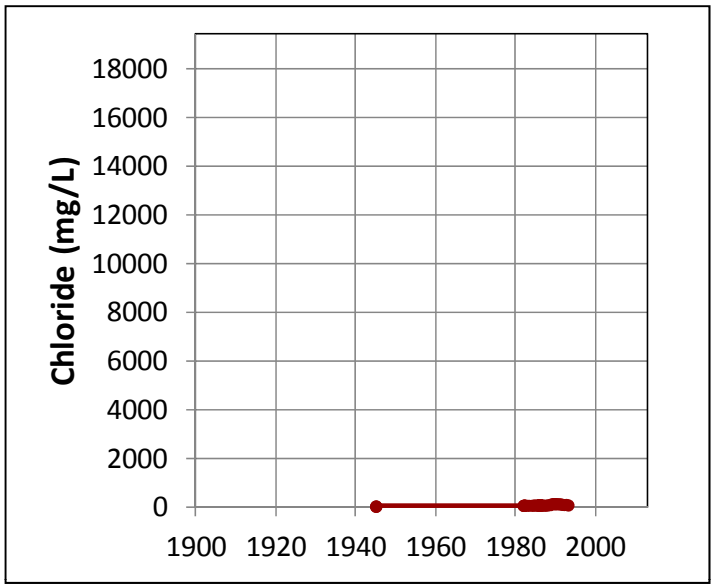

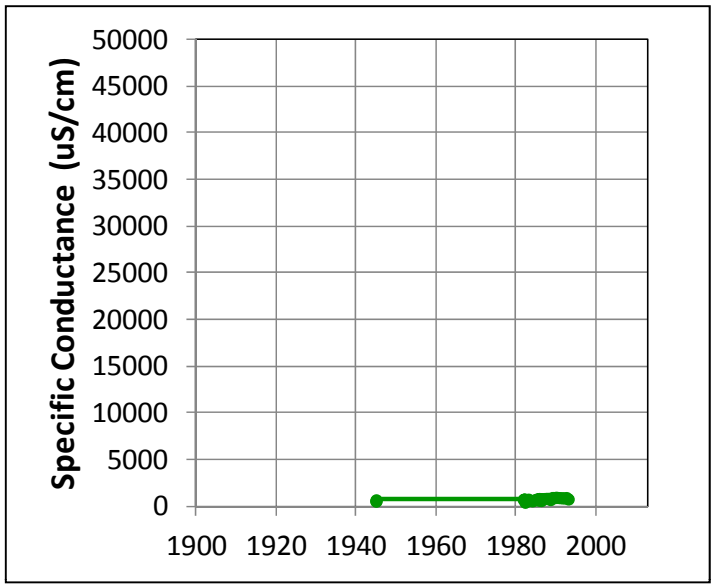

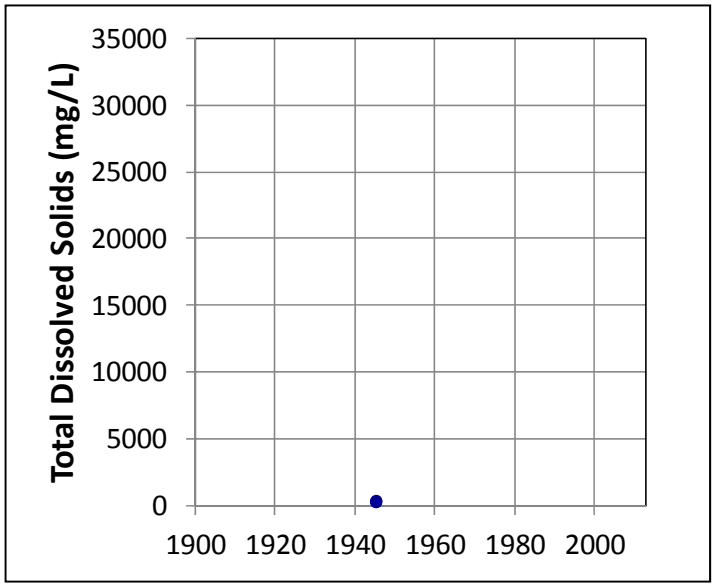

	Chloride (mg/L)	Specific Conductance (uS/cm)	Total Dissolved Solids (mg/L)
Number of Points	39	39	65
Mann Kendall Trend	Statistically significant upward	Statistically significant upward	Insufficient Data
Sen's Slope (per year)	3.12	17.09	-
40-Year Change	125	684	-
40-Year Change as % of Seawater	0.6%	1.4%	-

Notes:

This well is open in the Surficial Aquifer System.

Top of y-axis scales are assumed seawater characteristics 19,400 mg/L Chloride; 50,000 uS/cm Specific Conductance; 35,000 mg/L TDS

Data source: www.waterqualitydata.us

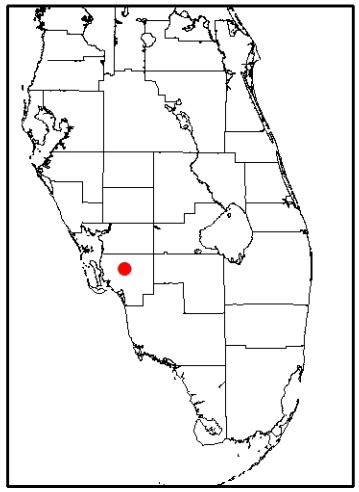

SALINITY VARIATIONS AT USGS-263802081493501

REGIONAL MODEL PRODUCTION SCENARIO REPORT

Figure 2.32

June 2013

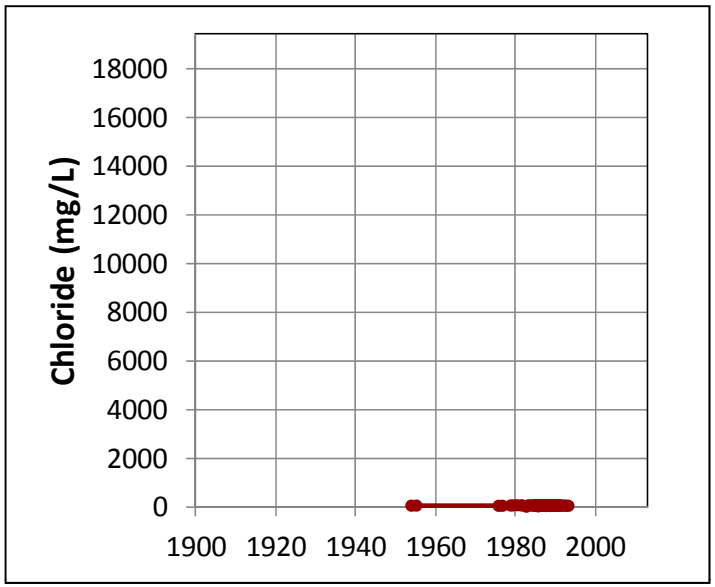

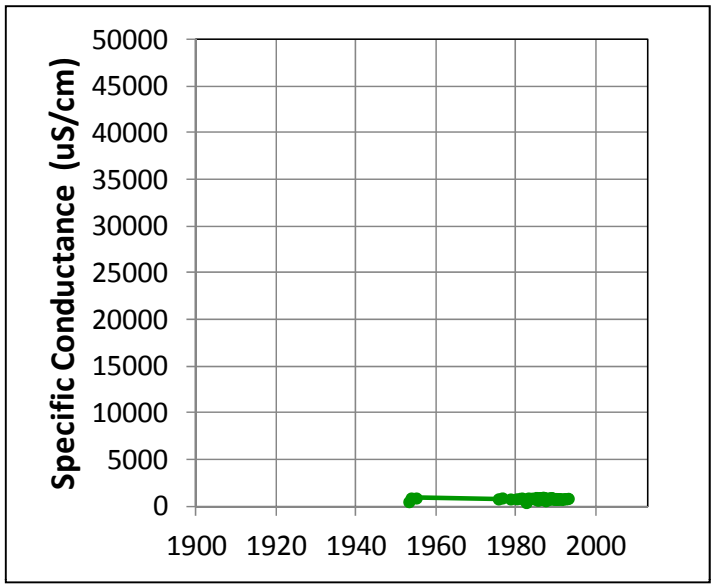

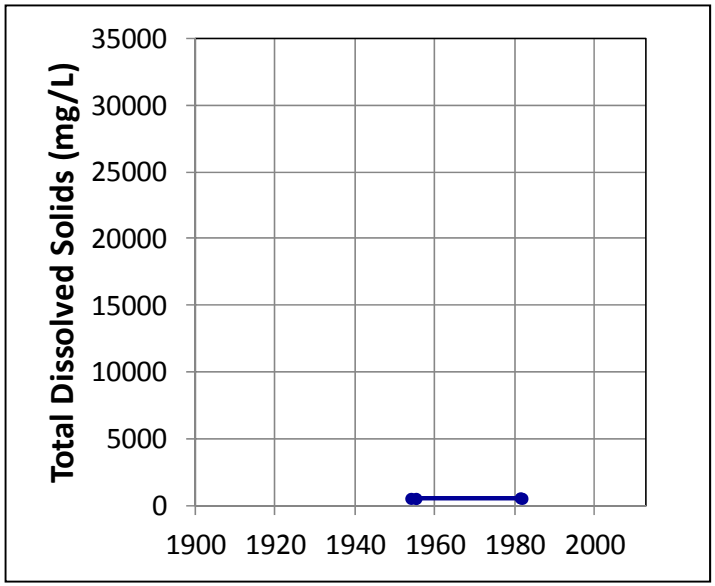

	Chloride (mg/L)	Specific Conductance (uS/cm)	Total Dissolved Solids (mg/L)
Number of Points	88	88	4
Mann Kendall Trend	No statis-tically signif-icant trend	Statistically significant downward	No statis-tically signif-icant trend
Sen's Slope (per year)	-	-2.95	-
40-Year Change	-	-118	-
40-Year Change as % of Seawater	-	-0.2%	-

Notes:

This well is open in the Surficial Aquifer System.

Top of y-axis scales are assumed seawater characteristics 19,400 mg/L Chloride; 50,000 uS/cm Specific Conductance; 35,000 mg/L TDS

Data source: www.waterqualitydata.us

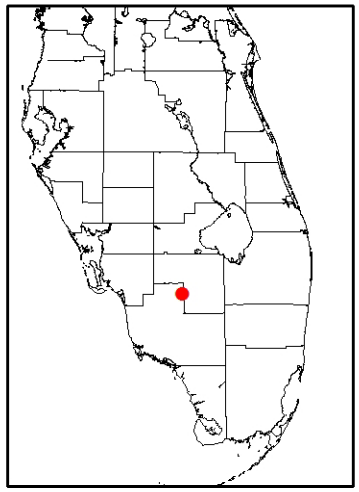

SALINITY VARIATIONS AT USGS-262521081161901

REGIONAL MODEL PRODUCTION SCENARIO REPORT

Figure 2.33

June 2013

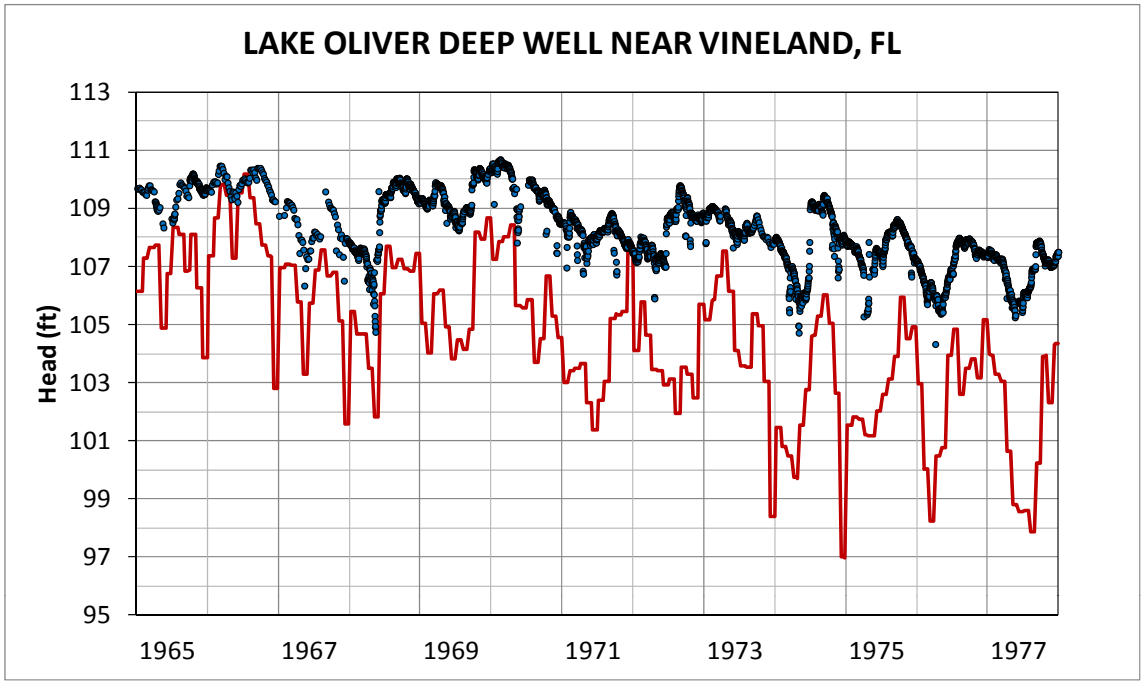

Plot Legend

- Observed Heads
- Model Result – Layer 7 (UF)

Statistics Abbreviations:

ME = Mean Error
MAE = Mean Absolute Error
RMS = Root Mean Square Error
(See text for definitions)

Observed Head and Well Construction data from USGS:
http://waterdata.usgs.gov/nwis/gw

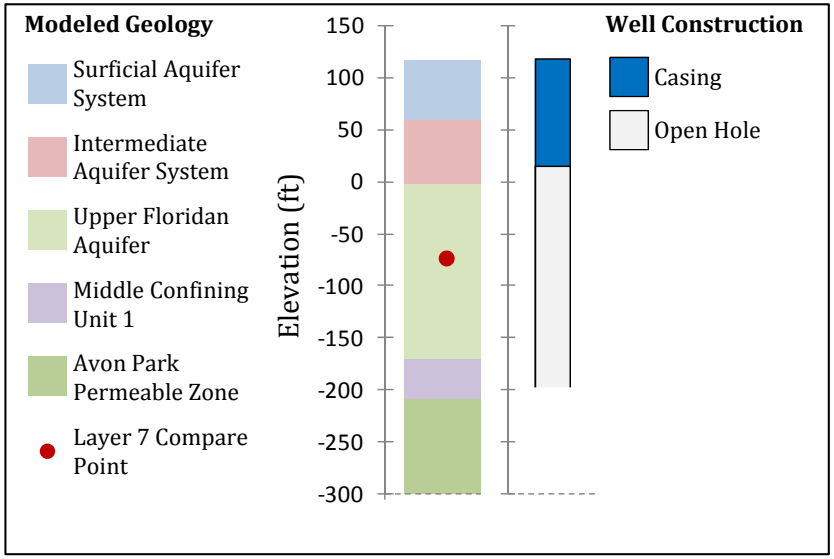

Statistics	
Obs. Count	3631
Obs. Range	6.36
ME	4.14
MAE	4.14
RMS	6.36
RMS as % of Range	71%

Well Location:

Comparison of no-ASR Modeled Results to Head Data: Lake Oliver Deep Well

Regional Model Production Scenario Report

Figure 2.34

June 2013

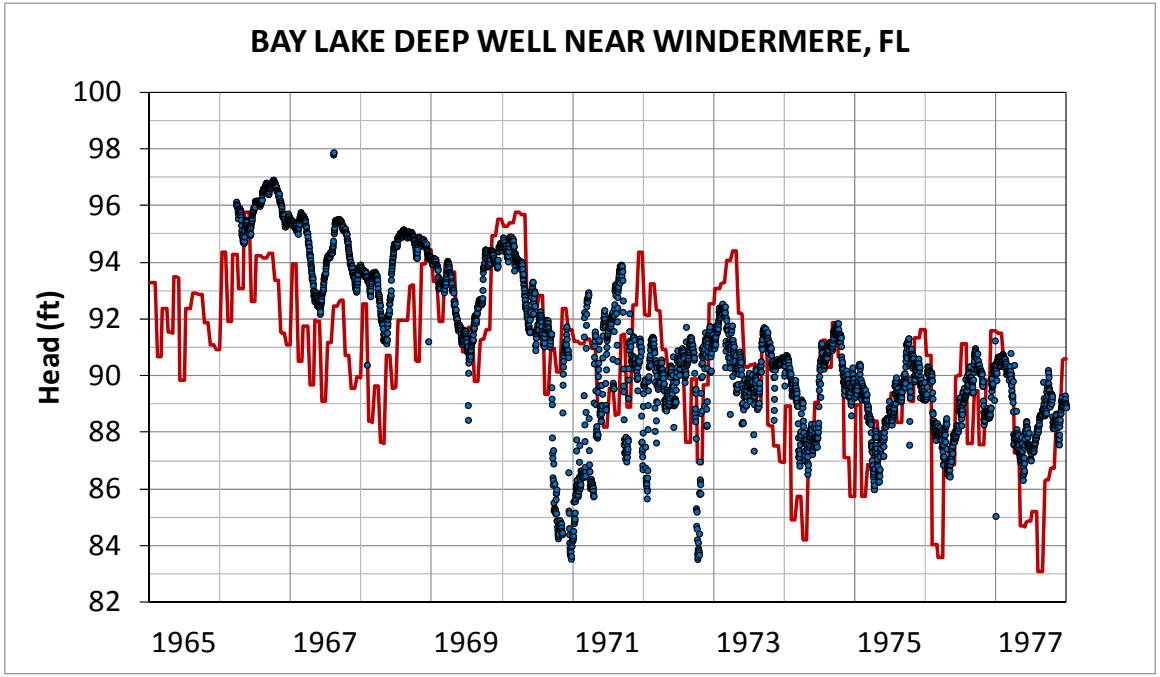

Plot Legend

- Observed Heads
- Model Result – Layer 7 (UF)

Statistics Abbreviations:

ME = Mean Error
MAE = Mean Absolute Error
RMS = Root Mean Square Error
(See text for definitions)

Observed Head and Well Construction data from USGS:
http://waterdata.usgs.gov/nwis/gw

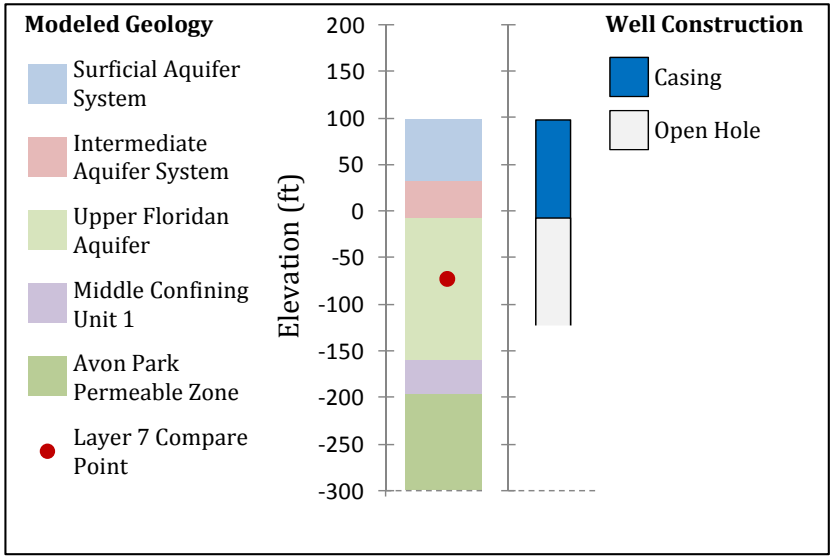

Statistics	
Obs. Count	4300
Obs. Range	14.35
ME	-0.71
MAE	2.10
RMS	2.60
RMS as % of Range	18%

Well Location:

Comparison of no-ASR Modeled Results to Head Data: Bay Lake Deep Well

Regional Model Production Scenario Report

Figure 2.35

June 2013

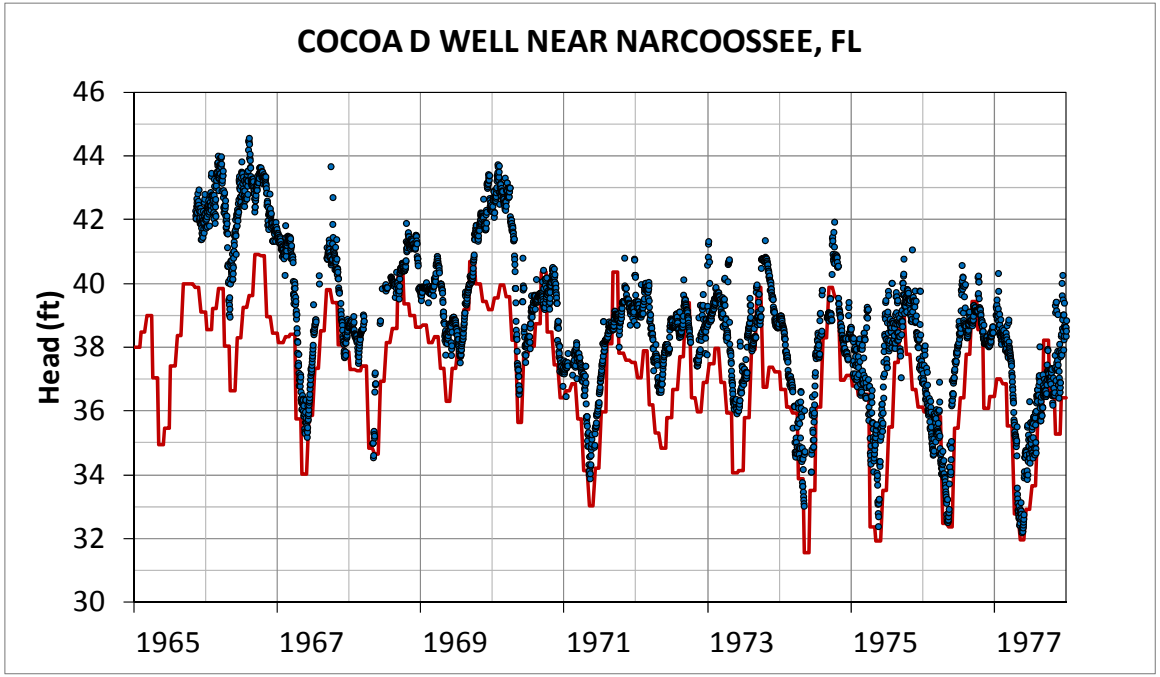

Plot Legend

- Observed Heads
- Model Result – Layer 7 (UF)

Statistics Abbreviations:

ME = Mean Error
MAE = Mean Absolute Error
RMS = Root Mean Square Error
(See text for definitions)

Observed Head and Well Construction data from USGS:
http://waterdata.usgs.gov/nwis/gw

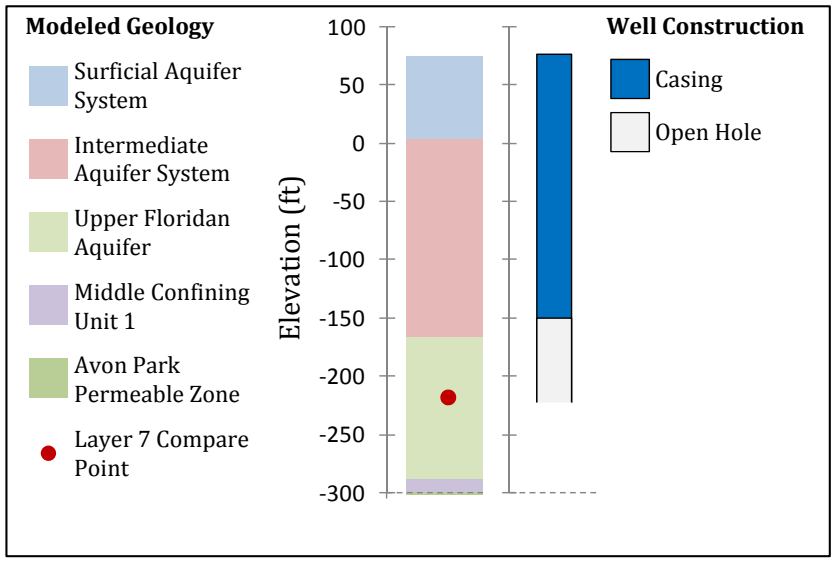

Statistics	
Obs. Count	4089
Obs. Range	12.37
ME	-1.72
MAE	1.83
RMS	2.13
RMS as % of Range	17%

Well Location:

Comparison of no-ASR Modeled Results to Head Data: Cocoa D Well

Regional Model Production Scenario Report

Figure 2.36

June 2013

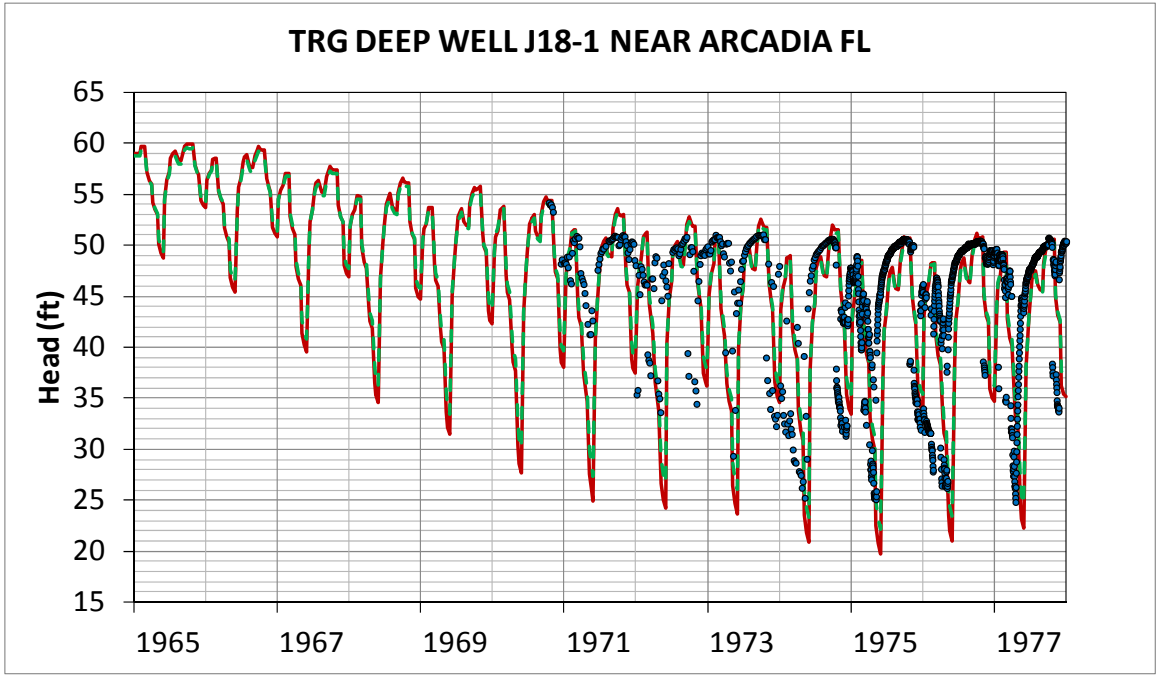

Plot Legend

- Observed Heads
- Model Result – Layer 7 (UF)
- Model Result – Layer 11 (MC1)

Statistics Abbreviations:

ME = Mean Error
MAE = Mean Absolute Error
RMS = Root Mean Square Error
(See text for definitions)

Observed Head and Well Construction data from USGS:
http://waterdata.usgs.gov/nwis/gw

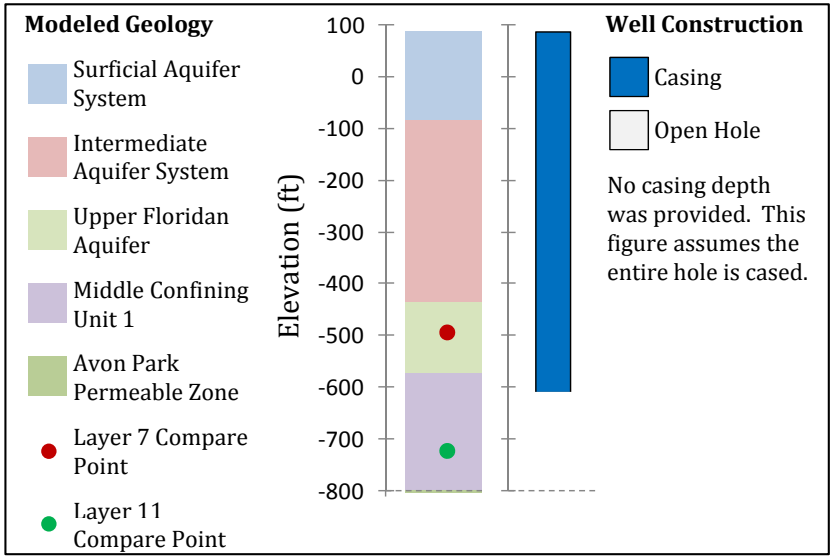

Statistics (Layer 7 Comparison)	
Obs. Count	1452
Obs. Range	29.36
ME	-2.26
MAE	6.41
RMS	8.85
RMS as % of Range	30%

Well Location:

Comparison of no-ASR Modeled Results to Head Data: TRG Deep Well J18-1

Regional Model Production Scenario Report

Figure 2.37

June 2013

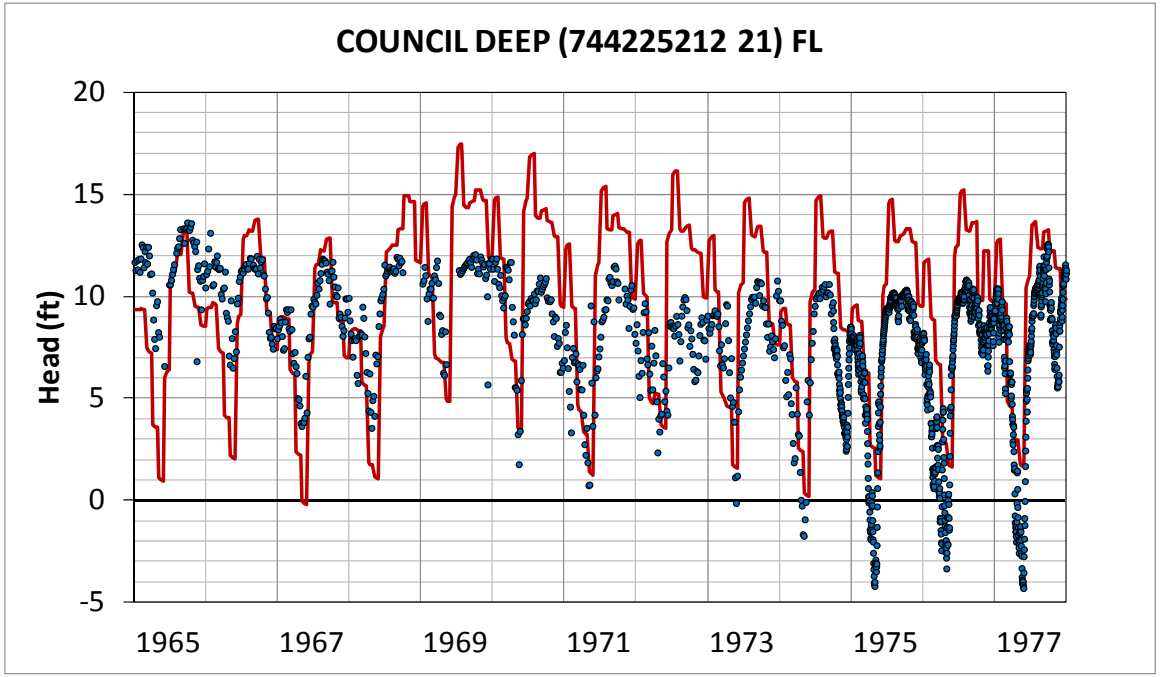

Plot Legend

- Observed Heads
- Model Result – Layer 7 (UF)

Statistics Abbreviations:

ME = Mean Error
MAE = Mean Absolute Error
RMS = Root Mean Square Error
(See text for definitions)

Observed Head and Well Construction data from USGS:
http://waterdata.usgs.gov/nwis/gw

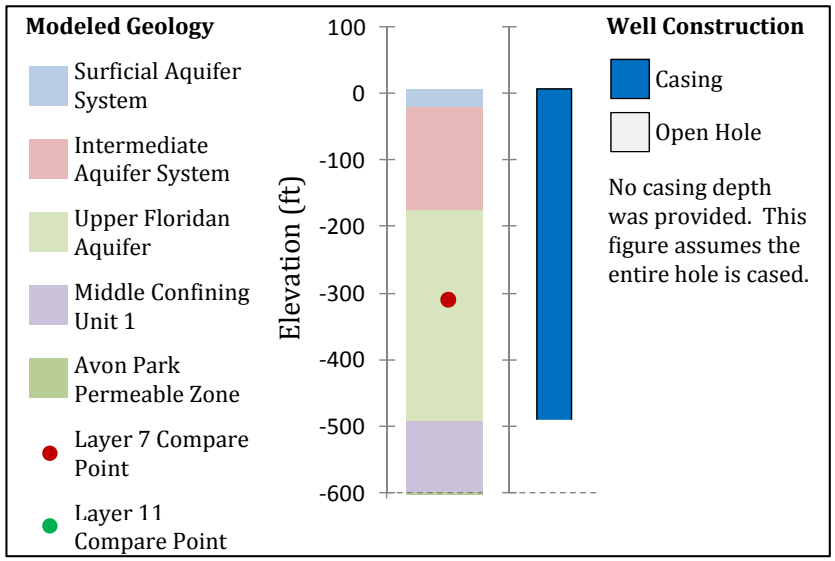

Statistics	
Obs. Count	1843
Obs. Range	17.92
ME	2.20
MAE	3.11
RMS	3.56
RMS as % of Range	20%

Well Location:

Comparison of no-ASR Modeled Results to Head Data: Council Deep

Regional Model Production Scenario Report

Figure 2.38

June 2013

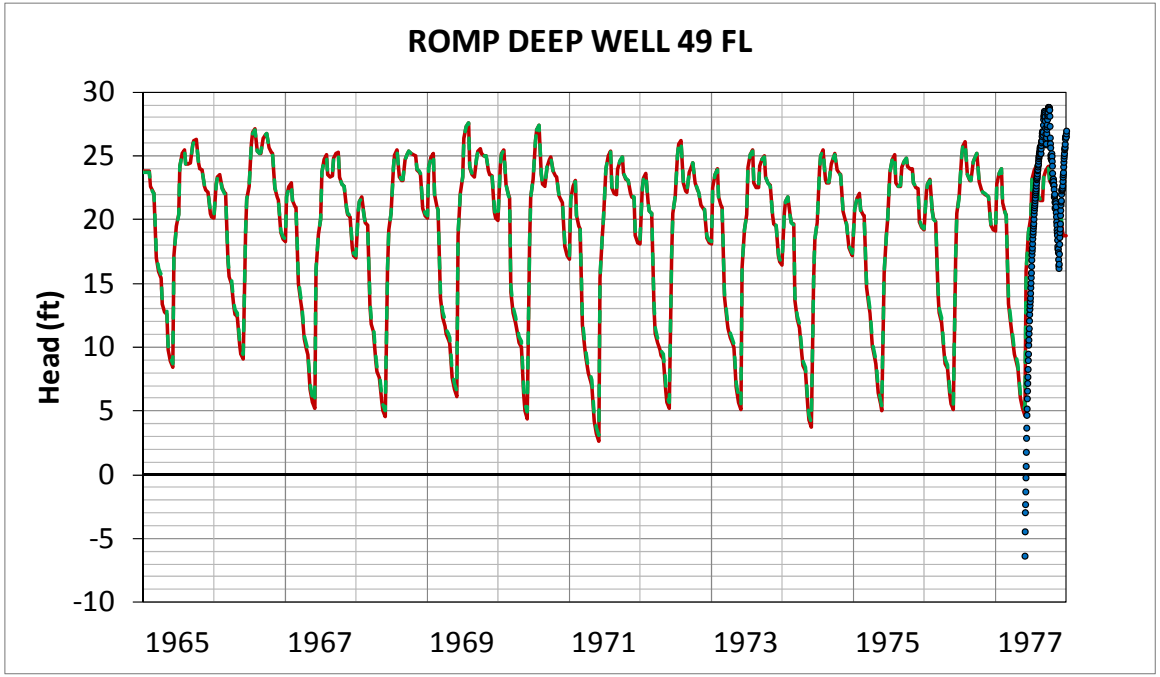

Plot Legend

- Observed Heads
- Model Result – Layer 7 (UF)
- Model Result – Layer 11 (MC1)

Statistics Abbreviations:

ME = Mean Error
MAE = Mean Absolute Error
RMS = Root Mean Square Error
(See text for definitions)

Observed Head and Well Construction data from USGS:
http://waterdata.usgs.gov/nwis/gw

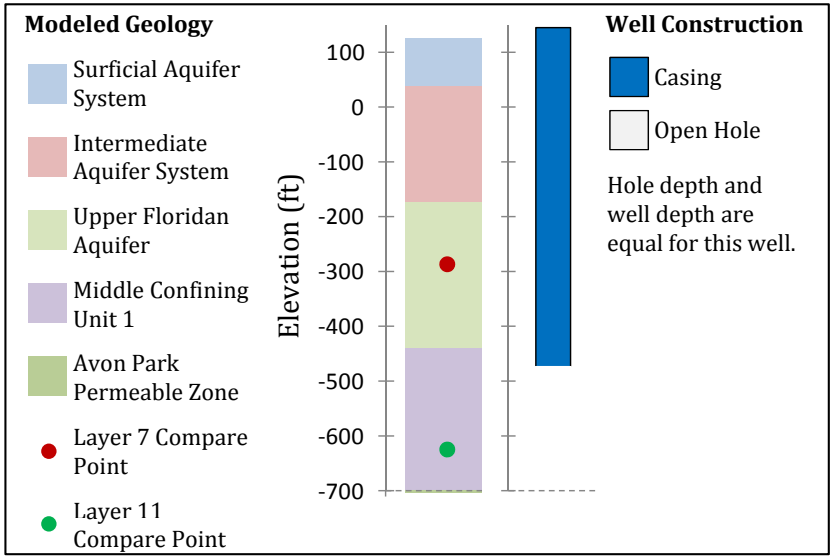

Statistics (Layer 7 Comparison)	
Obs. Count	215
Obs. Range	35.19
ME	0.03
MAE	4.18
RMS	5.01
RMS as % of Range	14%

Well Location:

Comparison of no-ASR Modeled Results to Head Data: ROMP Deep Well 49

Regional Model Production Scenario Report

Figure 2.39

June 2013

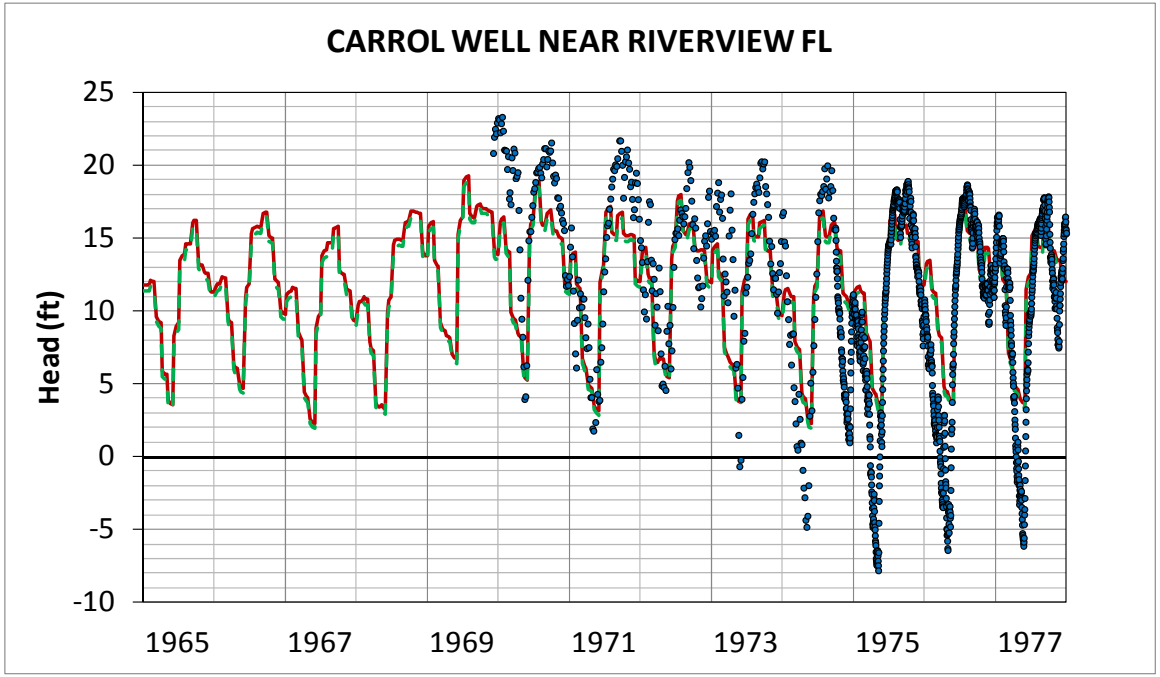

Plot Legend

- Observed Heads
- Model Result – Layer 7 (UF)
- Model Result – Layer 11 (MC1)

Statistics Abbreviations:

ME = Mean Error
MAE = Mean Absolute Error
RMS = Root Mean Square Error
(See text for definitions)

Observed Head and Well Construction data from USGS:
http://waterdata.usgs.gov/nwis/gw

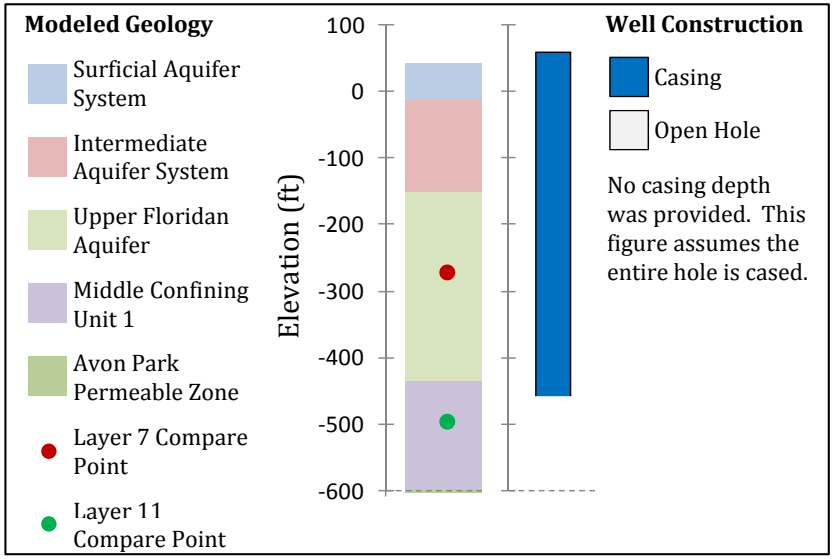

Statistics (Layer 7 Comparison)	
Obs. Count	1533
Obs. Range	31.11
ME	1.24
MAE	3.30
RMS	4.29
RMS as % of Range	14%

Well Location:

Comparison of no-ASR Modeled Results to Head Data: Carrol Well

Regional Model Production Scenario Report

Figure 2.40

June 2013

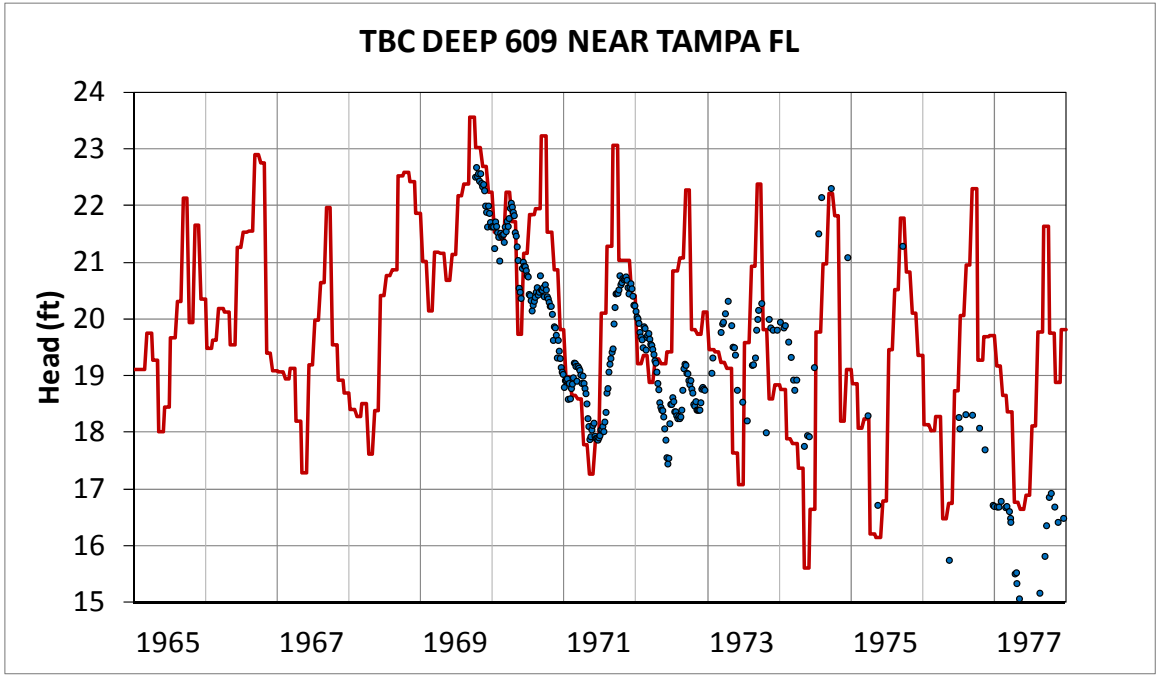

Plot Legend

- Observed Heads
- Model Result – Layer 7 (UF)

Statistics Abbreviations:

ME = Mean Error
MAE = Mean Absolute Error
RMS = Root Mean Square Error
(See text for definitions)

Observed Head and Well Construction data from USGS:
http://waterdata.usgs.gov/nwis/gw

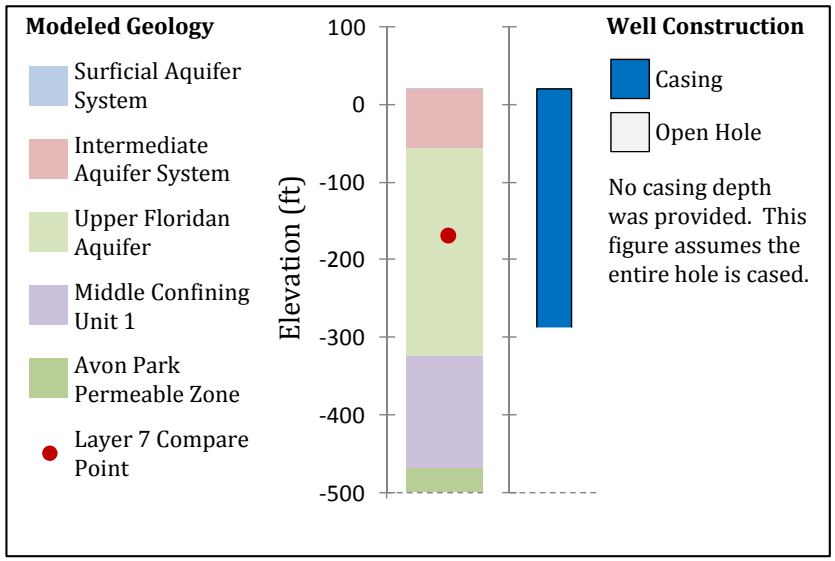

Statistics	
Obs. Count	312
Obs. Range	8.76
ME	0.75
MAE	1.22
RMS	1.57
RMS as % of Range	18%

Well Location:

Comparison of no-ASR Modeled Results to Head Data: TBC Deep 609

Regional Model Production Scenario Report

Figure 2.41

June 2013

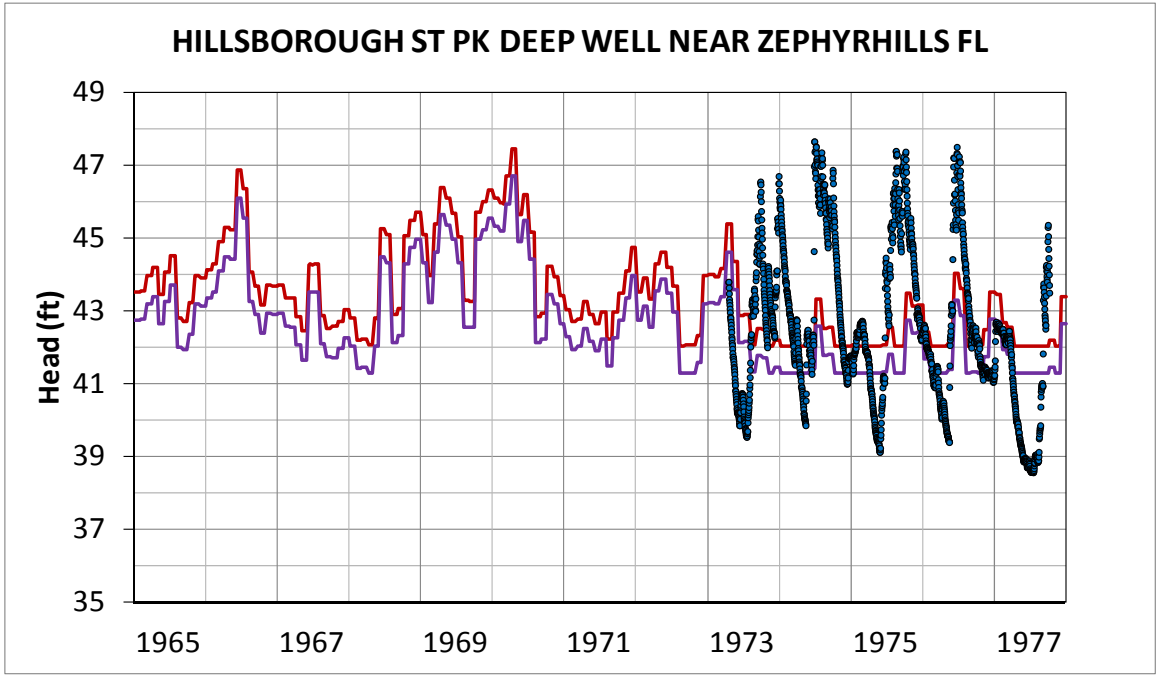

Plot Legend

- Observed Heads
- Model Result – Layer 7 (UF)
- Model Result – Layer 4 (IAS)

Statistics Abbreviations:

ME = Mean Error
MAE = Mean Absolute Error
RMS = Root Mean Square Error
(See text for definitions)

Observed Head and Well Construction data from USGS:
http://waterdata.usgs.gov/nwis/gw

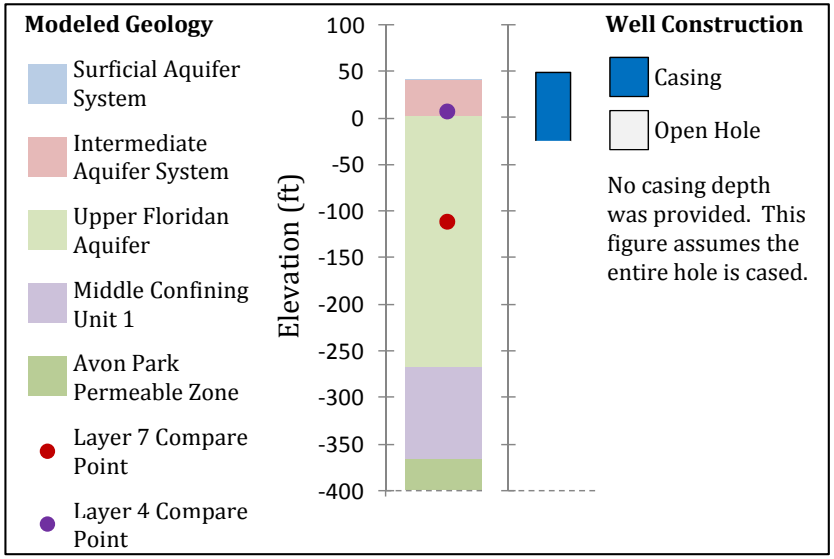

Statistics (Layer 7 Comparison)	
Obs. Count	1635
Obs. Range	9.08
ME	-0.11
MAE	1.72
RMS	2.12
RMS as % of Range	23%

Well Location:

Comparison of no-ASR Modeled Results to Head Data: Hillsborough St Pk Deep Well

Regional Model Production Scenario Report

Figure 2.42

June 2013

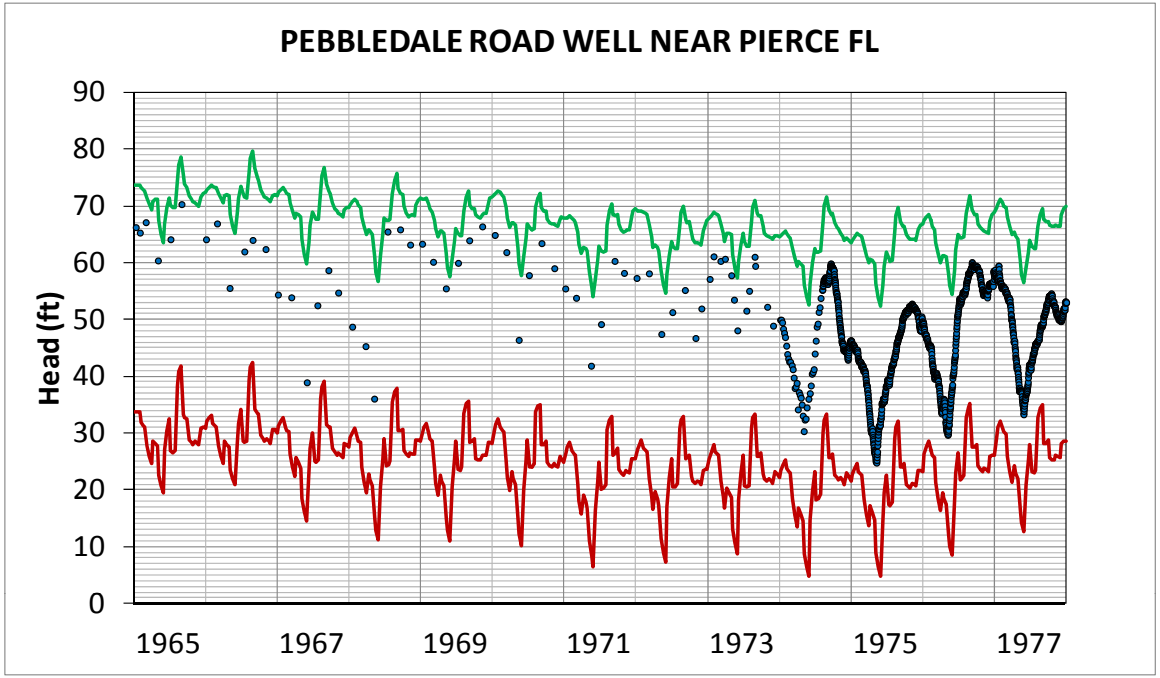

Plot Legend

- Observed Heads
- Model Result – Layer 4 (IAS)
- Model Result – Layer 7 (UF)

Statistics Abbreviations:

ME = Mean Error
MAE = Mean Absolute Error
RMS = Root Mean Square Error
(See text for definitions)

Observed Head and Well Construction data from USGS:
http://waterdata.usgs.gov/nwis/gw

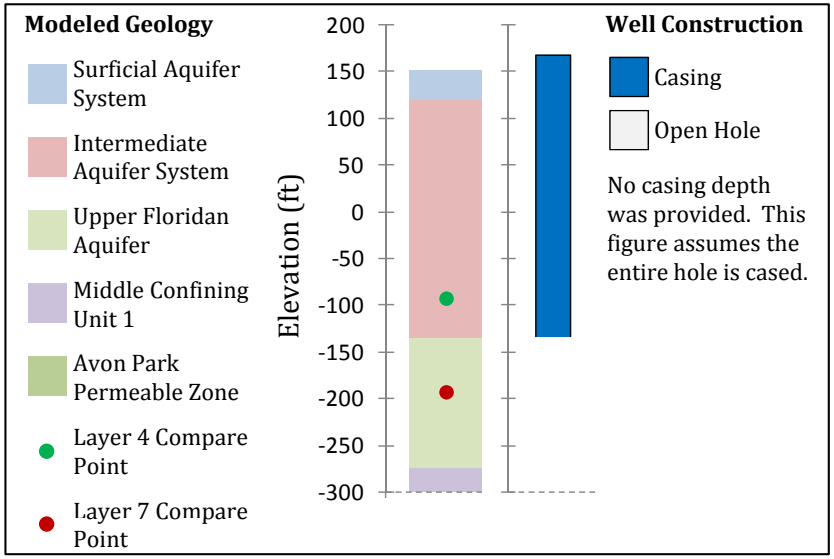

Statistics		
Compare Layer	7 (UF)	4 (IAS)
Obs. Count	1345	
Obs. Range	45.50	
ME	-24.25	17.33
MAE	24.25	17.33
RMS	24.95	18.23
RMS as % of Range	55%	40%

Well Location:

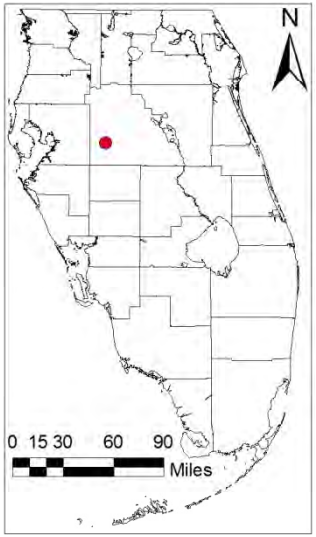

Comparison of no-ASR Modeled Results to Head Data: Pebbledale Road Well

Regional Model Production Scenario Report

Figure 2.43

June 2013

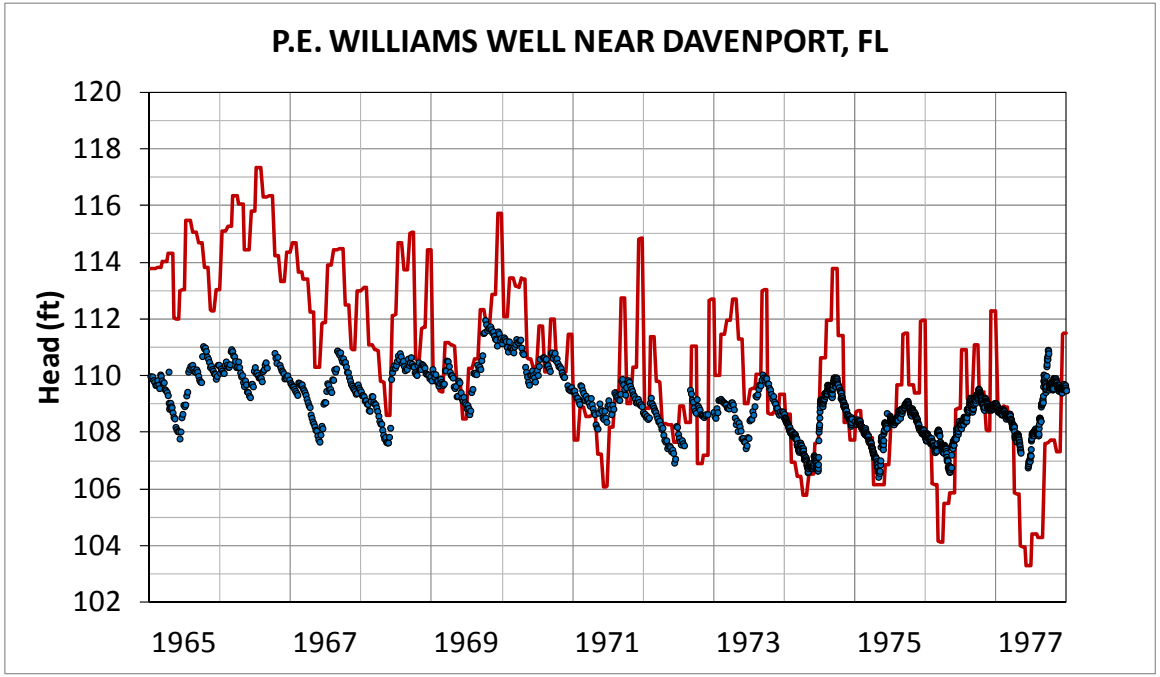

Plot Legend

- Observed Heads
- Model Result – Layer 7 (UF)

Statistics Abbreviations:

ME = Mean Error
MAE = Mean Absolute Error
RMS = Root Mean Square Error
(See text for definitions)

Observed Head and Well Construction data from USGS:
http://waterdata.usgs.gov/nwis/gw

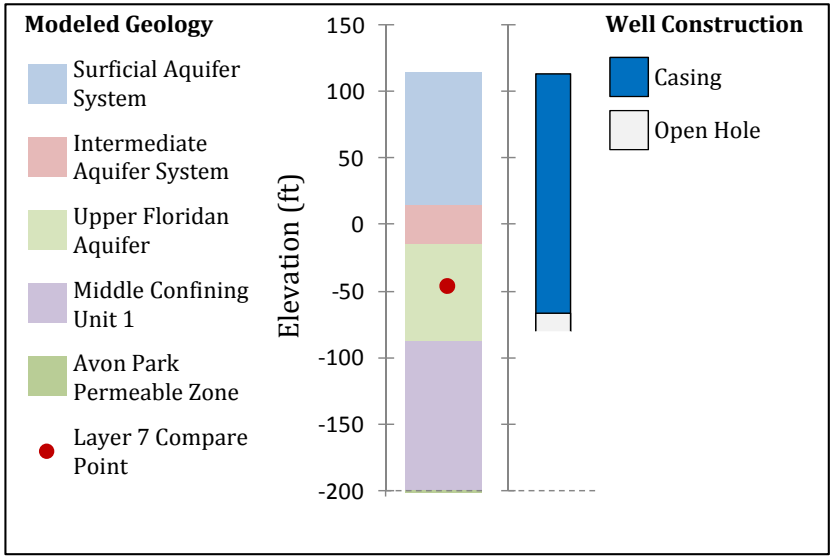

Statistics	
Obs. Count	2000
Obs. Range	5.53
ME	0.62
MAE	1.77
RMS	2.32
RMS as % of Range	42%

Well Location:

COMPARISON OF NO-ASR MODELED RESULTS TO HEAD DATA: P.E. WILLIAMS WELL

REGIONAL MODEL PRODUCTION SCENARIO REPORT

Figure 2.44

June 2013

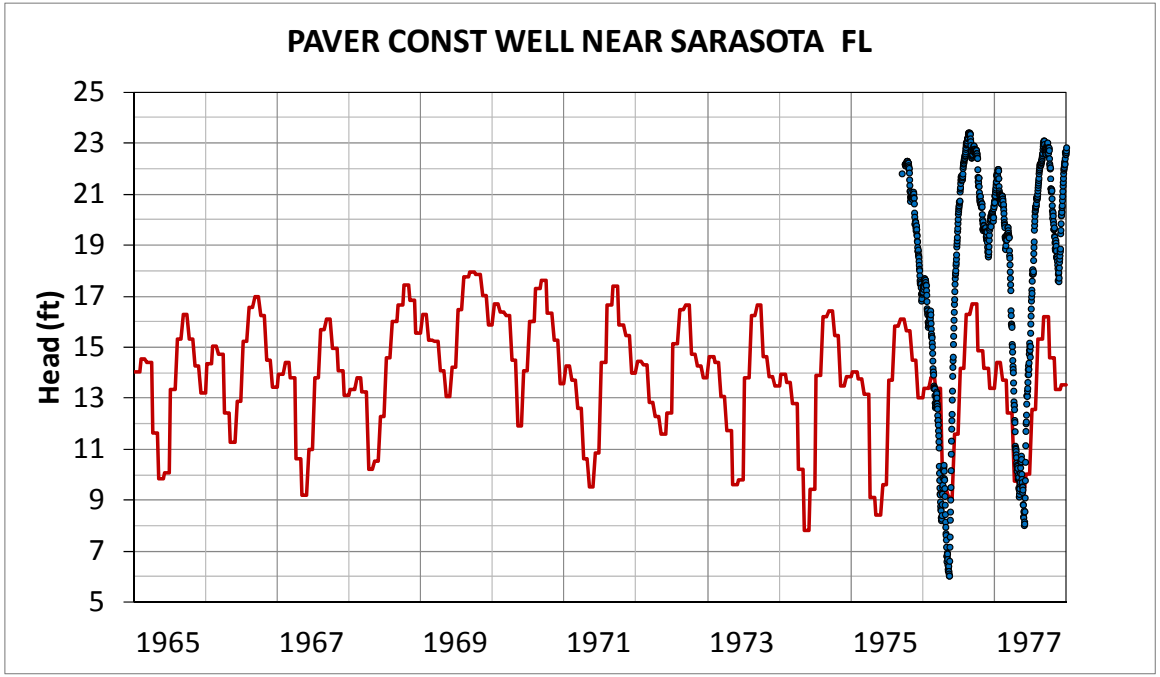

Plot Legend

- Observed Heads
- Model Result – Layer 7 (UF)

Statistics Abbreviations:

ME = Mean Error
MAE = Mean Absolute Error
RMS = Root Mean Square Error
(See text for definitions)

Observed Head and Well Construction data from USGS:
http://waterdata.usgs.gov/nwis/gw

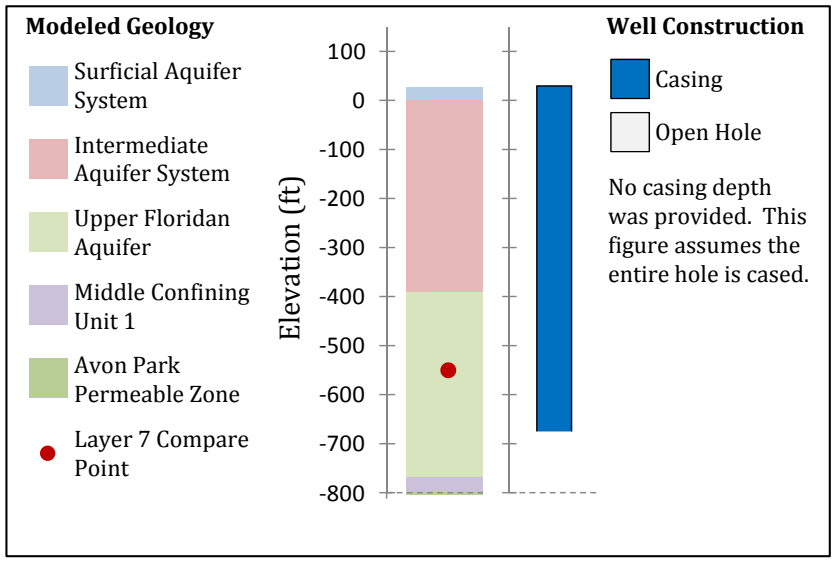

Statistics	
Obs. Count	824
Obs. Range	17.37
ME	-4.69
MAE	5.06
RMS	5.56
RMS as % of Range	32%

Well Location:

Comparison of no-ASR Modeled Results to Head Data: Paver Const Well

Regional Model Production Scenario Report

Figure 2.45

June 2013

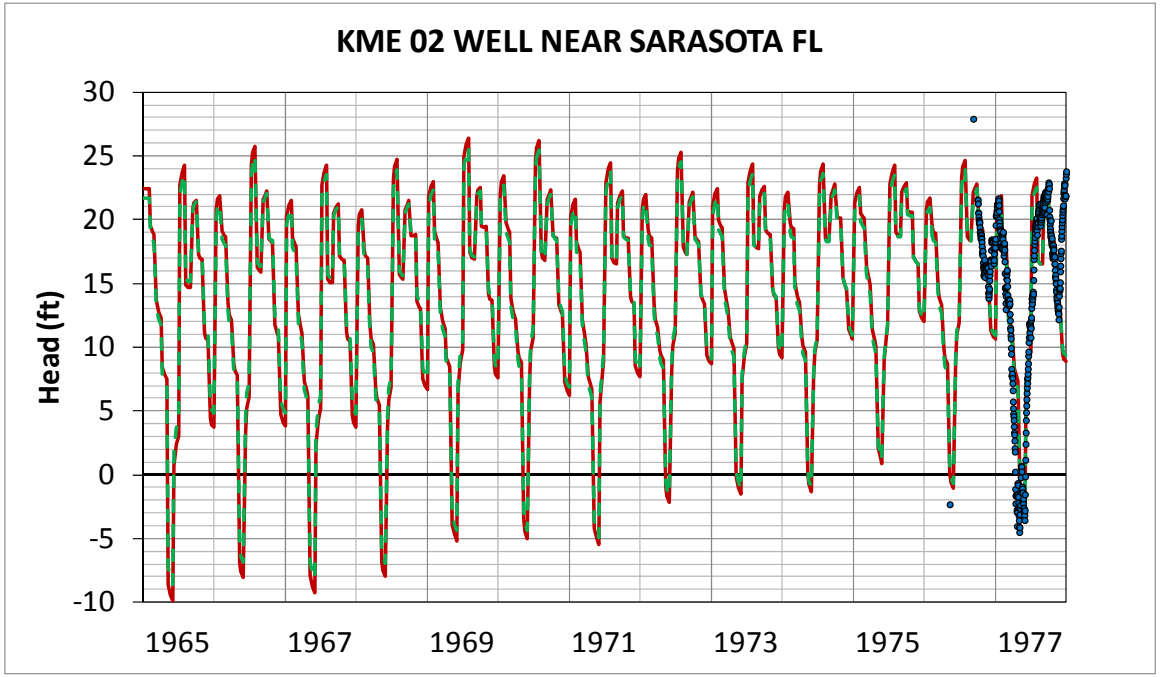

Plot Legend

- Observed Heads
- Model Result – Layer 7 (UF)
- Model Result – Layer 11 (MC1)

Statistics Abbreviations:

ME = Mean Error
MAE = Mean Absolute Error
RMS = Root Mean Square Error
(See text for definitions)

Observed Head and Well Construction data from USGS:
http://waterdata.usgs.gov/nwis/gw

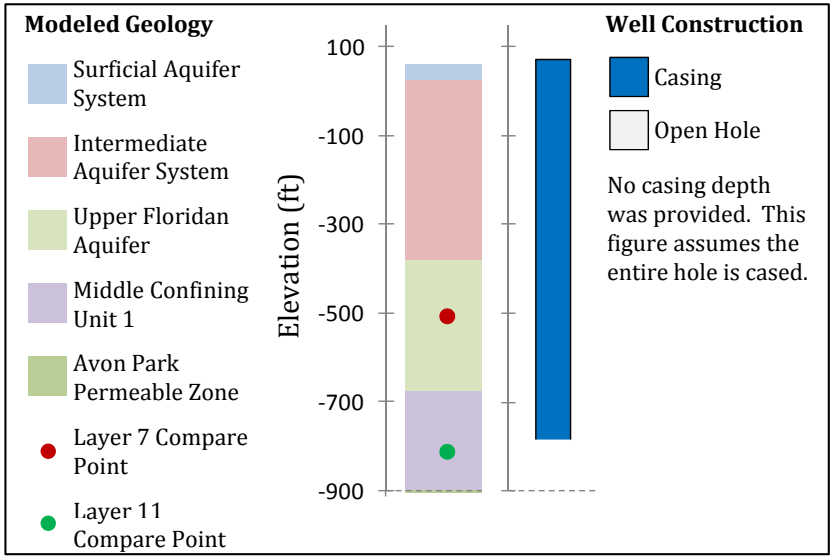

Statistics (Layer 7 Comparison)	
Obs. Count	460
Obs. Range	53.66
ME	-0.38
MAE	3.26
RMS	4.83
RMS as % of Range	9%

Well Location:

Comparison of no-ASR Modeled Results to Head Data: KME 02 Well

Regional Model Production Scenario Report

Figure 2.46

June 2013

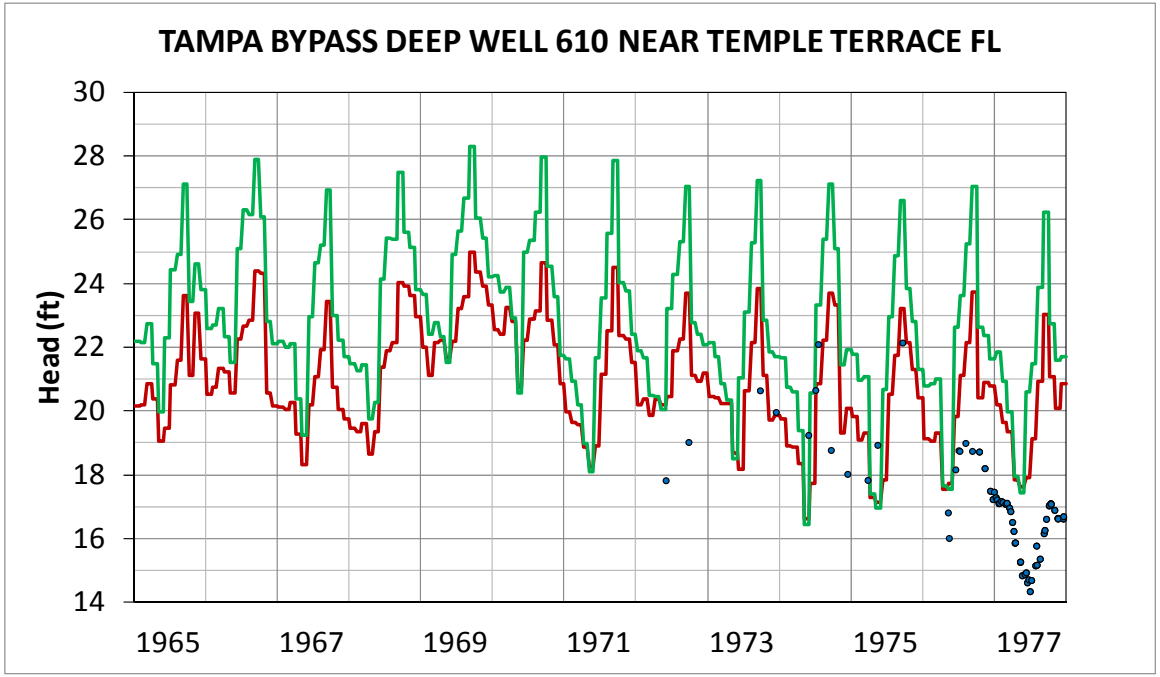

Plot Legend

- Observed Heads
- Model Result – Layer 7 (UF)
- Model Result – Layer 14 (APPZ)

Statistics Abbreviations:

ME = Mean Error
MAE = Mean Absolute Error
RMS = Root Mean Square Error
(See text for definitions)

Observed Head and Well Construction data from USGS:
http://waterdata.usgs.gov/nwis/gw

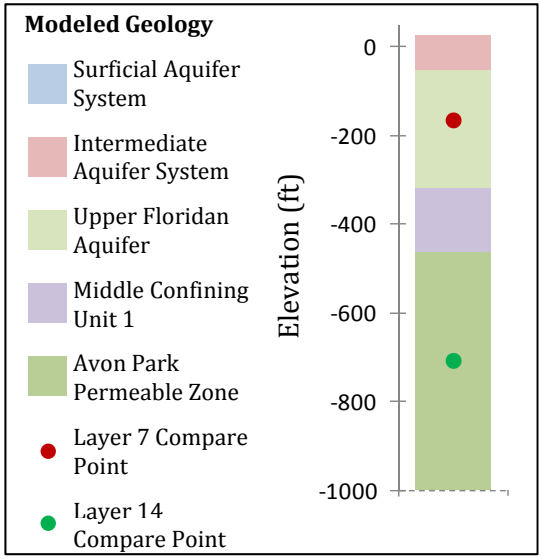

No depth information is provided for this well. USGS reports that it is completed in the Floridan Aquifer System.

Statistics		
Compare Layer	7 (UF)	14 (APPZ)
Obs. Count	109	
Obs. Range	7.80	
ME	3.09	4.70
MAE	3.23	4.79
RMS	3.48	5.23
RMS as % of Range	45%	67%

Well Location:

Comparison of no-ASR Modeled Results to Head Data: Tampa Bypass Deep Well 610

Regional Model Production Scenario Report

Figure 2.47

June 2013

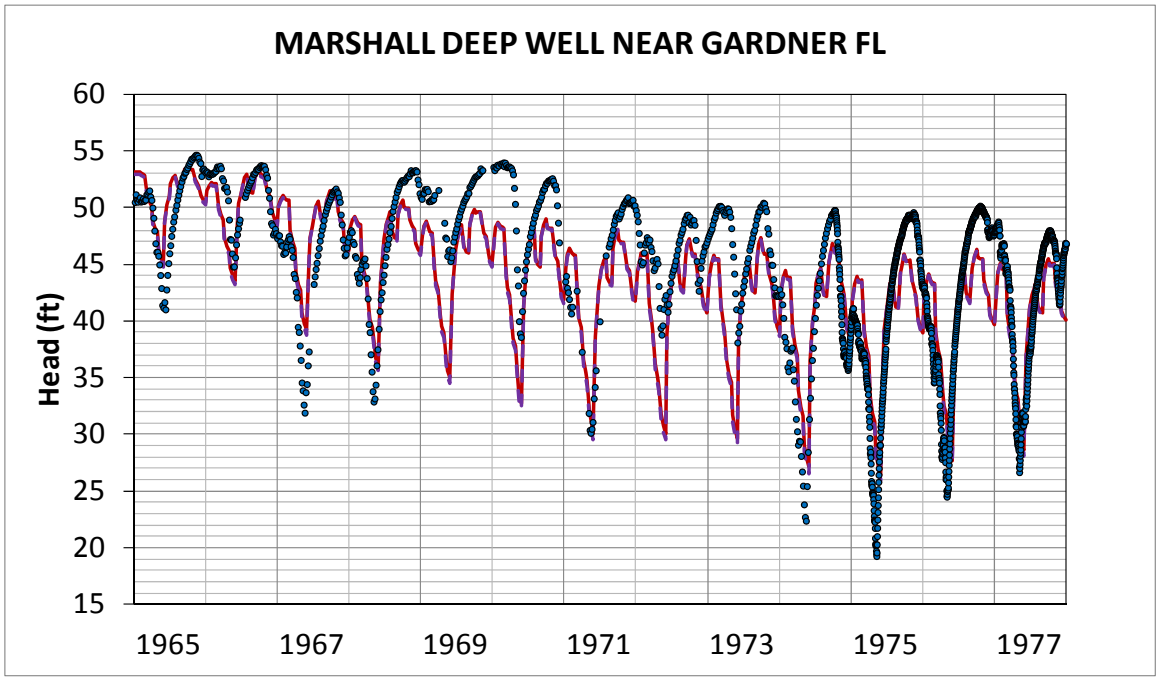

Plot Legend

- Observed Heads
- Model Result – Layer 7 (UF)
- Model Result – Layer 4 (IAS)

Statistics Abbreviations:

ME = Mean Error
MAE = Mean Absolute Error
RMS = Root Mean Square Error
(See text for definitions)

Observed Head and Well Construction data from USGS:
http://waterdata.usgs.gov/nwis/gw

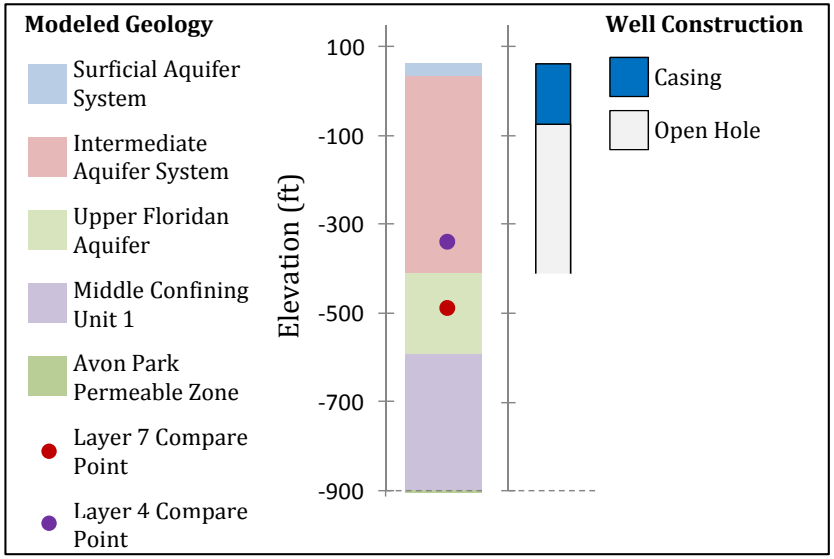

Statistics (Layer 7 Comparison)	
Obs. Count	1834
Obs. Range	35.40
ME	-0.94
MAE	3.57
RMS	4.32
RMS as % of Range	12%

Well Location:

COMPARISON OF NO-ASR MODELED RESULTS TO HEAD DATA: MARSHALL DEEP WELL

REGIONAL MODEL PRODUCTION SCENARIO REPORT

Figure 2.48

June 2013

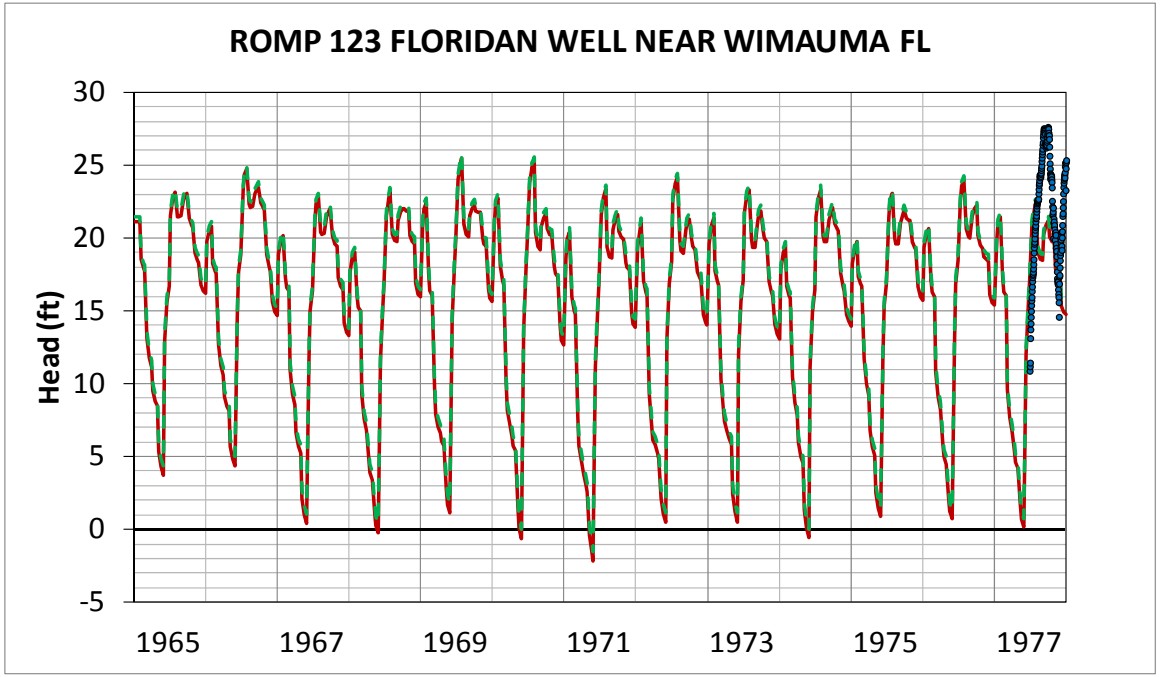

Plot Legend

- Observed Heads
- Model Result – Layer 7 (UF)
- Model Result – Layer 11 (MC1)

Statistics Abbreviations:

ME = Mean Error
MAE = Mean Absolute Error
RMS = Root Mean Square Error
(See text for definitions)

Observed Head and Well Construction data from USGS:
http://waterdata.usgs.gov/nwis/gw

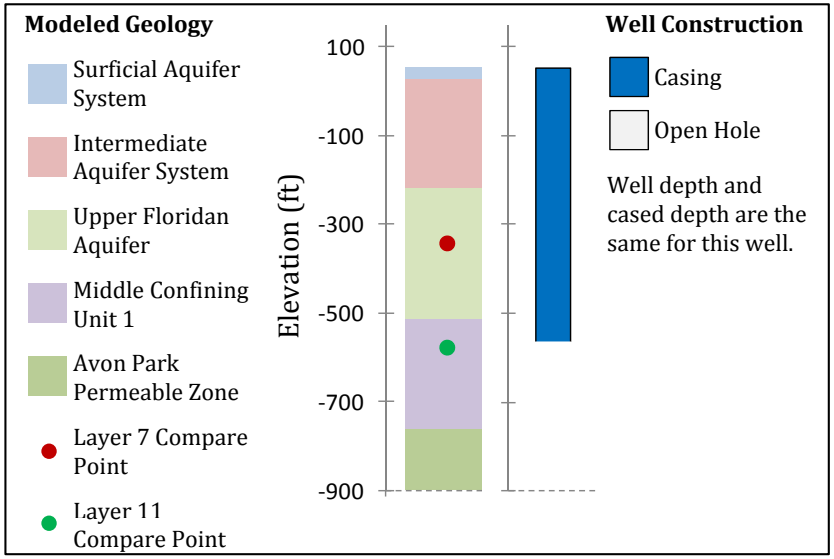

Statistics (Layer 7 Comparison)	
Obs. Count	187
Obs. Range	16.73
ME	-3.03
MAE	4.34
RMS	5.10
RMS as % of Range	30%

Well Location:

Comparison of no-ASR Modeled Results to Head Data: ROMP 123 Floridan Well

Regional Model Production Scenario Report

Figure 2.49

June 2013

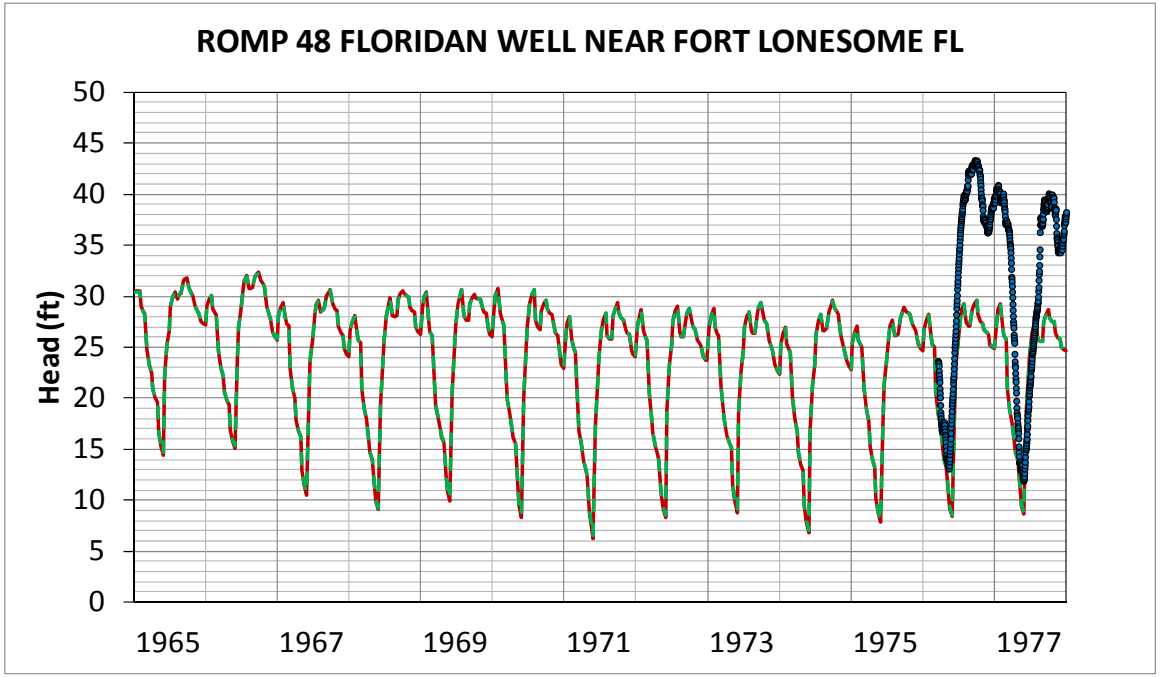

Plot Legend

- Observed Heads
- Model Result – Layer 7 (UF)
- Model Result – Layer 11 (MC1)

Statistics Abbreviations:

ME = Mean Error
MAE = Mean Absolute Error
RMS = Root Mean Square Error
(See text for definitions)

Observed Head and Well Construction data from USGS:
http://waterdata.usgs.gov/nwis/gw

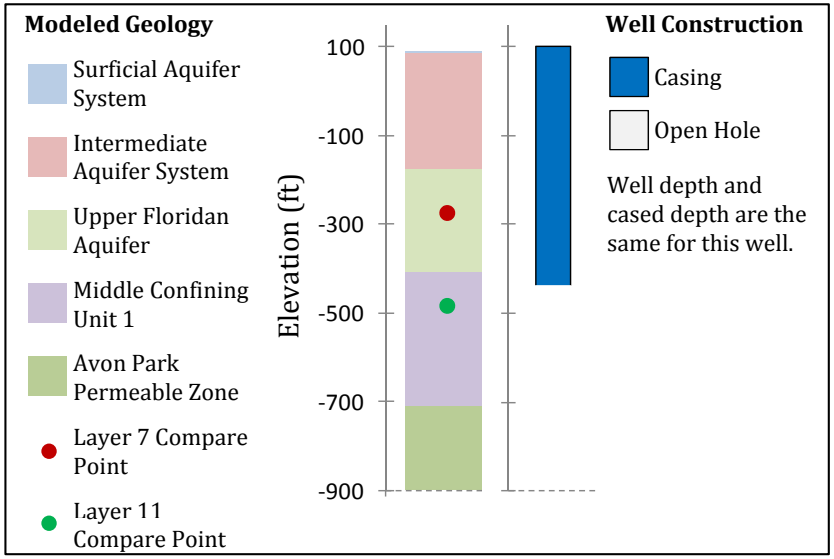

Statistics (Layer 7 Comparison)	
Obs. Count	654
Obs. Range	31.41
ME	-8.73
MAE	9.08
RMS	10.12
RMS as % of Range	32%

Well Location:

Comparison of no-ASR Modeled Results to Head Data: ROMP 48 Floridan Well

Regional Model Production Scenario Report

Figure 2.50

June 2013

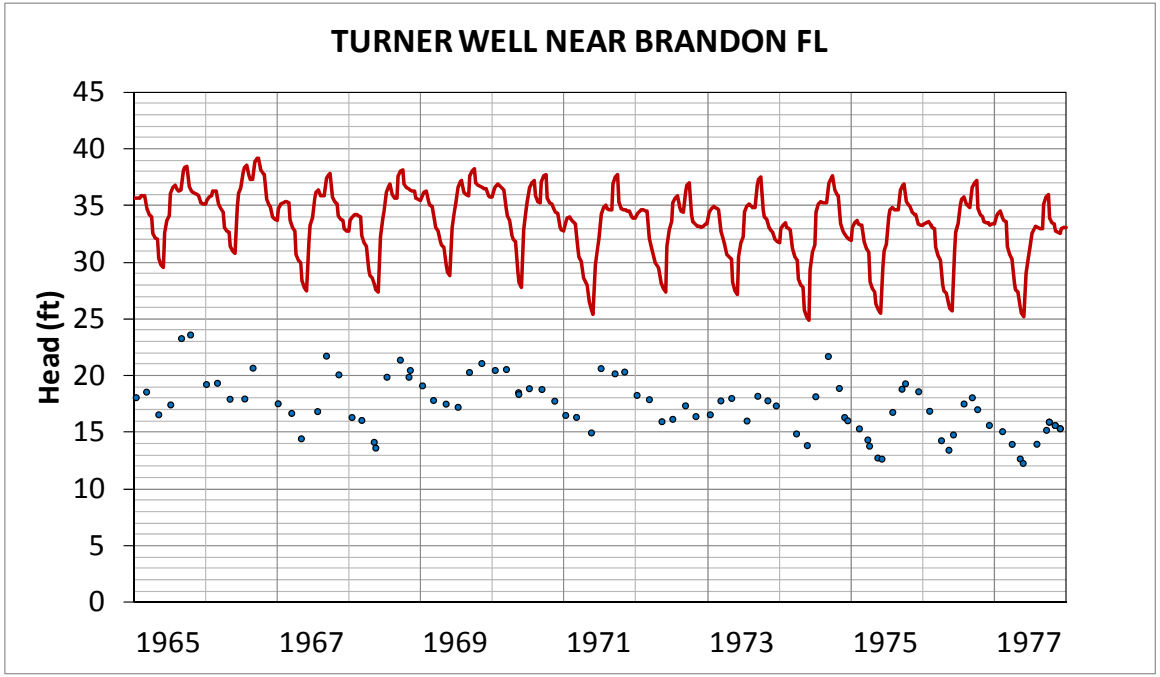

Plot Legend

- Observed Heads
- Model Result – Layer 7 (UF)

Statistics Abbreviations:

ME = Mean Error
MAE = Mean Absolute Error
RMS = Root Mean Square Error
(See text for definitions)

Observed Head and Well Construction data from USGS:
http://waterdata.usgs.gov/nwis/gw

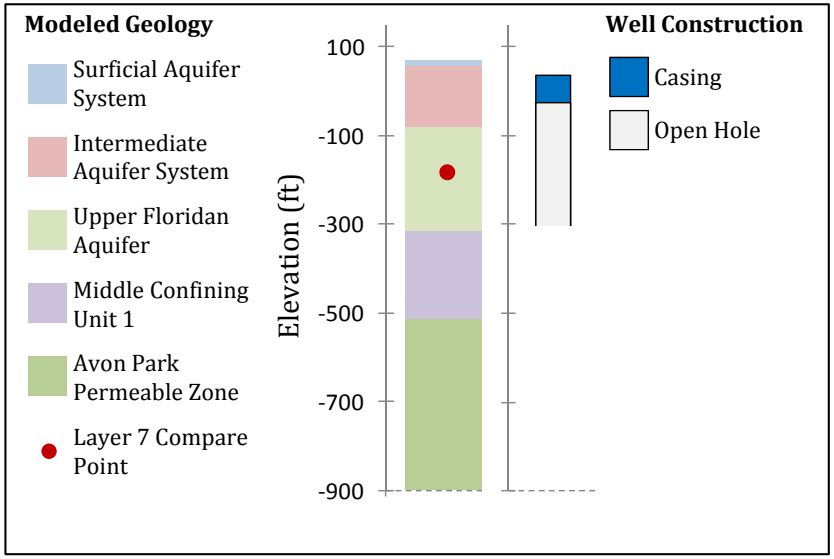

Statistics	
Obs. Count	93
Obs. Range	11.33
ME	16.01
MAE	16.01
RMS	16.17
RMS as % of Range	143%

Well Location:

COMPARISON OF NO-ASR MODELED RESULTS TO HEAD DATA: TURNER WELL

REGIONAL MODEL PRODUCTION SCENARIO REPORT

Figure 2.51

June 2013

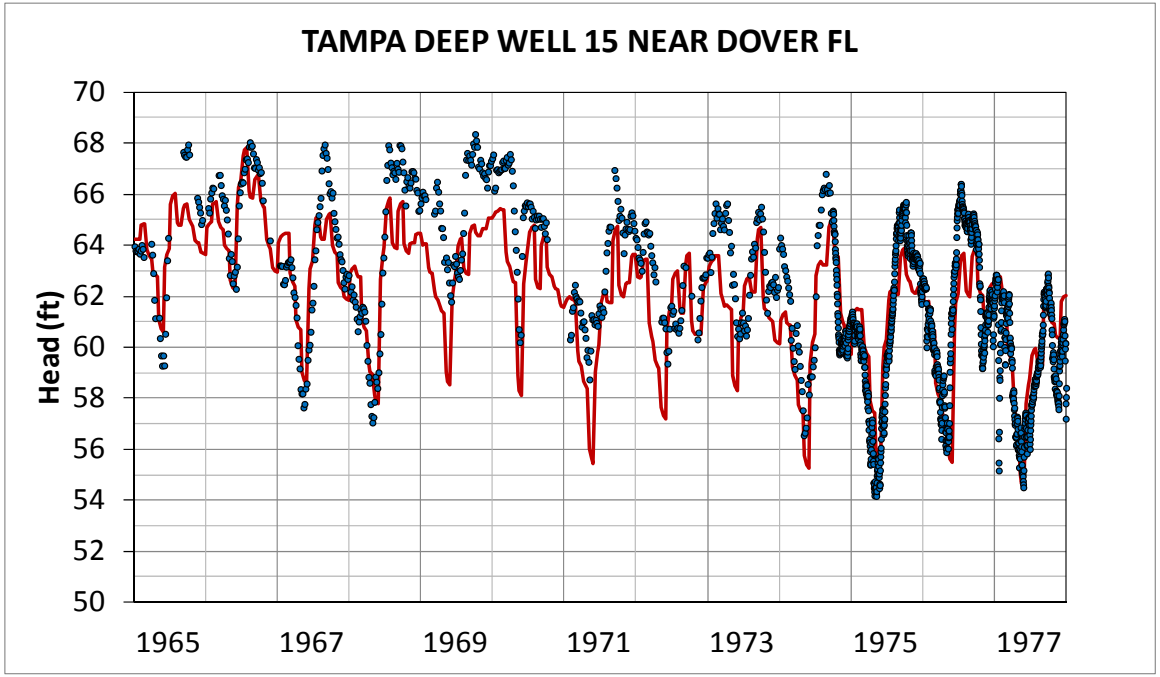

Plot Legend

- Observed Heads
- Model Result – Layer 7 (UF)

Statistics Abbreviations:

ME = Mean Error
MAE = Mean Absolute Error
RMS = Root Mean Square Error
(See text for definitions)

Observed Head and Well Construction data from USGS:
http://waterdata.usgs.gov/nwis/gw

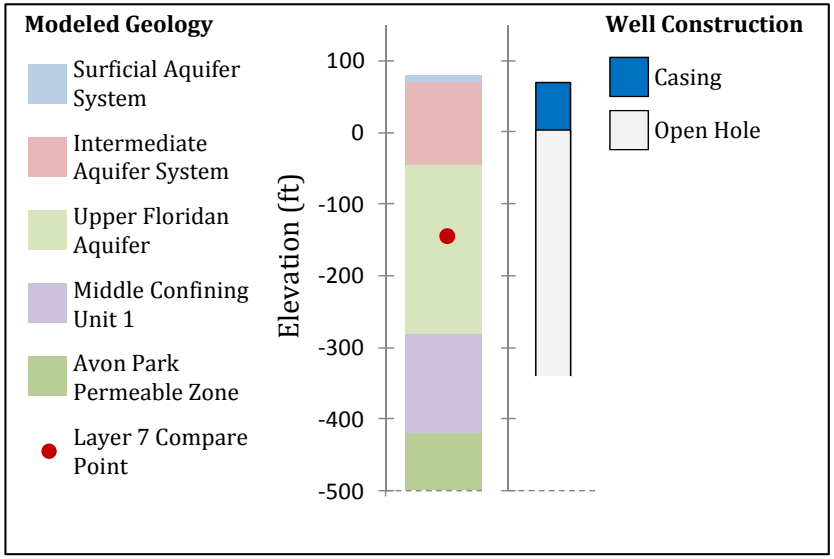

Statistics	
Obs. Count	1783
Obs. Range	14.19
ME	-0.36
MAE	1.43
RMS	1.79
RMS as % of Range	13%

Well Location:

Comparison of no-ASR Modeled Results to Head Data: Tampa Deep Well 15

Regional Model Production Scenario Report

Figure 2.52

June 2013

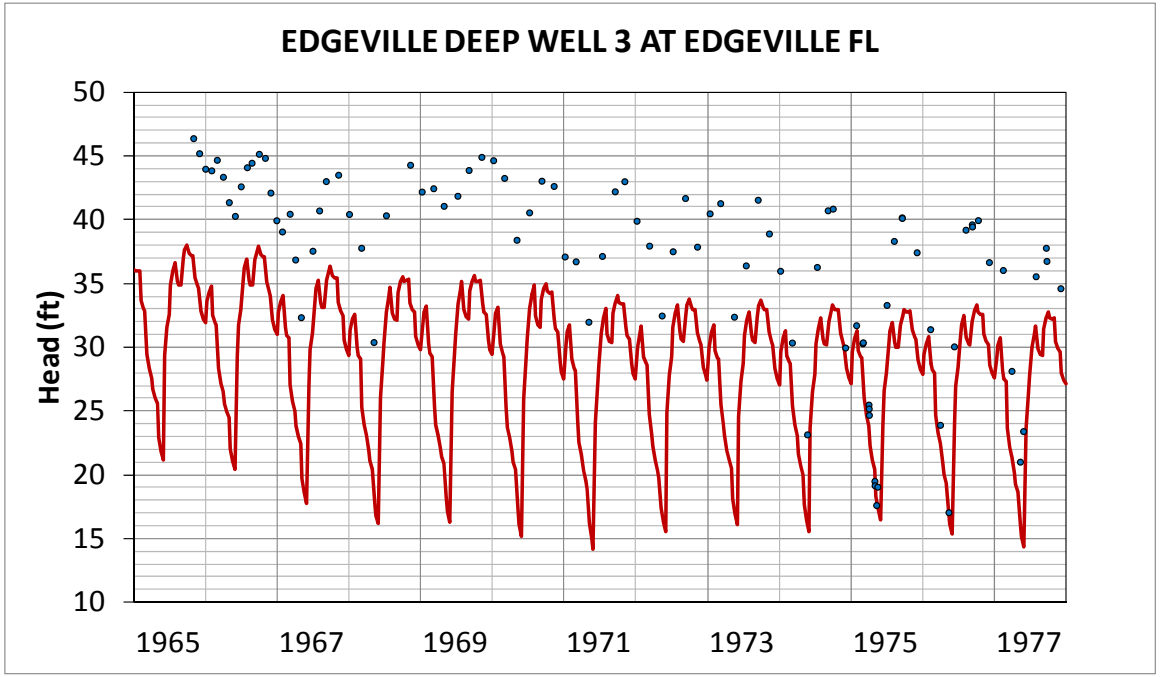

Plot Legend

- Observed Heads
- Model Result – Layer 7 (UF)

Statistics Abbreviations:

ME = Mean Error
MAE = Mean Absolute Error
RMS = Root Mean Square Error
(See text for definitions)

Observed Head and Well Construction data from USGS:
http://waterdata.usgs.gov/nwis/gw

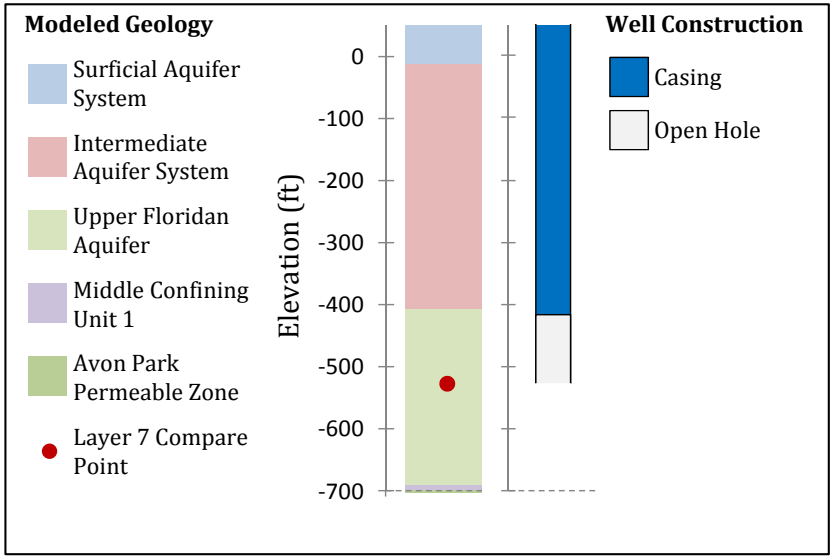

Statistics	
Obs. Count	97
Obs. Range	29.33
ME	-8.28
MAE	8.34
RMS	9.44
RMS as % of Range	32%

Well Location:

Comparison of no-ASR Modeled Results to Head Data: Hillsborough Rd State Park DP

Regional Model Production Scenario Report

Figure 2.53

June 2013

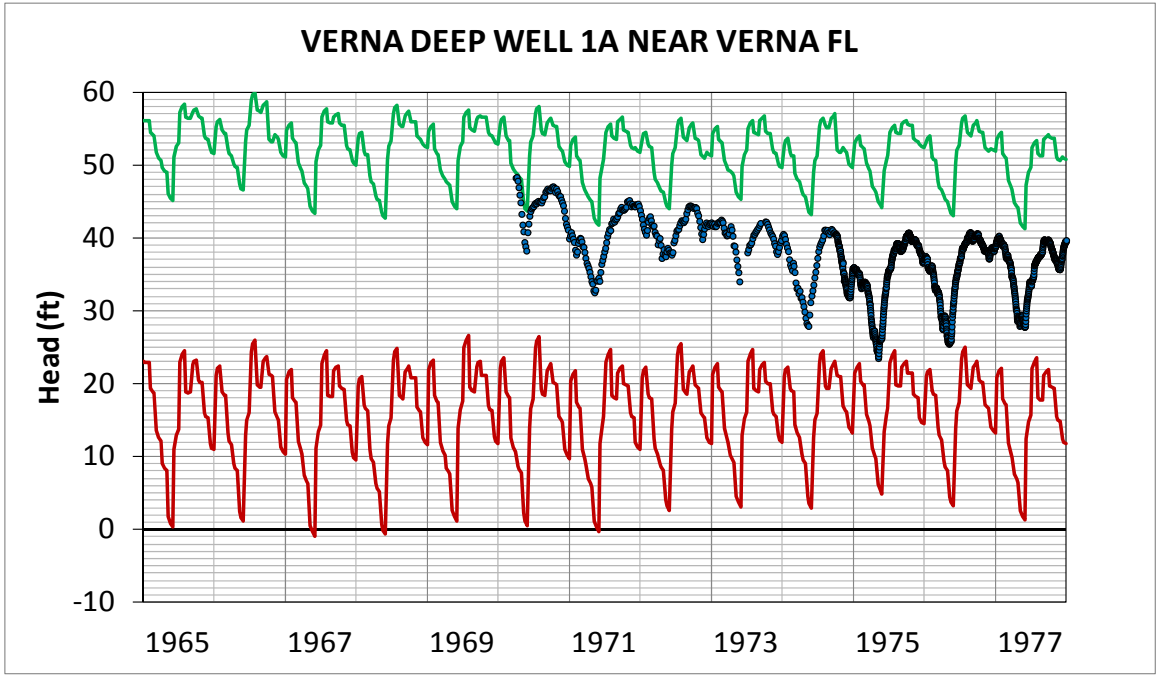

Plot Legend

- Observed Heads
- Model Result – Layer 7 (UF)
- Model Result – Layer 2 (IAS)

Statistics Abbreviations:

ME = Mean Error
MAE = Mean Absolute Error
RMS = Root Mean Square Error
(See text for definitions)

Observed Head and Well Construction data from USGS:
http://waterdata.usgs.gov/nwis/gw

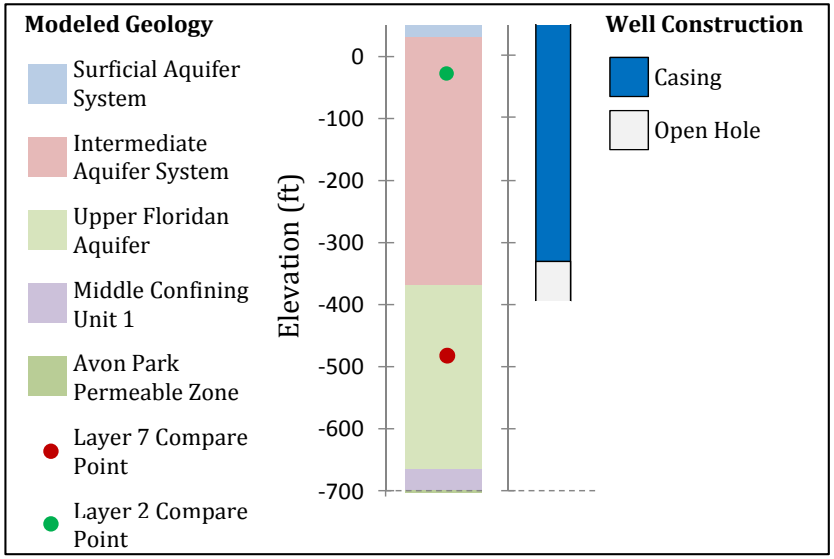

Statistics (Layer 7 Comparison)	
Obs. Count	1502
Obs. Range	24.84
ME	-20.27
MAE	20.27
RMS	24.84
RMS as % of Range	84%

Well Location:

Comparison of no-ASR Modeled Results to Head Data: Verna Deep Well 1A

Regional Model Production Scenario Report

Figure 2.54

June 2013

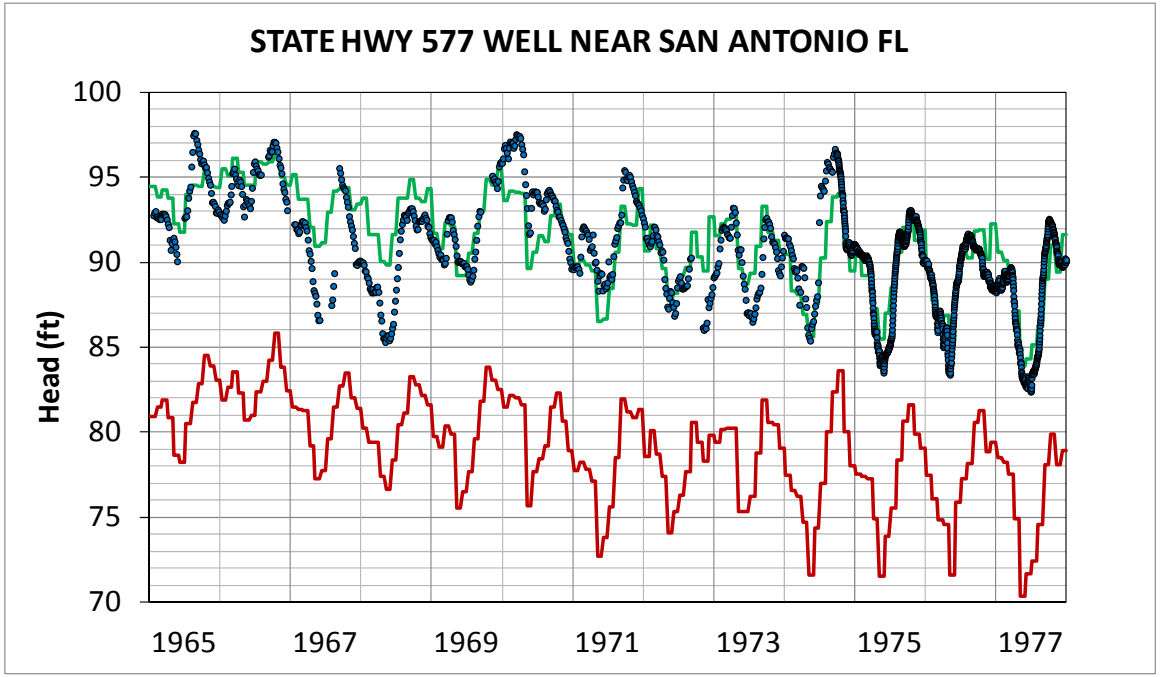

Plot Legend

- Observed Heads
- Model Result – Layer 7 (UF)
- Model Result – Layer 3 (IAS)

Statistics Abbreviations:

ME = Mean Error
MAE = Mean Absolute Error
RMS = Root Mean Square Error
(See text for definitions)

Observed Head and Well Construction data from USGS:
http://waterdata.usgs.gov/nwis/gw

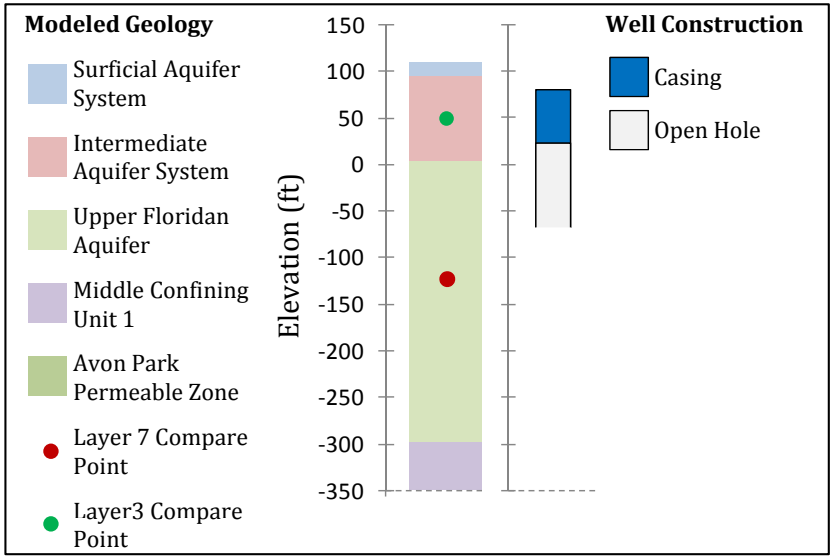

Statistics		
Compare Layer	7 (UF)	3 (IAS)
Obs. Count	1832	
Obs. Range	15.21	
ME	-11.83	0.35
MAE	11.83	1.32
RMS	11.94	1.65
RMS as % of Range	78%	11%

Well Location:

Comparison of no-ASR Modeled Results to Head Data: State Hwy 577 Well

Regional Model Production Scenario Report

Figure 2.55

June 2013

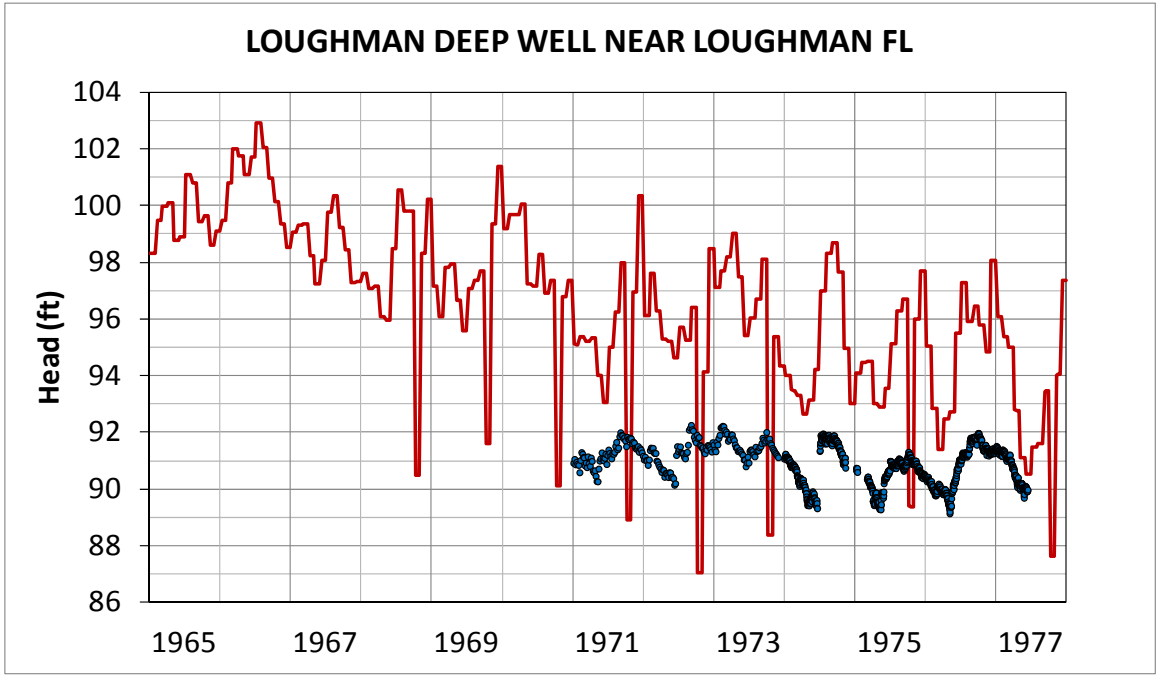

Plot Legend

- Observed Heads
- Model Result – Layer 7 (UF)

Statistics Abbreviations:

ME = Mean Error
MAE = Mean Absolute Error
RMS = Root Mean Square Error
(See text for definitions)

Observed Head and Well Construction data from USGS:
http://waterdata.usgs.gov/nwis/gw

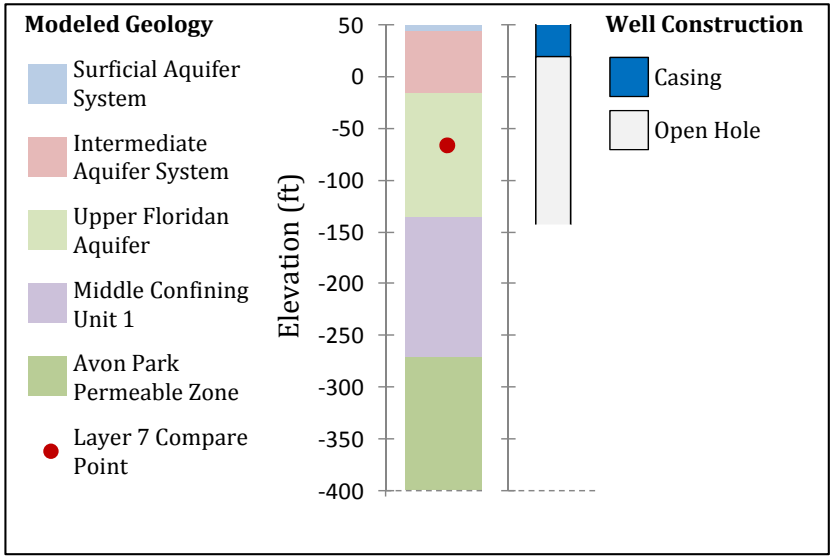

Statistics	
Obs. Count	1353
Obs. Range	3.12
ME	4.05
MAE	4.18
RMS	4.47
RMS as % of Range	143%

Well Location:

COMPARISON OF NO-ASR MODELED RESULTS TO HEAD DATA: LOUGHMAN DEEP WELL

REGIONAL MODEL PRODUCTION SCENARIO REPORT

Figure 2.56

June 2013

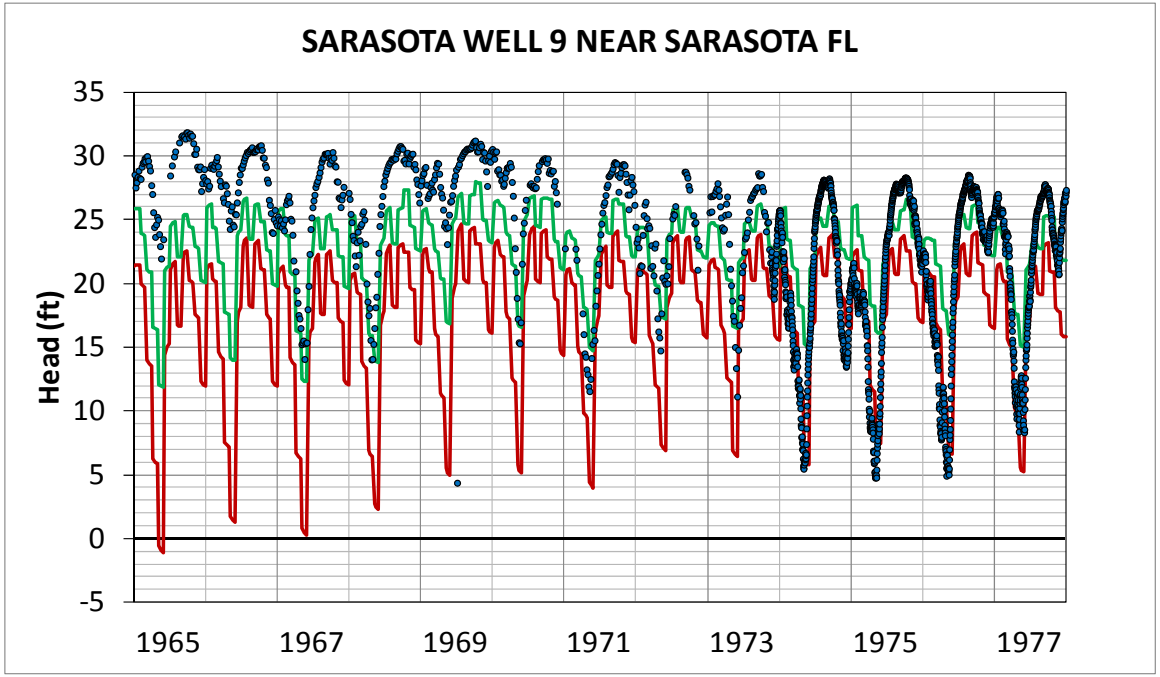

Plot Legend

- Observed Heads
- Model Result – Layer 7 (UF)
- Model Result – Layer 2 (IAS)

Statistics Abbreviations:

ME = Mean Error
MAE = Mean Absolute Error
RMS = Root Mean Square Error
(See text for definitions)

Observed Head and Well Construction data from USGS:
http://waterdata.usgs.gov/nwis/gw

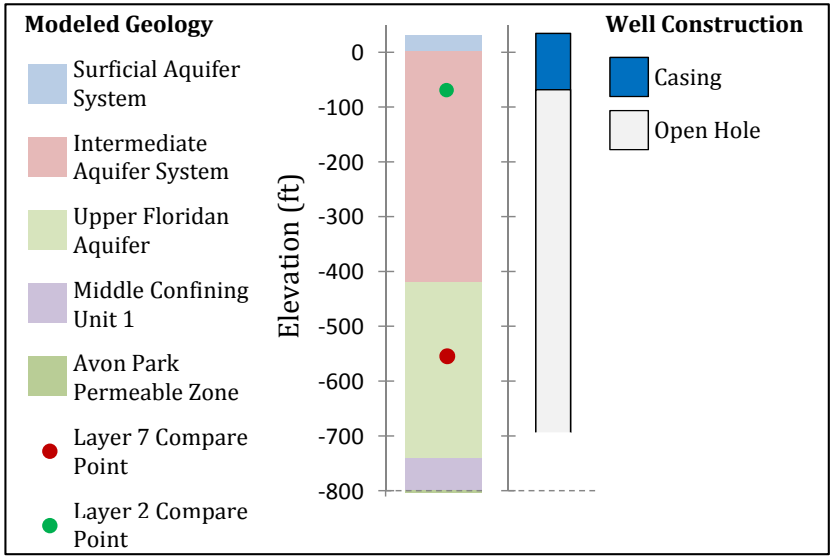

Statistics		
Compare Layer	7 (UF)	2 (IAS)
Obs. Count	2071	
Obs. Range	27.48	
ME	-4.30	0.46
MAE	5.40	3.72
RMS	6.55	4.72
RMS as % of Range	24%	17%

Well Location:

COMPARISON OF NO-ASR MODELED RESULTS TO HEAD DATA: SARASOTA WELL 9

REGIONAL MODEL PRODUCTION SCENARIO REPORT

Figure 2.57

June 2013

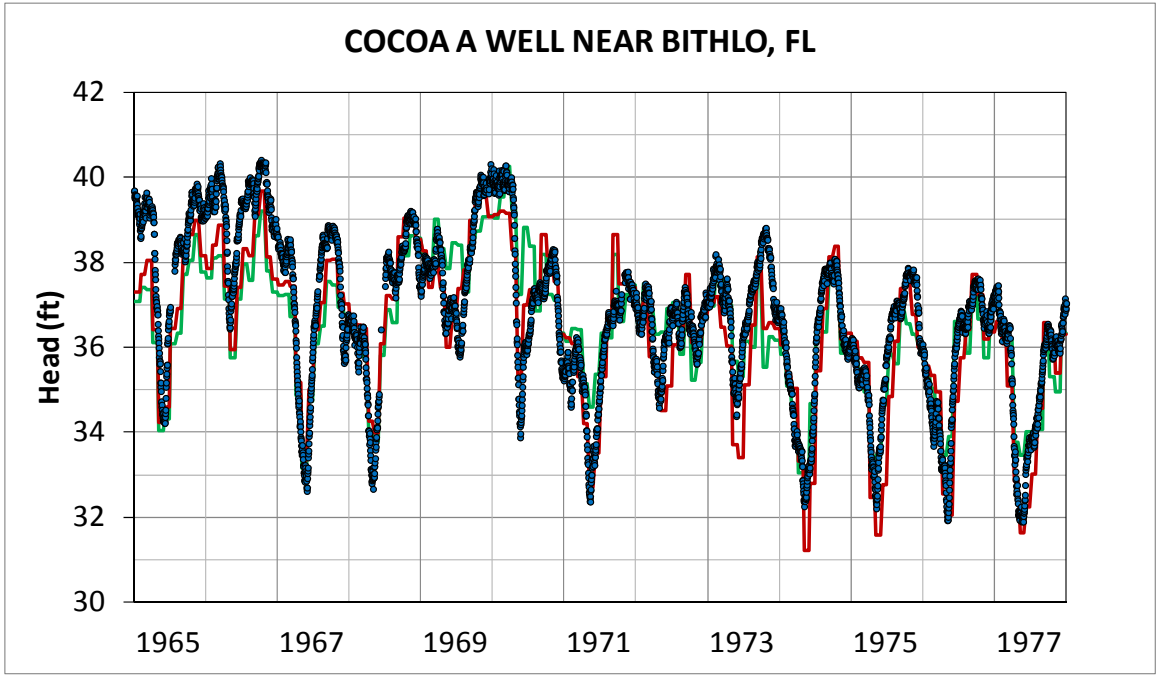

Plot Legend

- Observed Heads
- Model Result – Layer 7 (UF)
- Model Result – Layer 14 (APPZ)

Statistics Abbreviations:

ME = Mean Error
MAE = Mean Absolute Error
RMS = Root Mean Square Error
(See text for definitions)

Observed Head and Well Construction data from USGS:
http://waterdata.usgs.gov/nwis/gw

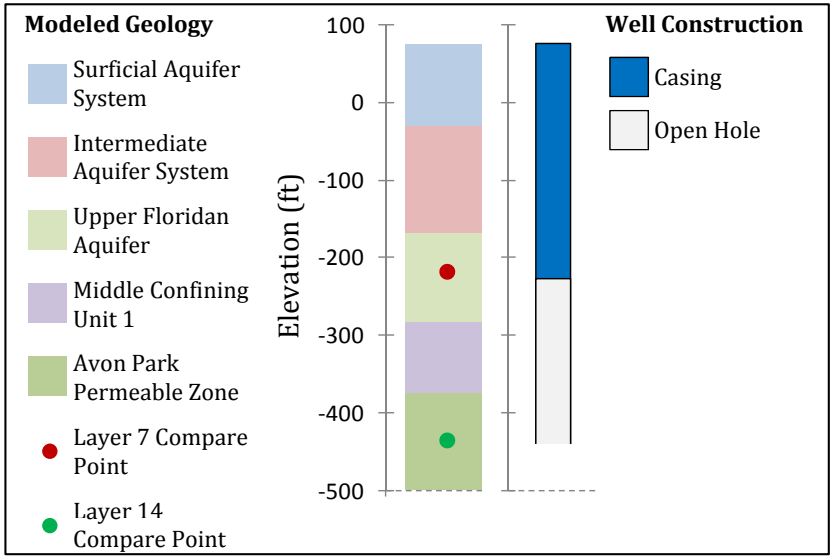

Statistics		
Compare Layer	7 (UF)	14 (APPZ)
Obs. Count	4659	
Obs. Range	8.51	
ME	-0.38	-0.28
MAE	0.74	0.82
RMS	0.92	1.04
RMS as % of Range	11%	12%

Well Location:

Comparison of no-ASR Modeled Results to Head Data: Cocoa A Well

Regional Model Production Scenario Report

Figure 2.58

June 2013

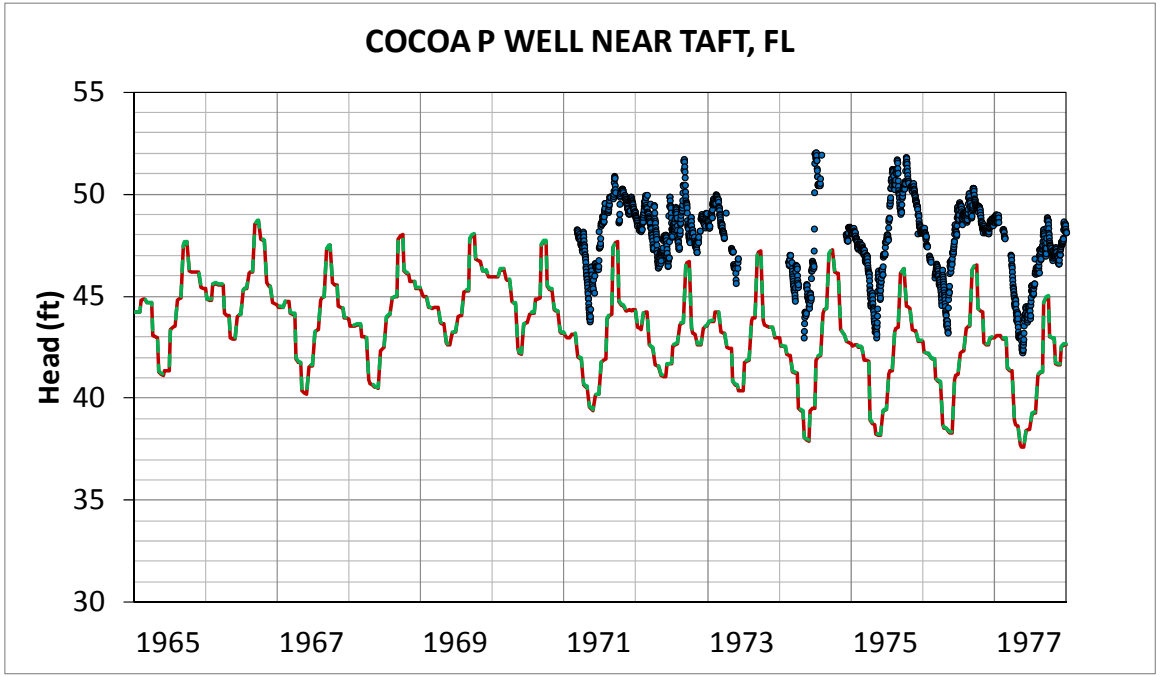

Plot Legend

- Observed Heads
- Model Result – Layer 7 (UF)
- Model Result – Layer 11 (MC1)

Statistics Abbreviations:

ME = Mean Error
MAE = Mean Absolute Error
RMS = Root Mean Square Error
(See text for definitions)

Observed Head and Well Construction data from USGS:
http://waterdata.usgs.gov/nwis/gw

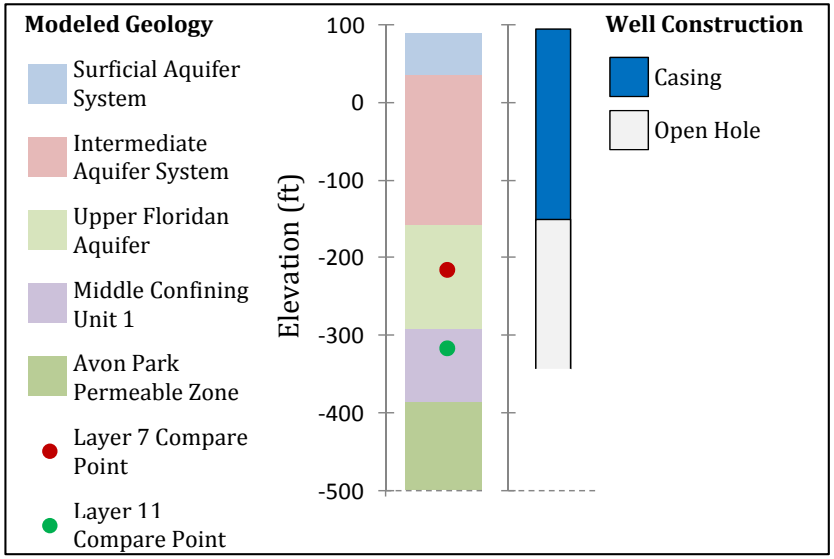

Statistics (Layer 7 Comparison)	
Obs. Count	1851
Obs. Range	9.80
ME	-5.71
MAE	5.71
RMS	5.86
RMS as % of Range	60%

Well Location:

Comparison of no-ASR Modeled Results to Head Data: Cocoa P Well

Regional Model Production Scenario Report

Figure 2.59

June 2013

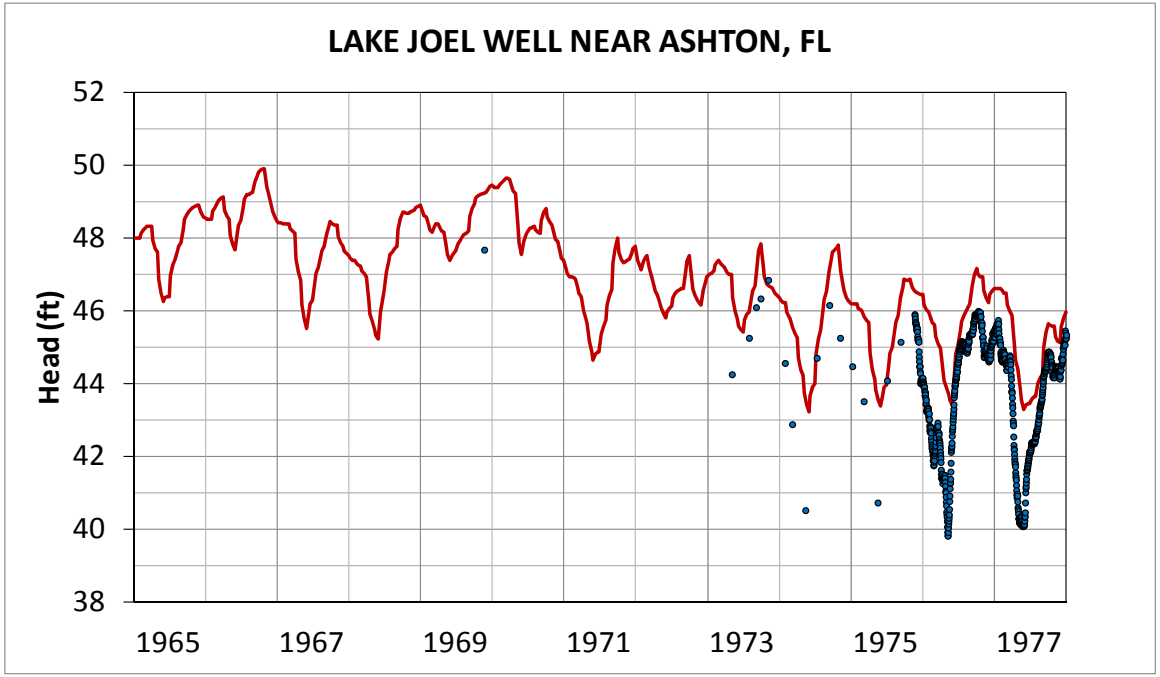

Plot Legend

- Observed Heads
- Model Result – Layer 14 (APPZ)

Statistics Abbreviations:

ME = Mean Error
MAE = Mean Absolute Error
RMS = Root Mean Square Error
(See text for definitions)

Observed Head and Well Construction data from USGS:
http://waterdata.usgs.gov/nwis/gw

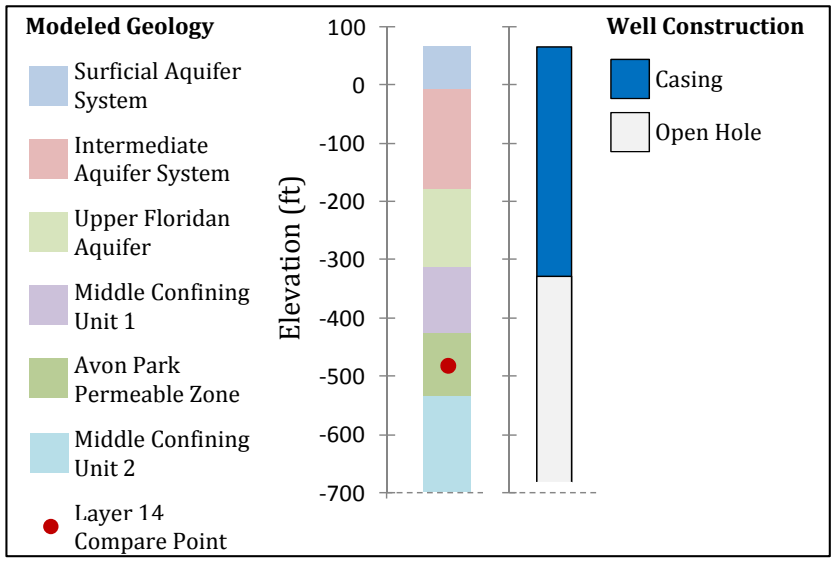

Statistics	
Obs. Count	790
Obs. Range	7.85
ME	1.67
MAE	1.67
RMS	1.93
RMS as % of Range	25%

Well Location:

Comparison of no-ASR Modeled Results to Head Data: Lake Joel Well

Regional Model Production Scenario Report

Figure 2.60

June 2013

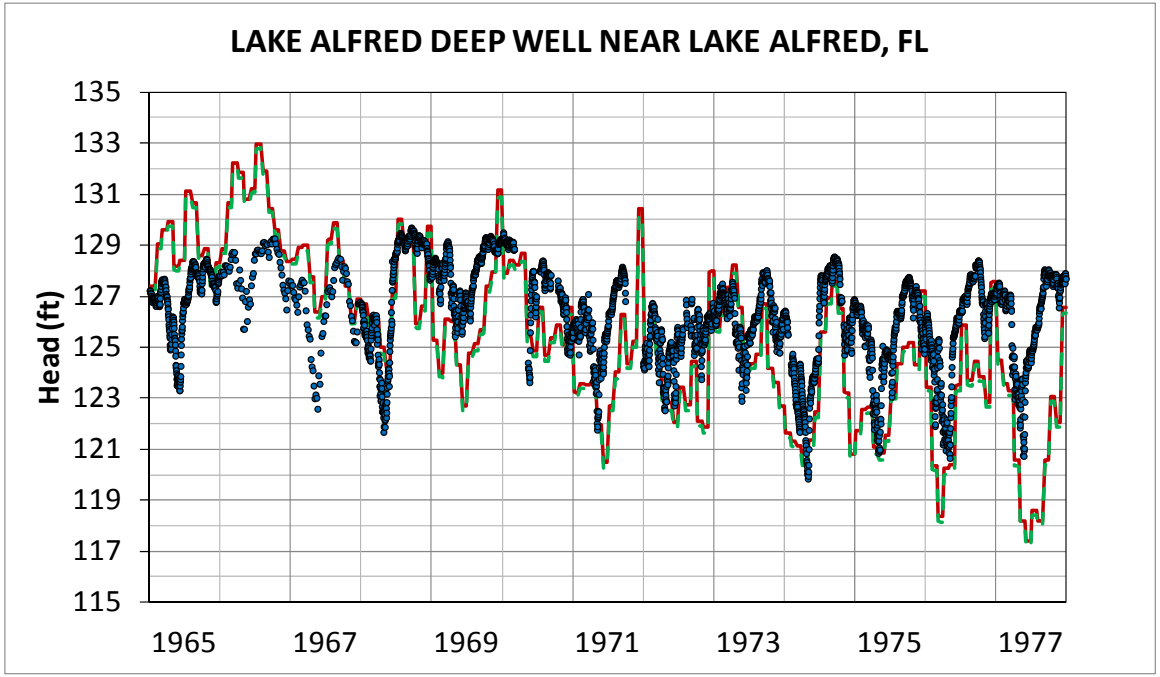

Plot Legend

- Observed Heads
- Model Result – Layer 7 (UF)
- Model Result – Layer 12 (MC1)

Statistics Abbreviations:

ME = Mean Error
MAE = Mean Absolute Error
RMS = Root Mean Square Error
(See text for definitions)

Observed Head and Well Construction data from USGS:
http://waterdata.usgs.gov/nwis/gw

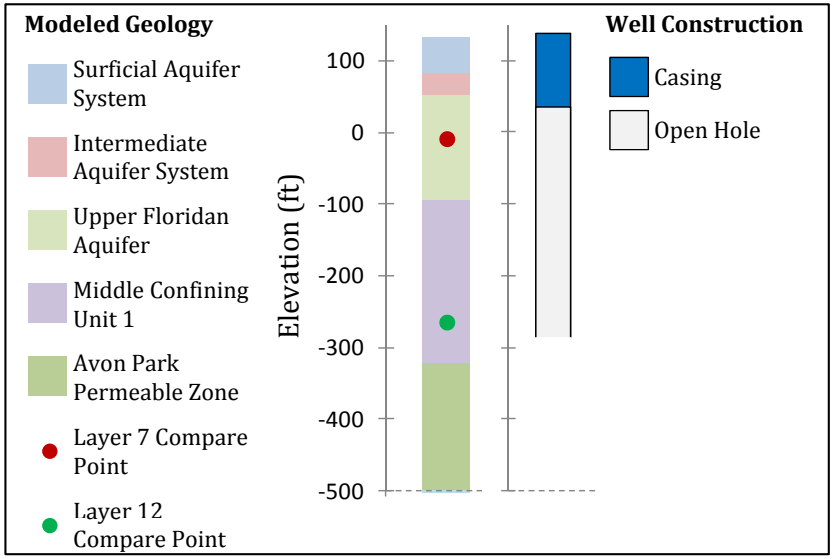

Statistics (Layer 7 Comparison)	
Obs. Count	3875
Obs. Range	9.84
ME	-1.45
MAE	2.30
RMS	2.81
RMS as % of Range	29%

Well Location:

Comparison of no-ASR Modeled Results to Head Data: Lake Alfred Deep Well

Regional Model Production Scenario Report

Figure 2.61

June 2013

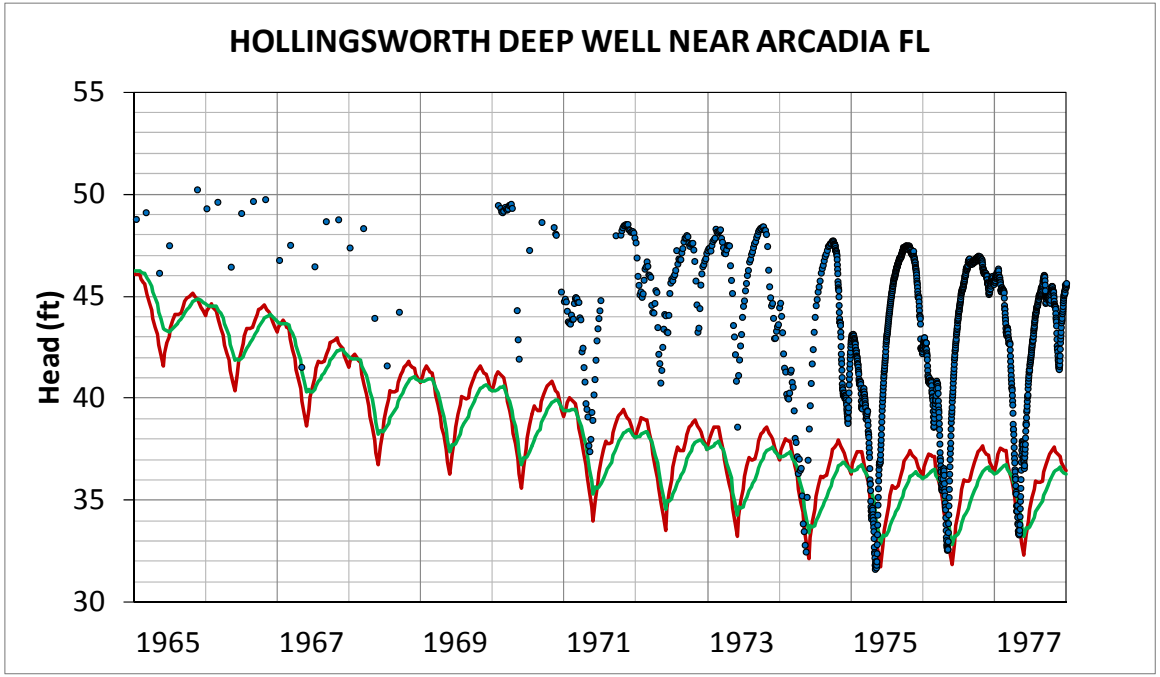

Plot Legend

- Observed Heads
- Model Result – Layer 14 (APPZ)
- Model Result – Layer 7 (UF)

Statistics Abbreviations:

ME = Mean Error
MAE = Mean Absolute Error
RMS = Root Mean Square Error
(See text for definitions)

Observed Head and Well Construction data from USGS:
http://waterdata.usgs.gov/nwis/gw

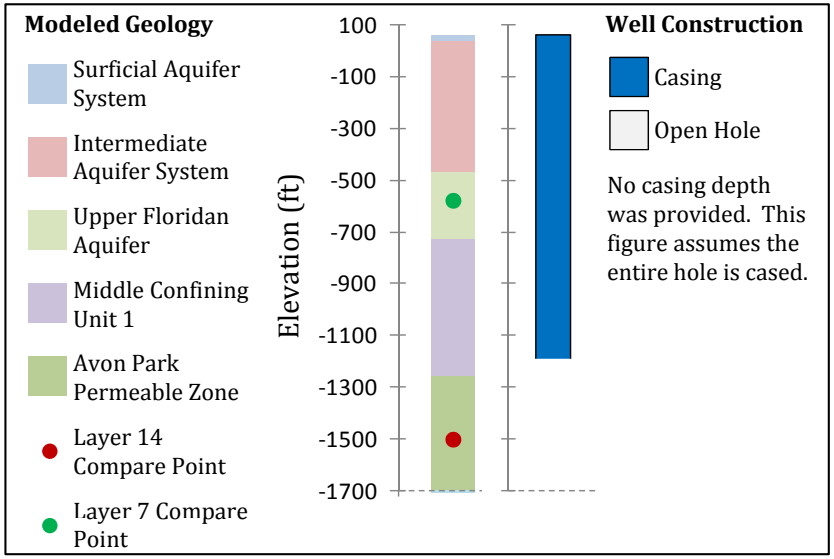

Statistics (Layer 14 Comparison)	
Obs. Count	1486
Obs. Range	18.60
ME	-6.77
MAE	6.83
RMS	7.49
RMS as % of Range	40%

Well Location:

COMPARISON OF NO-ASR MODELED RESULTS TO HEAD DATA:
HOLLINGSWORTH DEEP WELL

REGIONAL MODEL PRODUCTION SCENARIO REPORT

Figure 2.62

June 2013

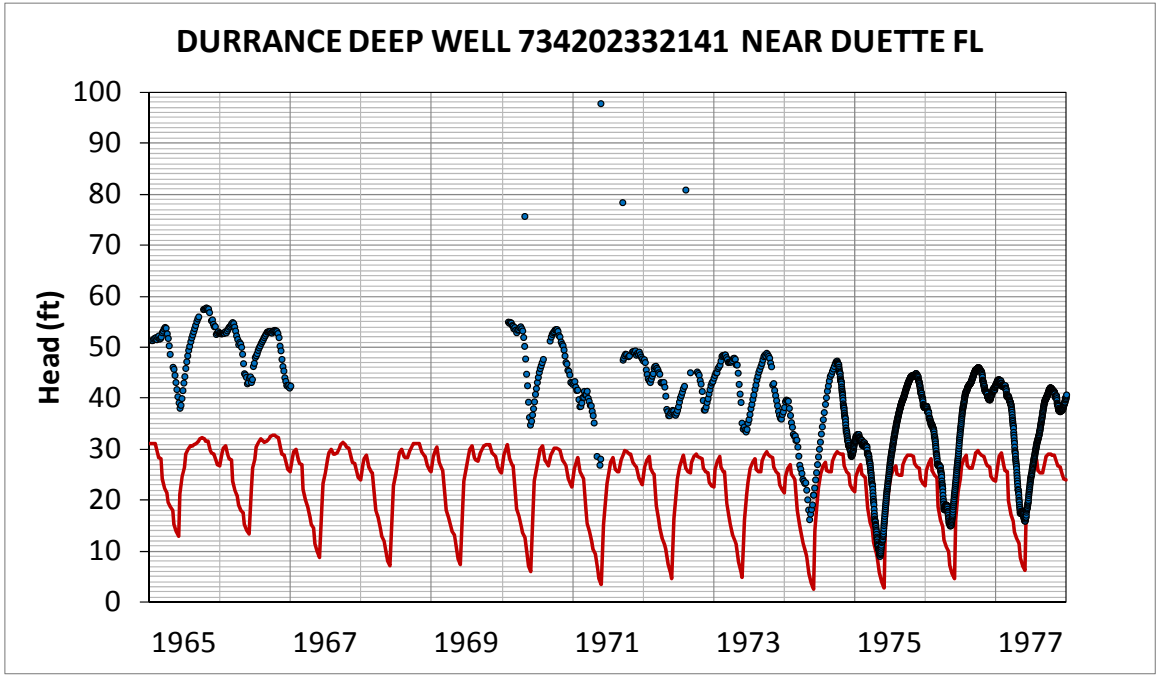

Plot Legend

- Observed Heads
- Model Result – Layer 14 (APPZ)

Statistics Abbreviations:

ME = Mean Error
MAE = Mean Absolute Error
RMS = Root Mean Square Error
(See text for definitions)

Observed Head and Well Construction data from USGS:
http://waterdata.usgs.gov/nwis/gw

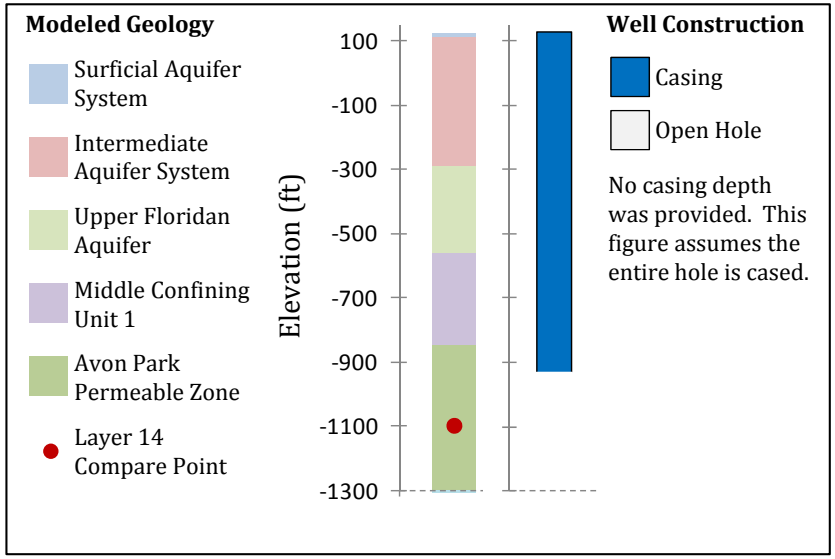

Statistics	
Obs. Count	1622
Obs. Range	88.76
ME	-13.87
MAE	13.87
RMS	15.75
RMS as % of Range	18%

Well Location:

Comparison of no-ASR Modeled Results to Head Data: Durrance Deep Well

Regional Model Production Scenario Report

Figure 2.63

June 2013

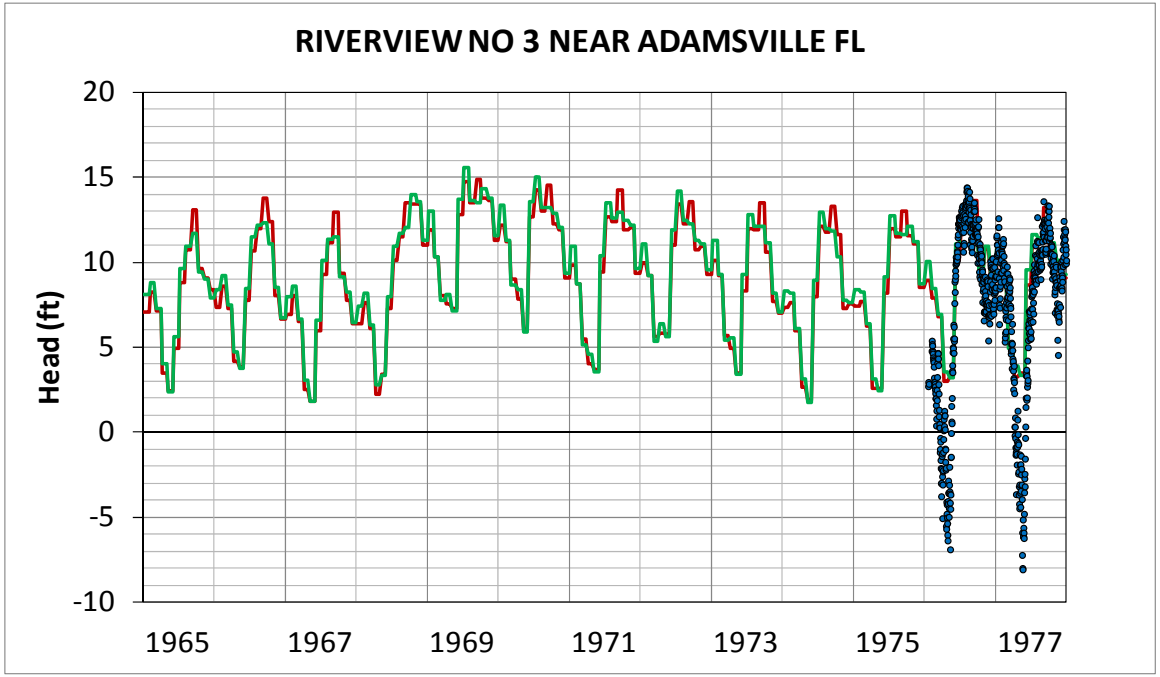

Plot Legend

- Observed Heads
- Model Result – Layer 14 (APPZ)
- Model Result – Layer 7 (UF)

Statistics Abbreviations:

ME = Mean Error
MAE = Mean Absolute Error
RMS = Root Mean Square Error
(See text for definitions)

Observed Head and Well Construction data from USGS:
http://waterdata.usgs.gov/nwis/gw

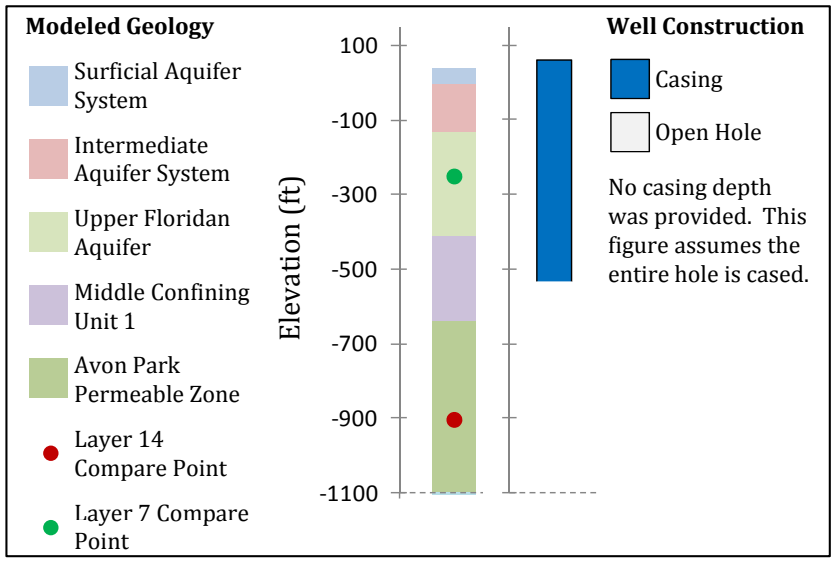

Statistics (Layer 14 Comparison)	
Obs. Count	698
Obs. Range	22.46
ME	1.80
MAE	2.51
RMS	3.45
RMS as % of Range	15%

Well Location:

Comparison of no-ASR Modeled Results to Head Data: Riverview No. 3 Well

Regional Model Production Scenario Report

Figure 2.64

June 2013

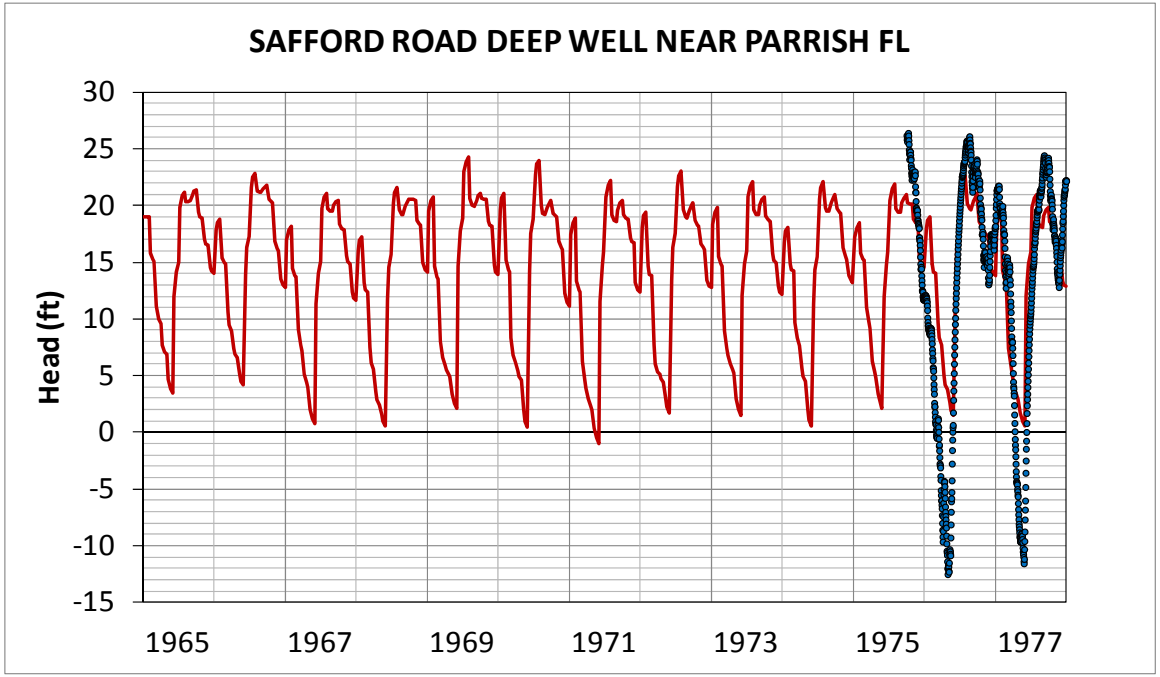

Plot Legend

- Observed Heads
- Model Result – Layer 14 (APPZ)

Statistics Abbreviations:

ME = Mean Error
MAE = Mean Absolute Error
RMS = Root Mean Square Error
(See text for definitions)

Observed Head and Well Construction data from USGS:
http://waterdata.usgs.gov/nwis/gw

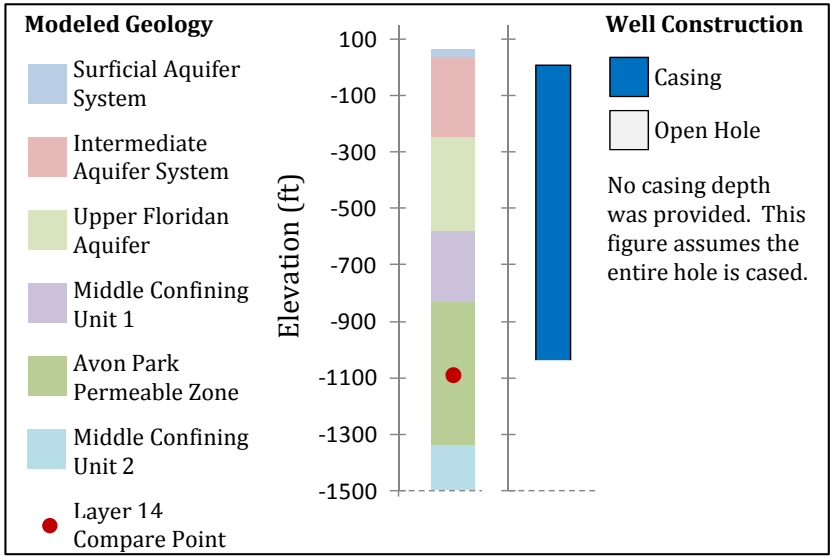

Statistics	
Obs. Count	824
Obs. Range	38.92
ME	1.56
MAE	4.82
RMS	6.21
RMS as % of Range	16%

Well Location:

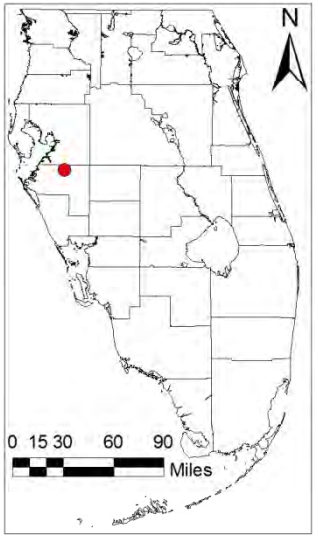

Comparison of no-ASR Modeled Results to Head Data: Safford Road Deep Well

Regional Model Production Scenario Report

Figure 2.65

June 2013

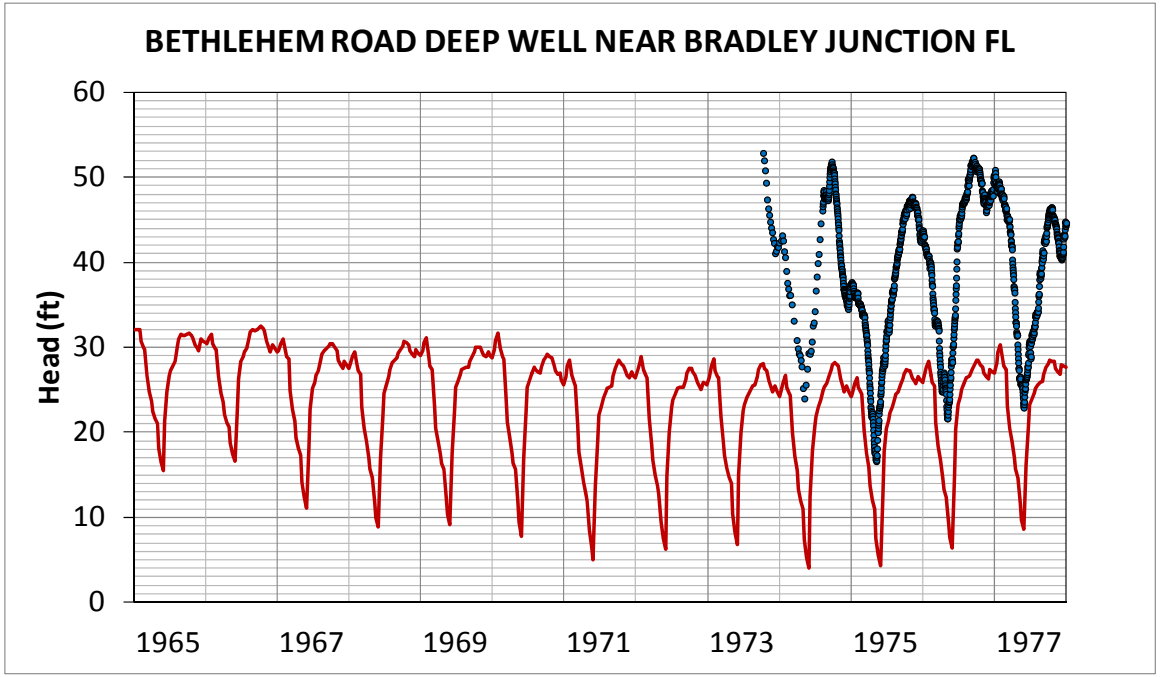

Plot Legend

- Observed Heads
- Model Result – Layer 14 (APPZ)

Statistics Abbreviations:

ME = Mean Error
MAE = Mean Absolute Error
RMS = Root Mean Square Error
(See text for definitions)

Observed Head and Well Construction data from USGS:
http://waterdata.usgs.gov/nwis/gw

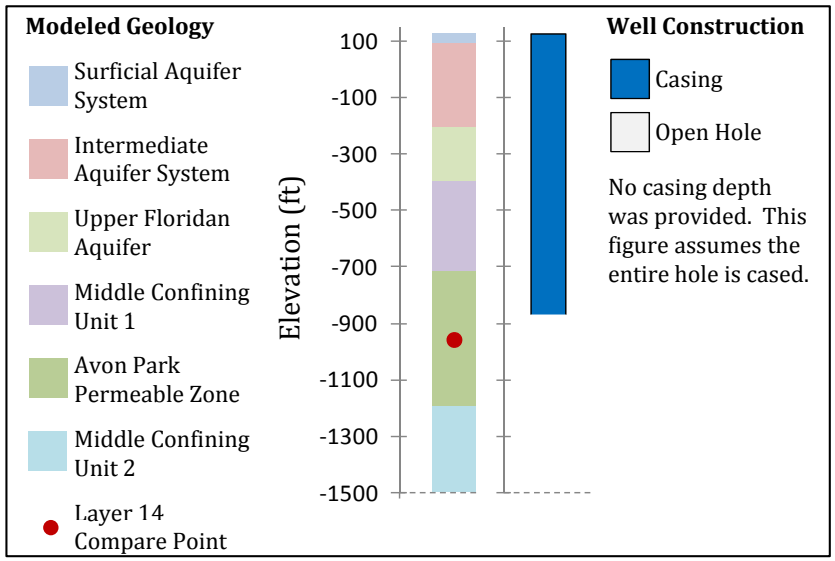

Statistics	
Obs. Count	1295
Obs. Range	36.54
ME	-16.20
MAE	16.20
RMS	16.87
RMS as % of Range	46%

Well Location:

Comparison of no-ASR Modeled Results to Head Data: Bethlehem Road Deep Well

Regional Model Production Scenario Report

Figure 2.66

June 2013

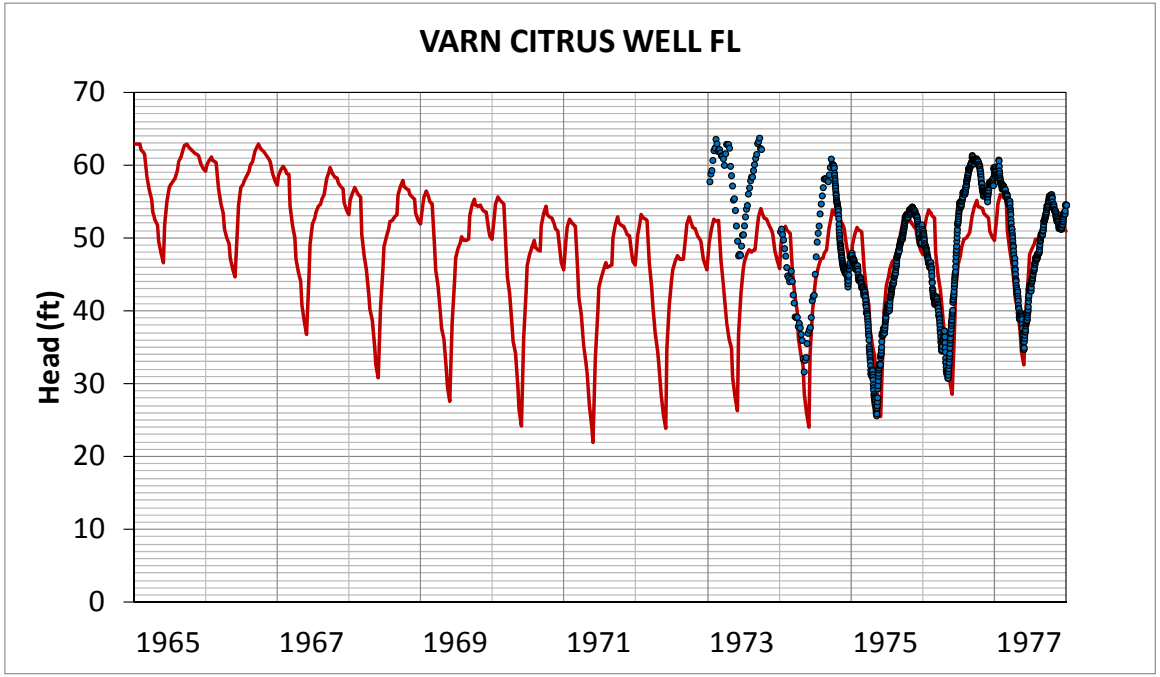

Plot Legend

- Observed Heads
- Model Result – Layer 14 (APPZ)

Statistics Abbreviations:

ME = Mean Error
MAE = Mean Absolute Error
RMS = Root Mean Square Error
(See text for definitions)

Observed Head and Well Construction data from USGS:
http://waterdata.usgs.gov/nwis/gw

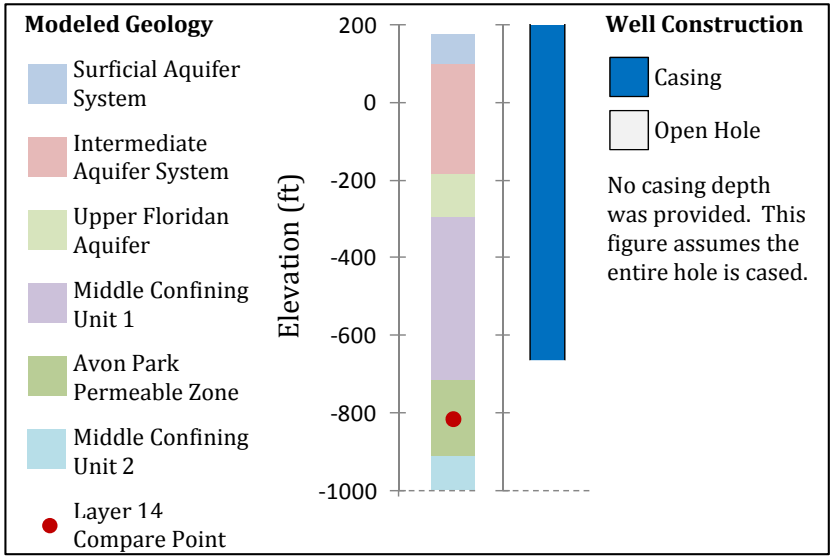

Statistics	
Obs. Count	1296
Obs. Range	38.10
ME	-1.04
MAE	4.29
RMS	5.57
RMS as % of Range	15%

Well Location:

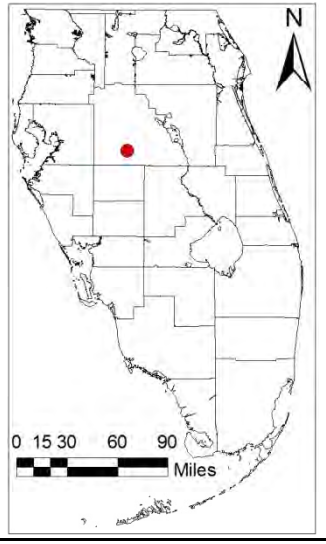

Comparison of no-ASR Modeled Results to Head Data: Varn Citrus Well

Regional Model Production Scenario Report

Figure 2.67

June 2013

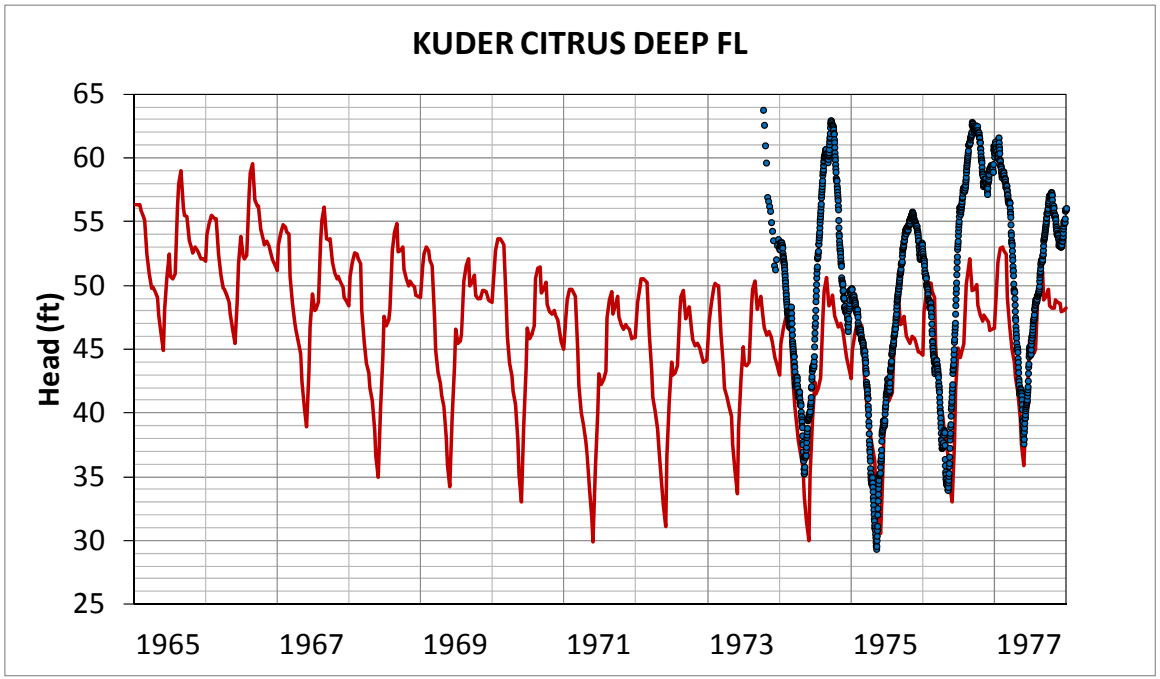

Plot Legend

- Observed Heads
- Model Result – Layer 14 (APPZ)

Statistics Abbreviations:

ME = Mean Error
MAE = Mean Absolute Error
RMS = Root Mean Square Error
(See text for definitions)

Observed Head and Well Construction data from USGS:
http://waterdata.usgs.gov/nwis/gw

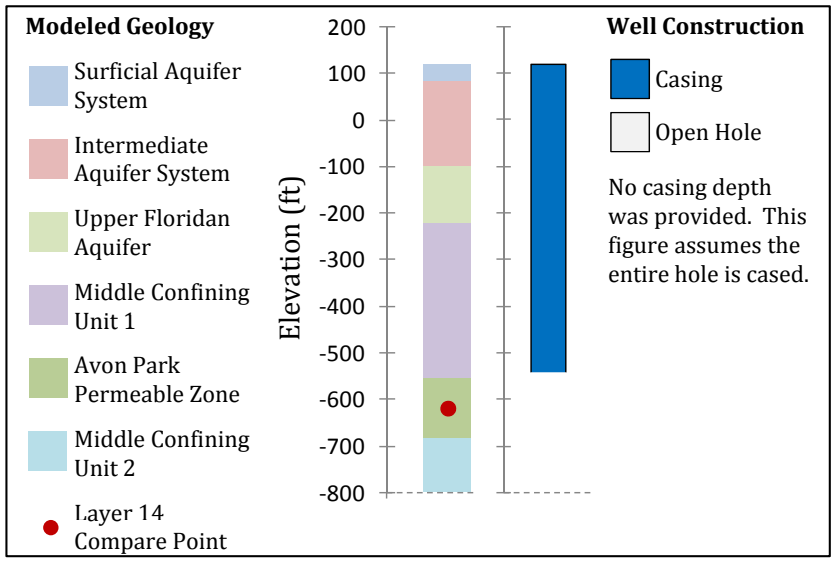

Statistics	
Obs. Count	1479
Obs. Range	34.82
ME	-5.27
MAE	5.85
RMS	7.14
RMS as % of Range	21%

Well Location:

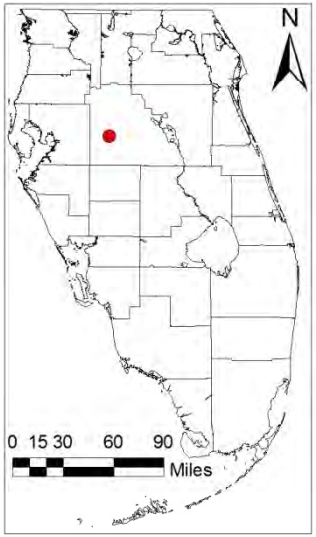

Comparison of no-ASR Modeled Results to Head Data: Kuder Citrus Deep Well

Regional Model Production Scenario Report

Figure 2.68

June 2013

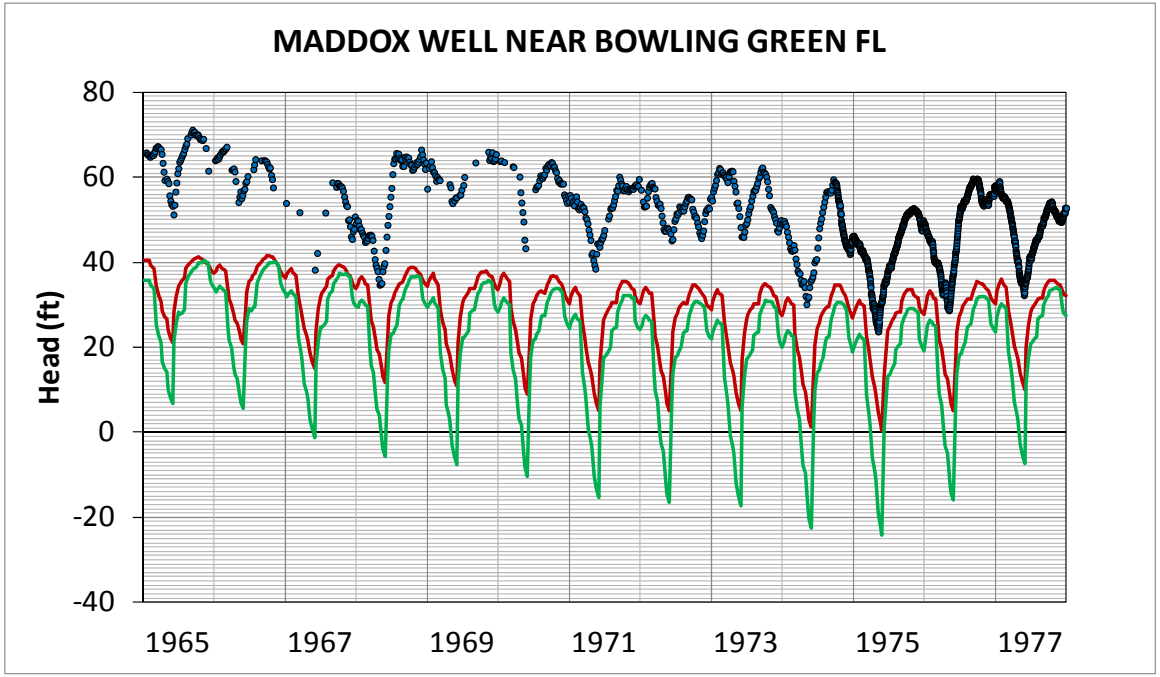

Plot Legend

- Observed Heads
- Model Result – Layer 14 (APPZ)
- Model Result – Layer 7 (UF)

Statistics Abbreviations:

ME = Mean Error
MAE = Mean Absolute Error
RMS = Root Mean Square Error
(See text for definitions)

Observed Head and Well Construction data from USGS:
http://waterdata.usgs.gov/nwis/gw

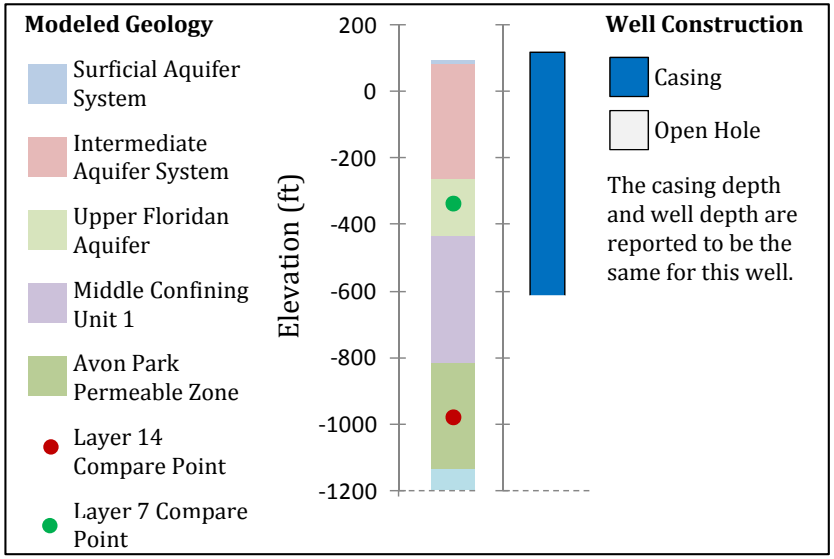

Statistics		
Compare Layer	14 (APPZ)	7 (UF)
Obs. Count	1734	
Obs. Range	47.47	
ME	-21.21	-29.54
MAE	21.21	29.54
RMS	22.11	30.99
RMS as % of Range	47%	65%

Well Location:

Comparison of no-ASR Modeled Results to Head Data: Maddox Well

Regional Model Production Scenario Report

Figure 2.69

June 2013

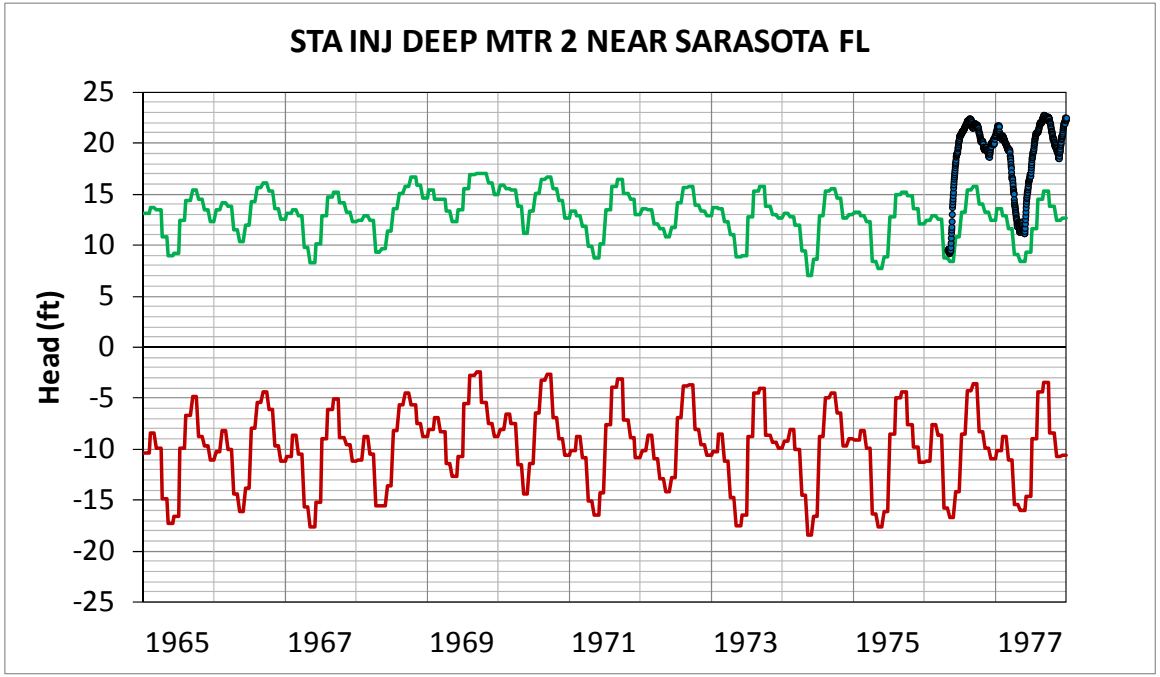

Plot Legend

- Observed Heads
- Model Result – Layer 14 (APPZ)
- Model Result – Layer 7 (UF)

Statistics Abbreviations:

ME = Mean Error
MAE = Mean Absolute Error
RMS = Root Mean Square Error
(See text for definitions)

Observed Head and Well Construction data from USGS:
http://waterdata.usgs.gov/nwis/gw

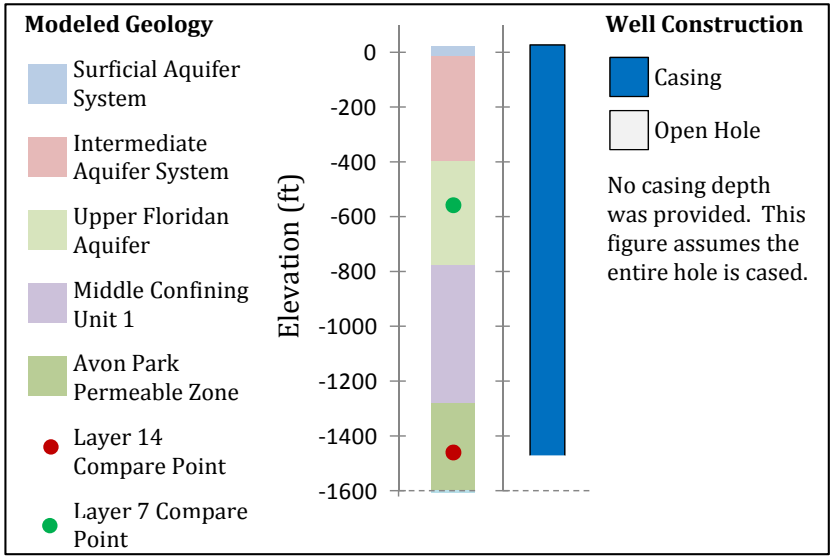

Statistics		
Compare Layer	14 (APPZ)	7 (UF)
Obs. Count	613	
Obs. Range	13.57	
ME	-29.03	-6.64
MAE	29.03	6.64
RMS	29.11	6.89
RMS as % of Range	215%	51%

Well Location:

Comparison of no-ASR Modeled Results to Head Data: STA Injection Deep MTR 2

Regional Model Production Scenario Report

Figure 2.70

June 2013

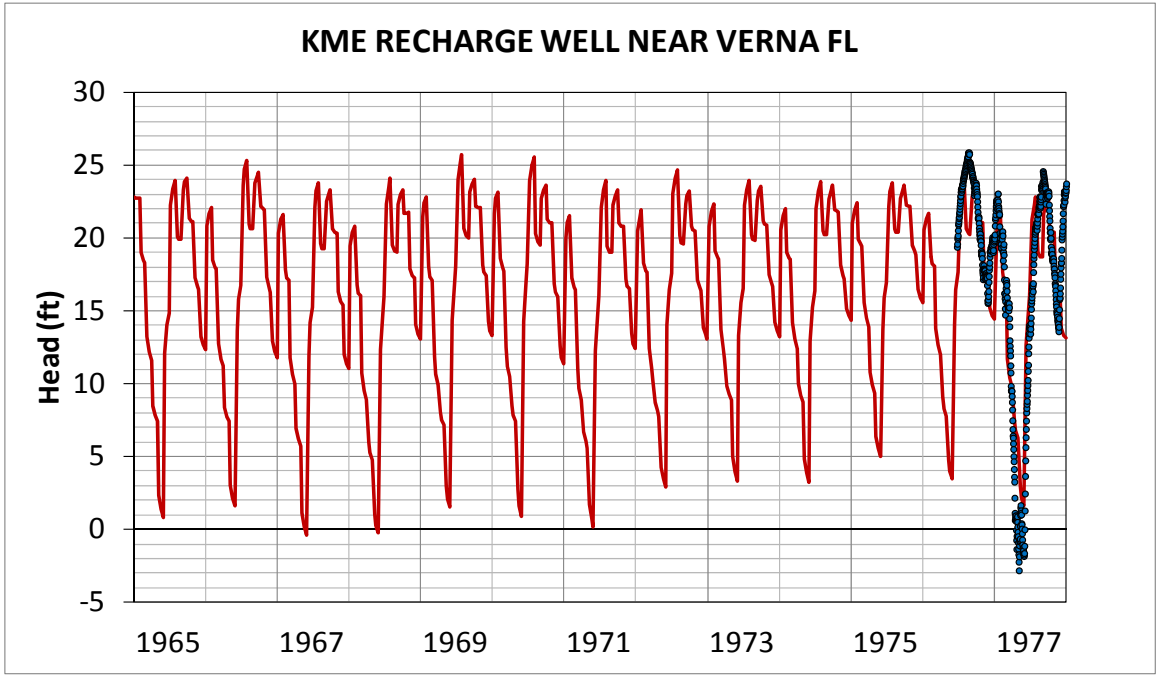

Plot Legend

- Observed Heads
- Model Result – Layer 14 (APPZ)

Statistics Abbreviations:

ME = Mean Error
MAE = Mean Absolute Error
RMS = Root Mean Square Error
(See text for definitions)

Observed Head and Well Construction data from USGS:
http://waterdata.usgs.gov/nwis/gw

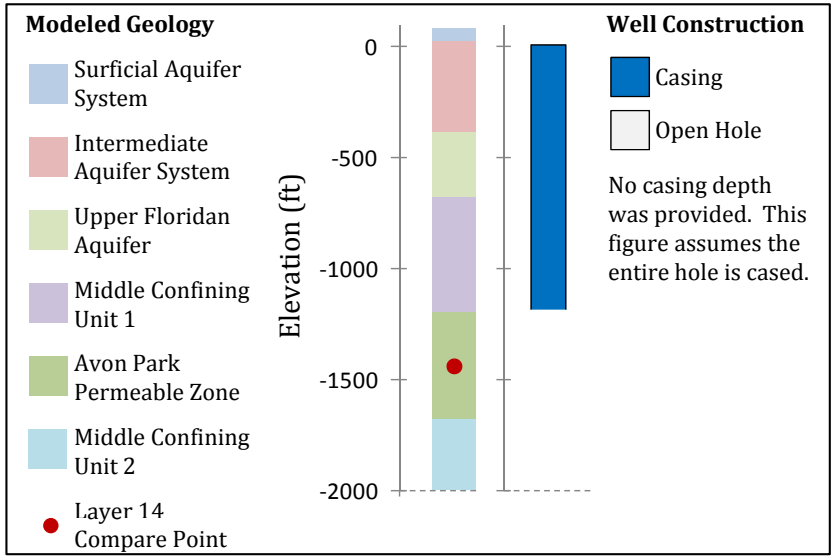

Statistics	
Obs. Count	559
Obs. Range	28.67
ME	-0.34
MAE	2.73
RMS	3.51
RMS as % of Range	12%

Well Location:

Comparison of no-ASR Modeled Results to Head Data: KME Recharge Well

Regional Model Production Scenario Report

Figure 2.71

June 2013

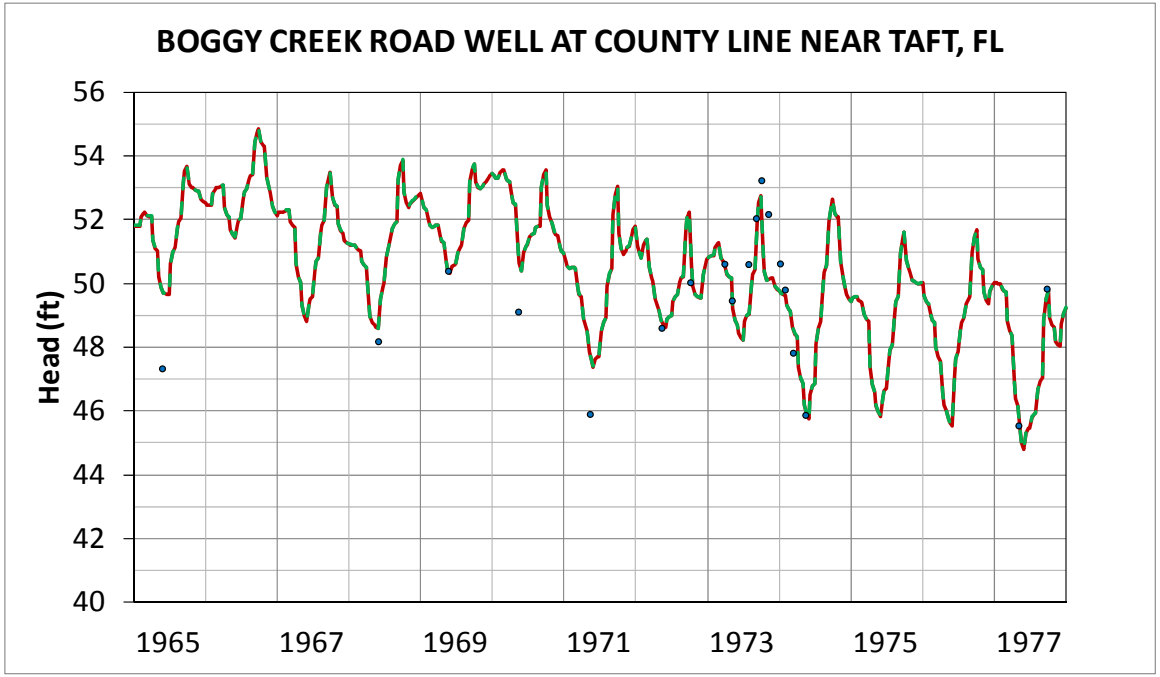

Plot Legend

- Observed Heads
- Model Result – Layer 7 (UF)
- Model Result – Layer 14 (APPZ)

Statistics Abbreviations:

ME = Mean Error
MAE = Mean Absolute Error
RMS = Root Mean Square Error
(See text for definitions)

Observed Head and Well Construction data from USGS:
http://waterdata.usgs.gov/nwis/gw

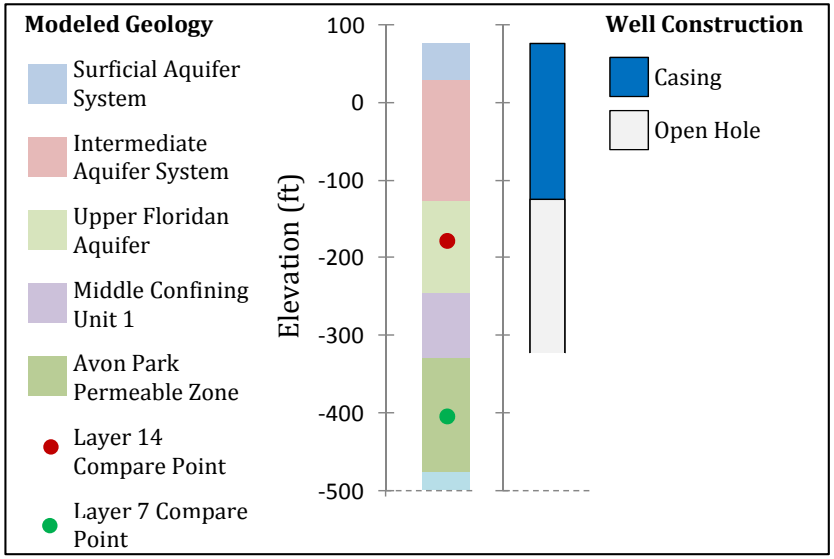

Statistics (Layer 7 Comparison)	
Obs. Count	19
Obs. Range	7.69
ME	0.18
MAE	0.89
RMS	1.17
RMS as % of Range	15%

Well Location:

Comparison of no-ASR Modeled Results to Head Data: Boggy Creek Road Well

Regional Model Production Scenario Report

Figure 2.72

June 2013

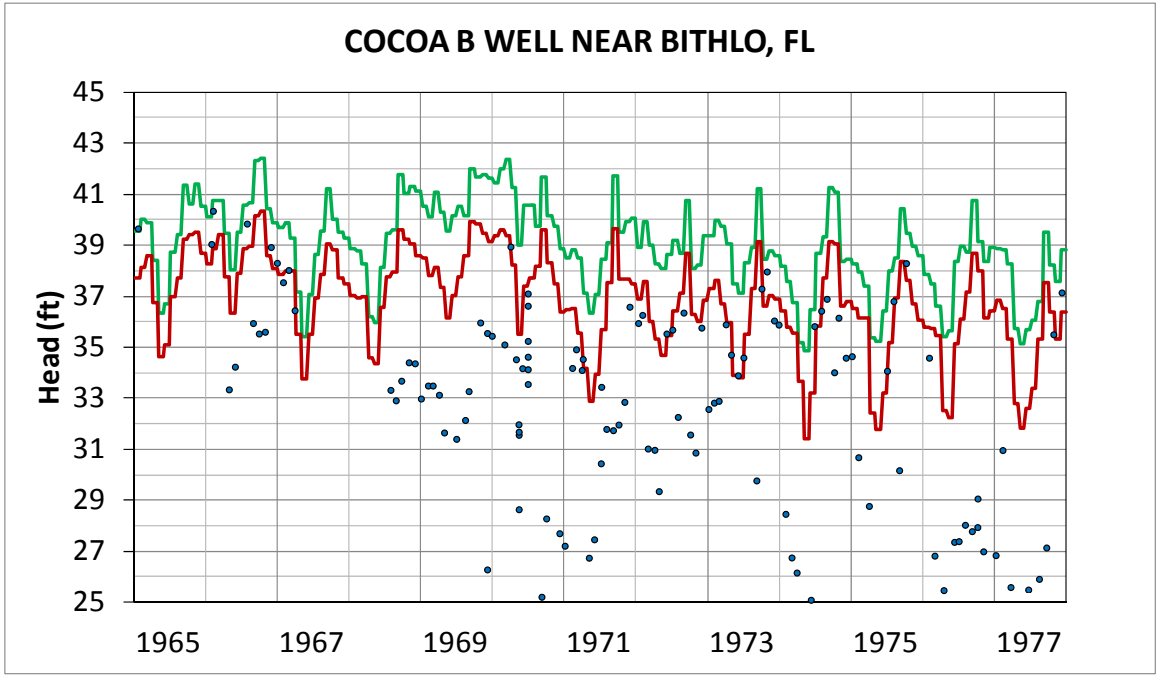

Plot Legend

- Observed Heads
- Model Result – Layer 7 (UF)
- Model Result – Layer 14 (APPZ)

Statistics Abbreviations:

ME = Mean Error
MAE = Mean Absolute Error
RMS = Root Mean Square Error
(See text for definitions)

Observed Head and Well Construction data from USGS:
http://waterdata.usgs.gov/nwis/gw

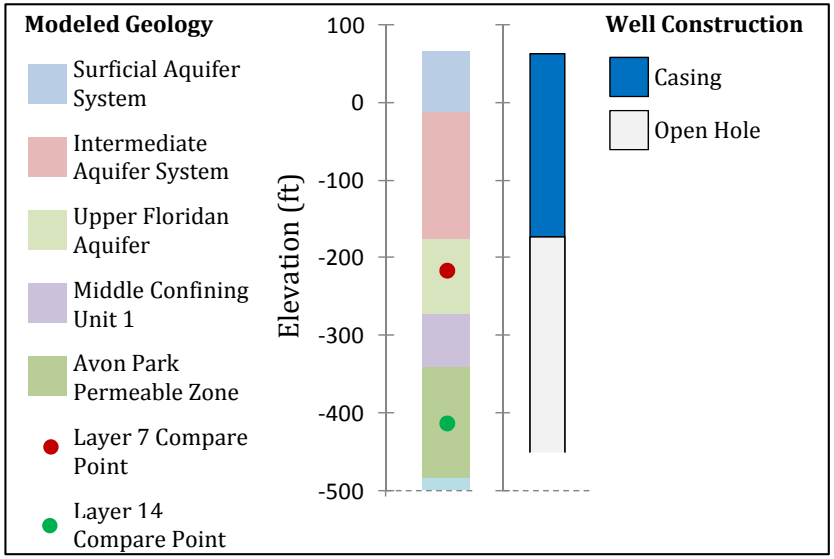

Statistics		
Compare Layer	7 (UF)	14 (APPZ)
Obs. Count	127	
Obs. Range	18.43	
ME	4.36	6.73
MAE	4.57	6.73
RMS	5.71	7.67
RMS as % of Range	31%	42%

Well Location:

Comparison of no-ASR Modeled Results to Head Data: Cocoa B Well

Regional Model Production Scenario Report

Figure 2.73

June 2013

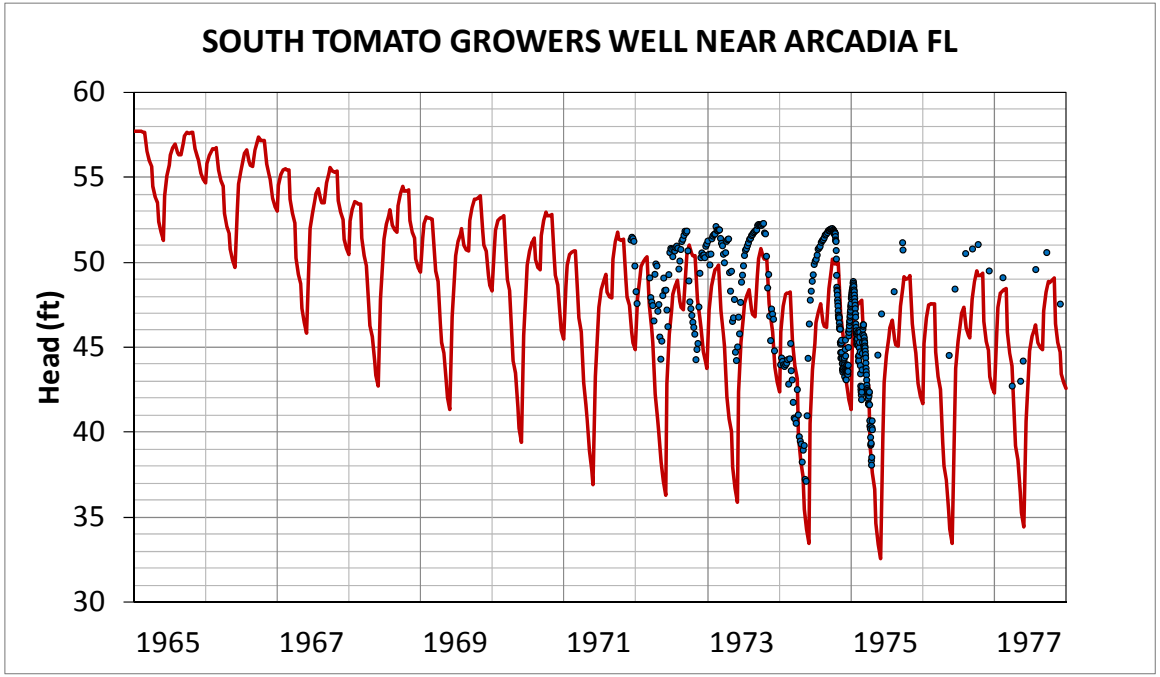

Plot Legend

- Observed Heads
- Model Result – Layer 14 (APPZ)

Statistics Abbreviations:

ME = Mean Error
MAE = Mean Absolute Error
RMS = Root Mean Square Error
(See text for definitions)

Observed Head and Well Construction data from USGS:
http://waterdata.usgs.gov/nwis/gw

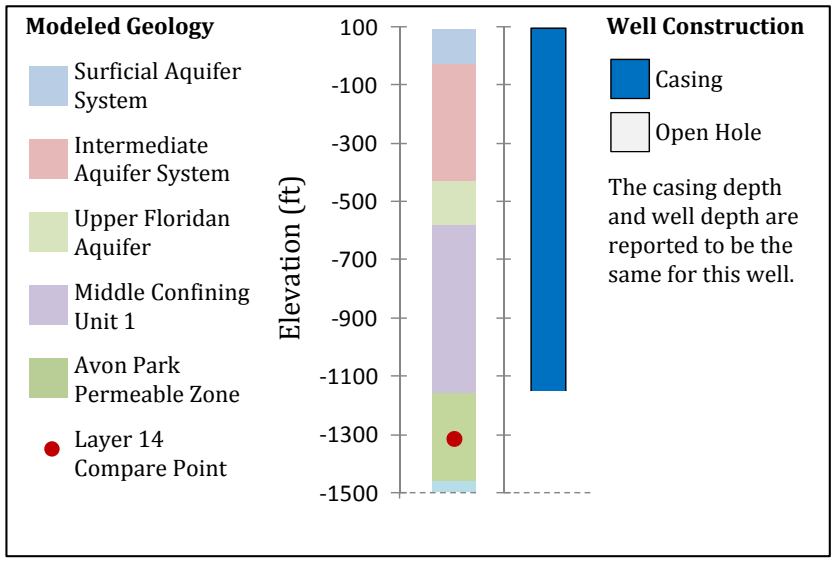

Statistics	
Obs. Count	405
Obs. Range	15.16
ME	-1.55
MAE	3.16
RMS	4.01
RMS as % of Range	26%

Well Location:

Comparison of no-ASR Modeled Results to Head Data: South Tomato Growers' Well

Regional Model Production Scenario Report

Figure 2.74

June 2013

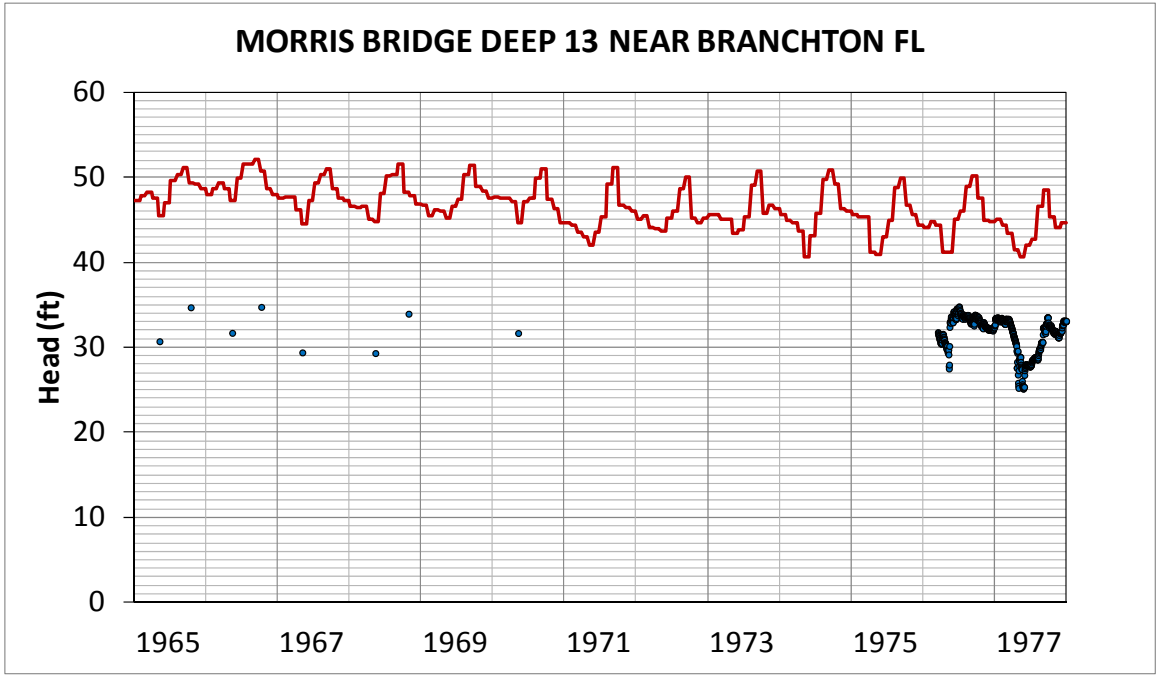

Plot Legend

- Observed Heads
- Model Result – Layer 14 (APPZ)

Statistics Abbreviations:

ME = Mean Error
MAE = Mean Absolute Error
RMS = Root Mean Square Error
(See text for definitions)

Observed Head and Well Construction data from USGS:
http://waterdata.usgs.gov/nwis/gw

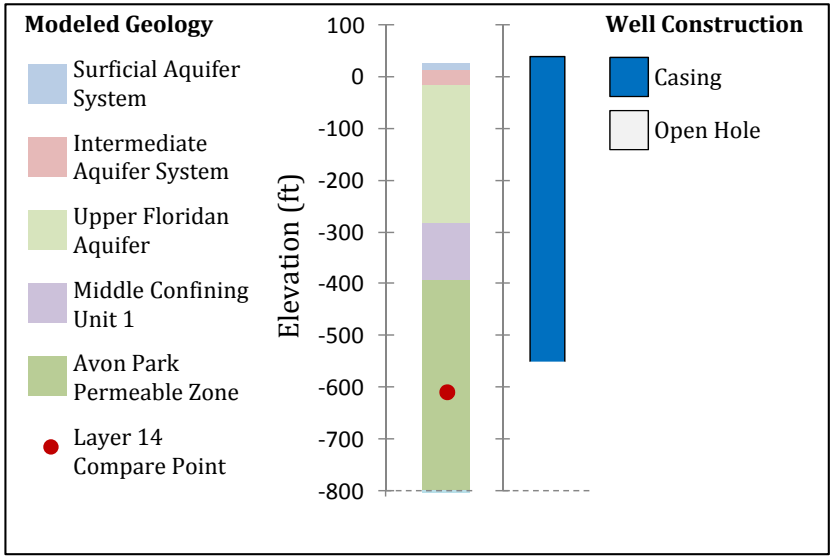

Statistics	
Obs. Count	664
Obs. Range	9.68
ME	13.01
MAE	13.01
RMS	13.18
RMS as % of Range	136%

Well Location:

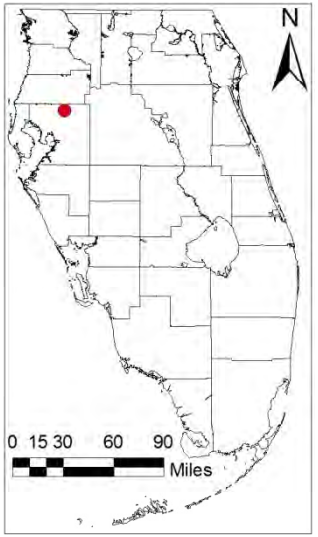

Comparison of no-ASR Modeled Results to Head Data: Morris Bridge Deep 13 Well

Regional Model Production Scenario Report

Figure 2.75

June 2013

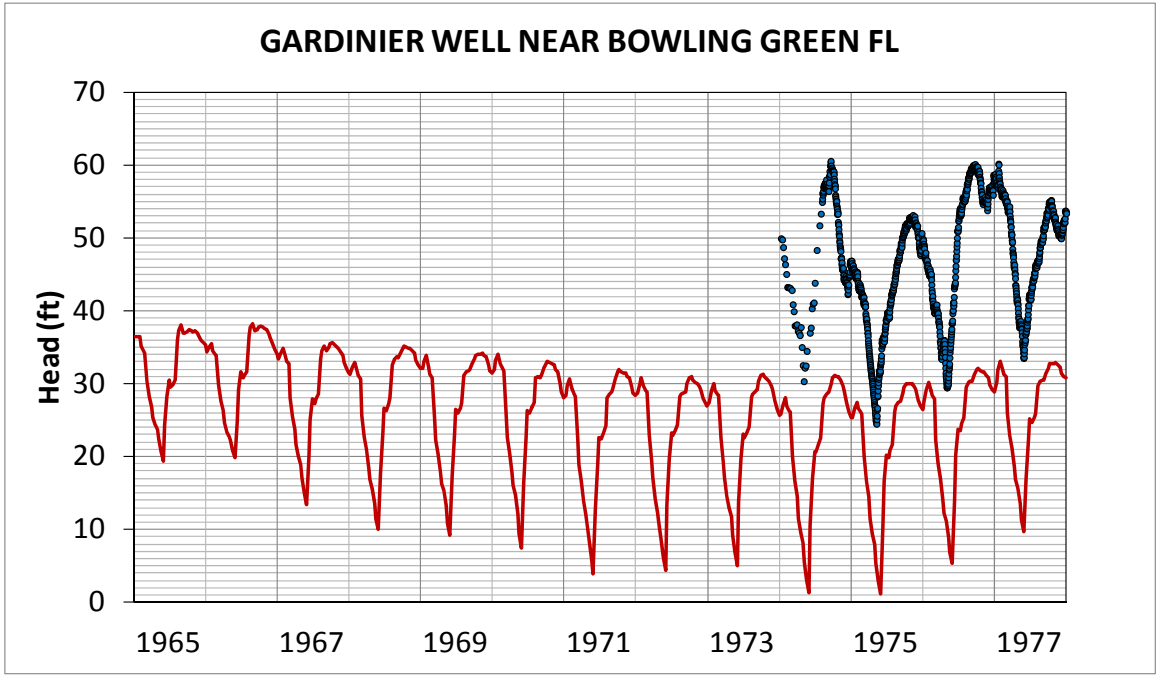

Plot Legend

- Observed Heads
- Model Result – Layer 14 (APPZ)

Statistics Abbreviations:

ME = Mean Error
MAE = Mean Absolute Error
RMS = Root Mean Square Error
(See text for definitions)

Observed Head and Well Construction data from USGS:
http://waterdata.usgs.gov/nwis/gw

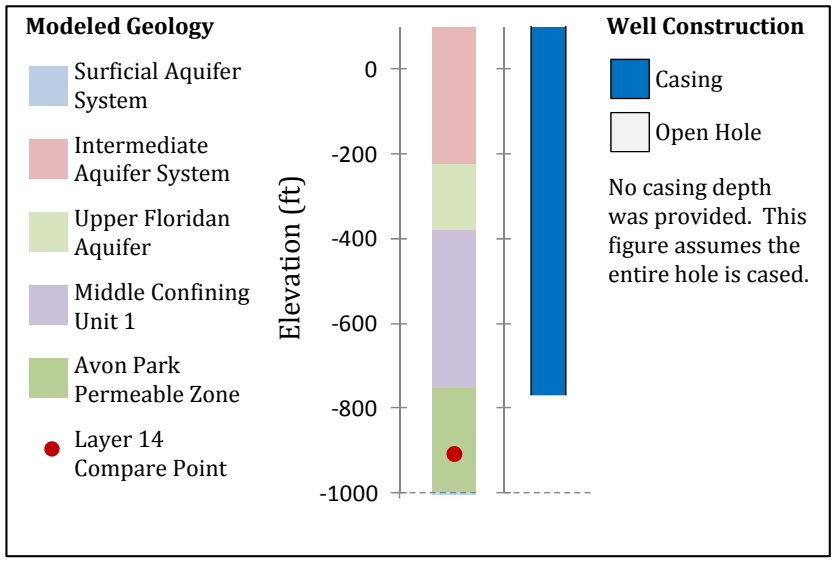

Statistics	
Obs. Count	1280
Obs. Range	36.07
ME	-22.66
MAE	22.66
RMS	23.09
RMS as % of Range	64%

Well Location:

Comparison of no-ASR Modeled Results to Head Data: Gardinier Well

Regional Model Production Scenario Report

Figure 2.76

June 2013

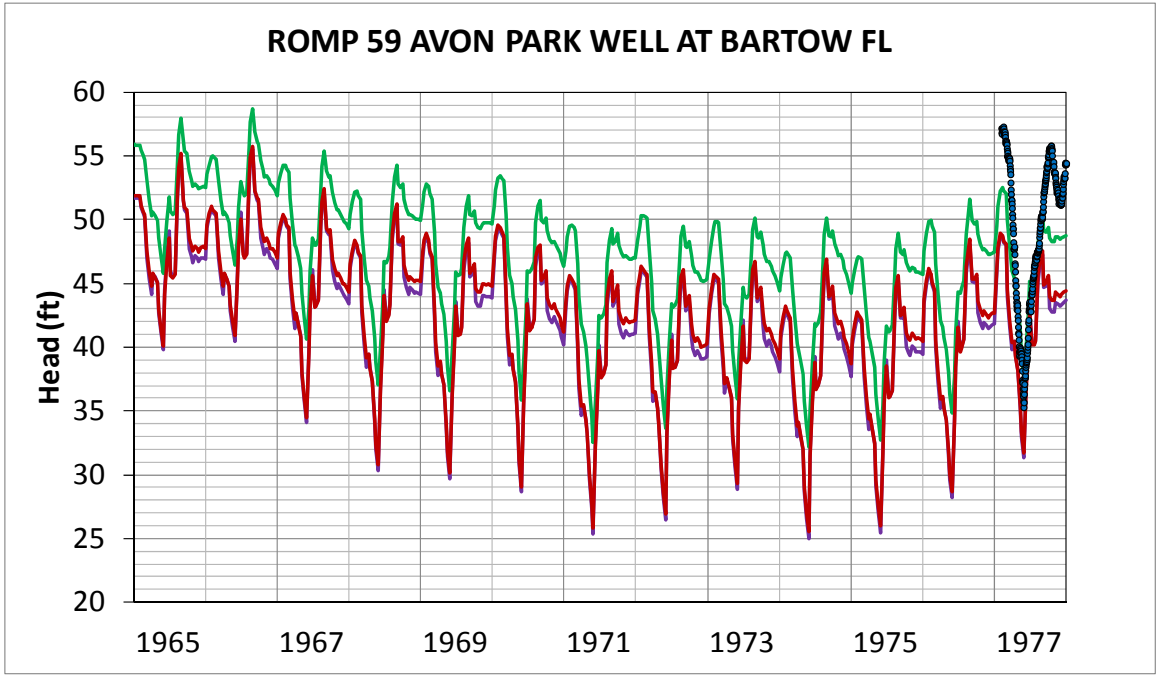

Plot Legend

- Observed Heads
- Model Result – Layer 7 (UF)
- Model Result – Layer 14 (APPZ)
- Model Result – Layer 16 (MC2)

Statistics Abbreviations:

ME = Mean Error
MAE = Mean Absolute Error
RMS = Root Mean Square Error
(See text for definitions)

Observed Head and Well Construction data from USGS:
http://waterdata.usgs.gov/nwis/gw

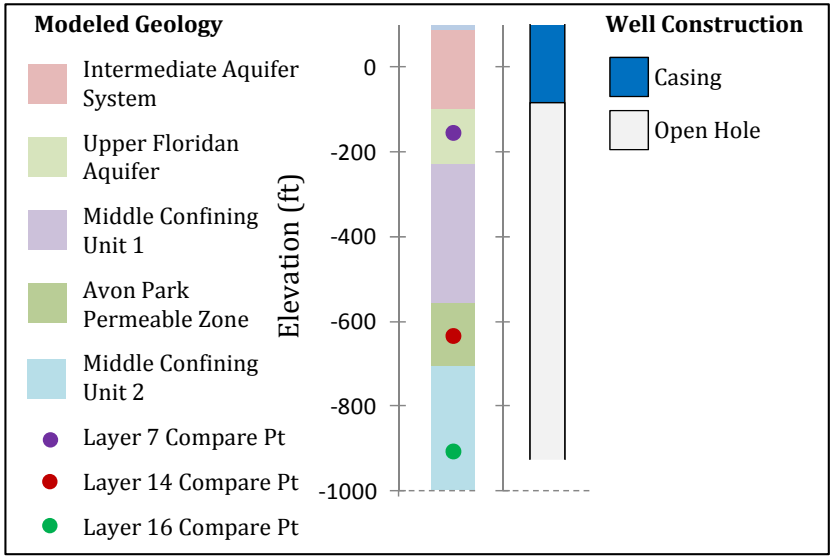

Statistics		
Compare Layer	14 (APPZ)	16 (MC2)
Obs. Count	333	
Obs. Range	22.01	
ME	-6.76	-2.40
MAE	6.76	3.09
RMS	7.42	3.70
RMS as % of Range	34%	17%

Well Location:

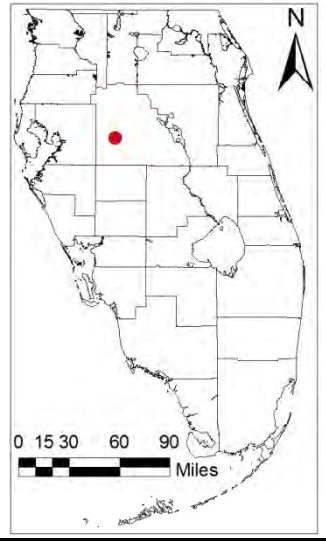

Comparison of no-ASR Modeled Results to Head Data: ROMP 59 Avon Park Well

Regional Model Production Scenario Report

Figure 2.77

June 2013

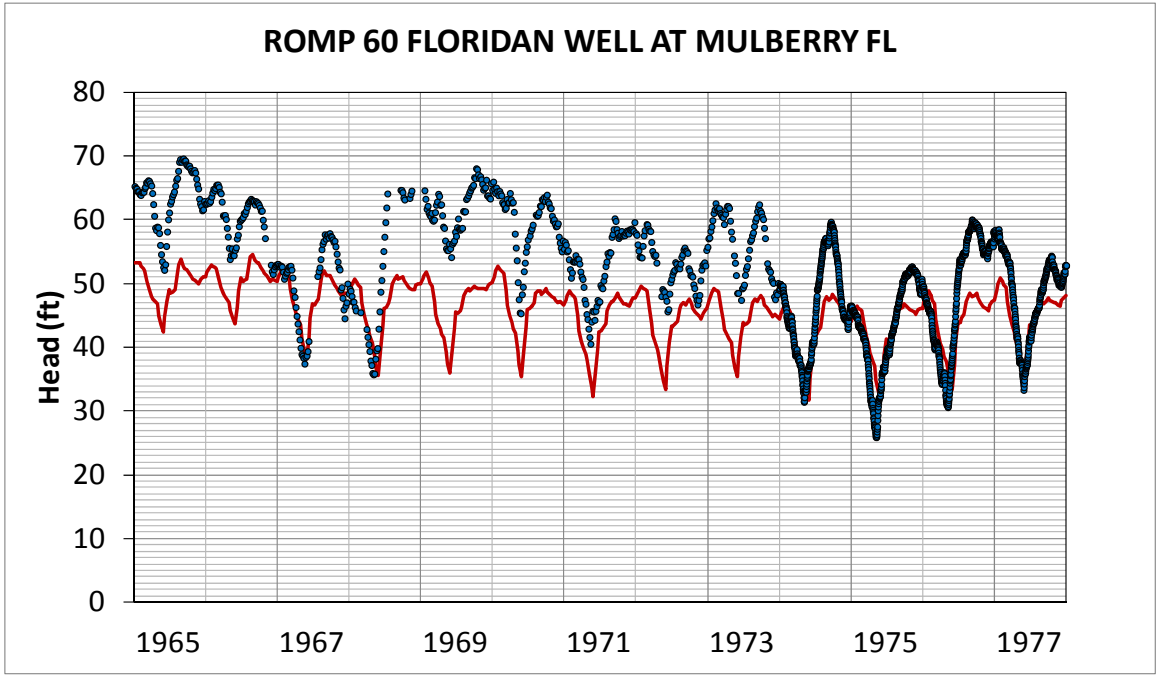

Plot Legend

- Observed Heads
- Model Result – Layer 14 (APPZ)

Statistics Abbreviations:

ME = Mean Error
MAE = Mean Absolute Error
RMS = Root Mean Square Error
(See text for definitions)

Observed Head and Well Construction data from USGS:
http://waterdata.usgs.gov/nwis/gw

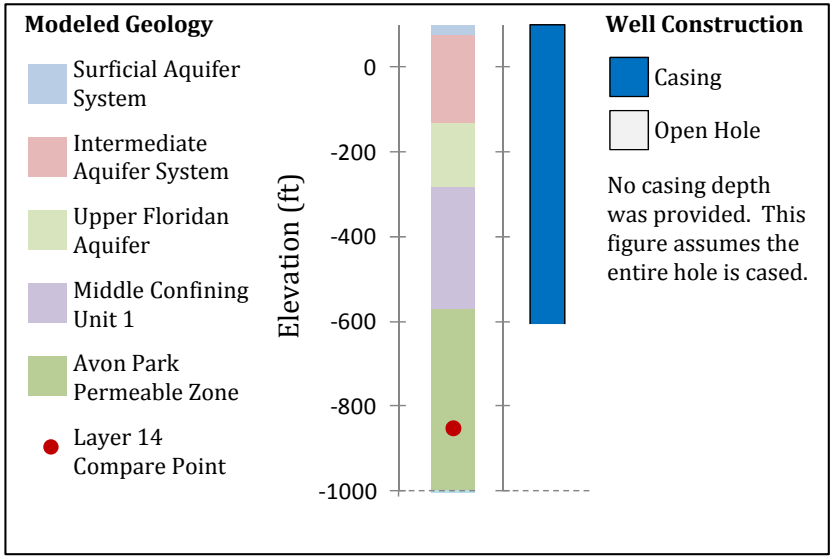

Statistics	
Obs. Count	2047
Obs. Range	43.71
ME	-4.79
MAE	6.20
RMS	7.71
RMS as % of Range	18%

Well Location:

Comparison of no-ASR Modeled Results to Head Data: ROMP 60 Floridan Well

Regional Model Production Scenario Report

Figure 2.78

June 2013

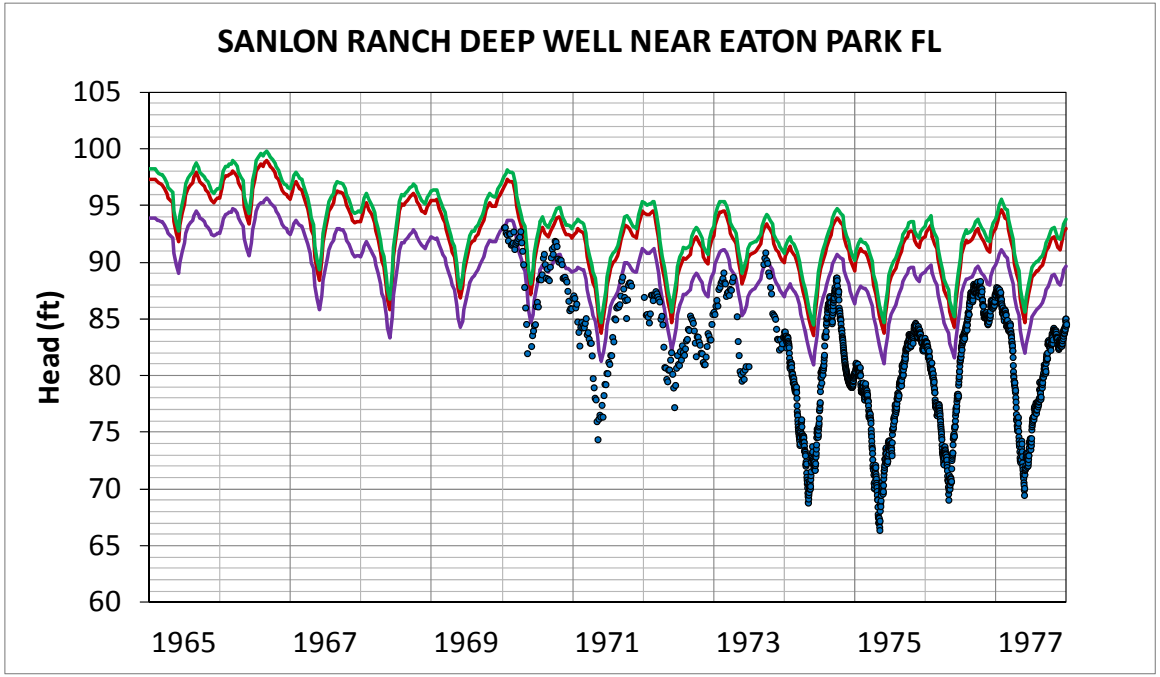

Plot Legend

- Observed Heads
- Model Result – Layer 7 (UF)
- Model Result – Layer 14 (APPZ)
- Model Result – Layer 16 (MC2)

Statistics Abbreviations:

ME = Mean Error
MAE = Mean Absolute Error
RMS = Root Mean Square Error
(See text for definitions)

Observed Head and Well Construction data from USGS:
http://waterdata.usgs.gov/nwis/gw

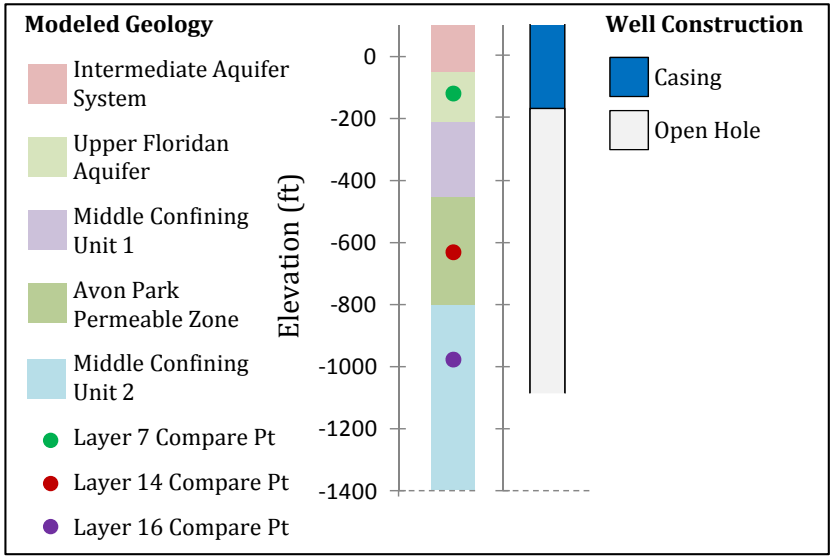

Statistics		
Compare Layer	14 (APPZ)	16 (MC2)
Obs. Count	1713	
Obs. Range	26.72	
ME	9.77	6.63
MAE	9.77	6.65
RMS	10.33	7.47
RMS as % of Range	39%	28%

Well Location:

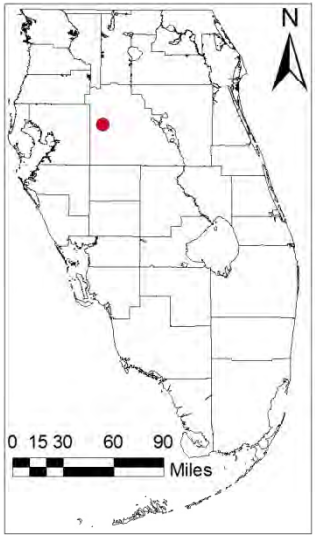

Comparison of no-ASR Modeled Results to Head Data: Sanlon Ranch Deep Well

Regional Model Production Scenario Report

Figure 2.79

June 2013

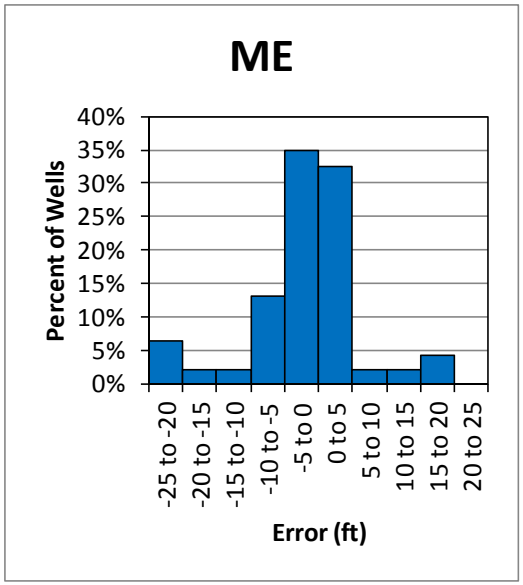

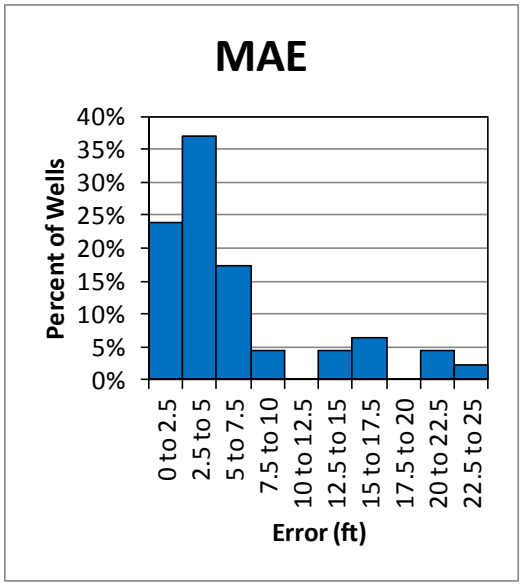

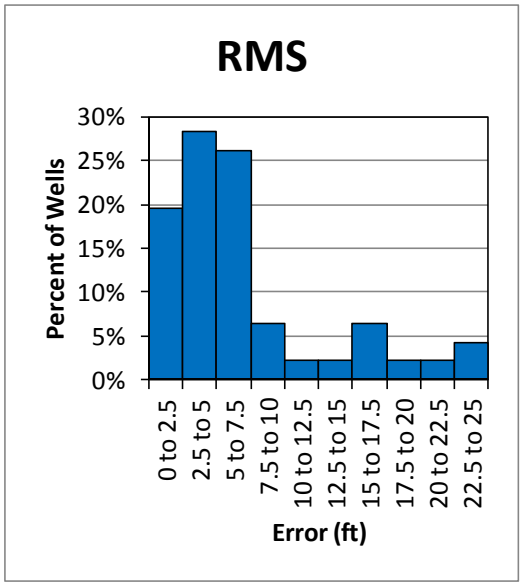

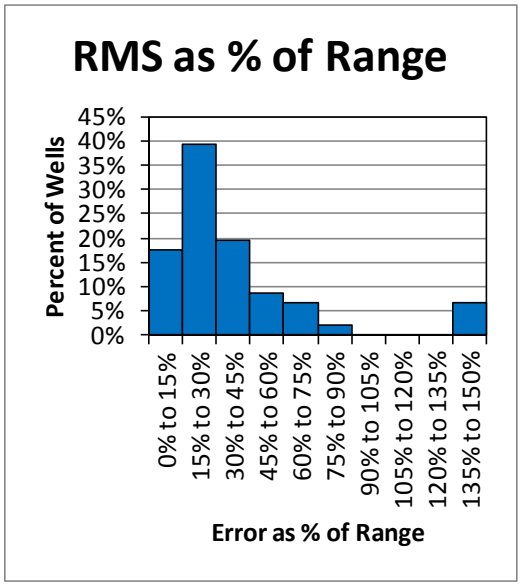

Notes:

This figure is a summary of the information presented in Figures 2.34 – 2.79. Statistics from the tables on each figure have been combined to form these histograms.

Statistics Abbreviations:

ME = Mean Error
MAE = Mean Absolute Error
RMS = Root Mean Square Error
(See text for definitions)

Observed Head and Well Construction data from USGS:
http://waterdata.usgs.gov/nwis/gw

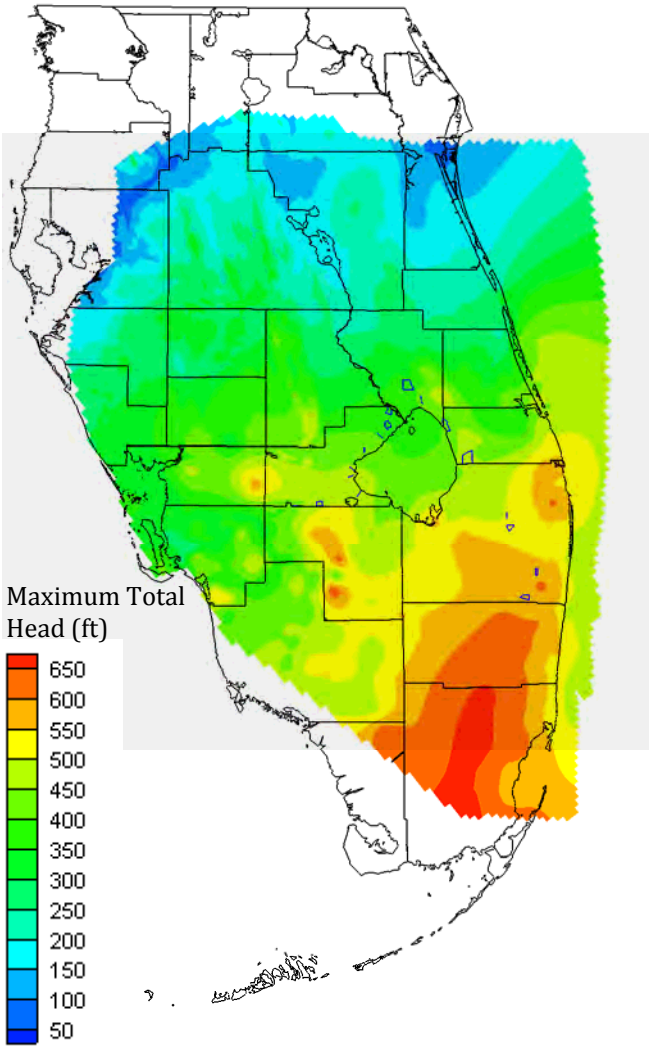

Upper Floridan Aquifer

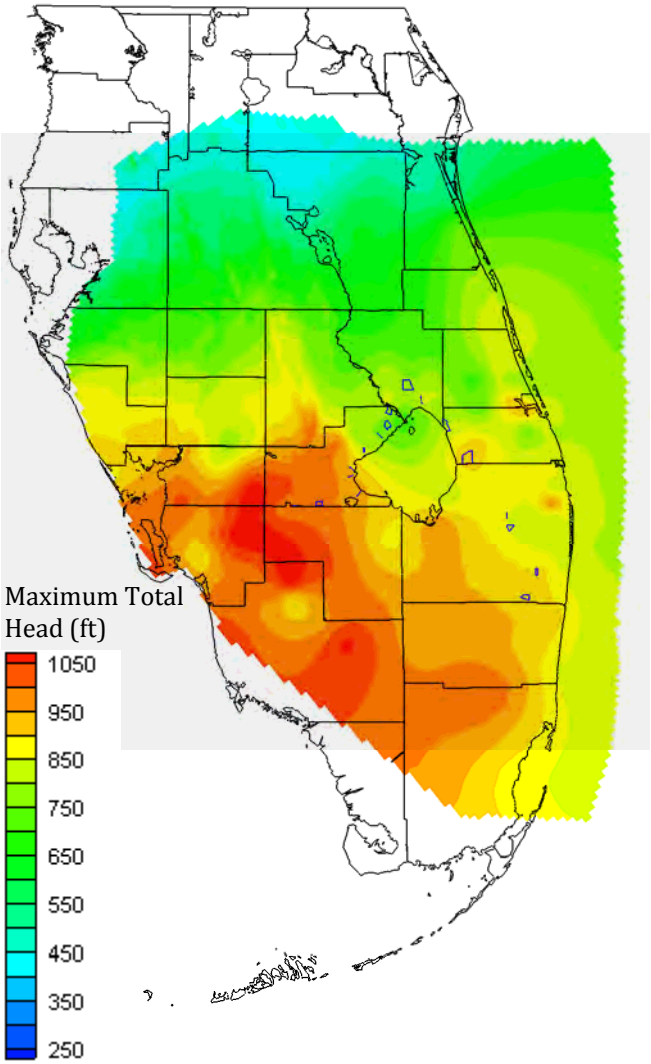

Avon Park Permeable Zone

Proposed ASR Sites

Notes:

These maps show the maximum allowable total head in the UF and APPZ which will preclude rock fracturing. The calculations are based on the Tensile Method in Geibel, 2012.

Assumptions:

- Ambient pre-fracture water pressure estimated as pressure from steady state February 2004 calibration model
- Specific weight of water: 62.4 lb/ft^3
- Specific weight of all materials: 130 lb/ft^3
- Angle of internal friction: 28.9°

ROCK FRACTURE POTENTIAL
MAXIMUM TOTAL HEAD

REGIONAL MODEL PRODUCTION SCENARIO REPORT

FIGURE 3.1

JUNE 2013

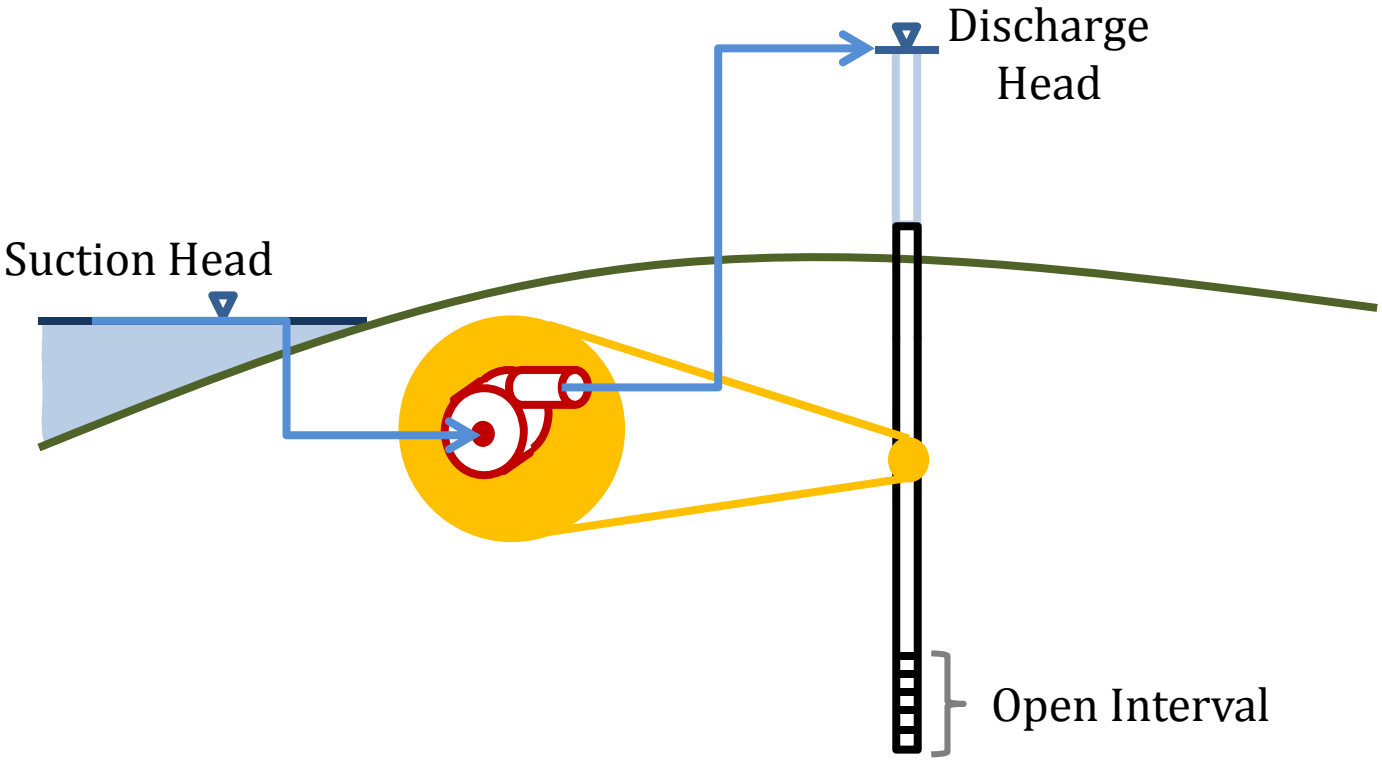

Notes:

This figure shows a simplified schematic of an ASR well pump when it is injecting into an artesian aquifer from a surface water body.

The head the pump must overcome is the difference between the discharge head and the suction head. The discharge head is the model-calculated head in the aquifer at the ASR site. The suction head is estimated to be the ground surface elevation at the ASR well. This assumes that the source water body is near the ASR well site and that there are no headlosses.

ASR Injection Well Schematic (Artesian Aquifer)

Figure 3.2

Regional Model Production Scenario Report

June 2013

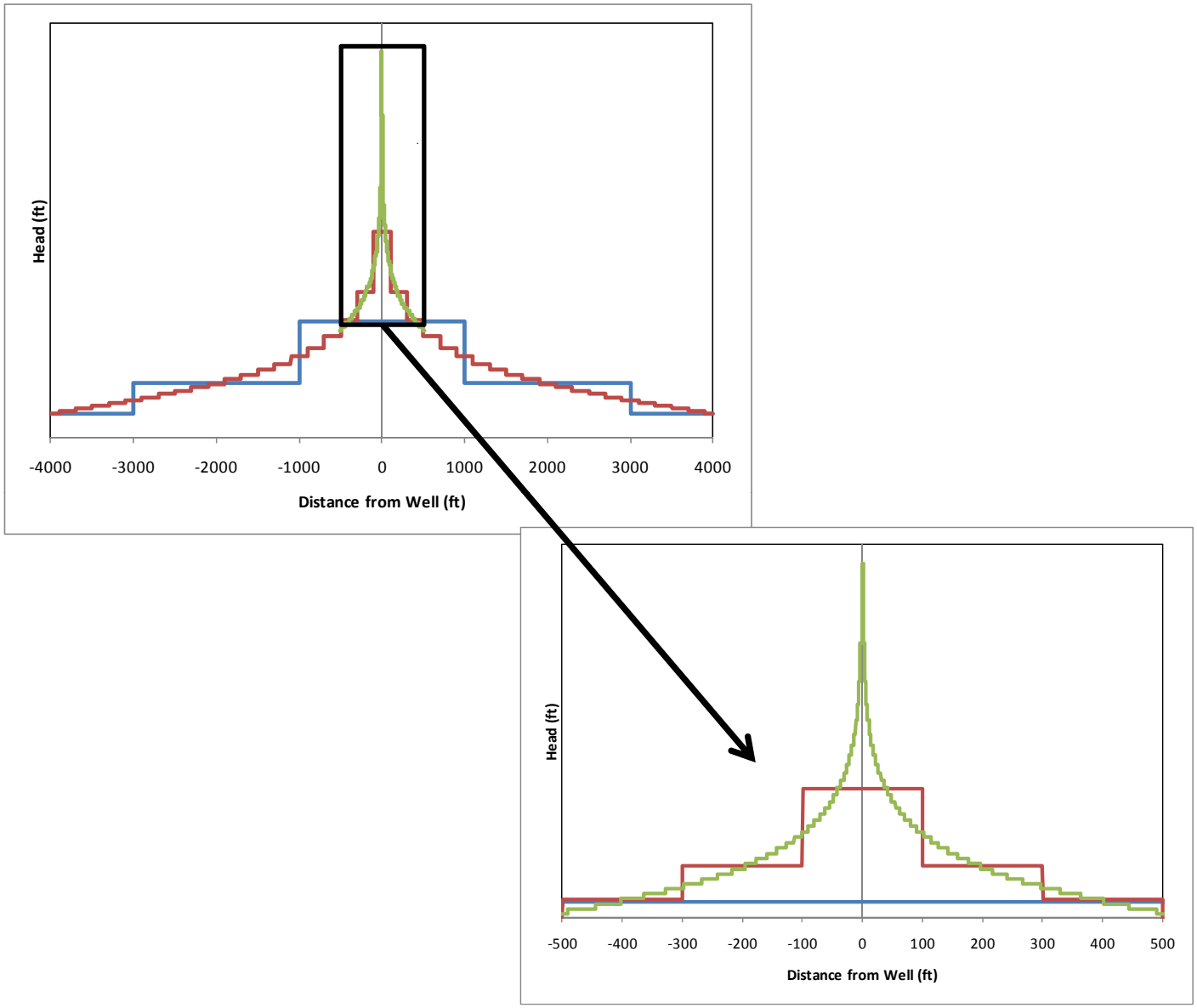

Legend

- Uniform Grid; 2000-ft cells
- Uniform Grid; 20-ft Cells
- Variably Sized Grid Cells; 2-ft Cells at Well Location

Notes:

These plots show the effects of grid resolution on the model results near an injection well. Each line represents the results of the same model run on a different grid. Note that the grid with the smallest cells (green line) has a significantly higher head at the well location than either of the two coarser grids.

Since the RASRSM has 2000-ft cells at most of the ASR sites, the head computed at the ASR cells is quite a bit lower than what would be experienced by the pump.

Note that both plots show the same information, but the lower right plot is zoomed in.

GRID RESOLUTION EFFECTS NEAR INJECTION WELL

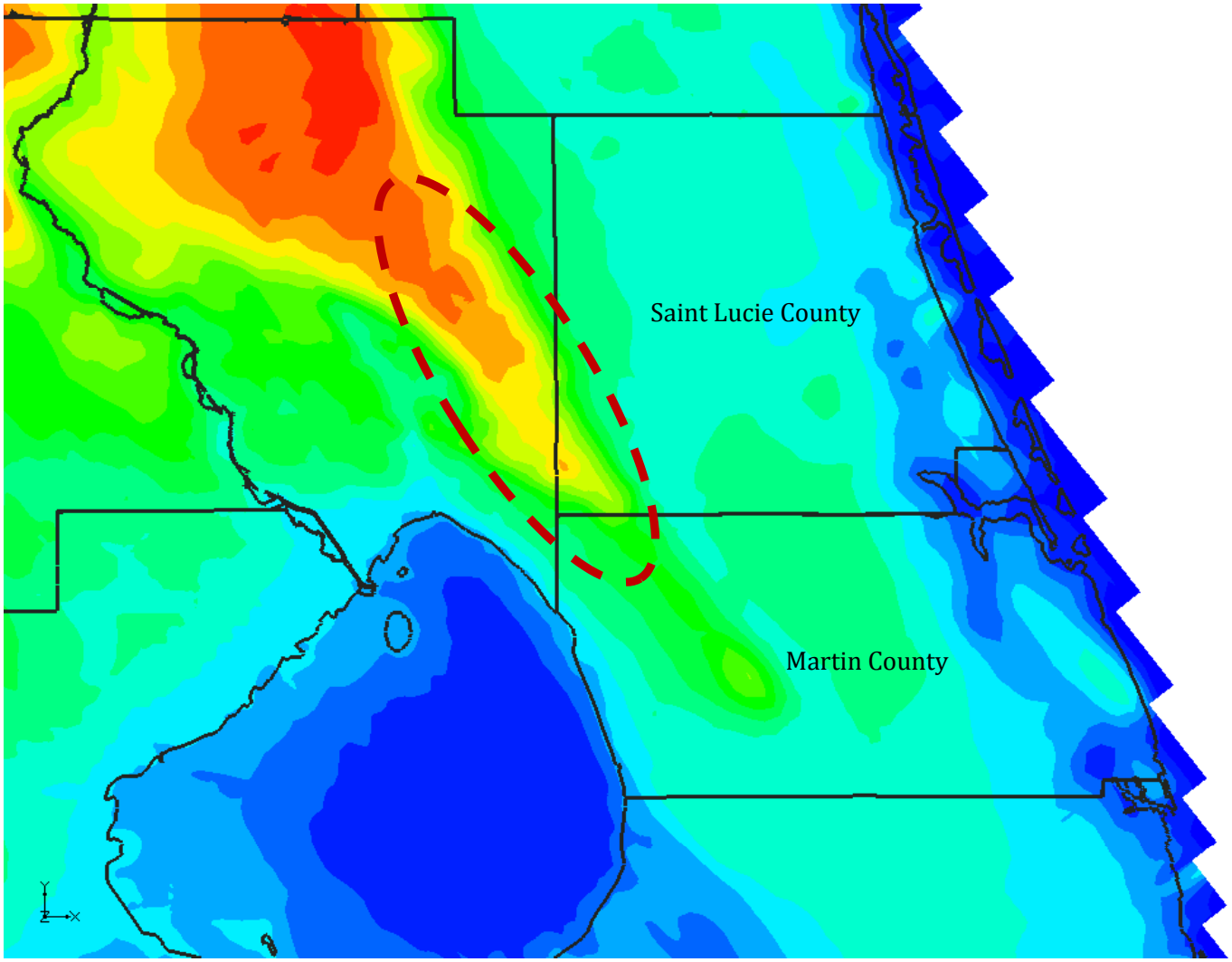

Ground Surface Elevation
(ft NGVD29)

70
65
60
55
50
45
40
35
30
25
20
15
10
5

Notes:

This figure shows the ground surface elevations for St. Lucie and Martin Counties and the surrounding areas. A ridge coming down through Okeechobee County through the corner of St. Lucie County and into Martin County is indicated with a dotted red oval.

Because of this ridge, the calibration model does not predict artesian conditions along the top of this ridge, and only slightly artesian conditions are indicated along the side slopes.

Readers should keep in mind that even small ASR pumping can greatly affect artesian conditions near this ridge.

GROUND SURFACE ELEVATIONS IN SAINT LUCIE AND MARTIN COUNTIES AND SURROUNDINGS

REGIONAL MODEL PRODUCTION SCENARIO REPORT

FIGURE 3.4

JUNE 2013

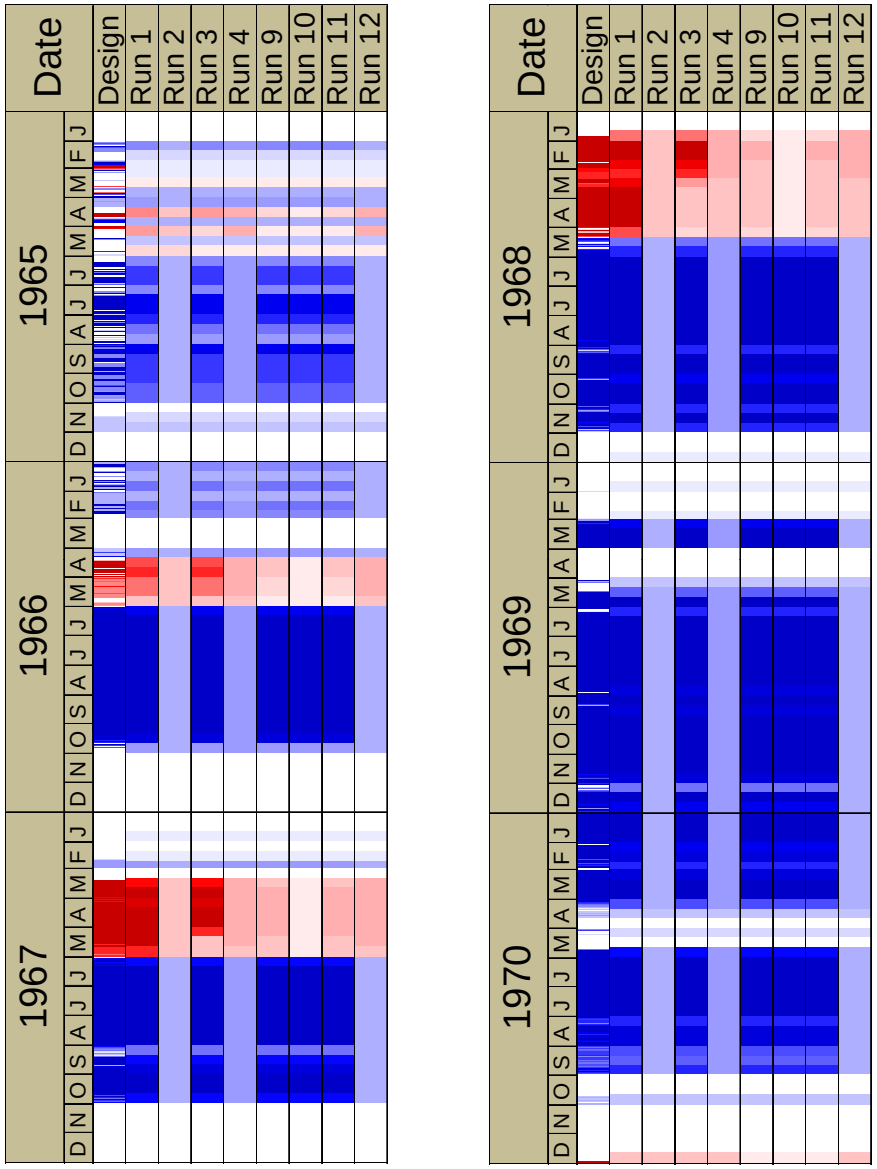

Notes:

These plots show the pump rates for the ASR wells in the SFWMM-D13R design and in each of the production scenarios for the RASRSM-D13R. Each day is designated with a small stripe, with the earliest part of the year (January) at the top of each box.

Note that the model scenarios were run with 10-day stress periods, requiring constant pumping during each 10-day time period. This accounts for the thicker stripes in the model run columns.

Darker colors indicate greater pumping rates. Blue indicates recharge(injection); red indicates recovery (extraction).

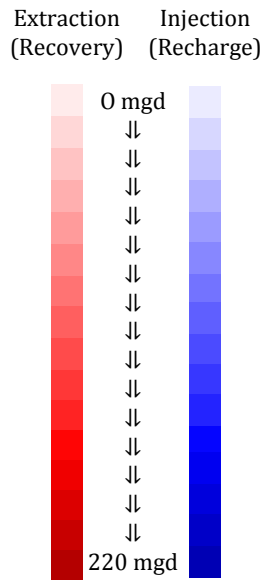

CALOOSAHATCHEE BASIN ASR PUMPING COMPARED FOR D13R SCENARIOS (1965-1970)

REGIONAL MODEL PRODUCTION SCENARIO REPORT

FIGURE 4.1

JUNE 2013

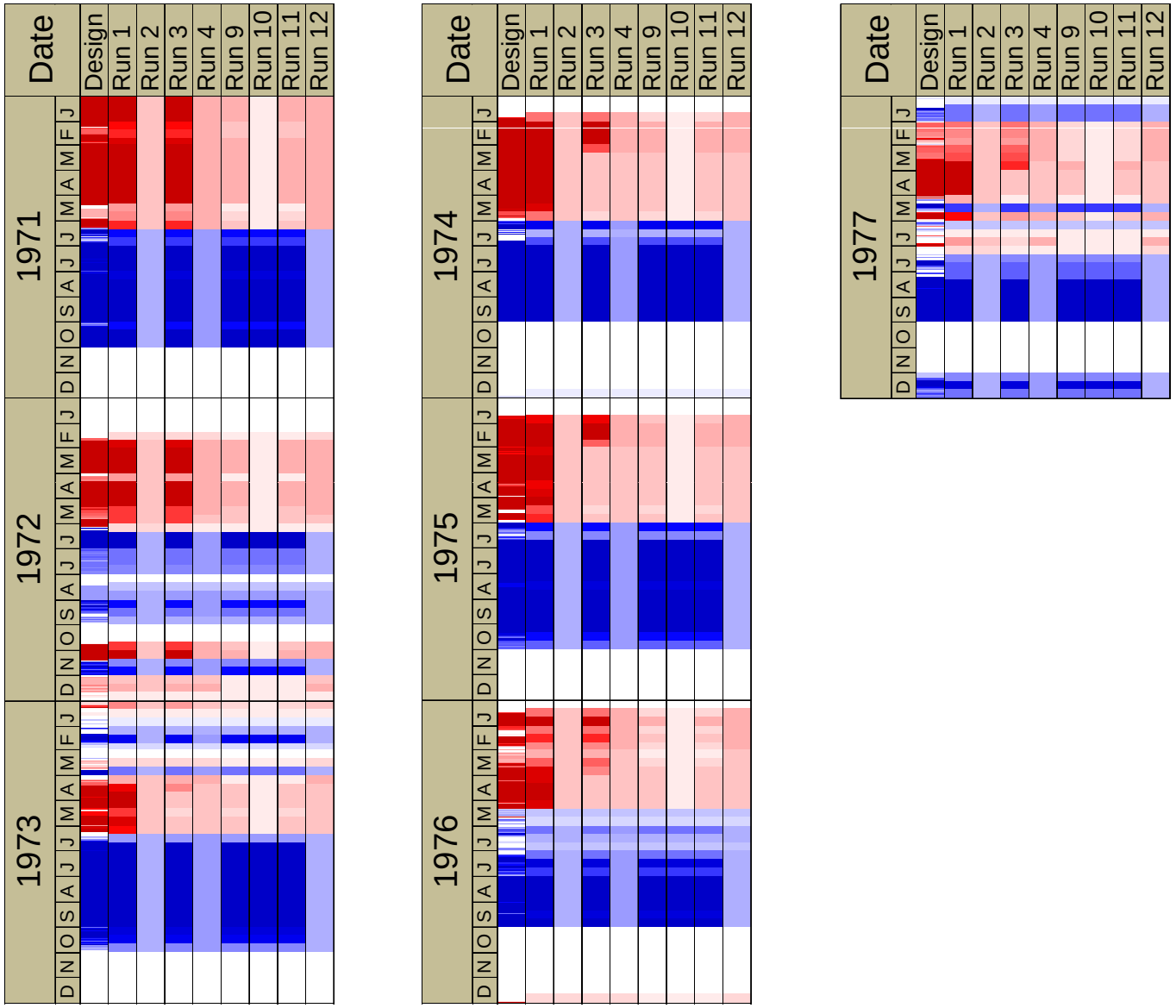

Notes:

These plots show the pump rates for the ASR wells in the SFWMM-D13R design and in each of the production scenarios for the RASRSM-D13R. Each day is designated with a small stripe, with the earliest part of the year (January) at the top of each box.

Note that the model scenarios were run with 10-day stress periods, requiring constant pumping during each 10-day time period. This accounts for the thicker stripes in the model run columns.

Darker colors indicate greater pumping rates. Blue indicates recharge(injection); red indicates recovery (extraction).

CALOOSAHATCHEE BASIN ASR PUMPING COMPARED FOR D13R SCENARIOS (1971-1977)

REGIONAL MODEL PRODUCTION SCENARIO REPORT

FIGURE 4.2

JUNE 2013

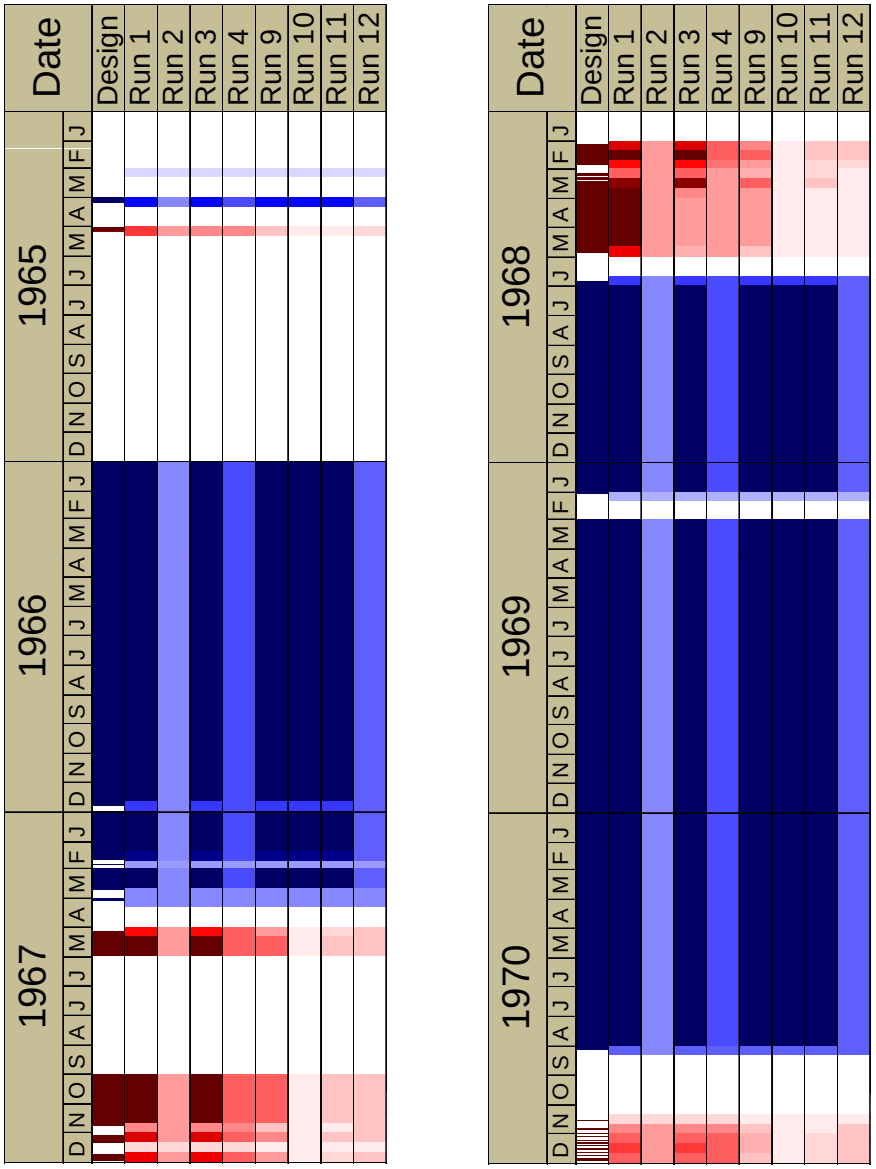

Notes:

These plots show the pump rates for the ASR wells in the SFWMM-D13R design and in each of the production scenarios for the RASRSM-D13R. Each day is designated with a small stripe, with the earliest part of the year (January) at the top of each box.

Note that the model scenarios were run with 10-day stress periods, requiring constant pumping during each 10-day time period. This accounts for the thicker stripes in the model run columns.

Darker colors indicate greater pumping rates. Blue indicates recharge(injection); red indicates recovery (extraction).

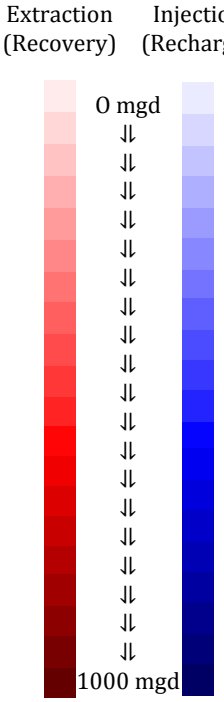

LAKE OKEECHOBEE BASIN ASR PUMPING COMPARED FOR D13R SCENARIOS (1965-1970)

REGIONAL MODEL PRODUCTION SCENARIO REPORT

FIGURE 4.3

JUNE 2013

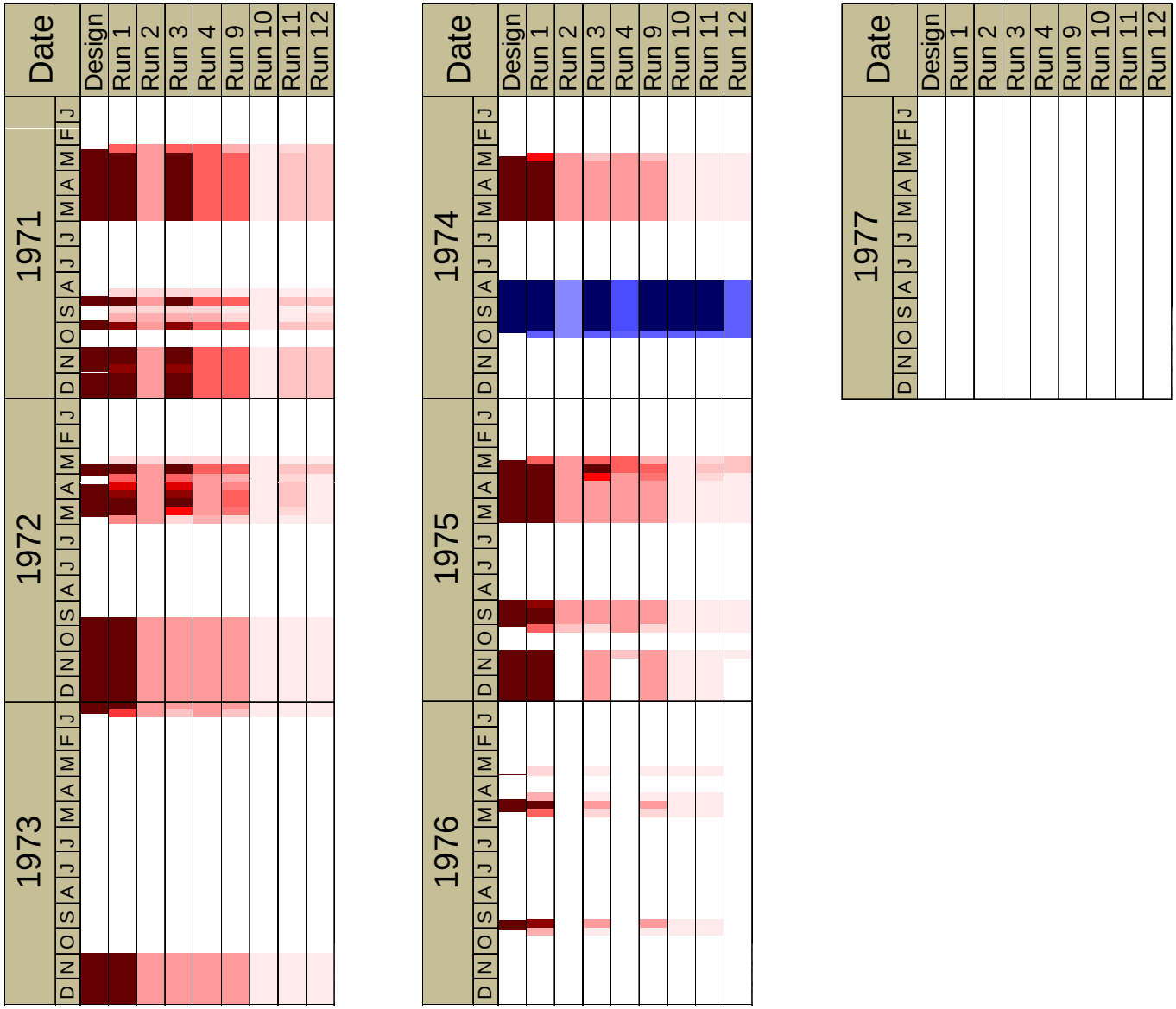

Notes:

These plots show the pump rates for the ASR wells in the SFWMM-D13R design and in each of the production scenarios for the RASRSM-D13R. Each day is designated with a small stripe, with the earliest part of the year (January) at the top of each box.

Note that the model scenarios were run with 10-day stress periods, requiring constant pumping during each 10-day time period. This accounts for the thicker stripes in the model run columns.

Darker colors indicate greater pumping rates. Blue indicates recharge(injection); red indicates recovery (extraction).

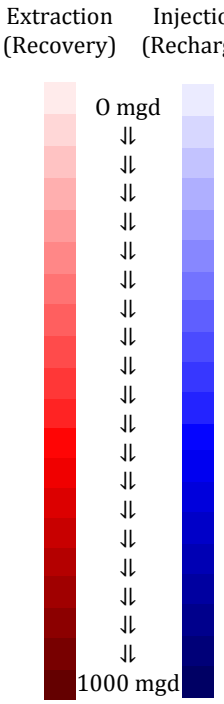

LAKE OKEECHOBEE BASIN ASR PUMPING COMPARED FOR D13R SCENARIOS (1971-1977)

REGIONAL MODEL PRODUCTION SCENARIO REPORT

FIGURE 4.4

JUNE 2013

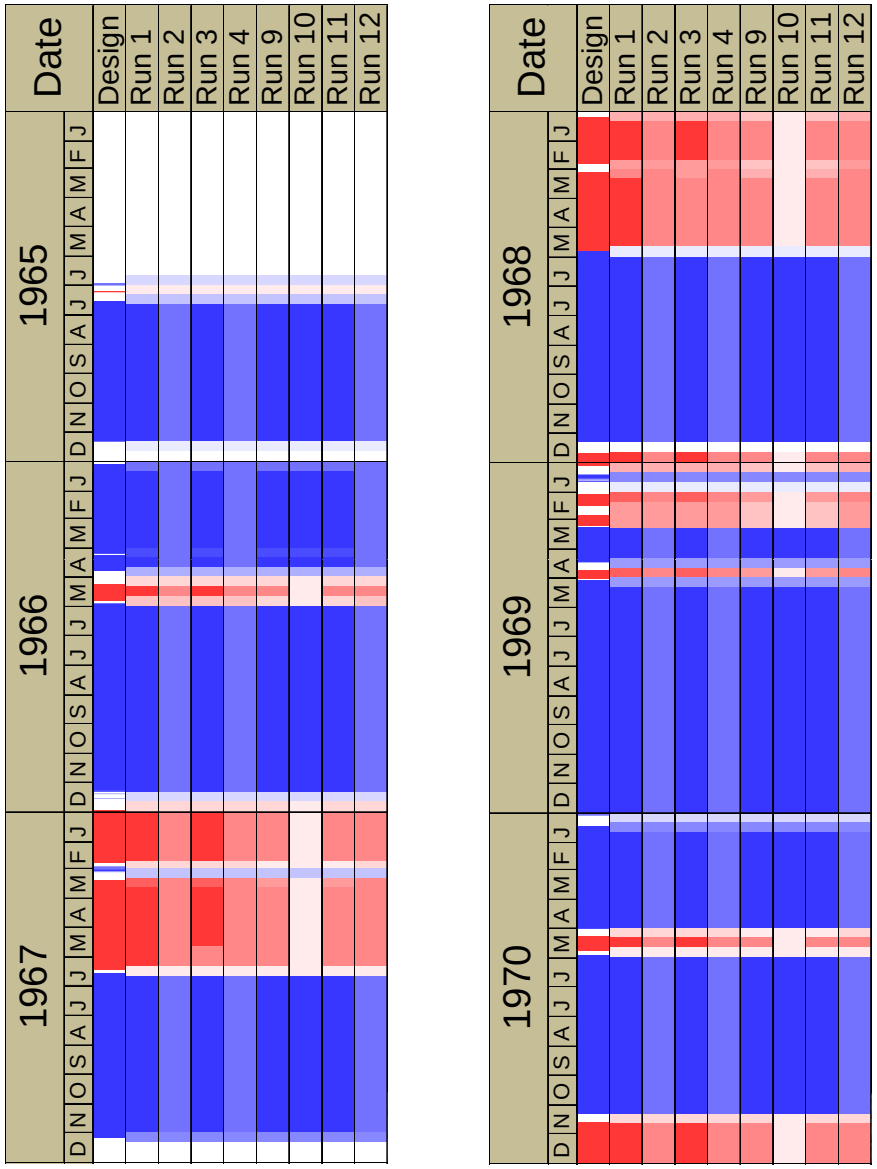

Notes:

These plots show the pump rates for the ASR wells in the SFWMM-D13R design and in each of the production scenarios for the RASRSM-D13R. Each day is designated with a small stripe, with the earliest part of the year (January) at the top of each box.

Note that the model scenarios were run with 10-day stress periods, requiring constant pumping during each 10-day time period. This accounts for the thicker stripes in the model run columns.

Darker colors indicate greater pumping rates. Blue indicates recharge(injection); red indicates recovery (extraction).

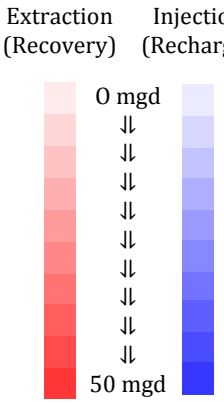

L-8 ASR Pumping Compared for D13R Scenarios (1965-1970)

Regional Model Production Scenario Report

Figure 4.5

June 2013

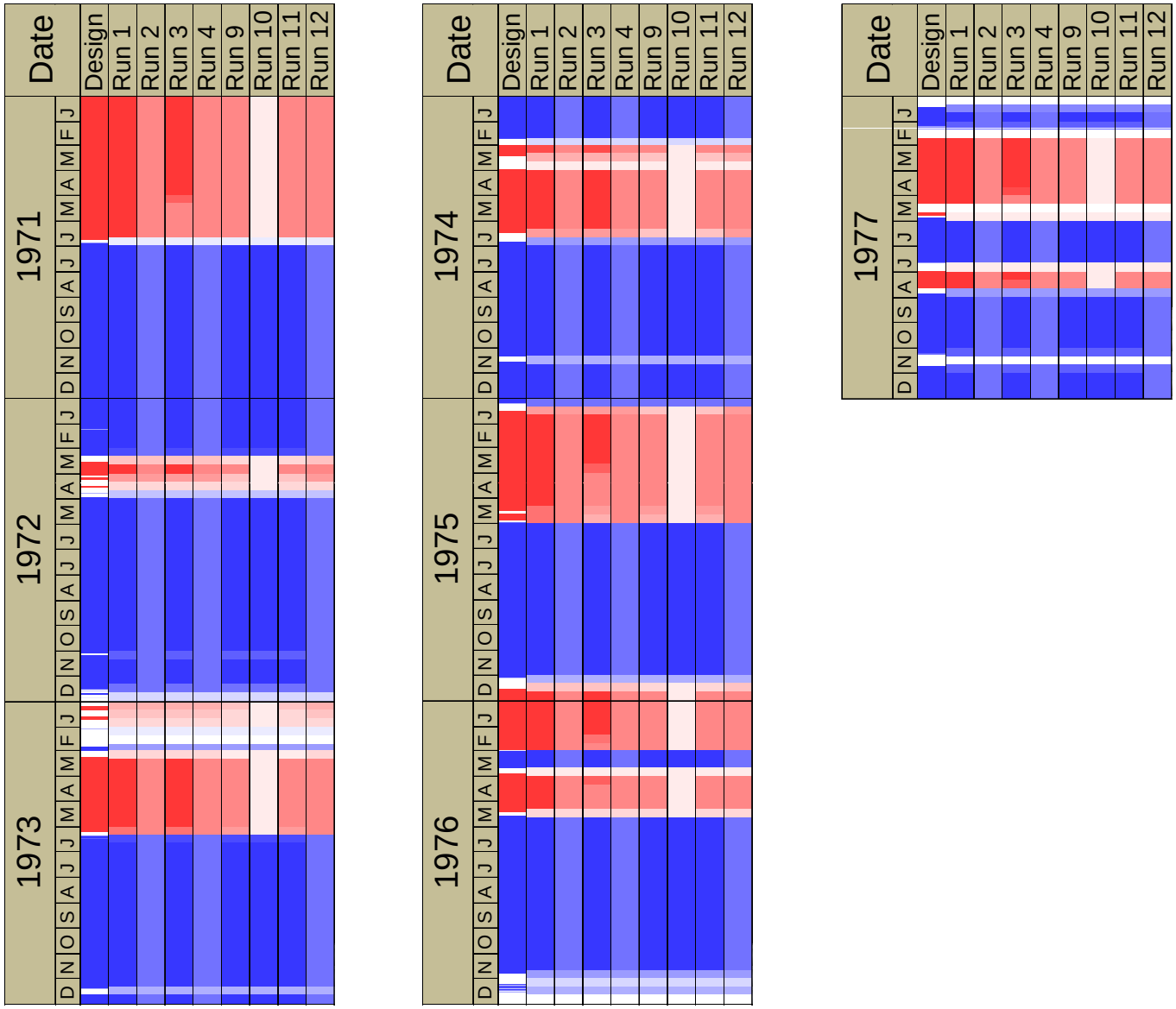

Notes:

These plots show the pump rates for the ASR wells in the SFWMM-D13R design and in each of the production scenarios for the RASRSM-D13R. Each day is designated with a small stripe, with the earliest part of the year (January) at the top of each box.

Note that the model scenarios were run with 10-day stress periods, requiring constant pumping during each 10-day time period. This accounts for the thicker stripes in the model run columns.

Darker colors indicate greater pumping rates. Blue indicates recharge(injection); red indicates recovery (extraction).

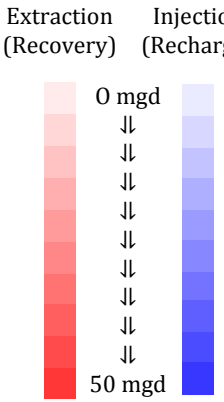

L-8 ASR Pumping Compared for D13R Scenarios (1971-1977)

Regional Model Production Scenario Report

Figure 4.6

June 2013

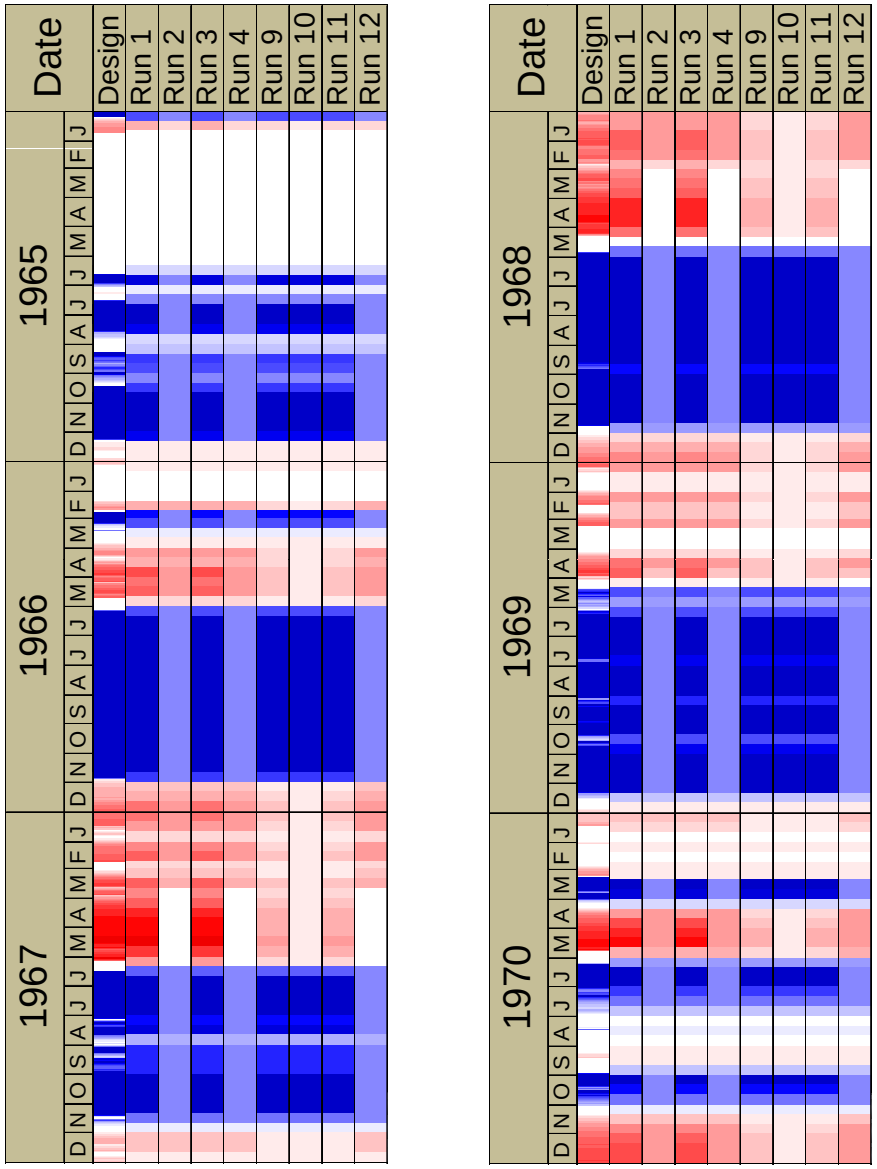

Notes:

These plots show the pump rates for the ASR wells in the SFWMM-D13R design and in each of the production scenarios for the RASRSM-D13R. Each day is designated with a small stripe, with the earliest part of the year (January) at the top of each box.

Note that the model scenarios were run with 10-day stress periods, requiring constant pumping during each 10-day time period. This accounts for the thicker stripes in the model run columns.

Darker colors indicate greater pumping rates. Blue indicates recharge(injection); red indicates recovery (extraction).

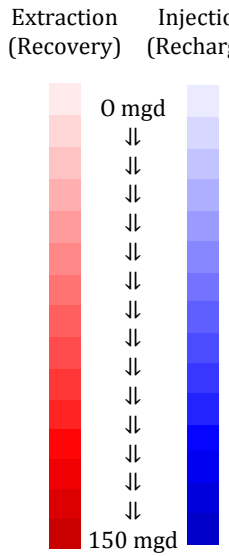

HILLSBORO (SITE 1) ASR PUMPING COMPARED FOR D13R SCENARIOS (1965-1970)

REGIONAL MODEL PRODUCTION SCENARIO REPORT

FIGURE 4.7

JUNE 2013

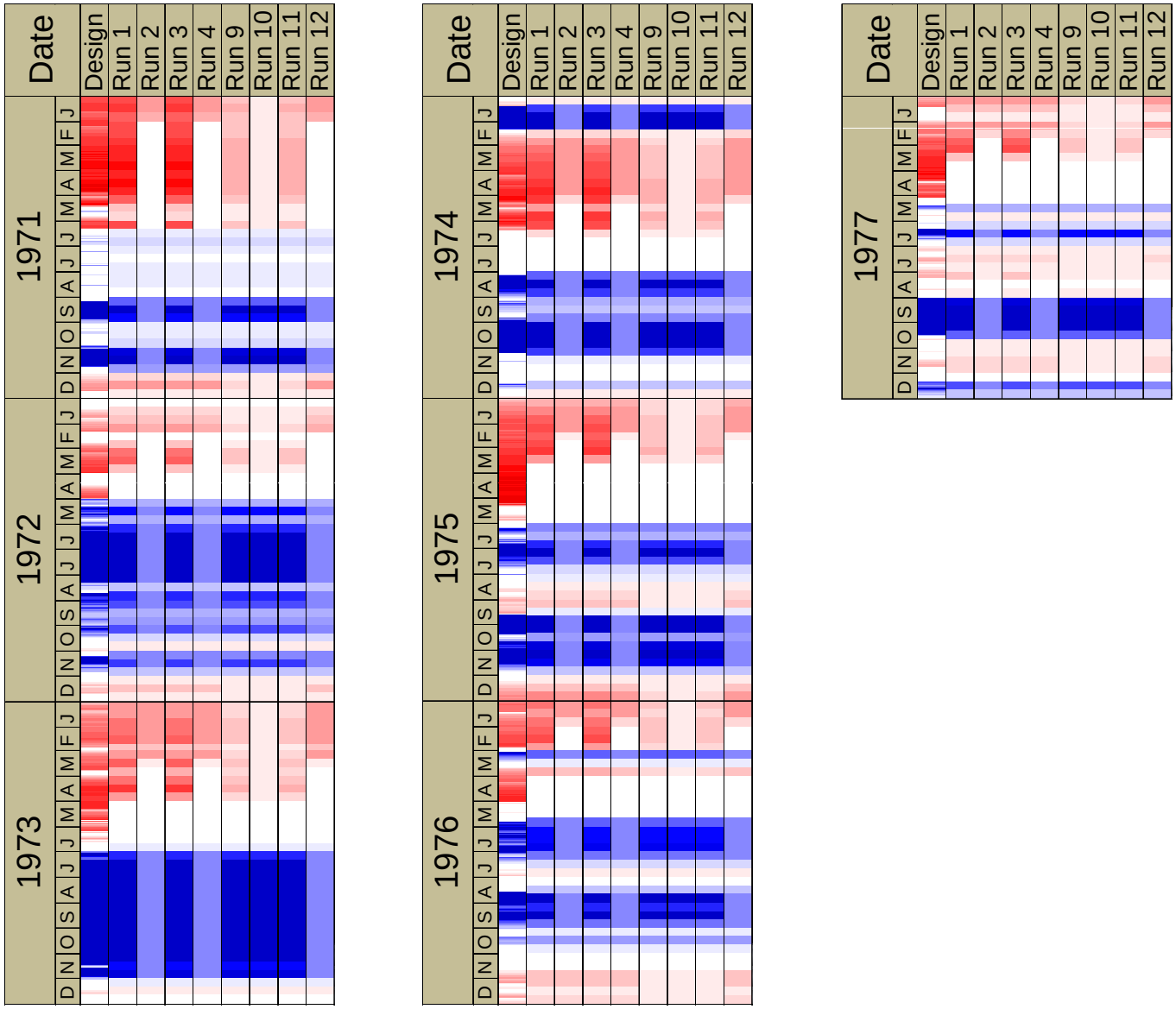

Notes:

These plots show the pump rates for the ASR wells in the SFWMM-D13R design and in each of the production scenarios for the RASRSM-D13R. Each day is designated with a small stripe, with the earliest part of the year (January) at the top of each box.

Note that the model scenarios were run with 10-day stress periods, requiring constant pumping during each 10-day time period. This accounts for the thicker stripes in the model run columns.

Darker colors indicate greater pumping rates. Blue indicates recharge(injection); red indicates recovery (extraction).

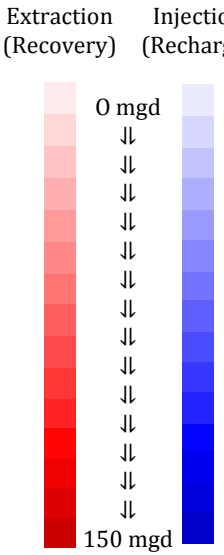

HILLSBORO (SITE 1) ASR PUMPING COMPARED FOR D13R SCENARIOS (1971-1977)

REGIONAL MODEL PRODUCTION SCENARIO REPORT

FIGURE 4.8

JUNE 2013

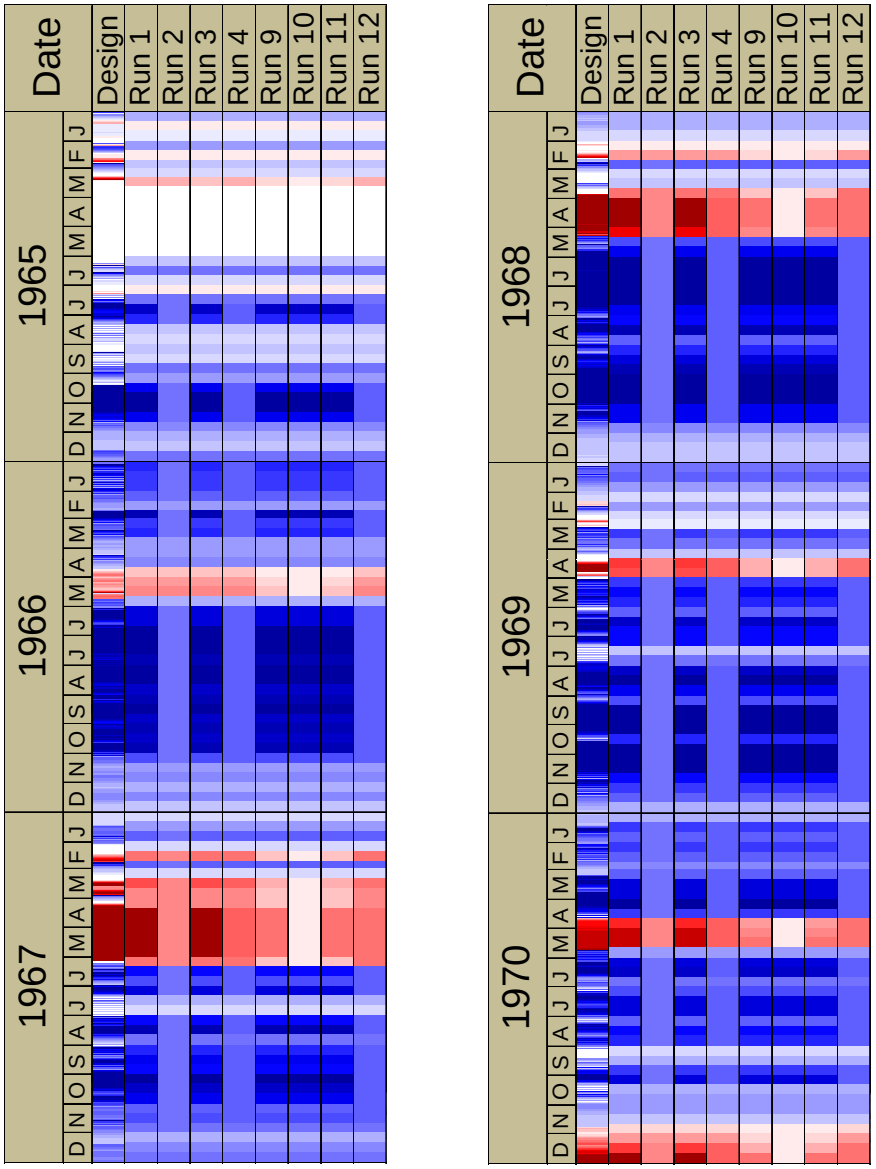

Notes:

These plots show the pump rates for the ASR wells in the SFWMM-D13R design and in each of the production scenarios for the RASRSM-D13R. Each day is designated with a small stripe, with the earliest part of the year (January) at the top of each box.

Note that the model scenarios were run with 10-day stress periods, requiring constant pumping during each 10-day time period. This accounts for the thicker stripes in the model run columns.

Darker colors indicate greater pumping rates. Blue indicates recharge(injection); red indicates recovery (extraction).

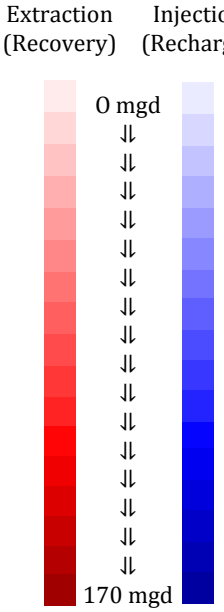

C-51 Canal ASR Pumping Compared for D13R Scenarios (1965-1970)

Regional Model Production Scenario Report

Figure 4.9

June 2013

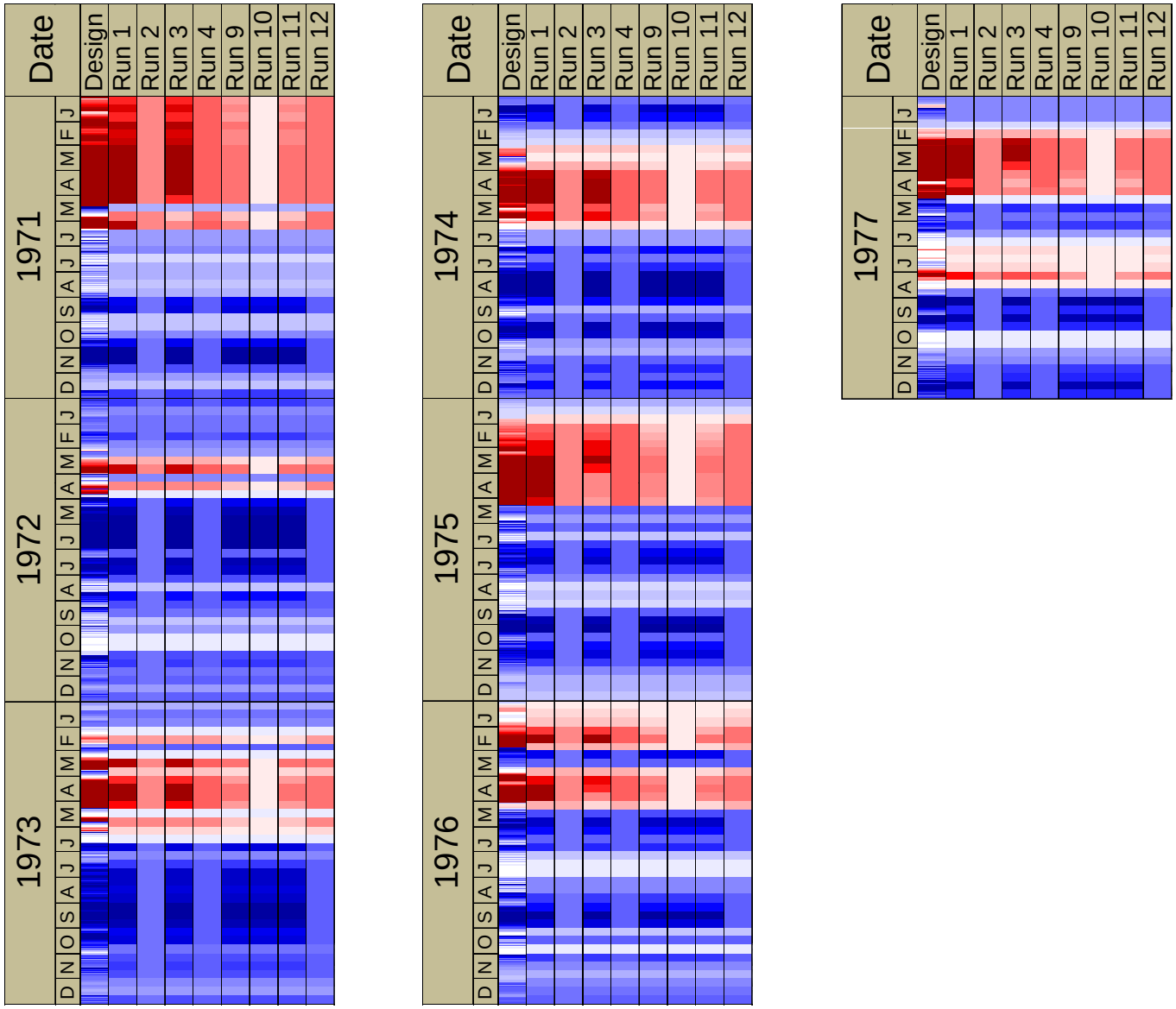

Notes:

These plots show the pump rates for the ASR wells in the SFWMM-D13R design and in each of the production scenarios for the RASRSM-D13R. Each day is designated with a small stripe, with the earliest part of the year (January) at the top of each box.

Note that the model scenarios were run with 10-day stress periods, requiring constant pumping during each 10-day time period. This accounts for the thicker stripes in the model run columns.

Darker colors indicate greater pumping rates. Blue indicates recharge(injection); red indicates recovery (extraction).

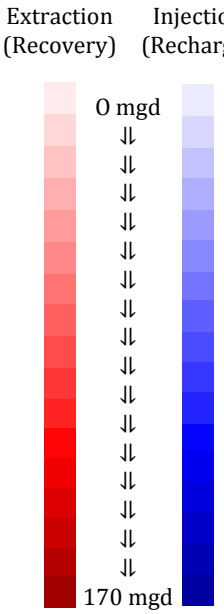

C-51 Pumping Compared for D13R Scenarios (1971-1977)

Regional Model Production Scenario Report

Figure 4.10

June 2013

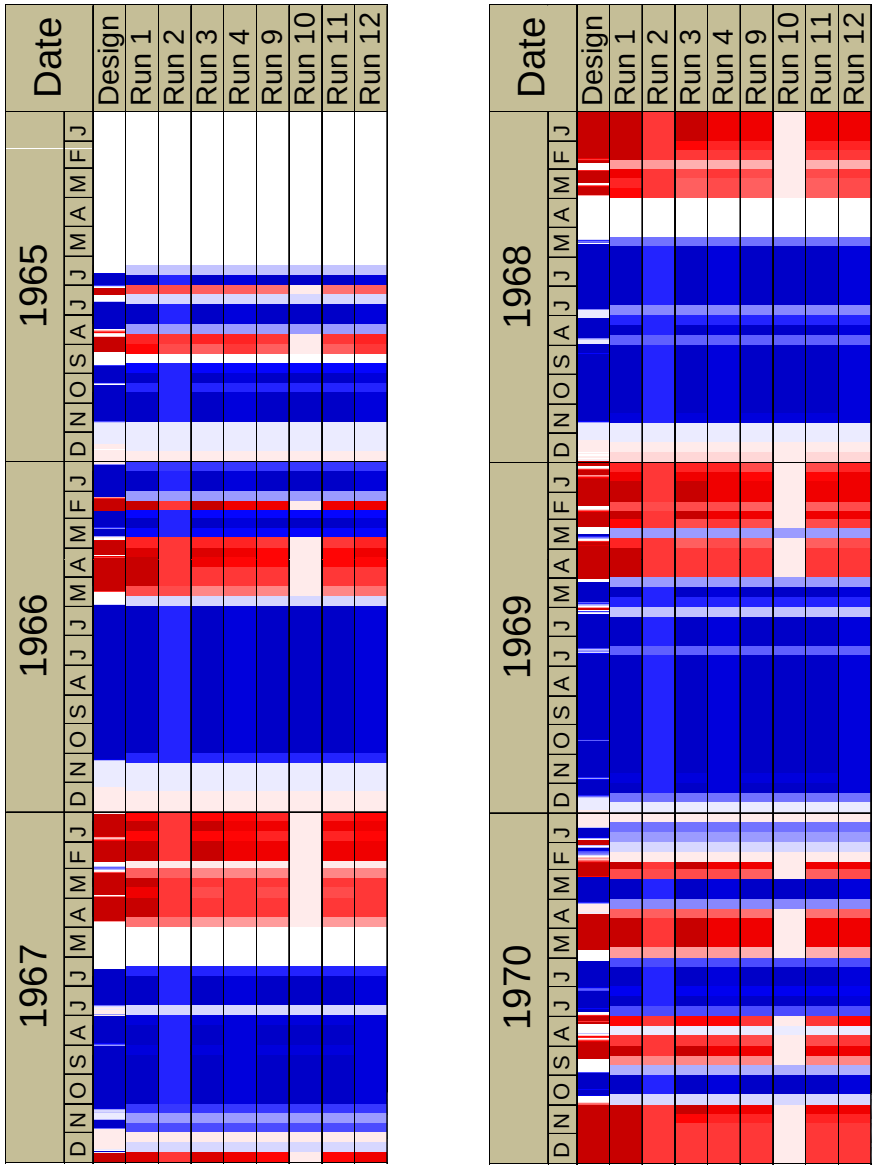

Notes:

These plots show the pump rates for the ASR wells in the SFWMM-D13R design and in each of the production scenarios for the RASRSM-D13R. Each day is designated with a small stripe, with the earliest part of the year (January) at the top of each box.

Note that the model scenarios were run with 10-day stress periods, requiring constant pumping during each 10-day time period. This accounts for the thicker stripes in the model run columns.

Darker colors indicate greater pumping rates. Blue indicates recharge(injection); red indicates recovery (extraction).

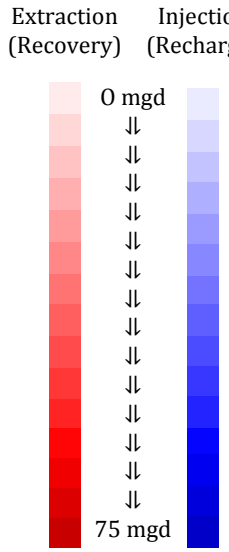

CENTRAL PALM BEACH ASR PUMPING COMPARED FOR D13R SCENARIOS (1965-1970)

REGIONAL MODEL PRODUCTION SCENARIO REPORT

FIGURE 4.11

JUNE 2013

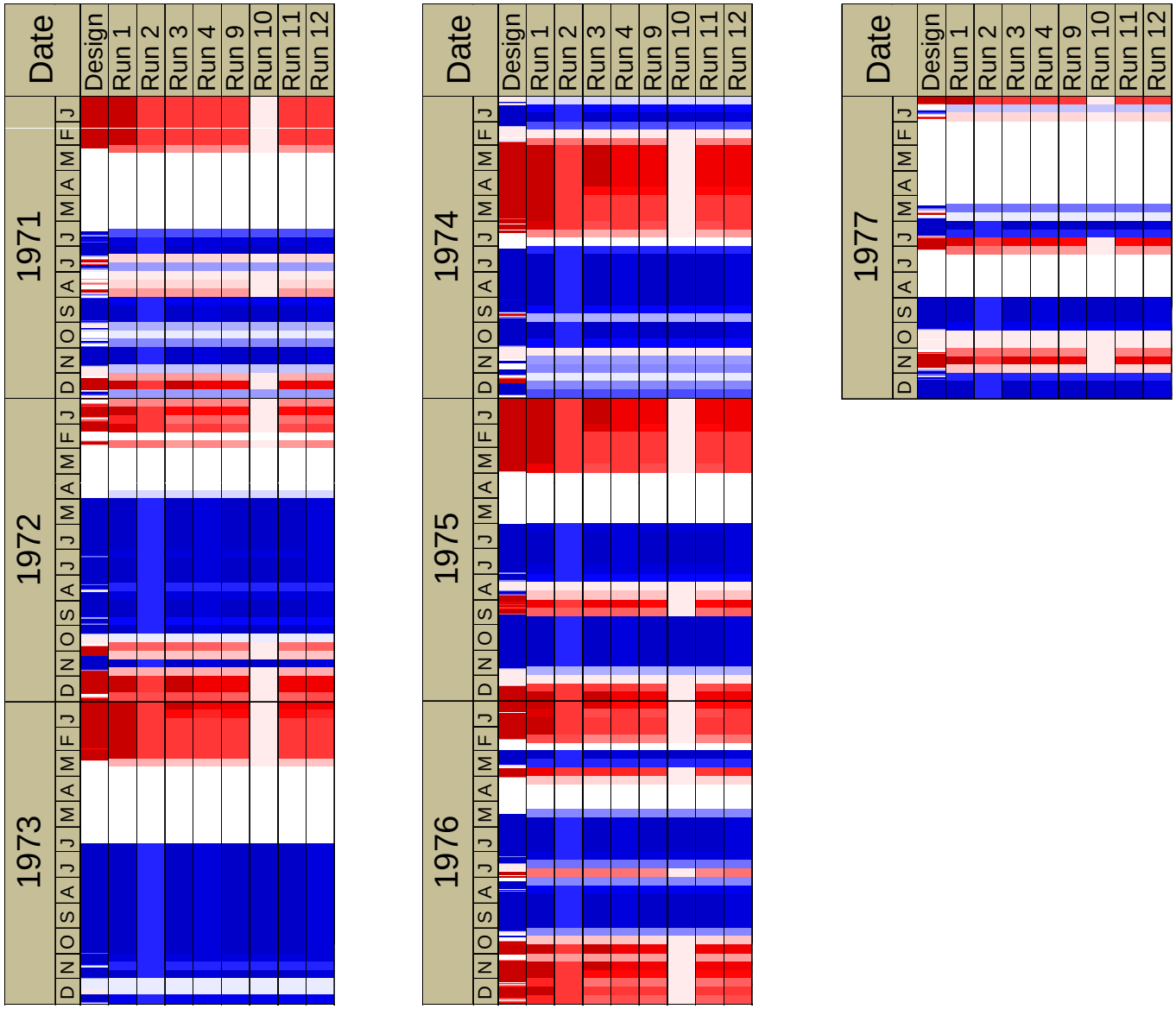

Notes:

These plots show the pump rates for the ASR wells in the SFWMM-D13R design and in each of the production scenarios for the RASRSM-D13R. Each day is designated with a small stripe, with the earliest part of the year (January) at the top of each box.

Note that the model scenarios were run with 10-day stress periods, requiring constant pumping during each 10-day time period. This accounts for the thicker stripes in the model run columns.

Darker colors indicate greater pumping rates. Blue indicates recharge(injection); red indicates recovery (extraction).

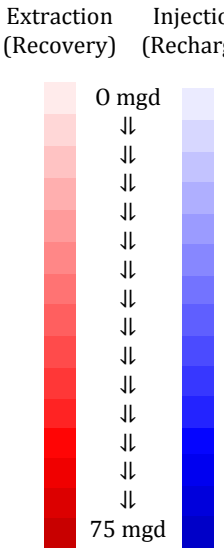

CENTRAL PALM BEACH ASR PUMPING COMPARED FOR D13R SCENARIOS (1971-1977)

REGIONAL MODEL PRODUCTION SCENARIO REPORT

FIGURE 4.12

JUNE 2013

		UF		APPZ		BZ		Total # Wells	Target # Wells
		Number of Wells	Recovery Efficiency	Number of Wells	Recovery Efficiency	Number of Wells	Recovery Efficiency		
Caloosahatchee Basin	Moore Haven	16	70%	0	30%	0	10%		
	River Bend	8	70%	0	30%	0	10%		
	Flaghole	20	70%	0	30%	0	10%		
	Basin Total	44		0		0		44	44
Lake Okeechobee Basin	Nicodemus Slough	10	70%	0	30%	0	10%		
	C-41 Canal	10	70%	0	30%	0	10%		
	C-40 Canal	10	70%	0	30%	0	10%		
	North Lake Okeechobee	20	70%	0	30%	0	10%		
	Kissimmee R./Paradise Run	75	70%	0	30%	0	10%		
	Taylor Creek	20	70%	0	30%	0	10%		
	L-63N	15	70%	0	30%	0	10%		
	Lakeside Ranch	20	70%	0	30%	0	10%		
	Port Mayaca	20	70%	0	30%	0	10%		
	Basin Total	200		0		0		200	200
L-8		10	70%	0	30%	0	10%	10	10
C-51		34	70%	0	30%	0	10%	34	34
Central Palm Beach		15	70%	0	30%	0	10%	15	15
Site 1 (Hillsboro)		30	40%	0	40%	0	10%	30	30
Total		333		0		0		333	333

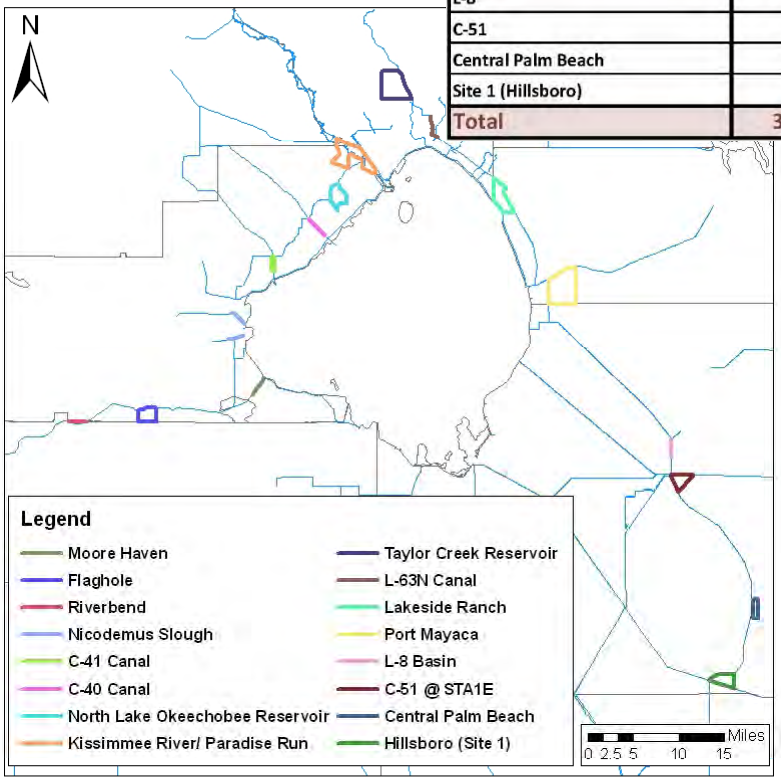

Notes:

Scenario 1 includes all of the 333 ASR wells specified by the SFWMM-D13R design. All are fully penetrating in the UF Aquifer.

Flow rates are divided evenly among the wells in each basin. Maximum flow rate for any one well is 5 mgd.

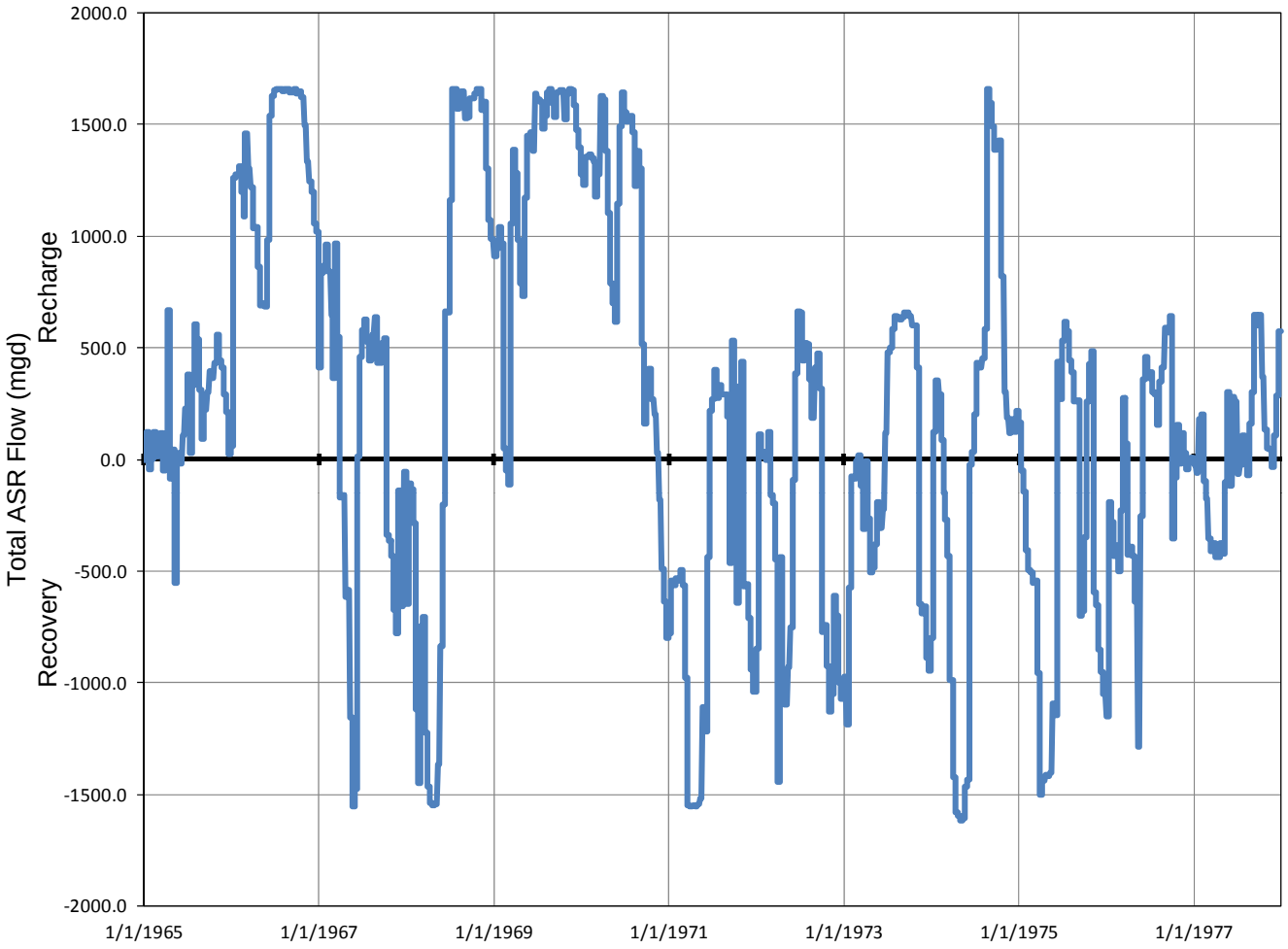

Legend

Scenario 1 – ASR Flux

Notes:

Scenario 1 includes all of the 333 ASR wells specified by the SFWMM-D13R design. All are fully penetrating in the UF Aquifer.

This plot shows the extraction and injection rates for all wells at all sites for Scenario 1. Positive rates are recharge (injection), while negative rates are recovery (extraction).

SCENARIO 1 – ASR WELL FLUXES

REGIONAL MODEL PRODUCTION SCENARIO REPORT

FIGURE 4.14

JUNE 2013

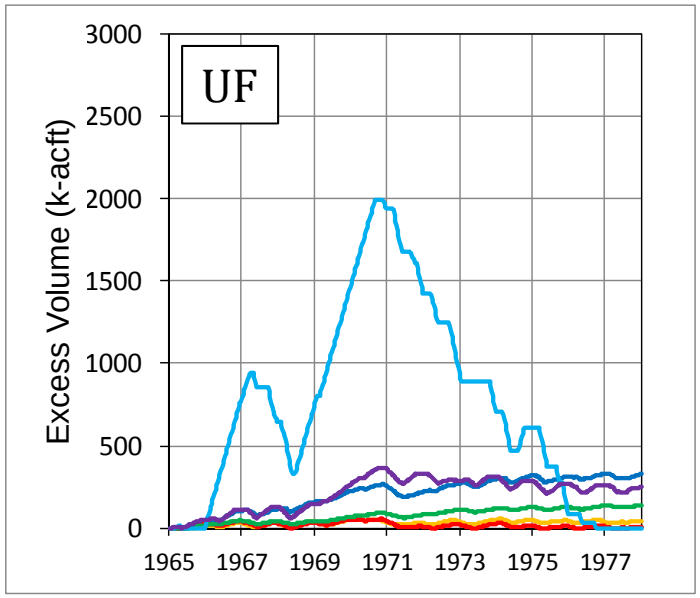

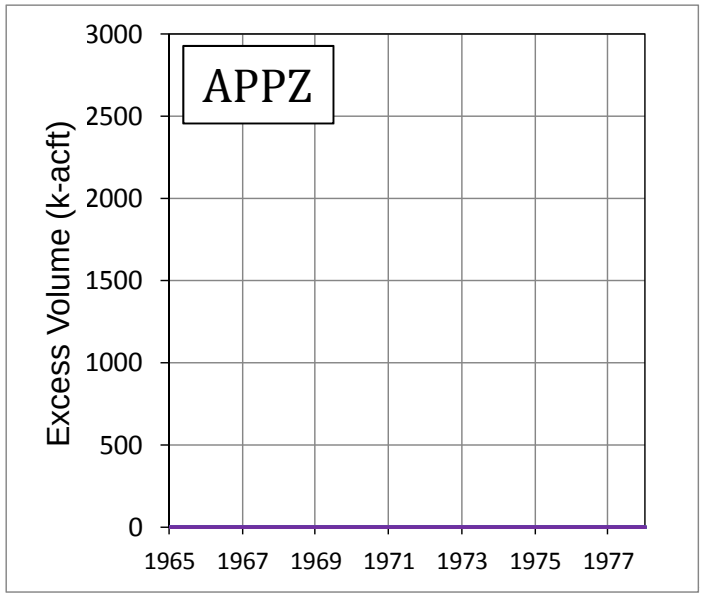

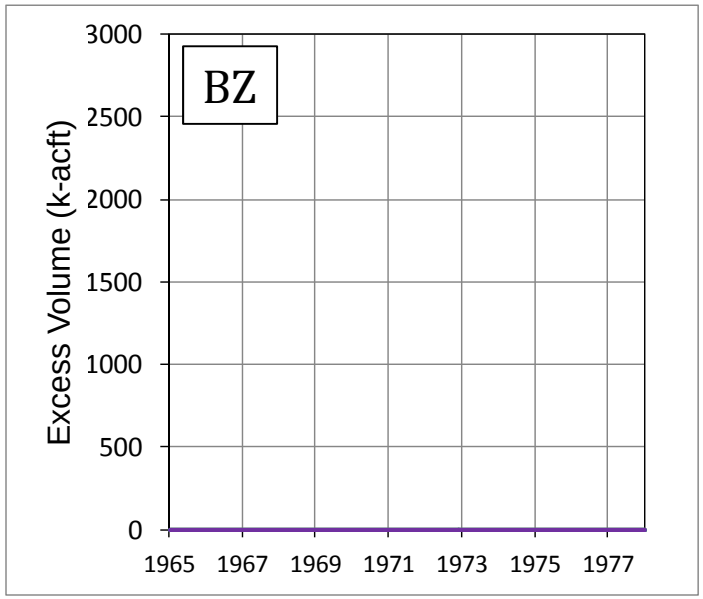

Legend

- Central Palm Beach
- C-51
- Hillsboro
- L-8
- Lake Okeechobee
- Caloosahatchee River

Notes:

Scenario 1 includes all of the 333 ASR wells specified by the SFWMM-D13R design. All are fully penetrating in the UF Aquifer.

These plots show the excess volume of fresh water remaining in each aquifer at each ASR basin. Excess volume is calculated by adding injected volume times recovery efficiency and subtracting extracted volume. The calculation is cumulative.

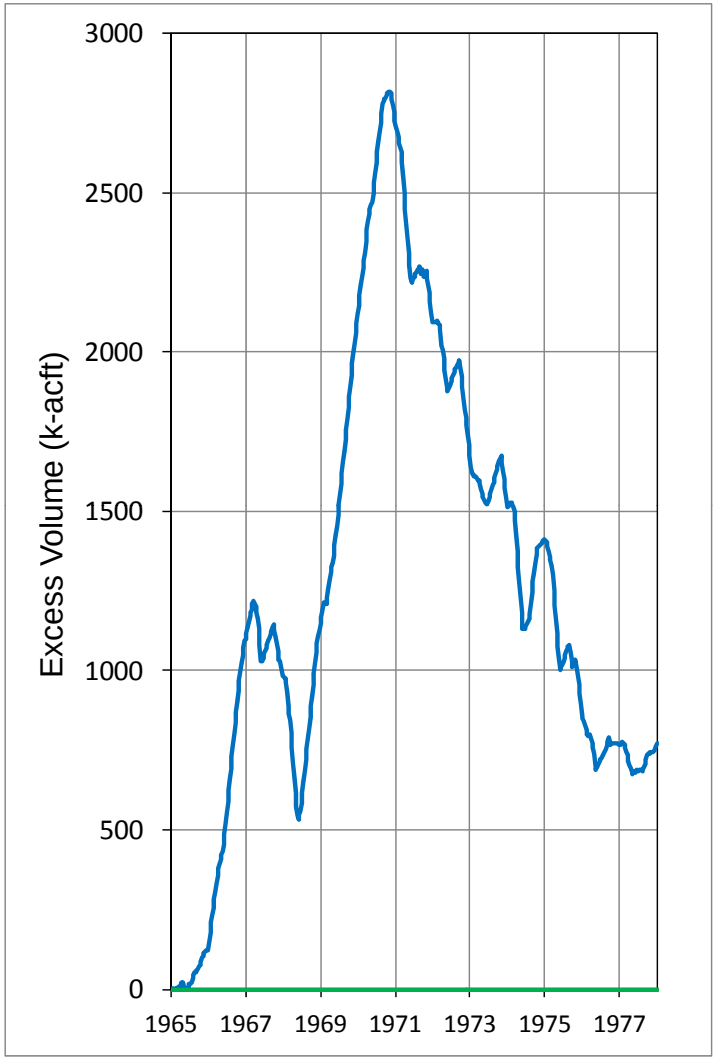

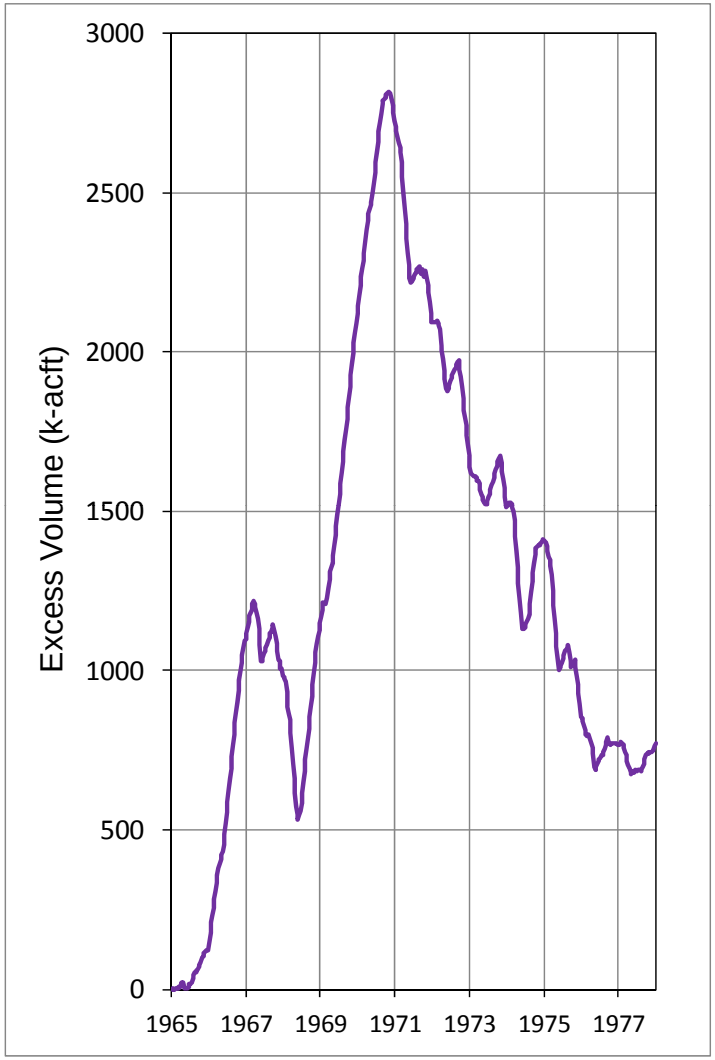

Legend

- Total UF
- Total APPZ
- Total BZ
- Total (All Aquifers)

Notes:

Scenario 1 includes all of the 333 ASR wells specified by the SFWMM-D13R design. All are fully penetrating in the UF Aquifer.

These plots show the total excess volume of fresh water remaining in each aquifer and in all aquifers. Excess volume is calculated by adding injected volume times recovery efficiency and subtracting extracted volume. The calculation is cumulative.

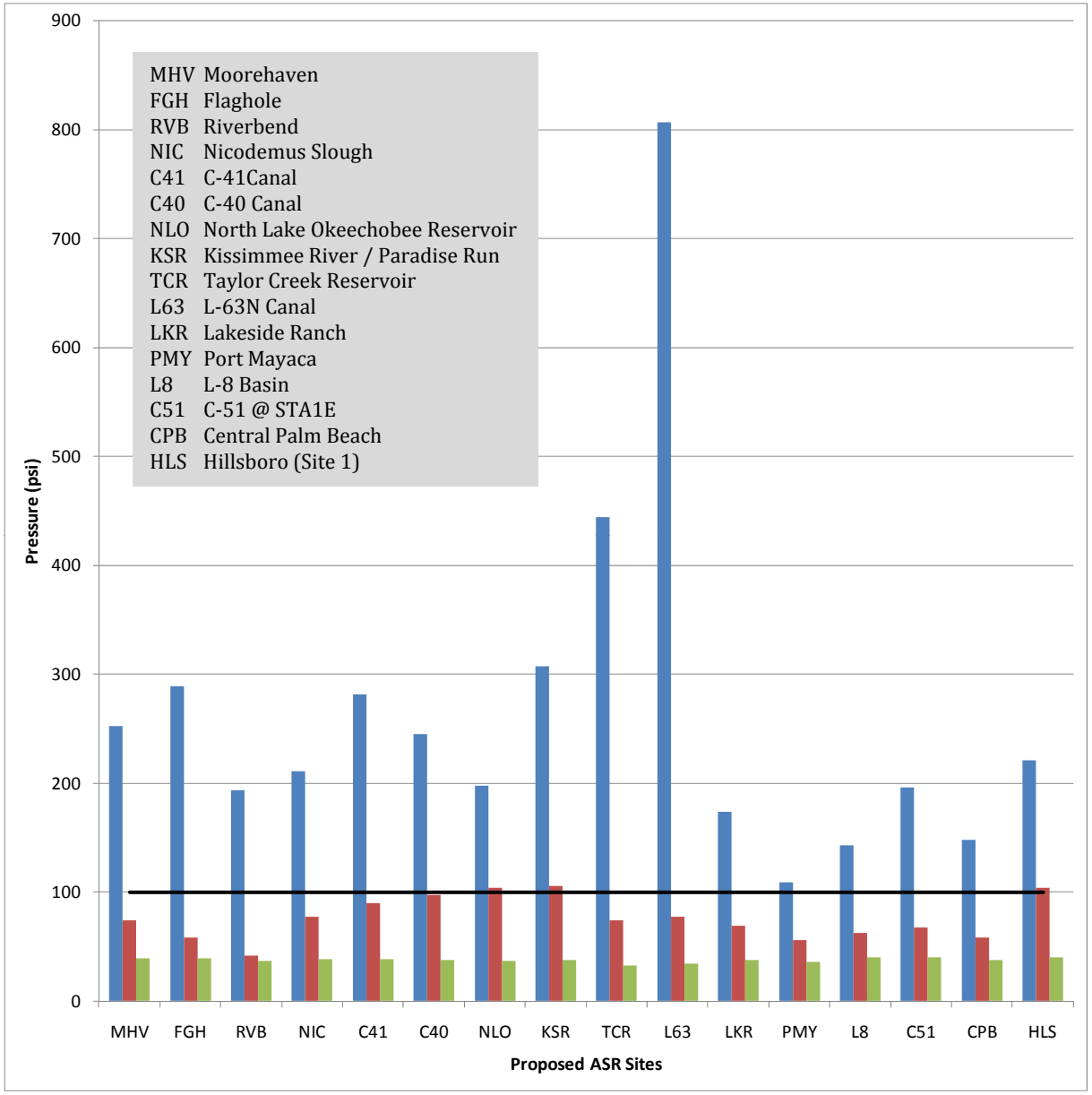

Legend

- Upper Floridan Aquifer
- Avon Park Permeable Zone
- Boulder Zone
- 100 psi Limit

Notes:

Scenario 1 includes all of the 333 ASR wells specified by the SFWMM-D13R design. All are fully penetrating in the UF Aquifer.

This plot shows the highest pressure at each site which the pump would need to overcome in order to inject storage water during the 13-year simulation.

The PDT determined that it would be important to keep this pressure below 100 psi (indicated by the heavy black line).

Note that maximum pressures are shown for all aquifers and all sites even if ASR pumps are not located there for the current scenario.

SCENARIO 1 – MAXIMUM PUMP PRESSURE REQUIREMENTS

FIGURE 4.17

REGIONAL MODEL PRODUCTION SCENARIO REPORT

JUNE 2013

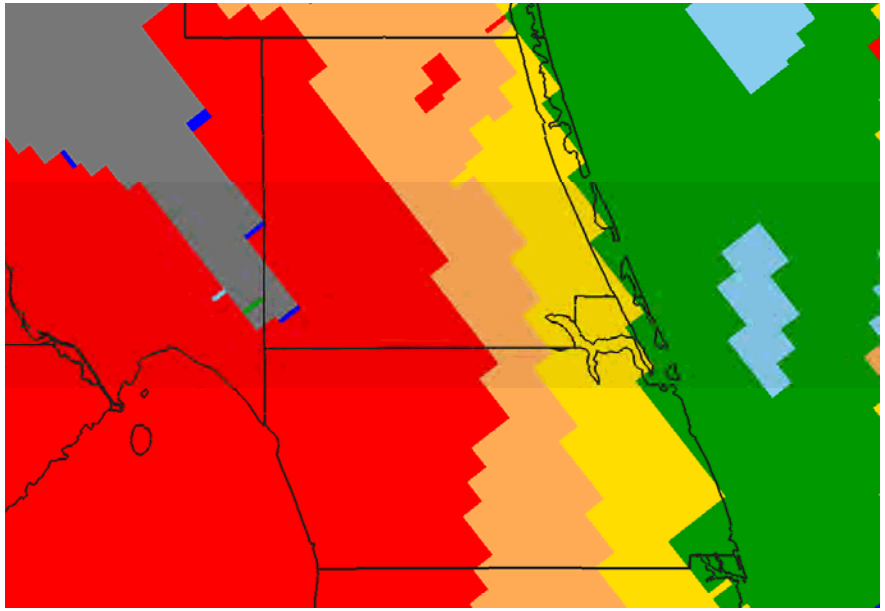

Upper Floridan Aquifer

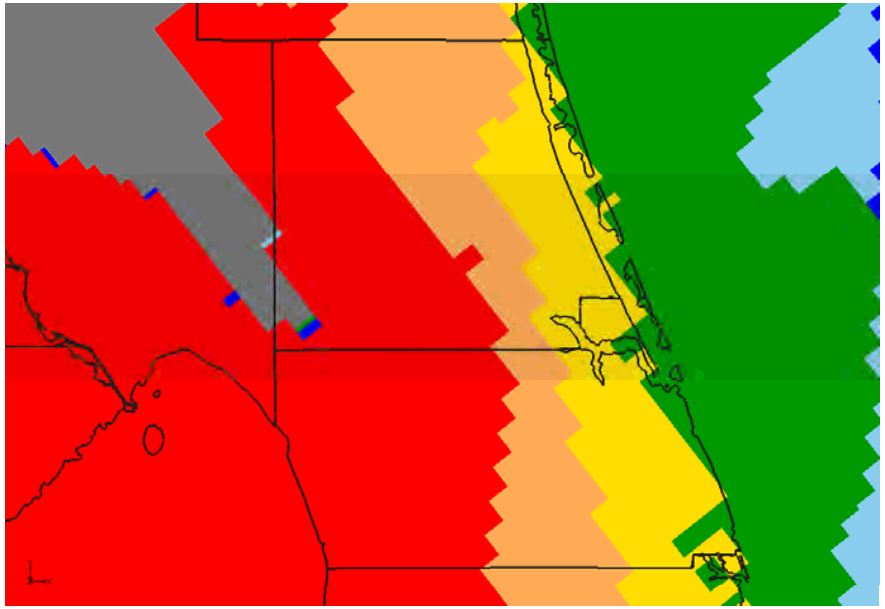

Avon Park Permeable Zone

Legend

- Not artesian
- < 5%
- 5% - 10%
- 10% - 20%
- 20% - 50%
- 50% - 100%
- Loses artesian condition

Notes:

Scenario 1 includes all of the 333 ASR wells specified by the SFWMM-D13R design. All are fully penetrating in the UF Aquifer.

These plots show the maximum reduction in artesian flow at each model cell as a percentage when compared to the flow expected without the ASR project.

Permit rules require that the reduction in Saint Lucie and Martin Counties be less than 10%.

Note the gray area in the northwest corner of the figures, which coincides with a ridge and does not normally have artesian conditions.

SCENARIO 1 – MAXIMUM REDUCTION IN ARTESIAN FLOW CAPACITY

REGIONAL MODEL PRODUCTION SCENARIO REPORT

FIGURE 4.18

JUNE 2013

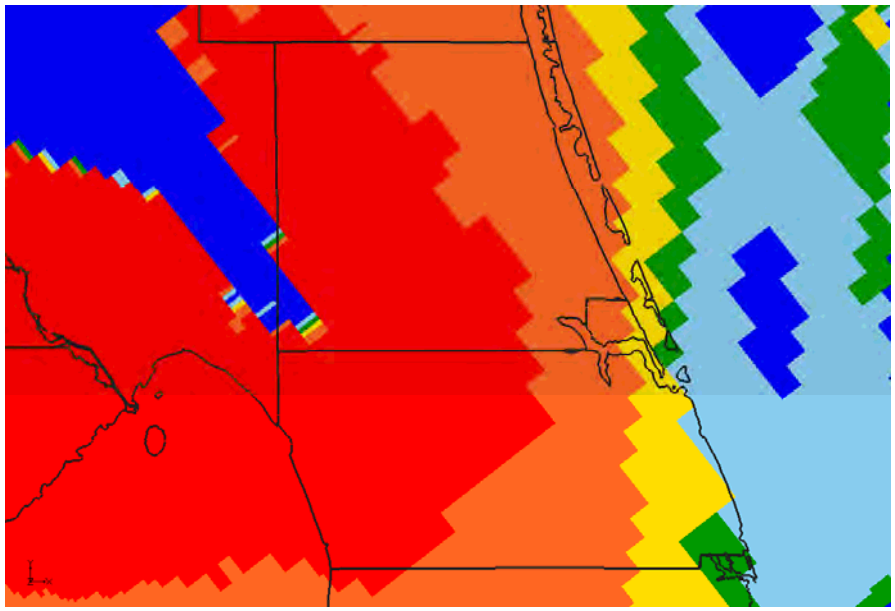

Upper Floridan Aquifer

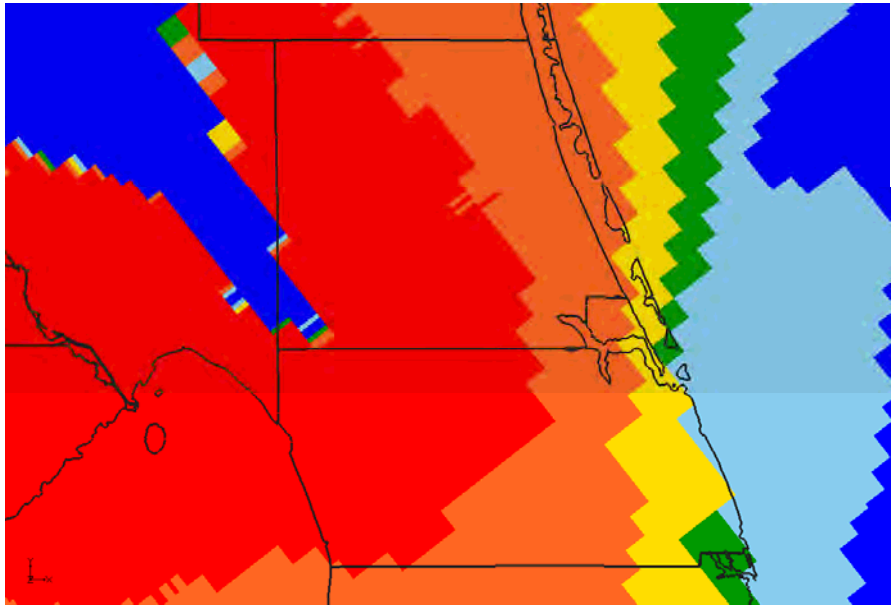

Avon Park Permeable Zone

Legend

- 0 days
- 1 – 250 days
- 250 – 500 days
- 500 – 1000 days
- 1000 – 2000 days
- > 2000 days

Notes:

Scenario 1 includes all of the 333 ASR wells specified by the SFWMM-D13R design. All are fully penetrating in the UF Aquifer.

These plots indicate the severity of the loss of artesian pressure due to ASR extraction pumping.

Permit rules require that the reduction in Saint Lucie and Martin Counties be less than 10%. This plot indicates the number of days during the simulation in which the flow reduction was greater than 10%. There are 4748 days in the 13-year model simulation period.

Note the blue area in the northwest corner of the figures, which coincides with a ridge and does not normally have artesian conditions.

SCENARIO 1 – NUMBER OF DAYS (OUT OF 13 YEARS) WITH FLOW REDUCTION EXCEEDING 10%

REGIONAL MODEL PRODUCTION SCENARIO REPORT

FIGURE 4.19

JUNE 2013

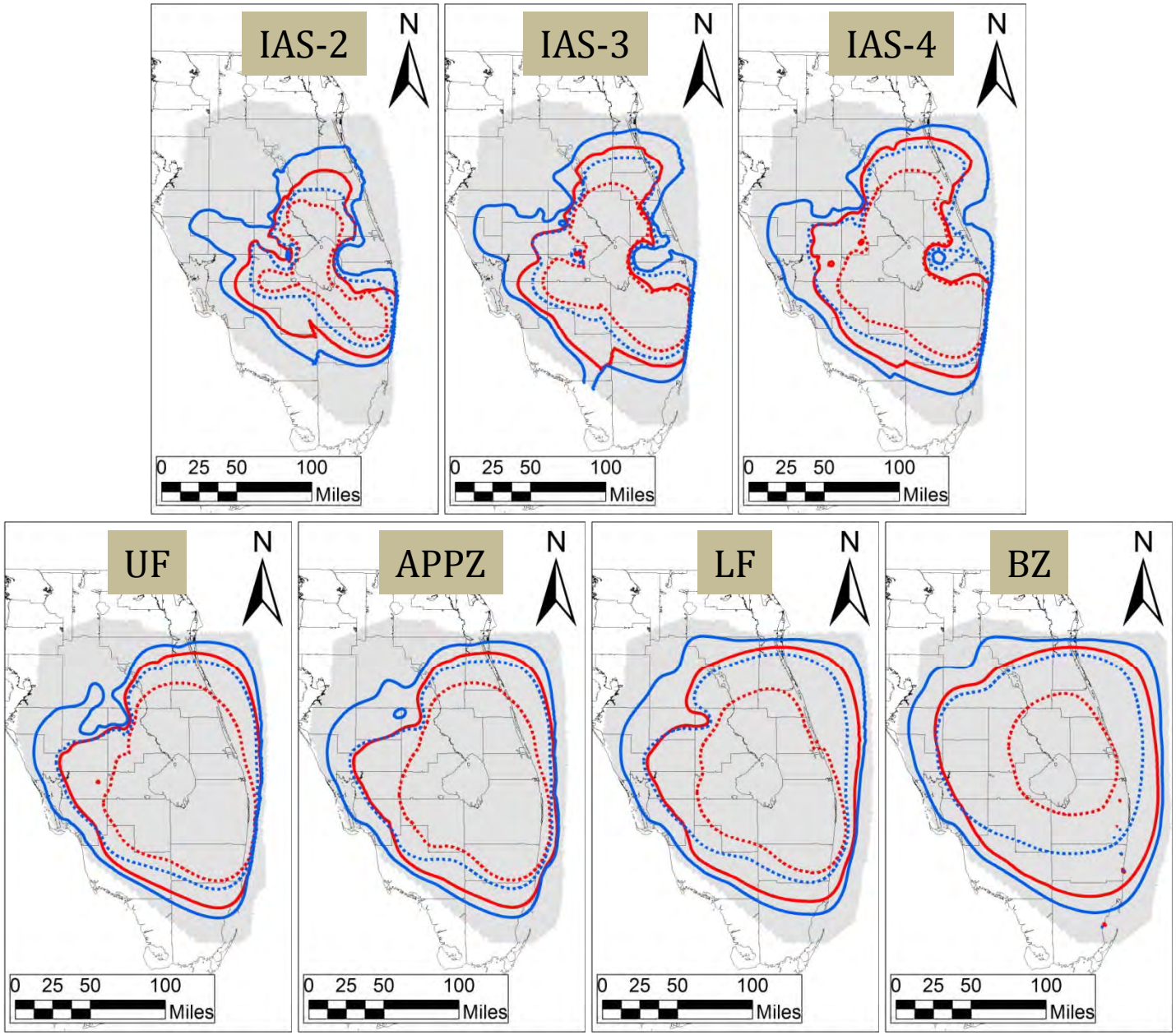

Legend

Maximum Drawdown
- 1 foot
- 5 feet

Maximum "Drawup"
- 1 foot
- 5 feet

Model Domain

Notes:

Scenario 1 includes all of the 333 ASR wells specified by the SFWMM-D13R design. All are fully penetrating in the UF Aquifer.

These figures show the extent of the areas where the maximum drawdown or "drawup" is greater than 1 foot or 5 feet.

The maximum condition does not necessarily occur at the same time for all regions of the model.

Scenario 1 – Maximum Drawdown and "Drawup" by Aquifer

Regional Model Production Scenario Report

Figure 4.20

June 2013

5-Mile Distance

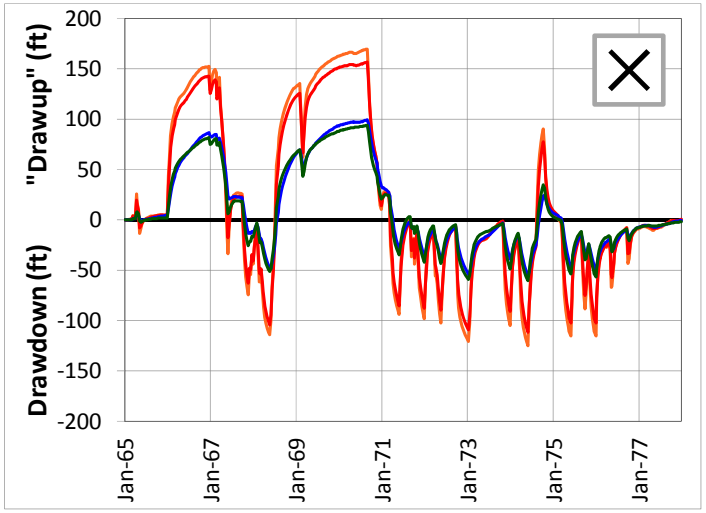

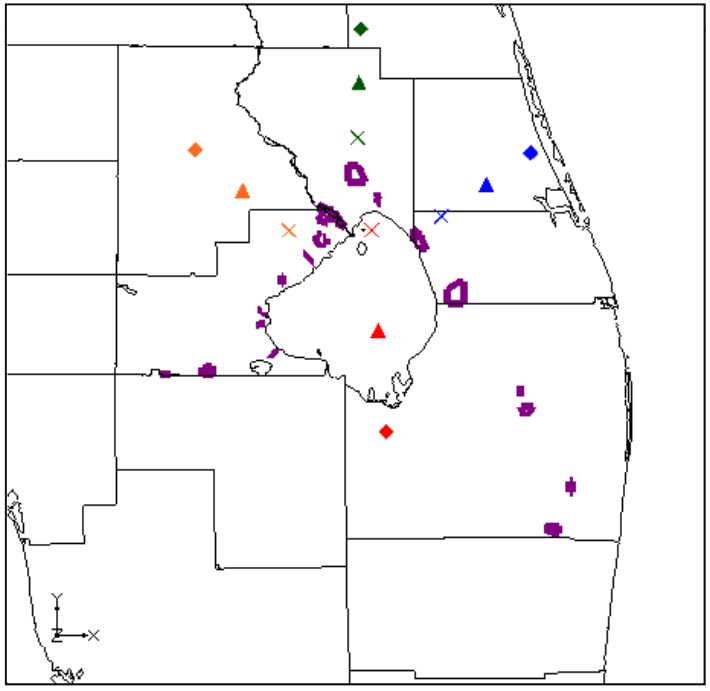

15-Mile Distance

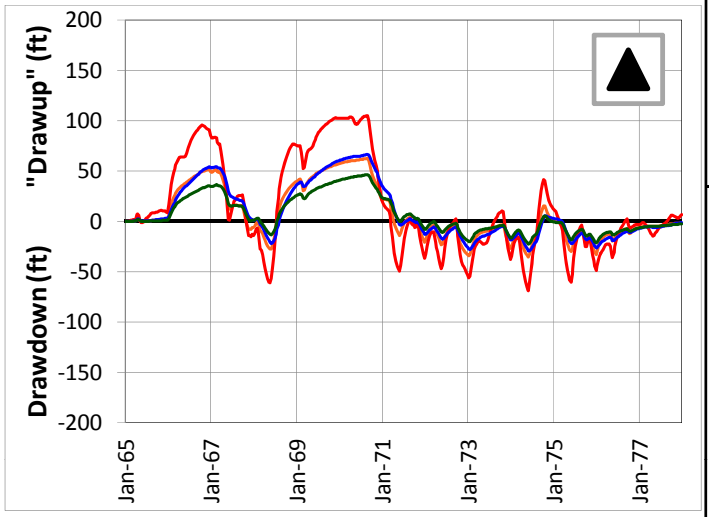

25-Mile Distance

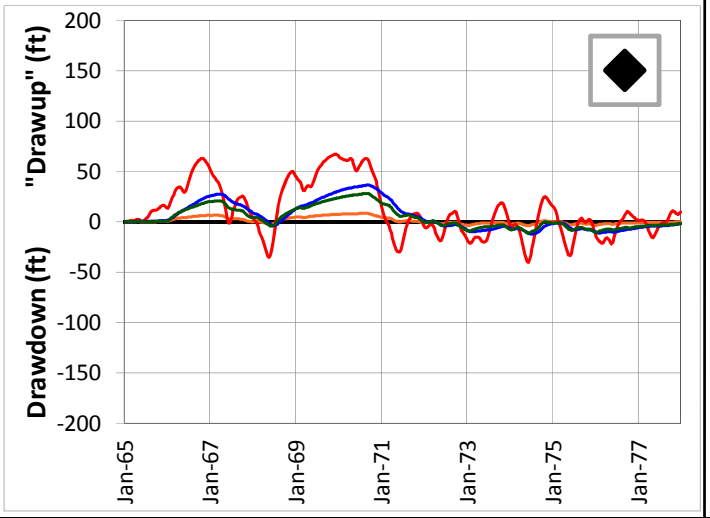

Legend

- CERP ASR Sites
- ✕ 5-Mile Distance Locations
- ▲ 15-Mile Distance Locations
- ◆ 25-Mile Distance Locations

Notes:

Scenario 1 includes all of the 333 ASR wells specified by the SFWMM-D13R design. All are fully penetrating in the UF Aquifer.

A number of individual sites were chosen from the UF Aquifer at distances of 5, 15 and 25 miles from the proposed ASR well sites. This figure shows the drawdown and "drawup" at each output time step for 12 of these sites.

The plots were calculated by subtracting the heads calculated by the D13R model from those calculated by the no project run. This results in a positive value for "drawup" and a negative value for drawdown.

The colors of the points on the map correspond to the colors of the lines on the plots.

The symbols on the map (x, triangle and diamond) indicate the distance from the ASR sites.

5-Mile Distance

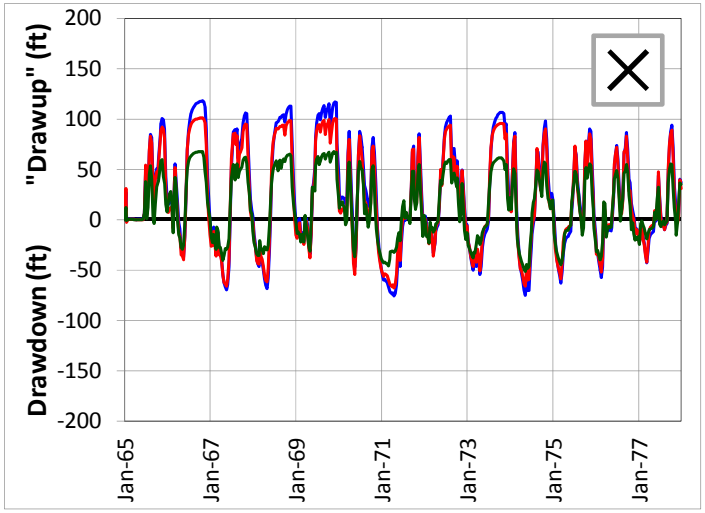

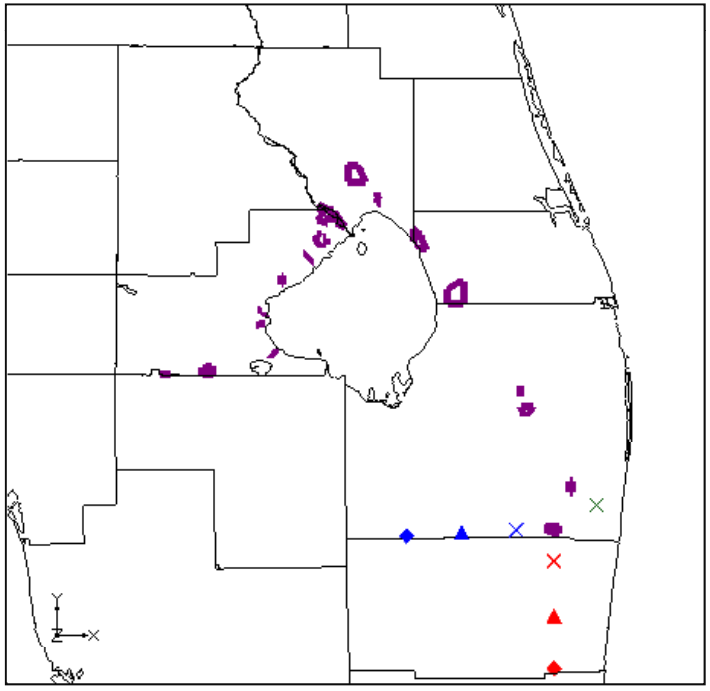

15-Mile Distance

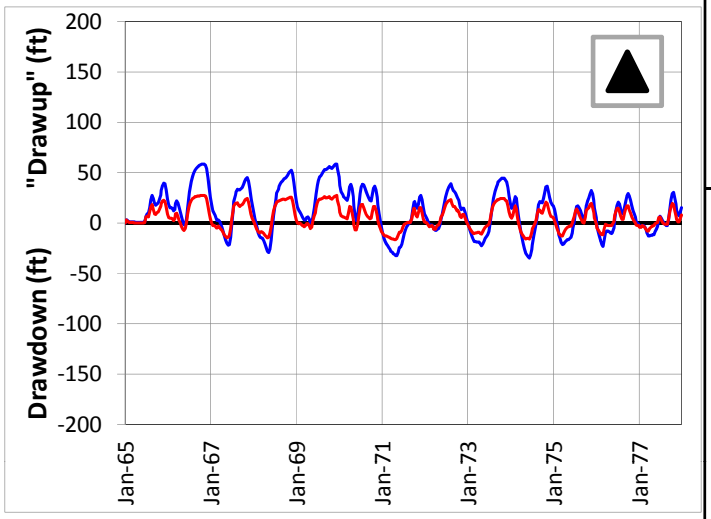

25-Mile Distance

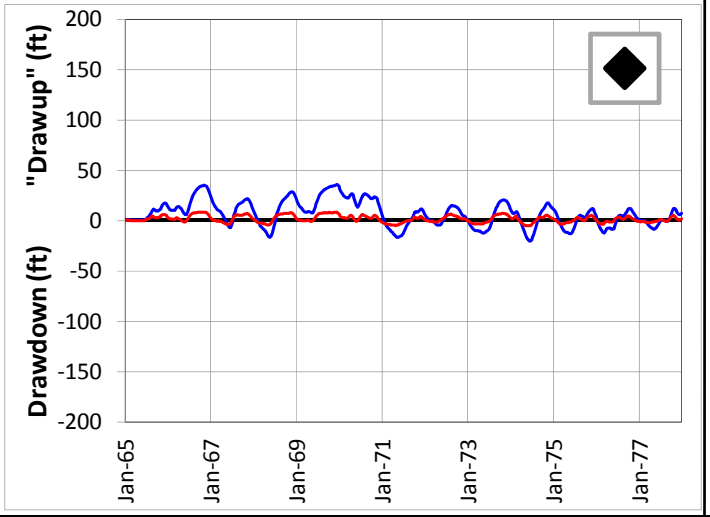

Legend

- CERP ASR Sites
- ✕ 5-Mile Distance Locations
- ▲ 15-Mile Distance Locations
- ◆ 25-Mile Distance Locations

Notes:

Scenario 1 includes all of the 333 ASR wells specified by the SFWMM-D13R design. All are fully penetrating in the UF Aquifer.

A number of individual sites were chosen from the UF Aquifer at distances of 5, 15 and 25 miles from the proposed ASR well sites. This figure shows the drawdown and "drawup" at each output time step for 7 of these sites.

The plots were calculated by subtracting the heads calculated by the D13R model from those calculated by the no project run. This results in a positive value for "drawup" and a negative value for drawdown.

The colors of the points on the map correspond to the colors of the lines on the plots.

The symbols on the map (x, triangle and diamond) indicate the distance from the ASR sites.

5-Mile Distance

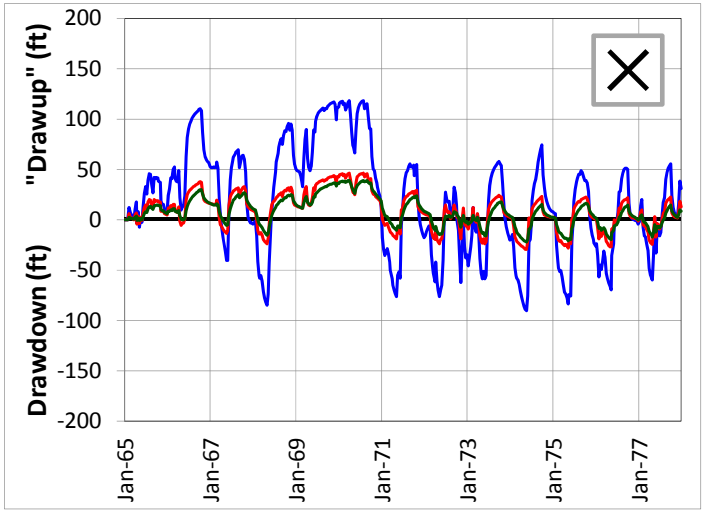

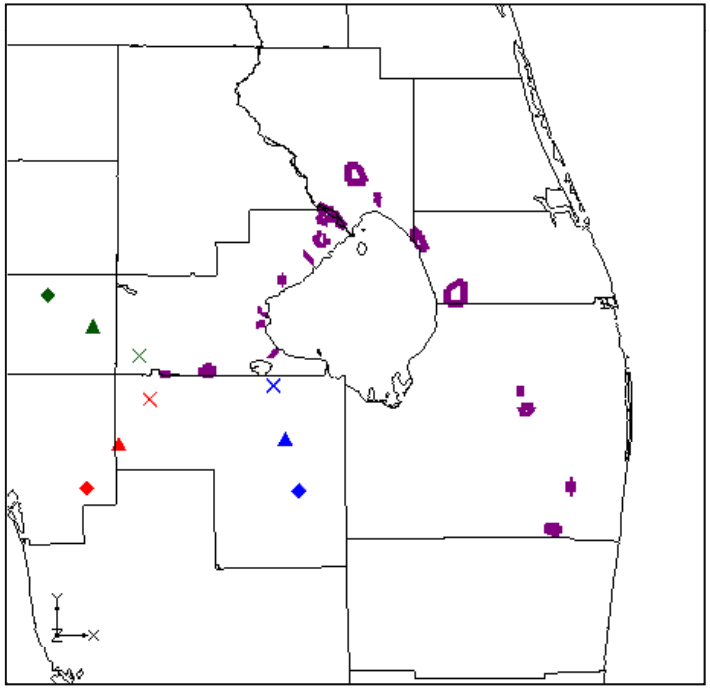

15-Mile Distance

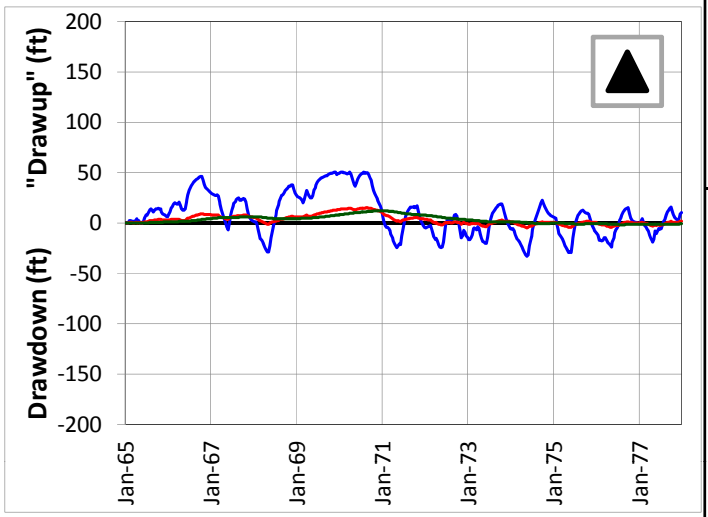

25-Mile Distance

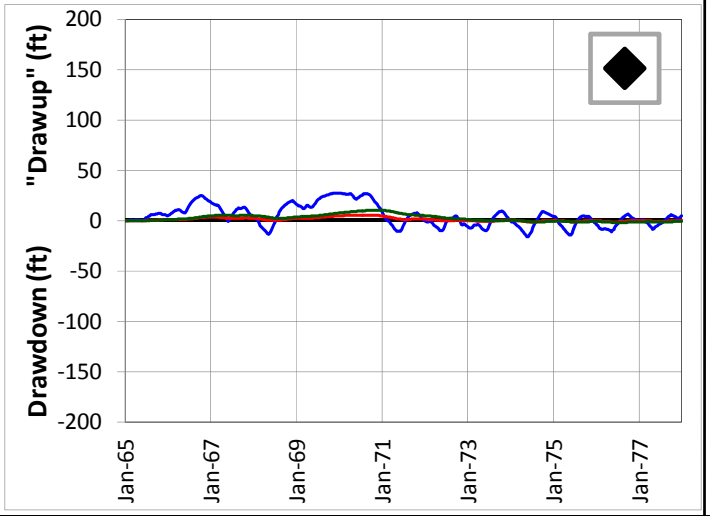

Legend

- CERP ASR Sites
- ✕ 5-Mile Distance Locations
- ▲ 15-Mile Distance Locations
- ◆ 25-Mile Distance Locations

Notes:

Scenario 1 includes all of the 333 ASR wells specified by the D13R scenario of the SFWMM. All are fully penetrating in the Upper Floridan Aquifer.

A number of individual sites were chosen from the UF Aquifer at distances of 5, 15 and 25 miles from the proposed ASR well sites. This figure shows the drawdown and "drawup" at each output time step for 9 of these sites.

The plots were calculated by subtracting the heads calculated by the D13R model from those calculated by the no project run. This results in a positive value for "drawup" and a negative value for drawdown.

The colors of the points on the map correspond to the colors of the lines on the plots.

The symbols on the map (x, triangle and diamond) indicate the distance from the ASR sites.

5-Mile Distance

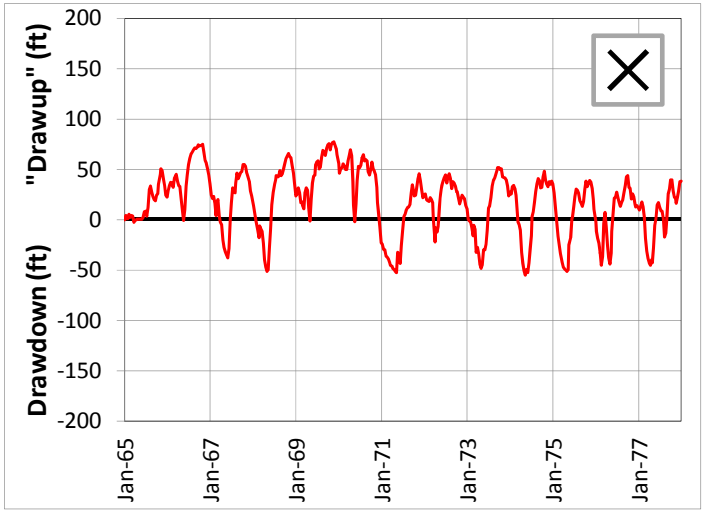

15-Mile Distance

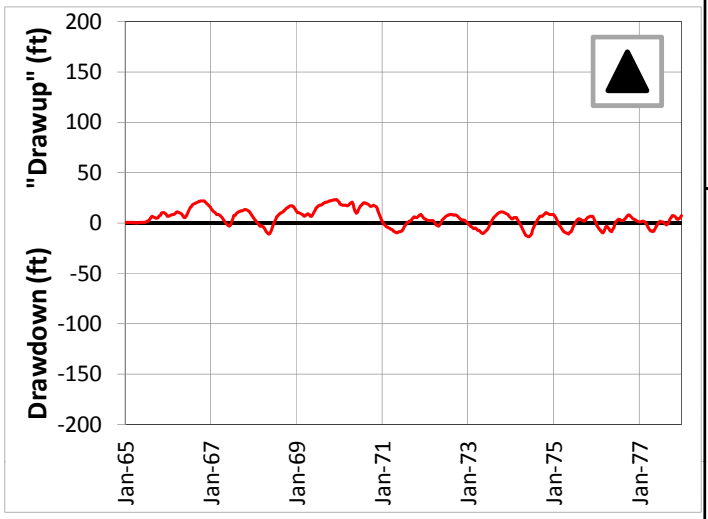

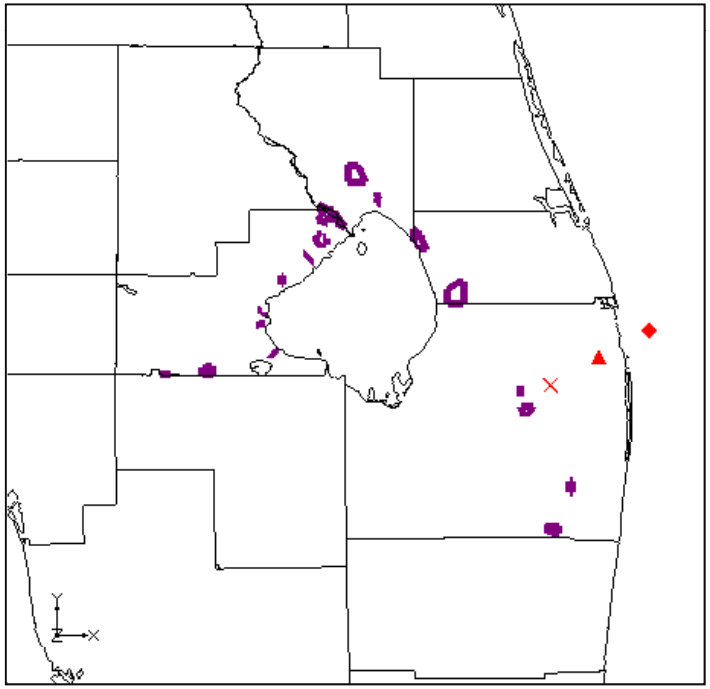

25-Mile Distance

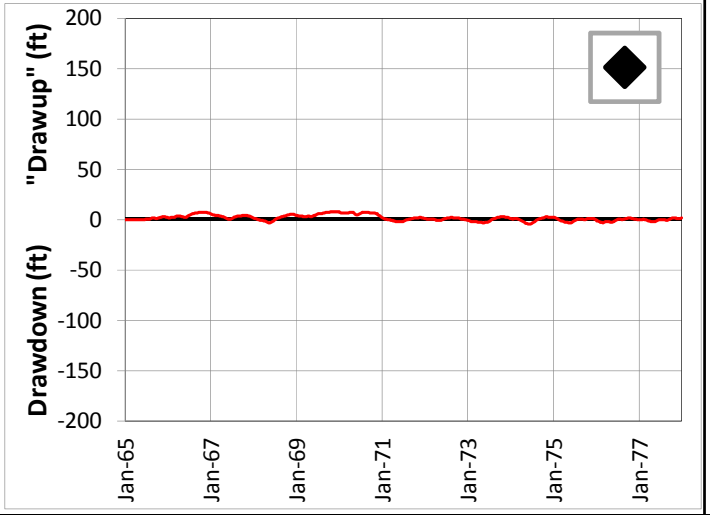

Legend

- CERP ASR Sites
- 5-Mile Distance Locations
- 15-Mile Distance Locations
- 25-Mile Distance Locations

Notes:

Scenario 1 includes all of the 333 ASR wells specified by the SFWMM-D13R design. All are fully penetrating in the UF Aquifer.

A number of individual sites were chosen from the UF Aquifer at distances of 5, 15 and 25 miles from the proposed ASR well sites. This figure shows the drawdown and "drawup" at each output time step for 3 of these sites.

The plots were calculated by subtracting the heads calculated by the D13R model from those calculated by the no project run. This results in a positive value for "drawup" and a negative value for drawdown.

The colors of the points on the map correspond to the colors of the lines on the plots.

The symbols on the map (x, triangle and diamond) indicate the distance from the ASR sites.

5-Mile Distance

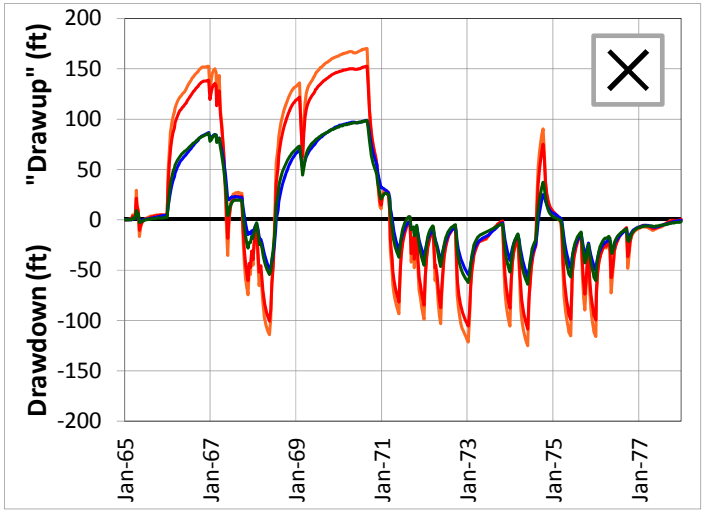

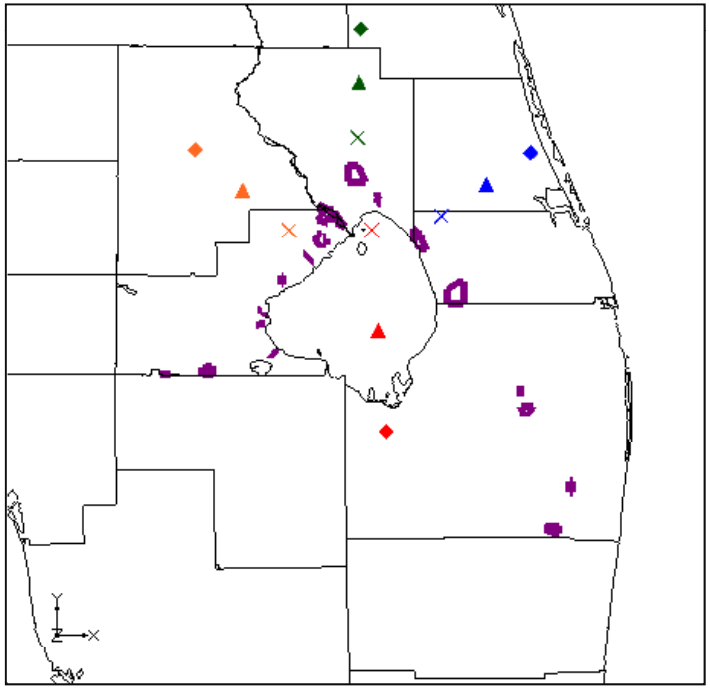

15-Mile Distance

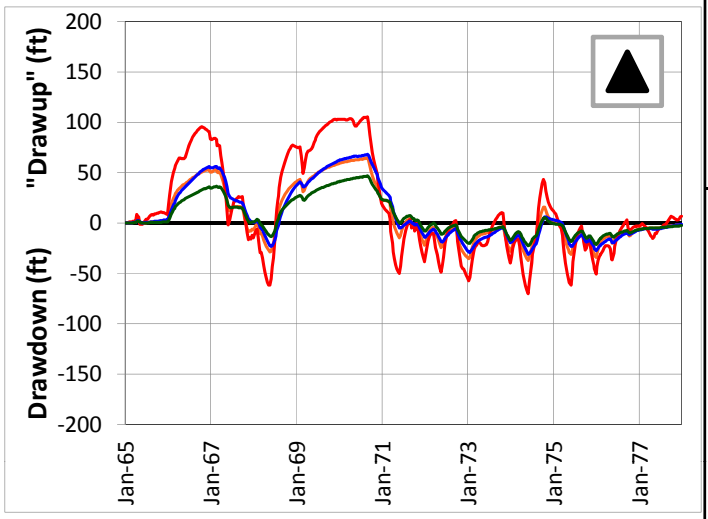

25-Mile Distance

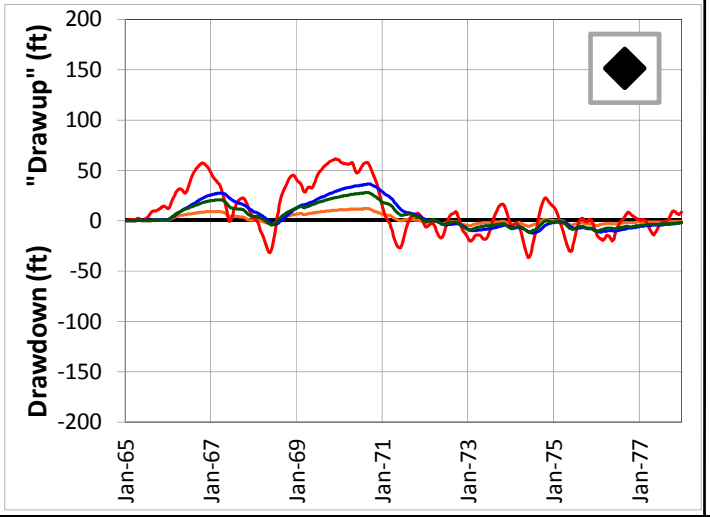

Legend

- CERP ASR Sites
- ✕ 5-Mile Distance Locations
- ▲ 15-Mile Distance Locations
- ◆ 25-Mile Distance Locations

Notes:

Scenario 1 includes all of the 333 ASR wells specified by the SFWMM-D13R design. All are fully penetrating in the UF Aquifer.

A number of individual sites were chosen from the APPZ Aquifer at distances of 5, 15 and 25 miles from the proposed ASR well sites. This figure shows the drawdown and "drawup" at each output time step for 12 of these sites.

The plots were calculated by subtracting the heads calculated by the D13R model from those calculated by the no project run. This results in a positive value for "drawup" and a negative value for drawdown.

The colors of the points on the map correspond to the colors of the lines on the plots.

The symbols on the map (x, triangle and diamond) indicate the distance from the ASR sites.

5-Mile Distance

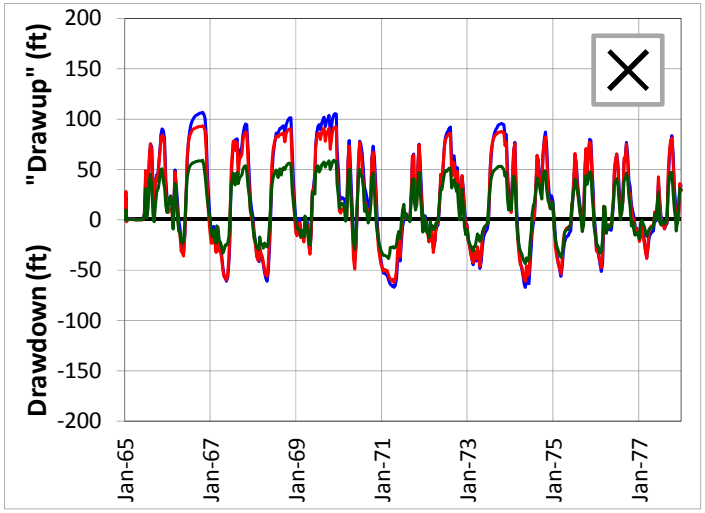

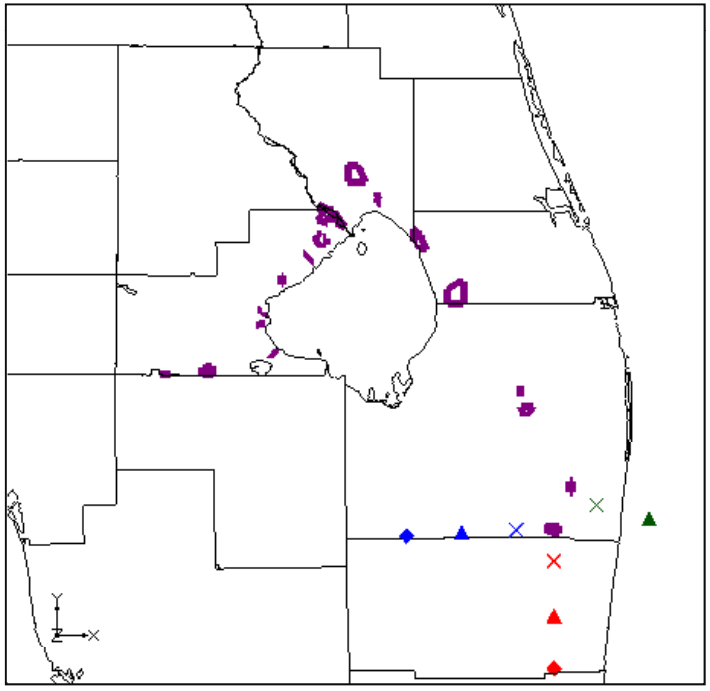

15-Mile Distance

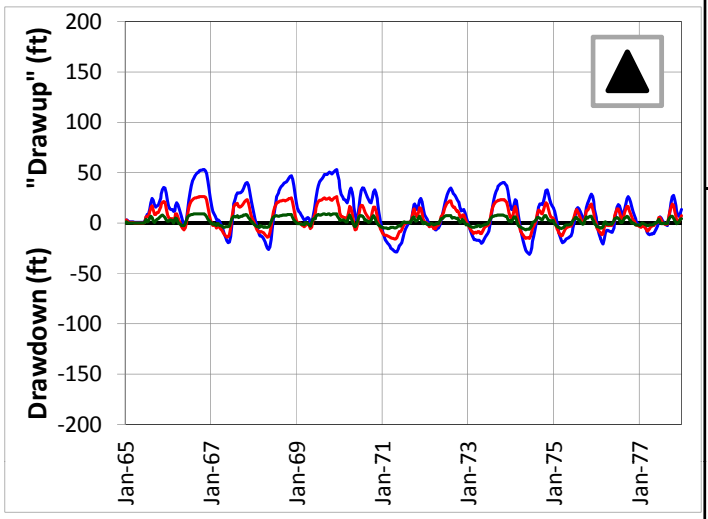

25-Mile Distance

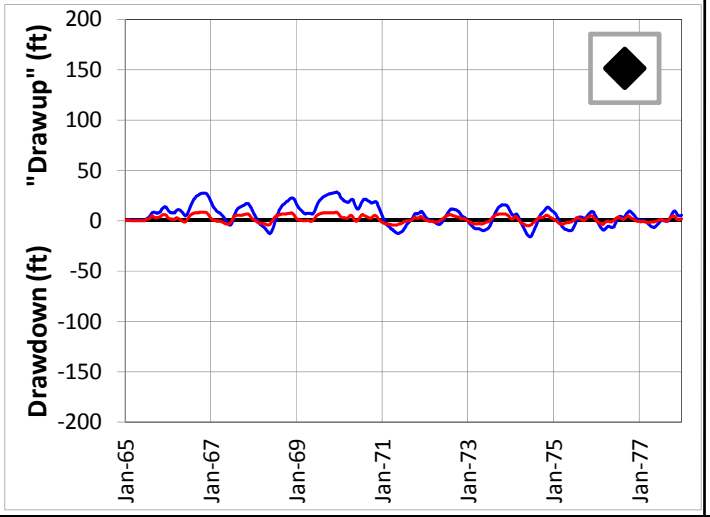

Legend

- CERP ASR Sites
- 5-Mile Distance Locations
- 15-Mile Distance Locations
- 25-Mile Distance Locations

Notes:

Scenario 1 includes all of the 333 ASR wells specified by the SFWMM-D13R design. All are fully penetrating in the UF Aquifer.

A number of individual sites were chosen from the APPZ Aquifer at distances of 5, 15 and 25 miles from the proposed ASR well sites. This figure shows the drawdown and "drawup" at each output time step for 8 of these sites.

The plots were calculated by subtracting the heads calculated by the D13R model from those calculated by the no project run. This results in a positive value for "drawup" and a negative value for drawdown.

The colors of the points on the map correspond to the colors of the lines on the plots.

The symbols on the map (x, triangle and diamond) indicate the distance from the ASR sites.

5-Mile Distance

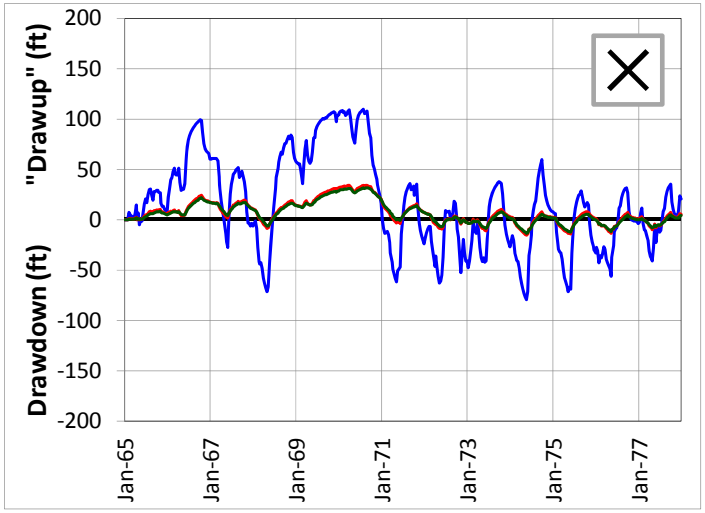

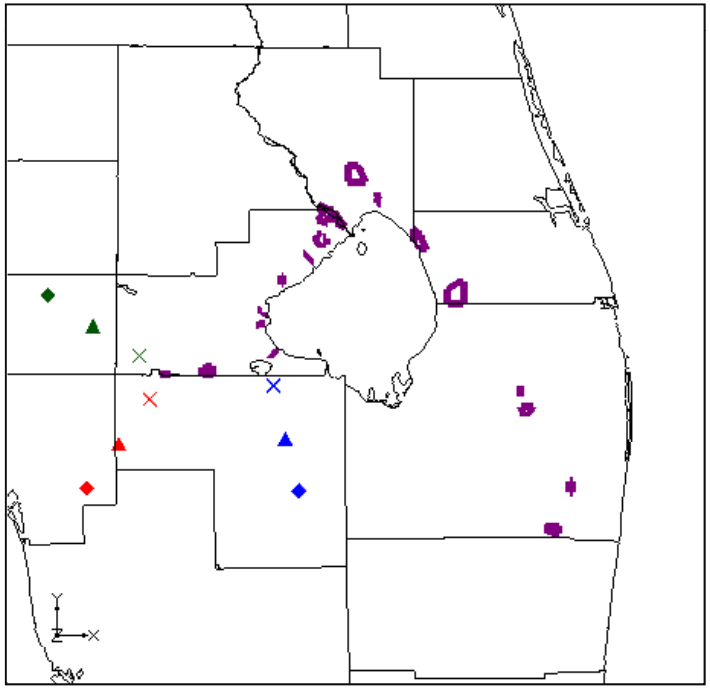

15-Mile Distance

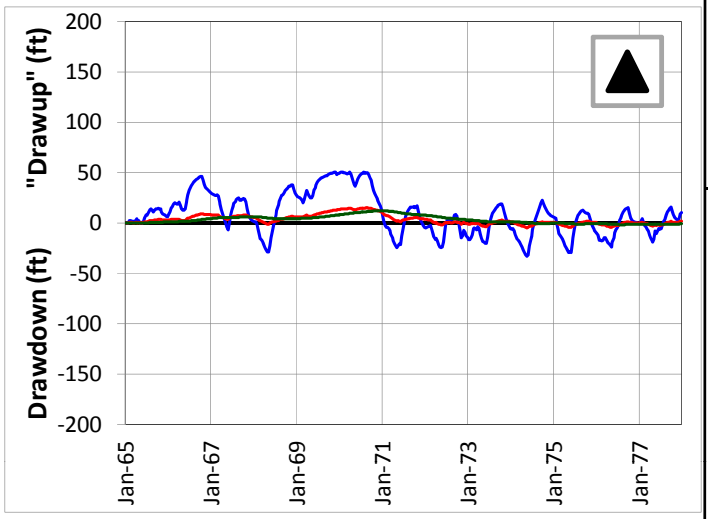

25-Mile Distance

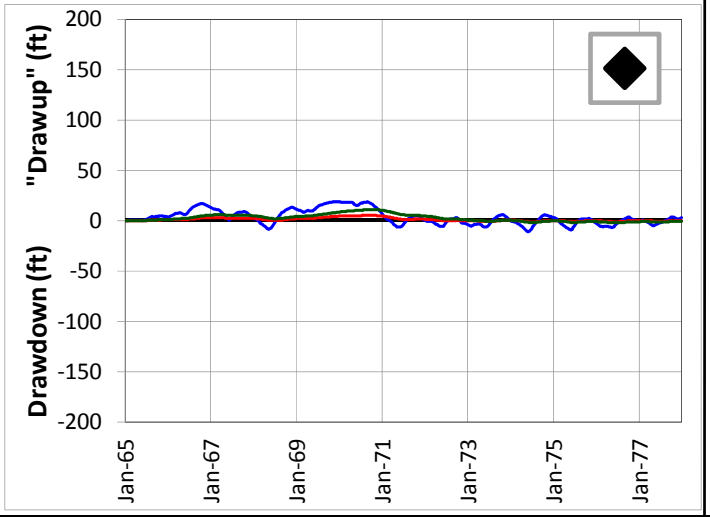

Legend

- CERP ASR Sites
- ✕ 5-Mile Distance Locations
- ▲ 15-Mile Distance Locations
- ◆ 25-Mile Distance Locations

Notes:

Scenario 1 includes all of the 333 ASR wells specified by the SFWMM-D13R design. All are fully penetrating in the UF Aquifer.

A number of individual sites were chosen from the APPZ Aquifer at distances of 5, 15 and 25 miles from the proposed ASR well sites. This figure shows the drawdown and "drawup" at each output time step for 9 of these sites.

The plots were calculated by subtracting the heads calculated by the D13R model from those calculated by the no project run. This results in a positive value for "drawup" and a negative value for drawdown.

The colors of the points on the map correspond to the colors of the lines on the plots.

The symbols on the map (x, triangle and diamond) indicate the distance from the ASR sites.

5-Mile Distance

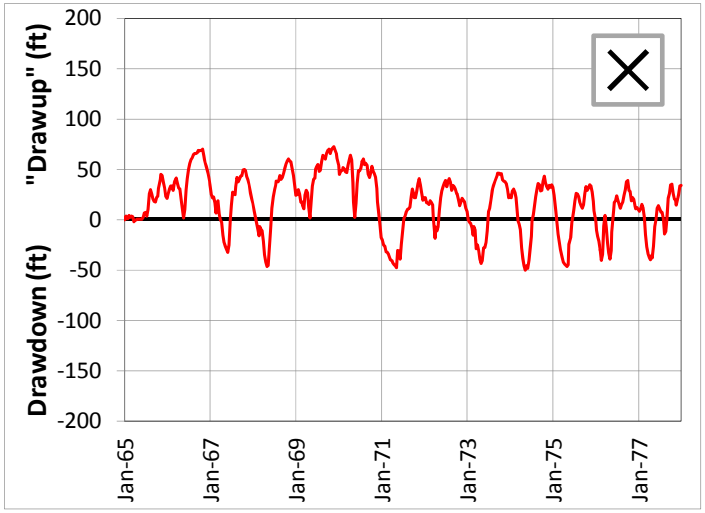

15-Mile Distance

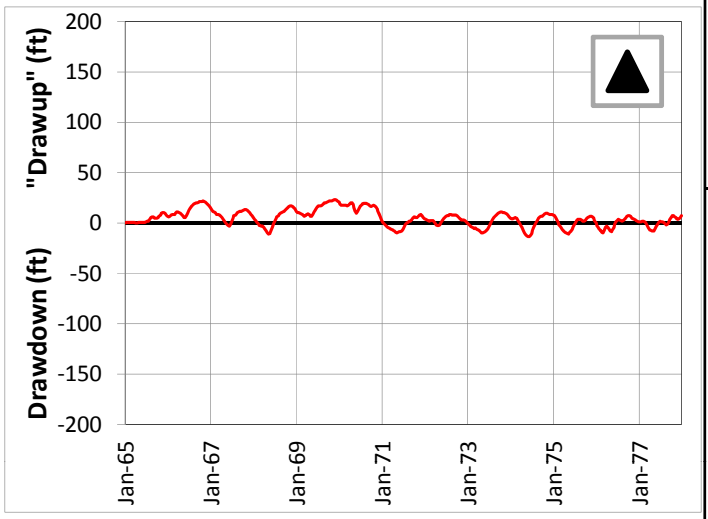

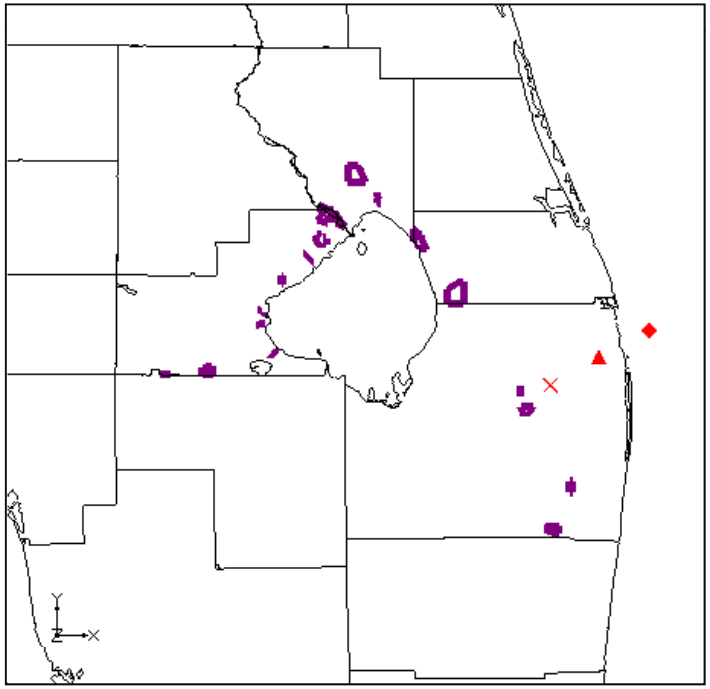

25-Mile Distance

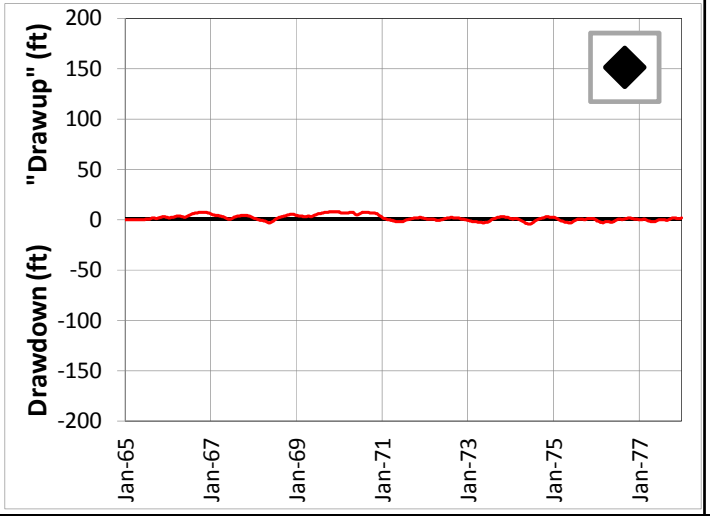

Legend

- CERP ASR Sites
- 5-Mile Distance Locations
- 15-Mile Distance Locations
- 25-Mile Distance Locations

Notes:

Scenario 1 includes all of the 333 ASR wells specified by the SFWMM-D13R design. All are fully penetrating in the UF Aquifer.

A number of individual sites were chosen from the APPZ Aquifer at distances of 5, 15 and 25 miles from the proposed ASR well sites. This figure shows the drawdown and "drawup" at each output time step for 3 of these sites.

The plots were calculated by subtracting the heads calculated by the D13R model from those calculated by the no project run. This results in a positive value for "drawup" and a negative value for drawdown.

The colors of the points on the map correspond to the colors of the lines on the plots.

The symbols on the map (x, triangle and diamond) indicate the distance from the ASR sites.

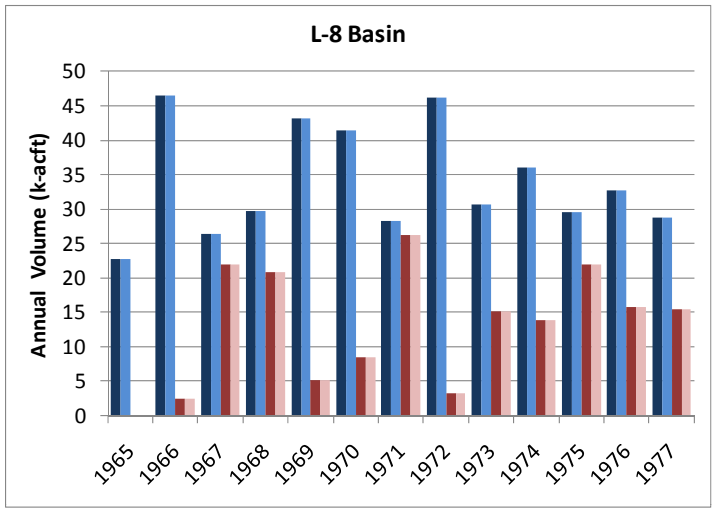

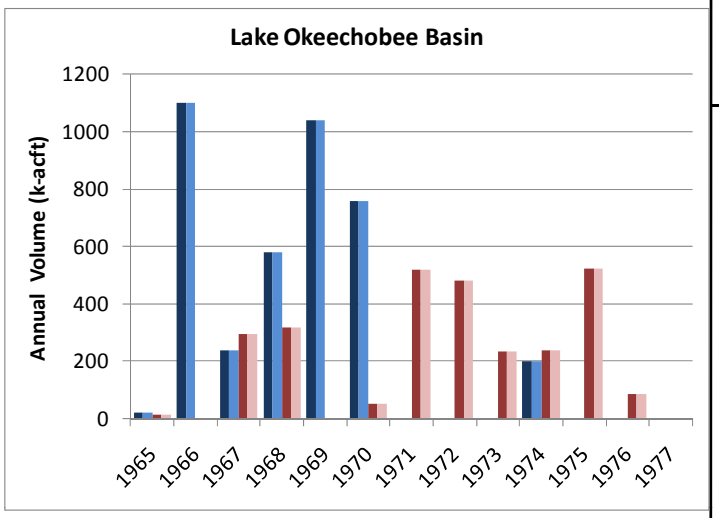

	L-8		Lake Okeechobee		Caloosahatchee	
	In %	Out %	In %	Out %	In %	Out %
1965	100%	100%	100%	100%	100%	100%
1966	100%	100%	100%	--	100%	100%
1967	100%	100%	100%	100%	100%	100%
1968	100%	100%	100%	100%	100%	100%
1969	100%	100%	100%	--	100%	--
1970	100%	100%	100%	100%	100%	100%
1971	100%	100%	--	100%	100%	100%
1972	100%	100%	--	100%	100%	100%
1973	100%	100%	--	100%	100%	100%
1974	100%	100%	100%	100%	100%	100%
1975	100%	100%	--	100%	100%	100%
1976	100%	100%	--	100%	100%	100%
1977	100%	100%	--	--	100%	100%

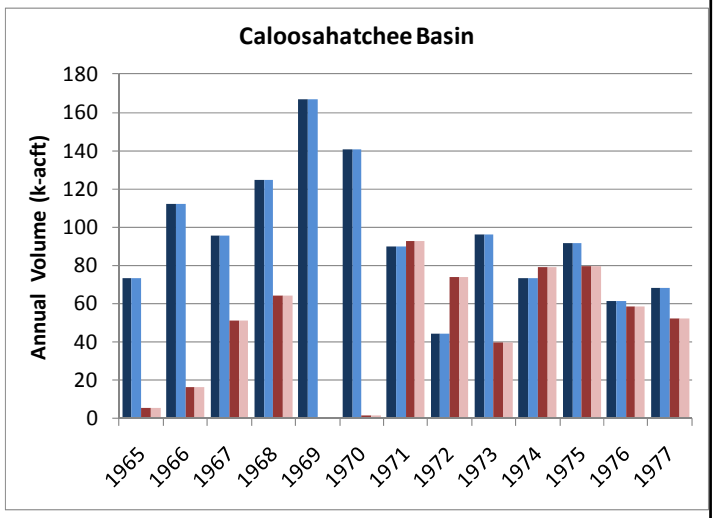

Legend

- Design Storage (injection)
- Modeled Storage (injection)
- Design Recovery (extraction)
- Modeled Recovery (extraction)

Notes:

Scenario 1 includes all of the 333 ASR wells specified by the SFWMM-D13R design. All are fully penetrating in the UF Aquifer.

These three plots show the comparison between the SFWMM-D13R designed annual injection and extraction volumes at the ASR wells and the actual assigned rates for the RASRSM-D13R for three of the basins.

The table presents the percentage of SFWMM-D13R annual flow rates that are included in this scenario of the RASRSM-D13R. These percentages are not recovery efficiencies.

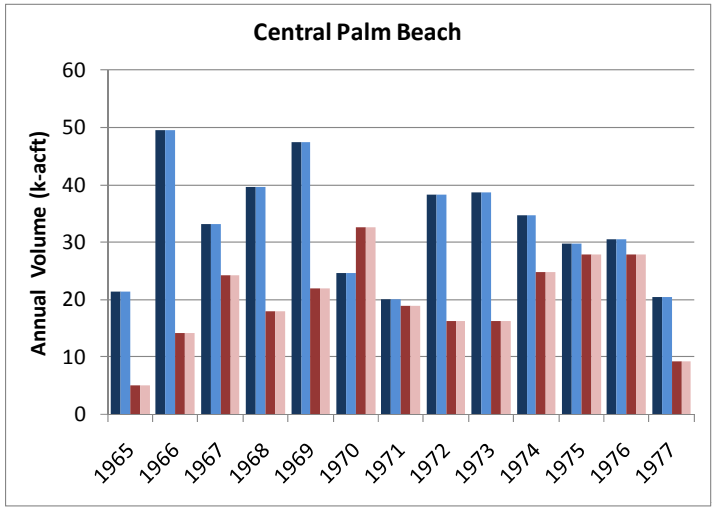

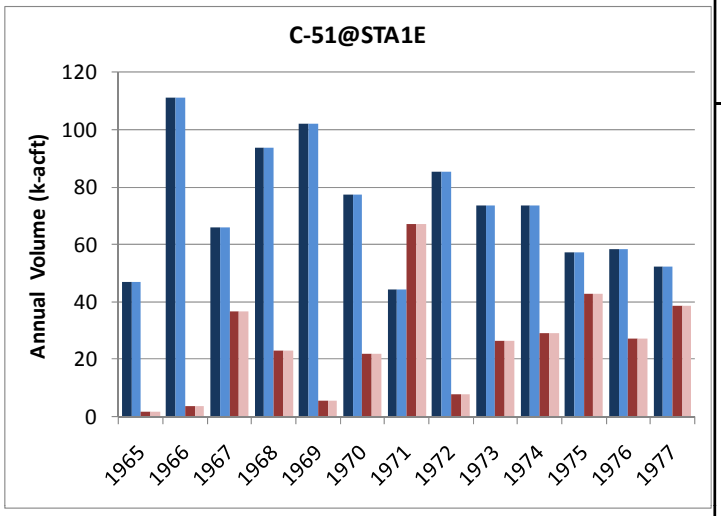

	CPB		C-51		Hillsboro	
	In %	Out %	In %	Out %	In %	Out %
1965	100%	100%	100%	100%	100%	66%
1966	100%	100%	100%	100%	100%	100%
1967	100%	100%	100%	100%	100%	100%
1968	100%	100%	100%	100%	100%	99%
1969	100%	100%	100%	100%	100%	100%
1970	100%	100%	100%	100%	100%	100%
1971	100%	100%	100%	100%	100%	100%
1972	100%	100%	100%	100%	100%	68%
1973	100%	100%	100%	100%	100%	68%
1974	100%	100%	100%	100%	100%	100%
1975	100%	100%	100%	100%	100%	50%
1976	100%	100%	100%	100%	100%	64%
1977	100%	100%	100%	100%	100%	49%

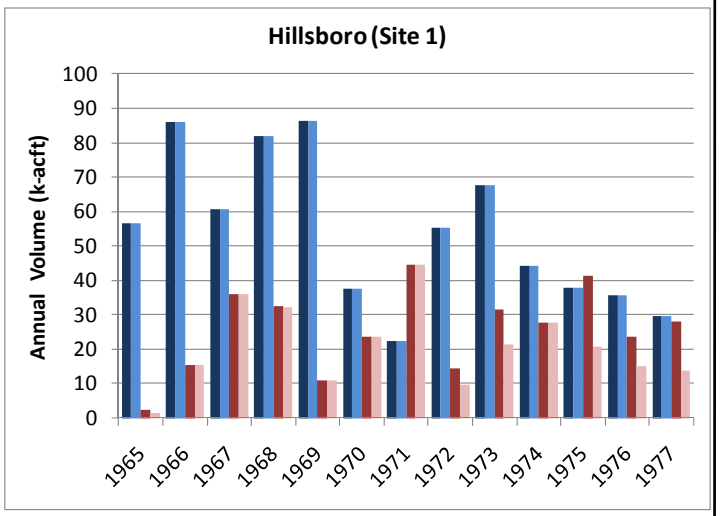

Legend

- Design Storage (injection)
- Modeled Storage (injection)
- Design Recovery (extraction)
- Modeled Recovery (extraction)

Notes:

Scenario 1 includes all of the 333 ASR wells specified by the SFWMM-D13R design. All are fully penetrating in the UF Aquifer.

These three plots show the comparison between the SFWMM-D13R designed annual injection and extraction volumes at the ASR wells and the actual assigned rates for the RASRSM-D13R for three of the basins.

The table presents the percentage of SFWMM-D13R annual flow rates that are included in this scenario of the RASRSM-D13R. These percentages are not recovery efficiencies.

	Total	
	In %	Out %
1965	100%	97%
1966	100%	100%
1967	100%	100%
1968	100%	100%
1969	100%	100%
1970	100%	100%
1971	100%	100%
1972	100%	99%
1973	100%	97%
1974	100%	100%
1975	100%	97%
1976	100%	96%
1977	100%	90%

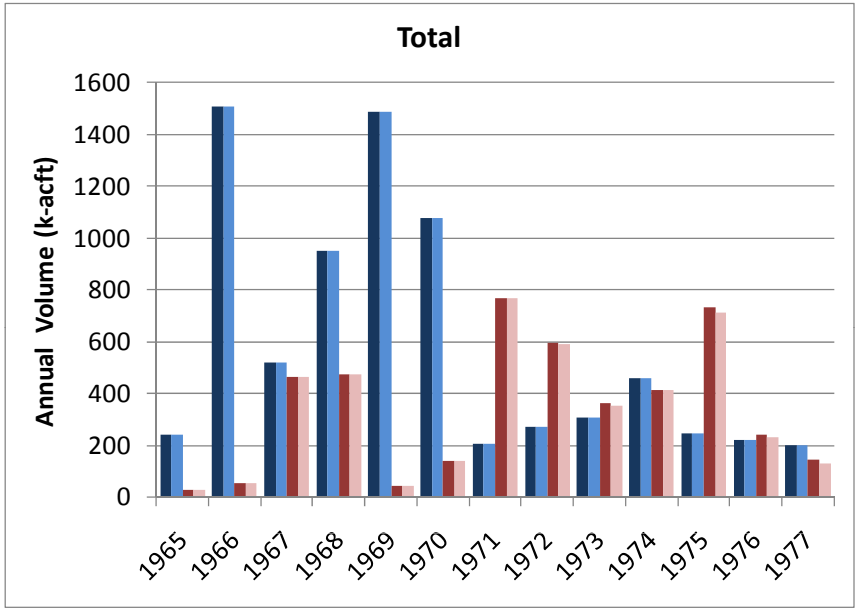

Legend

- Design Storage (injection)
- Modeled Storage (injection)
- Design Recovery (extraction)
- Modeled Recovery (extraction)

Notes:

Scenario 1 includes all of the 333 ASR wells specified by the SFWMM-D13R design. All are fully penetrating in the UF Aquifer.

This plot shows the comparison between the SFWMM-D13R designed annual injection and extraction volumes at the ASR wells and the actual assigned rates for the RASRSM-D13R for all basins.

The table presents the percentage of SFWMM-D13R annual flow rates that are included in this scenario of the RASRSM-D13R. These percentages are not recovery efficiencies.

SCENARIO 1 – COMPARISON OF DESIGNED AND MODELED ASR FLOW RATES

REGIONAL MODEL PRODUCTION SCENARIO REPORT

FIGURE 4.31

JUNE 2013

		UF		APPZ		BZ		Total # Wells	Target # Wells
		Number of Wells	Recovery Efficiency	Number of Wells	Recovery Efficiency	Number of Wells	Recovery Efficiency		
Caloosahatchee Basin	Moore Haven	4	70%	0	30%	0	10%		
	River Bend	3	70%	0	30%	0	10%		
	Flaghole	2	70%	0	30%	0	10%		
	Basin Total	9		0		0		9	44
Lake Okeechobee Basin	Nicodemus Slough	0	70%	0	30%	0	10%		
	C-41 Canal	1	70%	0	30%	0	10%		
	C-40 Canal	2	70%	0	30%	0	10%		
	North Lake Okeechobee	8	70%	0	30%	0	10%		
	Kissimmee R./Paradise Run	15	70%	0	30%	0	10%		
	Taylor Creek	0	70%	0	30%	0	10%		
	L-63N	0	70%	0	30%	0	10%		
	Lakeside Ranch	5	70%	0	30%	0	10%		
	Port Mayaca	19	70%	0	30%	0	10%		
	Basin Total	50		0		0		50	200
L-8		6	70%	0	30%	0	10%	6	10
C-51		12	70%	0	30%	0	10%	12	34
Central Palm Beach		10	70%	0	30%	0	10%	10	15
Site 1 (Hillsboro)		10	40%	0	40%	0	10%	10	30
Total		97		0		0		97	333

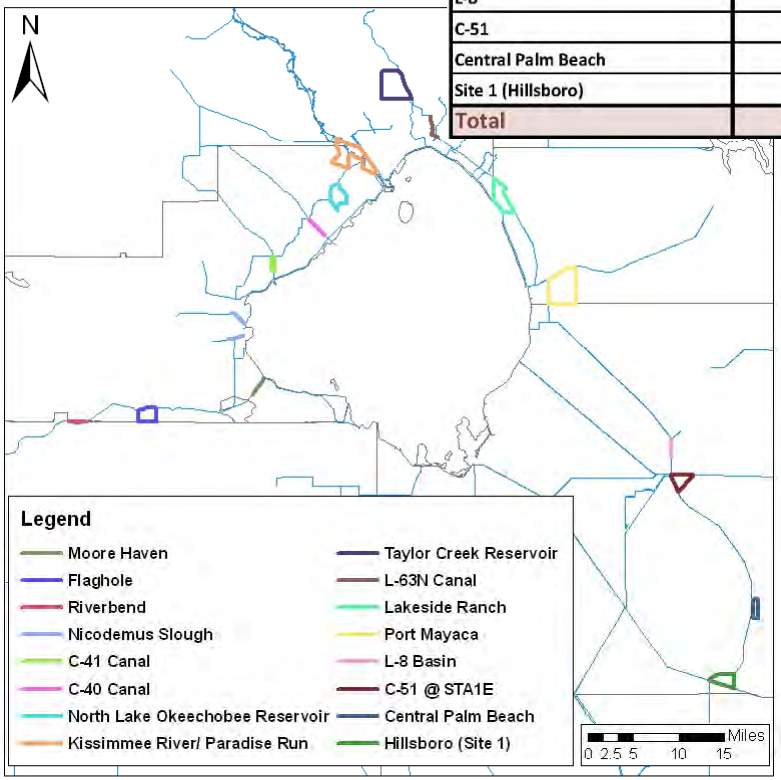

Notes:

Scenario 2 is scaled back from Scenario 1 to keep pump pressure below or near 100 psi. All wells are fully penetrating in the UF Aquifer.

Flow rates are divided evenly among the wells in each basin. Maximum flow rate for any one well is 5 mgd.

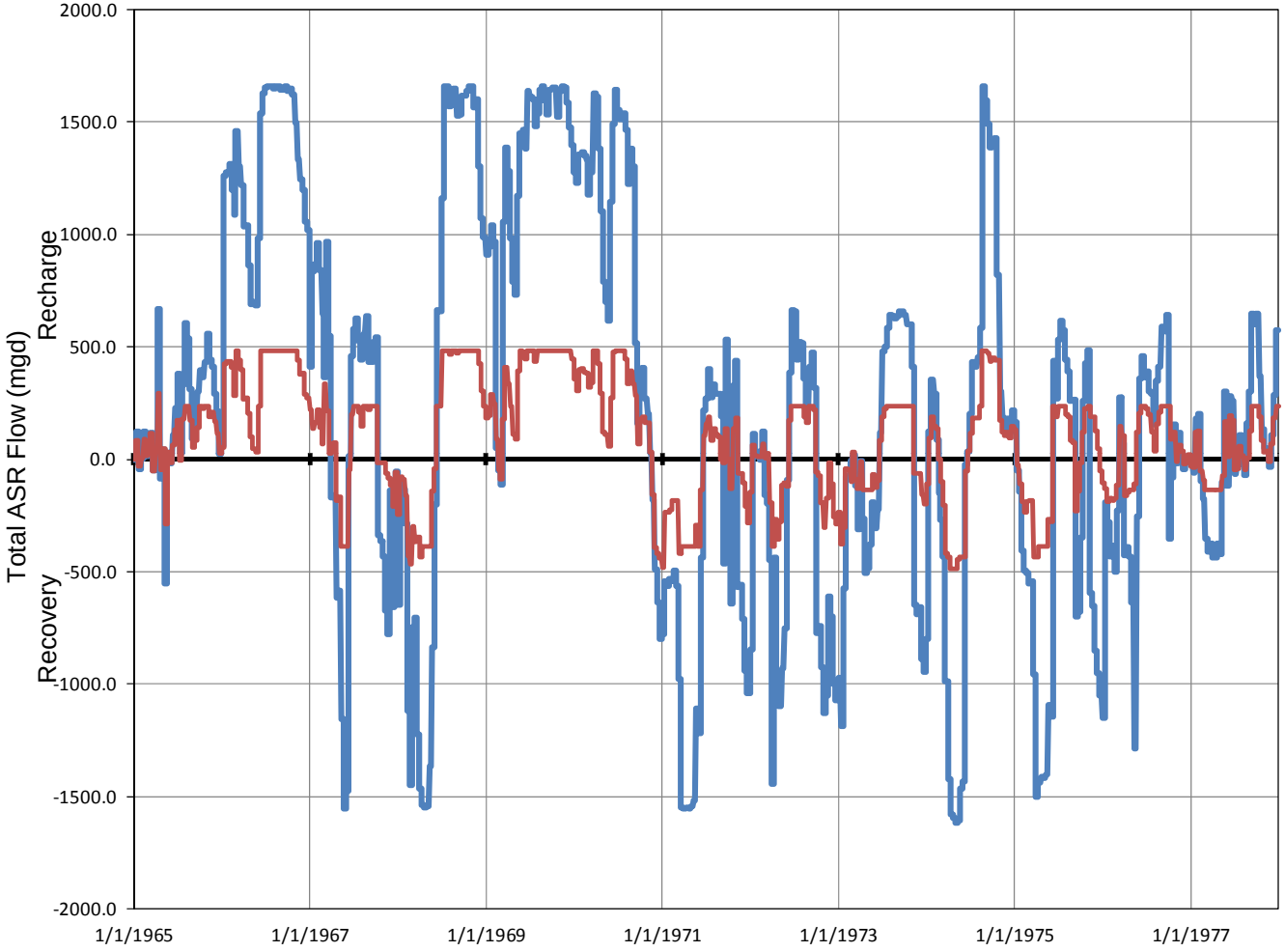

Legend

- Scenario 1 – ASR Flux
- Scenario 2 – ASR Flux

Notes:

Scenario 2 is scaled back from Scenario 1 to keep pump pressure below or near 100 psi. All wells are fully penetrating in the UF Aquifer.

This plot shows the extraction and injection rates for all wells at all sites for Scenario 1 and Scenario 2. Positive rates are recharge (injection), while negative rates are recovery (extraction).

Scenario 2 – ASR Well Fluxes (Compared to Scenario 1)

Regional Model Production Scenario Report

Figure 4.33

June 2013

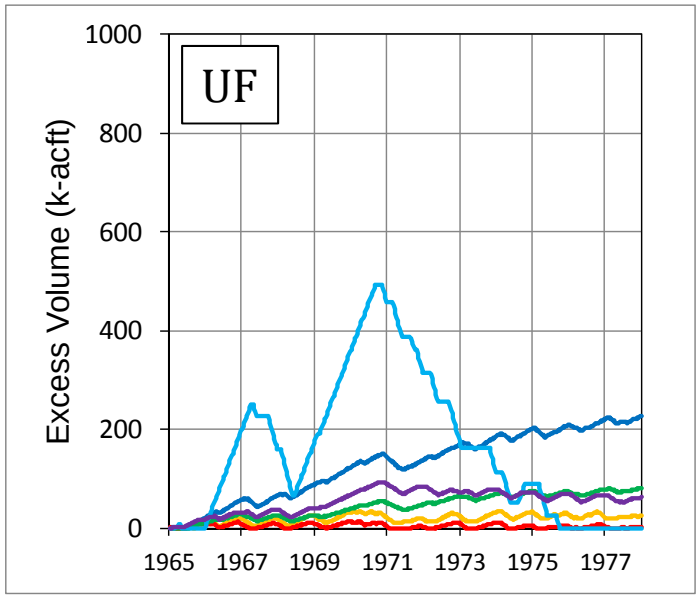

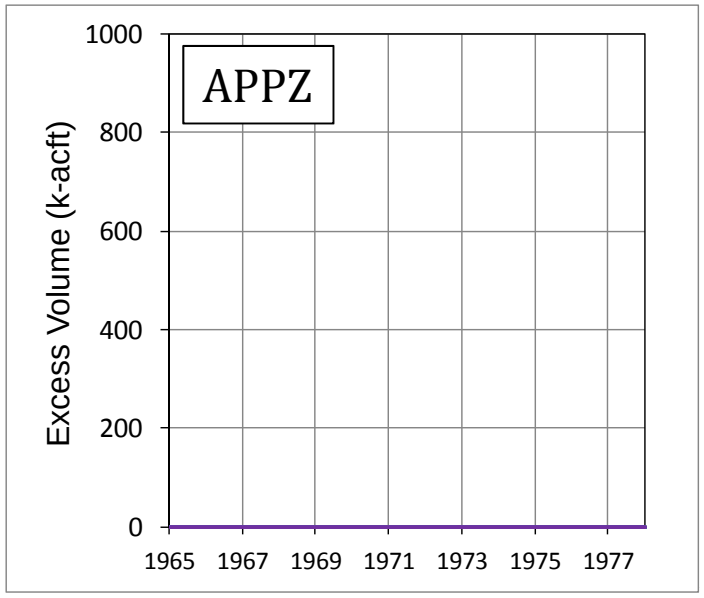

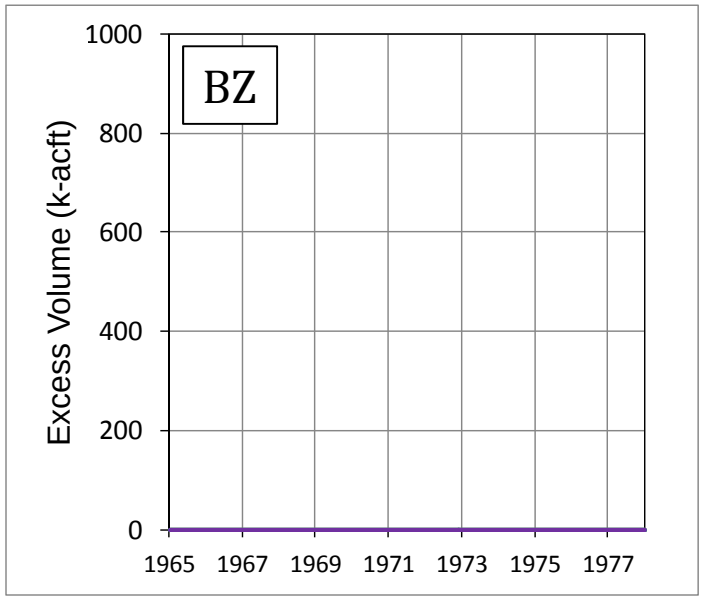

Legend

- Central Palm Beach
- C-51
- Hillsboro
- L-8
- Lake Okeechobee
- Caloosahatchee River

Notes:

Scenario 2 is scaled back from Scenario 1 to keep pump pressure below or near 100 psi. All wells are fully penetrating in the UF Aquifer.

These plots show the excess volume of fresh water remaining in each aquifer at each ASR basin. Excess volume is calculated by adding injected volume times recovery efficiency and subtracting extracted volume. The calculation is cumulative.

SCENARIO 2 – EXCESS VOLUME OF FRESH WATER

FIGURE 4.34

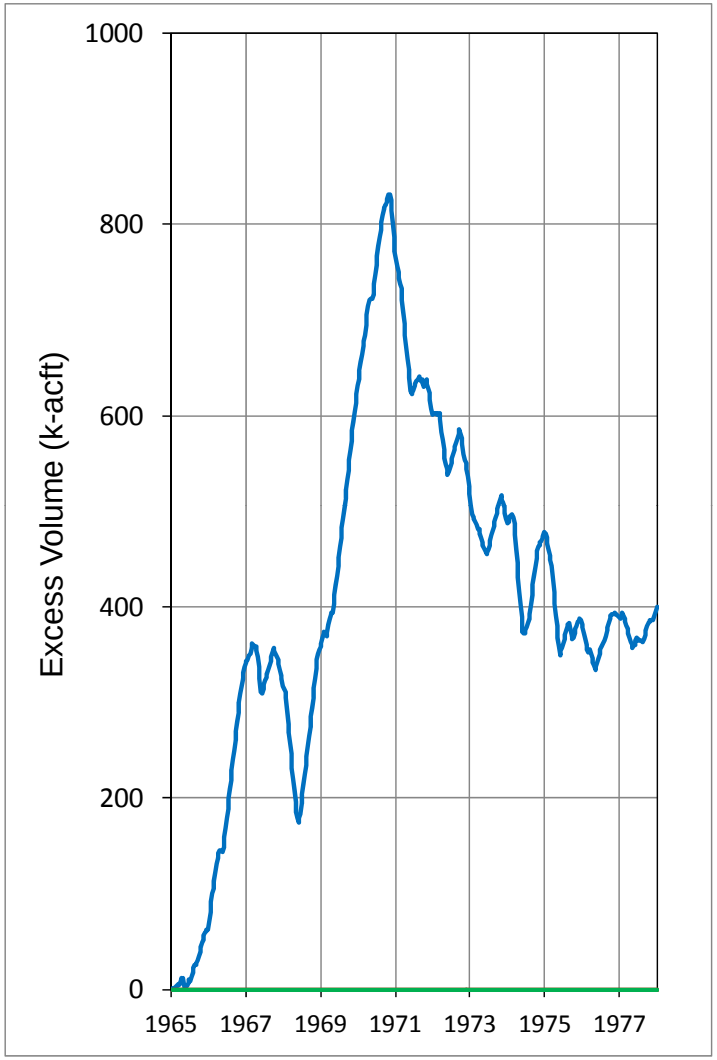

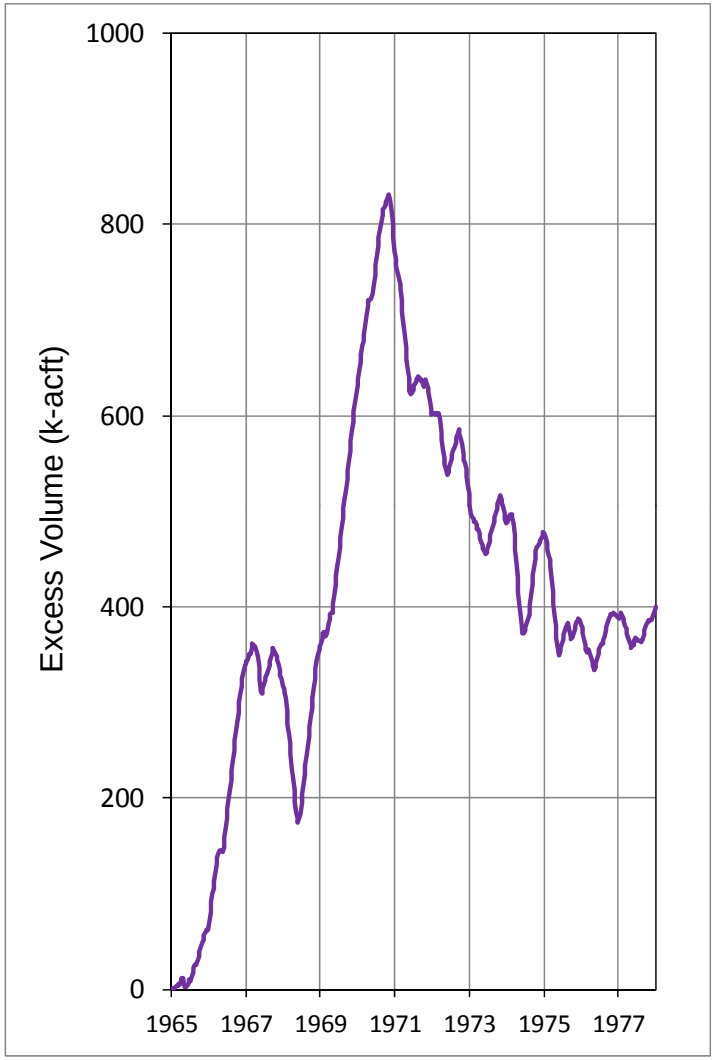

Legend

- Total UF
- Total APPZ
- Total BZ
- Total (All Aquifers)

Notes:

Scenario 2 is scaled back from Scenario 1 to keep pump pressure below or near 100 psi. All wells are fully penetrating in the UF Aquifer.

These plots show the total excess volume of fresh water remaining in each aquifer and in all aquifers. Excess volume is calculated by adding injected volume times recovery efficiency and subtracting extracted volume. The calculation is cumulative.

SCENARIO 2 – EXCESS VOLUME OF FRESH WATER

REGIONAL MODEL PRODUCTION SCENARIO REPORT

FIGURE 4.35

JUNE 2013

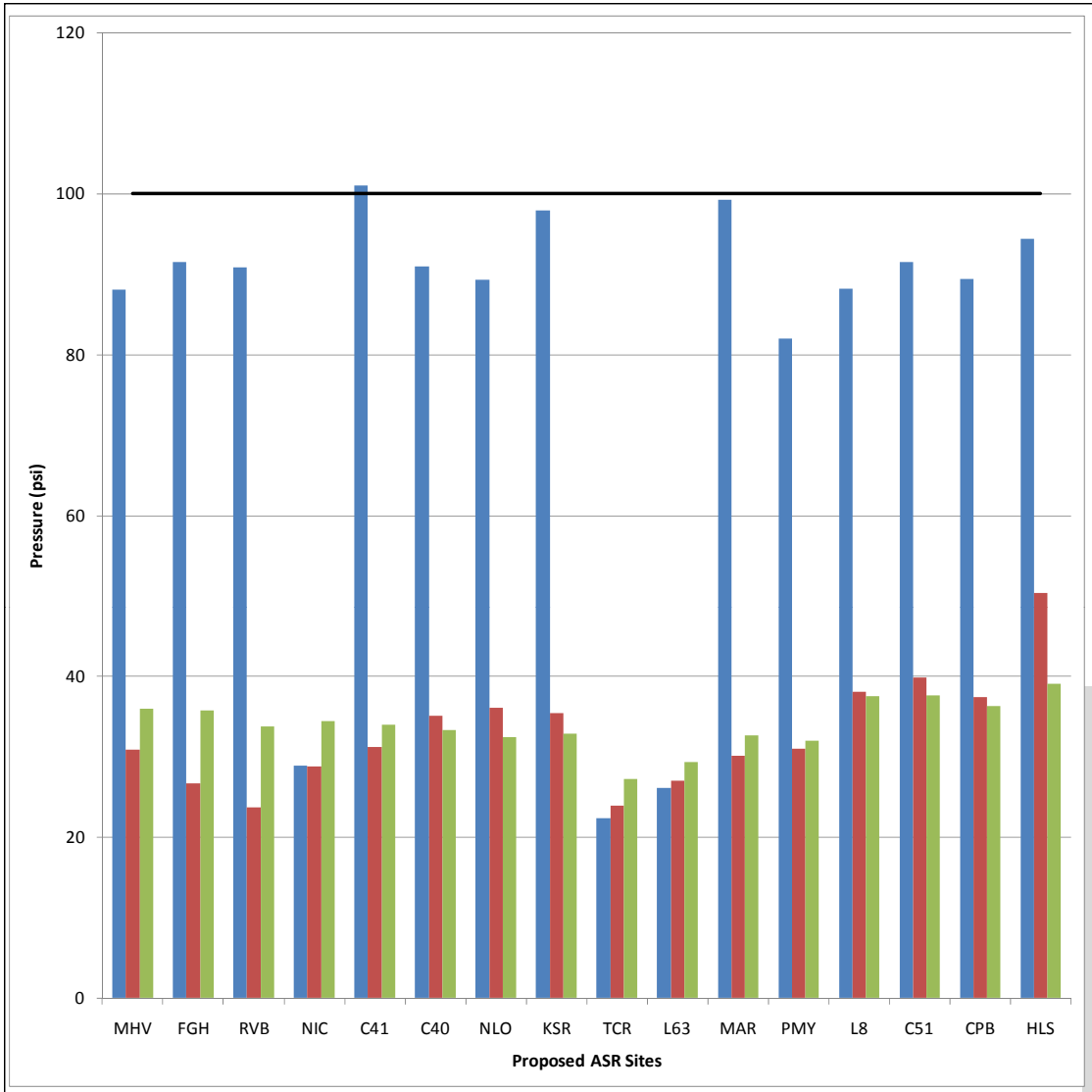

MHV	Moorehaven
FGH	Flaghole
RVB	Riverbend
NIC	Nicodemus Slough
C41	C-41Canal
C40	C-40 Canal
NLO	North Lake Okeechobee Reservoir
KSR	Kissimmee River / Paradise Run
TCR	Taylor Creek Reservoir
L63	L-63N Canal
LKR	Lakeside Ranch
PMY	Port Mayaca
L8	L-8 Basin
C51	C-51 @ STA1E
CPB	Central Palm Beach
HLS	Hillsboro (Site 1)

Legend

- Upper Floridan Aquifer
- Avon Park Permeable Zone
- Boulder Zone
- 100 psi Limit

Notes:

Scenario 2 is scaled back from Scenario 1 to keep pump pressure below or near 100 psi. All wells are fully penetrating in the UF Aquifer.

This plot shows the highest pressure at each site which the pump would need to overcome in order to inject storage water during the 13-year simulation.

The PDT determined that it would be important to keep this pressure below 100 psi (indicated by the heavy black line).

Note that maximum pressures are shown for all aquifers and all sites even if ASR pumps are not located there for the current scenario.

SCENARIO 2 – MAXIMUM PUMP PRESSURE REQUIREMENTS

REGIONAL MODEL PRODUCTION SCENARIO REPORT

FIGURE 4.36

JUNE 2013

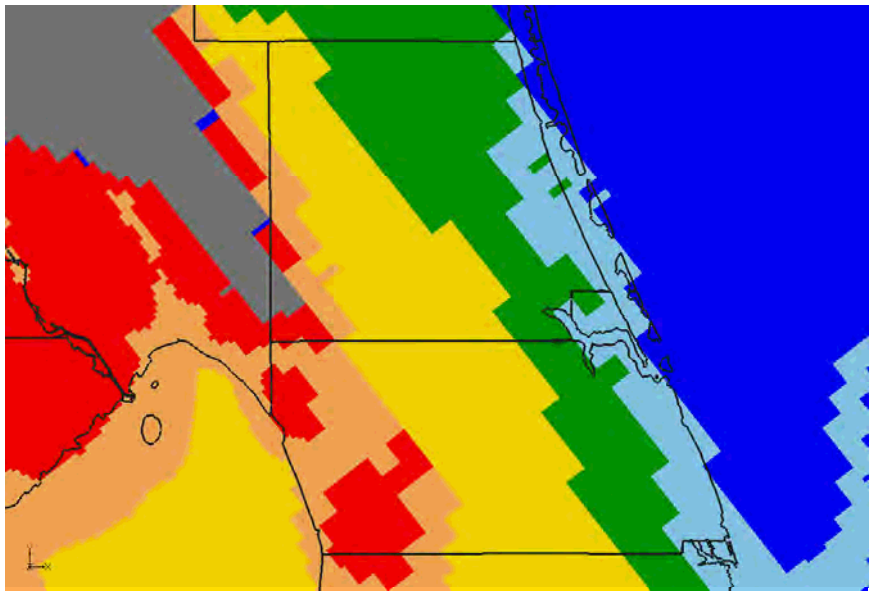

Upper Floridan Aquifer

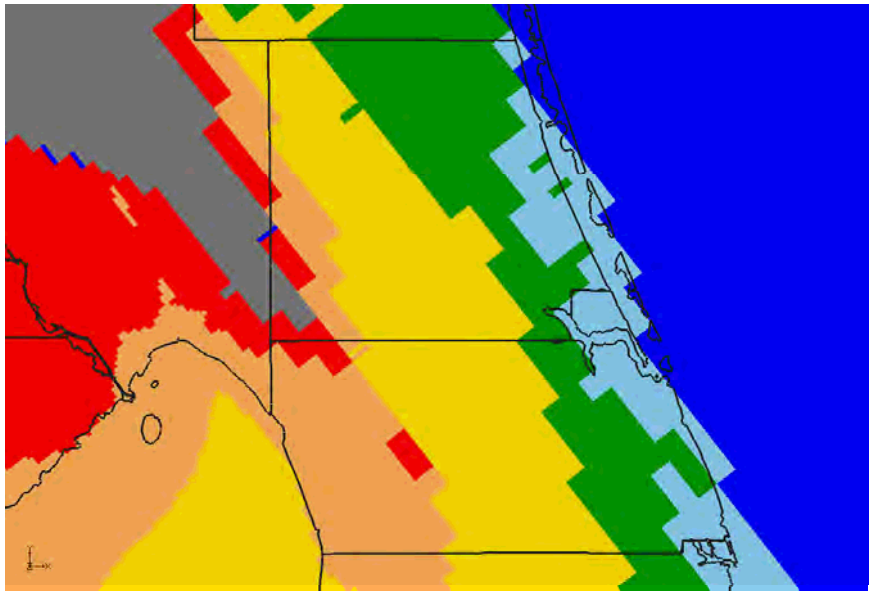

Avon Park Permeable Zone

Legend

- Not artesian
- < 5%
- 5% - 10%
- 10% - 20%
- 20% - 50%
- 50% - 100%
- Loses artesian condition

Notes:

Scenario 2 is scaled back from Scenario 1 to keep pump pressure below or near 100 psi. All wells are fully penetrating in the UF Aquifer.

These plots show the maximum reduction in artesian flow at each model cell as a percentage when compared to the flow expected without the ASR project.

Permit rules require that the reduction in Saint Lucie and Martin Counties be less than 10%.

Note the gray area in the northwest corner of the figures, which coincides with a ridge and does not normally have artesian conditions.

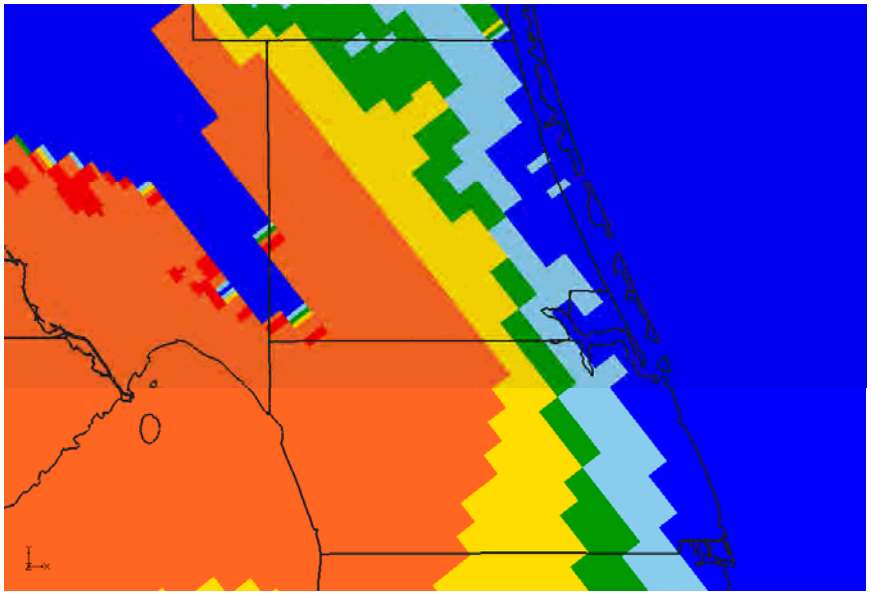

Upper Floridan Aquifer

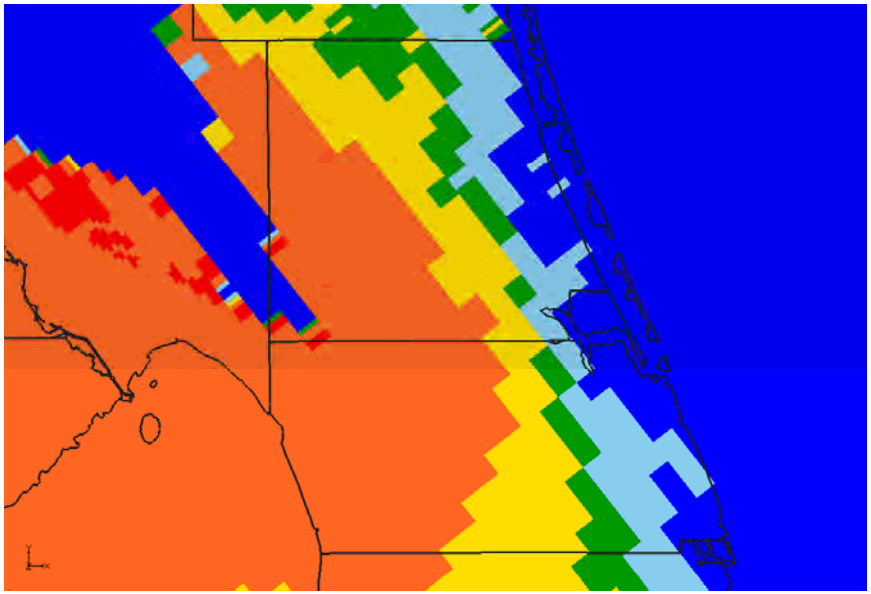

Avon Park Permeable Zone

Legend

- 0 days
- 1 – 250 days
- 250 – 500 days
- 500 – 1000 days
- 1000 – 2000 days
- > 2000 days

Notes:

Scenario 2 is scaled back from Scenario 1 to keep pump pressure below or near 100 psi. All wells are fully penetrating in the UF Aquifer.

These plots indicate the severity of the loss of artesian pressure due to ASR extraction pumping.

Permit rules require that the reduction in Saint Lucie and Martin Counties be less than 10%. This plot indicates the number of days during the simulation in which the flow reduction was greater than 10%. There are 4748 days in the 13-year model simulation period.

Note the blue area in the northwest corner of the figures, which coincides with a ridge and does not normally have artesian conditions.

SCENARIO 2 – NUMBER OF DAYS (OUT OF 13 YEARS) WITH FLOW REDUCTION EXCEEDING 10%

REGIONAL MODEL PRODUCTION SCENARIO REPORT

FIGURE 4.38

JUNE 2013

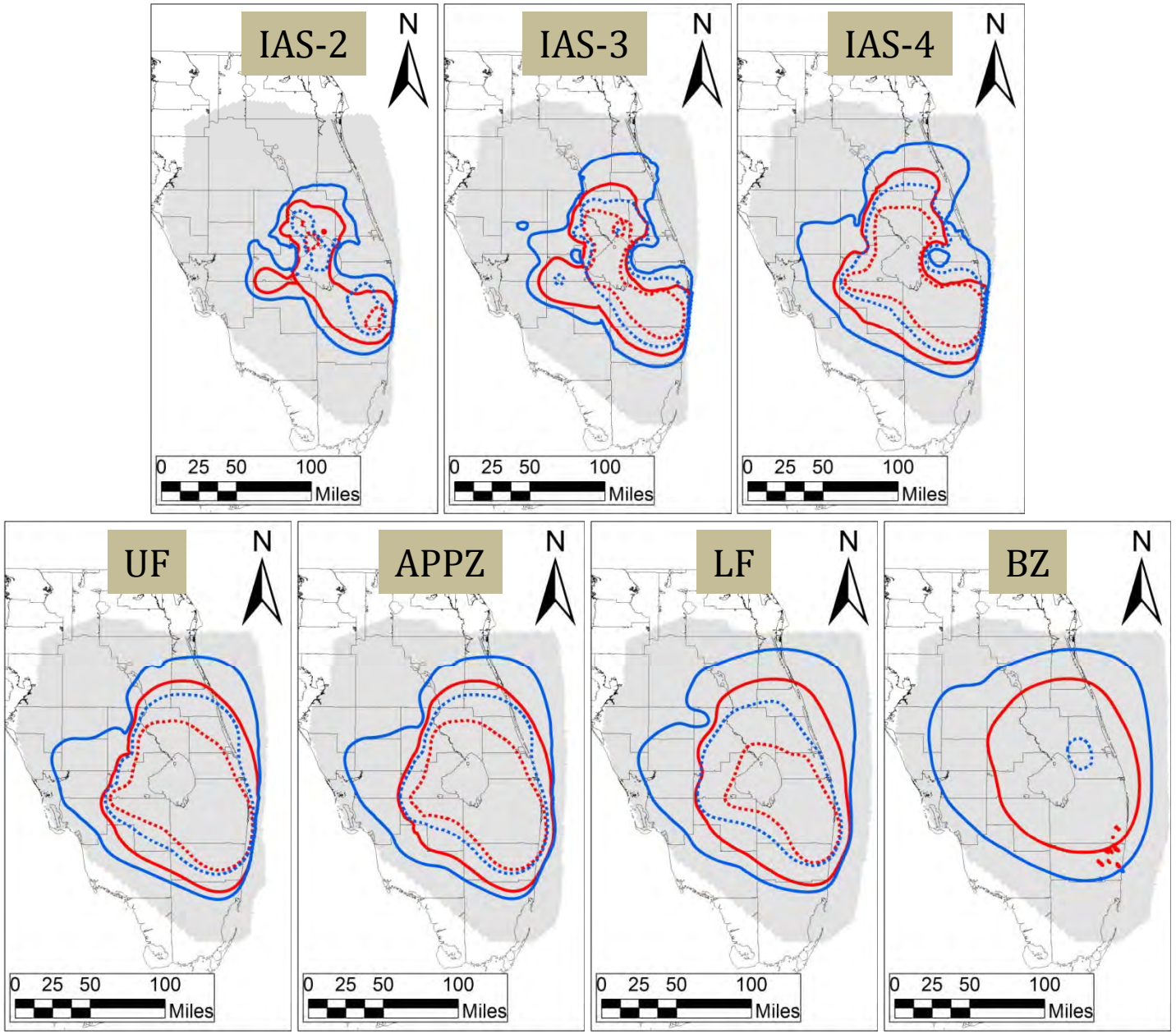

Legend

Maximum Drawdown
- 1 foot
- 5 feet

Maximum "Drawup"
- 1 foot
- 5 feet

Model Domain

Notes:

Scenario 2 is scaled back from Scenario 1 to keep pump pressure below or near 100 psi. All wells are fully penetrating in the UF Aquifer.

These figures show the extent of the areas where the maximum drawdown or "drawup" is greater than 1 foot or 5 feet.

The maximum condition does not necessarily occur at the same time for all regions of the model.

SCENARIO 2 – MAXIMUM DRAWDOWN AND "DRAWUP" BY AQUIFER

REGIONAL MODEL PRODUCTION SCENARIO REPORT

FIGURE 4.39

JUNE 2013

5-Mile Distance

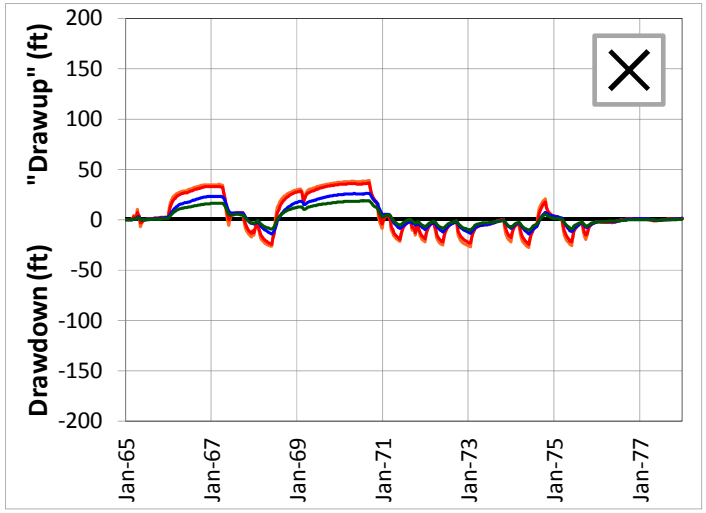

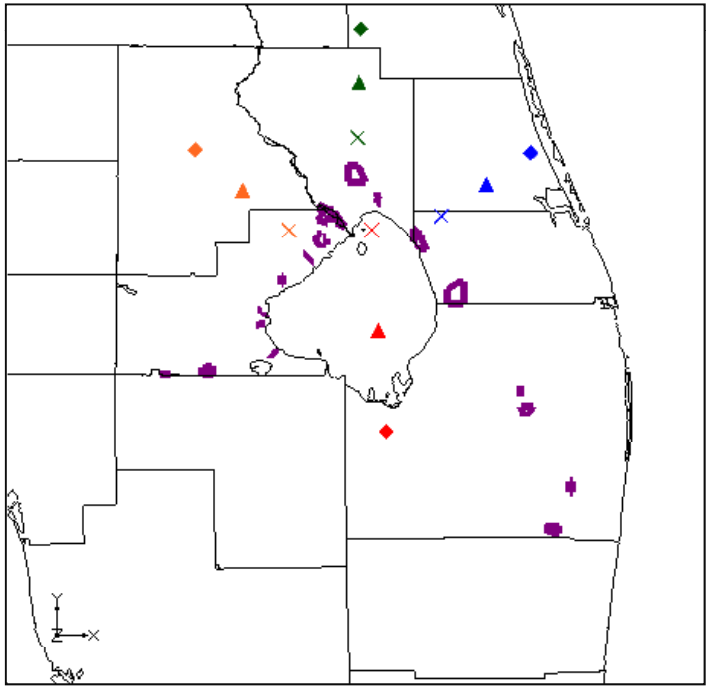

15-Mile Distance

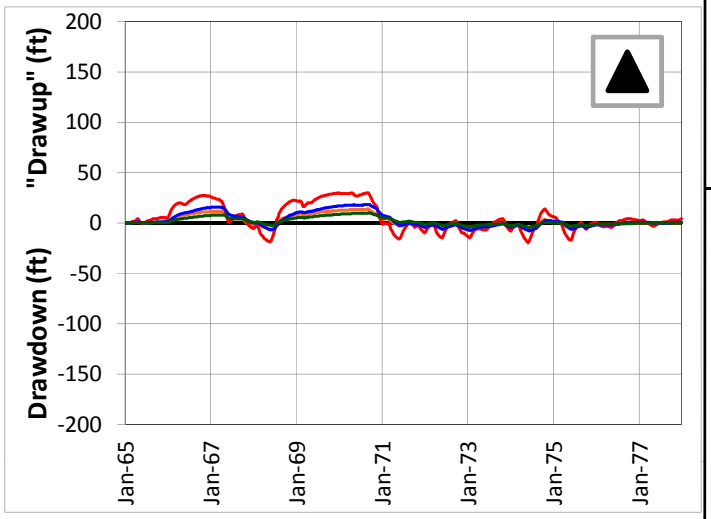

25-Mile Distance

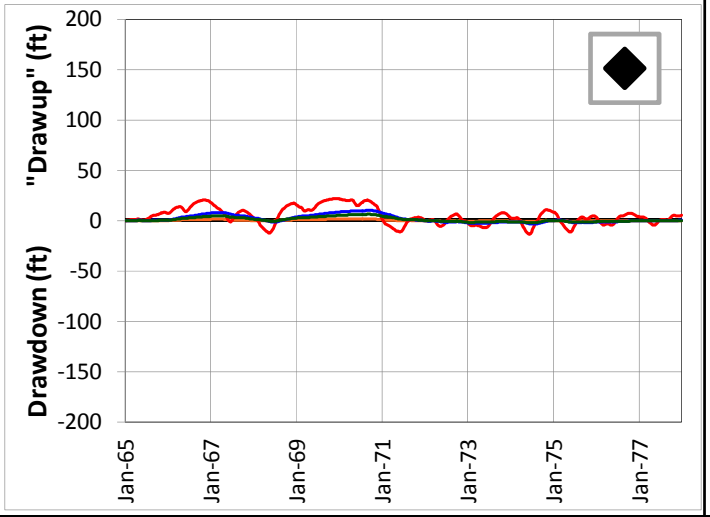

Legend

- CERP ASR Sites
- 5-Mile Distance Locations
- 15-Mile Distance Locations
- 25-Mile Distance Locations

Notes:

Scenario 2 is scaled back from Scenario 1 to keep pump pressure below or near 100 psi. All wells are fully penetrating in the UF Aquifer.

A number of individual sites were chosen from the UF Aquifer at distances of 5, 15 and 25 miles from the proposed ASR well sites. This figure shows the drawdown and "drawup" at each output time step for 12 of these sites.

The plots were calculated by subtracting the heads calculated by the D13R model from those calculated by the no project run. This results in a positive value for "drawup" and a negative value for drawdown.

The colors of the points on the map correspond to the colors of the lines on the plots.

The symbols on the map (x, triangle and diamond) indicate the distance from the ASR sites.

5-Mile Distance

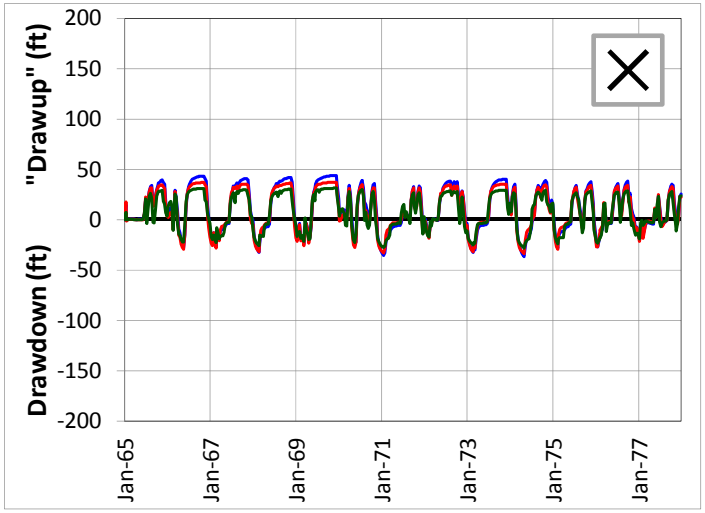

15-Mile Distance

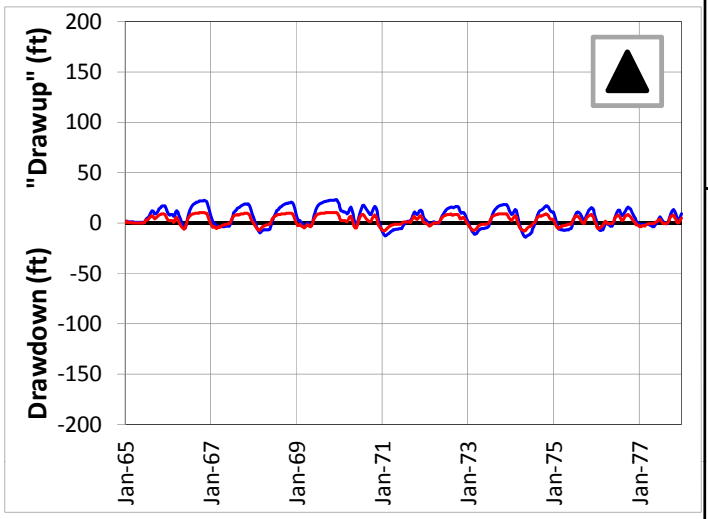

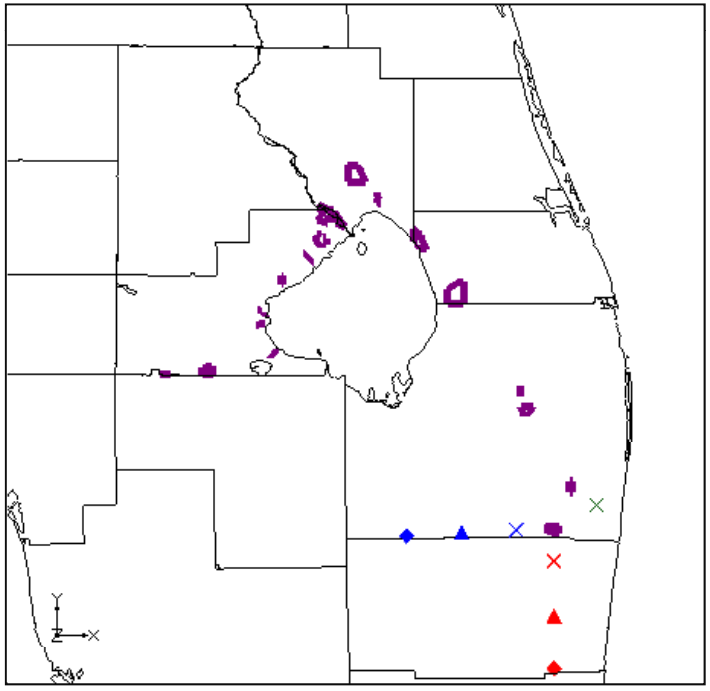

25-Mile Distance

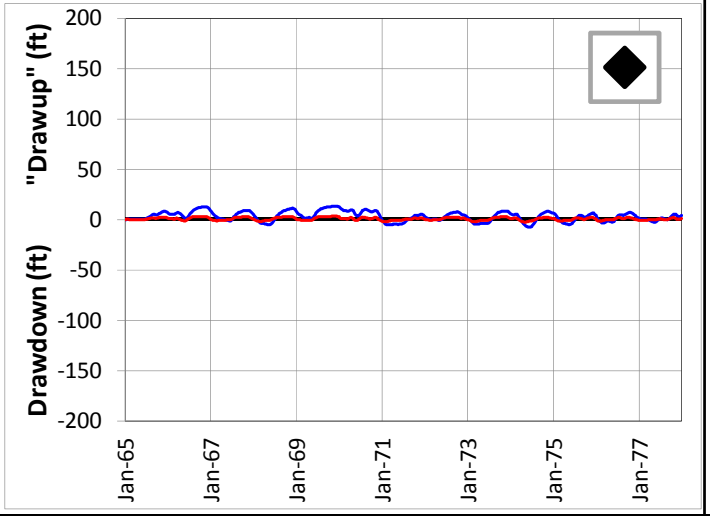

Legend

- CERP ASR Sites
- 5-Mile Distance Locations
- 15-Mile Distance Locations
- 25-Mile Distance Locations

Notes:

Scenario 2 is scaled back from Scenario 1 to keep pump pressure below or near 100 psi. All wells are fully penetrating in the UF Aquifer.

A number of individual sites were chosen from the UF Aquifer at distances of 5, 15 and 25 miles from the proposed ASR well sites. This figure shows the drawdown and "drawup" at each output time step for 7 of these sites.

The plots were calculated by subtracting the heads calculated by the D13R model from those calculated by the no project run. This results in a positive value for "drawup" and a negative value for drawdown.

The colors of the points on the map correspond to the colors of the lines on the plots.

The symbols on the map (x, triangle and diamond) indicate the distance from the ASR sites.

5-Mile Distance

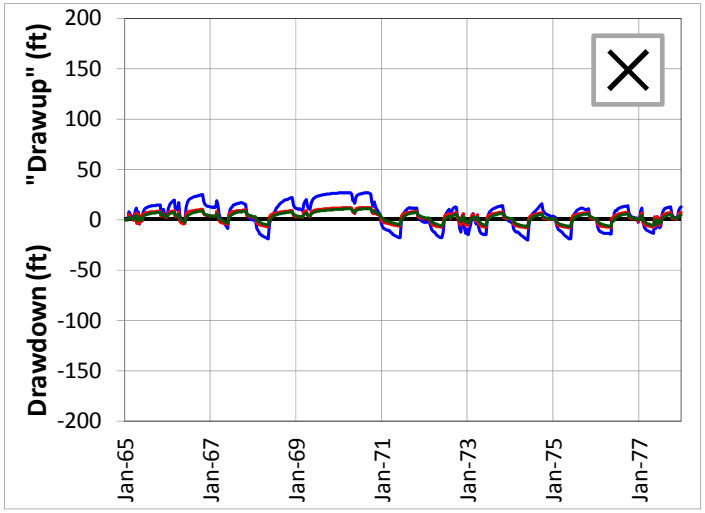

15-Mile Distance

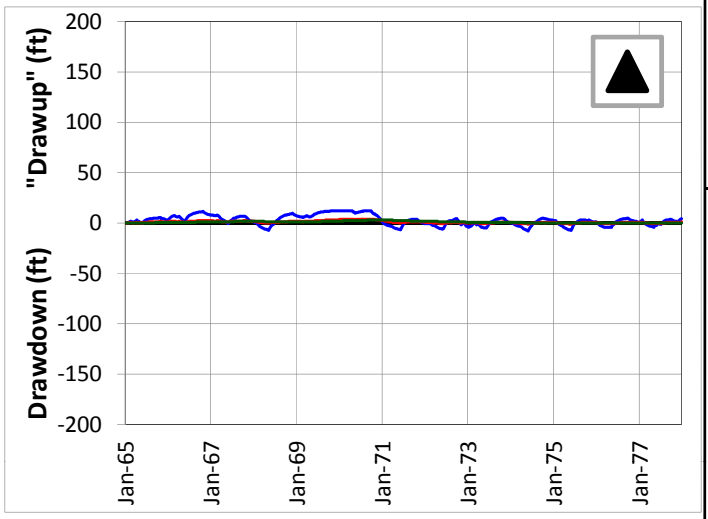

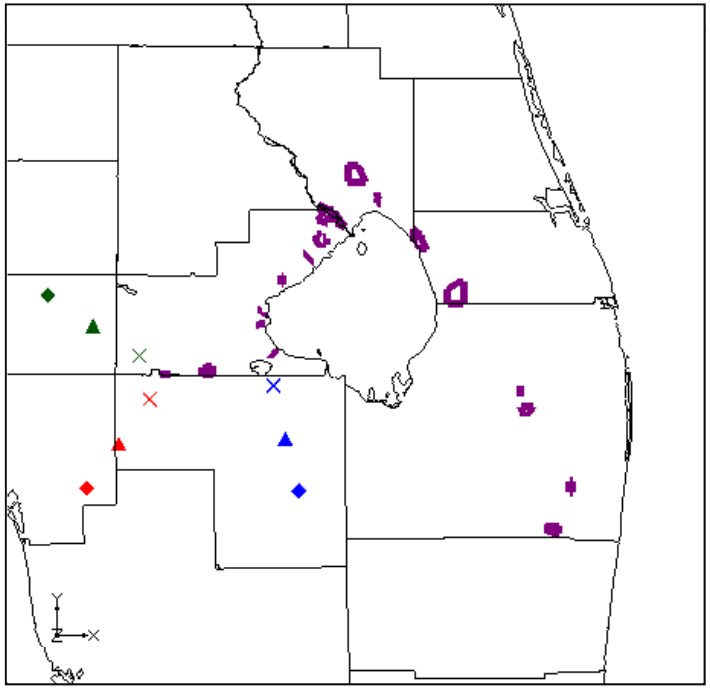

25-Mile Distance

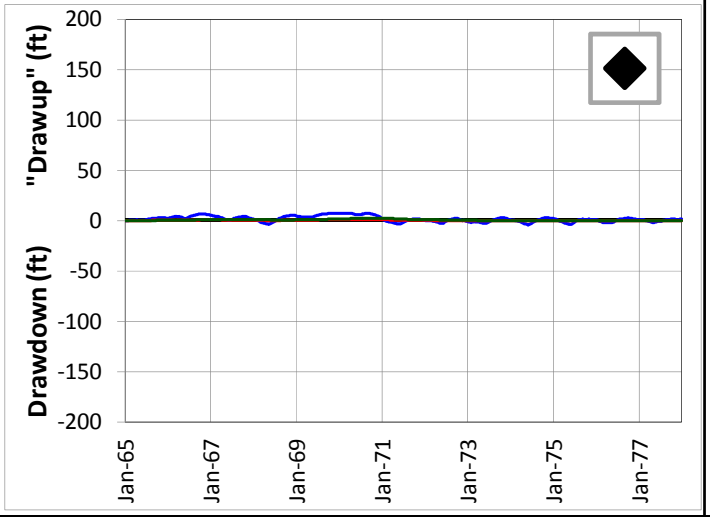

Legend

- CERP ASR Sites
- 5-Mile Distance Locations
- 15-Mile Distance Locations
- 25-Mile Distance Locations

Notes:

Scenario 2 is scaled back from Scenario 1 to keep pump pressure below or near 100 psi. All wells are fully penetrating in the UF Aquifer.

A number of individual sites were chosen from the UF Aquifer at distances of 5, 15 and 25 miles from the proposed ASR well sites. This figure shows the drawdown and "drawup" at each output time step for 9 of these sites.

The plots were calculated by subtracting the heads calculated by the D13R model from those calculated by the no project run. This results in a positive value for "drawup" and a negative value for drawdown.

The colors of the points on the map correspond to the colors of the lines on the plots.

The symbols on the map (x, triangle and diamond) indicate the distance from the ASR sites.

5-Mile Distance

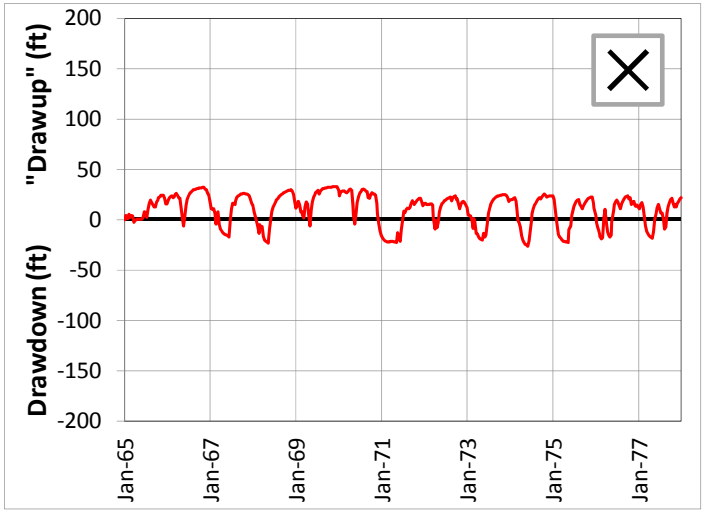

15-Mile Distance

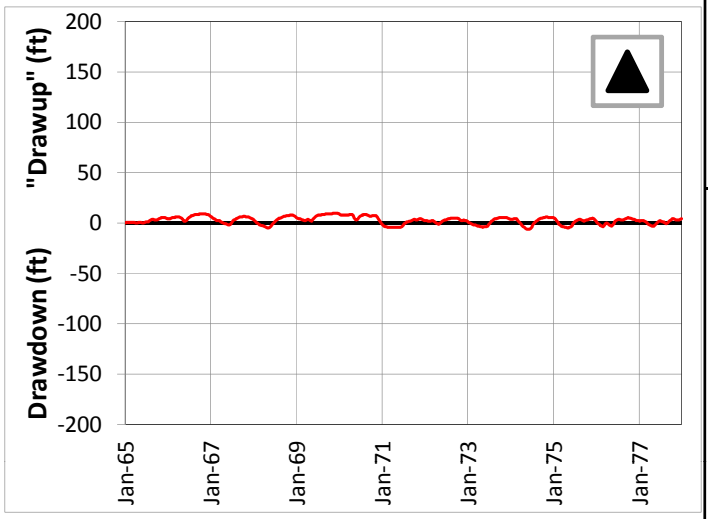

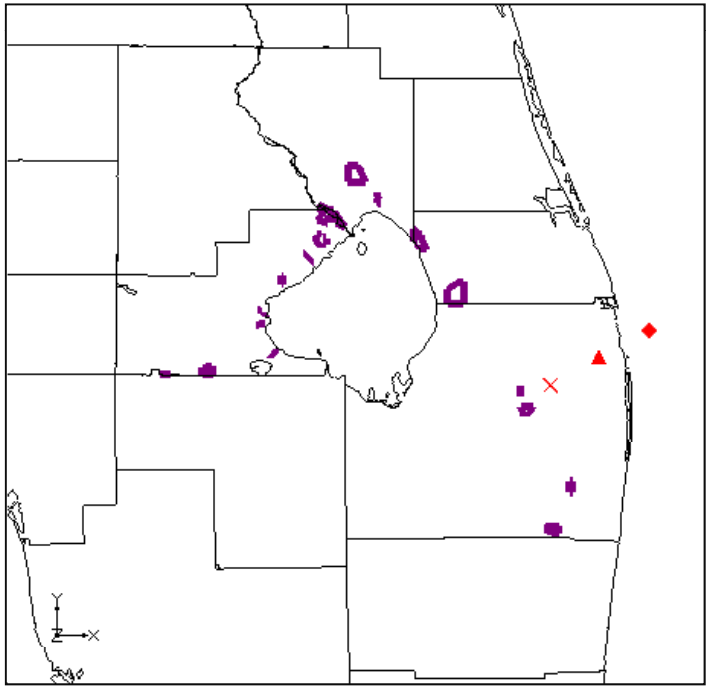

25-Mile Distance

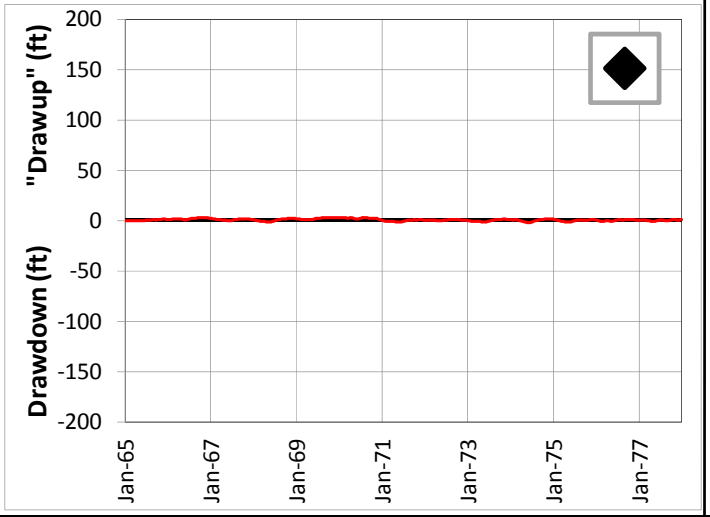

Legend

- CERP ASR Sites
- 5-Mile Distance Locations
- 15-Mile Distance Locations
- 25-Mile Distance Locations

Notes:

Scenario 2 is scaled back from Scenario 1 to keep pump pressure below or near 100 psi. All wells are fully penetrating in the UF Aquifer.

A number of individual sites were chosen from the UF Aquifer at distances of 5, 15 and 25 miles from the proposed ASR well sites. This figure shows the drawdown and "drawup" at each output time step for 3 of these sites.

The plots were calculated by subtracting the heads calculated by the D13R model from those calculated by the no project run. This results in a positive value for "drawup" and a negative value for drawdown.

The colors of the points on the map correspond to the colors of the lines on the plots.

The symbols on the map (x, triangle and diamond) indicate the distance from the ASR sites.

SCENARIO 2 – DRAWDOWN AND "DRAWUP" – UF

FIGURE 4.43

5-Mile Distance

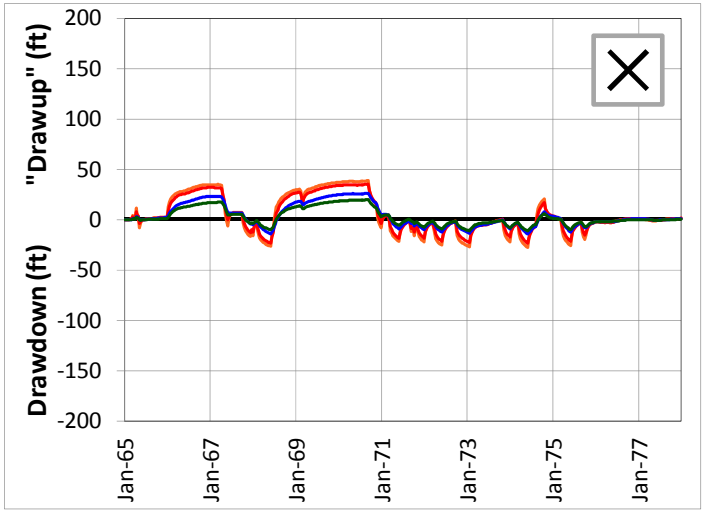

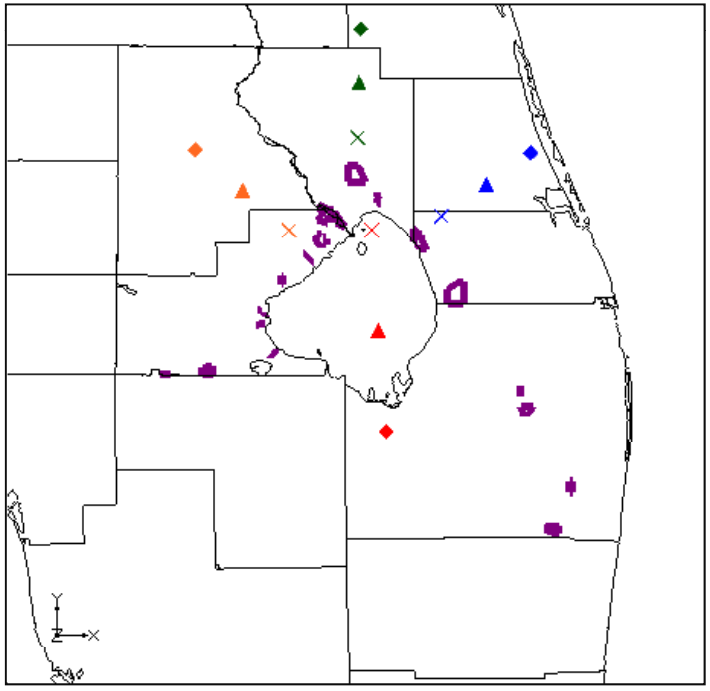

15-Mile Distance

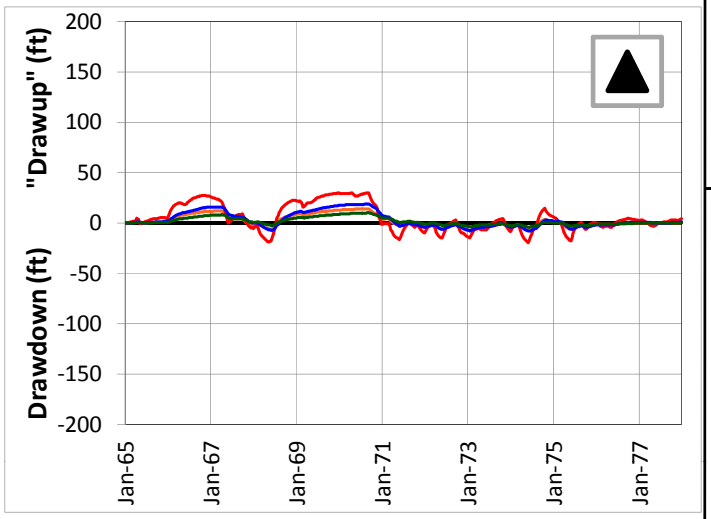

25-Mile Distance

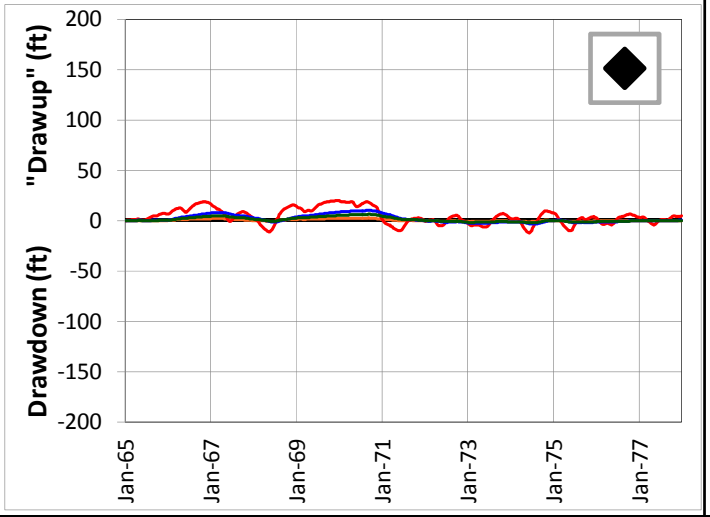

Legend

- CERP ASR Sites
- ✕ 5-Mile Distance Locations
- ▲ 15-Mile Distance Locations
- ◆ 25-Mile Distance Locations

Notes:

Scenario 2 is scaled back from Scenario 1 to keep pump pressure below or near 100 psi. All wells are fully penetrating in the UF Aquifer.

A number of individual sites were chosen from the APPZ Aquifer at distances of 5, 15 and 25 miles from the proposed ASR well sites. This figure shows the drawdown and "drawup" at each output time step for 12 of these sites.

The plots were calculated by subtracting the heads calculated by the D13R model from those calculated by the no project run. This results in a positive value for "drawup" and a negative value for drawdown.

The colors of the points on the map correspond to the colors of the lines on the plots.

The symbols on the map (x, triangle and diamond) indicate the distance from the ASR sites.

5-Mile Distance

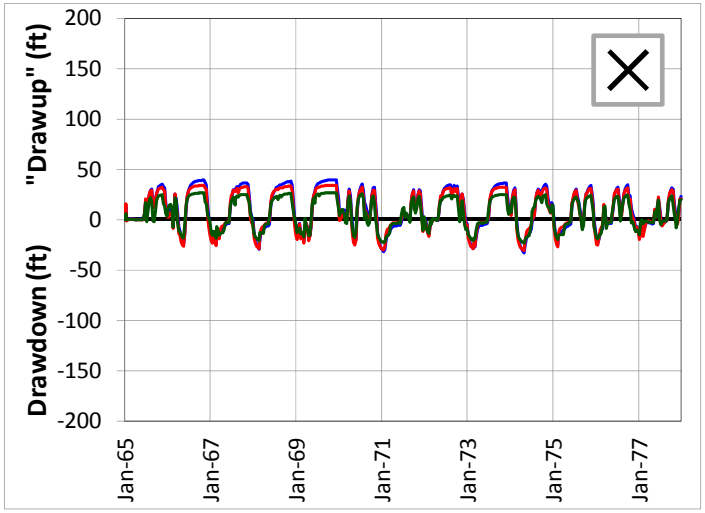

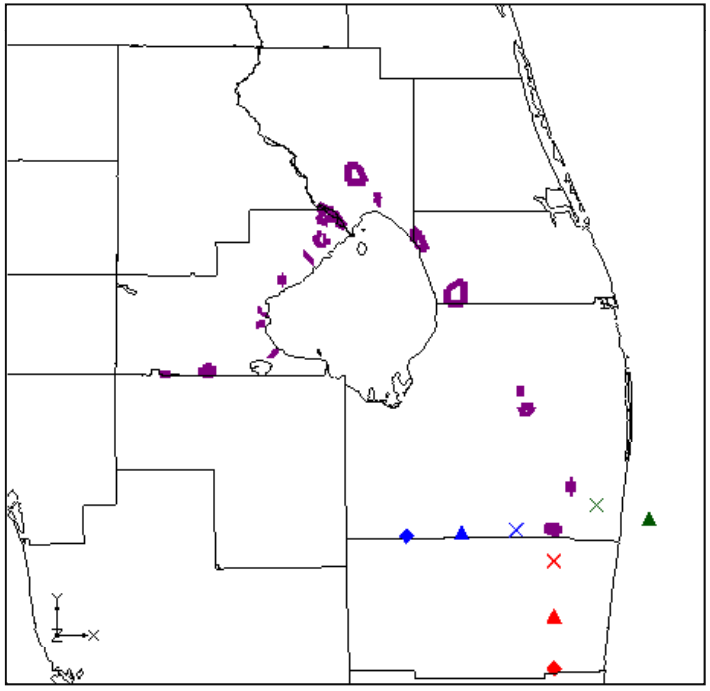

15-Mile Distance

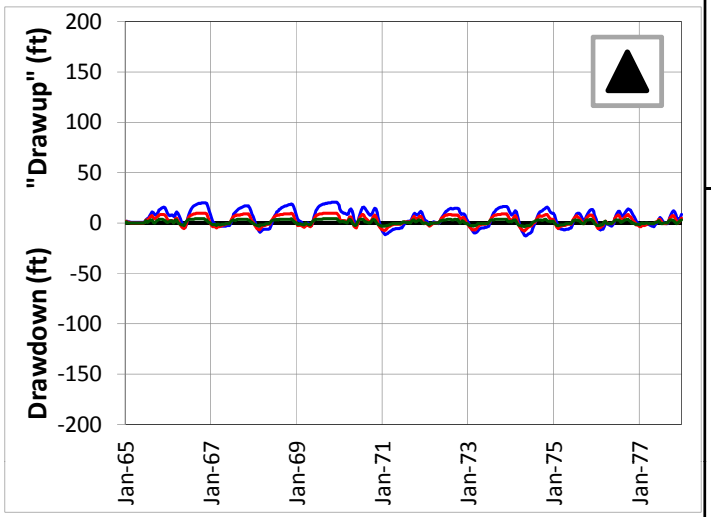

25-Mile Distance

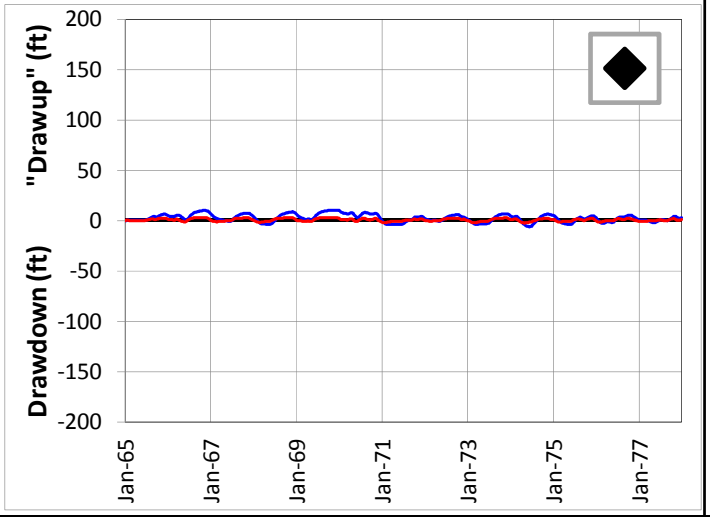

Legend

- CERP ASR Sites
- 5-Mile Distance Locations
- 15-Mile Distance Locations
- 25-Mile Distance Locations

Notes:

Scenario 2 is scaled back from Scenario 1 to keep pump pressure below or near 100 psi. All wells are fully penetrating in the UF Aquifer.

A number of individual sites were chosen from the APPZ Aquifer at distances of 5, 15 and 25 miles from the proposed ASR well sites. This figure shows the drawdown and "drawup" at each output time step for 8 of these sites.

The plots were calculated by subtracting the heads calculated by the D13R model from those calculated by the no project run. This results in a positive value for "drawup" and a negative value for drawdown.

The colors of the points on the map correspond to the colors of the lines on the plots.

The symbols on the map (x, triangle and diamond) indicate the distance from the ASR sites.

SCENARIO 2 – DRAWDOWN AND "DRAWUP" – APPZ

FIGURE 4.45

5-Mile Distance

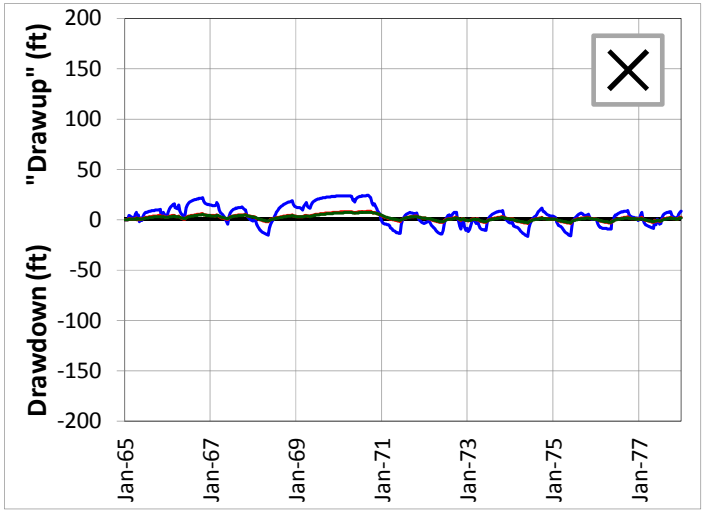

15-Mile Distance

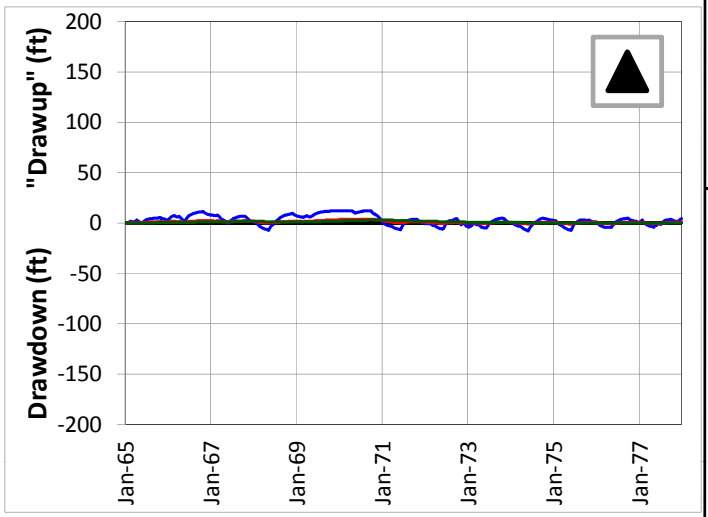

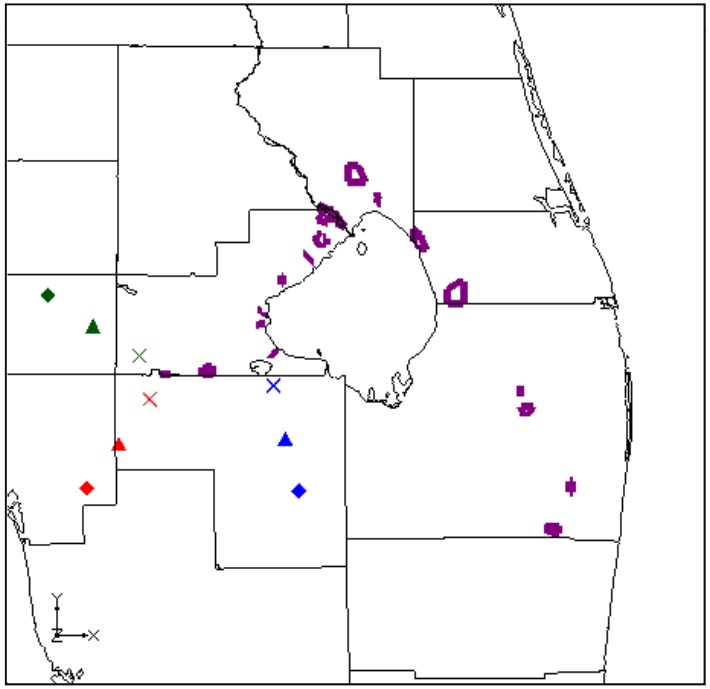

25-Mile Distance

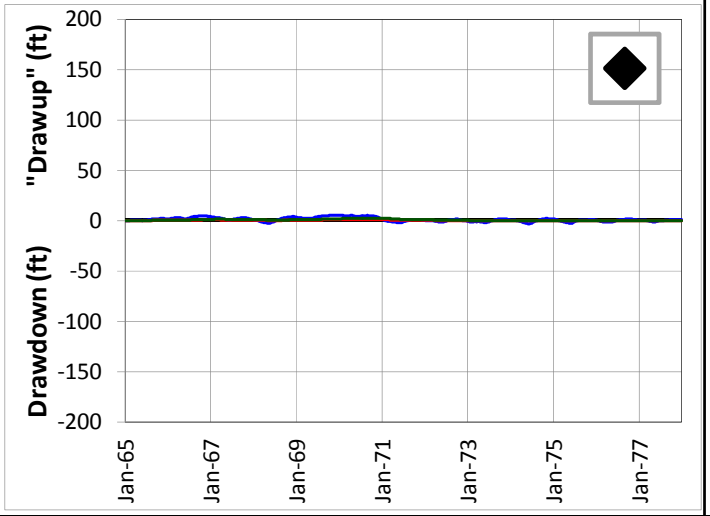

Legend

- CERP ASR Sites
- 5-Mile Distance Locations
- 15-Mile Distance Locations
- 25-Mile Distance Locations

Notes:

Scenario 2 is scaled back from Scenario 1 to keep pump pressure below or near 100 psi. All wells are fully penetrating in the UF Aquifer.

A number of individual sites were chosen from the APPZ Aquifer at distances of 5, 15 and 25 miles from the proposed ASR well sites. This figure shows the drawdown and "drawup" at each output time step for 9 of these sites.

The plots were calculated by subtracting the heads calculated by the D13R model from those calculated by the no project run. This results in a positive value for "drawup" and a negative value for drawdown.

The colors of the points on the map correspond to the colors of the lines on the plots.

The symbols on the map (x, triangle and diamond) indicate the distance from the ASR sites.

5-Mile Distance

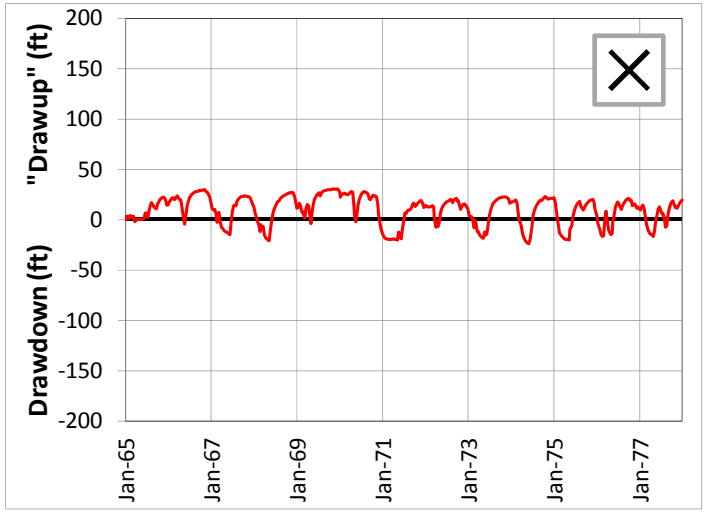

15-Mile Distance

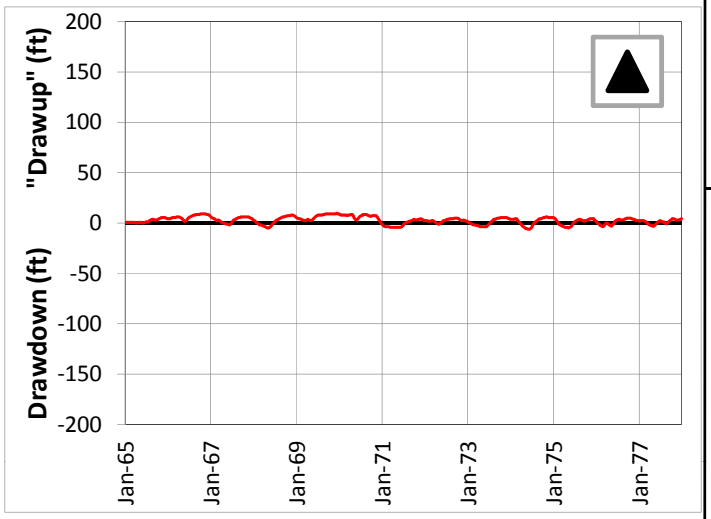

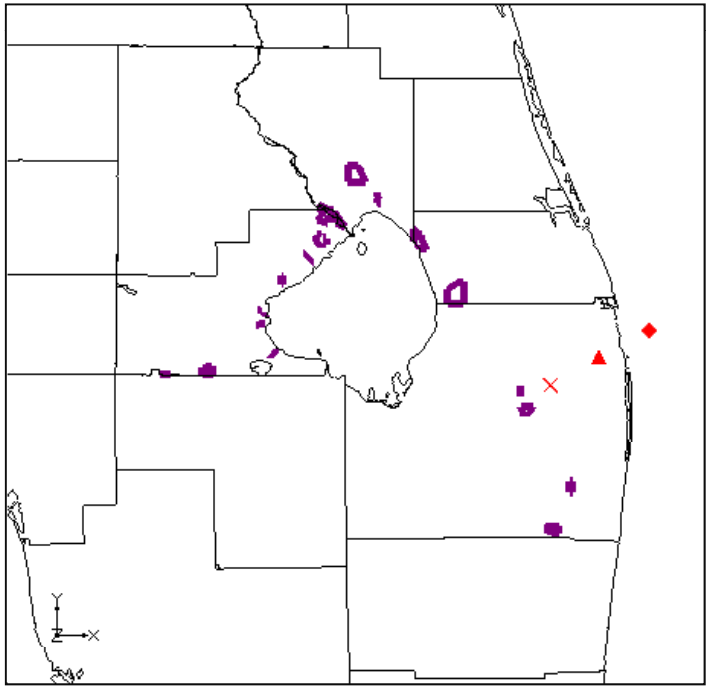

25-Mile Distance

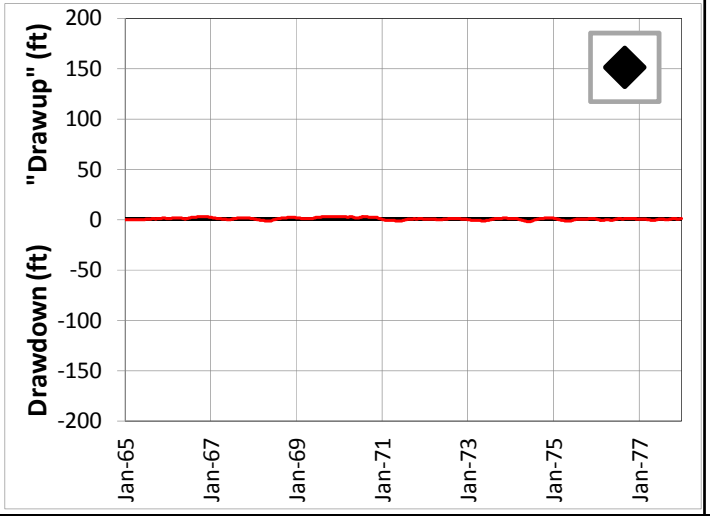

Legend

- CERP ASR Sites
- 5-Mile Distance Locations
- 15-Mile Distance Locations
- 25-Mile Distance Locations

Notes:

Scenario 2 is scaled back from Scenario 1 to keep pump pressure below or near 100 psi. All wells are fully penetrating in the UF Aquifer.

A number of individual sites were chosen from the APPZ Aquifer at distances of 5, 15 and 25 miles from the proposed ASR well sites. This figure shows the drawdown and "drawup" at each output time step for 3 of these sites.

The plots were calculated by subtracting the heads calculated by the D13R model from those calculated by the no project run. This results in a positive value for "drawup" and a negative value for drawdown.

The colors of the points on the map correspond to the colors of the lines on the plots.

The symbols on the map (x, triangle and diamond) indicate the distance from the ASR sites.

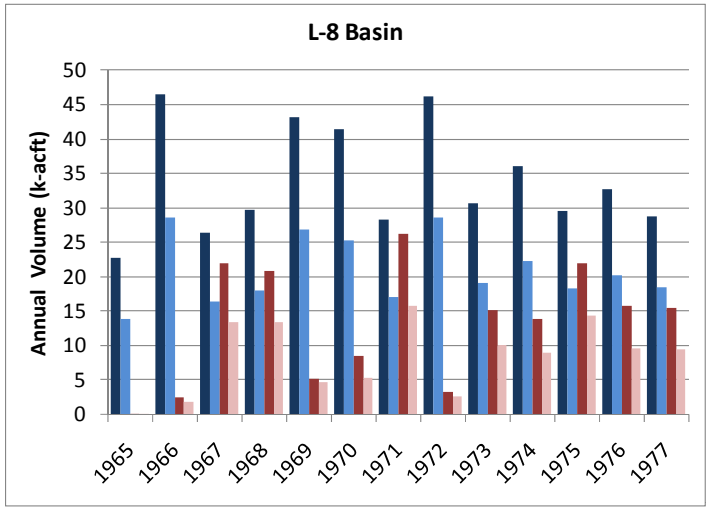

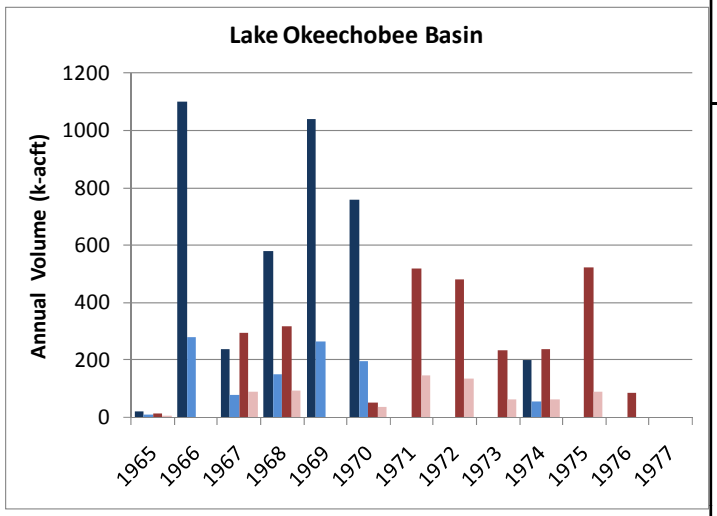

	L-8		Lake Okeechobee		Caloosahatchee	
	In %	Out %	In %	Out %	In %	Out %
1965	61%	100%	50%	50%	41%	67%
1966	62%	75%	25%	--	27%	42%
1967	62%	61%	32%	30%	24%	22%
1968	60%	65%	26%	29%	23%	24%
1969	62%	88%	25%	--	23%	--
1970	61%	63%	26%	66%	25%	100%
1971	60%	60%	--	28%	22%	24%
1972	62%	79%	--	28%	38%	29%
1973	62%	66%	--	27%	26%	30%
1974	62%	65%	27%	26%	23%	23%
1975	62%	65%	--	17%	23%	23%
1976	62%	61%	--	0%	30%	30%
1977	65%	61%	--	--	31%	33%

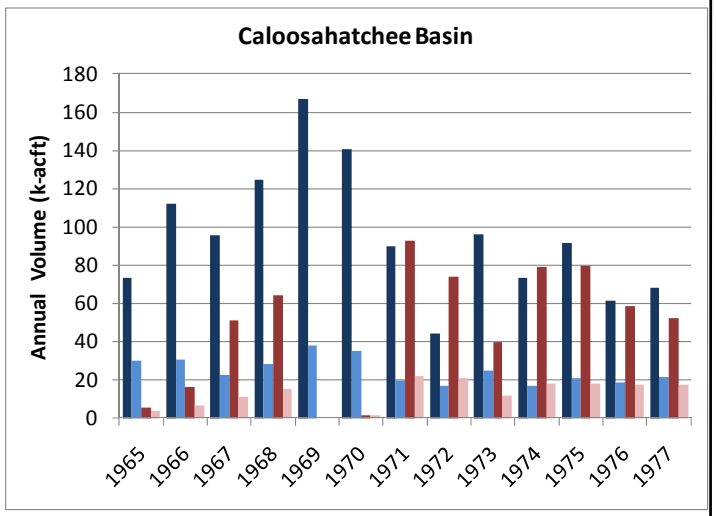

Legend

- Design Storage (injection)
- Modeled Storage (injection)
- Design Recovery (extraction)
- Modeled Recovery (extraction)

Notes:

Scenario 2 is scaled back from Scenario 1 to keep pump pressure below or near 100 psi. All wells are fully penetrating in the UF Aquifer.

These three plots show the comparison between the SFWMM-D13R designed annual injection and extraction volumes at the ASR wells and the actual assigned rates for the RASRSM-D13R for three of the basins.

The table presents the percentage of SFWMM-D13R annual flow rates that are included in this scenario of the RASRSM-D13R. These percentages are not recovery efficiencies.

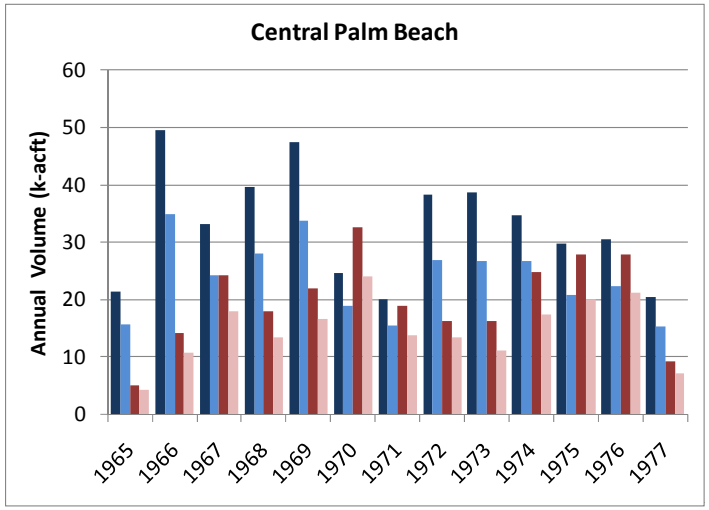

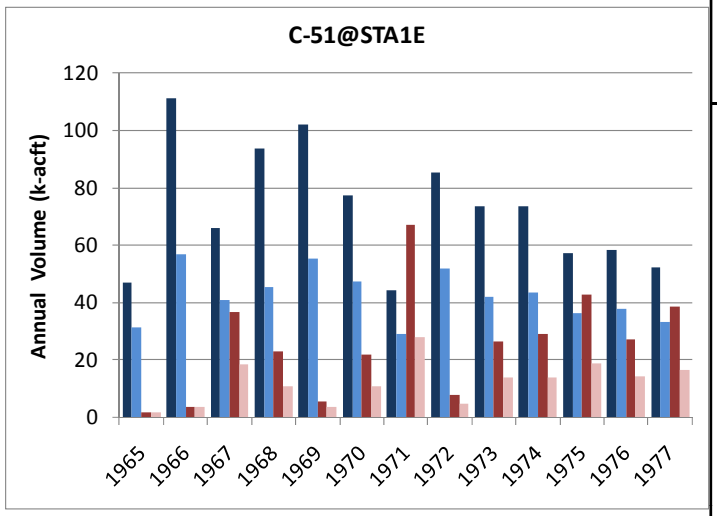

	CPB		C-51		Hillsboro	
	In %	Out %	In %	Out %	In %	Out %
1965	73%	88%	67%	100%	45%	46%
1966	71%	75%	51%	100%	36%	84%
1967	73%	74%	62%	50%	40%	28%
1968	71%	75%	49%	47%	36%	35%
1969	71%	76%	54%	69%	39%	80%
1970	76%	74%	61%	50%	48%	68%
1971	77%	72%	66%	41%	48%	14%
1972	70%	82%	61%	62%	49%	23%
1973	69%	68%	57%	52%	35%	32%
1974	77%	70%	59%	47%	45%	41%
1975	70%	72%	64%	44%	47%	23%
1976	74%	77%	65%	52%	52%	28%
1977	75%	78%	64%	43%	46%	23%

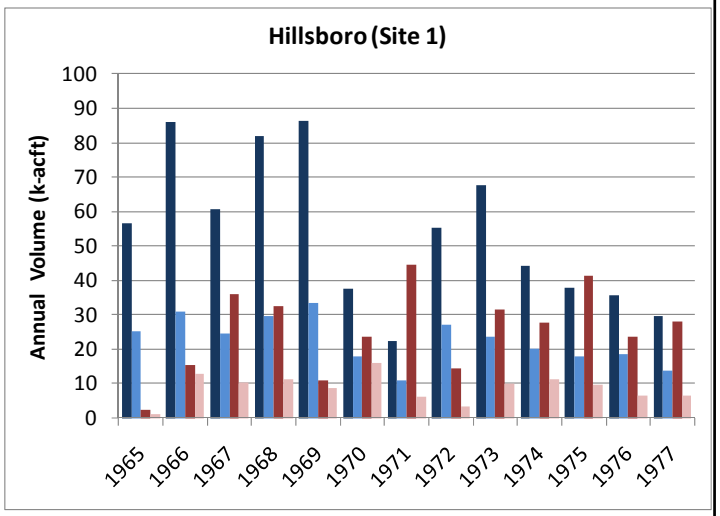

Legend

- Design Storage (injection)
- Modeled Storage (injection)
- Design Recovery (extraction)
- Modeled Recovery (extraction)

Notes:

Scenario 2 is scaled back from Scenario 1 to keep pump pressure below or near 100 psi. All wells are fully penetrating in the UF Aquifer.

These three plots show the comparison between the SFWMM-D13R designed annual injection and extraction volumes at the ASR wells and the actual assigned rates for the RASRSM-D13R for three of the basins.

The table presents the percentage of SFWMM-D13R annual flow rates that are included in this scenario of the RASRSM-D13R. These percentages are not recovery efficiencies.

Scenario 2 – Comparison of Designed and Modeled ASR Flow Rates

Regional Model Production Scenario Report

Figure 4.49

June 2013

	Total	
	In %	Out %
1965	52%	62%
1966	31%	69%
1967	39%	35%
1968	31%	33%
1969	30%	78%
1970	31%	66%
1971	45%	30%
1972	56%	30%
1973	44%	33%
1974	40%	32%
1975	47%	23%
1976	54%	29%
1977	51%	40%

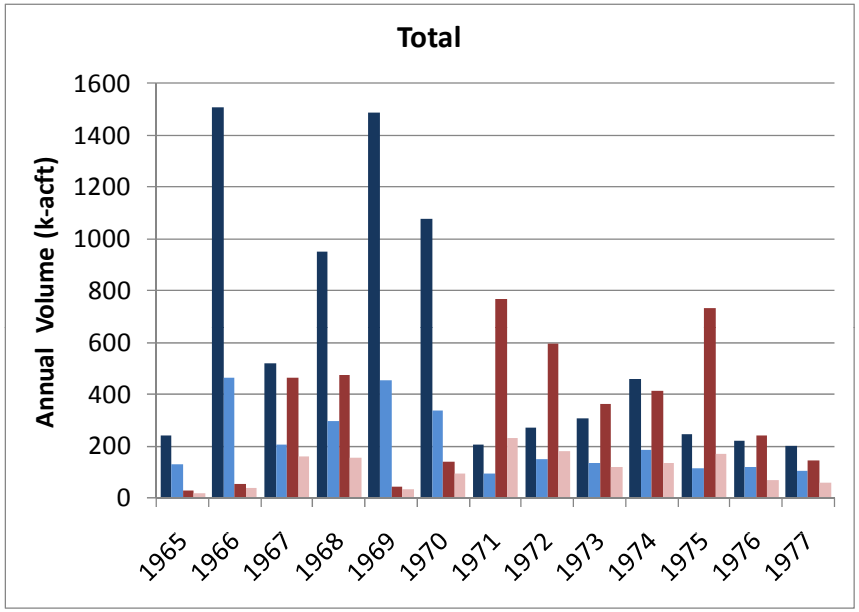

Legend

- Design Storage (injection)
- Modeled Storage (injection)
- Design Recovery (extraction)
- Modeled Recovery (extraction)

Notes:

Scenario 2 is scaled back from Scenario 1 to keep pump pressure below or near 100 psi. All wells are fully penetrating in the UF Aquifer.

This plot shows the comparison between the SFWMM-D13R designed annual injection and extraction volumes at the ASR wells and the actual assigned rates for the RASRSM-D13R for all basins.

The table presents the percentage of SFWMM-D13R annual flow rates that are included in this scenario of the RASRSM-D13R. These percentages are not recovery efficiencies.

		UF		APPZ		BZ		Total # Wells	Target # Wells
		Number of Wells	Recovery Efficiency	Number of Wells	Recovery Efficiency	Number of Wells	Recovery Efficiency		
Caloosahatchee Basin	Moore Haven	4	70%	12	30%	0	10%		
	River Bend	3	70%	5	30%	0	10%		
	Flaghole	2	70%	18	30%	0	10%		
	Basin Total	9		35		0		44	44
Lake Okeechobee Basin	Nicodemus Slough	0	70%	10	30%	0	10%		
	C-41 Canal	1	70%	9	30%	0	10%		
	C-40 Canal	2	70%	8	30%	0	10%		
	North Lake Okeechobee	8	70%	12	30%	0	10%		
	Kissimmee R./Paradise Run	15	70%	60	30%	0	10%		
	Taylor Creek	0	70%	20	30%	0	10%		
	L-63N	0	70%	15	30%	0	10%		
	Lakeside Ranch	5	70%	15	30%	0	10%		
	Port Mayaca	19	70%	1	30%	0	10%		
	Basin Total	50		150		0		200	200
L-8		6	70%	4	30%	0	10%	10	10
C-51		12	70%	22	30%	0	10%	34	34
Central Palm Beach		10	70%	5	30%	0	10%	15	15
Site 1 (Hillsboro)		10	40%	20	40%	0	10%	30	30
Total		97		236		0		333	333

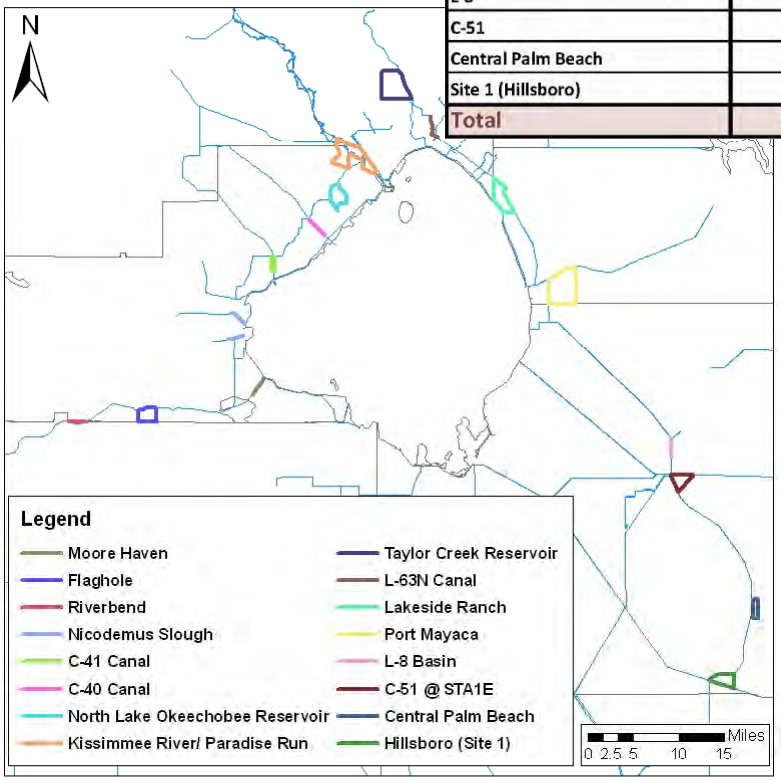

Notes:

Scenario 3 keeps all the wells from Scenario 2 in the UF and adds the remainder of the design wells into the APPZ. This allows the model to match the injection flows. Extraction flows are lower because of the lower assumed recovery efficiency in the APPZ. All wells are fully penetrating in their respective aquifers.

Flow rates are divided evenly among the wells in each basin. Maximum flow rate for any one well is 5 mgd.

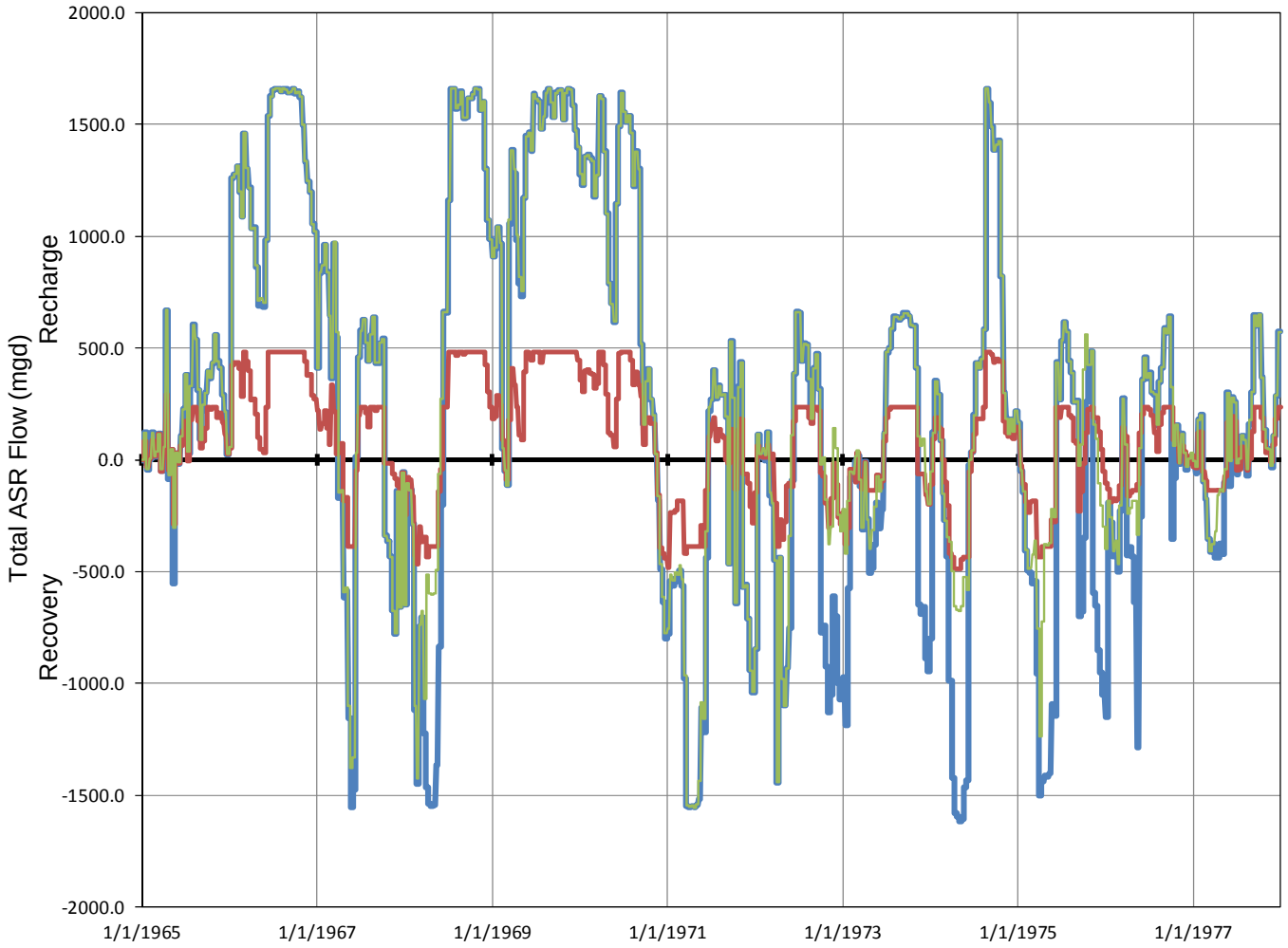

Legend

- Scenario 1 – ASR Flux
- Scenario 2 – ASR Flux
- Scenario 3 – ASR Flux

Notes:

Scenario 3 keeps all the wells from Scenario 2 in the UF and adds the remainder of the design wells into the APPZ. This allows the model to match the injection flows. Extraction flows are lower because of the lower assumed recovery efficiency in the APPZ. All wells are fully penetrating in their respective aquifers.

This plot shows the extraction and injection rates for all wells at all sites for Scenario 1, Scenario 2 and Scenario 3. Positive rates are recharge (injection), while negative rates are recovery (extraction).

Scenario 3 – ASR Well Fluxes (Compared to Scenarios 1 & 2)

Regional Model Production Scenario Report

Figure 4.52

June 2013

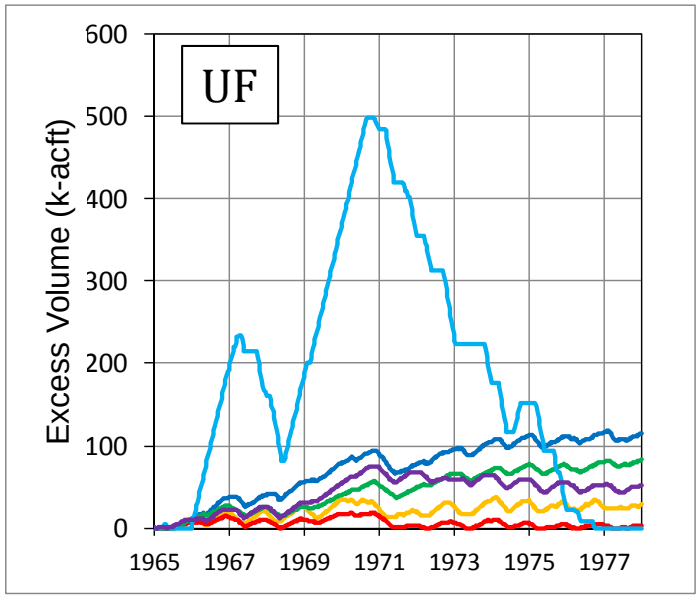

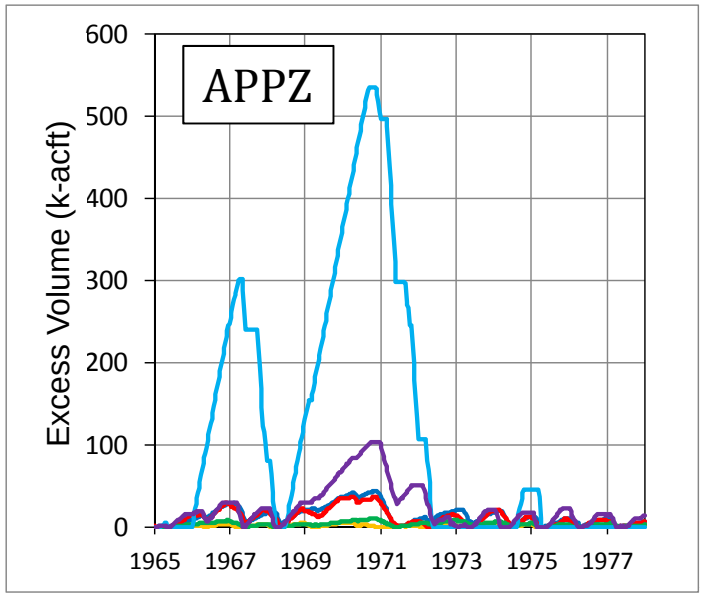

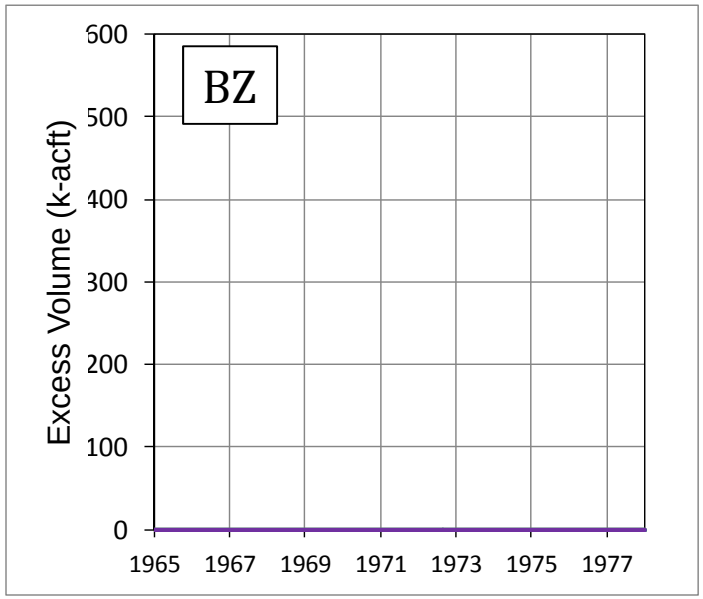

Legend

- Central Palm Beach
- C-51
- Hillsboro
- L-8
- Lake Okeechobee
- Caloosahatchee River

Notes:

Scenario 3 keeps all the wells from Scenario 2 in the UF and adds the remainder of the design wells into the APPZ. This allows the model to match the injection flows. Extraction flows are lower because of the lower assumed recovery efficiency in the APPZ. All wells are fully penetrating in their respective aquifers.

These plots show the excess volume of fresh water remaining in each aquifer at each ASR basin. Excess volume is calculated by adding injected volume times recovery efficiency and subtracting extracted volume. The calculation is cumulative.

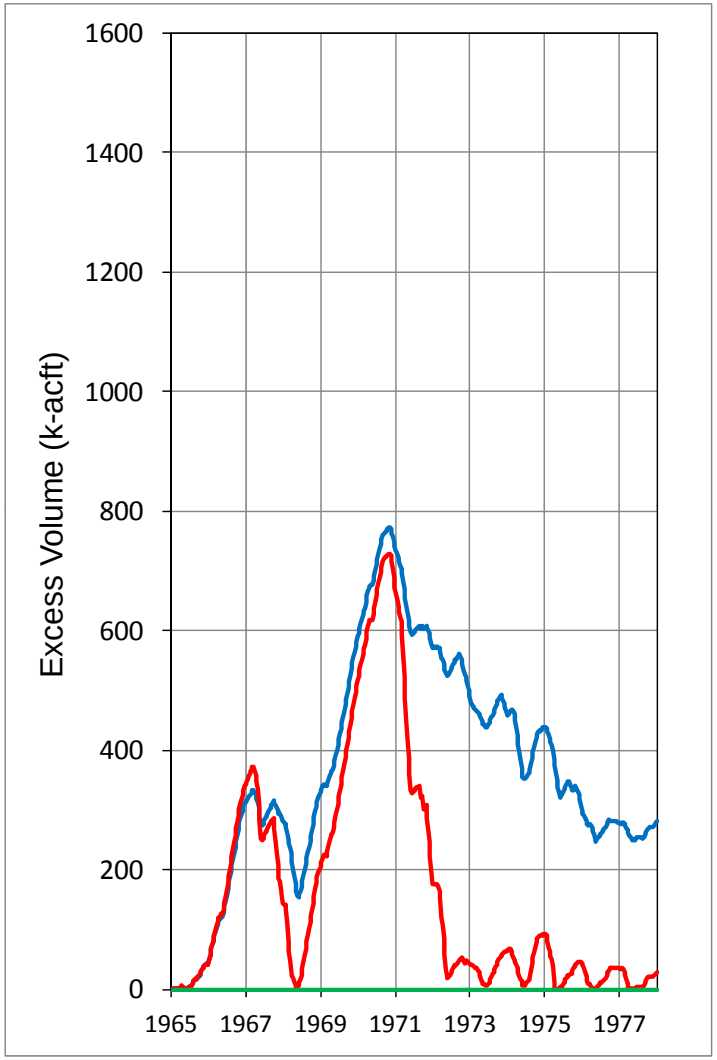

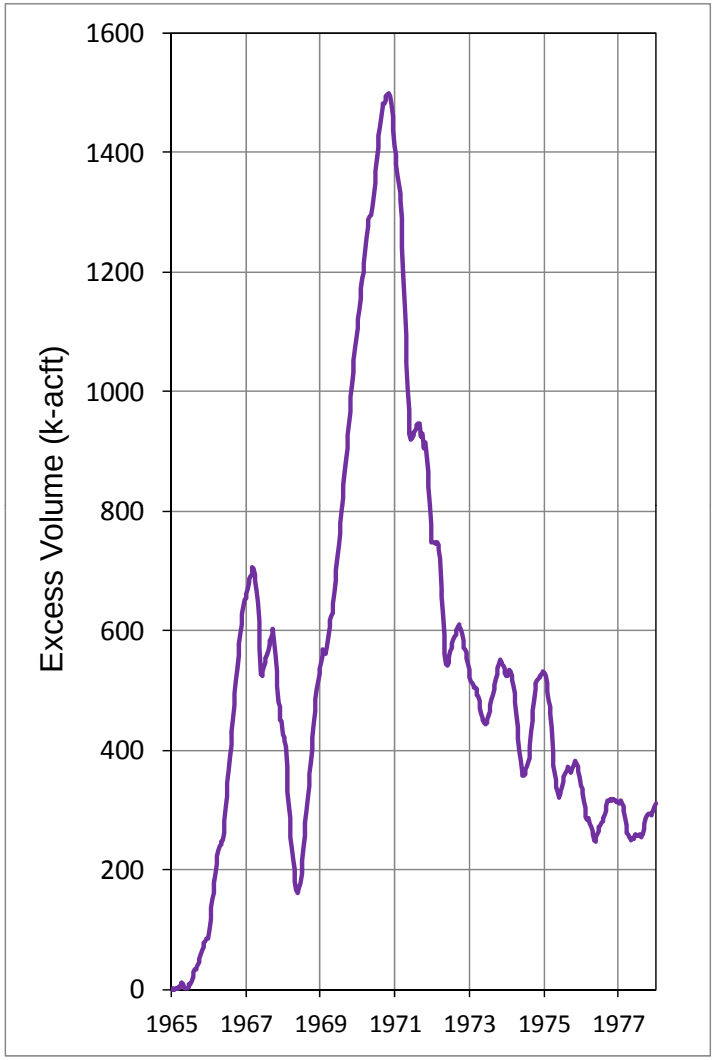

Legend

- Total UF
- Total APPZ
- Total BZ
- Total (All Aquifers)

Notes:

Scenario 3 keeps all the wells from Scenario 2 in the UF and adds the remainder of the design wells into the APPZ. This allows the model to match the injection flows. Extraction flows are lower because of the lower assumed recovery efficiency in the APPZ. All wells are fully penetrating in their respective aquifers.

These plots show the total excess volume of fresh water remaining in each aquifer and in all aquifers. Excess volume is calculated by adding injected volume times recovery efficiency and subtracting extracted volume. The calculation is cumulative.

SCENARIO 3 – EXCESS VOLUME OF FRESH WATER

REGIONAL MODEL PRODUCTION SCENARIO REPORT

FIGURE 4.54

JUNE 2013

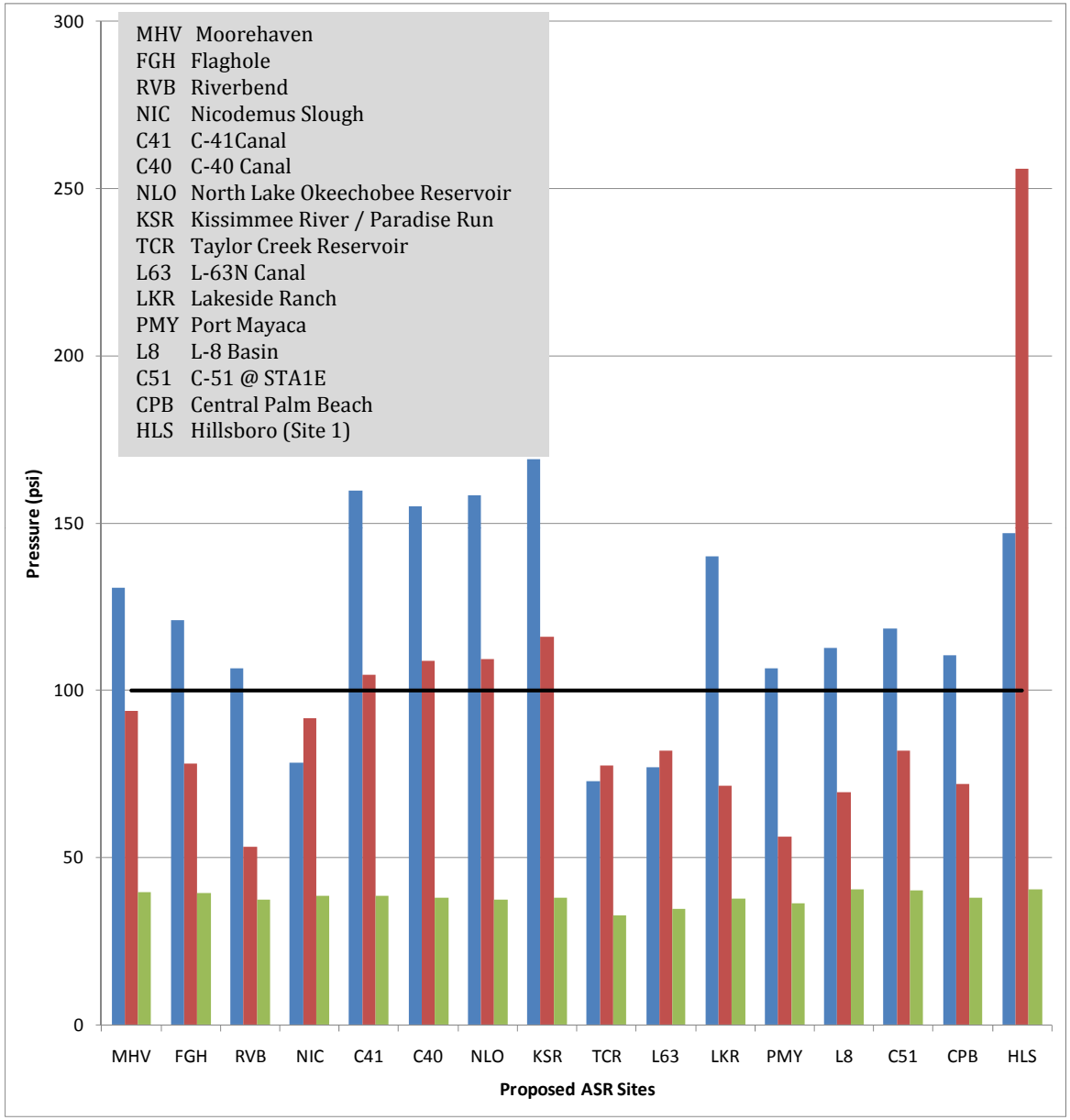

Legend

- Upper Floridan Aquifer
- Avon Park Permeable Zone
- Boulder Zone
- 100 psi Limit

Notes:

Scenario 3 keeps all the wells from Scenario 2 in the UF and adds the remainder of the design wells into the APPZ. This allows the model to match the injection flows. Extraction flows are lower because of the lower assumed recovery efficiency in the APPZ. All wells are fully penetrating in their respective aquifers.

This plot shows the highest pressure at each site which the pump would need to overcome in order to inject storage water during the 13-year simulation.

The PDT determined that it would be important to keep this pressure below 100 psi (indicated by the heavy black line).

Note that maximum pressures are shown for all aquifers and all sites even if ASR pumps are not located there for the current scenario.

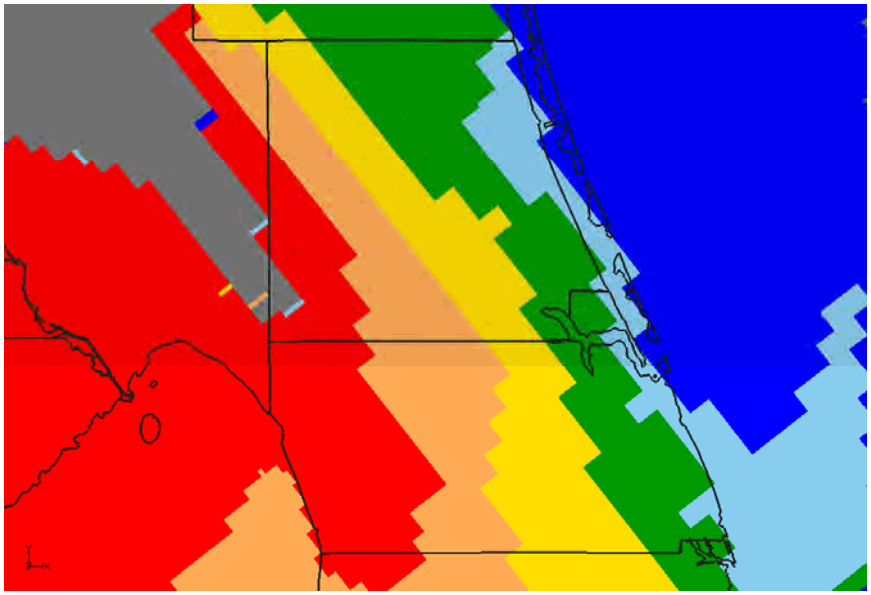

Upper Floridan Aquifer

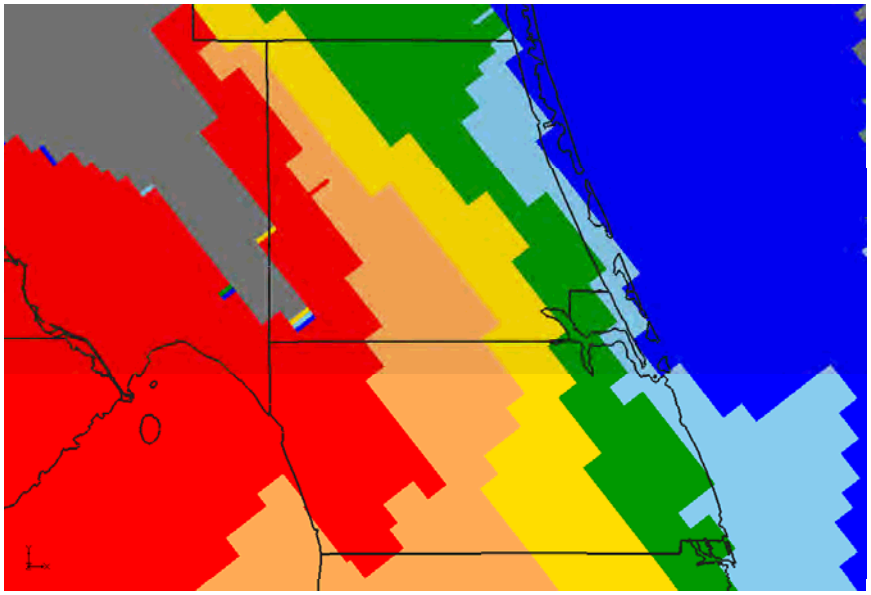

Avon Park Permeable Zone

Legend

- Not artesian
- < 5%
- 5% - 10%
- 10% - 20%
- 20% - 50%
- 50% - 100%
- Loses artesian condition

Notes:

Scenario 3 keeps all the wells from Scenario 2 in the UF and adds the remainder of the design wells into the APPZ. This allows the model to match the injection flows. Extraction flows are lower because of the lower assumed recovery efficiency in the APPZ. All wells are fully penetrating in their respective aquifers.

These plots show the maximum reduction in artesian flow at each model cell as a percentage when compared to the flow expected without the ASR project.

Permit rules require that the reduction in Saint Lucie and Martin Counties be less than 10%.

Note the gray area in the northwest corner of the figures, which coincides with a ridge and does not normally have artesian conditions.

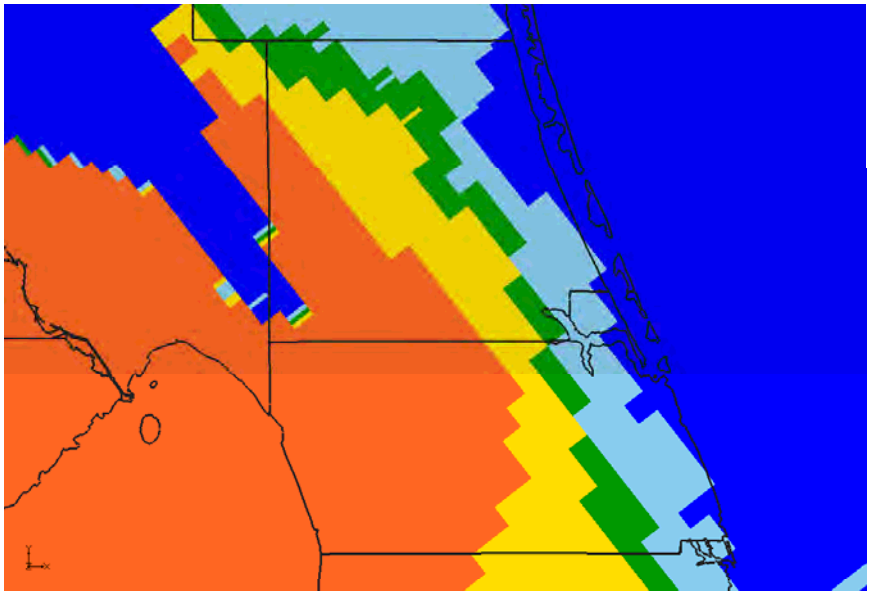

Upper Floridan Aquifer

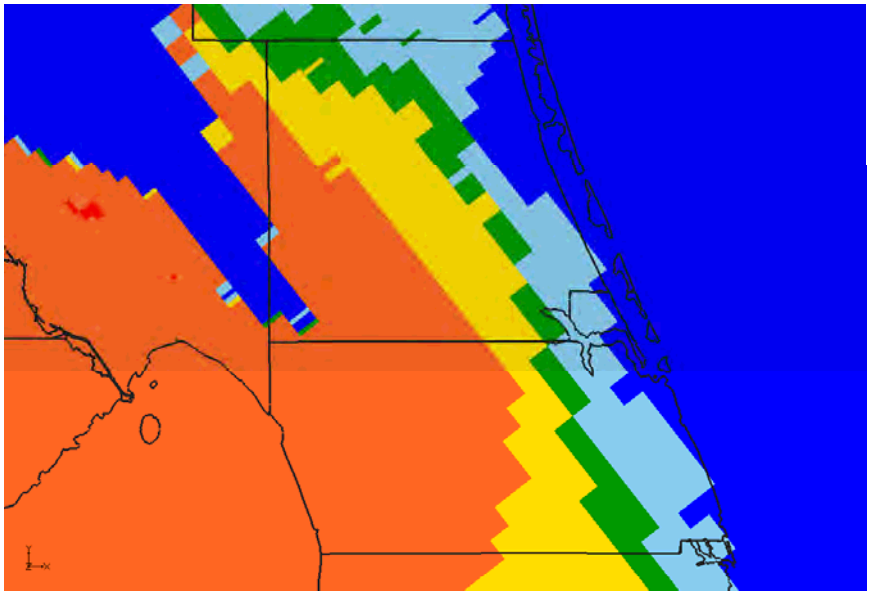

Avon Park Permeable Zone

Legend

- 0 days
- 1 – 250 days
- 250 – 500 days
- 500 – 1000 days
- 1000 – 2000 days
- > 2000 days

Notes:

Scenario 3 keeps all the wells from Scenario 2 in the UF and adds the remainder of the design wells into the APPZ. This allows the model to match the injection flows. Extraction flows are lower because of the lower assumed recovery efficiency in the APPZ. All wells are fully penetrating in their respective aquifers.

These plots indicate the severity of the loss of artesian pressure due to ASR extraction pumping.

Permit rules require that the reduction in Saint Lucie and Martin Counties be less than 10%. This plot indicates the number of days during the simulation in which the flow reduction was greater than 10%. There are 4748 days in the 13-year model simulation period.

Note the blue area in the northwest corner of the figures, which coincides with a ridge and does not normally have artesian conditions.

SCENARIO 3 – NUMBER OF DAYS (OUT OF 13 YEARS) WITH FLOW REDUCTION EXCEEDING 10%

REGIONAL MODEL PRODUCTION SCENARIO REPORT

FIGURE 4.57

JUNE 2013

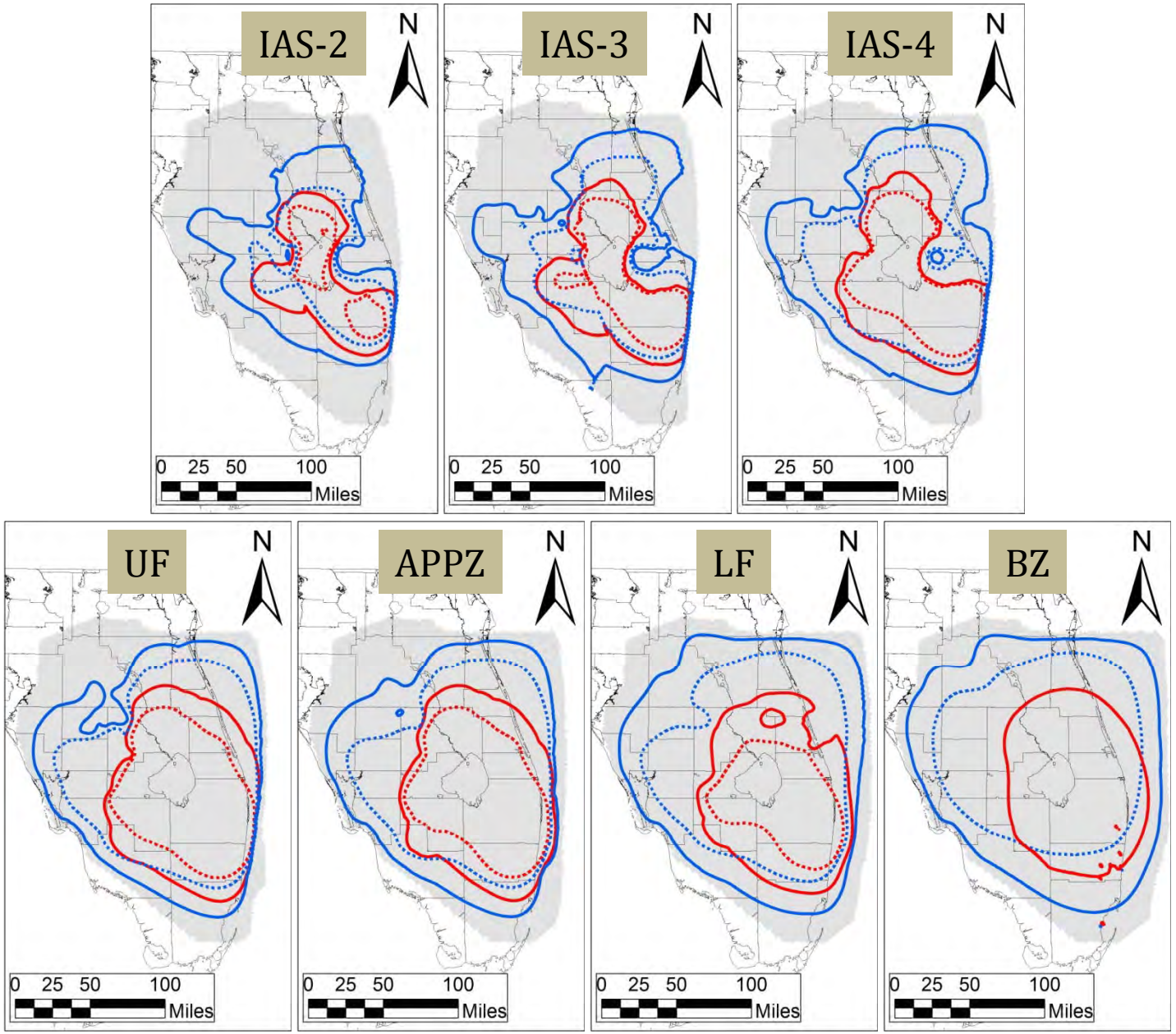

Legend

Maximum Drawdown
- 1 foot
- 5 feet

Maximum "Drawup"
- 1 foot
- 5 feet

Model Domain

Notes:

Scenario 3 keeps all the wells from Scenario 2 in the UF and adds the remainder of the design wells into the APPZ. This allows the model to match the injection flows. Extraction flows are lower because of the lower assumed recovery efficiency in the APPZ. All wells are fully penetrating in their respective aquifers.

These figures show the extent of the areas where the maximum drawdown or "drawup" is greater than 1 foot or 5 feet.

The maximum condition does not necessarily occur at the same time for all regions of the model.

SCENARIO 3 – MAXIMUM DRAWDOWN AND "DRAWUP" BY AQUIFER

REGIONAL MODEL PRODUCTION SCENARIO REPORT

FIGURE 4.58

JUNE 2013

5-Mile Distance

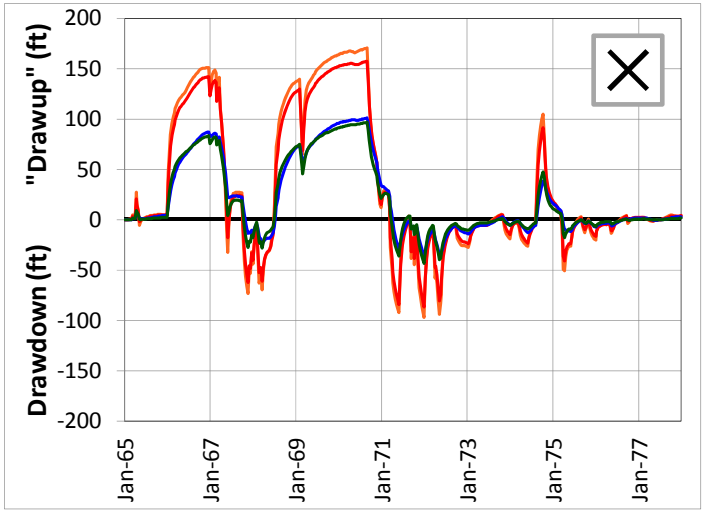

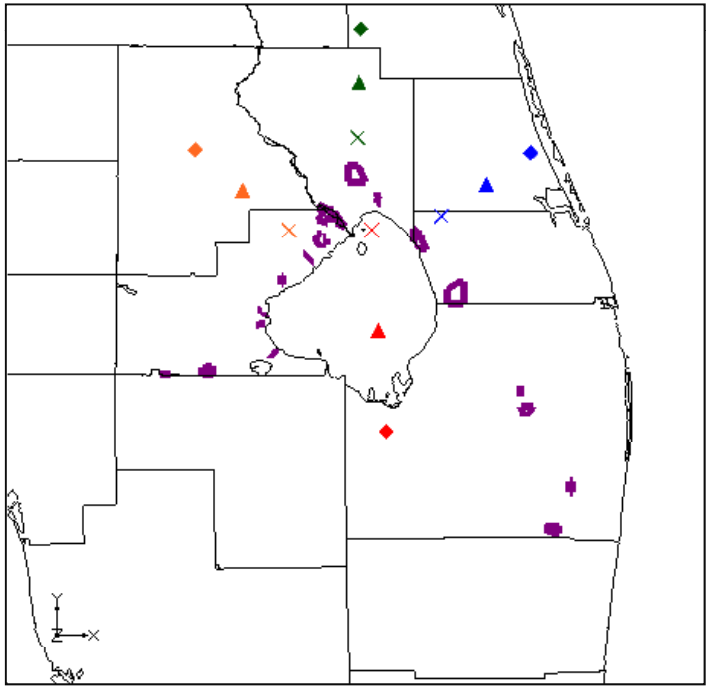

15-Mile Distance

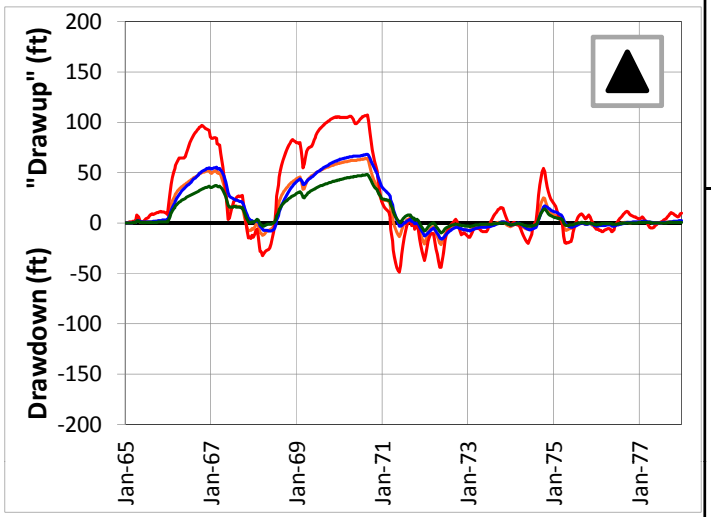

25-Mile Distance

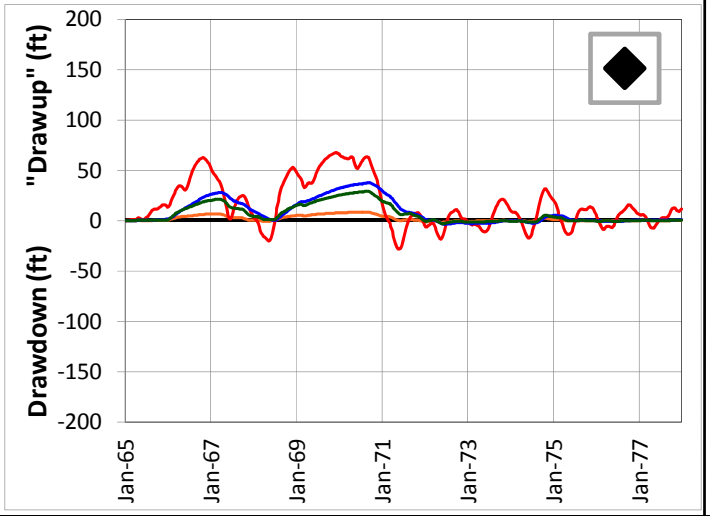

Legend

- CERP ASR Sites
- ✕ 5-Mile Distance Locations
- ▲ 15-Mile Distance Locations
- ◆ 25-Mile Distance Locations

Notes:

Scenario 3 keeps all the wells from Scenario 2 in the UF and adds the remainder of the design wells into the APPZ. This allows the model to match the injection flows. Extraction flows are lower because of the lower assumed recovery efficiency in the APPZ. All wells are fully penetrating in their respective aquifers.

A number of individual sites were chosen from the UF Aquifer at distances of 5, 15 and 25 miles from the proposed ASR well sites. This figure shows the drawdown and "drawup" at each output time step for 12 of these sites.

The plots were calculated by subtracting the heads calculated by the D13R model from those calculated by the no project run. This results in a positive value for "drawup" and a negative value for drawdown.

The colors of the points on the map correspond to the colors of the lines on the plots.

The symbols on the map (x, triangle and diamond) indicate the distance from the ASR sites.

5-Mile Distance

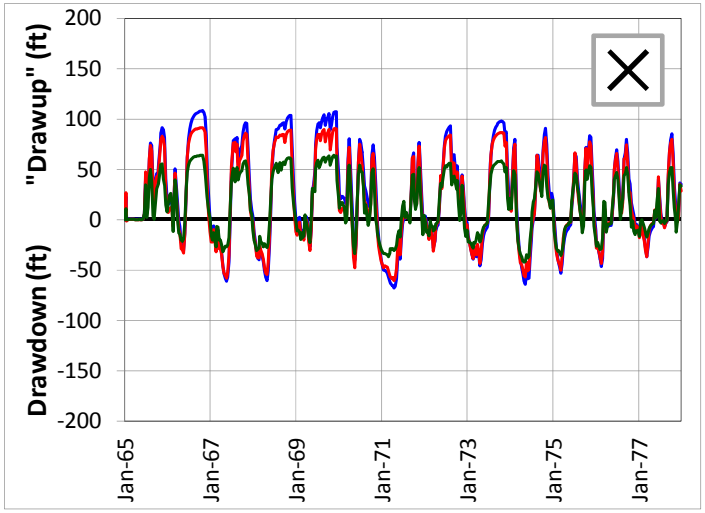

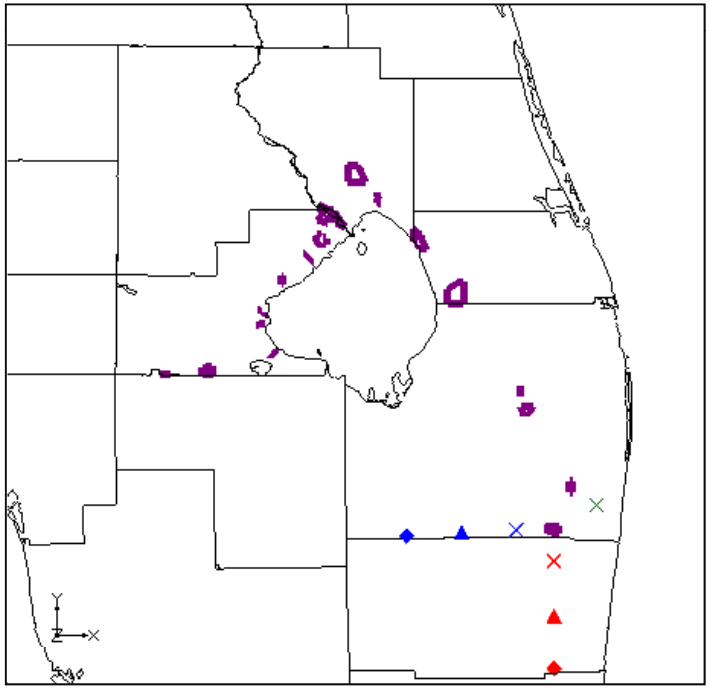

15-Mile Distance

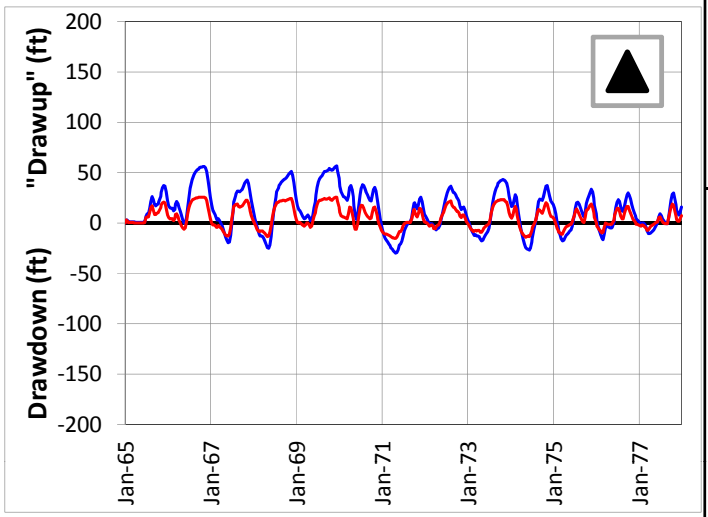

25-Mile Distance

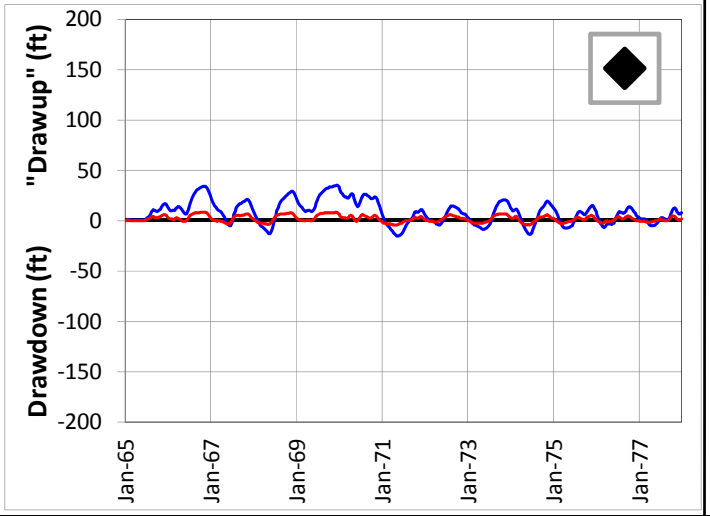

Legend

- CERP ASR Sites
- ✕ 5-Mile Distance Locations
- ▲ 15-Mile Distance Locations
- ◆ 25-Mile Distance Locations

Notes:

Scenario 3 keeps all the wells from Scenario 2 in the UF and adds the remainder of the design wells into the APPZ. This allows the model to match the injection flows. Extraction flows are lower because of the lower assumed recovery efficiency in the APPZ. All wells are fully penetrating in their respective aquifers.

A number of individual sites were chosen from the UF Aquifer at distances of 5, 15 and 25 miles from the proposed ASR well sites. This figure shows the drawdown and "drawup" at each output time step for 7 of these sites.

The plots were calculated by subtracting the heads calculated by the D13R model from those calculated by the no project run. This results in a positive value for "drawup" and a negative value for drawdown.

The colors of the points on the map correspond to the colors of the lines on the plots.

The symbols on the map (x, triangle and diamond) indicate the distance from the ASR sites.

5-Mile Distance

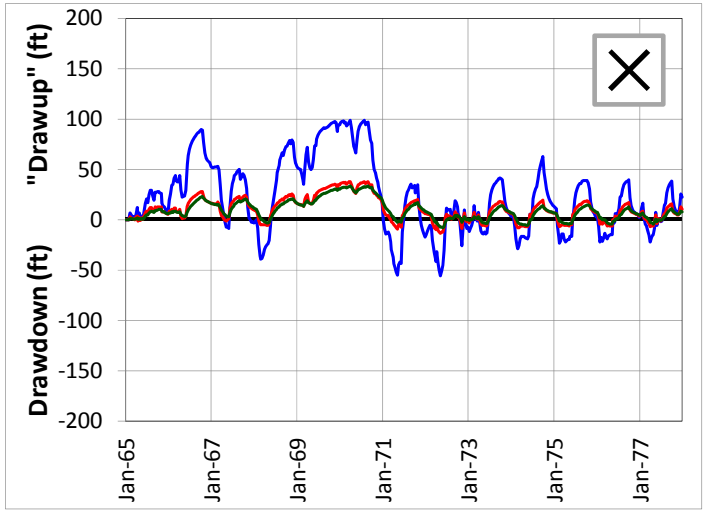

15-Mile Distance

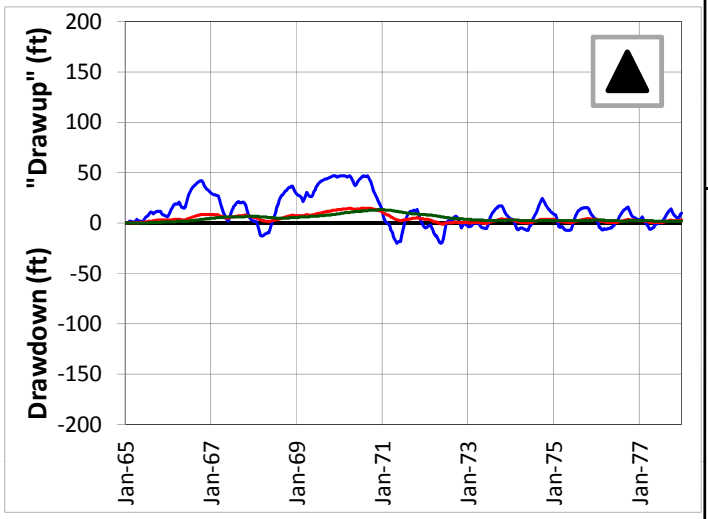

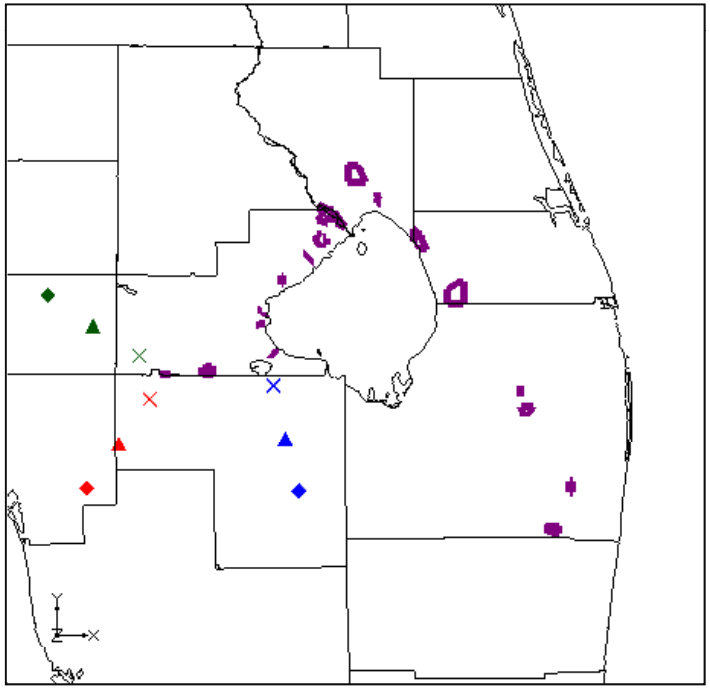

25-Mile Distance

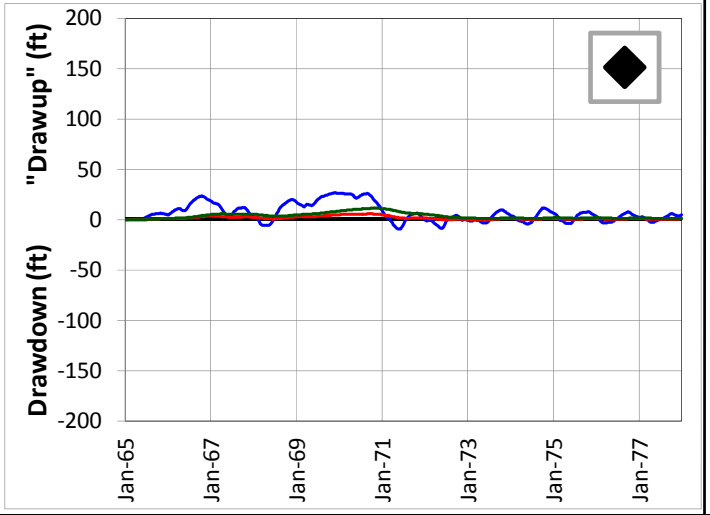

Legend

- CERP ASR Sites
- 5-Mile Distance Locations
- 15-Mile Distance Locations
- 25-Mile Distance Locations

Notes:

Scenario 3 keeps all the wells from Scenario 2 in the UF and adds the remainder of the design wells into the APPZ. This allows the model to match the injection flows. Extraction flows are lower because of the lower assumed recovery efficiency in the APPZ. All wells are fully penetrating in their respective aquifers.

A number of individual sites were chosen from the UF Aquifer at distances of 5, 15 and 25 miles from the proposed ASR well sites. This figure shows the drawdown and "drawup" at each output time step for 9 of these sites.

The plots were calculated by subtracting the heads calculated by the D13R model from those calculated by the no project run. This results in a positive value for "drawup" and a negative value for drawdown.

The colors of the points on the map correspond to the colors of the lines on the plots.

The symbols on the map (x, triangle and diamond) indicate the distance from the ASR sites.

5-Mile Distance

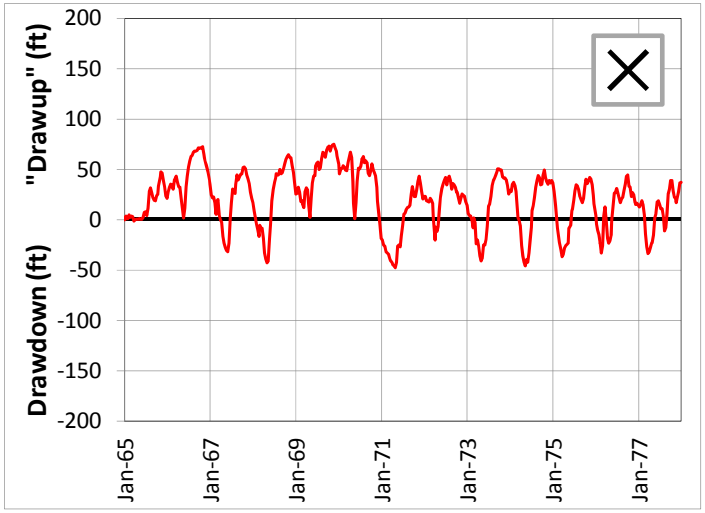

15-Mile Distance

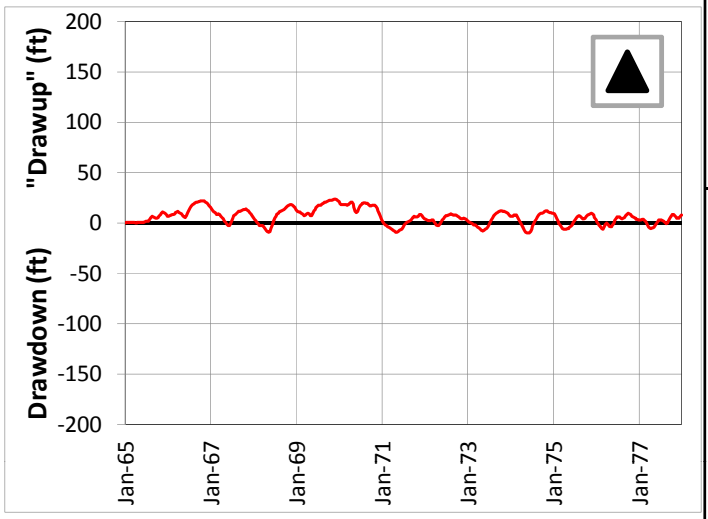

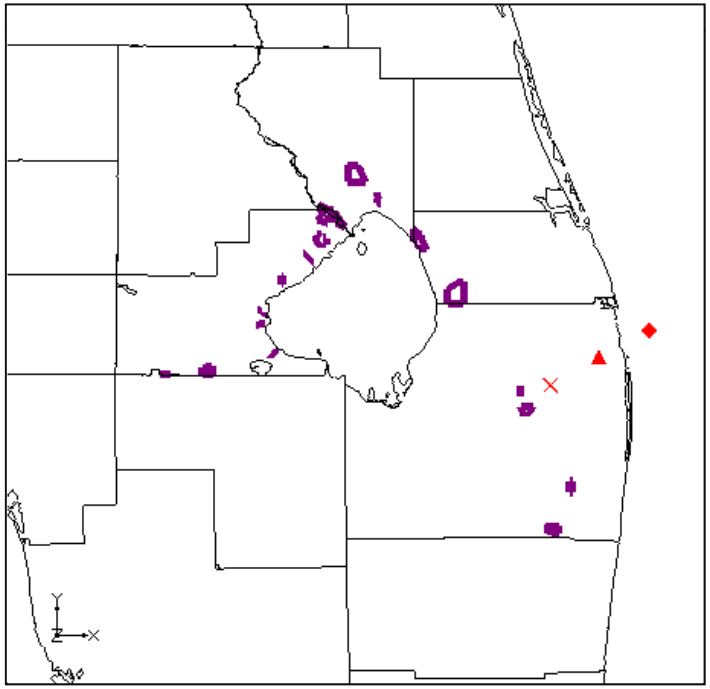

25-Mile Distance

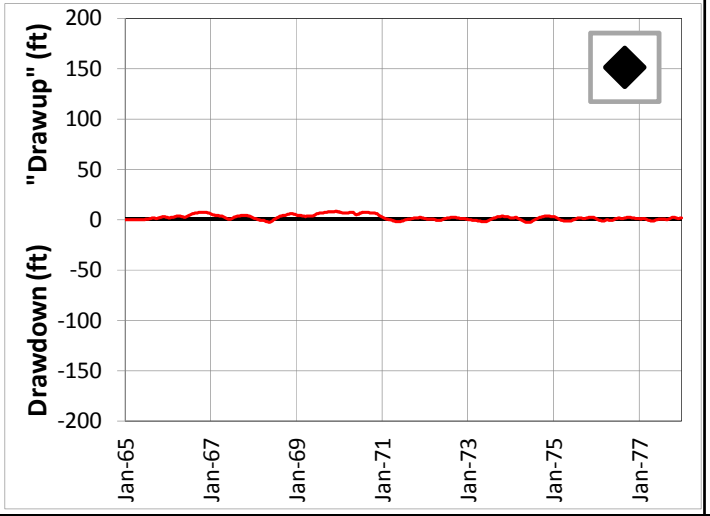

Legend

- CERP ASR Sites
- 5-Mile Distance Locations
- 15-Mile Distance Locations
- 25-Mile Distance Locations

Notes:

Scenario 3 keeps all the wells from Scenario 2 in the UF and adds the remainder of the design wells into the APPZ. This allows the model to match the injection flows. Extraction flows are lower because of the lower assumed recovery efficiency in the APPZ. All wells are fully penetrating in their respective aquifers.

A number of individual sites were chosen from the UF Aquifer at distances of 5, 15 and 25 miles from the proposed ASR well sites. This figure shows the drawdown and "drawup" at each output time step for 3 of these sites.

The plots were calculated by subtracting the heads calculated by the D13R model from those calculated by the no project run. This results in a positive value for "drawup" and a negative value for drawdown.

The colors of the points on the map correspond to the colors of the lines on the plots.

The symbols on the map (x, triangle and diamond) indicate the distance from the ASR sites.

5-Mile Distance

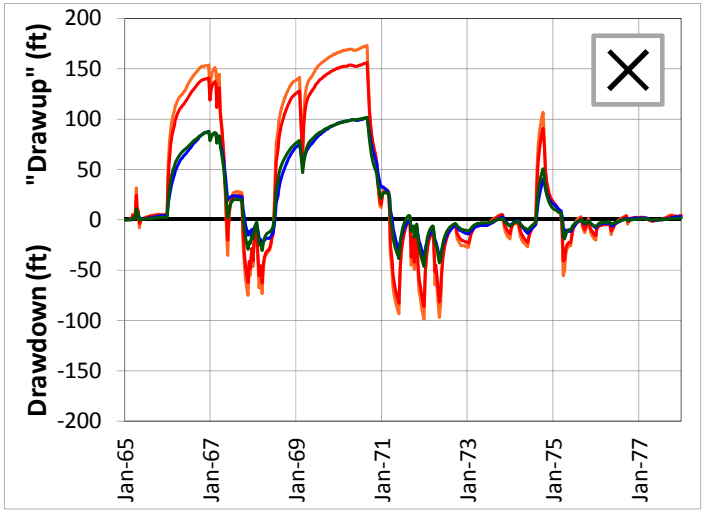

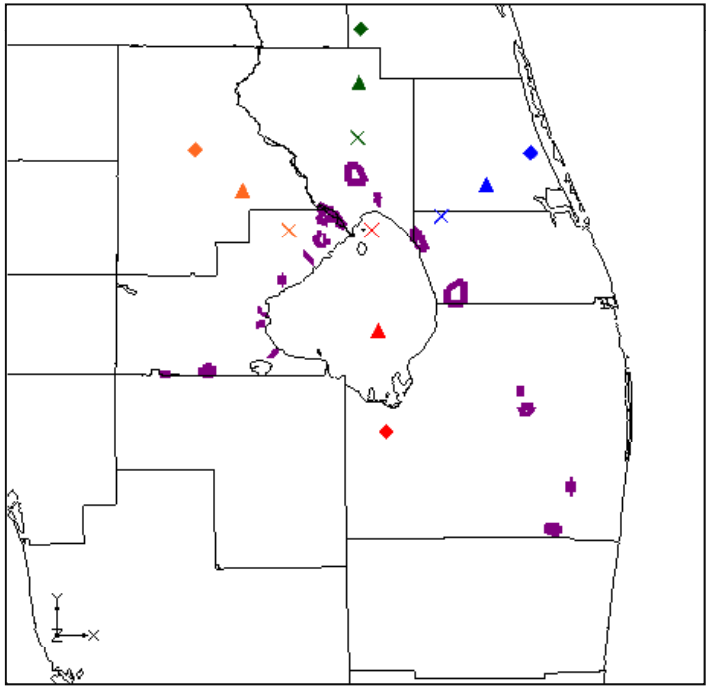

15-Mile Distance

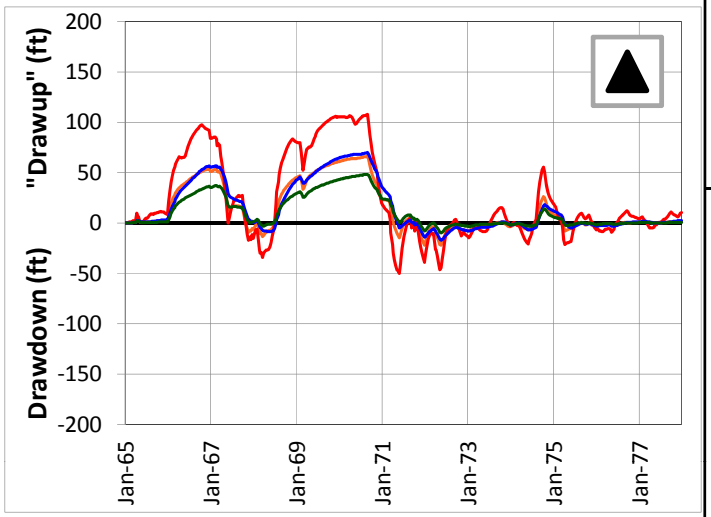

25-Mile Distance

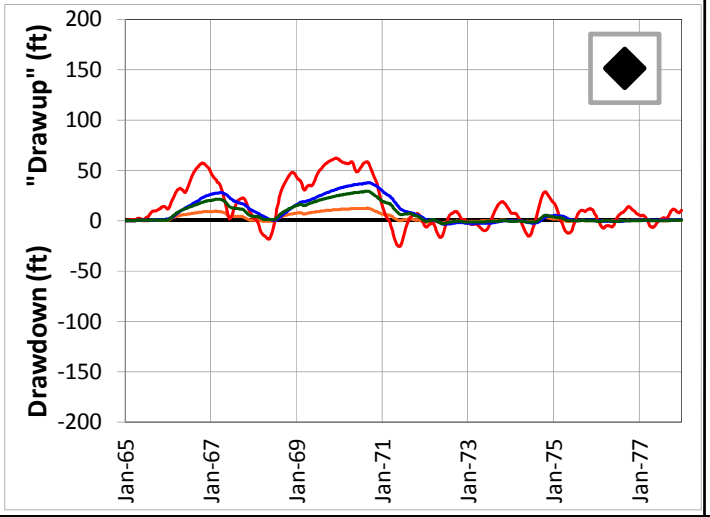

Legend

- CERP ASR Sites
- ✕ 5-Mile Distance Locations
- ▲ 15-Mile Distance Locations
- ◆ 25-Mile Distance Locations

Notes:

Scenario 3 keeps all the wells from Scenario 2 in the UF and adds the remainder of the design wells into the APPZ. This allows the model to match the injection flows. Extraction flows are lower because of the lower assumed recovery efficiency in the APPZ. All wells are fully penetrating in their respective aquifers.

A number of individual sites were chosen from the APPZ Aquifer at distances of 5, 15 and 25 miles from the proposed ASR well sites. This figure shows the drawdown and "drawup" at each output time step for 12 of these sites.

The plots were calculated by subtracting the heads calculated by the D13R model from those calculated by the no project run. This results in a positive value for "drawup" and a negative value for drawdown.

The colors of the points on the map correspond to the colors of the lines on the plots.

The symbols on the map (x, triangle and diamond) indicate the distance from the ASR sites.

5-Mile Distance

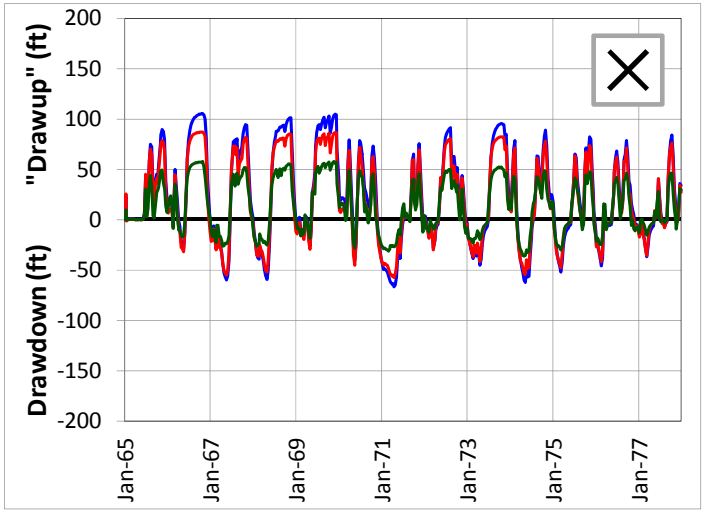

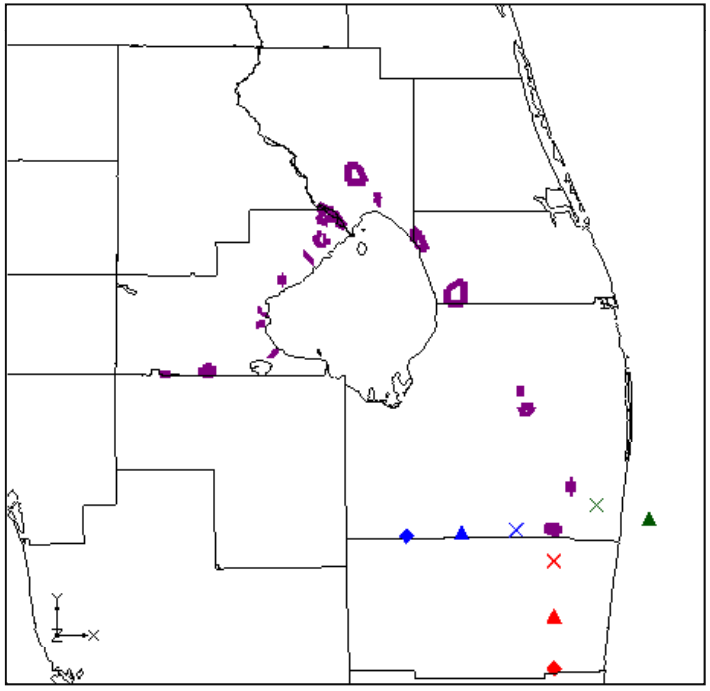

15-Mile Distance

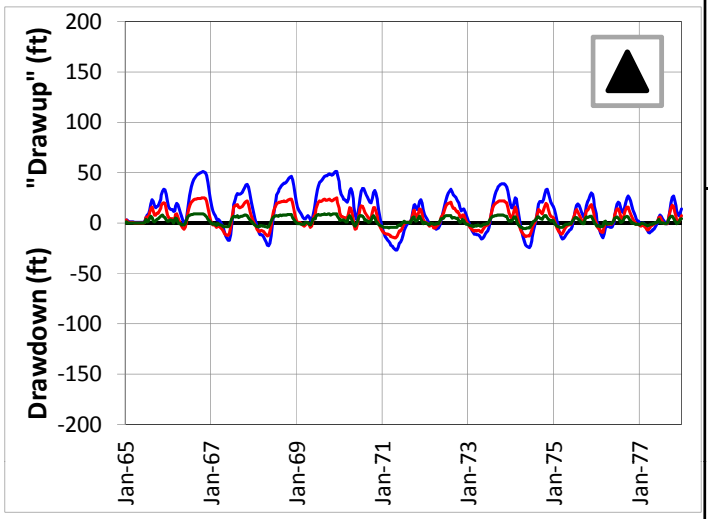

25-Mile Distance

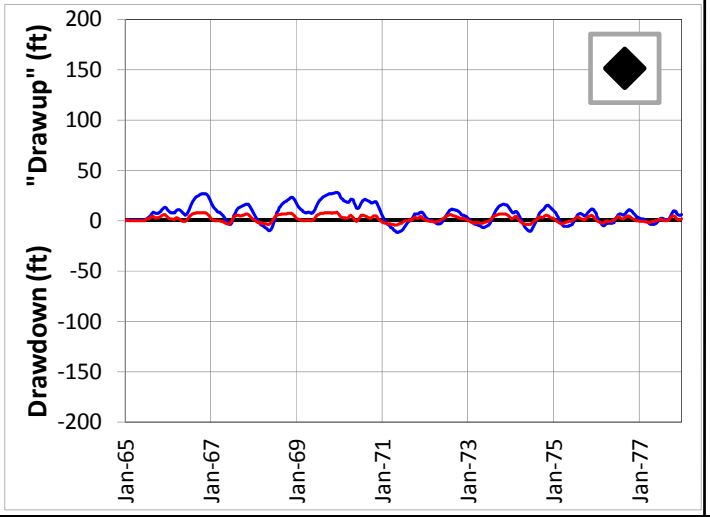

Legend

- CERP ASR Sites
- 5-Mile Distance Locations
- 15-Mile Distance Locations
- 25-Mile Distance Locations

Notes:

Scenario 3 keeps all the wells from Scenario 2 in the UF and adds the remainder of the design wells into the APPZ. This allows the model to match the injection flows. Extraction flows are lower because of the lower assumed recovery efficiency in the APPZ. All wells are fully penetrating in their respective aquifers.

A number of individual sites were chosen from the APPZ Aquifer at distances of 5, 15 and 25 miles from the proposed ASR well sites. This figure shows the drawdown and "drawup" at each output time step for 8 of these sites.

The plots were calculated by subtracting the heads calculated by the D13R model from those calculated by the no project run. This results in a positive value for "drawup" and a negative value for drawdown.

The colors of the points on the map correspond to the colors of the lines on the plots.

The symbols on the map (x, triangle and diamond) indicate the distance from the ASR sites.

5-Mile Distance

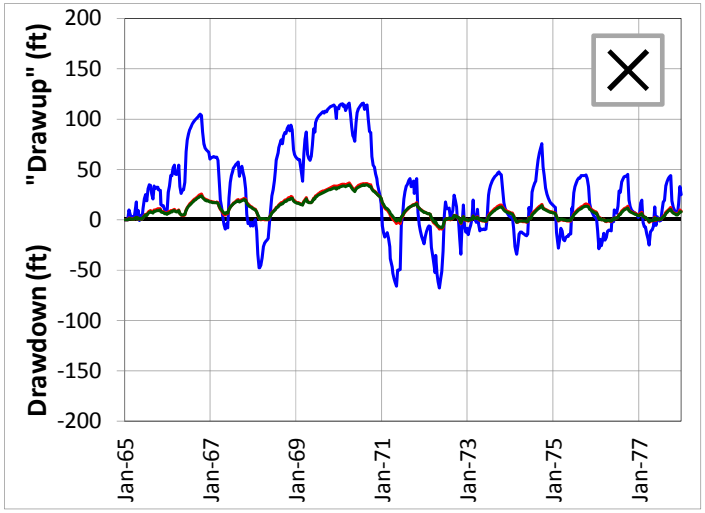

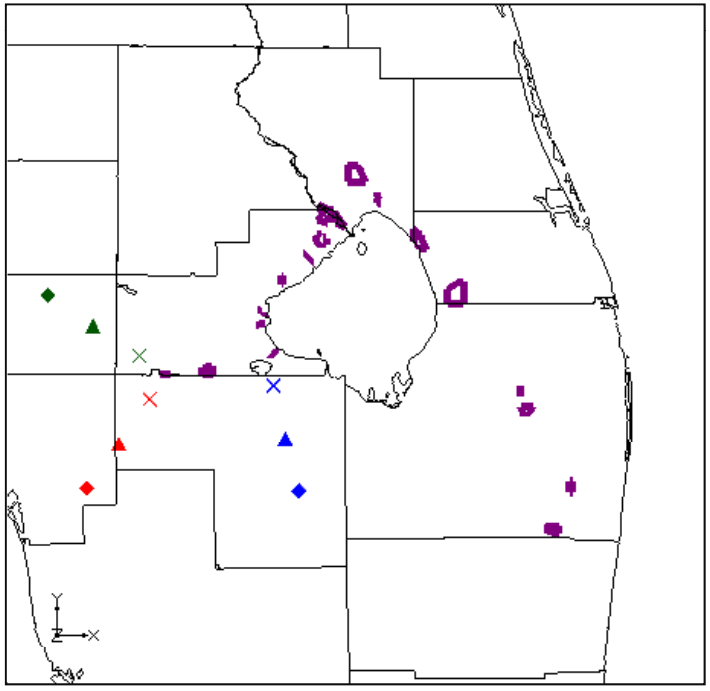

15-Mile Distance

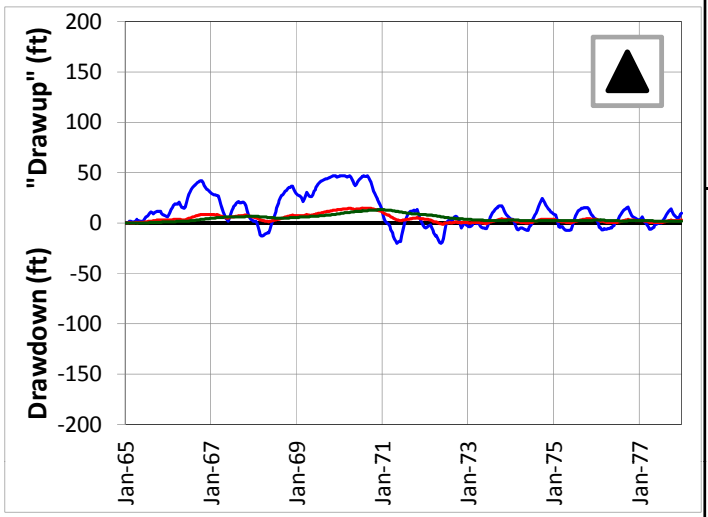

25-Mile Distance

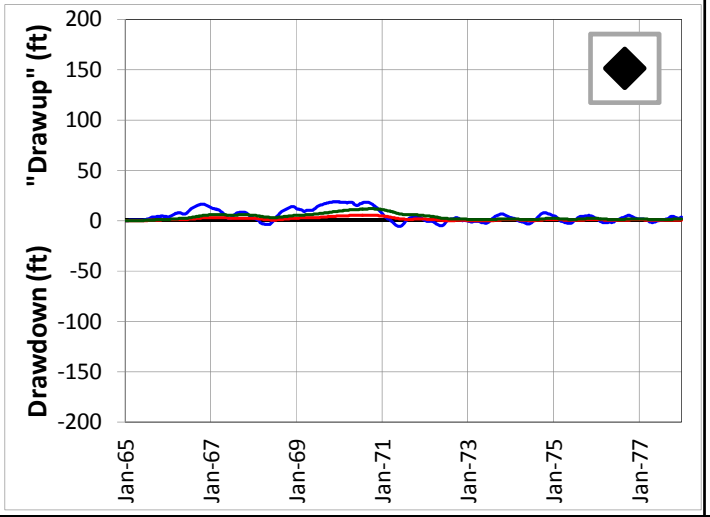

Legend

- CERP ASR Sites
- 5-Mile Distance Locations
- 15-Mile Distance Locations
- 25-Mile Distance Locations

Notes:

Scenario 3 keeps all the wells from Scenario 2 in the UF and adds the remainder of the design wells into the APPZ. This allows the model to match the injection flows. Extraction flows are lower because of the lower assumed recovery efficiency in the APPZ. All wells are fully penetrating in their respective aquifers.

A number of individual sites were chosen from the APPZ Aquifer at distances of 5, 15 and 25 miles from the proposed ASR well sites. This figure shows the drawdown and "drawup" at each output time step for 9 of these sites.

The plots were calculated by subtracting the heads calculated by the D13R model from those calculated by the no project run. This results in a positive value for "drawup" and a negative value for drawdown.

The colors of the points on the map correspond to the colors of the lines on the plots.

The symbols on the map (x, triangle and diamond) indicate the distance from the ASR sites.

5-Mile Distance

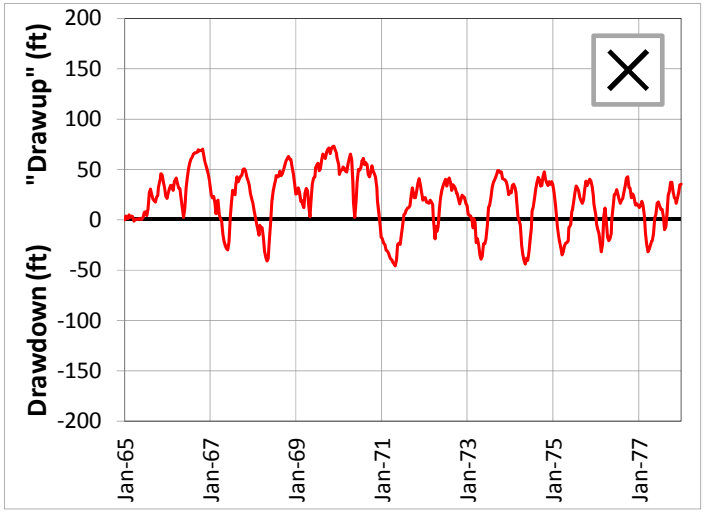

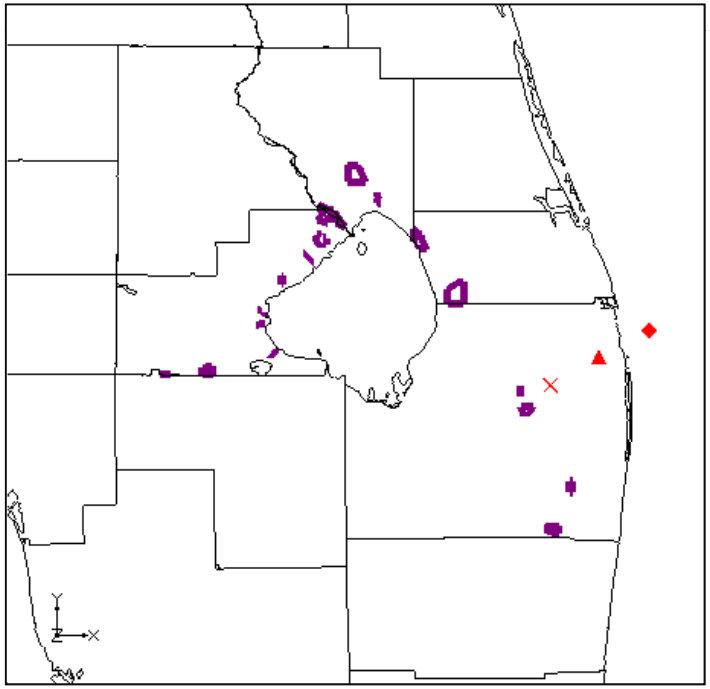

15-Mile Distance

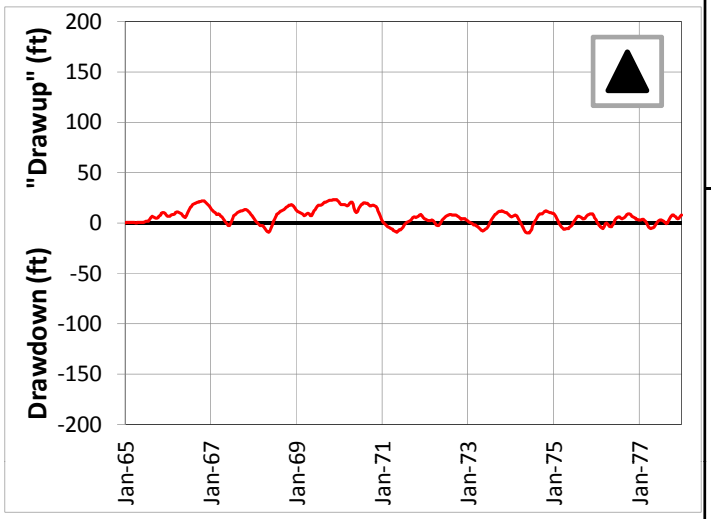

25-Mile Distance

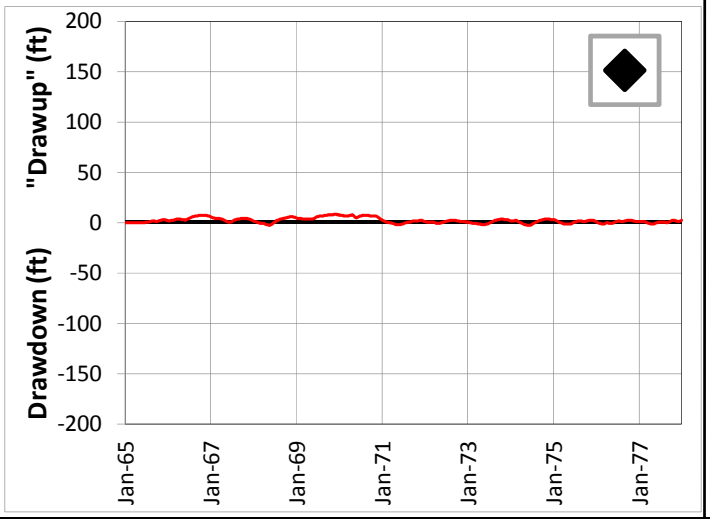

Legend

- CERP ASR Sites
- 5-Mile Distance Locations
- 15-Mile Distance Locations
- 25-Mile Distance Locations

Notes:

Scenario 3 keeps all the wells from Scenario 2 in the UF and adds the remainder of the design wells into the APPZ. This allows the model to match the injection flows. Extraction flows are lower because of the lower assumed recovery efficiency in the APPZ. All wells are fully penetrating in their respective aquifers.

A number of individual sites were chosen from the APPZ Aquifer at distances of 5, 15 and 25 miles from the proposed ASR well sites. This figure shows the drawdown and "drawup" at each output time step for 3 of these sites.

The plots were calculated by subtracting the heads calculated by the D13R model from those calculated by the no project run. This results in a positive value for "drawup" and a negative value for drawdown.

The colors of the points on the map correspond to the colors of the lines on the plots.

The symbols on the map (x, triangle and diamond) indicate the distance from the ASR sites.

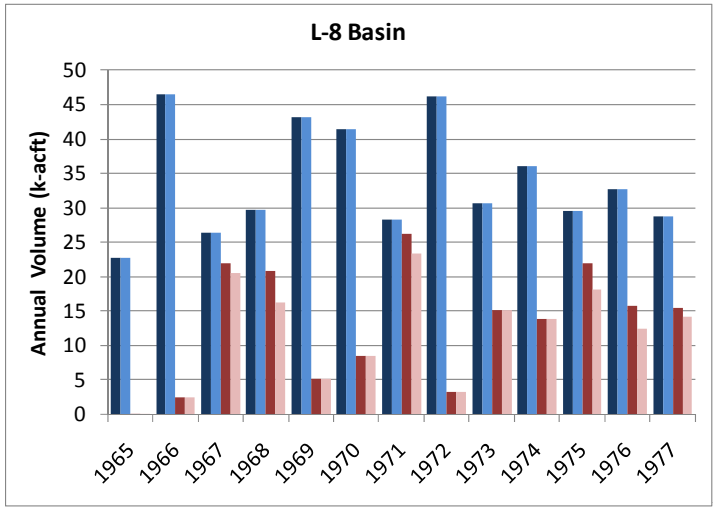

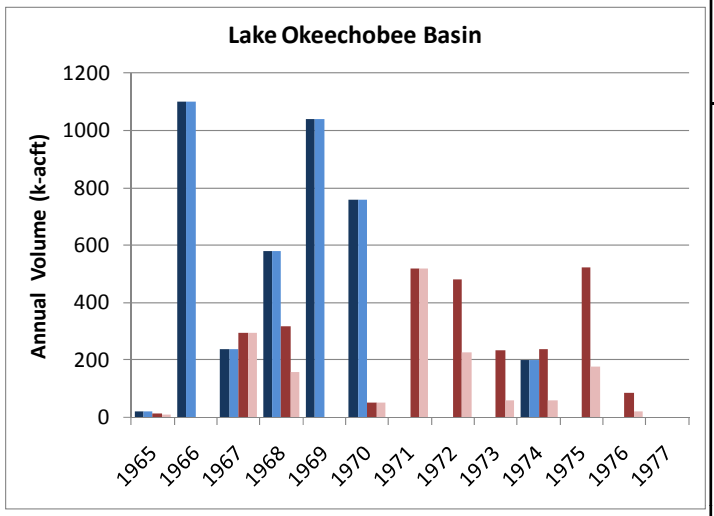

	L-8		Lake Okeechobee		Caloosahatchee	
	In %	Out %	In %	Out %	In %	Out %
1965	100%	80%	100%	57%	100%	63%
1966	100%	100%	100%	--	100%	100%
1967	100%	93%	100%	100%	100%	78%
1968	100%	78%	100%	51%	100%	55%
1969	100%	100%	100%	--	100%	--
1970	100%	100%	100%	100%	100%	100%
1971	100%	89%	--	100%	100%	100%
1972	100%	100%	--	47%	100%	100%
1973	100%	100%	--	25%	100%	31%
1974	100%	100%	100%	25%	100%	46%
1975	100%	83%	--	34%	100%	42%
1976	100%	78%	--	25%	100%	59%
1977	100%	92%	--	--	100%	53%

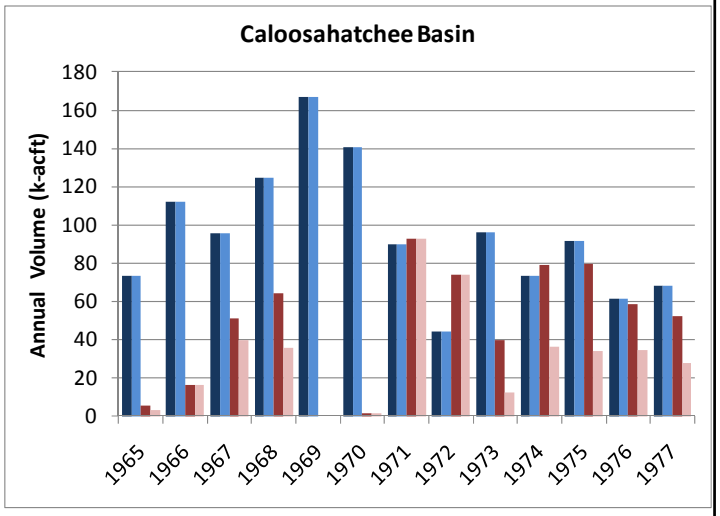

Legend

- Design Storage (injection)
- Modeled Storage (injection)
- Design Recovery (extraction)
- Modeled Recovery (extraction)

Notes:

Scenario 3 keeps all the wells from Scenario 2 in the UF and adds the remainder of the design wells into the APPZ. This allows the model to match the injection flows. Extraction flows are lower because of the lower assumed recovery efficiency in the APPZ. All wells are fully penetrating in their respective aquifers.

These three plots show the comparison between the SFWMM-D13R designed annual injection and extraction volumes at the ASR wells and the actual assigned rates for the RASRSM-D13R for three of the basins.

The table presents the percentage of SFWMM-D13R annual flow rates that are included in this scenario of the RASRSM-D13R. These percentages are not recovery efficiencies.

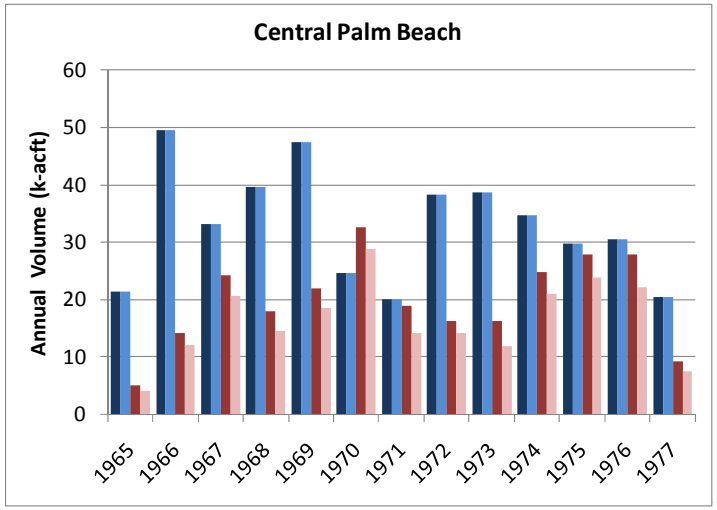

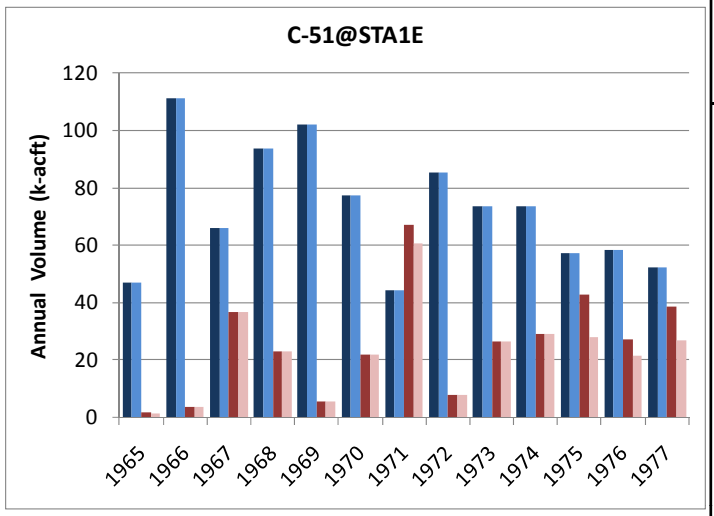

	CPB		C-51		Hillsboro	
	In %	Out %	In %	Out %	In %	Out %
1965	100%	84%	100%	84%	100%	66%
1966	100%	84%	100%	100%	100%	100%
1967	100%	85%	100%	100%	100%	100%
1968	100%	81%	100%	100%	100%	99%
1969	100%	85%	100%	100%	100%	100%
1970	100%	89%	100%	100%	100%	100%
1971	100%	74%	100%	91%	100%	100%
1972	100%	87%	100%	100%	100%	68%
1973	100%	73%	100%	100%	100%	68%
1974	100%	85%	100%	100%	100%	100%
1975	100%	86%	100%	65%	100%	50%
1976	100%	79%	100%	79%	100%	64%
1977	100%	82%	100%	70%	100%	49%

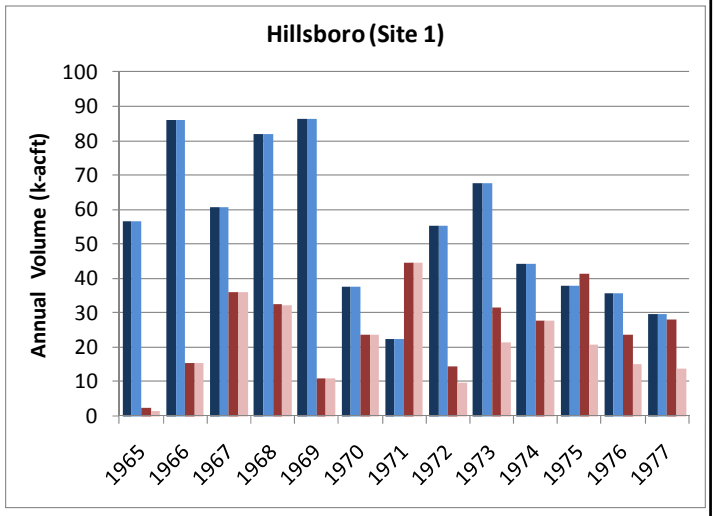

Legend

- Design Storage (injection)
- Modeled Storage (injection)
- Design Recovery (extraction)
- Modeled Recovery (extraction)

Notes:

Scenario 3 keeps all the wells from Scenario 2 in the UF and adds the remainder of the design wells into the APPZ. This allows the model to match the injection flows. Extraction flows are lower because of the lower assumed recovery efficiency in the APPZ. All wells are fully penetrating in their respective aquifers.

These three plots show the comparison between the SFWMM-D13R designed annual injection and extraction volumes at the ASR wells and the actual assigned rates for the RASRSM-D13R for three of the basins.

The table presents the percentage of SFWMM-D13R annual flow rates that are included in this scenario of the RASRSM-D13R. These percentages are not recovery efficiencies.

	Total	
	In %	Out %
1965	100%	65%
1966	100%	96%
1967	100%	97%
1968	100%	59%
1969	100%	92%
1970	100%	97%
1971	100%	98%
1972	100%	56%
1973	100%	40%
1974	100%	45%
1975	100%	41%
1976	100%	53%
1977	100%	63%

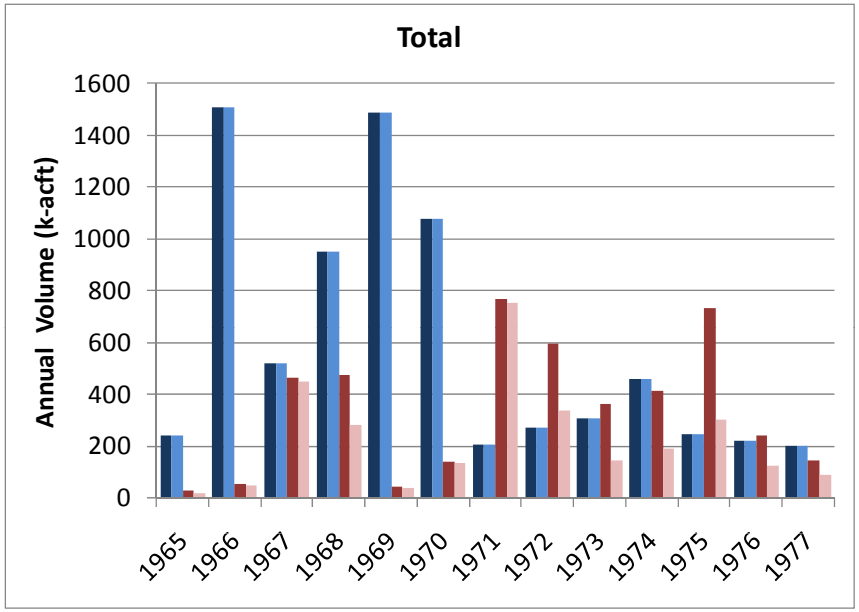

Legend

- Design Storage (injection)
- Modeled Storage (injection)
- Design Recovery (extraction)
- Modeled Recovery (extraction)

Notes:

Scenario 3 keeps all the wells from Scenario 2 in the UF and adds the remainder of the design wells into the APPZ. This allows the model to match the injection flows. Extraction flows are lower because of the lower assumed recovery efficiency in the APPZ. All wells are fully penetrating in their respective aquifers.

This plot shows the comparison between the SFWMM-D13R designed annual injection and extraction volumes at the ASR wells and the actual assigned rates for the RASRSM-D13R for all basins.

The table presents the percentage of SFWMM-D13R annual flow rates that are included in this scenario of the RASRSM-D13R. These percentages are not recovery efficiencies.

		UF		APPZ		BZ		Total # Wells	Target # Wells
		Number of Wells	Recovery Efficiency	Number of Wells	Recovery Efficiency	Number of Wells	Recovery Efficiency		
Caloosahatchee Basin	Moore Haven	4	70%	1	30%	0	10%		
	River Bend	3	70%	1	30%	0	10%		
	Flaghole	2	70%	1	30%	0	10%		
	Basin Total	9		3		0		12	44
Lake Okeechobee Basin	Nicodemus Slough	0	70%	10	30%	0	10%		
	C-41 Canal	0	70%	0	30%	0	10%		
	C-40 Canal	2	70%	0	30%	0	10%		
	North Lake Okeechobee	8	70%	2	30%	0	10%		
	Kissimmee R./Paradise Run	15	70%	0	30%	0	10%		
	Taylor Creek	0	70%	10	30%	0	10%		
	L-63N	0	70%	10	30%	0	10%		
	Lakeside Ranch	4	70%	0	30%	0	10%		
	Port Mayaca	19	70%	0	30%	0	10%		
	Basin Total	48		32		0		80	200
L-8		6	70%	0	30%	0	10%	6	10
C-51		12	70%	3	30%	0	10%	15	34
Central Palm Beach		10	70%	3	30%	0	10%	13	15
Site 1 (Hillsboro)		10	40%	0	40%	0	10%	10	30
Total		95		41		0		136	333

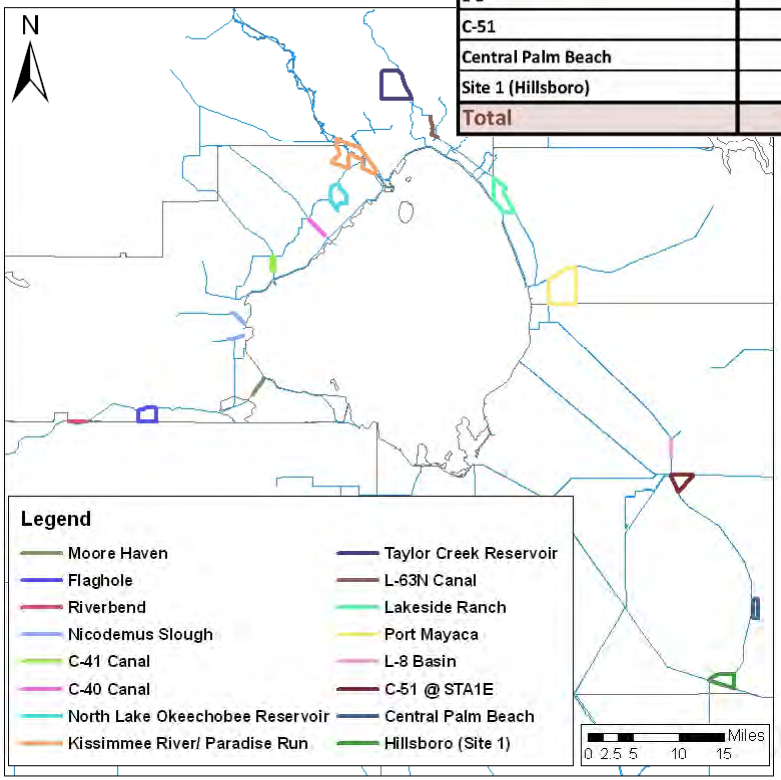

Notes:

Scenario 4 is a reduction of the wells from Scenario 3 which meets the requirements for pump pressure (100 psi). All wells are fully penetrating in their respective aquifers.

Flow rates are divided evenly among the wells in each basin. Maximum flow rate for any one well is 5 mgd.

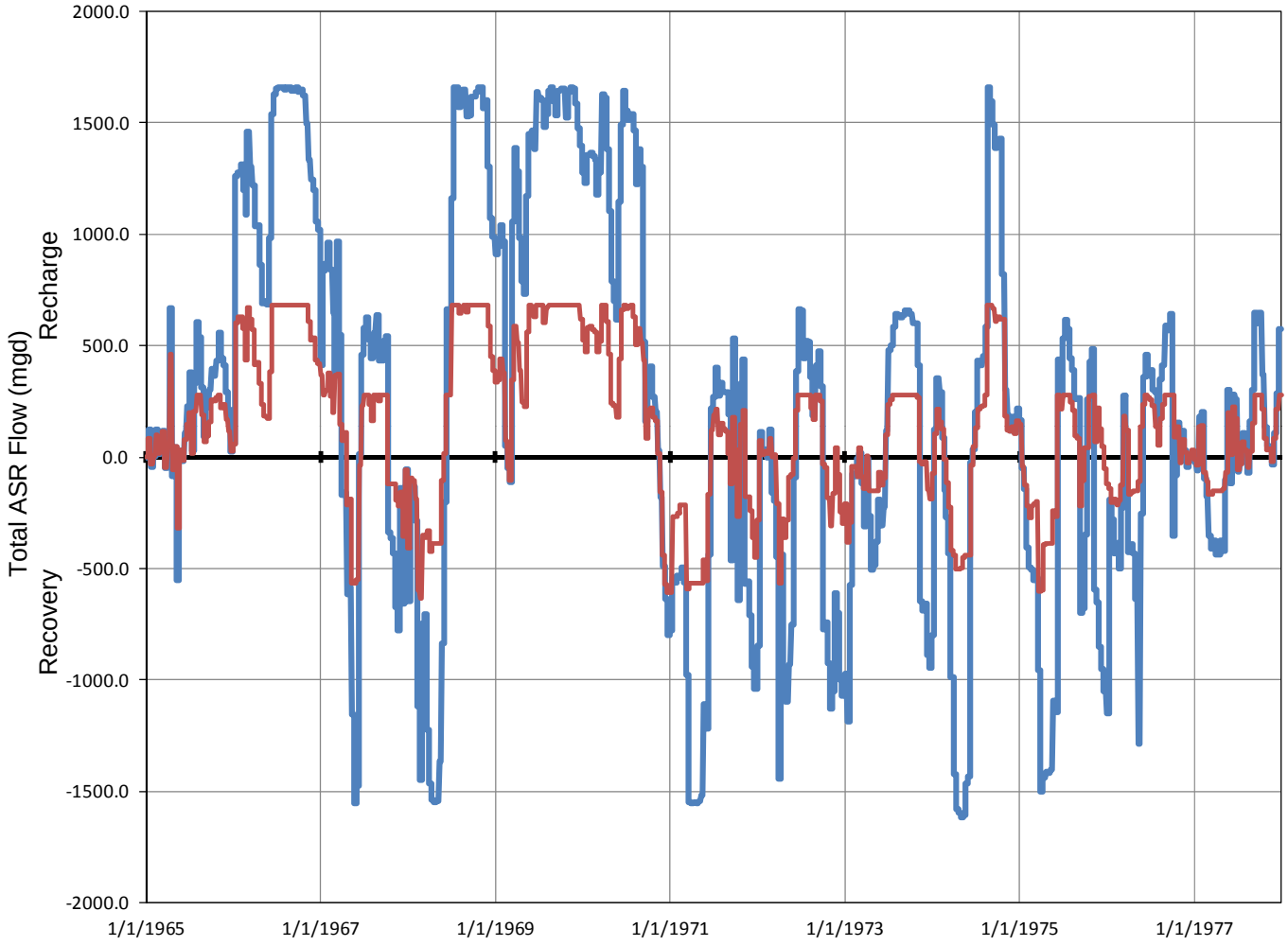

Legend

- Scenario 1 – ASR Flux
- Scenario 4 – ASR Flux

Notes:

Scenario 4 is a reduction of the wells from Scenario 3 which meets the requirements for pump pressure (100 psi). All wells are fully penetrating in their respective aquifers.

This plot shows the extraction and injection rates for all wells at all sites for Scenario 1 and Scenario 4. Positive rates are recharge (injection), while negative rates are recovery (extraction).

SCENARIO 4 – ASR WELL FLUXES (COMPARED TO RUN 1)

REGIONAL MODEL PRODUCTION SCENARIO REPORT

FIGURE 4.71

JUNE 2013

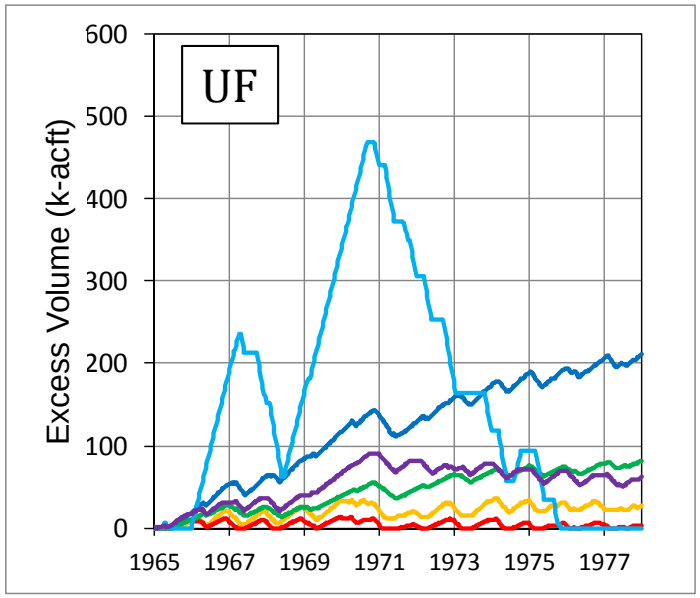

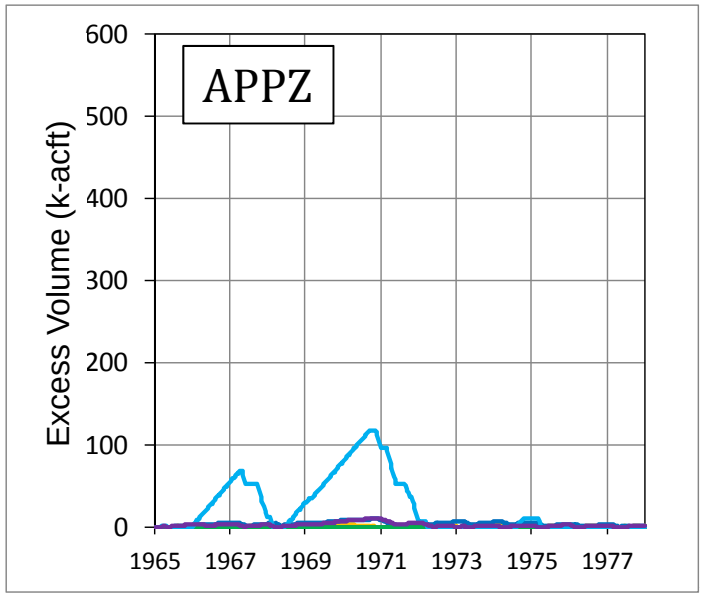

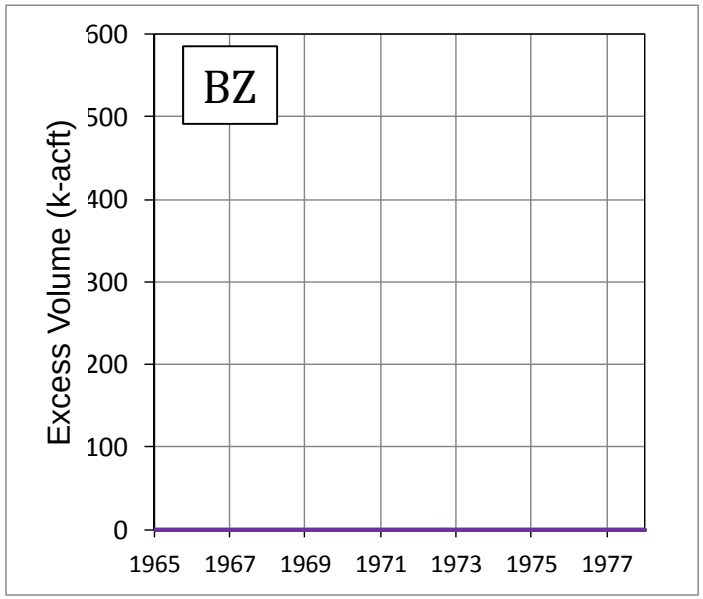

Legend

- Central Palm Beach
- C-51
- Hillsboro
- L-8
- Lake Okeechobee
- Caloosahatchee River

Notes:

Scenario 4 is a reduction of the wells from Scenario 3 which meets the requirements for pump pressure (100 psi). All wells are fully penetrating in their respective aquifers.

These plots show the excess volume of fresh water remaining in each aquifer at each ASR basin. Excess volume is calculated by adding injected volume times recovery efficiency and subtracting extracted volume. The calculation is cumulative.

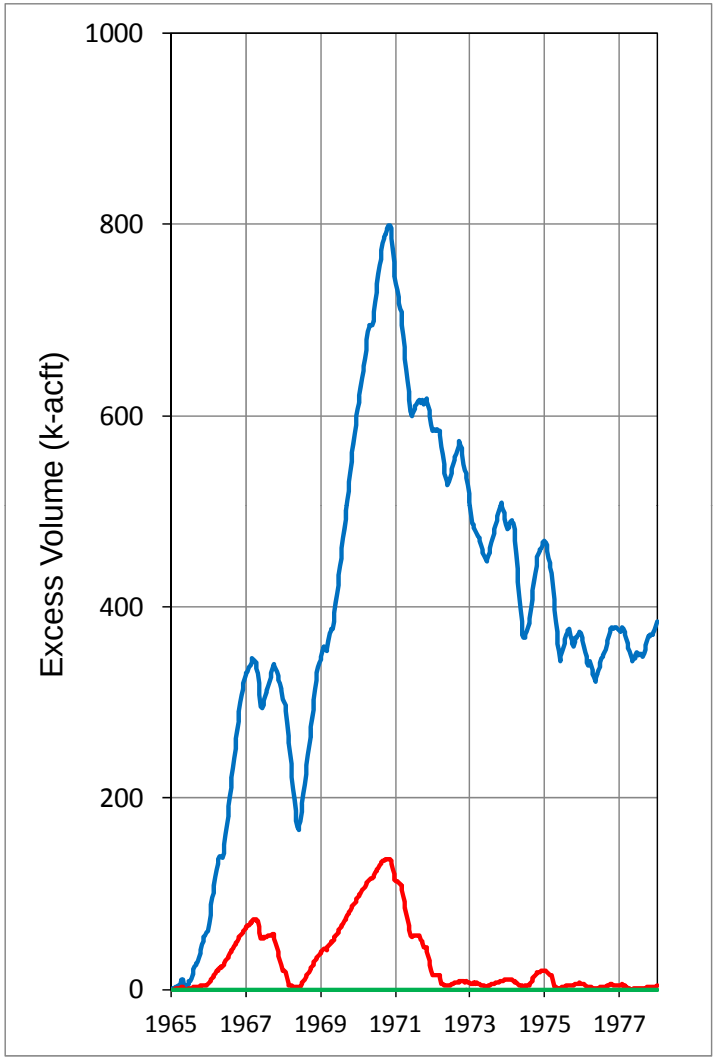

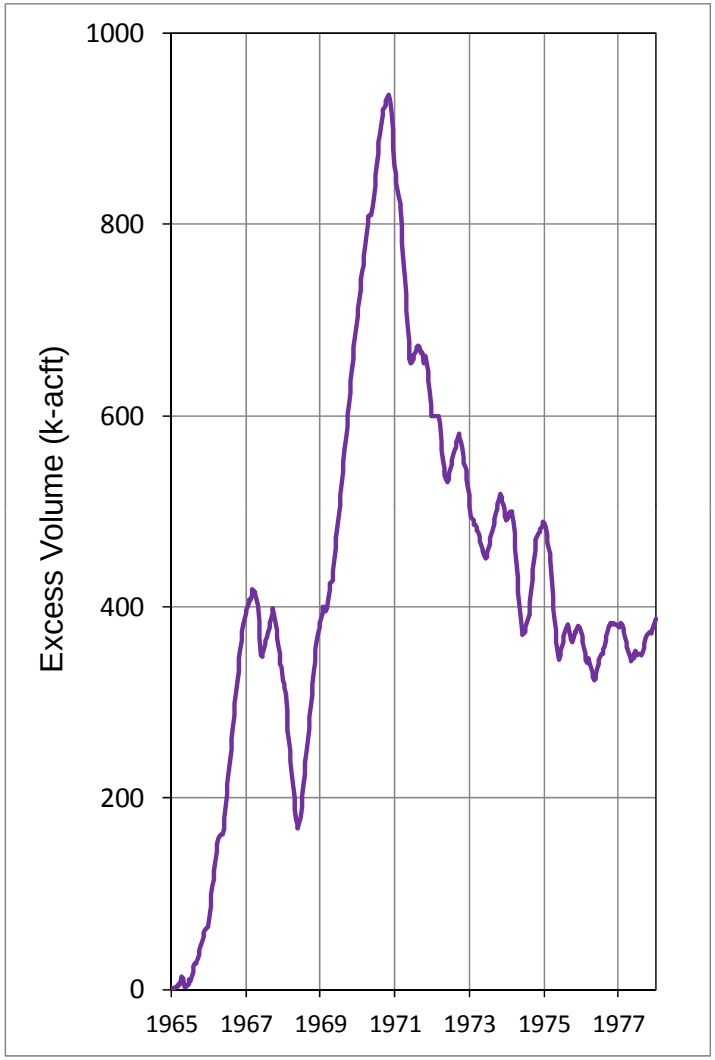

Legend

- Total UF
- Total APPZ
- Total BZ
- Total (All Aquifers)

Notes:

Scenario 4 is a reduction of the wells from Scenario 3 which meets the requirements for pump pressure (100 psi). All wells are fully penetrating in their respective aquifers.

These plots show the total excess volume of fresh water remaining in each aquifer and in all aquifers. Excess volume is calculated by adding injected volume times recovery efficiency and subtracting extracted volume. The calculation is cumulative.

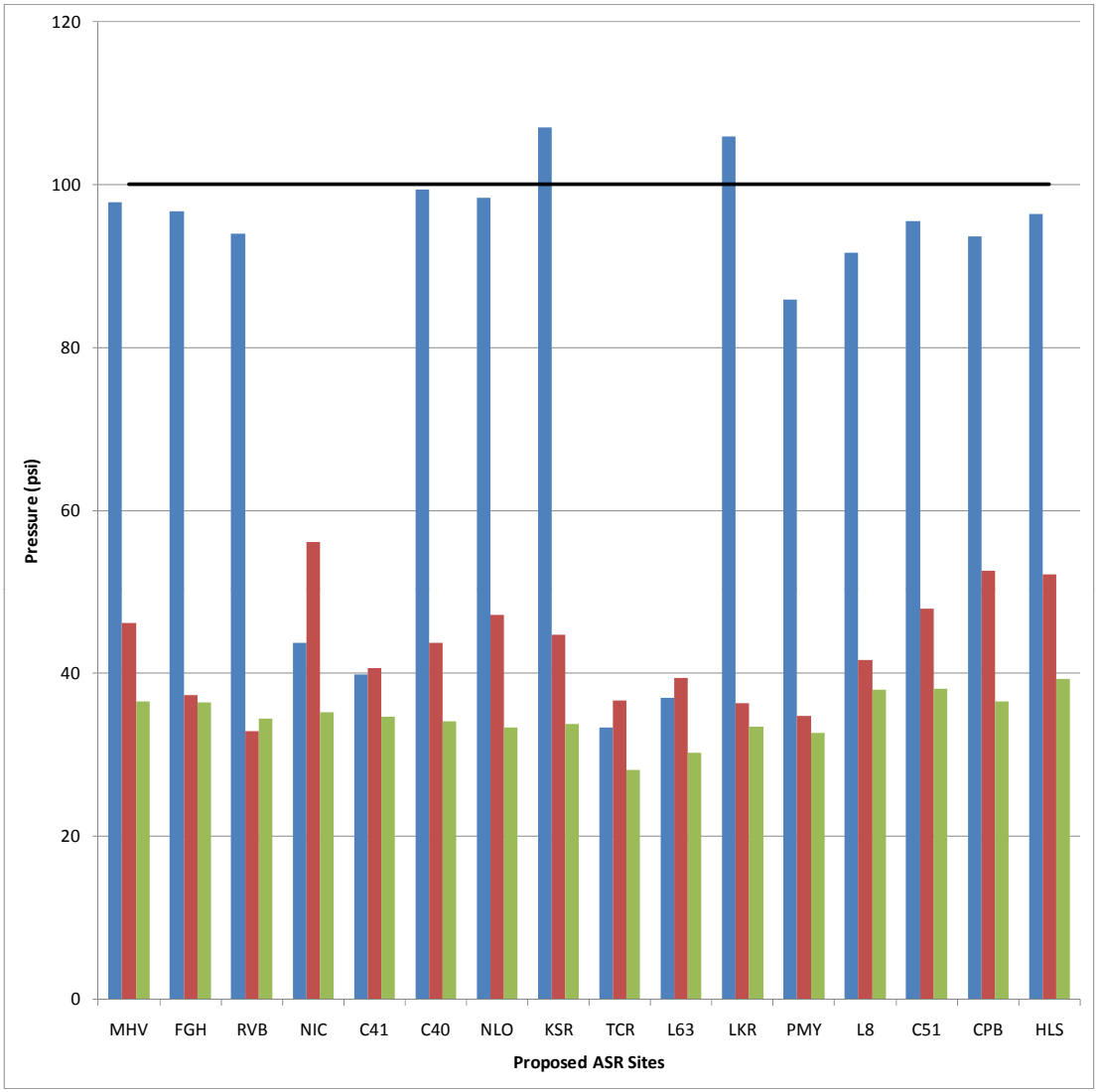

MHV	Moorehaven
FGH	Flaghole
RVB	Riverbend
NIC	Nicodemus Slough
C41	C-41Canal
C40	C-40 Canal
NLO	North Lake Okeechobee Reservoir
KSR	Kissimmee River / Paradise Run
TCR	Taylor Creek Reservoir
L63	L-63N Canal
LKR	Lakeside Ranch
PMY	Port Mayaca
L8	L-8 Basin
C51	C-51 @ STA1E
CPB	Central Palm Beach
HLS	Hillsboro (Site 1)

Legend

- Upper Floridan Aquifer
- Avon Park Permeable Zone
- Boulder Zone
- 100 psi Limit

Notes:

Scenario 4 is a reduction of the wells from Scenario 3 which meets the requirements for pump pressure (100 psi). All wells are fully penetrating in their respective aquifers.

This plot shows the highest pressure at each site which the pump would need to overcome in order to inject storage water during the 13-year simulation.

The PDT determined that it would be important to keep this pressure below 100 psi (indicated by the heavy black line).

Note that maximum pressures are shown for all aquifers and all sites even if ASR pumps are not located there for the current scenario.

SCENARIO 4 – MAXIMUM PUMP PRESSURE REQUIREMENTS

REGIONAL MODEL PRODUCTION SCENARIO REPORT

FIGURE 4.74

JUNE 2013

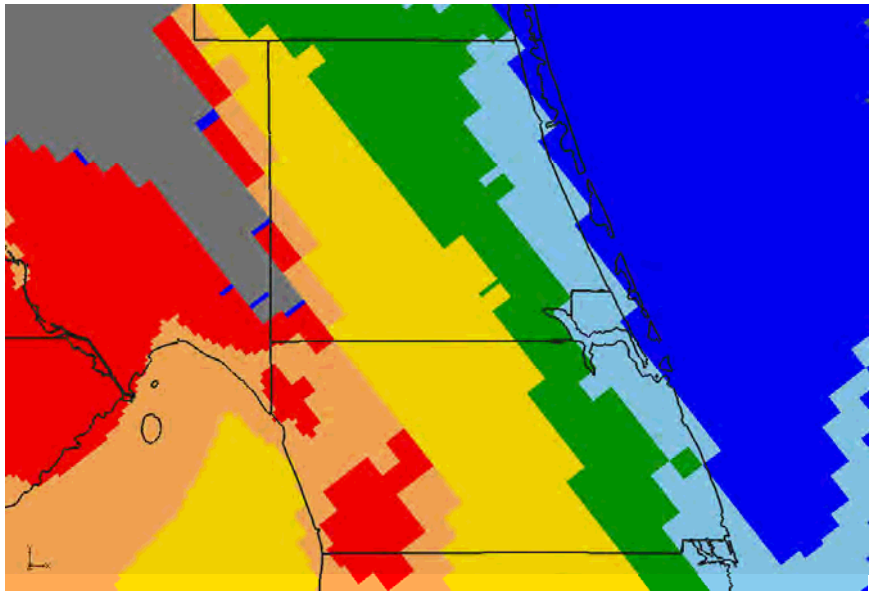

Upper Floridan Aquifer

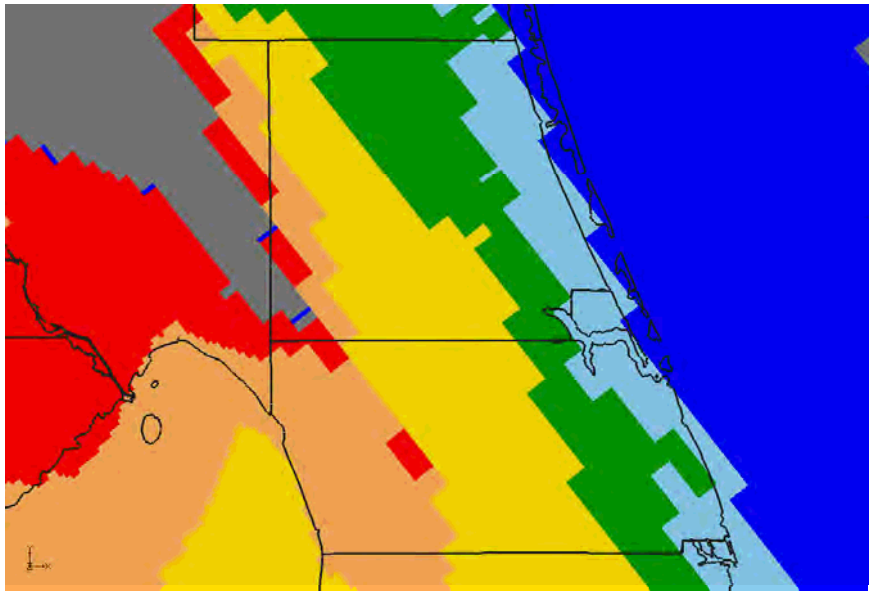

Avon Park Permeable Zone

Legend

- Not artesian
- < 5%
- 5% - 10%
- 10% - 20%
- 20% - 50%
- 50% - 100%
- Loses artesian condition

Notes:

Scenario 4 is a reduction of the wells from Scenario 3 which meets the requirements for pump pressure (100 psi). All wells are fully penetrating in their respective aquifers.

These plots show the maximum reduction in artesian flow at each model cell as a percentage when compared to the flow expected without the ASR project.

Permit rules require that the reduction in Saint Lucie and Martin Counties be less than 10%.

Note the gray area in the northwest corner of the figures, which coincides with a ridge and does not normally have artesian conditions.

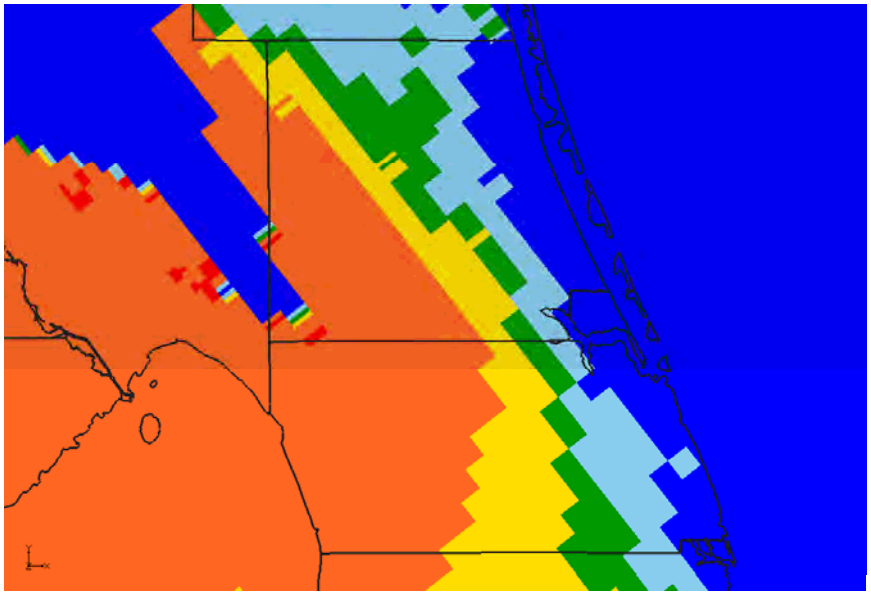

Upper Floridan Aquifer

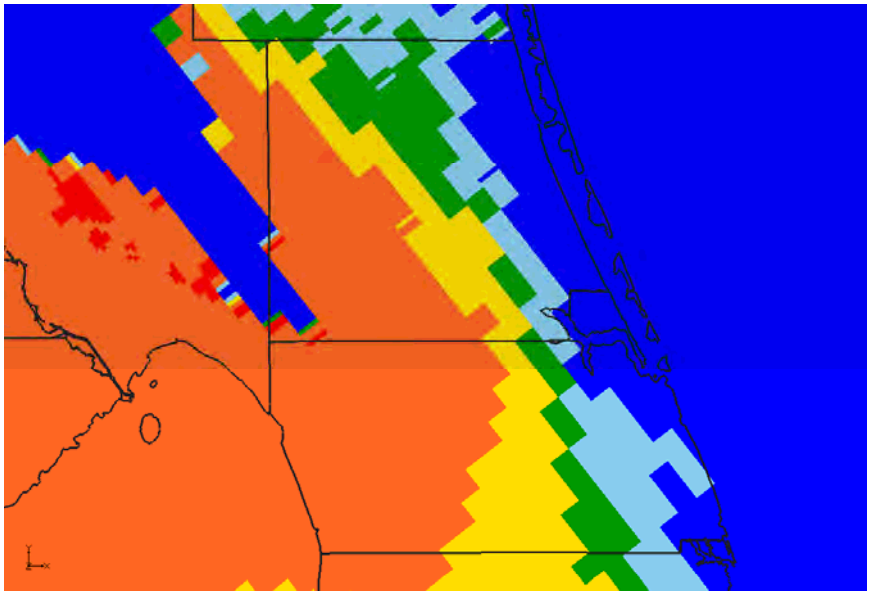

Avon Park Permeable Zone

Legend

- 0 days
- 1 – 250 days
- 250 – 500 days
- 500 – 1000 days
- 1000 – 2000 days
- > 2000 days

Notes:

Scenario 4 is a reduction of the wells from Scenario 3 which meets the requirements for pump pressure (100 psi). All wells are fully penetrating in their respective aquifers.

These plots indicate the severity of the loss of artesian pressure due to ASR extraction pumping.

Permit rules require that the reduction in Saint Lucie and Martin Counties be less than 10%. This plot indicates the number of days during the simulation in which the flow reduction was greater than 10%. There are 4748 days in the 13-year model simulation period.

Note the blue area in the northwest corner of the figures, which coincides with a ridge and does not normally have artesian conditions.

SCENARIO 4 – NUMBER OF DAYS (OUT OF 13 YEARS) WITH FLOW REDUCTION EXCEEDING 10%

REGIONAL MODEL PRODUCTION SCENARIO REPORT

FIGURE 4.76

JUNE 2013

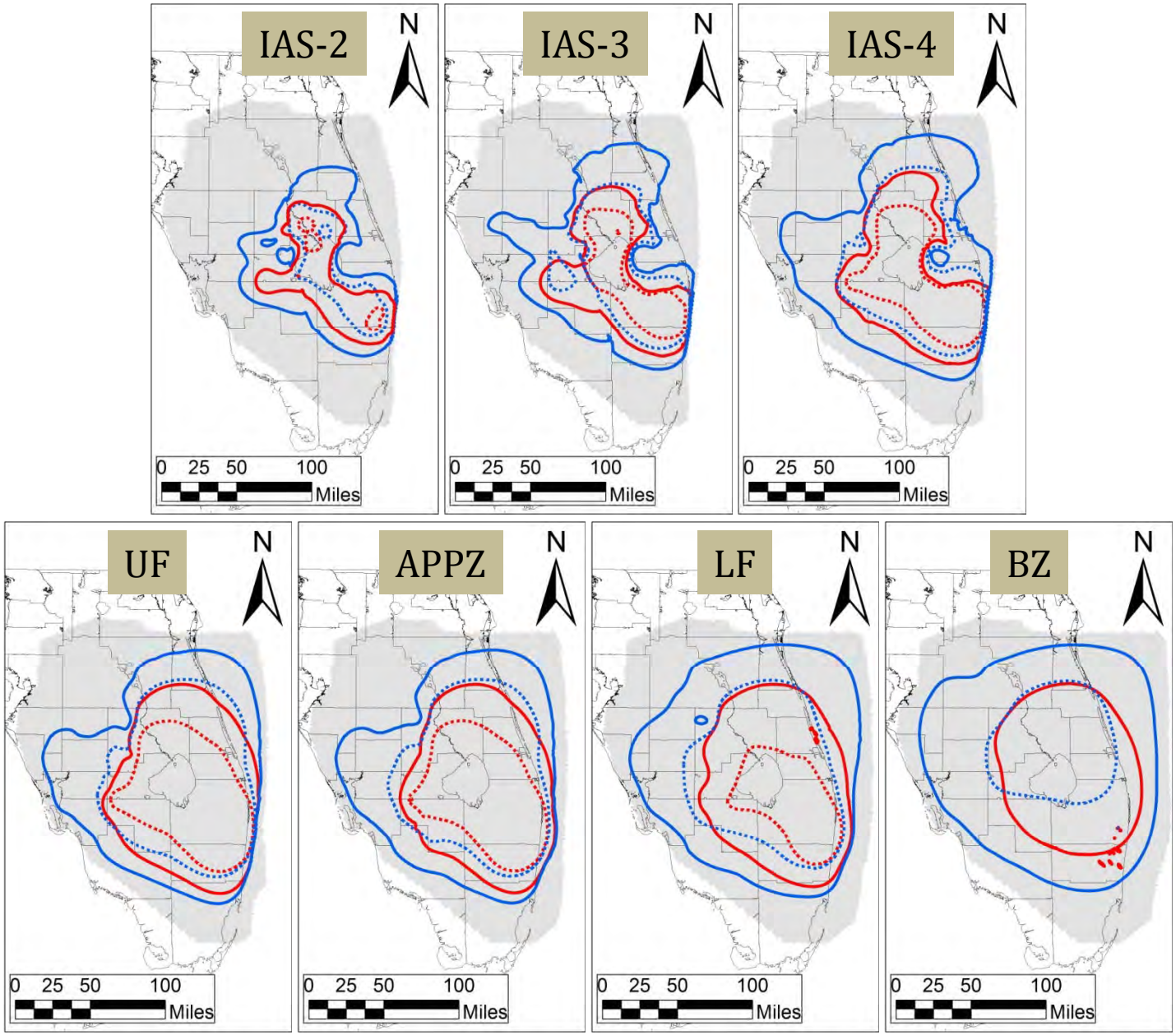

Legend

Maximum Drawdown
- 1 foot
- 5 feet

Maximum "Drawup"
- 1 foot
- 5 feet

Model Domain

Notes:

Scenario 4 is a reduction of the wells from Scenario 3 which meets the requirements for pump pressure (100 psi). All wells are fully penetrating in their respective aquifers.

These figures show the extent of the areas where the maximum drawdown or "drawup" is greater than 1 foot or 5 feet.

The maximum condition does not necessarily occur at the same time for all regions of the model.

SCENARIO 4 – MAXIMUM DRAWDOWN AND "DRAWUP" BY AQUIFER

REGIONAL MODEL PRODUCTION SCENARIO REPORT

FIGURE 4.77

JUNE 2013

5-Mile Distance

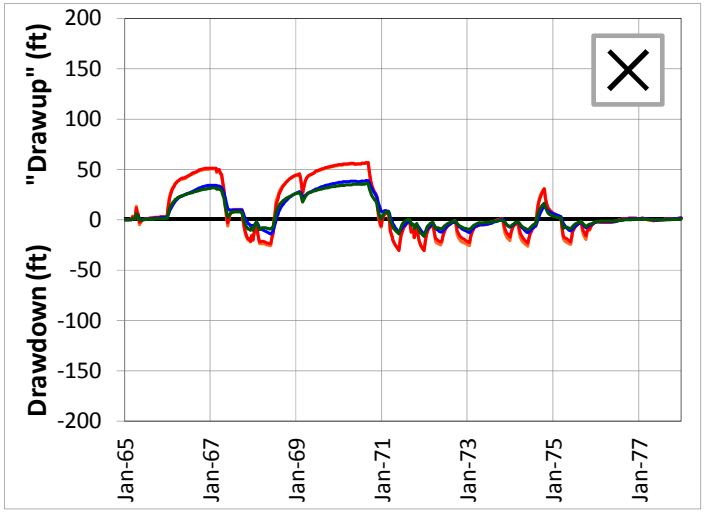

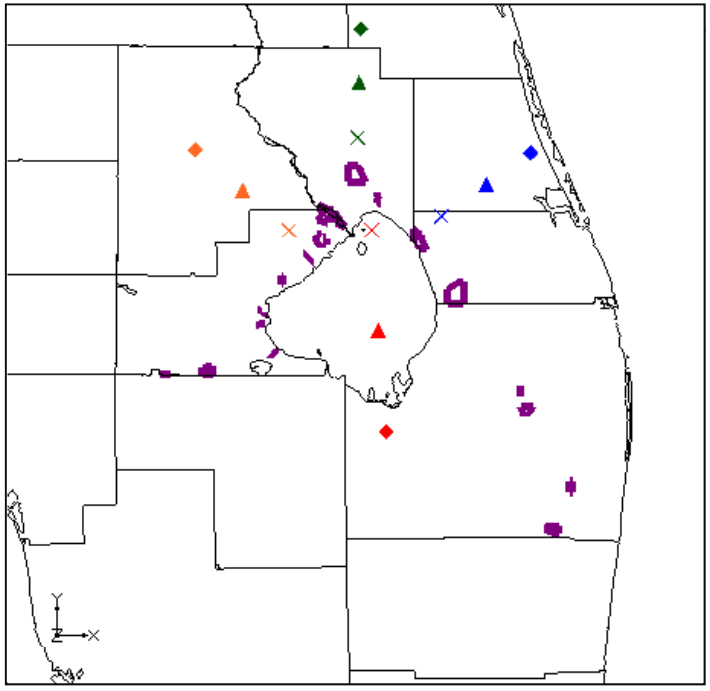

15-Mile Distance

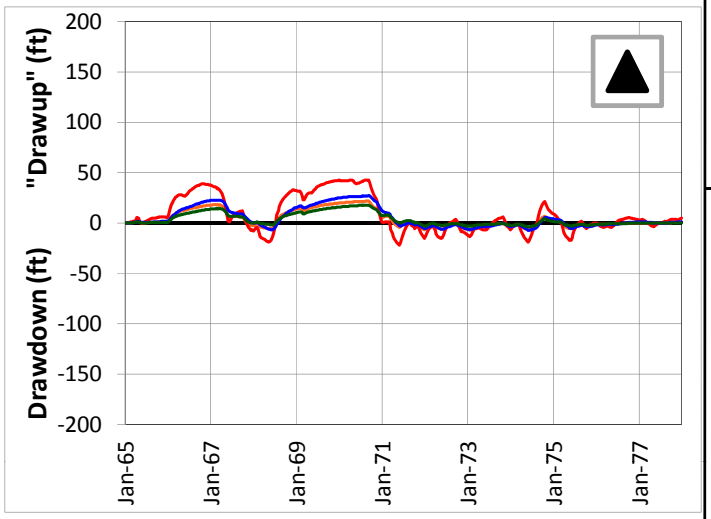

25-Mile Distance

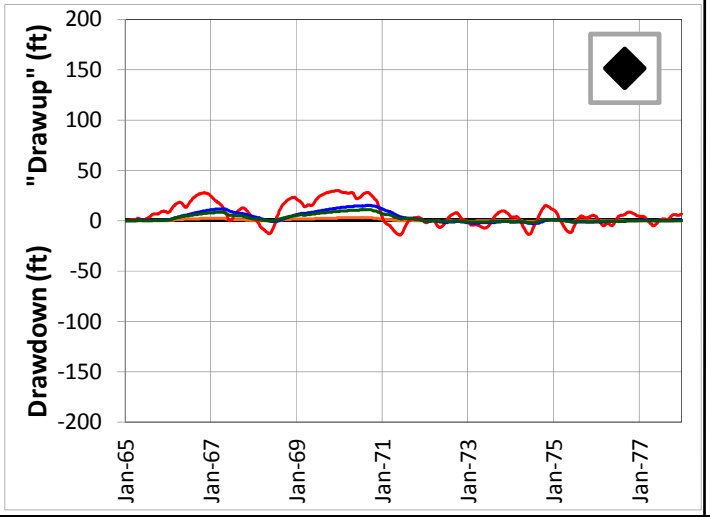

Legend

- CERP ASR Sites
- ✕ 5-Mile Distance Locations
- ▲ 15-Mile Distance Locations
- ◆ 25-Mile Distance Locations

Notes:

Scenario 4 is a reduction of the wells from Scenario 3 which meets the requirements for pump pressure (100 psi). All wells are fully penetrating in their respective aquifers.

A number of individual sites were chosen from the UF Aquifer at distances of 5, 15 and 25 miles from the proposed ASR well sites. This figure shows the drawdown and "drawup" at each output time step for 12 of these sites.

The plots were calculated by subtracting the heads calculated by the D13R model from those calculated by the no project run. This results in a positive value for "drawup" and a negative value for drawdown.

The colors of the points on the map correspond to the colors of the lines on the plots.

The symbols on the map (x, triangle and diamond) indicate the distance from the ASR sites.

5-Mile Distance

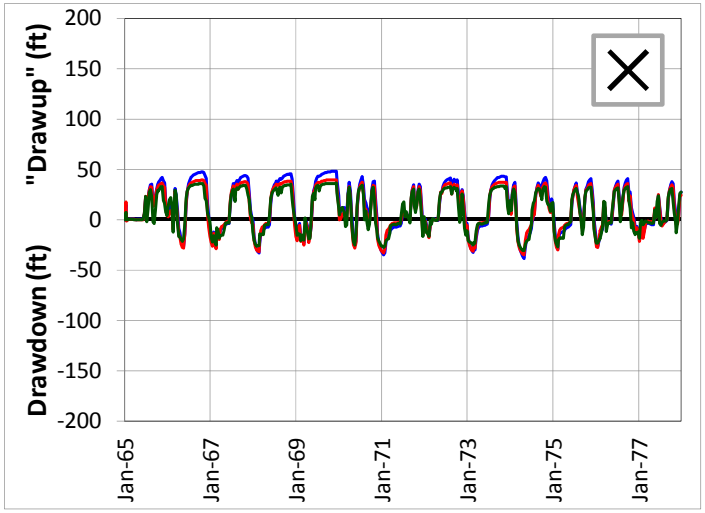

15-Mile Distance

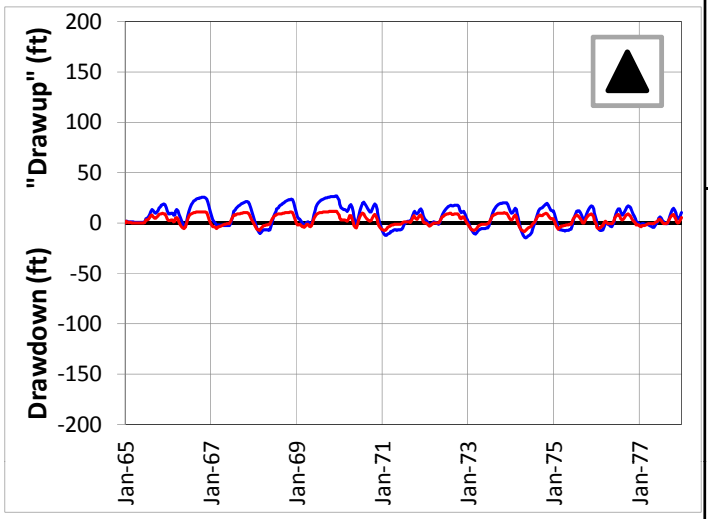

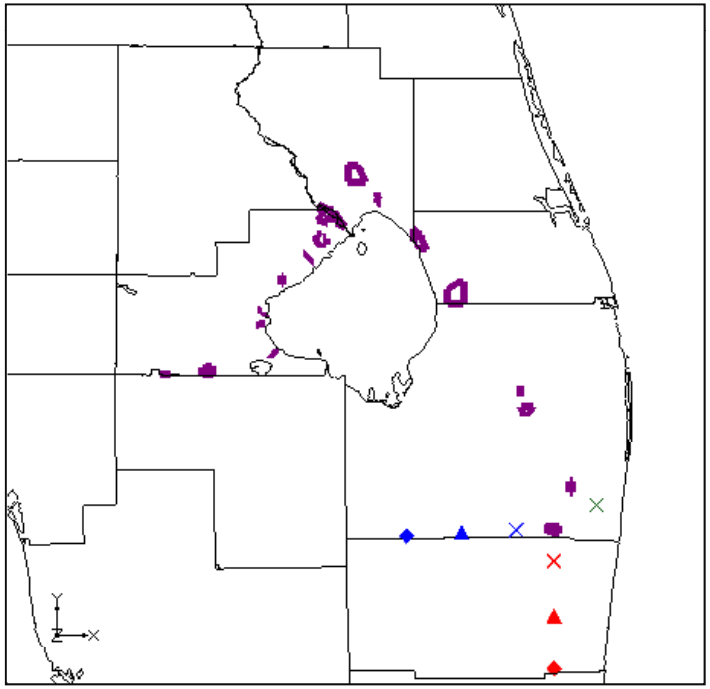

25-Mile Distance

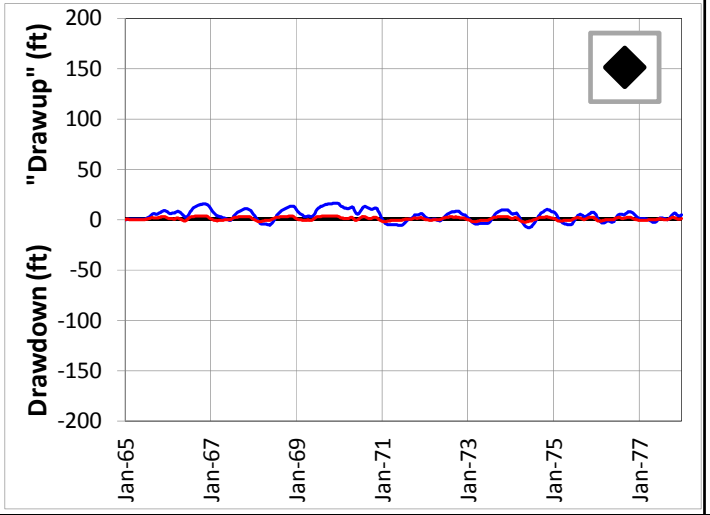

Legend

- CERP ASR Sites
- 5-Mile Distance Locations
- 15-Mile Distance Locations
- 25-Mile Distance Locations

Notes:

Scenario 4 is a reduction of the wells from Scenario 3 which meets the requirements for pump pressure (100 psi). All wells are fully penetrating in their respective aquifers.

A number of individual sites were chosen from the UF Aquifer at distances of 5, 15 and 25 miles from the proposed ASR well sites. This figure shows the drawdown and "drawup" at each output time step for 7 of these sites.

The plots were calculated by subtracting the heads calculated by the D13R model from those calculated by the no project run. This results in a positive value for "drawup" and a negative value for drawdown.

The colors of the points on the map correspond to the colors of the lines on the plots.

The symbols on the map (x, triangle and diamond) indicate the distance from the ASR sites.

5-Mile Distance

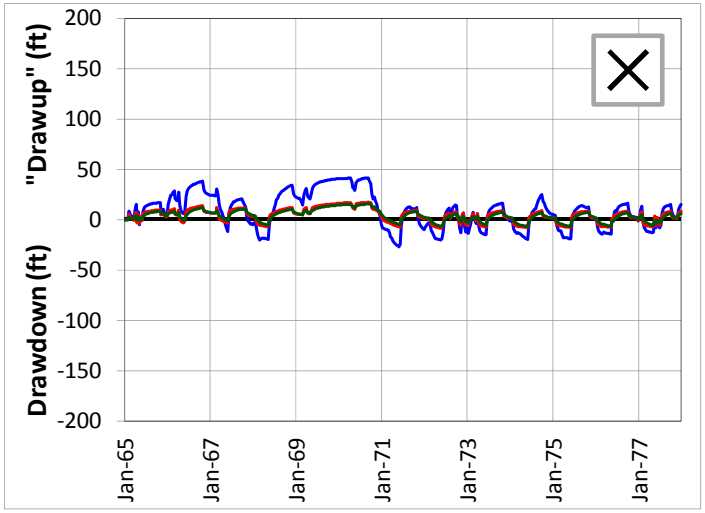

15-Mile Distance

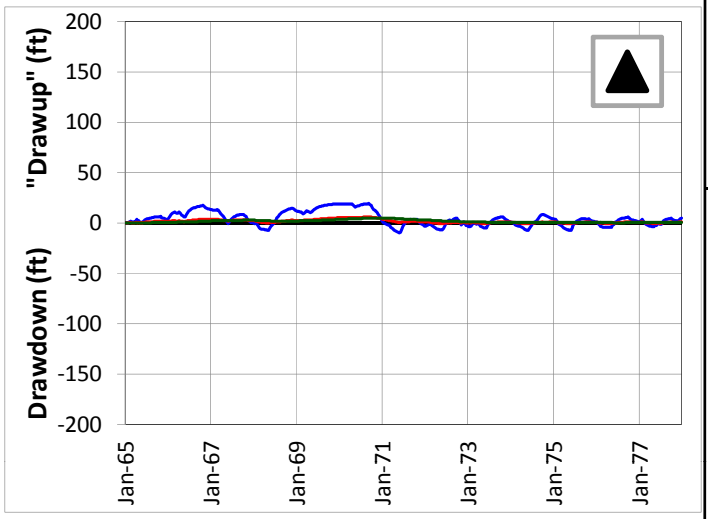

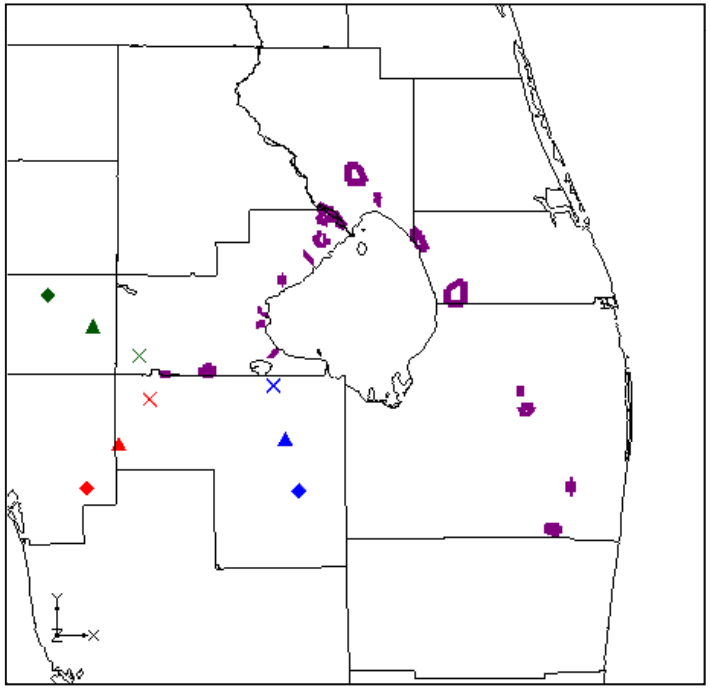

25-Mile Distance

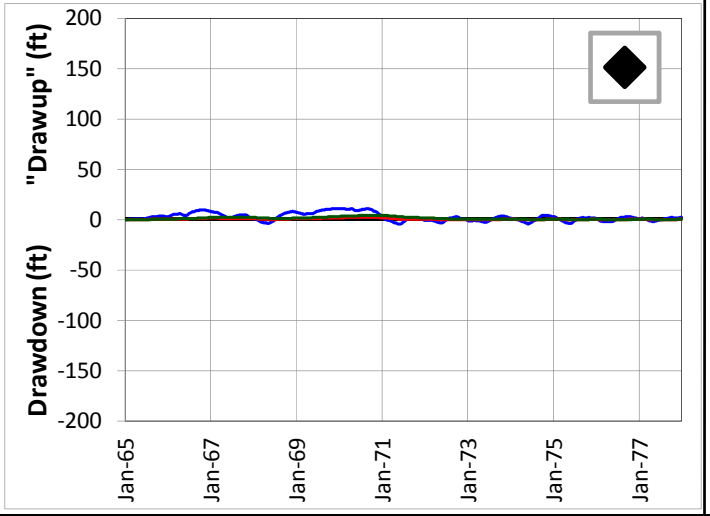

Legend

- CERP ASR Sites
- ✕ 5-Mile Distance Locations
- ▲ 15-Mile Distance Locations
- ◆ 25-Mile Distance Locations

Notes:

Scenario 4 is a reduction of the wells from Scenario 3 which meets the requirements for pump pressure (100 psi). All wells are fully penetrating in their respective aquifers.

A number of individual sites were chosen from the UF Aquifer at distances of 5, 15 and 25 miles from the proposed ASR well sites. This figure shows the drawdown and "drawup" at each output time step for 9 of these sites.

The plots were calculated by subtracting the heads calculated by the D13R model from those calculated by the no project run. This results in a positive value for "drawup" and a negative value for drawdown.

The colors of the points on the map correspond to the colors of the lines on the plots.

The symbols on the map (x, triangle and diamond) indicate the distance from the ASR sites.

5-Mile Distance

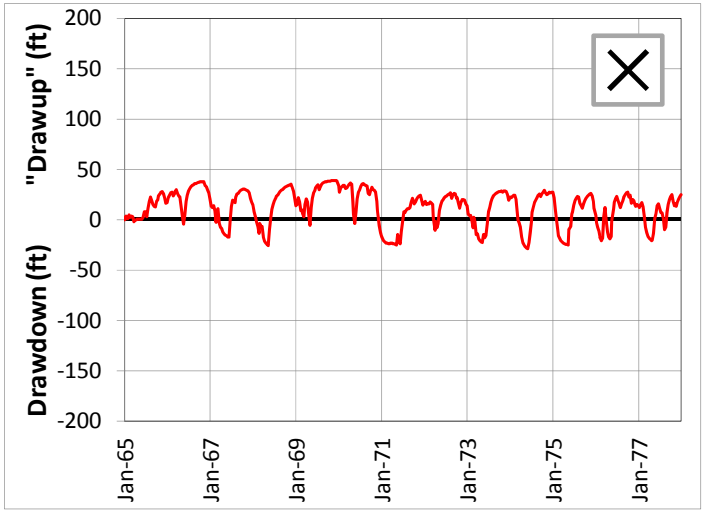

15-Mile Distance

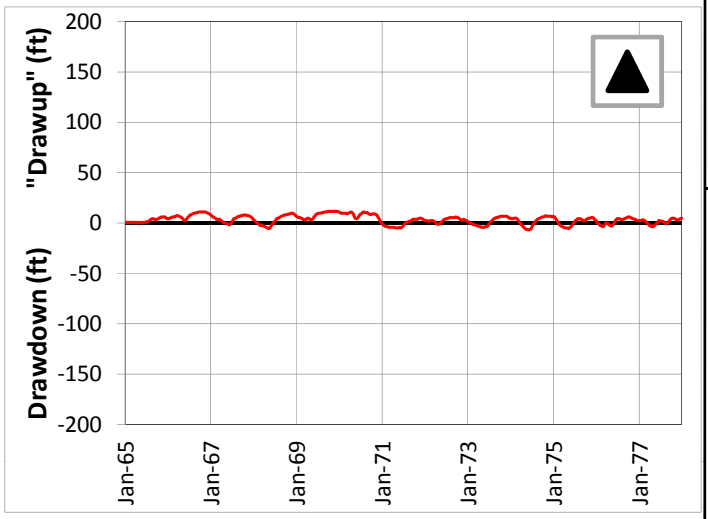

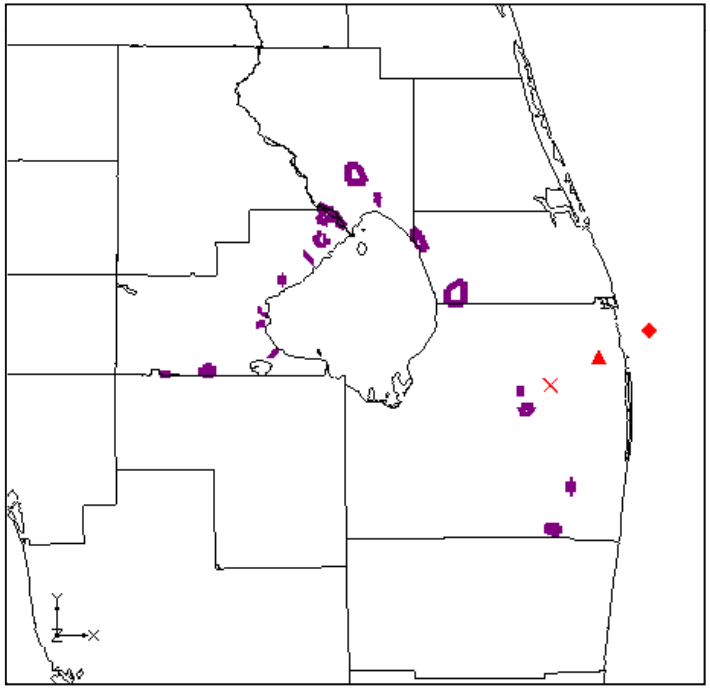

25-Mile Distance

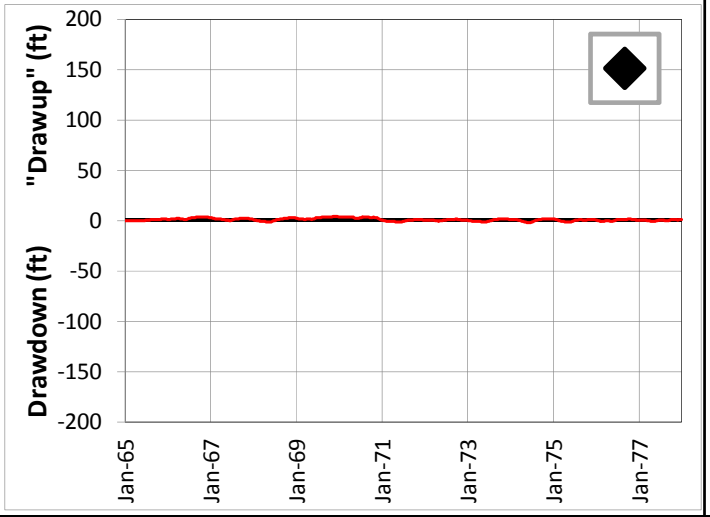

Legend

- CERP ASR Sites
- 5-Mile Distance Locations
- 15-Mile Distance Locations
- 25-Mile Distance Locations

Notes:

Scenario 4 is a reduction of the wells from Scenario 3 which meets the requirements for pump pressure (100 psi). All wells are fully penetrating in their respective aquifers.

A number of individual sites were chosen from the UF Aquifer at distances of 5, 15 and 25 miles from the proposed ASR well sites. This figure shows the drawdown and "drawup" at each output time step for 3 of these sites.

The plots were calculated by subtracting the heads calculated by the D13R model from those calculated by the no project run. This results in a positive value for "drawup" and a negative value for drawdown.

The colors of the points on the map correspond to the colors of the lines on the plots.

The symbols on the map (x, triangle and diamond) indicate the distance from the ASR sites.

5-Mile Distance

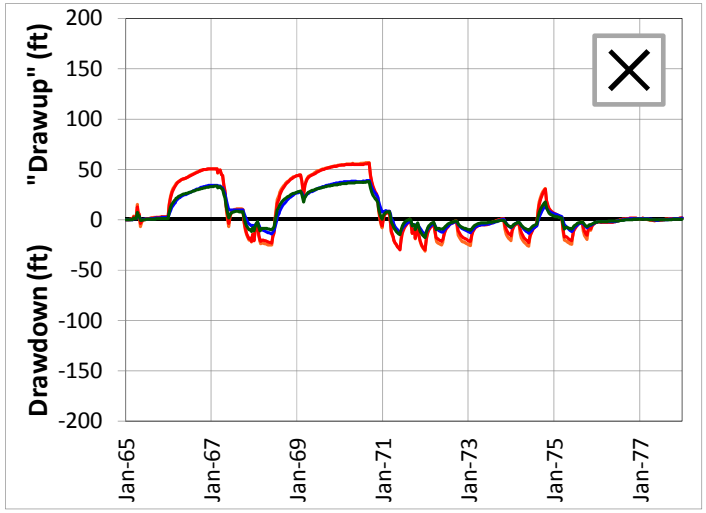

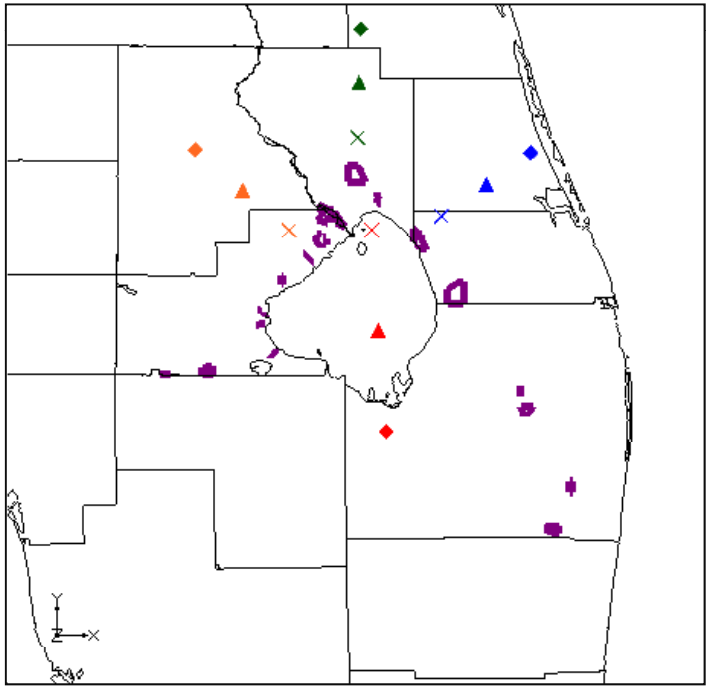

15-Mile Distance

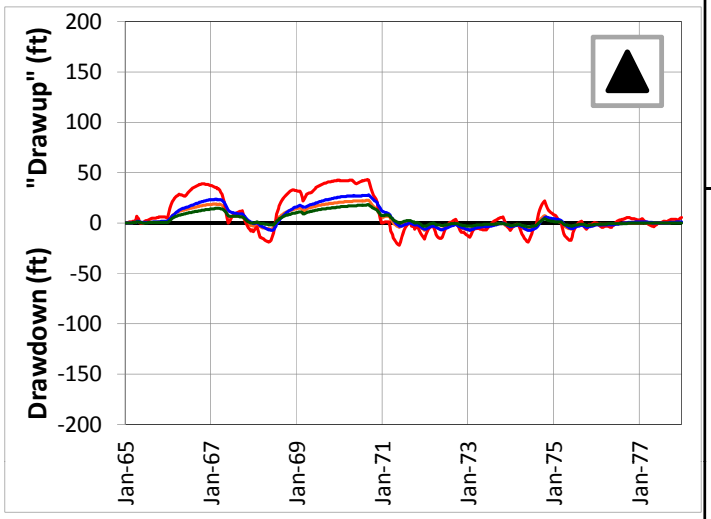

25-Mile Distance

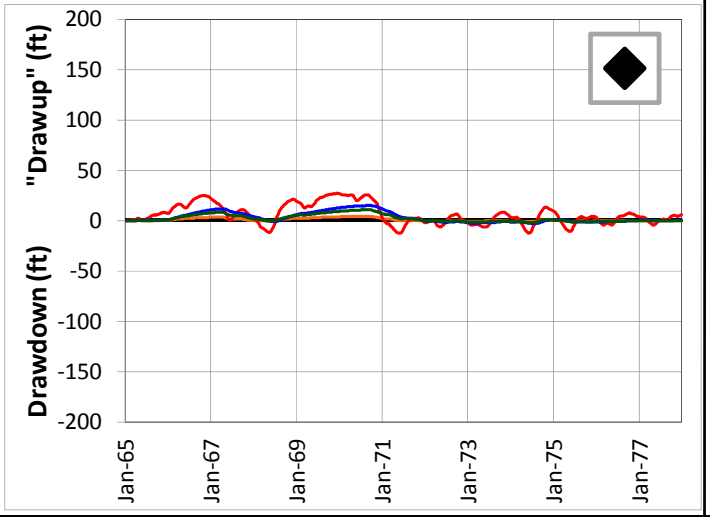

Legend

- CERP ASR Sites
- 5-Mile Distance Locations
- 15-Mile Distance Locations
- 25-Mile Distance Locations

Notes:

Scenario 4 is a reduction of the wells from Scenario 3 which meets the requirements for pump pressure (100 psi). All wells are fully penetrating in their respective aquifers.

A number of individual sites were chosen from the APPZ Aquifer at distances of 5, 15 and 25 miles from the proposed ASR well sites. This figure shows the drawdown and "drawup" at each output time step for 12 of these sites.

The plots were calculated by subtracting the heads calculated by the D13R model from those calculated by the no project run. This results in a positive value for "drawup" and a negative value for drawdown.

The colors of the points on the map correspond to the colors of the lines on the plots.

The symbols on the map (x, triangle and diamond) indicate the distance from the ASR sites.

5-Mile Distance

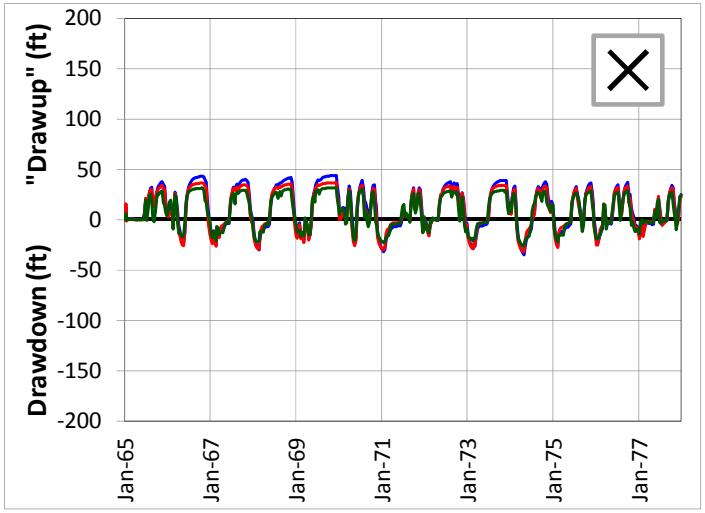

15-Mile Distance

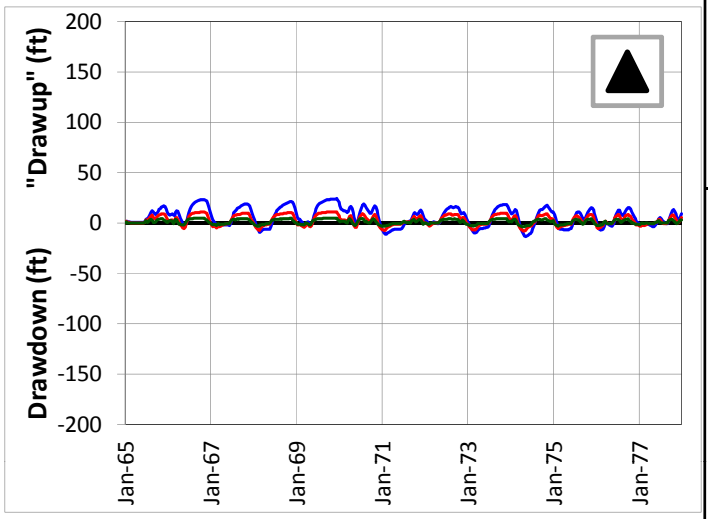

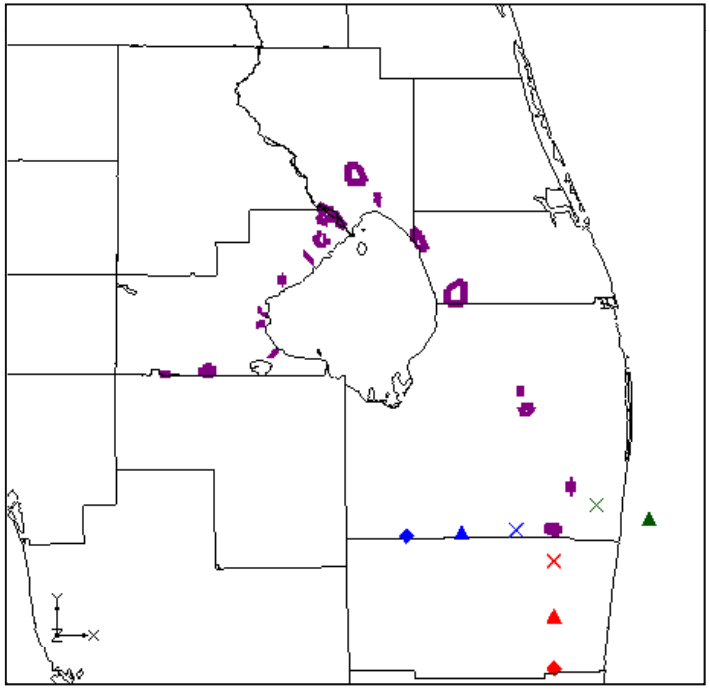

25-Mile Distance

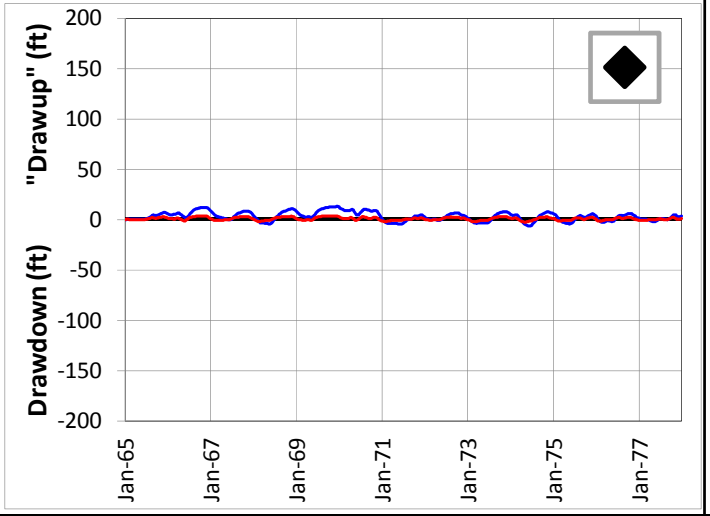

Legend

- CERP ASR Sites
- 5-Mile Distance Locations
- 15-Mile Distance Locations
- 25-Mile Distance Locations

Notes:

Scenario 4 is a reduction of the wells from Scenario 3 which meets the requirements for pump pressure (100 psi). All wells are fully penetrating in their respective aquifers.

A number of individual sites were chosen from the APPZ Aquifer at distances of 5, 15 and 25 miles from the proposed ASR well sites. This figure shows the drawdown and "drawup" at each output time step for 8 of these sites.

The plots were calculated by subtracting the heads calculated by the D13R model from those calculated by the no project run. This results in a positive value for "drawup" and a negative value for drawdown.

The colors of the points on the map correspond to the colors of the lines on the plots.

The symbols on the map (x, triangle and diamond) indicate the distance from the ASR sites.

SCENARIO 4 – DRAWDOWN AND "DRAWUP" – APPZ

FIGURE 4.83

5-Mile Distance

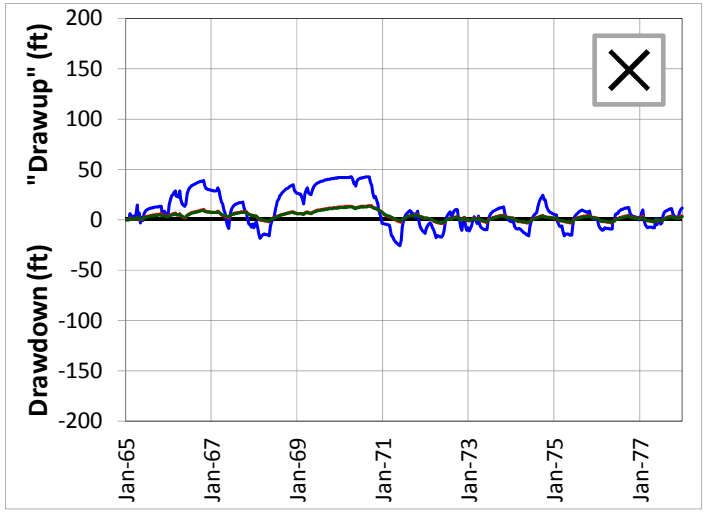

15-Mile Distance

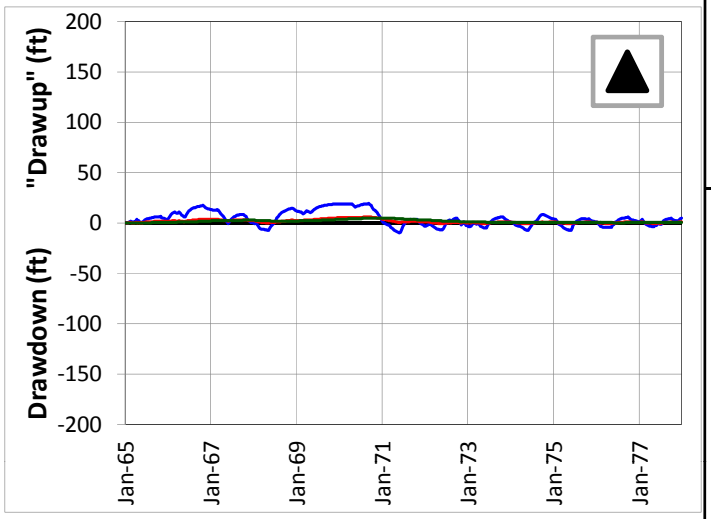

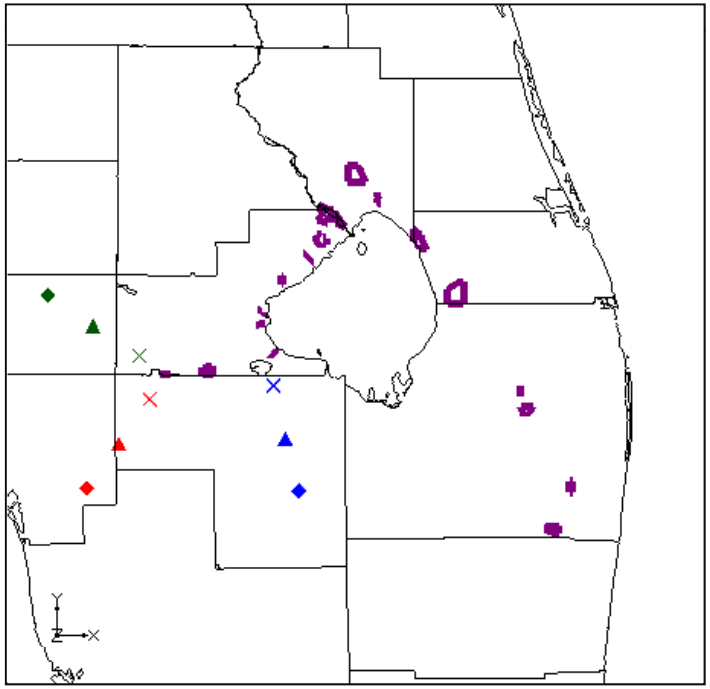

25-Mile Distance

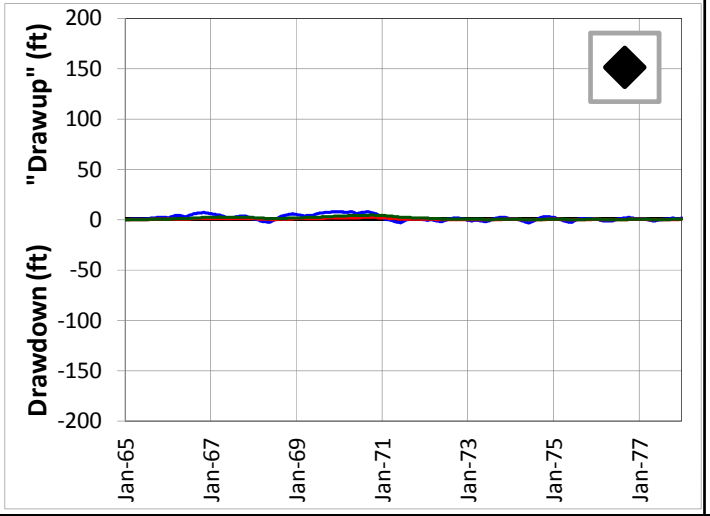

Legend

- CERP ASR Sites
- ✕ 5-Mile Distance Locations
- ▲ 15-Mile Distance Locations
- ◆ 25-Mile Distance Locations

Notes:

Scenario 4 is a reduction of the wells from Scenario 3 which meets the requirements for pump pressure (100 psi). All wells are fully penetrating in their respective aquifers.

A number of individual sites were chosen from the APPZ Aquifer at distances of 5, 15 and 25 miles from the proposed ASR well sites. This figure shows the drawdown and "drawup" at each output time step for 9 of these sites.

The plots were calculated by subtracting the heads calculated by the D13R model from those calculated by the no project run. This results in a positive value for "drawup" and a negative value for drawdown.

The colors of the points on the map correspond to the colors of the lines on the plots.

The symbols on the map (x, triangle and diamond) indicate the distance from the ASR sites.

5-Mile Distance

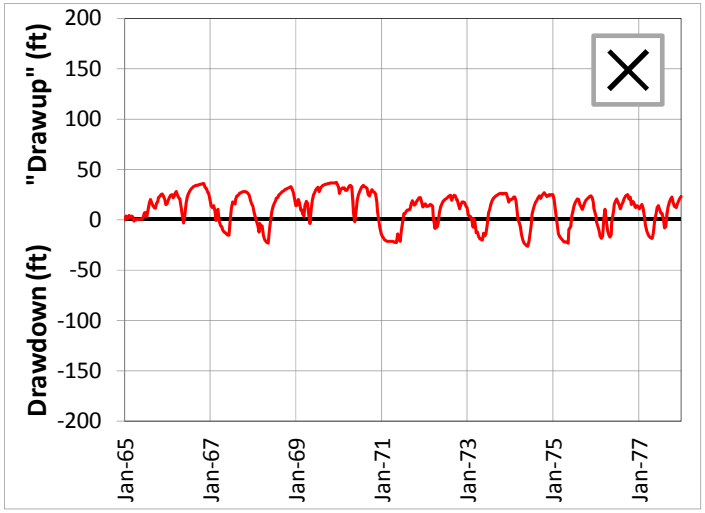

15-Mile Distance

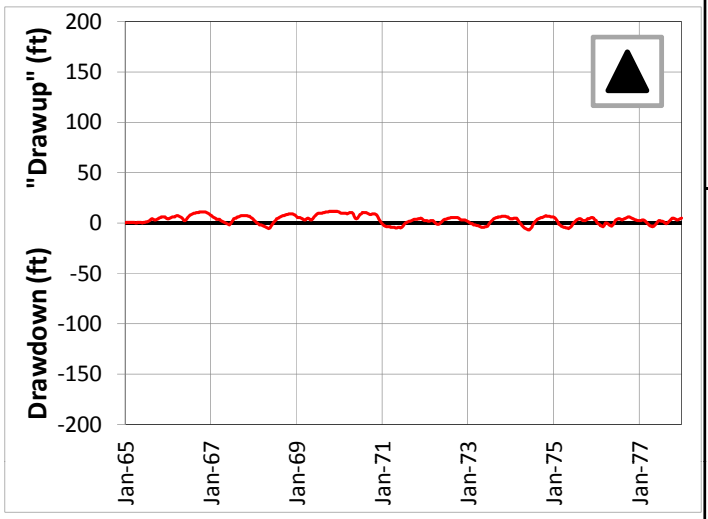

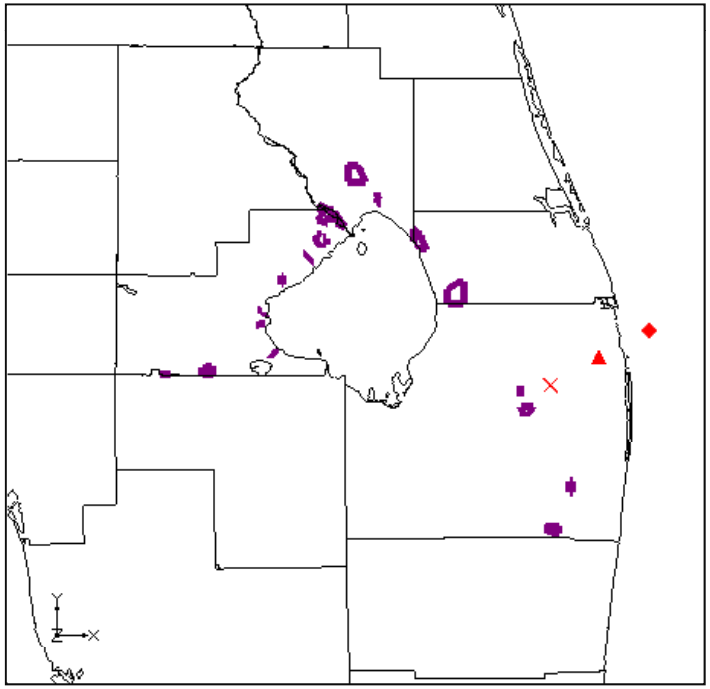

25-Mile Distance

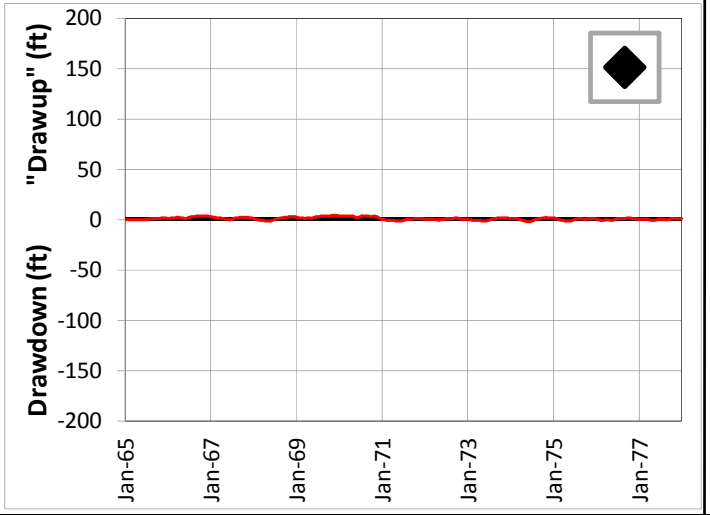

Legend

- CERP ASR Sites
- 5-Mile Distance Locations
- 15-Mile Distance Locations
- 25-Mile Distance Locations

Notes:

Scenario 4 is a reduction of the wells from Scenario 3 which meets the requirements for pump pressure (100 psi). All wells are fully penetrating in their respective aquifers.

A number of individual sites were chosen from the APPZ Aquifer at distances of 5, 15 and 25 miles from the proposed ASR well sites. This figure shows the drawdown and "drawup" at each output time step for 3 of these sites.

The plots were calculated by subtracting the heads calculated by the D13R model from those calculated by the no project run. This results in a positive value for "drawup" and a negative value for drawdown.

The colors of the points on the map correspond to the colors of the lines on the plots.

The symbols on the map (x, triangle and diamond) indicate the distance from the ASR sites.

SCENARIO 4 – DRAWDOWN AND "DRAWUP" – APPZ

FIGURE 4.85

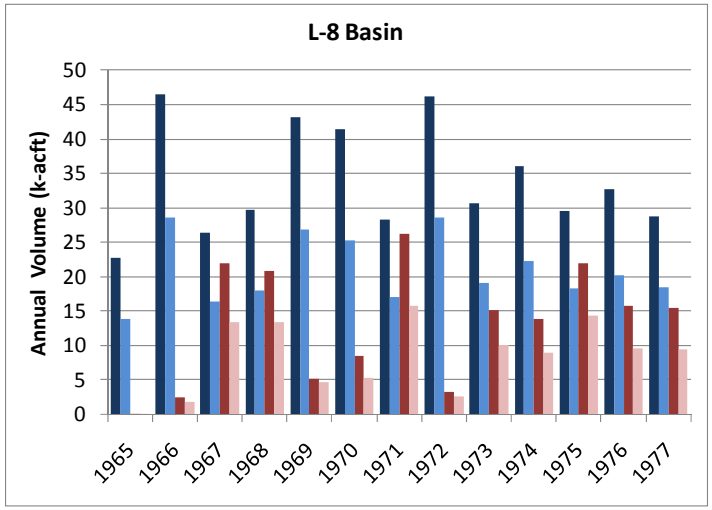

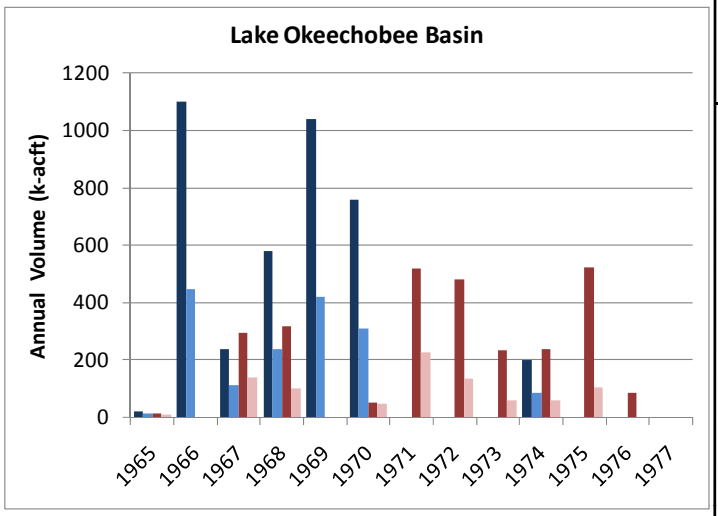

	L-8		Lake Okeechobee		Caloosahatchee	
	In %	Out %	In %	Out %	In %	Out %
1965	61%	100%	71%	55%	53%	75%
1966	62%	75%	41%	--	36%	53%
1967	62%	61%	47%	47%	31%	29%
1968	60%	65%	41%	32%	30%	27%
1969	62%	88%	40%	--	30%	--
1970	61%	63%	41%	94%	33%	100%
1971	60%	60%	--	43%	29%	32%
1972	62%	79%	--	28%	49%	35%
1973	62%	66%	--	26%	34%	30%
1974	62%	65%	44%	25%	31%	25%
1975	62%	65%	--	20%	31%	25%
1976	62%	61%	--	0%	38%	33%
1977	65%	61%	--	--	41%	36%

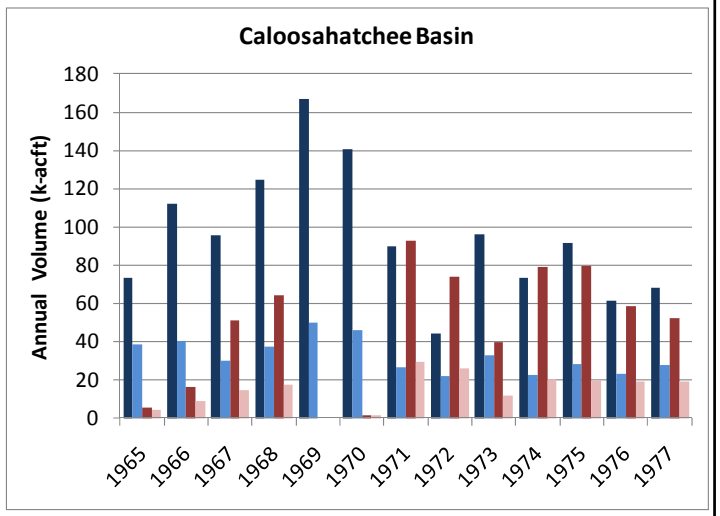

Legend

- Design Storage (injection)
- Modeled Storage (injection)
- Design Recovery (extraction)
- Modeled Recovery (extraction)

Notes:

Scenario 4 is a reduction of the wells from Scenario 3 which meets the requirements for pump pressure (100 psi). All wells are fully penetrating in their respective aquifers.

These three plots show the comparison between the SFWMM-D13R designed annual injection and extraction volumes at the ASR wells and the actual assigned rates for the RASRSM-D13R for three of the basins.

The table presents the percentage of SFWMM-D13R annual flow rates that are included in this scenario of the RASRSM-D13R. These percentages are not recovery efficiencies.

SCENARIO 4 – COMPARISON OF DESIGNED AND MODELED ASR FLOW RATES

REGIONAL MODEL PRODUCTION SCENARIO REPORT

FIGURE 4.86

JUNE 2013

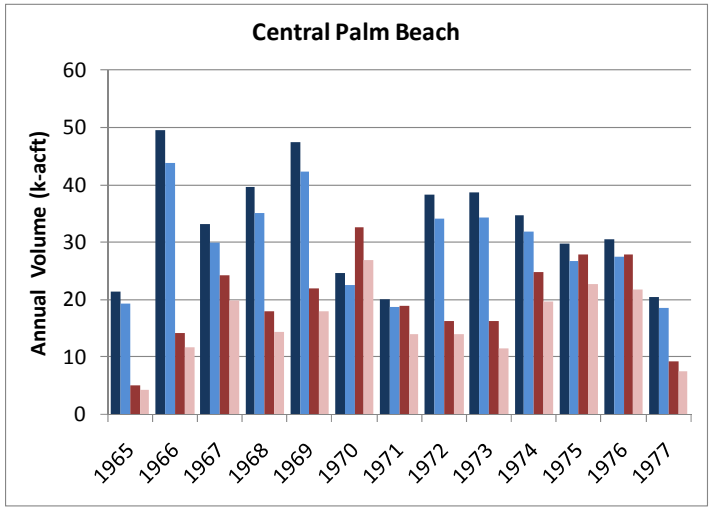

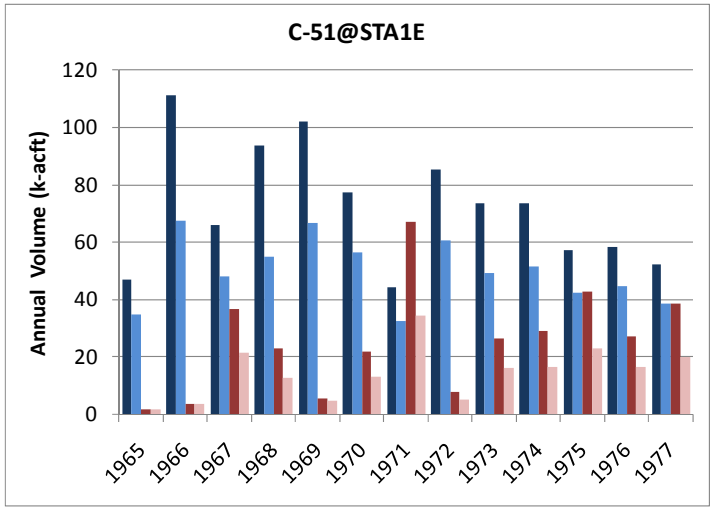

	CPB		C-51		Hillsboro	
	In %	Out %	In %	Out %	In %	Out %
1965	90%	88%	74%	95%	45%	46%
1966	89%	82%	61%	100%	36%	84%
1967	90%	82%	73%	59%	40%	28%
1968	89%	80%	59%	56%	36%	35%
1969	89%	82%	65%	86%	39%	80%
1970	91%	83%	73%	60%	48%	68%
1971	92%	73%	73%	51%	48%	14%
1972	89%	86%	71%	68%	49%	23%
1973	89%	71%	67%	61%	35%	32%
1974	92%	79%	70%	57%	45%	41%
1975	89%	82%	74%	54%	47%	23%
1976	90%	78%	76%	61%	52%	28%
1977	91%	81%	74%	52%	46%	23%

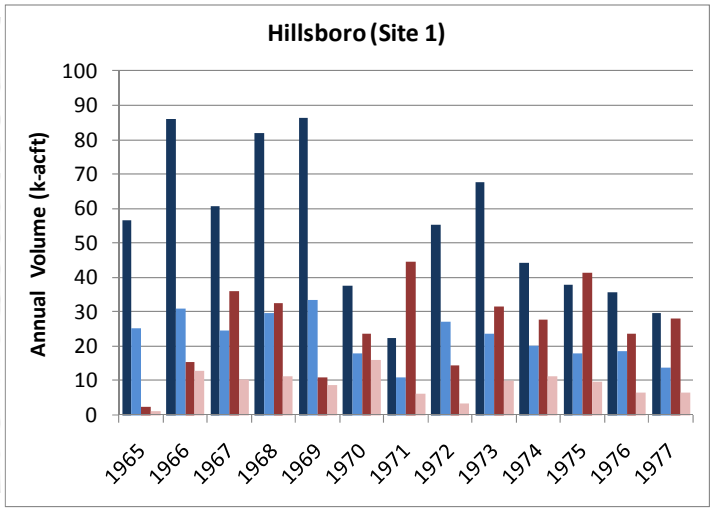

Legend

- Design Storage (injection)
- Modeled Storage (injection)
- Design Recovery (extraction)
- Modeled Recovery (extraction)

Notes:

Scenario 4 is a reduction of the wells from Scenario 3 which meets the requirements for pump pressure (100 psi). All wells are fully penetrating in their respective aquifers.

These three plots show the comparison between the SFWMM-D13R designed annual injection and extraction volumes at the ASR wells and the actual assigned rates for the RASRSM-D13R for three of the basins.

The table presents the percentage of SFWMM-D13R annual flow rates that are included in this scenario of the RASRSM-D13R. These percentages are not recovery efficiencies.

Scenario 4 – Comparison of Designed and Modeled ASR Flow Rates

Regional Model Production Scenario Report

Figure 4.87

June 2013

	Total	
	In %	Out %
1965	61%	66%
1966	44%	75%
1967	50%	47%
1968	44%	36%
1969	43%	83%
1970	44%	80%
1971	51%	42%
1972	64%	31%
1973	52%	33%
1974	51%	33%
1975	54%	26%
1976	61%	31%
1977	59%	43%

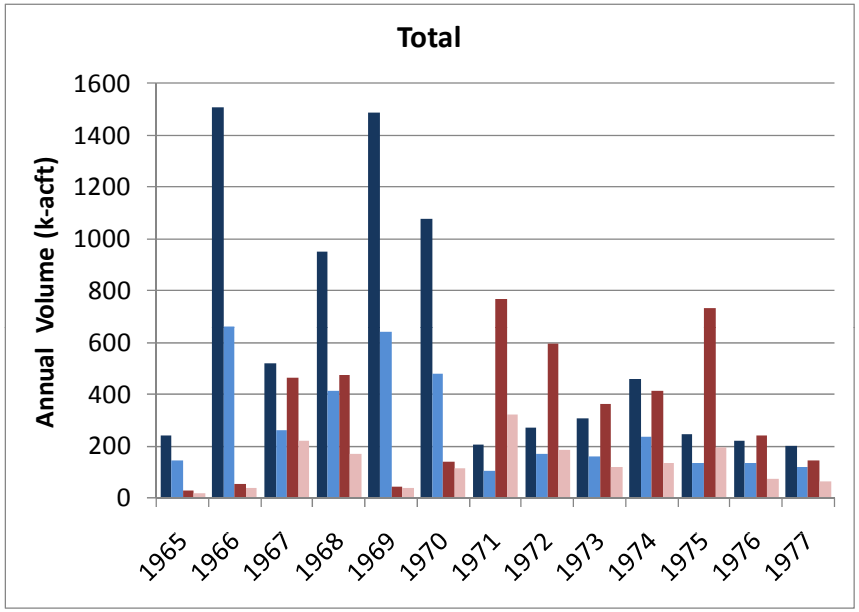

Legend

- Design Storage (injection)
- Modeled Storage (injection)
- Design Recovery (extraction)
- Modeled Recovery (extraction)

Notes:

Scenario 4 is a reduction of the wells from Scenario 3 which meets the requirements for pump pressure (100 psi). All wells are fully penetrating in their respective aquifers.

This plot shows the comparison between the SFWMM-D13R designed annual injection and extraction volumes at the ASR wells and the actual assigned rates for the RASRSM-D13R for all basins.

The table presents the percentage of SFWMM-D13R annual flow rates that are included in this scenario of the RASRSM-D13R. These percentages are not recovery efficiencies.

		UF		APPZ		BZ		Total # Wells	Target # Wells
		Number of Wells	Recovery Efficiency	Number of Wells	Recovery Efficiency	Number of Wells	Recovery Efficiency		
Caloosahatchee Basin	Moore Haven	4	70%	0	30%	6	0%		
	River Bend	3	70%	1	30%	2	0%		
	Flaghole	2	70%	0	30%	9	0%		
	Basin Total	9		1		17		27	44
Lake Okeechobee Basin	Nicodemus Slough	0	70%	10	30%	0	0%		
	C-41 Canal	0	70%	0	30%	5	0%		
	C-40 Canal	2	70%	0	30%	4	0%		
	North Lake Okeechobee	8	70%	2	30%	5	0%		
	Kissimmee R./Paradise Run	15	70%	0	30%	30	0%		
	Taylor Creek	0	70%	10	30%	5	0%		
	L-63N	0	70%	9	30%	3	0%		
	Lakeside Ranch	4	70%	0	30%	8	0%		
	Port Mayaca	18	70%	0	30%	1	0%		
	Basin Total	47		31		61		139	200
L-8		6	70%	0	30%	2	0%	8	10
C-51		12	70%	2	30%	10	0%	24	34
Central Palm Beach		10	70%	3	30%	1	0%	14	15
Site 1 (Hillsboro)		10	40%	0	40%	10	0%	20	30
Total		94		37		101		232	333

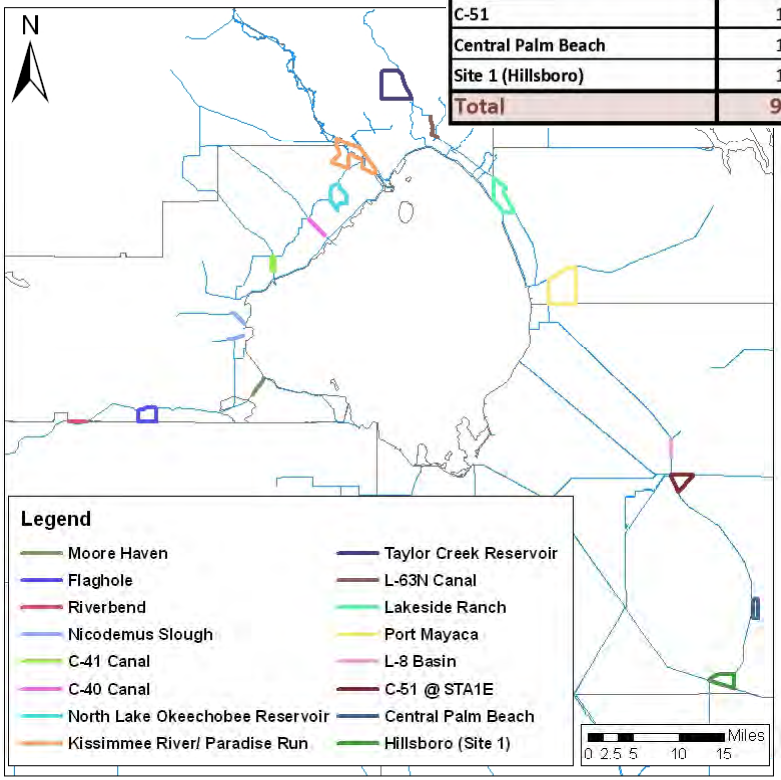

Notes:

Scenario 9 is similar to Scenario 5 except the BZ wells have been given a recovery efficiency of 0% (no recovery) and have been made 10 mgd wells. Therefore, there are half as many BZ wells. In a few sites, the numbers of wells in the UF or APPZ was adjusted slightly to prevent half wells in the BZ.

Flow rates are divided evenly among the wells in each basin. Maximum flow rate for any one well is 5 mgd in the UF and APPZ and 10 mgd in the BZ.

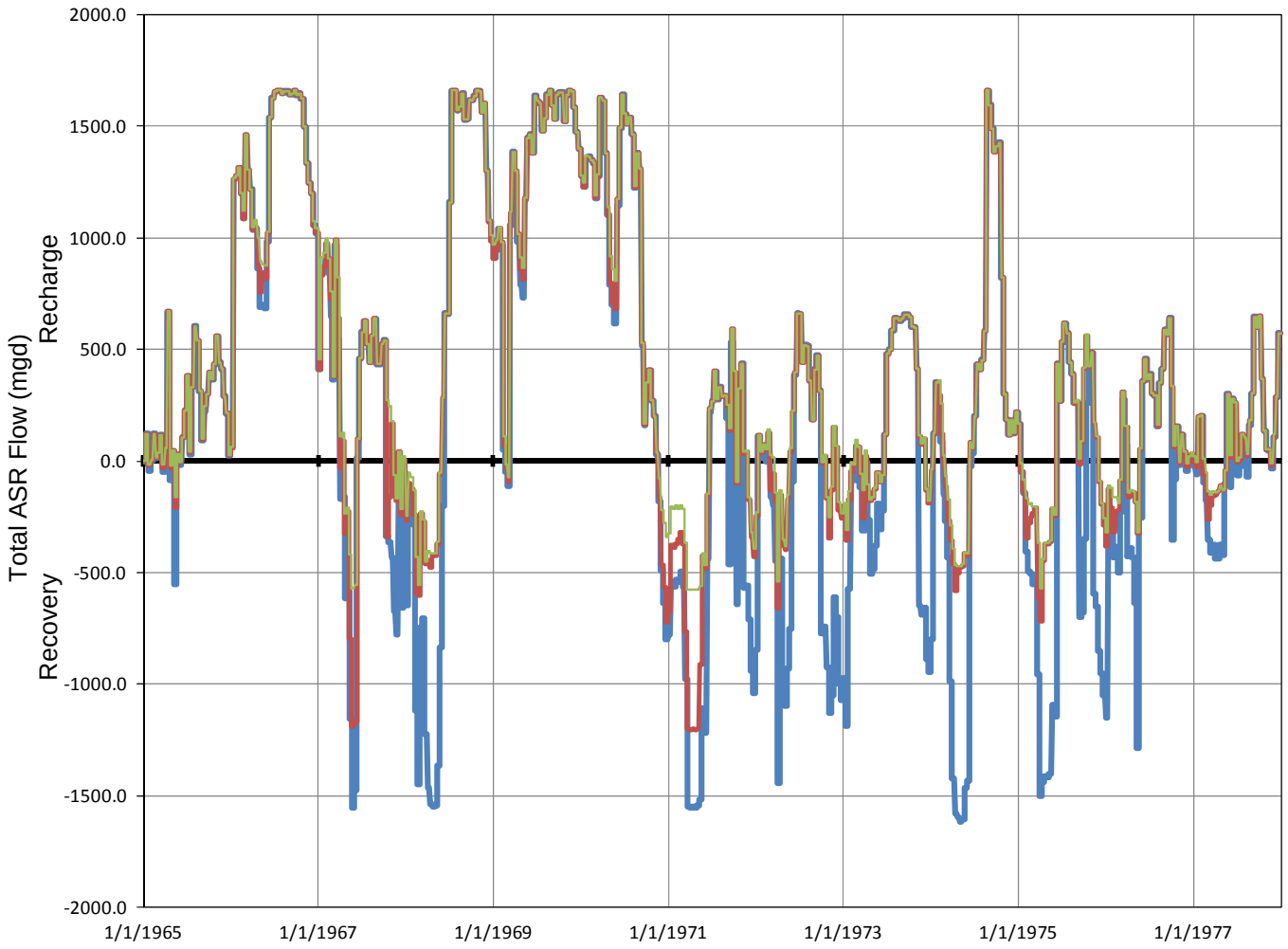

Legend

- Scenario 1 – ASR Flux
- Scenario 5 – ASR Flux
- Scenario 9 – ASR Flux

Notes:

Scenario 9 is similar to Scenario 5 except the BZ wells have been given a recovery efficiency of 0% (no recovery) and have been made 10 gpm wells. Therefore, there are half as many BZ wells. In a few sites, the numbers of wells in the UF or APPZ was adjusted slightly to prevent half wells in the BZ.

This plot shows the extraction and injection rates for all wells at all sites for Scenario 1, Scenario 5 and Scenario 9. Positive rates are recharge (injection), while negative rates are recovery (extraction).

Scenario 9 – ASR Well Fluxes (Compared to Runs 1 & 5)

Regional Model Production Scenario Report

Figure 4.90

June 2013

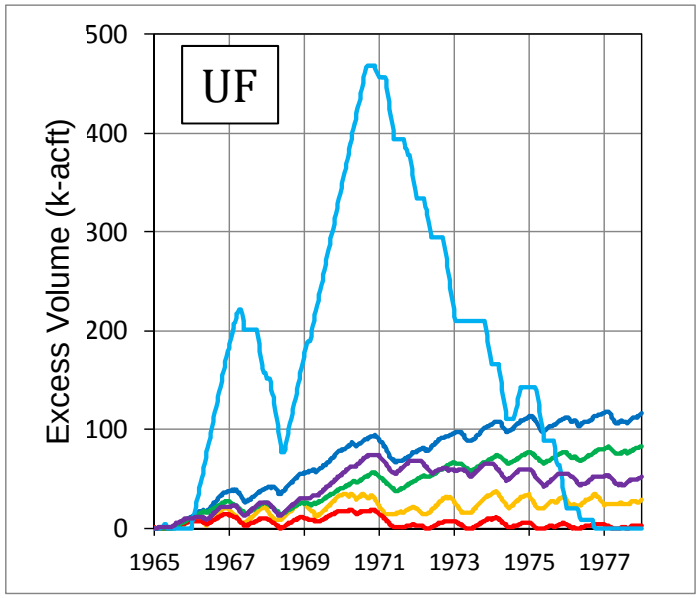

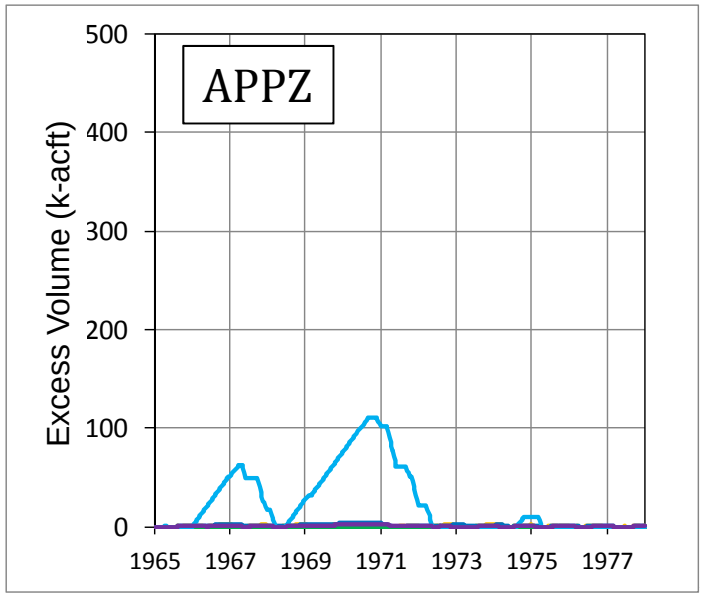

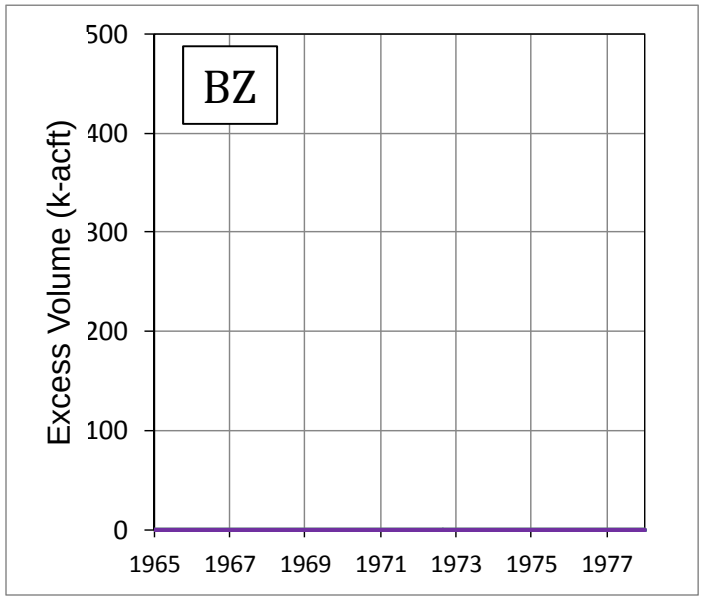

Legend

- Central Palm Beach
- C-51
- Hillsboro
- L-8
- Lake Okeechobee
- Caloosahatchee River

Notes:

Scenario 9 is similar to Scenario 5 except the BZ wells have been given a recovery efficiency of 0% (no recovery) and have been made 10 gpm wells. Therefore, there are half as many BZ wells. In a few sites, the numbers of wells in the UF or APPZ was adjusted slightly to prevent half wells in the BZ.

These plots show the excess volume of fresh water remaining in each aquifer at each ASR basin. Excess volume is calculated by adding injected volume times recovery efficiency and subtracting extracted volume. The calculation is cumulative.

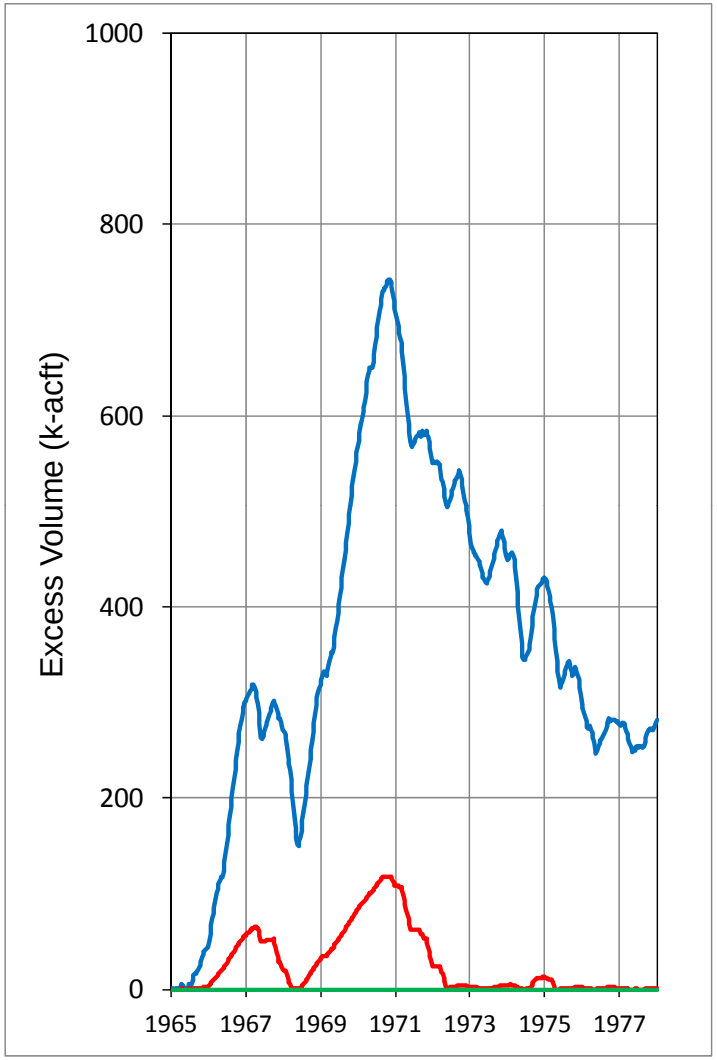

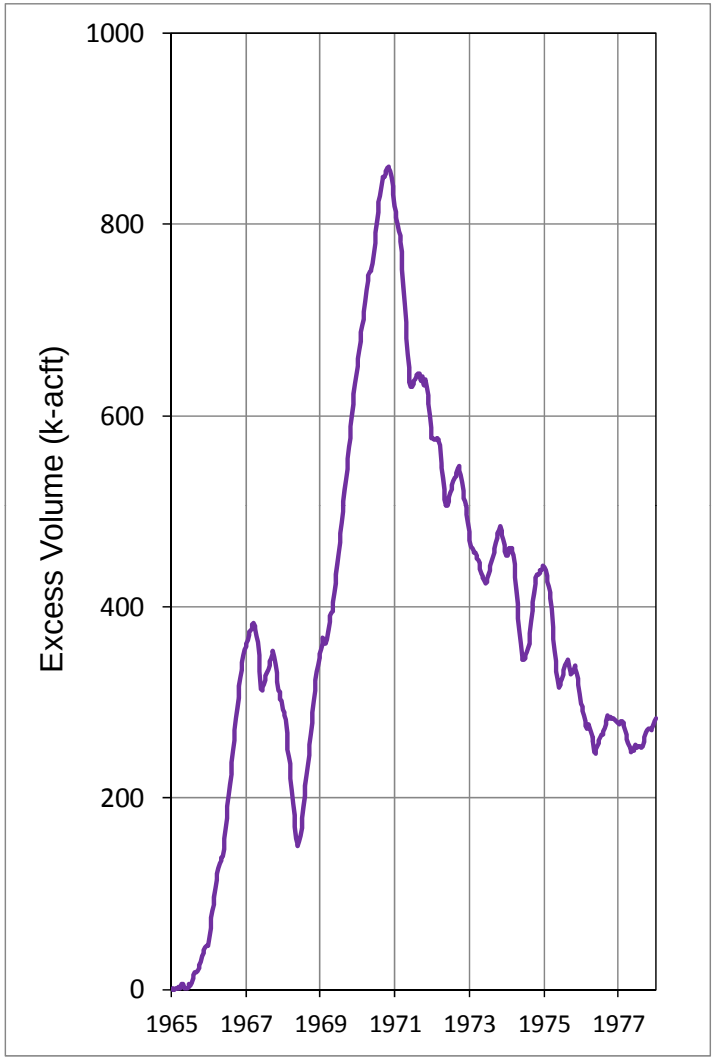

Legend

- Total UF
- Total APPZ
- Total BZ
- Total (All Aquifers)

Notes:

Scenario 9 is similar to Scenario 5 except the BZ wells have been given a recovery efficiency of 0% (no recovery) and have been made 10 gpm wells. Therefore, there are half as many BZ wells. In a few sites, the numbers of wells in the UF or APPZ was adjusted slightly to prevent half wells in the BZ.

These plots show the total excess volume of fresh water remaining in each aquifer and in all aquifers. Excess volume is calculated by adding injected volume times recovery efficiency and subtracting extracted volume. The calculation is cumulative.

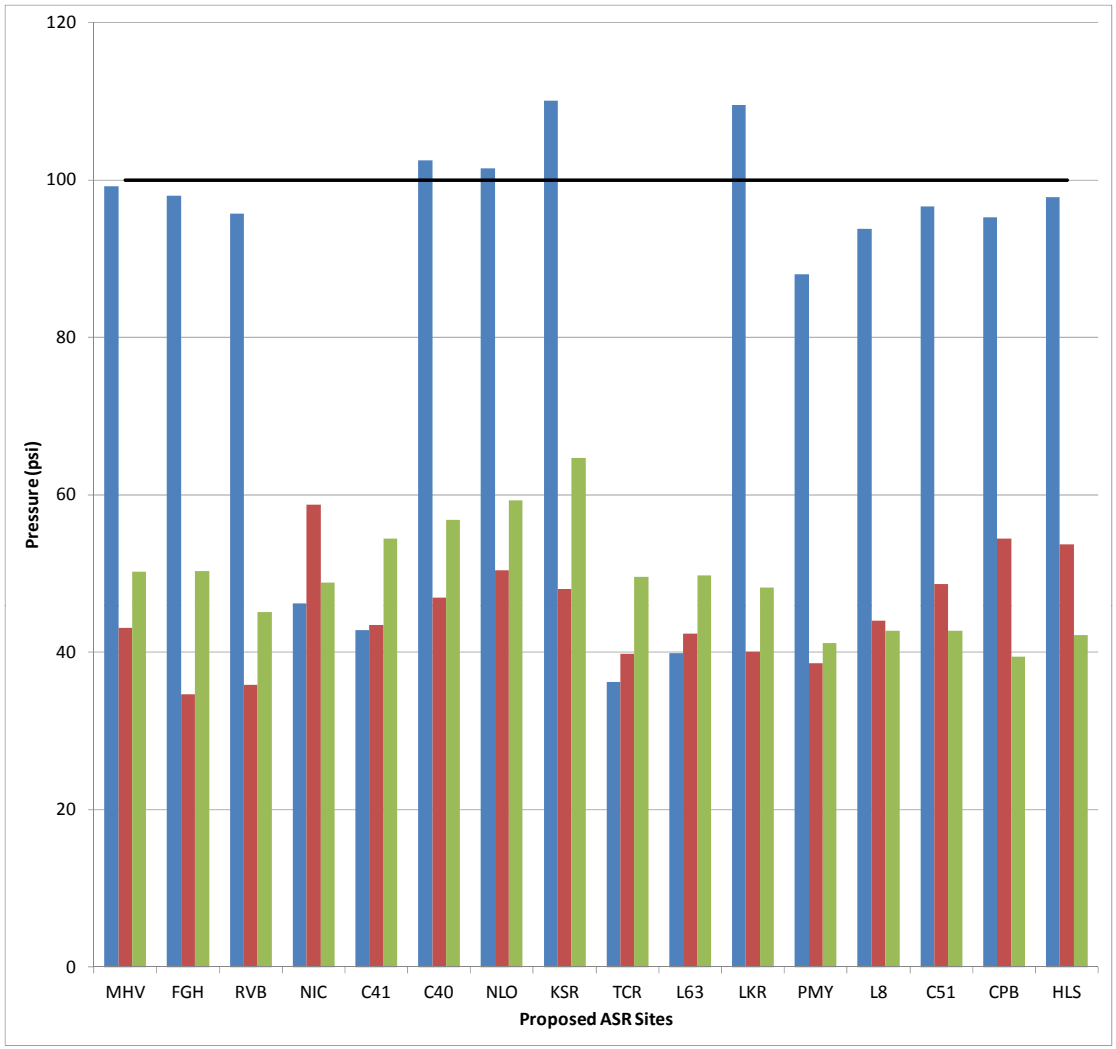

MHV	Moorehaven
FGH	Flaghole
RVB	Riverbend
NIC	Nicodemus Slough
C41	C-41Canal
C40	C-40 Canal
NLO	North Lake Okeechobee Reservoir
KSR	Kissimmee River / Paradise Run
TCR	Taylor Creek Reservoir
L63	L-63N Canal
LKR	Lakeside Ranch
PMY	Port Mayaca
L8	L-8 Basin
C51	C-51 @ STA1E
CPB	Central Palm Beach
HLS	Hillsboro (Site 1)

Legend

- Upper Floridan Aquifer
- Avon Park Permeable Zone
- Boulder Zone
- 100 psi Limit

Notes:

Scenario 9 is similar to Scenario 5 except the BZ wells have been given a recovery efficiency of 0% (no recovery) and have been made 10 gpm wells. Therefore, there are half as many BZ wells. In a few sites, the numbers of wells in the UF or APPZ was adjusted slightly to prevent half wells in the BZ.

This plot shows the highest pressure at each site which the pump would need to overcome in order to inject storage water during the 13-year simulation.

The PDT determined that it would be important to keep this pressure below 100 psi (indicated by the heavy black line).

Note that maximum pressures are shown for all aquifers and all sites even if ASR pumps are not located there for the current scenario.

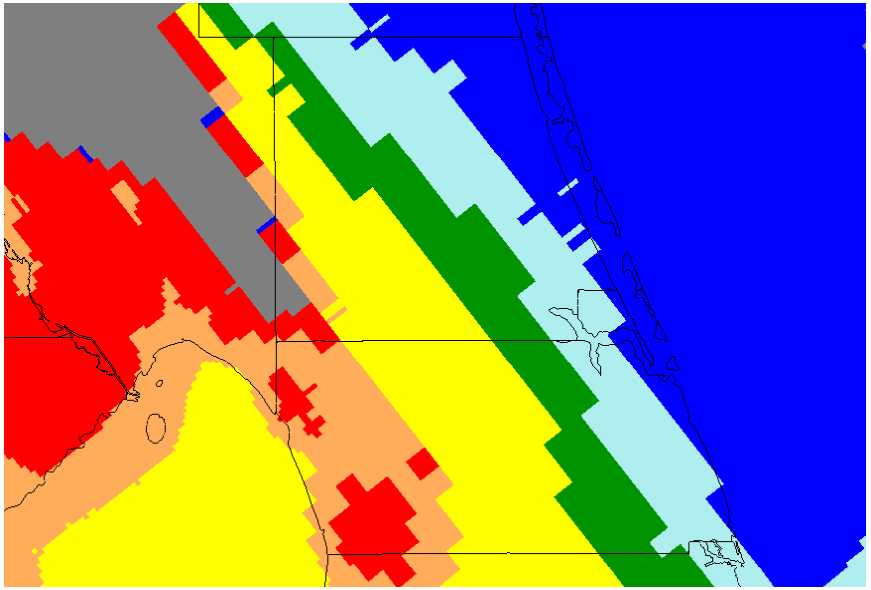

Upper Floridan Aquifer

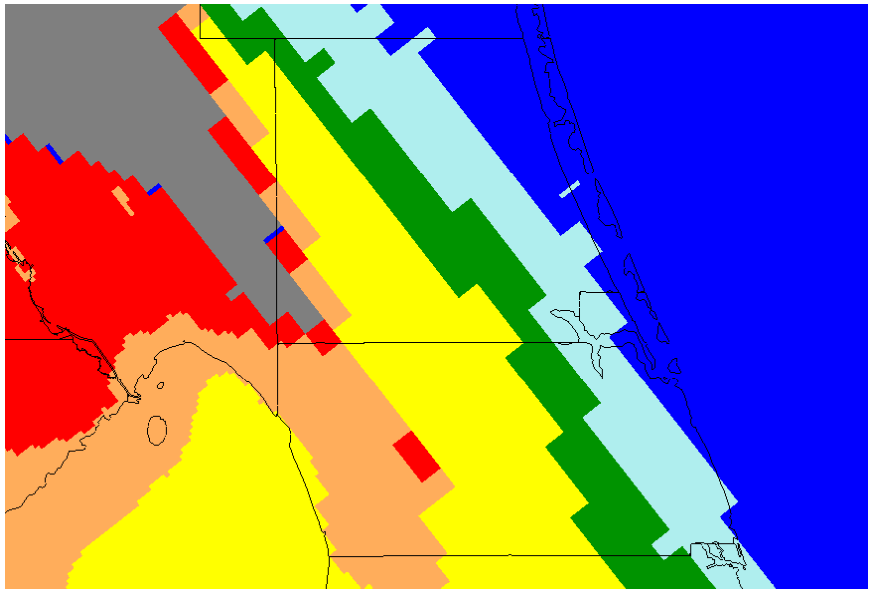

Avon Park Permeable Zone

Legend

- Not artesian or no reduction
- < 5%
- 5% - 10%
- 10% - 20%
- 20% - 50%
- 50% - 100%
- Loses artesian condition

Notes:

Scenario 9 is similar to Scenario 5 except the BZ wells have been given a recovery efficiency of 0% (no recovery) and have been made 10 gpm wells. Therefore, there are half as many BZ wells. In a few sites, the numbers of wells in the UF or APPZ was adjusted slightly to prevent half wells in the BZ.

These plots show the maximum reduction in artesian flow at each model cell as a percentage when compared to the flow expected without the ASR project.

Permit rules require that the reduction in Saint Lucie and Martin Counties be less than 10%.

Note the gray area in the northwest corner of the figures, which coincides with a ridge and does not normally have artesian conditions.

Scenario 9 – Maximum Reduction in Artesian Flow Capacity

Regional Model Production Scenario Report

Figure 4.94

June 2013

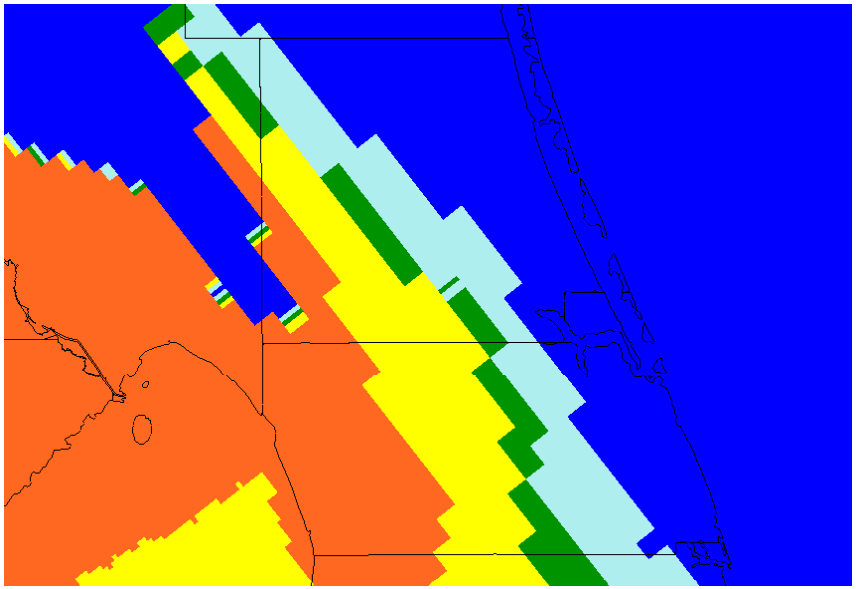

Upper Floridan Aquifer

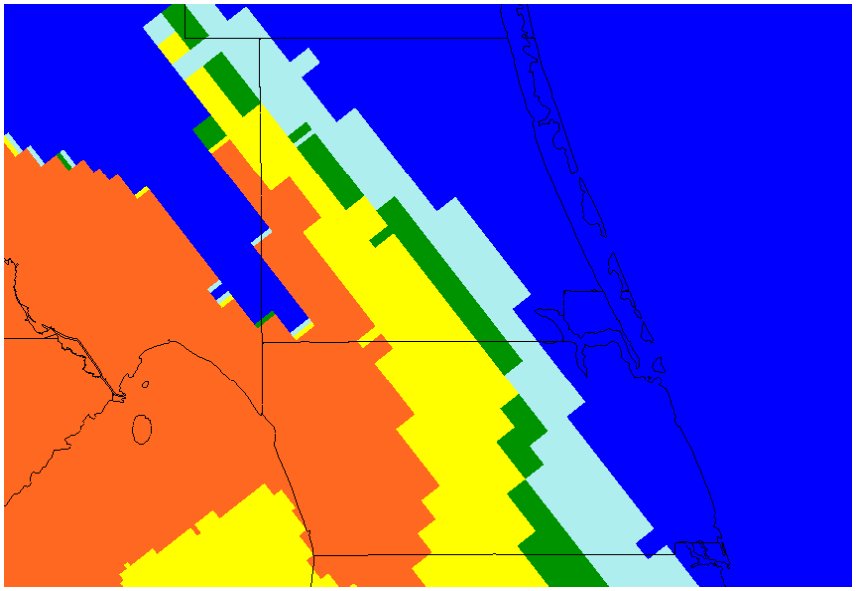

Avon Park Permeable Zone

Legend

- 0 days
- 1 – 250 days
- 250 – 500 days
- 500 – 1000 days
- 1000 – 2000 days
- > 2000 days

Notes:

Scenario 9 is similar to Scenario 5 except the BZ wells have been given a recovery efficiency of 0% (no recovery) and have been made 10 gpm wells. Therefore, there are half as many BZ wells. In a few sites, the numbers of wells in the UF or APPZ was adjusted slightly to prevent half wells in the BZ.

These plots indicate the severity of the loss of artesian pressure due to ASR extraction pumping.

Permit rules require that the reduction in Saint Lucie and Martin Counties be less than 10%. This plot indicates the number of days during the simulation in which the flow reduction was greater than 10%. There are 4748 days in the 13-year model simulation period.

Note the blue area in the northwest corner of the figures, which coincides with a ridge and does not normally have artesian conditions.

SCENARIO 9 – NUMBER OF DAYS (OUT OF 13 YEARS) WITH FLOW REDUCTION EXCEEDING 10%

REGIONAL MODEL PRODUCTION SCENARIO REPORT

FIGURE 4.95

JUNE 2013

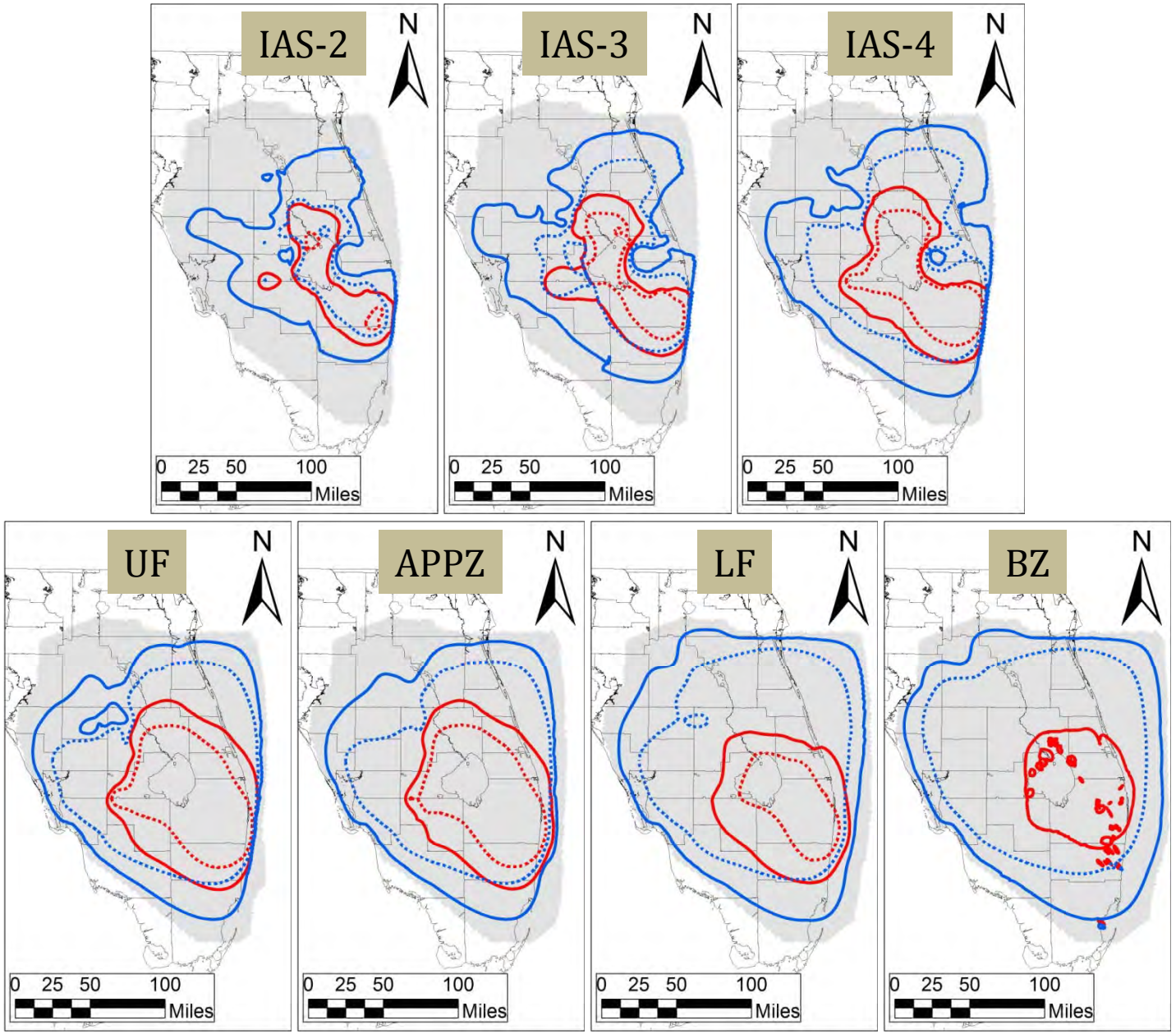

Legend

Maximum Drawdown
- 1 foot
- 5 feet

Maximum "Drawup"
- 1 foot
- 5 feet

Model Domain

Notes:

Scenario 9 is similar to Scenario 5 except the BZ wells have been given a recovery efficiency of 0% (no recovery) and have been made 10 gpm wells. Therefore, there are half as many BZ wells. In a few sites, the numbers of wells in the UF or APPZ was adjusted slightly to prevent half wells in the BZ.

These figures show the extent of the areas where the maximum drawdown or "drawup" is greater than 1 foot or 5 feet.

The maximum condition does not necessarily occur at the same time for all regions of the model.

SCENARIO 9 – MAXIMUM DRAWDOWN AND "DRAWUP" BY AQUIFER

REGIONAL MODEL PRODUCTION SCENARIO REPORT

FIGURE 4.96

JUNE 2013

5-Mile Distance

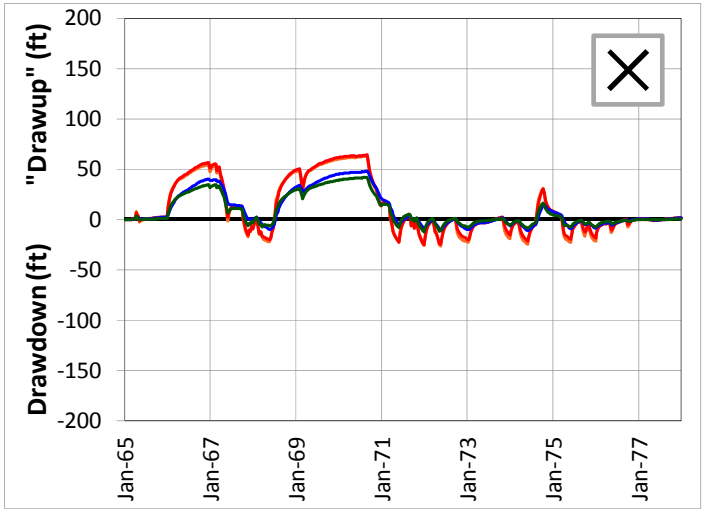

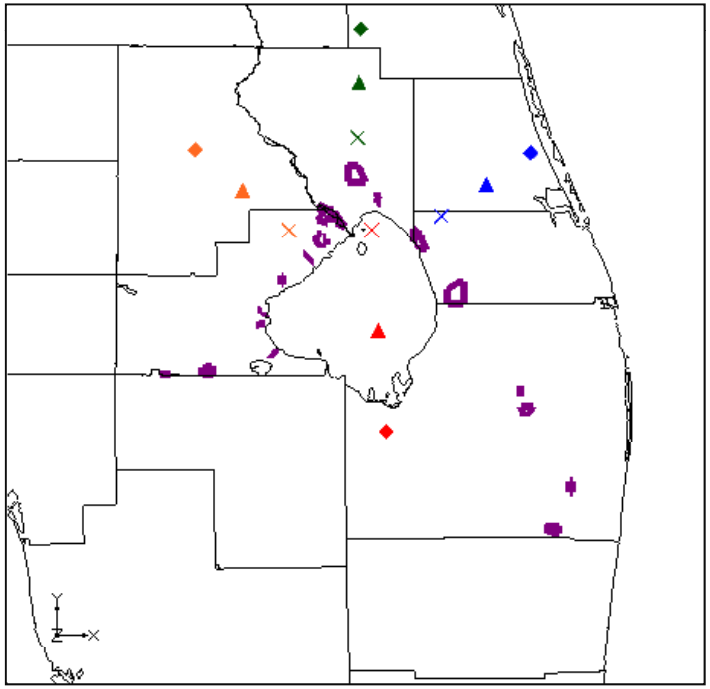

15-Mile Distance

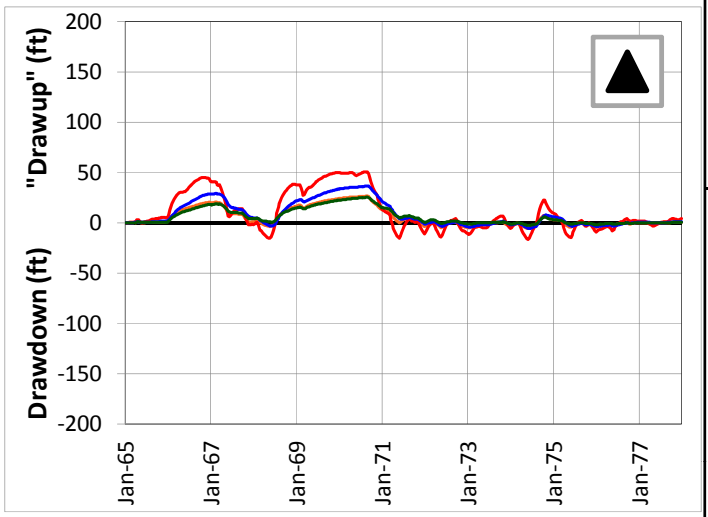

25-Mile Distance

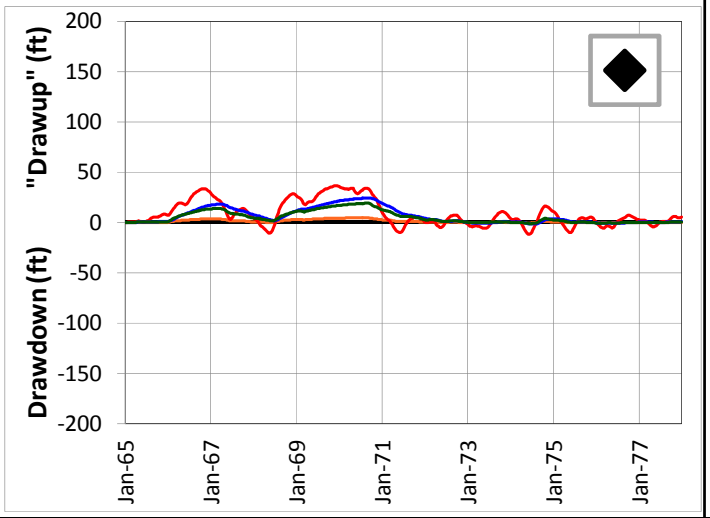

Legend

- CERP ASR Sites
- ✕ 5-Mile Distance Locations
- ▲ 15-Mile Distance Locations
- ◆ 25-Mile Distance Locations

Notes:

Scenario 9 is similar to Scenario 5 except the BZ wells have been given a recovery efficiency of 0% (no recovery) and have been made 10 gpm wells. Therefore, there are half as many BZ wells. In a few sites, the numbers of wells in the UF or APPZ was adjusted slightly to prevent half wells in the BZ.

A number of individual sites were chosen from the UF Aquifer at distances of 5, 15 and 25 miles from the proposed ASR well sites. This figure shows the drawdown and "drawup" at each output time step for 12 of these sites.

The plots were calculated by subtracting the heads calculated by the D13R model from those calculated by the no project run. This results in a positive value for "drawup" and a negative value for drawdown.

The colors of the points on the map correspond to the colors of the lines on the plots.

The symbols on the map (x, triangle and diamond) indicate the distance from the ASR sites.

5-Mile Distance

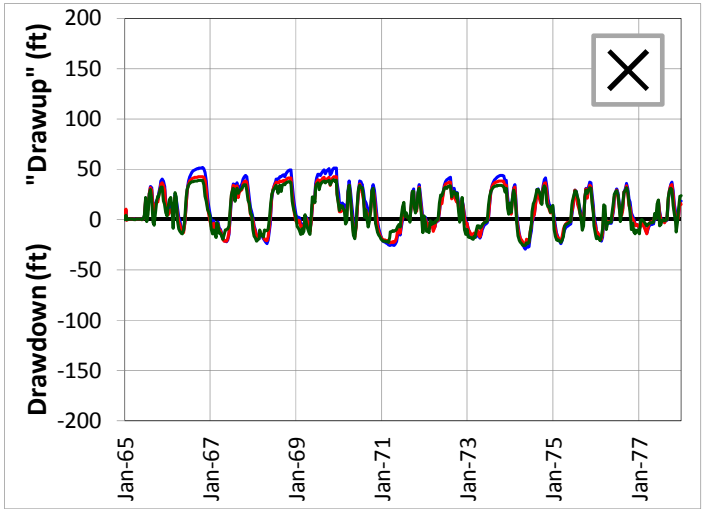

15-Mile Distance

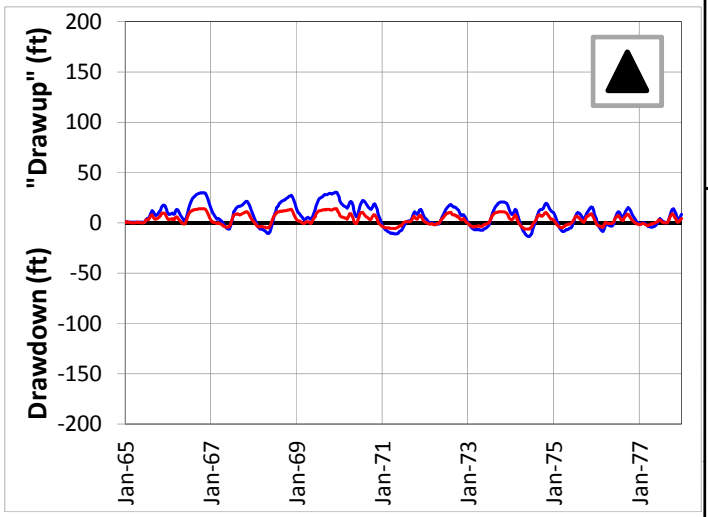

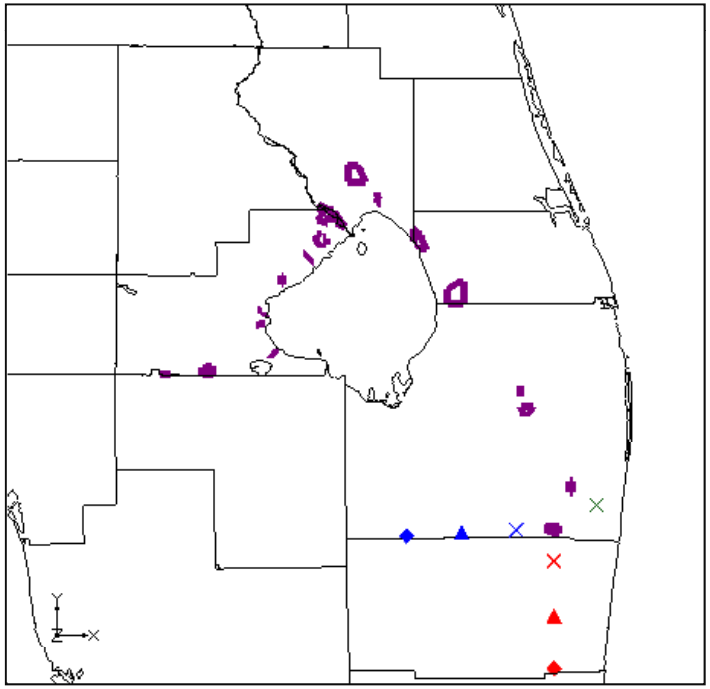

25-Mile Distance

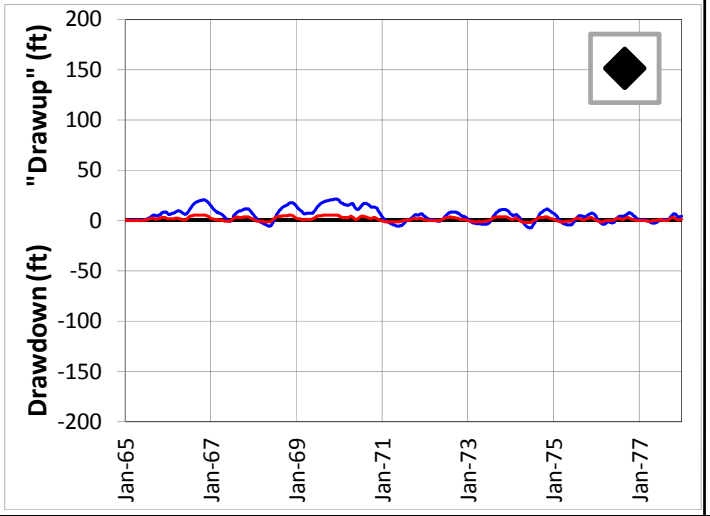

Legend

- CERP ASR Sites
- 5-Mile Distance Locations
- 15-Mile Distance Locations
- 25-Mile Distance Locations

Notes:

Scenario 9 is similar to Scenario 5 except the BZ wells have been given a recovery efficiency of 0% (no recovery) and have been made 10 gpm wells. Therefore, there are half as many BZ wells. In a few sites, the numbers of wells in the UF or APPZ was adjusted slightly to prevent half wells in the BZ.

A number of individual sites were chosen from the UF Aquifer at distances of 5, 15 and 25 miles from the proposed ASR well sites. This figure shows the drawdown and "drawup" at each output time step for 7 of these sites.

The plots were calculated by subtracting the heads calculated by the D13R model from those calculated by the no project run. This results in a positive value for "drawup" and a negative value for drawdown.

The colors of the points on the map correspond to the colors of the lines on the plots.

The symbols on the map (x, triangle and diamond) indicate the distance from the ASR sites.

5-Mile Distance

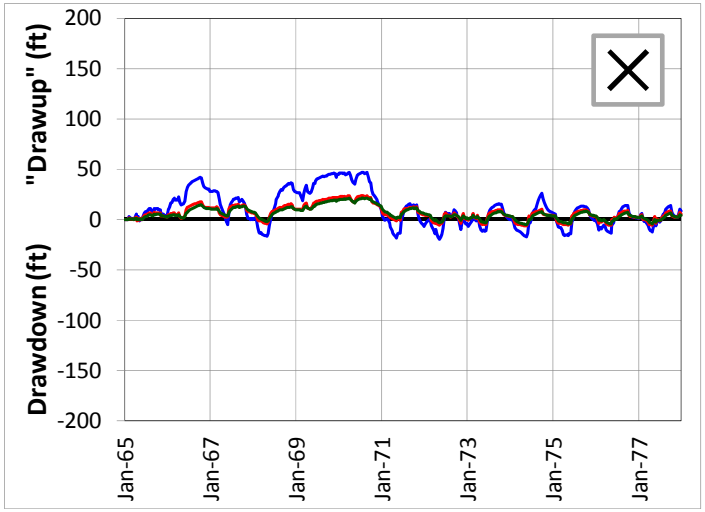

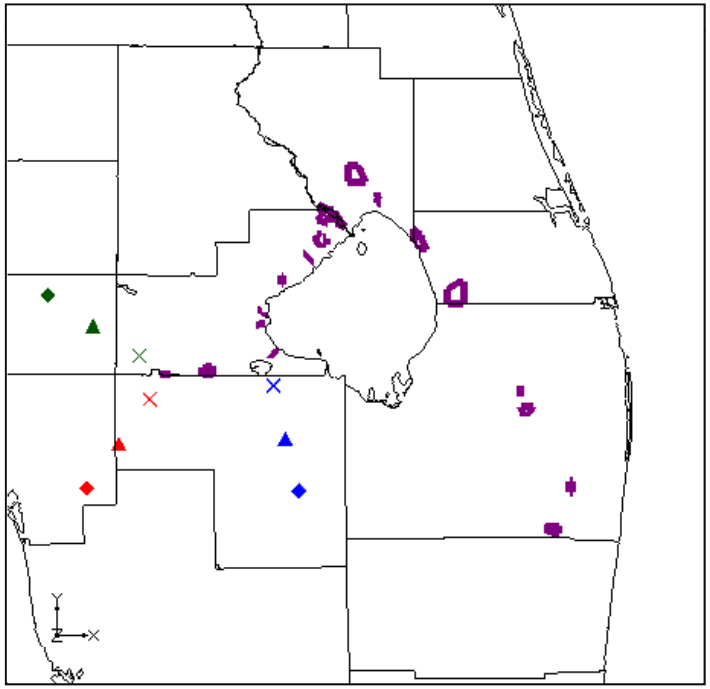

15-Mile Distance

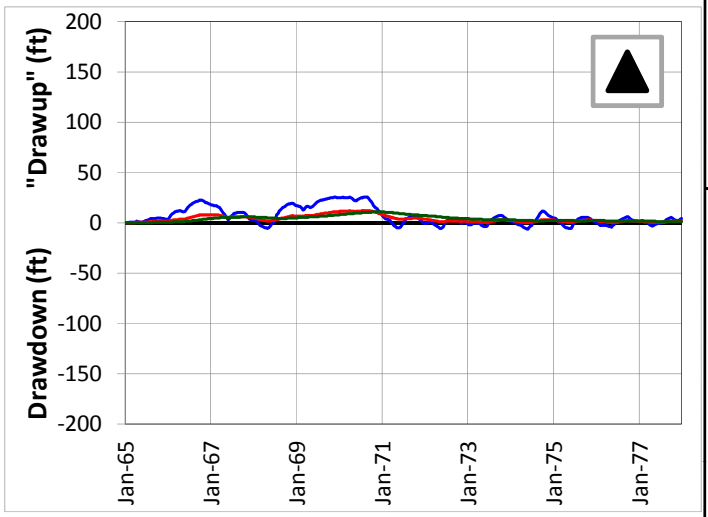

25-Mile Distance

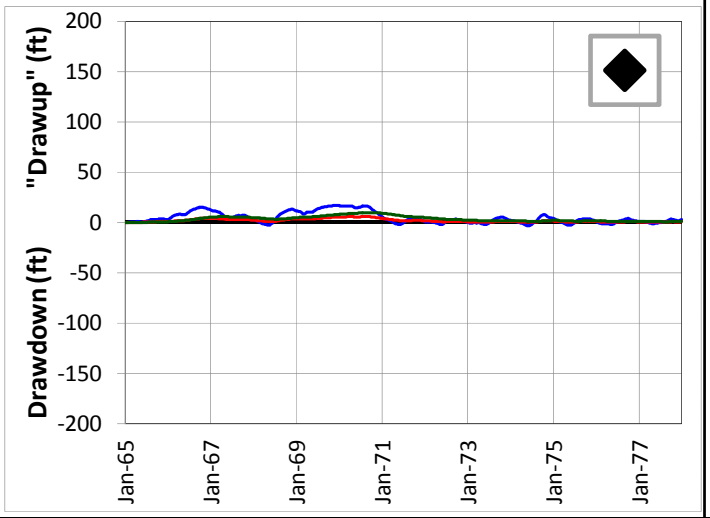

Legend

- CERP ASR Sites
- 5-Mile Distance Locations
- 15-Mile Distance Locations
- 25-Mile Distance Locations

Notes:

Scenario 9 is similar to Scenario 5 except the BZ wells have been given a recovery efficiency of 0% (no recovery) and have been made 10 gpm wells. Therefore, there are half as many BZ wells. In a few sites, the numbers of wells in the UF or APPZ was adjusted slightly to prevent half wells in the BZ.

A number of individual sites were chosen from the UF Aquifer at distances of 5, 15 and 25 miles from the proposed ASR well sites. This figure shows the drawdown and "drawup" at each output time step for 9 of these sites.

The plots were calculated by subtracting the heads calculated by the D13R model from those calculated by the no project run. This results in a positive value for "drawup" and a negative value for drawdown.

The colors of the points on the map correspond to the colors of the lines on the plots.

The symbols on the map (x, triangle and diamond) indicate the distance from the ASR sites.

5-Mile Distance

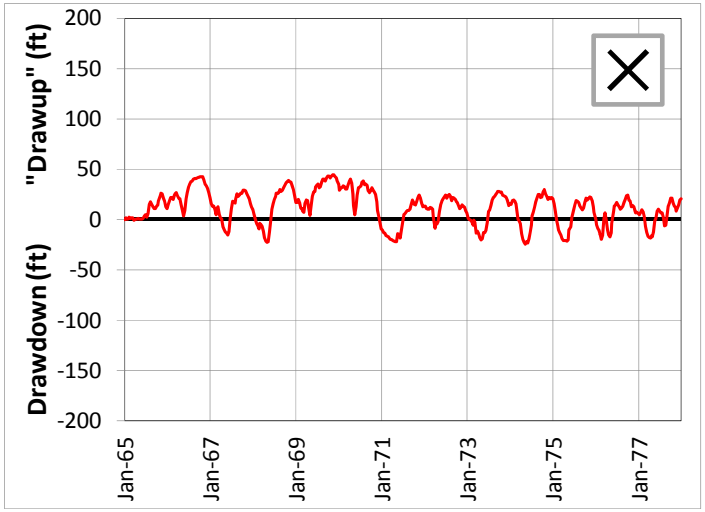

15-Mile Distance

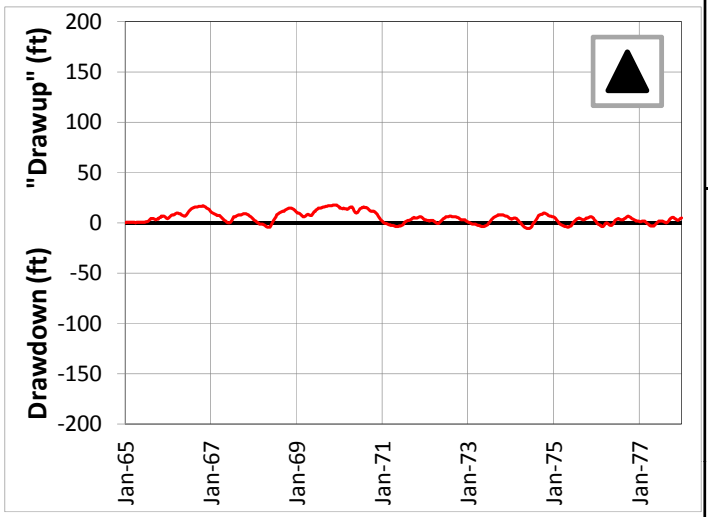

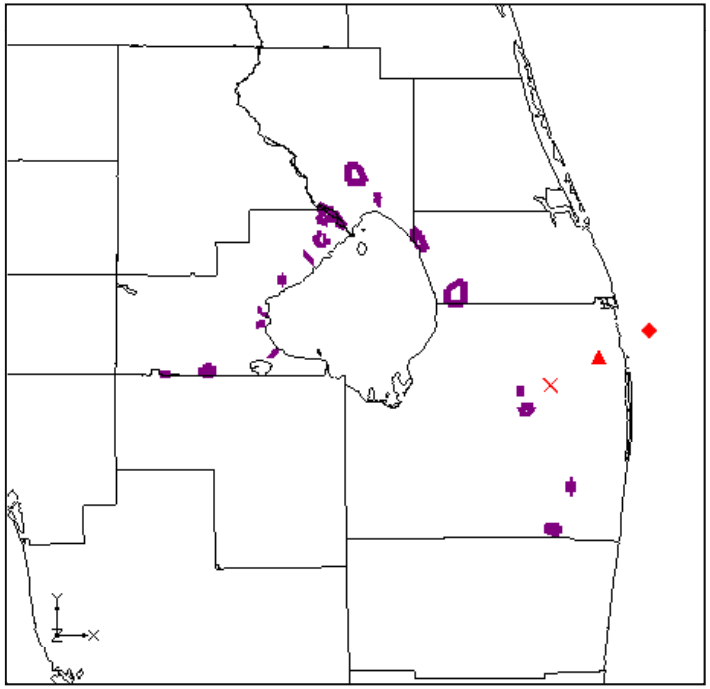

25-Mile Distance

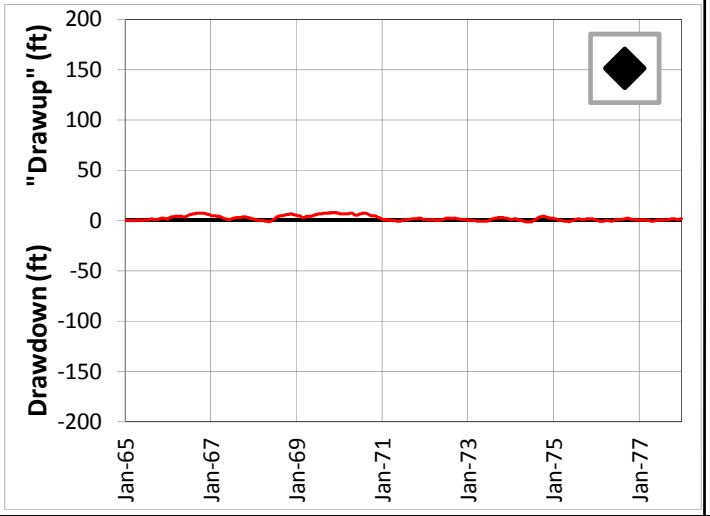

Legend

- CERP ASR Sites
- 5-Mile Distance Locations
- 15-Mile Distance Locations
- 25-Mile Distance Locations

Notes:

Scenario 9 is similar to Scenario 5 except the BZ wells have been given a recovery efficiency of 0% (no recovery) and have been made 10 gpm wells. Therefore, there are half as many BZ wells. In a few sites, the numbers of wells in the UF or APPZ was adjusted slightly to prevent half wells in the BZ.

A number of individual sites were chosen from the UF Aquifer at distances of 5, 15 and 25 miles from the proposed ASR well sites. This figure shows the drawdown and "drawup" at each output time step for 3 of these sites.

The plots were calculated by subtracting the heads calculated by the D13R model from those calculated by the no project run. This results in a positive value for "drawup" and a negative value for drawdown.

The colors of the points on the map correspond to the colors of the lines on the plots.

The symbols on the map (x, triangle and diamond) indicate the distance from the ASR sites.

5-Mile Distance

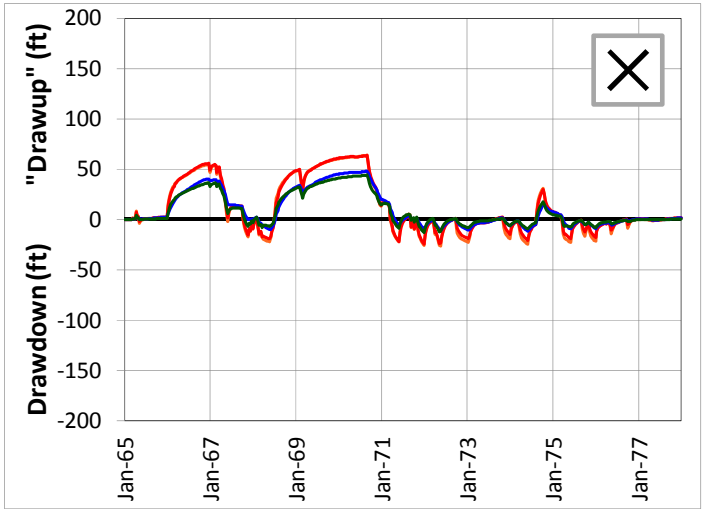

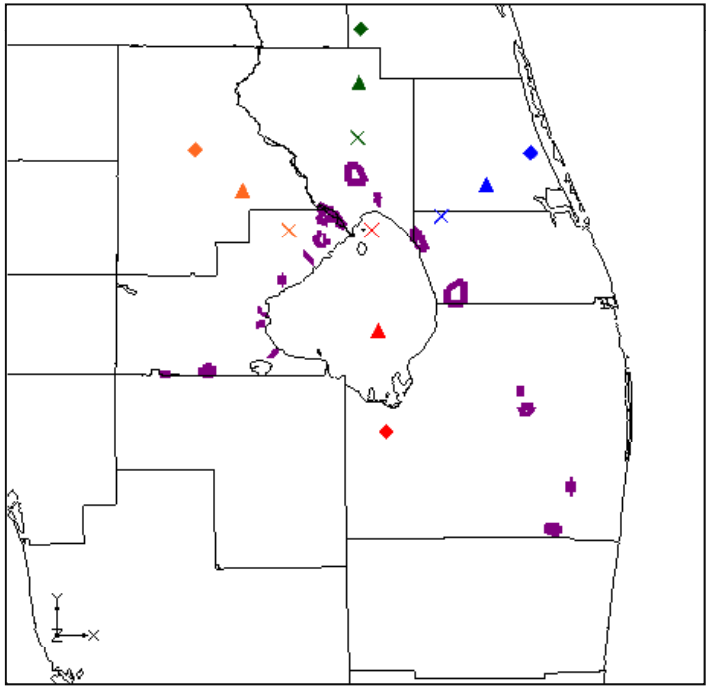

15-Mile Distance

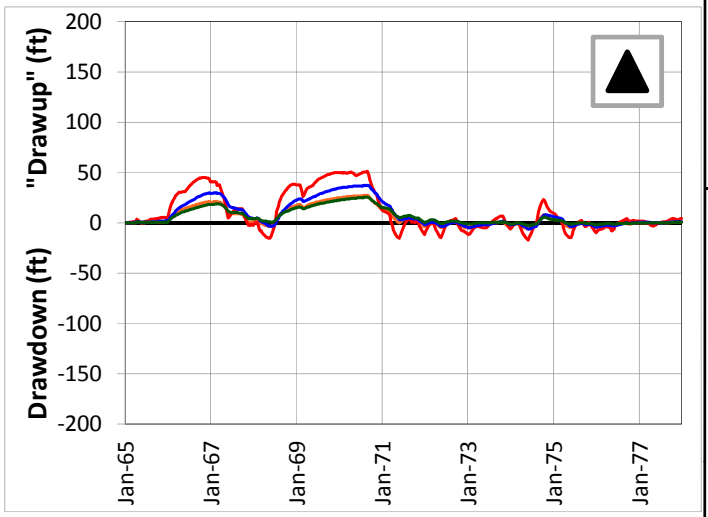

25-Mile Distance

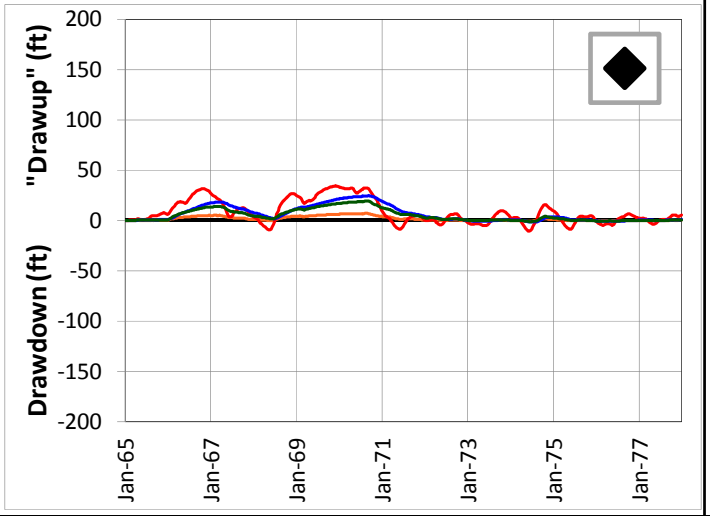

Legend

- CERP ASR Sites
- ✕ 5-Mile Distance Locations
- ▲ 15-Mile Distance Locations
- ◆ 25-Mile Distance Locations

Notes:

Scenario 9 is similar to Scenario 5 except the BZ wells have been given a recovery efficiency of 0% (no recovery) and have been made 10 gpm wells. Therefore, there are half as many BZ wells. In a few sites, the numbers of wells in the UF or APPZ was adjusted slightly to prevent half wells in the BZ.

A number of individual sites were chosen from the APPZ Aquifer at distances of 5, 15 and 25 miles from the proposed ASR well sites. This figure shows the drawdown and "drawup" at each output time step for 12 of these sites.

The plots were calculated by subtracting the heads calculated by the D13R model from those calculated by the no project run. This results in a positive value for "drawup" and a negative value for drawdown.

The colors of the points on the map correspond to the colors of the lines on the plots.

The symbols on the map (x, triangle and diamond) indicate the distance from the ASR sites.

5-Mile Distance

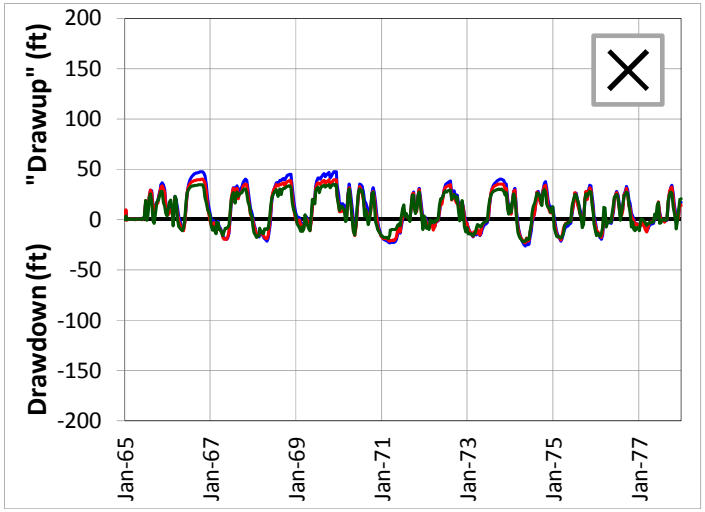

15-Mile Distance

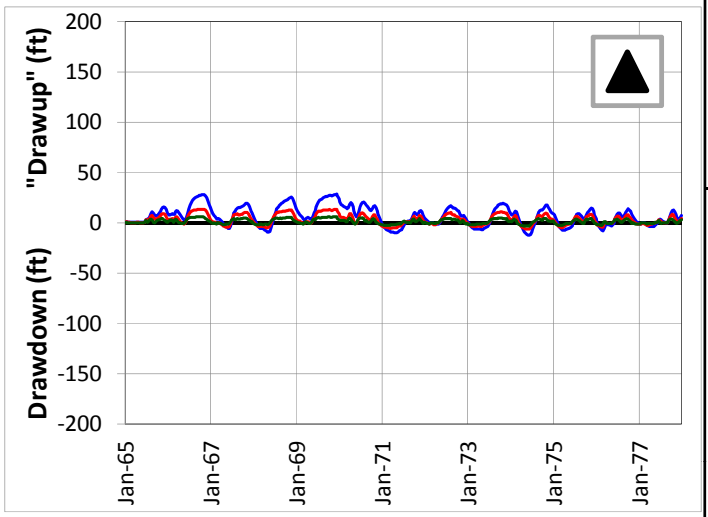

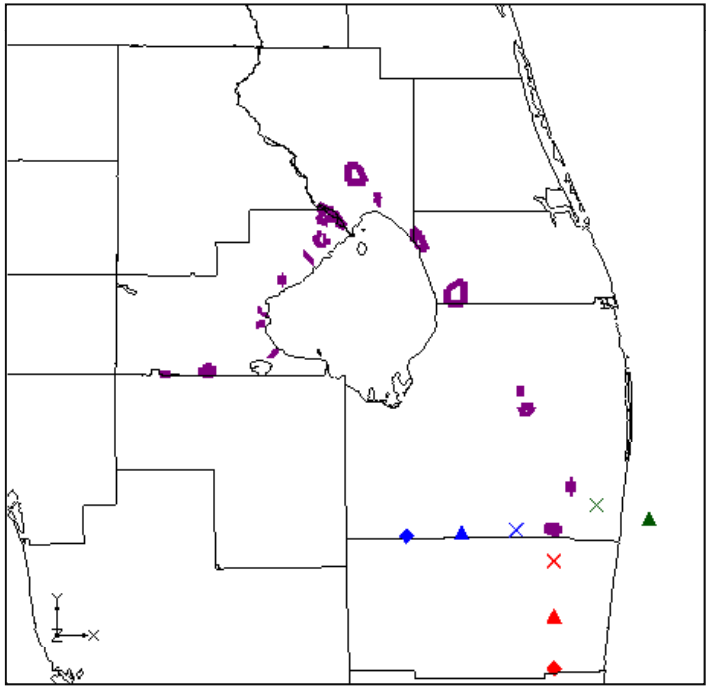

25-Mile Distance

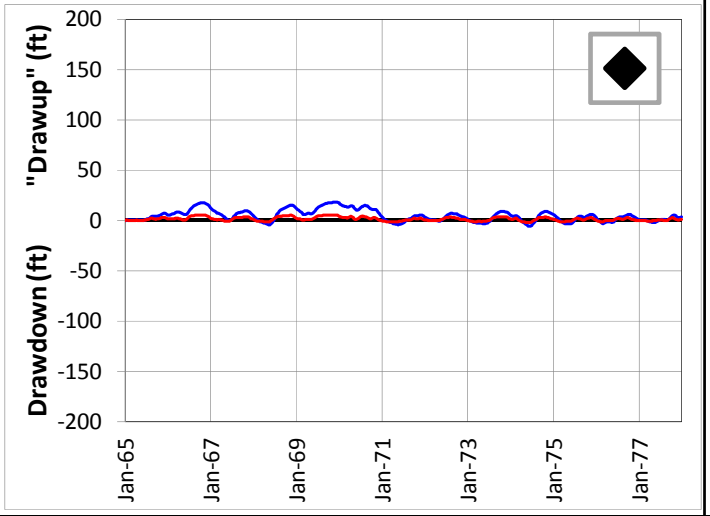

Legend

- CERP ASR Sites
- 5-Mile Distance Locations
- 15-Mile Distance Locations
- 25-Mile Distance Locations

Notes:

Scenario 9 is similar to Scenario 5 except the BZ wells have been given a recovery efficiency of 0% (no recovery) and have been made 10 gpm wells. Therefore, there are half as many BZ wells. In a few sites, the numbers of wells in the UF or APPZ was adjusted slightly to prevent half wells in the BZ.

A number of individual sites were chosen from the APPZ Aquifer at distances of 5, 15 and 25 miles from the proposed ASR well sites. This figure shows the drawdown and "drawup" at each output time step for 8 of these sites.

The plots were calculated by subtracting the heads calculated by the D13R model from those calculated by the no project run. This results in a positive value for "drawup" and a negative value for drawdown.

The colors of the points on the map correspond to the colors of the lines on the plots.

The symbols on the map (x, triangle and diamond) indicate the distance from the ASR sites.

SCENARIO 9 – DRAWDOWN AND "DRAWUP" – APPZ

REGIONAL MODEL PRODUCTION SCENARIO REPORT

FIGURE 4.102

JUNE 2013

5-Mile Distance

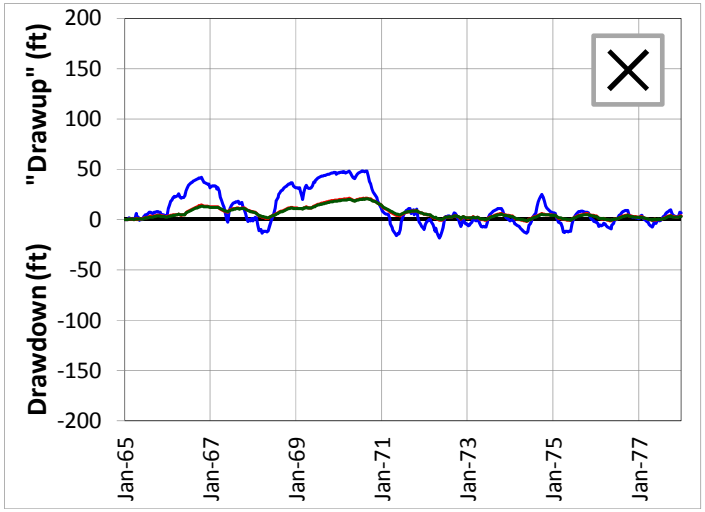

15-Mile Distance

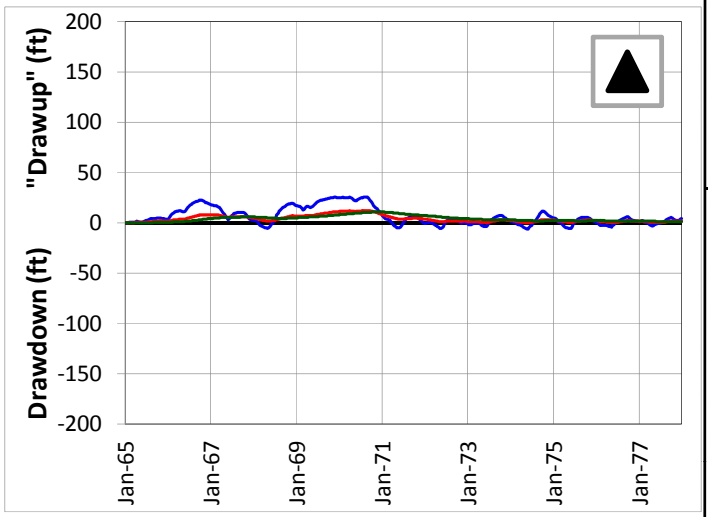

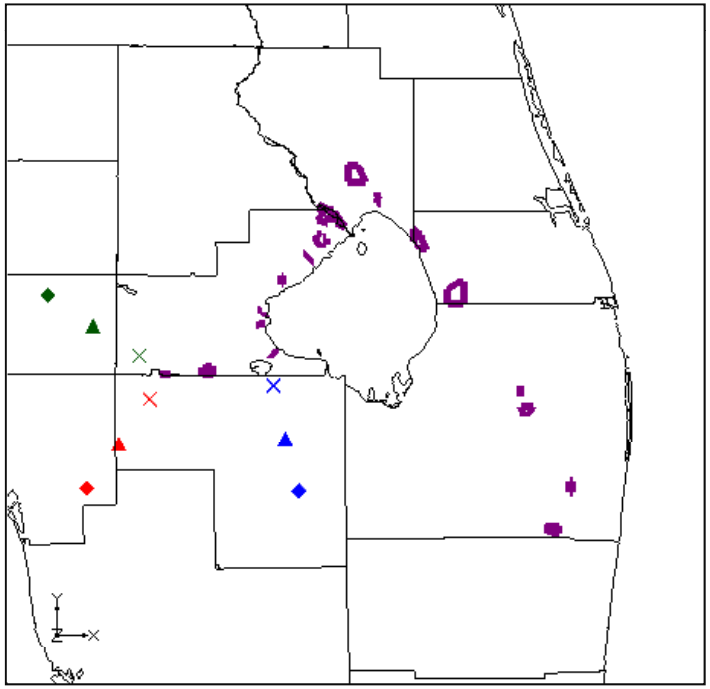

25-Mile Distance

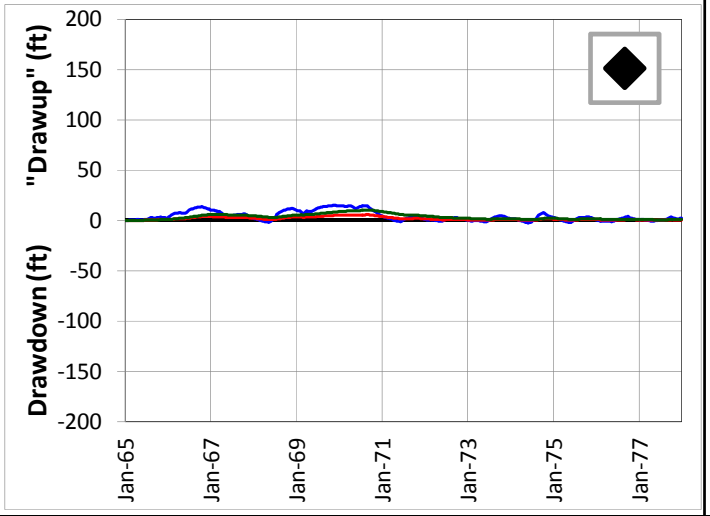

Legend

- CERP ASR Sites
- 5-Mile Distance Locations
- 15-Mile Distance Locations
- 25-Mile Distance Locations

Notes:

Scenario 9 is similar to Scenario 5 except the BZ wells have been given a recovery efficiency of 0% (no recovery) and have been made 10 gpm wells. Therefore, there are half as many BZ wells. In a few sites, the numbers of wells in the UF or APPZ was adjusted slightly to prevent half wells in the BZ.

A number of individual sites were chosen from the APPZ Aquifer at distances of 5, 15 and 25 miles from the proposed ASR well sites. This figure shows the drawdown and "drawup" at each output time step for 9 of these sites.

The plots were calculated by subtracting the heads calculated by the D13R model from those calculated by the no project run. This results in a positive value for "drawup" and a negative value for drawdown.

The colors of the points on the map correspond to the colors of the lines on the plots.

The symbols on the map (x, triangle and diamond) indicate the distance from the ASR sites.

5-Mile Distance

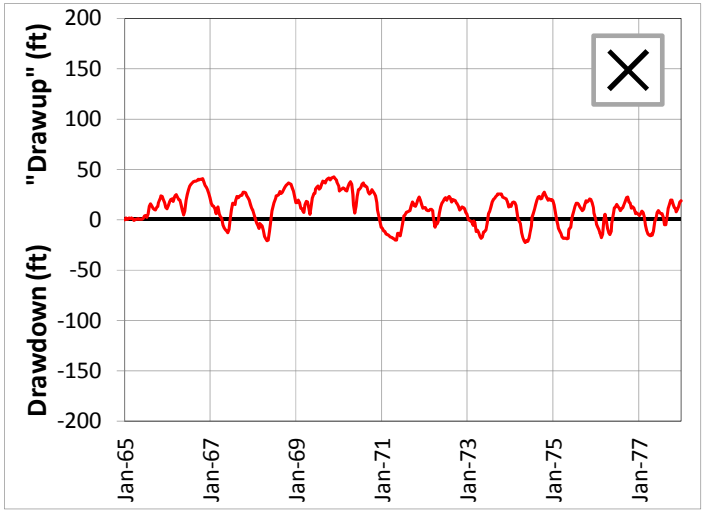

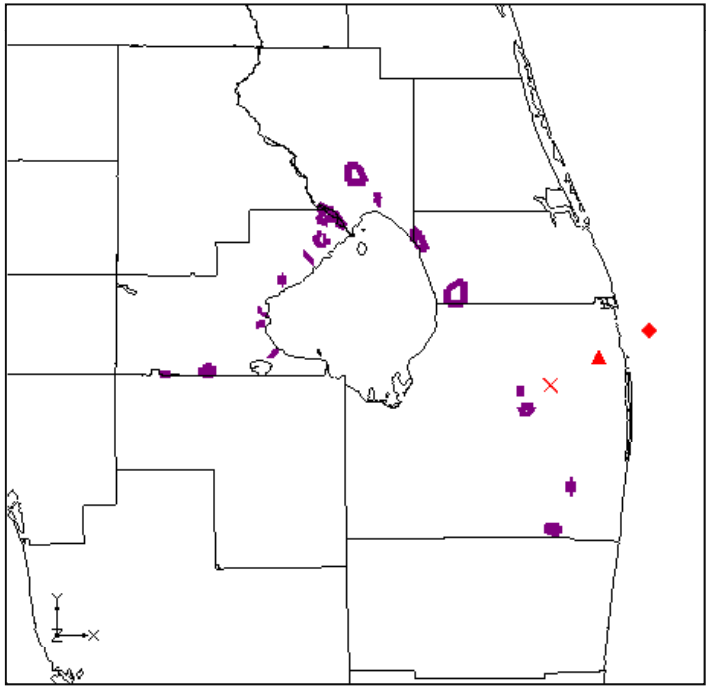

15-Mile Distance

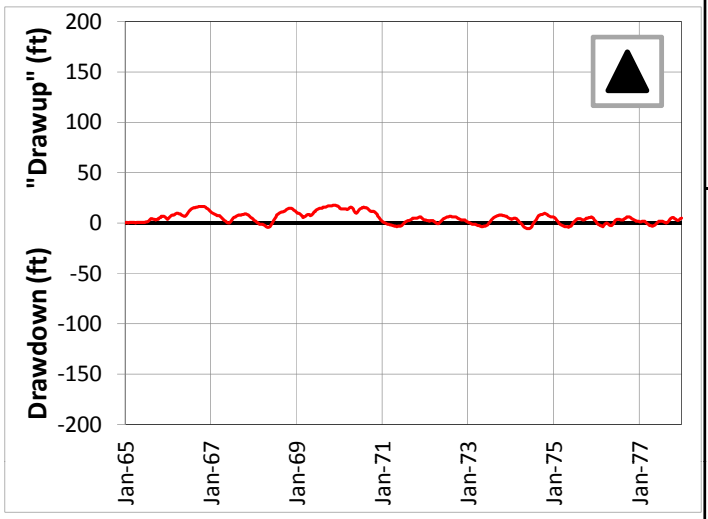

25-Mile Distance

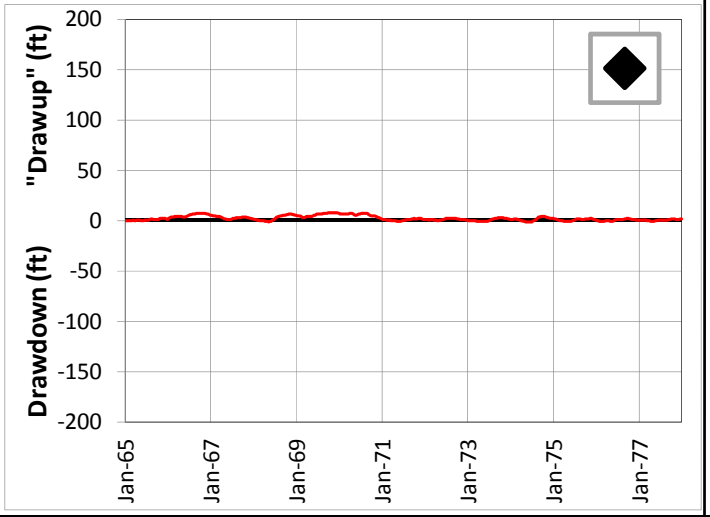

Legend

- CERP ASR Sites
- 5-Mile Distance Locations
- 15-Mile Distance Locations
- 25-Mile Distance Locations

Notes:

Scenario 9 is similar to Scenario 5 except the BZ wells have been given a recovery efficiency of 0% (no recovery) and have been made 10 gpm wells. Therefore, there are half as many BZ wells. In a few sites, the numbers of wells in the UF or APPZ was adjusted slightly to prevent half wells in the BZ.

A number of individual sites were chosen from the APPZ Aquifer at distances of 5, 15 and 25 miles from the proposed ASR well sites. This figure shows the drawdown and "drawup" at each output time step for 3 of these sites.

The plots were calculated by subtracting the heads calculated by the D13R model from those calculated by the no project run. This results in a positive value for "drawup" and a negative value for drawdown.

The colors of the points on the map correspond to the colors of the lines on the plots.

The symbols on the map (x, triangle and diamond) indicate the distance from the ASR sites.

SCENARIO 9 – DRAWDOWN AND "DRAWUP" – APPZ

FIGURE 4.104

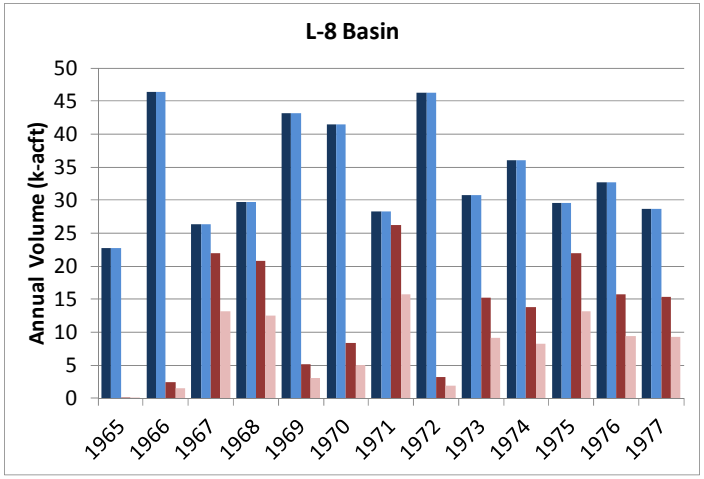

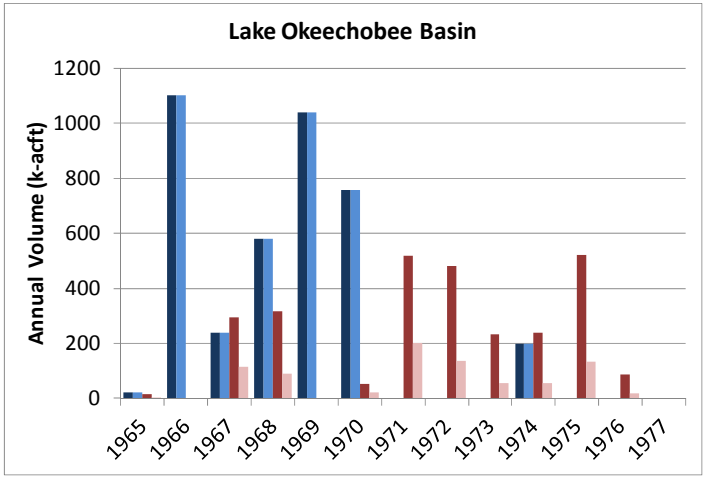

	L-8		Lake Okeechobee		Caloosahatchee	
	In %	Out %	In %	Out %	In %	Out %
1965	100%	60%	100%	30%	100%	22%
1966	100%	60%	100%	--	100%	23%
1967	100%	60%	100%	39%	100%	22%
1968	100%	60%	100%	29%	100%	21%
1969	100%	60%	100%	--	100%	--
1970	100%	60%	100%	39%	100%	23%
1971	100%	60%	--	39%	100%	23%
1972	100%	60%	--	28%	100%	23%
1973	100%	60%	--	24%	100%	21%
1974	100%	60%	100%	24%	100%	21%
1975	100%	60%	--	25%	100%	21%
1976	100%	60%	--	23%	100%	22%
1977	100%	60%	--	--	100%	21%

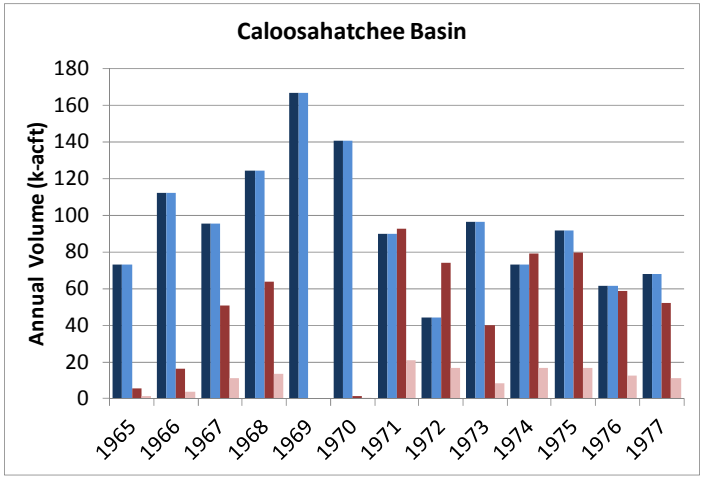

Legend

- Design Storage (injection)
- Modeled Storage (injection)
- Design Recovery (extraction)
- Modeled Recovery (extraction)

Notes:

Scenario 9 is similar to Scenario 5 except the BZ wells have been given a recovery efficiency of 0% (no recovery) and have been made 10 gpm wells. Therefore, there are half as many BZ wells. In a few sites, the numbers of wells in the UF or APPZ was adjusted slightly to prevent half wells in the BZ.

These three plots show the comparison between the SFWMM-D13R designed annual injection and extraction volumes at the ASR wells and the actual assigned rates for the RASRSM-D13R for three of the basins.

The table presents the percentage of SFWMM-D13R annual flow rates that are included in this scenario of the RASRSM-D13R. These percentages are not recovery efficiencies.

SCENARIO 9 – COMPARISON OF DESIGNED AND MODELED ASR FLOW RATES

REGIONAL MODEL PRODUCTION SCENARIO REPORT

FIGURE 4.105

JUNE 2013

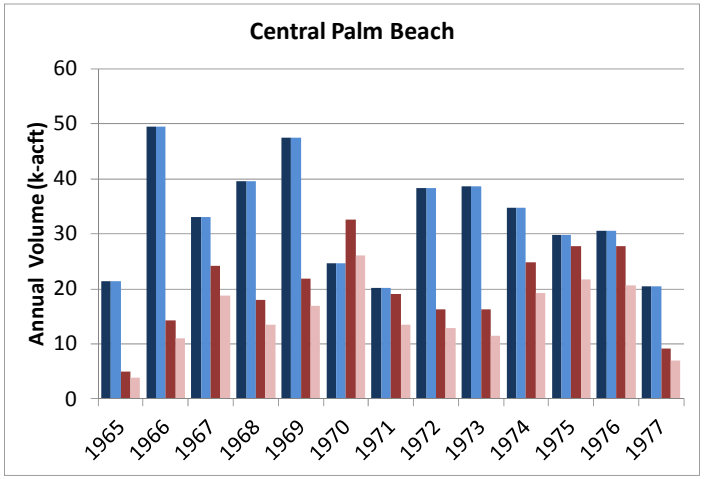

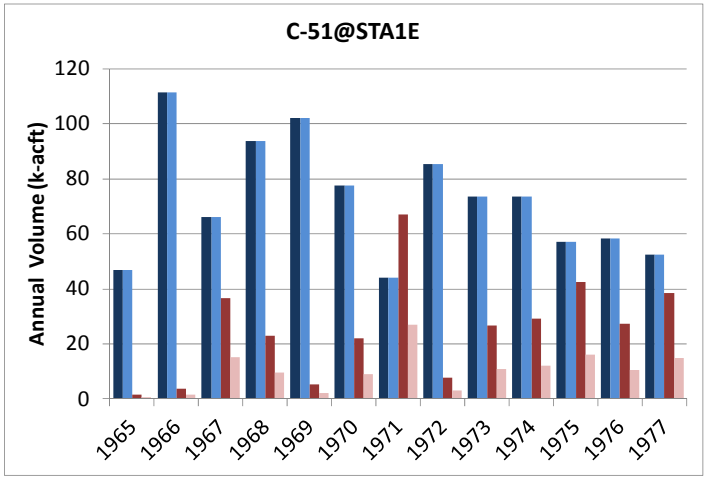

	CPB		C-51		Hillsboro	
	In %	Out %	In %	Out %	In %	Out %
1965	100%	77%	100%	40%	100%	22%
1966	100%	77%	100%	41%	100%	33%
1967	100%	78%	100%	41%	100%	33%
1968	100%	76%	100%	41%	100%	33%
1969	100%	77%	100%	41%	100%	33%
1970	100%	80%	100%	41%	100%	33%
1971	100%	71%	100%	40%	100%	33%
1972	100%	79%	100%	41%	100%	23%
1973	100%	71%	100%	41%	100%	23%
1974	100%	77%	100%	41%	100%	33%
1975	100%	78%	100%	38%	100%	17%
1976	100%	74%	100%	39%	100%	21%
1977	100%	76%	100%	38%	100%	16%

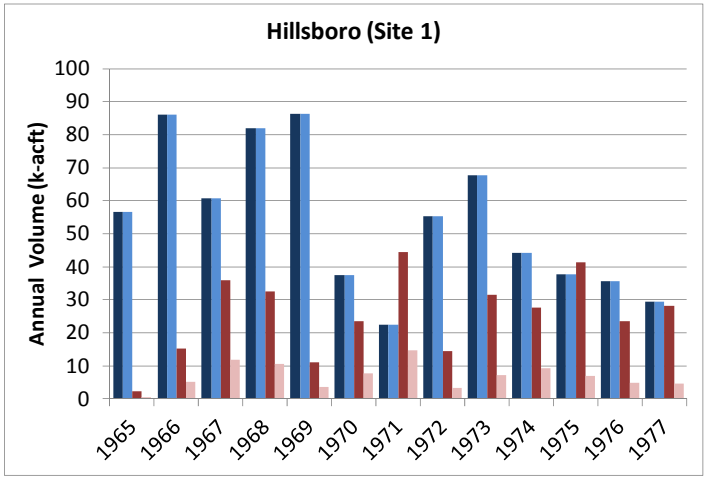

Legend

- Design Storage (injection)
- Modeled Storage (injection)
- Design Recovery (extraction)
- Modeled Recovery (extraction)

Notes:

Scenario 9 is similar to Scenario 5 except the BZ wells have been given a recovery efficiency of 0% (no recovery) and have been made 10 gpm wells. Therefore, there are half as many BZ wells. In a few sites, the numbers of wells in the UF or APPZ was adjusted slightly to prevent half wells in the BZ.

These three plots show the comparison between the SFWMM-D13R designed annual injection and extraction volumes at the ASR wells and the actual assigned rates for the RASRSM-D13R for three of the basins.

The table presents the percentage of SFWMM-D13R annual flow rates that are included in this scenario of the RASRSM-D13R. These percentages are not recovery efficiencies.

SCENARIO 9 – COMPARISON OF DESIGNED AND MODELED ASR FLOW RATES

REGIONAL MODEL PRODUCTION SCENARIO REPORT

FIGURE 4.106

JUNE 2013

	Total	
	In %	Out %
1965	100%	37%
1966	100%	44%
1967	100%	40%
1968	100%	32%
1969	100%	60%
1970	100%	49%
1971	100%	38%
1972	100%	29%
1973	100%	28%
1974	100%	29%
1975	100%	28%
1976	100%	33%
1977	100%	33%

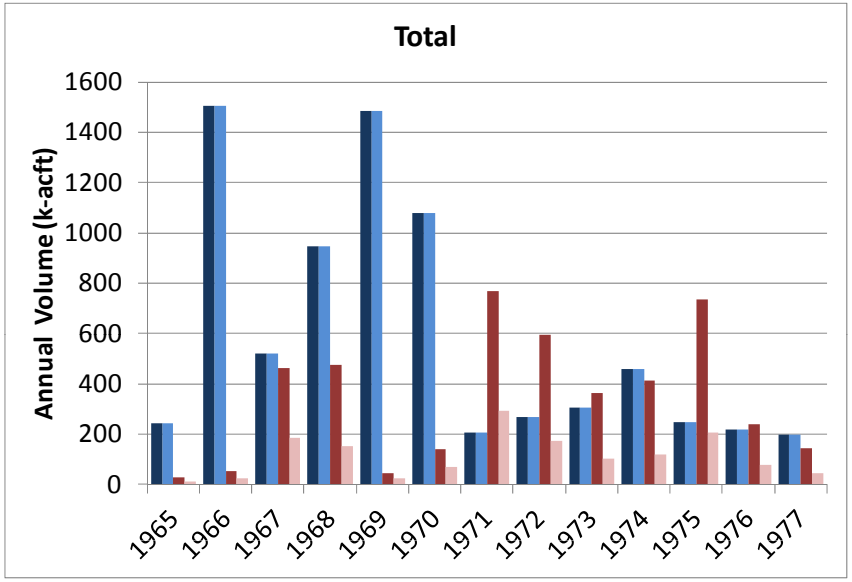

Legend

- Design Storage (injection)
- Modeled Storage (injection)
- Design Recovery (extraction)
- Modeled Recovery (extraction)

Notes:

Scenario 9 is similar to Scenario 5 except the BZ wells have been given a recovery efficiency of 0% (no recovery) and have been made 10 gpm wells. Therefore, there are half as many BZ wells. In a few sites, the numbers of wells in the UF or APPZ was adjusted slightly to prevent half wells in the BZ.

This plot shows the comparison between the SFWMM-D13R designed annual injection and extraction volumes at the ASR wells and the actual assigned rates for the RASRSM-D13R for all basins.

The table presents the percentage of SFWMM-D13R annual flow rates that are included in this scenario of the RASRSM-D13R. These percentages are not recovery efficiencies.

		UF		APPZ		BZ		Total # Wells	Target # Wells
		Number of Wells	Recovery Efficiency	Number of Wells	Recovery Efficiency	Number of Wells	Recovery Efficiency		
Caloosahatchee Basin	Moore Haven	4	70%	0	30%	6	0%		
	River Bend	3	70%	1	30%	2	0%		
	Flaghole	2	0%	0	30%	9	0%		
	Basin Total	9		1		17		27	44
Lake Okeechobee Basin	Nicodemus Slough	0	70%	10	30%	0	0%		
	C-41 Canal	0	70%	0	30%	5	0%		
	C-40 Canal	2	70%	0	30%	4	0%		
	North Lake Okeechobee	8	70%	2	30%	5	0%		
	Kissimmee R./Paradise Run	15	70%	0	30%	30	0%		
	Taylor Creek	0	70%	10	30%	5	0%		
	L-63N	0	70%	9	30%	3	0%		
	Lakeside Ranch	4	70%	0	30%	8	0%		
	Port Mayaca	18	70%	0	30%	1	0%		
	Basin Total	47		31		61		139	200
L-8		6	70%	0	30%	2	0%	8	10
C-51		12	70%	2	30%	10	0%	24	34
Central Palm Beach		10	70%	3	30%	1	0%	14	15
Site 1 (Hillsboro)		10	40%	0	40%	10	0%	20	30
Total		94		37		101		232	333

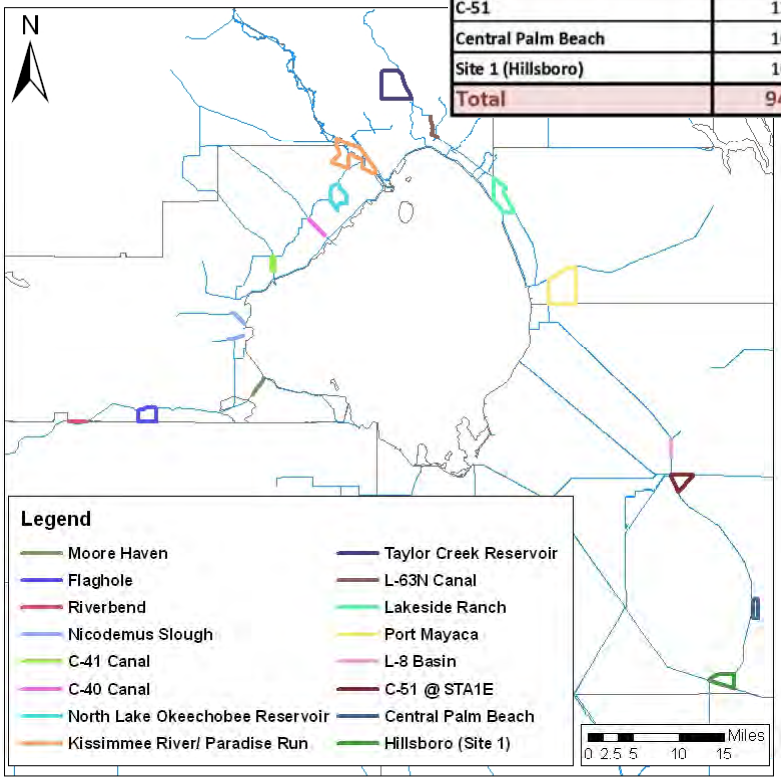

Extraction Percentage		
	UF	APPZ
Caloosahatchee Basin		
Moore Haven	7%	
River Bend	8%	20%
Flaghole	10%	
Lake Okeechobee Basin		
Nicodemus Slough		20%
C-41 Canal		
C-40 Canal	12%	
North Lake Okeechobee	5%	15%
Kissimmee R./Paradise Run	7%	
Taylor Creek		20%
L-63N		20%
Lakeside Ranch	20%	
Port Mayaca	6%	
L-8	3%	
C-51	2%	20%
Central Palm Beach	1%	10%
Site 1 (Hillsboro)	3%	

Notes:

Scenario 10 is a variation on Scenario 9. The numbers of wells and injection volumes are identical, but the extraction volumes have been cut back to reduce drawdown.

Reductions have been applied as a percentage of the Scenario 9 rates as shown in the lower table.

The extraction percentage is the percentage applied to the extraction rates to reduce drawdown effects. This is not the recovery efficiency.

Flow rates are divided evenly among the wells in each basin. Maximum flow rate for any one well is 5 mgd in the UF and APPZ and 10 mgd in the BZ.

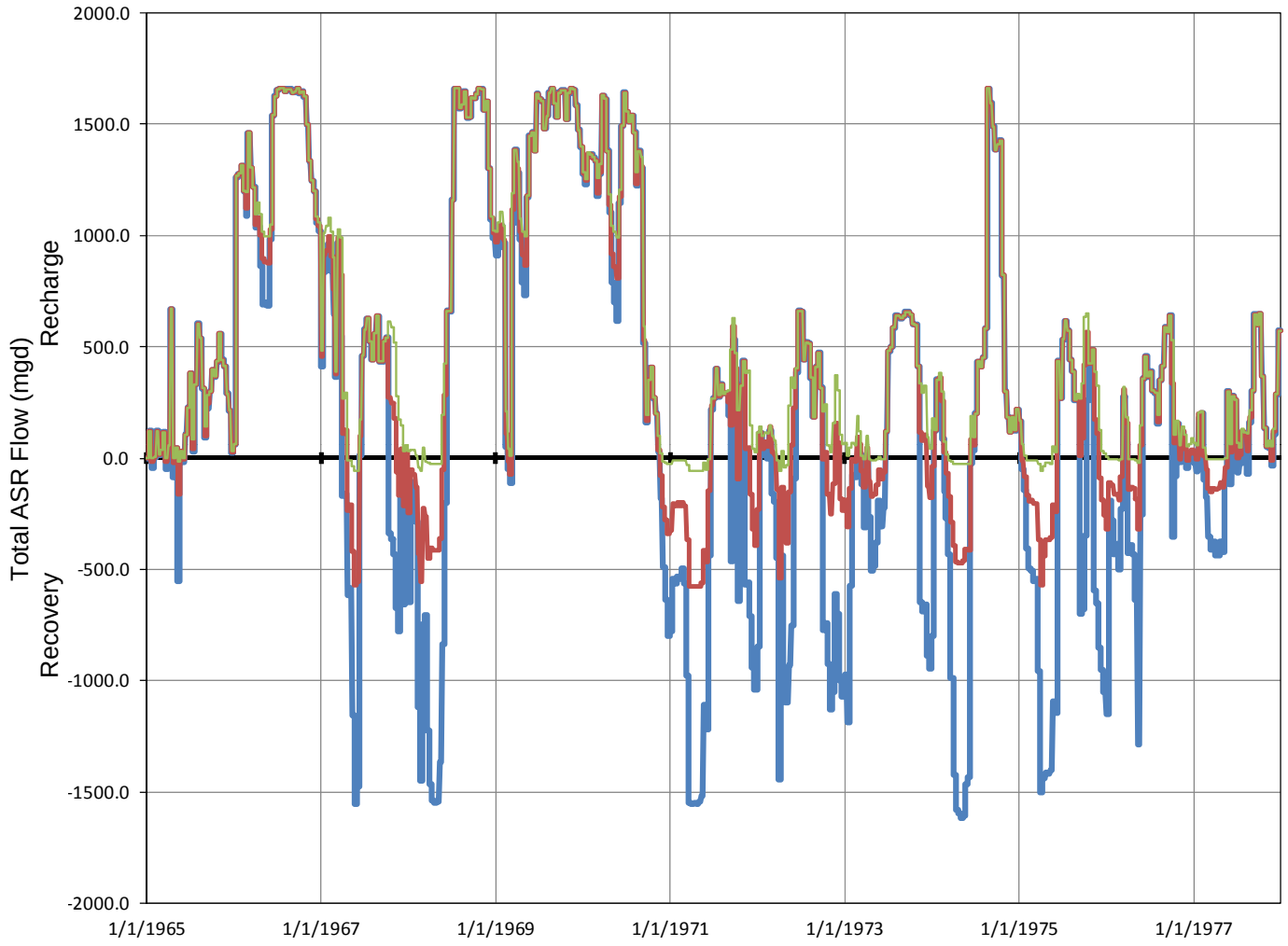

Legend

- Scenario 1 – ASR Flux
- Scenario 9 – ASR Flux
- Scenario10– ASR Flux

Notes:

Scenario 10 is a variation on Scenario 9. The numbers of wells and injection volumes are identical, but the extraction volumes have been cut back to reduce drawdown.

This plot shows the extraction and injection rates for all wells at all sites for Scenario 1, Scenario 9 and Scenario 10. Positive rates are recharge (injection), while negative rates are recovery (extraction).

Scenario 10 – ASR Well Fluxes (Compared to Scenarios 1 & 9)

Regional Model Production Scenario Report

Figure 4.109

June 2013

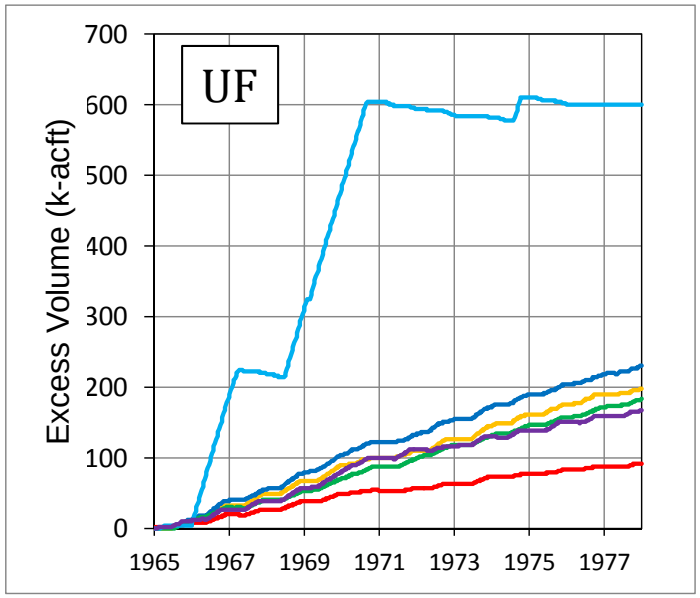

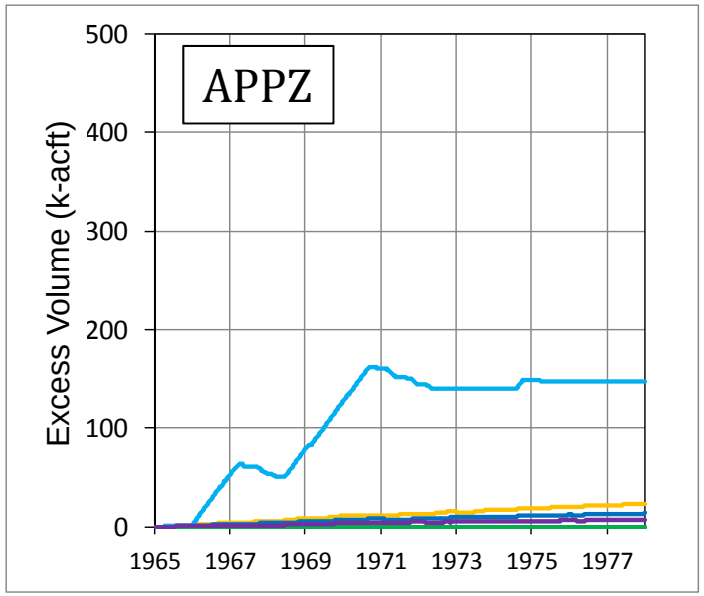

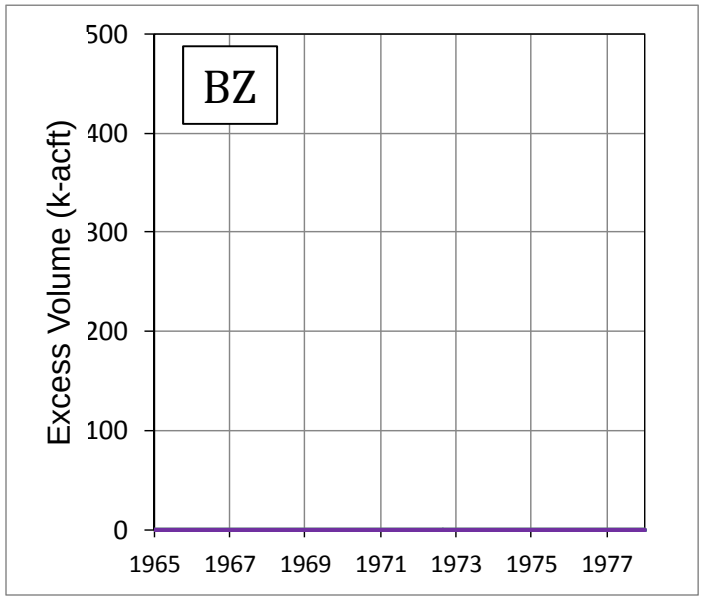

Legend

- Central Palm Beach
- C-51
- Hillsboro
- L-8
- Lake Okeechobee
- Caloosahatchee River

Notes:

Scenario 10 is a variation on Scenario 9. The numbers of wells and injection volumes are identical, but the extraction volumes have been cut back to reduce drawdown.

These plots show the excess volume of fresh water remaining in each aquifer at each ASR basin. Excess volume is calculated by adding injected volume times recovery efficiency and subtracting extracted volume. The calculation is cumulative.

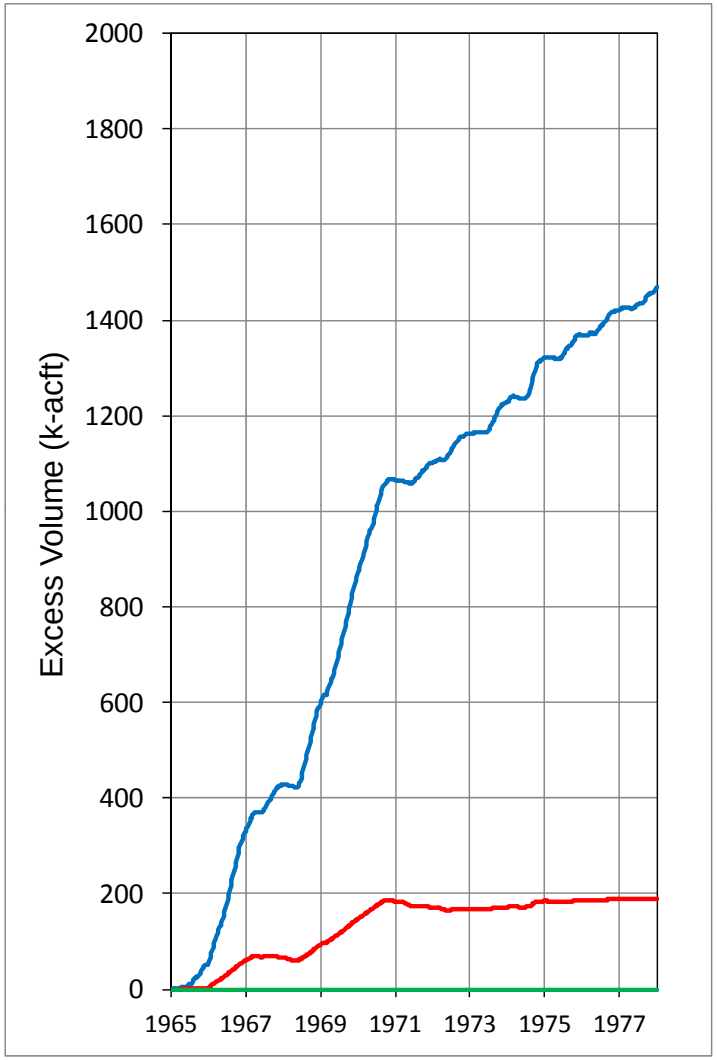

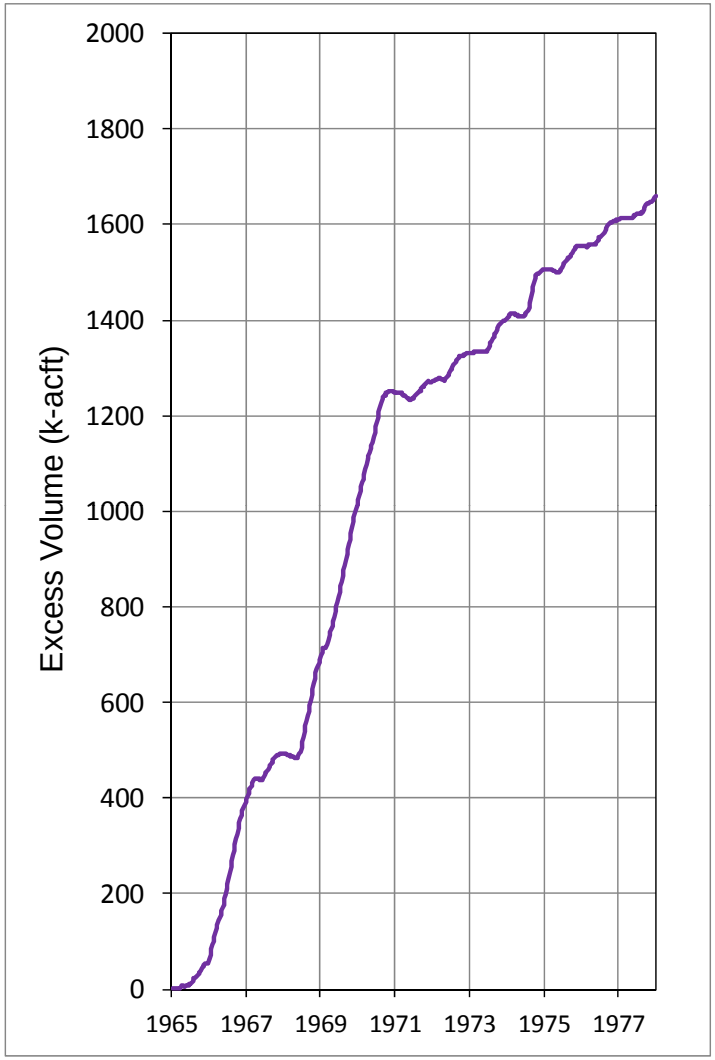

Legend

- Total UF
- Total APPZ
- Total BZ
- Total (All Aquifers)

Notes:

Scenario 10 is a variation on Scenario 9. The numbers of wells and injection volumes are identical, but the extraction volumes have been cut back to reduce drawdown.

These plots show the total excess volume of fresh water remaining in each aquifer and in all aquifers. Excess volume is calculated by adding injected volume times recovery efficiency and subtracting extracted volume. The calculation is cumulative.

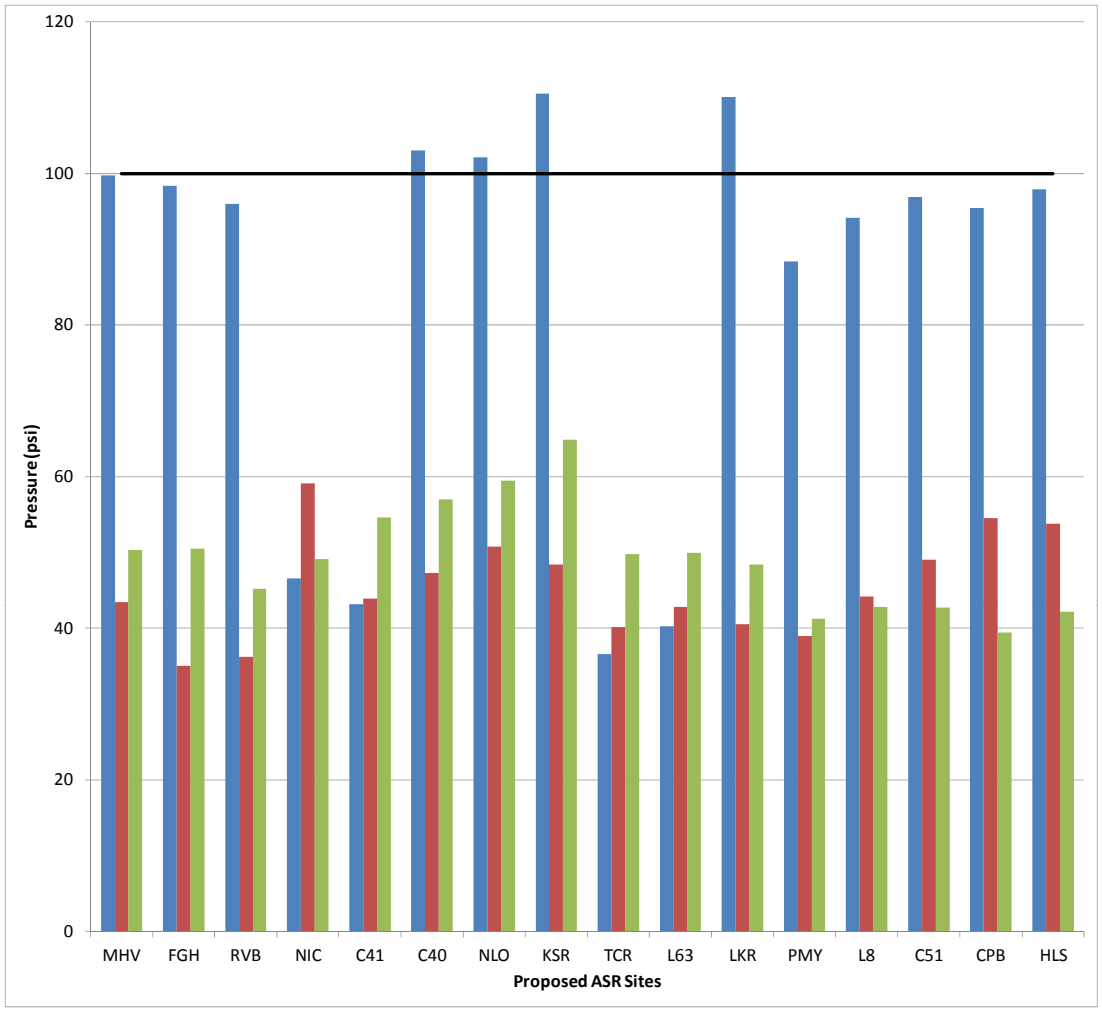

MHV	Moorehaven
FGH	Flaghole
RVB	Riverbend
NIC	Nicodemus Slough
C41	C-41Canal
C40	C-40 Canal
NLO	North Lake Okeechobee Reservoir
KSR	Kissimmee River / Paradise Run
TCR	Taylor Creek Reservoir
L63	L-63N Canal
LKR	Lakeside Ranch
PMY	Port Mayaca
L8	L-8 Basin
C51	C-51 @ STA1E
CPB	Central Palm Beach
HLS	Hillsboro (Site 1)

Legend

- Upper Floridan Aquifer
- Avon Park Permeable Zone
- Boulder Zone
- 100 psi Limit

Notes:

Scenario 10 is a variation on Scenario 9. The numbers of wells and injection volumes are identical, but the extraction volumes have been cut back to reduce drawdown.

This plot shows the highest pressure at each site which the pump would need to overcome in order to inject storage water during the 13-year simulation.

The PDT determined that it would be important to keep this pressure below 100 psi (indicated by the heavy black line).

Note that maximum pressures are shown for all aquifers and all sites even if ASR pumps are not located there for the current scenario.

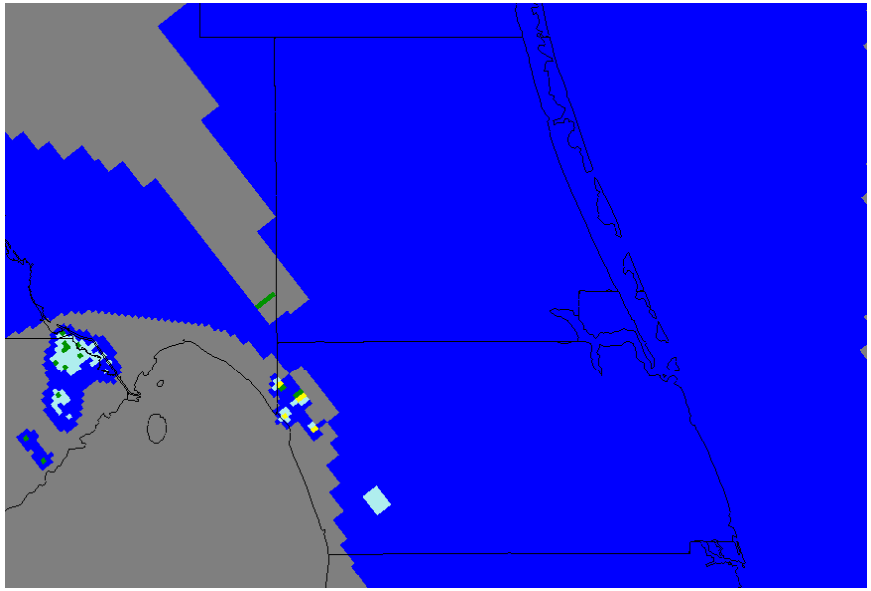

Upper Floridan Aquifer

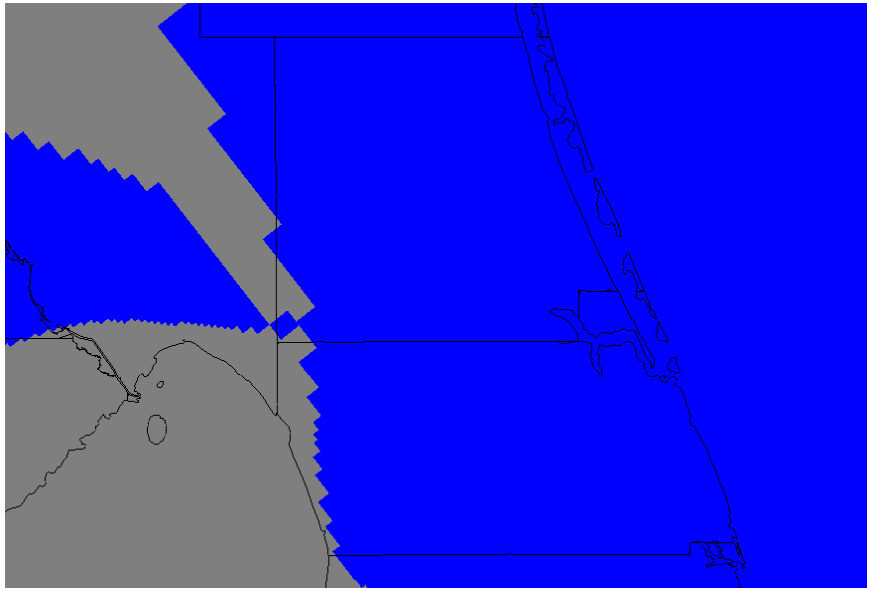

Avon Park Permeable Zone

Legend

- Not artesian or no reduction
- < 5%
- 5% - 10%
- 10% - 20%
- 20% - 50%
- 50% - 100%
- Loses artesian condition

Notes:

Scenario 10 is a variation on Scenario 9. The numbers of wells and injection volumes are identical, but the extraction volumes have been cut back to reduce drawdown.

These plots show the maximum reduction in artesian flow at each model cell as a percentage when compared to the flow expected without the ASR project.

Permit rules require that the reduction in Saint Lucie and Martin Counties be less than 10%.

Note the gray area in the northwest corner of the figures, which coincides with a ridge and does not normally have artesian conditions.

Scenario 10 – Maximum Reduction in Artesian Flow Capacity

Regional Model Production Scenario Report

Figure 4.113

June 2013

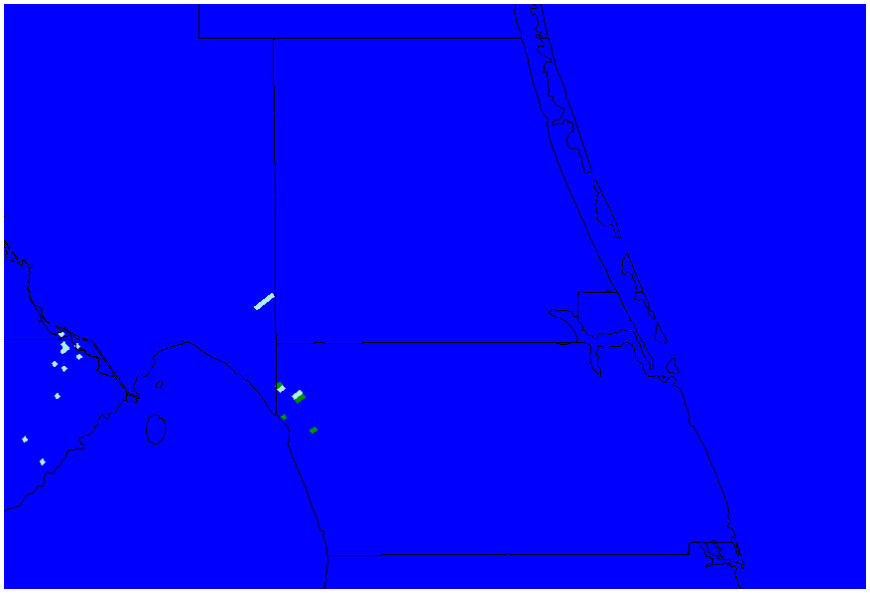

Upper Floridan Aquifer

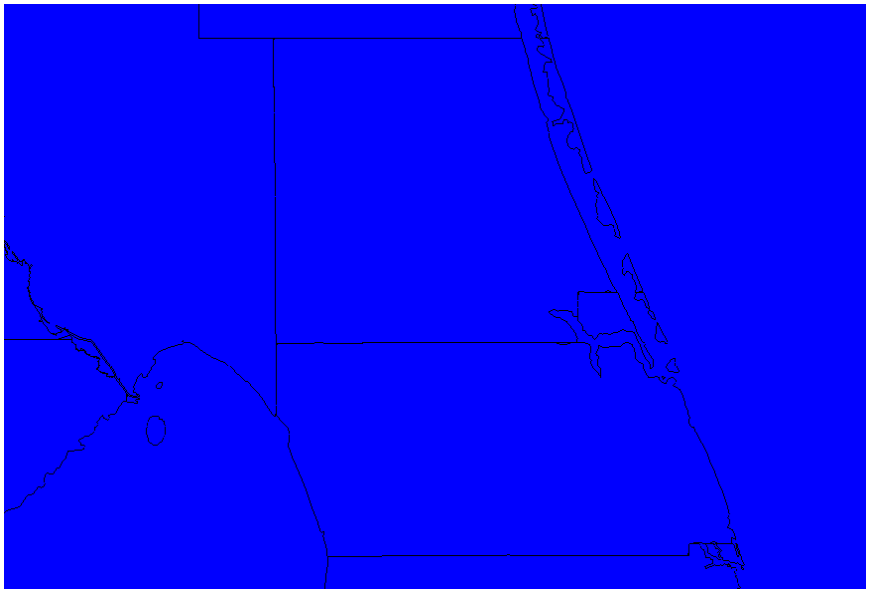

Avon Park Permeable Zone

Legend

- 0 days
- 1 – 250 days
- 250 – 500 days
- 500 – 1000 days
- 1000 – 2000 days
- > 2000 days

Notes:

Scenario 10 is a variation on Scenario 9. The numbers of wells and injection volumes are identical, but the extraction volumes have been cut back to reduce drawdown.

These plots indicate the severity of the loss of artesian pressure due to ASR extraction pumping.

Permit rules require that the reduction in Saint Lucie and Martin Counties be less than 10%. This plot indicates the number of days during the simulation in which the flow reduction was greater than 10%. There are 4748 days in the 13-year model simulation period.

SCENARIO 10 – NUMBER OF DAYS (OUT OF 13 YEARS) WITH FLOW REDUCTION EXCEEDING 10%

REGIONAL MODEL PRODUCTION SCENARIO REPORT

FIGURE 4.114

JUNE 2013

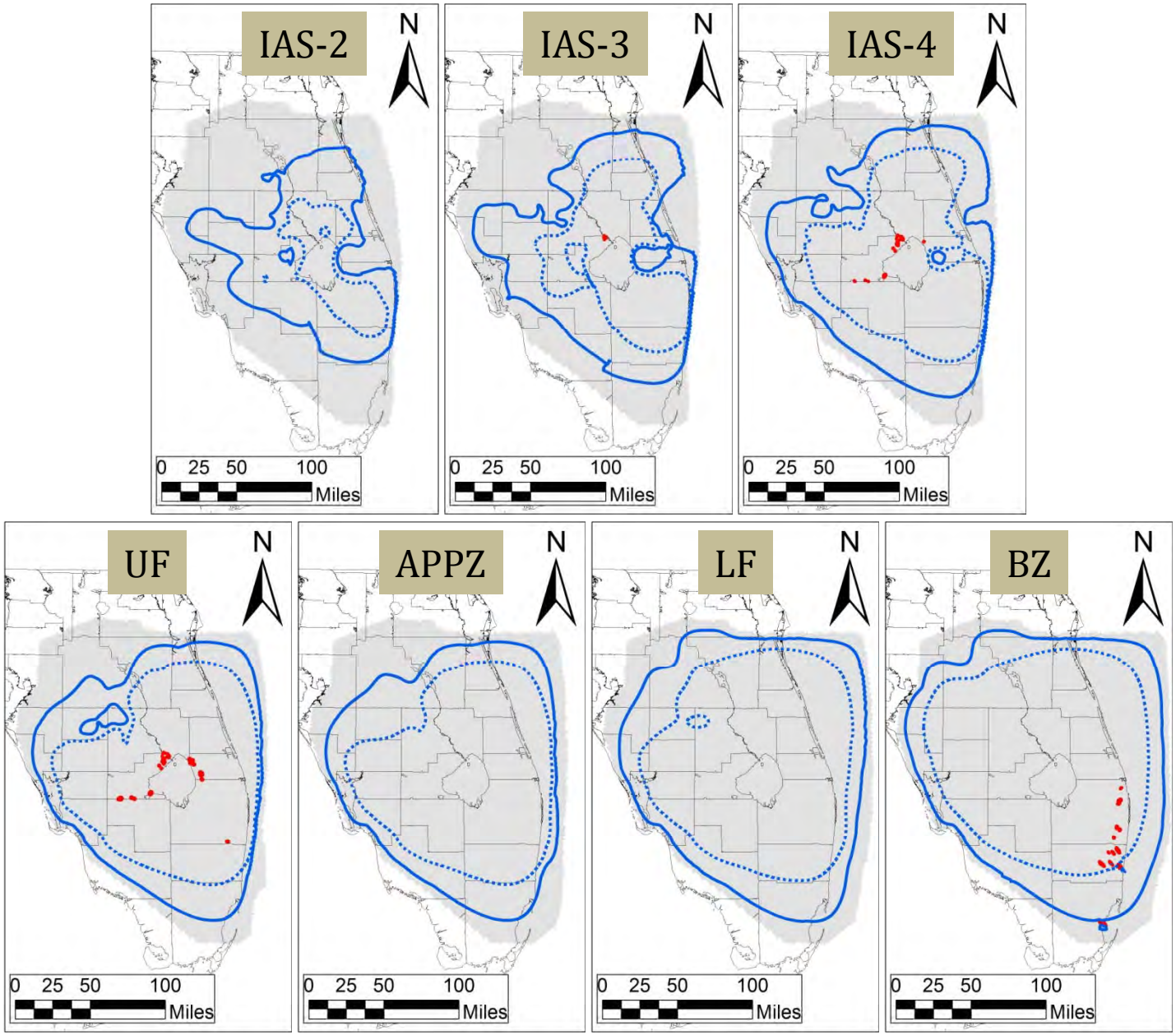

Legend

Maximum Drawdown
- 1 foot
- 5 feet

Maximum "Drawup"
- 1 foot
- 5 feet

Model Domain

Notes:

Scenario 10 is a variation on Scenario 9. The numbers of wells and injection volumes are identical, but the extraction volumes have been cut back to reduce drawdown.

These figures show the extent of the areas where the maximum drawdown or "drawup" is greater than 1 foot or 5 feet.

The maximum condition does not necessarily occur at the same time for all regions of the model.

SCENARIO 10 – MAXIMUM DRAWDOWN AND "DRAWUP" BY AQUIFER

REGIONAL MODEL PRODUCTION SCENARIO REPORT

FIGURE 4.115

JUNE 2013

5-Mile Distance

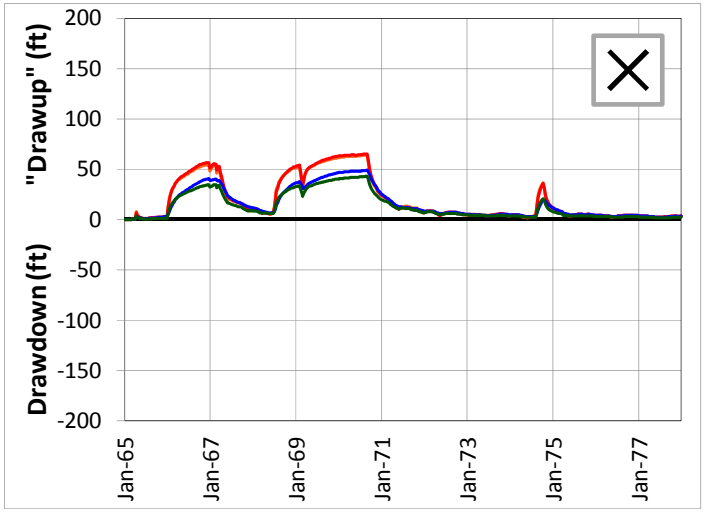

15-Mile Distance

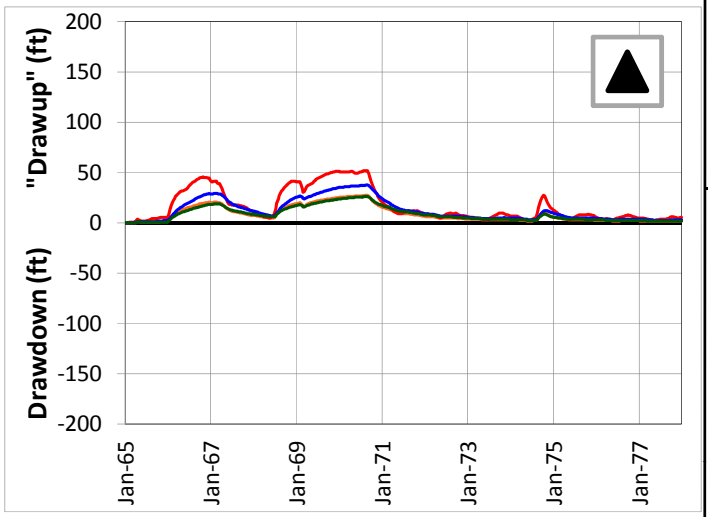

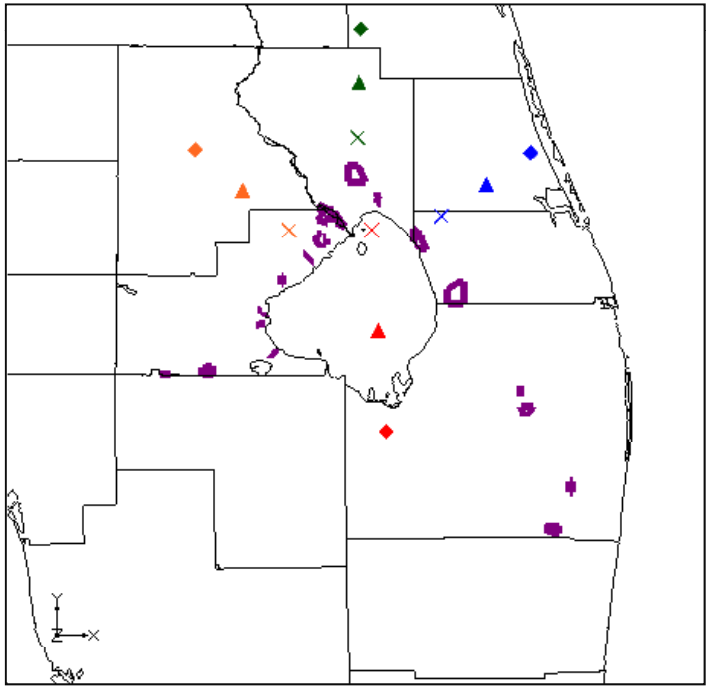

25-Mile Distance

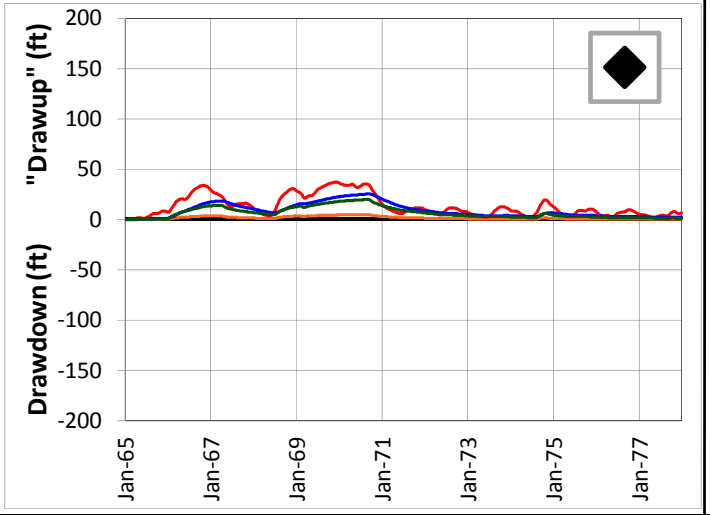

Legend

- CERP ASR Sites
- 5-Mile Distance Locations
- 15-Mile Distance Locations
- 25-Mile Distance Locations

Notes:

Scenario 10 is a variation on Scenario 9. The numbers of wells and injection volumes are identical, but the extraction volumes have been cut back to reduce drawdown.

A number of individual sites were chosen from the UF Aquifer at distances of 5, 15 and 25 miles from the proposed ASR well sites. This figure shows the drawdown and "drawup" at each output time step for 12 of these sites.

The plots were calculated by subtracting the heads calculated by the D13R model from those calculated by the no project run. This results in a positive value for "drawup" and a negative value for drawdown.

The colors of the points on the map correspond to the colors of the lines on the plots.

The symbols on the map (x, triangle and diamond) indicate the distance from the ASR sites.

5-Mile Distance

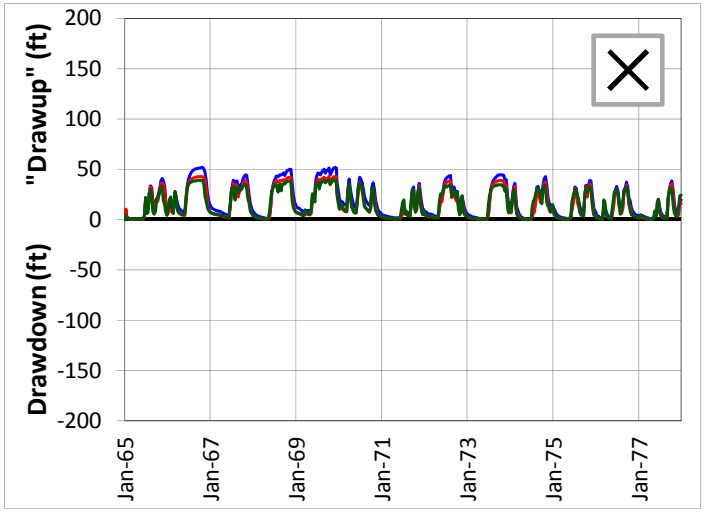

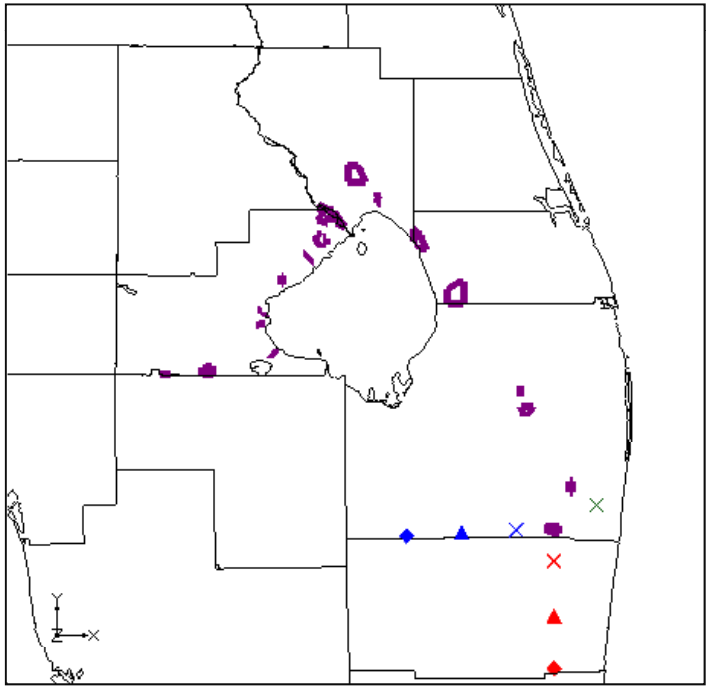

15-Mile Distance

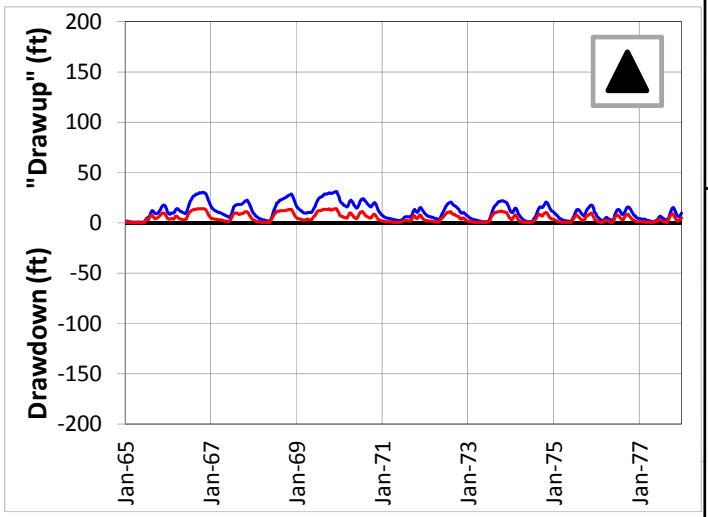

25-Mile Distance

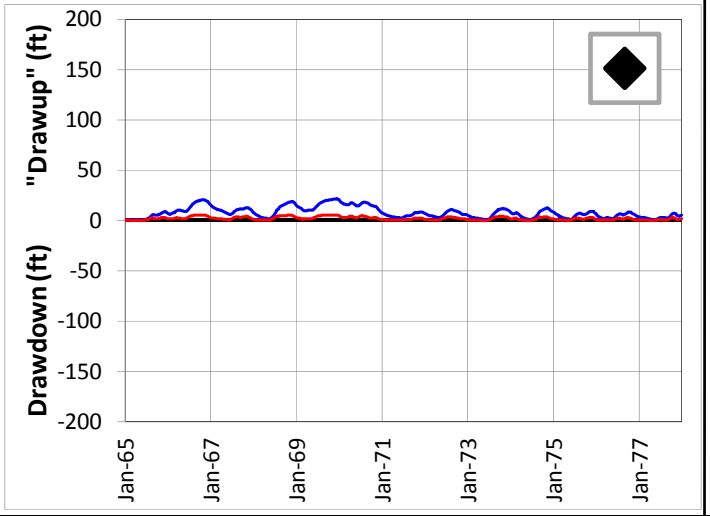

Legend

- CERP ASR Sites
- 5-Mile Distance Locations
- 15-Mile Distance Locations
- 25-Mile Distance Locations

Notes:

Scenario 10 is a variation on Scenario 9. The numbers of wells and injection volumes are identical, but the extraction volumes have been cut back to reduce drawdown.

A number of individual sites were chosen from the UF Aquifer at distances of 5, 15 and 25 miles from the proposed ASR well sites. This figure shows the drawdown and "drawup" at each output time step for 7 of these sites.

The plots were calculated by subtracting the heads calculated by the D13R model from those calculated by the no project run. This results in a positive value for "drawup" and a negative value for drawdown.

The colors of the points on the map correspond to the colors of the lines on the plots.

The symbols on the map (x, triangle and diamond) indicate the distance from the ASR sites.

5-Mile Distance

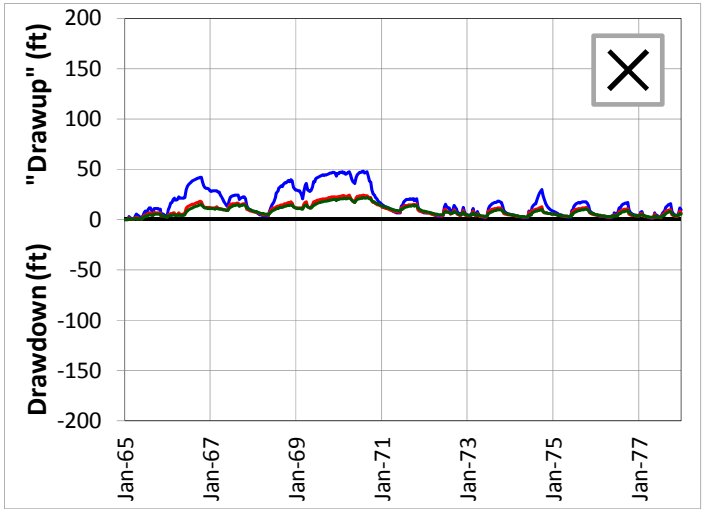

15-Mile Distance

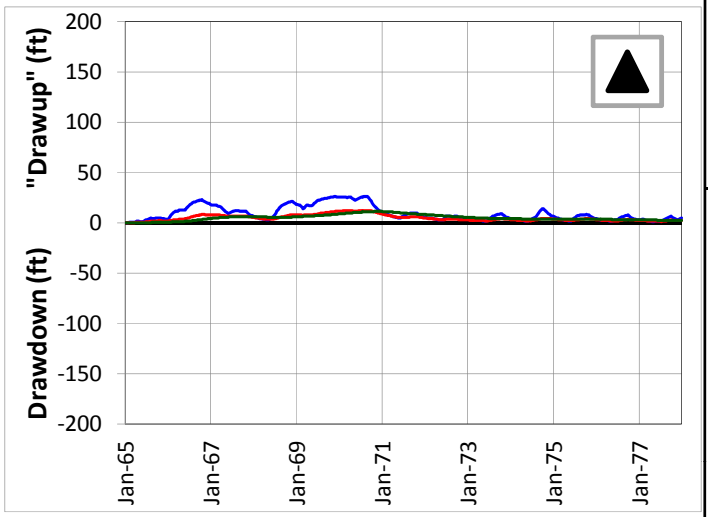

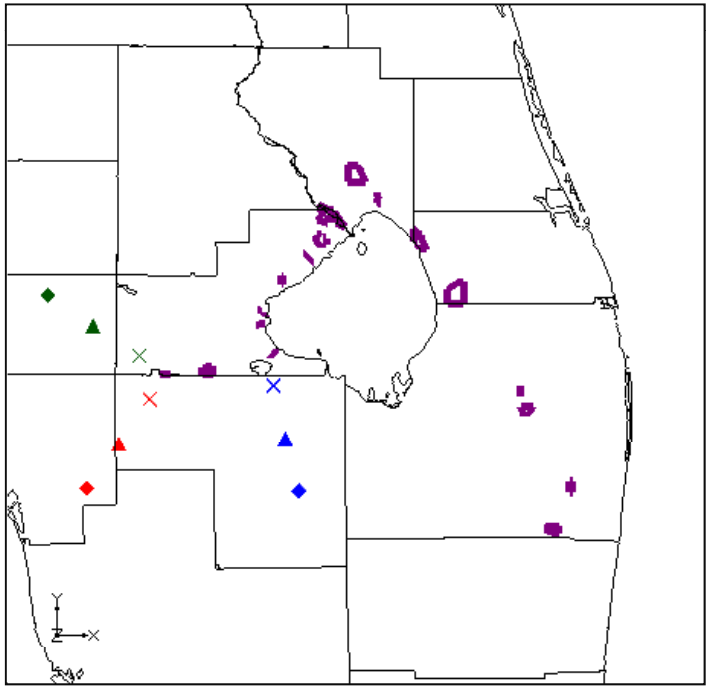

25-Mile Distance

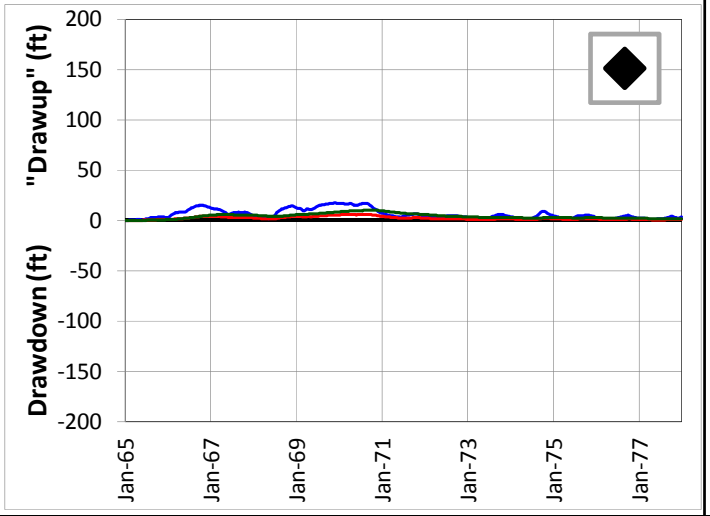

Legend

- CERP ASR Sites
- ✕ 5-Mile Distance Locations
- ▲ 15-Mile Distance Locations
- ◆ 25-Mile Distance Locations

Notes:

Scenario 10 is a variation on Scenario 9. The numbers of wells and injection volumes are identical, but the extraction volumes have been cut back to reduce drawdown.

A number of individual sites were chosen from the UF Aquifer at distances of 5, 15 and 25 miles from the proposed ASR well sites. This figure shows the drawdown and "drawup" at each output time step for 9 of these sites.

The plots were calculated by subtracting the heads calculated by the D13R model from those calculated by the no project run. This results in a positive value for "drawup" and a negative value for drawdown.

The colors of the points on the map correspond to the colors of the lines on the plots.

The symbols on the map (x, triangle and diamond) indicate the distance from the ASR sites.

SCENARIO 10 – DRAWDOWN AND "DRAWUP" – UF

REGIONAL MODEL PRODUCTION SCENARIO REPORT

FIGURE 4.118

JUNE 2013

5-Mile Distance

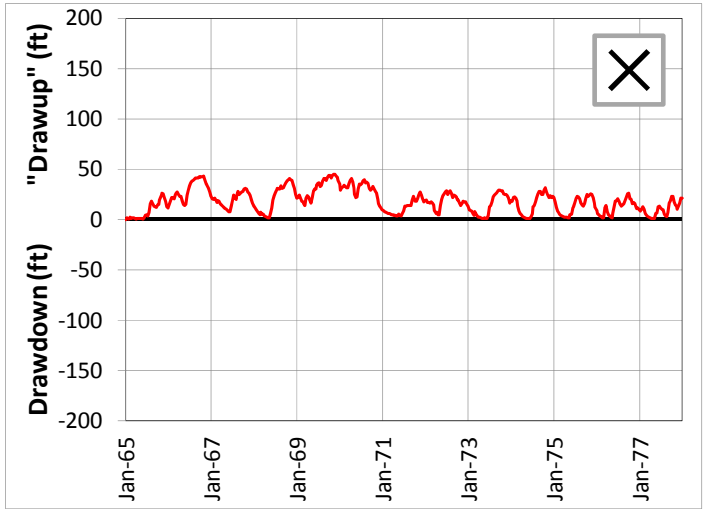

15-Mile Distance

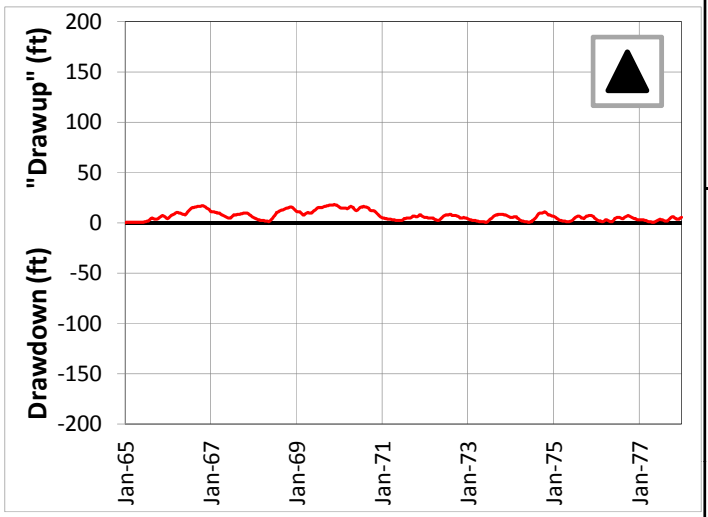

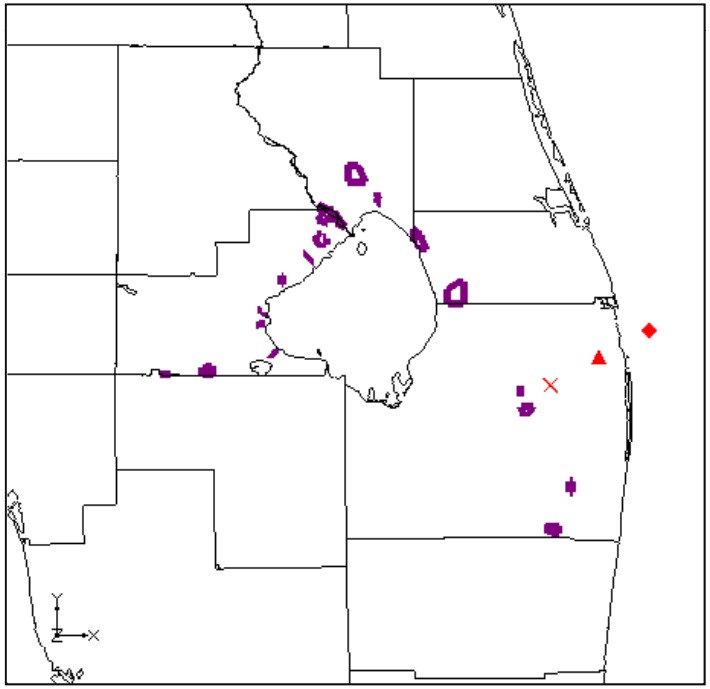

25-Mile Distance

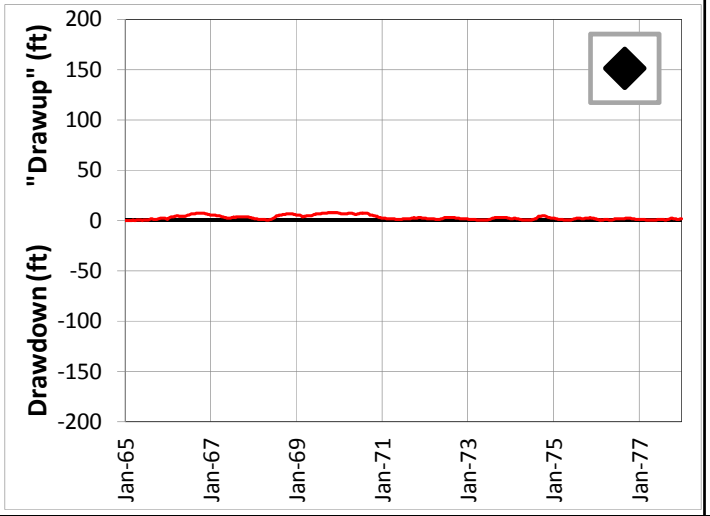

Legend

- CERP ASR Sites
- 5-Mile Distance Locations
- 15-Mile Distance Locations
- 25-Mile Distance Locations

Notes:

Scenario 10 is a variation on Scenario 9. The numbers of wells and injection volumes are identical, but the extraction volumes have been cut back to reduce drawdown.

A number of individual sites were chosen from the UF Aquifer at distances of 5, 15 and 25 miles from the proposed ASR well sites. This figure shows the drawdown and "drawup" at each output time step for 3 of these sites.

The plots were calculated by subtracting the heads calculated by the D13R model from those calculated by the no project run. This results in a positive value for "drawup" and a negative value for drawdown.

The colors of the points on the map correspond to the colors of the lines on the plots.

The symbols on the map (x, triangle and diamond) indicate the distance from the ASR sites.

5-Mile Distance

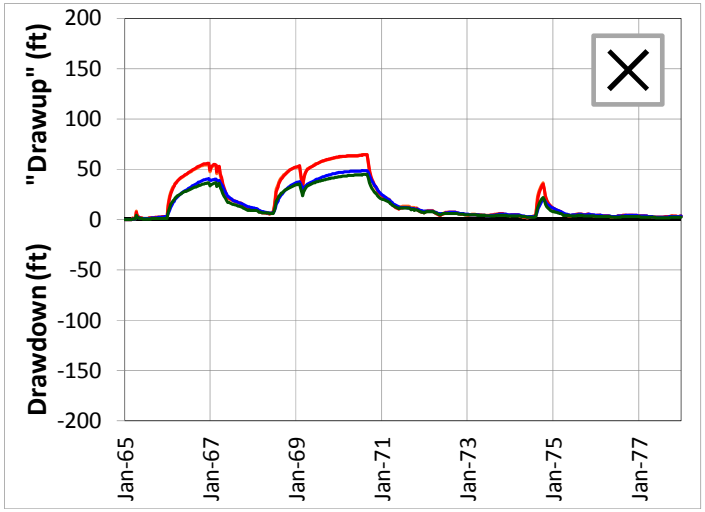

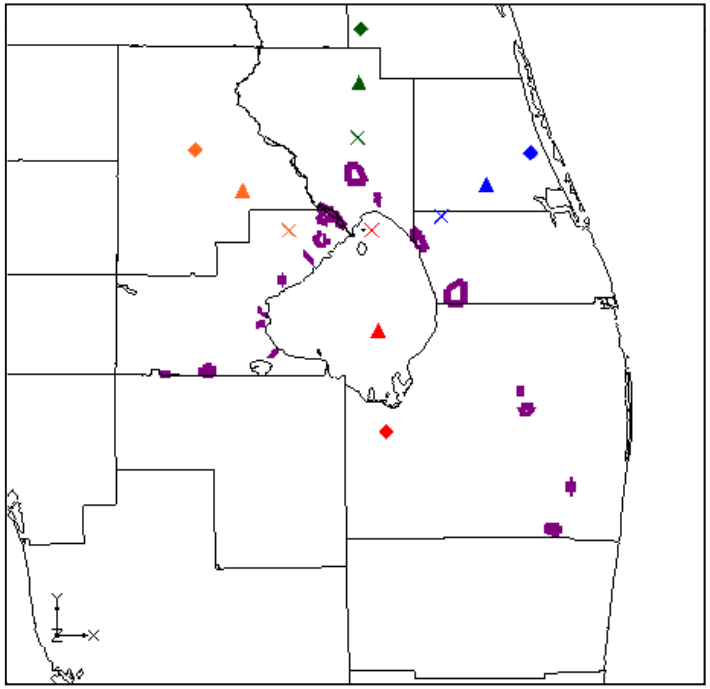

15-Mile Distance

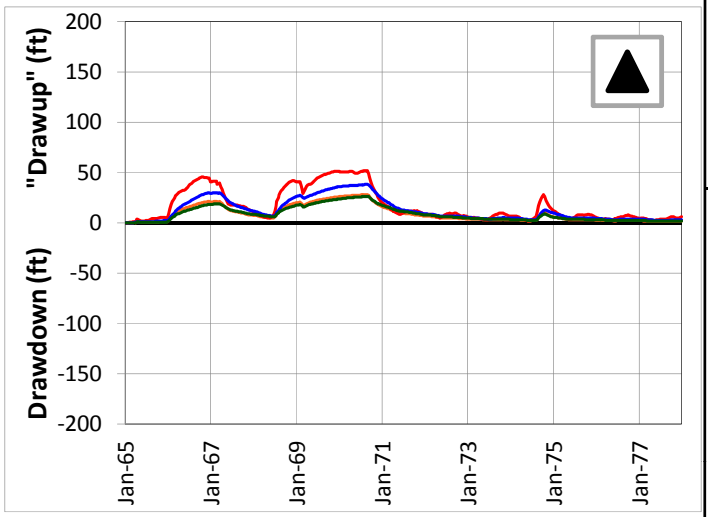

25-Mile Distance

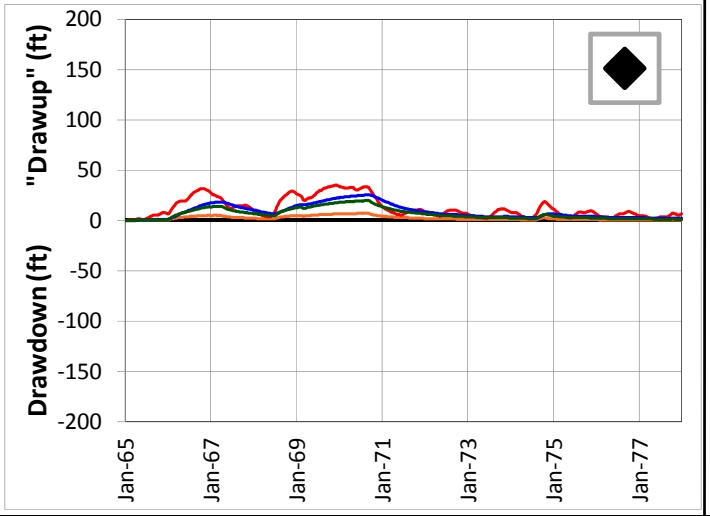

Legend

- CERP ASR Sites
- ✕ 5-Mile Distance Locations
- ▲ 15-Mile Distance Locations
- ◆ 25-Mile Distance Locations

Notes:

Scenario 10 is a variation on Scenario 9. The numbers of wells and injection volumes are identical, but the extraction volumes have been cut back to reduce drawdown.

A number of individual sites were chosen from the APPZ Aquifer at distances of 5, 15 and 25 miles from the proposed ASR well sites. This figure shows the drawdown and "drawup" at each output time step for 12 of these sites.

The plots were calculated by subtracting the heads calculated by the D13R model from those calculated by the no project run. This results in a positive value for "drawup" and a negative value for drawdown.

The colors of the points on the map correspond to the colors of the lines on the plots.

The symbols on the map (x, triangle and diamond) indicate the distance from the ASR sites.

5-Mile Distance

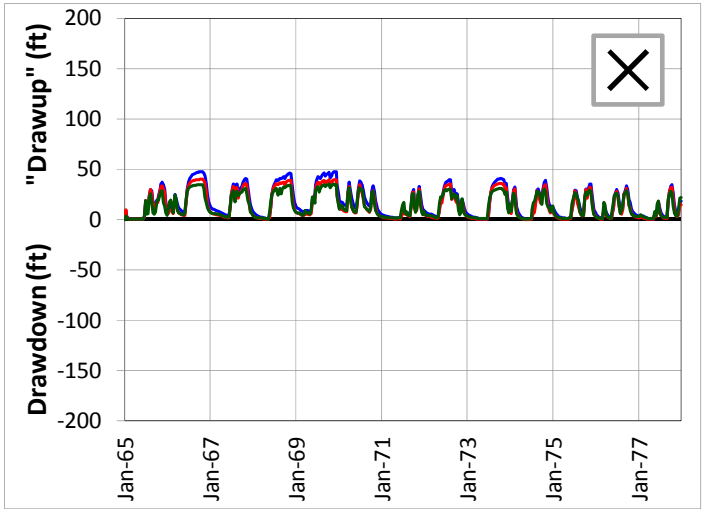

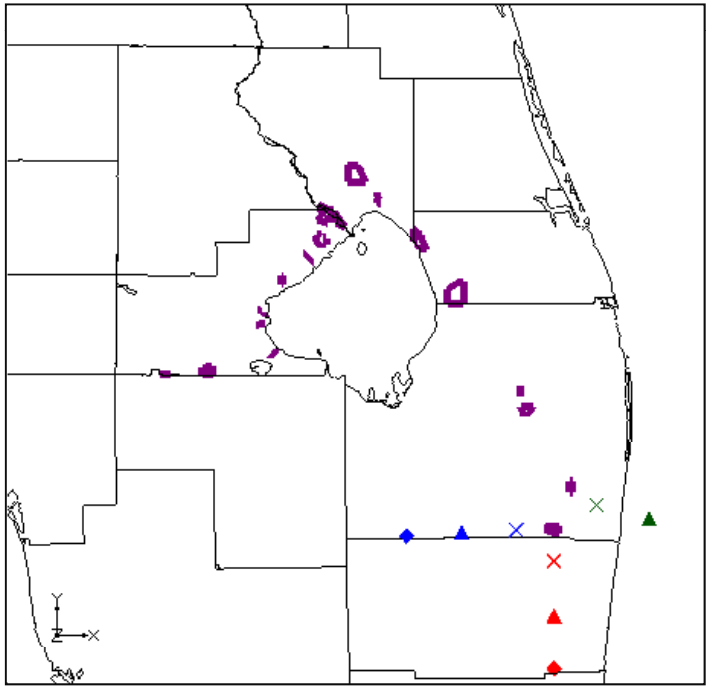

15-Mile Distance

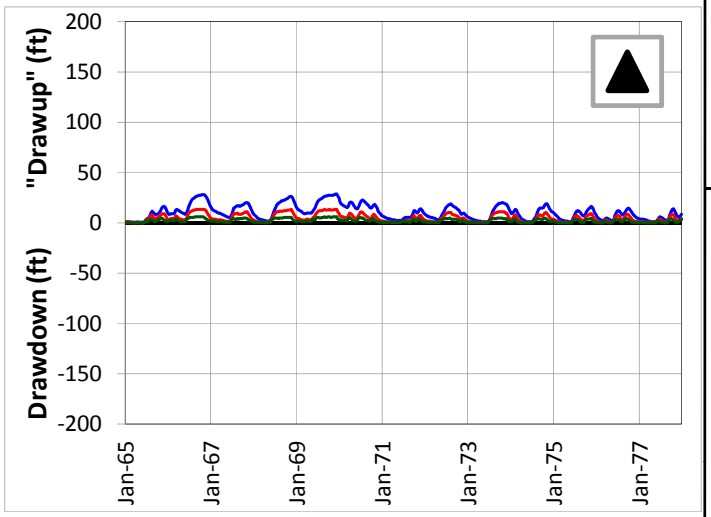

25-Mile Distance

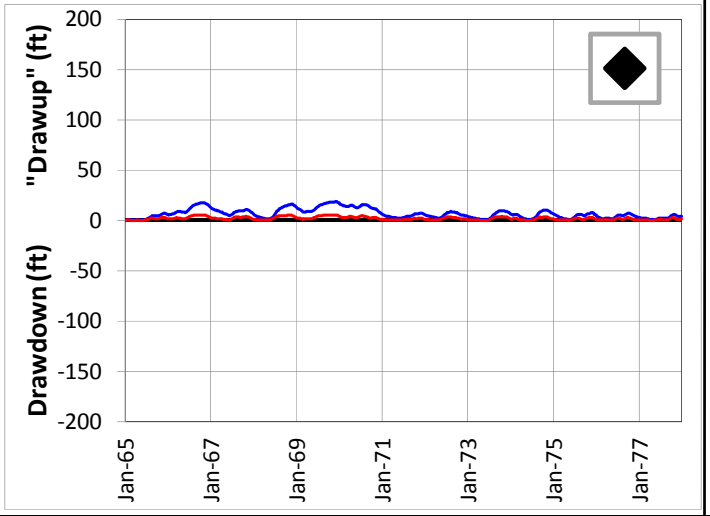

Legend

- CERP ASR Sites
- 5-Mile Distance Locations
- 15-Mile Distance Locations
- 25-Mile Distance Locations

Notes:

Scenario 10 is a variation on Scenario 9. The numbers of wells and injection volumes are identical, but the extraction volumes have been cut back to reduce drawdown.

A number of individual sites were chosen from the APPZ Aquifer at distances of 5, 15 and 25 miles from the proposed ASR well sites. This figure shows the drawdown and "drawup" at each output time step for 8 of these sites.

The plots were calculated by subtracting the heads calculated by the D13R model from those calculated by the no project run. This results in a positive value for "drawup" and a negative value for drawdown.

The colors of the points on the map correspond to the colors of the lines on the plots.

The symbols on the map (x, triangle and diamond) indicate the distance from the ASR sites.

SCENARIO 10 – DRAWDOWN AND "DRAWUP" – APPZ

REGIONAL MODEL PRODUCTION SCENARIO REPORT

FIGURE 4.121

JUNE 2013

5-Mile Distance

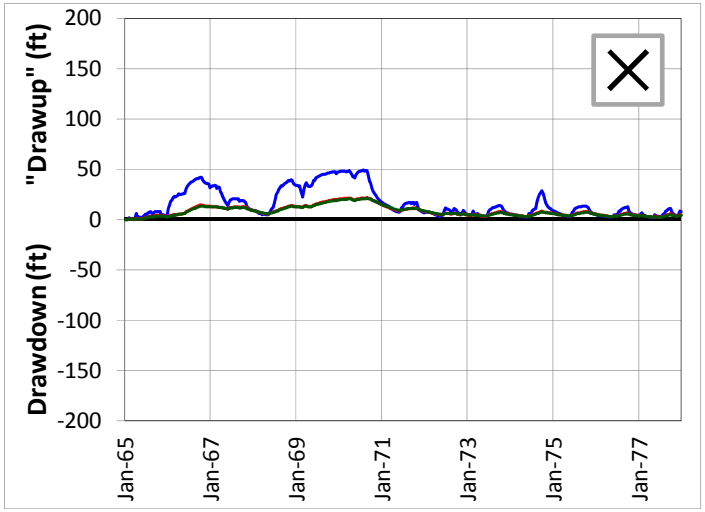

15-Mile Distance

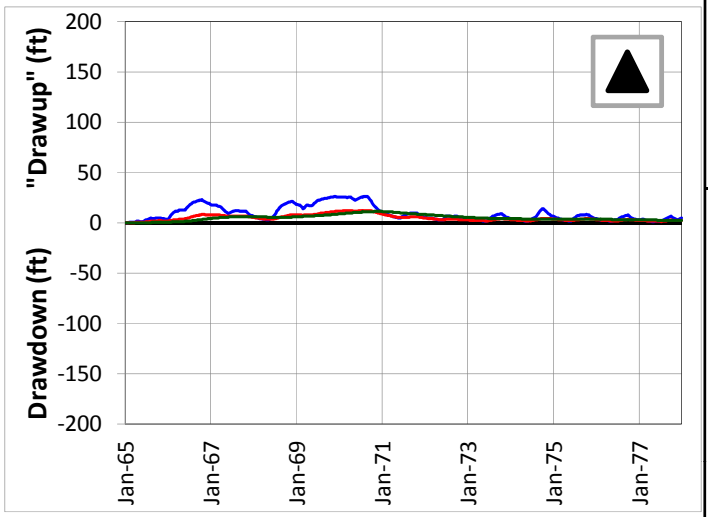

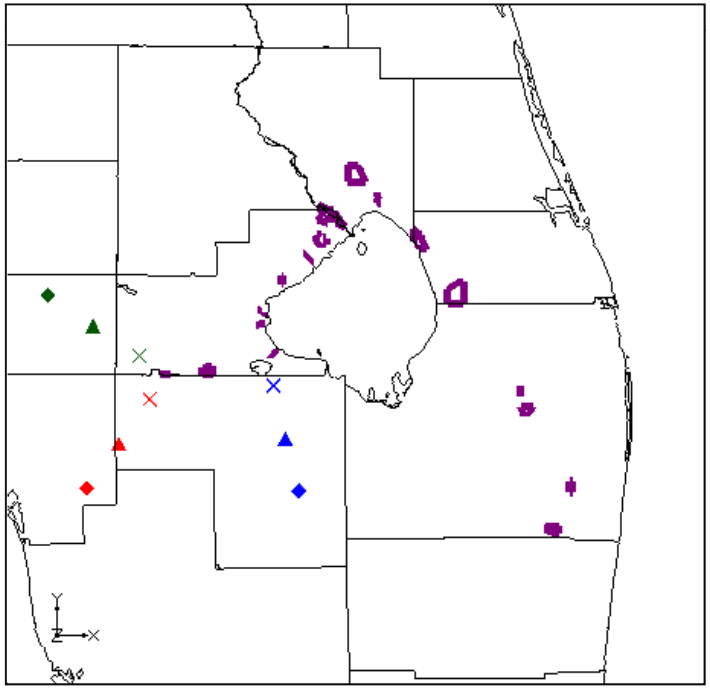

25-Mile Distance

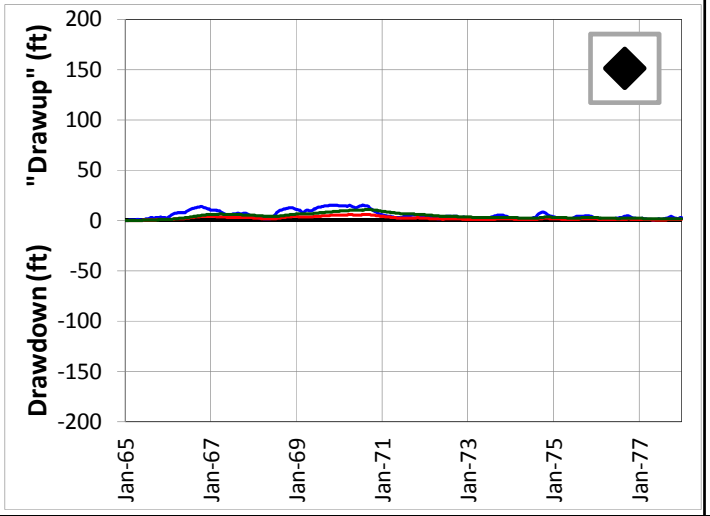

Legend

- CERP ASR Sites
- 5-Mile Distance Locations
- 15-Mile Distance Locations
- 25-Mile Distance Locations

Notes:

Scenario 10 is a variation on Scenario 9. The numbers of wells and injection volumes are identical, but the extraction volumes have been cut back to reduce drawdown.

A number of individual sites were chosen from the APPZ Aquifer at distances of 5, 15 and 25 miles from the proposed ASR well sites. This figure shows the drawdown and "drawup" at each output time step for 9 of these sites.

The plots were calculated by subtracting the heads calculated by the D13R model from those calculated by the no project run. This results in a positive value for "drawup" and a negative value for drawdown.

The colors of the points on the map correspond to the colors of the lines on the plots.

The symbols on the map (x, triangle and diamond) indicate the distance from the ASR sites.

5-Mile Distance

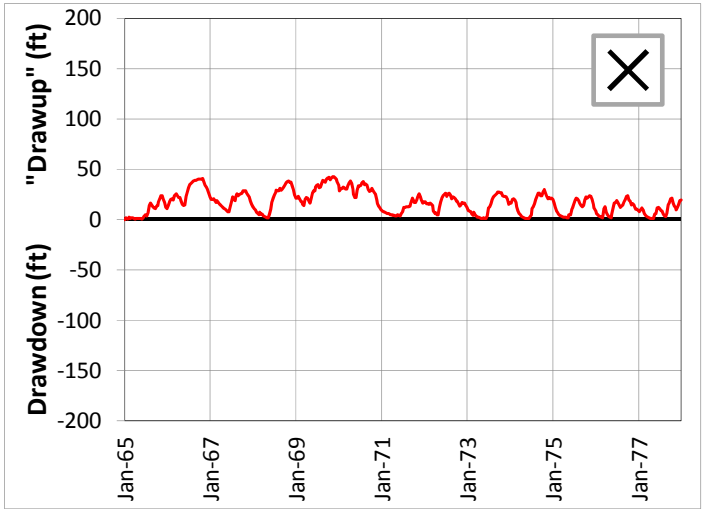

15-Mile Distance

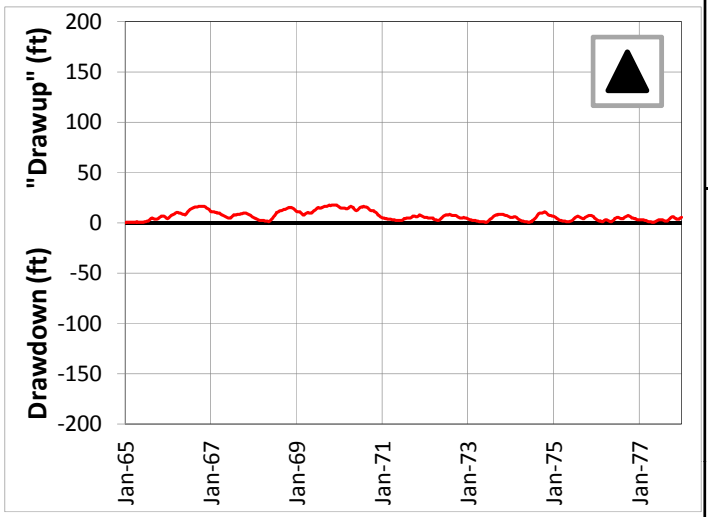

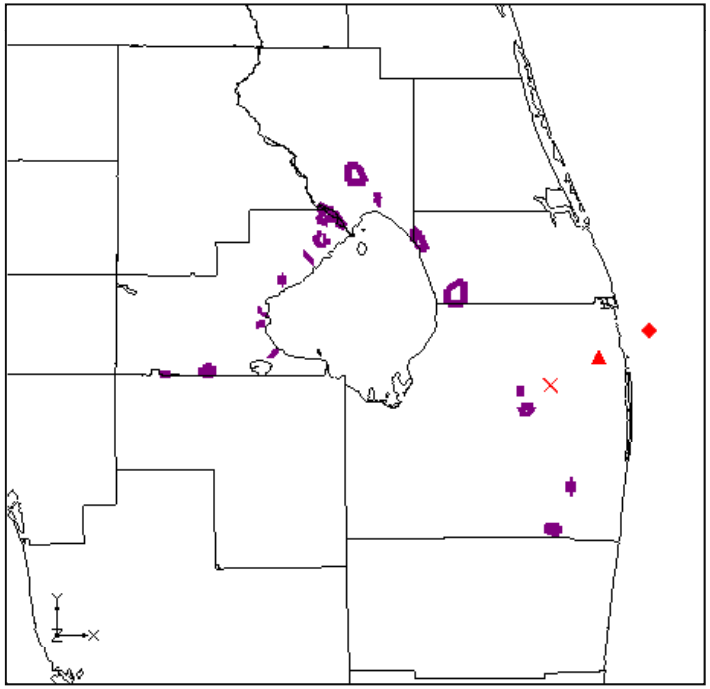

25-Mile Distance

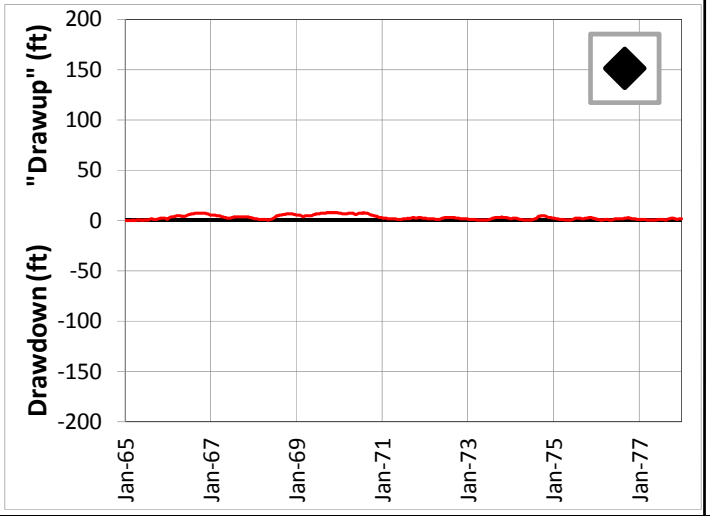

Legend

- CERP ASR Sites
- 5-Mile Distance Locations
- 15-Mile Distance Locations
- 25-Mile Distance Locations

Notes:

Scenario 10 is a variation on Scenario 9. The numbers of wells and injection volumes are identical, but the extraction volumes have been cut back to reduce drawdown.

A number of individual sites were chosen from the APPZ Aquifer at distances of 5, 15 and 25 miles from the proposed ASR well sites. This figure shows the drawdown and "drawup" at each output time step for 3 of these sites.

The plots were calculated by subtracting the heads calculated by the D13R model from those calculated by the no project run. This results in a positive value for "drawup" and a negative value for drawdown.

The colors of the points on the map correspond to the colors of the lines on the plots.

The symbols on the map (x, triangle and diamond) indicate the distance from the ASR sites.

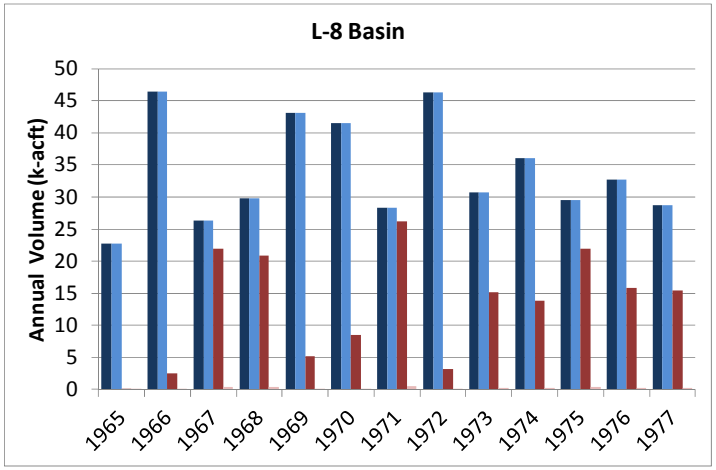

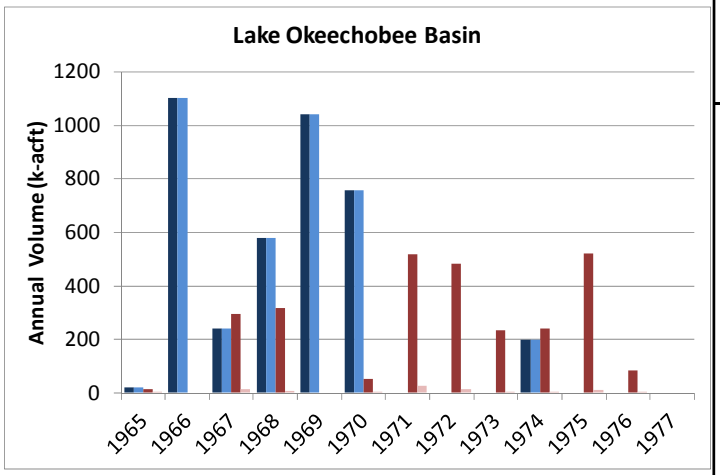

	L-8		Lake Okeechobee		Caloosahatchee	
	In %	Out %	In %	Out %	In %	Out %
1965	100%	2%	100%	3%	100%	2%
1966	100%	2%	100%	--	100%	2%
1967	100%	2%	100%	5%	100%	2%
1968	100%	2%	100%	3%	100%	2%
1969	100%	2%	100%	--	100%	--
1970	100%	2%	100%	5%	100%	2%
1971	100%	2%	--	5%	100%	2%
1972	100%	2%	--	3%	100%	2%
1973	100%	2%	--	2%	100%	2%
1974	100%	2%	100%	2%	100%	2%
1975	100%	2%	--	2%	100%	2%
1976	100%	2%	--	2%	100%	2%
1977	100%	2%	--	--	100%	2%

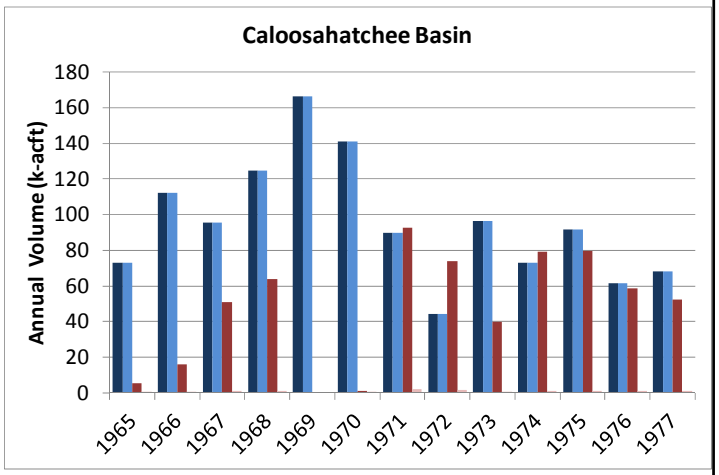

Legend

- Design Storage (injection)
- Modeled Storage (injection)
- Design Recovery (extraction)
- Modeled Recovery (extraction)

Notes:

Scenario 10 is a variation on Scenario 9. The numbers of wells and injection volumes are identical, but the extraction volumes have been cut back to reduce drawdown.

These three plots show the comparison between the SFWMM-D13R designed annual injection and extraction volumes at the ASR wells and the actual assigned rates for the RASRSM-D13R for three of the basins. The table presents the percentage of SFWMM-D13R annual flow rates that are included in the RASRSM-D13R.

Scenario 10 – Comparison of Designed and Modeled ASR Flow Rates

Regional Model Production Scenario Report

Figure 4.124

June 2013

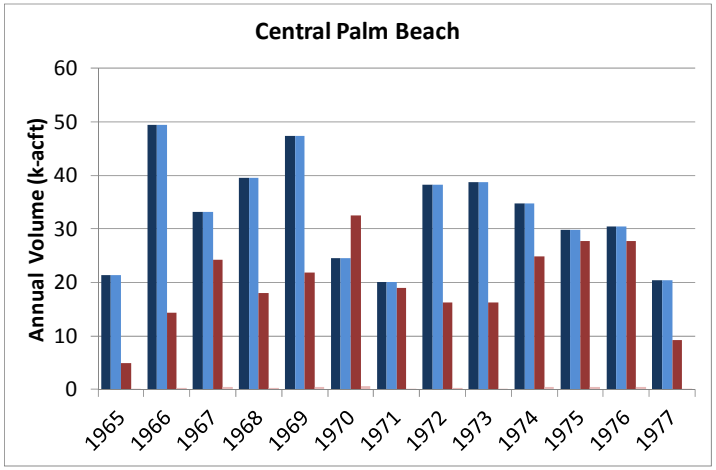

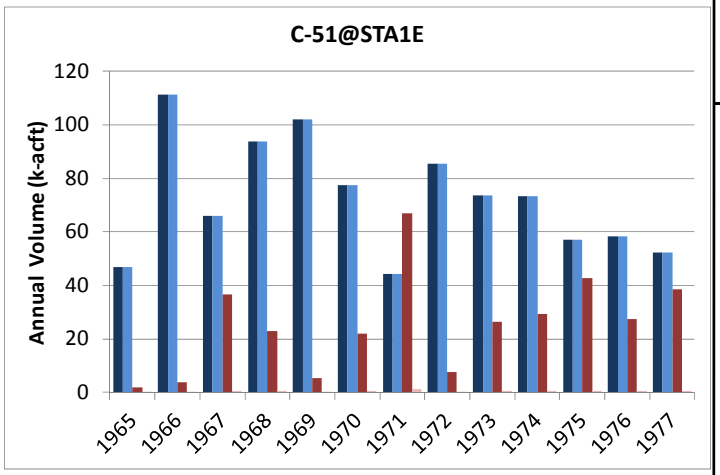

	CPB		C-51		Hillsboro	
	In %	Out %	In %	Out %	In %	Out %
1965	100%	2%	100%	2%	100%	1%
1966	100%	2%	100%	2%	100%	1%
1967	100%	2%	100%	2%	100%	1%
1968	100%	2%	100%	2%	100%	1%
1969	100%	2%	100%	2%	100%	1%
1970	100%	2%	100%	2%	100%	1%
1971	100%	1%	100%	2%	100%	1%
1972	100%	2%	100%	2%	100%	1%
1973	100%	1%	100%	2%	100%	1%
1974	100%	2%	100%	2%	100%	1%
1975	100%	2%	100%	1%	100%	0%
1976	100%	1%	100%	2%	100%	1%
1977	100%	2%	100%	1%	100%	0%

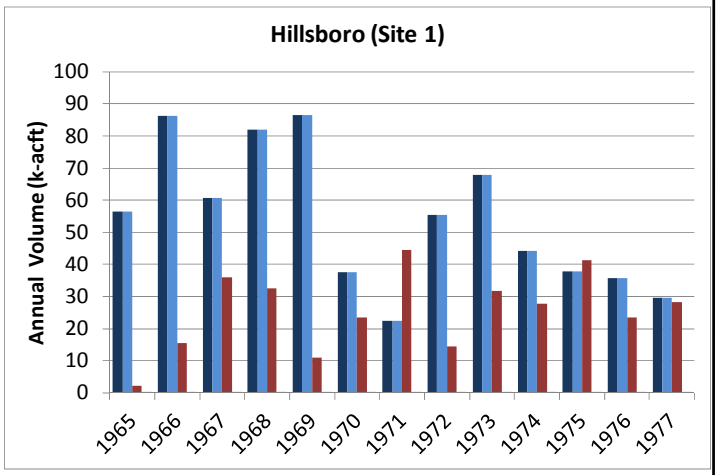

Legend

- Design Storage (injection)
- Modeled Storage (injection)
- Design Recovery (extraction)
- Modeled Recovery (extraction)

Notes:

Scenario 10 is a variation on Scenario 9. The numbers of wells and injection volumes are identical, but the extraction volumes have been cut back to reduce drawdown.

These three plots show the comparison between the SFWMM-D13R designed annual injection and extraction volumes at the ASR wells and the actual assigned rates for the RASRSM-D13R for three of the basins. The table presents the percentage of SFWMM-D13R annual flow rates that are included in the RASRSM-D13R.

Scenario 10 – Comparison of Designed and Modeled ASR Flow Rates

Regional Model Production Scenario Report

Figure 4.125

June 2013

	Total	
	In %	Out %
1965	100%	2%
1966	100%	2%
1967	100%	4%
1968	100%	2%
1969	100%	2%
1970	100%	3%
1971	100%	4%
1972	100%	3%
1973	100%	2%
1974	100%	2%
1975	100%	2%
1976	100%	2%
1977	100%	1%

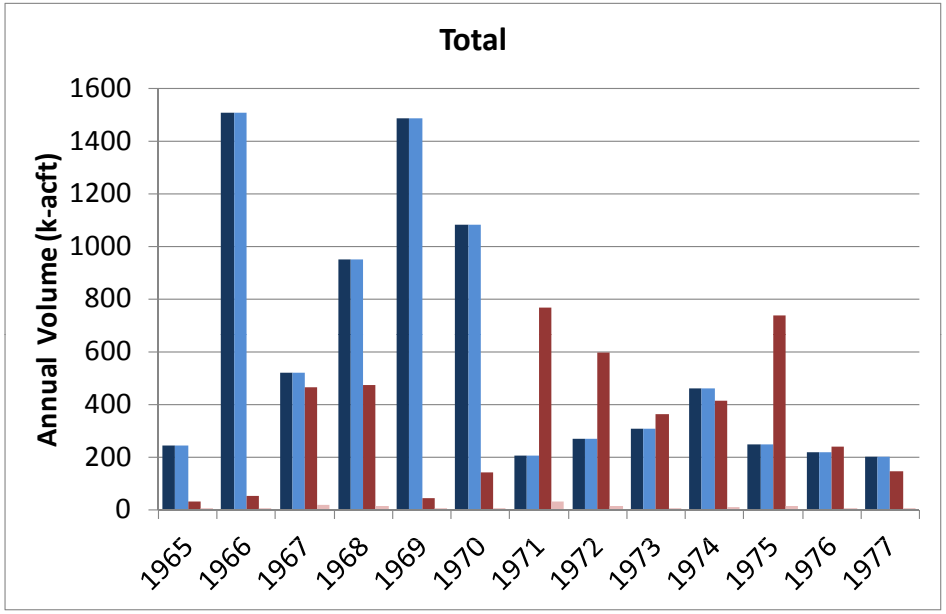

Legend

- Design Storage (injection)
- Modeled Storage (injection)
- Design Recovery (extraction)
- Modeled Recovery (extraction)

Notes:

Scenario 10 is a variation on Scenario 9. The numbers of wells and injection volumes are identical, but the extraction volumes have been cut back to reduce drawdown.

This plot shows the comparison between the SFWMM-D13R designed annual injection and extraction volumes at the ASR wells and the actual assigned rates for the RASRSM-D13R for all basins. The table presents the percentage of SFWMM-D13R annual flow rates that are included in the RASRSM-D13R.

		UF		APPZ		BZ		Total # Wells	Target # Wells
		Number of Wells	Recovery Efficiency	Number of Wells	Recovery Efficiency	Number of Wells	Recovery Efficiency		
Caloosahatchee Basin	Moore Haven	4	70%	0	30%	6	0%		
	River Bend	3	70%	1	30%	2	0%		
	Flaghole	2	0%	0	30%	9	0%		
	Basin Total	9		1		17		27	44
Lake Okeechobee Basin	Nicodemus Slough	0	70%	10	30%	0	0%		
	C-41 Canal	0	70%	0	30%	5	0%		
	C-40 Canal	2	70%	0	30%	4	0%		
	North Lake Okeechobee	8	70%	2	30%	5	0%		
	Kissimmee R./Paradise Run	15	70%	0	30%	30	0%		
	Taylor Creek	0	70%	10	30%	5	0%		
	L-63N	0	70%	9	30%	3	0%		
	Lakeside Ranch	4	70%	0	30%	8	0%		
	Port Mayaca	18	70%	0	30%	1	0%		
	Basin Total	47		31		61		139	200
L-8		6	70%	0	30%	2	0%	8	10
C-51		12	70%	2	30%	10	0%	24	34
Central Palm Beach		10	70%	3	30%	1	0%	14	15
Site 1 (Hillsboro)		10	40%	0	40%	10	0%	20	30
Total		94		37		101		232	333

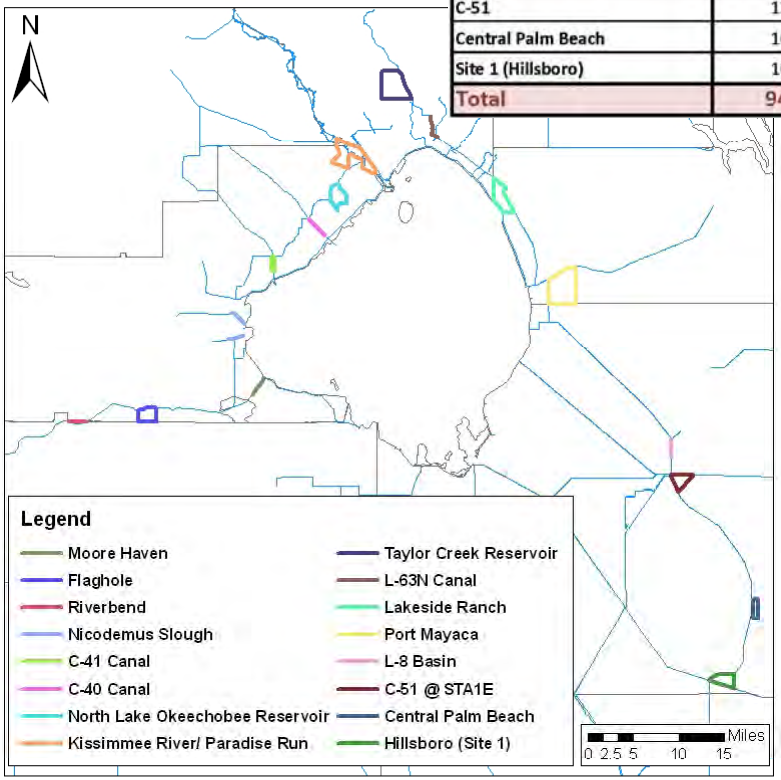

Extraction Percentage		
	UF	APPZ
Caloosahatchee Basin		
Moore Haven	100%	
River Bend	100%	100%
Flaghole	100%	
Lake Okeechobee Basin		
Nicodemus Slough		100%
C-41 Canal		
C-40 Canal	100%	
North Lake Okeechobee	25%	100%
Kissimmee R./Paradise Run	25%	
Taylor Creek		50%
L-63N		50%
Lakeside Ranch	0%	
Port Mayaca	0%	
L-8	100%	
C-51	100%	100%
Central Palm Beach	100%	100%
Site 1 (Hillsboro)	100%	

Notes:

Scenario 11 is a variation on Scenario 9. The numbers of wells and injection volumes are identical, but the extraction volumes have been reduced to meet the APPA performance measure.

Reductions have been applied as a percentage of the Scenario 9 rates as shown in the lower table.

The extraction percentage is the percentage applied to the extraction rates to reduce drawdown effects. This is not the recovery efficiency.

Flow rates are divided evenly among the wells in each basin. Maximum flow rate for any one well is 5 mgd in the UF and APPZ and 10 mgd in the BZ.

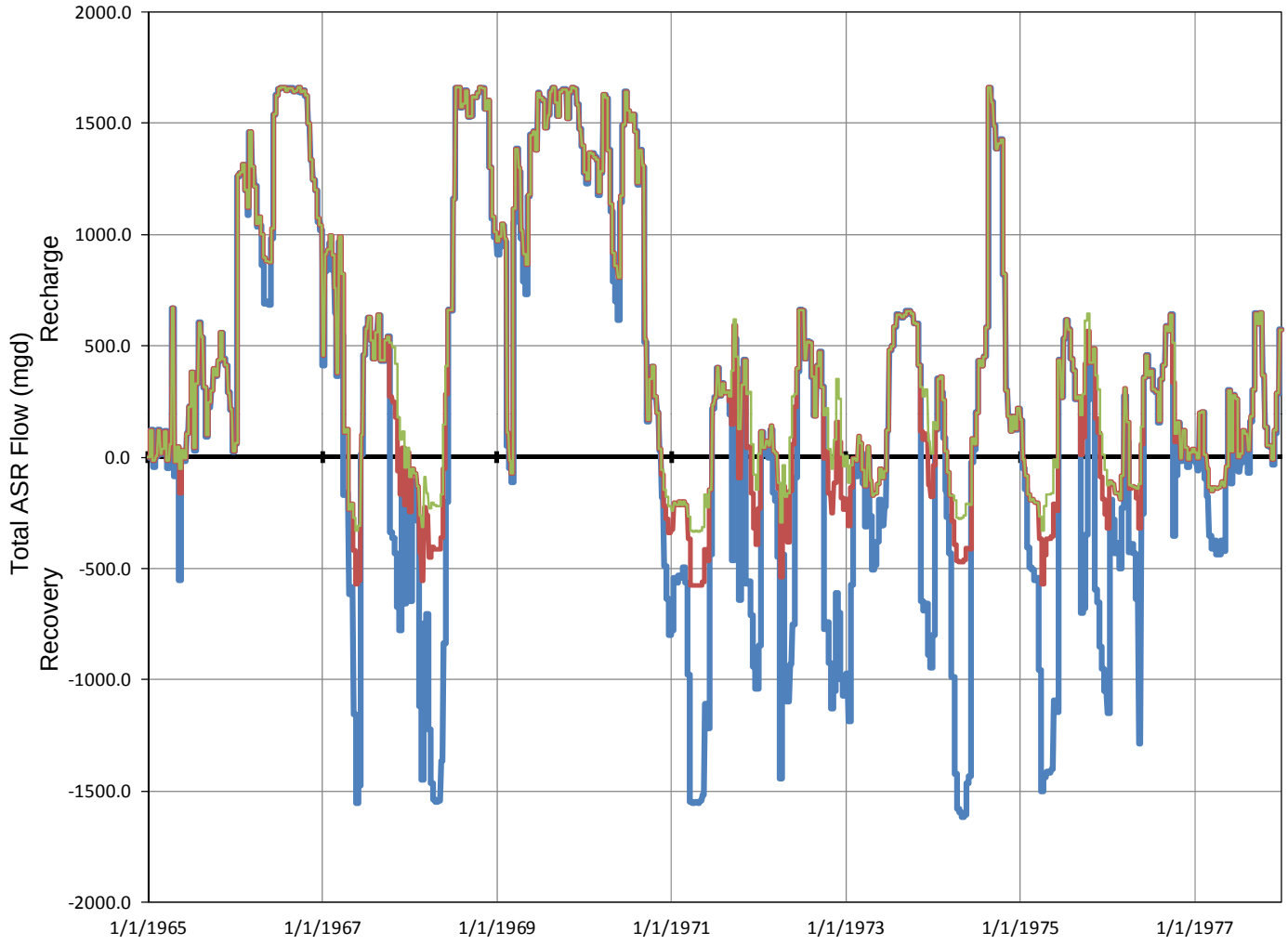

Legend

- Scenario 1 – ASR Flux
- Scenario 9 – ASR Flux
- Scenario11– ASR Flux

Notes:

Scenario 11 is a variation on Scenario 9. The numbers of wells and injection volumes are identical, but the extraction volumes have been reduced to meet the APPA performance measure.

This plot shows the extraction and injection rates for all wells at all sites for Scenario 1, Scenario 9 and Scenario 11. Positive rates are recharge (injection), while negative rates are recovery (extraction).

Scenario 11 – ASR Well Fluxes (Compared to Scenarios 1 & 9)

Regional Model Production Scenario Report

Figure 4.128

June 2013

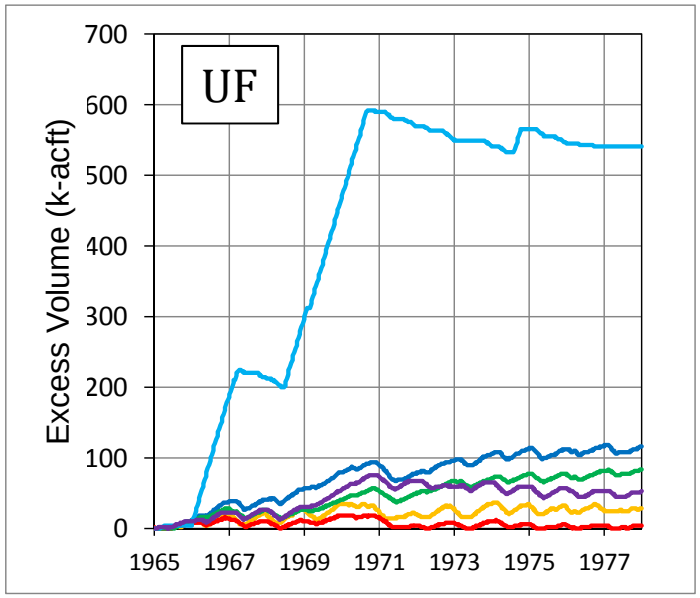

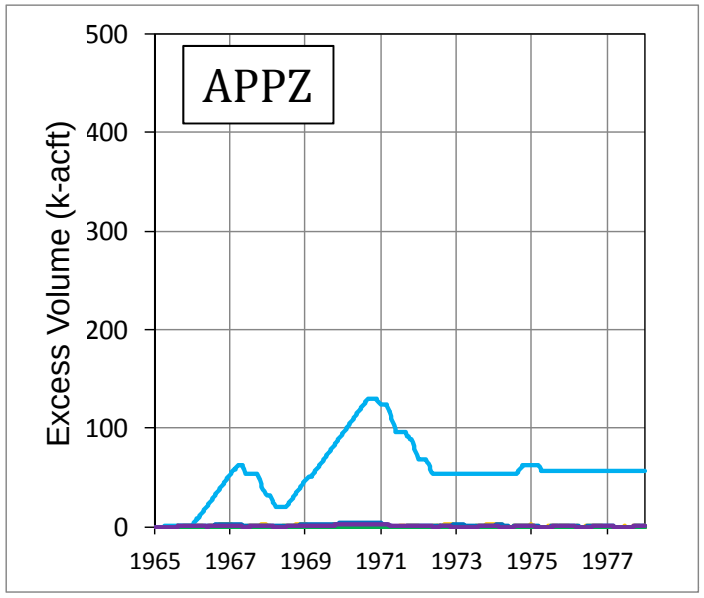

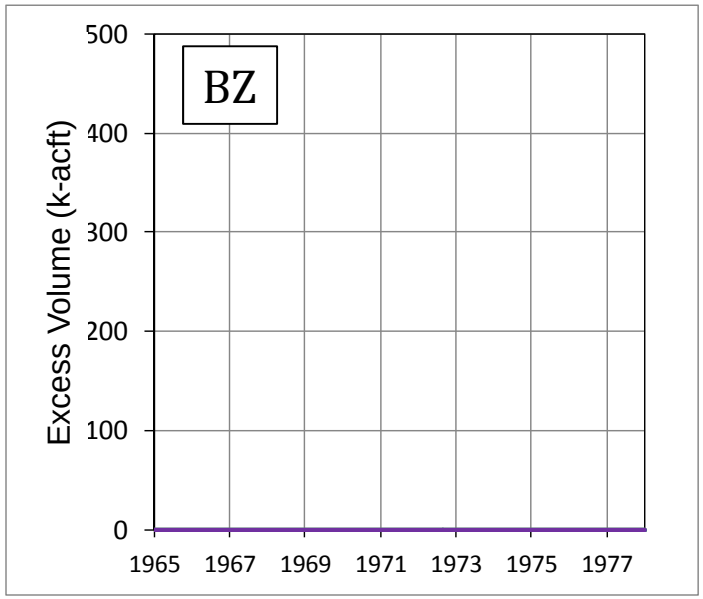

Legend

- Central Palm Beach
- C-51
- Hillsboro
- L-8
- Lake Okeechobee
- Caloosahatchee River

Notes:

Scenario 11 is a variation on Scenario 9. The numbers of wells and injection volumes are identical, but the extraction volumes have been reduced to meet the APPA performance measure.

These plots show the excess volume of fresh water remaining in each aquifer at each ASR basin. Excess volume is calculated by adding injected volume times recovery efficiency and subtracting extracted volume. The calculation is cumulative.

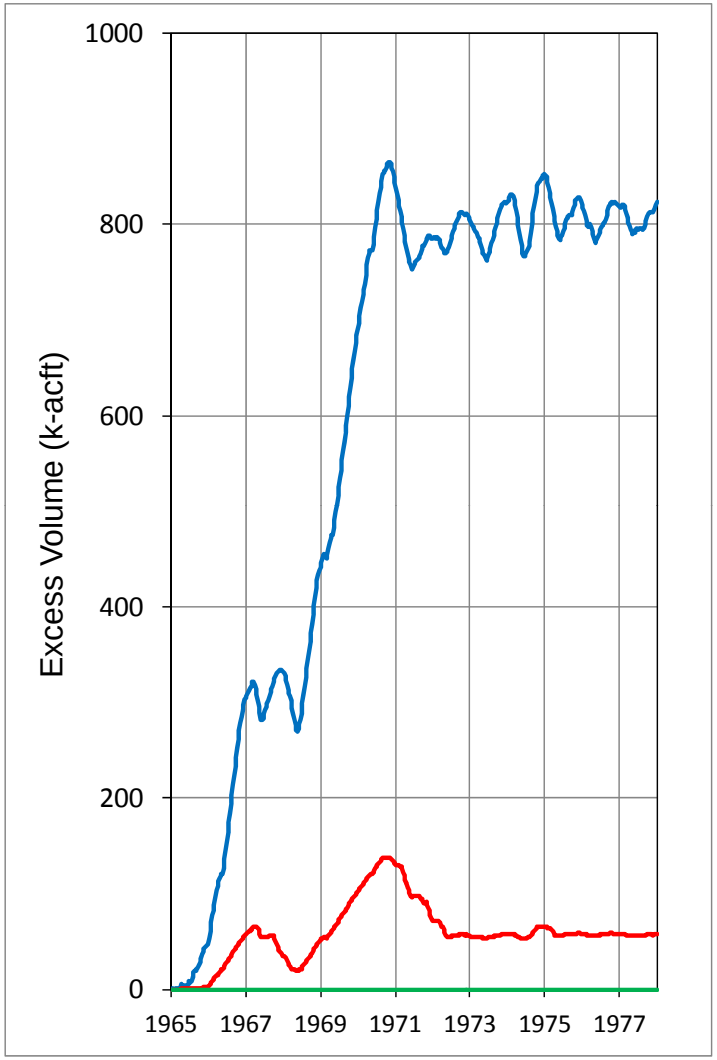

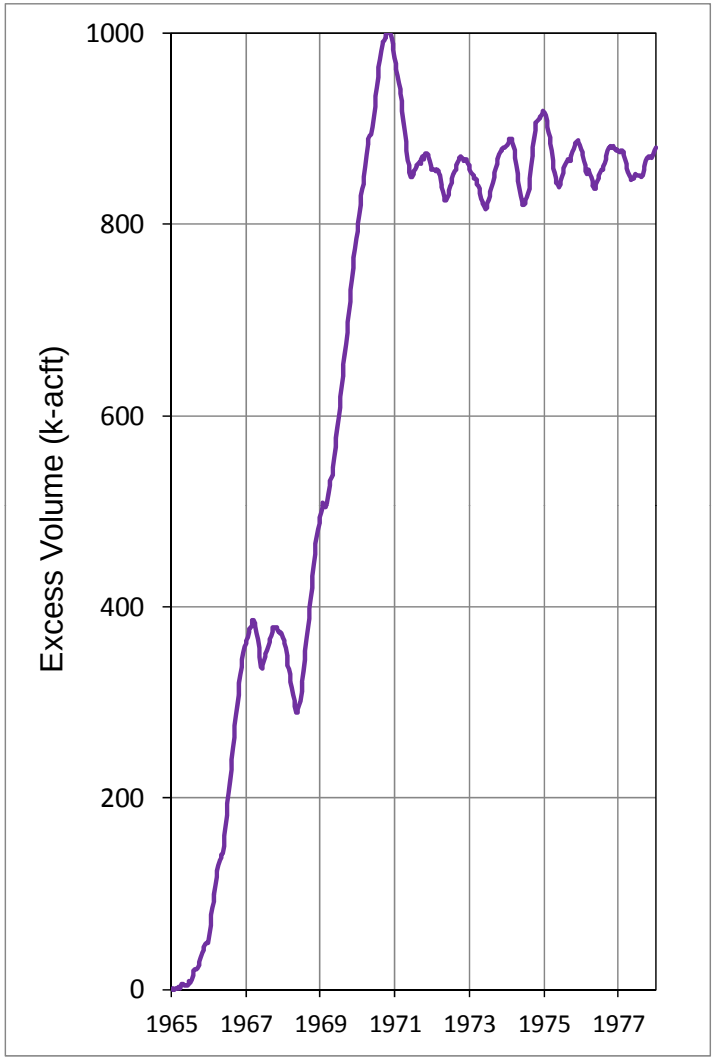

Legend

- Total UF
- Total APPZ
- Total BZ
- Total (All Aquifers)

Notes:

Scenario 11 is a variation on Scenario 9. The numbers of wells and injection volumes are identical, but the extraction volumes have been reduced to meet the APPA performance measure.

These plots show the total excess volume of fresh water remaining in each aquifer and in all aquifers. Excess volume is calculated by adding injected volume times recovery efficiency and subtracting extracted volume. The calculation is cumulative.

SCENARIO 11 – EXCESS VOLUME OF FRESH WATER

REGIONAL MODEL PRODUCTION SCENARIO REPORT

FIGURE 4.130

JUNE 2013

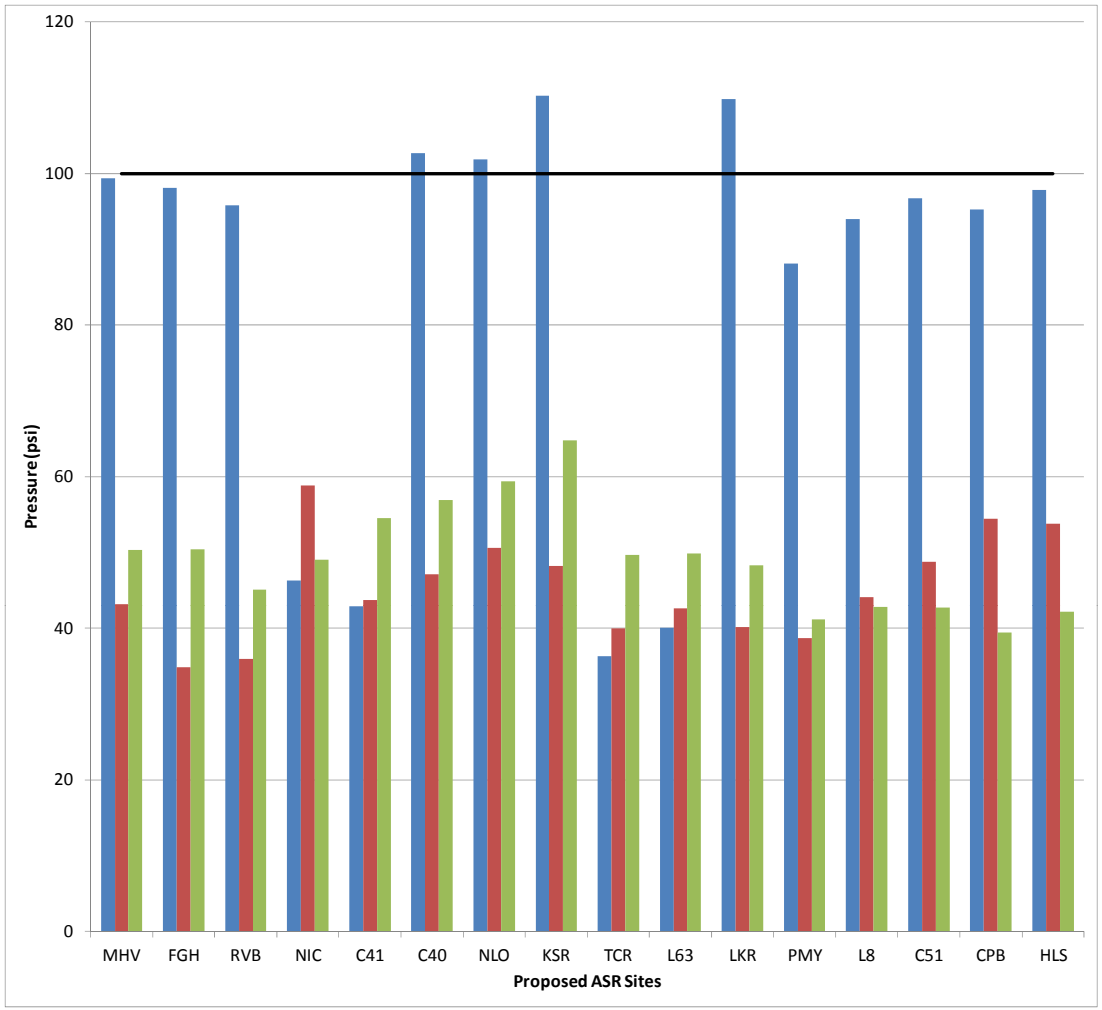

MHV	Moorehaven
FGH	Flaghole
RVB	Riverbend
NIC	Nicodemus Slough
C41	C-41Canal
C40	C-40 Canal
NLO	North Lake Okeechobee Reservoir
KSR	Kissimmee River / Paradise Run
TCR	Taylor Creek Reservoir
L63	L-63N Canal
LKR	Lakeside Ranch
PMY	Port Mayaca
L8	L-8 Basin
C51	C-51 @ STA1E
CPB	Central Palm Beach
HLS	Hillsboro (Site 1)

Legend

- Upper Floridan Aquifer
- Avon Park Permeable Zone
- Boulder Zone
- 100 psi Limit

Notes:

Scenario 11 is a variation on Scenario 9. The numbers of wells and injection volumes are identical, but the extraction volumes have been reduced to meet the APPA performance measure.

This plot shows the highest pressure at each site which the pump would need to overcome in order to inject storage water during the 13-year simulation.

The PDT determined that it would be important to keep this pressure below 100 psi (indicated by the heavy black line).

Note that maximum pressures are shown for all aquifers and all sites even if ASR pumps are not located there for the current scenario.

SCENARIO 11 – MAXIMUM PUMP PRESSURE REQUIREMENTS

REGIONAL MODEL PRODUCTION SCENARIO REPORT

FIGURE 4.131

JUNE 2013

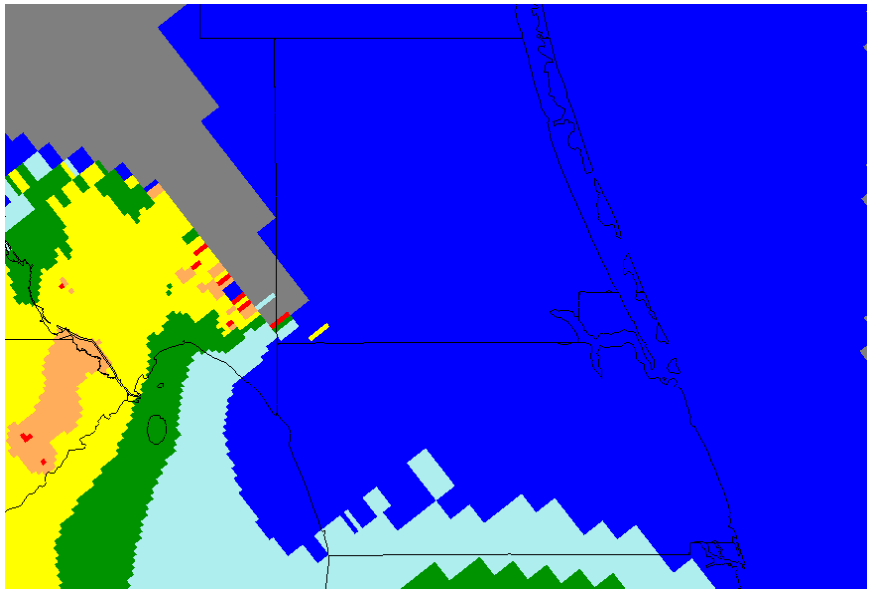

Upper Floridan Aquifer

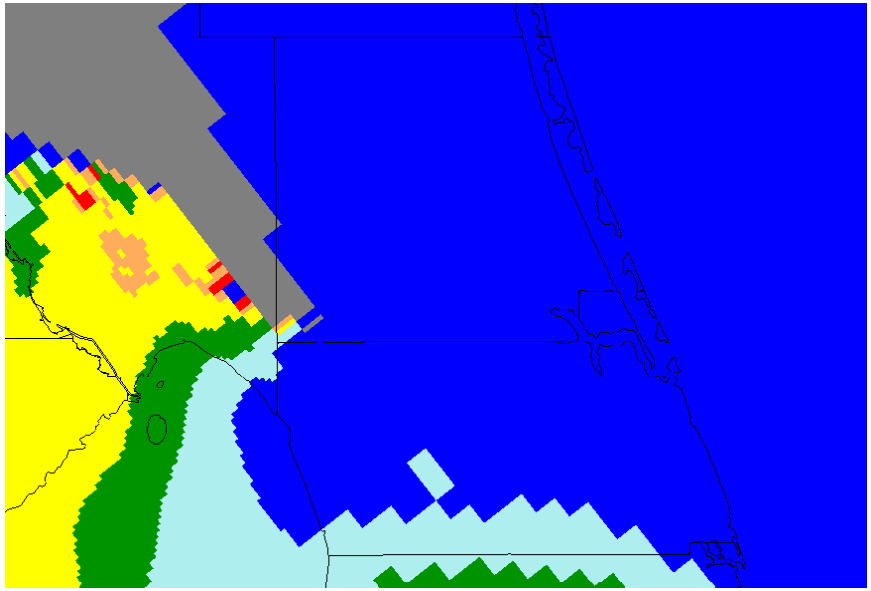

Avon Park Permeable Zone

Legend

- Not artesian or no reduction
- < 5%
- 5% - 10%
- 10% - 20%
- 20% - 50%
- 50% - 100%
- Loses artesian condition

Notes:

Scenario 11 is a variation on Scenario 9. The numbers of wells and injection volumes are identical, but the extraction volumes have been reduced to meet the APPA performance measure.

These plots show the maximum reduction in artesian flow at each model cell as a percentage when compared to the flow expected without the ASR project.

Permit rules require that the reduction in Saint Lucie and Martin Counties be less than 10%.

Note the gray area in the northwest corner of the figures, which coincides with a ridge and does not normally have artesian conditions.

Scenario 11 – Maximum Reduction in Artesian Flow Capacity

Regional Model Production Scenario Report

Figure 4.132

June 2013

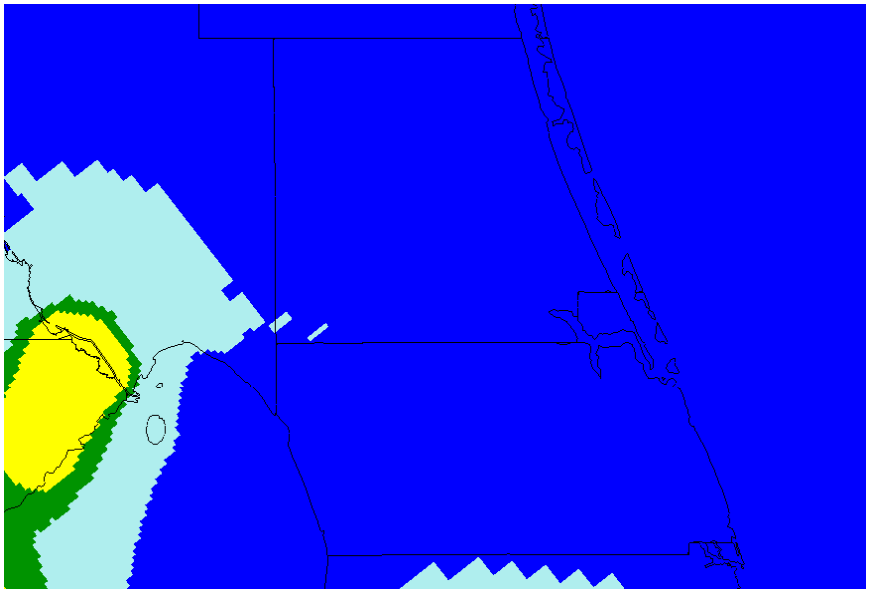

Upper Floridan Aquifer

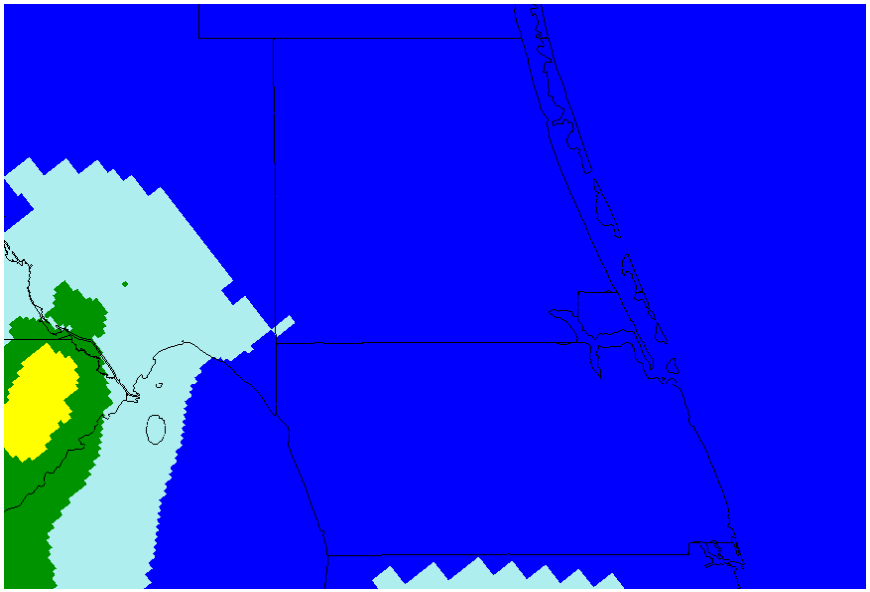

Avon Park Permeable Zone

Legend

- 0 days
- 1 – 250 days
- 250 – 500 days
- 500 – 1000 days
- 1000 – 2000 days
- > 2000 days

Notes:

Scenario 11 is a variation on Scenario 9. The numbers of wells and injection volumes are identical, but the extraction volumes have been reduced to meet the APPA performance measure.

These plots indicate the severity of the loss of artesian pressure due to ASR extraction pumping.

Permit rules require that the reduction in Saint Lucie and Martin Counties be less than 10%. This plot indicates the number of days during the simulation in which the flow reduction was greater than 10%. There are 4748 days in the 13-year model simulation period.

SCENARIO 11 – NUMBER OF DAYS (OUT OF 13 YEARS) WITH FLOW REDUCTION EXCEEDING 10%

REGIONAL MODEL PRODUCTION SCENARIO REPORT

FIGURE 4.133

JUNE 2013

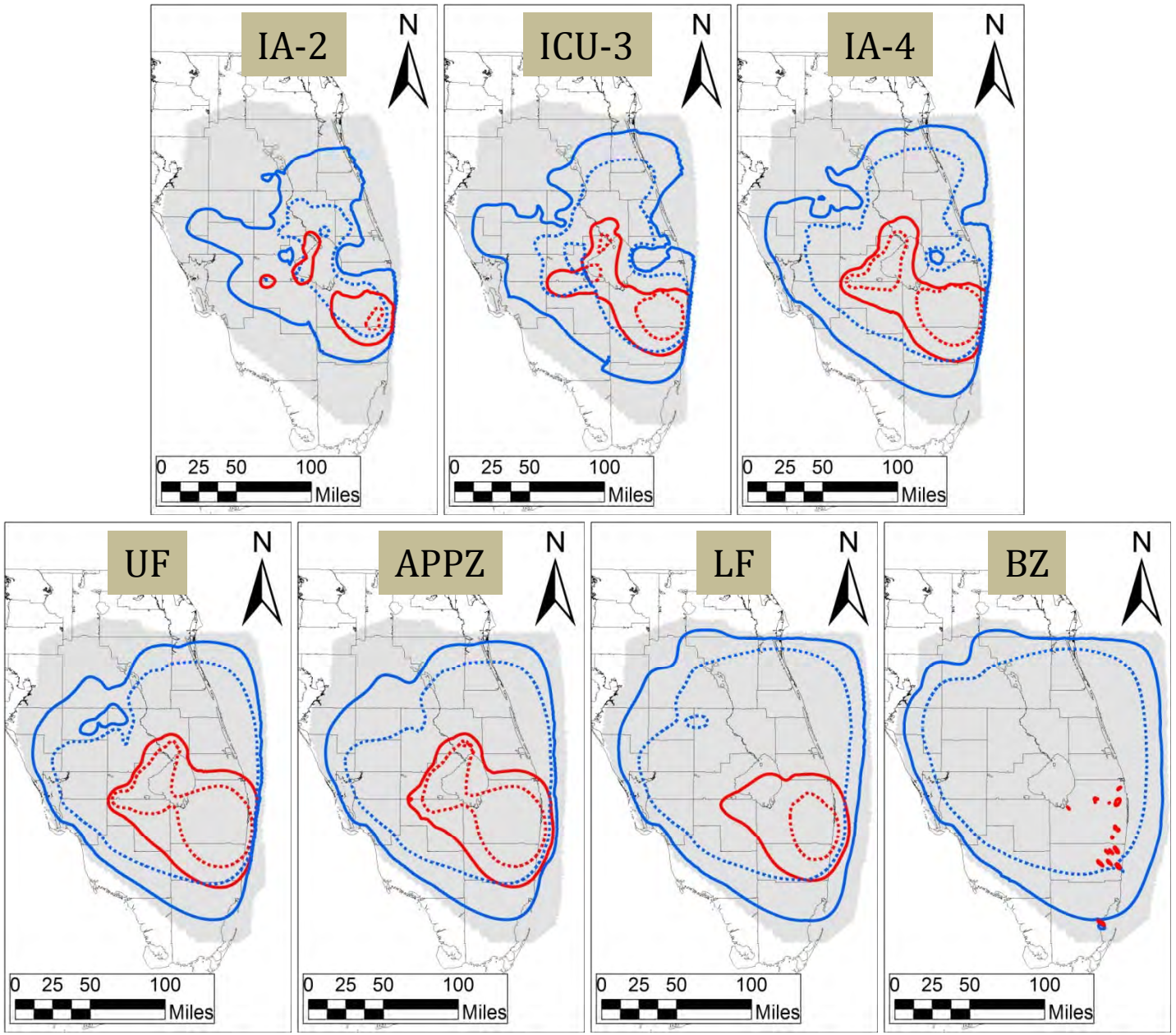

Legend

Maximum Drawdown
- 1 foot
- 5 feet

Maximum "Drawup"
- 1 foot
- 5 feet

Model Domain

Notes:

Scenario 11 is a variation on Scenario 9. The numbers of wells and injection volumes are identical, but the extraction volumes have been reduced to meet the APPA performance measure.

These figures show the extent of the areas where the maximum drawdown or "drawup" is greater than 1 foot or 5 feet.

The maximum condition does not necessarily occur at the same time for all regions of the model.

SCENARIO 11 – MAXIMUM DRAWDOWN AND "DRAWUP" BY AQUIFER

REGIONAL MODEL PRODUCTION SCENARIO REPORT

FIGURE 4.134

JUNE 2013

5-Mile Distance

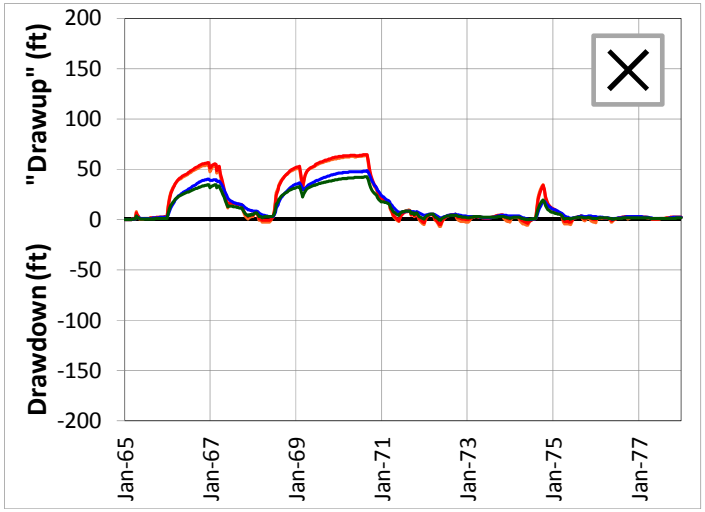

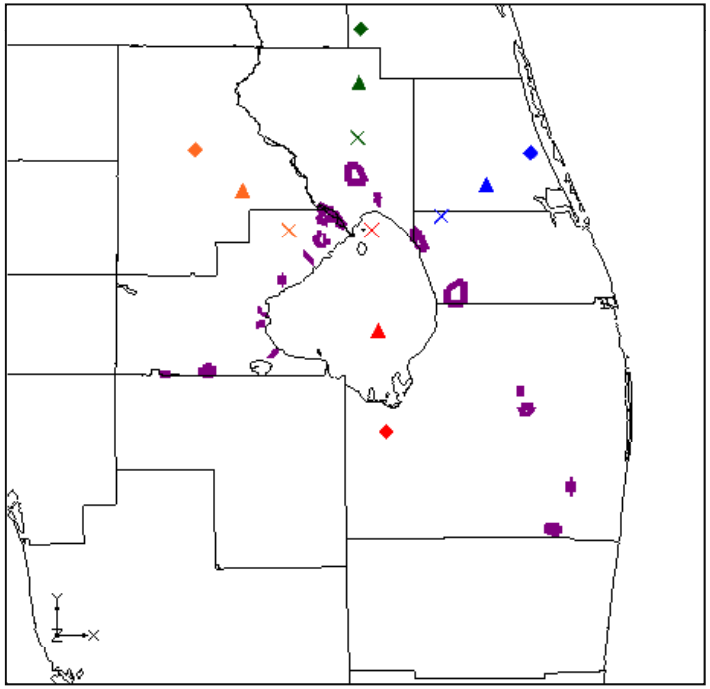

15-Mile Distance

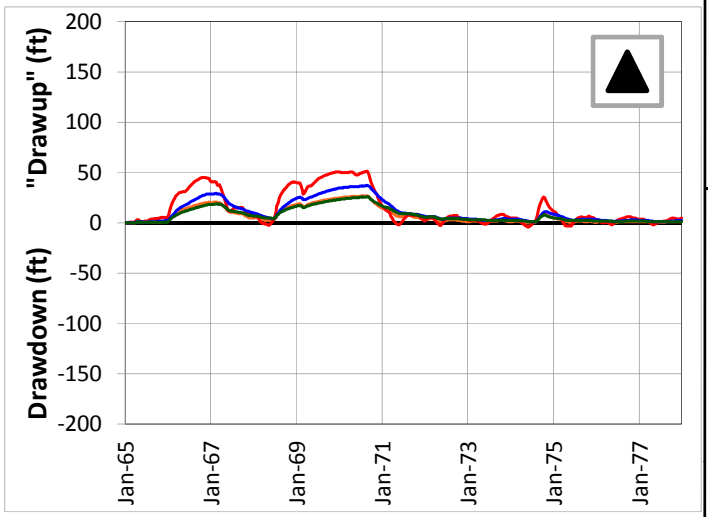

25-Mile Distance

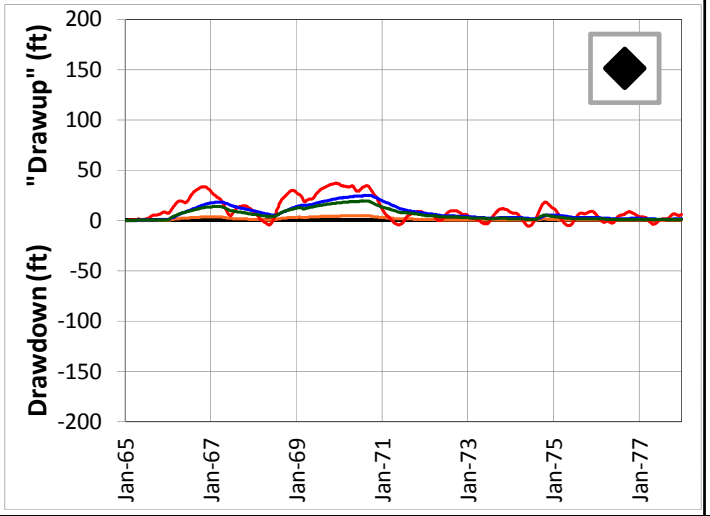

Legend

- CERP ASR Sites
- ✕ 5-Mile Distance Locations
- ▲ 15-Mile Distance Locations
- ◆ 25-Mile Distance Locations

Notes:

Scenario 11 is a variation on Scenario 9. The numbers of wells and injection volumes are identical, but the extraction volumes have been reduced to meet the APPA performance measure.

A number of individual sites were chosen from the UF Aquifer at distances of 5, 15 and 25 miles from the proposed ASR well sites. This figure shows the drawdown and "drawup" at each output time step for 12 of these sites.

The plots were calculated by subtracting the heads calculated by the D13R model from those calculated by the no project run. This results in a positive value for "drawup" and a negative value for drawdown.

The colors of the points on the map correspond to the colors of the lines on the plots.

The symbols on the map (x, triangle and diamond) indicate the distance from the ASR sites.

5-Mile Distance

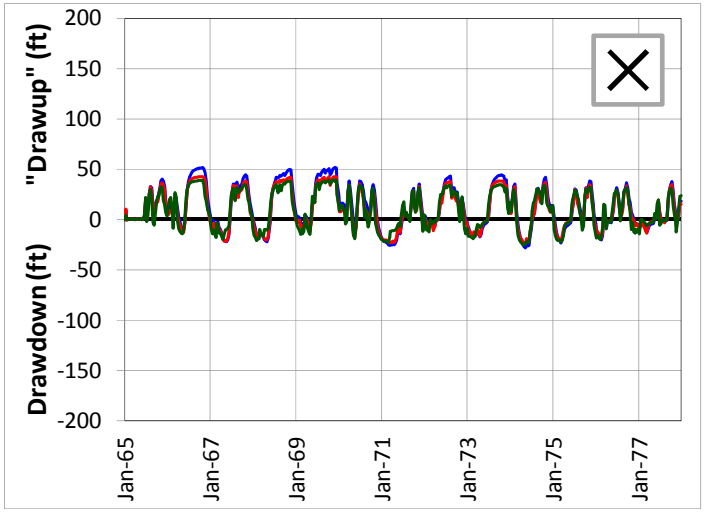

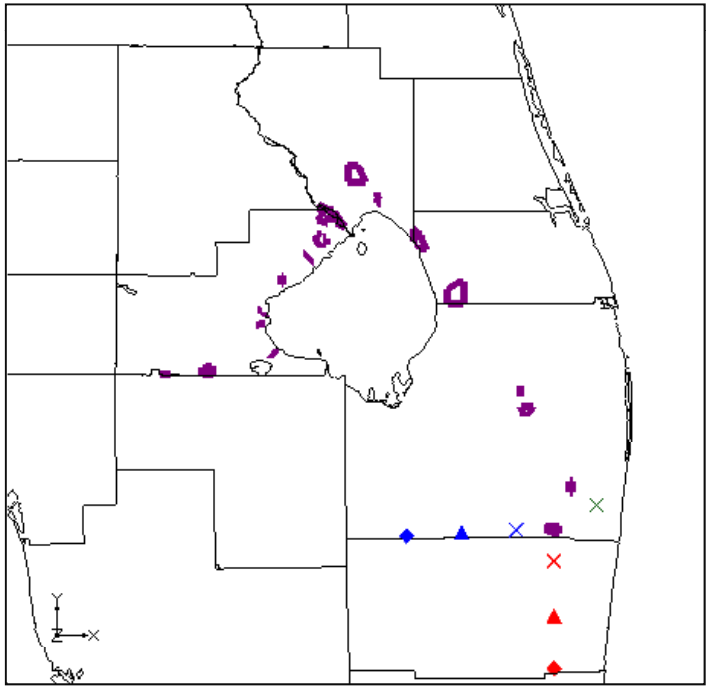

15-Mile Distance

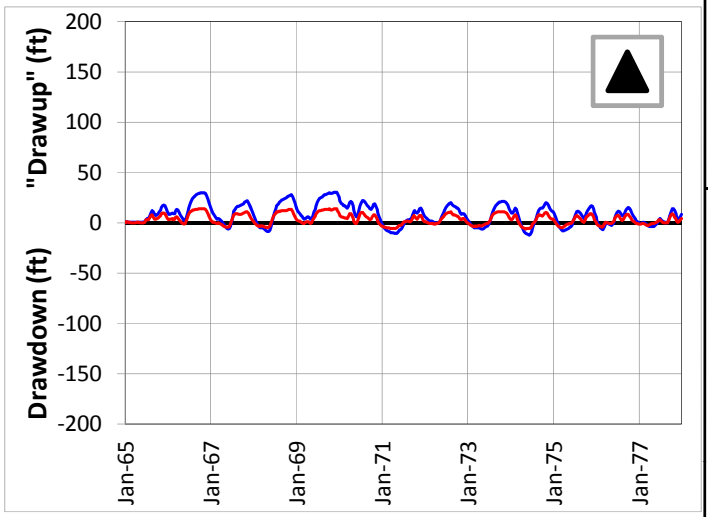

25-Mile Distance

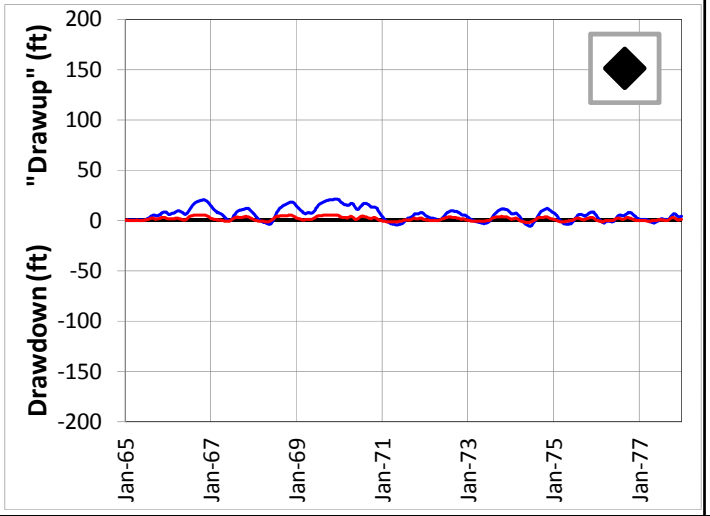

Legend

- CERP ASR Sites
- ✕ 5-Mile Distance Locations
- ▲ 15-Mile Distance Locations
- ◆ 25-Mile Distance Locations

Notes:

Scenario 11 is a variation on Scenario 9. The numbers of wells and injection volumes are identical, but the extraction volumes have been reduced to meet APPA performance measures.

A number of individual sites were chosen from the UF Aquifer at distances of 5, 15 and 25 miles from the proposed ASR well sites. This figure shows the drawdown and "drawup" at each output time step for 7 of these sites.

The plots were calculated by subtracting the heads calculated by the D13R model from those calculated by the no project run. This results in a positive value for "drawup" and a negative value for drawdown.

The colors of the points on the map correspond to the colors of the lines on the plots.

The symbols on the map (x, triangle and diamond) indicate the distance from the ASR sites.

5-Mile Distance

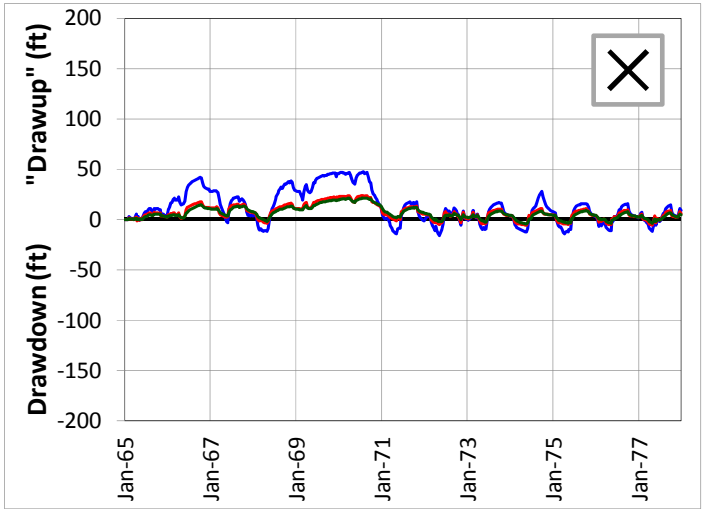

15-Mile Distance

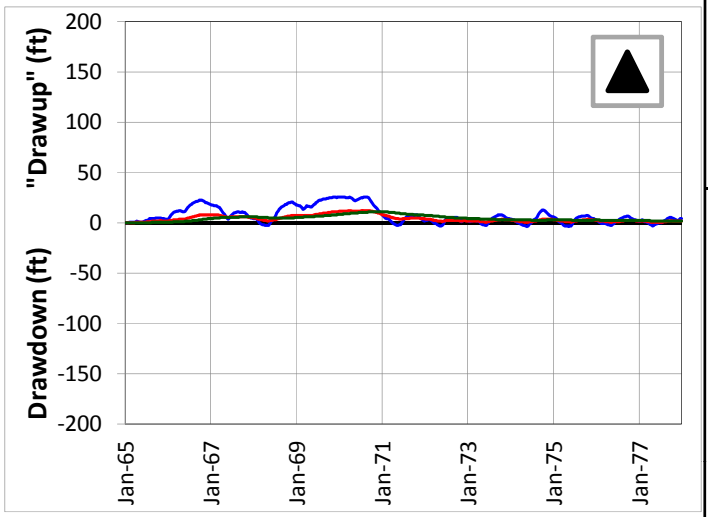

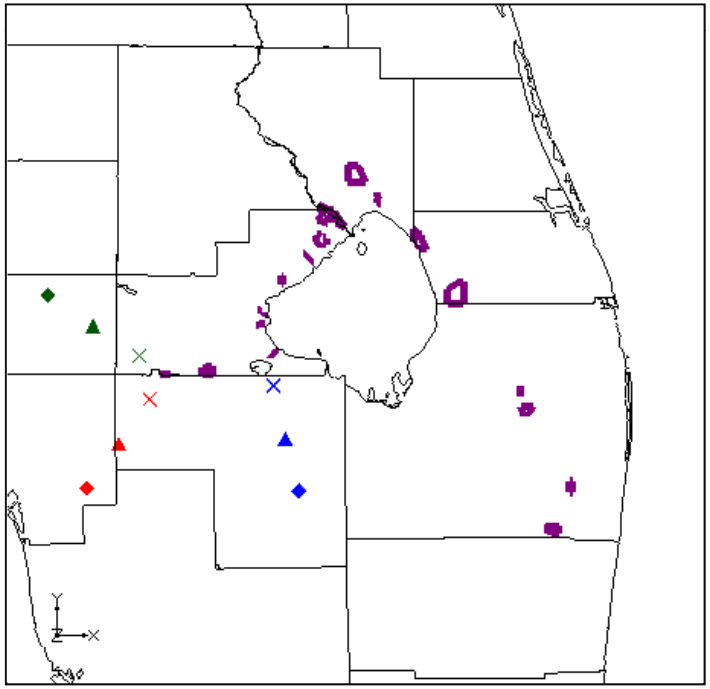

25-Mile Distance

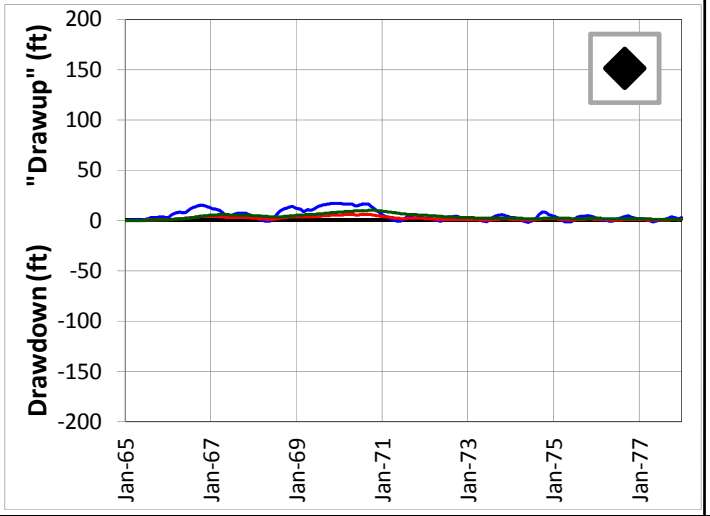

Legend

- CERP ASR Sites
- 5-Mile Distance Locations
- 15-Mile Distance Locations
- 25-Mile Distance Locations

Notes:

Scenario 11 is a variation on Scenario 9. The numbers of wells and injection volumes are identical, but the extraction volumes have been reduced to meet APPA performance measures.

A number of individual sites were chosen from the UF Aquifer at distances of 5, 15 and 25 miles from the proposed ASR well sites. This figure shows the drawdown and "drawup" at each output time step for 9 of these sites.

The plots were calculated by subtracting the heads calculated by the D13R model from those calculated by the no project run. This results in a positive value for "drawup" and a negative value for drawdown.

The colors of the points on the map correspond to the colors of the lines on the plots.

The symbols on the map (x, triangle and diamond) indicate the distance from the ASR sites.

5-Mile Distance

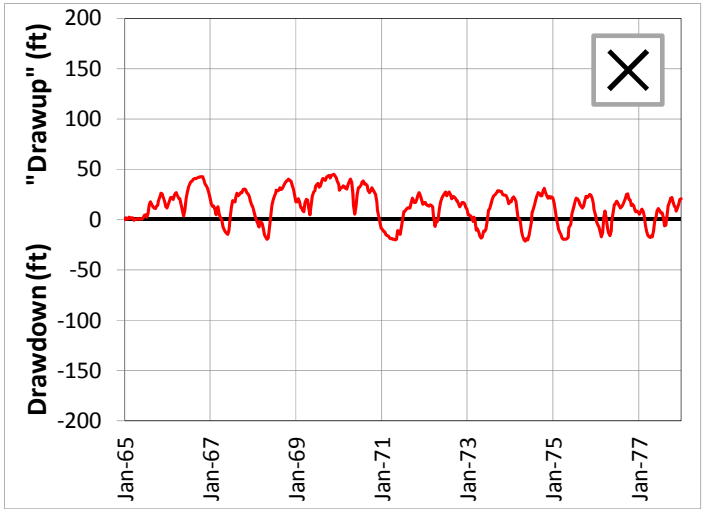

15-Mile Distance

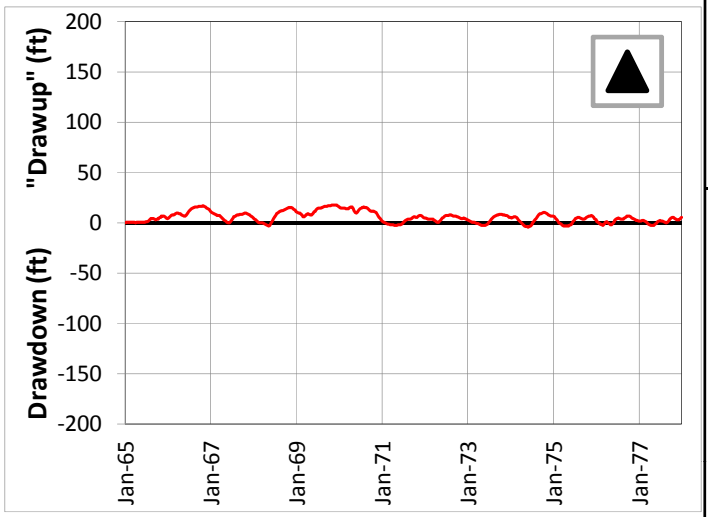

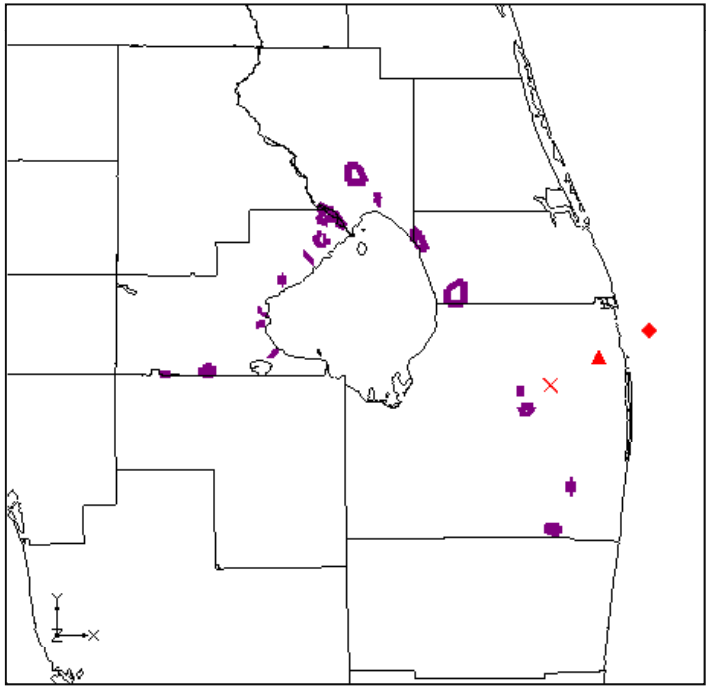

25-Mile Distance

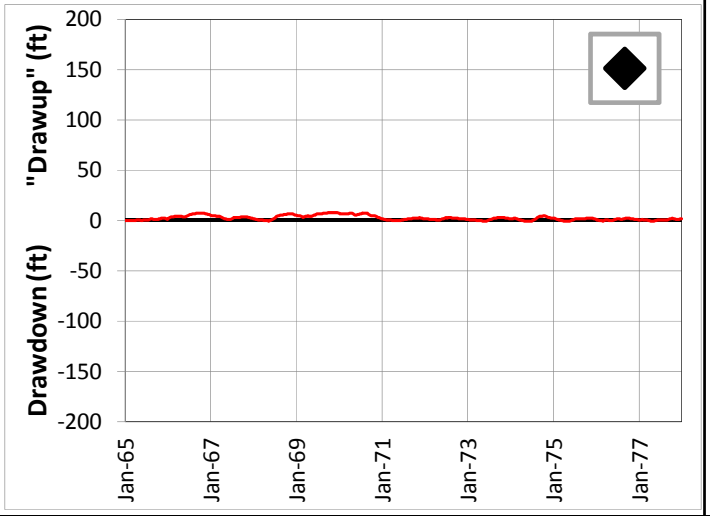

Legend

- CERP ASR Sites
- 5-Mile Distance Locations
- 15-Mile Distance Locations
- 25-Mile Distance Locations

Notes:

Scenario 11 is a variation on Scenario 9. The numbers of wells and injection volumes are identical, but the extraction volumes have been reduced to meet APPA performance measures.

A number of individual sites were chosen from the UF Aquifer at distances of 5, 15 and 25 miles from the proposed ASR well sites. This figure shows the drawdown and "drawup" at each output time step for 3 of these sites.

The plots were calculated by subtracting the heads calculated by the D13R model from those calculated by the no project run. This results in a positive value for "drawup" and a negative value for drawdown.

The colors of the points on the map correspond to the colors of the lines on the plots.

The symbols on the map (x, triangle and diamond) indicate the distance from the ASR sites.

5-Mile Distance

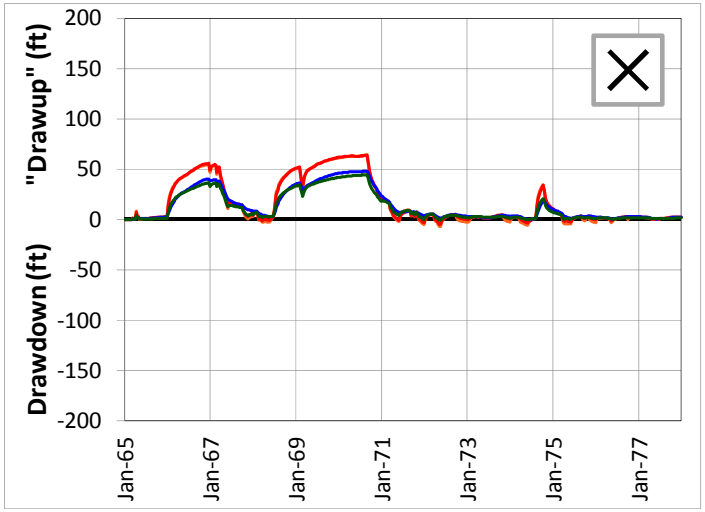

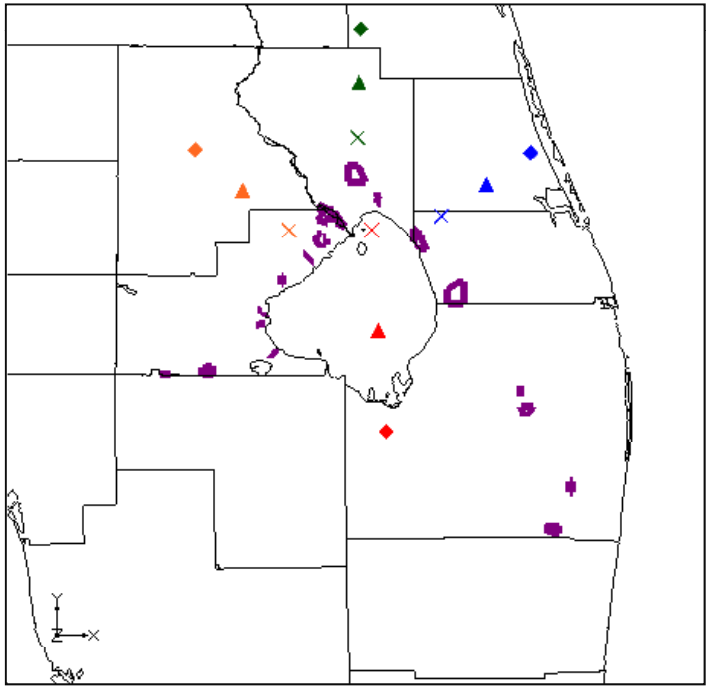

15-Mile Distance

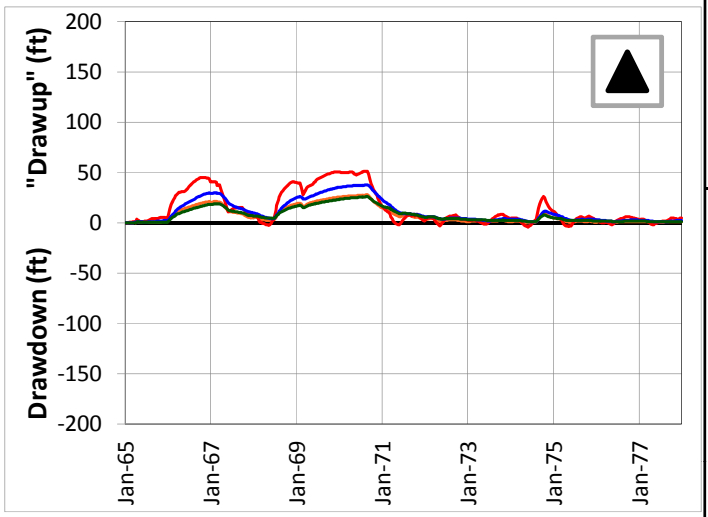

25-Mile Distance

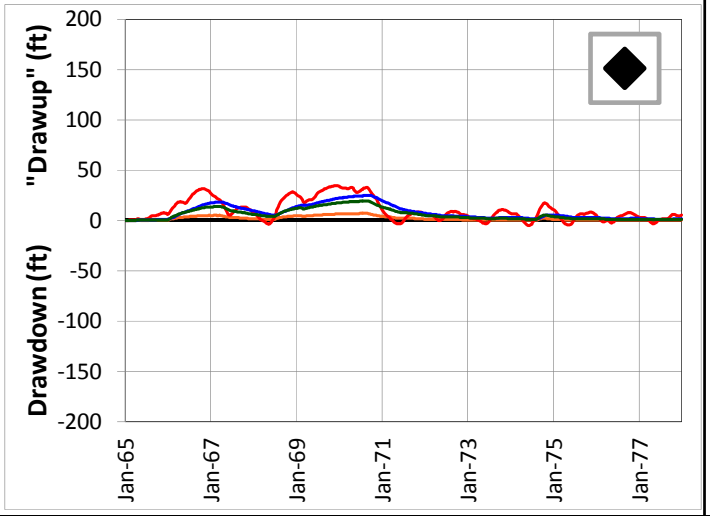

Legend

- CERP ASR Sites
- ✕ 5-Mile Distance Locations
- ▲ 15-Mile Distance Locations
- ◆ 25-Mile Distance Locations

Notes:

Scenario 11 is a variation on Scenario 9. The numbers of wells and injection volumes are identical, but the extraction volumes have been reduced to meet the APPA performance measure.

A number of individual sites were chosen from the APPZ Aquifer at distances of 5, 15 and 25 miles from the proposed ASR well sites. This figure shows the drawdown and "drawup" at each output time step for 12 of these sites.

The plots were calculated by subtracting the heads calculated by the D13R model from those calculated by the no project run. This results in a positive value for "drawup" and a negative value for drawdown.

The colors of the points on the map correspond to the colors of the lines on the plots.

The symbols on the map (x, triangle and diamond) indicate the distance from the ASR sites.

5-Mile Distance

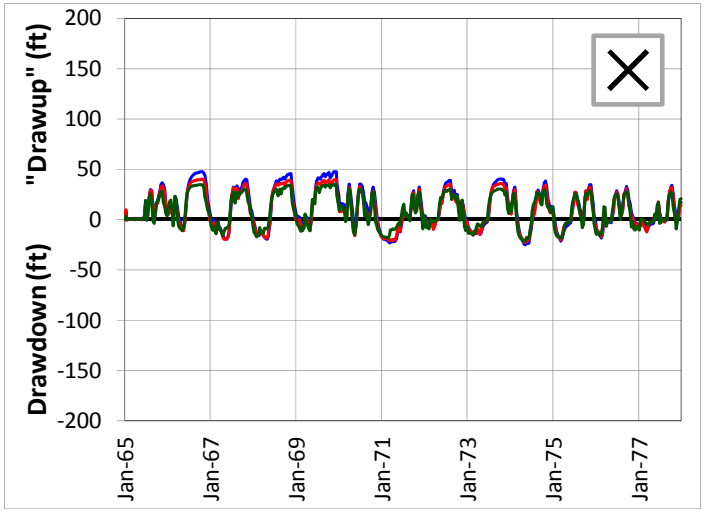

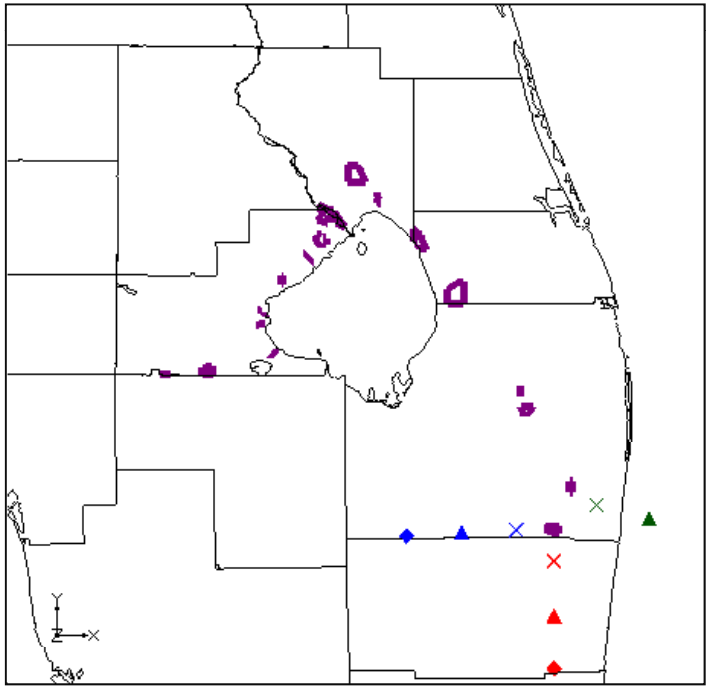

15-Mile Distance

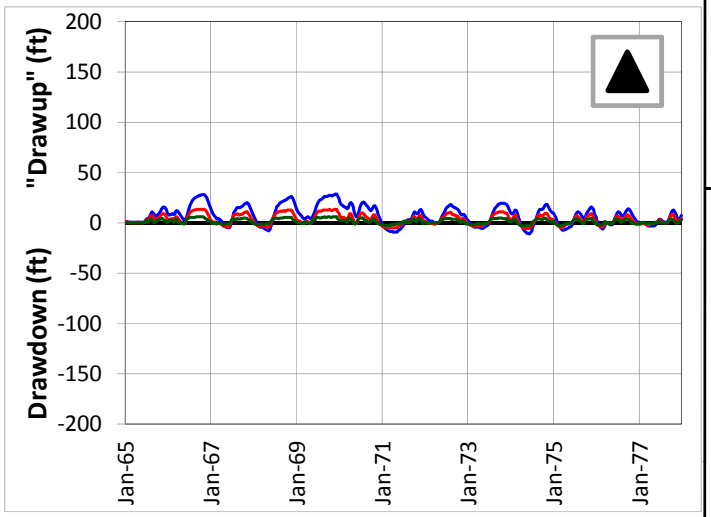

25-Mile Distance

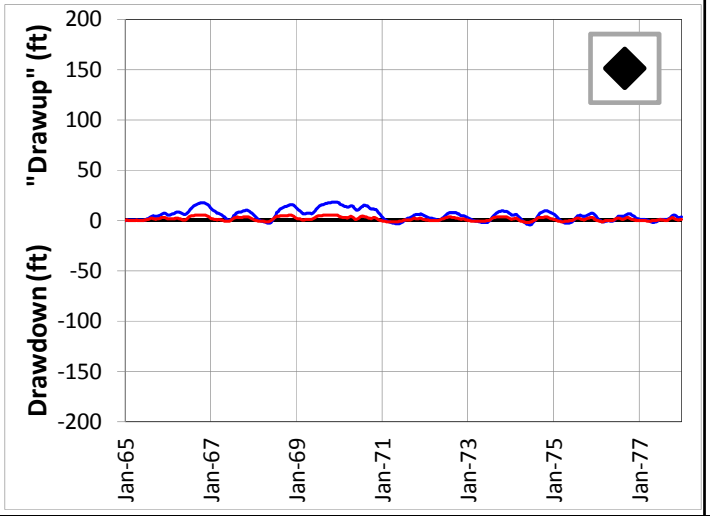

Legend

- CERP ASR Sites
- 5-Mile Distance Locations
- 15-Mile Distance Locations
- 25-Mile Distance Locations

Notes:

Scenario 11 is a variation on Scenario 9. The numbers of wells and injection volumes are identical, but the extraction volumes have been reduced to meet the APPA performance measure.

A number of individual sites were chosen from the APPZ Aquifer at distances of 5, 15 and 25 miles from the proposed ASR well sites. This figure shows the drawdown and "drawup" at each output time step for 8 of these sites.

The plots were calculated by subtracting the heads calculated by the D13R model from those calculated by the no project run. This results in a positive value for "drawup" and a negative value for drawdown.

The colors of the points on the map correspond to the colors of the lines on the plots.

The symbols on the map (x, triangle and diamond) indicate the distance from the ASR sites.

SCENARIO 11 – DRAWDOWN AND "DRAWUP" – APPZ

REGIONAL MODEL PRODUCTION SCENARIO REPORT

FIGURE 4.140

JUNE 2013

5-Mile Distance

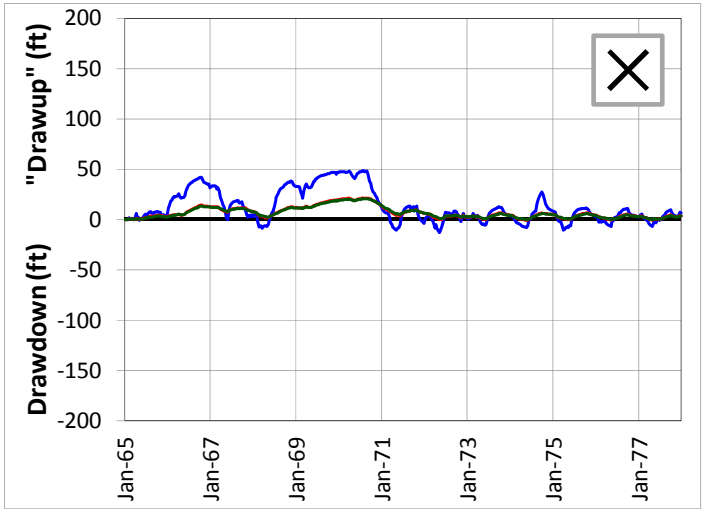

15-Mile Distance

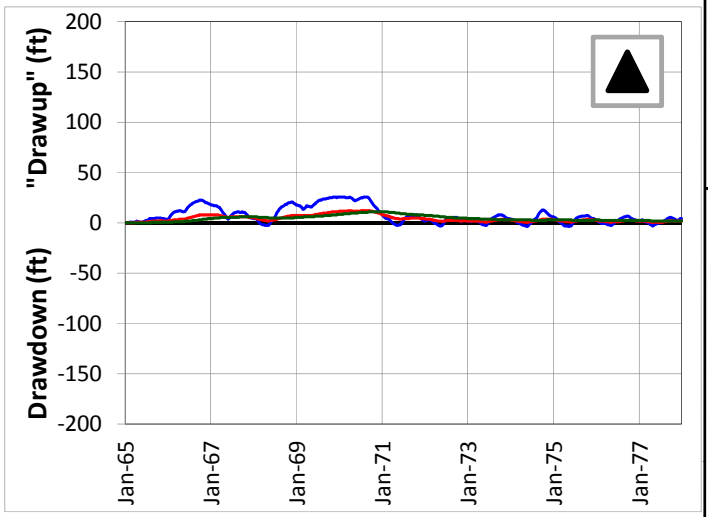

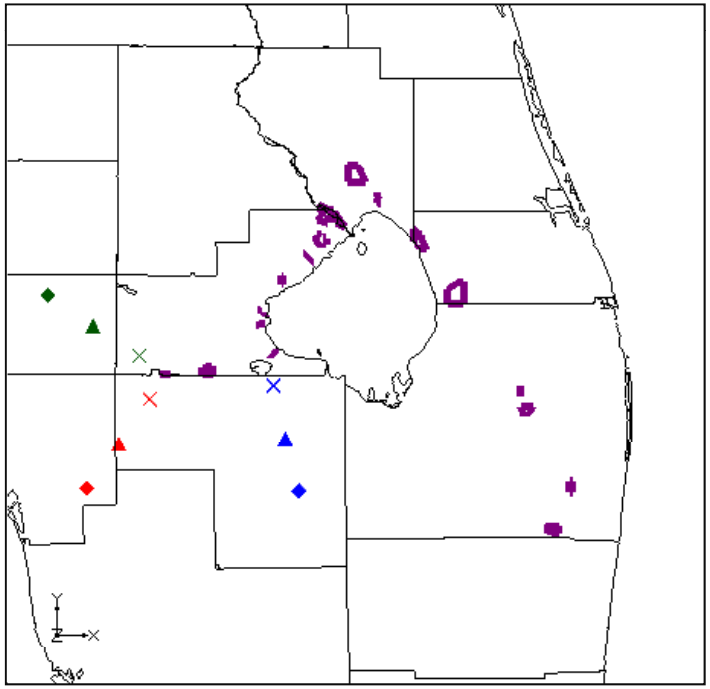

25-Mile Distance

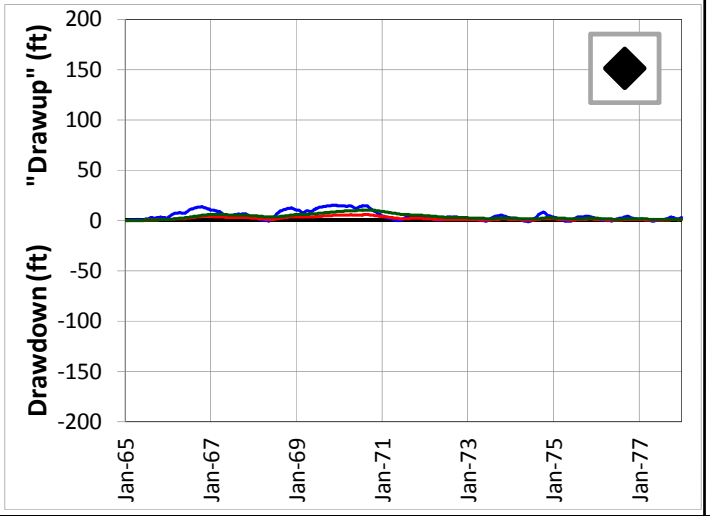

Legend

- CERP ASR Sites
- 5-Mile Distance Locations
- 15-Mile Distance Locations
- 25-Mile Distance Locations

Notes:

Scenario 11 is a variation on Scenario 9. The numbers of wells and injection volumes are identical, but the extraction volumes have been reduced to meet the APPA performance measure.

A number of individual sites were chosen from the APPZ Aquifer at distances of 5, 15 and 25 miles from the proposed ASR well sites. This figure shows the drawdown and "drawup" at each output time step for 9 of these sites.

The plots were calculated by subtracting the heads calculated by the D13R model from those calculated by the no project run. This results in a positive value for "drawup" and a negative value for drawdown.

The colors of the points on the map correspond to the colors of the lines on the plots.

The symbols on the map (x, triangle and diamond) indicate the distance from the ASR sites.

5-Mile Distance

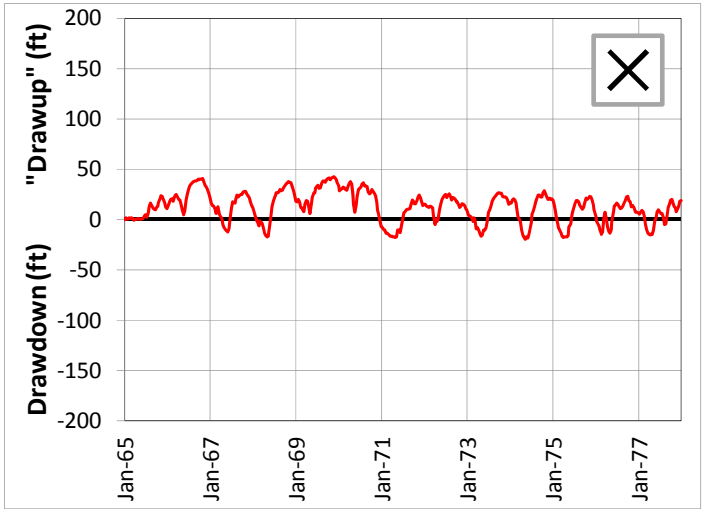

15-Mile Distance

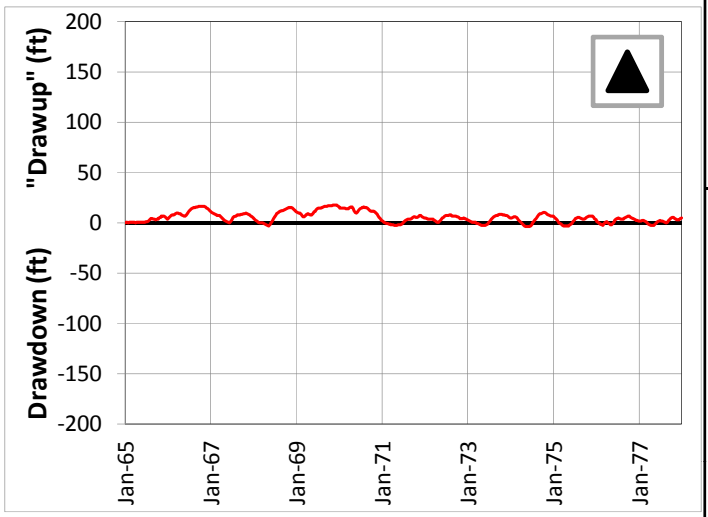

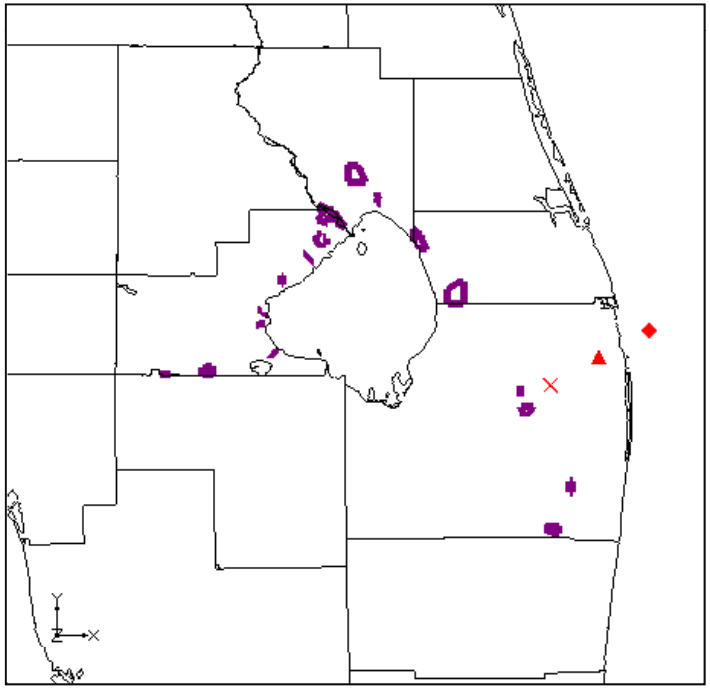

25-Mile Distance

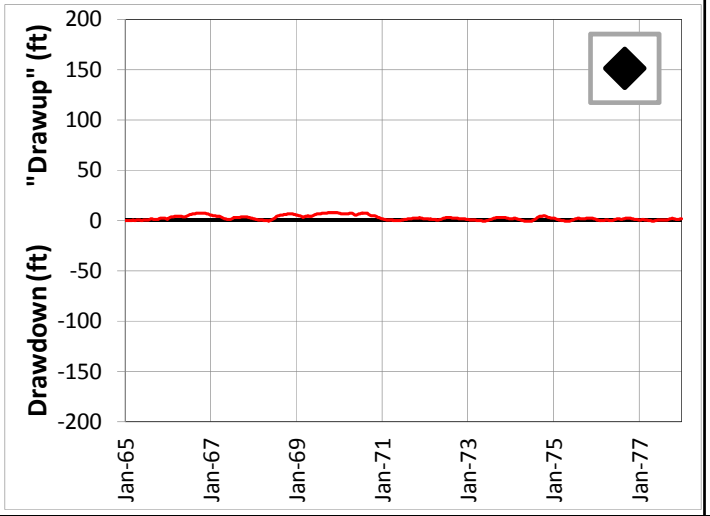

Legend

- CERP ASR Sites
- 5-Mile Distance Locations
- 15-Mile Distance Locations
- 25-Mile Distance Locations

Notes:

Scenario 11 is a variation on Scenario 9. The numbers of wells and injection volumes are identical, but the extraction volumes have been reduced to meet the APPA performance measure.

A number of individual sites were chosen from the APPZ Aquifer at distances of 5, 15 and 25 miles from the proposed ASR well sites. This figure shows the drawdown and "drawup" at each output time step for 3 of these sites.

The plots were calculated by subtracting the heads calculated by the D13R model from those calculated by the no project run. This results in a positive value for "drawup" and a negative value for drawdown.

The colors of the points on the map correspond to the colors of the lines on the plots.

The symbols on the map (x, triangle and diamond) indicate the distance from the ASR sites.

SCENARIO 11 – DRAWDOWN AND "DRAWUP" – APPZ

REGIONAL MODEL PRODUCTION SCENARIO REPORT

FIGURE 4.142

JUNE 2013

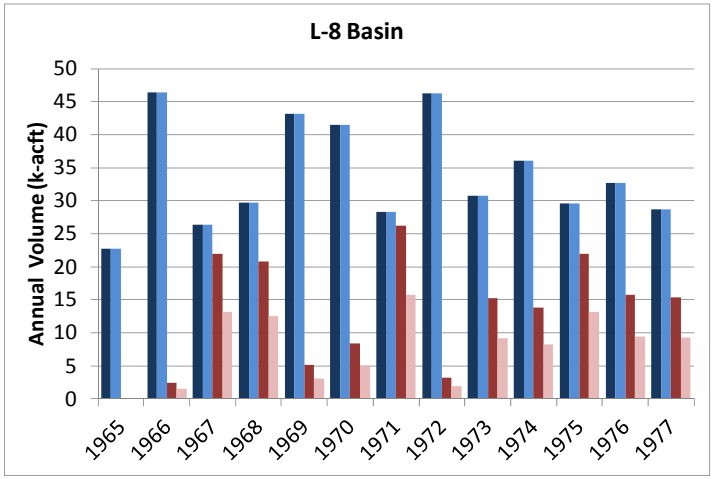

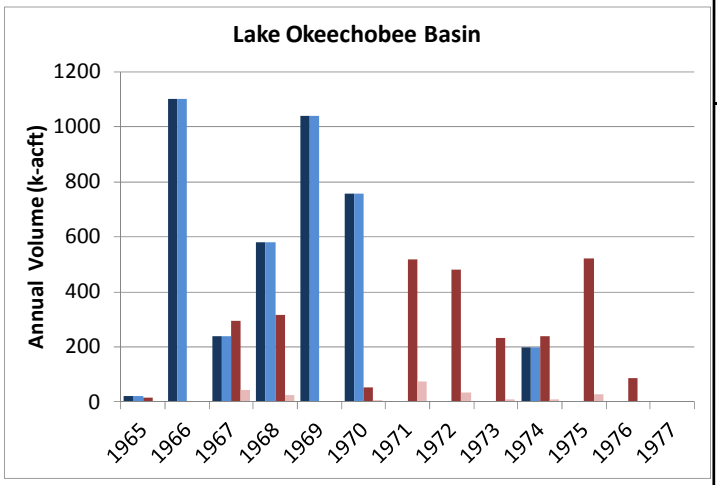

	L-8		Lake Okeechobee		Caloosahatchee	
	In %	Out %	In %	Out %	In %	Out %
1965	100%	60%	100%	8%	100%	22%
1966	100%	60%	100%	--	100%	23%
1967	100%	60%	100%	15%	100%	22%
1968	100%	60%	100%	8%	100%	21%
1969	100%	60%	100%	--	100%	--
1970	100%	60%	100%	15%	100%	23%
1971	100%	60%	--	15%	100%	23%
1972	100%	60%	--	7%	100%	23%
1973	100%	60%	--	4%	100%	21%
1974	100%	60%	100%	4%	100%	21%
1975	100%	60%	--	5%	100%	21%
1976	100%	60%	--	4%	100%	22%
1977	100%	60%	--	--	100%	21%

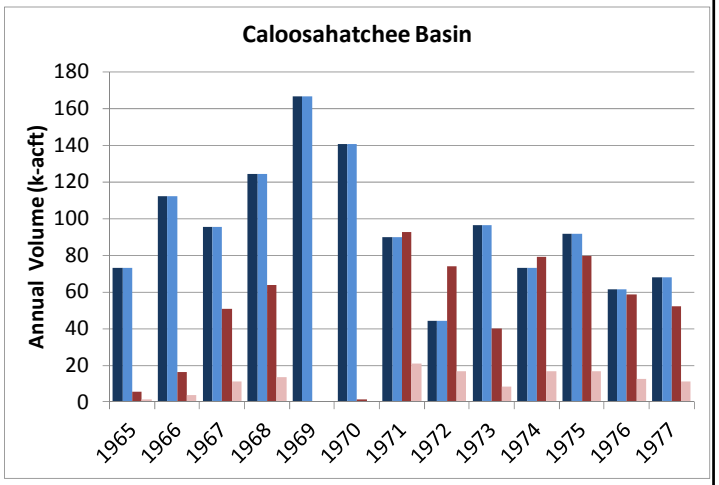

Legend

- Design Storage (injection)
- Modeled Storage (injection)
- Design Recovery (extraction)
- Modeled Recovery (extraction)

Notes:

Scenario 11 is a variation on Scenario 9. The numbers of wells and injection volumes are identical, but the extraction volumes have been reduced to meet the APPA performance measure.

These three plots show the comparison between the SFWMM-D13R designed annual injection and extraction volumes at the ASR wells and the actual assigned rates for the RASRSM-D13R for three of the basins. The table presents the percentage of SFWMM-D13R annual flow rates that are included in the RASRSM-D13R.

Scenario 11 – Comparison of Designed and Modeled ASR Flow Rates

Regional Model Production Scenario Report

Figure 4.143

June 2013

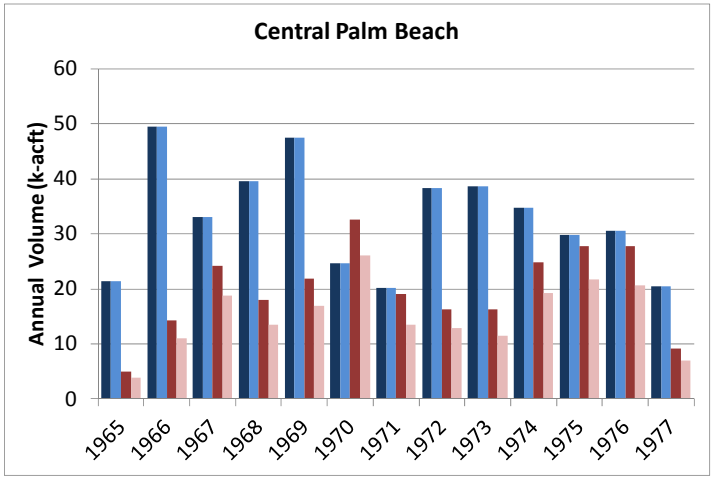

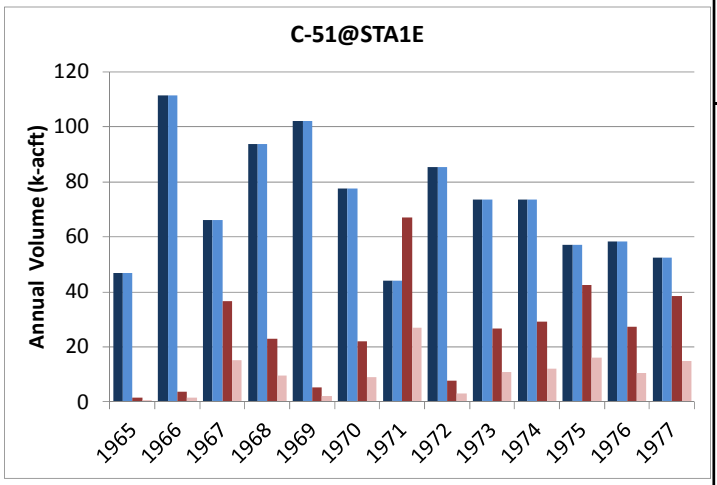

	CPB		C-51		Hillsboro	
	In %	Out %	In %	Out %	In %	Out %
1965	100%	77%	100%	40%	100%	22%
1966	100%	77%	100%	41%	100%	33%
1967	100%	78%	100%	41%	100%	33%
1968	100%	76%	100%	41%	100%	33%
1969	100%	77%	100%	41%	100%	33%
1970	100%	80%	100%	41%	100%	33%
1971	100%	71%	100%	40%	100%	33%
1972	100%	79%	100%	41%	100%	23%
1973	100%	71%	100%	41%	100%	23%
1974	100%	77%	100%	41%	100%	33%
1975	100%	78%	100%	38%	100%	17%
1976	100%	74%	100%	39%	100%	21%
1977	100%	76%	100%	38%	100%	16%

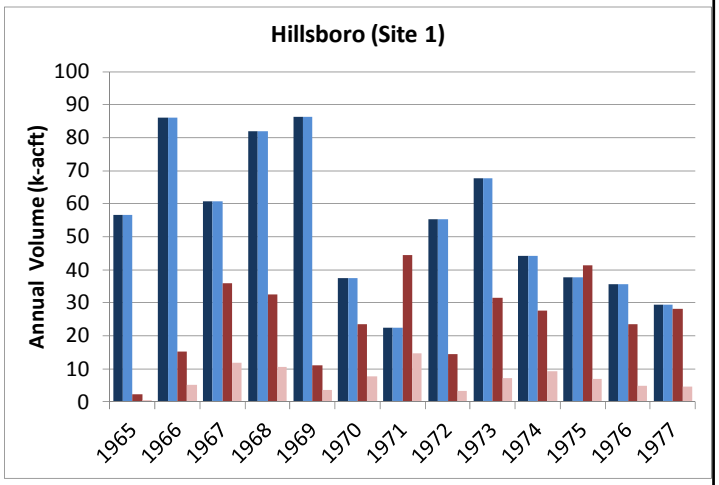

Legend

- Design Storage (injection)
- Modeled Storage (injection)
- Design Recovery (extraction)
- Modeled Recovery (extraction)

Notes:

Scenario 11 is a variation on Scenario 9. The numbers of wells and injection volumes are identical, but the extraction volumes have been reduced to meet the APPA performance measure.

These three plots show the comparison between the SFWMM-D13R designed annual injection and extraction volumes at the ASR wells and the actual assigned rates for the RASRSM-D13R for three of the basins. The table presents the percentage of SFWMM-D13R annual flow rates that are included in the RASRSM-D13R.

SCENARIO11 – COMPARISON OF DESIGNED AND MODELED ASR FLOW RATES

REGIONAL MODEL PRODUCTION SCENARIO REPORT

FIGURE 4.144

JUNE 2013

	Total	
	In %	Out %
1965	100%	25%
1966	100%	44%
1967	100%	24%
1968	100%	18%
1969	100%	60%
1970	100%	40%
1971	100%	22%
1972	100%	12%
1973	100%	15%
1974	100%	18%
1975	100%	14%
1976	100%	26%
1977	100%	33%

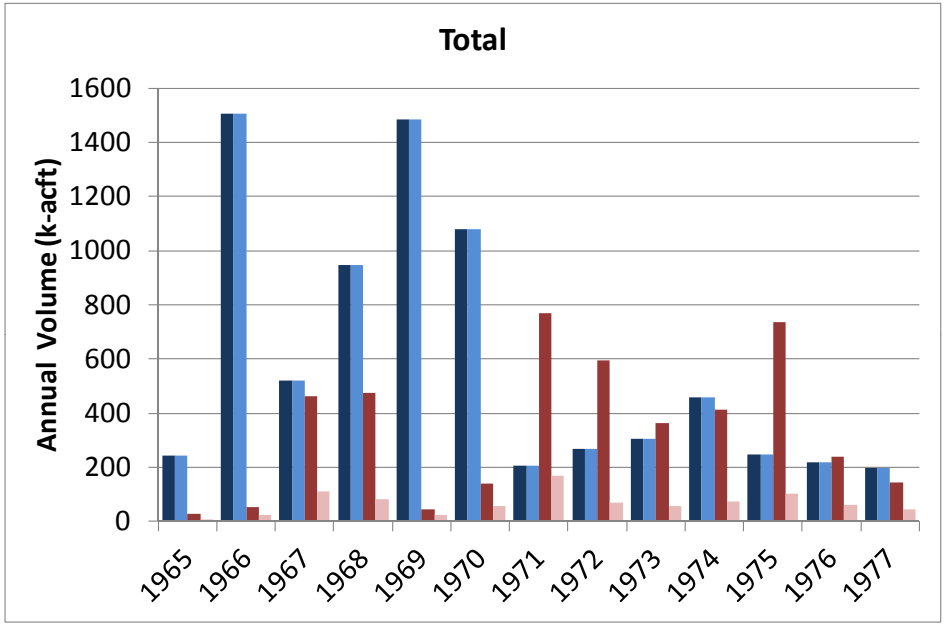

Legend

- Design Storage (injection)
- Modeled Storage (injection)
- Design Recovery (extraction)
- Modeled Recovery (extraction)

Notes:

Scenario 11 is a variation on Scenario 9. The numbers of wells and injection volumes are identical, but the extraction volumes have been reduced to meet the APPA performance measure.

This plot shows the comparison between the SFWMM-D13R designed annual injection and extraction volumes at the ASR wells and the actual assigned rates for the RASRSM-D13R for all basins. The table presents the percentage of SFWMM-D13R annual flow rates that are included in the RASRSM-D13R.

		UF		APPZ		BZ		Total # Wells	Target # Wells
		Number of Wells	Recovery Efficiency	Number of Wells	Recovery Efficiency	Number of Wells	Recovery Efficiency		
Caloosahatchee Basin	Moore Haven	4	70%	0	30%	0	0%		
	River Bend	3	70%	1	30%	0	0%		
	Flaghole	2	0%	0	30%	0	0%		
	Basin Total	9		1		0		10	44
Lake Okeechobee Basin	Nicodemus Slough	0	70%	10	30%	0	0%		
	C-41 Canal	0	70%	0	30%	0	0%		
	C-40 Canal	2	70%	0	30%	0	0%		
	North Lake Okeechobee	8	70%	2	30%	0	0%		
	Kissimmee R./Paradise Run	15	70%	0	30%	0	0%		
	Taylor Creek	0	70%	10	30%	0	0%		
	L-63N	0	70%	9	30%	0	0%		
	Lakeside Ranch	4	70%	0	30%	0	0%		
	Port Mayaca	18	70%	0	30%	0	0%		
	Basin Total	47		31		0		78	200
L-8		6	70%	0	30%	0	0%	6	10
C-51		12	70%	2	30%	0	0%	14	34
Central Palm Beach		10	70%	3	30%	0	0%	13	15
Site 1 (Hillsboro)		10	40%	0	40%	0	0%	10	30
Total		94		37		0		131	333

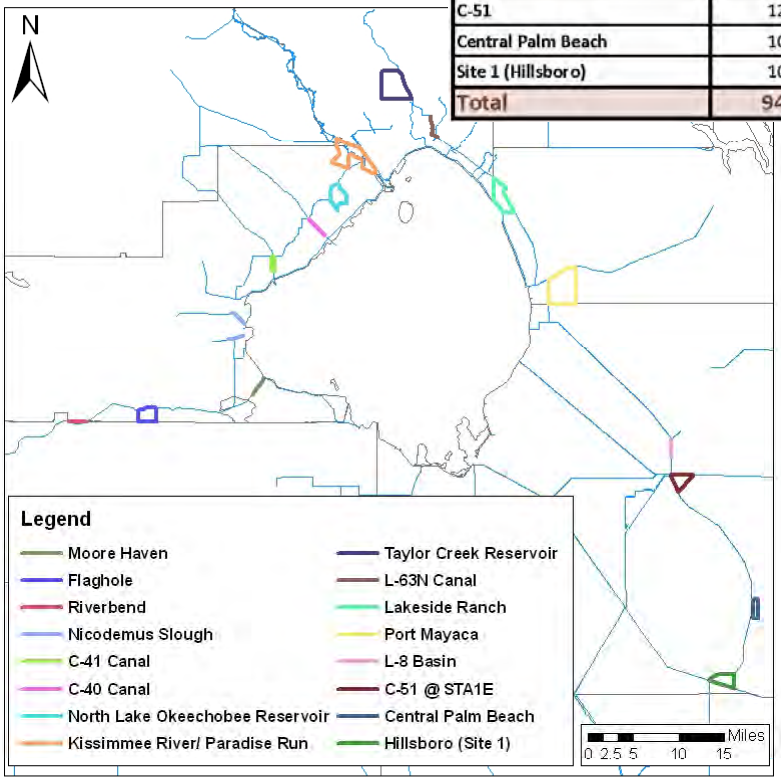

Extraction Percentage		
	UF	APPZ
Caloosahatchee Basin		
Moore Haven	100%	
River Bend	100%	100%
Flaghole	100%	
Lake Okeechobee Basin		
Nicodemus Slough		100%
C-41 Canal		
C-40 Canal	100%	
North Lake Okeechobee	25%	100%
Kissimmee R./Paradise Run	25%	
Taylor Creek		50%
L-63N		50%
Lakeside Ranch	0%	
Port Mayaca	0%	
L-8	100%	
C-51	100%	100%
Central Palm Beach	100%	100%
Site 1 (Hillsboro)	100%	

Notes:

Scenario 12 is the same as Scenario 11 but the BZ wells have been removed.

Reductions have been applied as a percentage of the Scenario 9 rates as shown in the lower table.

The extraction percentage is the percentage applied to the extraction rates to reduce drawdown effects. This is not the recovery efficiency.

Flow rates are divided evenly among the wells in each basin. Maximum flow rate for any one well is 5 mgd in the UF and APPZ and 10 mgd in the BZ.

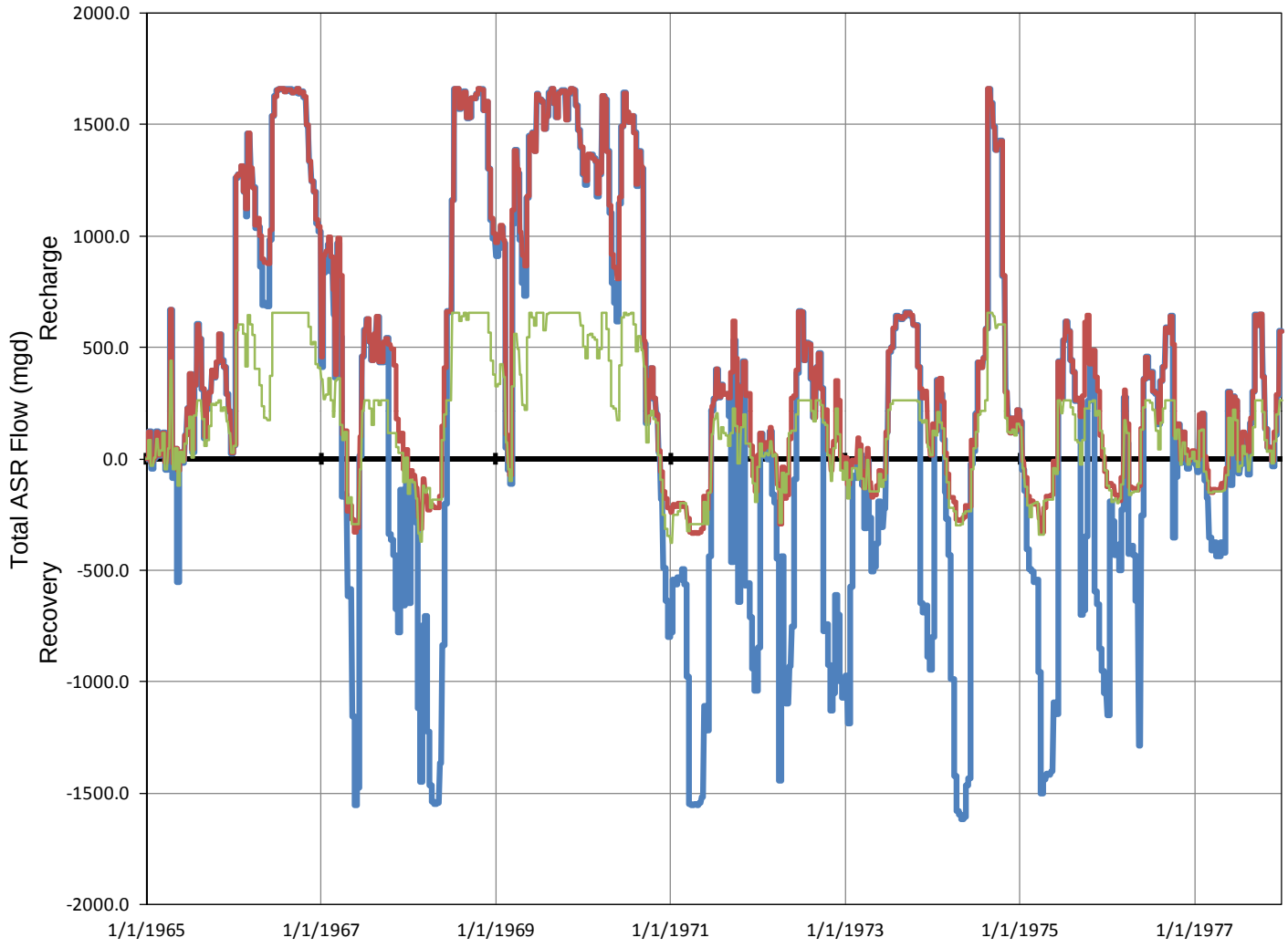

Legend

- Scenario 1 – ASR Flux
- Scenario 11 – ASR Flux
- Scenario12– ASR Flux

Notes:

Scenario 12 is the same as Scenario 11 but the BZ wells have been removed.

This plot shows the extraction and injection rates for all wells at all sites for Scenario 1, Scenario 9 and Scenario 11. Positive rates are recharge (injection), while negative rates are recovery (extraction).

Scenario 12 – ASR Well Fluxes (Compared to Scenarios 1 & 11)

Regional Model Production Scenario Report

Figure 4.147

June 2013

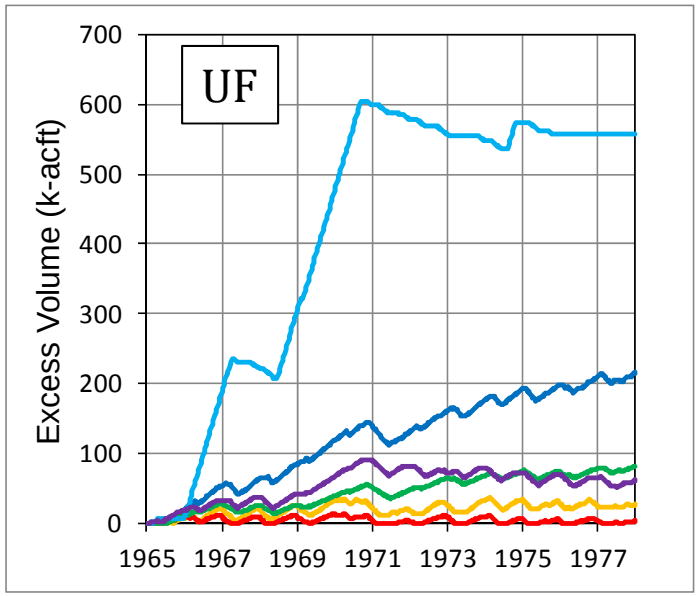

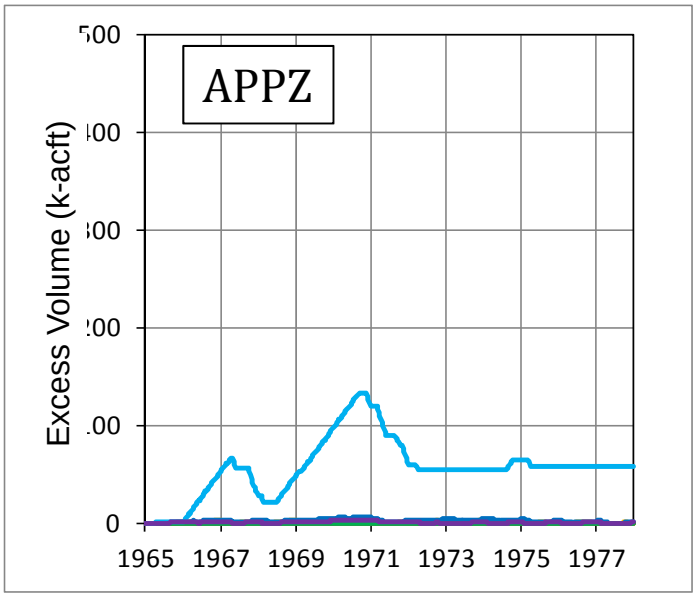

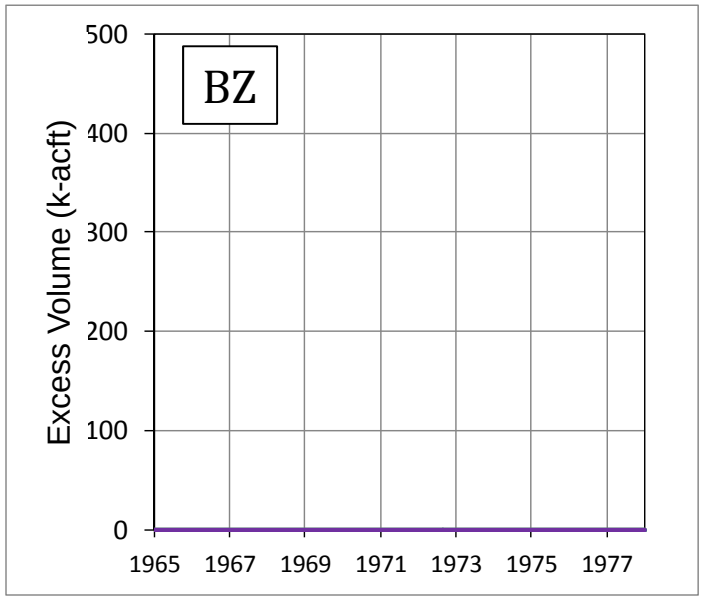

Legend

- Central Palm Beach
- C-51
- Hillsboro
- L-8
- Lake Okeechobee
- Caloosahatchee River

Notes:

Scenario 12 is the same as Scenario 11 but the BZ wells have been removed.

These plots show the excess volume of fresh water remaining in each aquifer at each ASR basin. Excess volume is calculated by adding injected volume times recovery efficiency and subtracting extracted volume. The calculation is cumulative.

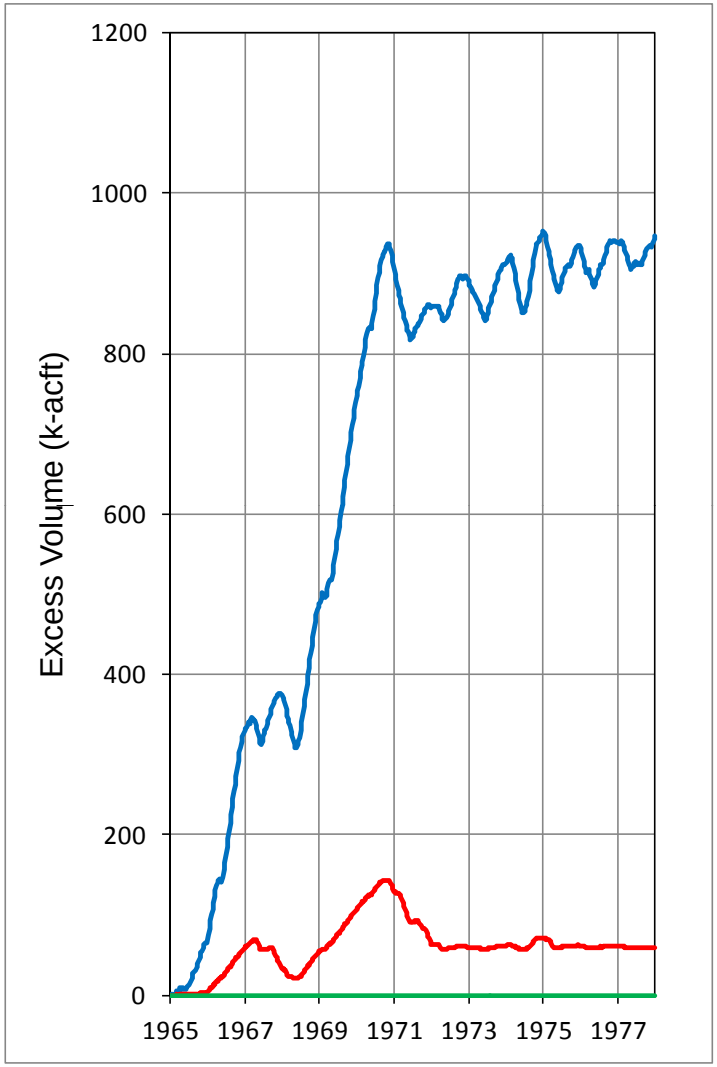

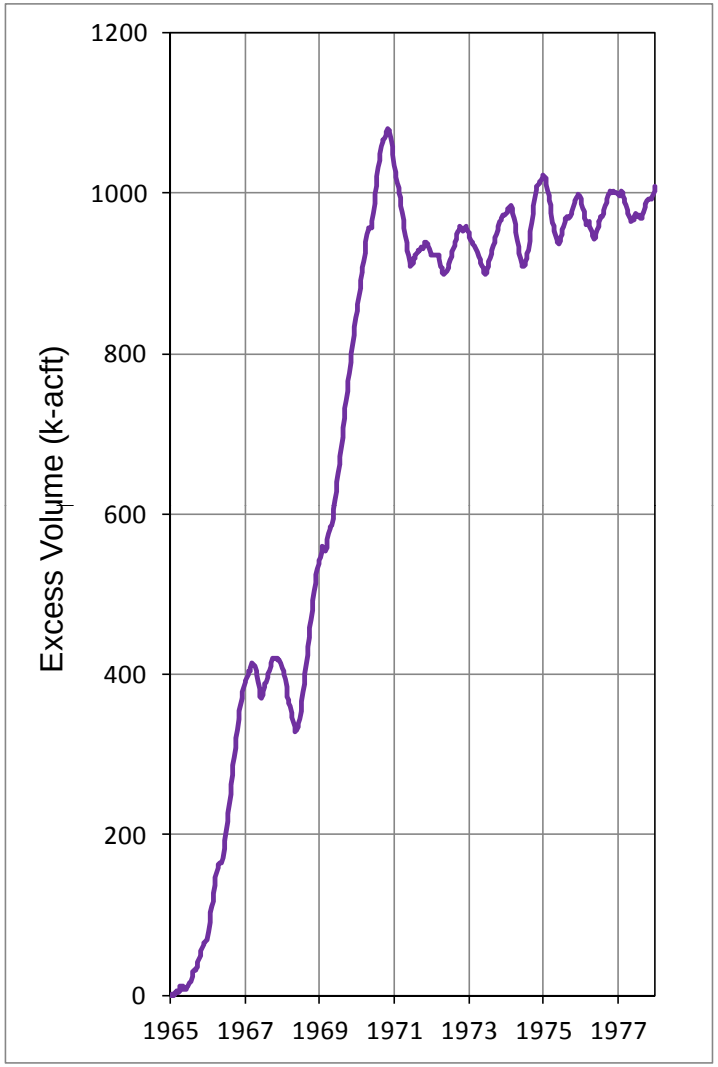

Legend

- Total UF
- Total APPZ
- Total BZ
- Total (All Aquifers)

Notes:

Scenario 12 is the same as Scenario 11 but the BZ wells have been removed.

These plots show the total excess volume of fresh water remaining in each aquifer and in all aquifers. Excess volume is calculated by adding injected volume times recovery efficiency and subtracting extracted volume. The calculation is cumulative.

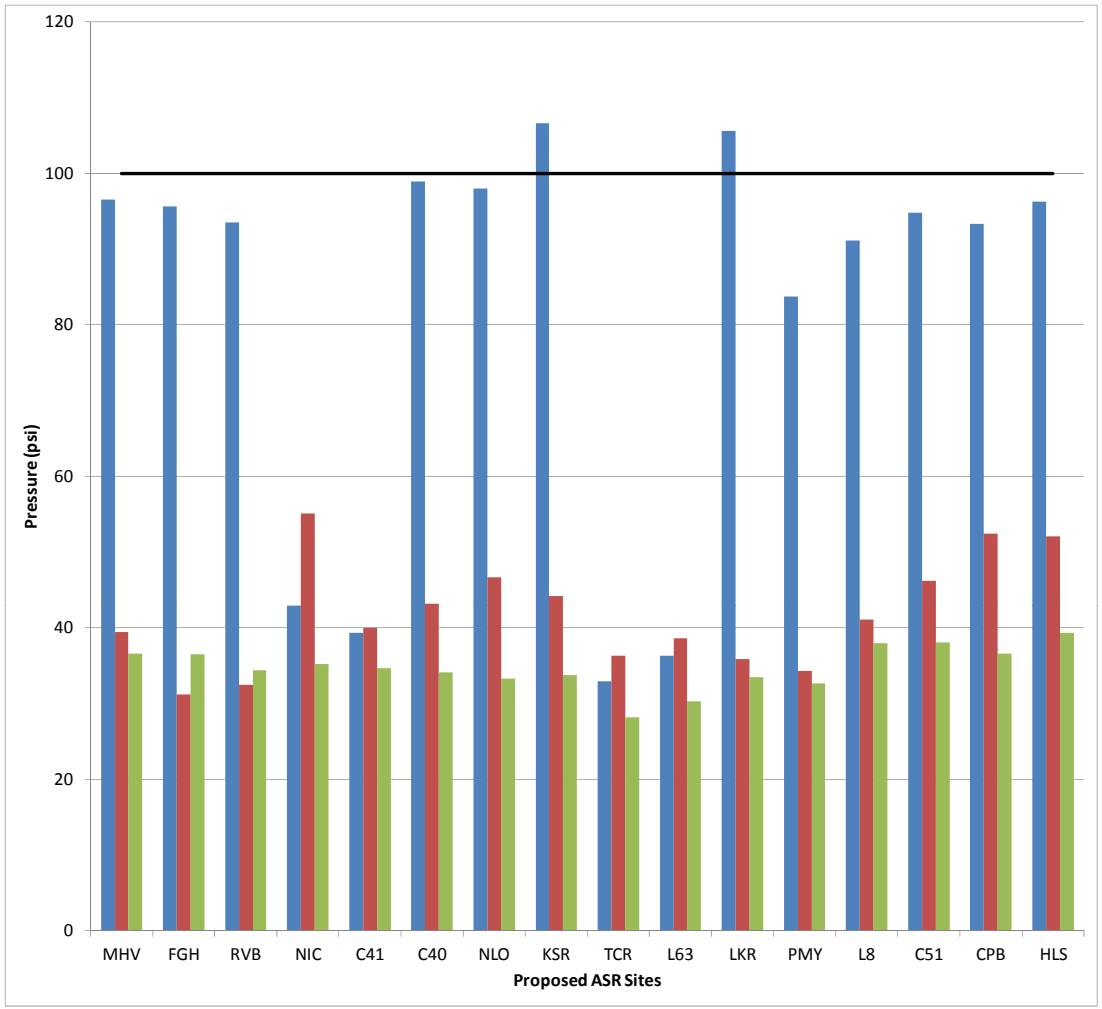

MHV	Moorehaven
FGH	Flaghole
RVB	Riverbend
NIC	Nicodemus Slough
C41	C-41Canal
C40	C-40 Canal
NLO	North Lake Okeechobee Reservoir
KSR	Kissimmee River / Paradise Run
TCR	Taylor Creek Reservoir
L63	L-63N Canal
LKR	Lakeside Ranch
PMY	Port Mayaca
L8	L-8 Basin
C51	C-51 @ STA1E
CPB	Central Palm Beach
HLS	Hillsboro (Site 1)

Legend

- Upper Floridan Aquifer
- Avon Park Permeable Zone
- Boulder Zone
- 100 psi Limit

Notes:

Scenario 12 is the same as Scenario 11 but the BZ wells have been removed.

This plot shows the highest pressure at each site which the pump would need to overcome in order to inject storage water during the 13-year simulation.

The PDT determined that it would be important to keep this pressure below 100 psi (indicated by the heavy black line).

Note that maximum pressures are shown for all aquifers and all sites even if ASR pumps are not located there for the current scenario.

SCENARIO 12 – MAXIMUM PUMP PRESSURE REQUIREMENTS

REGIONAL MODEL PRODUCTION SCENARIO REPORT

FIGURE 4.150

JUNE 2013

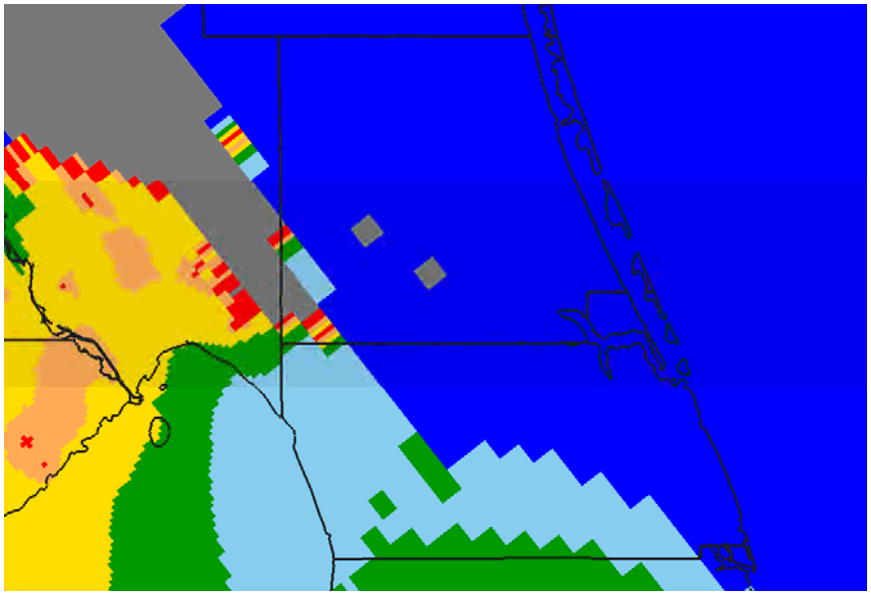

Upper Floridan Aquifer

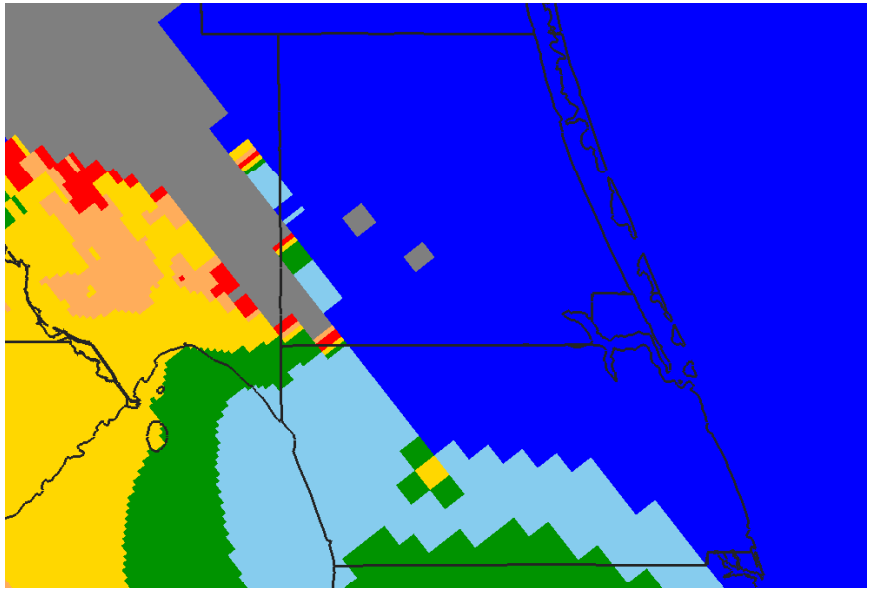

Avon Park Permeable Zone

Legend

- Not artesian or no reduction
- < 5%
- 5% - 10%
- 10% - 20%
- 20% - 50%
- 50% - 100%
- Loses artesian condition

Notes:

Scenario 12 is the same as Scenario 11 but the BZ wells have been removed.

These plots show the maximum reduction in artesian flow at each model cell as a percentage when compared to the flow expected without the ASR project.

Permit rules require that the reduction in Saint Lucie and Martin Counties be less than 10%.

Note the gray area in the northwest corner of the figures, which coincides with a ridge and does not normally have artesian conditions.

Scenario 12 – Maximum Reduction in Artesian Flow Capacity

Regional Model Production Scenario Report

Figure 4.151

June 2013

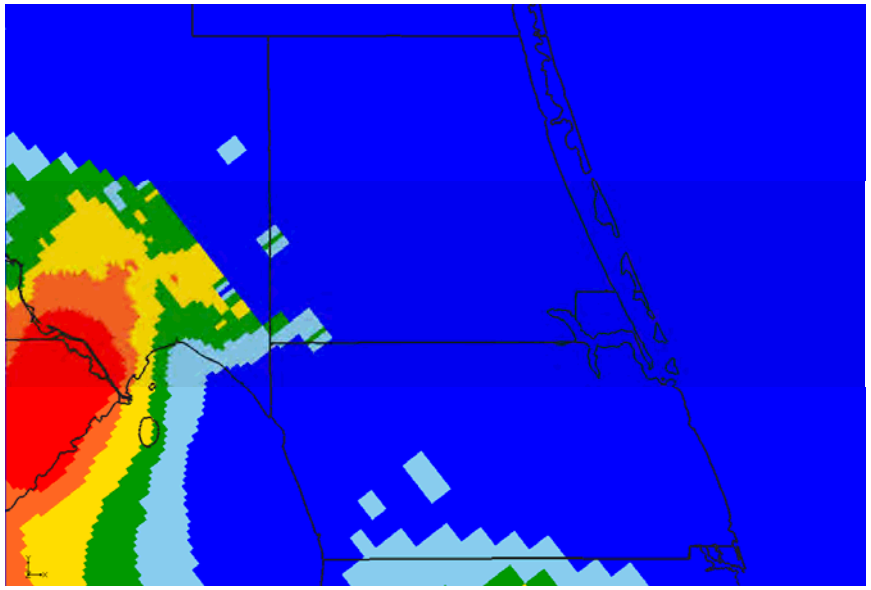

Upper Floridan Aquifer

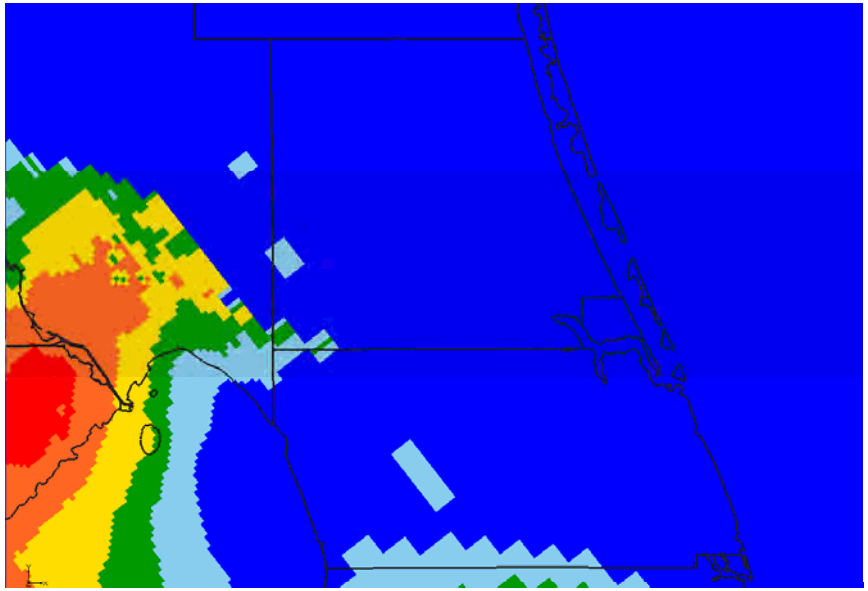

Avon Park Permeable Zone

Legend

- 0 days
- 1 – 250 days
- 250 – 500 days
- 500 – 1000 days
- 1000 – 2000 days
- > 2000 days

Notes:

Scenario 12 is the same as Scenario 11 but the BZ wells have been removed.

These plots indicate the severity of the loss of artesian pressure due to ASR extraction pumping.

Permit rules require that the reduction in Saint Lucie and Martin Counties be less than 10%. This plot indicates the number of days during the simulation in which the flow reduction was greater than 10%. There are 4748 days in the 13-year model simulation period.

SCENARIO 12 – NUMBER OF DAYS (OUT OF 13 YEARS) WITH FLOW REDUCTION EXCEEDING 10%

REGIONAL MODEL PRODUCTION SCENARIO REPORT

FIGURE 4.152

JUNE 2013

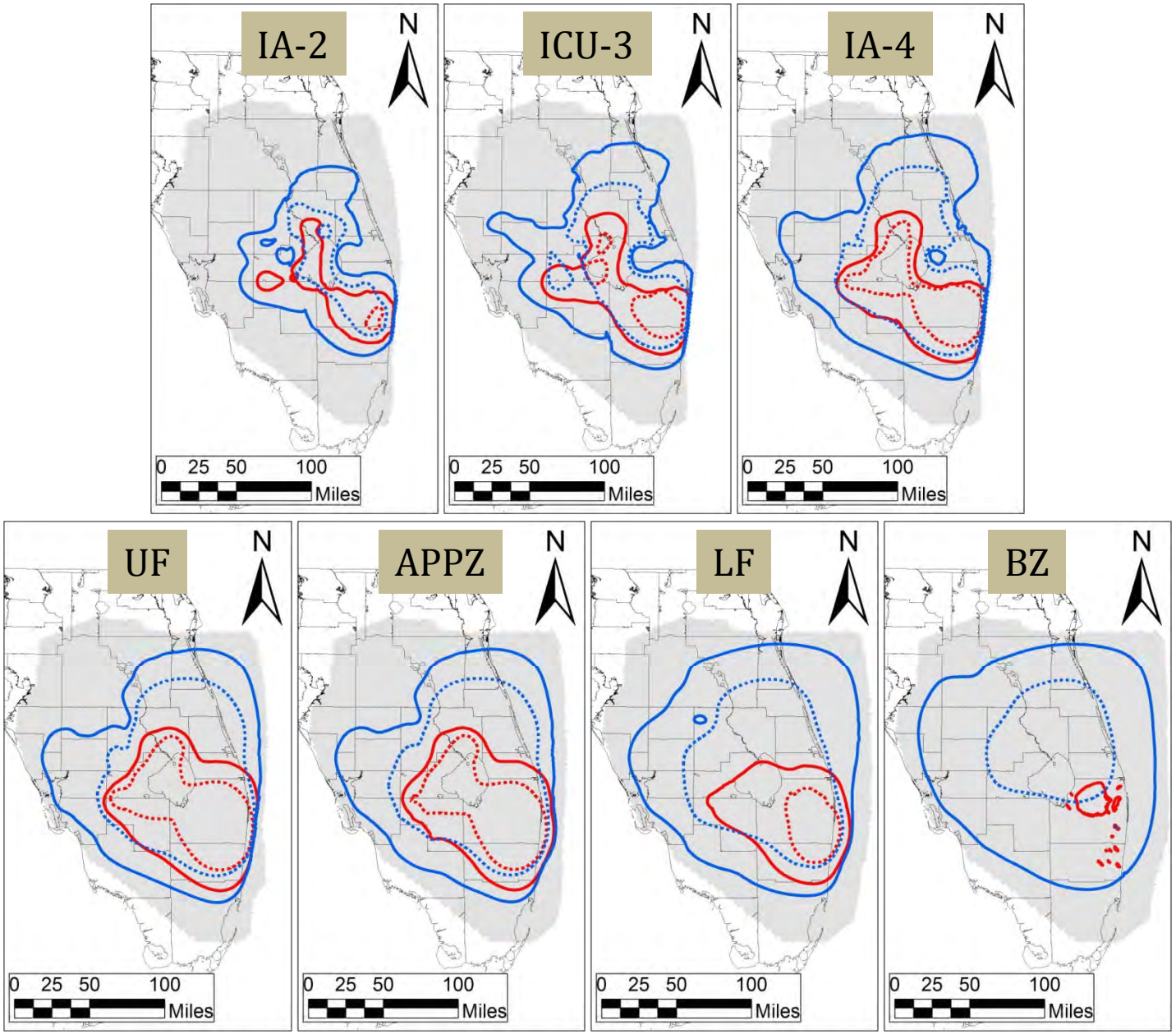

Legend

Maximum Drawdown
- 1 foot
- 5 feet

Maximum "Drawup"
- 1 foot
- 5 feet

Model Domain

Notes:

Scenario 12 is the same as Scenario 11 but the BZ wells have been removed.

These figures show the extent of the areas where the maximum drawdown or "drawup" is greater than 1 foot or 5 feet.

The maximum condition does not necessarily occur at the same time for all regions of the model.

SCENARIO 12 – MAXIMUM DRAWDOWN AND "DRAWUP" BY AQUIFER

REGIONAL MODEL PRODUCTION SCENARIO REPORT

FIGURE 4.153

JUNE 2013

5-Mile Distance

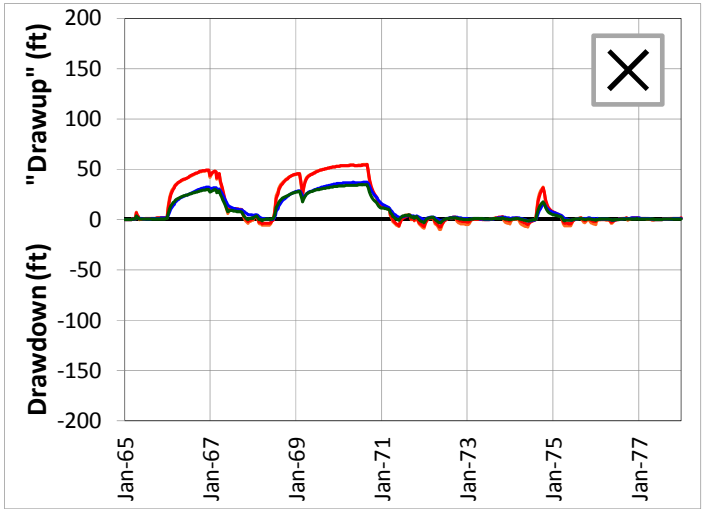

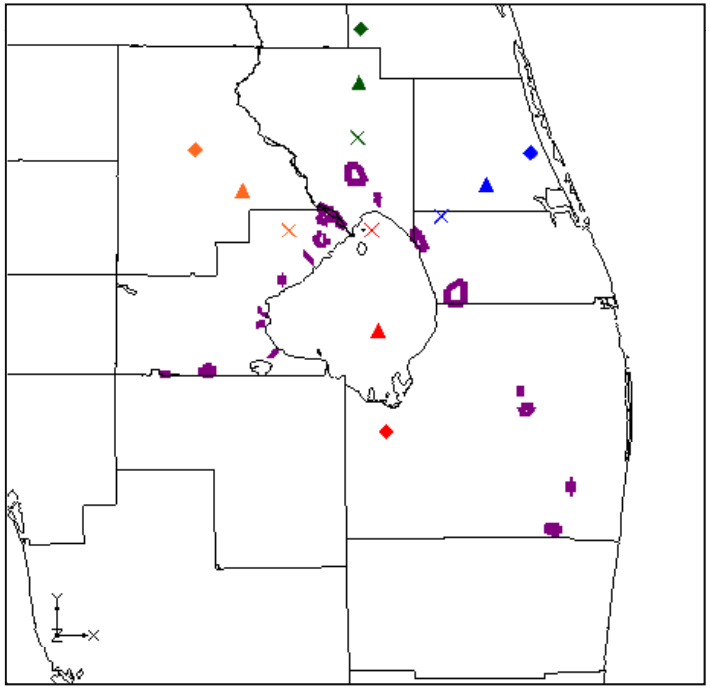

15-Mile Distance

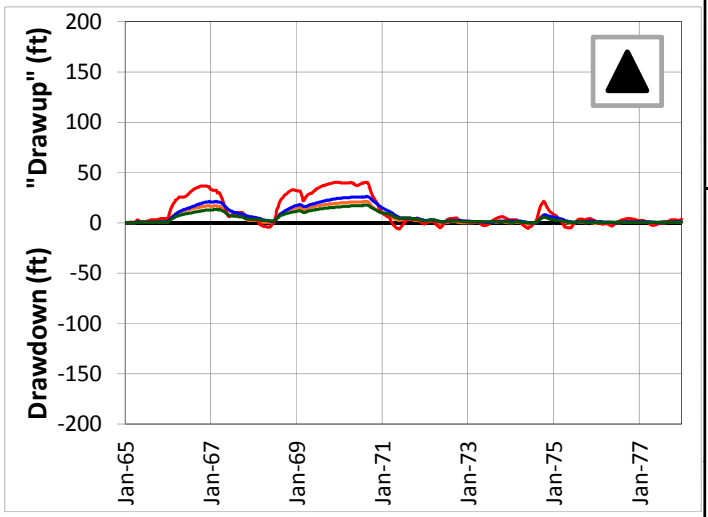

25-Mile Distance

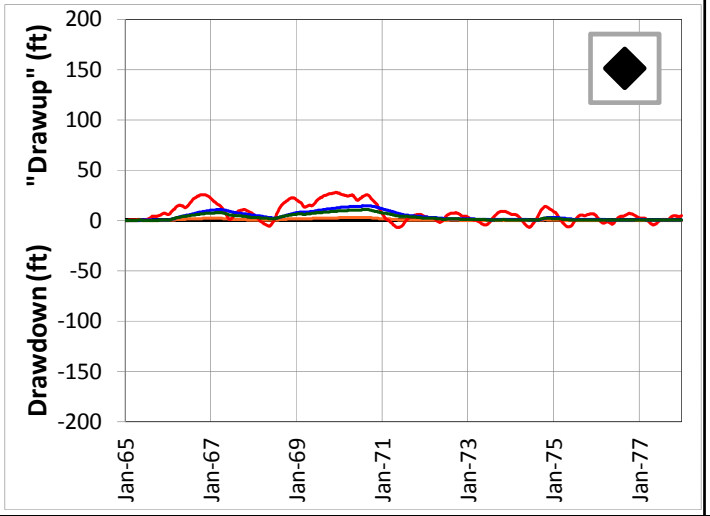

Legend

- CERP ASR Sites
- ✕ 5-Mile Distance Locations
- ▲ 15-Mile Distance Locations
- ◆ 25-Mile Distance Locations

Notes:

Scenario 12 is the same as Scenario 11 but the BZ wells have been removed.

A number of individual sites were chosen from the UF Aquifer at distances of 5, 15 and 25 miles from the proposed ASR well sites. This figure shows the drawdown and "drawup" at each output time step for 12 of these sites.

The plots were calculated by subtracting the heads calculated by the D13R model from those calculated by the no project run. This results in a positive value for "drawup" and a negative value for drawdown.

The colors of the points on the map correspond to the colors of the lines on the plots.

The symbols on the map (x, triangle and diamond) indicate the distance from the ASR sites.

5-Mile Distance

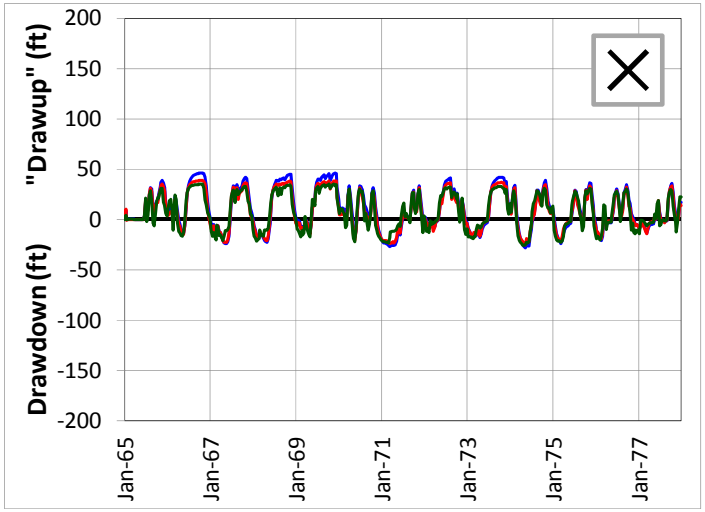

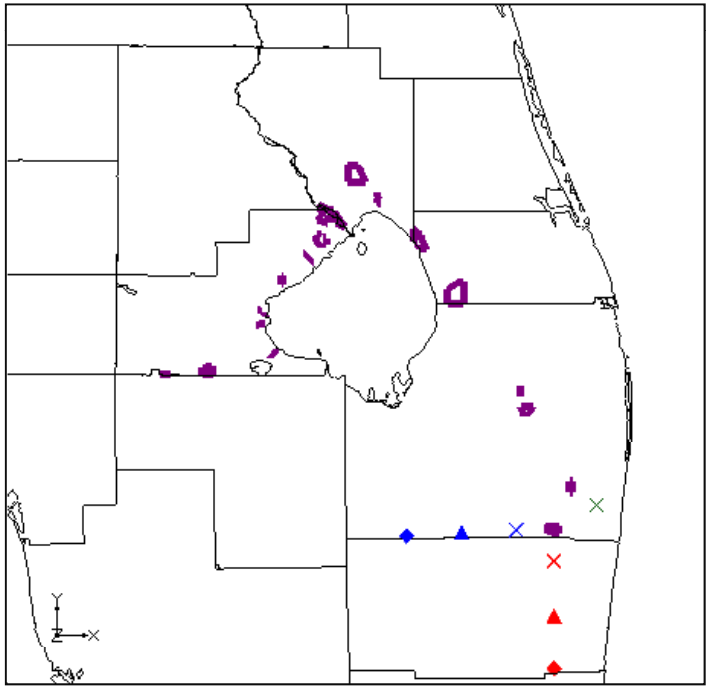

15-Mile Distance

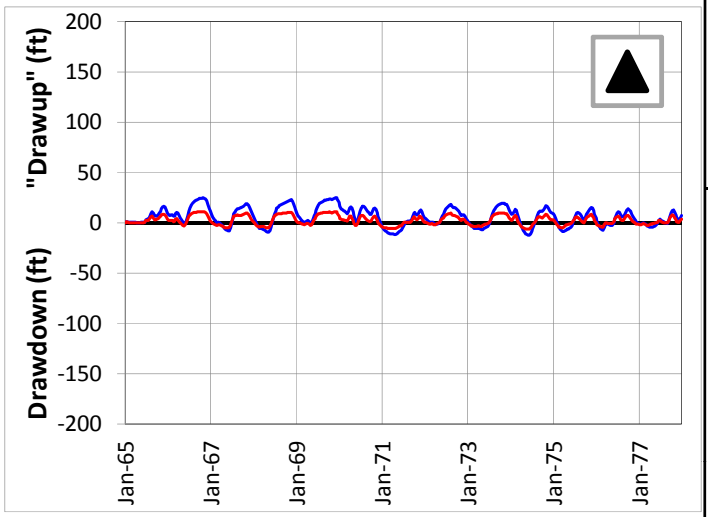

25-Mile Distance

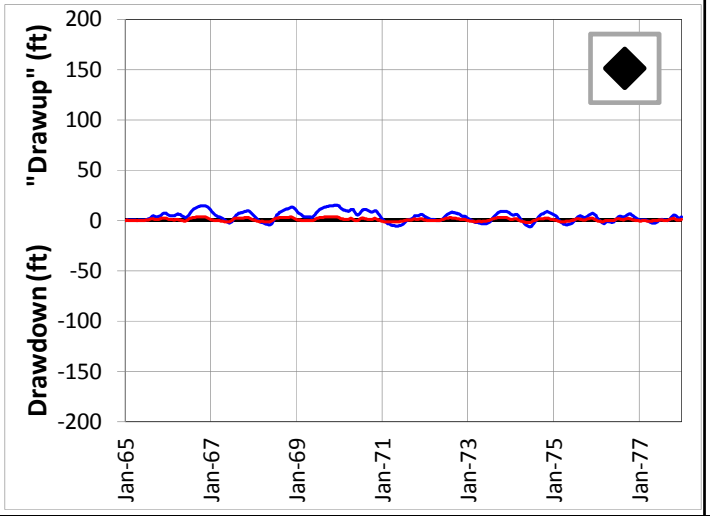

Legend

- CERP ASR Sites
- 5-Mile Distance Locations
- 15-Mile Distance Locations
- 25-Mile Distance Locations

Notes:

Scenario 12 is the same as Scenario 11 but the BZ wells have been removed.

A number of individual sites were chosen from the UF Aquifer at distances of 5, 15 and 25 miles from the proposed ASR well sites. This figure shows the drawdown and "drawup" at each output time step for 7 of these sites.

The plots were calculated by subtracting the heads calculated by the D13R model from those calculated by the no project run. This results in a positive value for "drawup" and a negative value for drawdown.

The colors of the points on the map correspond to the colors of the lines on the plots.

The symbols on the map (x, triangle and diamond) indicate the distance from the ASR sites.

5-Mile Distance

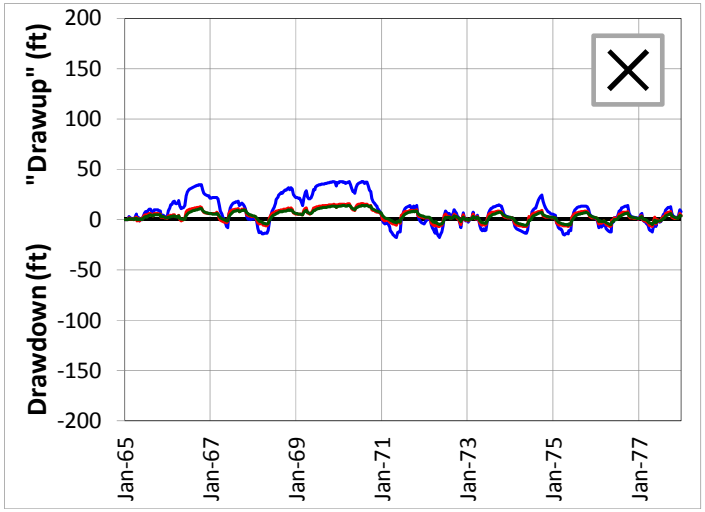

15-Mile Distance

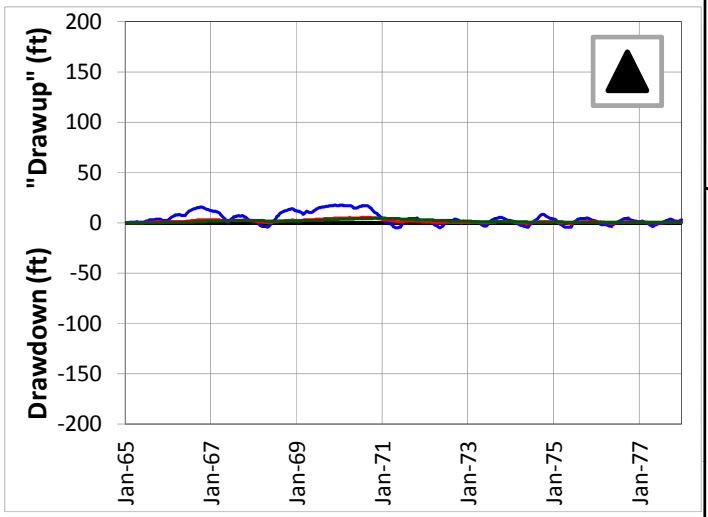

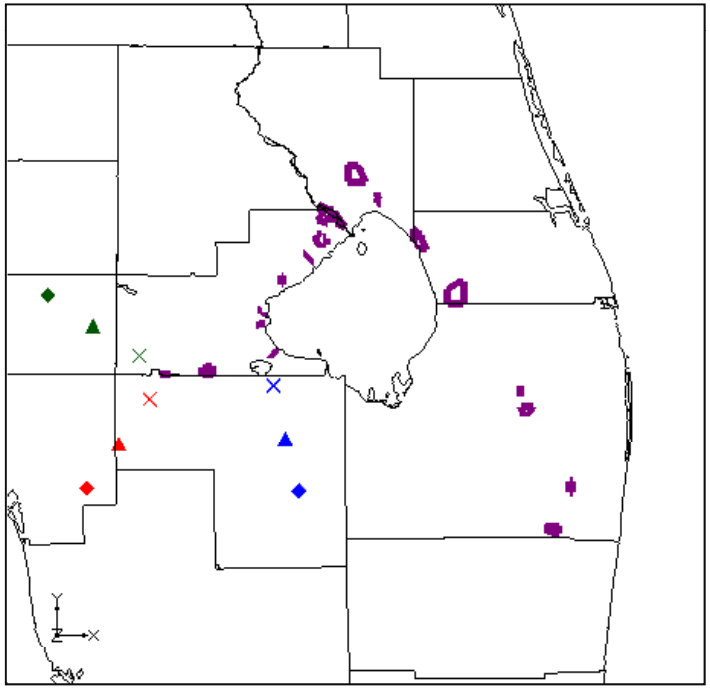

25-Mile Distance

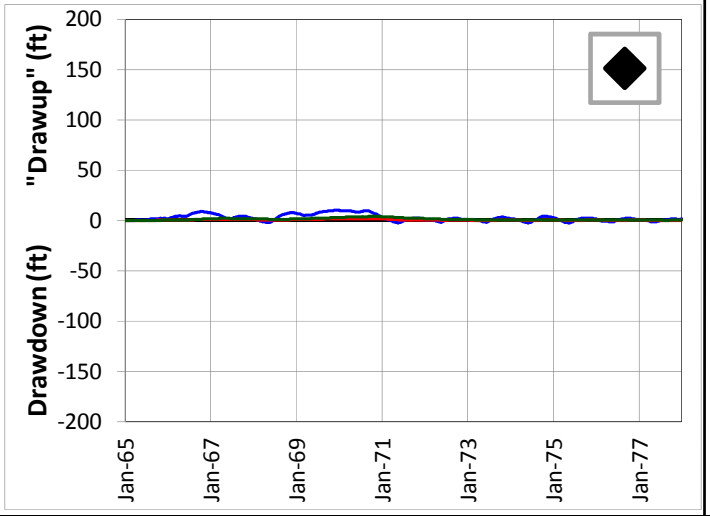

Legend

- CERP ASR Sites
- 5-Mile Distance Locations
- 15-Mile Distance Locations
- 25-Mile Distance Locations

Notes:

Scenario 12 is the same as Scenario 11 but the BZ wells have been removed.

A number of individual sites were chosen from the UF Aquifer at distances of 5, 15 and 25 miles from the proposed ASR well sites. This figure shows the drawdown and "drawup" at each output time step for 9 of these sites.

The plots were calculated by subtracting the heads calculated by the D13R model from those calculated by the no project run. This results in a positive value for "drawup" and a negative value for drawdown.

The colors of the points on the map correspond to the colors of the lines on the plots.

The symbols on the map (x, triangle and diamond) indicate the distance from the ASR sites.

Scenario 12 – Drawdown and "Drawup" – UF

Regional Model Production Scenario Report

Figure 4.156

June 2013

5-Mile Distance

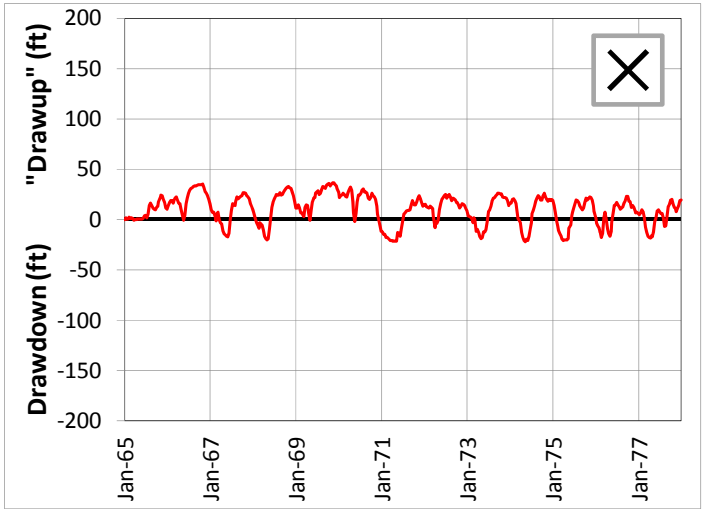

15-Mile Distance

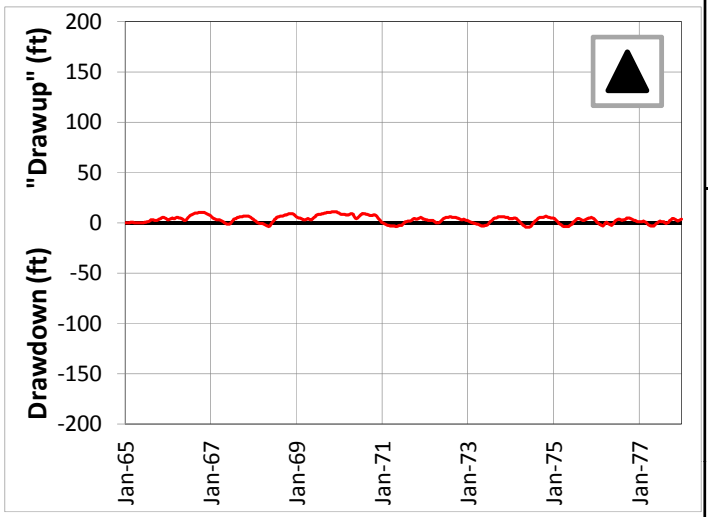

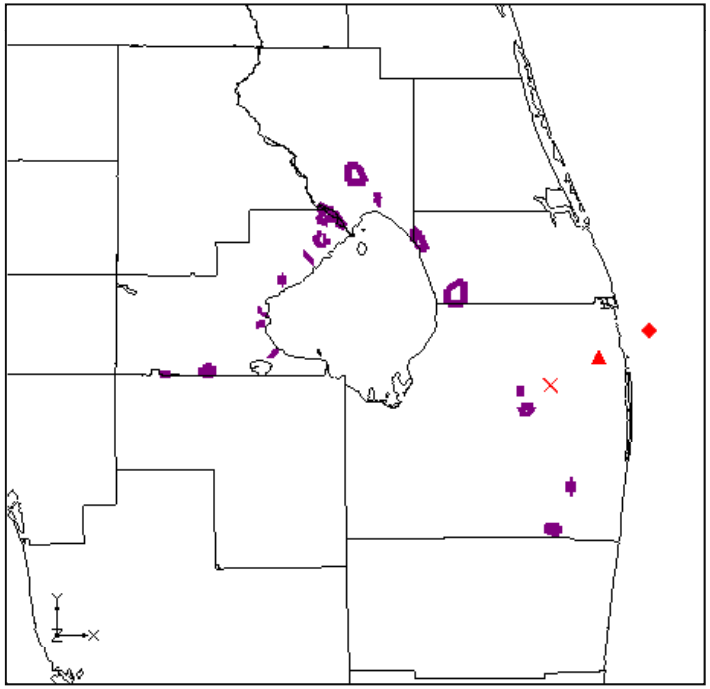

25-Mile Distance

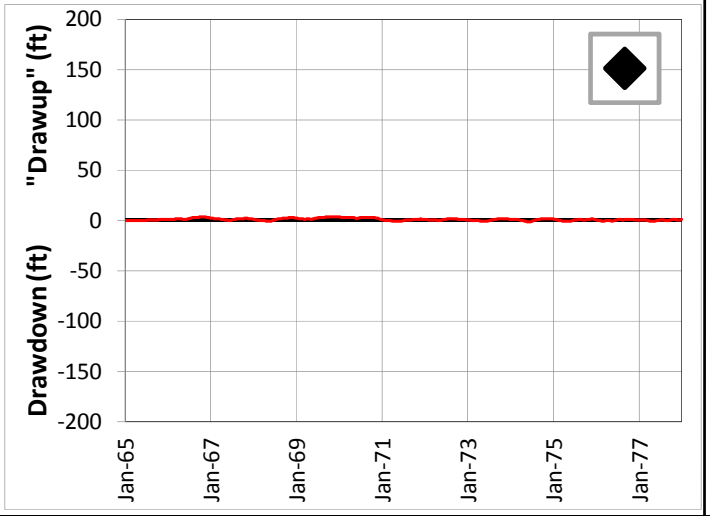

Legend

- CERP ASR Sites
- 5-Mile Distance Locations
- 15-Mile Distance Locations
- 25-Mile Distance Locations

Notes:

Scenario 12 is the same as Scenario 11 but the BZ wells have been removed.

A number of individual sites were chosen from the UF Aquifer at distances of 5, 15 and 25 miles from the proposed ASR well sites. This figure shows the drawdown and "drawup" at each output time step for 3 of these sites.

The plots were calculated by subtracting the heads calculated by the D13R model from those calculated by the no project run. This results in a positive value for "drawup" and a negative value for drawdown.

The colors of the points on the map correspond to the colors of the lines on the plots.

The symbols on the map (x, triangle and diamond) indicate the distance from the ASR sites.

5-Mile Distance

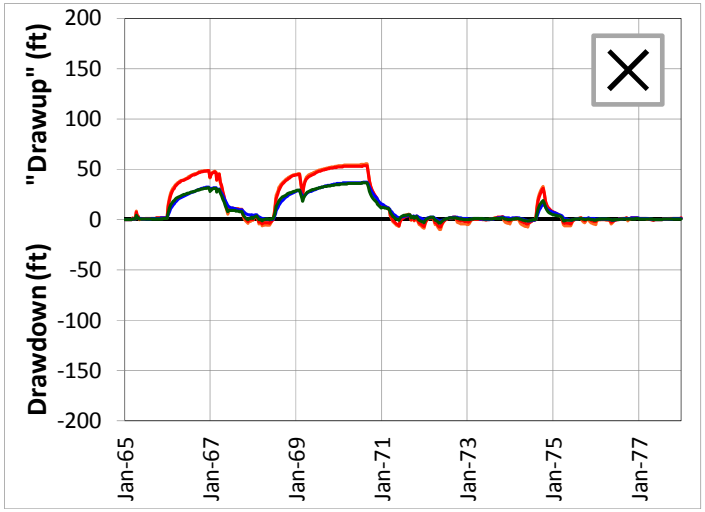

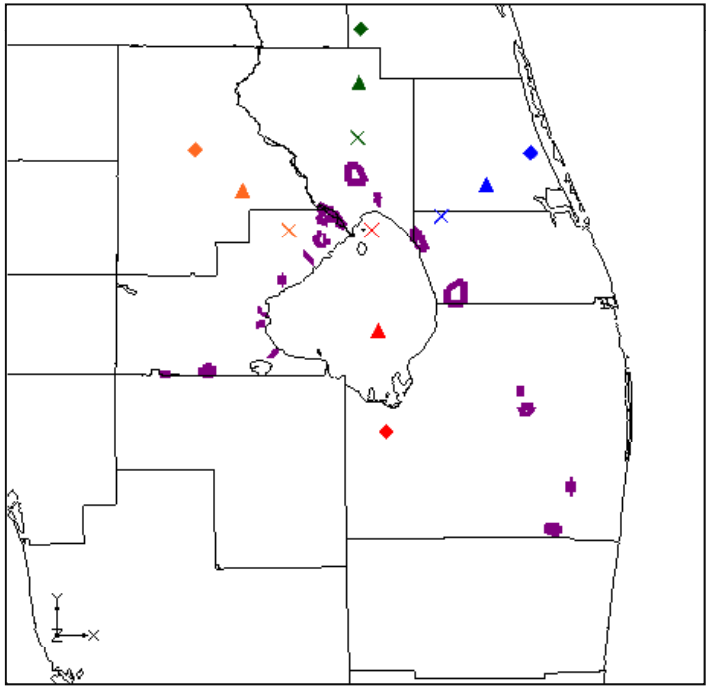

15-Mile Distance

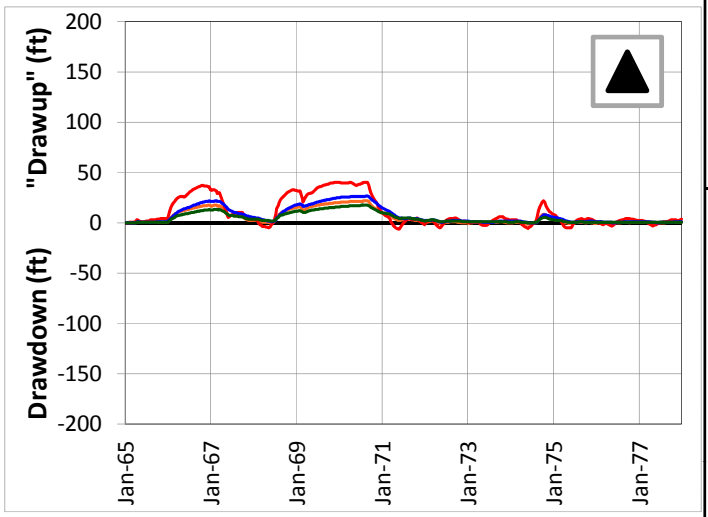

25-Mile Distance

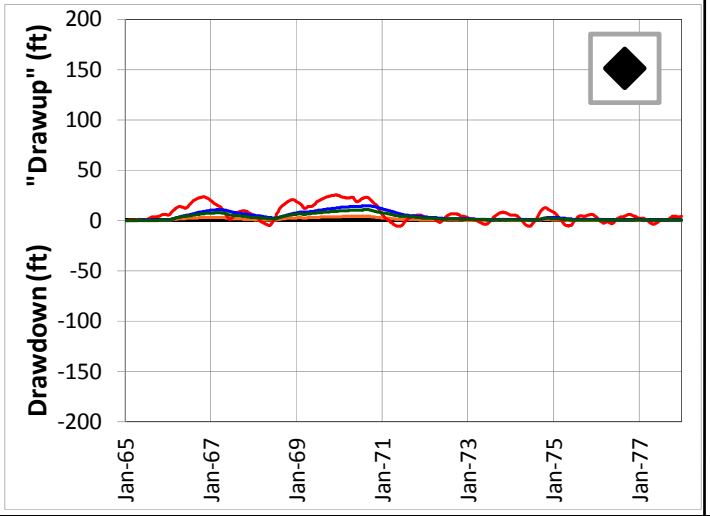

Legend

- CERP ASR Sites
- 5-Mile Distance Locations
- 15-Mile Distance Locations
- 25-Mile Distance Locations

Notes:

Scenario 12 is the same as Scenario 11 but the BZ wells have been removed.

A number of individual sites were chosen from the APPZ Aquifer at distances of 5, 15 and 25 miles from the proposed ASR well sites. This figure shows the drawdown and "drawup" at each output time step for 12 of these sites.

The plots were calculated by subtracting the heads calculated by the D13R model from those calculated by the no project run. This results in a positive value for "drawup" and a negative value for drawdown.

The colors of the points on the map correspond to the colors of the lines on the plots.

The symbols on the map (x, triangle and diamond) indicate the distance from the ASR sites.

5-Mile Distance

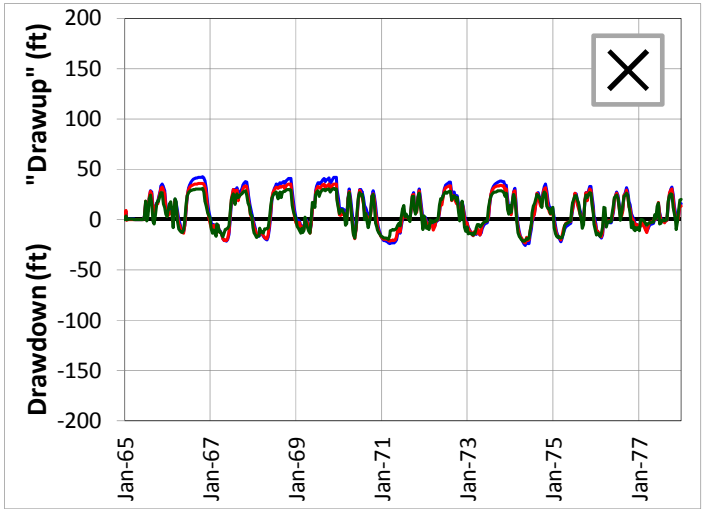

15-Mile Distance

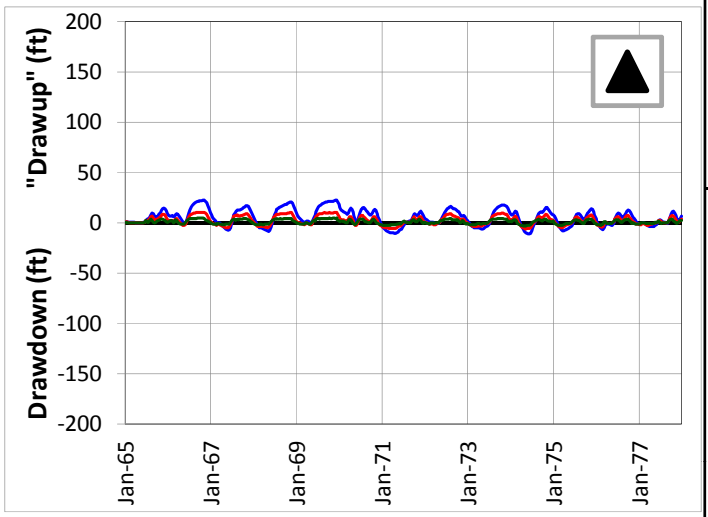

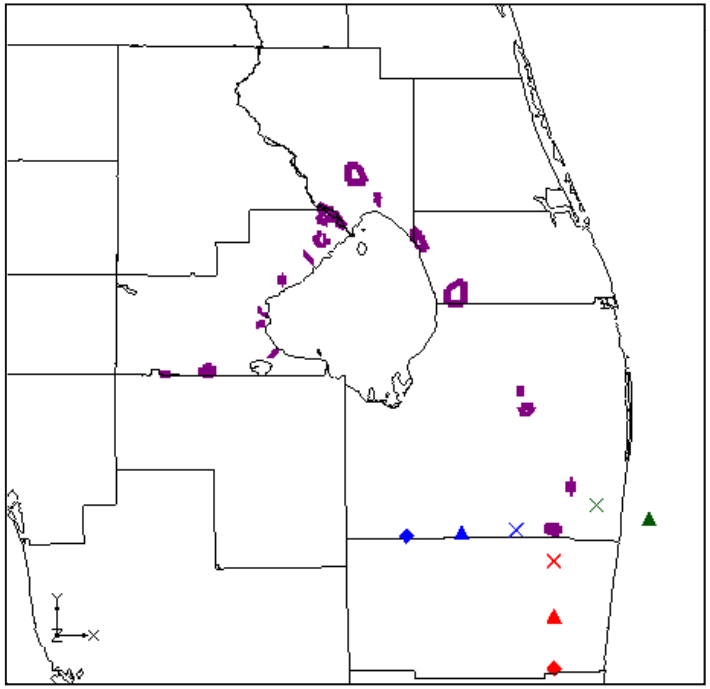

25-Mile Distance

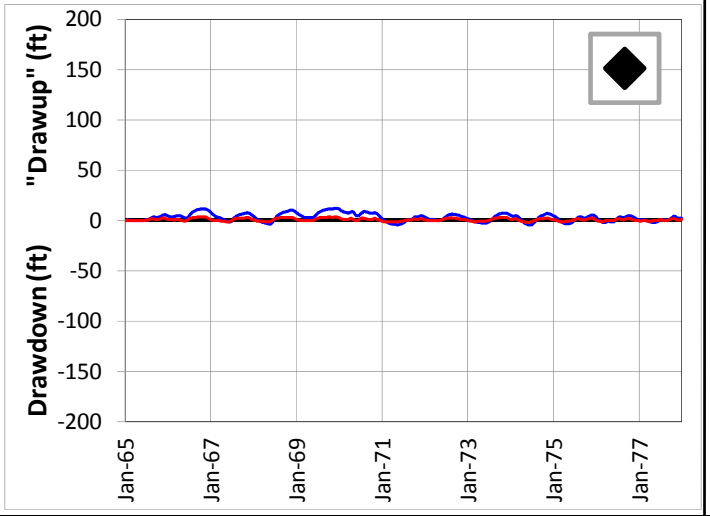

Legend

- CERP ASR Sites
- 5-Mile Distance Locations
- 15-Mile Distance Locations
- 25-Mile Distance Locations

Notes:

Scenario 12 is the same as Scenario 11 but the BZ wells have been removed.

A number of individual sites were chosen from the APPZ Aquifer at distances of 5, 15 and 25 miles from the proposed ASR well sites. This figure shows the drawdown and "drawup" at each output time step for 8 of these sites.

The plots were calculated by subtracting the heads calculated by the D13R model from those calculated by the no project run. This results in a positive value for "drawup" and a negative value for drawdown.

The colors of the points on the map correspond to the colors of the lines on the plots.

The symbols on the map (x, triangle and diamond) indicate the distance from the ASR sites.

5-Mile Distance

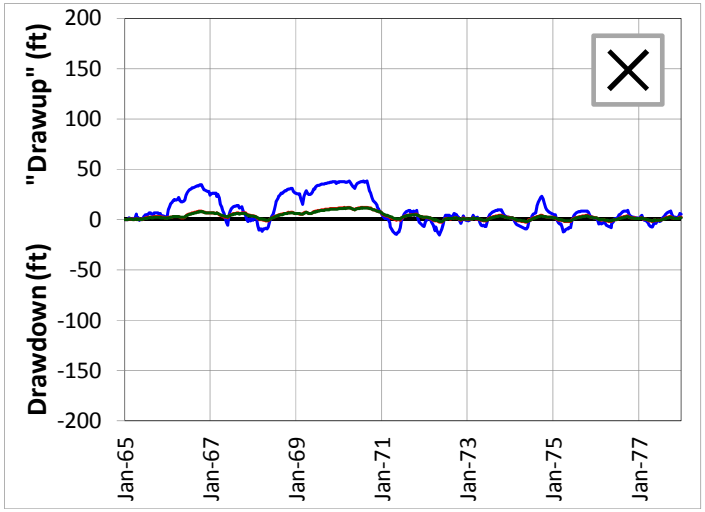

15-Mile Distance

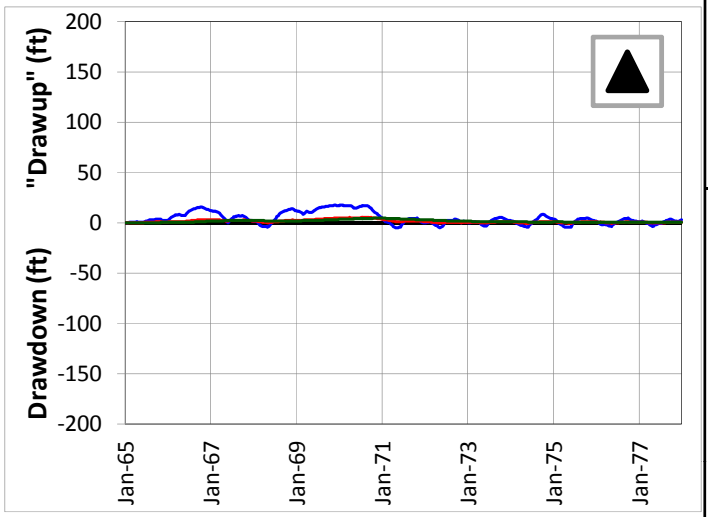

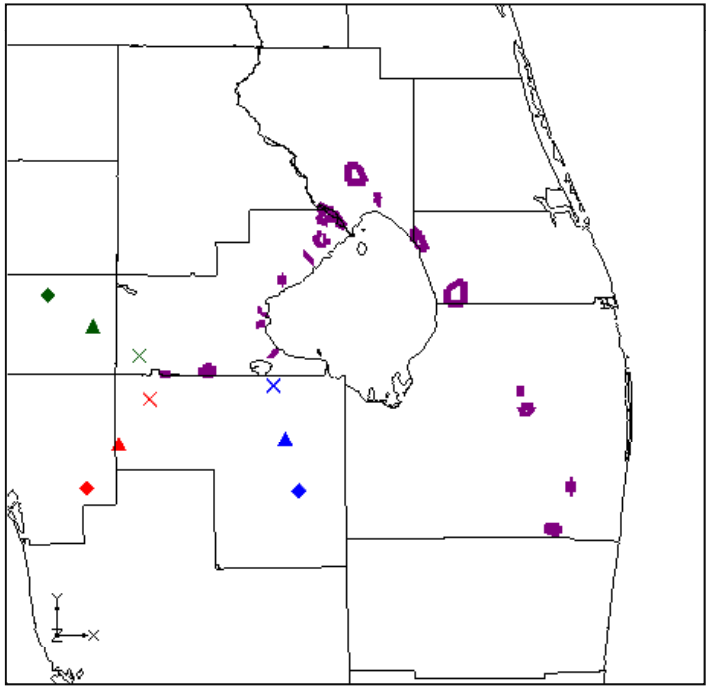

25-Mile Distance

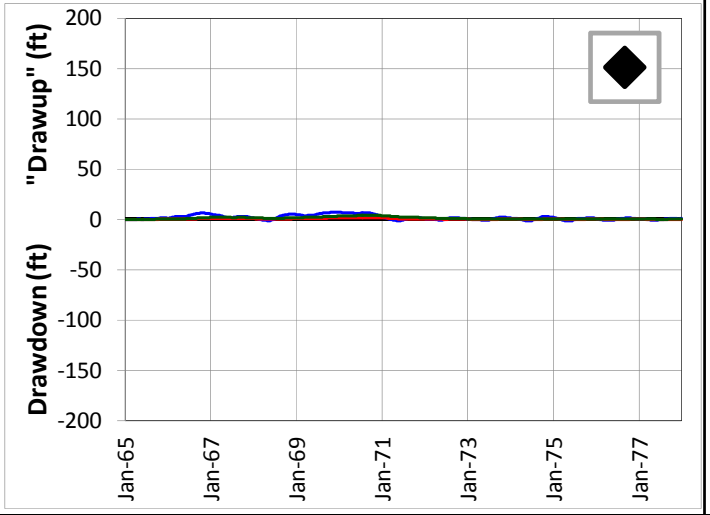

Legend

- CERP ASR Sites
- 5-Mile Distance Locations
- 15-Mile Distance Locations
- 25-Mile Distance Locations

Notes:

Scenario 12 is the same as Scenario 11 but the BZ wells have been removed.

A number of individual sites were chosen from the APPZ Aquifer at distances of 5, 15 and 25 miles from the proposed ASR well sites. This figure shows the drawdown and "drawup" at each output time step for 9 of these sites.

The plots were calculated by subtracting the heads calculated by the D13R model from those calculated by the no project run. This results in a positive value for "drawup" and a negative value for drawdown.

The colors of the points on the map correspond to the colors of the lines on the plots.

The symbols on the map (x, triangle and diamond) indicate the distance from the ASR sites.

SCENARIO 12 – DRAWDOWN AND "DRAWUP" – APPZ

REGIONAL MODEL PRODUCTION SCENARIO REPORT

FIGURE 4.160

JUNE 2013

5-Mile Distance

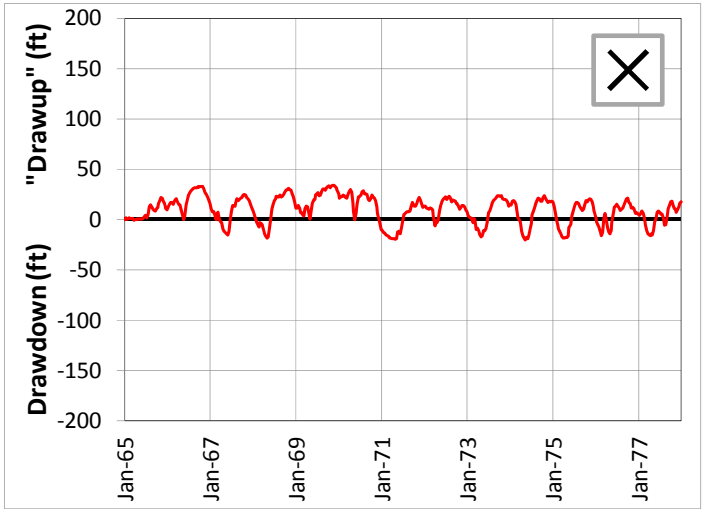

15-Mile Distance

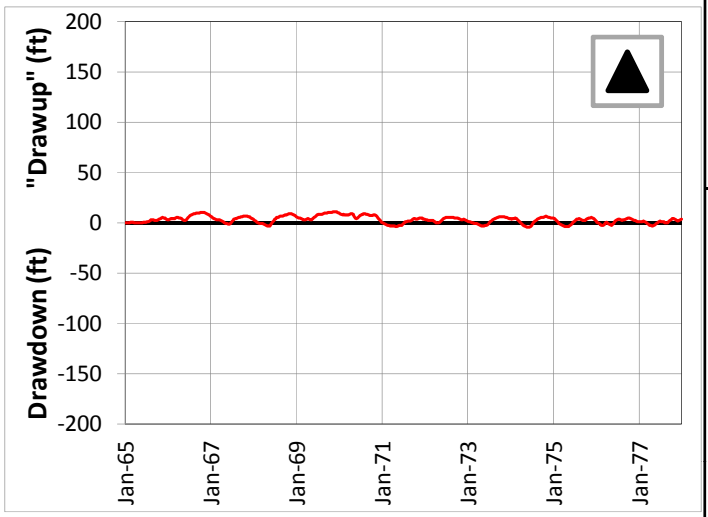

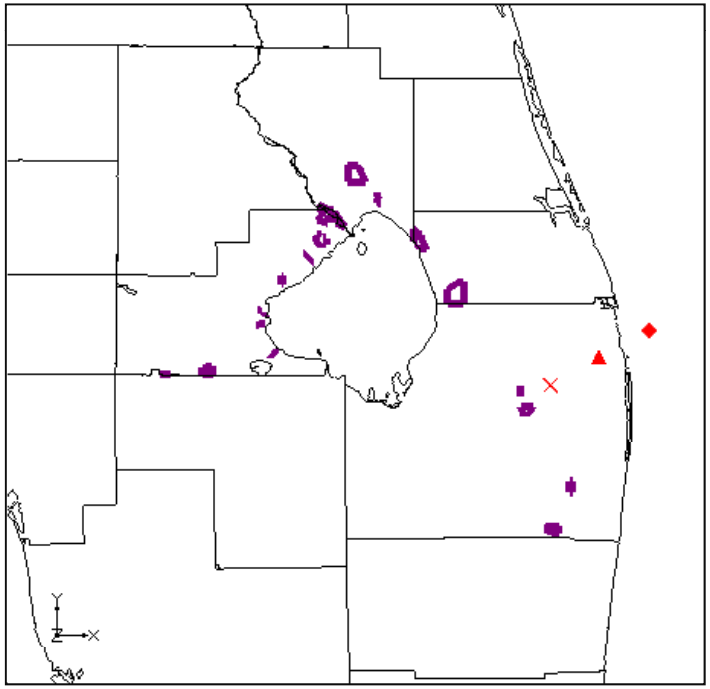

25-Mile Distance

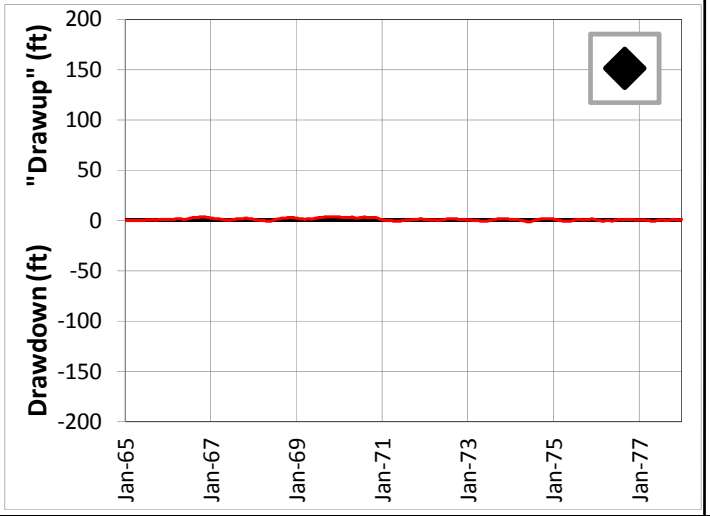

Legend

- CERP ASR Sites
- 5-Mile Distance Locations
- 15-Mile Distance Locations
- 25-Mile Distance Locations

Notes:

Scenario 12 is the same as Scenario 11 but the BZ wells have been removed.

A number of individual sites were chosen from the APPZ Aquifer at distances of 5, 15 and 25 miles from the proposed ASR well sites. This figure shows the drawdown and "drawup" at each output time step for 3 of these sites.

The plots were calculated by subtracting the heads calculated by the D13R model from those calculated by the no project run. This results in a positive value for "drawup" and a negative value for drawdown.

The colors of the points on the map correspond to the colors of the lines on the plots.

The symbols on the map (x, triangle and diamond) indicate the distance from the ASR sites.

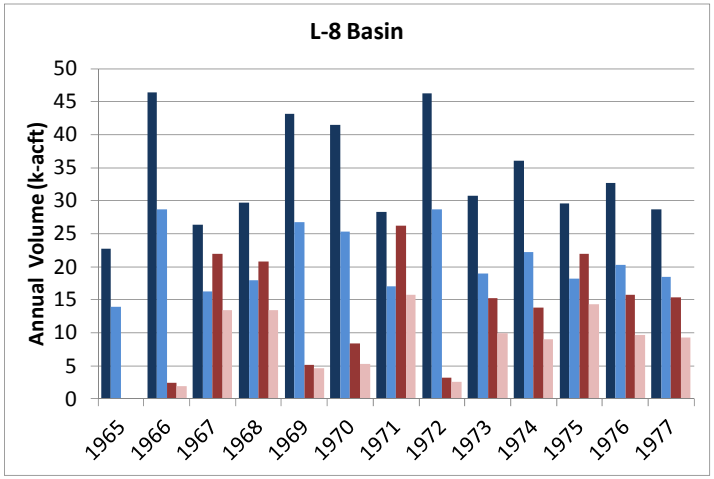

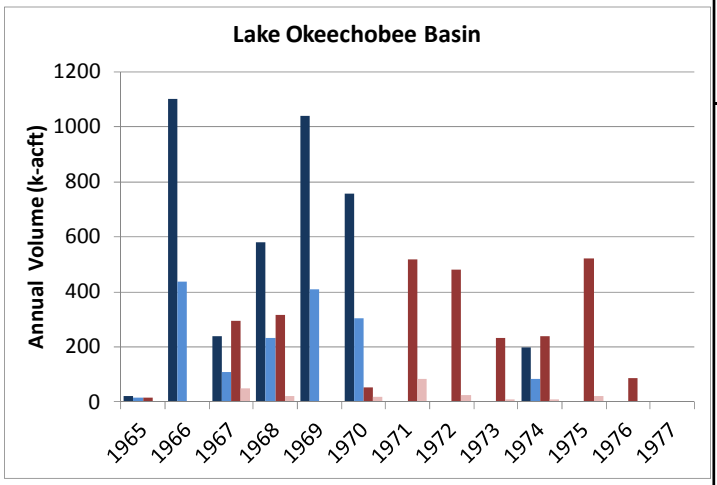

	L-8		Lake Okeechobee		Caloosahatchee	
	In %	Out %	In %	Out %	In %	Out %
1965	61%	100%	70%	15%	45%	69%
1966	62%	75%	40%	--	30%	46%
1967	62%	61%	46%	17%	26%	24%
1968	60%	65%	40%	7%	25%	25%
1969	62%	88%	39%	--	25%	--
1970	61%	63%	40%	35%	27%	100%
1971	60%	60%	--	16%	24%	27%
1972	62%	79%	--	5%	42%	31%
1973	62%	66%	--	4%	29%	30%
1974	62%	65%	43%	4%	26%	24%
1975	62%	65%	--	4%	26%	23%
1976	62%	61%	--	0%	33%	31%
1977	65%	61%	--	--	34%	34%

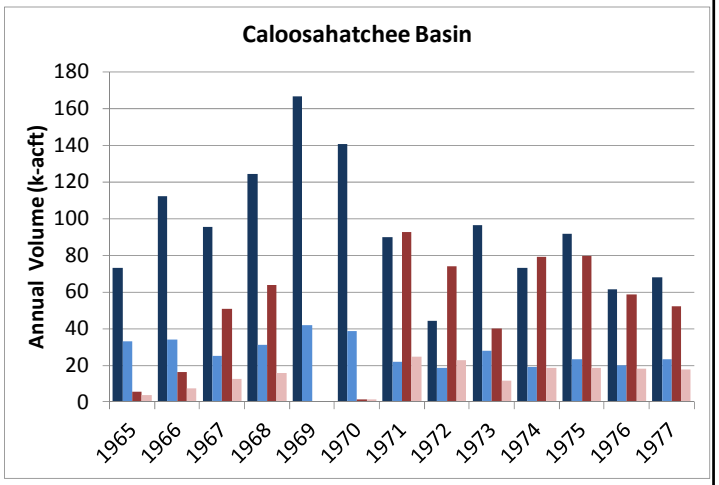

Legend

- Design Storage (injection)
- Modeled Storage (injection)
- Design Recovery (extraction)
- Modeled Recovery (extraction)

Notes:

Scenario 12 is the same as Scenario 11 but the BZ wells have been removed.

These three plots show the comparison between the SFWMM-D13R designed annual injection and extraction volumes at the ASR wells and the actual assigned rates for the RASRSM-D13R for three of the basins. The table presents the percentage of SFWMM-D13R annual flow rates that are included in the RASRSM-D13R.

Scenario 12 – Comparison of Designed and Modeled ASR Flow Rates

Regional Model Production Scenario Report

Figure 4.162

June 2013

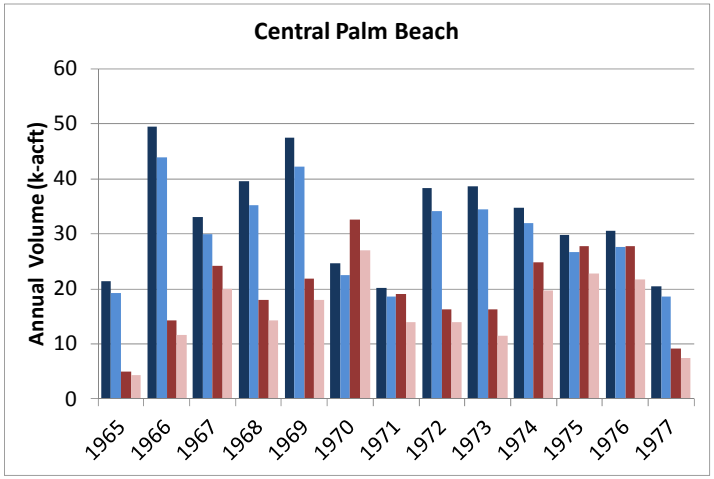

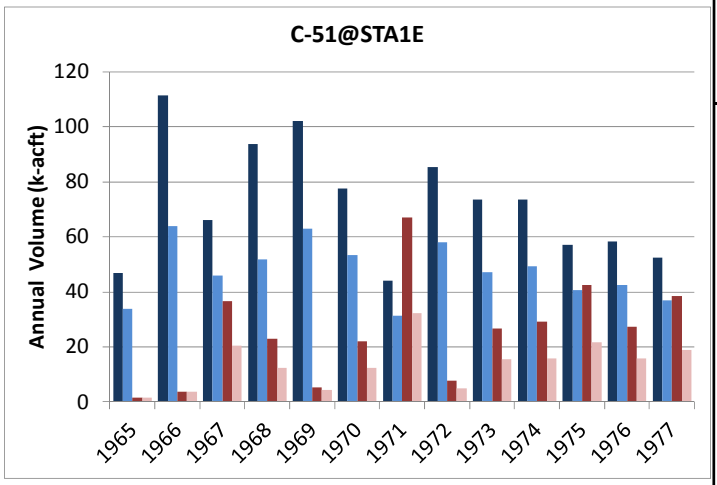

	CPB		C-51		Hillsboro	
	In %	Out %	In %	Out %	In %	Out %
1965	90%	88%	72%	96%	45%	46%
1966	89%	82%	58%	100%	36%	84%
1967	90%	82%	69%	56%	40%	28%
1968	89%	80%	55%	53%	36%	35%
1969	89%	82%	62%	80%	39%	80%
1970	91%	83%	69%	57%	48%	68%
1971	92%	73%	71%	48%	48%	14%
1972	89%	86%	68%	66%	49%	23%
1973	89%	71%	64%	58%	35%	32%
1974	92%	79%	67%	54%	45%	41%
1975	89%	82%	71%	51%	47%	23%
1976	90%	78%	73%	58%	52%	28%
1977	91%	81%	71%	49%	46%	23%

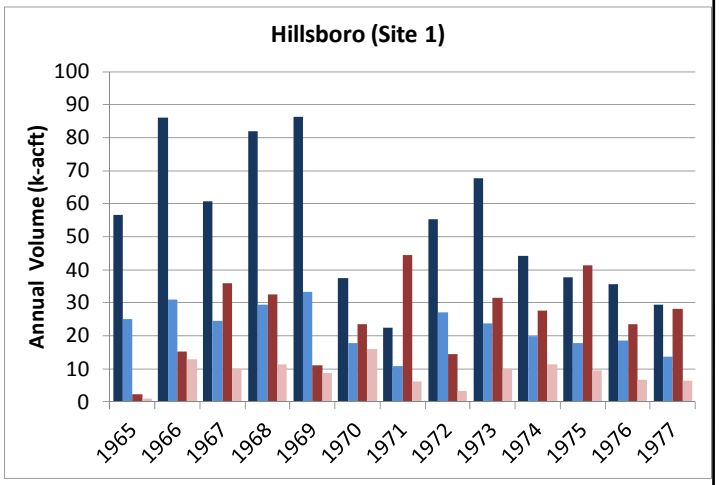

Legend

- Design Storage (injection)
- Modeled Storage (injection)
- Design Recovery (extraction)
- Modeled Recovery (extraction)

Notes:

Scenario 12 is the same as Scenario 11 but the BZ wells have been removed.

These three plots show the comparison between the SFWMM-D13R designed annual injection and extraction volumes at the ASR wells and the actual assigned rates for the RASRSM-D13R for three of the basins. The table presents the percentage of SFWMM-D13R annual flow rates that are included in the RASRSM-D13R.

SCENARIO12 – COMPARISON OF DESIGNED AND MODELED ASR FLOW RATES

REGIONAL MODEL PRODUCTION SCENARIO REPORT

FIGURE 4.163

JUNE 2013

	Total	
	In %	Out %
1965	58%	45%
1966	42%	72%
1967	48%	27%
1968	42%	19%
1969	42%	82%
1970	43%	57%
1971	49%	23%
1972	62%	12%
1973	49%	19%
1974	49%	20%
1975	52%	15%
1976	59%	30%
1977	56%	42%

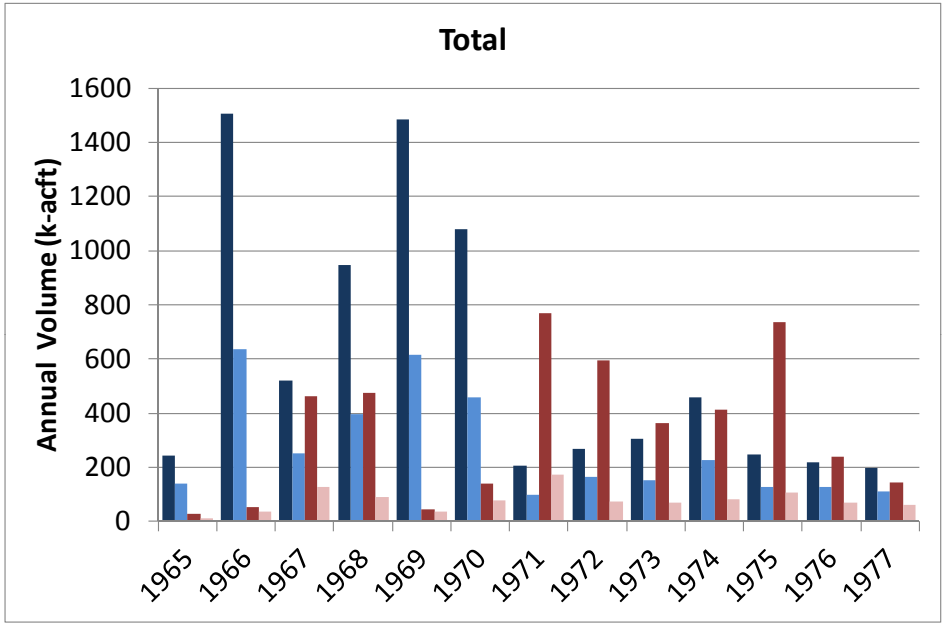

Legend

- Design Storage (injection)
- Modeled Storage (injection)
- Design Recovery (extraction)
- Modeled Recovery (extraction)

Notes:

Scenario 12 is the same as Scenario 11 but the BZ wells have been removed.

This plot shows the comparison between the SFWMM-D13R designed annual injection and extraction volumes at the ASR wells and the actual assigned rates for the RASRSM-D13R for all basins. The table presents the percentage of SFWMM-D13R annual flow rates that are included in the RASRSM-D13R.

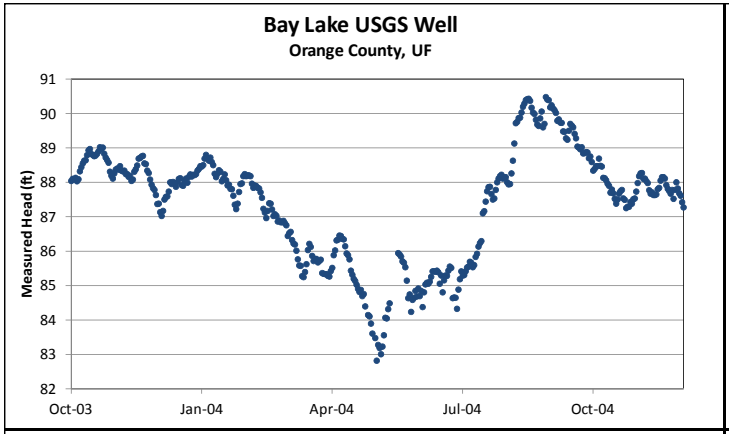

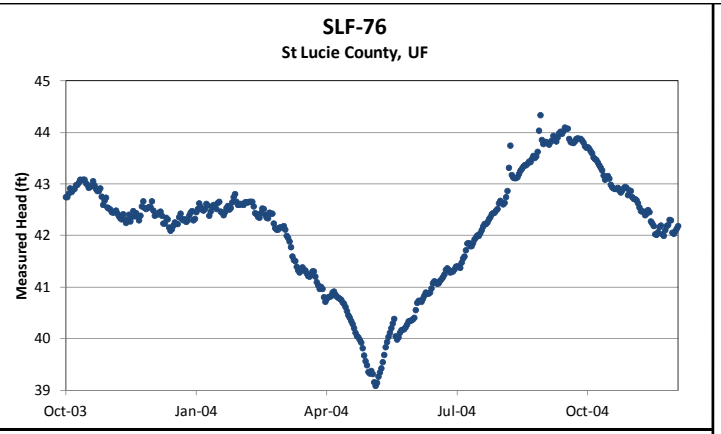

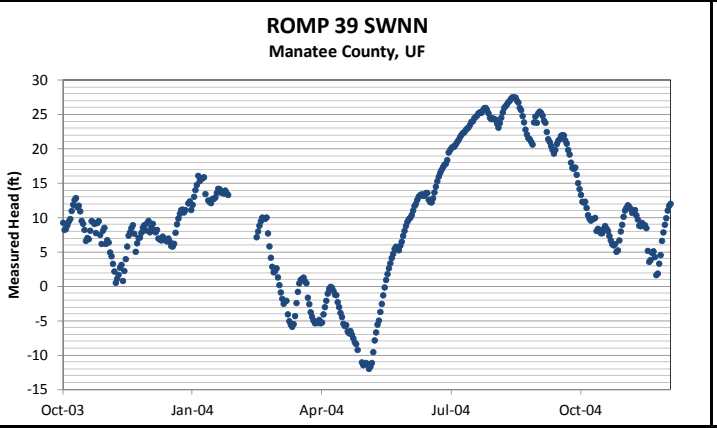

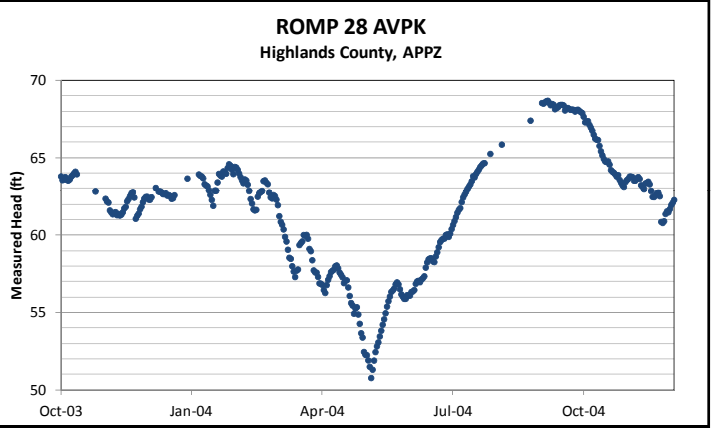

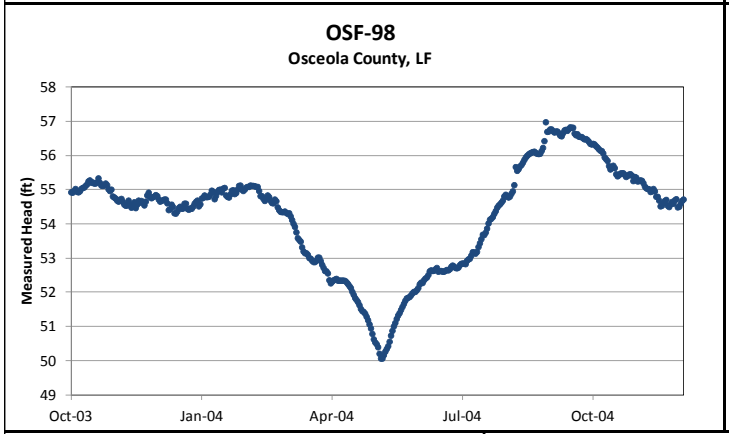

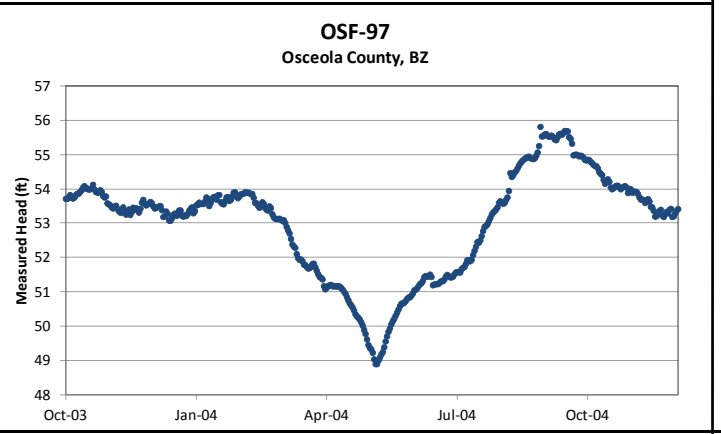

Notes:

These plots show the measured heads at six monitoring wells scattered across the regional domain in all four aquifers for the calibration period.

Notice that despite distances and confining units, all six wells have a steep decline down to a low head occurring between June 2 and June 4. Similarly, all six wells show a more gentle rise to a peak during the end of September 2004 and beginning of October 2004.

Each well has a different magnitude and range of heads and some have more damped responses to regional stresses, but all six have very similar head signatures during this time period.

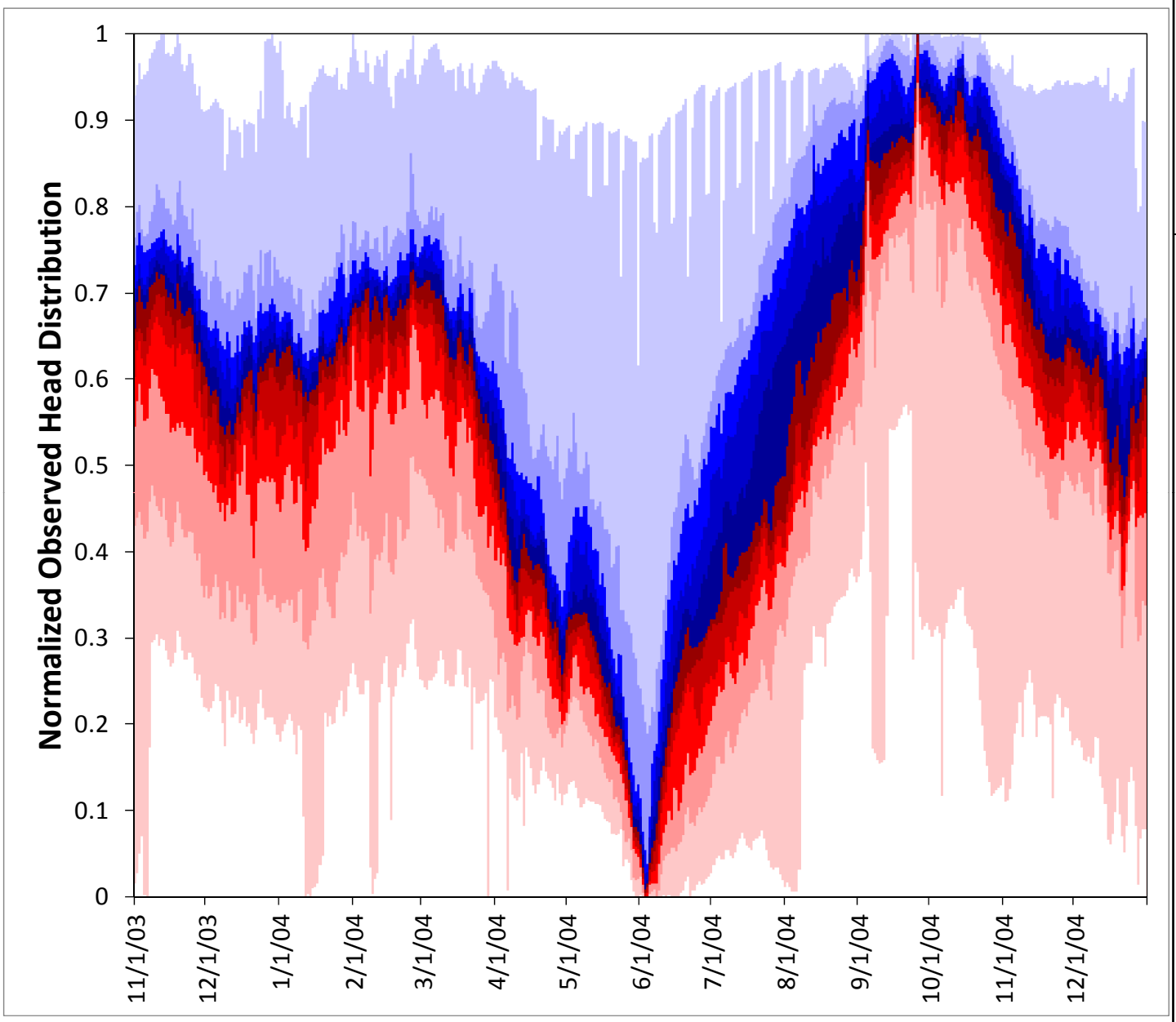

Normalized Observed Head

Maximum

Median

Minimum

10% of the values fall into each colored box.

Notes:

This plot was created by gathering the observed head plots for 74 observation points (see Figures 4.41 through 4.94 in the Calibration Report, NAP, 2011). Points were eliminated from the distribution only if there were fewer than 400 observations made between 10/31/2003 and 12/31/2004.

Heads at each point were normalized using the following formula:

$$H_N = \frac{H - H_{\min}}{H_{\max} - H_{\min}}$$

Here, H is the head and subscripts indicate normalized (N), minimum (min), and maximum (max). Minimums and maximums were computed over the 14 month period only. The normalized heads for each day of the period were then separated into bins of 10% and plotted as shown. Note the very narrow range of normalized heads for the middle 80% of the wells.

The head figures in the Calibration Report (NAP, 2011) show that some head plots have outliers, sudden shifts in head, and unusual local phenomena. These largely unexplained errata were not removed in the making of this plot and are the main explanation for the large, outer bands.

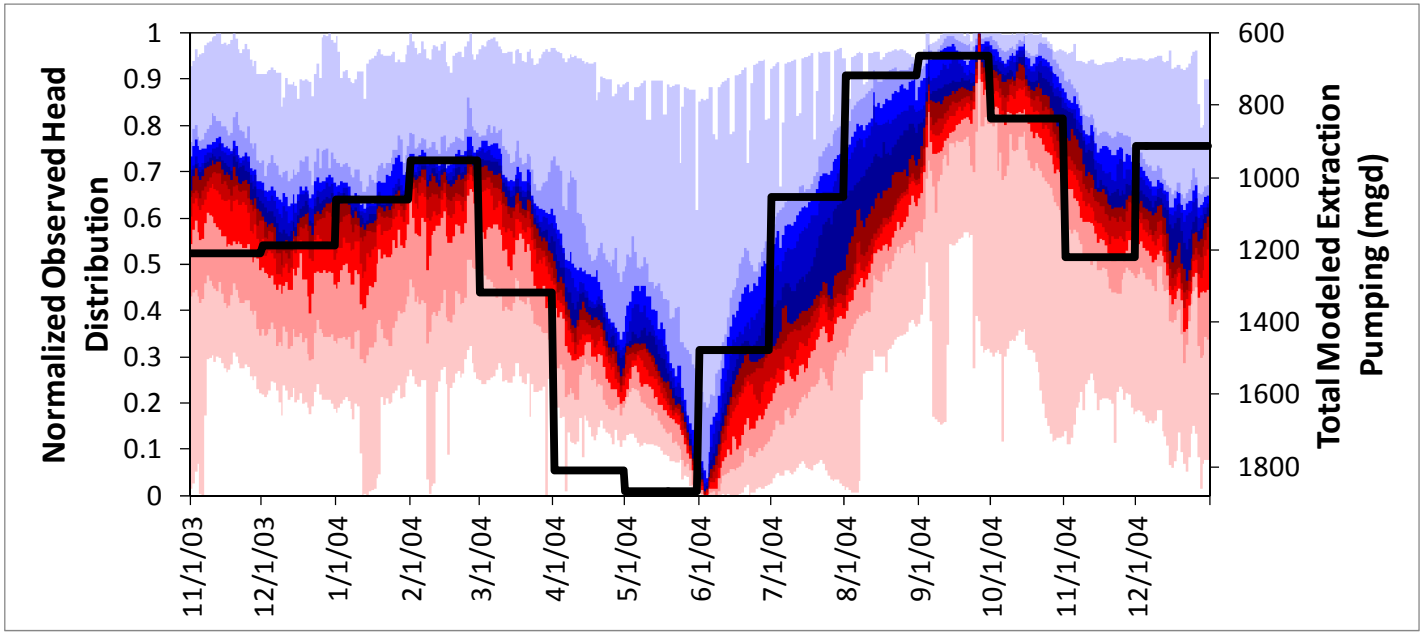

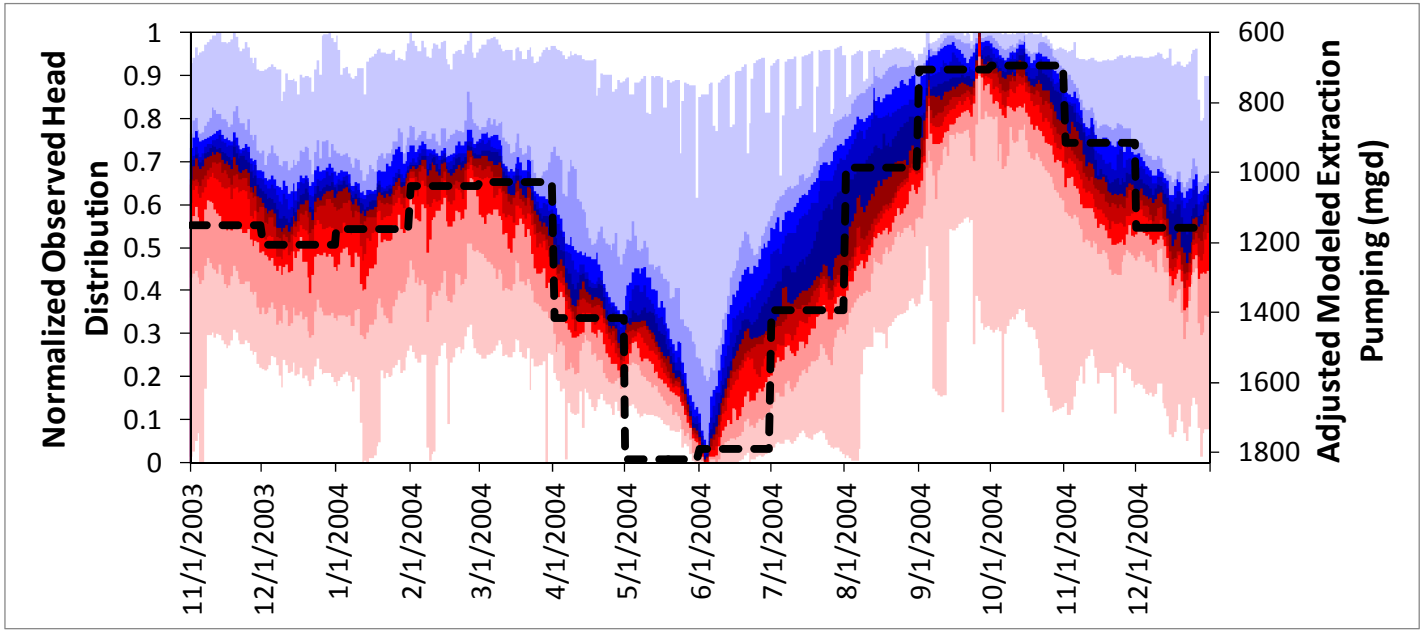

Normalized Observed Head

Maximum

Median

Minimum

10% of the values fall into each colored box.

Modeled Extraction Pumping

Adjusted Modeled Extraction Pumping

Notes:

The colored bars on these plots represent the distribution of normalized observed heads for 74 observation points. The development of these bars is described on Figure 4.166.

Each distribution is compared to the modeled extraction pumping. The solid black line (upper plot) represents the monthly averaged extraction pumping for all aquifers and all areas of the domain. Note the correlation to the median of the normalized observed heads is close, but slightly lagged.

The dotted black line (lower plot) is an adjustment of the monthly averaged plot. In this case, 80% of the previous month's pumping is added to 20% of the current month's pumping. Note the very close correlation between the heads measured in the field and the regional extraction pumping.

Note that the extraction rates are labeled on the right axis and the values are arranged in reverse order (high pumping at the bottom of the scale).

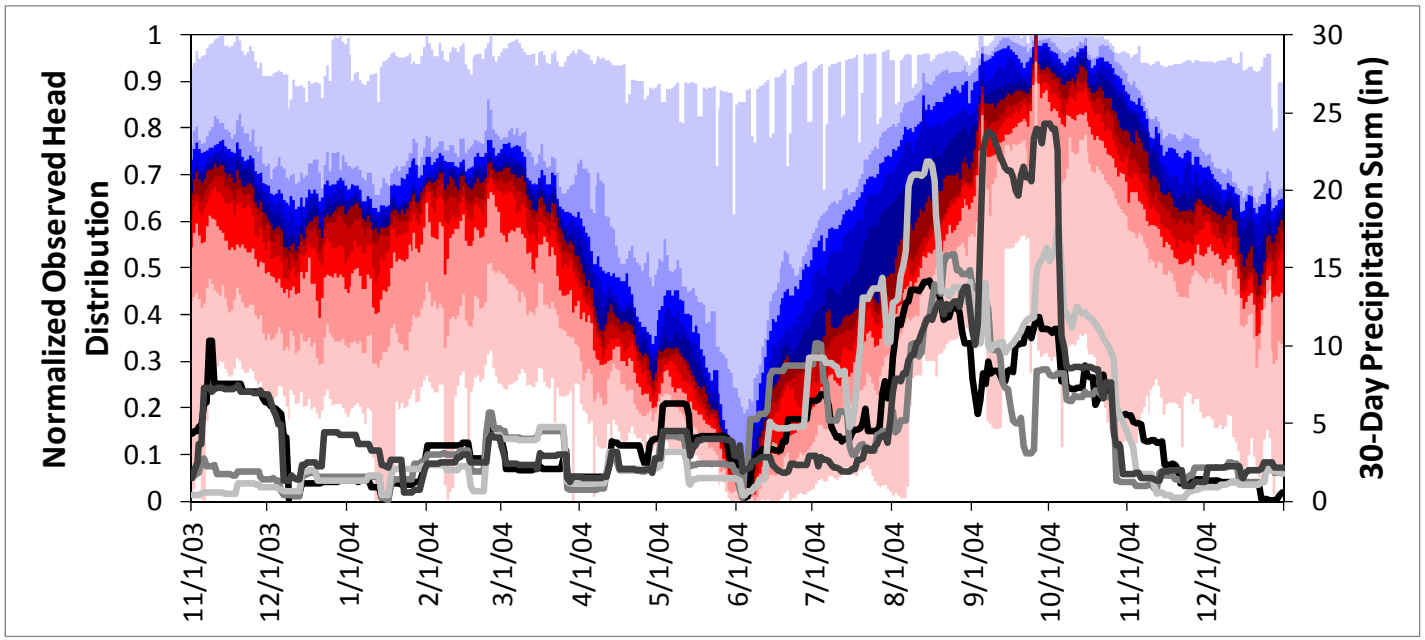

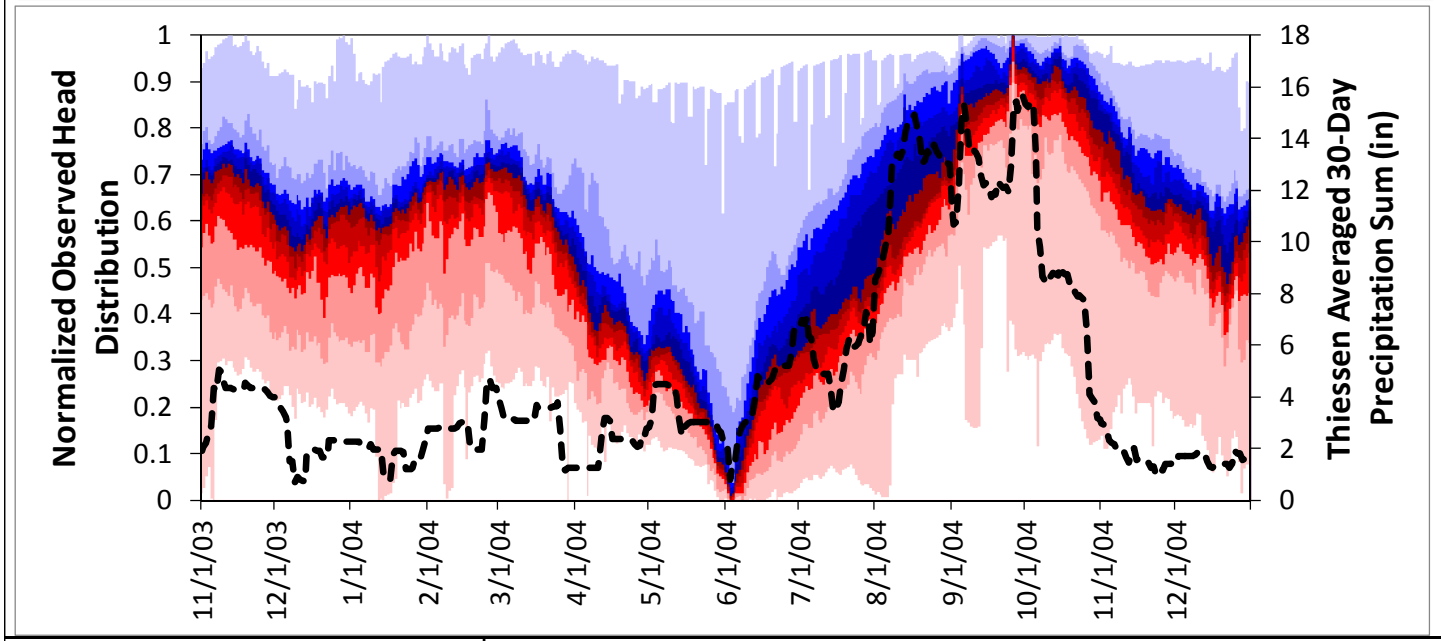

Normalized Observed Head

Maximum

Median

Minimum

10% of the values fall into each colored box.

30-day Precipitation Sums:

- Miami
- West Palm Beach
- Orlando
- Tampa
- Thiessen Average

Notes:

The colored bars on these plots represent the distribution of normalized observed heads for 74 observation points. The development of these bars is described on Figure 4.166.

Each distribution is compared to the precipitation. Daily precipitation data was available for four airports from National Climatic Data Center, 2012). Precipitation data has been smoothed by summing the previous 30 days of precipitation. The Thiessen average precipitation (lower plot) was calculated by comparing the Thiessen polygon areas (clipped to the model domain) to the total area of the model domain.

Note the poor correlation between head and precipitation during the winter and spring of 2004 and the fall of 2004. Good correlation is found during the summer of 2004. Precipitation is probably a major factor in the sudden rise in head seen at nearly all observation wells beginning in early June 2004.

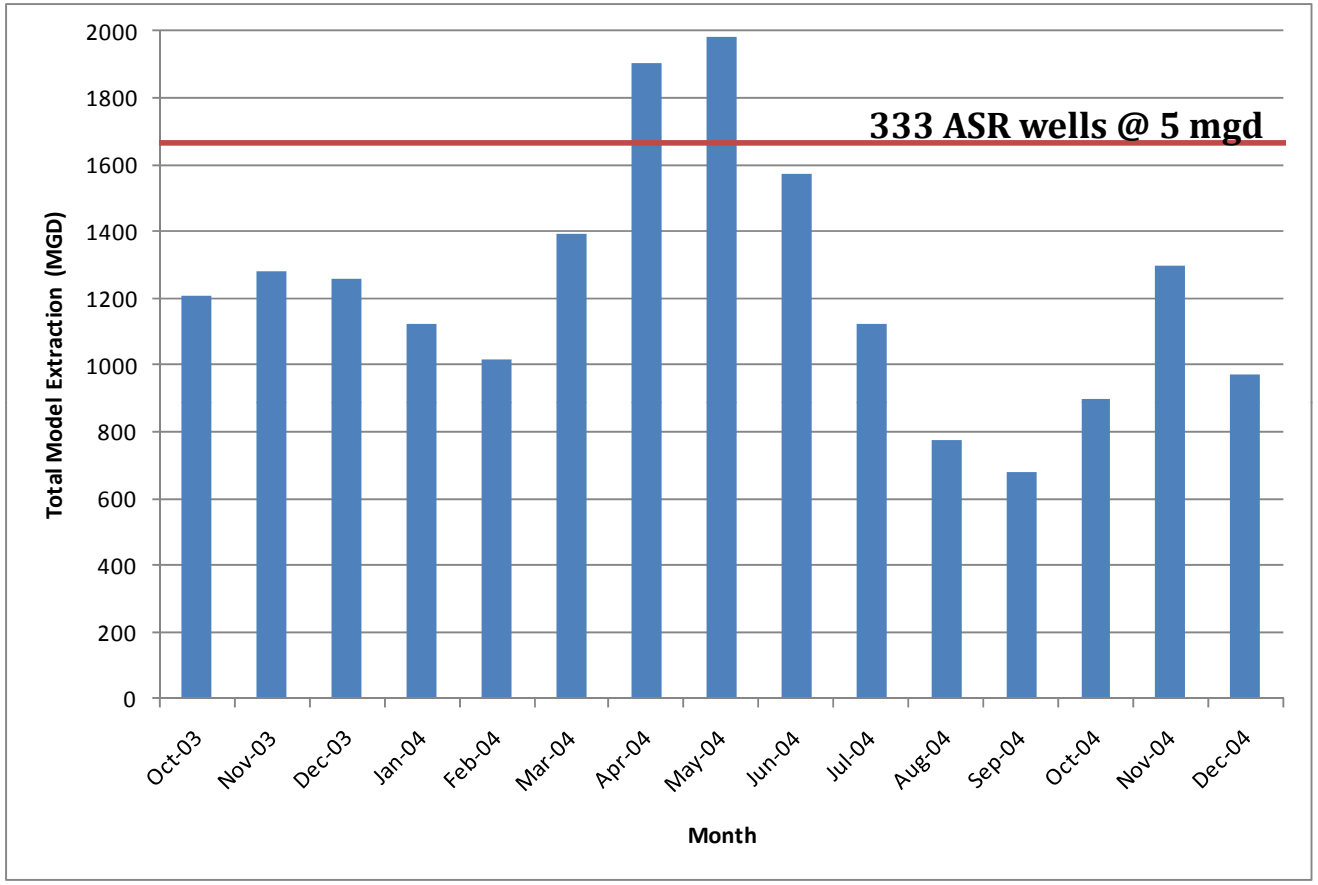

Notes:

This plot shows the total extraction volume from all regional pumping wells (agricultural, public water supply, industrial, etc.) for each month of the calibration period (October 2003 – December 2004) compared to the total extraction volume which would be realized if all 333 proposed ASR wells were to extract at full capacity together.

Note that the ASR system as proposed represents an enormous amount of water when compared to current water use in the Floridan aquifers.

COMPARISON OF PROPOSED ASR SYSTEM TO EXISTING REGIONAL GROUNDWATER USE

REGIONAL MODEL PRODUCTION SCENARIO REPORT

FIGURE 4.169

JUNE 2013

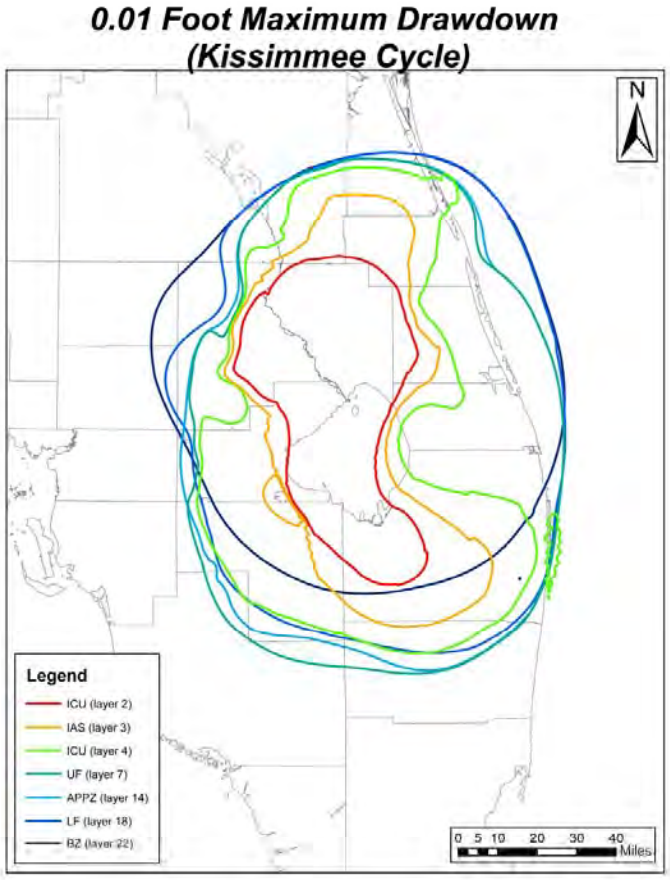

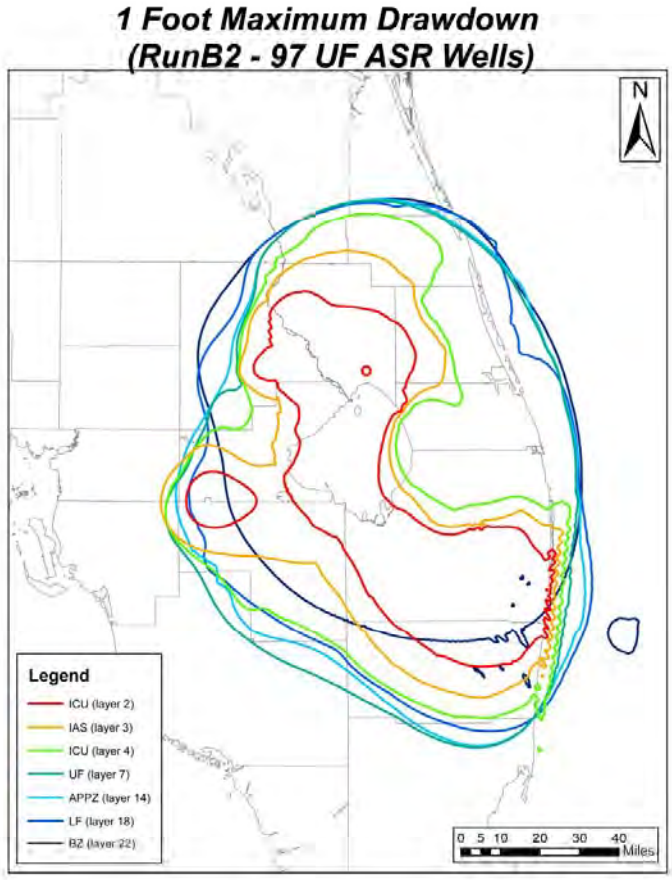

Notes:

These figures show the maximum drawdown for two runs on the RASRSM. On the left, the Kissimmee River pilot ASR was run with the pilot test pumping at 5 mgd. The contours show the location of the 0.01 foot maximum drawdown for each aquifer.

The figure on the right shows an early RASRSM-D13R simulation with 97 wells in the UF, divided among the proposed ASR sites. The maximum pump rate for each well is 5 mgd. In this figure, the lines are for the 1 foot maximum drawdown.

The RASRSM-D13R scenario (right) has nearly 100 times as many ASR wells as the cycle test model (left) and the maximum drawdown contours in the RASRSM-D13R figure (right) are 100 times the maximum drawdown contours on the cycle test figure (left). The areas impacted by the ASR wells as shown by the contour lines are similar. That is, the drawdown caused by 100 ASR wells is approximately 100 times the drawdown caused by 1 ASR well.

Differences in shape are caused primarily by the different distributions of wells in the two models.

COMPARISON OF DRAWDOWN AT KISSIMMEE PILOT SITE TO REGIONAL DRAWDOWN FOR D13R SCENARIO

REGIONAL MODEL PRODUCTION SCENARIO REPORT

FIGURE 4.170

JUNE 2013

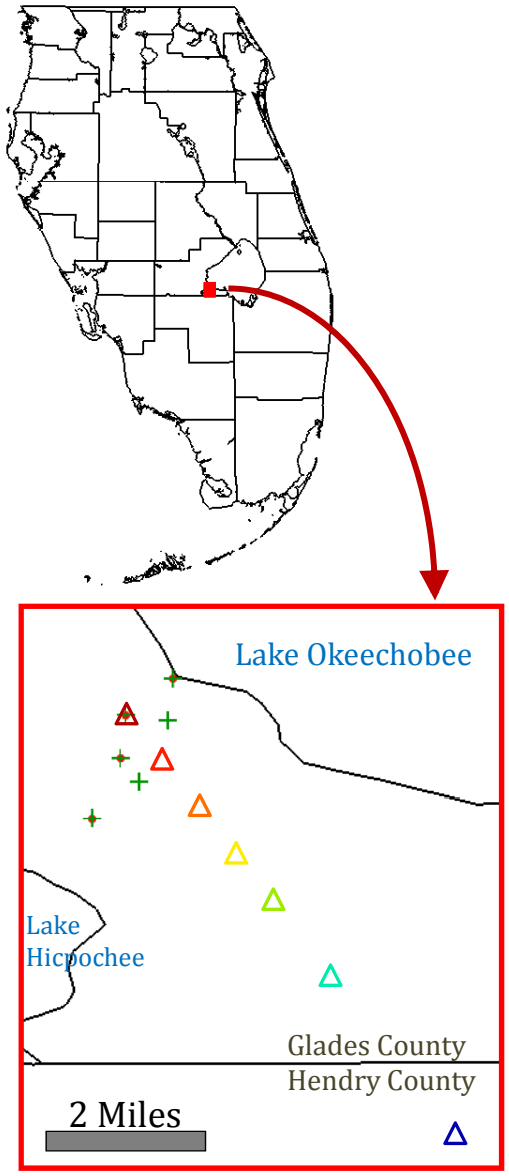

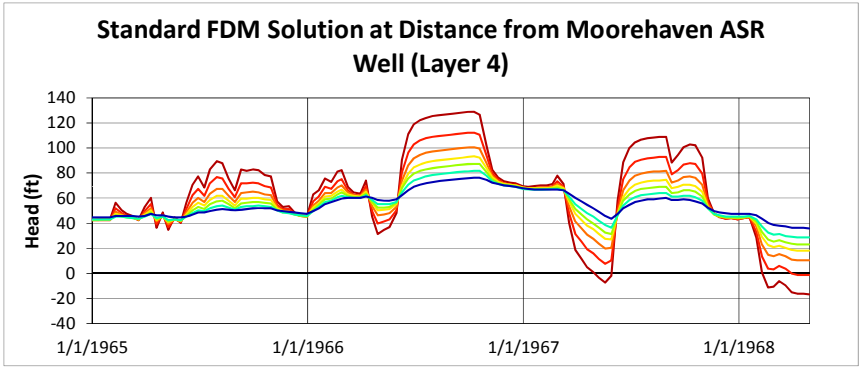

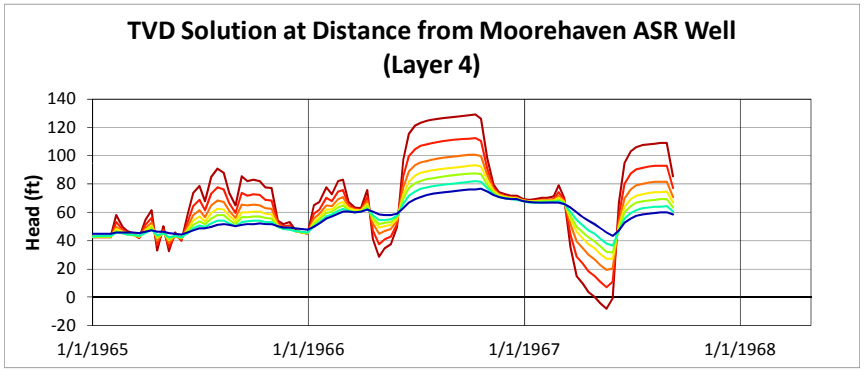

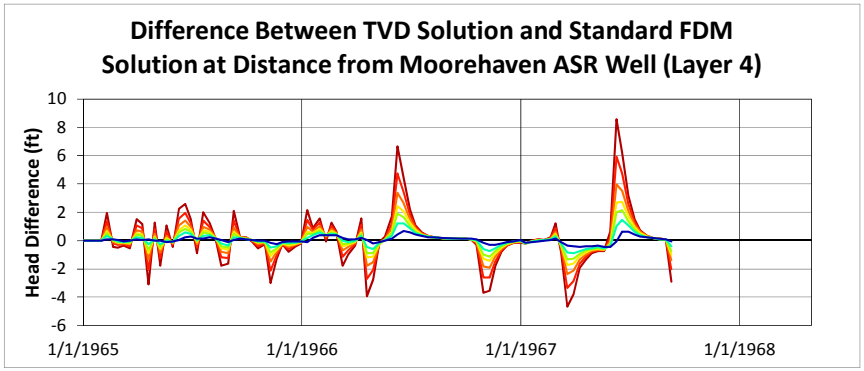

Legend

- ASR wells (UF)
- ASR wells (APPZ)
- ASR wells (BZ)
- Comparison points (color matches plot lines)

Notes:

These plots compare the heads calculated by the Standard FDM method (using upstream weighting) to those calculated by the TVD method (Courant Number = 0.2).

The map at left shows the comparison points and the relative positions of the Moorehaven site ASR wells, which are found in both the UF and BZ layers for Scenario 11.

These comparison points are placed in the ICU (layer 4 of the model). They are placed at varying distances with the nearest point (dark red) in the same cell as the ASR well and the furthest point (blue) nearly 7 miles southeast of the site.

Although there are no ASR wells in this layer of the model, the greatest difference between the two solution techniques is found in this layer at this site.

Note that as the impact of the ASR well is reduced with distance, so, the difference between the two solution methods is also reduced. Also, although the impact of the ASR wells continues throughout the pumping period, the differences between the methods drop off within a few weeks or months of the initial pumping change.

Comparison of Standard FDM to TVD Solution Moorehaven Site, ICU (Layer 4)

Regional Model Production Scenario Report

Figure 5.1

June 2013

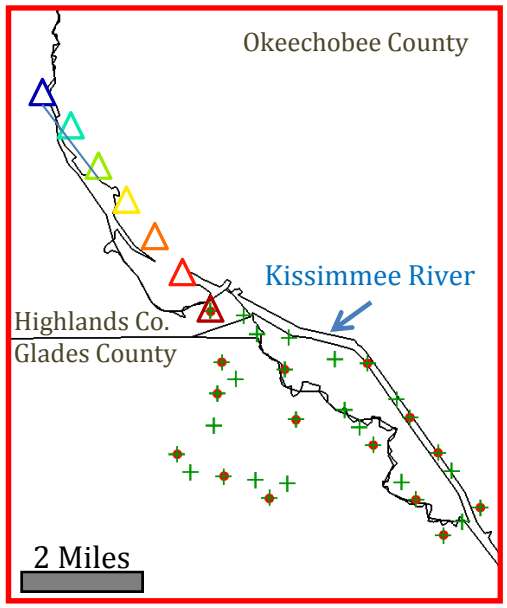

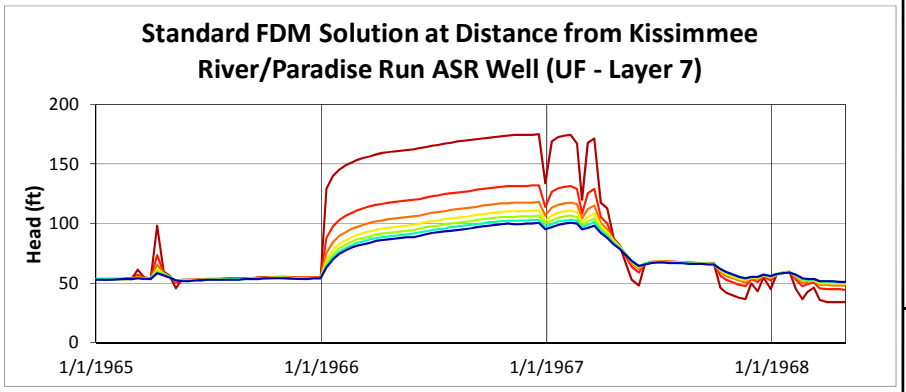

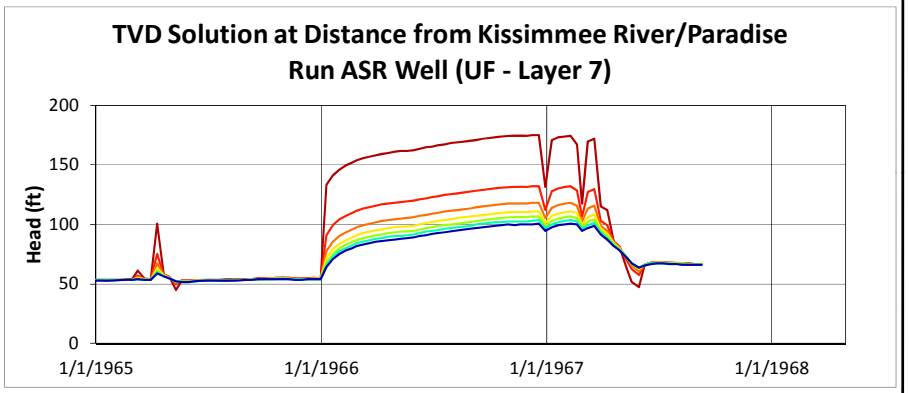

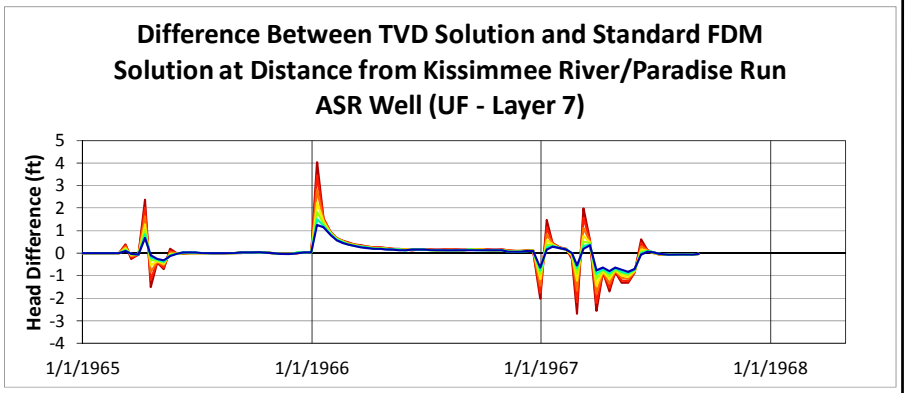

Legend

- ASR wells (UF)
- ASR wells (APPZ)
- ASR wells (BZ)
- Comparison points (color matches plot lines)

Notes:

These plots compare the heads calculated by the Standard FDM method (using upstream weighting) to those calculated by the TVD method (Courant Number = 0.2).

The map at left shows the comparison points and the relative positions of the Kissimmee River/Paradise Run site ASR wells, which are found in both the UF and BZ layers for Scenario 11.

These comparison points are placed in the UF (layer 7 of the model). They are placed at varying distances with the nearest point (dark red) in the same cell as the ASR well and the furthest point (blue) about 4.5 miles northwest of the site.

Note that as the impact of the ASR well is reduced with distance, so, the difference between the two solution methods is also reduced. Also, although the impact of the ASR wells continues throughout the pumping period, the differences between the methods drop off within a few weeks or months of the initial pumping change.

Comparison of Standard FDM to TVD Solution Kissimmee River/Paradise Run Site, UF (Layer 7)

Regional Model Production Scenario Report

Figure 5.2

June 2013

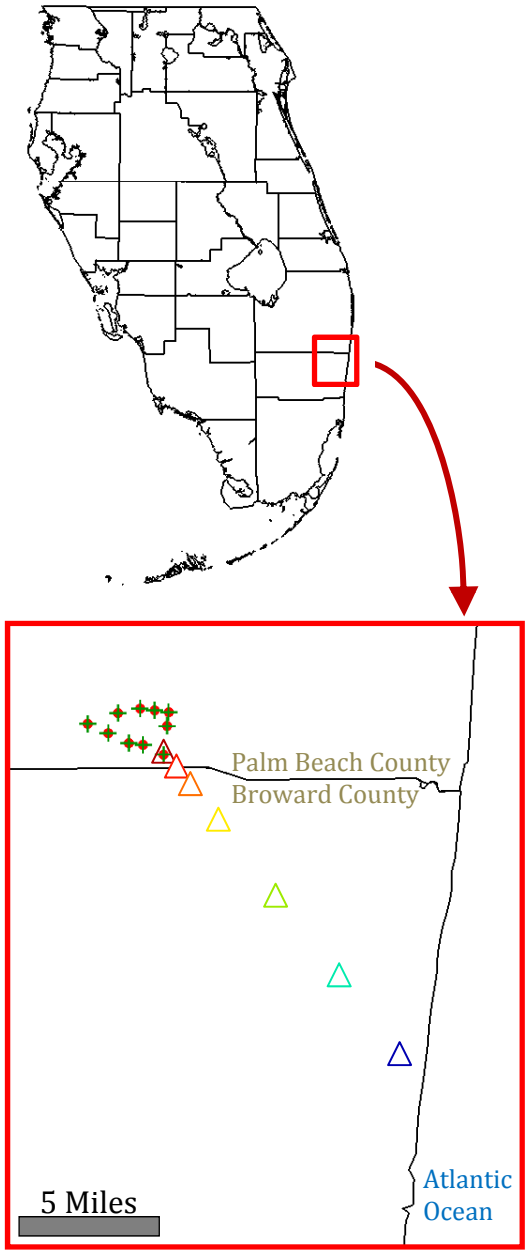

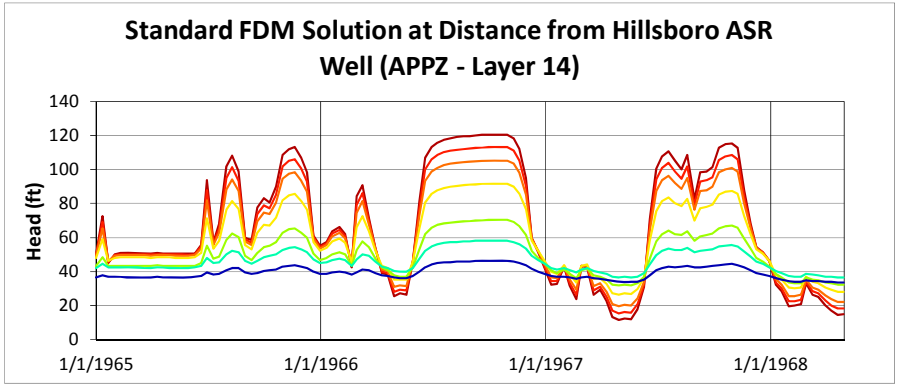

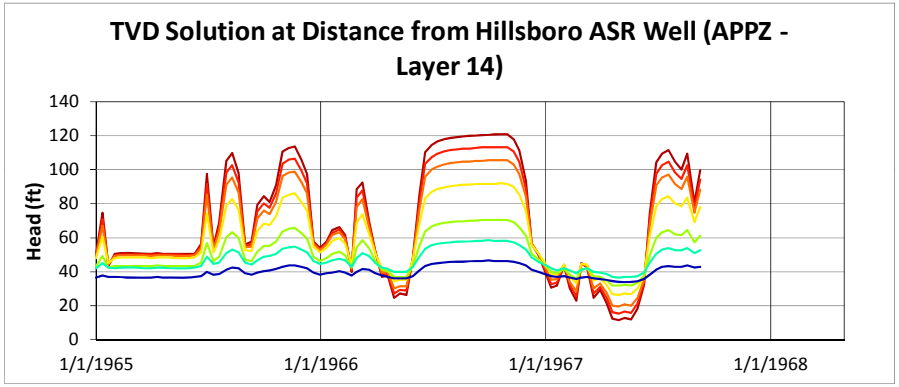

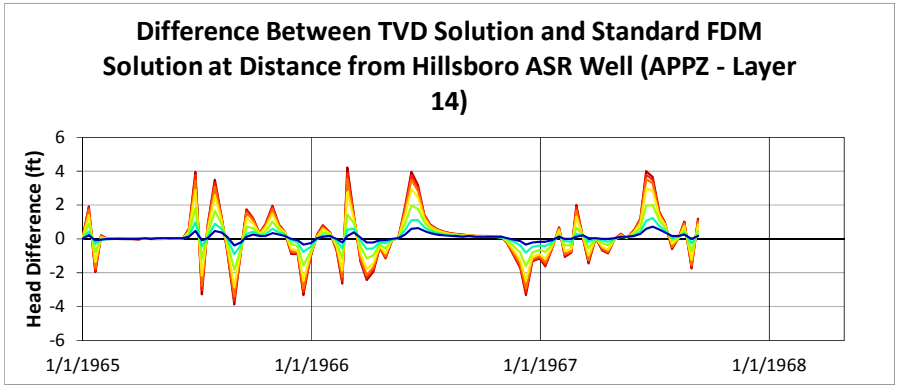

Legend

- ASR wells (UF)
- ASR wells (APPZ)
- ASR wells (BZ)
- Comparison points (color matches plot lines)

Notes:

These plots compare the heads calculated by the Standard FDM method (using upstream weighting) to those calculated by the TVD method (Courant Number = 0.2).

The map at left shows the comparison points and the relative positions of the Hillsboro site ASR wells, which are found in both the UF and BZ layers for Scenario 11.

These comparison points are placed in the APPZ (layer 14 of the model). They are placed at varying distances with the nearest point (dark red) in the same cell as the ASR well and the furthest point (blue) more than 14 miles southeast of the site.

Note that as the impact of the ASR well is reduced with distance, so, the difference between the two solution methods is also reduced. Also, although the impact of the ASR wells continues throughout the pumping period, the differences between the methods drop off within a few weeks or months of the initial pumping change.

Comparison of Standard FDM to TVD Solution Hillsboro Site, APPZ (Layer 14)

Regional Model Production Scenario Report

Figure 5.3

June 2013

Input Parameters

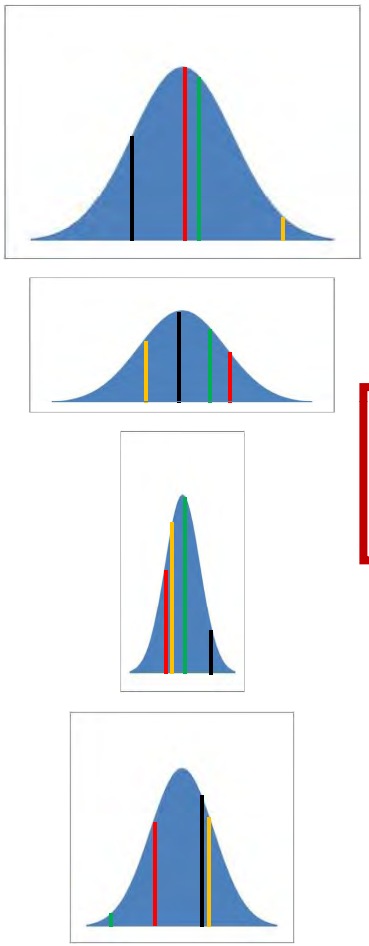

Numerous Model Runs

Model Output

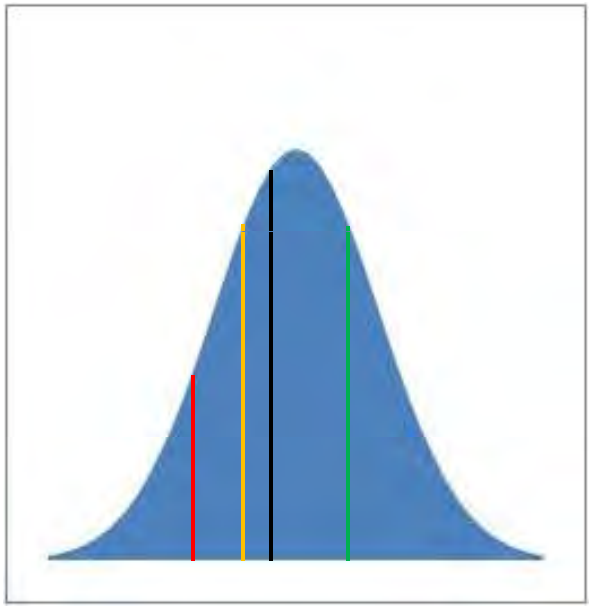

Notes:

In a Monte Carlo analysis, probability distributions are assigned to each input parameter. The computer randomly selects a value for each parameter based on the assigned distribution and then runs the model, resulting in a number of "equally probable" model results. With enough model runs, the probability distribution of the model output can be discerned. This allows the modeler to report a range or distribution of model output instead of a single "correct" result.

For example, in this cartoon, the blue bell curves are the distributions and the colored lines represent individual randomized model runs. Just four randomized runs have been pictured as colored lines, but when the model is run hundreds or thousands of times, the model output can also be presented as a probability distribution.

SCHEMATIC OF MONTE CARLO ANALYSIS

REGIONAL MODEL PRODUCTION SCENARIO REPORT

FIGURE 6.1

JUNE 2013

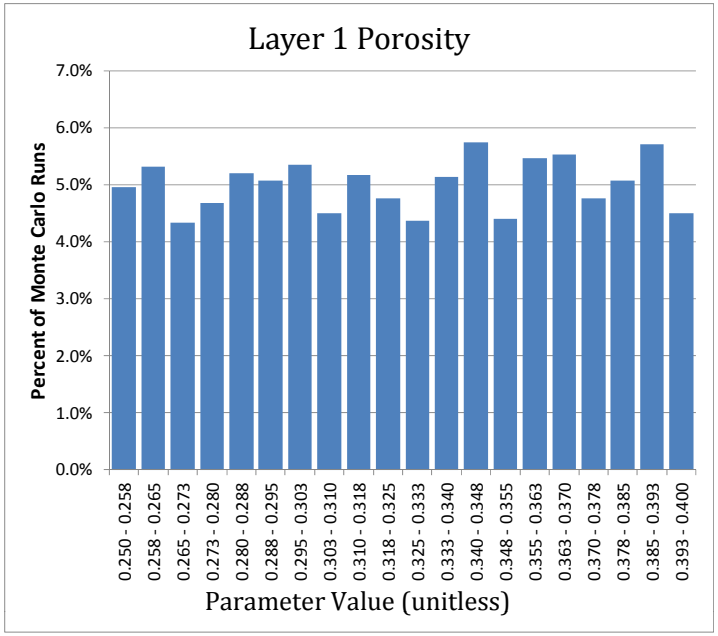

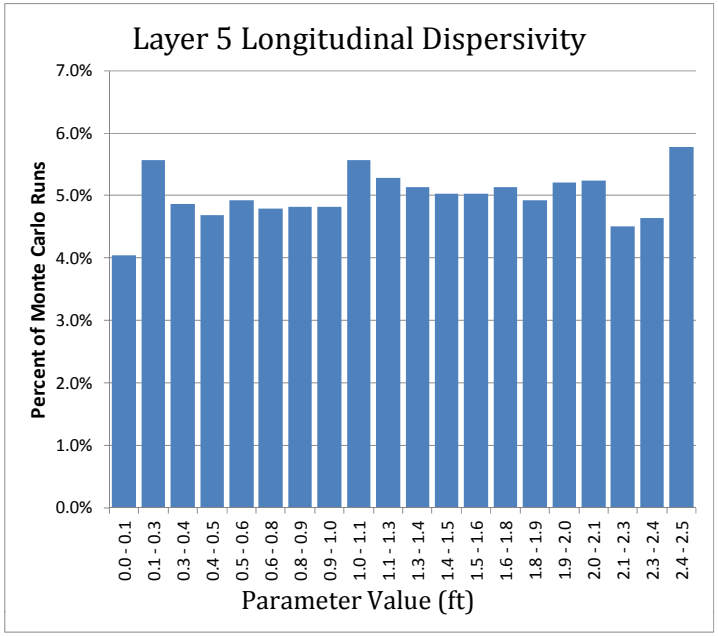

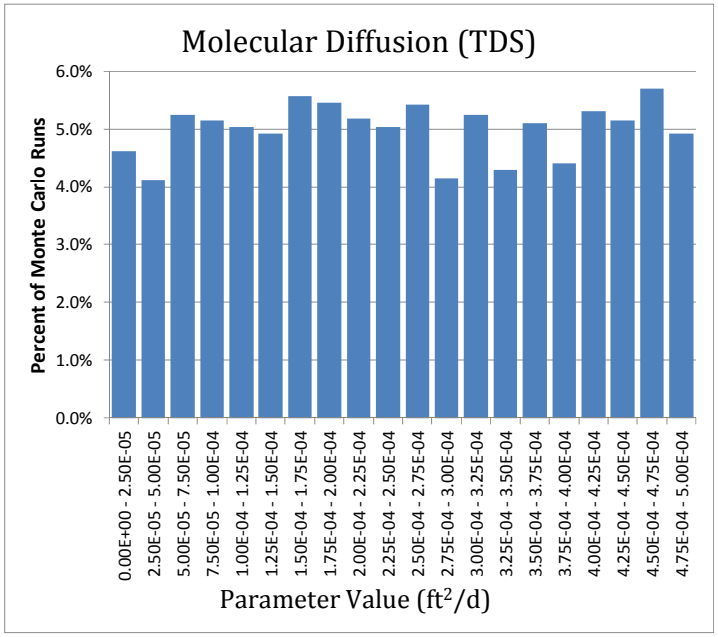

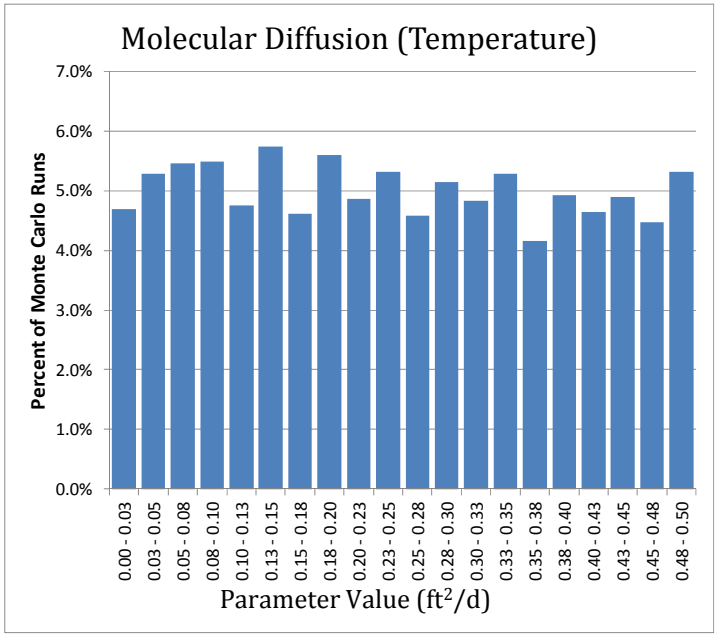

Notes:

Porosity, longitudinal dispersivity and molecular diffusion were given uniform distributions over a range of reasonable values in the Monte Carlo scenarios. The computer selected random values within the ranges for each of the 2892 Monte Carlo selections. These plots show examples of the resulting distributions and indicate a generally uniform distribution as expected.

Note that the plots are designed with 20 bins, so each bar would be at 5% if there were an infinite number of randomizations. As there are only 2892 randomizations, we can be content with the fact that each bar is between 4% and 6%.

Similar plots could be provided for porosity and longitudinal dispersivity in the other layers of the model; however, they are omitted for simplicity since they are quite similar to those presented.

EXAMPLES OF UNIFORM DISTRIBUTION PARAMETERS FOR MONTE CARLO ANALYSIS

REGIONAL MODEL PRODUCTION SCENARIO REPORT

FIGURE 6.2

JUNE 2013

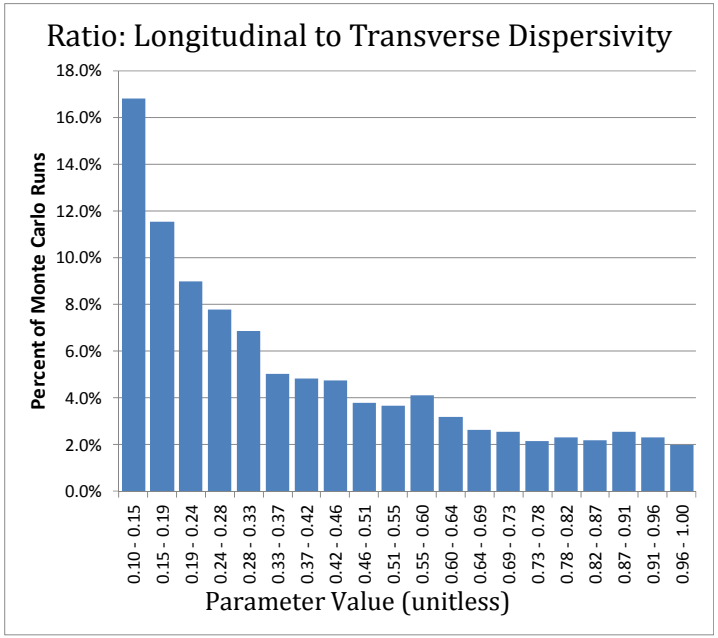

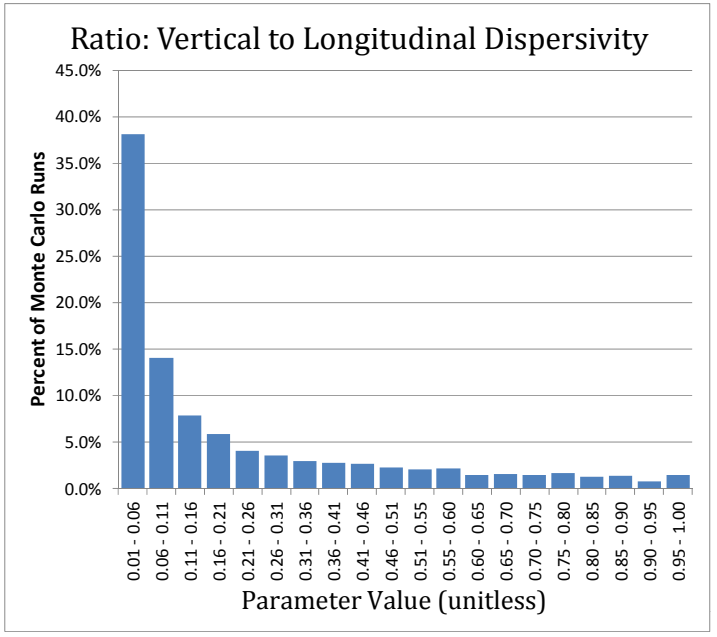

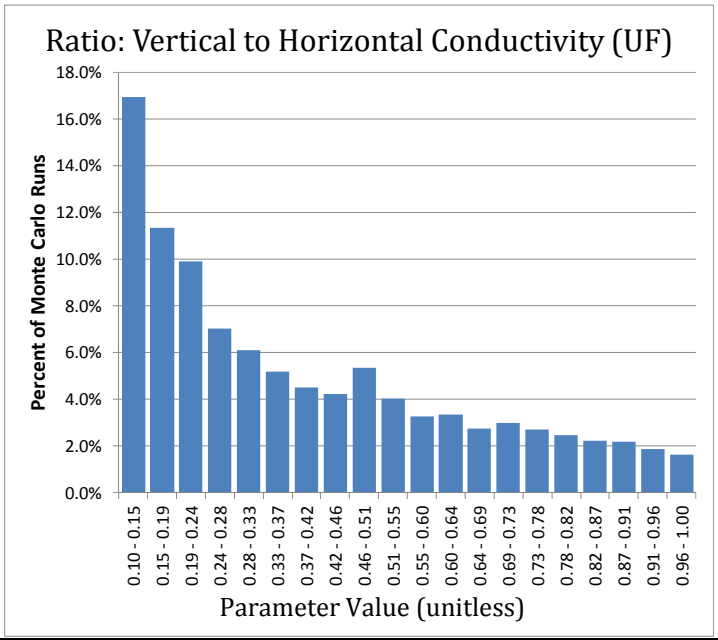

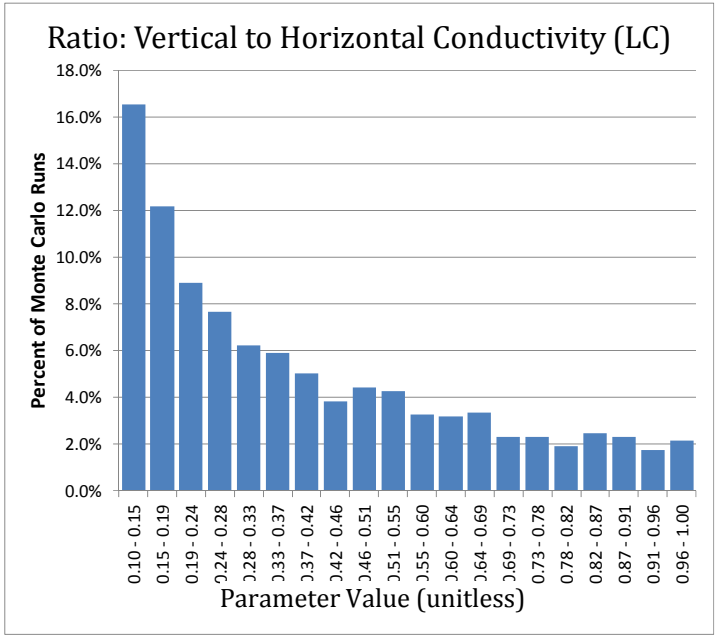

Notes:

Directional ratios for dispersivity and hydraulic conductivity were given log distributions over a range of reasonable values in the Monte Carlo scenarios. The computer selected random values within the ranges for each of the 2892 Monte Carlo selections. These plots show examples of the resulting distributions and indicate a clear log distribution as expected. The Monte Carlo simulation assumed that it was more likely that the values be on the lower end of these ranges and selected random values accordingly.

Similar plots could be provided for conductivity ratios for the other geologic units in the model; however, they are omitted for simplicity since they are quite similar to those presented.

EXAMPLES OF LOG DISTRIBUTION PARAMETERS FOR MONTE CARLO ANALYSIS

REGIONAL MODEL PRODUCTION SCENARIO REPORT

FIGURE 6.3

JUNE 2013

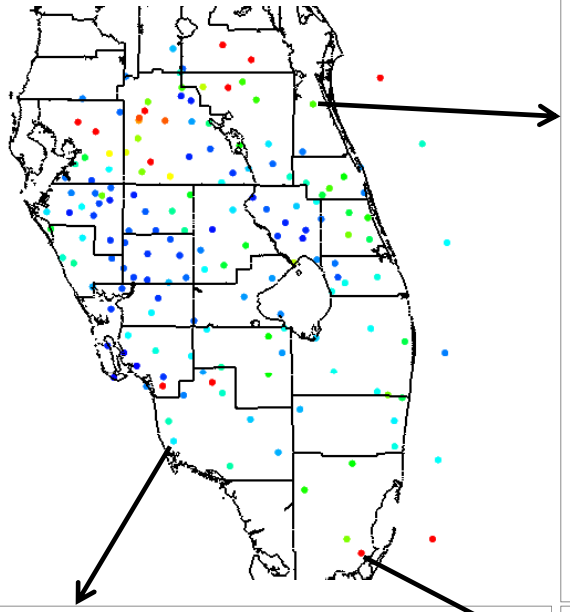

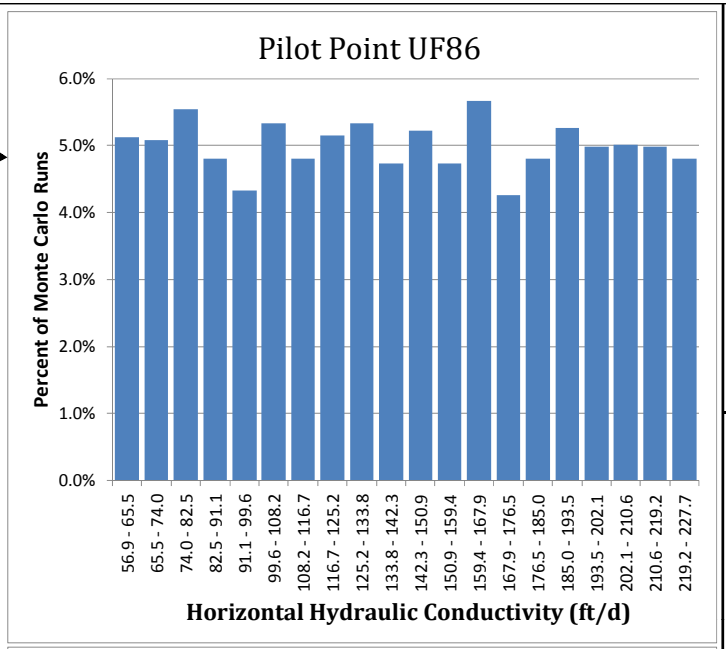

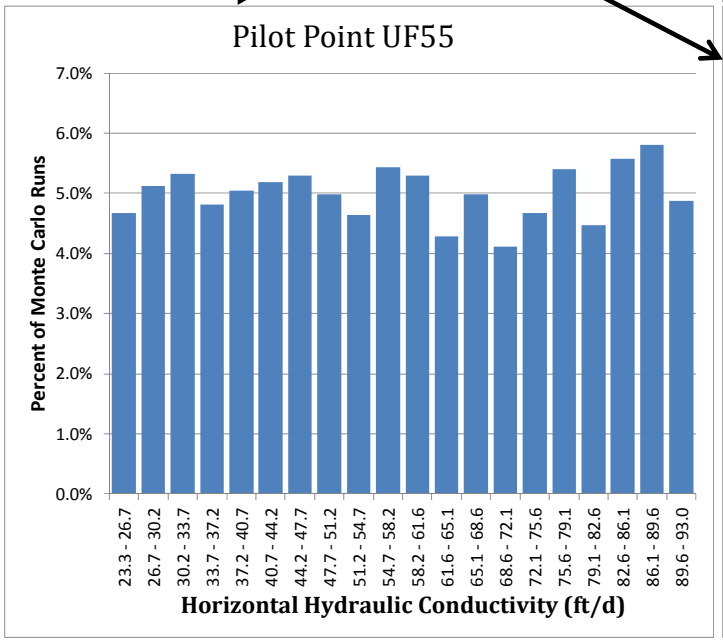

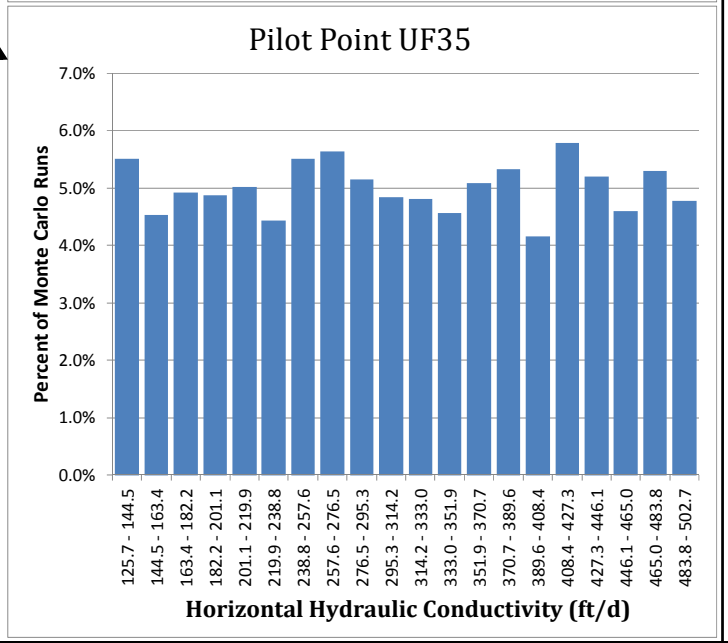

Horizontal Hydraulic Conductivity (ft/d)

- 1-20
- 20-40
- 40-60
- 60-80
- 80-100
- 100-120
- 120-140
- 140-160
- 160-180
- 180-200
- 200-500

Notes:

The map at upper left shows the pilot points used in the calibration model to set the horizontal hydraulic conductivity for the UF. Points are colored according to the calibrated hydraulic conductivity value.

During the Monte Carlo analysis, each pilot point was allowed to vary uniformly from half the calibrated value to twice the calibrated value. During each scenario, the computer randomly selected a value within the acceptable range for each point and then performed the krigging interpolation as shown on the following figure (6.5).

Plots like these could be presented for each pilot point in this layer and for those points in all other layers.

MONTE CARLO RANDOMIZATION OF HYDRAULIC CONDUCTIVITY - A

REGIONAL MODEL PRODUCTION SCENARIO REPORT

FIGURE 6.4

JUNE 2013

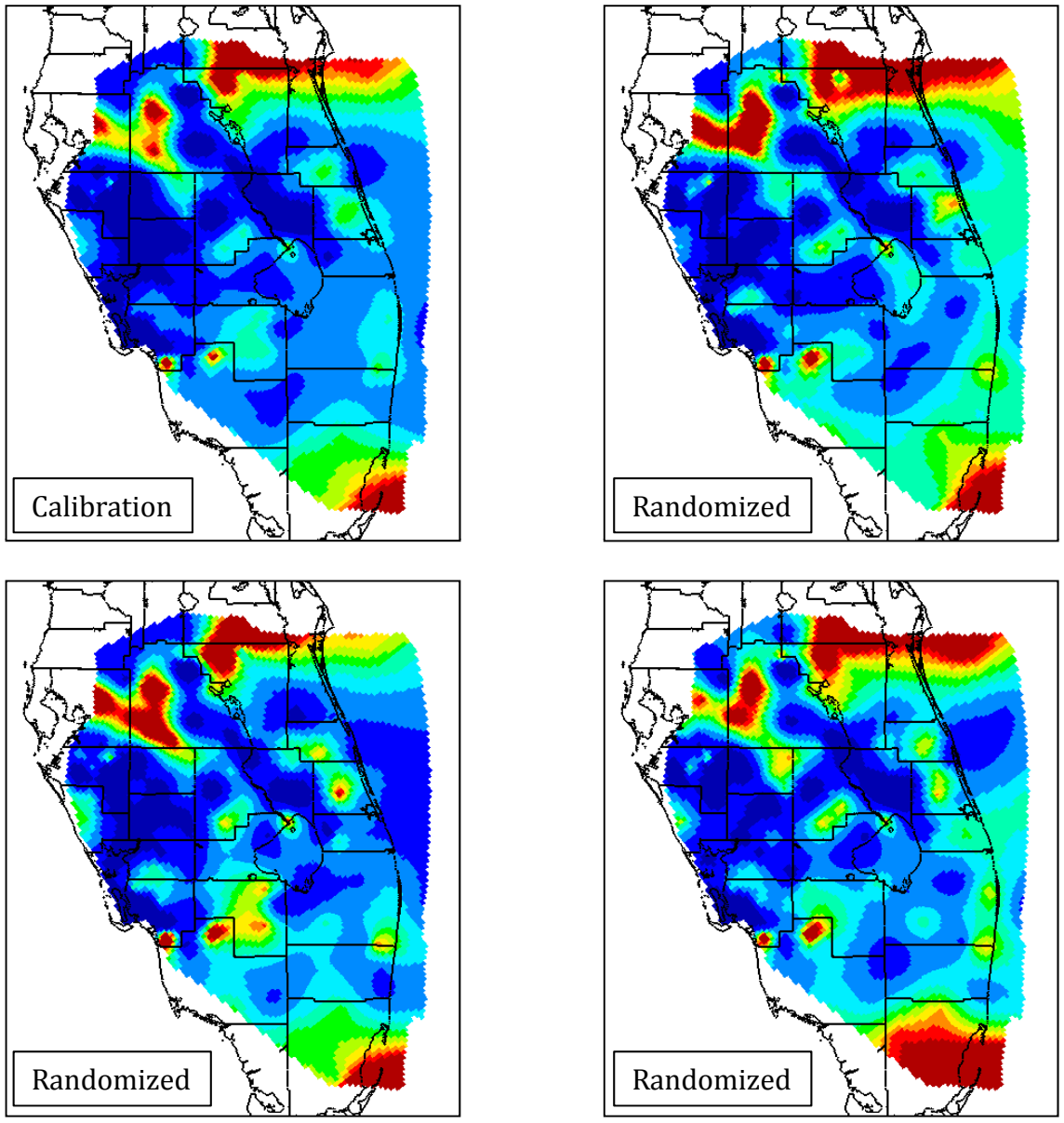

Horizontal Hydraulic Conductivity (ft/d)

- 1-20
- 20-40
- 40-60
- 60-80
- 80-100
- 100-120
- 120-140
- 140-160
- 160-180
- 180-200
- 200-500

Notes:

Once the randomized values had been assigned to each pilot point (see the previous figure, 6.4), the kriging was performed to yield a conductivity field for each Monte Carlo iteration.

The horizontal hydraulic conductivity distribution used in the calibrated model is shown here (top left) with three of the randomized distributions used in the Monte Carlo simulation.

Notice that general trends are unchanged and available data has been honored, but that each randomized distribution is slightly different.

Similar plots could be provided for other layers of the model or for other randomizations, but they are omitted for simplicity.

Monte Carlo Randomization of Hydraulic Conductivity - B

Regional Model Production Scenario Report

Figure 6.5

June 2013

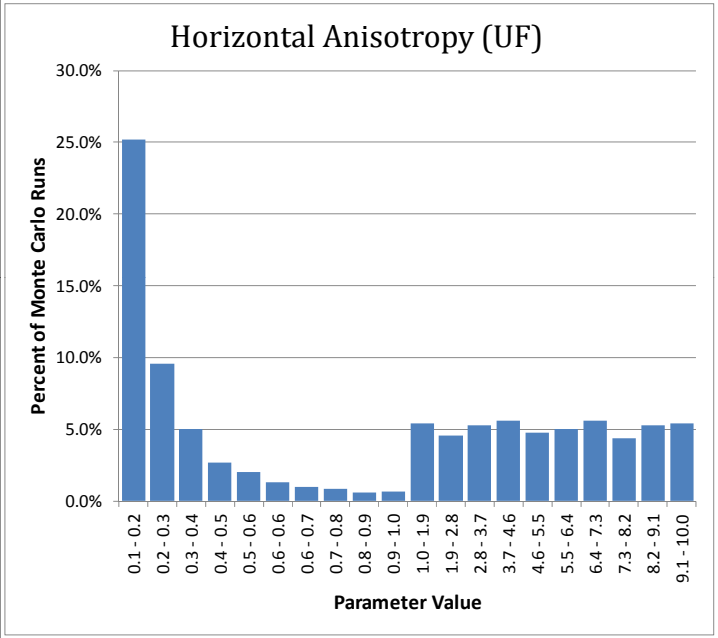

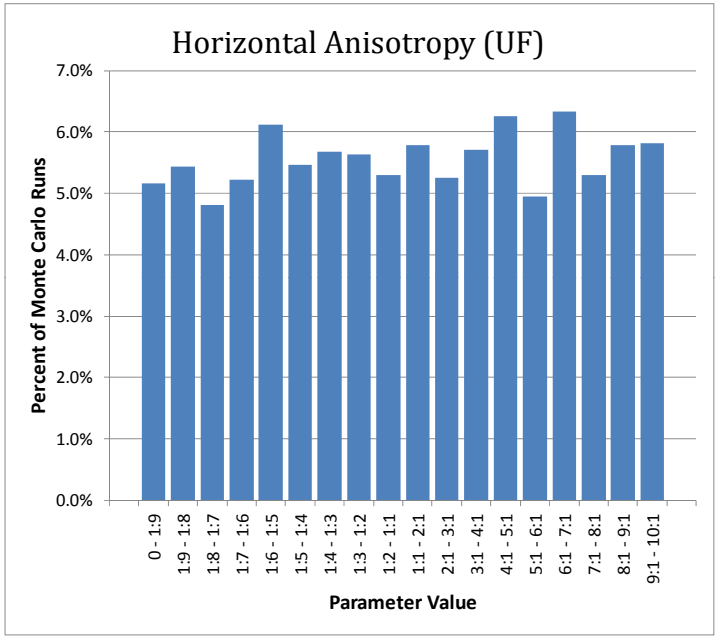

Notes:

These plots illustrate the results of an "inverted" uniform distribution used in the Monte Carlo analysis setup.

The details of the distribution development are given in Section 6.1.4.

These plots show the input distribution for the anisotropy of the UF aquifer. In SEAWAT, anisotropy is input as a decimal ratio of the hydraulic conductivity along the grid columns to that along the grid rows.

In the plot at left, the first 10 bins have sizes of 0.1, while the last 10 bins have sizes of 0.9. The left half of the plot seems to indicate a log distribution on anisotropy values which favor flow along the grid rows. The right half of the plot seems to indicate a uniform distribution on anisotropy values which favor flow along the grid columns.

When the bins are resized as ratios to unity, the entire range is uniformly distributed. It is just as likely, then, that the anisotropy will favor flow along the rows with a ratio of 1:5 as that it will favor flow along the columns with a ratio of 5:1.

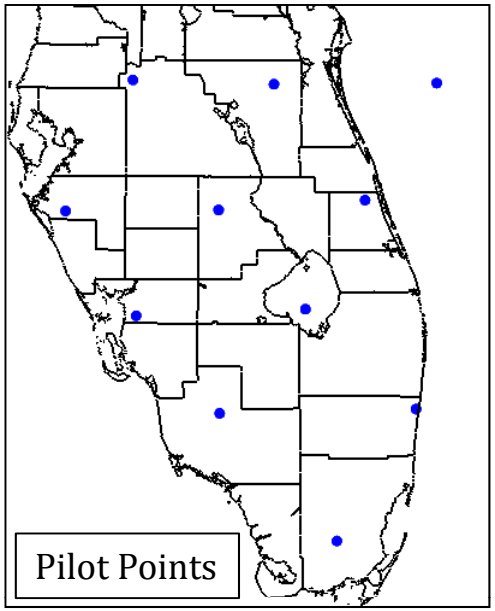

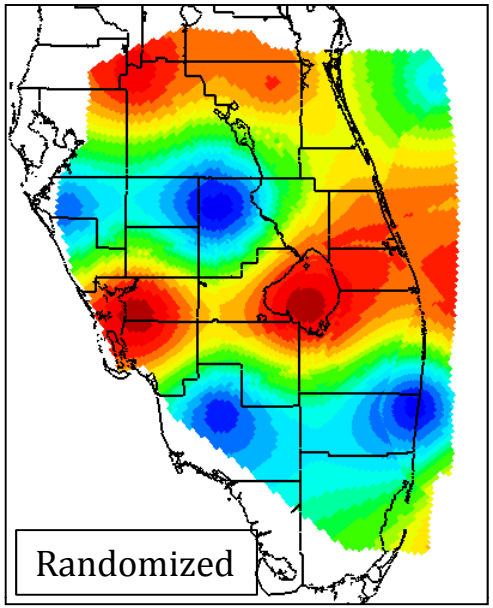

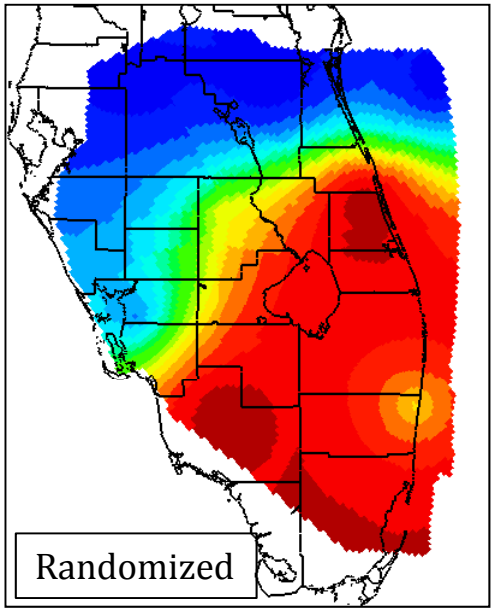

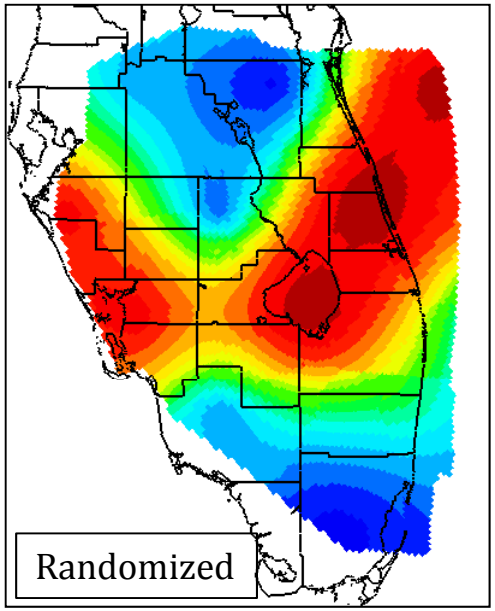

Horizontal Anisotropy

Ratio of

K_H along columns: K_H along rows

- 1:10 – 2:10
- 2:10 – 3:10
- 3:10 – 4:10
- 4:10 – 5:10
- 5:10 – 6:10
- 6:10 – 7:10
- 7:10 – 8:10
- 8:10 – 9:10
- 9:10 – 10:9
- 10:9 – 10:8
- 10:8 – 10:7
- 10:7 – 10:6
- 10:6 – 10:5
- 10:5 – 10:4
- 10:4 – 10:3
- 10:3 – 10:2
- 10:2 – 10:1

Preferential Flow Direction

Preferential Flow Direction

Notes:

Horizontal anisotropy was varied by applying an inverted uniform distribution to anisotropy values assigned to pilot points (see top left image).

Values were then kriged to cover the area and apply various anisotropy values.

These images show three examples of the randomized anisotropy applied to the UF.

MONTE CARLO RANDOMIZATIONS OF HORIZONTAL ANISOTROPY

REGIONAL MODEL PRODUCTION SCENARIO REPORT

FIGURE 6.7

JUNE 2013

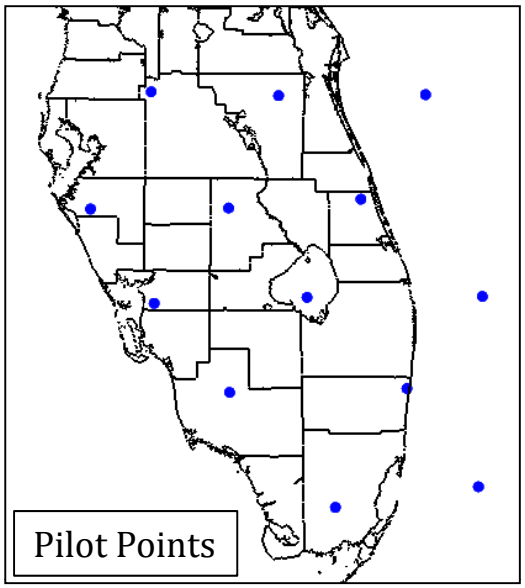

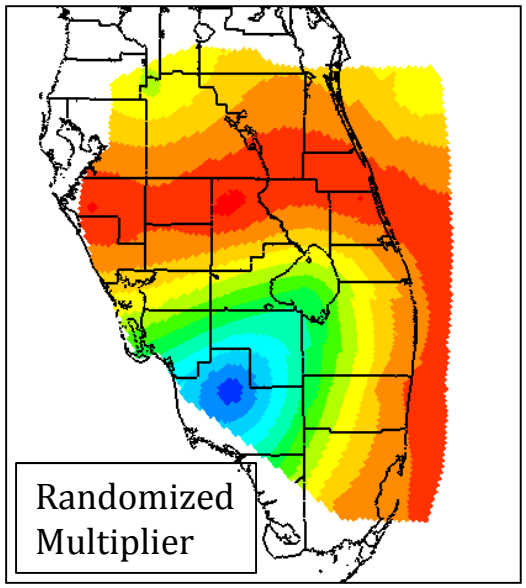

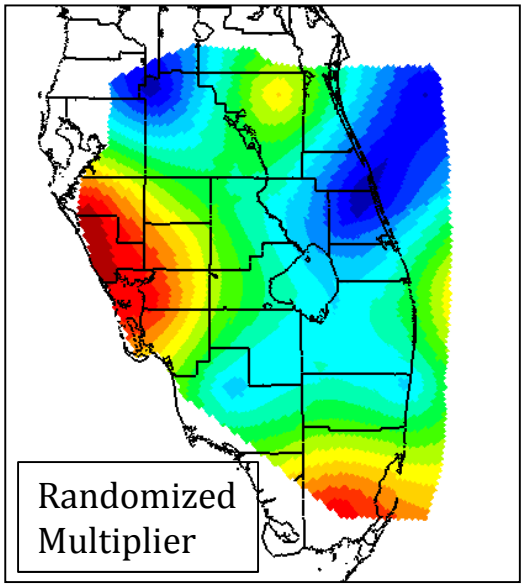

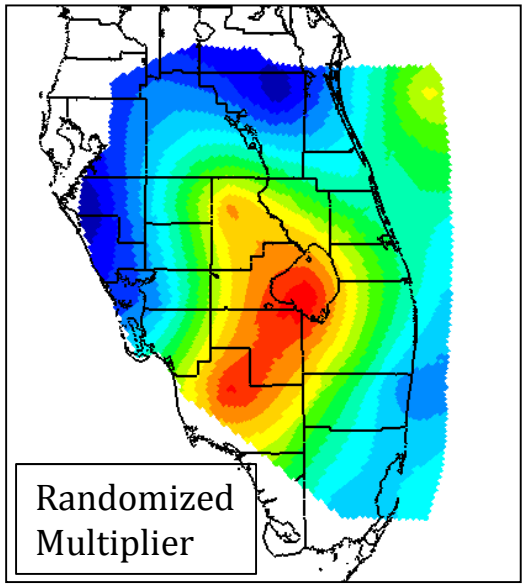

Multiplier

- 0.8 – 0.825
- 0.825 – 0.85
- 0.85 – 0875
- 0.875 – 0.9
- 0.9 – 0.925
- 0.925 – 0.95
- 0.95 – 0.975
- 0.975 – 1.0
- 1.0 – 1.025
- 1.025 – 1.05
- 1.05 – 1.075
- 1.075 – 1.1
- 1.1 – 1.125
- 1.125 – 1.15
- 1.15 – 1.175
- 1.175 – 1.2

Notes:

Starting conditions for TDS and temperature were set in a two-step process. A multiplier between 0.8 and 1.2 with a uniform distribution was assigned to each of a set of pilot points (shown at upper left).

The multipliers were interpolated to the cells of the grid using kriging. Three examples of the multiplier field are shown here.

The following figure (6.9) shows the resulting starting TDS fields for the APPZ.

MONTE CARLO RANDOMIZATIONS OF TDS STARTING CONDITION (STEP 1)

REGIONAL MODEL PRODUCTION SCENARIO REPORT

FIGURE 6.8

JUNE 2013

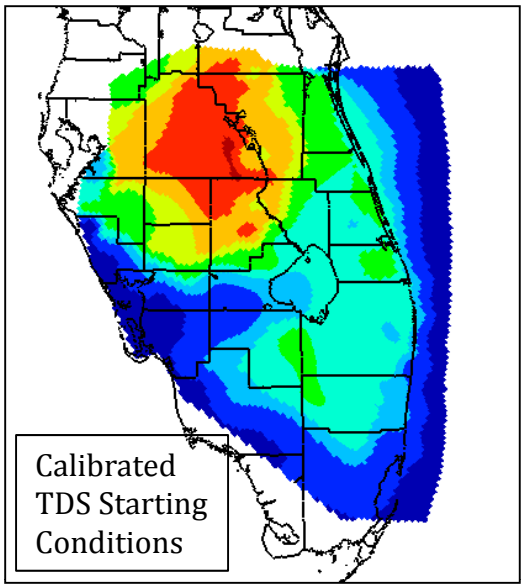

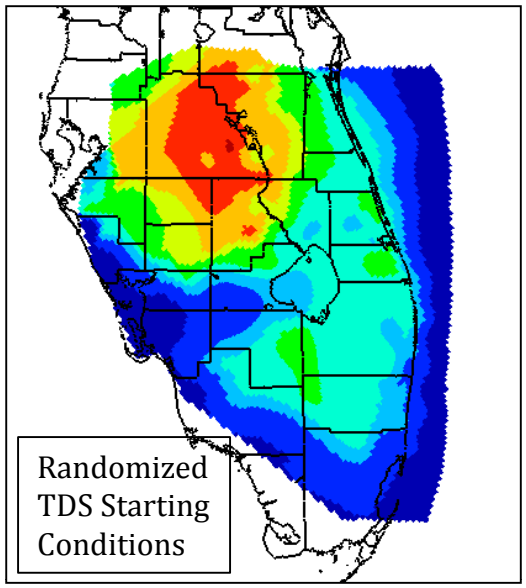

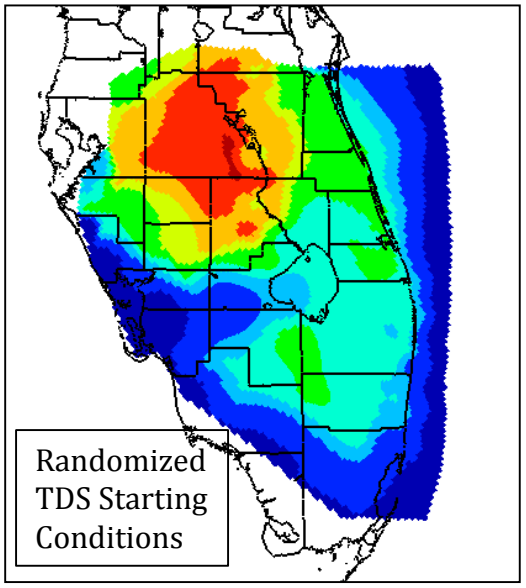

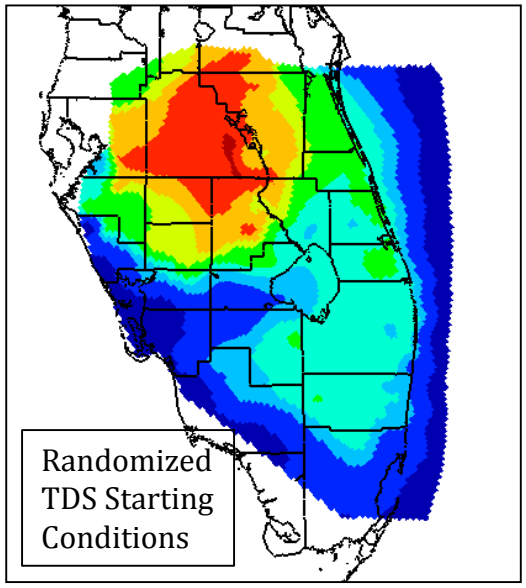

TDS (mg/L)

- <100
- 100 – 250
- 250 – 500
- 500 – 1000
- 1000 – 2500
- 2500 – 5000
- 5000 – 10000
- 10000 – 25000
- 25000 - 50000

Notes:

The starting conditions for TDS and temperature for the Monte Carlo analysis were set using a two-step method.

In the first step, shown on the previous figure (6.8), each cell in the model was assigned a multiplier between 0.8 and 1.2.

In the second step, shown here, the multiplier was applied to the calibrated TDS starting conditions to slightly change the condition.

Here, three randomizations of the starting conditions are compared to the calibrated condition (top left) for the APPZ.

A similar process was followed for the temperature starting conditions.

Note that only subtle changes have been introduced, allowing each Monte Carlo randomization to honor the available data.

MONTE CARLO RANDOMIZATION OF TDS STARTING CONDITIONS (STEP 2)

REGIONAL MODEL PRODUCTION SCENARIO REPORT

FIGURE 6.9

JUNE 2013

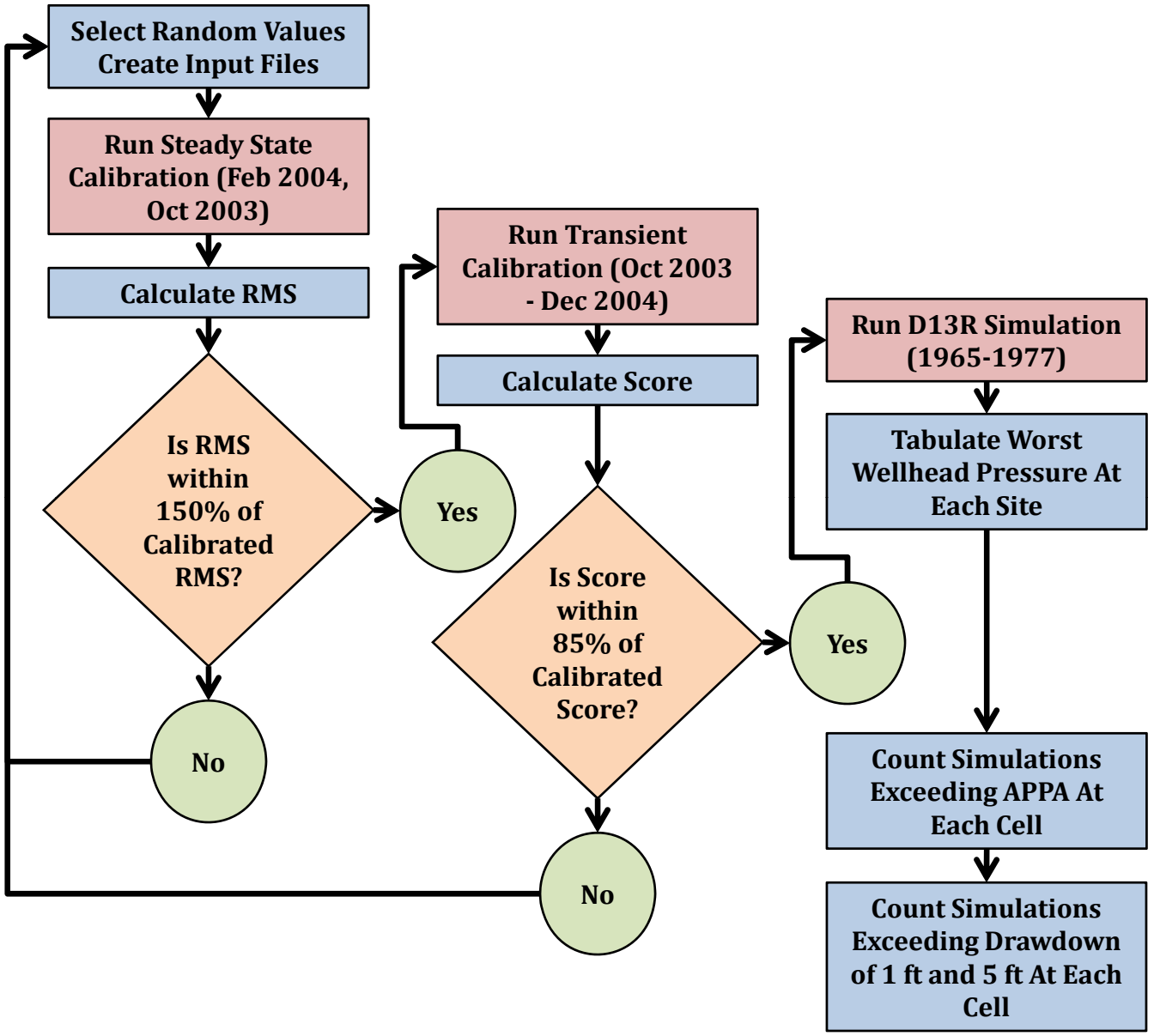

Notes:

This flow chart shows the process that was followed for each of the Monte Carlo simulations.

2836 sets of randomized parameters were developed and run through the steady state calibration models.

Of those, 1553 sets of randomized parameters met the steady state calibration standard and were run through the transient calibration model.

Of those, 825 met the transient calibration standard and were run through the RASRSM-D13R simulation.

The results of the performance measure analyses on the D13R results were tabulated to analyze the uncertainty in the results.

MONTE CARLO ANALYSIS FLOW CHART

FIGURE 6.10

REGIONAL MODEL PRODUCTION SCENARIO REPORT

JUNE 2013

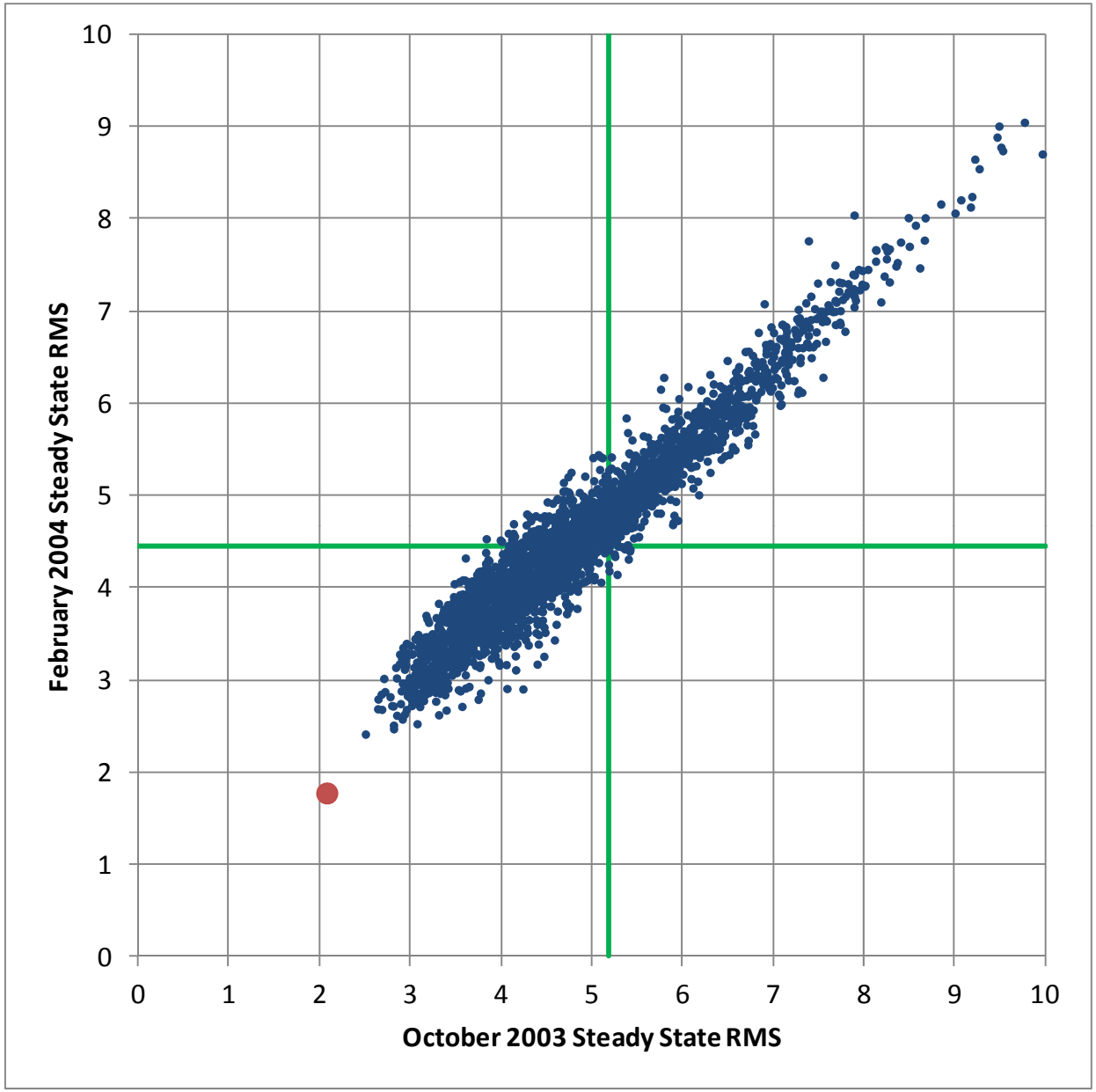

Legend

- Monte Carlo Randomized Scenario Results
- Calibrated Model Result
- RMS Requirements for Monte Carlo Simulation

Notes:

Each blue dot on this plot represents one randomized scenario tested for steady state calibration. In order to be selected for the next step, the dot must fall in the lower left quadrant, beyond the limits shown by the green lines.

The green lines represent a 150% change from the calibrated RMS values (indicated with the red dot).

STEADY STATE CALIBRATION TEST STATISTICS FOR MONTE CARLO ANALYSIS

REGIONAL MODEL PRODUCTION SCENARIO REPORT

FIGURE 6.11

JUNE 2013

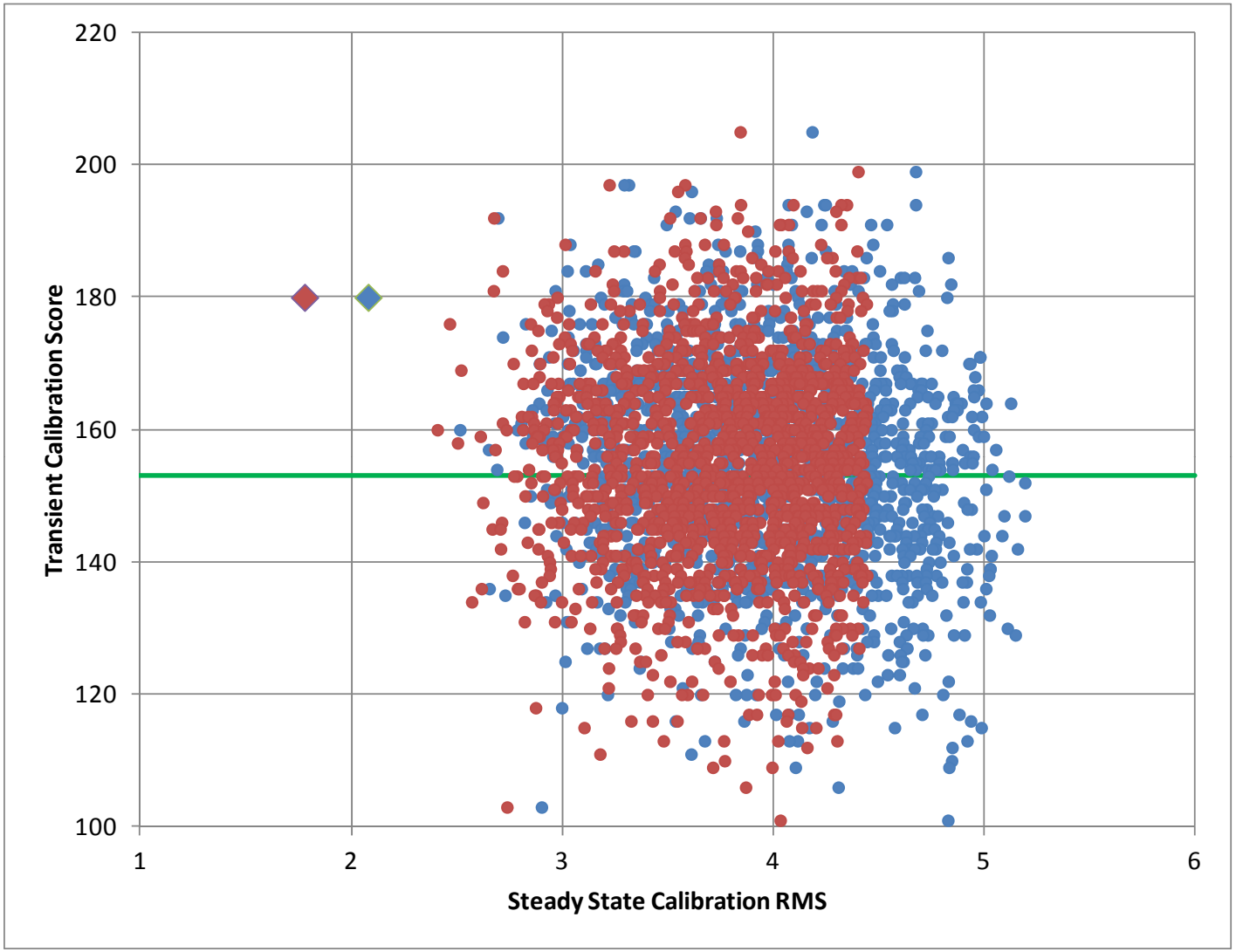

Legend

- Comparison of February Steady State RMS to Transient Calibration Score
- Comparison of October Steady State RMS to Transient Calibration Score
- Calibrated Model February Steady State RMS and Transient Calibration Score
- Calibrated Model October Steady State RMS and Transient Calibration Score

Notes:

This plot compares the steady state calibration RMS (for both October 2003 and February 2004) to the transient calibration score for all Monte Carlo randomizations that passed the steady state requirement (see Figure 6.11).

The green line indicates the transient calibration requirement. To be selected and continue to the D13R portion of the process, the transient calibration score must be above 153.

TRANSIENT CALIBRATION STATISTICS FOR MONTE CARLO ANALYSIS

REGIONAL MODEL PRODUCTION SCENARIO REPORT

FIGURE 6.12

JUNE 2013

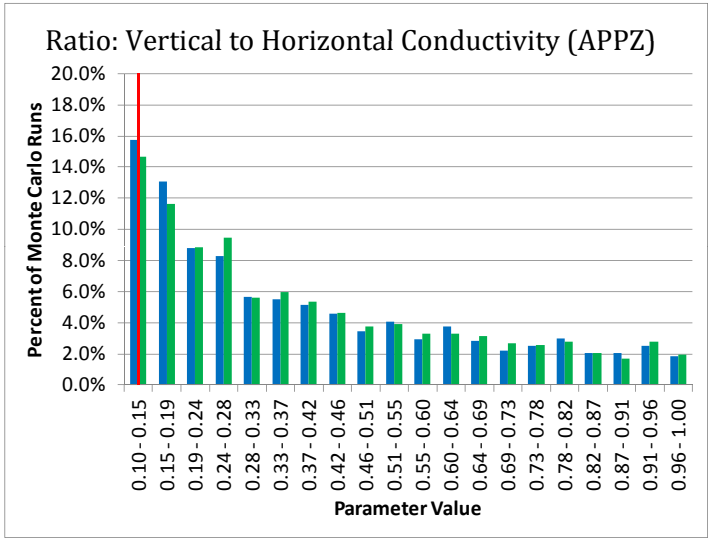

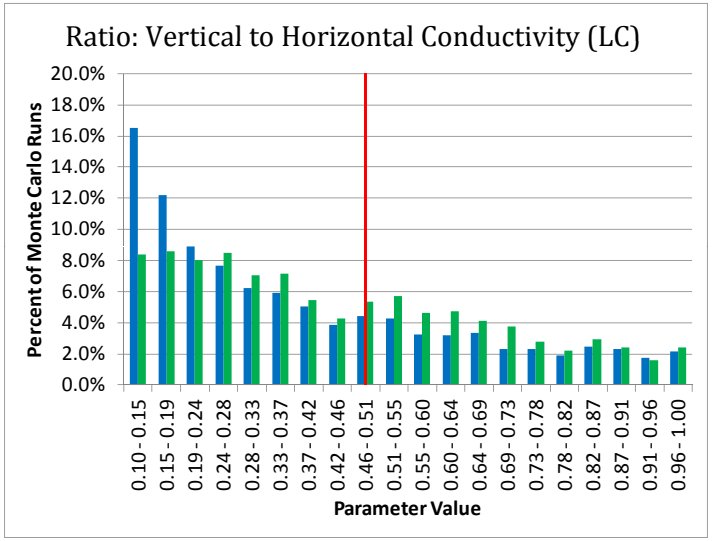

Legend

- Randomized Scenarios
- Acceptable Scenarios
- Calibrated Value

Notes:

Here the distributions of randomized values are compared to the distribution of parameter values in selected simulations, i.e., those that passed the steady state and transient calibration tests.

Also shown on each plot is the value used in the original calibration runs.

In the plot at left, the distribution of each set of parameters is very similar, with the most likely values falling near the calibration value.

In the plot at right, the calibration tests have eliminated some of the low parameter values which did not allow a good calibration. Since the input distribution was an error and did not match the calibrated value, this helped to improve the input parameter distributions

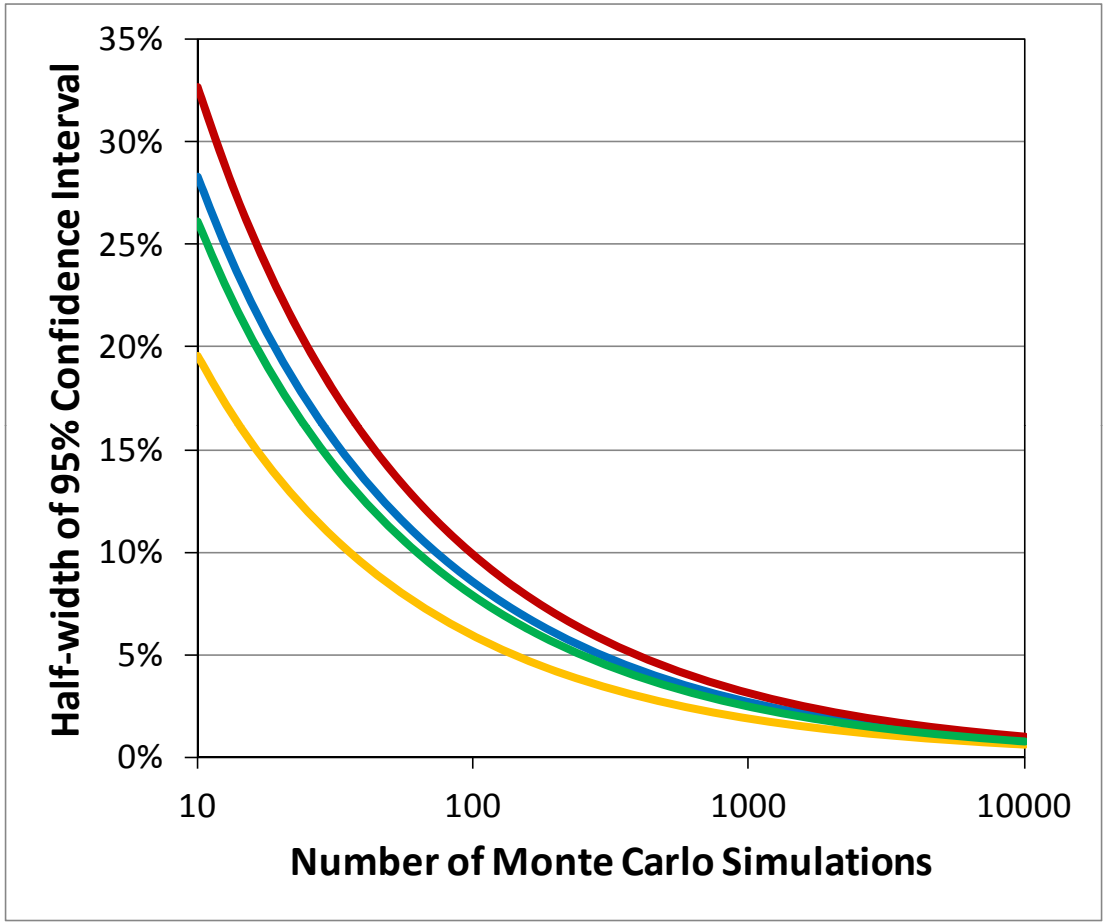

Legend

- 10% Pass Rate
- 25% Pass Rate
- 50% Pass Rate
- 80% Pass Rate

Notes:

Since the results of this Monte Carlo simulation are binary (either pass or fail), the half-width of the 95% confidence interval depends only on the percentage of Monte Carlo runs passing the requirement and the total number of simulations.

There were 825 simulations, so the largest 95% confidence interval half-width was 3.4%.

Note that the largest half-width occurs with 50% passing and the interval is smaller for both larger and smaller pass rates.

RELATIONSHIP BETWEEN NUMBER OF MONTE CARLO SIMULATIONS AND THE HALF-WIDTH OF THE 95% CONFIDENCE INTERVAL

REGIONAL MODEL PRODUCTION SCENARIO REPORT

FIGURE 6.14

JUNE 2013

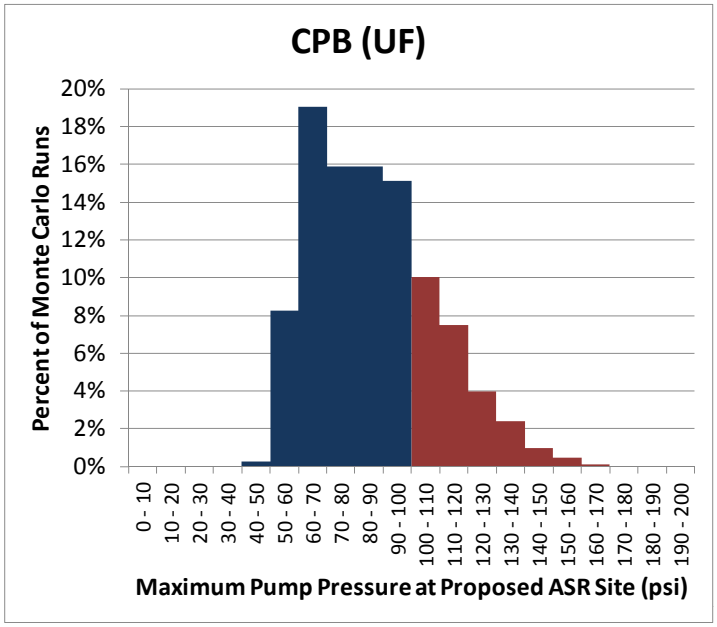

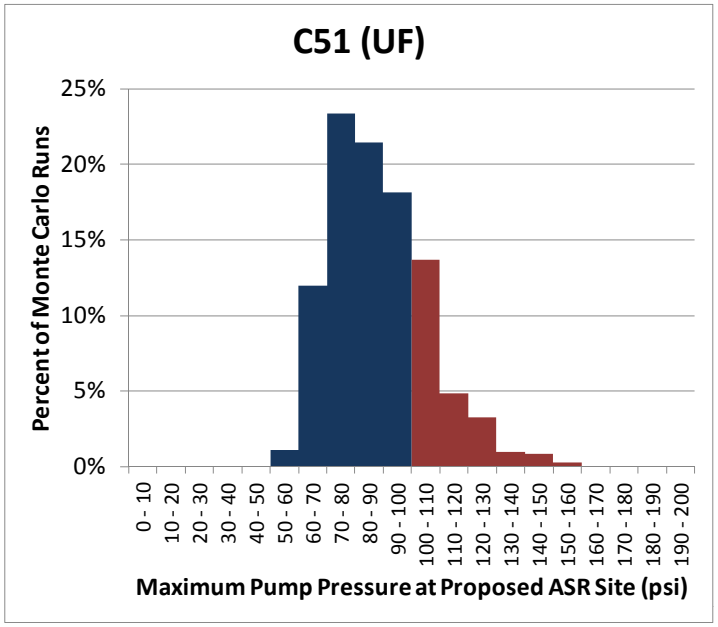

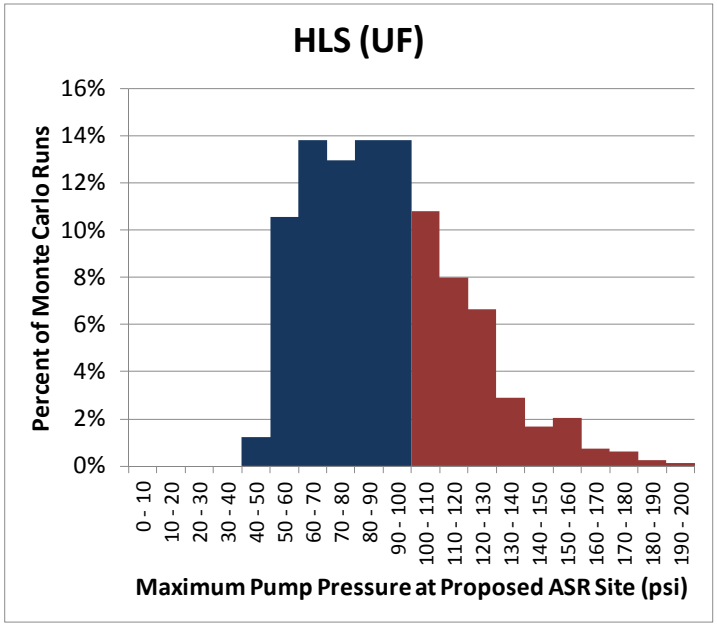

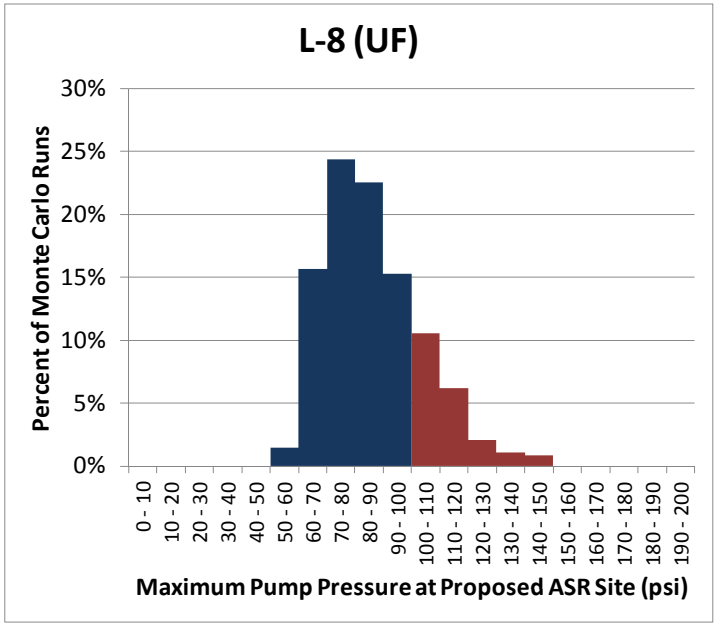

Legend

- Section of Histogram Meeting Pump Pressure Requirement
- Section of Histogram Not Meeting Pump Pressure Requirement

Notes:

These histograms show the distribution of Monte Carlo simulation results for maximum pump pressures at the sites designated. The performance measure required that the maximum pressure stay below 100 psi.

Key	Site
CPB	Central Palm Beach
C51	C-51 Canal
HLS	Hillsboro
L8	L-8 Canal

Monte Carlo Results – Pump Pressure Requirements

Regional Model Production Scenario Report

Figure 6.15

June 2013

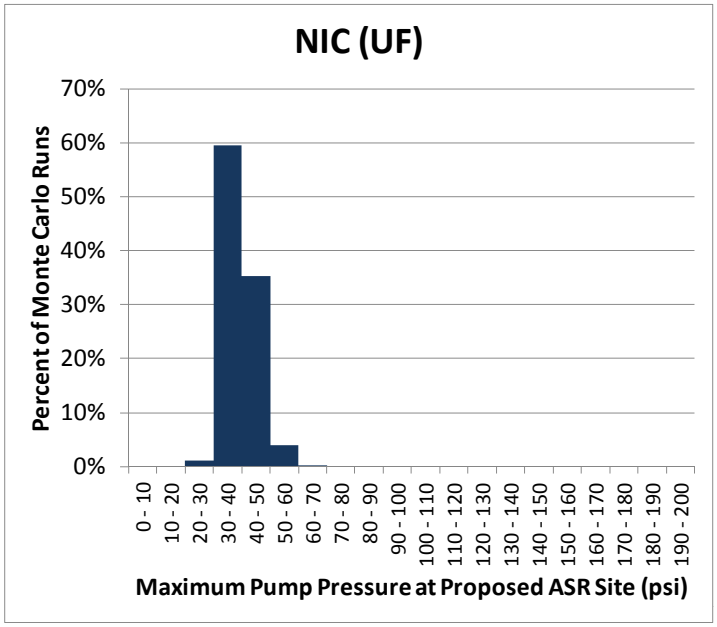

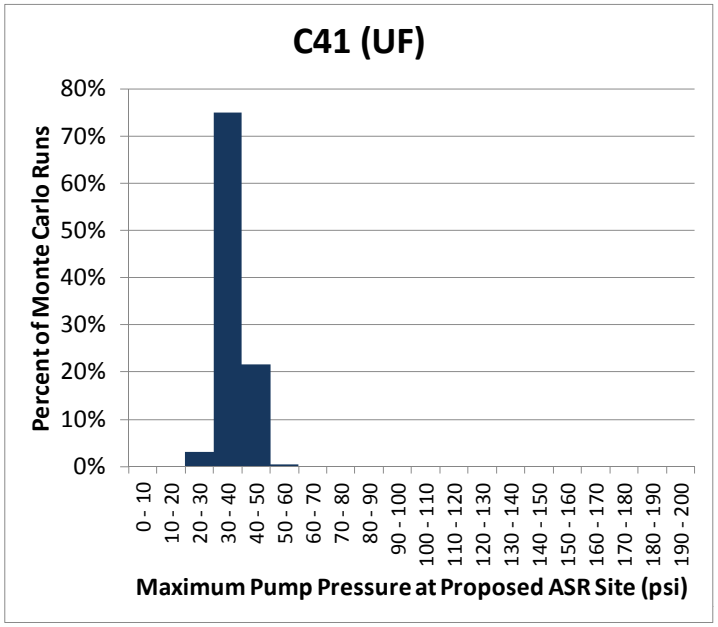

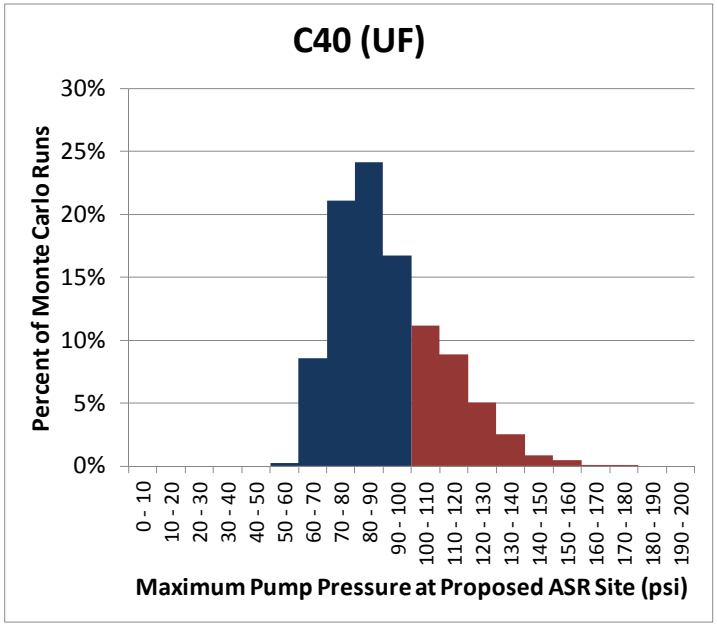

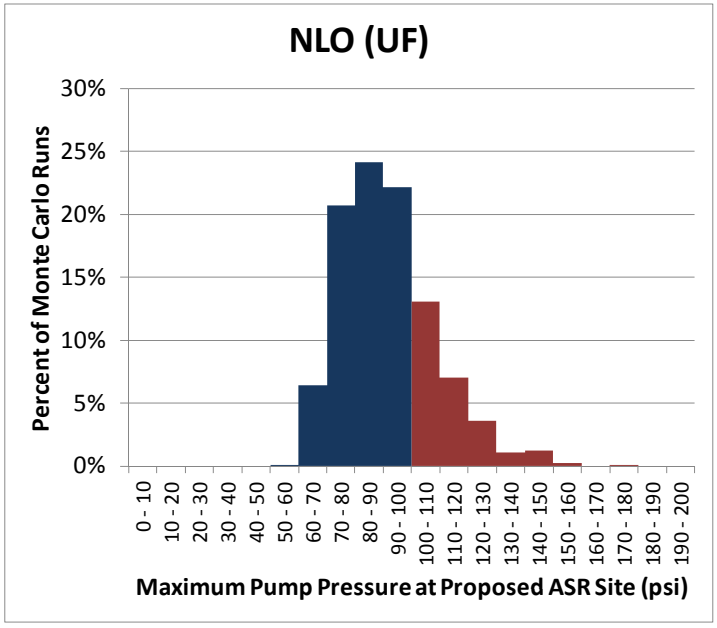

Legend

- Section of Histogram Meeting Pump Pressure Requirement
- Section of Histogram Not Meeting Pump Pressure Requirement

Notes:

These histograms show the distribution of Monte Carlo simulation results for maximum pump pressures at the sites designated. The performance measure required that the maximum pressure stay below 100 psi.

Key	Site
NIC	Nicodemus Slough
C41	C-41 Canal
C40	C-40 Canal
NLO	North Lake Okeechobee Reservoir

Monte Carlo Results – Pump Pressure Requirements

Regional Model Production Scenario Report

Figure 6.16

June 2013

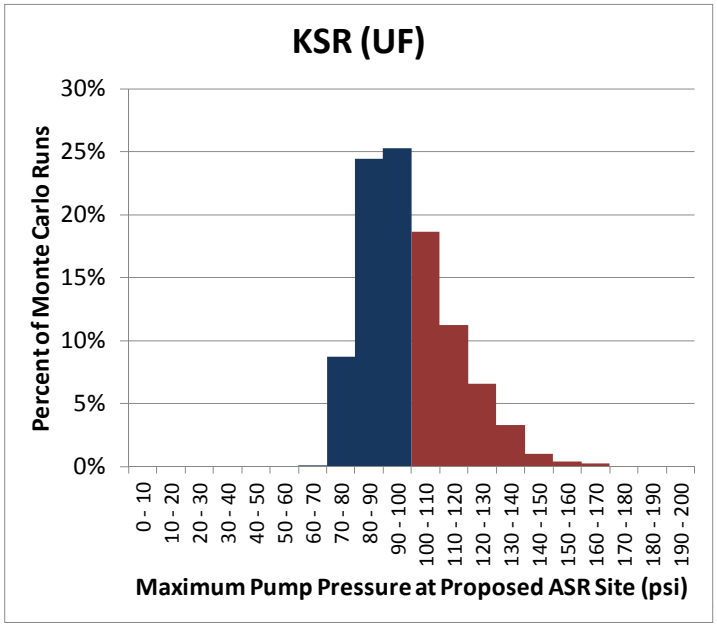

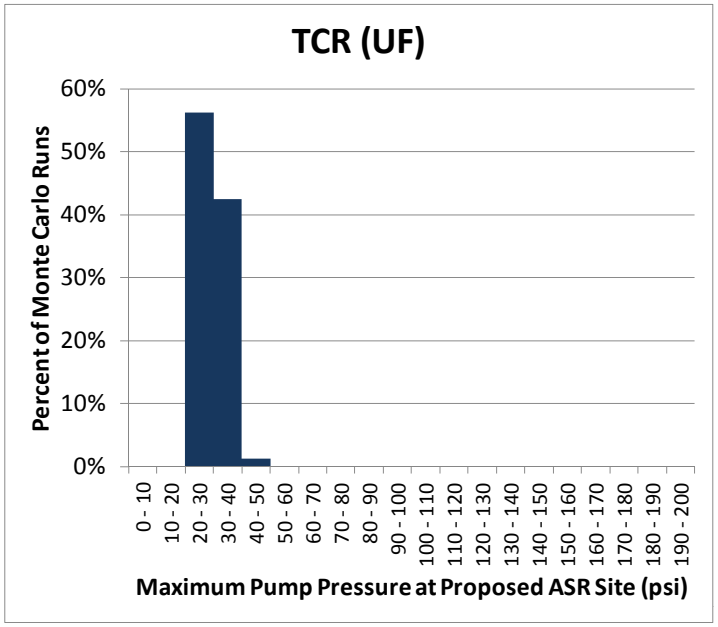

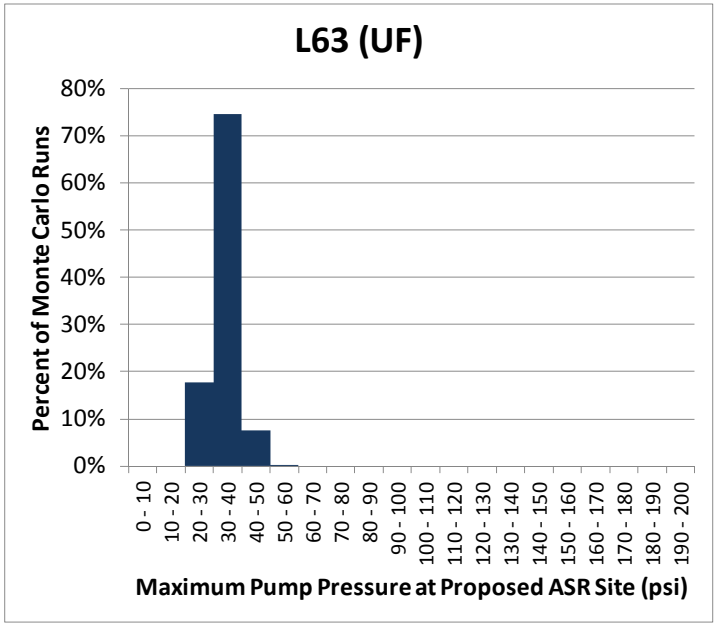

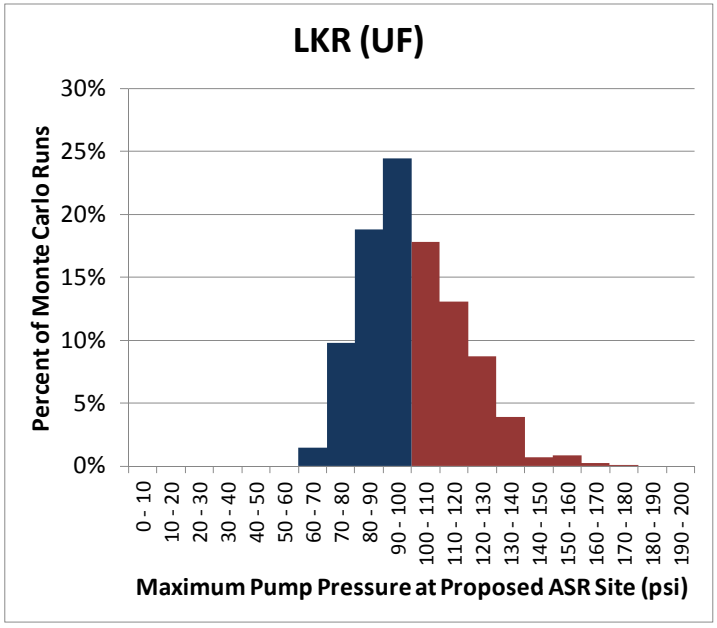

Legend

- Section of Histogram Meeting Pump Pressure Requirement
- Section of Histogram Not Meeting Pump Pressure Requirement

Notes:

These histograms show the distribution of Monte Carlo simulation results for maximum pump pressures at the sites designated. The performance measure required that the maximum pressure stay below 100 psi.

Key	Site
KSR	Kissimmee River / Paradise Run
TCR	Taylor Creek Reservoir
L63	L-63N Canal
LKR	Lakeside Ranch

MONTE CARLO RESULTS – PUMP PRESSURE REQUIREMENTS

REGIONAL MODEL PRODUCTION SCENARIO REPORT

FIGURE 6.17

JUNE 2013

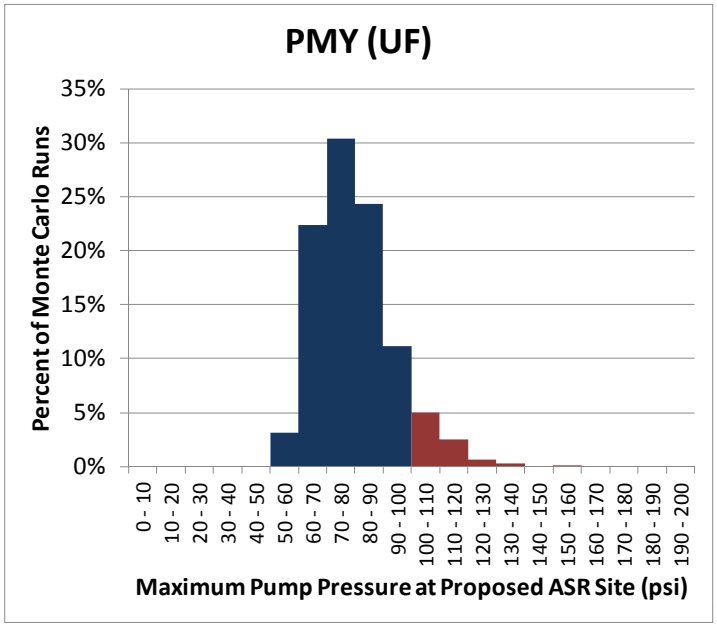

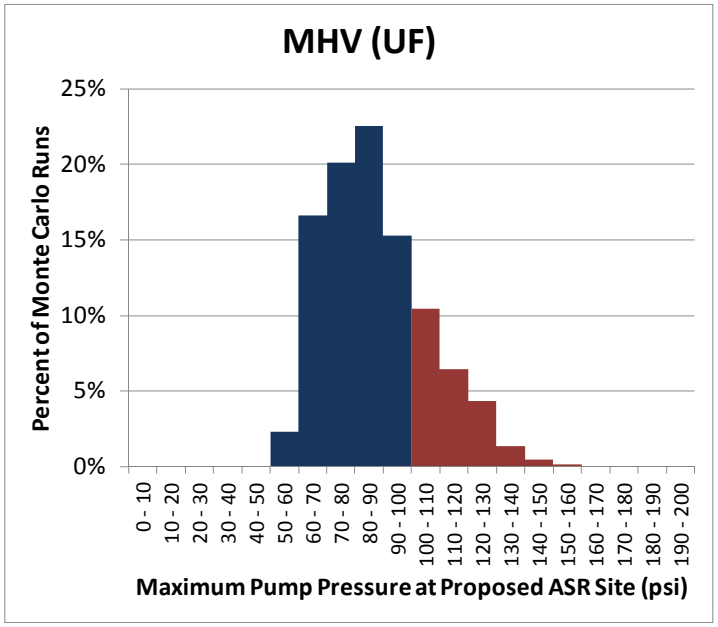

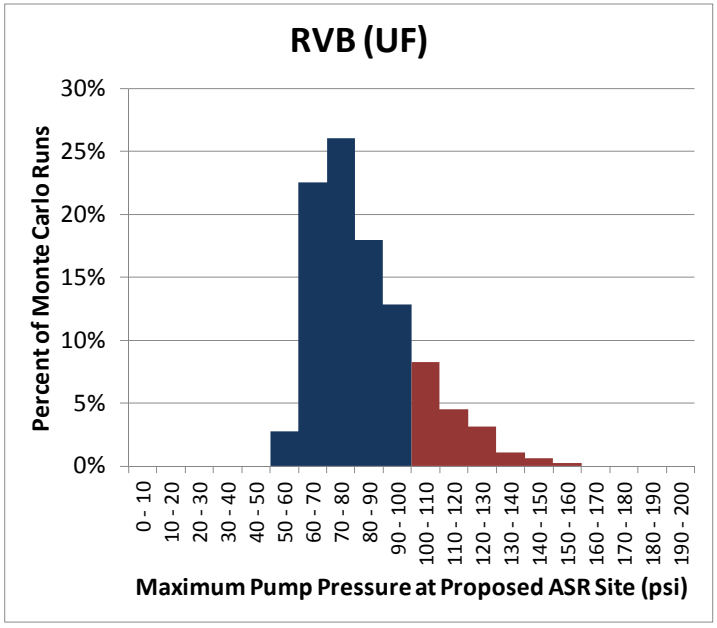

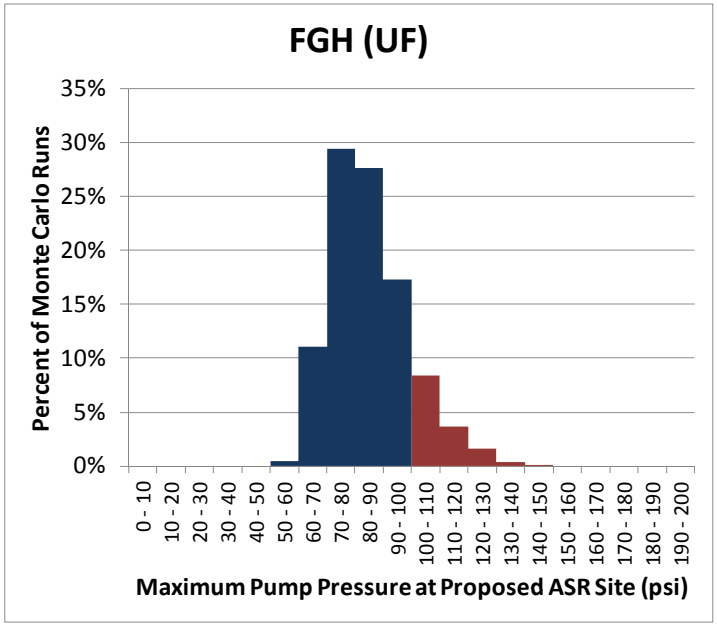

Legend

- Section of Histogram Meeting Pump Pressure Requirement
- Section of Histogram Not Meeting Pump Pressure Requirement

Notes:

These histograms show the distribution of Monte Carlo simulation results for maximum pump pressures at the sites designated. The performance measure required that the maximum pressure stay below 100 psi.

Key	Site
PMY	Port Mayaca
MHV	Moorehaven
RVB	Riverbend
FGH	Flaghole

MONTE CARLO RESULTS – PUMP PRESSURE REQUIREMENTS

REGIONAL MODEL PRODUCTION SCENARIO REPORT

FIGURE 6.18

JUNE 2013

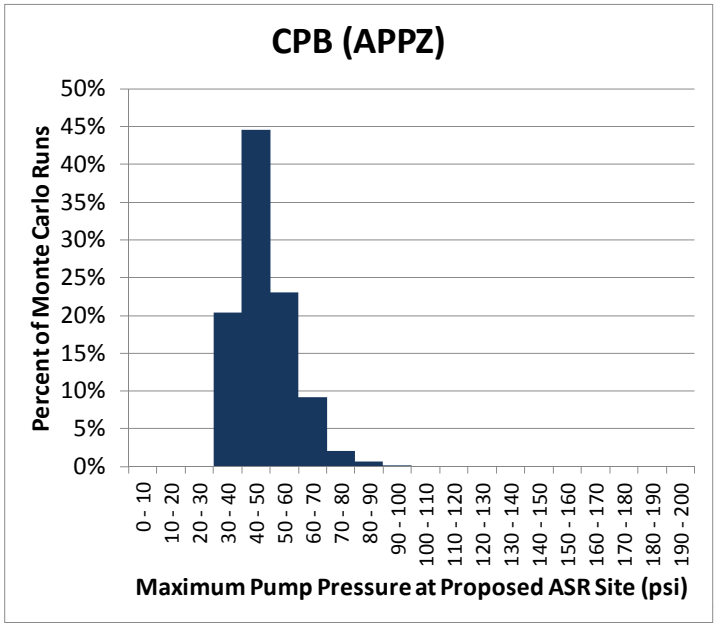

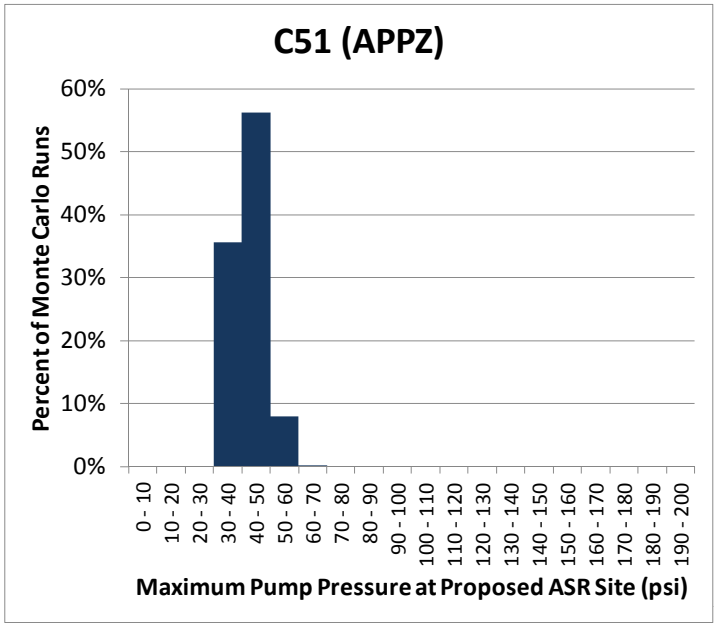

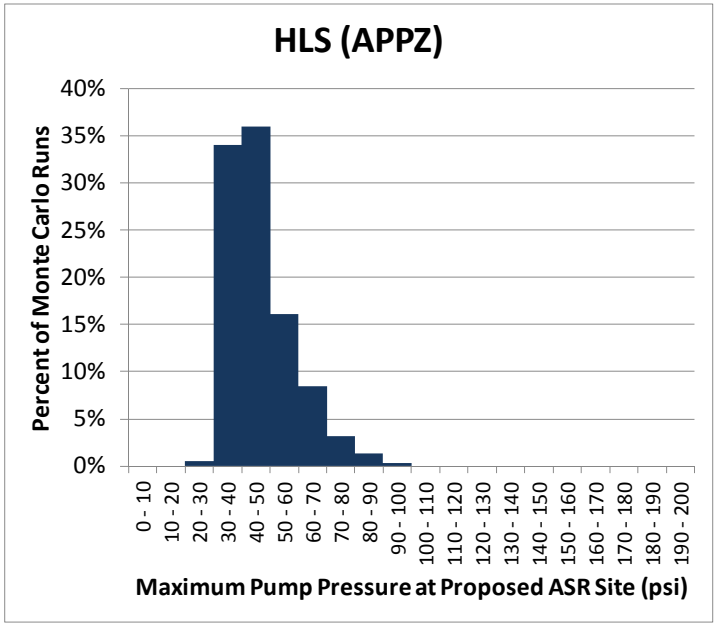

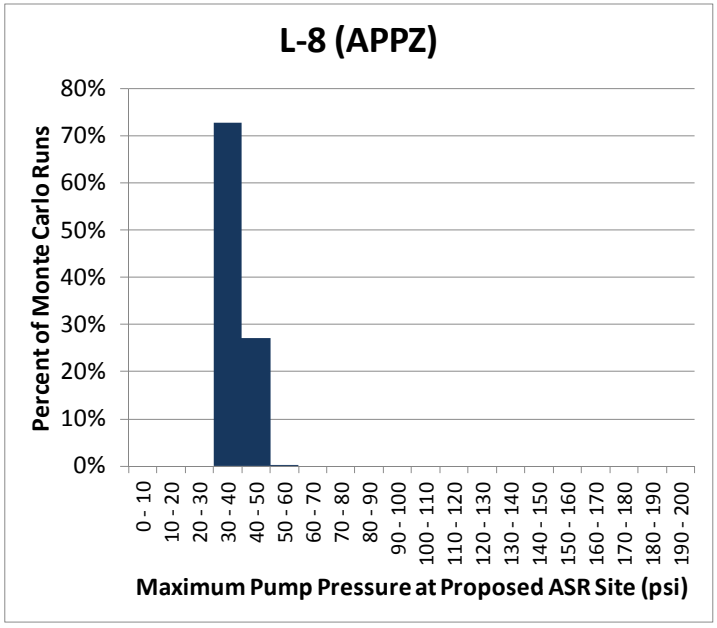

Legend

- Section of Histogram Meeting Pump Pressure Requirement
- Section of Histogram Not Meeting Pump Pressure Requirement

Notes:

These histograms show the distribution of Monte Carlo simulation results for maximum pump pressures at the sites designated. The performance measure required that the maximum pressure stay below 100 psi.

Key	Site
CPB	Central Palm Beach
C51	C-51 Canal
HLS	Hillsboro
L8	L-8 Canal

MONTE CARLO RESULTS – PUMP PRESSURE REQUIREMENTS

REGIONAL MODEL PRODUCTION SCENARIO REPORT

FIGURE 6.19

JUNE 2013

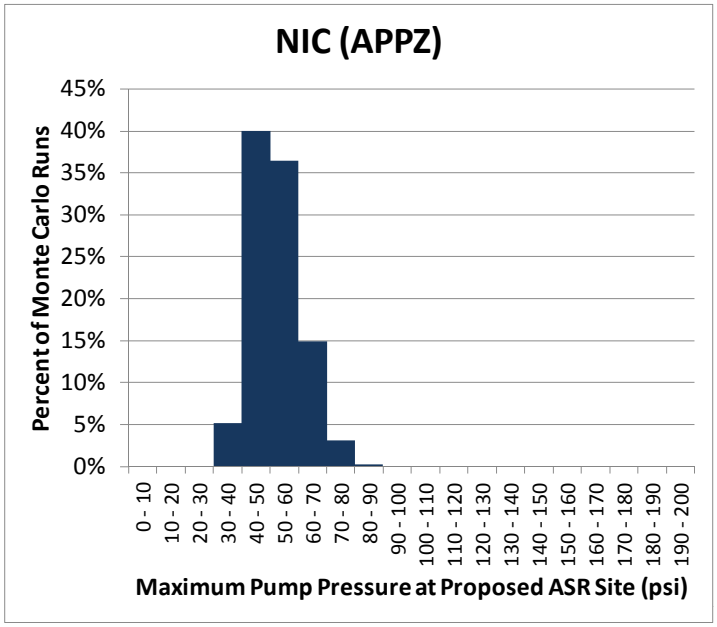

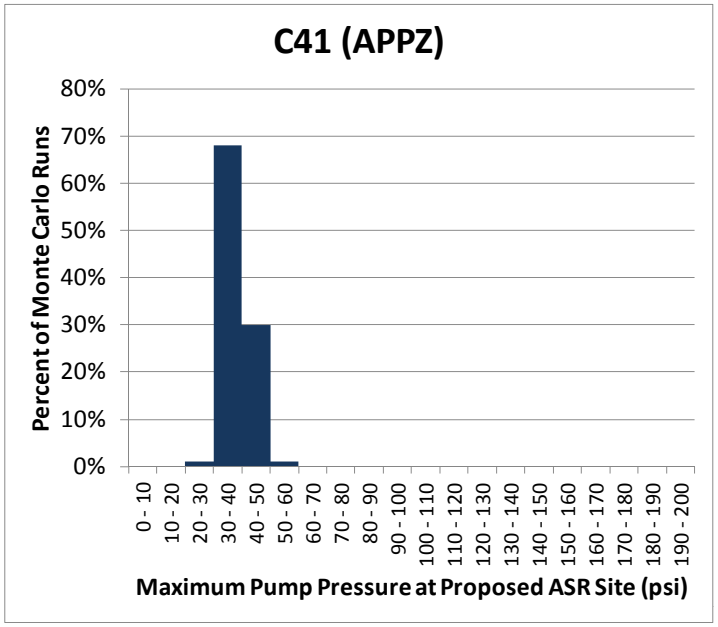

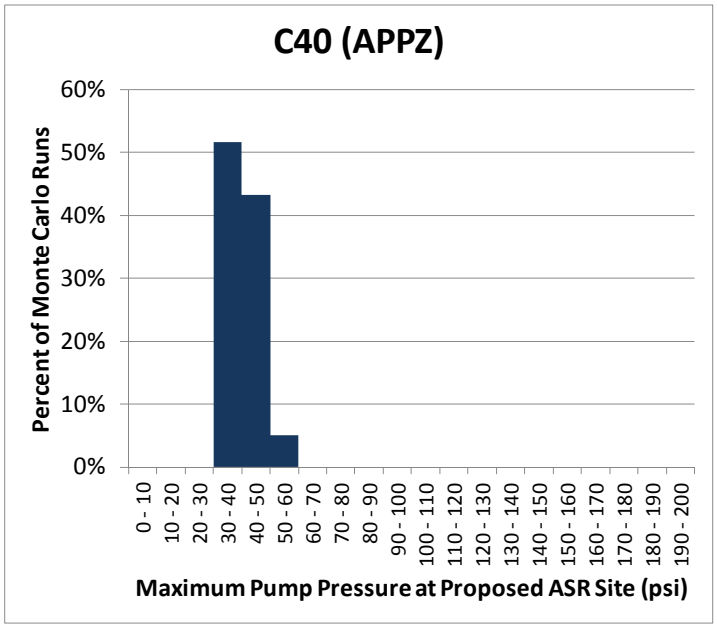

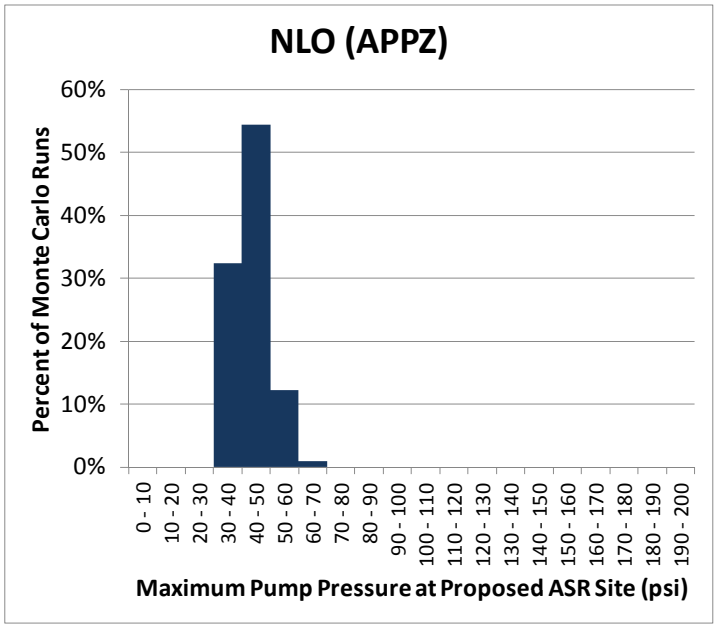

Legend

- Section of Histogram Meeting Pump Pressure Requirement
- Section of Histogram Not Meeting Pump Pressure Requirement

Notes:

These histograms show the distribution of Monte Carlo simulation results for maximum pump pressures at the sites designated. The performance measure required that the maximum pressure stay below 100 psi.

Key	Site
NIC	Nicodemus Slough
C41	C-41 Canal
C40	C-40 Canal
NLO	North Lake Okeechobee Reservoir

MONTE CARLO RESULTS – PUMP PRESSURE REQUIREMENTS

REGIONAL MODEL PRODUCTION SCENARIO REPORT

FIGURE 6.20

JUNE 2013

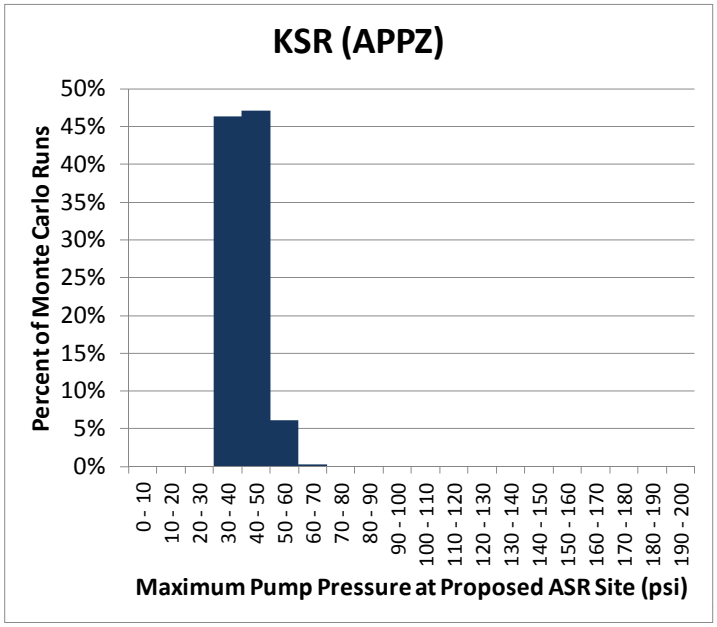

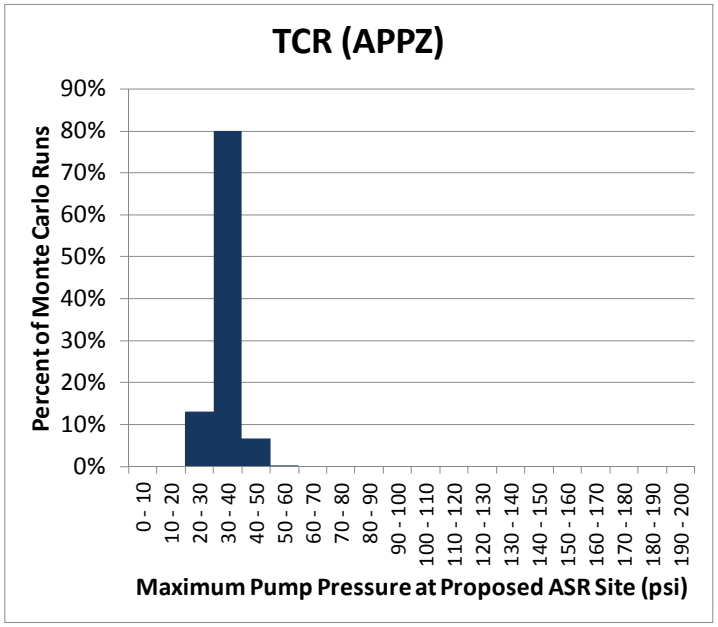

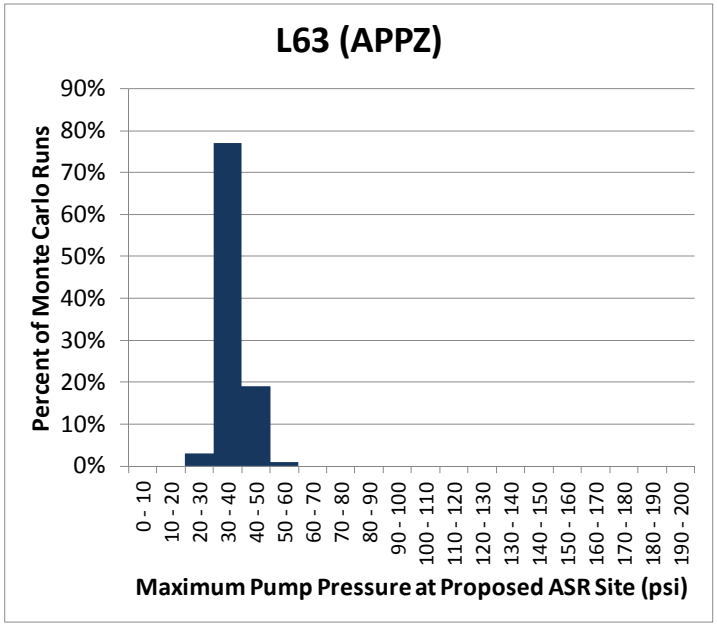

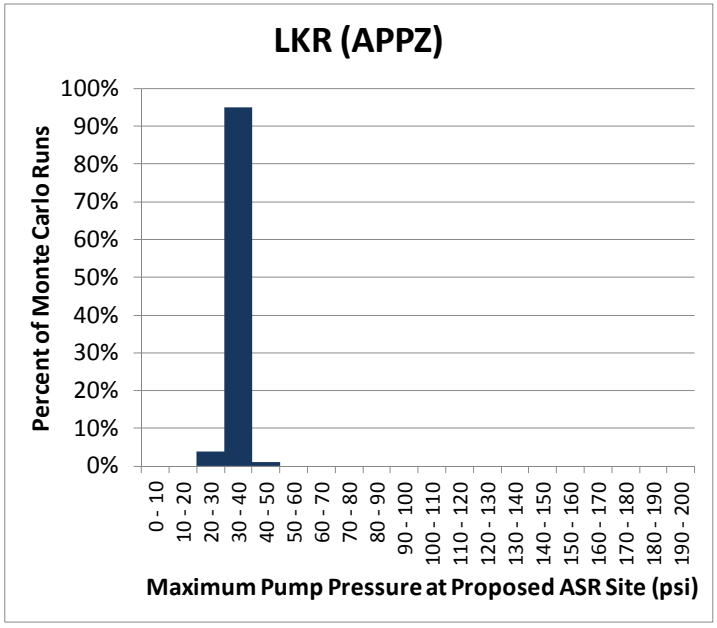

Legend

- Section of Histogram Meeting Pump Pressure Requirement
- Section of Histogram Not Meeting Pump Pressure Requirement

Notes:

These histograms show the distribution of Monte Carlo simulation results for maximum pump pressures at the sites designated. The performance measure required that the maximum pressure stay below 100 psi.

Key	Site
KSR	Kissimmee River / Paradise Run
TCR	Taylor Creek Reservoir
L63	L-63N Canal
LKR	Lakeside Ranch

MONTE CARLO RESULTS – PUMP PRESSURE REQUIREMENTS

REGIONAL MODEL PRODUCTION SCENARIO REPORT

FIGURE 6.21

JUNE 2013

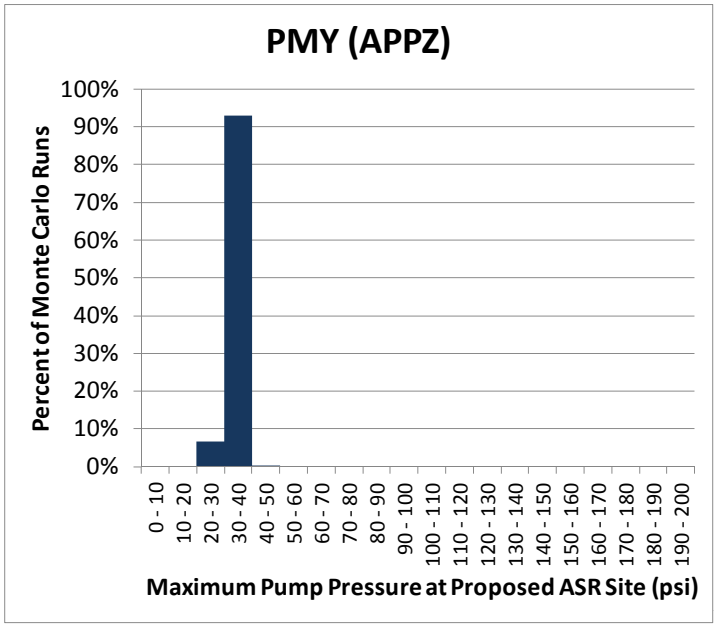

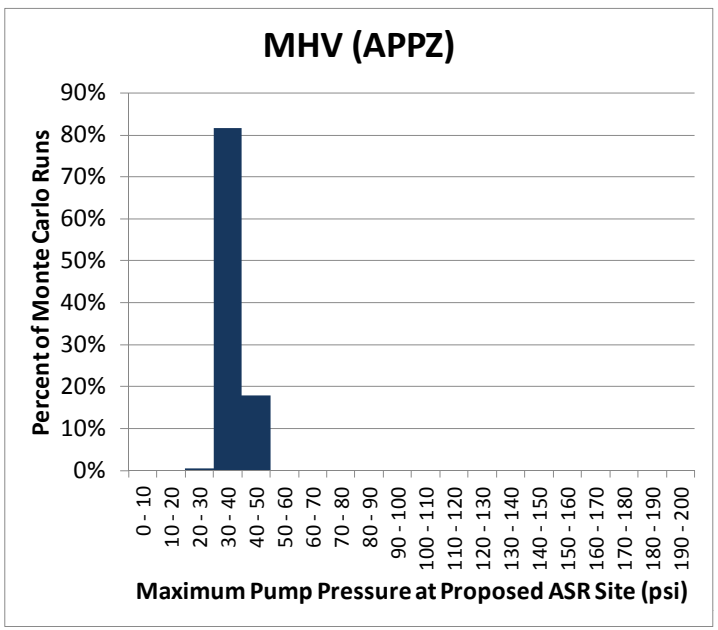

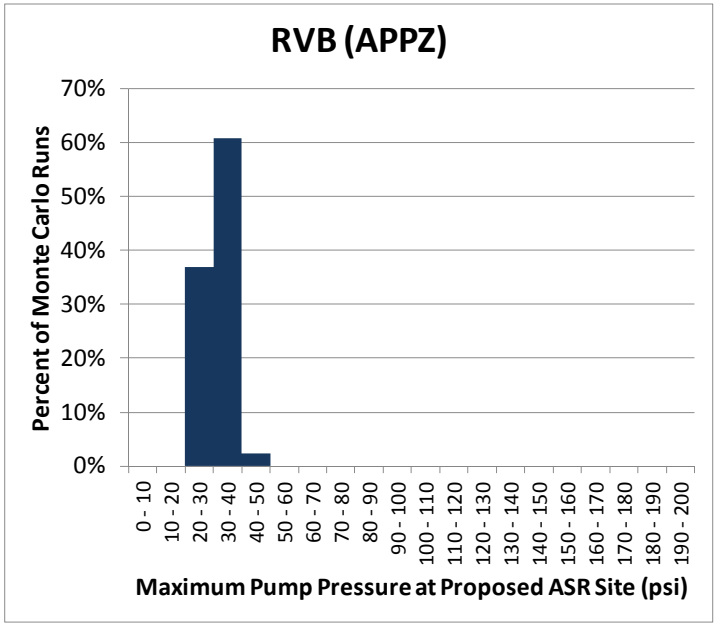

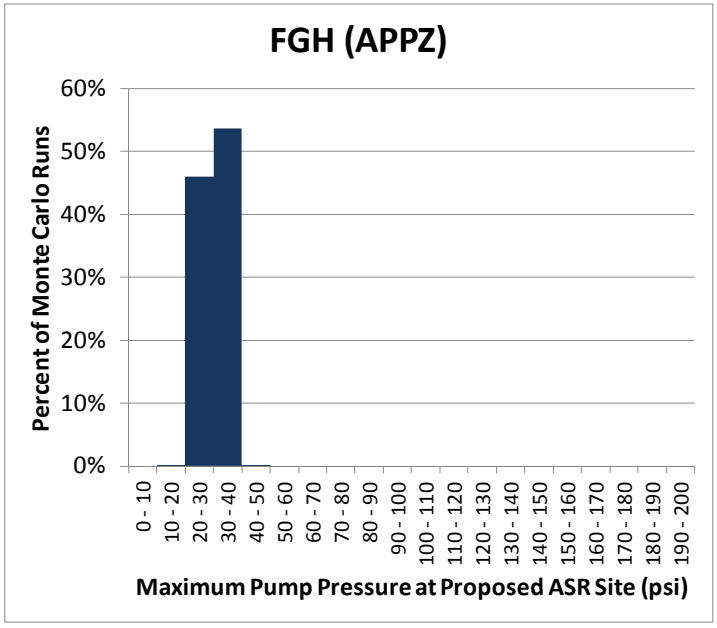

Legend

- Section of Histogram Meeting Pump Pressure Requirement
- Section of Histogram Not Meeting Pump Pressure Requirement

Notes:

These histograms show the distribution of Monte Carlo simulation results for maximum pump pressures at the sites designated. The performance measure required that the maximum pressure stay below 100 psi.

Key	Site
PMY	Port Mayaca
MHV	Moorehaven
RVB	Riverbend
FGH	Flaghole

MONTE CARLO RESULTS – PUMP PRESSURE REQUIREMENTS

REGIONAL MODEL PRODUCTION SCENARIO REPORT

FIGURE 6.22

JUNE 2013

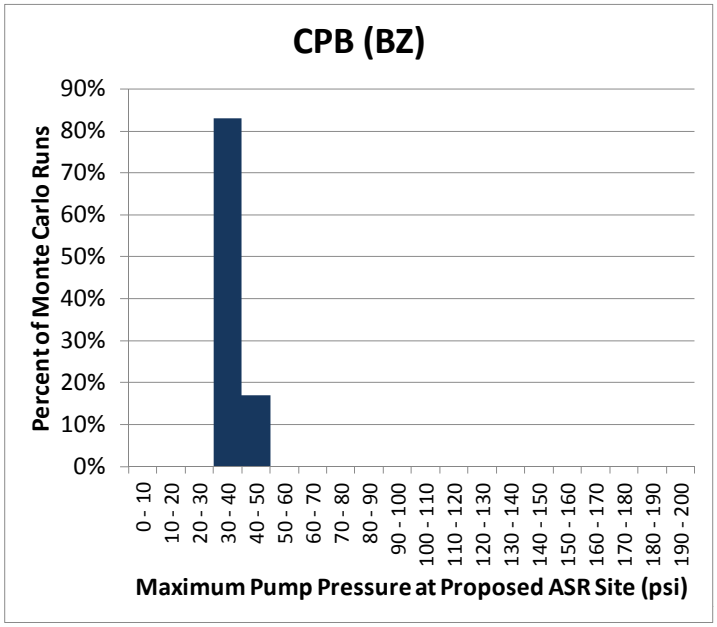

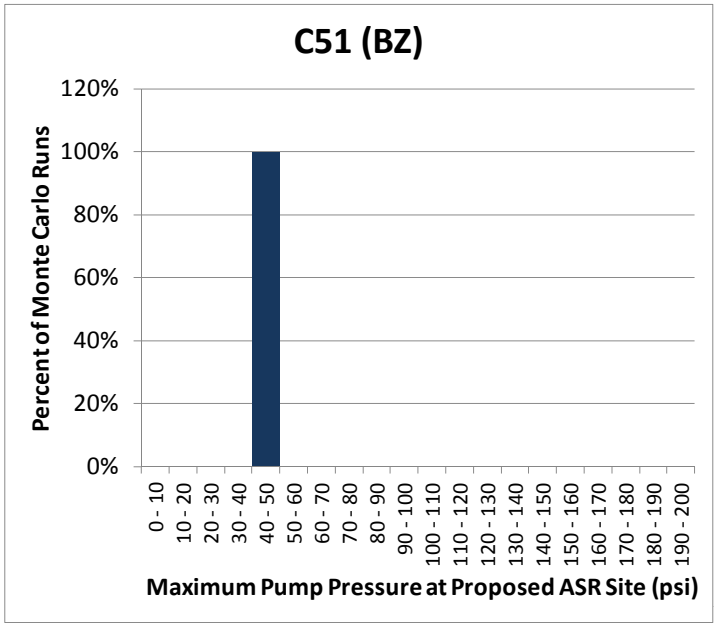

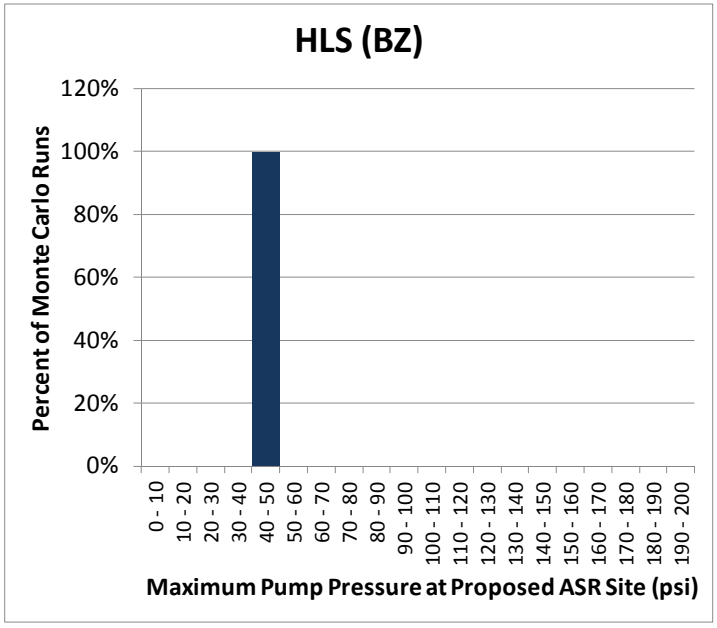

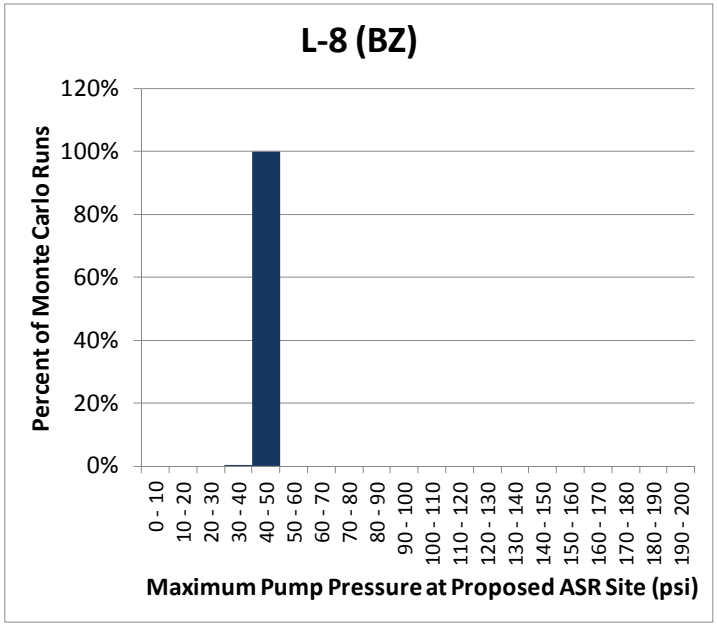

Legend

- Section of Histogram Meeting Pump Pressure Requirement
- Section of Histogram Not Meeting Pump Pressure Requirement

Notes:

These histograms show the distribution of Monte Carlo simulation results for maximum pump pressures at the sites designated. The performance measure required that the maximum pressure stay below 100 psi.

Key	Site
CPB	Central Palm Beach
C51	C-51 Canal
HLS	Hillsboro
L8	L-8 Canal

MONTE CARLO RESULTS – PUMP PRESSURE REQUIREMENTS

REGIONAL MODEL PRODUCTION SCENARIO REPORT

FIGURE 6.23

JUNE 2013

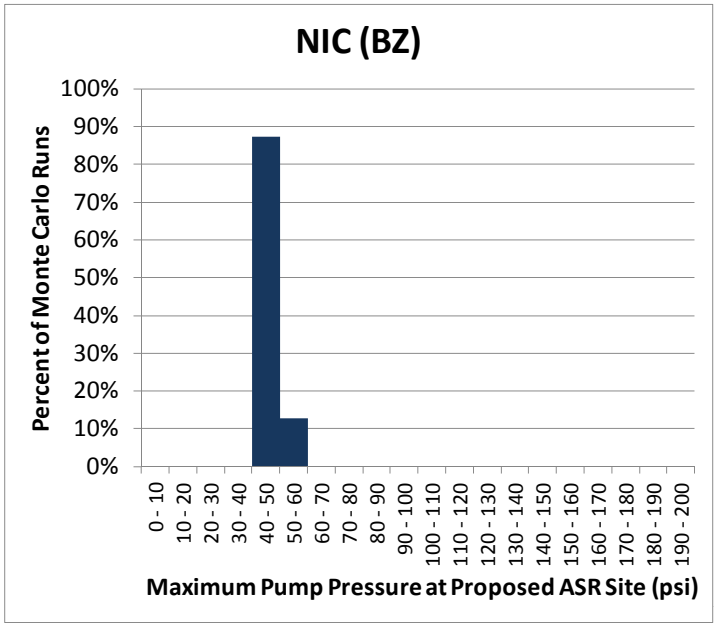

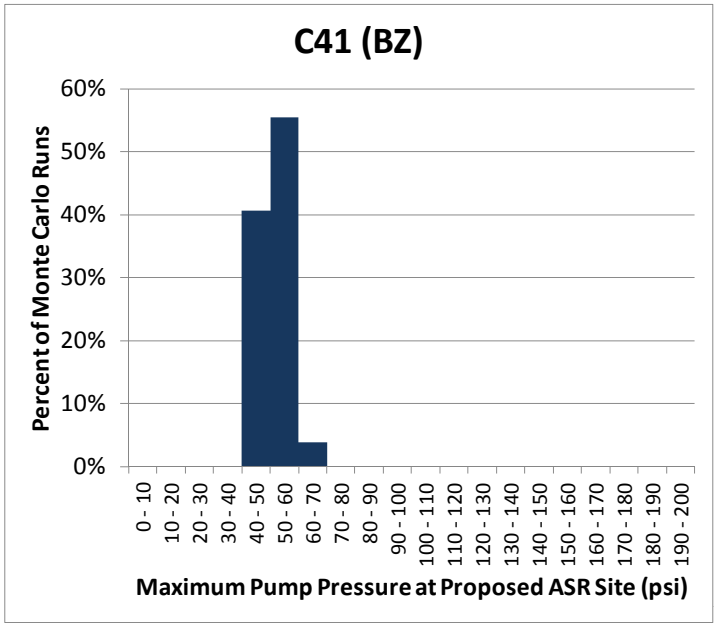

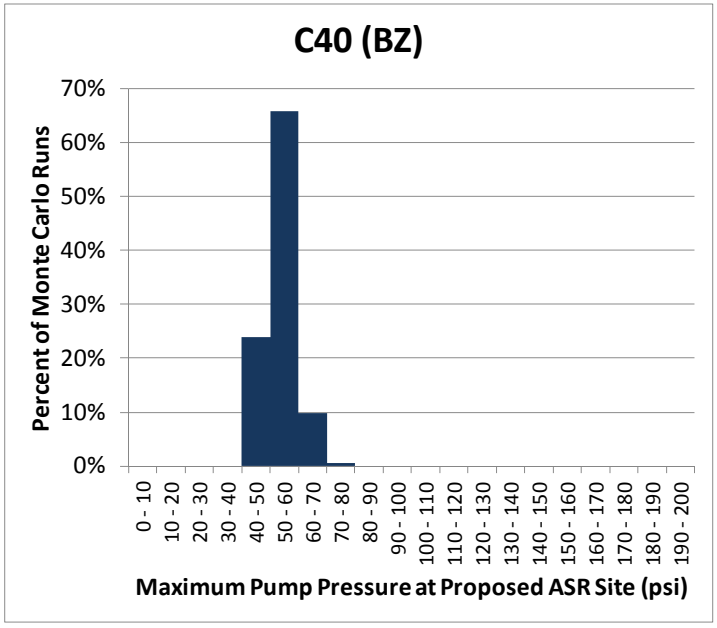

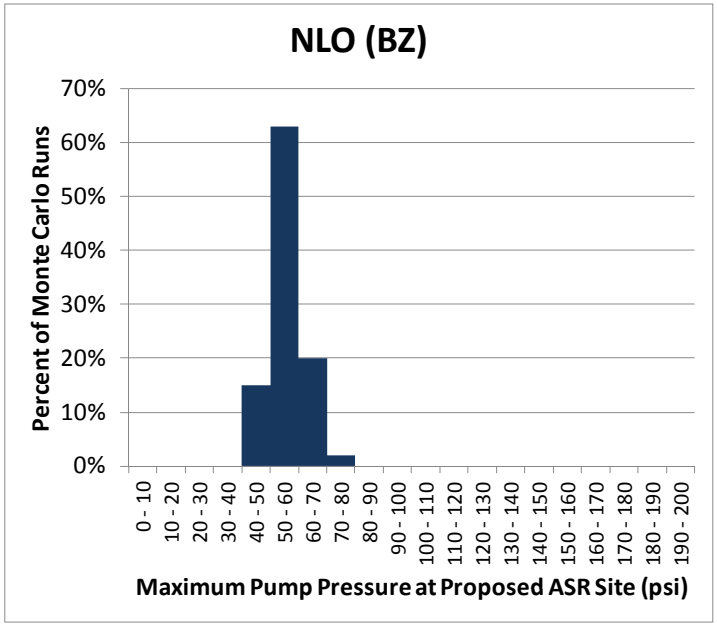

Legend

- Section of Histogram Meeting Pump Pressure Requirement
- Section of Histogram Not Meeting Pump Pressure Requirement

Notes:

These histograms show the distribution of Monte Carlo simulation results for maximum pump pressures at the sites designated. The performance measure required that the maximum pressure stay below 100 psi.

Key	Site
NIC	Nicodemus Slough
C41	C-41 Canal
C40	C-40 Canal
NLO	North Lake Okeechobee Reservoir

Monte Carlo Results – Pump Pressure Requirements

Regional Model Production Scenario Report

Figure 6.24

June 2013

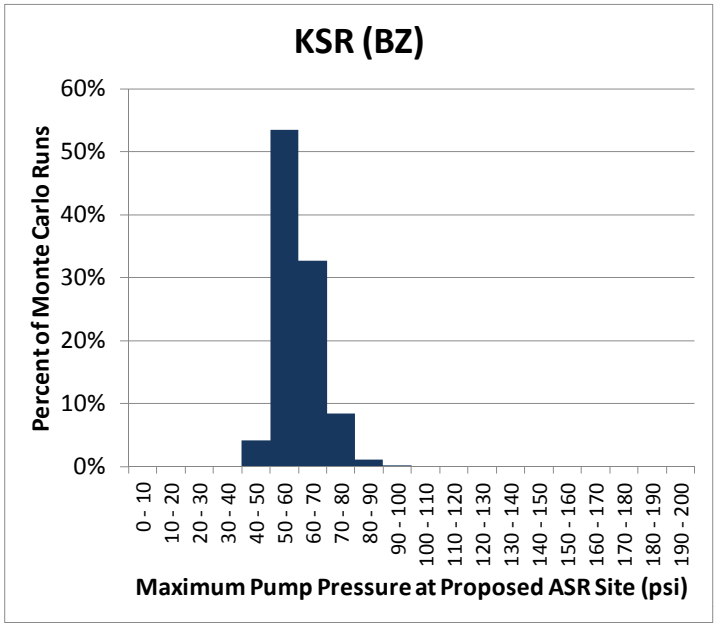

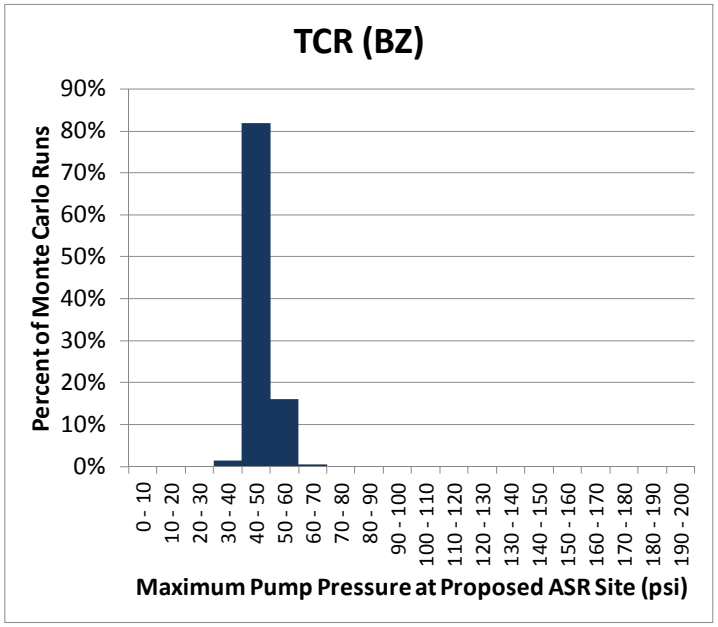

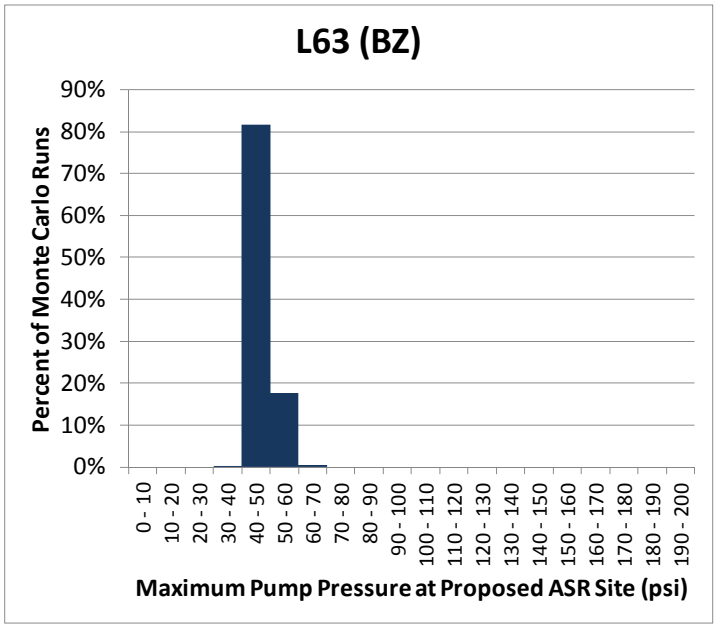

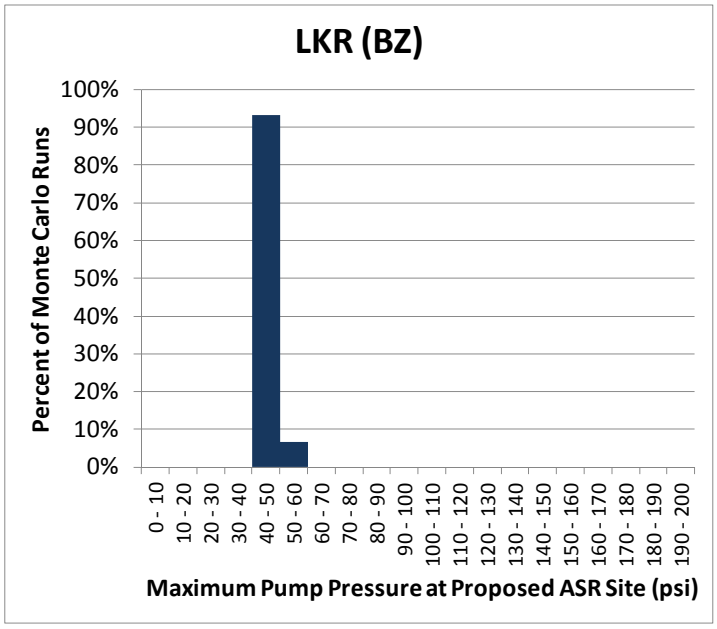

Legend

- Section of Histogram Meeting Pump Pressure Requirement
- Section of Histogram Not Meeting Pump Pressure Requirement

Notes:

These histograms show the distribution of Monte Carlo simulation results for maximum pump pressures at the sites designated. The performance measure required that the maximum pressure stay below 100 psi.

Key	Site
KSR	Kissimmee River / Paradise Run
TCR	Taylor Creek Reservoir
L63	L-63N Canal
LKR	Lakeside Ranch

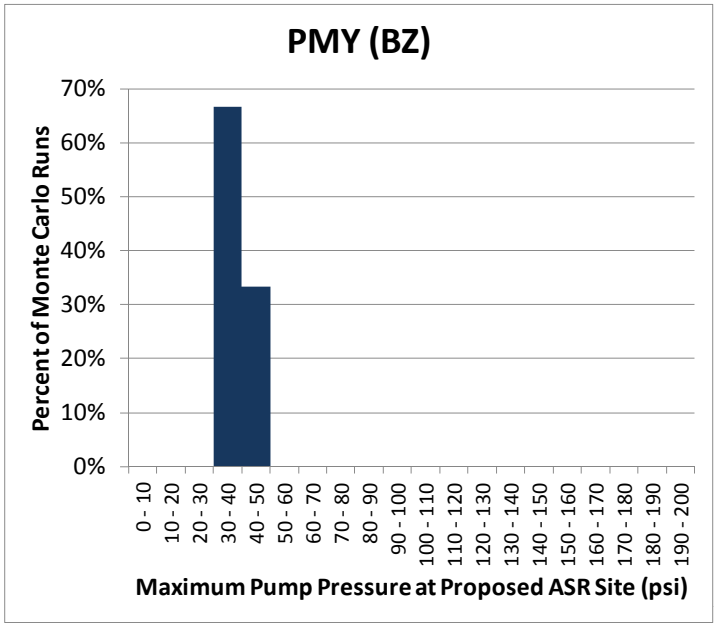

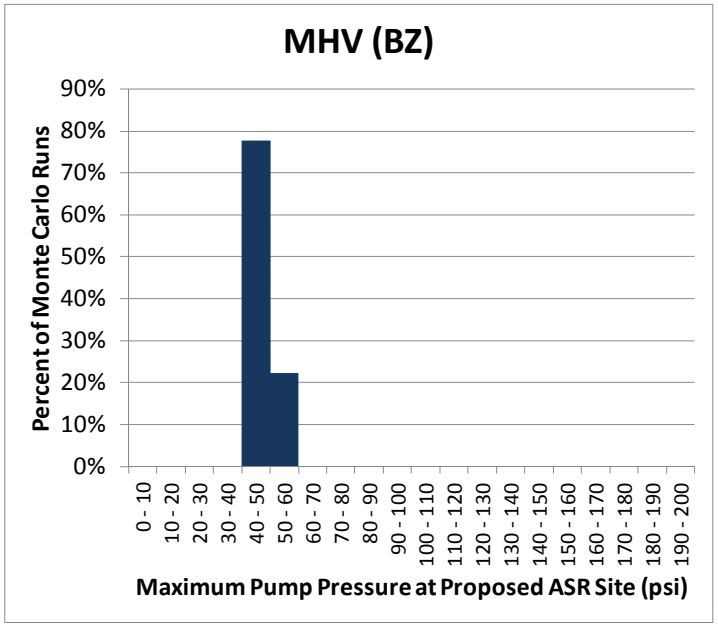

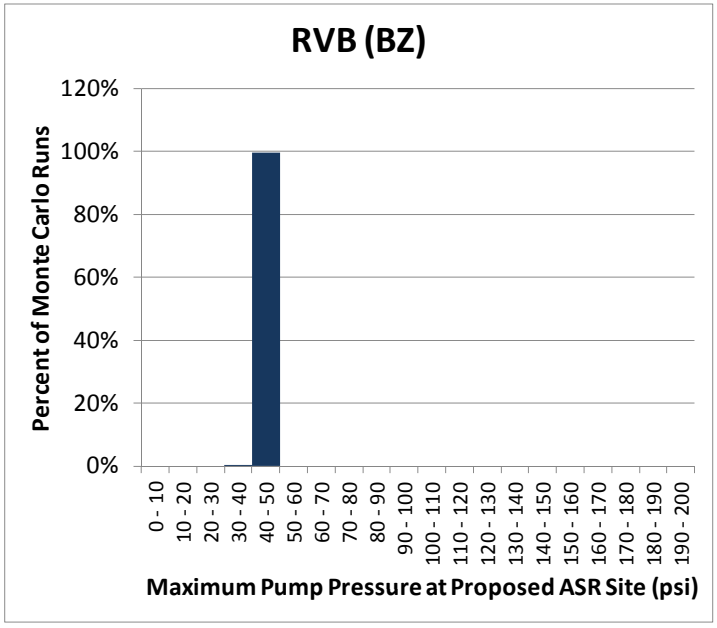

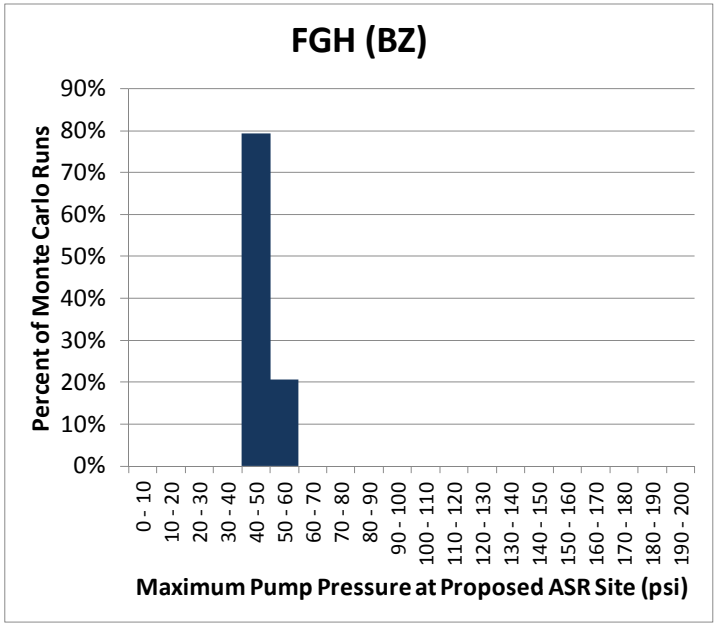

Legend

- Section of Histogram Meeting Pump Pressure Requirement
- Section of Histogram Not Meeting Pump Pressure Requirement

Notes:

These histograms show the distribution of Monte Carlo simulation results for maximum pump pressures at the sites designated. The performance measure required that the maximum pressure stay below 100 psi.

Key	Site
PMY	Port Mayaca
MHV	Moorehaven
RVB	Riverbend
FGH	Flaghole

MONTE CARLO RESULTS – PUMP PRESSURE REQUIREMENTS

REGIONAL MODEL PRODUCTION SCENARIO REPORT

FIGURE 6.26

JUNE 2013

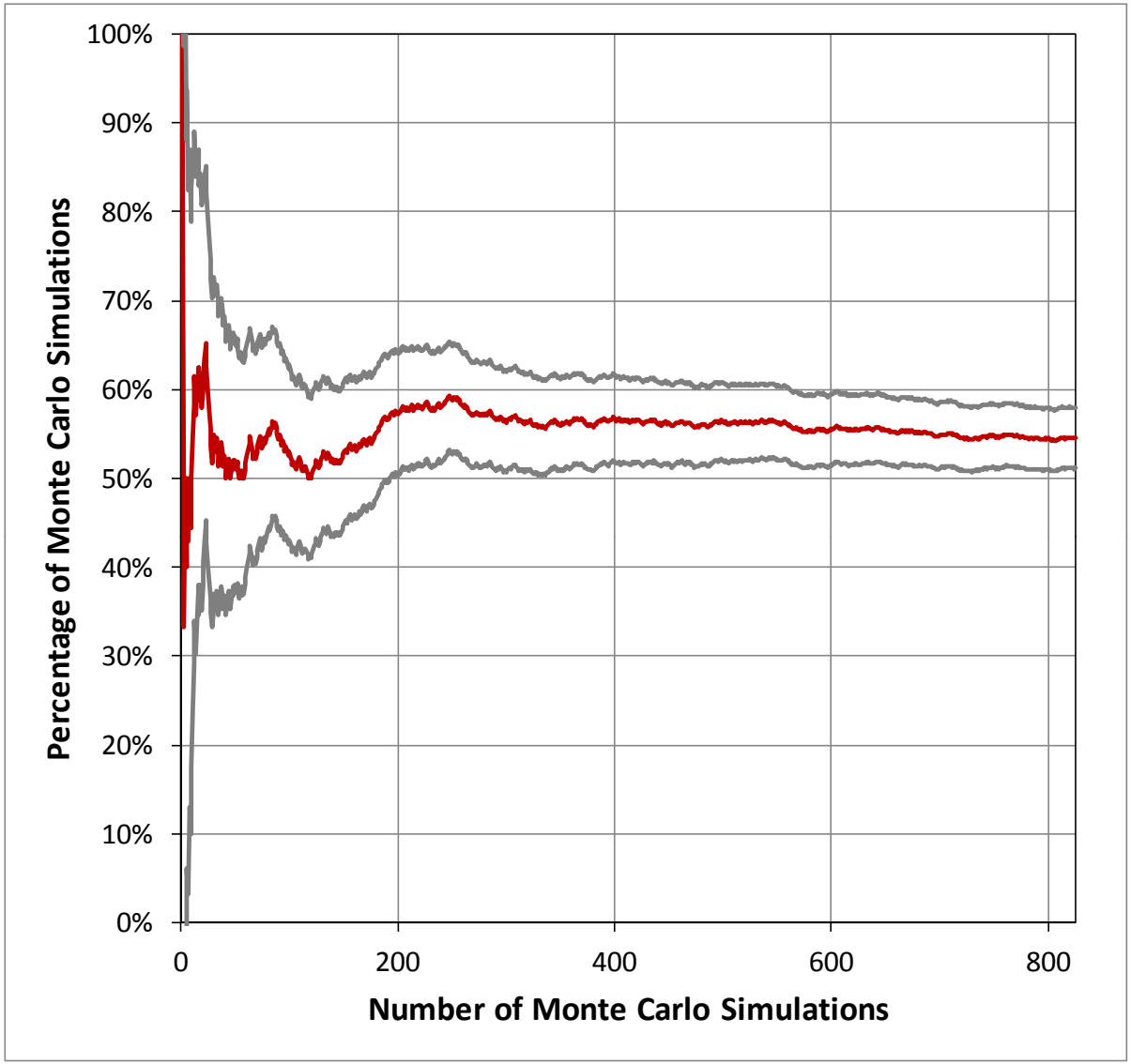

Legend

- Percent Passing
- Upper/Lower Bound 95% Confidence Interval

Notes:

This plot shows the change in percentage passing the pump pressure requirement with the 95% confidence interval at the Lakeside Ranch UF site as the Monte Carlo scenarios progressed.

As the number of Monte Carlo simulations increases, the stability of the red line improves and the confidence interval (between the gray lines) shrinks.

EXAMPLE: CHANGE IN PERCENTAGE PASSING AS NUMBER OF MONTE CARLO SIMULATIONS INCREASES (LAKESIDE RANCH, UF)

REGIONAL MODEL PRODUCTION SCENARIO REPORT

FIGURE 6.27

JUNE 2013

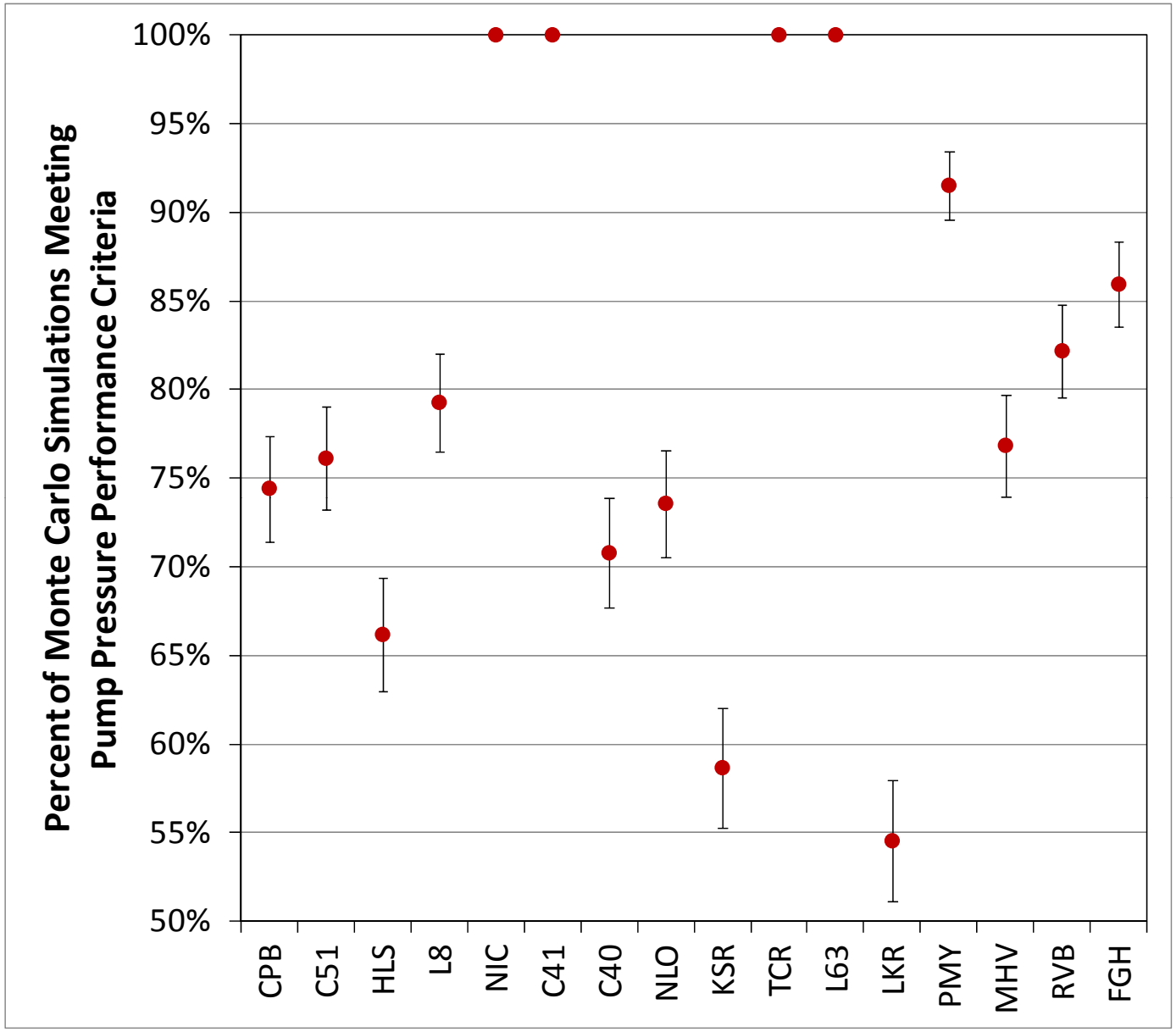

Percent of Monte Carlo Runs Meeting Performance Measure with 95% Confidence Interval

Notes:

This plot shows the percentage of 825 Monte Carlo scenarios which met the performance criteria for pump pressure in the UF. Each solution was analyzed to determine the maximum pressure at each site. If the maximum pressure was over 100 psi, it was considered to have failed the performance measure for that site.

The error bars indicate the 95% confidence interval on each point, which is dependent on the number of Monte Carlo runs and the pass rate.

Similar plots are not shown for the APPZ or BZ sites since all Monte Carlo runs met the criteria.

Key	Site
CPB	Central Palm Beach
C51	C-51 Canal
HLS	Hillsboro
L8	L-8 Canal
NIC	Nicodemus Slough
C41	C-41 Canal
C40	C-40 Canal
NLO	North Lake Okeechobee Reservoir
KSR	Kissimmee River/ Paradise Run
TCR	Taylor Creek Reservoir
L63	L-63N Canal
LKR	Lakeside Ranch
PMY	Port Mayaca
MHV	Moorehaven
RVB	Riverbend
FGH	Flaghole

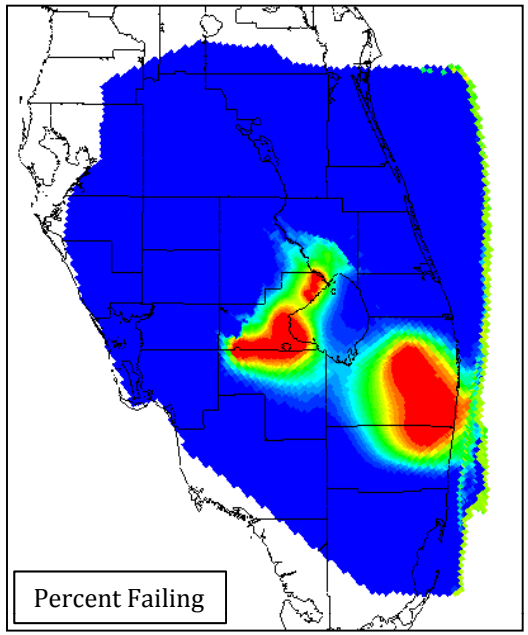

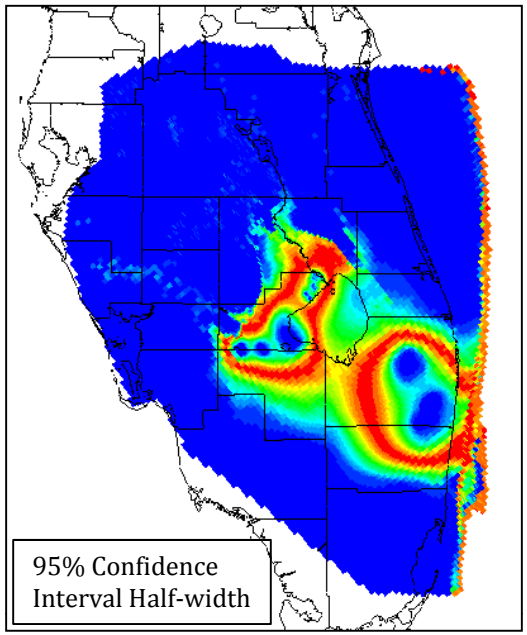

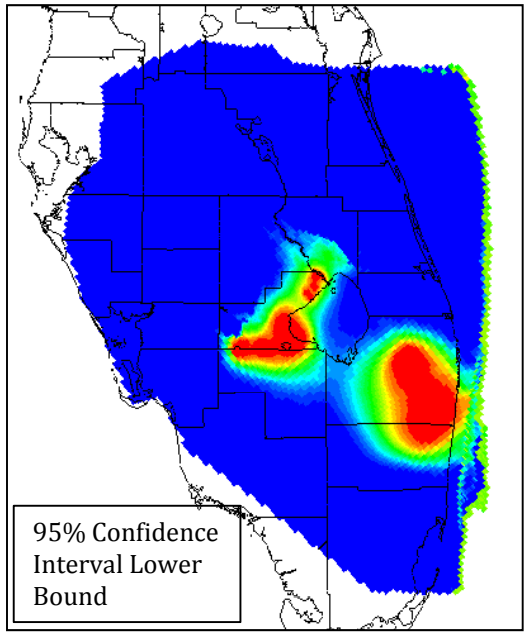

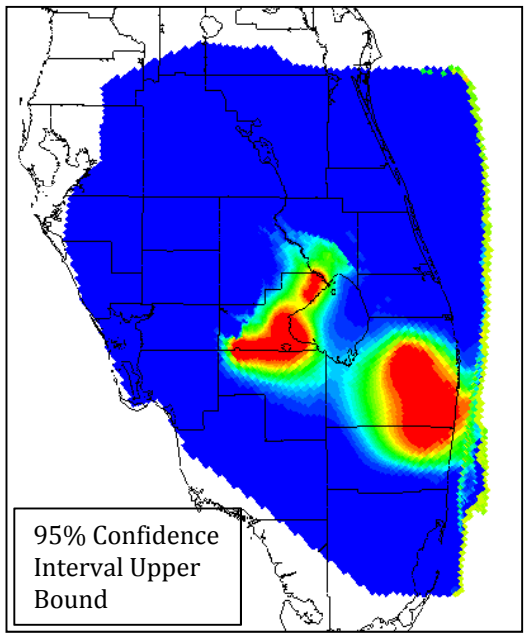

Legend

Percent Failing and Upper/ Lower Bounds

100%

0.0%

Confidence Interval Half-width

3.5%

0.0%

Notes:

The top left image shows the results of the Monte Carlo analysis for the loss of artesian pressure in the UF. Blue areas did not lose more than 10% of artesian pressure in any of the Monte Carlo runs. Red areas lost more than 10% of artesian pressure at least once in all Monte Carlo runs.

The top right image shows the half-width of the 95% confidence interval.

The bottom images show the upper and lower bounds calculated by adding and subtracting the half-width from the Monte Carlo results.

Monte Carlo Results – Less than 10% Artesian Pressure Loss (UF)

Regional Model Production Scenario Report

Figure 6.29

June 2013

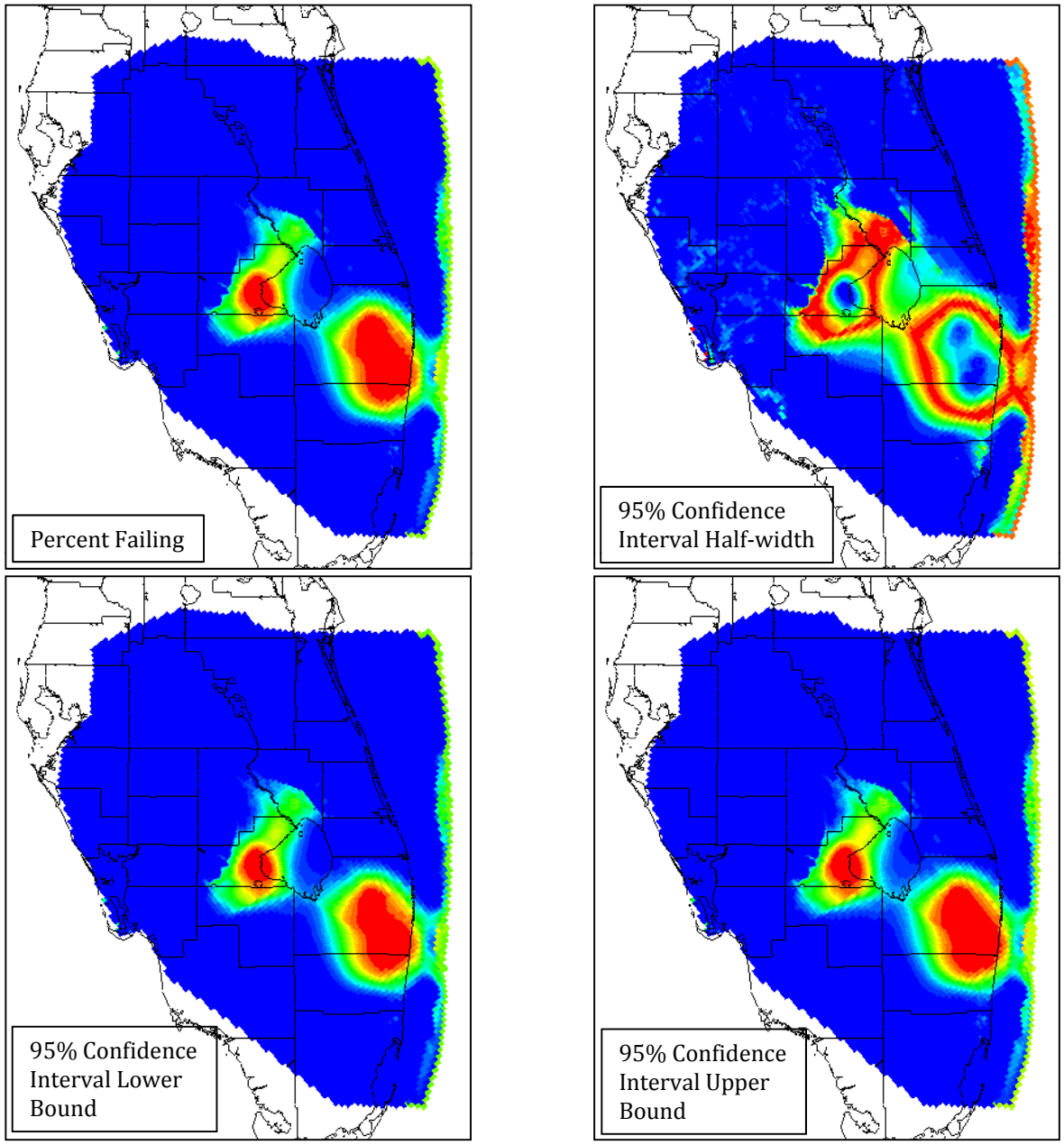

Legend

Percent Failing and Upper/ Lower Bounds

100%

0.0%

Confidence Interval Half-width

3.5%

0.0%

Notes:

The top left image shows the results of the Monte Carlo analysis for the loss of artesian pressure in the APPZ. Blue areas did not lose more than 10% of artesian pressure in any of the Monte Carlo runs. Red areas lost more than 10% of artesian pressure at least once in all Monte Carlo runs.

The top right image shows the half-width of the 95% confidence interval.

The bottom images show the upper and lower bounds calculated by adding and subtracting the half-width from the Monte Carlo results.

MONTE CARLO RESULTS – LESS THAN 10% ARTESIAN PRESSURE LOSS (APPZ)

REGIONAL MODEL PRODUCTION SCENARIO REPORT

FIGURE 6.30

JUNE 2013

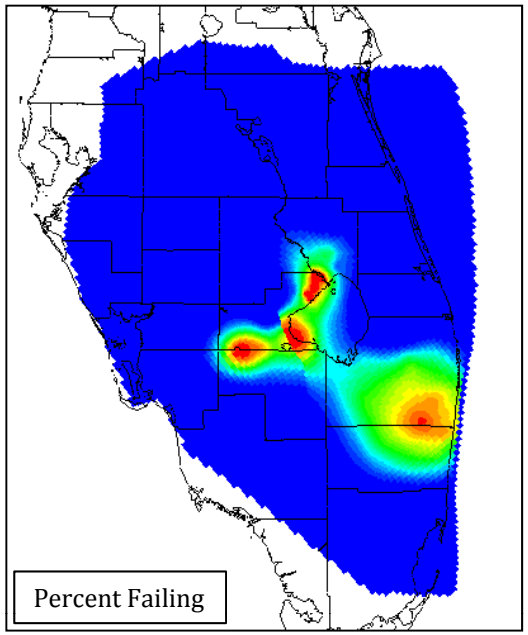

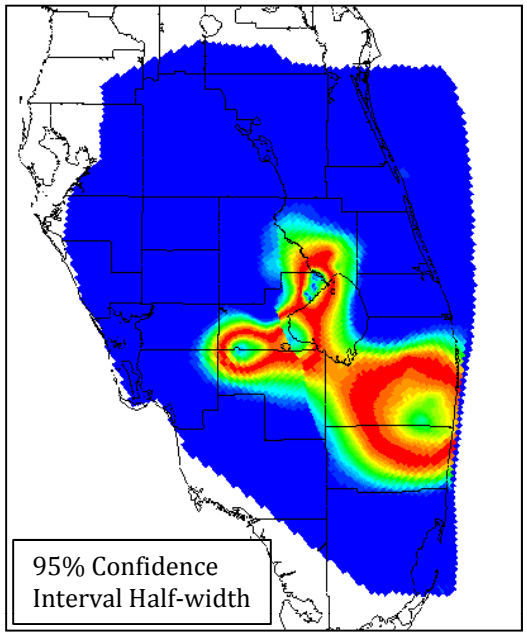

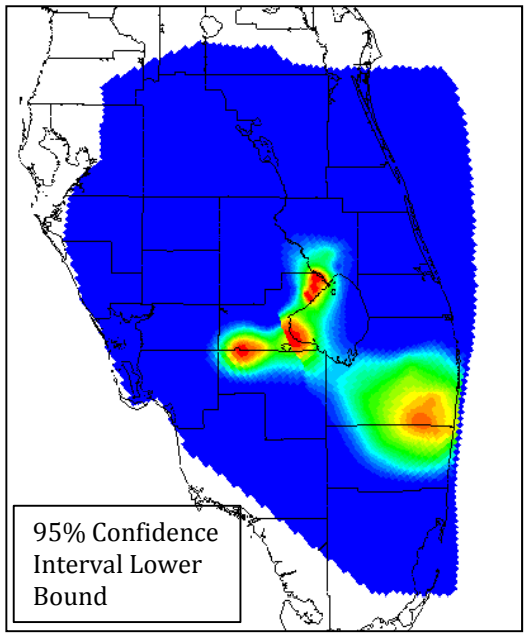

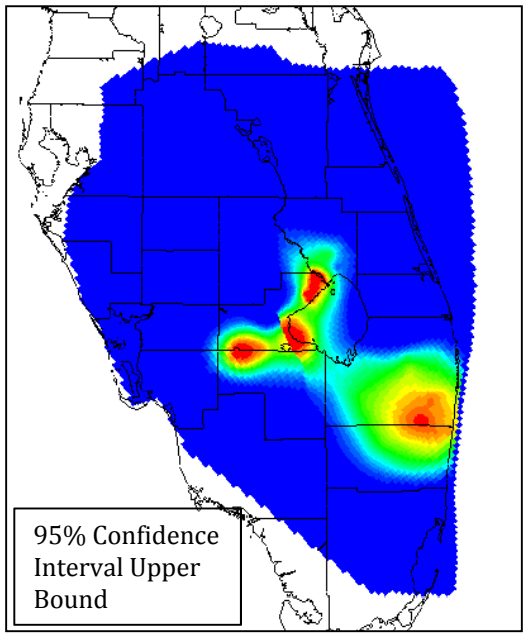

Legend

Percent Failing and Upper/ Lower Bounds

100%

0.0%

Confidence Interval Half-width

3.5%

0.0%

Notes:

The top left image shows the results of the Monte Carlo analysis for greater than 1-foot drawdown in the IAS/ICU (Layer 3). Blue areas did not see more than 1 foot drawdown in any of the Monte Carlo runs. Red areas saw more than 1 foot drawdown at least once in all Monte Carlo runs.

The top right image shows the half-width of the 95% confidence interval.

The bottom images show the upper and lower bounds calculated by adding and subtracting the half-width from the Monte Carlo results.

MONTE CARLO RESULTS – GREATER THAN 1 FOOT DRAWDOWN (IAS/ICU)

REGIONAL MODEL PRODUCTION SCENARIO REPORT

FIGURE 6.31

JUNE 2013

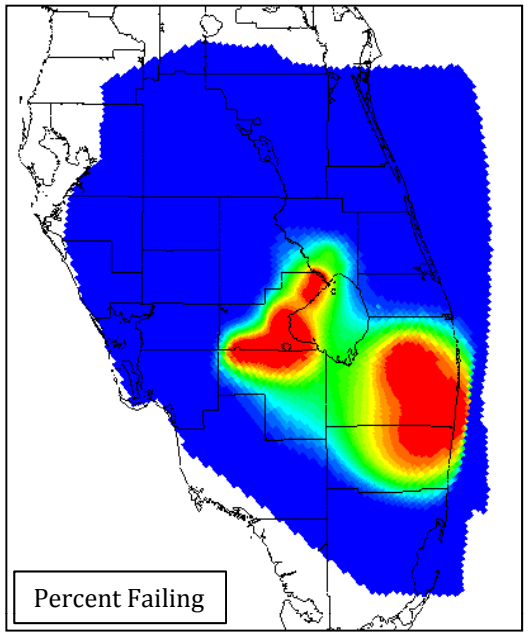

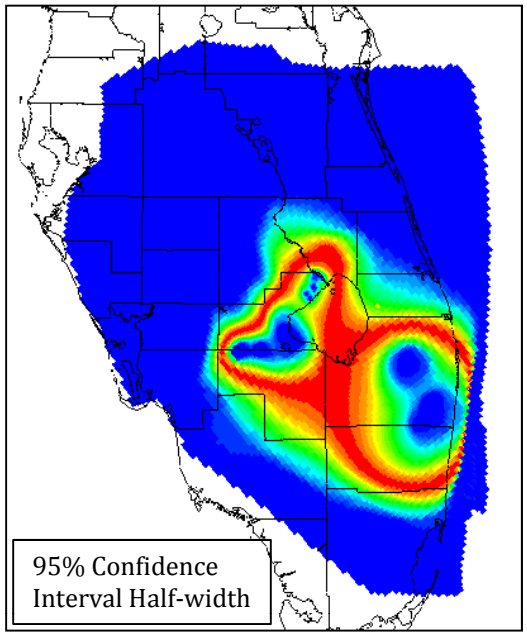

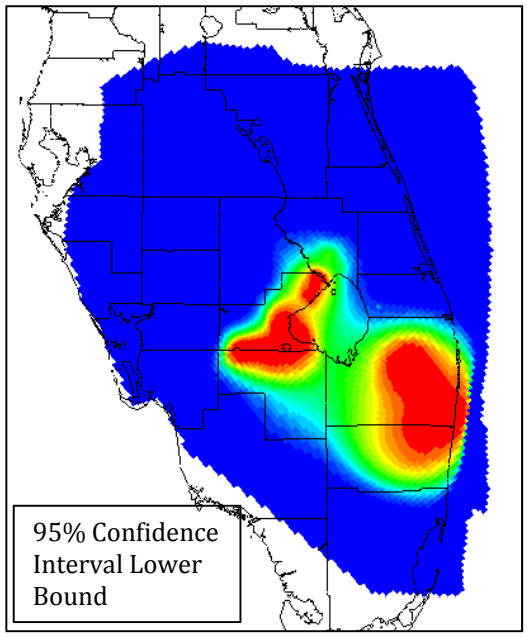

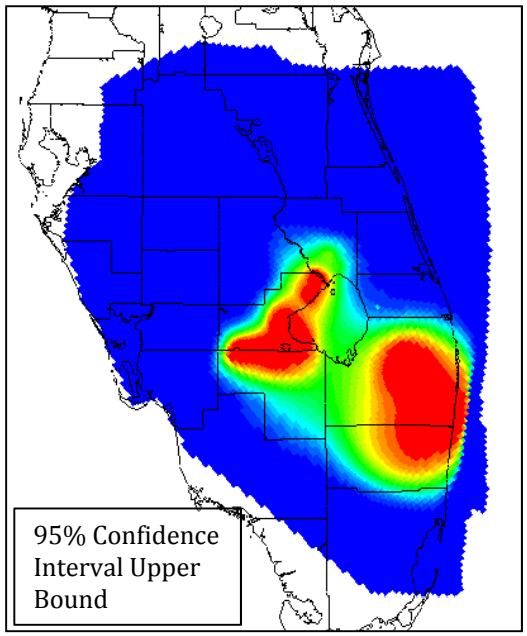

Legend

Percent Failing and Upper/ Lower Bounds

100%

0.0%

Confidence Interval Half-width

3.5%

0.0%

Notes:

The top left image shows the results of the Monte Carlo analysis for greater than 1-foot drawdown in the UF. Blue areas did not see more than 1 foot drawdown in any of the Monte Carlo runs. Red areas saw more than 1 foot drawdown at least once in all Monte Carlo runs.

The top right image shows the half-width of the 95% confidence interval.

The bottom images show the upper and lower bounds calculated by adding and subtracting the half-width from the Monte Carlo results.

MONTE CARLO RESULTS – GREATER THAN 1 FOOT DRAWDOWN (UF)

REGIONAL MODEL PRODUCTION SCENARIO REPORT

FIGURE 6.32

JUNE 2013

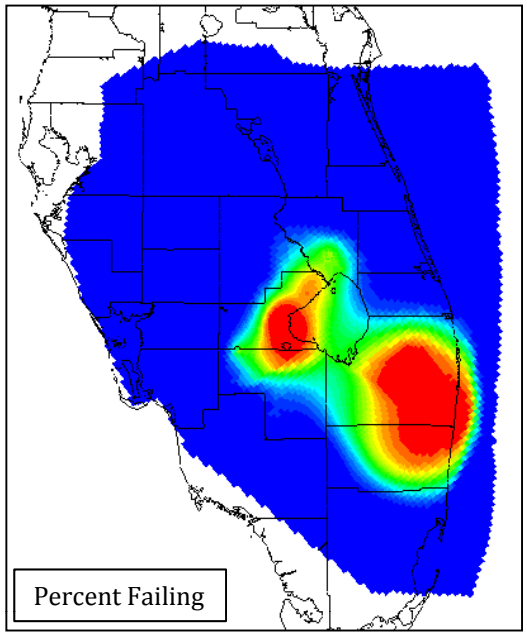

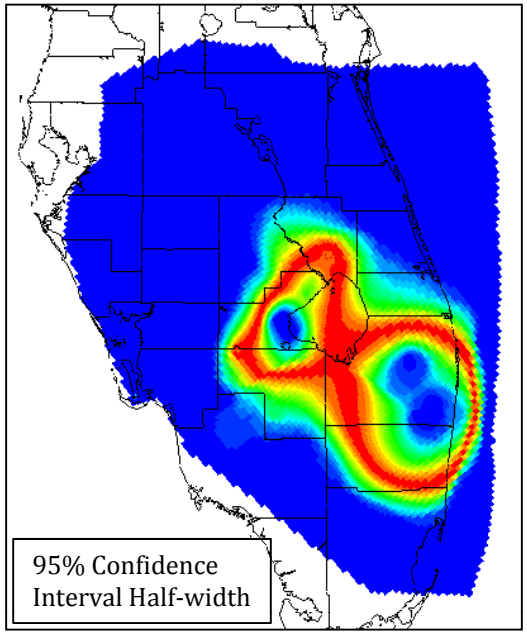

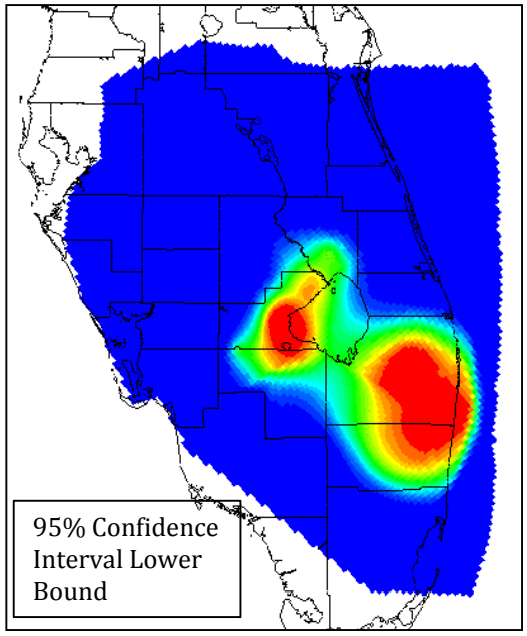

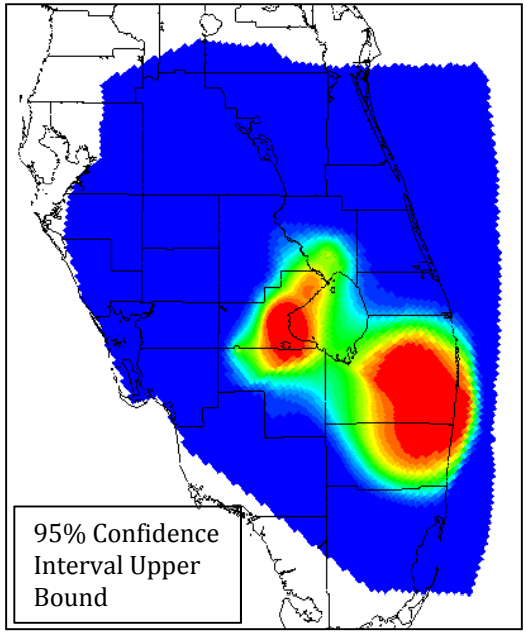

Legend

Percent Failing and Upper/ Lower Bounds

100%

0.0%

Confidence Interval Half-width

3.5%

0.0%

Notes:

The top left image shows the results of the Monte Carlo analysis for greater than 1-foot drawdown in the APPZ. Blue areas did not see more than 1 foot drawdown in any of the Monte Carlo runs. Red areas saw more than 1 foot drawdown at least once in all Monte Carlo runs.

The top right image shows the half-width of the 95% confidence interval.

The bottom images show the upper and lower bounds calculated by adding and subtracting the half-width from the Monte Carlo results.

MONTE CARLO RESULTS – GREATER THAN 1 FOOT DRAWDOWN (APPZ)

REGIONAL MODEL PRODUCTION SCENARIO REPORT

FIGURE 6.33

JUNE 2013

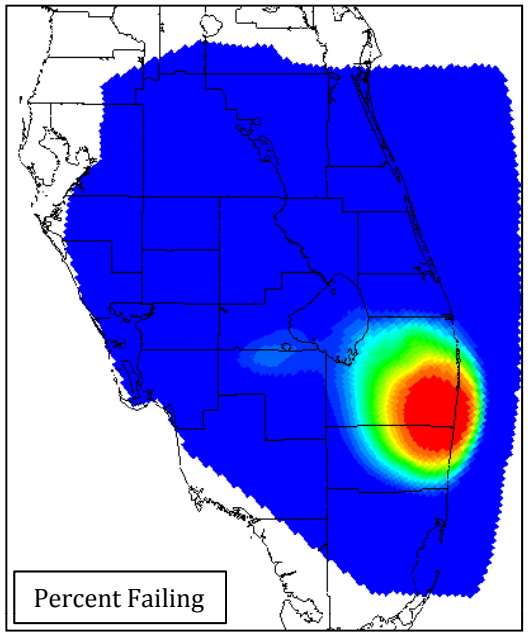

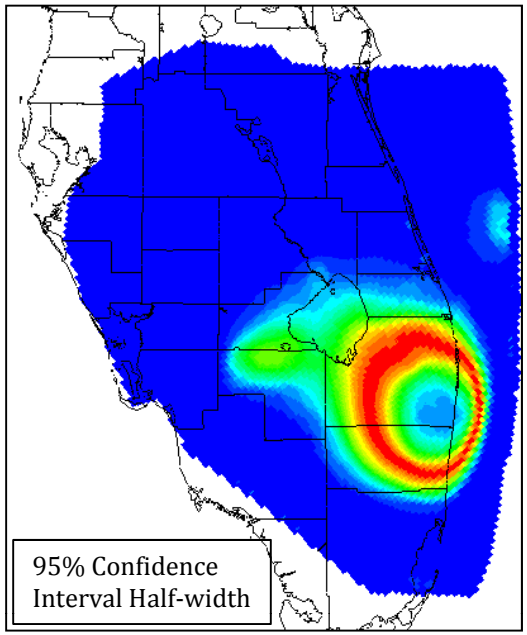

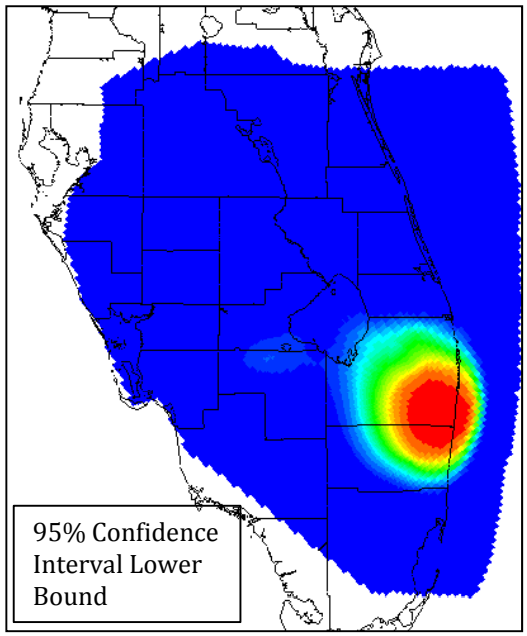

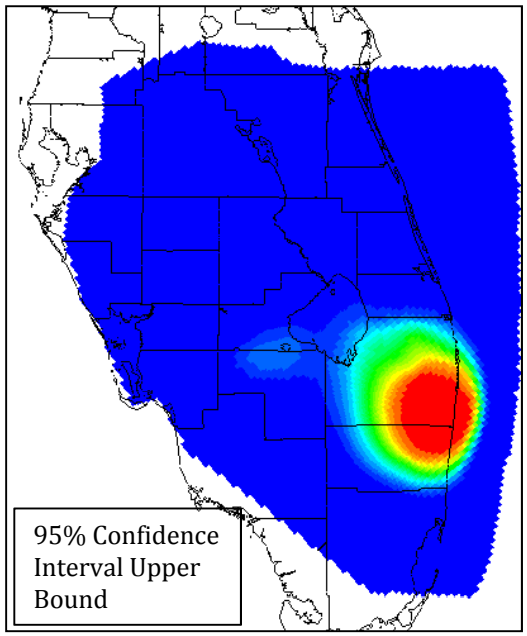

Legend

Percent Failing and Upper/ Lower Bounds

100%

0.0%

Confidence Interval Half-width

3.5%

0.0%

Notes:

The top left image shows the results of the Monte Carlo analysis for greater than 1-foot drawdown in the LF. Blue areas did not see more than 1 foot drawdown in any of the Monte Carlo runs. Red areas saw more than 1 foot drawdown at least once in all Monte Carlo runs.

The top right image shows the half-width of the 95% confidence interval.

The bottom images show the upper and lower bounds calculated by adding and subtracting the half-width from the Monte Carlo results.

MONTE CARLO RESULTS – GREATER THAN 1 FOOT DRAWDOWN (LF)

REGIONAL MODEL PRODUCTION SCENARIO REPORT

FIGURE 6.34

JUNE 2013

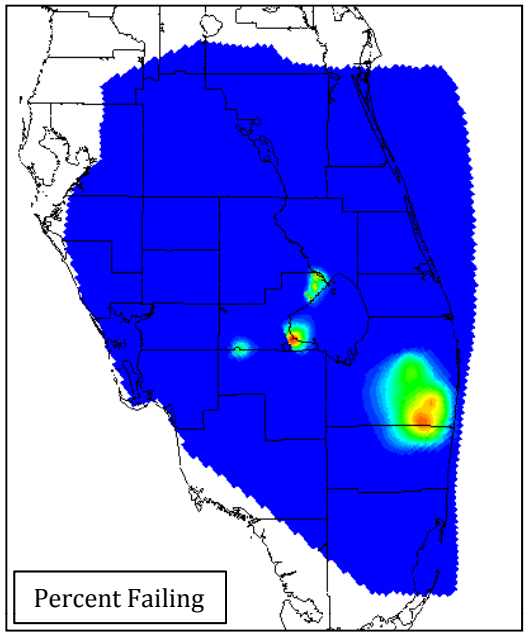

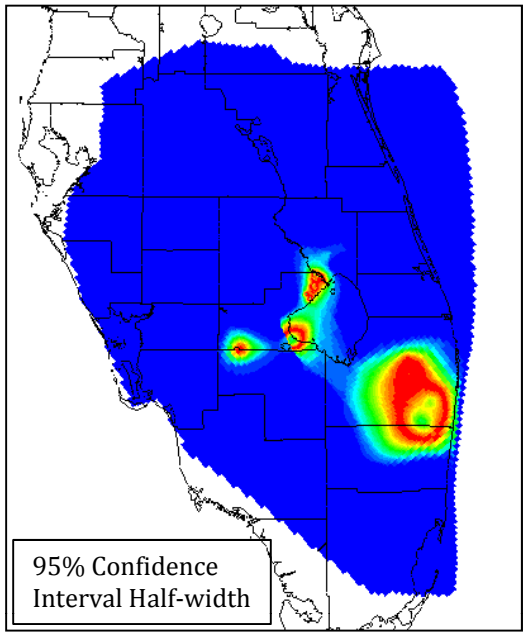

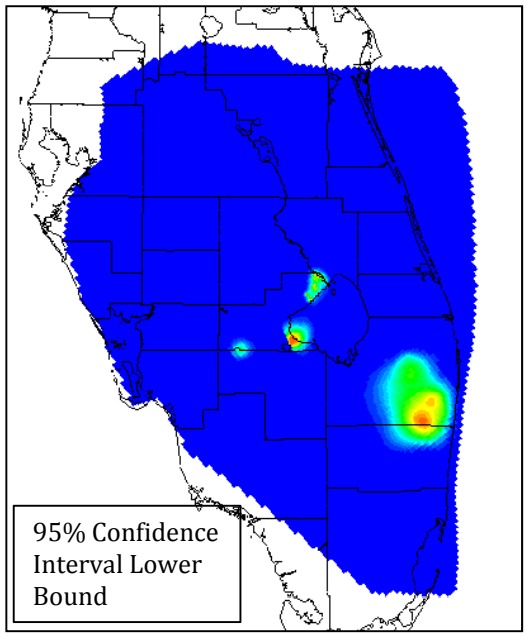

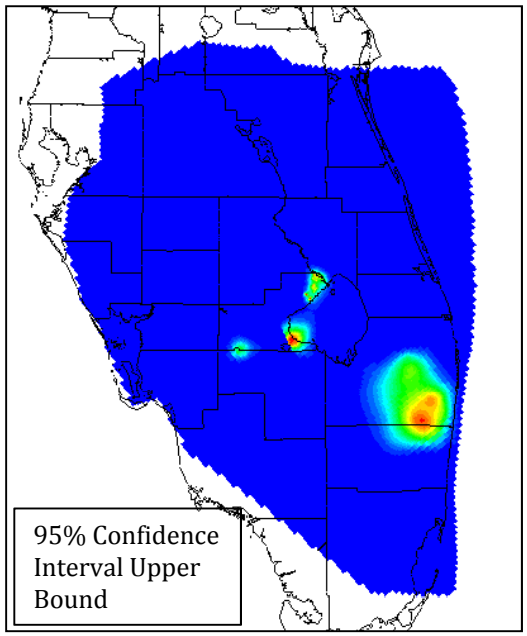

Legend

Percent Failing and Upper/ Lower Bounds

100%

0.0%

Confidence Interval Half-width

3.5%

0.0%

Notes:

The top left image shows the results of the Monte Carlo analysis for greater than 5-foot drawdown in the IAS/ICU (Layer 3). Blue areas did not see more than 5 foot drawdown in any of the Monte Carlo runs. Red areas saw more than 5 foot drawdown at least once in all Monte Carlo runs.

The top right image shows the half-width of the 95% confidence interval.

The bottom images show the upper and lower bounds calculated by adding and subtracting the half-width from the Monte Carlo results.

MONTE CARLO RESULTS – GREATER THAN 5 FOOT DRAWDOWN (IAS/ICU)

REGIONAL MODEL PRODUCTION SCENARIO REPORT

FIGURE 6.35

JUNE 2013

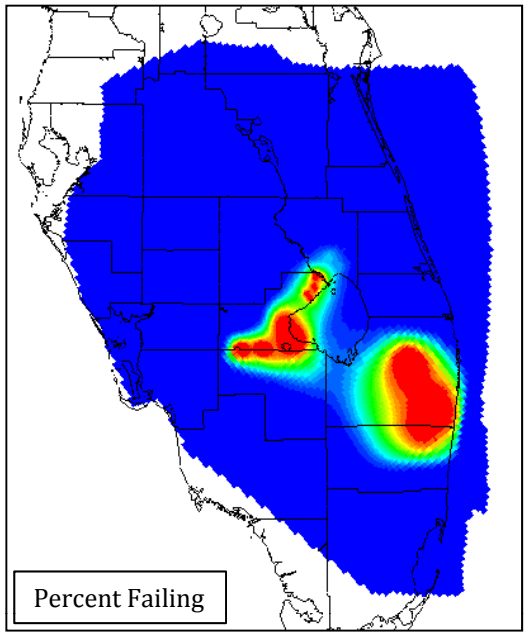

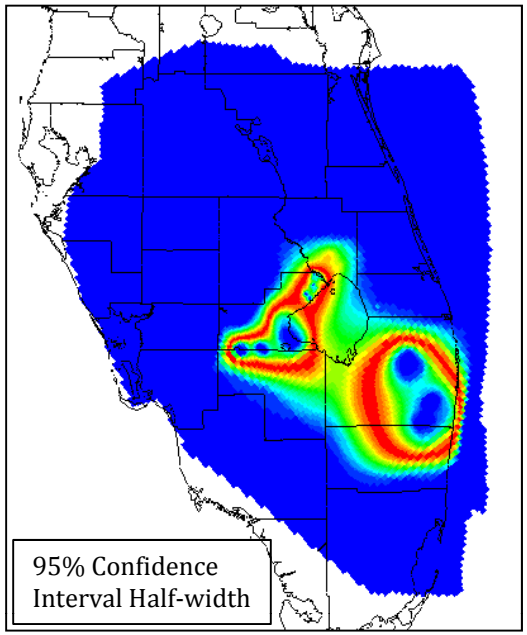

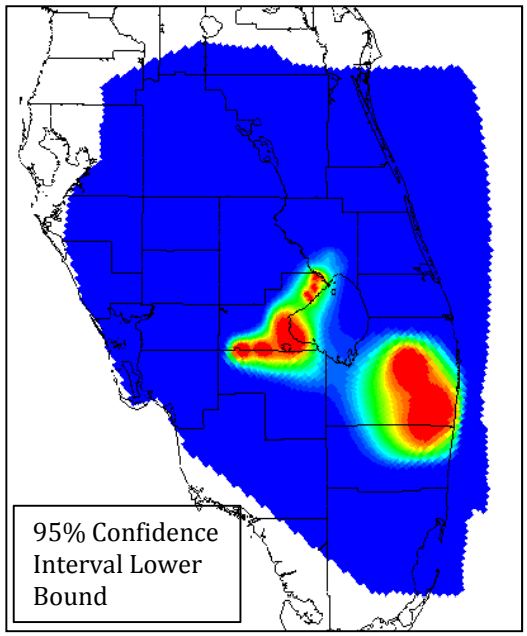

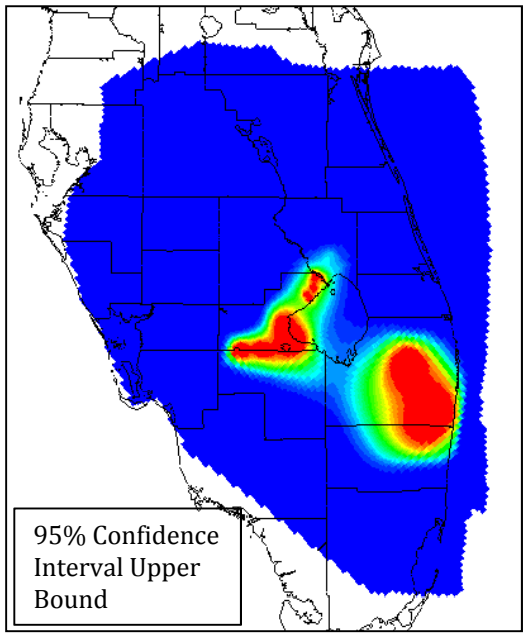

Legend

Percent Failing and Upper/ Lower Bounds

100%

0.0%

Confidence Interval Half-width

3.5%

0.0%

Notes:

The top left image shows the results of the Monte Carlo analysis for greater than 5-foot drawdown in the UF. Blue areas did not see more than 5 foot drawdown in any of the Monte Carlo runs. Red areas saw more than 5 foot drawdown at least once in all Monte Carlo runs.

The top right image shows the half-width of the 95% confidence interval.

The bottom images show the upper and lower bounds calculated by adding and subtracting the half-width from the Monte Carlo results.

MONTE CARLO RESULTS – GREATER THAN 5 FOOT DRAWDOWN (UF)

REGIONAL MODEL PRODUCTION SCENARIO REPORT

FIGURE 6.36

JUNE 2013

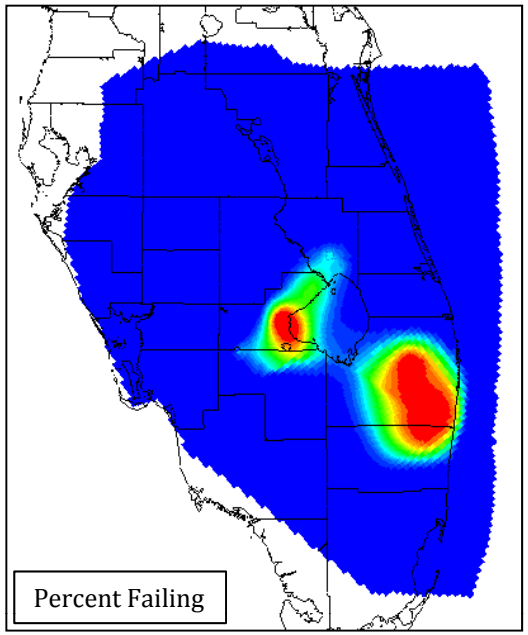

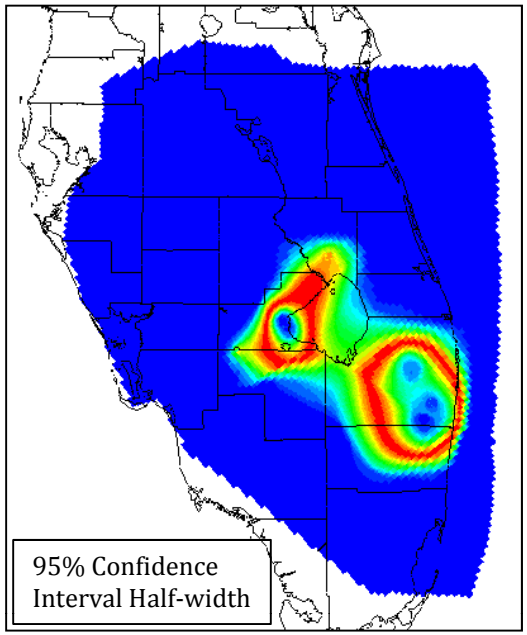

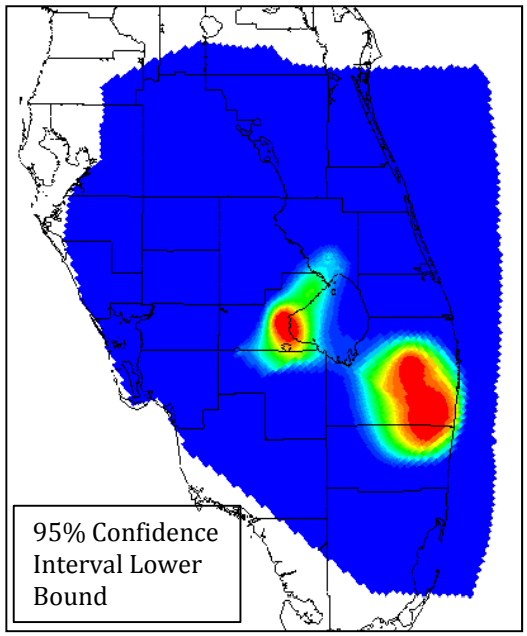

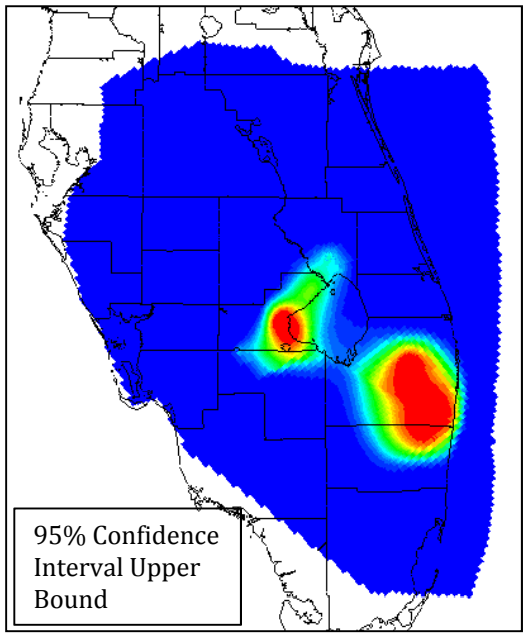

Legend

Percent Failing and Upper/ Lower Bounds

100%

0.0%

Confidence Interval Half-width

3.5%

0.0%

Notes:

The top left image shows the results of the Monte Carlo analysis for greater than 5-foot drawdown in the APPZ. Blue areas did not see more than 5 foot drawdown in any of the Monte Carlo runs. Red areas saw more than 5 foot drawdown at least once in all Monte Carlo runs.

The top right image shows the half-width of the 95% confidence interval.

The bottom images show the upper and lower bounds calculated by adding and subtracting the half-width from the Monte Carlo results.

MONTE CARLO RESULTS – GREATER THAN 5 FOOT DRAWDOWN (APPZ)

REGIONAL MODEL PRODUCTION SCENARIO REPORT

FIGURE 6.37

JUNE 2013

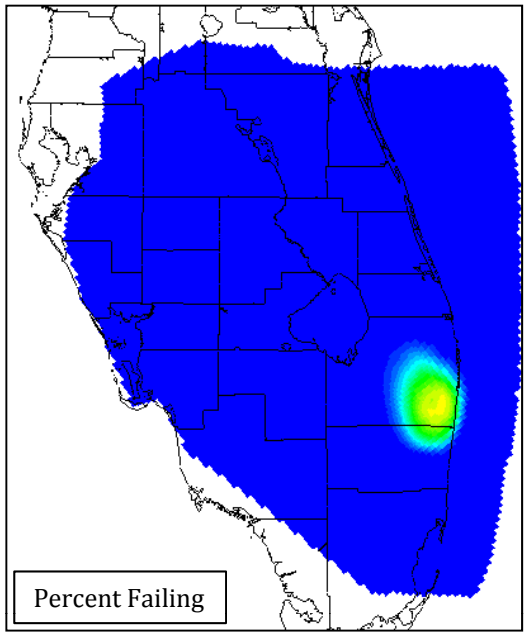

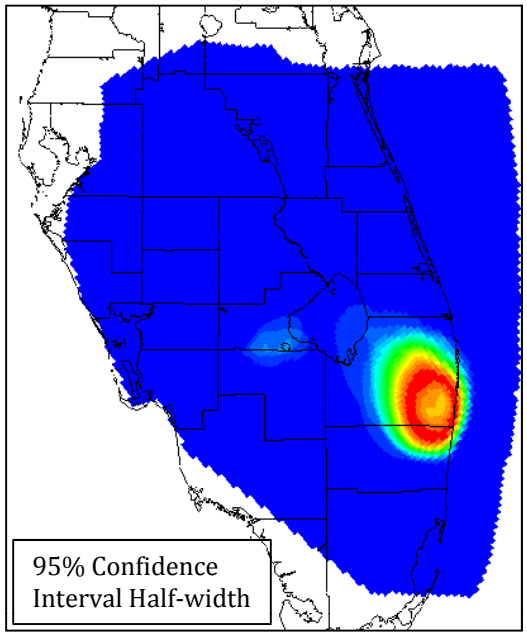

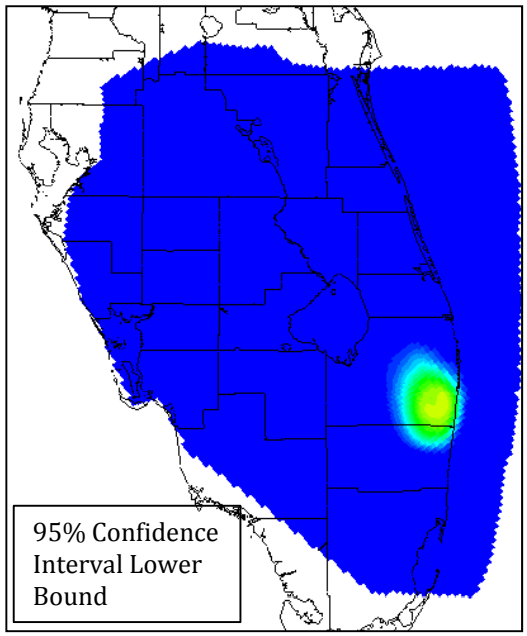

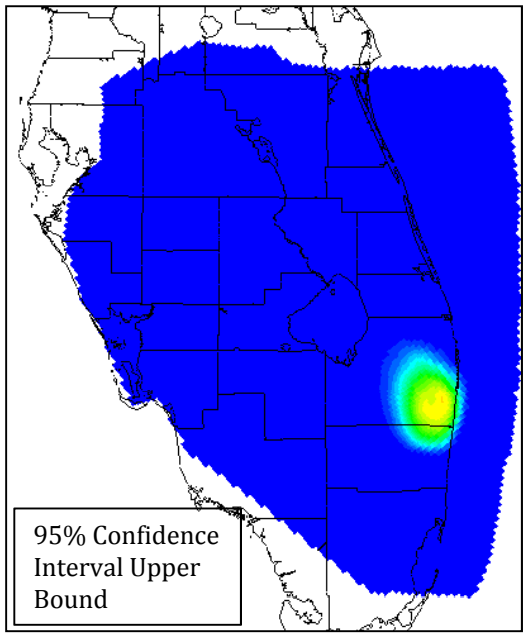

Legend

Percent Failing and Upper/ Lower Bounds

100%

0.0%

Confidence Interval Half-width

3.5%

0.0%

Notes:

The top left image shows the results of the Monte Carlo analysis for greater than 5-foot drawdown in the LF. Blue areas did not see more than 5 foot drawdown in any of the Monte Carlo runs. Red areas saw more than 5 foot drawdown at least once in all Monte Carlo runs.

The top right image shows the half-width of the 95% confidence interval.

The bottom images show the upper and lower bounds calculated by adding and subtracting the half-width from the Monte Carlo results.

MONTE CARLO RESULTS – GREATER THAN 5 FOOT DRAWDOWN (LF)

REGIONAL MODEL PRODUCTION SCENARIO REPORT

FIGURE 6.38

JUNE 2013

Table 2.1: Comparison of SFWMM and RASRASM

	South Florida Water Management Model	Regional ASR Study Model
Acronym	SFWMM	RASRSM
Code	In-house (SFWMD)	SEAWAT (USGS)
Scale	Regional	Regional
Area of Interest	Lake Okeechobee to Florida Bay	Orlando to the Everglades
Model Domain	Hydrologic Cycle and Water Management	Groundwater from the ground surface to the boulder zone (BZ)
Components	Rainfall, evapotranspiration, infiltration, overland and groundwater flow, canal flow, canal-groundwater seepage, levee seepage, groundwater pumping, water management structures, operational rules	Groundwater flow, with density dependence
D13R Period of Interest	1965-1995	1965-1977

Table 2.2: Methodology for setting regional pumping rates in D13R model from SAJ pumping database and USGS Historical water-use tables

Well Type Code in SAJ Pumping Database	Code Description when Provided by SAJ Database	Water Use Type from USGS Table	Notes
A	Agriculture	Agricultural	
AC	Air Conditioning / Withdrawal	Domestic	
ag	Agriculture	Agricultural	
AGR		Agricultural	
AGR CITRUS		Agricultural	
AQC	Aquaculture	Agricultural	
ASR	Aquifer Storage and Recovery	---	These wells were given a flowrate of zero. Only two of the ASR wells included in the SAJ database were drilled before 1977. The two that were drilled in 1974 did not pump during 1993 or 1994, so their flowrate in 1974-1977 cannot be accurately estimated using this method.
cattle	Irrigation for Cattle Pasture	Agricultural	
com/irr	Commercial and Irrigation	Agricultural	
C/I		Commercial-industrial-mining	
com	Commercial	Commercial-industrial-mining	
Commercial		Commercial-industrial-mining	
DAI	Dairy	Agricultural	

Well Type Code in SAJ Pumping Database	Code Description when Provided by SAJ Database	Water Use Type from USGS Table	Notes
DOM	Single Family	Domestic	
FIR	Fire	---	These flow rates were left unchanged for each year of the period. They account for 0.003% of the flow extracted from the model in the validation and calibration periods, so errors here will be minimal on a regional scale.
fire	Fire Protection	---	These flow rates were left unchanged for each year of the period. They account for 0.0002% of the flow extracted from the model in the validation and calibration periods, so errors here will be minimal on a regional scale.
FLOW		Total freshwater	The meaning of this code is unknown, so the rate was varied according to the total of all water uses. This well type accounts for 0.15% of the flow extracted from the model during the validation and calibration models, so errors here will be minimal on a regional scale.
FRZ	Freeze Protection	Agricultural	Although freeze protection was probably not intended to be part of the Agricultural water use type, the volumes of flow should rise and fall as the acreage of agricultural land rises and falls. These wells account for 0.12% of the flow extracted from the model during the validation and calibration models, so errors here will be minimal on a regional scale.
IC	Industrial / Commercial	Commercial-industrial-mining	
IND	Industrial	Commercial-industrial-mining	
INJ	Injection	Public supply	Although this type of well does not feed public supply, it is included with this water use type since injection of reclaimed wastewater may correlate with public water supply usage rates.
IRL	Irrigation Water Replacement	Agricultural	

Well Type Code in SAJ Pumping Database	Code Description when Provided by SAJ Database	Water Use Type from USGS Table	Notes
IRR	Irrigation	Agricultural	
irr/cattle	Irrigation for Cattle Pasture	Agricultural	
L DRAIN	Drains Stormwater	---	These drains are located in Orange County and the reported flow rates are loosely correlated with rainfall (R2=0.85). Rainfall data from 1965 – 1977 was used to estimate these flow rates. Combined, L DRAIN, R DRAIN, S DRAIN and W DRAIN wells constitute 0.09% of the injected flow in the validation and calibration models.
Large PWS		Public supply	
LIV	Livestock	Agricultural	
MD	Mining / Dewatering	Commercial-industrial-mining	
MND	Mining Dewatering	Commercial-industrial-mining	
N/A	Unspecified	Total freshwater	
OTR	Other	Total freshwater	
P	Public Supply	Public supply	
PH	Swimming Pool Heating /Withdrawal	Public supply	
PHR	Swimming Pool Heating / Injection	Public supply	
Private		Domestic	
PWS	Public Water Supply	Public supply	
R	Recreation	Recreational irrigation	
R DRAIN	Drains Stormwater	---	These drains are located in Orange County and the reported flow rates are loosely correlated with rainfall (R2=0.85). Rainfall data from 1965 – 1977 was used to estimate these flow rates. Combined, L DRAIN, R DRAIN, S DRAIN and W DRAIN wells constitute 0.09% of the injected flow in the validation and calibration models.
RCG	Recharge (unspecified)	Recreational irrigation	
rec	Recreational	Recreational	

Well Type Code in SAJ Pumping Database	Code Description when Provided by SAJ Database	Water Use Type from USGS Table	Notes
	Facility	irrigation	
REC GOLF COURSE		Recreational irrigation	
S DRAIN	Drains Stormwater	---	These drains are located in Orange County and the reported flow rates are loosely correlated with rainfall (R2=0.85). Rainfall data from 1965 – 1977 was used to estimate these flow rates. Combined, L DRAIN, R DRAIN, S DRAIN and W DRAIN wells constitute 0.09% of the injected flow in the validation and calibration models.
Small PWS		Public supply	
W DRAIN	Drains Stormwater	---	These drains are located in Orange County and the reported flow rates are loosely correlated with rainfall (R2=0.85). Rainfall data from 1965 – 1977 was used to estimate these flow rates. Combined, L DRAIN, R DRAIN, S DRAIN and W DRAIN wells constitute 0.09% of the injected flow in the validation and calibration models.
0	Unspecified	Total freshwater	
<Blank>	Unspecified	Total freshwater	

Table 2.3: Application of SFWMM D13R Structure Codes to Regional Model ASR Flows

Structure Code	Dictionary Definition	Regional Model Application	
		Basin	Flow Direction
CPBTAS	Injection of water from Central Palm Beach County Agri. reservoir to ASR wells	Central Palm Beach	Recharge
CPBTLW	Recovery from ASR wells in Central Palm Beach County Agri. reservoir to maintain E-1 and E-2 (LWD1 & LWD2 in model) in Lake Worth Drainage District	Central Palm Beach	Recovery
C51TAS	Injection of Excess water from C-51 into ASR wells	C-51	Recharge
C51FAS	Recovery from ASR wells to maintain C-51 during dry periods	C-51	Recovery
ST1TAS	Injection of water from proposed Site1 reservoir to proposed ASR wells	Hillsboro	Recharge
S1ATHL	Recovery from proposed ASR wells in Site1 area to Hillsboro Canal for water supply purposes	Hillsboro	Recovery
CATASR	Injection of water from WPB Catchment Area to ASR wells	L-8	Recharge
CTASRR	Recovery from ASR wells in the WPB Catchment Area	L-8	Recovery
LOKASR	Injection of excess Lake Okeechobee water into proposed Lake Okeechobee ASR wells	Lake Okeechobee	Recharge
ASRLOK	Recovery from proposed Lake Okeechobee ASR to Lake Okeechobee if stage in Lake Okeechobee is sufficiently low	Lake Okeechobee	Recovery
RESTASR	Caloos reservoir water injected into ASR	Caloosahatchee	Recharge
ASRTBASIN	Recovery of ASR water to meet basin demands	Caloosahatchee	Recovery
ASRTEST	Recovery of ASR water to meet remaining estuarine demands	Caloosahatchee	Recovery

Table 6.1: Monte Carlo Ranges for Parameters, Group 1

Parameter	Lower Bound	Upper Bound
Porosity (one value for each layer)	0.25	0.4
Longitudinal Dispersivity (one value for each layer)	0.0	2.5
Molecular Diffusion - TDS (single value for whole model)	0	5.0e-5
Molecular Diffusion – temperature (single value for whole model)	0.0	0.5

Table 6.2: Monte Carlo Ranges for Parameters, Group 2

Parameter	Lower Bound	Upper Bound
Ratio: Longitudinal to Transverse Dispersivity (single value for whole model)	0.1	1.0
Ratio: Longitudinal to Vertical Dispersivity (single value for whole model)	0.01	1.0
Ratio: Horizontal to Vertical Hydraulic Conductivity (one value for each geologic unit)	0.1	1.0

Table 6.3 : Comparison of Monte Carlo Randomization to Calibration

Nash-Sutcliffe statistic	Points
E > 0.75	4
0.5 < E < 0.75	3
0.25 < E < 0.5	2
0.05 < E < 0.25	1
-0.05 < E < 0.05	0
E < -0.05	-1

APPENDIX E

Supporting documents for Regional ASR Study groundwater model

Regional Model Production Scenarios Appendices to USACE (2013)

A. Analysis of Specified Head Boundary Condition Impacts to D13R Regional Model plus Figures

B. Interagency Modeling Center Comments to Draft Report with Responses and Figures

APPENDIX A

ANALYSIS OF SPECIFIED HEAD BOUNDARY CONDITION IMPACTS TO D13R REGIONAL MODEL

1 INTRODUCTION

As described in Section 3.3 and Appendix C of the Regional Groundwater Model Calibration Report (NAP, 2011), specified head boundary conditions were used to assign heads to the surface and the sides of all aquifers in the model. (See Figure A.1) This type of boundary condition assumes there is an infinite source or sink of water available at each boundary and allows the model to add or remove any volume of water necessary to match the user-specified heads at the boundary. This assumption is valid at the eastern boundary of the RASRSM, where the aquifer layers outcrop in the Atlantic Ocean since no reasonable amount of pumping in the model domain would result in a change to the ocean level.

Similarly, specified heads were set in all cells across the top surface of the model. The alternative would have been to gather precipitation, evapotranspiration and seepage data and apply a flux to the surface. This would have required additional vertical discretization of the upper hydrogeologic layers. Because of the likely sparse nature of both sets of data, the incoming flux at the surface of the model would have been used as additional calibration parameters, increasing the uncertainty in the calibration and the non-uniqueness of the solution. Further, the surface waters in southern Florida are highly engineered with a vast, complicated system of canals, reservoirs and stormwater treatment areas (STA). The inclusion of these features would have added unwarranted complexity to the surface system. Instead, the measured heads at the base of the Hawthorn unit were interpolated and applied to the surficial grid layer and the model was allowed to add or remove water as necessary to honor those measured heads. In effect, the model calculates the infiltration or exfiltration necessary to match the field measured heads in the SAS. This simplification was made to reduce data collection efforts and to save the majority of the computational energy for the areas near the ASR wells in the FAS. Since the source of ASR recharge water is the surface water system, increases in heads in the SAS caused by ASR pumping will only replaced water that has already been removed. Similarly, recovered ASR water is to be returned to the surface water system, replacing any loss of water caused by the ASR system. Because the SAS is so highly engineered, it can be assumed to act as an infinite source/sink of water.

There is, however, no infinite water source at the south, west or north boundaries of the model. Instead, the boundary heads were based on measured groundwater heads and the boundaries were set far from the proposed ASR sites to prevent ASR impacts to the boundaries. Other pumping closer to the boundaries may exist, but those impacts would be included in the measured groundwater heads. This simplification was made for several reasons:

- Extension of the northern boundary to a more suitable boundary location (likely at some distance) would have greatly increased the level of effort in data collection.
- Extension of the southern and western boundaries to ocean outcrops would have greatly increased the uncertainty in the model since the outcrop in the Gulf of Mexico is nearly 150 miles from the shore and there is little or no groundwater data available in that large area. All parameters would have had to be estimated or extrapolated from measurements in the peninsula.

- Extension of the boundaries in either location would have significantly increased the size of the model and the computational time required to solve the governing equations. Since the existing model already taxes the capabilities of available computers, the resolution of the model would have had to be reduced to include the additional area.
- Pumping at the proposed ASR locations was not expected to impact the boundaries since they were so far away.

The specified heads at the edges of the aquifers were set based on the assumption that the boundaries were far enough from the proposed ASR sites that the effects of the pumping would not impact the boundaries. However, the area of influence of the ASR wells could not be known until after the calibration was finished and the production runs were completed. At this point, it is generally too late to go back and extend the boundaries further. Plus, for the reasons listed above, it was not feasible to include the additional areas in the model, even if necessary.

With the completion of the RASRSM-D13R runs described in the main report, an analysis of the maximum drawdown and "drawup" was completed as part of the investigation of the performance of each scenario. As shown in Figures 4.20, 4.39, 4.58, 4.77, 4.96, 4.115, 4.134, and 4.153 of the main report, significant levels of head change extend to the western, southern and northern boundaries of most of the aquifers for all scenarios. This indicates that the assumptions implicit in the use of specified head boundary conditions at these locations may have been violated.

This appendix describes the analysis which was used to determine the degree of impact to the model results from these faulty boundary condition assumptions.

2 TEST MODEL

It is difficult to quantify the effects of the boundary conditions on the RASRSM since we don't know how the model would have behaved had the boundaries been extended to more suitable locations. Instead, a set of smaller test models were built to analyze the impacts. Although the test model cannot be directly used to determine the influence of the near boundary conditions, it can be used to assess trends and can lead to a better understanding of the conditions.

2.1 BASE MODEL SETUP

A set of five MODFLOW models of varying sizes were built. Each was a single-layered, square model centered at the same location and built of square cells 10 ft on a side. The layer thickness was 100 feet and the layer was assumed to be unconfined. No density dependence was included. All boundaries were set using a specified head condition. Figure A.2 shows the boundaries of each model. Individual data on each model is listed in the following table.

Table A.1: Test model sizes

Model Name	Size (ft x ft [acres])	Number of cells on each side	Total Number of Cells
Largest	2990 x 2990 [205]	299	89401
Larger	1990 x 1990 [91]	199	39601
Large	990 x 990 [23.5]	99	9801
Small	390 x 390 [3.5]	39	1521
Smallest	110 x 110 [0.3]	11	121

The boundaries of the "Largest" grid were assumed to coincide with an infinite water source, making the boundary condition valid. The model was imagined as an island in a large lake or ocean so that all heads around the island coast were equal (50 feet). This model is assumed to represent "truth" for the purposes of this test. The other four models were designed with boundaries set inland of the shore. These were intended to test the impacts of assigning specified head boundary conditions based on site measured conditions instead of true infinite water sources. The boundary conditions on these four models were set based on the steady state results of the "Largest" model. This process reproduces the methodology used in the regional ASR model to set the boundary condition heads based on measured data.

An ASR well was placed in the center of the models and it was assigned a short pumping cycle. The sizes of the models and the pump rates of the ASR well were developed so that the boundaries of the "Small" and "Smallest" models were clearly impacted by the ASR well, while the boundary of the "Larger" model was not.

Finally, a small area of constant recharge was added to the center of each model, around the ASR well. The purpose of this recharge was to add a small rise in the water table at the center of the model. In this way, the natural flow of water would be outward, towards the boundaries before the ASR well impacted the system. This was meant to match the general trend of water flow from the north of the regional ASR model towards the south, east and west boundaries.

The flow parameters were simple, with the hydraulic conductivity set to 10 ft/d everywhere and the specific yield set to 0.1.

The first stress period of each model was a steady state condition with the recharge but no ASR pumping. A recharge rate of 5 ft/d was applied to each of 24 grid cells in the center of the model. Since each grid cell had an area of 100 ft^2, this resulted in the addition of 12,000 ft^3/d of water to the model. The results of this first stress period are shown in Figure A.3. Since the boundary conditions for the four smaller models were set based on the solution from the "Largest" model, all heads are identical. This is to reproduce the conditions that would exist if the heads of the smaller models were set from field measurements.

Following the first stress period, the models were subjected to a 50-day pumping schedule for the center ASR well. The schedule consisted of 10 days of injection at a rate of 20,000 ft^3/d (about 0.15

mgd) followed by 10 days of rest, then 10 days of extraction at a rate of 10,000 ft^3/d (about 0.075 mgd), 10 days of rest and 10 days of injection at 20,000 ft^3/d.

2.2 Base Model Results

The head profiles from base model (described above) are shown in Figure A.4 for each of the grids at the end of the injection and extraction periods. Both the "Large" and "Larger" models closely match the head results from the "Largest" model, which represents reality and from which the boundary conditions were taken. The "Small" model is pretty accurate at the end of the extraction period, with a head error of less than 1 foot, but at the end of the injection period, error is somewhat higher, up to nearly 4 feet at the edge of the model. The errors on the "Smallest" model are even larger: about 4 feet at the end of extraction and over 8 feet at the end of injection.

Figures A.5 through A.8 show the results of this base model at different locations. The top half of each figure shows the heads as they change with time for each of the models. Note that head values are labeled on the left axis. Generally, the smaller models quickly reach a steady state condition, indicated by a flat (zero) slope on the head plots. The bottom half of each figure shows the boundary fluxes caused by the ASR well pumping. These are the boundary fluxes calculated by the model with the flux from recharge (12,000 ft^3/d) subtracted. The values, listed on the right axis, are positive for flow into the model and negative for flow out of the model. The steady state condition is recognized in these plots when the boundary fluxes equal to the ASR pump rates (10,000 ft^3/d for injection; -20,000 ft^3/d for extraction).

For this base model, the "Smallest" model reaches a steady state condition almost immediately after the pumping changes. The "Small" model also reaches a steady state condition, but it takes several days to reach this condition. None of the other three models reach this steady state condition. Heads for the "Large", "Larger", and "Largest" models are nearly indistinguishable, except for some minor differences in the "Large" model. Fluxes for the "Larger" and "Largest" model move only slightly. There is an impact to the boundary fluxes on the "Large" model, but it never reaches the level of the ASR pump rates and it is damped and delayed. Head impacts at other points in the model follow similar patterns, but the magnitudes of the head changes are smaller for locations further from the ASR well.

Generally, heads are underpredicted by the smaller models during the injection periods. Note that this is non-conservative. When allowed to run to steady state, heads are overpredicted by smaller models during extraction periods, but depending on previous conditions and the length of time for extraction, the heads can be slightly underpredicted, as well. The worst head differences generally occur at the end of pumping periods and the beginning of rest periods.

This test indicates that the changes in flux caused by the ASR wells can be used as a proxy for the head impacts of the boundary condition effects. When the flux signature changes immediately to the ASR pump rate, there is a significant impact on the model heads caused by the boundary conditions being too close to the ASR wells. When the flux signature is damped and delayed from the ASR pumping schedule, there is only a minor impact to model heads caused by the boundary condition problems.

2.3 Model Variations

After analyzing the results of the base test model, a few variations were run to investigate the effects of the model parameters on the head and flux variations caused by boundary effects.

2.3.1 Variation 1 – Reduce Hydraulic Conductivity

In the first variation, the horizontal hydraulic conductivity was reduced from 10 ft/d to 1 ft/d. The results are shown in Figures A.9 through A.12. The smaller conductivity value increases the effect of the recharge and the ASR well pumping. Thus, heads are much higher in this variation than in the base model. The boundary fluxes caused by the ASR well quickly reach steady state for the "Small" and "Smallest" models. There is no discernible impact to boundary flux for either the "Larger" or "Largest" models. The heads for the three largest models are indistinguishable on the plots.

The important conclusion from this variation is that when the conductivity is lower, the head errors caused by the nearer specified head conditions are greater but the boundary fluxes caused by ASR pumping decrease.

2.3.2 Variation 2 – Increase Aquifer Thickness

For the second variation, the thickness of the aquifer was increased by dropping the bottom elevation of the grid from 0 ft to -50 ft. These results are shown in Figures A.13 through A.16. The head impacts of the ASR pumping are smaller for these models because of the greater thickness of the aquifer. The impact of the ASR wells on boundary flux is slightly greater for the thicker aquifer runs but the head differences are slightly smaller.

2.3.3 Variation 3 – Increase Storage

For the last variation, the storage was increased by changing the specific yield from 0.1 to 0.5. Higher storage causes an increase in the time required for the model to reach a steady state condition. As concluded by the base model, significant head differences caused by boundary effects are found when the models reach steady state conditions.

2.4 Conclusions from Test Model

The purpose of this test model was to understand better the boundary effects from specified head boundaries on an ASR model. The models were also built to understand the relationship between head errors in the interior of the model due to boundary effects and the fluxes through the model boundary caused by the ASR wells. Conclusions from this exercise include:

- Head errors are greatest at the end of pumping periods and the beginning of rest periods.
- Heads are under-predicted by too-small models during injection.
- Heads are over-predicted by too-small models during extraction when the systems near steady state; head differences earlier in the pumping period are affected by previous conditions.
- Significant head errors in the interior of the model occur for models which reach steady state.
- Steady state conditions can be recognized both by a flattening of the heads and the arrival of boundary fluxes at the rate of ASR pumping.

- Generally, if the fluxes stay well below ASR pumping rates, the heads errors caused by the boundary effects are minor.
- When aquifer thickness is increased, boundary fluxes increase, but they are not matched by a similar increase in head errors in the interior of the model.
- When the conductivity is increased, boundary fluxes increase, but they are not matched by a similar increase in head errors in the interior of the model.
- When the storage term is decreased, steady state conditions are reached sooner, with the associated head impacts.

3 Regional Model Analysis

All of the performance measures used to assess the acceptability of the RASRSM-D13R scenarios were based on the head results of the model. Therefore, it is the impact of boundary effects on interior heads that are of greatest importance.

Because we cannot rerun the RASRSM-D13R with larger boundaries, we cannot directly determine the impact of the specified head boundary conditions on the head results of the model. However, by comparing the fluxes leaving the model through the boundaries with and without the ASR wells pumping, and using the lessons learned from the test models described in Section 2, we can draw some conclusions about the possible impact to the performance measure results.

For each specified head cell of the model, the impact of the ASR wells was quantified by comparing the flux to or from the model without the ASR wells to the flux with the ASR wells. The sign convention specifies that flux into the model be positive, while flux leaving the model is negative. The flux with ASR wells was subtracted from the flux without the ASR wells. A positive flux difference, then, indicates that flux out of the model has been increased by the ASR wells, flux into the model has been decreased or, an area which previously had flux into the model has now switched to flux leaving the model. Similarly, a negative flux difference indicates that flux out of the model has been decreased, flux into the model has been increased or an area which previously had flux out of the model has now switched to flux entering the model.

These flux differences were then summed up across “questionable” boundaries, which are defined as any non-ocean boundary where a specified head was assigned without the existence of a suitable infinite source/sink of water. These are the north, west and south boundaries of each of the aquifer units.

On Figures A.21 through A.25, the flux differences (changes to boundary fluxes caused by ASR pumping) at questionable boundaries are compared to the total ASR pumping throughout the 13-year period of the model. The total ASR pumping all ASR sites. Note that some sites may be injecting while others are extracting and the two rates have been summed with extraction rates being set to negative.

In Figure A.21, the questionable boundary flux differences in the IAS/ICU are depicted next to the total ASR pumping. Note that the total boundary flux differences never exceed 0.6 mgd, which is much less

than the pumping for a single ASR well (5 mgd). It is clear from the plot that there is a significant delay in the increase of the boundary flux and the flux is far from steady state. The low flux impact and the lack of steady state conditions indicate that the impacts to the model results are minimal in this unit.

Figure A.22 shows the questionable boundary flux differences in the UF along with the same plot of the total ASR pumping as in the previous figure. Again, the flux differences are small compared to the ASR pumping rates, with the maximum rate at approximately 13 mgd, less than three ASR wells. During most of the model period, the flux differences are below 5 mgd. As before, the plot shows no sign of steady state conditions, so the head impacts are likely minimal in the interior of the model.

The questionable boundary flux differences in the APPZ are shown in Figure A.23. Here, the maximum flux differences are nearly 11 mgd, slightly more than the capacity of two ASR wells. During most of the modeled period, the flux differences are below 3 mgd. There is no sign of steady state conditions, indicating minimal head impacts caused by the boundary conditions.

Figure A.24 shows the questionable boundary flux differences in the LF unit. In this unit, the boundary fluxes become more significant. The maximum difference between fluxes with and without the ASR wells is over 36 mgd, more than the capacity of seven ASR wells. Although the flux difference plot is still well below the total ASR pump rate and has not reached a steady state condition, there is clearly less damping in this unit. The head impacts are still expected to be minimal, but are probably more pronounced than in the upper aquifer units.

Finally, Figure A.25 shows the questionable boundary flux differences in the BZ. This unit shows the greatest flux difference caused by the ASR pumping with the maximum rate at nearly 435 mgd, the equivalent of almost 87 ASR wells. Although this seems like a significant flux difference, the plot still shows no evidence of arrival at steady state conditions. And the flow rate is still far below the maximum ASR pumping rate of over 1600 mgd. There is, however, a significant drop in the damping effects of the flux difference plot. Changes in flux occur quite rapidly after a change to the ASR pumping. The head impacts are expected to be minimal, but may be more pronounced than in the upper units.

Figure A.26 compares the boundary flux distributions across the 13-year period for each of the four aquifer units (UF, APPZ, LF, BZ). This plot reiterates the information from the previous plots.

It seems clear that there is no significant impact to heads in the IAS/ICU due to boundary condition effects. The confining unit in layer 4 of the model appears to cut off the ASR pumping from the western boundary of the IAS. This minimal impact is also apparent in the drawdown plots in Figure 4.134 of the main report. Significant head differences from the ASR system barely reach the western boundary of the model in a few places. No specified head boundary conditions are set on the north or south boundaries in these layers.

The impact to heads in the UF and APPZ is also likely insignificant. There is severe damping in the boundary flux difference plots and the flux differences are quite small compared to the ASR pumping. Impacts to heads are assumed to be within the error tolerance of the model.

The impacts to heads in the interior of the LF and BZ units could be larger. The damping observed in the upper units is less pronounced in these units. The magnitudes of the flux differences are also larger. However, neither unit reaches a steady state condition. Based on the test models described in Section 2, head impacts are not significant when the boundary flux differences are well below the ASR pumping rate and when they do not reach a steady state condition.

Further analysis of the model parameters in each of the layers can lend additional credence to the idea that head impacts are insignificant. Figure A.27 compares the aquifer thicknesses for each of the four aquifer units (UF, APPZ, LF, BZ). Note that the distributions are based on total area, not on total number of cells. One quarter of the model domain area fits into each section of the blue bar, with an additional quarter fitting into the black lined error bars above and below the blue bars. In Figure A.27, we see that the BZ thickness is 500 ft across the entire domain. The majority of each of the other aquifers is much thinner than 500 ft. One of the conclusions of the test model presented in Section 2 of this appendix was that an increased thickness can cause an increase in boundary flux differences without an associated increase in head errors. Thus, some of the large boundary flux differences experienced by the BZ may be the result of a thicker unit, not the result of additional error caused by the boundary condition selection.

Figure A.28 compares the horizontal hydraulic conductivities of each of the four units. Although there is a wide distribution of hydraulic conductivities in all units, the majority of the BZ has been assigned a hydraulic conductivity value that is at least one full order of magnitude higher than the majority of the values in the other units. The conductivity values in the LF are slightly higher than those in the APPZ and about an order of magnitude higher than those in the UF. One of the conclusions of the test model presented in Section 2 of this appendix was that higher conductivity values can have an impact on the boundary flux changes without having a parallel impact on interior head results. Some of the flux differences observed in the LF and BZ (shown in Figures A.24 and A.25) could be due to greater hydraulic conductivity, and not due to faulty boundary condition assignments.

Figure A.29 compares the specific storage values assigned to each of the four units. Note that the LF and the BZ have generally lower specific storage than the upper aquifer units. As described in Section 2 of this appendix, the smaller storage values result in a faster arrival at steady state conditions. This is seen in the regional model as a slight reduction in the damping effect of the boundary flux differences. However, since neither aquifer reaches any condition that appears to be steady state, there is little reason to suppose that head impacts in the interior of the model are significant.

4 CONCLUSIONS

A test model was built to investigate the relationship between flux differences at questionable boundaries due to ASR pumping and interior head differences caused by the specified head boundary conditions which did not correspond to infinite source/sinks of water. The table below lists the observations on the test model, the corresponding observations on the RASRSM and the conclusions that can be drawn.

Test Model Observations	RASRSM-D13R Observations	Conclusions
Head errors are greatest at the end of pumping periods and the beginning of rest periods.	The limiting factors on the performance measures generally occur at the end of the pumping periods when the head impacts from the ASR wells are greatest.	This is non-conservative for the RASRSM.
Heads are under-predicted by too-small models during injection.	N/A	This is non-conservative for the RASRSM.
Heads are over-predicted by too-small models during extraction when the systems near steady state; head differences earlier in the pumping period are affected by previous conditions.	N/A	This is non-conservative for the RASRSM.
Significant head errors in the interior of the model occur for models which reach steady state. Steady state conditions can be recognized both by a flattening of the heads and the arrival of boundary fluxes at the rate of ASR pumping.	The flux differences at the boundaries never reach steady state during the RASRSM run.	Head errors caused by the poorly defined boundary conditions are unlikely to be significant in the RASRSM.
Generally, if the fluxes remain below ASR pumping rates, the head errors caused by the boundary effects are minor.	The flux differences are far short of the ASR pumping rates in each aquifer unit of the model.	Head errors caused by the boundary effects are expected to be minor in all layers.
When aquifer thickness is increased, boundary fluxes increase, but they are not matched by a similar increase in head errors in the interior of the model.	The BZ, where the greatest flux differences were observed, is thicker than most areas of other units in the model.	Some of the boundary flux differences observed in the BZ are likely due to the increased unit thickness and do not indicate a significant head impact in the interior of the model.
When the conductivity is increased, boundary fluxes increase, but they are not matched by a similar increase in head errors in the interior of the model.	Hydraulic conductivities are generally greater in the LF and BZ layers of the model, where the greatest flux differences are observed.	Some of the boundary flux differences observed in the LF and BZ are likely due to greater hydraulic conductivity and do not indicate a significant head impact in the interior of the model.

Test Model Observations	RASRSM-D13R Observations	Conclusions
When the storage term is decreased, steady state conditions are reached sooner, with the associated head impacts.	The specific storage in the LF and BZ layers is generally smaller than in the UF and APPZ layers.	The smaller storage term in the LF and BZ account for the loss of some of the damping in the flux difference plots. However, a steady state condition is never reached in any of the layers.

The analysis and observations described in this appendix have led to the conclusion that the selection of specified head boundary conditions at areas interior of the ocean outcrop have not adversely affected the analysis of performance measures in the interior of the regional model. Any differences will be minor and within the error tolerance of the model.

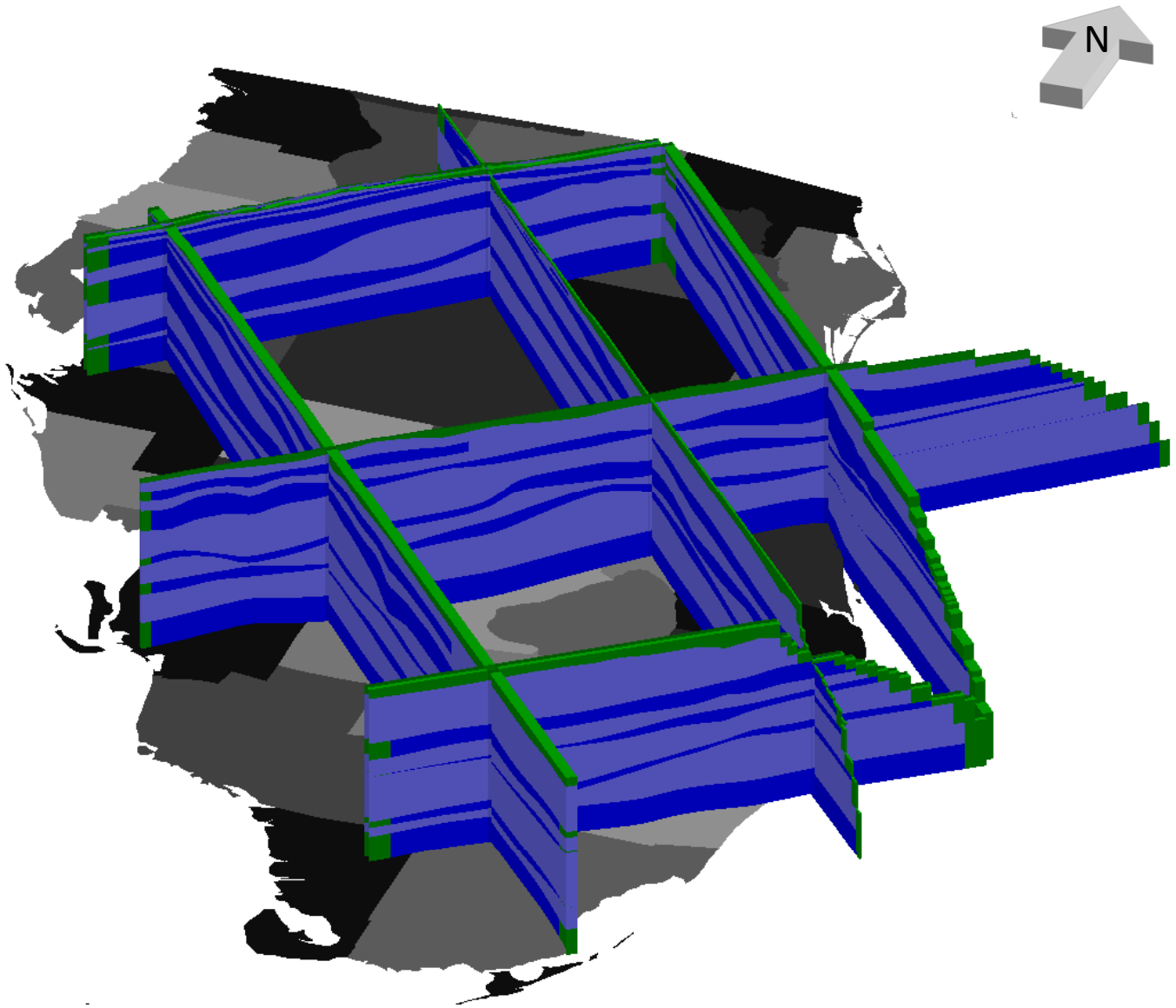

Legend

- Aquifer Layers
- Confining Units
- Specified Head Cells

Notes:

Specified head boundary conditions were applied to the top surface of the model, the Atlantic Ocean outcrop for all layers and the inland north, west, and south boundaries for aquifer layers.

Vertical exaggeration is 50.

SPECIFIED HEAD BOUNDARY CONDITIONS

DRAFT REGIONAL MODEL PRODUCTION SCENARIO REPORT

FIGURE A.1

JUNE 2013

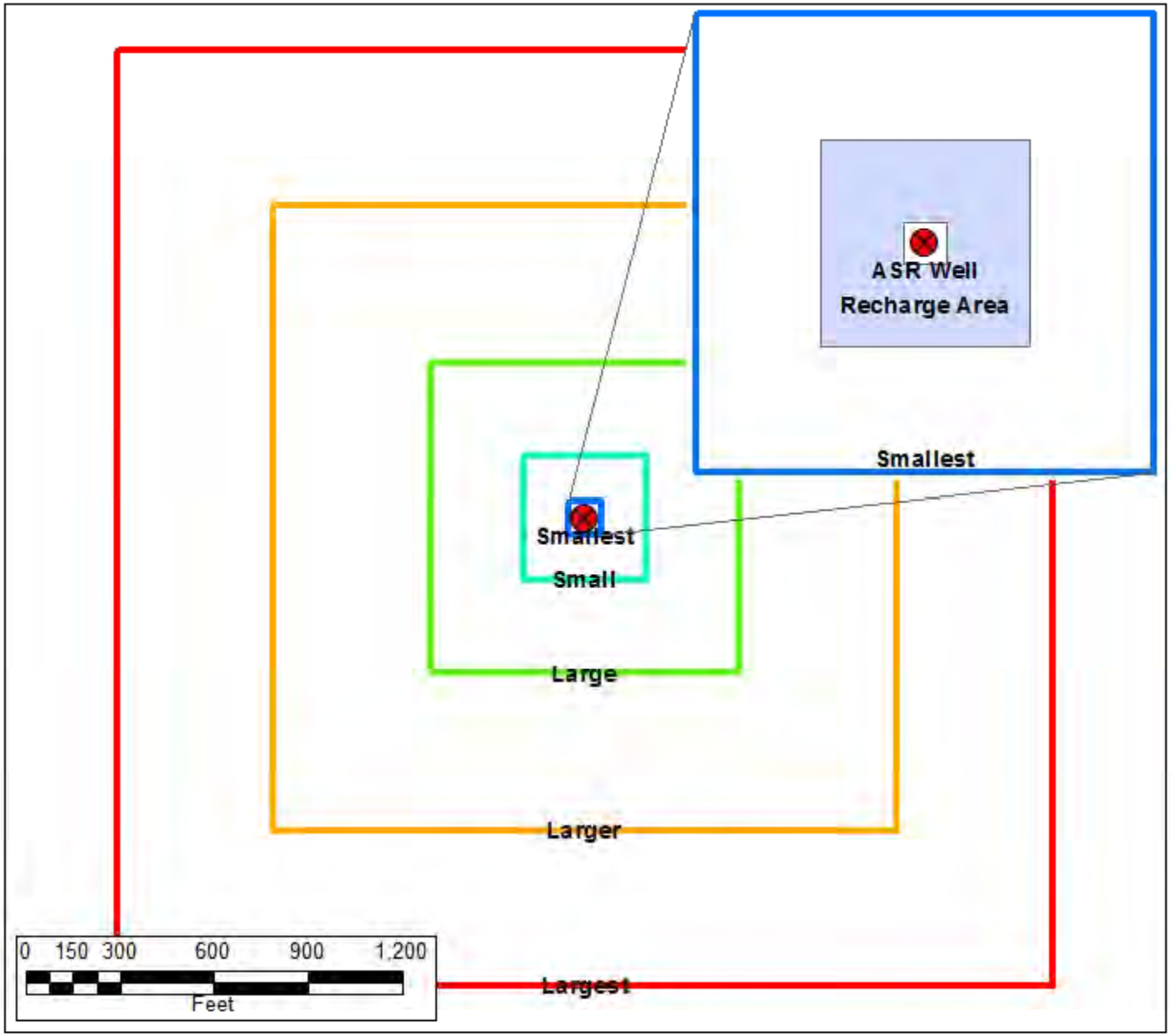

Notes:

The five test models were designed to be of varying sizes centered around the ASR well. A small area of recharge was set in the middle to produce a slightly raised water table with flow going out to all boundaries.

Each model consisted of 10 ft x 10 ft square cells and the thickness of the single layer was 100 ft.

The specified head boundary condition of 50 ft was set at the boundary of the "Largest" model. The steady state results of that model were then used to set the boundary conditions of all other models.

TEST MODEL BOUNDARIES

FIGURE A.2

DRAFT REGIONAL MODEL PRODUCTION SCENARIO REPORT

JUNE 2013

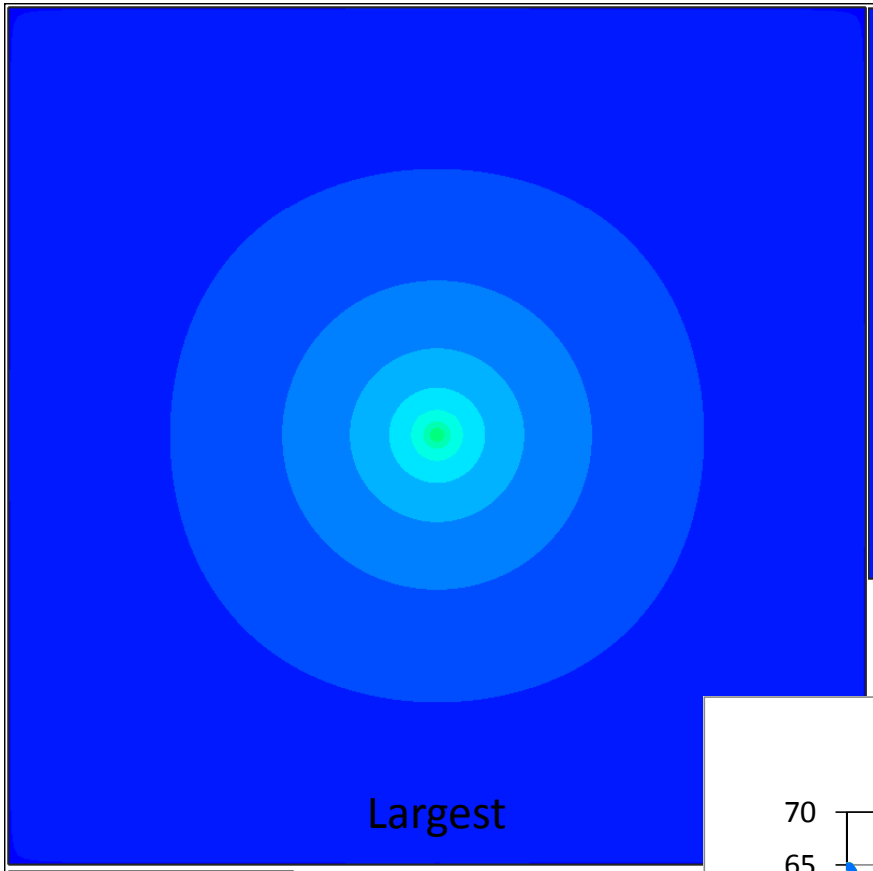

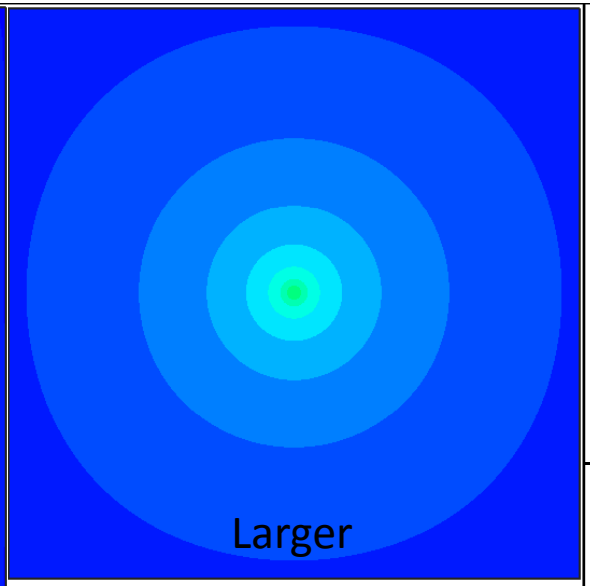

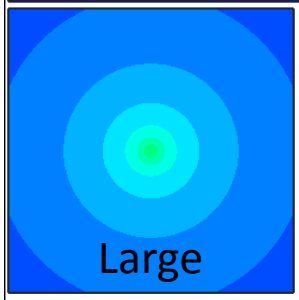

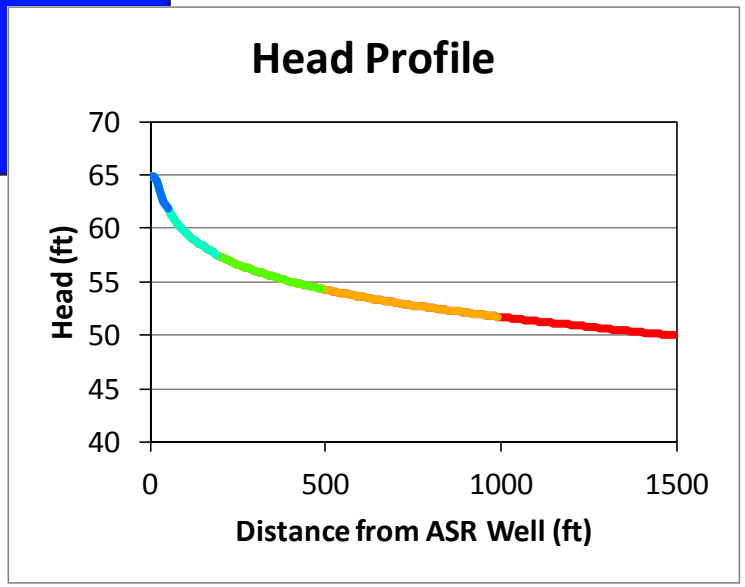

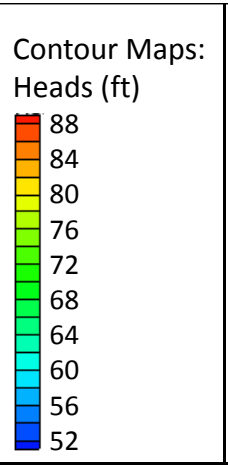

Notes:

These figures show the steady state condition used as a starting condition for the ASR test model. The "Largest" model has specified heads of 50 ft along the entire outside boundary and a small area of recharge near the center. The boundary conditions on the outside boundaries of the smaller four models are set from the "Largest" model and all have the same area of recharge near the center. The five images and the head profile plot show that the initial condition for each of the five models were identical.

STEADY STATE HEAD CONDITION

FIGURE A.3

DRAFT REGIONAL MODEL PRODUCTION SCENARIO REPORT

JUNE 2013

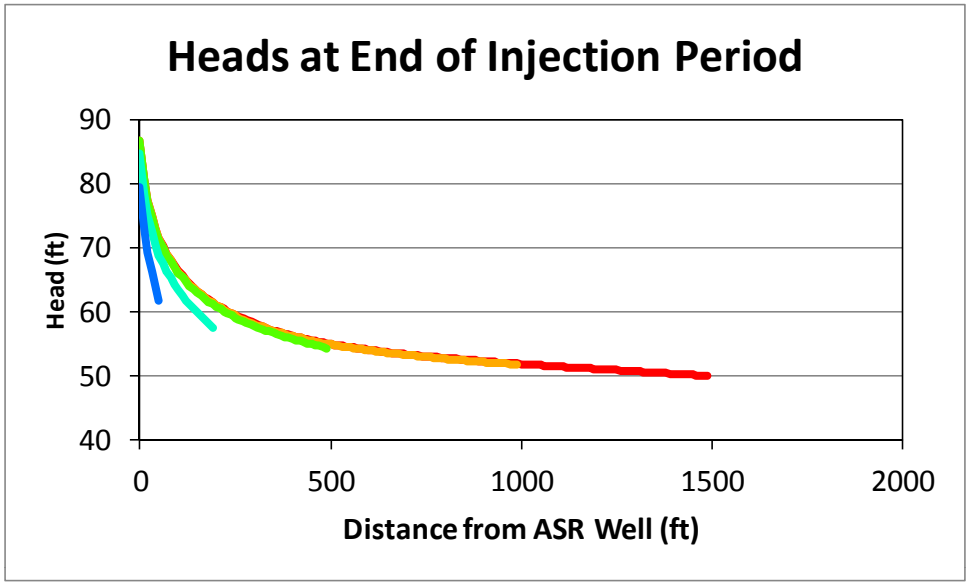

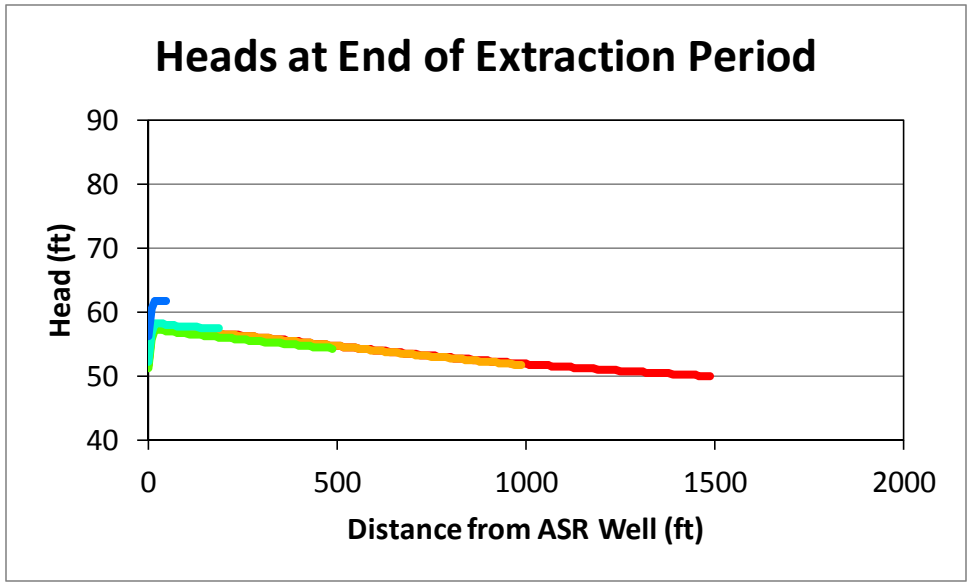

Smallest model
Small model
Large model
Larger model
Largest model

Notes:

These plots show the head profiles at the end of the injection and extraction periods for each of the base test models.

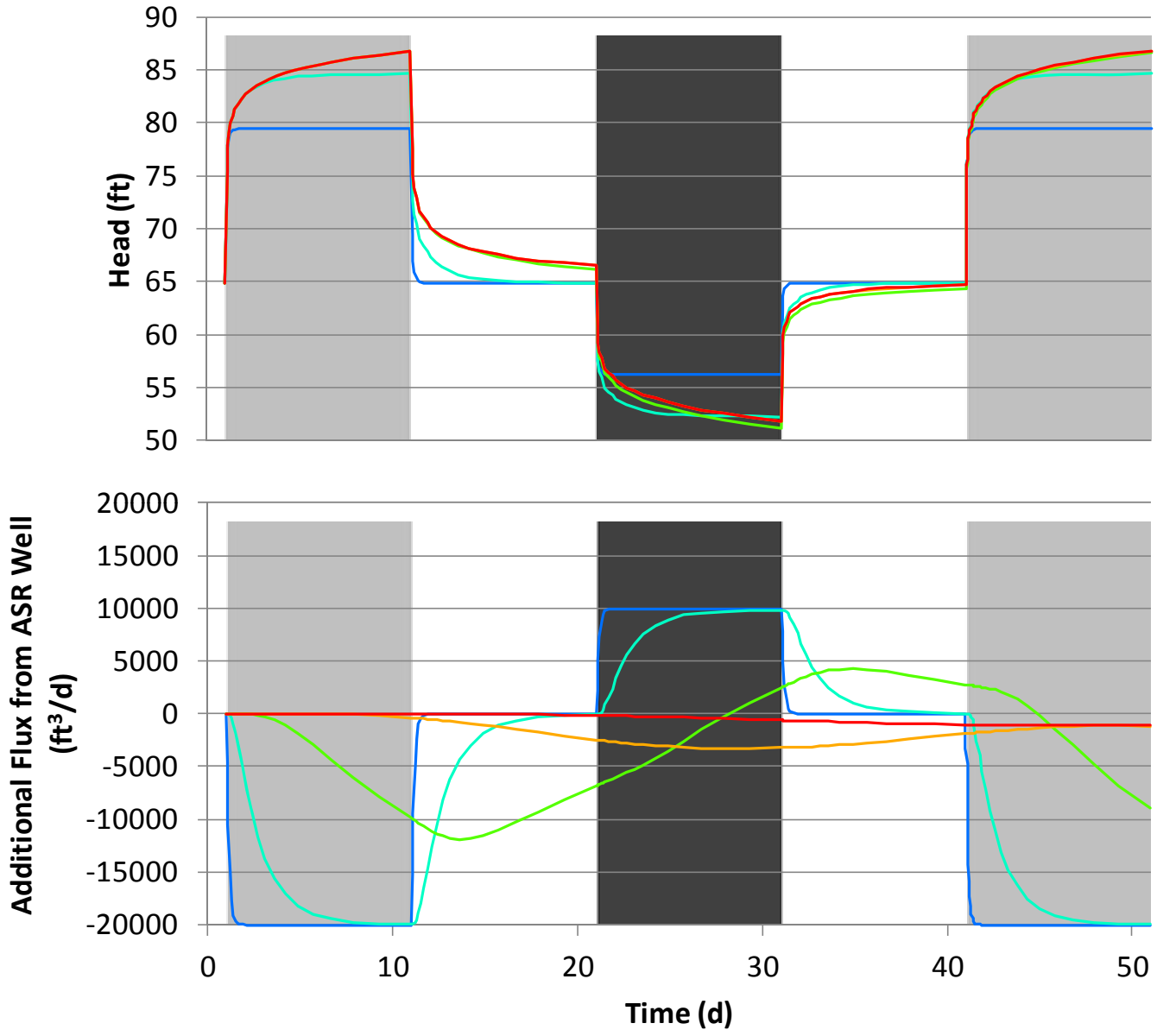

Smallest model
Small model
Large model
Larger model
Largest model

Injection Period
Extraction Period

Notes:

The upper plot shows the heads at the ASR well for each of the five base test models.

The lower plot shows the boundary flux changes (compared to the steady state flux) for each of the five base test models. Positive values indicate flow into the model; negative values indicate flow out of the model.

Note that the injection rate at the ASR well was 20,000 ft^3/d and the extraction rate was 10,000 ft^3/d.

BASE TEST MODEL RESULTS: HEADS AT THE ASR WELL AND BOUNDARY FLUXES

DRAFT REGIONAL MODEL PRODUCTION SCENARIO REPORT

FIGURE A.5

JUNE 2013

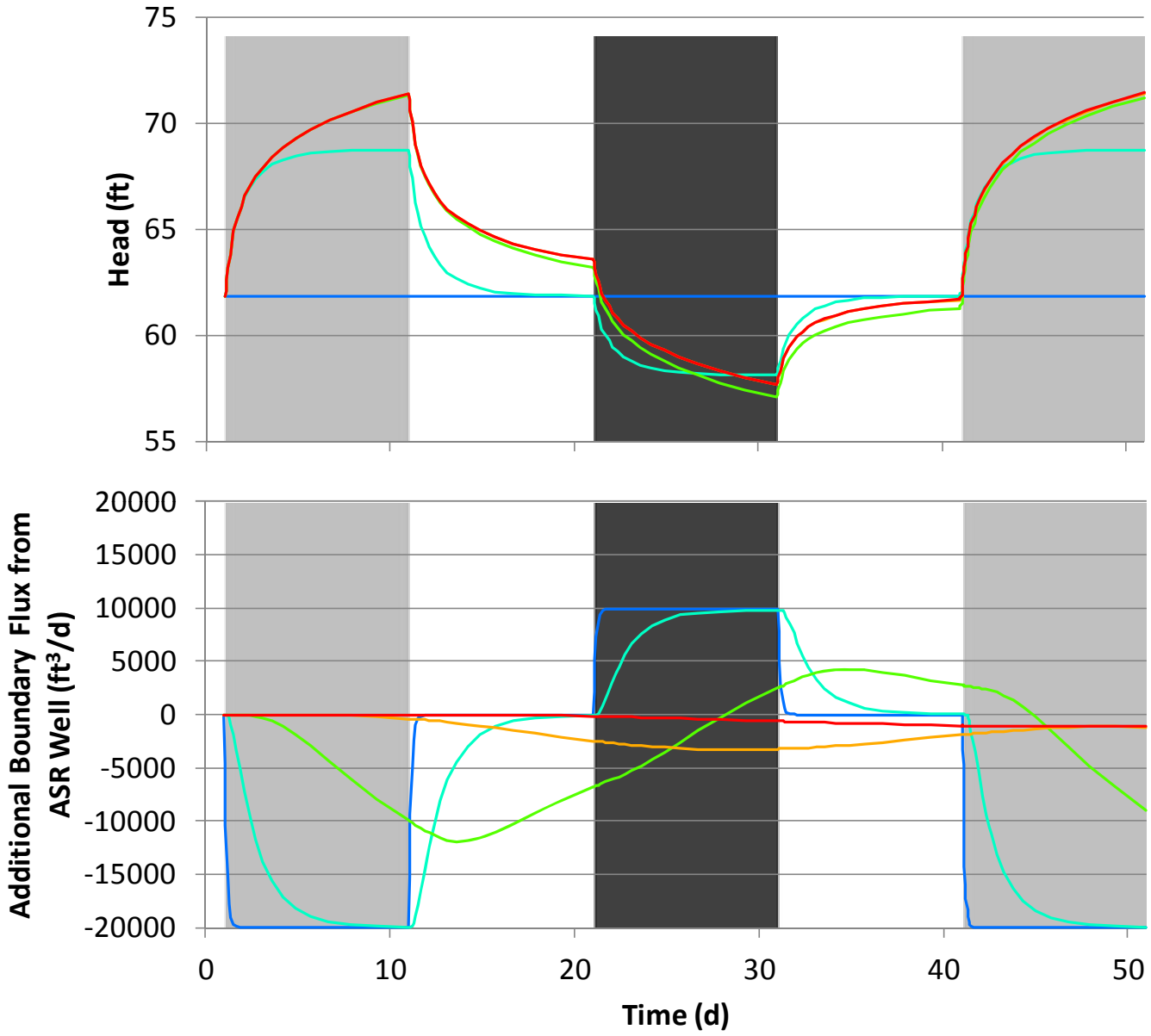

Smallest model
Small model
Large model
Larger model
Largest model

Injection Period
Extraction Period

Notes:

The upper plot shows the heads 50 ft from the ASR well for each of the five base test models.

The lower plot shows the boundary flux changes (compared to the steady state flux) for each of the five base test models. Positive values indicate flow into the model; negative values indicate flow out of the model.

Note that the injection rate at the ASR well was 20,000 ft^3/d and the extraction rate was 10,000 ft^3/d.

BASE TEST MODEL RESULTS: HEADS 50 FT FROM ASR WELL AND BOUNDARY FLUXES

DRAFT REGIONAL MODEL PRODUCTION SCENARIO REPORT

FIGURE A.6

JUNE 2013

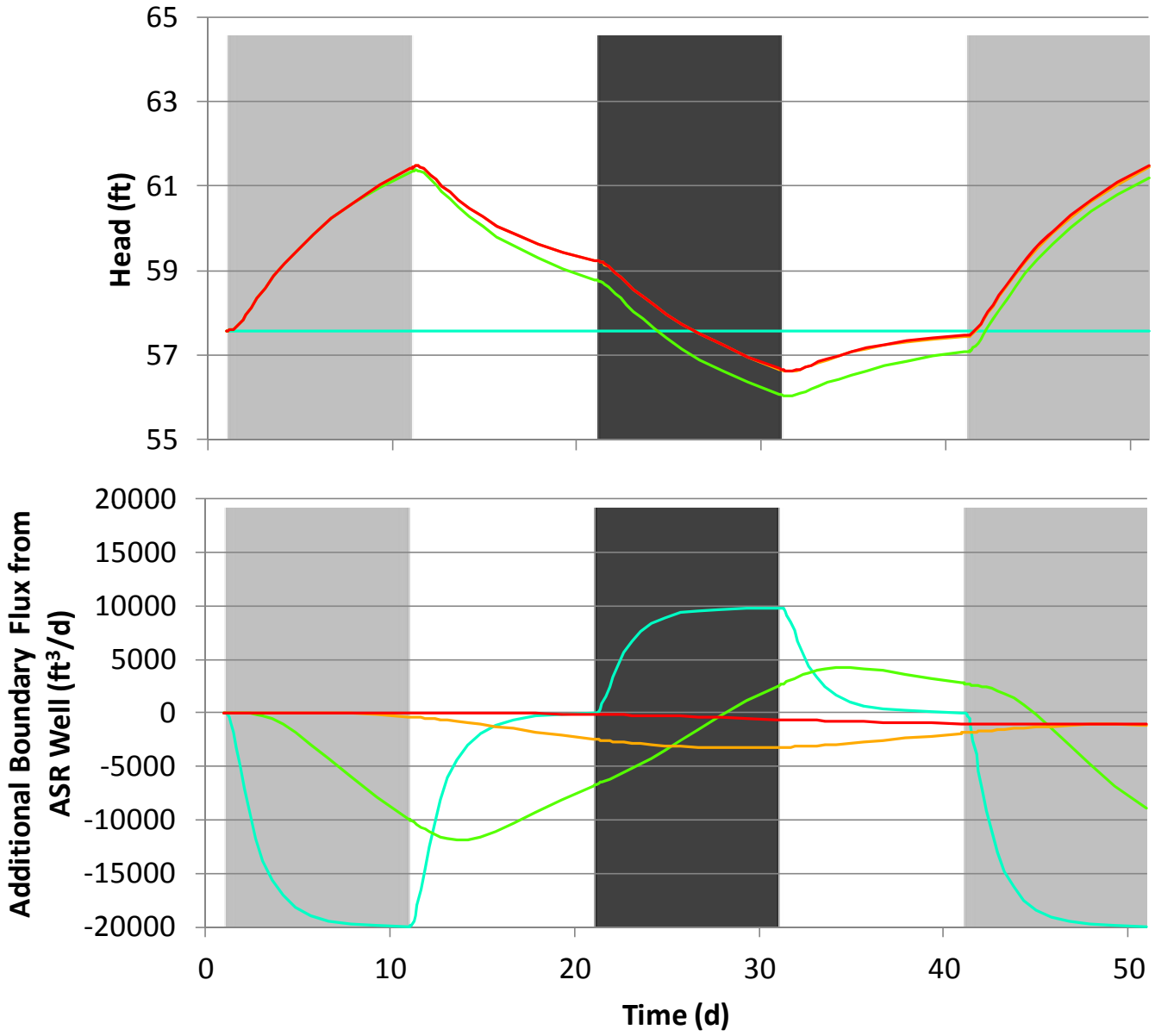

Small model
Large model
Larger model
Largest model

Injection Period
Extraction Period

Notes:

The upper plot shows the heads 190 ft from the ASR well for each of four base test models. (The smallest model is not large enough to provide results at a distance of 190 ft.)

The lower plot shows the boundary flux changes (compared to the steady state flux) for each of four base test models. Positive values indicate flow into the model; negative values indicate flow out of the model.

Note that the injection rate at the ASR well was 20,000 ft^3/d and the extraction rate was 10,000 ft^3/d.

BASE TEST MODEL RESULTS: HEADS 190 FT FROM ASR WELL AND BOUNDARY FLUXES

DRAFT REGIONAL MODEL PRODUCTION SCENARIO REPORT

FIGURE A.7

JUNE 2013

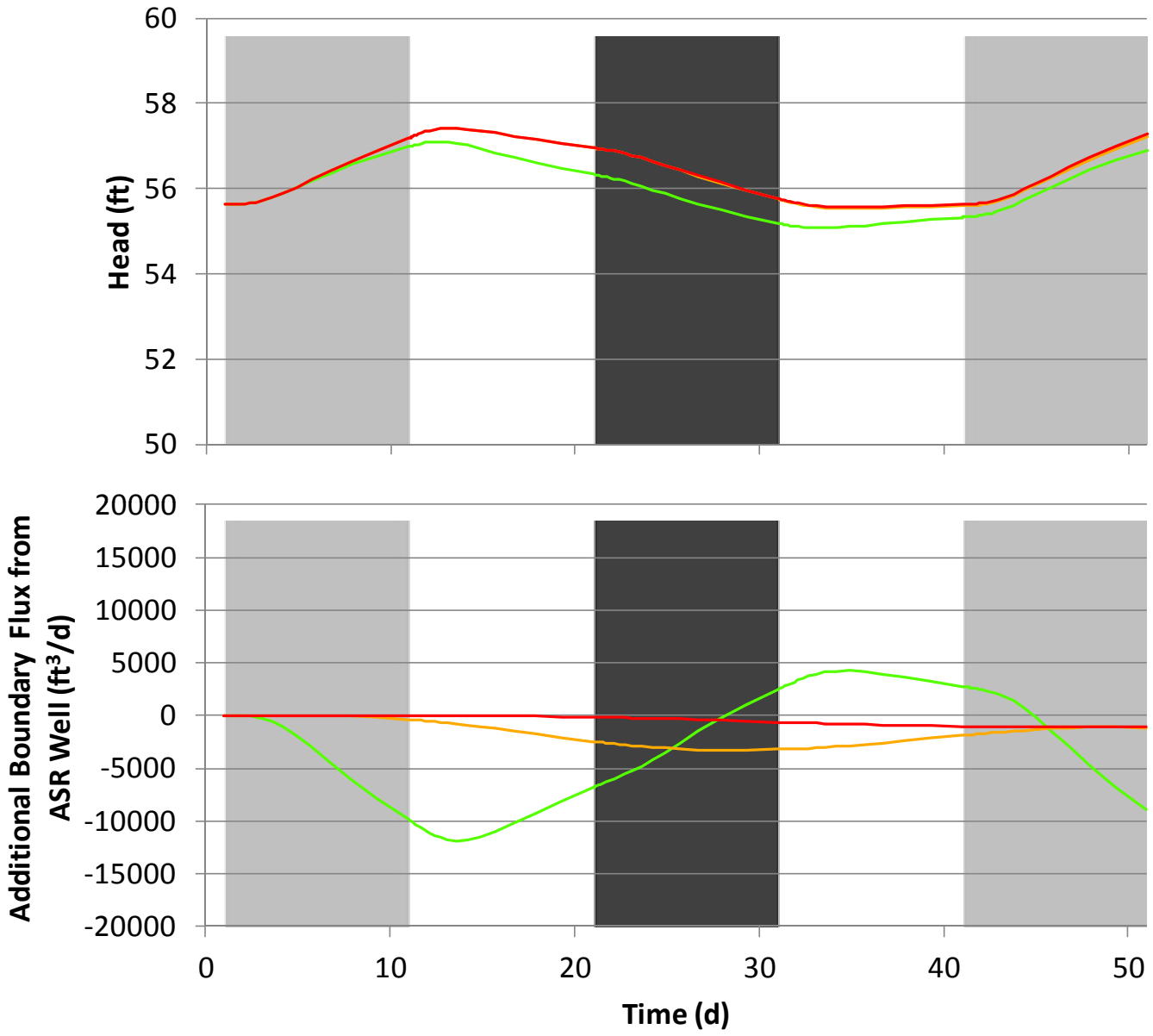

Large model
Larger model
Largest model

Injection Period
Extraction Period

Notes:

The upper plot shows the heads 340 ft from the ASR well for each of three base test models. (The small and smallest models are not large enough to provide results at a distance of 340 ft.)

The lower plot shows the boundary flux changes (compared to the steady state flux) for each of three base test models. Positive values indicate flow into the model; negative values indicate flow out of the model.

Note that the injection rate at the ASR well was 20,000 ft^3/d and the extraction rate was 10,000 ft^3/d.

BASE TEST MODEL RESULTS: HEADS 340 FT FROM ASR WELL AND BOUNDARY FLUXES

DRAFT REGIONAL MODEL PRODUCTION SCENARIO REPORT

FIGURE A.8

JUNE 2013

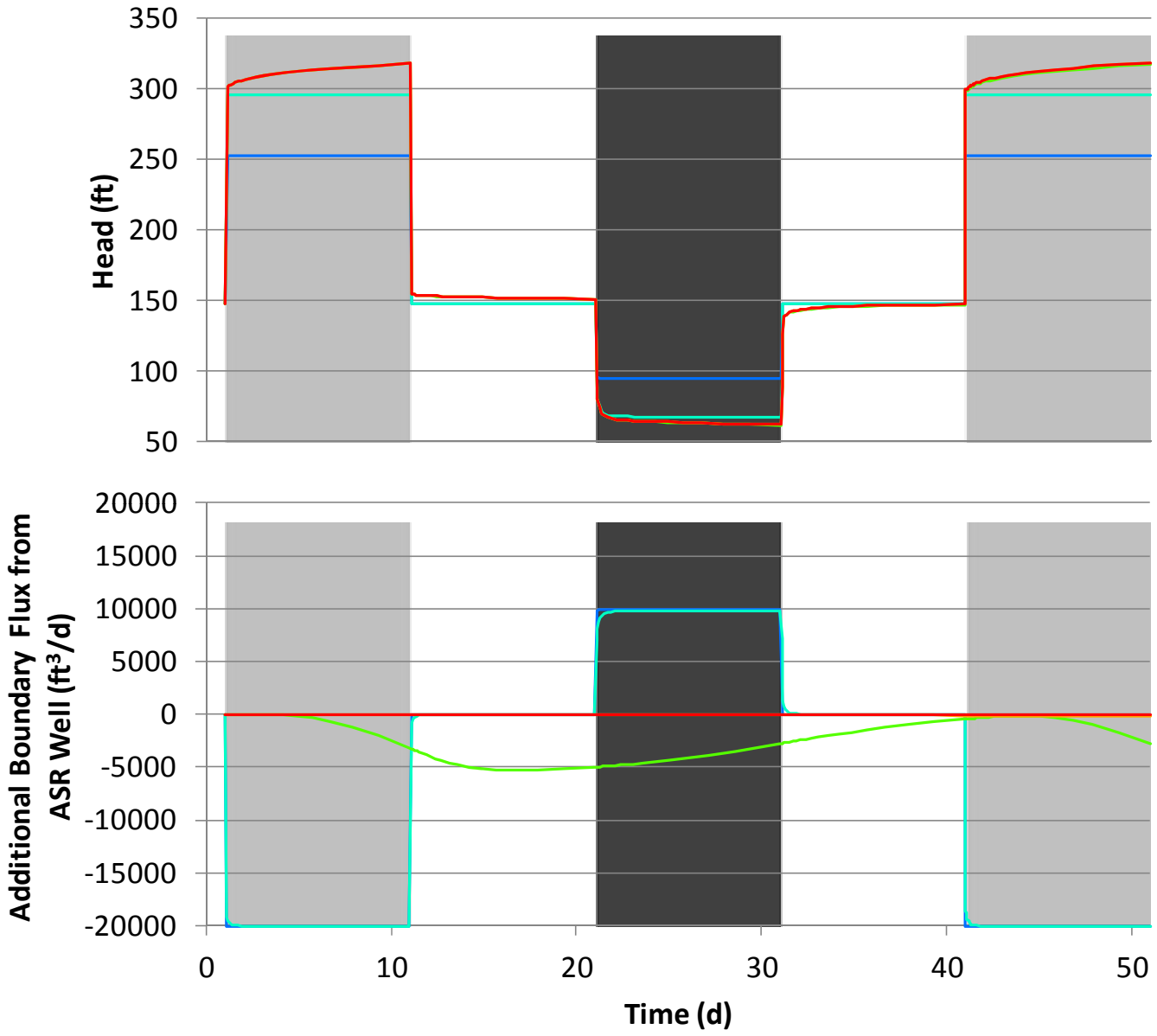

Smallest model
Small model
Large model
Larger model
Largest model

Injection Period
Extraction Period

Notes:

The upper plot shows the heads at the ASR well for each of the five decreased conductivity test models.

The lower plot shows the boundary flux changes (compared to the steady state flux) for each of the five decreased conductivity test models. Positive values indicate flow into the model; negative values indicate flow out of the model.

Note that the injection rate at the ASR well was 20,000 ft^3/d and the extraction rate was 10,000 ft^3/d.

DECREASED CONDUCTIVITY TEST MODEL RESULTS: HEADS AT THE ASR WELL AND BOUNDARY FLUXES

DRAFT REGIONAL MODEL PRODUCTION SCENARIO REPORT

FIGURE A.9

JUNE 2013

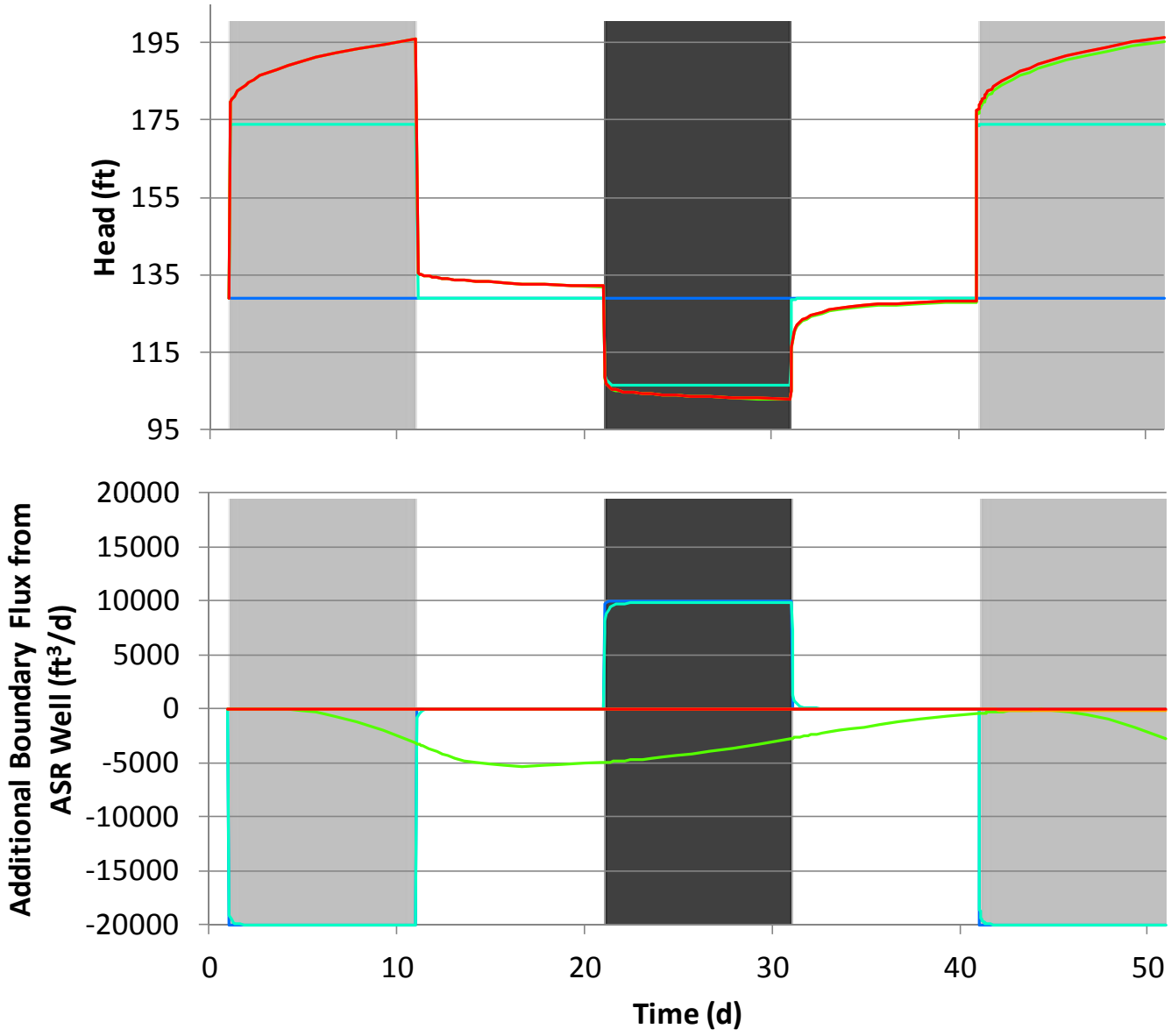

Smallest model
Small model
Large model
Larger model
Largest model

Injection Period
Extraction Period

Notes:

The upper plot shows the heads 50 ft from the ASR well for each of the five decreased conductivity test models.

The lower plot show the boundary flux changes (compared to the steady state flux) for each of the five decreased conductivity test models. Positive values indicate flow into the model; negative values indicate flow out of the model.

Note that the injection rate at the ASR well was 20,000 ft^3/d and the extraction rate was 10,000 ft^3/d.

DECREASED CONDUCTIVITY TEST MODEL RESULTS: HEADS 50 FT FROM ASR WELL AND BOUNDARY FLUXES

DRAFT REGIONAL MODEL PRODUCTION SCENARIO REPORT

FIGURE A.10

JUNE 2013

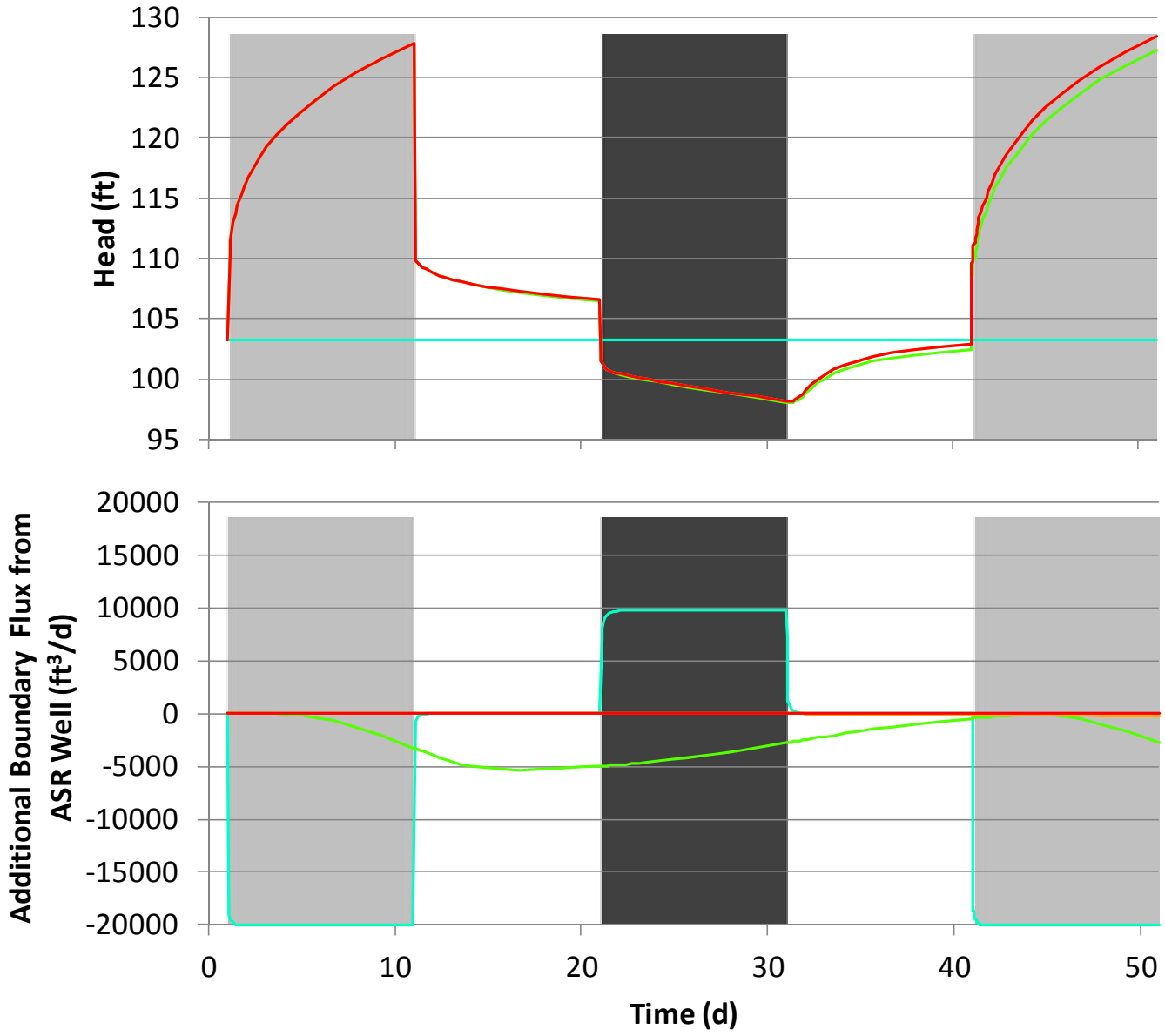

Small model
Large model
Larger model
Largest model

Injection Period
Extraction Period

Notes:

The upper plot shows the heads 190 ft from the ASR well for each of four decreased conductivity test models. (The smallest model is not large enough to provide results at a distance of 190 ft.)

The lower plot shows the boundary flux changes (compared to the steady state flux) for each of the five decreased conductivity test models. Positive values indicate flow into the model; negative values indicate flow out of the model.

Note that the injection rate at the ASR well was 20,000 ft^3/d and the extraction rate was 10,000 ft^3/d.

DECREASED CONDUCTIVITY TEST MODEL RESULTS: HEADS 190 FT FROM ASR WELL AND BOUNDARY FLUXES

DRAFT REGIONAL MODEL PRODUCTION SCENARIO REPORT

FIGURE A.11

JUNE 2013

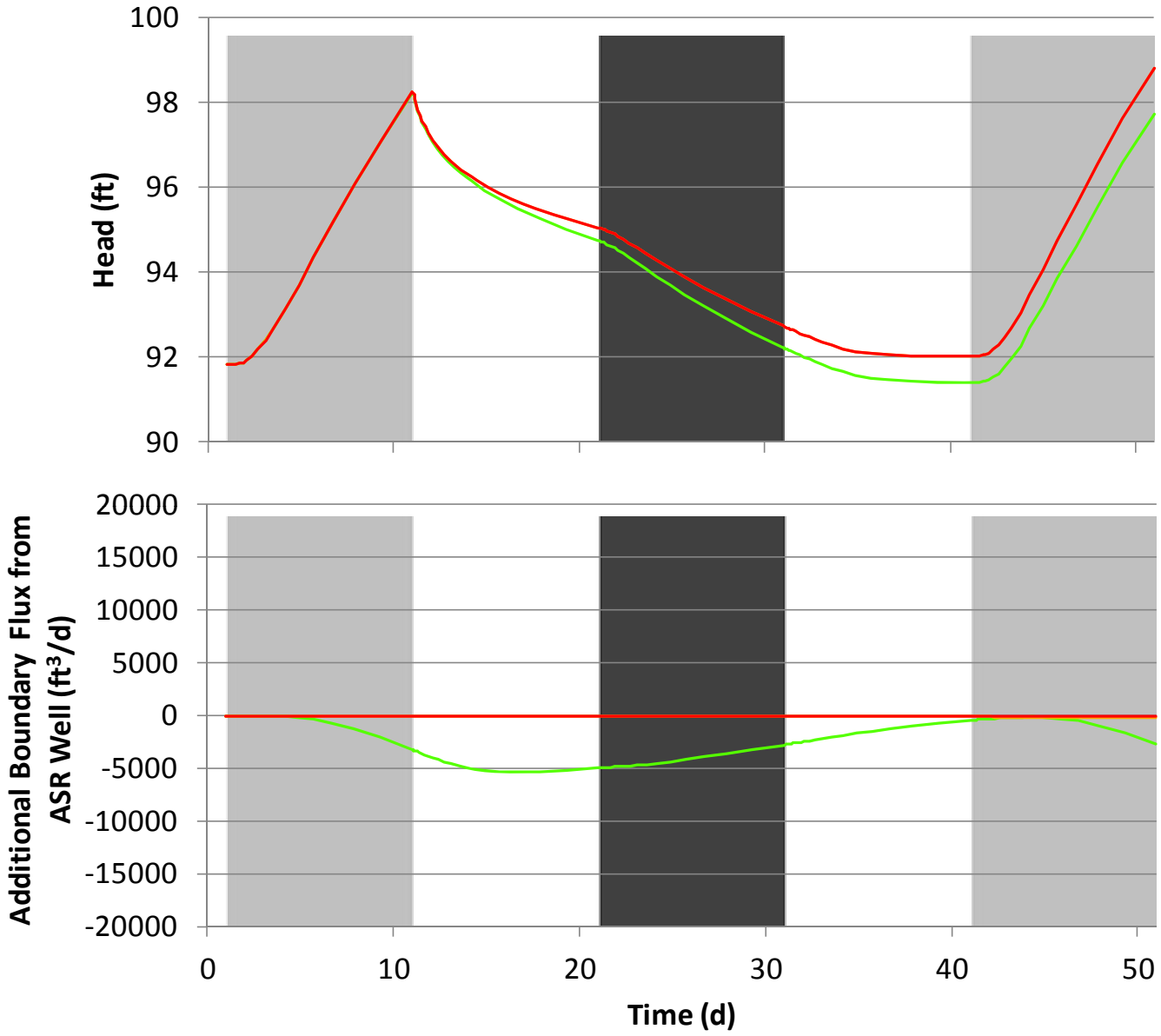

Large model
Larger model
Largest model

Injection Period
Extraction Period

Notes:

The upper plot shows the heads 340 ft from the ASR well for each of three decreased conductivity test models. (The small and smallest models are not large enough to provide results at a distance of 340 ft.)

The lower plot shows the boundary flux changes (compared to the steady state flux) for each of three decreased conductivity test models. Positive values indicate flow into the model; negative values indicate flow out of the model.

Note that the injection rate at the ASR well was 20,000 ft^3/d and the extraction rate was 10,000 ft^3/d.

DECREASED CONDUCTIVITY TEST MODEL RESULTS: HEADS 340 FT FROM ASR WELL AND BOUNDARY FLUXES

DRAFT REGIONAL MODEL PRODUCTION SCENARIO REPORT

FIGURE A.12

JUNE 2013

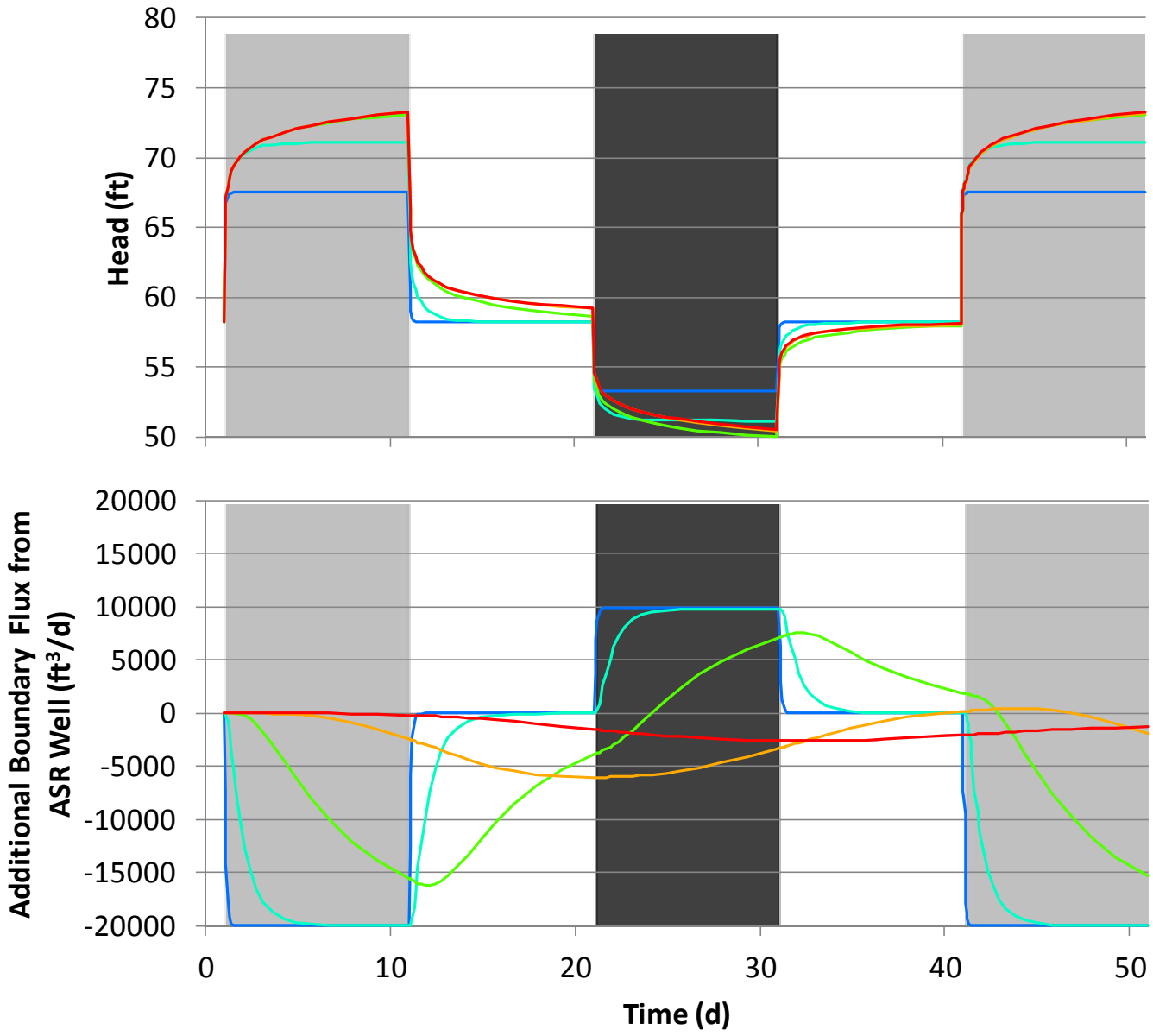

Smallest model
Small model
Large model
Larger model
Largest model

Injection Period
Extraction Period

Notes:

The upper plot shows the heads at the ASR well for each of the five increased thickness test models.

The lower plot shows the boundary flux changes (compared to the steady state flux) for each of the five increased thickness test models. Positive values indicate flow into the model; negative values indicate flow out of the model.

Note that the injection rate at the ASR well was 20,000 ft^3/d and the extraction rate was 10,000 ft^3/d.

INCREASED THICKNESS TEST MODEL RESULTS: HEADS AT THE ASR WELL AND BOUNDARY FLUXES

DRAFT REGIONAL MODEL PRODUCTION SCENARIO REPORT

FIGURE A.13

JUNE 2013

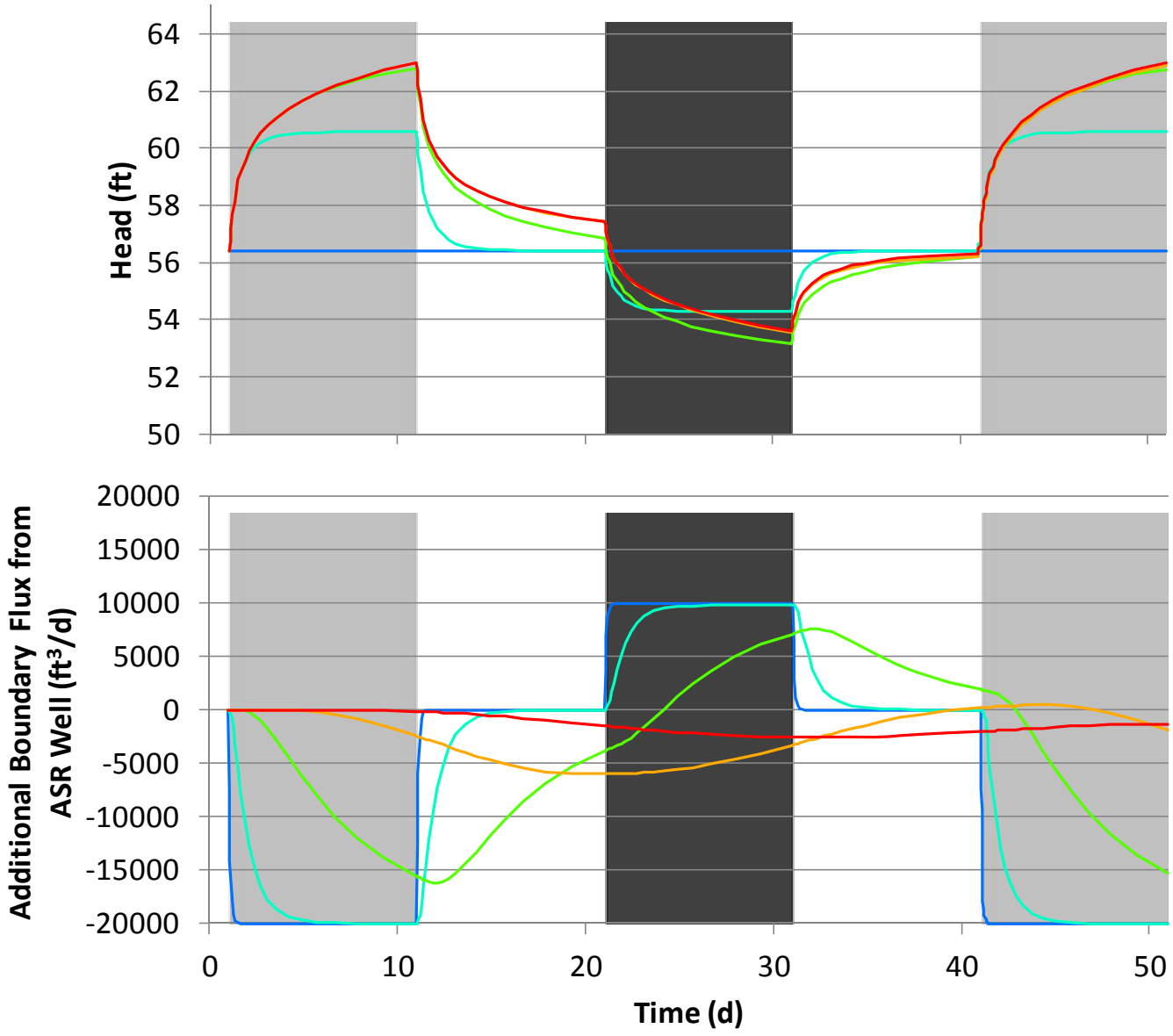

Smallest model
Small model
Large model
Larger model
Largest model

Injection Period
Extraction Period

Notes:

The upper plot shows the heads 50 ft from the ASR well for each of the five increased thickness test models.

The lower plot shows the boundary flux changes (compared to the steady state flux) for each of the five increased thickness test models. Positive values indicate flow into the model; negative values indicate flow out of the model.

Note that the injection rate at the ASR well was 20,000 ft^3/d and the extraction rate was 10,000 ft^3/d.

INCREASED THICKNESS TEST MODEL RESULTS: HEADS 50 FT FROM ASR WELL AND BOUNDARY FLUXES

DRAFT REGIONAL MODEL PRODUCTION SCENARIO REPORT

FIGURE A.14

JUNE 2013

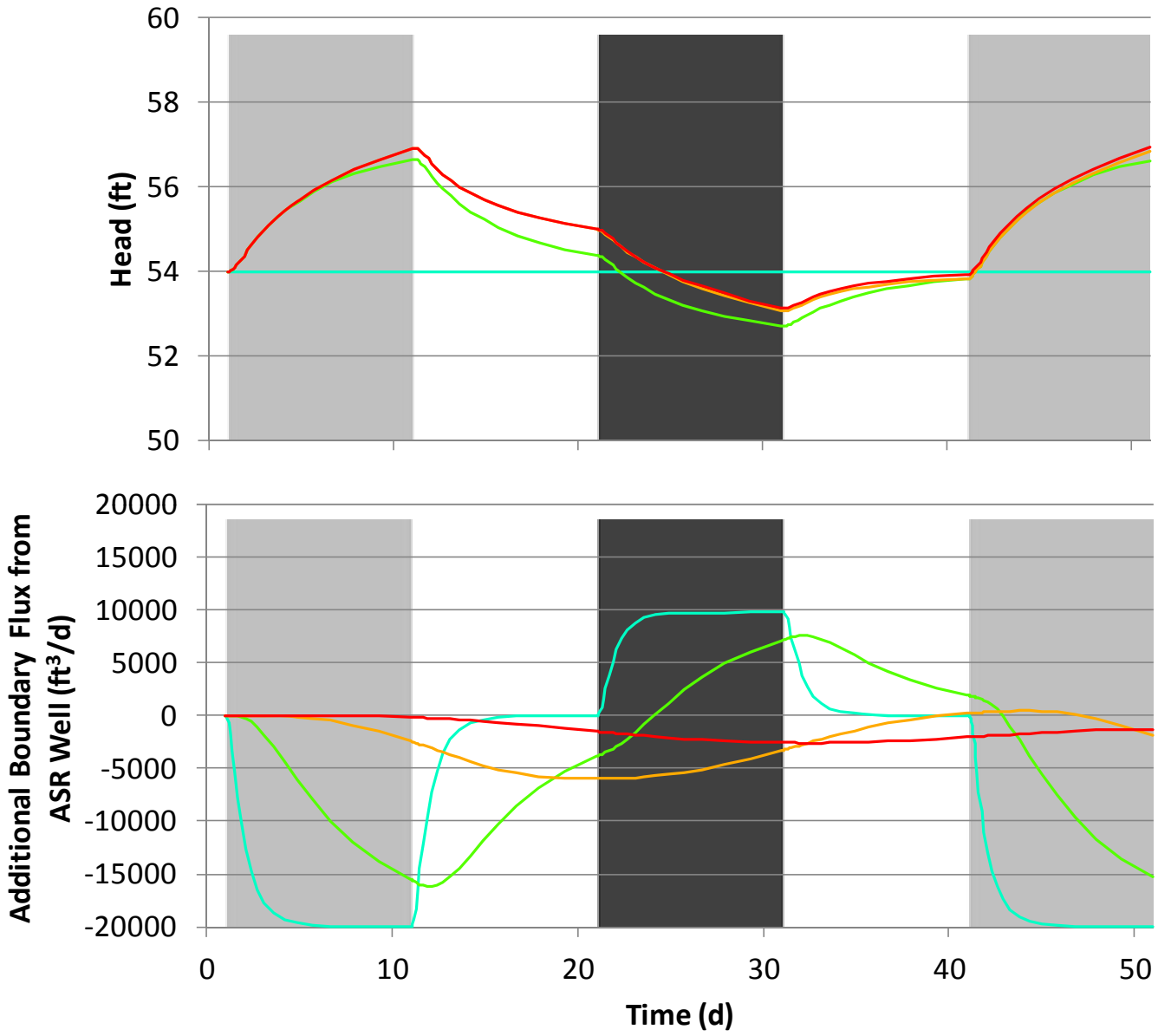

Small model
Large model
Larger model
Largest model

Injection Period
Extraction Period

Notes:

The upper plot shows the heads 190 ft from the ASR well for each of four increased thickness test models. (The smallest model is not large enough to provide results at a distance of 190 ft.)

The lower plot shows the boundary flux changes (compared to the steady state flux) for each of four increased thickness test models. Positive values indicate flow into the model; negative values indicate flow out of the model.

Note that the injection rate at the ASR well was 20,000 ft^3/d and the extraction rate was 10,000 ft^3/d.

INCREASED THICKNESS TEST MODEL RESULTS: HEADS 190 FT FROM ASR WELL AND BOUNDARY FLUXES

DRAFT REGIONAL MODEL PRODUCTION SCENARIO REPORT

FIGURE A.15

JUNE 2013

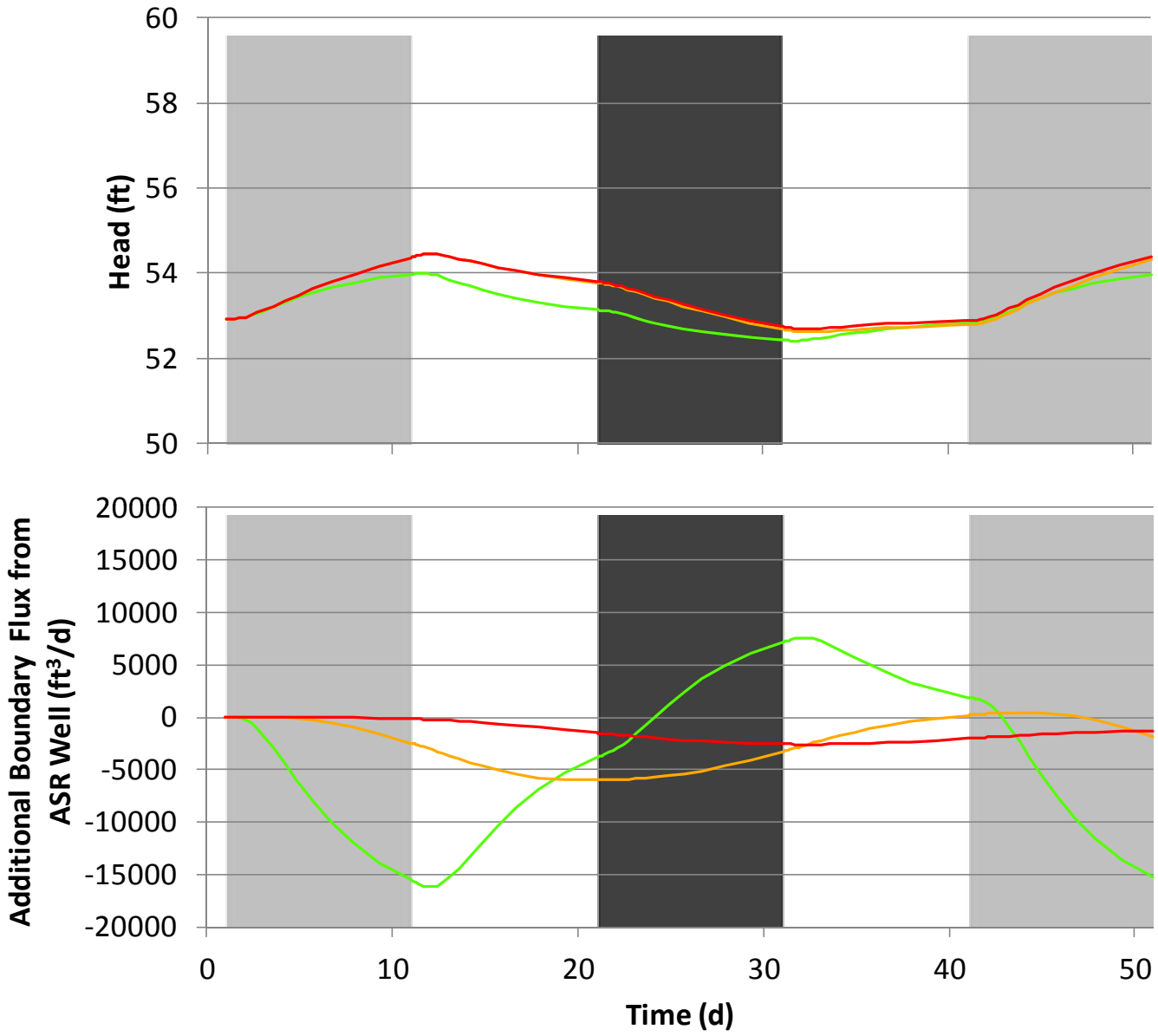

Large model
Larger model
Largest model

Injection Period
Extraction Period

Notes:

The upper plot shows the heads 340 ft from the ASR well for each of three increased thickness test models. (The small and smallest models are not large enough to provide results at a distance of 340 ft.)

The lower plot shows the boundary flux changes (compared to the steady state flux) for each of three increased thickness test models. Positive values indicate flow into the model; negative values indicate flow out of the model.

Note that the injection rate at the ASR well was 20,000 ft^3/d and the extraction rate was 10,000 ft^3/d.

INCREASED THICKNESS TEST MODEL RESULTS: HEADS 340 FT FROM ASR WELL AND BOUNDARY FLUXES

DRAFT REGIONAL MODEL PRODUCTION SCENARIO REPORT

FIGURE A.16

JUNE 2013

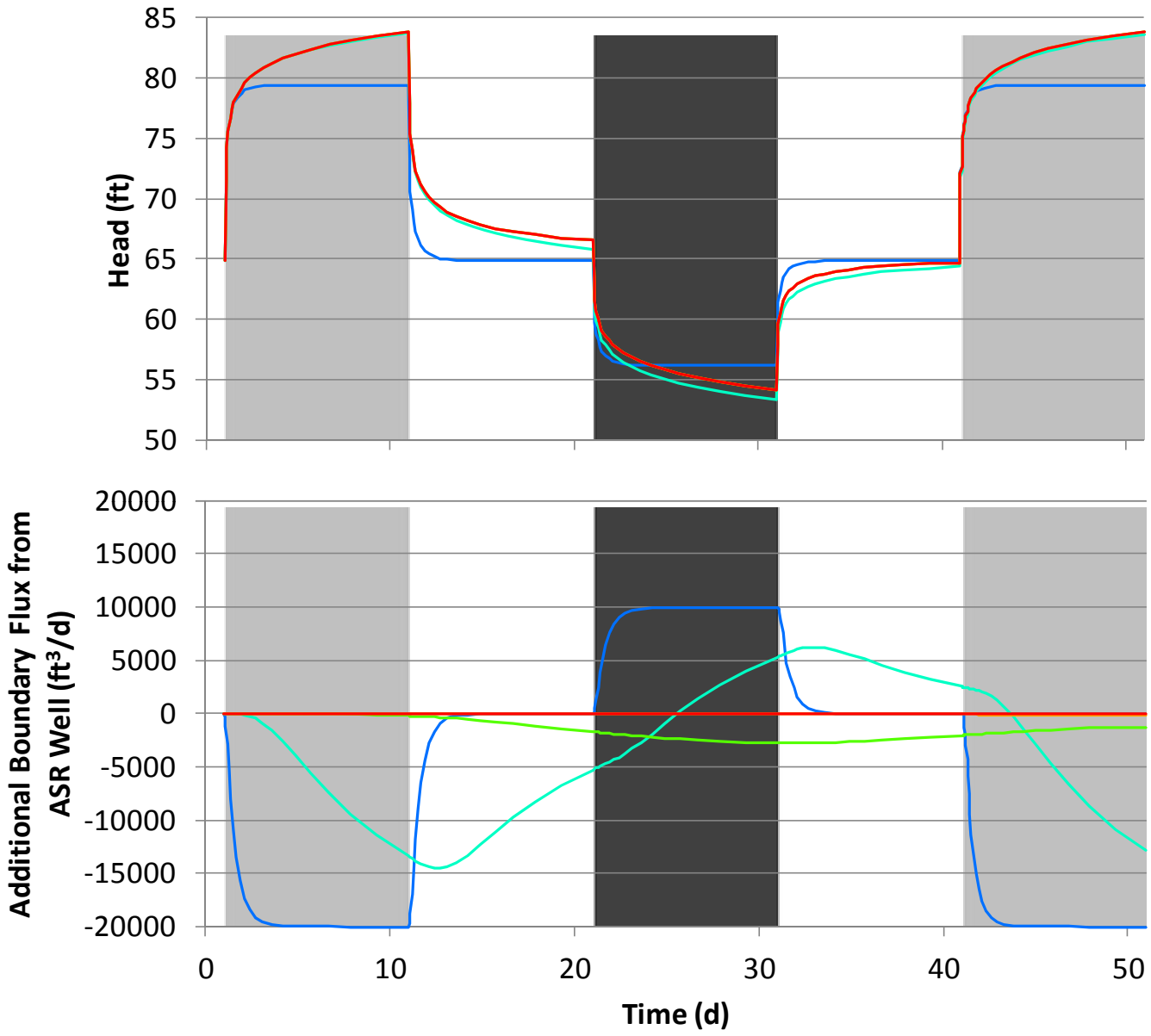

Smallest model
Small model
Large model
Larger model
Largest model

Injection Period
Extraction Period

Notes:

The upper plot shows the heads at the ASR well for each of the five increased storage test models.

The lower plot shows the boundary flux changes (compared to the steady state flux) for each of the five increased storage test models. Positive values indicate flow into the model; negative values indicate flow out of the model.

Note that the injection rate at the ASR well was 20,000 ft^3/d and the extraction rate was 10,000 ft^3/d.

INCREASED STORAGE TEST MODEL RESULTS: HEADS AT THE ASR WELL AND BOUNDARY FLUXES

DRAFT REGIONAL MODEL PRODUCTION SCENARIO REPORT

FIGURE A.17

JUNE 2013

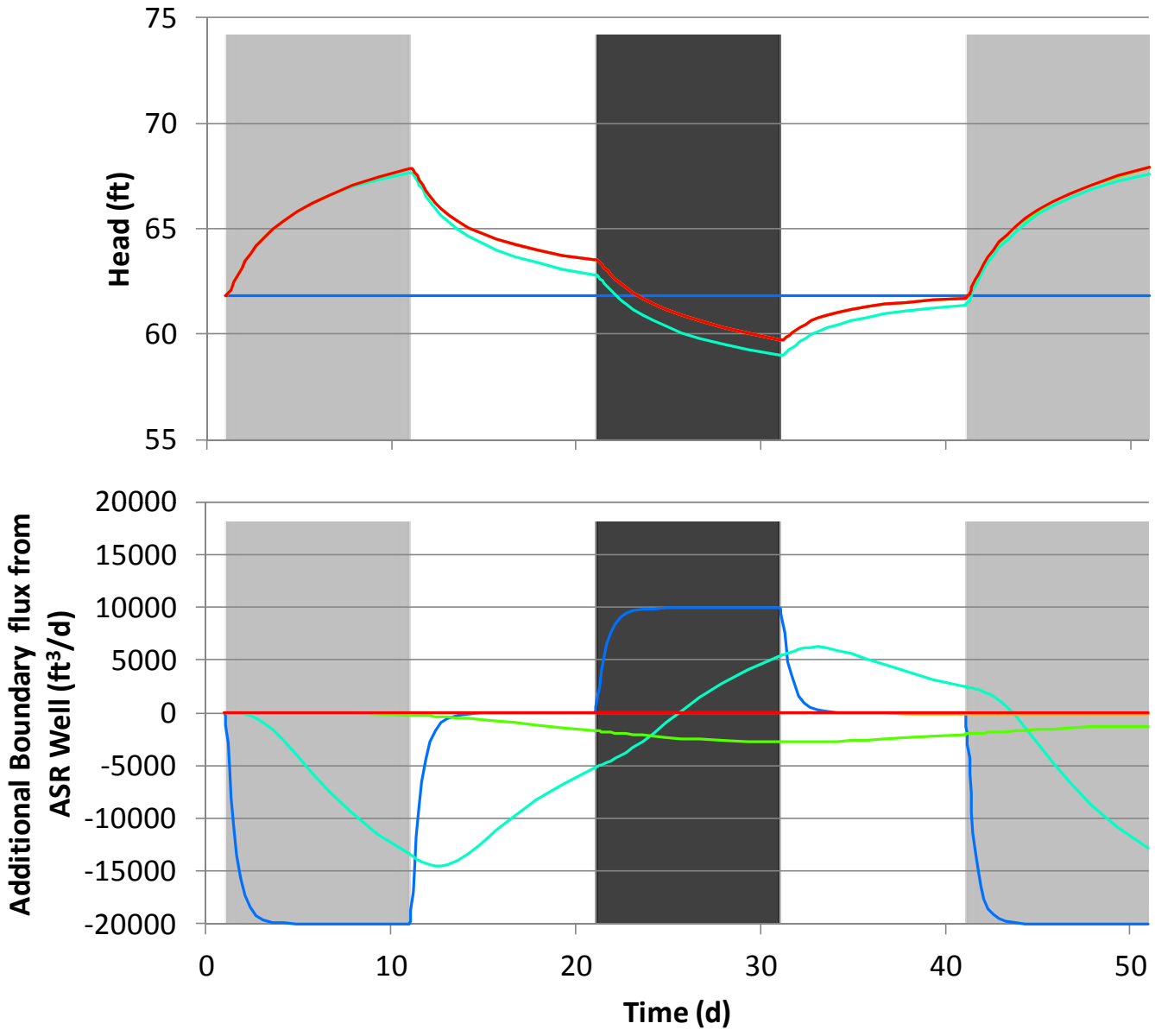

Smallest model
Small model
Large model
Larger model
Largest model

Injection Period
Extraction Period

Notes:

The upper plot shows the heads 50 ft from the ASR well for each of the five increased storage test models.

The lower plot shows the boundary flux changes (compared to the steady state flux) for each of the five increased storage test models. Positive values indicate flow into the model; negative values indicate flow out of the model.

Note that the injection rate at the ASR well was 20,000 ft^3/d and the extraction rate was 10,000 ft^3/d.

INCREASED STORAGE TEST MODEL RESULTS: HEADS 50 FT FROM ASR WELL AND BOUNDARY FLUXES

DRAFT REGIONAL MODEL PRODUCTION SCENARIO REPORT

FIGURE A.18

JUNE 2013

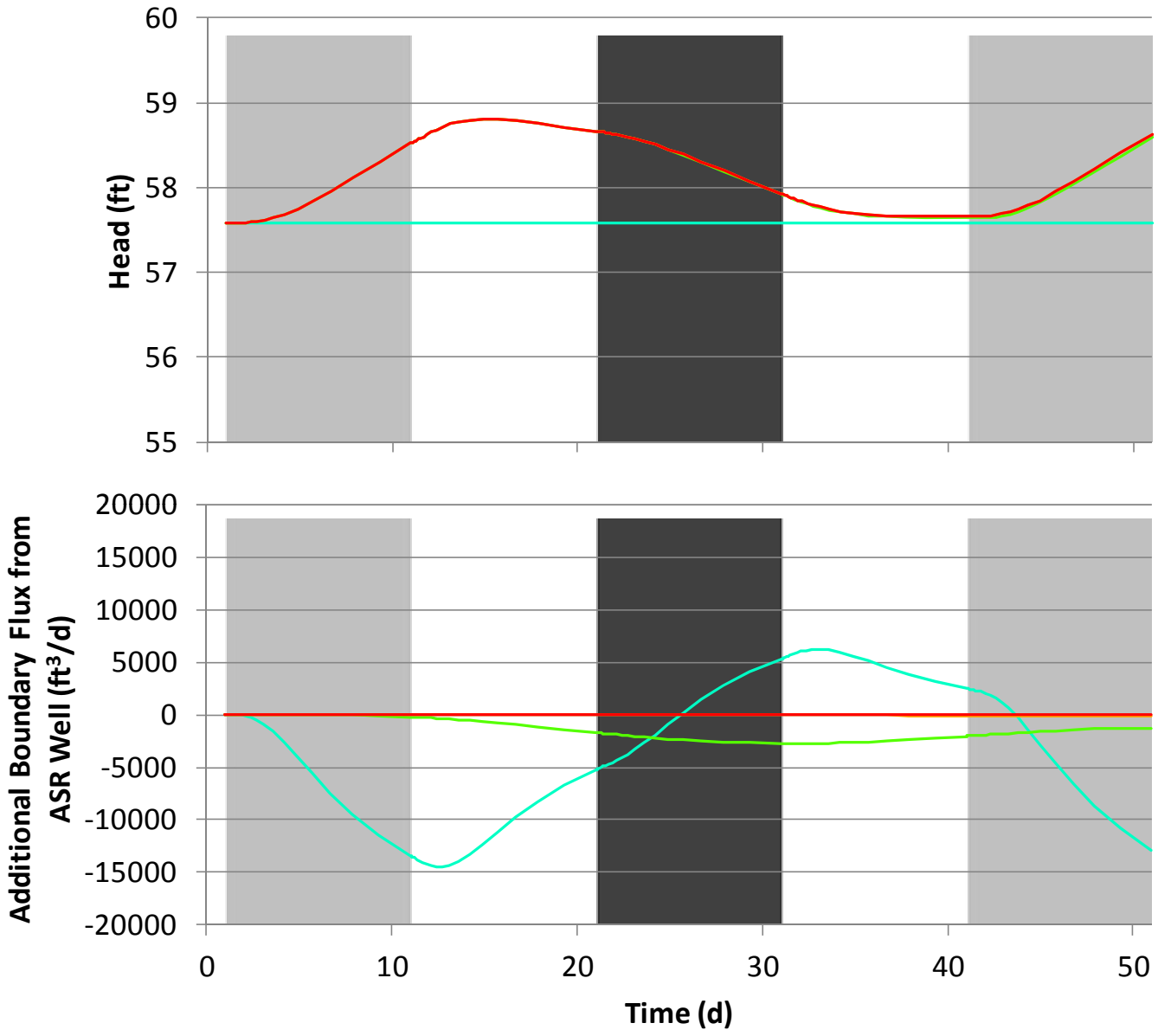

Small model
Large model
Larger model
Largest model

Injection Period
Extraction Period

Notes:

The upper plot shows the heads 190 ft from the ASR well for each of four increased storage test models. (The smallest model is not large enough to provide results at a distance of 190 ft.)

The lower plot shows the boundary flux changes (compared to the steady state flux) for each of four increased storage test models. Positive values indicate flow into the model; negative values indicate flow out of the model.

Note that the injection rate at the ASR well was 20,000 ft^3/d and the extraction rate was 10,000 ft^3/d.

INCREASED STORAGE TEST MODEL RESULTS: HEADS 190 FT FROM ASR WELL AND BOUNDARY FLUXES

DRAFT REGIONAL MODEL PRODUCTION SCENARIO REPORT

FIGURE A.19

JUNE 2013

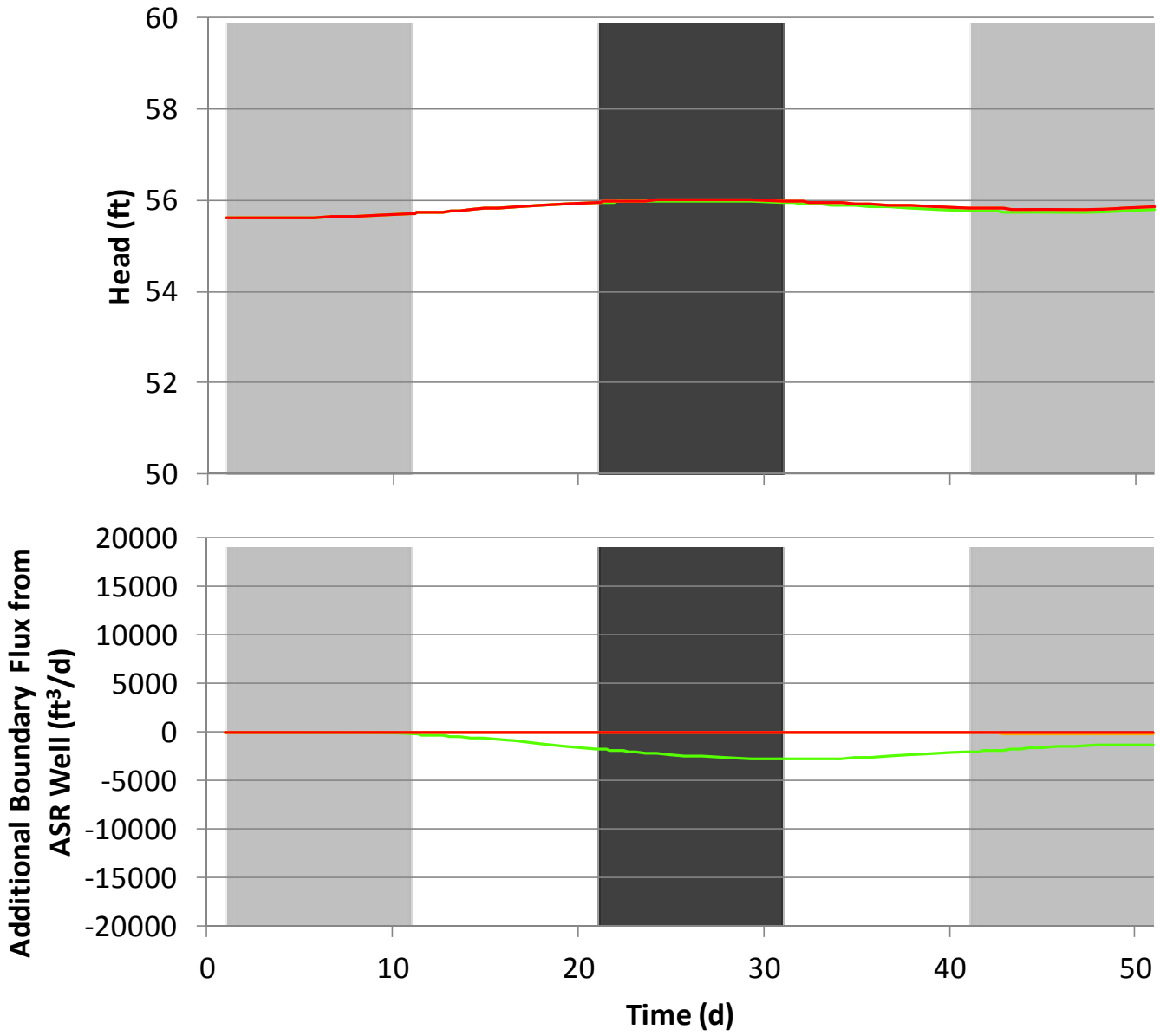

Large model
Larger model
Largest model

Injection Period
Extraction Period

Notes:

The upper plot shows the heads 340 ft from the ASR well for each of three increased storage test models. (The small and smallest models are not large enough to provide results at a distance of 340 ft.)

The lower plot shows the boundary flux changes (compared to the steady state flux) for each of three increased storage test models. Positive values indicate flow into the model; negative values indicate flow out of the model.

Note that the injection rate at the ASR well was 20,000 ft^3/d and the extraction rate was 10,000 ft^3/d.

INCREASED STORAGE TEST MODEL RESULTS: HEADS 340 FT FROM ASR WELL AND BOUNDARY FLUXES

DRAFT REGIONAL MODEL PRODUCTION SCENARIO REPORT

FIGURE A.20

JUNE 2013

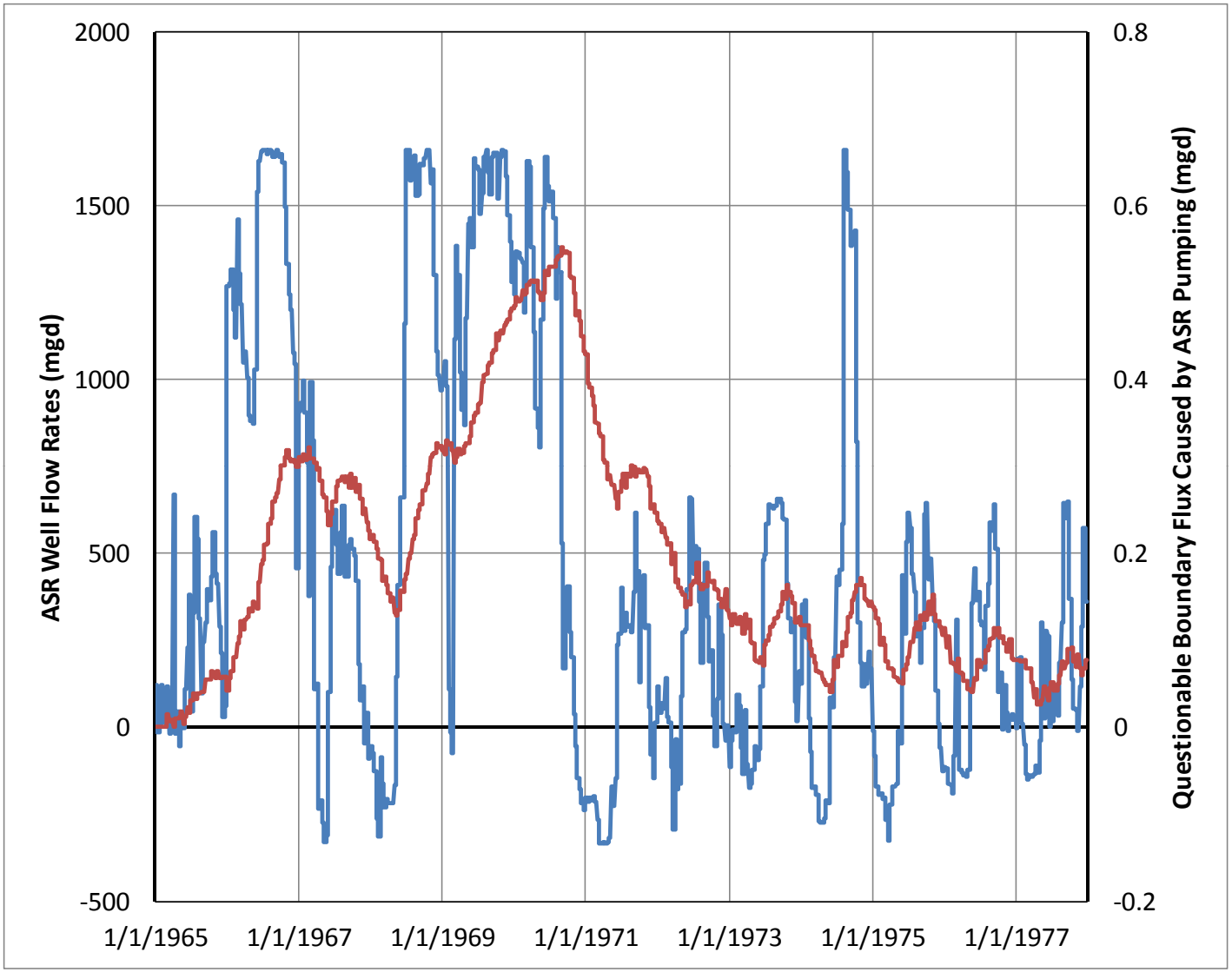

Legend

- Total ASR Pump Rate
- Questionable Boundary Flux Caused By ASR Wells

Notes:

This plot compares the ASR pumping schedule for Scenario 11 of the RASRSM-D13R, to the questionable boundary flux caused by this pumping in the IAS/ICU.

The blue line represents the total ASR pumping from all sites and all aquifers (left axis). Positive flow rates indicate injection (recharge); negative flow rates indicate extraction (recovery). Note that some sites could be injecting while others are extracting and the value shown here is the sum of the rates.

The red line represents the questionable boundary flux caused by the ASR wells in the IAS/ICU (right axis). The boundary flux caused by the ASR wells is calculated by subtracting the flux in a run including the ASR wells from that in the no-project run.

Questionable boundary flux is defined as flux through all non-ocean boundaries where specified heads were applied based on measured head data. Positive fluxes indicate an increase in water leaving the model or a decrease in water entering the model at the boundary.

QUESTIONABLE BOUNDARY FLUXES CAUSED BY ASR WELLS – IAS/ICU

DRAFT REGIONAL MODEL PRODUCTION SCENARIO REPORT

FIGURE A.21

JUNE 2013

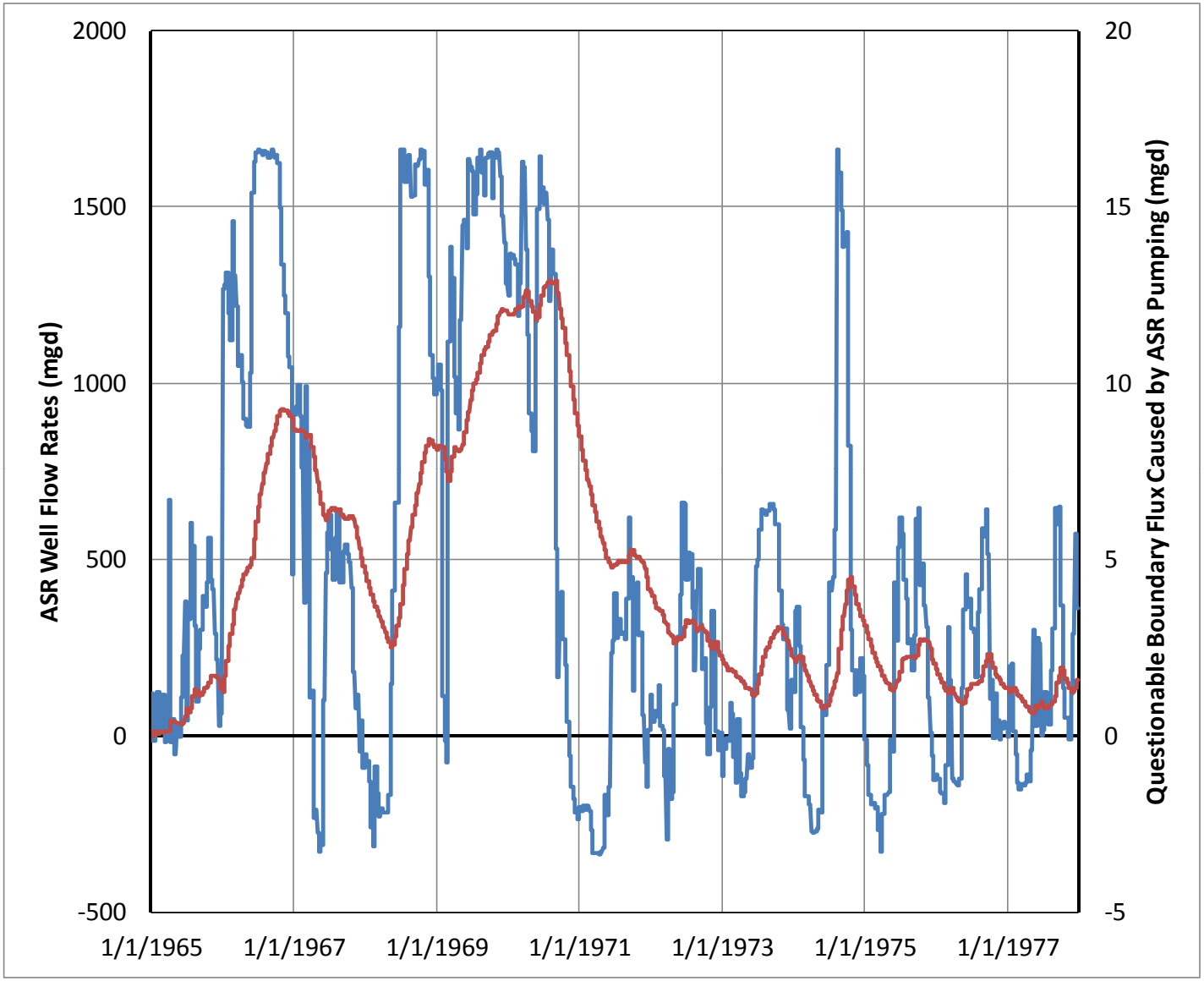

Legend

- Total ASR Pump Rate
- Questionable Boundary Flux Caused By ASR Wells

Notes:

This plot compares the ASR pumping schedule for Scenario 11 of the RASRSM-D13R, to the questionable boundary flux caused by this pumping in the UF.

The blue line represents the total ASR pumping from all sites and all aquifers (left axis). Positive flow rates indicate injection (recharge); negative flow rates indicate extraction (recovery). Note that some sites could be injecting while others are extracting and the value shown here is the sum of the rates.

The red line represents the questionable boundary flux caused by the ASR wells in the UF (right axis). The boundary flux caused by the ASR wells is calculated by subtracting the flux in a run including the ASR wells from that in the no-project run.

Questionable boundary flux is defined as flux through all non-ocean boundaries where specified heads were applied based on measured head data. Positive fluxes indicate an increase in water leaving the model or a decrease in water entering the model at the boundary.

Questionable Boundary Fluxes Caused by ASR Wells – UF

Figure A.22

Draft Regional Model Production Scenario Report

June 2013

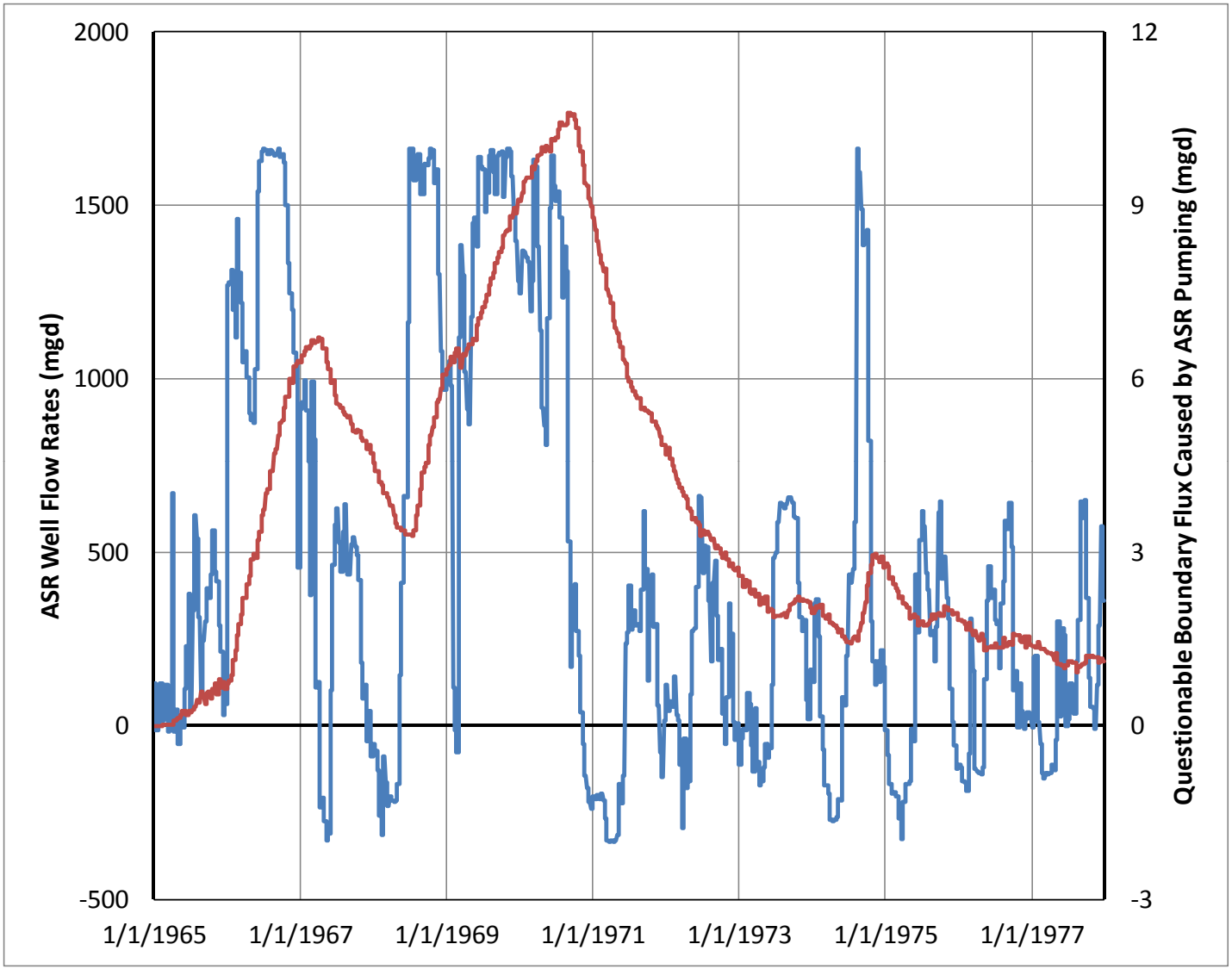

Legend

- Total ASR Pump Rate
- Questionable Boundary Flux Caused By ASR Wells

Notes:

This plot compares the ASR pumping schedule for Scenario 11 of the RASRSM-D13R, to the questionable boundary flux caused by this pumping in the APPZ.

The blue line represents the total ASR pumping from all sites and all aquifer (left axis). Positive flow rates indicate injection (recharge); negative flow rates indicate extraction (recovery). Note that some sites could be injecting while others are extracting and the value shown here is the sum of the rates.

The red line represents the questionable boundary flux caused by the ASR wells in the APPZ (right axis). The boundary flux caused by the ASR wells is calculated by subtracting the flux in a run including the ASR wells from that in the no-project run.

Questionable boundary flux is defined as flux through all non-ocean boundaries where specified heads were applied based on measured head data. Positive fluxes indicate an increase in water leaving the model or a decrease in water entering the model at the boundary.

QUESTIONABLE BOUNDARY FLUXES CAUSED BY ASR WELLS – APPZ

DRAFT REGIONAL MODEL PRODUCTION SCENARIO REPORT

FIGURE A.23

JUNE 2013

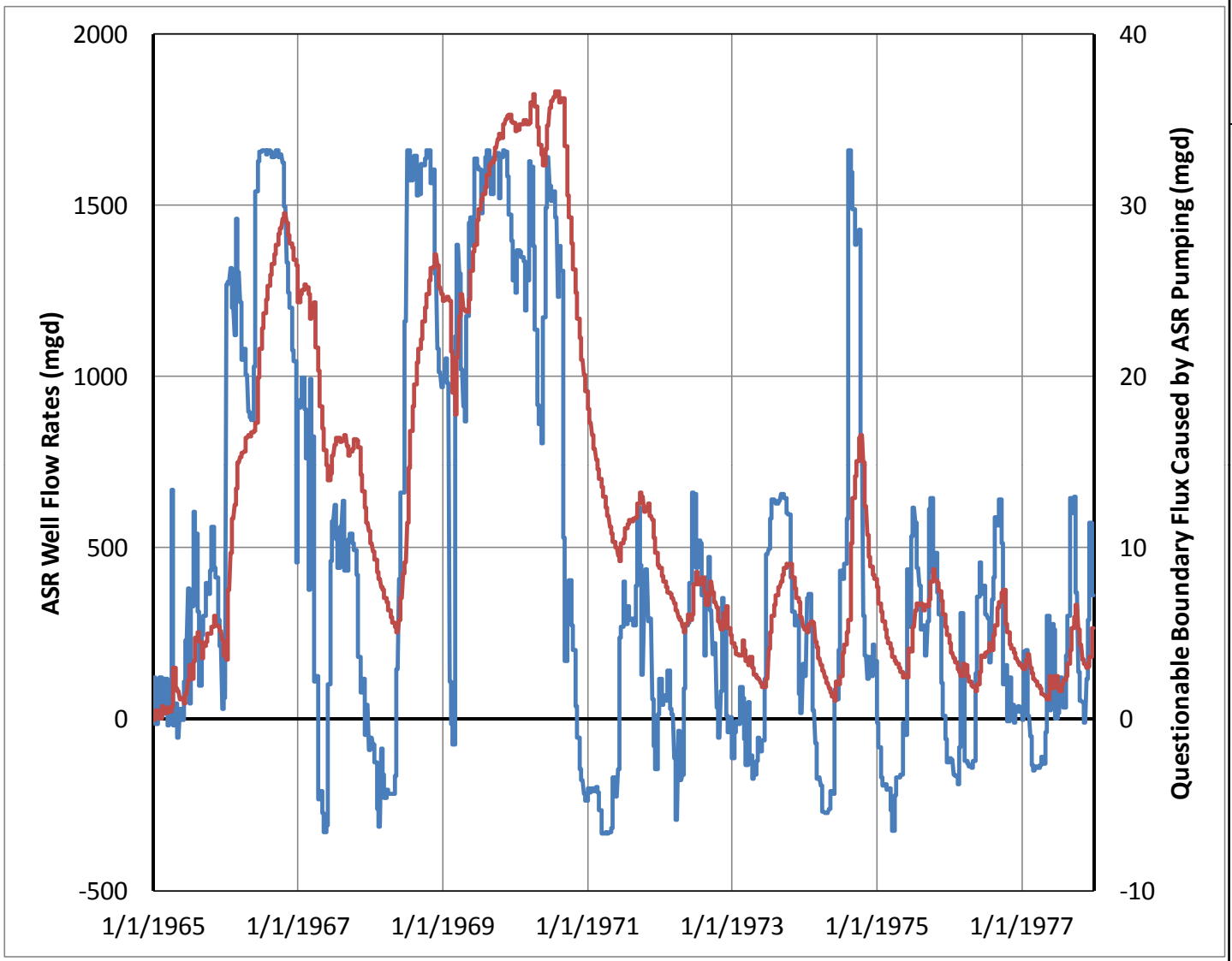

Legend

- Total ASR Pump Rate
- Questionable Boundary Flux Caused By ASR Wells

Notes:

This plot compares the ASR pumping schedule for Scenario 11 of the RASRSM-D13R, to the questionable boundary flux caused by this pumping in the LF.

The blue line represents the total ASR pumping from all sites and all aquifers (left axis). Positive flow rates indicate injection (recharge); negative flow rates indicate extraction (recovery). Note that some sites could be injecting while others are extracting and the value shown here is the sum of the rates.

The red line represents the questionable boundary flux caused by the ASR wells in the LF (right axis). The boundary flux caused by the ASR wells is calculated by subtracting the flux in a run including the ASR wells from that in the no-project run.

Questionable boundary flux is defined as flux through all non-ocean boundaries where specified heads were applied based on measured head data. Positive fluxes indicate an increase in water leaving the model or a decrease in water entering the model at the boundary.

QUESTIONABLE BOUNDARY FLUXES CAUSED BY ASR WELLS – LF

DRAFT REGIONAL MODEL PRODUCTION SCENARIO REPORT

FIGURE A.24

JUNE 2013

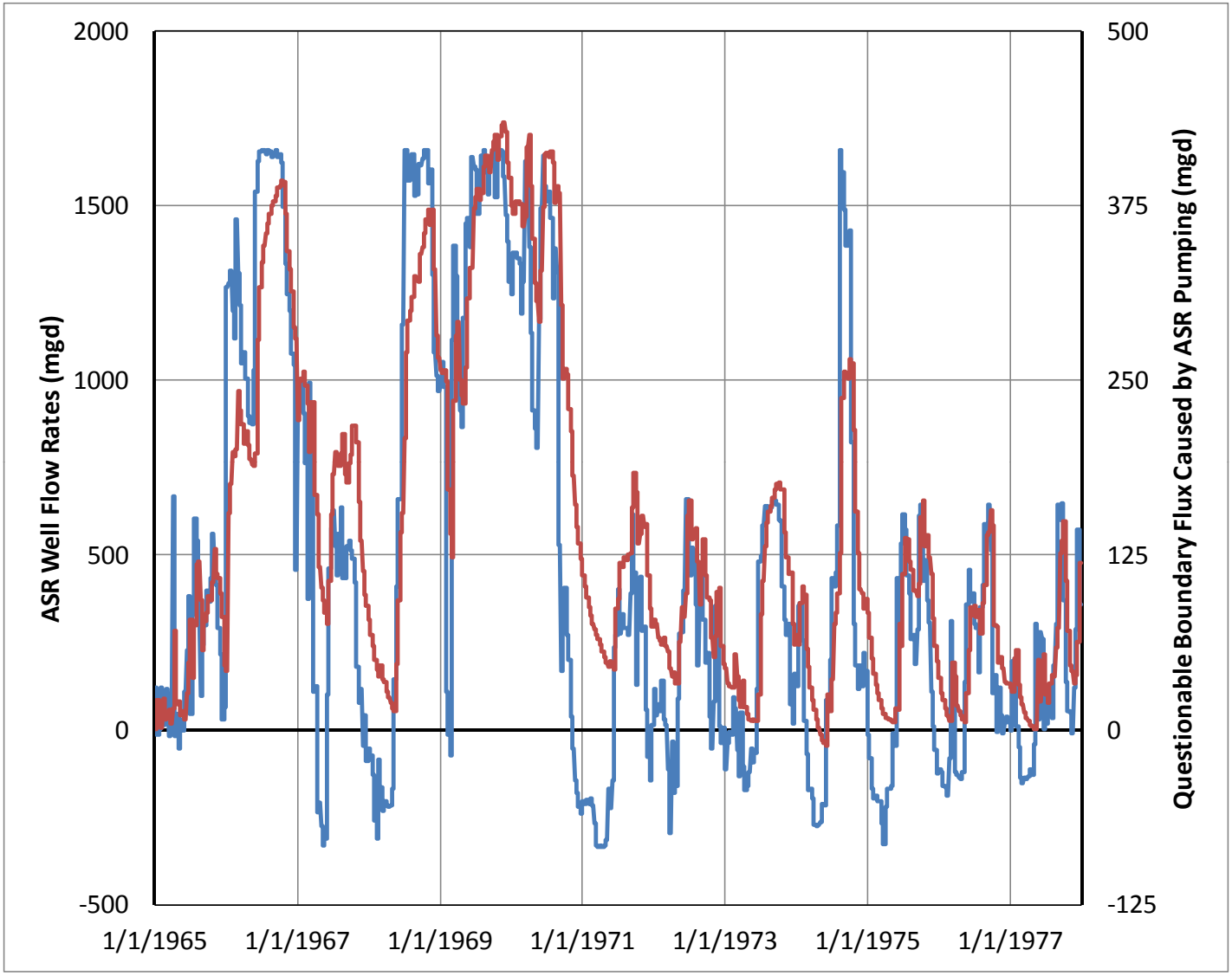

Legend

- Total ASR Pump Rate
- Questionable Boundary Flux Caused By ASR Wells

Notes:

This plot compares the ASR pumping schedule for Scenario 11 of the RASRSM-D13R, to the questionable boundary flux caused by this pumping in the BZ.

The blue line represents the total ASR pumping from all sites and all aquifers (left axis). Positive flow rates indicate injection (recharge); negative flow rates indicate extraction (recovery). Note that some sites could be injecting while others are extracting and the value shown here is the sum of the rates.

The red line represents the questionable boundary flux caused by the ASR wells in the BZ (right axis). The boundary flux caused by the ASR wells is calculated by subtracting the flux in a run including the ASR wells from that in the no-project run.

Questionable boundary flux is defined as flux through all non-ocean boundaries where specified heads were applied based on measured head data. Positive fluxes indicate an increase in water leaving the model or a decrease in water entering the model at the boundary.

Questionable Boundary Fluxes Caused by ASR Wells – BZ

Figure A.25

Draft Regional Model Production Scenario Report

June 2013

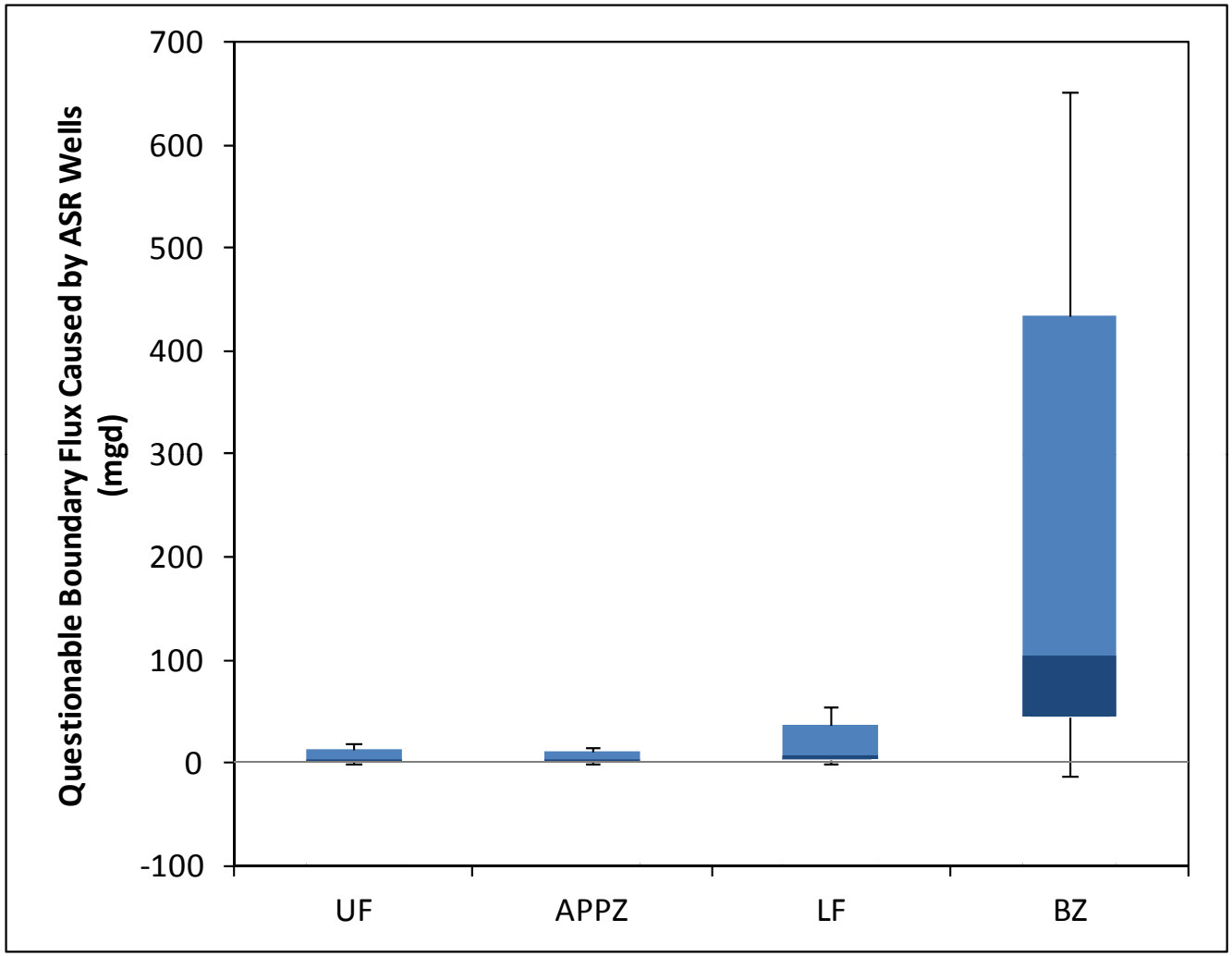

Questionable Boundary Fluxes

Maximum
Upper Quartile
Median
Lower Quartile
Minimum

Notes:

This plot shows the distribution of questionable boundary fluxes caused by ASR pumping in each of the main aquifers of the regional model over the 13-year model run time.

Note that in the UF and APPZ questionable boundary fluxes caused by the ASR wells are less than 15 mgd for the entire period and are usually less than 5 mgd.

Questionable boundary fluxes in the LF and, especially in the BZ, are more significant.

DISTRIBUTION OF QUESTIONABLE BOUNDARY FLUXES ACROSS 13-YEAR MODEL RUN PERIOD

DRAFT REGIONAL MODEL PRODUCTION SCENARIO REPORT

FIGURE A.26

JUNE 2013

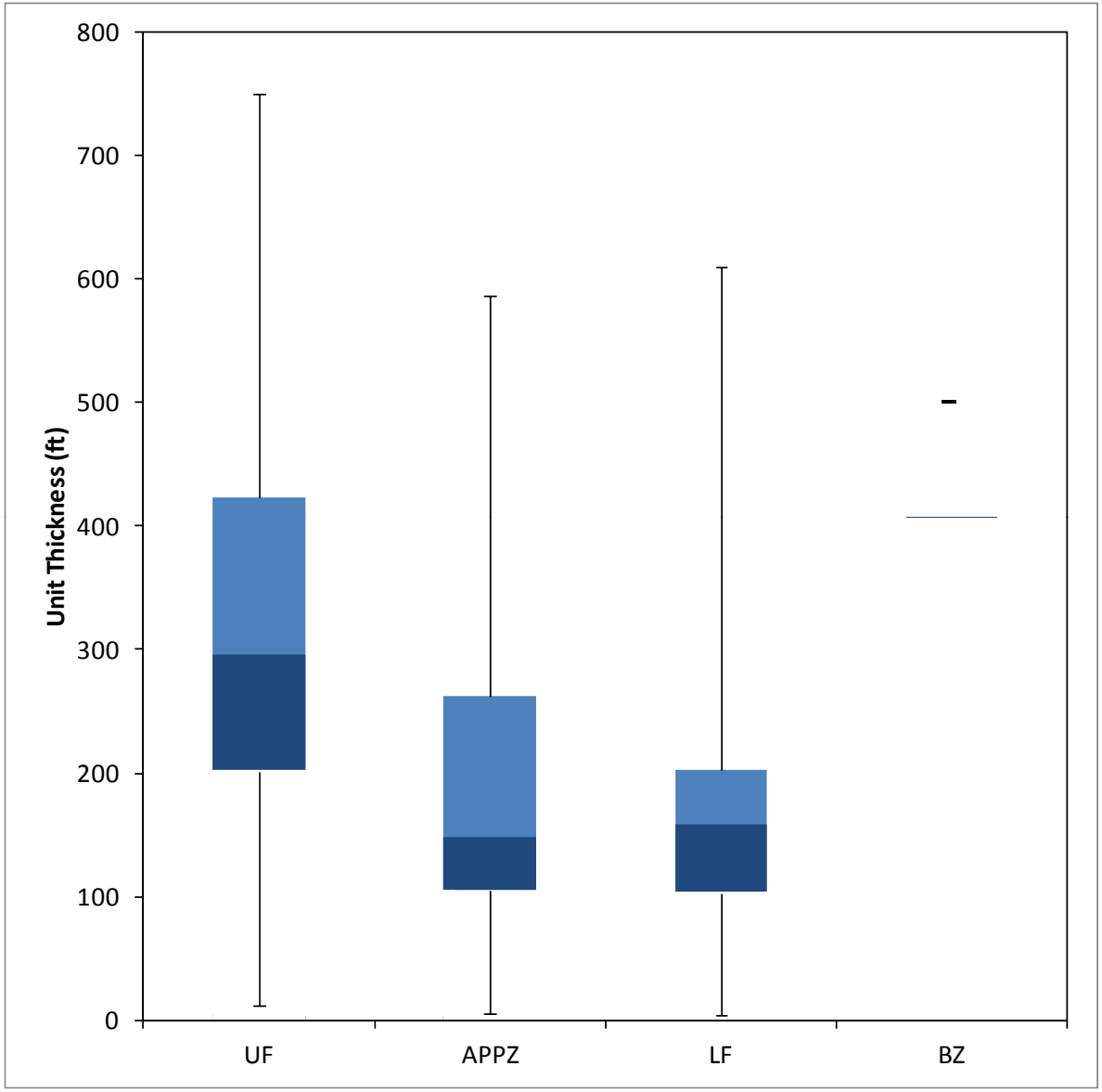

Unit Thickness

Maximum
Upper Quartile
Median
Lower Quartile
Minimum

Notes:

This plot depicts the varying thickness of each of the main aquifer units in the regional model.

The distributions are based on area, so one quarter of the area of the model domain fits into each blue box and into each black error bar above and below the blue boxes.

Note that the entire BZ was set to a constant thickness of 500 ft.

UNIT THICKNESS DISTRIBUTIONS BY AQUIFER UNIT

FIGURE A.27

DRAFT REGIONAL MODEL PRODUCTION SCENARIO REPORT

JUNE 2013

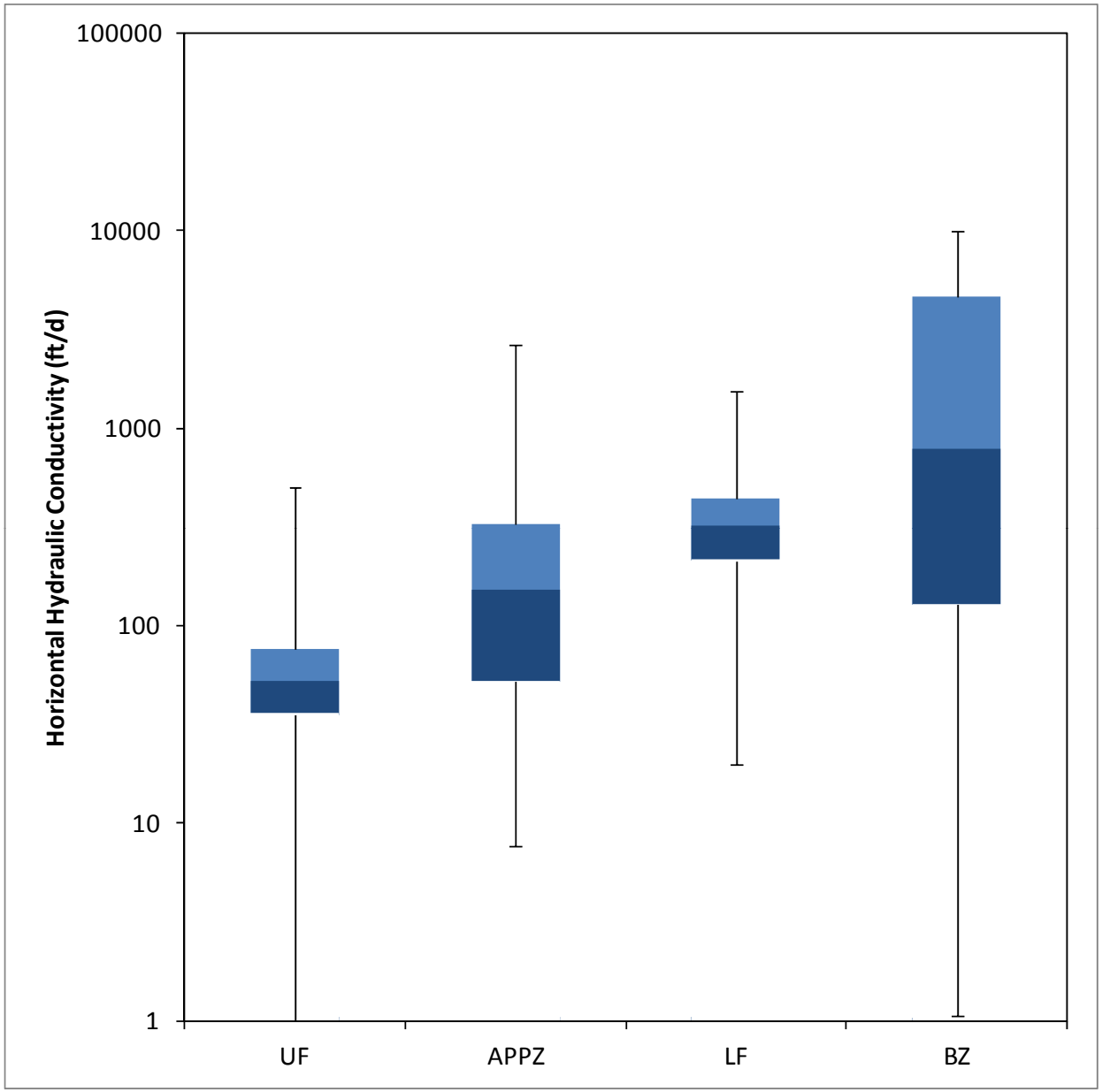

Horizontal Hydraulic Conductivity

Maximum
Upper Quartile
Median
Lower Quartile
Minimum

Notes:

This plot depicts the varying horizontal hydraulic conductivity of each of the main aquifer units in the regional model.

The distributions are based on area, so one quarter of the area of the model domain fits into each blue box and into each black error bar above and below the blue boxes.

HORIZONTAL HYDRAULIC CONDUCTIVITY DISTRIBUTIONS BY AQUIFER UNIT

DRAFT REGIONAL MODEL PRODUCTION SCENARIO REPORT

FIGURE A.28

JUNE 2013

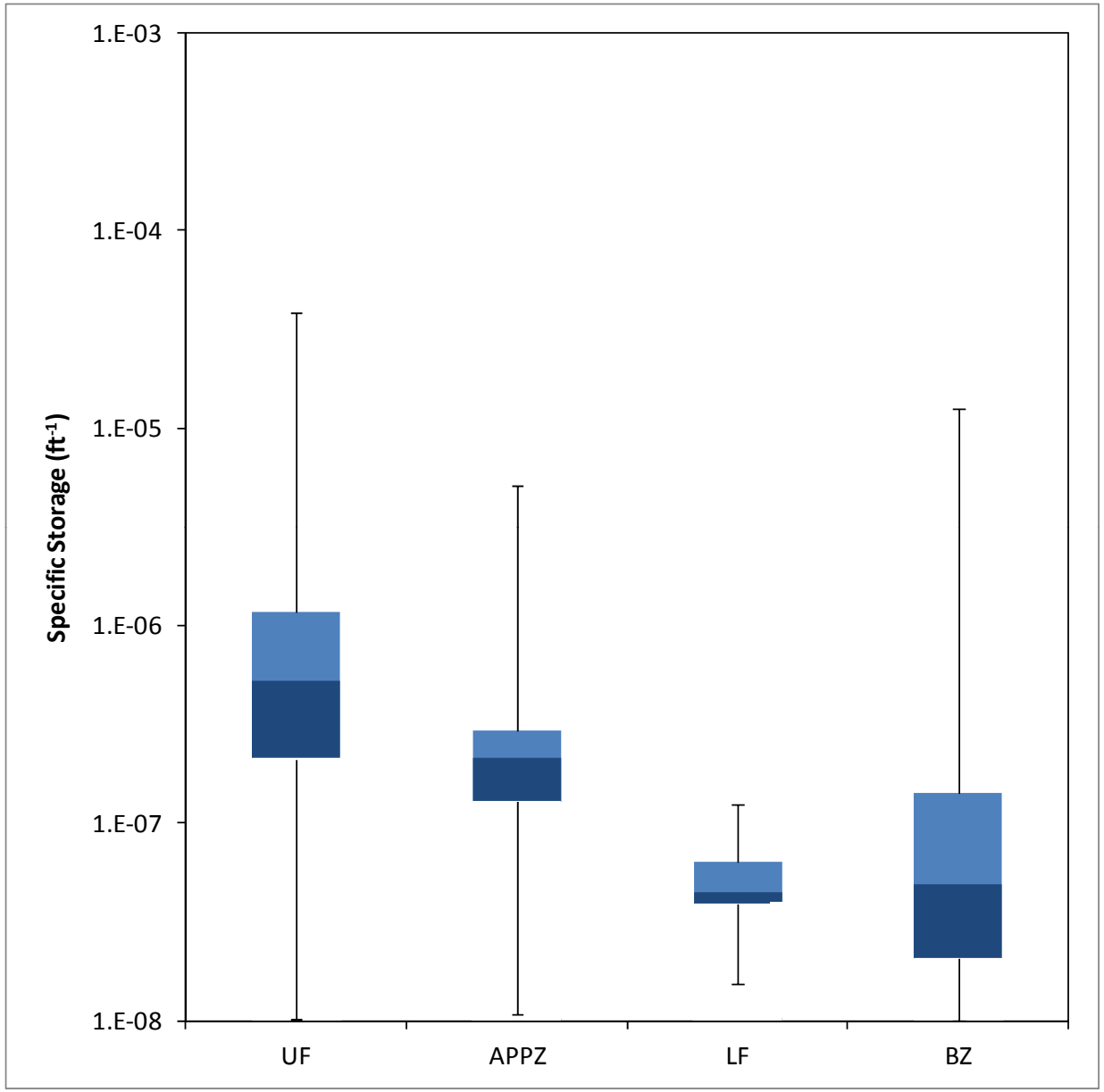

Specific Storage

Maximum
Upper Quartile
Median
Lower Quartile
Minimum

Notes:

This plot depicts the varying specific storage of each of the main aquifer units in the regional model.

The distributions are based on area, so one quarter of the area of the model domain fits into each blue box and into each black error bar above and below the blue boxes.

SPECIFIC STORAGE DISTRIBUTION BY AQUIFER UNIT

FIGURE A.29

APPENDIX B

IMC COMMENTS TO DRAFT REPORT WITH USACE RESPONSES

This appendix presents the comments from the IMC review of the Draft Production Scenario Report. The comments have been copied verbatim into the left column of this appendix. Comments have been divided into table rows for convenience. The right column of this appendix presents USACE responses to the comments, an indication of updates to the report and explanations where necessary.

IMC MSR 324 Task 4c -- Review of "Draft Regional Model Production Scenario Report Aquifer Storage and Recovery Regional Modeling Study"

Interagency Modeling Center (IMC)

IMC Comments	USACE Responses
Purpose The purpose of this document is to provide comments based upon the review of the report submitted in support of the Aquifer Storage and Recovery (ASR) modeling study based on the use of a calibrated regional model to analyze the effects of the proposed Comprehensive Everglades Restoration Plan (CERP) ASR system consisting of 333 ASR wells with the potential to inject or extract 5 mgd each. <u>Documents Reviewed</u> The document shown below was submitted for IMC review: • "Draft Regional Model Production Scenario Report, Aquifer Storage and Recovery Regional Modeling Study." US Army Corps of Engineers, September, 2012. Individual reviewers in some cases reviewed additional documents when certain parts of the report above needed further clarification. The technical comments made by the IMC review team on this document follow. **Technical Comments** The review was limited to the document above, and therefore does not extend to the model code, model input or model output files. The comments are listed following the review objectives agreed upon by the USACE and the IMC.	No response necessary.

IMC Comments	USACE Responses
1. Are the text and figures clear and understandable?	
In general, the text and figures are clear and understandable.	No comment necessary
The box and whisker plots in Figure 2.7 through Figure 2.9 do not seem appropriate to be within Section 2.2 (Choice of Time Period). A more appropriate section or subsection heading should be selected to suit precipitation analysis described in these figures.	The purpose of these box-and-whisker plots and the associated analysis was to support the decision to shorten the modeled time period from 30 years (like the SFWMM-D13R model) to just 13 years. As such, we feel this is the right place to include this analysis and the associated figures. Additional text and explanations have been added to Section 2.2 to clarify this purpose.
It would be helpful if the proposed ASR sites are shown in Figure 3.1(as was done in Figure 1.1) to understand better the rock fracture potential maximum total head in relation to the ASR well sites.	Figure has been updated.
In Figure 4.20 (Scenario 1 – Maximum Drawdown and "Drawup" by Aquifer) and subsequent figures for the other scenarios, it would be helpful to add the boundary locations of the model to these figures as these boundaries are relevant to the discussions in the appendix.	Figures have been updated.
In Figures 4.33, 4.52, and similar figures describing ASR well fluxes for the various scenarios, the legend uses Run1, Run 2, etc. Shouldn't these be Scenario 1, Scenario 2 etc?	Figures have been updated.
A correction should be made on the note section of Figure 4.108 from 10 gpm wells to 10 mgd wells.	Figure has been updated.
In Figure A.5 to Figure A.8, show the 0 (zero) line on the flux scale as this is a critical location in understanding the data.	Figures have been redesigned to show zero flux line.

IMC Comments	USACE Responses
Overall, the report is well organized. However, the report would be considered more complete if the model setup section had included setup and discussions of initial TDS/temperature and head conditions, how TDS/temperature was accounted for in the methodology on page 7 for boundary conditions, and detailed discussions of recovery efficiency uncertainty in Section 7.	Section 2.7 has been added to the document to describe the setup of the initial conditions (head, TDS and temperature). There was no need to account for TDS and temperature when developing the boundary conditions because SEAWAT allows the user to enter observed heads for the boundary conditions. During calculations, the model determines the effective freshwater head using the water quality and the observed head. SEAWAT does not have the capability to automatically stop extraction when the water quality reaches a certain threshold. In addition, this is a regional model and cannot be expected to accurately calculate near-field impacts of the wells – including water quality of extracted water. Recovery efficiency was an assumption and an input to the model. Assumed recovery efficiencies were based on hydraulic conductivity, existing water quality and experience at the two pilot sites as described in Section 2.6.1. The initial conditions set for the model did not impact decisions regarding assumed recovery efficiency.
2. Is the methodology used to convert the calibration model to the 1965-1977 time –period adequate to meet the goals of the projects?	
The modelers should state the reasons why it was necessary to develop the regional model production scenarios using the RASRSM-D13R model instead of using the SFWMM-D13R. The reasons should include the limitations of addressing the performance measures using SFWMM-D13R and the difference in the characteristics of the aquifer systems modeled using SFWMM-D13R and RASRSM-D13R.	Several new paragraphs have been added to Section 2 to describe the shortcomings of the SFWMM and the need for the RASRSM-D13R model.

IMC Comments	USACE Responses
Please explain in more detail why the RASRSM would not be able to cover the 30-year period. It was stated in the document that file-size limitation and run time made it difficult to run the RASRSM for the 30 year period. Was investment on additional computer resources considered?	Several new computers were acquired during this project and additional computers were borrowed from other projects during the Monte Carlo analysis. During the course of every model, the desired extent, resolution and detail must be balanced with the available time and computer resources. Because the first 13 years of the 30-year D13R period was considered to be representative, the purchase of even more computer resources was not considered to be likely to provide significantly better results. Additional text has been added to section 2.2 to better explain the constraints of the model.
To reduce run-time and file-size a possibility could have been shutting-off the density-dependent and transport part of SEAWAT and run it as a MODFLOW model to assume freshwater conditions since the injected water in the ASR is freshwater and the salinity in the UF might not have an effect on the performance measure analyses to determine the number of wells to be installed in the UF.	As explained in more detail below, the density dependence was very important to the model. Although the UF is not very deep or salty, the BZ is quite deep and salty and exerts a great force on the upper layers of the model. Without the density dependence, the model would not have yielded accurate results.
In the event that reducing the time period to 13 years was the most appropriate way to proceed with the analyses of the performance measures, the methodology used by the modelers to convert the calibrated RASRSM model to RASRM-D13R while considering ASR requirements used in the SFWMM-D13R model is reasonable. However, it is requested that the modelers clarify or explain the following modeling issues:	No comment necessary.

IMC Comments	USACE Responses
a) Please explain the methodology to convert the calibrated RASRSM to an earlier time period for the conversion of all the important parameters. This conversion is to some extent a validation process, since stresses and boundaries are redefined and applied to a calibrated model with calibrated parameters such as geological (i.e., aquifer tops and bottoms), hydrogeological (i.e., hydraulic conductivity, storativity) and transport (i.e., dispersivity) parameters. The modelers discussed and justified recharge and pumping stresses and head boundary conditions; however, initial conditions of heads and TDS concentrations were not mentioned and discussed in the report. As the modelers know, in a transient flow and transport model, initial conditions, especially TDS concentrations, are crucial. Transport process is not reversible, and initial TDS concentrations should be reasonably defined and discussed before running a model. Please discuss how initial conditions of head and TDS concentrations were converted to the back time period of 1965-1977.	A new section (2.7) has been added to describe the selection of initial conditions.

IMC Comments	USACE Responses
b) The modelers justified the conversion of model period to 1965-1977. The justifications look reasonable for the flow aspects but more information is needed for the contaminant transport aspects of the model. The modelers justified reducing the time period to a short 13-yr period due to file size limitations and computational run-time, choosing 1965 as the start time to minimize impact by previous injection periods, choosing 1977 as end time to include periods covered by SAJ Lake Okeechobee models and to incorporate the entire first cycle of Lake Okeechobee basin wells. Precipitations, annual extracted/injected volumes, boundary conditions, and regional pumping are also redefined and discussed for the shorter model time period 1965-1977. Model time steps and stress periods were adjusted to reduce computer run-time as well. Though all this looks reasonable, the reviewers were concerned that when you take into consideration the whole period 1965-1995, 1965-1977 was probably a period for which data is least accurate or insufficient. 1977 in Figure 2.2 showed a return to zero storage volume. With this observation, a later time period for example, 1983-1995 could produce more reliable data for ASR design since later times in the model period seem to have better data quality especially for pumping data. Please explain in the report why a later period, for example 1983-1995, was not used. Could the results have been significantly different for the performance measures if the period 1983-1995 have been used considering that the aquifer storage volumes shape in Figure 2.2 for 1965-1977 and 1983-1995 are quite different? Why or why not?	Figure 2.2 shows the storage volume only for the Lake Okeechobee ASR basin. Although this represents the largest volume in the CERP ASR system, there are 4 other basins with significant ASR flows which do not return to zero storage in 1977. Only the Lake Okeechobee and Central Palm Beach basins have zero storage at any period other than 1965. Further, running the RASRSM-D13R model from 1983-1995 would not have covered the time period used in the SAJ Lake Okeechobee models. The use of the period 1983-1995 might have had minor impacts on the performance measure results. The pump pressure limit is affected by the largest injection rate at the ASR wells. The maximum injection rates (5 mgd/well) is achieved in all basins during the 1965-1977 period. Some minor impacts might be caused by longer periods of injection or greater volumes injected over long periods of time. The maximum annual injection volume in the Lake Okeechobee basin during the 1965-1977 period is approximately 98% of the maximum annual injection volume for the period 1965-1995. The maximum annual injection volume in the Caloosahatchee basin during the 1965-1977 period is also about 98% of the 30-year maximum. For the Lower East Coast basins, the comparisons range from 81% to 87%. Possibly a small increase in these pump pressures might have been noted, but the difference would be within the error of the model because the maximum rate (5 mgd) was met on numerous occasions in all basins. The APPA performance measure results are affected by the extraction rates in a few sites on the east and northeast shore of Lake Okeechobee, mainly Lakeside Ranch, Port Mayaca, L-63N, Taylor Creek, North Lake Okeechobee and Kissimmee River/Paradise Run. As noted above, all of these sites achieve full extraction rates (5 mgd) during the 1965-1977 period. Some additional minor impacts might be felt if the extraction rates continue for long periods of time or if large volumes are extracted. However the maximum annual extraction volume for this basin, over the 30-year period, occurred in 1975, a year included in the shortened 13-year period used in the RASRSM-D13R scenarios. For these reasons, we feel that no additional justification is needed for the use of the shortened time period for the RASRSM-D13R.

IMC Comments	USACE Responses
d) On Page 19, it was mentioned "after the calibrated RASRM had been adjusted to reflect the 1965-1977 period…" Please explain how the adjusted model reflects the 1965-1977 hydrological and transport conditions. Are there any comparisons and statistics that show that the results from the adjusted model are reasonable especially for the transport conditions?	A new section, 2.8, has been added along with a number of figures showing good correlations between modeled output and available head data. Regarding comparisons to transport conditions, the reader is directed to Section 2.7 which explains the fact that salinity conditions are not expected to change drastically in most areas of the model on a time scale of 40 years.
3. Is the methodology used to calculate the required pump pressure adequate to meet the goals of the project? Are the results reasonable?	

IMC Comments	USACE Responses
The methodology is reasonable. It is the Theim equation for confined aquifers under steady state conditions. However, in transient conditions as in this model, it could be assume that after a short period of time, release of water from storage is negligible in the vicinity of the well and the Theim equation will apply. The modelers conducted useful numerical experiments with smaller grid sizes, showing that the pressure is inversely proportional to the distance to the pumping well. Also, the lesser the distance to the pumping well, the higher the pressure, and pressure becomes more similar as the distance from the well increases. However, since grid size is about 2000 ft and it is unrealistic to run a numerical model with a 2 ft grid size, the modelers used the Theim equation to estimate pressure around a pumping well by reducing the grid size to a smaller one (2 ft). The equation also includes the transmissivity of the aquifer, thus high pressure is found in an aquifer with low transmissivity. The report mentioned that the PDT determined that it would be important to keep pressure head below 100 psi but the justification of this pressure was not given. Please site a reference to justify that this pump pressure requirement is realistic for ASR wells or how the pressure limit for an ASR well could be determined. This criterion proved to be very important and is used to optimize the ASR design in each of the scenario runs.	An additional sentence has been added to the first paragraph of Section 3.2 to explain that permitted wells in the FAS are normally tested to a level of 100 psi. This includes the pilot study ASR wells at Kissimmee River and Hillsboro.

IMC Comments	USACE Responses
On page 4 of the calibration model report, it states, "For the Phase II study, SEAWAT modeling was performed using the variable-density flow with solute transport mode." On page 13, the modelers state that the head difference is converted to pressure using the density of water which is a constant. But the water in the UF is brackish water and it was stated in Section 2.1 of the ASR calibration report that there are substantial density variations in the groundwater thus requiring the use of a density-dependent groundwater modeling code. If this is so, why was the variability in density not taken into account in the pump pressure calculations?	It may have been more correct to take this into account when calculating the pump pressures. However, the impact of the decision not to include TDS in this calculation is minor for a few reasons: Although the variation in TDS in the model is large, the variation in TDS at the proposed UF ASR sites is small. Figure 3.18 in the calibration report shows a range of about 500 – 5000 ug/L TDS at the proposed sites in the UF. This translates into a change in density of 0.02 – 0.23 lb/ft3. Temperature variations are smaller: about 24-29 degrees F (see Figure 3.29 in the calibration report). This equates to an increase in density up to 0.02 (for temperature below 25 degrees F) or a decrease in density up to 0.07 (for temperature above 25 degrees). Thus, if freshwater density is 62.25 lb/ft3, the maximum groundwater density that would be seen at any UF ASR site would be 62.5 lb/ft3. See equation 2.1 in the calibration report for details on the calculations. At 100 psi, the head difference for the freshwater density would be 231.3 ft. For a density of 62.5 lb/ft3, the head difference would be 230.4 ft. This difference of 1.1 feet is within the error of the model. Note that in the APPZ and BZ, the TDS levels are higher and so the densities are also higher. This means there may be a greater error caused by using the freshwater densities in these calculations. However, the APPZ and BZ pressures are well below the 100 psi limit in all scenarios and so any error introduced in this way will not impact the number of wells recommended at each site.

IMC Comments	USACE Responses
The results on the maximum pump pressure computed for each proposed ASR site revealed that all sites would need to be able to overcome pressures much greater than 100 psi. This was a very useful finding as this performance measure revealed to the modelers right away that the 333 ASR wells in the UF proposed in CERP would exceed 100psi and the number of ASR wells in the UF would need to be reduced/.	No response necessary.
4. Is the methodology used to calculate the reduction in artesian pressure adequate to meet the goals of the project? Are the results reasonable?	
The methodology used to evaluate artesian pressure reduction in the UF and the APPZ aquifers in Saint Lucie and Martin counties is reasonable. It basically used the Jacob and Lohman flow equation. The flow equation given in the report has an error in one of its coefficients. It should be 2.25 and not 2.5. The reviewers hope that this is a typo. Please revisit the calculations as an error of this nature might have a significant impact on the artesian pressure calculations.	This value of 2.25 was a typo and has been corrected in equation 3.8 and 3.9. However, because the calculation is a comparison between flows with and without ASR, this coefficient and many of the other parameters are canceled out during the subsequent derivation. Note that Equation 3.14, which was used in the analysis does not include the 2.25 coefficient and is not dependent on it. No error was introduced by this typo.

IMC Comments	USACE Responses
The flow reduction is calculated from simulated head pressure before and after the ASR project. The modelers used a similar procedure by Merritt (1997) using the Jacob and Lohman equation to calculate flow from an artesian well in the UF over time. The equation includes aquifer transmissivity, well radius, storage coefficient and difference between aquifer head and ground surface elevation. The flow reduction is presented in two ways by the modelers: 1) maps of the UF and APPZ layer with the cells colored by maximum percent flow reduction across the time period and 2) maps of cells colored by the number of days within 13 years that the 10% rule is exceeded. The methods measured magnitudes and frequencies of flow reduction within most of the two counties. An exception is that a ridge coming from the northwest increases the ground surface elevations, making the Merritt equation invalid when evaluating artesian wells. The performance measure is used to evaluate the effect of ASR wells on the flow reduction of artesian wells in Saint Lucie and Martin counties.	No response necessary.
The results obtained from applying the methodology are reasonable if the coefficient of 2.25 was used and show that the effect on the artesian conditions in St. Lucie and Martin Counties are significant and that most areas loose over 10% of artesian flow for more than 40% of the model time period when all 333 ASR wells are used in the UF.	No response necessary.
5. Are the descriptions of the eight D13R scenarios clear and are their purposes explained well?	

IMC Comments	USACE Responses
The descriptions of the eight scenarios are clear and their purposes are also explained though the reviewers didn't see the significance of some of the scenarios. Please explain how the 333 ASR wells were determined by the SFWMM-D13R model. Note that the SFWMM models the unconfined surficial aquifer system (SAS) that is the topmost layer in the aquifer system. A link-node approach was used to simulate the ASR wells assuming an efficiency ratio. ASR wells for CERP purposes are supposed to be placed in the UF which is a confined aquifer below the SAS separated by a complete separation between the SAS and the UF.	Additional text has been added to Section 2 to explain the determination of the need for 333 ASR wells and to explain the differences in the groundwater calculations made in the SWFMM-D13R and the RASRSM-D13R models
In the RASRSM calibration report Figure 2.2 shows that the model includes five confined aquifers and five unconfined units (see p.7 of calibration report). It is also stated on page 7 of the calibration report "The SEAWAT grid also includes the SAS although no calculations are made there." The reason is because of the assumed complete separation between the SAS and the UF. Please explain how the 333 ASR wells were determined using the SFWMM (an SAS unconfined system). Please confirm if the original CERP assumption that 333 ASR wells could be used in the UF aquifer and aquifers below is valid.	Additional text has been added to Section 2 to explain the determination of the SFWMM-D13R of the need for 333 ASR wells. This determination was made solely on the volume of excess water which needed to be stored and the volume of additional water that needed to be supplied during dry seasons. The purpose of this RASRSM-D13R model was to determine if these 333 wells could be used from a regional hydrogeologic perspective.
Nonetheless, the scenarios started from a full D13R design from SFWMM, and then scaled back to meet performance measures such as pump pressure requirement. During model runs, some ASR wells were moved among aquifers and pump rates and recovery efficiency were adjusted in order to meet performance measures.	No response necessary.
6. Do the results of the eight D13R scenarios make sense conceptually?	

IMC Comments	USACE Responses
Before discussing whether the eight RASRSM-D13R scenarios make sense conceptually, the reviewers are recommending that two quick possible preliminary scenarios (Scenario 0a and 0b) should be run using the 30-year period RASRSM calibrated model with all 333 ASR wells in the UF but with important changes in the run mode of SEAWAT to avoid the runtime problems encountered by the modelers. *Scenario 0a:* Solve the RASRSM model as constant density flow and no solute transport with the additional 333 ASR wells. ➢ This simulation would determine the sensitivity to variable-density and solute transport to UF heads when compared to Scenario 1. ➢ In SEAWAT, turn off the switch for no density-dependent flow and no solute transport so that the simulation is done using MODFLOW only. ➢ Make a note of the UF heads for each cell in the UF layers. *Scenario 0b:* Solve the RASRSM model as a constant density flow and solute transport with the additional 333 ASR wells. ➢ This simulation would determine the density-dependence on UF heads when compared to Scenario 1. ➢ In SEAWAT, turn off the switch for the variable density component and solve as coupled flow and transport model. ➢ Make a note of the UF heads for each cell in the UF layers. Once these two scenarios are run, compare the difference in heads between each of the two scenarios and Scenario 1 for the UF in a difference map. If the UF heads in Scenario 1 are not significantly different from that of Scenario 0a, then all the analysis and scenarios discussed in this work could be performed using the RASRSM model for scenario 0a as the base model for scenarios 1 through 8. To show the advantage of doing this preliminary scenario analysis, consider the following results obtained with the SFWMD lower east coast (LEC) SEAWAT model. It has similar layers as the RASRSM. Each row and column was 2400 ft by 2400 ft; the active cells per layer were approximately 51,040; the total active cells were 714,520 and the time step was 1 month. A simulation similar to Scenario 0a for the LEC model took 1hr and 10 minutes for a 6 year stress period on a 3 GHz EMG4T processor machine with 8 GB RAM. Scenario 0b took 7hr and 25 minutes and Scenario 1 took 8 hours and 30 minutes. These results show that if variable density and TDS concentration do not affect significantly the heads in the UF, then the performance measures analyses could have been done using SEAWAT using Scenario 0a as the base model. The run time could have been reduced by an order of magnitude of about 8 and possibly the modelers would have had no need to limit the modeling period to 1965-1977.	Removal of density dependence as suggested by this commenter will result in significant changes to groundwater heads and flows. Note that Scenario 0a and 0b will result in the same head results. The only difference between the two is that a TDS concentration will be calculated for Scenario 0b but not for 0a. As shown in Figures B.1 through B.4, the steady state calibration of the RASRSM is greatly different when density dependence is removed. Note that in Figure B.1, the UF heads in the southern 2/3 of the model are significantly lower when density dependence is removed. Similar effects are seen in all other layers of the model. Figure B.5 shows the comparison between model calculated heads and observed heads. Note that where the heads are high (near the Polk County recharge area) the inclusion of density dependence makes no difference. But in other areas of the model, the difference is stark and many error values are greater than 20 feet. A similar effect is shown in Figures B.6 and B.7 where a few comparison points are shown from the transient calibration run. As expected, when density dependence is removed, points far from the recharge area have much lower heads than the measured heads. The measured heads in the southern portion of the model domain are high because of the pressure exerted by the high TDS, low temperature (high density) water in the ocean, which enters the BZ and pushes upward on the water above it. This cyclical movement of water is not only supported by the results of this model, but also in a number of references (Kohout, 1965, Kohout, 1988, Bittner, et al., 2008). Figures B.8 through B.11 show the impact of removal of density dependence for Scenario 1 as suggested by the reviewer. Note that large sections of both the UF and APPZ have head differences greater than 50 feet between the two runs. When post-processing is used to compare the results against the performance measures, the results are shown in Figures B.12 through B.14. Pump pressures estimated for the ASR sites are slightly lower when density dependence is removed (compare Figure B.12 to Figure 4.17 in the main report). The results of the APPA analysis are significantly different since most of St. Lucie and Martin Counties are no longer artesian even without the ASR wells (compare Figure B.13 to Figure 4.18 in the main report). Drawdown and "drawup" caused by the ASR wells is only slightly different (compare Figure B.14 to Figure 4.20 in the main report). The removal of density dependence affects more than just the head results. It completely changes the flow regime. Figures B.15 through B.29 show the results of a few particle tracking exercises. Note that in many places, the direction of flow is opposite for the two runs. Flow directions are summarized in the next few figures. Figures B.30 through B.32 show the comparison of vertical flow through each of the confining units. The sign of the vertical component of flow is shown with red for downward flow and blue for upward flow. In the LC, MC2 and MC1, the majority of the flow is downward without density dependence and upward with density dependence. Figures B.33 through B.36 show the direction of the horizontal component of flow in the aquifers. There are significant differences in the direction of flow in the two runs, especially in the southern half of the model domain. This shows that the entire flow regime has changed with the removal of the density dependence. The time savings of a simple MODFLOW model without water quality transport equations would have been useful, but the results would not have been accurate. Full SEAWAT calculations were necessary in this case.

IMC Comments	USACE Responses
The following comments below pertain to the scenarios that are modeled and presented in this report. Some of the scenarios are reasonable as they follow a logical sequence after discovering that the 333 ASR wells proposed by CERP for the UF wouldn't meet the requirements of the performance measures. Therefore the task after this discovery was to determine whether wells that could not be placed in the UF could be distributed within the other aquifers. However, it leaves the reviewers with two very important questions shown below.	No response necessary.

IMC Comments	USACE Responses
With the decision made to distribute some of the wells among other aquifer units, please explain the rationale of placing wells in the Boulder Zone (BZ), instead of the Lower Floridan aquifer (LF). The LF aquifer is a permeable unit above the Boulder Zone which is separated from the BZ by the Lower Floridan Confining unit. Installing wells in the LF would be a much better alternative to installing wells in the BZ. The Boulder Zone is difficult to drill into, having the same rough, shaking, grabbing effect on the drill system and drilling rig as boulders would. Also, the TDS concentrations in the BZ (that of salt water) and the depth from ground level, makes this a challenging zone to work with.	The process of developing the D13R scenarios began with the UF aquifer only, as was envisioned by CERP. When it became clear that the UF could not handle all 333 wells, it was a natural step to begin placing some in the APPZ. However, it was soon obvious that even with the two aquifers, the full injection and extraction volumes could not be achieved. As the PDT discussed the next steps, consideration of the BZ was introduced as a way to dispose of excess water, protecting the estuarine habitats from excess fresh water and reducing flooding in Lake Okeechobee and the canals. The PDT was aware of the expense and difficulty in working with the BZ. These wells were not considered to be true ASR wells because of the low recovery efficiency, but were considered to be disposal wells for the removal of excess water. This run was meant to get as close as possible to the D13R volumes, even though it might eventually turn out to be difficult or expensive to build. Further discussions with the PDT in January 2013 (after the release of the Draft version of this report, but before receipt of IMC comments) resulted in the addition of Scenario 12 which removes the BZ wells from Scenario 11. A section on Scenario 12 (4.12) was added to this report. Unfortunately, scheduling constraints do not allow the repeat of the Monte Carlo analysis, however, because of the high conductivity in the BZ, the results would be very similar.

IMC Comments	USACE Responses
Scenario 1: The modeling run made for this scenario using the RASRSM-D13R followed the injection and extraction schedules used in the SFWMM-D13R model as closely as possible. All the 333 recommended ASR wells were in the UF. The simulated results and calculated performance measures showed maximum pump pressure requirements at all ASR sites are above 100psi, and even approach more than 400 psi at Taylor Creek and 800 psi at the L-63N site. The effects on the artesian conditions in Saint Lucie and Martin counties were significant; maximum drawdown is greater than five feet in most of the modeled area. The regional effects of the system are widespread and significant, because all 333 ASR wells were assigned in the UF. This scenario didn't satisfy the performance measures.	No response necessary.
Scenario 2: Based on simulated results in Scenarios 1, the modelers developed a strategy by removing wells until the pump pressure requirement of 100 psi was met at each site. It was mentioned that removing some ASR wells is somewhat arbitrary, but we would suggest removing those wells located at areas with relatively low hydraulic conductivity, which will thus significantly reduce maximum pump pressures below 100 psi. As a result, the scenario provided less storage and recovery volume and reduced the total number of ASR wells from 333 to 97.	The process of removing the ASR wells was termed arbitrary because it was not based on any specific algorithm. Wells were removed from sites where the pressure was above 100 psi. Removal continued until the pressure was within the limit. Naturally, this would mean removal of most wells from areas of low hydraulic conductivity or areas of high ASR well density. Text has been adjusted to clarify this.

IMC Comments	USACE Responses
Scenario 3: Scenario 3 was developed by having 97 ASR wells in the UF and 236 ASR wells in the APPZ aquifer which consists mainly of the Middle Floridan aquifer (MF). The results showed an increase in pump pressure requirements in the UF but most of the wells that were already in the UF didn't violate the 100 psi pump pressure criteria. The 100 psi criterion for the APPZ was violated in most of the 232 wells in the APPZ. Only 41 wells in the APPZ met the 100 psi requirement.	No response necessary.
Scenario 4: In this scenario, the modelers ended up removing 191 wells from the APPZ in order to satisfy the 100 psi performance measure criteria for both the UF and the APPZ. They were able to successfully leave 41 wells in the APPZ because these 41 wells were mainly in areas that didn't have the UF as an upper confining unit. The implication of this scenario is that once the 97 ASR wells are already in place in the UF, it would be difficult to add wells in the APPZ without violating the pump pressure performance measure.	No response necessary.

IMC Comments	USACE Responses
Scenario 5: A scenario is recommended, referred to as (Scenario 4a) in this review report where the 191 wells removed from the APPZ should have been placed in the Lower Floridan aquifer (LF). It is not clear why this scenario was not tested or reported. Based on the familiarity of the reviewers with the Florida Aquifer System (FAS), this scenario would have ended with violation of the 100 psi requirement in the APPZ and UF in some of the wells that were already meeting this requirement under the previous scenarios because the aquifer is confined and pressure builds quickly under high pumping conditions. Thus, Scenario 5.	As mentioned in this comment, the addition of wells to the LF would probably not have resulted in a significant increase in available storage because of the hydraulic conditions of the aquifer. Because of the water quality conditions of the aquifer, recovery efficiency would have been low and only a small increase in recovery volumes would have been achieved. Once it was determined that the UF and APPZ together could not achieve the volumes set forth in the SFWMM-D13R, the PDT began looking for places to dispose of excess water, without expecting to be able to recover it. The BZ seemed like the best location for this.
The relevance of installing ASR wells in the BZ is not sufficiently explained. The BZ permeability is very high because of its cavernous nature and its anomalous extremely high permeability prevents pressure buildup in injection wells. However, the BZ is not suitable for ASR wells because the zone contains saltwater of concentration similar to that of seawater. The BZ has been used for years to store vast quantities of treated sewage injected into it in Miami, Fort Lauderdale, West Palm Beach and Stuart but the reviewers are not aware of anywhere where the BZ is being used to store fresh water.	As explained above, the recovery efficiency in the BZ is so low, that these wells cannot truly be considered ASR wells. These wells were meant to remove excess freshwater from the surface water system but were not expected to be able to store or provide freshwater when needed.

IMC Comments	USACE Responses
Due to the existence of the Floridan confining unit, and the lower middle confining unit which is located between the BZ and upper layers (UF and APPZ); and due to the cavernous nature of the BZ, the effect that ASR wells installed in the BZ may have on the upper layers is very limited as shown in the report. It is difficult to build up pressure in the BZ. Also, since TDS concentration in the BZ is similar to that of seawater, the assumption of 10% recovery efficiency is not reasonable. Thus total annual extraction rates will be even lower than estimated from the scenario. Is it consistent with the ASR objectives to pump freshwater into the BZ with TDS concentration close to or higher than seawater?	Scenario 5 has been removed from this report since it is so similar to Scenario 9. This removes the estimate of 10% recovery efficiency from the BZ and converts ASR wells in the BZ into disposal wells.
Scenarios 6-8: not detailed in the report as the PDT decided not to pursue these scenarios.	No response necessary.
Scenarios 9: In this scenario, the pump capacity was increased to 10 mgd at each ASR wells in the BZ in order to maintain the same total amount of injections. Recovery efficiency was reduced to 0% so that drawdowns decreased slightly. Again, because of the cavernous nature of the BZ increasing the pumping rate from 5 mgd to 10 mgd would have very little impact. The reason to develop this scenario for ASR is not clear.	With the removal of Scenario 5 (see above), Scenario 9 becomes more important.

IMC Comments	USACE Responses
Scenarios 10: Based on Scenario 9, the run simulated in this scenario further reduced recovery efficiency at each site so that the artesian pressure in the APPA area is less than 10% and maximum drawdown one mile each side is less than or equal to one (1) foot. In addition, recovery storage was reduced to between 1% and 4% of the SFWMM-D13R, so scenario 10 is more like storage system with no retrieval.	No response necessary.
Scenario 11: This is the final design that was selected by the PDT. According to the modelers, it meets all performance measure requirements other than the one (1) foot drawdown at one (1) mile distance from the well. This allowed to increase recovery efficiency at most sites so that total annual recovery storage increased between 12% and 60%. This scenario resulted in a design that located 94 ASR wells in the UF, 37 ASR wells in the APPZ, and 101 ASR wells in the BZ. The UF and APPZ wells will have 5 mgd each while the BZ wells will have 10 mgd capacity. Please describe what was the criteria to assign recovery efficiencies at each site. Also, based on the discussion, it seems that these efficiencies are different from recovery efficiencies expressed by the ratio of recovered over injected volume of water, please explain these differences. In Figure 4.146, recovery efficiency at Marcy and Port Mayaca (Lake Okeechobee basin) was reduced to 0%.	The assignment of recovery efficiencies to each proposed ASR site is described sufficiently in Section 2.6.1. The extraction percentages shown in Figure 4.146 are not recovery efficiencies. These are reductions to extraction rates which were used to reduce the impact to the APPA in St. Lucie and Martin Counties. These percentages were applied directly to the extraction rates and were unrelated to the injection rates or water quality. Although a 0% extraction percentage is equal to a 0% recovery efficiency, the reason for the reduction is different. Recovery efficiency is caused by poor water quality in the recovered water resulting the need to stop extracting. Extraction percentage is caused by the need to minimize drawdown impacts in St. Lucie and Martin Counties. Additional notes have been added to Figures 4.146 and 4.127 to clarify this.

IMC Comments	USACE Responses
Nevertheless, it is not clear about the rational of the PDT to select Scenario 11 as the final design. Is it required that 333 ASR wells must be installed as opposed to a number of wells that produce the same performance for CERP? Based on the analyses in this report, the reviewers concluded that ASR wells should only be installed in the UF and possibly the APPZ.	This analysis shows that installation of ASR wells at the specified sites in the UF and APPZ will not be able to fully meet the water storage needs of CERP or the water supplementation needs of CERP (as defined by SFWMM-D13R). Full water removal during wet periods can be achieved with the use of the BZ. No known number of ASR wells can be installed to produce the performance required for CERP while still meeting the regional hydraulic performance measures. This is explained in Section 8 of the report.
7. Does the analysis in Appendix A adequately address possible concerns with the location of the north, west, and south boundary of the model?	
The concern with the locations of the north, west, and south boundaries was previously provided to the modelers when the calibrated RASRM model was reviewed by the IMC. The review report from the IMC mentioned that when ASR wells are installed, some of the inland boundaries will be too close to the ASR wells and drawdown caused by ASR wells will extend to those boundaries. As mentioned in the report, in Figures 4.20, 4.39, 4.58, 4.77, 4.96, 4.115, 4.134 and 4.153, significant head changes extended to the western, southern and northern boundaries, indicating the use of inland specified head boundaries at these locations may be violated.	No response necessary.

IMC Comments	USACE Responses
However, as stated in the report, extension of western, southern and northern boundaries is not feasible for several reasons. Instead, the modelers conducted a series of numerical modeling, and calculated flux differences across these boundaries between the non-ASR well scenario and ASR well scenarios. The ideal situation would have been that there is no difference between these two conditions. However, Figures A.21 through 25 showed increases of flux across IAS/ICU, UF, APPZ, LF and BZ between the two conditions. This indicates that the inland specified head boundaries along the western, northern and southern boundaries do have effects on the interior heads of the model. The magnitudes of the increase are related to the magnitudes of the recharges and discharges of the ASR wells.	No response necessary.

IMC Comments	USACE Responses
As found in the numerical experiments, the flux change (increase / decrease) are larger when the model approaches steady state and larger where closer to ASR wells. Therefore, in addition to calculating flux changes across questionable boundaries, it is suggested cropping a smaller box around the area of interest (i.e., APPA) and calculating flux changes across the box boundaries between non-ASR and ASR conditions. Any quantifications and justifications about the magnitude of flux changes would be helpful.	When a specified head boundary condition is applied to a model boundary, the assumption is that there is an infinite source/sink of water at that location. The model removes or adds whatever volumes of water are necessary to ensure that the head remains at the specified value. If the boundary is set too close to the ASR wells, the specified head assumption is violated since the head will not remain constant. The purpose of this analysis was to determine the validity of the specified head boundary condition. If the fluxes through the boundary remained constant despite the addition of interior pumping, then we could be assured that the boundaries were set at a sufficient distance that they would not impact the head results inside the model. If the fluxes are calculated across the boundaries of a smaller box around the area of interest, as recommended by the reviewer, the fluxes would definitely be larger than at the model boundary, but this would not tell us anything about the validity of boundary conditions since the boundaries of a smaller box would not coincide with a model boundary. Since the heads at the location of a smaller box are allowed to vary, there is no violation of assumptions in allowing the flux to vary.
8. Is the Monte Carlo methodology (including the calibration checks) adequate for the reasonable analysis of model uncertainty?	

IMC Comments	USACE Responses
The Monte Carlo methodology is one of the widely used methods to characterize uncertainties in numerical models. The key point of the method is to use a large number of samples (or to run a number of simulations) so that realizations of the parameter fields using their probability density functions could be used to determined uncertainties in the predictive response of the model. To run a number of simulations, computational time is one of important factor to consider.	No response necessary.
The modelers did some checks before applying the method to the RASRSM-D13R model. If simulations pass steady state and transient model check (NAP, 2011), then the input files (selected parameters) will be valid for the RASRSM-D13R. Therefore, statistical analysis for uncertainties in the model will be based on these simulations. The reason for the check is that RASRSM-D13R cannot be explicitly calibrated but appears consistent with the calibrated RASRM model through the conversion process.	No response necessary.
9. Is the selection of parameters for variation (and their probability distributions) in the Monte Carlo simulation adequate for a reasonable analysis of model uncertainty?	
There were six (6) groups of parameter combination used in these analyses.	No response necessary.
a) Uniform distribution: Porosity, longitudinal dispersivity and molecular. However, according to previous studies (Gelhar, 1992), dispersivity is usually represented as a log distribution and not as a uniform distribution as used in the model.	The range of acceptable values for longitudinal dispersivity was quite small (0.1 to 2.5), only 1.4 times a log scale. It was felt that the linear distribution would be more appropriate for a small range. Also, a log scale would have put additional weight on small values, which was not desired.

IMC Comments	USACE Responses
b) Log Distribution: ratios of longitudinal to transverse dispersivity, longitudinal to vertical dispersivity and horizontal to vertical conductivity for each aquifer.	No comment necessary
c) Hydraulic conductivity and specific storage: The modelers included the most sensitive parameters into the calibration model as pilot points, which is reasonable and doable. However, the method to vary hydraulic conductivity is questionable. First, the range shouldn't be too narrow to make them close to calibrated values (only ½ to 2 times was used in the report). Uncertainty from these parameters could be investigated with a wider range. Second, uniform distribution can only be applied to log-transformed hydraulic conductivity and log-transformed specific storage but not to their original values directly.	The range was set to be very narrow because there was a great amount of field data used during the calibration of the model. (See Figures 3.8-3.10, 3.34, 3.36 and 3,38 in the Calibration Report.) The purpose of the Monte Carlo was to determine the uncertainty in the results caused by uncertainty in the input parameters. Thus, the ranges and distributions of the input parameters should reflect their uncertainty. Since there was quite a lot of APT data in each of the aquifers, the uncertainty in the hydraulic conductivity was low compared to many other model parameters. The narrow range ensures that this low uncertainty is communicated to the Monte Carlo analysis. Secondly, although a log transform is generally used for hydraulic conductivities, it was not used in this case because the range of values was less than one log cycle. Log distributions were applied to the specific storage values as explained in Section 6.1.3.
d) Invertible distribution: horizontal anisotropy of hydraulic conductivity.	No response necessary.

IMC Comments	USACE Responses
e) Initial (starting) conditions for TDS and temperature: The initial TDS concentrations and temperatures were not discussed in the model set-up section, but they are considered as one of the uncertainties in the numerical model. As mentioned before, initial TDS and temperature should be carefully determined before running a coupled variable-density transient flow and transport model. During randomizing the initial TDS and temperature, the values only vary between 80% and 120%, which means initial TDS and temperature used in the model are mostly close to their calibrated values. In addition, the model results would be very sensitive to the initial TDS concentration. The narrow range of variation of the value may be reasonable, but the question is how the initial TDS (and temperature) have been determined when running Scenario 1.	This comment was made previously and has been discussed above. In addition, a new section, 2.7, has been added to the report to discuss initial conditions, including TDS.
f) Multiplier (0.5 to2) was applied to change the thickness of the BZ.	No comment necessary.
For a specific model run, there is a combination of all input parameters such as hydraulic conductivity, storage, dispersivity, etc. some of them may be correlated. It is not clear how the modelers selected randomized values from each of the parameters and make a combination to run a simulation. It was mentioned that there were 1485 parameters, but detailed information about combining randomized parameters would be helpful.	No correlation of the parameters was assumed and no combinations were made. All values were randomized with their own unique random value, generated by FORTAN.

IMC Comments	USACE Responses
As to the number of Monte Carlo simulations, in Figure 6.14, it shows that when the number of Monte Carlo simulations increases, half-width of 95% Confidence Interval decreases, but it approaches a constant when certain number of simulations is run. This is the basis of the Monte Carlo method, which means a large number of simulations may be needed to reasonably characterize uncertainty of the model. From Figure 6.14, a number between 1000 and 10,000 would meet this requirement. So, it seems at least a doubled number (1,650) of simulations are needed if running time allows.	The half-width of the 95% confidence interval approaches zero without ever arriving at zero. When deciding the number of Monte Carlo simulations necessary, the required precision must be balanced with the available resources and time. The 825 simulations run for this project brought the half-width of the 95% confidence interval within 3.5%, which is likely within the error of the model. Sections 6.3.2, 6.3.3 and 6.3.4 show that this confidence interval is quite small compared to the results and continued Monte Carlo simulations would lend little additional precision to the results. At 825 simulations, the point of diminishing returns has been reached. Finishing with 10,000 Monte Carlo runs would reduce the half-width of the 95% confidence interval to less than 1%, but it would take 3 years with current computer resources. That is a very expensive 2.5% improvement.
10. Are there any sources of uncertainty or error that are not addressed in the report, but which might adversely impact the usefulness of the model results?	

IMC Comments	USACE Responses
The modelers discussed a number of uncertainties from model setup, conversion of calibration model to D13R model, ASR pumping data, and performance measures. One of the important uncertainties is the recovery efficiency. Throughout the report, the modelers did a series of numerical experiments to rearrange and renumber the ASR wells within aquifers and to assign various recovery efficiencies at ASR wells, in order to meet performance measures set by the PDT and to let the ASR system function properly. It is noticed that as much as 100% recovery efficiencies were assigned for a few ASR wells in the final scenario, but in reality, this 100% recovery efficiency is unreasonable, and it is likely that the water recharged into the aquifer system cannot be recovered or would disappear in fractures in the aquifer due to uncertainties in characterizing the aquifer system. Please clarify what these efficiencies represent.	No ASR wells were assigned 100% recovery efficiency. It is possible that the reviewer is referring either to extraction percentage (Figure 4.146) which is the comparison of actual extraction rates to assigned extraction rates, or to comparisons of SFWMM-D13R assigned rates and RASRSM-D13R assigned rates as shown on Figures 4.162, 4.163 and 4.164. Additional text and notes have been added to clarify this.
11. Does the reviewer agree with the conclusions and recommendations?	
The assumption of 333 ASR wells is based on CERP modeling with the SFWMM which is greatly limited because it assumes no interaction with the UF. The ASR wells are intended to be installed in the UF which is a confined aquifer system. A confined aquifer with 333 wells pumping at 5 mgd results in a cone of depression and drawdown of the aquifer system that could not be simulated with the SFWMM.	No response necessary.

IMC Comments	USACE Responses
No information was presented on the TDS concentration and temperature conversion that was done when the RASRSM-D13R was developed for the time period 1965-1977. On page 3 of the ASR calibration report which preceded the report currently under review, the modelers state "The regional model will provide planning level information to address large scale issues such as the regional effect of the ASR well clusters on saltwater intrusion……and water quality." In the ASR impact report under review, the modelers stated on page 17 that unfortunately, the regional model is not able to address water quality migration and salt water intrusion because it cannot accurately portray TDS transport near wells and that the salinity at locations far from the ASR wells are highly dependent on transport parameters such as dispersion, which could not be calibrated due to lack of TDS time series data. Please explain how TDS concentration and temperature conversion were done in RASRSM-D13R for 1965-1977 using data from the RASRSM calibrated model. The reviewers question would like to know details of the parameters of the contaminant transport component of the RASRSM-D13R.	Section 5.2 and 5.3 of the calibration report provide transport parameter values used in the calibration report. Tables 6.1 and 6.2 provide ranges and distributions for transport parameters values for the Monte Carlo analysis. A new section (2.7) has been added to this report to clarify the selection of initial TDS conditions.

IMC Comments	USACE Responses
The modelers did a series of numerical experiments on the converted RASRSM-D13R model, based on assumptions especially on recovery efficiency. Recovery efficiency, which is a very important uncertain parameter, is not included into the Monte Carlo analysis. The modelers mentioned in the end that the regional model made a few assumptions such as aquifer conditions and recovery efficiency, so that when predicting local effect of the ASR wells system it is necessary to analyze closely using pilot points at proposed ASR sites and using local scale models.	The inclusion of recovery efficiency in the model was not as simple as inputing a single value in a text file. A change to the recovery efficiency involved a detailed calculation of stored water volumes with comparisons to flow rates. Inclusion of recovery efficiency in the Monte Carlo was deemed far too complicated. However, recovery efficiency only impacts the length of time that extraction occurs. A small variation (5%-10%) of the recovery efficiency would likely only have impacted Lake Okeechobee and Central Palm Beach basins, since these are the basins that return to zero stored volume during the model period (see Figures 2.1 through 2.5). Further, because recovery efficiency only affects extraction and not injection, it would have only minor impacts on the pump pressure analysis or on the "drawup" results since these occur during injection periods. Although the loss of artesian pressure in the APPA is a result of extraction rates, all ASR sites near the APPA have had extraction rates dropped significantly below the recovery efficiency in order to meet the performance measure, so a small change to recovery efficiency in the Monte Carlo would not have affected that performance measure. The only measurable impact of a small variation to recovery efficiency would be to the drawdown areas. This performance measure did not impact the selection of ASR wells. As mentioned by the reviewer, recovery efficiency is an issue that should be studied in detail at each individual site using pilot projects and local scale models.
A final design was found with 94 wells in the UF, 37 ASR wells in the APPZ and 101 ASR wells in the BZ. The final design in our view should only include wells in the UF and possibly in the APPZ especially since the ASR wells are needed for water supply from the UF to supplement water from the SAS.	Scenario 12 has been added which removes the BZ wells from Scenario 11.

IMC Comments	USACE Responses
Additional Comments: 1. Limiting heads to prevent rock fracturing As mentioned in the report, the method of Nick Geibel of USACE Omaha District was used to analyze and estimate the limiting heads in each aquifer. A concern on the calculations is that the static total head was taken from the February 2004 calibration model. Why simulated heads from one of the scenario runs (e.g., full design run) was not used for the calculation? Adding 333 ASR injection wells will increase head pressure locally and/or globally.	This analysis is explained more clearly in the 2012 Geibel report and this document (section 3.1) has been adjusted to more closely resemble that explanation. The term "static total head" as used in this report is called "ambient pre-fracture water pressure" in the Geibel paper. We discussed this comment with Mr. Geibel and he assured us that this term refers to the aquifer conditions before pumping begins. The increased head caused by the injection from 333 ASR wells is compared to the result of Equation 3.6.
2. Can this model be used to determine the optimum number of ASR wells that can be located in the Upper Floridan aquifer while avoiding locating wells in the boulder zone?	Scenario 2 provides one possible answer to this question.

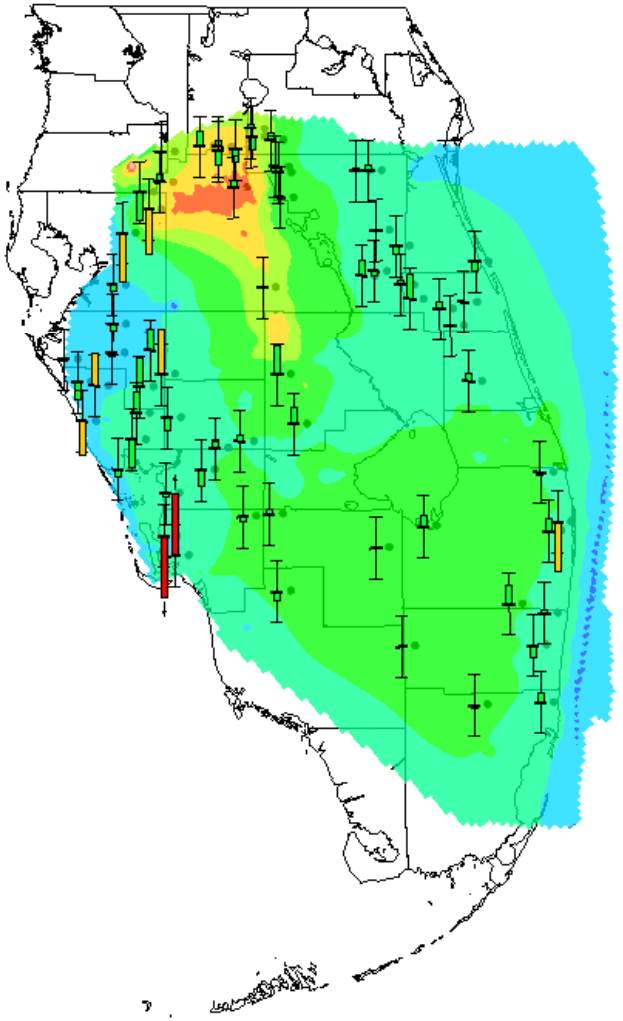

Original Feb 2004 Steady State Solution (With Density Dependent TDS/Temp Transport)

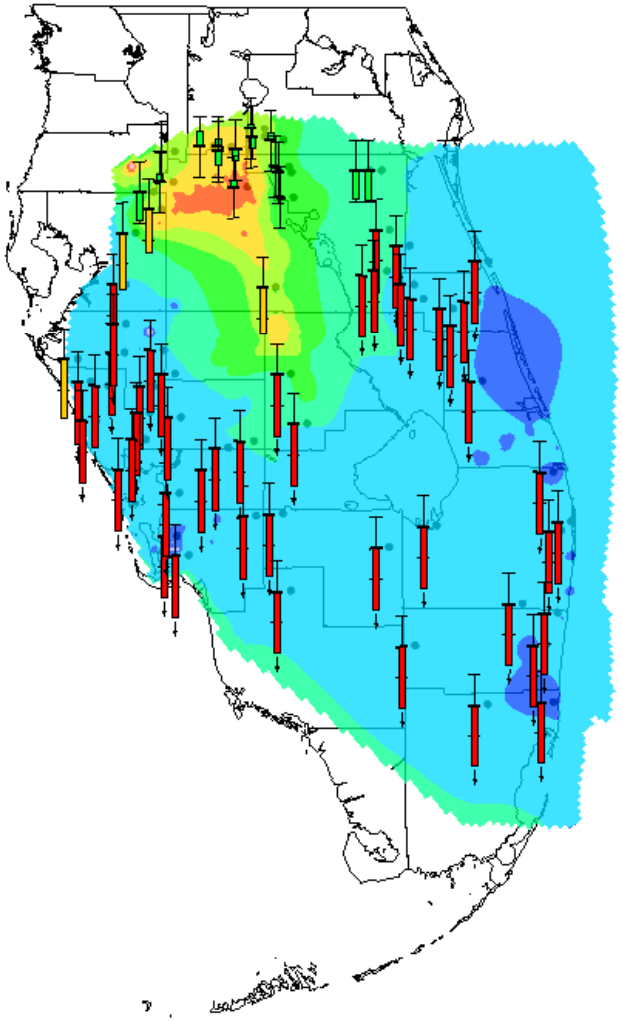

Sensitivity Feb 2004 Steady State Solution (Without TDS/Temp Transport)

Head (ft)

125
100
75
50
25
0

Notes:

At left is the original calibrated model (steady state, February 2004, UF layer) with density dependent flow TDS and temperature transport. At right is the same run made with density dependent flow and TDS and temperature transport turned off. Calibration targets show the comparison to measured heads. Green targets are within 2 feet of the measured head; yellow targets are within 4 feet of the measured head; red targets are more than 4 feet different from the measured head. The direction of the target indicates the sign of the error.

Impact of TDS and Temperature Transport on UF Head Solution

Response to Comments, Production Scenario Report

Figure B.1

June 2013

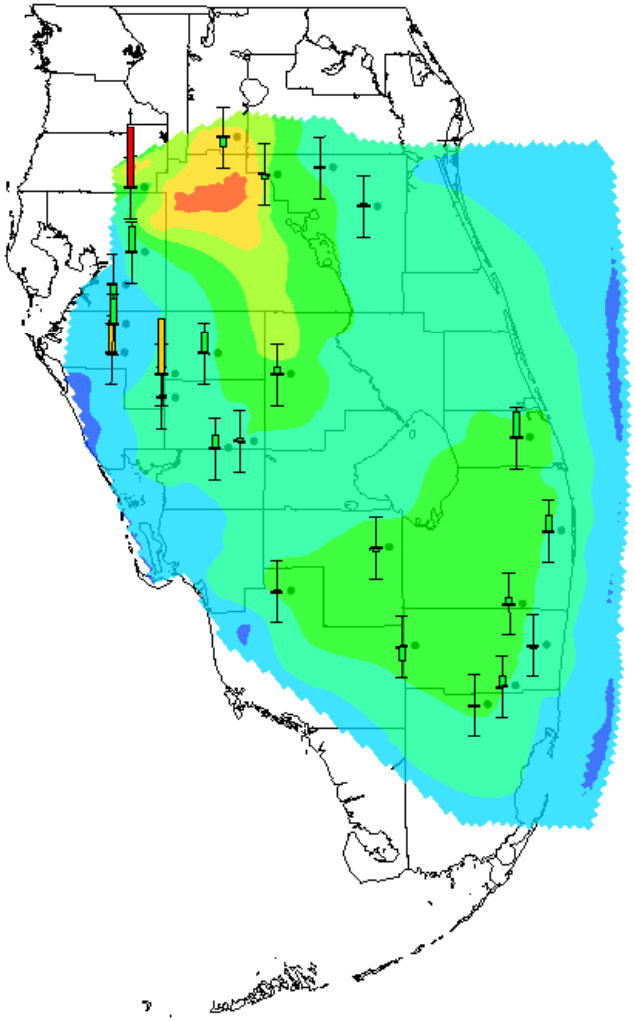

Original Feb 2004 Steady State Solution (With TDS and Temperature Transport)

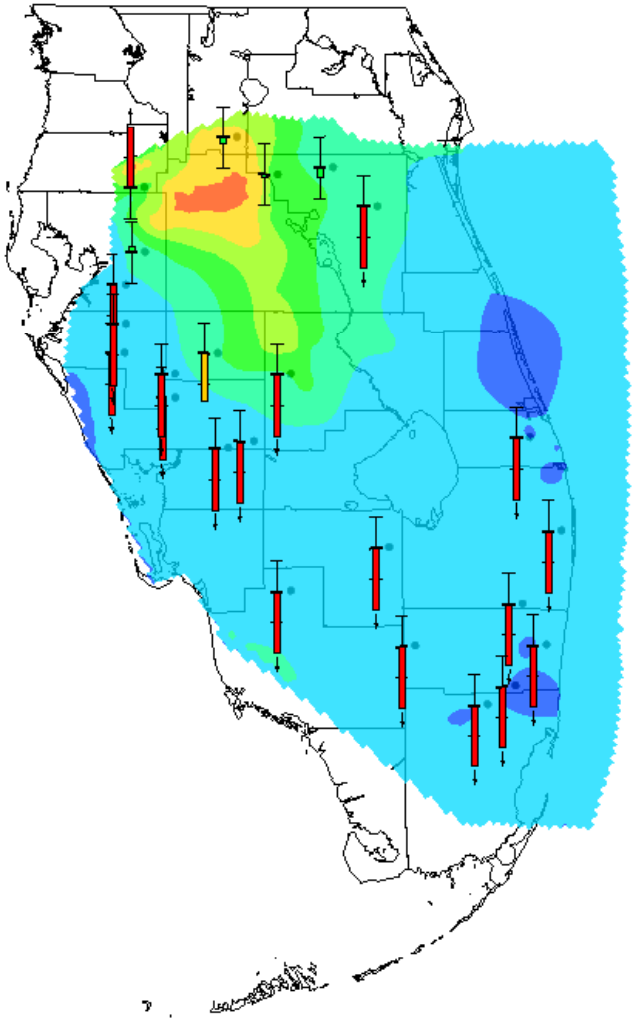

Sensitivity Feb 2004 Steady State Solution (Without TDS and Temperature Transport)

Head (ft)

125
100
75
50
25
0

Notes:

At left is the original calibrated model (steady state, February 2004, APPZ layer) with density dependent flow TDS and temperature transport. At right is the same run made with density dependent flow and TDS and temperature transport turned off. Calibration targets show the comparison to measured heads. Green targets are within 2 feet of the measured head; yellow targets are within 4 feet of the measured head; red targets are more than 4 feet different from the measured head. The direction of the target indicates the sign of the error.

Impact of TDS and Temperature Transport on APPZ Head Solution

Response to Comments, Production Scenario Report

Figure B.2

June 2013

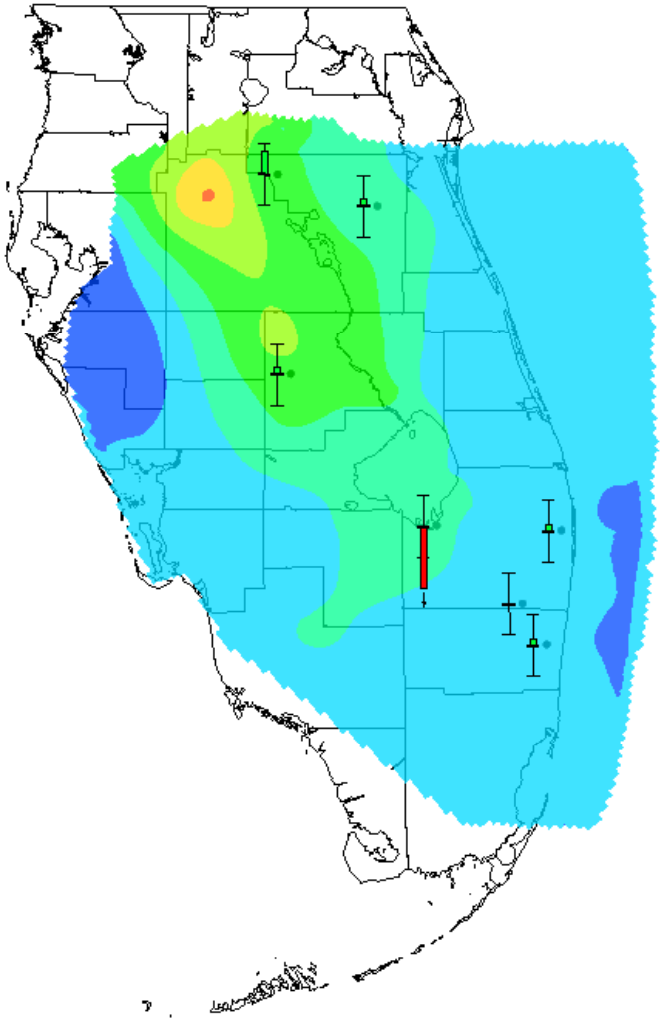

Original Feb 2004 Steady State Solution (With TDS and Temperature Transport)

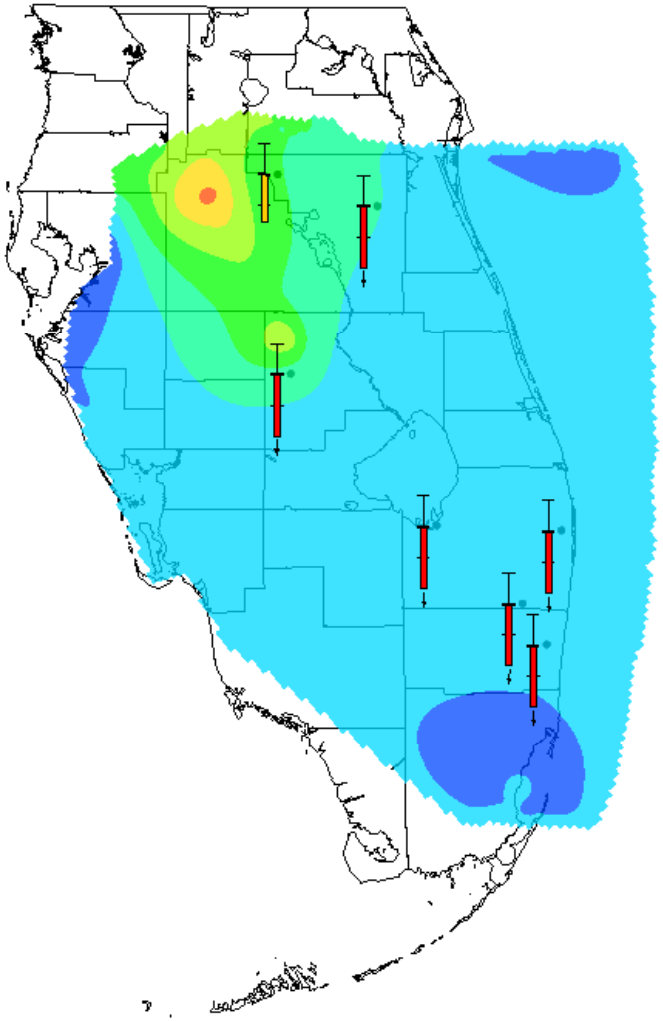

Sensitivity Feb 2004 Steady State Solution (Without TDS and Temperature Transport)

Head (ft)

125
100
75
50
25
0

Notes:

At left is the original calibrated model (steady state, February 2004, LF layer) with density dependent flow TDS and temperature transport. At right is the same run made with density dependent flow and TDS and temperature transport turned off. Calibration targets show the comparison to measured heads. Green targets are within 2 feet of the measured head; yellow targets are within 4 feet of the measured head; red targets are more than 4 feet different from the measured head. The direction of the target indicates the sign of the error.

Impact of TDS and Temperature Transport on LF Head Solution

Response to Comments, Production Scenario Report

Figure B.3

June 2013

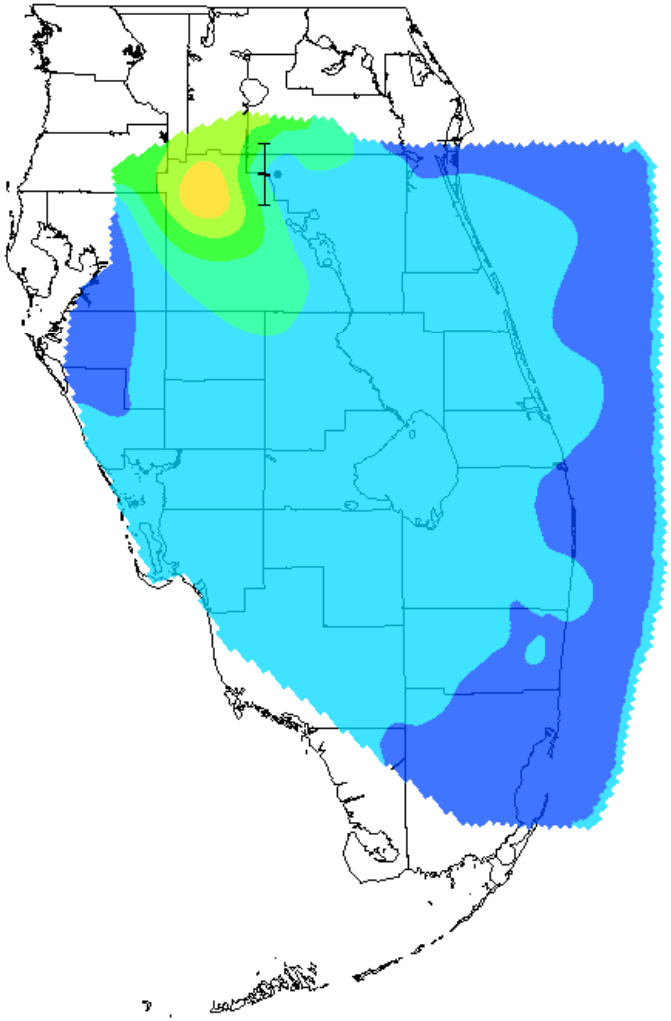

Original Feb 2004 Steady State Solution (With TDS and Temperature Transport)

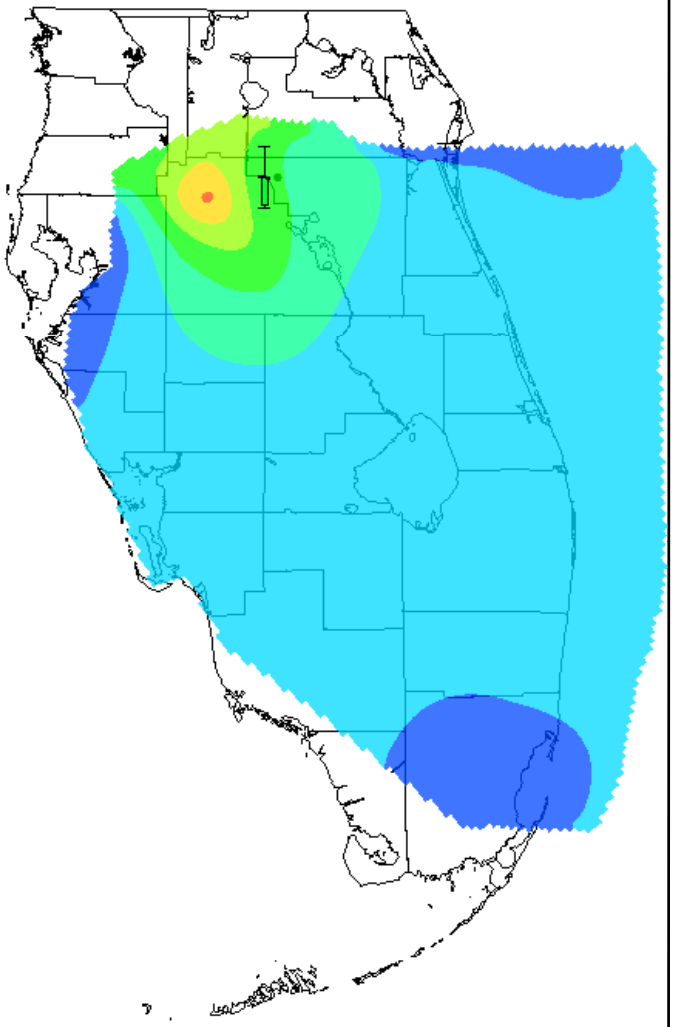

Sensitivity Feb 2004 Steady State Solution (Without TDS/Temperature Transport)

Head (ft)

125
100
75
50
25
0

Notes:

At left is the original calibrated model (steady state, February 2004, BZ layer) with density dependent flow TDS and temperature transport. At right is the same run made with density dependent flow and TDS and temperature transport turned off. Calibration targets show the comparison to measured heads. Green targets are within 2 feet of the measured head; yellow targets are within 4 feet of the measured head; red targets are more than 4 feet different from the measured head. The direction of the target indicates the sign of the error.

Impact of TDS and Temperature Transport on BZ Head Solution

Response to Comments, Production Scenario Report

Figure B.4

June 2013

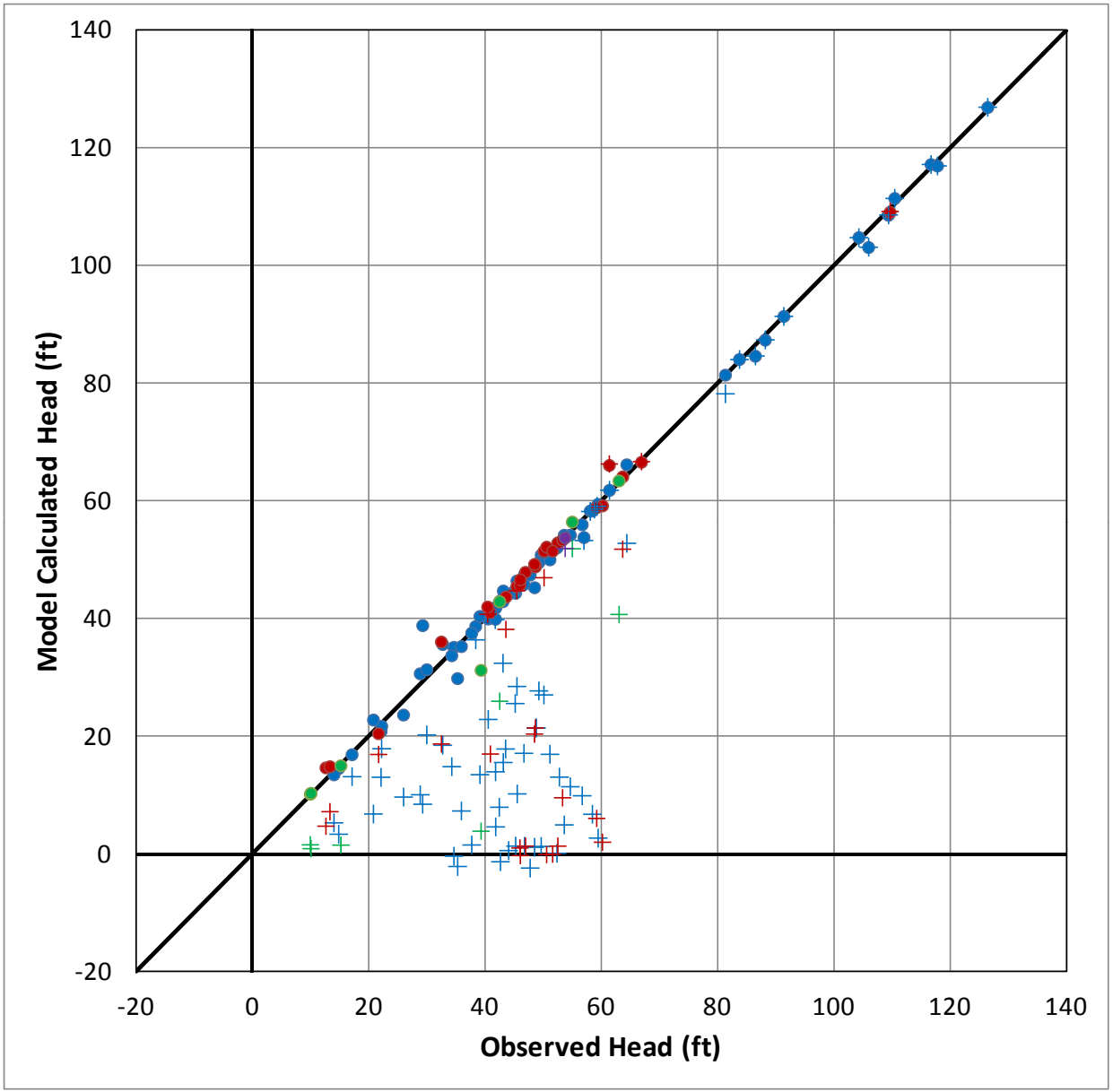

Original Run (with Density-Dependent TDS/Temp Transport)

- UF
- APPZ
- LF
- BZ

Sensitivity Run (no Transport)

- UF
- APPZ
- LF
- BZ

	With Density Dependence	Without Transport
ME	-0.182	21.116
MAE	1.042	21.299
RMS	1.819	28.009

ME = Mean Error
MAE = Mean Absolute Error
RMS = Root Mean Square Error

Impact of TDS and Temperature Transport on Head Solution (February 2004 Calibration Run)

Response to Comments, Production Scenario Report

Figure B.5

June 2013

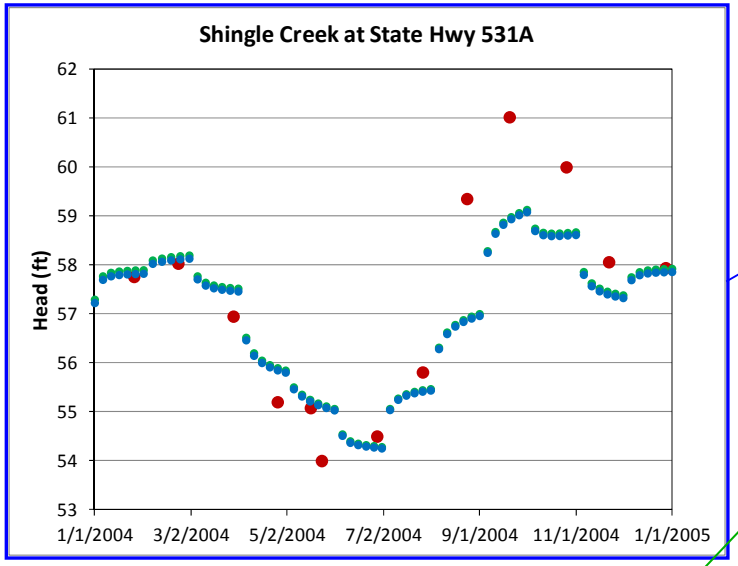

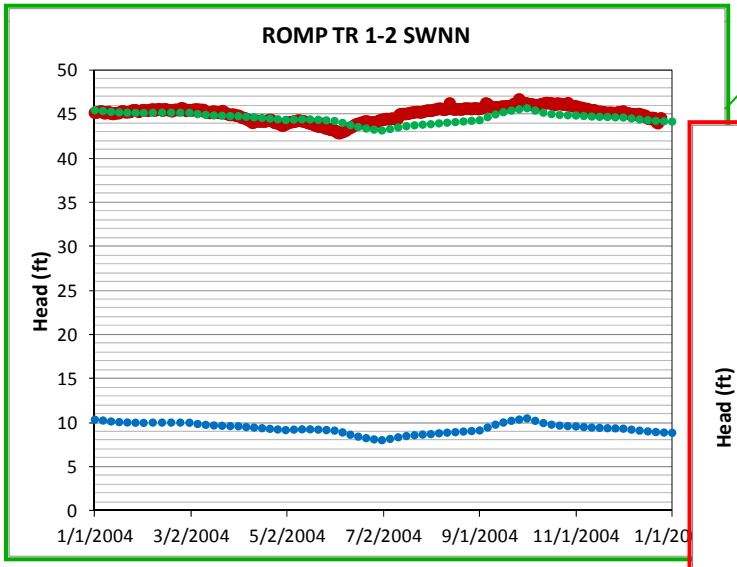

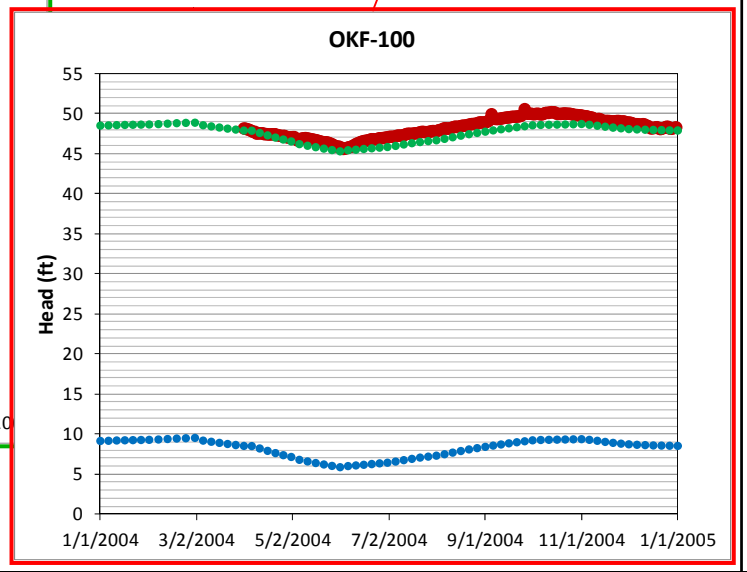

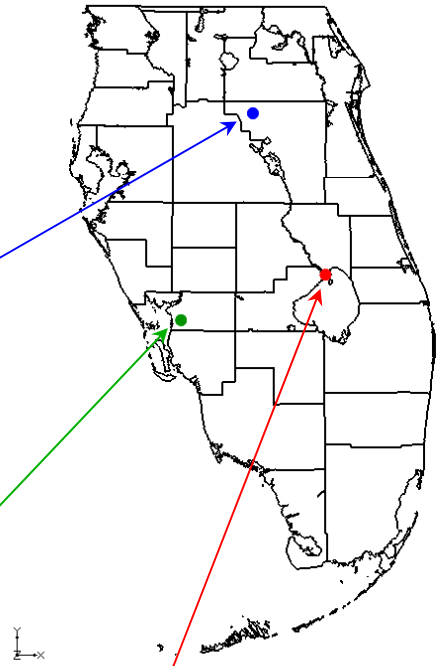

Legend (Plots)

- Observed Heads
- Model Result with Density Dependence
- Model Result without Density Dependence

Notes:

All three example wells are open in the UF aquifer.

There are numerous other observation wells which could be shown. All show stark differences between runs with and without density dependence except for a few wells near the Polk County recharge area (near the Shingle Creek well shown).

Impact of TDS and Temperature Transport on Head Solution (Transient Calibration Run)

Response to Comments, Production Scenario Report

Figure B.6

June 2013

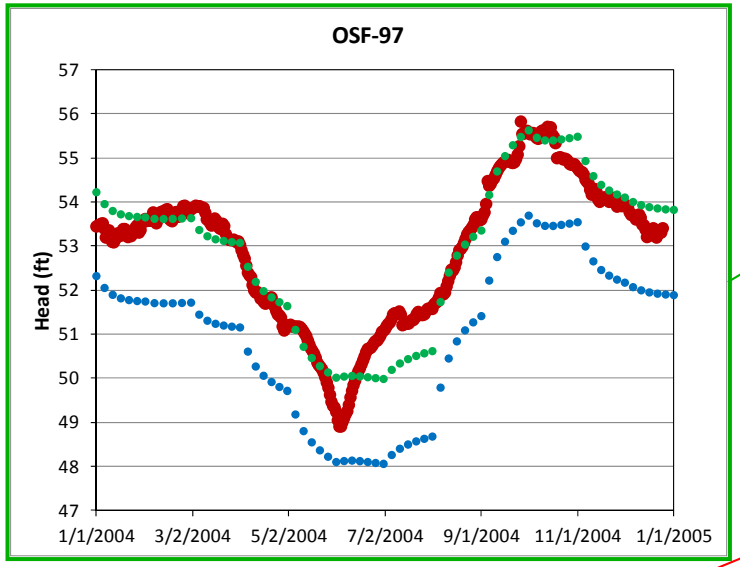

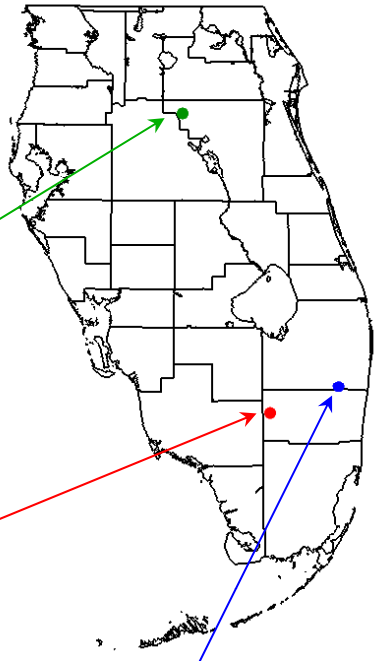

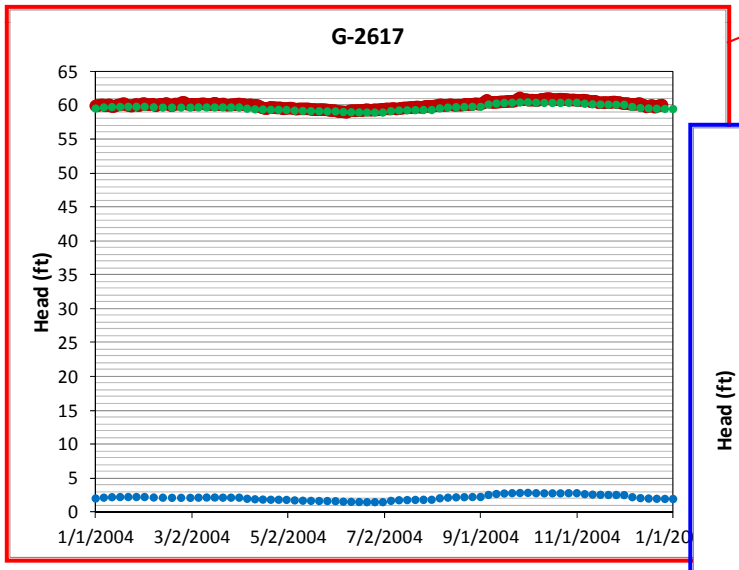

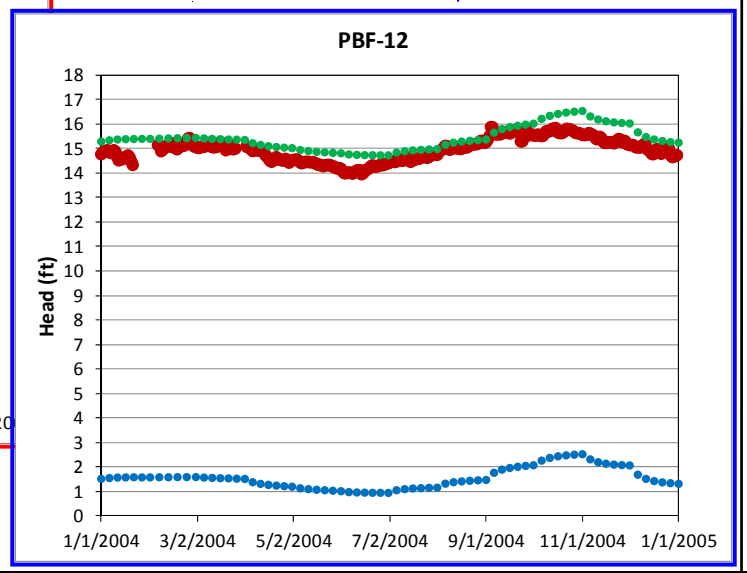

Legend (Plots)

- Observed Heads
- Model Result with Density Dependence)
- Model Result without Density Dependence

Notes:

OSF-97 is open in the BZ; G-2617 is open in the APPZ; PBF-12 is open in the LF aquifer.

There are numerous other observation wells which could be shown. All show stark differences between runs with and without density dependence except for a few wells near the Polk County recharge area (near OSF-97 shown).

Impact of TDS and Temperature Transport on Head Solution (Transient Calibration Run)

Response to Comments, Production Scenario Report

Figure B.7

June 2013

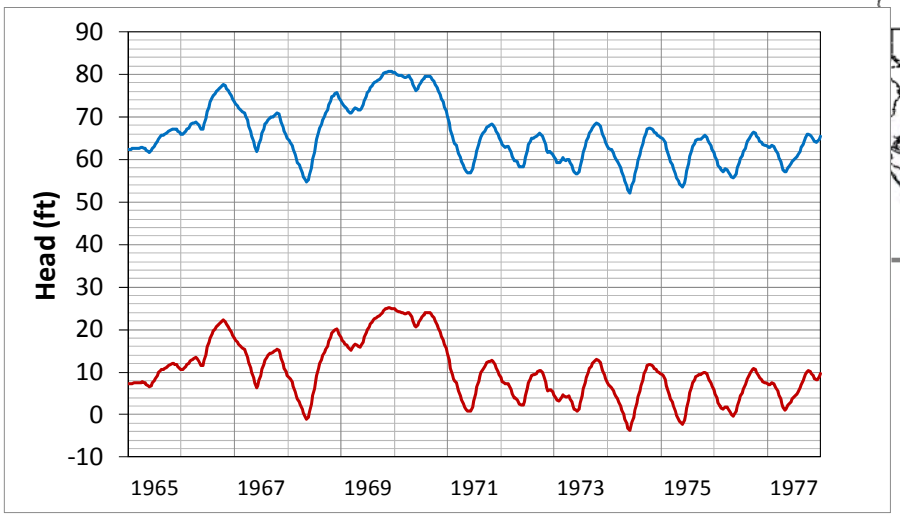

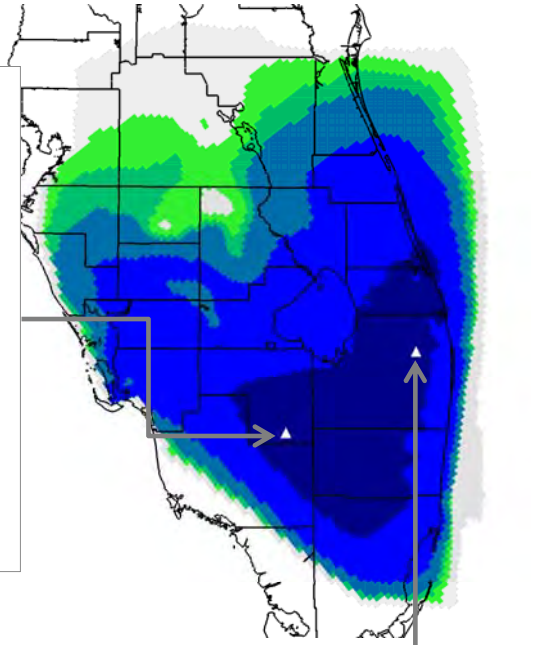

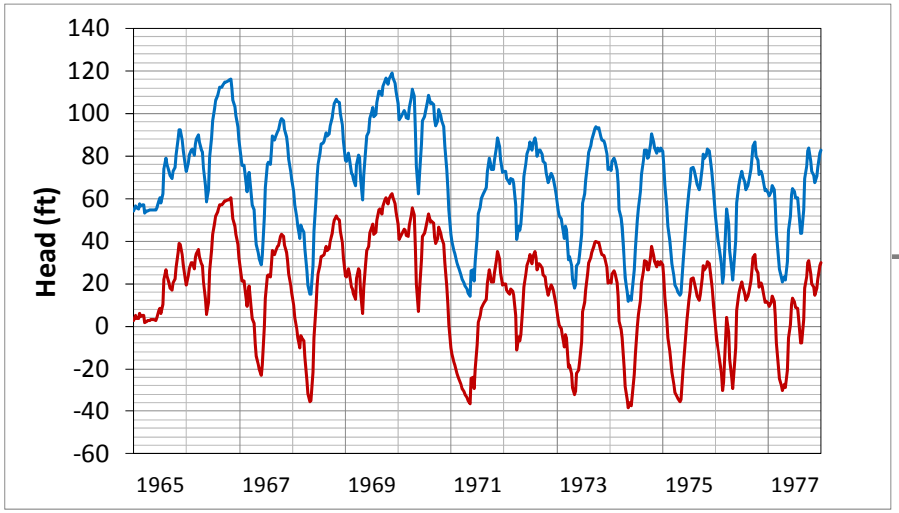

Average Head Difference (ft)

(Map Contours)

< - 50	1 to 5
-50 to -25	5 to 10
-25 - -10	10 to 25
-10 to -5	25 to 50
-5 to -1	> 50
-1 to 1	

Modeled Head (ft)

(Plot Lines)

- Scenario 1 (With Density Dependence)
- Scenario 0 (No Density Dependence)

Notes:

Map in upper right shows the average head difference in the UF for Scenario 1 when run with and without density dependence. The original run (with density dependence) was subtracted from the run without density dependence, so a negative number indicates that the removal of density dependence caused a drop in heads.

The head results at two locations are shown in the two time plots.

Impact of TDS and Temperature Transport on UF Head Solution (D13R Scenario 1)

Response to Comments, Production Scenario Report

Figure B.8

June 2013

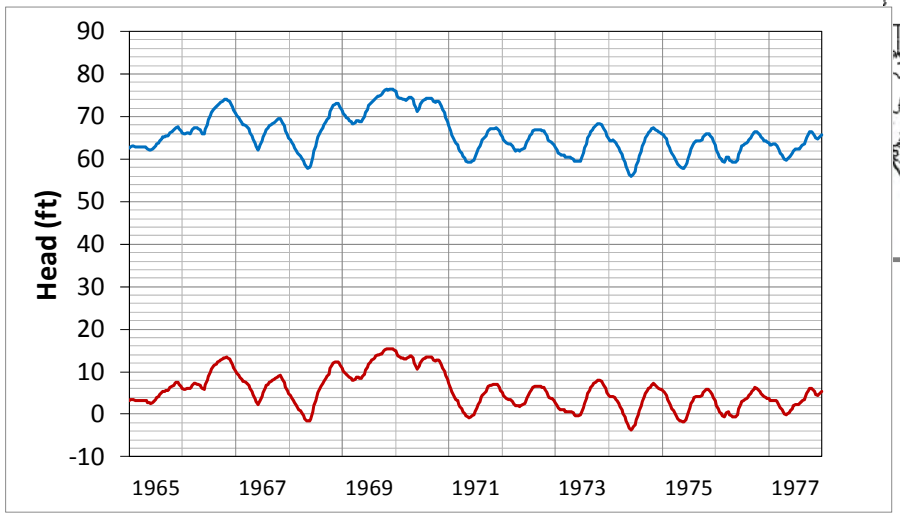

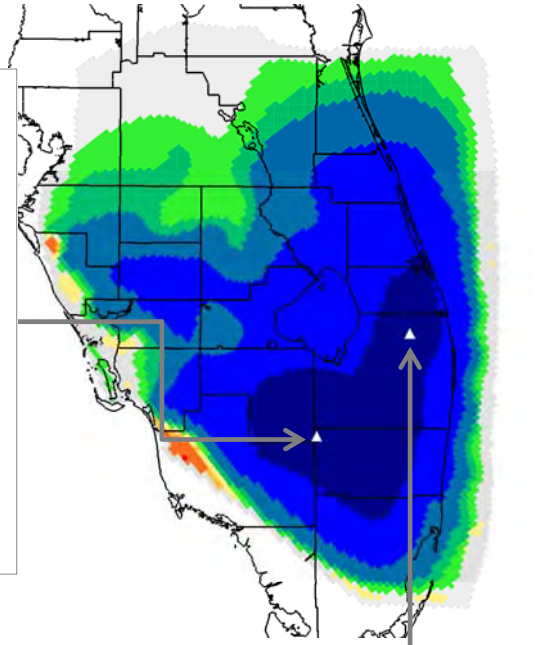

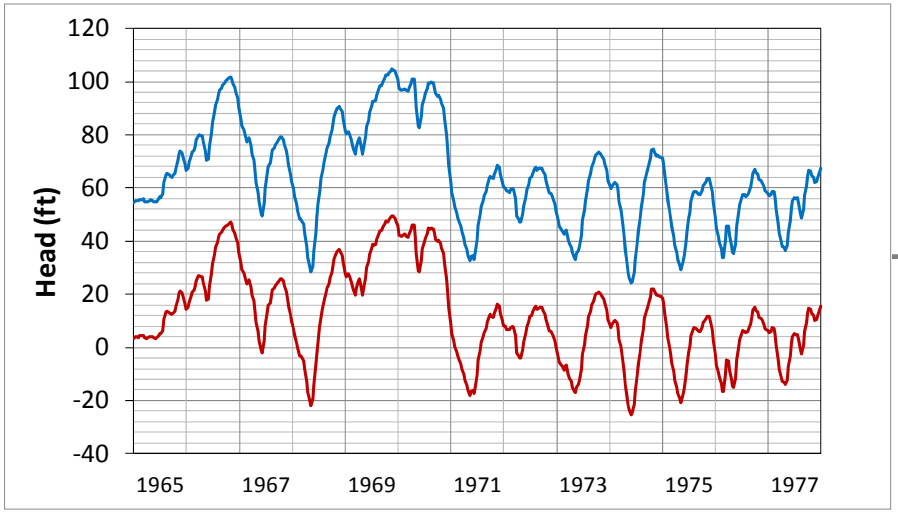

Average Head Difference (ft)

(Map Contours)

< - 50	1 to 5
-50 to -25	5 to 10
-25 - -10	10 to 25
-10 to -5	25 to 50
-5 to -1	> 50
-1 to 1	

Modeled Head (ft)

(Plot Lines)

- Scenario 1 (With Density Dependence)
- Scenario 0 (No Density Dependence)

Notes:

Map in upper right shows the average head difference in the APPZ for Scenario 1 when run with and without density dependence. The original run (with density dependence) was subtracted from the run without density dependence, so a negative number indicates that the removal of density dependence caused a drop in heads.

The head results at two locations are shown in the two time plots.

Impact of TDS and Temperature Transport on APPZ Head Solution (D13R Scenario 1)

Response to Comments, Production Scenario Report

Figure B.9

June 2013

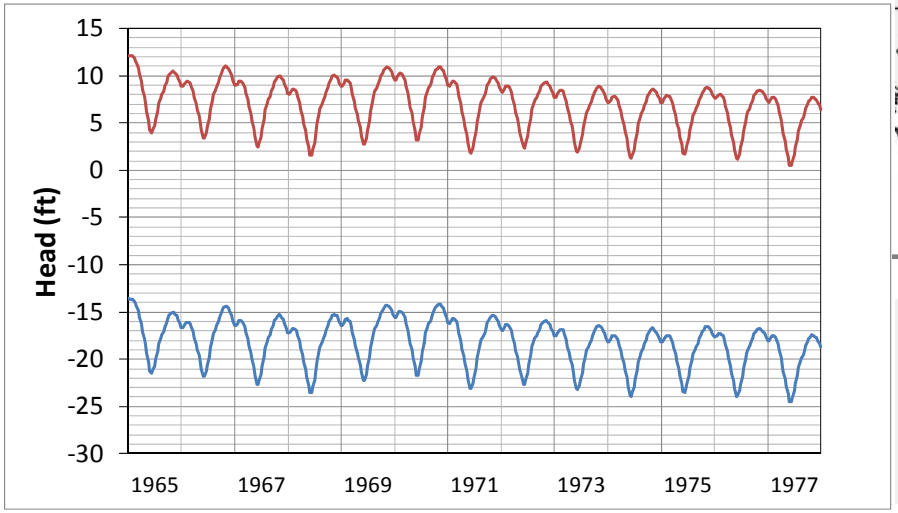

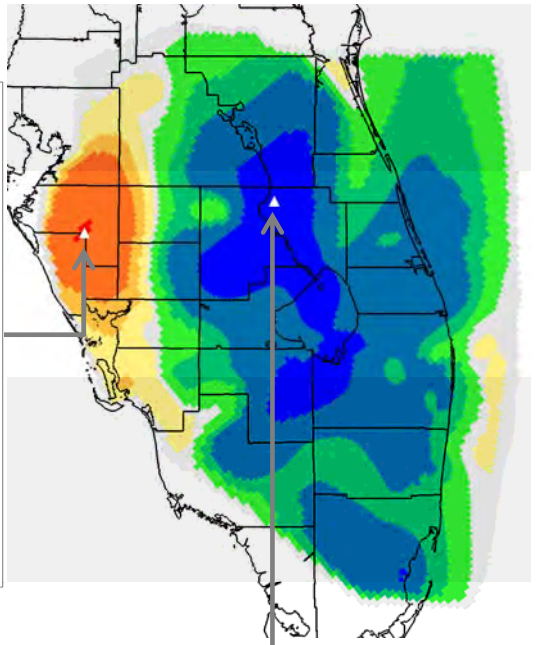

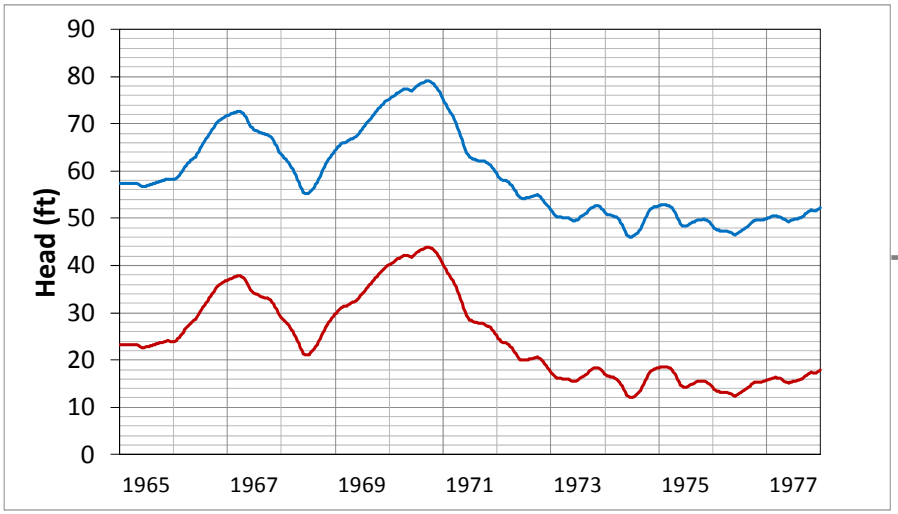

Average Head Difference (ft)

(Map Contours)

< - 50	1 to 5
-50 to -25	5 to 10
-25 - -10	10 to 25
-10 to -5	25 to 50
-5 to -1	> 50
-1 to 1	

Modeled Head (ft)

(Plot Lines)

- Scenario 1 (With Density Dependence)
- Scenario 0 (No Density Dependence)

Notes:

Map in upper right shows the average head difference in the LF for Scenario 1 when run with and without density dependence. The original run (with density dependence) was subtracted from the run without density dependence, so a negative number indicates that the removal of density dependence caused a drop in heads.

The head results at two locations are shown in the two time plots.

Impact of TDS and Temperature Transport on LF Head Solution (D13R Scenario 1)

Response to Comments, Production Scenario Report

Figure B.10

June 2013

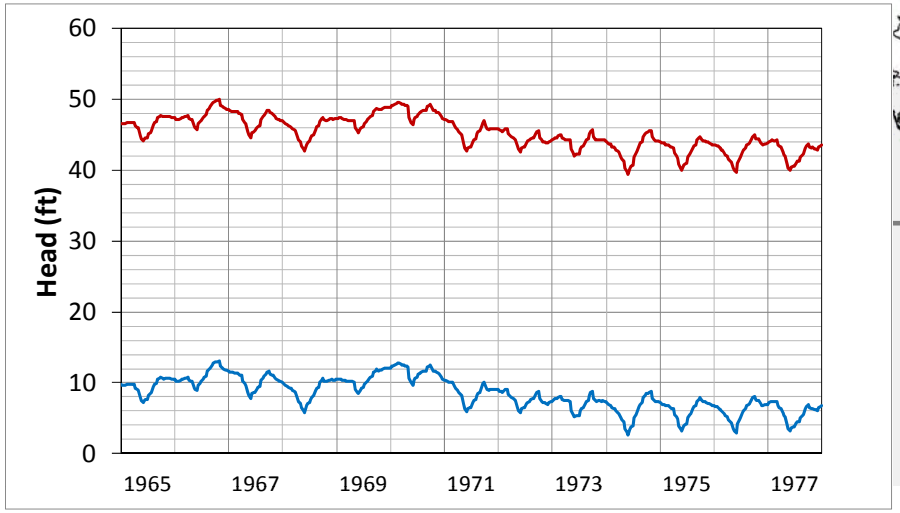

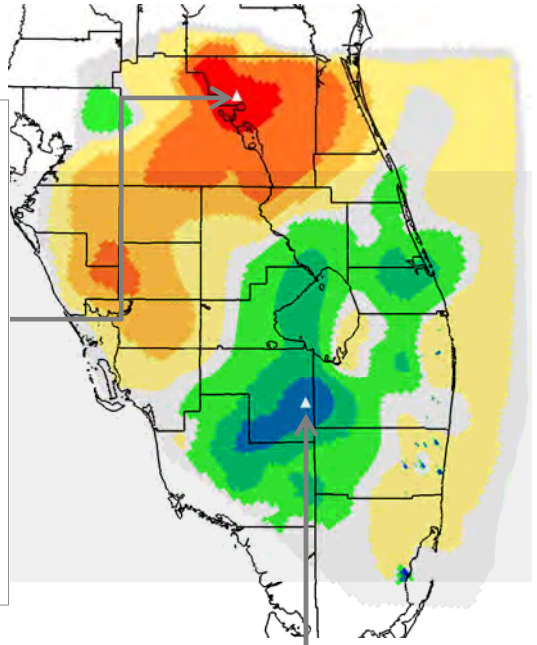

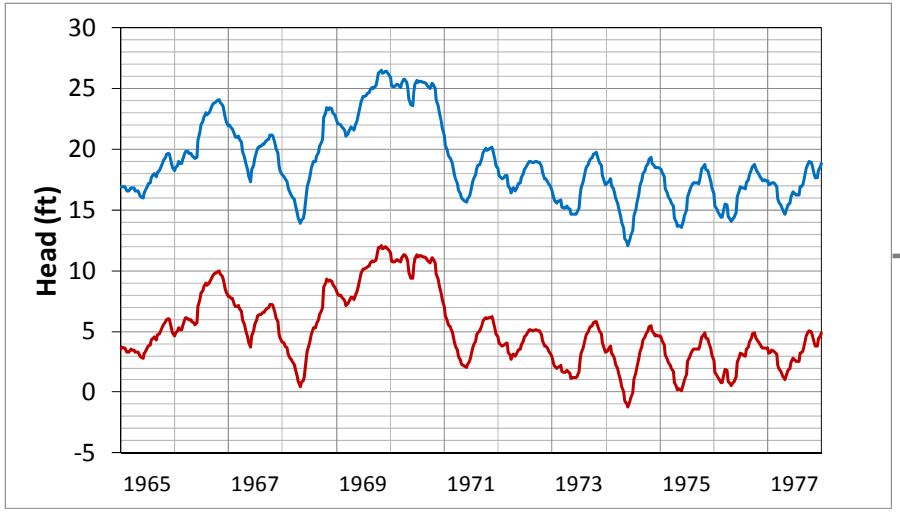

Average Head Difference (ft)

(Map Contours)

< - 50	1 to 5
-50 to -25	5 to 10
-25 - -10	10 to 25
-10 to -5	25 to 50
-5 to -1	> 50
-1 to 1	

Modeled Head (ft)

(Plot Lines)

- Scenario 1 (With Density Dependence)
- Scenario 0 (No Density Dependence)

Notes:

Map in upper right shows the average head difference in the BZ for Scenario 1 when run with and without density dependence. The original run (with density dependence) was subtracted from the run without density dependence, so a negative number indicates that the removal of density dependence caused a drop in heads.

The head results at two locations are shown in the two time plots.

Impact of TDS and Temperature Transport on BZ Head Solution (D13R Scenario 1)

Response to Comments, Production Scenario Report

Figure B.11

June 2013

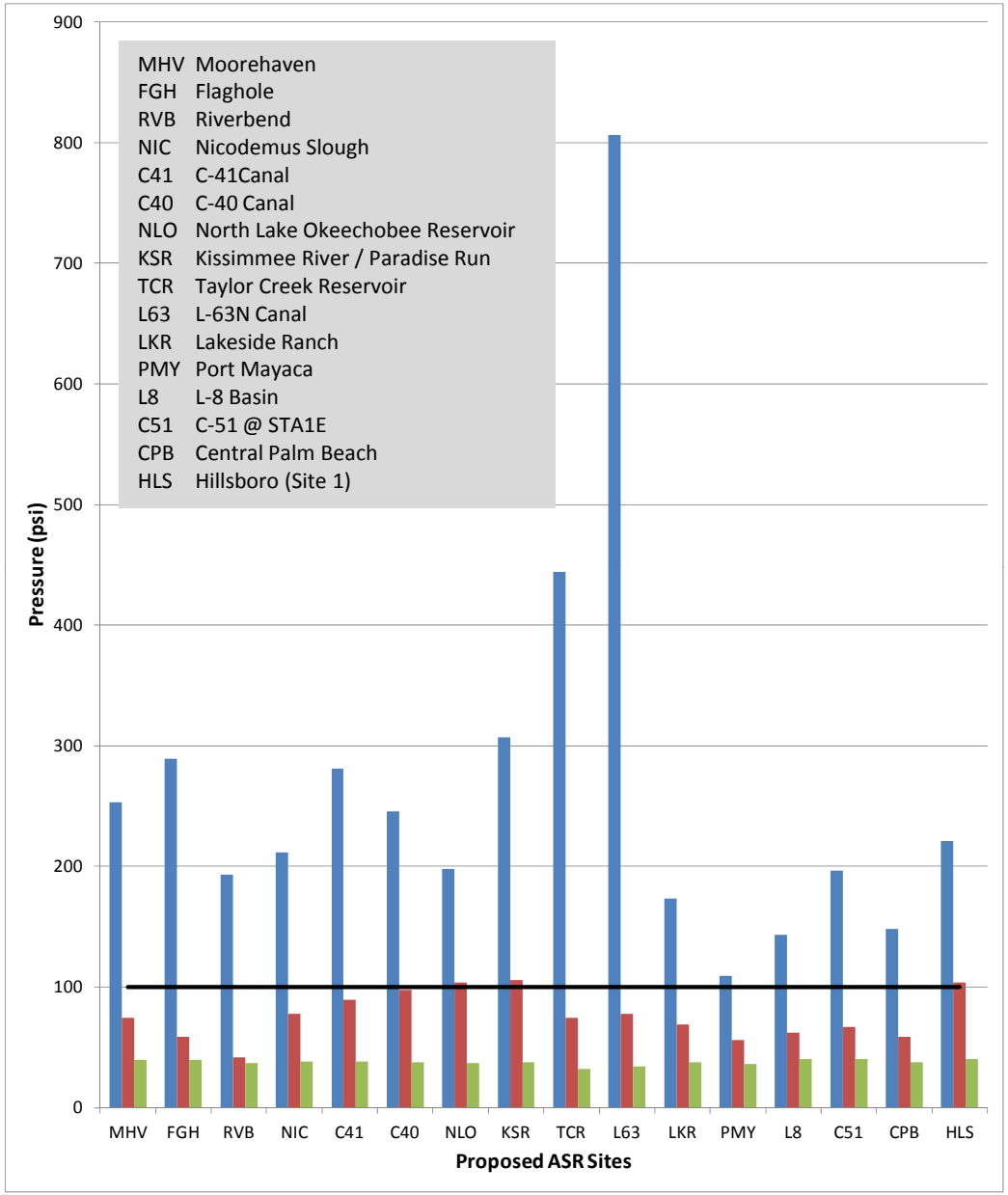

Legend

- Upper Floridan Aquifer
- Avon Park Permeable Zone
- Boulder Zone
- 100 psi Limit

Notes:

Scenario 0a includes all of the 333 ASR wells specified by the SFWMM-D13R design but no density dependence. All are fully penetrating in the UF Aquifer.

This plot shows the highest pressure at each site which the pump would need to overcome in order to inject storage water during the 13-year simulation.

The PDT determined that it would be important to keep this pressure below 100 psi (indicated by the heavy black line).

Note that maximum pressures are shown for all aquifers and all sites even if ASR pumps are not located there for the current scenario.

Compare to Figure 4.17 in the main report.

Impact of TDS and Temperature Transport on Pump Pressure Performance Measure (D13R Scenario 0a)

Response to Comments, Production Scenario Report

Figure B.12

June 2013

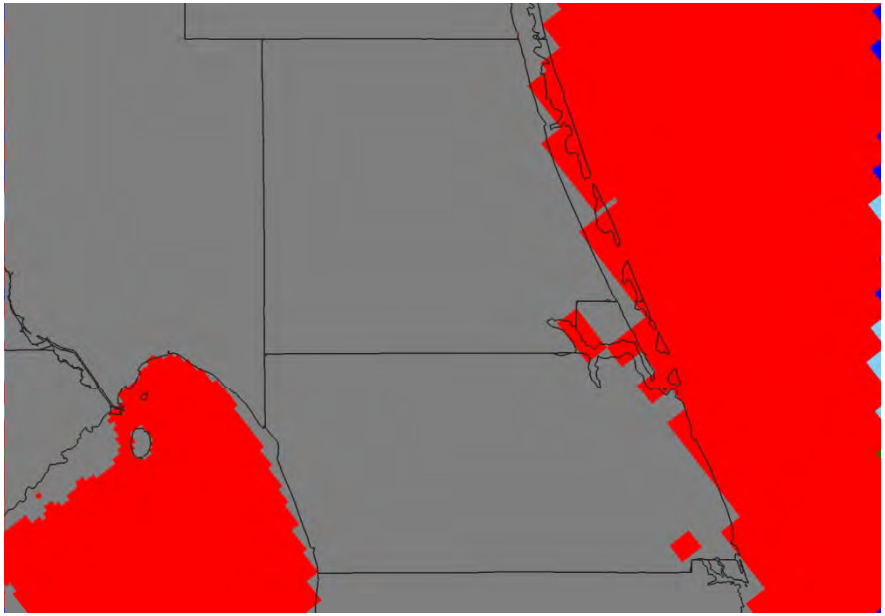

Upper Floridan Aquifer

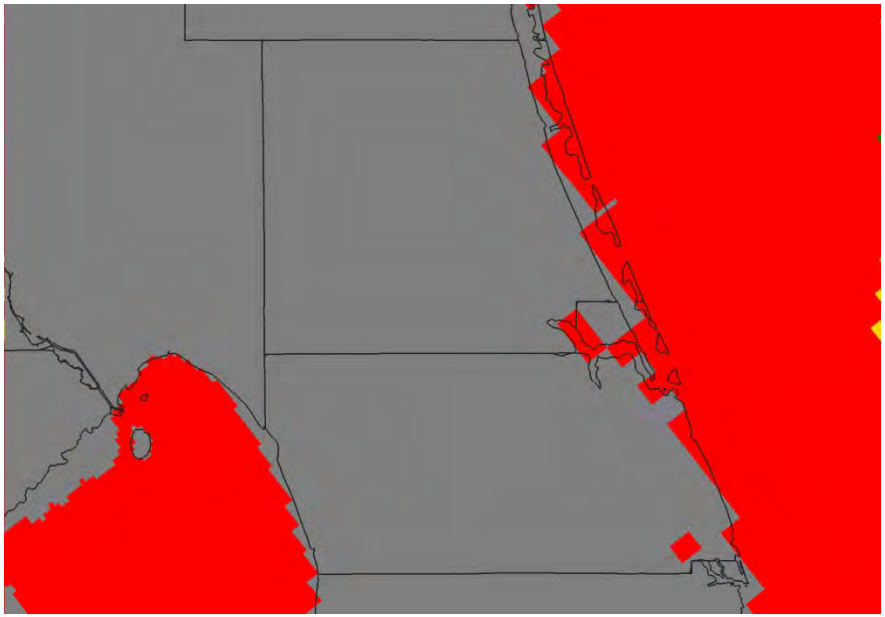

Avon Park Permeable Zone

Legend

- Not artesian
- < 5%
- 5% - 10%
- 10% - 20%
- 20% - 50%
- 50% - 100%
- Loses artesian condition

Notes:

Scenario 0a includes all of the 333 ASR wells specified by the SFWMM-D13R design but does not include density dependence. All are fully penetrating in the UF Aquifer.

These plots show the maximum reduction in artesian flow at each model cell as a percentage when compared to the flow expected without the ASR project.

Permit rules require that the reduction in Saint Lucie and Martin Counties be less than 10%.

Compare to Figure 4.18 in the main report.

Impact of TDS and Temperature Transport on APPA Performance Measure (D13R Scenario 0a)

Response to Comments, Production Scenario Report

Figure B.13

June 2013

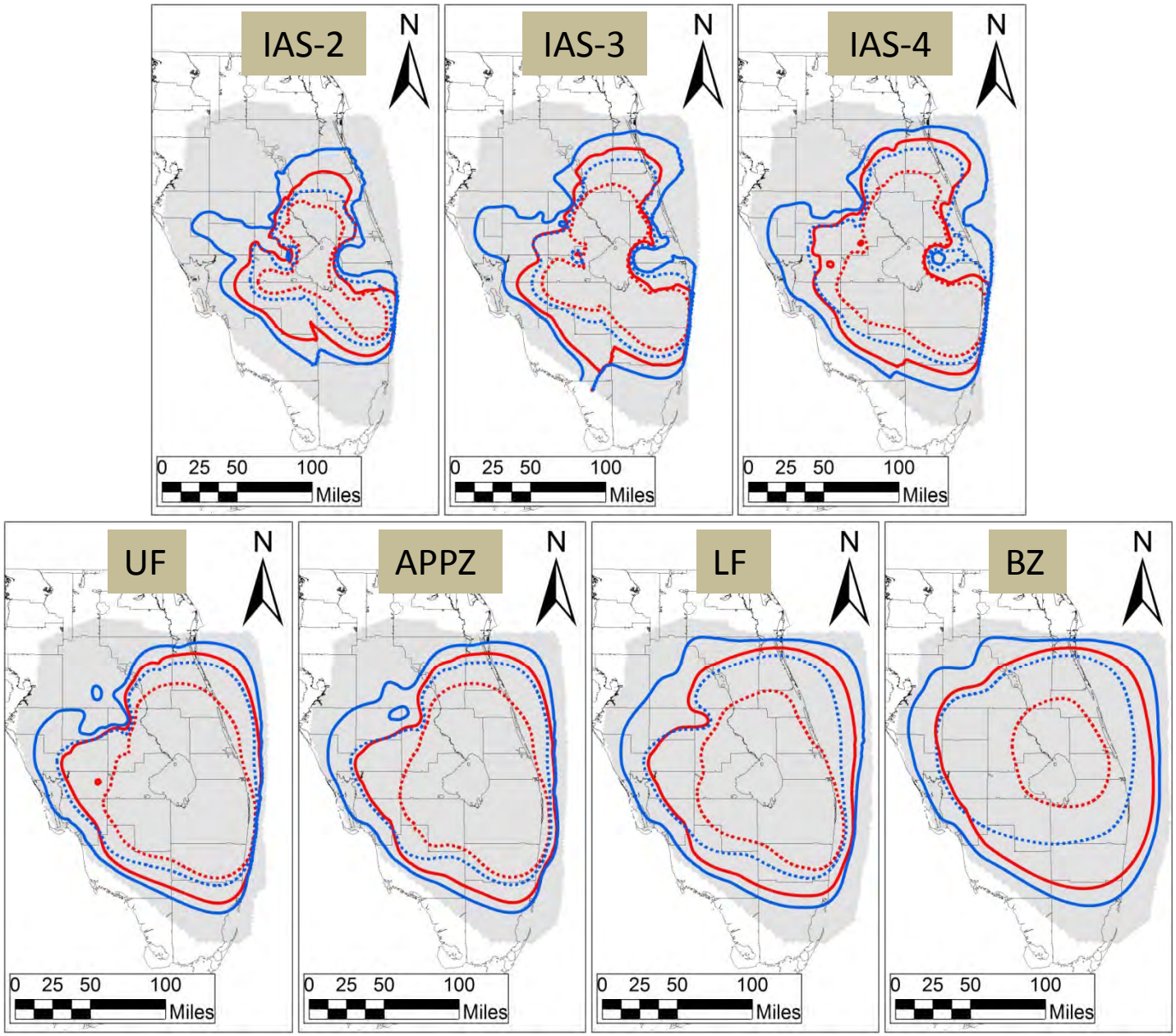

Legend

Maximum Drawdown
- 1 foot
- 5 feet

Maximum "Drawup"
- 1 foot
- 5 feet

Model Domain

Notes:

Scenario 0 includes all of the 333 ASR wells specified by the SFWMM-D13R design but does not include density dependence. All are fully penetrating in the UF Aquifer.

These figures show the extent of the areas where the maximum drawdown or "drawup" is greater than 1 foot or 5 feet.

The maximum condition does not necessarily occur at the same time for all regions of the model.

Compare to Figure 4.20 in the main report.

Impact of TDS and Temperature Transport on APPA Performance Measure (D13R Scenario 0a)

Response to Comments, Production Scenario Report

Figure B.14

June 2013

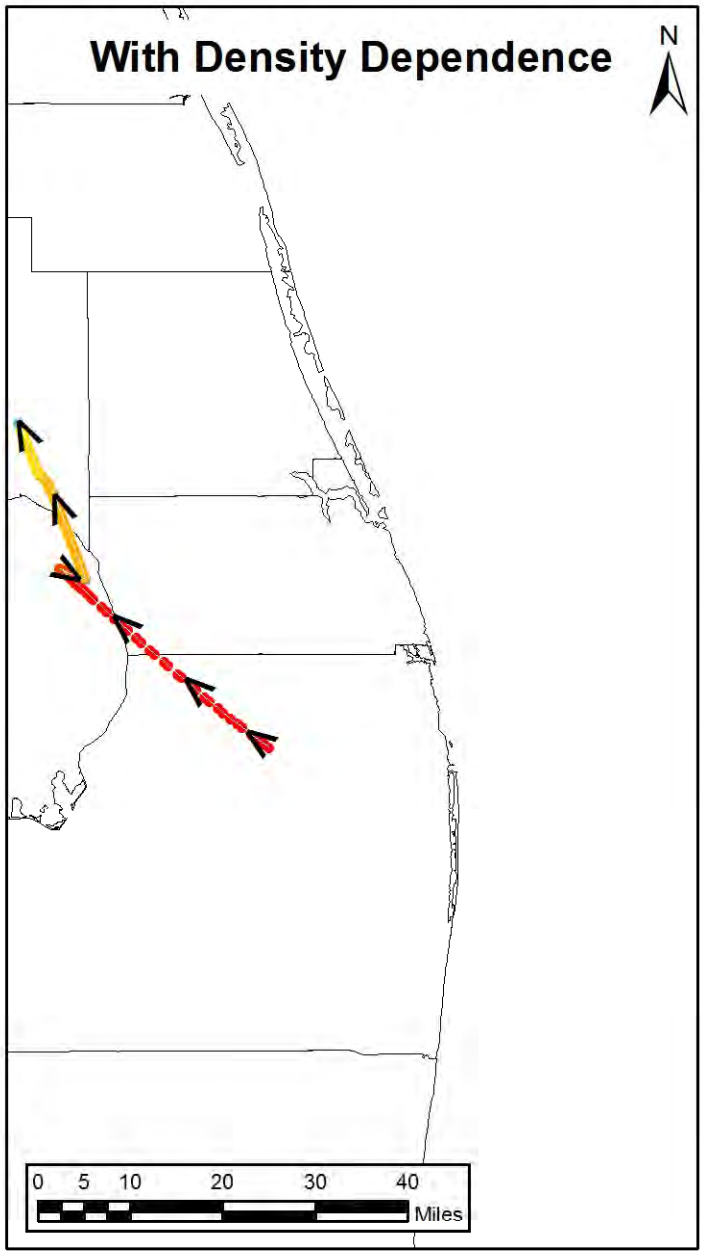

Particle Layer

- IAS
- UF
- APPZ
- LF
- BZ

Notes:

Using the February 2004 steady state calibration model and MODPATH, a particle was released in the BZ in northern Palm Beach County.

When the model was solved with density dependence, the particle moved to the northwest and rose to the upper layers of the model.

When the model was solved without density dependence, the particle moved to the east and stayed in the BZ.

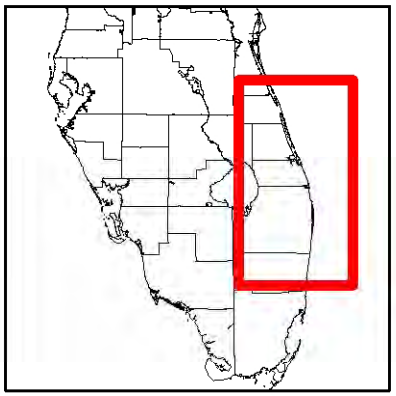

Impact of Density Dependence on Groundwater Flow Direction

Response to Comments, Production Scenario Report

Figure B.15

June 2013

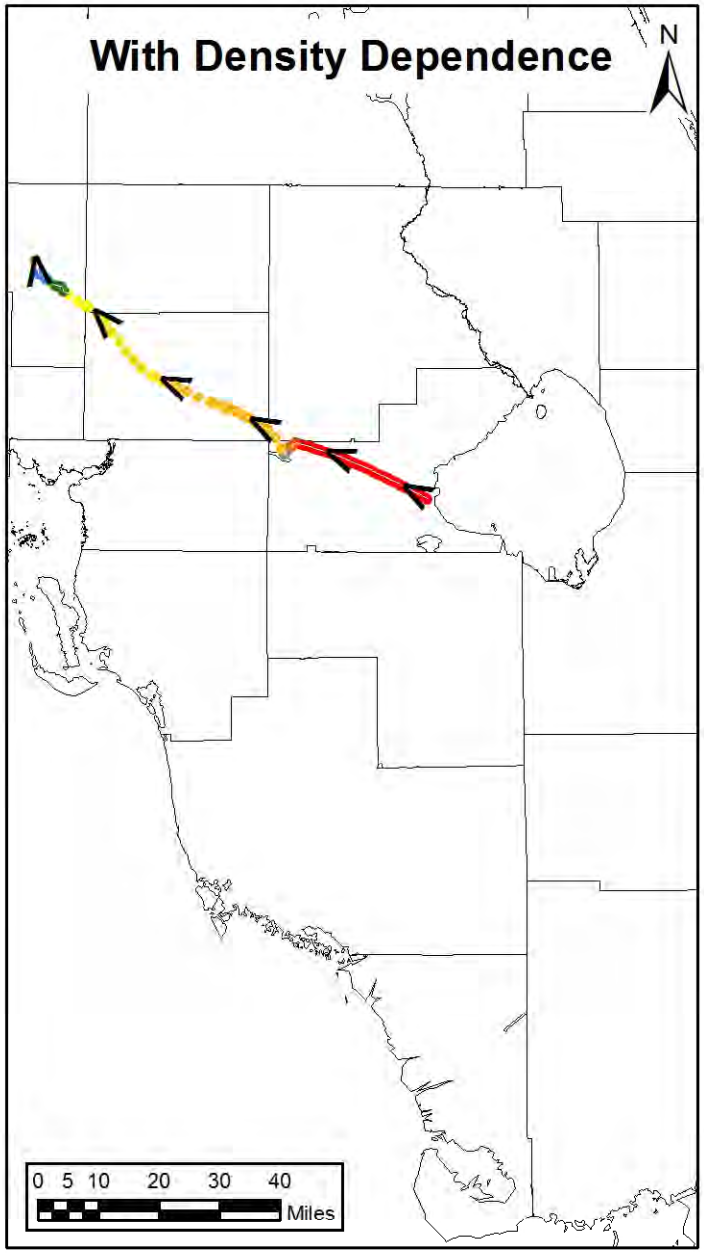

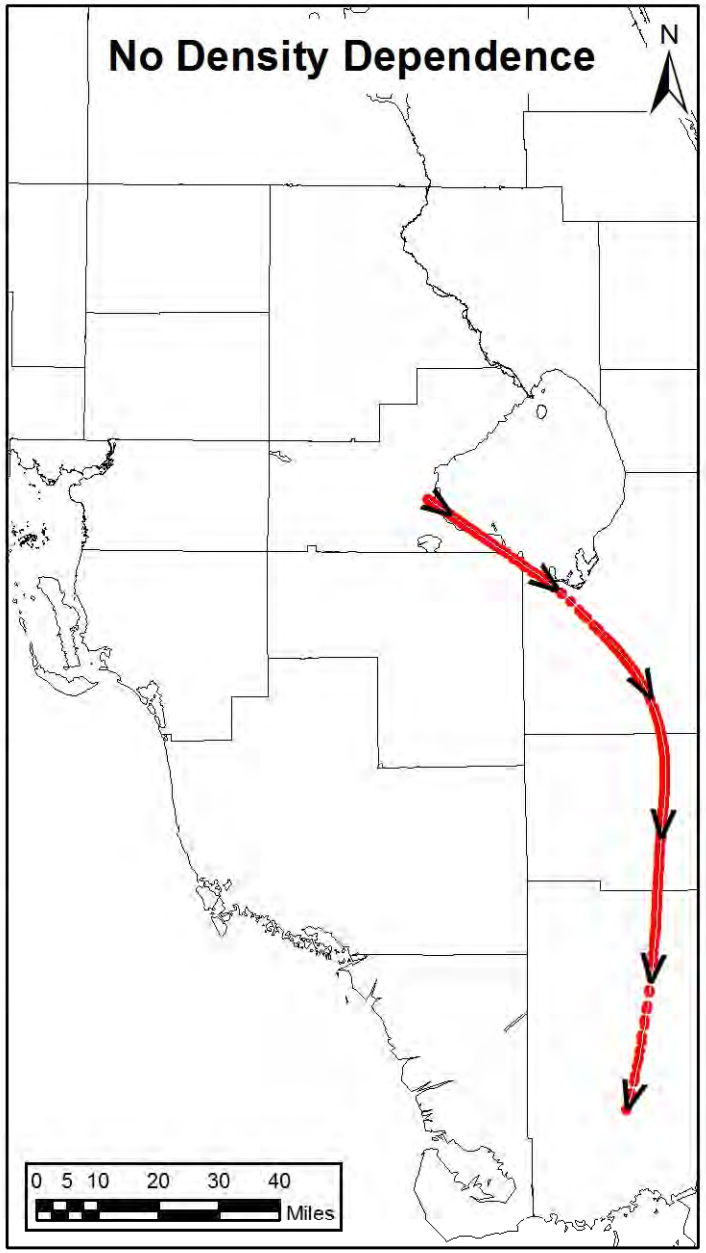

Particle Layer

- IAS
- UF
- APPZ
- LF
- BZ

Notes:

Using the February 2004 steady state calibration model and MODPATH, a particle was released in the BZ just west of Lake Okeechobee.

When the model was solved with density dependence, the particle moved to the northwest and rose to the upper layers of the model.

When the model was solved without density dependence, the particle moved to the south and stayed in the BZ.

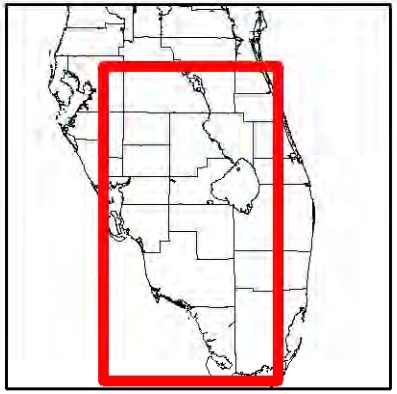

Impact of Density Dependence on Groundwater Flow Direction

Response to Comments, Production Scenario Report

Figure B.16

June 2013

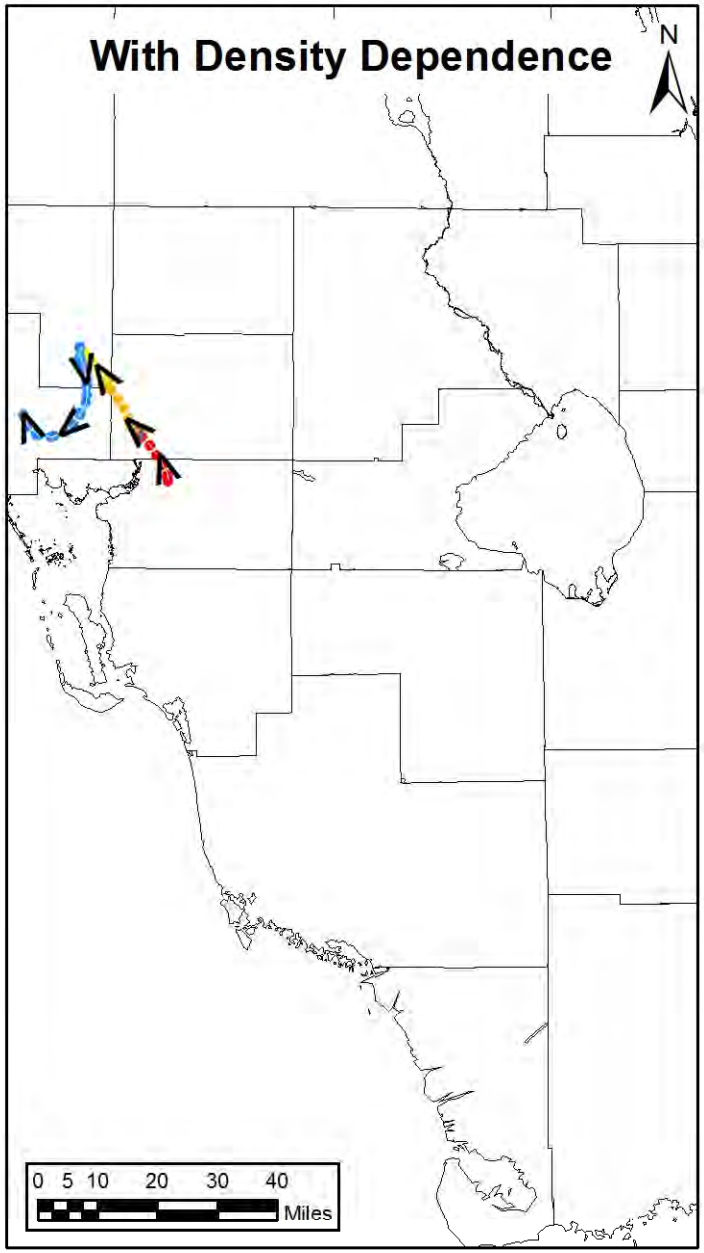

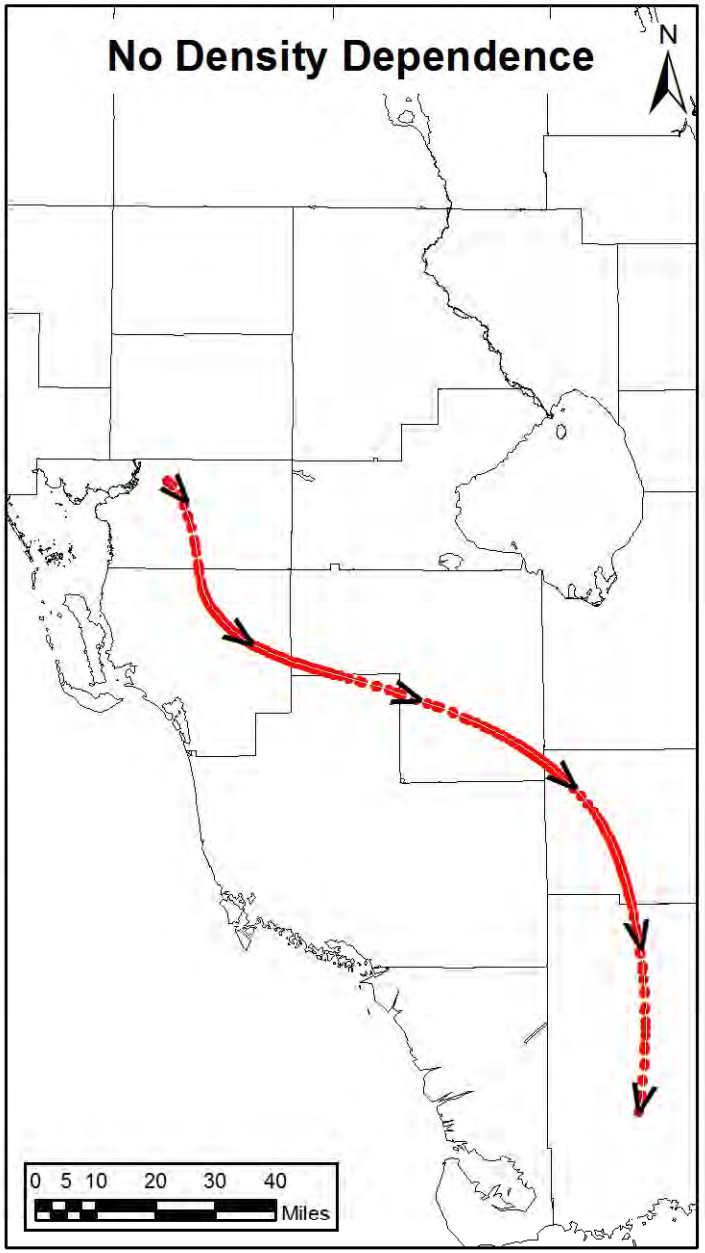

Particle Layer

- IAS
- UF
- APPZ
- LF
- BZ

Notes:

Using the February 2004 steady state calibration model and MODPATH, a particle was released in the BZ in Charlotte County.

When the model was solved with density dependence, the particle moved to the northwest and rose to the upper layers of the model, changing directions in the IAS.

When the model was solved without density dependence, the particle moved to the south east and stayed in the BZ.

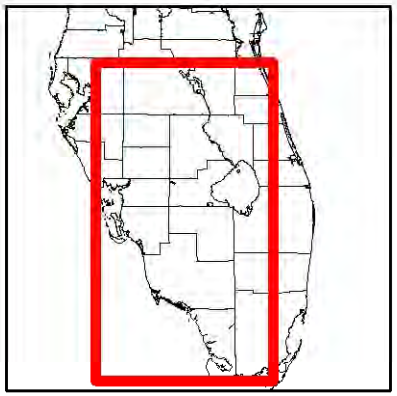

Impact of Density Dependence on Groundwater Flow Direction

Response to Comments, Production Scenario Report

Figure B.17

June 2013

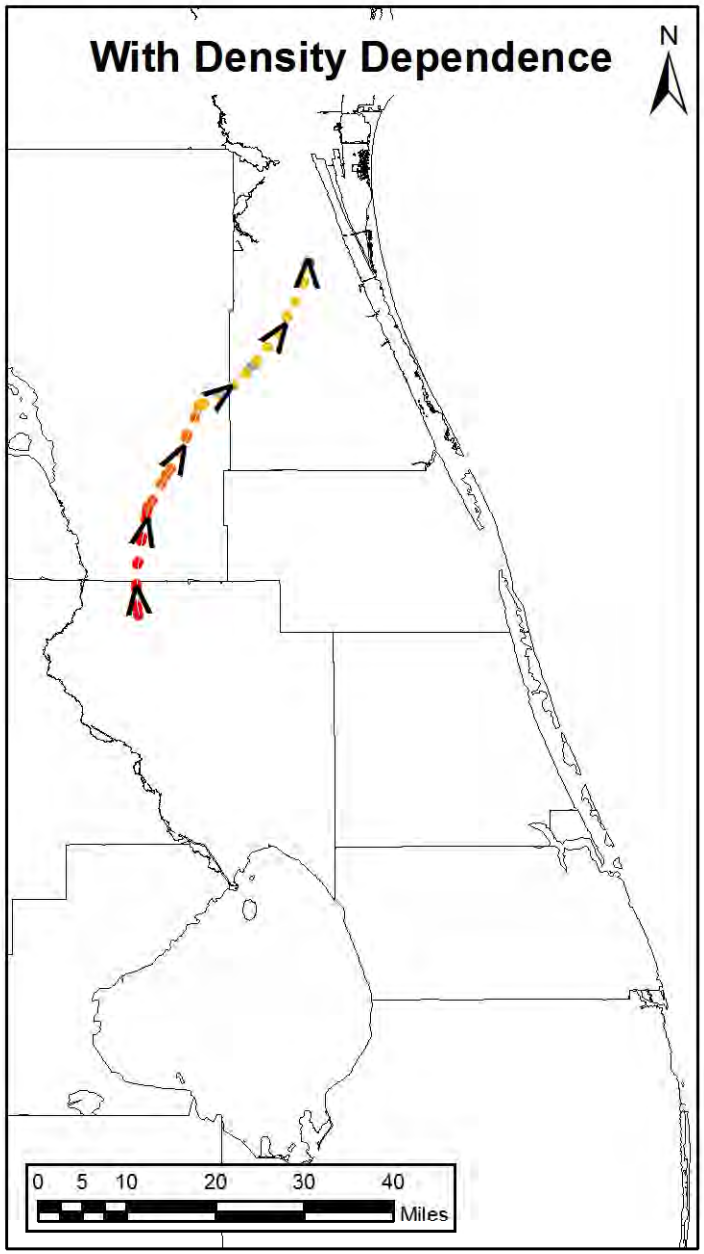

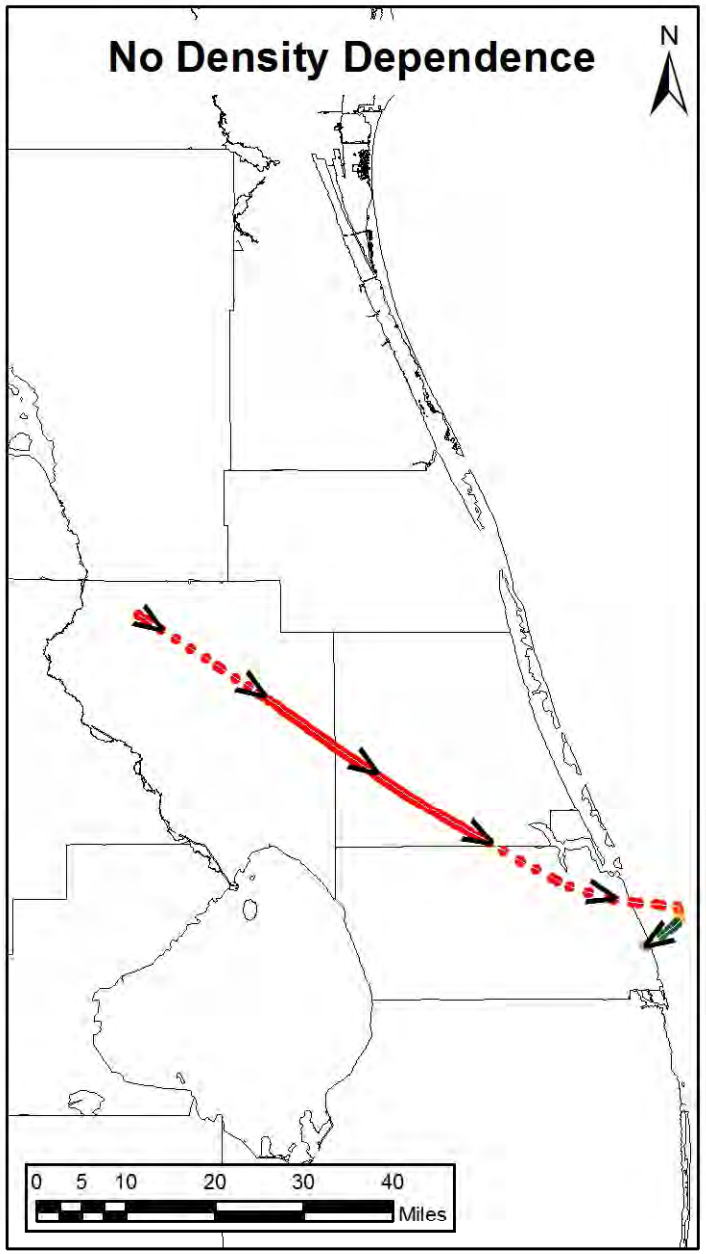

Particle Layer

- IAS
- UF
- APPZ
- LF
- BZ

Notes:

Using the February 2004 steady state calibration model and MODPATH, a particle was released in the BZ in northern Okeechobee County.

When the model was solved with density dependence, the particle moved to the north and rose to the upper layers of the model.

When the model was solved without density dependence, the particle moved to the south east and stayed in the BZ until rising to the UF offshore.

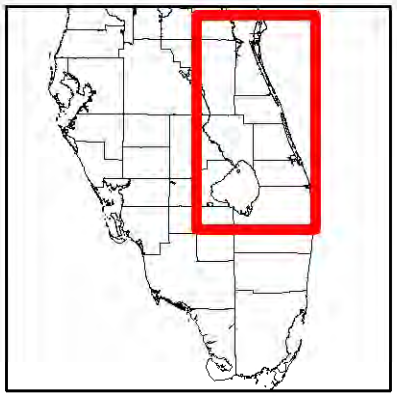

Impact of Density Dependence on Groundwater Flow Direction

Response to Comments, Production Scenario Report

Figure B.18

June 2013

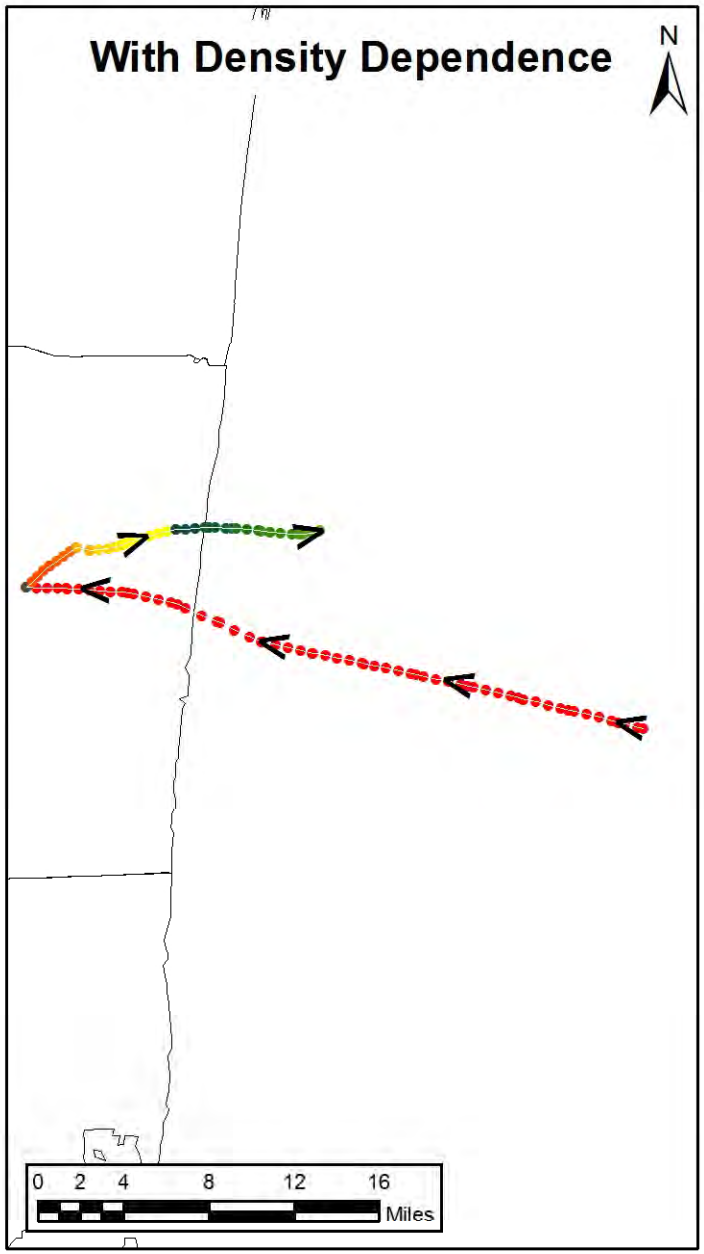

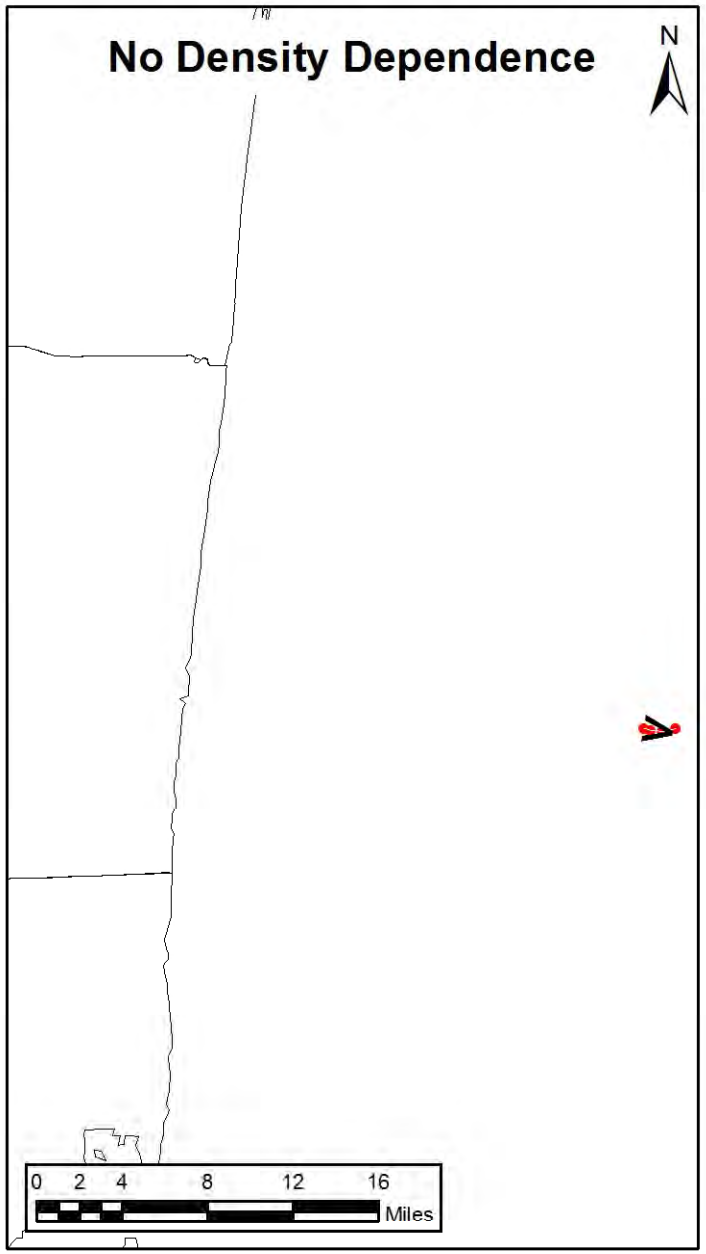

Particle Layer

- IAS
- UF
- APPZ
- LF
- BZ

Notes:

Using the February 2004 steady state calibration model and MODPATH, a particle was released in the BZ off the coast of Broward County.

When the model was solved with density dependence, the particle moved to the west and rose to the upper layers of the model, turning to the east in the LF.

When the model was solved without density dependence, the particle moved to the east, exiting to the ocean from the BZ.

Impact of Density Dependence on Groundwater Flow Direction

Response to Comments, Production Scenario Report

Figure B.19

June 2013

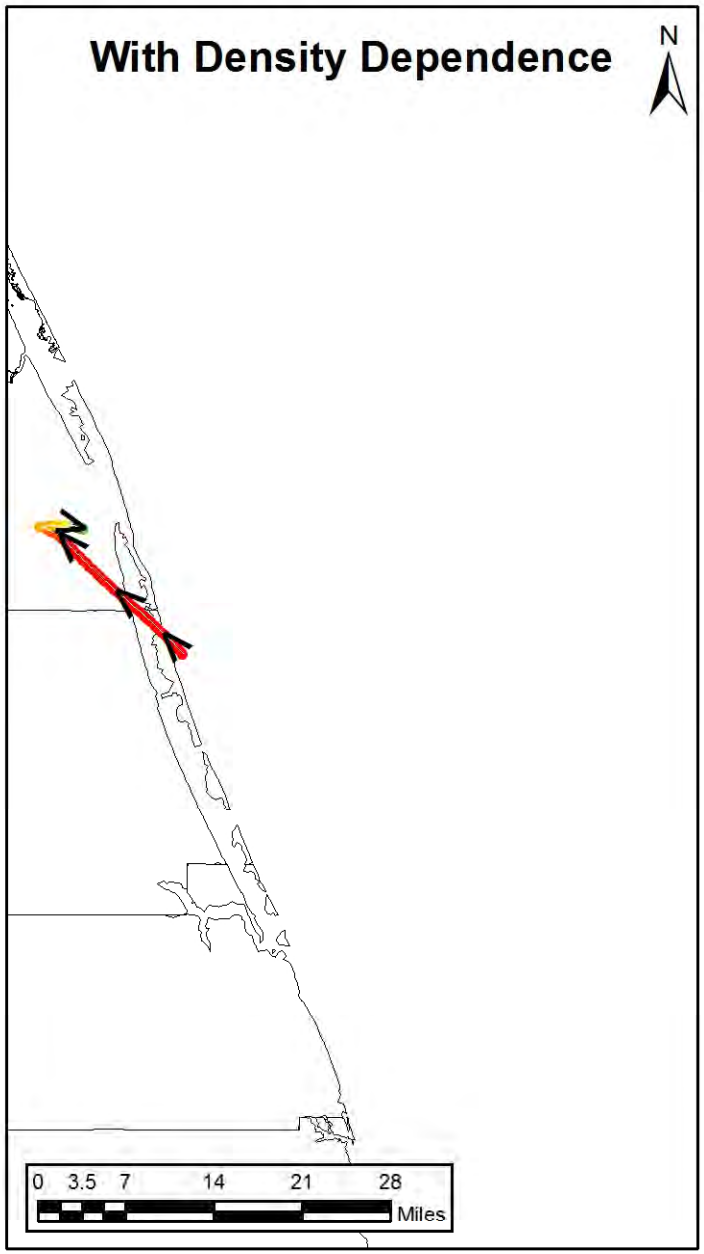

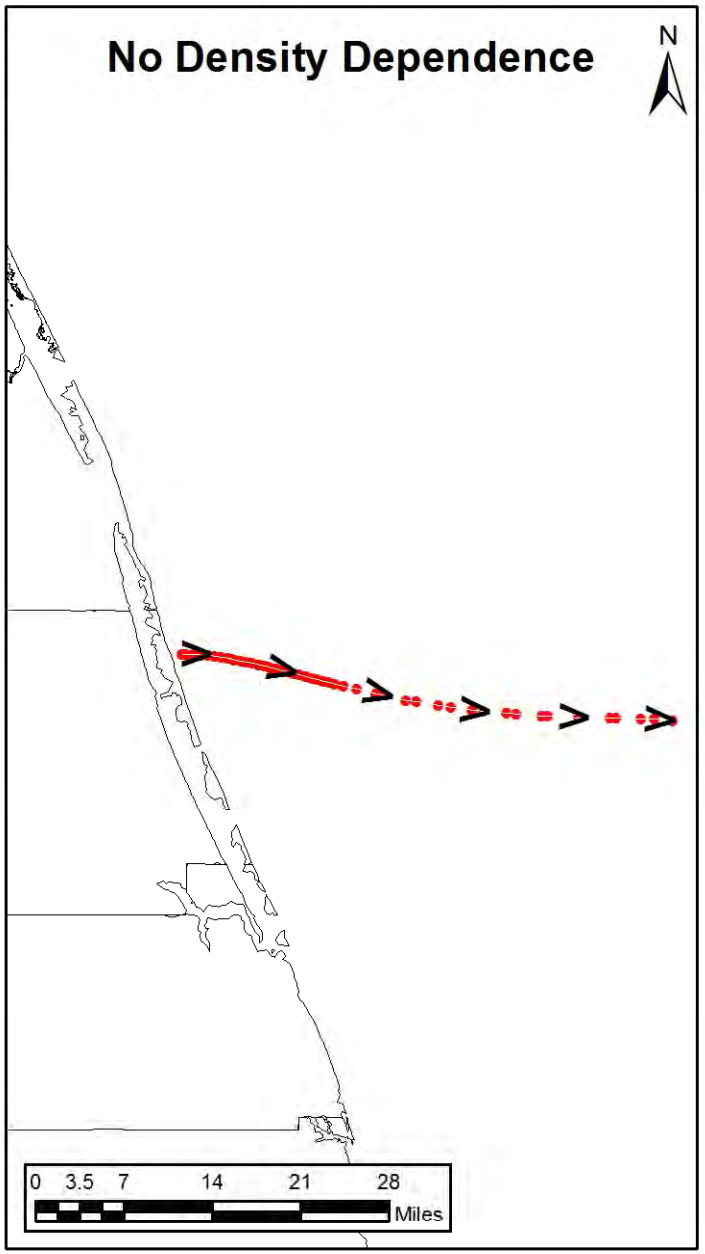

Particle Layer

- IAS
- UF
- APPZ
- LF
- BZ

Notes:

Using the February 2004 steady state calibration model and MODPATH, a particle was released in the BZ off the coast of St. Lucie County.

When the model was solved with density dependence, the particle moved to the northwest and rose to the upper layers of the model, turning to the east in the APPZ.

When the model was solved without density dependence, the particle moved to the east, exiting to the ocean from the BZ.

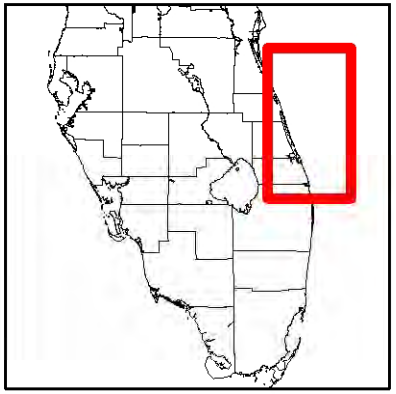

Impact of Density Dependence on Groundwater Flow Direction

Response to Comments, Production Scenario Report

Figure B.20

June 2013

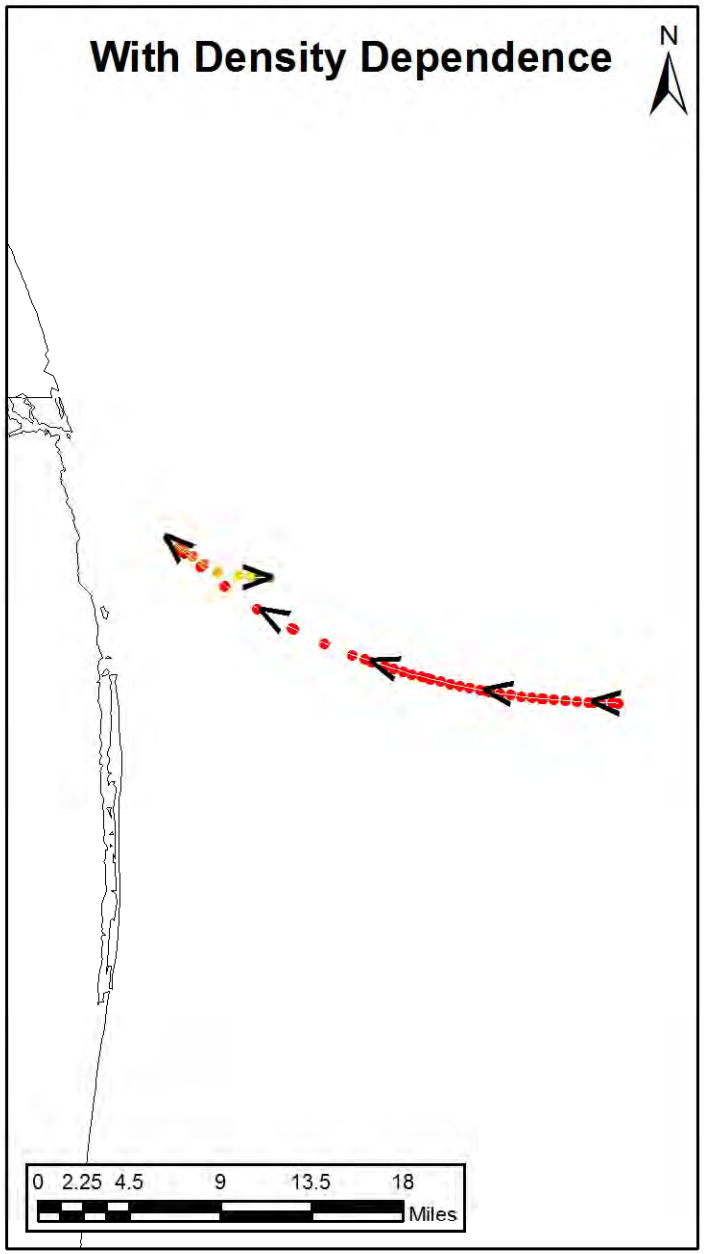

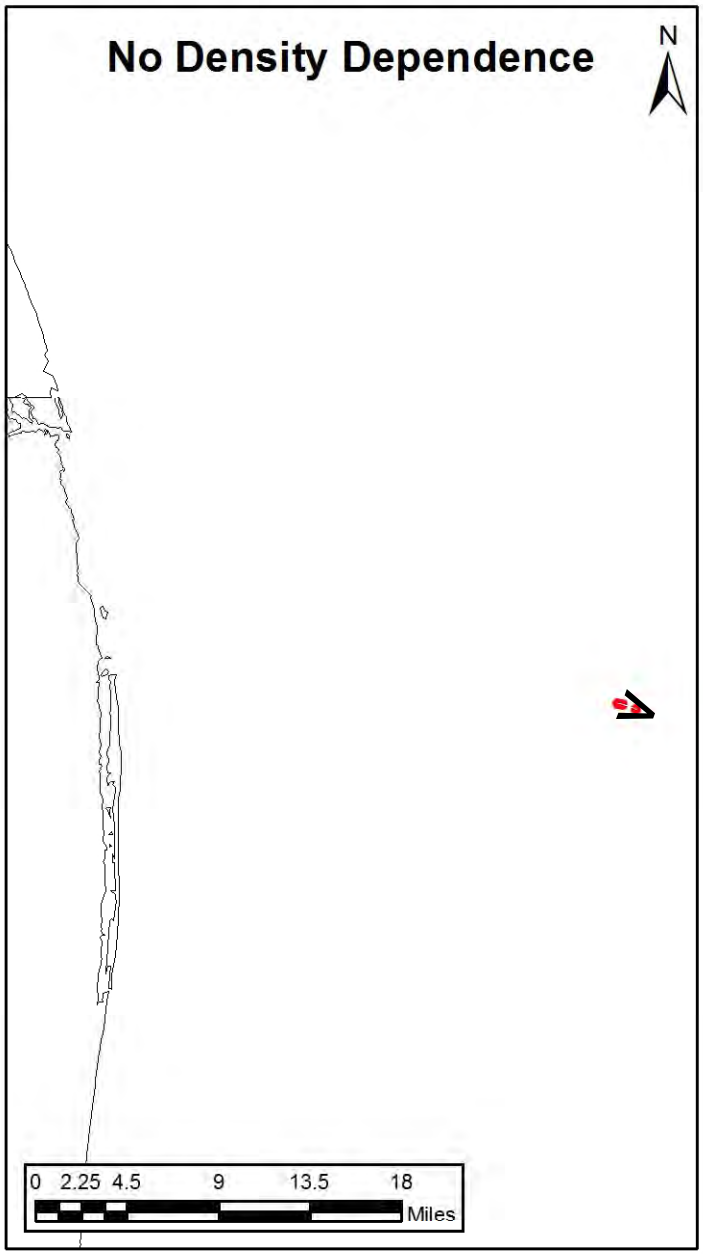

Particle Layer

- IAS
- UF
- APPZ
- LF
- BZ

Notes:

Using the February 2004 steady state calibration model and MODPATH, a particle was released in the BZ off the coast of Palm Beach County.

When the model was solved with density dependence, the particle moved to the west and rose to the upper layers of the model, turning to the east in the LF.

When the model was solved without density dependence, the particle moved to the east, exiting to the ocean from the BZ.

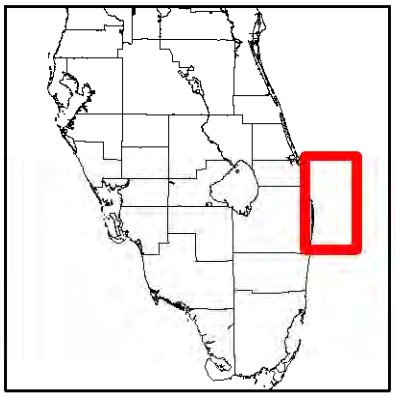

Impact of Density Dependence on Groundwater Flow Direction

Response to Comments, Production Scenario Report

Figure B.21

June 2013

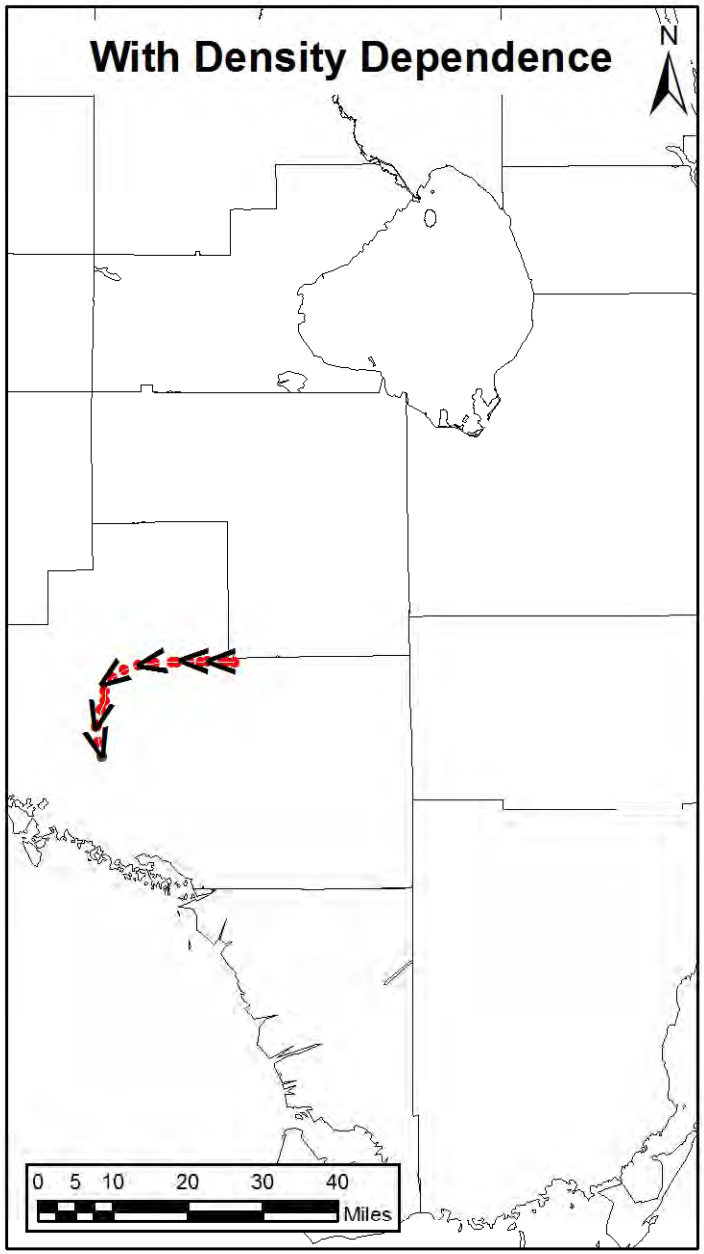

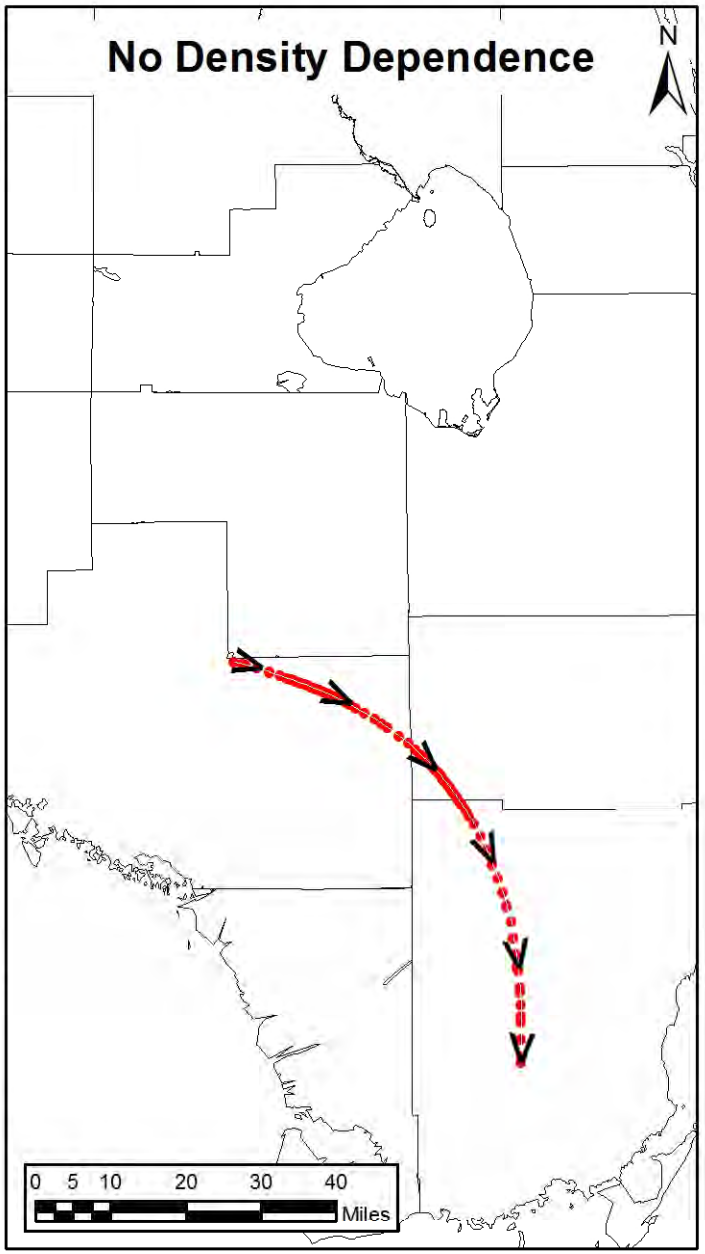

Particle Layer

- IAS
- UF
- APPZ
- LF
- BZ

Notes:

Using the February 2004 steady state calibration model and MODPATH, a particle was released in the BZ in the corner of Collier County.

When the model was solved with density dependence, the particle moved to the west then south, remaining in the BZ.

When the model was solved without density dependence, the particle moved to the east and then south, exiting to the ocean from the BZ.

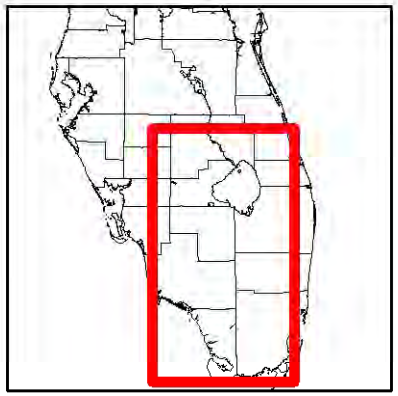

Impact of Density Dependence on Groundwater Flow Direction

Response to Comments, Production Scenario Report

Figure B.22

June 2013

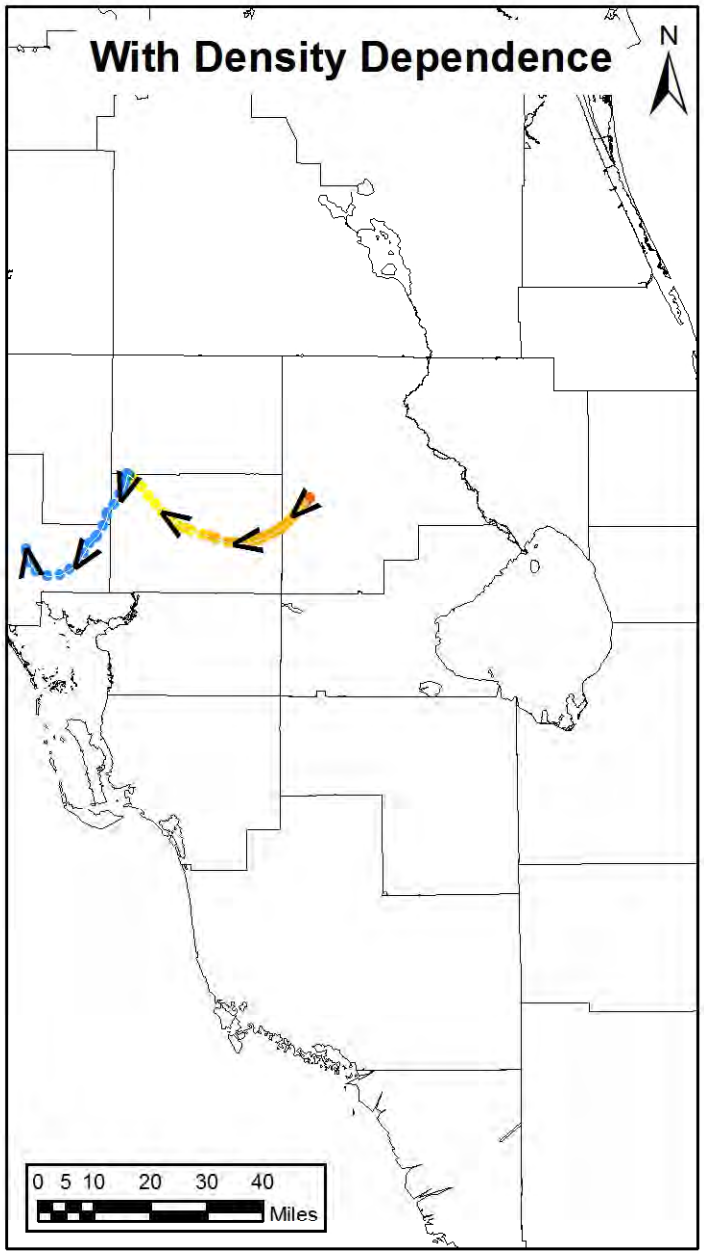

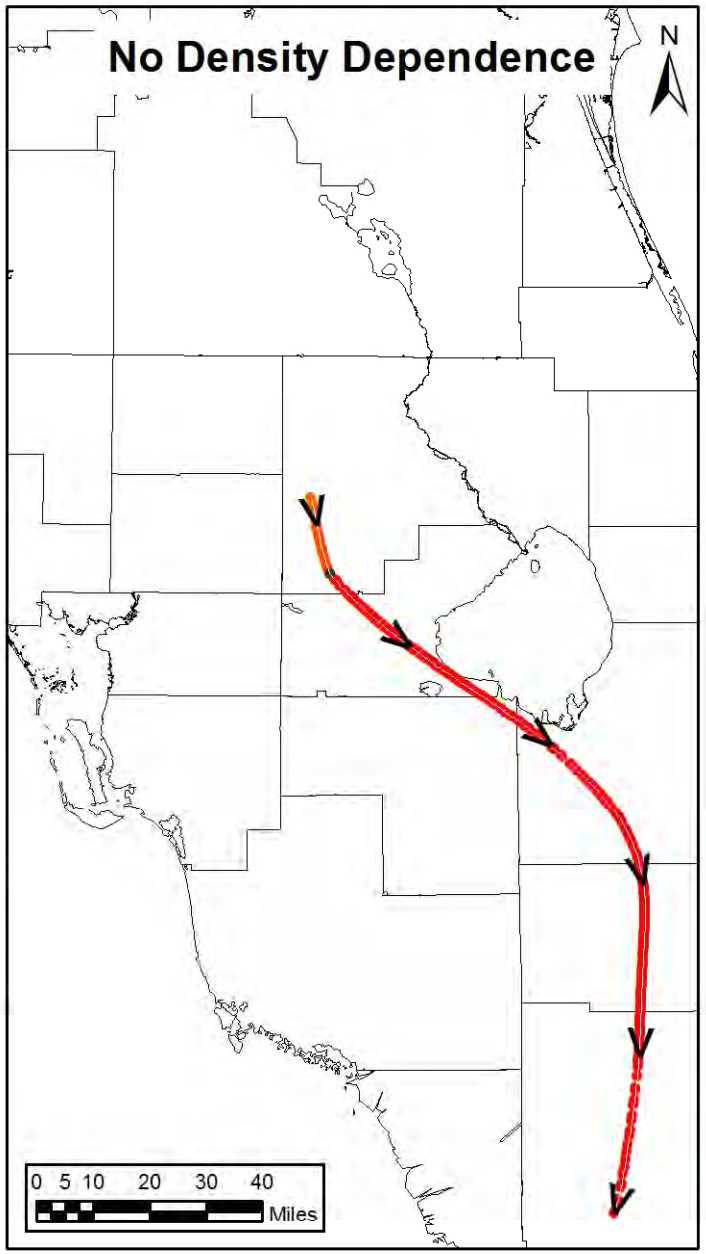

Particle Layer

- IAS
- UF
- APPZ
- LF
- BZ

Notes:

Using the February 2004 steady state calibration model and MODPATH, a particle was released in the LF in Highlands County.

When the model was solved with density dependence, the particle moved to the west, rising to the upper layers of the model and changing direction upon entering the IAS.

When the model was solved without density dependence, the particle moved to the south, dropping into the BZ.

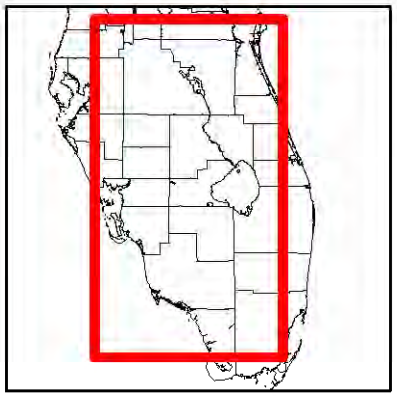

Impact of Density Dependence on Groundwater Flow Direction

Response to Comments, Production Scenario Report

Figure B.23

June 2013

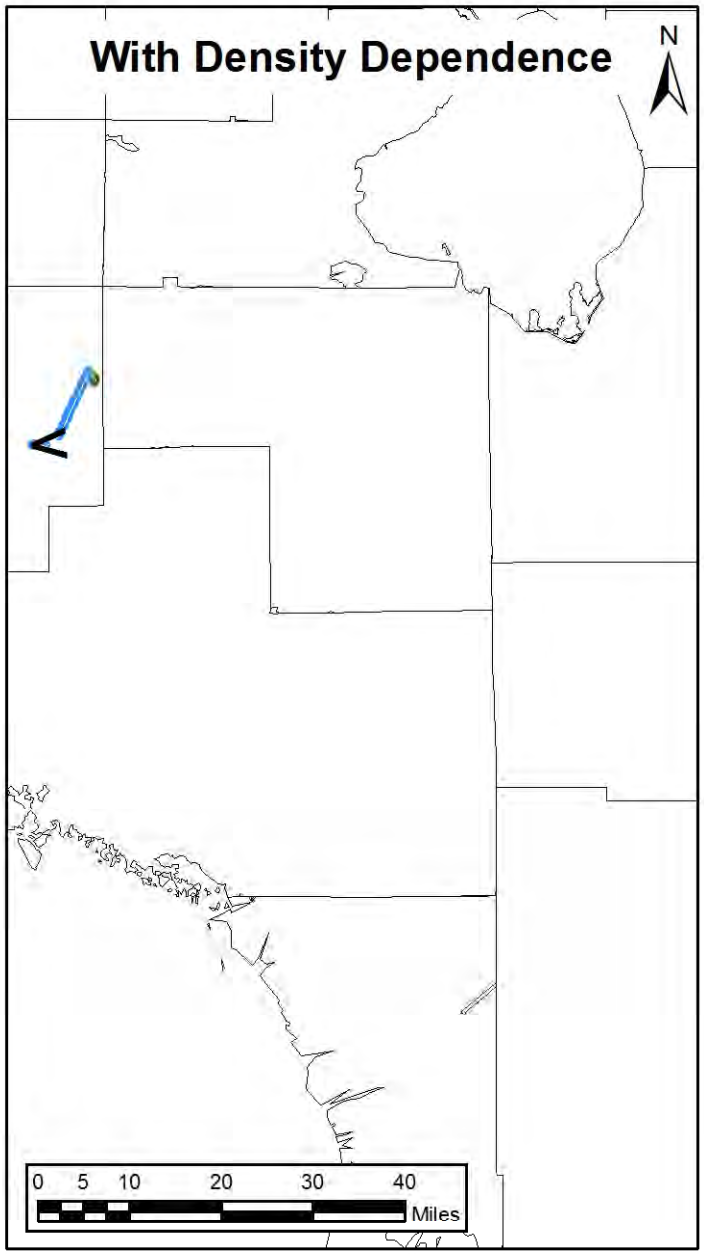

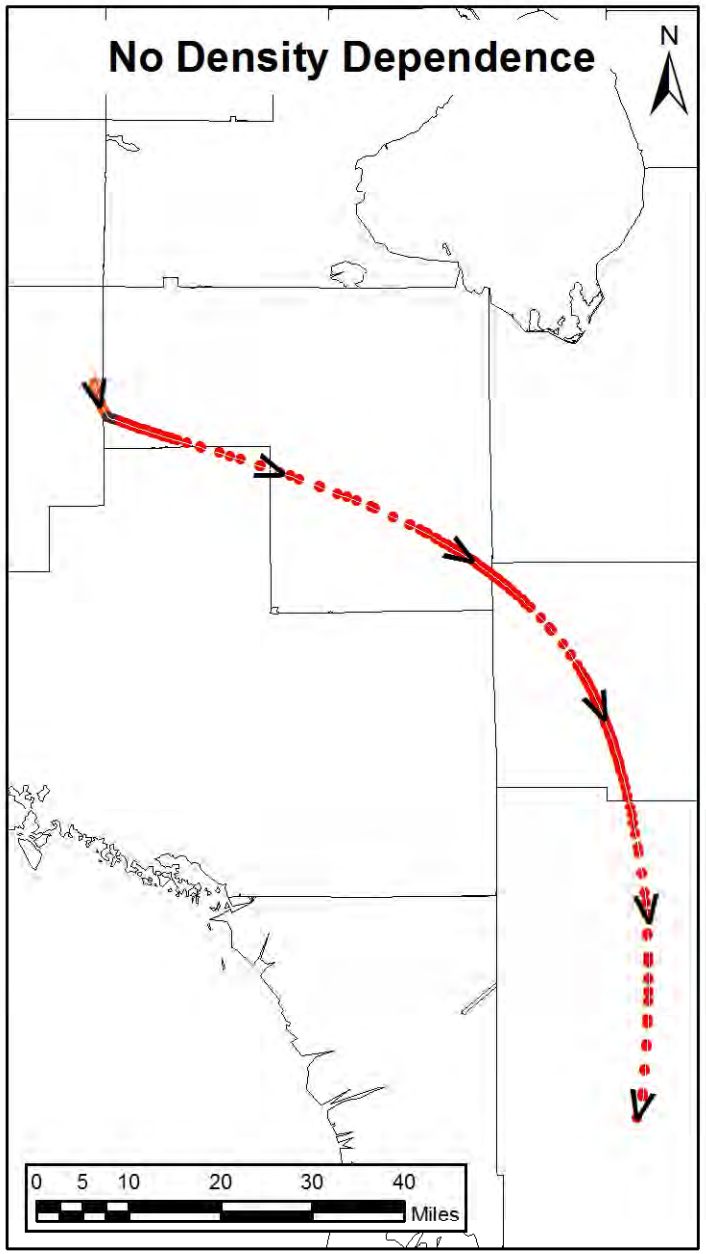

Particle Layer

- IAS
- UF
- APPZ
- LF
- BZ

Notes:

Using the February 2004 steady state calibration model and MODPATH, a particle was released near the eastern boundary of Lee County.

When the model was solved with density dependence, the particle rose quickly to the IAS and then moved to the southwest.

When the model was solved without density dependence, the particle dropped to the BZ and moved west and south.

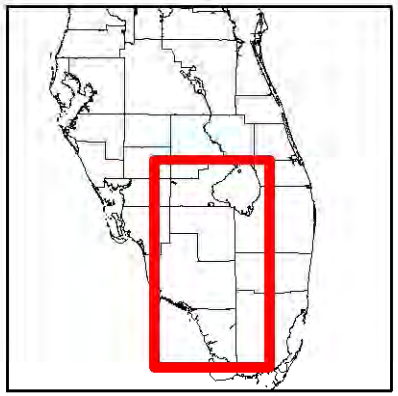

Impact of Density Dependence on Groundwater Flow Direction

Response to Comments, Production Scenario Report

Figure B.24

June 2013

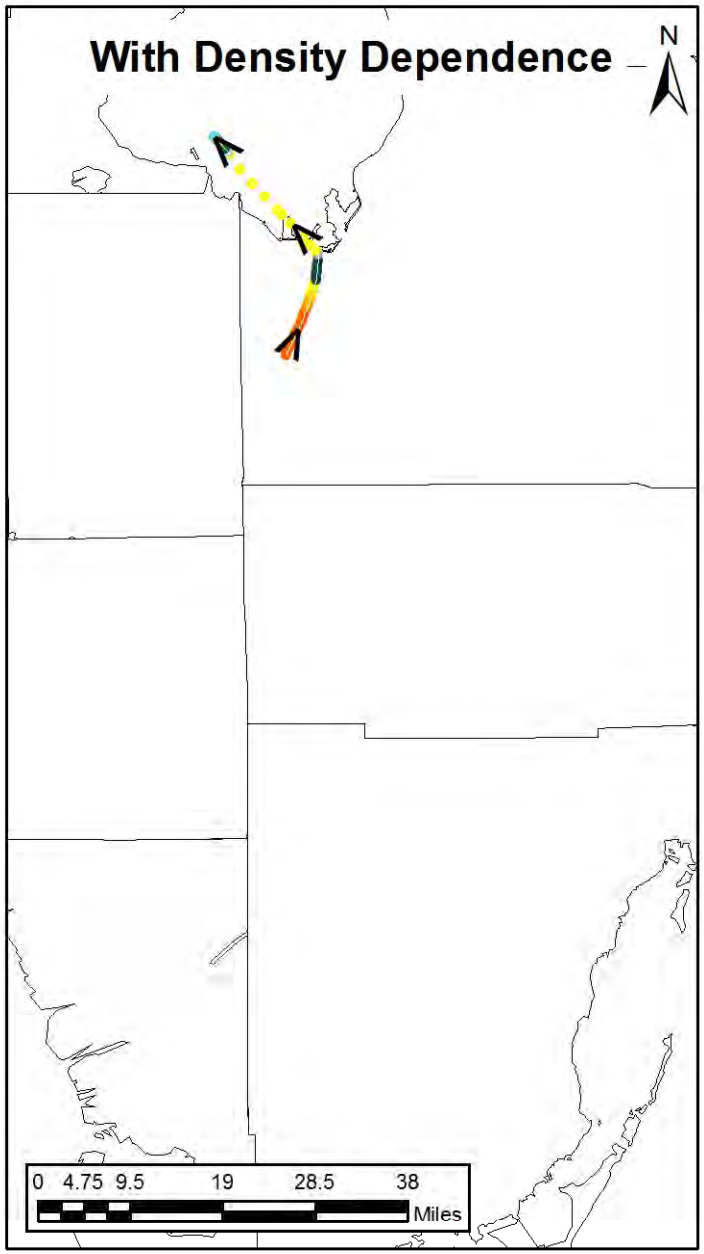

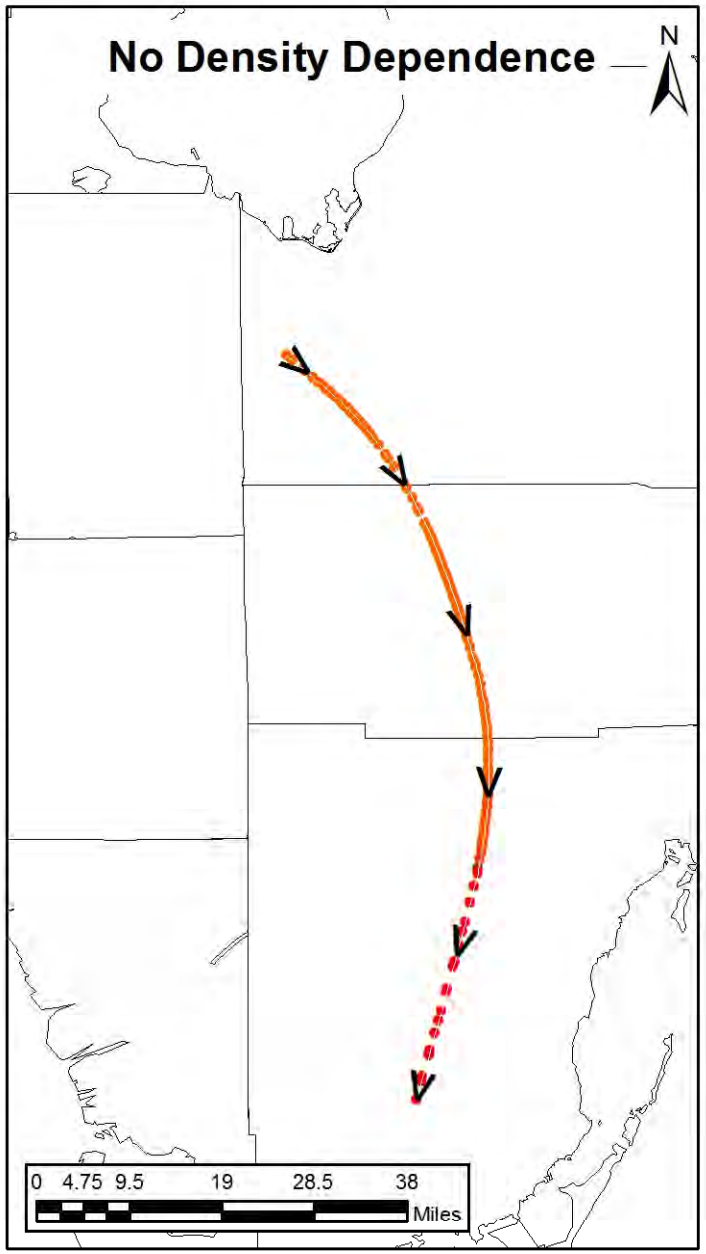

Particle Layer

- IAS
- UF
- APPZ
- LF
- BZ

Notes:

Using the February 2004 steady state calibration model and MODPATH, a particle was released just south of Lake Okeechobee in Palm Beach County.

When the model was solved with density dependence, the particle rose quickly to the UF, while moving north-northeast. The particle then dropped back to the APPZ and changed direction towards the northwest, rising back up and exiting the model from the surface.

When the model was solved without density dependence, the particle moved to the south and east, eventually dropping to the BZ.

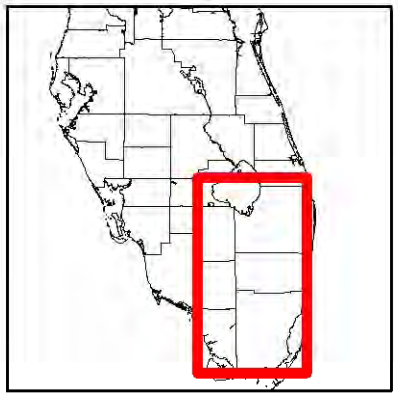

Impact of Density Dependence on Groundwater Flow Direction

Response to Comments, Production Scenario Report

Figure B.25

June 2013

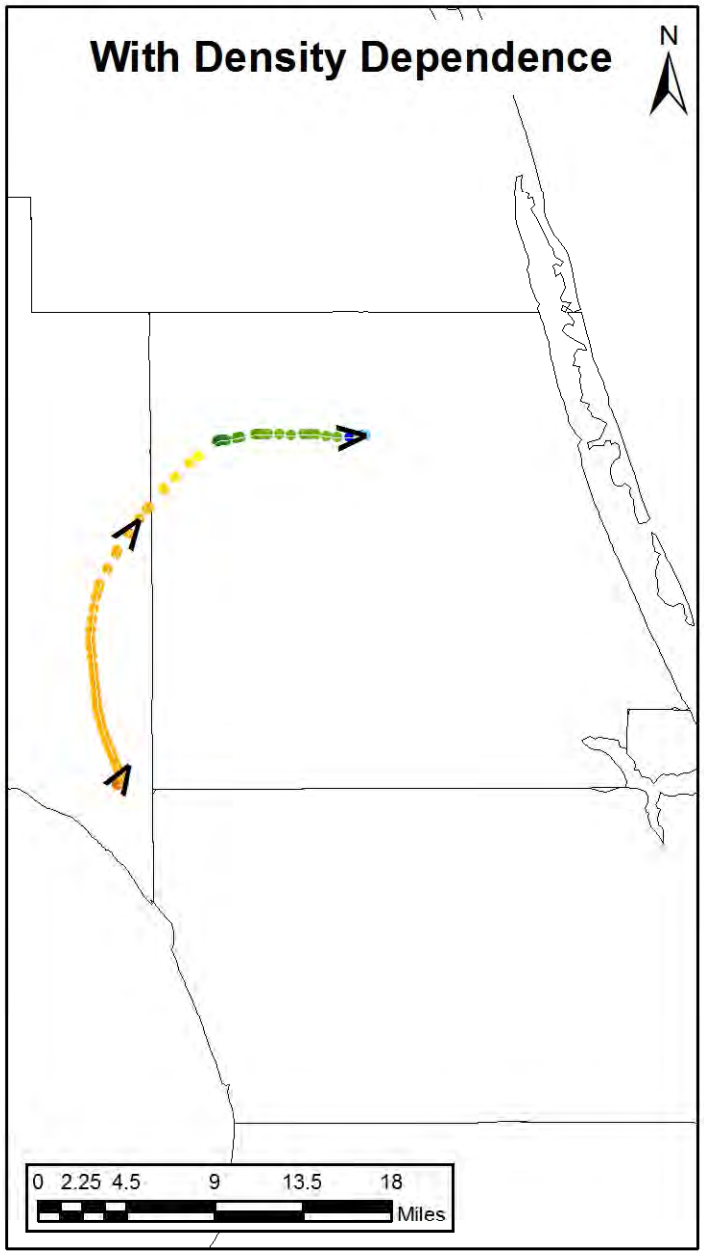

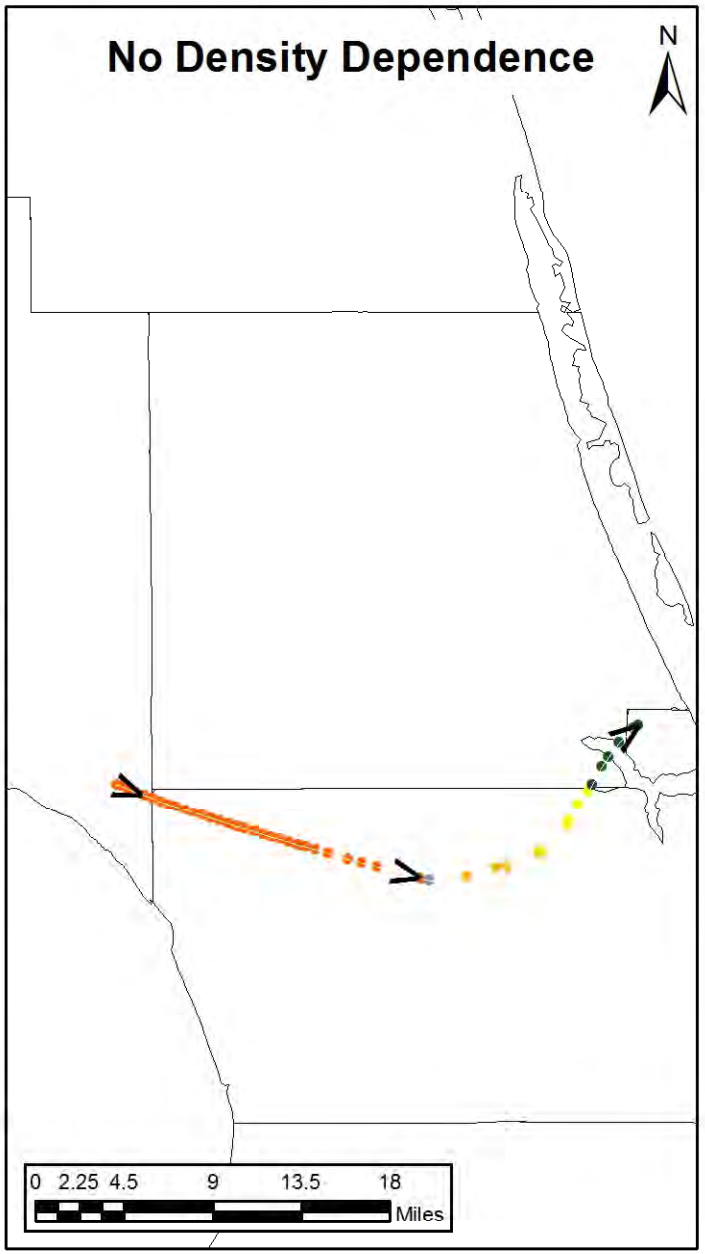

Particle Layer

- IAS
- UF
- APPZ
- LF
- BZ

Notes:

Using the February 2004 steady state calibration model and MODPATH, a particle was released in the southern corner of Okeechobee County.

When the model was solved with density dependence, the particle moved northward, eventually turning towards the east and rising to the IAS.

When the model was solved without density dependence, the particle moved in a east-southeasterly direction, turning slightly to the north as it rose to the UF.

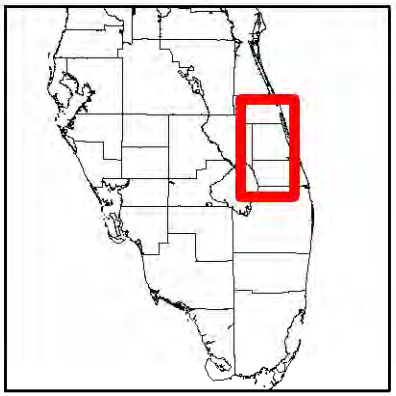

Impact of Density Dependence on Groundwater Flow Direction

Response to Comments, Production Scenario Report

Figure B.26

June 2013

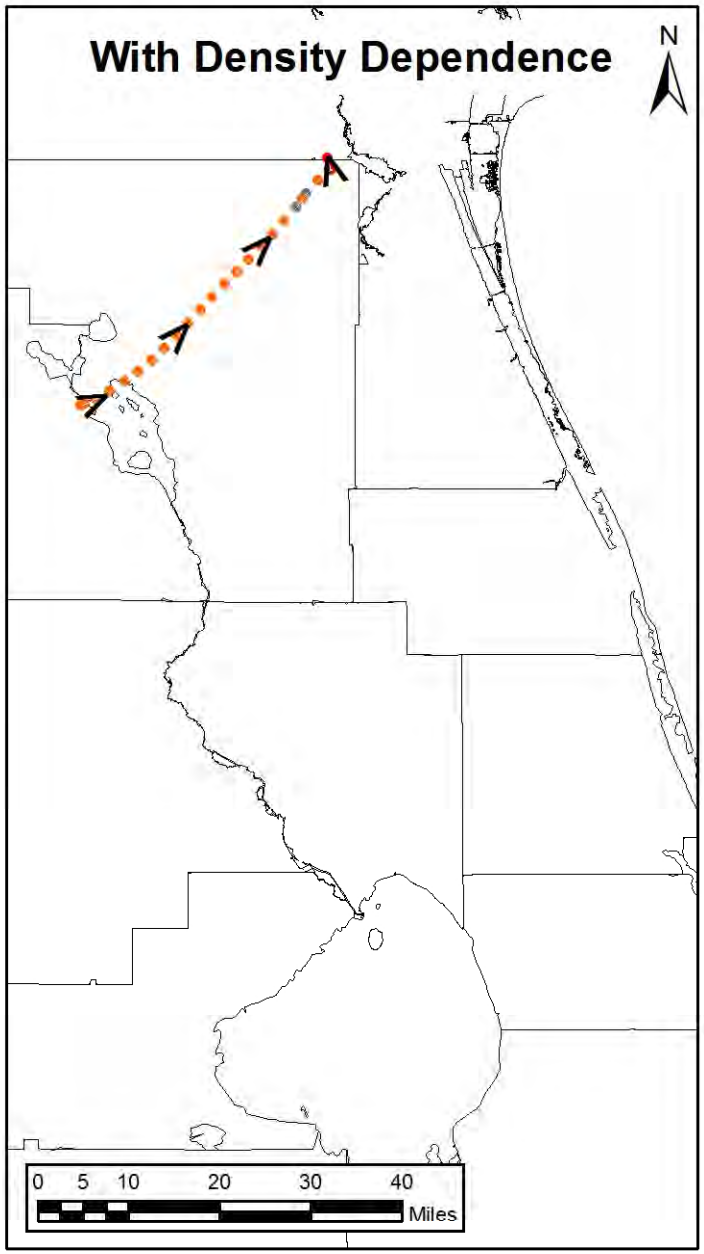

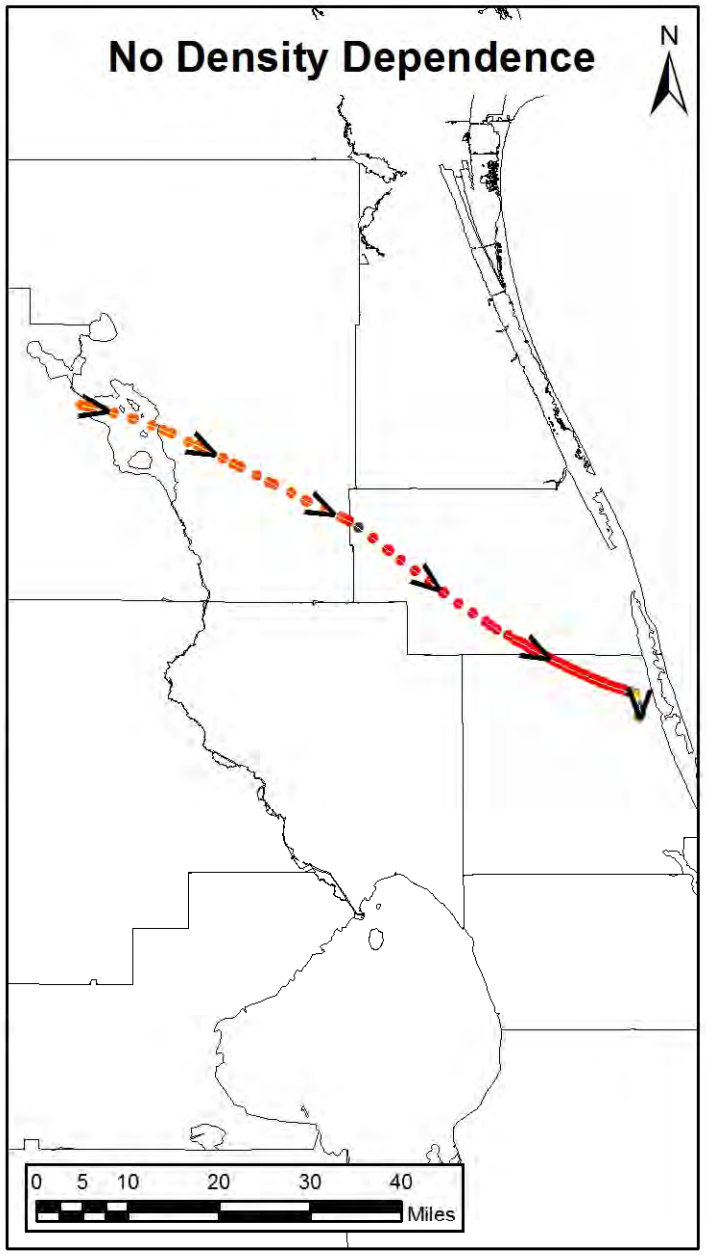

Particle Layer

- IAS
- UF
- APPZ
- LF
- BZ

Notes:

Using the February 2004 steady state calibration model and MODPATH, a particle was released near the eastern boundary of Polk County.

When the model was solved with density dependence, the particle moved to the northeast, eventually dropping to the BZ before exiting the model boundary.

When the model was solved without density dependence, the particle moved towards the southeast, dropping to the BZ and then quickly rising to the UF at the end of the track.

Impact of Density Dependence on Groundwater Flow Direction

Response to Comments, Production Scenario Report

Figure B.27

June 2013

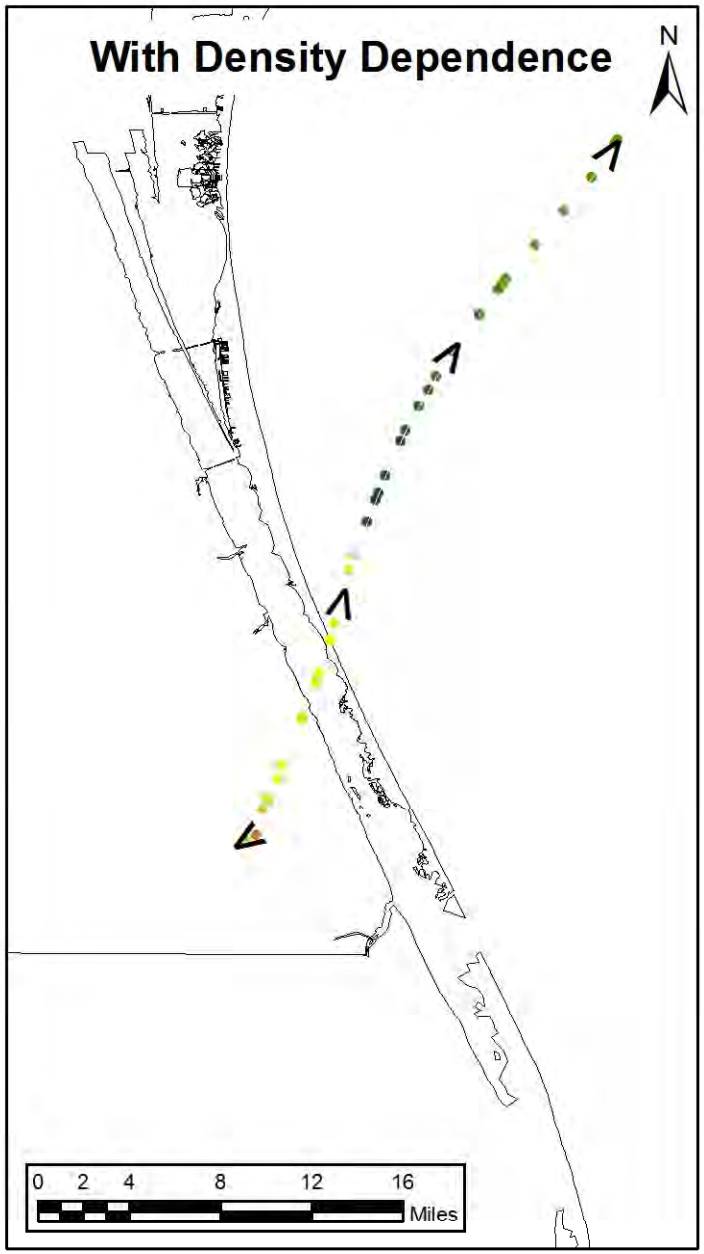

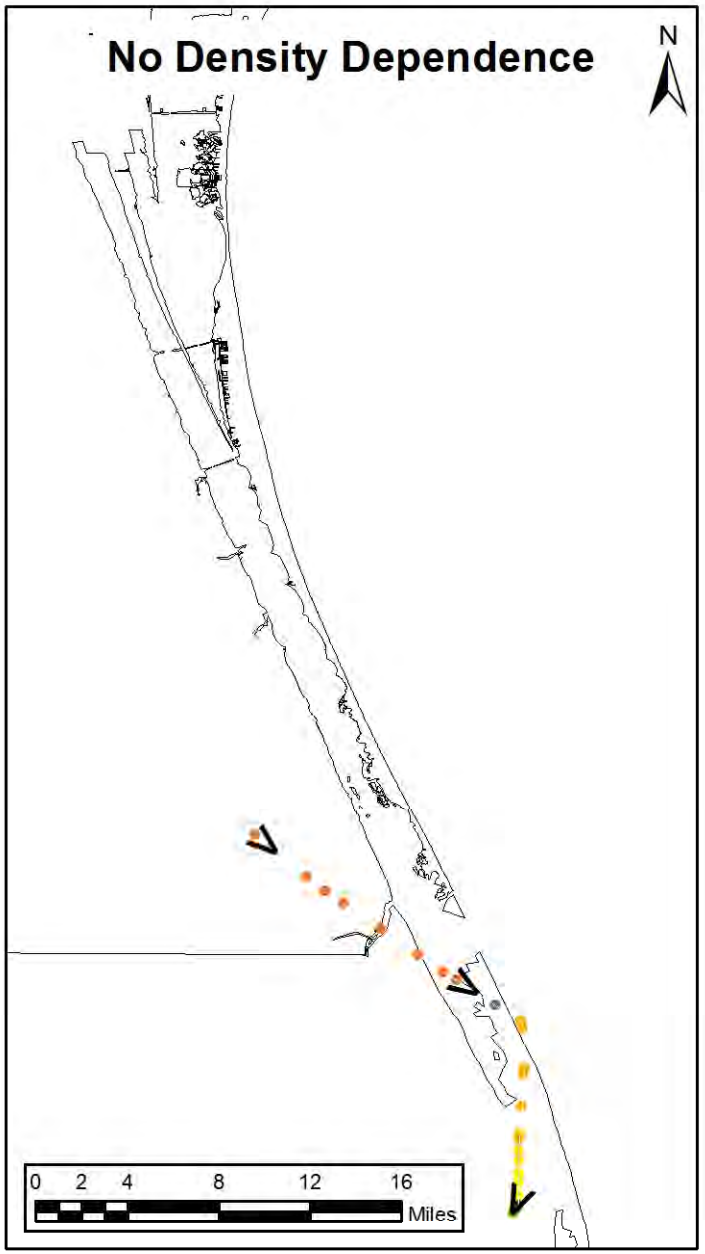

Particle Layer

- IAS
- UF
- APPZ
- LF
- BZ

Notes:

Using the February 2004 steady state calibration model and MODPATH, a particle was released near the eastern boundary of Polk County.

When the model was solved with density dependence, the initially moved to the west and then rose to the APPZ and changed directions to the northeast, eventually exiting to the ocean at the UF outcrop.

When the model was solved without density dependence, the particle moved to the southeast, rising to the UF.

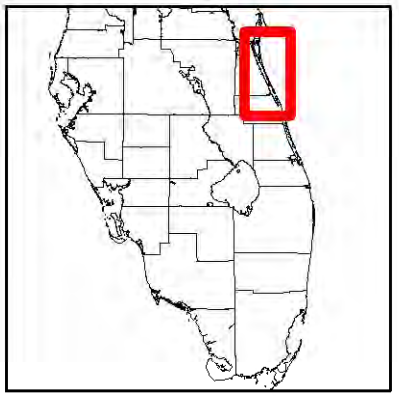

Impact of Density Dependence on Groundwater Flow Direction

Response to Comments, Production Scenario Report

Figure B.28

June 2013

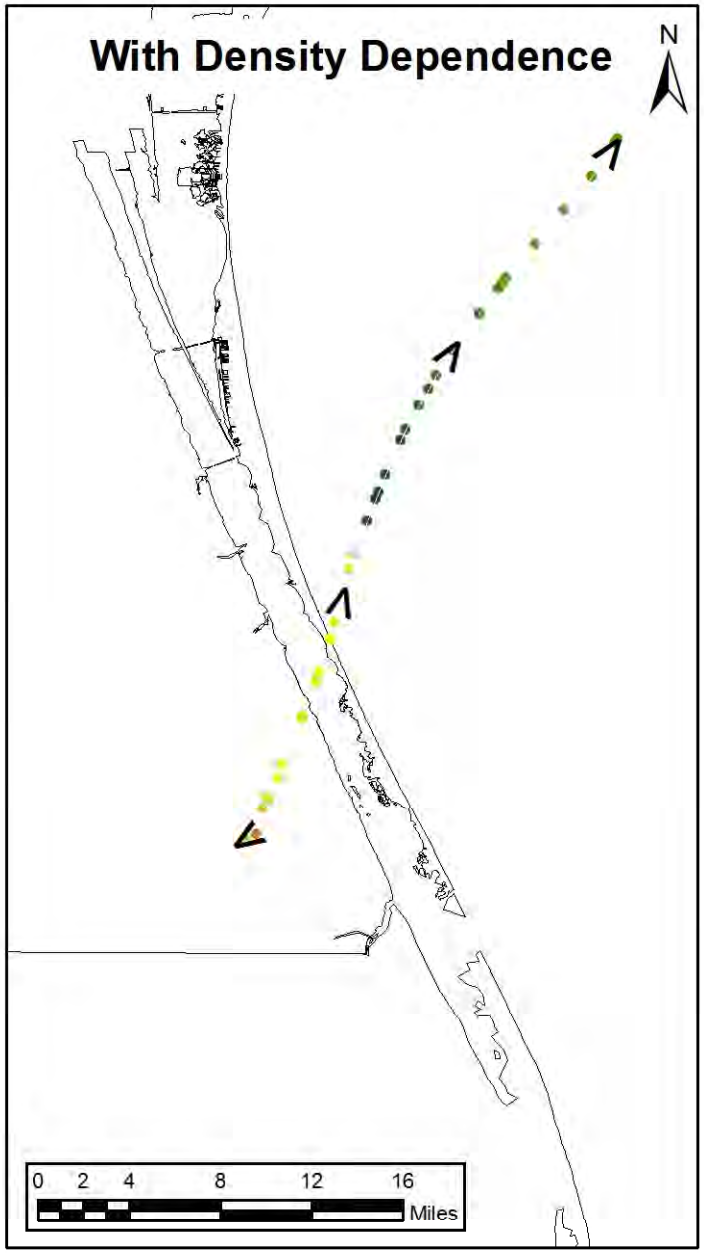

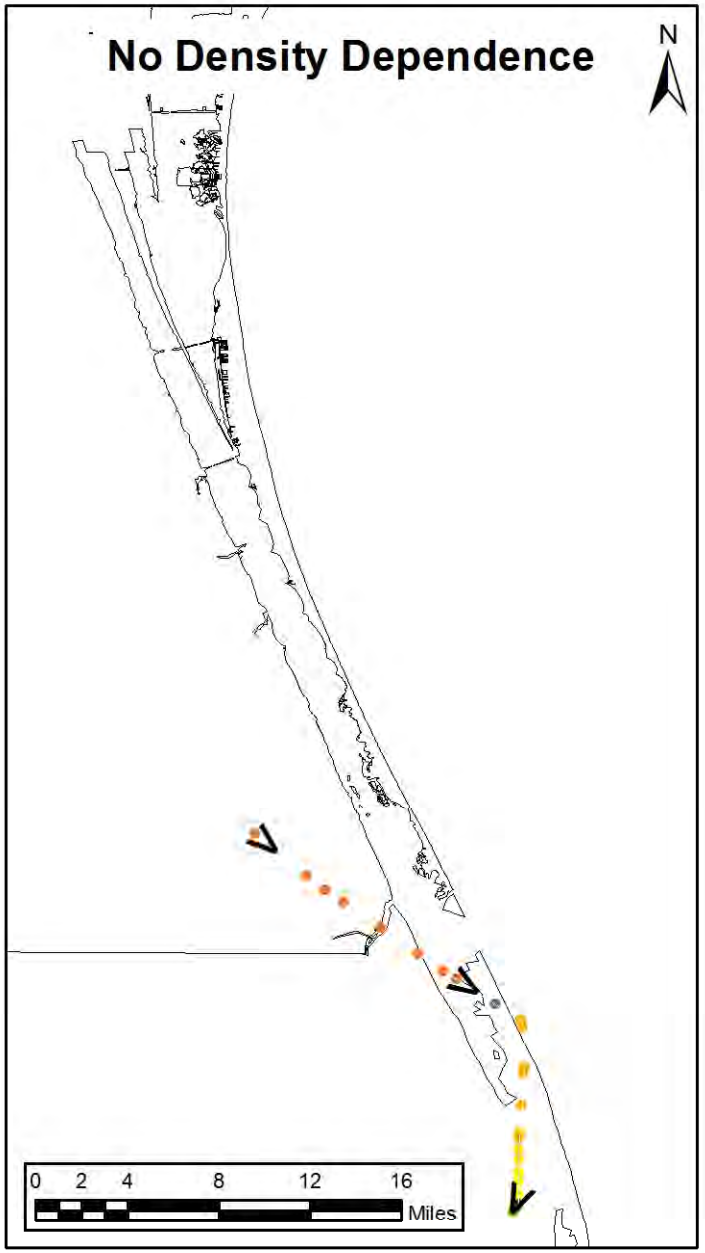

Particle Layer

- IAS
- UF
- APPZ
- LF
- BZ

Notes:

Using the February 2004 steady state calibration model and MODPATH, a particle was released near the eastern boundary of Polk County.

When the model was solved with density dependence, the initially moved to the west and then rose to the APPZ and changed directions to the northeast, eventually exiting to the ocean at the UF outcrop.

When the model was solved without density dependence, the particle moved to the southeast, rising to the UF.

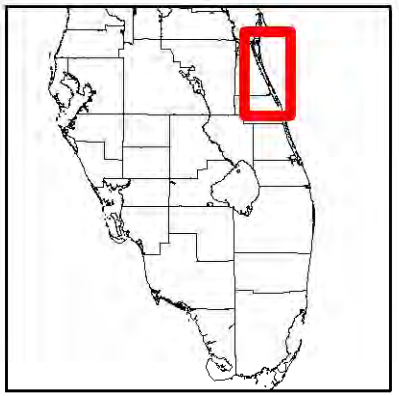

Impact of Density Dependence on Groundwater Flow Direction

Response to Comments, Production Scenario Report

Figure B.29

June 2013

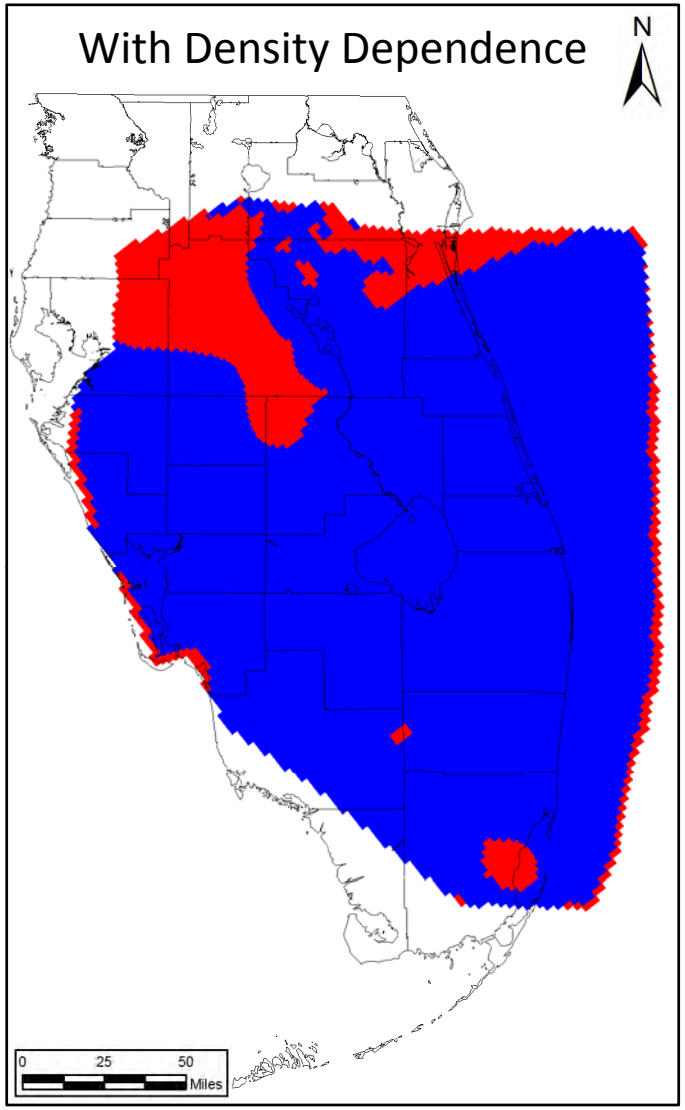

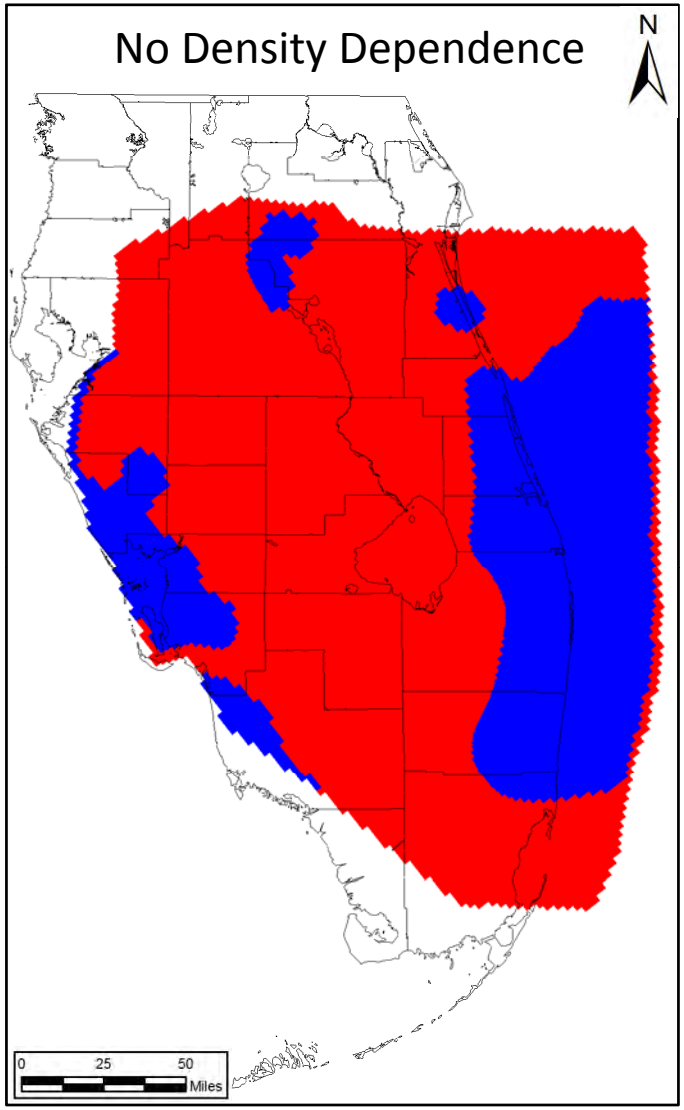

Legend

Downward Flow

Upward Flow

Notes:

This figure shows the locations of upward vs. downward flow in the LC when density dependence is included or removed in the February 2004 steady state calibration model.

When density dependence is included, the majority of the model domain has upward flow between the BZ and LF layers.

When the model is run without density dependence, the majority of the model domain has downward flow from the LF to the BZ.

Impact of Density Dependence on Groundwater Flow Direction - LC

Response to Comments, Production Scenario Report

Figure B.30

June 2013

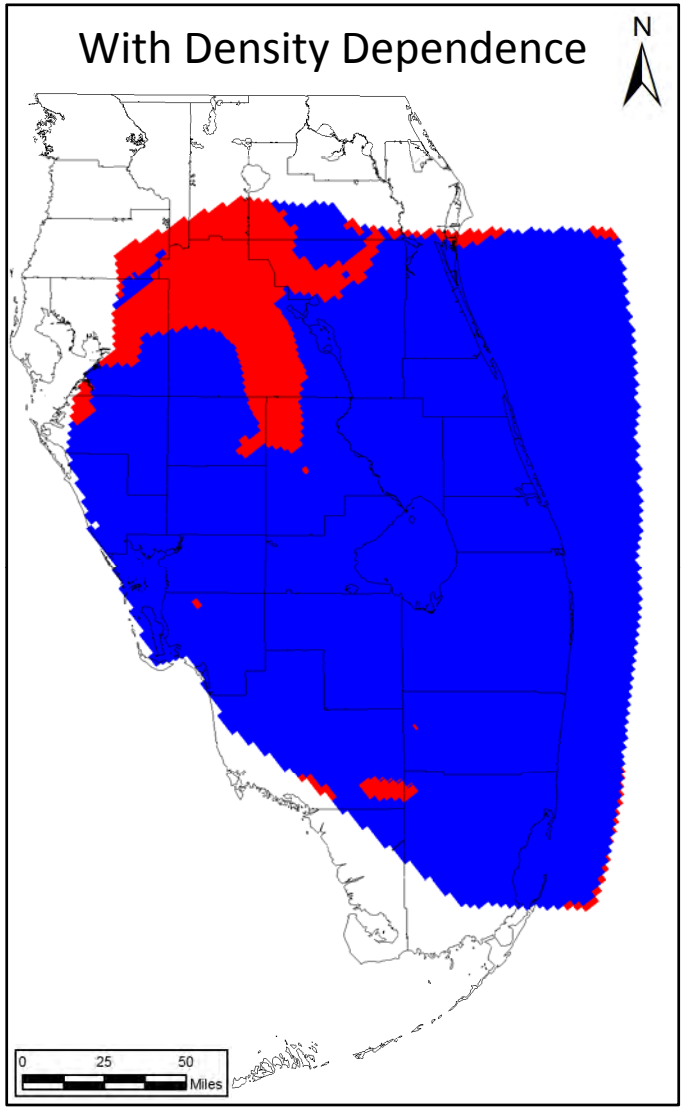

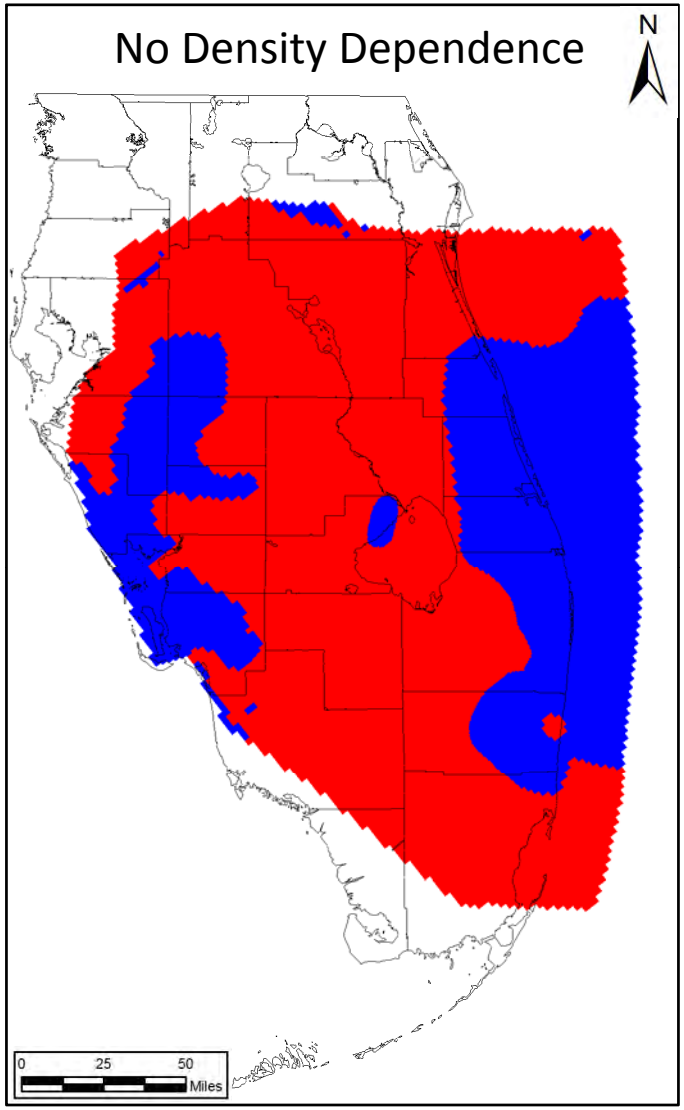

Legend

Downward Flow

Upward Flow

Notes:

This figure shows the locations of upward vs. downward flow in the MC2 when density dependence is included or removed in the February 2004 steady state calibration model.

When density dependence is included, the majority of the model domain has upward flow between the LF and APPZ layers.

When the model is run without density dependence, the majority of the model domain has downward flow from the APPZ to the LF.

Impact of Density Dependence on Groundwater Flow Direction – MC2

Response to Comments, Production Scenario Report

Figure B.31

June 2013

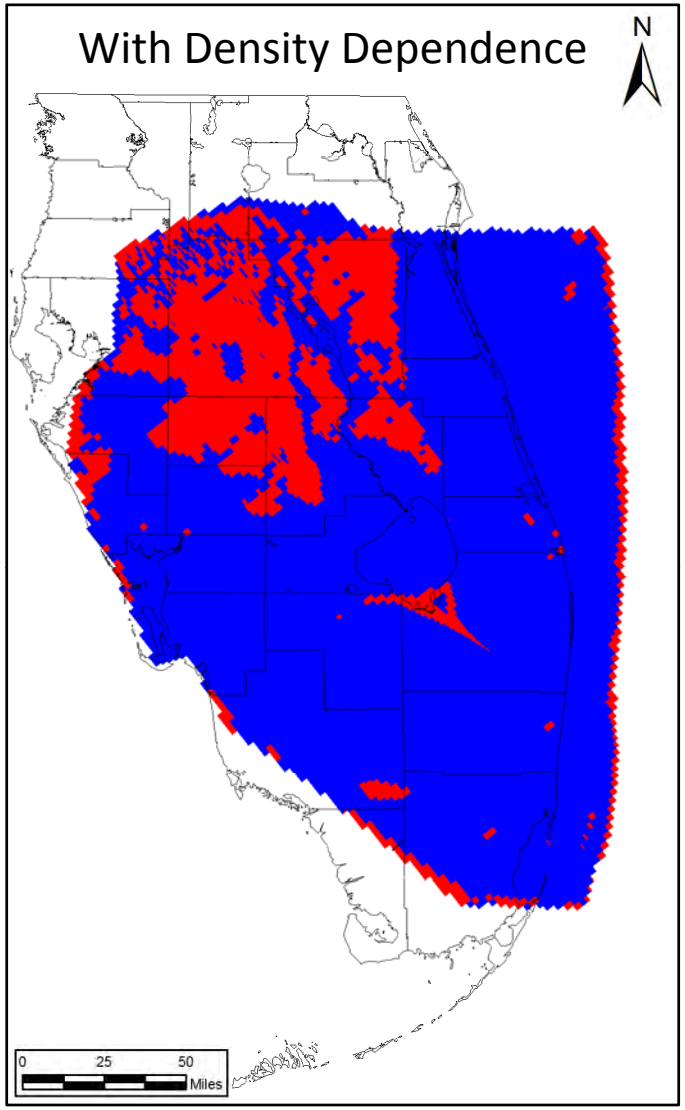

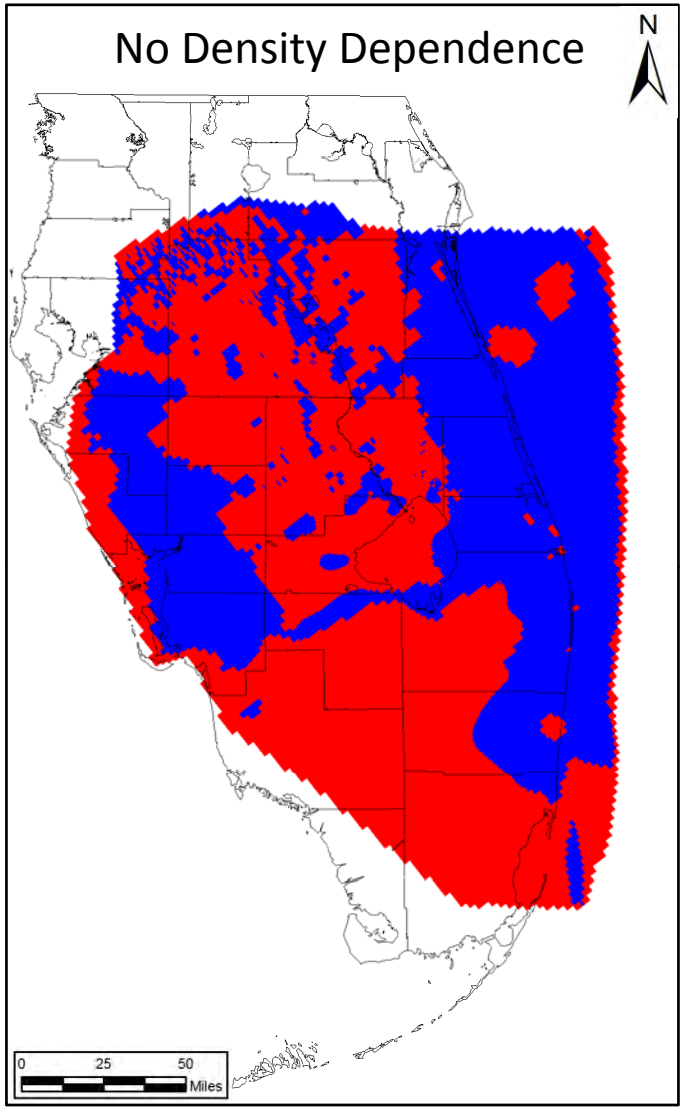

Legend

Downward Flow

Upward Flow

Notes:

This figure shows the locations of upward vs. downward flow in the MC1 when density dependence is included or removed in the February 2004 steady state calibration model.

When density dependence is included, the majority of the model domain has upward flow between the APPZ and UF layers.

When the model is run without density dependence, the majority of the model domain has downward flow from the UF to the APPZ.

Impact of Density Dependence on Groundwater Flow Direction – MC1

Response to Comments, Production Scenario Report

Figure B.32

June 2013

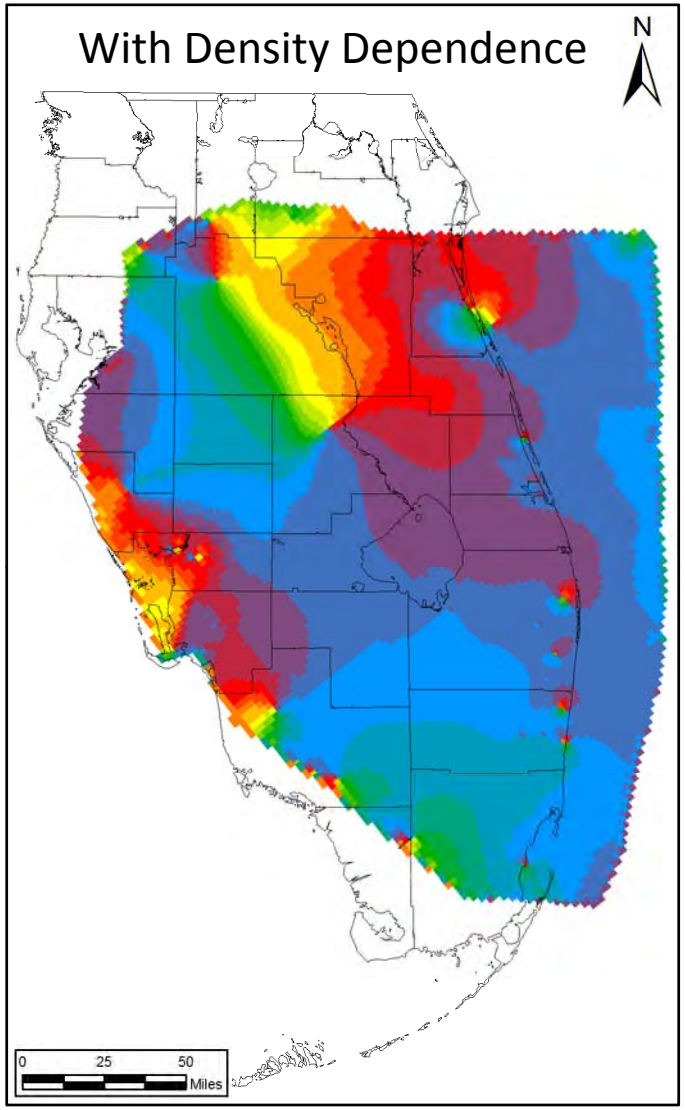

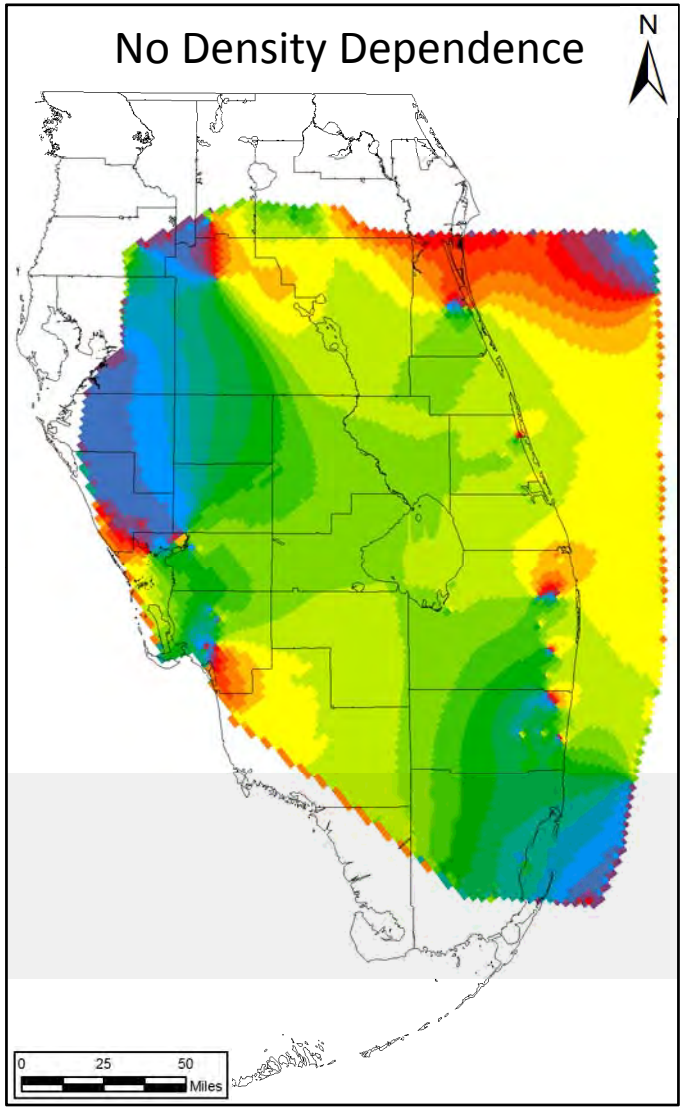

Horizontal Flow Directions

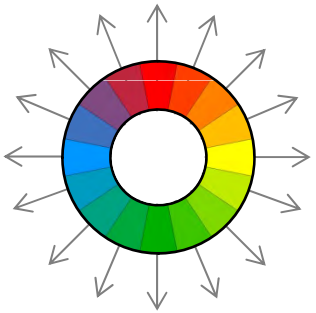

Notes:

This figure shows the horizontal flow directions for each cell of the with and without density dependence. The solution is from the February 2004 calibration model.

With density dependence, the majority of the model has flow towards the west and northwest, with some significant areas of northward flow. Without density dependence, nearly all the flow is towards the south, southeast and east.

Impact of Density Dependence on Groundwater Flow Direction – BZ

Response to Comments, Production Scenario Report

Figure B.33

June 2013

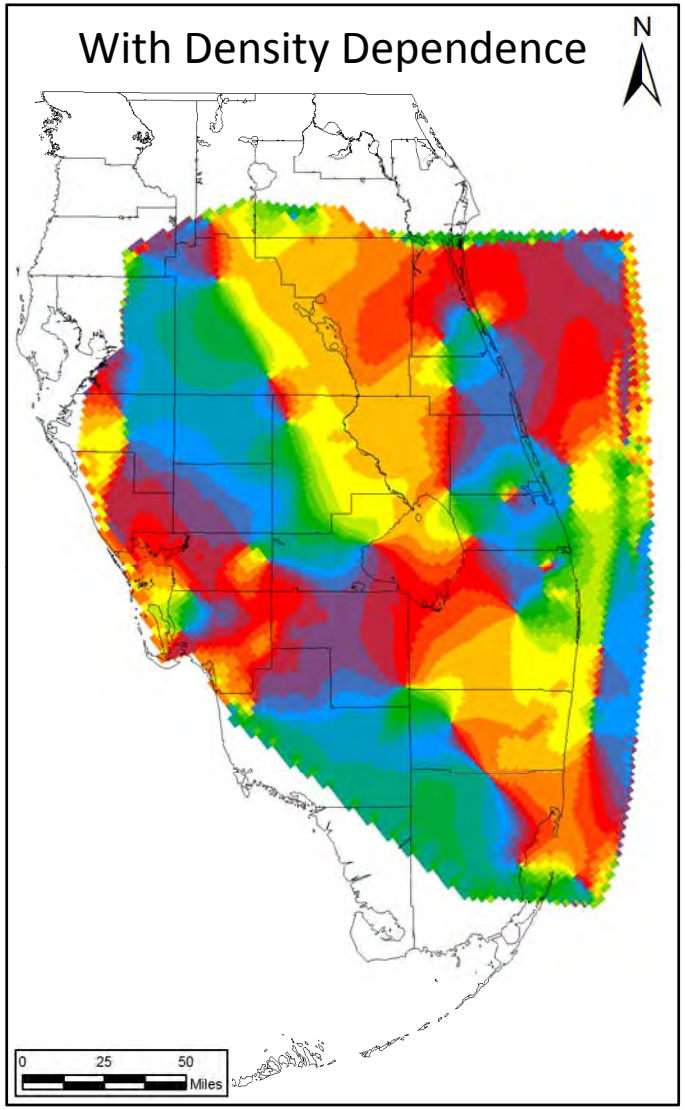

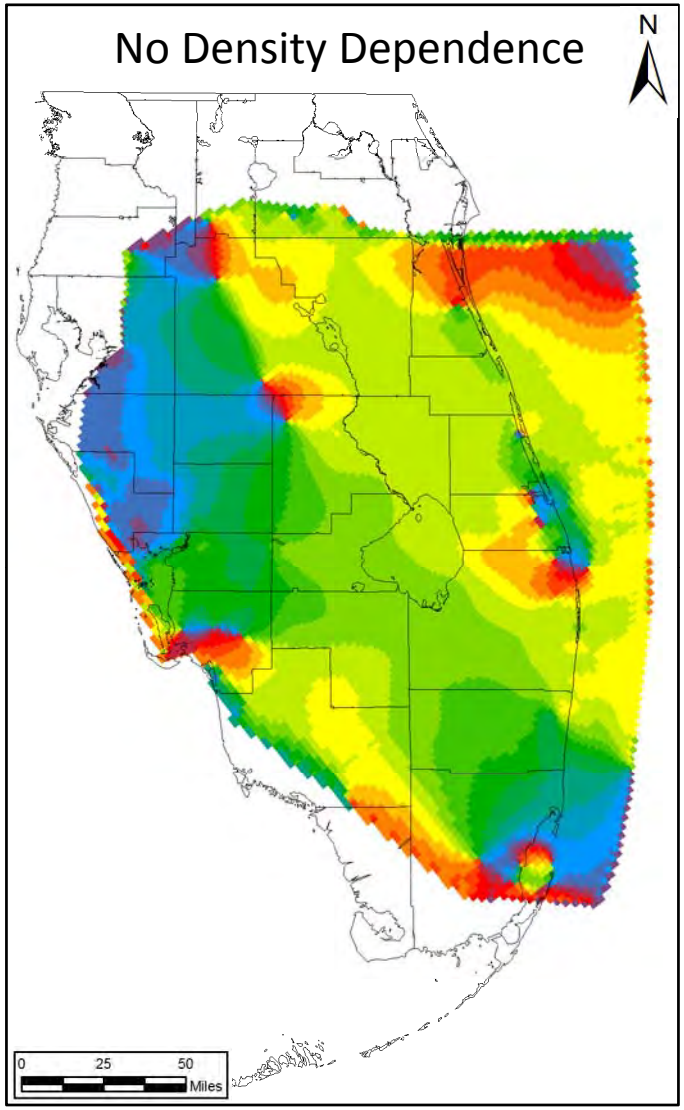

Horizontal Flow Directions

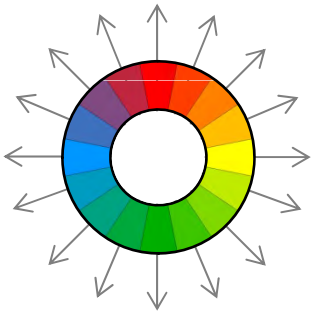

Notes:

This figure shows the horizontal flow directions for each cell of the LF (Layer 18) with and without density dependence. The solution is from the February 2004 calibration model.

Note that in western Polk County and many surrounding areas, density dependence does not impact flow directions. This is where the source of water is surface recharge and where the salinity is lowest.

The area around Lake Okeechobee shows a great difference in flow directions: with density dependence, the flow direction is mostly to the north and northwest; without density dependence it is mostly to the southeast.

Note that without density dependence a great majority of the flow is towards the south, southeast and east. Density dependence causes much more variability in flow directions.

Impact of Density Dependence on Groundwater Flow Direction – LF

Response to Comments, Production Scenario Report

Figure B.34

June 2013

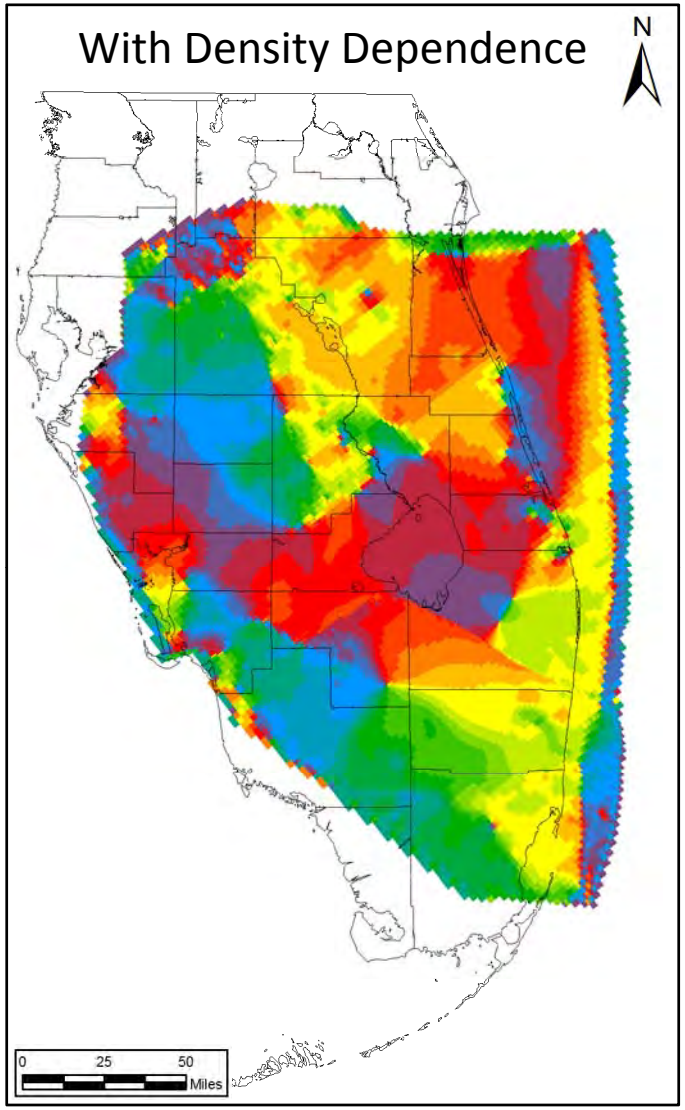

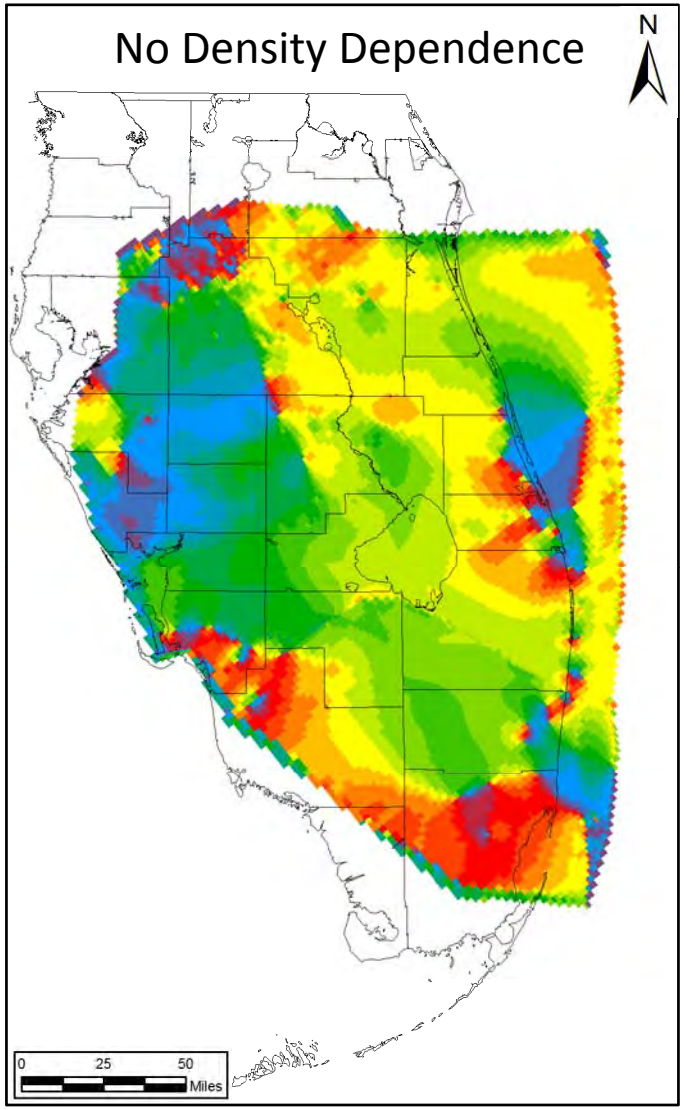

Horizontal Flow Directions

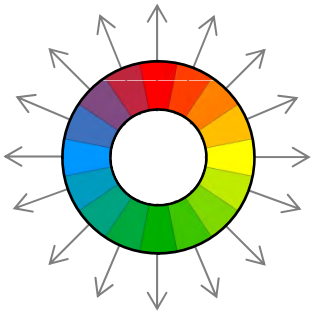

Notes:

This figure shows the horizontal flow directions for each cell of the APPZ (Layer 14) with and without density dependence. The solution is from the February 2004 calibration model.

Note that in Polk County and many surrounding areas, density dependence does not impact flow directions. This is where the source of water is surface recharge and where the salinity is lowest.

The area around Lake Okeechobee shows a great difference in flow directions: with density dependence, the flow direction is mostly to the north and northwest; without density dependence it is mostly to the southeast.

Similarly, the Everglades area, including Collier, Monroe and Miami-Dade Counties, the flow directions are mainly to the south and west with density dependence but are towards the north and northeast without density dependence.

Impact of Density Dependence on Groundwater Flow Direction – APPZ

Response to Comments, Production Scenario Report

Figure B.35

June 2013

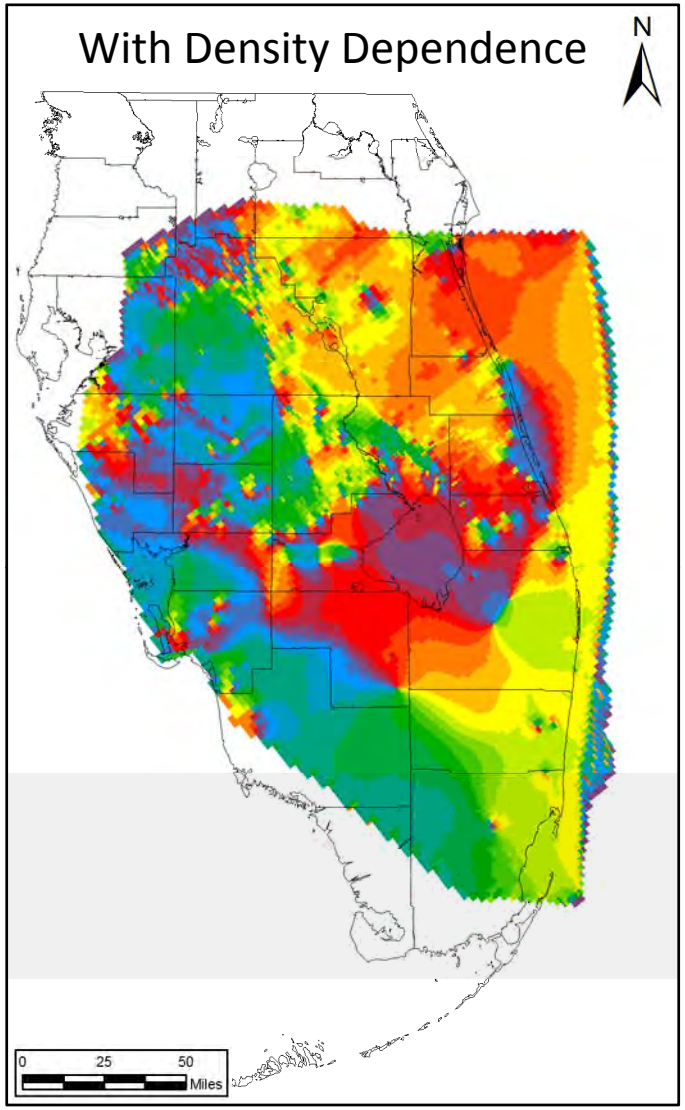

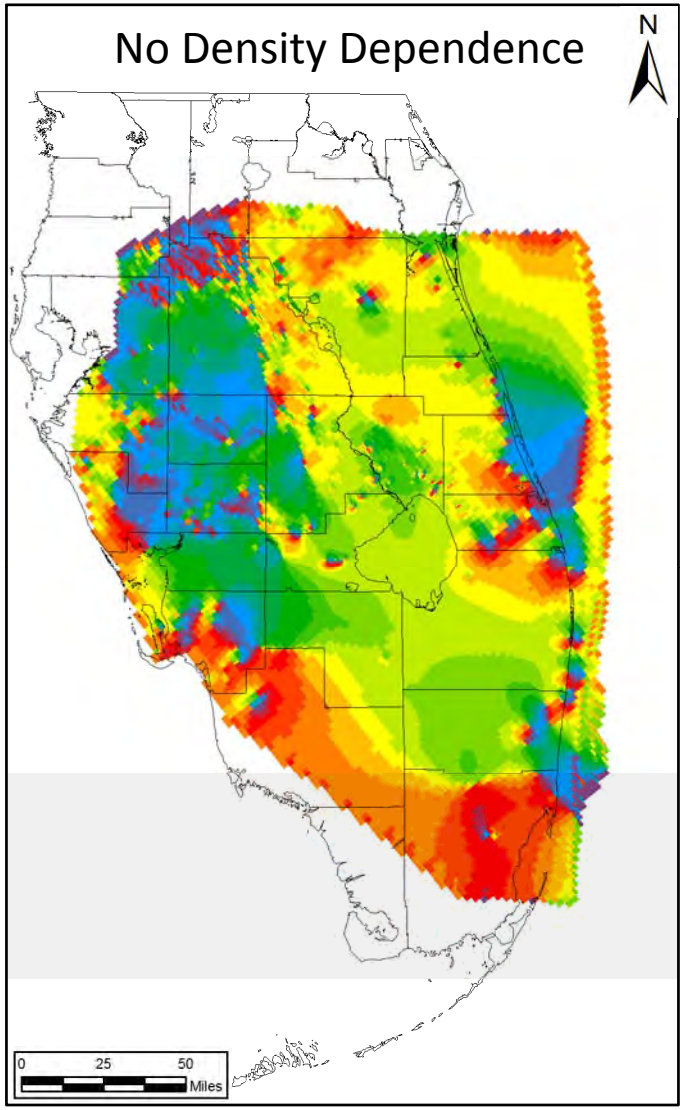

Horizontal Flow Directions

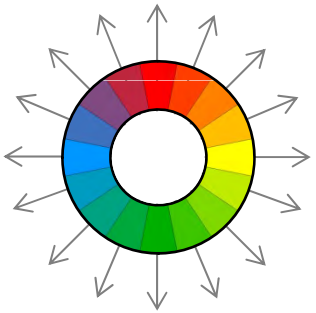

Notes:

This figure shows the horizontal flow directions for each cell of the UF (Layer 7) with and without density dependence. The solution is from the February 2004 calibration model.

Note that in Polk County and many surrounding areas, density dependence does not impact flow directions. This is where the source of water is surface recharge and where the salinity is lowest.

The area around Lake Okeechobee shows a great difference in flow directions: with density dependence, the flow direction is mostly to the north and northwest; without density dependence it is mostly to the southeast.

Similarly, the Everglades area, including Collier, Monroe and Miami-Dade Counties, the flow directions are mainly to the south and west with density dependence but are towards the north and northeast without density dependence.

Impact of Density Dependence on Groundwater Flow Direction – UF

Response to Comments, Production Scenario Report

Figure B.36

June 2013